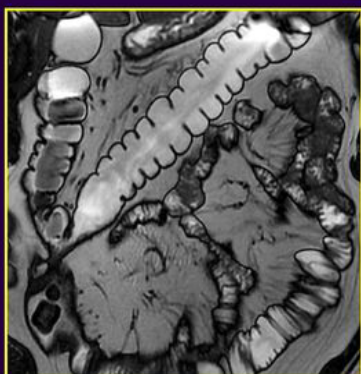


Get Full Access and More at

ExpertConsult.com

Textbook of Gastrointestinal Radiology

FOURTH EDITION



GORE & LEVINE

ELSEVIER
SAUNDERS

VOLUME 1

GORE & LEVINE

ELSEVIER
SAUNDERS

VOLUME 2

2-Volume Set

Don't Forget Your Online Access to

Expert | **CONSULT**

Built with **inking**

Elsevier | ExpertConsult.com

Enhanced eBooks for medical professionals

Compatible with PC, Mac®, most mobile devices, and eReaders, Expert Consult allows you to browse, search, and interact with this title – online *and* offline. Redeem your PIN at expertconsult.com today!

Continuously updated with the **results of late-breaking clinical trials, reviews of important new research publications, and updates on clinical practice**, masterfully selected and edited by **Dr. Eugene Braunwald**.

PIN REDEMPTION INSTRUCTIONS

Start using these innovative features today:

- Seamless, real-time integration between devices
- Straightforward navigation and search
- Notes and highlights sharing with other users through social media
- Enhanced Images with annotations, labels, and hot spots for zooming on specific details *
- Live streaming video and animations *
- Self-assessment tools such as questions embedded within the text and multiple-format quizzes *

** some features vary by title*

1. Login or Sign Up at ExpertConsult.com
2. Scratch off your PIN code below
3. Enter PIN into the "Redeem a Book Code" box
4. Click "Redeem"
5. Go to "My Library"

Use of the current edition of the electronic version of this book (eBook) is subject to the terms of the nontransferable, limited license granted on ExpertConsult.com. Access to the eBook is limited to the first individual who redeems the PIN, located on the inside cover of this book, at ExpertConsult.com and may not be transferred to another party by resale, lending, or other means.

For technical assistance: Email: online.help@elsevier.com;

Call: within the US and Canada: 800-401-9962;

outside the US and Canada: +1-314-447-8200

Textbook of Gastrointestinal Radiology

Textbook of Gastrointestinal Radiology

Fourth Edition

Richard M. Gore, MD

Chief of Gastrointestinal Radiology
NorthShore University HealthSystem
Evanston, Illinois
Professor of Radiology
Pritzker School of Medicine at the University of Chicago
Chicago, Illinois

Marc S. Levine, MD

Chief of Gastrointestinal Radiology
Hospital of the University of Pennsylvania
Professor of Radiology and Advisory Dean
Perelman School of Medicine at the University of Pennsylvania
Philadelphia, Pennsylvania

ELSEVIER
SAUNDERS

Copyright © 2015, 2008, 2000, 1994 by Saunders, an imprint of Elsevier Inc.

All rights reserved. No part of this publication may be reproduced or transmitted in any form or by any means, electronic or mechanical, including photocopying, recording, or any information storage and retrieval system, without permission in writing from the publisher. Details on how to seek permission, further information about the Publisher's permissions policies and our arrangements with organizations such as the Copyright Clearance Center and the Copyright Licensing Agency, can be found at our website: www.elsevier.com/permissions.

This book and the individual contributions contained in it are protected under copyright by the Publisher (other than as may be noted herein).

Notices

Knowledge and best practice in this field are constantly changing. As new research and experience broaden our understanding, changes in research methods, professional practices, or medical treatment may become necessary.

Practitioners and researchers must always rely on their own experience and knowledge in evaluating and using any information, methods, compounds, or experiments described herein. In using such information or methods they should be mindful of their own safety and the safety of others, including parties for whom they have a professional responsibility.

With respect to any drug or pharmaceutical products identified, readers are advised to check the most current information provided (i) on procedures featured or (ii) by the manufacturer of each product to be administered, to verify the recommended dose or formula, the method and duration of administration, and contraindications. It is the responsibility of practitioners, relying on their own experience and knowledge of their patients, to make diagnoses, to determine dosages and the best treatment for each individual patient, and to take all appropriate safety precautions.

To the fullest extent of the law, neither the Publisher nor the authors, contributors, or editors, assume any liability for any injury and/or damage to persons or property as a matter of products liability, negligence or otherwise, or from any use or operation of any methods, products, instructions, or ideas contained in the material herein.

Library of Congress Cataloging-in-Publication Data

Textbook of gastrointestinal radiology / [edited by] Richard M. Gore, Marc S. Levine. — Fourth edition.
p. ; cm.

Gastrointestinal radiology

Includes bibliographical references and index.

ISBN 978-1-4557-5117-4 (hardcover, 2 v. set : alk. paper)

I. Gore, Richard M., editor. II. Levine, Marc S., editor. III. Title: Gastrointestinal radiology.

[DNLM: 1. Gastrointestinal Diseases—diagnosis. 2. Gastrointestinal Diseases—radiography.

3. Digestive System—pathology. WI 141]

RC804.R6

616.3'407572—dc23

2014034661

Content Strategist: Helene Caprari

Content Development Specialist: Joanie Milnes

Publishing Services Manager: Patricia Tannian

Senior Project Manager: Claire Kramer

Design Direction: XiaoPei Chen

Printed in the United States

Last digit is the print number: 9 8 7 6 5 4 3 2 1



Working together
to grow libraries in
developing countries

www.elsevier.com • www.bookaid.org

*To Margaret and our children,
Diana, Elizabeth, and George*
RICHARD M. GORE

*To Deborah, my beautiful and amazing wife
and better half for 37 years and counting ...*
MARC S. LEVINE

CONTRIBUTORS

Jalil Afnan, MD, MRCS

Radiologist
Department of Radiology
Lahey Clinic Hospital and Medical Center
Burlington, Massachusetts
Assistant Professor of Radiology
Tufts University
School of Medicine
Boston, Massachusetts

Jeffrey A. Alexander, MD

Associate Professor of Medicine
Mayo Clinic School of Medicine
Rochester, Minnesota

Lauren F. Alexander, MD

Assistant Professor of Abdominal Imaging
Department of Radiology and Imaging Sciences
Emory University
Atlanta, Georgia

Surabhi Bajpai, MBBS, DMRD

Research Fellow
Department of Radiology
Division of Abdominal Imaging and Intervention
Massachusetts General Hospital
Boston, Massachusetts

Mark E. Baker, MD

Professor of Radiology
Cleveland Clinic Lerner College of Medicine
Case Western Reserve University
Imaging Institute
Cleveland Clinic
Staff Radiologist
Imaging Institute, Digestive Disease Institute, Cancer Institute
Cleveland Clinic
Cleveland, Ohio

Stephen R. Baker, MD, MPHIL

Professor and Chairman
Department of Radiology
Rutgers New Jersey Medical School
Chief
Department of Radiology
The University Hospital
Newark, New Jersey

Aparna Balachandran, MD

Associate Professor
Diagnostic Imaging
The University of Texas MD Anderson Cancer Center
Houston, Texas

Dennis M. Balfe, MD

Professor of Radiology
Washington University School of Medicine
St. Louis, Missouri

Emil J. Balthazar, MD

Professor Emeritus
Department of Radiology
New York University School of Medicine
Attending Consultant
Department of Radiology
Bellevue Hospital
New York, New York

Stuart A. Barnard, MA, MB, BS, MRCS, FRCR

Radiologist
Department of Radiology
Middlemore Hospital
Counties Manukau Health
Auckland, New Zealand

Ahmed Ba-Ssalamah, MD

Medical University of Vienna
Department of Biomedical Imaging and Image-Guided
Therapy
Vienna, Austria

Genevieve L. Bennett, MD

Assistant Professor of Radiology
Department of Radiology
Division of Abdominal Imaging
New York University School of Medicine
Assistant Professor of Radiology
Department of Radiology
Division of Abdominal Imaging
New York University Langone Medical Center
New York, New York

Senta Berggruen, MD

Department of Radiology
Northwestern Memorial Hospital
Chicago, Illinois

Jonathan W. Berlin, MD

Clinical Professor of Radiology
Department of Diagnostic Radiology
NorthShore University HealthSystem
Evanston, Illinois

George S. Bissett III, MD

Professor of Radiology and Pediatrics
Vice-Chairman
Department of Radiology
Duke University School of Medicine
Durham, North Carolina

Roi M. Bittane, MD

Radiology Resident
Department of Radiology
Winthrop University Hospital
Mineola, New York

Michael A. Blake, MB, MRCPI, FRCR, FFR(RCSI)

Associate Professor of Radiology
Harvard Medical School
Fellowship Director
Division of Abdominal Imaging
Massachusetts General Hospital
Boston, Massachusetts

Peyman Borghei, MD

Clinical Assistant Professor of Radiology
University of California at Irvine
Chief of Interventional Radiology
VA Hospital
Long Beach, California

Kevin P. Boyd, DO

Assistant Professor of Radiology
Children's Hospital of Wisconsin
Medical College of Wisconsin
Milwaukee, Wisconsin

Warren M. Brandwein, MD

Fellow
Body and Musculoskeletal Imaging Section
Department of Radiology
Northwestern University
Chicago, Illinois

David H. Bruining, MD

Associate Professor of Medicine
Mayo Clinic
Rochester, Minnesota

James L. Buck, MD

Professor
Department of Diagnostic Radiology
University of Kentucky College of Medicine
Lexington, Kentucky

Carina L. Butler, MD

Assistant Professor
Department of Diagnostic Radiology
University of Kentucky College of Medicine
University of Kentucky Chandler Medical Center
Lexington, Kentucky

Selim R. Butros, MD

Fellow in Abdominal Imaging and Interventional
Radiology
Department of Radiology
Massachusetts General Hospital
Boston, Massachusetts

Laura R. Carucci, MD

Professor of Radiology
Director of Computed Tomography and Magnetic Resonance
Imaging
Abdominal Imaging Section
Department of Radiology
Virginia Commonwealth University Medical Center
Richmond, Virginia

Wei-Chou Chang, MD

Department of Radiology
University of California
San Francisco, California

Raj R. Chinnappan, MD

Clinical Assistant
Abdominal and Interventional Radiology
Harvard Medical School
Massachusetts General Hospital
Boston, Massachusetts

Byung Ihn Choi, MD

Professor of Radiology
Department of Radiology
Seoul National University College of Medicine
Seoul National University Hospital
Seoul, Republic of Korea

**Peter L. Cooperberg, OBC, MDCM, FRCP(C),
FACR, FFR(RCSI)hon**

Professor Emeritus of Radiology
University of British Columbia
Vancouver, British Columbia, Canada

Abraham H. Dachman, MD

Professor of Radiology
Director, Fellowship Programs
Department of Radiology
The University of Chicago Medical Center
Chicago, Illinois

Alexander Ding, MD, MS

Department of Radiology
Division of Abdominal Imaging and Intervention
Harvard Medical School
Massachusetts General Hospital
Boston, Massachusetts

Carolyn K. Donaldson, MD, RPVI

Assistant Professor of Radiology
University of Chicago
NorthShore University HealthSystem
Evanston, Illinois

Ronald L. Eisenberg, MD, JD

Professor
Department of Radiology
Harvard Medical School
Radiologist
Beth Israel Deaconess Medical Center
Boston, Massachusetts

Sukru Mehmet Erturk, MD, PhD

Associate Professor of Radiology
Attending Radiologist
Administrative Director
Sisli Etfal Training and Research Hospital
Department of Radiology
Istanbul, Turkey

Thomas A. Farrell, MB, FRCR, MBA

Section Head, Interventional Radiology
NorthShore University Health System
Clinical Assistant Professor
University of Chicago Pritzker School of Medicine
Chicago, Illinois

Kate A. Feinstein, MD, FACR

Professor of Radiology and Surgery
Department of Radiology
University of Chicago Pritzker School of Medicine
Chicago, Illinois

Sandra K. Fernbach, MD

Professor of Radiology (Retired)
University of Chicago Pritzker School of Medicine
Chicago, Illinois

Hector Ferral, MD

Senior Clinical Educator
Department of Radiology
Section of Interventional Radiology
NorthShore University HealthSystem
Evanston, Illinois

Florian J. Fintelmann, MD, FRCPC

Clinical Assistant in Radiology
Department of Radiology
Massachusetts General Hospital
Boston, Massachusetts

Elliot K. Fishman, MD, FACR

Professor of Radiology
Departments of Oncology and Surgery
Johns Hopkins Hospital
Baltimore, Maryland

Joel G. Fletcher, MD

Professor of Radiology
Mayo Clinic
Rochester, Minnesota

Kathryn J. Fowler, MD

Assistant Professor
Director of Body Magnetic Resonance Imaging
Department of Radiology
Washington University
St. Louis, Missouri

Aletta A. Frazier, MD

Department of Diagnostic Radiology and Nuclear
Medicine
University of Maryland School of Medicine
Baltimore, Maryland

Ann S. Fulcher, MD

Professor and Chairman
Department of Radiology
Virginia Commonwealth University Medical Center
Richmond, Virginia

Helena Gabriel, MD

Associate Professor of Radiology
Department of Radiology
Northwestern University
Chicago, Illinois

Ana Maria Gaca, MD

Clinical Associate
Department of Radiology
Duke University Medical Center
Durham, North Carolina

Kirema Garcia-Reyes, MD

Department of Radiology
Duke University Medical Center
Durham, North Carolina

Gabriela Gayer, MD

Clinical Professor
Department of Radiology
Stanford Medical Center
Stanford, California
Department of Nuclear Medicine
Sheba Medical Center
Ramat Gan, Israel

Gary G. Ghahremani, MD, FACR

Clinical Professor of Radiology
University of California Medical Center
San Diego, California
Emeritus Professor of Radiology
Northwestern University
Chicago, Illinois

Seth N. Glick, MD

Clinical Professor of Radiology
University of Pennsylvania
Penn Presbyterian Medical Imaging
Philadelphia, Pennsylvania

Margaret D. Gore, MD

Clinical Assistant Professor of Radiology
Department of Diagnostic Radiology
NorthShore University HealthSystem
Evanston, Illinois

Richard M. Gore, MD

Chief of Gastrointestinal Radiology
NorthShore University HealthSystem
Evanston, Illinois
Professor of Radiology
Pritzker School of Medicine at the University of Chicago
Chicago, Illinois

Sofia Gourtsoyianni, MD, PhD

Consultant Radiologist
Guy's and St Thomas' National Health Service
Foundation Trust
London, United Kingdom

Nicholas C. Gourtsoyiannis, MD

Professor
Department of Radiology
University of Crete Medical School
Chairman
Department of Radiology
University Hospital of Heraklion
Heraklion, Crete, Greece

Jared R. Green, MD

Assistant Professor
Department of Medical Imaging
Ann & Robert H. Lurie Children's Hospital of Chicago
Chicago, Illinois

Gianfranco Gualdi, MD

Professor of Radiology
Director of DEA Radiology Department
Sapienza University
Rome, Italy

Rajan T. Gupta, MD

Assistant Professor of Radiology
Director of the Abdominal Imaging Fellowship Program
Department of Radiology
Duke University Medical Center
Durham, North Carolina

Ravi Guttikonda, MD

Body Imaging Fellow
Northwestern Memorial Hospital
Hudson, Ohio

Robert A. Halvorsen, MD

Professor of Radiology
Medical College of Virginia Hospitals
Virginia Commonwealth University
Richmond, Virginia

Nancy A. Hammond, MD

Associate Professor of Radiology
Director of the School of Ultrasound
Northwestern University
Chicago, Illinois

Mukesh G. Harisinghani, MD

Professor of Radiology
Harvard Medical School
Massachusetts General Hospital
Boston, Massachusetts

Sandeep S. Hedgire, MD

Division of Abdominal Imaging and Intervention
Massachusetts General Hospital
Boston, Massachusetts

Frederick L. Hoff, MD

Associate Professor
Department of Radiology
Northwestern University Feinberg School of Medicine
Chicago, Illinois

Caroline L. Hollingsworth, MD, MPH

Assistant Professor
Department of Radiology
Division of Pediatric Radiology
Duke University School of Medicine
Durham, North Carolina

Karen M. Horton, MD

Professor
Russell H. Morgan Department of Radiology and
Radiological Science
Johns Hopkins Medical Institutions
Baltimore, Maryland

Steven Y. Huang, MD

Assistant Professor
Department of Interventional Radiology
The University of Texas MD Anderson Cancer Center
Houston, Texas

James E. Huprich, MD

Emeritus Associate Professor of Radiology
Mayo Clinic Rochester
Rochester, Minnesota

Aleksandar M. Ivanovic, MD

Assistant Professor
Center for Radiology and Magnetic Resonance
Imaging
Clinical Center of Serbia
Faculty of Medicine
Belgrade, Serbia

Jill E. Jacobs, MD

Professor of Radiology
New York School of Medicine
New York, New York

Bruce R. Javors, MD

Professor of Clinical Radiology (Retired)
Albert Einstein College of Medicine
New York, New York

Bronwyn Jones, MB, BS, FRACP, FRCR

Professor of Radiology
Johns Hopkins University School of Medicine
Baltimore, Maryland

Naveen Kalra, MD

Professor of Radiology
Postgraduate Institute of Medical Education and
Research
Chandigarh, India

Avinash Kambadakone, MD, FRCR

Assistant Professor
Department of Radiology
Harvard Medical School
Massachusetts General Hospital
Boston, Massachusetts

Mariam M. Kappil, MD, BS, DABR

Pediatric Radiologist
Ann & Robert H. Lurie Children's Hospital of Chicago
Chicago, Illinois

Ana L. Keppke, MD

Radiologist
Kettering Network Radiologists, Inc.
Kettering, Ohio

David H. Kim, MD, FACP

Professor of Radiology
Vice-Chair of Education
Residency Program Director
University of Wisconsin School of Medicine and Public Health
Section of Abdominal Imaging
Madison, Wisconsin

Stanley Taeson Kim, MD

Instructor
Department of Radiology
Northwestern University Feinberg School of Medicine
Interventional Radiologist
Department of Radiology
Northwestern Memorial Hospital
Interventional Radiologist
Department of Medical Imaging
Children's Memorial Hospital
Chicago, Illinois

Douglas R. Kitchin, MD

Clinical Instructor
Department of Radiology
University of Wisconsin
Madison, Wisconsin

Michael L. Kochman, MD

Wilmott Family Professor of Medicine
Vice-Chair of Medicine for Clinical Services Center for
Endoscopic Innovation Research and Training
University of Pennsylvania
Philadelphia, Pennsylvania

Dow-Mu Koh, MD, MBBS, FRCR

Consultant Radiologist in Functional Imaging
Department of Radiology
Royal Marsden Hospital
Surrey, United Kingdom

J. Satheesh Krishna, MD

Postgraduate Institute of Medical Education and Research
Chandigarh, India

Naveen Kulkarni, MD

Department of Radiology
Harvard Medical School
Massachusetts General Hospital
Boston, Massachusetts

John C. Lappas, MD, FACP

Professor
Department of Radiology and Imaging Sciences
Indiana University School of Medicine
Indianapolis, Indiana

†Igor Laufer, MD

Professor of Radiology
Perelman School of Medicine at the University of Pennsylvania
Philadelphia, Pennsylvania

Fred T. Lee, Jr, MD

Robert Turrell Professor of Imaging Science
Department of Radiology
University of Wisconsin School of Medicine and Public Health
Madison, Wisconsin

Jeong Min Lee, MD

Associate Professor
Department of Radiology
Seoul National University
Seoul National University Hospital
Seoul, Republic of South Korea

Marc S. Levine, MD

Chief of Gastrointestinal Radiology
Hospital of the University of Pennsylvania
Professor of Radiology and Advisory Dean
Perelman School of Medicine at the University of Pennsylvania
Philadelphia, Pennsylvania

Angela D. Levy, MD

Professor of Radiology
Department of Radiology
Medstar Georgetown University Hospital
Washington, District of Columbia

Jennifer E. Lim-Dunham, MD

Associate Professor
Departments of Radiology and Pediatrics
Loyola University Medical Center
Stritch School of Medicine
Maywood, Illinois

Mark D. Little, MD

Assistant Professor
Department of Radiology
University of Alabama
Birmingham, Alabama

†Deceased.

Russell N. Low, MD

Medical Director
Sharp and Children's MRI Center
Sharp Memorial Hospital
San Diego, California

Dean D. T. Maglinte, MD

Distinguished Professor
Department of Radiology and Imaging Sciences
Indiana University School of Medicine
Indianapolis, Indiana

Abdullah Mahmutoglu, MD

Attending Radiologist
Department of Radiology
Sisli Etfal Training and Research Hospital
Istanbul, Turkey

Maria A. Manning, MD

Assistant Professor of Diagnostic Radiology
University of Maryland School of Medicine
Section Chief of Gastrointestinal Radiology
American Institute of Radiologic Pathology
Baltimore, Maryland

Charles S. Marn, MD

Professor of Radiology and Gastroenterology
Chair of the Quality Assurance Committee
Department of Radiology
Medical College of Wisconsin
Milwaukee, Wisconsin

Gabriele Masselli, MD, PhD

Consultant Radiologist
Associate Professor in Radiology and Nuclear Medicine
Department of Radiology
Sapienza University
Rome, Italy

Shaunagh McDermott, MB, BCh, BAO

Department of Abdominal Imaging
Massachusetts General Hospital
Boston, Massachusetts

Alec J. Megibow, MD, MPH, FACR

Professor of Radiology
New York University Langone Medical Center
New York, New York

Uday K. Mehta, MD

Assistant Professor of Radiology
Department of Radiology
NorthShore University HealthSystem
Evanston, Illinois

Vincent M. Mellnick, MD

Assistant Professor of Radiology
Mallinckrodt Institute of Radiology
Washington University School of Medicine
St. Louis, Missouri

Christine O. Menias, MD

Professor of Radiology
Mayo Clinic College of Medicine
Scottsdale, Arizona

Joseph Meranda, MD

Radiologist
Abdominal Imaging
Riverside Radiology and Interventional Associates
Columbus, Ohio

James M. Messmer, MD, MEd, FACR

Professor Emeritus of Radiology
Virginia Commonwealth University School of Medicine
Richmond, Virginia

Arthur B. Meyers, MD

Assistant Professor of Radiology
Children's Hospital of Wisconsin
Medical College of Wisconsin
Milwaukee, Wisconsin

Morton A. Meyers, MD, FACR, FACG

Distinguished Professor
Department of Radiology and Internal Medicine
Stony Brook School of Medicine
Stony Brook, New York

Frank H. Miller, MD

Professor of Radiology
Northwestern University Feinberg School of Medicine
Chief of Body Imaging Section and Fellowship Program
Chief of Gastrointestinal Radiology
Medical Director of Magnetic Resonance Imaging
Northwestern Memorial Hospital
Chicago, Illinois

Tara Morgan, MD

Assistant Professor
Department of Radiology and Biomedical Imaging
University of California
San Francisco, California

Koenraad J. Mortelet, MD

Associate Professor of Radiology
Harvard Medical School
Director of the Division of Clinical Magnetic
Resonance Imaging
Staff Radiologist
Department of Radiology
Beth Israel Deaconess Medical Center
Boston, Massachusetts

Peter R. Mueller, MD

Professor of Radiology
Massachusetts General Hospital
Boston, Massachusetts

Brian P. Mullan, MD

Assistant Professor of Radiology
Department of Radiology
Mayo Clinic
Rochester, Minnesota

Vamsi Narra, MD, FACR, FRCR

Professor of Radiology
 Chief of Abdominal Imaging Section
 Chief of Radiology
 Barnes-Jewish West County Hospital
 Washington University
 St. Louis, Missouri

Albert A. Nemcek, Jr, MD

Professor
 Department of Radiology
 Northwestern University Feinberg School of Medicine
 Staff Interventional Radiologist
 Northwestern Memorial Hospital
 Chicago, Illinois

Geraldine Mogavero Newmark, MD

Vice Chairman
 Outpatient Imaging
 Department of Radiology
 NorthShore University HealthSystem
 Evanston, Illinois

Jennifer L. Nicholas, MD, MHA, MA

Pediatric Radiologist
 Medical Imaging
 Ann & Robert H. Lurie Children's Hospital
 Assistant Professor
 Department of Radiology
 Northwestern University Feinberg School of Medicine
 Chicago, Illinois

Paul Nikolaidis, MD

Associate Professor of Radiology
 Northwestern University
 Chicago, Illinois

David J. Ott, MD

Professor Emeritus
 Department of Radiology
 Wake Forest University Medical Center
 Winston-Salem, North Carolina

Joseph Owen, MD

Department of Radiology
 Washington University School of Medicine
 St. Louis, Missouri

Orhan S. Ozkan, MD

Professor of Radiology
 Department of Radiology
 University of Wisconsin School of Medicine and Public Health
 Madison, Wisconsin

Nickolas Papanikolaou, PhD

Affiliated Researcher
 Department of Magnetic Resonance Imaging
 Huddinge Hospital
 Karolinska Institute
 Stockholm, Sweden

Mikin V. Patel, MD, MBA

Department of Radiology
 University of Chicago Pritzker School of Medicine
 Chicago, Illinois

Pritesh Patel, MD

Assistant Professor of Radiology
 University of Chicago
 Chicago, Illinois

Erik K. Paulson, MD

Professor of Radiology
 Chairman
 Department of Radiology
 Duke University School of Medicine
 Durham, North Carolina

Christine M. Peterson, MD

Associate Professor of Radiology
 Milton S. Hershey Penn State Medical Center
 Hershey, Pennsylvania

Perry J. Pickhardt, MD

Professor of Radiology
 Chief of Gastrointestinal Imaging
 University of Wisconsin School of Medicine and Public Health
 Madison, Wisconsin

Aliya Qayyum, MBBS, MRCP, FRCR

Professor of Radiology
 Section Chief of Abdominal Imaging
 The University of Texas MD Anderson Cancer Center
 Houston, Texas

David N. Rabin, MD

Assistant Professor of Radiology
 University of Chicago Pritzker School of Medicine
 NorthShore University HealthSystem
 Evanston, Illinois

Siva P. Raman, MD

Assistant Professor
 Department of Radiology
 Johns Hopkins University
 Baltimore, Maryland

Peter M. Rodgers, MB, BS, FRCR

Consultant Radiologist
 Leicester Royal Infirmary
 University Hospitals of Leicester National Health Service Trust
 Leicester, United Kingdom

Pablo R. Ros, MD, MPH, PhD

Radiologist-in-Chief
 University Hospitals Health System
 Theodore J. Castle University
 Professor and Chairman
 Department of Radiology
 Professor of Pathology
 Case Western Reserve University
 University Hospitals Case Medical Center
 Cleveland, Ohio

Stephen E. Rubesin, MD

Professor of Radiology
Department of Radiology
Hospital of the University of Pennsylvania
Philadelphia, Pennsylvania

Tara Sagebiel, MD

Assistant Professor
Department of Diagnostic Radiology
The University of Texas MD Anderson Cancer Center
Houston, Texas

Dushyant V. Sahani, MD

Director of Computed Tomography
Assistant Radiologist
Department of Radiology
Massachusetts General Hospital
Associate Professor of Radiology
Department of Radiology
Harvard Medical School
Boston, Massachusetts

Sanjay Saini, MD

Professor of Radiology
Harvard Medical School
Vice-Chair for Finance
Massachusetts General Hospital
Boston, Massachusetts

Martha Cotsen Saker, MD

Department of Medical Imaging
Ann & Robert H. Lurie Children's Hospital of Chicago
Department of Medical Imaging
Shriners Hospitals for Children
Chicago, Illinois

Riad Salem, MD

Associate Professor
Department of Radiology
Division of Interventional Radiology
Northwestern University
Chicago, Illinois

Kumar Sandrasegaran, MD

Associate Professor
Department of Radiology
Indiana University School of Medicine
Indianapolis, Indiana

Rupan Sanyal, MD

Assistant Professor
Department of Radiology
University of Alabama at Birmingham
Birmingham, Alabama

Christopher D. Scheirey, MD

Radiologist
Department of Radiology
Lahey Clinic Hospital and Medical Center
Burlington, Massachusetts
Assistant Professor of Radiology
Tufts University School of Medicine
Boston, Massachusetts

Francis J. Scholz, MD

Radiologist
Department of Radiology
Lahey Clinic Hospital and Medical Center
Burlington, Massachusetts
Professor of Radiology
Tufts University School of Medicine
Boston, Massachusetts

Adeel R. Seyal, MD

Department of Radiology
Northwestern University Feinberg School of Medicine
Chicago, Illinois

Martin J. Shelly, MB, BCh, BAO, MRCSI, FFRRCSI

Consultant Radiologist
Cavan Monaghan Hospital
Royal College of Surgeons in Ireland Healthcare Group
County Westmeath, Ireland

Linda C. Sherbahn, MD, MS, BA

Clinical Assistant Professor of Radiology
NorthShore University HealthSystem
Evanston, Illinois

Ali Shirkhoda, MD, FACR

Clinical Professor of Radiology
University of California at Irvine
Attending Radiologist
Veterans Affairs Hospital
Long Beach, California

Ana Catarina Silva, MD

Radiology Assistant
Department of Radiology
Unidade Local de Saúde de Matosinhos
Porto, Portugal

Paul M. Silverman, MD

Department of Radiology
Division of Diagnostic Imaging
The University of Texas MD Anderson Cancer Center
Houston, Texas

Stuart G. Silverman, MD

Professor
Department of Radiology
Harvard Medical School
Director, Abdominal Imaging and Intervention
Director, CT Scan
Director, Cross-Sectional Imaging Service
Department of Radiology
Brigham and Women's Hospital
Boston, Massachusetts

Robert I. Silvers, MD

Clinical Assistant Professor
Department of Radiology
Section Chief of Body Imaging
NorthShore University Health System
Assistant Professor of Radiology
University of Chicago Pritzker School of Medicine
Chicago, Illinois

Ajay K. Singh, MD

Associate Director
Division of Emergency Radiology
Massachusetts General Hospital
Boston, Massachusetts

Jovitas Skucas, MD

Professor Emeritus
Department of Imaging Sciences
University of Rochester Medical Center
Rochester, New York

Gail S. Smith, MD

Clinical Assistant Professor
Department of Diagnostic Radiology
NorthShore University HealthSystem
Evanston, Illinois

Sat Somers, MB, ChB (Sheffield), FRCPC, FFRCSI(Hon.), FACR

Professor
Department of Radiology
McMaster University
Hamilton, Ontario, Canada

Anthony W. Stanson, MD

Professor Emeritus of Radiology
Mayo Clinic College of Medicine
Department of Radiology
Mayo Clinic
Rochester, Minnesota

Allison L. Summers, MD

Department of Radiology
Northwestern Memorial Hospital
Chicago, Illinois

Richard A. Szucs, MD

Chairman of Radiology
Bon Secours St. Mary's Hospital
Richmond, Virginia

Mark Talamonti, MD

Professor and Chairman
Department of Surgery
NorthShore University HealthSystem
Evanston, Illinois

Andrew J. Taylor, MD

Professor
Department of Radiology
University of Minnesota
Minneapolis, Minnesota

Darshit J. Thakrar, MD, DNB, DABR

Attending Radiologist
Ann & Robert H. Lurie Children's Hospital of Chicago
Chicago, Illinois

Kiran H. Thakrar, MD

Clinical Assistant Professor
Department of Diagnostic Radiology
NorthShore University HealthSystem
Evanston, Illinois

Yee Liang Thian, MBBS, FRCR

Consultant
Department of Diagnostic Imaging
National University Hospital
Singapore

Ruedi F. Thoeni, MD

Professor of Radiology
Chief of Abdominal Imaging
San Francisco General Hospital
Department of Radiology and Biomedical Imaging
University of California
San Francisco, California

Stephen Thomas, MD

Assistant Professor of Radiology
University of Chicago
Chicago, Illinois

William Moreau Thompson, MD, BA

Professor and Vice Chair
Department of Radiology
University of New Mexico
Albuquerque, New Mexico

Temel Tirkes, MD

Assistant Professor of Radiology
Division of Diagnostic Radiology
University of Indiana School of Medicine
Indianapolis, Indiana

Mary Ann Turner, MD

Professor and Vice-Chair
Department of Radiology
Director and Chief of Gastrointestinal Radiology
Virginia Commonwealth University Medical Center
Richmond, Virginia

Jennifer W. Uyeda, MD

Clinical Assistant
Abdominal and Interventional Radiology
Harvard Medical School
Massachusetts General Hospital
Boston, Massachusetts

Fauzia Q. Vandermeer, MD

Assistant Professor of Diagnostic Radiology
Department of Diagnostic Radiology and Nuclear
Medicine
University of Maryland School of Medicine
Baltimore, Maryland

Robert L. Vogelzang, MD

Professor of Radiology
Northwestern Feinberg School of Medicine
Chicago, Illinois

Patrick M. Vos, MD, FRCPC

Clinical Associate Professor
Department of Radiology
University of British Columbia
Vancouver, British Columbia, Canada

Natasha Wehrli, MD

Assistant Professor of Radiology
Weill-Cornell Imaging at New York Presbyterian Hospital
New York, New York

Daniel R. Wenzke, MD

Clinical Assistant Professor of Radiology
NorthShore University HealthSystem
University of Chicago Pritzker School of Medicine
Evanston, Illinois

Ellen L. Wolf, MD

Professor of Clinical Radiology
Department of Radiology
Albert Einstein College of Medicine
Montefiore Medical Center
Bronx, New York

Jade J. Wong-You-Cheong, MD, MBChB(Hons)

Professor
Department of Diagnostic Radiology and Nuclear Medicine
University of Maryland School of Medicine
Baltimore, Maryland

Cecil G. Wood III, MD

Clinical Instructor
Department of Radiology
Northwestern University Feinberg School of Medicine
Chicago, Illinois

Michael A. Woods, MD

Assistant Professor of Radiology
Department of Radiology
University of Wisconsin School of Medicine and Public
Health
Madison, Wisconsin

Vahid Yaghmai, MD, MS

Professor
Department of Radiology
Northwestern University Feinberg School of Medicine
Medical Director of Computed Tomography Imaging
Department of Radiology
Northwestern Memorial Hospital
Chicago, Illinois

Benjamin M. Yeh, MD

Professor of Radiology
Radiology and Biomedical Imaging
University of California
San Francisco, California

PREFACE

In the 20 years since the publication of the first edition of *Textbook of Gastrointestinal Radiology*, much has changed in our discipline. Technologic advances have dramatically improved the capabilities of computed tomography (CT), magnetic resonance imaging (MRI), ultrasonography, fluoroscopy, angiography, and interventional radiology for abdominal and pelvic imaging and therapy. The extraordinary anatomic resolution achieved with modern imaging techniques has been complemented by the introduction and maturation of metabolic, functional, and molecular imaging, which provide new opportunities for staging and follow-up and monitoring tumor response to therapy in the oncology patient.

To keep pace with these amazing technologic, imaging, and therapeutic advances, every chapter of the fourth edition has been updated and revised. Several new chapters on molecular and functional imaging have also been included. Moreover, new authors have been recruited for nearly one third of the chapters to provide these chapters with fresh insight and perspective.

In this new edition, we have taken great care to maintain the objective of the first three editions—namely, to provide complete and up-to-date coverage on the state of the art of gastrointestinal radiology in a practical and usable form.

As in the first three editions, our basic organizing principle is the integration of rapidly changing information, common sense, and good judgment for the development of a rational and useful approach for radiologic diagnosis and treatment. To this end, the text contains sections on general radiologic principles

for evaluating the hollow viscera and solid organs and for performing and applying specific imaging and therapeutic techniques. Other sections present the clinical, radiologic, and pathologic aspects of disease in the various gastrointestinal organs. The chapters in these sections are designed to illustrate and integrate the spectrum of abnormalities seen with all diagnostic modalities available to the radiologist, including conventional radiography, barium studies, cholangiography, multidetector CT (MDCT), ultrasonography, MRI, positron emission tomography/computed tomography (PET/CT), positron emission tomography/magnetic resonance (PET/MR), angiography, diffusion-weighted MRI, and CT and MR perfusion imaging.

Once again, we have been able to assemble an outstanding group of internationally recognized authors for the fourth edition. Their time, effort, and expertise are truly appreciated. As editors, we have tried to strike a balance between uniformity of style and author individuality so that each contributor is able to speak in his or her own unique voice.

We trust that the collective efforts of the authors of the 127 chapters in this text, as well as our own, have enabled us to accomplish our goal of providing students and practitioners of gastrointestinal radiology a valuable educational resource that is clear, interesting, and enjoyable to read.

Richard M. Gore

Marc S. Levine

Volume 1

SECTION **I** **General Radiologic Principles 1**

- 1 Imaging Contrast Agents and Pharmacoradiology 3
JOVITAS SKUCAS
- 2 Barium Studies: Single and Double Contrast 23
MARC S. LEVINE | DAVID J. OTT | IGOR LAUFER
- 3 Pictorial Glossary of Double-Contrast Radiology 40
STEPHEN E. RUBESIN
- 4 Ultrasound of the Hollow Viscera 56
PETER M. RODGERS
- 5 Multidetector Computed Tomography of the Gastrointestinal Tract: Principles of Interpretation 67
RICHARD M. GORE | MARK E. BAKER
- 6 Magnetic Resonance Imaging of the Hollow Viscera 79
RUSSELL N. LOW
- 7 Positron Emission Tomography and Computed Tomography of the Hollow Viscera 96
SELIM R. BUTROS | SHAUNAGH McDERMOTT | MARTIN J. SHELLY | MICHAEL A. BLAKE
- 8 Angiography and Interventional Radiology of the Hollow Viscera 112
STANLEY TAESON KIM | ALBERT A. NEMCEK, JR. | HECTOR FERRAL | ROBERT L. VOGELZANG
- 9 Abdominal Computed Tomography Angiography 135
VAHID YAGHMAI | WARREN M. BRANDWEIN
- 10 Magnetic Resonance Angiography of the Mesenteric Vasculature 149
JOSEPH OWEN | KATHRYN J. FOWLER | VAMSI NARRA

SECTION **II** **Abdominal Radiography 163**

- 11 Abdomen: Normal Anatomy and Examination Techniques 165
WILLIAM MOREAU THOMPSON
- 12 Gas and Soft Tissue Abnormalities 178
JAMES M. MESSMER | MARC S. LEVINE

- 13 Abdominal Calcifications 197
STEPHEN R. BAKER

SECTION **III** **Pharynx 205**
STEPHEN E. RUBESIN, SECTION EDITOR

- 14 Pharynx: Normal Anatomy and Examination Techniques 207
STEPHEN E. RUBESIN
- 15 Abnormalities of Pharyngeal Function 222
BRONWYN JONES
- 16 Structural Abnormalities of the Pharynx 237
STEPHEN E. RUBESIN

SECTION **IV** **Esophagus 267**

- 17 Barium Studies of the Upper Gastrointestinal Tract 269
MARC S. LEVINE | IGOR LAUFER
- 18 Motility Disorders of the Esophagus 279
DAVID J. OTT | MARC S. LEVINE
- 19 Gastroesophageal Reflux Disease 291
MARC S. LEVINE
- 20 Infectious Esophagitis 312
MARC S. LEVINE
- 21 Other Esophagitides 326
MARC S. LEVINE
- 22 Benign Tumors of the Esophagus 350
MARC S. LEVINE
- 23 Carcinoma of the Esophagus 366
MARC S. LEVINE | ROBERT A. HALVORSEN
- 24 Other Malignant Tumors of the Esophagus 394
MARC S. LEVINE
- 25 Miscellaneous Abnormalities of the Esophagus 412
MARC S. LEVINE
- 26 Abnormalities of the Gastroesophageal Junction 438
MARC S. LEVINE

- 27 Postoperative Esophagus 449
STEPHEN E. RUBESIN

- 28 Esophagus: Differential Diagnosis 462
MARC S. LEVINE

SECTION V Stomach and Duodenum 465

- 29 Peptic Ulcers 467
MARC S. LEVINE

- 30 Inflammatory Conditions of the Stomach and Duodenum 496
MARC S. LEVINE

- 31 Benign Tumors of the Stomach and Duodenum 523
MARC S. LEVINE

- 32 Carcinoma of the Stomach and Duodenum 546
MARC S. LEVINE | ALEC J. MEGIBOW |
MICHAEL L. KOCHMAN

- 33 Other Malignant Tumors of the Stomach and Duodenum 571
MARC S. LEVINE | ALEC J. MEGIBOW

- 34 Miscellaneous Abnormalities of the Stomach and Duodenum 603
RONALD L. EISENBERG | MARC S. LEVINE

- 35 Postoperative Stomach and Duodenum 630
LAURA R. CARUCCI

- 36 Stomach and Duodenum: Differential Diagnosis 657
MARC S. LEVINE

SECTION VI Small Bowel 663

STEPHEN E. RUBESIN, SECTION EDITOR

- 37 Barium Examinations of the Small Intestine 665
STEPHEN E. RUBESIN

- 38 Computed Tomography Enterography 684
JOEL G. FLETCHER | DAVID H. BRUINING

- 39 Computed Tomography Enteroclysis 694
ANA CATARINA SILVA | DEAN D. T. MAGLINTE

- 40 Magnetic Resonance Enterography 710
GABRIELE MASSELLI | GIANFRANCO GUALDI

- 41 Crohn's Disease of the Small Bowel 725
MARK E. BAKER | RICHARD M. GORE

- 42 Inflammatory Disorders of the Small Bowel Other Than Crohn's Disease 756
STEPHEN E. RUBESIN

- 43 Malabsorption 773
STEPHEN E. RUBESIN

- 44 Benign Tumors of the Small Bowel 789
TEMEL TIRKES | JOHN C. LAPPAS

- 45 Malignant Tumors of the Small Bowel 796
KUMAR SANDRASEGARAN | CHRISTINE O. MENIAS

- 46 Small Bowel Obstruction 806
STEPHEN E. RUBESIN | RICHARD M. GORE

- 47 Vascular Disorders of the Small Intestine 827
SIVA P. RAMAN | KAREN M. HORTON |
ELLIOT K. FISHMAN

- 48 Postoperative Small Bowel 851
TEMEL TIRKES | JOHN C. LAPPAS

- 49 Miscellaneous Abnormalities of the Small Bowel 861
STEPHEN E. RUBESIN

- 50 Small Intestine: Differential Diagnosis 870
STEPHEN E. RUBESIN

SECTION VII Colon 877

- 51 Barium Studies of the Colon 879
MARC S. LEVINE | IGOR LAUFER

- 52 Functional Imaging of Anorectal and Pelvic Floor Dysfunction 890
SAT SOMERS | DEAN D. T. MAGLINTE

- 53 Computed Tomography Colonography 905
DAVID H. KIM | PERRY J. PICKHARDT

- 54 Magnetic Resonance Colonography 928
SOFIA GOURTSOYIANNI | NICKOLAS PAPANIKOLAOU |
NICHOLAS C. GOURTSOYIANNIS

- 55 Diverticular Disease of the Colon 934
KIRAN H. THAKRAR | RICHARD M. GORE |
VAHID YAGHMAI | EMIL J. BALTHAZAR

- 56 Diseases of the Appendix 955
DANIEL R. WENZKE | JILL E. JACOBS |
EMIL J. BALTHAZAR | NATASHA WEHRLI

- 57 Ulcerative and Granulomatous Colitis: Idiopathic Inflammatory Bowel Disease 984
RICHARD M. GORE | JONATHAN W. BERLIN |
ALEKSANDAR M. IVANOVIC

58 Other Inflammatory Conditions of the Colon 1017

RICHARD M. GORE | SETH N. GLICK |
ALEKSANDAR M. IVANOVIC

59 Polyps and Colon Cancer 1027

RUEDI F. THOENI

60 Other Tumors of the Colon 1074

STEPHEN E. RUBESIN

61 Polyposis Syndromes 1089

ANGELA D. LEVY | CARINA L. BUTLER | JAMES L. BUCK

62 Miscellaneous Abnormalities of the Colon 1102

RICHARD M. GORE | RICHARD A. SZUCS |
ELLEN L. WOLF | FRANCIS J. SCHOLZ |
RONALD L. EISENBERG | STEPHEN E. RUBESIN

63 Postoperative Colon 1133

CHRISTOPHER D. SCHEIREY | JAUL AFNAN |
FRANCIS J. SCHOLZ

64 Colon: Differential Diagnosis 1144

RICHARD M. GORE

Volume 2

SECTION VIII General Radiologic Principles for Imaging and Intervention of the Solid Viscera 1153

65 Computed Tomography of the Solid Abdominal Organs 1155

CECIL G. WOOD III | SENTA BERGGREEN

66 Ultrasound Examination of the Solid Abdominal Viscera 1169

STUART A. BARNARD | PATRICK M. VOS |
PETER L. COOPERBERG

67 Magnetic Resonance Imaging of the Solid Parenchymal Organs 1183

JENNIFER W. UYEDA | SANDEEP S. HEDGIRE |
MUKESH G. HARISINGHANI | RAJ R. CHINNAPPAN |
PRITESH PATEL

68 Positron Emission Tomography/Computed Tomography of the Solid Parenchymal Organs 1202

SHAUNAGH McDERMOTT | SELIM R. BUTROS |
MICHAEL A. BLAKE

69 Diffusion-Weighted Imaging of the Abdomen 1215

YEE LIANG THIAN | DOW-MU KOH

70 Perfusion Computed Tomography and Magnetic Resonance Imaging in the Abdomen and Pelvis 1230

SURABHI BAJPAI | DUSHYANT V. SAHANI |
AVINASH KAMBADAKONE

71 Techniques of Percutaneous Tissue Acquisition 1239

STEVEN Y. HUANG | ERIK K. PAULSON

72 Abdominal Abscess 1254

AVINASH KAMBADAKONE | PETER R. MUELLER

SECTION IX Gallbladder and Biliary Tract 1279

73 Gallbladder and Biliary Tract: Normal Anatomy and Examination Techniques 1281

MARY ANN TURNER | ANN S. FULCHER

74 Endoscopic Retrograde Cholangiopancreatography 1303

ANDREW J. TAYLOR

75 Magnetic Resonance Cholangiopancreatography 1325

ANN S. FULCHER | MARY ANN TURNER

76 Anomalies and Anatomic Variants of the Gallbladder and Biliary Tract 1340

RICHARD M. GORE | ANDREW J. TAYLOR |
GARY G. GHAHREMANI

77 Cholelithiasis, Cholecystitis, Choledocholithiasis, and Hyperplastic Cholecystoses 1348

GENEVIEVE L. BENNETT

78 Interventional Radiology of the Gallbladder and Biliary Tract 1392

THOMAS A. FARRELL | MIKIN V. PATEL

79 Neoplasms of the Gallbladder and Biliary Tract 1402

BYUNG IHN CHOI | JEONG MIN LEE

80 Inflammatory Disorders of the Biliary Tract 1427

BENJAMIN M. YEH | WEI-CHOU CHANG

81 Postsurgical and Traumatic Lesions of the Biliary Tract 1442

SIVA P. RAMAN | ELLIOT K. FISHMAN | GABRIELA GAYER

82 Gallbladder and Biliary Tract: Differential Diagnosis 1460

RICHARD M. GORE

SECTION X Liver 1469

83 Liver: Normal Anatomy and Examination Techniques 1471

ALEXANDER DING | NAVEEN KULKARNI |
FLORIAN J. FINTELMANN | SANJAY SAINI

84 Interventional Radiology of the Liver 1498MICHAEL A. WOODS | DOUGLAS R. KITCHIN |
ORHAN S. OZKAN | FRED T. LEE, JR**85 Anomalies and Anatomic Variants of the Liver 1520**

ALI SHIRKHODA | RICHARD M. GORE

86 Benign Tumors of the Liver 1528

PABLO R. ROS | SUKRU MEHMET ERTURK

87 Malignant Tumors of the Liver 1561

PABLO R. ROS | SUKRU MEHMET ERTURK

88 Focal Hepatic Infections 1608PABLO R. ROS | SUKRU MEHMET ERTURK |
ABDULLAH MAHMUTOGLU**89 Diffuse Liver Disease 1629**

TARA MORGAN | ALIYA QAYYUM | RICHARD M. GORE

90 Vascular Disorders of the Liver and Splanchnic Circulation 1676

RICHARD M. GORE | AHMED BA-SSALAMAH

91 Hepatic Trauma, Surgery, and Liver-Directed Therapy 1706HELENA GABRIEL | NANCY A. HAMMOND |
MARK TALAMONTI | RIAD SALEM | RICHARD M. GORE**92 Liver Transplantation Imaging 1737**LAUREN F. ALEXANDER | MARK D. LITTLE |
RUPAN SANYAL**93 Liver: Differential Diagnosis 1756**

RICHARD M. GORE

SECTION XI Pancreas 1769**94 Pancreas: Normal Anatomy and Examination Techniques 1771**NANCY A. HAMMOND | FREDERICK L. HOFF |
RAVI GUTTIKONDA | HELENA GABRIEL |
RICHARD M. GORE**95 Interventional Radiology of the Pancreas 1785**

KOENRAAD J. MORTELE | STUART G. SILVERMAN

96 Anomalies and Anatomic Variants of the Pancreas 1797

ALI SHIRKHODA | PEYMAN BORGHEI | RICHARD M. GORE

97 Pancreatitis 1809

FRANK H. MILLER | ANA L. KEPPKE | EMIL J. BALTHAZAR

98 Pancreatic Neoplasms 1838

ALEC J. MEGIBOW

99 Pancreatic Trauma and Surgery 1856PAUL NIKOLAIDIS | JOSEPH MERANDA |
FRANK H. MILLER | ALLISON L. SUMMERS |
HELENA GABRIEL | MARK TALAMONTI | RICHARD M. GORE**100 Pancreatic Transplantation Imaging 1872**FAUZIA Q. VANDERMEER | MARIA A. MANNING |
ALETIA A. FRAZIER | JADE J. WONG-YOU-CHEONG**101 Pancreas: Differential Diagnosis 1889**

RICHARD M. GORE

SECTION XII Spleen 1895**102 Spleen: Normal Anatomy and Examination Techniques 1897**

STEPHEN THOMAS | ABRAHAM H. DACHMAN

103 Angiography and Interventional Radiology of the Spleen 1905

J. SATHEESH KRISHNA | NAVEEN KALRA | AJAY K. SINGH

104 Anomalies and Anatomic Variants of the Spleen 1912

STEPHEN THOMAS | ABRAHAM H. DACHMAN

105 Benign and Malignant Lesions of the Spleen 1923PATRICK M. VOS | STUART A. BARNARD |
PETER L. COOPERBERG**106 Splenic Trauma and Surgery 1965**

VAHID YAGHMAI | ADEEL R. SEYAL

107 Spleen: Differential Diagnosis 1977

RICHARD M. GORE

SECTION XIII Peritoneal Cavity 1981**108 Anatomy and Imaging of the Peritoneum and Retroperitoneum 1983**VINCENT M. MELLNICK | DENNIS M. BALFE |
CHRISTINE M. PETERSON**109 Pathways of Abdominal and Pelvic Disease Spread 2006**RICHARD M. GORE | MORTON A. MEYERS |
DAVID N. RABIN**110 Ascites and Peritoneal Fluid Collections 2024**RICHARD M. GORE | ROBERT I. SILVERS |
GERALDINE MOGAVERO NEWMARK | MARGARET D. GORE**111 Mesenteric and Omental Lesions 2036**APARNA BALACHANDRAN | TARA SAGEBIEL |
PAUL M. SILVERMAN

112 Hernias and Abdominal Wall Pathology 2053

RICHARD M. GORE | GARY G. GHahremani |
CAROLYN K. DONALDSON | GAIL S. SMITH |
LINDA C. SHERBAHN | CHARLES S. MARN

SECTION XIV Pediatric Disease 2077
113 Applied Embryology of the Gastrointestinal Tract 2079

BRUCE R. JAVORS | ROI M. BITTANE

114 Neonatal Gastrointestinal Radiology 2095

KATE A. FEINSTEIN | SANDRA K. FERNBACH

115 Diseases of the Pediatric Esophagus 2125

JENNIFER E. LIM-DUNHAM | SANDRA K. FERNBACH

116 Diseases of the Pediatric Stomach and Duodenum 2141

JENNIFER E. LIM-DUNHAM | RICHARD M. GORE

117 Diseases of the Pediatric Small Bowel 2158

JENNIFER E. LIM-DUNHAM | SANDRA K. FERNBACH

118 Diseases of the Pediatric Colon 2164

KATE A. FEINSTEIN | SANDRA K. FERNBACH

119 Diseases of the Pediatric Gallbladder and Biliary Tract 2180

JENNIFER L. NICHOLAS

120 Diseases of the Pediatric Liver 2200

JENNIFER L. NICHOLAS | CAROLINE L. HOLLINGSWORTH

121 Diseases of the Pediatric Pancreas 2216

MARIAM M. KAPIL | DARSHIT J. THAKRAR

122 Diseases of the Pediatric Spleen 2228

JARED R. GREEN | MARTHA COTSEN SAKER

123 Diseases of the Pediatric Abdominal Wall, Peritoneum, and Mesentery 2241

KEVIN P. BOYD | ARTHUR B. MEYERS |
ANA MARIA GACA | GEORGE S. BISSETT III

SECTION XV Common Clinical Problems 2253
124 The Acute Abdomen 2255

RICHARD M. GORE | KIRAN H. THAKRAR |
DANIEL R. WENZKE | ROBERT I. SILVERS |
UDAY K. MEHTA | GERALDINE MOGAVERO NEWMARK |
JONATHAN W. BERLIN

125 Gastrointestinal Hemorrhage 2271

JAMES E. HUPRICH | JEFFREY A. ALEXANDER |
BRIAN P. MULLAN | ANTHONY W. STANSON

126 Abdominal Trauma 2282

RAJAN T. GUPTA | KIREMA GARCIA-REYES

127 Monitoring Gastrointestinal Tumor Response to Therapy 2295

KUMAR SANDRASEGARAN

VIDEO CONTENTS

38 Computed Tomography Enterography

Video 38-1: Enterography Demonstrating Both Jejunal and Ileal Crohn's Enteric Inflammation

53 Computed Tomography Colonography

Video 53-1: CTC Interpretation

Video 53-2: 2D Detection Pitfall

Video 53-3: 2D Detection Pitfall

Video 53-4: 3D Detection Pitfall

Video 53-5: Characterization Pitfall

SECTION

I

General Radiologic Principles

Imaging Contrast Agents and Pharmacoradiology

JOVITAS SKUCAS

CHAPTER OUTLINE

Intravascular Contrast Agents

Iodinated Water-Soluble Agents

Iodinated Oil

Other Agents

Gastrointestinal Contrast Agents

Barium Sulfate

Pharyngographic Agents

Upper Gastrointestinal Tract Studies

Small Bowel Studies

Barium Enema

Water-Soluble Contrast Agents

Negative Contrast Agents

Gastrointestinal Computed Tomography Agents

Adverse Reactions

Cholangiographic Contrast Agents

Magnetic Resonance Imaging Contrast Agents

Intravascular Agents

Gastrointestinal Agents

Pharmacoradiology

Vasoconstrictors

Vasodilators

Gastrointestinal Agents That Produce Hypotonia

Gastrointestinal Agents That Increase Bowel Motility

Mixed Action Agents

Drugs Affecting the Biliary Tract and Pancreas

Only a basic introduction and overview about contrast agent use in medical imaging are presented in this introductory chapter. These agents can be subdivided into intravascular contrast agents for computed tomography (CT) and angiography, intraluminal gastrointestinal (GI) tract agents, cholangiographic agents and a unique group of agents useful in magnetic resonance imaging (MRI). The currently active research field of contrast agent–assisted, image-guided therapy will be discussed briefly. In addition, there is a section on pharmacologic agents useful in GI radiology.

Intravascular Contrast Agents

IODINATED WATER-SOLUBLE AGENTS

Basic Properties

With the exception of MRI, all current intravascular contrast agents use iodine for x-ray absorption. Theoretically, sodium iodide is ideal, but its toxicity and iodism preclude its use. The complex delivery molecules developed over the years represent

an attempt to deliver the greatest iodine concentration with the least toxicity. From a simplistic viewpoint, the intravascular contrast agents can be viewed merely as vehicles for delivering iodine to a blood vessel or structure. These water-soluble intravascular contrast agents can be subdivided into the following categories: (1) ionic, high osmolality, roughly five times the osmolality of blood; (2) nonionic, low osmolality, roughly twice or slightly more than the osmolality of blood; and (3) isotonic agents—nonionic dimers. The basic structures and physicochemical characteristics of available contrast agents are not covered here; these topics are discussed in appropriate specialized publications.¹

At the x-ray energies used in CT, the mass attenuation coefficient for iodine is considerably greater than that of surrounding soft tissues and blood. After the intravascular injection of iodinated contrast, initial CT images reveal aortic and major arterial enhancement, followed by a capillary or parenchymal “blush” and eventual venous opacification. The rate of contrast injection and timing of subsequent CT scans determine the structures enhanced on any one image. Compared with earlier scanners, multidetector CT (MDCT) scanners require shorter injection rates because of the short scanning times; as a result, faster injection rates of more concentrated contrast agents are necessary, and a contrast’s viscosity has a dominant role. Various techniques of intravascular contrast agent administration are discussed elsewhere in this text.

A number of drugs, especially more acidic ones, are incompatible to mixing with contrast agents, an incompatibility less evident with nonionic agents. Nevertheless, as a general safety precaution, a drug probably should not be mixed with a contrast agent, and a catheter should be flushed if used for both drug and contrast injection.

Ionic Agents

Acetylation of aminotriiodobenzoic acid and further structural changes led to the development of ionic contrast agents. These agents are formulated as salts and consist of a cation and anion. Two commonly used cations are sodium and meglumine. The anion portion of the molecule consists of a benzene ring containing iodine substituted at positions 2, 4, and 6, plus a number of other side chains. These side chains determine water solubility and indirectly affect resultant toxicity. The benzene ring can be viewed as a scaffold for attaching iodine and side chains. When the molecule dissociates, three iodine atoms are available for every two particles in solution, or a ratio of 1.5:1.

Further refinements of ionic contrast media consist of the attachment of two monomer triiodinated benzene rings at one of the side groups. Such a dimer, containing two benzene rings, with each having three iodine atoms and only one cation particle, has six iodine atoms per two particles, or a ratio of 3:1.

Ionic contrast agents are hypertonic at the concentrations used for vascular opacification; considerable effort has been spent in an attempt to decrease their osmolality. In general, the viscosity of a sodium salt is less than that of a corresponding meglumine salt, but the sodium salt tends to be more toxic. Toxicity and viscosity limitations during intra-arterial injections are not as relevant for the intravenous (IV) injections used with CT.

Nonionic Agents

If the carboxyl group in position 1 on the benzene ring is replaced with a stable side group, the molecule no longer dissociates when in solution, and each particle in solution has three iodine atoms, or a ratio of 3:1. A dimer structure can also be achieved by linking two triiodobenzoic acid molecules (ioxaglic acid), formulated as a meglumine sodium salt, another contrast agent with a ratio of 3:1. A contrast agent with a ratio of 6:1 has also been developed (iodixanol) and is often referred to as being iso-osmolar.

Various manufacturers have taken different approaches to the type of side chains used with ionic and nonionic contrast agents. As a result, these compounds differ in their viscosities and other properties. The interaction with other molecules also differs between ionic and nonionic agents and is affected by the type of side branches present. Within limits, however, for each group of contrast agents, viscosity varies directly with iodine concentration.

Commercial contrast agents also contain chelating agents, usually calcium edetate disodium, to chelate impurities and buffering agents to achieve an acceptable pH. Their action is more important during contrast agent manufacture than during clinical use.

The American College of Radiology (ACR) has published criteria for situations in which nonionic agents are preferred,² although in many practices this is a nonissue because nonionic agents are used almost exclusively. The nonionic agents are associated with less patient discomfort and thus result in less motion artifacts; this is an evident advantage, especially with complex examinations such as three-dimensional (3D) reconstruction.

Pharmacokinetics

After a bolus intravascular injection, the initial plasma iodine concentration is determined by contrast agent iodine concentration and injected volume. Ionic and nonionic contrast agents are eventually distributed throughout the extravascular, extracellular space, with intravascular and extravascular equilibrium achieved within 10 minutes after intravascular injection. They are excreted mostly by renal glomerular filtration.

After injection, the relative plasma iodine concentration in a particular vessel depends on dilution by blood, extravascular diffusion, and renal excretion; the first factor is most important during arterial and venous phase imaging, with extravascular diffusion playing a larger role during the parenchymal phase. In theory, a contrast agent can be designed to have fast or slow extravascular diffusion and rapid or slow renal clearance; an ideal blood pool agent should have slow extravascular diffusion. In practice, with an equivalent iodine dose, nonionic agents achieve greater initial peak vascular enhancement than ionic agents, but subsequent blood iodine concentrations and parenchymal opacification are similar for the two types of agents (except renal visualization). Ionic and

nonionic agents have similar extravascular diffusion rates. Extensive literature is available on relative time-dependent blood iodine concentrations and renal excretion of various contrast agents.

Dynamic CT scanning after a single bolus injection relies on the enhancement of vascular structures above baseline. Correct arterial phase timing is obtained by injecting an initial test dose or using automatic bolus tracking. One mg iodine per gram of tissue corresponds roughly to an increase of 30 Hounsfield units (HU), which is about the limit for detection. In general, it is desirable to have sufficient iodine concentration in the vascular structures of interest to elevate them above baseline by up to 100 HU. With this degree of enhancement, major vessel thrombi are detected and vascular fistulas and related conditions evaluated. Whether early dynamic scanning (arterial phase) is superior to portal venous phase or even delayed scanning after contrast equilibration depends on the organ in question and information sought. For the liver, these arterial and portal phase time window are roughly 20 to 30 seconds. These short time intervals are readily achieved with MDCT.

A typical CT examination consists of a precontrast scan, followed by scanning after the initial bolus reaches the structure of interest. A relatively large-caliber venous catheter and power injector provide reproducible injection rates, keeping in mind that prediction of bolus arrival is somewhat empiric because, among other factors, decreased cardiac output can prolong vascular flow times.

Intravascular contrast agents cross the placenta, are excreted in breast milk, and affect fetal and infant thyroid function. If feasible, alternate studies should be considered during pregnancy. Breast-feeding should be stopped for 1 to 2 days after contrast injection.

Acute Adverse Reactions

Only a brief summary of contrast reactions and their therapy are provided here. More detailed information is available from ACR² and European Society of Urogenital Radiology (ESUR)³ publications.

The nonionic contrast agents have a considerably lower osmolality than the ionic agents; adverse reactions caused by hyperosmolality are therefore reduced with the nonionic agents. Hyperosmolality is also related to vasodilation of the involved capillaries. Nonionic contrast agents induce less hypotension than ionic agents.

Risk factors for acute renal failure include diabetes mellitus with decreased renal function, renal insufficiency, dehydration, and use of a high dose. Atopy confers an increased risk to contrast reactions, but allergies to shellfish appear not to increase the risk of reaction.⁴ Iodinated contrast agents are contraindicated in patients with obvious hyperthyroidism. Also, these agents should be avoided for 2 months prior to thyroid isotope imaging or radioactive thyroid therapy.⁴

Types of Reactions. Acute reactions vary from minor effects to severe and life-threatening. Sensations of warmth, nausea, and vomiting appear to be a direct side effect to contrast. Reactions such as mild changes in blood pressure or mild wheezing are often self-limiting or may progress to more severe reactions. An arbitrary but useful grading of contrast reactions is mild, moderate, severe, and fatal. Compilations of reactions to ionic contrast agents in the 1970s and 1980s revealed a risk of severe

reaction to be 1 in 1000 to 4000 studies. Types of reactions are similar with ionic and nonionic agents. In general, the risk of adverse reactions varies with contrast osmolality, so fewer reactions occur with nonionic agents than with ionic agents. In particular, the risk of severe adverse reactions is lower with nonionic contrast agents.⁵ Deaths have occurred with both ionic and nonionic agents.

At times, urticaria and even more severe reactions do not represent a classic antigen-antibody reaction but are secondary to histamine or serotonin release induced directly by the contrast agent. However, histamine release is probably not the only factor involved in serious contrast reactions. Among other effects, contrast agents activate the complement system, which acts as a host defense, and is related to coagulation abnormalities and bradykinin release. Overall, only a minority of unpredictable reactions mimics immunoglobulin E (IgE) hypersensitivity, probably secondary to an antigen-antibody reaction. How to classify the rare bowel wall edema is not clear.⁶ Iodide mumps is a rare delayed reaction to iodine-containing contrast media.

Some reactions are disease specific. IV contrast agents in the presence of a pheochromocytoma can lead to catecholamine release and acute hypertension. In this setting, the onset of such hypertension should suggest a pheochromocytoma.

Over the years, many radiologists have avoided the use of intravascular contrast agents in patients with sickle cell disease, although the prevalence of adverse reactions has not been established. Over an extended period, bottled hyperosmolar contrast agents can leach allergens from rubber stoppers. As a rule, contrast-containing vials and bottles should be stored in an upright position.

Premedication. The specific allergen responsible for iodinated contrast sensitization is unknown. It is difficult to prove that iodine is responsible for hypersensitive contrast reactions, a common assumption. A myosin protein rather than iodine is believed to be the allergen responsible in shellfish. Rather than ask a patient about iodine allergies, a more appropriate question appears to be whether drug allergies are present. On a practical level, the cause of an adverse reaction is often not sought, and the reaction is simply labeled as allergic, hypersensitive, or anaphylactic.

No reliable blood test detects patients who are allergic to contrast media. Risk factors associated with a contrast reaction include asthma and a history of prior reaction to contrast. However, even these are unpredictable, and a patient manifesting a severe reaction may have had prior intravascular contrast with no adverse reaction. Although patients with urticaria-like reactions have increased plasma levels of prekalikrein and α_2 -macroglobulin and lower levels of C1-esterase inhibitor, their predictive value is limited because of normal variation.⁷ Pretesting with a small dose of contrast was once popular but has been abandoned as having little or no value. Acute reactions have developed after less than 1 mL of administered contrast.

In a multi-institutional study involving ionic contrast agents, pretreatment with methylprednisolone, 32 mg, 12 hours and 2 hours before contrast injection, significantly reduced the risk of reactions.⁸ With this two-dose regimen, the number of reactions in patients receiving ionic contrast agents approximated those seen with nonionic agents and no pretreatment. Premedication is often considered for patients who have had

a previous reaction to a contrast agent. Regimens that have been proposed range from 3 days to immediately before a scan. At the University of Rochester, we recommend that patients who have had a significant prior reaction to IV contrast agents be pretreated with 50 mg of prednisone orally every 12 hours, for a total of three doses, with the last dose given approximately 1 hour before the examination, and 25 to 50 mg of diphenhydramine hydrochloride (Benadryl) orally, 2 hours before the examination.

The prevalence of seizures after IV contrast injection is increased in patients with brain metastases. Capillaries in brain metastases do not exhibit normal blood-brain barrier integrity and are permeable to a contrast agent. To decrease the risk of seizures, it has been suggested that these patients be premedicated with diazepam, 5 mg IV, before contrast administration.⁹

Treatment of Reactions. Any physician injecting a contrast agent intravascularly can expect to encounter a broad spectrum of reactions, from mild to severe, and must be prepared to deal with them. In general, mild reactions such as flushing or mild urticaria require no treatment, and most reactions resolve spontaneously. Similarly, nausea and vomiting require general support and observation only. If symptoms occur before all the contrast agent has been administered, the rate of injection should be slowed or the injection postponed until symptoms clear.

Early IV access should be established. The catheter used for contrast injection should be kept in place, ensuring intravascular access until the possibility of a reaction has passed. With progressive hypotension, it becomes increasingly difficult to cannulate a peripheral vein.

Moderate urticaria developing in the absence of other significant symptoms can be treated with diphenhydramine, 25 to 50 mg, orally or injected. With more severe urticaria, one should also consider an H₂ blocking agent such as cimetidine (Tagamet), 300 mg injected slowly (diluted) IV. For severe urticaria, epinephrine, 0.1 to 0.3 mL (1:1000) should be given subcutaneously unless contraindicated. If needed, the dose can be repeated in 15 minutes. Epinephrine should be used with caution in older patients who have underlying cardiovascular disease; electrocardiographic monitoring should be considered for these patients.

Severe reactions, such as severe bronchospasm, convulsions, or significant cardiopulmonary reactions, require prompt and vigorous therapy. Bronchospasm and laryngeal edema generally respond to subcutaneous epinephrine. If needed, the epinephrine dose can be repeated. Diphenhydramine and corticosteroids, such as hydrocortisone, 100 to 300 mg IV, are also often used. Oxygen should be administered by mask or nasal cannula. Beta agonist inhalers alone may be beneficial for mild bronchospasm or can be used in conjunction with aminophylline therapy. With refractory bronchospasm, aminophylline, 250 to 400 mg diluted in dextrose and water, can be administered IV over a 10- to 20-minute period. Aminophylline should be used with caution because it could exacerbate coexisting hypotension. Tracheal intubation should be considered early in the course of these symptoms; later, severe laryngeal edema may make intubation difficult if not impossible.

Because the treatment of hypotension in the settings of tachycardia and bradycardia is different, the pulse rate should

be monitored. A pulse may not be palpable in a hypotensive patient; cardiac auscultation or electrocardiographic monitoring may be necessary.

Hypotension in the absence of other major signs of an anaphylactic reaction should initially be treated with oxygen, leg elevation, and rapid administration of IV fluids. Epinephrine should be considered, keeping in mind that fluid therapy alone may be sufficient therapy. Although subcutaneous epinephrine injections are adequate for a mild to moderate reaction, IV administration is needed for moderate to severe hypotension. For IV administration, epinephrine should be diluted to 1:10,000 and 1.0 to 3.0 mL administered slowly. The dose can be repeated in 15 minutes, and the rate of injection can be titrated to achieve the desired result. A vasopressor agent such as dopamine, 2 to 5 $\mu\text{g/kg/min}$, can be added to sustain blood pressure. For unresponsive hypotension, other agents are available for treatment of underlying shock. An H₂ blocker such as cimetidine can be added, 300 mg in dextrose and water, infused slowly. Similarly, diphenhydramine, 25 to 50 mg, can be injected IV. Corticosteroids are also often used, with a typical dose of hydrocortisone being 500 mg IV. Steroids probably have no immediate effect on a reaction; their main use is to decrease delayed reactions.

At times, hypotension can be corrected with vigorous hydration alone, keeping in mind that overhydration of patients with possible underlying cardiovascular and/or renal disease also carries a risk. Thus, the initiation of therapy by adequate hydration is reasonable, but appropriate pharmacologic therapy should be instituted without undue delay.

Hypotension in the presence of bradycardia suggests a vagal reaction. Some patients respond to being placed in a Trendelenburg position. Hypotension in these patients should be treated with rapid IV infusion of isotonic saline. Oxygen should be administered. Bradycardia can be treated with atropine (0.5 to 1.0 mg IV), with the dose repeated every 5 minutes, to a maximal total dose of 3.0 mg.

Some patients receive long-term therapy with a beta blocker such as propranolol. A contrast reaction in these patients can be confusing because, even in the setting of anaphylactic shock, a beta blocker–induced bradycardia can persist. IV glucagon, 1.0 mg or more, may be useful for bradycardia. Dopamine is also effective. Doses of epinephrine that are usually administered may not be effective in reversing this hypotension.

Emergency cardiopulmonary resuscitation is necessary for cardiovascular collapse. Refractory seizures are treated with IV diazepam (Valium) and/or phenobarbital.

Contrast extravasation is treated by extremity elevation, warm or cold compresses and, if extensive, a plastic surgery consultation. Hyaluronidase, an enzyme that breaks down interstitial barriers, has been injected into the extravasation site by some investigators, but its impact on tissue healing is still not clear.

This discussion is only meant to be a guide. The treatment of all reactions should be individualized.

Contrast-Induced Nephropathy. The pathogenesis of contrast-induced nephrotoxicity is incompletely understood, but it is believed that a number of intrinsic renal events lead to renal medullary ischemia, usually augmented by a reduced intravascular volume.¹⁰ Direct cytotoxicity, oxidative tissue damage, and apoptosis are contributing factors. This nephrotoxicity is manifested by a significant rise in the serum creatinine level.

Various authors use different definitions of significant, with the ESUR guidelines using a creatinine level increase of more than 25%, or 44 $\mu\text{mol/L}$ (0.5 mg/dL), within 3 days.³ A transient nonoliguric decrease in renal function lasting up to 3 weeks is more common than the more ominous oliguric manifestation, which may require hemodialysis.

Risk factors for nephrotoxicity appear to be multifactorial and include preexisting renal insufficiency, diabetes, dehydration, cardiovascular disease, advanced age, myeloma, hypertension, hyperuricemia, and possibly contrast osmolality and dose. Patients at the greatest risk for acute renal failure are diabetics with preexisting renal insufficiency. Precaution is also necessary with treatment by agents such as nonsteroidal anti-inflammatory drugs (NSAIDs), aminoglycosides, cyclosporin, or even sulfonamides; underlying nephrotoxicity is a common pathway.

In diabetics with underlying cardiovascular or renal insufficiency, metformin, a biguanide antihyperglycemic agent, is associated with lactic acidosis and resultant increased mortality. This association appears to be indirect and probably involves underlying renal insufficiency. However, enough patients taking metformin and receiving IV contrast have developed lactic acidosis to prompt the U. S. Food and Drug Administration (FDA) to issue a warning—metformin should be discontinued before or at the time of contrast use for 48 hours after the procedure and reinstated only if renal function remains normal. However, substantial inconsistencies exist in the guidelines.¹¹ Adequate hydration should be maintained.

Because iodinated contrast agents are not protein-bound (except for cholangiographic agents), they can be dialyzed. In patients on hemodialysis, additional hemodialysis sessions are generally not necessary.

The most important preventive measure is to ensure that the patient is well hydrated. If IV hydration is necessary, some evidence suggests that the IV use of sodium bicarbonate hydration is superior to sodium chloride.^{12,13} Other guidelines include the use of low-osmolar contrast, discontinuing nephrotoxic drugs for at least 24 hours, and consideration of alternate imaging in high-risk patients. The osmotic diuretic mannitol does not provide any benefit; this loop diuretic furosemide exacerbates renal dysfunction.² Currently, it is probably safe to assume that diuretics do not offer any protective effect, and anecdotal evidence even suggests that diuretics should be stopped prior to a contrast study.¹⁴

N-acetylcysteine, an antioxidant, appears to diminish contrast-induced renal toxicity,^{15,16} although some have questioned its renal benefit.¹⁷ Many of these studies have involved coronary angiography and differ in methodology from contrast CT. The role for theophylline is less well established.

Hemodialysis after contrast use in preexisting renal failure patients is not thought to be warranted. Hemofiltration in chronic renal failure patients, on the other hand, has caused less creatinine level increase than in controls.¹⁸ The complexity of this procedure and the cost of hemofiltration limit its use to select patients.

IODINATED OIL

Intra-arterial iodized poppy seed oil (Ethiodol or Lipiodol) is used for several indications:

1. As a CT diagnostic agent for liver tumor detection, especially hepatocellular carcinoma.

Often used as a gold standard, it detects more tumors than other imaging modalities. Nevertheless, a study of explanted livers revealed that pretransplantation iodized oil CT tumor sensitivity is still rather low. Also, one should keep in mind that iodized oil is retained by some benign tumors, even hemangiomas.

2. Ethiodol is often included as a chemoembolization ingredient when injecting into a tumor feeding artery.

This acts as a chemotherapeutic agent carrier and, because of its high viscosity, is a temporary embolizing material that prolongs chemotherapeutic agent contact with a tumor. Ethiodol remains within tumor neovascularity much longer than in normal liver parenchyma and thus acts as a marker.

3. Occasionally, ethiodol is injected during percutaneous radiofrequency ablation of hepatocellular carcinomas.¹⁹

This aids in the CT delineation of extent of coagulation necrosis.

For a number of reasons, intra-arterial iodized oil is considerably more popular in the Far East than in the West.

OTHER AGENTS

Several reports have described the use of gadolinium (Gd)-based contrast agents for CT imaging in patients with renal insufficiency or prior severe reaction to an iodinated agent. One should keep in mind, however, that the pharmacokinetic properties of gadopentetate dimeglumine (Gd-DTPA), with only one gadolinium ion, are similar to iodinated agents containing three to six iodine atoms. Also, the toxicity of gadolinium agents, at doses achieving equivalent x-ray stopping power, is greater than that of nonionic iodinated agents. This is in distinction to the use of approved lower gadolinium MRI doses, which are insufficient for useful x-ray contrast, but have negligible nephrotoxicity.³ The ESUR position is that gadolinium-based contrast agents are more nephrotoxic than iodinated contrast agents in equivalent x-ray attenuation doses.³

Carbon dioxide is a viable angiographic contrast agent for certain digital vascular indications in the abdomen. It has been used as a guide for vascular interventional procedures. It displaces blood, forms a gaseous column, and is cleared by the lungs.

Apart from MR, viable abdominal reticuloendothelial contrast agents have eluded clinical development. The first such agent, thorium dioxide (Thorotrast), used until the 1950s, has left a painful and sorry legacy. Iodinated oily emulsions accumulate in the liver, spleen, bone marrow and, to a lesser extent, in other organs, long enough to permit CT imaging, but high toxicity and low specificity led to their abandonment. Colloidal iodine or emulsified perfluorooctyl bromide particles are also incorporated in reticuloendothelial cells. Most studies of emulsified perfluorooctyl bromide took place in the 1980s, and its use has lost favor since then.

Liposomes are taken up by the reticuloendothelial system, and considerable effort has been expended to encapsulate water-soluble iodinated contrast agents inside liposomes. Research activity peaked during the 1990s but, in spite of occasional more recent papers, pronounced adverse reactions limit the use of liposomal CT contrast agents in humans. Most current reticuloendothelial contrast research revolves around MRI agents.

Gastrointestinal Contrast Agents

BARIUM SULFATE

Barium sulfate is a white crystalline powder having a molecular weight of 233. Because of its specific gravity of 4.5, patients tend to comment that a cup of barium suspension is "heavy." The terms *thick* and *thin* should only be used when referring to viscosity. They should not be used to signify radiodensity, which has many other causative factors.

Although barium sulfate itself is inert and does not support bacterial growth, some additives in commercial preparations are organic. When a container is opened or reconstituted with tap water, the suspension should be refrigerated if it is to be kept overnight. Although many commercial formulations contain preservatives, bacterial contamination can and does occur.

Certain commercial formulations are advertised as being applicable throughout the GI tract. Invariably, these represent a compromise. The GI tract varies in pH, in composition of mucus, and in type of mucosa, and optimal coating in one part does not mean that a similar coating can be expected in another. Coating the mucosa with barium or simply opacifying the lumen requires different barium formulations.²⁰ The large-particle, high-density barium suspensions designed for double-contrast use should not be simply diluted and used for single-contrast studies. Ingesting such a diluted suspension causes rapid barium particle sedimentation, with the nondependent lumen containing little barium; lesions on the nondependent wall can therefore be missed. Products designed primarily for single-contrast examinations, on the other hand, can be diluted considerably before any settling occurs, mainly because they contain relatively small barium particles.

Ingestion of a barium sulfate suspension tends to be constipating. Currently, commercial barium products have additives that minimize this effect, and the formation of a bariolith is rare.

PHARYNGOGRAPHIC AGENTS

Pharyngeal radiography was already established in the 1960s, when cineradiography became popular to evaluate dysphagia. Although conventional or digital radiography produces high anatomic resolution, dynamic swallowing is best evaluated with video fluoroscopy or cineradiography. This pharyngogram, commonly called a modified barium swallow, evaluates oropharynx anatomy and function using contrast agents of varying consistencies.

After a stroke, appropriate patient feeding without inducing aspiration can be determined by using barium suspensions of different viscosities and barium-coated food. Contrast consistencies used range from barium-coated crackers to a viscosity approaching that of water. To improve patient acceptance, some investigators have developed their own contrast agents such as barium pudding or barium honey. Anatomic detail is best studied with high-density barium products such as the 250% w/v suspensions designed for gastric double-contrast examinations. Fistulas are also best studied with this type of contrast agent. A barium paste can also be used to study anatomy, but the high paste viscosity limits its application in fistula detection. The volume of barium used should be individualized. Thus, with suspected aspiration, a several-milliliter bolus is swallowed

initially; if no aspiration is detected, the bolus is gradually increased in volume.

The oropharynx handles high- and low-viscosity liquids differently, so pharyngeal function should be studied with high- and low-viscosity barium suspensions. The low-viscosity suspension should have a viscosity approaching that of water, whereas the high-viscosity suspension should be similar to a thick milkshake. It should be emphasized that some high-density double-contrast barium products are relatively fluid and are not applicable as high-viscosity preparations.

A tracheoesophageal fistula is easier to detect fluoroscopically with the patient in the lateral position. With the patient in a frontal position, it may not be possible to determine whether barium in the trachea was aspirated or flowed through a fistula.

UPPER GASTROINTESTINAL TRACT STUDIES

Studies of the esophagus consist of single-contrast, double-contrast, and mucosal relief views, together with fluoroscopic evaluation of motility. Normal esophageal tonicity leads to lumen collapse when a primary peristaltic wave has passed. Therefore, regardless of which method is used, the study must be performed reasonably quickly.

Some patient symptoms are reproduced by using a cold contrast suspension or acidic contrast. Although some have found acidified contrast useful, it is not commonly used.

Sufficient air is introduced into the esophagus for a double-contrast study in some patients with poor esophageal motility or those with gastroesophageal reflux. In most patients, however, an additional negative contrast agent is necessary to obtain double-contrast views. Solid gas-producing tablets, powder, or liquid effervescent agents are used. These contain sodium bicarbonate and an acid, such as tartaric acid or citric acid, which, in the presence of a liquid, produce carbon dioxide. About 400 to 500 mL of gas is necessary for adequate esophageal and gastric distention. One technique is to have the patient drink, in quick succession, first one and then another liquid effervescent solution, followed immediately by 60 to 120 mL of a barium suspension. The two effervescent agents distend the esophagus by releasing carbon dioxide, and barium then coats the esophageal mucosa.

The high-density, low-viscosity barium products designed for the stomach and duodenum also coat the esophagus wall. Visualization of the esophagus is impaired if barium is ingested before effervescent agents. On the other hand, the quality of the gastric mucosal coating is improved if the barium suspension is given first. The sequence of ingestion can be tailored to the patient's symptoms—if esophageal disease is suspected, the effervescent agents are given first; if gastroduodenal disease is suggested, the barium suspension is given first.

Esophageal varices tend to be more prominent and their detection easier if the esophageal lumen is collapsed. Although high-density, low-viscosity barium products detect larger esophageal varices, commercially available barium pastes are recommended. Some of these pastes are too viscous and tend to flow in a bolus; these should be diluted with water so the paste viscosity is similar to that of honey.

In a patient with acute dysphagia, an esophagram can be therapeutic. With the patient upright, the weight of a barium column can dislodge a foreign body into the stomach. Liquid effervescent agents increase the intraluminal esophageal

pressure and may also push a foreign body into the stomach. This technique should be performed with care to avoid perforation. Glucagon has also been proposed to help relieve spasm, although it is not clear whether pharmacoradiology has a significant role in acute dysphagia.

Commercial barium sulfate tablets with a diameter of 12 mm are available and are useful to evaluate subtle esophageal strictures. For results to be meaningful, the patient should be at least in a 45-degree upright position and at least 60 mL of water should be ingested with the tablet. Tablet transit time through the esophagus normally is less than 20 seconds. These tablets contain 650 mg of barium sulfate plus additives. The tablets dissolve in the esophagus or stomach (Fig. 1-1). Relatively fresh tablets should be used because older tablets take longer to dissolve.

It has been proposed that barium tablets be administered routinely during chest radiography because tablet retention in the esophagus is associated with the presence of structural or functional esophageal abnormalities, but this technique is not widely used.

In patients with suspected esophageal perforation, study of the esophagus with a water-soluble agent may not detect a subtle leak. Thus, administration of higher density barium sulfate enables detection of leaks that might otherwise be missed.²¹ For this part of the examination, barium suspensions varying from 35% to 80% w/v are used. Residual barium in the mediastinum does not result in clinically detectable

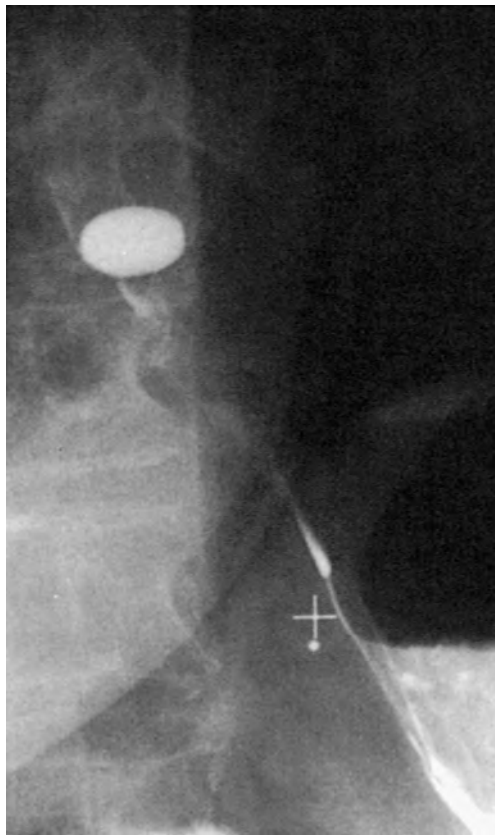


Figure 1-1 Barium sulfate tablet proximal to a stricture. A previous esophagram suggested narrowing at this site, and the tablet confirms this finding. (From Schabel SI, Skucas J: Esophageal obstruction following administration of "aged" barium sulfate tablets—a warning. *Radiology* 122:835–836, 1977.)

mediastinitis and does not interfere with subsequent radiographic evaluation.

High-density, low-viscosity barium preparations specifically designed for the upper GI tract produce best double-contrast results. A volume of 60 to 120 mL of a 250% w/v suspension is generally sufficient. A good barium formulation should result in routine identification of the *areae gastricae*. Small cancers, ulcers, gastritis, and duodenitis are readily detected during a high-quality examination.

When appropriate double-contrast gastric views have been obtained, a lower density barium suspension is ingested for subsequent single-contrast evaluation. For this part of the examination, barium suspensions varying from 35% to 80% w/v are used. Various external compression paddles are available and are helpful in obtaining mucosal relief views.

SMALL BOWEL STUDIES

A number of techniques have been developed to study the small bowel, such as conventional antegrade study, enteroclysis, retrograde ileography, peroral pneumocolon, and CT and MR enterography. The type of examination performed varies with clinical indication. Specific contrast agents have been developed for each type of study.

An antegrade examination is the simplest and most traditional way of studying the small bowel. Serial small bowel radiographs are obtained after the patient ingests a barium suspension. The primary contrast agent requirement is that it does not flocculate or precipitate during transit. The barium does not coat the mucosa; visualization is obtained primarily by filling the bowel lumen with the barium suspension. A 40% to 60% w/v suspension is typical. Many radiologists prefer a volume of 500 to 800 mL.

Contraindications to an antegrade barium study are suspected colonic obstruction or bowel perforation. A number of clinicians hesitate to request a barium study in the setting of small bowel obstruction and prefer to wait until the obstruction clears. Such an approach is analogous to obtaining a chest radiograph only after a pneumonia clears. Small bowel obstruction is not a contraindication. Barium proximal to a small bowel obstruction continues to stay in suspension, and barium inspissation does not occur. With a small bowel obstruction, an antegrade study with barium is safe and not only can detect the site of obstruction but also suggest a cause.

In enteroclysis (small bowel enema), contrast is injected through a steerable catheter directly into the small bowel, so the flow-limiting function of the pylorus is bypassed. The barium suspension can be infused by gravity, hand-held syringes, or an infusion pump. Typical infusion rates are 75 to 100 mL/min, although the flow rate should be individualized. If the rate is too slow, excessive peristalsis results in a study similar to a conventional antegrade small bowel examination. With a flow rate that is too high, overdistention leads to bowel atonia and lack of progression.

It is debatable whether single-contrast or double-contrast enteroclysis yields better results. For the double-contrast portion, many U.S. investigators use a solution of methylcellulose in water ($\geq 0.5\%$). Methylcellulose helps propel a barium suspension ahead of it. Water can be used as the second contrast agent, although water tends to wash off barium adhering to the mucosa. The total volume of the two contrast agents is tailored for each examination; in some patients, up to 2 L are required.

The contrast agents are instilled until a lesion is detected or contrast reaches the right colon. If needed, glucagon is administered to induce hypotonia.

Air as a second enteroclysis contrast agent, used more commonly in Japan and Europe, results in considerably more radiographic contrast than obtained with methylcellulose. Air does not propel the barium ahead of it as quickly as methylcellulose; it tends to percolate through barium-filled loops of bowel. Nevertheless, with overlapping bowel loops, as is common in the pelvis, infusion of air is often helpful. Air bubbles can be confusing, although some think that better diagnostic results can be achieved with air, even in patients with inflammatory bowel disease.

Several tubeless enteroclysis techniques have been described. One simple method is to initially perform a conventional small bowel study, but when barium approaches the cecum, the patient swallows additional effervescent agents, turns prone, and the table is turned into a 20- to 40-degree Trendelenburg position. Efflux of gas results in a double-contrast small bowel study. A tubeless double-contrast small bowel technique consists of effervescent granules coated with an acid-resistant lacquer. Gas is released directly into the small bowel lumen.

Barium formulations specifically designed for enteroclysis provide the best results and are commercially available. For a single-contrast study, a barium suspension having a specific gravity of about 1.25 (equivalent to $\approx 35\%$ w/v) is typical. For a double-contrast study, the barium suspension should be in the range of 50% to 95% w/v.

Retrograde ileography consists initially of a single-contrast barium enema, but infusion of barium is then continued retrograde into the ileum. Because flow is controlled by the examiner, the ileum can be readily studied without overlapping loops from the more proximal small bowel. Barium is instilled until the region in question is reached. Premedication with glucagon increases patient comfort and also relaxes the ileocecal valve. If a redundant sigmoid colon obscures part of the small bowel, the barium enema can be followed by a saline enema; such a solution pushes barium ahead of it and results in a see-through effect. A 20% to 25% w/v barium suspension is typical for such a study.

It is not unusual to achieve a double-contrast study of the terminal ileum during a double-contrast barium enema, especially if glucagon is used. This type of study is useful in suspected ileal Crohn's disease or gynecologic malignancies involving the ileum.

A peroral pneumocolon, consisting of antegrade and retrograde components, is designed to evaluate the distal ileum or right colon. Initially, a conventional antegrade small bowel examination is performed. When barium outlines the terminal ileum, air is instilled through the rectum to obtain double-contrast views of the distal small bowel or proximal colon. This study can also be combined with enteroclysis. Routine use of a hypotonic agent is helpful.

BARIUM ENEMA

Single-contrast and double-contrast techniques are well established methods of evaluating the colon. Numerous studies have compared the relative accuracy of a single-contrast versus double-contrast barium enema. Some radiologists prefer a single-contrast study in older or debilitated patients.

Dry and liquid barium formulations are commercially available. If dry barium-prefilled enema bags are used, the amount of water added and degree of subsequent shaking to achieve wettability should be standardized. The level marking on the enema bag should not be used to gauge the amount of water needed; resultant dilutions tend to be erratic. Liquid barium-filled enema bags should be kept on their sides because considerable settling can occur if bags are stored before use.

A 12% to 25% w/v barium suspension is commonly used for single-contrast barium enemas. The main requirement of the barium suspension is that it neither flocculates nor settles during the examination. Because the sedimentation rate depends, in part, on the amount and type of additives present, some products that are well suspended at higher concentrations settle readily when diluted. If there is doubt about a commercial product's sedimentation rate, a radiograph obtained with a horizontal x-ray beam should reveal any settling tendencies.

Double-contrast barium enema suspensions should consist of relatively high barium concentrations but should still be sufficiently fluid to flow readily through enema tubing. Their viscosity is greater than that of the lower concentration barium formulations designed for single-contrast studies. The resultant mucosal coating should be uniform, without undue artifacts. The suspension should not dry out while an examination is in progress. These barium formulations are generally in the range of 60% to 120% w/v, with 85% being typical.

Even when all conditions are standardized, the subsequent mucosal coating can vary among practices because of variations in local water hardness and type of water used (distilled water or cold or hot tap water). Premixed liquid formulations are available to avoid these variations. The barium suspension is simply poured into an enema bag without further dilution.

Some radiologists perform colonic lavage before a barium enema. This lavage invariably results in water retention and subsequent dilution of the barium suspension. Barium manufacturers recognize this difference and market two different preparations; the one designed to be used after colonic lavage has a barium suspension with a slightly greater specific gravity.

Tumors can be difficult to detect in a segment involved by severe diverticulosis. This segment can be further studied if the double-contrast barium enema is followed by a methylcellulose enema.

WATER-SOLUBLE CONTRAST AGENTS

Indications

Water-soluble organic iodine compounds designed for the GI tract were introduced in the 1950s. Ever since, controversy has surrounded the relative merit and role of these agents. These compounds do not coat the GI mucosa; rather, they provide bowel visualization simply by passive filling of the intestinal lumen.

For most bowel examinations, experienced radiologists prefer barium suspensions. Some surgeons, however, are still being taught about the purported dangers of barium and insist on the use of water-soluble agents. Stimulation of peristalsis in postoperative patients and lack of radiographically visible sequelae of spill from the GI tract are reasons cited by some surgeons for their preference for water-soluble agents.

Water-soluble agents are indicated if an acute perforation is suspected. The examination generally confirms or excludes a

perforation, with the realization that small perforations can be missed. Similarly, walled-off perforations or a perforation in an area of spasm can be difficult to detect, and it may be necessary to complete the examination with barium.

With a chronic or loculated perforation, the higher radiographic visibility of barium often yields more information than that obtained with water-soluble contrast agents. Thus, a chronic abscess or other cavity in continuity with the bowel lumen can be safely studied with barium. If there is a possible communication with the peritoneal cavity, however, water-soluble agents are preferred.

Meconium ileus and meconium plug syndrome can be treated with an iodinated contrast enema. The patient should be well-hydrated.

Some surgeons treat postoperative adynamic ileus with oral, full-strength, ionic contrast agents, but studies on these types of agents have been limited. Also, a hypertonic fluid proximal to a mechanical obstruction results in further distention.

Contrast Agents

In general, to achieve adequate radiographic opacification of most GI structures, at least a 60% solution of an ionic contrast agent is needed. The resultant iodine concentration is 282 to 292 mg/mL for the more commonly used commercial products, with a resultant osmolality of about 1500 mOsm/kg, or approximately five times that of serum. Because of this hyperosmolality, fluid is drawn into the bowel lumen, and diarrhea is common after their use. These agents stimulate intestinal peristalsis, so faster visualization of the distal small bowel can be achieved than with barium sulfate. The need for a faster examination should be balanced against decreased radiographic contrast obtained with these agents. In general, intraluminal dilution leads to poor visualization of the small bowel.

Some commercial ionic contrast agents designed for oral use, such as the diatrizoate meglumine preparations Gastrografin and oral Hypaque, contain flavoring agents. These are preferred to the nonflavored products, which are designed primarily for IV use.

Nonionic contrast agents with an iodine concentration of approximately 300 mg/mL have an osmolality of 600 to 710 mOsm/kg, which is less than 50% of that of ionic agents. At this concentration, however, they are still hyperosmolar compared with serum.

Ideally, one of the nonionic agents should be used whenever a water-soluble agent is indicated for evaluation of the GI tract; for certain examinations, some radiologists use nonionic agents. If a perforation into the pleural or peritoneal cavity is suspected in an adult and aspiration is not a consideration, nonionic agents probably do not offer any major advantage over their ionic counterparts. Nevertheless, some leaks are better defined with barium than water-soluble agents. In studies of the GI tract in infants and children, in whom perforation is not an issue, barium rather than a water-soluble is the preferred contrast agent.

NEGATIVE CONTRAST AGENTS

When performing double-contrast GI studies, the cheapest second contrast agent is air. Excellent double-contrast esophageal views can be obtained if the patient swallows air together with the barium preparation.

One commercial preparation incorporated carbon dioxide directly in the barium suspension; when the patient drank this “bubbly barium,” carbon dioxide was released into the esophagus and stomach. The effect was similar to that of drinking a bottle of club soda, and this product did not achieve ready acceptance.

Effervescent tablets, granules, and powders are commercially available. They produce carbon dioxide on contact with water and most are satisfactory in achieving adequate gastric and duodenal distention. There is, however, considerable variation in their dissolution time. Most commercial effervescent powders and granules come in single-dose packages. In clinical use, the patient places the effervescent agent in the mouth and uses small amounts of water to wash it down. This is immediately followed by a barium suspension. The swallowed gas is used for double-contrast views of the stomach and duodenum.

Liquid effervescent agents, consisting of separate acid and base solutions, can be prepared locally by a hospital pharmacy. The acid portion consists of citric and tartaric acids and the base portion is sodium bicarbonate. A dose of 12 to 15 mL is satisfactory for most patients.

Carbon dioxide is used by some in place of air for double-contrast barium enemas and CT colonography. Carbon dioxide is absorbed faster than air. Whether a gas or air is used probably does not influence examination quality although, with all other factors remaining constant, colonic distention is less with carbon dioxide compared with air.

Some double-contrast preparations result in excessive gas bubbles. An antifoam agent should be added empirically if these occur on a regular basis. Although many commercial barium preparations already include such an agent, in some areas the amount is not sufficient. A commonly used antifoam agent is dimethyl polysiloxane (simethicone); the addition of 1.5 mL of simethicone (equivalent to 100 mg) is often sufficient to eliminate bubbles.

GASTROINTESTINAL COMPUTED TOMOGRAPHY AGENTS

The term *double-contrast abdominal CT* is used by some to signify the use of IV and oral contrast. However, this is a misuse of the traditional connotation of double contrast and is best avoided to prevent confusion.

Full-strength barium preparations should not be diluted to the low concentrations needed for CT. The barium particles settle out after ingestion of such a dilute solution, leading to inhomogeneous bowel lumen opacification. The uppermost part of a loop of bowel may not contain enough barium for visualization, and excess barium in the dependent portion results in streak artifacts.

Stable but low-concentration barium formulations specifically designed for CT are commercially available, with most of these brand names ending in *-cat*. Most CT barium products contain small particles that resist settling. Additives selected also prevent barium sedimentation. At the low barium concentrations used, barium particles do not coat the mucosa but simply provide lumen opacification.

An esophagus marked with a contrast agent aids in evaluating the mediastinum during chest CT. The low-concentration CT agents used in the rest of the GI tract do not opacify the esophagus long enough, although one option is to have the patient drink small sips of a conventional CT contrast agent

before each scan. More convenient is a high-viscosity, low-concentration barium paste, which provides prolonged esophageal coating.²² Mucosal adherence by such a paste is long enough to allow a typical CT examination to be completed. Ingested water is often a useful and satisfactory contrast agent for evaluation of the GI tract during helical CT.

The traditional method of opacifying the stomach and small bowel is to have the patient drink approximately 500 mL of a dilute CT contrast agent several hours before the examination, with a similar amount ingested immediately before scanning. Ideally, such an agent should differentiate bowel from surrounding structures without introducing artifacts. Use of a dilute iodine solution or a barium suspension is generally a personal preference. A 1% to 3% w/v barium sulfate suspension or a 2% to 5% solution of Gastrografin or similar iodinated agent is typical. One refinement (granted, little practiced) is to use a 2.0% barium concentration for jejunal opacification and a slightly lower concentration for pelvic structures. With slower CT units, an iodine solution produces fewer streak artifacts than barium, a problem of little consequence with multislice CT. Commercial barium suspensions tend to taste better than iodine solutions, a factor when examining children and nausea-prone cancer patients.

The iodine taste can be masked by adding sugar and various fruit extracts; although essentially sugar-free iodine contrast is available, barium products, in general, contain less sugar than corresponding iodine contrasts. At the dilutions used, the iodinated solutions are hypoosmolar, but some patients still develop diarrhea. The poor taste and hence poor acceptance of iodinated agents by patients can be partly overcome by the empiric addition of a flavored juice such as Kool-Aid.²³ At the dilutions used in CT, nonionic contrast agents do not have any real advantage over ionic agents.

With suspected pelvic disease, a contrast agent can be ingested the evening before the examination. Even if full-strength Gastrografin is ingested, overnight dilution in the bowel is sufficient to eliminate most streak artifacts. Better rectosigmoid opacification is obtained after ingestion of such a full-strength contrast agent than dilute barium, probably because hyperperistalsis is induced by the iodinated agent. Nevertheless, identifying the large bowel is less of a problem than identifying fluid-filled loops of small bowel on abdominal CT.

Both CT and MR enterography can detect Crohn's disease with somewhat similar accuracy.²⁴ Adequate CT bowel opacification can be achieved by using a 2% flavored barium suspension.

CT enteroclysis consists of bowel intubation and instillation of an iodinated contrast agent, dilute barium suspension, or methylcellulose suspension. Whether a positive or water-density agent is superior is not clear; an IV contrast agent to opacify bowel mucosa aids in lesion detection. Negative oral contrast agents designed specifically for CT enteroclysis have also become available. Also, with MDCT and coronal reconstruction now more readily available, retained bowel fluid often provides a sufficient marker, especially in dilated bowel loops.

If the imaging study is performed to evaluate a rectal lesion, a high-viscosity, low-volume barium paste may suffice; approximately 100 mL of a 3.6% w/v carboxymethylcellulose and 2% w/v barium sulfate paste mixture has been proposed in this clinical setting.²⁵

A basic question when protocoling an examination on multidetector CT is whether intraluminal water-density or

fat-density contrast, or even a gas, is superior to a positive contrast agent. Positive bowel contrast creates artifacts, especially with maximal intensity projection images of vascular structures. Also, bowel wall enhancement by IV contrast is useful for detecting bowel wall thickening, and a positive intraluminal contrast can obscure subtle lesions. As a result, MDCT studies can be performed with oral water-density or even negative contrast agents. Although adequate for gastric and duodenal distention because of its absorption from the bowel, ingested water does not readily distend the distal small bowel; use of a carboxymethylcellulose or polyethylene glycol solution inhibits absorption and improves distention (compared to water). A preliminary study of simethicone-coated cellulose (SonoRx, Bracco Diagnostics, Monroe Township, NJ), developed for oral use in upper abdominal ultrasonography, found no significant advantage over oral water in abdominal CT.²⁶

In the past, a number of fat density products, such as mineral oil, corn oil, and milk, and even a paraffin emulsion, were proposed for CT use, but these have had limited application. Residual bowel gas often serves as a marker, especially in the colon. If a nasogastric tube is in place, air can be injected into the stomach and small bowel. If excessive amounts of gas are present, imaging with window settings slightly wider than usual is helpful. 2D colonography and 3D virtual colonoscopy require colonic distention with a contrast agent; typically, air is used, and carbon dioxide is used less often.

ADVERSE REACTIONS

Barium Sulfate

Barium sulfate is poorly soluble in water. The constipating tendency of barium products is well known to most radiologists. Through the judicious use of additives, this side effect is minimized in most current formulations, although barium impaction in the colon is still occasionally encountered.

Aspiration of small amounts of commercial barium formulations is of little clinical significance. After barium aspiration, most is cleared from major bronchi and trachea within hours, although some is retained in the interstitium and in macrophages. This residue is generally not visualized on radiographs. Alveolarization of barium, however, can result in prolonged retention. If aspiration is suspected clinically, nonionic, sterile, iso-osmolar iodinated contrast can be used rather than barium.

Hypersensitivity reactions during GI examinations are rare, although they have been known to occur. Although barium sulfate is inert, commercial formulations contain numerous known proprietary additives.²⁷ These include stabilizing, flavoring, coating, and viscosity-varying agents and range from natural flavors and gums, such as lemon, pectin, and guar, to synthetic products, such as various methylcelluloses. Some radiologists may still be familiar with chocolate-flavored barium products, which are no longer used because of common allergies to chocolate. Anaphylaxis can be caused by carboxymethyl. Methylparaben and similar compounds, used as preservatives, can induce hypersensitivity reactions, but barium manufacturers have replaced them with more innocuous preservatives in most commercial barium products.

Reactions appear to be more common during double-contrast than single-contrast studies. Most reactions are mild and consist of urticaria or pruritus, although erythema

multiforme, respiratory complications, anaphylaxis, GI angioedema, and even death have occurred. Patients with asthma and severe food allergies appear to be at a slightly increased risk for these reactions, but the average radiologist will probably not encounter a hypersensitivity reaction to a barium product in a lifetime of practice.

The cause of hypersensitivity reactions during most barium studies is not known. In general, the incriminating agent is not sought and no testing performed in most patients who develop a reaction.

Esophageal perforation and spillage of barium into the mediastinum result in an inflammatory reaction, with barium persisting in the mediastinum for a prolonged period. Such prior extravasation can often be recognized radiographically as dense linear radiopacities, but no strong evidence exists that these sequelae have any clinical significance for the patient.

Most perforations associated with a barium enema occur in the rectum and are not immediately detected by fluoroscopy. Rectal perforations tend to result from injudicious insufflation of an enema balloon. A British survey over a 3-year period between 1992 and 1994 revealed a complication rate of 1 in 9000 and a death rate of 1 in 57,000.²⁸ Although 10% of patients with a bowel perforation died (3 of 30), the mortality was 56% (9 of 16) in patients developing a cardiac arrhythmia.

Spillage of barium into the peritoneal cavity can be secondary to a preprocedure perforation, such as in patients with ulcers. Some perforations, however, are associated with a barium study and can occur during an upper GI examination or barium enema, and even during enteroclysis. Initially, leukocytes are drawn into the peritoneal cavity, together with an inpouring of fluid. Profound hypovolemia develops if massive inpouring of fluid into the peritoneal cavity is untreated. Bacterial contamination during a perforation can result in overwhelming sepsis and shock within hours.

Immediate management of barium peritonitis includes infusion of large volumes of IV fluid. Antibiotics are administered because of associated bacterial contamination. Most patients undergo surgery, with an attempt made to evacuate barium from the peritoneal cavity. Invariably, barium crystals embedded on the peritoneal surface resist dislodgment. Attempts to remove barium particles with a wet sponge simply induces diffuse peritoneal bleeding.

Barium crystals incite an inflammatory reaction; eventually, these crystals become coated by a fibrin membrane, and extensive fibrosis and granulomatous tissue develop. Dense fibrosis can involve adjacent structures and, depending on location, subsequent ureteral obstruction or bowel deformity and stenosis develop. Perirectal fibrosis can narrow the rectosigmoid lumen and even mimic a carcinoma. Residual barium is identified with conventional radiography or CT. No evidence suggests that barium in soft tissues is a carcinogen (Fig. 1-2).

The barium intravasation can involve systemic veins and the portal venous system.^{29,30} Some patients have no predisposing factors to account for intravasation. Overall, barium intravasation is associated with a mortality rate of more than 50%.

Water-Soluble Agents

The risk of sensitivity reactions to oral iodinated contrast agents is considerably less than with intravascular injection. In young children and adults with hypovolemia, however, the introduction of large volumes of a hypertonic agent into the GI tract

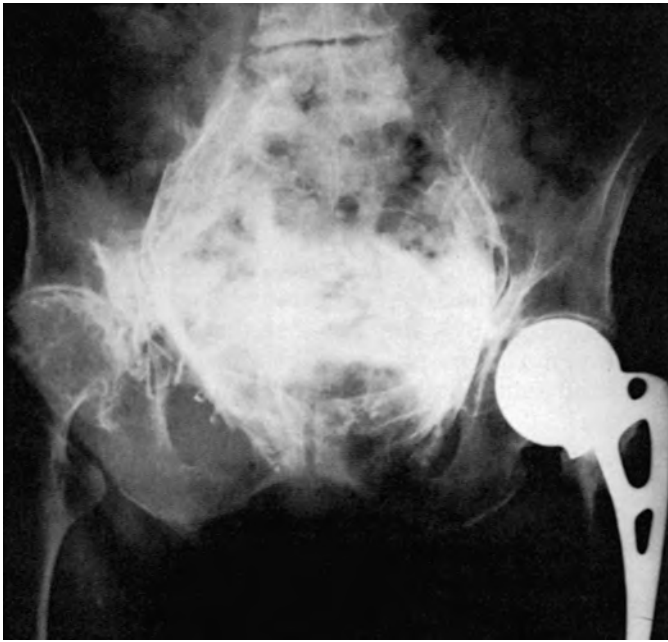


Figure 1-2 Prior colonic perforation during a barium enema. Barium crystals are encased by dense adhesions that also involve bowel. (From Miller RE, Skucas J: *Radiographic Contrast Agents*. Baltimore, University Park Press, 1977, p 137.)

can result in hypovolemia, shock, and possibly death. In such a setting, adequate intravascular fluid replacement and the use of a nonionic contrast agent should be considered.

If aspiration or a tracheoesophageal fistula is suspected, hyperosmolar ionic contrast agents are contraindicated because they can induce pneumonia, pulmonary edema, or death. The nonionic agents are reasonable substitutes. In most adults, however, barium sulfate is the preferred contrast of choice.

Other Contrast Agents

Some reactions occur even before a contrast agent is instilled. Latex, used in some enema balloons, has been implicated in some reactions. The offending antigen in latex is believed to be a water-soluble, heat-stable protein. It is found on the surface of cured latex and probably is a contaminant of natural latex when it is obtained from the *Hevea brasiliensis* tree. In sensitive individuals, contact with skin leads to urticaria; contact with mucous membranes can result in more severe anaphylactic reactions. Currently, nonlatex and synthetic latex products are available.

Cholangiographic Contrast Agents

With normal renal function, only about 1% of an ionic or nonionic contrast agent dose undergoes hepatic excretion, which is insufficient for CT bile duct visualization. In the setting of renal failure, however, it is not unusual to detect gallbladder opacification, even with conventional radiography.

Cholecystography using oral cholecystographic agents has been supplanted by other imaging modalities and currently is rarely performed. Several commercial cholecystographic agents are available. To ensure oral absorption, they have hydrophilic and lipophilic properties; in blood, they are bound to albumin and, theoretically, should have high toxicity, but in

actual practice, adverse reactions are uncommon. They undergo enterohepatic circulation and occasionally delayed reactions are encountered.

IV cholangiographic agents undergo hepatocyte uptake and biliary excretion by active transport. They are excreted unchanged or after conjugation with glucuronic acid. These hepatocyte-specific liver contrast agents consist of triiodobenzene compounds which, by means of benzene ring substitutions, have had their hydrophilicity decreased to the point that they can now pass through membranes. Iodipamide meglumine (Cholografin) is the only agent available in the United States. Most of the injected contrast is bound to albumin; biliary visualization is generally evident about 15 minutes after the start of IV injection. One might assume that because cholangiographic agents undergo hepatocyte uptake, they would make useful CT liver contrast agents; in actual practice, however, hepatocyte uptake is too slow and excretion too fast for them to serve this function.

Toxicity and allergic reactions are more severe with iodipamide than with more typical intravascular contrast agents. Nephrotoxicity is dose dependent. In part because of this toxicity, cholangiography has been supplanted by other imaging, including MRI and direct cholangiopancreatography. The latter is achieved by percutaneous transhepatic cholangiography, an endoscopic retrograde approach, or injection through a surgically placed tube.

Direct cholangiography is generally performed with full-strength contrast concentrations (≈ 300 mg iodine/mL). In particular, when searching for subtle leaks, a high iodine concentration is advantageous. Also, when injecting proximal to an obstruction, a high iodine concentration allows for dilution by residual bile. When searching for stones, however, dilution of contrast with an equal volume of water appears useful; subtle stones can be missed in markedly opacified bile ducts. Contrast overinjection during direct cholangiography should be avoided. In the United States, syringe injection is common, but in Europe, a drip infusion technique is more popular. The study should be terminated if the pancreatic duct begins to opacify—acute pancreatitis is a complication of this study. Earlier studies suggested that meglumine salts of ionic contrast agents resulted in less bile duct epithelial damage than corresponding sodium salts; the use of nonionic contrast makes this point moot.

Indications for CT cholangiography have been evolving. CT cholecystography is performed 10 to 12 hours after oral administration of a cholecystographic contrast agent (iopanoic acid). Another approach is slow infusion of a cholangiographic contrast agent, resulting in biliary images superior to those obtained with conventional IV cholangiography. Major intrahepatic ducts are visualized in most individuals. Preliminary evidence has suggested that CT cholangiography is somewhat superior to MR cholangiopancreatography (MRCP) in visualizing small biliary stones. It is not useful in jaundiced patients because insufficient contrast is excreted into bile ducts.

MRCP is a noninvasive imaging technique for visualizing biliary and pancreatic ducts. It has evolved as an alternative to diagnostic endoscopic retrograde cholangiopancreatography (ERCP) and diagnostic percutaneous cholangiography. Two approaches are feasible—an IV contrast-assisted technique and a technique without contrast using heavily T2-weighted images to make nonflowing fluid hyperintense. The former uses primarily hepatobiliary MR agents (see later); contrast-containing

bile is hyperintense on T1-weighted sequences. A limitation of this procedure is that reasonable hepatocyte function is required to accumulate enough biliary contrast to be imaged. The contrast-less technique, often simply called MRCP, has none of these limitations and has become the primary imaging study for visualizing bile ducts.

Magnetic Resonance Imaging Contrast Agents

INTRAVASCULAR AGENTS

The term *contrast agent* has a different meaning in MRI than usually applied to barium sulfate or iodinated agents. MRI contrast agents are not visualized directly; rather, their primary function is to alter water proton relaxation times. These agents have considerable variation in diffusion and renal clearance, thus leading to the use of a specific contrast agent for a specific application. Although MRI contrast agents are more complex and serve a more varied function than CT contrast agents, they are used for the same primary purpose—to improve lesion detection and characterization by increasing contrast tissue signal intensity differences because of different effects on tissue proton relaxation. These differences vary with time and depend on the degree of lesion vascularity. Much current MRI contrast agent research has focused on improving their specificity.

MRI contrast agents are often classified by their metal component. A more useful classification is based on their distribution, with the realization that many agents overlap between categories; many are initially blood pool agents but subsequent distribution depends on their molecular configuration:

1. Conventional gadolinium chelates (extracellular agents)
2. Macrophage-monocytic phagocytic (reticuloendothelial) agents
3. Primarily hepatobiliary agents (intracellular agents)
4. Primarily blood pool agents

All currently available MRI contrast agents shorten tissue T1 and T2 relaxation times. The paramagnetic gadolinium and manganese contrast agents primarily shorten T1 and thus increase signal intensity (enhancement) of normal parenchyma on T1-weighted images. The superparamagnetic iron oxides primarily shorten T2, thus decreasing signal intensity on T2-weighted images and, depending on the sequence used, increase the T1 signal. These metal ions are chelated to other structures, such as DTPA, to reduce their toxicity.

Gadolinium Chelates

The most often used vascular MRI contrast agents are gadolinium chelates. These mostly hydrophilic compounds are chelated to “mask” the toxic gadolinium ion. Their biodistribution and perfusion-related issues are similar to iodine-containing contrast agents. To take full advantage of these MRI contrast agents, dynamic imaging must be performed shortly after contrast injection (arterial to portal venous phases); later, these agents equilibrate with the extracellular space, and lesions become isointense to parenchyma. Liver tumor detection with these agents relies on differences in blood flow between tumor and normal tissue. A more recent application of these agents is in MR angiography (MRA) as a substitute for abdominal digital subtraction angiography (DSA). Image processing allows for the separation of arteries and veins.

At recommended doses, gadolinium chelates have a lower adverse reaction rate than iodinated contrast agents, but anaphylactic reactions and even cardiopulmonary arrest, including fatal ones, do occur. Risk factors for reactions are not well defined but appear to be similar to those for iodine contrast. Unlike iodine-related reactions, gadolinium-related reactions tend to be delayed, at times occurring even 1 hour or more later. These agents are excreted by glomerular filtration and, in the usual doses, nephrotoxicity is uncommon, although nephrogenic systemic fibrosis has been reported in some patients with renal disease.³¹

In patients on hemodialysis, about 80% of gadolinium is dialyzed after the first and essentially all after the fourth dialysis. A normal dose has been used in hemodialysis patients.

Gadolinium agents exhibit poor water relaxivity at higher magnetic fields (>4 T). Undoubtedly, new MRI agents will be developed for use with high field strength magnets.

Reticuloendothelial Agents

Larger superparamagnetic iron oxide (SPIO) particles are taken up by the reticuloendothelial system (RES) and, among other effects, result in decreased liver and spleen parenchymal enhancement on T2-weighted images. Uptake is also present in lymph nodes and bone marrow. Ferumoxides (Endorem, Guerbet, Villepinte, France) is an SPIO agent consisting of a colloidal mixture of ferrous and ferric oxide. Tissues lacking reticuloendothelial (RES) cells, such as metastases, have little or no signal loss and thus appear hyperintense to the resultant hypointense, normal RES-containing liver or spleen parenchyma. Not only are known tumors better identified but, compared with unenhanced MRI sequences, more tumors are detected. This differentiation is not absolute, however, because some well-differentiated neoplasms contain RES cells and thus take up iron oxide particles. These SPIO-induced changes differ among various tumors, potentially providing tissue characterization of different tumors. SPIO enhancement is impaired in diffuse liver disease. Nevertheless, imaging interpretations with these compounds is complex; some of the particles are ultrasmall, and T1-weighted gradient-echo sequences result in imaging patterns similar to those with Gd chelates and ultrasmall SPIO particles.

These agents have a longer intravascular half-life than gadolinium chelates. A prolonged scanning window is available once these particles are within the RES; eventually, free iron is used in normal iron metabolism. Their role in clinical imaging has not yet been clearly defined. Disadvantages include prolonged scanning times and an increased false-positive rate.

Hepatobiliary Agents (Intracellular Agents)

Several hepatobiliary-specific paramagnetic contrast agents, such as Gd-EOB-DTPA (Eovist, Bayer Imaging, Whippany, NJ) and Gd-BOPTA (MultiHance, Bracco Diagnostics) are initially extracellular and then undergo hepatocyte uptake. Early dynamic perfusion imaging is similar to that with conventional gadolinium chelates, but this can be followed by delayed hepatic imaging; each phase yields different information. Image interpretation differs from conventional gadolinium scans; thus, with Gd-BOPTA, a hepatocellular carcinoma shows early peripheral enhancement, but parenchymal phase images reveal an isointense or even hypointense tumor.³²

These agents are eliminated by biliary and renal pathways. Eovist achieves greater liver enhancement than MultiHance, has

a biliary excretion rate of about 50% of the injected dose, and a delayed biliary phase is evident. Gd-BOPTA exhibits a T1 relaxivity roughly double that of conventional gadolinium agents, probably secondary to its binding to albumin, which decreases extravascular leakage. Although only a small percentage is taken up by hepatocytes, this has a prolonged effect on liver signal intensity.

Mn-DPDP (Teslascan, GE Healthcare AS, Buckinghamshire, England) dissociates partly in plasma, with free Mn^{2+} taken up by hepatocytes and other tissues, including the pancreas. Non-dissociated Mn-DPDP is eventually eliminated by the kidneys. It is often considered to be a hepatobiliary-specific paramagnetic contrast agent, having an effect lasting for several hours, thus permitting delayed imaging. It is injected by slow IV infusion, so dynamic imaging is not feasible. On T1-weighted images, this agent selectively enhances normal liver parenchyma and hepatocyte-containing tumors such as focal nodular hyperplasia, regenerative nodules, and hepatocellular adenomas and carcinomas, but shows little or no enhancement of metastases, cysts, and hemangiomas. This agent differentiates hepatocellular carcinomas from metastases, with metastases of nonhepatocyte origin becoming more conspicuous because of an increased signal from surrounding normal liver parenchyma. An exception is metastatic neuroendocrine tumors; occasionally, these tumors enhance with Mn-DPDP. A possible use is during MRI-guided thermal tumor ablation when prolonged tumor visualization is beneficial³³; Mn-DPDP identifies more focal tumors in cirrhotic and noncirrhotic livers than detected on precontrast images. It appears useful in defining intrahepatic biliary anatomic variants, such as in pretransplantation liver lobe donors. Because it does not differentiate between benign and malignant primary liver neoplasms, its diagnostic impact is not clear.

Manganese is excreted in bile, but excretion is inhibited in biliary stasis. It is contraindicated in severe liver failure. Mn-DPDP's overall safety appears to be similar to that of the other hepatocyte gadolinium products.

Blood Pool Agents

Ultrasound superparamagnetic iron oxide (USPIO) particles, unlike most MRI contrast agents, shorten T1 and T2 relaxation times, with a few exceptions. Initially conceived as MRI lymphographic agents, their current role has evolved mostly into blood pool agents. They have a blood half-life measured in hours. One disadvantage is the superimposition of arteries and veins, although image processing techniques such as subtraction and phase contrast can differentiate these structures. These iron oxide contrast agents appear useful in differentiating highly vascular lesions, such as hemangiomas, from solid neoplasms. Also, their prolonged reduction of intravascular T1 values makes them useful for MR angiographic interventional procedures without need for repeat contrast injection. Their relaxivity increases at lower field strengths, and they are therefore suitable for use in open magnets.

Iron oxide particles smaller than 10 nm pass through capillaries and are eventually cleared by liver, spleen, bone marrow, and lymph node reticuloendothelial cells, resulting in homogeneous signal loss in these structures. These agents therefore can potentially identify lymph node metastasis independently of node size; normal nodes lose signal intensity but nodes (or regions of nodes) containing metastases do not take up these particles.³⁴

A potential use for iron oxide agents is to label them with a target-specific drug, such as cholecystokinin, with receptors in the pancreas. Development of such agents is still in its infancy.

A separate group of blood pool contrast agents consists of gadolinium-based products bound to albumin, dextran, or another similarly large molecule (also called macromolecular MRI contrast agents); imaging using Gd-BOPTA has already been discussed (see earlier). Biodegradable polymeric MRI contrast agents have been reported.³⁵ Tight albumin binding prolongs blood pool time. The clinical role of these agents presumably will be similar to that of USPIO agents.

Carbon dioxide is a blood pool MRI contrast agent. An intravascular column of carbon dioxide leads to signal loss and results in a black blood MR angiography technique.

More complex applications of MRI contrast agents involve combining two agents (sometimes called double-contrast MRI imaging). For example, more information is obtained about a focal tumor by combining perfusion data of a gadolinium chelate with its RES status obtained with a SPIO agent than is possible with a single agent alone. Such combined contrast agent use is mostly experimental.

Another research approach involves excitation-based, frequency-labeled, exchange transfer imaging to separate tissue magnetization transfer contrast components by using a paramagnetic chemical exchange saturation transfer agent.³⁶ MRA of hepatic vessels appears comparable to DSA and superior to portal vein images for evaluating liver arteries.

GASTROINTESTINAL AGENTS

An oral MRI bowel contrast agent identifies the bowel lumen and differentiates the normal bowel wall from an abnormal process. Bowel distention can be obtained by injecting contrast via a nasojejunal catheter (enteroclysis) or having the patient drink a large quantity of fluid (enterography). An oral contrast agent aids in identifying a soft tissue tumor in the bowel wall and in adjacent organs.

Oral MRI contrast agents are subdivided into positive contrast agents, which predominantly shorten T1 and increase MRI signal intensity on T1-weighted images, and negative contrast agents, which shorten T2 and decrease signal intensity or simply lack hydrogen protons and water-density contrast. Positive contrast agents consist of various iron, manganese, and gadolinium paramagnetic compounds; they are useful in detecting sinus tracts. On the other hand, they mask intraluminal content and make bowel wall visualization difficult.

A distinction between positive and negative contrast agents is not absolute, and some agents change properties with dilution and the MRI sequence used. Gadolinium is a positive contrast agent that shortens T1 in the small bowel but, when concentrated in the colon, it acts as a negative contrast agent. Ferric ammonium citrate is hyperintense on T1- and T2-weighted images at concentrations lower than 45 mg/mL; at higher concentrations, and at 10 to 20 mg/mL, bowel loops become hypointense on T2-weighted images. A more relevant issue is whether such contrast improves lesion detection; current results are not clear.

A dilute barium sulfate suspension is a useful negative agent. Perfluorocarbons lack hydrogen protons and do not produce an MRI signal on T1- or T2-weighted images, but their role as oral agents is not established. Methylcellulose, polyethylene glycol, and dilute magnesium sulfate³⁷ have been evaluated. Air and

water are also MR contrast agents. Nonabsorbable water-density agents are similar to those used for CT (see earlier).

Positive contrast agents accentuate motion artifacts. However, contrast artifacts are more pronounced with negative agents, but bowel wall abnormalities are better evaluated with negative agents. Antiperistaltic pharmacologic agents have been used; they reduce motion artifacts, even with a high field strength unit.

MR colonography is performed using water, a gadolinium solution, or a barium suspension as a luminal contrast agent. Evaluation can include surface-rendered, virtual endoscopic endoluminal views, orthogonal sections in three planes, and water-sensitive images.³⁸ A preliminary report has suggested that MR proctography is inferior to barium proctography for detecting pelvic floor abnormalities.³⁹

Pharmacoradiology

Pharmacologic agents useful in GI radiology will be discussed in this section. Included are those having an intravascular effect (vasoconstrictors and vasodilators), those modifying gut motility, and those affecting bile flow. Excluded are experimental agents, agents designed for molecular imaging, and therapeutic materials.

From a radiologist's viewpoint, most gut motility agents can be divided into those that increase GI tonicity and motility and those that decrease these functions. Some agents have different effects on different parts of the GI tract; they are discussed separately in the section on mixed action agents.

Bowel tonicity is not the same as peristalsis. In general, however, pharmacologic agents that increase bowel tonicity also result in increased peristalsis. For example, agents inducing gastric hypertonia tend to result in faster gastric emptying and hypertonic small bowel agents result in faster small bowel transit. Hypotonic agents have an opposite effect.

One exception to this classification is famotidine, which suppresses gastric secretions. A preliminary report suggested that famotidine may be useful prior to an upper GI examination; the decreased gastric secretion improved the quality of the examination.⁴⁰

VASOCONSTRICTORS

The primary use of vasoactive drugs in abdominal imaging is to alter blood flow in a way designed to increase diagnostic accuracy. Some drugs aid delivery of chemotherapeutic agents to neoplasms. All side effects must be acceptable. Vasoconstrictors aid primarily in detecting and characterizing neoplasms; they constrict normal blood vessels but have little if any effect on malignant vessels.

Epinephrine, an adrenergic hormone, stimulates α and β receptors and, depending on specific innervation, results in vasoconstriction or dilation. Initially used in renal arteriography, epinephrine decreases contrast opacification of normal renal parenchyma, thus accentuating renal cell carcinoma vasculature. Limitations for the use of epinephrine include a variable dose response and the ability of some inflammatory tissue neovascularity to respond similarly to neoplastic neovascularity. Hepatic and splenic arterial injection results in spasm of these vessels but little constriction of normal hepatic, gastric, duodenal, and pancreatic small vessels. Also, normal mesenteric vessels do not respond appreciably to epinephrine.

Propranolol blocks β -adrenergic vasodilation and, when used in conjunction with epinephrine, results in mesenteric vessel vasoconstriction.

Norepinephrine has α receptor stimulation similar to that of epinephrine but lacks β receptor stimulation. It has been less well studied for imaging use than epinephrine.

Patients with a pheochromocytoma have increased epinephrine or norepinephrine levels after contrast injection; it thus appears prudent to premedicate these patients with α - and β -adrenoceptor antagonists to control symptoms and prevent an adrenergic crisis, although this may not be necessary when using some nonionic contrast agents.

Angiotensin, a hormone family with vasoconstrictive activity, is a potent vasoconstrictor acting on normal vessel smooth muscle. Similar to epinephrine, it tends to enhance visualization of malignant neoplasms by a selective increase in tumor blood flow.

Vasopressin in pharmacologic doses has a pressor effect and constricts normal splanchnic small vessels (including capillaries), thus decreasing portal blood flow. It has little effect on hepatic artery flow. Transcatheter vasopressin infusion controls some GI hemorrhage, keeping in mind that intra-arterial administration may cause mesenteric infarction or small bowel necrosis.

Bombesin, a gut peptide, releases endogenous gastrin, which activates gastric mucosal sensory neurons, which in turn increase gastric mucosal blood flow and thus protect the mucosa against damage. Somatostatin negates this bombesin-induced gastroprotection. Although bombesin is not used in radiology, the somatostatin analogue, octreotide, has been used for therapy of esophageal and gastric variceal bleeding. Gut neuroendocrine tumors also contain somatostatin receptors, and octreotide is useful for diagnosis and palliation of these tumors. It suppresses carcinoid tumor symptoms.

VASODILATORS

Vasodilators increase blood flow in a selective vascular bed. Their effects differ in normal and neoplastic vessels, but vasodilators are less suitable than vasoconstrictors for outlining small neoplasms; increased normal vascularity tends to obscure a small tumor. Occasionally helpful is a high-calorie meal, which accentuates superior mesenteric artery and portal vein blood flow.

Tolazoline, an adrenergic alpha receptor blocking agent and synthetic vasodilator, aids in the angiographic visualization of small vessels. Direct mesenteric artery injection leads to improved venous visualization. Its effect on neoplasm visualization is mixed. Whether tolazoline has a role in intra-arterial provocative mesenteric angiography to identify GI bleeding is not clear. Infusion therapy with tolazoline and heparin has been used to treat nonocclusive mesenteric ischemia.⁴¹ Intra-arterial verapamil and tolazoline appear to be comparable in their vasodilatory efficacy.⁴²

Bradykinin is a nonapeptide, produced from decapeptide kallidin, normally present in blood in an inactive form. Bradykinin is a plasma kinin, potent vasodilator, and one of the mediators of anaphylaxis released from cytotoxic antibody-coated mast cells. Radiographically, bradykinin injected into the superior mesenteric artery improves portal vein visualization.

Acetylcholine, a parasympathetic hormone, is a vasodilator previously used mostly to evaluate renal artery stenosis.

Dopamine, a potent renal artery dilator, is similar to acetylcholine; it has also been studied mostly in renal vessels. Preliminary work has suggested that dopamine decreases contrast-induced nephrotoxicity, but further studies found that it may have a deleterious effect.⁴³

Prostaglandins have variable vascular effects, depending on their chemical composition and specific use. Prostaglandin therapy is used in neonates with cyanotic congenital heart disease. Prostaglandin E1 (PGE1) has a similar effect on splanchnic vasculature as acetylcholine and tolazoline, resulting in increased portal vein blood flow. Thus, superior mesenteric artery injection of PGE1 during CT hepatic arteriography results in increased conspicuity between hepatocellular carcinoma nodules and surrounding parenchyma.⁴⁴ Also, the use of PGE1 during CT hepatic arteriography helps reduce the number of pseudolesions around the gallbladder bed.⁴⁵ Preliminary work has suggested that it may reduce contrast-induced nephropathy, but this is associated with a number of side effects, and its role is not clear. PGF2 α dilates normal colonic vessels but vasoconstricts inflammatory and neoplastic colon vessels.

Persistent, usually asymptomatic, gastric distention, detected on radiographs, is a complication of prostaglandin therapy. Distention usually resolves after cessation of therapy. Superficially, this condition resembles pyloric stenosis, although imaging shows gastric mucosal thickening and distal antral and pyloric elongation, but no muscular wall thickening.

Papaverine is a vasodilator of large and small vessels. Similar to other vasodilators, it improves portal vein visualization during mesenteric angiography. It is not degraded in a single pass through the liver, and repeated injections can lead to systemic hypotension.

Secretin increases pancreatic blood flow. At times, selective venous sampling after intra-arterial secretin injection aids in detecting gastrinomas. IV secretin, however, does not appear reliable enough for detecting chronic pancreatitis or a pancreatic adenocarcinoma.

GASTROINTESTINAL AGENTS THAT PRODUCE HYPOTONIA

Bowel hypotonia is helpful in a number of settings. For example, a spasmolytic agent dilates a segment of spastic colon that otherwise might mimic a benign stricture or malignancy. Similarly, polyps and diverticula in the small bowel can be detected more readily if the bowel is dilated and atonic. Spasmolytic pharmacologic agents can be divided into hormonal agents (e.g., glucagon) and anticholinergic agents. Agents evaluated for use in the GI tract include morphine, propantheline bromide (Pro-Banthine), atropine, and related compounds. With some agents, after initial enthusiasm, recognition of toxicity and undesirable side effects led to their abandonment.

Glucagon

Human glucagon is a single-chain polypeptide containing 29 amino acid residues, with a molecular weight of 3483. It is generated by α cells in the islets of Langerhans. In some species, glucagon is also produced in the stomach; whether any gastric glucagon is produced in humans is controversial. The glucagon amino acid sequence in animals ranges from one similar to that in humans to completely different sequences. Identical amino acid sequences are found in humans, pigs, and cattle; this was once significant, when glucagon was obtained from animal

pancreatic tissue, but became a moot issue when a synthetic product was developed. Injectable glucagon is produced by the expression of recombinant DNA. The chemical structure of this synthetic glucagon is identical to that of human glucagon.

Glucagon is a hormone that has significant metabolic influence on a number of organs. It binds at specific receptor cell membranes in target organs. In the liver, it stimulates glucose output and hepatic ketogenesis. It lyses adipose tissue and leads to a reduction of circulating cholesterol and triglyceride levels. It stimulates insulin release and appears to be involved in liver regeneration, but its full role in the liver is not clear. Glucagon increases blood flow to the kidneys. Specific effects are also present in the adrenal glands and heart. It is metabolized in the liver and kidney. Glucagon is degraded by gastric secretions and therefore is ineffective when given orally.

In smooth muscle, glucagon is a relatively potent spasmolytic agent, and it is this spasmolytic action that accounts for its use in radiology. Pharmacologic doses are used. Smooth muscle in different GI tract segments varies in sensitivity to glucagon (Table 1-1). For example, 0.1 mg IV is sufficient to induce gastroduodenal hypotonia in most adults, but such a small dose is inadequate for colonic hypotonia, for which a dose several times greater is needed.

Intravascular glucagon is also a vasodilator. It improves portal vein visualization during mesenteric arteriography, although it has been replaced by other vasodilators because of its propensity to induce nausea and vomiting at the doses required for vasodilation.

Gastrointestinal Tract. Acute esophageal obstruction caused by food impaction is often related to an underlying stricture or spasm. Spasmolytic drugs have been recommended if spasm is suspected, but in a multicenter, double-blind study of glucagon and diazepam, no significant difference in disimpaction was evident between spasmolytic agents and placebo.⁴⁷ Effervescent agents have also been used to treat esophageal food impaction, with varying success.

The main advantage of glucagon over anticholinergic agents in inducing upper GI tract hypotonicity is its lack of side effects. In the United States, glucagon is generally used to induce hypotonia; in some countries, the anticholinergic agent scopolamine butylbromide (Buscopan) is used more often. One reason for using an anticholinergic agent is the higher cost of glucagon, although the price ratio of glucagon to Buscopan fluctuates considerably worldwide.

Glucagon decreases intragastric and intraduodenal mean pressures. Some studies suggest that barium mucosal coating in

TABLE 1-1 Spasmolytic Effect of Intravenous Glucagon: Average Duration of Atonicity (min)

Location and Response	GLUCAGON DOSE (mg)			
	0.25	0.5	1	2
Stomach	4.9	8.7	10.1	15.1
Duodenal bulb	7.5	10.1	12.5	16.7
Duodenum	7.8	10.1	12.5	16.1
Proximal small bowel	8.3	9.4	13.7	19.7
Distal small bowel	8.6	9.4	14.0	19.7

From Miller RE, Chernish SM, Brunelle RL, et al: Double-blind radiographic study of dose response to intravenous glucagon for hypotonic duodenography. *Radiology* 127:55-59, 1978.

the stomach and duodenum is improved more with anticholinergic agents than with glucagon, the rationale being that anticholinergics also decrease gastric secretions, whereas glucagon has no such effect. In actual practice, Buscopan and glucagon produce essentially equal distention and barium coating of the stomach and duodenum. A more basic question is whether induced gastric and duodenal hypotonia improves the ability to detect lesions. The diagnostic quality with and without glucagon does not appear to differ significantly. Radiologists in the United States tend not use a hypotonic agent during upper GI studies.

In enteroclysis, barium is instilled until a lesion or obstruction is reached, or the terminal ileum is filled. Glucagon is helpful if it is deemed desirable to slow down barium progression, such as when a suspicious region is identified. In general, 0.25 mg IV is sufficient to induce hypotonia, permitting a leisurely study of the region in question.

During a barium enema, glucagon relaxes the ileocecal valve and allows easier barium reflux into the distal small bowel. Thus, if retrograde ileography is being performed for suspected distal ileal disease, it appears reasonable to administer glucagon. Anticholinergics have little effect on the ileocecal valve.

In select patients, a peroral pneumocolon examination allows double-contrast study of the terminal ileum and right colon. Barium is introduced via a conventional oral examination or enteroclysis approach, and air is added through an enema tip. Because glucagon relaxes the ileocecal valve, it may increase the success rate of this examination.

Colon hypotonia is achieved by injecting 2 mg of glucagon intramuscularly. Hypotonia begins within several minutes and lasts about 15 minutes. Hypotonia can also be achieved with 0.25 to 0.5 mg of glucagon IV, although in some patients up to 1.0 mg may be necessary; the onset of hypotonia with an IV injection is almost immediate and lasts approximately 10 minutes. In general, the smaller IV dose is used because of cost considerations. In infants and children, an IV dose of 0.8 to 1.25 µg/kg has been recommended.⁴⁸

Few studies have evaluated whether the use of glucagon results in a more accurate diagnosis, and whether glucagon is injected during a barium enema varies considerably among radiologists. It is more commonly used in hospitalized, older, and ill patients. In some practices, it is injected routinely for double-contrast barium enemas but individualized with single-contrast studies. In an outpatient setting, many radiologists use glucagon when a patient has painful spasm or spasm interfering with the examination, is unable to retain the enema, or has suspected colitis or diverticulitis. Glucagon decreases the extent and severity of colonic spasm during a barium enema and makes patients more comfortable.

Occasionally, colonic spasm persists despite administration of glucagon. It has been my empiric observation that patients with long-standing diabetes have more glucagon-resistant colonic spasm than nondiabetic patients, but the reason for this decreased response in diabetics is not known. Many diabetics already have high blood glucagon levels, although these levels are in the physiologic rather than pharmacologic range. The presence of autonomic neuropathy in some diabetics may be a factor. At times, refilling the colon several minutes later results in a marked decrease of spasm.

Reduction of Intussusception. Because of its spasmolytic effect and tendency to relax the ileocecal valve, it was thought

that glucagon might have a role in ileocolic intussusception reduction. A number of reports described intussusception reduction after the administration of glucagon, but such empiric use does not imply that any eventual reduction can be attributed to glucagon; even a second or third attempt at reduction improves the overall success rate. Controlled studies have found similar success rates for intussusception reduction with and without glucagon.

Current controversy centers not on whether glucagon is useful in intussusception reduction, but whether the contrast agent should be barium, a saline solution, or air, and whether fluoroscopy or sonography is the preferred imaging modality.

Preferred Imaging Modality with Glucagon

In Computed Tomography. In spite of glucagon's diverse effects in the liver, it does not appear to influence hepatic CT enhancement. With older scanners, glucagon and somatostatin were used to decrease motion artifacts. There is little need to induce bowel hypotonia with multidetector scanners, but the ability to maintain bowel distention with a hypotonic agent aids gastric and bowel wall evaluation. Although some studies suggest that glucagon prior to CT colonography does not improve colonic distention,⁴⁹ others find an antispasmodic agent useful in maintaining hypotonia during air insufflation and scanning. Spasm developing during the study can be decreased by the judicious use of glucagon.

In Ultrasonography. Occasionally, bowel atonia is helpful in abdominal ultrasonography. An acoustic window to the biliary tract can sometimes be obtained by filling the stomach with fluid and inducing hypotonia of the surrounding GI structures.

In Magnetic Resonance Imaging. Currently, glucagon is used infrequently in MRI, although it may have a role if oral MRI contrasts agents and bowel distention are used. When evaluating mural and serosal disease, IV glucagon allows better visualization of normal bowel loops and bowel wall thickening.⁵⁰ Glucagon also helps eliminate ghost images of positive contrast-opacified bowel.

Contraindications and Side Effects

A myth persists that glucagon should not be given to diabetic patients. It should be pointed out that glucagon is used to treat hypoglycemic reactions in diabetics. On the other hand, in the setting of hyperglycemia and ketoacidosis, temporary additional glucose level elevation induced by glucagon is of limited importance. The diabetic patient can safely receive glucagon whenever clinically indicated prior to an imaging study.

Side effects of glucagon are less than those with atropine or propantheline. In one study, the side effects with glucagon were similar to those seen with a placebo. The prevalence of nausea and vomiting after injection of glucagon is dose dependent.⁵¹ When given IV, glucagon slowly decreases these reactions.

Because commercially available glucagon has an amino acid residue similar to human glucagon, allergic reactions should not occur, although rare ones have been reported. In these patients, an allergy to the preservative used, rather than to glucagon, should be considered. Glucagon is a naturally occurring polypeptide and, in pure form, should not result in hypersensitivity reactions. Previously, commercial glucagon contained bovine or porcine insulins, protoinsulins, other nonglucagon

protein contaminants, and preservatives, and any of these may be associated with a hypersensitivity reaction. A rash, periorbital edema, erythema multiforme, respiratory distress, and hypotension have been reported. Currently used genetically engineered glucagon should be associated with few anaphylactic reactions.

Contraindications to glucagon include prior sensitivity, suspected pheochromocytoma, or insulinoma. Glucagon can release catecholamines from a pheochromocytoma and result in the sudden onset of life-threatening hypertension. Such hypertension can be countered with the α -adrenergic blocking agent phentolamine mesylate (Regitine). In adults, a dose of 5 mg IV appears useful, although considerable variability exists in treatment requirements. Glucagon can also stimulate insulin release from an insulinoma, resulting in severe hypoglycemia; this condition is treated with glucose.

Anticholinergic Agents

Anticholinergic agents as a group are effective in tissues with receptors supplied by cholinergic postganglionic autonomic nerves. They block the effect of acetylcholine liberated from nerve endings. They reduce GI tract motility, decrease tonicity in the urinary tract, and may also have a hypotonic effect on the bile ducts. These agents also decrease salivary and bronchial secretions, dilate pupils, and increase heart rate, with the duration of action and specific effect on various target organs dependent on the specific compound and dose. Their action on tonicity and motility is similar to glucagon, but, unlike glucagon, they also reduce secretions. Current evidence suggests that the latter effect is insignificant in imaging studies.

Some of these agents have been used in peptic ulcer disease therapy in conjunction with antacids and H₂ receptor antagonists, although these applications have been inconclusive and controversial. They also play a role in the treatment of irritable bowel syndrome and have been used as supplemental therapy in treating biliary and ureteral colic to relax smooth muscle spasm; results here also are inconsistent.

Useful Agents. The most widely known anticholinergic agent is atropine sulfate. It is available in tablets and as a parenteral injectable liquid. Radiologists in North America may still remember the anticholinergic agent propantheline bromide, in vogue in the 1960s and early 1970s as a GI hypotonic agent. Currently, atropine and propantheline have been supplanted by other agents.

In many countries, the short-acting anticholinergic agent scopolamine butylbromide is used, but it is not available in the United States. It is administered IV; the usual dose is 20 mg before an upper GI examination. Its hypotonic effect lasts for 15 to 20 minutes. It does not induce gastroesophageal reflux, nor does it have any significant effect on the visualization of a hiatal hernia. It may be useful with CT and MRI in evaluating suspected gastric cancers.⁵² One study found that it improves colonic distention during CT colonography (compared with controls), and the authors recommended its use.⁵³

Pirenzepine, an antimuscarinic drug, shows promise as a hypotonic agent without the adverse effects of scopolamine.

Although other anticholinergic agents are available, their side effects and longer duration of action limit their application in radiology. For example, scopolamine hydrobromide is available but is not used in radiologic examinations because of its adverse side effects.

Oral hyoscyamine sulfate is a potential hypotonic agent, having actions and contraindications similar to those of atropine and other anticholinergic agents. It appears to provide no benefit when used as pain premedication during a barium enema, although it aids in achieving distention during CT colonography.

Complications. In patients predisposed to glaucoma, increased intraocular pressure induced by anticholinergic drugs may precipitate an acute attack. Although most patients with a history of glaucoma have chronic glaucoma, a patient may have acute angle-closure glaucoma and not be aware of it. Acute glaucoma should be suspected if eye pain or loss of vision develops after administration of an anticholinergic agent. Buscopan use can result in blurred vision.

The effect on the autonomic nervous system can lead to urinary retention. This complication is exacerbated in patients with prostatic hypertrophy or other predisposition to urine retention. Allergic reactions to anticholinergic agents are uncommon.

GASTROINTESTINAL AGENTS THAT INCREASE BOWEL MOTILITY

In some patients, the rate of gastric emptying is increased if the barium volume used is increased. A cold suspension is not only better tolerated but also leads to faster gastric emptying. Faster small bowel transit can be achieved by adding a hyperosmolar product to a barium suspension; a small amount of diatrizoate meglumine (Gastrografin) can be added to an oral barium suspension.

High-osmolality sorbitol added to oral CT contrast will accelerate bowel opacification. Some manufacturers add sorbitol to their barium sulfate products.

Metoclopramide

Metoclopramide is an antiemetic agent and is also useful in treating diabetic gastroparesis. Its primary effects in the GI tract are an increase in gastric peristalsis, pyloric relaxation, and increase in small bowel peristalsis. It has no major effect on the colon. Metoclopramide appears to decrease gastric secretions but has little effect on mucosal barium coating. A typical dose is 10 to 20 mg parenterally or orally. It is a relatively safe drug, although extrapyramidal side effects, such as acute dystonia and tardive dyskinesia, develop occasionally.

Oral metoclopramide reduces small bowel transit time. It can be given shortly before a small bowel study or up to 90 minutes before the procedure. Administered orally before a CT scan, metoclopramide improves opacification of the ileum, right colon, and transverse colon but not the more proximal bowel. Longitudinal contractions and foreshortening of ileal loops tend to elevate the ileum out of the pelvis. Metoclopramide also appears to improve visualization of the pancreas in abdominal sonography, with its primary benefit being decreased gastric and duodenal gas artifacts.

Domperidone

Domperidone, a potent dopamine antagonist, increases gastric emptying and accelerates small bowel transit. Although it decreases small bowel transit time, its effect on the small bowel appears to be less than that with metoclopramide.⁵⁴ It has been used for the treatment of diabetic gastroparesis. Domperidone

may increase serum levels of prolactin in patients with a pituitary prolactin-releasing tumor. It has also been associated with sudden cardiac death.⁵⁵

Cisapride

Cisapride is a prokinetic substance that induces antral contractility, enhances gastric emptying, and promotes small bowel peristalsis. It also enhances lower esophageal sphincter tone and is a relatively potent esophageal motor stimulator. It has been proposed for the treatment of diabetic patients with gastroparesis and as an antigastroesophageal reflux agent. It has had limited application in radiology. Its use has been discontinued in the United States because of associated cardiac arrhythmias and deaths.⁵⁶

Neostigmine

Neostigmine methyl sulfate is a cholinesterase inhibitor that promotes gastric and small bowel peristalsis and leads to faster gastric emptying and shorter small bowel transit time. It promotes peristalsis when activity is depressed by cholinergic stimulation. It is useful in treating colonic pseudo-obstruction (Ogilvie's syndrome),⁵⁷ but is contraindicated with mechanical bowel obstruction and in some settings of adynamic ileus.⁵⁸ It has led to colon perforation.

Erythromycin

Erythromycin, primarily an antibiotic, improves gastric motility and promotes gastric emptying. It is used as an aid in postoperative gastroparesis and for the treatment of diabetic gastroparesis, but has had little application in radiology.

MIXED ACTION AGENTS

Morphine

Some radiologists may undoubtedly remember using morphine sulfate for hypotonic duodenography, a procedure relegated to history. Currently, morphine has a role in nuclear medicine and a possible role in MRCP (see later).

Cholecystokinin

Cholecystokinin, a peptide hormone, has myriad functions; it induces gallbladder contraction and increases bowel peristalsis, resulting in faster small bowel transit. It also regulates pancreatic enzyme secretion, inhibits gastric acid secretion, affects satiety signaling, and acts as a neurotransmitter. It stimulates aldosterone secretion from human adrenocortical cells. From a radiologic viewpoint, cholecystokinin induces simultaneous contraction of the sphincter of Oddi and gallbladder; thus, most of the bile from the gallbladder refluxes into the intrahepatic bile ducts and reenters the gallbladder after hormone infusion stops.

Secretion of cholecystokinin is impaired in celiac disease and bulimia nervosa. Untreated celiacs have low postprandial cholecystokinin levels. It is overexpressed in certain neuroendocrine tumors and in medullary thyroid carcinomas.

Generally, only the COOH-terminal octapeptide of cholecystokinin is used. This fragment is more potent than the entire molecule.

Ceruletide

Ceruletide is a synthetic compound similar to cholecystokinin in its pharmacologic effects—namely, it delays gastric emptying

and induces gallbladder contraction, duodenal hypoperistalsis, and hyperperistalsis of the jejunum, ileum, and colon. It reverses bowel aperistalsis induced by drugs acting on enteric neural or smooth muscle.

In the early 1980s, ceruletide appeared to be a promising agent to increase small bowel peristalsis and thus shorten the duration of a small bowel examination, but radiologists lost interest in this agent; given IV, ceruletide induces nausea, vomiting, and abdominal cramps. For accelerating small bowel transit, a usual dose of 0.25 to 0.3 µg/kg is administered. Whether the shorter small bowel transit time leads to a better small bowel study is debatable; pronounced contractions tend to obscure anatomic detail, particularly in the distal ileum.

Because ceruletide induces gastric hypotonia, it should not be administered prior to significant amounts of barium reaching the jejunum. Such gastric stasis can be overcome by also administering metoclopramide.

DRUGS AFFECTING THE BILIARY TRACT AND PANCREAS

Bile flow into the duodenum is regulated by bile production in the liver and gallbladder tonicity. Agents affecting only the latter are considered in this section.

Inhibition of gallbladder contractions can be achieved by glucagon, atropine, and other cholinergic drugs, somatostatin, some calcium channel antagonists, and several other less studied drugs, keeping in mind that contractions are also inhibited in obesity, diabetes mellitus, celiac disease, and autonomic neuropathy.

Gallbladder contraction is stimulated by cholecystokinin, ceruletide, motilin, prostigmine, erythromycin, and possibly by cisapride and cholestyramine.

Glucagon relaxes the gallbladder. Glucagon also decreases papilla of Vater mean pressures. Currently, little clinical use has been made of these findings. Glucagon is of limited use in percutaneous transhepatic cholangiography or various biliary drainage procedures. In an occasional patient with persistent distal common bile duct narrowing, in the sphincter of Oddi region, glucagon aids in differentiating a tumor, impacted stone, and spasm. In most patients, however, judicious use of fluoroscopy is sufficient.

Glucagon improves bile duct visualization during MRCP.⁵⁹ Because incomplete duct visualization may lead to a repeat study or even an invasive procedure such as ERCP, glucagon is routinely used at some centers. Although earlier studies suggested that glucagon improves the quality of operative cholangiography, a double-blind prospective study found no improvement.⁶⁰ Use of fentanyl during surgery is associated with sphincter of Oddi spasm and, in these patients, glucagon may have a role.

Hypotonic agents are commonly used during ERCP to induce duodenal hypotonia, inhibit contractions of the sphincter of Oddi, and aid ampullary cannulation. In the United States, glucagon is used almost exclusively for this purpose; in other countries, an anticholinergic drug such as scopolamine is used more often.

Neostigmine, together with morphine, has been proposed as a provocative test in hepatobiliary scintigraphy for evaluation of sphincter of Oddi dyskinesia in postcholecystectomy patients.⁶¹

Morphine may have a role in MR cholangiography; IV morphine constricts the sphincter of Oddi, thus distending the biliary and pancreatic ducts.⁶² It may also improve duct visualization in primary sclerosing cholangitis. An interval of 10 to 20 minutes between morphine injection and imaging appears useful.

Cholecystokinin's effect on the gallbladder has been used to increase radiographic contrast during oral cholecystography; it also aids in evaluating gallbladder function. The gallbladder ejection fraction is typically determined with hepatobiliary scintigraphy but less often with ultrasonography; MR cholangiography uses an infusion of cholecystokinin as an alternate method.

A provocative test using a cholecystokinin derivative (Sin-calide) to identify acalculous cholecystitis patients likely to benefit from cholecystectomy has not achieved general clinical acceptance. Cholecystokinin relaxes the sphincter of Oddi and appears to assist in the passage of bile duct stones. On the other hand, a cholecystokinin receptor antagonist provides pain relief in patients with biliary colic.⁶³ Interestingly, cholecystokinin does not induce its usual sphincter of Oddi inhibitory effect after a cholecystectomy. Cholecystokinin is also useful as a diagnostic test of pancreatic function.

Ceruletide has an effect on the gallbladder similar to that of cholecystokinin or a fatty meal.⁶⁴ In patients with recurrent symptoms after cholecystectomy, an ultrasonographically detected increase in extrahepatic bile duct dilation following ceruletide injection suggests sphincter of Oddi dysfunction.

The cholecystokinin-secretin pancreatic exocrine function test is used to detect pancreatic exocrine insufficiency but does not differentiate between chronic pancreatitis and pancreatic carcinoma. MRI can also evaluate pancreatic exocrine function by measuring duodenal filling after stimulation with secretin.⁶⁵ Secretin improves pancreatic duct visualization and aids in detecting abnormalities during MR pancreatography.⁶⁶ Pancreas divisum and other abnormalities are more readily detected after secretin, potentially obviating the need for ERCP. MR pancreatography is best performed within 5 minutes after secretin injection.⁶⁷ Secretin-augmented MR pancreatography and MRI perfusion are useful for detecting graft dysfunction after pancreatic transplantation.⁶⁸

Analysis of duodenal aspirations of pancreatic juice after cholecystokinin-octapeptide stimulation can detect pancreatic insufficiency in patients with chronic pancreatitis. However, the analogous secretin test is more commonly used.

REFERENCES

- Krause W, Schneider PW: Chemistry of x-ray contrast agents. In Majoral J-P, editor: *Topics in Current Chemistry*, vol 222, Heidelberg, Germany, 2002, Springer-Verlag.
- American College of Radiology: *Manual on Contrast Media*, ed 4, Reston, VA, 1998, American College of Radiology.
- European Society of Urogenital Radiology: *Guidelines on contrast media*, version 4.0, 2004. <http://www.esur.org>.
- Schabelman E, Witting M: The relationship of radiocontrast, iodine, and seafood allergies: A medical myth exposed. *J Emerg Med* 39:701–707, 2010.
- Lawrence V, Matthai W, Hartmaier S: Comparative safety of high-osmolality and low-osmolality radiographic contrast agents. Report of a multidisciplinary working group. *Invest Radiol* 27:2–28, 1992.
- Park SW, Bae IY, Eun HW, et al: Small-bowel angioedema during screening computed tomography due to intravascular contrast material. *J Comput Assist Tomogr* 35:549–552, 2011.
- Mikkonen R, Aronen HJ, Kivisaari L, et al: Plasma levels of prekallikrein, alpha-2-macroglobulin and C1-esterase inhibitor in patients with urticarial reaction to contrast media. *Acta Radiol* 38:466–473, 1997.
- Lasser EC, Berry CC, Talner LB, et al: Pretreatment with corticosteroids to alleviate reactions to intravenous contrast material. *N Engl J Med* 317:845–849, 1987.
- Pagani JJ, Hayman LA, Bigelow RH, et al: Diazepam prophylaxis of contrast media-induced seizures during computed tomography of patients with brain metastases. *AJR* 140:67–72, 1983.
- Gleeson TG, Bulugahapitiya S: Contrast-induced nephropathy [review]. *AJR* 183:1673–1689, 2004.
- Goergen SK, Rumbold G, Compton G, Harris C: Systematic review of current guidelines, and their evidence base, on risk of lactic acidosis after administration of contrast medium for patients receiving metformin. *Radiology* 254:261–269, 2010.
- Merten GJ, Burgess WP, Gray LV, et al: Prevention of contrast-induced nephropathy with sodium bicarbonate: A randomized trial. *JAMA* 291:2328–2334, 2004.
- Jang JS: Sodium bicarbonate therapy for the prevention of contrast-induced acute kidney failure. *Circ J* 76:2255–2265, 2012.
- Kramer BK, Kamerl M, Schweda F, Schreiber M: A primer in radiocontrast-induced nephropathy. *Nephrol Dial Transplant* 14:2830–2834, 1999.
- Mueller C: Prevention of contrast nephropathy in critically ill patients using acetylcysteine and theophylline. *Internat J Artificial Organs* 27:1066–1069, 2004.
- Kelly AM, Dwamena B, Cronin P, et al: Effectiveness of drugs for preventing contrast-induced nephropathy. *Ann Intern Med* 148:284–294, 2008.
- Weisbord SD, Palevsky PM: Strategies for the prevention of contrast-induced acute kidney injury. *Curr Opin Nephrol Hypertens* 19:539–549, 2010.
- Marenzi G, Marana I, Lauri G, et al: The prevention of radiocontrast agent-induced nephropathy by hemofiltration. *N Engl J Med* 349:1333–1340, 2003.
- Kurokouchi K, Masaki T, Miyauchi Y, et al: Efficacy of combination therapies of percutaneous or laparoscopic ethanol-lipiodol injection and radiofrequency ablation. *Int J Oncol* 25:1737–1743, 2004.
- Skucas J: Barium sulfate: Clinical application. In Skucas J, editor: *Radiographic Contrast Agents*, ed 2, Rockville, MD, 1989, Aspen, pp 14–17.
- Buecker A, Wein BB, Neuerburg JM, Guenther RW: Esophageal perforation: Comparison of use of aqueous and barium-containing contrast media. *Radiology* 202:683–686, 1997.
- Noda Y, Ogawa Y, Nishioka A, et al: New barium paste mixture for helical (slip-ring) CT evaluation of the esophagus. *J Comput Assist Tomogr* 20:773–776, 1996.
- Quagliano PV, Austin RF, Jr: Oral contrast agents for CT: A taste test survey. *J Comput Assist Tomogr* 21:720–722, 1997.
- Grand DJ, Beland MD, Machan JT, Mayo-Smith WW: Detection of Crohn's disease: Comparison of CT and MR enterography without antiperistaltic agents performed on the same day. *Eur J Radiol* 81:1735, 1741, 2012.
- Ogawa Y, Noda Y, Nishioka A, et al: New barium paste mixture for helical (slip-ring) CT evaluation of rectal carcinoma. *J Comput Assist Tomogr* 21:398–401, 1997.
- Sahani DV, Jhaveri KS, D'Souza RV, et al: Evaluation of simethicone-coated cellulose as a negative oral contrast agent for abdominal CT. *Acad Radiol* 10:491–496, 2003.
- Skucas J: Anaphylactoid reactions with gastrointestinal contrast media. *AJR* 168:962–964, 1997.
- Blakeborough A, Sheridan MB, Chapman AH: Complications of barium enema examinations: A survey of UK Consultant Radiologists 1992 to 1994. *Clin Radiol* 52:142–148, 1997.
- Zalev AH: Venous barium embolization, a rare, potentially fatal complication of barium enema: 2 case reports. *Can Assoc Radiol J* 48:323–326, 1997.
- Murphy KD, Poster RB, Marx WH, et al: Upper gastrointestinal examination complicated by venous intravasation and portal vein thrombosis. *AJR* 169:501–503, 1997.
- Parazella MA: Current status of gadolinium toxicity in patients with kidney disease. *Clin J Am Soc Nephrol* 4:461–469, 2009.
- Manfredi R, Maresca G, Baron RL, et al: Delayed MR imaging of hepatocellular carcinoma enhanced by gadobenate dimeglumine (Gd-BOPTA). *J Magn Reson Imaging* 9:704–710, 1999.

33. Joarder R, de Jode M, Lamb GA, Gedroyc WM: The value of MnDPDP enhancement during MR guided laser interstitial thermoablation of liver tumors. *J Magn Reson Imaging* 13:37–41, 2001.
34. Harisinghani MG, Dixon WT, Saksena MA, et al: MR lymphangiography: Imaging strategies to optimize the imaging of lymph nodes with ferumoxtran-10. *Radiographics* 24:867–878, 2004.
35. Wen X, Jackson EF, Price RE, et al: Synthesis and characterization of poly(L-glutamic acid) gadolinium chelate: A new biodegradable MRI contrast agent. *Bioconjugate Chem* 15:1408–1415, 2004.
36. Lin CY, Yadav NN, Ratnakar J, et al: In vivo imaging of paraCEST agents using frequency labeled exchange transfer MRI. *Magn Reson Med* 71:286–293, 2014.
37. Shi H, Liu C, Ding HY, Li CW: Magnesium sulfate as an oral contrast medium in magnetic resonance imaging of the small intestine. *Eur J Radiol* 81:e370–e375, 2012.
38. Luboldt W, Bauerfeind P, Wildermuth S, et al: Colonic masses: Detection with MR colonography. *Radiology* 216:383–388, 2000.
39. Pilkington SA, Nugent KP, Brenner J, et al: Barium proctography vs magnetic resonance proctography for pelvic floor disorders. *Colorectal Dis* 14:1224–1230, 2012.
40. Tanioka H, Araki T, Sasaki Y, et al: Famotidine for gastric radiography. *Radiat Med* 11:12–16, 1993.
41. Huwer H, Winning J, Straub U, et al: Clinically diagnosed nonocclusive mesenteric ischemia after cardiopulmonary bypass: Retrospective study. *Vascular* 12:114–120, 2004.
42. Stoeckelhuber BM, Suttman I, Stoeckelhuber M, Kueffer G: Comparison of the vasodilating effect of nitroglycerin, verapamil, and tolazoline in hand angiography. *J Vasc Intervent Radiol* 14:749–754, 2003.
43. Chamsuddin AA, Kowalik KJ, Bjarnason H, et al: Using a dopamine type 1A receptor agonist in high-risk patients to ameliorate contrast-associated nephropathy. *AJR* 179:591–596, 2002.
44. Yamagami T, Nakamura T, Iida S, et al: Effects of prostaglandin E(1) injection through the superior mesenteric artery on the hemodynamics of hepatocellular carcinoma. *AJR* 178:349–352, 2002.
45. Yamagami T, Nakamura T, Sato O, et al: Value of intra-arterial prostaglandin E(1) injection during CT hepatic arteriography. *AJR* 177:115–119, 2001.
46. Miller RE, Chernish SM, Brunelle RL, et al: Double-blind radiographic study of dose response to intravenous glucagon for hypotonic duodenography. *Radiology* 127:55–59, 1978.
47. Tibbling L, Bjorkhoel A, Jansson E, Stenkvist M: Effect of spasmolytic drugs on esophageal foreign bodies. *Dysphagia* 10:126–127, 1995.
48. Ratcliffe JF: Glucagon in barium examinations in infants and children: Special reference to dosage. *Br J Radiol* 53:860–862, 1980.
49. Morrin MM, Farrell RJ, Keogan MT, et al: CT colonography: Colonic distention improved by dual positioning but not intravenous glucagon. *Eur Radiol* 12:525–530, 2002.
50. Low RN, Francis IR: MR imaging of the gastrointestinal tract with IV gadolinium and diluted barium oral contrast media compared with unenhanced MR imaging and CT. *AJR* 169:1051–1059, 1997.
51. Chernish SM, Maglinte DDT: Glucagon: Common untoward reactions—review and recommendations. *Radiology* 177:145–146, 1990.
52. Sohn KM, Lee JM, Lee SY, et al: Comparing MR imaging and CT in the staging of gastric carcinoma. *AJR* 174:1551–1557, 2000.
53. Taylor SA, Halligan S, Goh V, et al: Optimizing colonic distention for multi-detector row CT colonography: Effect of hyoscine butylbromide and rectal balloon catheter. *Radiology* 229:99–108, 2003.
54. Morewood DJW, Whitehouse GH: A comparison of three methods for performing barium follow-through studies of the small intestine. *Br J Radiol* 59:971–973, 1986.
55. Michaud V, Turgeon J: Domperidone and sudden cardiac death: How much longer should we wait? *J Cardiovasc Pharmacol* 61:215–217, 2013.
56. Quigley EM: Cisapride: What can we learn from the rise and fall of a prokinetic? *J Dig Dis* 12:147–156, 2011.
57. Eisner JL, Smith JM, Ensor CR: Intravenous neostigmine for postoperative acute colonic pseudo-obstruction. *Ann Pharmacother* 46:430–435, 2012.
58. St John PH, Radcliffe AG: Contraindication for the use of neostigmine in colonic pseudo-obstruction [letter]. *Brit J Surg* 84:1481–1482, 1997.
59. Dalal PU, Howlett DC, Sallomi DF, et al: Does intravenous glucagon improve common bile duct visualization during magnetic resonance cholangiopancreatography? Results in 42 patients. *Eur J Radiol* 49:258–261, 2004.
60. Cofer JB, Barnett RM, Major GR, et al: Effect of intravenous glucagon on intraoperative cholangiography. *South Med J* 81:455–456, 1988.
61. Madacsy L, Velosy B, Lonovics J, et al: Evaluation of results of the prostigmine-morphine test with quantitative hepatobiliary scintigraphy: A new method for the diagnosis of sphincter of Oddi dyskinesia. *Eur J Nucl Med* 22:227–232, 1995.
62. Silva AC, Friese JL, Hara AK, Liu PT: MR cholangiopancreatography: Improved ductal distention with intravenous morphine administration. *Radiographics* 24:677–687, 2004.
63. Malesci A, Pezzilli R, D'Amato M, Rovati L: CCK-1 receptor blockade for treatment of biliary colic: A pilot study. *Aliment Pharmacol Ther* 18:333–337, 2003.
64. Muraca M, Cianci V, Vilei MT, et al: Ultrasonic evaluation of gallbladder emptying with ceruletide. *Ital J Gastroenterol* 28:38–39, 1996.
65. Haverhagen JT, Muller D, Battmann A, et al: MR hydrometry to assess exocrine function of the pancreas: Initial results of noninvasive quantification of secretion. *Radiology* 218:61–67, 2001.
66. Monill J, Pernas J, Clavero J, et al: Pancreatic duct after pancreatoduodenectomy: Morphologic and functional evaluation with secretin-stimulated MR pancreatography. *AJR* 183:1267–1274, 2004.
67. Fukukura Y, Fujiyoshi F, Sasaki M, Nakajo M: Pancreatic duct: Morphologic evaluation with MR cholangiopancreatography after secretin stimulation. *Radiology* 222:674–680, 2002.
68. Haverhagen JT, Wagner HJ, Ebel H, et al: Pancreatic transplants: Noninvasive evaluation with secretin-augmented MR pancreatography and MR perfusion measurements—preliminary results. *Radiology* 233:273–280, 2004.

Barium Studies: Single and Double Contrast

MARC S. LEVINE | DAVID J. OTT | IGOR LAUFER

CHAPTER OUTLINE

Single-Contrast Studies

Diagnostic Principles
Equipment
Barium Suspensions
Quality Controls
Esophagography
Upper Gastrointestinal Series
Small Bowel
Barium Enema

Double-Contrast Studies

Performance
Interpretation
Artifacts

Since the 1980s, advances in cross-sectional imaging and endoscopy have led to a gradual but steady decline in the number of barium studies performed in the United States.^{1,2} Although barium studies no longer reign supreme in the diagnosis of gastrointestinal (GI) disease, single- and double-contrast examinations continue to have a role in modern radiology practice. In general terms, barium studies can demonstrate GI abnormalities in three ways:

1. Mucosal relief views of the collapsed or partially collapsed lumen obtained with a small volume of barium. These views enable visualization of the folds in various portions of the GI tract (Fig. 2-1A). Because the folds contain a submucosal core, these views are particularly useful for showing abnormalities involving the submucosa, such as esophageal varices.
2. Single-contrast views of the filled lumen obtained with a large volume of low-density barium (Fig. 2-1B). These views enable visualization of contour abnormalities, strictures, and large polypoid defects.
3. Double-contrast views obtained after the mucosal surface has been coated with a thin layer of high-density barium and the lumen has been distended with gas (Fig. 2-1C). These views enable visualization of subtle mucosal lesions, such as the early changes of inflammatory bowel disease and early neoplastic lesions.

Although these three types of views are incorporated to varying degrees in both single- and double-contrast examinations, single-contrast studies rely more heavily on diagnostic fluoroscopy, mucosal relief, and barium filling,³ whereas double-contrast studies emphasize the interpretation of double-contrast images supplemented by barium filling and mucosal relief.

In the past, there was considerable controversy about the relative virtues of single-contrast and double-contrast techniques.^{4,5} Currently, however, most authors believe that double-contrast techniques provide superior mucosal detail and allow earlier detection of subtle lesions than single-contrast techniques. As a result, it is generally recommended that double-contrast studies be performed on patients who are young enough and healthy enough to undergo this type of examination. In contrast, single-contrast barium studies are most appropriate in older or debilitated patients who are unable to cooperate for a double-contrast examination.^{6,7}

This chapter discusses the principles for performing and interpreting single- and double-contrast barium studies.⁸ These principles are illustrated with examples drawn from throughout the GI tract.

Single-Contrast Studies

DIAGNOSTIC PRINCIPLES

Depending on the organ examined, single-contrast techniques may include observation of function (e.g., pharyngeal and esophageal motility), compression imaging, full-column distention, mucosal relief views, and limited air-contrast images.⁹⁻¹¹ The use of compression during fluoroscopy is a critical component of the single-contrast examination. Small lesions (e.g., small ulcers, polypoid neoplasms) are often visible only when the barium pool is adequately thinned or displaced by manual compression. The barium suspension must also be adequately diluted if lesions (especially small lesions) are to be detected in the thinned-out barium pool.

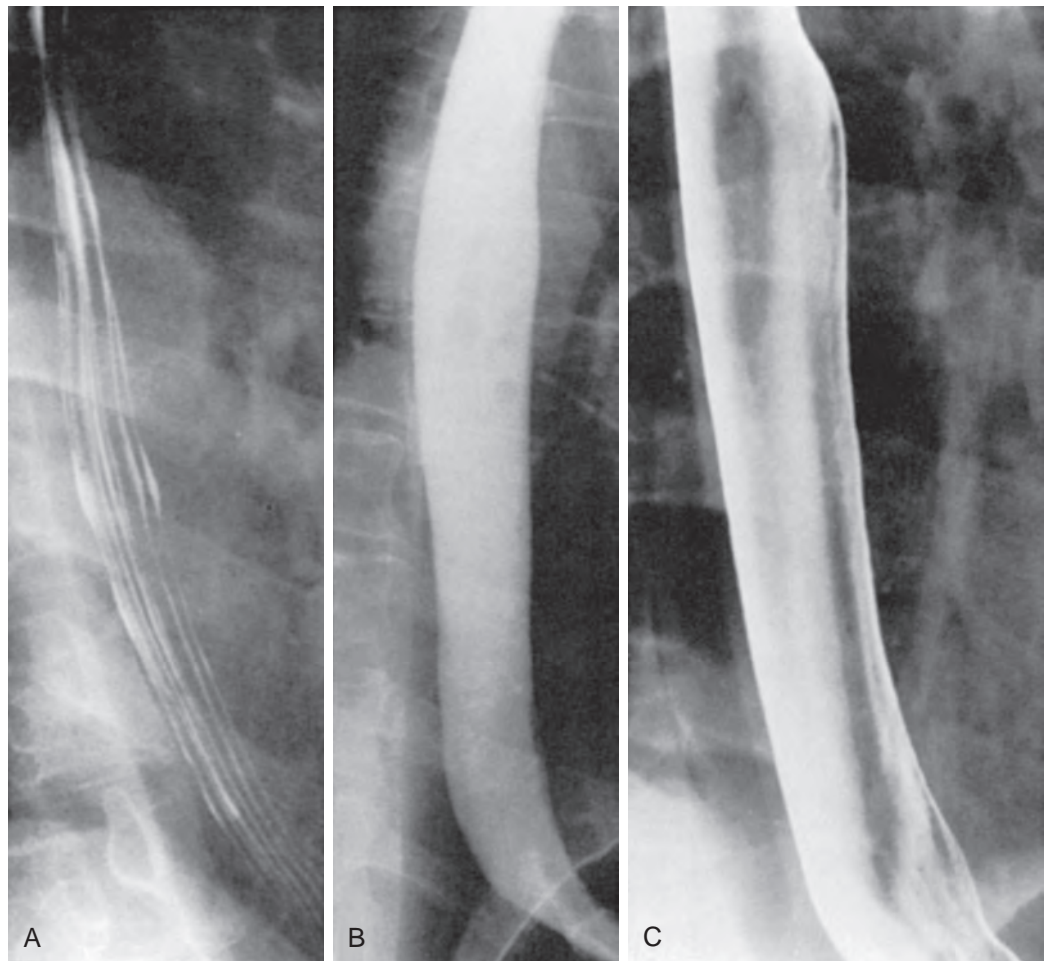
Full-column distention of the lumen is ideal for showing strictures, large neoplasms, and lesions projecting tangentially, such as ulcers or diverticula. Full-column views of barium-filled structures in various projections enable depiction of large ulcers and tumors. However, small lesions may be visible on full-column views only when viewed in profile. In such cases, mucosal techniques are required to supplement the barium-filled views.

EQUIPMENT

Fluoroscopic equipment has evolved dramatically with the transition from analogue cassette-based radiography to digital imaging and viewing on picture archiving and communications system (PACS) workstations.¹²⁻¹⁵ Regardless of the imaging technology, single-contrast examinations can be performed with conventional or remote control fluoroscopic units.¹² The ability to obtain optimal compression views is a major prerequisite of any well-designed fluoroscope. Compression can be performed manually or with a variety of hand-held devices on

Figure 2-1 Three types of views for visualizing the gastrointestinal tract, as illustrated in the esophagus.

A. Mucosal relief view. With the esophagus collapsed and coated, the normal longitudinal folds are seen. **B.** Single-contrast view. With the patient continuously drinking barium in the prone position, the barium-filled esophagus is demonstrated. **C.** Double-contrast view. With the patient in the upright position, the smooth, featureless surface of the esophagus is seen.



a conventional unit; alternatively, the plastic cone on the spot image device of the fluoroscope can be used for applying compression.

On remote control equipment, compression is easily performed with a vertical movable device incorporated into the machine, facilitated by the ability to angle the x-ray tube. Remote control units often contain a compression device that allows graded compression and tube angulation with compression. Nevertheless, many radiologists prefer standard fluoroscopic units rather than remote control units because it is generally easier to move, turn, and compress the patient when the fluoroscopist performing the procedure is at the table side.

BARIUM SUSPENSIONS

Numerous barium products are available commercially; a number are formulated for specific purposes, whereas others can be used for a variety of examinations.^{16,17} Barium suspensions for single-contrast studies should be of moderate density (50%-100% w/v) when not diluted. The optimal barium suspension for a particular study depends on the structure being examined and the type of examination being performed. For example, an esophagogram requires a moderately dense barium suspension that provides full-column and mucosal relief imaging; a high-density barium suspension or paste may also be needed for optimal mucosal coating. A similar barium suspension can be used for an upper GI series, in

which compression views, mucosal relief views, and limited double-contrast views are required. A standard peroral small bowel follow-through study can be performed with the same barium suspension used for the upper GI series. A single-contrast enteroclysis study requires a 15% to 20% w/v barium suspension, although somewhat denser solutions have been recommended.^{18,19} Finally, a 15% to 20% w/v barium suspension is used for a single-contrast barium enema, because this is the optimal suspension for obtaining compression views of the colon.

QUALITY CONTROLS

Quality control for single-contrast examinations requires balancing the barium density, kilovoltage, and width of the barium column to achieve adequate translucency of the barium-filled bowel. This permits radiographic penetration of the barium suspension to visualize lesions that might otherwise be obscured by barium in the lumen.^{6,10,11} The visibility of skeletal shadows through the barium column indicates that small filling defects are more likely to be seen, which is particularly important for the detection of colonic polyps.

Another quality control consideration, especially during the barium enema and small bowel follow-through, is the ability to see through overlapping loops of bowel.^{6,20} On barium enemas, a tortuous sigmoid colon may have overlapping loops, even with appropriate compression. Similarly, on small bowel

follow-throughs, overlapping small bowel loops in the pelvis may compromise the fluoroscopist's ability to detect abnormalities in the distal ileum. In such cases, pelvic loops can be better visualized by placing the patient in a prone position while he or she lies on a bolster or inflated balloon to lift these loops superiorly from the pelvis.²¹

ESOPHAGOGRAPHY

Routine single-contrast esophagography includes fluoroscopic observation of the esophagus supplemented by motion recordings, full-column views, and mucosal relief views.^{22,23} Full-column (barium-filled views) and mucosal relief views constitute the single-contrast phase of the examination. Motion recordings can be used to document pharyngeal function and esophageal motility using analog or digital recordings or rapid sequence solid-state recordings built into modern digital fluoroscopes.¹²⁻¹⁵

Depending on the imaging options of the fluoroscopic equipment, full-column technique is performed by obtaining partial or full-length views of the esophagus distended with barium. These views allow detection of esophageal carcinoma (Fig. 2-2) and other abnormalities at the gastroesophageal junction such as hiatal hernias, peptic strictures, and lower esophageal rings.²² Lower esophageal rings are best visualized on prone views of the barium-filled lower esophagus, sometimes supplemented with a solid bolus such as a marshmallow or barium tablet.²²⁻²⁴

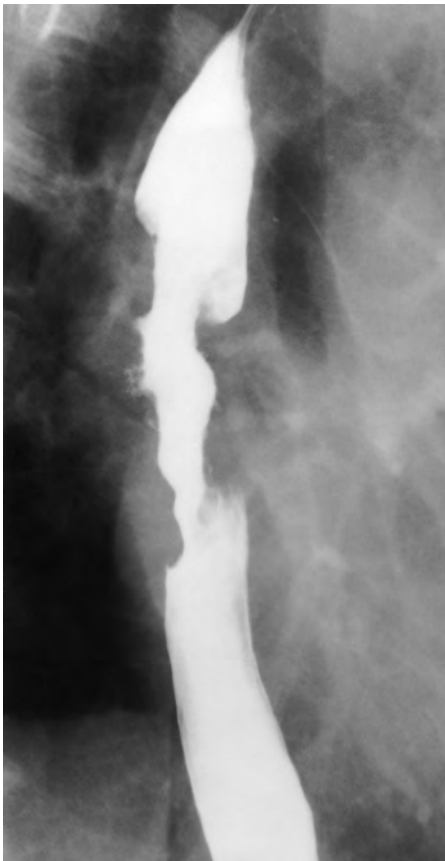


Figure 2-2 Annular carcinoma of the midesophagus. The lesion is well shown on the full-column portion of the barium esophagogram.

Full-column images of the esophagus are usually obtained with the patient on the fluoroscopic table in the prone, right anterior oblique position; a bolster may be used to increase intra-abdominal pressure. Esophageal peristalsis is inhibited by rapid swallowing of barium, allowing the esophagus to distend fully. Multiple images of the esophagus should be obtained at all levels; these images may be full-length views of the esophagus or coned-down views at different levels, depending on the imaging options of the fluoroscopic equipment.

Maximal distention of the esophagogastric region is required for optimal detection of hiatal hernias and lower esophageal rings (Fig. 2-3).^{22,24} Rapid ingestion of the barium suspension followed by deep inspiration (or a Valsalva maneuver) promotes distention of the gastroesophageal junction. Careful fluoroscopic observation is required to visualize lesions only seen when this region is optimally distended.

Full-column views are complemented by mucosal relief views of the collapsed esophagus, with coating of the longitudinal folds by the barium suspension.²³ A high-density barium suspension (e.g., that used for a double-contrast upper GI series) is ideal for this purpose. The patient takes one or several swallows of high-density barium to coat the esophageal folds with barium. These mucosal relief views may reveal thickened, irregular folds, small esophageal neoplasms, and reflux or infectious esophagitis (Fig. 2-4). Nevertheless, double-contrast views are better for showing the plaques of *Candida* esophagitis, the small ulcers of herpes esophagitis, and the giant ulcers of cytomegalovirus (CMV) or human immunodeficiency virus (HIV) esophagitis.²⁵

Single-contrast mucosal relief views are also best for detecting esophageal varices.^{23,26} The patient takes several swallows of the barium suspension, which coats the lower esophagus, and is then asked not to swallow to inhibit peristalsis. Intermittent fluoroscopic observation is performed for several minutes to visualize the varices optimally as they become more distended.

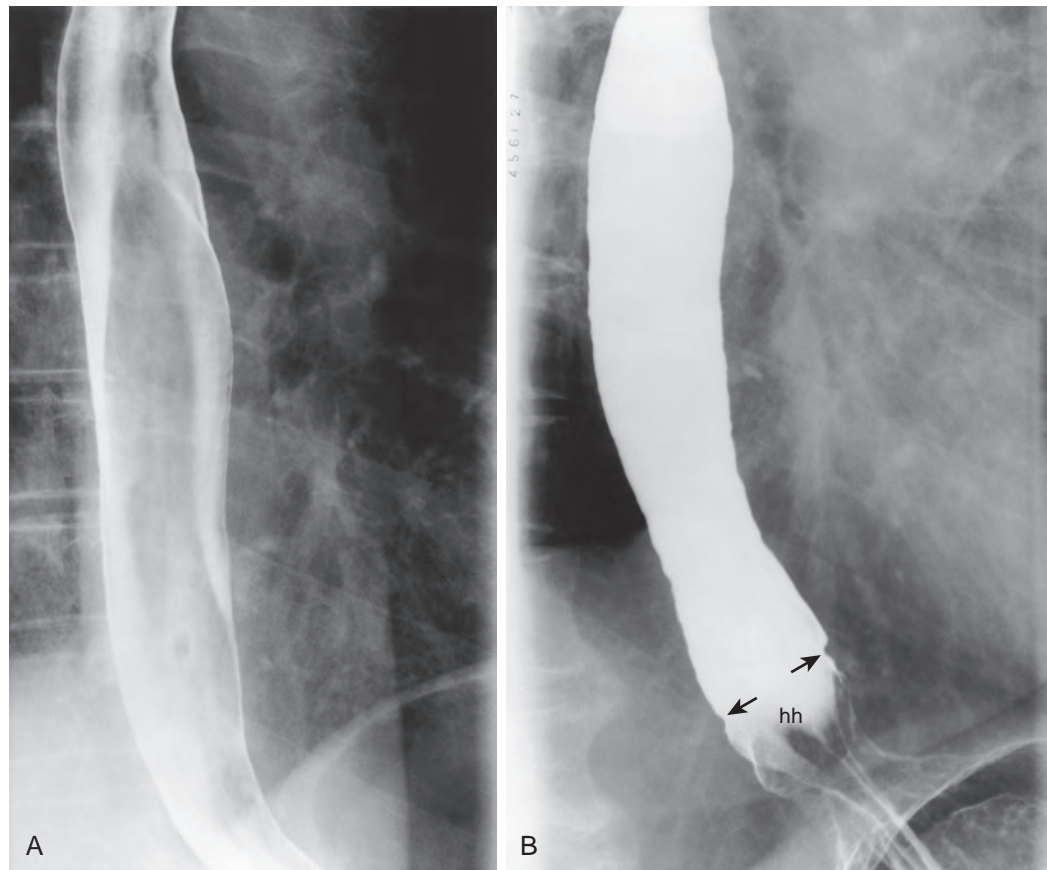
Fluoroscopic observation is an integral part of the radiographic evaluation of the esophagus and is usually adequate to assess esophageal function.^{9,23} Motion recording methods greatly aid in evaluating oropharyngeal swallowing disorders because of the rapid events that occur with deglutition, and may also be used to assess esophageal motility. Motion recordings should be obtained while the patient takes multiple discrete swallows of barium, because rapid swallowing causes reflex inhibition of esophageal peristalsis. With the use of single swallows, the single-contrast esophagogram is an excellent technique for evaluating esophageal motility.⁹

UPPER GASTROINTESTINAL SERIES

The single-contrast upper GI series is a complex examination requiring fluoroscopic observation, abdominal compression, and the use of multiple techniques for examining the esophagus, stomach, and duodenum.^{11,27} The study can be performed quickly and is tolerated even by patients who are immobile or unable to cooperate fully.

The examination starts with the table upright. After the patient ingests several swallows of barium, the stomach is compressed with a compression paddle or the cone on the fluoroscope to demonstrate the rugal folds, assess the pliability of the gastric wall, and detect focal areas of rigidity secondary to

Figure 2-3 Hiatal hernia and lower esophageal ring seen only on prone single-contrast esophagogram. **A.** Upright double-contrast view of the esophagus shows no abnormalities. **B.** Prone full-column view of the esophagogastric region in the same patient shows a hiatal hernia (hh) and a widely patent lower esophageal mucosal ring (arrows).



tumor or scarring. If the stomach empties, the barium-filled duodenal bulb can also be examined by compression in the upright position.

The table is then lowered to the horizontal position, and mucosal relief views of the stomach are obtained, first with the patient in a supine position and then after the patient turns into a prone position. These views supplement the upright compression views and can sometimes show small polyps, erosions, or ulcers that are later obscured in the barium-filled stomach (Fig. 2-5).^{4,28,29}

With the patient in the prone, right anterior oblique position, the esophagus is then examined using the same techniques described previously (see earlier, “Esophagography”). The gastric antrum and duodenal bulb usually fill with barium in this position, so prone compression views of the antrum and duodenal bulb should be obtained using an inflatable balloon placed beneath the patient to thin out the barium pool, enabling detection of anterior wall lesions in the antrum and duodenal bulb (Fig. 2-6).²⁷

With the patient in the supine, left posterior oblique position, air in the stomach rises into the gastric antrum and duodenal bulb, so limited double-contrast images of these areas can be obtained (Fig. 2-7). Compression can be used to displace the barium suspension, separate antroduodenal structures, and improve distention with air. The fluoroscopic portion of the examination is completed at this time. Some radiologists may then choose to obtain a standard set of overhead radiographs of the stomach and duodenum with the patient in prone, supine, right anterior oblique, and right lateral positions.

SMALL BOWEL

The small bowel can be examined by single-contrast technique with a small bowel follow-through, enteroclysis, or retrograde study via an ostomy or reflux from the colon.^{18,19,21} A peroral small bowel follow-through may be performed after a single-contrast upper GI series or as a separate study. A large volume (≥ 500 mL) of barium is recommended to promote gastric emptying, accelerate small bowel transit, and optimally distend small bowel loops. Fluoroscopic imaging and compression of all small bowel loops is a critical component of the examination because focal lesions are easily obscured by overlapping loops of small bowel unless compression is applied to separate these loops and ensure an adequate examination.

A small bowel follow-through typically requires a minimum of 500 mL of orally ingested barium, which can be the same product used for a single-contrast upper GI series. Prone overhead or low-magnification digital images of the small intestine are taken at timed intervals (e.g., every 30 minutes) until barium fills the right side of the colon. Depending on the barium product used, transit time through the small bowel is typically 60 to 90 minutes. Fluoroscopic spot imaging with manual compression should be performed at regular intervals during the examination. Compression of all loops and appropriate imaging of the entire small bowel is required to optimize detection of abnormalities (Fig. 2-8). When the barium suspension has reached the colon, compression views of the terminal ileum are obtained (typically with the patient in a supine or left posterior oblique position) for optimal visualization of this region.

Clear delineation of pelvic loops of small bowel, which often overlap, is not always possible, but several maneuvers may be performed to improve visualization of these loops.²¹ First, the patient should be told not to void during the examination because a full bladder elevates pelvic small bowel loops, enabling them to be separated with manual compression. A



Figure 2-4 Reflux esophagitis on mucosal relief view of the esophagus. Mucosal relief view from single-contrast esophagogram shows crenulated, irregular folds in the distal esophagus, suggesting esophagitis. Reflux esophagitis was confirmed at endoscopy.

similar effect may be achieved by instilling air into the rectum. The patient can also be placed in a prone Trendelenburg position with an inflated balloon beneath the lower abdomen and pelvis to displace pelvic small bowel loops superiorly for better visualization of these loops. If a remote control unit is available, the tube can be angulated to further separate these loops (Fig. 2-9).

Enteroclysis

An intubation small bowel study (enteroclysis) may be performed via a tube placed in the duodenum or jejunum.^{19,21,30} Several enteroclysis catheters are available commercially. The patient can be intubated via the mouth or the nose, with each approach having advantages and drawbacks. When single-contrast enteroclysis is performed, jejunal intubation is preferred to prevent duodenogastric reflux and emesis of barium.

Approximately 800 mL of a 15% to 20% w/v barium suspension is placed in an enema bag, which is hung on an adjustable vertical stand or IV pole. A water-soluble contrast agent may be added to stimulate intestinal peristalsis and shorten the length of the examination.^{16,17,21} The barium suspension is allowed to flow through the tube by gravity, and the rate of flow is regulated by adjusting the height of the enema bag. If the barium suspension flows too slowly, adequate distention is not achieved. Conversely, rapid flow rates may cause reflex paralysis of the small intestine, with slow transit and excessive duodenogastric reflux. Initially, the enema bag is placed about 2 feet above the table; the bag can be raised or lowered during the examination to adjust the flow rate for optimal distention of small bowel loops (Fig. 2-10).

The examination is performed under fluoroscopic guidance with the patient in a supine position. Careful compression spot images of all loops of small intestine are obtained under fluoroscopic guidance as bowel segments become fully distended to depict even subtle abnormalities (Fig. 2-11). When the entire small intestine has been opacified, overhead radiographs or low-magnification digital images of the small bowel are obtained; the patient can then be placed in a prone position to aid in separating small bowel loops in the pelvis.

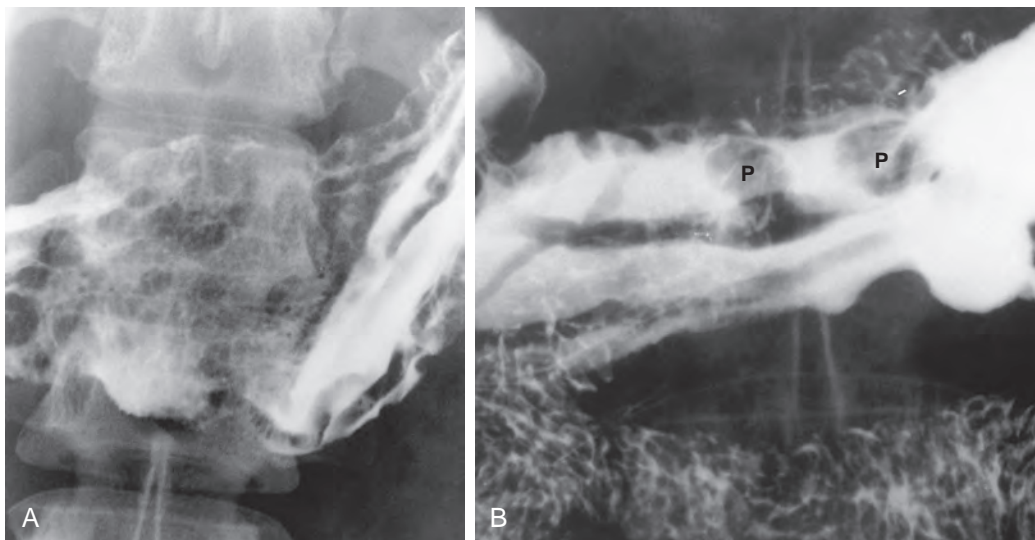


Figure 2-5 Recumbent compression views for detecting lesions in the stomach. **A.** Compression view of the gastric antrum shows antral erosions as multiple tiny nodules containing punctate collections of barium. **B.** In another patient, compression view of the antrum shows several small polyps (P) as filling defects in the barium pool. The findings in **A** and **B** were not well shown on double-contrast views but were confirmed at endoscopy.

Figure 2-6 Prone compression view of the duodenal bulb showing an anterior wall ulcer.

A. Prone view of the duodenal bulb (a balloon paddle compression device was used) shows an anterior wall ulcer (U) with surrounding edema.

B. Supine oblique air-contrast view of the duodenal bulb in the same patient shows a ring shadow (R) because of barium coating the rim of the unfilled anterior wall ulcer crater.

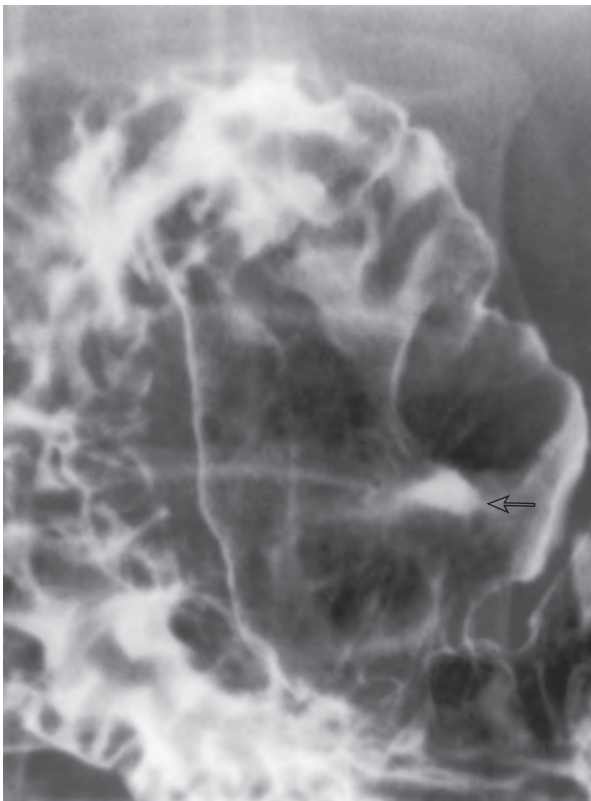
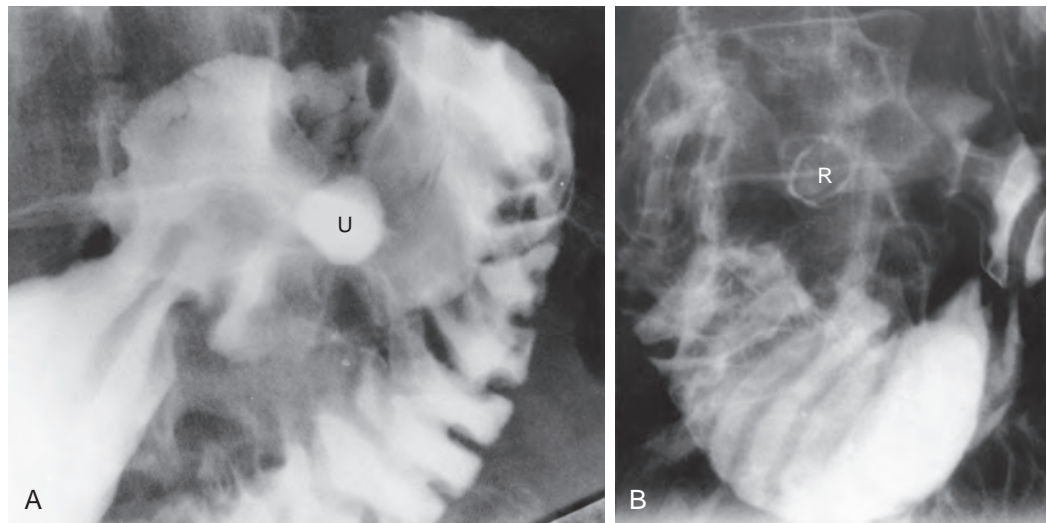


Figure 2-7 Posterior wall duodenal ulcer on air-contrast view of the bulb. Supine oblique air-contrast view of the duodenal bulb with compression shows a small posterior wall ulcer (arrow), emphasizing the importance of obtaining limited double-contrast views as part of a thorough single-contrast upper gastrointestinal examination.



Figure 2-8 Compression spot image of the small bowel showing a Meckel's diverticulum. A peroral small bowel follow-through study was performed in a patient with gastrointestinal bleeding. Compression spot image of the right lower quadrant shows a Meckel's diverticulum (M) as the cause of the patient's bleeding. The diverticulum was removed at surgery.

BARIUM ENEMA

Fluoroscopic observation, careful imaging with graded compression, and knowledge of appropriate technical factors enables detection of a variety of lesions in the barium-filled colon on single-contrast examinations.^{20,31} Although single-contrast barium enemas are less sensitive than double-contrast examinations for detecting small polypoid lesions

and for evaluation of inflammatory bowel disease,^{6,20,32} the single-contrast barium enema can be performed quickly and is usually a better choice for patients who are immobile, older, or incontinent.^{6,7}

Preparation of the large bowel is the most important prerequisite for an accurate single- or double-contrast barium enema.^{4,27} The diagnosis of neoplasms, including small polyps,

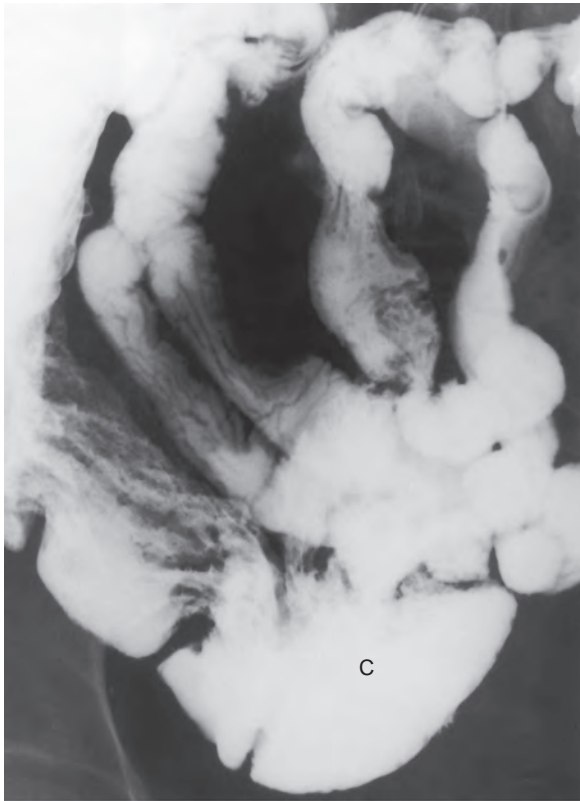


Figure 2-9 Peroral small bowel follow-through study in a posthysterectomy patient with pelvic small bowel loops lying deep within the pelvis. A prone image of the pelvis with a bolster placed beneath the patient and x-ray tube angulation clearly shows the cecum (C) and ileocecal junction. Note how pelvic loops of ileum are well separated and visualized.



Figure 2-10 Single-contrast enteroclysis. Normal small bowel loops are well distended, with the folds in a parallel arrangement. The use of a dilute barium suspension permits a see-through effect for visualization of overlapping loops of small bowel.

is easier and more reliable in a well-cleansed colon. Conversely, the presence of stool invariably limits the detection of polyps and is the most common cause of errors when interpreting the images.^{4,31}

A variety of colon-cleansing protocols can be used to obtain a thoroughly clean colon in the vast majority of patients.^{31,33} One recommended bowel preparation regimen includes the following:

1. A 24-hour clear liquid diet
2. One glass of water hourly the day before the examination
3. A saline cathartic such as magnesium citrate at 4:00 PM the day before the examination
4. 60 mL of a flavored castor oil or other irritant cathartic at 8:00 PM the day before the examination
5. An optional 1500-mL tap water cleansing enema the morning of the barium enema examination, although the need for a water enema is controversial³⁴

If a tap water enema is administered, the patient needs to wait at least 30 minutes before the single-contrast barium enema is performed to avoid excess fluid in the colon, which might further dilute the barium suspension and degrade the quality of the study.^{31,33,35}

A thorough examination protocol must be followed to ensure that an adequate single-contrast barium enema is obtained.^{6,20,31} All portions of the colon must be adequately visualized and imaged without overlapping segments to increase the fluoroscopist's confidence that suspected lesions are real

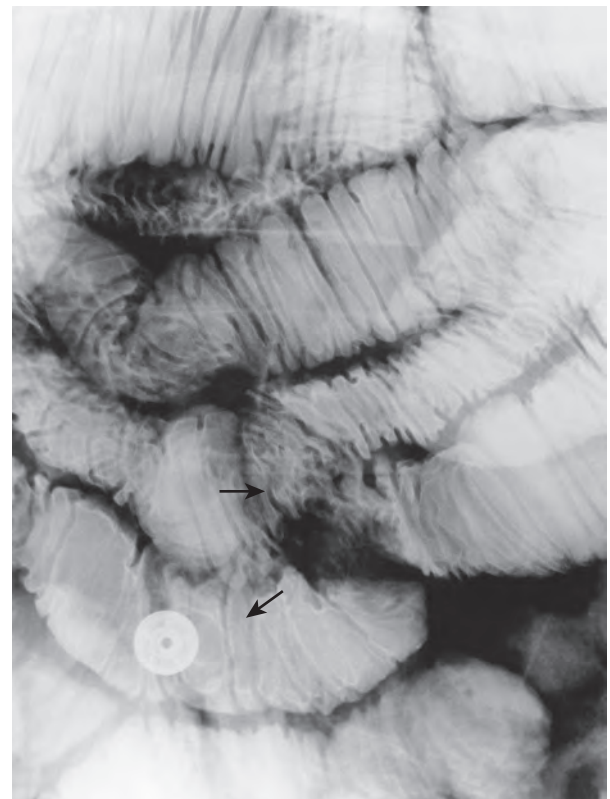


Figure 2-11 Nonobstructing adhesions on single-contrast enteroclysis with compression. Compression view of the mid small bowel shows focal nonobstructing adhesions (arrows) with angulation of the affected bowel and an inability to separate adjacent loops.

(Fig. 2-12). As in the small bowel follow-through, manual compression of the colon is a critical component of the examination because polyps and polypoid cancers protruding into the lumen may only be visualized with adequate thinning of the barium column (Fig. 2-13).^{20,31} Overhead radiographs may be obtained at the end of the examination, followed by a postevacuation radiograph.

The following technique can be used for performing a thorough single-contrast barium enema.³¹ After insertion of the rectal tip, the patient is placed in the left posterior oblique position, the flow of the barium suspension is started slowly, and a spot image of the rectosigmoid region is obtained while distention is minimal. Because the rectum cannot be compressed, this early image allows smaller lesions to be detected more easily. The rectosigmoid region is again imaged when fully distended. An appropriate number of views are obtained to demonstrate the sigmoid colon without overlapping loops. The entire colon is then opacified to the cecum, avoiding ileal reflux, if possible. Compression spot images of the remaining segments of colon are then obtained. After the fluoroscopic examination has been completed, overhead radiographs may be obtained. When using a remote control unit, the overheads may be taken during the fluoroscopic portion of the examination. A reasonable sequence of overheads includes a left lateral view of the rectum, prone and supine views of the colon, supine left and right anterior oblique views of the colon, and a prone angled view of the rectosigmoid.

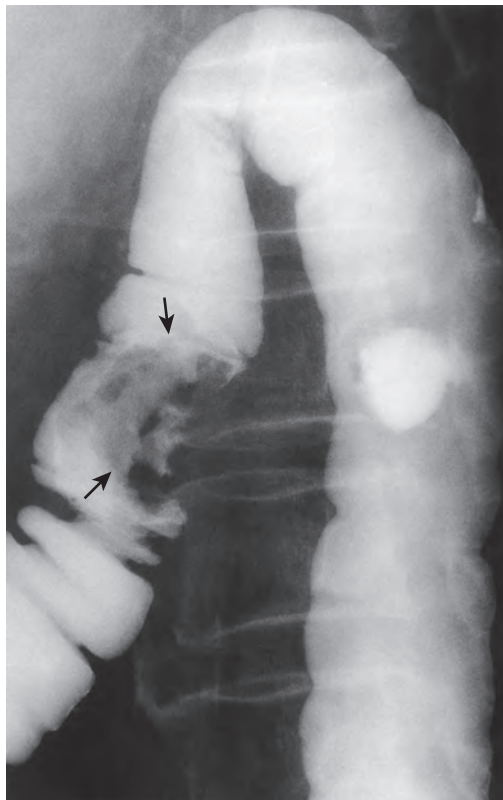


Figure 2-12 Colonic carcinoma on single-contrast barium enema. This oblique compression spot image of the splenic flexure shows a polypoid, ulcerated carcinoma (arrows) of the distal transverse colon. Careful patient positioning and the use of compression are critical components of this examination.

A postevacuation radiograph is generally obtained at the end of the study to document colonic emptying and rule out gross colonic dysmotility. The postevacuation radiograph may also show that a filling defect seen on earlier barium-filled views persists or disappears, thereby indicating whether this finding was caused by a true polyp or residual stool (Fig. 2-14).

Double-Contrast Studies

PERFORMANCE

The yield of diagnostic information from double-contrast studies can be maximized only with meticulous attention to the technical aspects of the examination. The major principles of performance include mucosal coating, distention, and projection.

Mucosal Coating

The diagnostic quality of double-contrast studies depends on the quality of mucosal coating. In the absence of good coating, lesions can be missed or patchy coating can be mistaken for a lesion. Good mucosal coating requires optimal interaction between the barium suspension and mucosal surface. An appropriate barium suspension must be chosen; it must be prepared properly,³⁶ and the mucosal surface must be clean enough to enable adequate coating. Even when the mucosal coating is only slightly impaired, major abnormalities can be missed (Fig. 2-15).

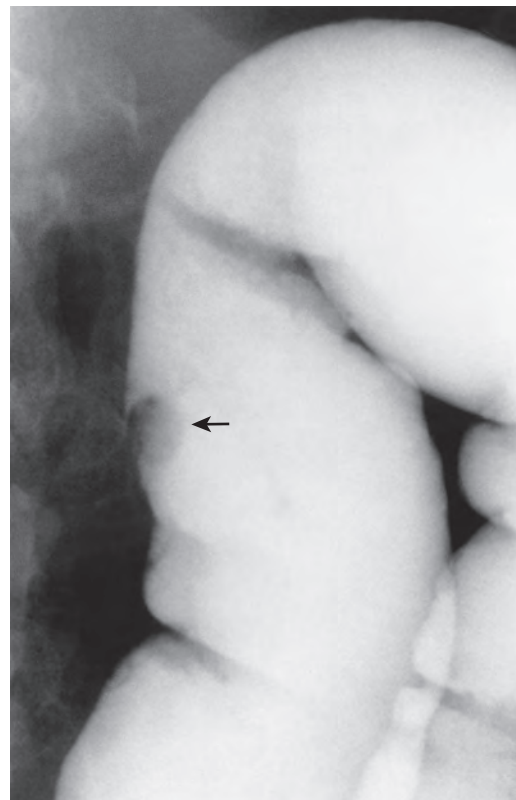


Figure 2-13 Small colonic polyp on compression spot image from a single-contrast barium enema. Oblique compression spot image of the splenic flexure shows an 8-mm colonic polyp (arrow). This small polyp was not seen on other images of the same area when compression was not applied.

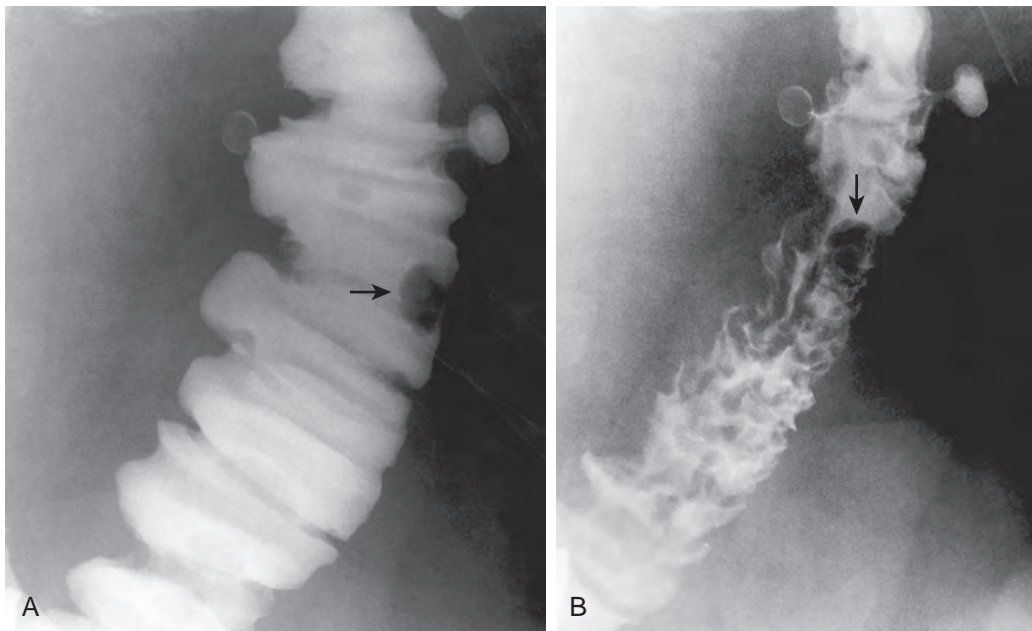


Figure 2-14 Value of postevacuation radiographs for detecting colonic polyps.

A. Compression spot image shows a small (<1 cm) filling defect (arrow) in the descending colon on a single-contrast barium enema. Diverticula are also present in this region. The filling defect was not clearly present on other views. **B.** Postevacuation compression spot image of the descending colon (note the location of the previously seen diverticula) again shows this small filling defect (arrow), indicating that it is a true polyp. A small adenoma was removed at colonoscopy.

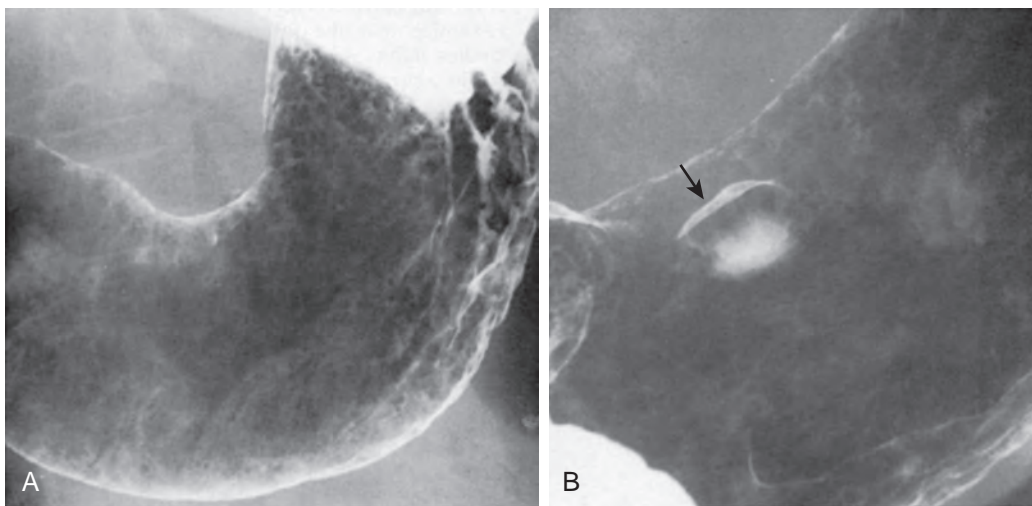


Figure 2-15 Risk of suboptimal coating. **A.** On the initial radiograph, an ulcer crater is barely recognizable along the lesser curvature of the stomach. **B.** With additional rotation and improved coating, the large ulcer crater (arrow) is clearly seen.

Distention

Normal folds are soft and pliable and are therefore effaced with moderate distention. The optimal degree of distention is that which just effaces the normal folds. Inadequate distention may conceal lesions, but overdistention can also obscure lesions such as shallow ulcers. Varying degrees of distention may therefore be required for optimal visualization of complex or subtle lesions. Overdistention may accentuate areas of rigidity, whereas partial collapse may accentuate abnormalities of the folds. The final diagnosis represents a synthesis of the information obtained with these various views (Fig. 2-16).

Projection

An adequate number of views should be obtained, so each loop of bowel is projected free of overlapping loops. Ideally, each segment of bowel should also be demonstrated in profile. In practice, however, these goals cannot always be achieved. It is

therefore important to assess overlapping loops of bowel and be able to recognize abnormalities that are viewed en face as well as in profile. This is particularly important for recognition of short, annular lesions in the colon because it may be difficult to demonstrate every colonic bend in profile (Fig. 2-17).

INTERPRETATION

After every effort is made to obtain excellent images, it is important to extract all of the diagnostic information available on these images. The interpretation of double-contrast studies also differs substantially from the interpretation of single-contrast studies.

Dependent and Nondependent Surfaces

The distinction between the dependent and nondependent surfaces must be understood. The nondependent surface has a thin coating of barium because all the free barium falls onto the

Figure 2-16 Adenocarcinoma in Barrett's esophagus. **A.** Double-contrast view shows ulceration and slight rigidity of the contour in the lower esophagus. **B.** Mucosal relief view shows the polypoid nature of the lesion. (From Laufer I, Levine MS [eds]: *Double Contrast Gastrointestinal Radiology*, 2nd ed. Philadelphia, WB Saunders, 1992.)

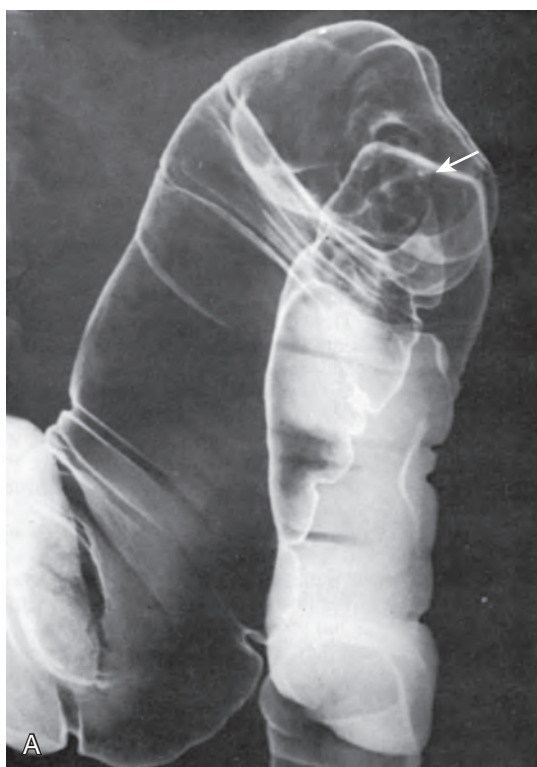
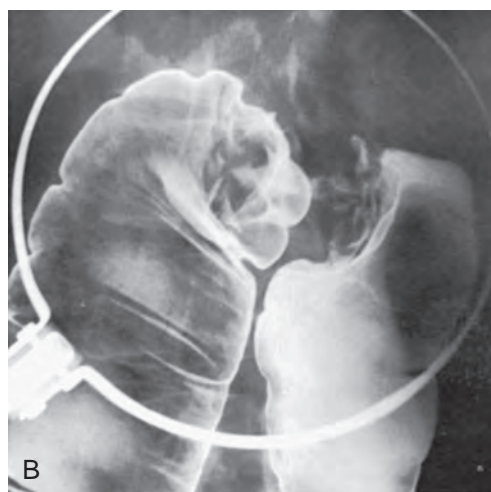


Figure 2-17 Annular carcinoma seen en face and in profile. **A.** There is irregularity of the lumen seen end-on (arrow) caused by an annular carcinoma. **B.** The annular lesion is readily apparent when viewed in profile on an appropriate oblique projection. (From Laufer I, Levine MS [eds]: *Double Contrast Gastrointestinal Radiology*, 2nd ed. Philadelphia, WB Saunders, 1992.)



dependent surface. As a result, the dependent surface has a thicker coating of barium, and the barium pool accumulates in any depression or concavity. The usual double-contrast image obtained with a vertical beam results in superimposition of the dependent and nondependent surfaces and any barium pool that might be present. The distinction between these surfaces is more clearly demonstrated on horizontal beam radiographs (Fig. 2-18).

Lesions in the GI tract can generally be classified as protruded or depressed, and their appearance depends on whether they are located on dependent or nondependent surfaces. Their appearance can also be affected or even masked by the barium pool.

Protrusions

Protrusions into the lumen of a hollow viscus can be normal structures such as folds or pathologic lesions such as polypoid tumors. The radiographic principles underlying the appearance



Figure 2-18 Dependent and nondependent surfaces. The distinction between the dependent and nondependent surfaces is clearly shown on this horizontal beam radiograph of the colon. The nondependent surface has a thin coating of barium, whereas the dependent surface contains the barium pool.

of protrusions are illustrated in Figure 2-19, which represents a cross-section through the stomach with rugal folds on its anterior and posterior walls. With the patient in the supine position, the posterior wall is dependent and the anterior wall is nondependent.

A protrusion on the dependent surface displaces barium from the barium pool and is therefore seen as a radiolucent filling defect. A protrusion on the nondependent surface is coated with barium, and the x-ray beam catches the edges of the protrusion, which are then etched in white. Figure 2-20 illustrates the different appearances of a lesion when it is located on the dependent surface and then on the nondependent surface.

In general, the density of the etching depends on the thickness of the lesion, so the etching of a slightly protruded or plaque-like lesion may be extremely faint. Such lesions are best demonstrated on the dependent surface in the presence of a shallow barium pool. Flow technique is particularly valuable for detecting these lesions.³⁷

Several other appearances are associated with protruded lesions. The stalactite phenomenon represents a droplet of barium hanging from a protrusion on the nondependent surface (Fig. 2-21).³⁸ These barium droplets can be differentiated from ulcers because they are almost always associated with protrusions on the nondependent surface and disappear as the droplet falls away. Nevertheless, it is important to recognize these stalactites because they may be the only clue to the presence of a protruded lesion on the nondependent surface.³⁹

The so-called bowler hat sign may be seen with a polypoid lesion or diverticulum. With a diverticulum, however, the dome of the hat points outward from the long axis of the bowel (Fig. 2-22A), whereas with a polyp, the dome of the hat points toward the lumen (Fig. 2-22B).⁴⁰ The so-called Mexican hat sign represents a pedunculated polyp hanging from the nondependent surface. The outer ring represents the head of the polyp, and the inner ring represents the stalk seen end-on through the head (Fig. 2-23).

Depressed Lesions

Depressed lesions are lesions such as ulcers or diverticula that extend beyond the normal contour of the bowel. When located

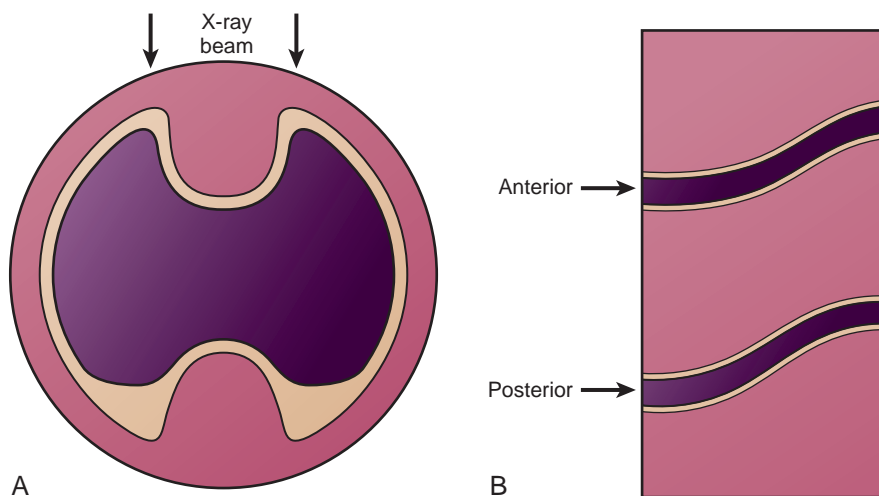


Figure 2-19 Principles underlying the appearance of protrusions. A, B. Diagrammatic representations of the appearance of a rugal fold on the anterior and posterior walls of the stomach. (From Laufer I, Levine MS [eds]: *Double Contrast Gastrointestinal Radiology*, 2nd ed. Philadelphia, WB Saunders, 1992.)

Figure 2-20 Effect of position on the appearance of a rectal carcinoma. **A.** With the patient in the supine position, there is a lobulated filling defect in the distal rectum. The plaque-like carcinoma is therefore on the dependent (posterior) wall. **B.** With the patient turned into the prone position, the carcinoma is now etched in white because it is on the nondependent (anterior) surface.

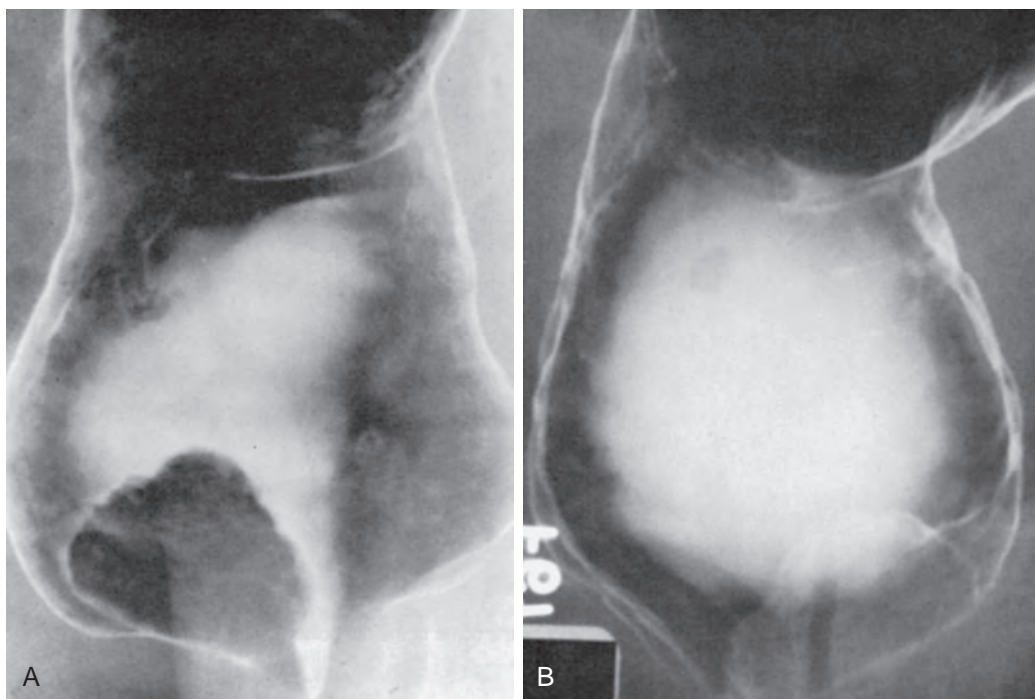


Figure 2-21 The stalactite phenomenon. Radiograph of the colon with the patient in the upright position shows a long droplet of barium (arrow) hanging from a haustral fold. (From Laufer I, Levine MS [eds]: *Double Contrast Gastrointestinal Radiology*, 2nd ed. Philadelphia, WB Saunders, 1992.)

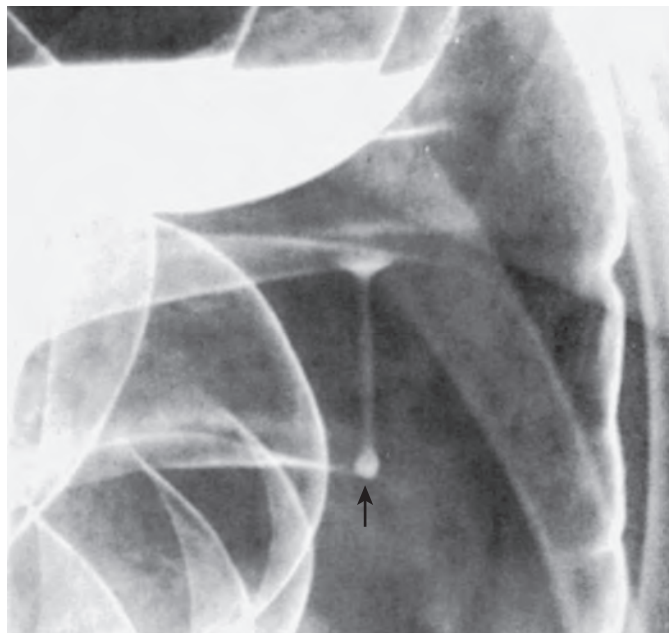


Figure 2-22 Bowler hat: polyp or diverticulum? **A.** When the dome of the hat (arrow) points away from the long axis of the bowel, it is a diverticulum. **B.** When the dome of the hat points toward the lumen of the bowel, it is a polyp. (From Laufer I, Levine MS [eds]: *Double Contrast Gastrointestinal Radiology*, 2nd ed. Philadelphia, WB Saunders, 1992.)

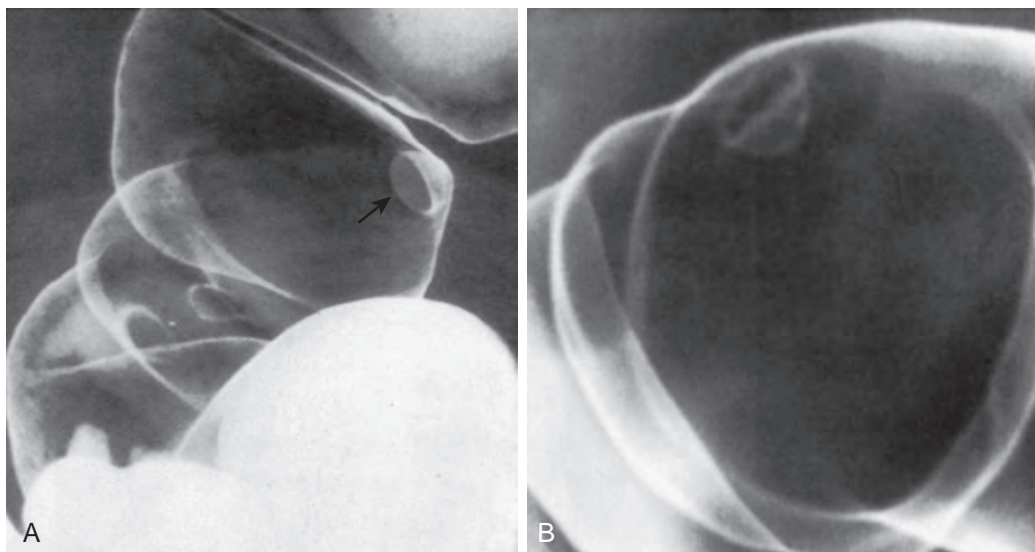




Figure 2-23 Mexican hat sign. Typical appearance of a pedunculated polyp seen end-on. The outer ring represents the head of the polyp, and the inner ring represents the stalk.

on the dependent surface, they trap barium and are therefore seen as focal barium collections (Fig. 2-24A). Conversely, when located on the nondependent surface, they empty of barium. If there is adequate coating of the sides of a depressed lesion, however, it can be recognized as a ring shadow (Figs. 2-24B and C). In patients with colonic diverticulosis, the appearance of these lesions therefore depends on their location in the bowel; diverticula on the dependent surface tend to fill with barium, whereas diverticula on the nondependent surface usually appear as ring shadows (Fig. 2-25).

This concept is particularly important for the recognition of anterior wall duodenal ulcers. With the patient in the supine or supine left posterior oblique position, the ulcer may be manifested by a ring shadow or crescent because of barium coating the rim of the unfilled, nondependent ulcer crater (see Fig. 2-24B). When the patient is placed in the prone position, however, the ulcer fills with barium (see Fig. 2-24C).

Barium Pool

The barium pool is the “paint” of the radiologic artist. In essence, the double-contrast examination requires manipulation of the barium pool to paint or coat the entire mucosal surface. At the same time, the barium pool may compromise the study in various ways (Fig. 2-26). It can cover over and submerge a lesion on the dependent surface. Even a small barium pool on the dependent surface can also obscure the etching of a lesion on the nondependent surface (Fig. 2-27). Finally, the barium pool in an overlapping loop of bowel can obscure lesions in the loop of interest.

In general terms, lesions on the dependent surface are best demonstrated with an extremely shallow barium pool, whereas recognition of lesions on the nondependent surface requires that the barium pool on the dependent surface be entirely eliminated. These varying requirements can be met by use of

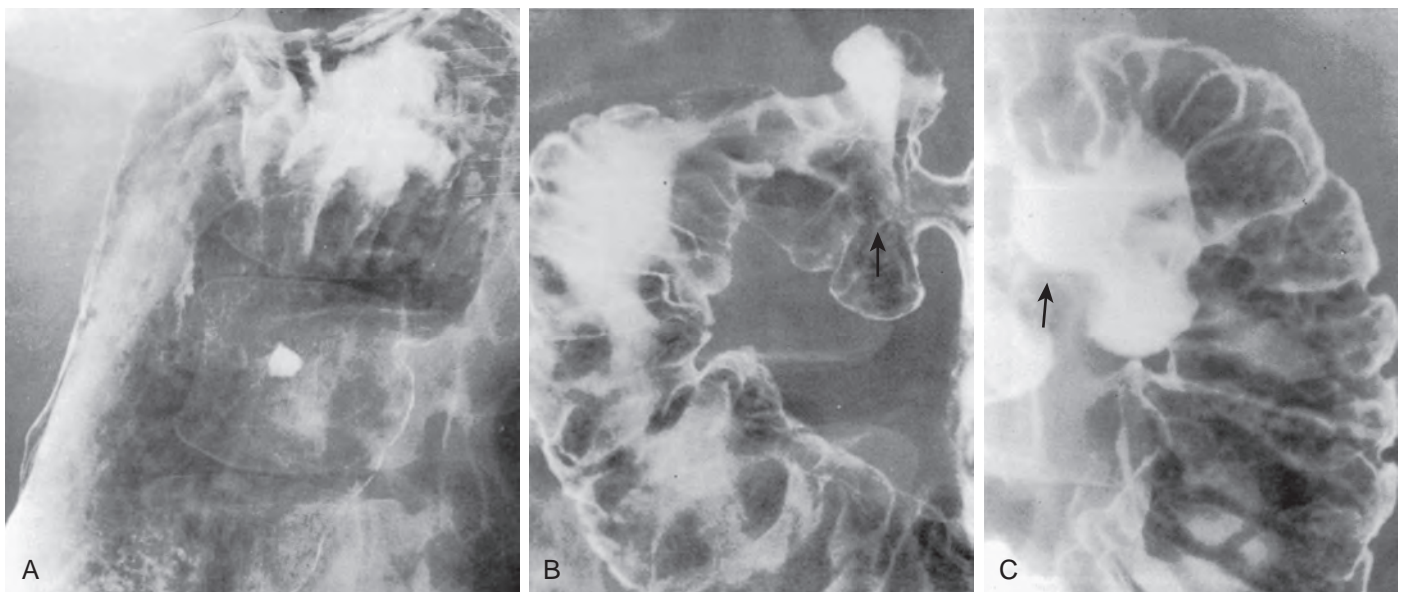


Figure 2-24 Depressed lesions. **A.** Dependent wall ulcer. Radiograph of the stomach in the right posterior oblique projection shows a high ulcer on the lesser curvature. **B.** Anterior wall ulcer. This spot image in the supine left posterior oblique projection shows a ring shadow (arrow) representing the nondependent ulcer crater etched in white on the anterior wall of a deformed duodenal bulb. **C.** With the patient in the prone position, the ring shadow fills with barium (arrow), indicating an anterior wall duodenal ulcer. (From Laufer I, Levine MS [eds]: *Double Contrast Gastrointestinal Radiology*, 2nd ed. Philadelphia, WB Saunders, 1992.)



Figure 2-25 Depressed lesions on the dependent and nondependent surfaces. In a segment of colonic diverticulosis, diverticula on the dependent surface are filled with barium, whereas diverticula on the nondependent surface are etched in white.

flow technique (Fig. 2-28).³⁷ As the patient is turned under fluoroscopic control, the flow of the barium pool across the dependent surface is observed. In this way, shallow lesions can be demonstrated on the dependent surface and, as the barium pool flows away, lesions can also be seen on the nondependent surface. The concept of flow technique is important for demonstrating subtle lesions and avoiding diagnostic error.

ARTIFACTS

Many of the artifactual appearances associated with double-contrast studies are obvious to the radiologist.⁴¹ These artifacts include findings caused by barium precipitates (Fig. 2-29A), patchy mucosal coating, and extraneous debris. However, some artifacts may be confusing if they closely resemble pathologic states.

In the colon, some barium suspensions may crack or flake, producing an appearance suggestive of inflammatory bowel disease (Fig. 2-29B). In other patients, there may not be enough distention of the lumen to separate the anterior and posterior walls. The area of apposition is manifested by a so-called kissing artifact, which can simulate a mass lesion (Fig. 2-30A). Kissing artifact can also result from extrinsic compression of the lumen, causing the anterior and posterior walls to become apposed (Fig. 2-30B). In such cases, the appropriate projection should be obtained to identify an extrinsic mass compressing the lumen.

Because the air-filled bowel is translucent, structures in front of or behind the bowel may be projected over the lumen, so they simulate lesions arising from the bowel. It is particularly important to recognize the true nature of barium-filled diverticula and calcified structures overlying the bowel and not to mistake them for polypoid or ulcerated lesions (Fig. 2-31). Other double-contrast artifacts are discussed elsewhere in this text in chapters dealing with specific organs.

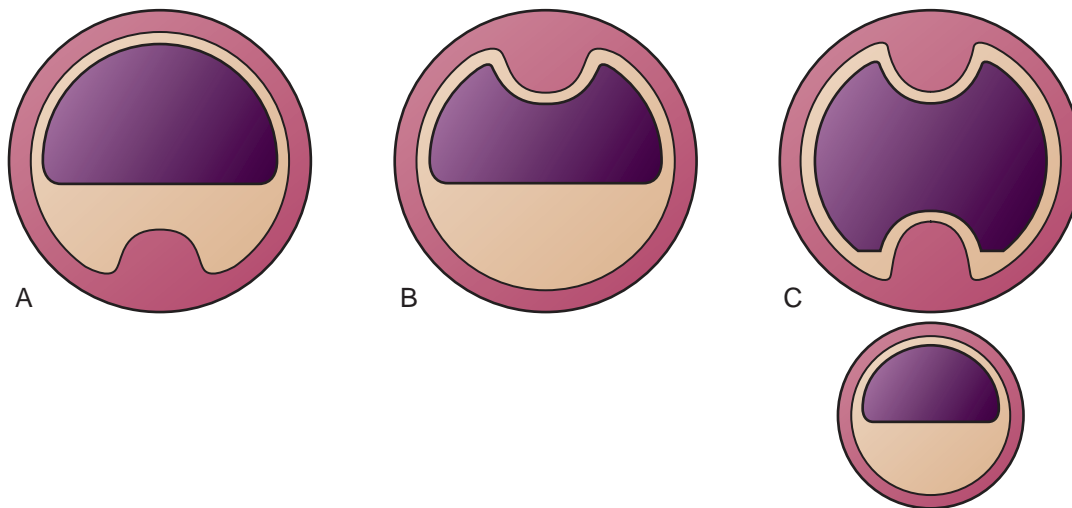


Figure 2-26 Diagrammatic representation of the hazards of the barium pool. **A.** The barium pool obscures a lesion on the dependent surface. **B.** The barium pool obscures the fine white etching of a lesion on the nondependent surface. **C.** The barium pool in an overlapping loop of bowel can obscure a lesion on the dependent or nondependent surface. (A and B from Laufer I, Levine MS [eds]: *Double Contrast Gastrointestinal Radiology*, 2nd ed. Philadelphia, WB Saunders, 1992.)

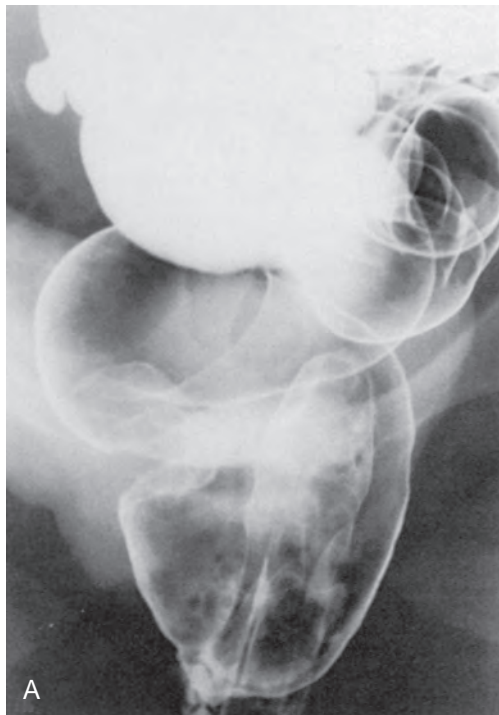


Figure 2-27 Barium pool obscuring a lesion on the nondependent surface. **A.** In the frontal projection, a polypoid carcinoma is seen along the right lateral wall of the rectum. **B.** In the left lateral projection, the rectal carcinoma is on the nondependent surface (right lateral wall) of the rectum, so the lesion is obscured by the barium pool on the dependent surface (left lateral wall).

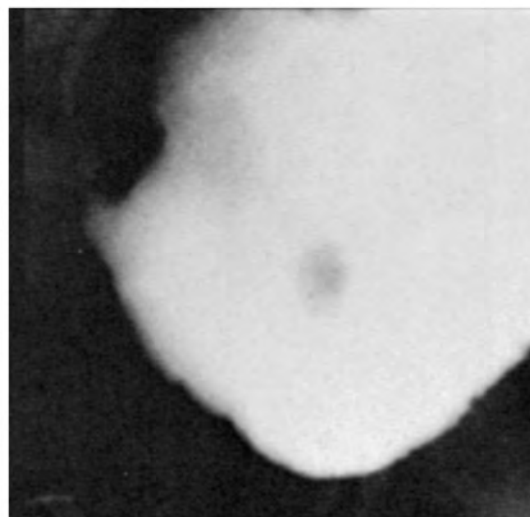
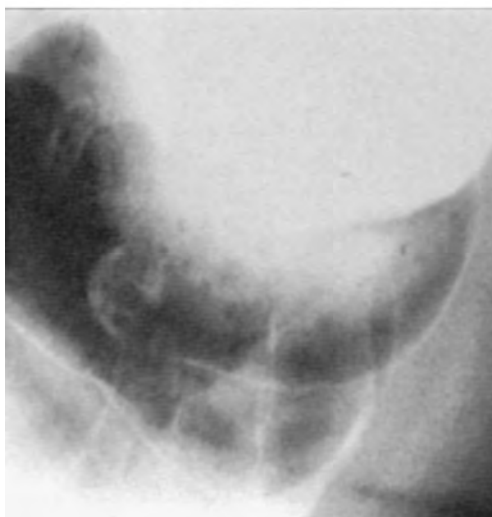
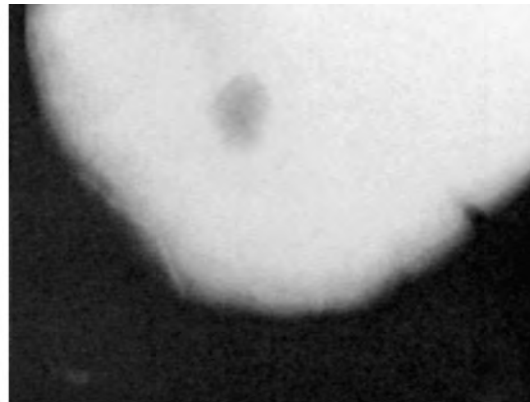
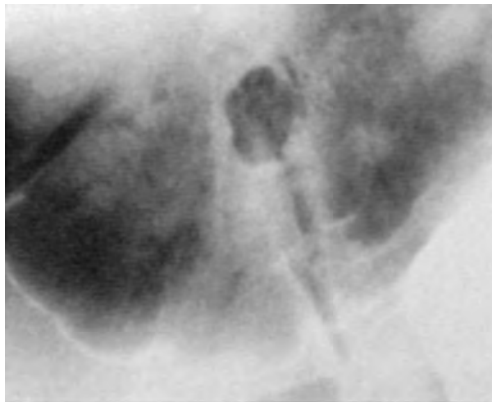
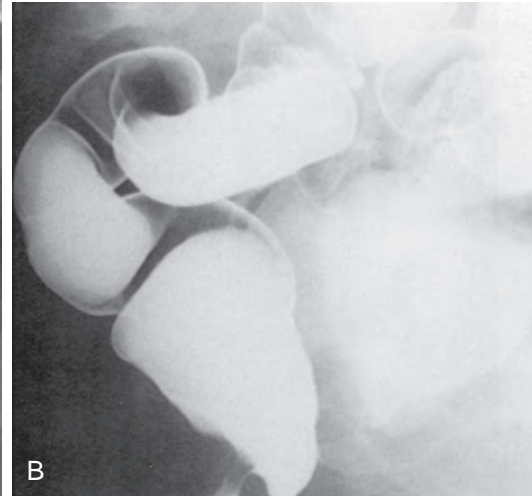


Figure 2-28 Flow technique. There is a 1-cm sessile polyp in the cecum. The appearance of this small protruded lesion varies as barium flows across the dependent surface of the cecum.

Figure 2-29 Double-contrast artifacts. **A.** Barium precipitates are recognized as sharp, dense barium collections on the mucosal surface. **B.** Flaking of the barium suspension simulates inflammatory bowel disease. (**B** from Laufer I: Air contrast studies of the colon in inflammatory bowel disease. *Crit Rev Diagn Imaging* 9:421–447, 1977.)

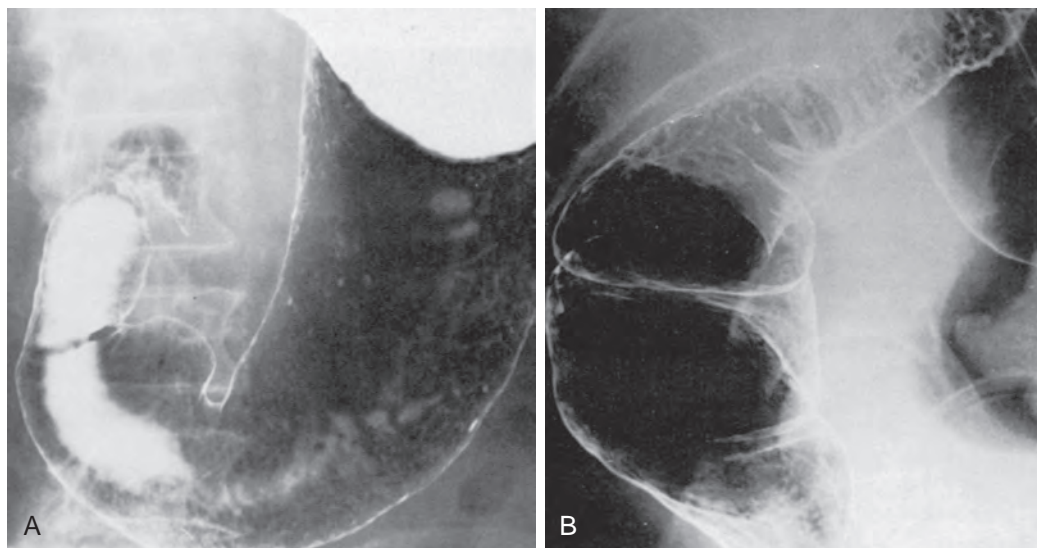


Figure 2-30 Kissing artifacts. **A.** A kissing artifact is seen near the lesser curvature of the stomach, simulating a polypoid lesion (arrow). **B.** This kissing artifact results from compression of the stomach by the abdominal aorta (straight arrows). The curved arrow indicates calcification in the wall of the aorta.

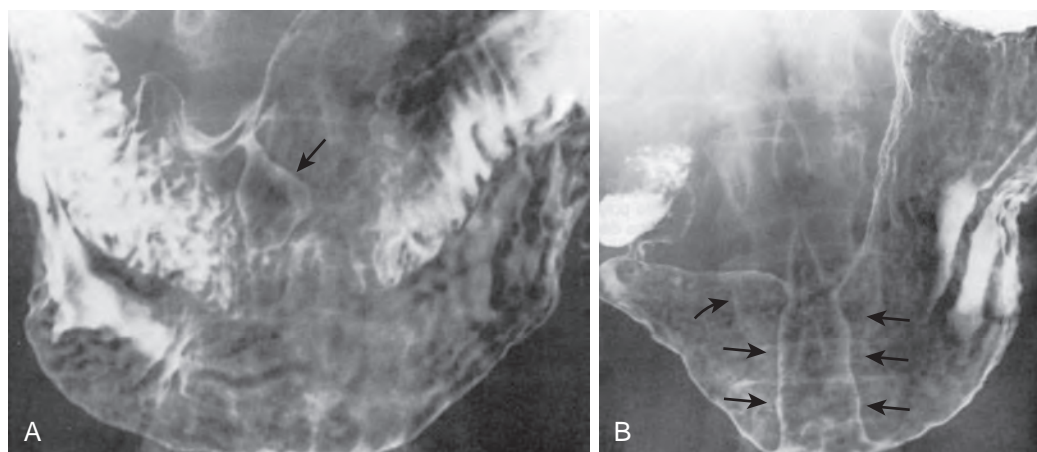
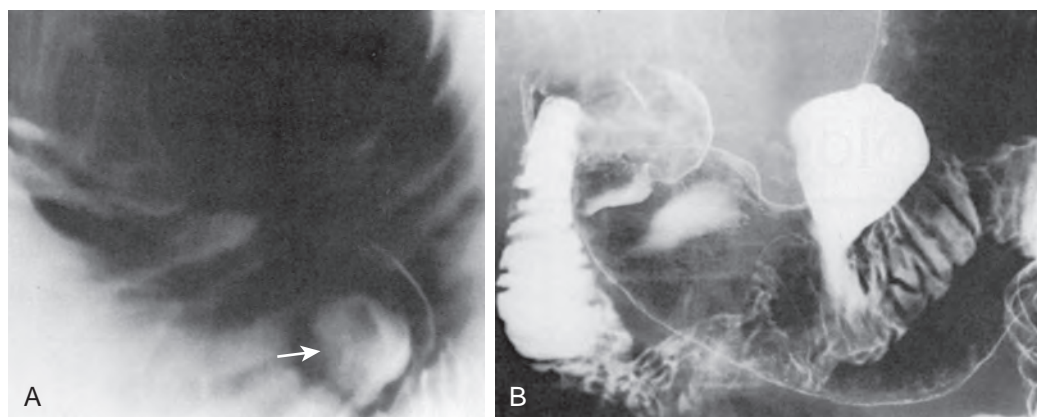


Figure 2-31 Duodenal diverticulum simulating a gastric ulcer. **A.** Compression radiograph of the stomach shows a large barium collection (arrow) suggestive of a gastric ulcer. **B.** Supine double-contrast radiograph shows that the barium-filled structure is a large diverticulum arising from the fourth portion of the duodenum.



REFERENCES

1. Gelfand DW, Ott DJ, Chen YM: Decreasing numbers of gastrointestinal studies: Report of data from 69 radiologic practices. *AJR* 148:1133–1136, 1987.
2. Ott DJ, Gelfand DW: The future of barium radiology. *Br J Radiol* 70:S171–S176, 1997.
3. Dekker W, Op den Orth JO: Biphasic radiologic examination and endoscopy of the upper gastrointestinal tract: A comparative study. *J Clin Gastroenterol* 10:461–465, 1988.
4. Gelfand DW, Chen YM, Ott DJ: Multiphasic examinations of the stomach: Efficacy of individual techniques and combinations of techniques in detecting 153 lesions. *Radiology* 162: 829–834, 1987.
5. Gelfand DW, Ott DJ: Single vs. double-contrast gastrointestinal studies: Critical analysis of reported statistics. *AJR* 137:523–528, 1981.

6. Gelfand DW, Chen YM, Ott DJ: Detection of colonic polyps on single-contrast barium enema study: Emphasis on the elderly. *Radiology* 164: 333–337, 1987.
7. Frederick MG, Ott DJ, Gelfand DW, et al: Gastrointestinal fluoroscopy in difficult patients. *Appl Radiol* 26:12–22, 1997.
8. Laufer I, Kressel HY: Principles of double contrast diagnosis. In Laufer I, Levine MS, editors: *Double Contrast Gastrointestinal Radiology*, ed 2, Philadelphia, 1992, WB Saunders, pp 9–54.
9. Ott DJ, Chen YM, Hewson EG, et al: Esophageal motility: Assessment with synchronous video tape fluoroscopy and manometry. *Radiology* 173:419–422, 1989.
10. Gelfand DW, Ott DJ, Chen MYM: Compression filming with high-density barium suspensions. *Abdom Imaging* 18:320–322, 1993.
11. Gelfand DW: The multiphasic upper gastrointestinal examination. *Radiol Clin North Am* 32:1067–1081, 1994.
12. Gelfand DW: Fluoroscopic equipment. In Ott DJ, Gelfand DW, Chen MYM, editors: *Manual of Gastrointestinal Fluoroscopy—Performance of Procedures*, Springfield, IL, 1996, Charles C Thomas, pp 15–23.
13. Levine MS, Laufer I: The gastrointestinal tract: Dos and don'ts of digital imaging. *Radiology* 207:311–316, 1998.
14. Taylor AJ: Impact of digital spot imaging in gastrointestinal fluoroscopy. *AJR* 173:1065–1069, 1999.
15. Chawla S, Levine MS, Laufer I, et al: Gastrointestinal imaging: A systems analysis comparing digital and conventional techniques. *AJR* 172: 1279–1284, 1999.
16. Gelfand DW: Gastrointestinal contrast materials. In Ott DJ, Gelfand DW, Chen MYM, editors: *Manual of Gastrointestinal Fluoroscopy—Performance of Procedures*, Springfield, IL, 1996, Charles C Thomas, pp 3–14.
17. Skucas J: Contrast media. In Gore RM, Levine MS, editors: *Textbook of Gastrointestinal Radiology*, ed 2, Philadelphia, 2000, WB Saunders, pp 2–14.
18. Davidson JC, Einstein DM, Herts BR, et al: Comparison of two barium suspensions for dedicated small-bowel series. *AJR* 172:379–382, 1999.
19. Ott DJ, Chen YM, Gelfand DW, et al: Detailed per-oral small bowel examination vs. enteroclysis. Part I: Expenditures and radiation exposure. *Radiology* 155:29–31, 1985.
20. Ott DJ, Gelfand DW: How to improve the efficacy of the barium enema examination. *AJR* 160:491–495, 1993.
21. Chen MYM, Gelfand DW: Small bowel. In Ott DJ, Gelfand DW, Chen MYM, editors: *Manual of Gastrointestinal Fluoroscopy—Performance of Procedures*, Springfield, IL, 1996, Charles C Thomas, pp 69–90.
22. Chen YM, Ott DJ, Gelfand DW, Munitz HA: Multiphasic examination of the esophagogastric region for strictures, rings, and hiatal hernias: Evaluation of the individual techniques. *Gastrointest Radiol* 10:311–316, 1985.
23. Ott DJ: Pharynx and esophagus. In Ott DJ, Gelfand DW, Chen MYM, editors: *Manual of Gastrointestinal Fluoroscopy—Performance of Procedures*, Springfield, IL, 1996, Charles C Thomas, pp 24–51.
24. Smith DF, Ott DJ, Gelfand DW, Chen MYM: Lower esophageal mucosal ring: Correlation of referred symptoms with radiographic findings using a marshmallow bolus. *AJR* 171:1361–1365, 1998.
25. Levine MS: Radiology of esophagitis: A pattern approach. *Radiology* 179:1–7, 1991.
26. Levine MS: Varices. In Gore RM, Levine MS, editors: *Textbook of Gastrointestinal Radiology*, ed 2, Philadelphia, 2000, WB Saunders, pp 452–463.
27. Gelfand DW: Stomach and duodenum. In Ott DJ, Gelfand DW, Chen MYM, editors: *Manual of Gastrointestinal Fluoroscopy—Performance of Procedures*, Springfield, IL, 1996, Charles C Thomas, pp 52–68.
28. Gelfand DW, Dale WJ, Ott DJ, et al: The radiologic detection of duodenal ulcers: Effects of examiner variability, ulcer size and location, and technique. *AJR* 145:551–553, 1985.
29. Gelfand DW, Ott DJ, Chen MYM: Radiologic evaluation of gastritis and duodenitis. *AJR* 173: 357–361, 1999.
30. Herlinger H, Maglinte DDT, Yao T: Enteroclysis—technique and variations. In Herlinger H, Maglinte DDT, Birnbaum BA, editors: *Clinical Imaging of the Small Intestine*, ed 2, New York, 1999, Springer, pp 95–123.
31. Ott DJ: Large bowel. In Ott DJ, Gelfand DW, Chen MYM, editors: *Manual of Gastrointestinal Fluoroscopy—Performance of Procedures*, Springfield, IL, 1996, Charles C Thomas, pp 91–119.
32. Ott DJ: Accuracy of double-contrast barium enema in diagnosing colorectal polyps and cancer. *Semin Roentgenol* 35:333–341, 2000.
33. Gelfand DW, Chen MYM, Ott DJ: Preparing the colon for the barium enema examination. *Radiology* 178:609–613, 1991.
34. Hageman MJHH, Goei R: Cleansing enema prior to double-contrast barium enema examination: Is it necessary? *Radiology* 187:109–112, 1993.
35. Freimanis MG: Interval between cleansing enema and barium examination of the colon. *Gastrointest Radiol* 14:83–84, 1989.
36. Miller RE: Recipes for gastrointestinal examinations. *AJR* 137:1285–1286, 1981.
37. Kikuchi Y, Levine MS, Laufer I, et al: Value of flow technique for double-contrast examination of the stomach. *AJR* 147:1183–1184, 1986.
38. Op den Orth JO, Ploem S: The stalactite phenomenon in double contrast studies of the stomach. *Radiology* 117:523–525, 1975.
39. Aronchick J, Laufer I, Glick S: Barium stalactites: Observations on their nature and significance. *Radiology* 149:588–591, 1983.
40. Miller WT, Jr, Levine MS, Rubesin SE, et al: Bowler-hat sign: A simple principle for differentiating polyps from diverticula. *Radiology* 173: 615–617, 1989.
41. Gohel VK, Kressel HY, Laufer I: Double-contrast artifacts. *Gastrointest Radiol* 3:139–146, 1978.

Pictorial Glossary of Double-Contrast Radiology

STEPHEN E. RUBESIN

CHAPTER OUTLINE

Surface Patterns

Villous Pattern
Reticular Pattern
Granularity
Nodularity
Shaggy
Cobblestoning

Fold Patterns

Striae
Web
Coil Spring Sign
Radiating Folds
Polypoid Folds
Serpentine (Serpiginous) Folds
Stack of Coins Appearance
Tethering
Pleating

Protruding Lesions

Filling Defect
Contour Defect
Polyp

Plaque
Carpet Lesion
Ulcerated Mass
Annular Lesion
Submucosal Mass
Target Lesion
Pliability

Depressed Lesions

Erosion
Aphthoid Ulcer
Ulcer Niche (Crater)
Collar Button Ulcer
Exoenteric Mass
Tracking

Contour Abnormalities

Tapering
Linitis Plastica
Thumbprinting
Sacculation
Spiculation
Angulation

Careful use of descriptive terms aids in the radiologic analysis of perceived abnormalities. By describing the radiographic characteristics of a lesion, a radiologist can localize the lesion to the mucosa, bowel wall, or tissue extrinsic to bowel. This radiographic description, in conjunction with the site and size of the lesion, age of the patient, and clinical history, enables the radiologist to make a specific diagnosis or formulate a graded differential diagnosis of the most likely possibilities. In addition, precise use of descriptive terms enhances communication between the radiologist and clinician. A radiologist should be able to describe an abnormality so that the person reading or listening to the radiographic report can visualize the lesion without looking at the images.

This chapter is a pictorial glossary that visually defines common descriptive terms in gastrointestinal radiology. The terms are divided according to whether they refer to mucosal lesions, wall lesions (i.e., *submucosal*, *intramural*, or *extramucosal*), or extrinsic lesions.

Surface Patterns

VILLOUS PATTERN

The villi of the small intestine are at the radiographic limits of resolution. Some villi may be seen if the mucosa is well coated

and slightly magnified. This villous pattern is manifested as barely perceptible radiolucencies surrounded by barium in the interstices between villi (Fig. 3-1).

RETICULAR PATTERN

The term *reticular* means netlike (Fig. 3-2). This net is formed by barium in the interstices of normal columnar mucosa, such as the *areae gastricae* of the stomach (see Fig. 3-2A), or in the interstices of a mucosal lesion, such as a carpet lesion. The intervening radiolucent mucosa may be round, ovoid, or polygonal. A reticular pattern typically occurs in abnormalities arising in columnar mucosa. For example, a reticular pattern is seen in the columnar metaplasia of Barrett's esophagus or in a colonic urticarial pattern (see Fig. 3-2B).

GRANULARITY

Granularity implies subtle elevation of the mucosal surface seen en face as small radiolucencies in the shallow barium pool or as punctate dots of barium between lucencies (Fig. 3-3). The "granules" are barely perceptible elevations, with indistinct borders, as if salt had been sprinkled on a plate. Granularity implies mucosa elevated by edema, inflammatory exudate, or

tumor. Barium flocculated on an inflamed mucosal surface can mimic a granular mucosa.

NODULARITY

Mucosal nodules are relatively well-circumscribed elevations seen en face as round to ovoid radiolucencies in the barium pool or as small rings etched in white (Fig. 3-4). In profile, nodules are seen as small hemispheric or sharp-edged elevations of the contour. Nodules may arise in the mucosa itself, lamina propria, or adjacent submucosa. If a mucosal nodule involves a bowel fold, especially the rugae of the stomach or valvulae conniventes of the small bowel, the fold is eccentrically enlarged. Submucosal nodules involving a bowel fold, seen en face, symmetrically splay the parallel surfaces of the fold. Mucosal nodularity may be described as fine or coarse. The distinction between fine nodularity and mucosal granularity is somewhat arbitrary, although mucosal nodules are generally larger and more discrete than granules.

SHAGGY

Shaggy describes such severe mucosal disease that it is difficult to distinguish ulcerated mucosa from sloughed epithelium and inflammatory detritus (Fig. 3-5). In profile, the contour is jagged. En face, numerous lines reflect barium filling the interstices between ulcerated mucosa and debris. Shaggy is frequently used to describe the radiographic findings in severe *Candida* esophagitis (see Fig. 3-5) and ulcerative colitis.

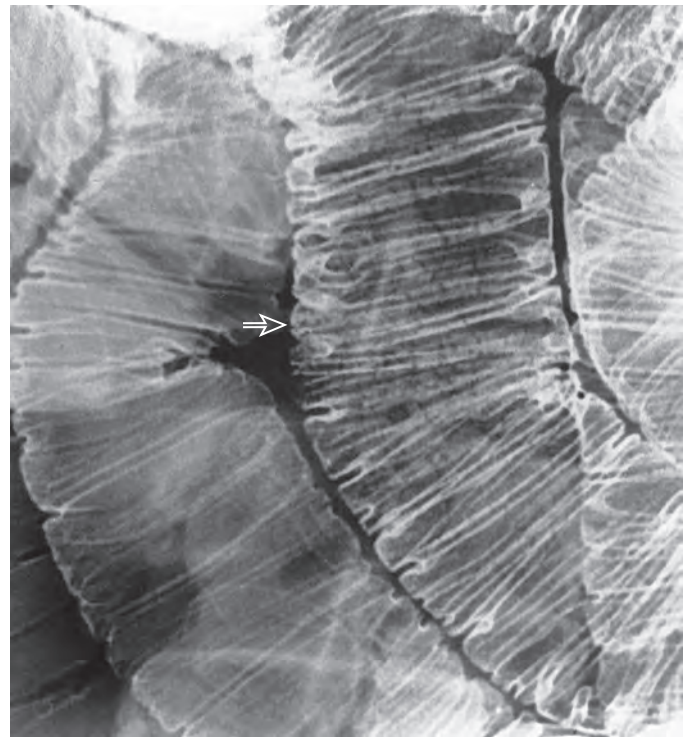


Figure 3-1 Villous pattern. This spot radiograph of the duodenal bulb shows multiple tiny radiolucencies surrounded by shallow, barium-filled grooves in a near-reticular pattern (arrow). The lucencies are the villi seen en face.

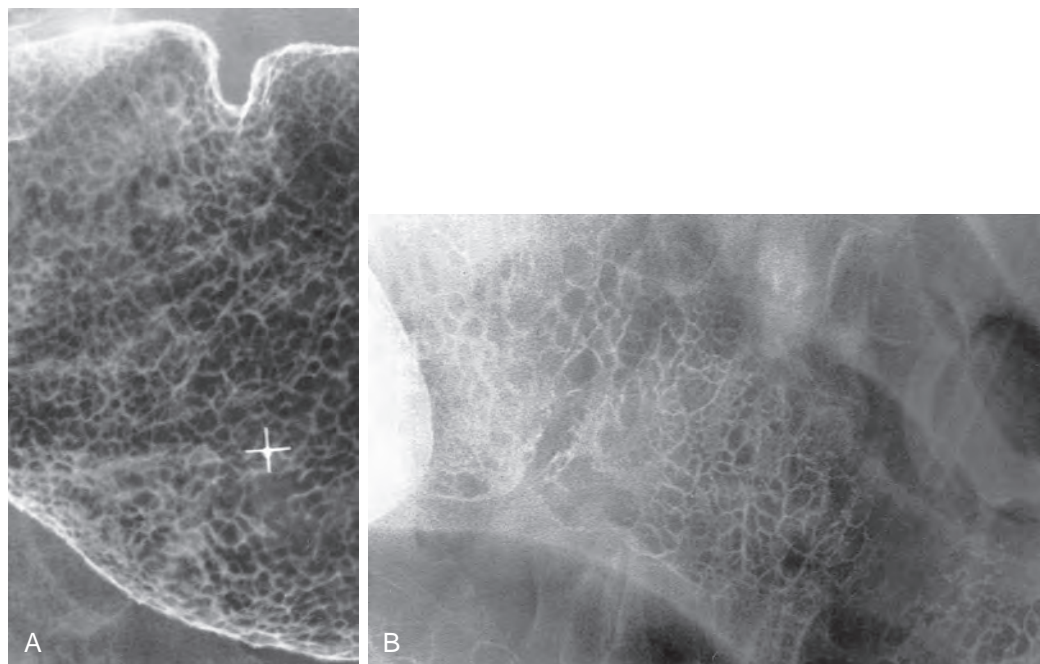


Figure 3-2 Reticular pattern. **A.** Areae gastricae. In general, columnar mucosa in the gastrointestinal tract is divided into islands of tissue surrounded by shallow grooves. This pattern is best exemplified in the areae gastricae of the stomach. The areae gastricae are seen as well-circumscribed, polygonal radiolucencies surrounded by barium-filled grooves. **B.** Urticarial pattern in the colon. When colonic mucosa is slightly elevated by edema and/or mild inflammation, the colonic surface may assume a reticular pattern. Barium etches sharply polygonal epithelial islands. This has been termed an *urticarial pattern* because it was first described in colonic urticaria. However, any disease that causes mild edema, inflammation, or ischemia of the mucosa may cause the columnar mucosa of the colon to assume an urticarial pattern, including ischemia caused by obstruction or adynamic ileus or inflammation caused by a viral infection. (**B** from Rubesin SE, Saul SH, Laufer I, et al: *Carpet lesions of the colon*. *RadioGraphics* 5:537–552, 1985.)

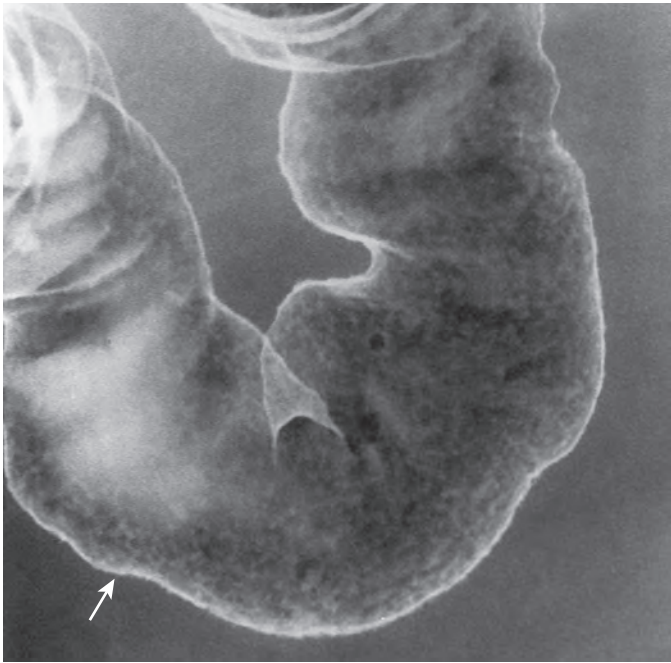


Figure 3-3 Granularity: ulcerative colitis. Numerous punctate dots of barium lie between radiolucent islands of mucosa (representative area identified by arrow). The splenic flexure has a tubular configuration, and the interhastral folds are absent.



Figure 3-4 Nodularity: squamous cell carcinoma of the epiglottis. The epiglottis is enlarged. The surface of the epiglottis is distorted by numerous small polygonal 1- to 2-mm radiolucent nodules outlined by barium in grooves between the nodules.

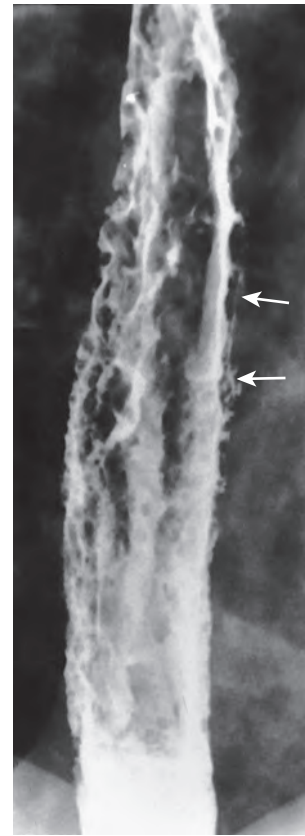


Figure 3-5 Shaggy. *Candida* esophagitis. The mucosal contour is markedly irregular or shaggy. Barium appears to be beneath the mucosal surface (arrows). In reality, this barium is trapped between sloughed epithelial debris and the ulcerated mucosa. En face, there are numerous variable-sized plaques.

COBBLESTONING

Transverse and longitudinal fissuring of the mucosal surface with extension of knifelike clefts into the submucosa and muscularis propria results in cobblestoning, typically seen in Crohn's disease (Fig. 3-6). The cobblestones appear as a carpet of nodules on the luminal surface. The cobblestones represent residual tissue between the transverse and longitudinal clefts.

Fold Patterns

The folds in the gastrointestinal (GI) tract are composed of mucosa—epithelium, lamina propria, and muscularis mucosae—and submucosa. When a radiograph demonstrates enlarged or nodular folds, the process therefore involves the mucosal or submucosal layers, or both. A desmoplastic process involving the serosa or adventitia of the bowel or the adjacent mesenteric or omental fat can secondarily pull on the bowel wall so that the smooth mucosal surface is thrown into an abnormal fold pattern.

STRIAE

When a viscus is less than fully distended, transverse striations may be seen perpendicular to the longitudinal axis of the bowel. Examples of this phenomenon include the so-called feline esophagus, gastric striae (Fig. 3-7), and innominate grooves of the colon.

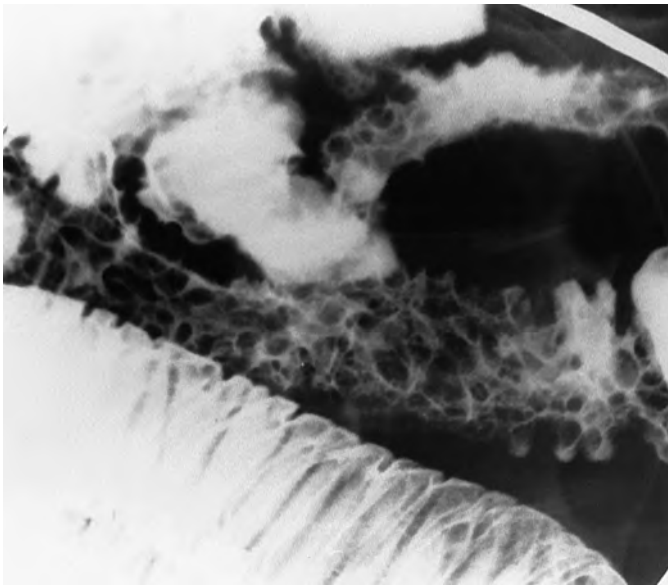


Figure 3-6 Cobblestoning: Crohn's disease involving the small intestine. Multiple round, ovoid, or polygonal radiolucencies are surrounded by barium-filled transverse and longitudinal fissures. This is also termed the *ulceronodular pattern* of Crohn's disease. The cobblestones represent the mildly inflamed residual mucosa and submucosa between the knifelike clefts. Narrowing of the bowel lumen reflects a transmural inflammatory reaction and bowel wall thickening. (From Rubesin SE, Laufer I, Dinsmore B: *Radiologic investigation of inflammatory bowel disease*. In MacDermott RP, Stenson WF [eds]: *Inflammatory Bowel Disease*. New York, Elsevier Science, 1992, pp 453–492.)



Figure 3-7 Gastric striae. Fine, barium-etched striae (arrows) perpendicularly cross the longitudinal axis of a slightly contracted gastric antrum. The striae are probably caused by contraction of the muscularis mucosae and have been described in patients with biopsy specimens showing normal mucosa or antral gastritis.

WEB

A web is a thin band of mucosa (with or without submucosa) that traverses a variable portion of the intestinal lumen. Webs vary from small shelflike lesions to hemispheric bars and circumferential rings (Fig. 3-8). Webs may be normal variants or the sequelae of inflammatory disease.



Figure 3-8 Web in distal esophagus. A thin radiolucent bar (arrows) is etched in white and crosses part of the circumference of the distal esophagus. Distal esophageal webs are usually related to gastroesophageal reflux disease. (A from Laufer I, Levine MS [eds]: *Double Contrast Gastrointestinal Radiology*, 2nd ed. Philadelphia, WB Saunders, 1992.)

COIL SPRING SIGN

If barium is forced between one loop of bowel intussuscepting into another loop, the barium may coat the mucosal folds of the outer loop. The result is the radiographic appearance of concentric rings of barium said to resemble a coil spring (Fig. 3-9).

RADIATING FOLDS

Folds that radiate to a focal site guide the radiologist's eye toward GI lesions. Radiographic analysis of the radiating folds aids in the differential diagnosis. Smooth folds radiating to a mucosal lesion indicate an active inflammatory process or scarring (Fig. 3-10A). Lobulated, pointed, or clubbed radiating folds indicate the presence of a malignant or severe inflammatory process (Fig. 3-10B).

POLYPOID FOLDS

Enlarged folds with a lobulated contour may appear polypoid (Fig. 3-11). Diseases that cause polypoid folds originate in the mucosa and submucosa and may also produce distinct polyps.

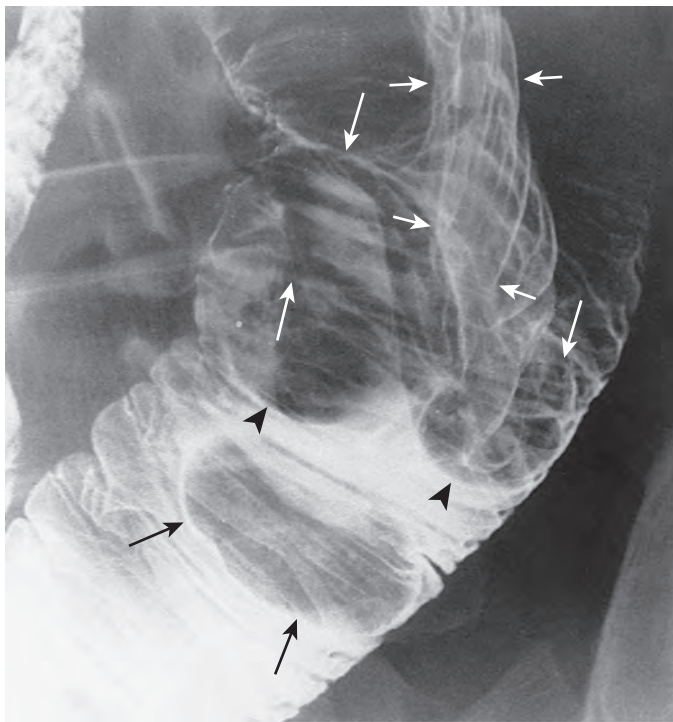


Figure 3-9 Coil spring sign: metastatic melanoma causing intussusception of the small bowel. Barium refluxes in a retrograde direction into the space between the prolapsing loop of the intussusception (intussusceptum) and the outer loop (intussusciens). The parallel folds of the coil spring (large white arrows) are identified. The intussusceptum is seen as a radiolucency (arrowheads) within the intussusciens. The lumen of the intussusceptum is narrow (small white arrows). The lead point of the intussusceptum is a polypoid mass (black arrows).

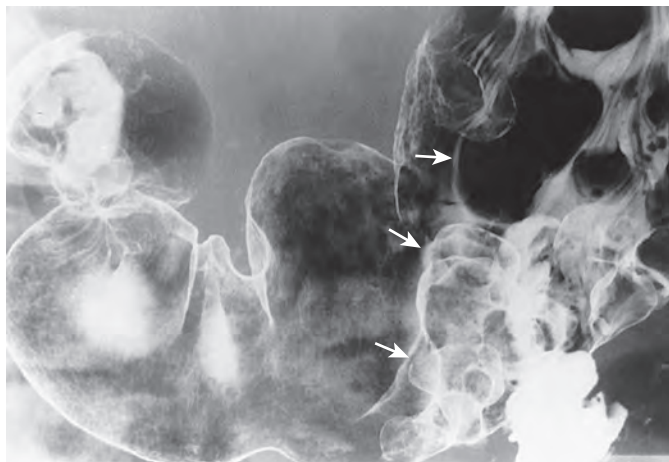


Figure 3-11 Polypoid folds. Large lobulated folds (arrows) are present along the greater curvature of the stomach. These thickened folds were caused by *Helicobacter pylori* gastritis.

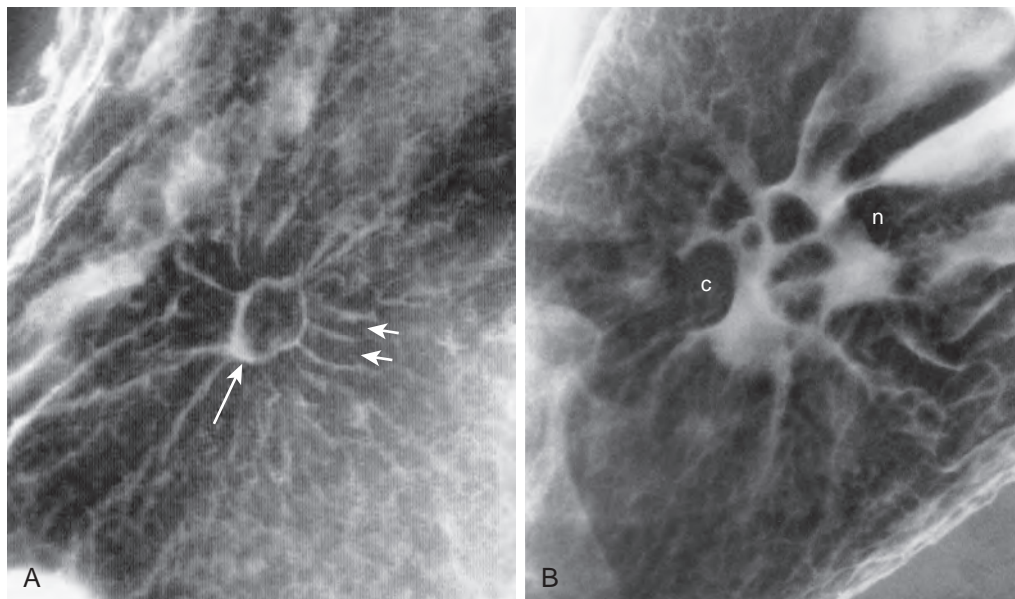


Figure 3-10 Radiating folds. A. Benign gastric ulcer. Smooth straight folds (short arrows) radiate toward the barium-etched rim of the ulcer (long arrow). **B.** Adenocarcinoma of the stomach. Abnormal folds radiate toward the center of the lesion. The folds are club-shaped (c) and nodular (n). Note the nodular mucosa in the center of the ulcer crater.



Figure 3-12 Serpentine (serpiginous) folds: esophageal varices. Smooth-surfaced, enlarged, sinuous radiolucent folds are parallel to the longitudinal axis of the esophagus

SERPENTINE (SERPIGINOUS) FOLDS

Serpentine (snakelike) and serpiginous (from the Latin, meaning “to creep”) folds are sinuous or wavy and are often aligned parallel to the longitudinal axis of the bowel. Serpentine folds are seen in mucosal and submucosal inflammatory or vascular processes (Fig. 3-12), especially varices.

STACK OF COINS APPEARANCE

Smooth, straight, enlarged folds perpendicular to the longitudinal axis of the small bowel resemble a stack of coins (Fig. 3-13). This appearance usually indicates submucosal edema or hemorrhage and, rarely, infiltrating tumor. Causes of submucosal hemorrhage include trauma, ischemia, radiation damage, and a bleeding diathesis caused by anticoagulants, hemophilia, and thrombocytopenic purpura.

TETHERING

Mucosal folds may be pulled toward an extrinsic process, resulting in tethering of the folds (Fig. 3-14).

PLEATING

If an extrinsic desmoplastic process extends into the bowel wall, the overlying mucosa may be thrown into thin folds, termed *pleating* (Fig. 3-15). In the colon, this finding suggests

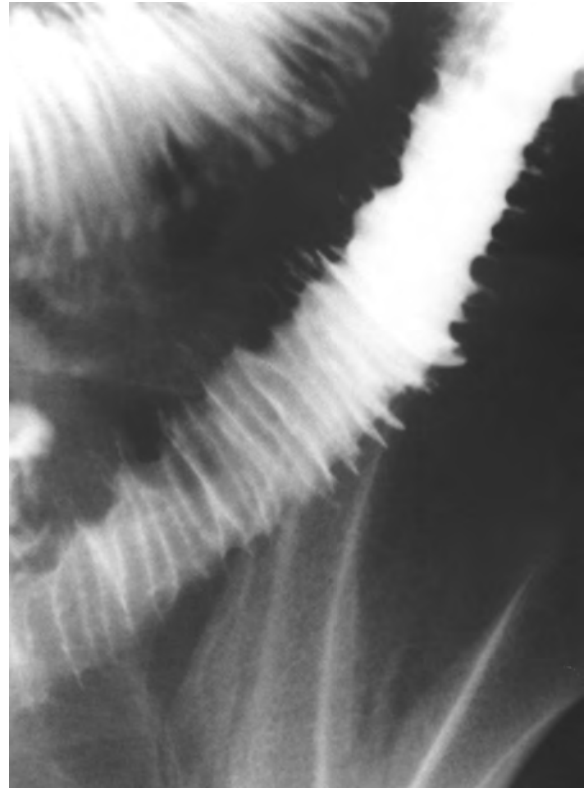


Figure 3-13 Stack of coins appearance: small bowel ischemia. Enlarged, smooth, straight parallel folds are perpendicular to the longitudinal axis of the jejunum. The folds are said to resemble a stack of coins or picket fence.

endometriosis or intraperitoneal metastases involving the serosal surface.

Protruding Lesions

FILLING DEFECT

A filling defect is a radiolucency in the barium pool caused by displacement of the barium by a protruding lesion (Fig. 3-16).

CONTOUR DEFECT

A contour defect is a disruption of the expected luminal contour by a sessile lesion protruding into the GI lumen (Fig. 3-17). A contour defect is not, in itself, a sign of malignancy. However, because the size of the contour defect is related to the size of the lesion, the larger the contour defect, the greater the likelihood of malignancy.

POLYP

A polyp is a protrusion from a mucous membrane. The term *polyp* is not histologically definitive and does not imply adenomatous (dysplastic) change. In general, the height of a polyp is comparable to its width, but a polyp is relatively tall in comparison to a mucosal plaque. Polyps may be seen as radiolucent filling defects on the dependent surface or may be etched in white on the nondependent surface

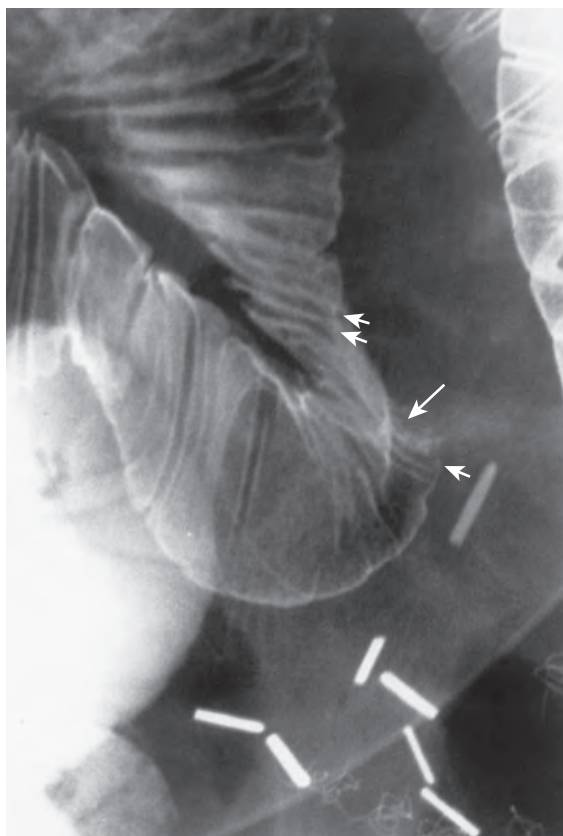


Figure 3-14 Tethering of mucosal folds: postoperative adhesions involving the pelvic ileum. Smooth mucosal folds (*short arrows*) are no longer perpendicular to the longitudinal axis of the ileum. The bowel is abruptly angulated at the site of adhesion (*long arrow*), and the lumen distal to the partially obstructive adhesion is narrowed.

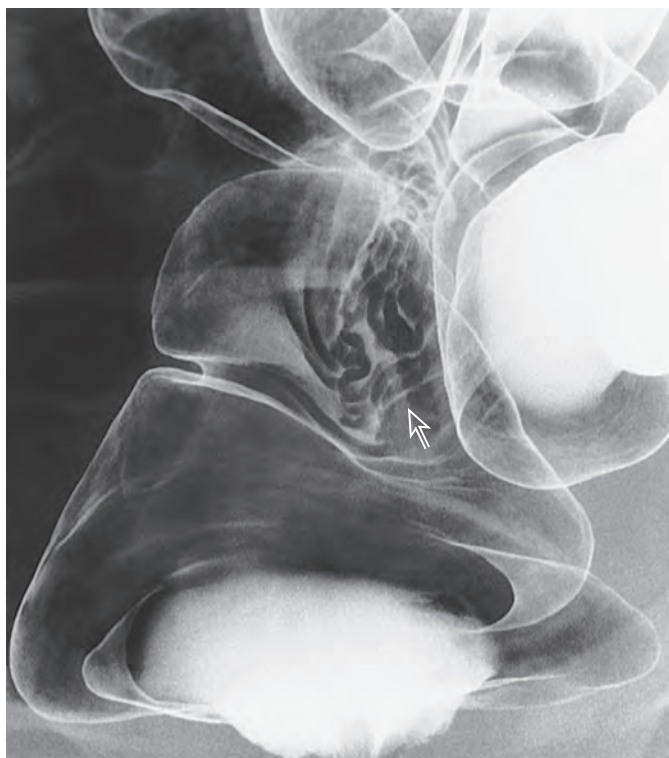


Figure 3-15 Pleating of the mucosa: endometriosis involving the rectosigmoid junction. The colonic mucosa is thrown into sinuous folds (*arrow*) by a desmoplastic process in the serosa and muscular layers.

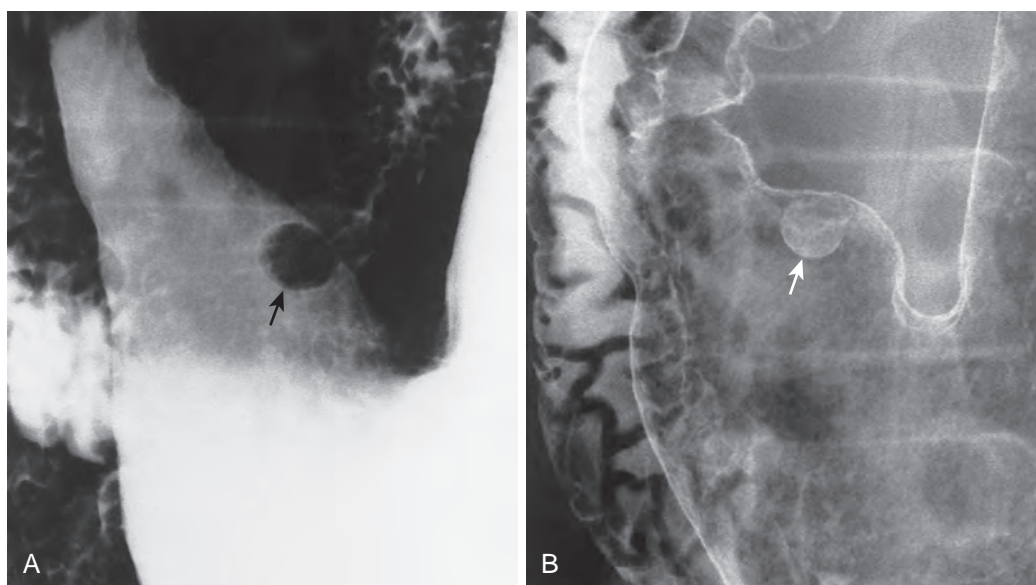


Figure 3-16 Filling defect. A. Hyperplastic polyp in the gastric antrum. A filling defect (*arrow*) is seen in the barium pool. **B.** The same polyp is seen in air contrast as a round, increased radiodensity etched in white (*arrow*). In **B**, the polyp is not described as a filling defect.

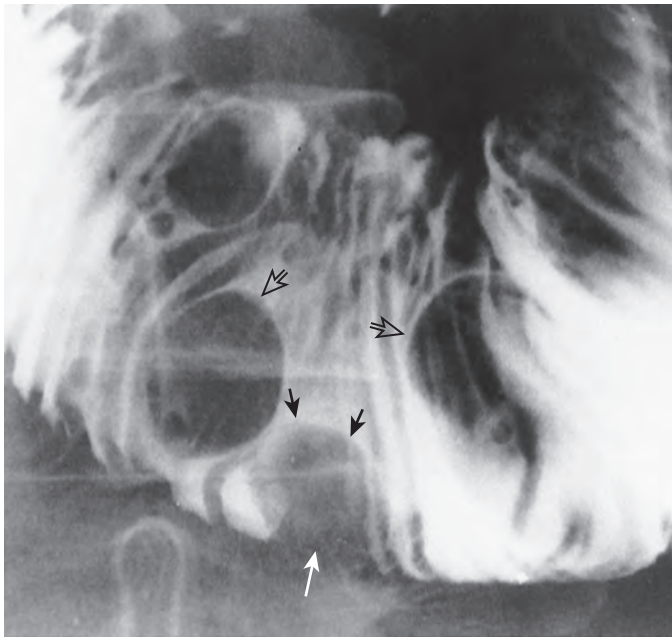


Figure 3-17 Contour defect: metastatic melanoma in the small intestine. A contour defect (white arrow) is seen as loss of the expected normal contour of the bowel. The contour of the lumen is pushed toward the center of the bowel loop. In this case, a submucosal metastasis is seen in profile (black arrows). Other metastases are seen en face as smooth-surfaced, ovoid filling defects (open arrows) in the barium pool.

(Fig. 3-18). They have many shapes and many radiographic appearances, depending on whether they are small or large, sessile or pedunculated, and smooth or nodular (see Fig. 3-18).

PLAQUE

A plaque is a shallow surface elevation, much broader than it is high. Plaques are so distinct that their margins are etched in white by barium trapped at the interface of the edges of the plaque and adjacent mucosa (Fig. 3-19). Plaques may vary greatly in size, from the small plaques of *Candida* esophagitis to plaque-like tumors.

CARPET LESION

Carpet lesions are focal, flat, well-circumscribed surface elevations. En face, the margin of the lesion is etched in white by barium (Fig. 3-20). When barium fills the interstices of the lesion, multiple small, polygonal radiolucent filling defects are seen surrounded by barium. In profile, the contour may be finely spiculated or nodular. The most characteristic carpet lesions are flat colonic adenomas.

ULCERATED MASS

Lesions that have both depressed and elevated components are typically ulcerated masses of mucosal or submucosal origin (Fig. 3-21).

ANNULAR LESION

Lesions that extend circumferentially around the bowel lumen are termed *annular lesions*. Circumferential spread around the lumen implies that the neoplastic or inflammatory process has spread at least into the submucosa. Annular configurations are seen in benign strictures caused by ischemia, radiation therapy, or diverticulitis or in malignancies such as primary tumors or metastases (Fig. 3-22).

SUBMUCOSAL MASS

The term *submucosal mass* refers to lesions arising in the submucosa and muscularis propria. These are typically benign or malignant tumors of smooth muscle, fat, or neural origin. Because the lesions arise in the submucosa or muscularis propria, they have also been referred to as intramural or extramucosal. The overlying mucosa is stretched and may be ulcerated.

In profile, a smooth-surfaced mass is seen forming right angles to the luminal contour (Fig. 3-23). En face, barium trapped in the abrupt margins results in a well-defined tumor. Central ulcers are seen in about 50% of all submucosal masses (see Fig. 3-24). Small submucosal masses involving a fold symmetrically splay the edges of the fold. Although the radiographic findings are distinctive for large lesions, small (0.5-2.0 cm) submucosal masses may be difficult to distinguish from mucosal polyps.

TARGET LESION

A target lesion or bull's-eye lesion is a mass with a central ulcer crater (Fig. 3-24). Target lesions are typically ulcerated submucosal masses caused by primary tumors such as GI stromal tumors or malignant tumors, especially metastatic melanoma, Kaposi's sarcoma, and disseminated lymphoma.

PLIABILITY

Change or lack of change in the size and shape of a lesion is a clue to its composition (Fig. 3-25). Lesions that change in size or shape, depending on the amount of luminal distention or manual compression, are often composed of fat, fluid, or blood.

Depressed Lesions

EROSION

An erosion is a defect in the mucosa that does not extend beneath the muscularis mucosae. Erosions are characterized by a small central barium collection and a surrounding radiolucent mound of edema (Fig. 3-26). The radiographic appearance is similar to that of aphthoid ulcers seen throughout the GI tract. In some cases, there is no known cause for erosive gastritis, but in most patients, the condition is caused by ingestion of aspirin or other nonsteroidal anti-inflammatory drugs (NSAIDs), viral infection, or alcohol ingestion.

APHTHOID ULCER

An aphthoid ulcer is a small ulcer occurring on a mucous membrane. This is a nonspecific pathologic term derived from the

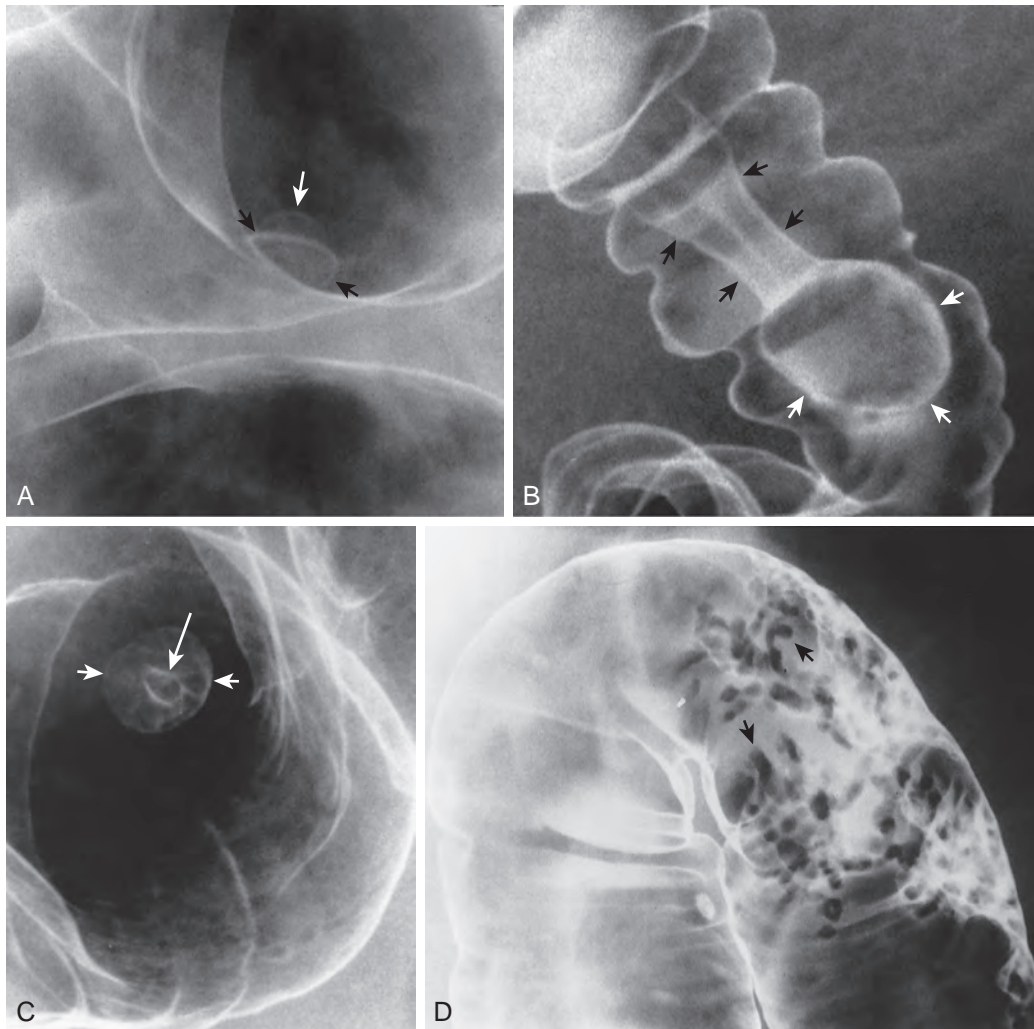


Figure 3-18 Polyp. **A.** Bowler hat polyp. Barium may be trapped between the edge of the polyp and intestinal lumen as the polyp is pulled against the adjacent wall by its stalk. If the surface and edge of the polyp are at the proper radiographic angle, the polyp appears similar to an English bowler hat. The ring (black arrows) of the polyp is the junction of the polyp and mucosal surface. The dome (white arrow) of the polyp points toward the longitudinal axis of the lumen. **B.** Pedunculated polyp. When a pedunculated polyp is seen in profile, the pedicle of the polyp appears as parallel barium-etched lines (black arrows) or as a tubular radiolucency in the barium pool. The head of the polyp (white arrows) is seen as a round or ovoid filling defect in the barium pool or is etched in white. **C.** Mexican hat polyp. If a pedunculated polyp is seen en face, the pedicle appears as a ring shadow (long arrow) central to the larger ring shadow of the head of the polyp (short arrows). These concentric ring shadows have been termed the *sombrero* or *Mexican hat* sign. **D.** Filiform polyp. A filiform polyp is a tubular or branched polyp, often with a clubbed head. Filiform polyps imply that there has been prior inflammatory disease involving the mucosal surface of the bowel. When residual inflamed, hyperplastic, or reparative tissue protrudes into the lumen, the resulting projections appear filiform. In this patient with quiescent Crohn's disease, numerous filiform polyps (arrows) are seen in the splenic flexure of the colon. (A from Miller WT, Levine MS, Rubesin SE, et al: Bowler-hat sign: A simple principle for differentiating polyps from diverticula. *Radiology* 173:615–617, 1989.)



Figure 3-19 Plaque. *Candida* esophagitis. Small, well-circumscribed radioluencies in the shallow barium pool (arrows) are aligned longitudinally along the esophageal mucosa. Note the normal intervening esophageal mucosa.

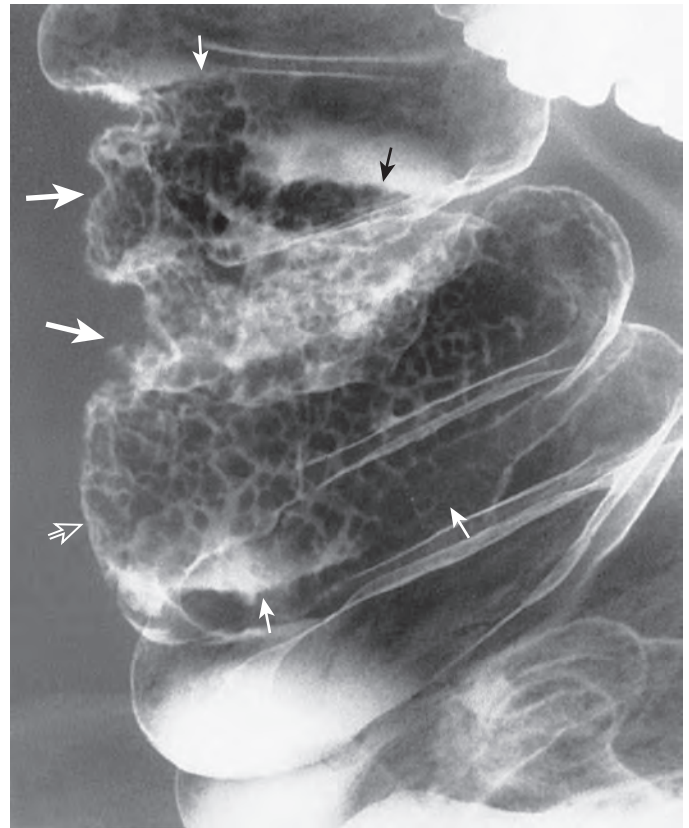


Figure 3-20 Carpet lesion: tubulovillous adenoma with carcinoma. A focal reticular network of barium lines crosses the lumen of the ascending colon (thin arrows). The contour of the colon is relatively maintained in one region (open arrow). In an area in which carcinoma is present, the contour is indented and angulated (thick arrows).

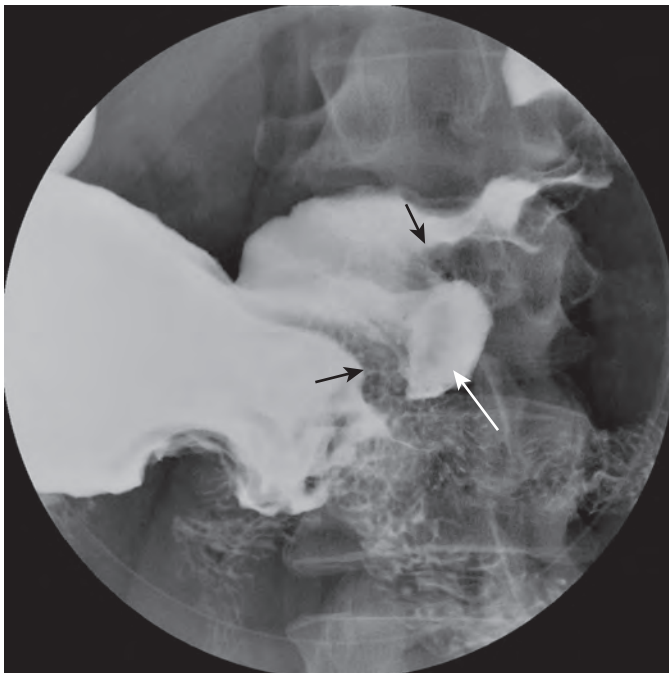


Figure 3-21 Ulcerated mass: adenocarcinoma involving the greater curvature of the stomach. A single-contrast compression view of the lesser curvature performed with the patient in a prone position shows an ulcerated mass as an ovoid barium collection (white arrow) within a radiolucent mass protruding into the gastric lumen. The mass has a coarsely nodular rim of tissue (black arrows).

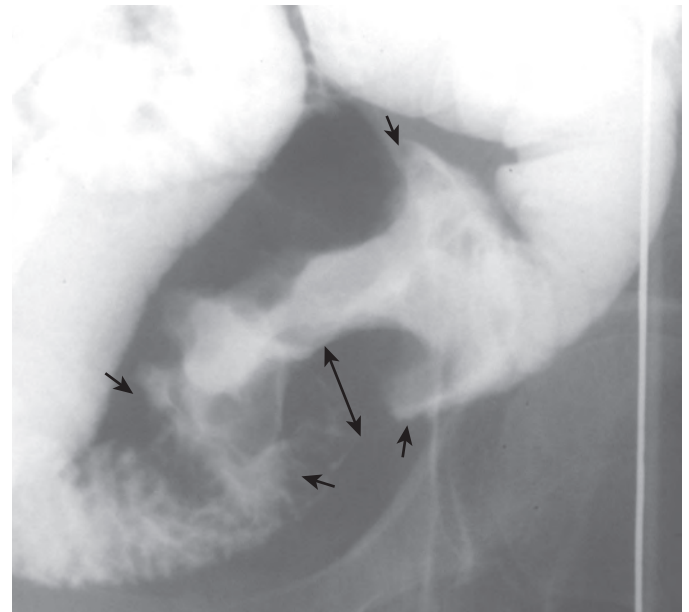


Figure 3-22 Annular lesion: adenocarcinoma of the mid small intestine. A focal annular lesion with abrupt shelflike margins (short arrows) and lobulated folds centrally is seen. The large amount of luminal narrowing (double-ended arrow) means that the tumor has spread at least into the muscularis propria.

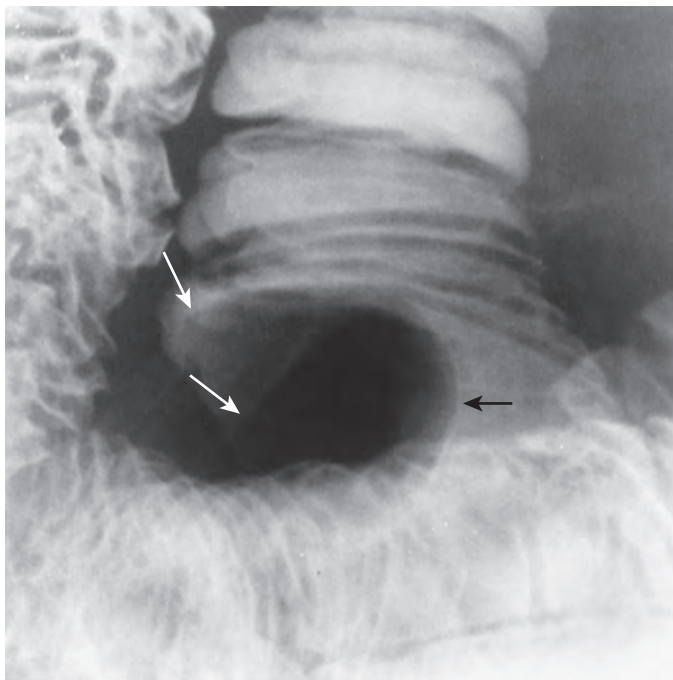


Figure 3-23 Submucosal mass: lipoma of the small intestine. A smooth-surfaced polypoid mass (black arrow) projects into the lumen of the mid small bowel. Note the abrupt angulation (white arrows) of the tumor margins and adjacent normal mucosa.



Figure 3-24 Target lesion: metastatic melanoma involving the ileum. Numerous ovoid, well-circumscribed or hemisphere-shaped radiolucent filling defects are seen in the intestine. Several lesions have large, irregularly shaped central barium collections (arrows). These lesions are said to resemble targets or bull's eyes.

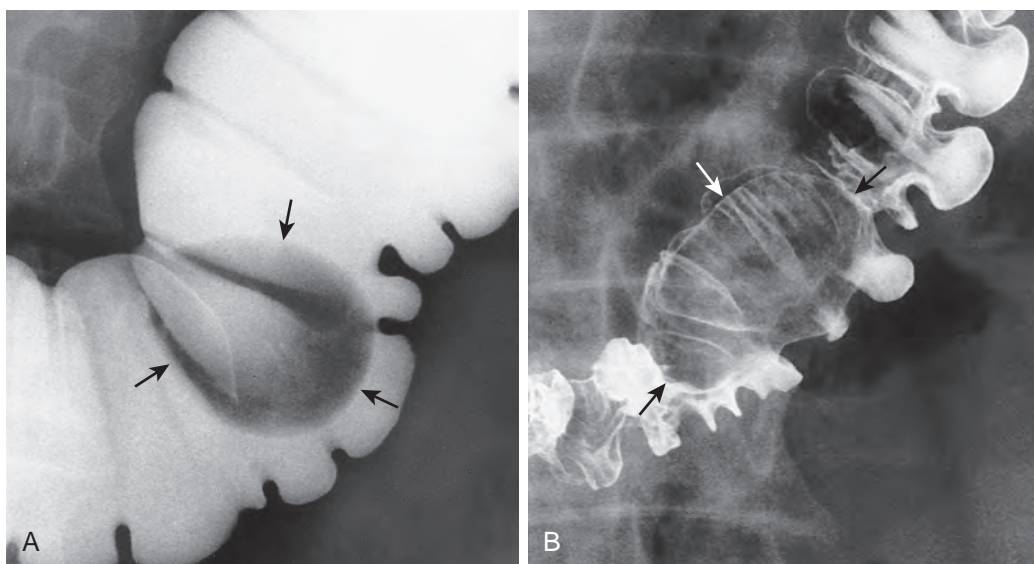


Figure 3-25 Pliability. A. Lipoma of the colon. A pear-shaped, smooth-surfaced filling defect (arrows) is seen in the barium column. **B.** A postevacuation radiograph shows that the polypoid mass has elongated (arrows) to conform to the collapsed lumen. These are classic findings of a colonic lipoma.

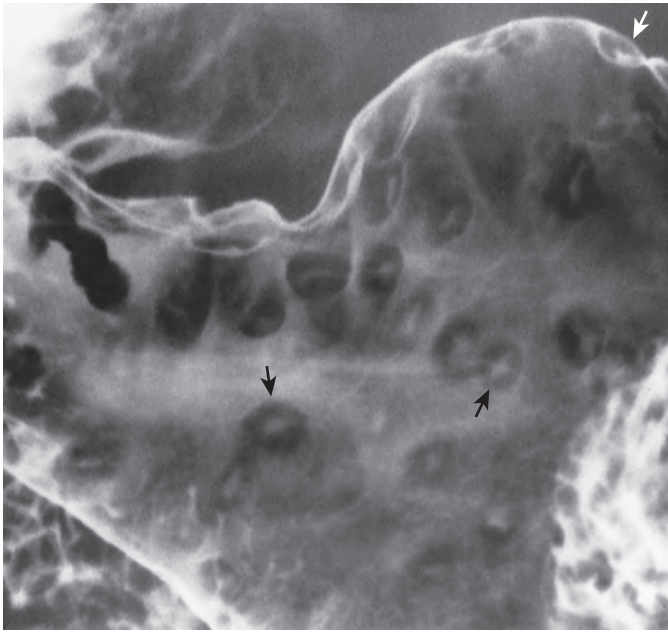


Figure 3-26 Erosions. Numerous linear and ovoid collections of barium (arrows) are surrounded by radiolucent halos of edema. This erosive gastritis was caused by aspirin use.

Greek root *aphthai* (meaning “to set on fire” or “to inflame”) and originally referred to the oral lesions of thrush, which are raised white plaques. The term was later used by the Greeks to refer to small ulcers on mucous membranes of the mouth (canker sores). Aphthoid means “resembling aphthae”; aphthous means “related to aphthae.” Radiologists use the terms *aphthoid ulcer* and *aphthous ulcer* interchangeably, but the preferred term is *aphthoid ulcer*. The most common causes of aphthoid ulcers are Crohn’s disease, viral infections, varioliform erosions, and amebiasis (Fig. 3-27). Erosions related to NSAIDs may appear identical to aphthoid ulcers.

ULCER NICHE (CRATER)

The term *niche* or *crater* refers to the defect or hole in the mucosal surface, representing an ulcer. The niche may be visualized in profile as a projection of barium extending beyond the luminal contour. Alternatively, the niche may be seen en face as a barium collection, or the edges of the crater may be etched in white (Fig. 3-28).

COLLAR BUTTON ULCER

Collar button ulcers are ulcers with a narrow neck and broad base (Fig. 3-29). These ulcers are formed when the inflammatory process spreads in the soft fat of the lamina propria and submucosa, parallel to the mucosal surface. This lateral extension gives the ulcer a relatively broad base in the submucosa and a narrow neck as it passes through the mucosa. In the colon, common causes of collar button ulcers are amebiasis, ulcerative colitis, and Crohn’s disease.

EXOENTERIC MASS

Exoenteric masses are masses of gastrointestinal origin that extend predominantly outside the bowel rather than into the

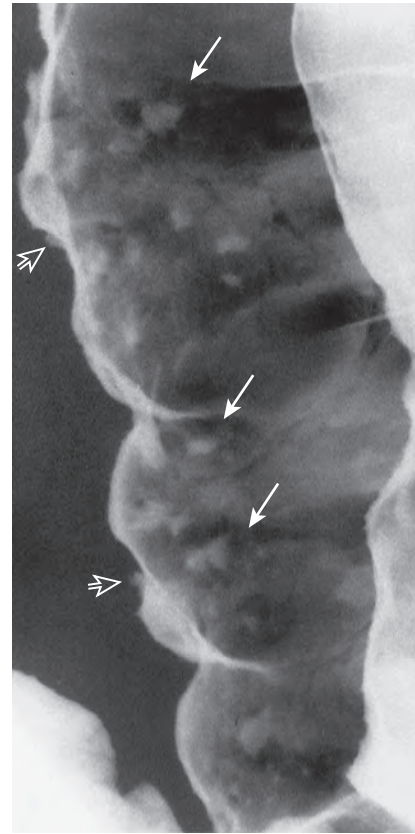


Figure 3-27 Aphthoid ulcers: Crohn’s disease involving the splenic flexure of the colon. Numerous aphthoid ulcers are seen en face as punctate barium collections surrounded by radiolucent halos of edema (white arrows). In profile, small ulcers are seen within edematous mounds of mucosa (open arrows).

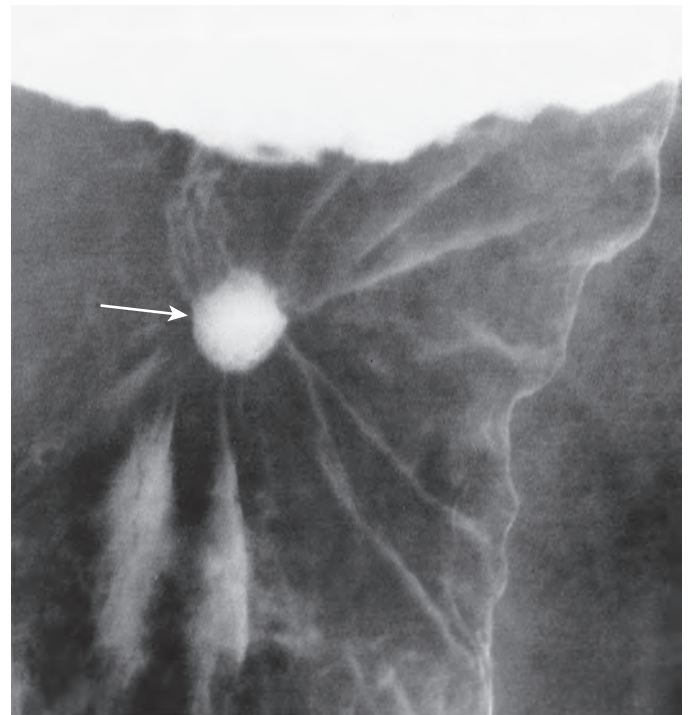


Figure 3-28 Ulcer niche (crater): benign gastric ulcer. The ulcer niche (crater) is seen as a focal barium collection (arrow). The benign nature of the lesion is indicated by smooth folds that radiate to the ulcer’s margin and lack of surrounding mass effect or mucosal nodularity.



Figure 3-29 Collar button ulcers: spectrum of inflammatory changes in ulcerative colitis. In the proximal transverse colon (T), there is relatively smooth mucosa. This progresses to a granular pattern (G). Distally, there is superficial ulceration (U). When the superficial ulcers penetrate the mucosa, lateral spread of inflammation in the submucosa results in collar button ulcers (arrows). (From Rubesin SE, Laufer I, Dinsmore B: *Radiologic investigation of inflammatory bowel disease*. In MacDermott RP, Stenson WF, [eds]: *Inflammatory Bowel Disease*. New York, Elsevier Science, 1992, pp 453–492.)

lumen of the bowel. They often extend into the mesentery or omentum. These lesions may cavitate, with the cavity extending outside the expected contour of the bowel (Fig. 3-30). The most common neoplastic masses include lymphoma, metastatic melanoma, and GI stromal tumors.

TRACKING

Linear collections of contrast medium within the bowel wall are termed *intramural tracks*. Linear collections of contrast medium outside the expected confines of the bowel are referred to as *extramural tracks*. Intramural tracks frequently course perpendicular to the longitudinal axis of the bowel (Fig. 3-31). Extramural tracks caused by diverticulitis often spread longitudinally in the pericolic fat. Tracks associated with radiation damage, trauma, Crohn's disease, or iatrogenic perforation may spread in any direction.

Contour Abnormalities

TAPERING

A shallow, smooth-surfaced, gradual narrowing of the contour of the bowel reflects a desmoplastic disease in the mucosa and submucosa that tapers the lumen. Tapering is usually caused by benign scarring from chronic inflammatory disease (Fig. 3-32). Occasionally, a neoplasm infiltrating the submucosa may incite a desmoplastic reaction that causes tapering.

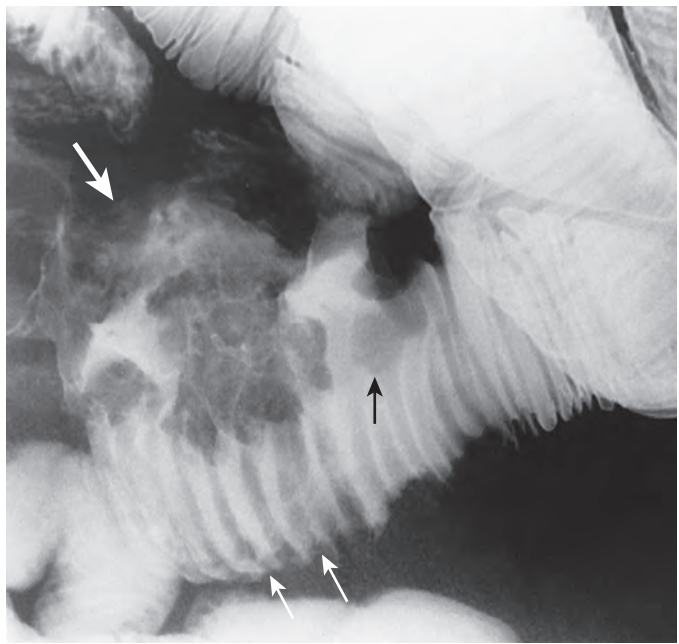


Figure 3-30 Exoenteric mass: primary lymphoma of the small intestine. A large barium-filled excavation (thick white arrow) projects from the mesenteric border of the small bowel. Note other radiographic findings of primary small bowel lymphoma, including thickened nodular folds (thin white arrows) and mucosal nodularity (black arrow).



Figure 3-31 Tracking. Crohn's disease involving the descending colon. Numerous intramural tracks (white arrows) extend from the colonic lumen into the pericolic space. The intramural tracks course perpendicular to the lumen through the muscularis propria. A large, linear, extramural barium collection (extramural track; open arrows) lies in the pericolic fat parallel to the lumen.



Figure 3-32 Tapering: benign radiation-induced stricture in the lower esophagus. A long, mild circumferential narrowing of the distal esophagus has a smooth tapered contour (*small arrows*) and smooth mucosa.

LINITIS PLASTICA

The term *linitis plastica* refers to diffuse narrowing and loss of pliability of a GI organ. The linitis pattern is usually seen in scirrhous carcinoma of the stomach ([Fig. 3-33](#)). This type of cancer is also seen in the colon, especially in patients with chronic ulcerative colitis. Both inflammatory and neoplastic processes, however, can result in a linitis appearance. For example, linitis plastica of the stomach may be caused by caustic ingestion or metastatic breast carcinoma. Because these infiltrative processes are primarily in a submucosal location, endoscopic biopsy specimens and brushings may be negative.

THUMBPRINTING

Submucosal hemorrhage or severe edema occurs to a greater degree along the mesenteric border of the small bowel and is manifested radiographically by what is termed *thumbprinting* ([Fig. 3-34](#)).

SACCULATION

Sacculation refers to broad-based outpouchings of the bowel wall. A relatively normal bowel wall may appear sacculated between folds radiating toward a neoplastic or desmoplastic process. This form of sacculation occurs on the bowel wall opposite the mesenteric changes of Crohn's disease ([Fig. 3-35A](#)), ischemia, or diverticulitis. These sacculations do not extend



Figure 3-33 Linitis plastica: adenocarcinoma of the stomach. The fundus and body of the stomach are diffusely narrowed. The luminal contour is altered by nodular, broad-based indentations (*arrows*), but the mucosa is relatively smooth. These findings indicate the submucosal location of the bulk of the infiltrating tumor.

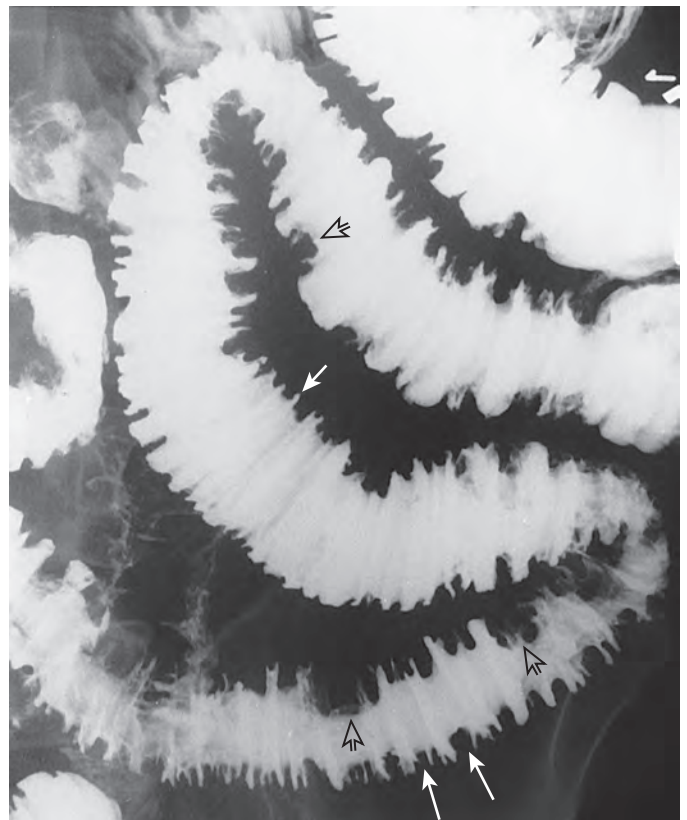


Figure 3-34 Thumbprinting. Polypoid projections (*open arrows*) are seen along the mesenteric border of the ileum. Note the abrupt angulation of the protrusions and smooth surfaces, radiographic findings typical of submucosal lesions. This thumbprinting reflects submucosal hemorrhage in a patient with small bowel vasculitis. Also note the smooth, straight, parallel folds (*long white arrows*)—stack of coins appearance—and interspace spikes (*short white arrow*).

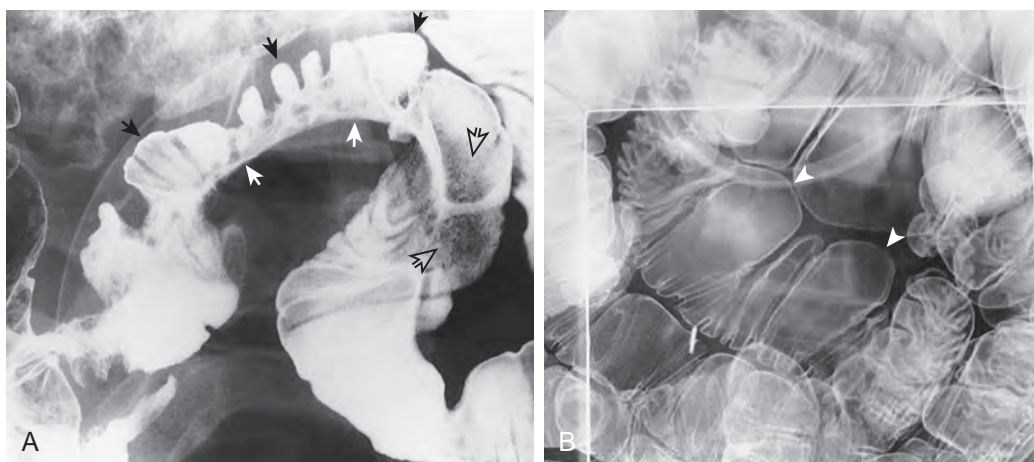


Figure 3-35 Sacculations. **A.** Crohn's disease involving the terminal ileum. The ileal contour is sacculated (black arrows) opposite a longitudinal ulcer (white arrows) on the mesenteric border. Note folds radiating toward the mesenteric border ulcer. Also note a reticular or granular mucosa (open arrows), reflecting mild mucosal changes. **B.** Scleroderma involving the small intestine. Large broad-based sacculations (arrowheads) protrude from the expected contour of the mesenteric border of the small bowel. (**A** courtesy Henrik DeGryse, MD, Antwerp, Belgium.)

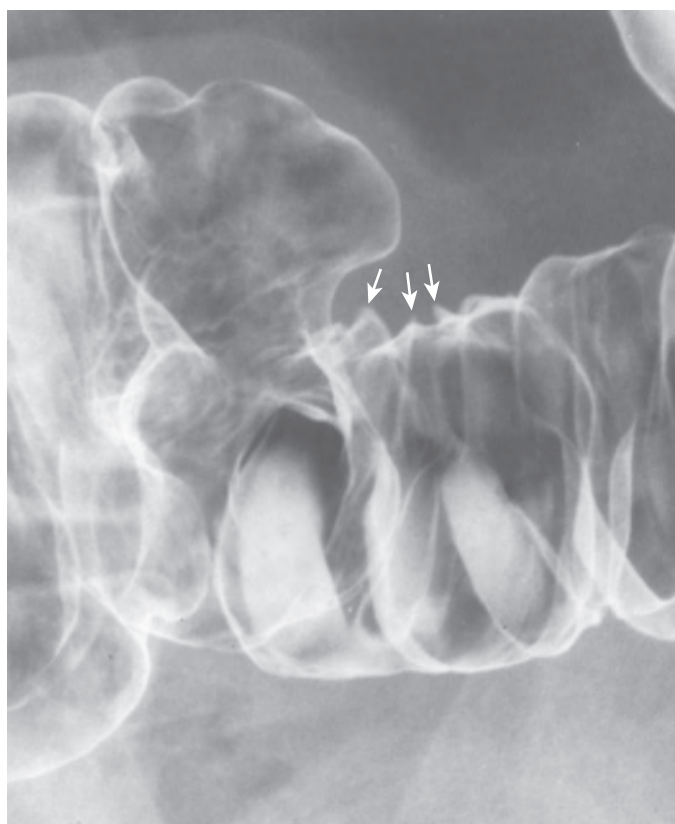


Figure 3-36 Spiculation: omental metastases from breast carcinoma infiltrating the serosa of the transverse colon. The superior border of the transverse colon is spiculated (arrows).

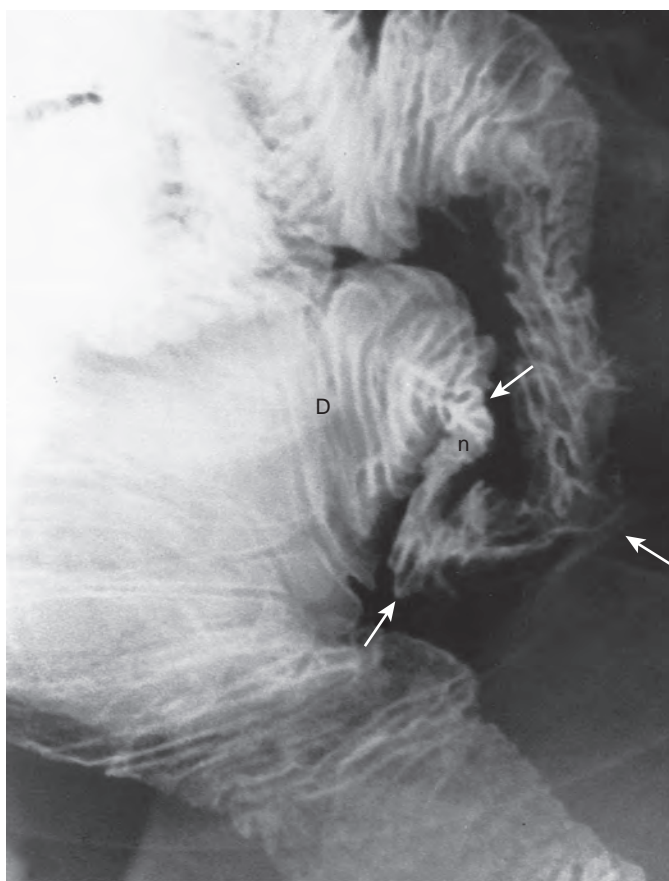


Figure 3-37 Angulation of bowel loops: adhesions involving the pelvic ileum. The small bowel is abruptly angulated (arrows) in several locations. Note narrowing of the lumen distal to the obstruction (n) and dilation of the lumen (D) proximal to the angulation. The mucosa is intact.

beyond the expected contour of the bowel. A bowel wall weakened by atrophy or fibrosis of the muscularis propria may also appear sacculated, especially in scleroderma (Fig. 3-35B). Saccululation related to weakening extends beyond the usual contour of the bowel.

SPICULATION

A desmoplastic process extrinsic to the bowel, resulting from inflammatory or neoplastic disease, may extend into the serosa

or muscularis propria and pull the luminal contour into spike-like points, termed *spiculation* (Fig. 3-36).

ANGULATION

Gross angulation of the bowel may occur when an extrinsic desmoplastic process tethers the bowel wall (Fig. 3-37).

Ultrasound of the Hollow Viscera

PETER M. RODGERS

CHAPTER OUTLINE

Ultrasound Features of the Normal Bowel

Ultrasound Findings of the Abnormal Bowel

Bowel Thickening
Bowel Wall Layers
Bowel Lumen
Bowel Plasticity, Mobility, and Peristalsis
Altered Blood Flow
Extramural and Mesenteric Changes

Ultrasound Technique

Graded Compression

Peritoneal, Mesenteric, and Omental Abnormalities

Acute Appendicitis
Diverticulitis
Inflammatory Bowel Disease
Mimics of Inflammatory Bowel Disease
Bowel Ischemia
Infectious Enterocolitides

Strategic Place for Ultrasound in Bowel Imaging

Transabdominal ultrasound (TAUS) allows the hollow viscera to be identified and characterized by anatomic location, morphology, and mesenteric attachments. At higher frequencies, TAUS and endoluminal probes resolve the bowel wall into multiple concentric layers approximating to the histologic strata¹ and usefully referred to as the sonographic gut signature.

This real-time capability, with patient interaction, to correlate symptoms, clinical signs, and imaging findings, makes TAUS a powerful diagnostic tool. Since the 1970s, the TAUS features of a broad range of common and uncommon gastrointestinal pathologic conditions have been documented in numerous original publications and review articles.²⁻⁴

Ultrasound Features of the Normal Bowel

At higher frequencies (5-17 MHz), the gut signature is comprised of five alternating bands of higher and lower echogenicity equating to serosa (bright), muscularis propria (very dark), submucosa (bright), deep mucosa (dark), and superficial mucosa-lumen interface (bright) (Fig. 4-1). The outer and inner bright bands are very fine and may not be visualized.

Healthy bowel wall is thin (<3 mm), varying with the state of contraction or distention. The muscle layer is the thickest and may be used as a yardstick for assessing relative changes in the mucosa and submucosa.

Ultrasound Findings of the Abnormal Bowel

BOWEL THICKENING

Thickening of the bowel wall is the most commonly identified pathologic feature. With improving technology, the threshold used to assess pathologic thickening has been lowered, from 5 to 3 mm. As the threshold is lowered, sensitivity increases at the cost of specificity.

Thickening may be caused by the presence of edema, hemorrhage, inflammation, tumor growth, or infiltration. Any of these may result in the classic ultrasound (US) feature of a hypoechoic circumferential thickening around a strong echogenic center (lumen), variously referred to as the target sign, ring sign, or pseudokidney sign (Fig. 4-2).

For more specific diagnostic indicators, thickened bowel must be characterized as focal or diffuse, circumferential or segmental, and solitary or multifocal. Tumors may grow into the bowel lumen to produce a polyp or polypoid mass (Fig. 4-3A) or away from the lumen into the peritoneal cavity (see Fig. 4-3B).

BOWEL WALL LAYERS

Changes in the gut signature within and adjacent to an observed bowel lesion should be carefully assessed. The high resolution of US provides a unique opportunity to identify the specific bowel layers affected, characterize the lesions, and diagnose the underlying process.

In pathologic conditions, the gut signature may be preserved, exaggerated, distorted, diminished, or obliterated. Focal alterations of the gut signature may allow identification of bowel lesions with borderline thickening (Fig. 4-4).

BOWEL LUMEN

Commonly, when the bowel wall is thickened, the bowel lumen is compromised, becoming narrowed or strictured. An uncommon exception to this is the aneurysmal dilation seen in lymphomas and gastrointestinal stromal tumors (GISTs), in which the lumen in the diseased segment enlarges.

Dilation of the bowel lumen is seen proximal to an obstructing lesion, where it is initially accompanied by increased peristalsis. Dilation with no peristalsis may be caused by late-stage obstruction or paralytic ileus, usually seen after abdominal surgery.

BOWEL PLASTICITY, MOBILITY, AND PERISTALSIS

TAUS resolution permits visualization of peristalsing small bowel folds, particularly as fluid passes along the lumen (Fig. 4-5A), and of rigid folds in dilated, fluid-filled obstructed loops

(Fig. 4-5B). Most disease processes result in stiffening of the affected bowel segment, which is observed sonographically as more rigid, less compressible, less easily displaced, and with reduced or absent peristalsis. Real-time scanning allows for the observation of other motility disorders, such as nonobstructive intussusceptions in celiac disease (Fig. 4-6).

ALTERED BLOOD FLOW

Doppler signals are negligible in normal bowel wall but assessment of flow in masses or thickened segments is essential. Color and power Doppler signals indicate hyperemia in actively inflamed segments or hypervascular lesions, and the absence of signals in a conspicuously thickened bowel segment may indicate ischemia. Most tumors have sparse Doppler signals but hypervascularity is a significant differentiator and should be routinely assessed (see Fig. 4-3B).

EXTRAMURAL AND MESENTERIC CHANGES

Bowel wall disease may extend to involve peri-intestinal structures, adjacent loops, or solid organs. Around inflammatory

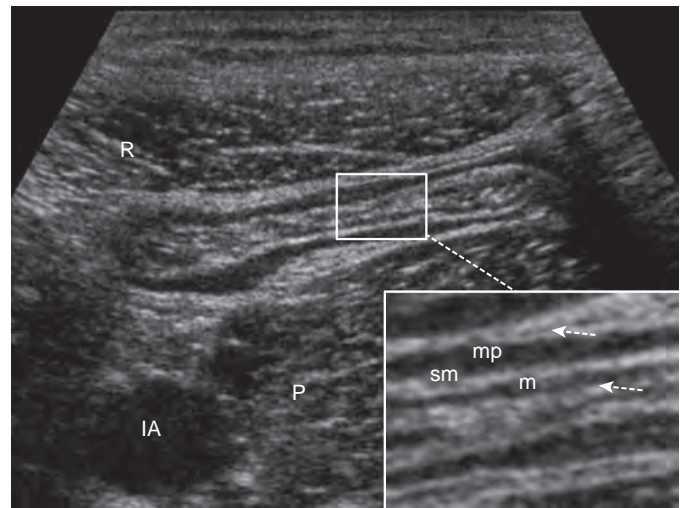


Figure 4-1 Sonographic gut signature. Shown is a compressed colon in the left iliac fossa between the rectus muscle (R), psoas muscle (P), and iliac artery (IA). *Inset*, Bowel wall detail of hypoechoic muscle proper (mp), echogenic submucosa (sm), and hypoechoic mucosa (m) between fine bright lines of serosa and mucosa (broken arrows).

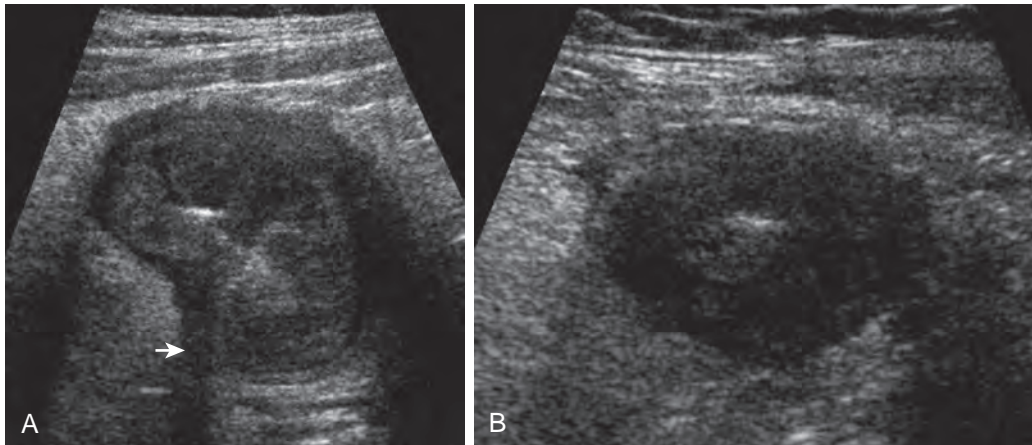


Figure 4-2 Pseudokidney and target signs. Inflammatory, neoplastic, and vascular diseases may all cause circumferential bowel thickening, with loss of gut signature, producing a low-echo wall around an echogenic center. This can result in the pseudokidney sign (A), a right colon cancer with acoustic shadowing from gas in the compressed lumen (arrow), or the target sign (B), acute ileitis with transmural inflammation.

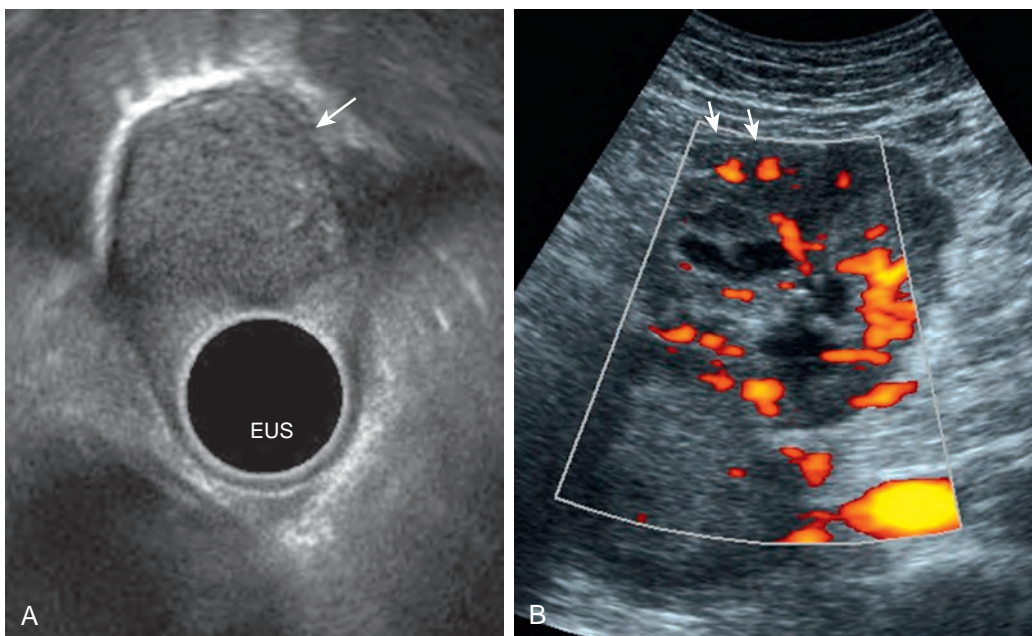


Figure 4-3 Focal masses. A. Distal esophageal polyp cancer with intact bowel signature (arrow). B. Bulky, intraperitoneal, dumbbell hypervascular GIST arising from small bowel (arrows). EUS, Endoscopic ultrasound.

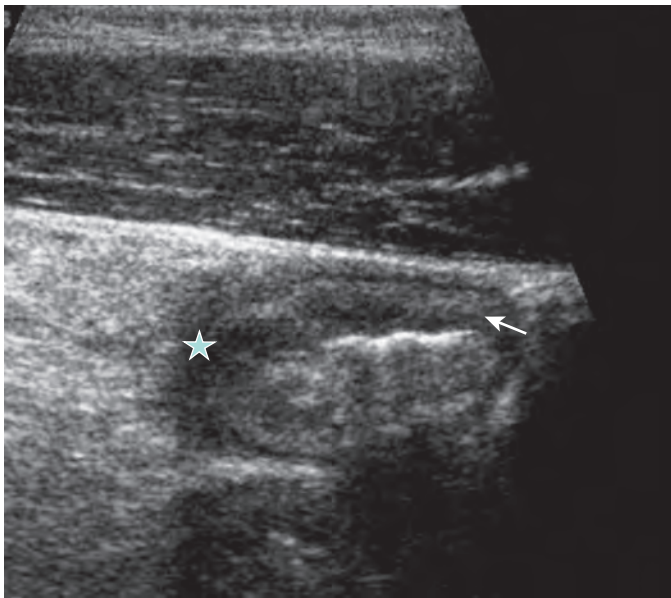


Figure 4-4 Altered gut signature—small bowel Crohn's disease. This axial image of a minimally thickened bowel shows blurring of identifiable layers (arrow), with focal signature obliteration (*) in the zone of transmurinal inflammation and with exudate on the serosal surface.

bowel lesions, collections, and abscesses, mesenteric fat becomes edematous (swollen and hyperechoic), displacing adjacent structures and increasing the conspicuity of the lesion (Fig. 4-7).

Changes in mesenteric lymph node size, shape (oval, round), echotexture, and surface should be documented. The initial identification of focal mesenteric lymphadenopathy should direct the search for a bowel abnormality.

Ultrasound Technique

TAUS is a well-tolerated, noninvasive technique. A 6-hour fast induces a quiescent intestinal state and reduces bowel gas; no other preparation is required. Focused bowel TAUS is preceded by a general examination of the abdomen and pelvis. Particular attention should be given to deeper recesses inaccessible to the higher frequency probes used for detailed investigation of the bowel wall.

Most bowel pathologic findings displace bowel gas and feces, making them stand out against normal bowel segments. Focal bowel masses, segments of wall thickening, or dilated loops may be apparent, even at lower frequencies, but high-frequency probes are essential to characterize changes in the layers of the bowel wall.

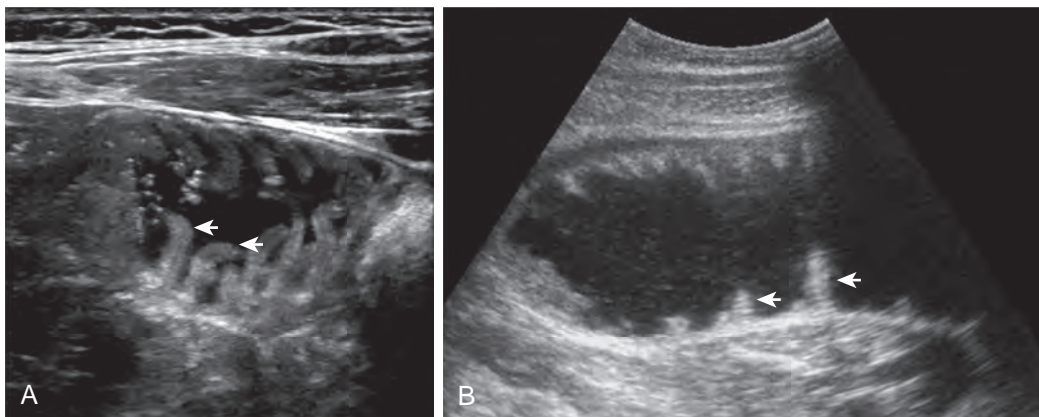


Figure 4-5 Small bowel folds. Valvulae conniventes are depicted (arrows) in the peristalsing jejunum (A) and in a patient with small bowel obstruction (B).

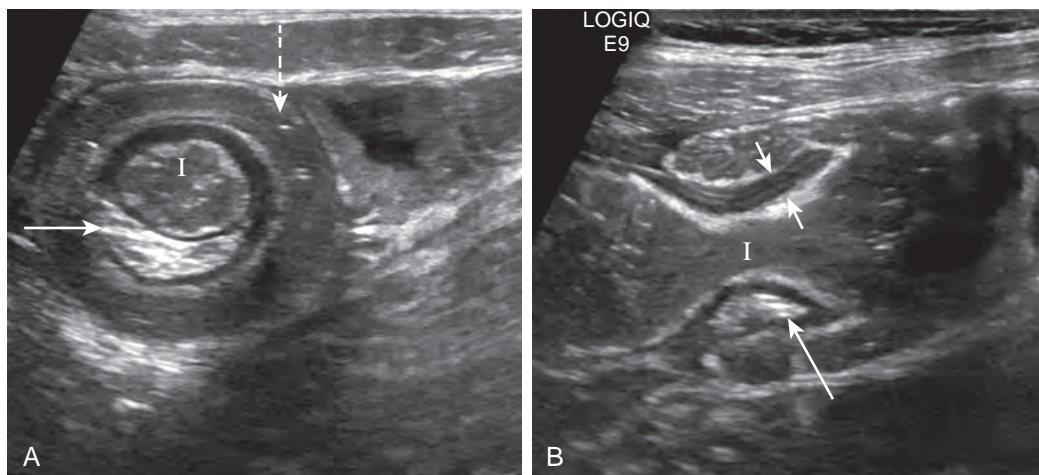


Figure 4-6 Abnormal motility. Spontaneous, nonobstructing, small bowel intussusception is demonstrated in a patient with celiac disease. Shown are axial (A) and longitudinal (B) images, with invaginated small bowel (I) and accompanying bright crescent of mesentery (solid arrows) within an outer bowel sleeve. Bright air bubbles are trapped between the outer layers (broken arrow).

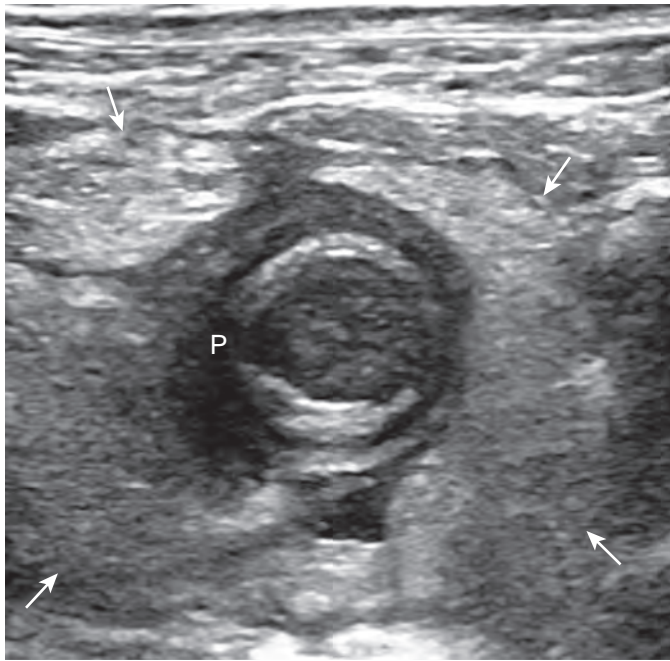


Figure 4-7 Extraintestinal changes. This axial image is of an inflamed appendix, with focal perforation (P) surrounded by edematous echogenic fat (arrows).

GRADED COMPRESSION

The term *graded compression* was introduced by Puylaert to describe the gradual progressive increase in pressure that the operator applies to the probe while making gentle sweeping movements.⁵ Done carefully to minimize discomfort, this is an essential technique for bringing the probe closer to the bowel, displacing bowel gas and overlying bowel loops and assessing the compressibility and rigidity of normal and abnormal bowel loops and mesenteric fat.

Mowing the Lawn

Surveying the entire intestine within the abdominal cavity requires a systematic technique. Puylaert recommended the use of overlapping vertical sweeps of a high-frequency probe up and down the abdomen, similar to the motion of a lawnmower.³ Additional operator techniques include posterior manual compression and scanning in the left lateral decubitus position to assess the retrocecal area.⁶

It is my practice to begin bowel scanning in the left iliac fossa (LIF), where the left colon is easily identified and compressed against the left psoas (see Fig. 4-1). This is an opportunity to optimize scanning parameters so that wall layers can be clearly identified, even in briskly peristalsing small bowel segments.

The distribution of bowel in the right iliac fossa (RIF) is variable. Several small bowel loops may be present, and the terminal ileum should only confidently be identified if continuity with the ileocecal valve is demonstrated. Reexamining the right iliac fossa with the patient in a left decubitus position allows movement of the mobile small bowel and cecum into different positions, redistribution of bowel gas, and improved access to a retrocecal appendix.

In adult female patients, transvaginal scanning may give excellent views of low pelvic bowel loops (Fig. 4-8).

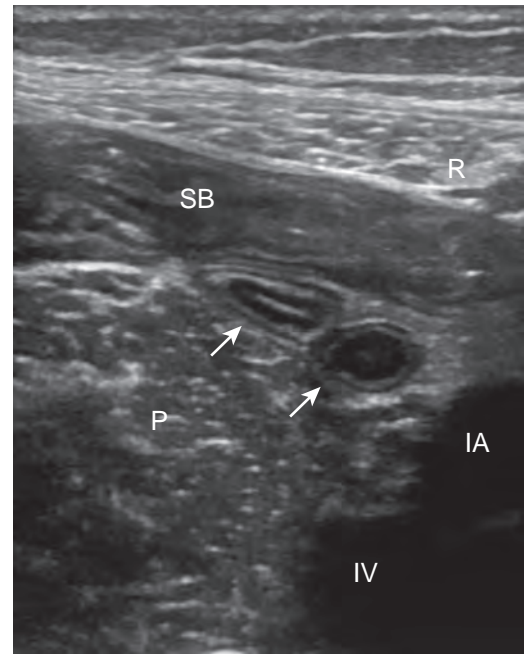


Figure 4-8 Normal appendix. Axial sections along the appendix (arrows) in the RIF lie coiled between the rectus (R) and psoas (P) beneath a loop of normal small bowel (SB). The appendiceal gut signature varies along its length. IA, Iliac artery; IV, iliac vein.

Peritoneal, Mesenteric, and Omental Abnormalities

ACUTE APPENDICITIS

Acute appendicitis is one of the most common causes of acute abdominal pain and is the most common indication for urgent abdominal surgery. It is more prevalent in older children and young adults.

Appendicitis is the result of luminal obstruction, usually by a fecalith or appendicolith. Less common causes include lymphoid hyperplasia, parasites, and primary and secondary tumors. The obstructed appendix is susceptible to mucosal ischemia and necrosis, which may progress to transmural inflammation, full-thickness infarction, and perforation (in ≈20% of cases).

The intention to preempt complications underpins the practice of early surgical intervention based on clinical assessment and laboratory tests. The “typical” clinical presentation is of vague central or epigastric abdominal pain with anorexia, progressing to nausea and vomiting, followed by migration of the pain to the right lower quadrant, and accompanied by fever, leukocytosis, and rebound tenderness. Any of these features may only be present to a variable degree or absent, so symptoms, signs, and laboratory tests are only moderately accurate for predicting appendicitis.

This strategy persists widely, although between one in three to five removed appendices will be healthy,^{7,8} in spite of over 20 years of evidence of the reduction in the number of unnecessary appendectomies using diagnostic imaging.^{9,10}

Sonography of the Normal Appendix

The normal appendix is elusive. It varies greatly in size (average, 8 cm; range, 1-24 cm) and position (pelvic and retrocecal

being the most common).¹¹ With TAUS, the appendix is identified as a thin, blind-ending tube, with a normal gut signature, in continuity with the cecal pole and arising several centimeters from the ileocecal valve.

Sonographic identification of the normal appendix is difficult and often only partial (see Fig. 4-8), because overlying loops must be compressed or displaced, and the healthy appendix is often coiled up. Identification rates for the normal appendix, in a population not presenting with suspected appendicitis, varies widely and is related to numerous factors, including technique, operator experience, examination time, and patient body habitus.

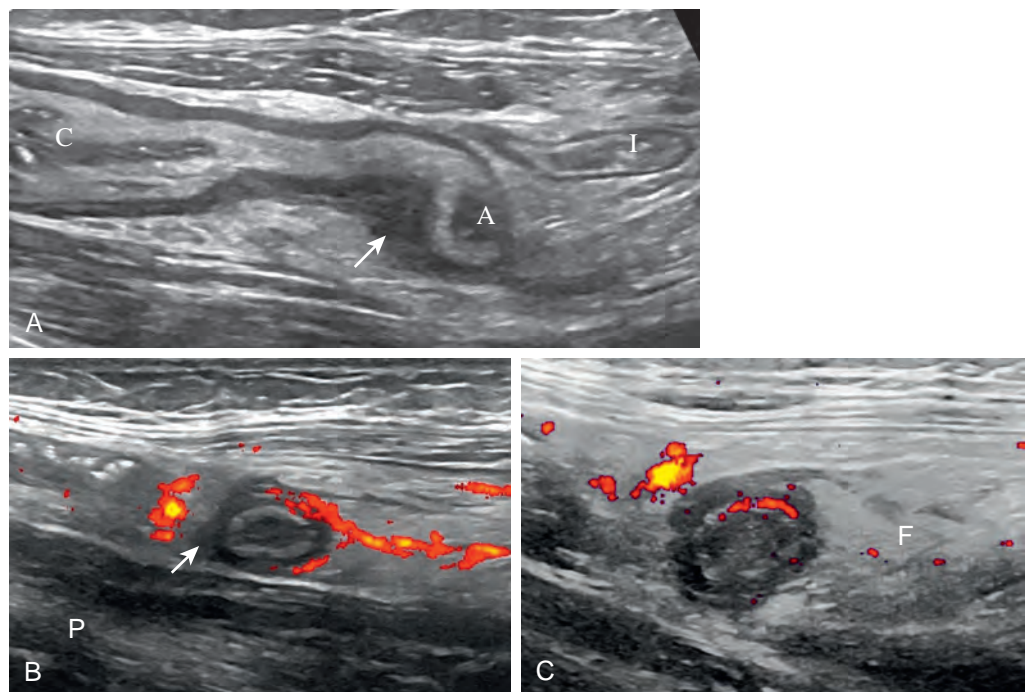
Sonography of Acute Appendicitis

The earliest sonographic descriptions of acute appendicitis identified the dominant diagnostic criteria as a noncompressible, blind-ending tube, with a maximum outside diameter (MOD) less than 6 mm. More recent studies have shown normal appendices with diameters of more than 6 mm and lumen distention by feces and/or air, confirming that this threshold diameter is unreliable unless included with other sonographic signs of appendiceal or extra-appendiceal inflammation^{12,13} (Box 4-1). Requiring a combination of these criteria to be present, together with significant clinical evidence of acute appendicitis, reduces the number of false-positive diagnoses (Fig. 4-9).

BOX 4-1 SONOGRAPHIC CRITERIA FOR APPENDICITIS

- Noncompressible blind-ending tube
- Lumen distention (MOD > 6 mm)
- Wall thickness > 3 mm
- Loss of gut signature
- Hyperemia on Doppler scanning
- Hyperechoic periappendiceal fat thickening
- Local transducer tenderness

Figure 4-9 Acute suppurative appendicitis. This 34-year-old woman presented with 3 days of RLQ (right lower quadrant) pain, with tenderness and guarding. **A.** Long view of thickened cecal pole (C) and appendix base (A) between the rectus (R) and psoas (P), with adjacent ileum (I). **B** and **C.** Axial power Doppler images of a hyperemic appendix on psoas (P) showing varying alterations in gut signature, local fat edema (F), and exudate on the serosal surface (arrow).



Appendicoliths are frequently identified in asymptomatic patients with otherwise normal US appearances and are not a reliable indicator of inflammation. In focal appendicitis, the MOD may not exceed 6 mm, and the diagnosis may be missed if the entire appendix is not visualized.^{14,15} The perforated appendix is even more elusive but may be most reliably identified by loss of the hyperechoic appendiceal wall layer (indicating transmural inflammation) and loculated periappendiceal or pelvic fluid collections.¹⁶ The negative predictive value of a scan in which the appendix is not identified differs widely across studies but is more reliable when the operator regularly identifies a normal or abnormal appendix.¹⁷

The strategic place for TAUS in the imaging of acute appendicitis is considered later.

Mimics of Acute Appendicitis

The imaging objectives for patients referred with suspected acute appendicitis are to identify the inflamed appendix or a normal appendix and any other cause of presentation. The most common differentials are acute diverticulitis, gynecologic causes, and mesenteric adenitis (in children), but prospective studies have identified a number of frequent and less frequent mimics (Box 4-2) and documented the relevant TAUS features.^{17,18}

These include a variety of conditions in which surgery is not indicated, and preoperative imaging diagnosis highly advantageous. In conditions such as epiploic appendagitis and rectus sheath hematoma, the sonographer has the diagnostic advantage of being guided to the point of tenderness.

DIVERTICULITIS

Acute colonic diverticulitis is a common cause for acute hospital admission.¹⁹ Patients are generally older adults but approximately 15% are younger than 40 years. The strongest clinical diagnostic indicators are left iliac fossa pain, absence of

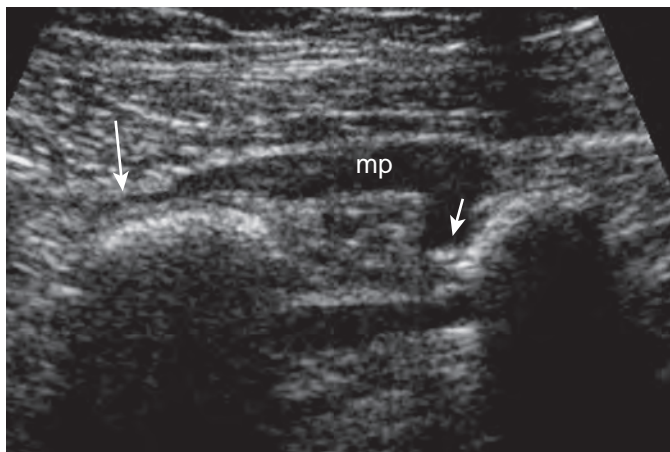


Figure 4-10 Colonic diverticula. Axial image of the left colon reveals a thickened muscle layer (mp) interrupted by an echogenic diverticular neck (short arrow). The wall of the diverticulum is thin, with no muscle layer (long arrow).

BOX 4-2 MIMICS OF APPENDICITIS

Mesenteric adenitis
 Infectious enterocolitis
 Epiploic appendagitis
 Omental infarction
 Right colonic diverticulitis
 Ileocecal Crohn's disease
 Intussusception
 Pelvic inflammatory disease
 Hemorrhagic ovarian cyst
 Urolithiasis
 Rectus sheath hematoma

Data from Mimics of Appendicitis: Alternative nonsurgical diagnosis with sonography and CT. AJR 186:1103–1112, 2006.

vomiting, and C-reactive protein (CRP) > 50, but all three are only present in 25% of presenters.²⁰ Computed tomography (CT) is routine in most cases for diagnostic certainty and to identify the complications of abscess, obstruction, fistula, and perforation. However, TAUS is highly sensitive and specific for uncomplicated acute diverticulitis and for the primary complication of pericolic abscess.²¹

Sonographic Features of Diverticula

Diverticula appear as bright “ears” outside the bowel wall, with acoustic shadowing caused by the presence of gas or inspissated feces. At higher probe frequencies, a thinned diverticular wall may be demonstrated with a reduced gut signature because of the absence of muscularis propria. The neck of a diverticulum may be identified as an echogenic band traversing hypoechoic circular muscle, which is often thickened (Fig. 4-10).

Sonographic Features of Diverticulitis

An isolated inflamed diverticulum²² is identified as an enlarged, echo-poor protrusion from the colon wall, with an ill-defined margin surrounded by echogenic noncompressible fat (Fig. 4-11). The gut signature is obliterated by the inflammation. Inspissated feces may be seen as a central shadowing echogenicity.

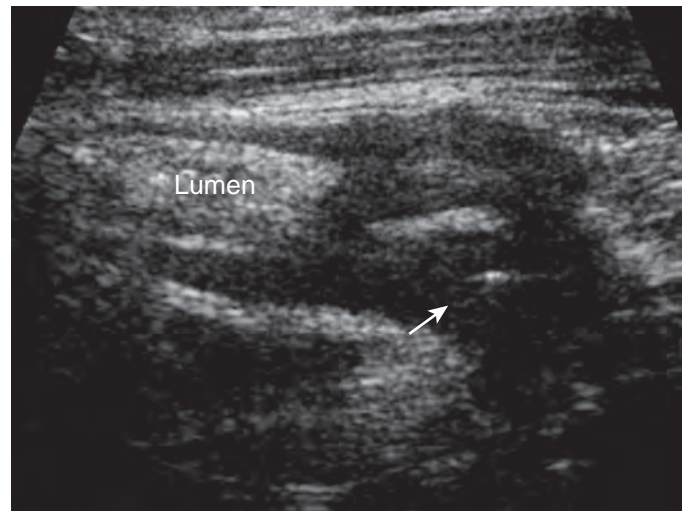


Figure 4-11 Acute diverticulitis. Axial image of the left colon showing asymmetric thickening of the echo-poor muscle layer around the echogenic lumen. A bright gas echo is demonstrated in the inflamed diverticulum (arrow).

Inflammation will commonly extend along the bowel, producing asymmetric or circumferential hypoechoic mural thickening that may be hyperemic on Doppler scanning. An intramural or pericolic abscess may be identified as an anechoic collection that may contain pockets of air or debris.

INFLAMMATORY BOWEL DISEASE

The prevalence of inflammatory bowel disease (IBD) in the United Kingdom is about 400/100,000, with ulcerative colitis (UC) almost twice as prevalent as Crohn's disease (CD). Most of these patients will require hospital assessment, and many will require acute admission: The lifetime risk for surgery is 20% to 30% for patients with UC and up to 70% to 80% for CD, depending on disease severity and location.²³

The diagnosis of IBD is made by clinical assessment, supported by a combination of laboratory tests, endoscopy and imaging. Establishing the location and extent of inflammatory lesions is critical to diagnosis, prognosis, and therapy. In CD, the behavior of disease at each site of involvement determines the likely clinical course. Penetrating disease producing fistulas and abscesses and stricturing disease results in episodes of obstruction. Although the location of disease is relatively stable over time, the course often changes.²⁴

Sonographic Evaluation

US is an accurate technique for the diagnosis of suspected IBD and evaluation of disease activity.^{25–27} It is less accurate for disease proximal to the ileum (L4) and for the rectum. However, over 70% CD patients have ileal or ileocolic disease at diagnosis.²⁴

As with all imaging modalities, the features of IBD overlap with those of a wide range of intestinal pathologic conditions. A specific diagnosis of UC or CD can seldom be made with confidence on imaging alone, but specific features such as skip lesions, longitudinal ulcers, and fat wrapping should be sought.

Bowel Wall Thickening. The primary imaging feature of IBD is bowel wall thickening (BWT). US has been shown to identify

Figure 4-12 Cobblestone mucosa in Crohn's disease. This is a long image of the ileum, with the lumen filled with edematous mucosal islands (M). The outer layers of the gut signature are preserved (arrows).

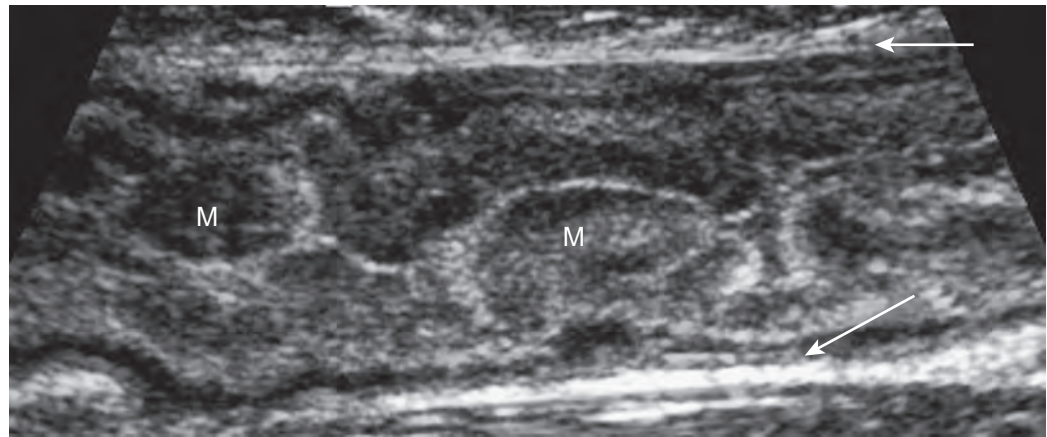
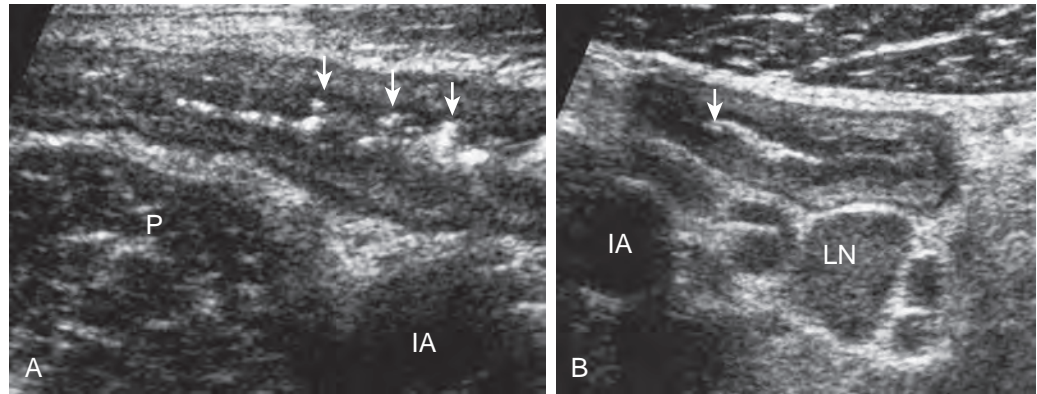


Figure 4-13 Acute ileitis in Crohn's disease. Shown are long (A) and axial (B) images of an ileal loop over the psoas (P) and iliac artery (IA). Gas-filled ulcers penetrate the thickened mucosa and submucosa (arrows). LN, Adjacent lymphadenopathy.



wall thickening in patients with suspected CD with a sensitivity of 88% and specificity of 93% at a BWT threshold of 3 mm or more and a sensitivity of 75% and specificity of 97% at a BWT threshold of more than 4 mm. In UC, BWT can be used to identify the extent and grade the severity of inflammation and the response to therapy.²⁸

Alteration in Gut Signature. The ability of TAUS to resolve the layers in a healthy bowel wall gives the potential to identify and characterize inflammatory behavior in wall layers, even at sub-threshold BWT. TAUS of inflamed segments may show the gut signature to be preserved, indistinct, or lost.²⁹

Isolated thickening of the mucosa may be accompanied by interruption of the lumen interface echo (layer 1) because of sloughing of the mucosal surface and/or tiny bright echoes caused by gas in the mucosal ulcers. In severe cases, the mucosa may be thinned by sloughing of necrotic tissue. The combination of ulcers and edematous mucosal islands produces the classic cobblestone appearance (Figs. 4-12 and 4-13).

In UC and CD, inflammation may be confined to the mucosa or mucosa and submucosa, resulting in thickening of these layers alone. Minimal thickening of the superficial layers may be judged in comparison with the muscularis propria, which is normally the thickest layer in all states of contraction.

In UC, severe inflammation extending into the submucosa reduces the echogenicity to the level of the adjacent muscle, producing a full-thickness hypoechoic ring. Hypoechoic wall thickening with complete loss of signature in CD indicates transmural inflammation, which may extend to produce an

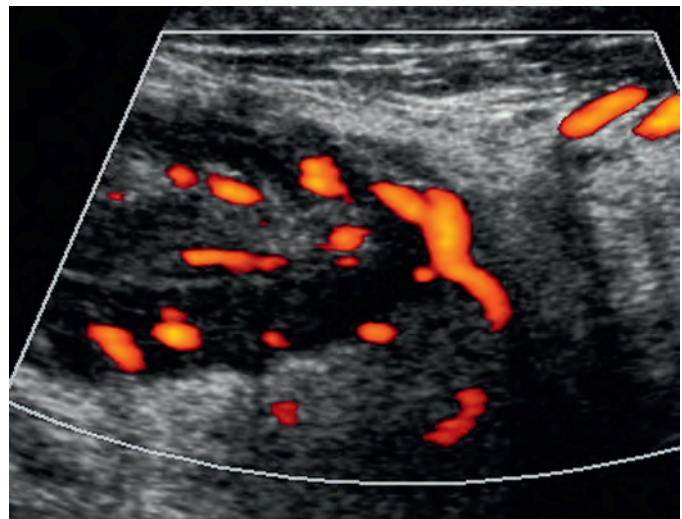


Figure 4-14 Acute ileitis in Crohn's disease. Power Doppler signals indicate hyperemia of acute, active, inflammatory CD ileitis.

irregular, mixed, hypoechoic inflammatory exudate on the serosal bowel surface. These changes may be circumferential or focal. Inflamed and normal bowel may be identified on the same axial circumference (skip lesion) that is strongly indicative of CD. Wedges of low-echo transmural inflammation on the mesenteric border have been shown to correlate with longitudinal ulcers (Fig. 4-14).³⁰ These are features of penetrating disease, with a high risk of abscess and fistulation.

Vascular Changes and Disease Activity. Actively inflamed bowel segments have an increased blood flow, which may be demonstrated with color Doppler or power Doppler imaging (see Fig. 4-14). Studies have shown this phenomenon to be helpful for distinguishing active inflammatory lesions from fibrotic strictures and monitoring response to medical therapies.³¹ Evidence indicates that the use of US contrast media may further increase the diagnostic confidence when assessing perfusion and help quantify this phenomenon.³²⁻³⁵

Fat Wrapping. Cytokines released in response to transmural inflammation stimulate proliferation of mesenteric or subserosal fat, which creeps or wraps around the inflamed bowel segment. This sign is determined to be present when more than 50% of the involved bowel circumference is encased and is a specific feature of transmural CD (Fig. 4-15). Fat wrapping correlates with histologic evidence of transmural inflammation and associated complications, such as fistulation. However, fat

wrapping is not a reliable indicator of the length of an involved CD segment because it does not occur over areas of more superficial disease.³⁶

Locoregional Lymphadenopathy. Active intestinal CD is usually accompanied by mild to moderate lymphadenopathy in the adjacent mesentery.

Stricturing Crohn's Disease. Narrowing of the bowel lumen sufficient to cause impaired intestinal function and obstructive symptoms may be seen in active inflammatory segments (hot strictures) and in segments in which fibrosis predominates (cold strictures). Spasm and edema contribute to the narrowing of active disease segments and may rapidly respond to medical therapy. Persistent symptomatic stricture is the most common indication for surgery.

In experienced hands, TAUS accurately detects bowel stenosis, particularly of more severely narrowed lesions likely to require surgical intervention, in which prestenotic dilation may make a short lesion conspicuous.³² Active inflammatory strictures are hyperemic compared with normal bowel and with fibrotic strictures. Color and power Doppler demonstrate no vascular activity in healthy bowel wall but both demonstrate increased flow in the inflamed bowel wall and inflammatory masses.

Penetrating Crohn's Disease. About one in six patients with CD have penetrating lesions (abscess, fistula, inflammatory mass) at the time of diagnosis.

Abscess and Phlegmon. Transmural inflammation extending out to and beyond the serosal surface may be seen with US as an irregular, mixed, low-echo inflammatory exudate on the serosal surface, a mixed low-echo inflammatory mass between bowel loops (phlegmon), or an irregularly thick and walled collection with a liquid center (abscess). Abscesses may form between bowel loops or in adjacent structures, such as the abdominal wall (see Fig. 4-15).

Fistula. Penetrating disease may progress beyond the serosal surface and interloop space to adjacent structures, creating an abnormal communication between the lumen of the disease bowel segment and adjacent bowel loops or any adjacent hollow organ (e.g., uterus, bladder).

With US, fistulas are identified as irregular tubular hypoechoic tracks, within which small hyperreflective air bubbles may occasionally be demonstrated. However, the presence of adjacent, indrawn, angulated bowel loops connected by mixed hypoechoic inflammatory exudate is highly suspicious of fistulation (Fig. 4-16).³⁷

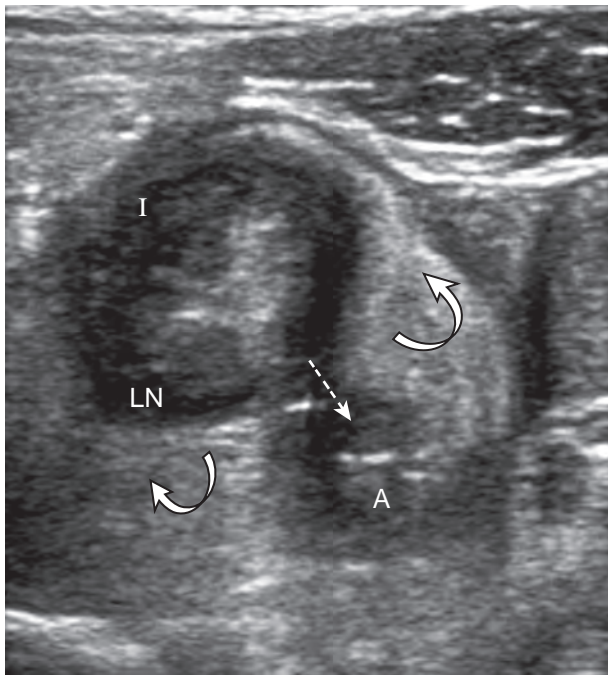


Figure 4-15 Penetrating Crohn's disease. Shown is an axial image of an inflamed ileum (I), with fat wrapping (curved arrows) and full-thickness penetration (broken arrow) extending to an adjacent abscess (A).

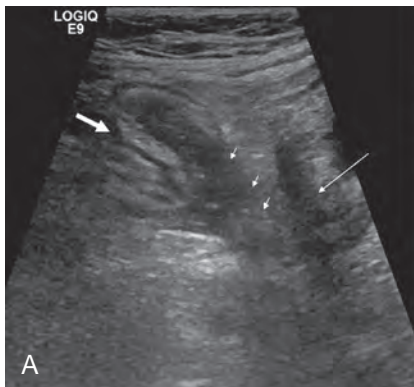


Figure 4-16 Crohn's disease fistula.

A. Ultrasound image of CD enterocolic fistula. Angulated ileal (short arrow) and colon (long arrow) loops are connected by echo-poor fistula (very small arrows) with moving, bright gas echoes in real time. **B.** CT scan of CD enterocolic fistula. This same-day CT scan confirms an inflammatory mass involving the small and large bowels extending onto the posterior pelvic brim. A tiny gas bubble marks the fistula (arrow). (From Rodgers PM, Verma R: Transabdominal ultrasound for bowel evaluation. *Radiol Clin North Am* 51:133-148, 2013.)

MIMICS OF INFLAMMATORY BOWEL DISEASE

Many of the imaging features of IBD are nonspecific and are shared with a wide range of pathologic conditions. The differential diagnoses relevant to the clinical presentation must be considered and imaging features sought to aid differentiation.

BOWEL ISCHEMIA

Bowel wall ischemia may result from impaired blood supply (embolic, stenotic, or diminished cardiac output) or drainage (mesenteric venous thrombosis). Depending on the cause, the injury may be focal or diffuse, range from superficial mucosal to full thickness, and vary in severity from mild to fulminant and life-threatening. The colon is more vulnerable to ischemic injury; the left colon is the most commonly affected segment.

The clinical picture is typically an older patient with abdominal pain, diarrhea, and rectal bleeding, with few clinical signs for the severity of symptoms. Ischemia produces mucosal and intramural necrosis, with associated edema and hemorrhage.

The chief sonographic features of bowel ischemia are marked circumferential thickening of a longer (>10 cm) bowel segment with reduced perfusion (little or no Doppler flow). The gut signature may be preserved in superficial injury, and the submucosal layer may be thickened by edema and hemorrhage. Full-thickness injury is more commonly accompanied by loss of the gut signature and peri-intestinal altered fat or fluid.^{38,39} Intramural air may be identified by highly echogenic reflectors with acoustic shadowing. US contrast agents can demonstrate persisting perfusion and predict likely recovery in those with less severe injury (Fig. 4-17).⁴⁰ Atypical presentations in younger patients with small bowel or more proximal gastrointestinal (GI) injury may be the result of autoimmune vasculitides, drugs (e.g., oral contraceptives, cocaine), fibromuscular dysplasia, and other rare conditions. These may mimic Crohn's lesions, so documenting the Doppler findings is critical.

INFECTIOUS ENTEROCOLITIDES

Pseudomembranous Colitis (PMC)

Pseudomembranous colitis (PMC) is a common, toxin-induced manifestation of intestinal infection *Clostridium difficile*. *C. difficile* is the cause in 15% to 25% of cases of antibiotic-associated diarrhea.⁴¹

Sonographically, PMC is characterized by diffuse large bowel, often so severe that it effaces the lumen. The mucosa and submucosa become indistinguishable, with a mixed heterogeneous striated echo pattern. The lumen and mucosal layer are interrupted by ulcers; and the coalescent slough of pseudomembranes is identified as linear echogenic structures in the lumen (Fig. 4-18). Ascites is a common feature.^{42,43}

Infectious Ileocolitis

Yersinia, *Campylobacter*, and *Salmonella* bacteria are well-known causes of acute, usually self-limiting, diarrheal illnesses but less commonly may produce an enteric infection confined to the ileocecal region. In such cases, patients present with right iliac fossa pain and tenderness, and diarrhea may be minimal or absent. In more acute cases, this may result in unnecessary appendectomy or more protracted cases may be mistaken for Crohn's disease or an appendix mass.

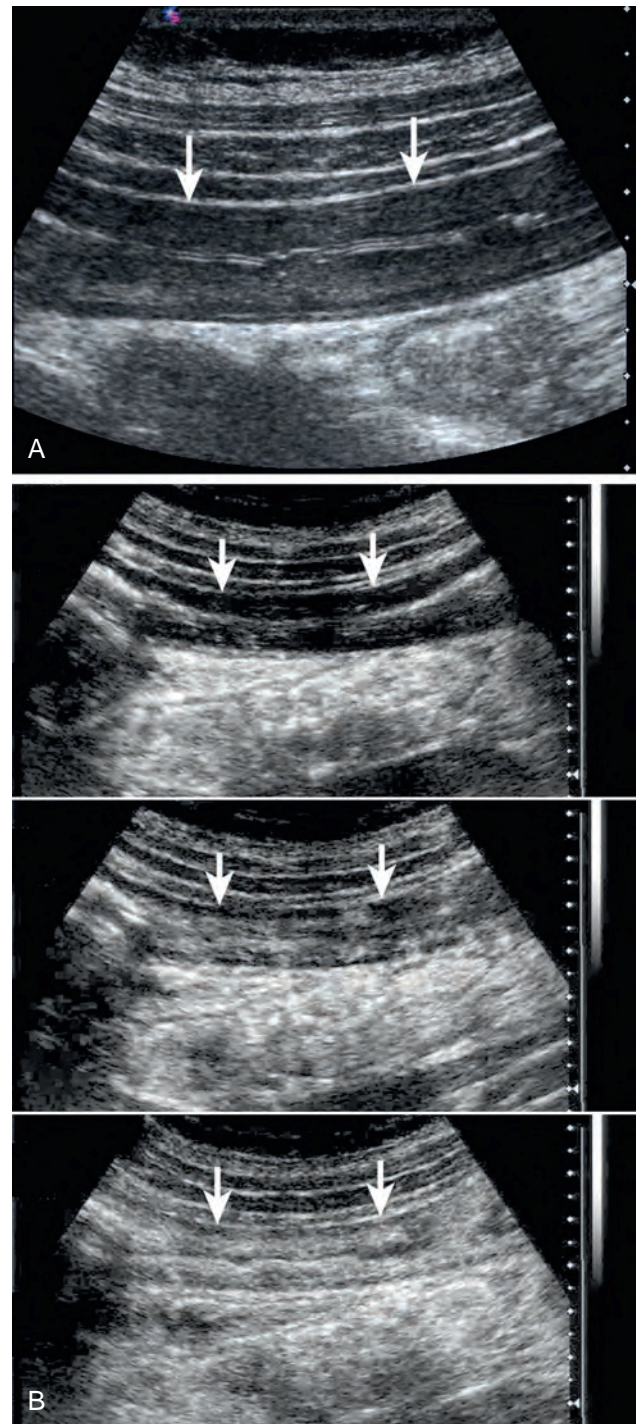


Figure 4-17 Ischemic bowel. **A.** Longitudinal section of the descending colon (arrows) shows hypoechoic wall thickening, with barely visible stratification. Color Doppler sonography (not shown) detected only minimal flow in the periphery of the bowel wall. **B.** Contrast-enhanced ultrasound clearly demonstrated vascularization of this segment (arrows), requiring no urgent surgical intervention. (From Hollerweger A: Colonic diseases: The value of US examination. *Eur J Radiol* 64:239–249, 2007.)

Ultrasound reveals a symmetric thickening of the wall of the terminal ileum and cecum confined to the mucosal and submucosal layers, with no extension to the muscularis or serosa, or beyond into the mesentery. It has been reported that the extent of cecal and colonic involvement may vary with the specific

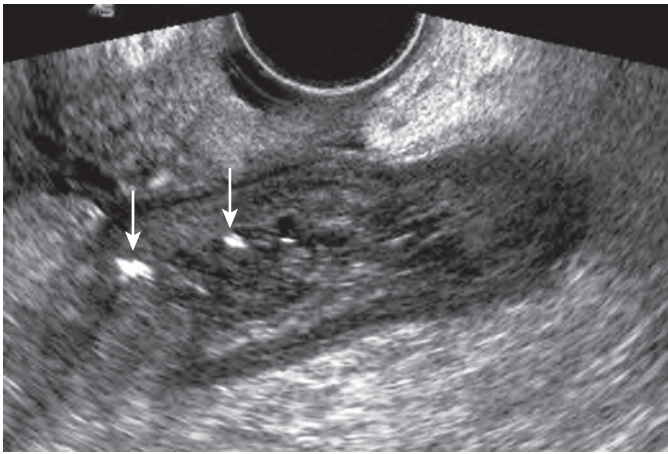


Figure 4-18 Pseudomembranous colitis. TVUS shows marked colon wall thickening, with mucosal breaks, blurred gut signature, and strong reflectors (pseudomembranes) formed by coalescing slough (arrows).

pathogen.⁴⁴ Local mesenteric lymph nodes are usually enlarged. The appendix is normal.

Intestinal Tuberculosis

Nonspecific symptoms such as abdominal pain, weight loss, anemia, and fever predominate, but patients may present with symptoms of intestinal obstruction or a palpable abdominal mass.⁴⁵ Tuberculosis usually involves the ileocecal segment but isolated ileal or jejunal disease does occur and is a particular feature of atypical varieties.

Ultrasound features include bowel thickening with luminal narrowing and superficial or deep ulcers, typically involving the terminal ileum, ileocecal valve, and cecum (Fig. 4-19). Lymphadenopathy is common and may form conglomerate masses. Bowel loops may be matted together by interloop exudates or abscesses. Ascites or peritoneal thickening may be identified.⁴⁶

Strategic Place for Ultrasound in Bowel Imaging

The current evidence-based consensus guidelines on imaging in IBD, produced jointly by ECCO (European Crohn's and Colitis Organization) and ESGAR (European Society of Gastrointestinal and Abdominal Radiology), document the significant contribution made by TAUS to the multimodality approach to IBD diagnosis and management.²⁷ Most of this is elective, and the high level of operator skills needed for bowel sonography can be matched to the specific clinical need. Emergent

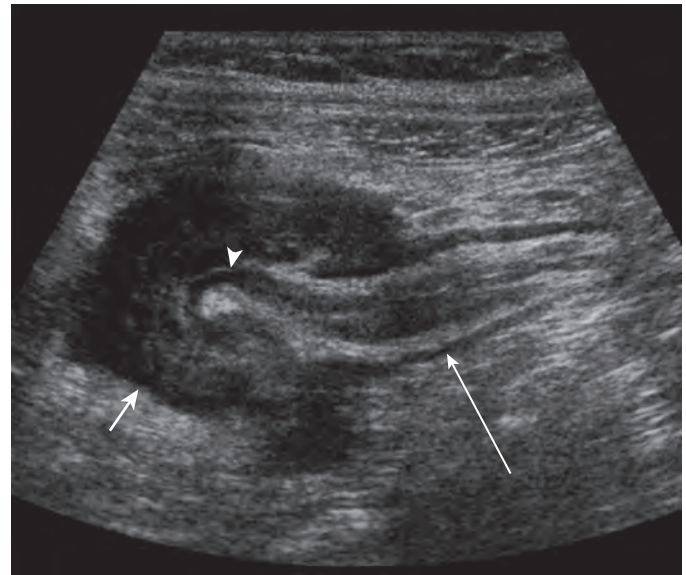


Figure 4-19 Ileocecal tuberculosis. There is an irregular, echo-poor contracted cecum (short arrow), ileocecal valve (arrowhead) and thickened terminal ileum, with preserved stratification (long arrow).

presentations are more likely to need management by CT, with the attendant concerns of radiation dose accruing over a lifetime of disease.

The role of TAUS in acute clinical presentations is more problematic, not least because of issues of training and availability outside of office hours. Prospective comparative studies of the performance of CT and US in acute appendicitis favor CT (diagnostic value of graded compression ultrasonography—summary sensitivity of 0.78, summary specificity of 0.83; diagnostic value of CT—summary sensitivity of 0.91, summary specificity of 0.90).⁴⁷ The authors of this meta-analysis and many others have only designated TAUS as a first-line test for children and younger or pregnant women to avoid exposure to ionizing radiation.^{48,49} However, equivocal CT findings are a significant problem, with up to one third of these individuals having acute appendicitis.⁵⁰ TAUS can be a useful adjunct to CT in equivocal cases.^{51,52}

A stratified approach commencing with ultrasound using a high-frequency probe and proceeding to CT for inconclusive cases has been recommended.⁵³⁻⁵⁵ Low-dose CT techniques and/or limited scan areas have been demonstrated as effective while reducing radiation.⁵⁶ The effectiveness of the locally adopted imaging protocols should be reflected in the local negative appendectomy rate, perforation rate, and radiation dose monitoring.

REFERENCES

1. Kimmey MB, Martin RW, Haggitt RC, et al: Histologic correlates of gastrointestinal ultrasound images. *Gastroenterology* 96(2 Pt 1):433-441, 1989.
2. Ledermann HP, Börner N, Strunk H, et al: Bowel wall thickening on transabdominal sonography. *AJR* 174:107-117, 2000.
3. Puylaert JB: Ultrasound of acute GI tract conditions. *Eur Radiol* 11:1867-1877, 2001.
4. O'Malley ME, Wilson SR: US of gastrointestinal tract abnormalities with CT correlation. *Radiographics* 23:59-72, 2003.
5. Puylaert JB: Acute appendicitis: US evaluation using graded compression. *Radiology* 158:355-360, 1986.
6. Lee J-H, Jeong YK, Hwang JC, et al: Graded compression sonography with adjuvant use of a posterior manual compression technique in the sonographic diagnosis of acute appendicitis. *AJR* 178:863-868, 2002.
7. Gilmore OJA, Browett JP, Griffin PH, et al: Appendicitis and mimicking conditions. *Lancet* 306:421-424, 1975.
8. Baigrie RJ, Dehn TC, Fowler SM, Dunn DC: Analysis of 8651 appendectomies in England and Wales during 1992. *Br J Surg* 82:933, 1995.

9. Jeffrey RB, Jr, Laing FC, Townsend RR: Acute appendicitis: sonographic criteria based on 250 cases. *Radiology* 167:327–329, 1988.
10. Puig S, Hörmann M, Rebhandl W, et al: US as a primary diagnostic tool in relation to negative appendectomy: Six years experience. *Radiology* 226:101–104, 2003.
11. Collins DC: The length and position of the vermiform appendix: A study of 4,680 specimens. *Ann Surg* 96:1044–1048, 1932.
12. Rettenbacher T, Hollerweger A, Macheiner P, et al: Outer diameter of the vermiform appendix as a sign of acute appendicitis: Evaluation at US. *Radiology* 218:757–762, 2001.
13. Park NH, Park CS, Lee EJ, et al: Ultrasonographic findings identifying the faecal-impacted appendix: Differential findings with acute appendicitis. *Br J Radiol* 80:872–877, 2007.
14. Lim HK, Lee WJ, Lee SJ, et al: Focal appendicitis confined to the tip: Diagnosis at US. *Radiology* 200:799–801, 1996.
15. Kessler N, Cyteval C, Gallix B, et al: Appendicitis: Evaluation of sensitivity, specificity, and predictive values of US, Doppler US, and laboratory findings. *Radiology* 230:472–478, 2004.
16. Quillin SP, Siegel MJ, Coffin CM: Acute appendicitis in children: value of sonography in detecting perforation. *AJR* 159:1265–1268, 1992.
17. Toorenvliet BR, Wiersma F, Bakker RFR, et al: Routine ultrasound and limited computed tomography for the diagnosis of acute appendicitis. *World J Surg* 34:2278–2285, 2010.
18. Van Breda Vriesman AC: Mimics of appendicitis: Alternative nonsurgical diagnoses with sonography and CT. *AJR* 186:1103–1112, 2006.
19. Etzioni DA, Mack TM, Beart RW, Jr, Kaiser AM: Diverticulitis in the United States, 1998–2005: Changing patterns of disease and treatment. *Ann Surg* 249:210–217, 2009.
20. Laméris W, van Randen A, van Gulik TM, et al: A clinical decision rule to establish the diagnosis of acute diverticulitis at the emergency department. *Dis Colon Rectum* 53:896–904, 2010.
21. Schwert WB, Schwarz S, Rothmund M: Sonography in acute colonic diverticulitis. *Dis Colon Rectum* 35:1077–1084, 1992.
22. Wilson SR, Toi A: The value of sonography in the diagnosis of acute diverticulitis of the colon. *AJR* 154:1199–1202, 1990.
23. Mowat C, Cole A, Windsor A, et al: Guidelines for the management of inflammatory bowel disease in adults. *Gut* 60:571–607, 2011.
24. Louis E, Collard A, Oger AF, et al: Behaviour of Crohn's disease according to the Vienna classification: Changing pattern over the course of the disease. *Gut* 49:777–782, 2001.
25. Fraquelli M, Colli A, Casazza G, et al: Role of US in detection of Crohn disease: Meta-analysis. *Radiology* 236:95–101, 2005.
26. Horsthuis K, Bipat S, Bennink RJ, Stoker J: Inflammatory bowel disease diagnosed with US, MR, scintigraphy, and CT: Meta-analysis of prospective studies. *Radiology* 247:64–79, 2008.
27. Panes J, Bouhnik Y, Reinisch W, et al: Imaging techniques for assessment of inflammatory bowel disease: Joint ECCO and ESGAR evidence-based consensus guidelines. *J Crohns Colitis* 7:556–585, 2013.
28. Parente F, Molteni M, Marino B, et al: Are colonoscopy and bowel ultrasound useful for assessing response to short-term therapy and predicting disease outcome of moderate-to-severe forms of ulcerative colitis? A prospective study. *Am J Gastroenterol* 105:1150–1157, 2010.
29. Hata J, Haruma K, Yamanaka H, et al: Ultrasonographic evaluation of the bowel wall in inflammatory bowel disease: comparison of in vivo and in vitro studies. *Abdom Imaging* 19:395–399, 1994.
30. Kunihiro K, Hata J, Haruma K, et al: Sonographic detection of longitudinal ulcers in Crohn disease. *Scand J Gastroenterol* 39:322–326, 2004.
31. Martínez MJ, Ripollés T, Paredes JM, et al: Assessment of the extension and the inflammatory activity in Crohn's disease: Comparison of ultrasound and MRI. *Abdom Imaging* 34:141–148, 2008.
32. Parente F, Maconi G, Bollani S, et al: Bowel ultrasound in assessment of Crohn's disease and detection of related small bowel strictures: A prospective comparative study versus x ray and intraoperative findings. *Gut* 50:490–495, 2002.
33. Ripollés T, Martínez MJ, Paredes JM, et al: Crohn disease: Correlation of findings at contrast-enhanced US with severity at endoscopy. *Radiology* 253:241–248, 2009.
34. Migaleddu V, Scanu AM, Quaia E, et al: Contrast-enhanced ultrasonographic evaluation of inflammatory activity in Crohn's disease. *Gastroenterology* 137:43–52, 2009.
35. Parente F, Molteni M, Marino B, et al: Are colonoscopy and bowel ultrasound useful for assessing response to short-term therapy and predicting disease outcome of moderate-to-severe forms of ulcerative colitis? A prospective study. *Am J Gastroenterol* 105:1150–1157, 2010.
36. Sheehan AL, Warren BF, Gear MW, Shepherd NA: Fat-wrapping in Crohn's disease: Pathological basis and relevance to surgical practice. *Br J Surg* 79:955–958, 1992.
37. Rodgers PM, Verma R: Transabdominal ultrasound for bowel evaluation. *Radiol Clin North Am* 51:133–148, 2013.
38. Ripollés T, Simó L, Martínez-Pérez MJ, et al: Sonographic findings in ischemic colitis in 58 patients. *AJR* 184:777–785, 2005.
39. Frisoli JK, Desser TS, Jeffrey RB: Thickened submucosal layer: A sonographic sign of acute gastrointestinal abnormality representing submucosal edema or hemorrhage. *AJR* 175:1595–1599, 2000.
40. Hollerweger A: Colonic diseases: The value of US examination. *Eur J Radiol* 64:239–249, 2007.
41. Bartlett JG, Gerding DN: Clinical recognition and diagnosis of *Clostridium difficile* infection. *Clin Infect Dis* 46(Suppl 1):S12–S18, 2008.
42. Downey DB, Wilson SR: Pseudomembranous colitis: sonographic features. *Radiology* 180:61–64, 1991.
43. Ramachandran I, Sinha R, Rodgers P: Pseudomembranous colitis revisited: Spectrum of imaging findings. *Clin Radiol* 61:535–544, 2006.
44. Puylaert J, Van der Zant FM, Mutsaers J: Infectious ileoceitis caused by *Yersinia*, *Campylobacter*, and *Salmonella*: Clinical, radiological and US findings. *Eur Radiol* 7:3–9, 1997.
45. Sharma MP, Bhatia V: Abdominal tuberculosis. *Indian J Med Res* 120:305–315, 2004.
46. Kedar RP, Shah PP, Shivde RS, Malde HM: Sonographic findings in gastrointestinal and peritoneal tuberculosis. *Clin Radiol* 49:24–29, 1994.
47. Van Randen A, Bipat S, Zwinderman AH, et al: Acute appendicitis: Meta-analysis of diagnostic performance of CT and graded compression US related to prevalence of disease. *Radiology* 249:97–106, 2008.
48. Jacobs JE: CT and sonography for suspected acute appendicitis: A commentary. *AJR* 186:1094–1096, 2006.
49. Rosen MP, Ding A, Blake MA, et al: ACR Appropriateness Criteria® right lower quadrant pain—suspected appendicitis. *J Am Coll Radiol* 8:749–755, 2011.
50. Rhea JT, Halpern EF, Ptak T, et al: The status of appendiceal CT in an urban medical center 5 years after its introduction: experience with 753 patients. *AJR* 184:1802–1808, 2005.
51. Jang KM, Lee K, Kim M-J, et al: What is the complementary role of ultrasound evaluation in the diagnosis of acute appendicitis after CT? *Eur J Radiol* 74:71–76, 2010.
52. Sim JY, Kim HJ, Yeon JW, et al: Added value of ultrasound re-evaluation for patients with equivocal CT findings of acute appendicitis: A preliminary study. *Eur Radiol* 23:1882–1890, 2013.
53. Van Breda Vriesman AC, Kole BJ, Puylaert JBCM, et al: Effect of ultrasonography and optional computed tomography on the outcome of appendectomy. *Eur Radiol* 13:2278–2282, 2003.
54. Krishnamoorthi R, Ramarajan N, Wang NE, et al: Effectiveness of a staged US and CT protocol for the diagnosis of pediatric appendicitis: Reducing radiation exposure in the age of ALARA. *Radiology* 259:231–239, 2011.
55. Poortman P, Oostvogel HJM, Bosma E, et al: Improving diagnosis of acute appendicitis: results of a diagnostic pathway with standard use of ultrasonography followed by selective use of CT. *J Am Coll Surg* 208:434–441, 2009.
56. Kim K, Kim YH, Kim SY, et al: Low-dose abdominal CT for evaluating suspected appendicitis. *N Engl J Med* 366:1596–1605, 2012.

Multidetector Computed Tomography of the Gastrointestinal Tract: Principles of Interpretation

RICHARD M. GORE | MARK E. BAKER

CHAPTER OUTLINE

Lumen Opacification

Positive Contrast Agents
Neutral Contrast Agents
Gas Contrast

Vascular Opacification

Normal Bowel Wall

Esophagus
Stomach
Small Bowel
Colon

Bowel Wall: Pathologic Changes

How to Examine the Bowel with MDCT
Evaluation of the Abnormal Gut

Mesenteric and Omental Fat Disease

Blood Vessels
Serosal and Subperitoneal Fat Density
Lymph Nodes
Calcifications

Multidetector computed tomography (MDCT) is currently the premier imaging technique for evaluating luminal, mural, and mesenteric abnormalities of the gastrointestinal tract. Although magnetic resonance (MR) enterography is rapidly gaining acceptance as the method of choice in evaluating patients with Crohn's disease, MDCT examinations of the entire abdomen and pelvis can be acquired in seconds with near-isotropic voxels, allowing for high-quality and clinically useful volume imaging. The CT datasets can be viewed in any plane, and 3D techniques can be used to display large datasets effectively and graphically in a user-friendly format that is understandable to referring physicians.¹⁻³

Lumen Opacification

Proper distention and marking of the bowel lumen are vital in detecting mural thickening and excluding mural masses and mesenteric and omental disease. There are a number of methods available to accomplish this goal; the choice depends on the clinical setting.

In the emergent setting, in which bowel obstruction or intestinal ischemia is suspected, the intestinal secretions are usually sufficient to highlight the lumen, especially in a high-grade

bowel obstruction. Orally administered contrast may be vomited and may remain in the stomach because of absent or diminished gastrointestinal motility. Finally, in cases of suspected ischemia, positive oral contrast media often hamper the creation of CT angiograms.

As part of a general survey examination of patients with no localizing signs or symptoms, a study performed with positive luminal contrast material is often obtained. As a caveat, the assessment of mural and mucosal enhancement of the gut may be compromised with the positive contrast material. Additionally, positive intraluminal contrast will interfere with CT angiography and some 3D techniques.

Air or carbon dioxide as an intraluminal contrast agent is used in the setting of CT gastroscopy and colonography.

POSITIVE CONTRAST AGENTS

Positive contrast opacification (>75-100 HU) of the gut is accomplished by giving 1% to 2% barium suspensions or 2% to 3% solutions of iodinated water-soluble agents (Fig. 5-1). The low percentage of barium requires commercial preparations made specifically for CT, in which additives are used to ensure that the barium remains in suspension.

In most patients, contrast material will reach the distal ileum within 45 minutes after initiation of drinking. Prolonged transit times are to be anticipated. Some common conditions altering the transit time include recent postoperative status, serum electrolyte disturbances, collagen vascular diseases (e.g., scleroderma), hypothyroidism, and intestinal obstruction. Conversely, patients who are hyperthyroid, have syndromes with associated increased intestinal motility (e.g., carcinoid, islet cell tumor), or have infections (e.g., cryptosporidiosis, giardiasis) will display a significantly accelerated intestinal transit time.

The choice between oral barium suspensions and water-soluble agents is dictated by the experience and preference of the radiologist. Water-soluble agents should be used exclusively for patients with abdominal trauma or a suspected perforated viscus, those who have a high likelihood of immediate surgery, and as an aid in percutaneous CT biopsy or other interventional procedures.

NEUTRAL CONTRAST AGENTS

Neutral contrast agents (0-25 HU) have several advantages over positive contrast agents for evaluating mucosal, mural, and serosal disease (Fig. 5-2).⁴⁻¹¹ They allow excellent depiction of mural enhancement of the gut without the algorithm under-shoot or overshoot that may accompany intraluminal high-attenuation, positive contrast, and low-attenuation gas. Neutral



Figure 5-1 Positive contrast opacification. Positive contrast within the lumen of the gut provides lumen distention and helps differentiate a collapsed bowel from masses, adenopathy, and abscesses. In this obese individual, the mesenteric vessels are well depicted.



Figure 5-2 Neutral contrast opacification. Neutral contrast not only distends the lumen but also provides for easier evaluation of mural enhancement and the mesenteric vessels.

contrast agents also facilitate the performance of CT angiography and other three-dimensional techniques. Neutral contrast agents include water, milk, lactulose, 0.1% solution of barium (VoLumen; Bracco Diagnostic, Princeton, NJ), and water with mannitol or polyethylene glycol. Water can be administered as an effective neutral contrast agent for the upper gastrointestinal tract, especially the stomach and duodenum. However, it is less effective in distending the more distal bowel because it is normally absorbed before reaching the distal ileum.

These neutral agents are also helpful when performing CT angiography for staging and preoperative evaluation of hepatic, biliary, and pancreatic malignancies. Regardless of the agent, consistent opacification and/or distention of the jejunum remains a challenge. Unlike the standard small bowel series, periodic overhead films are not obtained before a CT. Thus it is impossible to determine the best time to scan in relation to proximal small bowel opacification and distention.

GAS CONTRAST

Gaseous distention of the stomach is important when evaluating mucosal and mural disease. It has been used with great success in CT gastrography for the diagnosis and staging of upper gastrointestinal malignancies.¹²⁻¹⁴

For CT colonography, room air or carbon dioxide is insufflated per rectum (Fig. 5-3). Adequate gaseous distention of the colon is very important for image interpretation because significant lesions may be obscured in a collapsed segment of colon.¹⁵⁻¹⁹ A complete discussion of this technique is presented in Chapter 53.

Vascular Opacification

Opacification of the blood vessels is essential for complete evaluation of inflammatory, infectious, neoplastic, vascular, and traumatic diseases of the gastrointestinal tract. Obviously, this cannot be performed in all clinical settings (e.g., in cases of poor renal function or poor venous access). For general diagnostic cases, 100 to 150 mL (depending on concentration) of nonionic contrast is administered at a rate of 3 mL/s with a power injector. If CT angiography or other 3D techniques are to be performed, the rate is increased to 5 mL/s. Many sites use some form of bolus tracking as a method of timing the scan in relation to the level of arterial opacification.

One of the advantages of MDCT is that multiple datasets can be acquired with a single bolus of contrast. The following possible imaging times may be used when imaging the abdomen and pelvis—unenhanced, early arterial phase (20 seconds); late arterial-enteric phase (40 seconds); portal venous phase (70-90 seconds); equilibrium phase (210 seconds); and delayed phase (15-20 minutes).

For general survey abdominal imaging, obtaining scans during the portal venous phase is adequate. When assessing the viability of bowel, searching for a source of gastrointestinal hemorrhage, evaluating the cirrhotic liver, and searching for hypervascular metastases, it is useful to obtain noncontrast scans as well as scans during the later hepatic arterial and portal venous phases. When CT angiography is performed, scans should be obtained during the early arterial phase. The enteric phase corresponds to the late arterial phase and has been found useful for evaluating Crohn's disease activity.



Figure 5-3 Gas opacification. Distention of the lumen of the gut is an important part of CT colonography.

Normal Bowel Wall

Almost all significant pathology of the bowel wall results in mural thickening, which is often accompanied by changes in the attenuation of the bowel wall caused by edema, hemorrhage, tumor, fat, or gas. Two of the most common pitfalls in interpreting CT examinations of the gut are (1) confusing an insufficiently distended loop of bowel for pathologic thickening and (2) mistaking an inadequately opacified bowel loop for an abdominal mass. Techniques for achieving lumen distention are in the preceding section.

ESOPHAGUS

The esophagus has a length of 23 to 25 cm in the average adult. The wall of the distended esophagus is 3 mm in thickness (Fig. 5-4). When the esophagus is not distended, the wall may approach 5 to 7 mm. It may be very difficult to differentiate diffuse and even focal esophageal disease if the lumen is not distended (a common occurrence). Furthermore, a hiatal hernia commonly has the appearance of focal wall thickening. The cervical esophagus lies posterior to the trachea in the midline. It may normally bulge into the posterior aspect of the trachea because of the limited space of the neck.

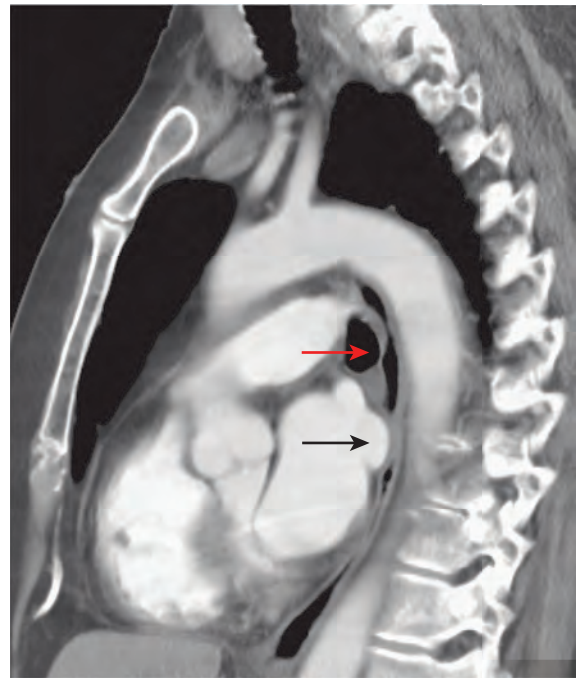


Figure 5-4 Normal esophagus. On this sagittal reformatted image of the thorax, the normal esophagus is depicted as a thin-walled tubular structure. Note that it courses posterior to the left mainstem bronchus (red arrow) and left atrial appendage (black arrow).

At the level of the thoracic inlet, the esophagus courses to the left of the midline and then lies adjacent to the left main stem bronchus and pericardium of the left atrium in the mid-thorax. More distally, the esophagus lies anterior to the descending aorta to the left of the midline as it enters the esophageal hiatus of the diaphragm. Normally, the thoracic esophagus should not indent the trachea, and there should be a triangle of fat between the aorta, spine, and esophagus distally. In patients with invasive esophageal carcinoma, the trachea is bowed along its posterior aspect by the esophageal tumor. More distally, invasive esophageal neoplasms obliterate the triangle of fat.

Contrast-enhanced examinations should show uniform mural enhancement of the esophagus, without mural stratification.

STOMACH

The stomach is a functionally and anatomically dynamic organ, and its appearance depends on the degree of luminal distention and gastric location (Fig. 5-5). For the well-distended, nondependent gastric fundus and body, a wall thickness of up to 5 mm is considered normal.²⁰ The mural thickness of the antrum, however, is affected by anatomic and functional factors that make it normally thicker than other portions of the stomach. The gastric smooth muscle, particularly the circular layer, is thicker and denser in the antrum compared with more proximal portions of the stomach. Periodic concentric and eccentric antral contractions, as seen fluoroscopically, also contribute to the apparent mural thickening of the stomach.

When the normal stomach is distended with neutral contrast, enhancement of the mucosa may be seen, highlighted against the lower attenuation mucosa and muscularis propria. Up to 25% of patients show linear submucosal low attenuation

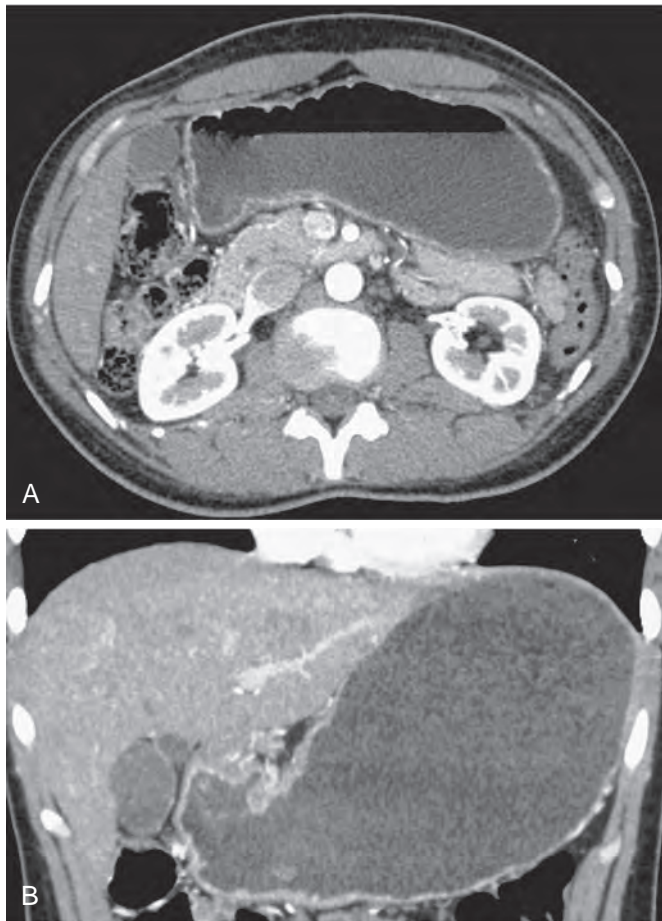


Figure 5-5 Normal stomach. Axial (A) and coronal reformatted (B) images show a thin gastric wall. Often, the antrum is slightly thicker than the more proximal stomach.

or mural stratification in the antrum on contrast-enhanced MDCT examination. This may be partly the result of fat deposition in the submucosa.

SMALL BOWEL

The normal small bowel is approximately 22 feet long and is suspended by a root that measures 6 to 9 inches and courses from the level of the ligament of Treitz caudally to the level of the ileocecal valve. As with conventional barium small bowel examinations, there are more valvulae conniventes in the jejunum than in the ileum. The normal small bowel wall measures between 1 and 2 mm when the lumen is well distended with a positive, neutral, or air contrast medium (Fig. 5-6). When collapsed, the normal mural thickness of the small bowel measures between 2 and 3 mm.

The normal small bowel wall appears to have the greatest level of enhancement during the enteric phase (approximately 40 seconds, after initiation of the contrast injection).²¹ This investigation did not take into account the location of the small bowel when assessing bowel wall enhancement. Some investigators think that this is the ideal time to scan in patients with Crohn's disease. Other investigators, using timed MR scanning after the injection of contrast, have shown that the maximal difference between normal and active inflammatory



Figure 5-6 Normal small bowel and colon. Coronal reformatted image shows nice distention of the small bowel and colon by positive contrast. The high-density intraluminal material limits assessment of the enhancement of the bowel wall.

small bowel Crohn's disease occurs much later, even several minutes after contrast injection.²² Furthermore, one investigation has shown that there is no significant difference in detecting the CT features of Crohn's disease at 40 and 70 seconds postcontrast.²³

Regardless, the wall of collapsed segments of the small bowel has a greater attenuation than the wall of distended loops. Also, because the duodenum has more folds than the jejunum and the jejunum has more than the ileum, the duodenum enhances more than the jejunum and the jejunum enhances more than the ileum.²⁴ Because collapsed small bowel loops have increased attenuation, similar to that of inflamed bowel loops, secondary findings of infectious or inflammatory small bowel disease (e.g., stratified enhancement pattern, engorged vasa recta, creeping fat of the mesentery, enlarged lymph nodes) should be considered (see Chapter 41).

COLON

The thickness of the colon wall as imaged on MDCT depends on the degree of distention. Fecal contents, fluid, colonic redundancy, and muscular hypertrophy (myochosis) make accurate determination of the true colonic wall thickness difficult. The normal colon wall (see Fig. 5-6) is normally less than 4 mm thick with proper distention. The normal wall is typically homogeneous in attenuation. With obesity becoming increasingly prevalent, submucosal fat is being identified in otherwise normal patients throughout the gut, but particularly in the colon.

Bowel Wall: Pathologic Changes

HOW TO EXAMINE THE BOWEL WITH MDCT

MDCT findings using thin section reconstructions (<1–2 mm), often overlapping, can be reconstructed in multiple planes. As in plain film radiography, orthogonal views are essential to assess the small bowel. We find that the axial and coronal planes are most helpful, with occasional sagittal reconstruction, especially if mesenteric artery occlusion is an important part of the investigation (i.e., ischemic bowel). Without orthogonal views, segments of the bowel may not be adequately assessed. Furthermore, in patients with Crohn's disease, strictures and fistulas may not be identified. As an added benefit, surgeons and gastroenterologists are more familiar with viewing the small bowel in the coronal plane.

When viewing MDCT depictions of the bowel, especially the small bowel, we find that the routine scrolling on a workstation from superior to inferior and back, as well as anterior to posterior, allows the radiologist to follow bowel loops from the jejunum to ileum in a continuous fashion. Also, viewing the images in this volume fashion, changing windows and levels as needed, can detect mural abnormalities and distinguish the small bowel from mesenteric processes. Viewing the bowel with narrow windows, similar to liver windowing and leveling, can facilitate detection of hypervascular small bowel tumors, vascular abnormalities of the bowel wall (arteriovenous malformations and Dieulafoy lesions), and the mural hyperenhancement identified in active, inflammatory Crohn's disease. Changing the window and level back to a soft tissue window after assessing the small bowel will facilitate identification of mesenteric abnormalities, which might have been missed using the narrow windowing and leveling. This dynamic volume interpretation is a demanding process but, once mastered on a modern interpreting workstation, can be performed rapidly and efficiently.

EVALUATION OF THE ABNORMAL GUT

Mural thickening is the pathologic hallmark of gastrointestinal disease. When evaluating the abnormal gut, the following features should be carefully analyzed: mural attenuation and enhancement patterns (Table 5-1); degree of mural thickening (Table 5-2); symmetry of bowel wall thickening (Table 5-3); and length of the diseased segment (Table 5-4). Wittenberg and colleagues described a classification system for the abnormal bowel wall as depicted by MDCT (Fig. 5-7).²⁵ Regardless of enhancement patterns, symmetry of the bowel wall thickening, and length of the diseased segment, the thicker the bowel wall, the more likely that neoplastic disease is present. As a good rule of thumb, confirmed in the literature as well as anecdotally, wall thickening of 1.5 cm or less is infectious and/or inflammatory and wall thickening more than 1.5 cm is neoplastic. Between 1 and 2 cm, there is overlap between the categories. Additionally, neoplastic disease tends to cause asymmetric wall thickening, but this general rule holds true for over 90% of cases.²⁶

White Attenuation Pattern

When the diseased segment of gut demonstrates contrast enhancement to a degree equal to or greater than that of venous opacification on the same scan, this indicates abnormal enhancement (Fig. 5-8A). Avid mural contrast enhancement is probably

TABLE
5-1

Patterns of Attenuation

- I. Homogeneous
 - A. Common
 1. Submucosal hemorrhage
 2. Lymphoma
 3. Small adenocarcinoma
 - B. Uncommon
 1. Infarcted bowel
 2. Pitfalls related to residual fluid
 3. Chronic Crohn's disease
 4. Chronic radiation injury
- II. Heterogeneous
 - A. Stratified attenuation
 1. Common
 - a. Ischemia
 - b. Infectious enterocolitis
 - c. Crohn's disease, ulcerative colitis
 - d. Vasculitis, lupus, Henoch-Schönlein purpura
 - e. Radiation
 - f. Bowel edema related to cirrhosis or low-protein state
 - g. Angioedema from angiotensin-converting enzyme (ACE) inhibitors
 2. Uncommon
 - a. Infiltrating scirrhous carcinoma (usually stomach or rectum)
 - b. Residual fluid and contrast material
 - c. Submucosal fat deposition
 - d. Pneumatosis
 - B. Mixed attenuation, common
 1. Large adenocarcinoma
 2. Gastrointestinal stromal tumor
 3. Mucinous adenocarcinoma

Modified from Macari M, Balthazar EJ: CT of bowel wall: Significance and pitfalls of interpretation. *AJR* 176:1105–1116, 2001; Appendix 1, p 1115.

TABLE
5-2

Degree of Mural Thickening

- I. Mild thickening (<2 cm)
 - A. Common
 1. Infectious enterocolitis
 2. Ulcerative colitis
 3. Crohn's disease
 4. Radiation injury
 5. Ischemia (generally <1 cm)
 6. Bowel edema in cirrhosis
 7. Submucosal hemorrhage (generally >1 cm)
 8. Angioedema from ACE inhibitors
 - B. Uncommon
 1. Adenocarcinoma
 2. Lymphoma
- II. Marked thickening (>2 cm)
 - A. Common
 1. Adenocarcinoma, gastrointestinal stromal tumor, metastases, lymphoma
 2. Severe colitis
 3. Systemic lupus erythematosus
 - B. Uncommon
 1. Crohn's disease, tuberculosis, histoplasmosis, cytomegalovirus
 2. Submucosal hemorrhage

Modified from Macari M, Balthazar EJ: CT of bowel wall: Significance and pitfalls of interpretation. *AJR* 176:1105–1116, 2001; Appendix 2, p 1116; and Macari M, Chandarana H, Balthazar E, Babb J: Intestinal ischemia vs intramural hemorrhage: CT evaluation. *AJR* 180:177–184, 2003.

TABLE 5-3 Symmetry of Mural Thickening

- I. Symmetric
 - A. Infections of the small and large bowel
 - B. Ulcerative colitis
 - C. Crohn's disease
 - D. Radiation injury
 - E. Ischemia
 - F. Bowel edema in cirrhosis
 - G. Lymphoma
 - H. Submucosal hemorrhage
- II. Asymmetric
 - A. Adenocarcinoma (mural or endoenteric)
 - B. Gastrointestinal stromal tumor (exoenteric)
 - C. Carcinoid tumor (mural or endoenteric)
 - D. Metastatic disease (mural or endoenteric)
 - E. Lymphoma (can be both symmetric and asymmetric)

Modified from Macari M, Balthazar EJ: CT of bowel wall: Significance and pitfalls of interpretation. *AJR* 176:1105–1116, 2001; Appendix 3, p 1116.

TABLE 5-4 Length of Mural Thickening

- I. Focal (<10 cm)
 - A. Common
 - 1. Diverticulitis, appendicitis
 - 2. Adenocarcinoma
 - B. Uncommon
 - 1. Lymphoma
 - 2. Tuberculosis
 - 3. Crohn's disease
- II. Segmental (10–30 cm)
 - A. Common
 - 1. Lymphoma
 - 2. Crohn's disease
 - 3. Infectious ileitis
 - 4. Radiation
 - 5. Submucosal hemorrhage (<15 cm, >1 cm thickness in relation to ischemia)
 - 6. Ischemia (>30 cm, <1 cm thickness in relation to hemorrhage)
 - B. Uncommon—systemic lupus erythematosus
- III. Diffuse
 - A. Common
 - 1. Ulcerative colitis
 - 2. Infectious enterocolitis
 - 3. Edema from low protein and cirrhosis
 - 4. Systemic lupus erythematosus
 - B. Uncommon—ischemia

Modified from Macari M, Balthazar EJ: CT of bowel wall: Significance and pitfalls of interpretation. *AJR* 176:1105–1116, 2001; Appendix 4, p 1116; and, Macari M, Chandarana H, Balthazar E, Babb J: Intestinal ischemia vs intramural hemorrhage: CT evaluation. *AJR* 180:177–184, 2003.

related to inflammation, vasodilation, and/or injury to intramural vessels with interstitial leakage of the contrast medium. This pattern of enhancement is usually seen in patients with acute inflammatory and infectious bowel disease, reflecting the hyperemic and hypervascular state found with acute inflammation and infection.

Vascular disorders such as shock bowel also may manifest with the white attenuation pattern. The increased vascular permeability and slowed perfusion that accompanies hypoperfusion permits the interstitial leakage of molecules of contrast material. Delayed venous drainage and altered vascular

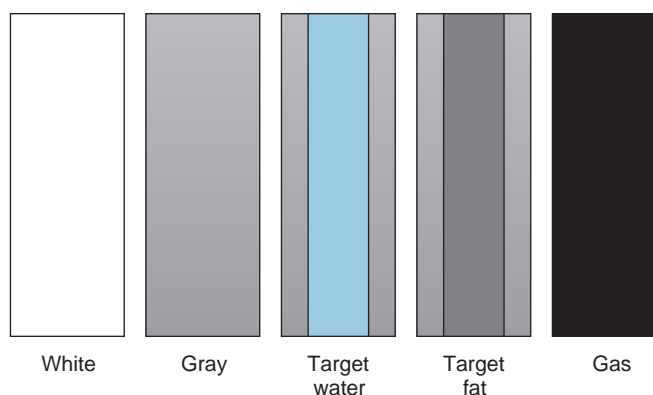


Figure 5-7 Classification scheme for mural thickening of the gastrointestinal tract.

permeability are also responsible for this sign in patients with bowel ischemia.

On non-contrast-enhanced scans, intramural hemorrhage will produce a hyperdense bowel wall (Fig. 5-8B).

Gray Attenuation Pattern

In this pattern, thickened bowel wall shows little enhancement and a homogeneous attenuation comparable with that of enhanced muscle (Fig. 5-9). This pattern should only be diagnosed if the intravascular contrast levels are adequate. Malignancy should be suspected in thickened segments of gut that show minimal enhancement and do not exhibit mural stratification.

Adenocarcinomas of the gastrointestinal tract are endoenteric lesions and usually show the uniform, gray enhancement pattern unless there are focal regions of necrosis. Lymphomas are also endoenteric and usually show a greater degree of wall thickening, generally more symmetric than adenocarcinoma, and are also homogeneous in attenuation. Gastrointestinal stromal tumors and metastases are exoenteric (the epicenter of the mass is outside the bowel wall and lumen) and often cause mural thickening, but are typically inhomogeneous in attenuation. They also commonly ulcerate.

In patients with Crohn's disease, the presence of a thick nonenhancing segment suggests the fibrostenotic disease. However, fibrostenotic disease is almost always associated with some level of inflammation, in which case there will often be some level of stratified hyperenhancement (see Chapter 41).

Water Halo Pattern

The water halo pattern is usually seen in patients with active infectious, inflammatory, ischemic disorders of the gastrointestinal tract (Fig. 5-10). The bowel, when viewed in the axial plane, has a target or bull's-eye appearance. An enhancing, central, higher density mucosal layer is surrounded by a water density submucosa that in turn is surrounded by a higher density muscularis propria.

Fat Halo Pattern

Fat in the submucosa of the gut produces the fat halo pattern (Fig. 5-11). It has lower attenuation than the grayer tone of the water halo sign. Although this finding can be seen in the small bowel and colon because of chronic Crohn's disease and in the colon because of ulcerative colitis, submucosal fat deposition in

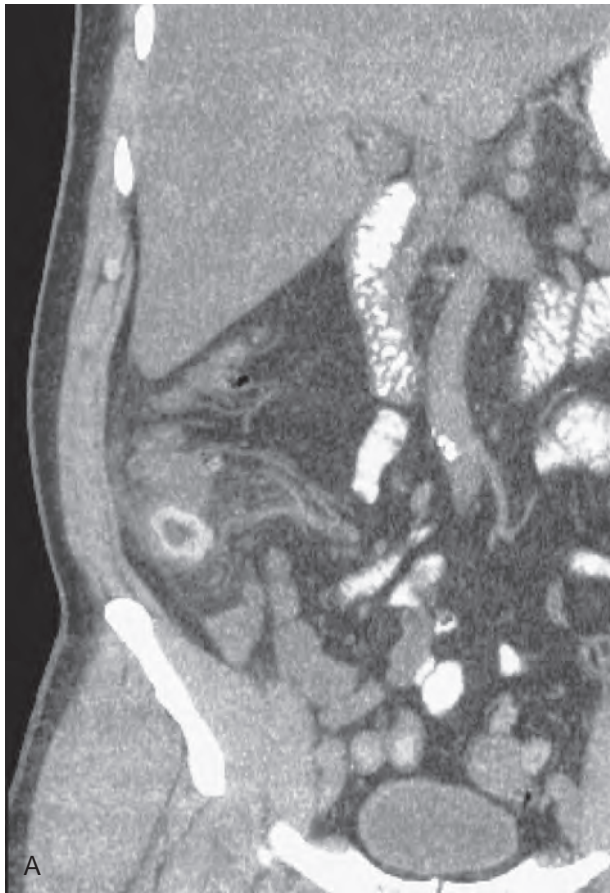


Figure 5-8 White enhancement pattern. **A.** Coronal reformatted image shows a uniformly, densely enhancing distal ileal loop caused by active Crohn's disease. There is disproportionate fat stranding surrounding this inflamed loop. Note the engorged vasa recta. This pattern is seen in patients with acute inflammatory bowel disease and shock bowel. **B.** On unenhanced scans, a hyperdense bowel wall (arrows) can be seen with intramural hemorrhage. A thickened segment of ileum is identified in this patient with systemic lupus erythematosus.



Figure 5-9 Gray enhancement pattern. The thickened wall of the gastric antrum in this patient with adenocarcinoma of the stomach shows uniform, gray enhancement. Malignancies do not typically demonstrate mural stratification.

the stomach, duodenum, small bowel, and colon is now understood to be a fairly common, benign finding, generally found in obese individuals.^{27,28} This finding may also be seen in patients who are not obviously obese (Fig. 5-12). The rapid accumulation of submucosal fat has also been reported in patients undergoing cytoreductive surgery for lymphoproliferative and myeloproliferative disorders and graft-versus-host disease.

Black Attenuation Pattern

Bowel pneumatosis should always be considered as a sign of acute injury—ischemic, infectious, or traumatic (Fig. 5-13). Any disease process that compromises the integrity of the mucosa can introduce intramural gas. The presence of intramural gas can herald an abdominal catastrophe and must be viewed with suspicion. It can be seen as a benign process in patients with pneumatosis cystoides intestinalis, scleroderma, or other connective tissue disease that weakens the integrity of the bowel wall and in the setting of enteral catheters (Fig. 5-14).

One must detect small intramural collections of gas and avoid confusing them with pseudopneumatosis. Gas bubbles can cling to the mucosa in the dependent portion of the bowel lumen, adjacent to the wall and not rising to the nondependent lumen, adjacent to the wall. Furthermore, in some patients with viscous intestinal secretions, gas may be displaced in the periphery of the lumen circumferentially. Differentiating this from pneumatosis at times can be very difficult. Careful scrutiny of the gas location in relation to the wall using wide, lunglike windows, is helpful in making this differentiation. Pneumatosis should be surrounded on all sides by the small bowel wall. Similar to the small bowel, gas bubbles in the colon may become trapped between fecal debris and mucosa.

Figure 5-10 Water halo enhancement pattern. **A.** Axial CT of the descending colon in a patient with cytomegalovirus colitis. **B.** Corresponding line diagram. Mural stratification with a target pattern is typical of acute infectious, inflammatory, and ischemic enterocolitides. There is an inner ring of enhancing mucosa surrounded by a hypodense ring caused by submucosal edema, which in turn is surrounded by enhancing muscularis propria.

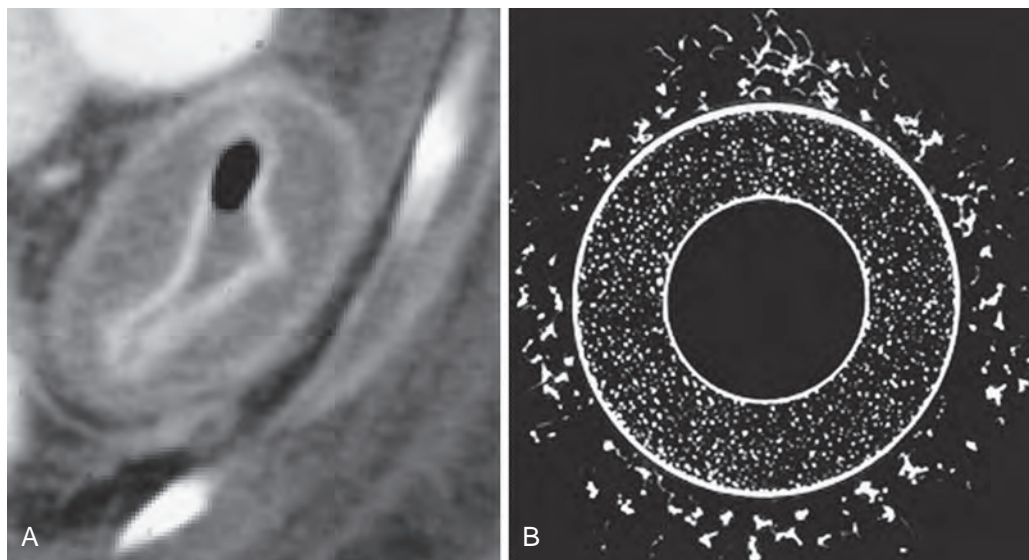


Figure 5-11 Fat halo enhancement pattern. In this patient with chronic ulcerative colitis, fat is present within the submucosa. The lumen of the rectum is narrow, and there is an increase in the presacral space because of fatty deposition.

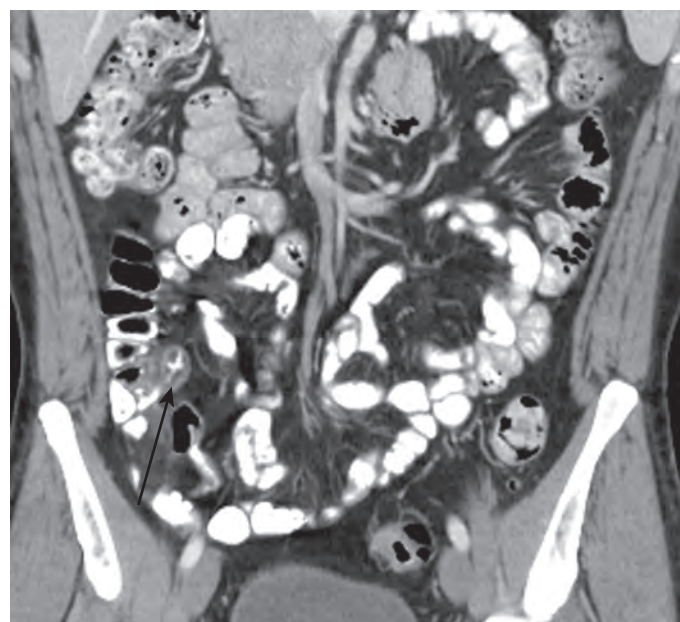


Figure 5-12 Fat halo enhancement pattern. This nonobese patient (body mass index [BMI] = 23.73) is not on steroids and does not have Crohn's disease. There is fat in the submucosa of the terminal ileum (arrow).

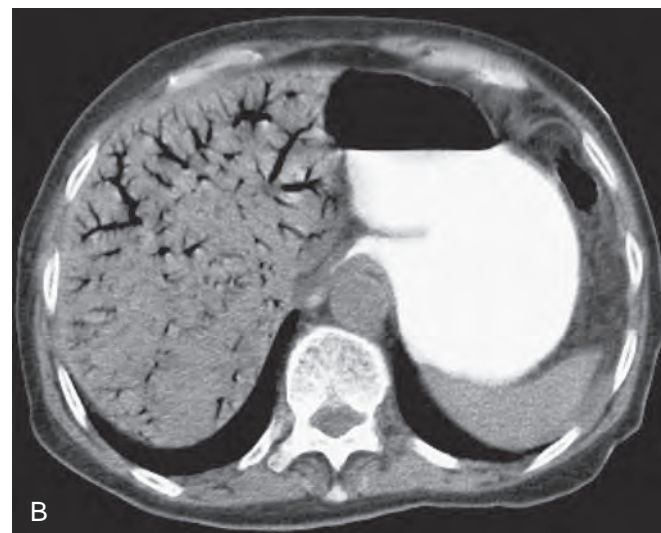


Figure 5-13 Black enhancement pattern. **A.** Scan of the pelvis displayed with lung windows shows intramural gas with ischemic necrosis of a segment of ileum. **B.** CT scan of the liver of this patient shows extensive portal venous gas.

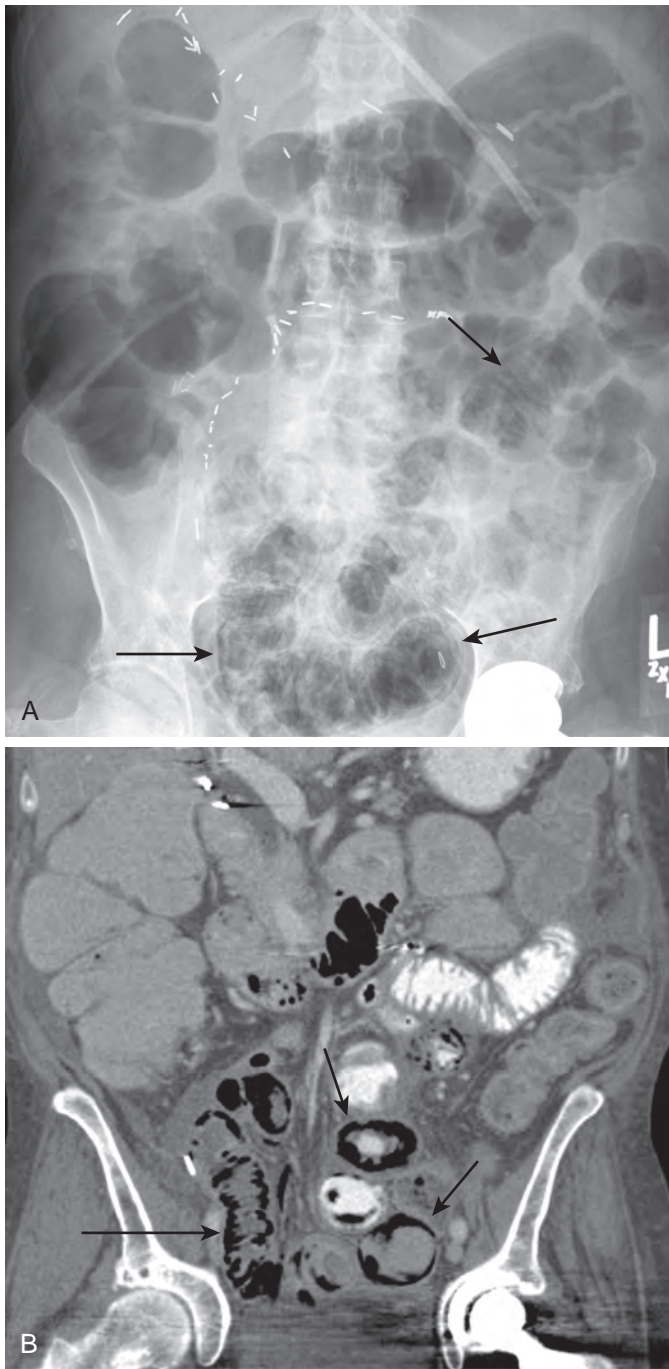


Figure 5-14 Black enhancement pattern. Plain abdominal x-ray (A) and MDCT scan (B) show intramural gas (arrows) in multiple loops of small bowel, 1 day after the operative placement of a jejunal feeding tube.

Mesenteric and Omental Fat Disease

Careful evaluation of the attenuation, vascularity, and lymph nodes of the fat within the subperitoneal spaces surrounding the gut provides important information about the disease in the adjacent bowel segment. There are six abdominal mesenteries—small bowel mesentery, transverse mesocolon, sigmoid mesocolon, ascending mesocolon, descending mesocolon, and mesoappendix. There are two omenta, the lesser and greater omentum. They may be involved by any number

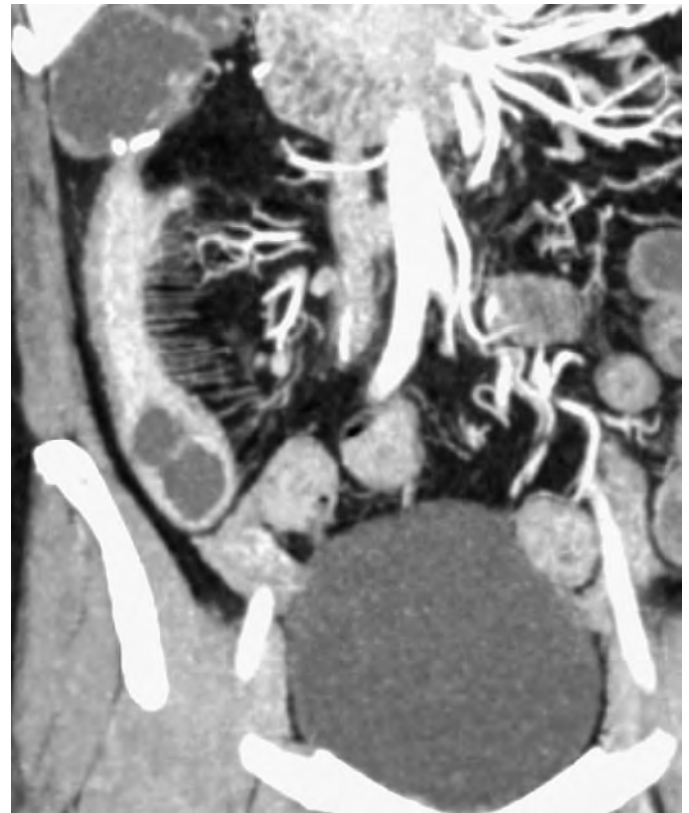


Figure 5-15 Engorged vasa recta. There is engorgement of the vasa rectae of the ileocolic mesentery in this patient with Crohn's disease, the so-called comb sign. Infectious and inflammatory enterocolitides tend to be more vascular than malignancies.

of ischemic, infectious, inflammatory, trauma, and malignant disorders.

BLOOD VESSELS

When a thickened segment of gut is supplied by engorged blood vessels (vasa recta along the mesenteric border), the disease most likely is infectious or inflammatory (Fig. 5-15). In the small bowel, mural thickening can be seen in Crohn's disease and lymphoma. If the vasa recta supplying the affected segment are engorged (often referred to as the comb sign), then the disease is most likely Crohn's disease. Similarly, in a patient with mural thickening of the sigmoid colon, the presence of engorged vasa recta (the caterpillar sign) is more suggestive of the diagnosis of diverticulitis as opposed to colon cancer.

SEROSAL AND SUBPERITONEAL FAT DENSITY

Comparing the degree of soft tissue stranding in the fat surrounding an abnormal segment of gut and the associated mural thickening is an important clue to diagnosing patients with acute abdomen. Inflammatory condition such as appendicitis, diverticulitis, epiploic appendagitis, and omental infarction are associated with disproportionate fat stranding (Fig. 5-16). In other words, the amount of fat stranding is greater than the degree of mural thickening.²⁹ In patients with small bowel obstruction, engorged vasa recta supplying the obstructed

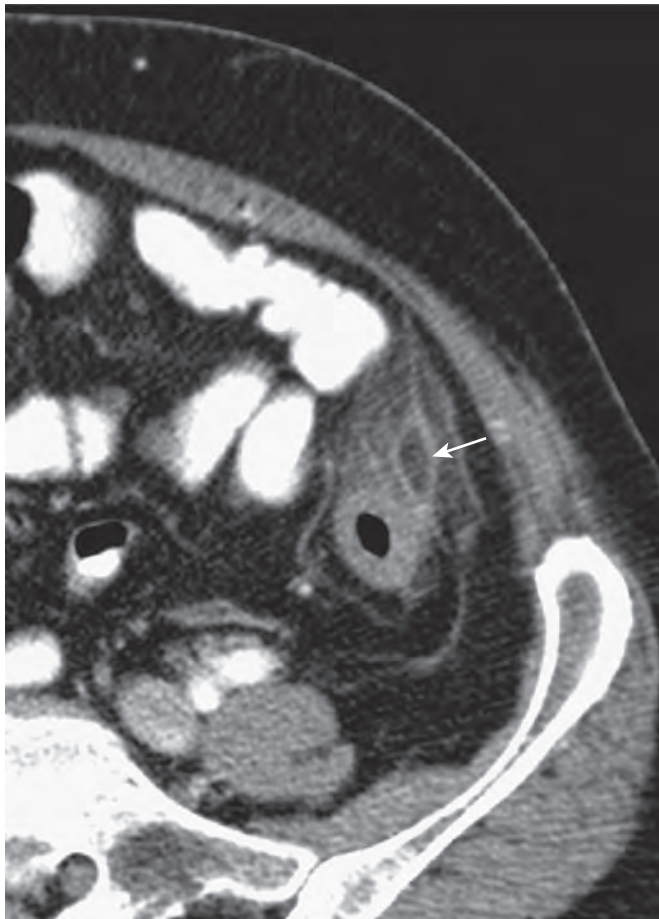


Figure 5-16 Disproportionate fat stranding: Epiploic appendagitis. There is an inflamed ischemic epiploic appendage (arrow) adjacent to a slightly thickened segment of descending colon. Note the stranding in the adjacent fat.

segment is a finding that can be seen in closed loop obstruction and in patients with venous compromise.

Creeping fat of the mesentery is a common finding in patients with Crohn's disease. This abnormal fat often demonstrates prominent lymph nodes and engorged vasa recta (see Chapter 38) and causes separation of bowel loops. Small bowel carcinoid tumors induce an intense desmoplastic reaction in the mesenteric fat. In classic cases, there is an enhancing, central soft tissue mass in the mesentery. There are radiating spokes from the mass extending peripherally in the mesenteric root, extending outward toward the small bowel, thickening the small bowel wall, and creating a retractile appearance on CT (see Fig. 5-15).

Neoplasms also produce changes in the subperitoneal fat of the adjacent mesentery or omentum. Tumor invasion into the pericolic fat results in more sharply defined and thicker dense strands than those found with inflammation and infection. Spikelike densities correlate with pathologic findings of tumor extension through the serosa into perienteric fat.

LYMPH NODES

The evaluation of mesenteric and omental lymph nodes is an important part of assessing abnormal bowel disease (Fig. 5-17). Mesenteric lymph nodes are enlarged if they exceed 5 mm in



Figure 5-17 Adenopathy. Enlarged lymph nodes are identified in the mesorectal fat in this patient with a thickened rectal wall caused by adenocarcinoma. The presence of adenopathy favors a malignant as opposed to a benign cause of the bowel wall thickening.

the short axis,³⁰ but mesenteric lymph nodes can be caused by infection, inflammation, and tumor (Fig. 5-18). As a general rule, when the lymph node size is disproportionately greater than the mesenteric or omental inflammatory response, a malignancy should be considered. The number and location of these lymph nodes is also another important consideration.³¹

In patients with mural thickening of the sigmoid colon, differentiating colon carcinoma from diverticulitis is a common clinical problem. Patients with carcinoma often have large lymph nodes in the sigmoid mesocolon and a greater degree of mural thickening, and tend to have acute, irregular, and eccentric margins. Diverticulitis produces disproportionate fat stranding, the length of involvement is longer, and lymph nodes are typically normal in size.

Patients with Crohn's disease will often have enlarged mesenteric lymph nodes (sometimes as large as 1.5 to 2 cm in the short axis, but generally <1.5 cm in the short axis) in the mesentery adjacent to the involved segment of gut. When patients with Crohn's disease have nodes more than 1.5 to 2 cm in the short axis, the radiologist must scrutinize the adjacent bowel wall for the possibility of a complicating adenocarcinoma or lymphoma (if the patient has been on long-term, anti-tumor necrosis factor [TNF] therapy). Gastrointestinal infections and mesenteric adenitis often produce mildly enlarged lymph nodes as well. However, adenopathy in these cases is less impressive than that found in patients with lymphoma.

The attenuation of the lymph nodes can also help narrow the differential diagnosis. A fat-containing lymph node can be



Figure 5-18 Calcifications. Mesenteric calcifications are identified in the ileocolic mesentery in this patient with an obstructing ileal carcinoid (arrow). Note the increased stranding of the mesentery resulting from the desmoplasia induced by the vasoactive peptides secreted by these tumors.

seen in patients with sprue and giant cavity lymph node syndrome. If the low-attenuation lymph node demonstrates a rim of contrast enhancement or calcifications, infections such as tuberculosis, other mycobacterial infections, and histoplasmosis should be considered. Mucinous tumors of the colon may also produce low-attenuation metastatic lymph nodes. In patients with acquired immunodeficiency syndrome (AIDS), high-attenuation lymph nodes suggest the diagnosis of Kaposi's sarcoma.

Carcinomas of the stomach, small bowel, and colon may only infiltrate a lymph node without necessarily increasing its size. Accordingly, any normal-sized lymph nodes near a gastrointestinal tract malignancy, especially if three or more in number, must be viewed with suspicion. Local lymph nodes associated with carcinoid tumors may calcify.

CALCIFICATIONS

Omental and mesenteric calcifications can develop in a number of benign and malignant disorders of the abdomen and pelvis. Carcinoid tumor often presents with a calcified mass in the mesentery associated with tethering of adjacent small bowel loops (see Fig. 5-18). The vasoactive peptides secreted by these tumors cause a local desmoplastic reaction, with retraction of the mesentery, kinking of the adjacent loops, and mural

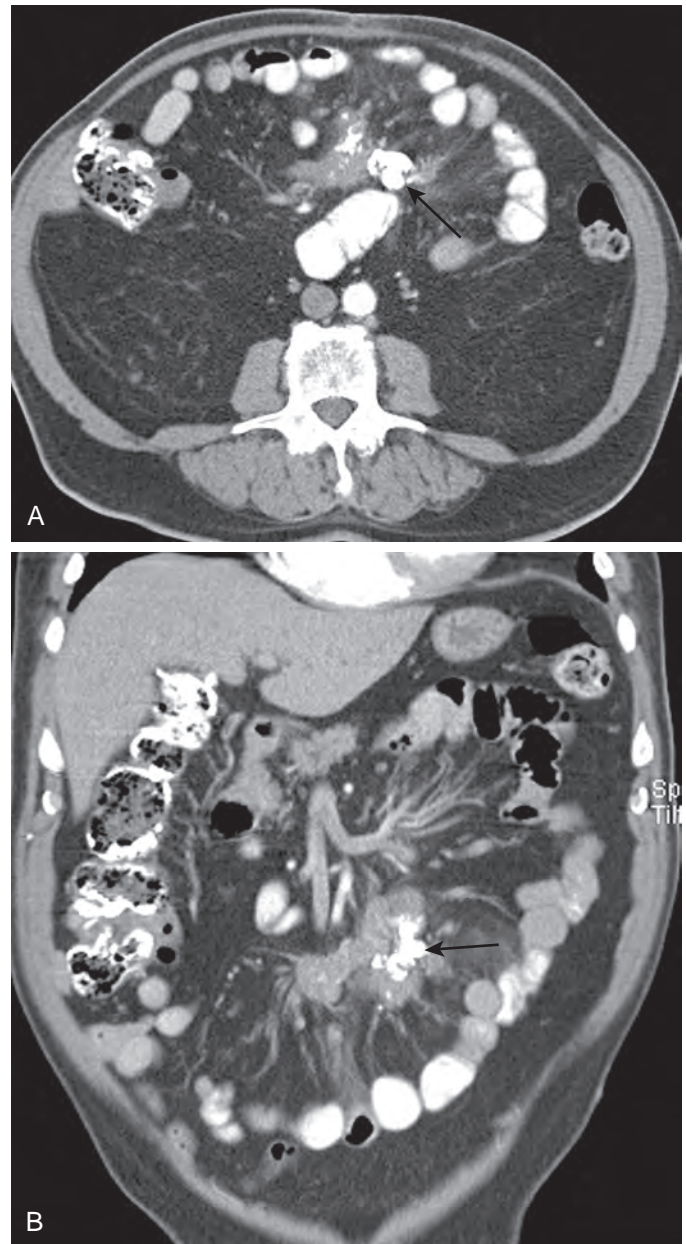


Figure 5-19 Calcifications. Axial (A) and coronal (B) MDCT scans show mesenteric calcifications within a soft tissue mesenteric mass caused by sclerosing mesenteritis. Although the calcification is more confluent and dense (arrow) than generally seen in carcinoid, only a biopsy can confirm the diagnosis.

thickening. Sclerosing mesenteritis is another entity commonly causing intense, often confluent, dense calcification in a mesenteric root mass (Fig. 5-19). It can be difficult to differentiate sclerosing mesenteritis from a carcinoid, but in general the calcification in sclerosing mesenteritis is much more dense and confluent. Biopsy is often the only way to make the differentiation. Foci of mesenteric and omental calcifications can also be seen in patients with metastatic mucinous ovarian and gastrointestinal tract neoplasms. Finally, calcified lymph nodes, generally rim-calcified, can be seen, often with an obscure cause. These are considered benign in most cases.

REFERENCES

- Nishino M, Kubo T, Kataoka ML, et al: Coronal reformations of the chest on 64-row multi-detector row CT: Evaluation of image quality in comparison with 16-, 8- and 4-row multi-detector row CT. *Eur J Radiol* 59:231–238, 2006.
- Macari M, Balthazar EJ: CT of bowel wall thickening: Significance and pitfalls of interpretation. *AJR* 176:1105–1116, 2001.
- Megibow AJ, Babb JS, Hecht EM, et al: Evaluation of bowel distention and bowel wall appearance by using neutral oral contrast agent for multi-detector row CT. *Radiology* 238:87–95, 2006.
- Arsalan H, Etlik O, Kayan M, et al: Peroral CT enterography with lactulose solution: Preliminary observations. *AJR* 185:1173–1179, 2005.
- Gollub MJ: Multidetector computed tomography enteroclysis of patients with small bowel obstruction: A volume-rendered “surgical perspective.” *J Comput Assist Tomogr* 29:401–407, 2005.
- Bodily KD, Fletcher JG, Solem CA, et al: Crohn disease: Mural attenuation and thickness at contrast-enhanced CT enterography—correlation with endoscopic and histologic findings of inflammation. *Radiology* 238:505–516, 2006.
- Hong SS, Kim AY, Byun JH, et al: MDCT of small-bowel disease: Value of 3D imaging. *AJR* 187:1212–1221, 2006.
- Boudiaf M, Jaff A, Soyer P, et al: Small-bowel diseases: Prospective evaluation of multi-detector row helical CT enteroclysis in 107 consecutive patients. *Radiology* 233:338–344, 2004.
- Kim JH, Eun HW, Goo DE, et al: Imaging of various gastric lesions with 2D MPR and CT gastrography performed with multidetector CT. *Radiographics* 26:1101–1116, 2006.
- Koo CW, Shah-Patel LR, Baer JW, Frager DH: Cost-effectiveness and patient tolerance of low-attenuation oral contrast material: Milk vs VoLumen. *AJR* 190:1307–1313, 2008.
- Fletcher JG: CT enterography technique: Theme and variations. *Abdom Imaging* 34:283–288, 2009.
- Umeoka S, Koyama T, Togashi K, et al: Esophageal cancer: Evaluation with triple-phase dynamic CT—initial experience. *Radiology* 239:777–783, 2006.
- Hur J, Park MS, Lee JH, et al: Diagnostic accuracy of multidetector row computed tomography in T and N staging of gastric cancer with histopathologic correlation. *J Comput Assist Tomogr* 30:372–377, 2006.
- Beer AJ, Wieder HA, Lordick F, et al: Adenocarcinomas of esophagogastric junction: Multi-detector row CT to evaluate early response to neoadjuvant chemotherapy. *Radiology* 239:472–480, 2006.
- Shi R, Schraedley-Desmond P, Napel S, et al: CT colonography: Influence of 3D viewing and polyp candidate features on interpretation with computer-aided detection. *Radiology* 239:768–776, 2006.
- Ash L, Baker ME, O'Malley CM, Jr, et al: Colonic abnormalities on CT in adult hospitalized patients with *Clostridium difficile* colitis: Prevalence and significance of findings. *AJR* 186:1393–1400, 2006.
- Taylor SA, Halligan S, Slater A, et al: Comparison of radiologists' confidence in excluding significant colorectal neoplasia with multidetector-row CT colonography compared with double contrast barium enema. *Br J Radiol* 79:208–215, 2006.
- Johnson KT, Johnson CD, Fletcher JG, et al: CT colonography using 360-degree virtual dissection: A feasibility study. *AJR* 186:90–95, 2006.
- Macari M, Bini EJ: CT colonography: Where have we been and where are we going? *Radiology* 237:819–833, 2005.
- Pickhardt PJ, Asher DB: Wall thickening of the gastric antrum as a normal finding: Multidetector CT with cadaveric comparison. *AJR* 181:973–979, 2003.
- Schindera ST, Nelson RC, DeLong DM, et al: Multi-detector row CT of the small bowel: Peak enhancement temporal window—initial experience. *Radiology* 243:438–444, 2007.
- Makanyanga J, Punwani S, Taylor SA: Assessment of wall inflammation and fibrosis in Crohn's disease: Value of T1-weighted gadolinium-enhanced MR imaging. *Abdom Imaging* 37:933–943, 2012.
- Vandenbroucke F, Mortele KJ, Tatli S, et al: Non-invasive multidetector computed tomography enterography in patients with small-bowel Crohn's disease: Is a 40-second delay better than 70 seconds? *Acta Radiol* 48:1052–1060, 2007.
- Baker ME, Walter J, Obuchowski NA, et al: Mural attenuation in normal small bowel and active inflammatory Crohn's disease on CT enterography: Location, absolute attenuation, relative attenuation and the effect of wall thickness. *AJR* 192:417–423, 2009.
- Wittenberg J, Harisinghani MG, Jhaveri K, et al: Algorithmic approach to CT diagnosis of the abnormal bowel wall. *Radiographics* 22:1093–1107, 2002.
- James S, Balfe DM, Le JKT, Picus D: Small-bowel disease: Categorization by CT examination. *AJR* 148:863–868, 1987.
- Harisinghani MG, Wittenberg J, Lee W, et al: Bowel wall fat halo sign in patients without intestinal disease. *AJR* 181:781–784, 2003.
- Ahualli J: The fat halo sign. *Radiology* 242:945–946, 2007.
- Pereira JM, Sirlin CB, Pinto PS, et al: Disproportionate fat stranding: A helpful CT sign in patients with acute abdominal pain. *Radiographics* 24:703–717, 2004.
- Lucey BC, Stuhlfaut JW, Soto JA: Mesenteric lymph nodes: Detection and significance on MDCT. *AJR* 184:41–44, 2005.
- Lucey BC, Stuhlfaut JW, Soto JA: Mesenteric lymph nodes seen at imaging: Causes and significance. *Radiographics* 25:351–365, 2005.

Magnetic Resonance Imaging of the Hollow Viscera

RUSSELL N. LOW

CHAPTER OUTLINE

Protocols for Magnetic Resonance Imaging of the Gastrointestinal Tract

Coil Selection

Patient Preparation and Intraluminal Contrast Material

Contrast Agents

Routes of Contrast Administration

Antiperistaltic Agents

Clinical Applications

Inflammatory Bowel Disease

Infectious Bowel Disease

Acute Appendicitis

Ischemic Bowel Disease

Gastrointestinal Malignancy

Summary

Magnetic resonance imaging (MRI) of the gastrointestinal tract takes advantage of the inherent outstanding soft tissue contrast of MRI to provide excellent depiction of inflammatory, infectious, ischemic, and neoplastic gastrointestinal diseases. By combining fast imaging pulse sequences with intraluminal and intravenous (IV) contrast agents, MRI can show the normal and diseased bowel wall as well as adjacent inflammatory and neoplastic changes involving the mesentery, peritoneum, and omentum.¹⁻⁵

Imaging the gastrointestinal tract presents significant challenges that can be met with current MRI techniques. In the past, slower MR pulse sequences required several minutes to acquire, resulting in degraded image quality because of bowel peristalsis and respiratory motion. Current high-field MR scanning represents a confluence of hardware and software development that has resulted in fast MRI scans, obtained in a few seconds. Breath-hold precontrast and dynamic breath-hold, contrast-enhanced MRI of the abdomen and pelvis can easily be performed, with outstanding image quality.

Extracellular IV MR contrast agents are relatively inexpensive and have a long track record of safety and efficacy for evaluating abdominal diseases. Intraluminal contrast agents can be administered using over-the-counter (OTC) agents or commercially available oral contrast material.

Protocols for Magnetic Resonance Imaging of the Gastrointestinal Tract

MRI of the gastrointestinal (GI) tract uses rapid breath-hold acquisitions to minimize motion artifacts. Each manufacturer

has pulse sequences available that can be optimized for MRI of the GI tract. Although they have different acronyms, similar pulse sequences and image types are available on scanners from all the major MR manufacturers. The specific pulse sequence parameters, however, will be vendor-specific.

For a general evaluation of the GI tract, we use breath-hold, single-shot (SS) rapid acquisition with relaxation enhancement (RARE) imaging in the axial and coronal planes.¹⁻³ This pulse sequence is known by a number of different acronyms, including single-shot fast spin-echo (SSFSE), single-shot turbo spin-echo (SSTSE), and half-Fourier acquisition single-shot turbo SE (HASTE). These single-slice images are breathing-independent and are thus insensitive to respiratory or peristaltic motion. They provide heavily T2-weighted images and an excellent overall abdominal and pelvic survey. Water-soluble intraluminal contrast material demonstrates high signal intensity, whereas the bowel wall is depicted as a thin, intermediate signal intensity line surrounding the bowel contents. Intestinal mural thickening is depicted on single-shot RARE images when the bowel wall measures more than 3 mm. Single-shot images are obtained without fat suppression.

Unenhanced T1-weighted images depict anatomic structures. 2D or 3D spoiled gradient-echo T1 sequences can be obtained with simultaneous acquisition of in-phase and opposed-phase images. Newer Dixon T1 sequences apply Dixon fat and water separation to the 3D gradient echo images, providing in-phase, opposed-phase, fat-only, and water-only images in a single breath-hold. The Dixon water image provides a precontrast fat-suppressed image that can be compared to the dynamic postcontrast images to assess inflammatory or malignant bowel wall enhancement. Depending on the vendor, Dixon MR sequences are known by the acronyms LAVA-Flex, m-Dixon, and 2-point Dixon.

Fat-suppressed, T2-weighted, fast spin-echo (FSE) images are obtained to distinguish intestinal mural edema from fibrosis. This important distinction may assist in differentiating an acute inflammatory process with wall thickening from a thickened wall caused by a chronic fibrotic stricture. An acute inflammatory stricture will show high signal intensity edema in the thickened bowel wall, whereas the thickened fibrotic wall of a chronic stricture will demonstrate low signal intensity. Fat-suppressed, T2-weighted images may be obtained with breath-holding or with respiratory triggering.

Diffusion-weighted imaging (DWI) uses fast, single-shot echo planar sequences, which are sensitive to the microscopic movement of water protons. Many benign and malignant diseases are characterized by restriction of diffusion and are displayed as areas of altered signal on DWI. DWI has become an integral part of body MRI protocols and is essential for GI imaging. The DWI sequence may be obtained during breath-holding or free breathing, or may be combined with respiratory

triggering. For GI imaging, an intermediate B value of 400 to 500 s/m² provides images with a good balance between adequate diffusion weighting and reasonable anatomic depiction. Higher B values will increase diffusion weighting at the expense of the image signal-to-noise ratio (SNR) and anatomic depiction. DW images are characterized by a high target to background signal, so that diseased bowel is seen with high contrast and conspicuity compared with the relatively suppressed background tissue and intraluminal contents.

Diffusion-weighted images may be displayed as a magnitude image, which is a combination of diffusion signal and T2-shine through, or as an apparent diffusion coefficient (ADC) map. On the ADC map, the T2 component of the image signal is removed so that only areas of true restricted diffusion are displayed. Quantitative measurements of ADC values on these images requires obtaining two or more different B values. I currently acquire three B values, at 20, 500, and 800 s/m². Quantitative measurements of ADC values may be useful to characterize GI masses and monitor the response of tumors to therapy.

Another sequence commonly used for GI tract imaging is balanced, steady-state free precession (SSFP) sequences.⁶ The image contrast is determined by T2* and T1 properties, depending heavily on repetition time (TR). The speed and relative motion insensitivity of this acquisition are useful features for GI imaging. On the balanced SSFP images, water-soluble intraluminal contrast material, blood, bile, ascites, and urine will all demonstrate high signal intensity.

Vendor acronyms for this pulse sequence include balanced turbo field-echo (b-TFE), and fast imaging employing steady-state acquisition (FIESTA), and true fast imaging with steady-state precession (true FISP). The balanced SSFP images show excellent homogeneity of luminal signal and visualization of the normal and diseased bowel wall. Compared to 3D gradient-echo images, the balanced SSFP images are less sensitive to motion artifact but show increased sensitivity to chemical shift and susceptibility artifacts.

Following the IV injection of gadolinium, two sets of axial, fat-suppressed, gradient-echo MR images are obtained through the abdomen and pelvis.⁴ One may use 2D or 3D gradient-echo imaging. The 2D gradient-echo images use a thicker slice thickness of 8 to 10 mm but are typically sharper and have a greater range of contrast than 3D gradient-echo images. The 3D images have a thinner slice thickness and provide more efficient coverage of the abdomen and pelvis. A typical slice thickness for 3D images is 4 mm. Some 3D acquisitions incorporate a fixed or variable slice overlap. The newer 3D Dixon sequences may be used for dynamic postcontrast imaging. The Dixon water image provides very homogeneous fat suppression, with higher SNR and reduced susceptibility artifact.

Water-soluble intraluminal contrast material demonstrates low signal intensity on the fat-suppressed, gadolinium-enhanced (GE) MR images. The bowel wall is shown as rings or lines surrounding the bowel lumen. The thickness of the normal bowel wall is 3 mm or less. The normal bowel wall will show gadolinium enhancement equal to or less than that of the liver parenchyma. Abnormal mural thickening or enhancement can be evaluated as signs of inflammatory or neoplastic intestinal disease.

Important features of the optimized GE MR image include fat suppression, image homogeneity, high-n plane resolution, and breath-hold imaging. In practice, we combine dynamic 3D gradient-echo imaging in the axial plane followed by coronal

and sagittal 3D GE imaging and delayed 2D gradient-echo imaging. The delayed 2D gradient-echo images are often most useful for depicting intestinal mural disease and adjacent disease of the peritoneum, showing excellent image sharpness and contrast conspicuity. The 2D images are also less susceptible to breathing artifacts, which may be more common at the end of the examination.

This MR examination of the GI tract can be performed in 20 to 25 minutes. Specific imaging parameters are listed in Table 6-1.

Coil Selection

Coil selection will depend on the availability of surface coils for a specific MR scanner. Dedicated surface coils, with larger areas of anatomic coverage, are now routinely available from all vendors. I typically require 48-cm coverage in the craniocaudal direction when imaging the abdomen and pelvis. There are now surface coils available that provide this extensive coverage, allowing for combined abdominal and pelvic imaging. One should be careful not to sacrifice image homogeneity when using a dedicated surface coil. Inhomogeneous images can create problems when assessing subtle GI tract or peritoneal disease. Some form of intensity correction algorithm should be used to maximize the homogeneity of the images. Ultimately, phased-array surface coils combined with parallel imaging provides optimal signal and speed of image acquisition.

Patient Preparation and Intraluminal Contrast Material

CONTRAST AGENTS

All patients are asked not to eat or drink for the 4 hours prior to their MRI appointment. If rectal water is to be administered, patients administer a Fleet's enema prior to the examination. If more thorough bowel cleansing is desired, patients are also asked to have a clear liquid diet starting for 12 hours prior to the MRI examination and to take four bisacodyl tablets orally the evening prior to the appointment.

The use of intraluminal contrast material is an essential element of the MRI protocol for GI tract imaging.^{4,7-16} Oral and/or rectal contrast material will distend the stomach, small intestines, and colon, improving the depiction of inflammatory or neoplastic mural disease. Subtle mural thickening can be easily masked by collapsed segments of bowel. Alternatively, incompletely distended bowel can mimic diseased bowel with apparent mural thickening, which will disappear when the bowel is adequately distended. In addition, well-distended bowel facilitates the depiction of an adjacent peritoneal, serosal, or omental tumor.

In my experience, a biphasic intraluminal contrast agent is optimal for GI tract imaging (Fig. 6-1). Water is the classic biphasic MR intraluminal agent, showing high signal intensity on T2-weighted images and low signal intensity on T1-weighted images. On fat-suppressed, GE T1-weighted spoiled gradient-echo (SGE) images, the water-soluble contrast material is low in signal intensity. This allows one to depict the normal bowel wall as a thin, linear, mildly enhancing structure surrounding the dark bowel lumen. Water can be used as an oral contrast agent. However, because water is absorbed through the small intestinal wall, its use as an oral agent for MRI often results in

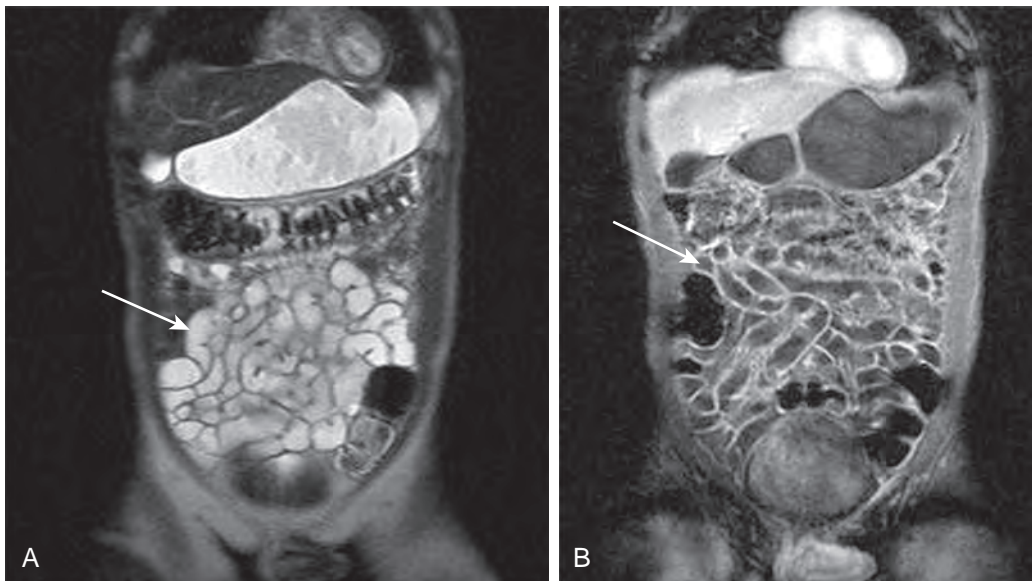


Figure 6-1 Oral contrast material. Coronal single-shot turbo spin-echo (SSTSE) (A) and gadolinium-enhanced 3D MR images (B) were obtained following oral administration of 1.5 L of Metamucil mixed with water. The water-soluble intraluminal contrast material demonstrates high signal intensity on the T2-weighted SSTSE images (arrow in A) and low signal intensity on the T1-weighted, 3D gradient-echo images (arrow in B).

TABLE 6-1

Protocol for Gastrointestinal Magnetic Resonance Imaging

Sequence	SSFSE	T1 GE	T2 SSFSE	DWI	Gad 3D GE	Gad 3D GE	Gad 3D GE	Delayed 2D GE
Plane	Coronal	Axial	Axial	Axial	Axial	Coronal	Sagittal	Axial
Anatomy	A & P	A & P	A & P	A & P	A & P	A & P	A & P	A & P
Scan time(s)	0.12	0.22	0.24	0.24	0.24	0.24	0.24	0.22
COIL: PHASED-ARRAY SURFACE COIL								
FOV (cm)	44	38	38	38	38	44	44	38
Phase FOV		0.8	0.8	1	0.8	1	0.8	0.8
TR (msec)	Min	172	Min	3750	4	4.4	4.4	100
TE (msec)	80	4.4/2.2	90	Min	1.7	1.7	1.7	Min full
Matrix	352 × 224	320 × 224	320 × 224	192 × 224	320 × 256	320 × 224	320 × 224	256 × 192
Nex	0.6	1	1	2	1	1	1	1
Slice thickness (mm)	8	4	8	8	4	4.4	4	8
Overlap		2			2	2.2	2.2	
Flip angle (degrees)	90	80	90	90	12	12	12	70
ASSET	2	2	2	2	2	2	2	2
Fat suppression	No	No	Yes	SPIR	Yes	Yes	Yes	Yes
B value (s/m ²)				20, 500				
ETL								
BW	83.3	83.3	83.3		125	125	83.3	31.25
Options	Pure	Pure	Pure	Pure 3 in 1	Pure	Pure	Pure	Pure, ZIP 512

A & P, Anterior and posterior; ASSET, Array Spatial Sensitivity Encoding Technique; BW, bandwidth; DWI, diffusion-weighted image; ETL, echo train length; FFE, fast field echo; FOV, field of view; Gad, gadolinium; GE, gradient-echo; Min, minimal; NSA, number of signal averages; REST, regional saturation technique; SE, spin-echo; SENSE, sensitivity encoding; SI, signal intensity; SPIR, spectral presaturation by inversion recovery; SSFSE, single-shot fast spin-echo; SSTSE, single-shot turbo spin-echo; TE, echo time; TFE, turbo field echo; TR, repetition time; TSE, turbo spin-echo.

unpredictable distention of the distal small bowel. For this reason, water-soluble contrast agents that are iso-osmolar are preferred because the ingested contrast will remain in the intestinal tract. In my practice, I have used different intraluminal agents for MRI. All the agents produce a biphasic appearance on MR images; they are readily available and relatively inexpensive. Other commercially available oral agents for MRI containing iron oxides and manganese have been described, but are not currently used in my practice.¹⁴⁻¹⁶

Dilute Barium Sulfate

Barium sulfate solution (Readi-CAT 2, Bracco Diagnostics, Monroe Township, NJ) is composed of 98% water and 2% barium and other additives. On MR images, dilute barium sulfate has a biphasic appearance, with low signal on T1-weighted images and high signal on T2-weighted images. Readi-CAT 2 is commonly used for helical CT scans of the abdomen and pelvis. Dilute barium sulfate will remain within the intestines and is very effective in distending the small bowel and colon. Patients

ingest 300 to 400 mL dilute barium, starting 1 hour before the MRI examination.^{4,5,7} Flavored versions of dilute barium sulfate (Readi-CAT 2 Smoothie, Bracco Diagnostics) are available and may be preferred by some patients.

Psyllium Fiber Mixed with Water

This is another water-soluble contrast agent that produces a biphasic appearance on T1-weighted and T2-weighted images (see Fig. 6-1).^{8,9} Metamucil (Proctor & Gamble, Cincinnati) is composed of psyllium fiber with orange flavoring. It is a dietary fiber supplement that can be purchased over the counter. Its active ingredient is psyllium husk, a natural plant fiber with a high percentage of soluble fiber. Because Metamucil is orange-flavored, it is typically preferred by patients and better tolerated than dilute barium sulfate. A total dose of 0.8 mg/kg body weight Metamucil is mixed in 1 to 1.5 L of water. I mix a half-scoop of Metamucil per 8-ounce glass of water and have patients ingest four or five glasses over 1 hour prior to the examination. To improve filling of the distal small bowel, I have patients drink two of the glasses of Metamucil at home before leaving for their appointment. Unlike the Readi-CAT 2, some of the water in the Metamucil is absorbed in the small intestine and will be excreted via the kidney.

VoLumen

VoLumen (Bracco Diagnostics) is a low-density barium sulfate contrast agent especially designed for MDCT (multidetector computed tomography), positron emission tomography (PET), and CT examinations to mark the bowel as a negative intraluminal contrast agent. It is an ultra-low-dose barium sulfate agent with only 10% of the barium sulfate of conventional CT barium oral contrast agents. With VoLumen, 0.1% with barium is combined with 3% sorbitol, a nonabsorbable sugar alcohol that promotes luminal distention and limits the resorption of water across the length of the small bowel. VoLumen can be used for MRI of the GI tract, providing a biphasic appearance similar to that obtained with dilute barium sulfate. Theoretical advantages of VoLumen might include better bowel distention and more rapid bowel transit because of the sorbitol.

I am unaware of any direct comparisons. In my experience, the degree of bowel distention is related more to the volume and timing of the administration of the oral contrast material.

Mannitol 2.5% Mixed with 2% Locust Bean Gum

This has been proposed as an effective iso-osmolar, water-soluble oral agent for MRI.^{10,11} Mannitol is a white, crystalline, water-soluble, slightly sweet alcohol, $C_6H_8(OH)_6$, used as a dietary supplement and dietetic sweetener. Mannitol comes in 500-mL bags mixed to a concentration of 20%. Mannitol 2.5% can be prepared by mixing 187.5 mL of 20% mannitol with enough tap water to achieve a volume of 1.5 L, and 3 g of locust bean gum (2%) is added to the mannitol solution to slow down the transit time through the intestinal tract. Locust bean gum, also called carob bean gum and Carubin, is extracted from the seed of the carob tree. It is used in ice cream, cultured dairy products, and cream cheese. The locust bean gum has been reported to decrease the diarrhea produced by orally ingested mannitol. The 1.5-L, 2.5% mannitol solution with locust bean gum is ingested over 1 hour prior to the MR examination. Sorbitol 2% can be used as an alternative to mannitol.¹⁰

Rectal Water

This can be administered to distend the rectum and colon. I administer 500 to 1000 mL of tap water through a balloon-tipped barium enema catheter. Slow administration will help maximize the amount of fluid tolerated by the patient. The balloon at the tip of the catheter should be filled with water to avoid the susceptibility artifact caused by air in the balloon.

ROUTES OF CONTRAST ADMINISTRATION

Intraluminal contrast material can be administered orally, with patients drinking 1 to 1.5 L of contrast material over 1 hour prior to the examination. Alternatively, contrast may be administered via a nasojunal tube, as has been described for CT and MR enteroclysis. The enteroclysis technique has the advantage of more controlled and consistent small bowel distention but obviously requires nasojunal intubation.¹⁷⁻¹⁹ Oral administration of intraluminal contrast material is effective in cooperative patients and can be combined with rectally administered water for simultaneous evaluation of the small bowel and colon.

ANTIPERISTALTIC AGENTS

Contrast-enhanced 3D GE images can be degraded by motion artifact related to bowel peristalsis. An antiperistaltic drug can markedly improve image quality. Glucagon, 1 mg, can be administered IV at the time of gadolinium injection. An alternative approach is to administer 0.25 mg hyoscyamine (Levsin) IV prior to the start of the examination. Levsin has a slower onset of action and longer duration compared with glucagon. In Europe, butylscopolamine (Buscopan) is commonly used to reduce bowel peristalsis. Users should consult the package insert to review contraindications prior to drug administration.

Clinical Applications

INFLAMMATORY BOWEL DISEASE

Crohn's Disease

MRI provides many unique advantages when evaluating the mural changes of Crohn's disease.^{7,20,21} Distending the bowel lumen with water-soluble contrast material allows one to depict the diseased bowel wall in the patient with active Crohn's disease. On MR images, one may assess the thickness of the bowel wall, its degree and pattern of enhancement, and presence of adjacent mesenteric inflammation. MDCT is equally effective in assessing bowel wall thickening but is more limited in its assessment of mural enhancement. Compared with MDCT, the degree of bowel wall enhancement is much more conspicuous on GE MRI. This marked enhancement of inflamed bowel segments on 2D or 3D GE MR images facilitates the detection of subtle Crohn's disease. A wall thickness greater than 3 mm is abnormal in a well-distended segment of bowel. Bowel wall thickening can be assessed on SS RARE images or fat-suppressed GE images.

Crohn's Disease Activity. Determining the activity of Crohn's disease has important clinical implications that affect the selection of appropriate treatment options. Patients with recurrent abdominal pain because of active Crohn's disease require treatment. However, patients commonly present with

symptoms that may be unrelated to reactivation of their Crohn's disease. This latter group of patients requires entirely different management. The activity of Crohn's disease may be determined from clinical parameters, including the Crohn's disease activity index, an assessment of acute-phase reactants (e.g., white blood cells [WBCs], erythrocyte sedimentation rate, C-reactive protein, orosomucoids), or clinical symptoms and physical findings. In practice, these clinical parameters may be misleading or inconclusive. The results of endoscopy and imaging studies can play an important role in determining the activity and extent of Crohn's disease.

The activity of Crohn's disease can be assessed by a number of different MRI parameters, including degree of bowel wall enhancement, pattern of enhancement, thickness and length of the involved diseased segment, and presence of edema in the bowel wall on T2-weighted images. Restricted diffusion within the diseased segments of bowel also indicates active inflammation. Perienteric changes, including enhancing lymph nodes, infiltration of mesenteric fat, and increased mesenteric vascularity, can also reflect active Crohn's disease.^{7,20-23}

Degree of Bowel Wall Enhancement. The degree of mural enhancement with IV gadolinium correlates with the activity of Crohn's disease.⁷ Enhancement of the thickened bowel wall can be assessed on the first set of GE images by comparing the bowel wall enhancement to the liver and intravascular gadolinium. The normal bowel wall enhances less than the liver parenchyma. Mural enhancement of thickened bowel greater than that of

the liver is abnormal, and mural enhancement equal to that of intravascular gadolinium is markedly abnormal. In chronic inactive Crohn's disease, the thickened bowel wall will show no enhancement or only mild enhancement (Fig. 6-2). Chronic fibrotic strictures will show a thickened bowel wall with minimal enhancement. Active Crohn's disease shows moderate to marked bowel wall enhancement (Fig. 6-3). In patients with a layered pattern of enhancement (see later), the enhancing mucosa should show moderate to marked enhancement.

Pattern of Bowel Wall Enhancement. A layered pattern of mural enhancement indicates active Crohn's inflammation (Fig. 6-4).²³ One will see marked mucosal and serosal enhancement with an intervening nonenhancing layer representing an edematous bowel wall. In one study, this layered pattern of mural enhancement was present in 7 of 24 bowel segments with active Crohn's disease and in no segments with inactive disease.²³ Full-thickness or diffuse enhancement of the thickened bowel wall will also represent active Crohn's disease if there is moderate to marked mural enhancement. Diffuse enhancement is the most common pattern of mural enhancement in active Crohn's disease. Mild diffuse enhancement can be seen in bowel segments with inactive Crohn's disease.

T2-Weighted Appearance of the Bowel Wall. Active Crohn's disease may show a high signal in the thickened bowel wall, indicating bowel wall edema and inflammation.²⁰ Chronic inactive Crohn's disease will show a less intense signal in the thickened bowel wall, usually equal to or less than that of muscle. A

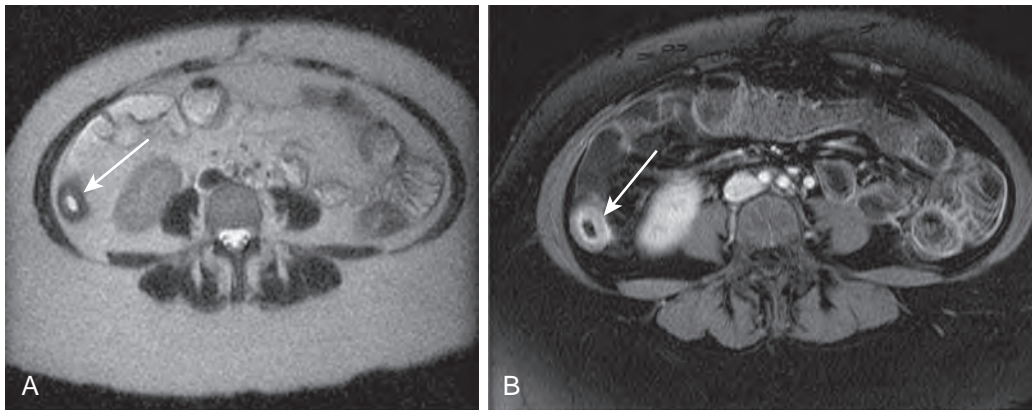


Figure 6-2 Inactive Crohn's disease. **A.** Axial single-shot fast spin-echo (SSFSE) image shows distal ileum with mural thickening (arrow). Note the low signal intensity of the thickening bowel wall. **B.** Immediate gadolinium-enhanced SGE image shows minimal enhancement of the thickened bowel wall (arrow). Absence of perienteric inflammation and stranding is also noted. Findings correlate with inactive Crohn's disease, which was confirmed at endoscopy.

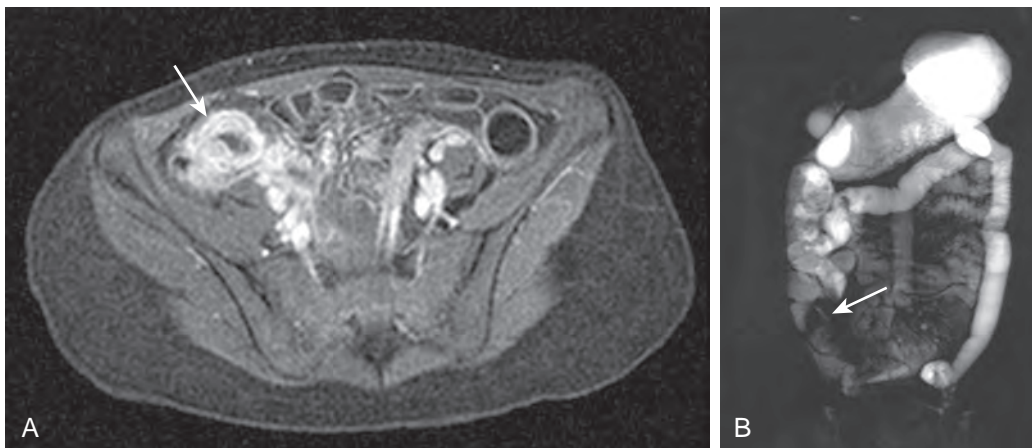


Figure 6-3 Active Crohn's disease with marked mural enhancement. **A.** Axial gadolinium-enhanced 3D GE image shows an abnormal terminal ileum (arrow) with moderate mural thickening and marked enhancement. The degree of enhancement indicates active Crohn's disease. **B.** Coronal MR hydrogram shows a stricture (arrow) of the terminal ileum.

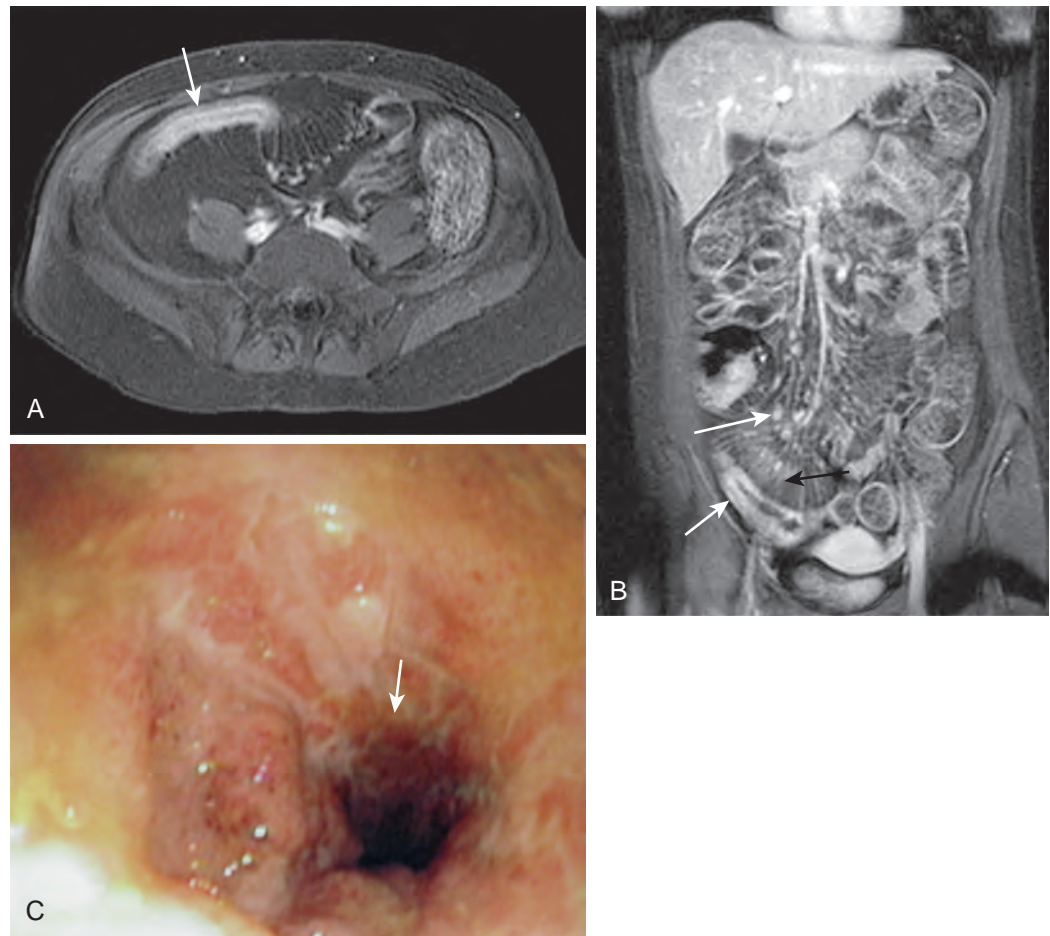


Figure 6-4 Active Crohn's disease with layered pattern of enhancement. **A.** Immediate axial gadolinium-enhanced 3D gradient-echo (GE) image shows an abnormally thickened terminal ileum (arrow) with a layered pattern of enhancement. **B.** Coronal gadolinium-enhanced 3D GE image confirms the diseased terminal ileum (short white arrow) and shows associated findings of acute Crohn's disease, including enhancing mesenteric lymph nodes (long white arrow) and mesenteric stranding (black arrow). **C.** Endoscopic view of the terminal ileum confirms active Crohn's disease, with mucosal inflammation (arrow).

fibrotic stricture can show a very low mural signal, similar to the psoas muscle. Fat-suppressed T2-weighted images are most useful to assess the signal intensity of the diseased segments of bowel. SS RARE images are useful for showing the segments of bowel but are less sensitive to the presence of bowel wall edema.

Diffusion-Weighted Imaging. Diffusion-weighted images obtained with an intermediate B value of 500 s/m² demonstrate restricted diffusion within the wall of diseased segments of bowel. The abnormal mural signal is demonstrated as areas of hyperintensity on magnitude DWI images or as areas of decreased signal on ADC maps. In my experience, this finding of restricted diffusion suggests active mural inflammation, which will resolve with effective therapy. Conversely, lack of restricted diffusion and mural edema on T2-weighted images indicate chronic disease without active inflammation.

Bowel Wall Thickness. In general, segments of bowel with active Crohn's disease will show greater mural thickness than segments with inactive disease.^{7,20,23} This assessment is affected by the degree of luminal distention. In one study, the mean thickness of segments with active Crohn's disease was 6.7 mm compared with 3.3 mm for segments with inactive disease. However, significant overlap exists between the mural thickness of the active and inactive groups.²³ Fibrotic strictures without active inflammation may show a moderately thickened bowel wall. In these cases, absence of moderate or marked mural enhancement will help characterize this as a chronic process, without active inflammation.⁷

Mesenteric Stranding. Infiltration of the adjacent mesentery and "whiskering" of the bowel wall are indirect indications of active Crohn's disease (see Fig. 6-4). This finding may be depicted on SS RARE images, true fast imaging with steady-state precession (FISP) images, or fat-suppressed, GE gradient-echo images as a linear signal or enhancement extending from the inflamed bowel into the adjacent small bowel or colonic mesentery.^{22,23}

Increased Mesenteric Vascularity. The vessels of the vasa recta supply the small bowel or colon. Increased prominence of the size and/or number of mesenteric vessels in the vasa recta can be an indication of active inflammation. In one study, increased mesenteric vascularity was present in 18 of 23 patients with active disease and 3 of 7 patients with inactive disease.²³

Enhancement of Mesenteric Lymph Nodes. Gadolinium enhancement of mesenteric lymph nodes is another strong indicator of active Crohn's disease (see Fig. 6-4).²² When comparing nodal signal intensity with that of adjacent fat, an enhancement ratio of 1:3 has been found to be a sensitive marker for active Crohn's disease. Mesenteric lymph nodes in patients with inactive Crohn's disease will not show significant enhancement. Lymph nodes are most conspicuous on diffusion-weighted images.

Monitoring Response to Treatment. Following patients with Crohn's disease on serial MR examinations is preferred to avoid the cumulative radiation exposure from repeated CT scanning.

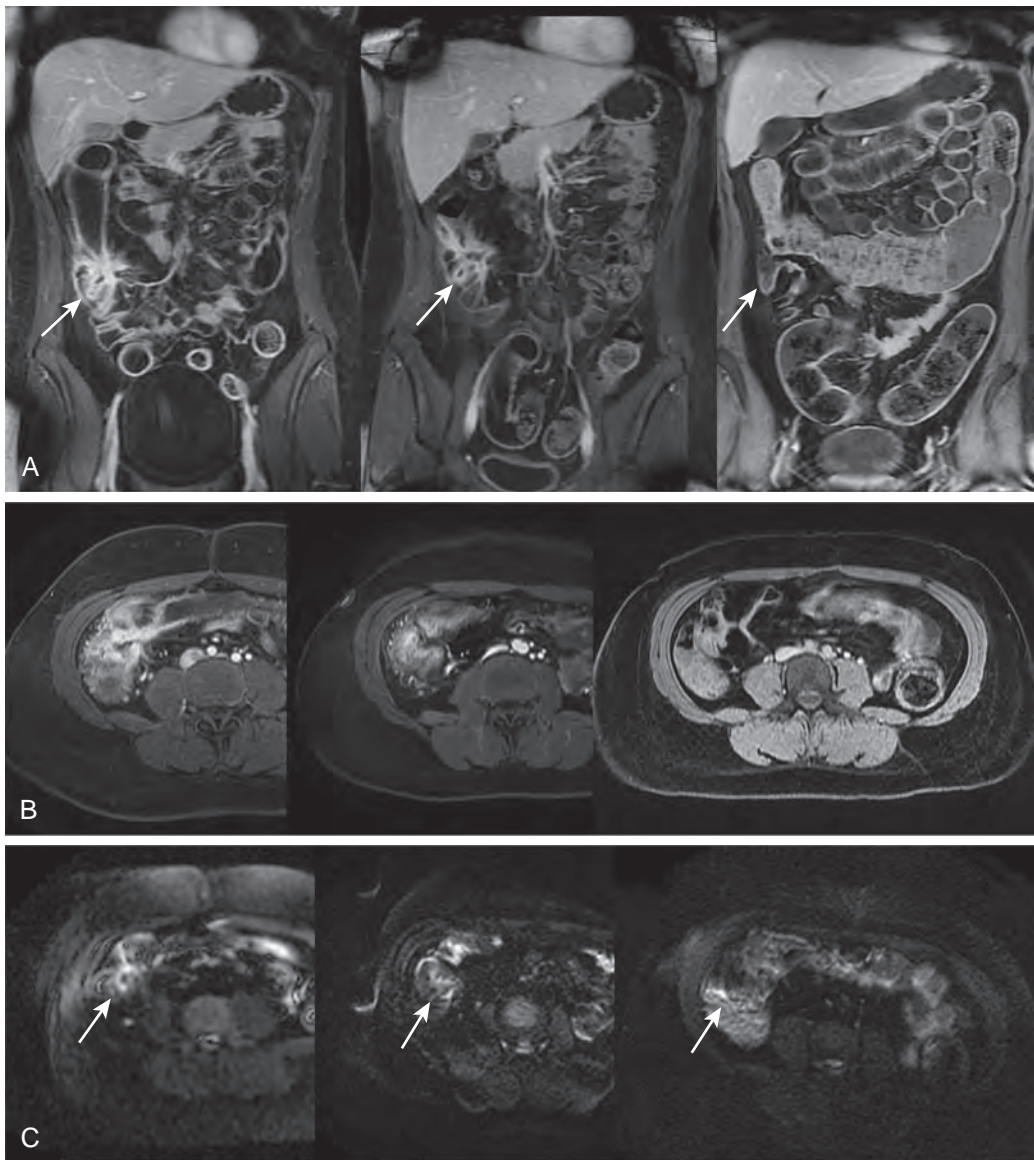


Figure 6-5 Crohn's disease. Response to therapy. Serial coronal (A) and axial (B) 3D GE gadolinium-enhanced images were obtained in 2005 (left), 2007 (middle), and 2009 (right). Inflammatory changes (arrows) in the right lower quadrant in 2005 show progressive resolution of serial follow-up examinations. **C.** Serial diffusion-weighted images, B value of 500 s/m², show initial large area of restricted diffusion in the right lower quadrant (2005) that resolved on subsequent examinations in 2007 and 2009.

With effective therapy, MR images of the diseased bowel segment demonstrate decreased restricted diffusion, decreased enhancement, and decreased mural edema on T2-weighted images (Fig. 6-5). Resolution of perienteric changes is also seen. Conversely, with relapse and recurrence of active inflammation, MR images show a reappearance of these same findings (Fig. 6-6). Therefore the findings on MRI will disappear and then reappear as they reflect response to treatment and subsequent recurrence of disease. This multiparametric approach to monitoring disease status on MRI allows one to distinguish segments of bowel with active inflammation from those with chronic disease and to characterize chronic fibrotic strictures with superimposed active inflammation accurately.

Complications of Crohn's Disease. Perienteric complications of Crohn's disease include abscess or phlegmon formation and fistulas. Abscesses are depicted on MR images as extraintestinal fluid collections, with a surrounding thick, enhancing abscess wall.⁷ Following administration of water-soluble intraluminal contrast material, the fluid content of an abscess may be

difficult to distinguish from bowel contents on T1- or T2-weighted images. However, on fat-suppressed GE MR images, the thick, enhancing abscess wall is easy to identify. The marked degree of enhancement of the abscess wall with gadolinium often makes the abscess easier to detect on MR images than on helical CT scans using iodinated contrast material (Fig. 6-7).

The development of fistulas in Crohn's disease is a common complication; it presents as abnormal connections between the diseased bowel and other organs or the skin. Enterointestinal fistulas occur between segments of bowel, whereas enterocutaneous fistulas occur between diseased bowel and the skin surface. Enterovesicular fistulas communicating with the bladder and enterovaginal fistulas extending from diseased intestines to the vagina are common complications of pelvic Crohn's disease.

With MRI, Crohn's fistulas are depicted as fluid- or air-containing tracts on fat-suppressed, T2-weighted images or as enhancing tracts on fat-suppressed, GE gradient-echo MR images.²⁴ High-resolution surface coil imaging with thin-section, short tau inversion recovery (STIR) or 3D GE images

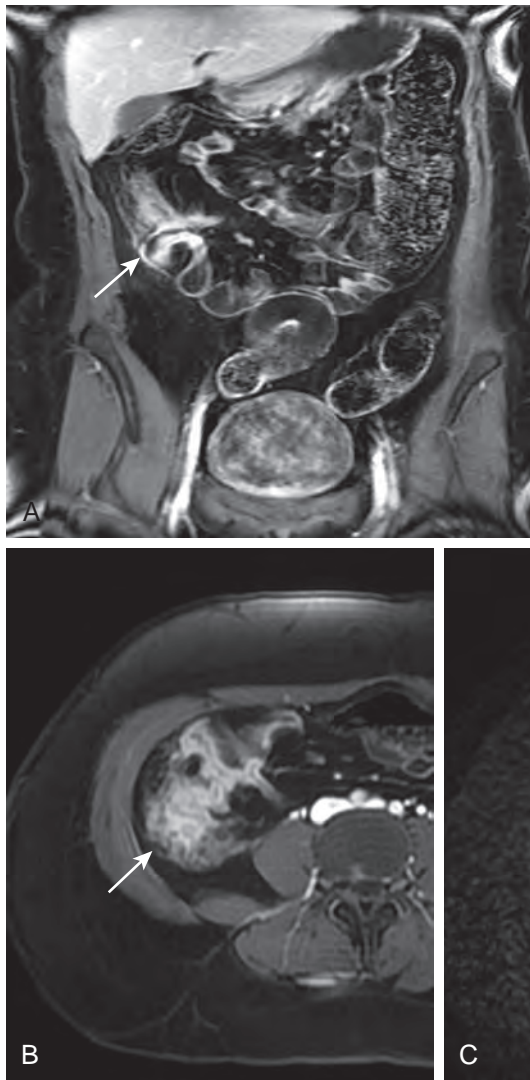


Figure 6-6 Crohn's disease recurrence (same patient as in Fig. 6-5). On a follow-up MR examination in 2012, the coronal (A) and axial (B) 3D GE gadolinium-enhanced images show interval recurrence of the right lower quadrant inflammatory changes (arrows). (C) A DWI, B value of 500 s/m², shows recurrence of the restricted diffusion (arrow) in the right lower quadrant.

are most useful to depict the fistulous communication. The accurate depiction of Crohn's fistulas is important when selecting patients for anti-tumor necrosis factor (TNF) therapy. Infliximab (Remicade) blocks the immune system's overproduction of a protein (TNF- α), with subsequent reduction in draining enterocutaneous and rectovaginal fistulas.

Ulcerative Colitis

Ulcerative colitis is depicted by MRI with colonic mural thickening and enhancement.²⁵ Unlike Crohn's disease, which can be discontinuous, with skip areas, ulcerative colitis is a continuous process that always begins in the distal colon and rectum and progresses proximally. Although the inflammation of ulcerative colitis should only involve the mucosa and submucosa, on MRI scans the entire colonic wall is thickened and shows enhancement. It is possible that with higher resolution MRI, combined with rapid and earlier dynamic imaging, one may be able to distinguish the superficial inflammatory changes of ulcerative colitis from the transmural inflammation of Crohn's disease. With current techniques, Crohn's disease with continuous pancolitis has a very similar appearance to that of ulcerative colitis.

Perirectal and perianal complications of ulcerative colitis include fistulas and abscess formation. Surface coil images of

the rectum can be obtained using thin-section images angled perpendicularly and parallel to the rectum and perianal area. Fat-suppressed STIR images and thin-section, 3D GE images are particularly useful to evaluate this anatomic region. Fistulous tracts will be depicted as high-signal linear tracts on the STIR images or as linear enhancing tracts extending between diseased bowel and adjacent structures on 2D or 3D GE images. An abscess will be shown as a pericolic or perirectal fluid collection, with an enhancing abscess wall. Surrounding inflammation will show similar enhancement with intravenous (IV) gadolinium.

INFECTIOUS BOWEL DISEASE

Infectious disease involving the stomach, small intestine, or colon may be caused by bacterial, viral, or parasitic organisms. Infectious enteritis or colitis will be depicted as segments of bowel with mural thickening and enhancement that are indistinguishable from those of inflammatory bowel disease. The infectious disease may be focal or may involve long segments of the small intestine or colon. Associated infiltration of the perintestinal fat is depicted as linear strands extending from the diseased bowel into the adjacent mesenteric fat on SS RARE and

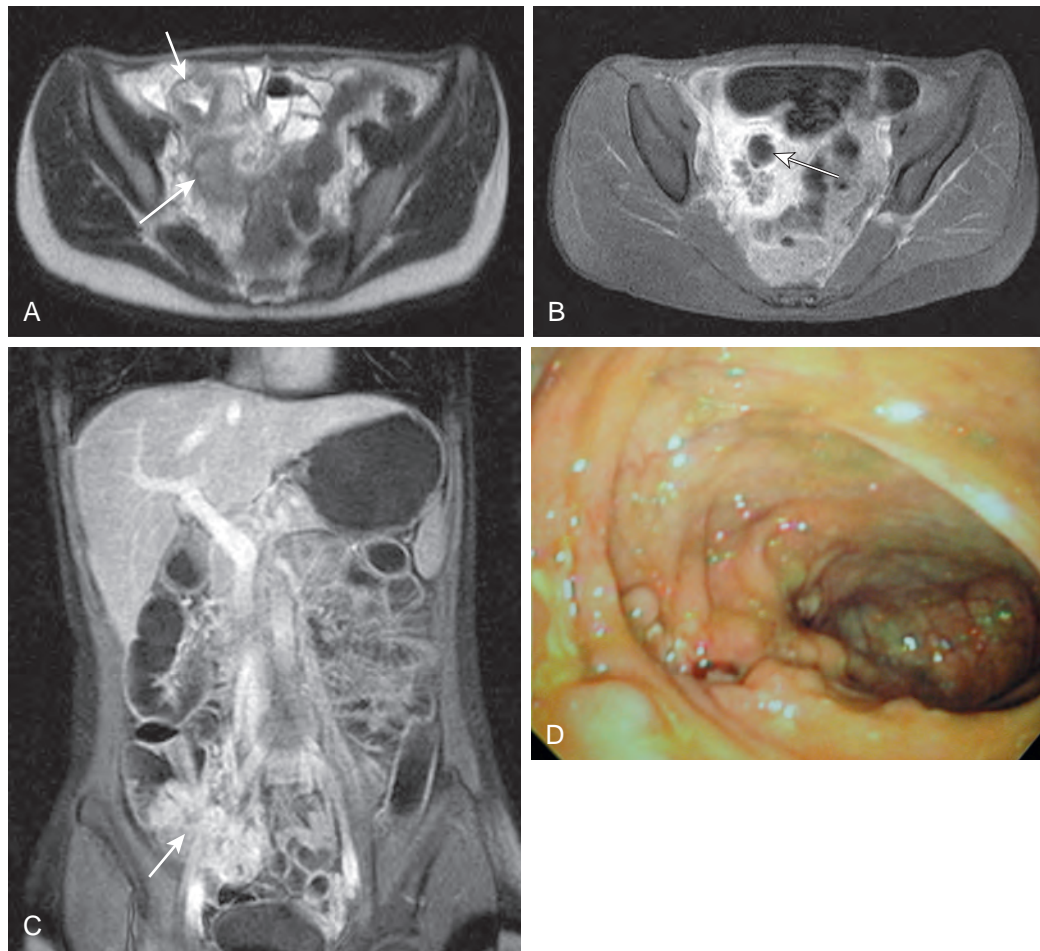


Figure 6-7 Crohn's phlegmon and abscess. **A.** Axial SSFSE image shows an abnormal small bowel (short white arrow) and a heterogeneous mass (long white arrow) in the right lower quadrant. **B.** Axial gadolinium-enhanced SGE image depicts a markedly enhancing phlegmon and central, nonenhancing abscess (arrow). **C.** Coronal gadolinium-enhanced SGE image confirms the thickened and enhancing terminal ileum (arrow). **D.** Endoscopic view of the terminal ileum shows a nodular inflamed mucosa. Biopsy confirmed active inflammation of Crohn's disease.

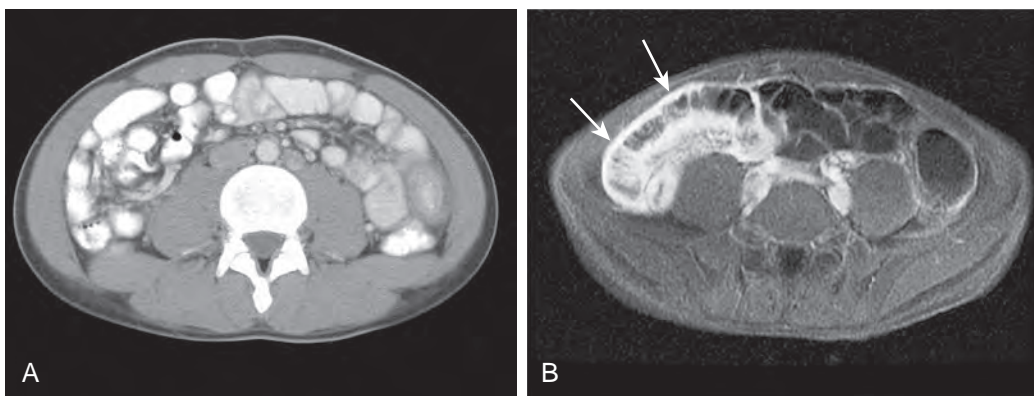


Figure 6-8 Infectious ileitis. **A.** Helical CT scan through the middle abdomen is unremarkable. **B.** GE fat-suppressed, SGE MR image with oral contrast material shows abnormally thickened and enhancing ileum (arrows) in the right side of the abdomen. MRI, the patient was treated for an infectious ileitis, with good clinical response.

fat-suppressed GE images. In the acute phase, there is marked mural enhancement of the diseased small bowel or colon (Fig. 6-8). Complications, including peri-intestinal abscess or phlegmon, are depicted on MR images as adjacent fluid collections with an enhancing abscess wall or as soft tissue inflammatory masses.

Pseudomembranous colitis is caused by *Clostridium difficile*, an anaerobic, gram-positive bacillus. Use of various antibiotics,

including clindamycin, broad-spectrum penicillins, and cephalosporins, alters the normal colonic flora, allowing for overgrowth of *C. difficile*. Toxins produced by pathogenic strains of *C. difficile* produce diarrhea and pseudomembranous colitis. With MRI, pseudomembranous colitis is depicted as marked colonic mural thickening and gadolinium enhancement. The descending and sigmoid colon is typically involved in pseudomembranous colitis. The degree of mural thickening can be

quite marked; the disease typically involves long segments of the colon. The marked mural thickening can help distinguish pseudomembranous colitis from other forms of infectious colitis.

ACUTE APPENDICITIS

Acute appendicitis can be depicted with MRI. The thick-walled, enlarged appendix shows moderate to marked enhancement on fat-suppressed GE MRI scans. DWIs show restricted diffusion within the abnormal appendix (Fig. 6-9). Fat-suppressed, T2-weighted images may show edema—ascites in the right lower quadrant. I do not use oral or rectal contrast in the clinical setting of suspected appendicitis. Additional thin-section, non-fat-suppressed, FSE T2-weighted images are obtained in the axial and coronal planes through the region of the appendix.

ISCHEMIC BOWEL DISEASE

Acute or chronic mesenteric ischemia is caused by insufficient blood supply through the mesenteric circulation supplying the GI tract. Chronic mesenteric ischemia develops slowly as a late-stage complication of atherosclerotic disease producing classic

so-called intestinal angina, with postprandial abdominal discomfort. Acute mesenteric ischemia results from a sudden decrease in mesenteric blood flow and is potentially life-threatening.

One may combine GE 3D MR angiography with anatomic images of the abdomen and pelvis.²⁶⁻³⁰ This approach allows one to visualize the mesenteric arteries directly and assess the small bowel and colon for secondary changes of mesenteric ischemia. In my experience, it is more common to see the secondary bowel wall changes with mural thickening and altered enhancement. In patients with acute arterial insufficiency, there will be diminished or absent enhancement within the thickened segments of ischemic bowel (Fig. 6-10). One can also see a layered appearance with mucosal and serosal enhancement but with decreased enhancement of the intervening submucosal and muscularis layers of the bowel wall. In the nonacute setting, the pattern of enhancement will be variable, depending on the degree of revascularization, fibrosis, or tissue necrosis. In my experience, the MRI findings can resolve very rapidly following spontaneous revascularization of the ischemic segment of bowel. An assessment of the degree of mural enhancement should be based on the first arterial phase set of images. On delayed images, the diseased bowel wall may enhance because of leaking, damaged capillaries.

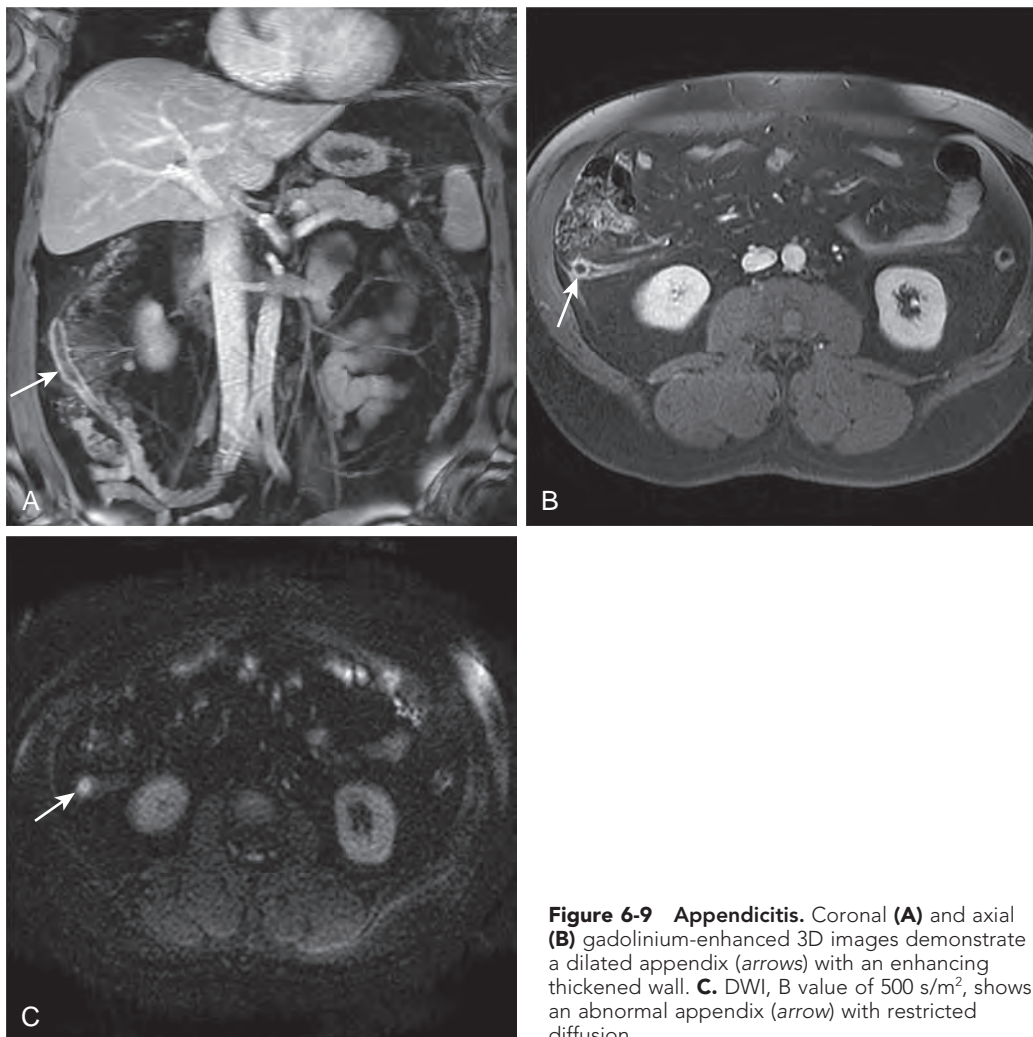


Figure 6-9 Appendicitis. Coronal (A) and axial (B) gadolinium-enhanced 3D images demonstrate a dilated appendix (arrows) with an enhancing thickened wall. C. DWI, B value of 500 s/m², shows an abnormal appendix (arrow) with restricted diffusion.

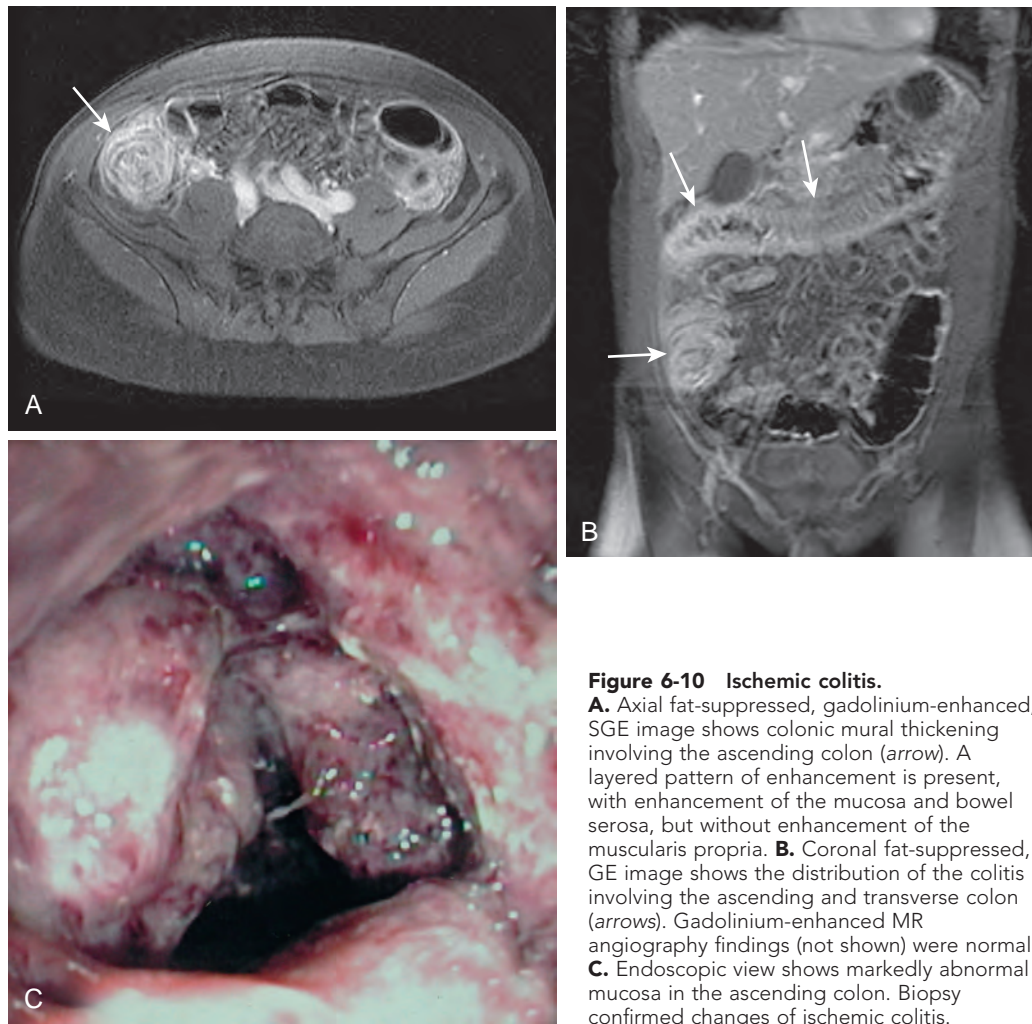


Figure 6-10 Ischemic colitis.

A. Axial fat-suppressed, gadolinium-enhanced, SGE image shows colonic mural thickening involving the ascending colon (arrow). A layered pattern of enhancement is present, with enhancement of the mucosa and bowel serosa, but without enhancement of the muscularis propria. **B.** Coronal fat-suppressed, GE image shows the distribution of the colitis involving the ascending and transverse colon (arrows). Gadolinium-enhanced MR angiography findings (not shown) were normal. **C.** Endoscopic view shows markedly abnormal mucosa in the ascending colon. Biopsy confirmed changes of ischemic colitis.

GASTROINTESTINAL MALIGNANCY

Stomach

The American Cancer Society estimated that in 2013 there would be 21,600 new cases of gastric cancer diagnosed in the United States, with 11,550 deaths from gastric cancer. The 5-year survival rate in the United States is 27%. Worldwide gastric cancer is the fourth most common cancer.³¹ Early diagnosis and accurate preoperative staging are critical for patient management and treatment.

MRI provides an elegant way to image gastric cancer.³²⁻³⁶ The depth of tumor penetration into the gastric wall can be accurately assessed with high-resolution T2-weighted images and GE MRI scans. Maximal distention of the gastric lumen with water-soluble oral contrast is essential to optimize depiction of the mural thickening or mass. Negative intraluminal agents on fat-suppressed, GE T1-weighted images are desirable because the dark lumen will help highlight the adjacent bowel wall and mural tumors. Large volumes of water or other oral agents should be ingested immediately before scanning. Pharmacologic agents can be administered to decrease peristalsis, but are not essential.

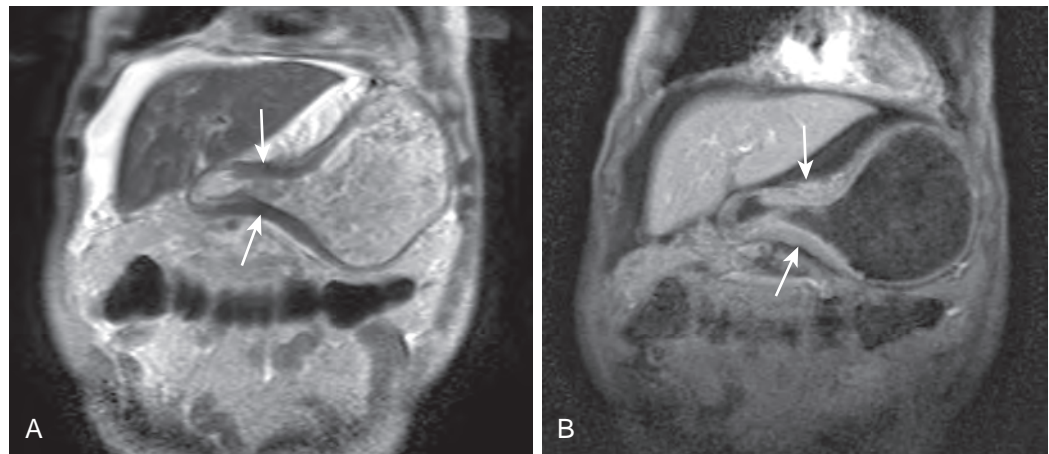
Thin-section, breath-hold, T2-weighted SS RARE images (SSTSE, SSFSE, HASTE), combined with fat-suppressed 3D GE

imaging, is most effective for depicting the transmural tumor extension used for tumor staging. The wall of the normal, well-distended stomach is depicted on unenhanced T1, T2, and SSFSE images as a thin, uniform, hypointense line typically measuring 2 to 3 mm in thickness. Prominent gastric rugal folds can increase the apparent thickness of the stomach wall. On dynamic GE images and delayed equilibrium phase images, the stomach wall will show only mild, uniform, and homogeneous enhancement.

Gastric cancers will be depicted on MR images as areas of focal mural thickening or as mural masses (Fig. 6-11). Superficial gastric cancer may not be visible on cross-sectional imaging. As they grow, they will be depicted as areas of focal mural thickening and eventually as a gastric mass. On dynamic GE MRI, gastric cancers will show more enhancement than the adjacent normal gastric wall. The presence of focal gastric mural thickening with a pattern of rapid enhancement is suggestive of gastric cancer. Linitis plastica will be depicted as a nondistensible stomach with a thickened, enhancing wall.

Transmural tumor invasion by a T3 or T4 tumor is indicated by disruption of this low-signal intensity band overlying the mural tumor, nodular tumor, or enhancing tumor masses and extending from the gastric wall into the surrounding perigastric fat.

Figure 6-11 Gastric cancer. Coronal SSTSE image (A) and gadolinium-enhanced 3D image (B) demonstrate moderate mural thickening of the distal gastric body and antrum (arrows). Ascites is also present. Note the distention of the gastric lumen with water, facilitating depiction of the mural thickening. Gastric cancer was confirmed at endoscopy and biopsy.



Nodal metastases are best shown on fat-suppressed T2-weighted images or DWI using a B value of 500 s/mm². In my experience, DWI is the most sensitive modality for depicting lymphadenopathy. Liver metastases are best shown on T1- and T2-weighted imaging and dynamic GE imaging. Peritoneal metastases commonly occur with GI malignancies and are best visualized on delayed, fat-suppressed, GE images. Osseous metastases can be visualized as high-signal intensity lesions on fat-suppressed T2-weighted images or as enhancing lesions on fat-suppressed GE images.

Small Intestine

Cancer arising in the small intestine is an uncommon malignancy, accounting for 2% of GI cancers. Cancer arising in the colon is 50 times more common than small bowel cancer. In the United States, the American Cancer Society estimated 8810 new cases of small bowel cancer in 2013, with 1070 associated deaths.³² Adenocarcinoma is the most common cell type, accounting for about one third of small bowel cancers. Other small bowel cancers include carcinoid tumors, leiomyosarcomas, and lymphomas.^{37,38}

Bowel distention is essential for MRI of small intestinal cancer. Intraluminal contrast may be administered orally with any of the oral contrast agents described earlier. Alternatively, small bowel enteroclysis may be performed with intraluminal contrast material infused through a nasojejunal tube providing maximal small bowel distention. On breath-hold SS FSE and fat-suppressed GE imaging, small bowel cancers will be depicted as areas of small intestinal mural thickening and masses. Because of their late clinical presentation, small bowel tumors are typically large tumor masses. Associated small bowel obstruction is indicated by distended loops of fluid-filled small bowel proximal to the obstructing mass.

Semelka and colleagues have described the appearance of small bowel tumors on MRI,³⁷ noting that small bowel tumors are isointense to small bowel on T1-weighted images. Malignant tumors showed moderate heterogeneous enhancement greater than that of the adjacent normal bowel on GE SGE imaging. Unenhanced T1-weighted and fat-suppressed, GE imaging are best for depicting tumor extent.

Colon and Rectum

Colorectal Cancer. Colorectal cancer is the third most commonly diagnosed malignancy in the United States and is the

second leading cause of cancer-related deaths. The American Cancer Society estimated that there would be about 142,820 new cases of colorectal cancer in 2013 in the United States, with an estimated 50,830 deaths.³⁹ The role of MRI for preoperative staging of colorectal cancer is well established and has been described in multiple studies.⁴⁰⁻⁵⁶

Different techniques have been proposed for MRI of colorectal cancer.⁴¹⁻⁴⁹ Endorectal coils or phased-array surface coils have been used to increase spatial resolution while maintaining an adequate SNR.⁴⁹⁻⁵¹ Some authors have advocated using positive or negative intraluminal contrast agents administered rectally to distend the rectosigmoid colon.⁵³⁻⁵⁵ In addition to the routine MR examination of the abdomen and pelvis described earlier, specific imaging sequences are used in the patient with colorectal cancer to assess local tumor extent and regional or distant metastases.

Thin-Section, High-Resolution, Angled T2-Weighted Turbo Spin-Echo Magnetic Resonance Imaging. High-resolution, phased-array surface coil images of rectal or colon cancer are obtained using thin-section, T2-weighted FSE images oriented perpendicularly and parallel to the cancer (Fig. 6-12).⁴¹⁻⁴³ These angled, T2-weighted images are prescribed from the sagittal T2-weighted images of the pelvis. Specific parameters for a rectal cancer MR protocol is shown in Table 6-2. These angled, T2-weighted images use a smaller field of view (FOV) and 3- to 4-mm slice thickness for detailed, high-resolution imaging of the rectal cancer. Higher signal averages combined with the phased-array surface coils are used to maintain an image SNR. Motion-corrected versions of the T2-weighted FSE sequences are available; these can reduce artifacts from patient or bowel motion. The motion-corrected sequences are known by the acronyms Propeller, Blade, Multivane, RADAR, and JET and are available from several different vendors.

Thin-section images are most useful for tumor staging, determining the depth of tumor penetration into the wall of the rectum or colon. The muscularis propria is easily depicted as a thin, low signal intensity linear structure. Disruption of the muscularis propria by tumor is evidence of T3 cancer, with transmural tumor extension. One may also use thinner slice sections (3 mm) with a smaller FOV by increasing the number of signal averages (NSA) to 8, with a corresponding increase in acquisition time.

Diffusion-Weighted Magnetic Resonance Imaging. I also use diffusion-weighted MRI (DW MRI) to evaluate colon and rectal

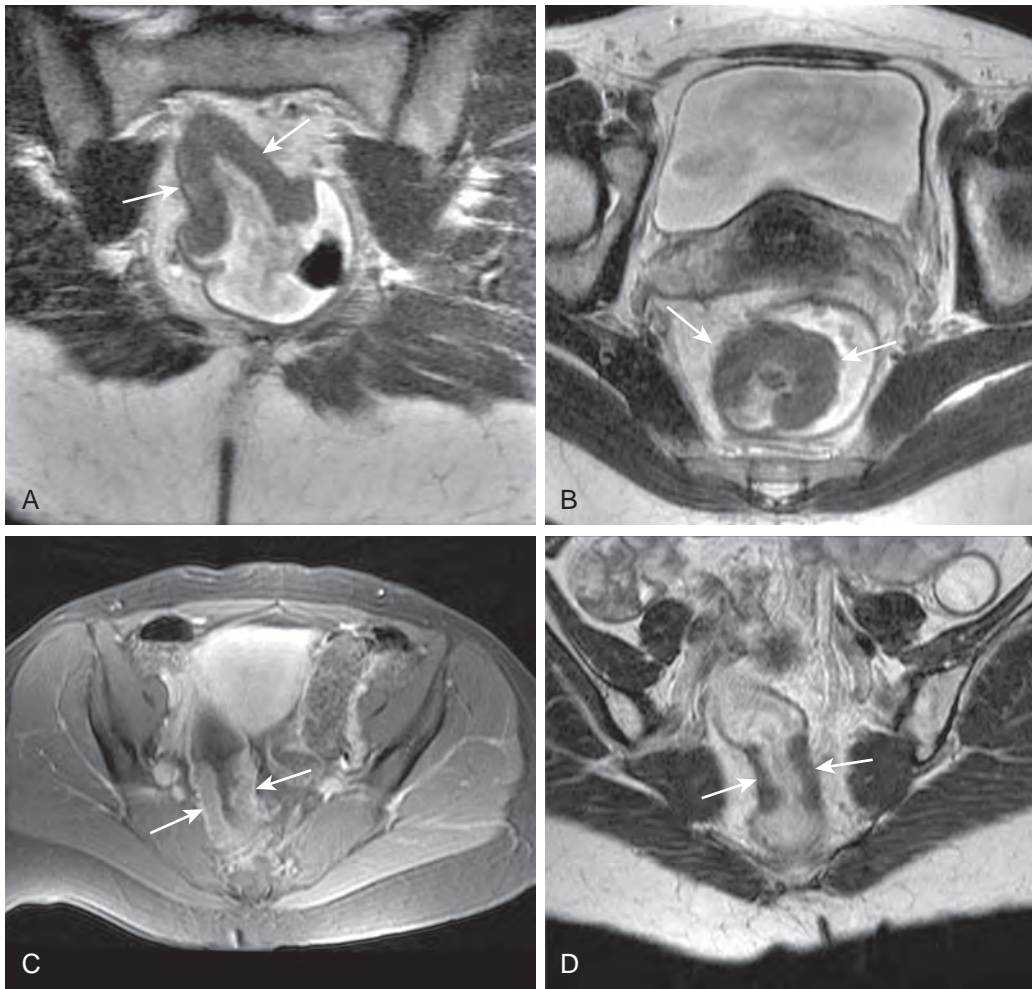


Figure 6-12 Rectal cancer. Coronal (A) and axial (B) surface coil, T2-weighted MR images angled parallel and perpendicular to rectal cancer depict a T3 rectal cancer (arrows) with extramural tumor extension. C. Axial gadolinium-enhanced SGE image shows the irregular rectal mass (arrows). D. Follow-up MRI scan obtained after chemotherapy shows response to treatment, with marked decrease in the rectal cancer (arrows).

TABLE 6-2

Angled T2-Weighted Imaging of Rectal Cancer

Sequence—2D FSE, SE propeller
Plane—oblique (angled perpendicularly and parallel to tumor)
TR, 3100 (shortest)
TE, 91
NSA, 4
FOV, 20-24 cm
Matrix, 352 × 352
ETL, 24
Flip angle, 160 degrees
Slice thickness, 4 mm, with 0.5-mm gap
24 slices
90% RFOV
Bandwidth: 83.3
ASSET, factor 2
Time: 4:00
Coil—phased-array surface coil

ASSET, Array Spatial Sensitivity Encoding Technique; ETL, echo train length; FOV, field of view; FSE, fast spin-echo; NSA, number of signal averages; RFOV, restricted field of view; SE, spin-echo; TE, echo time; TR, repetition time.

cancers. GI tract cancers show marked hyperintensity on diffusion-weighted images, improving their conspicuity (see Fig. 6-12).⁵⁷⁻⁶⁰ DW images are also very useful for the nodal staging of colon and rectal cancer. Small perirectal and pericolic nodal metastases are markedly hyperintense on DW images, facilitating their depiction (see Fig. 6-13). In patients

TABLE 6-3

Diffusion-Weighted Imaging of Colorectal Cancer

Sequence: single-shot spin-echo EPI
Plane: axial
Repetition time (TR): 2700
Echo time (TE): 58
NSA: 2
Matrix: 256 × 128
B value: 500
7 mm, skip 1 mm
No. of slices: 24
Senses: 2
Time: 20 s
Coil: phased-array surface coil

EPI, echo planar imaging; NSA, number of signal averages; sense, sensitivity encoding.

with locally advanced rectal cancer, the addition of DW MRI to conventional MRI can improve the depiction of tumor response to adjuvant chemotherapy and radiation therapy. Malignant gastrointestinal tract tumors have low ADC values, which increase after successful therapy.

I typically use a B value of 500 s/m² for extrahepatic DW imaging. With this B value, anatomic landmarks are still visible, whereas most intestinal fluid and ascites are suppressed. Specific MRI parameters for DWI are shown in Table 6-3.

Magnetic Resonance Staging of Colorectal Cancer. Preoperative MRI of colon and rectal cancers effectively determines local tumor extension, nodal metastases, and distant abdominal metastases.⁴¹⁻⁴⁹ These three features form the basis of TNM tumor staging. Stage I colon cancers are any T1 or T2 tumors without nodal or distant metastases. Stage II colon cancers are T3 or T4 tumors without nodal or distant metastases. Stage III colon cancers are any tumor with nodal involvement, and stage IV colon cancers are those with distant metastases. The overall MR staging accuracy for rectal cancer has ranged from 67% to 100%.⁴⁰

The information from preoperative MRI is used to direct patient management. Rectal cancer patients in whom MRI depicts stage III cancers with transmural tumor extension (T3 or T4) or stage IV cancers with nodal metastases undergo preoperative radiation therapy. After radiation therapy, follow-up MRI documents a reduction in tumor volume, resulting in an improved chance for successful surgical resection (see Fig. 6-12). In this scenario, the information from preoperative MRI is critical for directing management decisions of the patient with colorectal cancer.

Local Tumor Extension. Tumor staging determines the depth of mural penetration by the colon or rectal cancer. Tis (tumor in situ) indicates carcinoma in situ, T1 tumors invade the submucosa, T2 tumors invade the muscularis propria, T3 tumors extend through the muscularis propria onto the subserosa or nonperitonealized pericolic or perirectal tissues, and T4 tumors directly invade adjacent organs or structures.

The most challenging assessment is to distinguish T2 from borderline T3 cancers. Peritumoral fibrosis extending into the perirectal fat in a T2 tumor can be difficult to distinguish from early transmural extension from a T3 tumor. On the other

hand, nodular soft tissue extending through the disrupted rectal wall into the surrounding tissues confidently predicts a T3 or T4 cancer.

Nodal Metastases. Node staging is based on the presence or absence of local or regional nodal metastases. Although MRI can depict lymph nodes 2 to 3 mm in diameter, MRI assessment of nodal metastases remains limited to an evaluation of the size and number of lymph nodes (see Fig. 6-13). Morphologic criteria for evaluating lymph nodes pose obvious limitations. Microscopic metastases in normal-sized lymph nodes cannot be detected, and enlarged, inflammatory lymph nodes cannot be distinguished from nodal metastases. The accuracy of the detection of nodal metastases varies from 39% to 95%.⁴⁰ The use of ultrasmall superparamagnetic iron oxide (USPIO) contrast agents for depicting lymph node metastases has shown promise in early reports. The iron particles are phagocytosed by macrophages and taken up by the reticuloendothelial system. Normal lymph nodes will contain macrophages with iron particles and show loss of signal on GE MR images because of a susceptibility effect. Tumor deposits within lymph nodes displace the reticuloendothelial system and show areas of increased signal because of less uptake of the USPIO.

Distant Metastases. Metastasis staging is based on the presence or absence of distant metastases to the liver, peritoneum, mesentery, omentum, bowel serosa, lymph nodes, osseous structures, and lungs (Fig. 6-14).

Circumferential Resection Margin and the Mesorectal Fascia. Although TNM tumor staging provides important information, it is actually more important to determine the circumferential, tumor-free resection margin, which is the distance between the rectal tumor and surrounding mesorectal

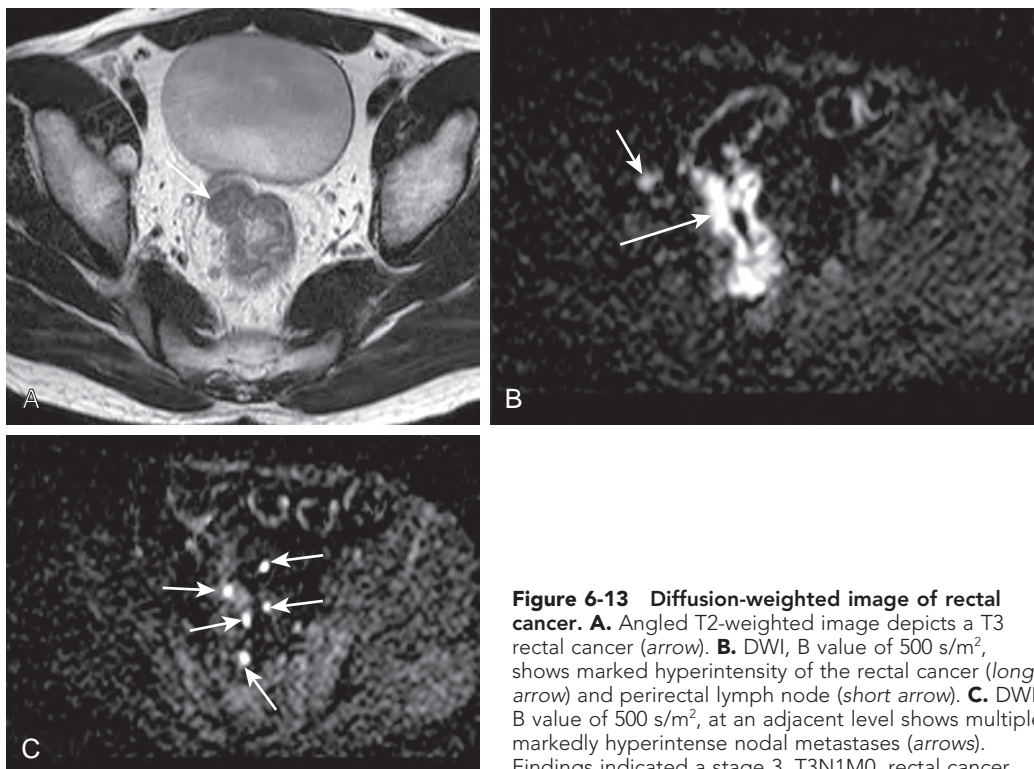


Figure 6-13 Diffusion-weighted image of rectal cancer. **A.** Angled T2-weighted image depicts a T3 rectal cancer (arrow). **B.** DWI, B value of 500 s/m², shows marked hyperintensity of the rectal cancer (long arrow) and perirectal lymph node (short arrow). **C.** DWI, B value of 500 s/m², at an adjacent level shows multiple markedly hyperintense nodal metastases (arrows). Findings indicated a stage 3, T3N1M0, rectal cancer.

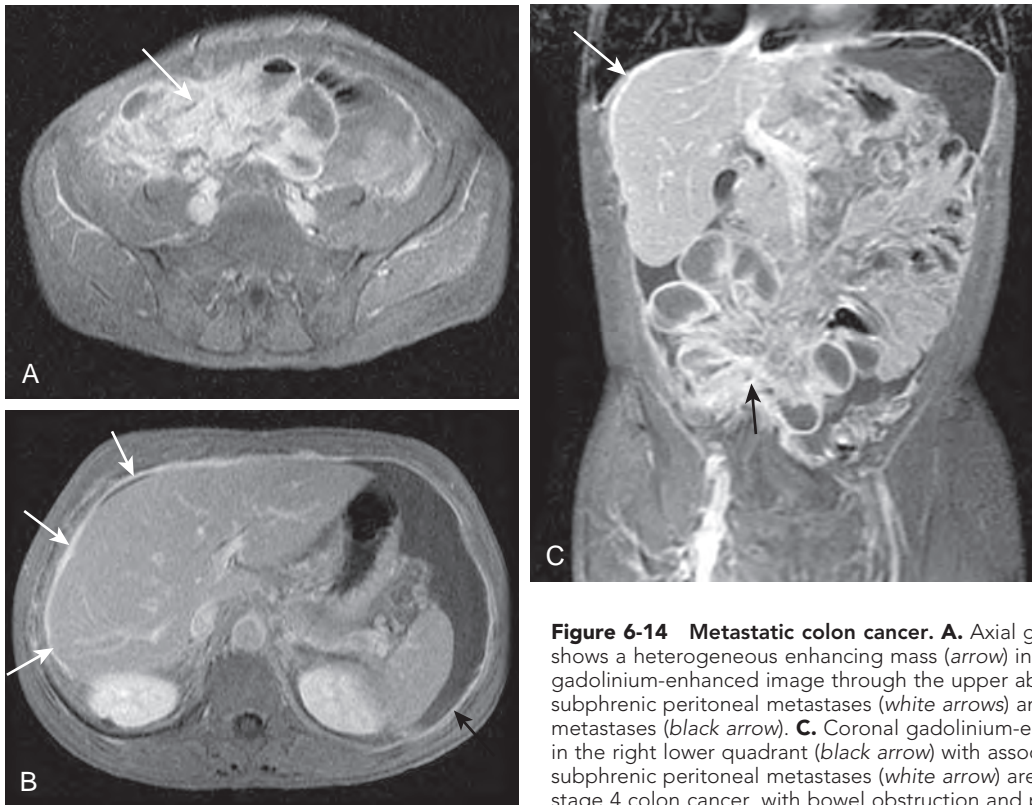


Figure 6-14 Metastatic colon cancer. **A.** Axial gadolinium-enhanced SGE image shows a heterogeneous enhancing mass (arrow) in the right lower quadrant. **B.** Axial gadolinium-enhanced image through the upper abdomen depicts enhancing right subphrenic peritoneal metastases (white arrows) and left subphrenic peritoneal metastases (black arrow). **C.** Coronal gadolinium-enhanced SGE image shows the mass in the right lower quadrant (black arrow) with associated bowel obstruction. Right subphrenic peritoneal metastases (white arrow) are confirmed. MR findings indicated a stage 4 colon cancer, with bowel obstruction and peritoneal metastases.

fascia.^{50,51} This tumor-free resection margin can be accurately and consistently predicted on high-resolution, phased-array, surface coil MR images.

The mesorectal fascia encloses the mesorectum, an anatomic unit comprised of the rectum, perirectal fat, superior hemorrhoidal vessels, nerves, and lymphatics. At surgery, patients undergo total mesorectal excision, with en bloc resection of the rectal cancer and surrounding tissues enclosed within the mesorectal fascia. This technique has resulted in a decrease in local tumor recurrence. With mesorectal excision, surgical failure resulting in local tumor recurrence is usually because of incomplete removal of the lateral spread of a tumor with microscopically positive resection margins.

Based on the MRI assessment of the circumferential resection margin (CRM), patients can be categorized and treated according to their risk of local recurrence. Superficial tumors may be treated with surgery alone. Operable T3 cancers with a wide CRM are treated with a short course of radiation therapy followed by mesorectal excision. Patients with locally advanced cancer in whom the tumor approaches or involves the resection margin are at greater risk for recurrence and will benefit from a more extended course of radiation therapy and chemotherapy, followed by surgical resection.

In a study of 76 patients with rectal cancer, Beets-Tan and associates evaluated the MRI assessment of the CRM compared with histopathology.⁵⁵ They noted that two observers correctly predicted a 0-mm resection margin in 12 of 12 patients with T4

cancers. In 29 patients with histologic resection margins of 10 mm or less, these observers correctly predicted a 10-mm resection margin in 27 and 28 patients. In a study of 98 patients with rectal cancer, Brown and co-workers reported 92% agreement between MRI and histologic findings for predicting the circumferential resection margin.⁴²

Locally advanced rectal cancers will extend beyond the mesorectal fascia and invade surrounding structures and organs. High-resolution surface coil MRI is more accurate than helical CT for depicting the invasion of adjacent structures by advanced rectal cancers. In one study of 26 patients, MRI had a 97% sensitivity and 98% specificity for local invasion compared with 70% and 85% for helical CT.⁵⁶

Summary

MRI offers unique advantages for evaluating inflammatory, infectious, ischemic, and malignant diseases of the GI tract. By combining readily available intraluminal and IV contrast agents with fast MRI techniques, one can reliably depict the wall of the stomach, small intestine, colon, and rectum. The inherent high-contrast resolution of MRI allows mural disease to be depicted confidently as areas of wall thickening and enhancement. MRI of the GI is a robust and versatile technique that can be applied to a wide variety of benign and malignant gastrointestinal diseases.

REFERENCES

- Regan F, Beall DP, Bohlman ME, et al: Fast MRI and the detection of small-bowel obstruction. *AJR* 170:1465–1469, 1988.
- Lee JKT, Marcos HB, Semelka RC: MRI of the small bowel using the HASTE sequence. *AJR* 170:1457–1463, 1998.
- Marcos HB, Semelka RC, Noone TC, et al: MRI of normal and abnormal duodenum using half-Fourier single-shot RARE and gadolinium-enhanced spoiled gradient echo sequences. *Magn Reson Imaging* 17:869–880, 1999.
- Low RN, Francis IR: MRI of the gastrointestinal tract with IV gadolinium and diluted barium oral contrast media compared with unenhanced MRI and CT. *AJR* 169:1051–1059, 1997.
- Low RN, Semelka RC, Worawattanakul S, et al: Extrahepatic abdominal imaging in patients with malignancy: Comparison of MRI and helical CT, with subsequent surgical correlation. *Radiology* 210:625–632, 1999.
- Gourtsoyiannis N, Papanikolaou N, Grammatikakis J, et al: MRI of the small bowel with a true-FISP sequence after enteroclysis with water solution. *Invest Radiol* 35:707–711, 2000.
- Low RN, Sebrechts CP, Politoske DA, et al: Crohn's disease with endoscopic correlation: Single-shot fast spin-echo and gadolinium-enhanced fat-suppressed spoiled gradient-echo MRI. *Radiology* 222:652–660, 2002.
- Maccioni F, Patak MA, Signore A, Laghi A: New frontiers of MRI in Crohn's disease: Motility imaging, diffusion-weighted imaging, perfusion MRI, MR spectroscopy, molecular imaging, and hybrid imaging (PET/MRI). *Abdom Imaging* 37:974–982, 2012.
- Frøehlich JM, Patak MA, von Weymarn C, et al: Small bowel motility assessment with magnetic resonance imaging. *J Magn Reson Imaging* 21:4370–4375, 2005.
- Ajay W, Goehd SC, Schneemann H, et al: Oral contrast agents for small bowel MRI: comparison of different additives to optimize bowel distention. *Eur Radiol* 14:458–464, 2004.
- Ajay W, Goehd SC, Schneemann H, et al: Dose optimization of mannitol solution for small bowel distension in MRI. *J Magn Reson Imaging* 20:648–653, 2004.
- Sood RS, Joubert I, Franklin H, et al: Small bowel MRI: Comparison of a polyethylene glycol preparation and water as oral contrast media. *J Magn Reson Imaging* 15:401–408, 2002.
- Laghi A, Carbone L, Catalano C, et al: Polyethylene glycol solution as an oral contrast agent for MRI of the small bowel. *AJR* 177:1333–1334, 2001.
- Johnson WK, Stoupis C, Torres GM, et al: Superparamagnetic iron oxide (SPIO) as an oral contrast agent in gastrointestinal (GI) magnetic resonance imaging (MRI): Comparison with state-of-the-art computed tomography (CT). *Magn Reson Imaging* 14:43–49, 2001.
- Holzknicht N, Helmlinger T, von Ritter C, et al: [MRI of the small intestine with rapid MRI sequences in Crohn disease after enteroclysis with oral iron particles.] *Radiologie* 38:29–36, 1998.
- Maccioni F, Viscido A, Marini M, Caprilli R: MRI evaluation of Crohn's disease of the small and large bowel with the use of negative superparamagnetic oral contrast agents. *Abdom Imaging* 27:384–393, 2002.
- Papanikolaou N, Prassopoulos P, Grammatikakis I, et al: Technical challenges and clinical applications of magnetic resonance enteroclysis. *Top Magn Reson Imaging* 13:397–408, 2002.
- Gourtsoyiannis N, Papanikolaou N, Grammatikakis J, et al: MR enteroclysis protocol optimization: Comparison between 3D FLASH with fat saturation after intravenous gadolinium injection and true FISP sequences. *Eur Radiol* 11:908–913, 2001.
- Umschaden HW, Gasser J: MR enteroclysis. *Radiol Clin North Am* 41:231–248, 2003.
- Maccioni F, Viscido A, Broglia L, et al: Evaluation of Crohn disease activity with magnetic resonance imaging. *Abdom Imaging* 25:219–228, 2000.
- Madsen SM, Thomsen HS, Schlichting P, et al: Evaluation of treatment response in active Crohn's disease by low-field magnetic resonance imaging. *Abdom Imaging* 24:232–239, 1999.
- Gourtsoyiannis N, Papanikolaou N, Grammatikakis J, et al: Assessment of Crohn's disease activity in the small bowel with MR and conventional enteroclysis: Preliminary results. *Eur Radiol* 14:1017–1024, 2004.
- Koh DM, Miao Y, Chinn RJS, et al: MRI evaluation of the activity of Crohn's disease. *AJR* 177:1325–1332, 2001.
- Maccioni F, Colaiacomo MC, Stasolla A, et al: Value of MRI performed with phased-array coil in the diagnosis and pre-operative classification of perianal and anal fistulae. *Radiol Med (Torino)* 104:58–67, 2002.
- Nozue T, Kobayashi A, Takagi Y, et al: Assessment of disease activity and extent by magnetic resonance imaging in ulcerative colitis. *Pediatr Int* 42:285–288, 2000.
- Chow LC, Chan FP, Li KP: A comprehensive approach to MRI of mesenteric ischemia. *Abdom Imaging* 27:507–516, 2002.
- Rha SE, Ha HK, Lee SH, et al: CT and MRI findings of bowel ischemia from various primary causes. *RadioGraphics* 20:29–42, 2000.
- Baden JG, Racy DJ, Grist TM: Contrast-enhanced three-dimensional magnetic resonance angiography of the mesenteric vasculature. *J Magn Reson Imaging* 10:369–375, 1999.
- Debatin JF: MR quantification of flow in abdominal vessels. *Abdom Imaging* 23:485–495, 1998.
- Lauenstein TC, Ajay W, Narin B, et al: MRI of apparent small-bowel perfusion for diagnosing mesenteric ischemia: Feasibility study. *Radiology* 234:569–575, 2005.
- American Cancer Society: What are the key statistics about stomach cancer? 2013. <http://www.cancer.org/cancer/stomachcancer/detailedguide/stomach-cancer-key-statistics>. Accessed January 26, 2014.
- Yamada I, Saito N, Takeshita K, et al: Early gastric carcinoma: Evaluation with high-spatial-resolution MRI in vitro. *Radiology* 220:115–121, 2001.
- Kim AY, Han JK, Seong CK, et al: MRI in staging advanced gastric cancer: Is it useful compared with spiral CT? *J Comput Assist Tomogr* 24:389–394, 2000.
- Sohn KM, Lee JM, Lee SY, et al: Comparing MRI and CT in the staging of gastric carcinoma. *AJR* 174:1551–1557, 2000.
- Oi H, Matsushita M, Murakami T, Nakamura H: Dynamic MRI for extraserosal invasion of advanced gastric cancer. *Abdom Imaging* 22:35–40, 1997.
- Motohara T, Semelka RC: MRI in staging of gastric cancer. *Abdom Imaging* 27:376–383, 2002.
- De Franco A, Celi G, Restaino G, et al: Imaging of small bowel tumors. *Rays* 27:35–50, 2002.
- Semelka RC, John G, Kelekis NL, et al: Small bowel neoplastic disease: Demonstration by MRI. *J Magn Reson Imaging* 6:855–860, 1996.
- American Cancer Society: Cancer Facts and Figures, 2005, Atlanta, 2005, American Cancer Society.
- Beets-Tan RGH, Beets GL: Rectal cancer: Review with emphasis on MRI. *Radiology* 232:335–346, 2004.
- Brown G, Richards CJ, Bourne MW, et al: Morphologic predictors of lymph node status in rectal cancer with use of high-spatial-resolution MRI with histopathologic comparison. *Radiology* 227:371–377, 2003.
- Brown G, Richards CJ, Newcombe RG, et al: Rectal carcinoma: Thin-section MRI for staging in 28 patients. *Radiology* 211:215–222, 1999.
- Kim NK, Kim MJ, Yun SH, et al: Comparative study of transrectal ultrasonography, pelvic computerized tomography, and magnetic resonance imaging in preoperative staging of rectal cancer. *Dis Colon Rectum* 42:770–775, 1999.
- Wallengren NO, Holtas S, Andren-Sandberg A, et al: Rectal carcinoma: Double-contrast MRI for preoperative staging. *Radiology* 215:108–114, 2000.
- Brown G, Radcliffe AG, Newcombe RG, et al: Preoperative assessment of prognostic factors in rectal cancer using high-resolution magnetic resonance imaging. *Br J Surg* 90:355–364, 2003.
- Matsuoka H, Nakamura A, Masaki T, et al: A prospective comparison between multidetector-row computed tomography and magnetic resonance imaging in the preoperative evaluation of rectal carcinoma. *Am J Surg* 185:556–559, 2003.
- Gagliardi G, Bayar S, Smith R, Salem RR: Preoperative staging of rectal cancer using magnetic resonance imaging with external phase-arrayed coils. *Arch Surg* 137:447–451, 2002.
- Kim NK, Kim MJ, Park JK, et al: Preoperative staging of rectal cancer with MRI: Accuracy and clinical usefulness. *Ann Surg Oncol* 7:732–737, 2000.
- Hunerbein M, Pegios W, Rau B, et al: Prospective comparison of endorectal ultrasound, three-dimensional endorectal ultrasound, and endorectal MRI in the preoperative evaluation of rectal tumors. Preliminary results. *Surg Endosc* 14:1005–1009, 2000.
- Matsuoka H, Nakamura A, Masaki T, et al: Comparison between endorectal coil and pelvic phased-array coil magnetic resonance imaging in patients with anorectal tumor. *Am J Surg* 185:328–332, 2003.
- Maldjian C, Smith R, Kilger A, et al: Endorectal surface coil MRI as a staging technique for rectal carcinoma: A comparison study to rectal endosonography. *Abdom Imaging* 25:75–80, 2000.
- Maier AG, Kersting-Sommerhoff B, Reiders JW, et al: Staging of rectal cancer by double-contrast MRI using the rectally administered superparamagnetic iron oxide contrast agent ferrioxene and IV gadodiamide injection: Results of a multicenter phase II trial. *J Magn Reson Imaging* 12:651–660, 2000.
- Low RN, McCue M, Barone R, et al: MR staging of primary colorectal carcinoma: Comparison to surgical and histopathologic findings. *Abdom Imaging* 28:784–793, 2003.

54. Low RN: MRI of colorectal cancer. *Abdom Imaging* 27:418–424, 2002.
55. Beets-Tan RGH, Beets GL, Vliegen RFA, et al: Accuracy of magnetic resonance imaging in prediction of tumor-free resection margin in rectal cancer surgery. *Lancet* 357:497–504, 2001.
56. Beets-Tan RG, Beets GL, Borstlap AC, et al: Preoperative assessment of local tumor extent in advanced rectal cancer: CT or high-resolution MRI? *Abdom Imaging* 25:533–541, 2000.
57. Curvo-Semedo L, Lambregts DMJ, Maas M, et al: Response to preoperative combined radiation therapy with chemotherapy—conventional MR volumetry versus diffusion-weighted MRI. *Radiology* 260:3734–3743, 2011.
58. Kim SH, Hong SH, Kim GH, et al: Locally advanced rectal cancer: Added value of diffusion-weighted MRI in the evaluation of tumor response to neoadjuvant chemo- and radiation therapy. *Radiology* 253:116–125, 2009.
59. Sinha R, Rajiah P, Ramachandran I, et al: Diffusion-weighted MRI of the gastrointestinal tract: Technique, indications, and imaging findings. *RadioGraphics* 33:655–676, 2013.
60. Song I, Kim SH, Lee SH, et al: Value of diffusion-weighted imaging in the detection of viable tumour after neoadjuvant chemoradiation therapy in patients with locally advanced rectal cancer: Comparison with T2-weighted and PET/CT imaging. *Br J Radiol* 85:577–586, 2012.

Positron Emission Tomography and Computed Tomography of the Hollow Viscera

SELIM R. BUTROS | SHAUNAGH McDERMOTT |
MARTIN J. SHELLY | MICHAEL A. BLAKE

CHAPTER OUTLINE

Protocol for Scanning

Patient Preparation and Scanning

Esophagus

Staging

Restaging and Treatment Response

Conclusion

Stomach

Small Bowel

Colon and Rectum

Staging

Restaging and Treatment Response

Positron emission tomography (PET) is a molecular imaging modality that has been increasingly used in clinical practice worldwide, especially in the oncologic population. It has gained widespread use for the diagnosis, staging, restaging, and monitoring treatment response of various malignancies.^{1,2} For years, computed tomography (CT), ultrasound (US), and magnetic resonance imaging (MRI) have been used for the detection and follow-up of tumors that grossly rely on the morphology or attenuation characteristics of pathologic tissue. PET has the ability to provide physiologic information by determining metabolic activity at a cellular level at an early phase, which is a shortcoming of cross-sectional imaging modalities. Thus, distinction of malignant versus benign lesions, detection of metabolic activity in organs that are not yet morphologically abnormal, and evaluation of the response of neoplasms to various treatments such as chemotherapy, radiation, or surgery have become possible with the use of PET.

PET imaging uses positron-emitting radionuclides produced in cyclotrons. Once the radiotracer is injected, the positron is emitted into the body. It travels a short distance, loses its energy, and interacts with electrons in tissue. This causes an annihilation reaction, which produces two 511-keV gamma rays that are emitted in opposite directions, approximately 180 degrees from each other. It is the localizing information provided by the coincidence of gamma photons, detected in opposite detectors in the ring of the PET scanner, that helps generate the image.³

The most commonly used radiopharmaceutical in PET imaging is the glucose analogue fluorine-18-deoxyglucose (fluoro-2-deoxyglucose; ¹⁸F-FDG). Just as with glucose, FDG is actively transported into the cell, mediated by glucose

transporters (GLUTs). Once intracellular, FDG is phosphorylated. However, in contrast to glucose, it cannot be dephosphorylated and remains trapped in the cell. This allows sufficient time for imaging before FDG is metabolized. The use of FDG for oncologic imaging relies mainly on increased glucose consumption and overexpression of GLUT proteins in neoplastic cells.

FDG distribution occurs in normal structures such as the brain and the heart and is excreted in the urinary system. There are regions in the body with variable physiologic FDG uptake, such as the digestive and genitourinary tracts.⁴ As a consequence, differentiating physiologic uptake from pathologic uptake may at times prove to be a diagnostic challenge. Increased FDG uptake is not specific to malignancy and can also be seen in various inflammatory or infectious benign pathologic processes as a result of the underlying hypermetabolism.⁵ It is therefore important to be aware of the various pitfalls and physiologic and varying FDG distribution patterns in the body during the interpretation of imaging findings so as not to confuse them with malignancy.

PET not only offers qualitative information but also offers quantification by measurement of radioactivity in a given voxel. SUV (standardized uptake value) is a semiquantitative index of FDG metabolism that is calculated and normalized for injected radiotracer amount and body weight or body surface area. SUV measurements are obtained by placing a region of interest (ROI) or cursor on the area of interest. The values are calculated and displayed by the software of a PET workstation. When repeated PET scans are obtained in the same scanner, with the same acquisition parameters, SUV can serve as a means to assess response to therapy.⁶ Maximum or mean values of SUV can be obtained; however, maximum SUV values are more commonly used in clinical practice because of their reliability and reproducibility compared with mean values.⁶ If FDG were distributed evenly throughout the body, the SUV would be 1.0. Traditionally, an SUV maximum cutoff of 2.5 or greater has been used to differentiate between benign and malignant lesions.⁷ However, the organ in which the measurement is obtained and its comparison to background should be taken into account when determining abnormality of SUV values.

The functional information provided by the PET scan is complementary to the anatomic and morphologic data obtained by the CT scan. PET is limited in regard to accurate anatomic localization of detected abnormal activity, which is especially more of a challenge for abdominal and pelvic imaging. Initial PET scanners provided anatomic registration—that is, superimposition of FDG activity from the PET scan with the corresponding anatomic structure—from CT scans via

separately acquired datasets fused with the aid of software.⁸ This method was easier and more accurate in organs such as the brain, but the same success was not achieved with body imaging, in which bowel peristalsis and motion from breathing caused frequent misregistration artifacts, complicating interpretation. Most of the current PET scans are hybrid units with built-in CT scans in the same hardware, providing immediately sequential acquisition and subsequent coregistration of data without moving the patient. Once the scan is completed, datasets from the PET and CT scans can be reviewed separately or as fused images. The first PET/CT scan became commercially available in 2001 and, since then, PET-only scanners have almost disappeared from the market. Currently, almost all manufacturers offer only hybrid PET/CT scanners.

Attenuation is the loss of the gamma photons emitted from the positron in the patient before they are detected by the scanner. Attenuation is a greater problem with PET imaging because both photons have to travel through the patient for greater distances compared with the traditional single-photon imaging used in nuclear medicine. Only approximately 10% of the photon pairs survive from a given source in the patient.³ As a result, attenuation correction is necessary to obtain high count, good-quality images. Earlier PET scans used external, long-lived radionuclide sources, such as germanium 68 (⁶⁸Ge) or cesium 137, and measured transmission using the same detectors to provide an attenuation map of the patient's body. However, obtaining transmission scans accounted for a significant portion of the scan time in PET-only units, and the length of the scan caused misalignment artifacts.⁹ Current PET/CT scans provide not only anatomic coregistration, but also attenuation correction, which reduces the statistical noise associated with ⁶⁸Ge transmission maps. They also enable a significant scan time reduction, down from 45 to 60 minutes with the PET-alone units to 20 to 30 minutes, thus enhancing patient throughput.

Protocol for Scanning

An agreed-on universal protocol for PET/CT scanning does not yet exist, given that it is still a relatively new and developing modality. Institutions have developed their own modifications to existing protocols to fit their own preferences. There are three main options regarding the CT component while performing a PET scan—to obtain a low-dose CT scan for attenuation correction and image coregistration, a standard-dose CT scan, or a combined standard-dose CT scan with intravenous (IV) and oral contrast. The advantage of the latter options is that they provide diagnostic quality CT scans at the expense of increased radiation dose. Use of a fully diagnostic CT scan using IV contrast is especially important in the evaluation of vascular structures, organ enhancement, and bowel disease, as well as for distinguishing lymphadenopathy and masses from small bowel loops. In our institution, we first obtain a low-dose, noncontrast CT scan followed by the whole-body FDG PET emission scan. Subsequently, a diagnostic quality transmission CT scan is obtained using IV and oral contrast agents, which maximizes diagnostic information and minimizes the risk of artifacts.

In CT imaging, contrast agents are administered to enhance tissue contrast and differentiation and improve lesion localization and characterization. However, protocol modifications are necessary to avoid artifacts and ensure accurate attenuation correction on PET scans.¹⁰⁻¹² Attenuation can be overestimated in PET in the presence of positive contrast agents.¹³⁻¹⁶ The

resulting overestimation of attenuation may lead to potential artifacts, with images demonstrating increased FDG uptake in areas of high contrast concentration. IV contrast causes artifacts that are mainly limited to venous vessels close to the injected bolus, whereas positive oral contrast agents may cause an overestimation of FDG uptake up to 20%; this may be even more problematic when the patient has poor peristalsis or an obstruction causing accumulation of contrast in the bowel.¹⁴ The same applies to metallic implants in the body, which frequently causes attenuation correction artifacts. Non-attenuation-corrected images and the CT scan can serve as problem-solving tools in these cases, because artifacts will be found only on the attenuation-corrected data.

Although much of the misregistration caused by bowel peristalsis and patient motion has been alleviated by the use of CT, respiratory misregistration represents a persistent problem in precluding optimal image fusion. The PET scan is acquired over approximately 30 minutes during shallow respiration, whereas the attenuation-corrected CT datasets are acquired in seconds, during which the patient is instructed to breathe quietly or perform a breath-hold maneuver. The ideal breathing protocol remains to be determined. Several investigators have suggested that optimal fusion occurs with limited expiratory breath holding,^{17,18} whereas others have suggested fusion images of equal quality with shallow breathing.¹⁹

Patient Preparation and Scanning

Our institutional protocol will be discussed here. Our patients are asked to fast for a minimum of 6 hours prior to PET/CT to optimize FDG uptake by tumors and minimize cardiac uptake. Instructions are given to avoid caffeinated beverages. However, water consumption and bladder emptying is encouraged, which aid in the urinary excretion of FDG and minimizes radiation dose to the bladder. FDG is a glucose analogue with a similar metabolism, as discussed earlier. Its uptake is affected by insulin and glucose levels in the blood. Hyperglycemia competes with and decreases FDG uptake by tumors; therefore, before the injection, a blood sugar measurement is obtained. The desired glucose level is below 200 mg/dL and the optimal level is below 150 mg/dL. Diabetic patients are instructed to avoid insulin injection within the 4 hours prior to the scan. In cases of higher glucose levels, measurement is repeated subsequent to light exercise, or sometimes even an injection of insulin is administered after an endocrine consultation.

After the IV injection of FDG (140 μ Ci/kg), patients are kept in a darkened room and encouraged to avoid excessive physical activity, as well as chewing and talking, until the time of the scan. Neutral oral contrast is given at the same time of injection for the subsequent diagnostic CT scan. We typically use two to three bottles (450 mL) of VoLumen (E-Z-EM, Lake Success, NY) for our neutral attenuation oral contrast agent. This is a low-density barium sulfate suspension that distends the bowel without increasing intraluminal attenuation. One hour after the administration of FDG, a static and emission PET scan is obtained. A transmission nonattenuation CT scan is obtained at the same time for attenuation correction at 120 kVp and 60 mAs during quiet breathing, with a slice thickness of 5 mm and overlap of 1.5 mm. A fully diagnostic helical CT scan using IV contrast is obtained subsequent to the emission PET scan during quiet breathing at approximately 140 kVp and 200 mAs, with a slice thickness and overlap of 5 mm.

Esophagus

Esophageal cancer is a leading cause of worldwide cancer mortality. The American Cancer Society (ACS) estimated 17,990 new diagnoses and 15,210 deaths from esophageal cancer in 2013. The lifetime risk of esophageal cancer in the United States is about 1 in 125 in men and about 1 in 435 in women.²⁰ Complete resection of the tumor is the only potentially curative treatment in patients who do not have distant metastases or locally advanced disease. Depending on the stage of the disease, various treatment options exist, ranging from endoscopic resection to primary surgical esophagectomy to chemotherapy and radiotherapy. These treatment modalities lead to substantial morbidity and mortality, which makes accurate staging and pretreatment planning crucial. PET is widely used in clinical practice in the management of patients with esophageal cancer. In the United States, the Centers for Medicare & Medicaid Services (CMS) have approved the use of PET and PET/CT in the diagnosis, staging, and restaging of esophageal cancer.

In the proximal and midesophagus, squamous cell carcinoma predominates, whereas adenocarcinoma is mostly seen in the distal esophagus and esophagogastric junction. In recent years, there has been a dramatic increase in the incidence of adenocarcinoma of the esophagus, but the incidence of squamous carcinoma has remained relatively stable. Whether squamous or adenocarcinoma, PET scanning does not indicate a distinct difference between the two as a diagnostic tool.²¹ The most significant risk factor for adenocarcinoma is gastroesophageal reflux disease, whereas alcohol consumption and smoking are the two major risk factors for squamous cell carcinoma.

PET has limited value as a screening modality and problem-solving tool in disease exclusion prompted by abnormal findings in other diagnostic modalities because of its low specificity.³ A variety of physiologic or benign entities can cause uptake of FDG in the esophagus.^{22,23} Low-intensity, linear physiologic uptake has been described and is thought to represent swallowed secretions or smooth muscle activity. In cases of reflux esophagitis, mild to moderate intensity linear uptake can be seen predominantly in the distal esophagus.²⁴ Radiation esophagitis can also lead to uptake of varying intensity, limited to the zone of radiation.²⁵ Barrett's esophagus, a precursor to adenocarcinoma, is columnar metaplasia of the distal esophagus. It is a complication of reflux esophagitis and has been associated with more intense uptake in the distal third of the esophagus. Other pitfalls include uptake in paraesophageal brown fat, atherosclerotic plaque in the adjacent aorta, and asymmetric uptake in the vocal cords.^{26,27} Recognizing these patterns because they are commonly seen pitfalls and correlating PET findings with the CT images to avoid misdiagnoses are important. However, when uptake is distinctly focal and intense, especially when a corresponding focal mass is seen on the CT scan, diagnosis is highly suspicious for esophageal cancer. In patients for whom the diagnosis is unknown or the PET scan is obtained for other reasons, it is reasonable to recommend endoscopic correlation.

STAGING

Accurate disease staging is critical in choosing the appropriate treatment option and determining the prognosis of esophageal cancer. PET/CT has been widely used for staging of esophageal cancer, especially for the detection of distant metastasis and to

determine whether patients are candidates for surgery. The clinical staging of esophageal cancer is assessed with the TNM staging system developed by the American Joint Committee on Cancer (AJCC) staging guidelines. The depth of tumor invasion through the layers of the esophagus determines the T (tumor) status of the disease, and the N (node) status of disease is determined by the presence (N1) or absence (N0) of regional lymph node metastasis. Detection of distant metastasis (M) determines the M status (M1 or M0) of disease.²⁸ Lymph node metastasis to the cervical lymph nodes in upper esophageal cancer and to the celiac axis lymph nodes in lower esophageal cancer is designated as an M1a status. All other distant lymph node metastases fall into the M1b category. This categorization has prognostic value because patients with M1a disease have a worse prognosis compared with those with N1 disease.²⁹

Detection rates of PET for primary tumor is greater compared with CT, ranging from 83% to 96% in various studies.³⁰⁻³² Patients with T1 (invasion of the lamina propria or submucosa) or T2 (invasion of the muscularis propria) disease primarily undergo surgical resection for curative treatment, whereas patients with T3 (invasion of the adventitia) or T4 (invasion of adjacent structures) disease usually require neoadjuvant chemotherapy or combined chemotherapy and radiation therapy. Although PET has a higher sensitivity in the detection rate of a primary tumor compared with CT, it is of limited value in T staging because it provides no data about the depth of invasion.^{30,33} PET is also limited in spatial resolution; thus, false-negative results occur in small tumors and in tumors that are well differentiated.³⁴ In a study evaluating the usefulness of PET in superficial esophageal cancers, Little and colleagues found that PET was able to detect only 45% of in situ lesions (Tis) and 69% of T1 lesions and was unable to differentiate between the two.³⁵ Endoscopic ultrasound (EUS), however, can accurately determine the T stage.³⁶ In one meta-analysis, which included 49 studies and 2558 patients, the pooled sensitivity and specificity of EUS for diagnosing the T stage were 81.6% and 99.4% in T1, 81.4% and 96.3% in T2, 91.4% and 94.4% in T3, and 92.4% and 97.4% in T4 disease, respectively.³⁷

Various studies have not shown a substantial added benefit of PET for the detection of regional lymph nodes, for which EUS is the standard diagnostic tool. In a prospective study conducted by Flamen and associates, PET had a sensitivity of only 33% in the detection of regional lymph node metastases compared with 81% for endoscopic ultrasound.³⁰ In the meta-analysis by Puli and co-workers, the sensitivity of EUS for diagnosing the N stage was 84.7%, which improved to 96.7% with the use of fine-needle aspiration (FNA).³⁷ In another prospective study of 42 patients, Lerut and colleagues found that PET had a lower accuracy for the diagnosis of locoregional nodes compared with combined CT and EUS (48% vs. 69%), with a significantly lower sensitivity (22% vs. 83%).³⁸ According to a meta-analysis of 12 studies conducted by van Westreenen and associates, the pooled sensitivity and specificity of PET for the detection of locoregional lymph node metastases were 51% and 84%, respectively.³⁹ Unlike other tumors, locoregional lymph node metastases of esophageal cancer are in close proximity to the primary tumor. It is believed that intense FDG uptake of the primary tumor can obscure the uptake of these immediately adjacent lymph nodes, thus creating difficulty in the differentiation of a primary tumor from locoregional lymph node metastasis.

The additional value of PET in the evaluation of nodal status may lie in its high specificity. In the study by Flamen

and co-workers,³⁰ the specificity of PET was 89% compared with 67% with EUS. In another prospective study by Kato and colleagues, PET had an incremental value over CT in the initial staging of esophageal carcinoma in 14% of patients by accurately showing nodal metastasis in six patients with no positive CT findings and absence of disease in six other patients with positive CT findings.⁴⁰ With PET/CT, anatomic and morphologic data obtained from CT are combined with functional information obtained from PET, thus improving detection rates of metastases. In esophageal cancer, metastatic involvement can be seen by histologic analysis in small lymph nodes and, conversely, benign causes of lymph node enlargement are commonly seen in the mediastinum. A morphologically abnormal or enlarged lymph node may show no FDG uptake; conversely, a small, normal-appearing lymph node may demonstrate FDG uptake. In this sense, PET and CT are supplemental to one another. When PET/CT is compared with PET in the assessment of locoregional lymph node metastasis, Yuan and colleagues showed an improved sensitivity of 94%, accuracy of 92%, and negative predictive value of 92% with PET/CT compared with 82%, 87%, and 86%, respectively, with PET only.⁴¹

The current sensitivity rates in detection of locoregional lymph nodes with PET deem its use for the classification of the N stage of disease not sufficient for accurate presurgical planning. A multimodality, multidisciplinary approach using PET, CT, and EUS should be followed for accurate staging of nodal status in patients with esophageal cancer.

The primary role of PET in the management of esophageal cancer is in its value for detecting distant lymph node or solid organ metastasis⁴² (Fig. 7-1). Although patients with M1a disease may benefit from neoadjuvant chemoradiation, radical surgery is contraindicated in patients with M1b disease. Patients with M1b disease are only offered palliative treatments and systemic chemotherapy.⁴³ PET is very useful for the detection of common sites of distant nodal metastases, such as cervical lymph node metastases in upper esophageal cancer and celiac axis lymph node metastases in lower esophageal cancer.^{38,44} In the study by Lerut and associates, the accuracy and specificity of FDG-PET for distant nodal metastasis (M1a) was significantly higher compared with the combined use of CT and EUS (86% vs. 62% and 90% vs. 69%, respectively). In the same study, FDG-PET scanning correctly upstaged 12% of the patients.³⁸

The most common solid organ metastasis of esophageal cancer is to the liver and lungs, followed by bone.⁴⁵ Metastatic disease is present in 20% to 30% of patients with esophageal cancer at initial presentation.⁴⁶ PET has shown to be more accurate and sensitive for the assessment of distant disease compared with CT and EUS.^{38,46-49} The meta-analysis conducted by van Westreenen and co-workers demonstrated a pooled sensitivity and specificity of 67% and 97%, respectively, for detection of distant metastases by PET.³⁹ PET/CT has been shown to prevent surgery by upstaging disease via identifying distant metastases not seen by CT in approximately 14% (5 of 36) of patients in a study by Flanagan and colleagues⁴⁶ and in 28% (7 of 25) of patients in another study by Rankin and associates.⁵⁰ Heeren and co-workers found that PET upstaged 15 patients (15 of 74; 20%) correctly as M1 disease, missed by CT and EUS, and correctly downstaged 4 patients (5%) from M1 to M0 disease, with an overall incremental value of 25%.⁵¹

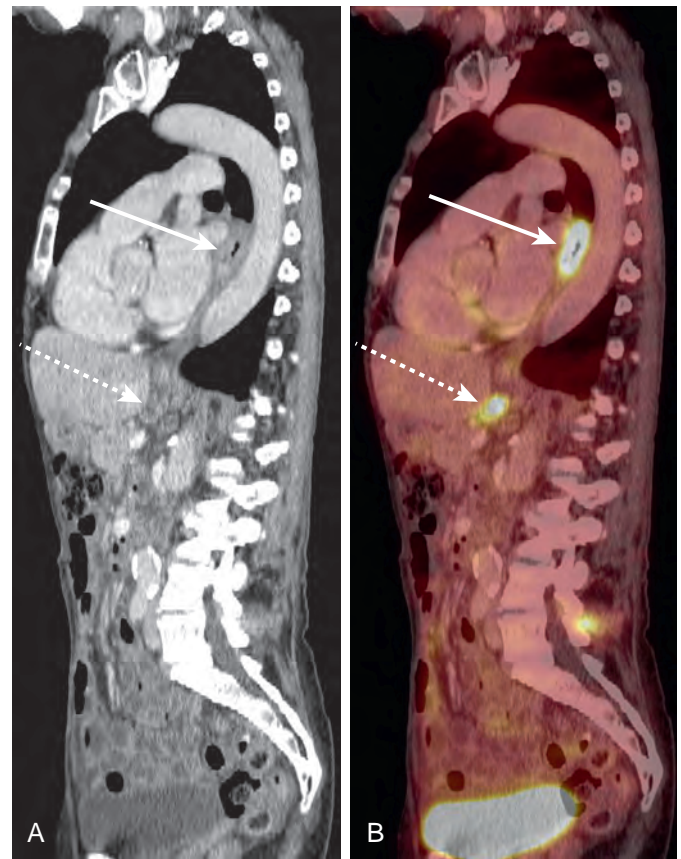


Figure 7-1 Midesophageal cancer. **A.** Sagittal contrast-enhanced CT scan demonstrates focal circumferential thickening of the midesophagus (solid arrow) suspicious for malignancy. A large, suspicious, low-density gastrohepatic lymph node (dashed arrow) is also seen. **B.** Corresponding sagittal fused PET/CT image shows intense FDG uptake in the midesophagus (solid arrow) and in a gastrohepatic lymph node (dashed arrow).

RESTAGING AND TREATMENT RESPONSE

The accuracy of CT for the detection of recurrent disease or evaluation of treatment response is limited because of the difficulty of differentiating post-treatment changes of inflammation and fibrosis from viable tumor. Morphologic changes do not always reflect tumor response because tumor size may remain stable, despite the viable tumor cells. Guo and colleagues⁵² evaluated PET/CT for disease recurrence and divided anatomic sites of recurrence to local, regional, and distant. The study demonstrated sensitivity values of 96.9%, 85.9%, and 90.5% and specificity values of 50%, 92.2%, and 89.9%, respectively. PET/CT was of low specificity for the evaluation of local recurrence. In the perianastomotic region, EUS is much more sensitive and specific for the detection of recurrence⁵³; however, in the post-treatment patient, the use of endoscopy may be limited because of scarring, inflammation, postradiation esophagitis, or luminal stenosis in the anastomotic region. Therefore, just as with initial staging, a multimodality approach should be applied for restaging esophageal cancer following treatment.

In a meta-analysis by Westterterp and associates⁵⁴ comparing the accuracy of CT, EUS, and PET in the assessment of response to neoadjuvant treatment, the maximum joint sensitivity and specificity values for CT, PET, and EUS were 54%, 85%, and 86%, respectively. PET and EUS had equivalent accuracy, but

the invasive nature and limitations of EUS in the post-treated esophagus were noted. EUS was not feasible in 6% and suboptimal in 14% of patients.

Another study conducted by Cerfolio and co-workers⁵⁵ investigated the accuracy of PET/CT, EUS with FNA, and CT for restaging following neoadjuvant chemotherapy and found that PET/CT accurately predicted complete response in 89% of patients compared with 67% with EUS-FNA and 71% with CT. The accuracy for detecting nodal disease was also superior with PET/CT, 93%, compared with 78% each with EUS-FNA and CT.

Response rates to neoadjuvant treatment are variable with esophageal cancer. Favorable response rates have ranged from 16% to 31% of patients in several published series.⁵⁶⁻⁵⁹ Patients who do not respond to neoadjuvant treatment may have a worse prognosis because of adverse effects of treatment or delay in surgery. Therefore it is crucial to have a test to select the pool of responders accurately and individualize treatment accordingly. PET has been widely used for this purpose.

Many studies have shown a strong correlation of FDG uptake with pathologic stage and survival in esophageal cancer.⁶⁰⁻⁶⁵ This has led to various studies investigating the use of the standardized uptake value (SUV) in determining the metabolic response to neoadjuvant treatment.

Ott and colleagues divided patients based on a predetermined rate of SUV reduction before and after neoadjuvant chemotherapy and classified them into metabolic responders and nonresponders in a prospective study of 65 patients. They found that metabolic response significantly correlated with pathologic response and median survival.⁶⁶

The Municon trial was a prospective study by Lordick and associates, which included 119 patients undergoing neoadjuvant chemotherapy, using PET to assess metabolic response rates in guiding treatment of distal esophageal adenocarcinoma.⁶⁷ On the basis of a cut-off of 35% reduction in the maximum SUV (SUV max), patients were divided into metabolic responders and nonresponders following neoadjuvant chemotherapy. A major histologic response was seen in 58% of metabolic responders compared with 0% in nonresponders. Event-free and overall survival rates were also significantly better in the responder group at 29.7 versus 14.1 months in nonresponders. This study confirmed the benefit of PET in the metabolic evaluation of treatment response in patients receiving neoadjuvant chemotherapy and the feasibility of PET-guided treatment algorithms.

For years, the World Health Organization (WHO) criteria and Response Evaluation Criteria in Solid Tumors (RECIST) have been used to follow treatment response in solid tumors, which used anatomic metrics based on tumor size reduction.^{68,69} However, it is known that metabolic response usually precedes and is more accurate than morphologic response.⁷⁰ With the introduction of molecularly targeted treatment options and the use of PET to assess the metabolic treatment response, these conventional evaluation methods have become of limited value. Recently, Wahl and co-workers introduced the PET Response Criteria in Solid Tumors (PERCIST), which is a new quantitative assessment of the metabolic response of tumors.⁷¹ Yanagawa and colleagues compared the use of RECIST to PERCIST and found that PERCIST was the strongest independent predictor of outcomes in patients receiving neoadjuvant chemotherapy for esophageal cancer.⁷²

PET/CT has also been used for radiation treatment planning. Calculating gross tumor volume in radiation therapy for the

accurate delineation of tumor margins to achieve the best conformity index, the ratio between target tumor volume and irradiated volume, is necessary to treat the tumor successfully while keeping treatment-related complications to a minimum. The use of PET leads to improved accuracy of tumor volume calculation, with up to 20% changes in the calculated tumor volume compared with CT.^{73,74} In a study by Leong and associates, the use of CT only compared with PET caused a geographic miss of gross tumor volume, predominantly in the longitudinal direction, in 31% of patients.⁷⁵ However, it is a developing method, and interobserver variability exists. More studies are needed before the use of PET/CT for radiotherapy planning gains widespread clinical use.

CONCLUSION

The main value of PET for the staging of esophageal cancer is its ability to detect distant lymph node and organ metastases otherwise not detected with other diagnostic modalities, thus altering the treatment in patients with more advanced disease status. Staging attempts should not be limited to PET because of its inherent limitations in T and N staging of disease. Ideal staging would use PET/CT for the detection of distant metastasis with precise anatomic localization and morphologic characterization provided by CT, supplemented by EUS for the improved detection of locoregional lymph nodes and assessment of depth of tumor invasion.

Another major strength of PET is its ability to evaluate treatment response more accurately by determining temporal changes in metabolic activity, thus providing the opportunity to identify those who do not respond to treatment and make alterations in their management. Standardization of scan timing, specific imaging protocols, and the establishment of PET treatment guidelines have yet to be determined. Further studies are needed to establish such standards.

Stomach

Gastric cancer is one of the most common primary gastrointestinal (GI) tract malignancies worldwide. It is often asymptomatic or causes nonspecific symptoms in its early stages. By the time symptoms occur, the cancer is often advanced and commonly metastatic, which accounts for its overall poor prognosis. As a result, gastric carcinoma, especially prevalent in Asian countries, is the second leading cause of cancer mortality, accounting for 600,000 deaths annually worldwide.⁷⁶ Cure can only be achieved by gastric and adequate regional lymph node resection.^{77,78} However, the prognosis remains poor and recurrence rates are high, despite surgical resection and neoadjuvant therapy. As with other cancers, accurate preoperative staging is crucial in determining the most appropriate treatment option and whether curative surgery should be attempted. The main use of PET in gastric cancer is primarily for the detection of distant metastases. It has limited use in the primary diagnosis and detection of lymph node status.

When interpreting PET images for gastric carcinoma or for incidental findings in studies performed for other causes, it is helpful to keep several pitfalls in mind to avoid misdiagnoses. Several benign inflammatory or infectious causes, such as gastritis secondary to medications or *Helicobacter pylori* infection, may frequently cause nonspecific, diffuse FDG uptake of the stomach. This may challenge interpretation because this pattern

of FDG uptake can also be seen in infiltrative primary or metastatic adenocarcinoma and lymphoma.⁷⁹⁻⁸¹ Physiologic uptake in a nondistended stomach with collapsed gastric folds may also accentuate background uptake; the use of water ingestion or low-density oral contrast to distend the stomach adequately before PET scanning is recommended by many to increase the accuracy of PET.⁸² In these cases, clinical correlation for the patient's symptoms of gastritis, recent endoscopy, or underlying primary malignancy may be helpful. In patients with unexplained diffuse or focal, moderate- to high-intensity uptake, correlation with endoscopy should be recommended.²³

Gastric cancer is staged by the standard TNM classification according to the depth of tumor invasion through the gastric wall (T), status and number of lymph nodes (N), and presence of metastasis (M).⁸³ Gastric cancer usually occurs at the gastroesophageal junction; the most common histologic type is adenocarcinoma (>90%) followed by less common types such as mucosa-associated lymphoid tissue (MALT) lymphoma, carcinoid tumor, and sarcomas. Currently, no routine screening programs exist in the United States for the prevention or detection of gastric cancer. Prompted by suspected clinical or imaging findings, the diagnosis is usually made with endoscopy, along with tissue sampling.

CT is the most commonly used modality for more locally advanced disease to stage and assess the extent of the primary tumor, to evaluate for spread to locoregional lymph nodes, and at the same time to determine metastatic status.⁸⁴ CT provides a rapid overall assessment of local and distant disease based on morphologic changes and tissue enhancement patterns. However, the use of CT, as for other cancers, is limited in the detection of nonenlarged local lymph nodes that may harbor tumor cells and has limited specificity because of benign entities that may cause lymph node enlargement. CT may also be limited for the detection of peritoneal and hematogenous metastases.^{85,86} Unfortunately, approximately 23% of patients who are otherwise not suspected to have metastases with conventional imaging modalities are found to have metastatic disease during surgery, precluding curative intent.⁸⁷ This has led several investigators to evaluate the value of PET/CT for detecting local and distant disease preoperatively.

In early gastric cancer, EUS can accurately T-stage mucosal and submucosal lesions, which are generally considered endoscopically resectable if limited to the gastric wall.⁸⁸ According to a study by Xi and co-workers, the overall accuracy of EUS for determination of the T stage was 80.0% and for T1, T2, T3, and T4 was 100%, 71.4%, 87.5% and 72.7%, respectively.⁸⁹ EUS is more accurate for assessing the depth of wall invasion in early cancer compared with other imaging modalities, including CT, but is limited in the assessment of locally advanced disease and the detection of distant metastases.⁹⁰ In a recent meta-analysis by Dassen and colleagues, the sensitivity of PET for the detection of the primary tumor ranged from 26% to 63% for early-stage gastric cancer and from 93% to 98% for locally advanced gastric cancer.⁹¹ Early-stage tumors are not detected at an equal sensitivity compared with more advanced tumors,^{92,93} which could be related to the difficulty in detecting focal uptake in a background of diffuse physiologic uptake or to the limited resolution of PET/CT.⁹⁴ Certain types of gastric cancers, such as MALT lymphoma (MALToma), mucinous carcinoma, and signet ring cell carcinoma, are also known to have low levels of FDG uptake, with limited sensitivity values.⁹⁵⁻⁹⁸ PET should not be used in the work-up of these patients. Kim and associates

have shown that signet ring cell gastric carcinoma has the lowest sensitivity for the detection on PET, 15%, whereas other types of gastric cancer have moderate sensitivity levels ranging from 30% to 71%.⁹⁹ According to a study by Stahl and co-workers, the sensitivity of PET also differs according to the histologic type of cancer, as described by the Lauren system, with a detection rate of 83% for the intestinal type versus 41% for the diffuse type.⁹⁵ Therefore it can be concluded that PET is of limited value in the detection and T staging of gastric cancer.

In a study by Chen and colleagues assessing the usefulness of PET for the preoperative staging of gastric carcinoma, the amount of FDG uptake correlated with macroscopic type, tumor size, lymph node metastasis, histologic type, and TNM stage of the tumor.¹⁰⁰ PET had an accuracy similar to that of CT for diagnosing local and distant lymph node metastases as well as peritoneal status; however, in assessing local lymph node status, PET had a higher specificity than CT (92% vs. 62%). Moreover, PET provided additional diagnostic value in 10 of 68 (15%) of patients by upstaging 4 (6%) and downstaging 6 (9%) patients. In a study by Namikawa and associates, the sensitivity, specificity, and accuracy of PET/CT in assessing regional lymph node metastasis were 64.5%, 85.7%, and 71.1%, respectively.⁹⁴ In another prospective study by Kim and co-workers, which included 73 patients with gastric cancer, the sensitivity, specificity, positive predictive value, and negative predictive value of PET for detecting lymph node metastases were 40%, 95%, 91%, and 56% respectively.⁹⁹ Currently, PET is considered to have low sensitivity and accuracy but high specificity for the detection of lymph node metastases. This is in part related to the low spatial resolution of PET and the difficulty in distinguishing uptake of the primary tumor or background physiologic uptake from the adjacent small perigastric lymph nodes, as discussed earlier for esophageal cancer. The benefit of PET over CT could be in its high specificity and positive predictive values for the assessment of locoregional lymph nodes as well as a theoretic increased accuracy for the detection of distant lymph node metastases (e.g., those in the retroperitoneum). To date, there have not been many studies comparing PET/CT to CT or PET alone for the evaluation of locoregional lymph nodes in gastric cancer. The added benefit of hybrid imaging with PET/CT has been well demonstrated in the preoperative evaluation of esophageal cancer and may have a role and added benefit for gastric cancer.⁴¹

Gastric cancer usually metastasizes to the liver, lungs, adrenal glands, and ovaries.¹⁰¹ The major advantage of PET is in the detection of these distant solid organ metastases, which may be metabolically active much sooner than they become morphologically apparent on CT. In one series, the overall sensitivity and specificity of PET to detect distant metastases was found to be 71% and 74%, respectively, with high values for liver and lung metastases but lower values for malignant ascites and malignant pleural effusion.¹⁰² Both CT and PET have limited sensitivity in the detection of peritoneal carcinomatosis, which is frequently diagnosed intraoperatively.^{103,104} Diffuse peritoneal FDG uptake or uptake in gross tumor deposits of omental caking can be seen; however, diffuse, small, nodular peritoneal deposits usually fall below the resolution of PET, although they can sometimes be detected by CT. Despite the added benefit of detecting distant unsuspected metastases in some cases with a high specificity,¹⁰⁵ the added value of PET/CT in the diagnosis and work-up of patients with gastric cancer has yet to be determined.

PET/CT is useful in the detection of recurrence subsequent to surgical resection and in the assessment of treatment response to preoperative chemotherapy. PET can frequently differentiate treatment-related morphologic changes seen on CT from tumor recurrence. In a recent meta-analysis, Zou and Zhao analyzed results from 8 studies, which included a total of 500 patients, and found that the pooled sensitivity and specificity of PET/CT for the detection of local gastric cancer recurrence following surgery were 86% and 88%, respectively.¹⁰⁶ Neoadjuvant therapy is frequently being used in the treatment of gastric cancer to improve survival with the subsequent surgical resection. Treatment response by CT is assessed with changes in tumor size following the RECIST criteria,⁶⁹ which may sometimes be sub-optimal. In some cases, the tumor may not reduce in size, despite no longer harboring tumor cells. PET can detect and separate treatment responders at an earlier phase than CT, thus reducing treatment-related morbidity and preventing delays in surgical treatment.⁸⁷ In this regard, PET also provides prognostic information, because patients who do not respond to chemotherapy usually have more aggressive tumor biology.

There has been increasing interest recently in a new radiotracer, ¹⁸F-fluorothymidine (FLT), in PET for the evaluation of gastric cancer, with the aim of acquiring more accurate diagnostic and staging information.¹⁰⁷ Herrmann and associates have compared the feasibility of FLT-PET to FDG-PET and found FLT-PET to have a sensitivity of 100% in primary tumor

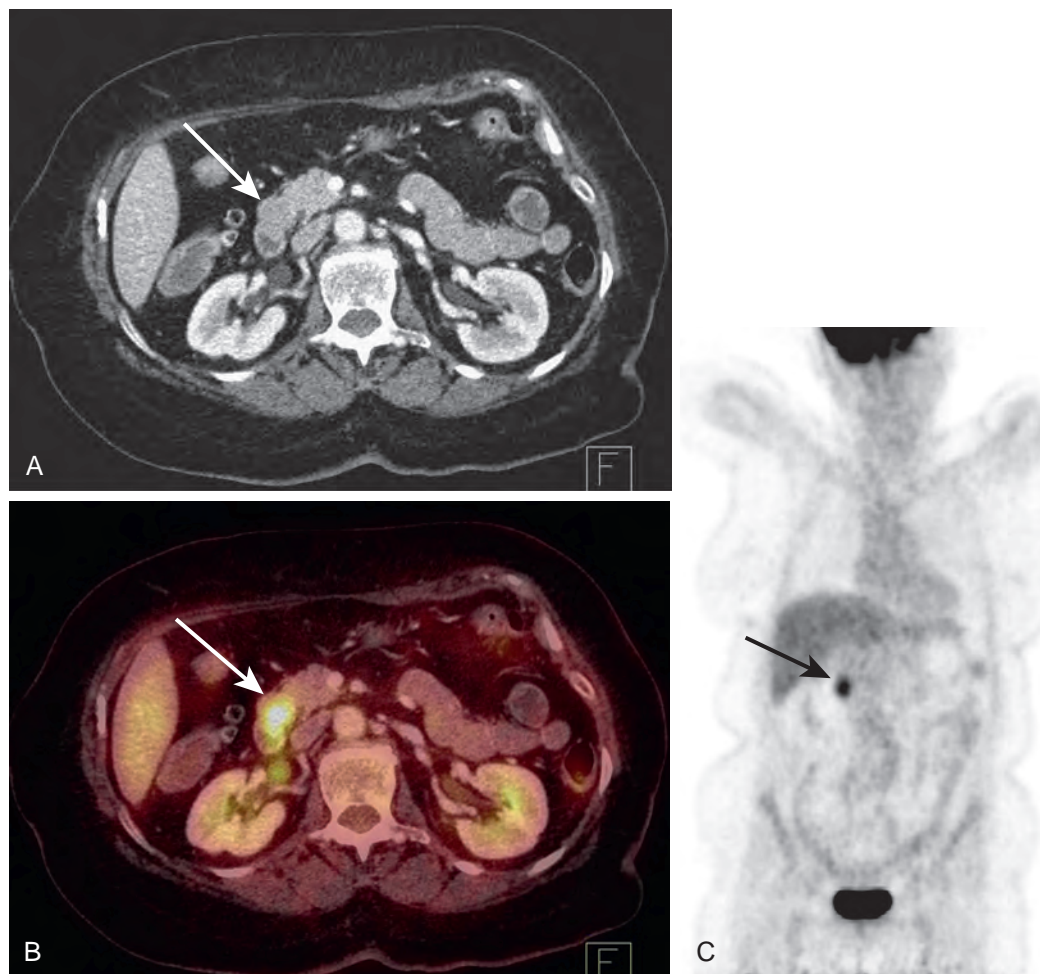
detection compared with 69% with FDG-PET.¹⁰⁸ These modalities are relatively new and warrant further investigation to gain acceptance in clinical practice.

To conclude, although PET may not have a role in the detection of the primary tumor and regional lymph nodes, it may provide valuable information with regard to increased specificity of findings, detection of distant metastases, and evaluation of treatment response. Fused PET/CT has been of additional value for various cancers, but its role in gastric cancer has yet to be fully determined. Initial results of studies investigating some new PET radiotracers appear promising.

Small Bowel

The most common small bowel cancer is adenocarcinoma which is mostly seen in the duodenum, followed by the jejunum, with the exception of patients with Crohn's disease, in whom the most common location is the ileum.^{109,110} Metastases to the small bowel can also occur, usually seen with malignant melanoma, followed by breast and lung cancers.^{111,112} Less commonly seen tumors of the small bowel include neuroendocrine tumors (NETs), gastrointestinal stromal tumors (GISTs), and sarcomas (Fig. 7-2). Some form of surgical treatment is offered with curative intent during early-stage cancer and for palliation, primarily to prevent obstruction in the more advanced stages. Neoadjuvant therapy is frequently used in

Figure 7-2 Duodenal neuroendocrine tumor. **A.** Axial contrast-enhanced CT scan shows a round mass at the junction of the descending and transverse duodenum (arrow). **B, C.** Corresponding axial fused PET/CT scan (**B**) and whole-body coronal maximum intensity projection (MIP) PET scan (**C**) demonstrate focal, intense FDG uptake in the mass (arrow). Also note the diffuse heterogeneous low-level uptake of the small bowel in the background.



more locally advanced disease, along with subsequent surgical resection, whereas systemic chemotherapy, which appears to provide a modest survival benefit, is offered to patients with more widespread disease.¹¹³ Given the variety of surgical and medical treatment options, accurate staging is crucial in deciding the optimal treatment to provide the most survival benefit to patients while minimizing unnecessary, treatment-related morbidity. Given the rarity of this type of cancer, the usefulness of PET/CT for the diagnosis and work-up of these patients has not been extensively investigated.

The most common appearance of small bowel carcinoma on PET/CT is focal or segmental wall thickening, with intense FDG uptake.¹¹⁰ However, potential pitfalls in interpretation exist and should be kept in mind to avoid misdiagnoses. The small bowel normally demonstrates diffuse, mildly heterogeneous FDG uptake, which may be more prominent in the pelvis, with multiple bowel loops overlying each other.²³ FDG uptake in the small bowel uptake is nonspecific and can be seen with various infectious and inflammatory causes, including Crohn's disease¹¹⁴ (Fig. 7-3). Primary and metastatic small bowel malignancies, GISTs, and lymphomatous involvement of the small bowel can also show FDG uptake. Interpretation of the PET scans should be made in conjunction with CT findings to localize and characterize focal unexpected FDG uptake accurately, because a variety of bowel wall-thickening patterns have been well described in the CT literature.^{115,116}

In patients suspected to have advanced disease, PET/CT would have the potential added benefit of staging the disease by identifying locoregional lymph node and distant metastases, evaluating treatment response, and restaging the disease

subsequent to treatment. PET/CT has been used successfully in the imaging of small bowel tumors, as reported in various studies.¹¹⁷⁻¹²⁰ PET/CT permits the detection and characterization of local and distant lymph node involvement and identification of unsuspected distant metastases, including the liver. Its added benefit has been proven in the work-up of patients with other GI tract malignancies, including esophageal, colorectal, and gastric cancers (see earlier). Currently, however, PET-CT's accuracy and added benefit for detecting local and distant metastatic disease from small bowel adenocarcinoma have not yet been studied sufficiently to allow for their accurate determination.

GISTs are nonepithelial neoplasms typically arising in the bowel wall, mesentery, or omentum. Most GISTs occur in the stomach, followed by the small bowel, accounting for approximately 10% to 15% of small bowel cancers. All GISTs have malignant potential, with a worse prognosis in those that are of nongastric origin, large in size, and with a high mitotic index.¹²¹ PET has been used for detecting the malignant potential of GISTs by the use of FDG uptake and for assessing metastatic disease before surgery for accurate staging.¹²²⁻¹²⁴ However, its full potential for the work-up of patients with GISTs, as well as the indications and the selection of patients for which PET/CT would be useful, are yet to be determined.

NETs are typically not FDG-avid, so novel PET radiotracers such as ⁶⁸gallium-DOTATATE, ⁶⁸gallium-DOTA-NOC, and ¹⁸F-L-DOPA are being developed for applications in NET evaluation and have shown highly promising results. In a study by Haug and co-workers, ⁶⁸gallium-DOTATATE PET/CT identified NET in 29 of 36 patients and excluded the presence of a NET in 61 of 68 non-NET patients in a pool of 104 patients suspected to have NET.¹²⁵ They reported a sensitivity of 81% and specificity of 90%. PET/CT had false-positive and false-negative results in 7 patients, with each indicating positive and negative predictive values of 81% and 90%, respectively, and an accuracy of 87%.^{125,126}

The use of PET/CT for the evaluation of small bowel tumors has yet to be determined, given the lack of sufficient data, which are restricted by the rarity of this type of cancer. Based on our experience, as well as extensive data obtained for other GISTs, PET/CT could be used as an adjunctive modality in the work-up of patients with small bowel tumors to detect local and advanced stages of the disease.

Colon and Rectum

Colorectal cancer is the third most common cancer in men and women and the second leading cause of cancer mortality in the United States. The National Cancer Institute estimated that approximately 142,000 new diagnoses would be made and 50,000 patients would die from colorectal cancer in 2013.¹²⁷ Surgery is the most common and only potentially curative treatment option for patients who do not have widespread distant metastases. Almost all patients with colon cancer undergo some form of surgery, whether an attempt for palliation or cure. Surgical resection of limited metastatic disease to the liver is also frequently performed. Patients with early-stage rectal cancer undergo local excision and/or radiation therapy, whereas for those with locally advanced disease, neoadjuvant chemoradiation followed by surgery is frequently used.

Although CMS has approved the use of PET and PET/CT in the diagnosis, staging, and restaging of colorectal cancer, the

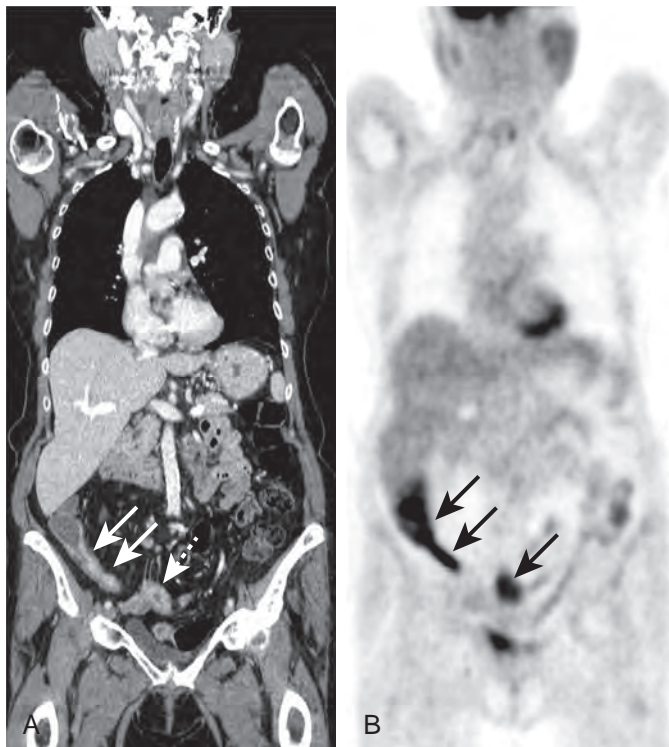


Figure 7-3 Crohn's disease. **A.** Coronal contrast-enhanced CT scan demonstrates bowel wall thickening and increased enhancement in the terminal ileum (solid arrows) and in the distal small bowel loops (dashed arrow). **B.** Corresponding whole-body MIP PET scan shows intense FDG uptake in the affected bowel loops (arrows).

main role of PET in the management of colorectal cancer is in the evaluation of locoregional lymph node and distant metastases. PET has limited value in the initial diagnosis and screening of colorectal cancer. In a study by Chen and colleagues investigating the use of PET as a screening tool in 3210 asymptomatic individuals, only 14 advanced adenoma (>1 cm) and 6 cancer diagnoses were made.¹²⁸ At present, radiation and cost considerations, as well as low positive predictive values, prohibit PET from gaining widespread acceptance as a screening tool.

FDG uptake in the colon is heterogeneous, and diffuse low intensity uptake is common. Focal, moderately intense physiologic uptake can also be seen, especially surrounding the ileocecal valve and in the right colon secondary to a high concentration of lymphoid tissue in this region.¹²⁹ Despite the high sensitivity of PET for the detection of primary tumors (95% to 100%), its specificity is limited because of a high number of benign pathologies that show focal, intense FDG uptake, such as diverticulitis, appendicitis, and abscess formation,^{23,130} which leads to a high number of false-positive studies. However, when there is focal and intense colonic uptake incidentally seen on the PET scan obtained for other indications, correlation with the CT scan is invaluable, because the diagnoses for benign causes of FDG uptake are readily made by CT. Clinical correlation for inflammatory or infectious causes of FDG uptake, such as inflammatory bowel disease or infectious colitis, should be made. In a study by Agress and Cooper, which reviewed the clinical significance of unexpected, abnormal, focal FDG uptake in 1750 patients with PET scans obtained to evaluate known or suspected malignancies, 26 patients with focal colorectal uptake were identified. Among these, 18 were found to be adenomas, 3 were cancers, 2 had benign causes, and 3 were found to be false-positives.¹³¹ Therefore in patients for whom there is no related known diagnosis and CT is unable to explain the uptake, or shows a distinct mass, findings should not be ignored, and endoscopic evaluation should be recommended.

Guidelines for screening of colorectal cancer in average-risk adults were last updated in 2008 in an evidence-based consensus statement that included the U.S. Multisociety Task Force (USMSTF) on Colorectal Cancer (which included the American College of Gastroenterology, American Gastroenterologic Association, and American Society for Gastrointestinal Endoscopy), ACS, and American College of Radiology (ACR). These recommendations were based on tests for cancer detection or tests for cancer and adenomatous polyp detection starting at the age of 50 years.¹³² The former included an annual, guaiac-based, fecal occult blood test, annual fecal immunochemical test, or stool DNA test, all tests with high sensitivity for cancer. The latter group included flexible sigmoidoscopy every 5 years, colonoscopy every 10 years, double-contrast barium enema every 5 years, and CT colonography every 5 years. The guidelines stated that all recommended tests were acceptable options and stressed shared, informed decision making with patients. PET/CT has no role in screening for colorectal cancer for these reasons and was not included in the guidelines.

STAGING

The AJCC recommends the TNM staging system for the clinical staging of colorectal cancer. Because surgery is frequently performed for curative purposes in the early stage of colon cancer, and for palliation or management of complications in the

advanced stage, current staging schemes are based on surgical and pathologic data.³ Although surgical staging is superior because of the evaluation of tumor depth in the bowel wall and microscopic involvement of regional lymph nodes on histopathology, attempts to determine accurate staging during the initial imaging evaluation are important to steer the nature of the surgery, whether it is palliative or curative in intent. The ACR has recommended CT scanning of the chest, abdomen, and pelvis as the initial pretreatment screening study for colon and rectal cancers.¹³³ CT provides speed, convenience, and an overall picture of disease status, permitting identification of complications such as obstruction or perforation from the tumor, which may not be clinically apparent. Accurate local and regional staging is even more important with rectal cancers because it determines the need for administering neoadjuvant chemoradiation. The added benefit of PET/CT in staging is appreciated most with more advanced disease.

The sensitivity of PET for the detection of the primary tumor is up to 100% in patients with a known diagnosis¹³⁴ (Fig. 7-4). A potential weakness of PET in primary tumor detection is that it may have a decreased sensitivity for lesions smaller than 1 cm because of limited spatial resolution and for certain tumor cells such as those of mucinous adenocarcinoma.^{135,136} Despite the strength of PET for the detection of the primary tumor, it does not provide sufficient detail about the depth of tumor penetration through the bowel layers to assess the T stage of disease, which is particularly important for treatment planning in rectal cancer. Patients with transmural disease undergo

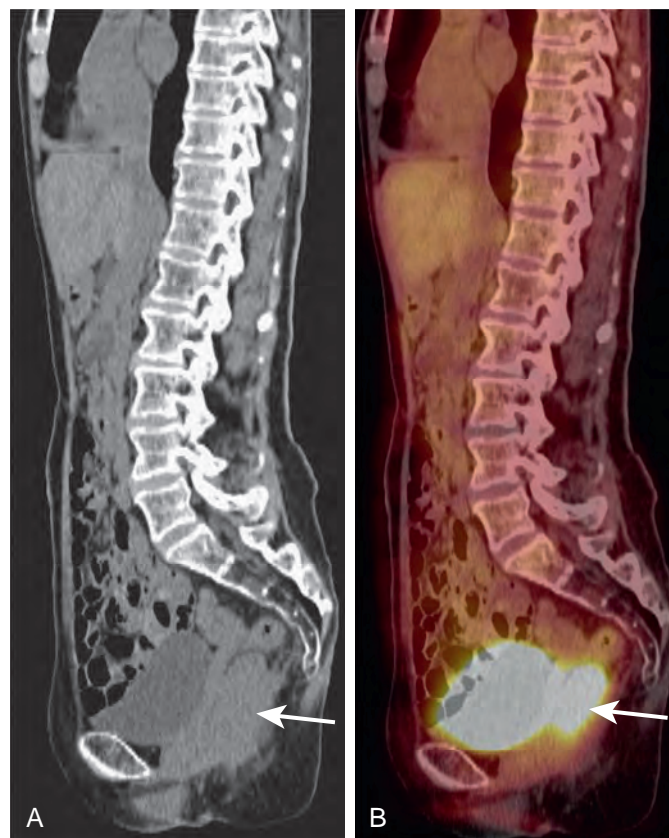


Figure 7-4 Rectal cancer. **A.** Sagittal non-contrast-enhanced CT scan shows a midrectal mass (arrow). **B.** Corresponding sagittal fused PET/CT image demonstrates intense FDG uptake in the mass (arrow).

neoadjuvant chemoradiation, whereas those with disease limited to the bowel wall undergo primary surgical resection.¹³⁷ CT cannot discriminate bowel layers either, and its accuracy is limited unless there is gross wall penetration or perirectal invasion by the tumor. A meta-analysis investigating the use of endorectal US, CT, and MRI for the assessment of perirectal invasion has reported a significantly higher sensitivity for US than for CT.¹³⁸ For small rectal tumors, the initial imaging recommendation to assess tumor depth is endorectal US. For large tumors, MRI of the pelvis with contrast is recommended, because endorectal US is very accurate for staging superficial T1 and T2 tumors, but less so for T3 and T4 tumors, which require evaluation of the perirectal fat and mesorectal fascia.^{139,140} All the conventional imaging modalities are limited, however, in the differentiation of peritumoral desmoplastic reaction from actual tumor.¹⁴¹

Because most patients undergo some form of colectomy, the extent of local disease can be histopathologically evaluated by the excision of pericolic and mesenteric lymph nodes. The intensity of uptake in the primary tumor may obscure adjacent small lymph nodes in PET/CT, and it may not detect microscopic involvement; therefore, it has limited value in the preoperative staging of local disease. In a recent meta-analysis by Lu and associates, PET/CT had a pooled sensitivity and specificity of 42.9% and 87.9%, respectively, for the detection of local lymph nodes.¹⁴² Although PET is less sensitive, it was shown to be more specific for the detection of locoregional lymph nodes compared with CT in various studies.^{134,143,144} Given its specificity, PET/CT could be used to improve the detection of finding metastatic lymph nodes that are not in the operative field depicted by other imaging modalities.

The main role of PET/CT in staging colorectal cancer is in the detection of distant metastases (Fig. 7-5). Colorectal cancer most commonly metastasizes to the liver and lungs, followed by

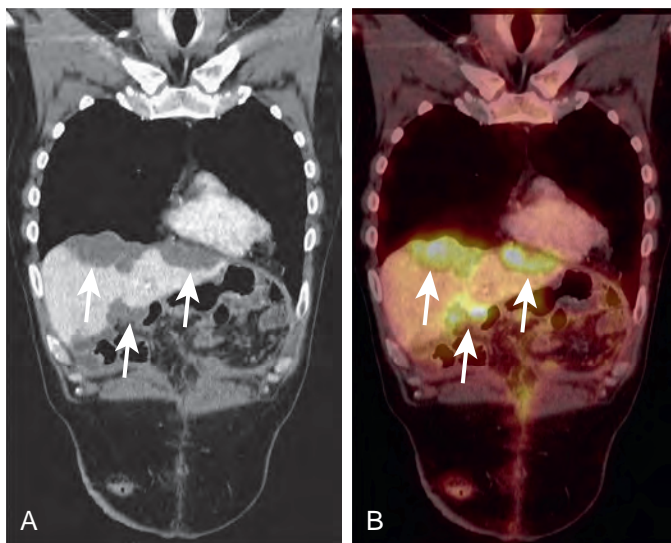


Figure 7-5 Metastatic colon cancer. **A.** Coronal contrast-enhanced CT scan demonstrates multiple, low-density peritoneal implants (arrows) along the surface of the liver in this patient with known mucinous adenocarcinoma of the colon. **B.** Corresponding coronal fused PET/CT shows intense FDG uptake in the peritoneal deposits (arrows). Mucinous tumors have variable and frequently low FDG uptake. However, in this patient, the metastases had intense FDG uptake.

retroperitoneal and iliac lymph nodes, bone, adrenal glands, and soft tissues. Hepatic metastases are most common and are present during initial presentation in approximately 30% of patients. Accurate detection and localization of hepatic metastases are very important, especially if resection of metastatic liver lesions is planned. Some patients may be deemed inoperable, whereas in others more extensive resections may be performed. Currently, contrast-enhanced CT is established as the primary imaging modality to detect and characterize focal liver lesions.¹⁴⁵ MRI is then recommended for further characterization of suspicious or equivocal lesions detected by CT. PET is limited in its ability to detect hepatic metastases smaller than 1 cm,¹⁴⁶ but it is more sensitive and specific compared with CT alone for the detection of hepatic and extrahepatic metastases. Among 43 patients who were evaluated with PET and CT prior to resection of colorectal liver metastases, PET identified additional lesions in 10 patients, which led to cancellation of the surgery in 6 of the patients.¹⁴⁷ In a recent meta-analysis, which included 3391 patients with colorectal cancer metastatic to the liver, the sensitivities of CT, MRI, and FDG-PET were 83.6%, 88.2%, and 94.1%, respectively.¹⁴⁸ When performing a PET/CT, the importance of obtaining a fully diagnostic CT scan, including the portal-venous phase, becomes paramount, especially for the detection of hypoenhancing lesions and potentially non-FDG-avid lesions, commonly seen in cancers of mucinous histology. With recent technologic advances, such as diffusion-weighted imaging and hepatobiliary-specific contrast agents, MRI is becoming increasingly valuable and even more sensitive, especially for the detection of subcentimeter liver metastases. Sahani and co-workers compared PET with MRI using a liver-specific contrast medium, mangafodipir trisodium, for the detection of liver metastases; MRI and FDG-PET had sensitivities of 96.6% and 93.3%, positive predictive values of 100% and 90.3%, and accuracies of 97.1% and 85.3%, respectively.¹⁴⁶ Of the 33 subcentimeter lesions (33 of 79), all were identified by MRI, whereas only 12 were detected by PET.

In a meta-analysis by Wiering and colleagues, the pooled sensitivity and specificity of FDG-PET for detecting hepatic lesions were 88.0% and 96.1%, respectively, and 91.5% and 95.4%, respectively, for extrahepatic disease in colorectal cancer.¹⁴⁹ In contrast with CT, the pooled sensitivity and specificity for hepatic lesions were 82.7% and 84.1%, respectively, and were 60.9% and 91.1%, respectively, for extrahepatic disease. PET resulted in a change of clinical management in 31.6% of patients. PET/CT was found to upstage 14%, downstage 17%, and alter management in approximately 12% of patients with primary rectal carcinoma compared with conventional imaging in a study by Davey and associates.¹⁵⁰ Another study by Gearhart and co-workers investigated the added benefit of PET/CT compared with transrectal US and CT, PET/CT identified discordant findings in 38% of patients, which resulted in a change of treatment plan in 27% of patients.¹⁵¹ These studies clearly indicate that the use of FDG-PET has added value in the diagnostic work-up of patients with colorectal cancer, especially in the evaluation of distant metastases.

RESTAGING AND TREATMENT RESPONSE

For the detection of recurrence in patients treated for colorectal cancer, routine surveillance is mandatory. The American Society of Clinical Oncology (ASCO) recommends annual CT of the chest, abdomen, and pelvis for 3 years, history and physical

examination every 3 to 6 months for the initial 3 years and every 6 months for years 4 and 5, determination of serum carcinoembryonic antigen (CEA) levels every 3 months postoperatively for 3 years, and colonoscopy at 3 years following surgery for surveillance of patients treated for colorectal cancer.¹⁵²

Most common sites of recurrence are locoregional or metastases in the liver. In a retrospective analysis of a total of 2657 patients who had curative resection for colonic cancer, a 5-year cumulative rate of 12.8% and 25.6% was found for local recurrence and distant metastases, respectively.¹⁵³ The most significant risk factor for recurrence was found to be the stage of disease at diagnosis. In a study investigating factors indicating improved survival and recurrence subsequent to resection of colorectal cancer, it was found that young age, general good health, surgery on an elective basis, and early-stage tumor at the time of resection helped improve 10-year survival of patients.¹⁵⁴ Another population-based analysis of 3375 patients with colon cancer found a 5-year cumulative rate of local recurrence of 7.6% in tumors resected for curative intent.¹⁵⁵ Rates of local recurrence are slightly higher with rectal cancer, especially lower rectal cancer, compared with colon cancer. Upper and midrectal cancers are successfully treated with total mesorectal excision, with low recurrence rates, whereas low rectal cancers have higher recurrence rates of up to 10% at 2 years.^{156,157} This is largely because of the scarcity of perirectal fat in the lower rectum, leading to challenges in obtaining an adequate, negative surgical margin during resection.

CT has its limitations in the detection of local recurrence because of distortion of anatomy in the post-treatment bed. Recurrence with extensive inflammatory changes and fibrosis secondary to surgery and radiation therapy may not be morphologically apparent until it is too late. Interpretation of post-treatment changes in the presacral space and pelvis following treatment for rectal cancer is especially challenging. Recurrence in this region reveals itself with very subtle soft tissue changes on CT scans over a long period. In cases of local recurrence, although only 20% of patients can have repeated, complete resection, early discrimination is important because it can enable prompt intervention and may affect patient survival.¹⁵⁸ Because PET is based on metabolic activity, it can better differentiate post-treatment changes from recurrent or residual tumor compared with CT. It is important, however, to keep in mind that in the immediate postsurgical or postradiation treatment period (within the first 3 months), false-positive FDG uptake can be seen.¹⁵⁹ PET has been shown to be more sensitive compared with CT in the presacral region, with a sensitivity and specificity of 100% and 96%, respectively.^{160,161} A recent meta-analysis, which included 510 patients, PET/CT had a pooled sensitivity of 94.1% and specificity of 77.2% in the detection of overall tumor recurrence for colorectal cancer.¹⁶²

In keeping with the ASCO recommendations, serum CEA levels are determined for routine surveillance.¹⁵² CEA levels can detect recurrence with a sensitivity of 59% and specificity of 84%.¹⁶³ CT is commonly used when there is suspected recurrence but has limitations in detecting recurrent metastatic disease when recurrence is in the peritoneum or small lymph nodes or if the tumor is metabolically active but not morphologically apparent. PET/CT can often find sites of disease in patients with abnormal CEA levels but no identifiable metastatic disease on conventional diagnostic work-up. A study by Hung and colleagues, which compared PET, CT, and serum CEA levels for the evaluation of recurrent disease demonstrated

sensitivity and specificity values of 100% and 83% for PET, 33% and 86% for serum CEA level elevation, and 78% and 61% for CT, respectively.¹⁶⁴ A recent study of PET/CT for the detection of recurrent or metastatic disease in patients with a history of colorectal cancer and elevated CEA levels found the sensitivity of PET/CT and CT to be 97.3% and 70.3%, with an equal specificity of 94.4%.¹⁶⁵ In a group of 84 patients, Votruba and associates found that the sensitivity, specificity, and overall accuracy of PET were 80%, 69%, and 75%, respectively, compared with 89%, 92%, and 90%, respectively, for PET/CT for the detection of hepatic and extrahepatic metastatic disease.¹⁶⁶ As with initial staging, distant metastatic disease is identified with a greater sensitivity and accuracy with PET/CT in patients with recurrence from colorectal cancer compared with conventional imaging modalities.

PET/CT is the most sensitive and specific method for detecting overall recurrence, especially at distant sites. Patients with advanced disease are usually treated with a combination of 5-fluorouracil with newer agents, such as irinotecan and oxaliplatin. The 5-year survival with chemotherapy alone is historically less than 1%, although two recent clinical trials using FOLFOX (folinic acid, 5-fluorouracil, and oxaliplatin), FOLFIRI (folinic acid, 5-fluorouracil, oxaliplatin, and irinotecan), or a combination of the two, reported 5-year survival rates of 5% to 10%.^{167,168} Earlier reports suggested that PET/CT is useful in monitoring treatment response to systemic chemotherapy in colorectal cancer and altering treatment when needed.¹⁶⁹ However, several studies have challenged the accuracy of PET/CT in patients who received chemotherapy. In a recent meta-analysis, the pooled sensitivity estimates of MRI, CT, PET, and PET/CT were 85.7%, 69.9%, 54.5%, and 51.7%, respectively, for the detection of colorectal liver metastases in patients treated with neoadjuvant chemotherapy; it was concluded that MRI was the most effective modality for this patient group.¹⁷⁰ Another study showed significantly decreased FDG uptake in colorectal liver metastases in patients treated preoperatively with chemotherapy, resulting in less efficient tumor detection.¹⁷¹ In this report, the explanation given for the decreased accuracy of PET was the significant decrease in hexokinase activity in the metastatic liver tumors following chemotherapy.

Despite advancements in systemic chemotherapy, liver resection is the most effective treatment for achieving long-term survival, offering the possibility of cure in advanced-stage disease confined to the liver.^{172,173} In a study by Selznert and co-workers, PET/CT was superior in establishing the diagnosis of intrahepatic recurrences in patients with hepatectomy, with a specificity of 100% versus 50% for CT.¹⁷⁴

Percutaneous thermal ablation is frequently used in the management of metastatic liver lesions in patients who are not operative candidates because of existing comorbidities. Thermal ablation in these patients has been shown to improve survival.^{175,176} Differentiation between postablation changes and residual disease may at times be challenging with morphologic imaging studies such as CT and MRI. PET can metabolically evaluate the ablation zone in equivocal cases on conventional imaging or in patients in whom additional hepatic or extrahepatic disease is suspected.¹⁷⁷⁻¹⁸⁰ Following ablation, FDG-avid lesions become photopenic, reflecting adequate treatment. Similar to contrast enhancement features of CT, focal areas of increased FDG uptake within the ablation zone suggest residual disease. Inflammatory reactive changes surrounding the

ablation zone usually show uniform, low-level uptake, whereas uptake in residual or recurrent disease is focal, nodular, and intense.¹⁸¹ Lesions that have no enhancement or diffuse peripheral enhancement on CT or MRI often have focal uptake on PET, which could be used to direct subsequent biopsy or repeated thermal ablation.

Numerous liver-directed therapies are available for treating unresectable liver metastases, including radioembolization with yttrium 90 microspheres (Y90) or transarterial chemoembolization. These are second- or third-line treatment algorithms administered to stabilize liver disease, with minimal toxicity, in patients for whom standard systemic chemotherapy regimens have failed. PET/CT has been used to evaluate treatment response to transcatheter arterial chemoembolization and radioembolization with Y90 microspheres.¹⁸² A study by Wong and colleagues showed that a metabolic response after 90Y treatment to one or both hepatic lobes was present in a significantly higher proportion of the lobes assessed by PET compared

with an anatomic response evaluated by CT or MRI.¹⁸³ Further studies are needed evaluating the accuracy and added benefit of PET in patients treated with transarterial, liver-directed therapies.

CT and MRI are more commonly used in current clinical practice for the evaluation of treatment response in the liver. At present, the optimal timing for imaging, cost concerns, and protocols for evaluating treatment response have not yet been established, which prohibit the use of PET/CT as a standard method for evaluating treatment response. However, PET/CT could be used as a problem-solving tool for patients in whom conventional imaging modalities do not provide sufficient information for critical decision making.

In summary, it has been found that PET/CT has the greatest impact for the detection of previously unrecognized sites of hepatic or extrahepatic metastases, detection of local recurrence in the treatment bed, and restaging in patients with suspected local or distant recurrent disease.

REFERENCES

- Ben-Haim S, Ell P: 18F-FDG PET and PET/CT in the evaluation of cancer treatment response. *J Nucl Med* 50:88–99, 2009.
- Kelloff GJ, Hoffman JM, Johnson B, et al: Progress and promise of FDG-PET imaging for cancer patient management and oncologic drug development. *Clin Cancer Res* 11:2785–2808, 2005.
- Rohren EM, Turkington TG, Coleman RE: Clinical applications of PET in oncology. *Radiology* 231:305–332, 2004.
- Shreve PD, Anzai Y, Wahl RL: Pitfalls in oncologic diagnosis with FDG PET imaging: physiologic and benign variants. *Radiographics* 19:61–77, 1999.
- Blake MA, Singh A, Setty BN, et al: Pearls and pitfalls in interpretation of abdominal and pelvic PET-CT. *Radiographics* 26:1335–1353, 2006.
- Adams MC, Turkington TG, Wilson JM, Wong TZ: A systematic review of the factors affecting accuracy of SUV measurements. *AJR* 195:310–320, 2010.
- Brady MJ, Thomas J, Wong TZ, et al: Adrenal nodules at FDG PET/CT in patients known to have or suspected of having lung cancer: A proposal for an efficient diagnostic algorithm. *Radiology* 250:523–530, 2009.
- Blodgett TM, Meltzer CC, Townsend DW: PET/CT: Form and function. *Radiology* 242:360–385, 2007.
- Bacharach SL: PET/CT attenuation correction: Breathing lessons. *J Nucl Med* 48:677–679, 2007.
- Antoch G, Freudenberg LS, Beyer T, et al: To enhance or not to enhance? 18F FDG and CT contrast agents in dual-modality 18F-FDG PET-CT. *J Nucl Med* 45(Suppl1):56S–65S, 2004.
- Antoch G, Freudenberg LS, Statta J, et al: Whole-body positron emission tomography-CT: optimized CT using oral and IV contrast materials. *AJR* 179:1555–1560, 2002.
- Dizendorf EV, Treyer V, von Schulthess GK, Hany TF: Application of oral contrast media in coregistered positron emission tomography-CT. *AJR* 179:477–481, 2002.
- Carney JP, Townsend DW: CT-based attenuation correction for PET/CT scanners. In Schulthess GV, editor: *Clinical PET, PET/CT and SPECT/CT: Combined Anatomic-Molecular Imaging*, Baltimore, 2002, Lippincott, Williams & Wilkins, pp 157–169.
- Cohade C, Osman M, Nakamoto Y, et al: Initial experience with oral contrast in PET/CT: Phantom and clinical studies. *J Nucl Med* 44:412–416, 2003.
- Dizendorf E, Hany TF, Buck A, et al: Cause and magnitude of the error induced by oral CT contrast agent in CT-based attenuation correction of PET emission studies. *J Nucl Med* 44:732–738, 2003.
- Nakamoto Y, Chin BB, Kraitchman DL, et al: Effects of nonionic intravenous contrast agents at PET/CT imaging: Phantom and canine studies. *Radiology* 227:817–824, 2003.
- de Juan R, Seifert B, Berthold T, et al: Clinical evaluation of a breathing protocol for PET/CT. *Eur Radiol* 14:1118–1123, 2004.
- Beyer T, Antoch G, Blodgett T, et al: Dual-modality PET/CT imaging: The effect of respiratory motion on combined image quality in clinical oncology. *Eur J Nucl Med Mol Imaging* 30:588–596, 2003.
- Gilman MD, Fischman AJ, Krishnasetty V, et al: Optimal CT breathing protocol for combined thoracic PET/CT. *AJR* 187:1357–1360, 2006.
- American Cancer Society: What are the key statistics about cancer of the esophagus? 2013. <http://www.cancer.org/cancer/esophagus-cancer/detailedguide/esophagus-cancer-key-statistics>.
- Yeung HW, Macapinlac HA, Mazumdar M, et al: FDG-PET in esophageal cancer: Incremental value over computed tomography. *Clin Positron Imaging* 2:255–260, 1999.
- Kostakoglu L, Hardoff R, Mirtcheva R, Goldsmith SJ: PET/CT fusion imaging in differentiating physiologic from pathologic FDG uptake. *Radiographics* 24:1411–1431, 2004.
- Prabhakar HB, Sahani DV, Fischman AJ, et al: Bowel hot spots at PET-CT. *Radiographics* 27:145–159, 2007.
- Bural GG, Kumar R, Mavi A, Alavi A: Reflux esophagitis secondary to chemotherapy detected by serial FDG-PET. *Clin Nucl Med* 30:182–183, 2005.
- Bhargava P, Reich P, Alavi A, Zhuang H: Radiation-induced esophagitis on FDG PET imaging. *Clin Nucl Med* 28:849–850, 2003.
- Heller MT, Meltzer CC, Fukui MB, et al: Superphysiologic FDG uptake in the nonparalyzed vocal cord: Resolution of a false-positive PET result with combined PET/CT imaging. *Clin Positron Imaging* 3:207–211, 2000.
- Truong MT, Erasmus JJ, Munden RF, et al: Focal FDG uptake in mediastinal brown fat mimicking malignancy: A potential pitfall resolved on PET/CT. *AJR* 183:1127–1132, 2004.
- Rice TW, Blackstone EH, Rusch VW: 7th edition of the AJCC Cancer Staging Manual: Esophagus and esophagogastric junction. *Ann Surg Oncol* 17:1721–1724, 2010.
- Eloubeidi MA, Wallace MB, Hoffman BJ, et al: Predictors of survival for esophageal cancer patients with and without celiac axis lymphadenopathy: Impact of staging endosonography. *Ann Thorac Surg* 72:212–229, 2001.
- Flamen P, Lerut A, Van Cutsem E, et al: Utility of positron emission tomography for the staging of patients with potentially operable esophageal carcinoma. *J Clin Oncol* 18:3202–3210, 2000.
- Kim K, Park SJ, Kim BT, et al: Evaluation of lymph node metastases in squamous cell carcinoma of the esophagus with positron emission tomography. *Ann Thorac Surg* 71:290–294, 2001.
- Rasanen JV, Sihvo EI, Knuuti MJ, et al: Prospective analysis of accuracy of positron emission tomography, computed tomography, and endoscopic ultrasonography in staging of adenocarcinoma of the esophagus and the esophagogastric junction. *Ann Surg Oncol* 10:954–960, 2003.

33. Fukunaga T, Okazumi S, Koide Y, et al: Evaluation of esophageal cancers using fluorine-18-fluorodeoxyglucose PET. *J Nucl Med* 39:1002–1007, 1998.
34. Wieder HA, Bernd J, Krause BJ, Herrmann K: PET and PET-CT in esophageal and gastric cancer. In Juweid ME, Hoekstra OS, editors: *Positron Emission Tomography (Methods in Molecular Biology, vol 727)*, Totowa, NJ, 2011, Humana Press, pp 59–76.
35. Little SG, Rice TW, Bybel B, et al: Is FDG-PET indicated for superficial esophageal cancer? *Eur J Cardiothoracic Surg* 31:791–796, 2007.
36. Cho JW: The role of endoscopic ultrasonography in T staging: Early gastric and esophageal cancer. *Clin Endosc* 46:239–242, 2013.
37. Puli SR, Reddy JB, Bechtold ML, et al: Staging accuracy of esophageal cancer by endoscopic ultrasound: A meta-analysis and systemic review. *World J Gastroenterol* 14:1479–1490, 2008.
38. Lerut T, Flamen P, Ectors N, et al: Histopathologic validation of lymph node staging with FDG-PET scan in cancer of the esophagus and gastroesophageal junction: A prospective study based on primary surgery with extensive lymphadenectomy. *Ann Surg* 232:743–752, 2000.
39. van Westreenen HL, Westerterp M, Bossuyt PM, et al: Systematic review of the staging performance of 18F-fluorodeoxyglucose positron emission tomography in esophageal cancer. *J Clin Oncol* 22:3805–3812, 2004.
40. Kato H, Miyazaki T, Nakajima M, et al: The incremental effect of positron emission tomography on diagnostic accuracy in the initial staging of esophageal carcinoma. *Cancer* 103:148–156, 2005.
41. Yuan S, Yu Y, Chao KS, et al: Additional value of PET/CT over PET in assessment of locoregional lymph nodes in thoracic esophageal squamous cell cancer. *J Nucl Med* 47:1255–1259, 2006.
42. Kim TJ, Kim HY, Lee KW, Kim MS: Multimodality assessment of esophageal cancer: Preoperative staging and monitoring of response to therapy. *Radiographics* 29:403–421, 2009.
43. Urschel JD, Vasan H: A meta-analysis of randomized controlled trials that compared neoadjuvant chemoradiation and surgery to surgery alone for resectable esophageal cancer. *Am J Surg* 185:538–543, 2003.
44. Kato H, Kuwano H, Nakajima M, et al: Comparison between positron emission tomography and computed tomography in the use of the assessment of esophageal carcinoma. *Cancer* 94:921–928, 2002.
45. Quint LE, Hepburn LM, Francis IR, et al: Incidence and distribution of distant metastases from newly diagnosed esophageal carcinoma. *Cancer* 76:1120–1125, 1995.
46. Flanagan FL, Dehdashti F, Siegel BA, et al: Staging of esophageal cancer with 18F-fluorodeoxyglucose positron emission tomography. *AJR* 168:417–424, 1997.
47. Meltzer CC, Luketich JD, Friedman D, et al: Whole-body FDG positron emission tomographic imaging for staging esophageal cancer comparison with computed tomography. *Clin Nucl Med* 25:882–887, 2000.
48. Luketich JD, Schauer PR, Meltzer CC, et al: Role of positron emission tomography in staging esophageal cancer. *Ann Thorac Surg* 64:76–79, 1997.
49. Rice TW: Clinical staging of esophageal carcinoma: CT, EUS, and PET. *Chest Surg Clin N Am* 10:471–485, 2000.
50. Rankin SC, Taylor H, Cook GJ, Mason R: Computed tomography and positron emission tomography in the pre-operative staging of oesophageal carcinoma. *Clin Radiol* 53:659–665, 1998.
51. Heeren PA, Jager PL, Bongaerts F, et al: Detection of distant metastases in esophageal cancer with (18)F-FDG PET. *J Nucl Med* 45:980–987, 2004.
52. Guo H, Zhu H, Xi Y, et al: Diagnostic and prognostic value of 18F-FDG PET/CT for patients with suspected recurrence from squamous cell carcinoma of the esophagus. *J Nucl Med* 48:1251–1258, 2007.
53. Flamen P, Lerut A, Van Cusem E, et al: The utility of positron emission tomography for the diagnosis and staging of recurrent esophageal cancer. *J Thorac Cardiovasc Surg* 120:1085–1092, 2000.
54. Westerterp M, van Westreenen HL, Reitsma JB, et al: Esophageal cancer: CT, endoscopic US, and FDG PET for assessment of response to neoadjuvant therapy—systematic review. *Radiology* 236:841–851, 2005.
55. Cerfolio RJ, Bryant AS, Ohja B, et al: The accuracy of endoscopic ultrasonography with fine-needle aspiration, integrated positron emission tomography with computed tomography, and computed tomography in restaging patients with esophageal cancer after neoadjuvant chemoradiotherapy. *J Thorac Cardiovasc Surg* 129:1232–1241, 2005.
56. Adham M, Baulieux J, Mornex F, et al: Combined chemotherapy and radiotherapy followed by surgery in the treatment of patients with squamous cell carcinoma of the esophagus—the Croix Rousse experiences. *Cancer* 89:946–954, 2000.
57. Mariette C, Piessen G, Lamblin A, et al: Impact of preoperative radiochemotherapy on postoperative course and survival in patients with locally advanced squamous cell oesophageal carcinoma. *Br J Surg* 93:1077–1083, 2006.
58. Rohatgi P, Swisher S, Correa A, et al: Histologic subtypes as determinants of outcome in esophageal carcinoma patients with pathologic complete response after preoperative chemoradiotherapy. *Cancer* 106:552–558, 2006.
59. Bedenne L, Michel P, Bouche O, et al: Chemoradiation followed by surgery compared with chemoradiation alone in squamous cancer of the esophagus: FFOCD 9102. *J Clin Oncol* 25:1160–1168, 2007.
60. Cerfolio RJ, Bryant AS: Maximum standardized uptake values on positron emission tomography of esophageal cancer predicts stage, tumor biology, and survival. *Ann Thorac Surg* 82:391–394, 2006.
61. Pan L, Gu P, Huang G, et al: Prognostic significance of SUV on PET/CT in patients with esophageal cancer: A systematic review and meta-analysis. *Eur J Gastroenterol Hepatol* 21:1008–1015, 2009.
62. Kato H, Kuwano H, Nakajima M, et al: Usefulness of positron emission tomography for assessing the response of neoadjuvant chemoradiotherapy in patients with esophageal cancer. *Am J Surg* 184:279–283, 2002.
63. Downey RJ, Akhurst T, Ilson D, et al: Whole body 18FDG-PET and the response of esophageal cancer to induction therapy: results of a prospective trial. *J Clin Oncol* 21:428–432, 2003.
64. Brucher BL, Weber W, Bauer M, et al: Neoadjuvant therapy of esophageal squamous cell carcinoma: Response evaluation by positron emission tomography. *Ann Surg* 233:300–309, 2001.
65. Weber WA, Ott K, Becker K, et al: Prediction of response to preoperative chemotherapy in adenocarcinomas of the esophagogastric junction by metabolic imaging. *J Clin Oncol* 19:3058–3065, 2001.
66. Ott K, Weber WA, Lordick F, et al: Metabolic imaging predicts response, survival, and recurrence in adenocarcinomas of the esophagogastric junction. *J Clin Oncol* 24:4692–4698, 2006.
67. Lordick F, Ott K, Krause BJ, et al: PET to assess early metabolic response and to guide treatment of adenocarcinoma of the oesophagogastric junction: The MUNICON phase II trial. *Lancet Oncol* 8:797–805, 2007.
68. Moertel CG, Hanley JA: The effect of measuring error on the results of therapeutic trials in advanced cancer. *Cancer* 38:388–394, 1976.
69. Eisenhauer EA, Therasse P, Bogaerts J, et al: New response evaluation criteria in solid tumours: Revised RECIST guideline (version 1.1). *Eur J Cancer* 45:228–247, 2009.
70. Michaelis LC, Ratain MJ: Measuring response in a post-RECIST world: From black and white to shades of grey. *Nat Rev Cancer* 6:409–414, 2006.
71. Wahl RL, Jacene H, Kasamon Y, Lodge MA: From RECIST to PERCIST: Evolving considerations for PET response criteria in solid tumors. *J Nucl Med* 50:122S–150S, 2009.
72. Yanagawa M, Tatsumi M, Miyata H, et al: Evaluation of response to neoadjuvant chemotherapy for esophageal cancer: PET response criteria in solid tumors versus response evaluation criteria in solid tumors. *J Nucl Med* 53:872–880, 2012.
73. Moureau-Zabotto L, Touboul E, Lerouge D, et al: Impact of CT and 18F-deoxyglucose positron emission tomography image fusion for conformal radiotherapy in esophageal carcinoma. *Int J Radiat Oncol Biol Phys* 63:340–345, 2005.
74. Muijs CT, Schreurs LM, Busz DM, et al: Consequences of additional use of PET information for target volume delineation and radiotherapy dose distribution for esophageal cancer. *Radiother Oncol* 93:447–453, 2009.
75. Leong T, Everitt C, Yuen K, et al: A prospective study to evaluate the impact of FDG-PET on CT-based radiotherapy treatment planning for oesophageal cancer. *Radiother Oncol* 78:254–261, 2006.
76. Yeoh KG: How do we improve outcomes for gastric cancer? *J Gastroenterol Hepatol* 22:970–972, 2007.
77. Gore RM: Gastric cancer: Clinical and pathologic features. *Radiol Clin North Am* 35:295–310, 1997.
78. Kim JP: Surgical results in gastric cancer. *Semin Surg Oncol* 17:132–138, 1999.
79. Bhandari S, Shim CS, Kim JH, et al: Usefulness of three-dimensional, multidetector row CT (virtual gastroscopy and multiplanar reconstruction) in the evaluation of gastric cancer: A comparison with conventional endoscopy, EUS, and histopathology. *Gastrointest Endosc* 59:619–626, 2004.
80. Habermann CR, Weiss F, Riecken R, et al: Preoperative staging of gastric adenocarcinoma: Comparison of helical CT and endoscopic US. *Radiology* 230:465–471, 2004.
81. Harisankar CN, Kashyap R, Bhattacharya A, Mittal BR: Fluoro-deoxy-glucose positron emission tomography/computed tomography pattern in a patient with linitis plastica of the

- stomach caused by primary signet cell adenocarcinoma. *World J Nucl Med* 11:26–27, 2012.
82. Lee SJ, Lee WW, Yoon HJ, et al: Regional PET/CT after water gastric inflation for evaluating loco-regional disease of gastric cancer. *Eur J Radiol* 82:935–942, 2013.
 83. Washington K: 7th edition of the AJCC cancer staging manual: Stomach. *Ann Surg Oncol* 17:3077–3079, 2010.
 84. Hasegawa S, Yoshikawa T, Shirai J, et al: A prospective validation study to diagnose serosal invasion and nodal metastases of gastric cancer by multidetector-row CT. *Ann Surg Oncol* 20:2016–2202, 2013.
 85. Lee KR, Levine E, Moffat RE, et al: Computed tomographic staging of malignant gastric neoplasms. *Radiology* 133:151–155, 1979.
 86. Komaki S, Toyoshima S: CT's capability in detecting advanced gastric cancer. *Gastrointest Radiol* 8:307–313, 1983.
 87. Ott K, Fink U, Becker K, et al: Prediction of response to preoperative chemotherapy in gastric carcinoma by metabolic imaging: Results of a prospective trial. *J Clin Oncol* 21:4604–4610, 2003.
 88. Cho JW: The role of endoscopic ultrasonography in T staging: Early gastric and esophageal cancer. *Clin Endosc* 46:239–242, 2013.
 89. Xi WD, Zhao C, Ren GS: Endoscopic ultrasonography in preoperative staging of gastric cancer: Determination of tumor invasion depth, nodal involvement and surgical resectability. *World J Gastroenterol* 9:254–257, 2003.
 90. Botet JF, Lightdale CJ, Zauber AG, et al: Preoperative staging of gastric cancer: Comparison of endoscopic US and dynamic CT. *Radiology* 181:426–432, 1991.
 91. Dassen AE, Lips DJ, Hoekstra CJ, et al: FDG-PET has no definite role in preoperative imaging in gastric cancer. *Eur J Surg Oncol* 35:449–455, 2009.
 92. Yun M, Lim JS, Noh SH, et al: Lymph node staging of gastric cancer using (18)F-FDG PET: A comparison study with CT. *J Nucl Med* 46:1582–1588, 2005.
 93. Mukai K, Ishida Y, Okajima K, et al: Usefulness of preoperative FDG-PET for detection of gastric cancer. *Gastric Cancer* 9:192–196, 2006.
 94. Namikawa T, Okabayashi T, Nogami M, et al: Assessment of ¹⁸F-fluorodeoxyglucose positron emission tomography combined with computed tomography in the preoperative management of patients with gastric cancer. *Int J Clin Oncol* 2013. [Epub ahead of print.]
 95. Stahl A, Ott K, Weber WA, et al: FDG PET imaging of locally advanced gastric carcinomas: Correlation with endoscopic and histopathologic findings. *Eur J Nucl Med Mol Imaging* 30:288–295, 2003.
 96. Yoshioka T, Yamaguchi K, Kubota K, et al: Evaluation of 18F-FDG PET in patients with advanced, metastatic, or recurrent gastric cancer. *J Nucl Med* 44:690–699, 2003.
 97. Enomoto K, Hamada K, Inohara H, et al: Mucosa-associated lymphoid tissue lymphoma studied with FDG-PET: A comparison with CT and endoscopic findings. *Ann Nucl Med* 22:261–267, 2008.
 98. Hoffmann M, Kletter K, Diemling M, et al: Positron emission tomography with fluorine-18-2-fluoro-2-deoxy-D-glucose (F18-FDG) does not visualize extranodal B-cell lymphoma of the mucosa-associated lymphoid tissue (MALT)-type. *Ann Oncol* 10:1185–1189, 1999.
 99. Kim SK, Kang KW, Lee JS, et al: Assessment of lymph node metastases using 18F-FDG PET in patients with advanced gastric cancer. *Eur J Nucl Med Mol Imaging* 33:148–155, 2006.
 100. Chen J, Cheong JH, Yun MJ, et al: Improvement in preoperative staging of gastric adenocarcinoma with positron emission tomography. *Cancer* 103:2383–2390, 2005.
 101. Lim JS, Yun MJ, Kim MJ, et al: CT and PET in stomach cancer: Preoperative staging and monitoring of response to therapy. *Radiographics* 26:143–156, 2006.
 102. Kim J, Lim ST, Na CJ, et al: Pretreatment F-18 FDG PET/CT parameters to evaluate progression-free survival in gastric cancer. *Nucl Med Mol Imaging* 48:33–40, 2014.
 103. Chang MC, Chen JH, Liang JA, et al: PET or PET/CT for detection of peritoneal carcinomatosis: A meta-analysis. *Clin Nucl Med* 38:623–629, 2013.
 104. Dalal KM, Woo Y, Kelly K, et al: Detection of micrometastases in peritoneal washings of gastric cancer patients by the reverse transcriptase polymerase chain reaction. *Gastric Cancer* 11:206–213, 2008.
 105. Rosenbaum SJ, Stergar H, Antoch G, et al: Staging and follow-up of gastrointestinal tumors with PET/CT. *Abdom Imaging* 31:25–35, 2006.
 106. Zou H, Zhao Y: 18FDG PET/CT for detecting gastric cancer recurrence after surgical resection: A meta-analysis. *Surg Oncol* 22:162–166, 2013.
 107. Staniuk T, Zegarski W, Małkowski B, et al: Evaluation of FLT-PET/CT usefulness in diagnosis and qualification for surgical treatment of gastric cancer. *Contemp Oncol (Pozn)* 17:165–170, 2013.
 108. Herrmann K, Ott K, Buck AK, et al: Imaging gastric cancer with PET and the radiotracers 18F-FLT and 18F-FDG: A comparative analysis. *J Nucl Med* 48:1945–1950, 2007.
 109. North JH, Pack MS: Malignant tumors of the small intestine: A review of 144 cases. *Am Surg* 66:46–51, 2000.
 110. Cronin CG, Scott J, Kambadakone A, et al: Utility of positron emission tomography/CT in the evaluation of small bowel pathology. *Br J Radiol* 85:1211–1221, 2012.
 111. Bender GN, Maglinte DD, McLarney JH, et al: Malignant melanoma: Patterns of metastasis to the small bowel, reliability of imaging studies, and clinical relevance. *Am J Gastroenterol* 96:2392–2400, 2001.
 112. Tulchinsky M, Coquia S, Wagner H, Jr: Small bowel metastasis from lung cancer detected on FDG PET/CT. *Clin Nucl Med* 34:446–448, 2009.
 113. Overman MJ: Recent advances in the management of adenocarcinoma of the small intestine. *Gastrointest Cancer Res* 3:90–96, 2009.
 114. Neurath MF, Vehling D, Schunk K, et al: Non-invasive assessment of Crohn's disease activity: A comparison of 18F-fluorodeoxyglucose positron emission tomography, hydromagnetic resonance imaging, and granulocyte scintigraphy with labeled antibodies. *Am J Gastroenterol* 97:1978–1985, 2002.
 115. Horton KM, Fishman EK: Multidetector-row computed tomography and 3-dimensional computed tomography imaging of small bowel neoplasms: Current concept in diagnosis. *J Comput Assist Tomogr* 28:106–116, 2004.
 116. Buckley JA, Fishman EK: CT evaluation of small bowel neoplasms: Spectrum of disease. *Radiographics* 18:379–392, 1998.
 117. Watanabe N, Hayashi S, Kato H, et al: FDG-PET imaging in duodenal cancer. *Ann Nucl Med* 18:351–353, 2004.
 118. Sperti C, Pasquali C, Fiore V, et al: Clinical usefulness of 18-fluorodeoxyglucose positron emission tomography in the management of patients with nonpancreatic periampullary neoplasms. *Am J Surg* 191:743–748, 2006.
 119. Han EJ, Yoo IeR, Choi WH, Lee KY: Adenocarcinoma arising in Meckel's diverticulum on 18F-FDG PET/CT. *Clin Nucl Med* 38:e157–e159, 2013.
 120. Choda Y, Ninomiya M, Fujiwara Y, et al: A case report of multiple adenocarcinoma in small intestine after total gastrectomy by Roux-en-Y re-construction. *Gan to Kagaku Ryoho* 38:2042–2044, 2011.
 121. Rutkowski P, Wozniak A, Dębiec-Rychter M, et al: Clinical utility of the new American Joint Committee on Cancer staging system for gastrointestinal stromal tumors: Current overall survival after primary tumor resection. *Cancer* 117:4916–4924, 2011.
 122. Yoshikawa K, Shimada M, Kurita N, et al: The efficacy of PET/CT for predicting the malignant potential of gastrointestinal stromal tumors. *Surg Today* 43:1162–1167, 2013.
 123. Yamada M, Niwa Y, Matsuura T, et al: Gastric GIST malignancy evaluated by 18FDG-PET as compared with EUS-FNA and endoscopic biopsy. *Scand J Gastroenterol* 42:633–641, 2007.
 124. Kalkmann J, Zeile M, Antoch G, et al: German GIST Imaging Working Group: Consensus report on the radiologic management of patients with gastrointestinal stromal tumours (GIST): Recommendations of the German GIST Imaging Working Group. *Cancer Imaging* 12:126–135, 2012.
 125. Haug AR, Cindea-Drimus R, Auernhammer CJ, et al: The role of ⁶⁸Ga-DOTATATE PET/CT in suspected neuroendocrine tumors. *J Nucl Med* 53:1686–1692, 2012.
 126. Sundin A, Garske U, Orlefors H: Nuclear imaging of neuroendocrine tumours. *Best Pract Res Clin Endocrinol Metab* 21:69–85, 2007.
 127. National Cancer Institute: Colon and rectal cancer, 2013. <http://www.cancer.gov/cancertopics/types/colon-and-rectal>. Accessed January 31, 2014.
 128. Chen YK, Kao CH, Liao AC, et al: Colorectal cancer screening in asymptomatic adults: The role of FDG PET scan. *Anticancer Res* 23:4357–4361, 2003.
 129. Abouzied MM, Crawford ES, Nabi HA: 18F-FDG imaging: Pitfalls and artifacts. *J Nucl Med Technol* 33:145–155, 2005.
 130. Israel O, Yefremov N, Bar-Shalom R, et al: PET/CT detection of unexpected gastrointestinal foci of 18F-FDG uptake: Incidence, localization patterns, and clinical significance. *J Nucl Med* 46:758–762, 2005.
 131. Agress H, Jr, Cooper BZ: Detection of clinically unexpected malignant and premalignant tumors with whole-body FDG PET: Histopathologic comparison. *Radiology* 230:417–422, 2004.
 132. Levin B, Lieberman DA, McFarland B, et al: Screening and surveillance for the early detection of colorectal cancer and adenomatous polyps, 2008: A joint guideline from the American Cancer Society, the US Multi-Society Task Force on Colorectal Cancer, and the American College of Radiology. *CA Cancer J Clin* 58:130–160, 2008.

133. Dewhurst C, Rosen MP, Blake MA, et al: ACR appropriateness criteria pretreatment staging of colorectal cancer. *J Am Coll Radiol* 9:775–781, 2012.
134. Abdel-Nabi H, Doerr RJ, Lamonica DM, et al: Staging of primary colorectal carcinomas with fluorine-18 fluorodeoxyglucose whole-body PET: Correlation with histopathologic and CT findings. *Radiology* 206:755–760, 1998.
135. Berger KL, Nicholson SA, Dehdashti F, Siegel BA: FDG PET evaluation of mucinous neoplasms: Correlation of FDG uptake with histopathologic features. *AJR* 174:1005–1008, 2000.
136. Whiteford MH, Whiteford HM, Yee LF, et al: Usefulness of FDG-PET scan in the assessment of suspected metastatic or recurrent adenocarcinoma of the colon and rectum. *Dis Colon Rectum* 43:759–770, 2000.
137. Allaix ME, Fichera A: Modern rectal cancer multidisciplinary treatment: The role of radiation and surgery. *Ann Surg Oncol* 20:2921–2928, 2013.
138. Bipat S, Glas AS, Slors FJM, et al: Rectal cancer: Local staging and assessment of lymph node involvement with endoluminal US, CT, and MR imaging—a meta-analysis. *Radiology* 232:773–783, 2004.
139. Garcia-Aguilar J, Pollack J, Lee SH, et al: Accuracy of endorectal ultrasonography in preoperative staging of rectal tumors. *Dis Colon Rectum* 45:10–15, 2002.
140. Mercury Study Group: Extramural depth of tumor invasion at thin-section MR in patients with rectal cancer: Results of the Mercury study. *Radiology* 243:132–139, 2007.
141. Dinter DJ, Hofheinz RD, Hartel M, et al: Preoperative staging of rectal tumors: Comparison of endorectal ultrasound, hydro-CT, and high-resolution endorectal MRI. *Onkologie* 31:230–235, 2008.
142. Lu YY, Chen JH, Ding HJ, et al: A systematic review and meta-analysis of pretherapeutic lymph node staging of colorectal cancer by 18F-FDG PET or PET/CT. *Nucl Med Commun* 33:1127–1133, 2012.
143. Uchiyama S, Haruyama Y, Asada T, et al: Role of the standardized uptake value of 18-fluorodeoxyglucose positron emission tomography-computed tomography in detecting the primary tumor and lymph node metastasis in colorectal cancers. *Surg Today* 42:956–961, 2012.
144. Kwak JY, Kim JS, Kim HJ, et al: Diagnostic value of FDG-PET/CT for lymph node metastasis of colorectal cancer. *World J Surg* 36:1898–1905, 2012.
145. Valls C, Andia E, Sanchez A, et al: Hepatic metastases from colorectal cancer: Preoperative detection and assessment of respectability with helical CT. *Radiology* 218:55–60, 2001.
146. Sahani DV, Kalva SP, Fischman AJ, et al: Detection of liver metastases from adenocarcinoma of the colon and pancreas: Comparison of mangafodipir trisodium-enhanced liver MRI and whole-body FDG PET. *AJR* 185:239–246, 2005.
147. Strasberg SM, Dehdashti F, Siegel BA, et al: Survival of patients evaluated by FDG-PET before hepatic resection for metastatic colorectal carcinoma: A prospective database study. *Ann Surg* 233:293–299, 2001.
148. Nickel MC, Bipat S, Stoker J: Diagnostic imaging of colorectal liver metastases with CT, MR imaging, FDG PET, and/or FDG PET/CT: A meta-analysis of prospective studies including patients who have not previously undergone treatment. *Radiology* 257:674–684, 2010.
149. Wiering B, Krabbe PF, Jager GJ, et al: The impact of fluor-18-deoxyglucose-positron emission tomography in the management of colorectal liver metastases. *Cancer* 104:2658–2670, 2005.
150. Davey K, Heriot AG, Mackay J, et al: The impact of 18-fluorodeoxyglucose positron emission tomography-computed tomography on the staging and management of primary rectal cancer. *Dis Colon Rectum* 51:997–1003, 2008.
151. Gearhart SL, Frassica D, Rosen R, et al: Improved staging with pretreatment positron emission tomography/computed tomography in low rectal cancer. *Ann Surg Oncol* 13:397–404, 2006.
152. Desch CE, Benson AB, 3rd, Somerfield MR, et al; American Society of Clinical Oncology: Colorectal cancer surveillance: 2005 update of an American Society of Clinical Oncology practice guideline. *J Clin Oncol* 23:8512–8519, 2005.
153. Manfredi S, Bouvier AM, Lepage C, et al: Incidence and patterns of recurrence after resection for cure of colonic cancer in a well-defined population. *Br J Surg* 93:1115–1122, 2006.
154. Ueberrueck T, Wurst C, Rauffuss F, et al: What factors influence 10-year survival after curative resection of a colorectal carcinoma? *World J Surg* 37:2476–2482, 2013.
155. Cortet M, Grimaud A, Cheynel N, et al: Patterns of recurrence of obstructing colon cancers after surgery for cure: A population-based study. *Colorectal Dis* 15:1100–1106, 2013.
156. Nagtegaal ID, van de Velde CJ, Marijnen CA, et al; Dutch Colorectal Cancer Group, Pathology Review Committee: Low rectal cancer: A call for a change of approach in abdominoperineal resection. *J Clin Oncol* 23:9257–9264, 2005.
157. Kapiteijn E, Marijnen CAM, Nagtegaal ID, et al: Preoperative radiotherapy combined with total mesorectal excision for resectable rectal cancer. *N Engl J Med* 345:638–646, 2001.
158. Brethauer SA, Magrino TJ, Riffenburgh RH, Johnstone PAS: Management of recurrent colorectal carcinoma. *Colorectal Dis* 4:246–253, 2002.
159. Greven KM, Williams DW, III, Keyes JW, Jr, et al: Positron emission tomography of patients with head and neck carcinoma before and after high-dose irradiation. *Cancer* 74:1355–1359, 1994.
160. Even-Sapir E, Parag Y, Lerman H, et al: Detection of recurrence in patients with rectal cancer: PET/CT after abdominoperineal or anterior resection. *Radiology* 232:815–822, 2004.
161. Imdahl A, Reinhardt MJ, Nitzsche EU, et al: Impact of 18F-FDG-positron emission tomography for decision making in colorectal cancer recurrences. *Langenbecks Arch Surg* 385:129–134, 2000.
162. Lu YY, Chen JH, Chien CR, et al: Use of FDG-PET or PET/CT to detect recurrent colorectal cancer in patients with elevated CEA: A systematic review and meta-analysis. *Int J Colorectal Dis* 28:1039–1047, 2013.
163. Moertel CG, Fleming TR, Macdonald JS, et al: An evaluation of the carcinoembryonic antigen (CEA) test for monitoring patients with resected colon cancer. *JAMA* 270:943–947, 1993.
164. Hung GU, Shiau YC, Tsai SC, et al: Value of 18F-fluoro-2-deoxyglucose positron emission tomography in the evaluation of recurrent colorectal cancer. *Anticancer Res* 21:1375–1378, 2001.
165. Metser U, You J, McSweeney S, et al: Assessment of tumor recurrence in patients with colorectal cancer and elevated carcinoembryonic antigen level: FDG PET/CT versus contrast-enhanced 64-MDCT of the chest and abdomen. *Am J Roentgenol* 194:766–771, 2010.
166. Votruba J, Belohlavek O, Jaruskova M, et al: The role of FDG-PET/CT in the detection of recurrent colorectal cancer. *Eur J Nucl Med Mol Imaging* 33:779–784, 2006.
167. Masi G, Vasile E, Loupakis F, et al: Randomized trial of two induction chemotherapy regimens in metastatic colorectal cancer: An updated analysis. *J Natl Cancer Inst* 103:21–30, 2011.
168. Sanoff HK, Sargent DJ, Campbell ME, et al: Five-year data and prognostic factor analysis of oxaliplatin and irinotecan combinations for advanced colorectal cancer: N9741. *J Clin Oncol* 26:5721–5727, 2008.
169. Guillem JG, Calle JPL, Akhurst T, et al: Prospective assessment of primary rectal cancer response to preoperative radiation and chemotherapy using 18-fluorodeoxyglucose positron emission tomography. *Dis Colon Rectum* 43:18–24, 2000.
170. van Kessel CS, Buckens CF, van den Bosch MA, et al: Preoperative imaging of colorectal liver metastases after neoadjuvant chemotherapy: A meta-analysis. *Ann Surg Oncol* 19:2805–2813, 2012.
171. Akhurst T, Kates TJ, Mazumdar M, et al: Recent chemotherapy reduces the sensitivity of [18F]fluorodeoxyglucose positron emission tomography in the detection of colorectal metastases. *J Clin Oncol* 23:8713–8716, 2005.
172. Gallinger S, Biagi JJ, Fletcher GG, et al: Liver resection for colorectal cancer metastases. *Curr Oncol* 20:e255–e265, 2013.
173. Stangl R, Altendorf-Hofmann A, Charnley RM, Scheele J: Factors influencing the natural history of colorectal liver metastases. *Lancet* 343:1405–1410, 1994.
174. Selzner M, Hany TF, Wildbrett P, et al: Does the novel PET/CT imaging modality impact on the treatment of patients with metastatic colorectal cancer of the liver? *Ann Surg* 240:1027–1034, 2004.
175. Gillams AR, Lees WR: Five-year survival following radiofrequency ablation of small, solitary, hepatic colorectal metastases. *J Vasc Interv Radiol* 19:712–717, 2008.
176. Solbiati L, Livraghi T, Goldberg SN, et al: Percutaneous radio-frequency ablation of hepatic metastases from colorectal cancer: Long-term results in 117 patients. *Radiology* 221:159–166, 2001.
177. Liu ZY, Chang ZH, Lu ZM, Guo QY: Early PET/CT after radiofrequency ablation in colorectal cancer liver metastases: Is it useful? *Chin Med J (Engl)* 123:1690–1694, 2010.
178. Kuehl H, Antoch G, Stergar H, et al: Comparison of FDG-PET, PET/CT and MRI for follow-up of colorectal liver metastases treated with radiofrequency ablation: Initial results. *Eur J Radiol* 67:362–371, 2008.
179. Veit P, Antoch G, Stergar H, et al: Detection of residual tumor after radiofrequency ablation of liver metastasis with dual-modality PET/CT: Initial results. *Eur Radiol* 16:80–87, 2006.

180. Barker DW, Zagoria RJ, Morton KA, et al: Evaluation of liver metastases after radiofrequency ablation: Utility of 18F-FDG PET and PET/CT. *AJR* 184:1096–1102, 2005.
181. Purandare NC, Rangarajan V, Shah SA, et al: Therapeutic response to radiofrequency ablation of neoplastic lesions: FDG PET/CT findings. *Radiographics* 31:201–213, 2011.
182. Vitola JV, Delbeke D, Meranze SG, et al: Positron emission tomography with F-18-fluorodeoxyglucose to evaluate the results of hepatic chemoembolization. *Cancer* 78:2216–2222, 1996.
183. Wong CY, Salem R, Raman S, et al: Evaluating 90Y-glass microsphere treatment response of unresectable colorectal liver metastases by [18F]FDG PET: A comparison with CT or MRI. *Eur J Nucl Med Mol Imaging* 29:815–820, 2002.

Angiography and Interventional Radiology of the Hollow Viscera

STANLEY TAESON KIM | ALBERT A. NEMCEK, JR |
HECTOR FERRAL | ROBERT L. VOGELZANG

CHAPTER OUTLINE

Preparation of Patients

Technical Factors

Vascular Access

Catheter Selection

Equipment

Angiography of the Major Visceral Vessels

Arterial Anatomy of Specific Segments of the Gut

Esophagus

Stomach

Small Bowel

Colon and Rectum

Venous Anatomy

Vascular Diagnosis and Intervention in the Gastrointestinal Tract

Primary Vascular Disease

Tumors

Inflammatory Disorders

Angiodysplasia of the Colon

Miscellaneous Vascular Disorders

Acute Gastrointestinal Bleeding

Acute Mesenteric Ischemia

Clinical and Angiographic Features

Thrombolytic Therapy for Mesenteric Vascular Occlusion

Bowel Interventions

Reasons for Placement of Needles or Catheters into the Gastrointestinal Tract

Diagnostic Biopsy of Bowel Masses

Enteric Puncture for Diagnostic or Therapeutic Access

Over the past 2 decades, the applications of angiography and interventional radiology in hollow abdominal viscera have dramatically changed.^{1,2} Multidetector computed tomography (MDCT) angiography and magnetic resonance (MR) angiography have replaced much of the diagnostic angiography that had been performed for investigating mesenteric ischemia, diagnosing abdominal masses, and detecting gastrointestinal (GI) tract bleeding sites.³⁻⁷ Interventional applications in the GI tract, however, have dramatically increased. In this chapter, new developments in angiography and interventional radiology of the hollow viscera are addressed.

Preparation of Patients

Certain preprocedural steps can enhance the diagnostic quality of a visceral angiogram. For elective studies, a standard bowel cleansing should be considered to delineate vessels and pathologic findings more clearly. Intravenous (IV) glucagon (1.0 mg) given at the time of the procedure, helps reduce the effects of bowel motion, particularly in studies with digital subtraction.

A Foley catheter is useful for studies of the inferior mesenteric artery because a contrast agent filling the bladder can obscure its branches. It also increases the patient's comfort and helps prevent unnecessary delays during long examinations.

Unless contraindicated, we routinely premedicate patients undergoing visceral angiography with fentanyl (Sublimaze) and midazolam (Versed) in an attempt to achieve the analgesic, anxiolytic, and amnesic effects of these combined agents while maintaining the patient's ability to cooperate. All patients have intraprocedural monitoring of pulse, electrocardiogram, arterial oxygenation (via a pulse oximeter), and blood pressure.

Technical Factors

VASCULAR ACCESS

In general, the femoral arterial route of catheterization is used for abdominal aortography and selective visceral angiography; the safety and ease of this approach are well established. Brachial or axillary access may be used in cases of difficult femoral access or when there is a need to advance a catheter more deeply into a vessel that has a steep caudal course.

CATHETER SELECTION

Our catheter of choice for celiac and superior mesenteric arteriography is a simple angled visceral hook, with a single side hole. For inferior mesenteric arteriography, we prefer a catheter with a short curved tip. For most indications, 5-Fr catheters are used to minimize puncture site complications. An angiographic sheath with a check flow valve is placed to secure vascular access.

Advances in guidewire and catheter technology have made subselective catheterization of visceral vessels easier. These include the development of flexible, hydrophilic, torque control guidewires and catheters that have low coefficients of friction, which allow them to follow wires around complex or tight curves more readily. The addition of microcatheters, microwires in 0.018-inch systems, microcoils, and embolic microspheres has allowed the interventionalist to manage acute GI bleeding, regardless of the source of bleeding.⁸

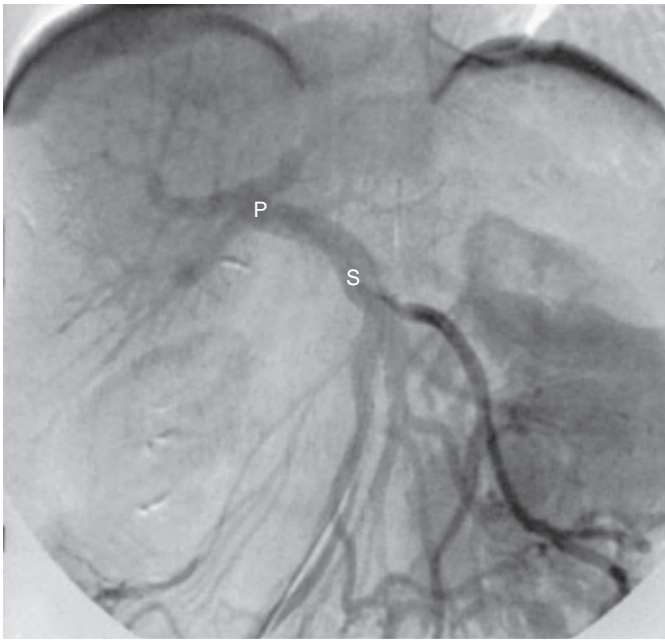


Figure 8-1 Arterial portography obtained during digital subtraction angiography. Excellent opacification of the mesenteric and portal venous system is achieved after superior mesenteric arterial injection. P, Portal vein; S, superior mesenteric vein.

EQUIPMENT

Digital subtraction angiography (DSA) is the preferred technique for visceral angiography (Fig. 8-1). In addition, digital image processing features greatly facilitate the guidance of complex vascular catheterizations and interventions. The improvement of digital subtraction systems has allowed the performance of angiography with carbon dioxide, providing exquisite angiographic images and minimizing the risk of contrast-induced nephropathy.⁹

Angiography of the Major Visceral Vessels

Visceral angiography begins with injection of the aorta or one of the three major visceral vessels—the celiac artery, superior mesenteric artery (SMA), or inferior mesenteric artery (IMA). Aortic injection is usually limited to situations that pose a risk for selective catheterization, such as suspicion of severe narrowing or occlusion of one or more of the origins of the major visceral vessels, especially in patients with clinical evidence of intestinal ischemia or those with severe aortic atherosclerosis.

The order of examination of the visceral vessels depends on the clinical situation. Thus, in GI bleeding, angiography should begin with the vessel most likely to be bleeding based on clinical history and the results of prior diagnostic studies.

Selective catheterization of the visceral arteries can be performed as an initial step or after aortography. The celiac artery generally arises from the aorta anteriorly, at the middle T12 or upper L1 vertebral level. The SMA originates slightly caudal to the celiac trunk. Generally, 5 to 7 mL/s of contrast medium is injected into these arteries, for a total of 15 to

35 mL; the rate is based on test injections. For the IMA, which usually arises to the left of midline from the abdominal aorta at the lower aspect of the L3 vertebral body, injection at a rate of 3 to 4 mL/s for a total of 12 to 16 mL is generally appropriate. Injection rates are proportionately decreased for the mesenteric branches.

Angiography using carbon dioxide requires a different technique. It is important to remember that carbon dioxide displaces blood and does not mix with it. This causes carbon dioxide images to appear incomplete or “cut.” Most current digital subtraction systems are now equipped with software for carbon dioxide angiography. The use of stacking software is essential to postprocess the original images obtained during carbon dioxide angiography. When performing carbon dioxide angiography, it is essential to use a “closed” carbon dioxide delivery or injection system to minimize the risk of air contamination.¹⁰ The new CO₂mmander system (AngioAdvancements, Fort Myers, FL) is a U.S. Food and Drug Administration (FDA)–registered portable carbon dioxide delivery system. It is composed of a converter, which is connected to a cartridge that holds up to 10,000 mL of medical grade carbon dioxide. The converter is connected to the delivery tubing, which has one-way valves to direct flow in the correct direction. The system safely delivers carbon dioxide at a low pressure and avoids air contamination and explosive delivery. Once the carbon dioxide is loaded in the injection syringe, it is gently injected into the selected artery using an end-hole or multi-perforated catheter. As a general rule, no more than 200 mL of carbon dioxide should be injected within a period of 5 minutes to prevent a vapor lock effect, which is a known complication of excessive carbon dioxide injection into the arterial system.¹¹

Arterial Anatomy of Specific Segments of the Gut

The vascular anatomy of the hollow abdominal viscera is complex. We have used a number of excellent general references in preparing this chapter; the reader is referred to these for more detailed discussions of angiographic and gross anatomy and the embryologic basis for many of the observed anatomic variations.

ESOPHAGUS

From a practical standpoint, only the distal esophageal arterial supply is important for angiographers. The gastroesophageal junction is a reasonably common site of arterial hemorrhage potentially treatable by embolization or vasopressin infusion. This region is typically supplied by branches of the left gastric artery (see later) or the left inferior phrenic artery (Figs. 8-2 and 8-3).

Catheterization of the upper and middle portions of the arteries that supply the esophagus is difficult but, fortunately, rarely necessary. The cervical esophagus typically receives its arterial supply from the inferior thyroid arteries (branches of the subclavian arteries), with predominant supply from the right. Subclavian, common carotid, or aortic branches may also supply this segment. The thoracic esophageal arteries arise directly from the aorta or as branches of the intercostal or bronchial arteries. Esophageal arteries anastomose along the length of the esophagus.

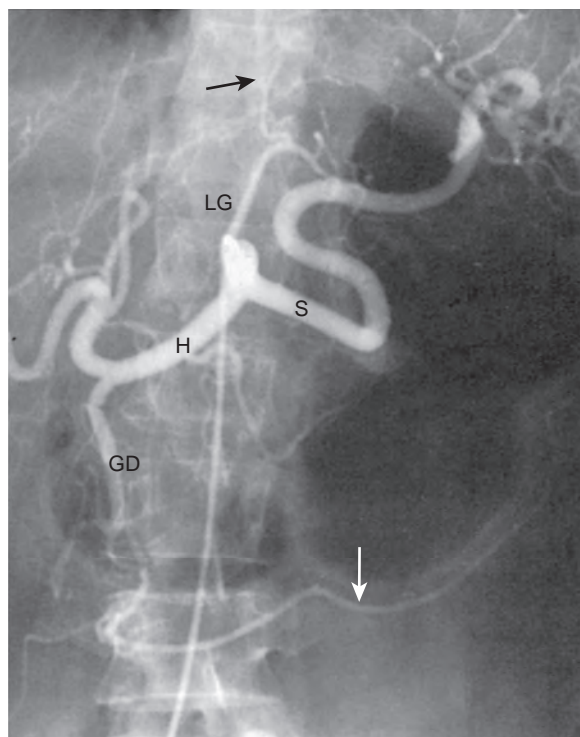


Figure 8-2 Celiac arteriogram. GD, Gastroduodenal artery; H, common hepatic artery; LG, left gastric artery; S, splenic artery; black arrow, branches of the left gastric artery supplying the lower esophagus; white arrow, right gastro-omental artery.

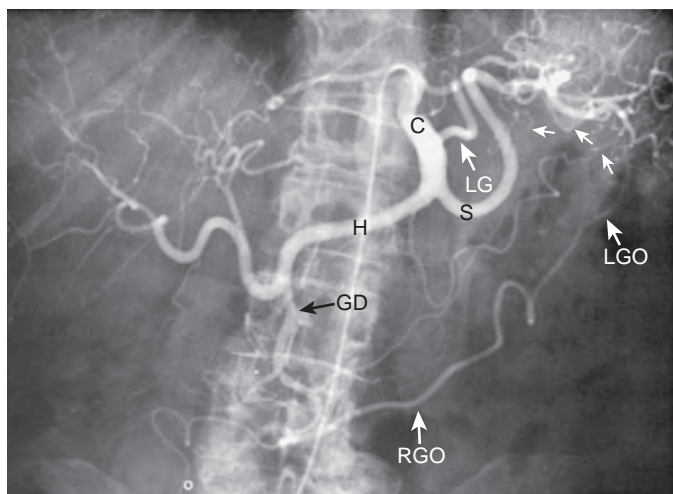


Figure 8-4 Celiac arteriogram. A well-formed gastro-omental anastomosis is present. C, Celiac artery; GD, gastroduodenal artery; H, common hepatic artery; LG, left gastric artery; LGO, left gastro-omental artery; RGO, right gastro-omental artery; S, splenic artery; small white arrows, short gastric branches.

STOMACH

The stomach has two major vascular arcades, one along the lesser curve formed by the right and left gastric arteries and the other along the greater curve, consisting of the right and left gastro-omental (gastroepiploic) arteries.

The left gastric artery usually arises as one of the three major branches of the celiac trunk, originating anywhere from the orifice of the trunk to the hepatic-splenic bifurcation (Figs. 8-4 to 8-6; see also Figs. 8-2 and 8-3). In 2% to 6% of patients, this vessel arises separately from the aorta.^{1,2}

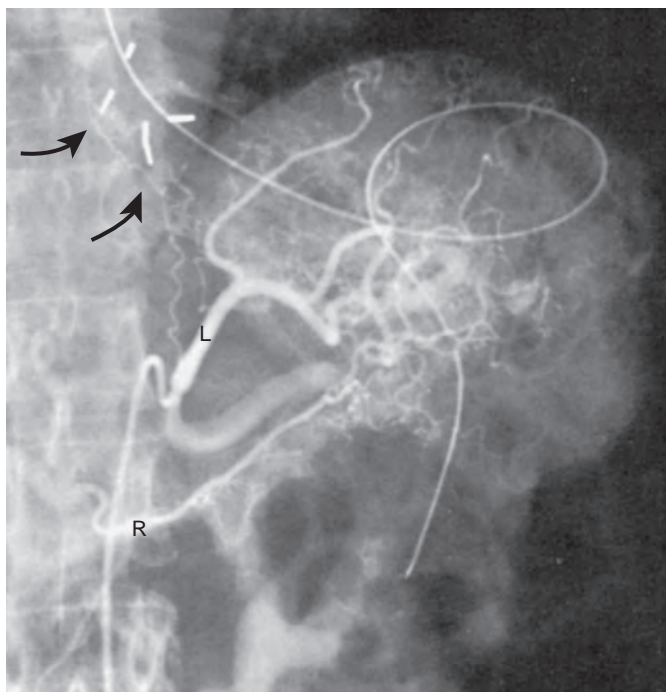


Figure 8-3 Selective left gastric artery injection. L, Left gastric artery; R, right gastric artery (filling retrograde via the left gastric branches); arrows, branches of the left gastric artery supplying the lower esophagus.

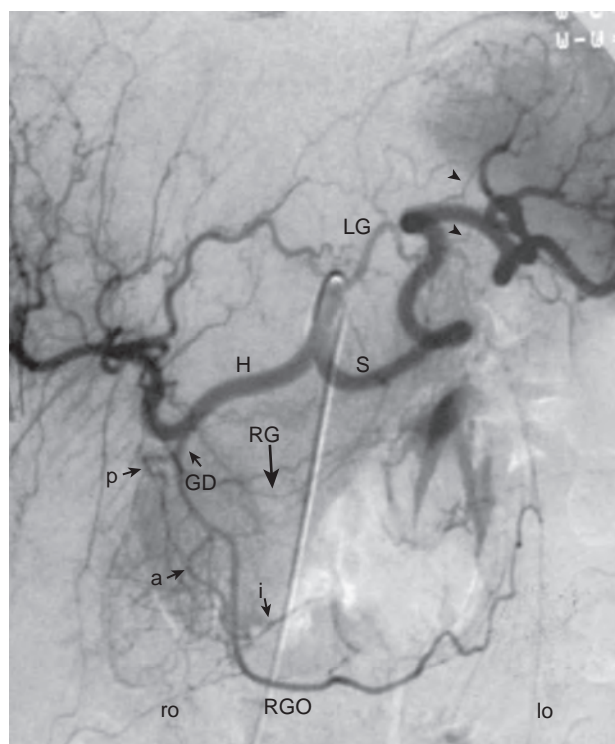


Figure 8-5 Celiac arteriogram. a, Anterosuperior pancreaticoduodenal branch; GD, gastroduodenal artery; H, common hepatic artery; i, inferior pancreaticoduodenal branch (filling retrograde via the pancreaticoduodenal arcades); LG, left gastric artery; lo, left omental branch; p, posterior superior pancreaticoduodenal branch; RGO, right gastro-omental artery (the left gastro-omental artery is not well opacified); ro, right omental branch; S, splenic artery; arrowheads, short gastric branches.

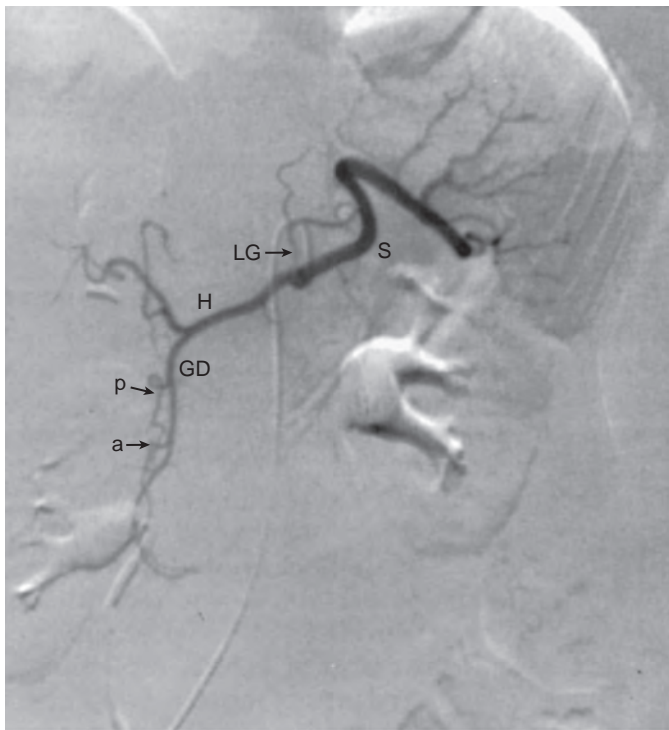


Figure 8-6 Early arterial phase, celiac arteriogram. *a*, Anterior superior pancreaticoduodenal branch; *GD*, gastrooduodenal artery; *H*, common hepatic artery; *LG*, left gastric artery; *p*, posterior superior pancreaticoduodenal branch; *S*, splenic artery.

A replaced or accessory left hepatic artery arises from the left gastric artery in 20% to 30% of cases.^{1,2} This has important clinical implications in patients for whom embolization or infusion therapy of hepatic or gastric arteries is anticipated. When this variant is present, the relative blood supply to the stomach and liver can vary, so that minimal supply to either may be present. In about 5% of cases, one or both inferior phrenic arteries arise from the left gastric trunk; this association is much higher when the left gastric artery arises as a separate aortic branch. The importance of this variant is emphasized by the reported association of hypertension and cardiac arrhythmias with vasopressin infusion into the phrenic artery. Accessory left gastric arteries are common.^{1,2}

Because most gastric angiography is performed for GI bleeding, and left gastric arterial ramifications account for about 85% of gastric hemorrhages, this is clearly an important vessel for subselective catheterization. Unfortunately, whereas the celiac artery is most readily catheterized with a caudally directed catheter, the course of the left gastric artery is cephalad. This may make selective catheterization difficult. A number of articles and texts have detailed methods that facilitate catheterization of this sometimes elusive vessel. The basic principle of these procedures is initial selection of the celiac artery with a catheter that has a caudally directed tip, followed by intraceliac exchange for, conversion to, or coaxial insertion of a catheter with a tip that points upward.^{1,2}

The right gastric artery arises at or distal to the common hepatic artery bifurcation, usually from the proper hepatic (57%) but occasionally from the left (17%) or right hepatic (2%) branches or at the origin or proximal portion of the gastroduodenal artery (10%). It has generally been considered an

unimportant vessel for arteriographers, along with the cystic and falciform arteries; however, these small vessels are found to be of increasing concern with the evolution of transarterial chemoembolization and arterial brachytherapy. Because the right gastric and cystic arteries have variable origins, these vessels increase the possibility of nontarget embolization, with subsequent tissue necrosis and/or inflammation (e.g., mucosal ulceration, cholecystitis, skin necrosis).^{1,2}

The right gastro-omental (gastroepiploic) artery is typically the larger of the two gastro-omental vessels (see Figs. 8-2, 8-4, and 8-5). It is the terminal branch of the gastroduodenal artery. The left gastro-omental (gastroepiploic) artery arises from the splenic artery or in conjunction with its inferior splenic branch (see Fig. 8-4). The gastro-omental arteries anastomose in a well-formed arcade along the greater curve of the stomach in 65% to 75% of cases; in most other cases, an anastomosis is still present but is not as well developed. In slightly fewer than 50% of individuals, a parallel anastomotic arcade called the arc of Barkow is present in the greater omentum, joining the right and left omental arteries, branches (respectively) of the right and left gastro-omental arteries (see Figs. 8-4 and 8-5).^{1,2}

The supply from the gastric and gastro-omental arcades is supplemented by other branches. A variable number of short gastric arteries supply the fundus and superior aspect of the greater curve of the stomach, usually arising from splenic hilar vessels (see Figs. 8-4 and 8-5). In 36% to 60% of individuals, a posterior gastric artery arises from the main splenic artery to supply the posterior wall of the stomach and parts of the fundus and gastroesophageal junction. The pyloric region typically receives part of its supply via branches of the gastroduodenal artery.^{1,2}

SMALL BOWEL

Much of the blood supply to the duodenum is via a series of freely anastomosing vessels; the anterior and posterior pancreaticoduodenal arcades provide a rich source of collaterals for the duodenum and head of the pancreas and between the celiac artery and SMA. These arcades (usually dual) form a continuous loop along the descending and transverse duodenum and the pancreatic head. The superior origin of this complex is usually dual, with both branches arising from the gastroduodenal artery and the posterior arcade typically arising more cephalad than the anterior (Fig. 8-7; see also Figs. 8-5 and 8-6). The inferior origin is usually a single trunk, usually arising from the SMA or its first or second jejunal branch (see Figs. 8-5 and 8-7).

Other sources of duodenal perfusion are branches of the right gastro-omental artery, supraduodenal artery (which has many possible origins, including the hepatic artery, gastroduodenal artery, posterior pancreaticoduodenal arcade, and right gastric artery), and smaller gastroduodenal branches.

In addition to the pancreaticoduodenal arcades, another potential collateral route between the celiac and superior mesenteric territories is the arc of Buhler, which represents persistence of an embryologic anastomosis between the celiac and superior mesenteric trunks.

The jejunum and ileum are supplied primarily by multiple branches arising from the left side of the SMA (Figs. 8-8 and 8-9); the level of the ileocolic artery origin is a good general indicator of the division between jejunal and ileal territories. The distal ileum also receives blood from the ileocolic artery (see later). An extensive network of vascular arcades connects

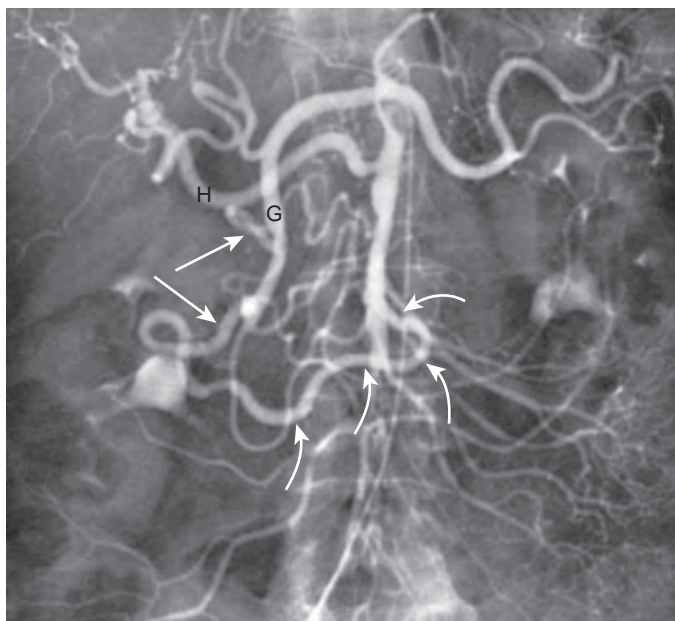


Figure 8-7 Superior mesenteric arteriogram. Enlarged pancreaticoduodenal arcades provide collaterals to the celiac territory in a patient with occlusion of the proximal celiac artery. Inferior pancreaticoduodenal branch (*curved arrows*) arises from the superior mesenteric artery and anastomoses with superior pancreaticoduodenal branches (*straight arrows*) to reconstitute the gastroduodenal artery (G). H, Replaced right hepatic artery arising from the superior mesenteric artery.

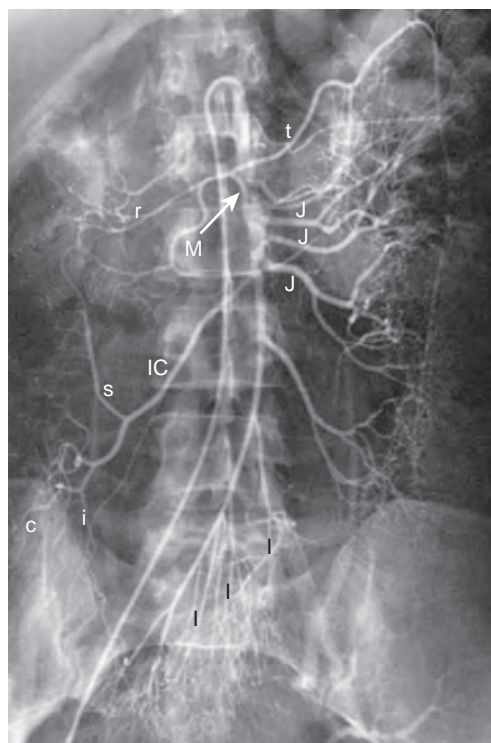


Figure 8-8 Superior mesenteric arteriogram. c, Cecal branches of the ileocolic artery; i, ileal branch of the ileocolic artery, anastomosing with terminal branches of the main superior mesenteric trunk; l, ileal branches; IC, ileocolic artery; J, jejunal branches; M, middle colic artery, with branches to the right colonic flexure (r) and the transverse colon (t); s, superior colic branch of the ileocolic artery, supplying the ascending colon and anastomosing with branches of the middle colic artery.

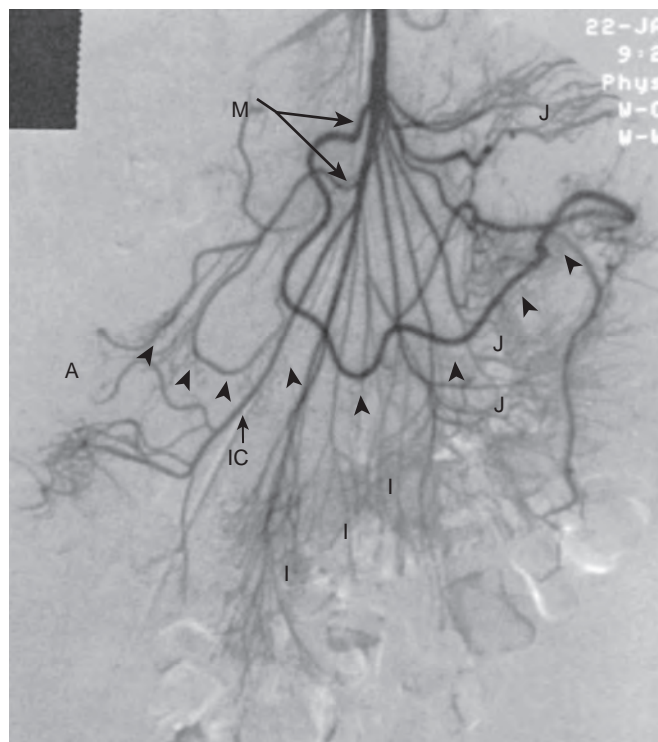


Figure 8-9 Superior mesenteric arteriogram. The middle colic territory (*arrowheads*) is supplied by two anastomosing superior mesenteric branches (M, *arrows*), one of which supplies the right colonic flexure and the other the mid to distal transverse colon. No discrete right colic artery to the ascending colon is present. A, Position of the ascending colon; I, ileal branches; IC, ileocolic artery; J, jejunal branches.

the jejunal and ileal branches; along the mesenteric border of the small bowel, the distal arcades give rise to multiple straight vasa recta that enter the bowel wall. The number of arcades increases, and the length of the vasa recta decreases more distally in the small bowel; these anatomic factors must be considered when performing small bowel embolization.

An important anatomic variant is a persistent vitelline artery, indicating the presence of Meckel's diverticulum. This vessel has a characteristic appearance—a relatively long vessel arising in the ileal region, without anastomoses to other ileal branches and with a network of irregular small distal branches (*Fig. 8-10*). Meckel's diverticulum may also be supplied by ileal branches without a well-defined vitelline artery, although this is less common. A dense mucosal stain at the tip of the diverticulum suggests the presence of ectopic gastric mucosa.

COLON AND RECTUM

The right colon and transverse colon are usually supplied by the SMA. Classically, this supply is described and diagrammed as consisting of three main branches arising independently from the SMA—the ileocolic, right colic, and middle colic arteries. Although the ileocolic is a constant vessel, a true right colic artery (arising independently from the SMA) is uncommon, and the middle colic “artery” is frequently variable in extent and branching pattern, consisting of one or more of five distinct vessels. The discrepancy between the classic description of three main independent branches and the most common situation,

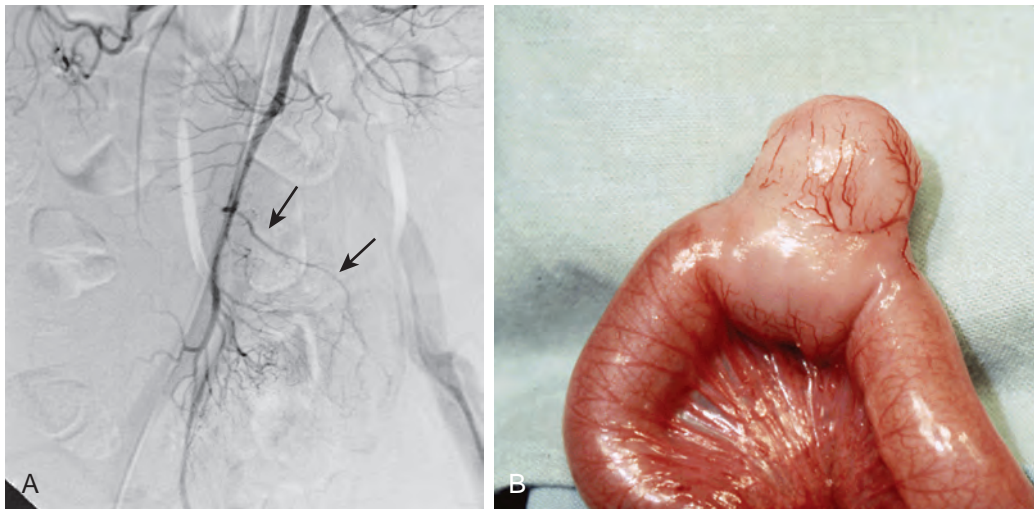


Figure 8-10 Persistent vitelline artery and Meckel's diverticulum. **A.** Selective superior mesenteric angiogram in a patient with recurrent GI hemorrhage shows a characteristic elongated artery (arrows) without anastomoses to adjacent ileal vessels. More proximal vessels show an abrupt change in direction relative to this vessel, reflecting intussusception (inversion) of the Meckel diverticulum. **B.** Surgical specimen of an inverted Meckel's diverticulum.

in which there are two independent branches, has given rise to some confusion and has caused the termination of the SMA to be labeled as the ileocolic artery on angiograms in various anatomic texts. It should be emphasized that the SMA termination is not a colic artery: its branches supply the ileum, and its final terminus joins the ileal branch of the ileocolic artery in a vascular arcade at the ileocecal junction.

The ileocolic artery supplies the transition between the small bowel and colon, with branches to the terminal ileum, cecum, ascending colon, and appendix (see Figs. 8-8 and 8-9). It is the last branch arising from the right side of the superior mesenteric trunk, and its constancy makes it a very important angiographic landmark. Most often, it consists of a main stem branching into two cecal branches distally, with anastomotic branches arising along the main stem. A nearly constant branch of the ileocolic artery is the superior colic, which anastomoses with the next colic artery arising from the SMA, whether the right colic or part of the middle colic complex.

The designation of right colic artery should apply only to an independent branch arising directly from the superior mesenteric trunk that supplies the middle portion of the ascending colon. The midportion of the ascending colon is usually supplied via an arcade formed between the ileocolic artery and middle colic system.

The middle colic artery has been classically described as the major proximal branch of the SMA, which supplies the right colonic flexure and transverse colon. A true middle colic artery is actually seen in slightly fewer than 50% of cases. In other cases, variant arteries or combinations of these arteries supply the vascular territory between the ileocolic or right colic artery and the left colic artery; a single vessel is present 75% of the time (see Figs. 8-8 and 8-9).^{1,2}

The middle colic artery or accessory arteries to the middle colic territory can arise from the celiac, splenic, hepatic, or pancreatic arteries (especially the dorsal pancreatic artery; Fig. 8-11). Thus, angiography of the entire colon may require injection of the celiac artery or its branches.

In unusual situations, portions of the blood supply to the colon can arise directly from the aorta between the origins of the SMA and IMA. In two publications,^{2,3} such a variant has been called the middle mesenteric artery, although in one report the artery supplied the distal transverse and proximal

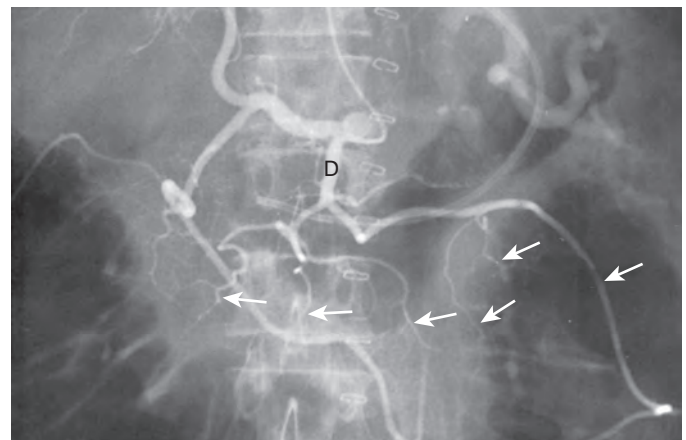


Figure 8-11 Variant middle colic supply. Celiac injection reveals an enlarged dorsal pancreatic artery (D), from which branches (arrows) arise that course to the middle colic territory and transverse mesocolon.

descending colon, and in the other the artery supplied the entire proximal colon, up to and including the splenic flexure.^{2,3}

The IMA usually supplies the splenic flexure, descending colon, sigmoid colon, and upper rectum IMA (Figs. 8-12 to 8-15). However, the boundary between the parts of the colon supplied by the SMA and IMA can be variable—proximal or distal to the splenic flexure. The IMA terminates in two superior rectal (hemorrhoidal) branches (see Figs. 8-12 and 8-13). It gives off branches from its left side. The first is the left colic artery, which courses toward the splenic flexure (see Figs. 8-12, 8-14, and 8-15). Its branches anastomose with branches of the middle colic territory (see Figs. 8-12 and 8-15). The left colic artery is frequently absent if there is an accessory left colic vessel arising as a portion of the middle colic supply. Other branches arise from the left colic artery or IMA trunk proximal to the superior rectal arteries to supply the descending and sigmoid colon and upper rectum. A colosigmoid artery or branch (see Figs. 8-13 and 8-14) can usually be identified as a large dominant vessel supplying the transition between the descending colon and sigmoid.

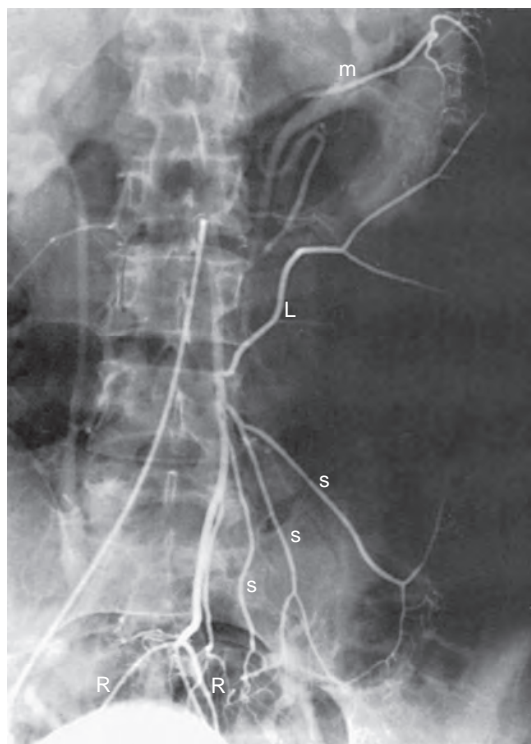


Figure 8-12 Inferior mesenteric arteriogram. *L*, Left colic artery; *m*, partial filling of the middle colic territory via the marginal artery; *R*, superior rectal (hemorrhoidal) arteries; *s*, sigmoid branches.

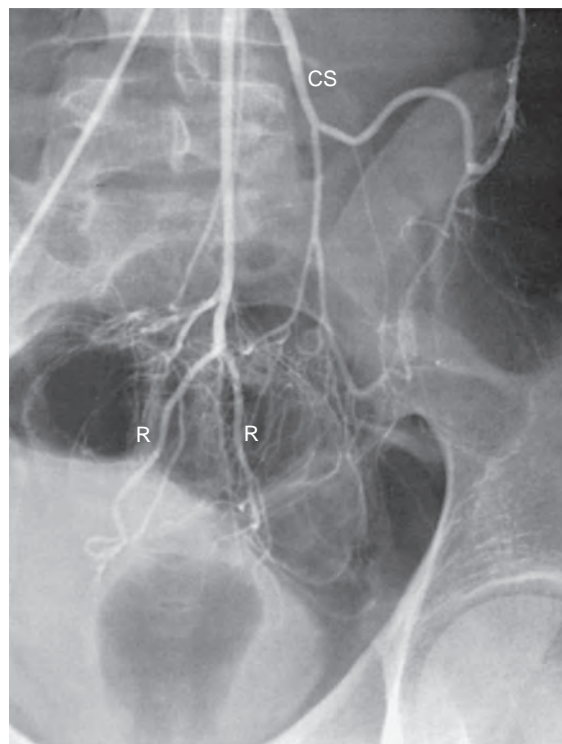


Figure 8-13 Caudal branches of the inferior mesenteric trunk. *CS*, Colosigmoid trunk; *R*, superior rectal (hemorrhoidal) arteries.

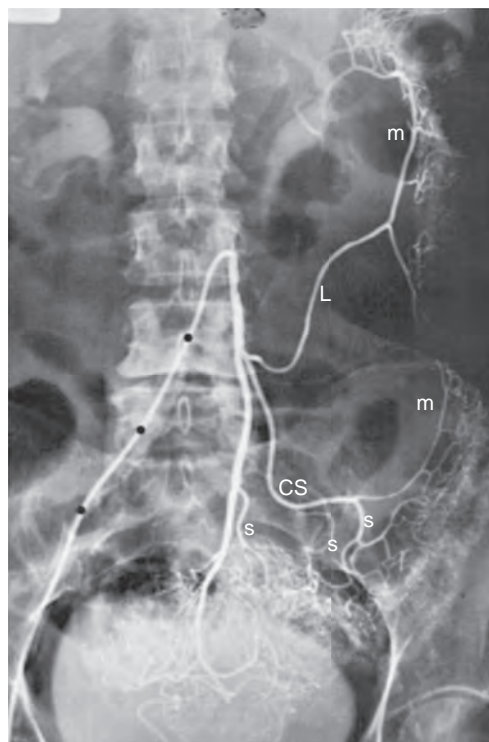


Figure 8-14 Inferior mesenteric arteriogram. *CS*, Colosigmoid branch; *L*, left colic artery; *m*, marginal artery; *s*, sigmoid branches; *black dots*, selective catheter.

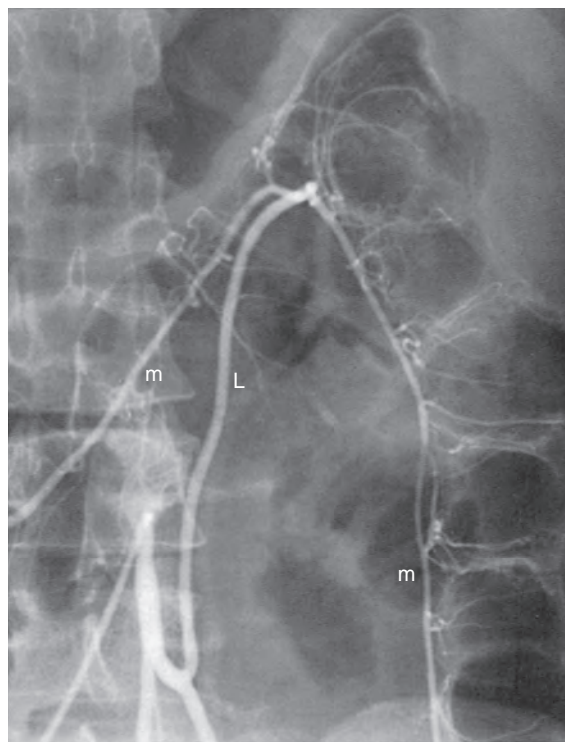


Figure 8-15 Inferior mesenteric injection. The left colic artery (*L*) ascends toward the left colonic flexure, and the marginal artery (*m*) is opacified in a continuous fashion from the transverse colon to the descending colon.

The marginal artery of Drummond designates a vascular arcade that runs along the mesenteric border of the colon, where it gives off its nutrient vessels (Figs. 8-16 and 8-17; also see Figs. 8-12, 8-14, and 8-15). Defined in this way, the major colic arteries can parallel the marginal artery or constitute part of it; the paracolic arcade can be considered part of the generalized system of paraintestinal arcades present throughout the abdominal GI tract. An enlarged marginal artery frequently provides a collateral pathway between the SMA and IMA territories (see Figs. 8-16 and 8-17). The marginal artery is not always reliably complete along its entire length. Griffith's point, for example, represents a watershed area of a potentially poor anastomotic connection between the SMA territory and marginal artery of the descending colon at the splenic flexure; it is

an area susceptible to ischemic injury when its marginal artery is poorly developed. The arc of Rioloan refers to a more central anastomotic loop that lies within the mesentery, joining the IMA and SMA territories. The term *meandering mesenteric artery* has also been used. This actually represents an enlarged and tortuous left colic artery acting as part of a collateral pathway (see Figs. 8-16 and 8-17).

The more distal rectum is supplied by branches of the internal iliac territory, the middle rectal and inferior rectal arteries. As is the case with the most proximal portion of the gut, angiography of this region is infrequently performed. Collateralization via the rectal arteries between the IMA and internal iliac system can become important in occlusive disease of the aorta and common iliac arteries.



Figure 8-16 Collateral blood supply of the colon. Early (A) and delayed (B) radiographs from an abdominal aortogram show a dilated marginal artery fed by the middle colic artery, which courses along the transverse and proximal descending colon (straight arrows) and reconstitutes the inferior mesenteric artery via the left colic artery (arrowheads in B). Stenosis of the abdominal aorta is present between the origins of the superior and inferior mesenteric arteries (curved arrow in A) and may contribute to diminished flow at the origin of the inferior mesenteric artery.

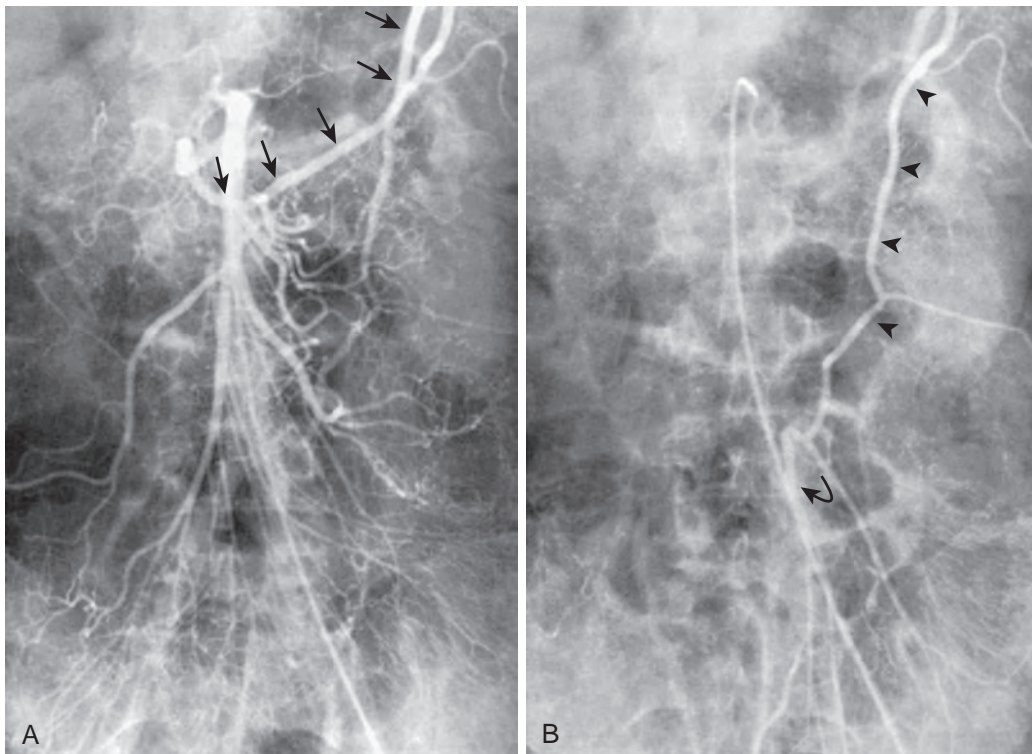


Figure 8-17 Collateral blood supply of the colon. Early (A) and delayed (B) radiographs from a superior mesenteric arteriogram demonstrate an enlarged marginal artery arising from the middle colic in A (arrows). B. The marginal artery fills the left colic artery (arrowheads) in a retrograde fashion, allowing reconstitution of the inferior mesenteric trunk (curved arrow). The dilated, tortuous collateral pathway has been called a meandering mesenteric artery.

VENOUS ANATOMY

The mesenteric venous system is studied for two main indications: (1) evaluation of the patency of the mesenteric veins in the setting of suspected acute mesenteric ischemia; and (2) evaluation of the patency and direction of flow in the mesenteric, splenic, and portal veins and potential collateral pathways in portal hypertension. Angiography in patients with portal hypertension may be difficult to interpret, and images of high quality are essential. A very good mesenteric venous phase can be obtained using a total volume of 35 mL of nonionic contrast at an injection rate of 5 to 7 mL/s. The use of glucagon (1-mg IV bolus) to slow down the peristalsis and vasodilators to increase the flow improve the quality of the images. Vasodilators may include papaverine (30-mg intra-arterial bolus, followed by a 10-mL saline flush to prevent papaverine crystallization) or tolazoline (Priscoline), 25 mg diluted in 10 mL of normal saline solution, injected slowly for 2 minutes. Contrast medium injection and filming begin immediately after drug administration.

The most important gastric vein is the left gastric, or coronary vein, which courses along the lesser curve of the stomach and joins the splenic-portal venous system at variable sites. It is a frequent pathway for portosystemic collateralization in portal hypertension and splenoportal collateralization in splenic vein occlusion. Gastro-omental and short gastric veins parallel their respective arteries and can be important collateral pathways as well. The superior mesenteric and inferior mesenteric veins run to the right of, parallel to, and drain the respective territories of the SMA and IMA. The superior mesenteric vein joins the splenic vein behind the pancreatic neck to form the portal vein (see Fig. 8-1); the inferior mesenteric vein can join the splenic or superior mesenteric vein or their confluence (Fig. 8-18).

Vascular Diagnosis and Intervention in the Gastrointestinal Tract

PRIMARY VASCULAR DISEASE

Atherosclerotic involvement of the visceral arteries is common, and the angiographic appearance is typical of atherosclerosis in other locations—irregular plaque formation, eccentric or concentric stenosis, and occlusion. Visceral artery stenoses can also occur in other primary vascular disorders, including fibromuscular dysplasia, Takayasu's arteritis, and Behçet's disease, or as the result of response to extrinsic agents, such as ergot preparations. It has been stated that in cases of celiac or SMA fibromuscular dysplasia, the classic string of beads appearance of this entity is less common than that of a tubular stenosis.

Although visceral artery aneurysms usually involve the splenic and hepatic arteries, they can occur in any of the mesenteric arteries. Causes of such aneurysms include arteriosclerosis, medial degeneration, infection (particularly common in the SMA territory), inflammation (particularly pancreatitis), dissection, connective tissue disorders (e.g., Ehler-Danlos type IV), vasculitides such as polyarteritis nodosa (which involves the GI tract in about 50% of cases), IV drug abuse, trauma, and other more unusual conditions (Fig. 8-19). Many are discovered during work-up for GI and intraperitoneal hemorrhage. Aneurysms of the GI tract vasculature may also thrombose and, as a result, present with mesenteric ischemia. Therapy for visceral

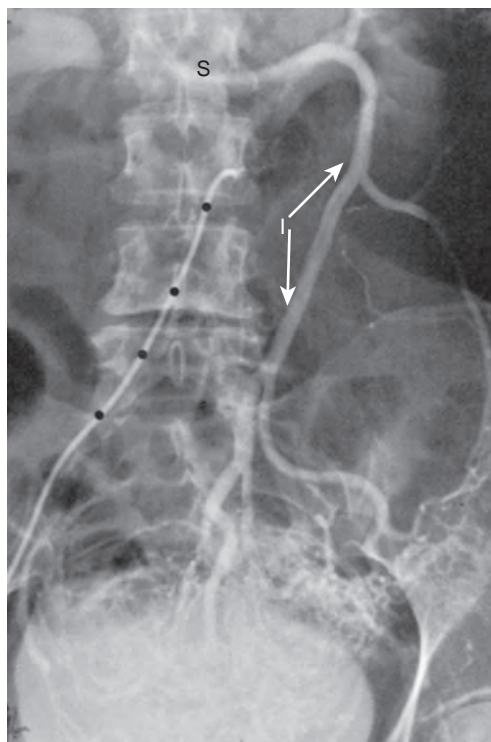


Figure 8-18 Venous phase of inferior mesenteric artery injection. The inferior mesenteric vein (I) joins the splenic vein (S). Black dots indicate that the catheter is placed selectively into the inferior mesenteric artery.

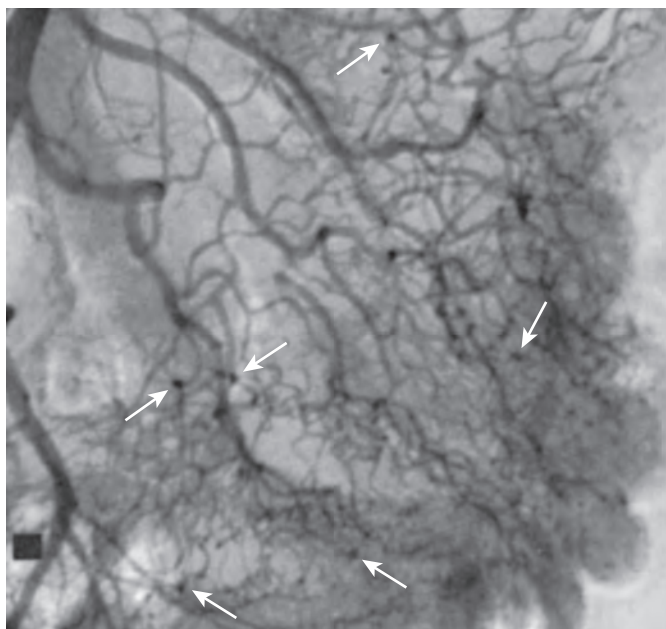


Figure 8-19 Polyarteritis nodosa. Multiple small aneurysms, some of which are indicated by arrows, arise from superior mesenteric branches in a patient with polyarteritis nodosa.

aneurysms has traditionally been surgical, but catheter embolization has been used successfully.¹²⁻¹⁷

Aneurysms of the superior mesenteric vein have also been described. Congenital, traumatic, and inflammatory causes have been proposed. Although rare, they may cause abdominal pain, GI bleeding, or compression of adjacent structures.

Arteriovenous malformations, characterized by dilated, tortuous feeding arteries, capillary blush, and prominent venous drainage, can occur throughout the GI tract. Thought to be developmental in origin, they are often seen in younger adults or children. They can be an elusive cause of GI hemorrhage, often discovered only on its angiographic work-up. MDCT has proven useful in the depiction of some of these vascular malformations.

Vascular malformations of the GI tract may also occur in association with systemic disorders such as pseudoxanthoma elasticum, hereditary hemorrhagic telangiectasia, and Klippel-Trenaunay-Weber syndrome. Pseudoxanthoma elasticum is a hereditary, autosomal recessive disorder of connective tissue that involves systemic abnormalities of elastic fibers. Patients display characteristic ocular and cutaneous lesions. Cardiovascular manifestations occur because of fragmentation, degeneration, and calcification of the arterial elastic laminae and premature atherosclerosis. A variety of splanchnic angiographic abnormalities have been described, including angiomatous malformations, vascular tortuosity, segments of vascular narrowing and occlusion, and small aneurysms. Upper GI tract bleeding is common and probably results from submucosal vascular degeneration and inability of the abnormal vessels to constrict at sites adjacent to areas of erosion and hemorrhage. Embolization has been used to treat hemorrhage in this disorder.¹²⁻¹⁸

Patients with hereditary hemorrhagic telangiectasia (Osler-Weber-Rendu disease) have multiple systemic vascular lesions involving the skin, mucous membranes, and gut. Abnormalities on abdominal visceral angiography include tangled masses of tortuous vessels with early venous filling, direct arteriovenous fistulas, arterial aneurysms, localized venous dilations, and small focal accumulations of contrast medium representing angiomatous lesions that are visualized during the arterial phase of injection of the contrast medium. Thin fragile walls are characteristic of these vascular lesions and help explain their propensity to bleed; recurrent GI hemorrhage is common.

Arteriovenous fistulas of the mesenteric vessels can be congenital or can result from penetrating trauma or from prior abdominal surgery. Successful transcatheter embolization of fistulas involving main mesenteric trunks or branches has been described.

TUMORS

Although rarely used in the primary diagnosis of tumors of the GI tract, angiography will occasionally detect neoplasms as incidental abnormalities or as the cause of active or occult GI bleeding. GISTs (gastrointestinal stromal tumors) are common neoplasms of the upper GI tract and small bowel that have a tendency to bleed. They are typically hypervascular and well defined on angiography (Fig. 8-20); venous shunting is common in GISTs of the small bowel but not typical of those in the stomach. Carcinoid tumors elicit a fibrotic response in the adjacent mesentery that is reflected in a characteristic angiographic appearance of stellate crowding, kinking, and an irregular contour of mesenteric branches. The neoplasm itself is hypovascular but can cause smooth arterial narrowings and occlusions. Venous drainage is typically via multiple collaterals. As might be expected, other processes resulting in mesenteric fibrosis may have a similar appearance.

Adenocarcinomas of the small bowel tend to show signs of encasement without tumor vascularity; in the colon, lesions may be hypervascular. Adenomatous polyps of the colon are hypovascular in most cases, whereas villous adenomas tend to be vascular lesions, with enlarged feeding arteries and draining veins and contrast staining in the parenchymal phase.

Other primary and metastatic upper GI tract tumors, depending on their pathology, may demonstrate nonspecific signs of neoplasia, including neovascularity, vascular encasement, vascular displacement and stretching, and arteriovenous shunting.

INFLAMMATORY DISORDERS

Angiography is seldom used in the work-up of inflammatory lesions such as ulcerative colitis, Crohn's disease, or diverticulitis. Acute inflammation usually produces nonspecific findings, such as increased vascularity with enlargement of feeding arteries, dense capillary blush of the bowel wall, and enlargement and sometimes early opacification of draining veins. In the colon, these findings overlap with those found in early ischemic colitis and may even be normal in the postprandial state. As Crohn's disease progresses, arterial occlusions, irregular arterial

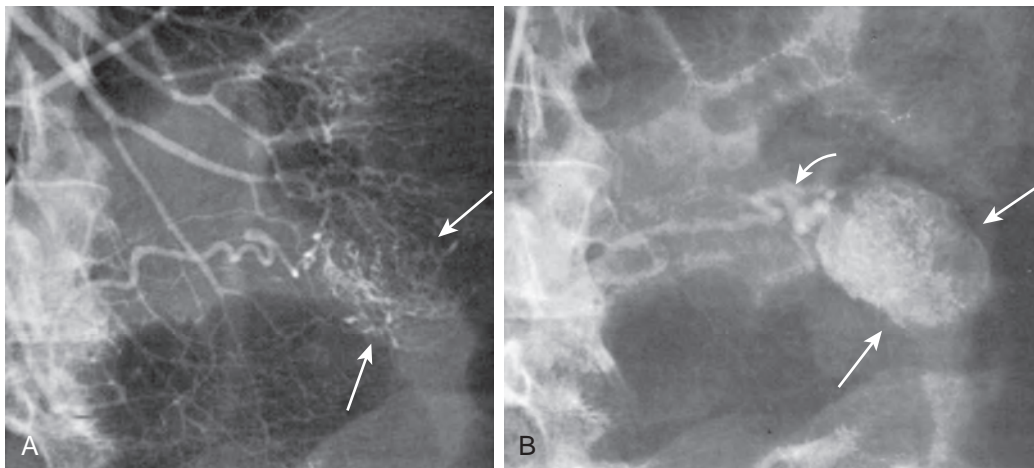


Figure 8-20. Superior mesenteric arteriography in a patient with intermittent arterial bleeding. **A.** Increased vascularity (arrows) is noted in a portion of the jejunum in the arterial phase. **B.** In the late arterial phase, a well-defined tumor stain (straight arrows) is noted, with a dilated early draining vein (curved arrow). A gastrointestinal stromal tumor was diagnosed.

narrowing, and hypovascularity may develop in the involved segment.

ANGIODYSPLASIA OF THE COLON

Angiodysplasia (vascular ectasia) of the colon is a vascular disorder that usually affects the right colon in older individuals. It has a number of characteristic angiographic features, which depend on the stage and size of the lesion—intense and prolonged opacification of a dilated and tortuous mural colonic vein (the earliest sign), vascular tufts (small, densely staining clusters of vessels), and tortuous feeding (Fig. 8-21). To ensure that the early opacification of the draining vein is not simply the result of prolonged arterial injection, it helps to limit the duration of injection of contrast medium to 4 seconds or less.

Although the exact cause is unknown, angiodysplasia may be the result of a degenerative process in which intermittent intramural venous obstruction leads to venous dilation and, later, to direct arteriovenous communication. There is an association of colonic vascular ectasia and aortic stenosis.

MISCELLANEOUS VASCULAR DISORDERS

The effects of radiation therapy on the mesenteric vasculature depend on the time course relative to such therapy. In the subacute phase, a hyperemic blush associated with early venous drainage has been described, correlating with an inflammatory response. In the more chronic setting, radiation enteritis may

produce obliterative findings, with irregular stenoses or occlusions of mesenteric branches, as well as findings related to shortening of bowel length, including tortuosity and vascular crowding.

Abnormalities of bowel position, although not typically diagnosed by angiography, may also be observed in the angiographic work-up of abdominal symptoms. Findings in conditions such as intussusception, internal hernias, and volvulus include unusual displacement of vessels, abrupt angulation and overlapping of branches, and abrupt changes in vessel caliber.

ACUTE GASTROINTESTINAL BLEEDING

The management of acute GI bleeding has become common practice in any active interventional radiology service. Diagnostic and therapeutic angiography is generally used after endoscopic techniques have failed to control the bleeding source. Acute upper GI bleeding is better evaluated first by endoscopy. In a large percentage of cases, endoscopy will be effective in controlling the acute problem. If endoscopic techniques fail for any reason, the endovascular option is the next step; however, the diagnostic input from the endoscopic procedure is essential to the interventionalist. For example, if endoscopy shows a large, uncontrollable variceal bleed, the option of choice will probably be a transjugular intrahepatic portosystemic shunt (TIPS) procedure or a balloon-occluded retrograde transvenous obliteration (BRTO). If the source of bleeding is an esophageal tear or gastric or duodenal ulcer, arterial evaluation is in

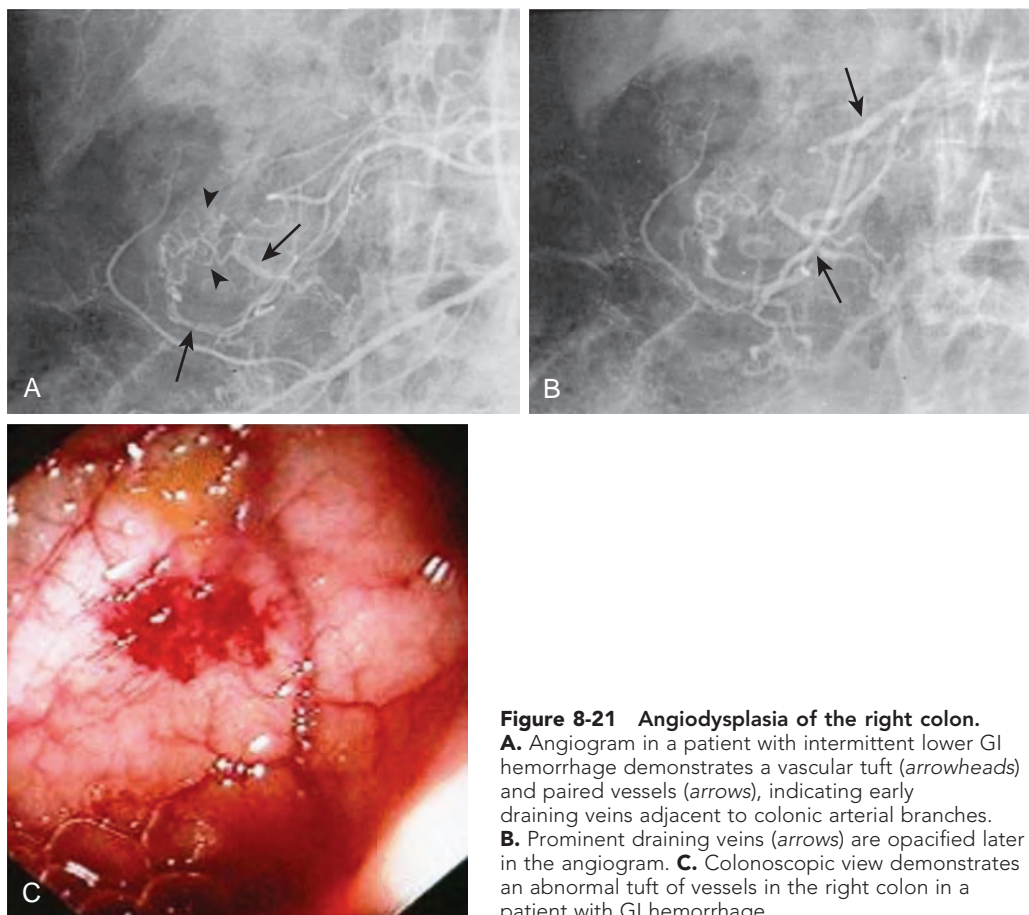


Figure 8-21 Angiodysplasia of the right colon.

A. Angiogram in a patient with intermittent lower GI hemorrhage demonstrates a vascular tuft (arrowheads) and paired vessels (arrows), indicating early draining veins adjacent to colonic arterial branches. **B.** Prominent draining veins (arrows) are opacified later in the angiogram. **C.** Colonoscopic view demonstrates an abnormal tuft of vessels in the right colon in a patient with GI hemorrhage.

order. Gastric ulcers may be managed with superselective embolization of the left gastric artery and esophageal ulcers and Mallory-Weiss tears by assessment of the lower esophageal arteries; duodenal ulcers are usually managed with assessment of the gastroduodenal artery.

Lower GI bleeding requires a different approach. Acute lower GI bleeding may be difficult to evaluate endoscopically without the proper patient preparation; in those cases, diagnostic and therapeutic arteriography may be the first choice. Small bowel and colonic bleeds are managed with superselective transcatheter embolization of the vasa recta of the affected field.¹⁹⁻²¹ Lower GI bleeds demand more technical skill and require superselective embolization of the vasa recta of the involved territory (Fig. 8-22). The use of microcatheters, microcoils (0.018-inch systems), and microparticles (polyvinyl alcohol [PVA] and spheres) has allowed the interventional specialist to manage these difficult and clinically challenging cases, with a success rate that ranges from 80% to 100% and low recurrence rates ranging between 5% and 15%.^{19,21}

Acute Mesenteric Ischemia

CLINICAL AND ANGIOGRAPHIC FEATURES

MDCT has become the major imaging method for assessing patients with acute abdominal pain. Because it can evaluate the bowel wall, the surrounding mesentery, and major vascular structures, MDCT can often suggest the presence of mesenteric ischemia or infarction and depict the thrombus if it is sufficiently large and central. Angiography provides detailed anatomic and etiologic information necessary for the urgent management of mesenteric ischemia and, in addition, allows for the initiation of selective transcatheter therapy, when appropriate.

Lateral abdominal aortography reveals the status of the proximal mesenteric vessels and should be the initial step in the angiographic evaluation of mesenteric ischemia. If the proximal

portion of the SMA is patent, selective arteriography of this vessel is performed for a detailed study of the superior mesenteric trunk and its branches and of the mesenteric venous drainage. Acute mesenteric ischemia is primarily a disorder of the SMA territory, and selective celiac and inferior mesenteric injections are not usually necessary. However, these further studies can provide information about the presence and extent of collateral supply to the superior mesenteric territory, particularly when the chronicity of a superior mesenteric occlusion is questioned. This additional angiography can also be considered if clinical data strongly suggest involvement of the stomach, duodenum, or segment of colon supplied by the IMA.

Major causes of acute mesenteric ischemia are SMA thrombosis or embolism, mesenteric venous thrombosis, and the non-occlusive form of ischemia. Vasculitis, aortic or mesenteric arterial dissection, trauma, bowel strangulation, and other disorders are less common causes of mesenteric ischemia. Involvement of all or most of the SMA territory typically produces severe and life-threatening mesenteric ischemia. Focal ischemia can result from more limited or segmental forms of the previously mentioned causes and has less severe clinical manifestations.²²⁻²⁷

SMA occlusion with embolism is more common than thrombosis (Figs. 8-23 to 8-26). The angiographic distinction between these two entities can be difficult. Multiple filling defects, tracking of contrast medium at the lateral aspects of a filling defect, and convex menisci protruding into the opacified vascular lumen suggest emboli. Emboli also tend to lodge at vascular branch points, generally more distally than an occlusive thrombus, which typically forms in the vicinity of a preexistent atherosclerotic stenosis of the proximal SMA. At times, however, emboli can lodge at proximal stenoses, or an embolus can initiate more proximal or distal propagation of thrombus. Extramesenteric emboli are common in cases of embolic mesenteric ischemia.²²⁻²⁷

Mesenteric venous thrombosis accounts for up to 10% to 20% of cases of acute mesenteric ischemia. Causes of this

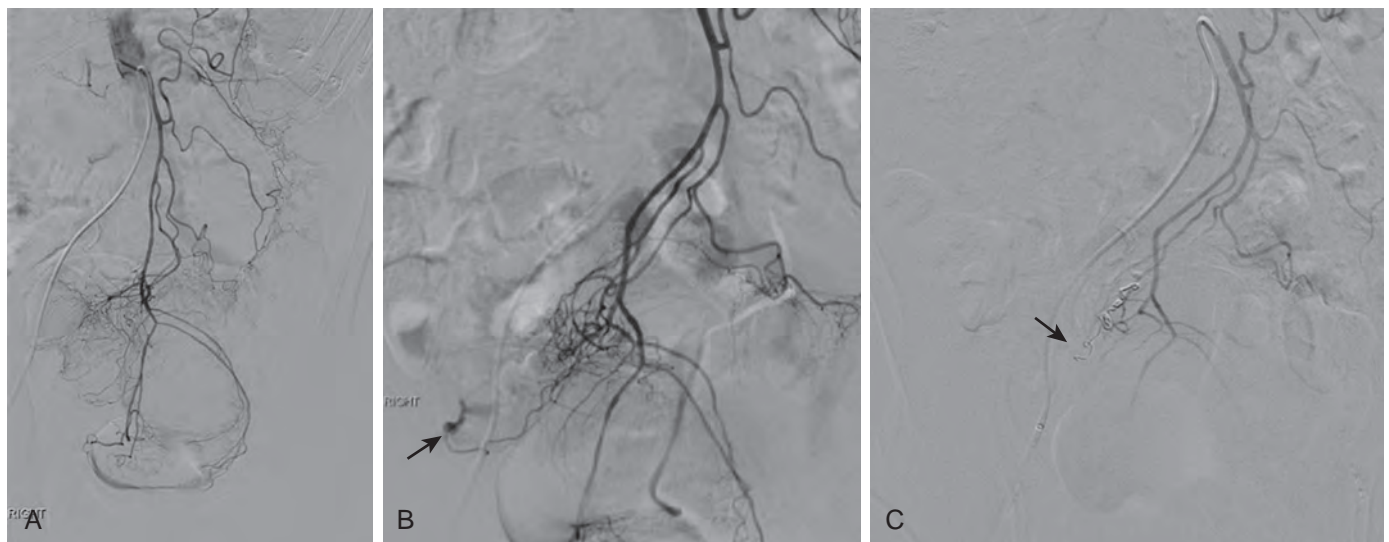


Figure 8-22 Acute diverticular bleed in the sigmoid colon. **A.** Selective inferior mesenteric angiogram in a patient with acute lower GI bleed. The selective IMA injection shows no active bleeding. **B.** Repeat selective injection of contrast shows a definite area of extravasation in the superior hemorrhoidal territory (arrow). **C.** Arteriogram obtained after superselective embolization with a single 6-mm × 7-cm Nester, 0.018-inch microcoil (Cook, Bloomington, IN) shows no further extravasation (arrow).



Figure 8-23 Superior mesenteric embolus. A nearly occlusive filling defect (arrow) is present in the main superior mesenteric artery trunk, with tracking of contrast medium around it and patency of the more distal superior mesenteric artery.



Figure 8-25 Superior mesenteric embolus. Abrupt occlusion (arrow) of the superior mesenteric trunk is present distal to jejunal branches in a patient with atrial fibrillation.

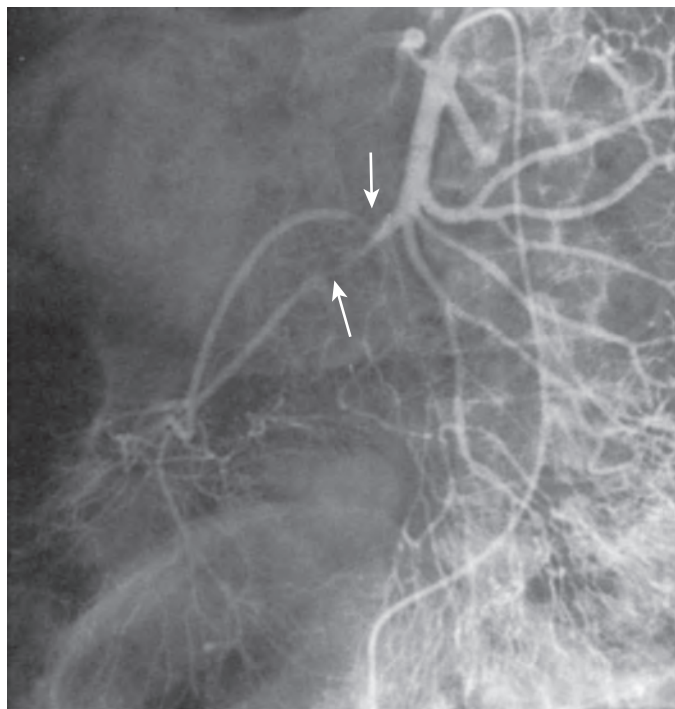


Figure 8-24 Superior mesenteric emboli. Multiple filling defects (arrows) are present in the superior mesenteric artery branches in a patient with atrial fibrillation.

disorder include bowel obstruction, hypercoagulable states, portal hypertension, abdominal inflammatory disease, previous surgery (particularly splenectomy), and trauma. Often, no predisposing condition is identified. Patients may present with less severe illness than in other forms of acute mesenteric ischemia; recognition that major venous occlusion does not always result in ischemia has increased as more cases of mesenteric venous thrombosis have been identified with the use of cross-sectional imaging. MDCT has excellent sensitivity for the diagnosis. However, angiographic recognition remains important as part of the favored algorithm for acute mesenteric ischemia. On superior mesenteric arteriography, slowing of arterial flow is noted, with prolonged staining of the bowel wall and smaller mesenteric arterial branches. Arterial vasoconstriction may be present. Normal mesenteric veins fail to opacify or show filling defects; venous collaterals may be visualized.²²⁻²⁷

Anatomic vascular obstruction need not be present for mesenteric ischemia and infarction to occur. Diminished cardiac output, systemic hypotension or hypovolemia, and some pharmacologic agents, particularly digitalis, can result in severely diminished intestinal blood flow, presumably mediated by vasoconstriction of the mesenteric arteries. Nonocclusive mesenteric ischemia accounts for a substantial proportion of cases of acute mesenteric ischemia (see Fig. 8-26). On angiography, intense vasospasm is characteristic. Spasm is frequently irregular or segmental, with more severe areas of narrowing often seen at the origins of arterial branches. Regular and diffuse spasm can also occur. Contrast medium flows sluggishly through mesenteric vessels, causing delayed opacification of peripheral and mural branches. In this regard, the findings are similar to those of mesenteric venous thrombosis, although normal veins eventually fill in most cases of nonocclusive ischemia. Increased reflux of contrast medium into the aorta can also be seen,

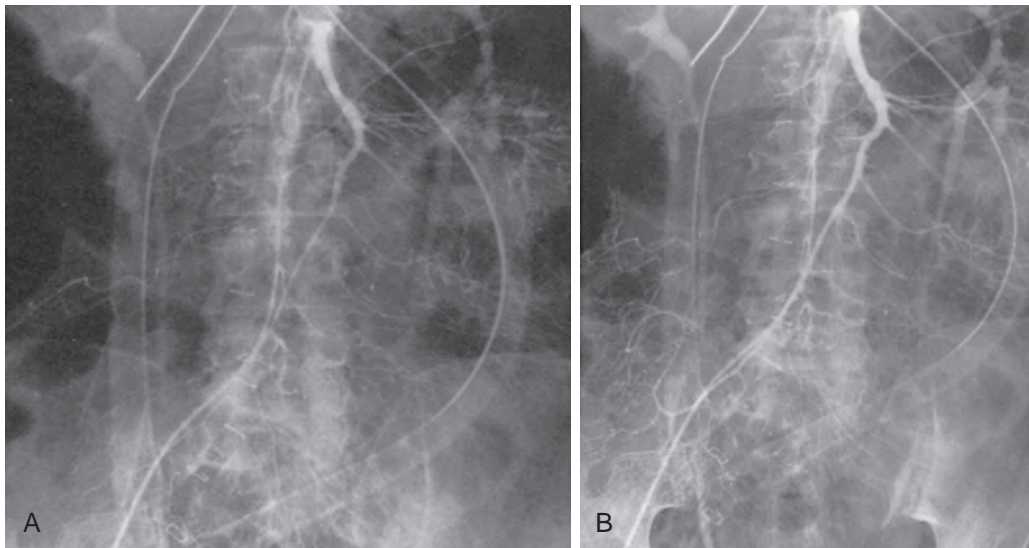


Figure 8-26 Nonocclusive mesenteric ischemia. **A.** Diffuse mesenteric arterial spasm is present, with poor filling of smaller arterial branches. **B.** Improvement in the spasm is noted after initiation of an intra-arterial papaverine infusion.

reflecting increased impedance to mesenteric flow. In practice, this finding is usually judged subjectively, although more objective and quantitative means of assessing superior mesenteric flow based on aortic reflux have been described.

Despite improved methods of diagnosis and therapy for acute mesenteric ischemia, this disorder continues to be associated with a high mortality rate. In the late 1970s, Boley and colleagues²¹ described their aggressive approach to acute mesenteric ischemia that remains the standard of care. Although about 50% of patients presenting with the full syndrome of acute mesenteric ischemia still die, this approach represents a distinct improvement compared with earlier controlled studies that showed only 10% to 30% survival; in addition, the aggressive approach may allow more bowel to be salvaged in those who survive. Key features of this approach include maintenance of a high level of suspicion for the disorder, followed by prompt diagnosis and therapy with emergency angiography.²²⁻²⁷

Another feature of the aggressive algorithm is the selective infusion of vasodilators into the SMA, the rationale being that vasospasm is associated with acute mesenteric ischemia, not only the nonocclusive variety but also occlusive forms (see Fig. 8-26). When mesenteric angiography reveals vasospasm or arterial occlusion, a test dose of a vasodilator should be given.

THROMBOLYTIC THERAPY FOR MESENTERIC VASCULAR OCCLUSION

In most cases of acute mesenteric ischemia with major vascular occlusion, the rapid deterioration of bowel status with time and the need to resect infarcted bowel mandate prompt surgical therapy (Fig. 8-27). However, a number of case reports have suggested a potential role for transcatheter thrombolytic therapy or mechanical thrombectomy (via a transhepatic route) in selected cases of recent mesenteric vascular occlusion, either alone or, as with vasodilator therapy, as part of a combined treatment approach. Candidates for this therapy have included patients deemed unlikely to survive major surgery because of coexistent disease, those with minor or partial vascular occlusions or mild symptoms (who, it could be argued, might need only observation, conservative therapy, and possibly

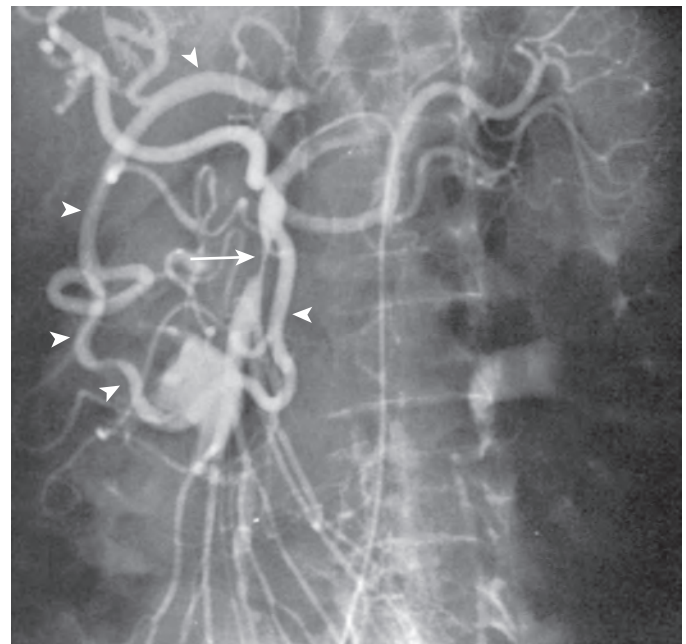


Figure 8-27 Chronic mesenteric ischemia. Superior mesenteric arteriogram of a 62-year-old woman with intermittent episodes of abdominal pain reveals a severe superior mesenteric artery stenosis (arrow). There is filling of the celiac territory via an enlarged pancreaticoduodenal arcade (arrowheads; the inferior pancreaticoduodenal artery arises from the superior mesenteric artery proximal to the stenosis). The presence of the collateral flow attests to the occlusion of the celiac origin, as also noted with lateral aortography. Symptomatic relief occurred after patch angioplasty of the superior mesenteric artery and aorta to celiac artery bypass with an autologous vein.

anticoagulation), those with extensive portal or mesenteric venous thrombosis precluding surgical thrombectomy or bypass, and those who develop occlusion of mesenteric arterial grafts. The presence of peritoneal signs suggesting bowel necrosis is considered a contraindication to thrombolytic therapy alone.

Chronic Mesenteric Ischemia

Chronic mesenteric ischemia is characterized by the presence of severe abdominal pain, typically 30 to 40 minutes after meals. This abdominal pain results in significant weight loss secondary to decreased food intake. Typically, the patients complain of so-called eating fear. In most cases, these patients undergo extensive diagnostic work-ups to investigate the cause of abdominal pain, including upper and lower endoscopies, MDCT, and abdominal ultrasounds, which are negative or disclose no reasonable cause of the pain presented by the patient. A vascular cause for the abdominal pain is typically a diagnosis of exclusion and is usually demonstrated on MDCT or magnetic resonance imaging (MRI) obtained to investigate the abdominal pain.

Most authors agree that at least two major vessels have to be involved or affected (celiac trunk, superior mesenteric artery, or inferior mesenteric artery) to consider that the patient's abdominal pain is actually caused by a vascular problem, but in some cases only one vessel is involved and treatment of a single artery may be sufficient to palliate or improve the patient's symptoms (Fig. 8-28). Angioplasty of celiac or SMA stenotic lesions has been replaced by repair using endovascular stents. The technical success rate for endovascular stent placement in the celiac trunk and/or SMA approaches 100%, with a clinical success approaching 85%. As in other vascular territories, stent stenosis may develop, and these patients require frequent surveillance of their stents.

A very interesting entity is arcuate compression of the celiac trunk, or median arcuate ligament syndrome. This is more common in young women and is characterized by nausea, diarrhea, weight loss, and postprandial abdominal pain. The characteristic picture is that of a compression of the cranial aspect of the celiac trunk, approximately 1 to 1.5 cm distal to the ostium of the artery (Fig. 8-29). This anatomic compression of the celiac trunk may be identified by CT, MRI, or angiography.

Angiographic diagnosis is classic for this entity; a two-view lateral aortogram is performed, one view in inspiration (which releases the compression and almost gives the artery a normal appearance) and a second view with the patient in full expiration (which tightens the compression and makes the stenosis evident; see Fig. 8-29). The clinical significance of this anatomic finding is controversial because only a single vessel is involved. The management is surgical; endovascular techniques are not indicated. The clinical response to surgery, in highly selected patients, is 60% to 70%. Angioplasty or stent placement may have a role if a stenosis of the celiac trunk persists after surgery.

Bowel Interventions

REASONS FOR PLACEMENT OF NEEDLES OR CATHETERS INTO THE GASTROINTESTINAL TRACT

This section is presented as a response to the question of why radiologists might place needles or catheters into or through portions of the GI tract.

Inadvertent Catheterization of the Bowel

This relates not to a specific indication but to a complication that has been described in the setting of various abdominal interventions, specifically unintentional puncture and placement of tubes into or through the bowel. The underlying principle of management (see later) is that given intrinsically normal bowel with no distal obstruction, intestinal contents will flow preferentially along the intestinal lumen. When inadvertent catheterization occurs, treatment of the complication should include drainage of any adjacent infected fluid. Antibiotics, bowel rest, and extended catheter drainage (to allow an organized tract to form) should permit safe catheter withdrawal; at this point, the site of perforation should seal readily because of muscular contraction of the bowel wall.

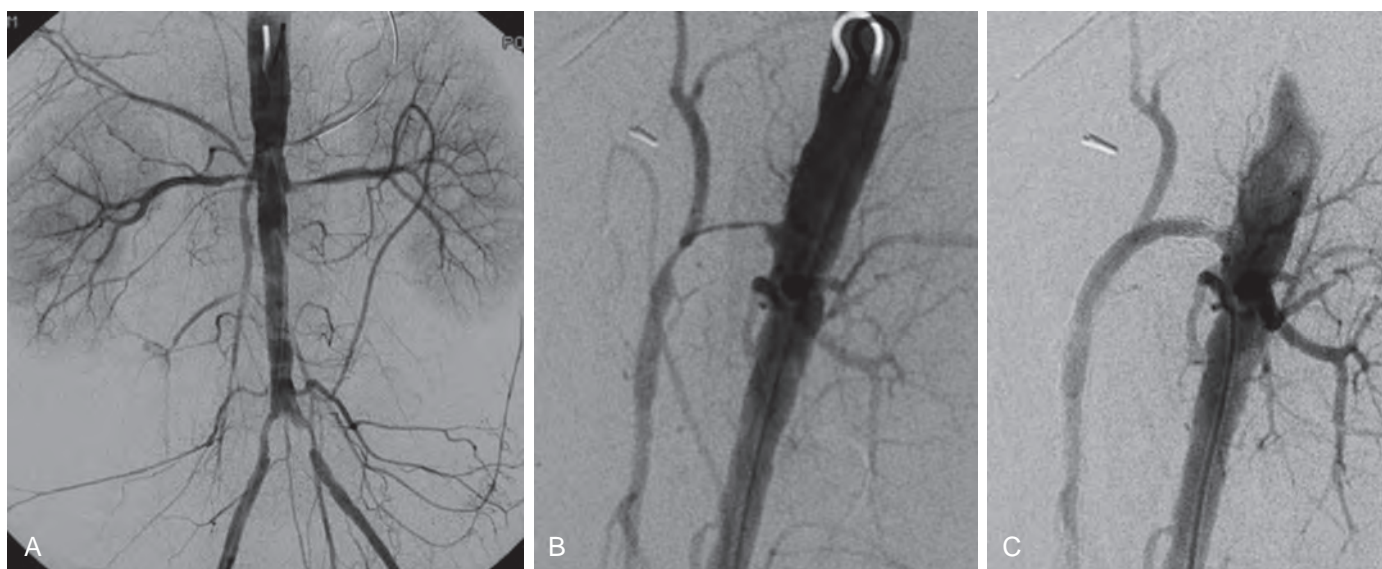


Figure 8-28 Chronic mesenteric ischemia—endovascular stent placement. **A.** Digital subtraction aortogram in a 67-year-old man with severe abdominal pain and a history of 25-pound weight loss. The arteriogram shows a prominent arc of Riolan, bilateral common iliac artery stenosis, and bilateral renal artery stenosis. **B.** Lateral aortogram confirms the presence of a severe stenosis of the superior mesenteric artery. **C.** Lateral aortogram after a successful endovascular stent placement shows an excellent angiographic result.

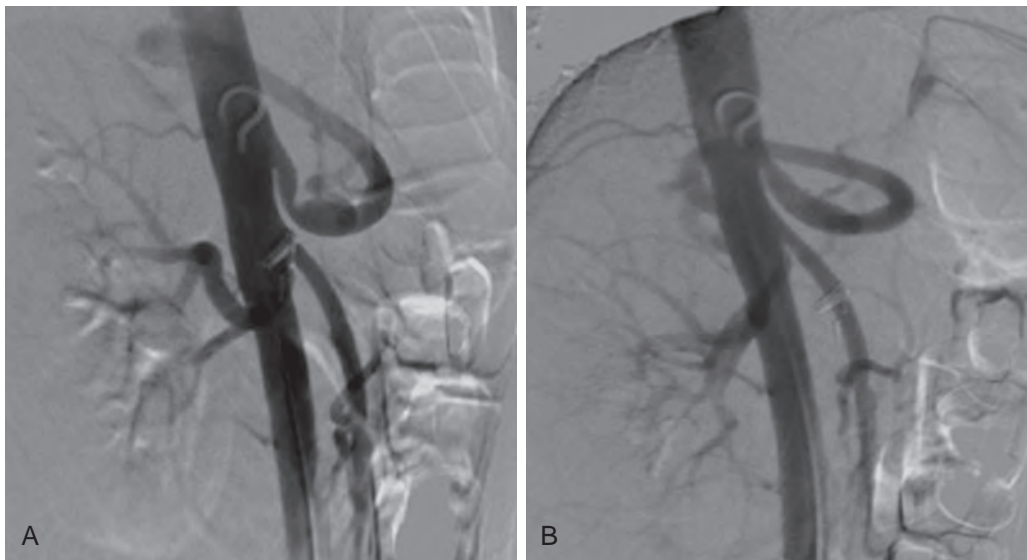


Figure 8-29 Celiac artery compression. Nonselective lateral aortograms in expiration (**A**) and inspiration (**B**) show the typical appearance of celiac artery compression by the arcuate ligament. Note how the compression of the celiac trunk is barely noticeable in the inspiration arteriogram.

Transenteric Biopsy and Fluid Aspiration

Frequently, the bowel is interposed along potential paths for percutaneous diagnostic aspiration of fluid collections or biopsy of masses. Transgression of the bowel in these cases, as well as during therapeutic drainage, can sometimes be avoided by injecting physiologic saline solution or carbon dioxide to displace structures. Nevertheless, avoidance of the bowel is not always possible. Because the aspirating needle passes through a colonized space, with increasing bacterial counts the more distal the segment of the GI tract, the potential for contamination must be acknowledged; confounding of culture results in fluid aspiration or leakage of contaminated contents along the path of the needle. The former may be aided by Gram stain of fluid because a contaminated sample will tend not to have a cellular response. With regard to the latter, considerable clinical and laboratory experience seems to indicate that transgression of the bowel wall with fine needles rarely leads to clinically evident infectious complications. As with any interventional procedure, the risks of bowel puncture should be balanced against the risks of alternate diagnostic methods and the need to obtain a pathologic or microbiologic diagnosis. Although it seems prudent to choose an approach that avoids the bowel, particularly the colon, and although it seems reasonable to avoid larger cutting needles if the bowel must be punctured, the need to pass a needle through the bowel does not in itself constitute a contraindication to needle aspiration. Possible exceptions would include passage through an obstructed loop or through the bowel in an immunosuppressed patient, although little hard data exist in these settings.

Puncture of Bowel to Confirm Identity

At times, nonopacified bowel loops may mimic abnormal fluid collections; conversely, collapsed loops may mimic masses (e.g., in the case of afferent loops in patients with a history of GI malignancy). Percutaneous puncture of such indeterminate structures with thin needles and injection of water-soluble contrast medium can be invaluable in guiding further diagnosis and therapy. Contrast medium is injected through one of the needles as it is withdrawn; if the bowel has been crossed, the needles can be withdrawn and another path chosen.

Drainage of Fluid Collections Shielded by Bowel

Taking the concept of transenteric diagnostic aspiration a step farther, and mimicking traditional surgical therapy (e.g., pseudocystogastrostomy) to some extent, transenteric drainage of infected or inflammatory fluid collections has been proposed (Figs. 8-30 to 8-33). This has been an area of particular interest in the setting of pancreatitis, which is often associated with lesser sac collections unapproachable for percutaneous drainage, except through the stomach. Although this approach is controversial, its advocates argue that it can help avoid spillage of pancreatic enzymes around the drainage site and prevent formation of pancreaticocutaneous fistulas. Along the same lines, there is growing favorable experience with transrectal drainage of pelvic collections by standard catheter placement or a one-step, complete aspiration. This approach offers increased patient comfort and possibly decreased complications compared with the more standard transgluteal drainage route.

DIAGNOSTIC BIOPSY OF BOWEL MASSES

Several investigators have found sonographic and fluoroscopic (via barium studies) biopsy of pathologic processes directly involving the bowel wall to be effective and safe. Indications for this approach include the following: (1) lesions yielding no diagnostic tissue via endoscopic biopsy (a common problem with submucosal lesions); (2) lesions in patients who are poor candidates for endoscopy or open exploration; (3) lesions that because of their location are not accessible endoscopically; and (4) lesions that if proved malignant will obviate the need for further investigation or change in therapy.^{28,29}

ENTERIC PUNCTURE FOR DIAGNOSTIC OR THERAPEUTIC ACCESS

An uncommon but potentially very useful application of transenteric access is to allow diagnostic or therapeutic access to various structures. One example of this is access to GI tract strictures difficult to reach via a nasenteric or rectal approach. Another novel approach involved placement of a percutaneous

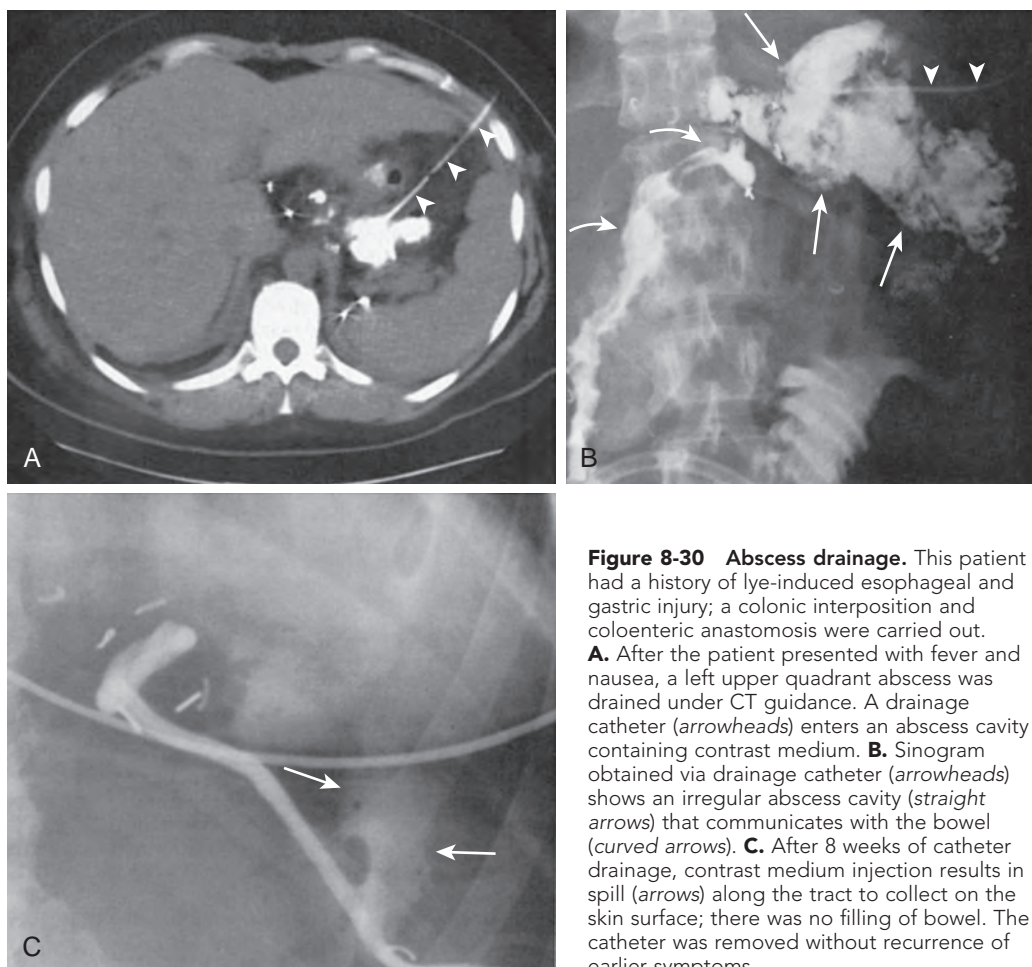


Figure 8-30 Abscess drainage. This patient had a history of lye-induced esophageal and gastric injury; a colonic interposition and coloenteric anastomosis were carried out.

A. After the patient presented with fever and nausea, a left upper quadrant abscess was drained under CT guidance. A drainage catheter (arrowheads) enters an abscess cavity containing contrast medium. **B.** Sinogram obtained via drainage catheter (arrowheads) shows an irregular abscess cavity (straight arrows) that communicates with the bowel (curved arrows). **C.** After 8 weeks of catheter drainage, contrast medium injection results in spill (arrows) along the tract to collect on the skin surface; there was no filling of bowel. The catheter was removed without recurrence of earlier symptoms.

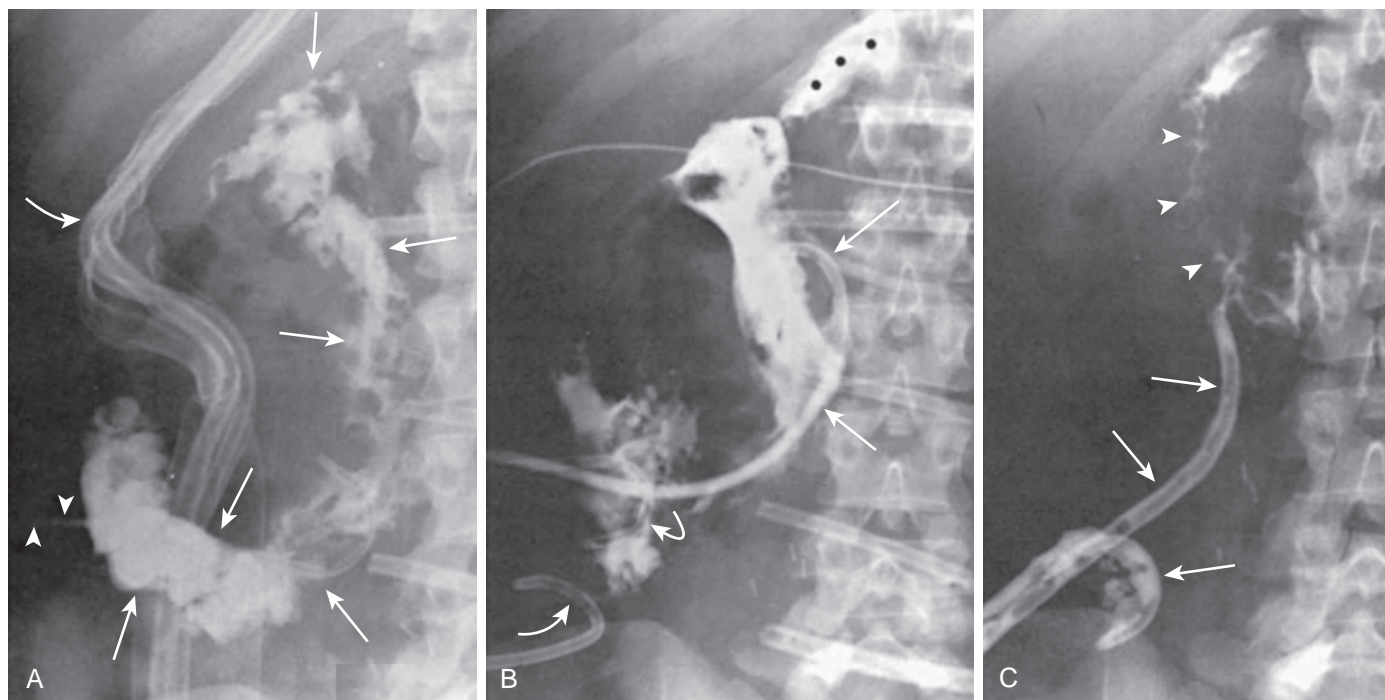


Figure 8-31 Abscess drainage, multiple catheters. Bowel injury was discovered at laparotomy in a patient who had abdominal trauma.

A. Sinogram obtained immediately after abscess drainage. The drainage catheter (arrowheads) enters an irregular cavity (straight arrows); no filling of bowel is noted on initial injection. The curved arrow indicates a surgical drain. **B.** Three drainage catheters have been placed 10 days later, two in the lower portion of the abscess cavity (curved arrows) and one in its cephalad aspect (straight arrow). Filling of the bowel (black dots) is now apparent. **C.** The abscess cavity has almost completely collapsed 3 months later, but a fistula to the bowel (arrowheads) is still present. Two catheters remain in place (arrows). With continued drainage, the fistula eventually closed and the catheters were removed.

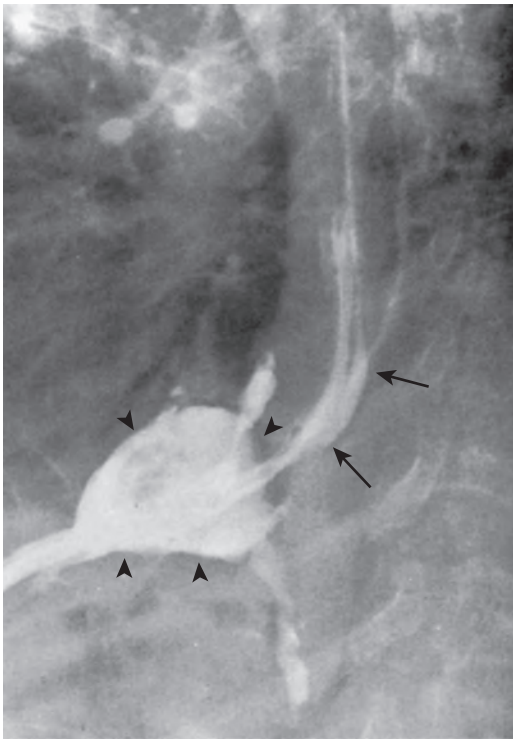


Figure 8-32 Percutaneous drainage of an esophageal leak. Sinography performed after CT-guided drainage of a juxtalesural fluid collection (arrowheads) shows communication with the esophagus (arrows).

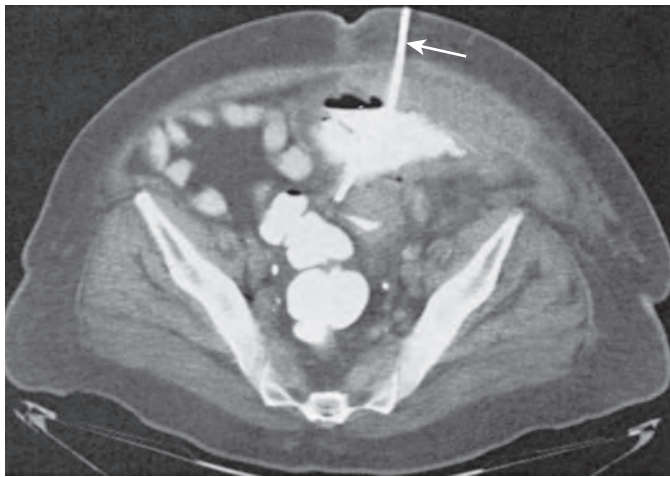


Figure 8-33 Percutaneous drainage of a diverticular abscess. A drain (arrow) courses through the anterior abdominal wall and enters the abscess, which has been opacified with contrast medium. The patient underwent a single-stage surgical resection after successful abscess drainage.

cecostomy tube to allow diagnostic and therapeutic endoscopy of the small bowel in a patient who was bleeding from ileal angiodysplasia.

Transenteric access to the biliary tract can be used in those in whom a choledochojejunostomy or hepaticojejunostomy was previously performed. Advantages of this approach are that it allows repeated access to the biliary tract without the need to traverse liver parenchyma, it gives a mechanical advantage for patients in whom multiple sites of disease need to be treated

(e.g., sclerosing cholangitis), and it allows easier access when the biliary tract is nondilated. Surgical techniques anticipating these advantages have been designed to allow easier access to the relevant bowel loop. Initially, this consisted of a formal jejunostomy, or so-called Hutson-Russell loop. Although access to the bowel was guaranteed, problems with skin excoriation caused by leakage of bile or mucus developed. Subcutaneous tacking of the jejunal loop was another option, but this was plagued by subcutaneous inflammation in the early postoperative period and by peristomal hernias later on. Consequently, the favored approach at this time is subparietal tacking of the loop, whose site can be marked with surgical clips.

Puncture is generally performed with fluoroscopic guidance (by identification of the gas within the loop), although opacification could potentially be obtained with manipulation of a nasoenteric tube.

Enteral Access for Bowel Decompression

Whereas percutaneous gastrostomy is most frequently used to provide a route for enteral alimentation, it can also serve as an effective means of decompressing the bowel in patients with chronic intestinal obstruction and symptoms of nausea and vomiting, eliminating most of the complications associated with long-term nasogastric intubation. However, this subset of patients may present unique technical problems, mainly the result of more limited access to the stomach because of diffuse peritoneal carcinomatosis, adhesions from prior radiation or surgical therapy, or ascites. Gastrostomy has also been used to provide symptomatic relief in patients with gastroparesis or delayed gastric emptying in the absence of a fixed anatomic obstruction.

Direct, percutaneous, small bowel catheterization has also been used to treat symptoms of enteric obstruction or stasis in cases in which gastric decompression alone would not suffice. These situations usually require surgery, but percutaneous management can be considered an alternative for patients who are poor surgical candidates. Maneuvers designed to distend or fix the bowel are often not possible, nor are they likely to be necessary because significant intrinsic distention of bowel is present. Acute palliation and long-term prevention of recurrence of closed loop obstruction in a patient with metastatic colon carcinoma have been described. Symptoms of blind or afferent loop stasis have also been relieved by this method. An alternative approach in afferent loop syndromes has been percutaneous management; a drainage tube can be passed percutaneously into the liver or gallbladder and through the biliary tree into the affected bowel limb (Fig. 8-34). A possible benefit of this route is simultaneous drainage of the biliary tract because these patients may have associated biliary stasis or cholangitis. The occurrence of delayed septic shock in one patient in whom transhepatic treatment of an afferent loop was performed suggests that placement of a separate biliary drain may be advisable. In appropriate circumstances, feeding tubes have been placed via a transhepatic biliary route. It is important in such cases to infuse feeding solutions through a tube placed well beyond the native or postsurgical biliary-enteric junction.

In nonobstructive colonic distention, the cecum is usually the most severely involved segment. This finding demonstrates the Laplace law, in which the portion of colon with the greatest diameter (the cecum) responds first with further distention once intraluminal pressure begins to increase. Cecal ileus refers to the situation in which cecal distention develops out of

proportion to that of the remainder of the colon. These patients have a mobile cecum suspended on a mesentery. When the patient is in the supine position, the cecum can rotate anteriorly, leading to progressive distention.

Massive colonic distention, when left untreated, may lead to colonic perforation, ischemia, peritonitis, and death. Once massive distention (≥ 9 cm) of the cecum occurs, the risk of perforation seems less related to the absolute degree of distention than to the duration of distention. Therefore early recognition and therapy for this condition are critical.

The initial treatment of nonobstructive colonic distention is conservative; it includes placement of a nasogastric tube, withholding of oral intake, and treatment of underlying metabolic and other medical disorders. If the distention fails to improve, colonoscopy and colonic decompression tube placement should be attempted; a fluoroscopic approach to decompression using

a coaxial steerable system for intubation has been described. These methods may prove ineffective because of thick retained stool. Distention may recur after initial colonoscopic success.

After unsuccessful colonoscopic decompression, surgical cecostomy has been the next therapeutic approach. However, surgery in these patients, who are often seriously ill, can be risky. Consequently, a number of investigators have attempted percutaneous decompression of the massively dilated but unobstructed cecum. Successful decompression has been achieved with simple aspiration and drainage tube placement. Reports of percutaneous decompression of the mechanically obstructed colon have also appeared.

A variety of approaches, methods, and tube sizes have been used for percutaneous cecostomy (Fig. 8-35). Usually, fluoroscopy provides sufficient guidance, although CT may be helpful if there are questions about the approach. Both the trocar and Seldinger methods of tube placement are feasible for these patients. Although further experience with percutaneous cecostomy is necessary to assess risks fully and evaluate optimal technique and indications, this is an alternative method of colonic decompression in severely ill and debilitated patients. Also, cecostomy has also been used to treat fecal incontinence in children by allowing antegrade cleansing enemas to be administered.³⁰⁻³²

Enteral Access for Alimentation

The last but not most common and important indication for radiologic enteric access is for nutritional support. Most of these procedures are percutaneous gastrostomies and gastrojejunostomies, but percutaneous jejunostomy and duodenostomy have been used in increasing numbers.³³⁻³⁸

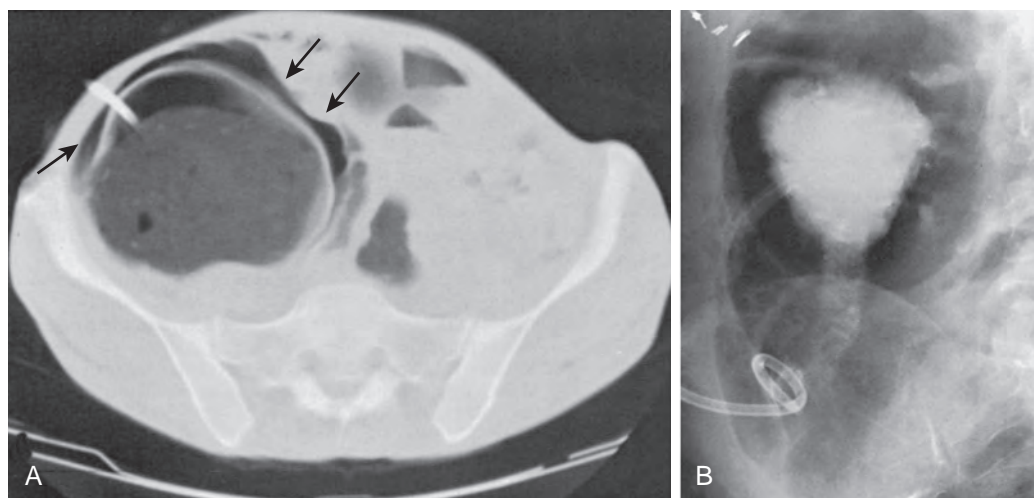
In the short term, nasoenteric tubes can be used effectively for alimentation. However, longer term use is associated with a variety of problems. These tubes are uncomfortable and often psychologically untenable for patients. Also, they predispose the patient to gastroesophageal reflux, esophagitis, and stricture formation, and the luminal diameter of most nasoenteric tubes is small, predisposing them to occlusion.

Total parenteral nutrition is another option for feeding patients. It is particularly useful for patients who are unable to assimilate enteric nutrients or require bowel rest. As a general method for alimentation, however, it has disadvantages



Figure 8-34 Percutaneous cholecystostomy. Patient with pancreatic carcinoma, after Roux-en-Y cholecystojejunostomy and gastrojejunostomy, who developed abdominal pain, elevated serum bilirubin level, and septicemia. CT revealed a dilated afferent bowel loop anastomosed to the gallbladder. Percutaneous cholecystostomy with passage of a catheter via the gallbladder (arrow) and into the jejunal loop (arrowheads) resulted in improvement of symptoms.

Figure 8-35 Percutaneous cecostomy. A transperitoneal approach was used. **A.** CT scan. **B.** Abdominal plain film. Air (arrows in **A**) was introduced into the peritoneal cavity during the procedure.



compared with the enteral route. It is more costly than the enteral alternative. Over the long term, it is associated with several complications, including small bowel atrophy, abnormalities of hepatic function, and electrolyte disturbances. The need for prolonged venous access also places the patient at high risk for the development of venous thromboses and stenoses.

Enteral access, on the other hand, is associated with few complications once it is established and is less expensive than total parenteral nutrition. Thus, enteral alimentation is indicated for patients with longer term nutritional requirements who, because of mechanical, functional, or psychological disorders, are unable to meet their nutritional needs without assistance but can still assimilate enterically administered nutrients.

In the past, gastrostomy tubes were placed surgically. However, many patients who require gastrostomy tubes are poor operative risks because of malnutrition, debilitation, and coexistent illnesses. Gastrostomy has increasingly been performed using less invasive techniques, such as radiologic, endoscopic (percutaneous endoscopic gastrostomy), and laparoscopic methods. Although each method has certain advantages and disadvantages, there has been little randomized prospective comparison among them. As much as in any area of interventional radiology, local referral patterns, politics, and expertise may result in widely variable patterns of practice among institutions.

There are several other technical differences. Radiologic gastrostomy or gastrojejunostomy appears to be less costly than the surgical alternative, does not require general anesthesia, and has less associated postprocedural ileus. The endoscopic method does not require exposure to ionizing radiation and can be performed easily and rapidly at the bedside. Although bedside placement using ultrasonography or portable fluoroscopy is possible, it is rarely performed. Endoscopic placement may be difficult or impossible when there is obstruction or high-grade narrowing of the esophagus or pharynx, leaving imaging-guided placement as the only feasible nonoperative alternative. Imaging guidance may also be critical for delineating and avoiding interposed structures (e.g., the colon) between the anterior abdominal wall and stomach. In patients prone to aspiration, imaging guidance is usually preferable because endoscopy may require heavy sedation and may be a lengthy procedure if tube placement into the jejunum is required. Tubes placed under imaging guidance seem less likely to give rise to stomal wound infections than those inserted endoscopically. The endoscope must pass through the contaminated oral cavity rather than the scrubbed anterior abdominal wall. Finally, endoscopic placement offers the possibility of biopsy and other diagnostic methods when appropriate.

Percutaneous gastrostomy can be performed by a variety of methods. Before the procedure, the patient should be given nothing by mouth for at least 12 hours to minimize risks of aspiration and peritoneal leakage. Prophylactic antibiotics are usually not necessary. Only mild sedation combined with local anesthesia at the puncture site is generally required, although general anesthesia offers advantages in infants and younger children.

An entry site is chosen in the anterior left upper quadrant, which allows direct puncture of the stomach, with no transgression of bowel, liver, or vascular structures. Preprocedural ultrasonography or CT delineates these structures (Fig. 8-36). Ultrasound is quickly and easily performed in the fluoroscopy

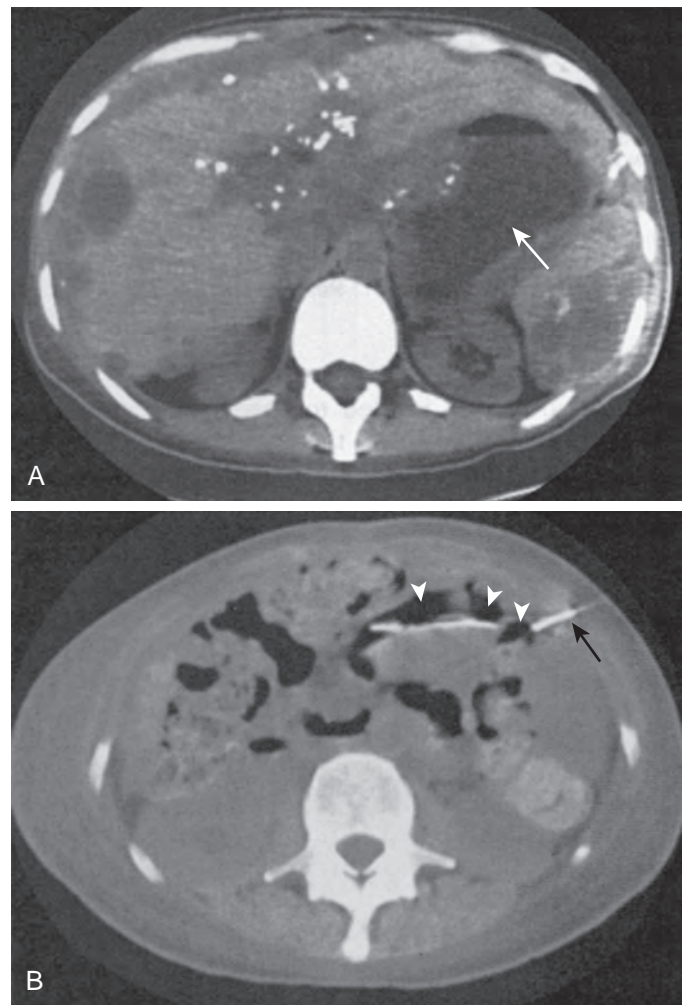


Figure 8-36 CT-guided percutaneous gastrostomy. **A.** CT scan of the upper abdomen in a patient with pseudomyxoma peritonei attributable to ovarian carcinoma shows the stomach (arrow) surrounded by adjacent organs and peritoneal metastases. **B.** At a more caudal level, a safe window to the stomach is present. Percutaneous gastrostomy was successfully performed under CT guidance. Arrowheads, Gastric lumen; black arrow, initial puncture needle.

suite and is often used routinely to demarcate a safe window on the skin surface. Another helpful adjunct in patients who have no obstruction or altered enteric motility is the administration of oral contrast medium the night before the examination, which provides good opacification of the colon at the time of the procedure.

One potential hazard of percutaneous gastrostomy is injury to the inferior epigastric artery, which lies at the junction of the medial two thirds and lateral third of the rectus abdominis. Therefore skin puncture should be made at a site lateral to this muscle or close to the midline of the abdomen, depending on the position of the stomach. A subcostal puncture site usually provides good access to the stomach, is more comfortable for the patient, and avoids pleural and pulmonary complications.

Gastric distention makes it easier to pierce the gastric wall, which tends to invaginate and move away from the puncture needle. Distention also helps bring the stomach closer to the anterior abdominal wall and displaces any interposed bowel.

Distention is provided by insufflation of the stomach with several hundred milliliters of room air administered via a previously placed nasogastric tube. If a nasogastric tube cannot be placed, the stomach can be punctured with a Seldinger needle, and air can be injected through its lumen. Another means of providing distention is the oral administration of effervescent granules that produce carbon dioxide. IV glucagon (1.0 mg in adults, 0.14 mg/kg in children) can be used to augment these measures by diminishing gastric peristalsis and decreasing passage of air through the pylorus. If fluoroscopic puncture proves difficult because of interposed structures or variant anatomy, inability to pass a nasogastric tube, or inability to tolerate gastric distention, cross-sectional imaging can also be used for guidance (see Fig. 8-36).

Another option for providing distention is intragastric inflation of a latex balloon attached to the end of a nasogastric tube. The balloon is inflated with diluted contrast medium or air, providing an easily visualized and stable target for fluoroscopically or sonographically guided puncture. Bursting of the balloon confirms intragastric positioning of the needle tip. Although this device can be difficult for some patients to tolerate and is usually unnecessary, it may be helpful when simple insufflation is unsuccessful in providing gastric distention, as seen in patients with a partial gastrectomy.

The anterior wall of the stomach is usually punctured in its middle third, toward the side of the greater curvature (Fig. 8-37). The greater and lesser curvatures should be avoided because the larger vascular arcades of the stomach are located in these regions. Lateral fluoroscopy is used to access the

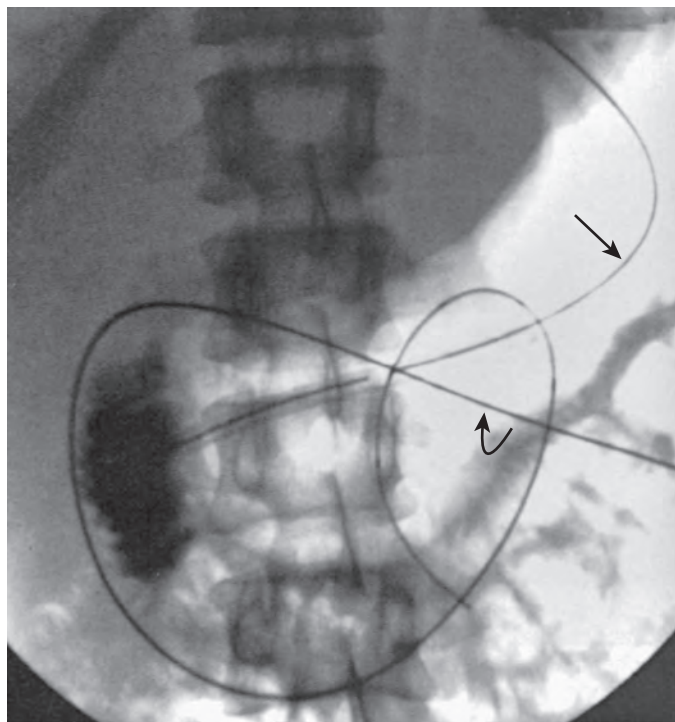


Figure 8-37 Fluoroscopically guided percutaneous gastrostomy. The midbody of the gas-filled stomach has been punctured with an 18-gauge Seldinger needle (*curved arrow*). It is angulated toward the pylorus, and a wire has been manipulated into the proximal jejunum. A gastrojejunostomy tube was subsequently placed. A nasogastric tube was used for insufflation of air (*straight arrow*).

proximity of the anterior gastric wall to the skin surface. If initial or delayed small bowel catheterization is anticipated, a downhill puncture angled toward the pyloric region makes manipulations of the guidewire and catheter easier. Too great an angle, however, makes tract dilation and catheter exchange difficult. If the tube is being placed for decompressive purposes only, it can be angled somewhat more vertically and toward the gastric fundus. Once the gastric wall is indented by the puncture needle, a short vigorous thrust is used to pierce its muscular layers.

Final catheter placement can be achieved by a variety of methods. One is the Seldinger technique and its variants, in which initial puncture is made with an 18- to 22-gauge Seldinger needle or a small sheathed needle. A wire is passed through the sheath or cannula, and successive guidewire and catheter exchange is used to place a final gastrostomy tube. Techniques using a trocar, an instrument consisting of a catheter or sheath mounted on the puncture needle, have also been successfully used in placing gastrostomy tubes. The trocar technique allows larger and softer tubes to be inserted at the time of the initial procedure and requires fewer catheter and wire exchanges, each of which may result in loss of gastric access. The initial puncture, however, may be difficult and risky with trocars, which are usually larger devices.

When the Seldinger technique is used, a peel-away sheath may facilitate insertion if catheter exchange is difficult or placement of a soft catheter or catheter without an end hole is desired. In addition, removal of the peel-away sheath may correct any gastric wall invagination that has occurred. During passage of catheters or dilators, the stabilizing guidewire has a free end within the GI tract and must not be displaced out of the gastric lumen. A method of preventing this problem in children has been described. The free end of the wire is secured and pulled from the stomach to the mouth by a wire basket or snare, allowing stable control of both ends of the wire in a manner analogous to that of endoscopic methods. In general, however, these maneuvers are unnecessary.

The use of fixation devices as an adjunct to percutaneous gastrostomy has generated some controversy. These devices are fasteners that can be placed through a small needle to affix the anterior gastric wall to the anterior abdominal wall at one or more sites. Advocates of these devices have cited a number of potential advantages, including reduced intraperitoneal leakage of gastric contents, facilitation of guidewire and catheter exchange and immediate placement of large catheters, increased safety in patients expected to have difficulty with track maturation (e.g., patients on corticosteroid therapy), easy reinsertion in cases of early catheter dislodgment (of greater concern in uncooperative patients), and possible tamponade of gastric hemorrhage induced at the gastrostomy site. Theoretical disadvantages of gastric fixation are interference with gastric peristalsis and excessive traction on the gastric wall, resulting in pressure necrosis, bleeding, infection, or catheter dislodgment. Problems related to excessive traction are not unique to the use of fixation devices. Other potential disadvantages that can be obviated by careful technique include anchor misplacement into the peritoneal cavity and difficulty with tube passage immediately adjacent to the anchor. Most of the controversy, however, has arisen because of extensive clinical and laboratory experience with percutaneous gastrostomy accomplished without fixation devices, which suggests that the procedure can be performed easily, safely, and less expensively in most cases.

without their use. No large prospective comparisons have yet been made.³³⁻³⁸

Massive ascites is generally considered a contraindication to percutaneous gastrostomy. Large quantities of peritoneal fluid make gastric puncture difficult and can lead to tube dislodgment, gastropexy breakdown, peritonitis, and skin breakdown. However, gastrostomies have been safely placed and managed in patients with smaller amounts of ascites via a combination of gastropexy, preprocedural paracentesis, and regular postprocedural paracentesis to allow the enterostomy track to mature.

Another area of controversy is the final position of the tube. Some practitioners prefer that the tube be manipulated into the proximal jejunum at the time of the initial procedure. This allows for immediate catheter feeding, diminishes the risks of gastroesophageal reflux and aspiration of gastric contents, and provides additional insurance against catheter dislodgment. Other practitioners have maintained that routine gastrojejunostomy is not indicated, and they have reserved jejunal placement for patients who are prone to reflux or aspiration, have impaired gastric motility, or have partial gastric obstruction. Scintigraphy has been reported to be helpful in determining whether a patient can safely tolerate a gastrostomy tube without risk of reflux and aspiration. Even if the tube is left in the stomach initially, subsequent conversion to a gastrojejunostomy tube can usually be accomplished without difficulty as long as the original angle of puncture is toward the pylorus. If not, a stiff sheath can frequently be used to redirect the tube, although in cases of severe unfavorable angulation, a new access site may be the best approach. A large variety of tubes have been used for percutaneous gastrostomy, including simple Cope loop catheters, Foley catheters, and catheters specially designed for percutaneous gastrostomy and gastrojejunostomy. Catheter sizes usually range from about 12 to 20 Fr. Because of its ease of insertion, the Cope loop is preferred by many investigators, except in patients who require gastrojejunostomy.

Altered gastric anatomy caused by prior surgery, although it may sometimes preclude percutaneous gastrostomy, should not be considered an absolute contraindication. However, a full understanding of the postsurgical anatomy is important. Generally, gastrostomy can be performed with minor modifications of standard methods, such as the use of longer needles and craniocaudal fluoroscopy. Other techniques reported to be helpful in this setting include gastric balloon support and the use of a transhepatic catheter route guided by CT.

Potential complications of percutaneous gastrostomy include catheter dislodgment, pericatheter leakage, peritonitis, sepsis, pain, hemorrhage, inadvertent puncture of other organs, pulmonary aspiration, subcutaneous inflammation, and wound infection. Although patients should be observed carefully after percutaneous gastrostomy for signs of complications, it should be noted that a number of postprocedural radiologic findings are common and should not by themselves cause alarm or prompt laparotomy. These findings include pneumoperitoneum and small abdominal wall and gastric hematomas. Subcutaneous emphysema, gastric pneumatosis, free or loculated intraperitoneal fluid, and pneumoperitoneum that increases in volume are uncommon and should be viewed with more concern (Fig. 8-38).

Long-term care of percutaneous gastrostomy catheters includes keeping the catheter entry site clean and maintaining tube patency after feeding with injection of saline solution. A

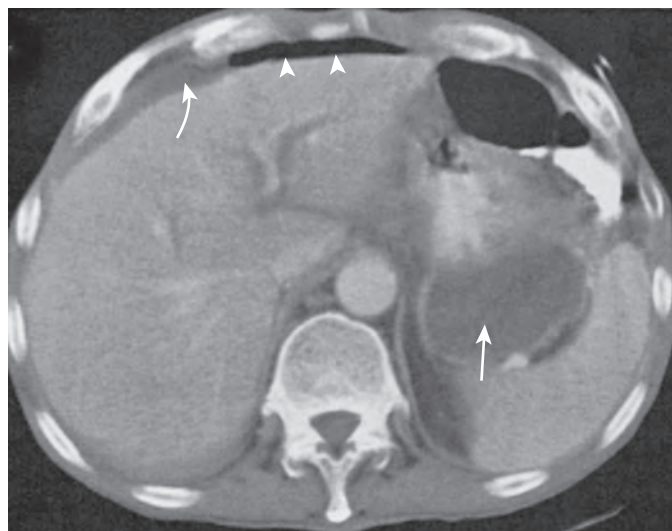


Figure 8-38 Percutaneous gastrostomy: complication. CT scan obtained 3 days after percutaneous gastrostomy. Although pneumoperitoneum (arrowheads) is often seen in the absence of clinically apparent complications, findings of loculated (straight arrow) and free (curved arrow) intraperitoneal fluid are atypical and are cause for concern. Peritoneal spillage in this case resulted from intraperitoneal positioning of a side hole of the gastrostomy tube. The patient required surgical treatment.

tract between the abdominal wall and gastric lumen is usually well established in about 7 days, and exchange of an occluded tube or replacement of a recently dislodged tube after this time is generally easy. If the tube is inadvertently removed at an earlier time, an attempt can be made to recatheterize the tract, but it is less likely to be successful. As noted earlier, one possible advantage to using gastric fixation devices is that it facilitates tube replacement or repeated puncture of the stomach in this early period. If pericatheter leakage is noted, the problem may respond to replacement of the tube with one that is slightly larger. Delayed pericatheter hemorrhage, presumably attributable to erosion into an adjacent vessel, has been described. Successful tamponade and long-term control of the bleeding can be achieved with gentle traction by a Foley catheter against the gastric wall. Another delayed complication, occurring from days to months after gastrostomy placement, is perforation of the GI tract by the tube. Perforations can be managed with nonsurgical means, including tube replacement, antibiotic therapy, drainage of associated abscesses, and gastric compression.

Direct percutaneous catheterization of the small bowel has been performed much less often than percutaneous gastrostomy. The procedure is made difficult by the mobility and compliance of small bowel loops and by the difficulty associated with providing and maintaining their distention. Although fluoroscopic guidance has been used in many cases, CT and ultrasonography have also proved useful for localization and puncture of the small bowel.³⁹

Indications for percutaneous jejunostomy include the need for prolonged enteric feeding in patients in whom a gastrostomy by the percutaneous or endoscopic route is not possible. This can occur, for example, when a large hiatal hernia is present or in postsurgical patients after a gastric

pull-up procedure or partial gastrectomy with a small and high-positioned gastric remnant. Other potential indications include chronic aspiration, gastric outlet or duodenal obstruction, recurrent dislodgment of previously placed gastrostomies, retrograde gastrojejunostomy dislodgment back into the stomach, or premature dislodgment of a jejunostomy.

Adequate distention of the jejunum is an important facet of the procedure. Transnasal or transoral intubation of the small bowel can provide access for small bowel distention with air, contrast medium, or supportive balloons. Direct fine-needle puncture and air insufflation into the left upper quadrant can also be used to identify the jejunum.³⁹

REFERENCES

- Kessel D, Robertson I: Diagnostic Imaging: Interventional Procedures, Salt Lake City, 2013, Airsys.
- Wicke L: Atlas of Radiologic Anatomy, ed 7, Philadelphia, 2004, Saunders.
- Gümüş H, Bükte Y, Özdemir E, et al: Variations of the celiac trunk and hepatic arteries: A study with 64-detector computed tomographic angiography. *Eur Rev Med Pharmacol Sci* 17:1636–1641, 2013.
- Hellinger JC: Evaluating mesenteric ischemia with multidetector-row CT angiography. *Tech Vasc Interv Radiol* 7:160–166, 2004.
- Chicoskie C, Tello R: Gadolinium-enhanced MDCT angiography of the abdomen: Feasibility and limitations. *AJR* 184:1821–1828, 2005.
- Vosshenrich R, Fischer U: Contrast-enhanced MR angiography of abdominal vessels: Is there still a role for angiography? *Eur Radiol* 12:218–230, 2002.
- Sabach AS, Bruno M, Kim D, et al: Gadofosveset trisodium: Abdominal and peripheral vascular applications. *AJR* 200:1378–1386, 2013.
- Funaki B: Microcatheter embolization of lower gastrointestinal hemorrhage: An old idea whose time has come. *Cardiovasc Interv Radiol* 27:591–599, 2004.
- Hawkins IF, Cho KJ, Caridi JG: Carbon dioxide in angiography to reduce the risk of contrast-induced nephropathy. *Radiol Clin North Am* 47:813–825, 2009.
- Hawkins IF, Jr, Caridi JG, Klioze SD, Mladinich CR: Modified plastic bag system with O-ring fitting connection for carbon dioxide angiography. *AJR* 176:229–232, 2001.
- Caridi JG, Hawkins IF, Jr: CO₂ digital subtraction angiography: Potential complications and their prevention. *J Vasc Interv Radiol* 8:383–391, 1997.
- Haage P, Krings T, Schmitz-Rode T: Nontraumatic vascular emergencies: Imaging and intervention in acute venous occlusion. *Eur Radiol* 12:2627–2643, 2002.
- Sachdev U, Baril DT, Ellozy SH, et al: Management of aneurysms involving branches of the celiac and superior mesenteric arteries: A comparison of surgical and endovascular therapy. *J Vasc Surg* 44:718–724, 2006.
- Connell JM, Han DC: Celiac artery aneurysms: A case report and review of the literature. *Am Surg* 72:746–749, 2006.
- Chang SH, Lien WC, Liu YP, et al: Isolated superior mesenteric artery dissection in a patient without risk factors or aortic dissection. *Am J Emerg Med* 24:385–387, 2006.
- Kang UR, Kim YH, Lee YH: Endovascular stent graft for treatment of complicated spontaneous dissection of celiac artery: Report of two cases. *Korean J Radiol* 14:460–464, 2013.
- Kobayashi M, Morishita S, Okabayashi T, et al: Preoperative assessment of vascular anatomy of inferior mesenteric artery by volume-rendered 3D-CT for laparoscopic lymph node dissection with left colic artery preservation in lower sigmoid and rectal cancer. *World J Gastroenterol* 12:553–555, 2006.
- Saikia N, Talukdar R, Mazumder S, et al: Polyarteritis nodosa presenting as massive upper gastrointestinal hemorrhage. *Gastrointest Endosc* 63:868–870, 2006.
- Navuluri R, Kang L, Patel J, Van Ha T: Acute lower gastrointestinal bleeding. *Semin Intervent Radiol* 29:178–186, 2012.
- Yi WS, Garg G, Sava JA: Localization and definitive control of lower gastrointestinal bleeding with angiography and embolization. *Am Surg* 79:375–380, 2013.
- Boley SJ, Brandt LJ, Sammartano RJ: History of mesenteric ischemia. The evolution of a diagnosis and management. *Surg Clin North Am* 77:275–288, 1997.
- Strate LL: Lower GI bleeding: Epidemiology and diagnosis. *Gastroenterol Clin North Am* 34:643–664, 2005.
- Silva JA, White CJ: Ischemic bowel syndromes. *Prim Care* 40:153–167, 2013.
- Haage P, Krings T, Schmitz-Rode T: Nontraumatic vascular emergencies: Imaging and intervention in acute venous occlusion. *Eur Radiol* 12:2627–2643, 2002.
- Horton KM, Talamini MA, Fishman EK: Median arcuate ligament syndrome: Evaluation with CT angiography. *Radiographics* 25:1177–1182, 2005.
- Strate LL: Lower GI bleeding: Epidemiology and diagnosis. *Gastroenterol Clin North Am* 34:643–664, 2005.
- Siersema PD: Therapeutic esophageal interventions for dysphagia and bleeding. *Curr Opin Gastroenterol* 22:442–447, 2006.
- Yang Z, Wu Q, Wang F, et al: A systematic review and meta-analysis of randomized trials and prospective studies comparing covered and bare self-expandable metal stents for the treatment of malignant obstruction in the digestive tract. *Int J Med Sci* 10:825–835, 2013.
- Mitton D, Ackroyd R: Oesophageal stenting. *Scand J Gastroenterol* 40:1–14, 2005.
- Gillman LM, Latosinsky S: Anterograde colonic stent placement via a cecostomy tube site. *Can J Gastroenterol* 20:425–426, 2006.
- De Ceglie A, Filiberti R, Baron TH, et al: A meta-analysis of endoscopic stenting as bridge to surgery versus emergency surgery for left-sided colorectal cancer obstruction. *Crit Rev Oncol Hematol* 88:387–403, 2013.
- Lynch CR, Jones RG, Hilden K, et al: Percutaneous endoscopic cecostomy in adults: A case series. *Gastrointest Endosc* 64:279–282, 2006.
- Burke DT, El Shami A, Heinle E, et al: Comparison of gastrostomy tube replacement verification using air insufflation versus Gastrografin. *Arch Phys Med Rehabil* 87:1530–1533, 2006.
- Chio A, Galletti R, Finocchiaro C, et al: Percutaneous radiological gastrostomy: A safe and effective method of nutritional tube placement in advanced ALS. *J Neurol Neurosurg Psychiatry* 75:645–647, 2004.
- Desport JC, Mabrouk T, Bouillet P, et al: Complications and survival following radiologically and endoscopically guided gastrostomy in patients with amyotrophic lateral sclerosis. *Amyotroph Lateral Scler Other Motor Neuron Disord* 6:88–93, 2005.
- Shaw AS, Ampong MA, Rio A, et al: Entristar skin-level gastrostomy tube: Primary placement with radiologic guidance in patients with amyotrophic lateral sclerosis. *Radiology* 233:392–399, 2004.
- Thornton FJ, Varghese JC, Haslam PJ, et al: Percutaneous gastrostomy in patients who fail or are unsuitable for endoscopic gastrostomy. *Cardiovasc Intervent Radiol* 23:279–284, 2000.
- Wollman B, D'Agostino HB: Percutaneous radiologic and endoscopic gastrostomy: A 3-year institutional analysis of procedure performance. *AJR* 169:1551–1553, 1997.
- Covarrubias DA, O'Connor OJ, McDermott S, et al: Radiologic percutaneous gastrostomy: Review of potential complications and approach to managing the unexpected outcome. *AJR* 200:921–931, 2013.

Abdominal Computed Tomography Angiography

VAHID YAGHMAI | WARREN M. BRANDWEIN

CHAPTER OUTLINE

Technical Considerations

Image Processing

Anatomy

Clinical Applications

Abdominal Aorta

Pancreas

Kidneys

Liver

Mesenteric Vasculature

Summary

Computed tomography angiography (CTA) revolutionized vascular imaging when vessels smaller than 1 mm in diameter were imaged with single-slice spiral CT.¹⁻⁵ However, because of the small volume of coverage and limitations in the speed of image processing, CTA did not become widely used until the introduction of multidetector CT (MDCT) in 1998.⁶⁻⁸ With the advent of MDCT, temporal and spatial resolution of the scanners significantly improved.^{9,10} Gantry rotation times of 0.33 to 0.5 second, with slice thicknesses of 0.5 to 0.75 mm, are now available on most MDCT scanners.

CTA uses several parallel detectors along the z-axis with multiple channels of data (currently up to 320), allowing significant improvement in z-axis resolution. This allows isotropic resolution for most vascular applications with images obtained during a single, short breath-hold. The result has been elimination of the trade-off between spatial resolution (z-axis) and scanning range, a significant limitation of single-detector spiral CT.^{11,12} Hence, a significant benefit has been a paradigm shift from single-slice to volumetric data acquisition. This, in turn, has made imaging of different vascular phases with a single contrast bolus a reality.⁷

Other than its limited invasiveness, advantages of CTA include lower cost and a potential reduction in the total volume of contrast material administered. With the fastest scanners currently available (16, 64, 256 slice), abdominal CTA can be performed with as little as 50 mL of contrast material using a saline flush.^{13,14} This requires meticulous attention to the timing of contrast bolus (see later). In the evaluation of life-threatening vascular disease, such as traumatic aortic injury or pulmonary embolus, CTA has clear advantage because of short acquisition times.¹⁵

An important advantage of CTA over catheter angiography is its ability to examine the vessel wall, as well as its lumen. The adjacent organs can also be evaluated (e.g., staging of pancreatic adenocarcinoma). Another advantage of CTA is its ability to

evaluate a vessel in projections that cannot be obtained with conventional techniques.

The increased use of CT has led to significant increases in radiation exposure and concerns about its effects.¹⁶ CT currently accounts for approximately 75% of the total radiation dose delivered by medical imaging.¹⁷ A number of techniques have been developed to help reduce radiation exposure from abdominal CTA. These technologic innovations address the issue in several ways, including collimation of x-ray beams to reduce exposure from over beaming, newer reconstruction algorithms, automatic tube current modulation, and use of lower tube potential settings.¹⁶ Automatic tube current modulation automatically adjusts the current during scanning to decrease the amount of radiation in anatomic regions that do not require higher current (e.g., lung bases or above the iliac crest) while maintaining image quality.¹⁶ In the appropriate setting, abdominal CTA may be performed with a reduced kilovoltage (kV) setting to decrease radiation to the patient and improve signal-to-noise ratio.¹⁸ For example, recent studies have demonstrated that lowering the kVp setting from 140 to 80 kVp significantly reduces patient dose and improves the contrast-to-noise ratio in the aorta while maintaining an acceptable level of image noise.¹⁹ Scanning with lower tube voltage may facilitate reduction of intravenous contrast dose because of an improved contrast-to-noise ratio.²⁰⁻²³

Technical Considerations

Until the introduction of 16- and 64-slice CT scanners, improvement in spatial resolution came at the cost of temporal resolution. Now, with faster gantry rotation time (0.27 to 0.5 second) and an increase in the number of detector rows, isotropic voxel acquisition independent of the length of coverage is possible. The newer CT scanners use very complex spiral cone beam reconstruction algorithms instead of the filtered back projection mathematical reconstruction algorithm that was used in older scanners. These mathematical reconstruction algorithms are a byproduct of significant advances in computer technology. A combination of all these advances has made isotropic scanning of the abdominal aorta and its branches in a single breath-hold a clinical reality.^{7,12,24}

The latest generation of image reconstruction brings many other benefits in addition to improved spatial and temporal resolution. Although filtered back projection is a widespread and fast reconstruction algorithm used to create CT images, this technique produces relatively noisy images when the tube current or voltage is lowered. Iterative reconstruction (IR), the newest improvement in reconstruction algorithms in CT, can remove the noise from low-dose images using mathematical models.²⁵ IR has shown the potential to improve image quality, allowing substantial reduction in patient dose compared

with the filtered back projection techniques (Fig. 9-1).²⁵⁻³¹ More recent studies have demonstrated that IR facilitates a reduction in administered contrast dose while maintaining image quality when using a low-dose technique.²¹

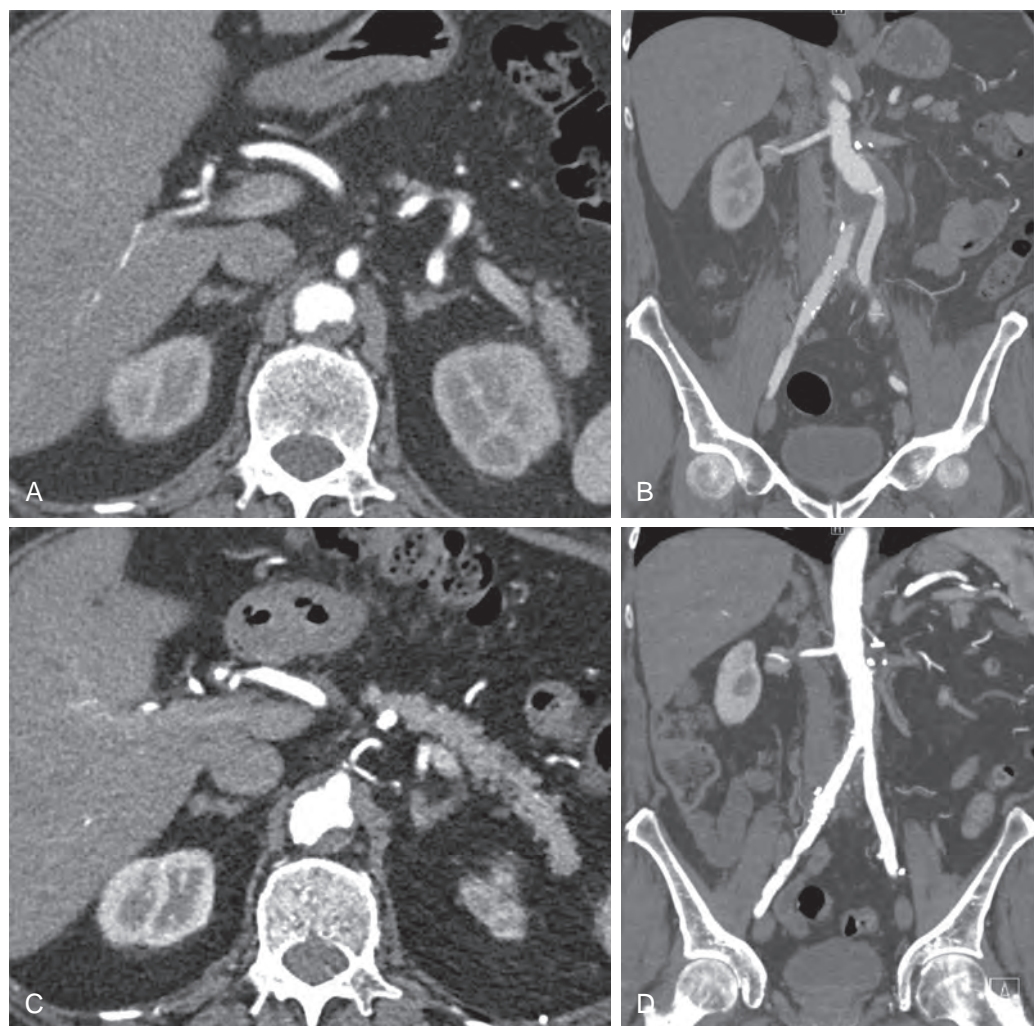
With shortened acquisition times of the multislice scanners, optimizing and maximizing vascular enhancement has become more challenging.^{32,33} CT angiography requires excellent contrast enhancement of the targeted vessels. A good-quality CT angiogram requires an arterial density value greater than 200 Hounsfield units (HU).^{34,35} This should be achieved rapidly, and the peak should coincide with the acquisition interval. Therefore it is crucial to time the contrast bolus correctly. However, rapid administration of contrast material shortens the plateau phase of contrast enhancement, thus creating a further challenge for correct timing of the study.^{32,33,36} For most abdominal CTA applications, an injection rate of 4 to 5 mL/s yields optimal vascular enhancement.

For achieving rapid intravenous (IV) administration of contrast material, excellent IV access (18- or 20-gauge needle) and a dual-head power injector are required. A saline bolus via a dual-head injector following contrast administration prolongs and improves arterial enhancement; it also decreases the amount of contrast required by using the residual contrast in the tubing, patient's arm veins, and superior vena cava.^{14,37,38}

There are several factors that affect time to peak from the start of a contrast bolus. These include the iodine content of contrast material, injection rate, and patient's cardiac status.^{32,33,37,39} A faster injection rate, for example, can achieve a higher density in the targeted vessel and results in a higher quality CTA. It also separates the arterial from the portal venous phase and thus results in excellent image quality without cross-contamination by different phases.³² Contrast material with a higher iodine concentration improves vascular enhancement if all other parameters are held constant.^{32,40} Because several factors affect time to peak enhancement in the aorta, a fixed timing delay for image acquisition is not advised.

All modern CT scanners provide software for calculating the optimal time to start scanning after the administration of a test bolus, a so-called test bolus injection (Fig. 9-2A) or allow automatic image acquisition once a preset HU threshold in the target vessel has been reached, known as bolus triggering (Fig. 9-2B). An important consideration with the 16- and 64-slice scanners is the possibility of outrunning the contrast bolus in patients with low cardiac output or in cases that require long z-axis coverage (e.g., combination of extremity and abdominal CTA). To overcome this problem, one can slow down the scanner by increasing the gantry rotation time and slowing the table speed.^{41,42}

Figure 9-1 CT angiography of the abdominal aorta with lower kV and iterative reconstruction algorithm. **A, B.** Axial and coronal maximum intensity projection images of the abdominal aorta obtained with 120 kV, tube current modulation, and filtered back projection reconstruction algorithm before aortic graft revision. Density of the aorta is 312 HU, with an image noise of 33. The dose-length product is 631 mGy • cm. **C, D.** Follow-up study after revision of the aortic graft was obtained with 80 kV, tube current modulation, and an iterative reconstruction algorithm. The density of the aorta has increased substantially to 574 HU whereas the image noise is similar, at 33. The dose-length product has decreased to 301 mGy • cm.



ROI	Peak (HU)	Times to peak(s)	Sample (HU) at 18.0 s
1	147.3	18.0	147.3

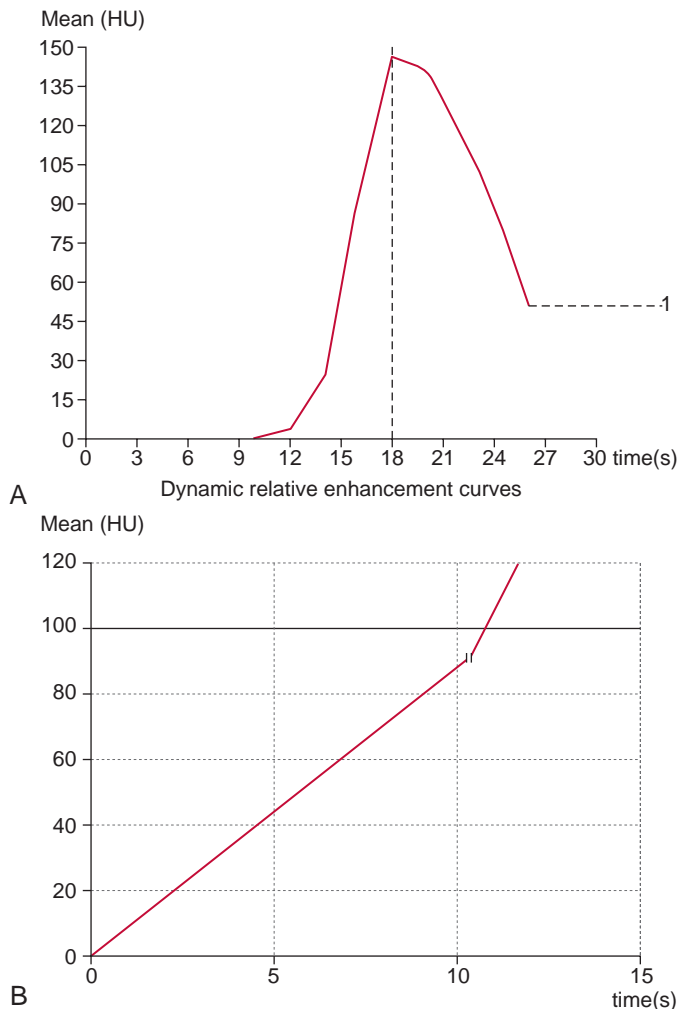


Figure 9-2 Graphic depictions of contrast bolus timing methods.

A. Test bolus injection technique. With this technique, a small bolus of contrast material (usually 15 to 20 mL) is administered, followed by a saline chase of similar volume. Time to peak is calculated after the acquisition of several images, with the region of interest placed on the target vessel. **B.** Bolus triggering technique.

A region of interest is placed on the target vessel and injection of contrast material is started. After reaching the preset threshold (100 HU in this case), the scanner automatically instructs the patient to hold his or her breath and image acquisition takes place automatically. With the bolus triggering technique, less contrast material is used because a test bolus is not needed.

As noted, the new multislice scanners, in combination with dual-head injectors, allow for a marked decrease in the amount of contrast used for routine CTA. However, the total volume of contrast administered for a routine abdominal CT (usually 150 mL of contrast material at a concentration of 300 mg/mL) should not change if solid organs, such as the liver, are evaluated in conjunction with CTA. Lowering the total volume of contrast may potentially reduce the sensitivity of lesion detection.^{12,40}

Many authors had previously reported the use of gadolinium chelates for CTA in patients who have diminished renal

function.⁴³⁻⁴⁶ Although gadolinium is radiodense and may be used as a contrast agent with an x-ray, many gadolinium-based products have higher osmolality than iodine-based contrast media and are therefore potentially more nephrotoxic. More importantly, there have been several reports of nephrogenic systemic fibrosis leading to serious physical disability in patients with end-stage renal disease who had been receiving gadolinium-containing contrast agents.⁴⁷⁻⁴⁹

Image Processing

Thinner slice acquisition with CTA has resulted in a significant increase in the number of images acquired. Hence, data overload has been a direct side effect of isotropic and near-isotropic scanning. CTA of the abdominal aorta and its branches on the newest scanners generates over 1000 images.⁵⁰ As the volume of data significantly increases, the processing power of many of the current image processing workstations is pushed to its limits. The strain on the fiberoptic networks and image processing workstations has become a significant challenge for many institutions that have installed the fastest CT scanners. Workflow and image transfer issues are significant byproducts of CTA that are beyond the scope of this discussion but are important to consider when upgrading to the latest CT technology.

Postprocessing of the source data not only improves visualization of the vascular structures and their relationship to the adjacent organs, but also decreases the number of slices needed for review of the dataset.^{51,52} Images can be processed on the scanner or a free-standing image processing workstation. Thicker slices may be produced for review of the axial images on the picture archiving and communications system (PACS).⁵³ Volume rendering, maximum intensity projection (MIP) rendering, or multiplanar reconstructions are routinely used to display large datasets.^{7,54} Volume-rendering techniques use attenuation thresholds to create a volumetric display of data and allow visualization of different tissue types simply by changing threshold settings. MIP rendering does not provide spatial depth but improves visualization of smaller vessels. Most institutions, including ours, routinely use a combination of the MIP and volume-rendered display of data for CTA because these two are complementary. Although volume rendering is useful for the display of soft tissues and three-dimensional relationships, MIP provides a more detailed view of the vessels within the slab of data and is less operator-dependent.⁵⁴

Anatomy

The major branches of the abdominal aorta are readily visible on helical CT and CTA. However, to evaluate vascular disease, CTA with thin sections and sufficient contrast enhancement is required. The typical branching of the celiac artery to the common hepatic, left gastric, and splenic arteries can routinely be appreciated on CTA. The smaller branches arising from the common hepatic artery may also be evaluated by CTA if thin slices are acquired and contrast enhancement is optimized by bolus timing or tracking techniques. The superior mesenteric artery and its branching are also easily evaluated by CTA. A significant portion of patients studied with CTA demonstrate variations in the branching of the abdominal aorta.⁵⁵⁻⁵⁸

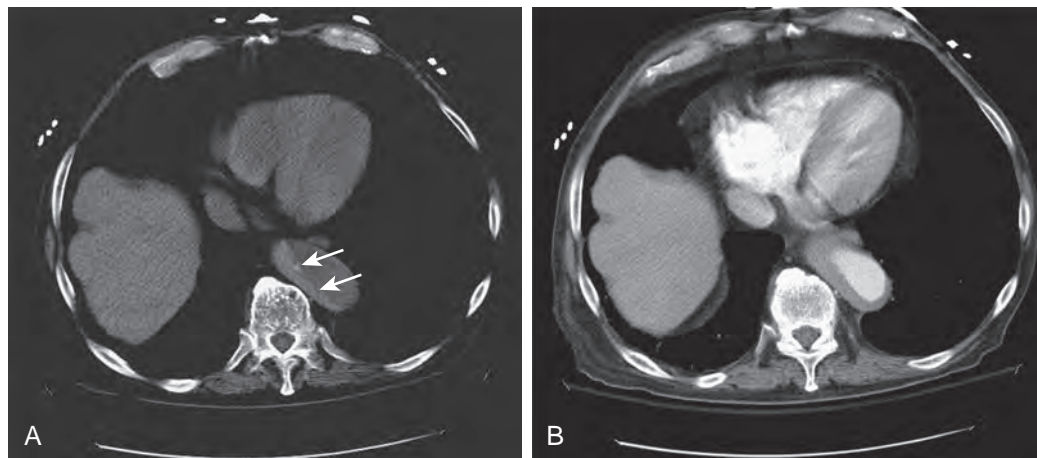
The renal arteries arise at approximately the L1-2 level, caudal to the origin of the superior mesenteric artery and cephalad to the origin of the inferior mesenteric artery. In approximately 28% of patients, there are multiple renal arteries.⁵⁹

The venous structures in the abdomen can also be evaluated by CTA. However, timing of scanning will be different, depending on the venous structure imaged. Renal veins will rapidly enhance as they return blood to the inferior vena cava. This, in combination with unopacified blood from the lower extremities, can create a pseudothrombus in the inferior vena cava. For optimal imaging of the portal vein, a delay of 65 seconds after the start of contrast administration is required. Therefore, to perform CTA and CT portography, one has to scan the abdomen successively with the newest multichannel scanners because these scanners, in combination with the rapid administration of contrast material, allow complete separation of the arterial and venous phases of hepatic enhancement. This separation of phases is more difficult with single- and four-slice MDCT because of lower temporal and spatial resolution. With the latest 16- and 64-channel scanners, early and late arterial enhancement of the liver can be imaged separately.

The portal vein arises from the confluence of the superior mesenteric and splenic veins and branches into right and left branches at the hepatic hilum. The right portal vein divides into anterior and posterior branches. The left portal vein defines the boundaries of the segments II, III, IVa, and IVb. When portal hypertension is present, numerous venous collaterals may be visible on MIP and volume-rendered images. The inferior mesenteric vein can be followed parallel to the course of superior mesenteric vein in the lower abdomen, coursing anterior to the left renal vein and draining into the splenic vein.

Anatomic variations of the major branches of the abdominal aorta, inferior vena cava, portal vein, and renal veins are common and are visible on CTA. For example, an accessory hepatic vein may be seen between segments V and VI. Single retroaortic or duplicated left renal veins are seen in 2.5% and 9% of the population, respectively. CTA allows accurate mapping of these variants.^{55,60,61} Assessment for these variations is essential when evaluating for hepatic segmentectomy, using the Whipple procedure, hepatic or renal donor assessment, or bowel resection. This is discussed in detail later in this chapter.

Figure 9-3 Intramural hematoma. **A.** Unenhanced image of the upper abdomen shows hyperattenuating aortic intramural hematoma (arrows). **B.** Enhanced image of the upper abdomen shows thrombus in the aortic wall, which can mimic chronic aortic thrombus or periaortic fluid.



Clinical Applications

Common abdominal applications of CTA include evaluation of the abdominal aorta, preoperative and postoperative assessment for renal and liver transplantation, preoperative planning for hepatic segmentectomy and pancreatic surgery, mesenteric ischemia, and gastrointestinal (GI) hemorrhage. Other applications include cholecystectomy and splenectomy planning, as well as assessment for renal arterial disease in the evaluation of hypertension. The protocols for each application should be individually tailored to optimize imaging of the targeted vascular structures. For example, planning a Whipple procedure should include arterial and portal venous phase images.

ABDOMINAL AORTA

MDCT has revolutionized imaging of the abdominal aorta because of its excellent spatial resolution and advantages over direct catheter angiography (DCA) (described earlier). Because of these advantages, CTA is usually the preferred imaging modality for evaluation of the abdominal aorta in acute and nonemergent settings.^{9,10,62,63}

Aortic Dissection

CTA allows accurate depiction of intimal separation from the adventitia and its extension into branch vessels. The site of intimal tear and its extension determine prognosis. Most institutions use the Stanford classification to assess prognosis as type A dissections (involving the ascending aorta), which require surgical management, and type B dissections (confined to the descending aorta), which are often managed conservatively.

Full assessment of aortic dissection by CTA requires unenhanced CT followed by contrast-enhanced CT. Unenhanced CT is useful because the detection of a dense intramural hematoma may be mistaken for chronic thrombus on enhanced images (Fig. 9-3). On enhanced images, extension of the intimal flap to the aortic side branches and perfusion of organs affected by dissection should be assessed. Although quite variable, the true lumen is usually anterior to the false lumen in the upper abdominal aorta. At the level of the renal arteries, the false lumen usually supplies the left renal artery. The false lumen can also be distinguished from the true lumen by its larger diameter, which also shows lower attenuation if images are acquired during peak arterial enhancement. If there are iatrogenic or

spontaneous fenestrations of the intima, the false lumen may show enhancement similar to that of the true lumen (Fig. 9-4). Complications of aortic dissection include hemorrhage, hypoperfusion of the involved organs, and aneurysm formation.

Aortic Aneurysm

An abdominal aortic aneurysm (AAA) is a fusiform or focal saccular dilation, usually of the infrarenal portion of the aorta, more than 4 cm in external anterior-posterior diameter.⁶⁴ About 90% of AAA are infrarenal, with most limited to the abdominal aorta, but extension to the common iliac arteries does occur. Accessory renal arteries may arise from an infrarenal aneurysm, thus affecting management. About 10% of aneurysms are juxtarenal, involving the main renal arteries, or suprarenal, involving the celiac or superior mesenteric arteries. Suprarenal and infrarenal aortic aneurysms together form a dumbbell configuration.

Aortic aneurysms are frequent in the older population and can be a cause of sudden death if they rupture.⁶⁵ The prevalence of AAA is estimated at 1.5% of those older than 50 years and 5% to 8% of men older than 65 years.^{66,67} Because rupture of an aortic aneurysm can be catastrophic, aggressive screening and treatment have been advocated.⁶⁸ An untreated AAA larger than 5 cm in diameter has a 20% likelihood of rupture in 5 years.⁶⁹

Ultrasound has been advocated as the imaging modality of choice for AAA screening.^{70,71} However, it has several shortcomings, including variability in transverse dimensions of the aneurysm, limitations in aneurysm neck assessment, and limited visualization of luminal thrombus.⁷² Because of the inherent limitations of ultrasound, CTA is preferred for confirming diagnosis, characterizing the aneurysm, and preoperative planning.^{73,74}

Currently, there are two accepted methods of treatment for AAA, open surgical repair and an endovascular approach.⁶⁵ Open surgical repair is associated with significant risk, including a 6% to 10% mortality rate that is commonly caused by myocardial infarction.^{67,75,76} Endovascular aneurysm repair (EVAR) is a technique that was first described by Parodi and colleagues in 1991.⁷⁷ This method excludes the aneurysm by traversing it with a stent graft, thus reducing pressure on the aortic wall.⁷⁸ The results of this less invasive treatment have been excellent, with fewer complications and more rapid recovery.^{79,80}

Preoperative assessment of the aorta is preferably performed with multislice CTA because accurate measurement of the diameter of the aneurysm, its length, and its relationship to major vessels (e.g., renal arteries) is essential.⁸¹⁻⁸³ For EVAR planning, the diameter and angle of the aneurysm neck, as well as its relationship to the renal arteries, is evaluated. Also, the amount of luminal clot may affect treatment. Three-dimensional evaluation of the aneurysm is particularly helpful for treatment planning (Fig. 9-5).⁸⁴ CTA provides useful information regarding femoral access sites and aortic accessibility.⁸³ Orthogonal measurements of the aneurysm using a center line provide accurate measurements for preoperative planning. CTA has been shown to be extremely accurate for measuring vessel lengths, diameters, and angles and for assessing occlusive disease and calcification.⁸⁵

Patients treated with EVAR undergo frequent imaging by CTA to monitor for endoleaks, stent migration, fracture, and stability of aneurysm size (Fig. 9-6).⁸⁶ An increase in the diameter of an aneurysm is associated with endoleak. Evaluation of an endoleak historically required imaging with unenhanced CT and imaging during the arterial and venous phases of contrast enhancement (Fig. 9-7). Unenhanced images are used to detect

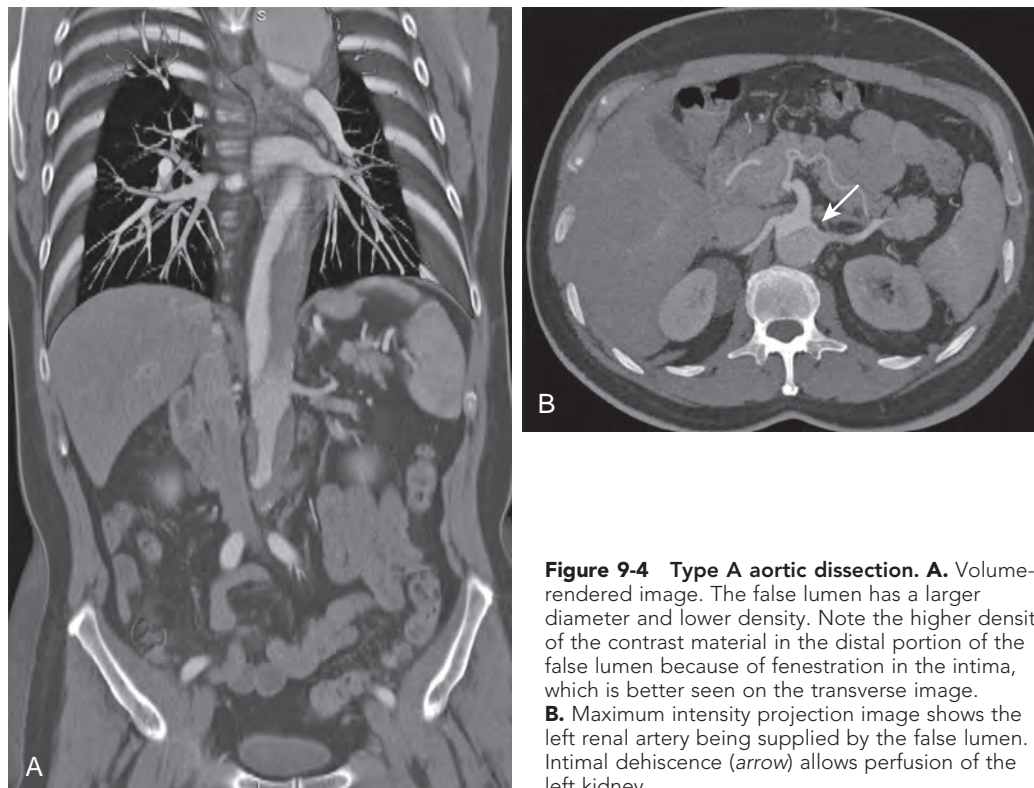


Figure 9-4 Type A aortic dissection. **A.** Volume-rendered image. The false lumen has a larger diameter and lower density. Note the higher density of the contrast material in the distal portion of the false lumen because of fenestration in the intima, which is better seen on the transverse image. **B.** Maximum intensity projection image shows the left renal artery being supplied by the false lumen. Intimal dehiscence (arrow) allows perfusion of the left kidney.



Figure 9-5 Infrarenal abdominal aortic aneurysm. Volume-rendered image shows relationship of the aneurysm neck to the renal arteries (arrows). The distance from the renal arteries using vessel analysis software and center line measurements should be calculated before EVAR. Incidentally noted is the replaced left hepatic artery arising from the left gastric artery (arrowhead).

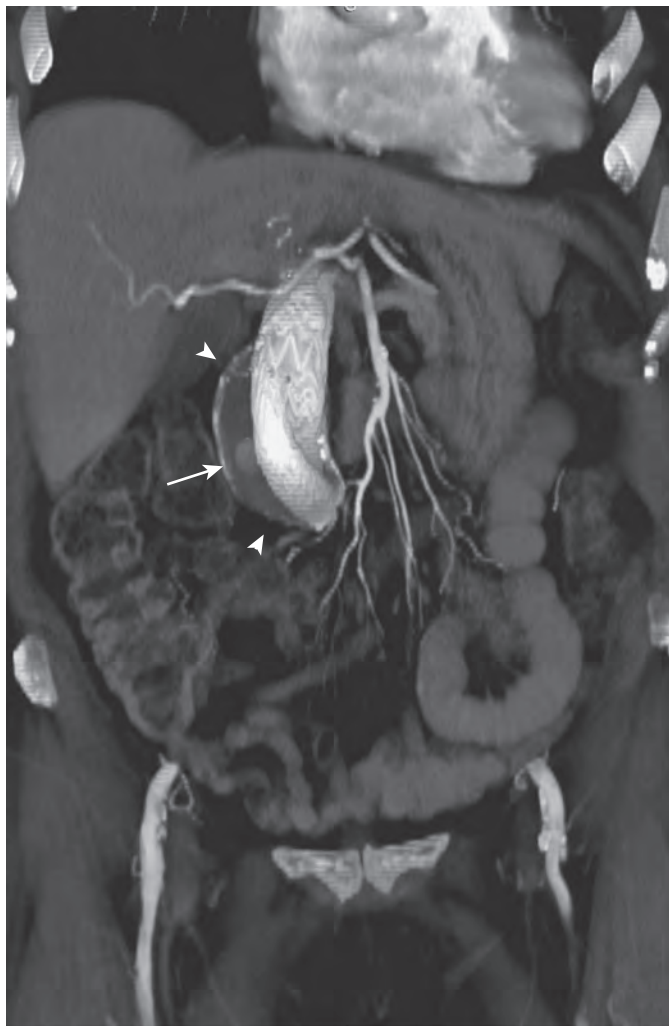


Figure 9-7 Stent graft placement for abdominal aortic aneurysm. There is opacification of the excluded portion of the abdominal aortic aneurysm (arrowheads) by a type II endoleak (arrow). The endoleak may be better visualized during the venous phase of the study.

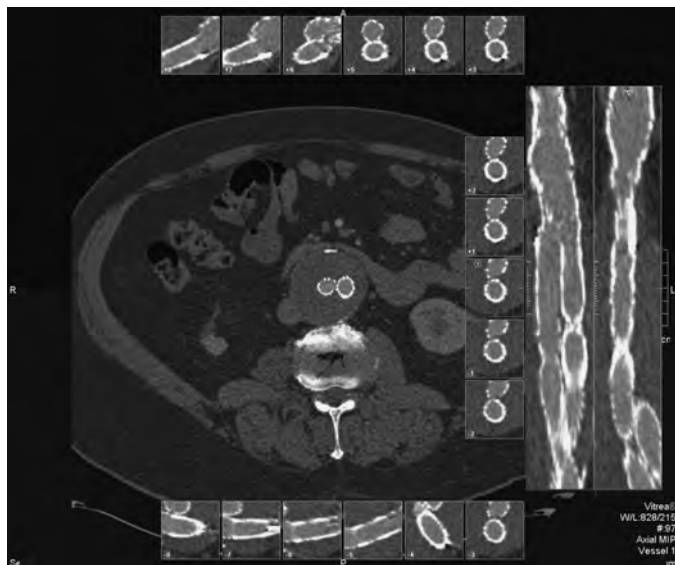


Figure 9-6 Endovascular stent graft. Orthogonal images allow assessment of the stent lumen.

artifacts from calcification or embolization material that may mimic endoleak on enhanced images. Venous phase images have been shown to enhance detection rate of endoleaks. In a type I endoleak, there is a leak in the proximal or distal end of the graft. Type II endoleaks are caused by retrograde flow from aortic side branches, commonly the inferior mesenteric or lumbar arteries. Type III endoleaks are related to separation of the graft components and require immediate treatment. Type IV endoleaks have been associated with leakage through the graft pores and are usually transient. Reintervention is recommended for any type I or III leak⁸⁷; type II endoleaks are characterized by lower flow and thus tend to be monitored regularly with intervention only if there is a significant increase in aneurysm size.^{88,89}

More recent studies on EVAR follow-up with CTA have focused on methods for radiation dose reduction. Although monitoring has typically involved triphasic protocols, some have suggested that the arterial phase can be eliminated, using only unenhanced and venous phases. This technique has been shown to depict and classify endoleaks accurately, with a significant dose reduction.^{90,91} Dual-energy CT is another more

recently described alternative for endoleak detection that may lead to lower radiation exposure.⁹¹⁻⁹³ Dual-source CT scanners contain two x-ray tubes with two corresponding detectors arranged on the gantry at a 90-degree angular offset.⁹⁴ When used in the dual-energy mode, the two x-ray tubes operate at different peak voltages, enabling reconstruction of virtual unenhanced images from a single venous phase acquisition.⁹⁵

PANCREAS

Staging of pancreatic cancer with multiphasic CT is now the standard of care in many institutions.⁹⁶ It requires arterial, parenchymal, and portal venous phase images to evaluate the solid organs and mesentery (Fig. 9-8).⁹⁷⁻⁹⁹ Addition of a noncontrast phase allows detection of parenchymal and vascular calcifications. Neutral oral contrast agents help distend the bowel and improve visualization of the bowel wall. Positive oral contrast agents (e.g., iodine-based agents) obscure vascular detail and should be avoided in all abdominal CTA procedures.

Although curved multiplanar reformations of the pancreas improve visualization of the parenchyma and pancreatic duct, MIP and volume-rendered images are needed for vascular analysis (Fig. 9-9).^{100,101} The newest generation of scanners allows rapid multiplanar and MIPs on the scanner, thus obviating the need for routine data transfer to an independent image processing workstation.

Staging of the pancreatic carcinoma is discussed in detail in Chapter 98. Because of the frequent variations of vascular anatomy that can affect the surgical approach, close evaluation of the anatomic variants, in addition to tumor encasement of the adjacent vasculature, is essential. For example, the presence of a replaced right hepatic artery originating from the superior mesenteric artery can significantly alter the planning for a Whipple procedure because this vessel traverses posteriorly to the pancreatic head (Fig. 9-10). Similarly, preoperative knowledge of a replaced left hepatic artery facilitates ligation during a left hepatectomy because this major branch does not need to be identified in the porta hepatis.¹⁰²

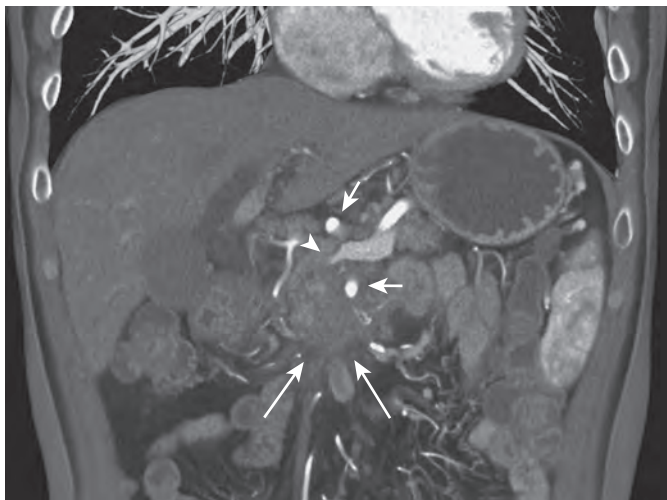


Figure 9-8 CT angiogram for the staging of pancreatic carcinoma. A large infiltrating pancreatic mass (large arrows) is encasing the superior mesenteric and common hepatic arteries (small arrows) and occluding the splenic vein (arrowhead). Note the perigastric collateral veins.

KIDNEYS

CTA is routinely used for the preoperative planning for nephrectomy, diagnosing renal artery stenosis, and evaluating renal artery in-stent restenosis and ureteropelvic junction obstruction.¹⁰³⁻¹⁰⁶ CTA has been shown to be extremely accurate for the assessment of renal artery stenosis and other renal vascular pathologies. Although CTA and magnetic resonance angiography (MRA) are equally accurate for the assessment of significant renal artery stenosis,¹⁰⁷ MRA cannot accurately assess the lumen of most renal artery stents because of susceptibility artifacts or regional flow dephasing, even with contrast administration.¹⁰⁸⁻¹¹⁰ Furthermore, contrast-enhanced MRA in patients with impaired renal function is limited by the risk of nephrogenic systemic fibrosis and the difficulties

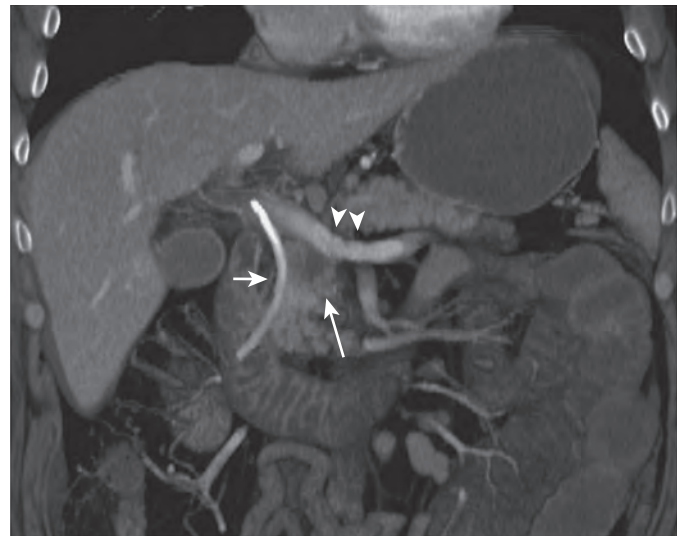


Figure 9-9 Volume-rendered image of pancreatic carcinoma (long arrow) with involvement of the portal vein. Note irregularity and subtle narrowing of the portal vein (arrowheads). A biliary stent is in place (short arrow).

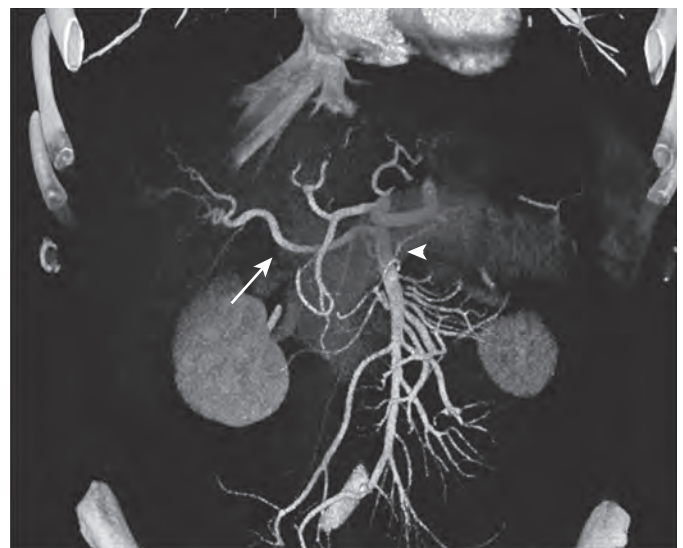


Figure 9-10 CT angiogram for staging of pancreatic head carcinoma. Shown is the replaced right hepatic artery (arrow) arising from the superior mesenteric artery (arrowhead).

in evaluating vascular calcifications.¹¹¹ However, the application of 64-slice CT to renal artery angiography has been reported to yield excellent results for the detection of native renal artery stenosis¹¹² and renal artery in-stent restenosis.^{106,113}

CTA is useful when evaluating potential renal transplant recipients through the use of multiplanar reformations, MIP images, and volume rendering.¹¹⁴ To perform an arterial anastomosis, a site without significant arteriosclerosis must be chosen. In nondialysis patients with significant chronic renal insufficiency and patients receiving peritoneal dialysis, only nonenhanced scanning is performed because residual renal function may be damaged by the use of IV contrast. MIP imaging is useful for showing vascular calcifications, leading to the production of a vascular map. Conversely, in patients on hemodialysis, nonenhanced and arterial phase imaging are performed. MIP images permit visualization of small branch vessels, but luminal narrowing can be overestimated because of vascular calcifications.¹¹⁵ Thus, MIP images are compared with the acquired axial images to determine the true degree of stenosis.¹¹⁶ Volume rendering allows better demonstration of a vascular map in these patients because vessel lumen and mural calcifications can be individually defined¹¹⁷; therefore the degree of stenosis can be accurately measured.¹¹⁸ Volume rendering also allows color display, which may improve comprehension of the 3D relationships of different anatomic structures.¹¹⁹

CTA is the imaging technique of choice for the evaluation of potential renal donors.¹²⁰ Its role is to assess vascular anatomy and evaluate for renal pathology (Fig. 9-11). A comprehensive examination includes noncontrast images to evaluate for renal calculi and vascular calcification and the arterial phase to detect vascular anatomic variants and anomalies, nephrographic phase

to detect renal parenchymal abnormalities, and excretory phase to evaluate the collecting systems and ureters.^{61,104,121,122} Coronal, thin slab MIP images are useful for optimal visualization of the renal arteries.¹²³ Because MIP images do not provide spatial depth, volume-rendered images are also beneficial (Fig. 9-12). It is feasible to scan the renal vasculature with 50 mL of non-ionic iodinated contrast material and a saline chase using a dual injector on a 16- or 64-slice CT, with excellent results.¹⁴ To improve opacification of the ureters, however, a saline bolus or diuretics may be beneficial.¹²⁴

LIVER

Vascular complications are a significant contributor to morbidity following hepatic surgery. The hepatic surgeon greatly benefits from vascular mapping of the liver when planning tumor resection, laparoscopic surgery, or transplantation (Fig. 9-13). Until rather recently, catheter angiography was the standard diagnostic method for preoperative planning of hepatic surgery. However, its associated morbidity and suboptimal visualization of the venous structures have made CTA the new standard in many institutions. CTA provides exquisite hepatic vascular detail and allows evaluation of the liver parenchyma and other organs.^{55,56}

When planning any type of hepatic surgery or locoregional therapy, knowledge of the vascular anatomy variation is essential. Accessory and aberrant hepatic venous and arterial branches are common and are easily visualized by CTA.^{55,125} CTA has been shown to be as effective as catheter angiography in planning a selective hepatic arterial infusion of chemotherapy.⁵⁷

MESENTERIC VASCULATURE

CTA allows excellent visualization of the mesenteric vasculature (Fig. 9-14).¹²⁶ Aneurysms, thrombosis, stenosis, dissection, and inflammatory processes affecting the mesenteric vasculature

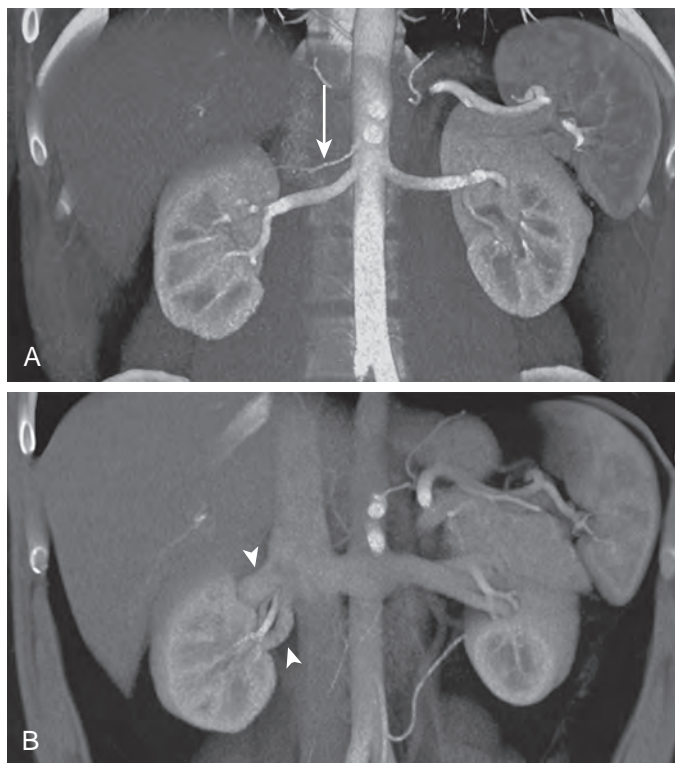


Figure 9-11 CT angiogram for evaluation of potential renal donor. **A.** Small accessory right renal artery (arrow). **B.** There are also two right renal veins (arrowheads).



Figure 9-12 Volume-rendered images of CTA performed for renal donor evaluation. There are two left renal arteries (arrows). Also, note the replaced common hepatic artery arising from the superior mesenteric artery, as well as a small accessory left hepatic artery arising directly from the aorta (arrowheads).

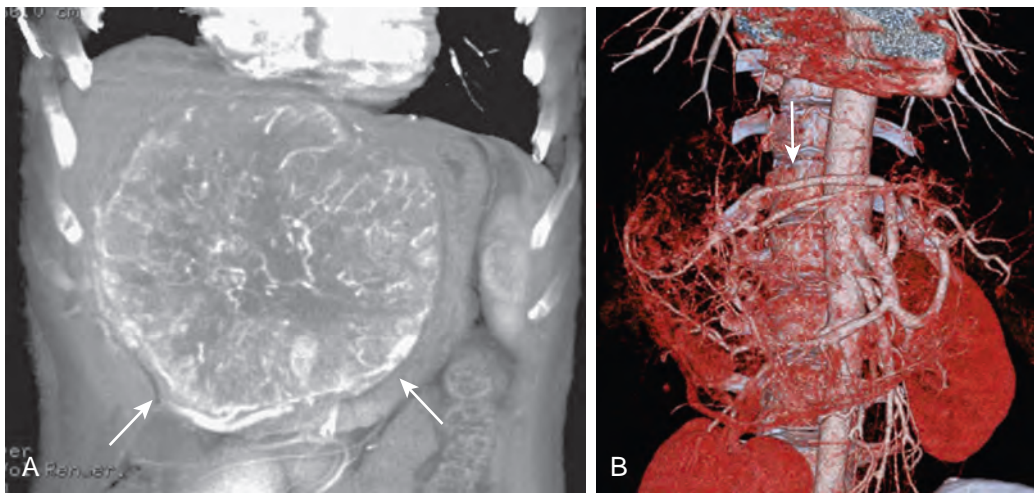


Figure 9-13 Patient with metastatic hemangiopericytoma evaluated for resection. **A.** A large very vascular hepatic mass (arrows) is displacing the stomach. **B.** The mass is supplied by a replaced left hepatic artery (arrow) arising from the left gastric artery. Accurate vascular mapping resulted in uneventful resection of the mass.



Figure 9-14 CT angiogram of the mesenteric vessels.

have been evaluated by MDCT. CTA is a robust method for evaluation of acute and chronic bowel ischemia (Fig. 9-15). However, because of its high temporal resolution, it may be necessary to scan the region of interest twice because a “pure” arterial phase does not allow evaluation of the venous structures. This is necessary because incomplete enhancement of the mesenteric venous branches during the late arterial phase may mimic thrombosis.

Atherosclerotic disease is a common cause of chronic mesenteric ischemia and is better assessed with CTA than with contrast-enhanced MRA because of its high spatial and temporal resolution.¹²⁷ Chronic mesenteric ischemia has many

different nonatherosclerotic causes, such as fibromuscular dysplasia, median arcuate ligament syndrome, many forms of vasculitis (including Takayasu’s arteritis, polyarteritis nodosa, and segmental mediolytic arteriopathy), and connective tissue diseases, such as Ehlers-Danlos syndrome. CTA is an excellent modality when evaluating vasculitides because of its ability to assess luminal narrowing, including stenosis and occlusion, aneurysmal dilation, and vascular wall changes such as wall thickening and enhancement.¹²⁷ Compression of the celiac axis by the median arcuate ligament is referred to as median arcuate ligament syndrome and may cause abdominal angina (Fig. 9-16). Also, this entity has been reported to predispose patients who have undergone orthotopic liver transplantation to develop hepatic artery thrombosis. Although surgical treatment can lead to clinical improvement in symptomatic patients, the importance of celiac artery compression in asymptomatic patients has not been established. If median arcuate ligament syndrome is suspected, imaging should be obtained during full inspiration to avoid artifactual stenosis.^{128,129} Celiac and mesenteric stenoses are best visualized by sagittal thin slab MIP or volume-rendered images (Fig. 9-17). Thin slab coronal MIP images also provide an excellent overview of the mesenteric vascular structures and the bowel loops.¹³⁰ The use of neutral oral contrast agents is important when evaluating the mesentery to improve visualization of the bowel mucosa.

Acute mesenteric ischemia is a life-threatening event that may have various causes. These include embolic phenomena, severe hypoperfusion, thrombosis of stenotic vessels, dissection, hypercoagulable states, and vasculitis. As noted, the diagnosis of mesenteric venous thrombosis requires delayed images to avoid early-phase, incomplete enhancement. Unenhanced images are also beneficial because they may show a hyperdense thrombus.^{7,131} The classic angiographic hallmark of an embolic occlusion—the abrupt termination of a vessel (cutoff sign)—and a luminal filling defect, indicating a nonocclusive thrombus, are both demonstrable with CTA. Mesenteric CTA is helpful when evaluating acute superior mesenteric artery (SMA) ischemia by localizing the site of occlusion, thus indicating the underlying cause of ischemia, because thrombosis of the SMA typically occurs within 2 cm of its origin, whereas embolic occlusions occur more distally.¹²⁷

When evaluating for mesenteric vascular pathology, close attention to the morphology of the bowel is important because

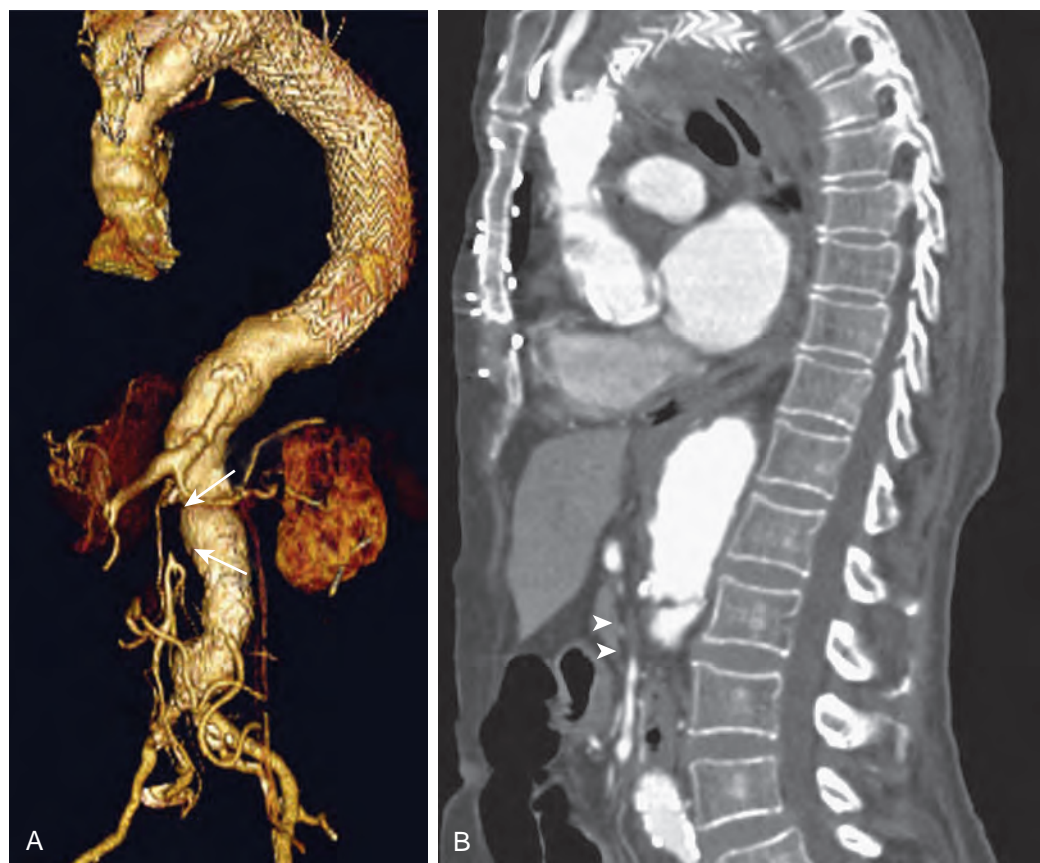


Figure 9-15 Occlusive thrombus in the superior mesenteric artery. **A.** Volume rendering shows defect in the superior mesenteric artery (arrows). Note the aortic stent graft. **B.** Sagittal reformatted image better demonstrates the occlusive thrombus (arrowheads) in the superior mesenteric artery.



Figure 9-16 Compression of the celiac artery by the median arcuate ligament (arrow).



Figure 9-17 Thrombus in the superior mesenteric artery (arrow) in a patient with acute abdominal pain.

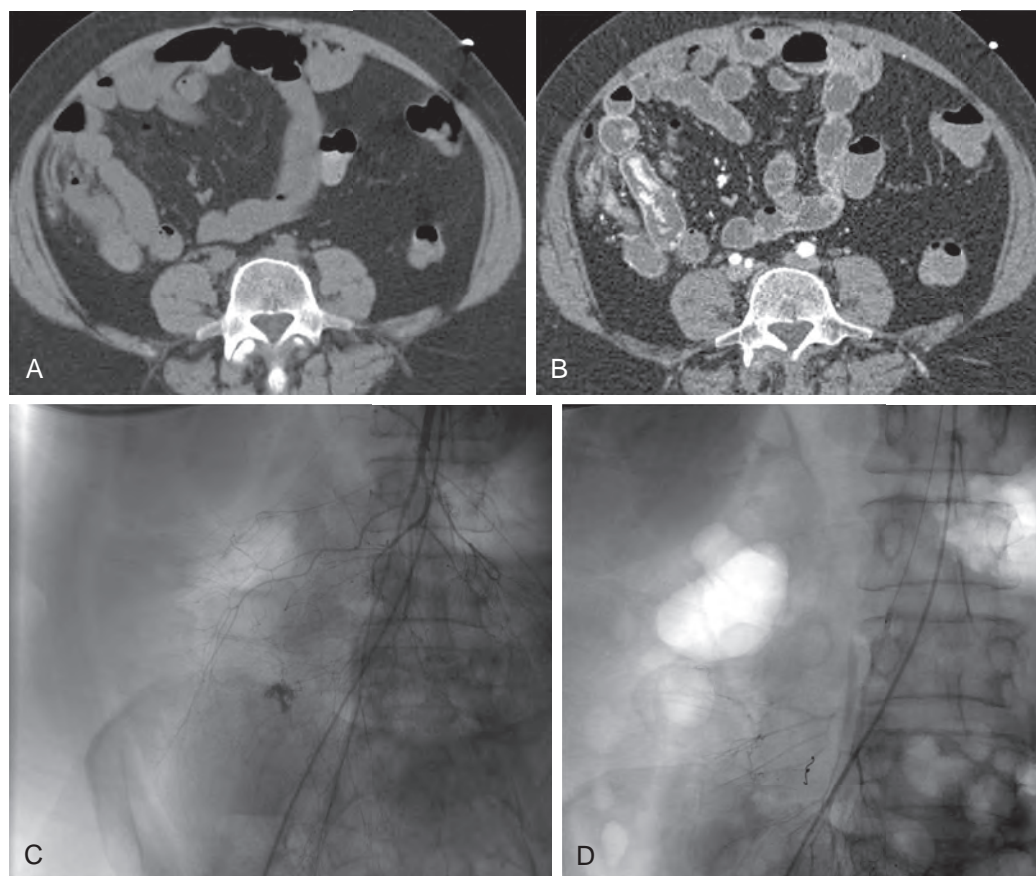


Figure 9-18 CT angiography in a patient with recent gastrointestinal hemorrhage and normal colonoscopy.

A. Unenhanced CT image shows no radiodense material in the small bowel. **B.** Arterial phase of CT angiography shows active hemorrhage into an ileal loop. **C.** Conventional angiography confirms active bleeding from a small ileocolic arcade branch. **D.** Successful coil embolization of the ileocolic arcade branch.

thickened bowel loops with pneumatosis or altered enhancement (hyper- or hypoenhancement of the affected bowel) are signs of ischemia.

CTA has been shown to be a promising first-line modality for the diagnosis or exclusion of active GI hemorrhage (see Chapter 124). Mesenteric CTA allows accurate localization of the bleeding site, thus facilitating interventional planning.^{132,133} CTA may also provide information about causative factors, which in cases of lower GI bleeding can direct treatment by differentiating among colonic diverticulosis, angiodysplasia, neoplasms, and colitis. The diagnosis of active GI bleeding is made when hyperattenuating, extravasated contrast material is identified within the bowel lumen. An unenhanced scan is obtained immediately prior to CTA, and comparison with unenhanced images allows for the differentiation of active hemorrhage from any preexisting hyperattenuating areas that may

be present within the bowel lumen at the time of evaluation (Fig. 9-18). Coronal MIP reformatted images are useful for localizing the site of hemorrhage and are used in conjunction with the axial images to evaluate the proximal femoral vasculature when intravascular treatment is anticipated. Sagittal MIP reformats are useful for evaluating the rectum and origins of the celiac artery, SMA, and inferior mesenteric artery (IMA).¹³⁴

Summary

CTA is the byproduct of rapid advances in CT technology and has replaced diagnostic catheter angiography for many indications. Image acquisition and processing techniques can significantly affect diagnostic image quality. A thorough knowledge of the scanner hardware and contrast optimization methods is therefore essential.

REFERENCES

1. Rubin GD, Dake MD, Napel SA, et al: Three-dimensional spiral CT angiography of the abdomen: Initial clinical experience. *Radiology* 186:147–152, 1993.
2. Adachi H, Ino T, Mizuhara A, et al: Assessment of aortic disease using three-dimensional CT angiography. *J Card Surg* 9:673–678, 1994.
3. Napel S, Marks MP, Rubin GD, et al: CT angiography with spiral CT and maximum intensity projection. *Radiology* 185:607–610, 1992.
4. Dillon EH, van Leeuwen MS, Fernandez MA, Mali WP: Spiral CT angiography. *AJR* 160: 1273–1278, 1993.
5. Galanski M, Prokop M, Chavan A, et al: Renal arterial stenoses: Spiral CT angiography. *Radiology* 189:185–192, 1993.
6. Rydberg J, Buckwalter KA, Caldemeyer KS, et al: Multisection CT: Scanning techniques and clinical applications. *Radiographics* 20: 1787–1806, 2000.
7. Fishman EK: From the RSNA Refresher Courses: CT angiography: Clinical applications in the abdomen. *Radiographics* 21:S3–S16, 2001.
8. Lawler LP, Fishman EK: Three-dimensional CT angiography with multidetector CT data: Study optimization, protocol design, and clinical applications in the abdomen. *Crit Rev Comput Tomogr* 43:77–141, 2002.

9. Rubin GD: MDCT imaging of the aorta and peripheral vessels. *Eur J Radiol* 45(Suppl 1): S42–S49, 2003.
10. Rubin GD, Shiau MC, Leung AN, et al: Aorta and iliac arteries: Single versus multiple detector-row helical CT angiography. *Radiology* 215:670–676, 2000.
11. Vrtiska TJ, Fletcher JG, McCollough CH: State-of-the-art imaging with 64-channel multi-detector CT angiography. *Perspect Vasc Surg Endovasc Ther* 17:3–8, 2005.
12. Saini S: Multi-detector row CT: Principles and practice for abdominal applications. *Radiology* 233:323–327, 2004.
13. Schoellnast H, Tillich M, Deutschmann MJ, et al: Aortoiliac enhancement during computed tomography angiography with reduced contrast material dose and saline solution flush: Influence on magnitude and uniformity of the contrast column. *Invest Radiol* 39:20–26, 2004.
14. Utsunomiya D, Awai K, Tamura Y, et al: 16-MDCT aortography with a low-dose contrast material protocol. *AJR* 186:374–378, 2006.
15. Anderson SW, Lucey BC, Varghese JC, Soto JA: Sixty-four multi-detector row computed tomography in multitrauma patient imaging: Early experience. *Curr Probl Diagn Radiol* 35:188–198, 2006.
16. Kalra MK, Maher MM, Toth TL, et al: Strategies for CT radiation dose optimization. *Radiology* 230:619–628, 2004.
17. Mettler FA, Wiest PW, Locken JA, Kelsey CA: CT scanning: Patterns of use and dose. *J Radiol Prot* 20:353–359, 2000.
18. Wintersperger B, Jakobs T, Herzog P, et al: Aorto-iliac multidetector-row CT angiography with low kV settings: Improved vessel enhancement and simultaneous reduction of radiation dose. *Eur Radiol* 15:334–341, 2005.
19. Marin D, Nelson RC, Schindera ST, et al: Low-tube-voltage, high-tube-current multidetector abdominal CT: Improved image quality and decreased radiation dose with adaptive statistical iterative reconstruction algorithm—initial clinical experience. *Radiology* 254:145–153, 2010.
20. Hunsaker AR, Oliva IB, Cai T, et al: Contrast opacification using a reduced volume of iodinated contrast material and low peak kilovoltage in pulmonary CT angiography: Objective and subjective evaluation. *AJR* 195:W118–W124, 2010.
21. Nakaura T, Nakamura S, Maruyama N, et al: Low contrast agent and radiation dose protocol for hepatic dynamic CT of thin adults at 256-detector row CT: Effect of low tube voltage and hybrid iterative reconstruction algorithm on image quality. *Radiology* 264:445–454, 2012.
22. Nakayama Y, Awai K, Funama Y, et al: Lower tube voltage reduces contrast material and radiation doses on 16-MDCT aortography. *AJR* 187:W490–W497, 2006.
23. Utsunomiya D, Oda S, Funama Y, et al: Comparison of standard- and low-tube voltage MDCT angiography in patients with peripheral arterial disease. *Eur Radiol* 20:2758–2765, 2010.
24. Brink JA: Contrast optimization and scan timing for single and multidetector-row computed tomography. *J Comput Assist Tomogr* 27(Suppl 1):S3–S8, 2003.
25. Cornfeld D, Israel G, Detroy E, et al: Impact of adaptive statistical iterative reconstruction (ASIR) on radiation dose and image quality in aortic dissection studies: A qualitative and quantitative analysis. *AJR* 196:W336–W340, 2011.
26. Elbakri IA, Fessler JA: Statistical image reconstruction for polyenergetic x-ray computed tomography. *IEEE Trans Med Imaging* 21: 89–99, 2002.
27. Fessler JA, Ficano EP, Clinthorne NH, Lange K: Grouped-coordinate ascent algorithms for penalized-likelihood transmission image reconstruction. *IEEE Trans Med Imaging* 16: 166–175, 1997.
28. Lasio GM, Whiting BR, Williamson JF: Statistical reconstruction for x-ray computed tomography using energy-integrating detectors. *Phys Med Biol* 52:2247–2266, 2007.
29. Nuyts J, De Man B, Dupont P, et al: Iterative reconstruction for helical CT: A simulation study. *Phys Med Biol* 43:729–737, 1998.
30. McCollough CH, Primak AN, Braun N, et al: Strategies for reducing radiation dose in CT. *Radiol Clin North Am* 47:27–40, 2009.
31. Hara AK, Paden RG, Silva AC, et al: Iterative reconstruction technique for reducing body radiation dose at CT: Feasibility study. *AJR* 193:764–771, 2009.
32. Bae KT: Peak contrast enhancement in CT and MR angiography: When does it occur and why? *Pharmacokinetic study in a porcine model. Radiology* 227:809–816, 2003.
33. Bae KT, Tran HQ, Heiken JP: Uniform vascular contrast enhancement and reduced contrast medium volume achieved by using exponentially decelerated contrast material injection method. *Radiology* 231:732–736, 2004.
34. Macari M, Israel GM, Berman P, et al: Infrarenal abdominal aortic aneurysms at multidetector row CT angiography: Intravascular enhancement without a timing acquisition. *Radiology* 220:519–523, 2001.
35. Johnson PT, Fishman EK: IV Contrast selection for MDCT: Current thoughts and practice. *AJR* 186:406–415, 2006.
36. Kim M-J, Chung YE, Kim KW, et al: Variation of the time to aortic enhancement of fixed-duration versus fixed-rate injection protocols. *AJR* 186:185–192, 2006.
37. Fleischmann D: Use of high concentration contrast media: Principles and rationale—vascular district. *Eur J Radiol* 45(Suppl 1):S88–S93, 2003.
38. Hittmair K, Fleischmann D: Accuracy of predicting and controlling time-dependent aortic enhancement from a test bolus injection. *J Comput Assist Tomogr* 25:287–294, 2001.
39. Fleischmann D, Rubin GD, Bankier AA, Hittmair K: Improved uniformity of aortic enhancement with customized contrast medium injection protocols at CT angiography. *Radiology* 214:363–371, 2000.
40. Furuta A, Ito K, Fujita T, et al: Hepatic enhancement in multiphasic contrast-enhanced MDCT: Comparison of high- and low-iodine-concentration contrast medium in same patients with chronic liver disease. *AJR* 183: 157–162, 2004.
41. Fleischmann D, Hallett RL, Rubin GD: CT angiography of peripheral arterial disease. *J Vasc Interv Radiol* 17:3–26, 2006.
42. Fleischmann D, Rubin GD: Quantification of intravenously administered contrast medium transit through the peripheral arteries: Implications for CT angiography. *Radiology* 236: 1076–1082, 2005.
43. Karcaaltincaba M, Foley WD: Gadolinium-enhanced multidetector CT angiography of the thoracoabdominal aorta. *J Comput Assist Tomogr* 26:875–878, 2002.
44. Pena CS, Kaufman JA, Geller SC, Waltman AC: Gadopentetate dimeglumine: A possible alternative contrast agent for CT angiography of the aorta. *J Comput Assist Tomogr* 23:23–24, 1999.
45. Chicoskie C, Tello R: Gadolinium-enhanced MDCT angiography of the abdomen: Feasibility and limitations. *AJR* 184:1821–1828, 2005.
46. Wicky S, Greenfield A, Fan C-M, et al: Aortoiliac gadolinium-enhanced CT angiography: Improved results with a 16-detector row scanner compared with a four-detector row scanner. *J Vasc Interv Radiol* 15:947–954, 2004.
47. Grobner T: Gadolinium—a specific trigger for the development of nephrogenic fibrosing dermopathy and nephrogenic systemic fibrosis? *Nephrol Dial Transplant* 21:1104–1108, 2006.
48. Thomsen HS: Nephrogenic systemic fibrosis: A serious late adverse reaction to gadodiamide. *Eur Radiol* 16:2619–2621, 2006.
49. Khurana A, Greene JF, Jr, High WA: Quantification of gadolinium in nephrogenic systemic fibrosis: Re-examination of a reported cohort with analysis of clinical factors. *J Am Acad Dermatol* 59:218–224, 2008.
50. Rubin GD: Data explosion: The challenge of multidetector-row CT. *Eur J Radiol* 36:74–80, 2000.
51. Yaghami V, Nikolaidis P, Hammond NA, et al: Multidetector-row computed tomography diagnosis of small bowel obstruction: Can coronal reformations replace axial images? *Emerg Radiol* 13:69–72, 2006.
52. Cody DD: AAPM/RSNA physics tutorial for residents: Topics in CT: Image processing in CT. *Radiographics* 22:1255–1268, 2002.
53. Prokop M: General principles of MDCT. *Eur J Radiol* 45(Suppl 1):S4–S10, 2003.
54. Shirai K, Nishiyama K, Katsuda T, et al: Phantom and clinical study of differences in cone beam computed registration when aligned to maximum and average intensity projection. *In J Radiat Oncol Biol Phys* 88:189–194, 2014.
55. Sahani D, Mehta A, Blake M, et al: Preoperative hepatic vascular evaluation with CT and MR angiography: Implications for surgery. *Radiographics* 24:1367–1380, 2004.
56. Sahani D, Saini S, Pena C, et al: Using multidetector CT for preoperative vascular evaluation of liver neoplasms: Technique and results. *AJR* 179:53–59, 2002.
57. Sahani DV, Krishnamurthy SK, Kalva S, et al: Multidetector-row computed tomography angiography for planning intra-arterial chemotherapy pump placement in patients with colorectal metastases to the liver. *J Comput Assist Tomogr* 28:478–484, 2004.
58. Winter TC, 3rd, Freeny PC, Nghiem HV, et al: Hepatic arterial anatomy in transplantation candidates: Evaluation with three-dimensional CT arteriography. *Radiology* 195:363–370, 1995.
59. Pollak R, Prusak BF, Mozes MF: Anatomic abnormalities of cadaver kidneys procured for purposes of transplantation. *Am Surg* 52:233–235, 1986.
60. Kawamoto S, Montgomery RA, Lawler LP, et al: Multidetector CT angiography for preoperative evaluation of living laparoscopic kidney donors. *AJR* 180:1633–1638, 2003.
61. Raman SS, Pojchamarnwiputh S, Muangsombon K, et al: Utility of 16-MDCT angiography for comprehensive preoperative vascular

- evaluation of laparoscopic renal donors. *AJR* 186:1630–1638, 2006.
62. Stueckle CA, Haegele KF, Jendreck M, et al: Multislice computed tomography angiography of the abdominal arteries: Comparison between computed tomography angiography and digital subtraction angiography findings in 52 cases. *Australas Radiol* 48:142–147, 2004.
 63. Romano M, Mainenti PP, Imbriaco M, et al: Multidetector row CT angiography of the abdominal aorta and lower extremities in patients with peripheral arterial occlusive disease: Diagnostic accuracy and interobserver agreement. *Eur J Radiol* 50:303–308, 2004.
 64. Lederle FA, Wilson SE, Johnson GR, et al: Design of the abdominal aortic aneurysm Detection and Management Study. ADAM VA Cooperative Study Group. *J Vasc Surg* 20:296–303, 1994.
 65. Daly KJ, Torella F, Ashleigh R, McCollum CN: Screening, diagnosis and advances in aortic aneurysm surgery. *Gerontology* 50:349–359, 2004.
 66. Scott RA, Vardulaki KA, Walker NM, et al: The long-term benefits of a single scan for abdominal aortic aneurysm (AAA) at age 65. *Eur J Vasc Endovasc Surg* 21:535–540, 2001.
 67. Ashton HA, Buxton MJ, Day NE, et al: The Multicentre Aneurysm Screening Study (MASS) into the effect of abdominal aortic aneurysm screening on mortality in men: A randomised controlled trial. *Lancet* 360:1531–1539, 2002.
 68. The United Kingdom Small Aneurysm Trial Participants: Health service costs and quality of life for early elective surgery or ultrasonographic surveillance for small abdominal aortic aneurysms. *Lancet* 352:1656–1660, 1998.
 69. Guirguis EM, Barber GG: The natural history of abdominal aortic aneurysms. *Am J Surg* 162:481–483, 1991.
 70. Powell JT, Brady AR: Detection, management, and prospects for the medical treatment of small abdominal aortic aneurysms. *Arterioscler Thromb Vasc Biol* 24:241–245, 2004.
 71. Longo C, Upchurch GR: Abdominal aortic aneurysm screening: Recommendations and controversies. *Vasc Endovascular Surg* 39:213–219, 2005.
 72. Ellis M, Powell JT, Greenhalgh RM: Limitations of ultrasonography in surveillance of small abdominal aortic aneurysms. *Br J Surg* 78:614–616, 1991.
 73. Ouriel K, Srivastava SD, Sarac TP, et al: Disparate outcome after endovascular treatment of small versus large abdominal aortic aneurysm. *J Vasc Surg* 37:1206–1212, 2003.
 74. Ng CS, Watson CJE, Palmer CR, et al: Evaluation of early abdominopelvic computed tomography in patients with acute abdominal pain of unknown cause: Prospective randomised study. *BMJ* 325:1387, 2002.
 75. Brady AR, Fowkes FG, Greenhalgh RM, et al: Risk factors for postoperative death following elective surgical repair of abdominal aortic aneurysm: Results from the UK Small Aneurysm Trial. On behalf of the UK Small Aneurysm Trial participants. *Br J Surg* 87:742–749, 2000.
 76. Benoit AG, Campbell BI, Tanner JR, et al: Risk factors and prevalence of perioperative cognitive dysfunction in abdominal aneurysm patients. *J Vasc Surg* 42:884–890, 2005.
 77. Parodi JC, Palmaz JC, Barone HD: Transfemoral intraluminal graft implantation for abdominal aortic aneurysms. *Ann Vasc Surg* 5:491–499, 1991.
 78. Vignali C, Cioni R, Neri E, et al: Endoluminal treatment of abdominal aortic aneurysms. *Abdominal Imaging* 26:461–468, 2001.
 79. Blankenstein JD, de Jong SECA, Prinssen M, et al: Two-year outcomes after conventional or endovascular repair of abdominal aortic aneurysms. *N Engl J Med* 352:2398–2405, 2005.
 80. Buth J, van Marrewijk CJ, Harris PL, et al: Outcome of endovascular abdominal aortic aneurysm repair in patients with conditions considered unfit for an open procedure: A report on the EUROSTAR experience. *J Vasc Surg* 35:211–221, 2002.
 81. Qanadli SD, Mesurolle B, Coggia M, et al: Abdominal aortic aneurysm: Pretherapy assessment with dual-slice helical CT angiography. *AJR* 174:181–187, 2000.
 82. Resch T, Ivancev K, Lindh M, et al: Abdominal aortic aneurysm morphology in candidates for endovascular repair evaluated with spiral computed tomography and digital subtraction angiography. *J Endovasc Surg* 6:227–232, 1999.
 83. Morasch MD: Percutaneous thoracic and abdominal aortic aneurysm repair. *Ann Vasc Surg* 19:585–589, 2005.
 84. White RA, Donayre CE, Walot I, et al: Preliminary clinical outcome and imaging criterion for endovascular prosthesis development in high-risk patients who have aortoiliac and traumatic arterial lesions. *J Vasc Surg* 24:556–569, 1996.
 85. Armerding MD, Rubin GD, Beaulieu CF, et al: Aortic aneurysmal disease: Assessment of stent-graft treatment—CT versus conventional angiography. *Radiology* 215:138–146, 2000.
 86. Goltzarian J, Valenti D: Endoleakage after endovascular treatment of abdominal aortic aneurysms: Diagnosis, significance and treatment. *Eur Radiol* 16:2849–2857, 2006.
 87. Iezzi R, Cotroneo AR, Marano R, et al: Endovascular treatment of thoracic aortic diseases: Follow-up and complications with multidetector computed tomography angiography. *Eur J Radiol* 65:365–376, 2008.
 88. Cohen EI, Weinreb DB, Siegelbaum RH, et al: Time-resolved MR angiography for the classification of endoleaks after endovascular aneurysm repair. *J Magn Reson Imaging* 27:500–503, 2008.
 89. Sommer WH, Becker CR, Haack M, et al: Time-resolved CT angiography for the detection and classification of endoleaks. *Radiology* 263:917–926, 2012.
 90. Macari M, Chandarana H, Schmidt B, et al: Abdominal aortic aneurysm: Can the arterial phase at CT evaluation after endovascular repair be eliminated to reduce radiation dose? *Radiology* 241:908–914, 2006.
 91. Stolzmann P, Frauenfelder T, Pfammatter T, et al: Endoleaks after endovascular abdominal aortic aneurysm repair: Detection with dual-energy dual-source CT. *Radiology* 249:682–691, 2008.
 92. Chandarana H, Godoy MC, Vlahos I, et al: Abdominal aorta: Evaluation with dual-source dual-energy multidetector CT after endovascular repair of aneurysms—initial observations. *Radiology* 249:692–700, 2008.
 93. Ascenti G, Mazziotti S, Lamberto S, et al: Dual-energy CT for detection of endoleaks after endovascular abdominal aneurysm repair: Usefulness of colored iodine overlay. *AJR* 196:1408–1414, 2011.
 94. Yeh BM, Shepherd JA, Wang ZJ, et al: Dual-energy and low-kVp CT in the abdomen. *AJR* 193:47–54, 2009.
 95. Scheffel H, Stolzmann P, Frauenfelder T, et al: Dual-energy contrast-enhanced computed tomography for the detection of urinary stone disease. *Invest Radiol* 42:823–829, 2007.
 96. Brugel M, Link TM, Rummeny EJ, et al: Assessment of vascular invasion in pancreatic head cancer with multislice spiral CT: Value of multiplanar reconstructions. *Eur Radiol* 14:1188–1195, 2004.
 97. Foley WD, Mallisee TA, Hohenwarter MD, et al: Multiphase hepatic CT with a multirow detector CT scanner. *AJR* 175:679–685, 2000.
 98. Foley WD: Special focus session: Multidetector CT: Abdominal visceral imaging. *Radiographics* 22:701–719, 2002.
 99. Fletcher JG, Wiersma MJ, Farrell MA, et al: Pancreatic malignancy: Value of arterial, pancreatic, and hepatic phase imaging with multidetector row CT. *Radiology* 229:81–90, 2003.
 100. Nino-Murcia M, Jeffrey RB, Jr, Beaulieu CF, et al: Multidetector CT of the pancreas and bile duct system: Value of curved planar reformations. *AJR* 176:689–693, 2001.
 101. Vargas R, Nino-Murcia M, Trueblood W, Jeffrey RB, Jr: MDCT in pancreatic adenocarcinoma: Prediction of vascular invasion and resectability using a multiphase technique with curved planar reformations. *AJR* 182:419–425, 2004.
 102. Winston CB, Lee NA, Jarnagin WR, et al: CT angiography for delineation of celiac and superior mesenteric artery variants in patients undergoing hepatobiliary and pancreatic surgery. *AJR* 189:W13–W19, 2007.
 103. Rouviere O, Lyonnet D, Berger P, et al: Ureteropelvic junction obstruction: Use of helical CT for preoperative assessment—comparison with intraarterial angiography. *Radiology* 213:668–673, 1999.
 104. Urban BA, Ratner LE, Fishman EK: Three-dimensional volume-rendered CT angiography of the renal arteries and veins: Normal anatomy, variants, and clinical applications. *Radiographics* 21:373–386, 2001.
 105. Kaatee R, Beek FJ, de Lange EE, et al: Renal artery stenosis: Detection and quantification with spiral CT angiography versus optimized digital subtraction angiography. *Radiology* 205:121–127, 1997.
 106. Steinwender C, Schutzenberger W, Fellner F, et al: 64-detector CT angiography in renal artery stenosis: Prospective comparison with selective catheter angiography. *Radiology* 252:299–305, 2009.
 107. Willmann JK, Wildermuth S, Pfammatter T, et al: Aortoiliac and renal arteries: Prospective intraindividual comparison of contrast-enhanced three-dimensional MR angiography and multi-detector row CT angiography. *Radiology* 226:798–811, 2003.
 108. Drevet D, Beck F, Streichenberger T, et al: Magnetic resonance angiography of stents. *J Radiol* 81:965–970, 2000.
 109. Letourneau-Guillon L, Soulez G, Beaudoin G, et al: CT and MR imaging of nitinol stents with radiopaque distal markers. *J Vasc Interv Radiol* 15:615–624, 2004.
 110. Trost DW, Zhang HL, Prince MR, et al: Three-dimensional MR angiography in imaging platinum alloy stents. *J Magn Reson Imaging* 20:975–980, 2004.
 111. Heinz-Peer G, Neruda A, Watschinger B, et al: Prevalence of NSF following intravenous

- gadolinium-contrast media administration in dialysis patients with endstage renal disease. *Eur J Radiol* 76:129–134, 2010.
112. Prokop M: Multislice CT angiography. *Eur J Radiol* 36:86–96, 2000.
 113. Raza SA, Chughtai AR, Wahba M, et al: Multislice CT angiography in renal artery stent evaluation: Prospective comparison with intra-arterial digital subtraction angiography. *Cardiovasc Intervent Radiol* 27:9–15, 2004.
 114. Catala V, Marti T, Diaz JM, et al: Use of multi-detector CT in presurgical evaluation of potential kidney transplant recipients. *Radiographics* 30:517–531, 2010.
 115. Fishman EK, Ney DR, Heath DG, et al: Volume rendering versus maximum intensity projection in CT angiography: What works best, when, and why. *Radiographics* 26:905–922, 2006.
 116. Ofer A, Nitecki SS, Linn S, et al: Multidetector CT angiography of peripheral vascular disease: A prospective comparison with intraarterial digital subtraction angiography. *AJR* 180:719–724, 2003.
 117. Heath DG, Soyer PA, Kuszyk BS, et al: Three-dimensional spiral CT during arterial portography: Comparison of three rendering techniques. *Radiographics* 15:1001–1011, 1995.
 118. Johnson PT, Halpern EJ, Kuszyk BS, et al: Renal artery stenosis: CT angiography—comparison of real-time volume-rendering and maximum intensity projection algorithms. *Radiology* 211:337–343, 1999.
 119. Dalrymple NC, Prasad SR, Freckleton MW, Chintapalli KN: Informatics in radiology (infoRAD): Introduction to the language of three-dimensional imaging with multidetector CT. *Radiographics* 25:1409–1428, 2005.
 120. Tsuda K, Murakami T, Kim T, et al: Helical CT angiography of living renal donors: Comparison with 3D Fourier transformation phase contrast MRA. *J Comput Assist Tomogr* 22:186–193, 1998.
 121. Patil UD, Ragavan A, Nadaraj R, et al: Helical CT angiography in evaluation of live kidney donors. *Nephrol Dial Transplant* 16:1900–1904, 2001.
 122. Kim J-K, Park S-Y, Kim H-J, et al: Living donor kidneys: Usefulness of multi-detector row CT for comprehensive evaluation. *Radiology* 229:869–876, 2003.
 123. Kim JK, Kim JH, Bae S-J, Cho K-S: CT angiography for evaluation of living renal donors: Comparison of four reconstruction methods. *AJR* 183:471–477, 2004.
 124. Noroozian M, Cohan RH, Caoili EM, et al: Multislice CT urography: State of the art. *Br J Radiol* 77(Suppl 1):S74–S86, 2004.
 125. Ishigami K, Yoshimitsu K, Irie H, et al: Accessory left gastric artery from left hepatic artery shown on MDCT and conventional angiography: Correlation with CT hepatic arteriography. *AJR* 187:1002–1009, 2006.
 126. Laghi A, Iannaccone R, Catalano C, Passariello R: Multislice spiral computed tomography angiography of mesenteric arteries. *Lancet* 358:638–639, 2001.
 127. Shih MC, Haghspeil KD: CTA and MRA in mesenteric ischemia: Part 1. Role in diagnosis and differential diagnosis. *AJR* 188:452–461, 2007.
 128. Lee VS, Morgan JN, Tan AGS, et al: Celiac artery compression by the median arcuate ligament: A pitfall of end-expiratory MR imaging. *Radiology* 228:437–442, 2003.
 129. Horton KM, Talamini MA, Fishman EK: Median arcuate ligament syndrome: Evaluation with CT angiography. *Radiographics* 25:1177–1182, 2005.
 130. Kirkpatrick IDC, Kroeker MA, Greenberg HM: Biphasic CT with mesenteric CT angiography in the evaluation of acute mesenteric ischemia: Initial experience. *Radiology* 229:91–98, 2003.
 131. Bradbury MS, Kavanagh PV, Bechtold RE, et al: Mesenteric venous thrombosis: Diagnosis and noninvasive imaging. *Radiographics* 22:527–541, 2002.
 132. Laing CJ, Tobias T, Rosenblum DI, et al: Acute gastrointestinal bleeding: Emerging role of multidetector CT angiography and review of current imaging techniques. *Radiographics* 27:1055–1070, 2007.
 133. Yoon W, Jeong YY, Shin SS, et al: Acute massive gastrointestinal bleeding: Detection and localization with arterial phase multidetector row helical CT. *Radiology* 239:160–167, 2006.
 134. Tochetto S, Yaghmai V: CT enterography: Concept, technique, and interpretation. *Radiol Clin North Am* 47:117–132, 2009.

Magnetic Resonance Angiography of the Mesenteric Vasculature

JOSEPH OWEN | KATHRYN J. FOWLER | VAMSI NARRA

CHAPTER OUTLINE

Magnetic Resonance Angiography Techniques

Nonenhanced Magnetic Resonance Angiography Techniques

Contrast-Enhanced Magnetic Resonance Angiography Techniques

Image Postprocessing and Display

Subtraction

Multiplanar Reformat

Maximum Intensity Projection

Shaded Surface Display

Volume Rendering

Clinical Applications of Abdominal Magnetic Resonance Angiography

Chronic Mesenteric Ischemia

Median Arcuate Ligament Syndrome

Splanchnic Artery Dissection

Visceral Artery Aneurysms

Segmental Arterial Mediolysis

Evaluation of Hepatic Vasculature

Magnetic Resonance Portography

Diseases of the Inferior Vena Cava

Magnetic Resonance Angiography Pitfalls

Summary

Magnetic resonance angiography (MRA) is a noninvasive technique that has been used as an alternate to conventional angiography. Noncontrast and contrast-enhanced techniques have been used historically to evaluate the visceral vessels. The most widely used noncontrast methods include time-of-flight (TOF) and phase contrast (PC) MRA, which have been validated most extensively for renal MRA. Advances in MR technology have facilitated the implementation of three-dimensional, contrast-enhanced MRA (CE MRA), which significantly expanded the role of MR angiography in imaging of the abdomen. New developments have led to time-resolved, contrast-enhanced MRA, which in addition to providing static arterial or venous phase images, provides hemodynamic information by allowing multiple rapid 3D acquisitions during the first pass of contrast. In addition, blood pool gadolinium contrast allows for steady-state imaging of the aorta and visceral vessels. In this chapter, we briefly discuss the various MR angiographic techniques, with emphasis on contrast-enhanced MR angiography. Included are approaches to patient preparation, imaging protocols, and image postprocessing techniques used in the evaluation of visceral vasculature with MRA. Various clinical applications of MRA in the abdomen are illustrated through a discussion of specific disease entities.

Magnetic Resonance Angiography Techniques

NONENHANCED MAGNETIC RESONANCE ANGIOGRAPHY TECHNIQUES

Time-of-Flight

Time-of-flight (TOF) is the oldest MRA technique for the evaluation of vasculature. This technique exploits blood motion to visualize vascular structures directly without the use of intravenous contrast material. It is performed using a gradient-refocused sequence in which the stationary tissues are saturated, resulting in low background signal intensity. In contrast, the blood moving into the imaging volume is unsaturated, with full longitudinal magnetization, which when excited gives a bright signal compared to the stationary, saturated background tissues. There are limitations with the TOF technique. The most important is that TOF is time-consuming and requires patient cooperation. Long acquisition times limit its use during a breath-hold. In addition, this technique is susceptible to in-plane saturation and phase dispersion, preventing the application of TOF for routine evaluation of the visceral vasculature. TOF may still provide diagnostic images in the evaluation of large vessels such as the abdominal aorta, proximal portions of the celiac and superior mesenteric arteries, large venous structures such as the inferior vena cava (IVC), portal vein, superior mesenteric vein, and portosystemic collaterals.^{1,2} Diseased vessels or small arteries such as the proper hepatic, gastroduodenal, and branches of the superior mesenteric arteries are not well evaluated with this technique.^{1,4} The direction of portal venous blood flow can be assessed using the TOF technique by simply applying a saturation band over the portal vein. Contrast-enhanced and nonenhanced techniques have mainly replaced TOF imaging in the abdomen.

Phase Contrast Technique

The phase contrast (PC) technique uses phase shifts of the flowing protons in the vascular structures to create MRA images. Phase shifts of stationary tissues are compensated by using bipolar gradient. Two imaging acquisitions are performed, in which the first has a positive bipolar gradient and the second has a negative bipolar gradient. The data from these two acquisitions are subtracted in k space to eliminate phase shift induced by other sequence parameters. The net effect is an image of flowing spins. The amount of phase difference that remains after subtraction is proportional to the velocity of the moving spins. The flow sensitivity can be adjusted by setting the velocity encoding value, $V(\text{enc})$. $V(\text{enc})$ determines the highest and lowest detectable velocities encoded by a phase-contrast sequence. For example, $V(\text{enc}) = 100 \text{ cm/s}$ is ideal for a phase contrast MRA with a measurable range

of flow velocities of ± 100 cm/s. PC MRA allows for the functional assessment of mesenteric circulation and has been shown to be helpful for diagnosing mesenteric ischemia.⁵⁻⁷ The information from phase contrast measurements can be processed into magnitude (bright blood and anatomic) images or phase contrast (velocity) images. A major disadvantage of the PC technique is long acquisition times, requiring patient cooperation. Because the final image relies on subtraction, patient motion can be problematic. Turbulent flow distal to a region of stenosis may result in dephasing and signal loss, overestimating the stenosis grade. As a result of these many limitations, this technique is not typically used as a primary imaging tool for anatomic assessment of the visceral arteries or portal system.

Balanced Steady-State Free Precession

Balanced steady-state free precession (b-SSFP) is a rapid imaging technique that provides a very high signal-to-noise ratio with T2*/T1-weighted image contrast. The different T2*/T1 ratios of blood and surrounding tissue are beneficial for angiographic imaging.⁸ This technique is not flow-dependent, so venous structures demonstrate as bright a signal intensity as arterial structures. Clotted blood is low in signal intensity, depending on the clotting stage and composition of blood products. b-SSFP is best suited for morphologic imaging of the vessels. It allows a rough anatomic preview and visualization of background tissues, such as mural thrombus and vascular wall, which may not be optimally evaluated when using a contrast-enhanced MRA sequence alone. The drawback of this technique is the banding artifacts caused by magnetic field inhomogeneity. One solution to this problem is to use a very short repetition time (TR) to eliminate the artifacts from the regions of interest. Given the high signal-to-noise ratio of b-SSFP sequences, the bright signal intensity of fat can obscure anatomic structures. In such cases, effective fat suppression can be used to improve the image quality.

Other Techniques

Other procedures for noncontrast MRA are available, such as fresh blood imaging (FBI), NATIVE, and flow prep, which are based primarily on electrocardiogram (ECG), gated, fast spin-echo (FSE) sequences. This general technique relies on high signal during diastole and flow void during systole within the arteries secondary to differential velocity, which allows for images depicting only arteries or veins following subtraction. Although in principle this technique seems simple, it requires expertise on the part of the technologist and, because it relies on differential flow between systole and diastole, it does not perform well in the setting of severe disease. ECG-gated FSE sequences have been used primarily for peripheral vascular disease and aortic imaging, with little published experience in mesenteric imaging.

In addition to ECG-gated FSE sequences, another new technique is the quiescent-interval single-shot (QISS) sequence. This has demonstrated promise for peripheral vascular disease and also may be used to image the abdominal aorta and origins of the major visceral vessels.⁹ QISS is an ECG-gated slice selective 2D b-SSFP sequence that uses a tracking saturation pulse to eliminate venous signals. Images are acquired during the quiescent interval, coinciding with arterial inflow during systole. This new technique has yet to be thoroughly tested for application in mesenteric MRA.

CONTRAST-ENHANCED MAGNETIC RESONANCE ANGIOGRAPHY TECHNIQUES

CE MRA is the preferred MR technique for anatomic evaluation of the arterial and venous systems in the abdomen and pelvis. The image contrast is based on the differences in the T1 relaxation time of blood and the surrounding tissues. Gadolinium chelate is administered to significantly shorten the T1 relaxation time of blood and T1-weighted images are obtained, often with precontrast images obtained for reference and subtraction. Conventional 3D CE MRA techniques requiring bolus timing often provide good anatomic detail. Time-resolved techniques minimize the need for bolus timing and allow for the assessment of flow dynamics using high temporal resolution. Steady state high resolution imaging with blood pool agents can provide exquisite anatomic detail not previously attainable with extracellular agents.

Conventional Three-Dimensional Contrast-Enhanced Magnetic Resonance Angiography

CE MRA requires bolus timing with pre- and postcontrast 3D spoiled gradient-echo technique (3D SPGR/3D fast low-angle shot [FLASH]) using very short echo times (TEs) and repetition times (TRs) in combination with a relatively high excitation flip angle (25 to 40 degrees). No special preparation for the scan is required. Some studies indicate that a mesenteric MRA is better performed postprandially because there is increased splanchnic circulation.

After the patient is positioned supine on the table and centered for the midabdomen, the basic imaging protocol for mesenteric MRA generally starts with multiplane scout images of the abdomen. Coronal and axial true fast imaging with steady-state precession (FISP; balanced SSFP) images of the abdomen are acquired to provide anatomic assessment of the outer wall of the vessel and an additional set of localizers to position the subsequent test bolus and 3D MRA slab. A precontrast 3D MRA sequence is performed in the coronal plane for most applications; consider sagittal for celiac and superior mesenteric pathologies such as the median arcuate ligament or superior mesenteric artery (SMA) syndrome. To achieve the best image quality, use the shortest possible TR to shorten the acquisition time and a minimized TE to decrease the dephasing artifact and T2* effects. An appropriate flip angle is between 25 and 40 degrees. The thicknesses of slabs and sections vary, depending on the patient, to cover all the mesenteric vessels, including the hepatic arteries, superior mesenteric arteries, and branches. One should aim for a slice thickness of 1 to 1.5 mm after interpolation; however, for larger vessels, thicker slices may be sufficient and allow greater coverage.

If using the test bolus technique (see later), a timing bolus sequence (turbo FLASH sequences: acquisition speed = 1 image/s) of the abdominal aorta is performed in the sagittal plane using a test injection of gadolinium chelate (≈ 1 -2 mL, injected at a rate of 2-3 mL/s). If there is an aortic aneurysm, the estimated contrast arrival time should be timed at the distal part of the aneurysm. After the administration of contrast (0.1-0.2 mmol/kg, 2-3 mL/s) at an appropriate delay time (as calculated, or automatically triggered) followed by a saline flush solution of 15 to 20 mL at the same rate, two imaging sets are consecutively acquired postcontrast. The imaging time for each sequence should be less than 20 to 25 seconds to permit breath holding.

Contrast Material Dosage and Injection Rate. Appropriate timing of contrast material injection is critical in obtaining a good conventional 3D CE MRA, without significant venous contamination, for evaluation of the arterial system. The volume of contrast material and chasing saline solution, delivery rate, and scan delay time are important parameters that are to be adjusted to optimize image quality.

The arterial and venous enhancement pattern after the rapid contrast injection is shown in Figure 10-1.¹⁰ To achieve excellent image contrast and signal-to-noise ratio, the imaging sequence has to be timed so that the acquisition of the central portion of the k space (low-frequency data lines) corresponds with the plateau phase of maximum concentration of contrast material in the vessels of interest. If the central portion of the k space is filled prior to the peak of the contrast concentration, ringing or banding artifacts occur (Fig. 10-2). However, if images are acquired too, late venous contamination may obscure the arterial anatomy.

Injection rate and duration of injection also have a significant effect on the pattern of arterial enhancement. A faster injection rate leads to a sharper arterial peak and higher maximum arterial signal intensity, whereas a slower injection rate results in a lower and broader arterial peak and lower maximum arterial signal intensity.¹⁰ Contrary to the arterial enhancement pattern, the degree of venous enhancement does not vary substantially with the injection rate but primarily depends on the total dose of contrast material when using an extracellular contrast agent. Thus, a larger amount of contrast material leads to higher intravascular signal intensity when performing gadolinium-enhanced portography or venography.¹¹ The time to peak for venous enhancement is longer with a slower injection rate, and image acquisition should be delayed proportionally to obtain the best contrast enhancement in the venous structures.

As the technique of CE MRA imaging was first introduced, the images were acquired as non-breath-holds, with acquisition times of 3 to 5 minutes. Under these circumstances, the gadolinium chelate was preferably infused at a slow uniform

rate over the entire scan duration to prolong the window of preferential arterial to venous enhancement.¹² Now, high-speed gradient MR systems and improved sequences permit shorter acquisition times, typically shorter than 20 seconds, which allows data acquisition during the first pass of contrast material in a single breath-hold. Therefore a rapid bolus injection with an automatic MR-compatible power injector is preferred.

Many different approaches have been used to optimize the injection rate and dosage of contrast material for MR angiography. The dosage of extracellular contrast agents used for performing abdominal MR angiography usually varies from a single to a triple dose (0.1 to 0.3 mmol/kg). Although some studies have shown that a single dose of contrast is sufficient for diagnostic assessment of the aorta and its major branches with CE MRA,¹³⁻¹⁵ some investigators have reported that image quality, vessel delineation, and confidence in diagnosis improve with the use of a higher dose (double^{16,17} or triple dose¹⁸). However, double- and triple-dose methods have fallen out of favor because of the association of nephrogenic systemic fibrosis with gadolinium contrast agents.¹⁹ With regard to injection rate, a faster injection allows for a greater degree of preferential arterial to venous enhancement,¹⁰ and the interval between arterial and venous peaks tend to be longer with a higher injection rate.¹¹ Hence, venous contamination is diminished with a high-rate injection protocol. For mesenteric MRA, we use a single dose and inject at a rate of 2 to 3 mL/s, followed by a 20-mL normal saline flush at the same rate.

Bolus Timing Methods. Because the image quality of CE MRA depends primarily on the distribution and concentration of gadolinium during the acquisition of the center of the k space, proper timing is paramount to achieving a good MRA image, particularly when using fast imaging techniques. There are several ways to synchronize the arterial peak enhancement with the center of k space data acquisition.

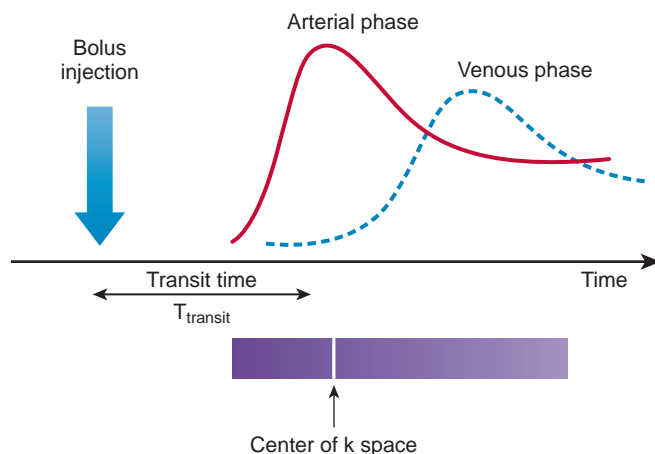


Figure 10-1 Arterial and venous enhancement pattern after a bolus injection. For the best MR angiographic quality to be achieved without venous contamination, the data at the center of k space should be acquired during peak arterial enhancement, when there is still no contrast in the venous structures. The transit time is a delayed time after the bolus injection to when the data at center of k space is acquired.

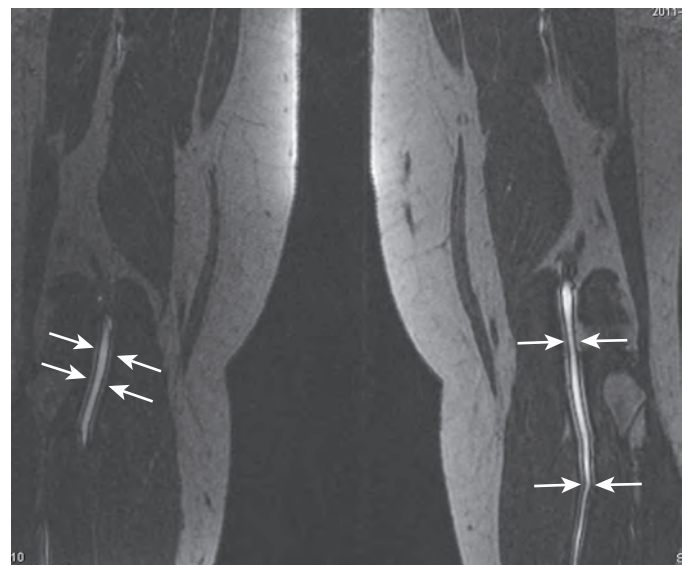


Figure 10-2 Ringing or banding artifact. The image demonstrates ringing or banding artifacts (arrows), which occur when the central portion of k space is filled prior to the peak of the contrast concentration during rapid changing of the contrast concentration.

“Best Guess” Technique. This is the simplest timing method; it is performed by using an estimated contrast travel time from the injection site to the vascular structure of interest with sequential (linear) order of k space acquisition. The variation in contrast travel time depends on age, gender, injection site, injection rate, and other clinical parameters, such as cardiac output status and vascular anatomy. In general, the estimated contrast travel time from an antecubital vein to the abdominal aorta is approximately 15 to 18 seconds in a healthy young patient and 20 to 25 seconds in a healthy older patient. In patients with decreased cardiac output or a large aortic aneurysm, the estimated contrast travel time may vary widely, from 25 to 50 seconds.²⁰

Test Bolus Technique. This is a more precise timing method performed by injecting a small amount of contrast material (1 to 2 mL) followed by normal saline flush (10 to 20 mL) at the same injection rate as in the planned contrast-enhanced MRA study. The vascular structure of interest is imaged with a timing bolus acquisition (single-slice, fast 2D gradient-echo sequence) acquired at a rate of one image every second. Time to peak of contrast enhancement is determined visually or by drawing a region of interest over the vessel. When using a sequential (linear) order of k space acquisition in the 3D MRA sequence, the scan delay time is calculated as follows:

$$\begin{aligned} &\text{Imaging delay time or scan delay} \\ &= (\text{time to peak of contrast enhancement}) \\ &\quad + (\text{injection duration time}/2) \\ &\quad - (\text{time to center of k space}) \end{aligned}$$

If a centrally reordered k space acquisition sequence is used, the estimated scan delay is equal to the time to peak of contrast enhancement. This technique is robust and reliable and offers the advantage of making sure that the intravenous access is in good working condition before the main contrast bolus is injected. The drawback of this technique is that there is no guarantee that the imaging bolus will behave identically to the test bolus because of the differences in the total volume of injection, especially in the setting of poor cardiac function.

Automatic Triggering Technique. The automatic triggering technique (SmartPrep, GE Medical Systems, Waukesha, Wis.; ABLE, Siemens, Munich, Germany) is another technique to optimize the imaging delay time by automatically synchronizing the bolus arrival and image acquisition. In this technique, a tracker volume is placed over the desired vascular structure, typically at a level slightly proximal to the area of interest. The signal level of the tracker volume is obtained repeatedly and rapidly using a tracker sequence during the contrast injection. When the signal intensity reaches a threshold value (usually 2-3 standard deviations [SDs] or 15%-30% above the mean signal level), the 3D MRA sequence (3D SPGR sequence with centric reordering of k space) is triggered. In general, there is a 4- to 5-second delay between the detection of bolus and the start of 3D acquisition, which allows contrast to reach the peak and also gives enough time to suspend respiration. This method ensures that peak arterial and central k space data acquisition occur simultaneously.²¹ The disadvantages of this technique is that if the size of the tracker volume ($\approx 2 \times 2 \times 2.5$ cm) is larger than the arterial structure of interest and overlaps an

adjacent vascular structure, the bolus may be missed or inappropriately timed.

Magnetic Resonance Fluoroscopy. Magnetic resonance fluoroscopy (CARE bolus, Siemens) is a fluoroscopic triggering technique. Similar to the automatic triggering technique, the entire volume of contrast is injected. Using a fast 2D gradient-echo technique, rapid images are acquired in real time over the vessel of interest. As the contrast arrives in the vessel of interest, the 3D MRA sequence is triggered by the operator. The operator-triggered approach has some advantages. For example, in the evaluation of cases with asymmetric flow patterns, or in cases in which there is displacement of the monitoring plane because of patient motion, an experienced operator can adapt and initiate the triggering accordingly.²²

3D Time-Resolved, Contrast-Enhanced Magnetic Resonance Angiography

This allows for the rapid acquisition of volumetric data sets throughout the contrast bolus, which are then commonly displayed as sequential 3D subtracted maximum intensity projections. To make time-resolved MRA feasible, k space filling must occur in a few seconds or less. Bolus timing becomes less important because multiple phases of contrast are obtained and an arterial phase without venous contamination can be selected for review. Capturing multiple phases of contrast provides hemodynamic information similar to that obtained with digital subtraction angiography (DSA), adding new diagnostic capabilities not previously available with conventional 3D CE MRA.

In TR MRA, reduction in acquisition time is achieved through spatial and temporal undersampling of k space and subsequent Fourier interpolation and/or k space sharing. Multiple proprietary algorithms for k space filling have been developed to allow rapid volumetric data acquisition including TRICKS,²³ TREAT,²⁴ and TWIST.²⁵ In general, the periphery of k space (high spatial frequencies) is undersampled relative to the center of k space (low spatial frequencies), which maintains contrast resolution at the expense of spatial resolution. During sequence optimization, the primary trade-off is spatial versus temporal resolution. The background structures and vessel location do not change substantially during a contrast bolus, so undersampling, interpolating, or k space sharing can be used to maintain spatial resolution while reducing acquisition time. The high-contrast resolution volumetric datasets can then be displayed as maximum intensity projections and viewed in a sequential manner to evaluate hemodynamics. Temporal resolutions on the order of 2 to 4 seconds are optimal for capturing the hemodynamics of the mesenteric arterial system. Our current method uses k space sharing using TWIST, with an injection of the entire contrast bolus at 2 mL/s, followed by the acquisition of TR MRA over multiple measurements (usually spanning at least 2.5 minutes). Because this method relies on subtraction, it can be repeated at multiple stations or with split boluses, if needed. If a blood pool agent is used, pre- and post-contrast traditional 3D CE MRA sequences can be obtained in addition to TR MRA to provide higher resolution subtractions and maximum intensity projections (MIPs). The addition of fat-suppressed, T1-weighted, postcontrast sequences, such as a 2D FLASH (perhaps better suited for patients in whom bowel pathology is sought to limit motion blurring), or a 3D volumetric interpolated breath-hold examination (VIBE), may provide further anatomic detail of organs of interest.

Steady-State, High-Resolution, Contrast-Enhanced Magnetic Resonance Angiography

This is now feasible with the advent of blood pool gadolinium contrast agents. Gadofosveset trisodium (Ablavar) is a U.S. Food and Drug Administration (FDA)–approved MR imaging (MRI) blood pool contrast agent, specifically designed for MRA and approved for aortoiliac occlusive disease. After intravenous administration, Ablavar is 80% to 96% bound strongly but reversibly to serum albumin, resulting in a long intravascular elimination half-life. According to studies performed in rabbits and nonhuman primates, Ablavar is eliminated primarily through the renal system, and its intravascular half-time is approximately 2 to 3 hours.^{26,27} The binding of Ablavar to plasma proteins exhibits T1 relaxivity 6 to 10 times higher than that of extracellular gadolinium chelate compounds. This results in a strong persistent intravascular T1 shortening, giving an acquisition window of approximately 1 hour.²⁶ Thus, these blood pool contrast agents allow excellent vascular enhancement during dynamic and steady-state MRA.²⁸ Moreover, the longer imaging window facilitates the higher spatial resolution MR acquisition than would be possible with conventional extracellular gadolinium chelate contrast agents. This longer imaging window is also more forgiving in cases in which first-pass bolus timing is suboptimal.

Blood pool gadolinium agents may prove to be the ideal contrast agent for mesenteric MRA. This is because they function as well as extracellular agents in conventional 3D CE MRA and time-resolved MRA while providing improved opacification of venous structures for venography and allowing steady-state, high-resolution, 3D MRA. A sample mesenteric MRA protocol with a blood pool agent starts with a variable scout and then a partial half-Fourier acquisition single-shot turbo spin-echo (HASTE), with a coronal breath-hold and axial non-breath-hold. Then b-SSFP with fat saturation in the coronal and axial planes is obtained to provide background anatomic detail, including vessel walls and the presence of an intraluminal or intramural thrombus. Precontrast 2D FLASH with fat saturation in the axial plane with breath holding, and precontrast 3D spoiled gradient-echo images with breath holding in a coronal plane, with the posterior end of the slab positioned just behind the aorta, are obtained for subtraction with subsequent steady-state, high-resolution sequences. A test bolus or preferred bolus timing method is performed. Then a single dose of Ablavar is administered at 1 to 2 mL/s with an MR-compatible power injector. Two sequential 3D spoiled gradient-echo images with breath holding in a coronal plane are obtained postcontrast. 3D spoiled gradient-echo images with breath holding are then obtained in a sagittal plane (for celiac and superior mesenteric artery indications). Finally, 2D FLASH with fat saturation in an axial plane with breath holding is performed for high-resolution, steady-state postcontrast images. Postprocessing is performed to create subtraction images from pre- and postcontrast sequences, and 3D MIPs are reconstructed (Fig. 10-3A).²⁹

Image Postprocessing and Display

3D contrast-enhanced MRA produces a contiguous volume of image data so that it can be easily reformatted in any desired plane or reconstructed using various 3D reconstruction algorithms for better demonstration of targeted vessels.

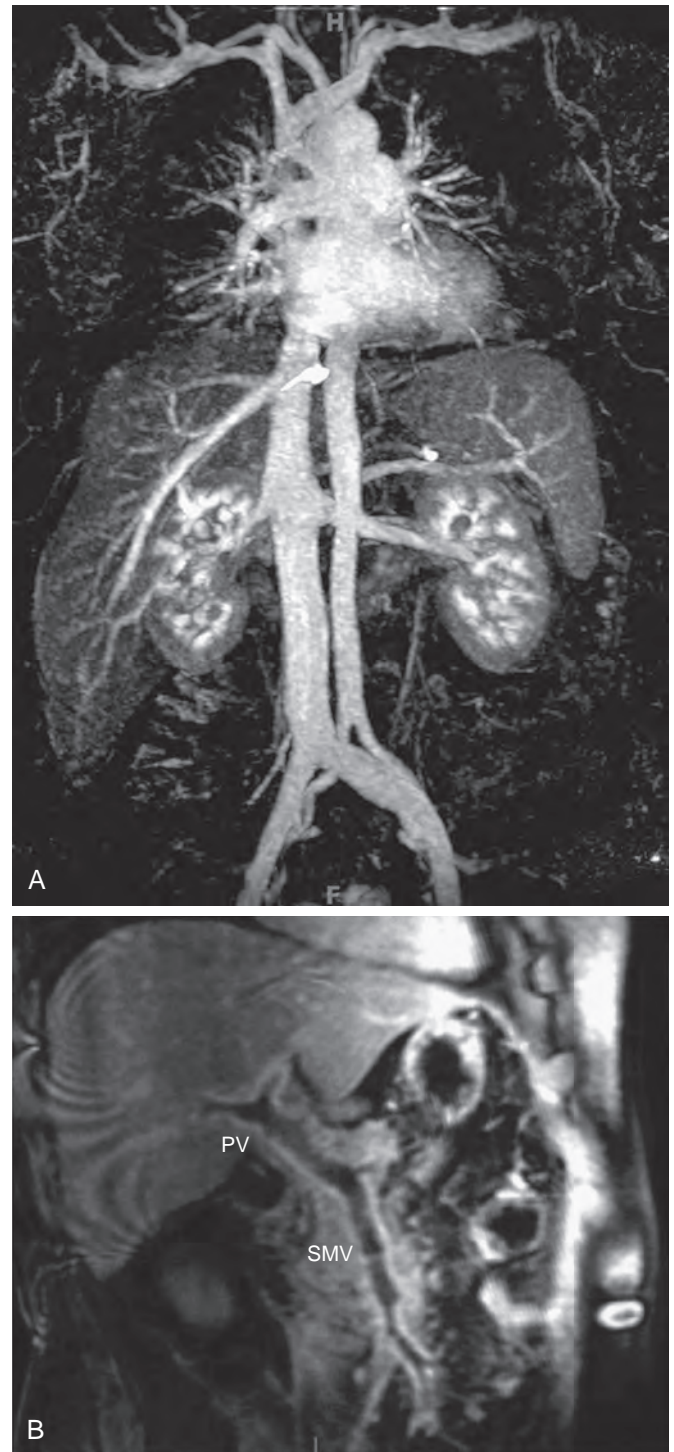


Figure 10-3 Reconstruction techniques. A. Thick MIP reconstructions from subtracted steady-state CE MRA with Ablavar show normal venous and artery anatomy. **B.** Curved MPR of the CE MR portography in a different patient demonstrates an extensive thrombus in the portal vein (PV) and superior mesenteric vein (SMV).

SUBTRACTION

This is a simple postprocessing technique that allows elimination of the background tissue signal such as fat. To achieve subtraction, postcontrast images are subtracted from the pre-contrast images, resulting in a new subtracted dataset. The

subtracted dataset can be further postprocessed using any of the techniques described here.

MULTIPLANAR REFORMAT

Multipolar reformat (MPR) is the reconstruction of images in arbitrary orientations, such as orthogonal, oblique, or curved planes. This method allows the viewer to slide through a given volume in any plane in real time. These reformatted slices remain thin, eliminating overlapping structures and unfolding tortuous vessels. The reformatted images frequently provide better demonstration and additional diagnostic information, particularly in the evaluation of complex anatomic structures or areas that are traditionally difficult to evaluate on axial source images (Fig. 10-3B). For best MPR results, images should be as close to isotropic (the same size in all three voxel dimensions) as possible. This can be achieved easily during high-resolution, steady-state imaging with Ablavar. It should be noted, however, that the acquisition time of isotropic 3D datasets is long and generally cannot be acquired during a single breath-hold. The motion related to respiration does create significant blurring or distortion of the anterior half of the abdomen, but the aorta and proximal visceral vessels are generally well depicted because they are less susceptible to motion during respiration.

MAXIMUM INTENSITY PROJECTION

Maximum intensity projection (MIP) is the projection of pixels with highest intensity onto an arbitrarily oriented plane. MIP images have an aspect similar to that of conventional angiograms and are commonly used for angiographic display because vascular signal is much greater than background signal. The image data can be reconstructed in a full-volumetric MIP (Figs. 10-4 to 10-6) or subvolumetric MIP (Figs. 10-7 and 10-8), in which only a small portion of the slab is reconstructed. The thickness of the slab and desired viewing plane can be adjusted. A drawback of MIP images is the lack of depth information, so that objects lying in the same projection plane of high-intensity structures cannot be visualized.³⁰ For example, stationary tissues that have greater signal intensity than vascular structures, such as fat, hemorrhage, or metallic susceptibility artifact, can lead to mapping of these nonvascular structures to the projection image and cause a discontinuity in the vessel signal, potentially mimicking stenosis or occlusion.³¹ On the other hand, eccentrically located stenoses may remain undetected.³² Careful evaluations with multiple angle projections, as well as use of the subvolumetric MIP reconstruction technique, can help minimize the chance of diagnostic errors incurred by full-volumetric MIP images. Given the potential pitfalls, MIP images should be used as a road map, whereas source images and MPR are used preferably for definitive diagnosis.^{17,30,33}

SHADED SURFACE DISPLAY

Shaded surface display (SSD) is the three-dimensional display of a surface from a series of contiguous slices using variable threshold settings. The 3D objects can be rotated and tilted in real time. The unwanted overlying structures can be easily eliminated using volume segmentation and confinement. Because SSD allows 3D visualization, it provides a clear 3D understanding of the patient's anatomy for improved surgical and treatment planning (Figs. 10-9 and 10-10).

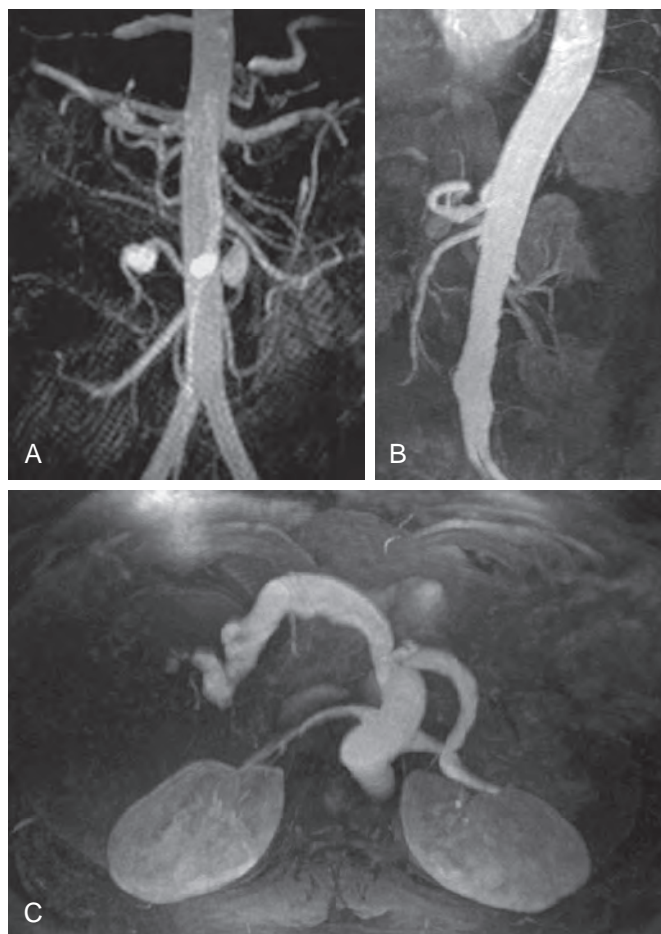


Figure 10-4 Visceral artery aneurysms. **A.** Full volumetric coronal MIP image with contrast-enhanced abdominal MRA in an 18-year-old woman who presented with a duodenal hemorrhage reveals multiple aneurysmal dilation of the superior mesenteric artery. **B.** Sagittal thick MIP subtraction images from MRA with Ablavar demonstrate an isolated celiac aneurysm in a patient with a history of aortic dissection. **C.** Axial thin MIP images with abdominal MRA demonstrate fusiform dilation of the celiac trunk and hepatic artery in a different patient.

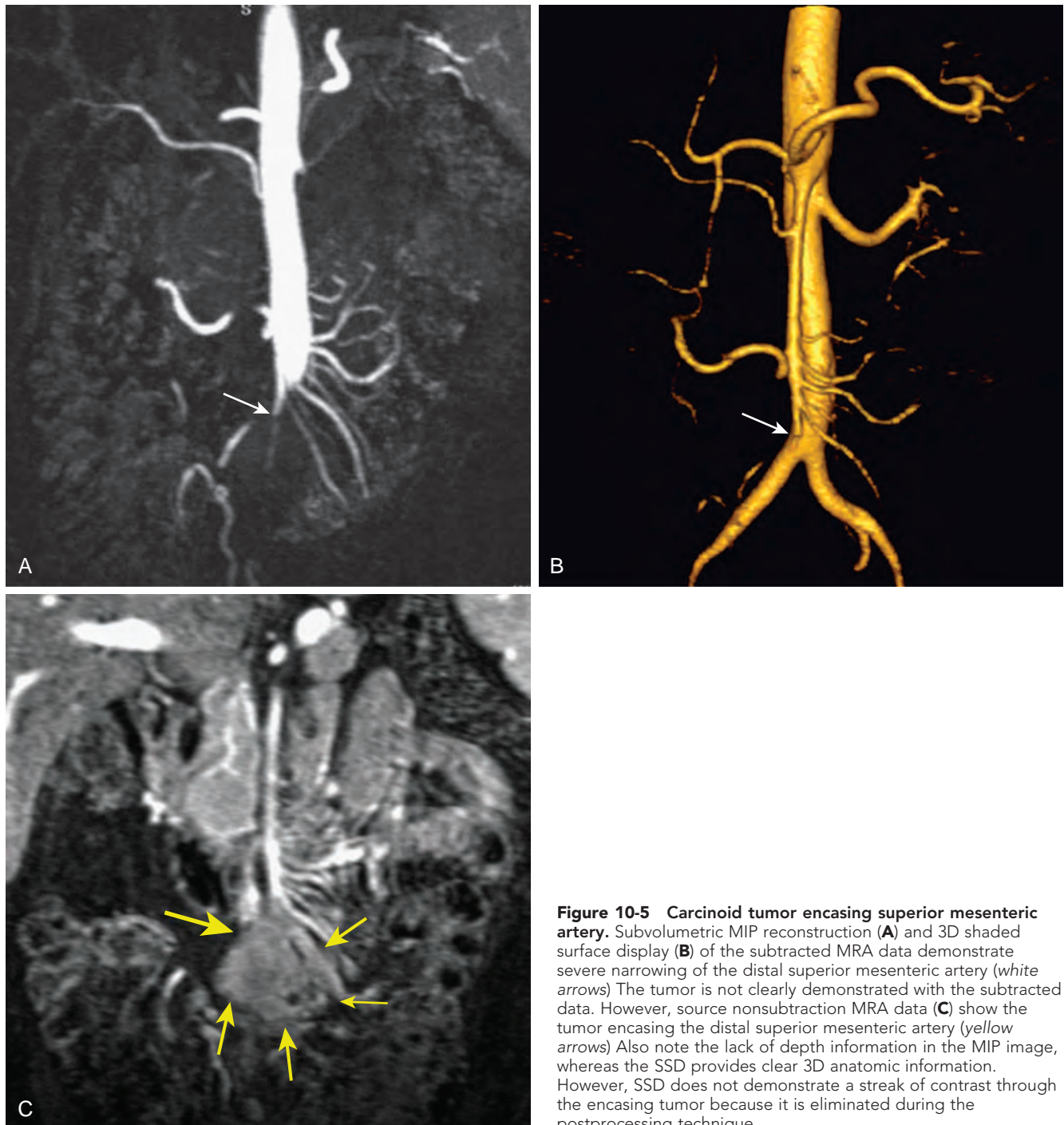
VOLUME RENDERING

Volume rendering (VR) is another 3D visualization tool. In contrast to SSD, not only is the surface displayed, but VR also allows the entire range of signal intensity within a volume data set to be illustrated. Objects with high signal intensity are opaque, and objects with low signal intensity are transparent. Thus, tissue differentiation is more feasible and the internal structures that would normally be hidden when using SSD can be demonstrated using VR. The display parameters, including window width, window level, opacity, and brightness, can be manipulated to obtain the optimal visualization of the areas of interest.

Clinical Applications of Abdominal Magnetic Resonance Angiography

CHRONIC MESENTERIC ISCHEMIA

Chronic mesenteric ischemia (CMI) is a gradual occlusive process, mostly caused by atherosclerotic changes of the



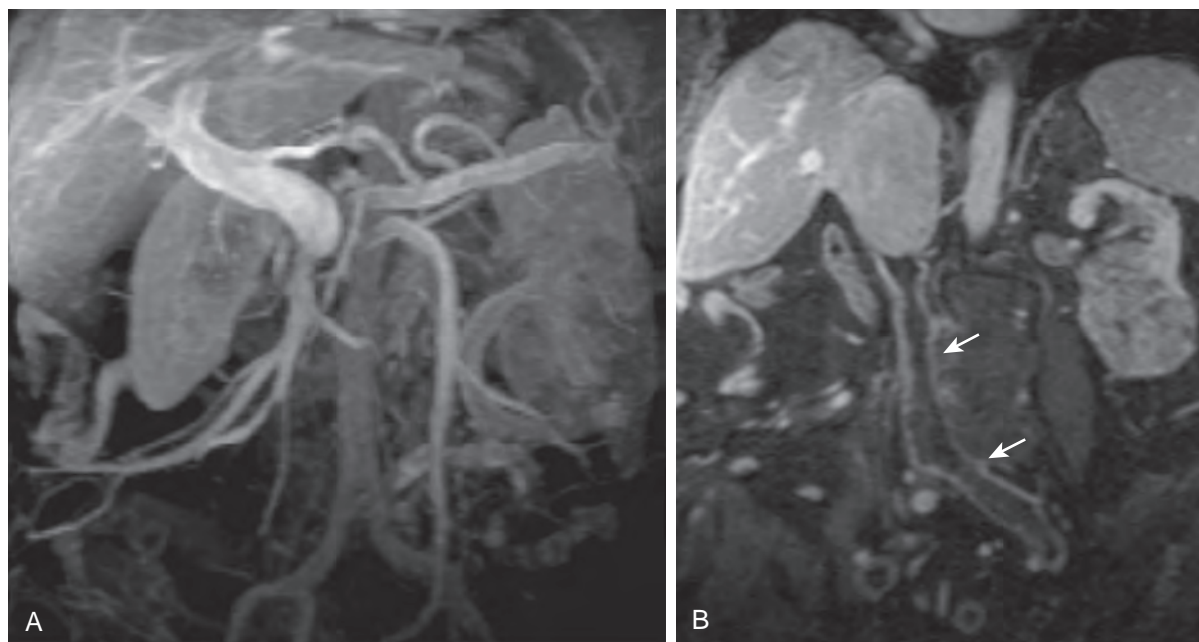


Figure 10-6 Inferior vena cava and iliac vein thrombosis. **A.** Coronal full volumetric MIP reconstruction of contrast-enhanced MR venography demonstrates no opacification of the inferior vena cava. **B.** Coronal reformatting reveals an extensive thrombus within the inferior vena cava and left iliac vein (arrows).

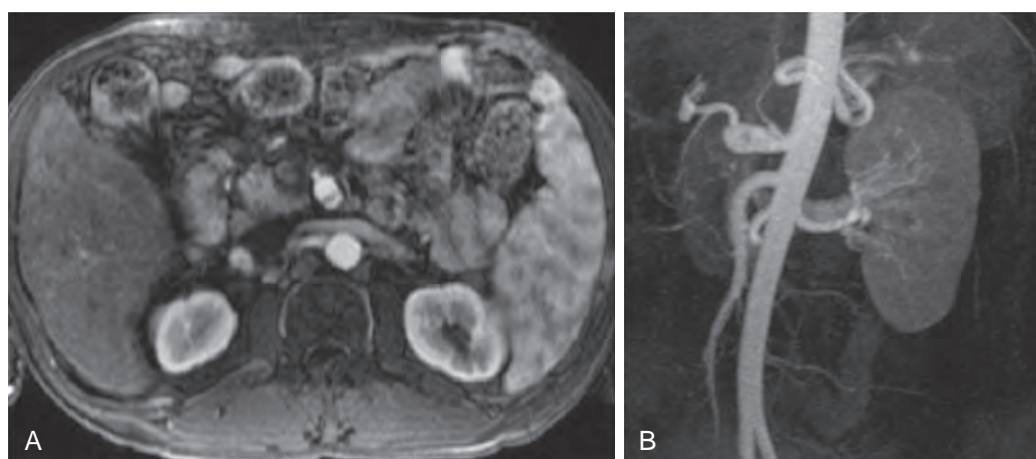


Figure 10-7 Celiac artery dissection. **A.** Axial spoiled gradient-echo postgadolinium MRI image demonstrates a dissecting flap within the celiac trunk. **B.** In a different patient, coronal thick MIP reconstruction from subtraction abdominal MRA with Ablavar demonstrates a celiac artery aneurysm with isolated celiac dissection.

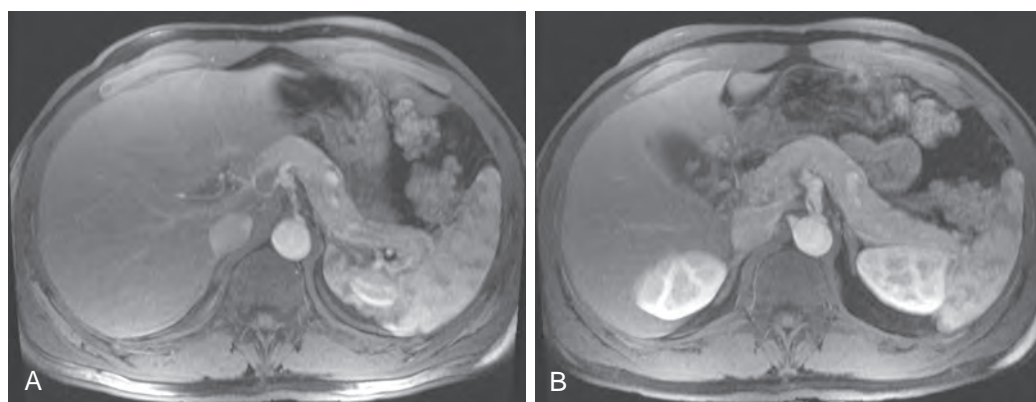


Figure 10-8 Segmental arterial mediolysis. Transaxial thin MIP postgadolinium spoiled gradient-echo images in this 51-year-old man demonstrated multifocal narrowing and beaded irregularity of the celiac axis (**A**), with aneurysmal dilation and dissection of the superior mesenteric artery (**B**).

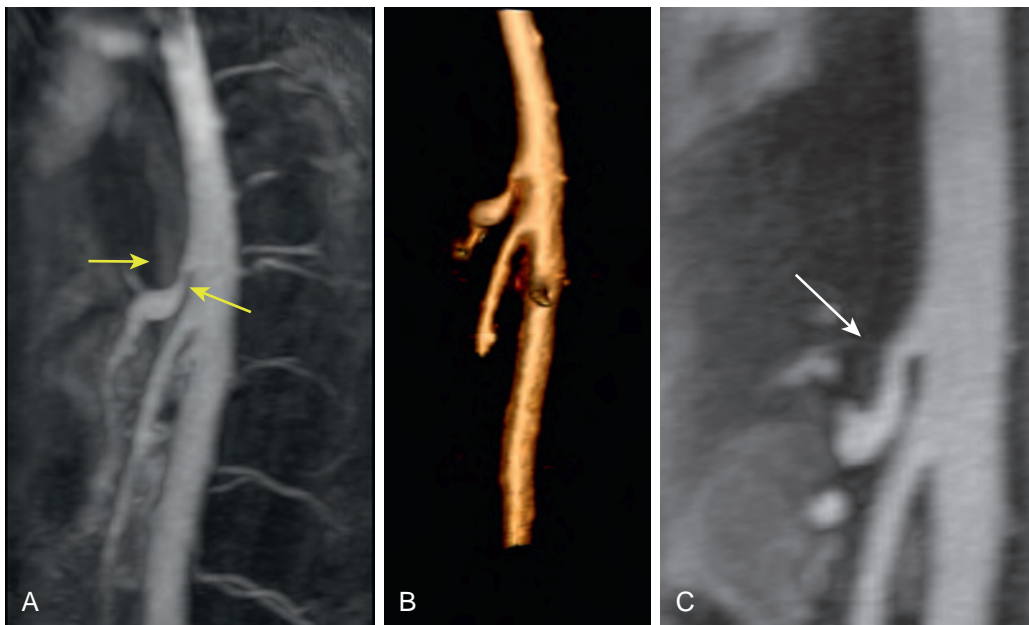


Figure 10-9 Median arcuate ligament syndrome. Sagittal MIP reconstruction of abdominal MRA (**A**) and surface-rendered sagittal reconstructions (**B**) in a 29-year-old man demonstrate external superior indentation with narrowing of the celiac trunk (anterior arrow) with poststenotic dilation caused by median arcuate ligament (posterior arrow) compression. **C.** Sagittal MIP reconstruction after median arcuate ligament release and reconstruction shows resolution of the celiac stenosis (arrow).



Figure 10-10 Portal hypertension with spontaneous splenorenal shunt. Full volumetric axial MIP image with 3D contrast-enhanced MR portography reveals a large portosystemic collateral pathway from the splenic to left renal vein, secondary to portal hypertension.

splanchnic arteries.^{34,35} The bowel remains viable but its blood supply is inadequate to support its metabolic and functional demands. The classic symptoms of CMI include postprandial abdominal pain, weight loss, and food avoidance.^{36,37} The diagnosis of CMI is made by a combination of appropriate clinical symptoms and the demonstration of significant stenosis in two or three of the three main mesenteric vessels.³⁷ Contrast-enhanced 3D MRA provides anatomic information similar to that of conventional angiography (Figs. 10-11 and 10-12). Its effectiveness in evaluation of mesenteric circulation has been well documented.³⁸⁻⁴⁰ A 100% sensitivity of CE 3D MRA to detect stenoses of the celiac artery (CA) and SMA was reported

in a prospective study of 125 patients.⁴⁰ Meaney and colleagues³⁸ reported a sensitivity of 100% and specificity of 87% in the overall detection of visceral artery stenosis. Unfortunately, its accuracy is lower in evaluation of the small peripheral branches. Shirkhoda and associates³⁹ found that correct assessment was obtained in 75% of first-order branching, 60% of second-order branching, and 50% of third-order branching vessels of the SMA.

Mesenteric circulation is often supported by extensive arterial collateral vessels that develop over time, because the occlusive process is gradual in onset. Thus, the significant stenosis of two or three of the major mesenteric vessels can be seen in patients who are completely asymptomatic.^{34,36} Many investigators⁵⁻⁷ have proposed MR flow quantification using cine phase contrast MRI for the diagnosis of CMI. It allows for the functional evaluation and quantification of mesenteric vascular flow, which can be measured separately in the main mesenteric arteries^{5,6} (CA, SMA, and inferior mesenteric artery [IMA]) or superior mesenteric vein.^{6,7} In healthy volunteers, there is an expected postprandial increase in mesenteric blood flow, whereas there is diminished postprandial flow augmentation in the diseased patient. The greatest difference in flow rates between normal and diseased patients is achieved when measurements are made 30 minutes postprandial.⁷

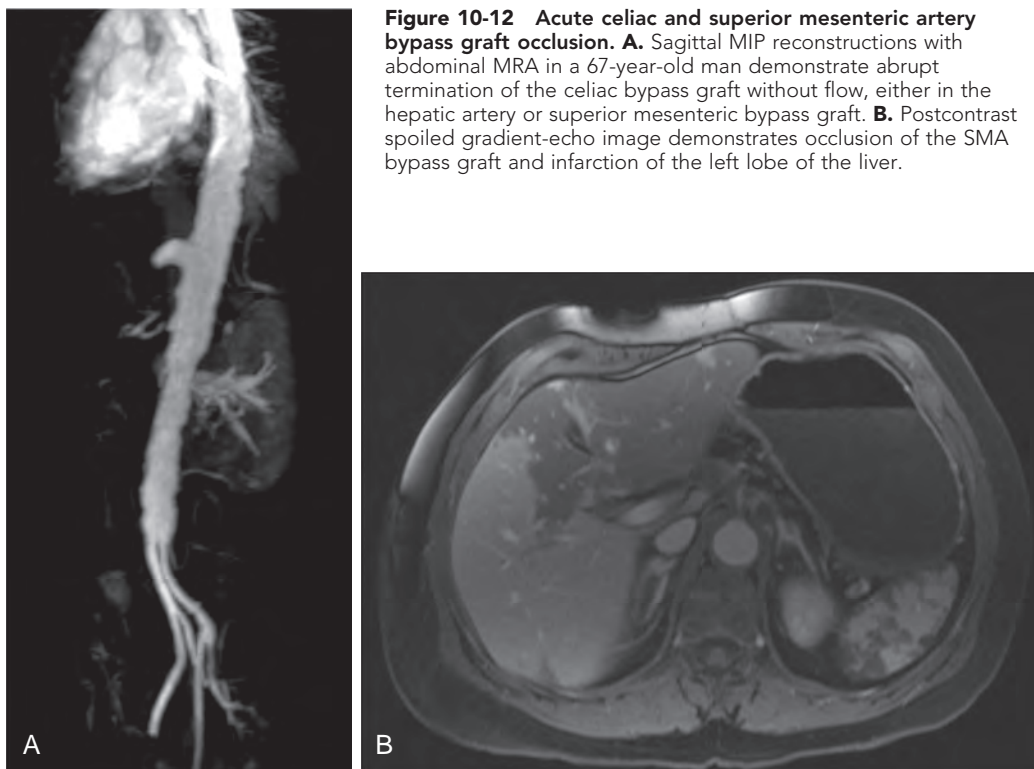
MEDIAN ARCUATE LIGAMENT SYNDROME

Median arcuate ligament syndrome (see Fig. 10-9) results from compression of the celiac artery by the median arcuate ligament and is a well-documented anatomic variant, seen in 12.5% to 49.7% of patients^{41,42} and resulting in intestinal angina in some cases.⁴³ The clinical symptoms include postprandial pain and an abdominal bruit on physical examination. The compression of the celiac axis varies with respiration. During inspiration, the aorta and celiac axis move downward with the abdominal viscera, whereas in expiration, the vessels move cephalad, resulting in maximal external compression. As a result, the MRA images obtained during end-expiration may accentuate the

Figure 10-11 Chronic mesenteric ischemia. Coronal (A) and sagittal (B) MIP reconstruction with abdominal MRA demonstrates atherosclerotic changes of the abdominal aorta and segmental occlusion at the origin of the superior mesenteric artery (arrow) in a 65-year-old man. Note that the distal part of the superior mesenteric artery is revascularized by collaterals arising from the left marginal artery (arrowhead).



Figure 10-12 Acute celiac and superior mesenteric artery bypass graft occlusion. A. Sagittal MIP reconstructions with abdominal MRA in a 67-year-old man demonstrate abrupt termination of the celiac bypass graft without flow, either in the hepatic artery or superior mesenteric bypass graft. B. Postcontrast spoiled gradient-echo image demonstrates occlusion of the SMA bypass graft and infarction of the left lobe of the liver.



celiac artery compression and can give rise to a potential interpretation pitfall. Thus, when median arcuate ligament syndrome is suspected on the basis of end-expiratory imaging, findings should be correlated with the clinical history and physical examination or confirmed with end-inspiration imaging. In general, MRA should be performed at end-inspiration in patients suspected of having intestinal ischemia.⁴⁴

SPLANCHNIC ARTERY DISSECTION

Splanchnic artery dissection (including the celiac axis, hepatic artery, SMA, and splenic artery) (see Fig. 10-7) can be

spontaneous and isolated,⁴⁵⁻⁴⁷ but most occur secondary to dissection of the aorta. The extension of aortic dissection into abdominal branch vessels can lead to visceral organ ischemia. There are two types of visceral artery involvement. More commonly, the intimal flap extends into the visceral artery, separating the vessel into two lumens, one of which is supplied by the true lumen and the other by the false lumen. In these cases, thrombosis of the false lumen or compression of the true lumen can lead to luminal compromise, resulting in ischemia and infarction. Less often, the branching arteries may be supplied exclusively by the false lumen. In these cases, compromise of vascular supply to the internal organs occurs less frequently.⁴⁸

VISCERAL ARTERY ANEURYSMS

Visceral artery aneurysms (see Fig. 10-4) are uncommon; nevertheless, they hold a high clinical significance because of their potential for rupture, resulting in life-threatening hemorrhage. Formerly, the most commonly affected vessel was believed to be the splenic artery.⁴⁹ However, an increasing incidence of hepatic artery pseudoaneurysms has recently been reported because of the increased use of percutaneous diagnostic and therapeutic procedures.⁵⁰ The other commonly affected vessels, in decreasing order, include the superior mesenteric, celiac, gastric, gastropiploic, ileocolic, and pancreatoduodenal arteries.^{50,51} When an aneurysm is thrombosed, it can be overlooked on MRA MIP images. This potential pitfall can be avoided by reviewing the MRA source images.

SEGMENTAL ARTERIAL MEDIOLYSIS

Segmental arterial mediolysis (SAM), initially described as segmental mediolytic arteritis,^{52,53} occurs because of mediolysis in the muscular arteries of the abdomen, with subsequent separation of the muscular layer from the adventitia. Radiologically, it manifests as arterial dilation, a single aneurysm or multiple aneurysms creating a string of beads, dissecting hematomas, arterial stenosis, and arterial occlusion (see Fig. 10-8), which occur segmentally in single or grouped abdominal arteries. Diagnosis is often made after a clinical presentation of intra-abdominal hemorrhage from an aneurysm rupture or as an incidental finding. It has been proposed that SAM is a precursor to fibromuscular dysplasia⁵⁵ because of its pattern of distribution, but there is no definitive evidence linking the two entities.⁵⁴

EVALUATION OF HEPATIC VASCULATURE

This is frequently requested for pre- and post-transplantation assessment and to evaluate for postprocedural complications (Fig. 10-13; see Fig. 10-10). Although basic anatomic variants and thrombus can be assessed with standard postcontrast spoiled gradient-echo imaging, MRA of the hepatic vasculature, including arteries, portal vein, and hepatic veins, is feasible and may provide additional information when unexpected pathology is encountered or for living donor pre-explantation evaluation. For this indication, the recipient and donor should be preoperatively evaluated for anatomic variations that might alter the surgical approach or exclude patients for whom surgery is not feasible. For example, in recipients, the small-caliber native hepatic artery increases the surgical complexity of creating a patent and durable anastomosis between the donor and recipient artery.⁵⁶ A stenosed celiac artery might precipitate post-transplantation ischemia and require an arterial bypass. A replaced or accessory left hepatic artery arising from a left gastric artery has to be ligated at its origin during removal of the native liver to prevent bleeding. CE MRA is also an excellent method for preoperative portal vein assessment (MR portography), including evaluation of portal hypertension, portosystemic shunts, portal vein thrombosis, and portal vein invasion by tumors.

For evaluation of living related liver donors, MRI can be used as the sole imaging technique for preoperative evaluation. Other than detection of liver lesions and biliary anomalies, MRA of the hepatic vasculature is needed to determine the patency and anatomy of the hepatic arteries, portal veins, and hepatic veins. Although not all vascular variants are surgically significant, there are some features that one should take into consideration

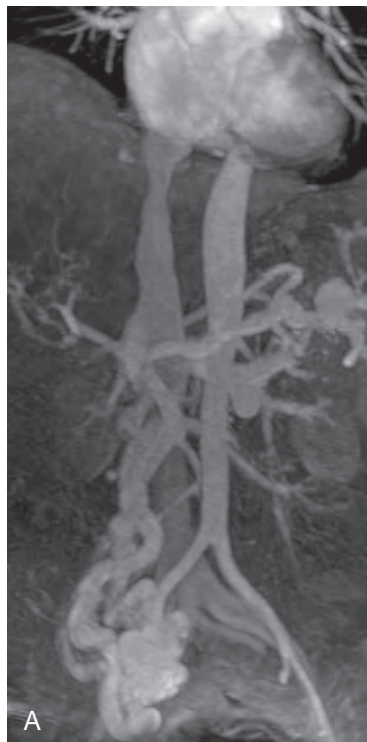
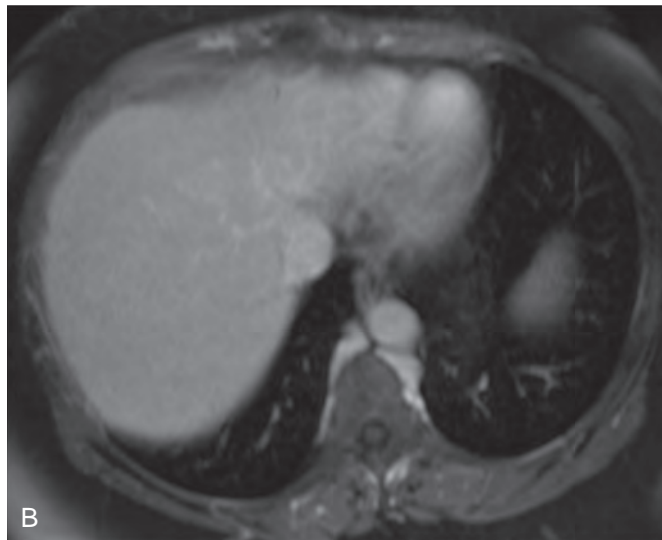


Figure 10-13 Budd Chiari syndrome and portosystemic shunts. A. Coronal MIP reconstructions from subtracted steady-state MRA with Ablavar demonstrate lack of visualization of the hepatic veins with a large superior mesenteric vein to gonadal vein varix in the setting of Budd Chiari syndrome. **B.** Axial 2D postgadolinium spoiled gradient-echo steady-state image through the liver shows absence of normal hepatic veins.



prior to surgery, especially in patients at risk for liver failure. For example, the origin and location of the artery supplying segment 4 (middle hepatic artery) of the liver should be identified preoperatively because it should be left intact in the donor to prevent parenchymal damage to the medial segment of the liver. Thus, if the middle hepatic artery arises from the right hepatic artery, this variant may not be important for an adult to child liver donor because only the lateral segment of the left lobe would be taken. On the other hand, in an adult to adult liver donor, for whom the right lobe of the liver would be taken out, the resection line typically crosses the arterial supply of segment 4, leading to ischemic damage of the residual liver. Similarly, for left lobe donors, the replaced left hepatic artery arising from the left gastric artery should be identified preoperatively. For portal venous variations, such as the trifurcation of portal veins into right anterior, right posterior, and left portal venous branches, is a surgically significant finding that has to be evaluated preoperatively before contemplating surgical resection. Hepatic venous anatomic variants such as accessory hepatic veins and the anatomy of the hepatic venous confluence should be evaluated preoperatively because accidental transection can result in bleeding and atrophy of the supplied hepatic segment.⁵⁷

MAGNETIC RESONANCE PORTOGRAPHY

This was formerly performed with nonenhanced MRA using TOF and phase contrast techniques (see Fig. 10-6). These techniques are primarily limited by long data acquisition time, motion, flow artifacts, and in-plane saturation effects. Alternatively, CE MR portography is excellent for the evaluation of the portal venous system and various pathologic conditions, such as portosystemic shunt, portal vein thrombosis, cavernous transformation, and tumor invasion of the portal vein (Fig. 10-14).⁵⁸ The principle of contrast-enhanced MR portography



Figure 10-14 Normal contrast-enhanced portal venography. Coronal subvolumetric MIP reconstruction of the 3D contrast-enhanced MR portography scan demonstrates normal opacification of the portal, splenic, and superior mesenteric veins.

is to image a high concentration of contrast material circulating in the portal venous system. Boeve and co-workers⁵⁹ found that optimal portal venous enhancement is mostly achieved at 30 seconds after maximum arterial enhancement. Practically, after gadolinium injection, three or four 3D MRA datasets are obtained. The first dataset acquired after contrast administration is usually an arterial phase, which can be used as a mask for image subtraction. Contrast-enhanced 3D MR portograms can then be created by reconstructing images of the portal phase (usually the second or third 3D dataset acquired after contrast administration) with MIP. A subtraction technique can be used to eliminate arterial enhancement when such enhancement conceals the portal venous anatomy.⁶⁰

The major limitation of CE MR portography is its inability to provide hemodynamic data regarding flow direction in the portal venous system. Portal venous flow direction can be assessed by using phase contrast MRA or 2D gradient-echo TOF sequences with a saturation band placed across the proximal aspect of the portal vein, with another saturation band placed transversely above the hepatic dome to eliminate signal within the hepatic artery. In normal hepatopetal flow, the distal portal vein beyond the first saturation band should lose the signal intensity. Bright signal intensity beyond the first saturation band indicates an abnormal hepatofugal flow.⁶¹

DISEASES OF THE INFERIOR VENA CAVA

Diseases of the IVC (see Fig. 10-6) and iliac veins can be evaluated with the 2D TOF technique with a superior traveling saturation band to suppress the arterial signal. Many prior studies⁶²⁻⁶⁵ have shown high accuracy and high sensitivity of TOF MRA for detecting thrombosis in the abdominal and pelvic vessels. 3D CE MR venography (MRV) is also a sensitive technique for evaluation of the IVC. The best delineation of venous structures is obtained by using a blood pool contrast agent and imaging during the steady state. This technique allows for higher spatial resolution images to evaluate for venous stenosis, webs, and neoplasms. Also, 3D data can be reconstructed into any desired plane to achieve the best anatomic delineation, especially when acquired as a 3D isotropic dataset.

Magnetic Resonance Angiography Pitfalls

MRA has several potential pitfalls. Some diagnostic problems are caused by improper scan technique. For example, inappropriate positioning of the imaging volume may produce false-positive occlusion of the vessels by elimination of structures from the imaging volume. Banding or ringing artifacts result from suboptimal timing when the center of k space data is acquired before the peak of contrast enhancement. This can result in a dark signal with the vessel and can mimic dissection or occlusion of the vessel. Some MRA pitfalls result from subtraction and reconstruction techniques. For example, the aneurysm with a mural thrombus may be misinterpreted as a normal vessel because MIP images only depict the opacified lumen. Also, MIP may cause overestimation or underestimation of stenosis because of partial volume effects or poor spatial resolution. Because MIP is generated by projecting only the pixel with the highest attenuation along a ray projected through

the dataset, the signal intensity within the volume-averaged pixels may simply be below the MIP threshold and may be erroneously excluded from the final image, resulting in an overestimation of the stenosis. Conversely, if the stenotic segment extends equally into two pixels, the signal intensity would be averaged over the two pixels, and each pixel would appear in the MIP image as part of the lumen, resulting in underestimation of the stenosis.^{66,67} Metallic artifacts from vascular stents and surgical clips may obscure the adjacent vascular structures and simulate stenosis. However, most MRA interpretation pitfalls can be avoided by cautiously reviewing the source images.

Summary

Evaluation of mesenteric vessel patency and flow dynamics can be achieved with high spatial and contrast resolution images using CE MRA techniques. In particular, time-resolved methods allow for the evaluation of hemodynamics similar to that seen on DSA. With the use of blood pool contrast, steady-state imaging for venous pathology and for high-resolution isotropic dataset acquisition can be carried out. Thus, MRA provides a noninvasive and nonionizing radiation method for the evaluation of the mesenteric vessels and, when performed in combination with anatomic sequences, also provides end-organ information.

REFERENCES

- Artioli D, Tagliabue M, Aseni P, et al: Detection of biliary and vascular anatomy in living liver donors: Value of gadobenate dimeglumine enhanced MR and MDCT angiography. *Eur J Radiol* 76:e1–e5, 2010.
- Bian J, Sha L, Yang C, et al: Three-dimensional dynamic contrast-enhanced MR angiography for evaluating recipient vessels in orthotopic liver transplantation. *Hepatobiliary Pancreat Dis Int* 7(5):476–480, 2008.
- Reference deleted in proofs.
- Bian J, Sha L, Yang C, et al: Three-dimensional dynamic contrast-enhanced MR angiography for evaluating recipient vessels in orthotopic liver transplantation. *Hepatobiliary Pancreat Dis Int* 7:476–480, 2008.
- Burkart DJ, Johnson CD, Reading CC, et al: MR measurements of mesenteric venous flow: Prospective evaluation in healthy volunteers and patients with suspected chronic mesenteric ischemia. *Radiology* 194:801–806, 1995.
- Shih MC, Hagspiel KD: CTA and MRA in mesenteric ischemia: Part 1. Role in diagnosis and differential diagnosis. *AJR* 188:452–461, 2007.
- Li KC, Whitney WS, McDonnell CH, et al: Chronic mesenteric ischemia: Evaluation with phase-contrast cine-MR imaging. *Radiology* 190:175–179, 1994.
- Scheffler K, Lehnhardt S: Principles and applications of balanced SSFP techniques. *Eur Radiol* 13:2409–2418, 2003.
- Edelman RR, Sheehan JJ, Dunkle E, et al: Quiescent-interval single-shot unenhanced magnetic resonance angiography of peripheral vascular disease: Technical considerations and clinical feasibility. *Magn Reson Med* 63:951–958, 2010.
- Strouse PJ, Prince MR, Chenevert TL: Effect of the rate of gadopentetate dimeglumine administration on abdominal vascular and soft-tissue MR imaging enhancement patterns. *Radiology* 201:809–816, 1996.
- Mitsuzaki K, Yamashita Y, Ogata I, et al: Optimal protocol for injection of contrast material at MR angiography: Study of healthy volunteers. *Radiology* 213:913–918, 1999.
- Prince MR, Yucel EK, Kaufman JA, et al: Dynamic gadolinium-enhanced three-dimensional abdominal MR arteriography. *J Magn Reson Imaging* 3:877–881, 1993.
- Angeretti M, Lumia D, Cani A, et al: Non-enhanced MR angiography of renal arteries: Comparison with contrast-enhanced MR angiography. *Acta Radiol* 54:749–756, 2013.
- Suh GY, Choi G, Draney MT, et al: Respiratory-induced 3D deformations of the renal arteries quantified with geometric modeling during inspiration and expiration breath-holds of magnetic resonance angiography. *J Magn Reson Imaging* 38:1325–1332, 2013.
- Shetty AN, Bis KG, Vrachliotis TG, et al: Contrast-enhanced 3D MRA with centric ordering in k space: A preliminary clinical experience in imaging the abdominal aorta and renal and peripheral arterial vasculature. *J Magn Reson Imaging* 8:603–615, 1998.
- Prince MR, Grist TM, Debatin JF: 3D Contrast MR angiography, ed 2, Berlin, 1999, Springer-Verlag.
- Thurnher SA, Capelastegui A, Del Olmo FH, et al: Safety and effectiveness of single- versus triple-dose gadodiamide injection-enhanced MR angiography of the abdomen: A phase III double-blind multicenter study. *Radiology* 219:137–146, 2001.
- Krinsky GA, Reuss PM, Lee VS, et al: Thoracic aorta: Comparison of single-dose breath-hold and double-dose non-breath-hold gadolinium-enhanced three-dimensional MR angiography. *AJR* 173:145–150, 1999.
- Marckmann P, Skov L, Rossen K, et al: Nephrogenic systemic fibrosis: Suspected causative role of gadodiamide used for contrast-enhanced magnetic resonance imaging. *J Am Soc Nephrol* 17:2359–2362, 2006.
- Maki JH, Chenevert TL, Prince MR: Contrast-enhanced MR angiography. *Abdom Imaging* 23:469–484, 1998.
- Foo TK, Saranathan M, Prince MR, Chenevert TL: Automated detection of bolus arrival and initiation of data acquisition in fast, three-dimensional, gadolinium-enhanced MR angiography. *Radiology* 203:275–280, 1997.
- Riederer SJ, Bernstein MA, Breen JE, et al: Three-dimensional contrast-enhanced MR angiography with real-time fluoroscopic triggering: Design specifications and technical reliability in 330 patient studies. *Radiology* 215:584–593, 2000.
- Korosec FR, Frayne R, Grist TM, Mistretta CA: Time-resolved contrast-enhanced 3D MR angiography. *Magn Reson Med* 36:345–351, 1996.
- Pinto C, Hickey R, Carroll TJ, et al: Time-resolved MR angiography with generalized autocalibrating partially parallel acquisition and time-resolved echo-sharing angiographic technique for hemodialysis arteriovenous fistulas and grafts. *J Vasc Interv Radiol* 17:1003–1009, 2006.
- Ayache JB, Collins JD: MR angiography of the abdomen and pelvis. *Radiol Clin North Am* 52:839–859, 2014.
- Lauffer RB, Parmelee DJ, Dunham SU, et al: MS-325: Albumin-targeted contrast agent for MR angiography. *Radiology* 207:529–538, 1998.
- Parmelee DJ, Walovitch RC, Ouellet JS, Lauffer RB: Preclinical evaluation of the pharmacokinetics, biodistribution, and elimination of MS-325, a blood pool agent for magnetic resonance imaging. *Invest Radiol* 32:741–747, 1997.
- Grist TM, Korosec FR, Peters DC, et al: Steady-state and dynamic MR angiography with MS-325: Initial experience in humans. *Radiology* 207:539–544, 1998.
- Keese M, Schmitz-Rixen T, Schmandra T: Chronic mesenteric ischemia: Time to remember open revascularization. *World J Gastroenterol* 19:1333–1337, 2013.
- Saloner D: MRA: Principles and display. In Higgins CB, Hricak J, Jelms CA, editors: *Magnetic Resonance Imaging of the Body*, Philadelphia, 1997, Lippincott-Raven, pp 1345–1368.
- Pecoraro F, Rancic Z, Lachat M, et al: Chronic mesenteric ischemia: Critical review and guidelines for management. *Ann Vasc Surg* 27:113–122, 2013.
- Upponi S, Harvey JJ, Uberoi R, et al: The role of radiology in the diagnosis and treatment of mesenteric ischaemia. *Postgrad Med J* 89:165–172, 2013.
- Sharafuddin MJ, Stolpen AH, Dang YM, et al: Comparison of MS-325 and gadodiamide-enhanced MR venography of ilioacaval veins. *J Vasc Interv Radiol* 13:1021–1027, 2002.
- Weber DG, Bendinelli C, Balogh ZJ: Damage control for abdominal emergencies. *Br J Surg* 101:e109–e118, 2014.
- Hagspiel KD, Leung DA, Angle JF, et al: MR angiography of the mesenteric vasculature. *Radiol Clin North Am* 40:867–886, 2002.
- Pecoraro F, Rancic Z, Lachat M, et al: Chronic mesenteric ischemia: Critical review and guidelines for management. *Ann Vasc Surg* 27:113–122, 2013.
- Upponi S, Harvey JJ, Uberoi R, et al: The role of radiology in the diagnosis and treatment of mesenteric ischaemia. *Postgrad Med J* 89:165–172, 2013.
- Meaney JFM, Prince MR, Nostrand TT, et al: Gadolinium-enhanced magnetic resonance angiography in patients with suspected chronic mesenteric ischemia. *J Magn Reson Imaging* 7:171–176, 1997.
- Shirkhoda A, Konez O, Shetty AN, et al: Mesenteric circulation: Three-dimensional MR angiography with a gadolinium-enhanced multiecho gradient-echo technique. *Radiology* 202:257–261, 1997.
- Gaa J, Laub G, Edelmann RR, et al: First clinical results of ultrafast, contrast-enhanced 2-phase

- 3D magnetic resonance angiography technique for imaging visceral abdominal arteries and veins. *Invest Radiol* 35:111–117, 2000.
41. Balderi A, Antonietti A, Pedrazzini F, et al: Treatment of visceral aneurysm using multilayer stent: Two-year follow-up results in five consecutive patients. *Cardiovasc Intervent Radiol* 36:1256–1261, 2013.
 42. Bron KM, Redman HC: Splanchnic artery stenosis and occlusion: Incidence, arteriographic and clinical manifestations. *Radiology* 92:323–328, 1969.
 43. Jimenez JC, Harlander-Locke M, Dutson EP: Open and laparoscopic treatment of median arcuate ligament syndrome. *J Vasc Surg* 56:869–873, 2012.
 44. Lee VS, Morgan JN, Tan AG, et al: Celiac artery compression by the median arcuate ligament: A pitfall of end-expiratory MR imaging. *Radiology* 228:437–442, 2003.
 45. Gehlen JM, Heeren PA, Verhagen PF, et al: Visceral artery aneurysms. *Vasc Endovascular Surg* 45:681–687, 2011.
 46. Balderi A, Antonietti A, Pedrazzini F, et al: Treatment of visceral aneurysm using multilayer stent: Two-year follow-up results in five consecutive patients. *Cardiovasc Intervent Radiol* 36:1256–1261, 2013.
 47. Takeda J, Matsunaga N, Sakamoto I: Spontaneous dissection of the celiac and hepatic arteries treated by transcatheter embolisation. *AJR* 165: 1288–1289, 1995.
 48. Laissy JP, Trillaud J, Douek P: MR angiography: Noninvasive vascular imaging of the abdomen. *Abdom Imaging* 27:488–506, 2002.
 49. Song Q, Zeng M, Chen C, et al: Non-contrast-enhanced magnetic resonance angiography using T2-weighted 3-dimensional fat-suppressed turbo spin echo (SPACE): Diagnostic performance and comparison with contrast-enhanced magnetic resonance angiography using volume interpolated breath-hold examination in the detection of portosystemic and portohepatic collaterals. *J Comput Assist Tomogr* 36:675–680, 2012.
 50. Cron DC, Coleman DM, Sheetz KH, et al: Aneurysm in abdominal organ transplant recipients. *J Vasc Surg* 59:594–598, 2014.
 51. Shimada K, Isoda H, Okada T, et al: Unenhanced MR portography with a half-Fourier fast spin-echo sequence and time-space labeling inversion pulses: Preliminary results. *AJR* 193: 106–112, 2009.
 52. Horsley-Silva JL, Ngamruenphong S, Frey GT, et al: Segmental arterial mediolysis: A case of mistaken hemorrhagic pancreatitis and review of the literature. *JOP* 15:72–77, 2014.
 53. Pillai AK, Iqbal SI, Liu RW, et al: Segmental arterial mediolysis. *Cardiovasc Intervent Radiol* 37:604–612, 2014.
 54. Huang SY, Kim CY, Miller MJ, et al: Abdominopelvic and lower extremity deep venous thrombosis: Evaluation with contrast-enhanced MR venography with a blood-pool agent. *AJR* 201: 208–214, 2013.
 55. Mu X, Wang H, Ma Q, et al: Contrast-enhanced magnetic resonance angiography for the preoperative evaluation of hepatic vascular anatomy in living liver donors: A meta-analysis. *Acad Radiol* 21:743–749, 2014.
 56. Ishigami K, Zhang Y, Rayhill S, et al: Does variant hepatic artery anatomy in a liver transplant recipient increase the risk of hepatic artery complications after transplantation? *AJR* 183: 1577–1584, 2004.
 57. Sahani D, Souza RD, Kadavigere R, et al: Evaluation of living liver transplant donors: Method for precise anatomic definition by using a dedicated contrast-enhanced MR imaging protocol. *Radiographics* 24:957–967, 2004.
 58. Turgutalp K, Kiykim A, Özhan O, et al: Comparison of diagnostic accuracy of Doppler USG and contrast-enhanced magnetic resonance angiography and selective renal arteriography in patients with atherosclerotic renal artery stenosis. *Med Sci Monit* 19:475–482, 2013.
 59. Boeve WJ, Sluiter WJ, Kamman RL: Optimization of scantiming in abdominal breath-hold contrast-enhanced MRA: An empirical guideline. *Magn Reson Imaging* 19:193–200, 2001.
 60. Hwang J, Kim YK, Lee WJ, et al: Unenhanced magnetic resonance portography using repetitive arterial or vein labeling method at 3.0-T. *J Comput Assist Tomogr* 37:856–861, 2013.
 61. Leyendecker JR, Brown JJ: *Practical Guide to Abdominal and Pelvic MRI*, Philadelphia, 2004, Lippincott Williams & Wilkins.
 62. Laissy JP, Cinqualbre A, Loshkajian A, et al: Assessment of deep venous thrombosis in the lower limbs and pelvis: MR venography versus duplex Doppler sonography. *AJR* 167:971–975, 1996.
 63. Huang SY, Kim CY, Miller MJ, et al: Abdominopelvic and lower extremity deep venous thrombosis: Evaluation with contrast-enhanced MR venography with a blood-pool agent. *AJR Am J Roentgenol* 201:208–214, 2013.
 64. Evans JA, Sostman HD, Knelson MH: Detection of deep venous thrombosis. Prospective comparison of MR imaging with contrast venography. *AJR* 161:131–135, 1993.
 65. Salvador SJ, Ottero RR, Salvador BL: Puerperal ovarian vein thrombosis: evaluation with CT US and MR imaging. *Radiology* 167:637–639, 1988.
 66. Turski P: Sources of variability in measuring carotid stenosis on time-resolved contrast-enhanced MR angiograms. *AJNR Am J Neuroradiol* 23:178–179, 2002.
 67. Turgutalp K, Kiykim A, Özhan O, et al: Comparison of diagnostic accuracy of Doppler USG and contrast-enhanced magnetic resonance angiography and selective renal arteriography in patients with atherosclerotic renal artery stenosis. *Med Sci Monit* 19:475–482, 2013.

SECTION

II

Abdominal Plain Images

Abdomen: Normal Anatomy and Examination Techniques

WILLIAM MOREAU THOMPSON

CHAPTER OUTLINE

Technique

Standard Projections

Supplemental Projections

Normal Anatomy

Peritoneal Cavity

Retroperitoneum and Abdominal Wall

Pelvis

From the 1970s to 1990s, the abdominal radiograph traditionally served as the initial radiologic means of evaluating patients with suspected abdominal pathology. During the past two decades, however, computed tomography (CT) has become the major imaging procedure in patients with suspected acute abdominal pathology.¹⁻³ When abdominal radiography was performed as a screening test, the diagnostic yield of this examination was low and most abnormalities that were detected were nonspecific.⁴⁻⁶ In a review of 1780 screening abdominal radiographs, important abnormalities were found in only 10% of cases.⁵ No clinically significant disease would have been missed if abdominal radiographs had been obtained only in patients with a strong clinical suspicion of disease and/or moderate to severe abdominal symptoms. Abdominal radiographs have the greatest value in patients in whom bowel obstruction or perforation, urinary calculi, or bowel ischemia is suggested on clinical grounds.^{2,3,7-9} In patients with mild or nonspecific symptoms, however, abdominal radiographs have a low diagnostic yield. The major value of a normal abdominal series is the exclusion of bowel obstruction or free air secondary to bowel perforation.⁷⁻⁹ Despite the increasing use of CT and the declining role of abdominal radiography, this examination is still performed in many patients, especially those who have undergone recent surgery and those who have some form of catheter, tube, or drain in the abdomen. Emergency department physicians may also order abdominal radiographs in patients with a low clinical suspicion of disease to ensure that a major abdominal disorder is not overlooked and to calm a concerned patient.

Technique

STANDARD PROJECTIONS

An anteroposterior radiograph taken with the patient in a supine position is the most common plain film examination of the abdomen (Fig. 11-1). Whether one uses conventional film or digital techniques, the patient should be positioned

comfortably on his or her back, without rotation of the pelvis. Maximal relaxation of the abdominal musculature is important in reducing artifact caused by motion; this is facilitated by supporting and slightly flexing the patient's knees. The film or field of view for digital imaging should be positioned with its lower edge at the symphysis pubis and the x-ray beam centered at the iliac crest. Both the lung bases and symphysis pubis should be included on the radiograph. The exposure is made during expiration and should begin 1 to 2 seconds after respiration is suspended.¹⁰

Delineation of intra-abdominal soft tissues on abdominal radiographs depends on the inherent contrast provided by soft tissues, fat, and intraluminal gas. Subject contrast on the radiograph is caused by differential attenuation of the x-ray beam in the patient.¹¹ Most abdominal radiographs are taken using routine equipment exposed at a low kilovoltage (60-75 kV), depending on the size of the patient.¹⁰ A short exposure time is desirable to avoid motion unsharpness. Also, an increase in peak kilovoltage increases scattered radiation, which degrades soft tissue contrast. Thus, the lowest possible peak kilovoltage that can penetrate the patient and has an acceptable exposure time should be used. With conventional films, a reciprocating (Potter-Bucky) grid and careful collimation are used to reduce scatter.¹⁰ In males with reproductive potential, gonadal shielding should be used if the gonads lie within 5 cm of the primary beam and if such shielding does not compromise the clinical objectives of the examination.

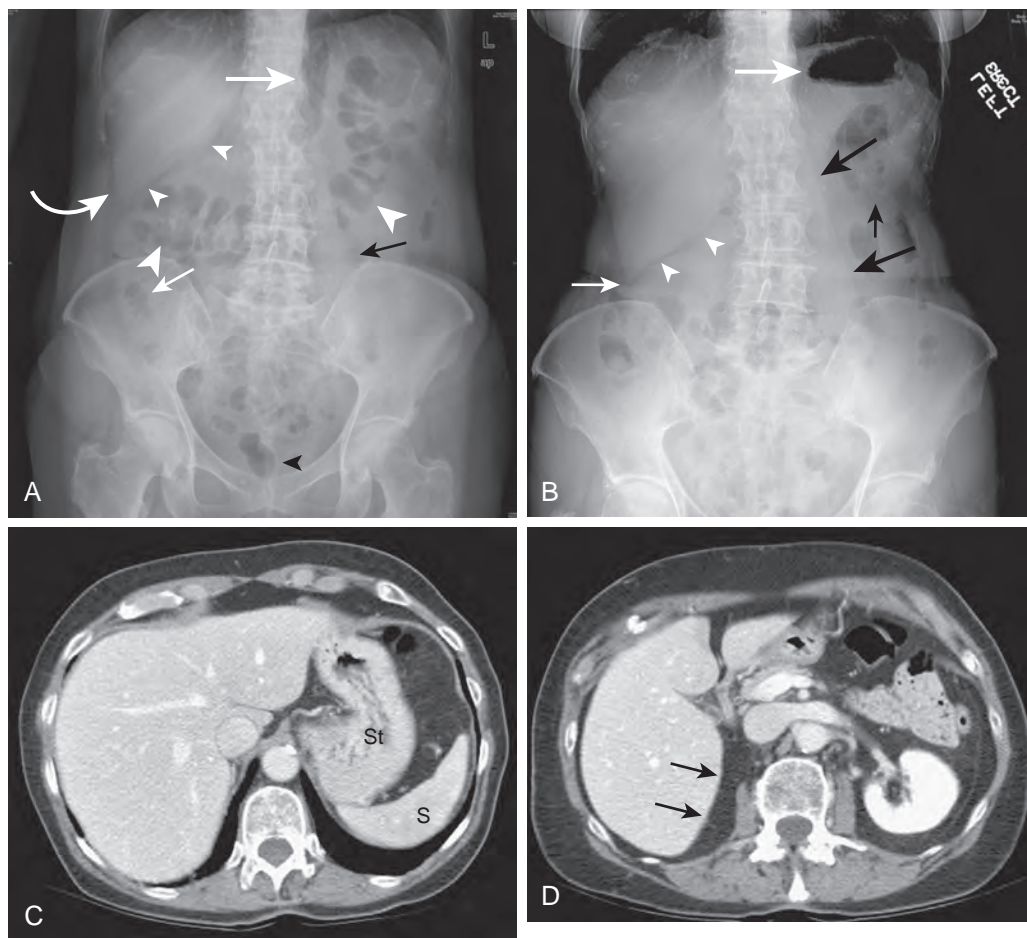
Portable abdominal radiographs may be obtained in hospitalized, extremely ill patients; however, these radiographs are usually of lower quality than standard abdominal radiographs obtained in the radiology department. Such patients are usually too ill to breath-hold, and most portable x-ray units have fixed milliamperage settings, which may necessitate using techniques of higher peak kilovoltage, resulting in reduced contrast. In addition, a stationary grid, rather than a Potter-Bucky grid, must be used to control scatter, and when these grids are poorly positioned, the image may be degraded secondary to grid cutoff. Whenever possible, abdominal radiographs should therefore be obtained using standard x-ray equipment in the radiology department.

SUPPLEMENTAL PROJECTIONS

In addition to the standard anteroposterior supine view, other projections may help in specific clinical situations and are frequently used as part of a routine abdominal series. In patients with abdominal pain, upright posteroanterior abdominal or chest radiographs may be useful to facilitate detection of small amounts of free intraperitoneal air, small bowel obstruction, and unsuspected thoracic disease that is causing abdominal pain (Fig. 11-2; see Fig. 11-1B).

Figure 11-1 Normal supine and upright abdominal radiographs.

A. Supine abdominal radiograph shows a normal bowel gas pattern with gas in the stomach (large white arrow), small bowel (small white arrow), colon (large white arrowheads), and rectum (black arrowhead). The hepatic angle (curved white arrow) is outlined by extraperitoneal fat, and the posteromedial surface of the right lobe of the liver is outlined by perirenal fat (small white arrowheads). The left psoas muscle (black arrow) is also seen. **B.** Upright abdominal radiograph shows a normal air-fluid level in the stomach (large white arrow). Note the hepatic angle (small white arrow), posteromedial surface of the right lobe of the liver (arrowheads), left psoas muscle (large black arrows), and splenic tip (small black arrow). **C.** Axial CT scan of the upper abdomen shows fat outlining the wall of the stomach (St) and spleen (S). **D.** Another more caudad axial CT scan shows the posteromedial surface of the right lobe of the liver outlined by perirenal fat (arrows).



An upright abdominal radiograph is often ordered on a routine basis, but some authors believe that it does not contribute significant information in many patients. Mirvis and colleagues reviewed the emergency department radiographs of 252 patients, which included supine and upright abdominal radiographs and upright chest radiographs.⁶ The upright abdominal radiographs did not contribute to the treatment of any patients with acute abdominal conditions in their series. The authors concluded that this view could be omitted to reduce the time and cost of the examination without sacrificing important diagnostic information. However, upright abdominal radiographs may be helpful in patients with suspected bowel obstruction who have a gasless abdomen on supine radiographs to assess the appearance of gas and fluid in the small bowel further (see Fig. 11-2A and B). Alternatively, this information could be obtained on abdominal radiographs taken with the patient in the lateral decubitus position. For extremely ill patients who cannot stand easily, a lateral decubitus view may be more helpful than a suboptimal upright radiograph.

Miller and Nelson showed that when a perforated viscus is suspected on clinical grounds, a specific sequence of exposures is most likely to demonstrate extraluminal gas.¹² They recommended that the patient be placed in the left side down position for at least 10 minutes before a left lateral decubitus view is obtained. This allows gas to rise and accumulate over the right margin of the liver and, occasionally, beneath the iliac crest. If the patient is unable to stand, an abdominal radiograph should

be obtained with the patient in the left lateral decubitus position with a horizontal beam, using a short exposure technique. This results in underpenetration of the abdominal viscera but good visualization of extra-alimentary gas between the non-dependent lateral abdominal wall and liver (Fig. 11-3). If the patient is able to stand, the table is tilted upright and an upright posteroanterior chest radiograph is obtained. In one study, lateral chest radiographs were found to be superior to frontal radiographs in detecting subtle pneumoperitoneum.¹³ Radiographs of the abdomen in upright and supine positions are also obtained to complete the so-called perforation series (see Fig. 11-2C and D).¹⁴ Even tiny amounts of free air can be detected with use of the proper technique (see Fig. 11-2E). Some authors have reported that upright posteroanterior chest radiographs are more sensitive for detecting pneumoperitoneum than upright abdominal radiographs.¹² This difference in sensitivity probably occurs because the x-ray beam is centered at the iliac crest on abdominal radiographs, so that it penetrates air beneath the diaphragm obliquely rather than tangentially, making small gas collections more difficult to detect. The higher exposure techniques required to penetrate the abdomen also result in excessive penetration at the lung interface, sometimes obscuring small collections of free intraperitoneal air. Nevertheless, most experts believe that upright and supine abdominal radiographs are a useful part of the abdominal series for detecting intra-abdominal disease in these patients.^{14,15}

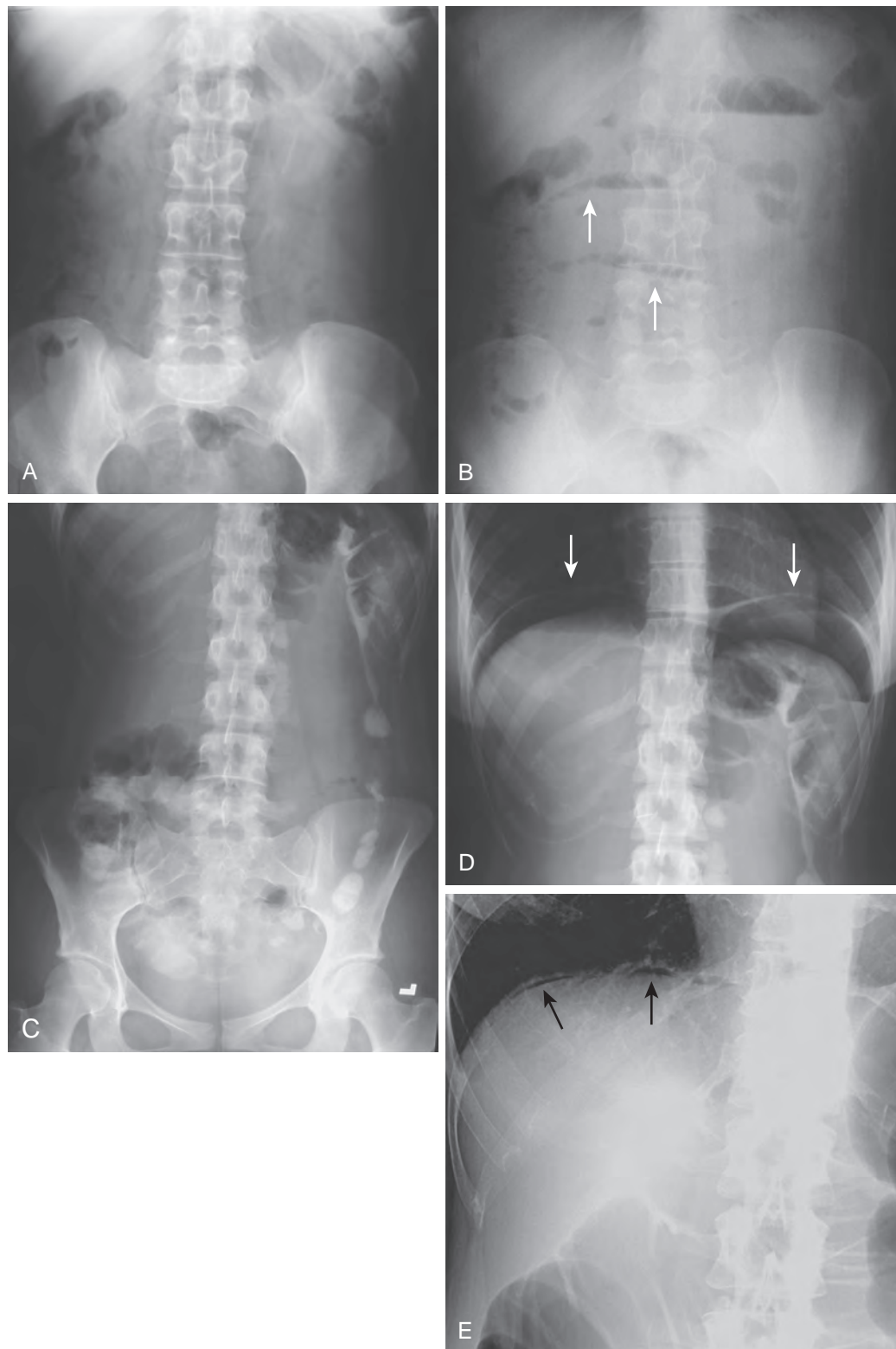
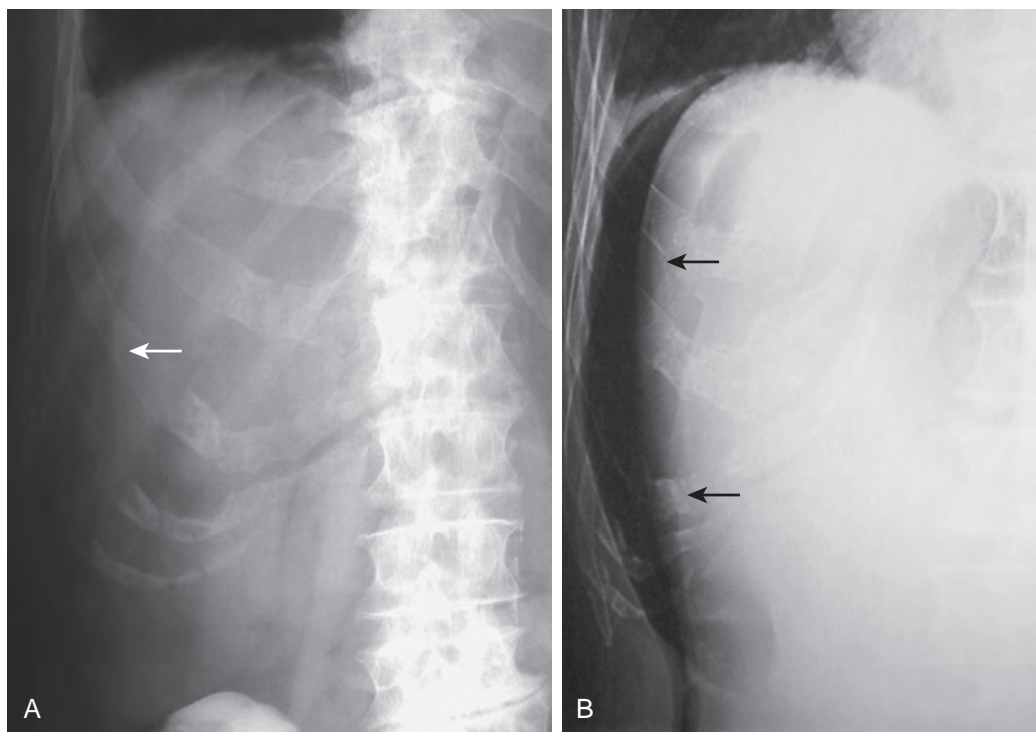


Figure 11-2 Value of upright abdominal radiograph in patients with small bowel obstruction or intestinal perforation. **A.** Supine abdominal radiograph shows a relatively gasless abdomen in a patient with signs and symptoms of intestinal obstruction. **B.** Upright radiograph shows multiple tiny air-fluid levels (arrows) caused by fluid-filled loops of dilated small bowel with trapping of air superiorly in these loops (producing the string of pearls sign). The patient was found at surgery to have a closed loop small bowel obstruction due to adhesions. **C.** Supine abdominal radiograph in another patient with abdominal pain shows no evidence of pneumoperitoneum. Note residual contrast material in the colon from a prior study. **D.** Upright abdominal radiograph in the same patient as in **C** shows a large amount of free intraperitoneal air (arrows) beneath both hemidiaphragms. **E.** Upright radiograph in another patient shows a tiny amount of free air (arrows) between the liver and right hemidiaphragm.

Figure 11-3 Value of left lateral decubitus radiograph of the abdomen in a patient with pneumoperitoneum.
A. Coned-down view of the right upper quadrant from a supine abdominal radiograph shows a vague radiolucency in the right lateral portion of the abdomen (arrow) but no definite free intraperitoneal air. **B.** Coned-down view of the right upper quadrant from a left lateral decubitus radiograph shows obvious free intraperitoneal air (arrows) between the liver and right lateral abdominal wall.



Additional projections such as prone, oblique, lateral, or coned views may be helpful in some clinical situations for better defining and localizing mass lesions, calcifications, or hernias. When distal colonic obstruction is suspected, prone abdominal radiographs are more helpful than supine radiographs because colonic gas occupies the more anterior transverse and sigmoid segments of the colon with the patient in the supine position (Fig. 11-4A, C, and D). As a result, a distal colonic obstruction may be difficult to distinguish from an ileus or pseudo-obstruction on supine and upright views of the abdomen. In this situation, a prone radiograph (Fig. 11-4B) or right lateral decubitus radiograph (Fig. 11-4E) may be useful because abdominal radiographs in these positions allow gas to fill the rectosigmoid colon if no mechanical obstruction is present.¹⁶

Normal Anatomy

Abdominal soft tissue planes and visceral surfaces are visible on abdominal radiographs because of the natural contrast created by surrounding fat. The best visualized interfaces are those that are smoothly margined and oriented in a sagittal or transverse plane tangential to the incident x-ray beam. Familiarity with the location of abdominal organs and the most commonly visualized tissue planes is helpful for identifying normal anatomic structures and recognizing and localizing pathologic processes.

PERITONEAL CAVITY

Liver

In the normal adult, the liver occupies the right upper quadrant of the abdomen. It measures 20 to 22 cm in its greatest transverse dimension and 15 to 17 cm in its greatest vertical

dimension near its right lateral border.¹⁷ There is considerable variation in the normal shape of the liver.¹⁸ With its most cephalad portion lying just beneath the dome of the right hemidiaphragm, the superior aspect of the liver is commonly S-shaped or concave. The inferior edge is usually triangular, with its apex directed caudad toward the right lower quadrant. Between 4% and 14% of the population has a prominent inferior extension of the right lower lobe, also known as *Riedel's lobe*. This lobe usually extends caudally below the iliac crest and does not by itself indicate hepatomegaly.

Although intraperitoneal fat is not always present around the liver, the right inferior edge of the liver (hepatic angle) is often visible on abdominal radiographs because it indents the extra-peritoneal fat in the parietal peritoneum (Fig. 11-5; see Fig. 11-1).¹⁸ This fat consists of posterior pararenal fat laterally and perirenal fat medially. The perirenal fat may outline not only the medial aspect of the hepatic angle but also the more cephalad portion of the posteromedial surface of the right lobe of the liver (see Fig. 11-1A). The hepatic angle may be obscured by effusions or blood that infiltrate the retroperitoneal fat or by ascites that displaces the liver edge away from the adjacent fat (Fig. 11-6).¹⁹ The posterior edge of the liver is visible on abdominal radiographs (see Fig. 11-1), whereas the anterior and left lateral margins of the liver are not. Because it is the anterior margin of an enlarged liver that is palpated on physical examination, a discrepancy may arise between clinical and radiographic measurements of the liver. On abdominal radiographs, hepatomegaly may be diagnosed by elevation of the right hemidiaphragm, visualization of the entire liver (not just a Riedel's lobe) extending into the lower abdomen, inferior displacement of the hepatic flexure of the colon, and lateral displacement of the lesser curvature of the stomach by an enlarged left lobe of the liver.²⁰

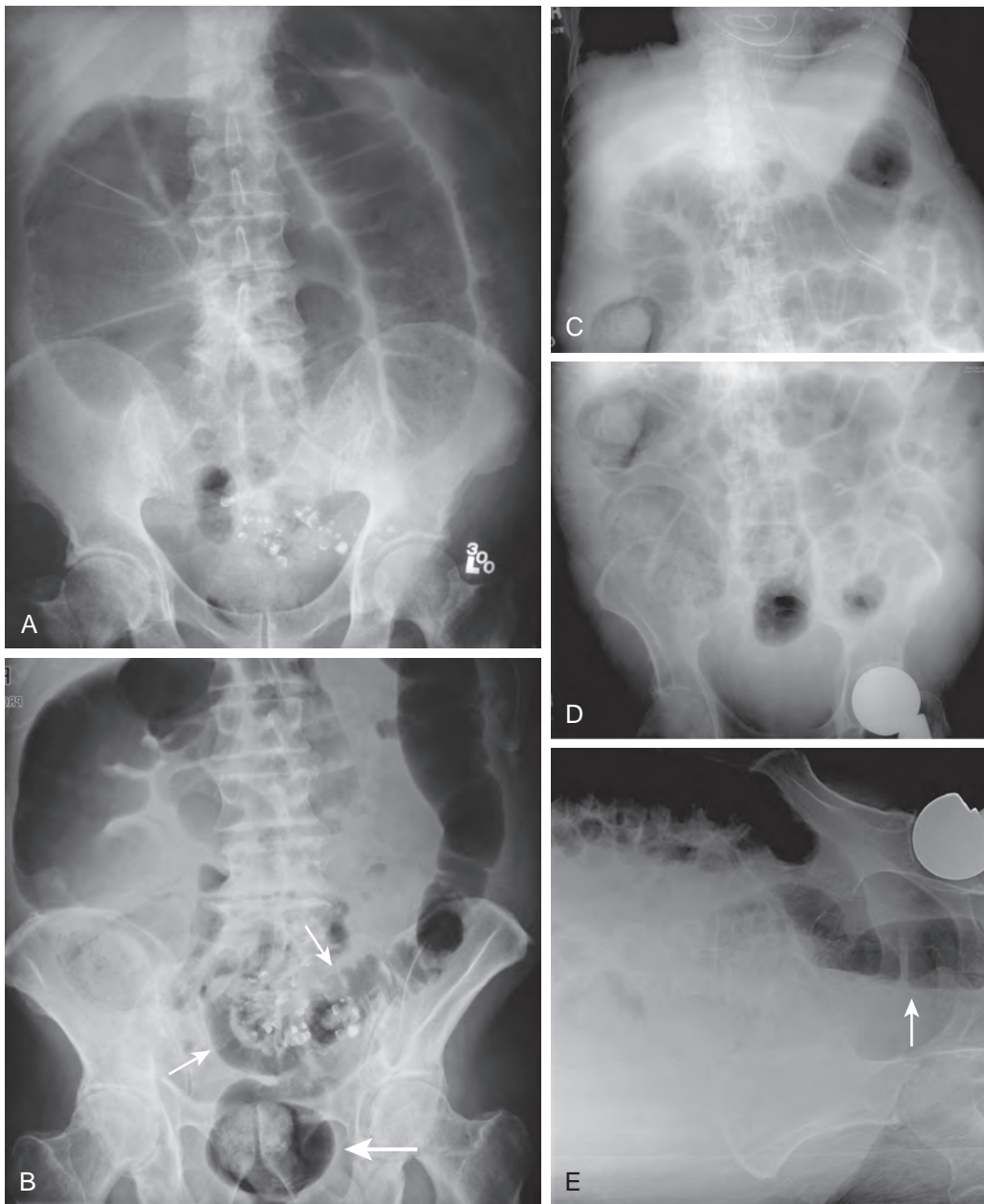


Figure 11-4 Value of prone and right lateral decubitus abdominal radiographs in patients with suspected colonic obstruction. **A.** Supine abdominal radiograph shows dilated colon to the level of the sigmoid with some stool but a paucity of gas in the rectum. Note residual barium in sigmoid diverticula. **B.** Prone abdominal radiograph in the same patient as in **A** shows gas in the sigmoid colon (small arrows) and rectum (large arrow), confirming that the patient does not have a distal colonic obstruction. **C, D.** Supine abdominal radiographs in another patient with abdominal distention show marked colonic dilation, with a paucity of gas in the rectum. **E.** Right lateral decubitus radiograph in the same patient as in **C** and **D** shows gas in the rectum (arrow), confirming that the patient does not have a distal colonic obstruction.

Gallbladder

The gallbladder occupies a shallow fossa on the inferior surface of the liver between the right and left lobes and is not usually visualized on abdominal radiographs.¹⁷ The gallbladder lies superior and lateral to the duodenal bulb and gastric antrum and superior to the proximal transverse colon. Occasionally, the fundus of the gallbladder may be visualized in normal patients if it indents the surrounding fat (Fig. 11-7; see Fig. 11-5A). Only about 15% of gallstones are sufficiently calcified to be seen on abdominal radiographs, so the abdominal series is a poor screening study for gallbladder disease.

Spleen

The spleen occupies the left upper quadrant of the peritoneal cavity beneath the left tenth rib and hemidiaphragm, posterolateral to the gastric fundus (see Figs. 11-1B and 11-5).²¹ The

normal adult spleen measures 12 cm in length and 7 cm in width.²⁰ The lower edge of its inferolateral surface often indents extraperitoneal fat, and the lower medial aspect is adjacent to the left kidney and may be outlined by perirenal fat, enabling it to be visualized on abdominal radiographs (see Figs. 11-1B and C and 11-5). The bulk of the spleen, however, extends medially behind the stomach, where it is not visible on abdominal radiographs, so splenomegaly cannot always be diagnosed on these radiographs. Nevertheless, an enlarged spleen should be suspected when abdominal radiographs show elevation of the left hemidiaphragm, medial displacement of the gastric air bubble, or the splenic tip below the left costal margin.²⁰

The most inferior surface of the spleen abuts the phrenicocolic ligament, a thick peritoneal fold that marks the anatomic splenic flexure of the colon. The left lateral pleural recess may extend inferiorly along the lateral margin of the spleen to the splenic tip.²¹

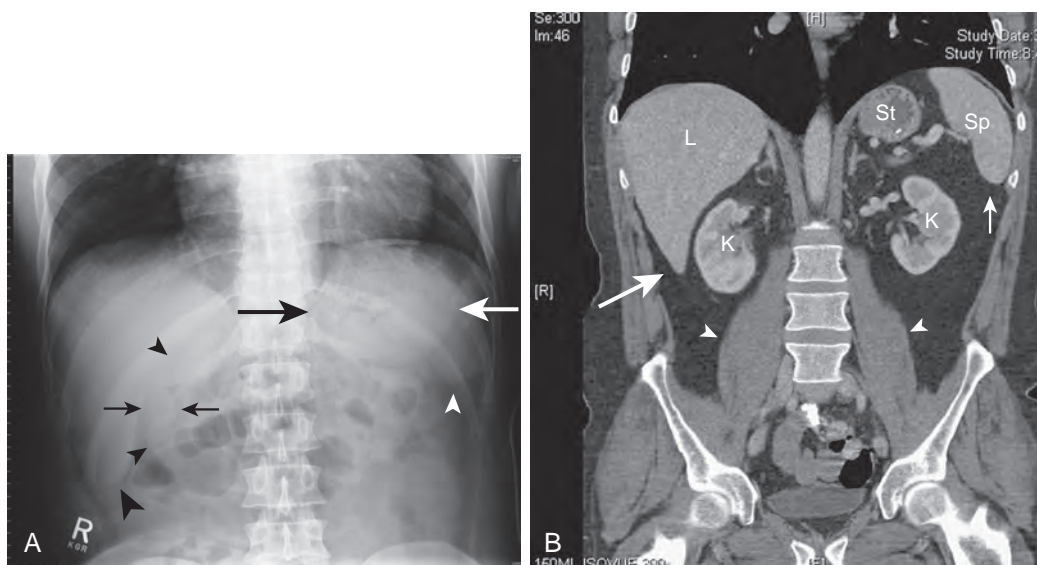


Figure 11-5 Gallbladder, liver, spleen, and stomach. **A.** Supine abdominal radiograph shows the gallbladder (small black arrows), hepatic angle (large black arrowhead), splenic tip (white arrowhead), and stomach (large black and white arrows). Note the partially visualized right kidney (small black arrowheads). **B.** Coronal CT scan of the abdomen shows the hepatic angle (large arrow) outlined by perirenal fat, splenic tip (small arrow), psoas muscles (arrowheads), and kidneys. L, liver; K, kidney; Sp, spleen; St, stomach.

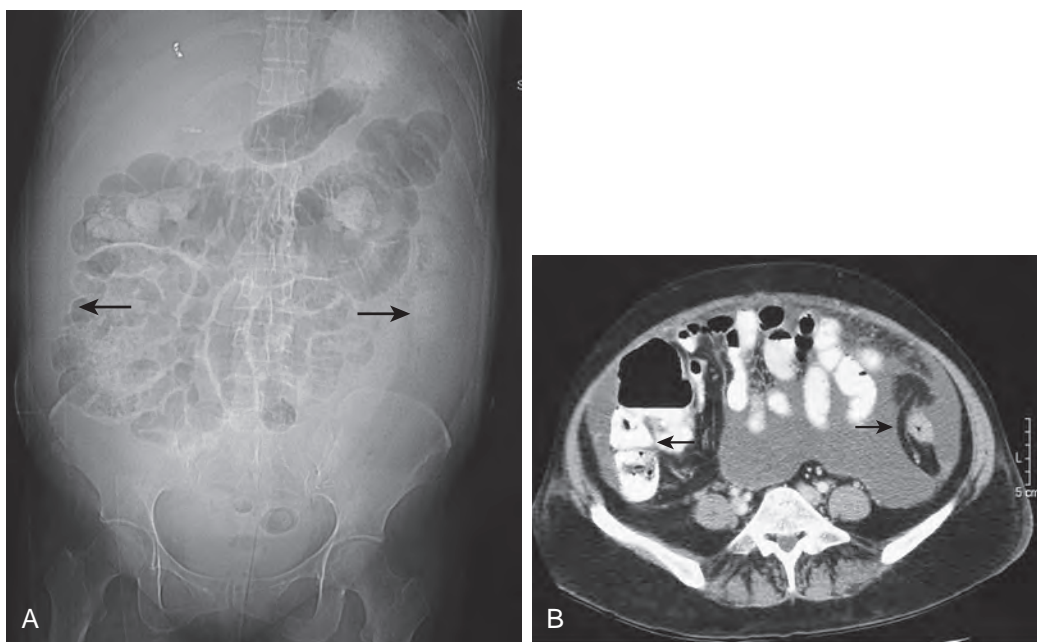


Figure 11-6 Intraperitoneal fluid (hemorrhage) in paracolic gutters. **A.** Supine abdominal radiograph in a patient with a traumatic liver laceration shows a large amount of fluid in both paracolic gutters (arrows) displacing bowel medially from the flank stripes. Also note loss of the hepatic angle normally outlined by extraperitoneal fat. The bleeding was controlled by embolization of the liver (note the radiopaque coil overlying the liver). **B.** Axial CT scan of the abdomen confirms the presence of ascitic fluid displacing adjacent bowel (arrows) from the paracolic gutters.

Stomach

The stomach usually contains air and fluid, so it can be recognized in the left upper quadrant by its characteristic location and the configuration of its rugal folds (see Fig. 11-1A). When the patient is in the supine position, gas in the stomach rises to the anteriorly located antrum, while fluid gravitates to the fundus. When the fluid-filled fundus is visible on abdominal

radiographs, it can occasionally be mistaken for a soft tissue mass (see Fig. 11-5A). However, confusion may be eliminated by the use of upright radiographs, which allow gas to enter the gastric fundus (see Fig. 11-1B). The stomach is a valuable landmark for identifying space-occupying lesions in surrounding structures such as the spleen laterally, the liver medially, and the lesser sac and pancreas posteriorly (see Figs. 11-1B and C and 11-5).¹⁷

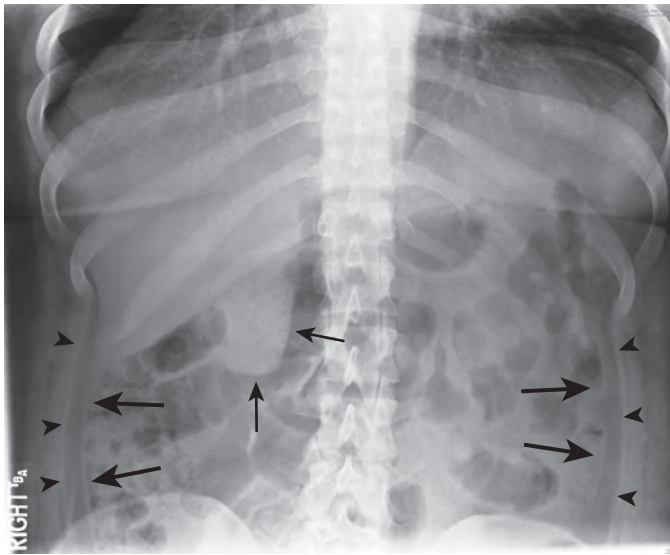


Figure 11-7 Paracolic gutters and lateral conal fascia. Coned-down view from supine abdominal radiograph shows the left and right paracolic gutters between the transversalis fascia (arrowheads) and lateral conal fascia (large arrows). Small arrows denote the gallbladder.

Small Intestine

The small bowel and its associated mesentery occupy the central portion of the peritoneal cavity.¹⁷ Although transit time through the small bowel is sufficiently rapid to prevent swallowed air from accumulating in normal small bowel loops, these loops may be visible on abdominal radiographs when they contain small amounts of gas (see Fig. 11-1A). In contrast, large amounts of air and fluid in a dilated small bowel indicate prolonged transit time caused by mechanical obstruction or an adynamic ileus. Scattered gas and fluid within normal to minimally dilated small bowel loops may occur in a variety of normal or pathologic conditions, including gastroenteritis, pancreatitis, inflammatory bowel disease, and aerophagia. Unfortunately, considerable interobserver variation occurs in interpretation of small bowel gas. The term *nonspecific gas pattern* has been used to describe abdominal radiographs showing more than the average amount of small bowel gas, without a clear indication of bowel obstruction. However, this term is vague or even misleading and is not helpful to the referring physician; therefore, it should not be used. Instead, radiologists should provide a clear description of the radiographic findings and the most reasonable diagnostic considerations. The gas-filled small bowel is distinguished from the colon by its more central location, smaller caliber, and typical mucosal folds, also known as the valvulae conniventes (see Fig. 11-1A). When visualized, the small bowel folds are usually thin and extend across the entire lumen of the bowel.

Colon

The adult colon usually contains some gas and fecal material and frames the abdomen, with the small bowel located more centrally. The more anterior transverse and sigmoid segments usually contain the greatest amount of gas when the patient is in the supine position. Unlike the valvulae conniventes of the small bowel, the colonic haustral folds are more widely spaced

and usually do not cross the entire lumen¹⁷ (see Fig. 11-1A). The caliber of the colon varies from 3 to 8 cm, with the largest diameter found in the cecum. Persistent cecal diameters of 9 to 10 cm or more may indicate a risk of impending perforation from mechanical obstruction or ileus.²²

The sigmoid and transverse colon are intraperitoneal structures suspended by the sigmoid mesentery and transverse mesocolon, respectively. Conversely, the ascending and descending colon and rectum are retroperitoneal structures, fixed to the posterior abdominal wall. In about 20% of the population, the cecum and a variable portion of the ascending colon have a persistent mesentery.²³ In such cases, the cecum is mobile and its position is more anterior and medial than usual. Although most of these patients are asymptomatic, this anatomic variation predisposes to an ileus, cecal bascule, and cecal volvulus.²⁴ The sigmoid colon is an intraperitoneal structure, but sigmoid diverticula are frequently oriented toward the sigmoid mesentery, so rupture of a diverticulum (with subsequent diverticulitis) usually results in the development of retroperitoneal gas rather than free intraperitoneal air.²³

On upright abdominal radiographs, air-fluid levels in the bowel can be interpreted as a sign of bowel obstruction. However, air-fluid levels in the small bowel and colon may occur in nonobstructive conditions and in normal patients. Air-fluid levels are particularly common in the right side of the colon after cathartic preparation.²⁵

Potential Intraperitoneal Spaces

The peritoneal reflections from the posterior abdominal wall over the viscera give rise to potential spaces in which blood, fluid, or pus may localize in the peritoneal cavity.¹⁷ In the normal abdomen, these compartments are not directly visible on abdominal radiographs, but their location can be inferred from the location of adjacent organs. The right subphrenic space is located between the right hemidiaphragm and liver. It is above the superior reflection of the right coronary ligament and continuous around the lateral edge of the liver with the right subhepatic space. The anterior subhepatic space lies just above the transverse colon and mesocolon and anterior to the right kidney and duodenum. The posterior subhepatic space, also known as Morison's pouch, continues posteriorly and superiorly to the inferior reflection of the coronary ligament. On abdominal radiographs, Morison's pouch overlies the superior pole of the right kidney.¹⁷ This is the most dependent portion of the upper peritoneal cavity with the patient in the supine position and is a frequent site of abscess formation. The subhepatic space is continuous with the right paracolic gutter between the ascending colon and properitoneal fat. The right paracolic gutter is deeper and wider than the left paracolic gutter. Fluid and abscesses are often visible here and can be recognized on abdominal radiographs by separation of the ascending and descending colon from the properitoneal fat (see Fig. 11-6). The left subphrenic space is separated from the right subphrenic space by the falciform ligament, which is a right midclavicular line structure in most patients. This space surrounds the left lobe of the liver and spleen and is limited inferiorly by the phrenicocolic ligament. Below the phrenicocolic ligament, the shallow left paracolic gutter extends inferiorly into the portion of the pelvis lateral to the descending colon (see Fig. 11-7).

The lesser sac of the peritoneal cavity is a potential space in the midabdomen, extending into the left upper quadrant. It is

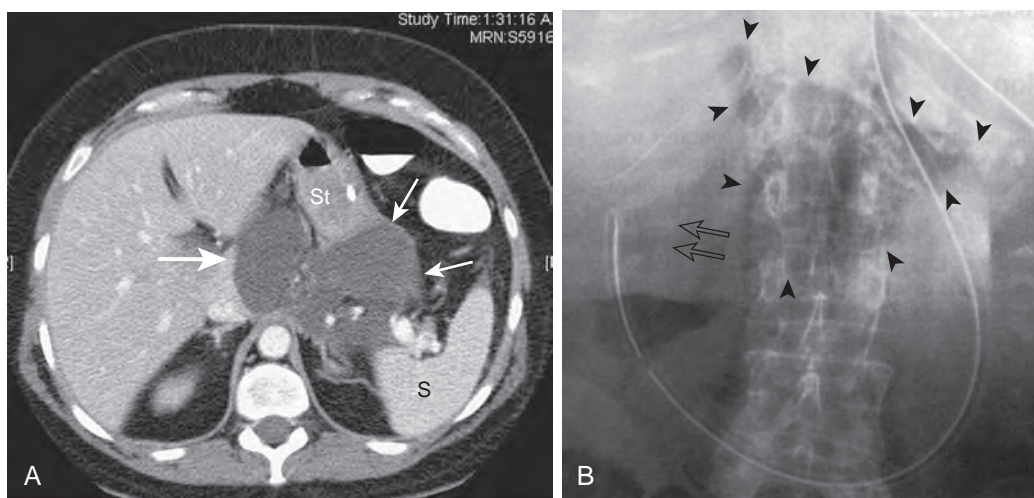


Figure 11-8 Lesser peritoneal sac. **A.** Axial CT scan of the abdomen in a patient with acute pancreatitis shows fluid posterior to the stomach in the lesser sac, extending into the superior medial recess (*large white arrow*). The fluid is contained on the left by the gastrosplenic ligament (*small arrows*). **B.** The boundaries of the lesser sac (*arrowheads*) are well delineated on a supine abdominal radiograph in another patient with gas in the lesser sac because of an abscess. The superior recess of the lesser sac extends toward the diaphragm just to the right of the spine. The foramen of Winslow is denoted by *open arrows*. A nasogastric tube is present in the stomach. S, spleen; St, stomach. (Courtesy Susan M. Williams, MD, Omaha.)

bounded superiorly by the left coronary ligament, posteriorly by the pancreas, anteriorly by the stomach, lesser omentum, and gastrocolic ligament, and inferiorly by the transverse colon and mesocolon¹⁷ (Fig. 11-8). Its left lateral borders are formed by the gastrosplenic and splenorenal ligaments. The lesser sac opens into the right subhepatic space via the foramen of Winslow at a site just posterior and superior to the duodenal bulb, beneath the free margin of the hepatoduodenal ligament. Dodds and associates described the lesser sac as an area defined by placing the right hand over the epigastrium, with the thumb extended over the midline toward the hilus of the liver and the fingers directed toward the hilum of the spleen.²⁶ The thumb represents the extension of the superior medial recess and the palm and fingers represent the main portion of the lesser sac. Space-occupying lesions or fluid collections in the lesser sac may displace the transverse colon inferiorly and the stomach superiorly, anteriorly, laterally, or medially (see Fig. 11-8).

RETROPERITONEUM AND ABDOMINAL WALL

The anatomy of the retroperitoneal space has been well described by Meyers.²³ It is posterior to the parietal peritoneum and anterior to the transversalis fascia. The retroperitoneal space is divided into three distinct compartments—the perirenal space, posterior pararenal space, and anterior pararenal space.

Perirenal Space: Kidneys and Adrenal Glands

The kidneys, adrenal glands, and abundant fat are located within the left and right perirenal spaces, which are confined by the anterior and posterior layers of renal fascia. It is the perirenal fat that allows visualization of some or all of the renal outlines on abdominal radiographs in most patients (see Fig. 11-5). On the other hand, the adrenal glands are small and not discernible unless they are calcified as a result of previous hemorrhage or granulomatous disease (Fig. 11-9). The upper half of the psoas muscle and the medial aspects of the hepatic and

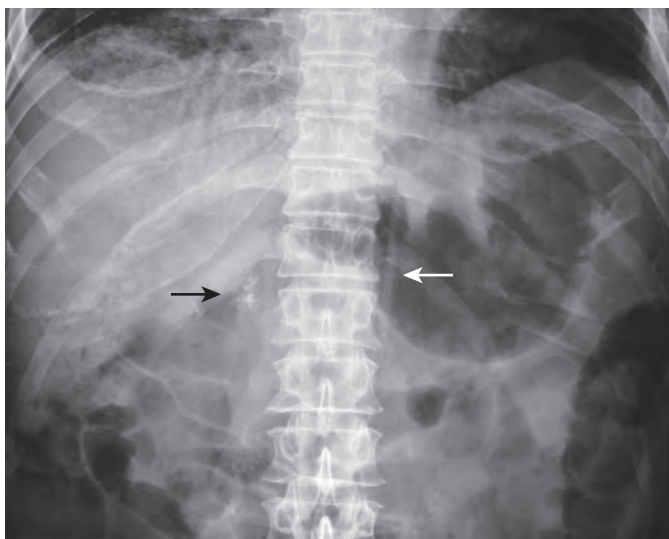


Figure 11-9 Diaphragmatic crus and calcified adrenal gland. Supine abdominal radiograph shows a calcified right adrenal gland (*black arrow*) and left diaphragmatic crus (*white arrow*). The right diaphragmatic crus is partially visualized just medial to the calcified right adrenal gland.

splenic angles are visualized on abdominal radiographs because of perirenal fat. Obliteration of the perirenal fat by inflammation, blood, or urine therefore obscures visualization of these structures. The medial perirenal space is continuous with the aorta and often fills with blood in patients with ruptured abdominal aortic aneurysms.²⁷ The anterior and posterior layers of perirenal fascia fuse laterally to form the lateroconal fascia, which continues laterally and ventrally to fuse with the parietal peritoneum along the lateral abdominal wall. In patients with abundant fat, the lateroconal fascia may be visible on abdominal radiographs as a thin line separating the posterior pararenal and anterior pararenal fat (Fig. 11-10).²⁸

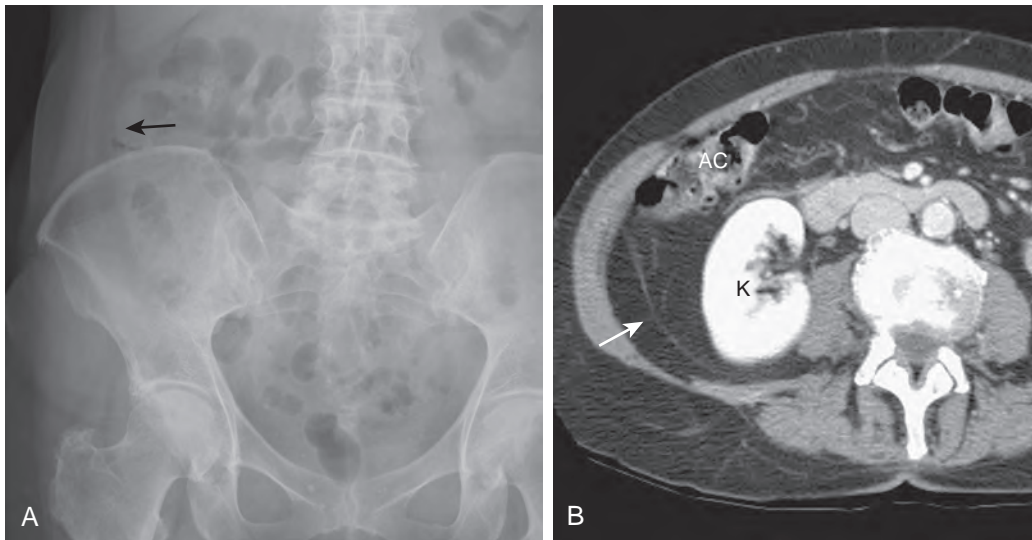


Figure 11-10 Lateroconal fascia. **A.** Supine abdominal radiograph shows the lateroconal fascia (arrow) along the paracolic gutter as a thin white line extending from the liver tip to the right lower quadrant. **B.** Axial CT scan shows the lateroconal fascia (arrow), which is composed of the anterior and posterior layers of the perirenal fascia that fuse laterally. The ascending colon (AC) is contained within the anterior pararenal space. K, kidney.

Posterior Pararenal Space

The posterior pararenal space is located posterior to the posterior perirenal and lateroconal fascia and is anterior to the transversalis fascia lining the abdominal wall (see Figs. 11-7 and 11-10).¹⁷ This space contains a variable amount of fat, but no organs. Medially, the posterior pararenal space originates at the lateral margin of the psoas muscle and is not continuous across the midline. Laterally, the posterior pararenal fat extends around the flank, joining the properitoneal fat of the lateral abdominal wall to form the so-called flank stripe (Fig. 11-11). The width of the flank stripe is variable and depends on body habitus. The posterior pararenal fat is continuous inferiorly with extraperitoneal fat in the pelvis.

Anterior Pararenal Space: Ascending and Descending Colon, Duodenum, and Pancreas

The anterior pararenal space, which lies anterior to the perirenal space and lateroconal fascia, contains the ascending and descending colon, retroperitoneal duodenum, and pancreas (see Fig. 11-10).¹⁷ In most patients, the ascending and descending colon can be identified by intraluminal fecal material and gas medial to the flank stripes (see Fig. 11-1). Semi-solid fecal material in the cecum and ascending colon often has a characteristic bubbly appearance. The retroperitoneal duodenum is usually not visible on abdominal radiographs unless it is filled with gas because of an ileus, proximal small bowel obstruction, or pancreatitis. The pancreas is also not visualized on abdominal radiographs because it has undulating, lobulated borders that are not outlined by fat. The normal location of the pancreas may be recognized on abdominal radiographs, however, if there is pancreatic calcification because of chronic pancreatitis (Fig. 11-12).

Psoas Muscle

The psoas muscle arises from the T12-L5 vertebrae and extends inferiorly to join the iliac muscle below the iliac crest. It continues as the iliopsoas muscle to the lesser trochanter.¹⁷ Perirenal fat superiorly and posterior pararenal fat below the level of the kidneys outline the lateral margin of the psoas muscle. In about 75% of patients, the psoas muscle is seen

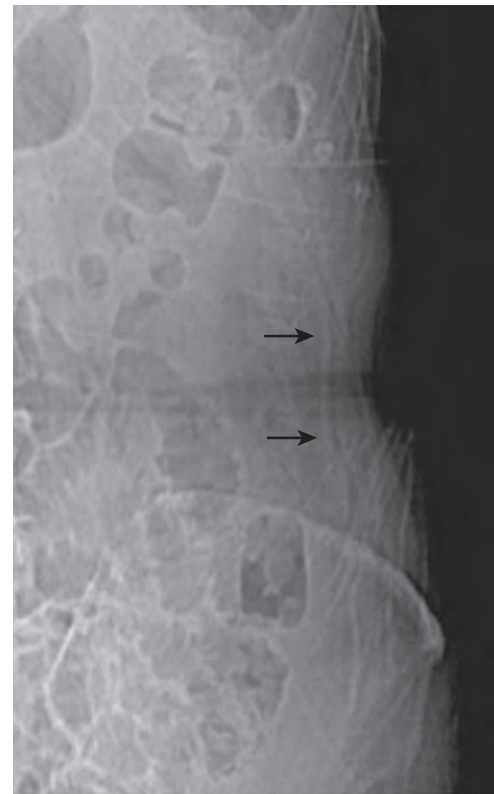


Figure 11-11 Flank stripe. Supine coned-down view of the left side of the abdomen shows the flank stripe (arrows) outlined by properitoneal fat just lateral to the descending colon. This fat is contiguous with the retroperitoneal fat in the posterior pararenal space. When there is no fluid in the left paracolic gutter, it is only a few millimeters in width.

to extend from the diaphragmatic crura to its junction with the iliac muscle (Fig. 11-13; see Fig. 11-1A and B).^{29,30} Fluid in the adjacent retroperitoneal fat may cause obliteration of the margin of the psoas muscle. Loss of one or both shadows of the psoas muscle is a common finding on abdominal

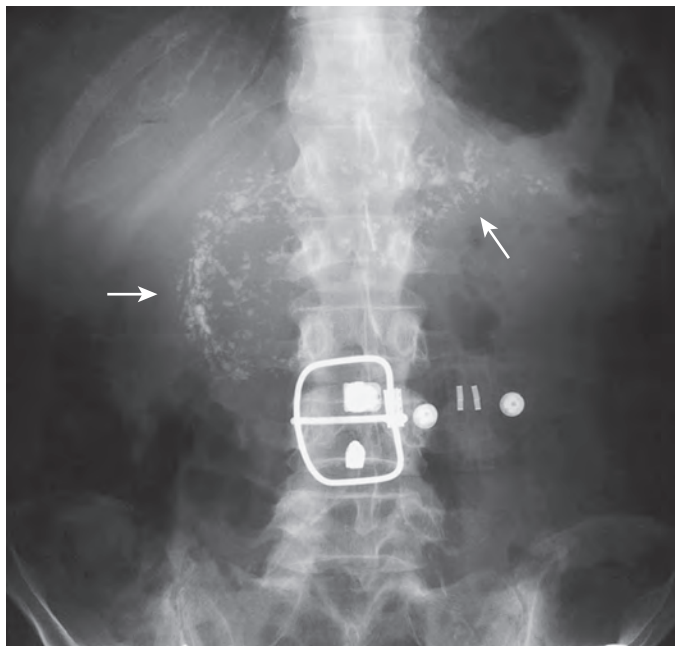


Figure 11-12 Pancreatic calcification. Supine abdominal radiograph shows multiple calcifications outlining the pancreas (arrows) caused by chronic pancreatitis. The pancreas normally is not visible on abdominal radiographs.



Figure 11-13 Psoas muscles. Supine abdominal radiograph shows both psoas muscles (arrows). The lateral margins of the psoas muscle extend inferiorly from the diaphragmatic crura to just below the iliac crest. The medial margins of the psoas muscles are also demonstrated. Note perivesical fat over the dome of the bladder (arrowheads). K, kidney.

radiographs when there is a ruptured abdominal aortic aneurysm, with blood infiltrating the perirenal and posterior paranrenal spaces.

The psoas muscle is optimally visualized when its lateral margin is straight and almost parallel to the x-ray beam. Non-visualization of the psoas margin on abdominal radiographs

must be interpreted with caution. A lumbar scoliosis may result in nonvisualization of the psoas shadow.³⁰ Rotation of the spinal column causes the psoas muscle on the concave side of the spine to assume a more flattened, horizontal configuration. The margin is then more perpendicular to the incident x-ray, so it may not be visible on abdominal radiographs. This phenomenon occurs not only in patients with a structural scoliosis but also in those with a positional scoliosis when muscle spasm causes contraction of the muscles in the flank. When there is a limited amount of retroperitoneal fat, the peritoneal cavity extends posteriorly, so fluid-filled bowel loops may come to lie directly adjacent to the psoas muscle, obscuring its margin. Occasionally, the kidney may also cause segmental nonvisualization of the psoas muscle, particularly in patients with an enlarged spleen that displaces the kidney medially.³⁰ Thus, retroperitoneal or intraperitoneal disease, scoliosis, or even a normal variation can obscure the psoas margin.

Quadratus Lumborum Muscle

Lateral and parallel to the psoas muscle is the lateral margin of the quadratus lumborum muscle, often seen to extend to its origin at the iliac crest. The quadratus lumborum muscle is part of the posterior abdominal wall and lies dorsal to the transversalis fascia, which passes between it and the psoas muscle.¹⁷ However, visualization of the quadratus lumborum muscle depends on the integrity of the posterior paranrenal fat, which outlines its lateral margin.

Diaphragmatic Crura

The diaphragmatic crura may outline retroperitoneal fat that is continuous with the origin of the psoas muscle (see Fig. 11-9). The crura are best seen on abdominal radiographs when the x-ray beam is centered near the level of the diaphragm.³¹ Occasionally, posterior paranrenal fat continues superiorly beneath the diaphragm, simulating pneumoperitoneum. In such cases, a left lateral decubitus view should differentiate pneumoperitoneum from paranrenal fat because the lucency associated with fat is not affected by changes in patient position.

PELVIS

Delineation of the various muscles and visceral structures in the pelvis is highly variable and depends on a variety of factors, including the amount of extraperitoneal pelvic fat, bowel contents, degree of bladder distention, position of the patient, and body habitus. As a result, these structures are not always identified, even in the absence of pelvic disease.

Piriformis Muscle

The piriformis muscle is in the superolateral posterior aspect of the pelvis.¹⁷ Its inferior margin can be visualized as a smooth convex interface passing from the sacrum to the greater sciatic foramen (Fig. 11-14). Just caudal to the piriformis muscle, the sciatic nerve passes out of the pelvis. Internal hernias can extend through the greater sciatic foramen into the buttocks; these hernias may contain bowel, bladder, or ureter.

Obturator Internus Muscle

The obturator internus muscle abuts the lateral pelvic sidewall and surrounds the greater portion of the obturator

foramen.¹⁷ It originates from the pubic ramus, ischium, and pelvic wall, and its tendon exits the pelvis at the lesser sciatic foramen, just below the sacrospinous ligament. The obturator internus muscle may be identified on abdominal radiographs as a result of subperitoneal fat that surrounds

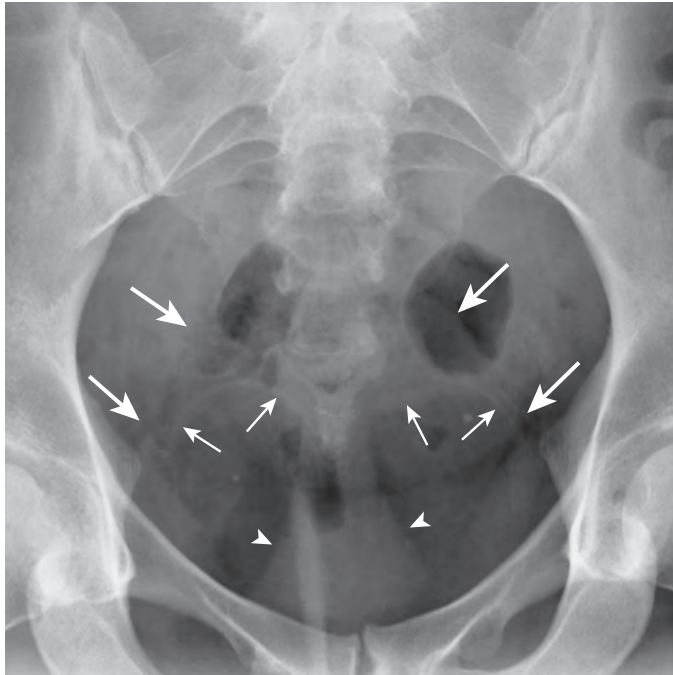


Figure 11-14 Piriformis muscle. Coned-down view of the pelvis from a supine abdominal radiograph shows the inferior margins of the piriformis muscles bilaterally (large arrows). Inferior to the piriformis muscles is the edge of the sacrospinous ligament and associated coccygeus muscles (small arrows) outlining the roof of the ischiorectal fossa. The perineum forms the medial boundary of the ischiorectal fossa (arrowheads).

it superiorly and ischiorectal fat that surrounds it inferiorly, below the origin of the levator ani muscle (Fig. 11-15). The obturator canal is located at the superolateral aspect of the obturator foramen; this canal transmits the obturator vessels and nerve.³² Hernias may occur at this site, particularly in older women (Fig. 11-16). These hernias often produce characteristic neuralgia in the thigh secondary to nerve compression.³²⁻³⁴

Sacrospinous Ligament and Coccygeus Muscle

The edge of the sacrospinous ligament and associated coccygeus muscle are outlined by underlying ischiorectal fat.¹⁷ These structures are located just inferior to the piriformis muscle and may be seen as a smooth band arching from the tip of the sacrum to the ischial spine (see Fig. 11-14).

Ischiorectal Fossa

The left and right ischiorectal fossae are wedge-shaped, subcutaneous fatty masses, with their bases at the perineum and their apices at the junction of the obturator internus and levator ani muscles.¹⁷ They are often visible on abdominal radiographs (see Fig. 11-14).

Gluteus Maximus Muscle

The gluteus maximus muscle forms the posterior border of the ischiorectal fossa.¹⁷ The medial edge of this muscle is outlined by subcutaneous fat, so it often appears on abdominal radiographs as a smooth line extending inferiorly and laterally from the tip of the sacrum.

Pelvic Viscera

The superior and lateral aspects of the urinary bladder are outlined by perivesical fat (Fig. 11-17; see Fig. 11-13). The uterus may also be visible in the pelvis just above this fat, particularly if the fundus is anteverted and indents the adjacent fat. This perivesical fat can be used to help identify fluid in

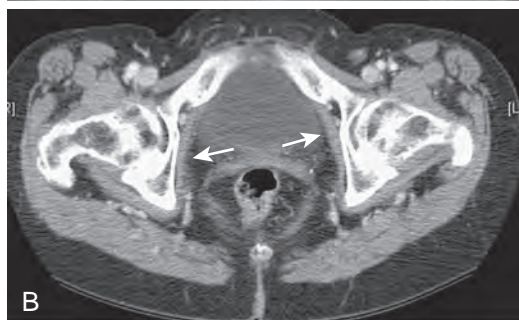
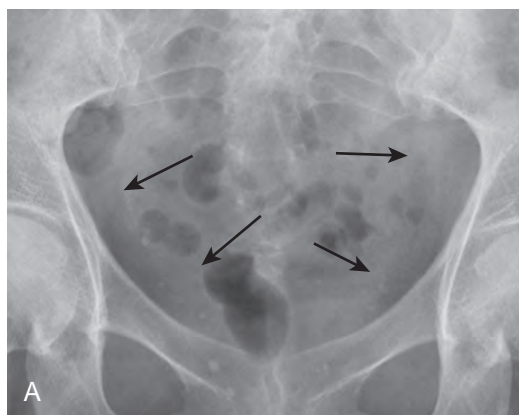
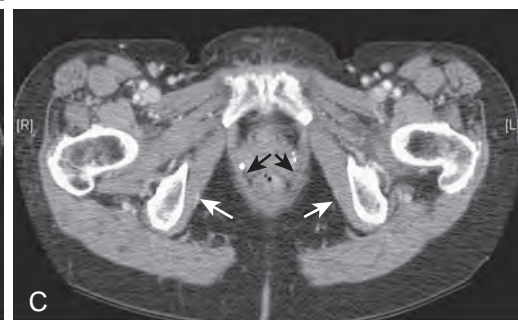


Figure 11-15 Obturator internus muscles.

A. Coned-down view of the pelvis from a supine abdominal radiograph shows the obturator internus muscles (arrows). **B.** Axial CT scan of the pelvis shows the superior portion of the obturator internus muscles (arrows) outlined by extra-peritoneal fat. **C.** Axial CT scan more caudally shows the obturator internus muscles (white arrows) outlined by ischiorectal fat. The left and right ischiorectal fossae are bounded by the levator ani muscles (black arrows) and obturator internus muscles.



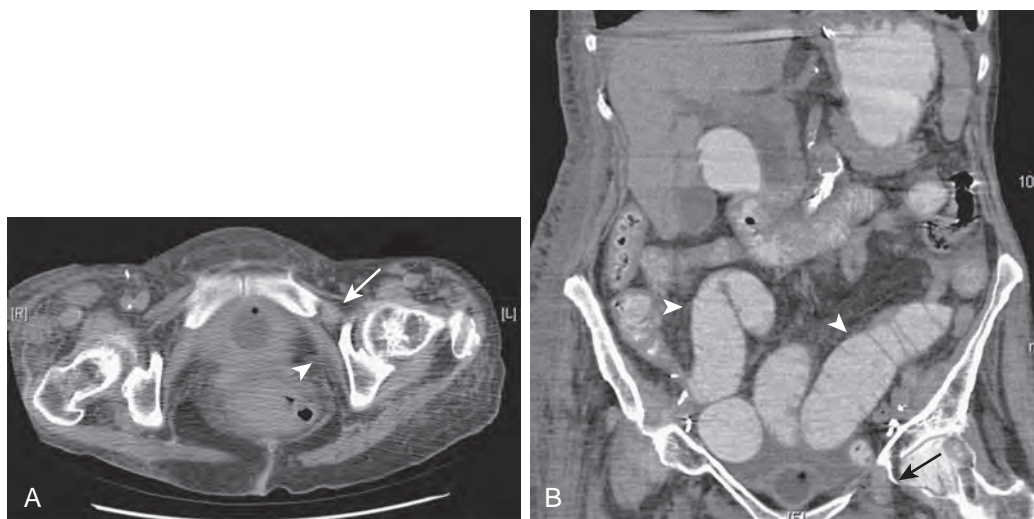


Figure 11-16 Obturator hernia causing small bowel obstruction. **A.** Axial CT of the pelvis in an older woman shows a left obturator hernia (arrow). Also note the left obturator internus muscle (arrowhead). **B.** Coronal CT of the pelvis shows the left obturator hernia (arrow), with dilated small bowel (arrowheads) proximal to the obstructing hernia.

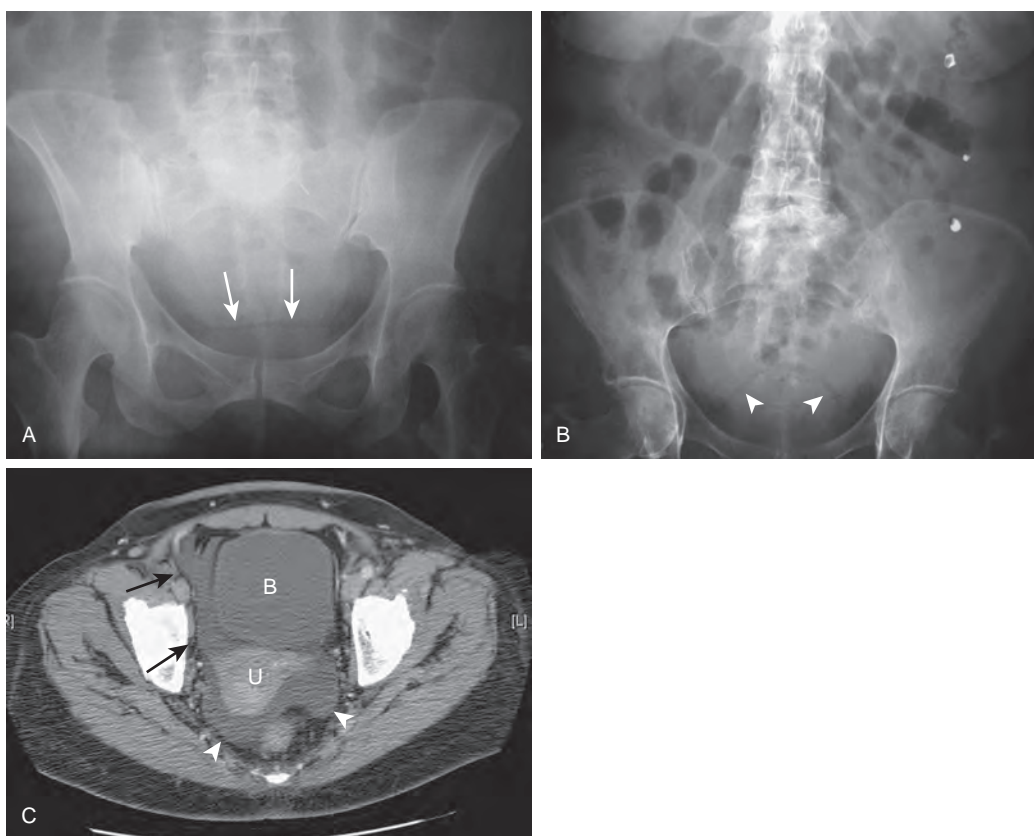


Figure 11-17 Ascites demarcated by perivesical fat. **A.** Coned-down view of pelvis from a supine abdominal radiograph shows evidence of ascites with increased density above the perivesical fat (arrows). Also note how the small bowel is displaced medially by ascitic fluid in the abdomen. **B.** Increased density is again seen in the paravesical spaces above the bladder on a supine abdominal radiograph in another patient with ascites. Note how the top of the bladder is outlined by perivesical fat (arrowheads). **C.** Axial CT of the pelvis in the same patient as in **B** confirms the presence of ascites (black arrows) around the bladder (B). Also note fluid (arrowheads) behind the bladder, surrounding the uterus (U).

the pelvis (see Fig. 11-17). Prostatic calculi will identify the position of the prostate gland, which is caudal to the urinary bladder and usually not seen on abdominal radiographs. Posterior to the bladder and uterus, the rectum can usually be recognized by the presence of intraluminal gas and stool (see Fig. 11-1).

Acknowledgment

The author would like to acknowledge and thank Susan M. Williams, MD, for giving permission to use parts of her excellent Chapter 10 from the second edition of this textbook.

REFERENCES

- Rosen MP, Sands DZ, Longmaid HE, III, et al: Impact of abdominal CT on the management of patients presenting to the emergency department with acute abdominal pain. *AJR* 174:1391–1396, 2000.
- Ahn SH, Mayo-Smith WW, Murphy BL, et al: Acute nontraumatic abdominal pain in adult patients: Abdominal radiography compared with CT evaluation. *Radiology* 225:159–164, 2002.
- MacKersie AB, Lane MJ, Gerhardt RT, et al: Nontraumatic acute abdominal pain: Unenhanced helical CT compared with three-view acute abdominal series. *Radiology* 237:114–122, 2005.
- Brewer RJ, Golden GT, Hitch DC, et al: Abdominal pain: An analysis of 1000 consecutive cases in a university hospital emergency room. *Am Surg* 131:219–224, 1976.
- Eisenberg RL, Heineken P, Hedgcock MW, et al: Evaluation of plain abdominal radiographs in the diagnosis of abdominal pain. *Ann Surg* 197:464–469, 1983.
- Mirvis SE, Young JWR, Keramati B, et al: Plain film evaluation of patients with abdominal pain: Are three radiographs necessary? *AJR* 147:501–503, 1986.
- Eisenberg RL, Hedgcock MW: Preliminary radiograph for barium enema examination: Is it necessary? *AJR* 136:115–116, 1981.
- Harned RK, Wolf GL, Williams SM: Preliminary abdominal films for gastrointestinal examinations: How efficacious? *Gastrointest Radiol* 5:343–347, 1980.
- Schwab FJ, Glick SN, Teplick SK, et al: The barium enema scout film: Cost-effectiveness and clinical efficacy. *Radiology* 160:619–622, 1986.
- Ballinger PW: Merrill's Atlas of Radiographic Positions and Radiologic Procedures, vol 2, ed 9, St. Louis, 1999, CV Mosby.
- Curry TS, Dowdey JE, Murry RC: Christensen's Physics of Diagnostic Radiology, ed 4, Philadelphia, 1990, Lea & Febiger.
- Miller RE, Nelson SW: The roentgenologic demonstration of tiny amounts of free intraperitoneal gas: Experimental and clinical studies. *AJR* 112:574–585, 1971.
- Woodring JH, Heiser J: Detection of pneumoperitoneum on chest radiographs: Comparison of upright lateral and posteroanterior projections. *AJR* 165:45–49, 1995.
- Baker SR: Imaging pneumoperitoneum. *Abdom Imaging* 21:413–416, 1996.
- Lappas JC, Reyes BL, Maglinte DD: Abdominal radiography findings in small-bowel obstruction: Relevance to triage for additional diagnostic imaging. *AJR* 176:167–174, 2001.
- Laufer I: The left lateral view in the plain film assessment of abdominal distention. *Radiology* 119:265–269, 1976.
- Gray H, Bannister LH, editors: Gray's Anatomy of the Human Body, ed 39, St. Louis, 2004, Mosby.
- Mould RF: An investigation of the variations in normal liver shape. *Br J Radiol* 45:586–590, 1972.
- Bundrick TJ, Cho SR, Brewer WH: Ascites: Comparison of plain film radiographs with ultrasonograms. *Radiology* 152:503–506, 1984.
- Riemenschneider PA, Whalen JP: The relative accuracy of estimation of enlargement of the liver and spleen by radiologic and clinical methods. *AJR* 94:462–468, 1965.
- Dodds WJ, Taylor AJ, Erickson SJ, et al: Radiologic imaging of splenic anomalies. *AJR* 155:805–810, 1990.
- Johnson CD, Rice RP, Kelvin FM, et al: The radiologic evaluation of gross cecal distension: Emphasis on cecal ileus. *AJR* 145:1211–1217, 1985.
- Meyers MA: Dynamic Radiology of the Abdomen, ed 4, New York, 1994, Springer-Verlag.
- Weinstein M: Volvulus of the cecum and ascending colon. *Am Surg* 107:248–259, 1938.
- Gammill SL, Nice CM: Air fluid levels: Their occurrence in normal patients and their role in the analysis of ileus. *Surgery* 71:771–780, 1972.
- Dodds WJ, Foley WD, Lawson TL: Anatomy and imaging of the lesser peritoneal sac. *AJR* 144:567–575, 1985.
- Loughran CF: A review of the plain abdominal radiograph in acute rupture of abdominal aortic aneurysms. *Clin Radiol* 37:383–387, 1986.
- Whalen JP, Berne AS, Riemenschneider PA: The extraperitoneal perivisceral fat pad. *Radiology* 92:466–480, 1969.
- Elkin M, Cohen G: Diagnostic value of the psoas shadow. *Clin Radiol* 13:210–217, 1962.
- Williams SM, Harned RK, Hultman SA, et al: The psoas sign: A reevaluation. *Radiographics* 5:525–536, 1985.
- Boyd DP: The anatomy and pathology of the subphrenic spaces. *Surg Clin North Am* 38:619–626, 1958.
- Wechsler RJ, Kurtz AB, Needleman L, et al: Cross-sectional imaging of abdominal wall hernias. *AJR* 153:517–521, 1989.
- Glicklich M, Eliasoph J: Incarcerated obturator hernia: Case diagnosed at barium enema fluoroscopy. *Radiology* 172:51–52, 1989.
- Baker SR, Cho KC: The Abdominal Plain Film with Correlative Imaging, ed 2, Norwalk, CT, 1999, Appleton & Lange.

Gas and Soft Tissue Abnormalities

JAMES M. MESSMER | MARC S. LEVINE

CHAPTER OUTLINE

Normal Bowel Gas Patterns

Abnormal Bowel Gas Patterns

Gastric Outlet Obstruction

Adynamic Ileus

Small Bowel Obstruction

Colonic Ileus

Colonic Obstruction

Closed Loop Obstruction

Volvulus

Appendicitis

Major Signs of Appendicitis

Toxic Megacolon

Pneumoperitoneum

Major Signs of Free Air

Pneumoretroperitoneum

Pneumobilia

Portal Venous Gas

Hepatic Arterial Gas

Intramural Gas (Pneumatosis)

Abscesses

Normal Soft Tissue Structures

Soft Tissue Abnormalities

Liver

Spleen

Kidneys

Other Structures

Ascites

Even with the widespread availability of cross-sectional imaging studies, abdominal radiography remains a common imaging test in modern radiology practice. Although CT and ultrasound provide more information about acute abdominal conditions, abdominal radiography has the advantages of relatively low cost and ease of acquisition and can readily be performed on acutely ill or debilitated patients, so it remains a valuable study for the trained and perceptive observer. The abdominal radiograph has also been called a KUB—*k*idneys, *u*reters (which are not visible), and *b*ladder. The term *flat plate of the abdomen* is dated and refers to a time when glass plates were used to produce images. Other terms include *plain film of the abdomen* and *abdominal plain film*, but with the widespread use of digital imaging and picture archiving communication systems (PACS) for interpretation of the images, *abdominal radiograph* has become the most appropriate term.

A wealth of diagnostic information can be obtained from correct interpretation of abdominal radiographs, and several excellent texts are available on the subject.¹⁻³ This chapter focuses on the abnormalities of gas and soft tissues that can be detected on abdominal radiographs.

Normal Bowel Gas Patterns

The intestinal tract in adults usually contains less than 200 mL of gas. Intestinal gas has three sources—swallowed air, bacterial production, and diffusion from the blood. In the supine patient, gas rises and accumulates in anteriorly placed segments of intestine, including the antrum and body of the stomach, transverse colon, and sigmoid colon. Gas may also be present in the remaining colon, particularly the rectum. Radiographic evaluation of intestinal gas should include the following: (1) identification of the bowel segments containing gas; (2) assessment of the caliber of these segments; (3) assessment of the most distal point of passage of gas; and (4) evaluation of the bowel contour outlined by gas.

The normal bowel gas pattern is readily visible on supine abdominal radiographs (Fig. 12-1). The first collection of gas encountered from the top of the radiograph is usually in the antrum and body of the stomach. Gas may also be seen in the transverse colon immediately inferior to the stomach. Gas in the ascending and descending portions of the colon usually occupies the lateral margins of the peritoneal cavity. The sigmoid colon occupies the inferior aspect of the abdomen and is often recognized by its characteristic shape and haustral folds. Rectal gas occupies a midline position in the pelvis and generally extends to the level of the pubic symphysis. The gas-filled small bowel tends to occupy the central portion of the abdomen and has a smaller caliber than the colon.

Although the location of intestinal gas is helpful in differentiating colon from small bowel, recognition of intestinal folds is also important. Haustral folds in the colon are normally 2 to 3 mm in width and occur at intervals of 1 cm, whereas the circular small bowel folds (also known as plicae circulares) are 1 to 2 mm in width and occur at intervals of 1 mm. In general, the small bowel is smaller than 3 cm in diameter and the colon is smaller than 5 cm in diameter.

Intestinal gas is a natural contrast agent for the interpretation of abdominal radiographs. When the patient is in the supine position, the gastric antrum and body tend to distend with air. A long narrowed segment of air-filled stomach may indicate an infiltrating process such as linitis plastica. Gastric ulcers and masses are also occasionally visible (Fig. 12-2A). In the colon, gas may outline a narrowed lumen from ulcerative or granulomatous colitis, thickened haustral folds from ischemia (Fig. 12-2B), or even a polypoid or annular carcinoma (see Fig. 12-5A).

Abnormal Bowel Gas Patterns

GASTRIC OUTLET OBSTRUCTION

Gastric outlet obstruction may be manifested on abdominal radiographs by a dilated stomach containing air, fluid, and/or debris. The amount of gastric distention depends not only on the degree of obstruction, but also on the duration of obstruction, position of the patient, and frequency of emesis. A dilated, air-filled stomach is usually recognized without difficulty because of its characteristic shape and location associated with

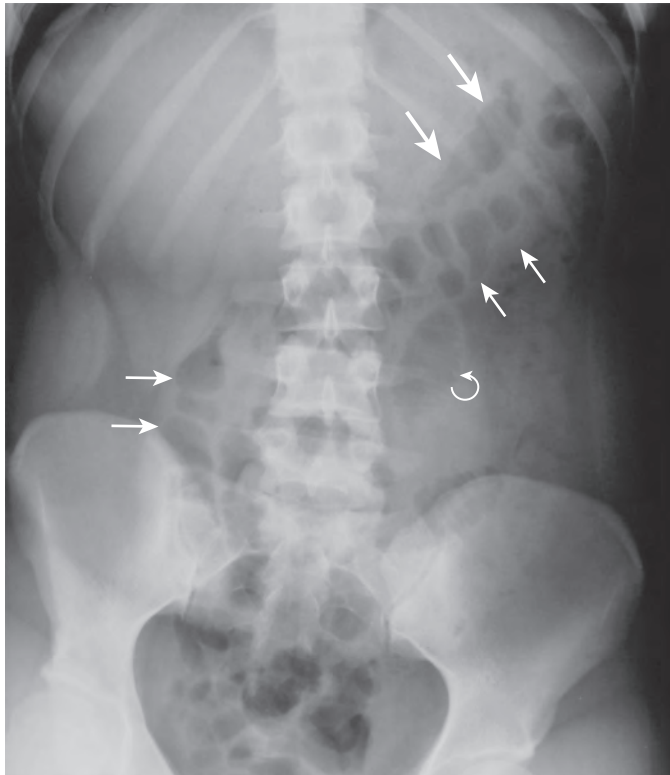


Figure 12-1 Normal bowel gas pattern. The most superior collection of intestinal gas is contained in the stomach (*large arrows*). Gas and stool outline the ascending and transverse colon (*small arrows*). Gas can also be seen in a portion of the small intestine (*curved arrow*).

inferior displacement of the transverse colon. Occasionally, a massively dilated, fluid-filled stomach can mimic the appearance of ascites or hepatomegaly. A small amount of air is almost always present within the stomach, however, so an upright radiograph of the chest or abdomen should demonstrate an air-fluid level within the gastric lumen.

The distal gastric antrum and pyloric region are the usual sites of gastric outlet obstruction. The most common causes of obstruction include acute edema and spasm from an ulcer in the distal antrum or pyloric channel or chronic antral narrowing secondary to scarring from a previous ulcer. Other causes of gastric outlet obstruction include an infiltrating antral carcinoma and, less commonly, scarring from granulomatous disease, radiation, or previous caustic ingestion.

Not all patients with gastric distention have mechanical obstruction. The stomach may also be dilated because of gastroparesis or gastric atony from diabetes (*gastroparesis diabetorum*), which is almost always associated with a peripheral neuropathy.⁴ Other causes of gastric dilation include morphine and other narcotic agents, hypokalemia, uremia, porphyria, lead poisoning, and previous truncal vagotomy. Pancreatitis or gastritis may also result in reflex gastric atony, and general anesthesia may occasionally cause marked gastric dilation.

Patients with obstructive lesions in the duodenum may also present with findings of gastric outlet obstruction. The duodenum may be filled with fluid, so it is not readily visible on supine radiographs. Left lateral decubitus views of the abdomen may allow air to enter the dilated duodenum, indicating that the obstruction is distal to the pylorus. When fluoroscopic barium studies are performed in patients with suspected gastric outlet obstruction, the duodenum should be carefully examined if the stomach appears normal.

ADYNAMIC ILEUS

The term *adynamic ileus* refers to dilated bowel in the absence of mechanical obstruction. It is used synonymously with the terms *paralytic ileus* and *nonobstructive ileus*. A more specific term, *postoperative ileus*, is limited to patients in whom recent abdominal surgery is responsible for this condition. All these terms refer to a state of decreased or absent intestinal peristalsis, causing swallowed air to accumulate in dilated bowel.⁵ An adynamic ileus is typically manifested on abdominal radiographs

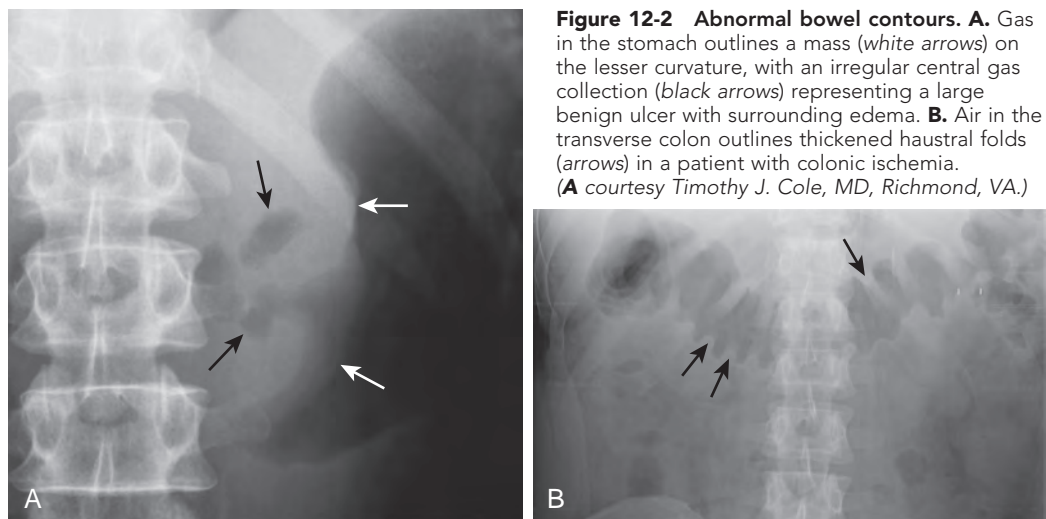


Figure 12-2 Abnormal bowel contours. A. Gas in the stomach outlines a mass (*white arrows*) on the lesser curvature, with an irregular central gas collection (*black arrows*) representing a large benign ulcer with surrounding edema. **B.** Air in the transverse colon outlines thickened haustral folds (*arrows*) in a patient with colonic ischemia. (*A* courtesy Timothy J. Cole, MD, Richmond, VA.)

by a dilated small bowel and colon, with multiple air-fluid levels on upright or horizontal beam decubitus views, so the presence of a dilated colon allows this condition to be differentiated from mechanical small bowel obstruction, in which only the small bowel is affected (see later, “[Small Bowel Obstruction](#)”). Sometimes, however, an adynamic ileus is confined to the small bowel, mimicking the findings of small bowel obstruction ([Fig. 12-3](#)), so the absence of colonic distention in no way excludes this condition. Apart from recent abdominal surgery, an adynamic ileus may result from a wide variety of causes, including electrolyte imbalances, sepsis, generalized peritonitis, blunt abdominal trauma, and infiltration of the mesentery by tumor.⁶

Other patients may have a localized ileus (also known as a sentinel ileus) related to acute inflammatory conditions in adjacent areas of the abdomen, including the right lower quadrant in patients with appendicitis, left lower quadrant in patients with diverticulitis, right upper quadrant in patients with cholecystitis, and mid upper abdomen or left upper quadrant in patients with pancreatitis.

Figure 12-3 Postoperative ileus mimicking small bowel obstruction. **A.** Supine abdominal radiograph shows multiple loops of dilated small bowel with a paucity of colonic gas. **B.** Upright radiograph shows differential air-fluid levels. Although the radiographic findings are suggestive of small bowel obstruction, this patient had a postoperative ileus involving the small bowel (note the longitudinal row of skin staples from recent abdominal surgery).

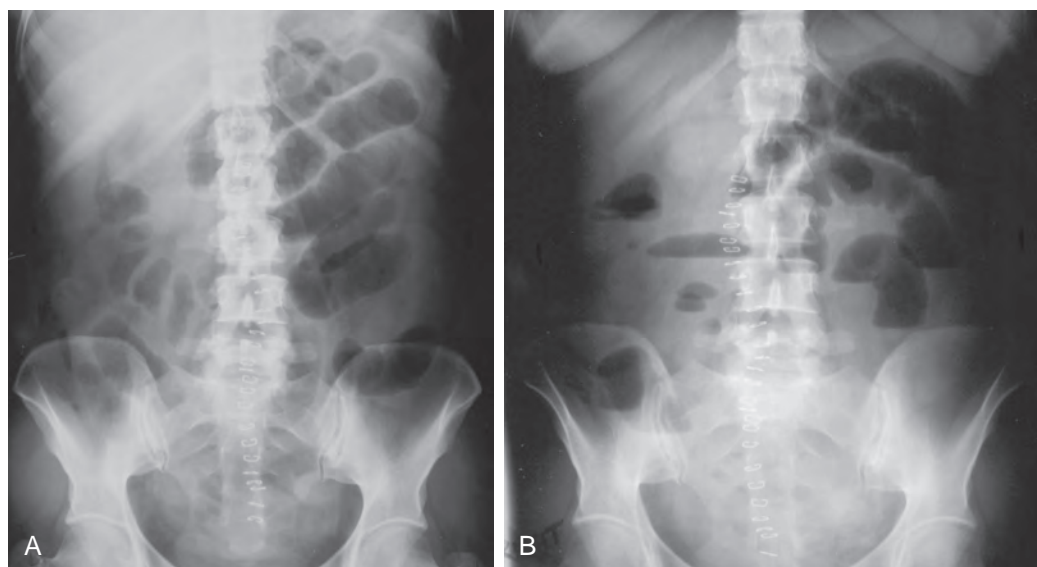
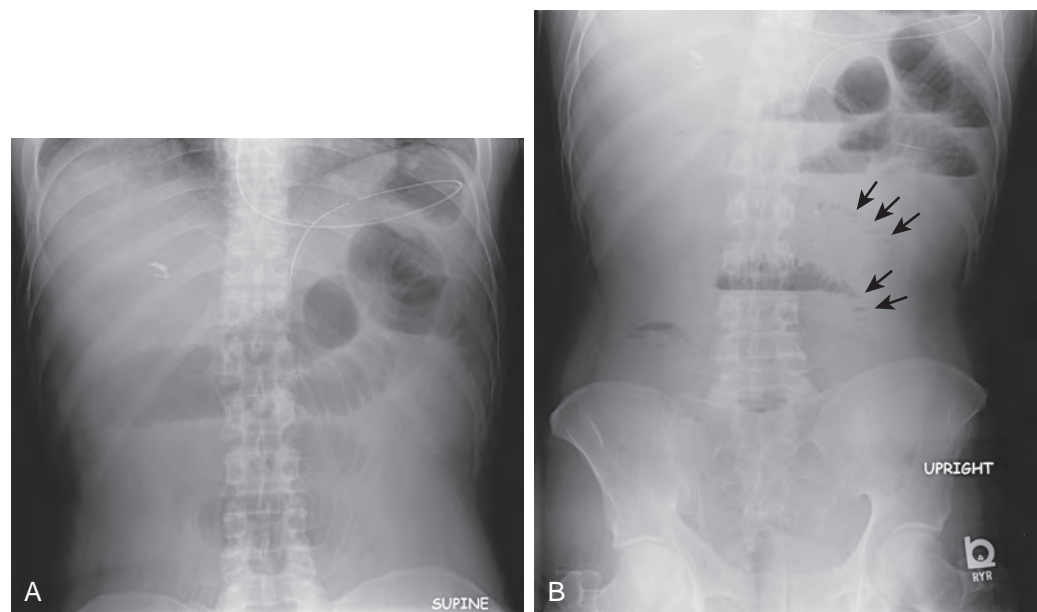


Figure 12-4 Small bowel obstruction. **A.** Supine radiograph shows dilated small bowel loops in the upper abdomen, with a paucity of colonic gas. **B.** Upright radiograph demonstrates multiple air-fluid levels. Small amounts of gas trapped between small bowel folds in the left midabdomen (arrows) produce the string of pearls sign.



SMALL BOWEL OBSTRUCTION

Small bowel obstruction is often difficult to diagnose on abdominal radiographs. False-positive and false-negative rates of 20% have been reported in the diagnosis of small bowel obstruction based solely on the radiographic findings.⁷ The diagnostic sensitivity can be increased by correlating the radiographs with the presence or absence of bowel sounds. Sequential radiographs over 12 to 24 hours may be helpful in demonstrating an evolving obstructive pattern.

When the small intestine becomes completely obstructed, accumulation of swallowed air and intestinal secretions causes proximal dilation of bowel. At the same time, intestinal peristalsis progressively eliminates bowel contents distal to the site of obstruction within 12 to 24 hours. As a result, small bowel obstruction is typically characterized on supine abdominal radiographs by dilated, gas-filled small bowel loops larger than 3 cm in diameter, with little or no gas in the colon or small bowel distal to the site of obstruction ([Fig. 12-4A](#)).

Upright and decubitus abdominal radiographs typically reveal multiple air-fluid levels in the dilated small bowel because of accumulation of gas and fluid proximal to the obstruction (Fig. 12-4B).

In his classic work on the acute abdomen, Frimann-Dahl stated that the presence of air-fluid levels at two different heights in the same loop of small bowel indicates a hyperperistaltic small intestine and is therefore a sign of small bowel obstruction.⁸ However, subsequent investigators have found that differential air-fluid levels may be present in any tubular viscus containing air and fluid. Thus, air-fluid levels should be recognized as a nonspecific finding that can be seen with a mechanical obstruction or adynamic ileus.

As small bowel obstruction progresses, gas-filled small bowel loops proximal to the site of obstruction become more dilated and tend to have a horizontal orientation in the central portion of the abdomen, producing a classic stepladder appearance. However, the amount of gaseous distention of these loops depends not only on the degree of obstruction, but also on the duration of obstruction, amount of air swallowing or emesis, and use of nasogastric suction for decompression. In some patients with small bowel obstruction who swallow relatively little air, supine abdominal radiographs may be unrevealing, whereas upright or decubitus abdominal radiographs (i.e., horizontal beam views) will show multiple air-fluid levels within small bowel loops proximal to the site of obstruction. In other patients, small amounts of gas trapped between the small bowel folds on upright or decubitus abdominal radiographs may be recognized by tiny bubbles of gas lined up along the nondependent surface of the bowel, also known as the **string of pearls or string of beads sign** (see Fig. 12-4B). This sign is seldom seen in patients with an adynamic ileus and should therefore suggest a mechanical small bowel obstruction. Finally, when patients swallow little or no air, abdominal radiographs may reveal multiple tubular, sausage-shaped soft tissue densities representing fluid-filled loops of small bowel without any intraluminal gas in the small bowel or colon, producing a so-called gasless abdomen. In general, the absence of colonic gas should suggest the possibility of a developing small bowel obstruction because gas is normally present in the colon in the absence of obstruction.

Most small bowel obstructions are caused by postoperative adhesions. Such adhesions may occur as early as 1 week after surgery, but more typically there is a remote history of surgery. In the absence of a surgical history, an obstructing hernia should be suspected. Of these hernias, 95% are external (inguinal, femoral, umbilical, or incisional). The presence of air-filled bowel below either pubic ramus should suggest the possibility of an obstructing inguinal hernia. Other less common causes of small bowel obstruction include small bowel tumors, ectopic gallstones, acute appendicitis and, occasionally, intestinal parasites or bezoars.⁹⁻¹³

It may not be possible to distinguish mechanical obstruction from an adynamic ileus on the basis of a single set of abdominal radiographs. If immediate surgery is not contemplated, further radiographic work-up with computed tomography (CT) is usually indicated.¹⁴ This topic is discussed in detail in Chapter 46. Barium studies may also be helpful when abdominal radiographs reveal findings of low-grade or partial small bowel obstruction.

COLONIC ILEUS

Acute colonic pseudo-obstruction (also known as Ogilvie's syndrome) was first described in 1948 by Ogilvie,¹⁵ who postulated that progressive colonic dilation is caused by interruption of sympathetic innervation with unopposed parasympathetic innervation of the colon. The most common clinical presentation is acute abdominal distention, usually occurring within 10 days of the onset of the precipitating pathologic process. Intra-abdominal inflammation, alcoholism, cardiac disease, burns, retroperitoneal disease, trauma, and pregnancy with spontaneous delivery or cesarean section have been described as causes of Ogilvie's syndrome.¹⁶⁻¹⁹

Abdominal radiographs may reveal marked colonic distention, which is typically confined to the cecum, ascending colon, and transverse colon. Occasionally, however, gas may extend to the level of the sigmoid colon. The underlying clinical condition and rapid onset of colonic distention usually suggest the diagnosis of colonic pseudo-obstruction, but a limited contrast enema may be required to rule out obstructing lesions in the colon.

Prediction of impending perforation of the cecum, as judged by cecal diameter, is fraught with difficulty because the risk of cecal perforation depends not only the degree of distention, but also on the duration—that is, the risk is considerably less in patients with long-standing cecal distention than in those with an acute increase in cecal caliber. Although some authors have indicated that a cecal diameter of 9 to 12 cm suggests impending perforation, cecal diameters of 15 to 20 cm are commonly observed in patients who recover spontaneously from Ogilvie's syndrome.^{18,20-22} Serial radiographs showing a change in cecal diameter at 12- to 24-hour intervals may be more helpful than a single radiograph showing a dilated cecum. Intravenous (IV) neostigmine is sometimes used for the initial treatment of these patients.^{23,24} Prolonged cecal distention beyond 2 to 3 days should prompt colonoscopic or surgical decompression.²⁵ The presence of intramural gas in the region of the dilated cecum should strongly suggest infarction and impending perforation.

COLONIC OBSTRUCTION

More than 50% of colonic obstructions are caused by annular carcinomas of the colon.^{26,27} The obstruction usually occurs in the sigmoid colon, where the bowel tends to have a narrower caliber and the stool is more solid. Conversely, cecal carcinomas and those in the ascending colon are less likely to cause obstruction because of the wider caliber of the bowel and more liquid character of the stool.

Colonic obstruction is typically manifested on abdominal radiographs by dilated, gas-filled loops of colon proximal to the site of obstruction and a paucity or absence of gas in the distal colon and rectum (Fig. 12-5A). Air-fluid levels may be seen on upright or decubitus views (Fig. 12-5B). Abdominal CT may be performed to confirm the presence of obstruction and determine its underlying cause (Fig. 12-5C). In patients with a competent ileocecal valve, the colon (especially the cecum) may become markedly dilated, and little or no gas may be seen in the small bowel. As the cecal diameter increases, the risk of perforation also increases. In various series, colonic perforation has been reported in as many as 7% of all large bowel obstructions and 2% of obstructing colonic carcinomas.²⁸⁻³⁰ Perforations sometimes occur at the site of obstruction, but usually

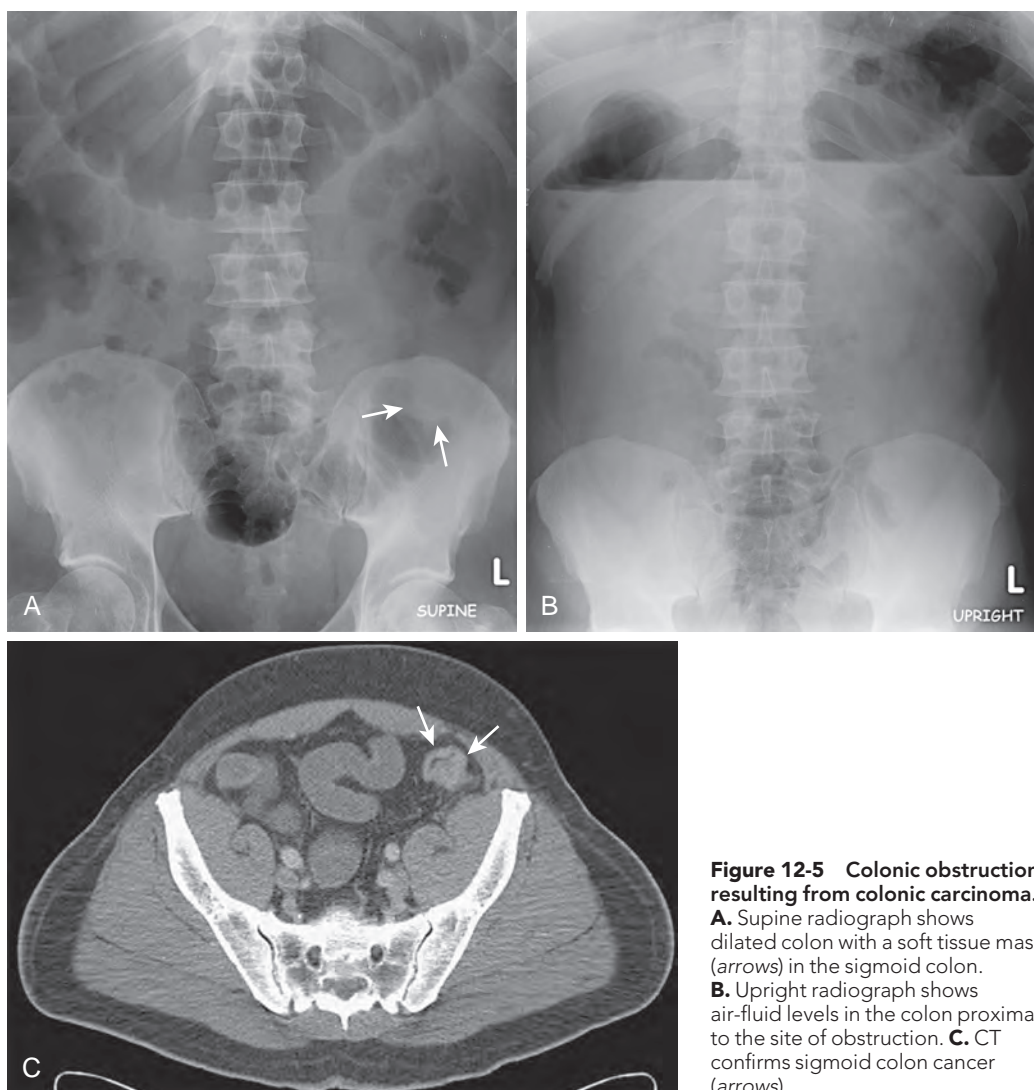


Figure 12-5 Colonic obstruction resulting from colonic carcinoma.
A. Supine radiograph shows dilated colon with a soft tissue mass (arrows) in the sigmoid colon.
B. Upright radiograph shows air-fluid levels in the colon proximal to the site of obstruction.
C. CT confirms sigmoid colon cancer (arrows).

result from progressive ischemia in the dilated colon or cecum proximal to the obstruction.³¹

An incompetent ileocecal valve allows gas to reflux into the small bowel, decompressing the colon, so the radiographic findings can mimic those of small bowel obstruction. Nevertheless, the distinction between colonic obstruction and small bowel obstruction has important implications because orally administered barium can inspissate above an unsuspected colonic obstruction. Abdominal CT or a single-contrast barium enema should therefore be considered in any patient with apparent obstruction of the distal small bowel on abdominal radiographs (especially an older patient who has no prior history of abdominal surgery) to rule out an underlying colonic or cecal carcinoma as the cause of obstruction.

CLOSED LOOP OBSTRUCTION

A closed loop obstruction refers to a segment of bowel that is obstructed at two points. Closed loop obstructions usually involve the small bowel and are caused by adhesions, internal hernias, or volvulus. The findings on abdominal radiographs are often nonspecific. Occasionally, there may be a disproportionately dilated, gas-filled loop of small bowel that has the

appearance of a coffee bean. Persistence of the dilated loop on sequential radiographs over several days should increase concern for a closed loop obstruction. Vascular compromise may lead to edema and thickening or effacement of the folds within this loop. If the obstructed segment fills with fluid, a rounded soft tissue density outlined by intra-abdominal fat produces a pseudotumor appearance. A history of intermittent, crampy abdominal pain replaced by steady, unrelenting pain should suggest a closed loop obstruction with vascular compromise. Nevertheless, a definitive diagnosis can be made only at surgery.

VOLVULUS

Any segment of intestine that has a mesenteric attachment has the potential to undergo a volvulus. Some patients may have intermittent intestinal twists associated with recurrent episodes of abdominal pain or emesis. If the twist is greater than 360 degrees, it is unlikely to resolve spontaneously. In some cases, air and intestinal contents may enter the twisted segment of bowel, producing abdominal distention and pain. The risk of vascular compromise in the twisted segment is more important than the mechanical effects of the volvulus. Severe vascular

compromise may result in necrosis and perforation of bowel, causing sepsis and death. Gastric volvulus is discussed in Chapter 34. Colonic volvulus may involve different segments of the colon, as discussed in the following sections.

Sigmoid Volvulus

Sigmoid volvulus constitutes 60% to 75% of all cases of colonic volvulus. Overall, sigmoid volvulus accounts for 1% to 2% of all intestinal obstructions in the United States.^{32,33} In some areas of South America and Africa, the incidence of sigmoid volvulus is extraordinarily high, reportedly because of a high-fiber diet and the resultant large, bulky stools, producing a chronically dilated, elongated sigmoid colon that predisposes patients to this type of volvulus. The incidence of sigmoid volvulus also appears to be higher in people living at higher altitudes in South America and Africa. In the United States, sigmoid volvulus tends to occur in older men and residents of nursing homes and mental hospitals, in whom chronic constipation and obtundation from medication are predisposing factors for gaseous distention of the sigmoid colon and stretching of the sigmoid mesocolon.

Patients with sigmoid volvulus typically present with abdominal pain and distention resulting from colonic obstruction. Obstipation and vomiting are also common findings. The symptoms are usually acute, but they may have a gradual onset in some patients.

Findings on abdominal radiographs are diagnostic of sigmoid volvulus in about 75% of patients with this condition. The classic radiographic appearance consists of a massively dilated loop of sigmoid colon that has an inverted U configuration and absent haustral folds and extends superiorly above the transverse colon into the left upper quadrant beneath the left hemidiaphragm (even elevating the diaphragm), with air-fluid levels in both the ascending and descending limbs of this loop. However, the dilated bowel can be in the midline or can even extend into the right upper quadrant (Fig. 12-6). Although there often is associated dilation of the more proximal colon, disproportionate dilation of the sigmoid in relation to the remaining colon and extension of the sigmoid colon superiorly above the transverse colon are important diagnostic features for differentiating sigmoid volvulus from simple colonic obstruction.³⁴ The apposed inner walls of the sigmoid colon may occasionally form a dense white line that points toward the pelvis. The absence of rectal gas is also an important differentiating feature. If prone or decubitus views of the pelvis show free passage of gas into the rectum, sigmoid volvulus therefore is extremely unlikely.

A contrast enema may occasionally be required in patients with suspected sigmoid volvulus. A low-pressure barium enema performed without inflation of a rectal balloon should demonstrate smooth, tapered narrowing, or beaking, at the rectosigmoid junction with associated obstruction.

Patients with sigmoid volvulus sometimes can be successfully treated by placement of a rectal tube for decompression of the dilated sigmoid loop. Patients who have persistent sigmoid dilation despite rectal tube placement and those who develop recurrent sigmoid volvulus may require surgical resection of the sigmoid colon for definitive treatment of this condition.

Cecal Volvulus

The term *cecal volvulus* refers to a condition caused by a rotational twist of the right colon on its long axis associated with



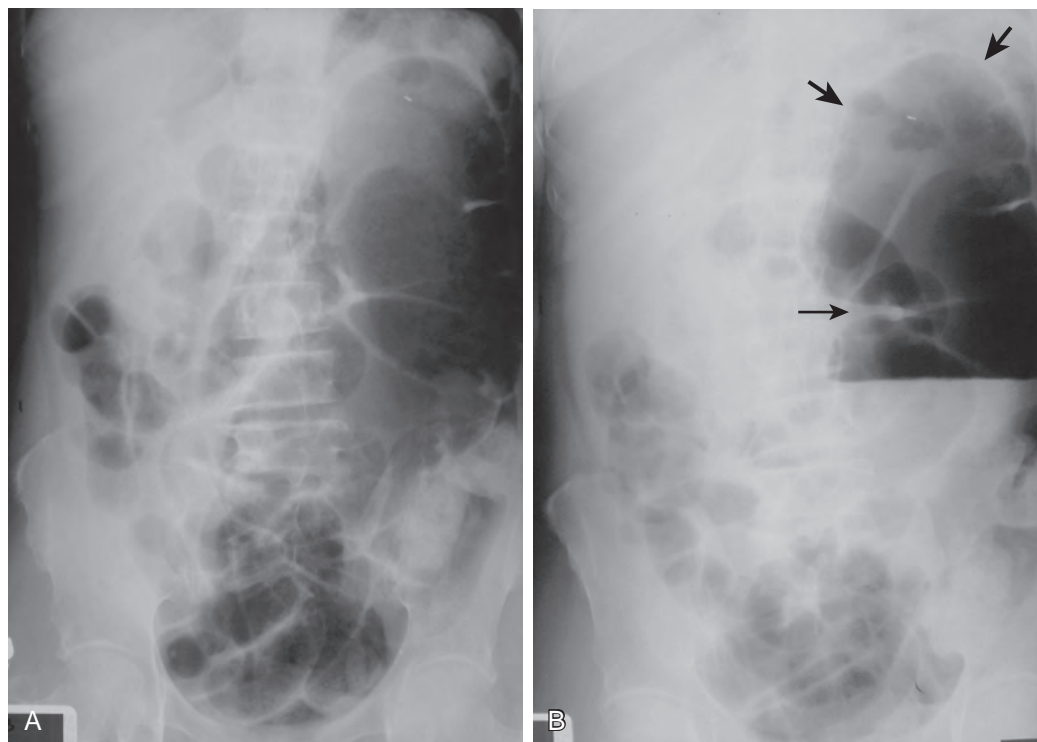
Figure 12-6 Sigmoid volvulus. Supine abdominal radiograph in a patient with sigmoid volvulus shows a massively dilated loop of sigmoid colon extending superiorly into the right upper quadrant and elevating the right hemidiaphragm, with no gas seen in the rectum.

mobility of the ascending colon, so the cecum flips into the midabdomen or left upper quadrant. Cecal volvulus can occur only when the right colon is incompletely fused to the posterior parietal peritoneum, an embryologic variant present in 10% to 37% of adults.³⁵⁻³⁷ These patients have a persistent mesentery on the ascending colon and, because of its greater mobility, the ascending colon can twist on its mesentery, producing a volvulus. Nevertheless, it should be recognized that the vast majority of patients with this embryologic variant never develop cecal volvulus. The term *cecal volvulus* is actually a misnomer because the twist is distal to the ileocecal valve. Cecal volvulus is less common than sigmoid volvulus, accounting for 2% to 3% of all colonic obstructions and about one third of all cases of colonic volvulus.

The characteristic findings of cecal volvulus, which are present on abdominal radiographs in about 75% of patients, consist of a markedly dilated, gas-filled cecum containing a single air-fluid level in an ectopic location (Fig. 12-7), usually with the cecal apex in the left upper quadrant. The medially placed ileocecal valve may produce a soft tissue indentation, so the gas-filled cecum has the appearance of a coffee bean or kidney. Usually, little gas is seen distally in the colon. If the ileocecal valve is incompetent, refluxed gas in the small bowel may erroneously suggest a small bowel obstruction. The diagnosis may be confirmed by a contrast enema or abdominal CT scan showing the typical beaking at the point of the volvulus in the mid-ascending colon.³⁸ Cecal volvulus may occur in a

Figure 12-7 Cecal volvulus.

A. Supine abdominal radiograph shows a markedly dilated viscus in the left upper quadrant, representing the obstructed cecum. Also note multiple loops of dilated small bowel. **B.** Upright radiograph shows the caput of the cecum superiorly (small thick arrows) and ileocecal valve (thin arrow), with a single air-fluid level in the dilated cecum.



variety of settings, including colonoscopy, barium enema, obstructive lesions in the distal colon, and pregnancy.³⁹⁻⁴¹

In 1938, Weinstein described a condition known as cecal bascule, which involved folding of the right colon without twisting, so the cecum occupied a position in the midabdomen.⁴² The term *bascule* is derived from *bascula*, the Latin word for “scale.”⁴¹ The point at which the ascending colon is folded represents the fulcrum of the scale. This entity also requires a persistent mesentery on the ascending colon.⁴³ The concept of a cecal bascule was challenged by Johnson and colleagues,²⁵ who believed that these patients have a focal adynamic ileus of the cecum. Of their patients, 20% had cecal perforation. They emphasized that the duration of cecal distention was more important than cecal diameter in predicting impending perforation. Whether cecal bascule represents an actual anatomic folding of the right colon or an adynamic ileus is not as important as the recognition that a dilated, ectopically located cecum may be a source of abdominal symptoms and potential cecal perforation.

Cecal volvulus should be differentiated from a prolonged colonic ileus in bedridden patients with a persistent mesentery on the ascending colon because the anteriorly located cecum in these patients may become disproportionately dilated, mimicking the appearance of a cecal volvulus. This has been described as cecal pseudovolvulus. Unlike patients with true cecal volvulus, however, cecal pseudovolvulus is associated with diffuse colonic distention, so it is usually possible to differentiate these conditions on the basis of the radiographic findings.

Transverse Colon Volvulus

Volvulus of the transverse colon is an uncommon condition, accounting for only about 4% of all cases of colonic volvulus in the United States.³³ As with sigmoid volvulus, elongation of the transverse mesocolon and close approximation of the hepatic

and splenic flexures may allow the transverse colon to twist on its mesenteric attachment. Failure of normal fixation of the mesentery may lead to increased mobility of the ascending colon and hepatic flexure, predisposing these patients to volvulus of the transverse colon.^{44,45} Compression of the duodenojejunal junction at the root of the mesentery may cause severe vomiting. Mortality rates as high as 33% have been reported in these individuals.⁴⁶

Abdominal radiographs are usually not helpful for patients with volvulus of the transverse colon and may erroneously suggest sigmoid volvulus. A barium enema may confirm the diagnosis if it shows typical beaking and obstruction at the level of the transverse colon. Two separate air-fluid levels can sometimes be seen in the dilated transverse colon, a finding that helps differentiate volvulus of the transverse colon from cecal volvulus.

Splenic Flexure Volvulus

Splenic flexure volvulus is the least common type of colonic volvulus. Postoperative adhesions, chronic constipation, and congenital or postsurgical absence of the normal peritoneal attachments of the splenic flexure may predispose patients to this uncommon condition.⁴⁷⁻⁵⁰ Abdominal radiographs may reveal a dilated, featureless, air-filled loop of bowel in the left upper quadrant that is separate from the stomach, with air-fluid levels in the transverse colon and cecum. When a splenic flexure volvulus is suspected, a single-contrast barium enema may be performed for a more definitive diagnosis.

Appendicitis

The development of acute appendicitis requires obliteration of the appendiceal lumen, usually by a concretion that may be visible on abdominal radiographs. The concretion has been

called a fecalith or coprolith, but the preferred term is *appendicolith*. This concretion forms around a nidus such as a piece of vegetable matter. Inspissated feces and calcium salts may adhere to the nidus, so it eventually reaches a size that occludes the appendiceal lumen. Accumulation of mucus proximal to the obstruction may distend the appendix, causing inflammation, ischemia, and perforation.

Some investigators believe that abdominal radiographs are of little value in patients with suspected appendicitis.^{51,52} Nevertheless, such radiographs are frequently obtained as the first imaging study in patients presenting to the emergency room with right lower quadrant pain.

MAJOR SIGNS OF APPENDICITIS

Signs of appendicitis on abdominal radiographs include the following:

Appendicolith. The presence of an appendicolith is the single most helpful sign of appendicitis on abdominal radiographs. Appendicoliths are found in about 10% of patients with acute appendicitis, typically appearing as round or ovoid calcified densities that are frequently laminated (Fig. 12-8). Most appendicoliths range from 1 to 2 cm in size, but some may be as large as 4 cm.⁵³⁻⁵⁶ They are usually in the right lower quadrant but can also be located in the pelvis or even in the right or left upper quadrant. The presence of an appendicolith has important implications for patients with appendicitis because it indicates a greater likelihood of superimposed perforation and abscess formation.



Figure 12-8 Acute appendicitis with partial small bowel obstruction. Supine abdominal radiograph shows a laminated appendicolith (arrows) in a patient with appendicitis. Also note a paucity of bowel gas in this region and dilated small bowel more proximally because of associated small bowel obstruction.

Abnormal Bowel Gas Pattern. About 25% of patients with appendicitis have an abnormal bowel gas pattern, usually an adynamic ileus, but occasionally a partial or even complete small bowel obstruction may be present (see Fig. 12-8).⁵⁷ An adynamic ileus occurs as a response to focal inflammation and may be localized to the right lower quadrant (also known as a sentinel ileus). Air-fluid levels in the jejunum have also been described in up to 50% of cases.⁵⁸ A dilated transverse colon may also be seen as an early sign of appendiceal perforation.⁵⁹ Mechanical obstruction may occur if the terminal ileum is compressed by the appendix or narrowed by adhesive bands.

Abnormal Cecum and Ascending Colon. Localized inflammation and edema may cause thickening of the cecal wall and widening of haustral folds in this region. An air-fluid level may also be present in the cecum on upright or decubitus abdominal radiographs, but this finding is transient and nonspecific.

Extraluminal Soft Tissue Mass. A soft tissue mass can be found in up to one third of patients with perforation. It may be caused by some combination of edema, fluid, and abscess formation in the right lower quadrant. The presence of mottled or loculated extraluminal gas within this soft tissue mass should strongly suggest an abscess.

Gas in the Appendix. This sign has been described as one of acute appendicitis, even though the pathophysiology of the disease would more likely result in an absence of appendiceal gas.⁶⁰ Usually, an air-filled appendix is a normal finding, simply reflecting the position of the appendix in relation to the cecum, because an ascending retrocecal appendix is more likely to contain gas.⁶¹

Free Intraperitoneal Air. A ruptured appendix rarely may lead to the development of a small amount of free intraperitoneal air. The obstructed appendiceal lumen prevents larger collections of gas from escaping into the peritoneal cavity, except in the case of a ruptured gas-containing abscess.^{62,63}

Obliteration of Normal Fat Planes. Inflammation and edema may alter the water content of surrounding fat and obscure the normal fat planes of the psoas muscle, obturator muscle, or properitoneal flank stripe. This finding is nonspecific and is usually associated with other signs of appendicitis on abdominal radiographs.

Scoliosis of the Lumbar Spine. Some patients with appendicitis may develop a lumbar scoliosis as a result of splinting. This finding is nonspecific, however, and can be related to patient positioning.

Surgeons have long believed that false-negative laparotomies are acceptable in some patients with right lower quadrant pain because of the serious, potentially life-threatening complications of untreated acute appendicitis. However, cross-sectional imaging studies such as CT and ultrasound have significantly improved the preoperative diagnosis of appendicitis (see Chapter 56).

Toxic Megacolon

Toxic megacolon, or toxic dilation of the colon, may be diagnosed on the basis of a dilated colon on abdominal radiographs

in patients with fever, tachycardia, and hypotension. Toxic megacolon is traditionally associated with ulcerative colitis, but it can also occur in patients with granulomatous colitis, amebiasis, cholera, pseudomembranous colitis, cytomegalovirus colitis, and ischemic colitis. Toxic megacolon develops in 5% to 10% of patients with ulcerative colitis, but in only 2% to 4% of patients with granulomatous colitis.⁶⁴⁻⁶⁷ The duration of the underlying disease has no relationship to the development of toxic megacolon. In fact, 70% of patients with toxic megacolon develop this complication during their first episode of colitis.

When toxic megacolon is suspected on clinical grounds, it is important to assess not only the degree of colonic dilation on abdominal radiographs, but also the appearance of the colonic mucosa outlined by air and the presence or absence of free intraperitoneal air. In general, the transverse and ascending portions of the colon tend to become disproportionately dilated, but this is more a reflection of their anterior position within the abdomen or their underlying capacity to dilate than of a greater predisposition to disease.⁶⁸ The upper limit of normal for the diameter of the transverse colon is about 6 cm, whereas the diameter of the transverse colon typically ranges from 6 to 15 cm in patients with toxic megacolon (Fig. 12-9).⁶⁹ A nodular mucosa may be visible in the dilated transverse colon as a result of inflammatory pseudopolyps in patients with ulcerative colitis (see Fig. 12-9).⁷⁰

Colonic perforation occurs in 30% to 50% of patients with toxic megacolon and is associated with a high mortality rate.^{66,71} Thus, a delayed diagnosis of toxic megacolon on



Figure 12-9 Toxic megacolon. There is marked colonic distention in a patient with ulcerative colitis and toxic megacolon. Note the nodular mucosal contour (arrows) in the transverse colon.

abdominal radiographs may have disastrous consequences for these individuals. An increased amount of gas in the small bowel in patients with severe colitis has also been associated with an increased likelihood of developing this condition.⁷²

The diagnosis of toxic megacolon usually is made based on a combination of the clinical and plain film findings, so a contrast enema does not need to be performed in these patients. Although some patients with suspected toxic megacolon have undergone barium enemas, most authors believe that such examinations are contraindicated because of the risk of perforation.⁷³ When toxic megacolon is suspected, CT may be performed to depict the underlying colitis and detect life-threatening complications such as colonic perforation.⁷⁴

Pneumoperitoneum

The presence of free intraperitoneal air (also known as pneumoperitoneum) is an important radiographic observation that usually indicates bowel perforation in patients with an acute abdomen. A classic experimental study by Miller and Nelson showed that as little as 1 mL of free air can be detected below the right hemidiaphragm on properly exposed upright chest radiographs.⁷⁵ They emphasized the importance of placing the patient in the left lateral decubitus position for 15 to 20 minutes before obtaining a radiograph with the patient in an upright position to maximize the possibility of detecting small amounts of free air. Radiographs obtained in midinspiration or midexpiration are even more likely to reveal subtle findings of pneumoperitoneum.⁷⁶ Chest radiographs obtained with the patient in an upright position are ideal for demonstrating free air because the x-ray beam strikes the diaphragms tangentially at their highest point. A posteroanterior view is usually obtained, but a lateral view of the chest may be even more sensitive.⁷⁷ Although properly performed upright chest radiographs are extremely sensitive for detecting pneumoperitoneum, abdominal CT has been shown to be even more sensitive for detecting tiny amounts of free air in patients with acute trauma.⁷⁸

In contrast, upright abdominal radiographs result in an oblique view of the hemidiaphragms that may obscure free air because the x-ray beam is centered more inferiorly. Left lateral decubitus views of the abdomen are better for detecting small amounts of free air interposed between the free edge of the liver and lateral wall of the peritoneal cavity. Care should be taken to include the upper abdomen, because air rises to the highest point in the abdomen, which frequently is beneath the lower ribs. Radiographs obtained with the patient in the right lateral decubitus position can also be helpful, but gas in the stomach or colon may obscure small amounts of free air. A cross-table lateral view of the abdomen with the patient in a supine position may demonstrate free air in those who are physically unable to roll onto their sides. Not surprisingly, CT also is more sensitive in detecting free air than left lateral decubitus radiographs.⁷⁹

Upright or left lateral decubitus abdominal radiographs are based on the principle that air rises to the highest point in the peritoneal cavity. If, however, horizontal beam views cannot be obtained in patients who are too sick or debilitated to stand or lie on their side, the radiologist must be able to recognize indirect signs of free intraperitoneal air on supine abdominal radiographs. In one study, one or more signs of pneumoperitoneum were present on these radiographs in 59% of patients.⁸⁰

MAJOR SIGNS OF FREE AIR

Major signs of free air on supine abdominal radiographs include the following:

Rigler's Sign. Gas normally outlines only the luminal surface of the bowel. Gas on both sides of the bowel, however, may outline the bowel wall as a thin linear stripe (Fig. 12-10A). Since its original description by Rigler in 1941,⁸¹ this sign has been recognized as an important finding of pneumoperitoneum, but a moderate amount of free air must be present in the abdomen. Extraluminal air trapped between adjacent loops of bowel may also have a characteristic triangular appearance in patients with pneumoperitoneum (Fig. 12-10B). Overlapping loops of small bowel in the central abdomen can mimic Rigler's sign, so it is helpful to evaluate the periphery of the radiograph. A pseudo-Rigler's sign may also result from Mach bands, a phenomenon in which there is the perception of a line at the interface between two areas of differing density (e.g., gas and soft tissue). However, the perceived line has almost no discernable thickness, whereas the bowel wall has a measurable thickness of 1 mm or more in patients with a true Rigler's sign.⁸⁰ Still other patients may have a pseudo-Rigler's sign caused by faint residual oral contrast material (usually from recent abdominal CT) coating the luminal surface of the bowel, so the increased density of the wall creates the erroneous impression that gas is present on both sides of the wall.

Increased Lucency in the Right Upper Quadrant. Air accumulating superiorly in the free space between the anterior aspect of the liver and the abdominal wall may cause increased lucency in the right upper quadrant (Fig. 12-11A). Depending on the habitus of the patient, the lateral border of the air collection may be linear. Small collections of air may be seen as subtle rounded lucencies overlying the liver.⁸² Linear collections of gas may also be seen in the subhepatic space, although the latter finding must be differentiated from subhepatic fat.⁸⁰

Visualization of the Undersurface of the Diaphragm. Air may be trapped anteriorly in the cupola of the diaphragm, permitting visualization of the undersurface of the central portion of the diaphragm or diaphragmatic muscle slips laterally. These findings depend on the amount of air present and on the orientation of the diaphragm.^{83,84}

Air in Morison's Pouch (Posterior Hepatorenal Space). Morison's pouch is an intraperitoneal recess bounded anteriorly by the liver and posteriorly by the right kidney. In the supine position, fluid may gravitate to this space. Air escaping from a perforated viscus may become loculated in this space because of surrounding inflammation. Air in Morison's pouch is characterized radiographically by a linear or triangular collection of gas in the medial aspect of the right upper quadrant outside the expected location of the bowel (Fig. 12-11B).⁸⁵⁻⁸⁷ The gallbladder may also be visualized.⁸⁸

Outline of the Normal Peritoneal Ligaments. Larger amounts of free air may occasionally outline the falciform ligament (Fig. 12-11C) or extrahepatic segment of the ligamentum teres in the right upper quadrant, the lateral umbilical ligaments (inverted V sign) in the lower abdomen, and the urachus.⁸⁹⁻⁹²

Football Sign. Originally described by Miller in infants, this sign is caused by a large amount of free air filling the oval-shaped peritoneal cavity, resembling an American football.⁹³ Occasionally, this sign may be seen in adults.

Air in the Lesser Sac of the Peritoneal Cavity. Intraperitoneal air that traverses the foramen of Winslow may become trapped in the lesser sac. Such gas may be manifested by an ill-defined lucency above the lesser curvature of the stomach.⁹⁴

The presence of pneumoperitoneum does not always indicate an acute abdominal condition. Various causes of free air are listed in Table 12-1.

Pneumoretroperitoneum

Gas that enters the retroperitoneal spaces (also known as pneumoretroperitoneum) can usually be distinguished from intraperitoneal gas. Because retroperitoneal gas is bound by fascial planes, it tends to collect in a linear fashion along the margins of the kidneys and psoas muscles and along the medial undersurface of the diaphragms (Fig. 12-12). Meyers has described the various pathways in which retroperitoneal gas can travel.⁹⁵ Perforation of the retroperitoneal portions of the intestines, such as the duodenum, ascending and descending colon, and rectum, usually accounts for this finding. In patients with sigmoid diverticulitis, gas can extend laterally along the left margin of the psoas muscle or, if the perforation involves the

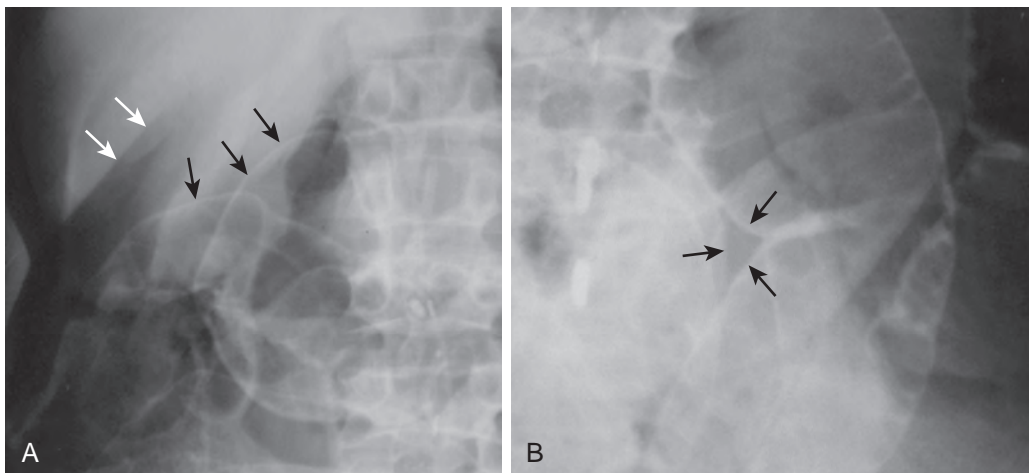


Figure 12-10
Pneumoperitoneum with Rigler's sign. **A.** Close-up view of the right upper quadrant in a patient with massive pneumoperitoneum shows a sharp liver edge (white arrows) with air outlining both sides of the bowel wall (black arrows). **B.** Extraluminal air trapped between adjacent loops of bowel has a characteristic triangular configuration (arrows).

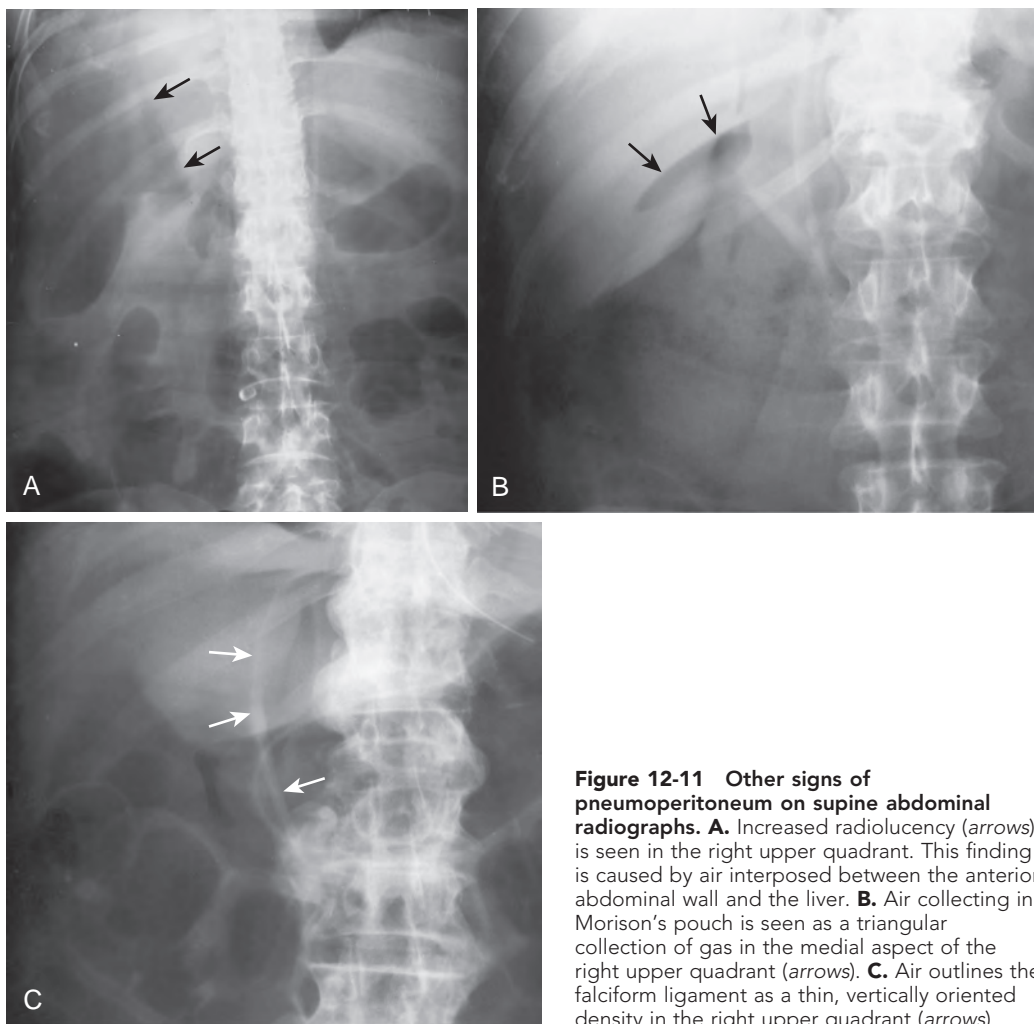


Figure 12-11 Other signs of pneumoperitoneum on supine abdominal radiographs. **A.** Increased radiolucency (arrows) is seen in the right upper quadrant. This finding is caused by air interposed between the anterior abdominal wall and the liver. **B.** Air collecting in Morison's pouch is seen as a triangular collection of gas in the medial aspect of the right upper quadrant (arrows). **C.** Air outlines the falciform ligament as a thin, vertically oriented density in the right upper quadrant (arrows).

TABLE
12-1

Causes of Pneumoperitoneum

BOWEL

Perforation of benign ulcer
Perforation of neoplasm
Perforation of appendix
Jejunal diverticulitis
Diverticulitis of sigmoid colon
Pneumatosis cystoides intestinalis
Pneumatosis coli
Foreign body perforation

TRAUMA

Abdominal surgery
Anastomotic leak
Peritoneal tap
Endoscopy or biopsy
Penetrating injury
Percutaneous endoscopic gastrostomy

FEMALE GENITAL TRACT

Rubin test
Sexual intercourse or cunnilingus
Pelvic examination
Athletic activities such as water skiing

root of the sigmoid mesocolon, along both margins of the psoas muscle.

The location of retroperitoneal gas may provide a clue to its site of origin. Gas escaping from duodenal perforations tends to be confined to the right anterior pararenal space. Gas may also extend medially across the anterior aspect of the psoas muscle, sparing its lateral margin. Less commonly, gas may enter the perirenal space and outline the right kidney. Duodenal ulcers, iatrogenic duodenal injuries, and blunt abdominal trauma are all possible causes of perforation of the extraperitoneal portion of the duodenum.⁹⁶

Gas from a rectal perforation may be confined to the perirectal space or may extend into the anterior and posterior retroperitoneal spaces and even superiorly into the mediastinum.⁹⁷ Iatrogenic trauma is a common cause of rectal perforation. Radiologists should always be aware of the potential risk of rectal perforation when insufflating a balloon during barium enemas.⁹⁸

Pneumobilia

Gas in the bile ducts, or *pneumobilia*, is characterized radiographically by thin, branching, tubular areas of lucency in the

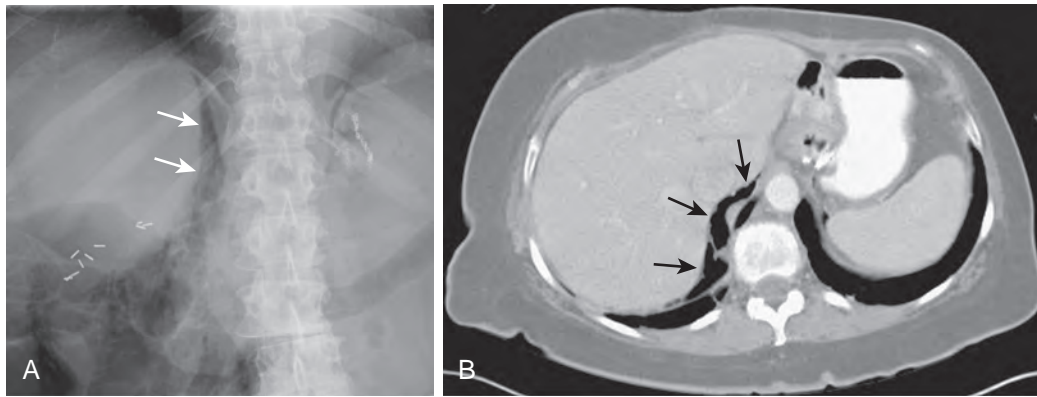


Figure 12-12 Retroperitoneal air in a patient with retroperitoneal perforation after endoscopy. **A.** Retroperitoneal air is manifested by linear gas collections (arrows) dissecting along the right margin of the psoas muscle in the upper retroperitoneum to the undersurface of the medial aspect of the right hemidiaphragm. **B.** CT confirms the retroperitoneal location of this extraluminal air (arrows). (Courtesy Laura R. Carucci, MD, Richmond, VA.)

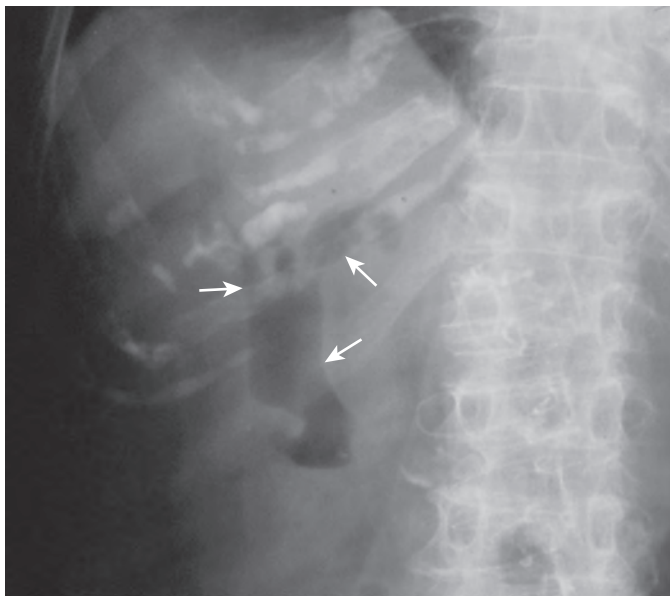


Figure 12-13 Pneumobilia. Air is seen collecting centrally in the biliary tree (arrows) in a patient who had a choledochojejunostomy.

central portion of the liver (Fig. 12-13). This central location is explained by the flow of bile from the periphery of the liver toward the porta hepatis.

Pneumobilia almost always results from some type of communication between the bile ducts and intestine. One of the most common causes is a surgically created biliary enteric fistula such as a choledochojejunostomy or cholecystojejunostomy (see Fig. 12-13). The most common nonsurgical cause of a choledochoduodenal fistula is a penetrating duodenal ulcer,⁹⁹ and the most common nonsurgical cause of a cholecystoduodenal fistula is a gallstone eroding into the duodenum. In some patients with a cholecystoduodenal fistula, a patent cystic duct may allow air to enter the intrahepatic bile ducts.^{100,101} If the ectopic gallstone is 2.5 cm or larger in diameter, it may obstruct the small bowel, usually at or near the ileocecal valve, and produce a so-called gallstone ileus; this is actually a misnomer because these patients have mechanical small bowel obstruction caused by a gallstone impacted in the distal ileum. The classic

triad (also known as Rigler's triad) of air in the biliary tree, small bowel obstruction, and an ectopic calcified gallstone is almost diagnostic of gallstone ileus on abdominal radiographs.¹⁰² An incompetent sphincter of Oddi, recent sphincterotomy or sphincteroplasty, anomalous insertions of the biliary tree, recent passage of a common duct stone, and infestation of the biliary tract by *Ascaris* are other causes of pneumobilia.^{103,104}

The radiographic appearance of pneumobilia is sufficiently characteristic to allow a confident diagnosis on the basis of the findings on abdominal radiographs. Occasionally, periportal fat or fat around the ligamentum teres hepatis may be manifested by a faint lucency over the liver, but its appearance is different from that of pneumobilia.^{105,106} The most important consideration in the differential diagnosis of pneumobilia is the presence of gas in the portal venous system (see later, "Portal Venous Gas").

Portal Venous Gas

Portal venous gas was originally described in adults by Susman and Senturia in 1960.¹⁰⁷ This ominous radiographic finding is manifested by thin, branching, tubular areas of lucency that occupy the periphery of the liver and extend almost to the liver surface (Fig. 12-14). The peripheral location of the gas reflects the hepatopetal flow of blood in the portal venous system away from the porta hepatis. In advanced cases, air can be seen outlining the more centrally located main portal vein, but this finding is less common. A left lateral decubitus radiograph of the abdomen may facilitate visualization of portal venous gas. Unless the gas has been introduced iatrogenically by vascular catheterization, endoscopic manipulation, or other iatrogenic causes, the source of the gas is almost invariably the intestine. Intraluminal intestinal air can breach a damaged mucosa, enter the bloodstream, and eventually reach the portal venous system of the liver.

The most important cause of portal venous gas is intestinal ischemia or infarction. In adults with ischemic bowel disease, death often occurs shortly after portal venous gas has been observed.^{108,109} The finding of portal venous gas should therefore lead to a careful search for gas in the wall of the bowel caused by intestinal infarction (see later, "Intramural Gas").

Portal venous gas may occasionally have benign causes. Dilation of the stomach and small bowel may allow air to enter the

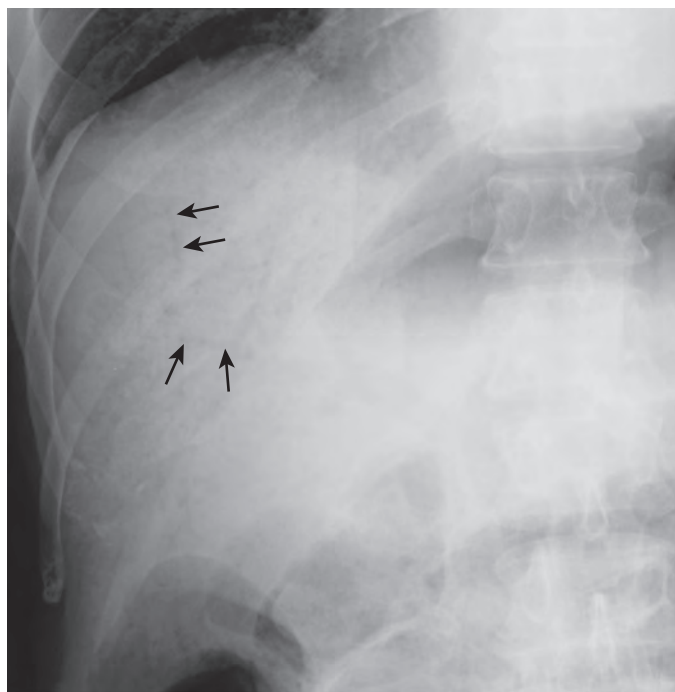


Figure 12-14 Portal venous gas. Tiny, branching gas collections (arrows) are seen extending toward the periphery of the liver.

intestinal mucosa, eventually reaching the liver.¹¹⁰ Nonfatal cases of portal venous gas have also been described in patients with diverticulitis and inflammatory bowel disease and in patients who have undergone a double-contrast barium enema or colonoscopy for inflammatory bowel disease.¹¹¹⁻¹¹⁴ Traumatic injury to the common bile duct as a complication of endoscopic retrograde cholangiopancreatography (ERCP) and endoscopic sphincterotomy has also been reported as a benign cause of portal venous gas.¹¹⁵ Portal venous gas has even been described as a transient finding on Doppler ultrasound during the early postoperative period after liver transplantation.¹¹⁶

Hepatic Arterial Gas

Gas in the hepatic artery has been reported anecdotally in a patient in whom the hepatic artery was ligated for the treatment of an unresectable hepatic adenoma.¹¹⁷ The smaller caliber of the hepatic artery and relative paucity of intrahepatic branches should differentiate this finding from portal venous gas. Hepatic arterial gas may be reported more frequently as the use of aggressive interventional radiographic techniques increases for the treatment of hepatic neoplasms.

Intramural Gas (Pneumatosis)

Gastric emphysema is a relatively benign form of pneumatosis usually resulting from iatrogenic injury to the mucosa at endoscopy or increased intraluminal pressure in the stomach associated with gastric outlet obstruction.^{118,119} This condition is characterized by linear collections of gas in the wall or stomach. In contrast, emphysematous gastritis is a rare fulminant variant of phlegmonous gastritis; hemolytic *Streptococcus* is the most commonly implicated organism.^{120,121} Underlying causes of this life-threatening condition include ingestion of caustic substances, severe gastroenteritis, and gastroduodenal surgery that

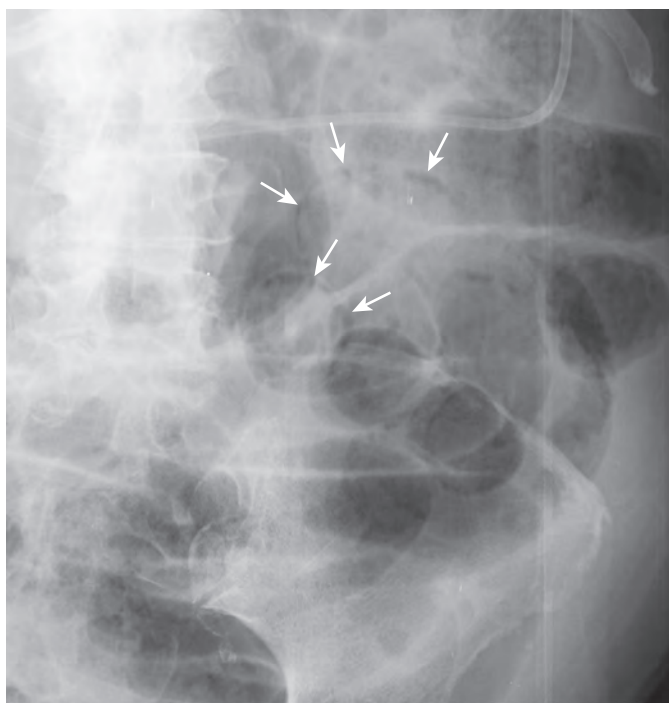


Figure 12-15 Infarcted bowel with intramural gas. Linear gas collections (arrows) are seen in the wall of several dilated small bowel loops in a patient with bowel infarction.

compromises the vascular supply of the stomach.^{120,121} Emphysematous gastritis is characterized by cystic, bubbly collections of gas in the gastric wall that have a very different appearance than that of the linear intramural collections seen in gastric emphysema.

Gas in the wall of the small bowel, which is termed *pneumatosis intestinalis*, is characterized by two radiographic patterns—a bubbly appearance or thin, linear streaks of gas.¹²² The bubbly appearance of intramural gas is easily mimicked by fecal material within the colon. In patients with this form of pneumatosis, close inspection may reveal small bubbles of gas outside the confines of the bowel, leading to the correct diagnosis. In contrast, linear gas collections tend to be more readily apparent and should always be considered an important finding on abdominal radiographs, regardless of their location (Fig. 12-15). In combination with portal venous gas (see earlier, “Portal Venous Gas”), linear gas collections in the intestinal wall are almost always a sign of bowel infarction in adult patients.¹²³ Other findings of bowel ischemia or infarction on abdominal radiographs include dilation of bowel and nodular thickening or thumbprinting of the bowel wall. CT may also reveal characteristic findings in patients with bowel ischemia or infarction.^{124,125} Pneumatosis is particularly well shown by CT, but does not always indicate infarction of the bowel unless the pneumatosis is associated with portomesenteric venous gas.¹²⁶ The linear pattern of pneumatosis identified on CT is more likely to be associated with transmural bowel infarction than the bubbly pattern.¹²⁷

Pneumatosis cystoides intestinalis and pneumatosis coli are rare benign conditions characterized by multiple gas-filled cysts or blebs in the wall of the small bowel and colon, respectively. The cysts appear radiographically as grapelike clusters of gas, usually segmental in distribution (Fig. 12-16). These cystic collections may protrude into the bowel lumen, giving the small

bowel or colon a scalloped appearance on barium studies. In the large intestine, the left colon tends to be involved more frequently than the right colon. Despite the dramatic radiographic findings, affected individuals may have mild abdominal pain or may even be asymptomatic. The cysts often resolve spontaneously, but oxygen inhalation therapy has been used to facilitate resolution of these lesions.¹²⁸⁻¹³⁰

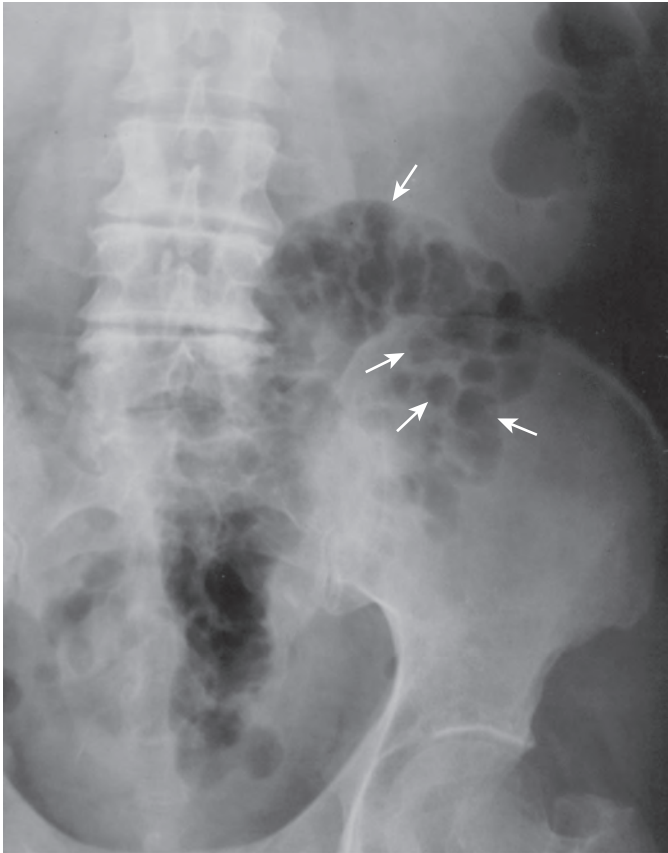


Figure 12-16 Pneumatosis coli. Multiple rounded, grapelike collections of gas (arrows) are seen in the wall of the sigmoid colon in a patient with benign pneumatosis coli.

Abscesses

Although CT is the most definitive radiologic test for diagnosing abscesses, abdominal radiographs may also be helpful for these patients.^{120,131,132} An abscess may be manifested by an extraluminal soft tissue mass that displaces adjacent bowel or by an extraluminal collection of gas. The most characteristic finding on abdominal radiographs is a mottled or bubbly gas collection within the abscess (Fig. 12-17A). Other patients may have a single rounded or ovoid collection of gas with an air-fluid level on horizontal beam views. Fecal material can mimic the appearance of a mottled gas collection but usually is distinguished by its location within the colon. A gastric or small bowel bezoar can also mimic an abscess.

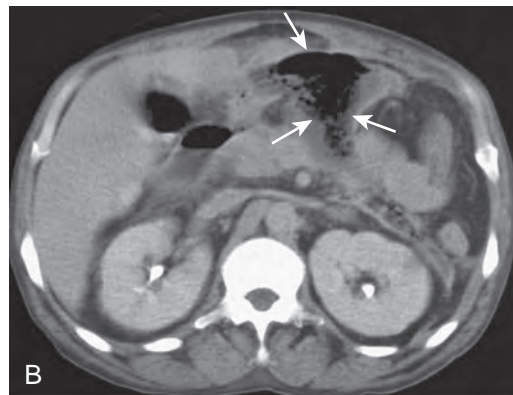
Infections of any intra-abdominal or retroperitoneal structure can result in the production of gas. Correlation of a linear or bubbly gas collection with knowledge of the anatomy is usually sufficient to localize the structure involved. The abdominal radiograph may be the initial study to suggest a gas-forming process, but CT is generally more useful in assessing the extent of disease and cause of the underlying pathology (Fig. 12-17B).¹³³

Normal Soft Tissue Structures

The ability to discern the edge of intra-abdominal organs on abdominal radiographs obtained with the patient in a supine position depends on the differences in x-ray attenuation between water density, fat density, and air. Intraperitoneal and retroperitoneal fat are present in varying degrees in even the thinnest patients. The liver, spleen, kidneys, psoas muscles, and urinary bladder can often be readily demonstrated because of surrounding fat (Fig. 12-18). In patients with sufficient fat, the serosal surface of the stomach may also appear as a faint edge. This subtle radiographic observation should not be confused with the much more distinct appearance of the serosa when it is outlined by air in patients with pneumoperitoneum. Fluid-filled loops of small and large bowel may also appear as tubular densities on a backdrop of abdominal fat. Recognition of organs is important because an abnormal contour or size of these organs may be the first indication of intra-abdominal disease.



Figure 12-17 Lesser sac abscess secondary to pancreatitis. **A.** A mottled collection of gas (arrows) is present in the left upper abdomen. **B.** CT shows gas and fluid (arrows) in the abscess cavity in a patient with pancreatitis.



Soft Tissue Abnormalities

LIVER

Liver size was estimated on abdominal radiographs by Pfahler as early as 1926.¹³⁴ Measurements of the liver on upright abdominal radiographs have been found to be reliable in detecting hepatomegaly.¹³⁵ The inferior tip of the liver usually does not extend below the iliac crest, except in asthenic individuals. Generalized hepatic enlargement tends to displace the hepatic flexure and transverse colon inferiorly and the stomach to the left (Fig. 12-19). Other signs of hepatic enlargement include the following: (1) extension of the inferior edge of the liver beyond



Figure 12-18 Normal soft tissue planes outlined by fat. The liver edge (large white arrows), left renal outline (small white arrows), margins of the psoas muscles (small black arrows), and splenic tip (large black arrow) can be identified.

the right margin of the psoas muscle; (2) displacement of the duodenal bulb below the L2 vertebral body or to the left of the midline; (3) inferior displacement of the right kidney; (4) enlargement or marked rounding of the hepatic angle; (5) elevation of the right hemidiaphragm, with decreased motion on respiration; (6) inferior or lateral displacement of the stomach with left lobe enlargement; and (7) anterior displacement of the duodenal bulb on lateral radiographs with caudate lobe enlargement.¹³⁶⁻¹³⁹ A small liver may result in reversal of some of these findings, with the right kidney higher than the left, the stomach displaced upward and to the right, and the duodenal bulb displaced above the level of the right 12th rib.

SPLEEN

Brogdon and Cros have found that the inferior tip of the spleen can be seen on abdominal radiographs in 44% of patients who had no evidence of splenomegaly.¹⁴⁰ The superior margin of the spleen normally lies just beneath the left hemidiaphragm, and its lateral edge approximates the lateral abdominal wall. As the spleen increases in size, its tip extends inferiorly below the 12th rib (Fig. 12-20). Displacement of the splenic flexure of the colon is an uncommon finding because the splenic flexure usually lies anterior to the spleen. A markedly enlarged spleen may also displace the stomach medially and anteriorly.

KIDNEYS

Because of surrounding fat, the renal outlines are visible on most abdominal radiographs. Moel studied 100 men and 100 women from 20 to 49 years of age and found that the average renal length on abdominal radiographs was 13.0 cm for men and 12.5 cm for women.¹⁴¹ Estimates of renal size must also take into account the foreshortening of the kidney that occurs because of angulation of this structure in normal individuals. Because of its retroperitoneal location, an enlarged kidney does not displace intra-abdominal organs, except in extreme cases. Renal cysts or tumors that produce contour abnormalities in the kidney may be readily apparent.

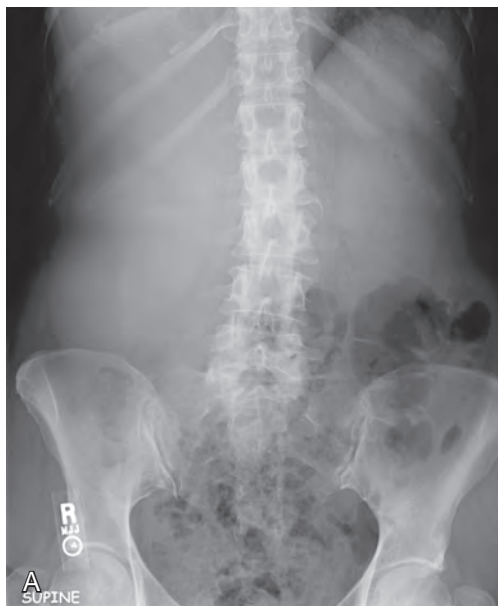
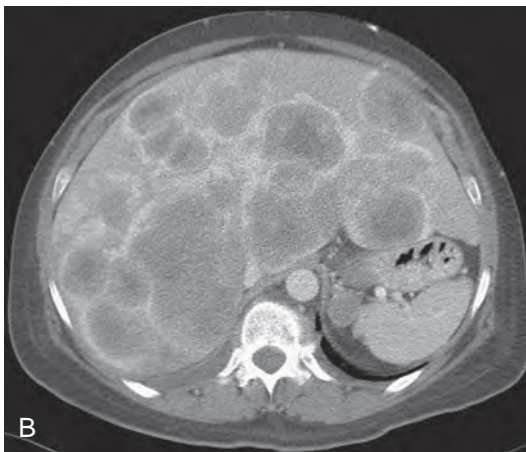


Figure 12-19 Hepatomegaly. **A.** Marked hepatic enlargement causes increased soft tissue density over the upper abdomen and displacement of bowel inferiorly. **B.** CT confirms hepatomegaly with multiple large metastases in the liver.



OTHER STRUCTURES

Retroperitoneal fat and intraperitoneal fat that permit visualization of adjacent water-density organs are helpful for evaluating contiguous pathologic processes in the abdomen. Surrounding inflammation may cause the fat to become edematous, so it takes in more water and approximates soft tissue density, thus obliterating contiguous planes. These changes are exemplified in patients with appendicitis because the normal margin of the psoas muscle and properitoneal fat planes demarcating the

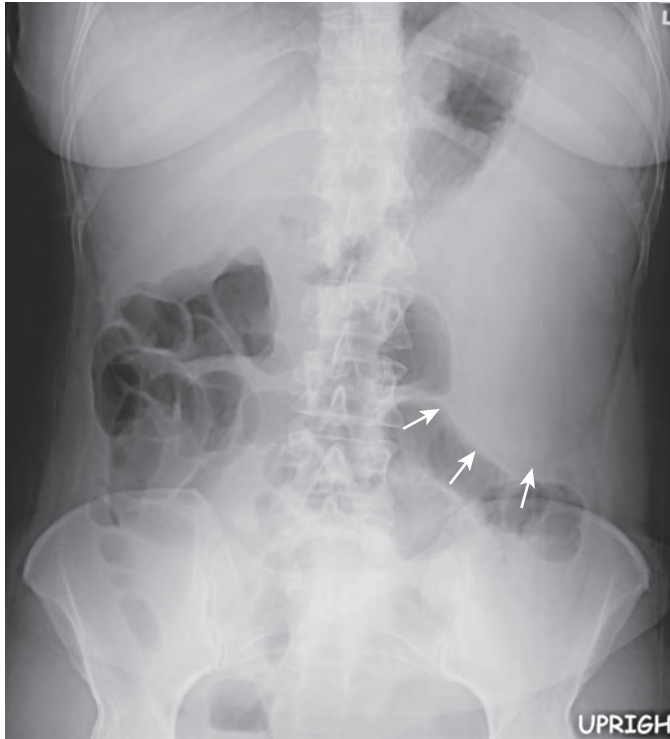


Figure 12-20 Splenomegaly. Supine abdominal radiograph shows marked splenic enlargement (arrows) with displacement of bowel inferiorly.

internal oblique, external oblique, and transversalis muscles of the abdomen may be obliterated. Although loss of these fat planes is an important sign of inflammation, it seldom occurs as an isolated finding, so it should be interpreted with caution and in conjunction with other signs of abdominal disease.

ASCITES

Because of the widespread use of abdominal CT and ultrasound, less emphasis is now placed on the findings of ascites on abdominal radiographs. It is still important to recognize these signs, however, because abdominal radiography is frequently one of the first imaging studies performed in patients with abdominal distention. In general, only large amounts of ascites can be identified on abdominal radiographs (Fig. 12-21).

Major Signs of Ascites

Major signs of ascites on abdominal radiographs include the following:

Obliteration of the Inferior Edge of the Liver. This sign can be extremely helpful (see Fig. 12-21A). Proper technique with the use of low kilovoltage is essential. The liver edge may be preserved in patients with loculated ascites, and excessive feces in the hepatic flexure of the colon may falsely obliterate the liver edge.¹⁴²

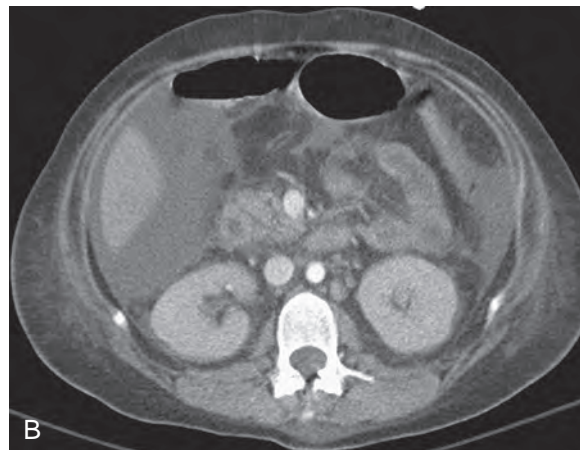
Widening of the Distance Between the Flank Stripe and Ascending Colon. This distance is normally 2 to 3 mm, but may increase as fluid fills the right paracolic gutter.

Medial Displacement of the Lateral Edge of the Liver (Hellmer's Sign). This finding usually requires a large amount of ascites and is more common with malignant ascites than with cirrhosis, probably because the fat content of the cirrhotic liver approximates the density of ascites.¹⁴³

Fluid Accumulation in the Pelvis. Intraperitoneal fluid tends to accumulate in the most inferior intraperitoneal recess, also known as the pouch of Douglas or cul de sac. A distended



Figure 12-21 Ascites. A. The normal liver edge is obscured. The bowel loops are centrally located in the abdomen, and there is separation of bowel loops. **B.** CT confirms the presence of perihepatic ascites.



bladder or rectum may impress centrally on this fluid, causing symmetric bulges that have been described as dog ears.

Separation of Bowel Loops. This sign is seldom seen as an isolated finding and requires a large amount of ascites (see Fig. 12-21A). It can easily be mimicked by a disproportionately large amount of fluid and smaller amount of air in juxtaposed bowel loops.

Centrally Located Bowel Loops with Bulging Flanks. With large amounts of ascites, bowel loops may float to the most nondependent central portion of the abdomen (see Fig. 12-21A).

Ground-Glass Appearance. This radiographic finding also requires large amounts of fluid and may erroneously be suggested by improper radiographic technique or marked obesity.

REFERENCES

- Baker SR, Cho KC: The Abdominal Plain Film with Correlative Imaging, East Norwalk, CT, 1999, Appleton & Lange.
- McCort JJ, editor: Abdominal Radiology, Baltimore, 1981, Williams & Wilkins.
- Welch JP: Bowel Obstruction: Differential Diagnosis and Clinical Management, Philadelphia, 1990, WB Saunders.
- Goyal RK, Spiro HM: Gastrointestinal manifestations of diabetes mellitus. *Med Clin North Am* 55:1031-1040, 1971.
- Seaman WB: Motor dysfunction of the gastrointestinal tract. *AJR* 116:235-248, 1972.
- Cantor MO: Ileus. *Am J Gastroenterol* 47:461-484, 1967.
- Tibblin S: Diagnosis of intestinal obstruction with special regard to plain roentgen examination of the abdomen. *Acta Chir Scand* 135:249-252, 1969.
- Frimann-Dahl J: Roentgen findings in intestinal knots. *Acta Radiol* 23:22-33, 1942.
- Holder LE, Schneider HJ: Spigelian hernias: Anatomy and roentgenographic manifestations. *Radiology* 112:309-313, 1974.
- Spiers TC, Rosenbloom MB, Palayew MJ: Spigelian hernia: Plain film diagnosis. *J Can Assoc Radiol* 31:147-148, 1980.
- Strauss S, Rubinstein ZJ, Shapiro Z: Food as a cause of small intestinal obstruction: A report of five cases without previous gastric surgery. *Gastrointest Radiol* 2:17-20, 1977.
- Weissberg DL, Berk RN: Ascariasis of the gastrointestinal tract. *Gastrointest Radiol* 3:415-418, 1978.
- Gupta S, Vaidya MP: Mechanical small bowel obstruction caused by acute appendicitis. *Am Surg* 35:670-674, 1969.
- Gollub MJ: Multidetector computed tomography enteroclysis of patients with small bowel obstruction: A volume-rendered "surgical perspective". *J Comput Assist Tomogr* 29:401-407, 2005.
- Ogilvie H: Large intestine colic due to sympathetic deprivation. *BMJ* 2:671-673, 1948.
- Lescher TJ, Teegarden DK, Pruitt BA: Acute pseudo-obstruction of the colon in thermally injured patients. *Dis Colon Rectum* 21:618-622, 1978.
- Caccese WJ, Bronzo RL, Wadler G, et al: Ogilvie's syndrome associated with herpes zoster infection. *J Clin Gastroenterol* 7:309-313, 1985.
- Nanni C, Garbini A, Luchetti P, et al: Ogilvie's syndrome (acute colonic pseudo-obstruction): Review of the literature and report of four additional cases. *Dis Colon Rectum* 25:157-166, 1982.
- Ravo B, Pollane M, Ger R: Pseudo-obstruction of the colon following caesarean section: A review. *Dis Colon Rectum* 26:440-444, 1983.
- Nakhgevan KB: Colonoscopic decompression of the colon in patients with Ogilvie's syndrome. *Am J Surg* 148:317-320, 1984.
- Shirazi KK, Agha FP, Strodel WE, et al: Nonobstructive colonic dilation: Radiologic findings in 50 patients following colonoscopic treatment. *J Can Assoc Radiol* 35:116-119, 1984.
- Strodel WE, Nostrant TT, Eckhauser FE, et al: Therapeutic and diagnostic colonoscopy in nonobstructive colonic dilatation. *Ann Surg* 197:416-421, 1983.
- Fazel A, Verne GN: New solutions to an old problem: Acute colonic pseudo-obstruction. *J Clin Gastroenterol* 39:17-20, 2005.
- Saunders MD: Acute colonic pseudo-obstruction. *Curr Gastroenterol Rep* 6:410-416, 2004.
- Johnson CD, Rice RP, Kelvin FM, et al: The radiological evaluation of gross cecal distensions: Emphasis on cecal ileus. *AJR* 145:1211-1217, 1985.
- Welch CE, Ottinger LW, Welch JP: Manual of Lower Gastrointestinal Surgery, New York, 1980, Springer-Verlag.
- Phillips RK, Hittinger R, Fry JS, et al: Malignant large bowel obstruction. *Br J Surg* 72:296-302, 1985.
- Albers JH, Smith LL, Carter R: Perforation of the cecum. *Ann Surg* 143:251-255, 1956.
- Crowder VH, Jr, Cohn I, Jr: Perforation in cancer of the colon and rectum. *Dis Colon Rectum* 10:415-420, 1967.
- Glenn F, McSherry CK: Obstruction and perforation in colorectal cancer. *Ann Surg* 173:983-992, 1971.
- Khan S, Pawlak SE, Eggenberger JC, et al: Acute colonic perforation associated with colorectal cancer. *Am Surg* 67:261-264, 2001.
- Ballantyne GH: Review of sigmoid volvulus: Clinical patterns and pathogenesis. *Dis Colon Rectum* 25:823-830, 1982.
- Ballantyne GH, Brandner MD, Beart RW, Jr, et al: Volvulus of the colon: Incidence and mortality. *Ann Surg* 202:83-92, 1985.
- Javors BR, Baker SR, Miller JA: The northern exposure sign: A newly described finding in sigmoid volvulus. *AJR* 173:571-574, 1999.
- Young WS: Further radiological observations in caecal volvulus. *Clin Radiol* 31:479-483, 1980.
- Anderson JR, Mills JOM: Cecal volvulus: A frequently missed diagnosis? *Clin Radiol* 35:65-69, 1985.
- Yang SH, Lin JK, Lee RC, et al: Cecal volvulus: Report of seven cases and literature review. *Zhonghua Yi Xue Za Zhi (Taipei)* 63:482-486, 2000.
- Moore CJ, Corl FM, Fishman EK: CT of cecal volvulus: Unraveling the image. *AJR* 177:95-98, 2001.
- Anderson JR, Spence RA, Wilson BG, et al: Gangrenous cecal volvulus after colonoscopy. *BMJ* 286:439-440, 1983.
- Hemingway AP: Cecal volvulus—a new twist to the barium enema. *Br J Radiol* 53:806-807, 1980.
- Howard RS, Catto J: Cecal volvulus: A case for non-resectional therapy. *Arch Surg* 115:273-277, 1980.
- Weinstein M: Volvulus of the cecum and ascending colon. *Ann Surg* 107:248-259, 1938.
- Bobroff LM, Messinger NH, Subbarao K, et al: The cecal bascule. *AJR* 115:249-252, 1972.
- Newton NA, Reines HD: Transverse colon volvulus: Case reports and review. *AJR* 128:69-72, 1977.
- Zinken LD, Katz LD, Rosin JD: Volvulus of the transverse colon: Report of a case and review of the literature. *Dis Colon Rectum* 22:492-496, 1979.
- Kerry RL, Ransom HK: Volvulus of the colon: Etiology, diagnosis, and treatment. *Arch Surg* 99:215-222, 1963.
- Ballantyne GH: Volvulus of the splenic flexure: Report of a case and review of the literature. *Dis Colon Rectum* 24:630-632, 1981.
- Lantieri R, Teplick SK, Labell MJ: Splenic flexure volvulus: Two case reports and review. *AJR* 132:463-464, 1979.
- Sachidanathan CK, Soehner B: Volvulus of the splenic flexure of the colon: Report of a case and review of the literature. *Dis Colon Rectum* 15:466-469, 1972.
- Mindelzun RE, Stone JM: Volvulus of the splenic flexure: Radiographic features. *Radiology* 181:221-223, 1991.
- Campbell JP, Gunn AA: Plain abdominal radiographs and acute abdominal pain. *Br J Surg* 75:554-556, 1988.
- Olutola PS: Plain film radiographic diagnosis of acute appendicitis: An evaluation of the signs. *Can Assoc Radiol J* 39:254-256, 1988.
- Nitecki S, Karmeli R, Sarr MG: Appendiceal calculi and fecaliths as indications for appendectomy. *Surg Gynecol Obstet* 171:185-188, 1990.
- Faegenburg D: Fecaliths of the appendix: Incidence and significance. *AJR* 89:752-759, 1963.
- Thomas SF: Appendiceal coproliths: Their surgical importance. *Radiology* 49:39-49, 1947.
- Bunch GH, Adcock DF: Giant faceted calculus. *Ann Surg* 109:143-146, 1939.
- Lewis FR, Holcroft JW, Boey J, et al: Appendicitis: A critical review of diagnosis and treatment in 1000 cases. *Arch Surg* 110:677-684, 1975.
- Mowji PJ, Jones MD, Cohen AJ: Localized ileus of the proximal jejunum: A new sign for acute appendicitis. *Gastrointest Radiol* 14:173-175, 1989.
- Hayden CK, Swischuk LE: Appendicitis with perforation: The dilated transverse colon sign. *AJR* 135:687-689, 1980.
- Killen DA, Brooks DW, Jr: Gas-filled appendix: A roentgen sign of acute appendicitis. *Ann Surg* 161:474-478, 1965.
- Lim MS: Gas-filled appendix: Lack of diagnostic specificity. *AJR* 128:209-210, 1977.

62. Farman J, Kassner EG, Dallemand S, et al: Pneumoperitoneum and appendicitis. *Gastrointest Radiol* 1:277-279, 1976.
63. McCort JJ: Extra-alimentary gas in perforated appendicitis: Report of six cases. *AJR* 77:647-651, 1977.
64. Greenstein AJ, Sachar DB, Gibas A, et al: Outcome of toxic dilatation in ulcerative colitis and Crohn's colitis. *J Clin Gastroenterol* 7:137-144, 1985.
65. Jalan KN, Sircus W, Card WL, et al: An experience of ulcerative colitis: I. Toxic dilatation in 55 cases. *Gastroenterology* 8:213-220, 1947.
66. Roys G, Kaplan MS, Juler GL: Surgical management of toxic megacolon. *Am J Gastroenterol* 68:161-166, 1977.
67. Katzka I, Katz S, Morris E: Management of toxic megacolon: The significance of early recognition in medical management. *J Clin Gastroenterol* 1:307-311, 1979.
68. Kramer P, Wittenberg J: Colonic gas distribution in toxic megacolon. *Gastroenterology* 80:433-437, 1981.
69. Norland CC, Kirsner JB: Toxic dilatation of the colon (toxic megacolon): Etiology, treatment and prognosis in 42 patients. *Medicine (Baltimore)* 48:229-250, 1969.
70. Halpert RD: Toxic dilatation of the colon. *Radiol Clin North Am* 25:147-155, 1987.
71. Greenstein AJ, Aufses AH: Differences in pathogenesis, incidence and outcome of perforation in inflammatory bowel disease. *Surg Gynecol Obstet* 160:63-69, 1985.
72. Caprilli R, Vernia P, Latella G, et al: Early recognition of toxic megacolon. *J Clin Gastroenterol* 9:160-164, 1987.
73. Wolf BS, Marshak RH: Toxic segmental dilatation of the colon during the course of fulminating ulcerative colitis: Roentgen findings. *AJR* 82:985-995, 1959.
74. Imbriaco M, Balthazar EJ: Toxic megacolon: Role of CT evaluation and detection of complications. *Clin Imaging* 25:349-354, 2001.
75. Miller RE, Nelson SW: The roentgenological demonstration of tiny amounts of free intraperitoneal gas: Experimental and clinical studies. *AJR* 112:574-585, 1971.
76. Miller RE, Becker GJ, Slabaugh RA: Detection of pneumoperitoneum: Optimum body position and respiratory phase. *AJR* 135:487-490, 1980.
77. Woodring JH, Heiser MJ: Detection of pneumoperitoneum on chest radiographs: Comparison of upright lateral and posteroanterior projections. *AJR* 165:45-47, 1995.
78. Stapakis JC, Thickman D: Diagnosis of pneumoperitoneum: Abdominal CT vs. upright chest film. *J Comput Assist Tomogr* 16:713-716, 1992.
79. Earls JP, Dachman AH, Colon E, et al: Prevalence and duration of postoperative pneumoperitoneum: Sensitivity of CT vs. left lateral decubitus radiography. *AJR* 161:781-785, 1993.
80. Levine MS, Scheiner JD, Rubesin SE, et al: Diagnosis of pneumoperitoneum on supine abdominal radiographs. *AJR* 156:731-735, 1991.
81. Rigler LG: Spontaneous pneumoperitoneum: A roentgenologic sign found in supine position. *Radiology* 37:604-607, 1941.
82. Cho KC, Baker SR, Lum C, Javors BR: Pneumoperitoneum: New observations on plain films and CT scans [abstract]. *Radiographics* 17(Suppl 2):1616-1620, 1997.
83. Mindelzun RE, McCort JJ: Cupola sign of pneumoperitoneum in the supine patient. *Gastrointest Radiol* 11:283-285, 1986.
84. Cho KC, Baker SR: Depiction of diaphragmatic muscle slips on supine plain radiographs: A sign of pneumoperitoneum. *Radiology* 203:431-433, 1997.
85. Hajdu N, de Lacy G: The Rutherford Morison pouch: A characteristic appearance on abdominal radiographs. *Br J Radiol* 43:706-709, 1970.
86. Brill PW, Olson SR, Winchester P: Neonatal necrotizing enterocolitis: Air in Morison pouch. *Radiology* 174:469-471, 1990.
87. Menuck L, Siemens PT: Pneumoperitoneum: Importance of right upper quadrant features. *AJR* 127:753-756, 1976.
88. Radin R, Van Allan RJ, Rosen RS: The visible gallbladder: A plain film sign of pneumoperitoneum. *AJR* 167:69-70, 1996.
89. Jelaso DV, Schultz EH, Jr: The urachus—an aid to the diagnosis of pneumoperitoneum. *Radiology* 92:295-296, 1969.
90. Weiner CI, Diaconis JN, Dennis JM: The "inverted V": A new sign of pneumoperitoneum. *Radiology* 107:47-48, 1973.
91. Cho KC, Baker SR: Air in the fissure for the ligamentum teres: New sign of intraperitoneal air on plain radiographs. *Radiology* 178:489-492, 1991.
92. Cho KC, Baker SR: Visualization of the extrahepatic segment of the ligamentum teres: A sign of free air on plain radiographs. *Radiology* 202:651-654, 1997.
93. Miller RE: Perforated viscus in infants: A new roentgen sign. *Radiology* 74:65-67, 1960.
94. Walker LA, Weens HS: Radiological observations on the lesser peritoneal sac. *Radiology* 80:727-737, 1963.
95. Meyers MA: Radiological features of the spread and localization of extraperitoneal gas and their relationship to its source: An anatomical approach. *Radiology* 111:17-26, 1974.
96. Walker CW, Purnell GL, Diner WC: Complications from extravasated retroperitoneal barium: Case report and review of the literature. *Radiology* 173:618-620, 1989.
97. Beerman PJ, Gelfand DW, Ott DJ: Pneumomediastinum after double-contrast barium enema examination: A sign of colonic perforation. *AJR* 136:197-198, 1981.
98. Peterson N, Rohrmann CA, Jr, Lennard ES: Diagnosis and treatment of retroperitoneal perforation complicating double-contrast barium enema examination. *Radiology* 144:249-252, 1982.
99. Balthazar EJ, Gurkin S: Cholecystoenteric fistulas: Significance and radiographic diagnosis. *Am J Gastroenterol* 65:168-173, 1976.
100. Balthazar EJ, Schecter LS: Air in gallbladder: A frequent finding in gallstone ileus. *AJR* 131:219-222, 1978.
101. Ulreich S, Massi J: Recurrent gallstone ileus. *AJR* 133:921-923, 1979.
102. Rigler LG, Borman DN, Noble JF: Gallstone obstruction: Pathogenesis and roentgen manifestations. *JAMA* 117:1753-1759, 1941.
103. Cremin BJ: Biliary parasites. *Br J Radiol* 42:506-508, 1969.
104. Mindelzun R, McCort JJ: Hepatic and perihepatic radiolucencies. *Radiol Clin North Am* 18:221-238, 1980.
105. Govoni AF, Meyers MD: Pseudopneumobilia. *Radiology* 118:526, 1976.
106. Halber MD, Daffner RH: Fat in the intrahepatic fissure. *AJR* 132:842-843, 1979.
107. Susman N, Senturia HR: Gas embolization of the portal venous system. *AJR* 83:847-850, 1960.
108. Sisk PB: Gas in the portal venous system. *Radiology* 77:103-107, 1981.
109. McCandless RL: Portal vein gas: A grave prognostic sign. *AJR* 92:1162-1165, 1964.
110. Benson MD: Adult survival with intrahepatic portal venous gas secondary to acute gastric dilatation, with a review of portal venous gas. *Clin Radiol* 36:441-443, 1985.
111. Graham GA, Bernstein RB, Gronner AT: Gas in the portal and inferior mesenteric veins caused by diverticulitis of the sigmoid colon: Report of a case with survival. *Radiology* 114:601-602, 1975.
112. Birnberg FA, Gore RM, Shragg B, et al: Hepatic portal venous gas: A benign finding in a patient with ulcerative colitis. *J Clin Gastroenterol* 5:89-91, 1983.
113. Sadler VK, Brennan RE, Madan V: Portal vein gas following air-contrast barium enema in granulomatous colitis: Report of a case. *Gastrointest Radiol* 4:163-164, 1979.
114. Haber I: Hepatic portal vein gas following colonoscopy in ulcerative colitis—report of a case. *Acta Gastroenterol Belg* 46:14-17, 1983.
115. Herman JB, Levine MS, Long WB: Portal venous gas as a complication of ERCP and endoscopic sphincterotomy. *Am J Gastroenterol* 90:828-829, 1995.
116. Chezmar JL, Nelson RC, Bernardino ME: Portal venous gas after hepatic transplantation: Sonographic detection and clinical significance. *AJR* 153:1203-1205, 1989.
117. Marks WM, Filly RA: Computed tomographic demonstration of intra-arterial air following hepatic artery ligation. *Radiology* 132:665-666, 1979.
118. Seaman WB, Fleming RJ: Intramural gastric emphysema. *AJR* 101:431-436, 1967.
119. Berens SV, Moskowitz H, Mellins HZ: Air within the wall of the stomach: Roentgen manifestations and a new roentgenographic sign. *AJR* 103:310-313, 1968.
120. Zweig GJ, Yuk-Pui L, Srinantaswamy S, et al: Gas-forming infections of the abdomen: Plain film findings. *Appl Radiol* 19:37-42, 1990.
121. Shipman PJ, Drury P: Emphysematous gastritis: Case report and literature review. *Australas Radiol* 45:64-66, 2001.
122. Pear BL: Pneumatosis intestinalis: A review. *Radiology* 207:13-19, 1998.
123. Tomchik FS, Wittenberg J, Ottinger LW: The roentgenographic spectrum of bowel infarction. *Radiology* 96:249-260, 1970.
124. Smerud MJ, Johnson CD, Stephens DH: Diagnosis of bowel infarction: A comparison of plain films and CT scans in 23 cases. *AJR* 154:99-103, 1990.
125. Lund EC, Han SY, Holley HC, et al: Intestinal ischemia: Comparison of plain radiographic and computed tomographic findings. *Radiographics* 8:1083-1108, 1988.
126. Kernagis LY, Levine MS, Jacobs JE: Pneumatosis intestinalis in patients with ischemia: Correlation of CT finding with viability of the bowel. *AJR* 180:733-736, 2003.
127. Wiesner W, Koenraad J, Morteale JN, et al: Pneumatosis intestinalis and portomesenteric venous gas in intestinal ischemia. *AJR* 177:1319-1323, 2003.
128. Marshak RH, Lindner AE, Milano AM: Pneumatosis coli. *Am J Gastroenterol* 56:68-73, 1971.

129. Bloch C: The natural history of pneumatosis coli. *Radiology* 123:311–314, 1977.
130. Simons NM, Hyman KE, Divertie MB, et al: Pneumatosis cystoides intestinalis: Treatment with oxygen via close-fitting mask. *JAMA* 231:1354–1356, 1975.
131. Sands WW: Extraluminal localized gas vesicles: An aid in the diagnosis of abdominal abscesses from plain roentgenograms. *AJR* 74:195–203, 1955.
132. Rice RP, Masters SJ: Intraabdominal abscess. *Semin Roentgenol* 8:365–374, 1973.
133. Grayson DE, Abbott RM, Levy AD, et al: Emphysematous infections of the abdomen and pelvis: A pictorial review. *Radiographics* 22:543–561, 2002.
134. Pfahler GE: Measurement of the liver by means of roentgen rays based upon a study of 502 subjects. *AJR* 16:558–564, 1926.
135. Unal B, Bilgili E, Kocacikli S, et al: Simple evaluation of liver size on erect abdominal plain radiography. *Clin Radiol* 59:1132–1135, 2004.
136. Gelfand DW: The liver: Plain film diagnosis. *Semin Roentgenol* 10:177–185, 1975.
137. Chon H, Arger PH, Miller WT: Displacement of duodenum by an enlarged liver. *AJR* 119:85–88, 1987.
138. Kattan KR, Moskowitz M: Position of the duodenal bulb and liver size. *AJR* 119:78–84, 1973.
139. Whalen JP, Evans JA, Meyers MS: Vector principle in the differential diagnosis of abdominal masses: II. Right upper quadrant. *AJR* 115:318–333, 1972.
140. Brogdon BG, Cros NE: Observations on the “normal” spleen. *Radiology* 72:412–414, 1959.
141. Moel H: Size of the normal kidneys. *Acta Radiol Diagn* 46:640, 1956.
142. Proto AV, Lane EJ: Visualization of differences in soft tissue densities: The liver in ascites. *Radiology* 121:19–23, 1976.
143. Wixson D, Kazam E, Whalen JP: Displaced lateral surface of the liver (Hellmer’s sign) secondary to an extraperitoneal fluid collection. *AJR* 127:679–682, 1976.

Abdominal Calcifications

STEPHEN R. BAKER

CHAPTER OUTLINE

Physiology

Morphology

Concretions

Conduit Wall Calcification

Cystic Calcification

Solid Mass Calcification

Difficulty in Classification

Location

Mobility

The abdomen is a closely packed space containing numerous conduits and organs related to each other in a complex spatial arrangement. Each of these structures is subject to a unique range of diseases, all having specific causes and characteristic manifestations. However, the spectrum of findings on abdominal radiographs is surprisingly limited. Important signs include displacement, enlargement, or atrophy of organs, distention of bowel, extraluminal gas, and calcification in parenchymal and supporting tissues. In many cases, the pattern of calcium deposition is the most informative and distinctive radiographic finding.

Calcification may occur in the wall of blood vessels or other conduits, the lumen of hollow structures, and the solid substance of viscera or neoplasms. Despite the variety of causes of abdominal calcification, a systematic evaluation of the morphologic features, location, and mobility of an abnormal opacity usually narrows the diagnostic considerations to just a few likely possibilities. In many cases, analysis of the appearance of an abdominal calcification on abdominal radiographs provides sufficient information for an unequivocal diagnosis without need for additional examinations. In other cases, careful assessment of the morphology, location, and mobility of an abdominal calcification helps focus the choice and sequence of subsequent imaging examinations.

Physiology

The precipitation of calcareous substances requires an alkaline medium and high local concentrations of ionic calcium. The term *metastatic calcification* refers to the deposition of calcium salts in normal tissues as the result of hypercalcemia and an elevated pH. Although the stomach and kidneys are the most frequent sites of metastatic calcification in the abdomen, the degree of parenchymal opacification in these organs is usually too faint to be detected on abdominal radiographs. The most common cause of radiographically detectable metastatic calcification is chronic renal failure with secondary

hyperparathyroidism.¹ As a result of this pathologic process, diffuse opacification of the kidneys is often accompanied by osteomalacia or osteoporosis.

The term *dystrophic calcification* refers to a phenomenon, far more frequent than metastatic calcification, that occurs despite normal serum levels of calcium. Dystrophic calcification may be caused by trauma, ischemia, infarction, or other pathologic processes, resulting in a predisposition to calcium deposition. In some tumors, the rapid breakdown of lipids releases fatty acids that bind calcium with particular avidity. Mucin-producing adenocarcinomas of the gastrointestinal (GI) tract possess a glycoprotein similar in chemical configuration to cartilage and share with it an affinity for calcium aggregation.² Although some structures in the abdomen have a propensity for dystrophic calcification, the mechanisms and kinetics of calcium deposition have not been fully elucidated.

Some devitalized or degenerative tissues are also associated with new bone formation. However, ossification is less common than dystrophic calcification. Calcified osteoid may be found as an isolated finding, or it may coexist with adjacent areas of calcium deposition that lack the histologic structure of bone. In either case, local tissue damage appears to be the precipitating factor. Ossification may occur in ovarian or retroperitoneal teratomas (Fig. 13-1), abdominal scars, particularly after gastric surgery or suprapubic bladder catheterization and, rarely, colonic and retroperitoneal neoplasms.

Papillary serous cystadenocarcinomas of the ovary often contain a distinctive form of calcification characterized by a psammomatous or cloudlike opacity attributable to intracellular deposition of calcium salts in the lesion (Fig. 13-2).³ In contrast, dystrophic calcification associated with other metastatic tumors is caused by extracellular precipitation of calcium salts. Psammomatous and dystrophic calcification may be manifested by amorphous, poorly outlined areas of increased density. When this finding occurs, the distribution of calcified metastases may narrow the differential diagnosis, sometimes leading to an unequivocal diagnosis.

Morphology

The recognition of specific abdominal calcifications has been aided by the attribution of vivid descriptive names to particular radiopacities. For example, a “staghorn calculus” is a large, branching opacity in the renal pelvis. Such appellations are highly evocative and easily remembered; however, they do not help generate a differential diagnosis from among the many causes of abdominal calcification. Unfortunately, most surveys of abdominal calcification have relied primarily on such descriptive designations and have failed to emphasize diagnostic features that might help organize the various opacities into categories with shared characteristics.

In this chapter, a logical scheme is presented for classifying almost all abdominal calcifications. They may be distinguished radiographically on the basis of various morphologic features, including contour, border, sharpness, marginal continuity, and internal architecture. Consideration of these features permits a grouping of calcifications into one of four classes: (1) concre-

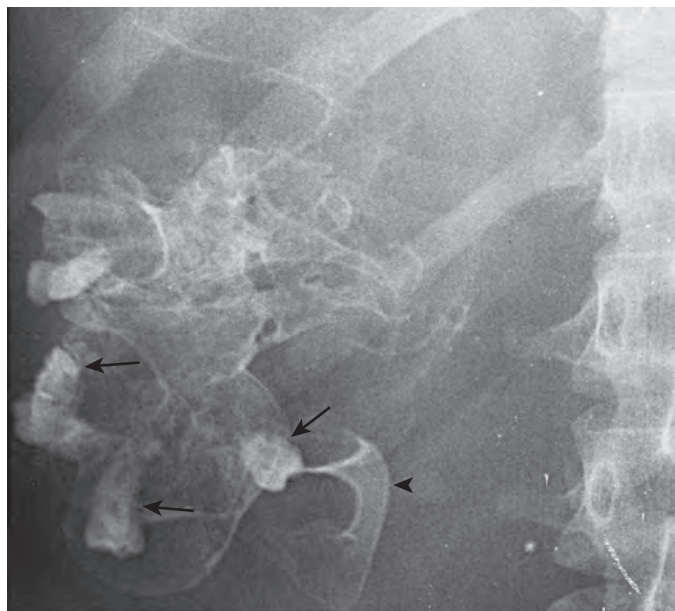


Figure 13-1 Retroperitoneal teratoma. Both teeth (*arrows*) and bone (*arrowhead*) are visualized. Note the cortex and trabecula in the disordered pattern of ossification.



Figure 13-2 Ovarian papillary serous cystadenocarcinoma. Patches of psammomatous calcification (*arrow*) are seen in the left abdomen in an intraperitoneal metastasis.

tions; (2) conduit wall calcification; (3) cystic calcification; and (4) solid mass calcification. In the following sections, the distinguishing features of each class are discussed in detail. Potential pitfalls and notable exceptions are also considered.

CONCRETIONS

Concretions are precipitates removed from solution in a liquid medium inside a vessel or hollow viscus. They often contain a central nidus, composed of an insoluble substance such as an inorganic foreign body, ingested vegetable matter, thrombus, or focal collection of pus and cellular debris. In pelvic veins and in the GI and genitourinary tracts, concretions are likely to calcify. They can be brightly or faintly opaque; the radiographic density depends on the size of the opacity and amount of calcium per unit volume. Concretions do not have a common shape. Biliary calculi are usually oval or rounded, whereas gallstones are often faceted (*Fig. 13-3*). Ureteral and pancreatic stones often have jagged edges, but in hollow viscera such as the urinary bladder and gallbladder, the concretions usually have smooth margins.

A sharply defined, continuous external margin is a unifying feature of concretions. Stones are almost always characterized by an uninterrupted edge of calcification throughout their entire perimeter, with no lucent gaps along the interface with the surrounding medium. This unique feature permits

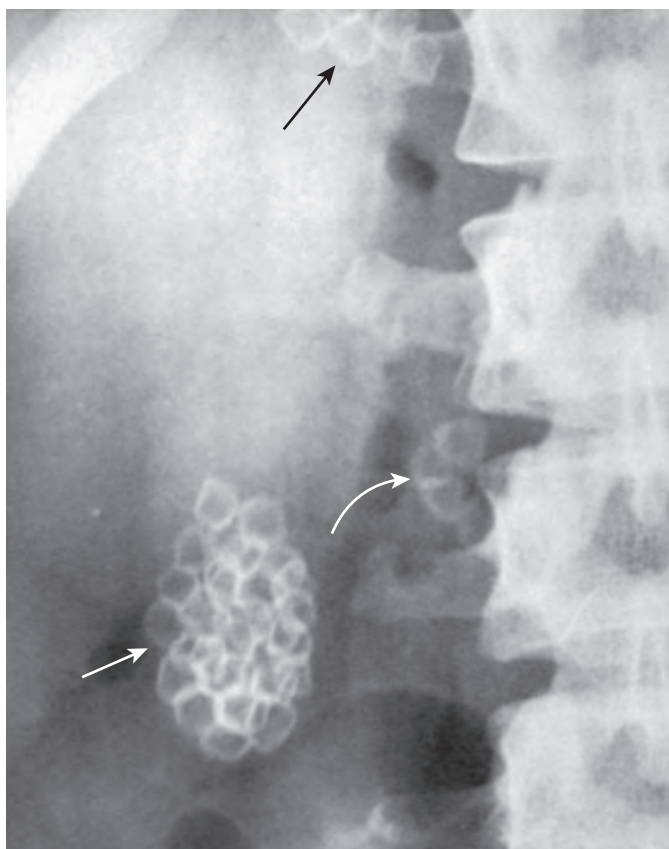


Figure 13-3 Biliary stones. Numerous stones are seen in the gallbladder (*straight white arrow*), cystic duct (*black arrow*), and common bile duct (*curved white arrow*). Note how the stones have faceted margins.



Figure 13-4 Ovarian vein phleboliths. Numerous phleboliths, each having a central lucency, are located within a dilated right ovarian vein.

differentiation of small stones with radiolucent centers from calcified vessels seen on end. The circumferential opacification of the perimeter of large stones also helps distinguish them from calcified cysts.

Concretions may vary greatly in their internal architecture. A stone may be homogeneously dense, a pattern often encountered in urinary calculi, or it may contain a slightly eccentric area of lucency, an appearance typical of phleboliths (Fig. 13-4). Concentric laminations are characteristic of gallstones, bladder concretions, and appendicoliths (Fig. 13-5). Each of these various internal configurations has a certain predictability and uniformity. A central lucency is often present. Stones seldom have a mottled, speckled, or patchy appearance. The deposition of calcium on only one surface of the stone is extremely rare.

Unlike calcified solid lesions or cysts, which are pathologic tumefactions that distort or displace normal organs and supporting structures, stones tend to be confined within preexisting vessels or fluid-filled viscera. When multiple stones are present, they may outline the course of a hollow tube or the dimensions of a distensible reservoir. Concretions appearing outside expected anatomic locations are unusual, such as multiple phleboliths in a hemangioma, ectopic gallstones in the distal small bowel in a patient with gallstone ileus, and appendicoliths from a ruptured appendix in the peritoneal cavity.

CONDUIT WALL CALCIFICATION

Conduits are fluid-conducting hollow tubes. In the abdomen, they include the ureter, urethra, vas deferens, pancreatic ducts, bile ducts, and vascular structures. The vast majority of



Figure 13-5 Lamellated appendicolith. Note the continuous margin of calcification, parallel lamina, and small medial bulge along the edge of this concretion.

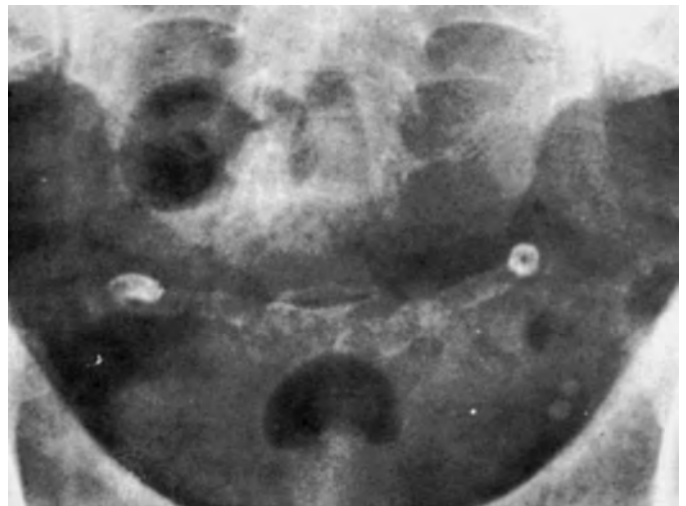


Figure 13-6 Conduit wall calcification in the vas deferens. Marginal opacities are seen en face and in profile.

conduit wall calcifications are located in the aorta and its branches. The tubular configuration characteristic of conduits is readily appreciated if the calcification is extensive and circumferential. When the vessel is parallel to the radiographic beam, a ringlike density is often observed (Fig. 13-6). In contrast to calculi, conduit wall calcifications often have gaps in the opaque ring. Because calcification in conduit walls is not uniform, alternating radiopaque and radiolucent areas may be seen along the course of the vessel. Internal radiopacities are not a feature of conduit wall calcifications, so

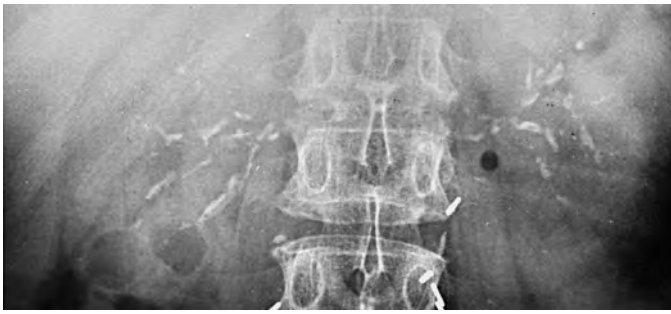


Figure 13-7 Calcification of the renal arteries and their intrarenal branches. These opacities have the typical configuration of conduit wall calcification.

the presence of central radiopaque areas brighter than the periphery of the agglomeration of a radiodensity should suggest another class of abdominal calcifications. Even when there is profuse mural calcification, the lateral walls of the conduit provide a longer path for the x-ray beam to traverse than the anterior or posterior walls, so they appear more opaque than the vessel wall oriented en face. As a result, a conduit wall calcification is usually manifest by parallel linear opacities when the vessel is aligned along the course of the x-ray beam or by a circle of radiopacity when the beam is directed perpendicular to the course of the conduit. A marginal branching pattern may be observed at the bifurcation of the abdominal aorta or in the intrarenal arteries (Fig. 13-7). Calcification of narrow-caliber vessels occasionally produces a stringlike appearance. In the female pelvis, calcification of the uterine artery may be evident by a horizontal or slightly undulating linear opacity or by a series of curvilinear stringlike densities.

Conduit wall calcification is clearly distinguishable only if deposition of calcium is extensive. A single fleck of calcification can simulate a small calculus or even a thin piece of cortical bone, particularly in the renal pelvis. Conversely, the lateral margin of the transverse process of a lumbar vertebra can mimic calcification in the renal artery. However, the lateral margin of the transverse process has a vertical orientation, whereas the renal artery is oriented horizontally (see Fig. 13-7).

Conduit wall calcification is usually found at the expected location of vessels. Thus, it is not seen at the lateral margin of the spleen or in other peripheral locations. As arteries become tortuous and dilated, however, their walls may eventually be displaced several centimeters or more from their expected location. Hence, the wall of a dilated calcified aorta may be seen to overlie the midline, or even to lie to the right of the spine on abdominal radiographs.

CYSTIC CALCIFICATION

Cystic calcification is characterized by the deposition of calcium in the wall of abnormal fluid-filled masses, a category encompassing true epithelial cysts, pseudocysts, and aneurysmally dilated arteries. Despite the diversity of cystic structures in the abdomen, cystic calcification exhibits remarkably uniform radiographic findings.

A cystic pattern of calcification is characterized by the presence of a smooth arcuate rim of radiopacity in the wall of the cyst (Fig. 13-8). Although opacities may be present in cysts and



Figure 13-8 Large echinococcus cyst in the liver. Note how the calcified wall of the cyst is flattened inferiorly.

conduits, the calcified rims of almost all cysts have a larger diameter than those of most conduits. Unlike stones, this calcified rim is often incomplete, and in many cases only a small section of the wall contains radiographically visible calcium. Moreover, morphologically uncomplicated cysts have only a single encircling wall, so when calcified, they do not have a laminated appearance. Cysts need not be perfectly round; some can be compressed on one side, producing an ovoid configuration (see Fig. 13-8).

The configuration of cysts depends on their location. They may displace and distort adjacent structures, or they themselves may be displaced by nearby solid organs or vessels. Usually, the differentiation of cystic calcification from the diffuse opacification of solid masses is not difficult. Nevertheless, solid uterine leiomyomas may contain curvilinear calcifications at their margins, mimicking the appearance of cystic calcification.

Unlike concretions and conduit wall calcifications, which appear at expected locations, the cystic pattern of calcification may be found almost anywhere in the abdomen. Cystic calcification usually occurs in abdominal aortic aneurysms. It is generally associated with conduit wall calcification in contiguous sections of the aorta and in the common iliac arteries. Cystic calcification may also occur in aneurysms of the splenic artery in the left upper quadrant. Also, cystic calcification is encountered in a variety of urinary tract lesions, including aneurysms of the renal artery, echinococcus cysts, perirenal hematomas, multicystic kidneys, adrenal cysts, and renal carcinomas. Echinococcal cysts are the most common cause of cystic calcification in the liver, but a calcified gallbladder (i.e., a so-called porcelain gallbladder) may occasionally produce similar findings.¹ Other causes of cystic calcification in the lower abdomen include mesenteric cysts, calcified appendiceal mucocoeles, and calcified benign tumors of the ovary.

SOLID MASS CALCIFICATION

Of all the classes of abdominal calcification, solid mass calcification includes the greatest variety of pathologic

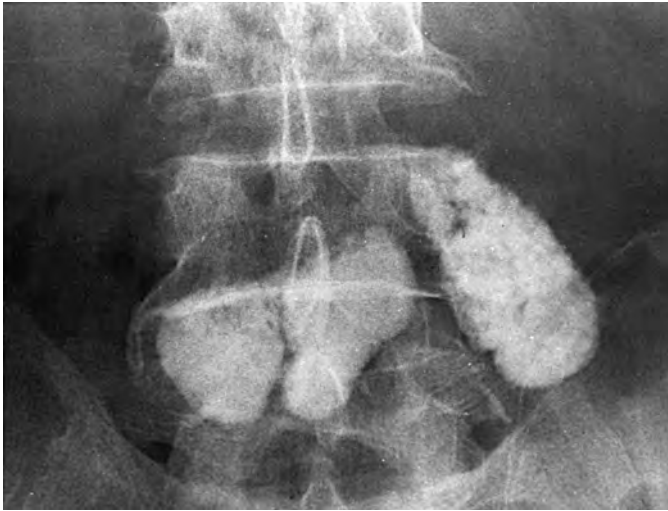


Figure 13-9 Calcified mesenteric nodes. Mottled interior and slightly irregular margins are typical of lymph node calcification.

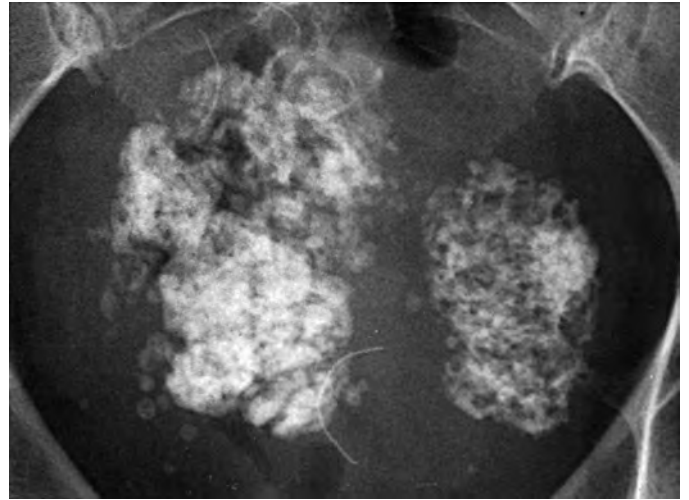


Figure 13-10 Calcified uterine leiomyomas. Two uterine fibroids are manifested by poorly defined, flocculent calcifications admixed with irregular lucencies.

abnormalities. Solid masses may appear as mottled densities with scattered radiolucencies on a calcified background, an appearance typical of calcified mesenteric lymph nodes (Fig. 13-9). A whorled configuration with incomplete bands and arcs of calcification is a feature of uterine leiomyomas. Calcified leiomyomas may also be manifested by numerous flocculent densities superimposed on a radiolucent background. Solid calcifications share the unifying feature of a nongeometric inner architecture and an irregular, often incomplete margin.

Calcified solid masses can be located anywhere in the abdomen. Calcified mesenteric lymph nodes are usually found in middle-aged or older individuals who at one time in life were infected by tuberculosis, even if they are now purified protein derivative–negative and exhibit no other manifestations of the disease. They tend to be located in a broad arc along the course of the mesentery of the small bowel from the left upper quadrant to the right lower quadrant of the abdomen. Multiple calcified nodes are often present, and individual nodes may vary widely in diameter.

Uterine leiomyomas are the most common calcified solid masses in the female pelvis. Some patients have multiple leiomyomas that may become calcified as they grow to enormous sizes (Fig. 13-10). Although leiomyomas are usually located in the pelvis, they may occasionally be found almost anywhere in the abdomen (Fig. 13-11).

All other types of solid mass calcification are much less common than calcified mesenteric lymph nodes or calcified uterine leiomyomas. A solid pattern of calcification may occasionally be found in adenomas, hamartomas, and carcinomas of the kidney as well as in tuberculous and chronic pyogenic abscesses of the kidney. Calcified pancreatic masses are rare and are usually associated with benign or malignant cystadenomas. Small, discretely outlined, calcified densities in the liver and spleen usually represent granulomas. In contradistinction, poorly defined radiopaque areas in the liver should be considered an indication of calcified metastases from colonic carcinoma until proven otherwise.



Figure 13-11 Multiple calcified leiomyomas. This patient has different patterns of calcification in leiomyomas extending from the pelvis to the midabdomen.

DIFFICULTY IN CLASSIFICATION

This classification scheme can be applied broadly to determine the nature of most abdominal calcifications. However, some cannot be separated into one of the four classes. If the density is too faint to have a definite inner architecture or margin, morphologic analysis is not possible. In addition, if the calcification is extremely small, a concretion may be

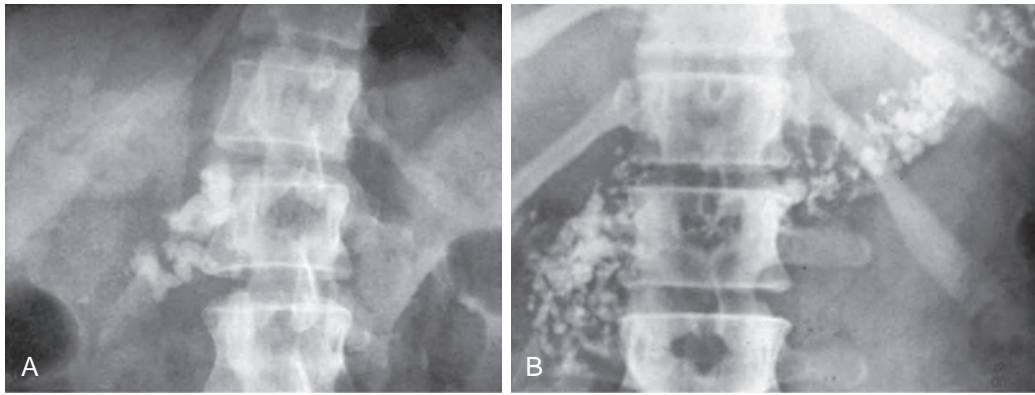


Figure 13-12 Two calcification patterns in pancreatic lithiasis. **A.** A conglomerate of stones filling larger ducts in the pancreatic head could be mistaken for calcification in conduits. **B.** Pancreatic stones can be seen throughout the pancreas. Each stone is located within a duct, but the cumulative appearance suggests diffuse acinar opacification.

difficult to distinguish from a solid opacity. Other calcifications may have an appearance suggestive of more than one morphologic class. For example, a collection of pancreatic stones clustered together may resemble a solid mass, although the area of radiopacity actually represents innumerable intra-ductal concretions with irregular margins (Fig. 13-12). Thus, one must be aware of potential pitfalls in the classification of abdominal calcifications. Nevertheless, a specific abdominal calcification can usually be classified into one of the four morphologic categories with a reasonable degree of confidence.

Location

The location of abdominal radiopacities also provides important clues about their identity. Most calcifications in the right upper quadrant are related to the gallbladder or right kidney. Gallstones are often multiple and are frequently laminated. Gallbladder wall calcification is much less common but can be clearly recognized by its marginal arcuate configuration. A transverse orientation and conduit morphologic features indicate calcification of the renal artery. Stones in the renal pelvis and ureters have a range of specific appearances and are oriented along the course of the urinary tract.

In both upper quadrants, adrenal calcification may assume various forms, including the solid opacities of calcified granulomas and eggshell calcification of cysts and pheochromocytomas. Multiple calcifications crossing the midline of the upper abdomen are characteristic of pancreatic lithiasis. Calcified mesenteric lymph nodes may also cross the midline but are usually situated more inferiorly along an oblique path extending from the left midabdomen to the right lower quadrant.

Appendicoliths typically appear as a single or tight grouping of several laminated calcifications in the right lower quadrant. However, the appendix may be located anywhere between the lower pelvis and right upper quadrant, so the diagnosis of an appendicolith should not be excluded simply because the concretion is found at a considerable distance from its expected location in the right iliac fossa.

In the lower abdomen and pelvis, calcifications that appear as concretions should arouse suspicion of ureteral calculi;

however, a small ureteral stone is often difficult to distinguish from a phlebolith on a single radiograph. Reference should therefore be made to previous or subsequent radiographs. Calculi may move freely within the ureteral lumen, whereas pelvic phleboliths are fixed in position unless displaced by an enlarging extraperitoneal mass. Bladder stones are usually readily recognizable by their location and configuration. Because of their protean manifestations, however, calcified uterine leiomyomas may be confused with other calcified lesions in the pelvis, such as ovarian tumors and mesenteric lymph nodes. Cystic teratomas of the ovary can frequently be recognized by the presence of teeth and bone, which are often accompanied by a large homogeneous lucency, indicating fat within the tumor.

Mobility

The movement of abdominal calcifications, during a single examination or over a longer period, provides additional information that may lead to a specific diagnosis. Gravity, respiration, peristaltic activity, and growth of masses may all result in changes in location. Stones located in a fluid medium may undergo layering on abdominal radiographs obtained in upright or decubitus projections. Such manipulation of position may be helpful in the diagnosis of gallstones or of calculi in hydronephrotic sacs. Epiploic appendices that have become amputated or appendicoliths that lie free in the peritoneal cavity may exhibit a great range of movement on sequential radiographs. Whereas mesenteric nodes move slightly with positional changes, ovarian teratomas may move considerably as the bladder fills and empties (Fig. 13-13). Because of the effects of peristalsis, stones in the lumen of the GI tract and pelviciceal system can migrate on successive radiographs. Consideration of this migration is particularly important in diagnosing ectopic gallstones and in differentiating distal ureteral calculi from stones in pelvic veins (Fig. 13-14). When images are obtained over a period of weeks or months, enlargement or shrinkage of abdominal masses may be recognized by the movement of calcifications or ossifications that lie within or adjacent to these lesions. Even pelvic phleboliths can be displaced by hematomas or other masses.⁴

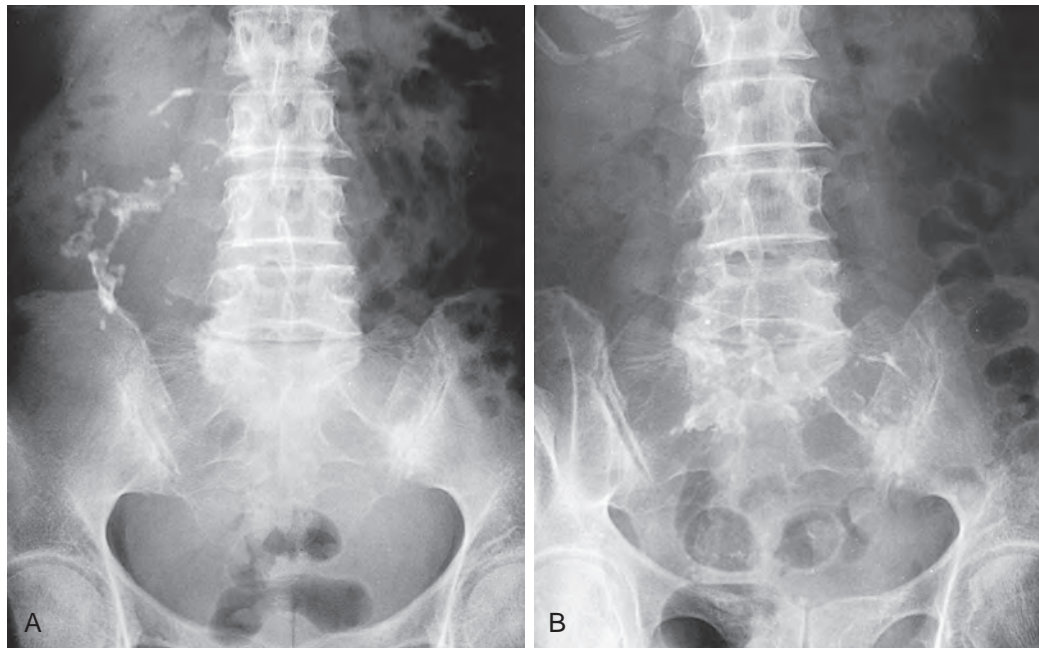


Figure 13-13 Mobility of ovarian dermoid. **A.** When the bladder is full, the tumor rises into the lower abdomen. **B.** When the bladder has been emptied, the calcified mass overlies the sacrum.

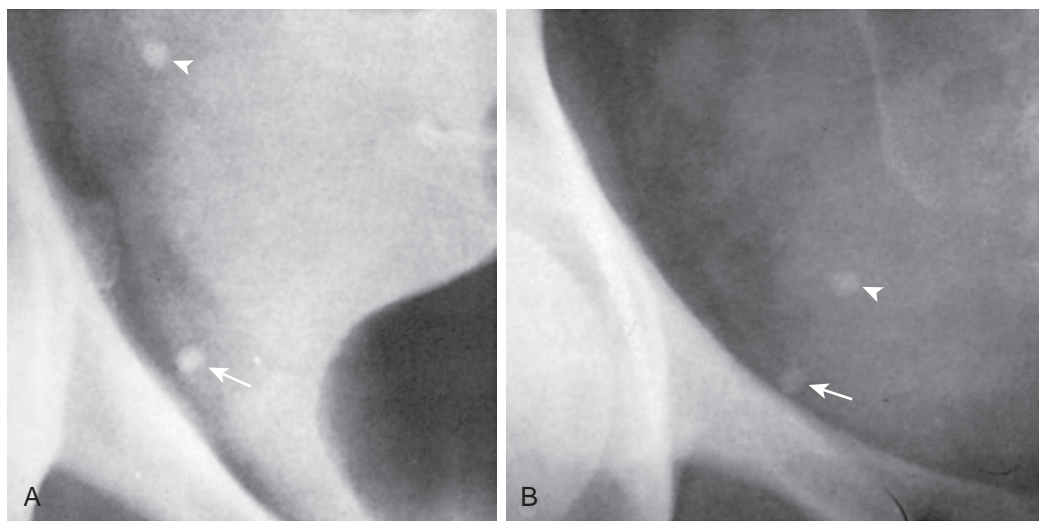


Figure 13-14 Mobility of ureteral calculus. **A.** A phlebolith (arrow) and ureteral calculus (arrowhead) are morphologically identical on the initial abdominal radiograph. **B.** However, the venous stone (arrow) maintains a fixed position, whereas the ureteral stone (arrowhead) has migrated distally on a subsequent radiograph.

REFERENCES

1. Hilbish TF, Bartter FC: Roentgen findings in abnormal deposition of calcium in tissues. *AJR* 87:1128–1129, 1962.
2. Kurturba P: A contribution to the problem of calcifications in malignant tumors: A case of late calcified retroperitoneal metastasis of an ovarian carcinoma. *Neoplasma* 11:633–642, 1964.
3. Widmann BF, Ostrum AW, Fried H: Practical aspects of calcification and ossification in the various body tissues. *Radiology* 30:598–609, 1938.
4. Steinbach HL: Identification of pelvic masses by phlebolith displacement. *AJR* 83:1063–1066, 1960.

SECTION
III

Pharynx

Pharynx: Normal Anatomy and Examination Techniques

STEPHEN E. RUBESIN

CHAPTER OUTLINE

Anatomy

Location

Basic Structures and Mucosal Surface Patterns

Divisions

Muscles

Principles of Technique

Preparation of Patients

Components of Routine Examination

Double-Contrast Interpretation

Motility Examination

Position of the Patient

Choice of Contrast Agents

Therapeutic Examination

The pharynx is the crossroads of respiration, speech, and swallowing. During respiration, the pharynx is an active conduit for the passage of air from the nasopharynx to the laryngeal aditus. During speech, the pharynx functions as a resonating chamber, changing size and shape to alter sounds. During swallowing, the pharynx directs the bolus into the esophagus and prevents the bolus from entering the tracheobronchial tree. Disorders of the pharynx may therefore be manifested by respiratory, speech, or swallowing dysfunction. Patients may complain of dysphagia, odynophagia, choking, or a feeling of a lump in the throat not associated with swallowing (a globus sensation). Soft palate insufficiency may be suggested by nasal regurgitation or a nasal voice quality. Recurrent pneumonia, asthma, chronic bronchitis, or coughing may indicate pharyngeal dysfunction. In this chapter, the focus is on the anatomy of the pharynx as a basis for understanding structural and motility disorders. The neurologic anatomy necessary for understanding motility disorders is presented in Chapter 15.

Anatomy

LOCATION

The pharynx is a funnel-shaped tube of skeletal muscle extending from the cranial base to the lower margin of the cricoid cartilage (Fig. 14-1). The pharynx lies anterior to the vertebral bodies of the cervical spine, prevertebral muscles, and loose connective tissue of the retropharyngeal space.^{1,2} The pharynx is confined laterally by the muscles of the neck, lateral portions of the hyoid bone and thyroid cartilage, and carotid sheath (Fig. 14-2). The pharynx and larynx are intimately related (Fig 14-3), in embryologic origin and anatomically. The epiglottis and

remainder of the supraglottis are of pharyngeal, not laryngeal origin.

BASIC STRUCTURES AND MUCOSAL SURFACE PATTERNS

The shape of the pharynx is determined by the underlying musculature, laryngeal cartilages, and supporting skeleton.³ Although the nasopharynx is primarily a respiratory tract structure, certain nasopharyngeal structures participate in the act of swallowing. The eustachian tube connects the middle ear with the nasopharynx, allowing equilibration of air pressures on the internal and external aspects of the tympanic membrane during swallowing.⁴ During breathing, however, the eustachian tube is closed. The eustachian tube cartilage bulges into the lateral nasopharyngeal wall at the torus tubarius.⁵ A C-shaped prominence is seen radiographically near the torus tubarius (Fig. 14-4).⁶ The salpingopharyngeal fold overlying the salpingopharyngeal muscle courses inferiorly from the torus along the lateral pharyngeal wall to the level of the soft palate.⁷ The posterior nasopharyngeal wall has a variably nodular surface because of underlying adenoidal tissue.⁸

The vertical (pharyngeal) surface of the base of the tongue is variably nodular because of underlying lymphoid tissue of the lingual tonsil (see Fig. 14-1A).⁹ The median glossoepiglottic fold overlies the glossoepiglottic ligament, which courses from the base of the tongue to the epiglottis. The median glossoepiglottic fold divides the space between the tongue and the epiglottis into two sacs, the valleculae (Fig. 14-5; see Fig. 14-1). The lateral glossoepiglottic folds form the lateral walls of the valleculae. The pharyngoepiglottic folds course from the posterolateral portion of the valleculae into the lateral pharyngeal wall (Fig. 14-6).¹ These folds overlie the paired stylopharyngeal muscles and form the posterior lateral wall of the valleculae. The valleculae are spaces at rest but disappear during swallowing when the epiglottis inverts and the space behind the base of the tongue communicates freely with the remainder of the oropharynx.¹⁰

The tonsillar fossa forms part of the lateral oropharyngeal wall. Each tonsillar fossa is bounded anteriorly by a palatoglossal fold (anterior tonsillar pillar; Fig. 14-7) and posteriorly by a palatopharyngeal fold (posterior tonsillar pillar) overlying the palatopharyngeal muscle (see Figs. 14-7 and 14-11).^{3,10}

The rounded epiglottic tip rises above the level of the valleculae (see Fig. 14-1B and 14-5).^{10,11} The aryepiglottic folds connect the epiglottis with the mucosa overlying the muscular processes of the arytenoid cartilages (see Fig. 14-5). Occasionally, round bulges are seen in the lower aryepiglottic folds, reflecting the small cuneiform and corniculate cartilages embedded in these folds.

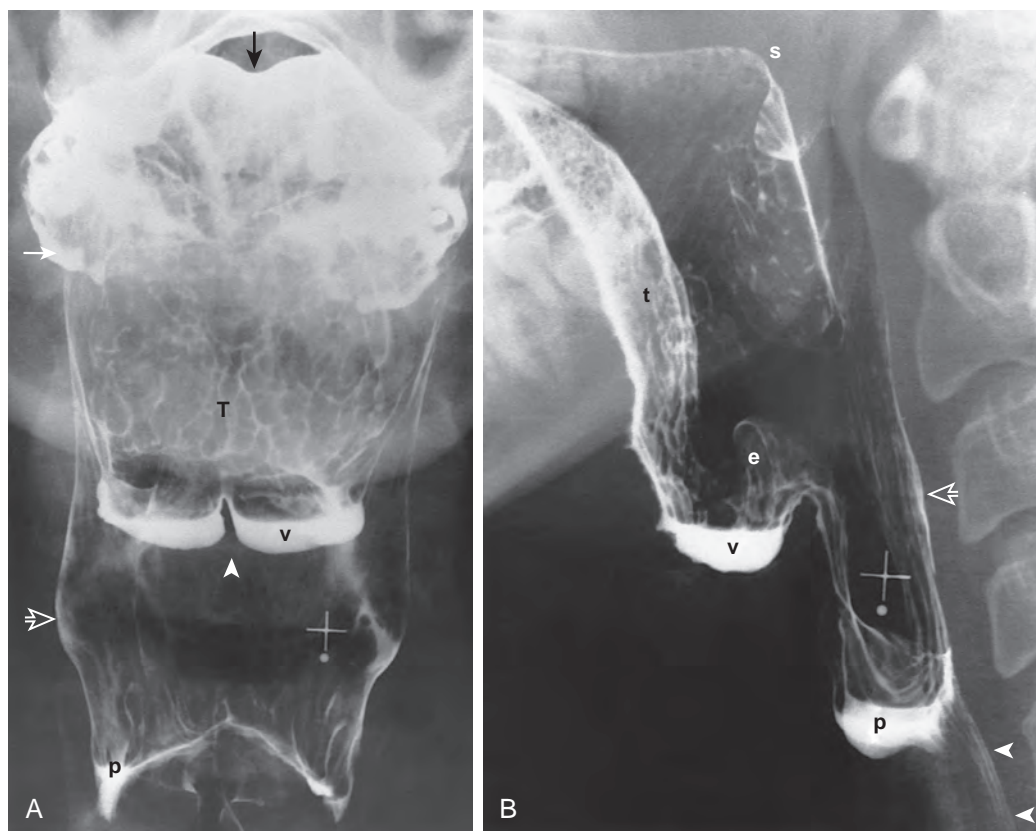


Figure 14-1 Basic structures of the normal pharynx. A. Double-contrast radiograph in the frontal view shows the contours of the superior surface of the tongue (*black arrow*), tonsillar fossa (right tonsillar fossa [*white arrow*]), valleculae (left vallecula [*v*]), and lateral wall (*open arrow*) of the piriform sinus (right piriform sinus [*p*]). The median glossoepiglottic fold (*arrowhead*) divides the space behind the tongue base into the two valleculae. The surface of the base of the tongue (*T*), seen en face, has a reticular appearance because of the underlying lingual tonsil.

B. Double-contrast radiograph in the lateral view (during phonation) shows the contours of the soft palate (*s*), base of the tongue (*t*), epiglottis (*e*), valleculae (*v*), posterior pharyngeal wall (*arrow*), barium pooling in the lower piriform sinus (*p*), and collapsed region of the pharyngoesophageal segment (*arrowheads*). Note the relative height of the soft palate with the C1 vertebral body and the thickness of the space behind the barium-coated pharyngeal mucosa, composed of pharyngeal musculature, fascial planes and prevertebral muscles, and anterior longitudinal ligament. (**B** from Rubesin SE, Jones B, Donner MW: *Contrast pharyngography: The importance of phonation*. *AJR* 148:269–272, 1987.)

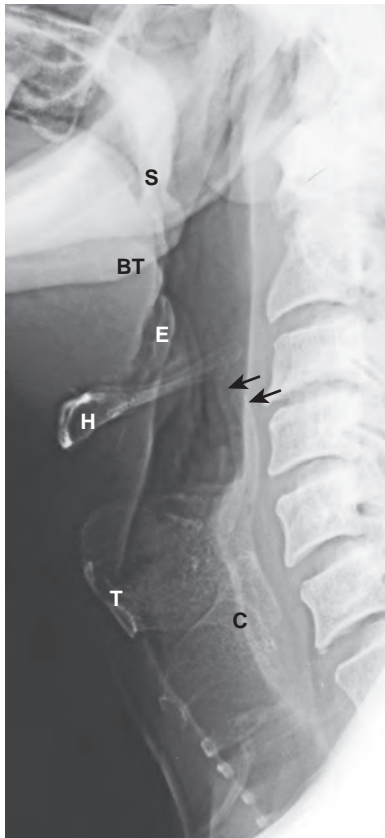


Figure 14-2 Laryngeal cartilages. Plain radiograph with patient in a lateral position shows the hyoid bone (H), tip of the epiglottis (E), calcified thyroid cartilage (T), calcified superior cornu of the thyroid cartilage (arrows), and calcified cricoid cartilage (C). The soft palate (S) and base of tongue (BT) are identified. The lower hypopharynx is devoid of air. A small amount of air is seen in the laryngeal ventricle. Note the normal width of the soft tissue posterior to the pharyngeal air column.

The shape of the hypopharynx is created primarily by its relationship to the posteriorly protruding larynx (see Figs. 14-3 and 14-6B). Protrusion of the larynx into the pharynx creates two grooves in the anterior lateral hypopharynx—the piriform sinuses (recesses), pear-shaped structures that open posteriorly into the hypopharynx (see Fig. 14-6). Each piriform sinus is bounded medially by the aryepiglottic fold and mucosa overlying the muscular process of the arytenoid cartilage and laterally by the hyoid bone, thyrohyoid membrane, and thyroid cartilage.^{1,3}

The lower end of the hypopharynx is collapsed, except during passage of a bolus. The posterior portion of the larynx (including the arytenoid cartilages, arytenoid muscles, and cricoid cartilage) protrudes deeply into the lower hypopharynx (see Fig. 14-3). The upper esophageal sphincter (formed predominantly by the cricopharyngeal muscle) is tonically contracted at rest, closing the pharyngoesophageal segment (see Fig. 14-1).¹² As a result, the lower hypopharynx is markedly constricted in an anteroposterior direction and is often not appreciated on a frontal radiograph. The arcuate lower border of the hypopharynx seen on the frontal view reflects only the protrusion of the larynx into the hypopharynx (see Fig. 14-3).³

The squamous mucosa of the lateral and posterior pharyngeal walls is closely apposed to the longitudinally striated inner

longitudinal muscle layer and its aponeurosis. Only a thin tunica propria separates the epithelium from the muscle or elastic tissue of the aponeurosis. On double-contrast views, longitudinally oriented lines may therefore be seen in the lateral and posterior pharyngeal walls, reflecting apposition of epithelium to muscle (Fig. 14-8).³

Transversely oriented lines are seen on the anterior hypopharyngeal wall, where redundant squamous mucosa and submucosa overlie the muscular processes of the arytenoid cartilages and cricoid cartilage. Transverse lines and tissue bulging from the anterior wall of the pharyngoesophageal segment had previously been described as a postcricoid venous plexus.¹³ However, these radiographic findings are mainly caused by redundant mucosa and submucosa on the anterior hypopharyngeal wall (Fig. 14-9).³ Demonstration of the redundant postcricoid mucosa on a pharyngogram identifies the location of the cricopharyngeal muscle.

DIVISIONS

The pharynx is arbitrarily divided into three parts—the nasopharynx (epipharynx), oropharynx (mesopharynx), and laryngopharynx (hypopharynx).¹⁴ The nasopharynx is primarily a respiratory tract structure continuous anteriorly with the nasal cavity. The superior and posterior walls of the nasopharynx abut the basisphenoid and basilar part of the occipital bone. The nasopharynx is separated inferiorly from the oropharynx by the soft palate (see Figs. 14-4 and 14-7). The velopharyngeal portal is the opening between the nasopharynx and oropharynx.¹⁵

The oropharynx and hypopharynx are the divisions of the pharynx that participate in swallowing. The oral cavity opens into the oropharynx at the palatoglossal isthmus at the level of the anterior tonsillar pillars (palatoglossal folds; see 14-7A). The oropharynx lies posterior to the oral cavity, extending cranio-caudally from the soft palate to its arbitrary division from the hypopharynx at the level of the hyoid bone. The three divisions of the pharynx are arbitrary because the soft palate and hyoid bone change position with phonation, swallowing, and respiration. Therefore, a better dividing line between the oropharynx and hypopharynx is the pharyngoepiglottic fold (see Fig. 14-6), a mucosal fold overlying the stylopharyngeal muscle.^{1,16} The base of the tongue (see Fig. 14-1B) forms the lower anterior wall of the oropharynx.

The hypopharynx lies behind and lateral to the larynx, extending from the level of the pharyngoepiglottic fold to the lower border of the cricopharyngeal muscle at the level of the inferior margin of the cricoid cartilage. The hypopharynx communicates with the larynx at the laryngeal aditus, formed by the epiglottis, aryepiglottic folds, and mucosa overlying the muscular process of the paired arytenoid cartilages (see Fig. 14-5B). The hypopharynx communicates with the cervical esophagus at the pharyngoesophageal segment, whose walls are surrounded by the posterior lamina of the cricoid cartilage and cricopharyngeal muscle (see Fig. 14-9).

MUSCLES

Pharyngeal function depends on coordinated, sequential contraction of the extrinsic muscles of the pharynx, which arise from the skull base, neck, tongue, mandible, and hyoid bone, and the intrinsic skeletal muscles of the pharynx and larynx

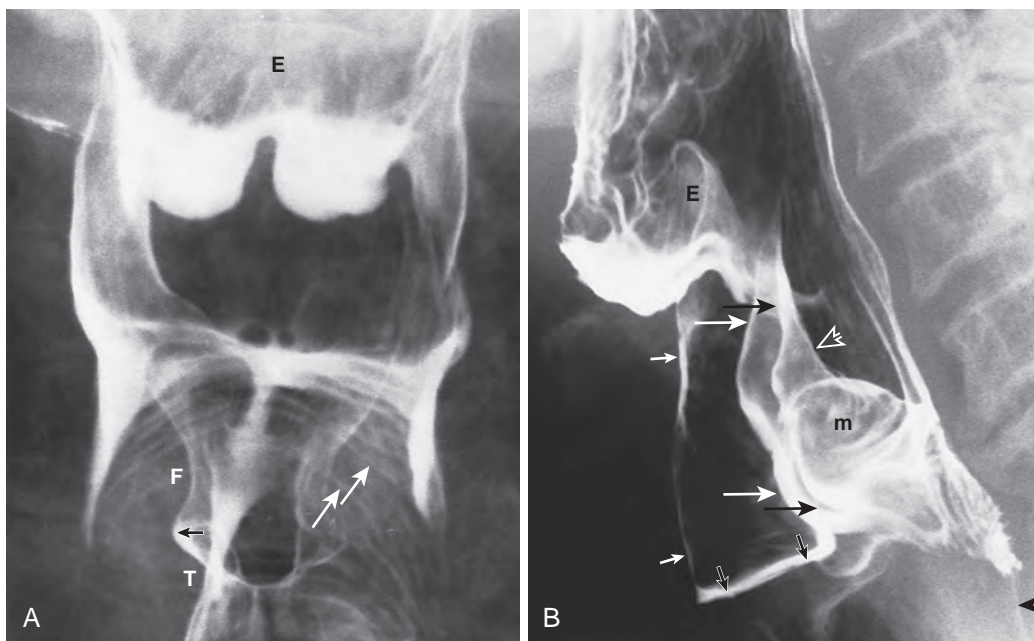


Figure 14-3 Relationship of larynx to pharynx. **A.** In a patient with laryngeal penetration, barium coats the false vocal cords (right false vocal cord, F), the true vocal cords (right true vocal cord, T), and the laryngeal ventricle (right laryngeal ventricle, *black arrow*). As the larynx protrudes into the midhypopharynx, arcuate lines (*white arrows*) are formed. **B.** The relationship of the barium-coated laryngeal vestibule (*small white arrows*) to the laryngeal ventricle (*small black arrows*) is shown. Note the angle of the laryngeal ventricle atop the true vocal cords and the tilt of the true vocal cords; the posterior portion of the cords is cranial to the anterior commissure. The anterior walls of the right piriform sinus (*large white arrows*) and left piriform sinus (*large black arrows*) are seen as anteriorly convex lines. The mucosa (m) overlying the muscular process of the arytenoid cartilages lies below the aryepiglottic fold (*open arrow*). The lower hypopharynx (*arrowhead*) is closed at rest. E, epiglottis. (**B** from Rubesin SE, Glick SN: *The tailored double-contrast pharyngogram*. *Crit Rev Diagn Imaging* 28:133–179, 1988.)

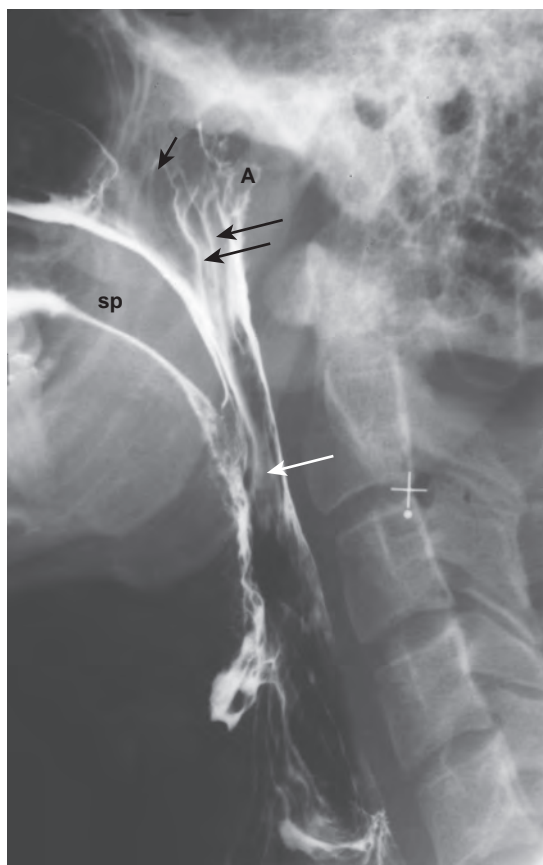


Figure 14-4 Salpingopharyngeal fold. Lateral view of the nasopharynx during phonation after intranasal instillation of 1 mL of barium shows the salpingopharyngeal folds (*long black arrows*). The paired salpingopharyngeal folds overlie the salpingopharyngeal muscles. The eustachian tube orifices (one orifice identified by *short black arrow*) are manifested as barium-coated, C-shaped lines. The posterior wall of the nasopharynx is slightly irregular because of the underlying adenoidal lymphoid tissue (A). The soft palate (sp) and one palatopharyngeal fold (*white arrow*) are also demonstrated.



Figure 14-5 Folds of the valleculae. Spot radiograph with the patient in a frontal position. The folds of the epiglottis and valleculae are accentuated by edema caused by chronic radiation changes. The median glossoepiglottic fold (*black arrowhead*) divides the retroglottic space into the two valleculae (right vallecula [V]). The pharyngoepiglottic folds (*large white arrow* identifies the left pharyngoepiglottic fold) overlie the paired stylopharyngeal muscles and form part of the posterior wall of the valleculae. Also shown are the epiglottic tip (E) and left aryepiglottic fold (*black arrow*). Barium coats the laryngeal surface of the epiglottis as a result of laryngeal penetration. The interarytenoid notch (*white arrowhead*) lies between swollen mucosa overlying the muscular processes of the arytenoid cartilages.

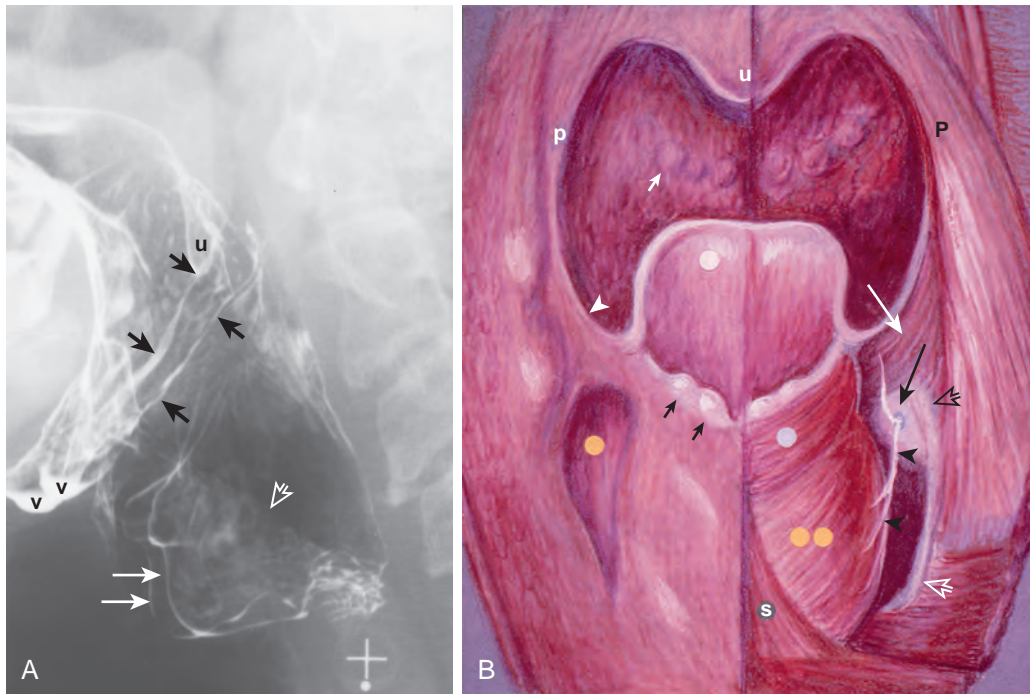


Figure 14-6 Pharyngoepiglottic folds. **A.** Spot image obtained in the lateral projection shows the paired pharyngoepiglottic folds (*thick arrows*) coursing as oblique lines across the lateral wall of the pharynx. The pharyngoepiglottic fold overlies the stylopharyngeal muscle, which extends from the styloid process to the posterior wall of the valleculae (*v*). The uvular tip (*u*) is seen. The anterior walls of the piriform sinuses (*thin arrows*) are well visualized. The mucosa overlying the muscular processes of the arytenoid cartilages (*open arrow*) is demonstrated. **B.** Posterior view of pharynx opened from behind. On the viewer's left, the mucosa has been left intact. The epiglottis rises above the level of the valleculae, hidden in this posterior view. The uvula (*u*), palatopharyngeal fold (*p*), piriform sinus (*left dot*), and laryngeal surface of the epiglottis (*uppermost dot*) are seen en face. The pharyngoepiglottic fold (*white arrowhead*) separates the oropharynx from the hypopharynx. Bulges in the aryepiglottic fold overlie the cuneiform and corniculate cartilages (*short black arrows*). The circumvallate papillae (*short white arrow*) form a V-shaped protuberance along the base of the tongue. On the viewer's right, the mucosa has been removed. The palatopharyngeal muscle (*P*) forms the palatopharyngeal fold. This muscle has been retracted laterally. The stylopharyngeal muscle (*long white arrow*) underlies the pharyngoepiglottic fold. The thyrohyoid membrane (*long black arrow*) and internal branch of the superior laryngeal nerve (*black arrowheads*) are identified. The transverse arytenoid muscle (*single dot on viewer's right*), posterior cricoarytenoid muscle (*two adjacent dots*), and suspensory ligament of the esophagus (*s*) are identified. (**B** from Rubesin S, Jesserun J, Robertson D, et al: *Lines of the pharynx*. Presented at the 71st Scientific Assembly and Annual Meeting, Radiological Society of North America, Chicago, 1985.)

(Fig. 14-10; Table 14-1).¹⁷ The pharynx and larynx are suspended as a unit from the skull base, tongue, mandible, and hyoid bone. The suspensory muscles of the hyoid bone (the suprahyoid muscles) include the following (with their cranial nerve innervations in parentheses): from the tongue, mandible, or both, the anterior belly of the digastric muscle (V3), geniohyoid muscle (XII, via C1-2), hyoglossal muscle (XII), and mylohyoid muscle (V3); and from the skull base, the posterior belly of the digastric muscle (VII) and stylohyoid muscle (VII).^{14-16,18} The major function of the suprahyoid muscle group related to swallowing is to elevate and fix the hyoid bone, a motion that contributes to elevating and widening the pharynx, tilting the epiglottis, and opening the pharyngoesophageal segment during passage of a bolus.¹⁶

The soft palate is formed by an interweaving of muscles from the skull base (tensor veli palatini and levator veli palatini), tongue (palatoglossus muscle), and pharynx (palatopharyngeal muscle) (Fig. 14-11; see Fig. 14-7B).^{1,16,19} The musculus uvulae is the only intrinsic muscle of the soft palate.

The tendon of the tensor veli palatini (V) forms the fibrous skeleton of the anterior portion of the soft palate.¹⁶ This muscle

depresses the anterior soft palate during swallowing. The levator veli palatini (X) suspends the midportion of the soft palate (see Figs. 14-7A and 14-11). During swallowing, the levator veli palatini pulls the mid-soft palate superiorly and posteriorly.¹⁹ The palatopharyngeal muscle (X) depresses the posterior lateral part of the soft palate, elevates the pharynx, and constricts the faucial isthmus. The palatoglossus muscle (X) pulls the soft palate and tongue toward each other. The musculus uvulae (X) shortens, thickens, and elevates the uvula.

The thyrohyoid muscle (XII, via C1-2) courses from the hyoid bone to the thyroid cartilage (see Fig. 14-10). Its major function is approximation of the hyoid bone and thyroid cartilage, an action that is partly responsible for closing the laryngeal vestibule.^{16,20} The infrahyoid depressors include the sternohyoid (C1-3), sternothyroid (C1-3), and omohyoid (C1-3) muscles.¹⁶

Epiglottic tilt is accomplished via contraction of the suprahyoid muscles, thyrohyoid muscle, and intrinsic epiglottic musculature.^{10,14,21} Contraction of the suprahyoid group pulls the hyoid bone superiorly and anteriorly up underneath the mandible. Hyoid motion pulls on the hyoepiglottic ligament that courses from the inferior anterior hyoid bone to the petiole

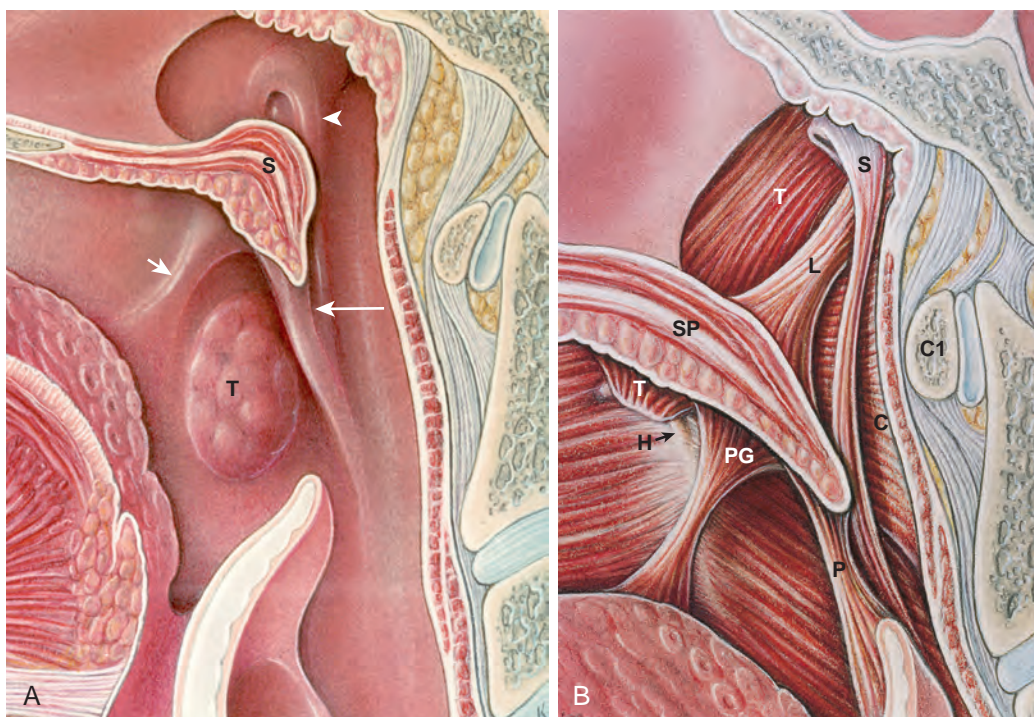


Figure 14-7 Tonsillar fossa. **A.** Lateral drawing demonstrates the tonsillar fossa during soft palate (S) elevation by phonation. The palatine tonsil (T) is surrounded by the palatoglossal fold (anterior tonsillar pillar; *short arrow*) and palatopharyngeal fold (posterior tonsillar pillar; *long arrow*). The salpingopharyngeal fold is also shown (*arrowhead*). **B.** Sagittal view of the nasopharynx and oropharynx after removal of the overlying mucosal layer demonstrates the muscles of the soft palate and tonsillar fossa. The palatoglossus muscle (PG) pulls the midtongue and mid-soft palate together and forms the palatoglossal fold. The palatopharyngeal muscle (P) forms the palatopharyngeal fold and constricts the lateral posterior pharyngeal space. The levator veli palatini (L) pulls the midportion of the soft palate (SP) superiorly and posteriorly. The relationship between the tensor veli palatini (T) and pterygoid hamulus (H) is shown. The salpingopharyngeal muscle (S) arises from the eustachian tube cartilage and forms the salpingopharyngeal fold. Also shown is the superior constrictor muscle (C). The anterior arch of the first cervical vertebra (C1) is identified. (**A** from Rubesin SE, Rabischong P, Bilaniuk LT, et al: Contrast examination of the soft palate with cross-sectional correlation. *RadioGraphics* 8:641–665, 1988.)

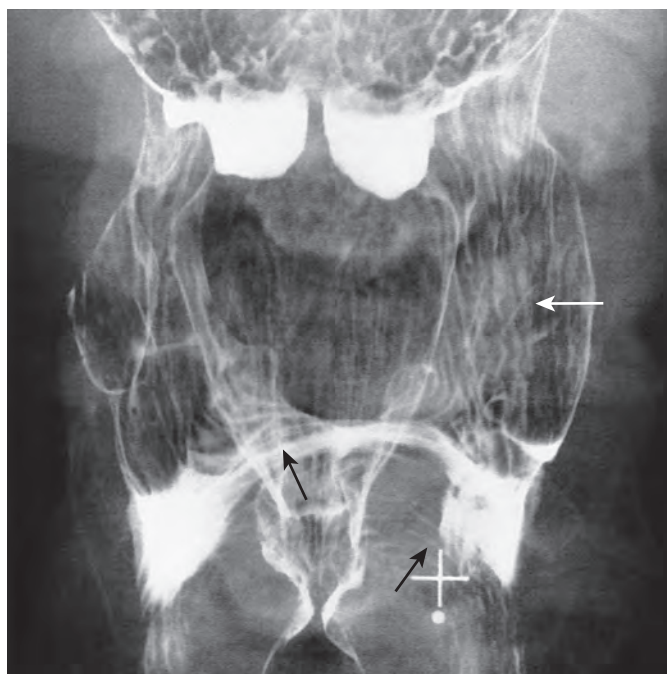


Figure 14-8 Lines of the pharynx. The longitudinally striated mucosa (*white arrow*) reflects close apposition of the squamous mucosa to the underlying longitudinal muscle layer of the pharynx. Arcuate lines of the anterior hypopharyngeal wall are identified (*black arrows*).

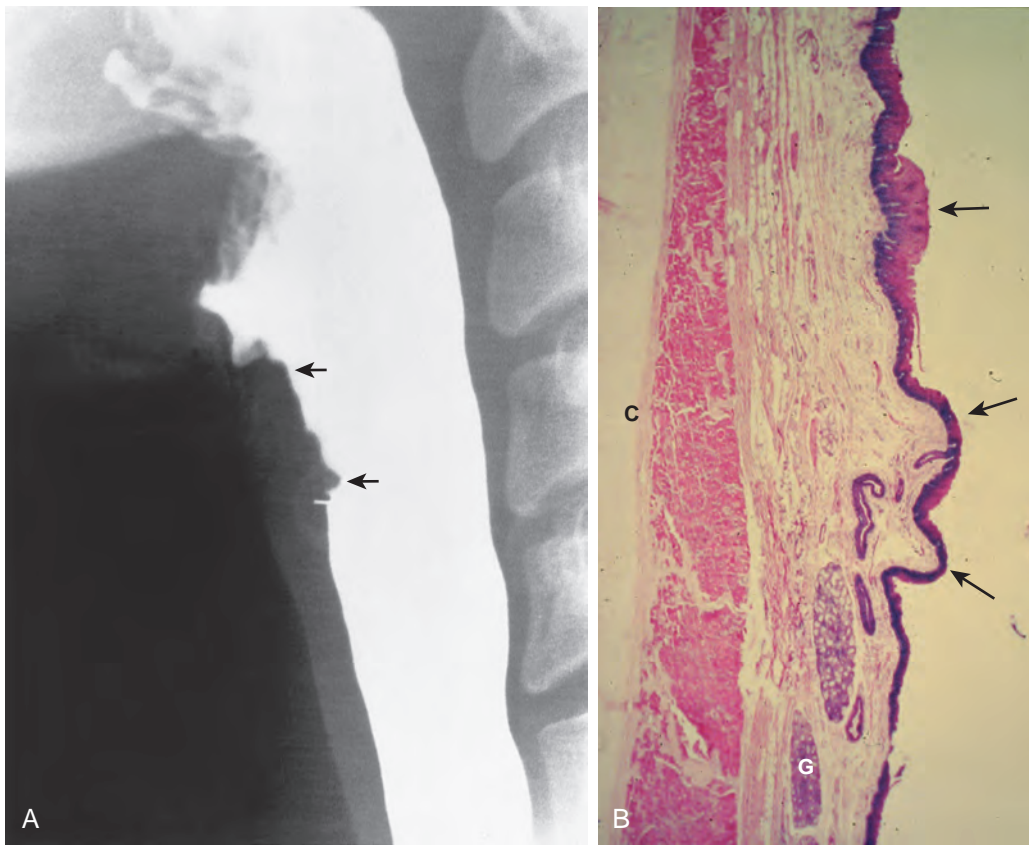


Figure 14-9. The postcricoid "defect." **A.** During swallowing, redundant mucosa along the anterior wall of the pharyngoesophageal segment just posterior to the cricoid cartilage may create an undulating or plaque-like contour (arrows). To rule out a subtle stricture, web, or infiltrating lesion, the radiologist must be certain that this mucosal nodularity changes size and shape and flattens during swallowing. **B.** Vertically oriented, low-power photomicrograph just posterior to the cricoid cartilage (C). The squamous epithelium has an undulating contour (arrows). The tunica propria is thick, with abundant fat and several minor salivary glands (H&E stain; $\times 10$).

(lower tip) of the epiglottis.¹⁶ Hyoid motion thus pulls the lower epiglottis anteriorly and superiorly, tilting the epiglottis toward a horizontal position, as if the epiglottis were on a fulcrum. Contraction of the paired aryepiglottic and oblique arytenoid muscles pulls the epiglottic tip inferiorly. Contraction of the thyroepiglottic muscles pulls the sides of the epiglottis and aryepiglottic folds laterally.¹⁶

Closure of the laryngeal aditus is not accomplished by epiglottic inversion alone. Thyrohyoid muscle contraction pulls the hyoid and thyroid cartilage together. Closure of the vocal cords and thyroarytenoid muscles helps close the laryngeal vestibule.²⁰ Contraction of the transverse arytenoid muscle and aryepiglottic-oblique arytenoids pulls together and elevates the mucosa overlying the muscular processes of the arytenoid cartilages.¹⁶

The muscular tube of the pharynx is surrounded by the buccopharyngeal fascia.¹⁴ The buccopharyngeal fascia is separated from the prevertebral muscles and fascia by the retropharyngeal space. The retropharyngeal space is an important site for the spread of malignant and inflammatory processes.

The muscular tube of the pharynx is formed by two layers, the inner longitudinal layer and outer circular (constrictor) layer. The constrictor muscle layer (X) forms a ring that is incomplete anteriorly. During swallowing, the constrictor muscles contract sequentially to help propel the bolus into the esophagus.¹² Contraction of the superior constrictor muscles also apposes the lateral pharyngeal wall with the soft palate, closing the lateral portion of the velopharyngeal portal.^{22,23} On a lateral view of the pharynx, the location of each paired constrictor muscle can be approximated by visible structures. The

superior constrictor extends from the level of the soft palate toward the mid and lower base of tongue. The lower portion of the middle constrictor angles slightly superiorly from the level of the hyoid bone; the upper portion of the middle constrictor is about one-and-a-half vertebral bodies superior to the level of the hyoid bone. The upper border of the thyropharyngeal muscle is just above the continuation of a line of the hyoid bone posteriorly; the lowermost fibers extend to the level of redundant mucosa behind the cricoid cartilage. The redundant mucosa posterior to posterior lamina of the cricoid cartilage identifies the location of the unpaired cricopharyngeal muscle.

The inner longitudinal muscle layer (see [Figs. 14-5 through 14-7](#)) includes the stylopharyngeal muscle (IX), salpingopharyngeal muscle (X), and palatopharyngeal muscle (X).^{1,16} During swallowing, contraction of the inner longitudinal muscles helps pull the pharynx up and over the descending bolus of food.¹⁸ The palatopharyngeal muscle also constricts the posterior portion of the pharynx, channeling the bolus into the hypopharynx and helping prevent nasal regurgitation. Transfer of the bolus through the pharynx results from the pressure of the bolus itself (gravity), closure of the palatoglossal isthmus, velopharyngeal portal and laryngeal aditus, tongue base retraction, elevation of the pharynx up over bolus, and contraction of the constrictor muscles.²⁴

The pharyngoesophageal segment is tonically contracted at rest.¹² Opening of the pharyngoesophageal segment (see [Fig. 14-9](#)) is caused by gravity and muscular contractions superior to it. Signals via the recurrent laryngeal nerve cause the cricopharyngeal muscle to relax. Elevation of the pharynx and larynx by the suprahyoid musculature, intrinsic pharyngeal elevators,

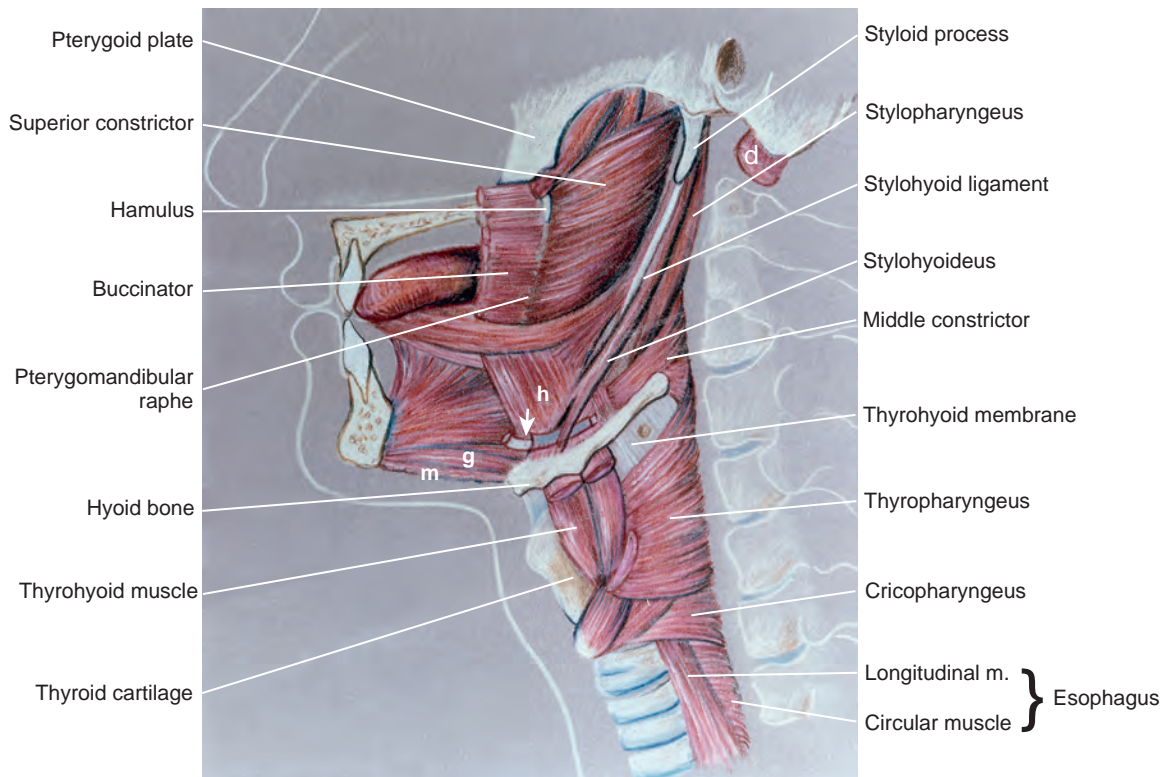


Figure 14-10 Lateral view of the muscles of the pharynx. The superficial muscles, nerves, arteries, and veins have been removed. The suspensory and constrictor muscles of the normal pharynx are demonstrated. The hyoid bone is suspended anteriorly by the geniohyoid muscle (g), mylohyoid muscle (m, cut in cross section), hyoglossus muscle (h), and anterior belly of the digastric muscle (resected; not shown). The tendon connecting the anterior and posterior belly of the digastric muscle is shown (arrow). The hyoid bone is suspended posteriorly by the stylohyoid ligament, stylohyoid muscle, and posterior belly of the digastric muscle (d) (resected; not shown). The thyrohyoid muscle and ligament suspend the thyroid cartilage from the hyoid bone. The overlying depressors of the hyoid bone, the omohyoid and sternohyoid muscles, have been resected. The paired constrictor muscles of the pharynx (superior, middle, and inferior) have a C shape when viewed from above and are incomplete anteriorly. The superior constrictor muscle originates at the pterygoid plate and hamulus, at the pterygomandibular raphe with the buccinator muscle, and in the longitudinal muscles of the tongue; it joins its partner posteriorly along the median raphe of the pharynx. The middle constrictor muscle originates on the greater and lesser horns of the hyoid bone and along the lower stylohyoid ligament; it joins its partner posteriorly at the median raphe of the pharynx. The thyropharyngeal muscle (upper portion of the inferior constrictor muscle) originates from the oblique line of the thyroid cartilage; it joins its partner in the posterior median raphe. The lower portion of the inferior constrictor muscle, the cricopharyngeal muscle, arises from the lateral surface of the cricoid cartilage, encircles the pharynx, and inserts on the opposite side of the cricoid cartilage. The cricopharyngeal muscle is a C-shaped muscle without a partner and has no posterior midline raphe. (From Rubesin S, Jessorun J, Robertson D, et al: *Lines of the pharynx*. Presented at the 71st Scientific Assembly and Annual Meeting, Radiological Society of North America, Chicago, 1985.)

and thyrohyoid muscle pull the anterior wall of the pharyngo-esophageal segment (the postcricoid mucosa) superiorly and anteriorly. Pressure (weight) of the bolus, tongue base retraction, and constrictor muscle contraction help push the pharyngo-esophageal segment open.¹²

Principles of Technique

PREPARATION OF PATIENTS

High-density barium adheres to dry pharyngeal mucosa.²⁵ Despite continuous salivary secretion, the pharynx should therefore be made as dry as possible during the examination.²⁶ As a result, patients are instructed not to eat or drink after midnight on the day of the examination.⁹ In the morning, regular oral medications may be taken with small amounts of water, but insulin-dependent diabetics should not take their insulin on the morning of examination. Oral antacid medications impair barium coating and should also be avoided. If

possible, the patient should refrain from activities that stimulate salivary secretion, such as sucking throat lozenges, smoking, or chewing gum. In some inpatients, in whom the swallowing study focuses on the pharyngeal function, we allow patients to rinse their mouths with water if their mouths are dry.

COMPONENTS OF ROUTINE EXAMINATION

Contrast examination of the pharynx may be dangerous in patients with suspected airway obstruction, especially in those with acute epiglottitis.^{27,28} Lateral radiographs of the neck should therefore be obtained if airway obstruction is suspected. Lateral radiographs are also obtained for suspected foreign bodies (Fig. 14-12), fistulas, abscesses, perforations, or palpable neck masses.

Routine examination of the pharynx and esophagus includes the following: (1) videofluoroscopy or DVD recording of the oral, pharyngeal, and esophageal phases of swallowing; (2) double-contrast spot images of the pharynx, esophagus, and

TABLE 14-1 Tongue and Pharyngeal Motor Function

Visualized Motion	Cranial Nerve	Muscle(s)
Lip closure	VII	Orbicularis oris m., four others
Mastication	V3	Masseter m. Temporalis m., lateral and medial pterygoid m.
Bolus holding posteriorly	VII IX V3 VII XII	Buccinator m. Palatoglossus Tensor veli palatini Lingualis (Sensory)
Tongue protrusion	XII	Genioglossus
Tongue tip elevation	XII	Genioglossus
Tongue forming inclined plane	XII	Genioglossus, lingualis
Tongue base retraction	XII	Styloglossus, hyoglossus
Velopharyngeal portal closure		
Soft palate elevation	X	Levator veli palatini m.
Lateral portal closure	X	Superior constrictor m.
Hyoid elevation (suprahyoid group)	V3 VII	Anterior belly digastric m., mylohyoid m. Stylohyoid m., posterior belly digastric m.
Thyrohyoid apposition	XII (via C1, C2)	Geniohyoid m.
Pharyngeal elevation	XII (via C1, C2)	Thyrohyoid m.
Suprahyoid group	See hyoid elevation.	
Intrinsic elevators	IX IX, X IX, X	Stylopharyngeus Palatopharyngeus Salpingopharyngeus
Epiglottic tilt		
Extrinsic muscles	V3, VII, XII, XII (C1, C2)	Suprahyoid group Thyrohyoid m.
Intrinsic muscles	X	Aryepiglottic m., thyroepiglottic m.
Laryngeal vestibule closure	X X	Oblique arytenoid m. Thyroarytenoid m., vocal cord muscles
Pharyngeal clearance	X	Superior, middle, inferior constrictor m.
	XII	Hyoglossus, styloglossus
Upper esophageal sphincter opening	V3, VII, XII IX, X X	Suprahyoid group Intrinsic elevators Constrictor muscles
Hyoid depression after swallow	C1, C2	Sternohyoid, omohyoid, sternothyroid m.

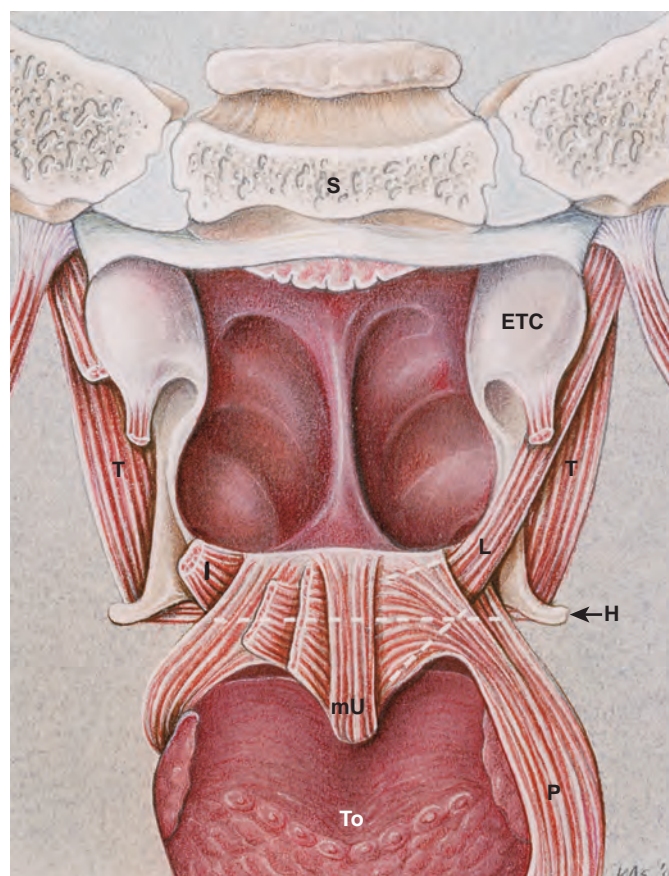


Figure 14-11 Muscles of the soft palate. The muscles forming the soft palate are viewed from behind, looking toward the tongue (To), nasal cavity, and sphenoid bone (S). The levator veli palatini (L) joins its partner (I; partly resected in drawing) from the opposite side to form a sling, which supports the mid-soft palate. The tensor veli palatini (T) forms a tendon that hooks around the pterygoid hamulus (H) to join its partner from the other side, forming the fibrous skeleton of the anterior soft palate. The musculus uvulae (mU), palatopharyngeal muscle (P), and eustachian tube cartilage (ETC) are also shown. (From Rubesin SE, Rabischong P, Bilaniuk LT, et al: Contrast examination of the soft palate with cross-sectional correlation. *RadioGraphics* 8:641–665, 1988.)

important. Both static and dynamic images are routinely obtained for the following reasons: (1) structural disorders often alter pharyngeal motility; (2) structural features of motility disorders are often well demonstrated on static images; and (3) structural lesions and motility disorders may coexist.

The oral and pharyngeal phases of swallowing should initially be evaluated if symptoms suggest an oral or pharyngeal disorder. If the clinical history and symptoms suggest thoracic esophageal disease, however, I only give one swallow of high-density barium in the frontal and lateral positions and then proceed to evaluate the esophagus. The radiologist should remember that the subjective sensation of dysphagia often cannot be localized accurately, and esophageal lesions may cause referred dysphagia to the neck or suprasternal region.³⁶ Furthermore, patients may have an esophageal disorder that secondarily affects pharyngeal function or a disease that involves both the pharynx and esophagus. Finally, some patients have more than one abnormality in the pharynx or esophagus, or in both.

gastric cardia; and (3) single-contrast and mucosal relief views of the esophagus (Table 14-2).²⁹⁻³⁴ The examination is tailored to the patient's clinical history, symptoms, and initial fluoroscopic findings. The pharyngoesophagogram is an interactive study; if a motility disorder is the major radiographic finding, dynamic techniques (e.g., videofluoroscopy, DVD recording) are emphasized.³⁵ If a structural abnormality is the major radiographic finding, double-contrast spot images become more



Figure 14-12 Scout radiograph prior to barium swallow. A lateral radiograph was obtained in a patient who swallowed a needle while sewing. The needle (arrow) lies adjacent to the posterior pharyngeal wall, with its sharp tip superiorly. The bulbous end of the needle is trapped just above the closed pharyngoesophageal segment.

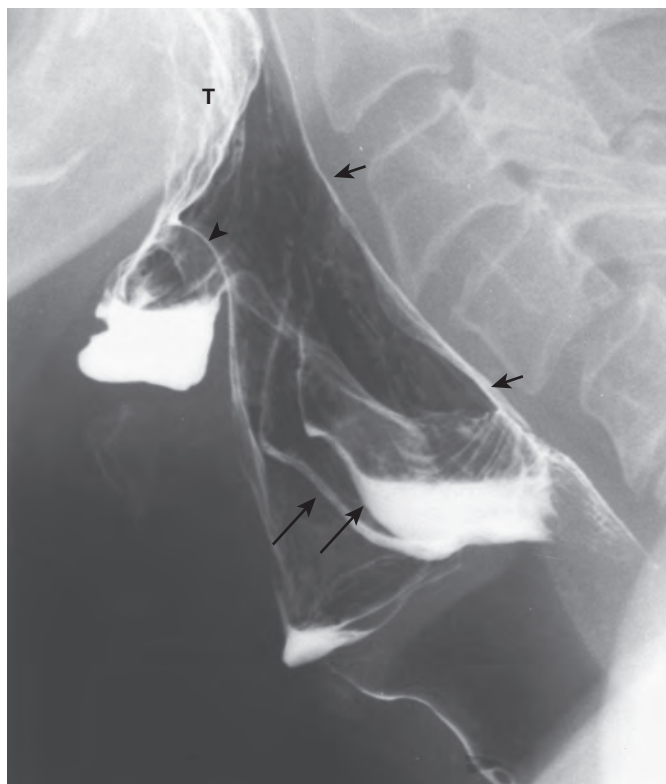


Figure 14-13 Radiograph of the pharynx with the patient in a right lateral position, facing the examiner. The lateral view is the best view to demonstrate the vertical surface of the tongue (T), epiglottic tip (arrowhead) and aryepiglottic folds, anterior walls of the piriform sinuses (long arrows), and posterior pharyngeal wall (short arrows). Opening of the pharyngoesophageal segment is shown only during swallowing. This static radiograph shows that swallowing is abnormal because barium fills the laryngeal ventricle and coats the proximal trachea; it does not demonstrate why barium entered the larynx.

TABLE
14-2

Routine Pharyngoesophagogram for Respiratory or Pharyngeal Symptoms

View	Technique	Organ
Erect, left lateral	Videofluoroscopy, double contrast in phonation	Pharynx
Erect, frontal	Videofluoroscopy, double contrast	Pharynx
Obliques	Video, rapid sequence images if PE segment not visualized on lateral view	Pharynx
EFFERVESCENT AGENT AND WATER*		
Erect, LPO	Double contrast	Esophagus
Prone, RAO	Videofluoroscopy, single contrast	Esophagus
Right lateral	Double contrast	Gastric cardia

*If no laryngeal penetration or esophageal obstruction.

LPO, left posterior oblique with respect to table top;

PE, pharyngoesophageal; RAO, right anterior oblique with respect to table top.

DOUBLE-CONTRAST INTERPRETATION

The principles of double-contrast interpretation for studying the pharynx are the same as those for studying structures elsewhere in the gastrointestinal (GI) tract.²⁵ The double-contrast examination requires adequate mucosal coating, a sufficient number of projections, and varying degrees of luminal distention.

Mucosal Coating

Adequate mucosal coating depends primarily on two factors, dry pharyngeal mucosa and properly prepared high-density

barium (250% w/v). If the barium is too thin, the barium is of insufficient radiodensity to outline the pharyngeal mucosa. If the barium is too thick, mucosal coating may be patchy or obscure mucosal detail. Barium that is too viscous may be unable to wash and scrub the mucosa, resulting in artifactual strands of mucus. Several swallows of high-density barium may be needed in each projection to achieve uniform coating.

Projections

The lateral view best demonstrates the tonsillar fossa en face and the contours of the soft palate, base of the tongue, posterior pharyngeal wall, epiglottis, aryepiglottic folds, anterior hypopharyngeal wall, and region of the cricopharyngeal muscle in profile (Fig. 14-13; see Figs. 14-1B and 14-3B).²⁵ The lateral view is also crucial for evaluating penetration of barium into the laryngeal vestibule (Fig. 14-14). In contrast, the frontal view shows the surface of the tongue base en face and the contours of the median and lateral glossoepiglottic folds, tonsillar fossa, valleculae, and hypopharynx in profile (see Figs. 14-1A and 14-3A). Oblique views are valuable in some patients for demonstrating the obliquely oriented aryepiglottic folds, anterior walls of the piriform sinuses, and region of the pharyngoesophageal segment.^{27,32,37} Spot images obtained in frontal and lateral projections are adequate for most examinations. If a portion of the

pharynx is not well seen in frontal and lateral projections, however, the patient is turned and oblique views are obtained.

Distention

Adequate distention is important for the demonstration of mucosal surface and contour. The pharynx cannot be distended by the use of effervescent agents or tube insufflation, as in other regions of the GI tract. Instead, pharyngeal distention is achieved with phonation (the long vowel sounds “eee” or “ooo”) or some form of modified Valsalva maneuver (blowing against pursed or closed lips or whistling).^{38,39}

Phonation with “eee” expands the pharynx, resulting in better visualization of the soft palate, tonsillar fossa, base of the tongue, valleculae, epiglottic tip, aryepiglottic folds, and mucosa overlying the muscular processes of the arytenoid cartilages on the lateral view (see Fig. 14-1B).³⁹ The distal 2 cm of hypopharynx, however, remain collapsed during phonation because the pharyngoesophageal sphincter remains contracted and the larynx impresses on this region. In contrast, the distal 2 cm of the hypopharynx, pharyngoesophageal segment, and proximal cervical esophagus is optimally distended during swallowing and therefore best visualized during the dynamic phase of the examination (see Fig. 14-9).

Pharyngeal distention on the frontal view is best obtained with a modified Valsalva procedure (Fig. 14-15).^{3,25} The patient is asked to whistle or blow air out of the mouth (as if blowing out a candle) or to blow out against pursed lips. To optimize visualization of pharyngeal structures, the patient is positioned so that the mandible and hard palate are superimposed over the occiput. Flexion or extension of the neck, or protrusion or retraction of the tongue, may improve visualization of various anatomic structures such as the uvula, epiglottic tip, and lateral walls of the hypopharynx.



Figure 14-14 Laryngeal penetration. In an image obtained during swallowing, barium can be seen entering the laryngeal vestibule (white arrow). Note apposition of the hyoid bone (h) to the calcified edge of the thyroid cartilage (black arrow). (From Laufer I, Levine MS [eds]: *Double-Contrast Gastrointestinal Radiology*, 2nd ed. Philadelphia, WB Saunders, 1992.)

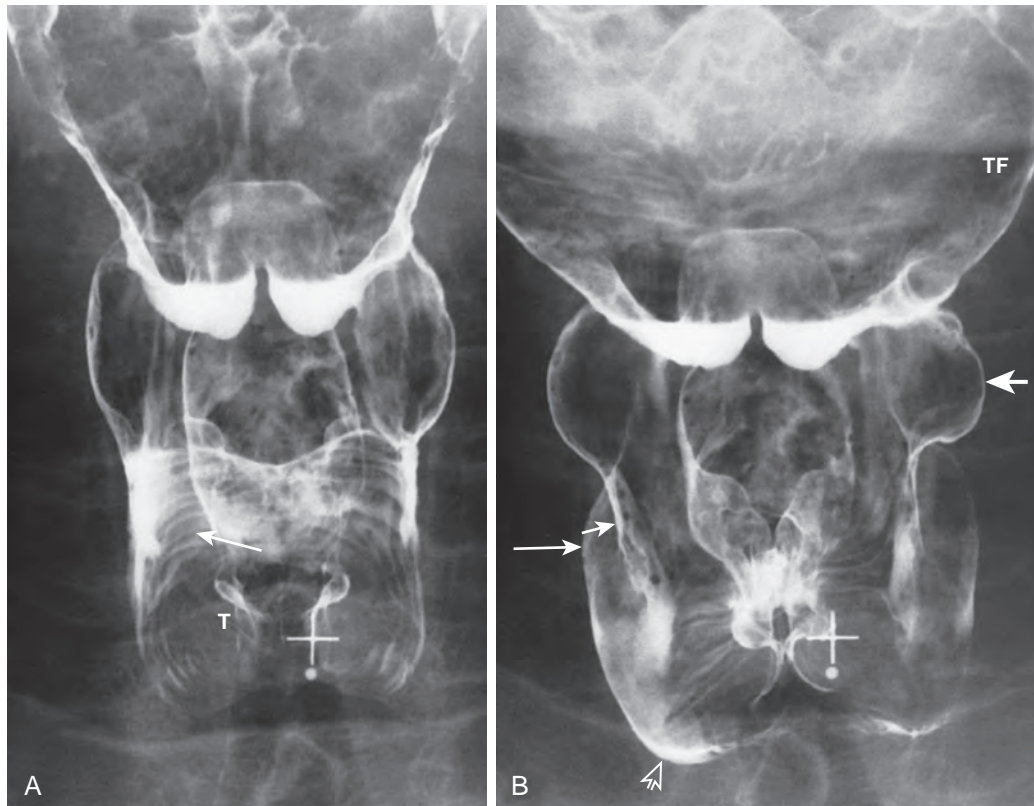


Figure 14-15 Modified Valsalva maneuver. **A.** During quiet inspiration, the right true cord (T) and false vocal cords are open. The pharynx is mildly distended. Note arcuate lines in the collapsed midhypopharynx (arrow). **B.** During a modified Valsalva, marked distention of the oral cavity and pharynx occurs. Note ballooning of the tonsillar fossae (left tonsillar fossae [TF]). Lateral pharyngeal pouches (left pouch, short thick arrow) protrude from the region of the thyrohyoid membrane. The lateral hypopharynx protrudes posterolaterally (long thin arrow) from the confines of the ala of the thyroid cartilage (short thin arrow). The lower hypopharynx, which was not apparent during inspiration, is now visible (open arrow). Protrusion of the lower hypopharynx is a sign of muscular weakness. (From Rubesin SE, Glick SN: *The tailored double-contrast pharyngogram*. *Crit Rev Diagn Imaging* 28:133–179, 1988.)

MOTILITY EXAMINATION

DVD recording and videofluoroscopy are the best methods for studying pharyngeal motility.^{29,30,40} Spot radiographs or rapid-sequence digital images are not adequate for detecting functional abnormalities. The dynamic portion of the pharyngoesophagogram focuses on patient posture and self-feeding, bolus holding anteriorly at the lips and posteriorly at the palatoglossal isthmus, tongue motion, hyoid, laryngeal, and pharyngeal elevation, soft palate elevation, formation of Passavant's cushion, pharyngeal constrictor motion, epiglottic tilt, laryngeal penetration, and cricopharyngeal muscle activity.^{31,32,40-45} An analysis of motility disorders is presented in Chapter 15.

POSITION OF THE PATIENT

The patient is first examined in the upright lateral position, which is the best position for visualizing entry of barium into the laryngeal vestibule during swallowing (penetration) or normal breathing (aspiration). If unable to stand, the patient is strapped and seated in a swallowing chair or on the footboard of the fluoroscope in a lateral position. If unable to sit, the patient is placed on the fluoroscopic table in as lateral a position as possible. Dentures are left in place because denture removal may alter swallowing dynamics. If a portable or fixed C-arm fluoroscope is available, patients may be studied while they are confined to a wheelchair or lying on a stretcher.⁴² Although the lateral view is the predominant position of the patient, the frontal view should be performed, even in debilitated patients. The frontal position demonstrates asymmetry of pharyngeal contraction and of epiglottic tilt (Fig. 14-16). Spot radiographs are performed in the frontal position, even in patients with motor disorders, because they may provide clues to the cause of a motor disorder (Fig. 14-17).³⁵

CHOICE OF CONTRAST AGENTS

In general, the pharynx manipulates a cohesive bolus more readily than a liquid bolus.^{26,43-45} Less laryngeal penetration is seen with thicker than thinner substances. Therefore, the pharyngeal phase of swallowing is usually safer with barium pudding than with thick barium and safer with thick barium than with thin barium. The caveat to "thick is safer" is that thin liquids are cleared from the pharynx better than thick liquids. Therefore, if the major abnormality is poor pharyngeal contraction leading to stasis in the piriform sinus (and epiglottic tilt is normal), a thin liquid is safer.

I usually begin an examination with thick, high-density barium because this barium best demonstrates morphologic characteristics of the pharynx. High-density barium is more visible during a review of dynamic images than thin barium. If a motility disorder is seen during fluoroscopy, swallows of thin barium are videotaped or digitally recorded in the lateral and frontal projections after double-contrast imaging of the pharynx and esophagus. Epiglottic motility is better assessed with thin barium because thick barium often obscures the epiglottic tip. Thin barium is also valuable because some patients show laryngeal penetration only with thin barium, not with thick barium or barium pudding.

If the examination is only concerned with the pharynx, I then often proceed to barium pudding or a thicker liquid



Figure 14-16 Asymmetric pharyngeal contraction demonstrated on frontal view during swallowing. Inbowing of the uppermost left lateral hypopharyngeal wall (*large arrow*) is the result of a normally contacting left thyropharyngeal muscle. The uppermost right lateral hypopharyngeal wall balloons outwardly at the level of the thyrohyoid membrane (*small arrow*), indicating lack of upper thyropharyngeal contraction.

(so-called nectar or honey) to stress the oral phase of swallowing or improve the pharyngeal phase. If the pharyngeal phase appears normal, I often stress the pharynx next with thin barium.

In general, the pharynx can manipulate small nonphysiologic boluses (2-5 mL) more safely than larger physiologic boluses (8-10 mL).^{46,47} I routinely ask outpatients to "take a normal-sized swallow of barium." If there are clinical signs of abnormal pharyngeal function, the patient should therefore be given small boluses first and then larger boluses. If I want to control the bolus size, measured amounts of barium are given with a teaspoon or small plastic measuring cup. Swallowing through a straw is relatively dangerous in a patient with abnormal oral bolus control and should be avoided until the patient is determined to be swallow-safe or to test if the patient is able to drink through a straw.

For the patient who is massively aspirating barium, the clinical status of the patient determines the number of barium swallows deemed safe for the examination. If there is aspiration of barium to or below the carina, the examination should generally be discontinued. Even with massive aspiration, views of one swallow in the lateral projection and one swallow in the frontal projection are usually obtained. A suction apparatus should be available for prompt removal of barium that enters the distal trachea.

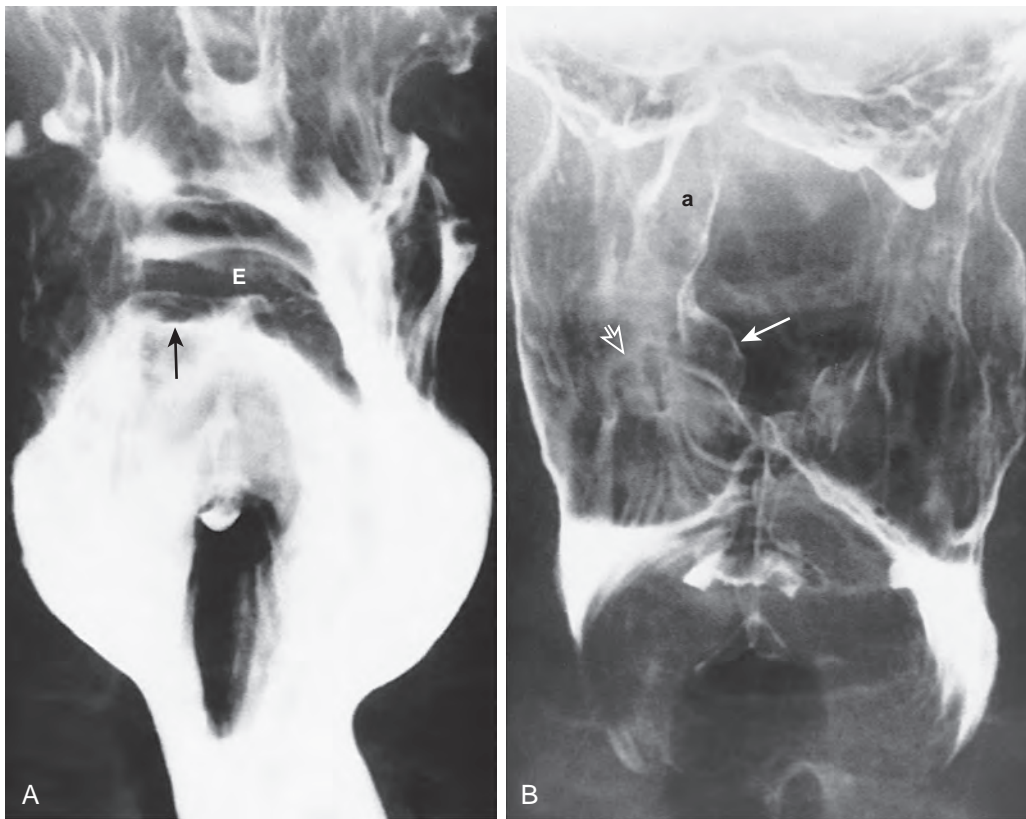


Figure 14-17 Abnormal epiglottic tilt caused by squamous cell carcinoma involving right aryepiglottic fold and the mucosa overlying the muscular process of the right arytenoid cartilage. **A.** During swallowing, tilt of the epiglottis (E) is diminished on the right (arrow). **B.** Frontal spot radiograph shows a small mass (arrow) and thickening of the aryepiglottic fold (a) and nodular mucosa (open arrow). A small squamous cell carcinoma was found to involve the aryepiglottic fold and mucosa overlying the muscular process of the right arytenoid cartilage. (From Rubesin SE: *Pharyngeal dysfunction*. In Gore R [ed]: *Syllabus for Categorical Course on Gastrointestinal Radiology*. Reston, VA, American College of Radiology, 1991, pp 1–9.)

THERAPEUTIC EXAMINATION

A therapeutic examination of the pharynx may be performed to use modifications of swallowing that prevent or diminish laryngeal penetration and educate patients about their swallowing function.⁴⁷⁻⁴⁹ This examination is usually performed in conjunction with a swallowing therapist from the department of rehabilitation medicine or speech pathology. During the therapeutic examination, various types of boluses, head positions, and breathing techniques are used to determine which foods can be safely swallowed. The swallowing team selects a technique based on a specific abnormality seen at fluoroscopy. Most strategies to improve swallowing are temporary measures while a treatable cause of the swallowing problem is discovered or the patient recovers from a cerebrovascular accident, surgery, or radiation therapy.²⁶

Compensatory Techniques

Compensatory techniques control bolus flow but do not improve swallowing physiology. These techniques include the following: (1) changes in posture; (2) increased sensory input; and (3) alterations in food volume or consistency.⁴⁸ Eliminating food consistencies that are difficult to swallow is a short-term strategy used while a patient recovers from a swallowing disorder. Continuation of swallowing in a limited fashion may help improve muscular function and give the patient some pleasure, although not necessarily maintaining adequate hydration or nutrition. The therapist tests the patient's ability to manage barium boluses of progressively larger size and of varying viscosity. If a patient has reduced tongue motion, strength, or coordination, a thin liquid is easier to swallow. If premature

spillage of the bolus from the oral cavity to the oropharynx is observed, a thick liquid or cohesive bolus (e.g., a barium pudding) may improve the timing between the oral and pharyngeal phases. A cohesive bolus may also decrease laryngeal penetration if there is poor timing between the oral and pharyngeal phases, abnormal epiglottic tilt, or abnormal glottic closure. Conversely, a thin liquid improves pharyngeal clearance if there is stasis in the piriform sinuses, thereby diminishing overflow aspiration. Although the use of thin liquids diminishes stasis, this practice results in decreased bolus control or laryngeal penetration in patients with abnormal epiglottic tilt or abnormal laryngeal closure. Thin liquids may also improve swallowing function in patients with isolated pharyngoesophageal segment dysfunction.

Postural techniques alter oral and pharyngeal relationships and redirect bolus flow. Commonly used head positions include chin-up, chin-down, and head rotation. When there is poor transfer of the bolus from the oral cavity to the oropharynx, the chin-up position causes gravity to help the bolus fall into the oropharynx. This position requires a relatively normal pharyngeal phase of swallowing to prevent laryngeal penetration.

The chin-down (chin tuck) position is used for patients with premature spill, abnormal tongue push, laryngeal penetration resulting from abnormal epiglottic tilt, or poor opening of the pharyngoesophageal segment. If the bolus prematurely spills from the oral cavity, tucking the chin widens the valleculae, providing a space for the prematurely spilled bolus to pool rather than enter the laryngeal vestibule. The chin tuck position also improves tongue push because the tongue is positioned more posteriorly. The chin tuck position also narrows the laryngeal aditus by elevating the larynx and pharynx and tilting the

epiglottis posteriorly, diminishing laryngeal vestibule penetration caused by abnormal epiglottic tilt. Finally, the chin tuck position pulls the anterior wall of the pharyngoesophageal segment anteriorly, helping improve clearance through a pharyngoesophageal segment that opens abnormally.

Rotating the head toward one side narrows the pharynx on that side and redirects the bolus toward the opposite swallowing channel. Head rotation is used for patients with unilateral pharyngeal paresis or asymmetric epiglottic tilt to guide the bolus away from the weak side. The head is turned toward the side of weakness. Head rotation may be combined with the chin tuck maneuver.

Therapeutic Techniques

Therapeutic techniques improve motion or strength of a structure or coordination of the timing of oral and pharyngeal events.^{47,49} These include range of motion or muscle-strengthening exercises, tactile stimulation, and swallowing maneuvers.

Swallowing maneuvers include the supraglottic swallow, supersupraglottic swallow, Mendelsohn maneuver, and effortful swallow. Such maneuvers require a patient to have enough cognitive and physical ability to follow the instructions for performing these examinations.

Both a supraglottic and supersupraglottic swallow may be tried in patients who have laryngeal penetration because of abnormal timing between the oral and pharyngeal phases of swallowing or abnormal closure of the laryngeal vestibule. In a supraglottic swallow, the patient takes a bolus into the mouth, takes a breath through the nose, consciously holds the breath, swallows, and then exhales or coughs. This sequence closes the true vocal cords before and during the swallow. Exhaling or coughing after the swallow helps expel any part of the bolus that has entered the laryngeal vestibule. A supersupraglottic swallow is similar to a supraglottic swallow but uses a consciously "hard" breath-hold, which closes the true vocal cords and tilts the arytenoids forward to help close the laryngeal aditus.

REFERENCES

- DuBrul EL: *Sicher's Oral Anatomy*, ed 7, St. Louis, 1980, CV Mosby, pp 319–350.
- Pernkopf E: *Anatomy*, vol 1, Head and Neck, ed 3, Baltimore, 1989, Urban & Schwarzenberg.
- Rubenstein SE, Jessurun J, Robertson D, et al: Lines of the pharynx. *Radiographics* 7:217–237, 1987.
- Sobotta J, Figge FHJ: *Atlas of Human Anatomy*, vol 2, Baltimore, 1977, Urban & Schwarzenberg.
- Silver AJ, Sane P, Hilal SK: CT of the nasopharyngeal region: Normal and pathologic anatomy. *Radiol Clin North Am* 22:161–176, 1984.
- Rubenstein SE: Pharyngeal morphology. In Ekberg O, editor: *Radiology of the Pharynx and Oesophagus*, Berlin, 2004, Springer-Verlag, pp 51–75.
- McMyn JK: The anatomy of the salpingopharyngeus muscle. *J Laryngol Otol* 55:1–22, 1940.
- Rubenstein SE, Jones B, Donner MW: Radiology of the adult soft palate. *Dysphagia* 2:8–17, 1987.
- Gromet M, Homer MJ, Carter BL: Lymphoid hyperplasia at the base of the tongue. *Radiology* 144:825–828, 1982.
- Ekberg O, Sigurjonsson S: Movements of the epiglottis during deglutition: A cineradiographic study. *Gastrointest Radiol* 7:101–107, 1982.
- Curtis DJ, Hudson T: Laryngotracheal aspiration: Analysis of specific neuromuscular factors. *Radiology* 149:517–522, 1983.
- Ekberg O, Lindstrom C: The upper esophageal sphincter area. *Acta Radiol* 28:173–176, 1987.
- Pitman RG, Fraser GM: The post-cricoid impression of the esophagus. *Clin Radiol* 16:34–39, 1965.
- Bosma JF, Donner MW, Tanaka E, et al: Anatomy of the pharynx, pertinent to swallowing. *Dysphagia* 1:23–33, 1986.
- Dickson DR: Anatomy of the normal velopharyngeal mechanism. *Clin Plast Surg* 2:235–248, 1975.
- Sinclair DC: Muscles and fasciae. In Romanes GJ, editor: *Cunningham's Textbook of Anatomy*, London, 1972, Oxford University Press, pp 286–299.
- Doty RW, Bosma JF: An electromyographic analysis of reflex deglutition. *J Neurophysiol* 19:44–60, 1956.
- Donner MW, Bosma JF, Robertson DL: Anatomy and physiology of the pharynx. *Gastrointest Radiol* 10:196–212, 1985.
- Rubenstein SE, Rabischong P, Bilaniuk LT, et al: Contrast examination of the soft palate with cross-sectional correlation. *Radiographics* 4:641–665, 1988.
- Ekberg O, Nylander G: Anatomy and physiology. In Ekberg O, editor: *Dysphagia: Diagnosis and Treatment*, Berlin, 2012, Springer-Verlag, pp 3–18.
- Curtis DJ, Sepulveda GU: Epiglottic motion: Video recording of muscular dysfunction. *Radiology* 148:473–477, 1983.
- Shprintzen RJ, McCall GN, Skolnick ML, et al: Selective movement of the lateral aspects of the pharyngeal walls during velopharyngeal closure for speech, blowing, and whistling in normals. *Cleft Palate J* 12:51–58, 1975.
- Skolnick ML, McCall GN, Barnes M: The sphincteric mechanism of velopharyngeal closure. *Cleft Palate J* 10:286–305, 1973.
- Rubenstein SE: Pharyngeal dysfunction. In Gore R, editor: *Syllabus for Categorical Course on Gastrointestinal Radiology*, Reston, VA, 1991, American College of Radiology, pp 1–9.
- Rubenstein SE, Laufer I: Pictorial review: Principles of double-contrast pharyngography. *Dysphagia* 6:170–178, 1991.
- Rubenstein SE, Stiles TD: Principles of performing a "modified barium swallow" examination. In Balfe DM, Levine MS, editors: *Categorical Course in Diagnostic Radiology: Gastrointestinal*, Oak Brook, IL, 1997, RSNA Publications, pp 7–20.
- Balfe DM, Heiken JP: Contrast evaluation of structural lesions of the pharynx. *Curr Probl Diagn Radiol* 15:73–160, 1986.
- Ott DJ, Gelfand DW: Gastrointestinal contrast agents: Indications, uses, risks. *JAMA* 249:2380–2384, 1984.
- Jones B, Donner MW: Examination of the patient with dysphagia. *Radiology* 167:319–326, 1988.
- Jones B, Kramer SS, Donner MW: Dynamic imaging of the pharynx. *Gastrointest Radiol* 10:213–224, 1985.
- Levine MS, Rubenstein SE: Radiologic investigation of dysphagia. *AJR* 154:1157–1163, 1990.
- Rubenstein SE, Glick SN: The tailored double-contrast pharyngogram. *Crit Rev Diagn Imaging* 28:133–179, 1988.
- Ekberg O, Nylander G: Double-contrast examination of the pharynx. *Gastrointest Radiol* 10:263–271, 1985.
- Logemann JA: *Manual for the Videofluorographic Study of Swallowing*, ed 2, Austin, TX, 1993, Pro-Ed.
- Rubenstein SE: Pharynx. In Levine MS, Ramchandani P, Rubenstein SE, editors: *Practical Fluoroscopy of the GI and GU Tracts*, Cambridge, England, 2012, Cambridge University Press, pp 1–22.
- Jones B, Ravich WJ, Donner MW, et al: Pharyngoesophageal inter-relationships: Observations and working concepts. *Gastrointest Radiol* 10:225–233, 1985.
- Taylor AJ, Dodds WJ, Stewart ET: Pharynx: Value of oblique projections for radiographic examination. *Radiology* 178:59–61, 1991.
- Jing BS: The pharynx and larynx: Roentgenographic technique. *Semin Roentgenol* 9:259–265, 1974.
- Rubenstein SE, Jones B, Donner MW: Contrast pharyngography: The importance of phonation. *AJR* 148:269–272, 1987.
- Dodds WJ, Logemann JA, Stewart ET: Radiologic assessment of abnormal oral and pharyngeal phases of swallowing. *AJR* 154:965–974, 1990.
- Ekberg O: Posture of the head and pharyngeal swallow. *Acta Radiol Diagn* 691–696, 1986.
- Davis M, Palmer P, Kelsey C: Use of C-arm fluoroscope to examine patients with swallowing disorders. *AJR* 155:986–988, 1990.
- Dantas RO, Dodds WJ, Massey BT, et al: The effect of high- vs. low-density barium preparations on the quantitative features of swallowing. *AJR* 153:1191–1195, 1989.

44. Curtis DJ, Cruess DF, Willgress ER: Abnormal solid bolus swallowing in the erect position. *Dysphagia* 2:46–49, 1987.
45. van Westen D, Ekberg O: Solid bolus swallowing in the radiologic evaluation of dysphagia. *Acta Radiol* 34:332–335, 1993.
46. Dodds WJ, Man KM, Cook IJ, et al: Influence of bolus volume on swallow-induced hyoid movement in normal subjects. *AJR* 150:1307–1309, 1988.
47. Logemann J: Anatomy and physiology of normal deglutition. In Logemann J, editor: *Evaluation and Treatment of Swallowing Disorders*, Austin, TX, 1983, Pro-Ed, pp 9–26.
48. Logemann JA: Rehabilitation of oropharyngeal swallowing disorders. *Acta Otorhinolaryngol Belg* 48:207–215, 1994.
49. Bilow M, Martin-Harris B: The therapeutic swallowing study. In Ekberg O, editor: *Dysphagia: Diagnosis and Treatment*, Berlin, 2012, Springer-Verlag, pp 411–424.

Abnormalities of Pharyngeal Function

BRONWYN JONES

CHAPTER OUTLINE

Analysis of the Functional Aspects of Swallowing

Neurophysiologic Control of Swallowing

Functional Components of Swallowing

Prevention of Aspiration

Adaptation, Compensation, and Decompensation

Functional Aspects of Zenker's Diverticulum

Interrelationships

Esophageal Distention and the Cricopharyngeus

Gastroesophageal Reflux and the Cricopharyngeus

Swallowing-Related Reflexes

Functional Changes After Radiation Therapy

Aging and Swallowing

Neurologic Disease and the Pharynx

Cerebrovascular Accident

Amyotrophic Lateral Sclerosis (Lou Gehrig's Disease)

Multiple Sclerosis

Neurodegenerative Disorders

Myasthenia Gravis and Related Disorders

Familial Dysautonomia (Riley-Day Syndrome)

Diseases of the Muscle

Infections

Medications

such as a web or laryngeal penetration may be visible on only one or two frames at 30 frames/s.

2. The entire swallowing chain must be examined. Such extensive examination is necessary because the level of symptoms is not a reliable indicator of the site of the abnormality,¹ several lesions could be causing dysphagia, and esophageal disease may result in pharyngeal disease.²

NEUROPHYSIOLOGIC CONTROL OF SWALLOWING

Swallowing involves the close cooperation of many muscles, six cranial nerves (trigeminal, facial, glossopharyngeal, vagus, spinal branch of accessory, and hypoglossal) and the first, second, and third cervical nerves (through the ansa cervicalis). Afferent sensory information is integrated in the swallowing center in the brain stem, and efferent signals originate in the motor ganglia of the cranial nerves; movements are then effected peripherally.³⁻⁸

The vagus nerve (cranial nerve [CN] X) supplies motor efferent fibers to all the intrinsic pharyngeal muscles (constrictors, palatopharyngeus, and salpingopharyngeus), except the stylopharyngeus, which is supplied by the glossopharyngeal nerve (CN IX). The vagus nerve also supplies motor efferent fibers to all the palatal muscles, except the tensor veli palatini, which is supplied by the trigeminal nerve (CN V). The trigeminal nerve also supplies the anterior digastricus and mylohyoides. The facial nerve (CN VII) supplies the posterior digastricus and stylohyoides. Although the vagus nerve carries the efferent fibers that innervate the striated pharyngeal musculature, most of these fibers probably emerge from the brain stem in the bulbar part of the accessory nerve (CN XI).

Pharyngeal branches of the glossopharyngeal and vagus nerves and rami of the sympathetic trunk and superior cervical ganglion form a plexus in the connective tissue outside the constrictor muscles (the pharyngeal plexus). In this plexus, autonomic (parasympathetic and sympathetic) and afferent and efferent branchial fibers intermingle and branch into the muscles and the mucosal lining. Damage to this plexus can produce dysphagia.^{9,10}

Pharyngeal sensation, including sensation of the tonsil and postsulcal part of the tongue, appears to be mediated by the glossopharyngeal nerve. This nerve also supplies motor innervation to the stylopharyngeus and parasympathetic secretomotor fibers to the parotid gland.

FUNCTIONAL COMPONENTS OF SWALLOWING

Oropharyngeal Phase

Tongue and Palate. Swallowing begins with the lips engulfing the bolus (Figs. 15-1 and 15-2). The bolus is then manipulated by the tongue and teeth until it is judged "swallowable." Two positions of the bolus preparatory to swallowing have been

Analysis of the Functional Aspects of Swallowing

In reviewing the pharyngeal swallow, the slow motion, reverse, and stop-frame capabilities of videofluorography are essential. With these capabilities, the movement of individual structures can be analyzed, first in isolation and then in combination with other structures, including the tongue, palate, epiglottis, hyoid bone, larynx, and cricopharyngeus. Esophageal peristalsis should also be evaluated, but discussion of this subject is beyond the scope of this chapter.

Familiarity with the anatomy, radiographic anatomy, and physiology of the pharynx and related structures is a necessity for abnormalities to be appreciated. Any lack of movement or abnormalities indicating compensation or decompensation must be noted.

Two important principles must be considered when reviewing pharyngeal studies:

1. Dynamic imaging is vital. Pharyngeal contraction occurs much faster than esophageal contraction (12-25 cm/s vs. 1-4 cm/s), which is why dynamic imaging is essential when examining the pharynx. In addition, an abnormality

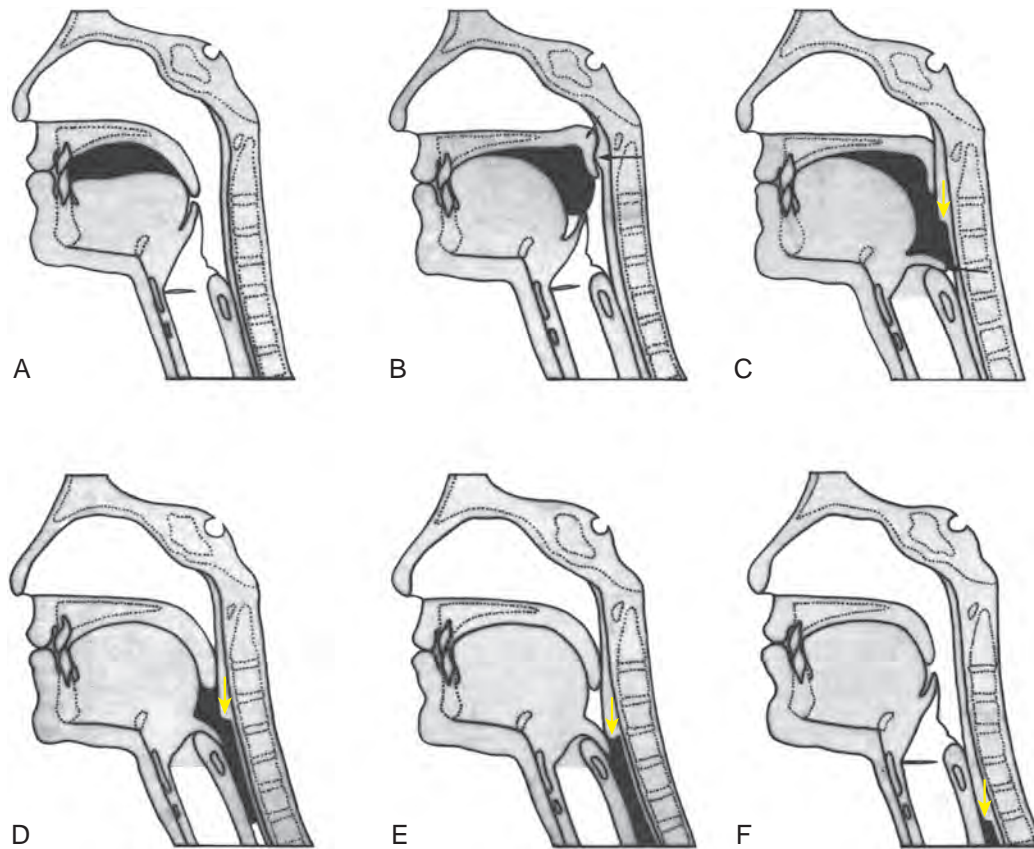


Figure 15-1 Line drawing of the normal swallow (lateral view). **A.** The bolus is held in the oral cavity by apposition of the soft palate and back of the tongue. **B.** As the bolus is presented to the oropharynx, the soft palate (short arrow) elevates to appose Passavant's cushion (long arrow) to prevent nasopharyngeal regurgitation. **C.** As the bolus passes through the pharynx, the beginning of the posterior pharyngeal stripping wave (yellow arrow) can be seen. The epiglottis (black arrow) is tilted to cover the laryngeal aditus, which is completely closed. **D.** As the bolus descends farther, the back of the tongue, soft palate, and pharyngeal stripping wave (arrow) continue to seal the nasopharyngeal inlet, the epiglottis remains tilted, and the larynx remains closed. The cricopharyngeus has opened completely to allow unimpeded bolus passage. **E.** As the bolus descends past the cricopharyngeal level, the tongue base begins to move forward, and the soft palate begins to elevate. **F.** As the bolus passes into the thoracic esophagus, the tongue base moves forward, the epiglottis flips up, and the larynx returns to its resting, open position. (From Donner MW, Bosma JF, Robertson DL: *Anatomy and physiology of the pharynx*. *Gastrointest Radiol* 10:196–212, 1985.)

identified: the tipper type (in which the bolus is held in the midline groove of the tongue) and the dipper type (in which the bolus is held anteriorly underneath the tongue in the floor of the mouth).¹¹

The back of the tongue blade and soft palate form a seal that prevents premature leakage into the pharynx before swallowing (see Figs. 15-1A and 15-2A). Weakness, atrophy, or resection of the tongue or soft palate can lead to aspiration before swallowing because of leakage of the bolus into the open, unprotected larynx. Viewed in the frontal position, unilateral leakage indicates decompensation on one side only.

As the bolus is propelled into the oropharynx by an upward backward movement of the tongue, the soft palate elevates to a right angle to appose the posterior pharyngeal wall, with Passavant's cushion moving anteriorly to complete the seal of the palatopharyngeal isthmus. Passavant's cushion results from focal contraction of the upper fibers of the superior pharyngeal constrictor muscle (Fig. 15-3; see also Figs. 15-1B, 15-2B, 15-10A, 15-11A, and 15-11B). Tongue thrust (involving first the blade and then the base of the tongue), combined with pharyngeal constriction and intrabolus pressure, result in bolus propulsion.

Pharynx. The constrictor stripping wave can be observed at the tail of the bolus in the lateral position as a progressive forward movement of the posterior pharyngeal wall (see Figs. 15-1C to F and 15-2C to E). In the frontal position, the wave can be appreciated as the lateral walls of the pharynx converge to the midline, completely obliterating the pharyngeal cavity behind the bolus. Unilateral weakness results in asymmetry on the frontal view, with one side moving to the midline and the other remaining still or bulging during the swallow. Sometimes, the contracting normal side can displace the bolus across to the atonic side, so the bolus passes down the paralyzed side. The contracting normal side may be misinterpreted as a mass, whereas the abnormality is actually on the noncontracting bulging side. Contraction of the constrictor muscles may be affected by intrinsic disease of the pharyngeal muscles (e.g., polymyositis), neuromuscular disorders (e.g., amyotrophic lateral sclerosis, cerebrovascular accident [CVA]), or local factors (e.g., scarring, radiation, cervical spine disease). Large osteophytes in the cervical spine may hinder or prevent epiglottic tilt.¹² Diseases that restrict laryngeal elevation (e.g., radiation, head and neck surgery) may compound the problem.

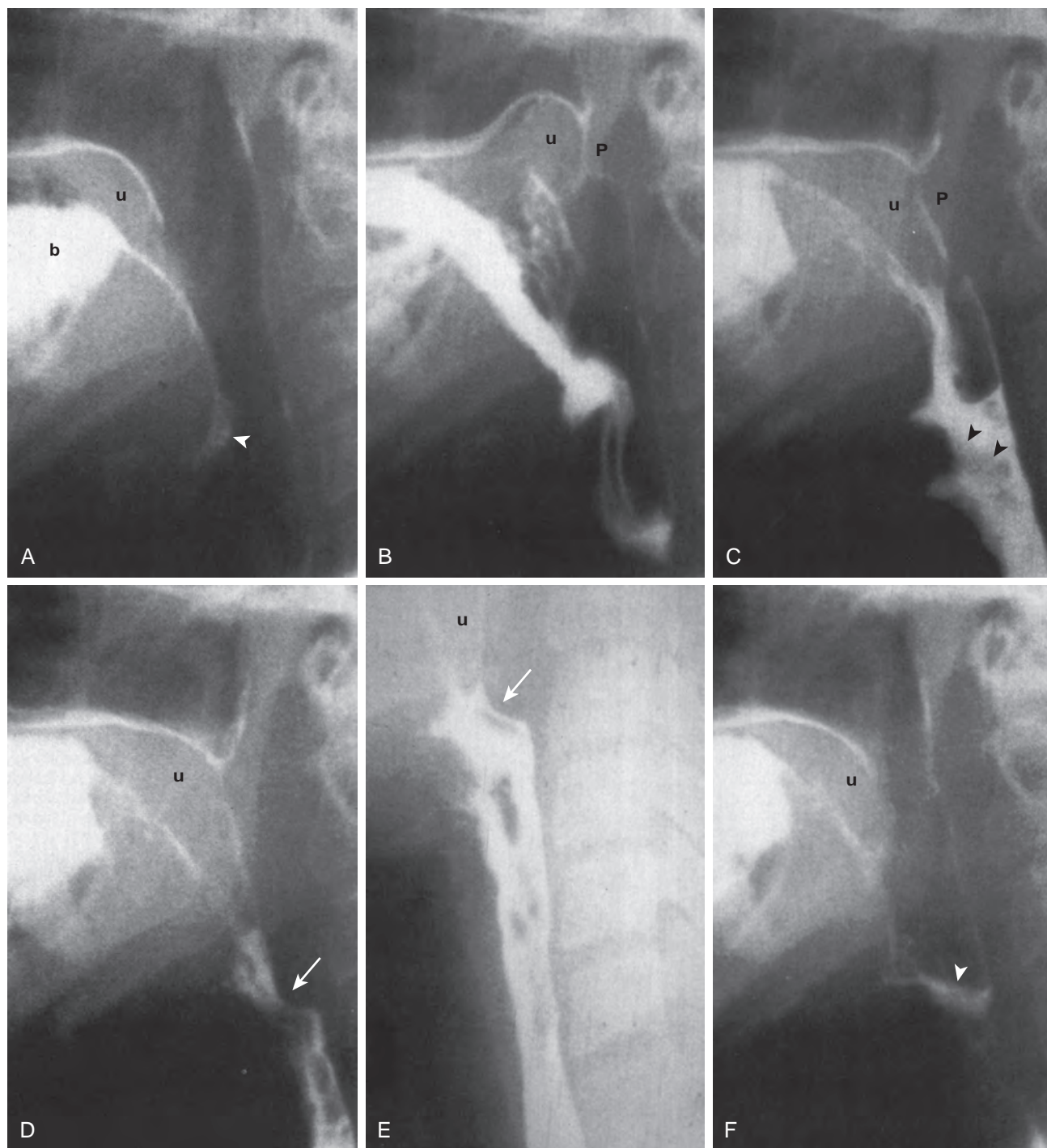


Figure 15-2 The normal swallow. **A** to **F.** A series of stop-frame prints from a cinepharyngoesophagogram shows the normal swallow as it appears on the dynamic imaging study in the lateral position. The epiglottis (*arrowheads*) and stripping wave (*arrow*) are identified. Note that the superior and posterior surfaces of the soft palate have been coated by intranasal injection of barium. **F.** The epiglottis is beginning to re-elevate but has not yet returned to its resting position. *b*, Bolus; *p*, Passavant's cushion; *u*, soft palate.

Laryngeal Dynamics and Hyoid Elevation

Respiration is suspended during swallowing and resumes after swallowing. As the bolus enters the oropharynx, the larynx begins to elevate, the hyoid bone moves upward and forward, and the true vocal folds, false vocal folds, and laryngeal vestibule close inferiorly to superiorly, with the vestibule closing last. Laryngeal elevation begins simultaneously with elevation of the

hyoid bone but continues for a short time after the hyoid bone has reached its peak elevation. Laryngeal movement can be appreciated by observing the hyoid bone rising to appose the angle of the mandible. There is an excellent review of laryngeal dynamics by Curtis.¹³ A direct correlation exists between hyoid bone excursion and bolus volume, with larger volumes producing more elevation.¹⁴ Hyoid bone elevation may occur in one step (20%) or in two steps (80%), whereas descent occurs in

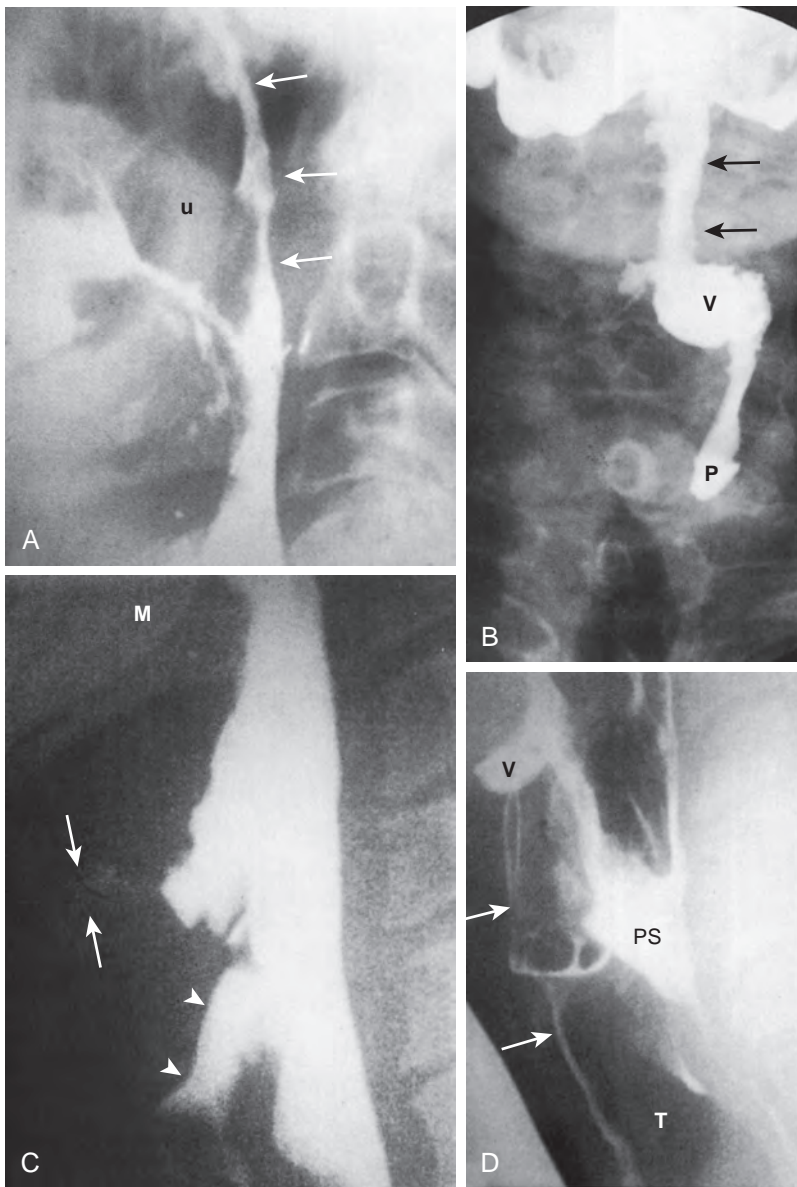


Figure 15-3 Multiple stop-frame prints from four different patients show multiple decompensations.

A. Somewhat magnified view of the lateral oropharynx and nasopharynx demonstrates incomplete elevation of the soft palate (u) and marked nasopharyngeal regurgitation (arrows). **B.** There is unilateral leakage over the back of the tongue (arrows) into the left vallecula (V) and then into the piriform sinus (P). **C.** Lateral view shows marked laryngeal penetration into the widely open larynx (arrowheads) and incomplete elevation of the hyoid bone (arrows); normally, the hyoid elevates almost to the angle of the mandible (M). **D.** There is marked retention in the valleculae (V) and piriform sinuses (PS) after swallowing and overflow aspiration (arrows) into the larynx and trachea (T). (B from Jones B, Donner MW: *Interpreting the study*. In Jones B, Donner MW [eds]: *Normal and Abnormal Swallowing: Imaging in Diagnosis and Therapy*. New York, Springer-Verlag, 1991, p 60.)

one step, simultaneously with return of the epiglottis to the upright position.¹⁵

A recent review of the literature of hyoid and laryngeal kinematics¹⁶ has revealed a large variability in the values reported for superior hyoid displacement, varying from 5.8¹⁷ to 25.0 mm.¹⁸ Anterior displacement similarly ranged from 7.6¹⁹ to 18 mm.²⁰ Another recent study²¹ has correlated hyoid displacement with cervical spine height (measuring from the anteroinferior border of C4 to the anteroinferior border of C2) and compared findings in men and women. When adjusted for height, the upward movements of the hyoid and larynx were similar in magnitude in men and women.

Epiglottic Tilt

Epiglottic tilt deflects food and liquid into the lateral food channels away from the larynx; when completely inverted, the epiglottis covers the laryngeal aperture. In many people, this movement occurs in two steps; the first movement (to a horizontal position) is probably a passive one caused by elevation

of the hyoid bone and the second movement (to complete inversion) is probably caused by contraction of the thyroepiglotticus.²² In a minority of people, the epiglottis fails to invert, tilting only to the horizontal or oblique position. In the frontal view, the completely inverted epiglottis produces a seagull-shaped filling defect. Flow of the bolus into the lateral food channels may also produce a flow defect, or pseudomass.

Cricopharyngeal Opening

Pharyngeal constriction must be coordinated with cricopharyngeal relaxation and opening. The cricopharyngeus must relax and open completely to allow unimpeded bolus passage.²³⁻³⁸ Opening of the lumen at the pharyngoesophageal junction results from several actions: (1) cricopharyngeal relaxation; (2) superior and anterior movement of the larynx, resulting in traction on the anterior wall of the lumen; (3) pharyngeal constriction, producing thrust; and (4) intrabolus pressure, producing thrust. Thus, cricopharyngeal prominence is often observed in patients with pharyngeal paresis or a frozen larynx.

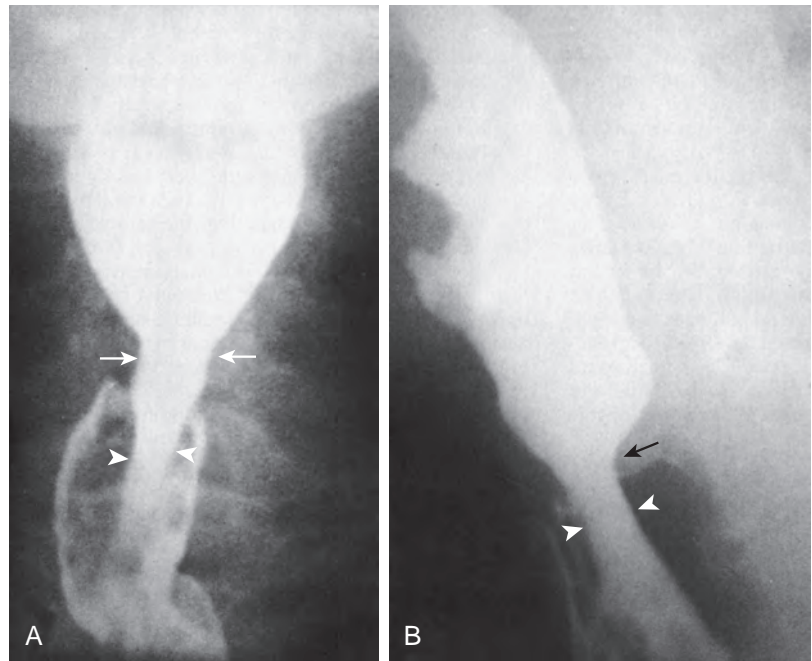


Figure 15-4 Cricopharyngeal prominence. Frontal (A) and lateral (B) radiographs show prominence of the cricopharyngeus (arrows). Note the jet effect below the narrowing (arrowheads), simulating a stenotic lesion, especially on the lateral view. The lumen of the cervical esophagus is actually dilated because the patient had achalasia. (From Jones B, Donner MW, Rubesin SE, et al: *Pharyngeal findings in 21 patients with achalasia of the esophagus*. *Dysphagia* 2:87–92, 1987.)

In such cases, the pharyngeal milieu, rather than the muscle itself, is abnormal.

Radiographically, one normally observes luminal opening, not cricopharyngeal relaxation; a radiographic report therefore should not comment on cricopharyngeal relaxation but only on cricopharyngeal opening. *Cricopharyngeal achalasia* is a manometric term referring to complete failure of cricopharyngeal relaxation, an unusual entity. Other common conditions associated with cricopharyngeal prominence include Zenker's diverticulum, advanced age, gastroesophageal reflux, and other esophageal motility disorders (e.g., diffuse esophageal spasm, achalasia; Fig. 15-4).² The resulting luminal compromise may be minimal or marked. In severe cases, there may be a horizontal bar. The luminal narrowing can be treated by endoscopic bougienage.

Pharyngeal Residue

The normal swallow should clear most of the bolus from the mouth and pharynx. (An exception is high-density barium designed to coat the gastrointestinal [GI] tract). A study by Dejaeger and colleagues in 1997³⁹ studied mechanisms involved in postdeglutition residue in older adults and found that retention in the valleculae and piriform sinuses was related to markedly reduced pharyngeal shortening, a low tongue-driving force, and diminished amplitude of pharyngeal contraction. Retention in the valleculae only is related to a low tongue-driving force and in the piriform sinuses only is related to reduced pharyngeal shortening.

Prevention of Aspiration

Many mechanisms protect the larynx from aspiration (see Figs. 15-3 and 15-11). Laryngeal elevation and closure of the vocal folds, arytenoid cartilages, and laryngeal vestibule all contribute, as does epiglottic tilt.⁴⁰ Thus, a frozen larynx can result in aspiration.

If aspiration is observed, all factors that prevent aspiration should be analyzed and the following questions asked:

- Does the epiglottis tilt, and does the larynx (hyoid bone) elevate adequately?
- Do the vocal cords and laryngeal vestibule close?

It should also be noted when the aspiration occurs in relation to swallowing. Laryngeal penetration or aspiration through the vocal folds may occur during swallowing, before swallowing (premature leakage from the mouth), or after swallowing (overflow aspiration of a retained bolus in the pharynx, or regurgitated of refluxed material). The timing and causes of aspiration have potential therapeutic implications.

Another important observation is whether the aspirated material precipitates a cough; this needs to be conveyed to the referring physician in the radiologic report. Some patients with chronic aspiration are silent aspirators, presumably because of loss of laryngeal sensation. Bedside evaluation of these patients for aspiration is notoriously unreliable. In fact, the so-called bedside evaluation underestimates the possibility of aspiration in many patients.^{41–44}

The important role that the mouth can play in aspiration was underestimated until two important studies highlighted the role of oral decompensation alone in aspiration.^{45,46} Feinberg and Ekberg studied a group of 50 patients with known aspiration; they found that aspiration was the result of oral decompensation alone in 23 patients, a combination of oral and pharyngeal decompensation in 17 patients, and pharyngeal decompensation alone in 10 patients.⁴⁵ The same authors studied oral decompensation in 75 patients who survived a near-fatal choking episode.⁴⁶ Abnormalities were found on videography in 58 of these 75 patients. Oral stage dysfunction was the predominant finding in 32 patients, with pharyngeal abnormalities in 19 and cricopharyngeal abnormalities in 28.

Reduced vertical excursion of the hyoid or larynx may contribute to incomplete airway closure and the risk of aspiration.⁴⁷ Reduced anterior displacement may result in reduced upper

esophageal sphincter (UES) and cricopharyngeal (CP) opening, contributing to piriform sinus residue.⁴⁸

Adaptation, Compensation, and Decompensation

The pharynx is an extremely flexible organ that must adapt to its various functions, including respiration, speech, and swallowing. In addition, the pharynx adapts to different stimuli, such as the size and consistency of the bolus and temperature of ingested liquids and food; the pharynx compensates when one of its parts is defective. The process of adjustment of normal swallowing to different stimuli is called *adaptation*.⁴⁹ The pharynx must adjust to the bolus, which may vary in volume, temperature, consistency, viscosity, and elasticity. The effect of different boluses can be seen with videofluoroscopy by watching the difference between a swallow of thin liquid barium and a swallow of the same volume of barium paste.⁵⁰

The effect of a carbonated bolus on the physiology of the swallow has been investigated.⁵¹ Carbonated liquids reduced penetration, aspiration, and pharyngeal retention, and pharyngeal transit time was shorter.

When signs of compensation are visible on dynamic studies, swallowing is already impaired.⁴⁹ Some types of compensation for impaired swallowing may be conscious and voluntary. For example, a patient may change the types of foods eaten, perhaps omitting solid food and substituting puréed food, or may even restrict the diet to liquids only. Certain postures such as flexing the neck (chin tuck) or turning the head may help a patient swallow more effectively, reducing laryngeal penetration or aspiration and clearing any retained bolus.

Swallowing can be considered to have five distinct stages, each of which has a characteristic pattern of compensation and decompensation.⁴⁹ The five stages include the following:

1. Control of the junction of the mouth and pharynx (palatoglossal seal; Fig. 15-5)
2. Closure of the palatopharyngeal isthmus (Fig. 15-6)

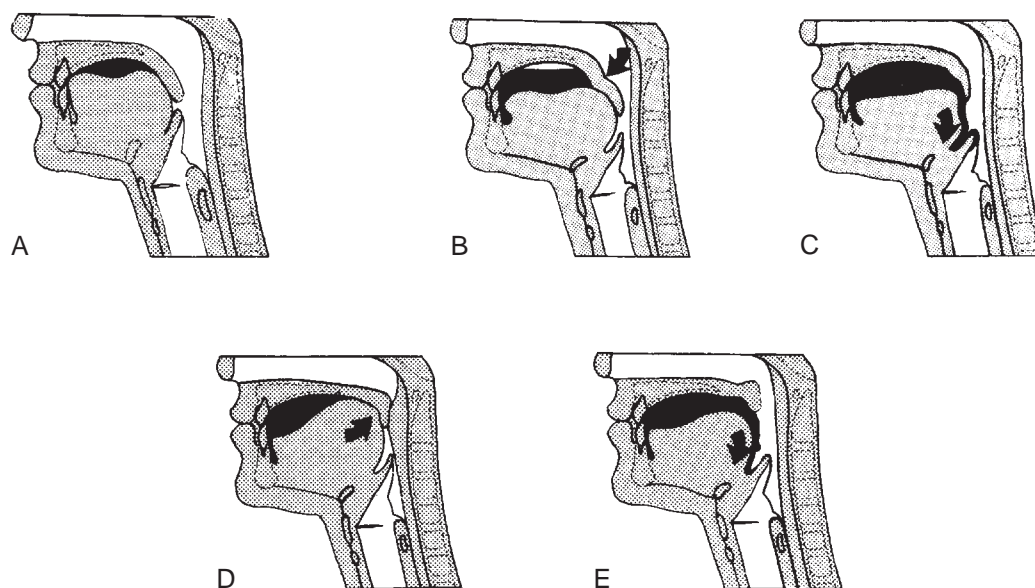


Figure 15-5 Control of the junction of the mouth and pharynx. **A.** Leakage from the back of the mouth is prevented in the normal patient when the soft palate abuts the posterior portion of the tongue. **B.** Deficiency of the tongue caused by atrophy, weakness, incoordination, or postsurgical defect may be compensated by downward displacement of the palate (arrow), with the palate “kinking” to appose the tongue. **D.** Conversely, palatal deficiency is compensated by upward displacement of the tongue (arrow). Note that the bolus is held further forward in the mouth under these circumstances. **C, E.** Decompensation, in which there is premature leakage of oral contents into the pharynx (arrow), with the potential for overflow aspiration. (From Buchholz DW, Bosma JF, Donner MW: *Adaptation, compensation, and decompensation of the pharyngeal swallow*. *Gastrointest Radiol* 10:235–240, 1985.)

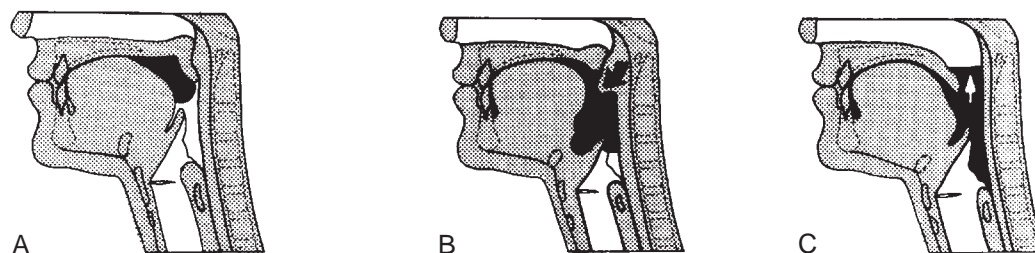


Figure 15-6 Closure of palatopharyngeal isthmus during swallowing. **A.** Normal closure, in which the soft palate has elevated to a right angle to abut Passavant’s cushion. **B.** Deficiency of the pharyngeal palate may be compensated by increasing convergence of the pharyngeal constrictor muscles (arrow), resulting in a very prominent Passavant’s cushion. **C.** Decompensation results in nasopharyngeal regurgitation through the palatopharyngeal isthmus (arrow). (From Buchholz DW, Bosma JF, Donner MW: *Adaptation, compensation, and decompensation of the pharyngeal swallow*. *Gastrointest Radiol* 10:235–240, 1985.)

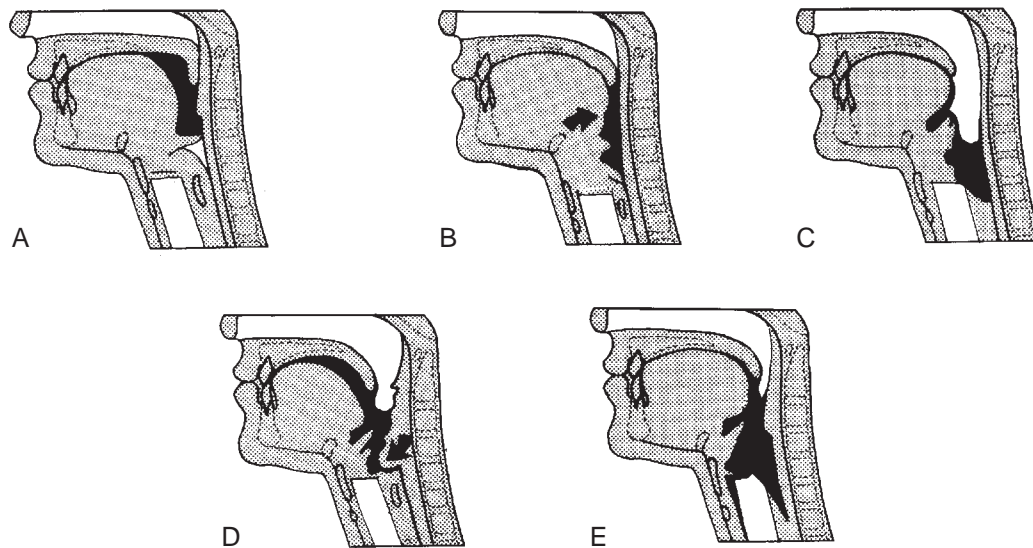


Figure 15-7 Compression of the bolus. **A.** Normal compression. **B.** Deficiency of the constrictor muscles may be compensated by increased upward and posterior displacement of the tongue and larynx (arrow). **D.** Deficiency of the tongue in bolus compression may be followed by more anterior displacement of the constrictor wall (arrow), resulting in a very prominent pharyngeal stripping wave. **C, E.** Decompensation caused by inadequate bolus compression results in bolus retention in the valleculae and piriform sinuses after swallowing, with the potential for overflow aspiration. (From Buchholz DW, Bosma JF, Donner MW: Adaptation, compensation, and decompensation of the pharyngeal swallow. *Gastrointest Radiol* 10:235–240, 1985.)

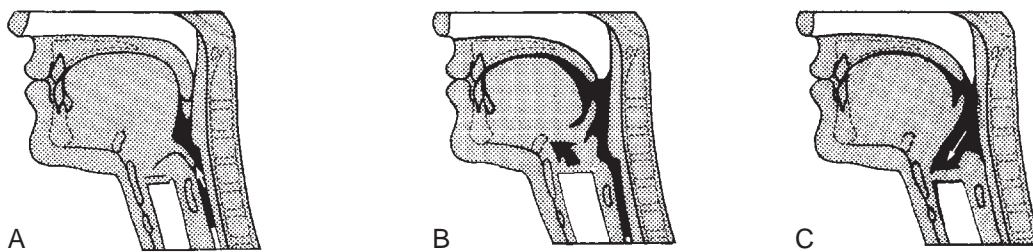


Figure 15-8 Closure of the larynx. **A.** The normal condition, in which the larynx is elevated and closed, and the epiglottis (arrow) is completely tilted down to cover the entrance to the laryngeal aditus. **B.** With deficiency of epiglottic tilting or glottic closure, there may be increased upward and anterior displacement of the larynx (arrow). Under these circumstances, the arytenoid masses may be enlarged as a sign of compensation (not illustrated). **C.** Failure of compensation results in penetration of bolus (arrow) into the laryngeal vestibule, and even through the incompletely closed cords, with aspiration. (From Buchholz DW, Bosma JF, Donner MW: Adaptation, compensation, and decompensation of the pharyngeal swallow. *Gastrointest Radiol* 10:235–240, 1985.)

3. Compression of the bolus (Fig. 15-7)
4. Closure of the larynx (Fig. 15-8)
5. Opening of the pharyngoesophageal segment (Fig. 15-9)

During the first stage, for example, downward placement of the soft palate may compensate for deficiencies of the tongue (resulting from atrophy, weakness, or surgical resection). Conversely, upward displacement of the tongue may compensate for weakness of the soft palate (see Figs. 15-5 to 15-9 for compensation occurring during other stages of swallowing). Another compensatory phenomenon is the development of a deeper pharyngeal stripping wave, which may be observed in the presence of a partially obstructing lesion in the cervical esophagus, such as a web or cricopharyngeal bar.

Any radiographic findings of compensation must be communicated to the referring physician so the patient can be informed that swallowing is impaired. The patient can then be instructed to take additional care when eating or drinking quickly—for example, in a restaurant or in other social situations.

Functional Aspects of Zenker's Diverticulum

Zenker's diverticulum is a pulsion diverticulum located at the level of the pharyngoesophageal junction; the most common site is between the oblique and horizontal fibers of the cricopharyngeal muscle through a triangular area known as Killian's dehiscence (Fig. 15-10). It is a posterior diverticulum that may fill during or after swallowing and, if large, may flop to one side or the other. Once swallowing is completed, the diverticulum may empty back into the pharynx, filling the piriform sinuses. This often precipitates a second swallow but also places the patient at risk for overflow aspiration.

The pathogenesis of Zenker's diverticulum remains unclear, but incoordination between pharyngeal contraction and cricopharyngeal opening may be a contributing factor.⁵²⁻⁵⁵ Manometric and cineradiographic studies have demonstrated premature sphincter closure in some patients with Zenker's

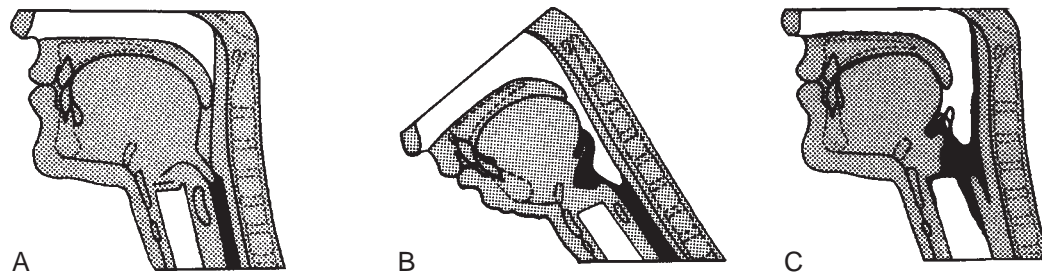


Figure 15-9 Opening of the pharyngoesophageal segment. **A.** Normal opening of pharyngoesophageal segment. **B.** Deficiency of upward laryngeal displacement, which contributes to opening of the pharyngoesophageal segment, results in flexion of the neck and/or forward thrusting of the jaw during swallowing. **C.** Failure of compensation results in poor pharyngoesophageal segment opening, with retention of the bolus in the piriform sinuses and the risk of overflow aspiration. (From Buchholz DW, Bosma JF, Donner MW: Adaptation, compensation, and decompensation of the pharyngeal swallow. *Gastrointest Radiol* 10:235–240, 1985.)

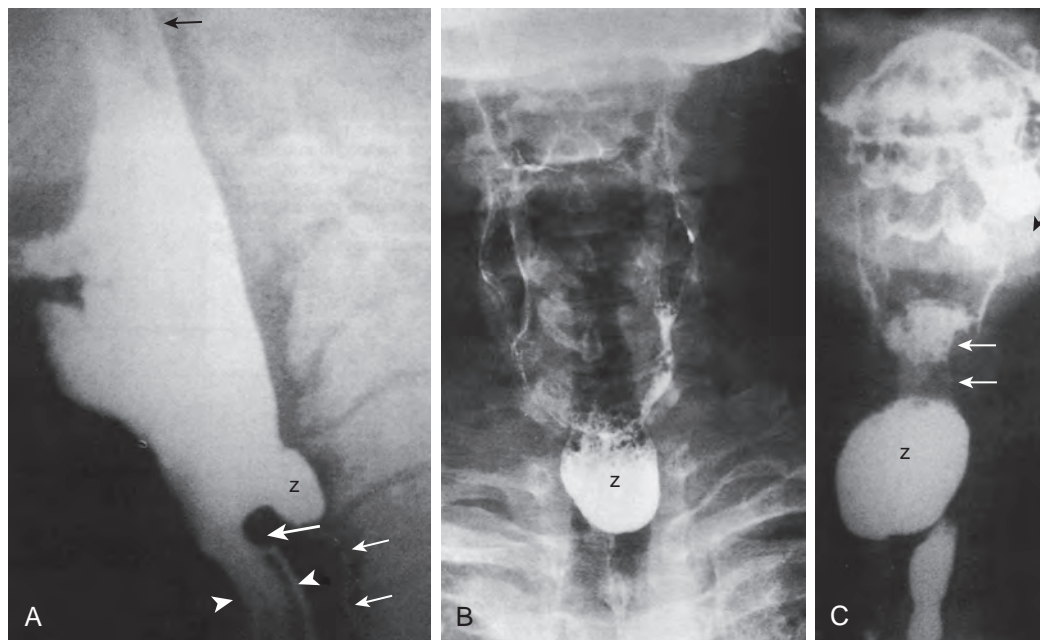


Figure 15-10. Zenker's diverticulum. **A.** Lateral view shows a small diverticulum (Z) above a very prominent cricopharyngeus (large white arrow) causing luminal narrowing of at least 50%, with a jet of barium (arrowheads) below it. The cervical esophageal lumen is actually abutting the spine (small white arrows). Also note nasopharyngeal regurgitation (black arrow) and marked degenerative changes in the cervical spine. **B.** After swallowing, Zenker's diverticulum (Z) remains filled. **C.** Frontal view in another patient shows emptying of the diverticulum (Z) back into the pharynx (arrows) after swallowing, placing this patient at risk for overflow aspiration. Also note the buccal pouch on the left side (arrowhead). (From Jones B, Donner MW [eds]: *Normal and Abnormal Swallowing: Imaging in Diagnosis and Therapy*. New York, Springer-Verlag, 1991.)

diverticulum. Other studies performed in patients with fully developed diverticula, however, have shown that the timing of pharyngeal contraction and cricopharyngeal relaxation may be normal.

Cook and associates demonstrated decreased compliance of the UES in a group of patients with Zenker's diverticulum, in whom inadequate sphincter opening resulted in increased intrabolus pressure.^{56–58} Shaw and co-workers subsequently demonstrated that with cricopharyngeal myotomy and pouch ablation, the intrabolus pressure fell and full UES opening was restored.^{59,60} They also observed structural abnormalities in muscle strips of the cricopharyngeus in 14 patients with Zenker's diverticulum.⁶¹ They found type 1

fiber predominance and greater fiber size variability. The muscles also demonstrated fibroadipose tissue replacement and fiber degeneration. These studies suggest that decreased UES compliance may have a major role in the development of Zenker's diverticulum.

Gastroesophageal reflux may also contribute to the development of Zenker's diverticulum.^{62–65} In an analysis of 67 patients with Zenker's diverticulum, 63 were found to have esophageal pathology such as gastroesophageal reflux, spasm, or hiatal hernia (T. Karaho, unpublished data, 1998).

Radiologically, Zenker's diverticulum is usually associated with prominence of the cricopharyngeus or a cricopharyngeal bar. Esophageal disease may produce prominence of the

cricopharyngeus, perhaps with decreased compliance, which in turn may raise intrapharyngeal and intrabolus pressure, necessitating more forceful contraction, with eventual bulging through a congenitally weak area. Further studies are necessary (including those addressing the early developmental stages of Zenker's diverticulum) before the pathophysiology can be fully understood.

Interrelationships

ESOPHAGEAL DISTENTION AND THE CRICOPHARYNGEUS

Intraluminal foreign bodies lodged in the hypopharynx or upper esophagus may produce cricopharyngeal spasm.⁶⁶ In cats, it has been shown that stimulation of afferent receptors in the hypopharynx or upper cervical esophagus evokes reflex contraction and spasm in the cricopharyngeal muscle, with an increase in intraluminal pressure in the sphincter segment. Similarly, esophageal distention by liquids or an intraluminal balloon in humans results in elevated pressure in the sphincter segment.⁶⁷⁻⁶⁹

GASTROESOPHAGEAL REFLUX AND THE CRICOPHARYNGEUS

There are variable reports in the manometric literature as to whether acid bathing the esophagus produces a rise in pressure in the UES. In the 1970s, studies in human volunteers using perfused catheters reported elevated pressures in the sphincter segment after infusion of the esophagus with saline or acid.^{70,71} The closer the infusion was to the UES, the greater the increase in pressure. In the late 1980s, a study using a modified sleeve sensor compared UES pressures in normal persons and patients with esophagitis⁷²; this study reported no UES response to acid reflux or acid perfusion. Another manometric study using solid-state catheters has shown many interactions among the lower esophageal sphincter, gastroesophageal reflux, intraesophageal pressure changes, and changes in pressure in the UES.⁷³

Several reflexes have been described, primarily by Shaker and co-workers⁷⁴⁻⁷⁸:

1. UES contractile response to gastroesophageal reflux. Torrico and colleagues compared UES pressure changes in normal controls and patients with reflux esophagitis⁷³; most of the controls and patients with reflux esophagitis had a significant increase in UES pressures in response to reflux episodes.
2. UES contractile response. Mechanical stimulation of the pharynx in cats and water stimulation in humans⁷⁵ results in an increase in UES resting tone. As little as 0.1 mL of water produced this reflex.
3. Esophagoglottal closure reflex. Esophageal distention during gastroesophageal reflux could overwhelm the UES, with the potential for overflow aspiration. A reflex has been described in humans⁷⁸ and cats⁷⁶ in which esophageal distention resulted in reflex closure of the glottis.
4. Pharyngoglottal adduction reflex. An injection of minute amounts of water into the pharynx resulted in brief closure of the vocal folds. This was thought to be a protective reflex to prevent aspiration.⁷⁸

SWALLOWING-RELATED REFLEXES

Many cardiorespiratory reflexes are related to swallowing, resulting from laryngeal, pharyngeal, or esophageal stimulation. Examples include syncope, change in heart rate, apnea, and bronchoconstriction leading to asthma.⁷⁹⁻⁸³ A review of swallowing-related reflexes is referenced for further reading.⁸⁴

Functional Changes After Radiation Therapy

Radiotherapy with or without chemotherapy is a common treatment for head and neck cancers. Dysphagia is a common result of the treatment. Approximately 80% of patients being treated with radiotherapy develop mucositis.⁸⁵ Mucositis is most marked over the arytenoids, but the epiglottis and posterior pharynx are also affected. Endothelial vasculitis results in localized ischemia, which in the long term may result in fibrosis.

Several studies of the long-term effect of radiation therapy on swallowing have been reported.^{86,87} Abnormalities included paresis of constrictor muscles, bolus retention, laryngeal penetration, and aspiration, often silent. Absent epiglottic tilt was common. Incomplete cricopharyngeal opening and reduced tongue base retraction was present.

Logemann and colleagues⁸⁸ reported on swallowing disorders in the first year after radiation and chemoradiation in 48 patients. Chemoradiation resulted in fewer functional swallows than radiation alone. The authors compared pretreatment videofluoroscopic swallowing study (VFSS) results with findings at 3 months and 12 months. All 48 patients had abnormal swallows pretreatment, probably related to the presence of the tumor. The most frequent abnormalities were reduced tongue base retraction, reduced tongue strength, and a delay in pharyngeal triggering. Other findings included delayed laryngeal closure and reduced laryngeal elevation. Two other studies compared the effects of chemoradiation on voice and swallowing.^{89,90}

Postradiation xerostomia often compounds swallowing difficulties. One study compared the findings in 15 cancer patients and 20 controls.⁹¹ Patients with xerostomia took almost twice as long to chew a shortbread cookie, but the duration of swallowing was unaffected. For liquid barium and paste, timing measures were the same for controls and for patients with xerostomia. Attempts are being made to modify radiotherapy regimens (organ preservation regimens) by collimating the radiation to avoid the pharyngeal constrictors and spare the parotids, so xerostomia is not as common a problem.

Aging and Swallowing

Swallowing in older individuals is called *presbyphagia*.⁹² Presbyphagia may be considered under two separate categories: (1) the effects of the normal aging process on swallowing (primary presbyphagia); and (2) the effects on swallowing of other diseases that affect older adults, such as CVAs and Parkinson's disease (secondary presbyphagia).

Prevalence studies have shown that the incidence of dysphagia is 12% to 13% in teaching hospitals and as high as 59% in nursing homes.⁹³ Up to 74% of nursing home residents

were reported to have feeding disorders.^{94,95} Although there is little loss of functional motor neurons before 60 years of age, a striking and progressive depletion of functioning motor neurons occurs after this age, with subsequent deterioration of connective tissue, loss of elasticity, and atrophy of fat.⁹⁶ In the oropharynx, the suspensory ligaments of all structures become lax, resulting in premature leakage, low positioning of the hyoid, squaring of the valleculae, and expansion of the pharyngeal cavity.⁹⁷⁻¹⁰¹ Loss of pliability may also result in incomplete inversion of the epiglottis and incomplete closure of the larynx.¹⁰²

In one study, defective closure of the laryngeal vestibule with laryngeal penetration was found in 70 of 101 patients over 80 years of age.¹⁰³ Thus, laryngeal penetration in older adults may be a normal finding. The laryngeal epithelium appears to become less sensitive to aspirated material with increasing age, which may explain why silent aspiration can be a problem.¹⁰⁴ In addition, airway protection may be further compromised by medications for depression, anxiety, or Parkinson's disease. One study found no significant change in the velocity of peristalsis with increasing age.¹⁰⁵ However, the oral and pharyngeal phases may become uncoupled, resulting in delayed initiation of pharyngeal contraction and early cricopharyngeal closure. With aging, there is also a decrease in how long the pharyngoesophageal segment remains open to allow bolus passage.⁹⁸

Borgstrom and Ekberg studied swallowing function in an asymptomatic group of 56 patients ranging from 72 to 93 years of age.¹⁰⁵ Normal deglutition (as defined in younger persons) was found in only 16% of patients. Oral abnormalities were found in 63%, pharyngeal abnormalities in 25%, and pharyngoesophageal segment abnormalities in 39%.

A review of dysphagia in older adults is recommended for further reading.¹⁰⁶ A discussion of changes in esophageal motility that occur with increasing age is beyond the scope of this chapter.

Neurologic Disease and the Pharynx

Neuromuscular disorders may cause dysphagia by affecting the afferent or efferent limbs of the swallowing reflex and by producing abnormalities at many levels, including the cerebral cortex, cranial nerve nuclei in the brain stem, cranial nerves themselves, pharyngeal plexus, neuromuscular junction, muscles, or sensory feedback mechanisms.¹⁰⁷⁻¹¹⁵ Dysphagia can be a minor or major symptom; occasionally, it may be the predominant or only complaint. For example, acute onset of dysphagia may signal focal brain stem stroke, and chronic dysphagia may be the presenting symptom of an unrecognized neuromuscular disease such as amyotrophic lateral sclerosis. At the Johns Hopkins Swallowing Center, approximately 30% of patients have dysphagia in the setting of neuromuscular disease; dysphagia was the predominant or only symptom in 10% of these patients. (B. Jones, personal observation).

CEREBROVASCULAR ACCIDENT

Formerly, it was thought that a unilateral abnormality of one corticobulbar tract did not produce a major swallowing deficit because each corticobulbar tract supplies both sides of the brain stem with cortical input. Despite the supposed bilateral

representation of swallowing, however, dysphagia occurs in 20% to 40% of patients with cerebrovascular accidents,¹¹⁰⁻¹¹⁸ including those with unilateral strokes. Robbins and co-workers have challenged the theory of bilateral representation of swallowing.^{119,120} They studied patients with unilateral cortical strokes (as diagnosed by computed tomography [CT]) and compared swallowing abnormalities in the group with infarcts in the right cerebral cortex to those in the group with infarcts in the left cerebral cortex. Initiation of the pharyngeal phase of swallowing was delayed in all patients. However, patients with left cortical strokes showed impaired oral stage function, difficulty initiating coordinated motor activity, and apraxia, whereas pharyngeal pooling, penetration, and aspiration were more prominent in patients with right cortical strokes.

In 1990, Alberts and associates studied the sensitivity of magnetic resonance imaging (MRI) for CVA.¹²¹ They found that 1.5-T imaging was positive in 66 of 71 patients with CVAs. They also evaluated the occurrence of aspiration after CVA in 38 patients and correlated the incidence of aspiration with the site of the lesion.¹²² The highest frequency of aspiration was found in large vessel pontine lesions (80%). Pontine infarctions of the middle cerebral artery (MCA), posterior cerebral artery (PCA), or cerebellum (large vessel) resulted in aspiration in approximately 66% of patients. Periventricular small vessel disease resulted in aspiration in slightly less than half (48%).

Two reviews on swallowing and functional MRI are suggested to the reader.^{123,124} MRI, however, is not infallible and may be negative in patients with focal strokes.^{125,126}

Wallenberg's syndrome is a CVA involving the medulla (lateral medullary infarction) in the distribution of the posterior inferior cerebellar artery. Traditional teaching had stressed that the resulting pharyngeal paresis was unilateral, but two studies found that the deficit is actually bilateral.^{127,128} Lateral medullary infarction can also lead to aphagia.¹²⁹

AMYOTROPHIC LATERAL SCLEROSIS (LOU GEHRIG'S DISEASE)

Amyotrophic lateral sclerosis, also known as motor neuron disease or Lou Gehrig's disease, can result in bulbar palsy, pseudobulbar palsy, or a combination of both. The disease may produce a wide spectrum of abnormal findings, including muscle weakness and atrophy of the lips, tongue, palate, and pharyngeal constrictors, with various degrees of retention of secretion.¹³⁰⁻¹³⁴ Weakness of the intrinsic laryngeal muscles leads to airway penetration and aspiration. The tongue, hyoid, and larynx are weak and ptotic in the upright position. The patient will often compensate by holding the head and neck in a position of sustained extension (swan neck) to help maintain the airway and facilitate swallowing.

MULTIPLE SCLEROSIS

Corresponding to the course of the disease itself, swallowing impairment in multiple sclerosis is relapsing and remitting.¹³⁵⁻¹³⁷ The radiographic appearance depends on the location and extent of the demyelination process. Abnormalities may vary from difficulty initiating swallowing to episodes of choking on liquids or sticking of solid particles. Sensory loss may compound the problem, and symptoms may be minimal or absent, even in the presence of severe decompensation.

NEURODEGENERATIVE DISORDERS

Parkinson's disease is associated with dysphagia in as many as 50% of patients. Delayed initiation of swallowing and oral transfer problems predominate. The findings include lingual tremor or rocking, squeezing of the bolus between the tongue and palate, piecemeal deglutition, and hesitancy to propel the bolus into the pharynx.¹³⁸⁻¹⁴¹

Huntington's disease,^{142,143} progressive supranuclear palsy,¹⁴⁴⁻¹⁴⁶ and Alzheimer's disease¹⁴⁷ may also produce dysphagia and feeding difficulties. The oropharyngeal findings simulate those of Parkinson's disease. Dementia, other cognitive problems, and uncontrolled movements may complicate feeding and rehabilitation.

Similarly, dystonia and dyskinesia may result in dysphagia or feeding difficulties because of involuntary localized muscle contractions.¹⁴⁸ In dystonia, the tonically contracted tongue, positioned in a tight mass in the back of the oral cavity, produces a characteristic appearance, the so-called fistled tongue. To swallow, the patient tilts his or her head into extreme extension and appears to decant the bolus into the pharynx by gravity.¹⁴⁸

MYASTHENIA GRAVIS AND RELATED DISORDERS

Myasthenia gravis^{149,150} and the Eaton-Lambert myasthenic-myopathic syndrome¹⁵¹ are myoneural junction disorders with diminished release or inadequate binding of acetylcholine. In addition to ocular and proximal limb weakness, there may be dysphagia or choking, characteristically appearing late in the day. Slowing of swallowing or decompensation after repetitive swallowing may suggest the diagnosis during dynamic imaging.

The Eaton-Lambert myasthenic-myopathic syndrome (carcinomatous neuropathy) is usually seen with oat cell carcinoma of the lung but has also been reported in association with carcinoma of the breast, prostate, stomach, and rectum.¹⁵¹ Diplopia, dysarthria, and dysphagia may accompany weakness of muscles of the trunk, pelvis, and shoulder girdle, the most common sites affected.

Botulism also affects transmission at the myoneuronal junction and may result in dysphagia. Interestingly, botulin toxin has been used to treat a variety of dystonias, including torticollis; dysphagia may occur as a side effect in a small number of patients because of diffusion of the toxin into the soft tissues of the neck and pharyngeal musculature.¹⁵²

FAMILIAL DYSAUTONOMIA (RILEY-DAY SYNDROME)

A characteristic finding is delayed cricopharyngeal opening with airway penetration.¹⁵³

Diseases of the Muscle

Diseases prominently affecting muscles may be caused by inflammatory disease (e.g., polymyositis, dermatomyositis, sarcoidosis)¹⁵⁴ metabolic or endocrine disease (e.g., mitochondrial myopathy or ragged red fiber disease),^{155,156} dysthyroid myopathy (e.g., hypothyroidism, hyperthyroidism), or muscular dystrophy.¹⁵⁷ Polymyositis or myopathy may

also be caused by a prolonged course of steroid therapy. Muscular dystrophies affecting the pharynx include myotonic dystrophy, Duchenne's muscular dystrophy, and oculopharyngeal dystrophy.¹⁵⁸⁻¹⁶¹ There is bilateral pharyngeal paresis with bolus retention; the cricopharyngeus may be prominent but closes with normal timing. The use of chilled barium accentuates the abnormalities in myotonic dystrophy.¹⁶¹

Infections

Viral infections of the nervous system may cause dysphagia. For example, a patient with bulbar poliomyelitis can present with pharyngeal paralysis, aspiration, and disturbance of vasomotor control when motor neurons in the medullary reticular formation, especially those in or near the nucleus ambiguus, are involved. Acute bulbar poliomyelitis is now rare in countries with mass vaccination but is still seen in areas where vaccination is not widespread.

A postpolio syndrome has been described, with symptoms of increasing weakness beginning 20 or more years after the acute attack of poliomyelitis; symptoms may include dysphagia.¹⁶²⁻¹⁶⁶ In a minority of patients, these symptoms are progressive; this has been called postpolio progressive muscle atrophy.¹⁶²⁻¹⁶⁶

Buchholz and Jones reported 13 patients with a remote history of acute poliomyelitis and dysphagia.¹⁶⁴ None of these 13 patients reported progressive dysphagia, and constrictor weakness was found in 11. Subsequently, Jones and co-workers reviewed the dynamic imaging studies of 20 patients with dysphagia and a remote history of polio.¹⁶⁵ Multiple abnormalities were present in these patients, including atrophy of prevertebral soft tissue, pharyngeal paresis or paralysis with bolus retention after swallowing, incomplete or absent epiglottic tilt, laryngeal penetration or aspiration, a cricopharyngeal bar, palatal weakness, incomplete laryngeal closure, and poor or absent laryngeal elevation (Fig. 15-11).

Sonies and Dalakas evaluated 32 postpolio patients with videofluoroscopy and ultrasound; 18 of these patients did not report dysphagia.¹⁶⁶ Despite the lack of symptoms, 17 of 18 patients had abnormalities of oropharyngeal function of varying severity.

Medications

Medications may cause localized pill-induced pharyngitis or esophagitis.¹⁶⁷ They may also induce or aggravate myasthenia gravis, dystonia, and myopathy or neuropathy.¹⁶⁸⁻¹⁸⁰ More than 30 medications in current clinical use may interfere with neuromuscular transmission, including antibiotics such as neomycin, streptomycin, and some tetracycline and immunosuppressive agents, such as adrenocorticotrophic hormone (ACTH), prednisone, and azathioprine. Sedatives, antipsychotic drugs, and antidepressants may produce extrapyramidal symptoms and signs of muscle spasm or dystonia or may unmask a latent neuromuscular disease. Ideally, such medications should be temporarily stopped for several days before a swallowing study. Tryptophan use has been associated with the development of an eosinophilia-myalgia syndrome.¹⁸¹⁻¹⁸³ Studies suggest that this association is caused by a chemical constituent related to the specific manufacturing conditions rather than to the tryptophan itself.¹⁸³

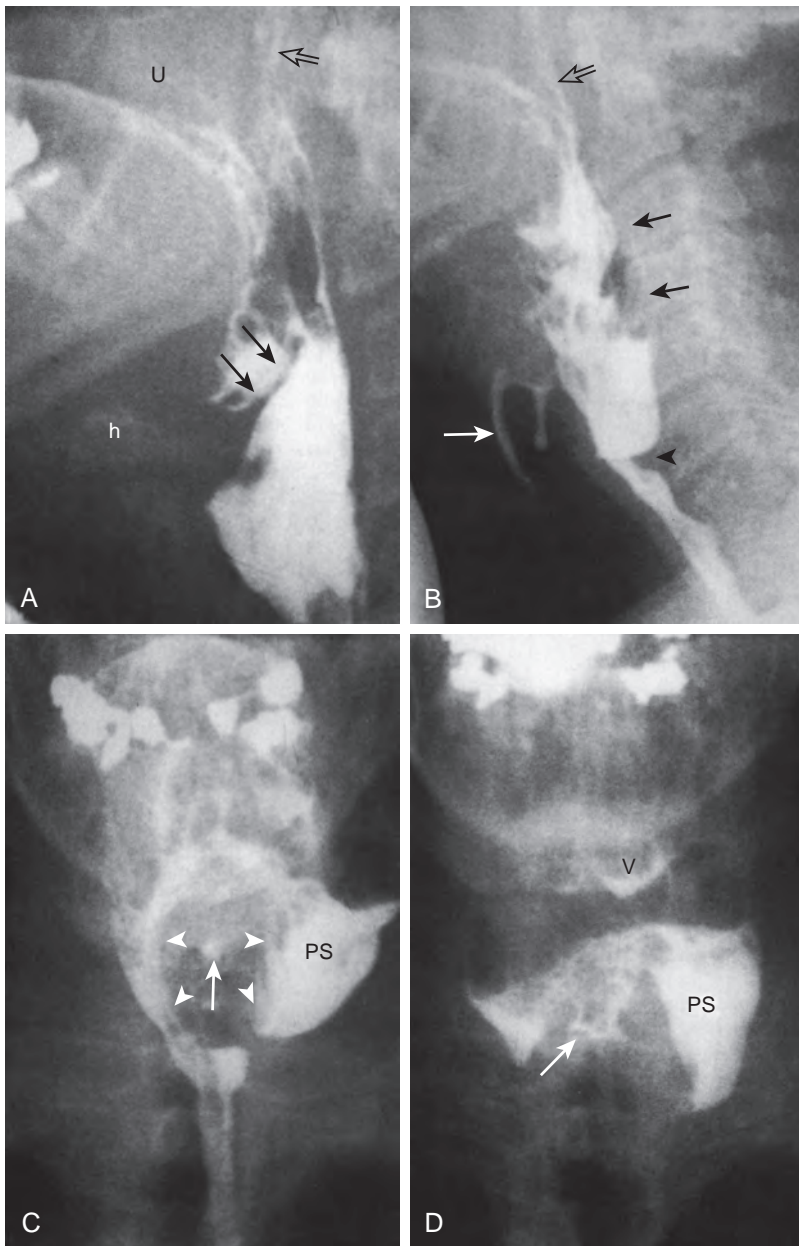


Figure 15-11 Postpolio dysphagia. **A.** Lateral view shows incomplete elevation of the soft palate (U) and minimal nasopharyngeal regurgitation (open arrow). Passavant's cushion is not evident. The bolus is past the epiglottis (solid arrows), which has remained almost completely upright, and there is incomplete elevation of the hyoid bone (h), which has not moved anteriorly. **B.** There is bulging of the pharynx, so it is overlapping the cervical spine (black arrows) with laryngeal penetration (white arrow). There is prominence of the cricopharyngeus (arrowhead) and poor distention of the cervical esophagus below the cricopharyngeus. Also note nasopharyngeal regurgitation (open black arrow). **C.** Frontal view shows asymmetric distention, with the left piriform sinus (PS) bulging much more than the right because of pharyngeal constrictor weakness. There is a small amount of barium in the laryngeal vestibule (arrow) and a moderate pseudomass effect caused by a flow defect (arrowheads). **D.** After passage of the bolus, there is marked retention in the left piriform sinus (PS), which is larger than the right, and mild retention in the right piriform sinus. There is also asymmetric retention in the vallecula on the left side (V). Barium is also seen in the laryngeal vestibule and ventricle (arrow).

REFERENCES

1. Edwards DAW: History and symptoms of esophageal disease of the esophagus. In Vantrappen G, Hellemans J, editors: *Diseases of the Esophagus*, New York, 1972, Springer-Verlag, pp 103–105.
2. Jones B, Ravich WJ, Donner MW, et al: Pharyngoesophageal inter-relationships: Observations and working concepts. *Gastrointest Radiol* 10:225–233, 1985.
3. Bosma JF: Deglutition: Pharyngeal stage. *Physiol Rev* 37:275–300, 1957.
4. Miller AJ: Deglutition. *Physiol Rev* 62:129–184, 1982.
5. Donner MW, Bosma JF, Robertson DL: Anatomy and physiology of the pharynx. *Gastrointest Radiol* 10:196–212, 1985.
6. Miller AJ: Neurophysiological basis of swallowing. *Dysphagia* 1:91–100, 1986.
7. Miller AJ: Swallowing: Neurophysiologic control of the esophageal phase. *Dysphagia* 2:72–82, 1987.
8. Dodds WJ, Stewart ET, Logemann JA: Physiology and radiology of the normal oral and pharyngeal phases of swallowing. *AJR* 154:953–963, 1990.
9. Buchholz DW, Jones B, Ravich WJ: Dysphagia following anterior cervical fusion. *Dysphagia* 8:390(A), 1993.
10. Ekberg O, Bergqvist D, Takolander R, et al: Pharyngeal function after carotid endarterectomy. *Dysphagia* 4:151–154, 1989.
11. Dodds WJ, Taylor AJ, Stewart ET, et al: Tipper and dipper types of oral swallows. *AJR* 153:1197–1199, 1989.
12. Zerhouni EA, Bosma JF, Donner MW: Relationship of cervical spine disorders to dysphagia. *Dysphagia* 1:129–144, 1987.
13. Curtis DJ: Laryngeal dynamics. *CRC Crit Rev Diagn Imaging* 19:29–80, 1982.
14. Dodds WJ, Man KM, Cook IJ, et al: Influence of bolus volume on swallow-induced hyoid movement in normal subjects. *AJR* 150:1307–1309, 1988.
15. Ekberg O: The normal movements of the hyoid bone during swallow. *Invest Radiol* 5:408–410, 1986.
16. Molfenter SM, Steele CM: Physiological variability in the deglutition literature: hyoid and laryngeal kinematics. *Dysphagia* 26:67–74, 2011.
17. Ishida R, Palmer JB, Hiimeae KM: Hyoid motion during swallowing: Factors affecting forward and upward displacement. *Dysphagia* 17:262–272, 2002.
18. Logemann JA, Pauloski BR, Rademaker AW, et al: Temporal and biomechanical

- characteristics of oropharyngeal swallow in younger and older men. *J Speech Lang Hear Res* 43:1264–1274, 2000.
19. Vandaele DJ, Perlman AL, Cassell MD: Intrinsic fibre architecture and attachments of the human epiglottis and their contributions to the mechanism of deglutition. *J Anat* 186:1–15, 1995.
 20. Kim Y, McCullough GH: Maximum hyoid displacement in normal swallowing. *Dysphagia* 23:274–279, 2008.
 21. Steele CM, Bailey GL, Chau T, et al: The relationship between hyoid and laryngeal displacement and swallowing impairment. *Clin Otolaryngol* 36:30–36, 2011.
 22. Ekberg O, Sigurjonsson S: Movements of the epiglottis during deglutition: A cineradiographic study. *Gastrointest Radiol* 7:101–107, 1982.
 23. Templeton RE, Kredel RA: Cricopharyngeal sphincter: Roentgenologic study. *Laryngoscope* 53:1–12, 1943.
 24. Crichlow TVL: Cricopharyngeus in radiography and cineradiography. *Br J Radiol* 29:546–556, 1956.
 25. Seaman WB: Cineroentgenographic observations of the cricopharyngeus. *AJR* 96:922–931, 1966.
 26. Sokol EM, Heitman P, Wolfe BS, et al: Simultaneous cineradiographic and manometric study of the pharynx, hypopharynx, and cervical esophagus. *Gastroenterology* 51:960–974, 1966.
 27. Seaman WB: Functional disorders of the pharyngoesophageal junction: Achalasia and chaliasia. *Radiol Clin North Am* 7:113–119, 1969.
 28. Palmer ED: Disorders of the cricopharyngeus muscle: A review. *Gastroenterology* 71:510–517, 1976.
 29. Roed-Peterson K: The pharyngoesophageal sphincter: A review of the literature. *Dan Med Bull* 26:275–281, 1979.
 30. Ekberg O, Nylander B: Dysfunction of the cricopharyngeal muscle. *Radiology* 143:481–486, 1982.
 31. Torres WE, Clements JL, Austin GE, Knight K: Cricopharyngeal muscle hypertrophy: Radiologic-anatomic correlation. *AJR* 141:927–930, 1984.
 32. Curtis DJ, Cruess DF, Berg T: The cricopharyngeal muscle: A video-recording review. *AJR* 142:497–500, 1984.
 33. Kahrilas PJ, Dodds WJ, Dent J, et al: Upper esophageal sphincter function during deglutition. *Gastroenterology* 95:52–62, 1988.
 34. Jacob P, Kahrilas PJ, Logemann JA, et al: Upper esophageal sphincter opening and modulation during swallowing. *Gastroenterology* 97:1469–1478, 1989.
 35. Olsson R, Ekberg O: Videomanometry of the pharynx in dysphagic patients with a posterior cricopharyngeal indentation. *Acad Radiol* 2:597–601, 1995.
 36. Brady AP, Stevenson GW, Somers S, et al: Premature contraction of the cricopharyngeus: A new sign of gastroesophageal reflux disease. *Abdom Imaging* 20:225–229, 1995.
 37. Ekberg O: Cricopharyngeal bar: Myth and reality. *Abdom Imaging* 20:179–180, 1995.
 38. Halum SL, Merati AL, Kulpa JJ, et al: Videofluoroscopic swallow studies in unilateral cricopharyngeal dysfunction. *Laryngoscope* 113:981–984, 2003.
 39. Dejaeger E, Pelemans W, Ponette E, Joosten E: Mechanisms involved in postdeglutition retention in the elderly. *Dysphagia* 12:63–67, 1997.
 40. Ekberg O, Hilderfors H: Defective closure of the laryngeal vestibule: Frequency of pulmonary complications. *AJR* 145:1159–1164, 1985.
 41. Linden P, Siebens AA: Dysphagia: Predicting laryngeal penetration. *Arch Phys Med Rehabil* 64:281–284, 1983.
 42. Linden P, Kuhlemeier KV, Patterson C: The probability of correctly predicting subglottic penetration from clinical observations. *Dysphagia* 8:170–179, 1993.
 43. McCullough GH, Wertz RT, Rosenbek JC: Sensitivity and specificity of clinical/bedside examination signs for detecting aspiration in adults subsequent to stroke. *J Commun Disord* 34:55–72, 2001.
 44. Ryu JS, Park SR, Choi KH: Prediction of laryngeal aspiration using voice analysis. *Am J Phys Med Rehabil* 83:753–757, 2004.
 45. Feinberg MJ, Ekberg O: Videofluoroscopy in elderly patients with aspiration: Importance of evaluating both oral and pharyngeal stages of deglutition. *AJR* 156:293–296, 1991.
 46. Feinberg MJ, Ekberg O: Deglutition after near-fatal choking episode: Radiologic evaluation. *Radiology* 176:637–640, 1995.
 47. Logemann JA, Kahrilas PJ, Cheng J, et al: Closure mechanisms of laryngeal vestibule during swallow. *Am J Physiol* 262:G338–G344, 1992.
 48. Jacob P, Kahrilas PJ, Logemann JA, et al: Upper esophageal sphincter opening and modulation during swallowing. *Gastroenterology* 97:1469–1478, 1989.
 49. Buchholz DW, Bosma JE, Donner MW: Adaptation, compensation, and decompensation of the pharyngeal swallow. *Gastrointest Radiol* 10:235–240, 1985.
 50. Dantas RO, Dodds WJ, Massey BT, Kern MK: The effect of high- vs low-density barium preparations on the quantitative features of swallowing. *AJR* 153:1191–1195, 1989.
 51. Bulow M, Olsson R, Ekberg O: Videoradiographic analysis of how carbonated thin liquids and thickened liquids affect the physiology of swallowing in subjects with aspiration on thin liquids. *Acta Radiol* 44:366–372, 2003.
 52. Dohlman G, Mattsson O: The role of the cricopharyngeal muscle in cases of hypopharyngeal diverticula. *AJR* 81:561–569, 1959.
 53. Knuff TE, Benjamin SB, Castell DO: Pharyngoesophageal (Zenker's) diverticulum: A reappraisal. *Gastroenterology* 82:734–736, 1982.
 54. Westrin KM, Ergun S, Carlsoo B: Zenker's diverticulum—a historical review and trends in therapy. *Acta Otolaryngol* 116:351–360, 1996.
 55. van Overbeek JJ: Pathogenesis and methods of treatment of Zenker's diverticulum. *Ann Otol Rhinol Laryngol* 112:583–593, 2003.
 56. Cook IJ, Gabb M, Panagopoulos V, et al: Zenker's diverticulum: A defect in upper esophageal sphincter compliance. *Gastroenterology* 96:A98, 1989.
 57. Cook IJ, Blumbergs P, Cash K, et al: Zenker's diverticulum: Evidence for a restrictive cricopharyngeal myopathy. *Gastroenterology* 96:A98, 1989.
 58. Cook IJ, Gabb M, Panagopoulos V, et al: Pharyngeal (Zenker's) diverticulum is a disorder of upper esophageal sphincter opening. *Gastroenterology* 103:1229–1235, 1992.
 59. Shaw DW, Cook IJ, Simula ME, et al: Restoration of normal upper esophageal sphincter compliance following cricopharyngeal myotomy in patients with Zenker's diverticulum. *Gastroenterology* 95:A122, 1990.
 60. Shaw DW, Cook IJ, Jamieson GG, et al: Influence of surgery on deglutitive upper oesophageal sphincter mechanics in Zenker's diverticulum. *Gut* 38:806–811, 1996.
 61. Cook IJ, Blumbergs P, Cash K, et al: Structural abnormalities of the cricopharyngeus muscle in patients with pharyngeal (Zenker's) diverticulum. *J Gastroenterol Hepatol* 7:556–562, 1992.
 62. Smiley TB, Caves PK, Porter DC: Relationship between posterior pharyngeal pouch and hiatus hernia. *Thorax* 25:725–731, 1970.
 63. Delahunty JE, Margulies SE, Alonso UA, et al: The relationship of reflux esophagitis to pharyngeal pouch (Zenker's diverticulum). *Laryngoscope* 81:570–577, 1971.
 64. Veenker EA, Anderson PE, Cohen JL: Cricopharyngeal spasm and Zenker's diverticulum. *Head Neck* 25:681–694, 2003.
 65. Murakami Y, Fukuda H, Kirchner JA: The cricopharyngeus muscle. *Acta Otolaryngol (Suppl)* (Stockh) 311:1–19, 1972.
 66. Creamer B, Schlegel J: Motor responses of the esophagus to distension. *J Appl Physiol* 10:498–504, 1957.
 67. Enzmann DR, Harell GS, Zboralske FF: Upper esophageal responses to intraluminal distention in man. *Gastroenterology* 72:1292–1298, 1977.
 68. Gerhardt DC, Shuck BS, Bordeaux RA, et al: Human upper esophageal sphincter: Response to volume, osmotic and acid stimuli. *Gastroenterology* 75:268–274, 1978.
 69. Rosenberg SJ, Harris LD: A single physiologic mechanism for changing strength of both esophageal sphincters [abstract]. *Gastroenterology* 60:798, 1971.
 70. Hunt PS, Connell AM, Smiley TB: The cricopharyngeal sphincter in gastric reflux. *Gut* 11:303–306, 1970.
 71. Stanciu C, Bennett JR: Upper esophageal sphincter yield pressure in normal subjects and in patients with gastroesophageal reflux. *Thorax* 29:459–462, 1974.
 72. Vakil NB, Kahrilas PJ, Dodds WJ, Vanagunas A: Absence of an upper esophageal sphincter response to acid reflux. *Gastroenterology* 84:606–610, 1989.
 73. Torrico S, Ren J, Sui Z, et al: Upper esophageal sphincter function during gastroesophageal reflux events. *Gastroenterology* 114:G3481, 1998.
 74. Medda BK, Lang IM, Layman R, et al: Characterization and quantification of a pharyngo-UES contractile reflex in cats. *Am J Physiol* 267:G972–G983, 1994.
 75. Shaker R, Ren J, Xie P, et al: Characterization of the pharyngo-UES contractile reflex in humans. *Am J Physiol* 273:G854–G858, 1997.
 76. Shaker R, Ren J, Medda B, et al: Identification and characterization of the esophagoglottal closure reflex in a feline model. *Am J Physiol* 266:G147–G153, 1994.
 77. Shaker R, Ren J, Kern M, et al: Mechanisms of airway protection and UES opening during belching. *Am J Physiol* 262:G621–G628, 1992.
 78. Ren J, Shaker R, Dua K, et al: Glottal adduction response to pharyngeal water stimulation: Evidence for a pharyngoglottal closure reflex. *Gastroenterology* 106:A558, 1994.
 79. Thach BT, Davies AM, Koenig JS, et al: Reflex induced apneas. In Issa FG, Suratt PM, Remmers JE, editors: *Sleep and Respiration*, New York, 1990, Wiley-Liss, pp 77–87.

80. Loughlin GM: Respiratory consequences of dysfunctional swallowing and aspiration. *Dysphagia* 3:126–130, 1989.
81. Levin B, Posner JB: Swallow syncope: Report of a case and review of the literature. *Neurology* 22:1086–1093, 1972.
82. Kalloo AN, Lewis JH, Maher K, et al: Swallowing: An unusual case of syncope. *Dig Dis Sci* 34:1117–1120, 1989.
83. Wright RA, Miller SA, Corsello BF: Acid-induced esophagobronchial-cardiac reflexes in humans. *Gastroenterology* 99:71–73, 1990.
84. Cunningham ET, Jr, Ravich WJ, Jones B, et al: Vagal reflexes referred from the upper aerodigestive tract: An infrequently recognized cause of common cardiorespiratory responses. *Ann Intern Med* 116:575–582, 1992.
85. Treister N, Sonis S: Mucositis: Biology and management. *Curr Opin Otolaryngol Head Neck Surg* 15:123–129, 2007.
86. Ekberg O, Nylander G: Pharyngeal dysfunction after treatment for pharyngeal cancer with surgery and radiotherapy. *Gastrointest Radiol* 8:97–104, 1983.
87. Eisbruch A, Lyden T, Bradford CR, et al: Objective assessment of swallowing dysfunction and aspiration after radiation concurrent with chemotherapy for head-and-neck cancer. *Int J Radiat Oncol Biol Phys* 53:23–28, 2002.
88. Logemann JA, Pauloski BR, Rademaker AW, et al: Swallowing disorders in the first year after radiation and chemoradiation. *Head Neck* 30:148–158, 2008.
89. Lazarus C, Logemann JA, Pauloski BR, et al: Effects of radiotherapy with or without chemotherapy on tongue strength and swallowing in patients with oral cancer. *Head Neck* 29:632–637, 2007.
90. Lazarus CL: Effects of chemoradiotherapy on voice and swallowing. *Curr Opin Otolaryngol Head Neck Surg* 17:172–178, 2009.
91. Hamlet S, Faull J, Klein B, et al: Mastication and swallowing in patients with postirradiation xerostomia. *Int J Radiat Oncol Biol Phys* 37:789–796, 1997.
92. Kashima HK: Presbyphagia, introduction. In Goldstein JC, Kashima HK, Koopmann CF, editors: *Geriatric Otorhinolaryngology*, Toronto, 1989, BC Decker.
93. Groher ME, Bukatman R: The prevalence of swallowing disorders in two teaching hospitals. *Dysphagia* 1:3–6, 1986.
94. Trupe EH, Siebens H, Siebens A: Prevalence of feeding-swallowing disorders in a nursing home. Presented at the Annual Meeting of the American Congress of Rehabilitation Medicine, Boston, 1984.
95. Siebens H, Trupe E, Siebens A, et al: Correlates and consequences of eating dependency in institutionalized elderly. *J Am Geriatric Soc* 34:192–198, 1986.
96. McComas AF, Upton AR, Sica RE: Motoneuron disease and aging. *Lancet* 2:1477–1480, 1973.
97. Baum BJ, Bodner L: Aging and oral motor function: Evidence for altered performance among older persons. *J Dent Res* 62:2–6, 1983.
98. Tracy JF, Logemann JA, Kahrilas PJ, et al: Preliminary observations on the effects of age on oropharyngeal deglutition. *Dysphagia* 4:90–94, 1989.
99. Ekberg O, Feinberg MJ: Altered swallowing function in elderly patients without dysphagia: Radiologic findings in 56 cases. *AJR* 156:1181–1184, 1991.
100. Shaker R, Dodds WJ, Hogan WJ, et al: Effect of aging on swallow-induced lingual palatal closure pressure. *Gastroenterology* 96:A464, 1989.
101. Sonies BC, Stone M, Shawker T: Speech and swallowing in the elderly. *Gerontology* 3:115–123, 1984.
102. Kahane JC: Postnatal development and aging of the human larynx. *Semin Speech Lang* 4:189–203, 1983.
103. Borgstrom PS, Ekberg O: Pharyngeal dysfunction in the elderly. *J Med Imaging* 2:74–81, 1988.
104. Pontoppidan H, Beecher HK: Progressive loss of protective reflexes in the airway with the advance of age. *JAMA* 174:2209–2213, 1960.
105. Borgstrom PS, Ekberg O: Speed of peristalsis in pharyngeal constrictor musculature: Correlations to age. *Dysphagia* 2:140–144, 1988.
106. Humbert IA, Robbins J: Dysphagia in the elderly. *Phys Med Rehabil Clin N Am* 19:853–866, 2008.
107. Buchholz D: Neurologic causes of dysphagia. *Dysphagia* 1:152–156, 1987.
108. Kirshner S: Causes of neurogenic dysphagia. *Dysphagia* 3:184–188, 1989.
109. Silbiger ML, Pikielney R, Donner MW: Neuromuscular disorders affecting the pharynx: Cineradiographic analysis. *Invest Radiol* 2:442–448, 1967.
110. Veis SL, Logemann JA: Swallowing disorders in persons with cerebrovascular accident. *Arch Phys Med Rehabil* 66:372–375, 1985.
111. Gordon C, Hewer RL, Wade DT: Dysphagia in acute stroke. *BMJ* 295:411–414, 1987.
112. Paciaroni M, Mazzotta G, Corea F, et al: Dysphagia following stroke. *Eur Neurol* 51:162–167, 2004. [Epub 2004.]
113. Parker C, Power M, Hamdy S, et al: Awareness of dysphagia by patients following stroke predicts swallowing performance. *Dysphagia* 19:28–35, 2004.
114. Smithard DG: Swallowing and stroke: Neurological effects and recovery. *Cerebrovasc Dis* 4:1–8, 2002.
115. Martino R, Terrault N, Ezerzer F, et al: Dysphagia in a patient with lateral medullary syndrome: Insight into the central control of swallowing. *Gastroenterology* 121:420–426, 2001.
116. Mann G, Hankey GJ: Initial clinical and demographic predictors of swallowing impairment following acute stroke. *Dysphagia* 16:208–215, 2001.
117. Han TR, Paik NJ, Park JW: Quantifying swallowing function after stroke: A functional dysphagia scale based on videofluoroscopic studies. *Arch Phys Med Rehabil* 82:677–682, 2001.
118. Nilsson H, Ekberg O, Olsson R, et al: Dysphagia in stroke: A prospective study of quantitative aspects of swallowing in dysphagic patients. *Dysphagia* 13:32–38, 1988.
119. Robbins JA, Levine RL: Swallowing after unilateral stroke of the cerebral cortex: Preliminary experience. *Dysphagia* 3:11–17, 1988.
120. Robbins JA, Levine RL, Maser A, et al: Swallowing after unilateral stroke of the cerebral cortex. *Arch Phys Med Rehabil* 74:1295–1300, 1993.
121. Alberts MJ, Faulstich M, Gray L: Sensitivity of magnetic resonance imaging in patients with acute stroke. *Ann Neurol* 28:258, 1990.
122. Alberts MJ, Horner J, Gray L, Brazer SR: Aspiration after stroke: Lesion analysis by brain MRI. *Dysphagia* 7:170–173, 1992.
123. Humbert IA, Robbins J: Normal swallowing and functional magnetic resonance imaging: A systematic review. *Dysphagia* 22:266–275, 2007.
124. Malandraki GA, Johnson S, Robbins J: Functional MRI of swallowing: From neurophysiology to neuroplasticity. *Head Neck* 33(Suppl 1):S14–S20, 2011.
125. Alberts MJ, Faulstich ME, Gray L: Stroke with negative brain magnetic resonance imaging. *Stroke* 23:663–667, 1992.
126. Buchholz DW: Clinically probable brain stem stroke presenting primarily as dysphagia and nonvisualized by MRI. *Dysphagia* 8:235–238, 1993.
127. Neumann S, Buchholz D, Wuttge-Hannig A, et al: Bilateral pharyngeal dysfunction after lateral medullary infarction (LMI). *Dysphagia* 9:263, 1994.
128. Neumann S, Buchholz D, Jones B, et al: Pharyngeal dysfunction after lateral medullary infarction is bilateral: Review of 15 additional cases. *Dysphagia* 10:136, 1995.
129. Buchholz D, Neumann S: Aphagia due to pharyngeal constrictor paresis from acute lateral medullary infarction. *Dysphagia* 14:187, 1999.
130. Garfinkle TJ, Kimmelman CP: Neurologic disorders: Amyotrophic lateral sclerosis, myasthenia gravis, multiple sclerosis and poliomyelitis. *Am J Otolaryngol* 3:204–212, 1982.
131. Kawai S, Tsukuda M, Mochimatsu I, et al: A study of the early stage of dysphagia in amyotrophic lateral sclerosis. *Dysphagia* 18:1–8, 2003.
132. Higo R, Tayama N, Watanabe T, et al: Videomanofluorometric study in amyotrophic lateral sclerosis. *Laryngoscope* 112:911–917, 2002.
133. Strand EA, Miller RM, Yorkston KM, et al: Management of oral-pharyngeal dysphagia symptoms in amyotrophic lateral sclerosis. *Dysphagia* 11:129–139, 1996.
134. Leighton SE, Burton MJ, Lund WS, et al: Swallowing in motor neuron disease. *J R Soc Med* 87:801–805, 1994.
135. Daly DD, Code CF, Anderson HA: Disturbances of swallowing and esophageal motility in patients with multiple sclerosis. *Neurology* 59:250–256, 1962.
136. Prossiegel M, Schelling A, Wagner-Sonntag E: Dysphagia and multiple sclerosis. *Int MS J* 11:22–31, 2004.
137. Wiesner W, Wetzel SG, Kappos L, et al: Swallowing abnormalities in multiple sclerosis: Correlation between videofluoroscopy and subjective symptoms. *Eur Radiol* 12:789–792, 2002.
138. Lieberman AN, Horowitz L, Redmond P, et al: Dysphagia in Parkinson's disease. *Am J Gastroenterol* 74:157–160, 1980.
139. Nagaya M, Kachi T, Yamada T, et al: Videofluorographic study of swallowing in Parkinson's disease. *Dysphagia* 13:95–100, 1998.
140. Leopold NA, Kagel MC: Pharyngoesophageal dysphagia in Parkinson's disease. *Dysphagia* 12:11–18, 1997.
141. Leopold NA, Kagel MC: Laryngeal deglutition movement in Parkinson's disease. *Neurology* 48:373–376, 1997.
142. Leopold NA, Kagel MC: Dysphagia in Huntington's disease. *Neurology* 42:57–60, 1985.
143. Kagel MC, Leopold NA: Dysphagia in Huntington's disease: 16-year retrospective. *Dysphagia* 7:106–114, 1992.
144. Neumann S, Reich S, Buchholz D, et al: Progressive supranuclear palsy (PSP): Characteristics of dysphagia in 14 patients. *Dysphagia* 11:164, 1996.

145. Johnston BT, Castell JA, Stumacher S, et al: Comparison of swallowing function in Parkinson's disease and progressive supranuclear palsy. *Mov Disord* 12:322–327, 1997.
146. Leopold NA, Kagel MC: Dysphagia in progressive supranuclear palsy: Radiologic features. *Dysphagia* 12:140–143, 1997.
147. Horner J, Alberts MJ, Dawson DV, et al: Swallowing in Alzheimer's disease. *Alzheimer Dis Assoc Disord* 8:177–189, 1994.
148. Bosma JF, Geoffrey VC, Thach BT, et al: A pattern of medication-induced persistent bulbar and cervical dystonia. *Int J Orofacial Myology* 8:5–18, 1982.
149. Murray JP: Deglutition in myasthenia gravis. *Br J Radiol* 35:43–52, 1962.
150. Llabres M, Molina-Martinez FJ, Miralles F: Dysphagia as the sole manifestation of myasthenia gravis. *Neurol Neurosurg Psychiatry* 76:1297–1300, 2005.
151. Eaton LM, Lambert EH: Electromyography and electric stimulation of nerves and diseases of motor unit: Observations on myasthenia syndrome associated with malignant tumors. *JAMA* 163:1117–1124, 1957.
152. Jankovic J, Brin MF: Therapeutic uses of botulinum toxin. *N Engl J Med* 324:1186–1194, 1991.
153. Margulies SI, Bruint PW, Donner MW, et al: Familial dysautonomia: A cineradiographic study of the swallowing mechanism. *Radiology* 90:107–112, 1968.
154. Ertekin C, Secil Y, Yuceyar N, et al: Oropharyngeal dysphagia in polymyositis/dermatomyositis. *Clin Neurol Neurosurg* 107:32–37, 2004.
155. Rimington DS, Chambers ST, Parkin PJ, et al: Inclusion body myositis presenting solely as dysphagia. *Neurology* 43:1241–1243, 1993.
156. Buchholz DW, Neumann S, Ravich W, et al: Inclusion body myositis presenting as dysphagia: Report of 3 cases. *Dysphagia* 12:110, 1997.
157. Siegel CI, Hendrix TR, Harvey JC: The swallowing disorder in myotonia dystrophica. *Gastroenterology* 50:541–550, 1966.
158. Duranceau A, Jamieson G, Clemont RJ: Oropharyngeal dysphagia in patients with oculopharyngeal muscular dystrophy. *Can J Surg* 21:326–329, 1978.
159. Castell JA, Castell DO, Duranceau CA, et al: Manometric characteristics of the pharynx, upper esophageal sphincter, esophagus, and lower esophageal sphincter in patients with oculopharyngeal muscular dystrophy. *Dysphagia* 10:22–26, 1995.
160. Perie S, Eymard B, Laccourreye L, et al: Dysphagia in oculopharyngeal muscular dystrophy: A series of 22 French cases. *Neuromuscul Disord* 7:S96–S99, 1997.
161. Bosma JF, Brodie DR: Cineradiographic demonstration of pharyngeal area myotonia in myotonic dystrophy patients. *Radiology* 92:104–109, 1969.
162. Dalakas MC, Elder G, Hallett M, et al: A long-term follow-up study of patients with post-polio myelitis neuromuscular symptoms. *N Engl J Med* 314:959–963, 1986.
163. Cashman NR, Maselli R, Wollmann RL, et al: Late denervation in patients with antecedent paralytic poliomyelitis. *N Engl J Med* 317:7–12, 1987.
164. Buchholz DW, Jones B: Dysphagia occurring after polio. *Dysphagia* 6:165–169, 1991.
165. Jones B, Buchholz DW, Ravich WJ, et al: Swallowing dysfunction in the post-polio syndrome: A cinefluorographic study. *AJR* 158:283–286, 1992.
166. Sonies BC, Dalakas MC: Dysphagia in patients with the post-polio syndrome. *N Engl J Med* 324:1162–1167, 1991.
167. Kikendall JW, Friedman AC, Oyewole MA, et al: Pill-induced esophageal injury: Case reports and review of the medical literature. *Dig Dis Sci* 28:174–182, 1983.
168. Swift TR: Disorders of neuromuscular transmission other than myasthenia gravis. *Muscle Nerve* 4:334–353, 1981.
169. Miller CD, Oleshansky MA, Gibson KE, et al: Procainamide-induced myasthenia-like weakness and dysphagia. *Ther Drug Monit* 15:251–254, 1993.
170. McQuillen MP, Cantor HE, O'Rourke JR, Jr: Myasthenic syndrome associated with antibiotics. *Arch Neurol* 18:402–415, 1968.
171. Pittinger CB, Eryase Y, Adamson R: Antibiotic-induced paralysis. *Anesth Analg* 49:487–501, 1970.
172. Stewart JT: Reversible dysphagia associated with neuroleptic treatment. *J Am Geriatr Soc* 49:1260–1261, 2001.
173. Hhayashi T, Nishikawa T, Koga I, et al: Life-threatening dysphagia following prolonged neuroleptic therapy. *Clin Neuropharmacol* 20:77–81, 1997.
174. Sokoloff LG, Pavlakovic R: Neuroleptic-induced dysphagia. *Dysphagia* 12:177–179, 1997.
175. Dantas RO, Nobre Souza MA: Dysphagia induced by chronic ingestion of benzodiazepine. *Am J Gastroenterol* 92:1194–1196, 1997.
176. Leopold NA: Dysphagia in drug-induced Parkinsonism: A case report. *Dysphagia* 11:151–153, 1996.
177. Buchholz D, Jones B, Neumann S, et al: Benzodiazepine-induced pharyngeal dysphagia: Report of two probable cases. *Dysphagia* 10:142, 1995.
178. Buchholz DW: Oropharyngeal dysphagia due to iatrogenic neurological dysfunction. *Dysphagia* 10:248–254, 1995.
179. Hughes TA, Shone G, Lindsay G, et al: Severe dysphagia associated with major tranquilizer treatment. *Postgrad Med J* 70:581–583, 1994.
180. Bazemore PH, Tonkonogy J, Ananth R: Dysphagia in psychiatric patients: Clinical and videofluoroscopic study. *Dysphagia* 6:2–5, 1996.
181. Hertzman PA, Blevins WL, Mayer J, et al: Association of the eosinophilia-myalgia syndrome with the ingestion of tryptophan. *N Engl J Med* 322:869–873, 1990.
182. Dicker RM, James N, Cunha BA: The eosinophilia-myalgia syndrome with neuritis associated with l-tryptophan use. *Ann Intern Med* 112:957–958, 1990.
183. Belongia EA, Hederg CW, Gleich GJ, et al: An investigation of the cause of the eosinophilia-myalgia syndrome associated with tryptophan use. *N Engl J Med* 323:357–365, 1990.

Structural Abnormalities of the Pharynx

STEPHEN E. RUBESIN

CHAPTER OUTLINE

Pharyngeal Pouches and Diverticula

Lateral Pharyngeal Pouches and Diverticula

Laryngoceles

Branchial Cleft Cysts, Branchial Cleft Fistulas, and Branchial Pouch Sinuses

Zenker's Diverticulum

Lateral Cervical Esophageal Pouches and Diverticula

Pharyngeal and Cervical Esophageal Webs

Inflammatory Lesions of the Pharynx

Lymphoid Hyperplasia of the Lingual and Palatine Tonsils

Benign Tumors of the Pharynx

Malignant Tumors of the Pharynx

Signs and Symptoms

Squamous Cell Carcinoma

Lymphoma

Rare Malignant Tumors

Pharyngeal Damage from Radiation

Postoperative Pharynx

Total Laryngectomy

Pharyngolaryngectomy

Esophageal Speech

Neck Dissection

Voice-Sparing Procedures

Surgery for Tongue and Oropharyngeal Cancers

Tracheostomy

Surgery for Zenker's Diverticulum and Pharyngeal Pouches

Cricopharyngeal Myotomy

Pharyngeal Pouches and Diverticula

LATERAL PHARYNGEAL POUCHES AND DIVERTICULA

The lateral pharyngeal wall may protrude beyond the normal expected contour of the pharynx in areas unsupported by muscle layers. The upper anterolateral pharyngeal wall is poorly supported in the region of the posterior and superior portions of the thyrohyoid membrane.¹ This region is bounded superiorly by the greater cornu of the hyoid bone, anteriorly by the thyrohyoid muscle, posteriorly by the superior cornu of the thyroid cartilage and stylopharyngeal muscle, and inferiorly by the ala of the thyroid cartilage.² This unsupported part of the thyrohyoid membrane is perforated by the superior laryngeal

artery and vein and the internal laryngeal branch of the superior laryngeal nerve.¹

Patients with lateral pharyngeal pouches usually have no symptoms. Approximately 5% of people with lateral pharyngeal pouches complain of dysphagia, choking, or regurgitation of undigested food.³⁻⁵ Lateral pharyngeal pouches are extremely common, and the frequency of their occurrence increases with age.¹ The pouches are usually bilateral.

On frontal views during swallowing, pouches appear as transient, hemispheric, contrast-filled protrusions from the lateral hypopharyngeal wall, below the hyoid bone and above the calcified edge of the thyroid cartilage (Fig. 16-1). The junction of the ala of the thyroid cartilage and thyrohyoid membrane is seen on frontal views as a notch in the lateral pharyngeal wall.² On double-contrast frontal views in which a modified Valsalva maneuver is performed, the pouches are seen as hemispheric, barium-coated protrusions above the notch in the lateral pharyngeal wall.² On lateral views, the pouches are seen as oval ring shadows (occasionally with an air-contrast level) below the hyoid bone at the level of the valleculae, just behind the epiglottic plate, along the anterior hypopharyngeal wall.^{1,2} Barium that is retained in pouches during swallowing spills into the ipsilateral piriform sinus after the bolus passes. This delayed spill may result in dysphagia or a choking sensation because of overflow aspiration.^{4,5}

In contrast, lateral pharyngeal diverticula are persistent protrusions of pharyngeal mucosa, usually through the thyrohyoid membrane or, rarely, through the tonsillar fossa.^{1,2} The diverticula are lined by nonkeratinizing squamous epithelium surrounded by loose areolar connective tissue, with many vascular spaces.³ These protrusions are commonly found in those who have increased intrapharyngeal pressure (e.g., wind instrument players, glass blowers, people with severe sneezing episodes). Clinical symptoms may include dysphagia, choking, cough, hoarseness, regurgitation of undigested food, or a painless neck mass.^{1,3} Radiographically, the diverticula are persistent, barium-filled sacs of various sizes connected to a bulging lateral hypopharyngeal wall by a narrow neck (Fig. 16-2). They are usually unilateral.

LARYNGOCELES

A lateral pharyngeal diverticulum is a protrusion of nonkeratinizing squamous mucosa originating in the pharynx. A laryngocele is a protrusion of ciliated pseudostratified columnar epithelium and loose areolar connective tissue arising from saccular dilation of the appendix of the laryngeal ventricle.^{6,7} If saccular dilation of the appendix is confined by the thyroid cartilage, it is termed an *internal laryngocele*. If the dilation extends above the thyroid cartilage and through the thyrohyoid membrane, the sac is termed *external*



Figure 16-1 Lateral pharyngeal pouches. Frontal view of the pharynx obtained as the bolus is passing through the lower pharynx and pharyngoesophageal segment. Barium is retained in the right and left lateral pharyngeal pouches (arrows). The pouches protrude through the region of the thyrohyoid membrane.

laryngocele. A combination of internal and external laryngocele is termed a *mixed laryngocele*.

Patients with laryngoceles and those with lateral pharyngeal diverticula have similar symptoms and physical findings. Most patients are asymptomatic and in the fifth to sixth decade of life.⁶ Patients with external or mixed laryngoceles may have a compressible lateral neck mass. Patients with internal laryngoceles may complain of hoarseness, dysphagia, or choking. Laryngoceles are seen in patients with increased intralaryngeal pressure, such as glass blowers and wind instrument players.

Frontal radiographs in patients with an external laryngocele may show an air-filled sac above and lateral to the ala of the thyroid cartilage. Lateral radiographs may show the air-filled sac anterior to the epiglottic plate, in contrast to a lateral pharyngeal diverticulum, which lies posterior to the epiglottic plate.¹ External and internal laryngoceles do not fill with barium on pharyngograms. However, barium studies may reveal enlargement of the aryepiglottic fold with a smooth overlying mucosa.

BRANCHIAL CLEFT CYSTS, BRANCHIAL CLEFT FISTULAS, AND BRANCHIAL POUCH SINUSES

In the 4-week-old embryo, paired grooves of ectodermal origin, termed *branchial clefts*, appear on both sides of the neck region.^{6,8} Branchial ridges (arches) lie between the branchial clefts. Four outpouchings from the pharynx grow to meet the branchial clefts. The pharyngeal outpouchings are of endodermal origin and are termed *branchial pouches*. The first branchial cleft forms the external auditory meatus. The second branchial cleft forms the middle ear, eustachian tube, and floor of the tonsillar fossa. The third and fourth branchial pouches form the piriform sinuses.⁸

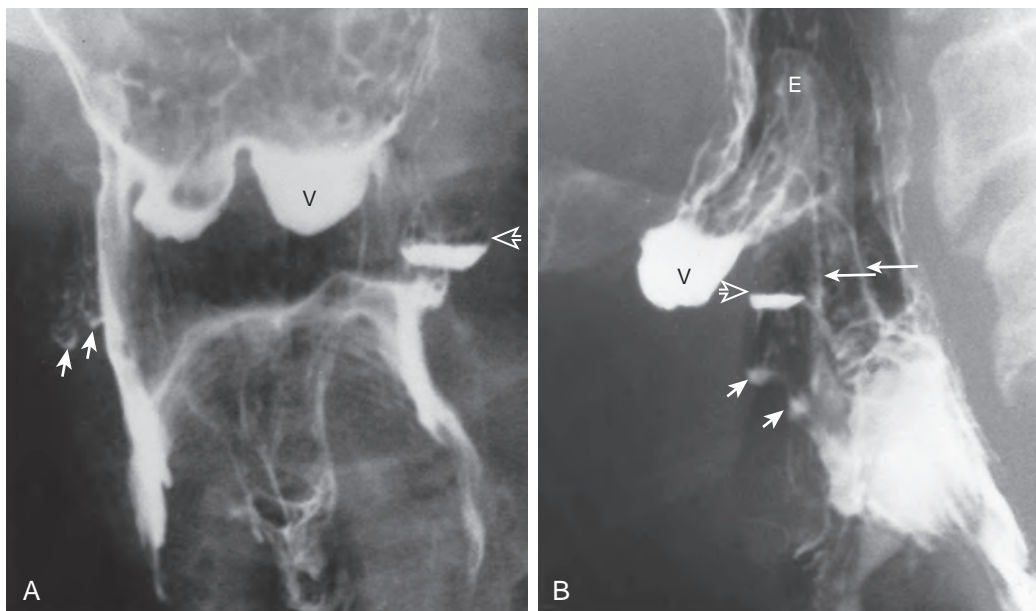


Figure 16-2 Lateral pharyngeal diverticula. **A.** Frontal view shows a round saclike structure (open arrow) protruding from the left lateral pharyngeal wall. This lateral pharyngeal diverticulum contains an air-contrast level. A right lateral diverticulum is faintly seen as a bilobed structure (solid arrows). V, Left vallecula. **B.** Lateral view shows that the left lateral pharyngeal diverticulum (open arrow) is behind and at the level of the vallecula (V). In this slightly tilted view, the bilobed right lateral pharyngeal diverticulum (short arrows) is faintly seen. Long arrows indicate the aryepiglottic folds. E, epiglottic tip. (A and B modified from Rubesin SE, Glick SN: *The tailored double-contrast pharyngogram*. Crit Rev Diagn Imaging 28:133–179, 1988.)

Persistence of branchial pouches or clefts results in the formation of sinus tracts or cysts. The most common branchial vestige is a cyst arising from the second branchial cleft. A second branchial cleft cyst is found at the level of the hyoid bone, deep to the sternocleidomastoid muscle.⁶ Pathologically, a unilocular cyst is lined by keratinizing, stratified, squamous epithelium and is filled with desquamated keratinaceous debris. A zone of lymphoid tissue surrounds the epithelium.⁶

Patients with second branchial cleft cysts usually present between the ages of 10 and 40 years with a painless or fluctuant mass in the upper neck along the upper third of the anterior border of the sternocleidomastoid muscle.⁹ When small, the cysts are anterior to the sternocleidomastoid muscle. When large, the cysts may extend posteriorly to the sternocleidomastoid muscle, displacing the carotid sheath.

Cross-sectional imaging of noninfected cysts may reveal a smooth, thin-walled mass with a homogeneous water core.¹⁰ If infected, the wall of the branchial cleft cyst becomes thickened and may enhance with the administration of intravenous contrast medium.¹⁰ The second branchial cleft cyst may extend between the internal and external carotid arteries at a level superior to their bifurcation. Rarely, branchial cleft cysts may communicate with the pharynx (branchial cleft fistulas), filling with barium during pharyngography.¹

Branchial pouch sinuses or fistulas are tracts that extend from the pharynx and end blindly in the soft tissues of the neck (sinus) or extend to the skin (fistulas). These tracts are lined by ciliated columnar epithelium. Branchial pouch sinuses arise from the tonsillar fossa (second pouch), upper anterolateral piriform fossa (third pouch), or lower anterolateral piriform sinus (fourth pouch; Fig. 16-3). Many of these fistulas are present at birth⁹ and communicate with the skin. Sinus tracts that end blindly are occasionally seen in adults.

ZENKER'S DIVERTICULUM

Zenker's diverticulum (posterior hypopharyngeal diverticulum) is an acquired mucosal herniation through an area of anatomic weakness in the region of the cricopharyngeal muscle (Killian's dehiscence). The inferior constrictor muscle is composed of the thyropharyngeal and cricopharyngeal muscles. The thyropharyngeal muscle arises from the lateral ala of the thyroid cartilage; it courses laterally and posteriorly to merge with its counterpart from the opposite side in a raphe in the posterior pharyngeal wall. The cricopharyngeal muscle constitutes the lower portion of the inferior constrictor muscle, arising from the lateral cricoid cartilage to encircle the lowermost hypopharynx. The cricopharyngeal muscle has no midline raphe. No overlap of fibers exists between the thyropharyngeal and cricopharyngeal muscles. Considerable variation is found in the arrangement of the muscle bundles of the thyropharyngeal and cricopharyngeal muscles. Killian's dehiscence has been variably described as arising between the thyropharyngeal and cricopharyngeal muscles or between the oblique and horizontal fibers of the cricopharyngeal muscle.^{11,12} This area of weakness occurs in one third of patients.¹³

The pathogenesis of Zenker's diverticulum is as controversial as the muscular anatomy. Some radiographic and manometric studies have suggested that spasm with elevated pressure of the upper esophageal sphincter or incoordination and abnormal relaxation of the upper esophageal sphincter (achalasia) are contributing factors. However, other manometric studies have

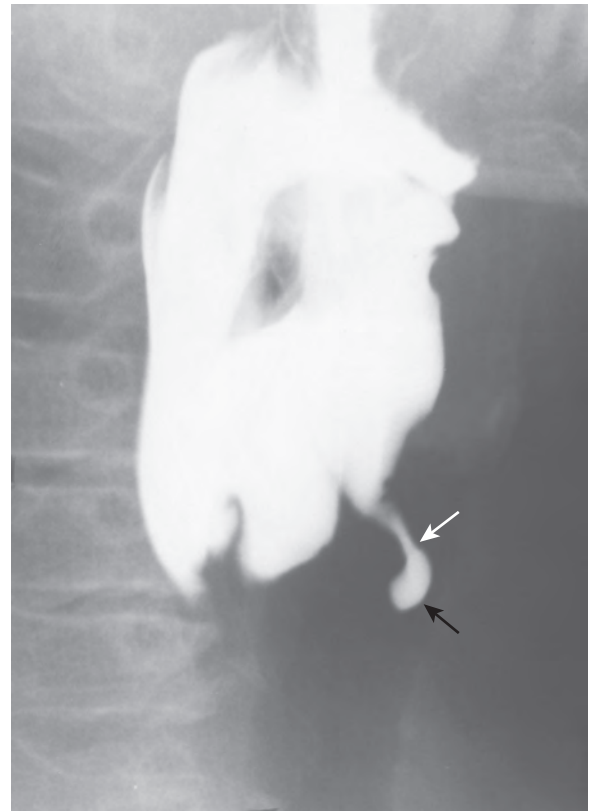


Figure 16-3 Fourth branchial pouch sinus. Spot radiograph of the pharynx obtained with patient in a left posterior oblique position shows a thin, 1.5-cm barium-filled track (white arrow) arising from the anterolateral wall of the lower left piriform sinus. The track has a saccular configuration at its termination (black arrow).

shown the following: (1) there is normal coordination between pharyngeal contraction and relaxation of the upper esophageal sphincter; (2) the upper esophageal sphincter relaxes completely during swallowing (i.e., there is no achalasia); and (3) the resting pressure of the upper esophageal sphincter is low (i.e., there is no spasm).^{14,15} The relationship between gastroesophageal reflux disease and Zenker's diverticulum is also controversial. Almost all patients with Zenker's diverticulum have an associated hiatal hernia,^{16,17} and many patients have radiographic evidence of gastroesophageal reflux, reflux esophagitis, or both. Whether gastroesophageal reflux predisposes patients with a large Killian dehiscence to the formation of Zenker's diverticulum is unknown.

Zenker's diverticulum is usually found in older patients who have dysphagia, regurgitation of undigested food, halitosis, choking, hoarseness, or a neck mass. Some patients with Zenker's diverticulum are asymptomatic.

During swallowing, Zenker's diverticulum appears as a posterior bulging of the lowermost hypopharyngeal wall above an anteriorly protruding pharyngoesophageal segment (cricopharyngeal muscle; Fig. 16-4). The neck of the Zenker's diverticulum can be very broad during swallowing. At rest, the barium-filled diverticulum extends below the level of the cricopharyngeal muscle posterior to the proximal cervical esophagus (Fig. 16-5). After swallowing, barium in the diverticulum is regurgitated into the hypopharynx. In some patients, this regurgitation of barium results in overflow aspiration.

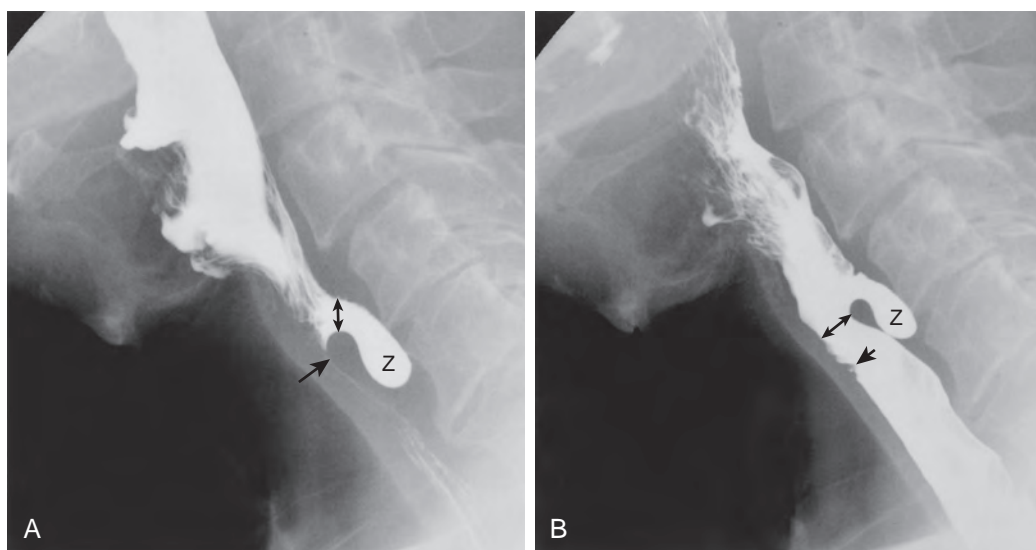
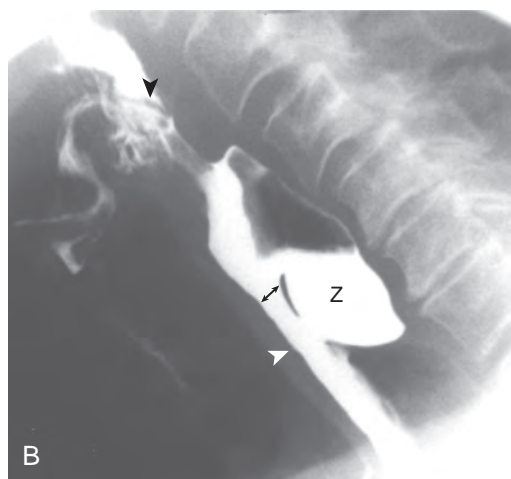


Figure 16-4 Zenker's diverticulum during swallowing. The relationship between the mouth of the Zenker's diverticulum and prominent cricopharyngeus is demonstrated. **A.** The bolus approaches the closed pharyngoesophageal segment (arrow), but barium has entered the mouth (double arrow) and lumen of the Zenker's diverticulum (Z). The mouth of a Zenker's diverticulum can be very broad, often larger than 1 cm. **B.** Most of the bolus has passed through the pharynx. The pharynx and larynx have continued to rise (≈ 3 mm), and the anterior wall of the trachea has been pulled forward slightly. The pharyngoesophageal segment is now open (double arrow). Redundant mucosa is seen in the postcricoid region (arrow). Opening of the pharyngoesophageal segment depends on elevation and anterior movement of the larynx, as well as the pressure of the bolus caused by gravity, tongue base thrust, and constrictor muscle contraction.



Figure 16-5 Zenker's diverticulum. **A.** Frontal view of the pharynx shows a 3- x 4-cm barium-filled sac (Z) midline below the tips of the piriform sinuses. Barium also coats the vocal cords because of an abnormal epiglottic tilt. **B.** A lateral view obtained while the patient is drinking shows the Zenker's diverticulum as a barium-filled sac (Z) posterior to the cervical esophagus (white arrowhead). The opening of the sac is superior to the posterior wall of the pharyngoesophageal segment (double arrow). The pharyngoesophageal segment is mildly narrowed. Also note diminished epiglottic tilt (black arrowhead) and laryngeal penetration.



A true Zenker's diverticulum may be confused with barium trapped above a cricopharyngeal muscle that has closed before the pharyngeal contraction wave has passed. This barium, trapped between downwardly progressing pharyngeal contraction and the cricopharyngeal muscle, is termed a *pseudo-Zenker's diverticulum* (Fig. 16-6). Barium may also be trapped above early closure of the upper cervical esophagus. Incomplete opening and early closure of the cricopharyngeal muscle, and early closure of the upper cervical esophagus, have been associated with gastroesophageal reflux disease.¹⁸

The complications of Zenker's diverticulum include bronchitis, bronchiectasis, lung abscess, diverticulitis, ulceration, fistula formation, and carcinoma.¹⁹ Any change in the character of dysphagia or bloody discharge in a patient known to have Zenker's diverticulum should suggest a complication.²⁰ On barium studies, irregularity of the contour of Zenker's diverticulum should suggest an inflammatory or neoplastic complication. Carcinoma arises in less than 1% of patients with Zenker's diverticulum,²⁰ but it is usually fatal.

LATERAL CERVICAL ESOPHAGEAL POUCHES AND DIVERTICULA

The Killian-Jamieson space is a triangular area of weakness in the cervical esophagus just below the cricopharyngeal muscle. This space is bounded superiorly by the inferior margin of the cricopharyngeal muscle, anteriorly by the inferior margin of the cricoid cartilage, and inferomedially by the suspensory ligament of the esophagus originating from the posterior wall of the cricoid cartilage, just before the tendon forms the longitudinal muscle of the esophagus.^{21,22}

Transient or persistent protrusions of the anterolateral cervical esophagus into the Killian-Jamieson space are termed *lateral cervical esophageal pouches* or *diverticula*, respectively. They are also known as *Killian-Jamieson pouches* or *Killian-Jamieson diverticula*. Most patients with Killian-Jamieson diverticula are asymptomatic, but some may complain of dysphagia or regurgitation.

These pouches and diverticula are relatively common and may be confused radiographically with Zenker's diverticulum. Killian-Jamieson diverticula can be bilateral or unilateral. If unilateral, the diverticula are usually found on the left side of the proximal cervical esophagus.²³ Radiographically, a small (3-20 mm in diameter), round to ovoid, smooth-surfaced out-pouching is seen just below the level of the cricopharyngeal muscle (Fig. 16-7).²³ On frontal views, pouches appear as small, round, or ovoid protrusions of the lateral upper esophageal wall that are filled late during swallowing and that empty after swallowing.²² Diverticula appear on frontal views as saccular protrusions that have narrow necks (see Fig. 16-7) and do not empty as quickly after swallowing. On lateral views, the anterior wall of the sac is anterior to the cervical esophagus, below the level of the cricopharyngeal muscle.²³ In contrast, the neck of Zenker's diverticulum is on the posterior hypopharyngeal wall, and the sac extends inferiorly behind the cervical esophagus.

Pharyngeal and Cervical Esophageal Webs

Webs are thin mucosal folds usually located along the anterior wall of the lower hypopharynx and proximal cervical

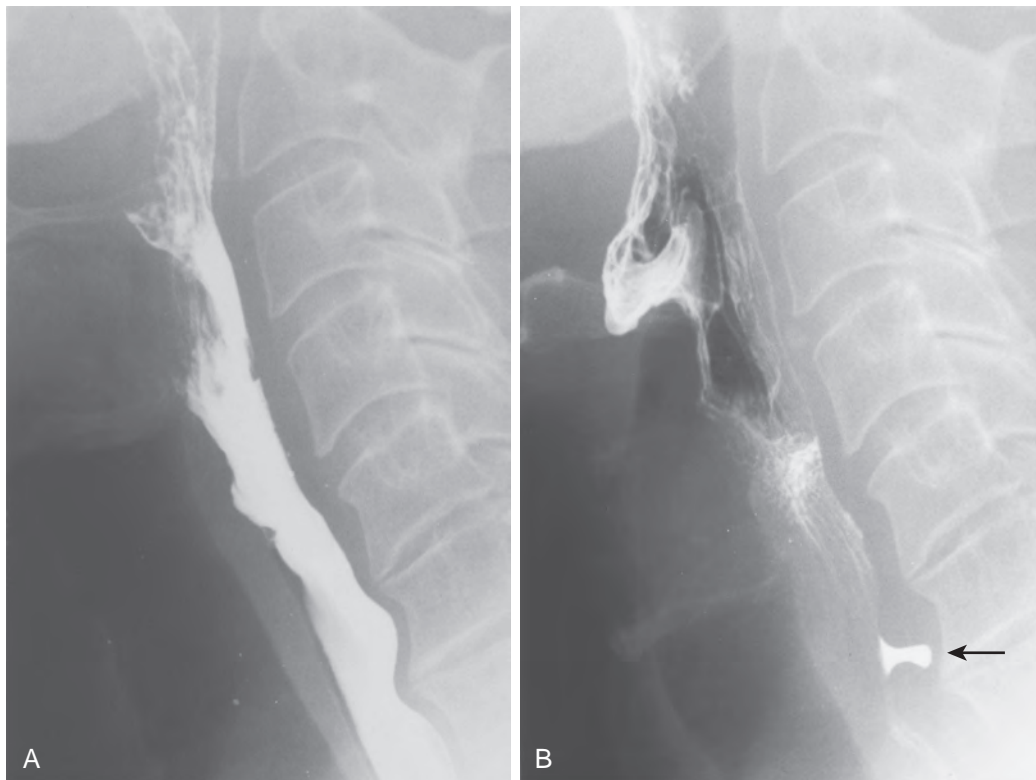


Figure 16-6 Pseudo-Zenker's diverticulum. **A.** During barium drinking, no pouch is seen as the bolus passes through the pharyngoesophageal segment. **B.** A view taken just after the swallow passes shows barium trapped (arrow) above an early-closing cricopharyngeal bar. This barium passed through the pharyngoesophageal segment seconds later.

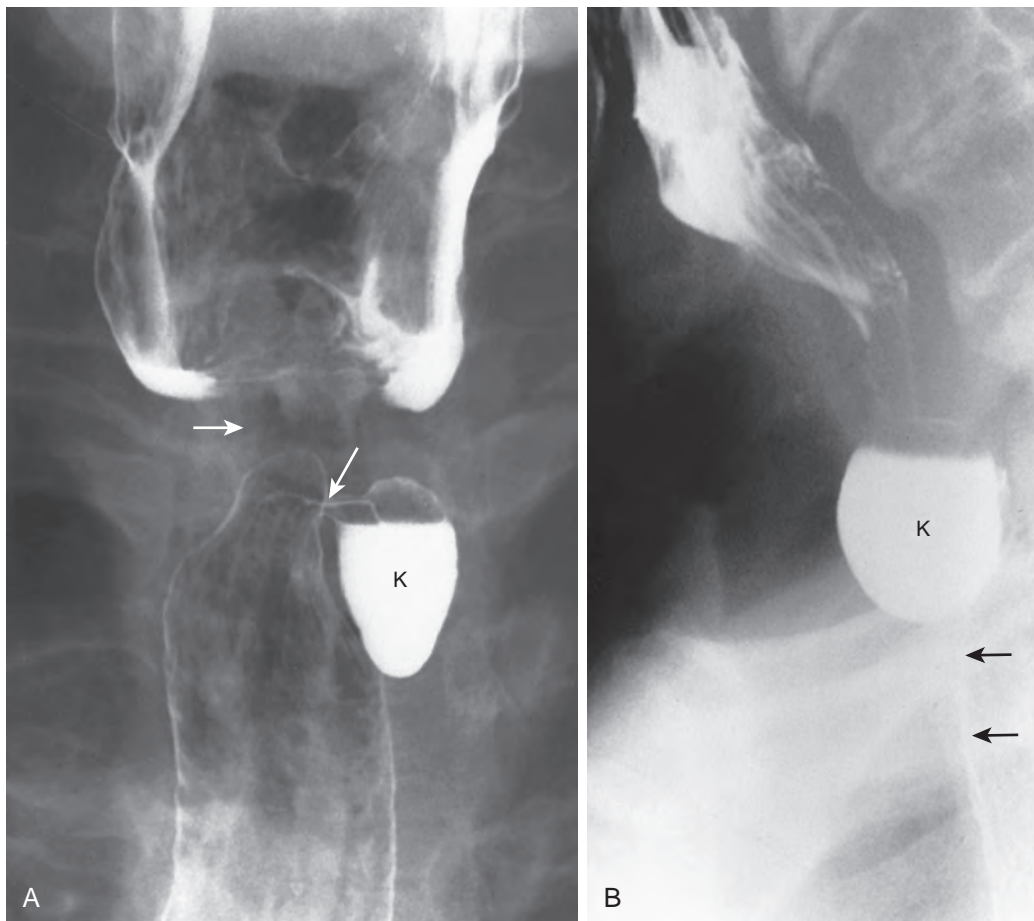


Figure 16-7 Killian-Jamieson diverticulum. **A.** Frontal view of the pharynx shows a barium-filled sac (K) to the left of the cervical esophagus. The neck of the diverticulum (long arrow) is below the level of the cricopharyngeal muscle (short arrow). **B.** Lateral view shows the diverticulum (K) protruding anterior to the course of the cervical esophagus (arrows). (From Rubesin SE: *Pharynx*. In Laufer I, Levine MS [eds]: *Double Contrast Gastrointestinal Radiology*, 2nd ed. Philadelphia, WB Saunders, 1992.)

esophagus. They are usually composed of normal epithelium and lamina propria.²⁴ Some webs show inflammatory changes.

The cause and clinical significance of webs are controversial. Most patients with cervical esophageal webs are asymptomatic. The webs are seen as isolated findings in 3% to 8% of patients undergoing upper GI barium studies.²⁵⁻²⁹ In one autopsy series, 16% of patients had incidental cervical esophageal webs.²⁴

Some pharyngeal and cervical esophageal webs are associated with diseases that cause inflammation and scarring, such as epidermolysis bullosa or benign mucous membrane pemphigoid. Several older northern European series showed an association of cervical esophageal webs, iron deficiency anemia, and pharyngeal or esophageal carcinoma.^{30,31} This association was termed *Plummer-Vinson syndrome* or *Paterson-Kelly syndrome*. In the United States, no strong association of cervical esophageal webs, iron deficiency anemia, and pharyngoesophageal carcinoma has been found. Webs in the distal esophagus have been associated with gastroesophageal reflux disease.²⁵ Some cervical esophageal webs may also be associated with gastroesophageal reflux.²⁷

Some webs are present in the valleculae or lower piriform sinus. These vallecular and piriform sinus webs are composed of mucosa, lamina propria, and underlying blood vessels. These webs are thought to be normal variants in the valleculae and piriform sinuses.³²

Webs appear radiographically as 1- to 2-mm wide, shelflike filling defects along the anterior wall of the hypopharynx or cervical esophagus (Fig. 16-8). The webs protrude to various depths into the esophageal lumen. Webs may extend laterally, and a few extend circumferentially. Circumferential webs appear as ringlike shelves in the cervical esophagus. With severe luminal narrowing, dysphagia may result, especially in patients with circumferential cervical esophageal webs. Partial obstruction is suggested by a jet phenomenon^{33,34} or by dilation of the esophagus or pharynx proximal to the web (see Fig. 16-10). A dynamic examination reveals a higher percentage of webs than spot images alone. Better demonstration of webs is also achieved with the use of large boluses of barium.²⁸

Webs may be confused radiographically with redundant mucosa in the anterior wall of the pharyngoesophageal segment at the level of the cricoid cartilage. This redundant mucosa has been termed the *postcricoid defect* and was previously attributed to a venous plexus in this region.³⁵ However, the postcricoid defect is probably related to redundancy of the mucosal and submucosal tissue in this area.² Webs also should not be confused with a prominent cricopharyngeal muscle, which appears as a round, broad-based protrusion from the posterior pharyngeal wall at the level of the pharyngoesophageal segment.

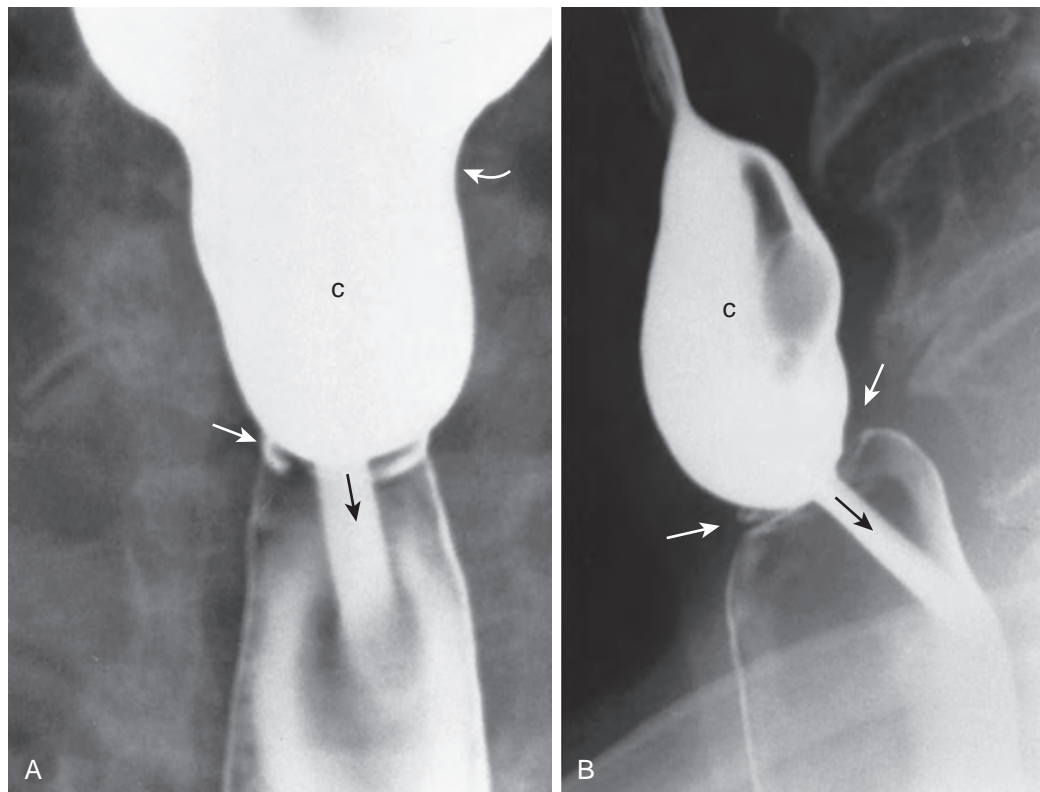


Figure 16-8 Partially obstructing cervical esophageal web. Frontal (A) and lateral (B) views show a circumferential radiolucent ring (white arrows) in the proximal cervical esophagus. Partial obstruction is suggested by a jet phenomenon (black arrows), with barium spurting through the ring, and by mild dilation of the proximal cervical esophagus (c). The level of the cricopharyngeus is identified (curved arrow in A). (From Rubesin SE: *Pharynx*. In Laufer I, Levine MS [eds]: *Double Contrast Gastrointestinal Radiology*, 2nd ed. Philadelphia, WB Saunders, 1992.)

Inflammatory Lesions of the Pharynx

Although acute epiglottitis usually affects children between 3 and 6 years of age, it occasionally causes severe stridor and sore throat in adults.³⁶ Plain radiographic diagnosis of acute epiglottitis is important (even in adults) because manipulation of the tongue or pharynx may exacerbate edema and respiratory distress. Neck radiographs may show smooth enlargement of the epiglottis and aryepiglottic folds. Barium studies are contraindicated because they may exacerbate edema, triggering an episode of acute respiratory arrest.³⁷

Barium studies of the pharynx are usually of limited value in patients with acute sore throat caused by viral, bacterial, or fungal infection.³⁷ Such patients usually demonstrate normal findings on pharyngograms or evidence of nonspecific lymphoid hyperplasia of the palatine or lingual tonsils.

In immunosuppressed patients with acute dysphagia, barium studies are directed toward the esophagus to demonstrate the presence, site, and type of esophagitis. However, double-contrast examination of the pharynx may demonstrate the plaques of *Candida* pharyngitis or the ulcers of herpes pharyngitis, particularly in patients with AIDS (Fig. 16-9).³⁸

In patients with chronic sore throat, barium studies may help determine whether underlying gastroesophageal reflux and reflux esophagitis are present. Inflammatory disorders of the pharynx or gastroesophageal reflux can alter pharyngeal elevation, epiglottic tilt, or closure of the vocal cords and laryngeal vestibule. Inflammation-induced dysmotility may result in laryngeal penetration and stasis.

Some diseases with diffuse mucous membrane ulceration affect the pharynx. Pharyngeal inflammation and ulceration may be seen in patients with Behçet's syndrome, Stevens-Johnson syndrome, Reiter's syndrome, epidermolysis bullosa,^{39,40} or bullous pemphigoid.⁴¹ Most of these patients have recurrent aphthous stomatitis and oropharyngeal ulceration. With severe ulceration, amputation of the uvula and tip of the epiglottis may be observed radiographically.⁴¹ Scarring may cause distortion of the pharyngeal contours. Severe ulceration with subsequent scarring may also be caused by lye ingestion (Fig. 16-10).⁴²

LYMPHOID HYPERPLASIA OF THE LINGUAL AND PALATINE TONSILS

The lingual tonsil is an aggregate of 30 to 100 follicles along the pharyngeal surface of the tongue, extending from the circumvallate papillae to the root of the epiglottis.⁴³ This lymphoid tissue causes the normal surface of the base of the tongue to be divided into small nodules of varying size.

Hypertrophy of the lingual tonsil frequently occurs after puberty, as a compensatory response after tonsillectomy, or as a nonspecific response to allergies or repeated infection.⁴³ Symptoms attributed to lymphoid hyperplasia of the lingual tonsil include throat discomfort, a globus sensation, and dysphagia. There are no criteria based on size for differentiating nodularity of the base of the tongue because of normal lingual tonsils from that resulting from reactive lymphoid hyperplasia. On frontal radiographs obtained in patients with lymphoid



Figure 16-9 Lymphoid hyperplasia of the base of the tongue. Frontal view shows large, smooth-surfaced, round to ovoid nodules (arrow) symmetrically distributed over the surface of the base of the tongue.

hyperplasia, multiple smooth, round, or ovoid nodules are symmetrically distributed over the surface of the base of the tongue (Fig. 16-11). On lateral radiographs, the base of the tongue may seem to protrude posteriorly. In lymphoid hyperplasia of the palatine tonsils, masslike enlargement of the palatine tonsils is seen in the frontal and lateral views (Fig. 16-12). With severe lymphoid hyperplasia of the base of the tongue, the nodules may extend into the valleculae, along the lingual surface of the epiglottis, or even into the upper hypopharynx. Lingual tonsil lymphoid hyperplasia can be coarsely nodular, asymmetrically distributed, or masslike. However, any asymmetrically distributed coarse nodularity or mass must be viewed with suspicion. The use of endoscopy and magnetic resonance imaging (MRI) may help exclude malignancy.

Benign Tumors of the Pharynx

A wide variety of benign tumors occur in the pharynx.⁶ Non-epithelial tumors arising from the supporting tissues of the pharynx are rare.^{44,45} However, tumor-like cysts of various histologic types are not uncommonly seen in the pharynx.⁴⁶ The most common benign lesions are retention cysts of the valleculae or aryepiglottic folds.

Symptoms are related primarily to the location and polypoid or sessile nature of the lesion. Patients with benign tumors of the base of the tongue may be asymptomatic or may

complain of throat irritation or dysphagia. Aryepiglottic fold nodules or mass lesions may cause dysphonia or respiratory symptoms such as stridor. Tumors of the epiglottis and aryepiglottic folds may also result in dysphagia, coughing, or choking because of laryngeal penetration. Rarely, pedunculated lesions (e.g., papillomas, lipomas,⁴⁷ fibrovascular polyps) may be coughed up into the mouth or may cause sudden death through asphyxiation.

Tumors of various histologic types tend to occur at specific locations in the pharynx. Retention cysts and granular cell tumors are the most common benign tumors of the base of the tongue (Fig. 16-13).⁴⁸ Ectopic thyroid tissue and thyroglossal duct cysts may occur at the tongue base but are rare. The tumor-like lesions that usually involve the aryepiglottic folds are retention cysts and saccular cysts. Retention cysts of the aryepiglottic folds are lined by squamous epithelium and filled with desquamated squamous debris (Fig. 16-14). In contrast, saccular cysts of the aryepiglottic folds arise from the mucus-secreting glands of the appendix of the laryngeal ventricle and are filled with mucoid secretions. True soft tissue tumors of the aryepiglottic folds, such as lipomas, neurofibromas, hamartomas,⁴⁵ granular cell tumors, and oncocytomas, are rare.⁶ Laryngeal involvement in neurofibromatosis (von Recklinghausen's disease) is rare but usually involves the region of the arytenoid cartilage and aryepiglottic folds.⁴⁹ Benign tumors arising from the minor mucoserous salivary glands are usually seen in the oropharynx in the region of the soft palate and base of the tongue. Benign cartilaginous tumors involving the pharynx (chondromas) usually arise from the posterior lamina of the cricoid cartilage.⁵⁰

Regardless of its underlying histologic characteristics, a benign pharyngeal tumor usually appears radiographically as a smooth, round, sharply circumscribed mass en face and as a hemispheric line with abrupt angulation in profile (see Figs. 16-16 and 16-17).^{37,48} Only rarely is a pedunculated polypoid lesion (e.g., papilloma, fibrovascular polyp) seen. The benign nature of these lesions should be confirmed by endoscopic examination. However, submucosal masses are sometimes missed at endoscopy.

Malignant Tumors of the Pharynx

Radiologists should be as familiar with pharyngeal carcinoma as they are with esophageal carcinoma. Squamous cell carcinomas of the head and neck (e.g., tongue, pharynx, larynx) constitute 5% of all cancers in the United States, whereas esophageal carcinomas constitute only 1% of all cancers. The radiologist may be the first physician to suggest a diagnosis of pharyngeal carcinoma (Fig. 16-15). Some tumors may be detected during barium studies performed for other reasons. Patients with pharyngeal symptoms or a palpable neck mass may undergo pharyngoesophagography as the initial diagnostic examination. In patients with known pharyngeal cancer, a contrast examination is of value to assist in planning proper work-up and therapy. A barium examination can also be used to rule out a second primary lesion in the esophagus. Furthermore, the examination can detect coexisting structural lesions (e.g., prominent cricopharyngeal muscle, Zenker's diverticulum, web, stricture) that may be difficult to circumvent safely at endoscopy. Barium studies reveal the size, extent, and inferior limit of pharyngeal tumors and the degree of functional impairment. The barium examination can also show areas behind

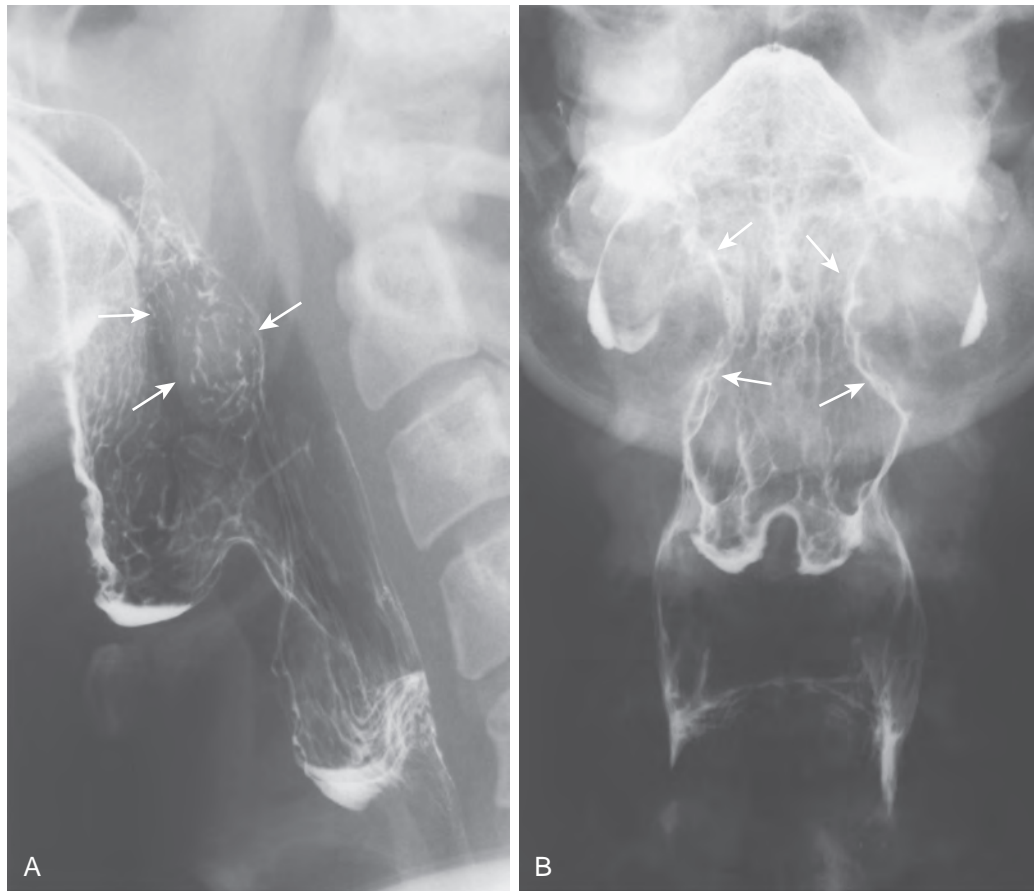


Figure 16-10 Lymphoid hyperplasia of the palatine tonsils. Frontal (A) and lateral (B) views of the pharynx show bilateral, symmetric enlargement of the palatine tonsils (arrows).

bulky tumors that are difficult to visualize by endoscopic examination.

Barium studies allow detection of more than 95% of structural lesions below the pharyngoesophageal fold.⁵¹ These studies are especially valuable in areas of the pharynx that are difficult to evaluate by endoscopy (e.g., lower base of the tongue, valleculae, lower hypopharynx, pharyngoesophageal segment).

SIGNS AND SYMPTOMS

The symptoms of pharyngeal carcinoma are nonspecific and usually of short duration (<4 months). They include sore throat, dysphagia, and odynophagia. Choking or coughing may be caused by laryngeal penetration during swallowing or aspiration of barium trapped in ulcerated tumors. Hoarseness occurs primarily in patients with laryngeal carcinoma, supraglottic carcinoma, or carcinoma of the medial piriform sinus infiltrating the arytenoid cartilage or cricoarytenoid joint. A referred earache may occur, especially when nasopharyngeal tumors block the eustachian tube.⁵² Some patients are asymptomatic but present with a palpable neck mass. Most patients with squamous cell carcinoma are 50 to 70 years of age.⁵² Almost all patients (>95%) are moderate to heavy abusers of alcohol and tobacco or have a tumor related to herpes virus.⁵³

SQUAMOUS CELL CARCINOMA

Pathology

Squamous cell carcinomas represent 90% of malignant lesions involving the oropharynx and hypopharynx.^{6,53} Most of these tumors are keratinizing squamous cell carcinomas. In general, they occur in two macroscopic forms: (1) exophytic tumors that spread over the mucosa; and (2) infiltrative or ulcerative tumors that penetrate deeply into surrounding soft tissue, cartilage, and bone.⁷ Multiple primary lesions of the oral cavity, pharynx, esophagus, and lung are seen in more than 20% of patients.⁵² Because such a strong association exists between head and neck squamous cell carcinoma and esophageal carcinoma,^{54,55} a major goal of a preoperative radiologic study is to rule out a synchronous primary esophageal cancer. Between 1% and 15% of patients with head and neck squamous cell carcinoma subsequently develop squamous cell carcinoma of the esophagus.^{54,55}

Radiographic Findings

The radiographic findings of pharyngeal cancer include an intraluminal mass, mucosal irregularity, and impairment or loss of normal mobility or distensibility (Fig. 16-16).^{37,56-59} An intraluminal mass may be manifested radiographically by obliteration of the normal luminal contour, extra

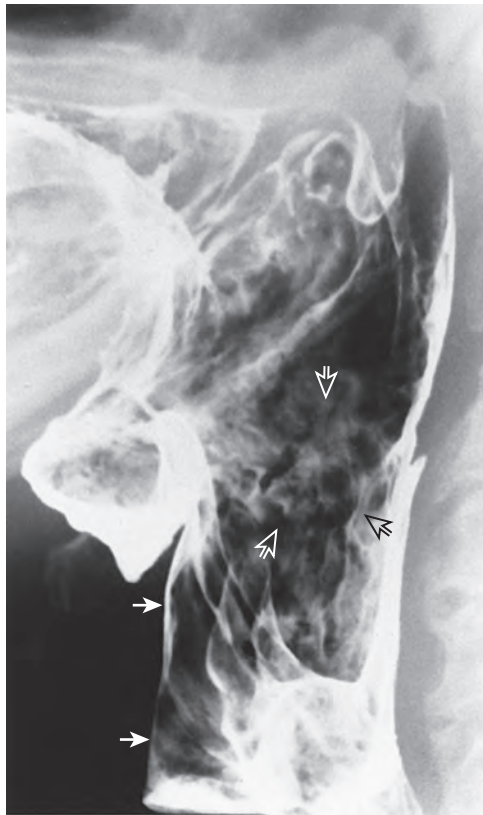


Figure 16-11 *Candida pharyngitis.* Lateral view of the pharynx shows well-circumscribed plaques (open arrows) at the level of the epiglottis. Note laryngeal vestibule penetration (solid arrows) resulting from abnormal pharyngeal motility associated with this inflammatory pharyngitis. (From Rubesin SE: Pharynx. In Laufer I, Levine MS [eds]: *Double Contrast Gastrointestinal Radiology*, 2nd ed. Philadelphia, WB Saunders, 1992.)

barium-coated lines protruding into the expected pharyngeal air column, a focal area of increased radiopacity, or a filling defect in the barium pool.^{37,38,56,59} Mucosal irregularity may be seen as abnormal barium collections resulting from surface ulceration or as a lobulated, finely nodular, or granular surface texture.⁵⁶ Asymmetrical distensibility is seen as flattening of the pharyngeal contour caused by fixation of structures by infiltrating tumor or by an extrinsic mass impinging on the pharynx.^{38,58,59}

Cross-sectional imaging studies are the examinations of choice for showing spread of tumor into the submucosa, intrinsic muscles, tissues extrinsic to the pharynx, and regional lymph nodes.⁶⁰ Computed tomography (CT) and MRI may occasionally reveal lesions (typically submucosal masses) that are not visible, even with modern endoscopes.

Specific Sites

Nasopharynx. Squamous cell carcinoma is the most common histologic type of nasopharyngeal malignant tumor. Many nasopharyngeal squamous cell cancers are undifferentiated tumors, and many have a reactive lymphoid stroma. The risk factors, age of presentation, and histologic type are more varied than those of the typical squamous cell carcinoma of the oropharynx and hypopharynx. In addition to alcohol and smoking abuse, poor ventilation, nasal balms, ingested carcinogens, and upper respiratory viruses such as the Epstein-Barr virus have been implicated as causative factors.⁶

Nasopharyngeal squamous cell carcinoma occurs at a relatively young age, with 20% of patients being younger than 30 years.⁶ Approximately 50% of patients complain of hearing loss because of eustachian tube involvement. About 50% of these patients are asymptomatic and present with a neck mass caused by cervical nodal metastases. Other signs and symptoms include nasal obstruction, epistaxis, pain,

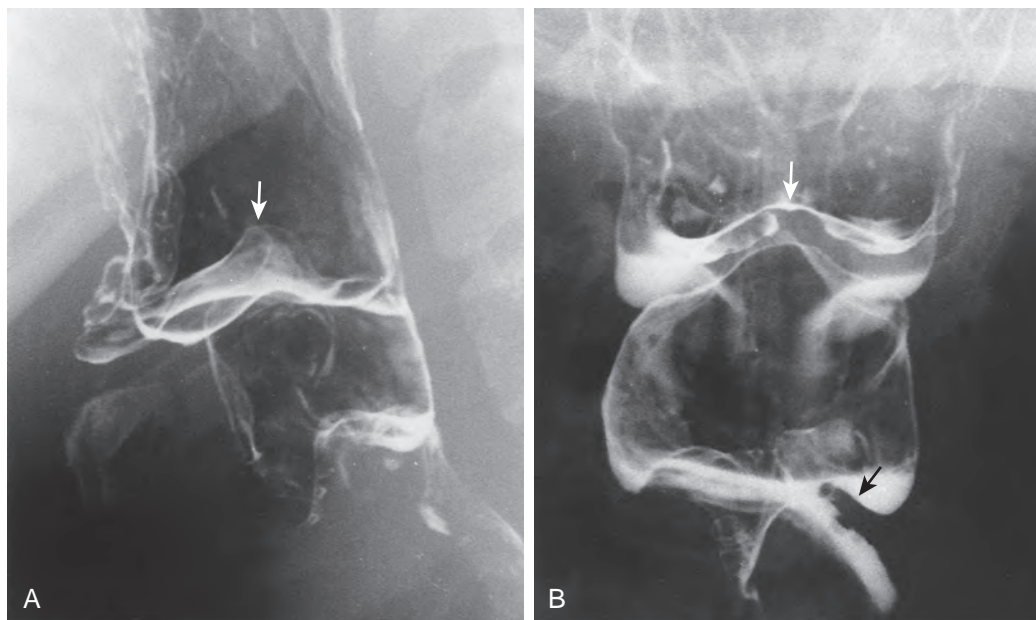


Figure 16-12 *Scarring caused by lye ingestion.* **A.** On the lateral view, the tip of the epiglottis (arrow) appears truncated. **B.** On the frontal view, the epiglottis (white arrow) is located inferior to its normal position. A scar in the inferior portion of the left piriform sinus is seen as a fold of tissue (black arrow).



Figure 16-13 Retention cyst at the base of the tongue. Lateral view shows a smooth-surfaced hemispheric mass (arrow) protruding posteriorly from the base of the tongue.

headache, and damage to the fifth cranial nerve. The 5-year survival rate varies from 76% for patients with localized tumors to 10% to 20% for patients with cervical lymph node metastases.

MRI is the method of choice for evaluating tumors of the nasopharynx.⁶¹ The radiologist carefully searches for spread to the nasal cavity, sinuses, and cranial base, especially for cranial nerve involvement. Barium studies are used primarily to evaluate the symptoms of nasal regurgitation and voice changes caused by soft palate insufficiency and to rule out a synchronous esophageal tumor.

Palatine Tonsil. Squamous cell carcinoma of the palatine tonsil is the most common malignant tumor arising in the pharynx.⁶ Well-differentiated tumors are usually exophytic and easily seen on barium studies (Fig. 16-17).³⁷ Poorly differentiated tumors are frequently of the ulcerative infiltrative type and may be obscured on barium studies by the underlying nodular lymphoid tissue of the palatine tonsil.³⁸ Tonsillar tumors may spread to the soft palate, base of the tongue, and posterior pharyngeal wall. Approximately 50% of patients develop cervical nodal metastases.³⁷

Base of the Tongue. Squamous cell carcinomas of the base of the tongue are poorly differentiated lesions that often present as advanced lesions with nodal metastases.^{6,62} These tumors infiltrate deeply into the intrinsic and extrinsic muscles of the tongue. Lymph node metastases are seen ipsilaterally or contralaterally in more than 70% of patients. The 5-year survival rate is 20% to 40%.³⁷ Patients with small lesions are

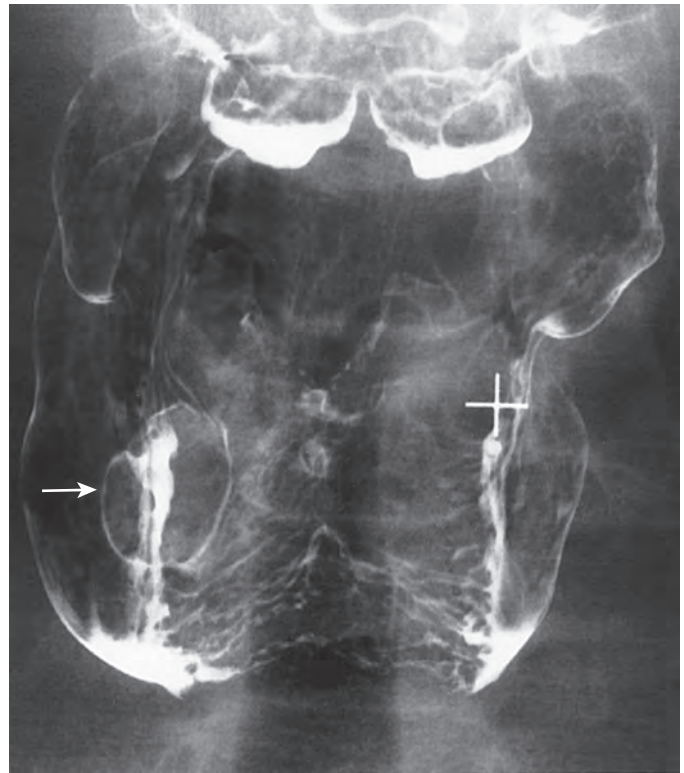


Figure 16-14 Retention cyst. A smooth-surfaced, well-circumscribed mass (arrow) is seen in the region of the mucosa overlying the muscular process of the right arytenoid cartilage. This 2.5-cm mass was not detected on endoscopy. After a repeat endoscopic examination confirmed the presence of the lesion, surgery was performed and pathologic evaluation revealed a retention cyst lined by squamous epithelium. (From Rubesin SE, Glick SN: *The tailored double-contrast pharyngogram*. *Crit Rev Diagn Imaging* 28:133–179, 1988.)

often asymptomatic but present with enlarged cervical nodes. Initial results of diagnostic endoscopy may be negative.⁶³ Small or predominantly submucosal lesions may be hidden in the valleculae or the recess between the tongue and tonsil (glossotonsillar recess). Barium, MRI, or CT studies may be extremely helpful in detecting clinically occult lesions with nodal metastases.

Radiographically, an exophytic lesion appears as a polypoid mass projecting into the oropharyngeal air space.^{63,64} An ulcerated lesion appears as an irregular barium collection disrupting the expected contour of the base of the tongue. Nodules of tumor may spread to the palatine tonsil, valleculae, or pharyngoepiglottic fold. Occasionally, a deeply infiltrating, primarily submucosal lesion may be manifested by subtle asymmetric enlargement of the tongue base. A small plaque-like or ulcerative lesion can easily be missed on barium or endoscopic studies but can be detected on MRI or CT studies.

Supraglottic Region. Squamous cell carcinomas that affect the epiglottis, aryepiglottic folds, mucosa overlying the arytenoid cartilages, false vocal cords, and laryngeal ventricles are defined as supraglottic carcinomas. These poorly differentiated or undifferentiated tumors spread rapidly to the entire supraglottic region and pre-epiglottic space.³⁷ Exophytic lesions are more

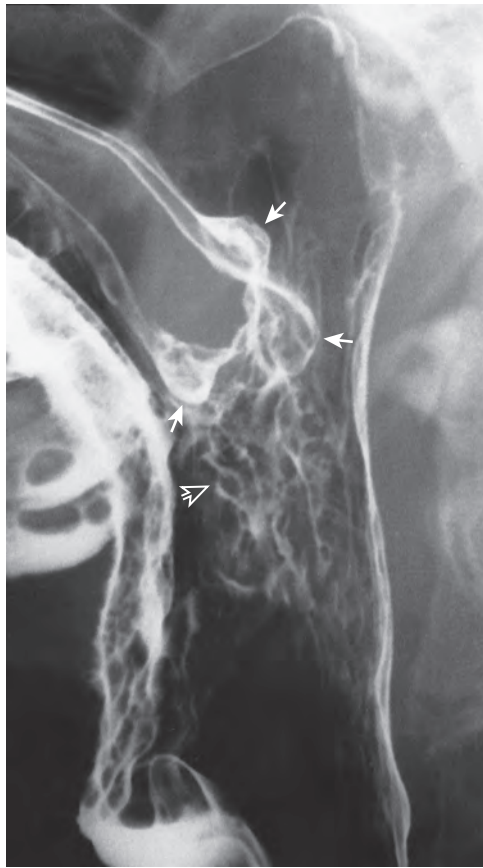


Figure 16-15 Unsuspected soft palate carcinoma. An 80-year-old patient with dementia underwent an upper GI examination for epigastric pain. Nasal regurgitation was observed during the initial double-contrast swallow. Lateral spot image of the pharynx shows obliteration of the contour of the lower soft palate, which is replaced by a lobulated mass (solid arrows). Nodular mucosa in the tonsillar fossa (open arrow) indicates spread of the tumor into this region. (From Rubesin SE, Rabischong P, Bilaniuk LT, et al: Contrast examination of the soft palate with cross-sectional correlation. *RadioGraphics* 8:641–665, 1988.)

common (Fig. 16-18).^{57,65} Ulcerative lesions may deeply penetrate the tongue and valleculae and invade the pre-epiglottic space (Fig. 16-19).⁵⁷ These tumors may spread laterally to the pharyngoepiglottic folds and lateral pharyngeal walls. Only rarely do these tumors extend through the laryngeal ventricles into the true vocal cords. Cervical nodal metastases are seen in one third to one half of patients.^{37,65} The 5-year survival rate is approximately 40%.

Piriform Sinus. Squamous cell carcinomas of the piriform sinuses are advanced lesions that spread quickly and metastasize widely.⁵⁶ Metastases to cervical lymph nodes are seen in 70% to 80% of patients.³⁷ The 5-year survival rate is 20% to 40%.⁶³

Tumors involving the medial wall of the piriform sinus have a slightly better prognosis than lateral wall tumors⁶⁶ because medial wall tumors present early with hoarseness when they infiltrate the aryepiglottic fold, arytenoid and cricoid cartilages, and paraglottic space.⁵⁶ Tumors involving the lateral wall present later as a neck mass when they infiltrate the thyrohyoid membrane, thyroid cartilage, and soft tissues of the neck, including the structures of the carotid sheath.^{37,67}



Figure 16-16 Radiographic findings in pharyngeal carcinoma. A frontal view shows loss of the normal contour of the left piriform sinus. Obliteration of the contour indicates that the lateral and inferior piriform sinus has been replaced by a soft tissue mass (black arrows). The left aryepiglottic fold (white arrow) is enlarged and has a nodular surface, indicating tumor infiltration. The mucosa overlying the muscular process of the left arytenoid cartilage is enlarged (white arrowhead) and deviated medially, crossing the midline. Thus, the hypopharyngeal tumor involves the lateral hypopharyngeal wall, left arytenoid region, and left aryepiglottic fold. Barium coating the vocal cords results from abnormal epiglottic tilt on the left caused by tumor infiltration.

Radiographically, an early lesion may appear as a subtle area of mucosal irregularity (Fig. 16-20). Advanced lesions are typically seen as bulky exophytic masses (Fig. 16-21). Occasionally, infiltrative masses are seen.

Posterior Pharyngeal Wall. Squamous cell carcinomas of the posterior pharyngeal wall are typically large fungating lesions more than 5 cm in length (Fig. 16-22), often spreading vertically into the nasopharynx or cervical esophagus. Approximately 50% of patients have jugular or retropharyngeal lymphatic metastases, or both, at the time of diagnosis.⁵² The 5-year survival rate is approximately 20%.⁵² Posterior pharyngeal squamous cell carcinoma is the type of pharyngeal cancer usually associated with a synchronous or metachronous malignant lesion in the oral cavity, pharynx, or esophagus.

Postcricoid Area. Postcricoid squamous cell carcinomas are rare, except in Scandinavia.⁵⁶ In Scandinavia, primary postcricoid carcinomas may be associated with iron deficiency anemia and cervical esophageal webs, the Plummer-Vinson syndrome. In the United States, however, only a rare association has been found between iron deficiency anemia and malignant

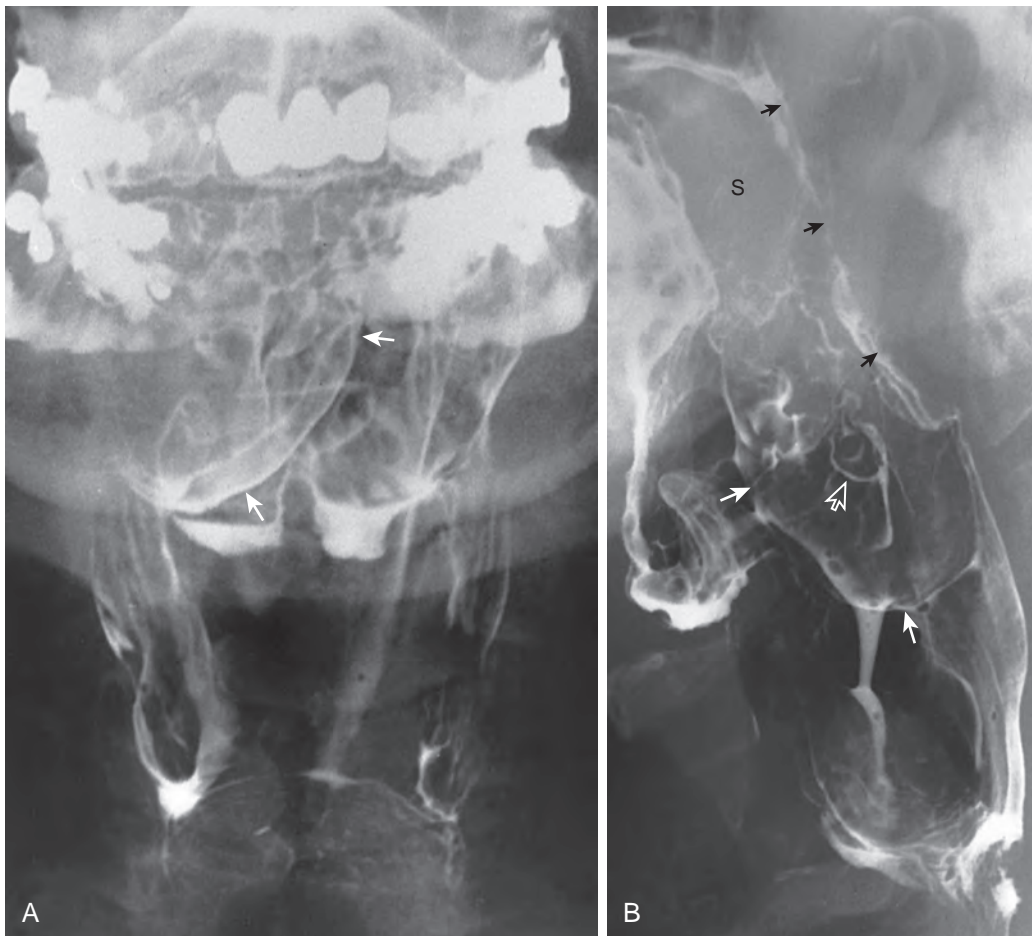


Figure 16-17 Squamous cell carcinoma of the right palatine tonsil. **A.** Frontal view shows a large polypoid mass (arrows) protruding into the oropharynx. The right lateral wall of the tonsillar fossa has been obliterated. **B.** Lateral view shows a large tonsillar fossa mass (white arrows) with a central ulcer (open arrow). Tumor infiltration of the posterior pharyngeal wall is manifested by enlargement of the soft tissue space in this region (black arrows). The soft palate (S) is also widened and has an irregular contour. (From Levine MS, Rubesin SE: *Radio-logic investigation of dysphagia*. AJR 154:1157–1163, 1990.)

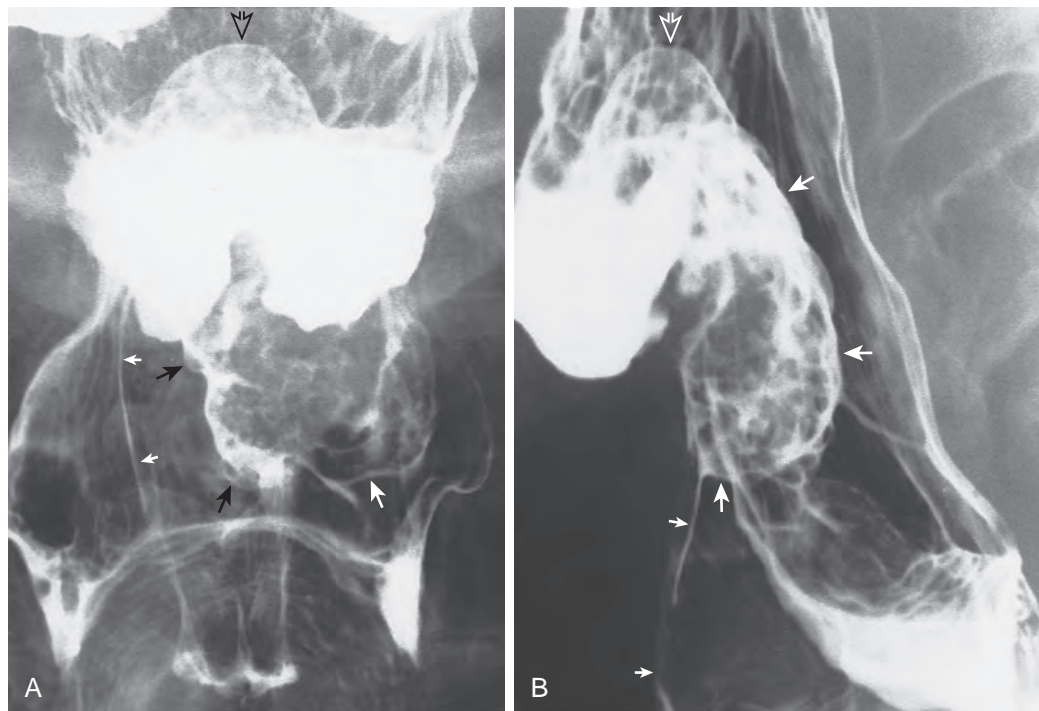


Figure 16-18 Polypoid squamous cell carcinoma of the epiglottis. **A.** Frontal view shows an enlarged, rounded epiglottic tip (open arrow) and an enlarged, nodular, left aryepiglottic fold (long white and black arrows). Note excessive pooling of barium in the valleculae. Laryngeal penetration has occurred, coating the laryngeal vestibule. This barium coating shows that the tumor has not spread to the lower right side of the epiglottis and right aryepiglottic fold (short white arrows). **B.** Lateral view shows a bulbous, enlarged, epiglottic tip (open arrow) and a large epiglottic mass (large arrows) extending down the aryepiglottic fold and along the anterior wall of the laryngeal vestibule. The lower portion of the laryngeal vestibule (small arrows) is not involved by tumor. (From Rubesin SE: *Pharynx*. In Laufer I, Levine MS [eds]: *Double Contrast Gastrointestinal Radiology*, 2nd ed. Philadelphia, WB Saunders, 1992.)

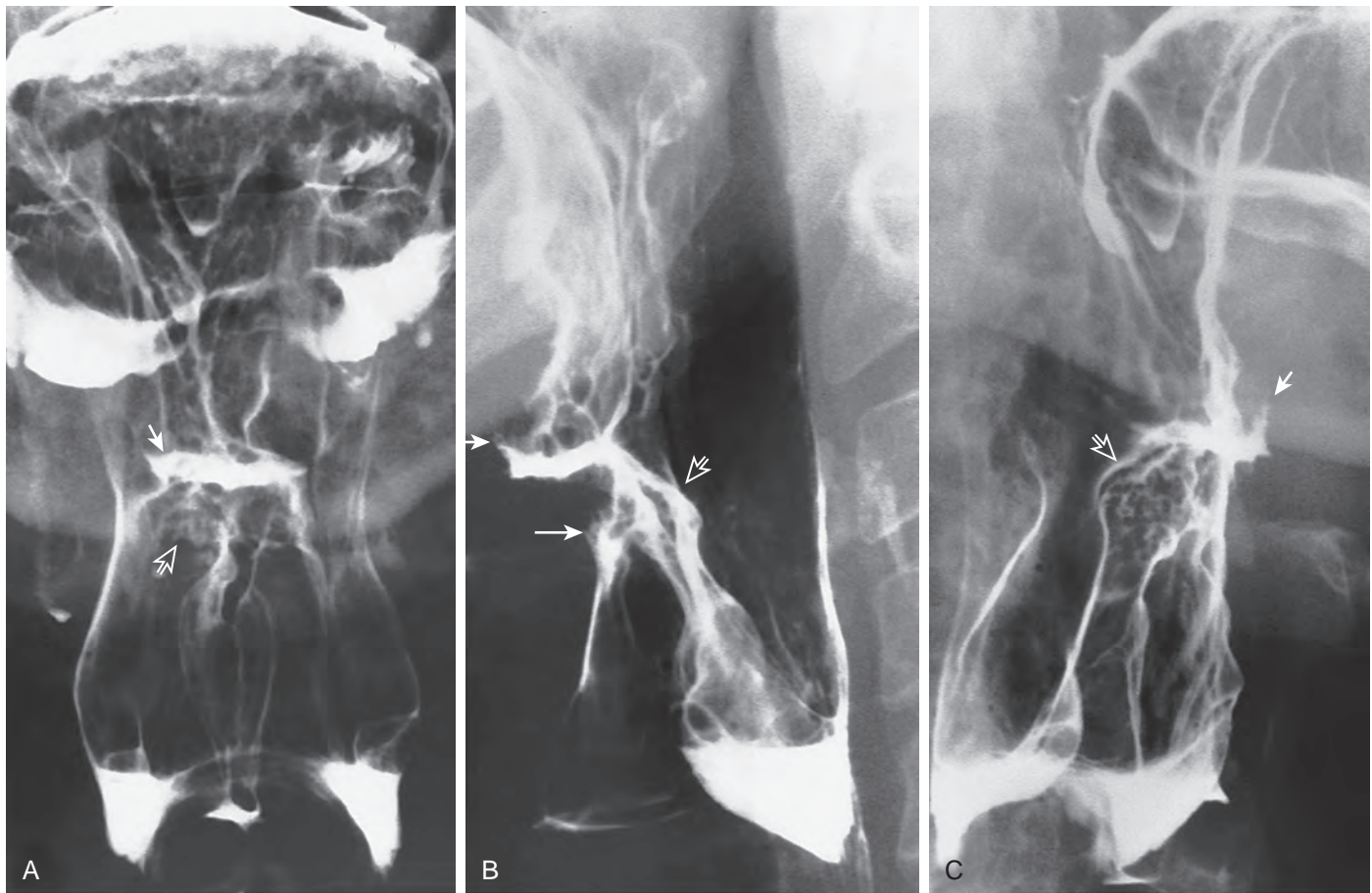


Figure 16-19 Ulcerative squamous cell carcinoma of the epiglottis and base of the tongue. Frontal (A), lateral (B), and left posterior oblique (C) views show that the epiglottic tip and median glossoepiglottic fold have been destroyed and are not visualized. The normal vallecular contour is not seen. Instead, an irregular barium collection is seen in the base of the tongue, with deep penetration into the contour of the tongue (short arrows). The tumor is manifest by finely nodular mucosa at the base of the tongue and in the upper right aryepiglottic fold (open arrows), as well as on the upper laryngeal surface of the residual epiglottis (long arrow in B).

pharyngeal tumors. The pharyngoesophageal segment is usually involved by direct extension of squamous cell cancer of the piriform sinus, posterior pharyngeal wall, or cervical esophagus.⁵⁶ Radiographically, postcricoid carcinomas appear as annular infiltrating lesions that may extend into the lower hypopharynx or cervical esophagus (Fig. 16-23).³⁷ These annular lesions are best detected while the pharyngoesophageal segment is fully distended with barium on video recordings or rapid-sequence spot images obtained during swallowing.

LYMPHOMA

Lymphomas of the pharynx represent approximately 10% of malignant pharyngeal tumors.^{6,68} Almost all pharyngeal lymphomas are of the non-Hodgkin's type, arising from Waldeyer's ring (i.e., the adenoids, palatine tonsils, and lingual tonsil). Hodgkin's lymphoma involving the pharynx is rare, despite the fact that Hodgkin's lymphoma often begins in cervical lymph nodes.⁶⁹ Pharyngeal involvement occurs in only 1% to 2% of all patients with Hodgkin's lymphoma, even those with disseminated tumor.

Most patients with pharyngeal lymphoma are in the fifth to sixth decade of life. Approximately 50% of patients have cervical lymphadenopathy as the initial clinical finding.⁶⁸ Cervical

lymph nodes are involved in more than 60% of patients.⁶⁸ At the time of diagnosis, only 10% of patients have involvement of extranodal sites (lung and bones). Approximately 50% of patients have symptoms related to local pharyngeal involvement, including nasal obstruction, earache, sore throat, or a lump in the throat.

The most frequent pharyngeal locations of lymphoma are the palatine tonsil (40%-60% of patients),^{6,68} nasopharynx (18%-28%),⁶⁸ and base of the tongue (10%). Approximately 25% of tumors involve multiple sites. Bilateral involvement of the palatine tonsils occurs in 15% of pharyngeal lymphomas.⁶⁸ Lymphomas only rarely arise in the hypopharynx.

Pharyngeal lymphomas are manifested radiographically as lobulated masses involving the nasopharynx, palatine tonsil (Fig. 16-24), base of the tongue (Fig. 16-25), or a combination of these sites. The normal lymphoid follicular pattern of the base of the tongue or palatine tonsil may be effaced by these bulging submucosal masses.

RARE MALIGNANT TUMORS

Carcinoma of the Minor Salivary Glands

Benign and malignant tumors arise from the minor mucous salivary glands located deep to the epithelial layer of the



Figure 16-20 Squamous cell carcinoma of the lateral wall of the right piriform sinus. Frontal view shows obliteration of the right lateral wall of the piriform sinus. There is a large polypoid mass (long arrows) protruding into the hypopharynx. The tip of the epiglottis (short arrow) is spared. (From Rubesin SE, Glick SN: *The tailored double-contrast pharyngogram*. *Crit Rev Diagn Imaging* 28:133–179, 1988.)

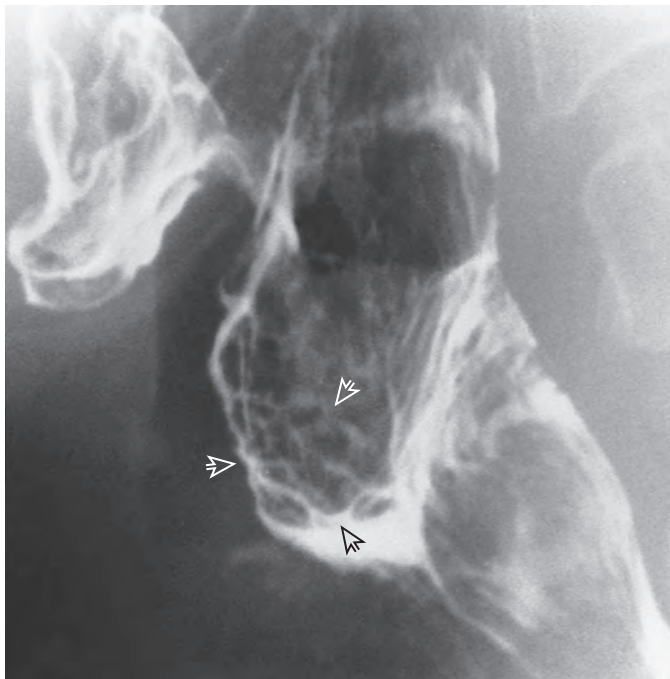


Figure 16-21 Early squamous cell carcinoma of the right piriform sinus extending into the submucosa. Lateral view of the pharynx shows a flat area of nodular mucosa (open arrows) along the lateral wall of the right piriform sinus. (From Levine MS, Rubesin SE, Ott DJ: *Update on esophageal radiology*. *AJR* 155:933–941, 1990.)

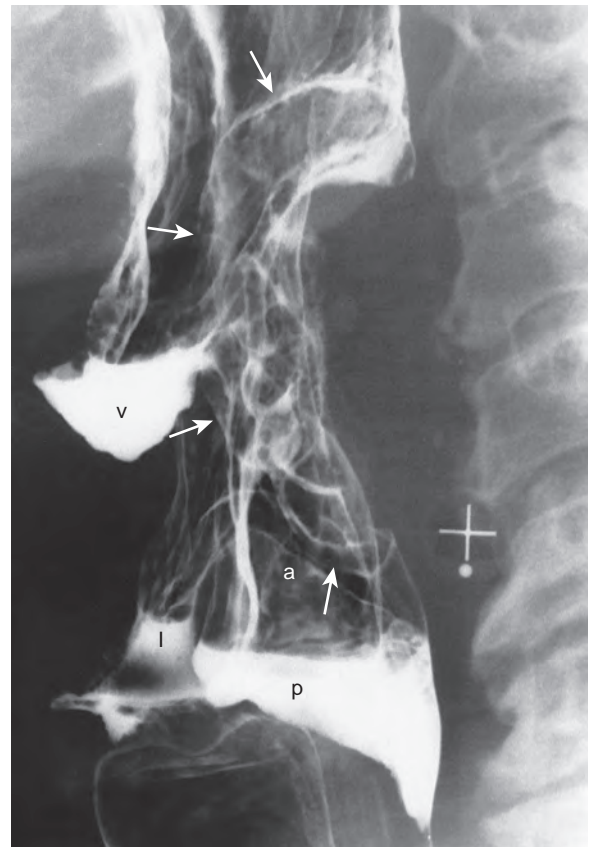


Figure 16-22 Squamous cell carcinoma of the posterior pharyngeal wall. Lateral spot image of the pharynx shows a large fungating mass (arrows) on the posterior pharyngeal wall, extending from the level of the uvula to the level of the muscular processes of the arytenoid cartilages (a). Note evidence of pharyngeal dysfunction with pooling of barium in the valleculae (v), piriform sinus (p), and laryngeal vestibule (l). (From Rubesin SE, Glick SN: *The tailored double-contrast pharyngogram*. *Crit Rev Diagn Imaging* 28:133–179, 1988.)

pharynx. Minor salivary gland tumors constitute 20% of all salivary gland tumors and have diverse histologic features and a diverse clinical course. Of minor salivary gland tumors, 65% to 88% are malignant.⁷⁰ The most frequent malignant types are adenoid cystic carcinoma (35%), solid adenocarcinoma (22%; Fig. 16-26), and mucoepidermoid carcinoma (16%).⁷⁰ The most common pharyngeal location of minor salivary gland tumors is the soft palate. Palatal salivary gland tumors are manifested clinically by painless masses near the junction of the hard and soft palates. Palatal salivary gland tumors spread to the tongue, submandibular gland, lingual and hypoglossal nerves, and mandible. In contrast to squamous cell carcinoma, cervical metastases are relatively infrequent, occurring in approximately 25% of malignant lesions.⁷⁰ Adenoid cystic carcinoma has a particular propensity for perineural tumor spread.

Sarcoma

Malignant fibrous histiocytoma (Fig. 16-27) and synovial sarcomas of the pharynx are extremely rare.^{71,72} Most patients with synovial sarcoma are 20 to 40 years of age and complain of a painless neck mass. At initial diagnosis, synovial sarcomas appear radiographically as large bulky tumors involving the

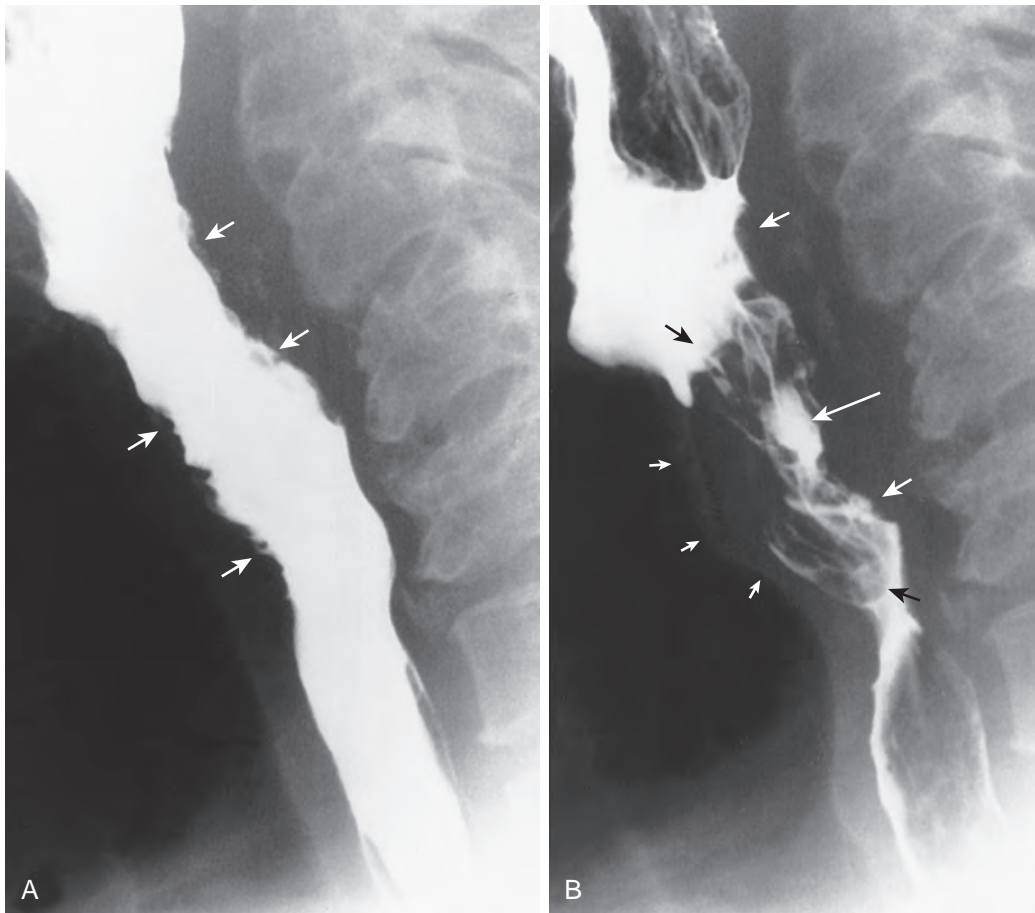


Figure 16-23 Squamous cell carcinoma of the postcricoid region. **A.** Lateral spot image obtained during swallowing shows a finely lobulated contour of the anterior and posterior walls of the pharyngoesophageal segment (arrows). **B.** Lateral spot image of the pharyngoesophageal segment during phonation shows an ulcerated mass. The central ulcer crater (large white arrow) is filled with barium. The mass is seen as a filling defect in the barium pool (black arrows) and as an irregular contour of the posterior pharyngeal wall (medium white arrows). The mass also causes a smooth extrinsic impression on the posterior wall of the trachea (small white arrows).

larynx, pharynx, and soft tissues of the neck.⁷² A clue that a bulky pharyngeal tumor is a sarcoma, not a squamous cell carcinoma, is marked enhancement during a CT or MRI examination of the neck.⁷¹

Cartilaginous Tumors

Primary cartilaginous tumors of the pharynx are extremely rare. The pharynx may be invaded secondarily by cartilaginous tumors (e.g., chondroma, osteochondroma, chondrosarcoma) arising in the larynx.⁷³ Cartilaginous tumors of the larynx are seen mainly in the fourth to sixth decade of life. Patients complain of hoarseness, poor voice, and dysphagia. Chondroid tumors usually arise from the cricoid cartilage.

Radiographically, a smooth-surfaced mass is usually seen in the posterior lamina of the cricoid cartilage, compressing and distorting the lower hypopharynx and pharyngoesophageal segment. Stippled calcification is seen in a central or peripheral location in more than 80% of patients.⁶

Kaposi's Sarcoma

Kaposi's sarcoma may arise anywhere in the GI tract in patients with AIDS. Kaposi's sarcoma involving the pharynx may cause dysphagia or odynophagia.⁷⁴ Radiographically, Kaposi's sarcoma

may be manifested by multiple small nodules or plaque-like lesions, small submucosal masses with or without central ulceration, or larger, bulky polypoid masses.⁷⁴

Pharyngeal Damage from Radiation

Radiation therapy may be used as a primary or adjunctive form of treatment for pharyngeal tumors such as squamous cell carcinoma and lymphoma. The pharynx is included within the radiation portal during irradiation of tumors of the larynx and cervical lymph nodes. In the past, the pharynx was also included in the radiation portal during treatment of thyrotoxicosis or tuberculous lymphadenitis.⁷⁵

Acute mucositis and edema occur early during the course of radiotherapy. Epithelial necrosis and ulceration result in a fibrinous exudate.⁷⁶⁻⁷⁸ Submucosal inflammation also occurs early. Over time, the mucosa atrophies and submucosal fibrosis may occur.⁷⁶ Most chronic radiation damage results from vascular changes, with thrombosis and fibrosis of capillaries and lymphatics and subintimal fibrosis and hyalinization of veins and arteries. Vascular damage leads to atrophy of the skin and to fibrosis of subcutaneous tissues, submucosal tissues, and muscle.⁷⁹ The most frequent localization of persistent edema is

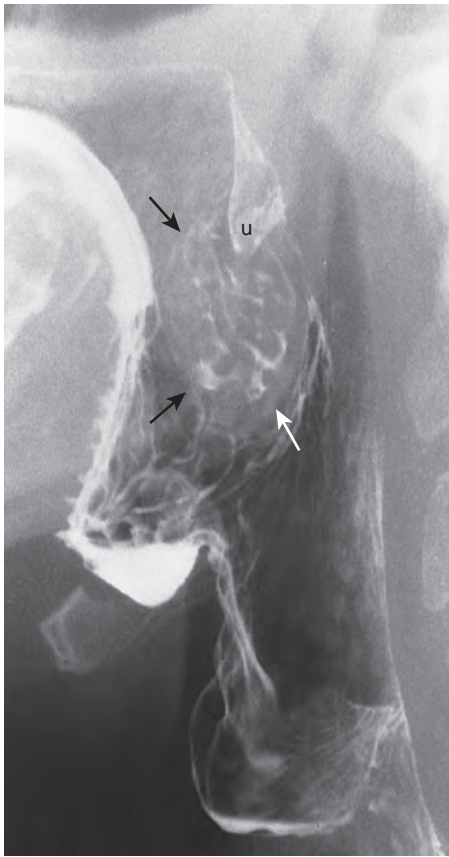


Figure 16-24 Non-Hodgkin's lymphoma of the palatine tonsil. A large lobulated mass is seen in the tonsillar fossa (arrows). The uvula (u) is identified.

in the glottis and mucosa overlying the arytenoid cartilages. Severe complications such as life-threatening osteomyelitis and chondronecrosis may occur.

Five to 10 days after initial radiotherapy, the patient may complain of local discomfort, hoarseness, dryness, dysphagia, or a lump in the throat. The peak occurrence of symptoms occurs near the end of the typical 6-week course of radiation treatment. Most symptoms gradually subside 2 to 6 weeks after cessation of radiotherapy.⁷⁷ However, a substantial number of patients have persistent symptoms. For example, 15% of patients have persistent edema after radiotherapy for carcinoma of the vocal cord.⁸⁰ If the parotid or other salivary glands have been damaged, xerostomia may cause persistent dysphagia. Persistent edema may suggest a serious underlying complication such as persistent carcinoma or the development of osteomyelitis or chondronecrosis.⁸⁰⁻⁸² Approximately 50% of patients with persistent edema have recurrent or persistent tumor.⁸⁰

The radiographic changes of radiation damage are seen in almost all patients after radiation therapy, with or without surgery.⁸³ Spot images typically show that the epiglottis and aryepiglottic folds are diffusely and smoothly enlarged (Fig. 16-28).^{38,84,85} The valleculae may be flattened, and the mucosa overlying the muscular processes of the arytenoid cartilages may be elevated. Soft tissue atrophy seen with chronic radiation change is manifested as a small soft palate and as loss of the muscular soft tissue between the barium-coated posterior pharyngeal wall and vertebral bodies of the cervical spine. Edema

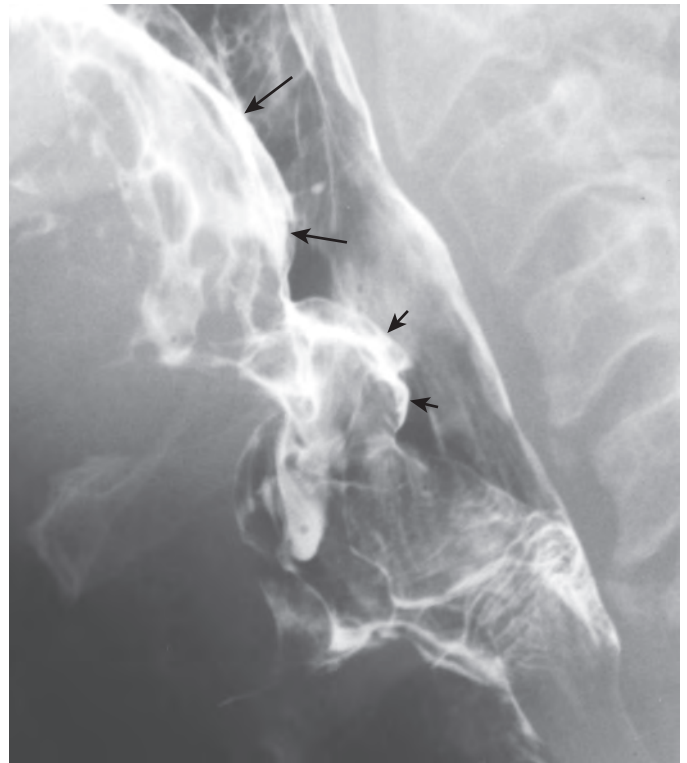


Figure 16-25 Lymphoma of the base of the tongue and epiglottic tip. Lateral view of the pharynx shows a large, lobulated mass involving the base of the tongue (large arrows) and tip of the epiglottis (small arrows). Note that the normal contours of the valleculae have been obliterated.

from radiation may be asymmetric, especially in the region of the original tumor. The most frequent dynamic findings are abnormal epiglottic tilt and poor closure of the laryngeal vestibule, resulting in laryngeal penetration, and pharyngeal paresis, resulting in stasis in the piriform sinuses, with the potential for overflow penetration.⁸³ Any surface irregularity on a post-radiation pharyngogram should suggest the possibility of persistent cancer, although radiation-induced ulceration may produce identical radiographic findings.^{2,84}

Postoperative Pharynx

The radiologist frequently studies the pharynx in the early and remote postoperative periods, testing a patient's ability to swallow and looking for complications. Ideally, the surgeon provides a clear description of the postoperative anatomy to the radiologist and states what information needs to be obtained from the postoperative pharyngogram. In reality, the radiologist must be familiar with the numerous operations performed for a wide variety of pharyngeal tumors, Zenker's diverticulum, and cricopharyngeal achalasia. The radiologist must also have a working knowledge of the spectrum of postoperative complications associated with these various procedures (Table 16-1).⁸⁶

TOTAL LARYNGECTOMY

Total laryngectomy is usually performed for advanced malignant tumors of the larynx, subglottic cancers, and small

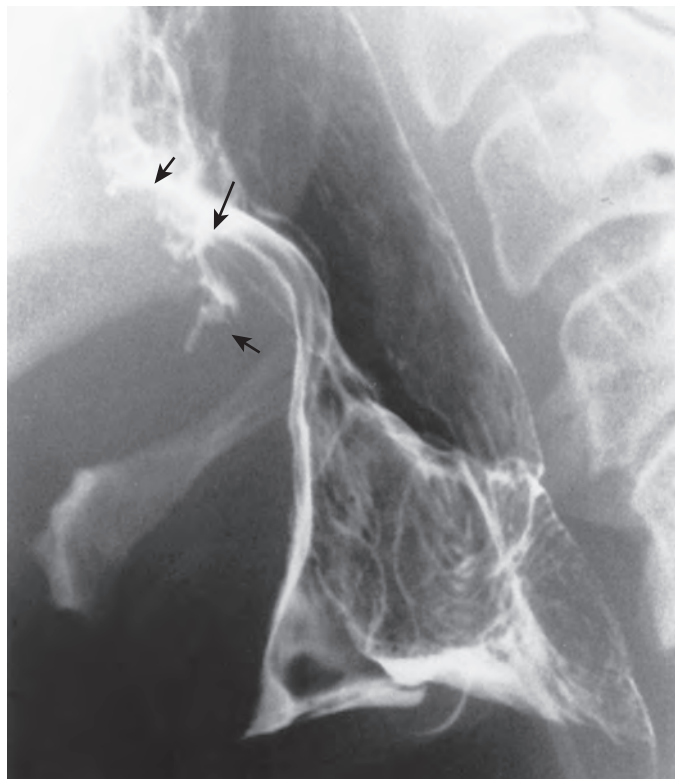


Figure 16-26 Adenocarcinoma of the minor salivary glands. The epiglottic tip (*long arrow*) is apposed to the base of the tongue, and its vallecular surface is ulcerated. The valleculae are obliterated and filled by a lobulated tumor (*short arrows*) arising from the tongue base. This adenocarcinoma is radiographically indistinguishable from a typical squamous cell carcinoma of the base of the tongue. The tumor presumably arose in minor salivary gland tissue.

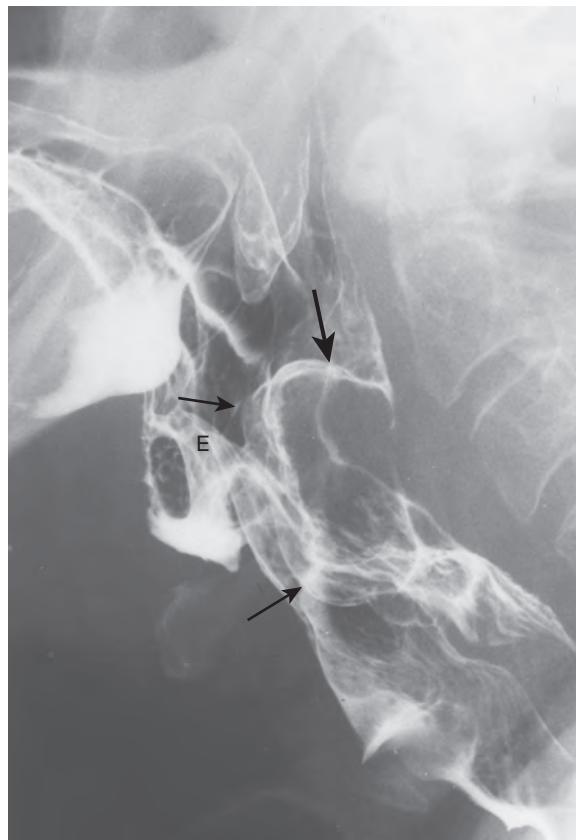


Figure 16-27 Malignant fibrous histiocytoma of the pharynx. Lateral view of the pharynx shows a 3-cm relatively smooth mass (*arrows*) protruding from the posterior wall of the upper hypopharynx. The surface is finely nodular anteriorly. Barium in the laryngeal vestibule and trachea resulted from poor closure of the laryngeal aditus when the epiglottis (E) was unable to tilt posteriorly.

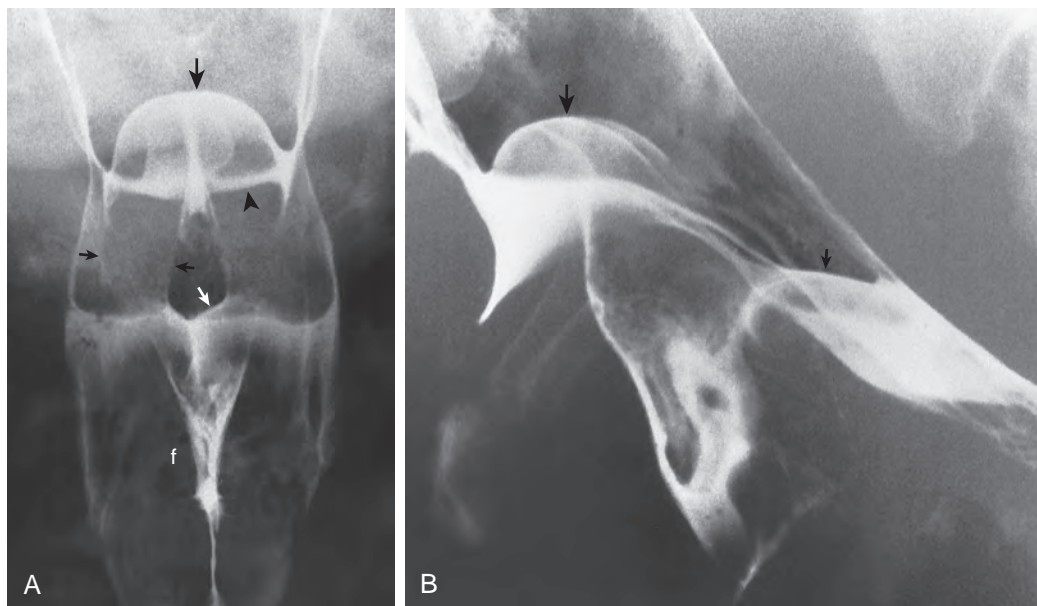


Figure 16-28 Radiation changes in the pharynx. **A.** Frontal view of the pharynx shows smooth, bulbous enlargement of the epiglottis (*large black arrow*) and flattening of the valleculae (*left vallecula, arrowhead*). Abnormal pharyngeal motility results in laryngeal penetration. Barium coating the laryngeal vestibule demonstrates enlargement of the epiglottis, wide aryepiglottic folds (*small black arrows*), elevation of the mucosa overlying the muscular process of the arytenoid cartilages (*white arrow*), and even edema of the false vocal cords (f). **B.** Lateral view of the pharynx shows smooth, bulbous enlargement of the epiglottis (*large arrow*) and elevation of the mucosa overlying the muscular processes of the arytenoid cartilages (*small arrow*).

TABLE 16-1
Common Postoperative Complications

Stage	Voice-Sparing Procedure	Laryngectomy
Early postoperative period	Wound breakdown	Wound breakdown*
	Fistula formation*	Fistula formation*
Late postoperative period	Abscess (wound or fistula)	Abscess (wound or fistula)
	Aspiration, pneumonia*	Constrictor dysfunction*
	Airway obstruction (edema)	Tongue dysfunction (partial resection, immobility; rarely, hypoglossal nerve damage)*
	Hematoma	Hematoma
	Mediastinitis	Mediastinitis
	Thoracic duct or carotid injury from radical neck dissection	Thoracic duct or carotid injury from radical neck dissection
	Hoarseness	Stricture*
	Aspiration*	Constrictor dysfunction*
	Recurrent tumor*	Recurrent tumor*
	Laryngeal stenosis*	Stomal stenosis
	Velopharyngeal incompetence*	Stomal tumor recurrence
	Failure of flap graft	Failure of flap graft or jejunal graft
		Hypothyroidism
		Hypoparathyroidism
		Abnormal vocalization*

From Rubesin SE, Eisele DW, Jones B: *Pharyngography in the postoperative patient*. In Jones B (ed): *Normal and Abnormal Swallowing. Imaging in Diagnosis and Therapy*. New York, Springer, 2003, pp 167–203.

*Pharyngography is helpful for evaluation.

carcinomas of the low tongue base and for failed irradiation or voice-conserving surgery for laryngeal cancer.^{87,88} Early glottic or supraglottic cancers are often treated by radiation therapy, endoscopic removal, or partial laryngectomy.⁸⁹ Cancers of the piriform sinuses, lateral and posterior pharyngeal walls, and postcricoid region are treated by total laryngectomy with partial pharyngectomy or laryngopharyngectomy, depending on the degree of retropharyngeal invasion.

During total laryngectomy, the larynx is removed, along with the epiglottic, thyroid, cricoid, and paired arytenoid cartilages. The hyoid bone may be removed or spared. Resection of the epiglottis, aryepiglottic folds, arytenoid cartilages, and anterior walls of the piriform sinuses results in the creation of a large gap in the anterior wall of the hypopharynx. Total laryngectomy also disrupts most of the muscles of the pharynx. The suprahyoid muscles (mylohyoid, geniohyoid, hyoglossus, and stylohyoid) and infrahyoid muscles (thyrohyoid, sternohyoid, sternothyroid, and omohyoid) are transected. The thyropharyngeus and cricopharyngeus are detached from their lateral origins on the thyroid and cricoid cartilages, respectively. A permanent tracheostoma is necessary. In some patients, the ipsilateral thyroid gland and its accompanying parathyroid glands are excised.

The gap in the anterior wall of the pharynx is closed by approximating the residual pharyngeal mucosa. The constrictor muscles may be joined anteriorly as an additional buttressing layer. A myocutaneous or free flap may be necessary to form the neopharyngeal tube if there is insufficient mucosa. A neck dissection may also be performed.

Radiographically, the normal neopharyngeal tube resembles an inverted cone with a smooth mucosal surface (Fig. 16-29).⁸⁷ On lateral views, the anterior wall of the neopharyngeal tube lies just below the skin of the neck, and the posterior wall of the tube abuts the vertebral column. On frontal views, the tube is within 0.5 cm of the midline.⁸⁹ The epiglottis, aryepiglottic folds, and extrinsic mass of the larynx on the

hypopharynx are no longer present. The hyoid bone may also be absent. At the closure site of the base of the tongue and anterior neopharyngeal tube, the contour may be angulated or sacculated. These postoperative sacculations at the tongue base are normal and resemble valleculae—hence, the term *pseudovalleculae*. A fold of tissue courses from each posterolateral wall of the oropharynx to the new base of the tongue, superficially resembling an epiglottis—hence, the term *pseudoepiglottis*.

The most common complication in the early postoperative period is the formation of a pharyngocutaneous fistula, occurring in 6% to 21% of patients (see Table 16-1).^{87,90,91} Fistulas develop at sites of mucosal closure, including the junction of the neopharyngeal tube with the tongue base, anterior aspect of the neopharyngeal tube (Fig. 16-30), margin of the flap (if one is used), and near the tracheal stoma. It is unknown whether radiation therapy increases the risk of fistula formation.⁹² Fistulas may end blindly in the subcutaneous tissue or extend to the skin and, rarely, may involve the carotid sheath. Most patients have signs of fistula formation within 10 to 14 days after surgery, including fever, wound erythema, swelling, and increased drainage from the wound.⁹³ Some patients with fistulas are asymptomatic. Most fistulas close spontaneously if feeding is delayed. The development of a fistula in the late postoperative period should suggest recurrent tumor. Radiographically, fistulas appear as contrast-filled tracks or collections arising from the anterior pharyngeal wall or base of the tongue.

Dysphagia is the most common symptom in the remote postoperative period. This symptom may be caused by benign strictures, retracted thyropharyngeal or cricopharyngeal muscle, or recurrent tumor. Some patients have no symptoms because they compensate for luminal narrowing by changing their diet and chewing patterns. Radiographically, benign strictures have a smooth contour and mucosal surface. Long (>3 cm) symmetric strictures involving a large portion of the neopharyngeal

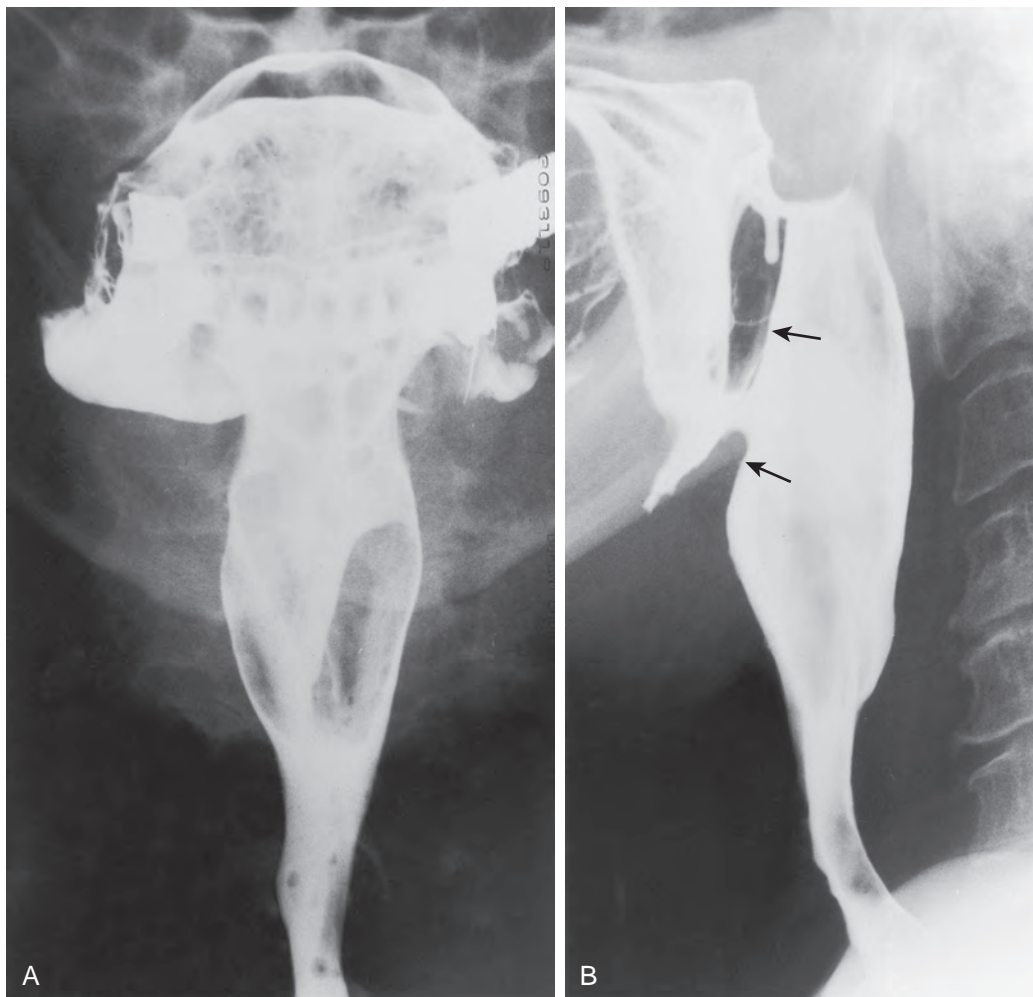


Figure 16-29 Total laryngectomy. **A.** Frontal view of the neopharynx shows a featureless tube that tapers distally. The tube is wider than 5 mm in each direction and the mucosa is smooth. The neopharyngeal tube is in the midline. **B.** Lateral view also shows a tubular structure that tapers inferiorly. Just behind the junction of the tongue and neopharyngeal tube, a tubular radiolucency (arrows) curves superiorly toward the lateral mid-oropharyngeal wall. This is a pair of folds created surgically on each side of the lateral pharyngeal wall. Because these folds mimic the course of the epiglottis, they have been termed a *pseudoepiglottis*. The hyoid bone, valleculae, epiglottis, and piriform sinuses are missing. (From Rubesin SE, Eisele DW, Jones B: *Pharyngography in the postoperative patient*. In Jones B [ed]: *Normal and Abnormal Swallowing. Imaging in Diagnosis and Therapy*, 2nd ed. New York, Springer, 2003, pp 167–204.)



Figure 16-30 Leak after total laryngectomy. Lateral view of the neopharynx after the patient swallows water-soluble contrast shows a linear contrast collection (*short arrow*) just anterior to the anterior wall of the neopharyngeal tube. The collection arises from a short track (*long arrow*). A nasogastric tube is in place. A tracheostomy tube is seen inferiorly. (From Rubesin SE: *Pharynx*. In Levine MS, Rubesin SE, Laufer I [eds]: *Double Contrast Gastrointestinal Radiology*, 3rd ed. Philadelphia, WB Saunders, 2000, pp 61–89.)

tube are usually the sequelae of radiation therapy or insufficient mucosa at the time of closure (Fig. 16-31).⁸⁷ Short (5 mm) weblike narrowings usually form at the upper or lower end of the closure line and are usually the sequelae of infection or fistula formation (Fig. 16-32).⁸⁷ Although some benign strictures have irregular contours, the presence of mucosal nodularity in the region of a stricture should suggest recurrent tumor. Deviation of the neopharyngeal tube from the midline is uncommon and should also suggest recurrent tumor.

After total laryngectomy, most of the muscles of the pharynx lose their normal bony or cartilaginous attachments and are partially or totally denervated. Dysphagia may result from abnormal muscular contraction. The thyropharyngeus and cricopharyngeus muscles, in particular, may not participate in a coordinated contraction wave with the spared superior constrictor muscle. Radiographically, abnormal inferior constrictor contraction is manifested by a smooth extrinsic mass impression on the posterior wall of the neopharyngeal tube (Fig. 16-33). Unlike recurrent tumor, this impression changes in size, shape, and position during swallowing. Stasis of barium and dilation of the oropharynx above a prominent cricopharyngeus are clues that postoperative dysphagia may be related to abnormal muscular contraction.

Foreign body impactions often occur in the neopharyngeal tube. Patients with head and neck cancers frequently have poor dentition or have had teeth removed before radiotherapy. These patients may have difficulty chewing vegetables and meats. As a result, solid food may become lodged in normal areas of postoperative sacculation at the base of the tongue, in a neopharynx that contracts poorly, or above strictures (Fig. 16-34).

Recurrent squamous cell carcinoma usually develops within 2 years after laryngectomy.⁹³ Radiographically, recurrent tumor may be manifested by a large (>1.5 cm) mass with a nodular or ulcerated surface or as a stricture with an irregular contour and irregular mucosal surface.^{2,86,94} The neopharynx may be deviated more than 1 cm from the midline, with narrowing of the neopharyngeal tube at the site of maximal deviation.⁸⁷

The hypoglossal nerves that lie superficially on the hyoglossus muscle may be damaged during surgery. Abnormal tongue motion may result from hypoglossal nerve damage, partial glossectomy, or postoperative scarring. Complications involving the tracheal stoma include stomal stenosis and recurrent tumor. Voice rehabilitation may be difficult because of a retracted cricopharyngeus, malpositioned tracheoesophageal voice prosthesis, gastroesophageal reflux, or esophageal motility disorder.

PHARYNGOLARYNGECTOMY

Resection of the larynx and hypopharynx may be required if cancer involves the posterior pharyngeal wall, postcricoid region, or large portions of a piriform sinus. The gap between the oropharynx and cervical esophagus may be bridged by a free jejunal graft or by a gastric pull-through.^{95,96} A defect in the anterolateral neopharyngeal wall may also be closed by a myocutaneous flap (pectoralis major or trapezius), free flap (radial forearm), or cutaneous skin flap (thigh).^{96,97}

Radiographically, flaps are atonic segments that form a portion of the walls of the pharynx. These flaps often protrude as masslike lesions into the expected lumen of the neopharynx. Complications of flaps include ischemic necrosis (Fig. 16-35) and leaks. Accumulation of hair and cutaneous debris on the luminal surface of a cutaneous flap (termed the *hirsute pharynx*) can cause mucosal nodularity and partial obstruction to the flow of liquids (Fig. 16-36).

In creating a jejunal free flap, a segment of proximal jejunum and its vascular arcade are autotransplanted into the neck and placed in a peristaltic direction. Jejunal contractions do not aid in bolus propulsion, however, because they occur at a slow rate of three contractions per minute and are not coordinated with swallowing. Clearance of the bolus from jejunal grafts is accomplished by gravity and pressure generated by tongue base push.⁹⁸ Complications of jejunal free grafts include fistula formation and ischemia. A normal jejunal free flap radiographically appears as a tubular segment of bowel, with a thin valvulae conniventes. No acute narrowing, angulation, or tethering of the tube should be seen.

ESOPHAGEAL SPEECH

Vocalization after total laryngectomy is accomplished by a buccal, oropharyngeal, or esophageal speech or voice prosthesis placed in a surgically created tracheoesophageal fistula. During esophageal speech, the patient swallows air into the esophagus

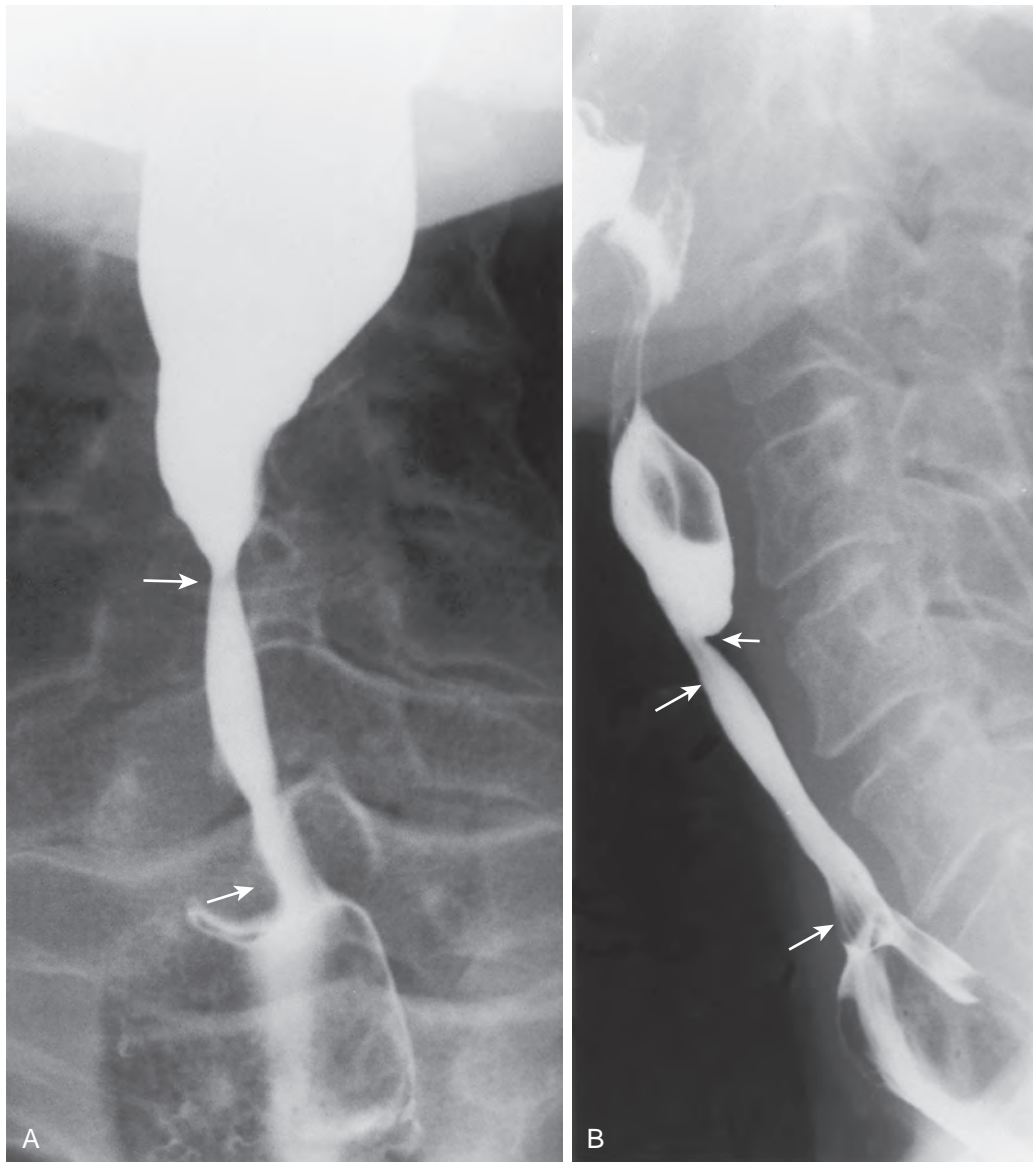


Figure 16-31 Stricture after total laryngectomy. Frontal (A) and lateral (B) views of the neck show diffuse narrowing of the neopharyngeal tube (long arrows). An even tighter weblike area of narrowing (small arrow) is seen proximally. Long strictures are usually attributed to radiation therapy or insufficient tissue to close the neopharynx. (From Rubesin SE: *Pharynx*. In Levine MS, Rubesin SE, Laufer I [eds]: *Double Contrast Gastrointestinal Radiology*, 3rd ed. Philadelphia, WB Saunders, 2000, pp 61–89.)



Figure 16-32 Short stricture after total laryngectomy. Lateral view shows a short circumferential stricture (*long arrow*) of the upper neopharyngeal tube. The anterior wall is undulating, caused by scarring. A pseudoepiglottis is identified (*short arrows*).

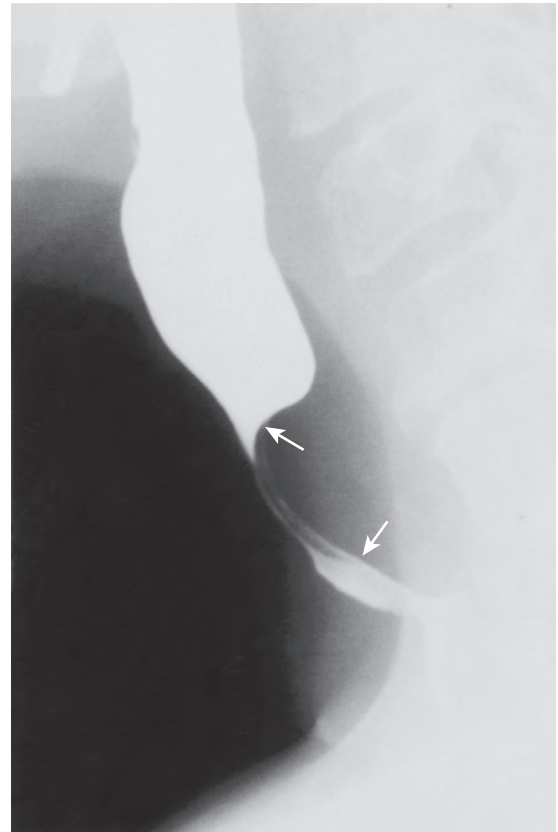


Figure 16-33 Incomplete opening of cricopharyngeus after total laryngectomy. Lateral view of the neck shows a smooth-surfaced protrusion (*arrows*) into the posterior wall of the lower neopharyngeal tube. During fluoroscopy, this indentation changed in size and shape because of prominence of the lower portion of the thyropharyngeus and cricopharyngeus.

and then expels the air through the cricopharyngeus into the neopharynx and oral cavity. The pharyngoesophageal segment narrowing varies in length and diameter during normal esophageal speech. Rapid change of configuration of the cricopharyngeus replaces the vibrations of the resected true vocal cords.

Pharyngoesophagography helps determine the causes of failure to attain esophageal speech.⁹⁹ Fixation and marked narrowing of the pharyngoesophageal segment may prevent esophageal speech.¹⁰⁰ Patients who have adequate quality of speech but diminished loudness may have a flaccid or strictured pharyngoesophageal segment.

NECK DISSECTION

A unilateral or bilateral neck dissection may be performed, depending on the initial location and size of the primary tumor and presence of clinically or radiographically suspected lymph node metastases. The submandibular gland, internal jugular vein, spinal accessory nerve, hypoglossal nerve, external carotid artery, and sternocleidomastoid muscle may be preserved or resected.

A chylous collection may form in the left lower neck because of thoracic duct damage or in the right lower neck because of accessory duct damage. Damage or resection of the hypoglossal nerve may lead to tongue dysfunction. Shoulder dysfunction may result from damage or resection of the spinal accessory nerve supplying the trapezius muscle.¹⁰¹

VOICE-SPARING PROCEDURES

Horizontal (Supraglottic) Laryngectomy

During supraglottic laryngectomy, the epiglottis, aryepiglottic folds, and false vocal cords are removed. The thyroid cartilage is transected at the level of the laryngeal ventricle.¹⁰² The voice is conserved because the true vocal cords and arytenoid cartilages are spared. In some patients, one arytenoid cartilage and part of the medial wall of the piriform sinus on the side of the tumor are resected.¹⁰³ The hyoid bone may be spared or partially or fully resected. A cricopharyngeal myotomy may be performed.¹⁰³ The remaining portion of the thyroid cartilage and larynx are pulled up to the base of tongue (or hyoid, if this structure is spared). The free anterior edge of the piriform sinus is pulled anteromedially, creating a fold superior to the vocal cord.¹⁰³

Radiographically, the epiglottis and aryepiglottic folds are absent (*Fig. 16-37*). Barium penetrating the remaining larynx outlines the true vocal cords. On lateral views, the vocal cords lie just inferior to the tongue base. Barium etches the mucosa overlying the muscular processes of the arytenoid cartilages. The folds of the piriform sinus tissue that have been pulled superior to the vocal cords are outlined by barium, termed *pseudocords*.¹⁰² The mucosa at the junction between the tongue base and true vocal cords may appear nodular. On frontal

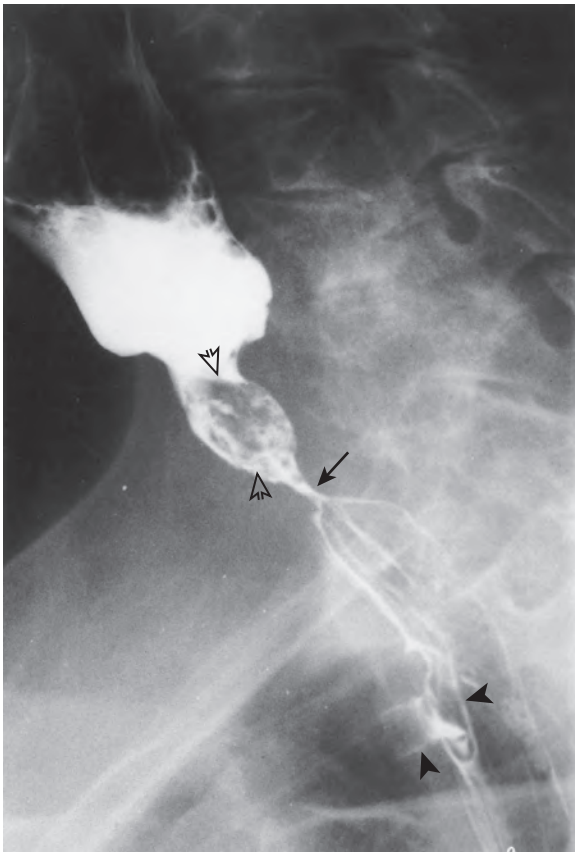


Figure 16-34 Foreign body impaction above stricture after total laryngectomy. Oblique view of the lower neck shows a 1-cm, finely lobulated, radiolucent filling defect (open arrows) in the lower neopharyngeal tube trapped above a 3-mm-long by 1- to 2-mm-diameter stricture (large arrow). This foreign body proved to be a piece of meat. A voice prosthesis is identified (arrowheads).

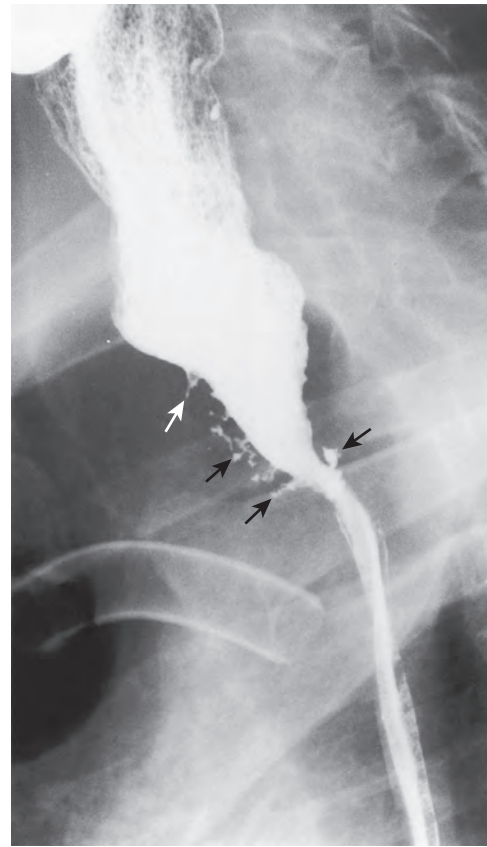


Figure 16-35 Partial breakdown of free flap. Oblique view shows numerous barium-filled tracks (arrows) extending into the interstices of the flap. (From Rubesin SE, Eisele DW, Jones B: *Pharyngography in the postoperative patient*. In Jones B [ed]: *Normal and Abnormal Swallowing. Imaging in Diagnosis and Therapy*, 2nd ed. New York, Springer, 2003, pp 167–204.)

views, the barium-etched vocal cords and arytenoid cartilages are seen. If one arytenoid cartilage has been removed, the neolarynx appears asymmetric. A concomitant neck dissection may result in ipsilateral flattening of the lateral pharyngeal wall.

Complications in the immediate postoperative period include aspiration, fistula formation, and airway obstruction caused by postoperative edema. A Zenker's diverticulum may develop (see Fig. 16-37). Edema and fibrosis are manifested radiographically by smooth, symmetric or asymmetric enlargement of the mucosa overlying the muscular processes of the arytenoid cartilages. Fistulas develop in approximately 15% of patients.¹⁰³ The most common complications in the late postoperative period are aspiration in over 40% of patients and recurrent tumor in up to one third of patients.¹⁰⁴ Recurrent tumor is manifested radiographically by a focal mass with a nodular mucosal surface.

Vertical Laryngectomy

Early glottic carcinomas may be treated by endoscopic surgery, radiotherapy, and open surgical procedures. Cancers of the anterior portion of the true vocal cords and anterior commissure can be treated by a variety of surgical procedures, including cordectomy, vertical partial laryngectomy, and vertical hemilaryngectomy.¹⁰⁵

Cordectomy. Cancers localized to the true vocal cord or cancer with limited extension to the contralateral anterior commissure may be treated by cordectomy.¹⁰⁶ The vocal cord and internal perichondrium of the thyroid cartilage are resected.

Vertical Partial Laryngectomy. Vertical partial laryngectomy is used to treat glottic cancers with local extension to the arytenoid and floor of the laryngeal ventricle or cancers that occur after radiotherapy.¹⁰⁷ The cancerous vocal cord and approximately one third of the thyroid cartilage on the side of the tumor are resected.¹⁰⁷ The epiglottis is preserved, and its base is reattached. The false vocal fold on the side of the tumor may be reattached to the remaining ipsilateral thyroid cartilage.

Vertical Hemilaryngectomy. The true vocal cord, false vocal cord, arytenoid cartilage, and thyroid cartilage on the side of the tumor are resected. This procedure is often complicated by laryngeal stenosis and aspiration.

The radiographic findings associated with the various forms of vertical laryngectomy depend on the extent of surgery. If a cordectomy has been performed and no laryngeal penetration occurs, the pharynx may appear relatively normal.¹⁰⁸ If a complete vertical hemilaryngectomy has been performed, aspiration usually occurs. The true and false vocal cords and arytenoid that

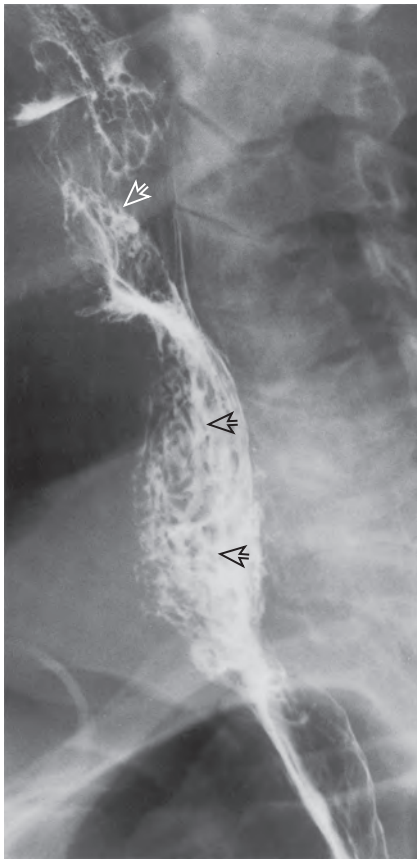


Figure 16-36 Hirsute neopharynx. Oblique view of the neck shows that the mucosa of the neopharynx is diffusely nodular (open arrows), which was caused by barium coating the skin and hair of this radial forearm flap. (From Rubesin SE, Eisele DW, Jones B: *Pharyngography in the postoperative patient*. In Jones B [ed]: *Normal and Abnormal Swallowing. Imaging in Diagnosis and Therapy*, 2nd ed. New York, Springer, 2003, pp 167–204.)

have been removed will be missing from the radiographs. The preserved contralateral true and false vocal cords will be etched by barium (Fig. 16-38).

A combination of endoscopy, cross-sectional imaging, and barium studies is helpful in the diagnosis of recurrent tumor.^{108,109} Recurrent tumor may be manifested radiographically by narrowing and irregularity of the residual laryngeal vestibule or subglottic region. However, postoperative deformity caused by edema or granulation tissue can mimic tumor recurrence.

SURGERY FOR TONGUE AND OROPHARYNGEAL CANCERS

Glossectomy

Surgical approaches to the tongue depend on the size, location, and spread of the primary tumor.¹¹⁰ Small lesions of the anterior tongue may be resected via a transoral approach. Larger lesions may require exposure via a mandibulotomy. Segmental mandibular resection is performed for lesions involving the mandible. Small lesions of the posterior tongue may be operated on via a transhyoid approach.

Large tumors of the posterior tongue may require near-total or total glossectomy. This procedure may include resection of tissue in the floor of the mouth, retromolar trigone, and lateral pharyngeal wall. A skin graft, tissue flap, or microvascular free flap can be used.¹¹¹ A concomitant cricopharyngeal myotomy may be performed as a drainage procedure. Approximately one third to one half of the tongue can be removed without resulting in significant swallowing disability.¹¹²

During a barium swallow, the radiologist evaluates collection and manipulation of the bolus by the residual tongue, stasis in the oral cavity, and premature spillage of the bolus into the hypopharynx. Abnormal tongue motion may reflect loss of tongue volume, adhesions, or damage to the hypoglossal nerve. A large proportion of the bolus may remain in the oral cavity. Abnormal elevation of the pharynx and larynx and abnormal epiglottic tilt may result from surgical transection of various suprahyoid muscles. Aspiration is detected in 10% to 33% of patients after total glossectomy.¹¹³ Postoperative deformity of the tongue is the norm (Fig. 16-39) but is difficult to distinguish from recurrent tumor. The diagnosis of recurrent tumor is best made by a combination of direct visualization and cross-sectional imaging.

Malignant Oropharyngeal Lesions

Surgical approaches to the oropharynx include the transoral route, lip splitting with or without mandibulotomy, mandibulotomy, or a transcervical approach. A neck dissection is often concomitantly performed. Surgical defects may be filled with a skin graft, myocutaneous flap, or free flap.¹¹⁴

Portions of the palate may be resected for primary squamous cell carcinoma, lymphoma, or minor salivary gland tumors or for contiguous tumors of the tonsil or retromolar trigone region secondarily invading the palate. Soft palate or tonsillar resection may result in hypernasal speech or nasal regurgitation. Partial palatotomy may also cause premature spillage of the bolus from the oral cavity into the oropharynx, resulting in poor timing of the swallow, with subsequent laryngeal penetration. Postoperative defects in the palate may result in an oronasal or sinonasal fistula. Flap or graft breakdown may result in an orocutaneous or pharyngocutaneous fistula. If the tongue base has been partially removed or is fixed by adhesions, the patient may have difficulty chewing or swallowing.

TRACHEOSTOMY

Patients with a tracheostomy (with or without laryngectomy) may develop dysphagia or aspiration caused by postoperative changes in the soft tissues of the neck, resulting in tethering of the trachea and pharynx, with subsequent diminished laryngeal and pharyngeal elevation.^{111,115} The presence of a tracheostomy may also result in poor coordination of laryngeal closure, with resultant aspiration during swallowing. A tracheostomy may also cause desensitization of the cough reflex.

SURGERY FOR ZENKER'S DIVERTICULUM AND PHARYNGEAL POUCHES

Various endoscopic and surgical procedures may be performed for treatment of Zenker's diverticulum. Some procedures alter

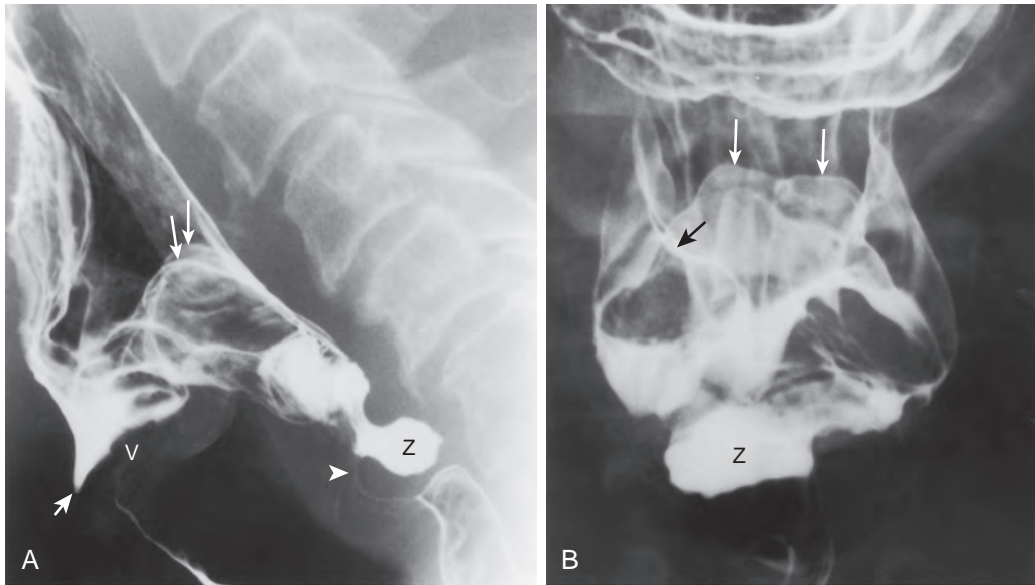


Figure 16-37 Zenker's diverticulum developing after horizontal hemilaryngectomy for epiglottic carcinoma. A. Lateral view of the pharynx shows that the hyoid bone, valleculae, epiglottis, and aryepiglottic folds are missing. Aspirated barium coats the true vocal cords (V) and anterior commissure (short arrow) that have been pulled up to the base of the tongue. The arytenoids (long arrows) are markedly elevated. The pharyngoesophageal segment is elevated, now opposite the anterior commissure. There is a Zenker's diverticulum (Z) and a prominent cricopharyngeal bar (arrowhead) that were not seen on preoperative images. **B.** Frontal view shows the prominent masslike arytenoids (white arrows). Folds of tissue arising from the lateral pharyngeal wall (right lateral fold identified by black arrow) have been pulled medially to cover the true vocal cords. The Zenker's diverticulum is a 1.5-cm midline ovoid barium collection (Z). (From Rubesin SE, Eisele DW, Jones B: *Pharyngography in the postoperative patient*. In Jones B [ed]: *Normal and Abnormal Swallowing. Imaging in Diagnosis and Therapy*, 2nd ed. New York, Springer, 2003, pp 167–204.)

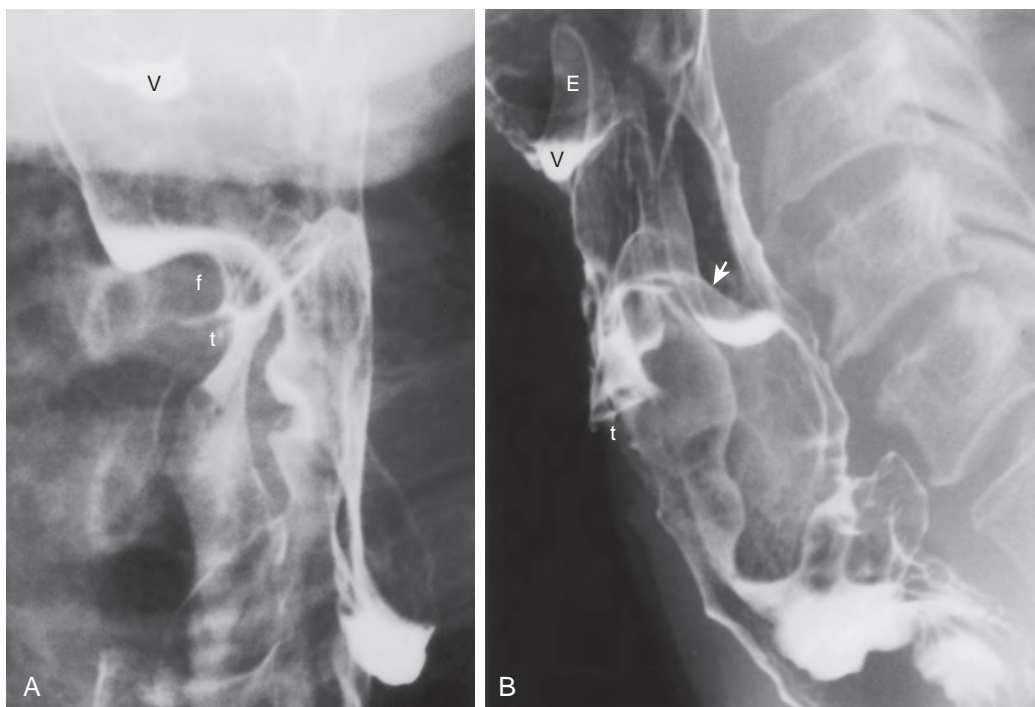


Figure 16-38 Vertical hemilaryngectomy. A. Frontal view shows that the right false (f) and right true (t) vocal cords remain. The presence of barium in the right vallecula (V) indicates that at least part of the epiglottis has been preserved. In contrast, the absence of the left vallecula indicates that the left side of the epiglottis has been resected. The left true and false vocal cords and left aryepiglottic fold are missing and have been resected. The remaining portion of the left side of the hypopharynx is dilated with barium stasis inferiorly in the pharyngoesophageal segment. **B.** Lateral view shows the epiglottic tip (E) and right vallecula (V). The anterior commissure is coated with aspirated barium, and one vocal cord (t) and arytenoid (arrow) remain. A kissing artifact is seen in the lower hypopharynx.

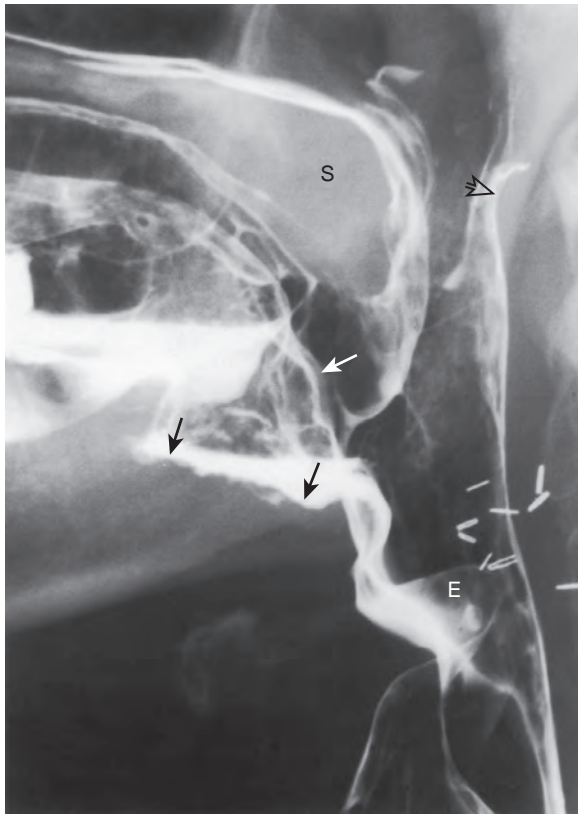


Figure 16-39 Partial glossectomy. A large barium-coated defect (black arrows) is seen at the tongue base. This defect and associated tongue dysfunction resulted in premature spill of the bolus into the oropharynx. The contralateral portion of the base of the tongue is intact (white arrow). It is impossible to determine whether there is recurrent tumor in the nodular tissue lining the tongue defect. Radiation-induced, smooth-surfaced enlargement of the soft palate (S) and epiglottis (E) is seen. Nasal regurgitation results in barium coating the superior surface of the soft palate. Soft palate elevation is abnormal because a gap remains between the soft palate and posterior pharyngeal wall, despite phonation. Passavant's cushion (open arrow) is demonstrated. Abnormal soft palate elevation may have resulted from scarring related to surgery or prior radiation therapy. (From Rubesin SE, Eisele DW, Jones B: *Pharyngography in the postoperative patient*. In Jones B [ed]: *Normal and Abnormal Swallowing. Imaging in Diagnosis and Therapy*, 2nd ed. New York, Springer, 2003, pp 167–204.)

the prominent cricopharyngeus, whereas others involve the diverticulum itself. The most successful procedure combines diverticulectomy with cricopharyngeal myotomy.

Endoscopic dilation of the prominent cricopharyngeus has been performed¹¹⁶ but is often unsuccessful because the upper esophageal sphincter is not damaged enough to improve hypopharyngeal clearance and because the pouch is left intact. Surgical cricopharyngeal myotomy alone also has a poor success rate.¹¹⁷

Transection of the cricopharyngeus may be performed endoscopically in debilitated and older patients who are poor operative candidates.¹¹⁸ The anterior lip of a specially designed endoscope is placed into the lumen of the pharyngoesophageal segment, and the posterior lip of the endoscope is inserted into the diverticulum.¹¹⁹ The endoscopist then divides the posterior

wall of the pharyngoesophageal segment between the lumen of the pharyngoesophageal segment–cervical esophagus and the lumen of the Zenker's diverticulum. The Zenker's diverticulum is left intact, but the prominent cricopharyngeus is transected. On a postoperative pharyngogram, the Zenker's diverticulum that remains intact should have less barium filling because there is improved drainage through an opened pharyngoesophageal segment. The barium-air level in the diverticulum should be lower in comparison to that in preoperative studies. The pharyngoesophageal segment should also open to a greater degree than was seen preoperatively.

Diverticulopexy is a surgical procedure performed in high-risk patients that avoids opening the pharynx. The apex of the Zenker's diverticulum is suspended from the prevertebral fascia superior to the diverticulum.^{120,121} A cricopharyngeal myotomy is performed. Although the diverticulum may partially fill during swallowing, it drains through the damaged cricopharyngeus, diminishing the risk of aspiration.

The most successful approach for the treatment of Zenker's diverticulum is diverticulectomy with cricopharyngeal myotomy. An extended myotomy is performed, including division of the lowermost thyropharyngeus. The Zenker's diverticulum is excised without removing the mucosa of the pharyngoesophageal segment.¹²⁰ During postoperative pharyngography, the Zenker's diverticulum should not be seen. The pharyngoesophageal segment should open widely. In one series, however, 3 of 13 patients had a continued saclike outpouching at the site of surgical excision.¹²² Postoperative pharyngography may demonstrate unsuspected leaks and a characteristic beaklike postoperative deformity.¹²²

CRICOPHARYNGEAL MYOTOMY

Cricopharyngeal myotomy is used as an isolated drainage procedure in patients with an abnormally functioning pharyngoesophageal segment caused by a global pharyngeal motor disorder or Zenker's diverticulum.^{121,123} Cricopharyngeal myotomy facilitates drainage from a neuromuscularly impaired pharynx, as does pyloroplasty in patients who develop abnormal gastric emptying because of vagotomy. Cricopharyngeal myotomy is not indicated in patients with globus symptoms alone.¹²¹ Because the upper esophageal sphincter normally prevents reflux of esophageal contents into the pharynx, surgical destruction of the sphincter can sometimes lead to aspiration of esophageal contents into the lungs. The surgeon therefore balances the risk of aspiration caused by pharyngeal stasis in an untreated patient with a neuromuscularly compromised pharynx with the risk of aspiration of esophageal contents from a cricopharyngeal myotomy. Given the operative risks of cricopharyngeal myotomy, some physicians have been injecting botulinum toxin into the cricopharyngeus as an alternative form of treatment for ameliorating symptoms.

After cricopharyngeal myotomy, pharyngography should demonstrate less stasis of barium in the hypopharynx. The cricopharyngeal bar should be absent, and there should be decreased or no luminal narrowing of the pharyngoesophageal segment in comparison to that in the preoperative pharyngogram. Complications include incomplete myotomy manifested as a persistent cricopharyngeal bar, fistula or abscess formation, and vocal cord paralysis because of recurrent laryngeal nerve damage.

REFERENCES

- Bachman AL, Seaman WB, Macken KL: Lateral pharyngeal diverticula. *Radiology* 91:774-782, 1968.
- Rubenstein SE, Jessurun J, Robertson D, et al: Lines of the pharynx. *Radiographics* 7:217-237, 1987.
- Norris CW: Pharyngoceles of the hypopharynx. *Laryngoscope* 89:1788-1807, 1979.
- Curtis DJ, Cruess DF, Crain M, et al: Lateral pharyngeal outpouchings: A comparison of dysphagic and asymptomatic patients. *Dysphagia* 2:156-161, 1988.
- Lindbichler F, Raith J, Uggowitz M, et al: Aspiration resulting from lateral hypopharyngeal pouches. *AJR* 170:129-132, 1998.
- Hyams VJ, Batsakis JG, Michaels L: Tumors of the upper respiratory tract and ear. In *Atlas of Tumor Pathology*, 2nd series, fascicle 25, Bethesda, MD, 1988, Armed Forces Institute of Pathology.
- Lindell MM, Jing BS, Fischer EP, et al: Laryngocele. *AJR* 131:259-262, 1978.
- Maran AGD, Buchanan DR: Branchial cysts, sinuses and fistulae. *Clin Otolaryngol* 3:77-92, 1978.
- Bhaskar SN, Bernier JL: Histogenesis of branchial cysts. *Am J Pathol* 35:407-414, 1959.
- Som PM, Sacher M, Lanzieri CF, et al: Parenchymal cysts of the lower neck. *Radiology* 157:399-406, 1985.
- Perrott JW: Anatomical aspects of hypopharyngeal diverticula. *Aust N Z J Surg* 31:307-317, 1962.
- Zaino C, Jacobson HG, Lepow H, et al: The pharyngoesophageal sphincter. *Radiology* 89:639-645, 1967.
- Zaino C, Jacobson HG, Lepow H, et al: The Pharyngoesophageal Sphincter, Springfield, IL, 1970, Charles C Thomas.
- Knuff TE, Benjamin SB, Castell DO: Pharyngoesophageal (Zenker's) diverticulum: A reappraisal. *Gastroenterology* 82:734-736, 1982.
- Frieling T, Berges W, Lubke HJ, et al: Upper esophageal sphincter function in patients with Zenker's diverticulum. *Dysphagia* 3:90-92, 1988.
- Smiley TB, Caves PK, Porter DC: Relationship between posterior pharyngeal pouch and hiatus hernia. *Thorax* 25:725-731, 1970.
- Delahunty JE, Margulies SE, Alonso UA, et al: The relationship of reflux esophagitis to pharyngeal pouch (Zenker's diverticulum). *Laryngoscope* 81:570-577, 1971.
- Brady AP, Stevenson GW, Somers S, et al: Premature contraction of the cricopharyngeus: New sign of gastroesophageal reflux disease. *Abdom Imaging* 20:225-229, 1995.
- Shirazi KK, Daffner RH, Gaede JT: Ulcer occurring in Zenker's diverticulum. *Gastrointest Radiol* 2:117-118, 1977.
- Wychulis AR, Gunnulaugsson GH, Clagett OT: Carcinoma arising in pharyngoesophageal diverticulum. *Surgery* 66:976-979, 1969.
- Jamieson JB: Illustrations of Living Anatomy, Set 2, 44, Edinburgh, 1934, Livingstone.
- Ekberg O, Nylander G: Lateral diverticula from the pharyngoesophageal junction area. *Radiology* 146:117-122, 1983.
- Rubenstein SE, Levine MS: Killian-Jamieson diverticula: Radiographic findings in 16 patients. *AJR* 177:85-89, 2001.
- Clements JL, Cox GW, Torres WE, et al: Cervical esophageal webs—a roentgen-anatomic correlation. *AJR* 121:221-231, 1974.
- Weaver JW, Kaude JV, Hamlin DJ: Webs of the lower esophagus: A complication of gastroesophageal reflux? *AJR* 142:289-292, 1984.
- Seaman WB: The significance of webs in the hypopharynx and upper esophagus. *Radiology* 89:32-38, 1967.
- Gordon AR, Levine MS, Redfern RO, et al: Cervical esophageal webs: Association with gastroesophageal reflux. *Abdom Imaging* 26:574-577, 2001.
- Ekberg O: Cervical oesophageal webs in patients with dysphagia. *Clin Radiol* 32:633-641, 1981.
- Ekberg O, Nylander G: Webs and web-like formations in the pharynx and cervical esophagus. *Diagn Imaging* 52:10-18, 1983.
- Waldenström J, Kjeulberg SR: The roentgenological diagnosis of sideropenic dysphagia (Plummer-Vinson's syndrome). *Acta Radiol* 20:618-638, 1939.
- McNab Jones RF: The Paterson-Brown-Kelly syndrome: Its relationship to iron deficiency and postcricoid carcinoma. *J Laryngol Otol* 71:529-561, 1961.
- Ekberg O, Birch-Lensen M, Lindstrom C: Mucosal folds in the valleculae. *Dysphagia* 1:68-72, 1986.
- Shauver IA, Phillips HE, Sequeira J: The jet phenomenon: A manifestation of esophageal web. *AJR* 129:747-748, 1977.
- Taylor AJ, Stewart ET, Dodds WJ: The esophageal jet phenomenon revisited. *AJR* 155:289-290, 1990.
- Pitman RG, Fraser GM: The post-cricoid impression on the oesophagus. *Clin Radiol* 16:34-39, 1965.
- Harris RD, Berdon WE, Baker DH: Roentgen diagnosis of acute epiglottitis in the adult. *J Can Assoc Radiol* 21:270-272, 1970.
- Balfe DM, Heiken JP: Contrast evaluation of structural lesions of the pharynx. *Curr Probl Diagn Radiol* 15:73-160, 1986.
- Rubenstein SE, Glick SN: The tailored double-contrast pharyngogram. *Crit Rev Diagn Imaging* 28:133-179, 1988.
- Kabakian HA, Dahmash MS: Pharyngoesophageal manifestations of epidermolysis bullosa. *Clin Radiol* 29:91-94, 1978.
- Agha FP, Francis IR, Ellis CN: Esophageal involvement in epidermolysis bullosa dystrophica: Clinical and roentgenographic manifestations. *Gastrointest Radiol* 8:111-117, 1983.
- Bosma JF, Gradowski EA, Trystad CW: Chronic ulcerative pharyngitis. *Arch Otolaryngol* 87:85-96, 1968.
- Scott JC, Jones B, Eisele DW, et al: Caustic ingestion injuries of the upper aerodigestive tract. *Laryngoscope* 102:1-8, 1992.
- Gromet M, Homer MJ, Carter BL: Lymphoid hyperplasia at the base of the tongue. *Radiology* 144:825-828, 1982.
- Mansson T, Wilske J, Kindblom L-G: Lipoma of the hypopharynx: A case report and a review of the literature. *J Laryngol Otol* 92:1037-1043, 1978.
- Patterson HC, Dickerson GR, Pilch BZ, et al: Hamartoma of the hypopharynx. *Arch Otolaryngol* 107:767-772, 1981.
- Bachman AL: Benign, non-neoplastic conditions of the larynx and pharynx. *Radiol Clin North Am* 16:273-290, 1978.
- DiBartolomeo JR, Olsen AR: Pedunculated lipoma of the epiglottis. *Arch Otolaryngol* 98:55-57, 1973.
- Woodfield C, Levine MS, Rubenstein SE, et al: Pharyngeal retention cysts: Radiographic findings in seven patients. *AJR* 184:793-796, 2005.
- Chang-Lo M: Laryngeal involvement in Von Recklinghausen's disease. *Laryngoscope* 87:435-442, 1977.
- Hyams VJ, Rabuzzi DD: Cartilaginous tumors of the larynx. *Laryngoscope* 80:755-767, 1970.
- Semenkovich JW, Balfe DM, Weyman PJ, et al: Barium pharyngography: Comparison of single and double contrast. *AJR* 144:715-720, 1985.
- Carpenter RJ, III, DeSanto LW, Devine KD, et al: Cancer of the hypopharynx. *Arch Otolaryngol* 102:716-721, 1976.
- Dockerty MD, Parkhill EM, Dahlin DC, et al: Tumors of the Oral Cavity and Pharynx, Washington, DC, 1968, Armed Forces Institute of Pathology.
- Goldstein HM, Zornoza J: Association of squamous cell carcinoma of the head and neck with cancer of the esophagus. *AJR* 131:791-794, 1978.
- Thompson WM, Oddson TA, Kelvin F, et al: Synchronous and metachronous squamous cell carcinoma of the head, neck, and esophagus. *Gastrointest Radiol* 3:123-127, 1978.
- Jing BS: Roentgen examination of the larynx and hypopharynx. *Radiol Clin North Am* 8:361-386, 1970.
- Seaman WB: Contrast radiography in neoplastic disease of the larynx and pharynx. *Semin Roentgenol* 9:301-309, 1974.
- Levine MS, Rubenstein SE, Ott DJ: Update on esophageal radiology. *AJR* 155:933-941, 1990.
- Rubenstein SE, Laufer I: Pictorial review: Principles of double contrast pharyngography. *Dysphagia* 6:170-178, 1991.
- Som PM, Urken ML, Biller H, et al: Imaging the postoperative neck. *Radiology* 187:593-603, 1997.
- Vogl T, Dresel S, Bilaniuk LT, et al: Tumors of the nasopharynx and adjacent areas: MR imaging with Gd-DTPA. *AJNR* 11:187-194, 1990.
- Strong EW: Carcinoma of the tongue. *Otolaryngol Clin North Am* 12:107-114, 1979.
- Jimenez JR: Roentgen examination of the oropharynx and oral cavity. *Radiol Clin North Am* 8:413-424, 1970.
- Apter AJ, Levine MS, Glick SN: Carcinomas of the base of the tongue: Diagnosis using double-contrast radiography of the pharynx. *Radiology* 151:123-126, 1984.
- Kirchner JA, Owen JR: Five hundred cancers of the larynx and pyriform sinus: Results of treatment by radiation and surgery. *Laryngoscope* 87:1288-1303, 1977.
- Zbaren P, Egger C: Growth patterns of pyriform sinus carcinomas. *Laryngoscope* 107:511-518, 1997.
- Johnson JT, Bacon GW, Meyers EN, et al: Medial vs. lateral wall pyriform sinus carcinomas: Implications for management of regional lymphatics. *Head Neck* 16:401-405, 1995.
- Banfi A, Bonadonna G, Carnevali G, et al: Lymphoreticular sarcomas with primary involvement of Waldeyer's ring. *Cancer* 26:341-351, 1970.
- Todd GB, Michaels L: Hodgkin's disease involving Waldeyer's lymphoid ring. *Cancer* 34:1769-1778, 1974.

70. Spiro RH, Koss LG, Hajdu SI, et al: Tumors of minor salivary origin. *Cancer* 31:117-129, 1973.
71. Lakhani P, Rubesin SE, Zhang PJ: Malignant fibrous histiocytoma of the pharynx. *AJR* 184:S12-S13, 2005.
72. Gatti WM, Strom CG, Orfei E: Synovial sarcoma of the laryngopharynx. *Arch Otolaryngol* 101:633-636, 1975.
73. Huizenga C, Balogh K: Cartilaginous tumors of the larynx. *Cancer* 26:201-210, 1970.
74. Emery CD, Wall S, Federle MP, et al: Pharyngeal Kaposi's sarcoma in patients with AIDS. *AJR* 147:919-922, 1986.
75. Goolden AWG: Pharyngeal malignancy following irradiation of the neck [abstract]. *Br J Radiol* 45:795, 1972.
76. Fajardo LF: Radiation-induced pathology of the alimentary tract. In Whitehead R, editor: *Gastrointestinal and Oesophageal Pathology*, Edinburgh, 1984, Churchill Livingstone, pp 813-814.
77. Chandler JR: Radiation fibrosis and necrosis of the larynx. *Ann Otol Rhinol Laryngol* 88:509-514, 1979.
78. Mukherji SK, Mancuso AA, Kotzur IM, et al: Radiologic appearance of the irradiated larynx. I. Expected changes. *Radiology* 193:141-148, 1994.
79. Keene M, Harwood AR, Bryce DP, et al: Histopathological study of radionecrosis in laryngeal carcinoma. *Laryngoscope* 92:173-180, 1982.
80. Fu KK, Woodhouse RJ, Quivey JM, et al: The significance of laryngeal edema following radiotherapy of carcinoma of the vocal cord. *Cancer* 49:655-658, 1982.
81. Larson DL, Lindberg RD, Lane E, et al: Major complications of radiotherapy in cancer of the oral cavity and oropharynx. A 10-year retrospective study. *Am J Surg* 146:531-536, 1983.
82. Bedwinek JM, Shukovsky LJ, Fletcher GH, et al: Osteonecrosis in patients treated with definitive therapy for squamous cell carcinomas of the oral cavity and naso- and oropharynx. *Radiology* 119:665-667, 1976.
83. Ekberg O, Nylander G: Pharyngeal dysfunction after treatment for pharyngeal cancer with surgery and radiotherapy. *Gastrointest Radiol* 8:97-104, 1983.
84. Goldstein HM, Rogers LF, Fletcher GH, et al: Radiological manifestations of radiation-induced injury to the normal upper gastrointestinal tract. *Radiology* 117:135-140, 1975.
85. Quillen SP, Balfe DM, Glick SN: Pharyngography after head and neck irradiation: Differentiation of postirradiation edema from recurrent tumor. *AJR* 161:1205-1208, 1993.
86. Rubesin SE, Eisele DW, Jones B: Pharyngography in the postoperative patient. In Jones B, editor: *Normal and Abnormal Swallowing*, ed 2, New York, 2003, Springer, pp 167-203.
87. Balfe DM, Koehler RE, Setzen M, et al: Barium examination of the esophagus after total laryngectomy. *Radiology* 143:501-508, 1982.
88. Wong F: Total Laryngectomy. In Bailey BJ, editor: *Atlas of Head & Neck Surgery—Otolaryngology*, Philadelphia, 1996, Lippincott-Raven, p 2000.
89. Balfe DM: Imaging of the pharynx after surgical therapy. In Jones B, Donner MW, editors: *Normal and Abnormal Swallowing*, New York, 1991, Springer-Verlag, pp 147-171.
90. Moses BL, Eisele DW, Jones B: Radiologic assessment of the early postoperative total laryngectomy patient. *Laryngoscope* 103:1157-1160, 1993.
91. Muller-Miny H, Eisele DW, Jones B: Dynamic radiographic imaging following total laryngectomy. *Head Neck* 15:342-347, 1993.
92. Hier M, Black MJ, Lafond G: Pharyngocutaneous fistulas after total laryngectomy: Incidence etiology and outcome analysis. *J Otolaryngol* 22:164-166, 1993.
93. DiSantis DJ, Balfe DM, Hayden RE, et al: The neck after total laryngectomy: CT study. *Radiology* 153:713-717, 1984.
94. Quillen SP, Balfe DM, Glick SN: Pharyngography after head and neck irradiation: Differentiation of postirradiation edema from recurrent tumor. *AJR* 161:1205-1208, 1993.
95. Stepnick DW, Hayden RE: Options for reconstruction of the pharyngoesophageal defect. *Otolaryngol Clin North Am* 27:1151-1158, 1994.
96. Haughey BH: The jejunal free flap in oral cavity and pharyngeal reconstruction. *Otolaryngol Clin North Am* 27:1159-1170, 1994.
97. Wong F: Total pharyngolaryngectomy. In Bailey BJ, editor: *Atlas of Head & Neck Surgery—Otolaryngology*, Philadelphia, 1996, Lippincott-Raven, pp 206-209.
98. Wilson JA, Maran AG, Pryde A, et al: The function of free jejunal autografts in the pharyngoesophageal segment. *J R Coll Surg Edinburgh* 40:363-366, 1995.
99. Sloane PM, Griffin JM, O'Dwyer TP: Esophageal insufflation and videofluoroscopy for evaluation of esophageal speech in laryngectomy patients: Clinical implications. *Radiology* 181:433-437, 1991.
100. Gatenby RA, Rosenblum JS, Leonard CM, et al: Esophageal speech: Double-contrast evaluation of the pharyngoesophageal segment. *Radiology* 157:127-131, 1985.
101. Medina JE: Radical neck dissection. In Bailey BJ, editor: *Atlas of Head & Neck Surgery—Otolaryngology*, Philadelphia, 1996, Lippincott-Raven Publishers, pp 140-143.
102. Niemeyer JH, Balfe DM, Hayden RE: Neck evaluation with barium-enhanced radiographs and CT scans after supraglottic subtotal laryngectomy. *Radiology* 162:493-498, 1987.
103. Wong F: Supraglottic laryngectomy (horizontal hemilaryngectomy). In Bailey BJ, editor: *Atlas of Head & Neck Surgery—Otolaryngology*, Philadelphia, 1996, Lippincott-Raven Publishers, pp 190-193.
104. Gregor RT, Oei SS, Baris G, et al: Supraglottic laryngectomy with neck dissection and postoperative radiation in the management of supraglottic laryngeal cancer. *Am J Otolaryngol* 17:316-321, 1996.
105. Roberson JB, Jr, Fee WE, Jr: Conservation surgery for laryngeal carcinoma. *Ann Acad Med* 20:656-664, 1991.
106. Rassekh CH: Laryngofissure and cordectomy. In Bailey BJ, editor: *Atlas of Head & Neck Surgery—Otolaryngology*, Philadelphia, 1996, Lippincott-Raven, pp 174-176.
107. Bailey BJ: Vertical partial laryngectomy. In Bailey BJ, editor: *Atlas of Head & Neck Surgery—Otolaryngology*, Philadelphia, 1996, Lippincott-Raven, pp 184-187.
108. DiSantis DJ, Balfe DM, Koehler RE, et al: Barium examination of the pharynx after vertical hemilaryngectomy. *AJR* 141:335-339, 1983.
109. DiSantis DJ, Balfe DM, Hayden R: The neck after vertical hemilaryngectomy: Computed tomographic study. *Radiology* 151:683-687, 1984.
110. Johnson RC: Near-total glossectomy. Total glossectomy. In Bailey BJ, editor: *Atlas of Head & Neck Surgery—Otolaryngology*, Philadelphia, 1996, Lippincott-Raven Publishers, pp 78-83.
111. Kronenberger MB, Meyers AD: Dysphagia following head and neck cancer surgery. *Dysphagia* 9:236-244, 1994.
112. Hirano M, Kuroiwa Y, Tanaka S, et al: Dysphagia following various degrees of surgical resection for oral cancer. *Ann Otol Rhinol Laryngol* 101:138-142, 1992.
113. Weber RS, Ohlms L, Bowman J, et al: Functional results after total or near-total glossectomy with laryngeal preservation. *Arch Otolaryngol Head Neck Surg* 117:512-516, 1991.
114. Waldron J: Surgery for malignant lesions of the oropharynx. In Bleach N, Milford C, Van Hasselt A, editors: *Operative Otorhinolaryngology*, Oxford, England, 1997, Blackwell Science, pp 357-362.
115. Nash M: Swallowing problems in the tracheotomized patient. *Otolaryngol Clin North Am* 21:701-709, 1988.
116. Ravich W, Neumann S, Jones B: Dilation as treatment of pharyngoesophageal segment (PES) prominence with hypopharyngeal (Zenker's) diverticulum. *Dysphagia* 15:103, 2000.
117. Schmit PJ, Zuckerbraun L: Treatment of Zenker's diverticula by cricopharyngeus myotomy under local anesthesia. *Am Surg* 18:710-716, 1992.
118. Hadley JM, Ridley N, Djazaeri B, et al: The radiological appearances after endoscopic cricopharyngeal myotomy: Dohlman's procedure. *Clin Radiol* 52:613-615, 1997.
119. Dohlman G, Mattsson O: The endoscopic operation for hypopharyngeal diverticula: A roentgen cinematographic study. *Arch Otolaryngol* 71:744-752, 1960.
120. Konowitz PM, Biller HF: Diverticulopexy and cricopharyngeal myotomy: Treatment for the high-risk patient with a pharyngoesophageal (Zenker's) diverticulum. *Otolaryngol Head Neck Surg* 100:146-153, 1989.
121. McKenna A, Dedo HH: Cricopharyngeal myotomy: Indications and technique. *Ann Otol Rhinol Laryngol* 101:216-221, 1992.
122. Sydow BD, Levine MS, Rubesin SE, et al: Radiographic findings and complications after surgical/endoscopic repair of Zenker's diverticulum in 16 patients. *AJR* 177:1067-1071, 2001.
123. Overbeek JJM: Upper esophageal sphincterotomy in dysphagic patients with and without a diverticulum. *Dysphagia* 6:228-234, 1991.

SECTION
IV

Esophagus

Barium Studies of the Upper Gastrointestinal Tract

MARC S. LEVINE | IGOR LAUFER

CHAPTER OUTLINE

General Principles

Components

Barium Suspensions
Effervescent Agents
Hypotonic Agents
Radiographic Components

Routine Technique

Anatomic Considerations

Esophagus
Stomach
Duodenum

Variations in Technique

Anterior Wall Lesions
Possible Perforation
Partial Gastrectomy
Gastric Outlet Obstruction
Esophageal Varices

There are different ways to perform an upper gastrointestinal (GI) barium study. In Chapter 2, a technique was described that relies primarily on barium filling and mucosal relief (i.e., single-contrast technique). The method described in this chapter relies primarily on double contrast, although it is actually a biphasic technique that combines the advantages of single and double contrast. Individual fluoroscopists generally develop their own routines and variations. Nevertheless, the techniques discussed in this chapter are representative of a reasonable approach for performing double-contrast upper GI examinations.^{1,2}

General Principles

Double-contrast upper GI studies are designed to coat the mucosal surface with a thin layer of high-density barium while the lumen is distended with gas. The routine examination should include the thoracic esophagus, stomach, and duodenum as far as the duodenojejunal junction. The examination should be performed quickly to maintain optimal mucosal coating and prevent barium filling of the duodenum and small bowel from obscuring the stomach. It is not critical that each segment of the upper GI tract be examined in anatomic sequence. For example, it may be preferable to examine the antrum, pylorus, and duodenum before significant overlap with the small bowel has occurred. Similarly, when the pharynx needs to be evaluated, it may be preferable to

perform this portion of the examination after the upper GI study has been completed. The technical and logistic details of the examination should also be tailored for individual studies based on the following: (1) the patient's presenting symptoms; (2) the anatomic configuration of the esophagus, stomach and duodenum; and (3) the specific abnormalities observed at fluoroscopy.

Components

BARIUM SUSPENSIONS

For the double-contrast examination, we use high-density 250% w/v barium (E-Z-HD; Bracco Diagnostics, Monroe Township, NJ). The preparation of the barium suspension is critical because slight deviations in concentration may impair the quality of mucosal coating and create artifacts.³

EFFERVESCENT AGENTS

Various effervescent agents are available in powder, granular, or liquid form.⁴ These agents release 300 to 400 mL of carbon dioxide on contact with fluid in the stomach.

HYPOTONIC AGENTS

The use of a hypotonic agent to relax the stomach and duodenum results in a better examination and allows the examiner additional time to achieve optimal mucosal coating. In the United States, the only suitable hypotonic agent is glucagon; an intravenous injection of 0.1 mg usually produces transient hypotonia of the stomach.⁵ In some patients, this hypotonic effect delays barium filling of the duodenum for several minutes, prolonging the examination. Anticholinergic agents may also be used to induce GI hypotonia,⁶ but these agents are contraindicated in patients with glaucoma, cardiac disease, and urinary retention.

RADIOGRAPHIC COMPONENTS

In modern radiology practice, fluoroscopic GI examinations are generally performed with digital fluoroscopy and spot imaging.⁷ The advantages of a digital system—better contrast resolution, shorter exposures, and faster examinations—more than compensate for a small decrease in spatial resolution. The study is reviewed at a computer workstation,⁸ with post-processing of the images for optimal interpretation.⁹ Afterward, the studies are archived on a central picture archiving and communications system (PACS), enabling easy electronic retrieval of prior studies for comparison with the current examinations.

Routine Technique

Selected views from a normal double-contrast upper GI study are shown in [Figure 17-1](#). We begin with a short review of the patient's history and symptoms. Special care is taken to ask whether the patient has had any previous surgery and whether the patient is taking any ulcerogenic medications. The examination usually starts with an intravenous injection of 0.1 mg of glucagon. After this injection, the patient ingests an

effervescent agent followed by 10 mL of water to facilitate the release of carbon dioxide in the stomach. The patient then stands in the left posterior oblique position and is asked to gulp the contents of a cup containing 120 mL of high-density barium as rapidly as possible while double-contrast views of the esophagus are obtained in rapid succession. These views should include the distal esophagus and gastroesophageal junction. Barium is often seen cascading into the gas-filled stomach (see [Fig. 17-1A](#)).

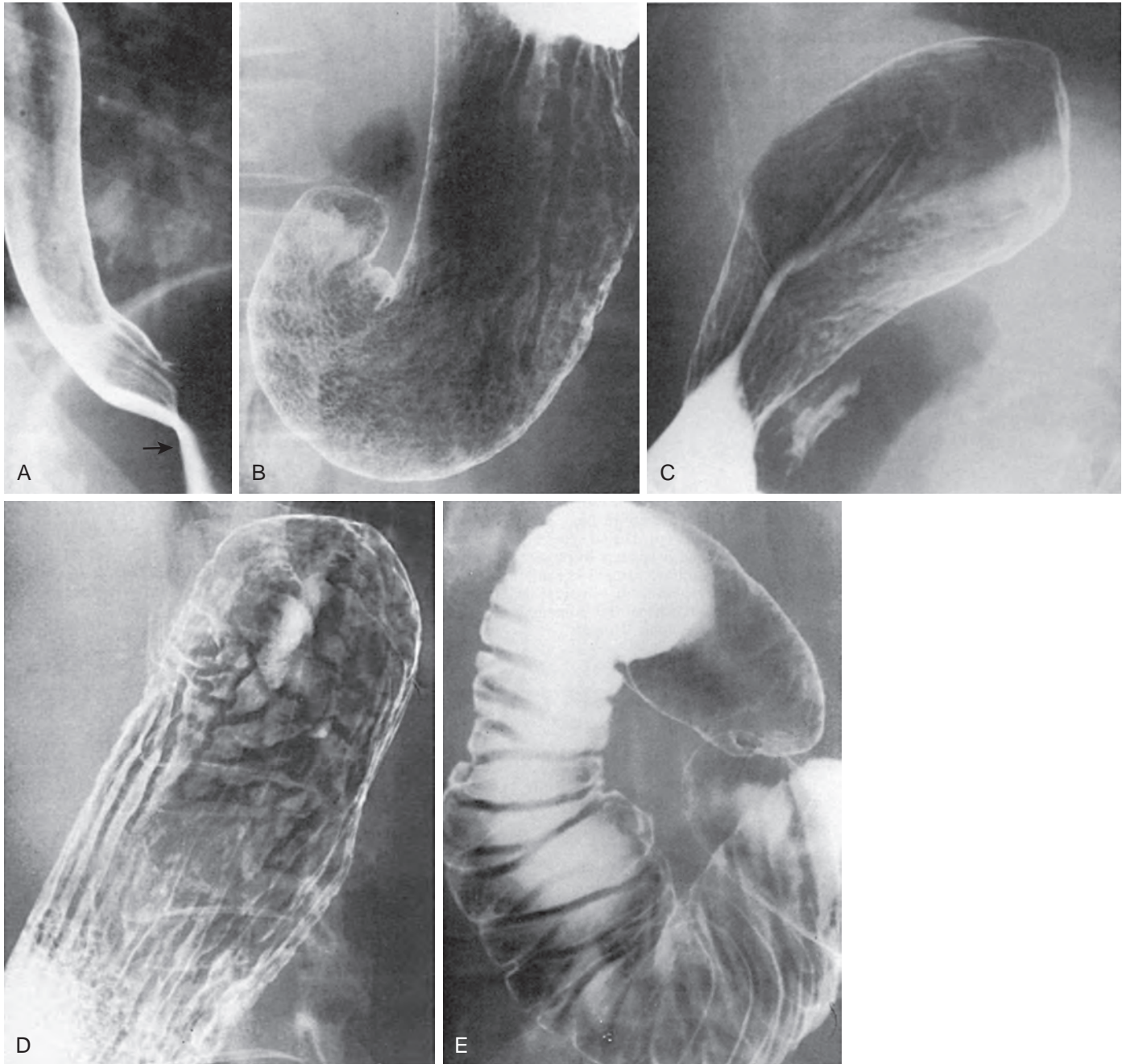


Figure 17-1 Representative images from a normal double-contrast upper GI study. **A.** Upright double-contrast view of the esophagus showing the distal esophagus with barium cascading (arrow) into the gas-filled stomach. **B.** Supine left posterior oblique view of the stomach showing normal areae gastricae in the gastric antrum and body and normal rugal folds along the greater curvature of the body. **C.** Right lateral view of the stomach with minimal filling of the duodenum. This view is particularly helpful for evaluating the cardia and retrogastric region. **D.** Semiupright right posterior oblique view of the high lesser curvature, upper body, and fundus. **E.** Supine left posterior oblique view of the duodenum showing the smooth, featureless appearance of the bulb. (**D** and **E** from Laufer I, Levine MS [eds]: *Double Contrast Gastrointestinal Radiology*, 2nd ed. Philadelphia, WB Saunders, 1992.)

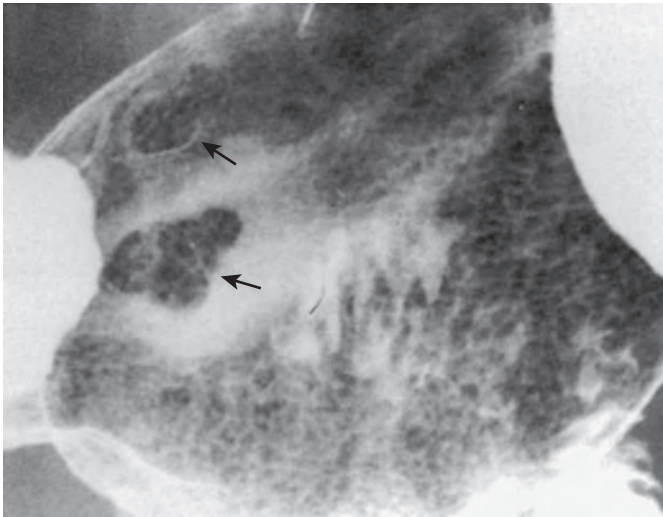


Figure 17-2 Flow technique. With barium flowing across the dependent surface of the stomach, two polypoid lesions (arrows) are identified on the posterior wall. This AIDS patient had biopsy-proven Kaposi's sarcoma in the stomach.

After the esophagus has been examined, the table is lowered into the horizontal position, and the patient is turned a full circle to achieve adequate barium coating of all surfaces of the stomach. Supine, left posterior oblique, and right posterior oblique views of the gastric antrum and body are then obtained (see Fig. 17-1B). The patient is next placed in the recumbent right side down position for a double-contrast view of the gastric cardia and fundus (see Fig. 17-1C). The patient is then placed in the semiupright, right posterior oblique position for a view of the high lesser curvature, upper body, and fundus (see Fig. 17-1D) and then in the supine, left posterior oblique position for double-contrast views of the duodenal bulb and sweep (see Fig. 17-1E). Flow technique is subsequently performed by slowly rotating the patient from side to side to manipulate a thin pool of barium over the posterior (dependent) gastric wall. Flow technique is extremely valuable for demonstrating shallow protruded or depressed lesions on the dependent surface (Fig. 17-2).¹⁰

After the double-contrast phase of the study has been completed, the patient is placed in a prone, right anterior oblique position and asked to take discrete swallows of a thin, low-density barium suspension to evaluate esophageal motility (see Chapter 18). The patient then rapidly gulps thin barium for single-contrast views of the optimally distended thoracic esophagus. Prone and upright compression views of the barium-filled stomach and duodenum are then obtained. Finally, the fluoroscopist tests for spontaneous gastroesophageal reflux or reflux induced by a Valsalva maneuver to increase intra-abdominal pressure. If there is no evidence of gastroesophageal reflux with this maneuver, a water siphon test is performed to increase the sensitivity of the fluoroscopic examination for reflux.¹¹ Our routine double-contrast upper GI study is summarized in Table 17-1.

Anatomic Considerations

Although the normal anatomy of the upper GI tract is well known, several anatomic variations that are particularly well

TABLE 17-1 Routine Upper Gastrointestinal Technique: Double Contrast

Position	Purpose
Upright, LPO	Esophagus, double contrast
Supine, LPO	Stomach, antrum and body, double contrast
Supine	Stomach, antrum and body, double contrast
Supine, RPO	Stomach, antrum and body, double contrast
Right side down lateral	Stomach, cardia and fundus, double contrast
Supine, LPO	Antrum, pylorus, duodenal bulb and sweep, double contrast
Supine and supine obliques	Antrum and body, flow technique
Semiupright, RPO	Stomach, high lesser curvature and fundus, double contrast
Prone, RAO	Esophagus, function and barium filling
Prone or prone, RAO	Antrum and duodenum, compression
Upright	Antrum, lesser curvature, and duodenum, compression
Recumbent	Test for gastroesophageal reflux

LPO, left posterior oblique; RAO, right anterior oblique; RPO, right posterior oblique.

demonstrated by the double-contrast technique should be stressed.

ESOPHAGUS

The normal mucosal surface of the esophagus is smooth and featureless (Fig. 17-3A). When the esophagus is partially collapsed, the normal longitudinal folds are seen as smooth, straight structures no more than 1 to 3 mm in width (Fig. 17-3B). In some patients, fine transverse folds may also be observed in the esophagus because of transient contraction of the longitudinally oriented muscularis mucosae (Fig. 17-3C). These folds are almost always found to be associated with gastroesophageal reflux.¹² In contrast, focally spiculated transverse folds may be detected as a normal variant in the upper thoracic esophagus at the junction of the striated and smooth muscle near the level of the aortic arch (Fig. 17-3D); these are thought to result from localized weakening of the amplitude of peristalsis in this region.¹³ Finally, in older patients, small nodules may be visible on the mucosal surface of the esophagus because of glycogenic acanthosis, a common degenerative condition of no clinical significance (Fig. 17-4).¹⁴

The esophagus may be indented by normal extrinsic impressions from the aortic arch, left main bronchus, and heart (Fig. 17-5A). A smooth, gently sloping indentation may also be seen on the right posterolateral wall of the upper thoracic esophagus between the thoracic inlet and aortic arch in about 10% of patients (see Chapter 25).¹⁵ This indentation represents a normal anatomic variant resulting from an unusually prominent right inferior supra-azygous recess of the mediastinum abutting the esophagus. This variation should not be mistaken for adenopathy or other masses in the mediastinum impinging on the esophagus.¹⁵ In contrast, abnormal impressions may be caused by enlargement of normal structures such as the heart and aorta or by abnormal structures such as enlarged lymph nodes, mediastinal masses, or large vertebral osteophytes (Fig. 17-5B).

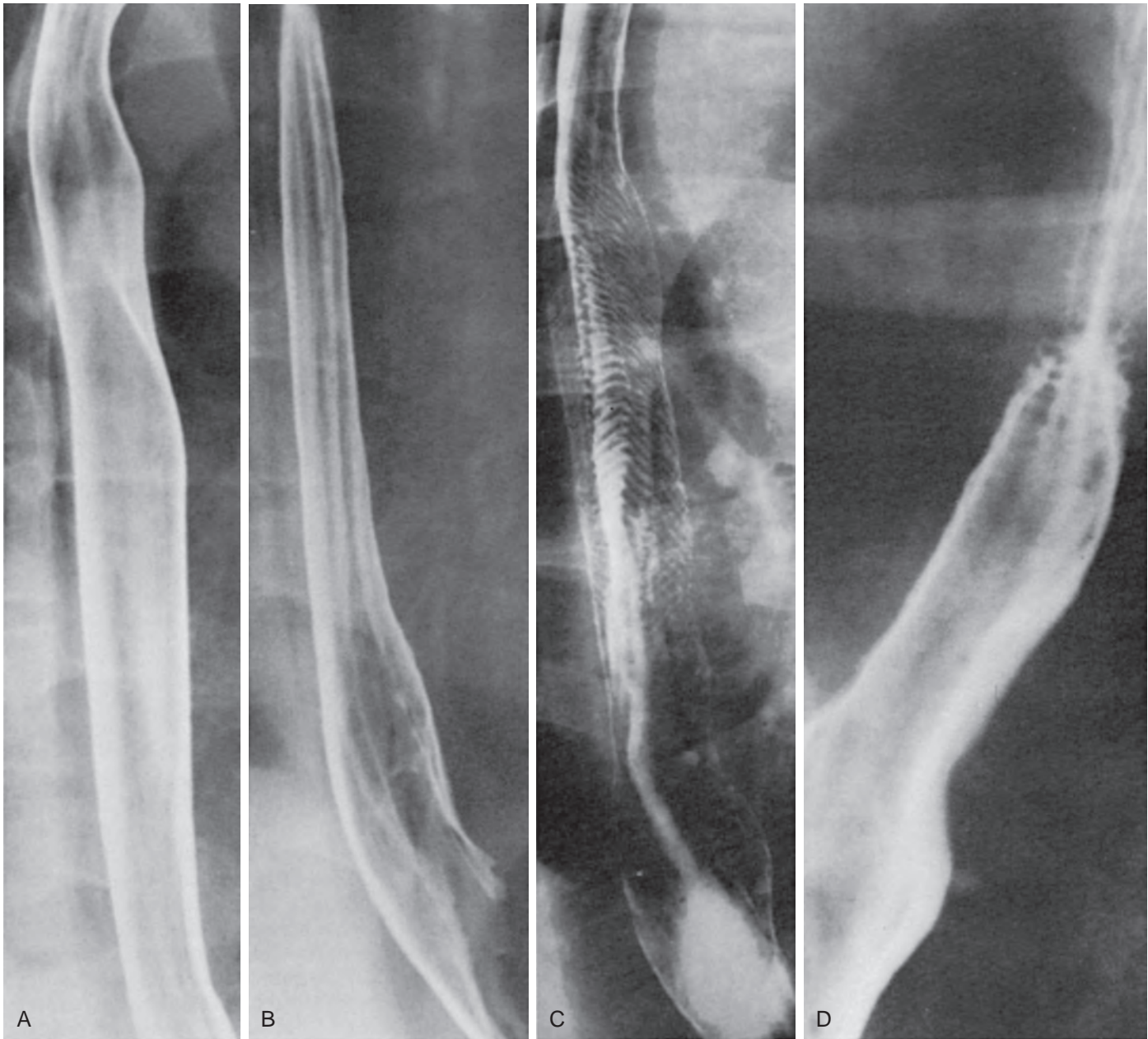


Figure 17-3 Normal esophagus. **A.** Double-contrast view. In the upright, left posterior oblique projection, the esophagus is thrown off the spine. Note the smooth, featureless appearance of the esophagus. **B.** Longitudinal folds. With the esophagus partially collapsed, the normal longitudinal folds are seen. **C.** Transverse folds. These transverse folds are thought to result from contraction of the longitudinally oriented muscularis mucosae and are almost always associated with gastroesophageal reflux. **D.** Spiculation of the upper thoracic esophagus caused by focally prominent, spiculated transverse folds. (**C** from Gohel VK, Edell SK, Laufer I, et al: *Transverse folds in the human esophagus*. *Radiology* 128:303–308, 1978.)

STOMACH

The surface of the stomach can be studied at several levels. The rugal folds are best seen when the stomach is incompletely distended and are most prominent along the greater curvature of the gastric body (Fig. 17-6A). Because rugal folds contain a submucosal core, any process (e.g., inflammatory cells or tumor) that infiltrates the submucosa may cause the folds to become thickened. Conversely, as the normal rugal folds are effaced with greater distention, a fine mucosal pattern, also known as the *areae gastricae*, can be visualized by

double-contrast technique (see Fig. 17-1B) and, occasionally, by single-contrast technique (see Fig. 17-6A).¹⁶ This reticulonodular mucosal pattern can become distorted by inflammatory or neoplastic lesions and also serves as a marker of the quality of mucosal coating. The *areae gastricae* are more likely to be visualized in older patients because of thinning of the mucous gel layer in the stomach with aging.¹⁷ Enlarged *areae gastricae* are sometimes observed in patients with increased acid secretion or chronic *Helicobacter pylori* gastritis.¹⁸ In other patients, fine transverse folds (also known as gastric striae) are seen in the gastric antrum as a sign of chronic antral gastritis

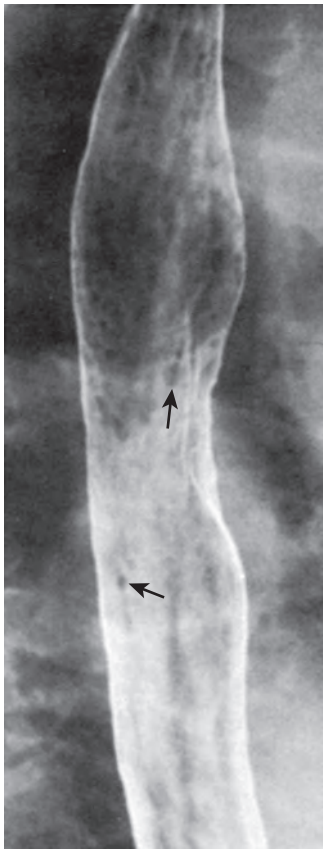


Figure 17-4 Glycogenic acanthosis. Small nodules (arrows) are seen on the mucosal surface of the midesophagus in an asymptomatic patient. These nodules result from a benign degenerative condition known as glycogenic acanthosis.

(Fig. 17-6B).¹⁹ In thin patients, the posterior wall of the stomach may be impressed by normal retrogastric structures (e.g., spleen and pancreas) that should not be mistaken for pathologic mass lesions (Fig. 17-6C). The gastric cardia may also be recognized on double-contrast views of the fundus by the presence of three or four stellate folds radiating to a central point at the gastroesophageal junction (also known as the cardiac rosette), sometimes associated with a hooding fold (Fig. 17-7).²⁰ In patients with ligamentous laxity and a small hiatal hernia, these anatomic landmarks may no longer be present. The cardiac rosette can also be distorted or obliterated by malignant tumors involving the cardia (see Chapters 26 and 32).

DUODENUM

The surface of the duodenal bulb is usually quite smooth. In some patients, double-contrast studies may reveal a fine feathery or velvety surface in the bulb, probably representing a normal villous pattern (Fig. 17-8A).²¹ In other patients, double-contrast studies may reveal small angular filling defects near the base of the duodenal bulb, a finding that is characteristic of heterotopic gastric mucosa (Fig. 17-8B).²² Still other patients may have a smooth round or ovoid mass with a central barium collection at the superior duodenal flexure (Fig. 17-8C). Although the appearance may resemble that of an ulcer with a surrounding mound of edema or even an ulcerated submucosal mass (i.e., a bull's-eye lesion), this finding actually results from

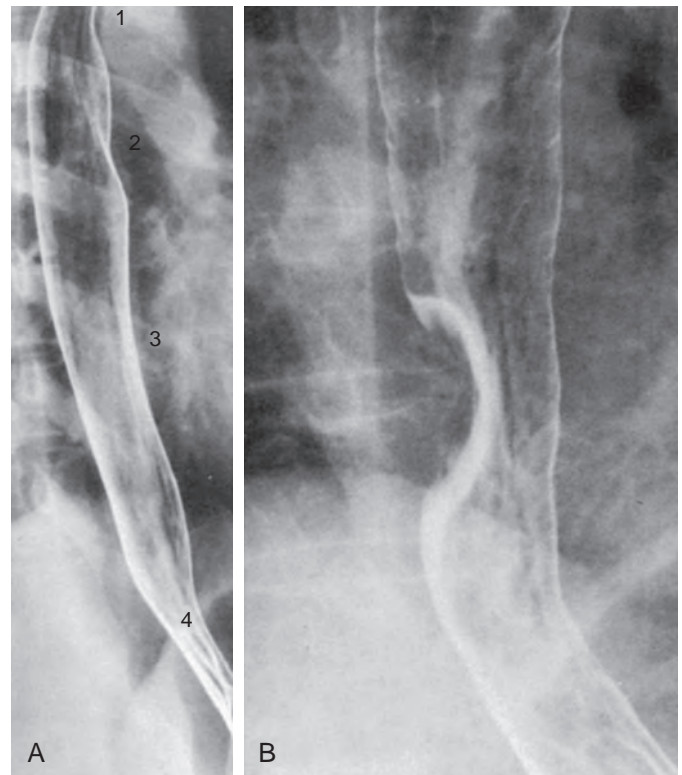


Figure 17-5 Extrinsic impressions on the esophagus. **A.** Normal impressions: 1, aortic arch; 2, left main bronchus; 3, heart; and 4, esophageal hiatus. **B.** Abnormal extrinsic impression on the posterior wall of the esophagus caused by a large thoracic osteophyte.

a normal anatomic variant in which there is an infolding of redundant mucosa at the superior duodenal flexure, also known as the duodenal pseudolesion or flexural fallacy.²³ Occasionally, the duodenal bulb contains tiny barium collections (Fig. 17-8D) representing normal pits in the duodenal mucosa that should not be mistaken for duodenal erosions.²⁴ However, these mucosal pits are not surrounded by radiolucent halos of edematous mucosa, whereas true erosions in the duodenum almost always have a varioliform appearance with surrounding mounds of edema. Finally, symmetric filling defects may be observed at the base of the duodenal bulb (abutting the medial and lateral margins of the pylorus) as a result of prolapsed antral mucosa, a finding of little or no clinical significance.

In the descending duodenum, the anatomy of the major papilla of Vater is particularly well demonstrated on double-contrast studies.²⁵ The major papilla is located on the medial wall of the descending duodenum and is usually associated with a longitudinal fold and a hooding fold (Fig. 17-9A). In contrast, the minor papilla is located on the anterior wall of the descending duodenum just proximal to the major papilla and is therefore best seen when the patient is in the prone position (Fig. 17-9B).

Variations in Technique

ANTERIOR WALL LESIONS

Routine double-contrast technique with the patient in a supine or supine oblique position is best for detecting protruded or depressed lesions on the posterior (dependent) wall of the

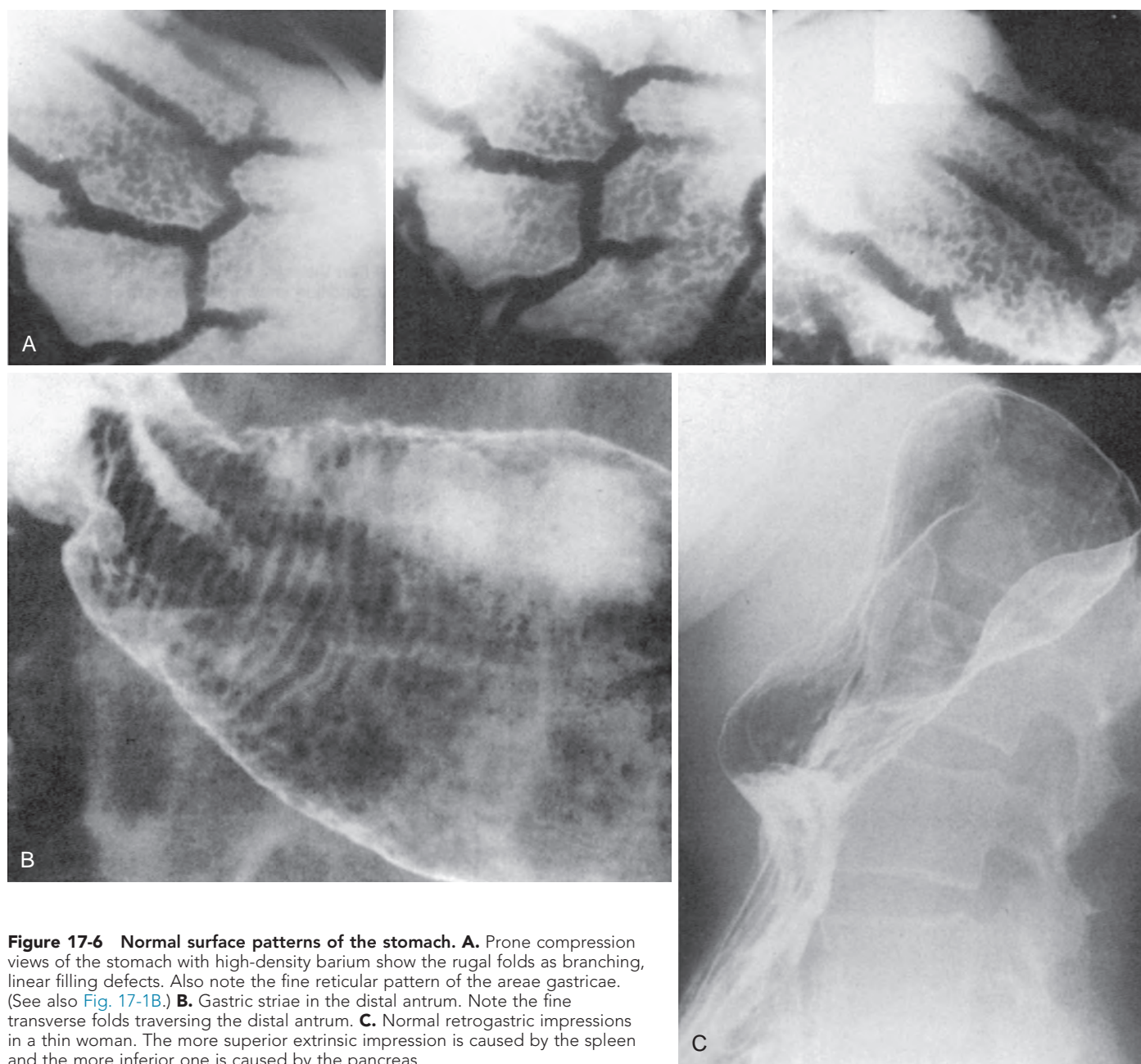


Figure 17-6 Normal surface patterns of the stomach. **A.** Prone compression views of the stomach with high-density barium show the rugal folds as branching, linear filling defects. Also note the fine reticular pattern of the areae gastricae. (See also [Fig. 17-1B](#).) **B.** Gastric striae in the distal antrum. Note the fine transverse folds traversing the distal antrum. **C.** Normal retrogastric impressions in a thin woman. The more superior extrinsic impression is caused by the spleen and the more inferior one is caused by the pancreas.

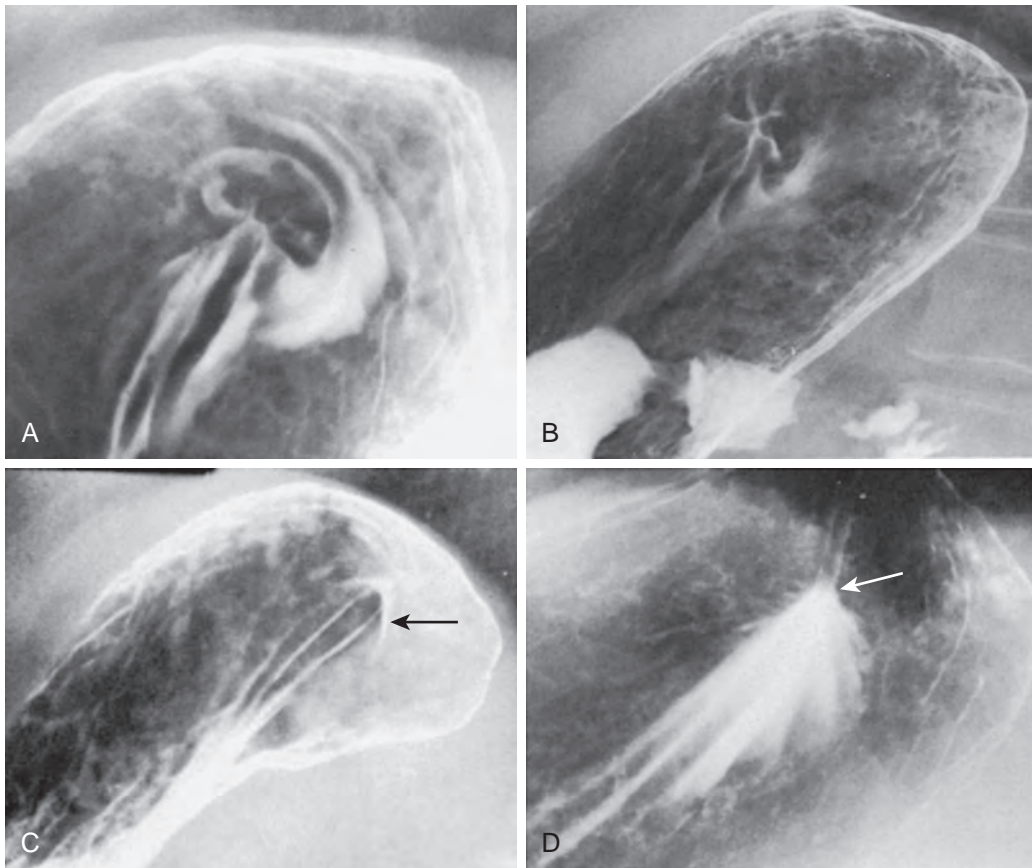


Figure 17-7 Normal cardia and its variations. **A.** Well-anchored cardia appears as a circular elevation with centrally radiating folds (the cardiac rosette). **B.** Stellate folds without the surrounding elevation caused by laxity of the ligamentous attachments. **C.** Further weakening of the ligaments with obliteration of the cardiac rosette. Note the crescentic line (arrow) crossing the area of the esophageal orifice. **D.** Severe ligamentous laxity with gastric folds converging superiorly (arrow) in a tiny hiatal hernia above the esophageal hiatus of the diaphragm. (From Laufer I, Levine MS [eds]: *Double Contrast Gastrointestinal Radiology*, 2nd ed. Philadelphia, WB Saunders, 1992.)

gastric antrum or body. In contrast, protruded or depressed lesions on the anterior wall may be seen as ring shadows etched in white on double-contrast views obtained with the patient in the supine position. Such lesions are usually visualized as filling defects (protruded lesions) or barium collections (depressed lesions) on compression views obtained with the patient in the prone position (Fig. 17-10). Double-contrast examination of the anterior wall of the stomach can also be performed with the patient in the prone position, turned slightly to the left, with the head of the table lowered.²⁶ Similarly, the anterior wall of the duodenum can be studied by double contrast with the patient in the prone position (see Fig. 17-9B).

POSSIBLE PERFORATION

When perforation of any portion of the GI tract is suspected because of underlying disease, surgery, or other iatrogenic causes, a water-soluble contrast agent such as diatrizoate meglumine and diatrizoate sodium (Gastroview; Mallinckrodt Pharmaceuticals, St. Louis) should be used.²⁷ If no extravasation of contrast material is demonstrated, the examination should be completed with high-density barium because the better definition achieved with this type of barium enables visualization of small leaks that cannot be detected with a water-soluble contrast agent.²⁸

PARTIAL GASTRECTOMY

After partial gastrectomy for ulcer disease or tumor, the double-contrast examination must be modified to compensate for the

absence of a pylorus (Fig. 17-11).²⁹ Important modifications include an increase in the dose of glucagon to at least 0.5 mg to delay emptying of barium from the remaining stomach and a smaller dose of an effervescent agent because there is less stomach to distend. In addition, the examination should not be started with the patient in the upright position because rapid emptying of barium in this position may prevent adequate visualization of the gastric remnant. Details of the examination are discussed in Chapter 35.

GASTRIC OUTLET OBSTRUCTION

When gastric outlet obstruction is suspected, the patient should initially be examined in the upright position to determine whether there is a fluid level in the stomach. If a fluid level is present, a single-contrast barium study should be performed to delineate the site and nature of the obstruction. In such cases, high-density barium should be used rather than thin barium, because high-density barium is more likely to traverse retained fluid or debris in the stomach and reach the site of obstruction.

ESOPHAGEAL VARICES

Esophageal varices are discussed in detail in Chapter 25. Esophageal varices are typically manifested by thickened, tortuous, or serpiginous longitudinal folds that are best demonstrated with the patient in the recumbent position, with coating of the esophageal mucosa by high-density barium or barium paste and the esophagus partially collapsed.³⁰

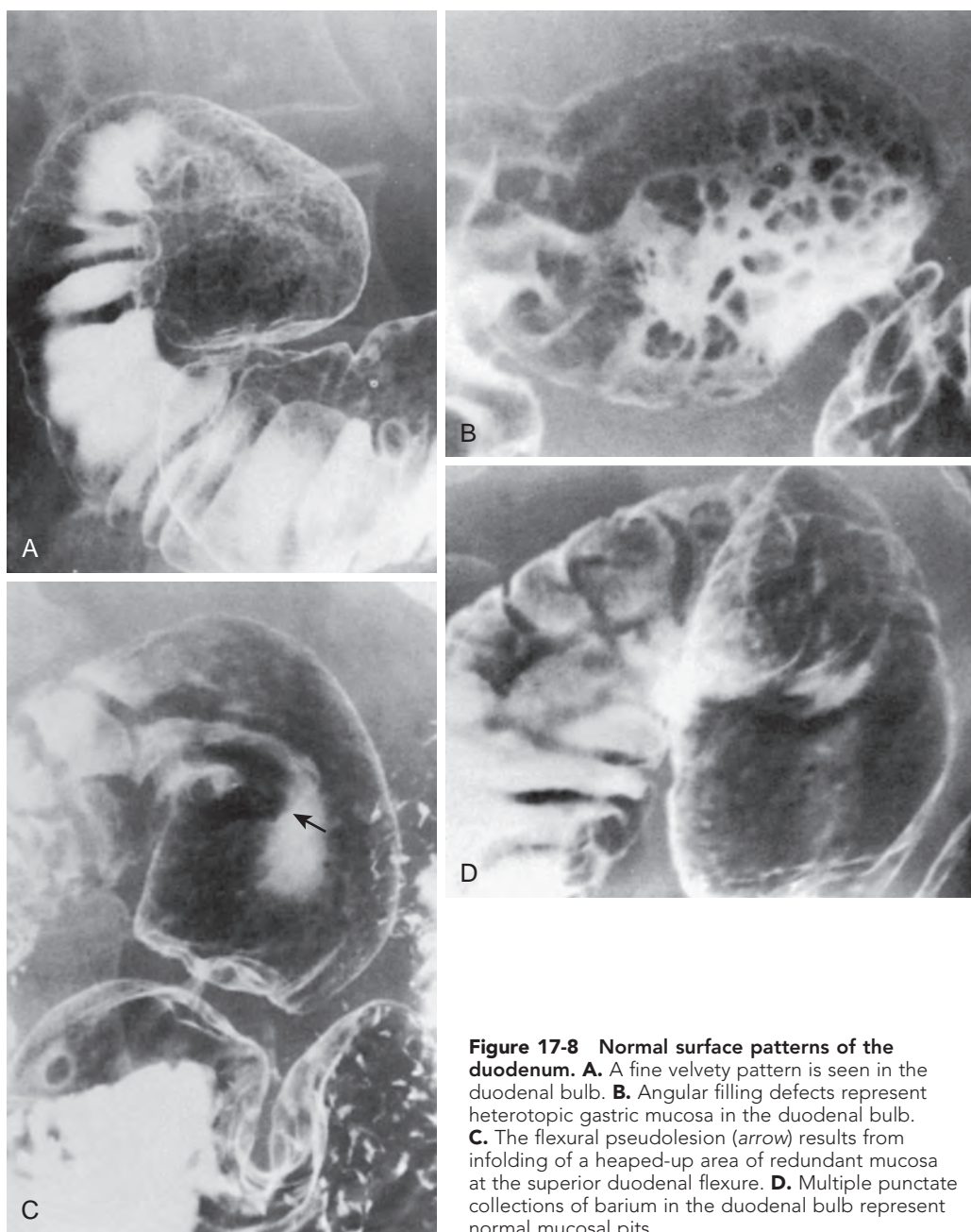


Figure 17-8 Normal surface patterns of the duodenum. **A.** A fine velvety pattern is seen in the duodenal bulb. **B.** Angular filling defects represent heterotopic gastric mucosa in the duodenal bulb. **C.** The flexural pseudolesion (arrow) results from infolding of a heaped-up area of redundant mucosa at the superior duodenal flexure. **D.** Multiple punctate collections of barium in the duodenal bulb represent normal mucosal pits.

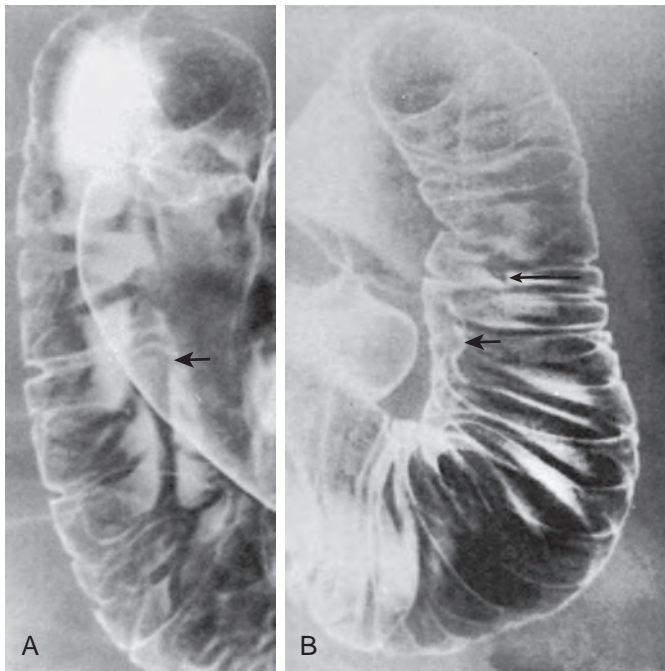


Figure 17-9 Descending duodenum. **A.** The descending duodenum is seen through the gas-filled antrum with the patient in the left posterior oblique position. Note the major papilla (arrow) and its associated folds. **B.** Prone view shows the major papilla (short arrow) on the medial wall of the descending duodenum, with the minor papilla (long arrow) seen anteriorly above this level. (**B** from Laufer I, Levine MS [ed]: *Double Contrast Gastrointestinal Radiology*, 2nd ed. Philadelphia, WB Saunders, 1992.)

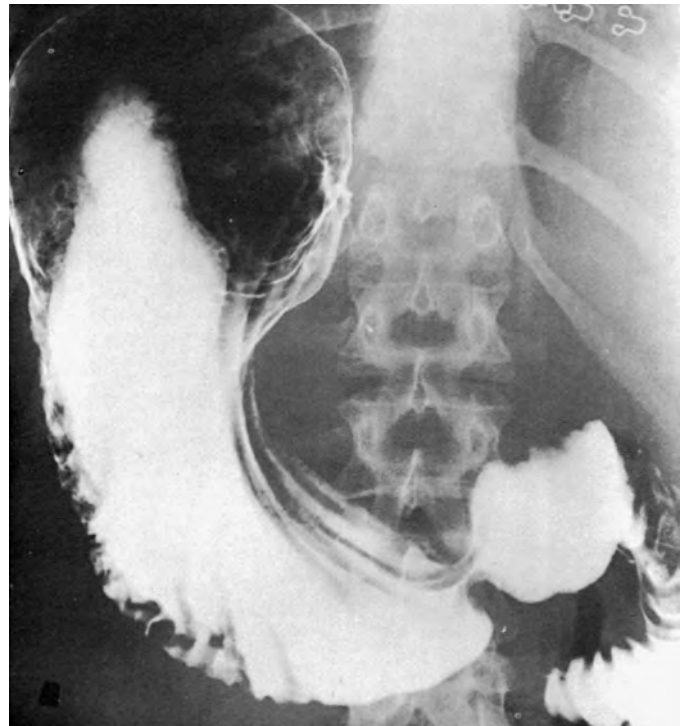


Figure 17-10 Examination of the anterior wall of the stomach. The rugal folds on the anterior wall of the stomach are clearly seen with the patient in the prone position. The fundus is filled with gas. (From Laufer I, Levine MS [eds]: *Double Contrast Gastrointestinal Radiology*, 2nd ed. Philadelphia, WB Saunders, 1992.)

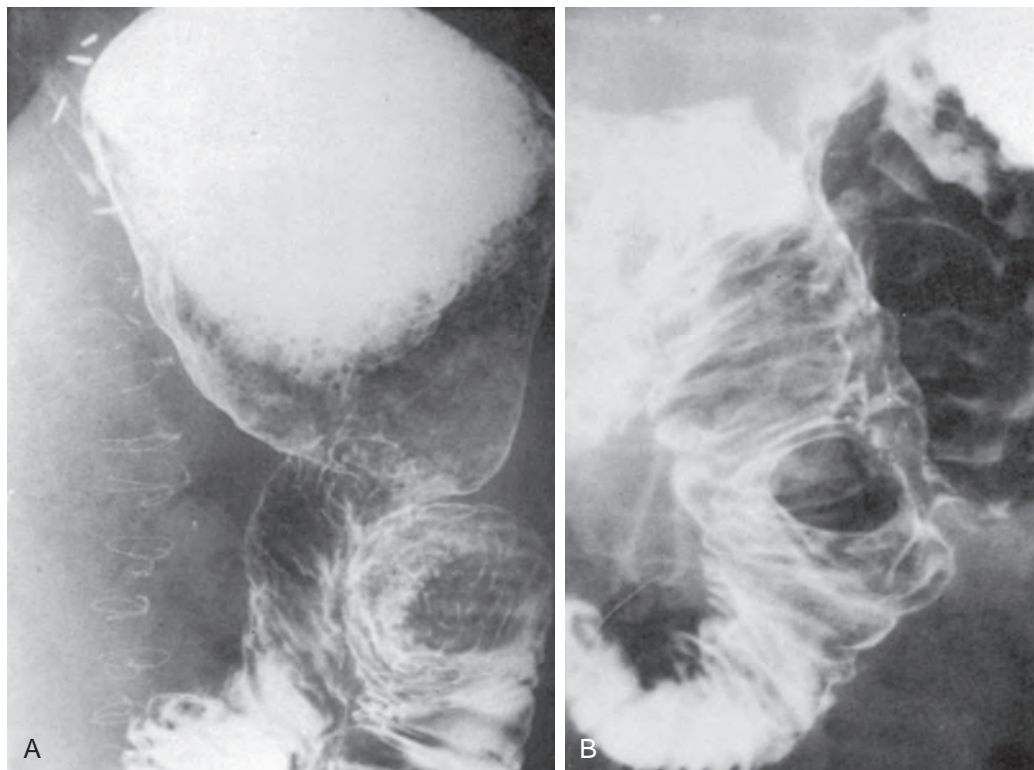


Figure 17-11 Postoperative stomach. **A.** Double-contrast view showing the normal postoperative appearance after a partial gastrectomy (Billroth II). **B.** Double-contrast view of the gastrojejunal anastomosis after a partial gastrectomy (Billroth II).

REFERENCES

1. Levine MS, Rubesin SE, Herlinger H, et al: Double-contrast upper gastrointestinal examination: Technique and interpretation. *Radiology* 168:593–602, 1988.
2. Levine MS: Examination of the esophagus, stomach, and duodenum: Techniques and normal anatomy. In Levine MS, Ramchandani P, Rubesin SE, editors: *Practical Fluoroscopy of the GI and GU Tracts*, Cambridge, 2013, Cambridge University Press, pp 23–39.
3. Rubesin SE, Herlinger H: The effect of barium suspension viscosity on the delineation of areae gastricae. *AJR* 146:35–38, 1986.
4. Koehler RE, Weyman PJ, Stanley RJ, et al: Evaluation of three effervescent agents for double-contrast upper gastrointestinal radiography. *Gastrointest Radiol* 6:111–114, 1981.
5. Maglinte DD, Caudill LD, Krol KL, et al: The minimum effective dose of glucagon in upper gastrointestinal radiography. *Gastrointest Radiol* 7:119–122, 1982.
6. Moeller G, Hughes JJ, Mangano FA, et al: Comparison of L-hyoscyamine, glucagon, and placebo for air-contrast upper gastrointestinal series. *Gastrointest Radiol* 17:195–198, 1992.
7. Kastan DJ, Ackerman LV, Feczko PJ: Digital gastrointestinal imaging: The effect of pixel size on detection of subtle mucosal abnormalities. *Radiology* 167:853–856, 1987.
8. Arenson RL, Chakraborty DP, Seshadri SB, et al: The digital imaging workstation. *Radiology* 176:303–315, 1990.
9. Levine MS, Laufer I: The gastrointestinal tract: Dos and don'ts of digital imaging (state of the art). *Radiology* 207:311–316, 1998.
10. Kikuchi Y, Levine MS, Laufer I, et al: Value of flow technique for double-contrast examination of the stomach. *AJR* 174:1183–1184, 1986.
11. Thompson JK, Koehler RE, Richter JE: Detection of gastroesophageal reflux: Value of barium studies compared with 24-hr pH monitoring. *AJR* 162:621–626, 1994.
12. Samadi F, Levine MS, Rubesin SE, et al: Feline esophagus and gastroesophageal reflux. *AJR* 194:972–976, 2010.
13. Levine MS, Low V, Laufer I, et al: Focal spiculation of the upper thoracic esophagus: A normal variant on double-contrast esophagography. *Radiology* 183:807–810, 1992.
14. Glick SN, Teplick SK, Goldstein J, et al: Glycogenic acanthosis of the esophagus. *AJR* 139:683–688, 1982.
15. Sam JW, Levine MS, Miller WT: The right inferior supraazygous recess: A cause of upper esophageal pseudomass on double-contrast esophagography. *AJR* 171:1583–1586, 1998.
16. Mackintosh CE, Kreel L: Anatomy and radiology of the areae gastricae. *Gut* 18:855–864, 1977.
17. Charagundla SR, Levine MS, Langlotz CP, et al: Visualization of areae gastricae on double-contrast upper gastrointestinal radiography: Relationship to age of patients. *AJR* 177:61–63, 2001.
18. Sohn J, Levine MS, Furth EE, et al: *Helicobacter pylori* gastritis: Radiographic findings. *Radiology* 195:763–767, 1995.
19. Cho KC, Gold BM, Printz DA: Multiple transverse folds in the gastric antrum. *Radiology* 164:339–341, 1987.
20. Herlinger H, Grossman R, Laufer I, et al: The gastric cardia in double-contrast study: Its dynamic image. *AJR* 135:21–29, 1980.
21. Glick SN, Gohel VK, Laufer I: Mucosal surface patterns of the duodenal bulb. *Radiology* 150:317–322, 1984.
22. Agha FP, Ghahremani GG, Tsang TK, et al: Heterotopic gastric mucosa in the duodenum: Radiographic findings. *AJR* 150:291–294, 1988.
23. Burrell M, Toffler R: Flexural pseudolesions of the duodenum. *Radiology* 120:313–315, 1976.
24. Bova JG, Kamath V, Tio FO, et al: The normal mucosal surface pattern of the duodenal bulb: Radiologic-histologic correlation. *AJR* 145:735–738, 1985.
25. Levine MS, Laufer I, Stevenson G: Duodenum. In Laufer I, Levine MS, editors: *Double Contrast Gastrointestinal Radiology*, ed 2, Philadelphia, 1992, WB Saunders, pp 321–361.
26. Goldsmith MR, Paul RE, Poplack WE, et al: Evaluation of routine double-contrast views of the anterior wall of the stomach. *AJR* 126:1159–1163, 1976.
27. Dodds WJ, Stewart ET, Vlymen WJ: Appropriate contrast media for evaluation of esophageal disruption. *Radiology* 144:439–441, 1982.
28. Swanson JO, Levine MS, Redfern RO, et al: Usefulness of high-density barium for detection of leaks after esophagogastrectomy, total gastrectomy, and total laryngectomy. *AJR* 181:415–420, 2003.
29. Woodfield CA, Levine MS: The postoperative stomach. *Eur J Radiol* 53:341–352, 2005.
30. Cockerill EM, Miller RE, Chernish SM, et al: Optimal visualization of esophageal varices. *AJR* 126:512–523, 1976.

Motility Disorders of the Esophagus

DAVID J. OTT | MARC S. LEVINE

CHAPTER OUTLINE

Normal Esophageal Anatomy

Normal Esophageal Physiology

Radiographic Evaluation

Esophageal Motility Disorders

Primary Motility Disorders

Nonspecific Esophageal Motility Disorder

Secondary Motility Disorders

Motility disorders of the esophagus are an important cause of esophageal complaints, especially when symptoms are not readily explained by a structural abnormality. An understanding of esophageal anatomy and physiology is required for proper radiographic evaluation of normal and abnormal esophageal function. This chapter reviews the normal anatomy and physiology of the esophagus before discussing the radiographic evaluation of esophageal motility and the various esophageal motility disorders.

Normal Esophageal Anatomy

The esophagus is a muscular tube measuring 20 to 24 cm in length; it is composed of outer longitudinal and inner circular muscle fibers and is lined by stratified squamous epithelium.¹ Striated muscle predominates in the upper third of the esophagus, with smooth muscle in the lower two thirds. The transition from striated to smooth muscle varies but usually occurs at the level of the aortic arch.^{1,2} Although this transitional zone is not evident on barium esophagography, certain motility disorders (e.g., collagen vascular diseases) may selectively involve the striated or smooth muscle portions of the esophagus.

Opening and closing of the upper and lower ends of the esophagus are regulated by the upper esophageal sphincter (UES) and lower esophageal sphincter (LES), respectively. The UES is located at the pharyngoesophageal junction and is formed primarily by the cricopharyngeal muscle, the horizontal portion of the inferior pharyngeal constrictor. The LES is not a distinct muscular entity but is defined manometrically as a high-pressure zone measuring 2 to 4 cm in length in the esophagogastric region.^{1,3} This physiologic sphincter corresponds in location to the anatomic esophageal vestibule.^{3,4}

Normal Esophageal Physiology

In the resting state, the esophageal body is normally collapsed, and the UES and LES are closed to prevent retrograde flow of esophageal and gastric contents.^{1,5} The major function of the esophagus is the transport of solids and liquids from the oral

cavity to the stomach. The chief mechanism of bolus transport is esophageal peristalsis, which is assisted by gravity in the upright position. Radiographic evaluation of esophageal peristalsis is therefore usually performed with the patient recumbent to eliminate the effect of gravity.

Primary esophageal peristalsis is initiated by swallowing. A rapid wave of inhibition (not apparent radiographically) is followed by a slower wave of contraction, which traverses the entire esophagus (Fig. 18-1). Relaxation of the UES occurs within 0.2 to 0.3 second of the initiation of swallowing, and relaxation of the LES occurs several seconds later.^{1,5,6} The LES remains relaxed as the oncoming bolus approaches the distal esophagus, returning to its contracted state shortly after the bolus reaches the stomach. The primary peristaltic contraction wave propagates through the esophagus in 6 to 8 seconds.

Secondary peristalsis and nonperistaltic contractions (NPCs) are other types of esophageal functional activity.^{1,6-9} Secondary peristalsis is initiated by local esophageal stimulation or distention, but is otherwise similar to primary peristalsis, propagating aborally. In contrast, NPCs (also known as tertiary contractions) are not propagated aborally. They typically involve the smooth muscle segment of the esophagus, occurring spontaneously or during swallowing. NPCs may be single or multiple, simultaneous or repetitive, and feeble or strong. Severe NPCs may narrow or obliterate the esophageal lumen, producing a characteristic corkscrew appearance on barium studies (Fig. 18-2). NPCs are nonspecific and may be related to a variety of motility disorders involving the esophagus.

Individual variations in esophageal function are primarily related to aging. In young adults, most wet swallows initiate a complete peristaltic sequence, followed invariably by LES relaxation.¹⁰ NPCs are rare in this age group. However, older patients often exhibit incomplete peristaltic sequences during swallowing, with occasional LES dysfunction and a higher prevalence and severity of NPCs, a condition known as presbyesophagus.¹⁰⁻¹³ The amplitude of peristalsis, as recorded manometrically, also decreases with age. Thus, mild functional disturbances of the esophagus that are observed in older adults must be interpreted with caution and correlated with the clinical findings.

Radiographic Evaluation

Radiographic evaluation of esophageal motility includes an examination of the esophageal body and both sphincters.^{1,4,7-9,14} During swallowing, the UES relaxes and the pharyngoesophageal segment opens in response to bolus distention. Incomplete relaxation of the UES may be manifested on barium studies by a persistent indentation on the posterior aspect of the pharyngoesophageal junction resulting from the contracted cricopharyngeal muscle (see Chapter 15).^{8,14} This finding is often associated with other signs of pharyngeal dysmotility, such as aspiration or stasis of barium within the valleculae and piriform sinuses. Motion-recording techniques (using videotape or

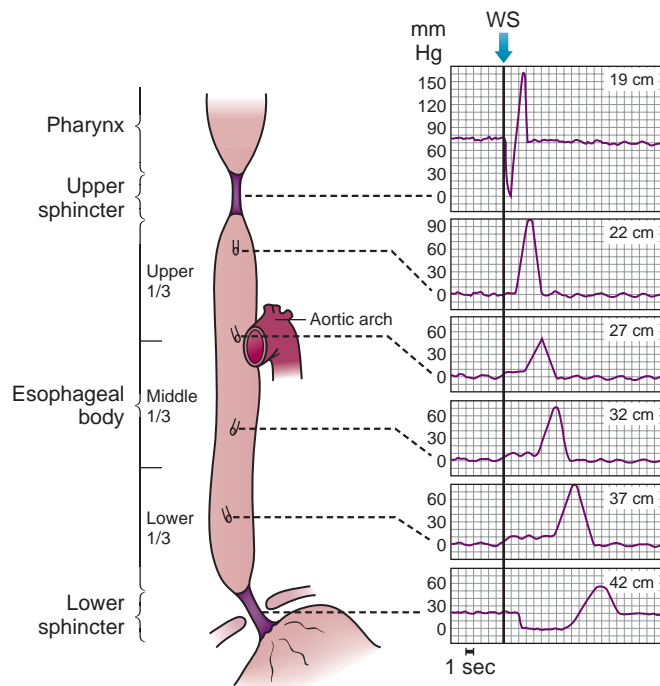


Figure 18-1 Manometric representation of normal esophageal peristalsis. Measurements are taken from multiple recording sites in the esophagus, including the upper esophageal sphincter (UES) and the lower esophageal sphincter (LES). After a wet swallow (WS), UES relaxation is followed almost immediately by prolonged LES relaxation. The primary peristaltic contraction wave is seen as an aborally progressing pressure peak. (From Dodds WJ: *Esophagus-radiology*. In Margulis AR, Burhenne HJ [eds]: *Alimentary Tract Radiology*, vol 1, 4th ed. St. Louis, CV Mosby, 1989, p 430.)

a digital recording device) facilitate evaluation of the pharynx and UES.

The fluoroscopic examination can be used to evaluate esophageal motility, but motion-recording techniques facilitate assessment of the findings. The patient is placed in the prone right anterior oblique (RAO) position and instructed to take single swallows of barium. At least five barium swallows are required for adequate evaluation of esophageal peristalsis and LES relaxation.^{4,7-9,15} Single swallows must be observed because a second swallow taken before completion of a primary contraction wave inhibits the propagating wave, so it can erroneously be mistaken for a peristaltic abnormality. In contrast, rapid, repetitive swallowing does not assess primary esophageal peristalsis but distends the esophagus maximally for structural evaluation (Fig. 18-3).

As barium is propelled into the esophagus through the relaxed UES, a normal primary peristaltic sequence is seen as an aboral contraction wave that obliterates the esophageal lumen and progressively strips the barium bolus from the esophagus (Fig. 18-4). This lumen-obliterating wave imparts an inverted V configuration to the top of the barium column, corresponding to the peristaltic pressure peak observed at manometry. In younger individuals, the peristaltic contraction wave normally strips all of the swallowed barium from the esophagus. Occasionally, so-called proximal escape of barium occurs at the level of the aortic arch (Fig. 18-5). This age-related phenomenon is caused by a low-amplitude pressure trough at the transition zone between the striated and smooth muscle portions of the esophagus, which prevents closure of the esophageal lumen

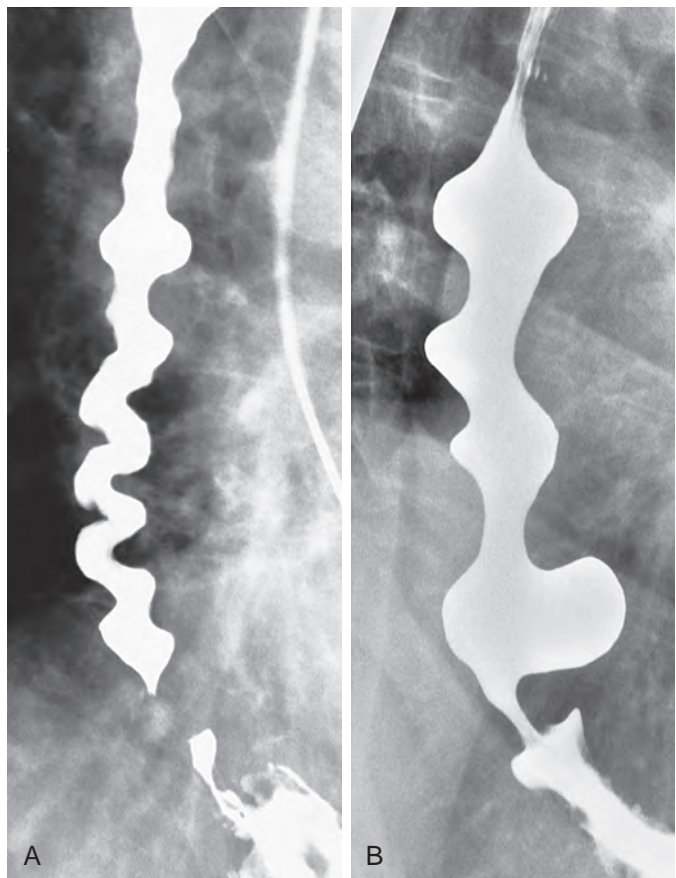


Figure 18-2 Nonperistaltic contractions in the esophagus.

A. Barium study of an 89-year-old man with dysphagia but no chest pain. The esophagus has a corkscrew appearance because of simultaneous nonperistaltic contractions. A nonspecific esophageal motility disorder was diagnosed on manometric examination. **B.** Another older man without esophageal symptoms has less severe simultaneous nonperistaltic contractions. (From Ott DJ: *Radiologic evaluation of esophageal dysphagia*. *Curr Probl Diagn Radiol* 17:1-33, 1988.)

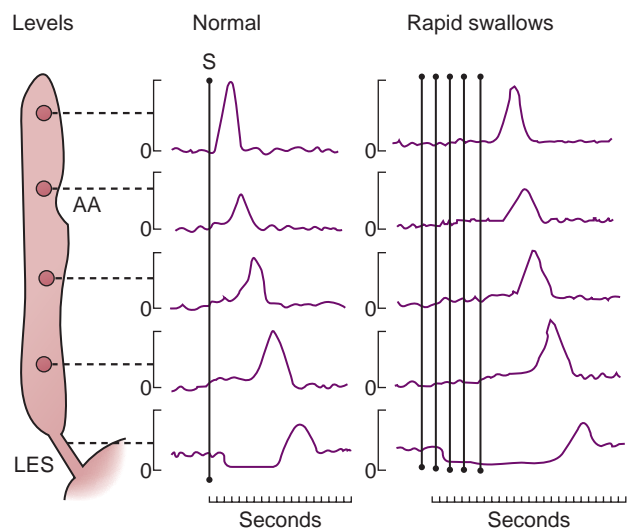


Figure 18-3 Manometric representation of normal esophageal peristalsis. Measurements are taken from multiple recording levels in the esophagus. Rapid swallows cause prolonged lower esophageal sphincter (LES) relaxation but do not generate a primary peristaltic sequence until the final swallow. AA, Aortic arch; S, swallow.

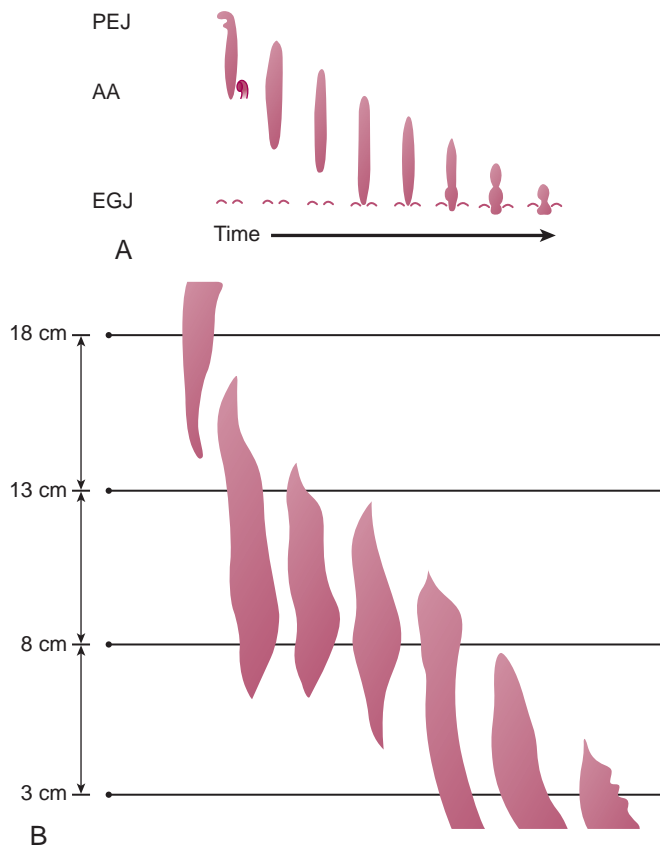


Figure 18-4 Normal primary peristalsis. **A.** Schematic representation of normal primary peristalsis with a lumen-obliterating contraction wave stripping all of the barium from the esophagus. **B.** Videotaped temporal tracings of a 5-mL barium bolus at 1-second intervals show normal primary peristalsis. The tapered tops of the barium column correspond to the peristaltic contraction wave seen during synchronous manometry. The numbers on the vertical axis represent the positions of the manometric catheter ports above the LES. AA, Aortic arch; EGJ, esophagogastric junction; PEJ, pharyngoesophageal junction. (**A** from Ott DJ: *Radiologic evaluation of esophageal dysphagia*. *Curr Probl Diagn Radiol* 17:1–33, 1988; **B** from Ott DJ, Chen YM, Hewson EG, et al: *Esophageal motility: Assessment with synchronous videotape fluoroscopy and manometry*. *Radiology* 173:419–422, 1989.)

and allows retrograde flow of barium.^{2,6,16} In almost all cases, proximal escape can readily be differentiated from true esophageal motility disorders.

Esophageal Motility Disorders

Esophageal motility disorders may be classified as primary or secondary (Table 18-1).^{1,5,7-9,17-19} Primary motility disorders mainly involve the esophagus, whereas secondary esophageal motility disorders result from a wide variety of systemic diseases or from physical or chemical injury of the esophagus. Esophageal motility disorders may also be classified manometrically into four groups: (1) inadequate LES relaxation (classic achalasia); (2) uncoordinated contraction (diffuse esophageal spasm); (3) hypercontraction (nutcracker esophagus and hypertensive LES); and (4) hypocontraction (nonspecific esophageal motility disorders, presbyesophagus, and secondary esophageal motility disorders).¹⁷⁻¹⁹ Because this classification of esophageal motility disorders is based on manometric findings that cannot be adequately quantified on barium

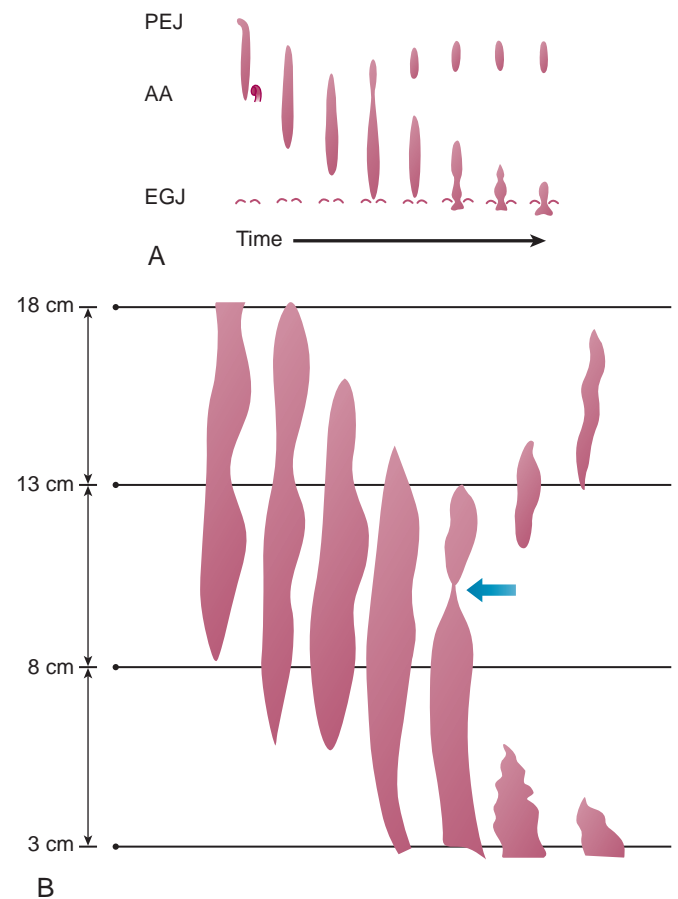


Figure 18-5 Proximal escape. **A.** Manometric representation shows normal primary peristalsis with proximal escape because the contraction wave fails to obliterate the lumen completely at the level of the aortic arch (AA). Note that the peristaltic sequence continues aborally. **B.** Videotaped temporal tracings of a 5-mL barium bolus at 1-second intervals show normal primary peristalsis associated with proximal escape (arrow). The lower esophagus is normally stripped of barium below the area of escape. The numbers on the vertical axis represent the positions of the manometric catheter ports above the LES. EGJ, Esophagogastric junction; PEJ, pharyngoesophageal junction. (**A** from Ott DJ: *Radiologic evaluation of esophageal dysphagia*. *Curr Probl Diagn Radiol* 17:1–33, 1988; **B** from Ott DJ, Chen YM, Hewson EG, et al: *Esophageal motility: Assessment with synchronous videotape fluoroscopy and manometry*. *Radiology* 173:419–422, 1989.)

studies, we have instead chosen to classify primary and secondary esophageal motility disorders conceptually in this chapter (see Table 18-1).

PRIMARY MOTILITY DISORDERS

Achalasia

Achalasia is a well-recognized esophageal motility disorder characterized by a combination of absent peristalsis in the esophagus and impaired LES opening in response to deglutition.^{1,7-9,17-21} Two forms of achalasia have been described, primary and secondary. Primary achalasia (also known as idiopathic achalasia) is caused by degeneration and loss of myenteric ganglia in the wall of the esophagus. The cause is unknown but is postulated to be secondary to viral or autoimmune disease.² In contrast, secondary achalasia (also known as pseudoachalasia) is a less common form caused by

TABLE 18-1 Classification of Esophageal Motility Disorders**PRIMARY MOTILITY DISORDERS (NEWER CLINICAL CATEGORIES)**

Achalasia and variants (inadequate lower esophageal sphincter relaxation)
 Diffuse esophageal spasm (uncoordinated contraction)
 Nutcracker esophagus (hypercontraction)
 Nonspecific esophageal motility disorder (hypocontraction)
 Presbyesophagus (questionable entity—hypocontraction)
 Hypertensive lower esophageal sphincter (hypercontraction)

SECONDARY MOTILITY DISORDERS (MANY WITH HYPOCONTRACTION)

Collagen-vascular disease
 Chemical or physical agents
 Reflux esophagitis
 Caustic esophagitis
 Radiation therapy
 Infectious causes
 Diabetes mellitus
 Alcoholism
 Endocrine disease
 Neuromuscular disorders
 Cerebrovascular disease
 Demyelinating disorders
 Chorea-related disorders
 Myasthenia gravis
 Muscular dystrophies
 Other rare causes
 Idiopathic intestinal pseudo-obstruction

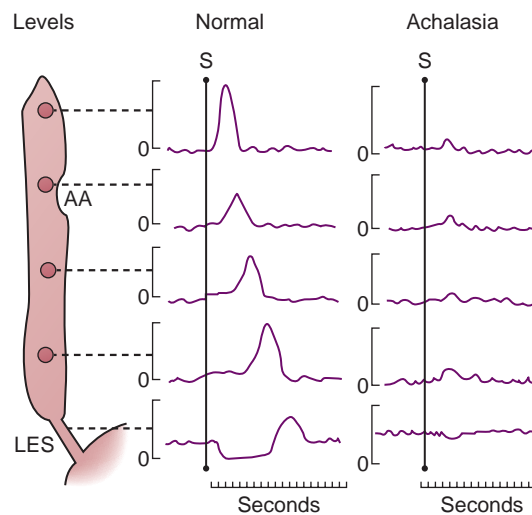


Figure 18-6 Manometric representation of normal peristalsis and achalasia. Measurements are taken from multiple recording levels in the esophagus. In this example of achalasia, peristalsis and lower esophageal sphincter (LES) relaxation are absent, and LES pressure is elevated. AA, Aortic arch; S, swallow.

extraesophageal conditions (usually malignant tumors) that induce an achalasia-like motility disorder by a variety of proposed mechanisms.^{3,4} Long-standing primary achalasia may also be a precursor of esophageal carcinoma. The association with carcinoma varies, but in one study the risk of carcinoma was 9 to 28 times greater than that in the general population.²² For the remainder of this chapter, the term *achalasia* is used to denote primary achalasia.

Achalasia occurs equally in both genders and usually affects patients during the middle decades of life.^{5,7,20,21} Most patients seek medical attention because of long-standing, slowly progressive dysphagia for solids and liquids, often associated with regurgitation of bland, undigested food and saliva.²³ Painful swallowing and chest pain are less common. Weight loss may occur in severe cases. Patients with chronic regurgitation may develop recurrent episodes of coughing, choking, and aspiration pneumonia. If dysphagia has a recent onset and is rapidly progressive in older patients with radiographic or manometric findings of achalasia, secondary achalasia caused by malignancy should be strongly suspected (see Chapter 24).^{7,20,23-25}

Achalasia is characterized manometrically by the absence of primary peristalsis, elevated or normal resting LES pressures, and incomplete or absent LES relaxation in response to deglutition (Fig. 18-6).^{5,7,9,20} However, the presence and degree of LES relaxation on manometry are unreliable because some patients with typical clinical and radiographic findings of achalasia are found to have complete manometric relaxation of the LES.²⁶ Other patients may have variants of achalasia, with atypical manometric findings. A debated variant, vigorous achalasia, is characterized by high-amplitude, simultaneous, and repetitive contractions.^{20,27,28} These patients may present with chest pain and have less esophageal dilation. Another controversial variant, early achalasia, is characterized by aperistalsis, with normal

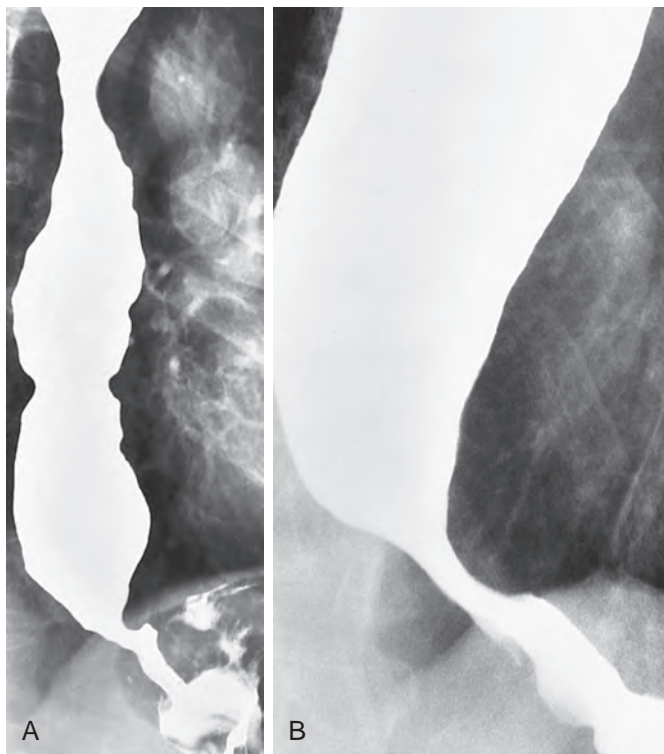


Figure 18-7 Achalasia. **A.** There is a dilated esophagus with smooth, tapered narrowing just above the level of the gastroesophageal junction. Esophageal peristalsis was absent at fluoroscopy. **B.** Close-up view shows smooth, beaklike tapering of the distal esophagus because of LES dysfunction.

LES relaxation.²⁹ Patients with early achalasia also have less esophageal dilation and tend to be younger. Both these variants may represent transitional motility disorders evolving toward classic achalasia.³⁰⁻³²

Achalasia is characterized on barium esophagography by the absence of primary peristalsis on all swallows.^{1,5,7-9,20} The distal esophagus typically has a smooth, tapered, beaklike appearance at the level of the esophageal hiatus (Fig. 18-7) because of LES

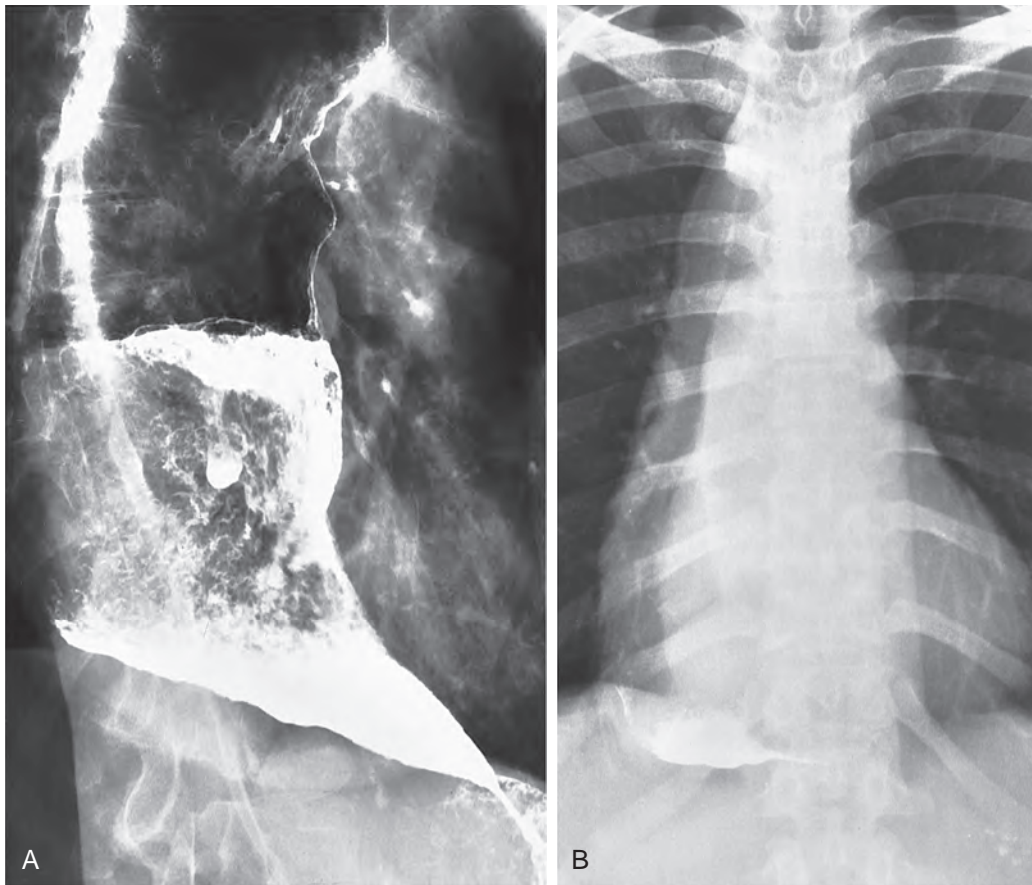


Figure 18-8 Advanced achalasia. **A.** There is a markedly dilated esophagus with tapered distal narrowing caused by incomplete opening of the LES. Note retained food in the esophagus. **B.** A double contour of the right mediastinal border is seen in another patient with advanced achalasia. The outer border represents the dilated esophagus projecting beyond the shadows of the aorta and heart. A small amount of retained barium is present in the distal esophagus. Also note the absence of gas in the proximal stomach.

dysfunction and failure of the barium bolus to distend the tonically contracted sphincter. The degree of esophageal dilation is variable, and some patients with early achalasia have little or no esophageal dilation.²⁹ Others with vigorous achalasia have repetitive NPCs associated with typical findings of achalasia.²⁷ Over time, the esophagus becomes increasingly distended, and retained food, secretions, and barium in the dilated esophagus (Fig. 18-8A) may obscure underlying esophagitis or even developing esophageal carcinomas. In such cases, the fluoroscopist can use a water flush technique in which the patient swallows tap water at the end of the fluoroscopic examination to clear residual barium from the distal esophagus and facilitate the detection of tumor.³³ Advanced achalasia may be recognized on chest radiographs when marked esophageal dilation produces a double contour of the right mediastinal border, and little or no gas enters the stomach (Fig. 18-8B). Eventually, some patients with long-standing disease develop a massively dilated esophagus that has a tortuous distal configuration, also known as the sigmoid esophagus of end-stage achalasia (Fig. 18-9).

Achalasia must be differentiated from other causes of narrowing in the distal esophagus (Table 18-2). In particular, an underlying carcinoma of the esophagogastric region must be excluded (Fig. 18-10).^{7-9,20,23-25} Although most malignant tumors in this region are characterized radiographically by mucosal irregularity or mass effect (see Fig. 18-10B), carcinoma of the cardia and other malignant tumors causing secondary achalasia may be manifested on barium studies by smooth, tapered narrowing of the distal esophagus and aperistalsis, mimicking the findings of primary achalasia (see Fig. 18-10A and Chapter 24).²³ Peptic strictures are another common cause of distal esophageal narrowing, but such strictures are rarely associated



Figure 18-9 Long-standing achalasia with a sigmoid esophagus. There is a massively dilated esophagus with a tortuous distal configuration and tapered narrowing (arrow) above the gastroesophageal junction caused by incomplete opening of the LES. The sigmoid esophagus is a sign of end-stage achalasia.

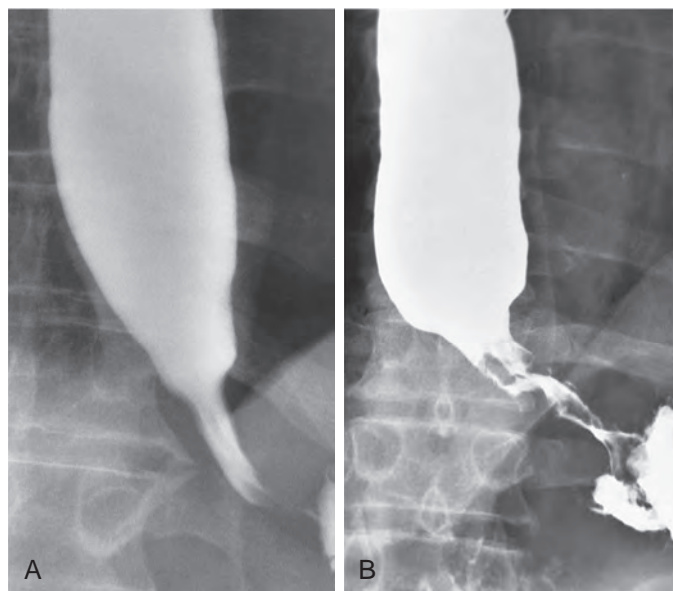


Figure 18-10 Secondary achalasia or pseudoachalasia. **A.** Smooth narrowing of the esophagogastric junction simulates achalasia. This patient had a scirrhous carcinoma of the proximal stomach invading the distal esophagus. **B.** Fluoroscopy in another patient revealed esophageal dilation and aperistalsis. However, there is irregular tapering of the esophagogastric region caused by gastric carcinoma. (**A** from Ott DJ: Radiologic evaluation of esophageal dysphagia. *Curr Probl Diagn Radiol* 17:1–33, 1988.)

TABLE 18-2 Differential Diagnosis of Achalasia

Chagas' disease
Complicated scleroderma
Extrinsic neoplasms
Intestinal pseudo-obstruction
Intrinsic neoplasms
Peptic stricture
Postvagotomy effect

with aperistalsis, and affected individuals almost always have accompanying hiatal hernias, an unusual finding in achalasia.³⁴ Scleroderma is another cause of marked esophageal dilation, but these patients typically have a patulous, gaping esophagogastric junction, enabling differentiation from achalasia. Occasionally, peptic strictures complicating scleroderma may produce an appearance simulating that of achalasia, but the correct diagnosis is usually suggested by the presence of an associated hiatal hernia.

Achalasia may be treated by botulinum toxin injection of the LES in older patients who are not candidates for more invasive therapy, but repeated injections are required because the relaxant effect of the botulinum toxin on the LES is relatively short term.³⁵ In contrast, younger patients with achalasia may have more effective long-term treatment of achalasia by pneumatic dilation or laparoscopic or surgical myotomy.^{36–38} Radiographic evaluation of the esophagus immediately after pneumatic dilation is helpful in detecting serious complications such as perforation,^{20,39–43} but is of little value for determining the long-term efficacy of the procedure because of edema and spasm of the distal esophagus in the early

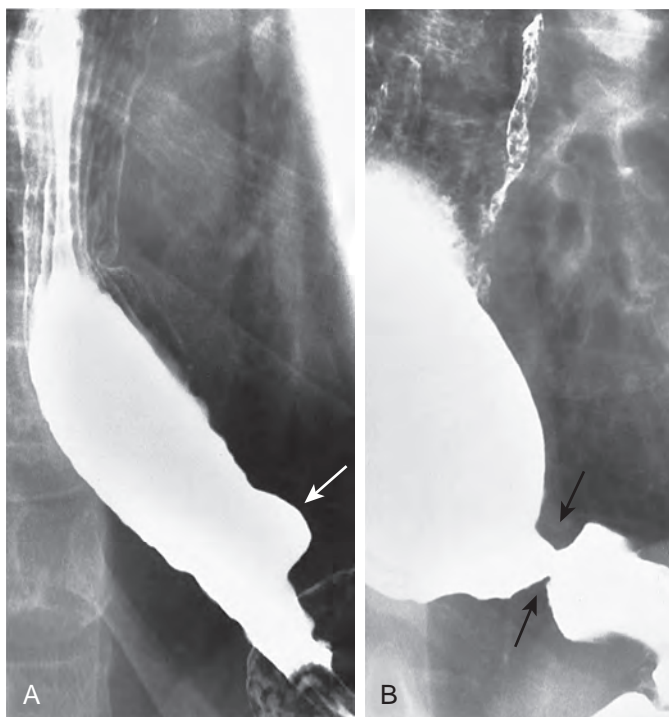


Figure 18-11 Complications of a Heller myotomy. **A.** There is a wide-mouthed outpouching or sacculation (arrow) of the distal esophagus caused by focal weakening of the wall at the site of a Heller myotomy for achalasia. **B.** A stricture (arrows) is present in the distal esophagus after a Heller myotomy in another patient with achalasia. The stricture was confirmed by endoscopy.

postoperative period.⁴³ After a Heller myotomy, a wide-mouthed outpouching or sacculation is typically present in the distal esophagus as a result of focal weakening of the wall in the region of the myotomy (Fig. 18-11A).⁴⁴ Successful treatment of achalasia may paradoxically be complicated by the development of gastroesophageal reflux, reflux esophagitis, and peptic strictures (Fig. 18-11B). For this reason, a “loose” or incomplete fundoplication is often performed at the time of the myotomy to prevent these complications.^{20,45,46} Occasionally, patients with intractable dysphagia from end-stage achalasia may require an esophagogastricectomy.^{5,8,20}

Radionuclide studies and timed barium swallows may aid in the diagnosis and management of achalasia.^{20,47,48} Radionuclide transit studies are particularly helpful for quantifying esophageal retention before and after therapy.⁴⁷ Similarly, timed barium swallows are simple to perform and enable ready quantification of esophageal emptying of barium for objective assessment of the patient's response to various forms of therapy.⁴⁸

Diffuse Esophageal Spasm

Diffuse esophageal spasm (DES) is an uncommon motility disorder of unknown cause that is characterized by chest pain, often accompanied by dysphagia, and intermittently abnormal esophageal motility.^{5,7–9,17,18,49} DES typically involves the smooth muscle portion of the esophagus. Some patients have marked smooth muscle hypertrophy with thickening of the esophageal wall,⁵⁰ whereas others have little or no wall thickening.^{51,52} DES is not classically thought to involve the LES, but recent studies have shown that DES is often associated with LES dysfunction.⁴⁹ As a result, some investigators believe that achalasia, vigorous

achalasia, and DES represent a spectrum of related esophageal motility disorders and that vigorous achalasia may occur as a transitional phase between DES and achalasia.^{5,7,17,49}

Patients with DES typically present with chest pain, often accompanied by dysphagia.^{5,17,18,49,52} Radiation of pain to the shoulder or back may simulate angina and may even be relieved by nitroglycerin. The pain is often spontaneous and not related to swallowing and can worsen during emotional stress. Other patients with DES may have dysphagia for solids or liquids without chest pain. Food impaction is a dramatic but unusual feature of this motility disorder.

The major manometric criteria for DES are simultaneous contractions on more than 10% of wet swallows and intermittently normal primary peristalsis.^{5,7,17,18,52} Associated findings include repetitive or prolonged-duration contractions, high-amplitude contractions, and frequent spontaneous contractions (Fig. 18-12). Some patients with DES have normal LES function, but others have incomplete LES relaxation during swallowing.^{17,18,49}

The radiographic features of DES reflect the manometric findings.^{1,7-9,49,52} Primary peristalsis is present in the cervical esophagus but intermittently absent in the thoracic esophagus. NPCs affect the smooth muscle portion of the esophagus, intermittently disrupting primary peristalsis (Fig. 18-13A). These NPCs are often repetitive and simultaneous and, if severe, may compartmentalize the esophageal lumen, producing a classic corkscrew appearance (Fig. 18-13B).^{7,8,52} In one study, however, lumen-obliterating NPCs were detected on esophagography in less than 15% of all patients with DES.⁴⁹ Instead, most patients had NPCs of mild to moderate magnitude that did not obliterate the esophageal lumen.⁴⁹ It should therefore be recognized that the severity of NPCs varies in patients with DES, and that the absence of a corkscrew esophagus on barium studies in no way excludes this diagnosis. It has also been shown that most patients with DES have impaired LES opening on barium studies, with the tapered, beaklike distal esophageal narrowing

typically associated with achalasia (Fig. 18-14).⁴⁹ Some patients with DES may develop pulsion diverticula or even giant epiphrenic diverticula as a complication of their esophageal dysmotility (Fig. 18-15).⁵³

Muscular thickening of the esophagus is uncommon in DES, but a wall thickness of 2 cm or more is occasionally seen (normal wall thickness is less than 4 mm).⁵⁰⁻⁵² Thickening of the esophageal wall can sometimes be estimated along the right lateral border of the upper thoracic esophagus on barium studies when the wall closely apposes the pleural reflection line. Alternatively, wall thickness can be evaluated directly by computed tomography (CT) or endoscopic ultrasound.^{50,51} In patients with DES, CT may reveal smooth circumferential wall thickening, predominantly in the distal esophagus (Fig. 18-16).⁵⁴ However, esophageal wall thickening on CT is a nonspecific imaging finding that may result from a variety of causes, including esophagitis and benign and malignant tumors involving the esophagus.⁵⁴

When patients with DES have chest pain because of high-amplitude esophageal contractions, drugs such as calcium channel blockers, long-acting nitrates, and anticholinergics have been shown to decrease the amplitude of these contractions, sometimes ameliorating the patient's symptoms.⁴⁹ However, patients who present with dysphagia because of

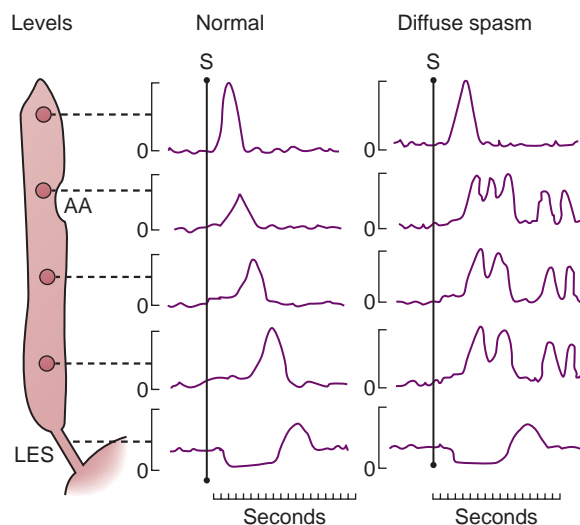


Figure 18-12 Manometric representation of normal peristalsis and diffuse esophageal spasm. Measurements are taken from multiple recording levels in the esophagus. Normal peristalsis is present in the upper esophagus but is replaced by simultaneous, repetitive contractions below the aortic arch (AA). Normal lower esophageal sphincter (LES) relaxation is seen. S, Swallow.

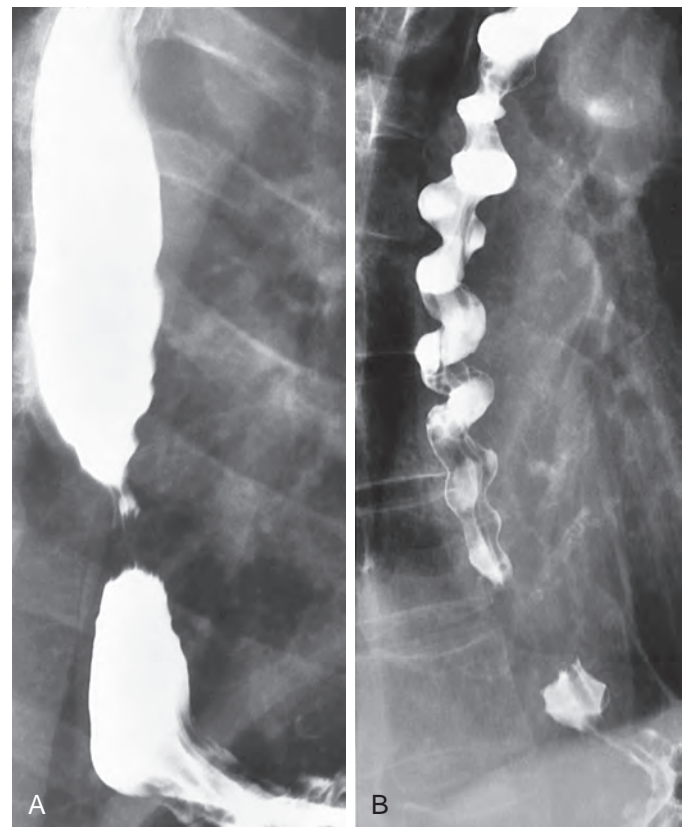


Figure 18-13 Diffuse esophageal spasm. **A.** This patient has diffuse esophageal spasm with intermittent disruption of primary peristalsis associated with a focally obliterated nonperistaltic contraction. **B.** Another patient has the typical corkscrew appearance of diffuse esophageal spasm. Clinical and manometric correlation is required to confirm the diagnosis because this appearance is nonspecific, especially in older adults. (From Levine MS, Rubesin SE, Ott DJ: Update on esophageal radiology. *AJR* 155:933-941, 1990.)

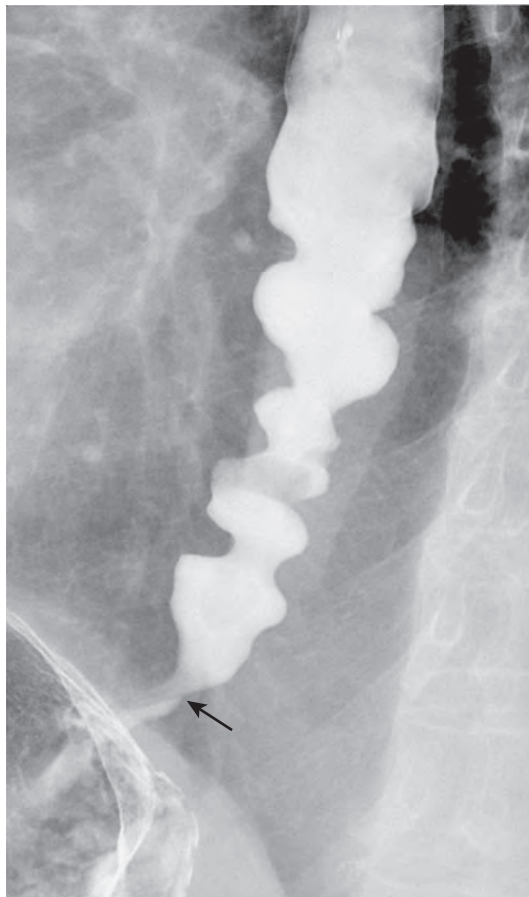


Figure 18-14 Diffuse esophageal spasm with LES dysfunction. This patient has diffuse esophageal spasm with multiple nonperistaltic contractions. There also is tapered narrowing of the distal esophagus (arrow) caused by incomplete opening of the LES.

impaired LES opening may have marked relief of dysphagia from endoscopic balloon dilation or botulinum toxin injection of the LES.⁴⁹ In the absence of symptoms, patients with manometric or radiographic findings of DES require no treatment.

Nutcracker Esophagus

Nutcracker esophagus is an esophageal motility disorder seen in some patients with chest pain or dysphagia.^{5,7,17,18,55-57} Manometric examination shows normal peristalsis, with distal contractions of abnormally high amplitude and prolonged duration (Fig. 18-17). The term *high-amplitude peristaltic esophageal contractions* has also been used to describe this entity. Debate has arisen over whether nutcracker esophagus is a true motility disorder or part of the normal spectrum of esophageal function.^{5,17,18,55-62}

Nutcracker esophagus is a manometric diagnosis made in patients with appropriate symptoms. The radiographic examination is normal or reveals only nonspecific findings such as nonperistaltic contractions.^{63,64} Nutcracker esophagus therefore is not a radiologic diagnosis.

NONSPECIFIC ESOPHAGEAL MOTILITY DISORDER

Nonspecific esophageal motility disorder (NEMD) is a catchall category used for patients with motility disturbances that do



Figure 18-15 Giant epiphrenic diverticulum. A giant diverticulum (arrows), also known as an epiphrenic diverticulum, is seen arising from the right lateral aspect of the distal esophagus. This usually develops as a pulsion diverticulum secondary to long-standing esophageal dysmotility.

not fit clinical, manometric, or radiographic criteria for classic motility disorders such as achalasia and DES.^{5,17,18,65,66} Patients with NEMD sometimes have dysphagia or chest pain, but symptoms may be minimal or absent. Manometric abnormalities include intermittent absence of peristalsis on 20% or more of wet swallows, low-amplitude peristalsis, prolonged duration of peristalsis, repetitive or triple-peaked contractions, and incomplete LES relaxation (Fig. 18-18).^{17,18,65} Esophagography may reveal disruption of primary peristalsis and a variable number of NPCs, mimicking other esophageal motility disorders such as DES and presbyesophagus (Fig. 18-19).⁷⁻⁹ Barium studies may also be normal in patients with NEMD who have only minor manometric abnormalities.⁷⁻⁹

Presbyesophagus

Presbyesophagus has become a controversial entity.^{7-9,11-14,67,68} As originally described, the term *presbyesophagus* referred to a form of esophageal motor dysfunction associated with aging that rarely causes esophageal symptoms such as chest pain or dysphagia.^{67,68} The major manometric criteria include a decreased frequency of normal peristalsis, increased frequency of simultaneous contractions and, less commonly, incomplete LES relaxation. Barium studies in these patients may also reveal intermittently weakened or absent peristalsis with a variable number of NPCs. In early reports of presbyesophagus, however, affected individuals often had underlying neurologic disorders or diabetes, which might have accounted for their esophageal dysmotility. Later manometric studies in older patients have shown only minor changes in esophageal motility with

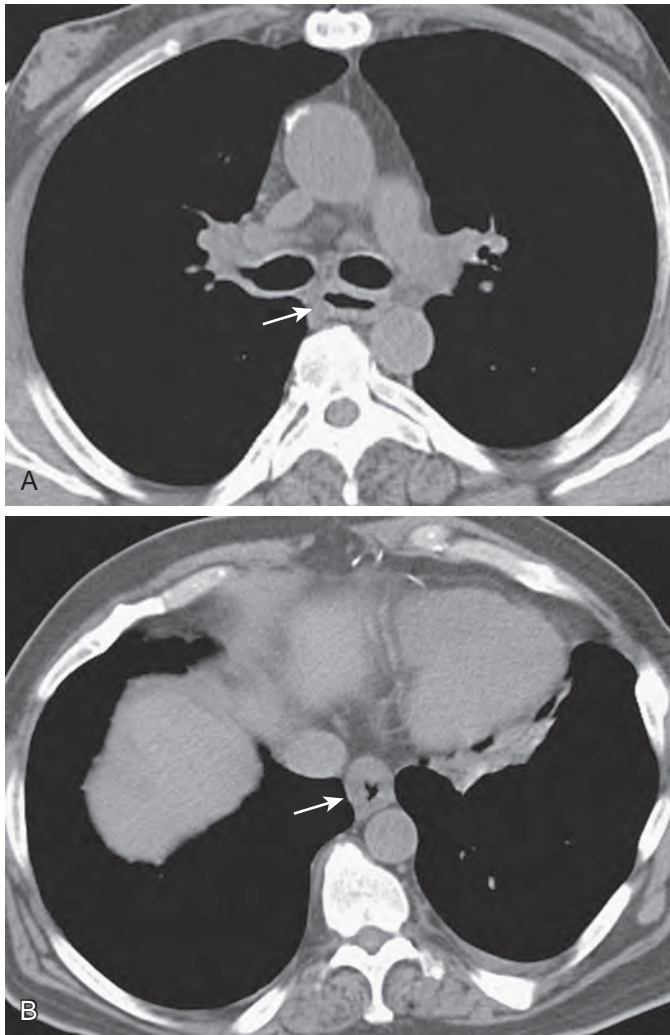


Figure 18-16 Diffuse esophageal spasm on CT. Axial contrast-enhanced CT images of the chest show moderate esophageal wall thickening (arrow) just below the carina (**A**) and even greater esophageal wall thickening (arrow) more distally (**B**). Barium esophagography revealed characteristic findings of diffuse esophageal spasm with multiple nonperistaltic contractions at fluoroscopy. Esophageal wall thickening is thought to result from progressive hypertrophy of the muscularis propria in these patients. (From Goldberg MF, Levine MS, Torigian DA: Diffuse esophageal spasm: CT findings in seven patients. *AJR* 191:758–763, 2008.)

aging.^{11–13} Furthermore, many of the manometric criteria for presbyesophagus are similar to those for NEMD, which may be the preferred radiologic term for this form of esophageal dysfunction. Whatever terminology is used, presbyesophagus is a clinically trivial condition that should be differentiated from DES and other motility disorders associated with chest pain or dysphagia.

Hypertensive Lower Esophageal Sphincter

Hypertensive LES was first described in patients with esophageal symptoms who had unusually high resting LES pressures.^{5,17,18,69} Almost all patients have chest pain, and many have dysphagia. The reported manometric criteria include a resting LES pressure greater than 40 mm Hg, with normal LES relaxation and esophageal peristalsis. Barium studies are usually normal in these patients.⁶⁹ Like nutcracker esophagus,

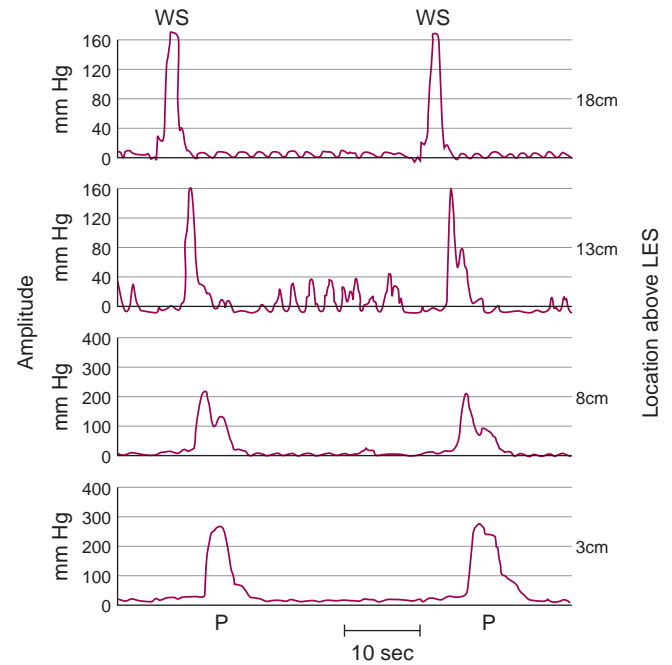


Figure 18-17 Manometric representation of nutcracker esophagus. This patient had a normal radiographic examination. There is normal peristalsis (P) manometrically, with high-amplitude contractions (>200 mm Hg, lower two leads). Accentuated baseline activity in the 13-cm lead is cardiac artifact. LES, Lower esophageal sphincter; WS, wet swallow. (Redrawn from Ott DJ, Richter JE, Chen YM, et al: Esophageal radiography and manometry: Correlation in 172 patients with dysphagia. *AJR* 149: 307–311, 1987.)

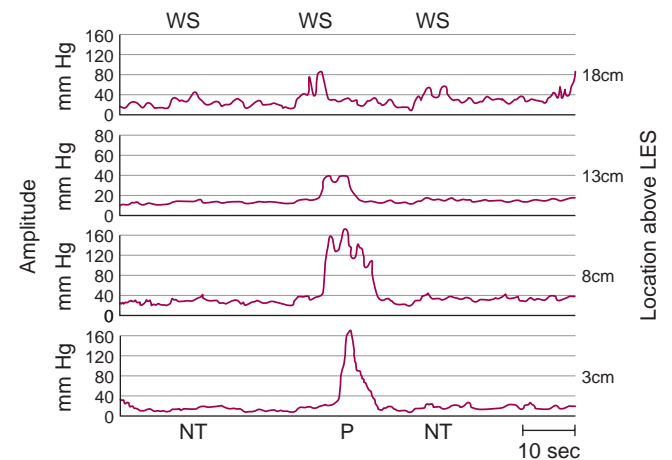


Figure 18-18 Manometric representation of nonspecific esophageal motility disorder. There is nontransmitted peristalsis (NT) in the lower leads and repetitive contractions during transmitted peristalsis (P). LES, Lower esophageal sphincter; WS, wet swallow. (Redrawn from Ott DJ, Richter JE, Chen YM, et al: Esophageal radiography and manometry: Correlation in 172 patients with dysphagia. *AJR* 149:307–311, 1987.)

hypertensive LES is thought to be a manometric diagnosis rather than a radiologic diagnosis.

SECONDARY MOTILITY DISORDERS

The causes of secondary esophageal motility disorders are numerous and varied (see Table 18-1).^{1,7–9,17–19,70} The radiographic findings are nonspecific and are often similar to those

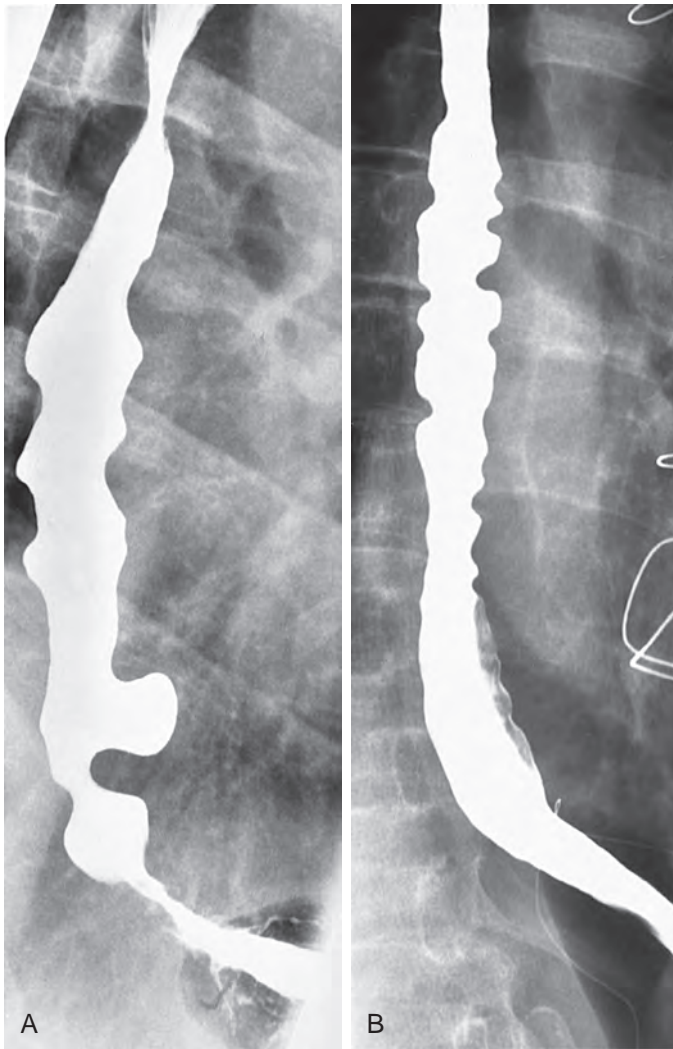


Figure 18-19 Nonspecific esophageal motility disorder. **A.** This asymptomatic patient had simultaneous nonperistaltic contractions. Primary peristalsis was disrupted intermittently at fluoroscopy. Nonspecific esophageal motility disorder was diagnosed by manometry. **B.** Multiple nonperistaltic contractions and disrupted primary peristalsis are seen in another patient with nonspecific esophageal motility disorder. Clinical and manometric correlation are needed to distinguish this condition from diffuse esophageal spasm. (From Levine MS, Rubesin SE, Ott DJ: Update on esophageal radiology. *AJR* 155:933–941, 1990.)

described for NEMD. Thus, clinical correlation is critical for the proper diagnosis of secondary esophageal motility disorders.

Gastroesophageal Reflux Disease

Patients with gastroesophageal reflux disease (GERD) often have esophageal dysmotility that is characterized on barium studies and manometry by intermittently decreased or absent primary peristalsis in the mid and lower esophagus, without accompanying NPCs.^{71,72} This form of esophageal dysmotility should be differentiated from DES, NEMD, and presbyesophagus, which are almost always associated with NPCs of variable number and severity. It is uncertain whether the dysmotility of GERD is caused by refluxed acid in the esophagus, physical injury from reflux esophagitis, or a combination of both.⁷³ Whatever the pathogenesis, abnormal peristalsis in patients with GERD impairs the clearance of refluxed acid from the

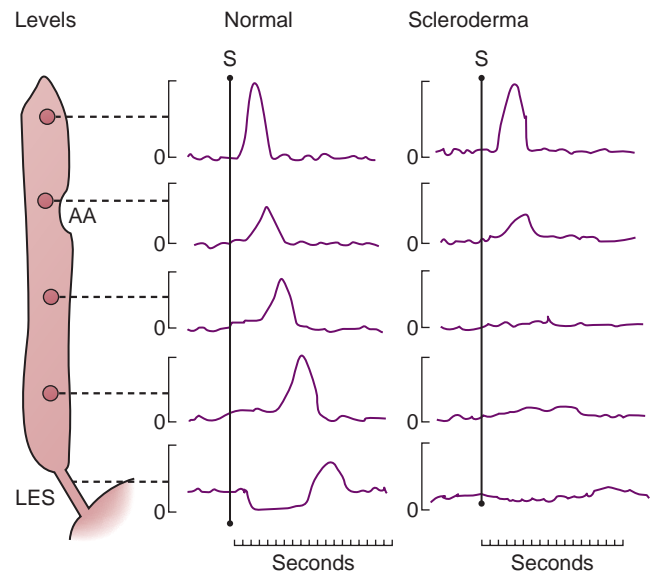


Figure 18-20 Manometric representation of normal peristalsis and scleroderma. Measurements are taken from multiple recording levels in the esophagus. Normal peristalsis is present in the upper esophagus, with absence of peristalsis in the smooth muscle segment. The lower esophageal sphincter (LES) also shows low resting pressure. AA, Aortic arch; S, swallow.

esophagus, leading to a vicious cycle, with progressively severe reflux esophagitis.⁷⁴ The presence of esophageal dysmotility without NPCs on barium studies should therefore elicit a careful search for GERD and its sequelae. Rarely, reflux esophagitis may be manifested on barium studies by esophageal aperistalsis.⁷⁵ It has been postulated that this severe form of esophageal dysmotility is secondary to neuronal damage in Auerbach's plexus from reflux esophagitis.⁷⁵

Collagen Vascular Diseases

Collagen vascular diseases are characterized by immunologic and inflammatory changes in connective tissue, typically involving multiple organ systems. The esophagus is often involved by collagen vascular disease, most commonly scleroderma, mixed connective tissue disease, dermatomyositis, and polymyositis.^{17-19,76} Although scleroderma and mixed connective tissue disease typically involve the lower two thirds of the esophagus, which contains smooth muscle in its wall, dermatomyositis and polymyositis usually involve the pharynx and upper third of the esophagus, which contain striated muscle.

Scleroderma is characterized by fibrosis and degenerative changes in the skin, synovium, and parenchyma of multiple organs, including the esophagus. Esophageal involvement occurs in most patients with scleroderma, with the smooth muscle portion and LES predominantly affected.^{17-19,76,77} Because of resulting LES incompetence, symptoms of gastroesophageal reflux are common. Affected individuals may subsequently develop dysphagia secondary to abnormal motility, reflux esophagitis, or peptic strictures. Manometric features of scleroderma include decreased or absent resting LES pressure and markedly weakened or absent peristalsis in the lower two thirds of the esophagus (Fig. 18-20).^{17-19,76,77} Barium studies typically reveal absent peristalsis in the smooth muscle portion of the esophagus, with a markedly dilated esophagus, patulous gastroesophageal junction, and free gastroesophageal reflux, with poor clearance of refluxed barium from the esophagus

after reflux occurs (Fig. 18-21A). As a result, these patients often develop severe reflux esophagitis and peptic strictures (Fig. 18-21B). The major consideration in the differential diagnosis for a dilated, aperistaltic esophagus is achalasia, but this condition is almost always associated with tapered distal esophageal narrowing, enabling differentiation from scleroderma. Occasionally, patients with scleroderma may develop superimposed *Candida* esophagitis secondary to stasis and colonization of the esophagus by the fungal organism.⁷⁸

Other Secondary Motility Disorders

A variety of conditions may be associated with motility disorders in the esophagus. Of the infectious causes, Chagas' disease has the most specific appearance.^{5,17-19} This infection occurs primarily in South America and is caused by a protozoan organism, *Trypanosoma cruzi*. The disease affects multiple organs, including the myenteric plexus of the gastrointestinal tract, and may produce esophageal abnormalities identical to those in achalasia.

A variety of metabolic and endocrine disorders may affect esophageal motor function. In diabetic patients with peripheral neuropathy, manometric and radiographic abnormalities of the esophagus are common.^{5,17-19} The most frequent findings on barium studies include decreased primary peristalsis, NPCs, and mild esophageal dilation. Esophageal dysmotility is also common in alcoholic patients, but this dysmotility may be reversed by withdrawal of alcohol.⁷⁹

Esophageal motility may also be affected by a variety of neuromuscular disorders that predominantly involve the pharynx and upper esophagus. Finally, idiopathic intestinal pseudo-obstruction is a poorly understood syndrome that is sometimes associated with esophageal dysmotility, producing a radiographic appearance indistinguishable from that of achalasia.¹⁷⁻¹⁹

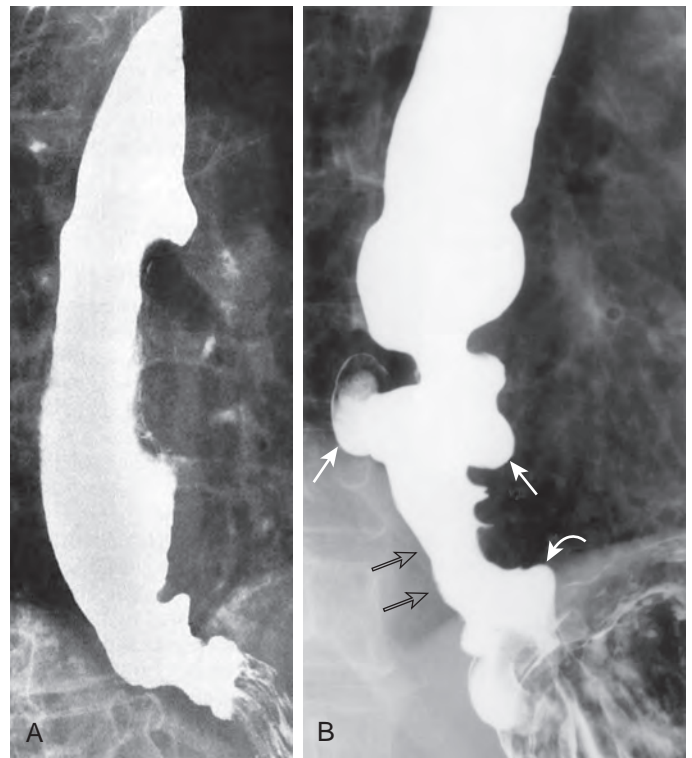


Figure 18-21 Esophageal involvement by scleroderma.

A. This patient has a dilated esophagus and a patulous esophagogastric junction. Esophageal peristalsis was absent at fluoroscopy. **B.** Another patient with scleroderma has developed a peptic stricture (open arrows) as a complication of reflux disease. Also note a small hiatal hernia (curved arrow) and sacculations (straight arrows) in the distal esophagus above the level of the stricture.

REFERENCES

- Dodds WJ: Esophagus-radiology. In Margulis AR, Burhenne HJ, editors: *Alimentary Tract Radiology*, vol 1, ed 4, St. Louis, 1989, CV Mosby, pp 427-500.
- Meyer GW, Austin RM, Brady CE, III, et al: Muscle anatomy of the human esophagus. *J Clin Gastroenterol* 8:131-134, 1986.
- Mittal RK, Balaban DH: The esophagogastric junction. *N Engl J Med* 336:924-932, 1997.
- Ott DJ: Pharynx and esophagus. In Ott DJ, Gelfand DW, Chen MYM, editors: *Manual of Gastrointestinal Fluoroscopy*, Springfield, IL, 1996, Charles C Thomas, pp 24-51.
- Clouse RE, Diamant NE: Esophageal motor and sensory function and motor disorders of the esophagus. In Feldman M, Friedman LS, Sleisenger MH, editors: *Gastrointestinal and Liver Disease*, vol 1, ed 7, Philadelphia, 2002, Saunders, pp 561-598.
- Goyal RK, Prasad M, Chang HY: Functional anatomy and physiology of swallowing and esophageal motility. In Castell DO, Richter JE, editors: *The Esophagus*, ed 4, Philadelphia, 2004, Lippincott Williams & Wilkins, pp 1-36.
- Ott DJ: Motility disorders of the esophagus. *Radiol Clin North Am* 32:1117-1134, 1994.
- Levine MS, Rubesin SE: Radiology of the pharynx and esophagus. In Castell DO, Richter RE, editors: *The Esophagus*, ed 4, Philadelphia, 2004, Lippincott Williams & Wilkins, pp 47-105.
- Schima W, Eisenhuber E: Radiologic evaluation of esophageal function. In Ekberg O, editor: *Radiology of the Pharynx and the Esophagus*, Berlin, 2004, Springer, pp 109-125.
- Ribeiro AC, Klingler PJ, Hinder RA, DeVault K: Esophageal manometry: A comparison of findings in younger and older patients. *Am J Gastroenterol* 93:706-710, 1998.
- Grande L, Lacima G, Ros E, et al: Deterioration of esophageal motility with age: A manometric study of 79 healthy subjects. *Am J Gastroenterol* 94:1795-1801, 1999.
- Shaker R, Lang IM: Effect of aging on the deglutitive oral, pharyngeal, and esophageal motor junction. *Dysphagia* 9:221-228, 1994.
- Grishaw EK, Ott DJ, Frederick MG, et al: Functional abnormalities of the esophagus: A prospective analysis of radiographic findings relative to age and symptoms. *AJR* 167:719-723, 1996.
- Ott DJ, Pikna LA: Clinical and videofluoroscopic evaluation of swallowing disorders. *AJR* 161:507-513, 1993.
- Ott DJ, Chen YM, Hewson EG, et al: Esophageal motility: Assessment with synchronous video tape fluoroscopy and manometry. *Radiology* 173:419-422, 1989.
- Clouse RE, Alrakawi A, Staiano A: Intersubject and interswallow variability in topography of esophageal motility. *Dig Dis Sci* 43:1978-1985, 1998.
- Spechler SJ, Castell DO: Nonachalasia esophageal motility abnormalities. In Castell DO, Richter RE, editors: *The Esophagus*, ed 4, Philadelphia, 2004, Lippincott Williams & Wilkins, pp 262-274.
- Alrakawi A, Clouse RE: The changing use of esophageal manometry in clinical practice. *Am J Gastroenterol* 93:2359-2362, 1998.
- Clouse RE, Staiano A, Alrakawi A, Haroian L: Application of topographical methods to clinical esophageal manometry. *Am J Gastroenterol* 95:2720-2730, 2000.
- Richter RE: Achalasia. In Castell DO, Richter RE, editors: *The Esophagus*, ed 4, Philadelphia, 2004, Lippincott Williams & Wilkins, pp 221-261.
- Goldblum JR, Whyte RI, Orringer MB, et al: Achalasia—a morphologic study of 42 resected specimens. *Am J Surg Pathol* 18:327-337, 1994.
- Sandler RS, Nyren O, Ekblom A, et al: The risk of esophageal cancer in patients with achalasia—a population-based study. *JAMA* 274:1359-1362, 1995.
- Woodfield CA, Levine MS, Rubesin SE, et al: Diagnosis of primary versus secondary achalasia: Reassessment of clinical and radiographic criteria. *AJR* 175:727-731, 2000.
- Tucker HJ, Snape WJ, Cohen S: Achalasia secondary to carcinoma: Manometric and clinical features. *Ann Intern Med* 89:315-318, 1978.

25. Parkman HP, Cohen S: Malignancy-induced secondary achalasia. *Dysphagia* 9:292–296, 1994.
26. Amaravadi R, Levine MS, Rubesin SE, et al: Achalasia with complete relaxation of lower esophageal sphincter: Radiographic-manometric correlation. *Radiology* 235:886–891, 2005.
27. Goldenberg SP, Burrell M, Fette GG, et al: Classic and vigorous achalasia: A comparison of manometric, radiographic, and clinical findings. *Gastroenterology* 101:743–748, 1991.
28. Todorcuk JR, Aliperti G, Staiano A, et al: Reevaluation of manometric criteria for vigorous achalasia—is this a distinct clinical disorder? *Dig Dis Sci* 36:274–278, 1991.
29. Ott DJ, Richter JE, Chen YM, et al: Radiographic and manometric correlation in achalasia with apparent relaxation of the lower esophageal sphincter. *Gastrointest Radiol* 14:1–5, 1989.
30. Vaezi MF, Richter JE: Diagnosis and management of achalasia. *Am J Gastroenterol* 94:3406–3412, 1999.
31. Blam ME, Delfyett W, Levine MS, et al: Achalasia: A disease of varied and subtle symptoms that do not correlate with radiographic findings. *Am J Gastroenterol* 97:1916–1923, 2002.
32. Nayar DS, Khandwala F, Achkar E, et al: Esophageal manometry: Assessment of interpreter consistency. *Clin Gastroenterol Hepatol* 3:218–224, 2005.
33. Hansford BG, Mitchell MT, Gasparaitis A: Water flush technique: A noninvasive method of optimizing visualization of the distal esophagus in patients with primary achalasia. *AJR* 200:818–821, 2013.
34. Ott DJ, Hodge RG, Chen MYM, et al: Achalasia associated with hiatal hernia: Prevalence and potential implications. *Abdom Imaging* 18:7–9, 1993.
35. Kolbasnik J, Waterfall WE, Fachnie B, et al: Long-term efficacy of botulinum toxin in classical achalasia: A prospective study. *Am J Gastroenterol* 94:3434–3439, 1999.
36. Katz PO, Gilbert J, Castell DO: Pneumatic dilatation is effective long-term treatment for achalasia. *Dig Dis Sci* 43:1973–1977, 1998.
37. West RL, Hirsch DP, Bartelsman JF, et al: Long term results of pneumatic dilation in achalasia followed for more than 5 years. *Am J Gastroenterol* 97:1346–1351, 2002.
38. Vela MF, Richter JE, Khandwala F, et al: The long-term efficacy of pneumatic dilatation and Heller myotomy for the treatment of achalasia. *Clin Gastroenterol Hepatol* 4:580–587, 2006.
39. Ott DJ, Donati D, Wu WC, et al: Radiographic evaluation of achalasia immediately after pneumatic dilatation with the Rigidflex dilator. *Gastrointest Radiol* 16:279–282, 1991.
40. Molina EG, Stollman N, Grauer L, et al: Conservative management of esophageal nontransmural tears after pneumatic dilation for achalasia. *Am J Gastroenterol* 91:15–18, 1995.
41. Metman E-H, Lagasse J-P, d'Altoche L, et al: Risk factors for immediate complications after progressive pneumatic dilation for achalasia. *Am J Gastroenterol* 94:1179–1185, 1999.
42. Ott DJ, Pineau BC, Chen MY: Intervention on the esophagus. In Ekberg O, editor: *Radiology of the Pharynx and the Esophagus*, Berlin, 2004, Springer, pp 153–166.
43. Yoo C, Levine MS, Redfern RO, et al: Laparoscopic Heller myotomy and fundoplication: Findings and predictive value of early postoperative radiographic studies. *Abdom Imaging* 29:643–647, 2004.
44. Rubesin SE, Kennedy M, Levine MS, et al: Distal esophageal ballooning following Heller myotomy. *Radiology* 167:345–347, 1988.
45. Ackroyd R, Watson DJ, Devitt PG, Jamieson GG: Laparoscopic cardiomyotomy and anterior partial fundoplication for achalasia. *Surg Endosc* 15:683–686, 2001.
46. Hui JM, Hunt DR, de Carle DJ, et al: Esophageal pneumatic dilation for postfundoplication dysphagia: Safety, efficacy, and predictors of outcome. *Am J Gastroenterol* 97:2986–2991, 2002.
47. Mariani G, Boni G, Barreca M, et al: Radionuclide gastroesophageal motor studies. *J Nucl Med* 45:1004–1028, 2004.
48. Vaezi MF, Baker ME, Achkar E, Richter JE: Timed barium oesophagram: Better predictor of long-term success after pneumatic dilation in achalasia than symptom assessment. *Gut* 50:765–770, 2002.
49. Prabhakar A, Levine MS, Rubesin S, et al: Relationship between diffuse esophageal spasm and lower esophageal sphincter dysfunction on barium studies and manometry in 14 patients. *AJR* 183:409–413, 2004.
50. Mittal RK, Kassab G, Puckett JL, Liu J: Hypertrophy of the muscularis propria of the lower esophageal sphincter and the body of the esophagus in patients with primary motility disorders of the esophagus. *Am J Gastroenterol* 98:1705–1712, 2003.
51. Loebeberg MJ, Lewis JH, Fleischer DE, et al: Endoscopic ultrasound (EUS) for evaluating esophageal wall thickness (EWT) in esophageal motility disorders (EMD) [abstract]. *Gastroenterology* 94:A267, 1989.
52. Chen YM, Ott DJ, Hewson EG, et al: Diffuse esophageal spasm: Radiographic and manometric correlation. *Radiology* 170:807–810, 1989.
53. Fasano NC, Levine MS, Rubesin SE, et al: Epiphrenic diverticulum: Clinical and radiographic findings in 27 patients. *Dysphagia* 18:9–15, 2003.
54. Goldberg MF, Levine MS, Torigian DA: Diffuse esophageal spasm: CT findings in seven patients. *AJR* 191:758–763, 2008.
55. Mujica VR, Mudipalli RS, Rao SSC: Pathophysiology of chest pain in patients with nutcracker esophagus. *Am J Gastroenterol* 96:1371–1377, 2001.
56. Pilhall M, Borjesson M, Rolny P, Mannheimer C: Diagnosis of nutcracker esophagus, segmental or diffuse hypertensive patterns, and clinical characteristics. *Dig Dis Sci* 47:1381–1388, 2002.
57. Melzer E, Ron Y, Tiomni E, et al: Assessment of the esophageal wall by endoscopic ultrasonography in patients with nutcracker esophagus. *Gastrointest Endosc* 46:223–225, 1997.
58. Lacima G, Grande L, Pera M, et al: Utility of ambulatory 24-hour esophageal pH and motility monitoring in noncardiac chest pain: Report of 90 patients and review of the literature. *Dig Dis Sci* 48:952–961, 2003.
59. Valori RM: Nutcracker, neurosis, or sampling bias? *Gut* 31:736–737, 1990.
60. Nevens F, Janssens J, Piessens J, et al: Prospective study on prevalence of esophageal chest pain in patients referred on an elective basis to a cardiac unit for suspected myocardial ischemia. *Dig Dis Sci* 36:229–235, 1991.
61. Tack J, Janssens J: The esophagus and noncardiac chest pain. In Castell DO, Richter RE, editors: *The Esophagus*, ed 4, Philadelphia, 2004, Lippincott Williams & Wilkins, pp 634–647.
62. Richter JE, Wu WC, Johns DN, et al: Esophageal manometry in 95 healthy adult volunteers. *Dig Dis Sci* 32:583–592, 1987.
63. Chobanian SJ, Curtis DJ, Benjamin SB, et al: Radiology of the nutcracker esophagus. *J Clin Gastroenterol* 8:230–232, 1986.
64. Ott DJ, Richter JE, Wu WC, et al: Radiologic and manometric correlation in “nutcracker esophagus.” *AJR* 147:692–695, 1986.
65. Freeman J, Hila A, Castell DO: Esophageal manometry. In Castell DO, Richter RE, editors: *The Esophagus*, ed 4, Philadelphia, 2004, Lippincott Williams & Wilkins, pp 115–134.
66. Hsu JJ, O'Connor MK, Kang YW, Kim CH: Nonspecific motor disorder of the esophagus: A real disorder or a manometric curiosity? *Gastroenterology* 104:1281–1284, 1993.
67. Ren J, Shaker R, Kusano M, et al: Effect of aging on the secondary esophageal peristalsis: Presbyesophagus revisited. *Am J Physiol* 268:G772–G779, 1995.
68. DeVault KR: Presbyesophagus: A reappraisal. *Curr Gastroenterol Rep* 4:193–199, 2002.
69. Waterman DC, Dalton CB, Ott DJ, et al: Hypertensive lower esophageal sphincter: What does it mean? *J Clin Gastroenterol* 11:139–146, 1989.
70. Wo JM: Esophageal involvement in systemic diseases. In Castell DO, Richter RE, editors: *The Esophagus*, ed 4, Philadelphia, 2004, Lippincott Williams & Wilkins, pp 611–633.
71. Campbell C, Levine MS, Rubesin SE, et al: Association between esophageal dysmotility and gastroesophageal reflux on barium studies. *Eur J Radiol* 59:88–92, 2006.
72. Kahrilas PJ, Dodds WJ, Hogan WJ, et al: Esophageal peristaltic dysfunction in peptic esophagitis. *Gastroenterology* 91:897–904, 1986.
73. Bontempo I, Piretta L, Corazzari E, et al: Effects of intraluminal acidification on oesophageal motor activity. *Gut* 35:84–90, 1995.
74. Lin S, Ke M, Xu J, et al: Impaired esophageal emptying in reflux disease. *Am J Gastroenterol* 89:1003–1006, 1994.
75. Simeone JF, Burrell M, Toffler R, et al: Aperistalsis and esophagitis. *Radiology* 82:463–467, 1964.
76. Campbell WL, Schultz JC: Specificity and sensitivity of esophageal motor abnormality in systemic sclerosis (scleroderma) and related diseases: A cineradiographic study. *Gastrointest Radiol* 11:218–222, 1986.
77. Klein HA, Wald A, Graham TO, et al: Comparative studies of esophageal function in systemic sclerosis. *Gastroenterology* 102:1551–1556, 1992.
78. Geffer WB, Laufer I, Edell S, et al: Candidiasis in the obstructed esophagus. *Radiology* 138:25–28, 1981.
79. Keshavarzian A, Iber FL, Ferguson Y: Esophageal manometry and radionuclide emptying in chronic alcoholics. *Gastroenterology* 92:651–657, 1987.

Gastroesophageal Reflux Disease

MARC S. LEVINE

CHAPTER OUTLINE

Reflux Esophagitis

Pathogenesis

Relationship Among Hiatal Hernia, Gastroesophageal Reflux, and Reflux Esophagitis

Clinical Findings

Diagnosis

Radiographic Findings

Differential Diagnosis

Barrett's Esophagus

Clinical Findings

Endoscopic and Histologic Findings

Radiographic Findings

Differential Diagnosis

Gastroesophageal reflux disease (GERD) is the most common inflammatory disease involving the esophagus, with a prevalence of 10% to 20% in the West.^{1,2} In the past, barium studies were advocated for patients with reflux symptoms primarily to show the presence of a hiatal hernia or gastroesophageal reflux (GER), detect complications such as deep ulcers or strictures, and rule out other organic or motor abnormalities in the esophagus that can mimic reflux disease. By permitting a more detailed assessment of the esophageal mucosa, however, double-contrast radiographic techniques have made it possible to detect superficial ulceration and other changes of mild or moderate esophagitis before the development of deep ulcers or strictures. Double-contrast esophagography is also a useful screening examination for Barrett's esophagus. With double-contrast techniques, barium studies therefore have a major role in the evaluation of patients with GERD.

Reflux Esophagitis

PATHOGENESIS

Reflux esophagitis is thought to be a multifactorial process related to the frequency and duration of reflux episodes, content of the refluxed material, and resistance of the esophageal mucosa.³⁻⁸ GER occurs when lower esophageal sphincter (LES) pressure is decreased or absent, so the major barrier to reflux is lost.^{3-5,9} In most patients, however, these reflux episodes result not from a sustained decrease in resting sphincter pressure but from multiple transient LES relaxations that frequently occur at night.^{6,10-12}

The severity of GERD depends not only on the frequency of reflux episodes but also on their duration. Because the duration of reflux is related to the efficacy of esophageal clearance by peristalsis, dysmotility exacerbates reflux disease and increases

the risk of developing esophagitis by prolonging exposure to refluxed acid.^{4,5} As a result, esophageal involvement by scleroderma often leads to severe esophagitis because of absent peristalsis and extremely poor clearance of peptic acid from the esophagus after reflux has occurred. In one study, 60% of patients with scleroderma who underwent endoscopy had evidence of reflux esophagitis.¹³

The severity of reflux disease also depends on the content of the refluxed material. Hydrochloric acid and pepsin are the noxious agents most responsible for injuring esophageal mucosa. These agents appear to have a synergistic effect, so reflux of acid and pepsin produces greater mucosal injury than reflux of acid alone.¹⁴ The concentration of refluxed acid is another important determinant of the degree of injury. Patients with Zollinger-Ellison syndrome are therefore more likely to develop severe esophagitis or strictures because of the high acidity of refluxed peptic juices into the esophagus.¹⁵⁻¹⁷

Finally, the severity of reflux esophagitis depends on the intrinsic resistance of the esophageal mucosa.^{4-6,8} Because mucosal resistance and esophageal motor function deteriorate with age, older patients are at greater risk for developing reflux esophagitis.

RELATIONSHIP AMONG HIATAL HERNIA, GASTROESOPHAGEAL REFLUX, AND REFLUX ESOPHAGITIS

Axial hiatal hernias occur more frequently in older patients because of progressive weakening of the ligaments that anchor the gastroesophageal junction to the surrounding esophageal hiatus of the diaphragm.^{4,18} There is considerable controversy about the relationship between a hiatal hernia and the subsequent development of GER or reflux esophagitis. Because most patients with clinically significant GERD have evidence of a hiatal hernia, it has been postulated that the presence of a hernia predisposes patients to the development of GER and reflux esophagitis.^{19,20} Nevertheless, many patients with a hiatal hernia have no evidence of GER, and many patients with GER have no evidence of a hernia.^{21,22} Thus, intrinsic LES dysfunction is probably the major factor in the development of GER, independent of the anatomic location of the sphincter above or below the diaphragm.^{3,5,21}

Although a hiatal hernia by itself is a poor predictor of GERD, most patients with severe reflux esophagitis or reflux-induced (peptic) strictures have hiatal hernias.^{5,23,24} There is evidence that marked acid reflux causes longitudinal esophageal shortening, disrupting the ligaments surrounding the gastroesophageal junction.²⁵ Thus, the hernia may represent an effect rather than a cause of esophagitis in these patients.

Similarly, GER is a poor predictor of reflux esophagitis because reflux may be demonstrated in some asymptomatic individuals but not in others with proven reflux esophagitis.^{4,5} Thus, the diagnosis of reflux esophagitis should be based not

on the presence or absence of a hiatal hernia or GER but on specific morphologic evidence of inflammatory changes in the esophagus.

CLINICAL FINDINGS

Patients with GERD classically present with heartburn—defined as retrosternal pain and burning that are worse after eating—and, less frequently, regurgitation.^{3,26,27} However, some patients may present with angina-like chest pain rather than heartburn. In one study, 43% of patients with chest pain of noncardiac origin were found to have GERD as the cause of their pain.²⁸ Others may present with epigastric pain or dyspepsia that is erroneously attributed to peptic ulcer disease.²⁹ Still others may have upper gastrointestinal (GI) bleeding, manifested by melena or guaiac-positive stool.³ However, major hemorrhage from reflux esophagitis is extremely uncommon.

An association between GERD and pulmonary problems has been well documented. Abnormal reflux has been reported in more than 80% of adult patients with asthma.³⁰ These patients typically present with nocturnal coughing or wheezing and do not have an allergic component to their asthma.²⁶ It has been postulated that this condition is caused by aspiration of refluxed acid into the airway or by vagally mediated bronchoconstriction secondary to reflux-induced irritation of the esophageal mucosa.³¹ Esophagopharyngeal reflux of peptic acid may also cause pharyngitis or laryngitis, manifested by a globus sensation, chronic cough, or hoarseness.^{26,32}

The perception of reflux symptoms depends on the degree and duration of exposure of the esophagus to refluxed acid.³³ Nevertheless, the severity of symptoms correlates poorly with the severity of reflux esophagitis on endoscopy.⁸ Some patients with marked reflux symptoms have normal endoscopic findings, whereas others with unequivocal endoscopic findings of esophagitis are asymptomatic. It has therefore been postulated that the development of reflux symptoms is sometimes related to an esophageal visceral hypersensitivity and inappropriately heightened perception because of underlying neuronal dysfunction rather than the actual degree of esophagitis in these patients.^{8,34}

The development of a peptic stricture is typically manifested by slowly progressive dysphagia for solids (followed by liquids) superimposed on a history of long-standing reflux symptoms.^{35,36} Nevertheless, 25% of patients with peptic strictures present with dysphagia as the initial manifestation of their disease.³⁶ Weight loss is usually minimal because patients with peptic strictures modify their diets to compensate for their dysphagia. Substantial weight loss should therefore raise concern about the possibility of a malignant esophageal stricture (see Chapter 23).

DIAGNOSIS

Patients with reflux symptoms may undergo various clinical tests to determine whether the symptoms are esophageal in origin and whether there are objective findings of GER or reflux esophagitis. GER may be assessed by radiologic, scintigraphic, manometric, or esophageal pH monitoring techniques. Esophagography or endoscopy is required to establish a diagnosis of reflux esophagitis. Barium studies are particularly useful for evaluating patients with GERD when surgical treatment is planned.³⁷

Gastroesophageal Reflux

Spontaneous GER is detected on barium studies in only 20% to 35% of patients with reflux esophagitis.^{5,24,38,39} Because GER often results from transient LES relaxations rather than from a sustained decrease in sphincter tone, intermittent episodes of reflux are easily missed during the brief period of fluoroscopic observation. Some radiologists advocate the use of the water siphon test (see Chapter 17), which increases the radiographic sensitivity for GER to 70%.³⁸ However, others do not favor the water siphon test, arguing that it is a physiologic technique with a low specificity for GER.^{22,40} Despite its limitations, I am a strong advocate of the water siphon test, which frequently permits detection of GER in patients in whom no reflux is observed spontaneously or with a Valsalva maneuver.

Gastroesophageal scintigraphy is an alternative technique for detecting and quantifying GER.^{41,42} Esophageal manometry can also be used to assess LES pressures, but many patients with normal resting sphincter pressures have intermittent GER secondary to transient LES relaxations.¹⁰⁻¹² Intraesophageal pH monitoring is thought to be the most accurate diagnostic test for GER,⁴³ but this test measures the acidity rather than the volume of refluxed material in the esophagus. Also, it has been shown that almost all patients with massive reflux on barium studies (defined as reflux of barium to or above the thoracic inlet with the patient in a recumbent position) have pathologic acid reflux on 24-hour esophageal pH monitoring.⁴⁴ Patients with massive GER on barium studies can therefore be further evaluated and treated for their reflux disease without need for pH monitoring.

Because the severity of GERD depends not only on the frequency of reflux episodes but also on their duration, esophageal clearance may be evaluated after reflux has occurred. Fluoroscopy, scintigraphy, intraesophageal pH monitoring, and manometry are tests used to evaluate esophageal clearance or motility.^{5,22,45,46}

Reflux Esophagitis

Conventional single-contrast esophagography has been considered to be an unreliable technique for detecting reflux esophagitis, with an overall sensitivity of only 50% to 75%.⁴⁷⁻⁵⁰ With the use of double-contrast technique, however, the radiographic sensitivity approaches 90%.^{48,50,51} A major advantage of double-contrast esophagography is that it permits a detailed assessment of the esophageal mucosa for superficial ulceration or other changes of mild or moderate esophagitis that cannot be detected with conventional barium studies. At the same time, single-contrast technique (with the patient in the prone position) is best for demonstrating areas of decreased distensibility in the distal esophagus caused by strictures or rings.⁵² A biphasic examination with upright double-contrast and prone single-contrast views of the esophagus therefore appears to be the best radiologic technique for evaluating patients with suspected reflux disease.

Endoscopy is generally advocated as the most definitive diagnostic test for reflux esophagitis. Various grading systems have been used to estimate the severity of esophagitis based on the endoscopic findings of erythema, friability, exudates, ulcers, and strictures.⁵³ Investigators have particularly focused on the importance of differentiating erosive esophagitis from nonerosive reflux disease.⁵⁴ Nevertheless, the use of endoscopy as the gold standard for reflux esophagitis is problematic because of

controversies about the endoscopic definition of esophagitis and interobserver reliability.⁵⁵⁻⁵⁷ In two studies, there was 50% or less agreement between the endoscopic and histologic findings of esophagitis.^{58,59} Thus, endoscopy is by no means an infallible technique for detecting this condition.

A definitive histologic diagnosis of reflux esophagitis can be made when endoscopic biopsy specimens reveal acute inflammatory changes with accumulation of neutrophils and eosinophils in the lamina propria. Basal cell hyperplasia of the squamous epithelium has also been recognized as an important sign of reflux disease, resulting from mucosal damage by refluxed acid and accelerated epithelial turnover in the esophagus.⁶⁰ Nevertheless, the histologic diagnosis of reflux esophagitis can be unreliable because of the patchy distribution of disease. In one study, 30% of patients with reflux symptoms had normal and abnormal biopsy specimens obtained from the same regions of the esophagus.⁶⁰ Some investigators have even questioned whether endoscopic biopsy specimens should be used as the gold standard for reflux esophagitis.⁶¹

RADIOGRAPHIC FINDINGS

Abnormal Motility

Between 25% and 50% of patients with reflux esophagitis have abnormal esophageal motility on manometry, manifested by weakening or disruption of primary peristalsis in the esophagus.^{4,62} In one study, esophagography revealed a distinct form of esophageal dysmotility in patients with GER in which there was intermittently weakened or absent peristalsis in the mid or lower esophagus without associated nonperistaltic contractions (NPCs).⁶³ In contrast, esophageal dysmotility associated with aging (also known as presbyesophagus) is characterized by a combination of weakened peristalsis and multiple repetitive NPCs of varying severity.⁶⁴ The presence of intermittently weakened or absent peristalsis without NPCs should therefore suggest underlying GERD on barium studies.⁶³

Much less frequently, esophageal aperistalsis may be the only radiographic finding in patients with reflux esophagitis.⁶⁵ In such cases, abnormal motility may be secondary to neuronal damage in Auerbach's plexus caused by the inflammatory process in the esophageal wall.⁶⁵ Conversely, preexisting esophageal dysmotility (e.g., that associated with scleroderma) may predispose patients to the development of reflux esophagitis by impairing clearance of refluxed acid from the esophagus. In either case, the combination of abnormal motility and GER results in a vicious cycle, sometimes leading to progressively severe esophagitis and stricture formation.⁵

Mucosal Nodularity

In the early stages of reflux esophagitis, mucosal edema and inflammation may be manifested on double-contrast images by a finely nodular or granular appearance in the distal third of the thoracic esophagus (Fig. 19-1).^{59,66-68} In one study, mucosal granularity was the most frequent and reliable sign of reflux esophagitis on double-contrast esophagograms, with a specificity and positive predictive value of about 90%.⁵⁹ This granularity is characterized by poorly defined lucencies that fade peripherally into the adjacent mucosa. Less frequently, reflux esophagitis may produce coarse nodularity of the mucosa. In almost all cases, this granularity or nodularity extends proximally from the gastroesophageal junction as a continuous area of disease.



Figure 19-1 Reflux esophagitis with a granular mucosa. There is a finely nodular or granular appearance of the mucosa extending proximally from the gastroesophageal junction as a continuous area of disease. (From Levine MS, Rubesin SE: *Diseases of the esophagus: Diagnosis with esophagography*. Radiology 237:414-427, 2005.)

More advanced reflux esophagitis may occasionally be associated with inflammatory exudates or pseudomembranes that resemble the plaquelike lesions of *Candida* esophagitis (Fig. 19-2),⁶⁹ but these patients usually present with reflux symptoms rather than odynophagia. A single large pseudomembrane can also be mistaken for a plaquelike carcinoma, particularly an adenocarcinoma arising in Barrett's mucosa.⁶⁹ However, pseudomembrane formation may be suggested by the presence of other satellite lesions or by changes in the size or shape of the lesions at fluoroscopy. When the radiographic findings are equivocal, endoscopy and biopsy should be performed for a definitive diagnosis.

Ulceration

Shallow ulcers and erosions associated with reflux esophagitis may appear on double-contrast barium studies as one or more tiny collections of barium in the distal esophagus at or near the gastroesophageal junction (Fig. 19-3).^{66,67} The ulcers can have a punctate, linear, stellate, or serpiginous configuration and are often associated with surrounding mounds of edematous mucosa, radiating folds, and puckering or saccululation of the adjacent esophageal wall (Fig. 19-4).^{66,67,70} Some patients may have diffuse ulceration of the distal third or even half of the thoracic esophagus. However, ulceration in reflux esophagitis tends to occur as a continuous area of disease extending proximally from the gastroesophageal junction, so the presence of



Figure 19-2 Reflux esophagitis with pseudomembranes. The pseudomembranes appear as discrete plaquelike defects indistinguishable from the plaques of candidiasis. (Courtesy Howard Kessler, MD, Philadelphia.)

one or more ulcers in the upper or middle thirds of the esophagus with sparing of the distal third should suggest another cause for the patient's disease.

Reflux esophagitis may also be manifested by a solitary ulcer in the distal esophagus at or near the gastroesophageal junction.⁷¹ These marginal ulcers may be recognized en face as discrete collections of barium (Fig. 19-5A) but are best visualized when the ulcers are viewed in profile (Fig. 19-5B). In one study, about 70% of these solitary reflux-induced ulcers were found to be located on the posterior wall of the esophagus (see Fig. 19-5B).⁷¹ Because GER often occurs during sleep, it has been postulated that patients who sleep primarily in the supine position are more likely to develop posterior wall ulcers as a result of prolonged exposure to refluxed acid that pools by gravity on the dependent (posterior) esophageal wall, causing maximal injury in this location.⁷¹

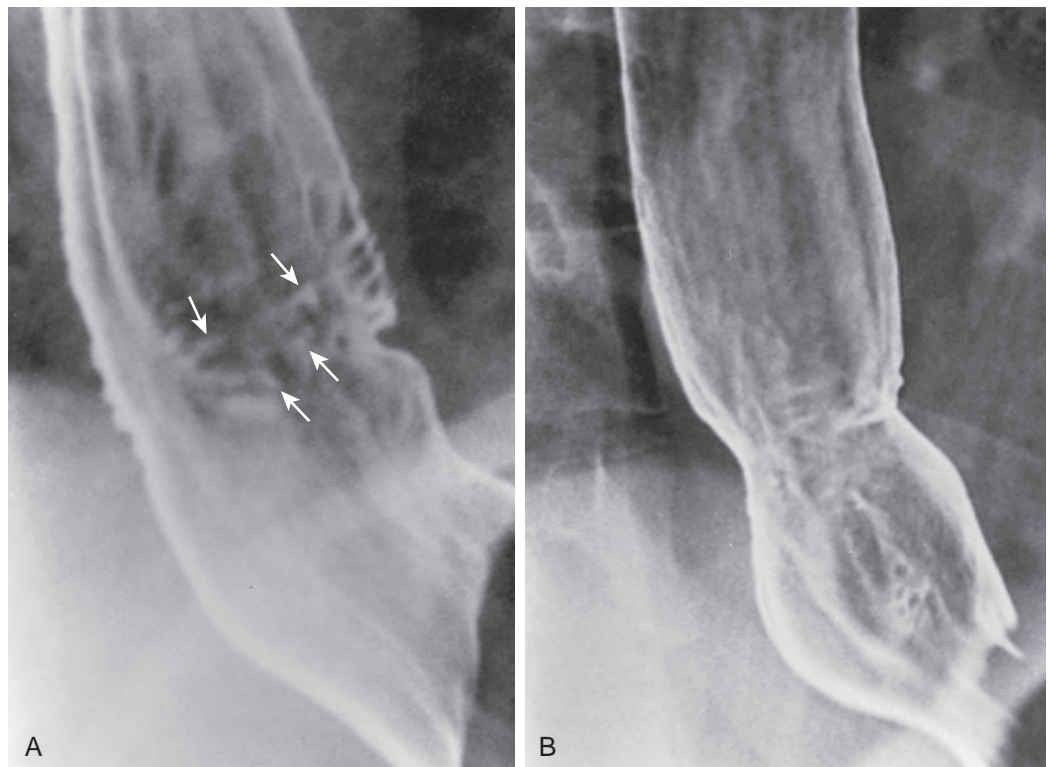
In advanced reflux esophagitis, the esophagus may have a grossly irregular contour with serrated or spiculated margins, wall thickening, and decreased distensibility secondary to extensive ulceration, edema, and spasm (Fig. 19-6).^{4,24,47,49} Occasionally, the narrowing and deformity associated with severe esophagitis can even mimic the appearance of an infiltrating carcinoma (Fig. 19-7). In such cases, endoscopy and biopsy are required for a definitive diagnosis.

Thickened Folds

In some patients with reflux esophagitis, submucosal edema and inflammation may lead to the development of thickened longitudinal folds (Fig. 19-8). Thickened folds are best seen on mucosal relief views of the collapsed or partially collapsed esophagus in which folds wider than 3 mm are thought to be abnormal.^{49,66} These thickened folds may have a smooth, nodular, scalloped, or crenulated appearance. Occasionally, they

Figure 19-3 Reflux esophagitis with superficial ulceration.

A. Multiple tiny ulcers (arrows) are seen en face in the distal esophagus near the gastroesophageal junction. Note radiating folds and puckering of the adjacent esophageal wall.
B. Another patient has punctate and linear ulcers in the distal esophagus.



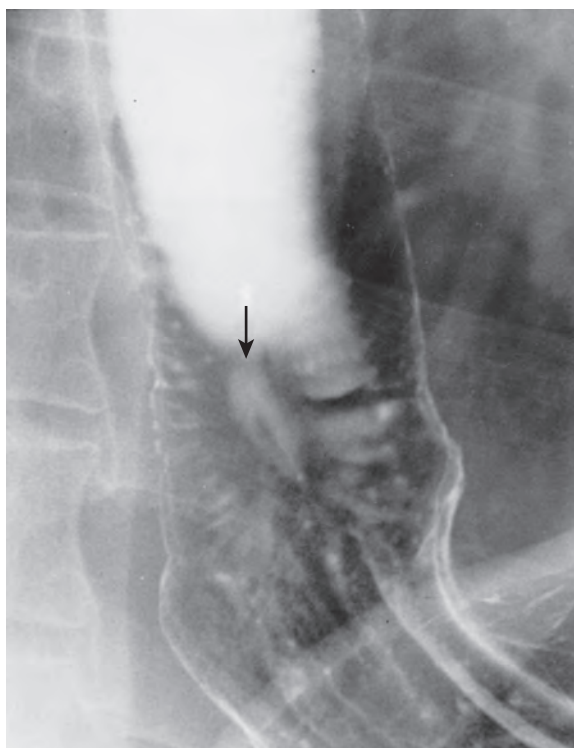


Figure 19-4 Reflux esophagitis with a linear ulcer. Note the radiolucent halo of edematous mucosa and folds radiating toward the ulcer crater (arrow). (From Laufer I, Levine MS [eds]: *Double Contrast Gastrointestinal Radiology*, 2nd ed. Philadelphia, WB Saunders, 1992.)

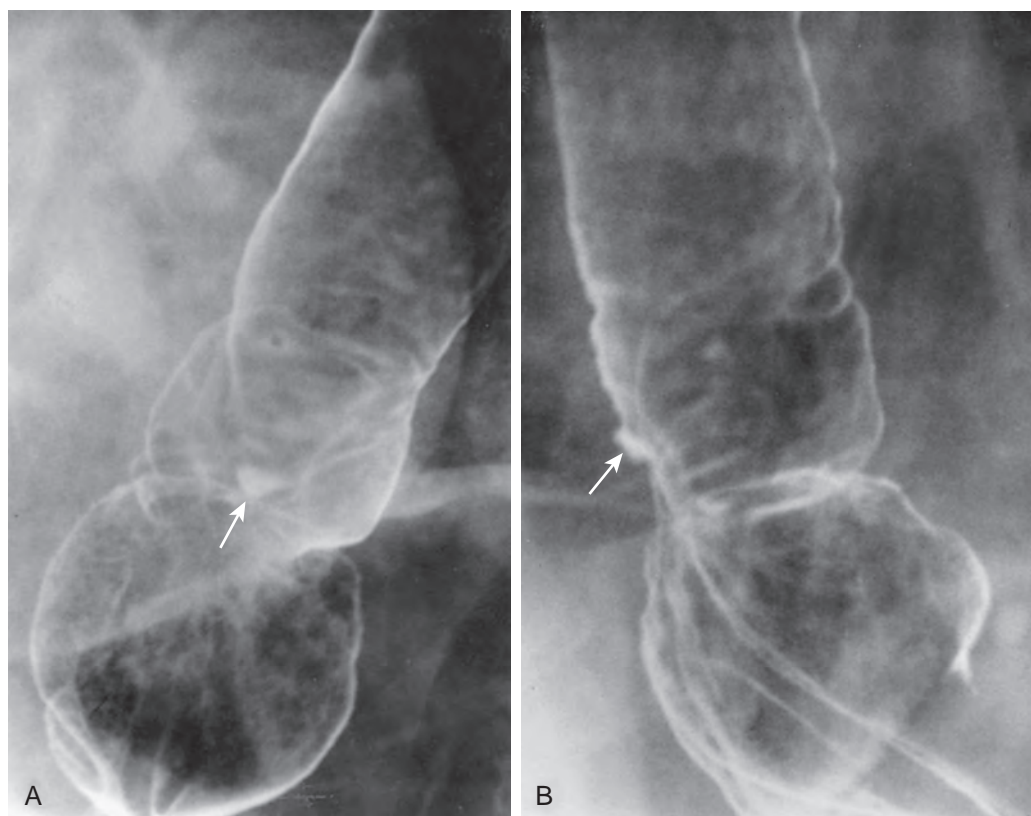


Figure 19-5 Reflux esophagitis with a discrete ulcer. This small ulcer (arrows) is seen both en face (**A**) and in profile (**B**) in the distal esophagus above a hiatal hernia. When viewed in profile (**B**), note how the ulcer is located on the right posterolateral wall of the distal esophagus. (From Laufer I, Levine MS [eds]: *Double Contrast Gastrointestinal Radiology*, 2nd ed. Philadelphia, WB Saunders, 1992.)

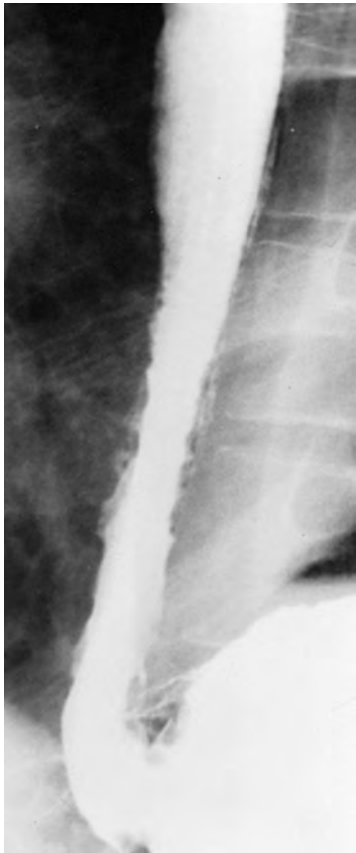


Figure 19-6 Advanced reflux esophagitis. There is decreased distensibility of the distal esophagus, which has an irregular, serrated contour because of extensive ulceration, edema, and spasm of the wall. (From Levine MS: *Radiology of the Esophagus*. Philadelphia, WB Saunders, 1989.)

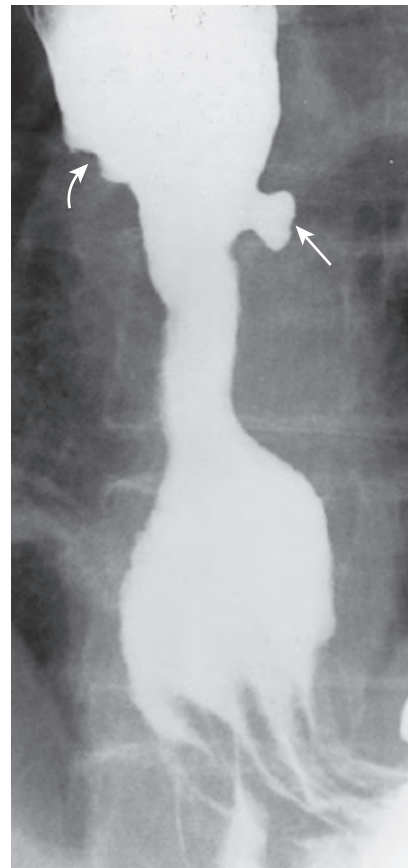


Figure 19-7 Reflux esophagitis with a deep ulcer (straight arrow). There is also asymmetric narrowing of the distal esophagus with a relatively abrupt cutoff (curved arrow) at the proximal border of the narrowed segment. These findings were caused by edema and spasm, but the possibility of malignant tumor cannot be excluded on this image. (From Levine MS: *Radiology of the Esophagus*. Philadelphia, WB Saunders, 1989.)

may be tortuous or serpiginous, mimicking the appearance of esophageal varices.⁷²

Multiple delicate transverse folds may also be found in patients with GERD (Fig. 19-9).⁷³⁻⁷⁶ In the past, this appearance has been described as the feline esophagus because transverse esophageal folds are normally found in cats. These delicate transverse striations are only 1 to 2 mm wide and extend completely across the esophagus without interruption.⁷⁴ The folds occur as a transient phenomenon resulting from contraction of the longitudinally oriented muscularis mucosae,⁷⁵ so they may be seen on only one of a number of spot images obtained during the radiologic examination (see Fig. 19-9). It has been shown that almost 100% of patients with a feline esophagus have associated GER.⁷⁶ In fact, these transverse folds are most often observed at fluoroscopy during reflux of barium from the stomach rather than during swallowing of barium.⁷⁶ Occasionally, the transverse folds may be thickened in patients with reflux esophagitis (Fig. 19-10).⁶⁶

Inflammatory Esophagogastric Polyps

Other patients with reflux esophagitis may develop inflammatory esophagogastric polyps consisting of inflammatory and granulation tissue.⁷⁷⁻⁷⁹ The polyps usually appear on barium

studies as smooth, ovoid, or club-shaped protuberances in the lower esophagus atop a single prominent fold that tapers distally at the gastroesophageal junction (Fig. 19-11).^{77,78} Inflammatory esophagogastric polyps frequently straddle a hiatal hernia and may be associated with other radiographic findings of reflux esophagitis. Because these lesions have no malignant potential, endoscopy is not warranted when a typical inflammatory esophagogastric polyp is found on barium study (see Fig. 19-11A).^{78,79} If the lesions have a lobulated or irregular appearance (see Fig. 19-11B), however, endoscopy and biopsy should be performed to rule out malignant tumor.

Scarring and Strictures

Scarring from reflux esophagitis may be manifested by a variety of findings on esophagography. It is sometimes possible to detect slight flattening or puckering of the esophageal wall, radiating folds, or both in the absence of an actual stricture (Fig. 19-12). Asymmetric scarring from reflux esophagitis may also lead to focal outpouching or sacculation of the distal esophagus as a result of outward ballooning of the wall between areas of fibrosis (Fig. 19-13). Although these sacculations may resemble ulcer craters, they can usually be differentiated from ulcers by their more rounded appearance and changeable configuration

at fluoroscopy. Sacculations are particularly likely to develop in patients with scleroderma involving the esophagus, presumably because of the severe esophagitis that occurs in these individuals. Much less frequently, patients with esophageal involvement by scleroderma may develop wide-mouthed outpouchings or sacculations in the absence of strictures as a result of asymmetric smooth muscle atrophy and fibrosis (Fig. 19-14).⁸⁰

Scarring from reflux esophagitis may also be manifested by fixed transverse folds in the distal esophagus, producing a characteristic stepladder appearance as a result of pooling of barium between the folds (Fig. 19-15).⁷⁰ These transverse folds are usually 2 to 5 mm wide and do not extend more than halfway across the esophagus. They tend to be few in number and cannot be obliterated with esophageal distention. In most cases, there is other evidence of scarring from reflux esophagitis, and these transverse folds extend proximally a variable distance from the site of a distal stricture or scar.⁷⁰ The folds probably represent areas of heaped-up or crinkled mucosa caused by simultaneous longitudinal scarring from reflux esophagitis. These fixed transverse folds should be distinguished from the thin transverse striations that are sometimes observed as a transient finding in patients with a feline esophagus (see Fig. 19-9).⁷³⁻⁷⁶

Between 10% and 20% of patients with reflux esophagitis develop peptic strictures as a result of circumferential scarring of the distal esophagus.^{50,81} Accurate radiographic diagnosis of these strictures requires continuous drinking of low-density barium in the prone position to distend the distal esophagus and optimally demonstrate mild or even moderate strictures that are not visible on upright double-contrast images



Figure 19-8 Reflux esophagitis with thickened longitudinal folds. (From Levine MS: *Radiology of the Esophagus*. Philadelphia, WB Saunders, 1989.)



Figure 19-9 Transverse folds (feline esophagus) occurring as a transient phenomenon.

A. Fine transverse folds are seen in the distal esophagus.
B. Another image moments later shows obliteration of the folds. (From Levine MS: *Radiology of the Esophagus*. Philadelphia, WB Saunders, 1989.)



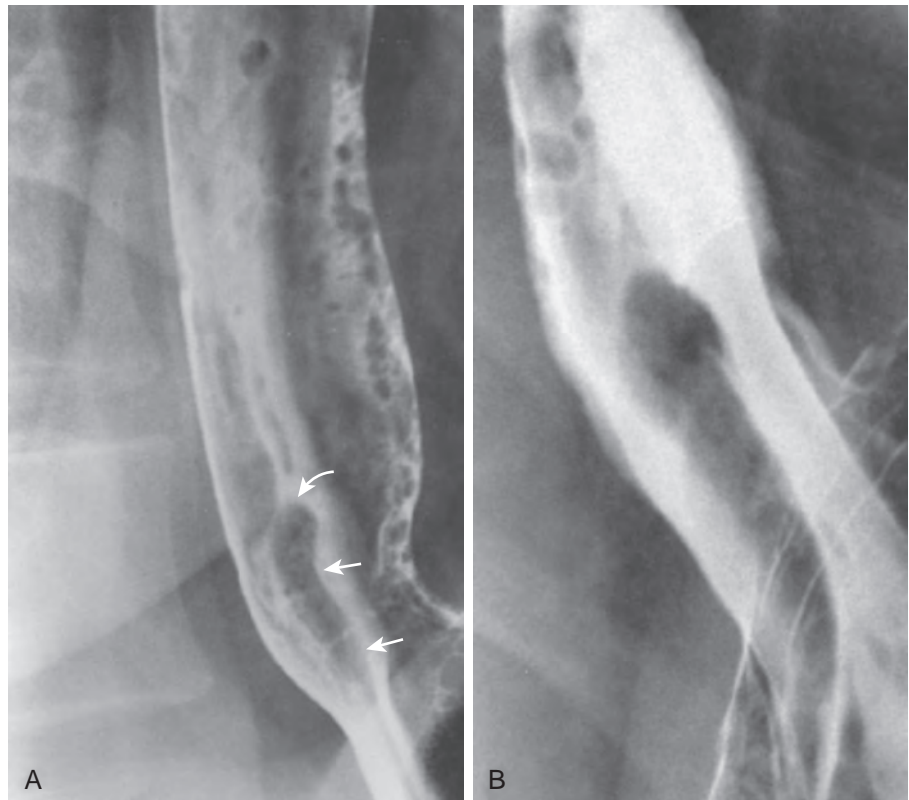
Figure 19-10 Reflux esophagitis with thickened transverse folds. There is also a peptic stricture (arrow) in the distal esophagus. (From Levine MS: *Radiology of the Esophagus*. Philadelphia, WB Saunders, 1989.)

(Fig. 19-16). With careful biphasic technique, barium studies have a sensitivity of almost 95% in detecting peptic strictures and may sometimes reveal strictures that are missed at endoscopy.^{82,83}

The vast majority of peptic strictures are located in the distal esophagus above an axial hiatal hernia (Fig. 19-17). Because many patients with GER or mild reflux esophagitis do not have a concomitant hernia, it has been postulated that scarring from reflux esophagitis leads not only to circumferential narrowing of the distal esophagus but also to longitudinal shortening and subsequent hernia formation.^{3,23,25} Whatever the explanation, a hiatal hernia is found on barium studies in more than 95% of patients with peptic strictures.²³ If the hernia fails to reduce below the diaphragm in the upright position and is a persistent finding at fluoroscopy, the patient is said to have developed a short esophagus. The latter finding has important implications for performing antireflux surgery because patients with a short esophagus may require an esophageal lengthening procedure such as a Collis gastroplasty at the time of Nissen fundoplication.⁸⁴ Conversely, when a hiatal hernia is not present in patients with distal esophageal strictures, the possibility of malignant tumor should be considered as a possible cause of these strictures because it is unlikely for a benign stricture to develop in the absence of a hernia.

The classic appearance of a smooth, tapered area of concentric narrowing in the distal esophagus above an axial hiatal hernia should be almost pathognomonic of a peptic stricture (see Fig. 19-17A).⁸⁵ Many peptic strictures have an asymmetric appearance, however, with puckering, deformity, or sacculation of one wall of the stricture caused by asymmetric scarring from reflux esophagitis (see Fig. 19-17B).⁸⁵ Other strictures may

Figure 19-11 Esophagogastric polyps. **A.** A prominent fold (straight arrows) is seen arising at the cardia and extending into the distal esophagus as a smooth polypoid protuberance (curved arrow). This appearance is characteristic of inflammatory polyps. **B.** An inflammatory esophagogastric polyp is seen in the distal esophagus in another patient. This lesion is more lobulated than most inflammatory polyps, so it cannot be differentiated from an adenomatous polyp or even an adenocarcinoma. (From Levine MS: *Radiology of the Esophagus*. Philadelphia, WB Saunders, 1989.)



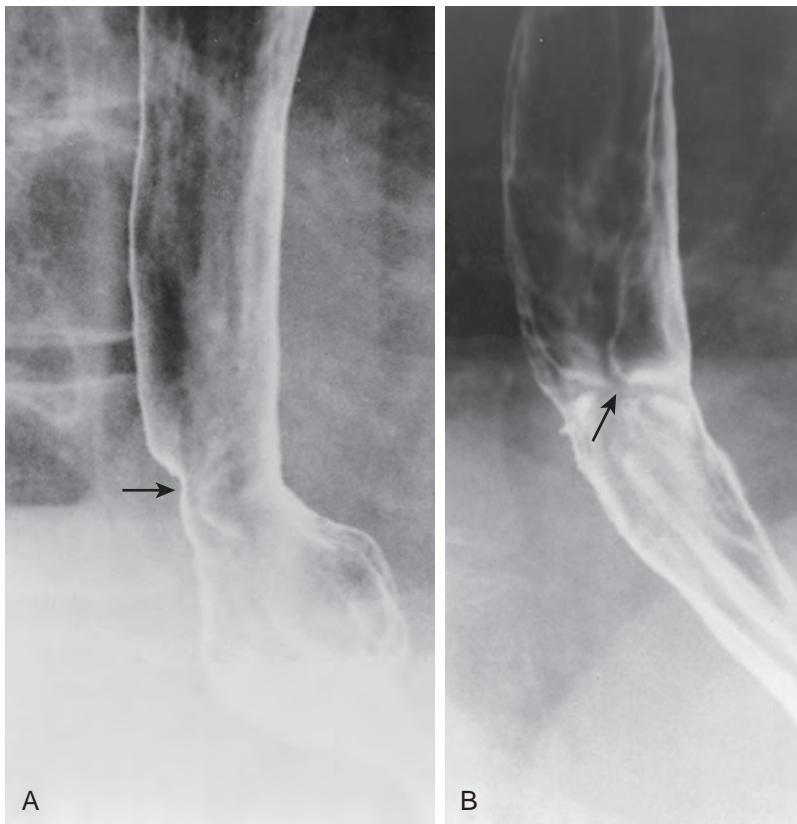


Figure 19-12 Mild peptic scarring in the distal esophagus. **A.** There is slight flattening and puckering of the distal esophagus (arrow) with radiating folds in this region as a result of scarring from reflux esophagitis. **B.** In another patient, folds are seen radiating to a central scar (arrow).

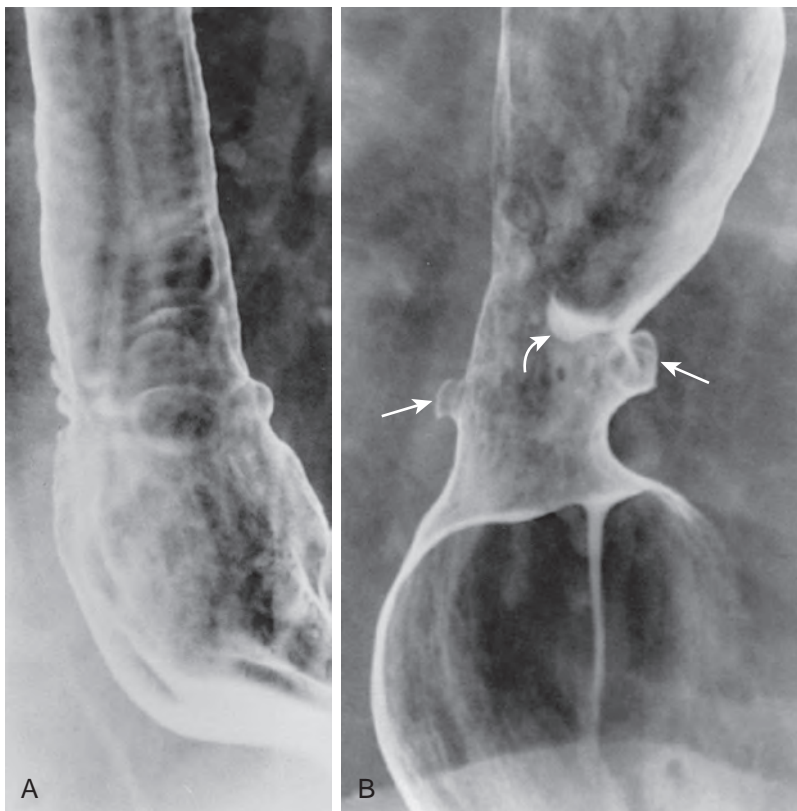


Figure 19-13 Scarring from reflux esophagitis with sacculations. **A.** There are sacculations and radiating folds in the distal esophagus without evidence of a stricture. **B.** In another patient with greater scarring, there is a peptic stricture with several large sacculations seen en face (curved arrow) and in profile (straight arrows) in the distal esophagus. (**B** from Laufer I, Levine MS [eds]: *Double Contrast Gastrointestinal Radiology*, 2nd ed. Philadelphia, WB Saunders, 1992.)

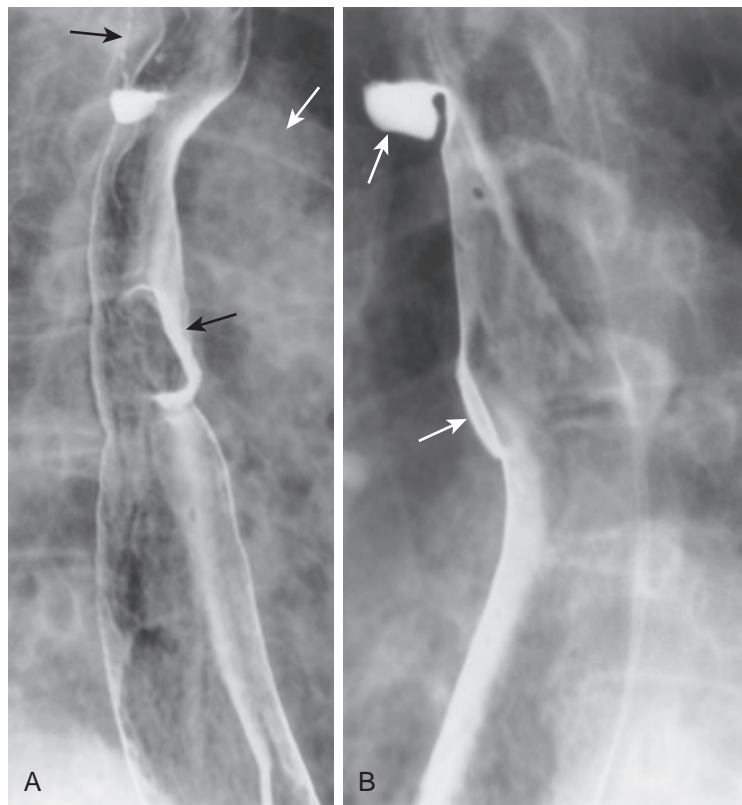


Figure 19-14 Wide-mouthed sacculations in scleroderma. **A.** Two large sacculations are seen en face (black arrows) in the upper and midesophagus. Note how the upper sacculation extends superiorly just above the level of the aortic arch (white arrow). **B.** Additional view with the patient turned 90 degrees shows the sacculations in profile (arrows). (From Coggins CA, Levine MS, Kesack CD, et al: *Wide-mouthed sacculations in the esophagus: A radiographic finding in scleroderma*. AJR 176:953–954, 2001.)

involve a longer segment of the distal esophagus and may have irregular margins because of associated reflux esophagitis (see Fig. 19-17C).⁸²

Most peptic strictures range from 1 to 4 cm in length and from 0.2 to 2.0 cm in width.^{82,86} These strictures rarely cause esophageal obstruction, but some patients may develop intermittent food impactions above the proximal end of the stricture.³⁶ As many as 40% of radiographically diagnosed peptic strictures appear as ringlike areas of narrowing at the gastroesophageal junction with slightly tapered margins and a length of only 0.4 to 1 cm (Fig. 19-18).⁸⁶ Schatzki rings may produce similar radiographic findings, but they usually range from 2 to 4 mm in length and have more abrupt, symmetric margins (see Chapter 26).⁸⁷ Despite these subtle distinctions, there probably is overlap between ringlike peptic strictures and Schatzki rings detected on barium studies or endoscopy.

Distal esophageal webs have also been recognized as a manifestation of scarring from reflux esophagitis.⁸⁸ These webs are almost always associated with peptic strictures and tend to occur several centimeters above the gastroesophageal junction, so they can usually be differentiated from Schatzki rings by their more proximal location (Fig. 19-19). Some investigators have also found an association between cervical esophageal webs and GER,⁸⁹ possibly secondary to chronic injury from refluxed acid in the cervical esophagus.

Longer peptic strictures involving the distal third of the thoracic esophagus are relatively unusual. Such strictures may occur as a result of nasogastric intubation, protracted vomiting, bile reflux after partial or total gastrectomy, and

Zollinger-Ellison syndrome (see Chapter 21).^{15-17,35,90-92} Occasionally, patients with Zollinger-Ellison syndrome may present with long strictures in the distal esophagus as the initial manifestation of their disease (Fig. 19-20).^{15,16}

Esophageal intramural pseudodiverticula can sometimes be detected in the region of a peptic stricture (Fig. 19-21; see Chapter 21).⁹³ The pseudodiverticula probably occur as a sequela of chronic reflux esophagitis, but it is unclear why so few patients with esophagitis have this finding.

Many gastroenterologists believe that endoscopy and biopsy are required to rule out malignant tumor in all patients with radiographically diagnosed peptic strictures because of difficulty differentiating benign peptic strictures from infiltrating esophageal carcinomas on esophagography.⁹⁴⁻⁹⁶ In a large retrospective study, however, no patients with unequivocally benign-appearing peptic strictures in the distal esophagus on double-contrast esophagograms were found to have malignant tumor on endoscopy,⁸⁶ so endoscopy is not required to rule out esophageal cancer in these patients. If, however, the strictures have irregular contours, more abrupt margins, or other suspicious radiographic features, endoscopy and biopsy should be performed to rule out malignant tumor, particularly an adenocarcinoma arising in Barrett's esophagus (see Chapter 23).

DIFFERENTIAL DIAGNOSIS

Artifacts

Various technical artifacts may simulate the appearance of small ulcers on double-contrast esophagography.^{66,97} When barium



Figure 19-15 Fixed transverse folds in the esophagus.

Multiple transverse folds in the distal esophagus produce a stepladder appearance caused by longitudinal scarring from reflux esophagitis. (From Levine MS, Goldstein HM: *Fixed transverse folds in the esophagus: A sign of reflux esophagitis*. *AJR* 143:275–278, 1984.)

agents are improperly prepared, barium precipitates can be mistaken for numerous tiny ulcers (Fig. 19-22A). A similar appearance may also result from transient mucosal crinkling because of incomplete esophageal distention. Occasionally, an irregular Z line at the squamocolumnar junction may resemble a focal area of superficial ulceration. Even prominent interstitial lung markings seen through the esophagus may create the erroneous impression of ulceration.

Apparent mucosal granularity or nodularity may be caused by undissolved effervescent agent, gas bubbles, or debris in the esophagus (Fig. 19-22B). As a result, the increased sensitivity of the double-contrast study has been compromised by the increased number of false-positive examinations with this technique.^{48,50} If an artifact is suspected, however, additional double-contrast images should be obtained to demonstrate the transient nature of these findings.

Mucosal Nodularity

Glycogenic acanthosis should be the major consideration in the differential diagnosis of a nodular esophageal mucosa. This benign, degenerative condition is manifested on esophagography by multiple small, rounded nodules or plaques in the esophagus that can resemble the nodular mucosa of reflux esophagitis (see Chapter 22).^{98,99} The nodules of glycogenic acanthosis tend to be more well defined than those of reflux esophagitis, however, and are usually more prominent in the midesophagus than in the distal esophagus. The clinical history

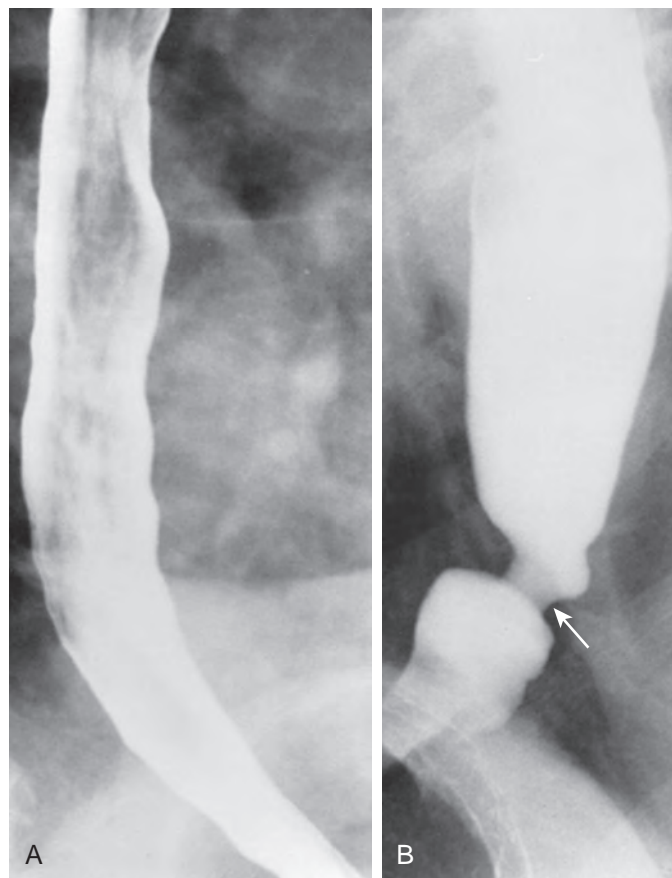


Figure 19-16 Peptic stricture seen only on prone single-contrast views of the esophagus.

A. Double-contrast view with the patient upright shows no evidence of narrowing in the distal esophagus. **B.** Single-contrast view from the same examination with the patient prone reveals an unequivocal peptic stricture (arrow) above a hiatal hernia. Even in retrospect, this short stricture was not visible on double-contrast views because of inadequate distention of this region.

is also helpful because patients with glycogenic acanthosis are almost always asymptomatic.⁹⁸

Candida esophagitis may occasionally produce a finely nodular or granular appearance in the esophagus, mimicking the appearance of reflux esophagitis (see Chapter 20). This form of *Candida* esophagitis has been observed more frequently in patients with AIDS.¹⁰⁰ Opportunistic esophagitis should be suggested by the typical history of odynophagia in an immunocompromised patient.

Rarely, superficial spreading carcinoma may produce a reticulonodular appearance of the mucosa, but the area of involvement is usually more localized than that in reflux esophagitis, and the distal esophagus is often spared.¹⁰¹ Finally, leukoplakia, squamous papillomatosis, and acanthosis nigricans are rare causes of mucosal nodularity in the esophagus; the diagnosis is usually made unexpectedly at endoscopy or autopsy in these patients (see Chapter 22).

Ulceration

Although reflux esophagitis is the most common cause of superficial ulceration in the esophagus, shallow ulcers and erosions may be caused by other types of esophagitis, including herpes esophagitis and drug-induced esophagitis.^{102,103} Unlike

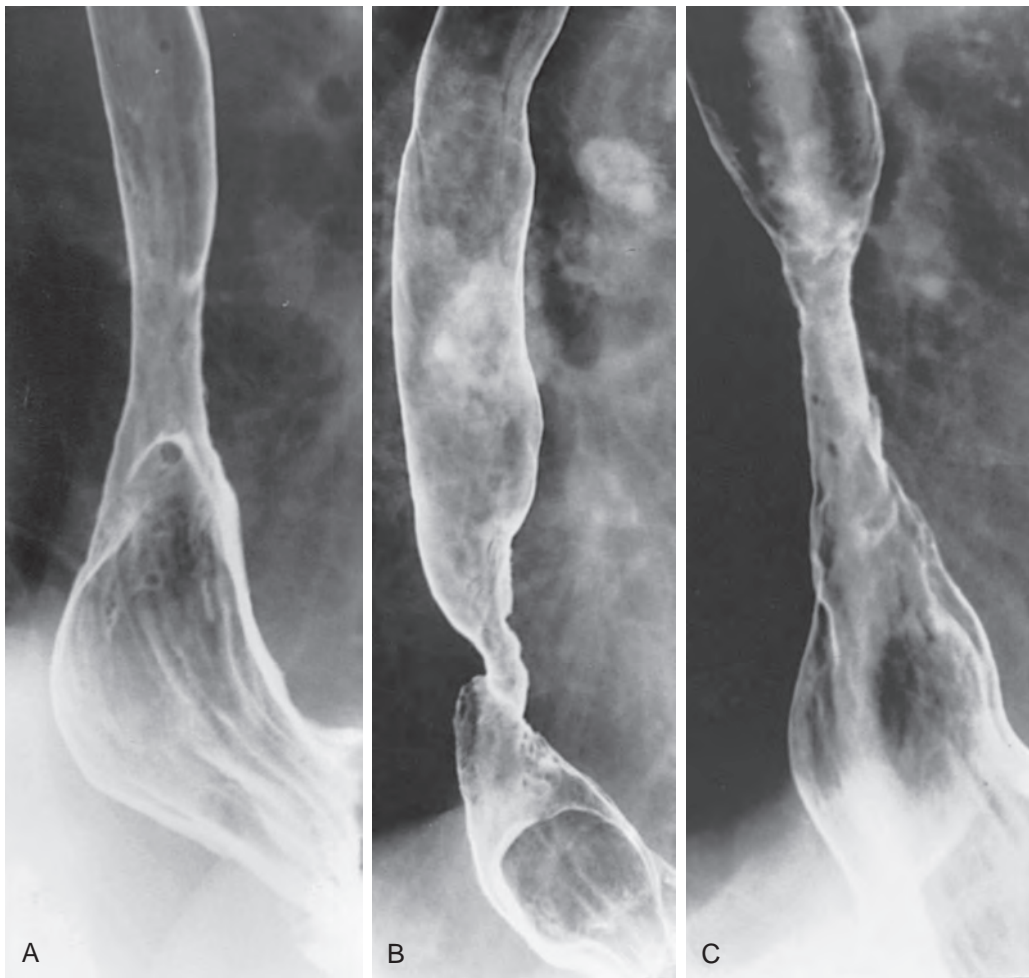


Figure 19-17 Peptic strictures. **A.** There is a concentric area of smooth, tapered narrowing in the distal esophagus above a hiatal hernia. This is the classic appearance of a peptic stricture. **B.** In another patient, there is an eccentric stricture with asymmetric narrowing and deformity of the distal esophagus. **C.** This peptic stricture involves a longer segment of the distal esophagus and has a more irregular contour. (**A** from Levine MS: *Radiology of the Esophagus*. Philadelphia, WB Saunders, 1989; **B** from Laufer I, Levine MS [eds]: *Double Contrast Gastrointestinal Radiology*, 2nd ed. Philadelphia, WB Saunders, 1992.)

reflux esophagitis, herpes esophagitis and drug-induced esophagitis tend to involve the upper or midesophagus with distal esophageal sparing (see Chapters 20 and 21), and are not usually associated with a hiatal hernia or GER. The correct diagnosis should also be suggested by a clinical history of odynophagia in immunocompromised patients or in those taking oral medications such as tetracycline.

Esophageal involvement by Crohn's disease may occasionally be manifested by tiny aphthoid ulcers, mimicking the findings of reflux esophagitis.¹⁰⁴ Esophageal Crohn's disease is uncommon, however, and these patients almost always have concomitant Crohn's disease in the small bowel or colon. More extensive ulceration may be caused by opportunistic infection, caustic ingestion, and mediastinal irradiation, but the correct diagnosis is usually suggested by the clinical history and presentation (see Chapters 20 and 21).

Thickened Folds

Thickened longitudinal folds in the esophagus may be caused by esophageal varices or by any inflammatory or neoplastic process that involves the submucosa. Although varices may occasionally resemble the thickened folds of esophagitis, they

tend to be more tortuous or serpiginous and can usually be effaced to a greater degree or even obliterated by esophageal distention. Rarely, varicoid carcinomas can also be mistaken for esophagitis on a single image.¹⁰⁵ Because the folds are infiltrated by tumor, however, they are unaffected by esophageal peristalsis and cannot be substantially effaced by esophageal distention. As a result, these entities can usually be differentiated at fluoroscopy.

Scarring and Strictures

Fixed transverse folds in the esophagus secondary to scarring from reflux esophagitis should be distinguished not only from the delicate transverse striations of the feline esophagus but also from the broad transverse bands associated with NPCs. The horizontal collections of barium pooled between these fixed transverse folds also should not be mistaken for linear ulcers. The regularity and symmetry of these folds should suggest the correct diagnosis.

A smooth, tapered area of concentric narrowing above a hiatal hernia poses little diagnostic dilemma, but not all peptic strictures have this classic appearance. If suspicious radiographic features such as asymmetry, abrupt margins, and

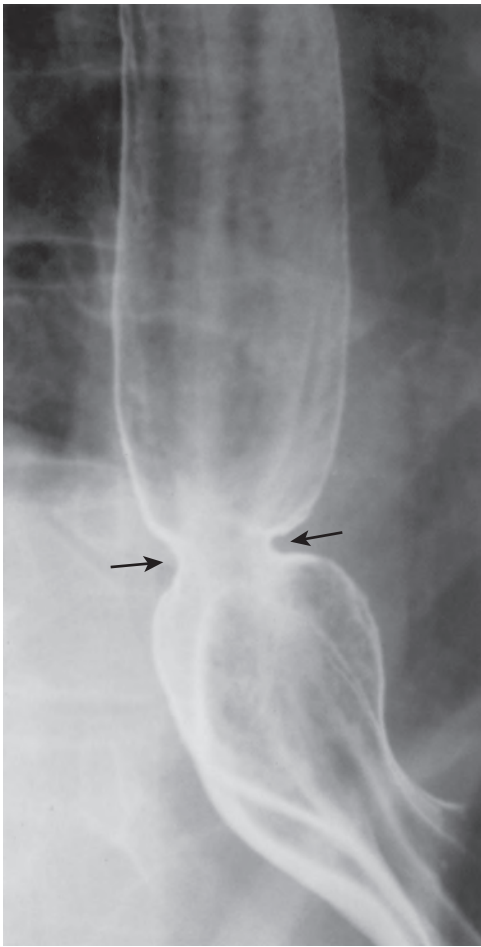


Figure 19-18 Ringlike peptic stricture. There is a ringlike stricture (arrows) in the distal esophagus above a hiatal hernia. Although this stricture could be mistaken for a Schatzki ring, it has a longer vertical height and more tapered margins than a true Schatzki ring. (From Luedtke P, Levine MS, Rubesin SE, et al: *Radiologic diagnosis of benign esophageal strictures: A pattern approach*. RadioGraphics 23:897–909, 2003.)

mucosal nodularity or ulceration are identified on the barium study, endoscopy and biopsy may be required to rule out an infiltrating carcinoma (Fig. 19-23).

Barrett's Esophagus

Barrett's esophagus is an acquired condition in which there is progressive columnar metaplasia of the distal esophagus secondary to long-standing GER and reflux esophagitis.¹⁰⁶⁻¹¹⁰ The diagnosis of Barrett's esophagus was traditionally reserved for patients who had endoscopic evidence of a columnar epithelium-lined esophagus extending more than 3 cm above the gastroesophageal junction and histopathologic findings of intestinal metaplasia on biopsy specimens.¹⁰⁸ In various studies, the prevalence of Barrett's esophagus in patients with reflux esophagitis has ranged from 5% to 15%, with an overall prevalence of about 10%.¹¹¹⁻¹¹⁵ These figures may underestimate the true prevalence of Barrett's esophagus in the general population. In one study, the number of cases of Barrett's esophagus at autopsy was 20 times greater than the number of cases at endoscopy.¹¹⁶ The findings in this study suggest that most cases



Figure 19-19 Peptic stricture with an associated web. The web (arrow) is located a greater distance from the gastroesophageal junction than expected for lower esophageal rings. (From Levine MS: *Radiology of the Esophagus*. Philadelphia, WB Saunders, 1989.)

of Barrett's esophagus remain undiagnosed because of the absence of esophageal symptoms. Nevertheless, Barrett's esophagus is being diagnosed with greater frequency as the number of patients who undergo endoscopy increases.

Despite its frequency, Barrett's esophagus would not be important if it were a benign entity. There is considerable evidence, however, that it is a premalignant condition associated with an increased risk of developing esophageal adenocarcinoma. These tumors evolve through a sequence of progressively severe epithelial dysplasia, eventually leading to the development of invasive carcinoma. In various studies, the prevalence of adenocarcinoma in patients with Barrett's esophagus has ranged from 2% to 46%, with an overall prevalence of about 10%.^{113,117,118} It should be recognized that prevalence data tend to exaggerate the risk of cancer by failing to identify all patients with underlying Barrett's esophagus. This problem is exacerbated by the fact that as many as 40% of patients with Barrett's esophagus remain asymptomatic until the development of a superimposed adenocarcinoma.¹¹⁹ In contrast, incidence data have shown that esophageal adenocarcinoma develops in only 0.1% to 0.5% of patients with Barrett's esophagus each year.^{120,121}

Whatever the precise cancer risk, the American College of Gastroenterology has recommended that patients with Barrett's esophagus undergo endoscopic surveillance at 2- to 3-year intervals to detect dysplastic changes before the development



Figure 19-20 Long peptic stricture caused by Zollinger-Ellison syndrome. There is a long area of narrowing in the distal esophagus with extensive ulceration in the region of the stricture. The unusual length of the strictures in these patients is presumably related to the higher acidity of refluxed peptic acid in Zollinger-Ellison syndrome. (From Levine MS: *Radiology of the Esophagus*. Philadelphia, WB Saunders, 1989.)

of overt cancer (see Chapter 23).¹²² The cost-effectiveness of endoscopic surveillance of patients with known Barrett's esophagus is supported by a Markov model showing that it compares favorably with other widely accepted screening strategies for cancer.¹²³ On the other hand, endoscopic surveillance of patients with Barrett's esophagus has not yet been shown to improve the mortality from esophageal adenocarcinoma. Thus, many questions remain about the role of endoscopic surveillance and its ultimate value in patients with Barrett's esophagus.

As our understanding of Barrett's esophagus has evolved, investigators have developed revised histopathologic criteria for this condition in which patients are classified as having long-segment (extending more than 3 cm from the gastroesophageal junction) or short-segment (extending 3 cm or less from the gastroesophageal junction) Barrett's esophagus based on the vertical extent of columnar metaplasia in the esophagus.¹²⁴ Short-segment Barrett's esophagus is even more common than long-segment Barrett's esophagus, with a reported prevalence of 10% to 15% at endoscopy.¹²⁵ Patients with short-segment Barrett's esophagus are more likely to develop dysplasia than the general population, but less likely to develop dysplasia than those with long-segment Barrett's esophagus.^{126,127} Although the cancer risk in these patients remains uncertain, some investigators believe that endoscopic surveillance is also warranted for patients with short-segment disease.¹²⁶⁻¹²⁹

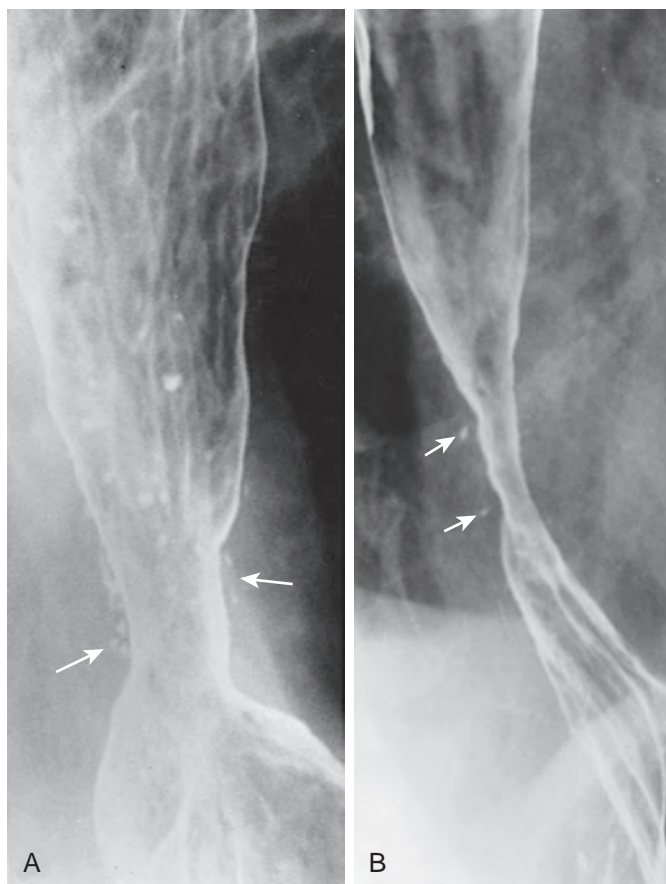


Figure 19-21 Peptic strictures with esophageal intramural pseudodiverticulosis. **A.** There is a mild peptic stricture in the distal esophagus with multiple intramural pseudodiverticula seen en face and in profile (arrows) in the region of the stricture. **B.** This patient has a more severe peptic stricture with several pseudodiverticula (arrows) adjacent to the stricture. Note how the pseudodiverticula seem to be floating outside the wall of the esophagus without apparent communication with the lumen. The latter feature is characteristic of these structures. (A from Levine MS: *Radiology of the Esophagus*. Philadelphia, WB Saunders, 1989.)

CLINICAL FINDINGS

The prevalence of Barrett's esophagus increases with age; the mean age is 55 to 60 years at the time of diagnosis.¹³⁰ This condition is more common in men than in women (2:1) and in whites than in blacks.¹³¹ Affected individuals may present with reflux symptoms because of their underlying reflux disease or with dysphagia because of the development of strictures. However, as many as 40% of patients with Barrett's esophagus are asymptomatic.¹²⁰ Such patients may not seek medical attention until the development of a superimposed esophageal adenocarcinoma (see Chapter 23). When patients with Barrett's esophagus do have reflux symptoms, they are usually treated with proton pump inhibitors or, if necessary, a laparoscopic fundoplication. It should be recognized, however, that medical or even surgical treatment of the underlying reflux disease does not cause this Barrett's epithelium to regress, so these individuals remain at risk for the development of esophageal adenocarcinoma even after a surgical fundoplication.¹³²



Figure 19-22 Double-contrast artifacts. **A.** Barium precipitates are present in the esophagus. These punctate collections of barium could be mistaken for tiny ulcers. **B.** In another patient, undissolved effervescent agent and gas bubbles in the esophagus cause apparent nodularity of the mucosa. If an artifact is suspected, additional double-contrast views should be obtained to demonstrate the transient nature of these findings. (**B** from Levine MS: *Radiology of the Esophagus*. Philadelphia, WB Saunders, 1989.)

ENDOSCOPIC AND HISTOLOGIC FINDINGS

Long-segment Barrett's esophagus can be recognized at endoscopy by the presence of velvety, pinkish red columnar mucosa (often seen as islands or tongues) extending more than 3 cm above the LES or an endoscopically identified hiatal hernia.¹⁰⁸ Endoscopy is reported to have a sensitivity greater than 90% in diagnosing Barrett's esophagus based solely on the endoscopic findings.¹³³ Conversely, short-segment Barrett's esophagus is defined as endoscopically visualized columnar epithelium in the distal esophagus extending 3 cm or less above the gastroesophageal junction.¹²⁴

In the past, the histopathologic criteria for Barrett's esophagus included the presence of columnar epithelium (including a junctional-type epithelium, gastric fundic-type epithelium, and specialized columnar epithelium or incomplete form of intestinal metaplasia) on endoscopic biopsy specimens more than 3 cm above the gastroesophageal junction.¹³⁴ Subsequently, however, investigators focused on the importance of intestinal metaplasia on endoscopic biopsy specimens anywhere from the esophagus as the major prerequisite for a histologic diagnosis of Barrett's esophagus.^{124,135} This intestinal metaplasia is

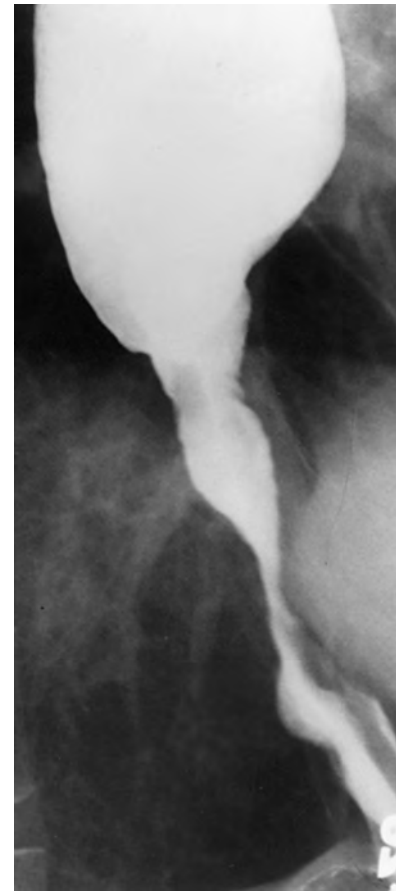


Figure 19-23 Esophageal carcinoma. There is a relatively long area of narrowing in the distal esophagus that could be mistaken for a benign peptic stricture. However, the asymmetric contour and relatively abrupt proximal margins of the narrowed segment should suggest the possibility of malignant tumor. (From Levine MS: *Radiology of the Esophagus*. Philadelphia, WB Saunders, 1989.)

characterized histologically by goblet cells with acidic mucin and, in some cases, enterocyte differentiation with brush border formation. The revised definition for Barrett's esophagus was based on an emerging consensus that intestinal metaplasia represents the major type of epithelium predisposing these individuals to esophageal adenocarcinoma.¹³⁵

RADIOGRAPHIC FINDINGS

Long-Segment Barrett's Esophagus

The classic radiologic features of long-segment Barrett's esophagus consist of a midesophageal stricture or ulcer, often associated with an axial hiatal hernia or GER.¹³⁶⁻¹³⁸ The unusually high location of these strictures or ulcers can be attributed to the fact that they often occur in the proximal zone of columnar metaplasia at or near the elevated squamocolumnar junction. The strictures may appear on barium studies as ringlike constrictions (Fig. 19-24A) or, less commonly, as tapered areas of narrowing (Fig. 19-24B) in the midesophagus.¹³⁶ Occasionally, early strictures may be recognized on double-contrast studies as subtle contour abnormalities with focal indentations or gently sloping concavities of one wall.¹³⁹ Barrett's ulcers typically appear as relatively deep ulcer craters within the columnar mucosa, occurring at a considerable distance from

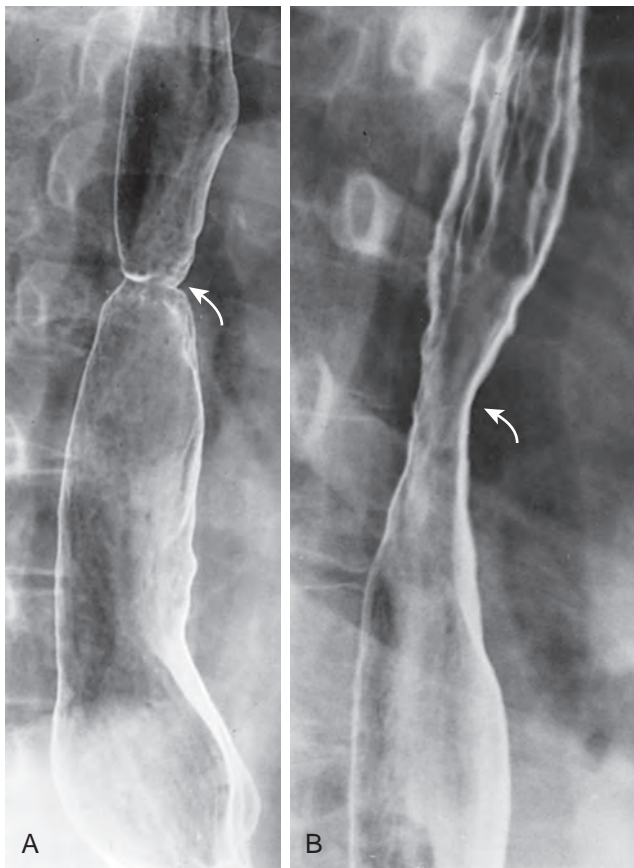


Figure 19-24 Barrett's esophagus with midesophageal strictures.

A. There is a ringlike constriction (arrow) in the midesophagus.

B. A smooth, tapered area of narrowing (arrow) is seen in the midesophagus. In the presence of a hiatal hernia and gastroesophageal reflux, a midesophageal stricture should be strongly suggestive of Barrett's esophagus. (From Levine MS: *Radiology of the Esophagus*. Philadelphia, WB Saunders, 1989.)



Figure 19-25 Barrett's esophagus with a high ulcer. There is a relatively deep ulcer crater (arrow) at a greater distance from the gastroesophageal junction than expected for uncomplicated reflux esophagitis. In the presence of a hiatal hernia and gastroesophageal reflux, a high ulcer should be strongly suggestive of Barrett's esophagus. (From Levine MS: *Radiology of the Esophagus*. Philadelphia, WB Saunders, 1989.)

the gastroesophageal junction (Fig. 19-25).¹⁴⁰ Because these findings are unusual in uncomplicated reflux disease, the presence of a midesophageal stricture or ulcer, particularly if associated with a hiatal hernia or GER, should be highly suggestive of Barrett's esophagus. However, studies have found that strictures are actually more common in the distal esophagus and that most cases do not fit the classic stereotype of a midesophageal stricture or ulcer.¹⁴¹⁻¹⁴⁴ Thus, esophagography is an inadequate screening examination for long-segment Barrett's esophagus when the diagnosis is made only in patients who have the classic radiologic features of this condition.

A reticular mucosal pattern has also been described as a relatively specific sign of long-segment Barrett's esophagus, particularly if located adjacent to a stricture.¹⁴² This delicate reticular pattern is characterized radiographically by innumerable tiny, barium-filled grooves or crevices on the esophageal mucosa, resembling the *areae gastricae* pattern found on double-contrast studies of the stomach (Fig. 19-26). In most cases, there is an adjacent stricture in the midesophagus or, less commonly, distal esophagus, with the reticular pattern seen extending distally a short but variable distance from the stricture.¹⁴² Occasionally, however, a reticular pattern of the mucosa may be observed as the only morphologic abnormality in

Barrett's esophagus without evidence of strictures.¹⁴⁵ Whether or not a stricture is present, a reticular pattern should be highly suggestive of Barrett's esophagus, and endoscopy and biopsy should be performed for a definitive diagnosis. Nevertheless, this finding has been observed in only 5% to 30% of patients with Barrett's esophagus,^{138,142-144,146} and its specificity has also been questioned.¹⁴⁷ Thus, most cases of long-segment Barrett's esophagus are missed on double-contrast esophagography if a reticular mucosal pattern is used as the primary radiologic criterion for diagnosing this condition.

Other common findings of reflux disease, such as hiatal hernias, GER, reflux esophagitis, and peptic strictures, can be detected on double-contrast esophagograms in more than 95% of patients with long-segment Barrett's esophagus (Fig. 19-27),^{137,138,141-144,146,148} but these findings frequently occur in patients with uncomplicated reflux disease in the absence of Barrett's esophagus. Thus, radiographic findings that are specific for Barrett's esophagus are not sensitive, and findings that are more sensitive are not specific. As a result, many investigators have traditionally believed that esophagography has limited value as a screening examination for Barrett's esophagus and that endoscopy and biopsy are required to diagnose this condition.

In 1988, Gilchrist and colleagues¹⁴⁹ introduced a novel approach for the diagnosis of long-segment Barrett's esophagus

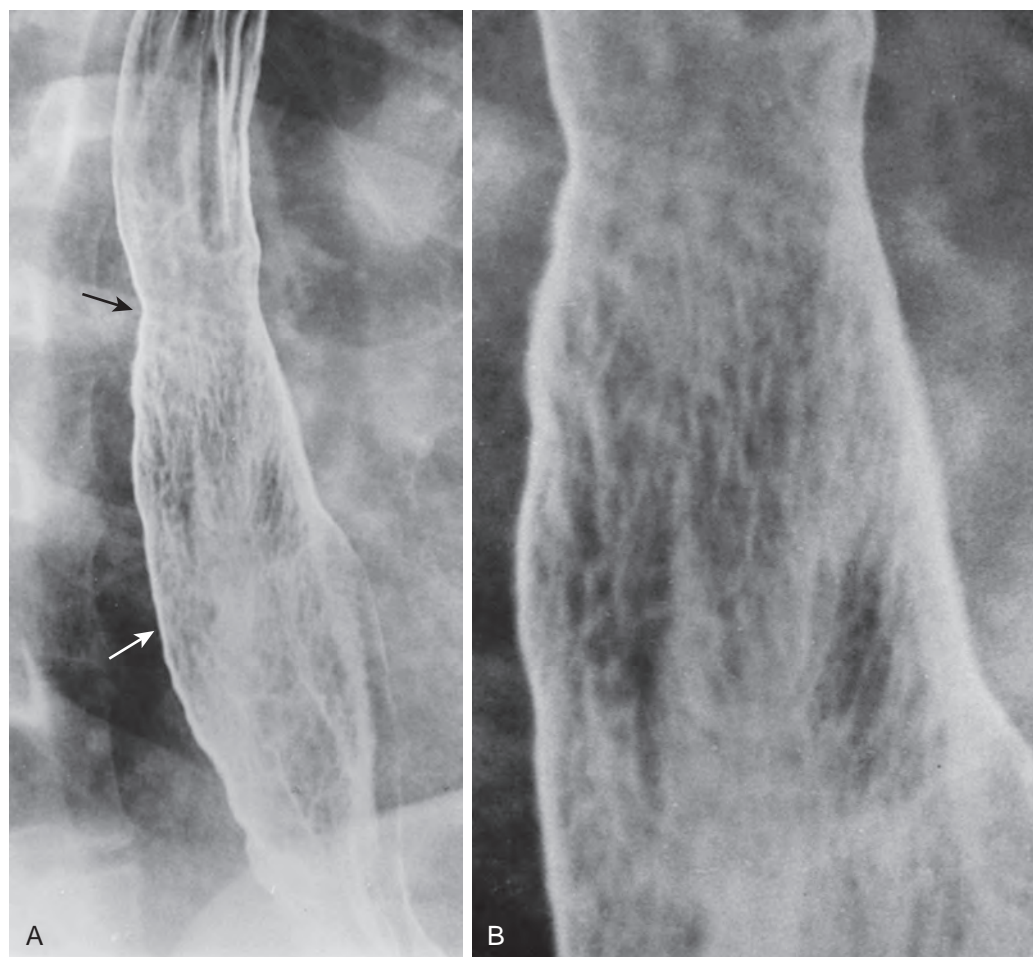


Figure 19-26 Barrett's esophagus with a reticular mucosal pattern. **A.** There is an early stricture (black arrow) in the midesophagus with a reticular pattern extending distally a considerable distance from the stricture (approximately to the level of the white arrow). **B.** A close-up view better delineates this delicate reticular pattern. (From Levine MS, Kressel HY, Caroline DF, et al: Barrett esophagus: Reticular pattern of the mucosa. *Radiology* 147:663–667, 1983.)

on double-contrast esophagography by stratifying patients with reflux symptoms based on the following radiologic criteria: patients were classified at high risk if the images revealed the classic findings of a midesophageal stricture or ulcer or a reticular mucosal pattern; at moderate risk if the images revealed reflux esophagitis or a distal peptic stricture (previous studies have found that 10% of patients with reflux esophagitis and as many as 40% with peptic strictures have Barrett's esophagus^{111–115,150}); and at low risk if the images revealed a normal-appearing esophagus. The vast majority of patients classified at high risk and approximately 15% classified at moderate risk for Barrett's esophagus on double-contrast esophagograms were found to have this condition. Conversely, fewer than 1% of patients classified at low risk for Barrett's esophagus because of the absence of esophagitis or strictures were found to have this condition. Thus, esophagitis or peptic scarring severe enough to cause Barrett's esophagus can almost always be detected on technically adequate double-contrast examinations.

On the basis of these data, the investigators concluded that patients found to be at high risk for Barrett's esophagus on double-contrast esophagograms because of a midesophageal

stricture or ulcer or reticular mucosal pattern should undergo endoscopy and biopsy for a definitive diagnosis.¹⁴⁹ A larger group of patients are found to be at moderate risk for Barrett's esophagus because of reflux esophagitis or peptic strictures in the distal esophagus, so clinical judgment should be used regarding the decision for endoscopy in this group based on the severity of reflux symptoms, age, and overall health of the patient (i.e., whether they are reasonable candidates for endoscopic surveillance). However, most patients are found to be at low risk for Barrett's esophagus because of the absence of esophagitis or strictures, and the risk of Barrett's esophagus is so low in this group that endoscopy does not appear to be warranted. Thus, the major value of double-contrast esophagography is its ability to separate patients into these various risk groups for Barrett's esophagus to determine the relative need for endoscopy and biopsy.

Short-Segment Barrett's Esophagus

Although the radiographic features of long-segment Barrett's esophagus have been well documented, much less is known about the findings in short-segment Barrett's esophagus. In a study by Yamamoto and associates,¹⁵¹ 70% of patients with

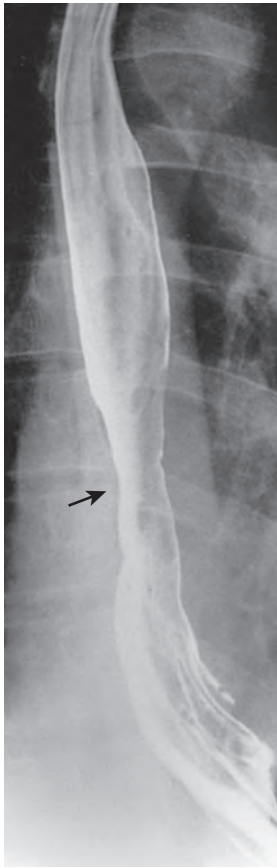


Figure 19-27 Barrett's esophagus with a distal stricture. There is a concentric area of narrowing (arrow) in the distal esophagus above a hiatal hernia. An ordinary peptic stricture without Barrett's esophagus could produce identical findings. (From Levine MS: *Radiology of the Esophagus*. Philadelphia, WB Saunders, 1989.)

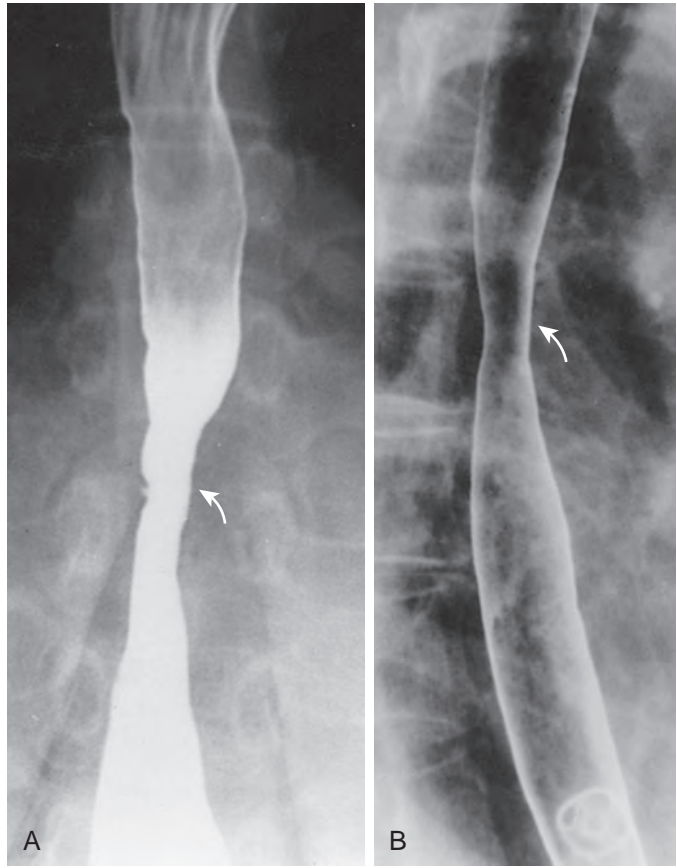


Figure 19-28 Other causes of midesophageal strictures. **A.** There is a segmental stricture (arrow) with shallow ulceration in the midesophagus secondary to previous lye ingestion. **B.** There is a smooth, tapered stricture (arrow) in the midesophagus caused by mediastinal irradiation. (From Levine MS: *Radiology of the Esophagus*. Philadelphia, WB Saunders, 1989.)

short-segment Barrett's esophagus had esophagitis or peptic scarring or strictures in the distal esophagus on double-contrast esophagograms, but the remaining 30% had hiatal hernias or GER as the only radiographic findings. Thus, the absence of reflux esophagitis or peptic strictures on double-contrast esophagograms does not exclude the possibility of short-segment Barrett's esophagus, and patients with short-segment Barrett's esophagus are far more likely to have a normal-appearing esophagus on double-contrast studies than those with long-segment disease. Nevertheless, the clinical importance of this observation remains uncertain because of the lower cancer risk of short-segment Barrett's esophagus compared with that associated with long-segment disease.^{126,127}

In the study by Yamamoto and co-workers,¹⁵¹ all the patients with short-segment Barrett's esophagus had disease confined to the distal third of the esophagus on barium studies, but the length of involvement of the distal esophagus by esophagitis or peptic scarring often extended more than 3 cm above the gastroesophageal junction, so the diseased segment on esophagography does not necessarily correspond to the vertical extent of columnar metaplasia in the esophagus.

DIFFERENTIAL DIAGNOSIS

Uncomplicated peptic strictures are almost always located in the distal esophagus, so the presence of a midesophageal stricture should strongly suggest the possibility of Barrett's esophagus, particularly if associated with a hiatal hernia and GER. Midesophageal strictures may also be caused by caustic ingestion (Fig. 19-28A), mediastinal irradiation (Fig. 19-28B), and malignant tumors, but these conditions can usually be differentiated from Barrett's esophagus by the clinical history and presentation.

The presence of a reticular mucosal pattern appears to be a relatively specific radiologic sign of Barrett's esophagus, particularly if located adjacent to the distal aspect of a midesophageal stricture.¹⁴² Although a reticulonodular appearance may occasionally be seen in patients with superficial spreading carcinoma, such lesions are not generally associated with strictures.¹⁰¹ *Candida* esophagitis may also be manifested by mucosal nodularity, but the discrete plaquelike lesions of candidiasis can usually be differentiated from the coalescent reticular pattern of Barrett's mucosa.

REFERENCES

- Locke GR, Talley NJ, Fett SL, et al: Prevalence and clinical spectrum of gastroesophageal reflux: A population-based study in Olmsted County, Minnesota. *Gastroenterology* 112:1448–1456, 1997.
- Lacy BE, Weiser K, Chertoff J, et al: The diagnosis of gastroesophageal reflux disease. *Am J Med* 123:583–592, 2010.
- Behar J: Reflux esophagitis: Pathogenesis, diagnosis, and management. *Arch Intern Med* 136:560–566, 1976.
- Dodds WJ: Current concepts of esophageal motor function: Clinical implications for radiology. *AJR* 128:549–561, 1977.
- Dodds WJ, Hogan WJ, Helm JE, et al: Pathogenesis of reflux esophagitis. *Gastroenterology* 81:376–394, 1981.
- Dodds WJ: The pathogenesis of gastroesophageal reflux disease. *AJR* 151:49–56, 1988.
- Pope CE: Acid-reflux disorders. *N Engl J Med* 331:656–660, 1994.
- Barlow WJ, Orlando RC: The pathogenesis of heartburn in nonerosive reflux disease: A unifying hypothesis. *Gastroenterology* 128:771–778, 2005.
- Pope CE: Pathophysiology and diagnosis of reflux esophagitis. *Gastroenterology* 70:445–454, 1976.
- Schoeman MN, Tippet MD, Akkermans LMA, et al: Mechanisms of gastroesophageal reflux in ambulant healthy human subjects. *Gastroenterology* 108:83–91, 1995.
- Mittal RK, Holloway RH, Penagini R, et al: Transient lower esophageal sphincter relaxation. *Gastroenterology* 109:601–610, 1995.
- Pandolfino JE, Zhang Q, Ghosh SK, et al: Transient lower esophageal sphincter relaxations and reflux: Mechanistic analysis using concurrent fluoroscopy and high-resolution manometry. *Gastroenterology* 131:1725–1733, 2006.
- Zamost BJ, Hirschberg J, Ippoliti AF, et al: Esophagitis in scleroderma: Prevalence and risk factors. *Gastroenterology* 92:421–428, 1987.
- Vaezi MF, Singh S, Richter JE: Role of acid and duodenogastric reflux in esophageal mucosal injury: A review of animal and human studies. *Gastroenterology* 108:1897–1907, 1995.
- Dodds WJ, Dehn TG, Hogan WJ, et al: Severe peptic esophagitis in a patient with Zollinger-Ellison syndrome. *AJR* 113:237–240, 1971.
- Smith HJ, Chapa HJ, Kilman WJ, et al: Zollinger-Ellison syndrome presenting as esophageal stricture. *Gastrointest Radiol* 4:349–351, 1979.
- Agha FP: Esophageal involvement in Zollinger-Ellison syndrome. *AJR* 144:721–725, 1985.
- Cohen S: The diagnosis and management of gastroesophageal reflux. *Adv Intern Med* 21:47–75, 1976.
- Wright RA, Hurwitz AL: Relationship of hiatal hernia to endoscopically proved reflux esophagitis. *Dig Dis Sci* 24:311–313, 1979.
- Ott DJ, Gelfand DW, Chen YM, et al: Predictive relationship of hiatal hernia to reflux esophagitis. *Gastrointest Radiol* 10:317–320, 1985.
- Cohen S, Harris LD: Does hiatus hernia affect competence of the gastroesophageal sphincter? *N Engl J Med* 284:1053–1056, 1971.
- Ellis FH: Current concepts: Esophageal hiatal hernia. *N Engl J Med* 287:646–649, 1972.
- Ho CS, Rodrigues PR: Lower esophageal strictures, benign or malignant? *J Can Assoc Radiol* 31:110–113, 1980.
- Ott DJ, Dodds WJ, Wu WC, et al: Current status of radiology in evaluating for gastroesophageal reflux disease. *J Clin Gastroenterol* 4:365–375, 1982.
- Paterson WG, Kolyn DM: Esophageal shortening induced by short-term intraluminal acid perfusion in opossum: A cause of hiatus hernia? *Gastroenterology* 107:1736–1740, 1994.
- Rex DK: Gastroesophageal reflux disease in adults: Pathophysiology, diagnosis, and management. *J Fam Pract* 35:673–681, 1992.
- DeVault KR, Castell DO: Guidelines for the diagnosis and treatment of gastroesophageal reflux disease. *Arch Intern Med* 155:2165–2172, 1995.
- Lam HGT, Dekker W, Kan G, et al: Acute non-cardiac chest pain in a coronary care unit. *Gastroenterology* 102:453–460, 1992.
- Boyd EJS: The prevalence of esophagitis in patients with duodenal ulcer or ulcer-like dyspepsia. *Am J Gastroenterol* 91:1539–1542, 1996.
- Sontag SJ, O'Connell S, Khandelwal S, et al: Most asthmatics have gastroesophageal reflux with or without bronchodilator therapy. *Gastroenterology* 99:613–620, 1990.
- Hamilos DL: Gastroesophageal reflux and sinusitis in asthma. *Clin Chest Med* 16:683–697, 1995.
- Deveney CW, Benner K, Cohen J: Gastroesophageal reflux and laryngeal disease. *Arch Surg* 128:1021–1027, 1993.
- Weusten BLAM, Akkermans LMA, van Berge-Henegouwen GP, et al: Symptom perception in gastroesophageal reflux disease is dependent on spatiotemporal reflux characteristics. *Gastroenterology* 108:1739–1744, 1995.
- Smith JL, Opekun AR, Larkai E, et al: Sensitivity of the esophageal mucosa to pH in gastroesophageal reflux disease. *Gastroenterology* 96:683–689, 1989.
- Bennett JR: Oesophageal strictures. *Clin Gastroenterol* 7:555–569, 1978.
- Marks RD, Richter JE: Peptic strictures of the esophagus. *Am J Gastroenterol* 88:1160–1172, 1993.
- Canon CL, Morgan DE, Einstein DM, et al: Surgical approach to gastroesophageal reflux disease: What the radiologist needs to know. *Radiographics* 25:1485–1499, 2005.
- Thompson JK, Koehler RE, Richter JE: Detection of gastroesophageal reflux: Value of barium studies compared with 24-hr pH monitoring. *AJR* 162:621–626, 1994.
- Ott DJ: Gastroesophageal reflux: What is the role of barium studies? *AJR* 162:627–629, 1994.
- Blumhagen JD, Christie DL: Gastroesophageal reflux in children: Evaluation of the water siphon test. *Radiology* 131:345–349, 1979.
- Blumhagen JD, Rudd TG, Christie DL: Gastroesophageal reflux in children: Radionuclide gastroesophagography. *AJR* 135:1001–1004, 1980.
- Malmud LS, Fisher RS: Gastroesophageal scintigraphy. *Gastrointest Radiol* 5:195–204, 1980.
- Kahrilas PJ, Quigley EMM: Clinical esophageal pH recording: A technical review for practice guideline development. *Gastroenterology* 110:1982–1996, 1996.
- Pan JJ, Levine MS, Redfern RO, et al: Gastroesophageal reflux: Comparison of barium studies with 24-h pH monitoring. *Eur J Radiol* 47:149–153, 2003.
- Booth DJ, Kemmerer WT, Skinner DB: Acid clearing from the distal esophagus. *Arch Surg* 96:731–734, 1968.
- Tolin RD, Malmud LS, Reilly J, et al: Esophageal scintigraphy to quantitate esophageal transit (quantitation of esophageal transit). *Gastroenterology* 76:1402–1408, 1979.
- Ott DJ, Gelfand DW, Wu WC: Reflux esophagitis: Radiographic and endoscopic correlation. *Radiology* 130:583–588, 1979.
- Koehler RE, Weyman PJ, Oakley HF: Single- and double-contrast techniques in esophagitis. *AJR* 135:15–19, 1980.
- Ott DJ, Wu WC, Gelfand DW: Reflux esophagitis revisited: Prospective analysis of radiologic accuracy. *Gastrointest Radiol* 6:1–7, 1981.
- Creteur V, Thoeni RF, Federle MP, et al: The role of single and double-contrast radiography in the diagnosis of reflux esophagitis. *Radiology* 147:71–75, 1983.
- Graziani L, De Nigris E, Pesaresi A, et al: Reflux esophagitis: Radiologic-endoscopic correlation in 39 symptomatic cases. *Gastrointest Radiol* 8:1–6, 1983.
- Chen YM, Ott DJ, Gelfand DW, et al: Multiphasic examination of the esophagogastric region for strictures, rings, and hiatal hernia: Evaluation of the individual techniques. *Gastrointest Radiol* 10:311–316, 1985.
- Gibbs D: Endoscopy in the assessment of reflux oesophagitis. *Clin Gastroenterol* 5:135–142, 1976.
- Fass R, Ofman JJ: Gastroesophageal reflux disease—should we adopt a new conceptual framework? *Am J Gastroenterol* 97:1901–1909, 2002.
- Bytzer P, Havelund T, Hansen JM: Interobserver variation in the endoscopic diagnosis of reflux esophagitis. *Scand J Gastroenterol* 28:119–125, 1993.
- Armstrong D, Bennett JR, Blum AL, et al: The endoscopic assessment of esophagitis: A progress report on observer agreement. *Gastroenterology* 111:85–92, 1996.
- Lundell LR, Dent J, Bennett JR, et al: Endoscopic assessment of oesophagitis: Clinical and functional correlates and further validation of the Los Angeles classification. *Gut* 45:72–180, 1999.
- Funch-Jensen P, Kock K, Christensen LA, et al: Microscopic appearance of the esophageal mucosa in a consecutive series of patients submitted to upper endoscopy: Correlation with gastroesophageal reflux symptoms and macroscopic findings. *Scand J Gastroenterol* 21:65–69, 1986.
- Dibble C, Levine MS, Rubesin SE, et al: Detection of reflux esophagitis on double-contrast esophagrams and endoscopy using the histologic findings as the gold standard. *Abdom Imaging* 29:421–425, 2004.
- Ismail-Beigi F, Horton PF, Pope CE: Histological consequences of gastroesophageal reflux. *Gastroenterology* 58:163–174, 1970.
- Schindlbeck NE, Wiebecke B, Klauser AG, et al: Diagnostic value of histology in nonerosive gastroesophageal reflux disease. *Gut* 39:151–154, 1996.
- Kahrilas PJ, Dodds WJ, Hogan WJ, et al: Esophageal peristaltic dysfunction in peptic esophagitis. *Gastroenterology* 91:897–904, 1986.
- Campbell C, Levine MS, Rubesin SE, et al: Association between esophageal dysmotility

- and gastroesophageal reflux on barium studies. *Eur J Radiol* 59:88–92, 2006.
64. Zboralske FF, Amberg JR, Soergel KH: Presbyesophagus: Cineradiographic manifestations. *Radiology* 82:463–467, 1964.
 65. Simeone JF, Burrell M, Toffler R, et al: Aperistalsis and esophagitis. *Radiology* 123:9–14, 1977.
 66. Kressel HY, Glick SN, Laufer I, et al: Radiologic features of esophagitis. *Gastrointest Radiol* 6:103–108, 1981.
 67. Laufer I: Radiology of esophagitis. *Radiol Clin North Am* 20:687–699, 1982.
 68. Graziani L, Bearzi I, Romagnoli A, et al: Significance of diffuse granularity and nodularity of the esophageal mucosa at double-contrast radiography. *Gastrointest Radiol* 10:1–6, 1985.
 69. Levine MS, Cajade AG, Herlinger H, et al: Pseudomembranes in reflux esophagitis. *Radiology* 159:43–45, 1986.
 70. Levine MS, Goldstein HM: Fixed transverse folds in the esophagus: A sign of reflux esophagitis. *AJR* 143:275–278, 1984.
 71. Hu C, Levine MS, Laufer I: Solitary ulcers in reflux esophagitis: Radiographic findings. *Abdom Imaging* 22:5–7, 1997.
 72. Rabin M, Schmamman IB: Reflux oesophagitis resembling varices. *S Afr Med J* 55:293–295, 1979.
 73. Gohel VK, Edell SL, Laufer I, et al: Transverse folds in the human esophagus. *Radiology* 128:303–308, 1978.
 74. Williams SM, Harned RK, Kaplan P, et al: Transverse striations of the esophagus: Association with gastroesophageal reflux. *Radiology* 146:25–27, 1983.
 75. Furth EE, Rubesin SE, Rose D: Feline esophagus. *AJR* 164:900, 1995.
 76. Samadi F, Levine MS, Rubesin SE, et al: Feline esophagus and gastroesophageal reflux. *AJR* 194:972–976, 2010.
 77. Bleshman MH, Banner MP, Johnson RC, et al: The inflammatory esophagogastric polyp and fold. *Radiology* 128:589–593, 1978.
 78. Ghahremani GG, Fisher MR, Rushovich AM: Prolapsing inflammatory pseudopolyp-fold complex of the oesophagogastric region. *Eur J Radiol* 4:47–51, 1984.
 79. Styles RA, Gibb SP, Tarshis A, et al: Esophagogastric polyps: Radiographic and endoscopic findings. *Radiology* 154:307–311, 1985.
 80. Coggins CA, Levine MS, Kesack CD, et al: Wide-mouthed sacculations in the esophagus: A radiographic finding in scleroderma. *AJR* 176:953–954, 2001.
 81. Palmer ED: The hiatus hernia-esophagitis-esophageal stricture complex: Twenty-year prospective study. *Am J Med* 44:566–579, 1968.
 82. Ott DJ, Gelfand DW, Lane TG, et al: Radiologic detection and spectrum of appearances of esophageal strictures. *J Clin Gastroenterol* 4:11–15, 1982.
 83. Ott DJ, Chen YM, Wu WC, et al: Endoscopic sensitivity in the detection of esophageal strictures. *J Clin Gastroenterol* 7:121–125, 1985.
 84. Baker ME, Einstein DM, Herts BR, et al: Gastroesophageal reflux: Integrating the barium esophagram before and after antireflux surgery. *Radiology* 243:329–339, 2007.
 85. Luedtke P, Levine MS, Rubesin SE, et al: Radiologic diagnosis of benign esophageal strictures: A pattern approach. *Radiographics* 23:897–909, 2003.
 86. Gupta S, Levine MS, Rubesin SE, et al: Usefulness of barium studies for differentiating benign and malignant strictures of the esophagus. *AJR* 180:737–744, 2003.
 87. Schatzki R, Gary JE: Dysphagia due to a diaphragm-like localized narrowing in the lower esophagus (“lower esophageal ring”). *AJR* 70:911–922, 1953.
 88. Weaver JW, Kaude JV, Hamlin DJ: Webs of the lower esophagus: A complication of gastroesophageal reflux? *AJR* 142:289–292, 1984.
 89. Gordon AR, Levine MS, Redfern RO, et al: Cervical esophageal webs: Association with gastroesophageal reflux. *Abdom Imaging* 26:574–577, 2001.
 90. Waldman I, Berlin L: Strictures of the esophagus due to nasogastric intubation. *Am J Roentgenol Radium Ther Nucl Med* 94:321–324, 1965.
 91. Banfield WJ, Hurwitz AL: Esophageal stricture associated with nasogastric intubation. *Arch Intern Med* 134:1083–1086, 1974.
 92. Levine MS, Fisher AR, Rubesin SE, et al: Complications after total gastrectomy and esophagojejunostomy: Radiologic evaluation. *AJR* 157:1189–1194, 1991.
 93. Levine MS, Moolten DN, Herlinger H, et al: Esophageal intramural pseudodiverticulosis: A reevaluation. *AJR* 147:1165–1170, 1986.
 94. Marks RD, Richter JE: Peptic strictures of the esophagus. *Am J Gastroenterol* 88:1160–1173, 1993.
 95. Castell DO, Katz PO: Approach to the patient with dysphagia and odynophagia. In Yamada T, editor: *Textbook of Gastroenterology*, ed 3, Philadelphia, 1999, Lippincott Williams & Wilkins, pp 683–693.
 96. O'Connor JB, Richter JE: Esophageal strictures. In Castell DO, Richter JE, editors: *The Esophagus*, ed 3, Philadelphia, 1999, Lippincott Williams & Wilkins, pp 473–483.
 97. Gohel VK, Kressel HY, Laufer I: Double contrast artifacts. *Gastrointest Radiol* 3:139–146, 1978.
 98. Glick SN, Teplick SK, Goldstein J, et al: Glycogenic acanthosis of the esophagus. *AJR* 139:683–688, 1982.
 99. Ghahremani GG, Rushovich AM: Glycogenic acanthosis of the esophagus: Radiographic and pathologic features. *Gastrointest Radiol* 9:93–98, 1984.
 100. Levine MS, Woldenberg R, Herlinger H, et al: Opportunistic esophagitis in AIDS: Radiographic diagnosis. *Radiology* 165:815–820, 1987.
 101. Itai Y, Kogure T, Okuyama Y, et al: Superficial esophageal carcinoma: Radiological findings in double-contrast studies. *Radiology* 126:597–601, 1978.
 102. Levine MS, Laufer I, Kressel HY, et al: Herpes esophagitis. *AJR* 136:863–866, 1981.
 103. Bova JG, Dutton NE, Goldstein HM, et al: Medication-induced esophagitis: Diagnosis by double-contrast esophagography. *AJR* 148:731–732, 1987.
 104. DeGryse HR, De Schepper AM: Aphthoid esophageal ulcers in Crohn's disease of ileum and colon. *Gastrointest Radiol* 9:197–201, 1984.
 105. Silver TM, Goldstein HM: Varicoid carcinoma of the esophagus. *Am J Dig Dis* 19:56–58, 1974.
 106. Bozymski EM, Herlihy KH, Orlando RC: Barrett's esophagus. *Ann Intern Med* 97:103–107, 1982.
 107. Sjogren RW, Jr, Johnson LF: Barrett's esophagus: A review. *Am J Med* 74:313–321, 1983.
 108. Spechler SJ, Goyal RK: Barrett's esophagus. *N Engl J Med* 315:362–371, 1986.
 109. Hassall E: Barrett's esophagus: Congenital or acquired? *Am J Gastroenterol* 88:819–824, 1993.
 110. Spechler SJ: Barrett's esophagus. *N Engl J Med* 346:836–842, 2002.
 111. Naef AP, Savary M, Ozello L: Columnar-lined lower esophagus: An acquired lesion with malignant predisposition. *J Thorac Cardiovasc Surg* 70:826–835, 1975.
 112. Starnes VA, Adkins RB, Ballinger JF, et al: Barrett's esophagus: A surgical entity. *Arch Surg* 119:563–567, 1984.
 113. Sarr MG, Hamilton SR, Marrone GC, et al: Barrett's esophagus: Its prevalence and association with adenocarcinoma in patients with symptoms of gastroesophageal reflux. *Am J Surg* 149:187–192, 1985.
 114. Levine MS, Herman JB, Furth EE: Barrett's esophagus and esophageal adenocarcinoma: The scope of the problem. *Abdom Imaging* 20:291–298, 1995.
 115. Shaheen N: Advances in Barrett's esophagus and esophageal adenocarcinoma. *Gastroenterology* 128:1554–1566, 2005.
 116. Cameron AJ, Zinsmeister AR, Ballard DJ, et al: Prevalence of columnar-lined (Barrett's) esophagus: Comparison of population-based clinical and autopsy findings. *Gastroenterology* 99:918–922, 1990.
 117. Reid BJ: Barrett's esophagus and esophageal adenocarcinoma. *Gastroenterol Clin North Am* 20:817–834, 1991.
 118. Duhaylongsod FG, Wolfe WG: Barrett's esophagus and adenocarcinoma of the esophagus and gastroesophageal junction. *J Thorac Cardiovasc Surg* 102:36–42, 1991.
 119. Lagergren J, Bergstrom R, Lindgren A, et al: Symptomatic gastroesophageal reflux as a risk factor for esophageal adenocarcinoma. *N Engl J Med* 340:825–831, 1999.
 120. Shaheen NJ, Crosby MA, Bozymski EM, et al: Is there publication bias in the reporting of cancer risk for esophageal adenocarcinoma. *Gastroenterology* 119:333–338, 2000.
 121. Hvid-Jensen F, Pedersen L, Drewes AM, et al: Incidence of adenocarcinoma among patients with Barrett's esophagus. *N Engl J Med* 365:1375–1383, 2011.
 122. Sampliner RE: Practice guidelines on the diagnosis, surveillance, and therapy of Barrett's esophagus. The Practice Parameters Committee on the American College of Gastroenterology. *Am J Gastroenterol* 93:1028–1032, 1998.
 123. Gerson LB, Groeneveld PW, Triadafilopoulos G: Cost-effectiveness model of endoscopic screening and surveillance in patients with gastroesophageal reflux disease. *Clin Gastroenterol Hepatol* 2:868–879, 2004.
 124. Sharma P, Morales TG, Sampliner RE: Short segment Barrett's esophagus—the need for standardization of the definition and of endoscopic criteria. *Am J Gastroenterol* 93:1033–1036, 1998.
 125. Hirota WK, Loughney TM, Lazas DJ, et al: Specialized intestinal metaplasia, dysplasia, and cancer of the esophagus and esophagogastric junction: Prevalence and clinical data. *Gastroenterology* 116:277–285, 1999.
 126. Sharma P, Morales TH, Bhattacharyya A, et al: Dysplasia in short-segment Barrett's esophagus: A prospective 3-year follow-up. *Am J Gastroenterol* 92:2012–2016, 1997.
 127. Weston AP, Krmpotich PT, Cherian R, et al: Prospective long-term endoscopic and histological follow-up of short-segment Barrett's esophagus: Comparison with traditional long-

- segment Barrett's esophagus. *Am J Gastroenterol* 92:407–413, 1997.
128. Donahue D, Navab F: Significance of short-segment Barrett's esophagus. *J Clin Gastroenterol* 25:480–484, 1997.
129. Sharma P: Recent advances in Barrett's esophagus: Short-segment Barrett's esophagus and cardia intestinal metaplasia. *Semin Gastrointest Dis* 10:93–102, 1999.
130. Cameron AJ, Lomboy CT: Barrett's esophagus: Age, prevalence, and extent of columnar epithelium. *Gastroenterology* 103:1241–1245, 1992.
131. Wong A, Fitzgerald RC: Epidemiologic risk factors for Barrett's esophagus and associated adenocarcinoma. *Clin Gastroenterol Hepatol* 3:1–10, 2005.
132. Tran T, Spechler SJ, Richardson PE, et al: Fundoplication and the risk of esophageal cancer in gastroesophageal reflux disease: A Veterans Affairs cohort study. *Am J Gastroenterol* 100:1002–1008, 2005.
133. Winters C, Spurling TJ, Chobanian SJ, et al: Barrett's esophagus: A prevalent, occult complication of gastroesophageal reflux disease. *Gastroenterology* 92:118–124, 1987.
134. Paull A, Trier JS, Dalton D, et al: The histologic spectrum of Barrett's esophagus. *N Engl J Med* 295:476–480, 1976.
135. Weinstein WM, Ippoliti AF: The diagnosis of Barrett's esophagus: Goblets, goblets, goblets. *Gastrointest Endosc* 44:91–95, 1996.
136. Missakian MM, Carlson HC, Andersen HA: The roentgenologic features of the columnar epithelial-lined lower esophagus. *AJR* 99:212–217, 1967.
137. Robbins AH, Hermos JA, Schimmel EM, et al: The columnar-lined esophagus: Analysis of 26 cases. *Radiology* 123:1–7, 1977.
138. Chen YM, Gelfand DW, Ott DJ, et al: Barrett esophagus as an extension of severe esophagitis: Analysis of radiologic signs in 29 cases. *AJR* 145:275–281, 1985.
139. Glick SN: Barium studies in patients with Barrett's esophagus: Importance of focal areas of esophageal deformity. *AJR* 163:65–67, 1994.
140. Adler RH: The lower esophagus lined by columnar epithelium: Its association with hiatal hernia, ulcer, stricture, and tumor. *J Thorac Cardiovasc Surg* 45:13–34, 1963.
141. Robbins AH, Vincent ME, Saini M, et al: Revised radiologic concepts of the Barrett esophagus. *Gastrointest Radiol* 3:377–381, 1978.
142. Levine MS, Kressel HY, Caroline DE, et al: Barrett esophagus: Reticular pattern of the mucosa. *Radiology* 147:663–667, 1983.
143. Shapir J, DuBrow R, Frank P: Barrett oesophagus: Analysis of 19 cases. *Br J Radiol* 58:491–493, 1985.
144. Agha FP: Radiologic diagnosis of Barrett's esophagus: Critical analysis of 65 cases. *Gastrointest Radiol* 11:123–130, 1986.
145. Glick SN, Teplick SK, Amenta PS, et al: The radiologic diagnosis of Barrett esophagus: Importance of mucosal surface abnormalities on air-contrast barium studies. *AJR* 157:951–954, 1991.
146. Chernin MM, Amberg JR, Kogan FJ, et al: Efficacy of radiologic studies in the detection of Barrett's esophagus. *AJR* 147:257–260, 1986.
147. Vincent ME, Robbins AH, Spechler SJ, et al: The reticular pattern as a radiographic sign of the Barrett esophagus: An assessment. *Radiology* 153:333–335, 1984.
148. Levine MS: Barrett esophagus: Update for radiologists. *Abdom Imaging* 30:133–141, 2005.
149. Gilchrist AM, Levine MS, Carr RF, et al: Barrett's esophagus: Diagnosis by double-contrast esophagography. *AJR* 150:97–102, 1988.
150. Spechler SJ, Sperber H, Doos WG, et al: The prevalence of Barrett's esophagus in patients with chronic peptic esophageal strictures. *Dig Dis Sci* 28:769–774, 1983.
151. Yamamoto AJ, Levine MS, Katzka DA, et al: Short-segment Barrett's esophagus: Findings on double-contrast esophagography in 20 patients. *AJR* 176:1173–1178, 2001.

Infectious Esophagitis

MARC S. LEVINE

CHAPTER OUTLINE

Candida Esophagitis

Pathogenesis
Clinical Findings
Endoscopic Findings
Radiographic Findings
Differential Diagnosis

Herpes Esophagitis

Pathogenesis
Clinical Findings
Endoscopic Findings
Radiographic Findings
Differential Diagnosis

Cytomegalovirus Esophagitis

Radiographic Findings

Human Immunodeficiency Virus Esophagitis

Clinical Findings
Radiographic Findings

Tuberculosis

Radiographic Findings

Actinomycosis

Other Infections

Because of the increased survival of immunocompromised patients with malignant neoplasms, organ transplants, and other debilitating diseases, infectious esophagitis has become an increasingly common problem in modern medical practice. *Candida albicans* is the usual offending organism, but herpes simplex virus and cytomegalovirus (CMV) have also been recognized with increased frequency as opportunistic esophageal invaders. Patients with AIDS may develop more fulminant forms of fungal and viral esophagitis (including human immunodeficiency virus [HIV] esophagitis), accentuating the need for early diagnosis and treatment.

Candida Esophagitis

PATHOGENESIS

Candidiasis is the most common cause of infectious esophagitis. *C. albicans* is almost always the offending organism.^{1,2} Because *C. albicans* is a commensal inhabitant of the pharynx, *Candida* esophagitis is presumably caused by downward spread of the fungus to the esophagus.³ Clinically significant infection occurs primarily in patients who are immunocompromised because of underlying malignant tumor, debilitating illness, diabetes, or treatment with radiation, steroids, or other cytotoxic agents.^{2,4-7}

Candida esophagitis is particularly prevalent in patients with AIDS, occurring in 15% to 20% of these individuals,⁶ although effective antiviral agents have substantially decreased the number of HIV-positive patients who develop AIDS.

Local esophageal stasis is another factor that predisposes patients to the development of *Candida* esophagitis. Esophageal stasis may be caused by mechanical obstruction from achalasia or strictures or by physiologic obstruction from scleroderma or other causes of esophageal aperistalsis.^{7,8} Delayed esophageal emptying in these patients permits the fungal organism to overgrow and colonize the esophagus with subsequent esophagitis.

Much less frequently, *Candida* esophagitis may develop in otherwise healthy individuals who have no underlying systemic or esophageal diseases.⁹ As a result, the possibility of fungal infection should not be excluded simply because the classic predisposing factors are not present in a particular patient.

CLINICAL FINDINGS

Most patients with *Candida* esophagitis have acute onset of dysphagia or, even more commonly, odynophagia, characterized by intense substernal pain during swallowing.¹⁻⁴ Others may have nonspecific findings such as chest pain, epigastric pain, or upper gastrointestinal bleeding, or they may be asymptomatic.^{1,2,5} Occasionally, patients with chronic *Candida* esophagitis may have persistent dysphagia because of the development of esophageal strictures.¹⁰⁻¹²

Despite the characteristic presentation, *Candida* esophagitis may be difficult to differentiate from viral esophagitis on clinical grounds. The presence of oropharyngeal candidiasis (i.e., thrush) is a helpful finding, but only 50% to 75% of patients with *Candida* esophagitis have fungal lesions in the oropharynx.^{2,13} Other patients with thrush may have herpes or CMV esophagitis, so the presence of oropharyngeal candidiasis does not preclude the development of viral esophagitis.¹⁴ Still other patients may have concomitant *Candida* and herpes esophagitis,^{2,15,16} most likely resulting from fungal superinfection of herpetic ulcers.¹⁶

Immunocompromised patients with *Candida* esophagitis require treatment with potent antifungal agents such as fluconazole.^{2,6,17} Affected individuals usually have a marked clinical response to antifungal therapy. In one study, however, recurrent *Candida* esophagitis occurred in 90% of successfully treated AIDS patients.¹⁸

ENDOSCOPIC FINDINGS

Candida esophagitis is usually characterized at endoscopy by patchy, white exudates covering a friable, erythematous mucosa.^{1,2} In more advanced disease, the mucosa becomes ulcerated and necrotic with extensive pseudomembrane formation. The presence of budding yeast cells, hyphae, and pseudohyphae on endoscopic biopsy specimens with silver stain, periodic

acid–Schiff stain, or Gram stain is diagnostic of *Candida* esophagitis.^{1,2}

RADIOGRAPHIC FINDINGS

Candida esophagitis tends to be a superficial disease with mucosal abnormalities that are difficult to recognize on conventional single-contrast barium studies. As a result, single-contrast esophagography has been an unreliable technique for detecting this condition, with a reported sensitivity of less than 50%.^{1,4,5,9} In contrast, double-contrast esophagography has a sensitivity of about 90% in diagnosing *Candida* esophagitis.^{7,19} The major advantage of this technique is its ability to demonstrate mucosal plaques that cannot easily be seen on single-contrast studies.

Candida esophagitis is usually manifested on double-contrast images by discrete plaquelike lesions consisting of small exudates and pseudomembranes on the mucosa. The lesions tend to be longitudinally oriented, appearing en face as discrete, linear or irregular filling defects with normal intervening mucosa (Fig. 20-1).^{7,14} The plaques are located predominantly in the upper or midesophagus, occasionally having a focal distribution (Fig. 20-2). In the appropriate clinical setting, discrete plaquelike lesions should be highly suggestive of *Candida* esophagitis.

In other patients, *Candida* esophagitis may be manifested by a finely nodular or granular appearance because of tiny plaques

on the mucosa (Fig. 20-3).^{14,20} Some plaques may contain central umbilications that collect barium, mimicking the appearance of tiny ulcers caused by herpes esophagitis.²¹ When larger plaques are present, the lesions may coalesce, producing a distinctive snakeskin appearance (Fig. 20-4).¹⁹ Occasionally, submucosal edema and inflammation may result in thickened longitudinal folds, a nonspecific manifestation of esophagitis.³ Thus, the classic radiographic features of *Candida* esophagitis are not present in all patients.

In severe candidiasis, the esophagus may have a grossly irregular or shaggy contour because of coalescent plaques and pseudomembranes, with trapping of barium between these lesions (Fig. 20-5).^{4,7,14,19,22} Some of these plaques and pseudomembranes may eventually slough, producing one or more deep ulcers superimposed on a background of diffuse plaque formation (see Fig. 20-5B). This fulminant form of candidiasis has been encountered primarily in patients with AIDS.¹⁴ As a result, the shaggy esophagus of *Candida* esophagitis has become a less common finding as more effective antiviral medications have become available to prevent the development of AIDS in HIV-positive patients. Nevertheless, the possibility of AIDS should be suspected when a shaggy esophagus is detected on barium studies, particularly in high-risk patients.

Candida esophagitis may occasionally produce other unusual radiographic findings. In some patients, barium may dissect

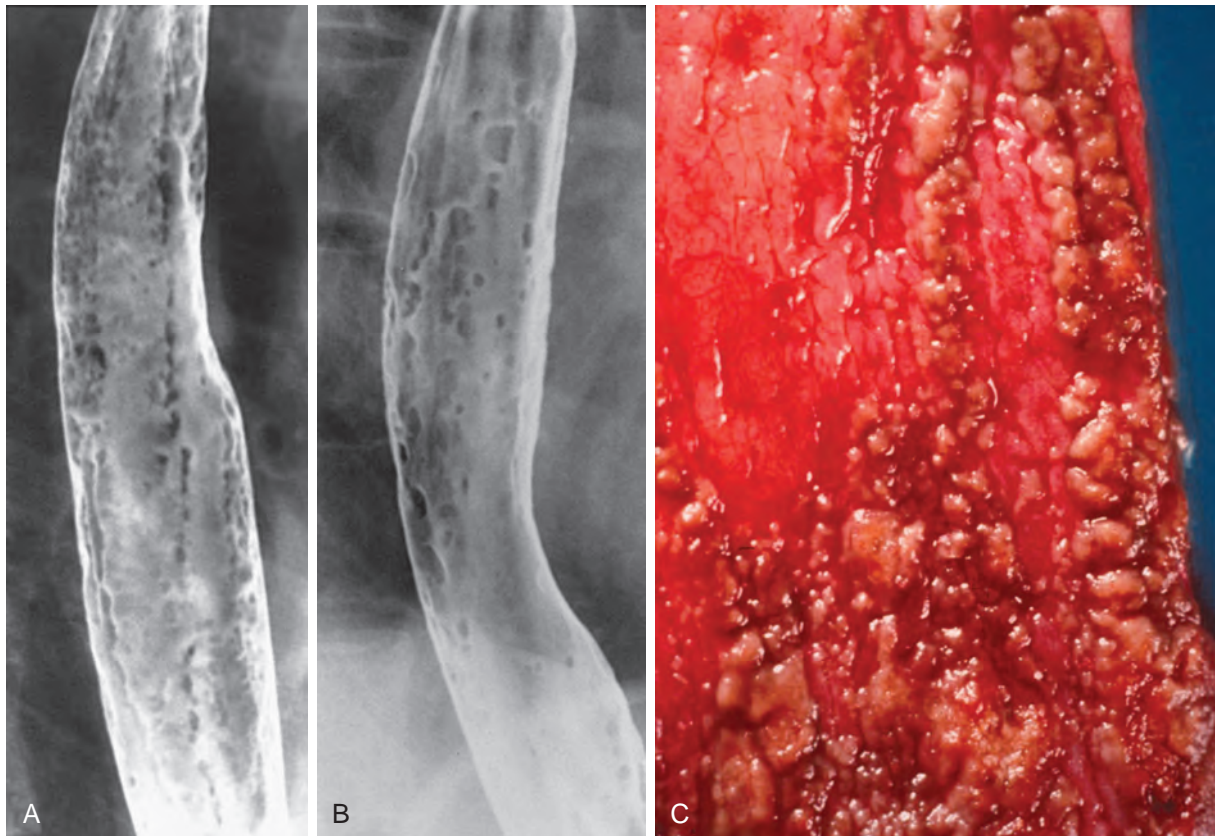


Figure 20-1 *Candida* esophagitis with discrete plaques. **A.** Multiple plaquelike lesions are present in the esophagus. The linear plaques have a characteristic appearance with discrete borders and a predominantly longitudinal orientation. **B.** In another patient, the plaques have a more irregular configuration. However, they are still seen as discrete lesions separated by normal mucosa. **C.** The gross specimen in another case shows how these plaquelike lesions represent heaped-up areas of necrotic epithelial debris and actual colonies of *C. albicans* on the mucosa. (**A** and **B** from Levine MS, Macones AJ, Laufer I: *Candida* esophagitis: Accuracy of radiographic diagnosis. *Radiology* 154:581–587, 1985.)



Figure 20-2 Localized *Candida* esophagitis. Discrete plaque-like lesions are clustered together in the midesophagus, with normal-appearing mucosa above and below this level.

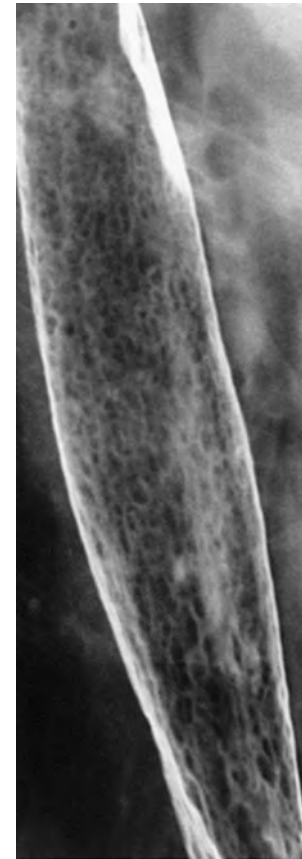


Figure 20-3 *Candida* esophagitis with a granular mucosa. This patient has innumerable tiny, nodular elevations in the esophagus rather than the typical plaque-like defects associated with candidiasis.

beneath plaques or pseudomembranes, producing an intramural track or double-barreled esophagus.²² Rarely, a coalescent mass of heaped-up necrotic debris and fungal mycelia (a fungus ball) may be indistinguishable from a polypoid esophageal carcinoma.²³⁻²⁵ Esophageal obstruction, perforation, and tracheoesophageal or aortoesophageal fistula formation are other rare but potentially life-threatening complications.²⁶⁻²⁸

Candida esophagitis usually responds quickly to antifungal therapy, but resolution of the radiographic findings sometimes lags behind the clinical recovery, so follow-up barium studies may still be abnormal in patients who are asymptomatic.²⁴ The immediate effects of antifungal therapy should therefore be assessed primarily on clinical grounds.

Although *Candida* esophagitis is usually self-limited with proper treatment, occasional cases of stricture formation have been reported.¹⁰⁻¹² These strictures typically appear as long, tapered areas of esophageal narrowing (Fig. 20-6).¹² Fungal-induced strictures should be distinguished from pseudostrictures caused by esophageal spasm or the patient's inability to swallow an adequate bolus of barium. Therefore a second examination may be necessary after treatment to determine if a true stricture is present.

Because of the effects of local esophageal stasis (see earlier, "Pathogenesis"), patients with conditions such as achalasia and scleroderma are at increased risk for developing *Candida* esophagitis.^{7,8} Such cases may be manifested on esophagography by tiny nodular defects, polypoid folds, or a distinctive lacy

appearance in the esophagus (Fig. 20-7).⁸ Because of esophageal stasis in patients with achalasia or scleroderma, these individuals may also develop a foamy esophagus characterized by innumerable tiny, rounded bubbles that settle out along the top of the barium column, producing a layer of foam (Fig. 20-8).²⁹ It has been postulated that this finding is caused by extensive production of carbon dioxide by a yeast form of the organism.²⁹ Whatever the explanation, *Candida* esophagitis should be suspected when a foamy esophagus is detected on esophagography, particularly in patients with achalasia or scleroderma.

Candida esophagitis is also known to be associated with esophageal intramural pseudodiverticulosis (see Chapter 21).³⁰⁻³² It has been postulated that the pseudodiverticula develop as a complication of fungal infection.³⁰ It is more widely believed, however, that the fungal organism is a secondary invader as a result of local stasis.^{31,32}

Patients with defects in their cell-mediated immune response to *C. albicans* may have an unusual disease known as chronic mucocutaneous candidiasis, in which there is persistent fungal infection of the skin, mucous membranes, and nails.³³ Although uncommon, esophageal involvement may lead to chronic esophageal candidiasis.³³ In contrast to acute *Candida* esophagitis, this entity is characterized by chronic scarring and stricture formation in the esophagus.³³ The presence of a long esophageal stricture in patients with chronic mucocutaneous candidiasis should therefore suggest the possibility of esophageal involvement by this disease.



Figure 20-4 *Candida* esophagitis with a cobblestone appearance. There is confluent involvement of the mucosa by innumerable round, oval, and polygonal plaques. (From Levine MS: *Radiology of the Esophagus*. Philadelphia, WB Saunders, 1989.)

DIFFERENTIAL DIAGNOSIS

Mucosal plaques or nodules may also be caused by herpes esophagitis, reflux esophagitis, glycogenic acanthosis, and superficial spreading carcinoma.^{20,34-39} Although herpes esophagitis is usually manifested by multiple small, discrete ulcers in the esophagus (see later, “*Herpes Esophagitis*”), advanced herpetic infection may lead to the development of plaquelike lesions indistinguishable from those in *Candida* esophagitis (Fig. 20-9).^{34,35}

Reflux esophagitis may also produce a nodular or granular appearance of the mucosa that resembles candidiasis.²⁰ However, the nodules of reflux esophagitis tend to have poorly defined borders that fade peripherally into the adjacent mucosa, whereas the plaques of candidiasis have more discrete borders. The nodular mucosa of reflux esophagitis also occurs as a continuous area of disease, extending proximally from the gastroesophageal junction, whereas *Candida* esophagitis often spares the distal esophagus. Rarely, severe reflux esophagitis may produce inflammatory exudates or pseudomembranes that are indistinguishable on double-contrast studies from the plaquelike lesions of candidiasis.³⁶

Glycogenic acanthosis may also be manifested by discrete plaques or nodules, mimicking the appearance of *Candida* esophagitis.³⁷ However, the nodules of glycogenic acanthosis tend to have a more rounded appearance, whereas the plaques of candidiasis usually have a more linear configuration. The clinical history is also helpful for differentiating these

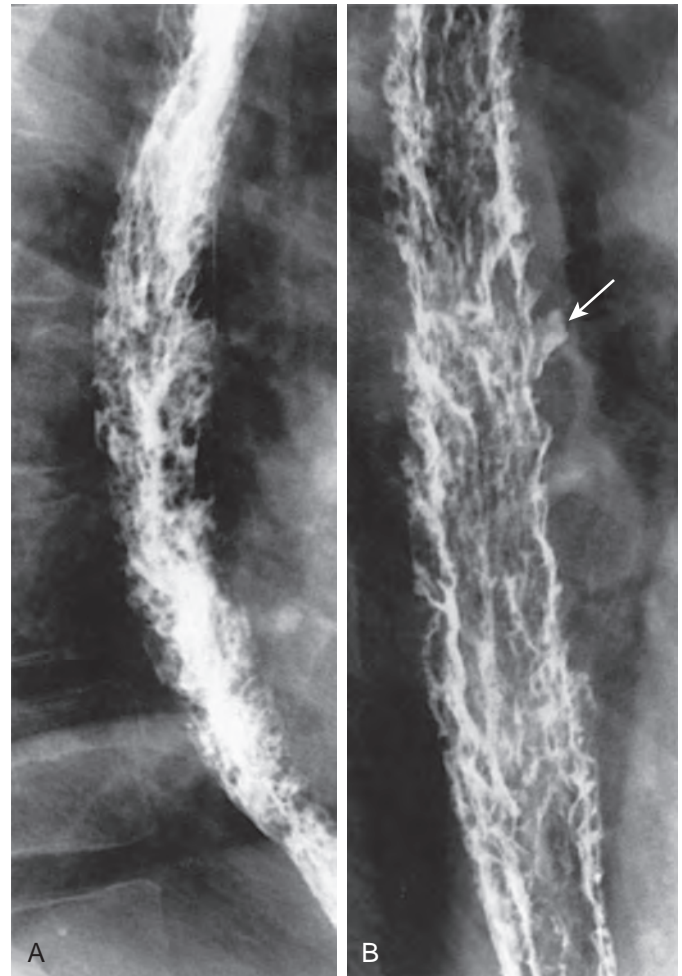


Figure 20-5 *Candida* esophagitis with a shaggy esophagus. **A, B.** The esophagus has a grossly irregular contour as a result of multiple plaques and pseudomembranes, with trapping of barium between these lesions. A deep area of ulceration (arrow) is also seen (**B**). Both patients had AIDS. (**A** from Levine MS: *Radiology of the Esophagus*. Philadelphia, WB Saunders, 1989; **B** from Levine MS, Woldenberg R, Herlinger H, et al: *Opportunistic esophagitis in AIDS: Radiographic diagnosis*. *Radiology* 165:815–820, 1987.)

conditions because patients with glycogenic acanthosis are almost always asymptomatic.³⁷

Superficial spreading carcinoma of the esophagus is characterized by focal nodularity of the mucosa that could be mistaken for a localized area of *Candida* esophagitis.^{38,39} However, candidiasis usually produces discrete plaquelike lesions separated by segments of normal intervening mucosa, whereas the plaques or nodules of superficial spreading carcinoma tend to coalesce, producing a continuous area of disease.^{38,39} Rarely, an advanced infiltrating carcinoma extending longitudinally in the wall can mimic the shaggy esophagus of candidiasis (Fig. 20-10).

Mucosal plaques may be simulated by technical artifacts on double-contrast studies, including air bubbles, debris, and undissolved effervescent agent (Fig. 20-11).^{20,40} When candidiasis is suspected on clinical grounds, double-contrast images of the esophagus should therefore be obtained before administration of an effervescent agent. If the radiographic findings are equivocal, additional double-contrast images may be obtained to demonstrate the transient nature of these artifacts.



Figure 20-6 *Candida*-induced esophageal stricture. A long, tapered stricture is seen in the distal esophagus as a result of scarring from severe *Candida* esophagitis. (From Levine MS: *Radiology of the Esophagus*. Philadelphia, WB Saunders, 1989.)



Figure 20-7 *Candida* esophagitis in a patient with scleroderma. Tiny nodular defects in the esophagus could be mistaken for retained debris. The esophagus is dilated because of underlying involvement by scleroderma.

Herpes Esophagitis

PATHOGENESIS

Herpes simplex virus type 1, a DNA core virus, has been recognized as another common cause of infectious esophagitis in patients who are immunocompromised because of underlying malignant tumor, debilitating illness, AIDS, or treatment with irradiation, chemotherapy, or steroids.^{14,41-43} This infection should be suspected in the same clinical setting as candidiasis. Occasionally, however, herpes esophagitis may occur as an acute, self-limited disease in otherwise healthy individuals who have no underlying immunologic problems.⁴⁴⁻⁴⁸ Thus, the diagnosis of herpes esophagitis should not be excluded because the patient has a normal immunologic status.

CLINICAL FINDINGS

Patients with herpes esophagitis typically present with acute odynophagia, characterized by severe substernal chest pain during swallowing.^{13,49} Other patients may have dysphagia, chest pain and, less commonly, upper gastrointestinal bleeding.^{50,51} In the appropriate clinical setting, the presence of herpetic lesions in the oropharynx should suggest a diagnosis of herpes esophagitis. Most patients do not have active infection of the oropharynx, however, so the absence of oropharyngeal lesions does not preclude this diagnosis.^{13,49} Furthermore, some patients with herpetic lesions in the oropharynx are found to

have *Candida* esophagitis. As a result, it can be extremely difficult to differentiate viral and fungal esophagitis on clinical grounds.

The natural history of herpes esophagitis is uncertain. In various autopsy series, it has been shown that immunocompromised hosts with herpes esophagitis may develop herpetic pneumonitis or even a disseminated herpetic infection.⁴³ However, most patients with herpes esophagitis recover spontaneously.^{49,52,53} These individuals are usually treated effectively with analgesics and, if necessary, antiviral agents such as acyclovir.⁵⁴

Otherwise healthy patients with herpes esophagitis have a characteristic clinical presentation. They typically are young men with a history of recent exposure to sexual partners with herpetic lesions on the lips or buccal mucosa.^{45,47} Most of these patients have a 3- to 10-day influenza-like prodrome characterized by fever, sore throat, upper respiratory tract infection, and myalgias.^{44,45,47,48} This prodrome is followed by acute onset of odynophagia, which prompts the patient to seek medical attention. Despite the dramatic presentation, these patients almost always have an acute, self-limited illness, with resolution of symptoms in less than 2 weeks.⁴⁴⁻⁴⁷

ENDOSCOPIC FINDINGS

Herpes esophagitis is initially manifested on endoscopy by esophageal vesicles that subsequently rupture to form discrete, punched-out ulcers.^{43,52,53,55} With further progression, the ulcers



Figure 20-8 *Candida* esophagitis with a foamy esophagus in two patients with achalasia. **A, B.** In both cases, innumerable tiny, rounded bubbles are seen to settle out along the top of the barium column, producing a layer of foam (white arrows). Also note tapered narrowing of the distal esophagus (black arrow) caused by underlying achalasia with incomplete opening of the lower esophageal sphincter (**B**).

may become covered by a fibrinous exudate.⁴³ Thus, early herpes esophagitis has a characteristic endoscopic appearance, whereas advanced herpes esophagitis may be indistinguishable from candidiasis. Whatever the stage of infection, the histologic or cytologic findings on endoscopic biopsy specimens or brushings are relatively specific for the herpesvirus group. The classic finding of Cowdry type A intranuclear inclusions in intact epithelial cells adjacent to ulcers is virtually pathognomonic of herpes.⁴³ The diagnosis of herpes esophagitis can also be confirmed by positive viral cultures from the esophagus or by direct immunofluorescent staining for the herpes simplex antigen.²

RADIOGRAPHIC FINDINGS

Herpes esophagitis is usually manifested on double-contrast esophagograms by multiple, small (<1 cm), superficial ulcers in the upper or midesophagus, without plaque formation.^{14,49,56-58} These ulcers are visible on double-contrast images in more than 50% of patients.⁵⁸ The ulcers may have a punctate, linear, ring-like, or stellate configuration and are often surrounded by radiolucent mounds of edema (Fig. 20-12).⁴⁹ Although ulceration may occasionally be seen in advanced *Candida* esophagitis, the ulcers in these patients almost always occur on a background of diffuse plaque formation.^{7,14} Thus, in the appropriate clinical

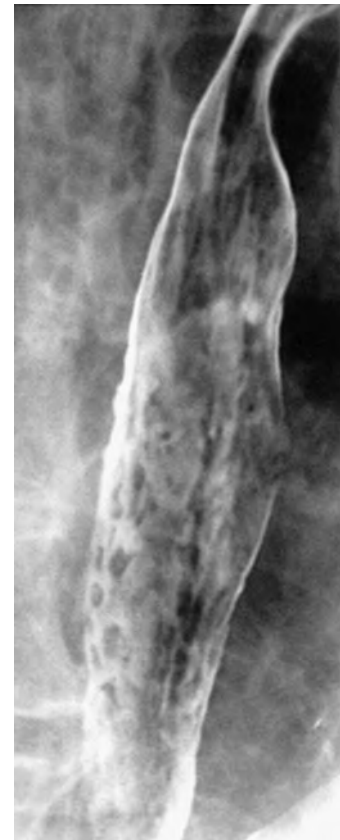


Figure 20-9 *Herpes* esophagitis. Multiple plaquelike lesions are seen in the midesophagus, mimicking the appearance of candidiasis.

setting, the presence of multiple small, discrete ulcers in the upper or midesophagus should be highly suggestive of herpes esophagitis. Nevertheless, endoscopy may be required for a definitive diagnosis if the radiographic findings are equivocal or if appropriate treatment with antiviral agents fails to produce an adequate clinical response.

More advanced herpes esophagitis may be associated with extensive ulceration, plaque formation, or a combination of ulcers and plaques (see Fig. 20-9).^{34,35,49,56,58} In such cases, the findings may be indistinguishable from those of advanced *Candida* esophagitis. Rarely, herpes esophagitis may be manifested by a giant ulcer, mimicking an ulcerated carcinoma.⁵⁸

Herpes esophagitis in otherwise healthy patients is usually manifested on double-contrast studies by innumerable tiny ulcers that tend to be clustered together in the midesophagus near the level of the left main bronchus (Fig. 20-13).^{59,60} The small size of the ulcers may be related to an intact immune system that contains the herpetic infection and prevents the ulcers from enlarging. Whatever the explanation, the diagnosis of herpes esophagitis in otherwise healthy patients can usually be suggested on the basis of the clinical and radiographic findings.⁶⁰

DIFFERENTIAL DIAGNOSIS

In the appropriate clinical setting, multiple small, discrete ulcers on an otherwise normal background mucosa should be pathognomonic of viral esophagitis. Although most cases are

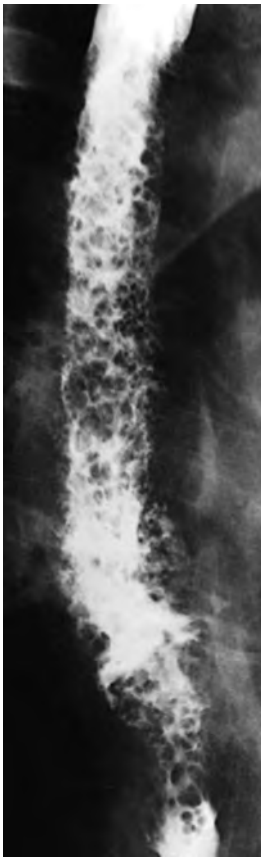


Figure 20-10 Advanced esophageal carcinoma. The esophagus has a grossly irregular or shaggy contour caused by a highly invasive carcinoma extending longitudinally in the wall. (Courtesy Hans Herlinger, MD, Philadelphia.)



Figure 20-11 Undissolved effervescent agent and bubbles in the esophagus. Although this appearance could be mistaken for *Candida* esophagitis on a single radiograph, the transient nature of these artifacts can easily be confirmed by obtaining additional views.

caused by the herpes simplex virus, CMV may occasionally produce similar findings. However, CMV esophagitis is more commonly manifested by the development of one or more giant ulcers in the esophagus (see later, “[Cytomegalovirus Esophagitis](#)”). Oral medications may also cause a focal contact esophagitis, manifested by multiple small, shallow ulcers indistinguishable from those in herpes esophagitis.^{61,62} The correct diagnosis should be suggested, however, by a temporal relationship between ingestion of the offending medication and the onset of esophagitis. Reflux esophagitis is a common cause of ulceration, but tends to involve the distal esophagus and is usually associated with a hiatal hernia or gastroesophageal reflux. Radiation esophagitis, caustic esophagitis and, rarely, Crohn’s disease involving the esophagus may cause superficial ulceration, but these entities can usually be differentiated from herpes esophagitis by the clinical history and presentation.

Cytomegalovirus Esophagitis

CMV is another member of the herpesvirus group that has been recognized as a cause of infectious esophagitis in AIDS patients.⁶³⁻⁶⁵ For reasons that are unclear, however, CMV esophagitis rarely occurs in other immunocompromised patients. Affected individuals usually present with severe odynophagia. Endoscopic examinations may demonstrate one or more ulcers in the esophagus. Characteristic features of CMV infection on endoscopic biopsy specimens include intranuclear inclusions

and, in contrast to herpes simplex virus, small cytoplasmic inclusions in endothelial cells or fibroblasts at or near the base of the ulcers.^{2,63,65} Endoscopic biopsy specimens, brushings, and viral cultures have a combined sensitivity of greater than 90% in detecting CMV esophagitis.⁶⁶⁻⁶⁸

RADIOGRAPHIC FINDINGS

CMV esophagitis may be manifested on esophagography by discrete, superficial ulcers indistinguishable from those in herpes esophagitis (Fig. 20-14).⁶³⁻⁶⁵ More commonly, however, CMV esophagitis is associated with the development of one or more giant (>1 cm), flat ulcers in the mid or distal esophagus.^{14,63,64,69} These giant ulcers may be recognized in profile or en face as ovoid, elongated, or diamond-shaped collections of barium surrounded by a thin, smooth radiolucent rim of edematous mucosa (Fig. 20-15). Because herpetic ulcers rarely become this large, the presence of one or more giant ulcers should suggest CMV esophagitis in patients with AIDS.

HIV has also been implicated as a cause of giant esophageal ulcers that are impossible to differentiate from CMV ulcers on radiographic criteria (see later, “[Human Immunodeficiency Virus Esophagitis](#)”). Endoscopy is therefore required to distinguish these infections. If endoscopic biopsy specimens or brushings reveal the characteristic cytoplasmic inclusions of CMV, or if viral cultures are positive for CMV, treatment can be initiated with potent antiviral agents such as ganciclovir.^{2,66}

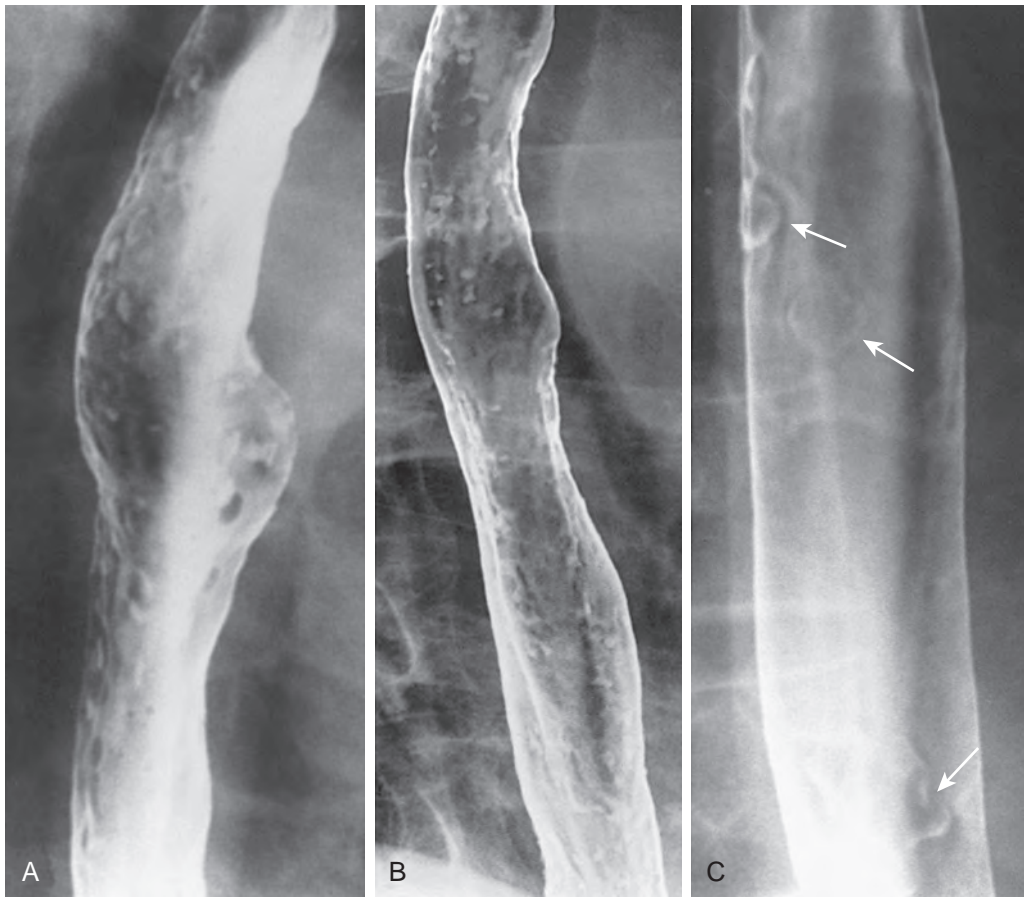


Figure 20-12 Herpes esophagitis with discrete ulcers. **A, B.** Multiple discrete, superficial ulcers are seen in the midesophagus. Many of the ulcers are surrounded by radiolucent mounds of edema. **C.** There are several widely separated ulcers (arrows) with a ringlike or stellate configuration. (**A** from Levine MS: *Radiology of esophagitis: A pattern approach*. Radiology 179:1–7, 1991; **B** courtesy Harvey M. Goldstein, MD, San Antonio, TX.)

However, ganciclovir may cause severe bone marrow suppression with neutropenia, thrombocytopenia, or anemia,^{2,70} so potentially toxic antiviral drugs should be used only if cytopathologic confirmation of CMV is obtained.

Human Immunodeficiency Virus Esophagitis

A clinical syndrome of odynophagia and giant esophageal ulcers has been recognized in patients with HIV infection.^{71–78} Biopsy specimens, brushings, and cultures from the esophagus have failed to reveal any signs of the usual fungal or viral organisms associated with infectious esophagitis in patients with AIDS. Furthermore, electron microscopy of biopsy specimens from these ulcers has demonstrated viral particles with morphologic features of HIV infection, directly implicating HIV as the cause of the ulcers.⁷⁴ These HIV ulcers (also called idiopathic ulcers^{76,77}) may develop in patients who have recently become HIV-positive or in patients who have been HIV-positive for extended periods and have other clinical signs of AIDS.^{2,73–76,78} Thus, giant esophageal ulcers may occur as a manifestation of acute or chronic HIV infection.

CLINICAL FINDINGS

Patients with HIV ulcers in the esophagus typically present with acute onset of severe odynophagia.^{72–76,78} The pain may be so intense that patients are unable to swallow their saliva.

Occasionally, these patients may develop hematemesis or other signs of upper gastrointestinal bleeding.⁷¹ The ulcers sometimes develop at or shortly after the time of HIV seroconversion.⁷⁴ As part of this seroconversion syndrome, there may be associated ulcers in the oropharynx and soft palate or a characteristic maculopapular rash involving the face, trunk, and upper extremities.^{72,73,76} In most cases, however, HIV ulcers in the esophagus occur after the patient has developed clinically overt AIDS with low CD4 counts.^{2,78}

Candida, herpes, and CMV esophagitis are other common causes of odynophagia in HIV-positive patients, but the possibility of HIV esophagitis should be suspected if these individuals have the characteristic maculopapular rash or develop symptoms at or near the time of seroconversion. HIV can sometimes be confirmed as the cause of the ulcers by electron microscopy and in situ DNA hybridization.^{74,76} Because these techniques are not widely available, however, HIV esophagitis has primarily been a diagnosis of exclusion when no cytopathologic findings of CMV or other opportunistic infections are present on endoscopic biopsy specimens or brushings.^{71,75,77,78}

RADIOGRAPHIC FINDINGS

HIV esophagitis is usually manifested on esophagography by the development of one or more giant (>1 cm), flat ulcers in the mid or distal esophagus, sometimes associated with small, satellite ulcers (Fig. 20-16).^{75,78} The ulcers may appear in profile or en face as ovoid, elongated, or diamond-shaped collections



Figure 20-13 Herpes esophagitis in an otherwise healthy patient. Multiple punctate and linear areas of ulceration are seen in the midesophagus below the level of the left main bronchus. This appearance is characteristic of herpes esophagitis in immunocompetent patients. (From DeGaeta L, Levine MS, Guglielmi GE, et al: *Herpes esophagitis in an otherwise healthy patient*. *AJR* 144:1205–1206, 1985.)

of barium, often surrounded by a thin, smooth radiolucent rim of edema.^{75,78} These HIV ulcers are therefore indistinguishable radiographically from CMV ulcers in the esophagus (see Fig. 20-15).^{75,78} Nevertheless, most giant esophageal ulcers in HIV-positive patients are caused by HIV rather than CMV.⁷⁸ In contrast to CMV ulcers, HIV ulcers in the esophagus may heal spontaneously or may respond to treatment with steroids, but do not require treatment with potentially toxic antiviral agents such as ganciclovir.^{2,72-74,78,79} Endoscopic biopsy specimens, brushings, and viral cultures are therefore required to differentiate HIV ulcers from CMV ulcers, so appropriate treatment can be instituted in these patients.

Rarely, HIV esophagitis may be associated with the development of esophagoesophageal or esophagogastric fistulas or focal perforation into the mediastinum.⁸⁰ Tuberculous esophagitis can also be associated with intramural sinus tracks and fistulas, but these tracks and fistulas tend to be located more proximally in the esophagus in patients with tuberculosis (see later, “**Tuberculosis**”).^{81,82} Other causes of giant ulcers include nasogastric intubation, endoscopic sclerotherapy, caustic ingestion, and oral medications such as quinidine, potassium chloride, and nonsteroidal anti-inflammatory drugs. The correct diagnosis is usually suggested by the clinical history and presentation. Thus, for all practical purposes, giant esophageal ulcers in HIV-positive patients are almost always caused by HIV or CMV.



Figure 20-14 Cytomegalovirus esophagitis. Multiple discrete, superficial ulcers are seen in the midesophagus. Herpes esophagitis could produce identical radiographic findings. (From Levine MS: *Radiology of the Esophagus*. Philadelphia, WB Saunders, 1989.)

Tuberculosis

Esophageal involvement by tuberculosis is extremely uncommon. When it occurs, these patients usually have advanced tuberculosis in the lungs or mediastinum.^{83,84} Both *Mycobacterium tuberculosis* and *Mycobacterium avium-intracellulare* have been implicated as causes of infectious esophagitis in patients with AIDS.^{81,82}

Esophageal involvement is usually caused by adjacent tuberculous nodes in the mediastinum that compress or erode into the esophagus, causing narrowing, ulceration, or fistula formation.^{81,84,85} In patients with active pulmonary tuberculosis, esophageal infection may also be caused by swallowed sputum containing the tubercle bacilli, particularly if there is a preexisting mucosal lesion or stricture in the esophagus. Rarely, hematogenous seeding of the esophagus may occur in patients with disseminated miliary tuberculosis.

Patients with tuberculous esophagitis may be asymptomatic, or they may present with dysphagia, odynophagia, or chest pain.⁸⁴ Although the clinical findings are nonspecific, the possibility of esophageal tuberculosis should be considered in patients with persistent dysphagia who have active pulmonary tuberculosis. In such cases, the diagnosis may be confirmed at endoscopy by the presence of tubercle bacilli or, rarely, caseating granulomas on endoscopic biopsy specimens or brushings from the esophagus.⁸⁶

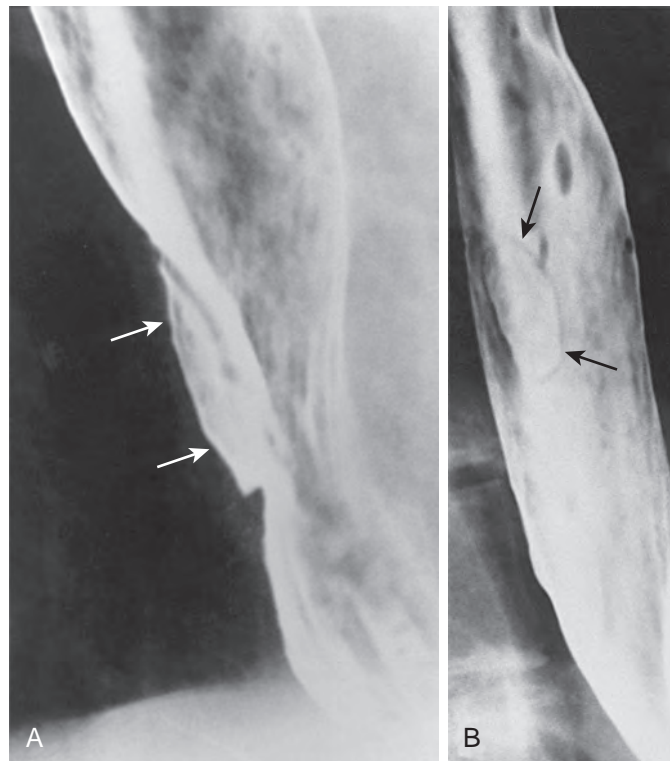


Figure 20-15 Cytomegalovirus esophagitis. **A.** A giant, relatively flat ulcer (arrows) is seen in profile in the distal esophagus. **B.** A large, ovoid ulcer (arrows) is seen en face in another patient. Note the thin radiolucent rim of edema surrounding the ulcer. Because herpetic ulcers rarely become this large, the presence of one or more giant esophageal ulcers should raise the possibility of cytomegalovirus esophagitis in patients with AIDS. (**A** courtesy Sidney W. Nelson, MD, Seattle; **B** courtesy Kyunghee C. Cho, MD, Newark, NJ.)

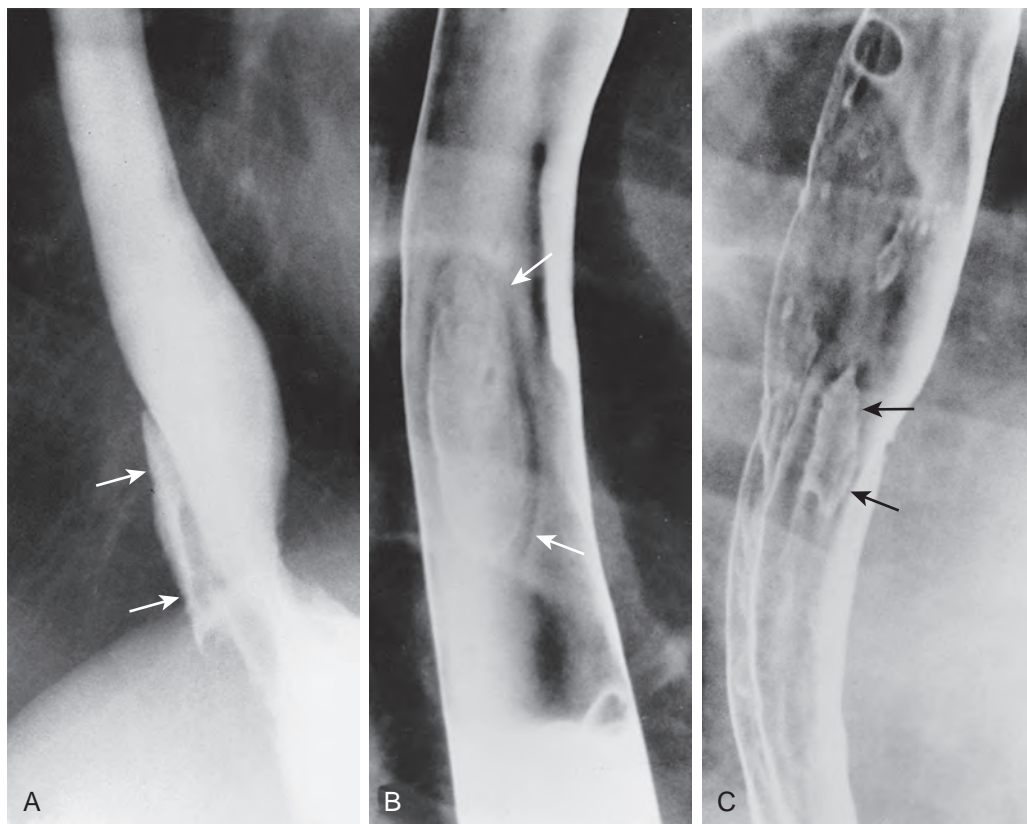


Figure 20-16 Human immunodeficiency virus (HIV) esophagitis. **A.** A giant, relatively flat ulcer (arrows) is seen in profile in the distal esophagus. This patient was HIV-positive. **B.** In another HIV-positive patient, a large ovoid ulcer (arrows) is seen en face with a thin surrounding rim of edema. **C.** In a third patient, a diamond-shaped ulcer (arrows) is seen in the midesophagus with a cluster of small satellite ulcers. All three cases are indistinguishable from the cytomegalovirus ulcers illustrated in [Figure 20-15](#). However, endoscopic biopsy specimens, brushings, and cultures were negative for cytomegalovirus in these patients. (From Levine MS, Loercher G, Katzka DA, et al: Giant, human immunodeficiency virus-related ulcers in the esophagus. *Radiology* 180:323–326, 1991.)



Figure 20-17 Tuberculous esophagitis. There is compression (black arrows) of the upper thoracic esophagus with associated ulceration (white arrow) caused by caseating tuberculous nodes that have eroded into the esophagus. (Courtesy Alan Grundy, MD, London.)

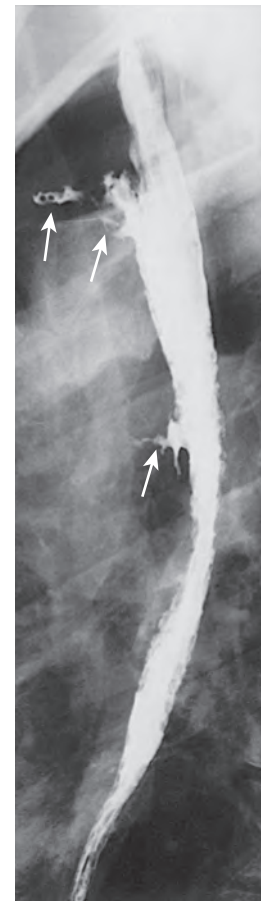


Figure 20-18 Tuberculous esophagitis in a patient with AIDS. There is diffuse esophagitis with several deep sinus tracks (arrows) extending anteriorly from the esophagus into the mediastinum. (From Goodman P, Pinero SS, Rance RM, et al: *Mycobacterial esophagitis in AIDS*. *Gastrointest Radiol* 14:103–105, 1989.)

RADIOGRAPHIC FINDINGS

Extrinsic esophageal involvement by tuberculous nodes in the mediastinum is usually manifested on esophagography by compression, displacement, or narrowing of the esophagus by an adjacent mediastinal mass.^{83,85,86} These patients may also develop strictures or traction diverticula, usually at the level of the carina.^{83,84} Occasionally, caseating nodes in the mediastinum may erode into the upper or midesophagus, producing superficial or deep areas of ulceration, longitudinal or transverse sinus tracks, or fistulas into the mediastinum or tracheobronchial tree (Fig. 20-17).^{83–85} Sinus tracks and fistulas have been recognized as particularly prominent features of tuberculous esophagitis in patients with AIDS (Fig. 20-18).^{81,82} Similar findings may be demonstrated in patients with Crohn's disease, trauma, radiation, and esophageal carcinoma, but the presence of pulmonary or mediastinal tuberculosis should suggest the correct diagnosis, particularly in patients with AIDS.

Intrinsic tuberculous esophagitis occurs much less frequently and is characterized on barium studies by mucosal irregularity, ulcers, plaques, fistulas and, eventually, strictures (Fig. 20-19).^{83,86} Rarely, esophageal tuberculosis can lead to the development of an intramural abscess, seen on esophagography as a smooth submucosal mass and on computed tomography (CT) as a well-margined cystic mass with an enhancing rim in the esophagus.⁸⁷ Tuberculous esophagitis

may be indistinguishable from severe esophagitis resulting from caustic ingestion, radiation, or other causes.

Actinomycosis

Actinomycosis is an indolent, suppurative infection caused by *Actinomyces israelii*, an anaerobic, gram-positive bacterium. Rarely, this organism may cause severe esophagitis in patients with AIDS.⁸⁸ Esophageal actinomycosis may be manifested on esophagography by deep ulcers with multiple longitudinal and transverse fistulas and intramural tracks (Fig. 20-20).⁸⁸ Although tuberculous esophagitis may also cause ulceration and fistula formation (see earlier, “Tuberculosis”), the presence of multiple intramural tracks parallel to the esophageal lumen should raise the possibility of esophageal actinomycosis in patients with AIDS.

Other Infections

Although infectious esophagitis is usually caused by fungal or viral organisms, other rare causes include *Staphylococcus*, *Streptococcus*, *Klebsiella*, *Blastomyces*, *Cryptosporidium*, *Torulopsis glabrata*, and *Lactobacillus acidophilus*.^{89–94}

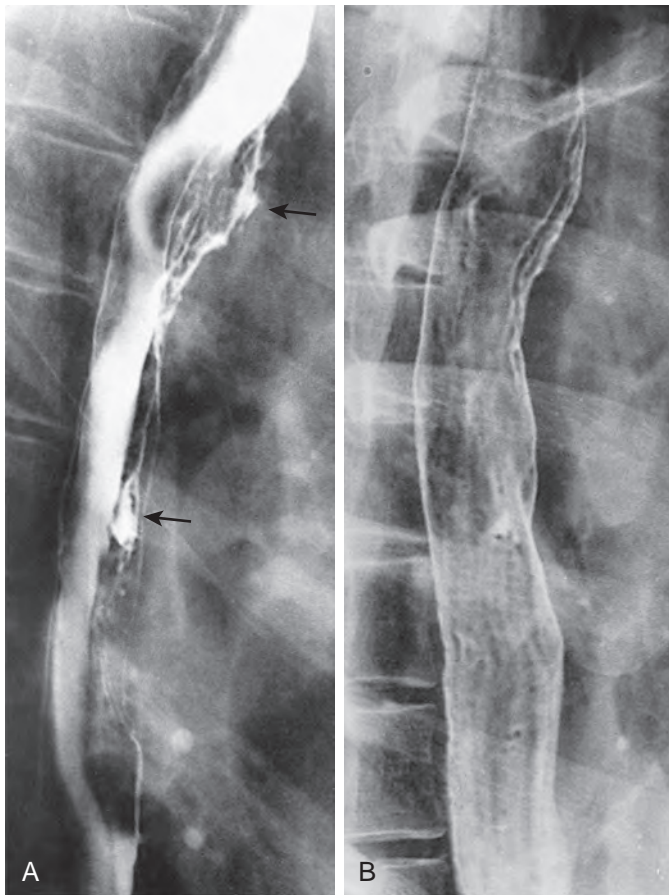


Figure 20-19 Tuberculous esophagitis. **A.** The initial esophagogram shows two areas of irregular ulceration (arrows) in the midesophagus caused by proven tuberculous esophagitis. **B.** Another esophagogram after 6 months of antituberculous therapy shows healing of the ulcers. (From Savage PE, Grundy A: *Oesophageal tuberculosis: An unusual cause of dysphagia*. *Br J Radiol* 57:1153–1155, 1984.)



Figure 20-20 Esophageal actinomycosis. Multiple longitudinal and transverse intramural tracks and fistulas are seen in the distal esophagus caused by actinomycosis involving the esophagus. This patient had AIDS. (Courtesy Emil J. Balthazar, MD, New York.)

REFERENCES

- Mathieson R, Dutta SK: *Candida* esophagitis. *Dig Dis Sci* 28:365–370, 1983.
- Baehr PH, McDonald GB: Esophageal infections: Risk factors, presentation, diagnosis, and treatment. *Gastroenterology* 106:509–532, 1994.
- Lewicki AM, Moore JP: Esophageal moniliasis. *AJR* 125:218–245, 1975.
- Sheft DJ, Shrager G: Esophageal moniliasis: The spectrum of the disease. *JAMA* 213:1859–1862, 1970.
- Eras P, Goldstein MJ, Sherlock P: *Candida* infection of the gastrointestinal tract. *Medicine (Baltimore)* 51:367–379, 1972.
- Barbaro G, Barbarini G, Calderon W, et al: Fluconazole versus itraconazole for *Candida* esophagitis in acquired immunodeficiency syndrome. *Gastroenterology* 111:1169–1177, 1996.
- Levine MS, Macones AJ, Laufer I: *Candida* esophagitis: Accuracy of radiographic diagnosis. *Radiology* 154:581–587, 1985.
- Geffert WB, Laufer I, Edell S, et al: Candidiasis in the obstructed esophagus. *Radiology* 138:25–28, 1981.
- Kodsi BE, Wickremesinghe PC, Kozinn PJ, et al: *Candida* esophagitis. *Gastroenterology* 71:715–719, 1976.
- Ott DJ, Gelfand DW: Esophageal stricture secondary to candidiasis. *Gastrointest Radiol* 2: 323–325, 1978.
- Kelvin FM, Clark WM, Thompson WM, et al: Chronic esophageal stricture due to moniliasis. *Br J Radiol* 51:826–828, 1978.
- Agha FP: Candidiasis-induced esophageal strictures. *Gastrointest Radiol* 9:283–286, 1984.
- Friedman HM, Gluckman SJ: Infections of the esophagus. In Cohen S, Soloway RD, editors: *Diseases of the Esophagus*, New York, 1982, Churchill Livingstone, pp 277–286.
- Levine MS, Woldenberg R, Herlinger H, et al: Opportunistic esophagitis in AIDS: radiographic diagnosis. *Radiology* 165:815–820, 1987.
- Brayko CM, Kozavek RA, Sanowski RA, et al: Type I herpes simplex esophagitis with concomitant esophageal moniliasis. *J Clin Gastroenterol* 4:351–355, 1982.
- Mirra SS, Bryan JA, Butz WC, et al: Concomitant herpes-monilial esophagitis: Case report with ultrastructural study. *Hum Pathol* 13:760–763, 1982.
- Wilcox CM, Alexander LN, Clark WS, et al: Fluconazole compared with endoscopy for human immunodeficiency virus-infected patients with esophageal symptoms. *Gastroenterology* 110: 1803–1809, 1996.
- Laine L: The natural history of esophageal candidiasis after successful treatment in patients with AIDS. *Gastroenterology* 107:744–746, 1994.
- Vahey TN, Maglinte DD, Chernish SM: State-of-the-art barium examination in opportunistic esophagitis. *Dig Dis Sci* 31:1192–1195, 1986.
- Kressel HY, Glick SN, Laufer I, et al: Radiologic features of esophagitis. *Gastrointest Radiol* 6: 103–108, 1981.
- Glick SN: Barium studies in patients with *Candida* esophagitis: Pseudo-ulcerations simulating viral esophagitis. *AJR* 163:349–352, 1994.
- Gonzalez G: Esophageal moniliasis. *AJR* 113: 233–236, 1971.
- Ho CS, Cullen JB, Gray RR: An unusual manifestation of esophageal moniliasis. *Radiology* 123:287–288, 1977.
- Roberts L, Gibbons R, Gibbons G, et al: Adult esophageal candidiasis: A radiographic spectrum. *Radiographics* 7:289–307, 1987.
- Farman J, Tivittian A, Rosenthal LE, et al: Focal esophageal candidiasis in acquired immunodeficiency syndrome (AIDS). *Gastrointest Radiol* 11:213–217, 1986.

26. Obrecht WF, Richter JE, Olympio GA, et al: Tracheoesophageal fistula: A serious complication of infectious esophagitis. *Gastroenterology* 87: 1174-1179, 1984.
27. Sehha S, Hazeghi K, Bajoghli M, et al: Oesophageal moniliasis causing fistula formation and lung abscess. *Thorax* 31:361-364, 1976.
28. Campero AA, Campbell GD: Complete oesophageal obstruction due to monilial infection. *Aust N Z J Surg* 43:244-246, 1973.
29. Sam JW, Levine MS, Rubesin SE, et al: The "foamy" esophagus: A radiographic sign of *Candida* esophagitis. *AJR* 174:999-1002, 2000.
30. Troupin RH: Intramural esophageal diverticulosis and moniliasis: A possible association. *AJR* 104:613-616, 1968.
31. Beauchamp JM, Nice CM, Belanger MA, et al: Esophageal intramural pseudodiverticulosis. *Radiology* 113:273-276, 1974.
32. Castillo S, Abvrashed A, Kimmelman J, et al: Diffuse intramural esophageal pseudodiverticulosis. *Gastroenterology* 72:541-545, 1977.
33. Rohrmann CA, Kidd R: Chronic mucocutaneous candidiasis: Radiologic abnormalities in the esophagus. *AJR* 130:473-476, 1978.
34. Meyers C, Durkin MG, Love L: Radiographic findings in herpetic esophagitis. *Radiology* 119:21-24, 1976.
35. Skucas J, Schrank WW, Meyer PC, et al: Herpes esophagitis: A case study by air-contrast esophagography. *AJR* 128:497-499, 1977.
36. Levine MS, Cajade AG, Herlinger H, et al: Pseudomembranes in reflux esophagitis. *Radiology* 159:43-45, 1986.
37. Glick SN, Teplick SK, Goldstein J, et al: Glycogenic acanthosis of the esophagus. *AJR* 139:683-688, 1982.
38. Itai Y, Kogure T, Okuyama Y, et al: Diffuse finely nodular lesions of the esophagus. *AJR* 128:563-566, 1977.
39. Itai Y, Kogure T, Okuyama Y, et al: Superficial esophageal carcinoma: Radiological findings in double-contrast studies. *Radiology* 126:597-601, 1978.
40. Gohel VK, Kressel HY, Laufer I: Double-contrast artifacts. *Gastrointest Radiol* 3:139-146, 1978.
41. Muller SA, Herrmann EC, Winkelman RK: Herpes simplex infections in hematologic malignancies. *Am J Med* 52:102-114, 1972.
42. Weiden PL, Schuffler MD: Herpes esophagitis complicating Hodgkin's disease. *Cancer* 33: 1100-1102, 1974.
43. Nash G, Ross JS: Herpetic esophagitis: A common cause of esophageal ulceration. *Hum Pathol* 5:339-345, 1974.
44. Depew WT, Prentice RS, Beck IT, et al: Herpes simplex ulcerative esophagitis in a healthy subject. *Am J Gastroenterol* 68:381-385, 1977.
45. Owensby LC, Stammer JL: Esophagitis associated with herpes simplex infection in an immunocompetent host. *Gastroenterology* 74:1305-1306, 1978.
46. Springer DJ, Da Costa LR, Beck IT: A syndrome of acute self-limiting ulcerative esophagitis in young adults probably due to herpes simplex virus. *Dig Dis Sci* 24:535-539, 1979.
47. Deshmukh M, Shah R, McCallum RW: Experience with herpes esophagitis in otherwise healthy patients. *Am J Gastroenterol* 79:173-176, 1984.
48. Desigan G, Schneider RP: Herpes simplex esophagitis in healthy adults. *South Med J* 78:1135-1137, 1985.
49. Levine MS, Laufer I, Kressel HY, et al: Herpes esophagitis. *AJR* 136:863-866, 1981.
50. Fishbein PG, Tuthill R, Kressel HY, et al: Herpes simplex esophagitis: A cause of upper gastrointestinal bleeding. *Am J Dig Dis* 24:540-544, 1979.
51. Rattner HM, Cooper DJ, Zaman MB: Severe bleeding from herpes esophagitis. *Am J Gastroenterol* 80:523-525, 1985.
52. Lightdale CJ, Wolf DJ, Marcucci RA, et al: Herpetic esophagitis in patients with cancer: Antemortem diagnosis by brush cytology. *Cancer* 39:243-246, 1977.
53. Lasser A: Herpes simplex virus esophagitis. *Acta Cytol (Baltimore)* 21:301-302, 1977.
54. Balfour HH: Antiviral drugs. *N Engl J Med* 340:1255-1268, 1999.
55. Klotz DA, Silverman L: Herpes virus esophagitis, consistent with herpes simplex, visualized endoscopically. *Gastrointest Endosc* 21:71-73, 1974.
56. Shortleeve MJ, Gauvin GP, Gardner RC, et al: Herpetic esophagitis. *Radiology* 141:611-617, 1981.
57. Agha FP, Lee HH, Nostrant TT: Herpetic esophagitis: A diagnostic challenge in immunocompromised patients. *Am J Gastroenterol* 81: 246-253, 1986.
58. Levine MS, Loevner LA, Saul SH, et al: Herpes esophagitis: Sensitivity of double-contrast esophagography. *AJR* 151:57-62, 1988.
59. DeGaeta L, Levine MS, Guglielmi GE, et al: Herpes esophagitis in an otherwise healthy patient. *AJR* 144:1205-1206, 1985.
60. Shortleeve MJ, Levine MS: Herpes esophagitis in otherwise healthy patients: Clinical and radiographic findings. *Radiology* 182:859-861, 1992.
61. Creteur V, Laufer I, Kressel HY, et al: Drug-induced esophagitis detected by double-contrast radiography. *Radiology* 147:365-368, 1983.
62. Bova JG, Dutton NE, Goldstein HM, et al: Medication-induced esophagitis: Diagnosis by double-contrast esophagography. *AJR* 148:731-732, 1987.
63. Balthazar EJ, Megibow AJ, Hulnick DH: Cytomegalovirus esophagitis and gastritis in AIDS. *AJR* 144:1201-1204, 1985.
64. Balthazar EJ, Megibow AJ, Hulnick D, et al: Cytomegalovirus esophagitis in AIDS: Radiographic features in 16 patients. *AJR* 149:919-923, 1987.
65. Teixidor HS, Honig CL, Norsoph E, et al: Cytomegalovirus infection of the alimentary canal: Radiologic findings with pathologic correlation. *Radiology* 163:317-323, 1987.
66. Wilcox CM, Diehl DL, Cello JP, et al: Cytomegalovirus esophagitis in patients with AIDS: A clinical, endoscopic, and pathologic correlation. *Ann Intern Med* 113:589-593, 1990.
67. Hackman RC, Wolford JL, Gieves CA, et al: Recognition and rapid diagnosis of upper gastrointestinal cytomegalovirus infection in marrow transplant recipients: A comparison of seven virologic methods. *Transplantation* 57: 231-237, 1994.
68. Wilcox CM, Rodgers W, Lazenby A: Prospective comparison of brush cytology, viral culture, and histology for the diagnosis of ulcerative esophagitis in AIDS. *Clin Gastroenterol Hepatol* 2:564-567, 2004.
69. Frager DH, Frager JD, Brandt LJ, et al: Gastrointestinal complications of AIDS: Radiologic features. *Radiology* 158:597-603, 1986.
70. Buhles WC, Mastre BJ, Tinker AJ, et al: Ganciclovir treatment of life- or sight-threatening cytomegalovirus infection: Experience in 314 immunocompromised patients. *Rev Infect Dis* 10(Suppl 3):495-506, 1988.
71. Kumar A, Posner G, Colby S, et al: Giant esophageal ulcers in AIDS-related complex. *Gastrointest Endosc* 34:153-154, 1988.
72. Bach MC, Valenti AJ, Howell DA, et al: Odynophagia from aphthous ulcers of the pharynx and esophagus in the acquired immunodeficiency syndrome (AIDS). *Ann Intern Med* 109:338-339, 1988.
73. Bach MC, Howell DA, Valenti AJ, et al: Aphthous ulceration of the gastrointestinal tract in patients with the acquired immunodeficiency syndrome (AIDS). *Ann Intern Med* 112:465-466, 1990.
74. Rabeneck L, Popovic M, Gartner S, et al: Acute HIV infection presenting with painful swallowing and esophageal ulcers. *JAMA* 263:2318-2324, 1990.
75. Levine MS, Loercher G, Katzka DA, et al: Giant, human immunodeficiency virus-related ulcers in the esophagus. *Radiology* 180:323-326, 1991.
76. Kotler DP, Reka S, Orenstein JM, et al: Chronic idiopathic esophageal ulceration in the acquired immunodeficiency syndrome: Characterization and treatment with corticosteroids. *J Clin Gastroenterol* 15:284-290, 1992.
77. Wilcox CM, Schwartz DA: Endoscopic characterization of idiopathic esophageal ulceration associated with human immunodeficiency virus infection. *J Clin Gastroenterol* 16:251-256, 1993.
78. Sor S, Levine MS, Kowalski TE, et al: Giant ulcers of the esophagus in patients with human immunodeficiency virus: Clinical, radiographic, and pathologic findings. *Radiology* 194:447-451, 1995.
79. Dretler RH, Rausher DB: Giant esophageal ulcer healed with steroid therapy in an AIDS patient. *Rev Infect Dis* 11:768-769, 1989.
80. Frager D, Kotler DP, Baer J: Idiopathic esophageal ulceration in the acquired immunodeficiency syndrome: Radiologic reappraisal in 10 patients. *Abdom Imaging* 19:2-5, 1994.
81. Goodman P, Pinero SS, Rance RM, et al: Mycobacterial esophagitis in AIDS. *Gastrointest Radiol* 14:103-105, 1989.
82. de Silva R, Stoopack PM, Raufman JP: Esophageal fistulas associated with mycobacterial infection in patients at risk for AIDS. *Radiology* 175:449-453, 1990.
83. Schneider R: Tuberculosis of the mediastinum. *Gastrointest Radiol* 1:143-145, 1976.
84. Williford ME, Thompson WM, Hamilton JD, et al: Esophageal tuberculosis: Findings on barium swallow and computed tomography. *Gastrointest Radiol* 8:119-124, 1983.
85. Ramakantan R, Shah P: Tuberculous fistulas of the pharynx and esophagus. *Gastrointest Radiol* 15:145-147, 1990.
86. Savage PE, Grundy A: Oesophageal tuberculosis: An unusual cause of dysphagia. *Br J Radiol* 57:1153-1155, 1984.
87. Kim HG: Esophageal tuberculosis manifesting as submucosal abscess. *AJR* 180:1482-1483, 2003.
88. Spencer GM, Roach D, Skucas J: Actinomycosis of the esophagus in a patient with AIDS: Findings on barium esophagograms. *AJR* 161:795-796, 1993.
89. Walsh TJ, Belitsos NJ, Hamilton SR: Bacterial esophagitis in immunocompromised patients. *Arch Intern Med* 146:1345-1348, 1986.

90. Miller JT, Slywka SW, Ellis JH: Staphylococcal esophagitis causing giant ulcers. *Abdom Imaging* 18:245–246, 1993.
91. McKenzie R, Khakoo R: Blastomycosis of the esophagus presenting with gastrointestinal bleeding. *Gastroenterology* 88:1271–1273, 1985.
92. Kazlow PG, Shah K, Benkov K, et al: Esophageal cryptosporidiosis in a child with acquired immune deficiency syndrome. *Gastroenterology* 91:1301–1303, 1986.
93. Bentlif PS, Widermann B: Esophagitis caused by *Torulopsis glabrata*. *Am J Gastroenterol* 71:395–397, 1979.
94. McManus JPA, Webb JN: A yeast-like infection of the esophagus caused by *Lactobacillus acidophilus*. *Gastroenterology* 68:583–586, 1975.

CHAPTER OUTLINE

Drug-Induced Esophagitis

Pathogenesis
Causative Agents
Clinical Findings
Radiographic Findings
Differential Diagnosis

Radiation Esophagitis

Pathogenesis
Clinical Findings
Radiographic Findings
Differential Diagnosis

Caustic Esophagitis

Pathogenesis
Clinical Findings
Diagnosis and Treatment
Radiographic Findings
Differential Diagnosis

Idiopathic Eosinophilic Esophagitis

Clinical Findings
Radiographic Findings
Differential Diagnosis

Crohn's Disease

Clinical Findings
Radiographic Findings
Differential Diagnosis

Epidermolysis Bullosa Dystrophica

Pathogenesis
Clinical Findings
Radiographic Findings

Pemphigoid

Clinical Findings
Radiographic Findings

Erythema Multiforme Major

Clinical Findings
Radiographic Findings

Nasogastric Intubation Esophagitis

Pathogenesis
Clinical Findings
Radiographic Findings

Alkaline Reflux Esophagitis

Clinical Findings
Radiographic Findings

Acute Alcohol-Induced Esophagitis

Clinical Findings
Radiographic Findings

Chronic Graft-Versus-Host Disease

Clinical Findings
Radiographic Findings

Glutaraldehyde-Induced Esophageal Injury**Behçet's Disease****Esophageal Intramural Pseudodiverticulosis**

Pathogenesis
Clinical Findings
Radiographic Findings
Differential Diagnosis

Drug-Induced Esophagitis

Since its original description in 1970,¹ drug-induced esophagitis has been recognized as a relatively common condition in today's pill-oriented society. The medications implicated most frequently include tetracycline, doxycycline, potassium chloride, quinidine, aspirin, other nonsteroidal anti-inflammatory drugs (NSAIDs), and alendronate sodium. These patients may have severe esophageal symptoms, but drug-induced esophagitis usually resolves after withdrawal of the offending agent. Although conventional single-contrast barium studies have limited value in detecting mucosal abnormalities associated with drug-induced esophagitis, double-contrast esophagography is a valuable technique for diagnosing this condition.

PATHOGENESIS

The type and degree of injury that occurs in drug-induced esophagitis depend not only on the properties of the

offending medication but also on the manner in which it is taken. Many patients have a history of ingesting the medication with little or no water before going to bed.²⁻⁴ As a result, the tablets or capsules may become lodged in the midesophagus, where they are compressed by the adjacent aortic arch or left main bronchus.² Drug-induced esophagitis is therefore believed to represent a focal contact esophagitis, with injury to the adjacent mucosa by the dissolving pills. Less frequently, prolonged retention of the medication may result from esophageal compression by an enlarged heart.⁵ Occasionally, drug-induced esophagitis may be caused by abnormal motility or preexisting strictures that delay transit of pills from the esophagus.^{6,7}

CAUSATIVE AGENTS*Tetracycline and Doxycycline*

Tetracycline and doxycycline, two widely used antibiotics, are responsible for at least 50% of all cases of drug-induced

esophagitis.² Because these medications are given in the form of capsules that are relatively acidic, prolonged retention of the capsules in the upper or midesophagus may cause superficial ulceration of the adjacent mucosa.^{2,8} Although doxycycline (pH 3.0) is slightly less acidic than tetracycline (pH 2.3), it dissolves more slowly and forms an adherent gel, presumably accounting for the high frequency of esophagitis in patients taking this agent.⁹ Affected individuals almost never develop strictures, however, because the ulcers caused by tetracycline and doxycycline are so small and superficial that they rarely cause enough scarring and fibrosis to produce a stricture.⁴

Potassium Chloride

Potassium chloride tablets may produce a severe form of drug-induced esophagitis.^{1,2,5,10-12} These patients often have mitral valvular disease with an enlarged left atrium compressing the distal esophagus, so passage of the potassium chloride tablets is impeded at this level. Subsequent release of potassium chloride over a localized area of esophageal mucosa may cause severe chemical injury with focal ulceration and stricture formation.^{5,11,12} As a result, potassium supplements are sometimes given in liquid form to patients with known cardiomegaly to prevent this complication. Even liquid potassium, however, has been described as a cause of drug-induced esophagitis.¹³

Quinidine

Because oral quinidine is often given for cardiac arrhythmias, these patients may have associated cardiomegaly, with compression of the distal esophagus by an enlarged left atrium or ventricle. Retained quinidine above this level may have a corrosive effect on the adjacent mucosa, causing ulceration and strictures.^{2,6,13}

Nonsteroidal Anti-inflammatory Drugs

Nonsteroidal anti-inflammatory drugs (NSAIDs) have been implicated with increasing frequency in the development of esophagitis. Major offending agents include aspirin, phenylbutazone, indomethacin (Indocin), ibuprofen (Motrin), naproxen (Naprosyn), piroxicam (Feldene), and sulindac (Clinoril).^{2,14-19} These NSAIDs not only may cause a focal contact esophagitis, but sometimes may lead to stricture formation.^{15,16}

Alendronate

Alendronate sodium (Fosamax) is an aminobisphosphonate, a selective inhibitor of osteoclast-mediated bone resorption, that has been used with increasing frequency in the non-hormonal treatment of postmenopausal osteoporosis. This agent may be associated with the development of a severe form of ulcerative esophagitis and stricture formation in the distal esophagus.²⁰⁻²³ The mechanism of injury is uncertain. Topical corrosive injury may be a contributing factor, but the high frequency of ulceration in the distal esophagus suggests that there is a reflux-mediated component in these patients.²⁰

Other Drugs

Other oral medications that have been implicated in the development of drug-induced esophagitis include emepronium bromide, ferrous sulfate, alprenolol chloride, ascorbic acid, theophylline, cromolyn sodium, and antibiotics such as clindamycin and lincomycin.^{2,7,24-29}

CLINICAL FINDINGS

Patients with drug-induced esophagitis typically present with odynophagia or unremitting chest pain accentuated by swallowing.² Others may present with signs of upper gastrointestinal (GI) bleeding.^{7,19} Symptoms usually develop within several hours to days after taking the medication.² The symptoms of drug-induced esophagitis also tend to resolve rapidly after withdrawal of the offending agent, so most patients are asymptomatic within 7 to 10 days after stopping the medication.⁸ Occasional patients may have progressive dysphagia because of the development of strictures.^{11,13,30}

RADIOGRAPHIC FINDINGS

The radiographic findings in drug-induced esophagitis depend on the nature of the offending medication. Tetracycline, doxycycline and, less commonly, other medications cause superficial ulceration in the esophagus without permanent sequelae. Double-contrast esophagography is a useful technique for detecting shallow ulcers that cannot easily be recognized on single-contrast studies. Affected individuals may have a solitary ulcer (Fig. 21-1A), several discrete ulcers (Fig. 21-1B), or multiple small ulcers on a normal background mucosa (Fig. 21-1C).^{4,31-33} The ulcers are usually clustered together in the midesophagus near the level of the aortic arch or left main bronchus. These ulcers may be recognized en face as punctate, linear, ovoid, stellate, or serpiginous collections of barium or in profile as shallow depressions (see Fig. 21-1).^{4,31-33} When esophageal ulcers are drug induced, a follow-up esophagogram 7 to 10 days after withdrawal of the offending agent often shows dramatic healing of the lesions.³¹

Potassium chloride, quinidine, NSAIDs, and alendronate tend to cause a more severe form of esophagitis, sometimes associated with stricture formation. Potassium chloride and quinidine may result in particularly large ulcers with considerable surrounding edema and inflammation, mimicking the appearance of an ulcerated carcinoma (Fig. 21-2A).^{13,31,34} Subsequent scarring and fibrosis occasionally lead to the development of strictures that typically appear as segmental areas of concentric narrowing above the level of an enlarged left atrium (Fig. 21-2B).^{5,12,13,18,30} In contrast, aspirin and other NSAIDs sometimes produce giant, flat ulcers that are several centimeters or longer (Fig. 21-3A).¹⁷ Healing of these ulcers may result in smooth, re-epithelialized depressions that are sometimes mistaken for active ulcer craters (Fig. 21-3B).¹⁷ Finally, alendronate may be associated with the development of severe ulcerative esophagitis and stricture formation in the distal esophagus (Fig. 21-4).²⁰⁻²²

DIFFERENTIAL DIAGNOSIS

Herpes esophagitis is the major consideration in the differential diagnosis for discrete, superficial ulcers in the upper or midesophagus.³⁵ Although viral ulcers may be indistinguishable from the ulcers of drug-induced esophagitis, the correct diagnosis can usually be suggested on the basis of the clinical history. Occasionally, however, herpes esophagitis may occur in otherwise healthy individuals who have no underlying immunologic problems (see Chapter 20).³⁶ The diagnosis of drug-induced esophagitis should therefore be

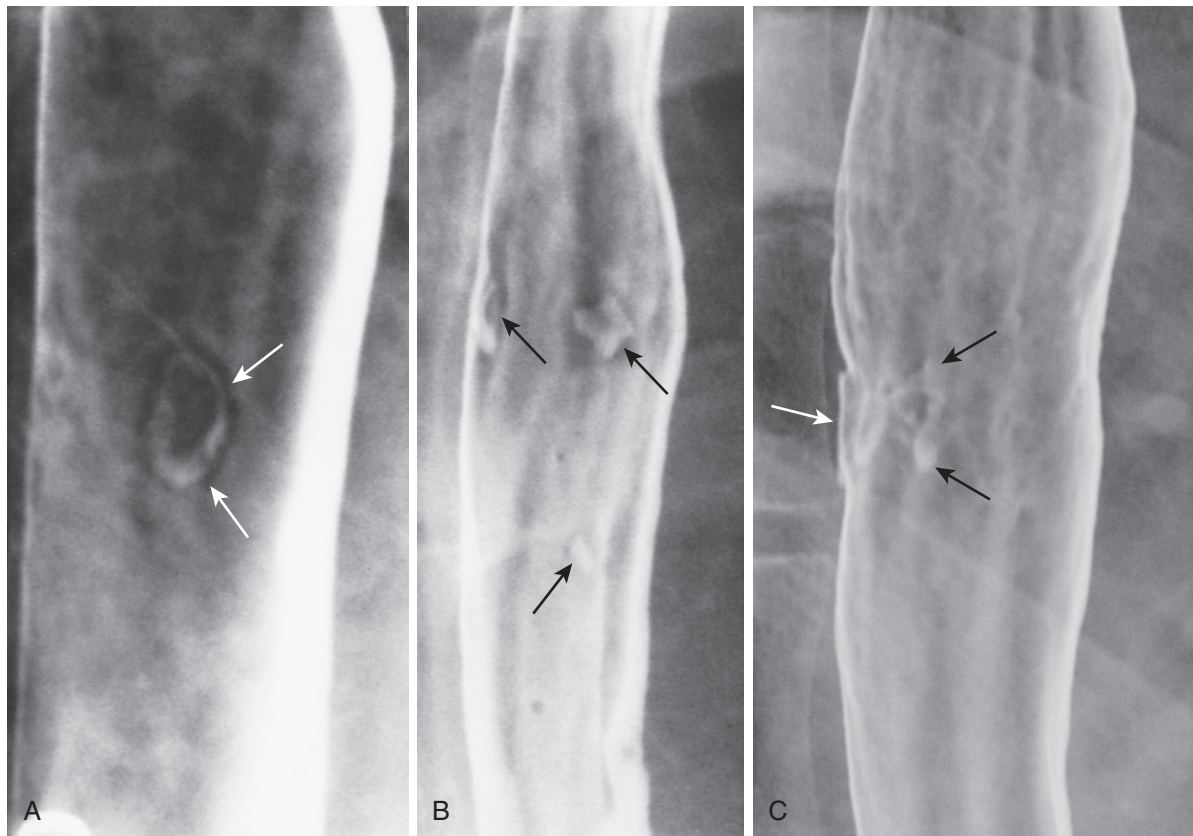


Figure 21-1 Drug-induced esophagitis with superficial ulcers. **A.** A solitary ringlike ulcer (arrows) is seen in the midesophagus. Note the thin radiolucent halo of edematous mucosa surrounding the ulcer. **B.** Several discrete ulcers (arrows) are seen in the midesophagus on a normal background mucosa. The largest ulcer has a stellate configuration. **C.** This patient has a flat ulcer (white arrow) on the right lateral wall of the midesophagus, with a cluster of small ulcers (black arrows) abutting the larger ulcer. The patient in **A** was taking doxycycline, the patient in **B** was taking tetracycline, and the patient in **C** was taking ibuprofen. (**A** and **B** from Levine MS: *Radiology of the Esophagus*. Philadelphia, WB Saunders, 1989.)

considered only when there is a definite temporal relationship between ingestion of the offending medication and the onset of esophagitis.

Reflux esophagitis is a more common cause of superficial ulceration, but the ulcers are almost always confined to the distal esophagus.³⁷ Mediastinal irradiation and caustic ingestion are other causes of ulceration, but the correct diagnosis is usually suggested on clinical grounds. Crohn's disease may also be associated with shallow ulcers in the esophagus, but these patients usually have advanced Crohn's disease in the small bowel or colon (see later, "[Crohn's Disease](#)"). Finally, giant drug-induced ulcers may be indistinguishable from ulcerated carcinomas or from cytomegalovirus or human immunodeficiency virus (HIV) ulcers in patients with AIDS (see Chapter 20).³⁸ However, these conditions can usually be differentiated by the clinical history and presentation.

Because drug-induced strictures are usually located at a considerable distance from the gastroesophageal junction, they must be differentiated from high esophageal strictures caused by Barrett's esophagus, mediastinal irradiation, caustic ingestion, eosinophilic esophagitis, and primary or metastatic tumors. However, the possibility of a drug-induced stricture should be suspected in patients with cardiomegaly who have a history of taking potassium chloride or quinidine.

Radiation Esophagitis

Malignant tumors involving the lungs, mediastinum, or thoracic spine are often treated by high-dose, external-beam radiation to the chest. The major limiting factor with this form of treatment is esophageal damage by ionizing radiation. Total doses of 45 to 60 Gy may lead to severe esophagitis, with irreversible damage and stricture formation.³⁹ Smaller doses (20 to 45 Gy) may cause a self-limited esophagitis without permanent sequelae. Most patients have clinical evidence of esophagitis shortly after the onset of radiation therapy, but barium studies are not usually performed during this period. Instead, esophagography has been used primarily to detect strictures or other signs of chronic radiation injury. Both the acute and the chronic forms of radiation esophagitis are considered in this chapter.

PATHOGENESIS

Experiments on laboratory animals have shown that high-dose radiation to the esophagus causes an acute, self-limited form of esophagitis within 1 to 3 weeks of the onset of radiation therapy.^{40,41} After the acute stage of radiation injury and subsequent epithelial repair, chronic radiation esophagitis is characterized by progressive submucosal scarring and fibrosis with

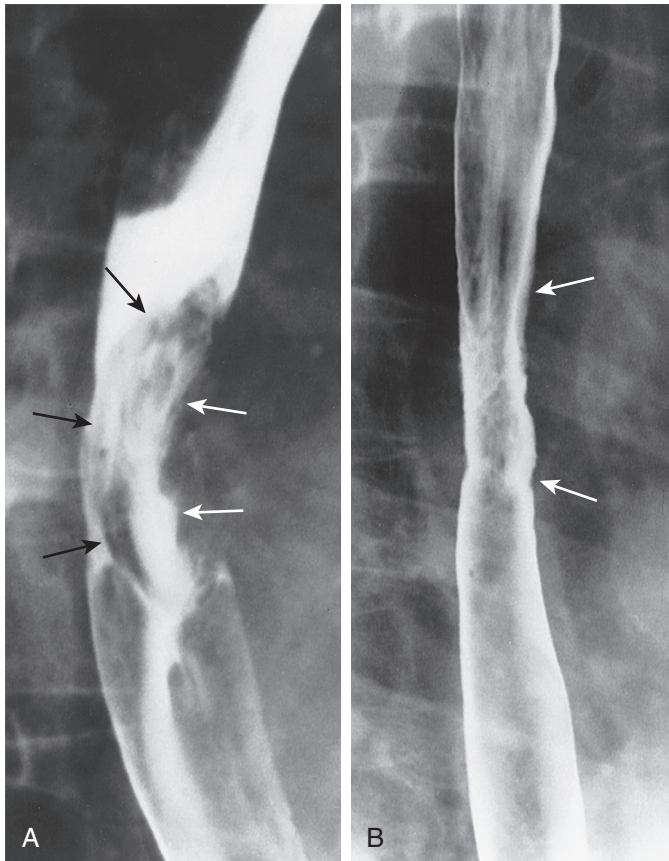


Figure 21-2 Spectrum of esophageal injury associated with potassium chloride ingestion. **A.** A giant ulcer (white arrows) is seen in the midesophagus with an associated area of mass effect (black arrows) caused by a surrounding mound of edema. This lesion could be mistaken for an ulcerated carcinoma. **B.** A midesophageal stricture (arrows) is seen in another patient who had been taking slow-release potassium chloride tablets. The stricture has relatively tapered borders. (B from Levine MS: *Radiology of the Esophagus*. Philadelphia, WB Saunders, 1989.)

the development of esophageal strictures 4 to 8 months after completion of radiation therapy at doses of 30 to 50 Gy.⁴² If the radiation dose is more than 60 Gy, esophageal strictures may develop within 3 to 4 months.⁴²

CLINICAL FINDINGS

Most patients who receive mediastinal irradiation develop a self-limited esophagitis, manifested by acute onset of substernal burning, odynophagia, or dysphagia within 1 to 3 weeks after the onset of radiation therapy.⁴³ The symptoms usually subside within 24 to 48 hours but may occasionally persist for several weeks.⁴³ Because these patients are immunocompromised, the development of odynophagia may erroneously be attributed to opportunistic esophagitis. The correct diagnosis should be suggested, however, by the temporal relationship between the onset of radiation therapy and onset of symptoms. When acute radiation esophagitis is suspected, these patients are usually treated empirically with viscous lidocaine and analgesics, so radiologic or endoscopic examinations are not often performed in this setting.

Chronic radiation injury to the esophagus may cause dysphagia within several months after completion of radiation therapy. Dysphagia may result from esophageal dysmotility or,

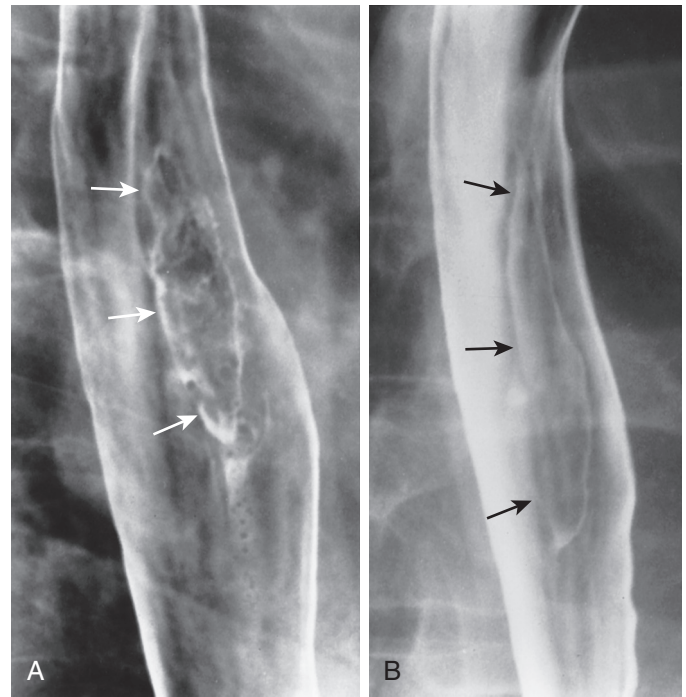


Figure 21-3 Drug-induced esophagitis with a giant esophageal ulcer. **A.** Initial double-contrast esophagogram shows a 7-cm-long, diamond-shaped ulcer (arrows) in the midesophagus below the level of the carina. The ulcer crater has irregular margins. This patient was taking sulindac (Clinoril), a nonsteroidal anti-inflammatory agent. **B.** Another esophagogram 6 months later shows a long, shallow depression with smooth borders (arrows) at the site of the previous ulcer. Endoscopy revealed that this was an ulcer scar with a re-epithelialized pit or depression. (From MS Levine, RD Rothstein, I Laufer: *Giant esophageal ulcer due to Clinoril*. *AJR* 156:955-956, 1991.)

less commonly, from the development of strictures.^{39,42} Mild radiation strictures may be successfully dilated, but more severe strictures necessitate feeding tube placement or other palliative measures. Occasionally, severe radiation injury may lead to life-threatening complications such as an esophageal airway fistula or esophageal perforation. However, these unusual complications of radiation therapy almost always occur in an area of the esophagus involved by tumor and rarely in normal irradiated tissue.^{42,44}

RADIOGRAPHIC FINDINGS

Although most patients with acute radiation esophagitis are treated empirically, barium studies are sometimes performed when the clinical diagnosis is uncertain. This condition may be manifested on double-contrast esophagography by a granular appearance of the mucosa and decreased distensibility from edema and inflammation of the irradiated segment (Fig. 21-5A).⁴⁵ Other patients with acute radiation esophagitis have multiple small, discrete ulcers within a known radiation portal (Fig. 21-6).^{41,45} With more severe disease, the esophagus may have a grossly irregular, serrated contour secondary to larger areas of ulceration and mucosal sloughing.

After the acute phase of radiation injury, the most frequent finding on barium studies is abnormal esophageal motility, which usually develops 4 to 8 weeks after completion of radiation therapy.^{39,42,46} This dysmotility is characterized by interruption of primary peristalsis at the superior border of the

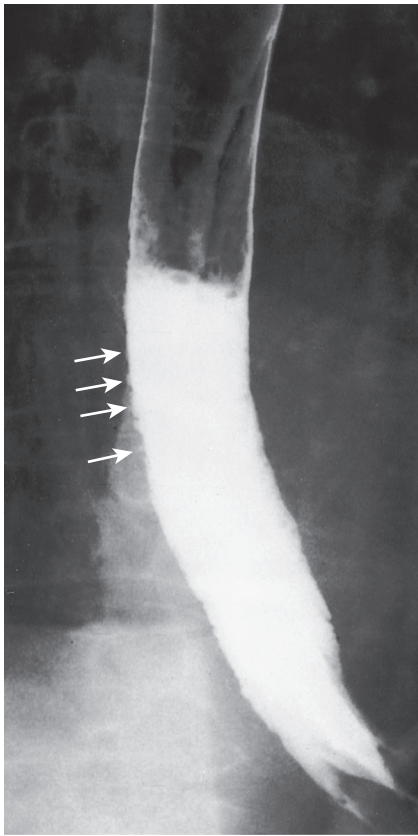


Figure 21-4 Alendronate-induced esophagitis. Multiple tiny ulcers (arrows) are seen in profile in the distal esophagus. This patient was taking alendronate (Fosamax) for the treatment of postmenopausal osteoporosis. (Courtesy Barbara Sabinsky, MD, Stamford, CT.)

radiation portal, with numerous nonperistaltic contractions distal to the point of disruption of the primary wave.^{39,42,46} Less commonly, the irradiated segment may be aperistaltic.⁴²

Radiation strictures in the esophagus usually develop 4 to 8 months after completion of radiation therapy.^{39,42} Higher doses of radiation may shorten the interval for developing a stricture but have no effect on its length or caliber. The strictures typically appear as relatively smooth, tapered areas of concentric narrowing in the upper or midesophagus within a preexisting radiation portal (Fig. 21-5B).^{39,42,44}

Tracheoesophageal and esophagobronchial fistulas are potentially life-threatening complications of mediastinal irradiation. These fistulas are usually caused by radiation necrosis, with erosion of tumor into the esophagus and adjacent airway.⁴⁴ The most frequent site of fistula formation is the left main bronchus, where it crosses the esophagus at the level of the fourth or fifth thoracic vertebra.⁴² When an esophageal airway fistula is suspected, the radiologic examination should be performed with barium sulfate because a water-soluble contrast agent may cause severe pulmonary edema if it enters the lungs via a fistula.⁴⁷

DIFFERENTIAL DIAGNOSIS

When acute odynophagia or dysphagia develops several weeks after mediastinal irradiation, the major diagnostic considerations are acute radiation esophagitis versus infectious esophagitis in an immunocompromised patient. *Candida*

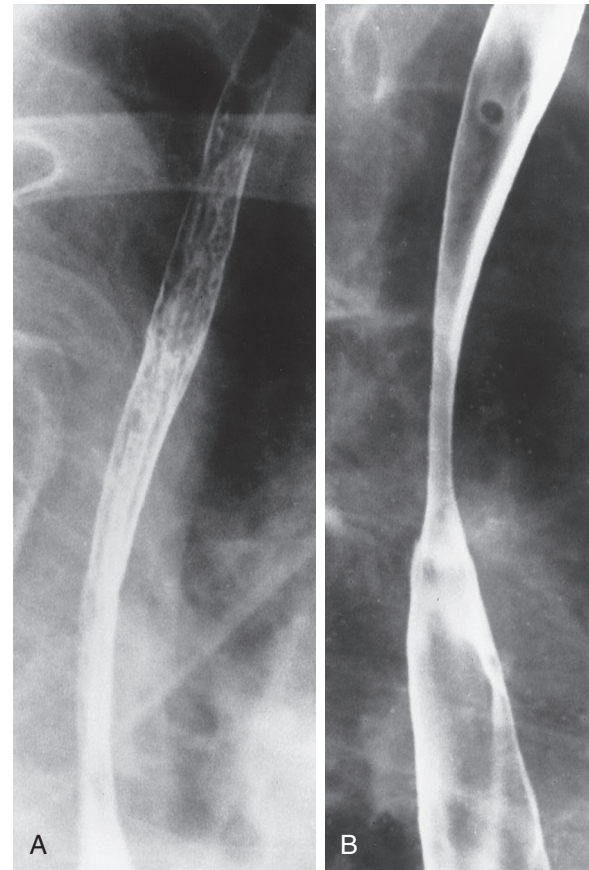


Figure 21-5 Acute radiation esophagitis with subsequent stricture formation. **A.** The mucosa has a granular appearance in the upper thoracic esophagus. Also note decreased distensibility of the irradiated segment. The patient presented with acute odynophagia 3 weeks after undergoing mediastinal irradiation for bronchogenic carcinoma. **B.** Another esophagogram 6 months later because of recurrent dysphagia shows a smooth, tapered stricture within the radiation portal.

esophagitis should be suggested on barium studies by mucosal plaques, whereas herpes esophagitis should be suggested by discrete superficial ulcers without plaque formation.³⁵ In contrast, radiation esophagitis may be manifested by a granular appearance or ulceration, but the area of involvement almost always conforms to a known radiation portal, with a sharp demarcation at the superior and inferior borders of the portal (see Fig. 21-6).

Although many conditions should be considered in the differential diagnosis for an upper or midesophageal stricture,⁴⁸ the major considerations after mediastinal irradiation should be a radiation stricture versus esophageal involvement by recurrent mediastinal tumor (see Chapter 24). A concentric area of smooth, tapered narrowing should favor the diagnosis of a radiation stricture, whereas irregular, eccentric narrowing with extrinsic mass effect should suggest a malignant tumor. When the radiographic findings are equivocal, computed tomography (CT) may be helpful for differentiating a radiation stricture from recurrent tumor in the mediastinum.

Caustic Esophagitis

Caustic esophagitis did not become a serious medical problem in the United States until 1967, when concentrated liquid lye

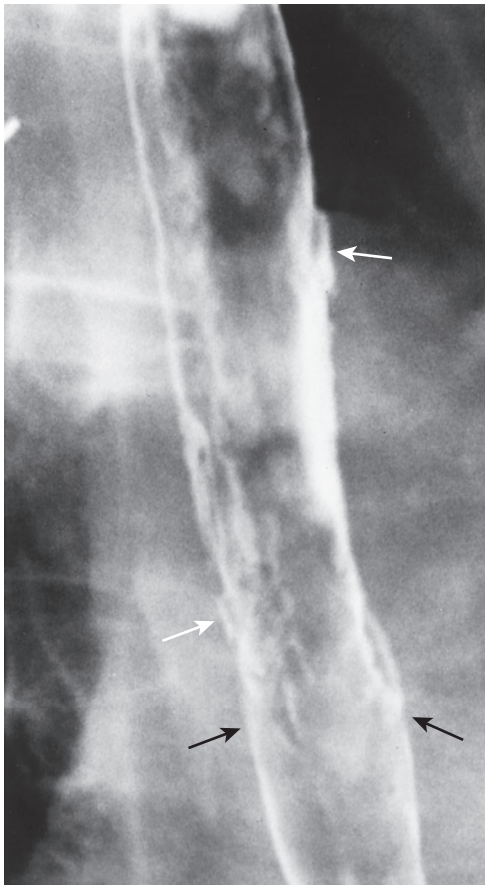


Figure 21-6 Acute radiation esophagitis. Multiple superficial ulcers are seen en face and in profile (white arrows) in the midesophagus. The area of ulceration has a relatively abrupt inferior demarcation (black arrows), which corresponds to the lower border of the radiation portal. This patient had undergone mediastinal irradiation for bronchogenic carcinoma several weeks earlier. (From Levine MS: *Radiology of the Esophagus*. Philadelphia, WB Saunders, 1989.)

solutions were made commercially available to the U.S. public for use as drain cleaners.⁴⁹ Because they could be swallowed rapidly, liquid corrosives exposed all surfaces of the upper GI tract to potentially life-threatening caustic injury. Thus, caustic esophagitis became an important clinical entity. Endoscopy has generally been advocated as the best means of assessing the extent and severity of esophageal injury, but radiologic studies may also provide valuable information during the acute and chronic stages of the disease.

PATHOGENESIS

Caustic injury to the esophagus may be caused by ingestion of alkali, acids, ammonium chloride, phenols, silver nitrate, and a variety of other common household products. Children usually ingest these corrosive substances accidentally, whereas adults take them intentionally to commit suicide. The degree of injury depends on the nature, concentration, and volume of the corrosive agent as well as the duration of tissue contact. In the United States, most patients with caustic esophagitis swallow some form of liquid lye (concentrated sodium hydroxide), which causes severe esophageal injury by liquefaction necrosis.^{50,51} In contrast, ingested acids cause tissue damage by coagulative necrosis, forming a protective eschar that tends to limit

further tissue penetration.^{50,51} Nevertheless, acidic agents may produce severe esophagitis and strictures comparable to those caused by lye.⁵²

Caustic esophagitis is characterized pathologically by three phases of injury—an acute necrotic phase, an ulceration-granulation phase, and a final phase of cicatrization and scarring.⁵³ The initial phase of acute cellular necrosis begins immediately after caustic ingestion. This acute phase usually lasts 1 to 4 days and is accompanied by an intense inflammatory reaction in the surrounding tissues.⁵³ The ulceration-granulation phase begins 3 to 5 days after caustic ingestion and is characterized by edema, ulceration, and sloughing of necrotic mucosa.⁵³ During the next 7 to 14 days, subsequent healing leads to the production of granulation tissue in areas of mucosal sloughing. The esophagus is thought to be weakest and therefore most vulnerable to perforation during this period. The final phase of cicatrization begins 3 to 4 weeks after caustic ingestion.⁵³ Depending on the degree of injury, this cicatrization process may lead to severe scarring and stricture formation.

CLINICAL FINDINGS

Acute caustic esophagitis may be manifested by odynophagia, chest pain, drooling, vomiting, or hematemesis.^{50,51,53} Severe substernal pain, fever, and shock usually indicate esophageal perforation and mediastinitis.^{50,51} Associated gastric perforation leads to the development of peritonitis. If patients survive the acute illness, there may be a latent period of several weeks, during which they are no longer symptomatic.^{50,51,53} Subsequently, however, these patients often develop severe dysphagia secondary to progressive stricture formation 1 to 3 months after the initial injury.^{50,51}

DIAGNOSIS AND TREATMENT

When caustic ingestion is suspected, examination of the mouth and oropharynx sometimes reveals obvious tissue injury, with ulceration of the lingual, buccal, or pharyngeal mucosa. Liquid corrosives may be swallowed rapidly, however, so caustic esophagitis often occurs without associated pharyngeal injury.^{50,51,53} Direct visualization of the esophagus is therefore required to confirm this diagnosis. A limited radiographic study may be performed with a water-soluble contrast agent to detect an esophageal or gastric perforation or other signs of caustic injury. However, most authors advocate endoscopy within 24 hours of caustic ingestion (assuming that there are no clinical or radiographic signs of perforation) to assess the extent and severity of esophageal injury.^{50,51,53}

Treatment of caustic esophagitis is generally aimed at preventing stricture formation. Some advocate early administration of steroids and antibiotics to inhibit collagen formation and decrease the risk of infection.^{54,55} Others believe that esophageal bougienage should be performed as early as 2 to 3 weeks after caustic ingestion. Despite such measures, 10% to 40% of patients with caustic esophagitis develop strictures.^{51,56} Some of these strictures may respond to periodic dilation procedures, but others eventually require an esophageal bypass operation, such as a colonic interposition (see Chapter 27). When strictures develop after caustic ingestion, barium studies may be used to determine the degree and extent of stricture formation as well as the response to treatment. Patients with lye strictures are also thought to have a substantially

increased risk of developing esophageal carcinoma 20 to 40 years after the initial caustic injury.^{57,58} This subject is discussed in detail in Chapter 23.

RADIOGRAPHIC FINDINGS

Chest and abdominal radiographs should be obtained routinely for patients who have ingested caustic agents. With severe esophageal injury, posteroanterior and lateral radiographs of the chest may show a dilated, gas-filled esophagus or, if esophageal perforation has occurred, mediastinal widening, pneumomediastinum, or pleural effusions.^{59,60} Similarly, abdominal radiographs may reveal pneumoperitoneum or a localized gas-containing abscess from gastric perforation.

When esophageal or gastric perforation is suspected in patients who have normal or equivocal chest and abdominal radiographs, a water-soluble contrast study should be performed to document the presence of a leak. Water-soluble contrast agents are used because barium in the mediastinum may cause mediastinal fibrosis, and barium in the peritoneal cavity may cause peritonitis.⁴⁷ If there is no evidence of esophageal or gastric perforation with a water-soluble contrast agent, however, barium should be given for a more detailed examination.

Acute caustic esophagitis may be manifested on esophagography by esophageal dysmotility with poor primary peristalsis, nonperistaltic contractions, diffuse esophageal spasm, or a dilated, atonic esophagus (Fig. 21-7).⁵⁹⁻⁶² Some authors believe

that the latter finding indicates diffuse muscular necrosis and that it is an ominous sign of impending esophageal perforation.⁵⁹ These various motor abnormalities have been attributed to edema, inflammation, or destruction of ganglion cells in Auerbach's plexus.^{61,63}

In other patients, acute caustic esophagitis may be manifested by multiple shallow, irregular ulcers (Fig. 21-8). With more severe caustic injury, the esophagus may be diffusely narrowed and may have a grossly irregular contour because of marked edema, spasm, and ulceration (Fig. 21-9).^{52,59,60} Occasionally, contrast material may dissect beneath partially sloughed mucosal fragments, producing a double-barreled appearance.⁵⁹

Subsequent cicatrization and fibrosis may lead to the development of one or more strictures in the esophagus 1 to 3 months after the acute injury. The strictures usually appear as relatively long areas of smooth, tapered narrowing in the upper or midesophagus; some strictures may have an irregular contour or eccentric areas of sacculation because of asymmetric scarring (Fig. 21-10).⁶⁰ With severe scarring, the entire thoracic esophagus may have a threadlike, filiform appearance (Fig. 21-11).⁶⁰ This finding should be highly suggestive of a caustic stricture because other conditions are rarely associated with such severe esophageal narrowing. When esophagography is performed after caustic ingestion, the stomach should also be evaluated to determine whether associated gastric injury is present. This subject is discussed in detail in Chapter 30.

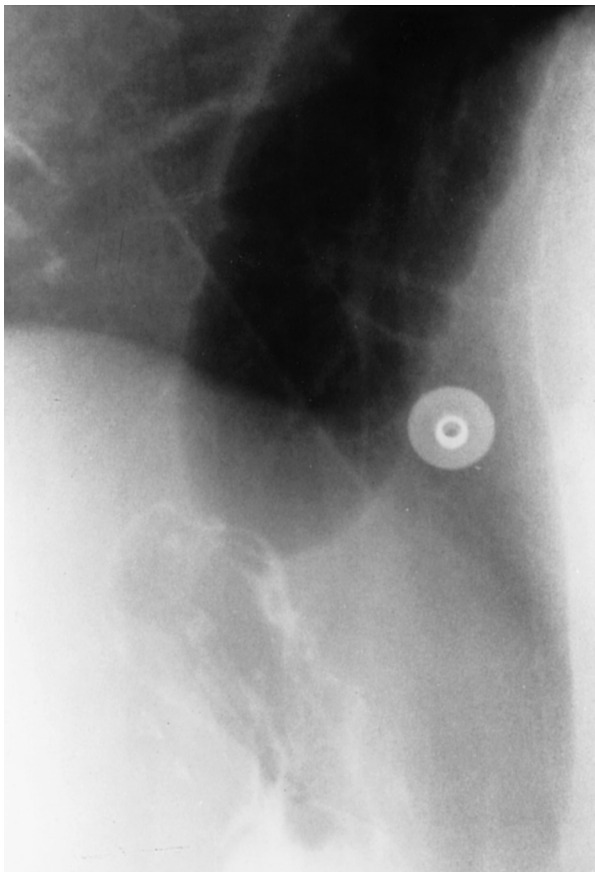


Figure 21-7 Acute caustic esophagitis with a dilated, atonic esophagus. There is a dilated, aperistaltic, gas-filled esophagus with a small amount of water-soluble contrast material in the stomach. This finding indicates a high risk of perforation.



Figure 21-8 Acute caustic esophagitis. Multiple shallow, irregular ulcers are seen en face and in profile in the midesophagus. This patient had taken concentrated potassium hydroxide in a suicide attempt. (From Levine MS: *Radiology of the Esophagus*. Philadelphia, WB Saunders, 1989.)

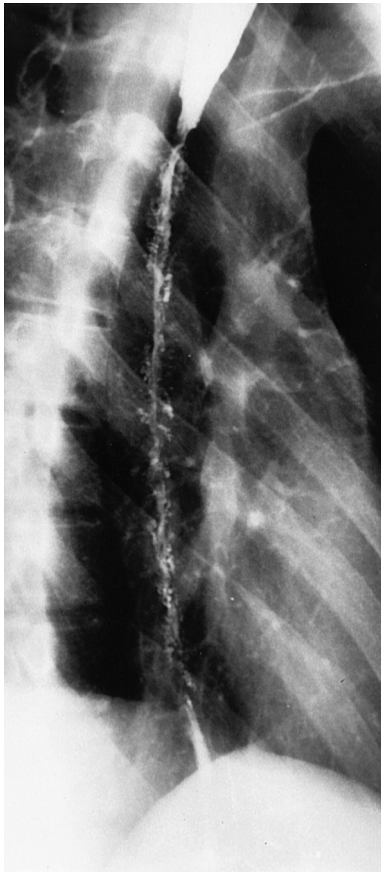


Figure 21-9 Severe caustic esophagitis. The thoracic esophagus is diffusely narrowed and has a grossly irregular contour with extensive ulceration because of ingestion of concentrated sodium hydroxide (liquid lye). (From Levine MS: *Radiology of the Esophagus*. Philadelphia, WB Saunders, 1989.)

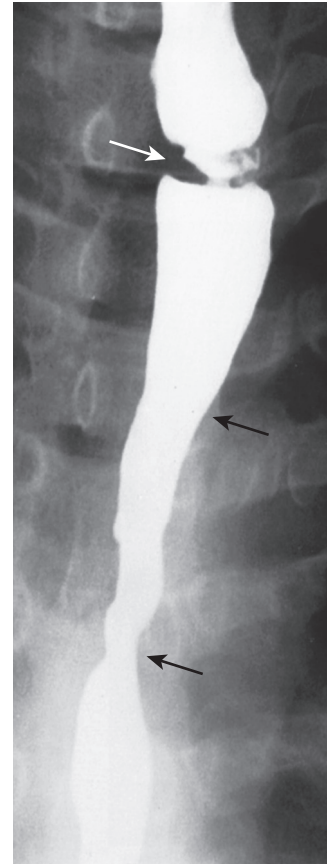


Figure 21-10 Lye strictures. A long, tapered stricture (black arrows) is seen in the upper thoracic esophagus. Another short, asymmetric stricture (white arrow) is seen more proximally at the thoracic inlet. The presence of one or more segmental strictures in the cervical or thoracic esophagus is characteristic of caustic injury. (From Levine MS: *Radiology of the Esophagus*. Philadelphia, WB Saunders, 1989.)

DIFFERENTIAL DIAGNOSIS

Acute caustic esophagitis may be difficult to differentiate from severe cases of reflux, infectious, drug-induced, or radiation esophagitis. However, reflux esophagitis tends to involve the distal esophagus, drug-induced esophagitis usually involves the midesophagus, and radiation esophagitis occurs within a pre-existing radiation portal. In contrast, the site of caustic injury in the esophagus is unpredictable because these patients may have segmental or diffuse esophagitis involving the cervical or thoracic esophagus. Whatever the radiographic findings, the diagnosis of caustic esophagitis is usually apparent from the clinical history.

The classic finding of a long, tapered stricture in the cervical or thoracic esophagus should suggest prior caustic ingestion. However, localized caustic strictures in the upper or mid-esophagus may be indistinguishable from high esophageal strictures from other causes, including Barrett's esophagus, mediastinal irradiation, oral medications, metastatic tumor or, rarely, dermatologic diseases such as epidermolysis bullosa dystrophica and benign mucous membrane pemphigoid. When a lye stricture has irregular margins or relatively abrupt borders, differentiation from an infiltrating carcinoma may also be difficult. The ability to distinguish benign from malignant lesions

is particularly important because of the increased risk of developing esophageal carcinoma in long-standing lye strictures (Fig. 21-12).^{57,58} Thus, endoscopy and biopsy may be required for a definitive diagnosis.

Idiopathic Eosinophilic Esophagitis

Since its original description by Attwood and associates in 1993,⁶⁴ eosinophilic esophagitis has been recognized as a chronic inflammatory disorder in children and adults.⁶⁵⁻⁶⁷ Eosinophilic esophagitis has been diagnosed with greater frequency over the past 2 decades, probably because of increasing awareness and increasing prevalence of this condition.⁶⁸ The diagnosis is established on pathologic grounds by an increased number of intraepithelial eosinophils (more than 20/high-power field) on endoscopic biopsy specimens from the esophagus.^{64,67} The cause is uncertain, but investigators believe that this condition develops as a result of an allergic immune response to ingested food items involving T-cell mediated hypersensitivity and immunoglobulin E (IgE)-mediated pathways, leading to eosinophilic activation, inflammation, and fibrosis.⁶⁹ Most patients with eosinophilic esophagitis do not have eosinophilic infiltration of the stomach and small bowel (eosinophilic gastroenteritis).

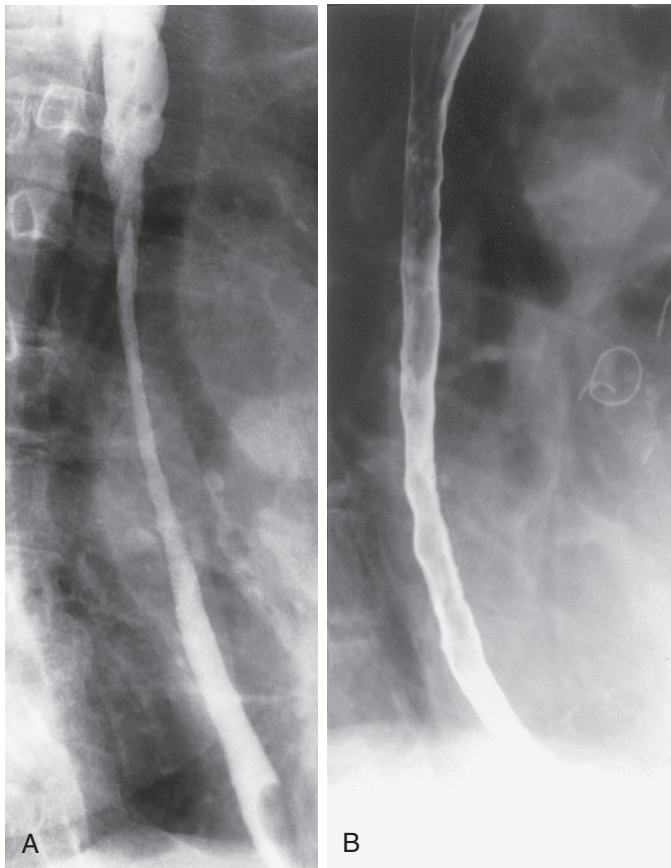


Figure 21-11 Advanced lye strictures. A, B. There is diffuse narrowing of the thoracic esophagus caused by extensive scarring and fibrosis in two patients with lye strictures. This appearance should suggest caustic injury because other conditions are rarely associated with such severe esophageal narrowing. (A from Levine MS: *Radiology of the Esophagus*. Philadelphia, WB Saunders, 1989.)

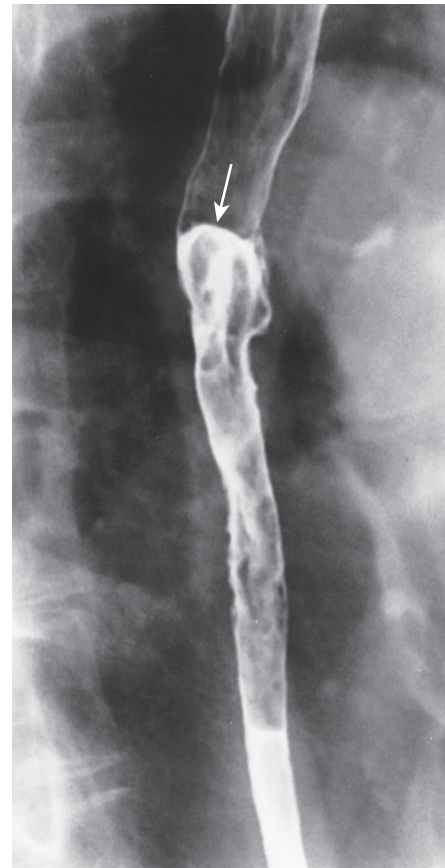


Figure 21-12 Esophageal carcinoma arising in a lye stricture. There is a long stricture in the thoracic esophagus caused by caustic ingestion many years earlier. The irregular appearance and abrupt proximal border (arrow) of the narrowed segment are caused by a superimposed carcinoma.

CLINICAL FINDINGS

Adults with eosinophilic esophagitis are typically young men who present with long-standing dysphagia and recurrent food impactions.⁶⁵⁻⁶⁷ These individuals may have an atopic history (e.g., asthma, allergic rhinitis, and other allergic conditions) and peripheral eosinophilia,⁷⁰ but eosinophilic esophagitis often occurs as an isolated condition in the absence of an allergic history or peripheral eosinophilia.^{67,71}

Based on the assumption that food allergens act as antigenic stimulation for eosinophilic inflammation of the esophagus, most patients are treated with antiallergy therapy, including oral steroids, topical steroids (swallowing metered doses of aerosolized steroid preparations), and elemental diets (i.e., protein-free diets) or elimination food diets (diets that exclude food items most commonly associated with food allergies), with varying degrees of success.⁷²⁻⁷⁵ Patients with strictures causing intractable dysphagia may undergo endoscopic dilation procedures, but these individuals often have only transient relief of dysphagia, so multiple dilations may be required.^{67,76}

RADIOGRAPHIC FINDINGS

Eosinophilic esophagitis may be manifested on esophagography by strictures, rings, diffuse esophageal narrowing, or some

combination of these findings. Not infrequently, affected patients develop one or more segmental strictures in the upper or midesophagus or, less commonly, distal esophagus.^{70,77-79} These strictures typically appear as relatively long segments of concentric narrowing with smooth contours and tapered margins, although strictures in the distal esophagus tend to be shorter than those in the upper or midesophagus (Fig. 21-13A).⁷⁹ Other patients may develop a so-called ringed esophagus, manifested on barium studies by distinctive ringlike indentations, with multiple closely spaced concentric rings traversing the lumen (see Fig. 21-13A).⁸⁰ The rings may be associated with strictures or a small-caliber esophagus (see later) or may occur as an isolated finding in the esophagus.^{79,80} Although the pathogenesis is uncertain, such rings have been well documented at endoscopy, producing a typical corrugated appearance.⁸¹⁻⁸³ Still other patients with eosinophilic esophagitis may have diffuse loss of caliber of most or all of the thoracic esophagus, resulting in a so-called small-caliber esophagus (Fig. 21-13B).⁷⁹ Paradoxically, these long segments of narrowing can be more difficult to recognize on barium studies than shorter segments of narrowing because of their long length, uniform luminal diameter, and smooth contour, without obvious demarcations from adjacent normal-caliber esophagus. Despite the frequent subtlety of this finding, eosinophilic esophagitis should be suspected when a small-caliber esophagus is detected on barium

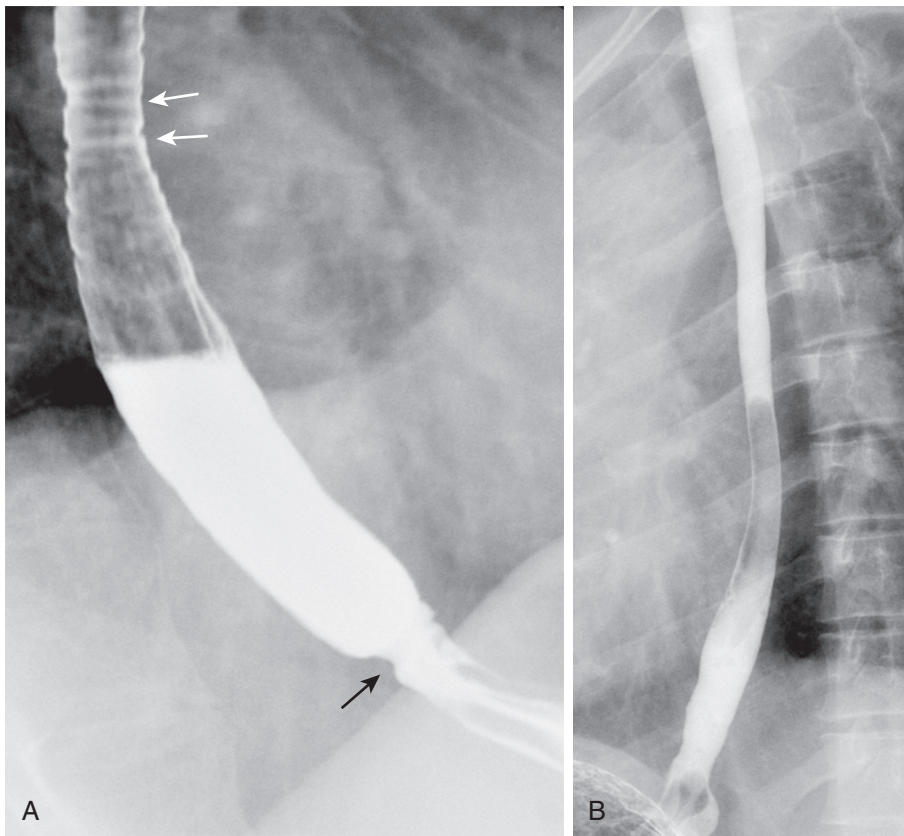


Figure 21-13 Eosinophilic esophagitis.

A. A mild area of tapered narrowing is seen in the midesophagus, with several distinctive ringlike indentations (*white arrows*) in the region of the stricture, producing a ringed esophagus. Note a second short stricture (*black arrow*) in the distal esophagus. **B.** In another patient, there is diffuse loss of distensibility of the entire thoracic esophagus, producing a small-caliber esophagus. The ringed esophagus and small-caliber esophagus are both characteristic of eosinophilic esophagitis.

studies in the proper clinical setting. In symptomatic patients, treatment with topical steroids can lead to improved esophageal diameter and relief of solid-food dysphagia.⁸⁴ It is therefore unclear whether the small-caliber esophagus results from actual fibrosis and stricture formation or other pathophysiologic mechanisms.

Other patients with eosinophilic esophagitis may have abnormal esophageal motility, with an increased frequency of nonperistaltic contractions or even an achalasia-like syndrome.^{77,85} Rarely, small, sessile eosinophilic polyps may be found in the esophagus.^{77,78}

DIFFERENTIAL DIAGNOSIS

Upper or midesophageal strictures in eosinophilic esophagitis cannot always be differentiated from high esophageal strictures caused by Barrett's esophagus, mediastinal irradiation, caustic ingestion, and metastatic tumor. The presence of an atopic history or peripheral eosinophilia, however, should suggest the correct diagnosis. In contrast, distal esophageal strictures in eosinophilic esophagitis may be impossible to differentiate from peptic strictures. Rarely, a long esophageal stricture or even a small-caliber esophagus may develop in patients with lichen planus involving the esophagus.⁸⁶

A ringed esophagus has also been described in patients with congenital esophageal stenosis. These patients may have corrugated esophageal strictures with multiple concentric rings indistinguishable from those in eosinophilic esophagitis.⁸⁷ Although congenital esophageal stenosis is usually not associated with an allergic history or peripheral eosinophilia, this condition also occurs in young men with long-standing

dysphagia, and biopsy specimens from the esophagus may also reveal increased numbers of intraepithelial eosinophils.⁸⁷ Because of the similarities in the clinical, radiographic, and pathologic findings of these conditions, some of the reported patients with congenital esophageal stenosis may have had unrecognized eosinophilic esophagitis as the cause of their symptoms.

The differential diagnosis of the ringed esophagus includes fixed transverse folds in patients with strictures, but these folds generally are incomplete and further apart, producing a characteristic stepladder appearance.⁸⁸ The feline esophagus could also conceivably be mistaken for the ringed esophagus of eosinophilic esophagitis, but these transverse striations occur as a transient phenomenon and are not associated with strictures.

Crohn's Disease

The esophagus is the least common site of involvement by Crohn's disease in the GI tract. When the esophagus is involved, these patients almost always have associated disease in the small bowel or colon. As a result, esophageal lesions are usually found after a clinical diagnosis of Crohn's disease has been established. Occasionally, however, the onset of esophageal Crohn's disease coincides with the onset of disease in the small bowel or colon, so these patients do not necessarily have known Crohn's disease when they seek medical attention. Rarely, isolated esophageal Crohn's disease may occur before the development of disease elsewhere in the GI tract.⁸⁹

A definitive diagnosis of esophageal Crohn's disease requires histologic confirmation, but endoscopic biopsy specimens often

fail to reveal granulomas because of the superficial nature of the biopsies and patchy distribution of the disease.⁹⁰ As a result, the absence of definitive histologic findings should not preclude a diagnosis of Crohn's disease if the clinical and radiographic findings suggest this condition.

CLINICAL FINDINGS

Most patients with esophageal Crohn's disease have advanced Crohn's disease in the lower GI tract, so the clinical presentation is dominated by their ileocolitis. Nevertheless, esophageal Crohn's disease may cause dysphagia or, less commonly, odynophagia or upper GI bleeding.⁹⁰⁻⁹² Because the esophagus is rarely involved by Crohn's disease as an isolated finding, the diagnosis should be considered only in patients with known Crohn's disease elsewhere in the GI tract who develop dysphagia or other esophageal symptoms. When esophageal Crohn's disease is present, the clinical course may parallel that of the patient's ileal or colonic disease, with remission of upper and lower GI symptoms after medical or surgical treatment.⁹¹

RADIOGRAPHIC FINDINGS

Although Crohn's disease primarily affects the small bowel or colon, esophageal involvement has been recognized with increased frequency on double-contrast esophagography. The major advantage of double-contrast technique is its ability to detect aphthoid ulcers, which are seen on double-contrast examinations in about 3% of patients with Crohn's disease in the small bowel or colon.⁹² As in other portions of the GI tract, the aphthoid ulcers appear as punctate, slitlike, or ringlike collections of barium surrounded by radiolucent halos of edematous mucosa (Fig. 21-14).⁹²⁻⁹⁴ These ulcers are usually few in number and are sporadically distributed throughout the esophagus with intervening normal mucosa (see Fig. 21-14A), but may occasionally be more numerous (see Fig. 21-14B).⁹⁴

As the disease progresses, barium studies may reveal more severe esophagitis characterized by larger areas of ulceration, thickened folds, pseudomembranes, or even a cobblestone appearance.^{91,95} Other patients may develop transverse or longitudinal intramural tracks (Fig. 21-15) or tracheoesophageal, esophagobronchial, esophagomediastinal, or esophagogastric fistulas.^{91,95} Progressive scarring may also lead to the development of strictures, usually in the distal esophagus (Fig. 21-16).⁹¹ Rarely, advanced esophageal Crohn's disease may be manifested by filiform polyposis of the esophagus, analogous to filiform polyposis of the colon in granulomatous colitis.⁹⁶

DIFFERENTIAL DIAGNOSIS

The aphthoid ulcers of esophageal Crohn's disease may be indistinguishable from discrete superficial ulcers associated with reflux, herpes, or drug-induced esophagitis. However, reflux esophagitis predominantly involves the distal esophagus and usually occurs in patients with reflux symptoms. Although herpetic ulcers may closely resemble aphthoid ulcers,³⁵ the correct diagnosis should be apparent in an immunocompromised patient with odynophagia. Drug-induced esophagitis may also be manifested by shallow ulcers, but they tend to be

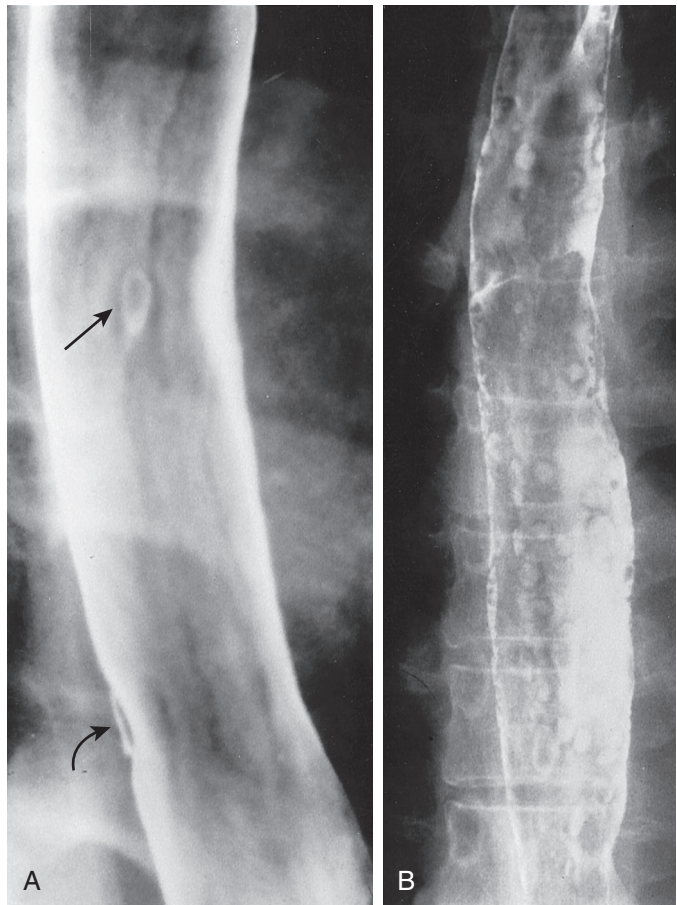


Figure 21-14 Esophageal Crohn's disease with aphthoid ulcers.

A. Discrete, widely separated aphthoid ulcers are seen en face (straight arrow) and in profile (curved arrow) as a result of early esophageal involvement by Crohn's disease. **B.** This patient has more advanced Crohn's disease, with multiple large aphthoid ulcers in the midesophagus and distal esophagus. The ulcers are surrounded by radiolucent mounds of edema. (**A** from Gohel V, Long BW, Richter G: Aphthous ulcers in the esophagus with Crohn colitis. *AJR* 137:872-873, 1981; **B** courtesy Peter J. Feczko, MD, Royal Oak, MI.)

clustered in the midesophagus near the aortic arch or left main bronchus, and there is usually a recent history of ingesting oral medications such as tetracycline or doxycycline.³¹⁻³³ Thus, the clinical history and presentation are extremely helpful for differentiating these conditions.

More advanced esophageal Crohn's disease may be indistinguishable from other types of severe esophagitis. When intramural tracks or fistulas are present, the differential diagnosis includes radiation, trauma, malignant tumor, tuberculosis, and esophageal intramural pseudodiverticulosis.⁹⁷⁻⁹⁹ Because esophageal Crohn's disease is much less common than other types of esophagitis, this diagnosis should be considered only in patients who have clinical or radiographic findings of Crohn's disease elsewhere in the GI tract.

Epidermolysis Bullosa Dystrophica

Epidermolysis bullosa is a rare hereditary skin disease in which minimal trauma causes separation of the epidermis and dermis, with subsequent bulla formation. Two forms of the disease,

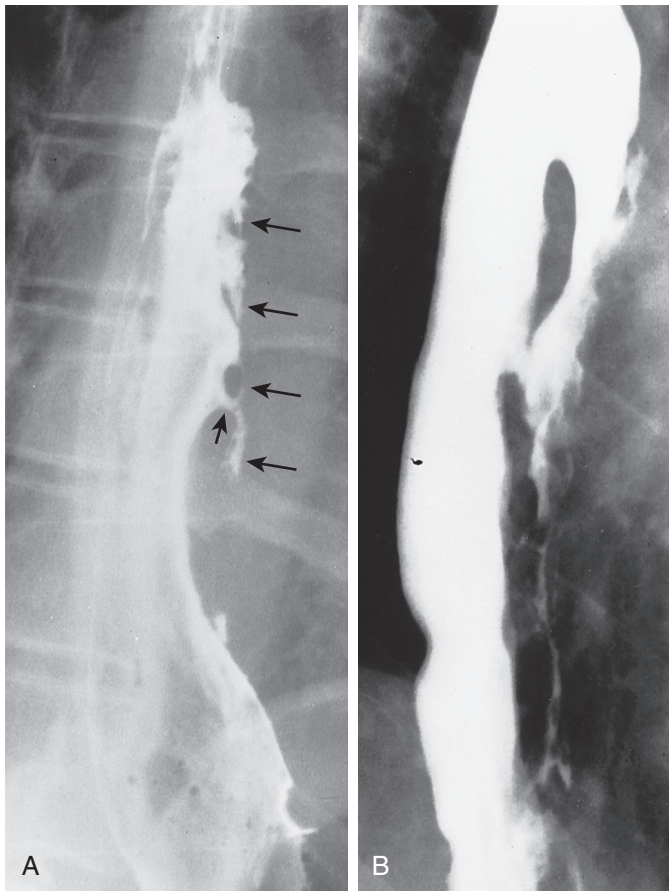


Figure 21-15 Esophageal Crohn's disease with intramural tracks. **A.** Longitudinal (long arrows) and transverse (short arrow) tracks are seen in the distal third of the esophagus because of transmural involvement by Crohn's disease. **B.** This patient has a so-called double-barreled esophagus with a long intramural track as a result of advanced esophageal Crohn's disease. (**A** courtesy Peter J. Feczko, MD, Royal Oak, MI; **B** courtesy Francis J. Scholz, MD, Burlington, MA.)

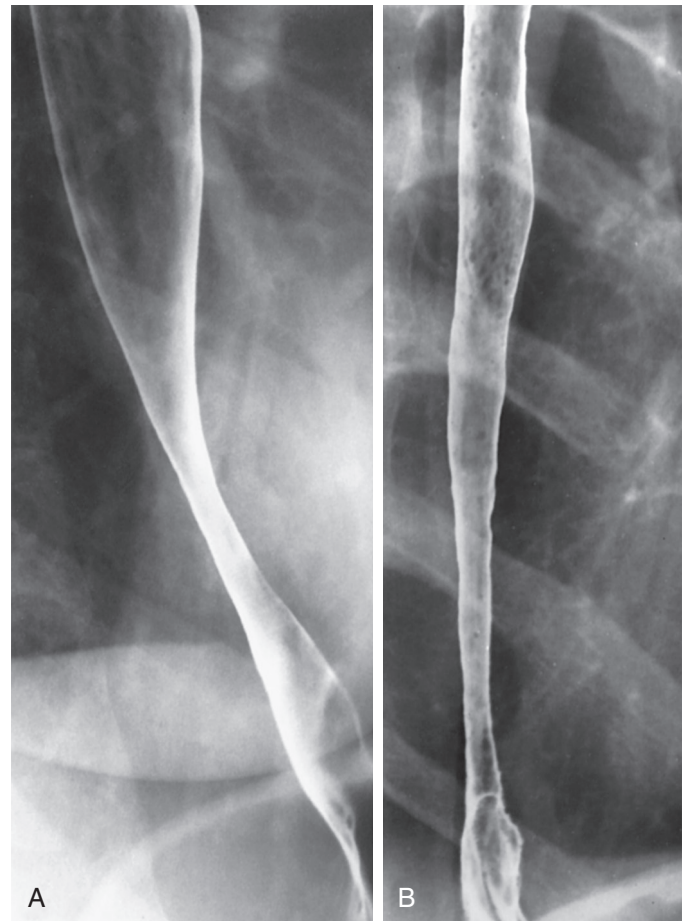


Figure 21-16 Esophageal Crohn's disease with strictures. **A, B.** Two patients have long strictures in the distal esophagus as a result of severe scarring from Crohn's disease. (**A** from Levine MS: *Radiology of the Esophagus*. Philadelphia, WB Saunders, 1989; **B** from Tishler JMA, Hellman CA: *Crohn's disease of the esophagus*. *Can Assoc Radiol J* 35:28–30, 1984.)

epidermolysis bullosa simplex and epidermolysis bullosa dystrophica, have been described. In epidermolysis bullosa simplex, the bullae heal without scarring, and the disease usually subsides at puberty. In contrast, epidermolysis bullosa dystrophica is a mutilating, potentially lethal condition manifested by progressive scarring and deformity throughout the body.¹⁰⁰ Epidermolysis bullosa dystrophica may be transmitted by autosomal dominant and autosomal recessive forms of inheritance. The autosomal dominant form involves only the skin, whereas the autosomal recessive form also involves mucous membranes in other squamous epithelium-lined organs such as the oropharynx, esophagus, and anus.¹⁰⁰

PATHOGENESIS

In patients with epidermolysis bullosa dystrophica, solid food in the esophagus repeatedly traumatizes an already fragile mucosa, causing extensive bulla formation.^{100,101} Some bullae rupture and heal without permanent sequelae, but others heal with severe scarring and stricture formation. Because these strictures further impede the passage of swallowed food, esophageal involvement may lead to a self-perpetuating cycle of blistering, scarring, and stenosis.¹⁰¹

CLINICAL FINDINGS

Skin involvement by epidermolysis bullosa dystrophica may be recognized at or shortly after birth. Other findings include flexion contractures of the hands and feet, webbed digits (syndactyly), dystrophic or absent nails, microstomia, retarded epiphyseal development, and overconstriction of long bones.¹⁰² These deformities can be disabling or even fatal.

Although the esophagus is usually affected during the first decade of life, clinical signs of esophageal involvement may not be seen until puberty.¹⁰³ Affected individuals may present with intermittent dysphagia or odynophagia because of recurrent bulla formation and healing.^{103,104} Subsequently, they may develop severe dysphagia as a result of irreversible scarring and stricture formation.^{101,103,104} Esophageal involvement should therefore be suspected in any patient with epidermolysis bullosa dystrophica who develops dysphagia or other esophageal symptoms.

Endoscopy should be avoided in patients with known or suspected epidermolysis bullosa dystrophica involving the esophagus because of the risk of further traumatizing an already fragile mucosa and causing bleeding, perforation, or further scarring and stenosis. Once strictures have developed, however,

balloon dilation or bougienage of the esophagus or, rarely, surgery may be required to alleviate symptoms.^{100,104}

RADIOGRAPHIC FINDINGS

Because of the risks associated with endoscopy, barium studies should be performed when esophageal involvement by epidermolysis bullosa dystrophica is suspected on clinical grounds. Early disease may be manifested by abnormal motility, bullae, or ulcers.^{103,105} Discrete bullae may be recognized as small, nodular filling defects in the esophagus, whereas extensive bulla formation may produce a diffusely serrated or spiculated esophageal contour.¹⁰³ Because of the reversible nature of the disease, these lesions may completely regress on follow-up examinations.

More advanced esophageal disease is characterized by scarring and stricture formation. The strictures tend to be located in the cervical or upper thoracic esophagus, appearing as concentric areas of segmental narrowing (Fig. 21-17).^{103,105-107} These strictures may be difficult to differentiate from those caused by Barrett's esophagus, mediastinal irradiation, and caustic ingestion. Other patients with epidermolysis bullosa dystrophica may develop esophageal webs, usually in the cervical esophagus near the cricopharyngeus.^{103,106} Esophageal involvement by epidermolysis bullosa dystrophica should be suspected when high esophageal strictures or webs are seen on barium

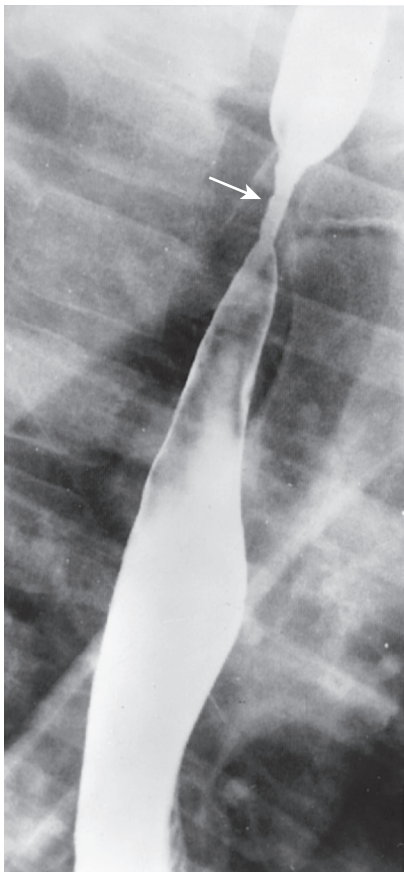


Figure 21-17 Epidermolysis bullosa dystrophica with a high esophageal stricture (arrow). (From Tishler JM, Han SY, Hellman CA: Esophageal involvement in epidermolysis bullosa dystrophica. *AJR* 141:1283-1286, 1983.)

studies in children or young adults with other clinical signs of this disease.

Pemphigoid

Pemphigoid is a dermatologic disease characterized by chronic, recurrent bullous eruptions of the skin and mucous membranes. Two forms of pemphigoid, benign mucous membrane pemphigoid and bullous pemphigoid, have been described. Benign mucous membrane pemphigoid is much more likely to involve mucous membranes, however, so esophageal abnormalities are primarily encountered in this form of the disease.

CLINICAL FINDINGS

Benign mucous membrane pemphigoid usually occurs in middle-aged patients and is twice as common in women.¹⁰⁸ About 75% of patients have involvement of the oral mucosa and conjunctiva, 50% have skin involvement, and 5% to 10% have esophageal involvement.¹⁰⁸⁻¹¹⁰ The most severe complications of this disease occur in the eye, in which conjunctival scarring causes corneal destruction and blindness in 25% of patients.¹⁰⁹ Thus, despite its name, benign mucous membrane pemphigoid should not be considered a benign condition.

Affected individuals usually present with dysphagia caused by edema, spasm, ulceration, or strictures.^{108,110} Severe esophageal involvement may occasionally result in massive sloughing of mucosa, with subsequent expulsion of a hollow membranous cast from the patient's mouth.¹¹¹ When these patients initially develop dysphagia, systemic administration of steroids may prevent further progression of esophageal disease and stricture formation. Once strictures have developed, however, one or more esophageal dilation procedures are usually required to alleviate symptoms.¹¹²

RADIOGRAPHIC FINDINGS

Although discrete bullae are rarely observed, barium studies may reveal superficial ulceration in the early stages of esophageal involvement by benign mucous membrane pemphigoid (Fig. 21-18).¹⁰⁸ Subsequent scarring may lead to the development of webs or strictures in the cervical or upper thoracic esophagus (Fig. 21-19) or, less commonly, the mid or lower thoracic esophagus.^{108,110,113,114} The strictures are of variable length and may be difficult to distinguish from those caused by Barrett's esophagus, mediastinal irradiation, and caustic ingestion. However, esophageal involvement by benign mucous membrane pemphigoid should be suspected in patients who have a history of bullous eruptions on the skin.

Erythema Multiforme Major

CLINICAL FINDINGS

Erythema multiforme is a hypersensitivity reaction characterized by a maculopapular or bullous rash that usually develops during the first 3 decades of life.¹¹⁵ Erythema multiforme minor is confined to the skin, but erythema multiforme major also involves mucous membranes of the eyes, oropharynx, genitalia, or anus and, rarely, the tracheobronchial tree or esophagus.¹¹⁵ Stevens-Johnson syndrome is a life-threatening form of

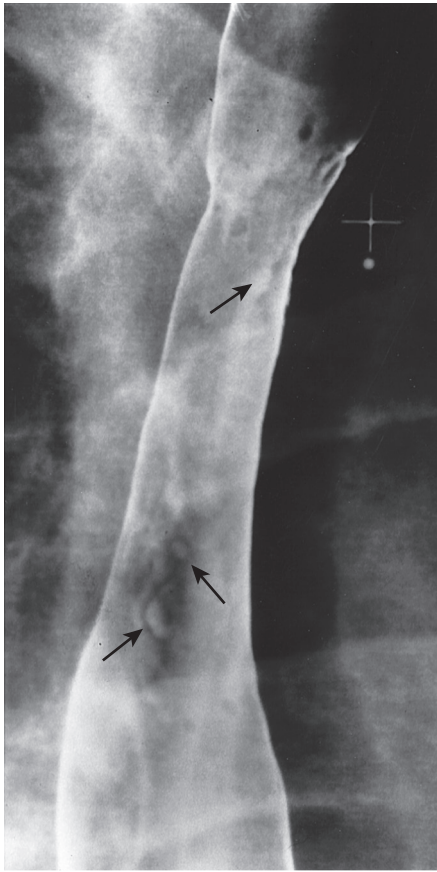


Figure 21-18 Benign mucous membrane pemphigoid with superficial ulceration. Multiple shallow ulcers (arrows) are seen in the midesophagus, with decreased distensibility of this region. (Courtesy Stephen E. Rubesin, MD, Philadelphia.)



Figure 21-19 Benign mucous membrane pemphigoid with a high esophageal stricture. A long asymmetric stricture is seen in the cervical and upper thoracic esophagus. (Courtesy John A. Bonavita, MD, Philadelphia.)

esophageal multiforme major, with associated constitutional symptoms.¹¹⁶

RADIOGRAPHIC FINDINGS

Esophageal involvement by erythema multiforme major is usually self-limited, but occasional children or adolescents have been reported with dysphagia caused by esophageal strictures, predominantly in the upper or midesophagus.¹¹⁶⁻¹¹⁸ Rarely, barium studies may reveal diffuse esophageal narrowing in children or adults with this condition.¹¹⁹ Other more common causes of long esophageal strictures include mediastinal irradiation and caustic ingestion, but esophageal involvement by erythema multiforme major should be suspected in patients with characteristic mucocutaneous lesions. Epidermolysis bullosa dystrophica and benign mucous membrane pemphigoid may also be associated with bullous lesions on the skin and esophageal strictures, but these patients usually have focal strictures or webs in the cervical or upper thoracic esophagus (see earlier, “Epidermolysis Bullosa Dystrophica” and “Pemphigoid”).

Nasogastric Intubation Esophagitis

Nasogastric intubation has been recognized as an unusual cause of esophagitis and strictures.^{120,121} Most patients develop strictures only after repeated or prolonged nasogastric intubation. These strictures may progress rapidly after removal of the tube,

causing severe dysphagia. When all causes of esophageal strictures are considered, nasogastric intubation is probably second only to caustic ingestion in terms of the length and severity of stricture formation.

PATHOGENESIS

The pathogenesis of esophageal injury is uncertain. Most patients who develop strictures have been intubated for 3 to 15 days.¹²¹ Some investigators believe that esophagitis results from uncontrolled gastroesophageal reflux around the lower end of the nasogastric tube, whereas others think that the tube occludes the lower esophageal sphincter, preventing clearance of refluxed acid from the esophagus.¹²² It has also been postulated that the irritant effect of the tube itself may cause a direct contact esophagitis.¹²³

CLINICAL FINDINGS

Most patients with esophageal injury develop symptoms several weeks to months after removal of the nasogastric tube.^{120,121} They may initially present with heartburn, chest pain, or odynophagia from severe esophagitis. Subsequently, they may develop progressive dysphagia as a result of rapid stricture formation.¹²¹ Despite the length and severity of the strictures, adequate relief from dysphagia may be obtained by periodic dilation procedures.

RADIOGRAPHIC FINDINGS

Nasogastric intubation esophagitis may be manifested by a long segment of extensive ulceration in the distal esophagus (Fig. 21-20).¹²³ Occasionally, large flat ulcers are associated with considerable mass effect because of an adjacent mound of edema, mimicking the appearance of an ulcerated esophageal carcinoma (Fig. 21-21). Subsequent stricture formation may be detected on esophagography 1 to 4 months after removal of the tube.^{120,121} Initially, the strictures may appear as smooth, tapered areas of concentric narrowing in the distal esophagus that are indistinguishable from ordinary peptic strictures. However, they tend to progress rapidly, increasing in length and severity within a relatively short period (Fig. 21-22). Because of the extent and severity of stricture formation, these patients may be suspected of ingesting caustic agents. However, nasogastric intubation strictures always involve the distal esophagus, so the presence of an unusually long or rapidly progressive stricture in the distal esophagus should suggest the correct diagnosis.

Alkaline Reflux Esophagitis

Alkaline reflux esophagitis is an unusual condition caused by reflux of bile and pancreatic secretions into the esophagus

after total or, less commonly, partial gastrectomy.¹²⁴ The development of esophagitis in these patients depends on the type of surgical reconstruction that is used. Alkaline reflux esophagitis is a common complication of total gastrectomy and simple loop esophagojejunostomy but rarely occurs after Roux-en-Y esophagojejunostomy.^{125,126} Most surgeons therefore perform a Roux-en-Y reconstruction, placing the jejunoejunal anastomosis 40 cm or more distal to the esophagojejunal anastomosis to prevent reflux of bile into the esophagus. Nevertheless, alkaline reflux esophagitis has occasionally been documented in these patients, so a Roux-en-Y reconstruction decreases the risk of esophagitis and stricture formation but does not completely eliminate these complications.¹²⁷ Some investigators have found that alkaline reflux esophagitis also predisposes to the development of Barrett's esophagus.^{128,129}

CLINICAL FINDINGS

Alkaline reflux esophagitis may initially be manifested by retrosternal burning, chest pain, and regurgitation of bile.¹²⁵ These patients may then develop worsening dysphagia within several months after surgery because of rapidly progressive stricture formation. In most cases, relief from dysphagia is obtained by mechanical dilation of the stricture.



Figure 21-20 Severe esophagitis caused by nasogastric intubation. There are multiple areas of superficial ulceration and associated narrowing of the distal esophagus caused by marked edema and spasm. A large hiatal hernia is also present. (From Levine MS: *Radiology of the Esophagus*. Philadelphia, WB Saunders, 1989.)

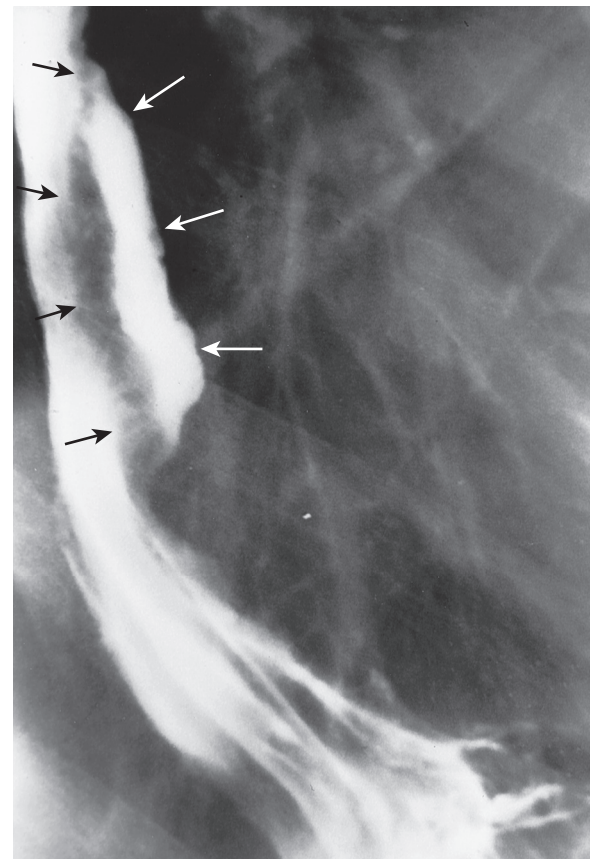


Figure 21-21 Giant esophageal ulcer caused by nasogastric intubation. A large, flat ulcer (white arrows) is seen in the distal esophagus; an associated area of mass effect (black arrows) is caused by an adjacent mound of edema. This appearance could be mistaken for that of an ulcerated esophageal carcinoma. (From Levine MS: *Radiology of the Esophagus*. Philadelphia, WB Saunders, 1989.)

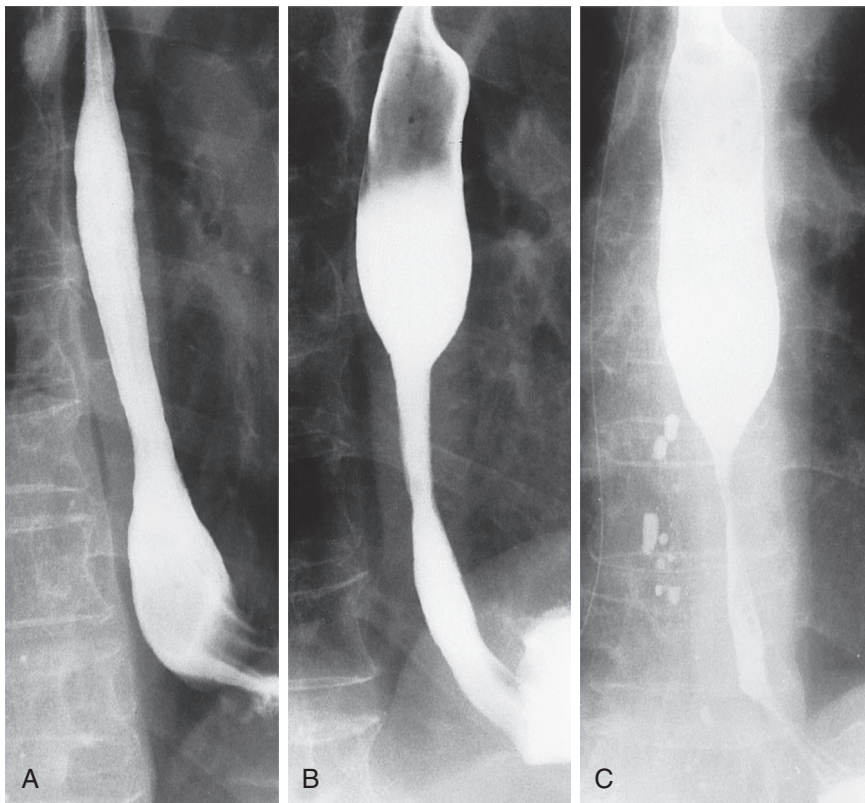


Figure 21-22 Rapidly progressive stricture caused by nasogastric intubation. **A.** Initial esophagogram shows moderately decreased distensibility of the distal esophagus shortly after removal of a nasogastric tube. **B.** Second esophagogram 3 weeks later shows rapid stricture formation with marked narrowing of the distal esophagus. **C.** Third esophagogram 6 weeks later shows further progression of the stricture. There is now evidence of esophageal obstruction. (Courtesy Vijay Gohel, MD, Philadelphia.)

RADIOGRAPHIC FINDINGS

Alkaline reflux esophagitis is characterized on esophagography by mucosal nodularity, thickened folds, and ulceration of the distal esophagus above the esophagojejunal anastomosis (Fig. 21-23).¹³⁰ Subsequent stricture formation may be detected as early as 1 to 3 months after surgery.¹³⁰ The strictures usually appear as smooth tapered areas of narrowing, often extending a considerable distance above the anastomosis.¹³⁰ These strictures must be differentiated from benign anastomotic strictures or recurrent tumor involving the distal esophagus. However, anastomotic strictures usually appear as focal areas of symmetric narrowing at the esophagojejunal anastomosis, whereas recurrent tumor is manifested by more irregular esophageal narrowing and an eccentric mass effect.¹³⁰ Because patients who undergo total or partial gastrectomy are usually intubated at the time of surgery, nasogastric intubation should be considered as another cause of rapidly developing strictures in these individuals.

Acute Alcohol-Induced Esophagitis

Alcohol abusers may occasionally develop an acute, transient esophagitis after an alcoholic binge.¹³¹ The cause is uncertain, but heavy alcohol consumption appears to have an effect on esophageal peristalsis and lower esophageal sphincter function. Several studies have shown that oral or intravenous ethanol in volunteers produces a reversible esophageal motor disturbance characterized by impaired primary peristalsis and decreased lower esophageal sphincter pressures.^{132,133} As a result, acute alcohol intoxication may promote gastroesophageal reflux with impaired clearance of refluxed peptic acid from the esophagus after reflux has occurred. Thus, alcohol-induced

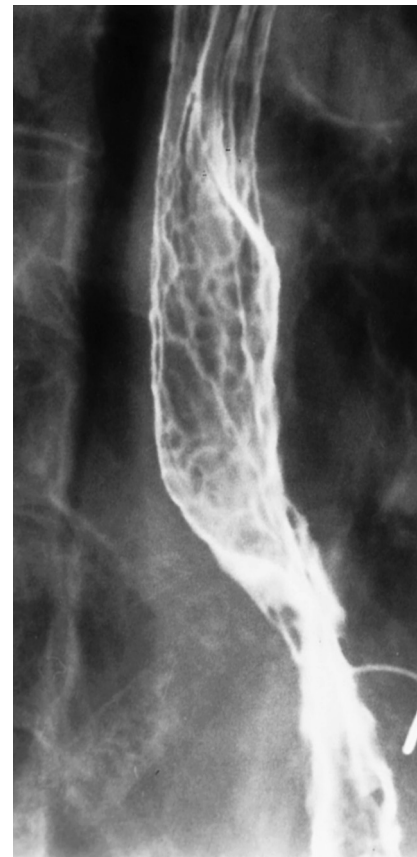


Figure 21-23 Alkaline reflux esophagitis. This patient has undergone a total gastrectomy and esophagojejunostomy. A nodular mucosa is seen in the distal esophagus above the anastomosis. (From Levine MS: *Radiology of the Esophagus*. Philadelphia, WB Saunders, 1989.)

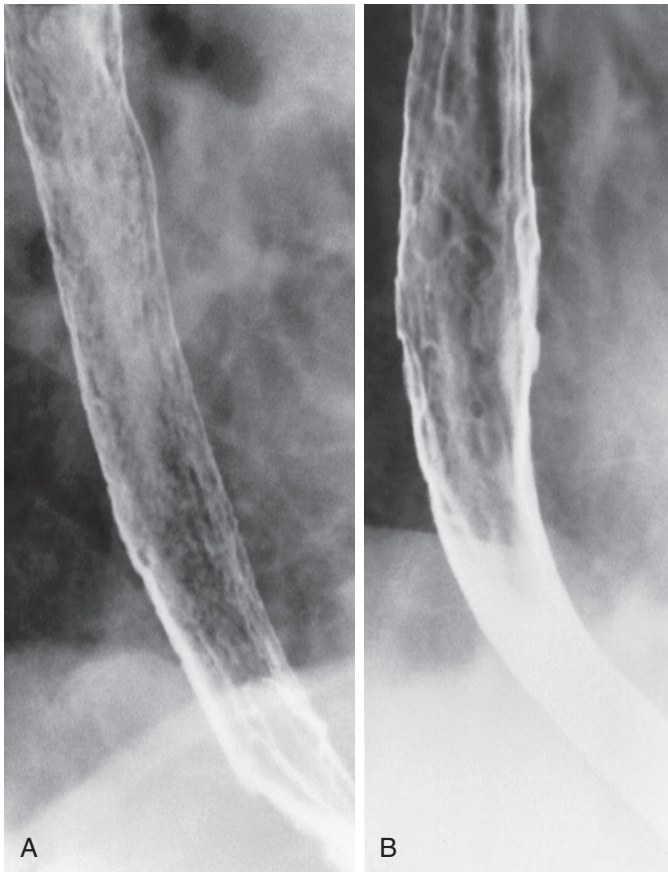


Figure 21-24 Acute alcohol-induced esophagitis. A, B. In both patients, multiple small, superficial ulcers are present in the midesophagus and distal esophagus. Reflux esophagitis could produce identical findings, but esophageal symptoms were precipitated by a recent alcoholic binge in both cases. (From O'Riordan D, Levine MS, Laufer I: *Acute alcoholic esophagitis*. *Can Assoc Radiol J* 37:54–55, 1986.)

esophagitis most likely represents a self-limited form of reflux esophagitis.

CLINICAL FINDINGS

Acute alcohol-induced esophagitis may be associated with abrupt onset of odynophagia, dysphagia, or hematemesis immediately after an alcoholic binge.¹³¹ Marked clinical improvement occurs within 1 to 2 weeks after withdrawal of alcohol.¹³¹ Although other conditions may have a similar presentation, the correct diagnosis is usually suggested by the temporal relationship between an alcoholic binge and the development of esophagitis.

RADIOGRAPHIC FINDINGS

Acute alcohol-induced esophagitis is manifested radiographically by multiple areas of superficial ulceration in the distal third of the esophagus (Fig. 21-24).¹³¹ Reflux esophagitis may produce identical radiographic findings. Nevertheless, the diagnosis should be suggested by the patient's recent drinking history.

Chronic Graft-Versus-Host Disease

Transplantation of bone marrow from matched sibling donors has become an accepted treatment for patients with aplastic anemia, acute leukemia, and other hematologic malignancies. Depending on the underlying disease, these patients have 5-year survival rates of 60% to 80% after marrow transplantation.¹³⁴ However, 30% of long-term survivors develop chronic graft-versus-host disease within 3 to 12 months after undergoing this procedure.¹³⁵ The disease is an immunologic disorder in which immunocompetent donor lymphocytes react against antigenic differences in host tissues, causing severe tissue damage. The most frequently involved target organs are the skin and liver, but the eyes, mucous membranes, and GI tract may also be affected.¹³⁴⁻¹³⁶

Esophageal involvement occurs in about 15% of patients with chronic graft-versus-host disease.¹³⁷ The immunologic process causes bulla formation, followed by desquamation and sloughing of the esophageal mucosa and subsequent stricture formation.¹³⁷⁻¹³⁹ The pathologic findings appear to be similar to those of epidermolysis bullosa dystrophica, benign mucous membrane pemphigoid, and other diseases associated with severe scarring and stricture formation in the esophagus.

CLINICAL FINDINGS

Symptoms of esophageal involvement by chronic graft-versus-host disease include dysphagia, odynophagia, substernal chest pain, and weight loss.^{135,137} Infectious esophagitis may produce similar findings in this clinical setting,¹⁴⁰ but opportunistic infection of the esophagus often develops within 1 to 8 weeks after marrow transplantation, whereas chronic graft-versus-host disease usually occurs later (3 to 12 months after transplantation).¹³⁷ The temporal relationship between marrow transplantation and the development of symptoms is therefore helpful for differentiating these conditions.

RADIOGRAPHIC FINDINGS

In early esophageal involvement by chronic graft-versus-host disease, the esophagus may have an irregular, serrated contour secondary to mucosal desquamation and sloughing.¹³⁷ With the development of scarring, barium studies may reveal webs or strictures in the esophagus. Webs are usually found in the cervical esophagus near the level of the cricopharynx (Fig. 21-25A).¹³⁷ These lesions cannot be differentiated from idiopathic webs or those associated with other conditions such as epidermolysis bullosa dystrophica and benign mucous membrane pemphigoid. Other patients may develop ringlike or smoothly tapered strictures in the upper, mid, or, less commonly, distal esophagus (Fig. 21-25B).^{135,137} The correct diagnosis should be suggested in patients who are known to have undergone marrow transplantation.

Glutaraldehyde-Induced Esophageal Injury

Glutaraldehyde is the agent most commonly used to disinfect endoscopic equipment. Outbreaks of hemorrhagic colitis in patients who underwent colonoscopy have been attributed to inadequate cleaning and rinsing of endoscopic equipment, with

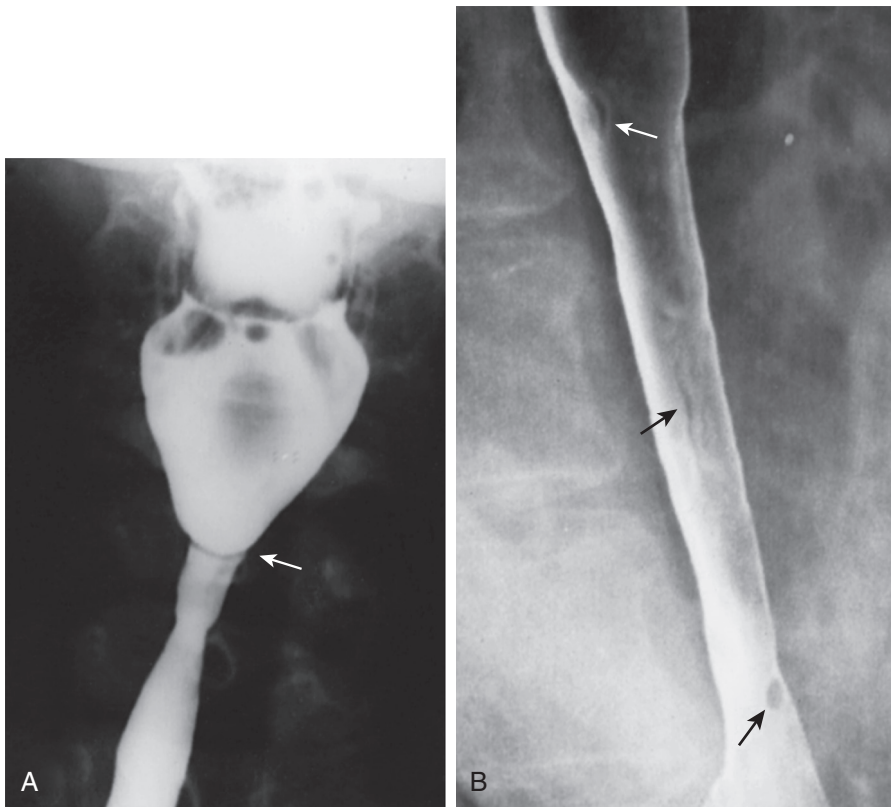


Figure 21-25 Chronic graft-versus-host disease with esophageal involvement.

A. A web is seen en face (arrow) in the cervical esophagus. **B.** A long tapered stricture is present in the distal esophagus in another patient. Nodular and linear filling defects (arrows) within the narrowed segment are caused by mucosal desquamation and sloughing. (**A** from McDonald GB, Sullivan KM, Plumley TF: Radiographic features of esophageal involvement in chronic graft-vs.-host disease. *AJR* 142:501–506, 1984; **B** courtesy Seth N. Glick, MD, Philadelphia.)

subsequent exposure of the colonic mucosa to residual glutaraldehyde.¹⁴¹ A study on laboratory rats has shown that glutaraldehyde also has a toxic effect on the esophagus, causing inflammation and segmental vasculitis.¹⁴² Rarely, esophageal strictures may develop in humans within several weeks of endoscopy, presumably because of exposure to glutaraldehyde-contaminated endoscopic equipment (Fig. 21-26).¹⁴² Exposure to glutaraldehyde should therefore be considered as a possible cause of esophagitis and rapidly progressive esophageal strictures in these patients.

Behçet's Disease

Behçet's disease was first described by Behçet in 1937 as the clinical triad of oral and genital ulceration and ocular inflammation. Behçet's disease is now recognized as a multisystem disorder characterized by a nonspecific vasculitis with resulting skin lesions, arthritis, colitis, thrombophlebitis, and, rarely, encephalitis.^{143,144} In the GI tract, Behçet's disease usually involves the colon, producing a localized or diffuse form of colitis in about 20% of patients.¹⁴³ Esophageal involvement has occasionally been reported.¹⁴⁴⁻¹⁴⁹ Affected individuals may present with substernal chest pain, dysphagia, and hematemesis.^{144,145} Double-contrast esophagography may reveal discrete superficial ulcers in the midesophagus (Fig. 21-27), widespread esophagitis, or strictures.¹⁴⁴ Rarely, a single giant ulcer may be observed.¹⁴⁶ Because Behçet's disease is often treated with steroids or other immunosuppressive agents, herpes esophagitis should be suspected as a more likely cause of esophageal ulcers in these patients. Endoscopic brushings, biopsy specimens, and cultures are therefore required to differentiate this condition from viral esophagitis.

Esophageal Intramural Pseudodiverticulosis

When esophageal intramural pseudodiverticulosis was first described in 1960, it was thought that mucosal herniation through defects in the esophageal wall produced true intramural diverticula, analogous to Rokitansky-Aschoff sinuses in the gallbladder.¹⁵⁰ Since that time, however, the pathologic basis for these structures has been well elucidated. Although esophageal intramural pseudodiverticulosis is a relatively uncommon condition, it has received considerable attention in the radiologic literature because of its often spectacular appearance on barium studies.

PATHOGENESIS

The esophagus normally contains about 200 deep mucous glands that occur in longitudinal rows parallel to the long axis of the esophagus.¹⁵¹ Within each gland, several short ducts converge to form a single main excretory duct that extends 2 to 5 mm through the esophageal wall, producing a small opening on the mucosa.¹⁵² Pathologic studies have shown that esophageal intramural pseudodiverticula represent dilated excretory ducts of these deep mucous glands.¹⁵³⁻¹⁵⁵

Although the anatomic basis of these structures has been well delineated, the explanation for this ductal dilation is unclear. One organism, *Candida albicans*, has been cultured from the esophagus in 34% to 50% of patients.^{151,156-158} It has therefore been postulated that *Candida* esophagitis predisposes to the development of esophageal intramural pseudodiverticulosis.¹⁵⁹ However, most investigators instead believe that the fungal organisms are secondary esophageal invaders and are not



Figure 21-26 Glutaraldehyde-induced esophageal stricture. A long, tapered stricture is seen in the thoracic esophagus. This stricture developed 1 month after endoscopy, presumably because of exposure to residual glutaraldehyde on the endoscopic equipment. Scarring from caustic ingestion could produce identical radiographic findings.

important causative factors in the development of this condition.^{154,160-162}

Others have postulated that ductal dilation results from plugging and obstruction of the ducts by thick, viscous mucus and inflammatory material.¹⁵²⁻¹⁵⁴ In various series, 80% to 90% of patients with pseudodiverticulosis have had endoscopic or histologic evidence of inflammatory disease in the esophagus.^{151,157} In one study, most patients also had scarring or strictures in the distal esophagus caused by reflux esophagitis.¹⁶³ Thus, esophageal intramural pseudodiverticulosis most likely occurs as a sequela of chronic esophagitis, particularly reflux esophagitis, but it is unclear why so few patients with esophagitis develop this condition.

About 90% of patients with esophageal intramural pseudodiverticulosis have associated strictures.^{151,156,157} It has therefore been suggested that increased intraluminal pressure or stasis above the stricture may cause ductal dilation.¹⁵² This theory is weakened, however, by the observation that the pseudodiverticula are often found below the level of the stricture.¹⁵¹ Conversely, stricture formation could be caused by the development of microabscesses in the ducts, resulting in perforation, peridiverticulitis, and scarring.^{162,164} This hypothesis would explain why there is often no other apparent cause for the development of esophageal strictures in these patients.

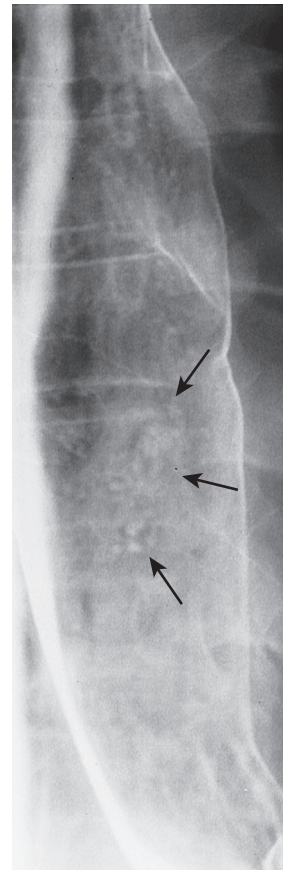


Figure 21-27 Behçet's disease with superficial ulceration. A cluster of tiny ulcers (arrows) is present in the midesophagus. Herpes esophagitis and drug-induced esophagitis are much more common causes of discrete ulcers in the midesophagus. (From Levine MS: *Radiology of the Esophagus*. Philadelphia, WB Saunders, 1989.)

CLINICAL FINDINGS

Esophageal intramural pseudodiverticulosis usually occurs in older adults and is slightly more common in men.^{151,156-158} About 20% of patients are diabetics, and 15% are alcoholics.^{143,144} Most patients present with intermittent or slowly progressive dysphagia resulting from the high prevalence of associated strictures.^{151,153,156,157,161,162}

Treatment is usually directed toward the underlying stricture because the pseudodiverticula themselves rarely cause symptoms. Dilation of strictures produces a marked clinical response in almost all patients.^{162,164} The pseudodiverticula may persist or disappear after treatment, but the fate of these structures has no relationship to the clinical course of the patient.

RADIOGRAPHIC FINDINGS

Esophageal intramural pseudodiverticulosis is diagnosed in fewer than 1% of all patients who undergo barium esophagograms.¹⁶³ Failure to visualize the pseudodiverticula may result from ductal obstruction by inflammatory material or debris that prevents barium from entering the ducts. Nevertheless, esophagography is more sensitive than endoscopy for detecting these lesions because the orifices of the

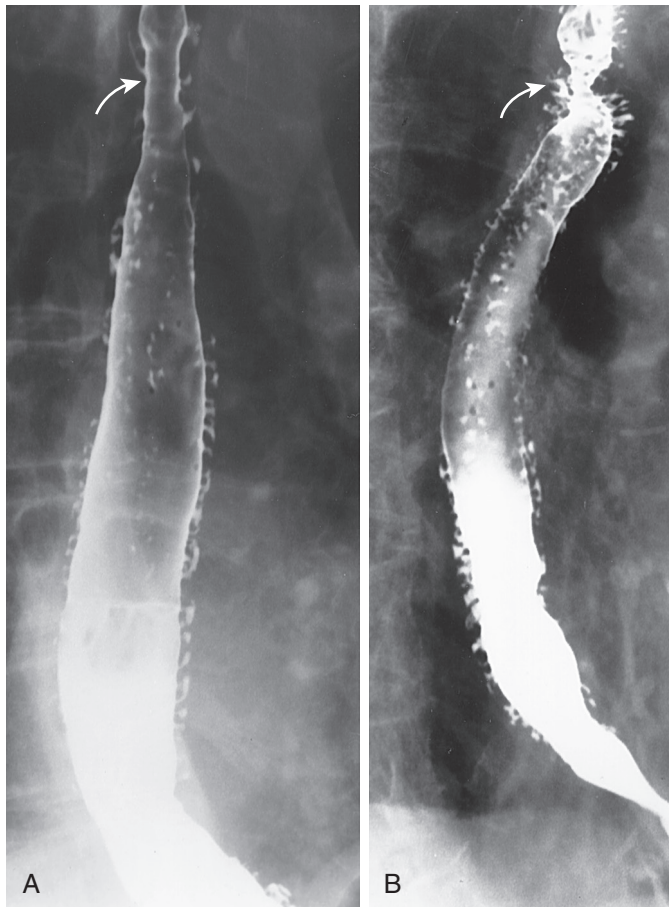


Figure 21-28 Esophageal intramural pseudodiverticulosis with high strictures. A, B. In both cases, the pseudodiverticula appear as characteristic outpouchings in longitudinal rows parallel to the long axis of the esophagus. Associated strictures (arrows) are seen in the upper thoracic esophagus. (**B** from Levine MS: *Radiology of the Esophagus*. Philadelphia, WB Saunders, 1989.)

dilated excretory ducts are extremely difficult to visualize at endoscopy.¹⁵⁶

Esophageal intramural pseudodiverticulosis is classically manifested by innumerable, tiny (1- to 4-mm), flask-shaped outpouchings in longitudinal rows parallel to the long axis of the esophagus (Fig. 21-28).^{151,153,156,157,160,164}

Because the necks of the pseudodiverticula are 1 mm or less in diameter, incomplete filling may erroneously suggest lack of communication with the esophageal lumen.¹⁶³ The pseudodiverticula may occasionally be recognized on CT by thickening of the esophageal wall, irregularity of the lumen, and intramural gas collections within these structures.¹⁶⁵

Bridging may sometimes occur between adjacent pseudodiverticula, resulting in discrete intramural tracks (Fig. 21-29).^{156,157,160} In one study, intramural tracking was detected on esophagography in 50% of patients with esophageal intramural pseudodiverticulosis.⁹⁹ These tracks may vary from short, thin connections between two or more pseudodiverticula to long intramural collections of barium paralleling the lumen.⁹⁹ Occasionally, these long tracks can be mistaken for large ulcers or even extraluminal collections associated

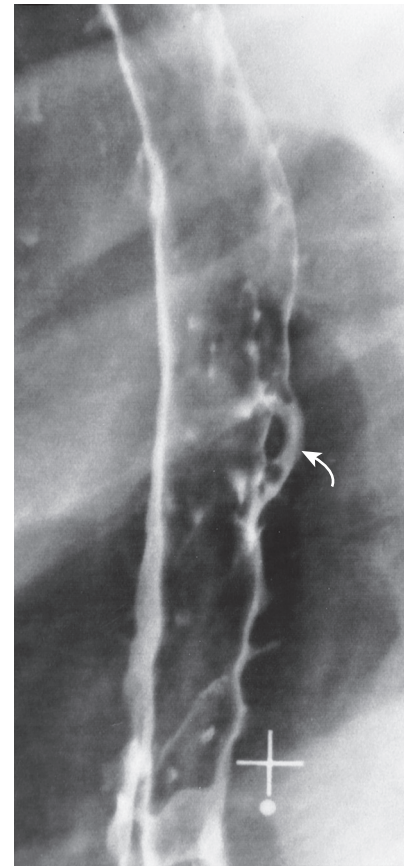


Figure 21-29 Esophageal intramural pseudodiverticulosis with an intramural track. This track (arrow) is caused by bridging of adjacent pseudodiverticula. Other pseudodiverticula seen en face could be mistaken for shallow ulcers. (Courtesy Stephen E. Rubesin, MD, Philadelphia.)

with an intramural esophageal dissection or contained perforation.⁹⁹

Half of the reported patients with esophageal intramural pseudodiverticulosis have diffuse disease, and the remaining 50% have segmental disease.^{151,156,157} About 90% of patients have associated strictures, usually in the distal esophagus, with a focal cluster of pseudodiverticula in the region of a peptic stricture (Fig. 21-30).¹⁶³ Other patients may have segmental strictures in the upper or middle third of the esophagus (see Fig. 21-28).^{151,156,157} In such cases, the pseudodiverticula often extend well above and below the level of the stricture.¹⁵⁶ Although most patients with esophageal intramural pseudodiverticulosis have esophagitis or strictures, pseudodiverticula may occasionally be observed in patients with an otherwise normal-appearing esophagus.¹⁶³

Esophageal intramural pseudodiverticulosis has also been reported in patients with esophageal carcinoma.¹⁶⁶ Such cases could conceivably result from malignant degeneration of preexisting peptic strictures in patients with Barrett's esophagus. Whatever the explanation, strictures associated with pseudodiverticulosis are not always benign, so these strictures should be evaluated individually for radiographic signs of malignancy.



Figure 21-30 Esophageal intramural pseudodiverticulosis with a peptic stricture. When viewed en face, the pseudodiverticula could be mistaken for tiny ulcers. When viewed in profile, however, the pseudodiverticula (arrows) do not appear to communicate with the esophageal lumen. This characteristic feature helps differentiate these structures from ulcers. There also is narrowing and deformity of the distal esophagus caused by an associated peptic stricture. (From Levine MS: *Radiology of the Esophagus*. Philadelphia, WB Saunders, 1989.)

Rarely, perforation of an esophageal intramural pseudodiverticulum may result in diverticulitis, with the development of a periesophageal inflammatory mass or abscess in the mediastinum.^{167,168} Affected individuals may present with chest pain, fever, leukocytosis, or other signs of mediastinitis.¹⁶⁸ In such cases, esophagography may reveal localized extravasation of contrast material into the mediastinum from the perforated pseudodiverticulum (Fig. 21-31).¹⁶⁸ CT may also reveal a periesophageal inflammatory mass with or without associated collections of gas.¹⁶⁷ In previously reported cases, the perforations have sealed off with parenteral nutrition and intravenous antibiotics.^{167,168} Thus, esophageal perforation caused by ruptured pseudodiverticula may be more likely to heal on conservative medical treatment than other types of esophageal perforations.

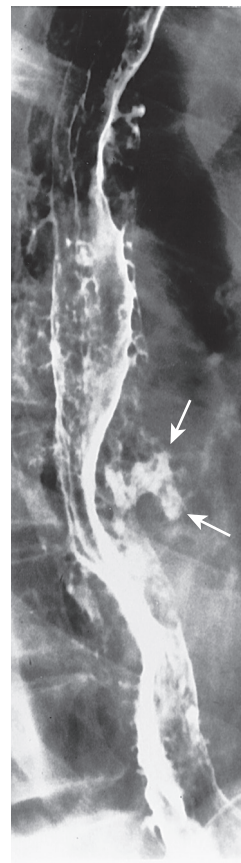


Figure 21-31 Esophageal intramural pseudodiverticulosis with associated diverticulitis. There is a large, irregular extraluminal barium collection (arrows), presumably caused by a sealed-off perforation of a pseudodiverticulum. (Courtesy Peter J. Feczko, MD, Royal Oak, MI.)

DIFFERENTIAL DIAGNOSIS

The radiographic findings of esophageal intramural pseudodiverticulosis are pathognomonic of this condition. Although pseudodiverticula can occasionally be confused with true diverticula, the latter structures are considerably larger and less numerous and should not pose a major diagnostic dilemma. When viewed en face, pseudodiverticula can also be mistaken for tiny ulcers associated with various types of esophagitis (see Fig. 21-30). When viewed in profile, however, the pseudodiverticula have a typical flask-shaped configuration and often seem to be floating outside the esophageal wall without any apparent communication with the lumen, whereas true ulcers almost always communicate directly with the lumen. The characteristic tangential appearance of the pseudodiverticula should therefore differentiate these structures from actual areas of ulceration.

REFERENCES

1. Pemberton J: Oesophageal obstruction and ulceration caused by oral potassium therapy. *Br Heart J* 32:267–268, 1970.
2. Kikendall JW, Friedman AC, Oyewole MA, et al: Pill-induced esophageal injury: Case reports and review of the medical literature. *Dig Dis Sci* 28:174–182, 1983.
3. Evans KT, Roberts GM: Where do all the tablets go? *Lancet* 2:1237–1239, 1976.
4. Levine MS: Drug-induced disorders of the esophagus. *Abdom Imaging* 24:3–8, 1999.
5. Whitney B, Croxon R: Dysphagia caused by cardiac enlargement. *Clin Radiol* 23:147–152, 1972.
6. Mason SJ, O'Meara TF: Drug-induced esophagitis. *J Clin Gastroenterol* 3:115–120, 1981.
7. Walta DC, Giddens JD, Johnson LF, et al: Localized proximal esophagitis secondary to ascorbic acid ingestion and esophageal motor disorder. *Gastroenterology* 70:766–769, 1976.

8. Bokey L, Hugh TB: Oesophageal ulceration associated with doxycycline therapy. *Med J Aust* 1:236–237, 1975.
9. Crowson TD, Head LH, Ferrante WA: Esophageal ulcers associated with tetracycline therapy. *JAMA* 235:2747–2748, 1976.
10. Rosenthal T, Adar R, Militianu J, et al: Esophageal ulceration and oral potassium chloride ingestion. *Chest* 65:463–465, 1974.
11. Lubbe WF, Cadogan ES, Kannemeyer AHR: Oesophageal ulceration due to slow-release potassium in the presence of left atrial enlargement. *N Z Med J* 90:377–379, 1979.
12. Peters JL: Benign oesophageal stricture following oral potassium chloride therapy. *Br J Surg* 63:698–699, 1976.
13. Teplick JG, Teplick SK, Ominsky SH, et al: Esophagitis caused by oral medication. *Radiology* 134:23–25, 1980.
14. Heller SR, Fellows IW, Ogilvie AL, et al: Non-steroidal anti-inflammatory drugs and benign oesophageal stricture. *BMJ* 285:167–168, 1982.
15. Coates AG, Nostrand TT, Wilson JAP, et al: Esophagitis caused by non-steroidal anti-inflammatory medication. *South Med J* 79:1094–1097, 1986.
16. Semble EL, Wu WC, Castell DO: Nonsteroidal antiinflammatory drugs and esophageal injury. *Semin Arthritis Rheum* 19:99–109, 1989.
17. Levine MS, Rothstein RD, Laufer I: Giant esophageal ulcer due to Clinoril. *AJR* 156:955–956, 1991.
18. Levine MS, Borislow SM, Rubesin SE, et al: Esophageal stricture caused by a Motrin tablet (ibuprofen). *Abdom Imaging* 19:6–7, 1994.
19. Sugawa C, Takekuma Y, Lucas CE, et al: Bleeding esophageal ulcers caused by NSAIDs. *Surg Endosc* 11:143–146, 1997.
20. de Groen PC, Lubbe DF, Hirsch LJ, et al: Esophagitis associated with the use of alendronate. *N Engl J Med* 335:1016–1021, 1996.
21. Colina RE, Smith M, Kikendall JW, et al: A new probable increasing cause of esophageal ulceration: Alendronate. *Am J Gastroenterol* 92:704–706, 1997.
22. Ryan JM, Kelsey P, Ryan BM, et al: Alendronate-induced esophagitis: Case report of a recently recognized form of severe esophagitis with esophageal stricture—radiographic features. *AJR* 206:389–391, 1998.
23. Lanza FL, Hunt RH, Thomson ABR, et al: Endoscopic comparison of esophageal and gastroduodenal effects of risedronate and alendronate in postmenopausal women. *Gastroenterology* 119:631–638, 2000.
24. Kavin H: Oesophageal ulceration due to emeprium bromide. *Lancet* 1:424–425, 1977.
25. Abbarah TR, Fredell JE, Ellenz GB: Ulceration by oral ferrous sulfate. *JAMA* 236:2320, 1976.
26. Stiris MG, Oyen D: Oesophagitis caused by oral ingestion of Aptin (alprenolol chloride) duresettes. *Eur J Radiol* 2:38–40, 1982.
27. Enzenauer RW, Bass JW, McDonnell JT: Esophageal ulceration associated with oral theophylline. *N Engl J Med* 310:261, 1984.
28. Israel RH, Wood J: Esophagitis related to cromolyn. *JAMA* 242:2758–2759, 1979.
29. Sutton DR, Gosnold JK: Oesophageal ulceration due to clindamycin. *BMJ* 1:1977, 1598.
30. Bonavina L, DeMeester TR, McChesney L, et al: Drug-induced esophageal strictures. *Ann Surg* 206:173–183, 1987.
31. Creteur V, Laufer I, Kressel HY, et al: Drug-induced esophagitis detected by double contrast radiography. *Radiology* 147:365–368, 1983.
32. Agha FP, Wilson JAP, Nostrand TT: Medication-induced esophagitis. *Gastrointest Radiol* 11:7–11, 1986.
33. Bova JG, Dutton NE, Goldstein HM, et al: Medication-induced esophagitis: Diagnosis by double-contrast esophagography. *AJR* 148:731–732, 1987.
34. Ravich WJ, Kashima H, Donner MW: Drug-induced esophagitis simulating esophageal carcinoma. *Dysphagia* 1:13–18, 1986.
35. Levine MS, Laufer I, Kressel HY, et al: Herpes esophagitis. *AJR* 136:863–866, 1981.
36. Shortsleeve MJ, Levine MS: Herpes esophagitis in otherwise healthy patients: Clinical and radiographic findings. *Radiology* 182:859–861, 1992.
37. Kressel HY, Glick SN, Laufer I, et al: Radiologic features of esophagitis. *Gastrointest Radiol* 6:103–108, 1981.
38. Levine MS, Loercher G, Katzka DA, et al: Giant, human immunodeficiency virus-related ulcers in the esophagus. *Radiology* 180:323–326, 1991.
39. Goldstein HM, Rogers LF, Fletcher GH, et al: Radiological manifestations of radiation-induced injury to the normal upper gastrointestinal tract. *Radiology* 117:135–140, 1975.
40. Phillips TL, Ross G: Time-dose relationships in the mouse esophagus. *Radiology* 113:435–440, 1974.
41. Northway MG, Libshitz HI, West JJ, et al: The opossum as an animal model for studying radiation esophagitis. *Radiology* 131:731–735, 1979.
42. Lepke RA, Libshitz HI: Radiation-induced injury of the esophagus. *Radiology* 148:375–378, 1983.
43. Roswit B: Complications of radiation therapy: The alimentary tract. *Semin Roentgenol* 9:51–63, 1974.
44. Rubin P: The radiographic expression of radiotherapeutic injury: An overview. *Semin Roentgenol* 9:5–13, 1974.
45. Collazzo LA, Levine MS, Rubesin SE, et al: Acute radiation esophagitis: Radiographic findings. *AJR* 169:1067–1070, 1997.
46. DuBrow RA: Radiation changes in hollow viscera. *Semin Roentgenol* 28:344–362, 1994.
47. Dodds WJ, Stewart ET, Vlymen WJ: Appropriate contrast media for evaluation of esophageal disruption. *Radiology* 144:439–441, 1982.
48. Karasick S, Lev-Toaff AS: Esophageal strictures: Findings on barium radiographs. *AJR* 165:561–565, 1995.
49. Leape LL, Ashcraft KW, Scarpelli DG, et al: Hazard to health: Liquid lye. *N Engl J Med* 284:587–591, 1971.
50. Kirsh MM, Ritter F: Caustic ingestion and subsequent damage to the oropharyngeal and digestive passages. *Ann Thorac Surg* 21:74–82, 1976.
51. Goldman LP, Weigert JM: Corrosive substance ingestion: A review. *Am J Gastroenterol* 79:85–90, 1984.
52. Muhlethaler CA, Gerlock AJ, de Soto L, et al: Acid corrosive esophagitis: Radiographic findings. *AJR* 134:1137–1140, 1980.
53. Citron BP, Pincus JJ, Geokas MC, et al: Chemical trauma of the esophagus and stomach. *Surg Clin North Am* 48:1303–1311, 1968.
54. Webb WR, Koutras P, Ecker RR: An evaluation of steroids and antibiotics in caustic burns of the esophagus. *Ann Thorac Surg* 9:95–102, 1970.
55. Cardona JC, Daly JF: Current management of corrosive esophagitis: An evaluation of results in 239 cases. *Ann Otol* 80:521–527, 1971.
56. Neimark S, Rogers AI: Chemical injury of the esophagus. In Berk JA, editor: *Bockus Gastroenterology*, ed 4, Philadelphia, 1985, WB Saunders, pp 769–776.
57. Appelqvist P, Salmo M: Lye corrosion carcinoma of the esophagus: A review of 63 cases. *Cancer* 45:2655–2685, 1980.
58. Hopkins RA, Postlethwait RW: Caustic burns and carcinoma of the esophagus. *Ann Surg* 194:146–148, 1981.
59. Martel W: Radiologic features of esophagitis secondary to extremely caustic agents. *Radiology* 103:31–36, 1972.
60. Franken EA: Caustic damage of the gastrointestinal tract: Roentgen features. *AJR* 118:77–85, 1973.
61. Guelrud M, Arocha M: Motor function abnormalities in acute caustic esophagitis. *J Clin Gastroenterol* 2:247–250, 1980.
62. Dantas RO, Mamede RCM: Esophageal motility in patients with esophageal caustic injury. *Am J Gastroenterol* 91:1157–1161, 1996.
63. Moody FG, Garrett JM: Esophageal achalasia following lye ingestion. *Ann Surg* 170:775–784, 1969.
64. Attwood SE, Smyrk TC, DeMeester TR, et al: Esophageal eosinophilia with dysphagia: A distinct clinicopathologic syndrome. *Dig Dis Sci* 38:109–116, 1993.
65. Fox VL, Nurko S, Furuta GT: Eosinophilic esophagitis: It's not just kid's stuff. *Gastrointest Endosc* 56:260–270, 2002.
66. Markowitz JE, Liacouras CA: Eosinophilic esophagitis. *Gastroenterol Clin North Am* 32:949–966, 2003.
67. Croese J, Fairley SK, Masson JW, et al: Clinical and endoscopic features of eosinophilic esophagitis in adults. *Gastrointest Endosc* 58:516–522, 2003.
68. Prasad GA, Alexander JA, Schleck CD, et al: Epidemiology of eosinophilic esophagitis over three decades in Olmsted County, Minnesota. *Clin Gastroenterol Hepatol* 7:1055–1061, 2009.
69. Aceves SS, Ackerman SJ: Relationships between eosinophilic inflammation, tissue remodeling, and fibrosis in eosinophilic esophagitis. *Immunol Allergy Clin North Am* 29:197–211, 2009.
70. Vitellas KM, Bennett WF, Bova JG, et al: Idiopathic eosinophilic esophagitis. *Radiology* 186:789–793, 1993.
71. Munitiz V, Martinez de Haro LF, Ortiz A, et al: Primary eosinophilic esophagitis. *Dis Esoph* 16:165–168, 2003.
72. Liacouras CA, Wenner WJ, Brown K, et al: Primary eosinophilic esophagitis in children: Successful treatment with oral corticosteroids. *J Pediatr Gastroenterol Nutr* 26:380–385, 1998.
73. Markowitz JE, Spergel JM, Ruchelli E, et al: Elemental diet is an effective treatment for eosinophilic esophagitis in children and adolescents. *Am J Gastroenterol* 98:777–782, 2003.
74. Arora AS, Perrault J, Smyrk TC: Topical corticosteroid treatment of dysphagia due to eosinophilic esophagitis in adults. *Mayo Clin Proc* 78:830–835, 2003.
75. Gonsalves N, Yang G-Y, Doerfler B: Elimination diet effectively treats eosinophilic esophagitis in adults: Food reintroduction identified causative factors. *Gastroenterology* 142:1451–1459, 2012.

76. Khan S, Orenstein SR, Di Lorenzo C, et al: Eosinophilic esophagitis: Strictures, impactions, dysphagia. *Dig Dis Sci* 48:22–29, 2003.
77. Picus D, Frank PH: Eosinophilic esophagitis. *AJR* 136:1001–1003, 1981.
78. Feczko PJ, Halpert RD, Zonca M: Radiographic abnormalities in eosinophilic esophagitis. *Gastrointest Radiol* 10:321–324, 1985.
79. White SB, Levine MS, Rubesin SE, et al: The small-caliber esophagus: Radiographic sign of idiopathic eosinophilic esophagitis. *Radiology* 256:127–134, 2010.
80. Zimmerman SL, Levine MS, Rubesin SE, et al: Idiopathic eosinophilic esophagitis in adults: The ringed esophagus. *Radiology* 236:159–165, 2005.
81. Bousvaros A, Antonioli DA, Winter HS: Ringed esophagus: An association with esophagitis. *Am J Gastroenterol* 87:1187–1190, 1992.
82. Siafakas CG, Ryan CK, Brown MR, et al: Multiple esophageal rings: An association with eosinophilic esophagitis. *Am J Gastroenterol* 95:1572–1575, 2000.
83. Kim HP, Vance B, Shaheen NJ, et al: The prevalence and diagnostic utility of endoscopic features of eosinophilic esophagitis: A meta-analysis. *Clin Gastroenterol Hepatol* 10:988–996, 2012.
84. Lee J, Huprich J, Kujath C, et al: Esophageal diameter is decreased in some patients with eosinophilic esophagitis and might increase with topical corticosteroid therapy. *Clin Gastroenterol Hepatol* 10:481–486, 2012.
85. Landres RT, Kuster GGR, Strum WB: Eosinophilic esophagitis in a patient with vigorous achalasia. *Gastroenterology* 74:1298–1301, 1978.
86. Katzka DA, Smyrk TC, Bruce AJ, et al: Variations in presentations of esophageal involvement in lichen planus. *Clin Gastroenterol Hepatol* 8:777–782, 2010.
87. Oh CH, Levine MS, Katzka DA, et al: Congenital esophageal stenosis in adults: Clinical and radiographic findings in seven patients. *AJR* 176:1179–1182, 2001.
88. Levine MS, Goldstein HM: Fixed transverse folds in the esophagus: A sign of reflux esophagitis. *AJR* 143:275–278, 1984.
89. LiVolsi VA, Jaretzki A: Granulomatous esophagitis: A case of Crohn's disease limited to the esophagus. *Gastroenterology* 64:313–319, 1973.
90. Weinstein T, Valderrama E, Pettei M, et al: Esophageal Crohn's disease: Medical management and correlation between clinical, endoscopic, and histologic features. *Inflamm Bowel Dis* 3:79–83, 1997.
91. Ghahremani GG, Gore RM, Breuer RI, et al: Esophageal manifestations of Crohn's disease. *Gastrointest Radiol* 7:199–203, 1982.
92. Tishler JMA, Helman CA: Crohn's disease of the esophagus. *J Can Assoc Radiol* 35:28–30, 1984.
93. Gohel V, Long BW, Richter G: Aphthoid ulcers in the esophagus with Crohn colitis. *AJR* 137:872–873, 1981.
94. Degryse HRM, De Schepper AM: Aphthoid esophageal ulcers in Crohn's disease of ileum and colon. *Gastrointest Radiol* 9:197–201, 1984.
95. Cynn WS, Chon H, Gureghian PA, et al: Crohn's disease of the esophagus. *AJR* 125:359–364, 1975.
96. Cockey BM, Jones B, Bayless TM, et al: Filiform polyps of the esophagus with inflammatory bowel disease. *AJR* 144:1207–1208, 1985.
97. Schneider R: Tuberculous esophagitis. *Gastrointest Radiol* 1:143–145, 1976.
98. Spalding AR, Burney DP, Richie RE: Acquired benign bronchoesophageal fistulas in the adult. *Ann Thorac Surg* 28:378–383, 1979.
99. Canon CL, Levine MS, Cherukuri R, et al: Intramural tracking: A feature of esophageal intramural pseudodiverticulosis. *AJR* 175:371–374, 2000.
100. Katz J, Gryboski JD, Rosenbaum HM, et al: Dysphagia in children with epidermolysis bullosa. *Gastroenterology* 52:259–262, 1967.
101. Nix TE, Christianson HB: Epidermolysis bullosa of the esophagus: Report of two cases and review of literature. *South Med J* 58:612–620, 1965.
102. Becker MH, Swinyard CA: Epidermolysis bullosa dystrophica in children: Radiologic manifestations. *Radiology* 90:124–128, 1968.
103. Agha FP, Francis IR, Ellis CN: Esophageal involvement in epidermolysis bullosa dystrophica: Clinical and roentgenographic manifestations. *Gastrointest Radiol* 8:111–117, 1983.
104. Schuman BM, Arciniegas E: The management of esophageal complications of epidermolysis bullosa. *Am J Dig Dis* 17:875–880, 1972.
105. Tishler JM, Han SY, Helman CA: Esophageal involvement in epidermolysis bullosa dystrophica. *AJR* 141:1283–1286, 1983.
106. Mauro MA, Parker LA, Hartley WS, et al: Epidermolysis bullosa: Radiographic findings in 16 cases. *AJR* 149:925–927, 1987.
107. Wong WL, Entwisle K, Pemberton J: Gastrointestinal manifestations in the Hallopeau-Siemens variant of recessive dystrophic epidermolysis bullosa. *Br J Radiol* 66:788–793, 1993.
108. Agha FP, Raji MR: Esophageal involvement in pemphigoid: Clinical and roentgen manifestations. *Gastrointest Radiol* 7:109–112, 1982.
109. Hardy KM, Perry HO, Pingree GC, et al: Benign mucous membrane pemphigoid. *Arch Dermatol* 104:467–475, 1971.
110. Al-kutoubi MA, Eliot C: Oesophageal involvement in benign mucous membrane pemphigoid. *Clin Radiol* 35:131–135, 1984.
111. Foroozan P, Enta T, Winship DH, et al: Loss and regeneration of esophageal mucosa in pemphigoid. *Gastroenterology* 52:548–558, 1967.
112. Soong C, Bynum TE: The endoscopic appearance of pemphigoid esophagitis. *Gastrointest Endosc* 19:17–18, 1972.
113. Karasick S, Mapp E, Karasick D: Esophageal involvement in benign mucous membrane pemphigoid. *J Can Assoc Radiol* 32:247–248, 1981.
114. Naylor MF, MacCarty RL, Rogers RS: Barium studies in esophageal cicatricial pemphigoid. *Abdom Imaging* 20:97–100, 1995.
115. Stampien TM, Schwartz RA: Erythema multiforme. *Am Fam Physician* 46:1171–1176, 1992.
116. Tan YM, Goh KL: Esophageal stricture as a late complication of Stevens-Johnson syndrome. *Gastrointest Endosc* 50:566–568, 1999.
117. Peters ME, Gourley G, Mann FA: Esophageal stricture and web secondary to Stevens-Johnson syndrome. *Pediatr Radiol* 13:290–291, 1983.
118. Howell CT, Mansberger JA, Parrish RA: Esophageal stricture secondary to Stevens-Johnson syndrome. *J Pediatr Surg* 22:994–995, 1987.
119. Carucci LR, Levine MS, Rubesin SE: Diffuse esophageal stricture caused by erythema multiforme major. *AJR* 180:749–750, 2003.
120. Waldman I, Berlin L: Stricture of the esophagus due to nasogastric intubation. *AJR* 94:321–324, 1965.
121. Banfield WJ, Hurwitz AL: Esophageal stricture associated with nasogastric intubation. *Arch Intern Med* 134:1083–1086, 1974.
122. Nagler R, Spiro HM: Persistent gastroesophageal reflux induced during prolonged gastric intubation. *N Engl J Med* 269:495–500, 1963.
123. Balkany TJ, Baker BB, Bloustein PA, et al: Cervical esophagostomy in dogs: Endoscopic, radiographic, and histopathologic evaluation of esophagitis induced by feeding tubes. *Ann Otol Rhinol Laryngol* 86:1–6, 1977.
124. Salo JA, Kivilaakso E: Role of bile salts and trypsin in the pathogenesis of experimental alkaline esophagitis. *Surgery* 93:525–532, 1983.
125. Morrow D, Passaro ER: Alkaline reflux esophagitis after total gastrectomy. *Am J Surg* 132:287–290, 1976.
126. Sanchez RE, Gordon HE: Complications of total gastrectomy. *Arch Surg* 100:136–139, 1970.
127. Salo J, Kivilaakso E: Failure of long limb Roux-en-Y reconstruction to prevent alkaline reflux esophagitis after total gastrectomy. *Endoscopy* 22:65–67, 1990.
128. Meyer W, Vollmar F, Bar W: Barrett-esophagus following total gastrectomy. *Endoscopy* 2:121–126, 1979.
129. Sandvik AK, Halvorsen TB: Barrett's esophagus after total gastrectomy. *J Clin Gastroenterol* 10:587–588, 1988.
130. Levine MS, Fisher AR, Rubesin SE, et al: Complications after total gastrectomy and esophagojejunostomy: Radiologic evaluation. *AJR* 157:1189–1194, 1991.
131. O'Riordan D, Levine MS, Laufer I: Acute alcoholic esophagitis. *J Can Assoc Radiol* 37:54–55, 1986.
132. Hogan WJ, De Andrade SR, Winship DH: Ethanol-induced acute esophageal motor dysfunction. *J Appl Physiol* 32:755–760, 1972.
133. Kaufman SE, Kay MD: Induction of gastroesophageal reflux by alcohol. *Gut* 19:336–338, 1978.
134. McDonald GB, Shulman HM, Sullivan KM, et al: Intestinal and hepatic complications of human bone marrow transplantation: I. Gastroenterology 90:460–477, 1986.
135. McDonald GB, Shulman HM, Sullivan KM, et al: Intestinal and hepatic complications of human bone marrow transplantation: II. Gastroenterology 90:770–784, 1986.
136. Rosenberg HK, Serota FT, Hock P, et al: Radiographic features of gastrointestinal graft-vs.-host disease. *Radiology* 138:371–374, 1981.
137. McDonald GB, Sullivan KM, Plumley TF: Radiographic features of esophageal involvement in chronic graft-vs.-host disease. *AJR* 142:501–506, 1984.
138. McDonald GB, Sullivan KM, Schuffler MD, et al: Esophageal abnormalities in chronic graft-vs.-host disease in humans. *Gastroenterology* 89:914–921, 1981.
139. Minocha A, Mandanas RA, Kida M, et al: Bullous esophagitis due to chronic graft-versus-host disease. *Am J Gastroenterol* 92:529–530, 1997.
140. McDonald GB, Sharma P, Hackman RC, et al: Esophageal infections in immunosuppressed patients after marrow transplantation. *Gastroenterology* 88:1111–1117, 1985.

141. Dolce P, Gordeau M, April N, et al: Outbreak of glutaraldehyde-induced proctocolitis. *Am J Infect Control* 23:34–39, 1995.
142. Isserow JA, Kumar N, Goldschmidt MH, et al: Glutaraldehyde-induced esophageal injury: Histologic study of laboratory rats. *Invest Radiol* 33:730–733, 1998.
143. O'Duffy JD: Suggested criteria for diagnosis of Behçet's disease [abstract]. *J Rheumatol* 1:18, 1974.
144. Chung SY, Ha HK, Kim JH, et al: Radiologic findings of Behçet syndrome involving the gastrointestinal tract. *Radiographics* 21:911–926, 2001.
145. Kaplinsky N, Neumann G, Harzahav Y, et al: Esophageal ulceration in Behçet's syndrome. *Gastrointest Endosc* 23:160, 1977.
146. Lebowitz O, Forde KA, Berdon WE, et al: Ulcerative esophagitis and colitis in a pediatric patient with Behçet's syndrome. *Am J Gastroenterol* 68:550–555, 1977.
147. Mori S, Yoshihira A, Kawamura H, et al: Esophageal involvement in Behçet's disease. *Am J Gastroenterol* 78:548–553, 1983.
148. Yashiro K, Nagasako K, Hasegawa K, et al: Esophageal lesions in intestinal Behçet's disease. *Endoscopy* 18:57–60, 1986.
149. Anti M, Marra G, Rapaccini GL, et al: Esophageal involvement in Behçet's syndrome. *J Clin Gastroenterol* 8:514–519, 1986.
150. Mendl K, McKay JM, Tanner CH: Intramural diverticulosis of the oesophagus and Rokitan-sky-Aschoff sinuses in the gallbladder. *Br J Radiol* 33:496–501, 1960.
151. Cho SR, Sanders MM, Turner MA, et al: Esophageal intramural pseudodiverticulosis. *Gastrointest Radiol* 6:9–16, 1981.
152. Hammon JW, Rice RP, Postlethwait RW, et al: Esophageal intramural diverticulosis. *Ann Thorac Surg* 17:260–267, 1974.
153. Wightman AJA, Wright EA: Intramural esophageal diverticulosis: A correlation of radiological and pathological findings. *Br J Radiol* 47:496–498, 1974.
154. Umlas J, Sakhuja R: The pathology of esophageal intramural pseudodiverticulosis. *Am J Clin Pathol* 65:314–320, 1976.
155. Medeiros LJ, Doos WG, Balogh K: Esophageal intramural pseudodiverticulosis: A report of two cases with analysis of similar, less extensive changes in "normal" autopsy esophagi. *Hum Pathol* 19:928–931, 1988.
156. Bruhlmann WF, Zollikofer CL, Maranta E, et al: Intramural pseudodiverticulosis of the esophagus: Report of seven cases and literature review. *Gastrointest Radiol* 6:199–208, 1981.
157. Sabanathan S, Salama FD, Morgan WE: Oesophageal intramural pseudodiverticulosis. *Thorax* 40:849–857, 1985.
158. Flora KD, Gordon MD, Lieberman D, et al: Esophageal intramural pseudodiverticulosis. *Dig Dis* 15:113–119, 1997.
159. Troupin RH: Intramural esophageal diverticulosis and moniliasis. *AJR* 104:613–616, 1968.
160. Boyd RM, Bogoch A, Greig JH, et al: Esophageal intramural pseudodiverticulosis. *Radiology* 113:267–270, 1974.
161. Beauchamp JM, Nice CM, Belanger MA, et al: Esophageal intramural pseudodiverticulosis. *Radiology* 113:273–276, 1974.
162. Castillo S, Aburashed A, Kimmelman J, et al: Diffuse intramural esophageal pseudodiverticulosis. *Gastroenterology* 72:541–545, 1977.
163. Levine MS, Moolten DN, Herlinger H, et al: Esophageal intramural pseudodiverticulosis: A reevaluation. *AJR* 147:1165–1170, 1986.
164. Graham DY, Goyal RK, Sparkman J, et al: Diffuse intramural esophageal diverticulosis. *Gastroenterology* 68:781–785, 1975.
165. Pearlberg JL, Sandler MA, Madrazo BL: Computed tomographic features of esophageal intramural pseudodiverticulosis. *Radiology* 147:189–190, 1983.
166. Plavsic BM, Chen MYM, Gelfand DW, et al: Intramural pseudodiverticulosis of the esophagus detected on barium esophagograms: Increased prevalence in patients with esophageal carcinoma. *AJR* 165:1381–1385, 1995.
167. Kim S, Choi C, Groskin SA: Esophageal intramural pseudodiverticulitis. *Radiology* 173:418–419, 1989.
168. Abrams LJ, Levine MS, Laufer I: Esophageal peridiverticulitis: An unusual complication of esophageal intramural pseudodiverticulosis. *Eur J Radiol* 19:139–141, 1995.

Benign Tumors of the Esophagus

MARC S. LEVINE

CHAPTER OUTLINE

Mucosal Lesions

Papilloma
Adenoma
Inflammatory Esophagogastric Polyp
Glycogenic Acanthosis
Leukoplakia
Acanthosis Nigricans

Submucosal Lesions

Leiomyoma
Gastrointestinal Stromal Tumor
Leiomyomatosis and Idiopathic Muscular Hypertrophy
Fibrovascular Polyp
Granular Cell Tumor
Lipoma
Hemangioma
Hamartoma
Other Mesenchymal Tumors
Cysts

Benign tumors of the esophagus constitute only about 20% of all esophageal neoplasms.¹ Most are small lesions that cause no symptoms and are discovered fortuitously on barium studies or endoscopy. Occasionally, however, these tumors may cause dysphagia, bleeding, or other symptoms, necessitating endoscopic or surgical removal. Depending on their site of origin, benign esophageal neoplasms may be classified as mucosal or submucosal lesions, which have typical radiographic and endoscopic features.

Mucosal Lesions

PAPILLOMA

Squamous papillomas (or simply, papillomas) are uncommon benign tumors, accounting for less than 5% of all esophageal neoplasms.² The lesions consist histologically of a central fibrovascular core with multiple finger-like projections covered by hyperplastic squamous epithelium.³ Papillomas usually appear grossly as coral-like excrescences from the mucosa. Although the pathogenesis of these tumors is uncertain, the human papillomavirus⁴ and chronic reflux esophagitis⁵ have been implicated as causative factors.

All papillomas in the esophagus reported thus far have been benign lesions. Nevertheless, malignant degeneration has been observed in experimentally induced esophageal papillomas in rats.⁶ Malignant transformation has also been documented in papillomas arising in the oral cavity, larynx, and uterine cervix.⁷⁻⁹ In some cases, benign papillomas can be mistaken on histologic examination for verrucous carcinoma, an

uncommon form of squamous cell carcinoma.¹⁰ Thus, some investigators believe that all papillomas in the esophagus should be resected because of the uncertain risk of malignant degeneration and potential confusion with verrucous carcinoma.¹¹

Papillomas in the esophagus usually occur as solitary lesions, ranging from 0.5 to 1.5 cm in size. Most patients are asymptomatic, but dysphagia is an occasional finding.^{3,11} Rarely, multiple papillomas may be present in the esophagus, a condition known as *esophageal papillomatosis*.¹²⁻¹⁴

Radiographic Findings

Papillomas are difficult to detect on single-contrast barium studies because of the small size of the lesions. In contrast, they can be recognized on double-contrast studies as small (<1 cm), sessile polyps that have a smooth or slightly lobulated contour (Fig. 22-1).¹⁵ Because early esophageal cancers may also appear as small polypoid lesions, endoscopy should be performed to exclude an early carcinoma. Occasionally, larger papillomas may be manifested by lobulated intraluminal masses that are indistinguishable from advanced esophageal carcinoma. Rarely, esophageal papillomas may have a bubbly appearance secondary to trapping of barium between the papillary fronds of the tumor (Fig. 22-2).¹⁶

Multiple papillomas may be demonstrated on esophagography in patients with esophageal papillomatosis.¹²⁻¹⁴ Despite its rarity, the diagnosis of papillomatosis should be suggested by the presence of multiple, discrete, lobulated protrusions on the mucosa (Fig. 22-3). Even when multiple papillomas are present, these lesions rarely cause obstruction.

ADENOMA

Adenomas account for less than 1% of all benign esophageal neoplasms.¹⁷ They are rarely found in the esophagus because it is lined by squamous rather than columnar epithelium. However, adenomas may develop in patients with Barrett's esophagus (see Chapter 19).^{18,19} These adenomas are important because of the risk of malignant degeneration via an adenoma-carcinoma sequence similar to that found in the colon.^{18,19} Esophageal adenomas should therefore be resected endoscopically or surgically, whenever feasible.

Radiographic Findings

Esophageal adenomas may appear on barium studies as sessile or pedunculated polyps in the esophagus (Fig. 22-4). Larger, more lobulated lesions have a greater likelihood of harboring adenocarcinoma. Most adenomas are located in the distal esophagus at or near the gastroesophageal junction.¹⁷⁻¹⁹ As a result, they can be mistaken for inflammatory esophagogastric polyps (see next section). Nodularity, lobulation, and the large size of the lesion should favor an adenoma or adenocarcinoma. When an adenoma is suspected on barium studies, endoscopy and biopsy should be performed for a definitive diagnosis.

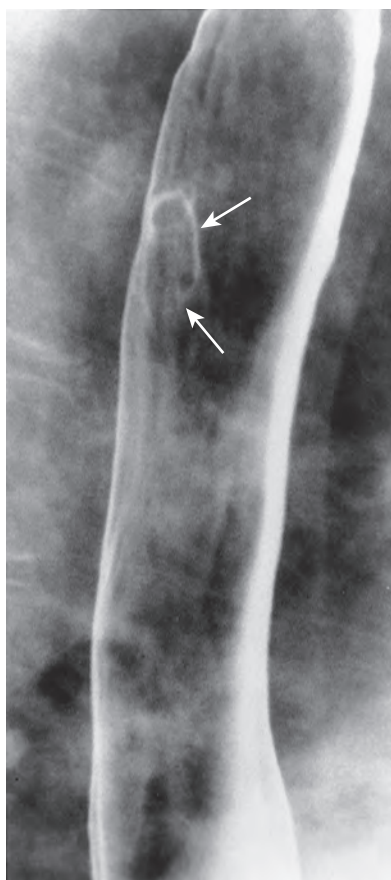


Figure 22-1 Papilloma. The lesion appears as a sessile, slightly lobulated polyp (arrows) in the midesophagus. An early esophageal carcinoma could produce similar findings.

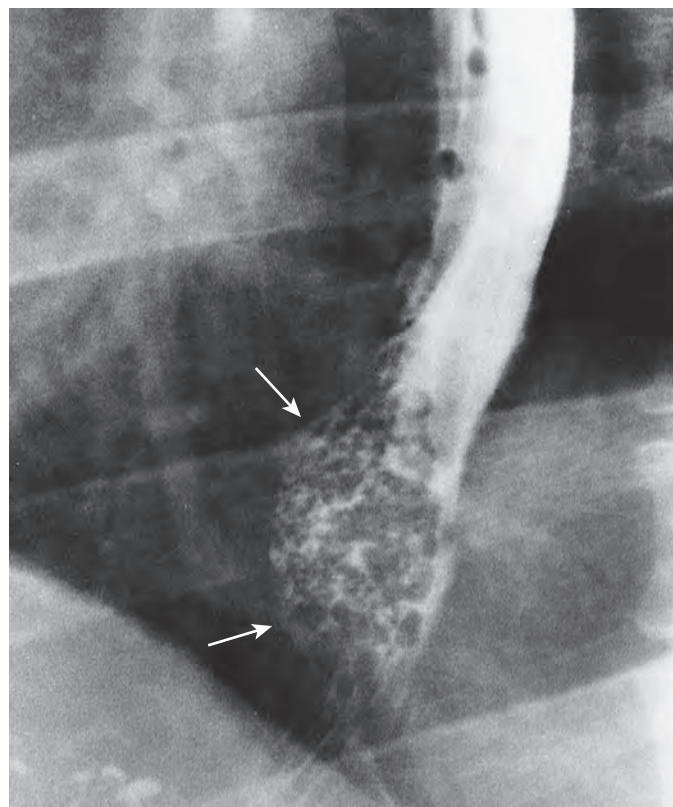


Figure 22-2 Giant esophageal papilloma. The lesion has a bubbly appearance (arrows) caused by trapping of barium between the papillary fronds of the tumor. (From Walker JH: *Giant papilloma of the thoracic esophagus*. AJR 131:519–520, 1978.)

INFLAMMATORY ESOPHAGOGASTRIC POLYP

Although inflammatory esophagogastric polyps are not neoplastic, they are included in this chapter because they are characterized by the presence of a polypoid protuberance in the distal esophagus abutting the gastroesophageal junction. The polyp represents the bulbous tip of a thickened gastric fold extending into the distal esophagus from the gastric fundus.^{20–24} The lesions are composed of inflammatory and granulation tissue and are thought to be a sequela of chronic reflux esophagitis (see Chapter 19).^{21,22} Affected individuals may therefore have clinical signs of chronic reflux disease. Because inflammatory esophagogastric polyps have no malignant potential, endoscopic resection is unwarranted.²⁴

Radiographic Findings

Inflammatory esophagogastric polyps are usually manifested on barium studies by a single prominent fold that arises in the gastric fundus and extends into the distal esophagus as a smooth, ovoid, or club-shaped protuberance (Fig. 22-5A).^{20,23,24} The lesions frequently straddle a hiatal hernia and may be associated with other findings of reflux esophagitis. When the characteristic features of these lesions are present on barium studies, endoscopic confirmation is unnecessary. Occasionally, however, the polyps may have a more irregular, nodular, or lobulated appearance, so a malignant lesion cannot be excluded

(Fig. 22-5B).²³ In such cases, endoscopy and biopsy are required for a definitive diagnosis.

GLYCOGENIC ACANTHOSIS

Since its original description in 1970,²⁵ glycogenic acanthosis has been recognized as a benign, non-neoplastic condition of unknown cause. Nevertheless, it is included in this chapter because it is manifested by mucosal nodules or plaques. Glycogenic acanthosis is characterized histologically by hyperplasia of squamous epithelial cells secondary to increased cytoplasmic glycogen.^{25,26} It is a common condition, with a prevalence of 3% to 15% at endoscopy.^{27–29} The lesions appear endoscopically as white mucosal plaques or nodules, ranging from 2 to 15 mm in size.^{27,28} A definitive diagnosis is made by demonstrating the characteristic glycogen-rich epithelial cells on biopsy specimens stained with periodic acid–Schiff stain.²⁵

Glycogenic acanthosis is a degenerative condition; the lesions first appear when patients are in their 40s and 50s and become larger and more numerous in patients over 60 years of age.³⁰ Glycogenic acanthosis rarely causes esophageal symptoms, and it is not associated with any known risk of malignant degeneration.³¹ This condition is therefore almost always discovered as an incidental finding on radiologic or endoscopic examination.

Radiographic Findings

Although the appearance of glycogenic acanthosis was not described on barium studies until 1981,³² it has since



Figure 22-3 Esophageal papillomatosis. There are innumerable wartlike excrescences on the esophageal mucosa. Despite the dramatic radiographic appearance, this patient had no esophageal symptoms. (Courtesy Harvey M. Goldstein, MD, San Antonio, TX.)

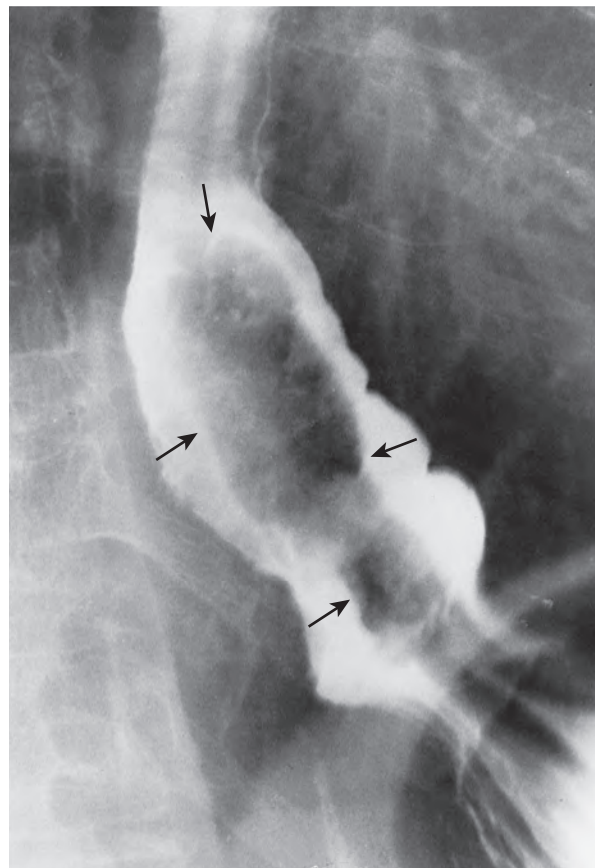


Figure 22-4 Adenomatous polyp in Barrett's esophagus. The polyp (arrows) originates at the gastroesophageal junction and extends into the distal esophagus above a hiatal hernia. Although this lesion could be mistaken for an inflammatory esophagogastric polyp, it is larger and more lobulated than most inflammatory polyps. The resected specimen contained a solitary focus of adenocarcinoma. (From Levine MS, Caroline D, Thompson JJ, et al: Adenocarcinoma of the esophagus: relationship to Barrett mucosa. *Radiology* 150:305–309, 1984.)

Figure 22-5 Inflammatory esophagogastric polyps. **A.** An inflammatory polyp is seen en face as a prominent fold (straight arrows) arising at the cardia and extending into the distal esophagus as a smooth, club-shaped mass (curved arrow). The radiographic findings are so characteristic that endoscopy is unwarranted. **B.** This inflammatory polyp has a more lobulated appearance (arrows), so it cannot be differentiated from an adenomatous polyp or even an adenocarcinoma (see Fig. 22-4). (B from Levine MS: *Radiology of the Esophagus*. Philadelphia, WB Saunders, 1989.)



been recognized as a frequent finding on double-contrast esophagography, occurring in up to 30% of patients.^{30,31} Glycogenic acanthosis is usually manifested on double-contrast radiographs by discrete, small, rounded nodules or plaques in the mid or distal esophagus (Fig. 22-6).³¹ The lesions tend to be more obvious in the midesophagus because the distal esophagus is often obscured by pooling of barium in this region. The nodules usually range from 2 to 3 mm in size, but occasional plaques may be 1 cm or larger.^{31,32}

Differential Diagnosis

Although glycogenic acanthosis has little clinical significance, it should be distinguished from other causes of mucosal nodularity, such as superficial spreading carcinoma and reflux or *Candida* esophagitis. However, superficial spreading carcinoma is characterized by poorly defined, confluent nodules and plaques (see Chapter 23), and reflux esophagitis is characterized by innumerable tiny nodules in the distal esophagus, producing a granular appearance (see Chapter 19). In contrast, the nodules of glycogenic acanthosis are more prominent in the midesophagus and have more discrete margins with normal intervening mucosa. Although the plaques of *Candida* esophagitis may be indistinguishable on double-contrast studies from those in glycogenic acanthosis (see Chapter 20), *Candida* esophagitis occurs in immunocompromised patients with

odynophagia or dysphagia, whereas glycogenic acanthosis occurs in older individuals who are not immunocompromised and have no esophageal symptoms. Thus, the clinical history and presentation are extremely helpful for differentiating these conditions.

LEUKOPLAKIA

Oral leukoplakia is a common condition characterized by white mucosal plaques that exhibit various combinations of hyperkeratosis, epithelial dysplasia, and frank carcinoma on histologic examination. In contrast, leukoplakia rarely involves the esophagus,³³⁻³⁵ and its malignant potential in this location is unknown. Endoscopy may reveal white mucosal plaques smaller than 1 cm.³³ Rarely, the lesions may be recognized on double-contrast esophagograms as tiny nodules or plaques.^{34,35} However, most asymptomatic patients with a nodular mucosa probably have glycogenic acanthosis.³¹ Esophageal leukoplakia should therefore be considered a histologic rather than a radiologic diagnosis.

ACANTHOSIS NIGRICANS

Acanthosis nigricans is a dermatologic disorder characterized by the triad of papillomatosis, pigmentation, and hyperkeratosis. Some patients have a malignant type of acanthosis nigricans associated with adenocarcinomas of the gastrointestinal tract, ovary, lung, or breast. Esophageal involvement has occasionally been reported in patients with the malignant form of the disease.^{35,36} The esophageal lesions appear on barium studies as numerous tiny nodules.^{35,36} Because this condition rarely involves the esophagus, the diagnosis should be suggested only in patients with known acanthosis nigricans involving the skin.

Submucosal Lesions

By definition, all submucosal lesions arising in the wall of the gastrointestinal tract are intramural. Not all intramural lesions are submucosal, however, because they can also arise from the muscularis propria or even the subserosa. Despite this distinction, the terms *submucosal* and *intramural* are used interchangeably in this text based on long-standing convention.

LEIOMYOMA

Leiomyomas are the most common mesenchymal tumors of the esophagus, accounting for more than 50% of all benign esophageal neoplasms.^{2,37-39} These lesions are composed of intersecting bands of smooth muscle and fibrous tissue in a well-defined capsule and consist histologically of an interlacing or palisading pattern of spindle cells with eosinophilic cytoplasm.³⁹ Leiomyomas are usually smaller than 3 cm,³⁸ but giant lesions as large as 20 cm have been reported.^{40,41} These tumors are predominantly located in the middle and lower thirds of the thoracic esophagus, because this is the portion of the esophagus lined by smooth muscle.³⁹ Leiomyomas usually appear grossly as discrete submucosal masses, but some lesions have an exophytic, intraluminal, or even circumferential pattern of growth.

Most leiomyomas in the esophagus occur as solitary lesions, but multiple leiomyomas are present in 3% to 4% of patients.^{42,43}

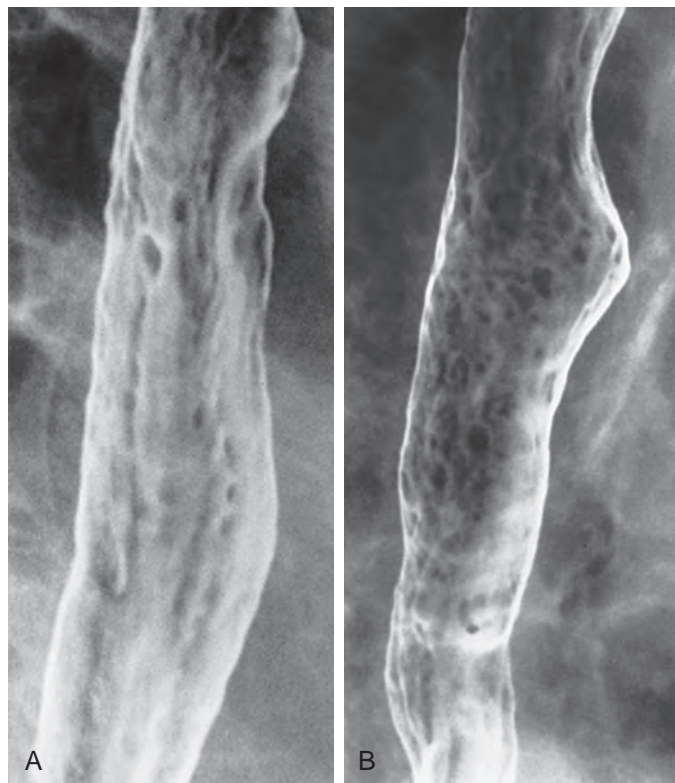


Figure 22-6 Glycogenic acanthosis. A, B. In both cases, this condition is manifested by multiple small plaques and nodules in the midesophagus. The lesions tend to have a rounded appearance. *Candida* esophagitis could produce similar findings, but patients with glycogenic acanthosis are almost always asymptomatic. (A from Levine MS, Macones AJ, Laufer I: *Candida* esophagitis: Accuracy of radiographic diagnosis. *Radiology* 154:581-587, 1985; B from Levine MS: *Radiology of the Esophagus*. Philadelphia, WB Saunders, 1989.)

Rarely, these tumors may be associated with uterine or vulvar leiomyomas, apparently on a familial basis.^{44,45} Esophageal leiomyomas have also been documented in patients with hypertrophic osteoarthropathy, a condition characterized by clubbed fingers and toes, swollen joints, and subperiosteal new bone formation in the extremities.⁴⁶

Clinical Findings

Most patients with esophageal leiomyomas are asymptomatic, but lesions that encroach on the lumen may cause slowly worsening dysphagia or other symptoms such as substernal discomfort, vomiting, and weight loss.^{39,47} Unlike gastrointestinal stromal tumors (GISTs) in the stomach, esophageal leiomyomas rarely ulcerate, so upper gastrointestinal bleeding is extremely uncommon.⁴⁷ Because of the slowly progressive nature of the lesions, symptoms may be present for several years before these patients seek medical attention. Rarely, affected individuals may present with signs and symptoms of acute esophageal obstruction.⁴⁸ The treatment of choice for symptomatic patients is surgical enucleation of the tumor, but larger lesions may necessitate a more extensive esophageal resection. Leiomyomas typically do not recur after surgery.³⁹

Although leiomyomas are relatively common lesions in the esophagus, their malignant counterparts, leiomyosarcomas, are rare (see Chapter 24). To date, sarcomatous degeneration of an esophageal leiomyoma has not been reported. In one series, esophageal leiomyomas were followed for as long as 15 years without evidence of malignant transformation.⁴⁹ Thus, surgical removal of small leiomyomas in asymptomatic patients is probably not warranted.

Radiographic Findings

Leiomyomas that grow exophytically into the mediastinum may be recognized on chest radiographs by the presence of a mediastinal mass.⁵⁰ Rarely, these tumors may contain amorphous or punctate calcification.^{51,52} Because calcification almost never occurs in other benign or malignant tumors of the esophagus, the presence of a calcified esophageal mass should suggest a leiomyoma, although one case of a densely calcified esophageal leiomyosarcoma has been reported.⁵³

On barium esophagography, leiomyomas usually appear in profile as smooth-surfaced submucosal masses (etched in white on double-contrast radiographs) that form right angles or slightly obtuse angles with the adjacent esophageal wall (Figs. 22-7 and 22-8A) and en face as round or ovoid filling defects with splitting of the barium column around the lesion and apparent widening of the lumen (Fig. 22-8B).³⁸ These tumors may gradually enlarge over time, but ulceration is rare. Leiomyomas typically appear on computed tomography (CT) scans as homogeneous soft tissue masses,⁵⁴ but differentiation from other esophageal tumors is difficult.

Although the vast majority of leiomyomas in the esophagus occur as solitary submucosal masses, esophagography may occasionally reveal multiple lesions^{42,43} or even annular lesions with varying degrees of obstruction.³⁹ Rarely, leiomyomas may be giant intraluminal masses that are attached to the upper thoracic or cervical esophagus by a long pedicle.⁵⁵ However, most pedunculated intraluminal tumors in the esophagus contain a variety of other mesenchymal elements; these tumors have therefore been classified together as fibrovascular polyps (see later, “Fibrovascular Polyp”). Rarely, distal esophageal

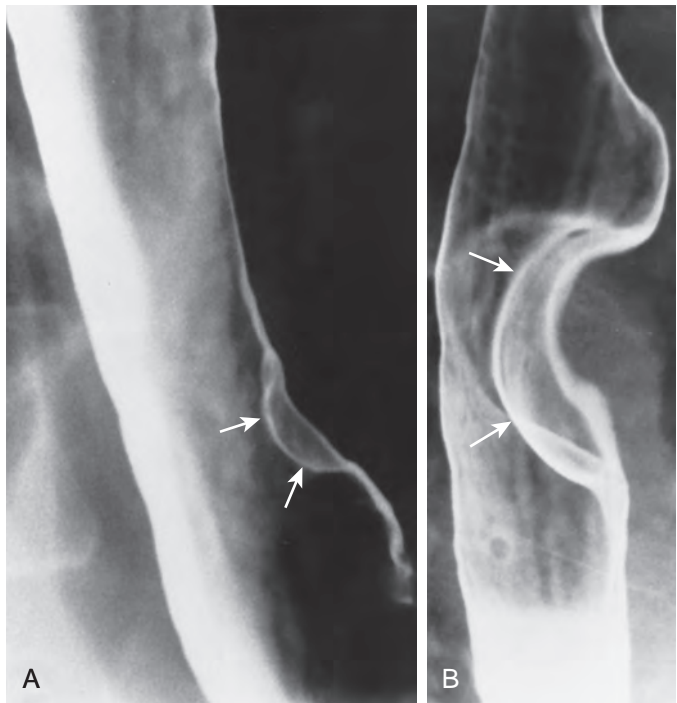


Figure 22-7 Esophageal leiomyomas. A, B. The lesions (arrows) have a smooth surface (etched in white) and slightly obtuse borders characteristic of submucosal masses.

leiomyomas may directly involve the gastric cardia and fundus.⁵⁶

Differential Diagnosis

Most submucosal masses in the esophagus are leiomyomas. However, other unusual intramural tumors such as granular cell tumors, lipomas, hemangiomas, and neurofibromas may produce identical radiographic findings (see later). Cystic lesions such as congenital duplication cysts and acquired retention cysts may also appear as submucosal masses on barium studies (see later, “Cysts”). Even an isolated esophageal varix may resemble a submucosal tumor, but effacement or obliteration of the lesion by esophageal distention should suggest its vascular origin (see Chapter 25). Because leiomyomas usually occur as solitary lesions in the esophagus, the presence of multiple submucosal masses should raise the possibility of multiple granular cell tumors or hemangiomas or malignant conditions such as lymphoma, leukemia, or Kaposi’s sarcoma involving the esophagus (see Chapter 24). In contrast, hematogenous metastases almost never involve the esophagus.

Leiomyomas should be distinguished from extramural lesions that are extrinsically compressing or indenting the esophagus. When viewed in profile, extrinsic lesions tend to have more obtuse, gently sloping borders than intramural lesions. Another useful criterion for differentiating these lesions is the spheroid sign, which is based on the principle that the estimated center of the mass should lie outside the projected contour of the esophagus for extramural lesions but inside the projected contour for intramural lesions.⁵⁷ When the radiographic findings are equivocal, CT may be helpful for differentiating a submucosal tumor from a mediastinal mass compressing the esophagus.⁵⁵

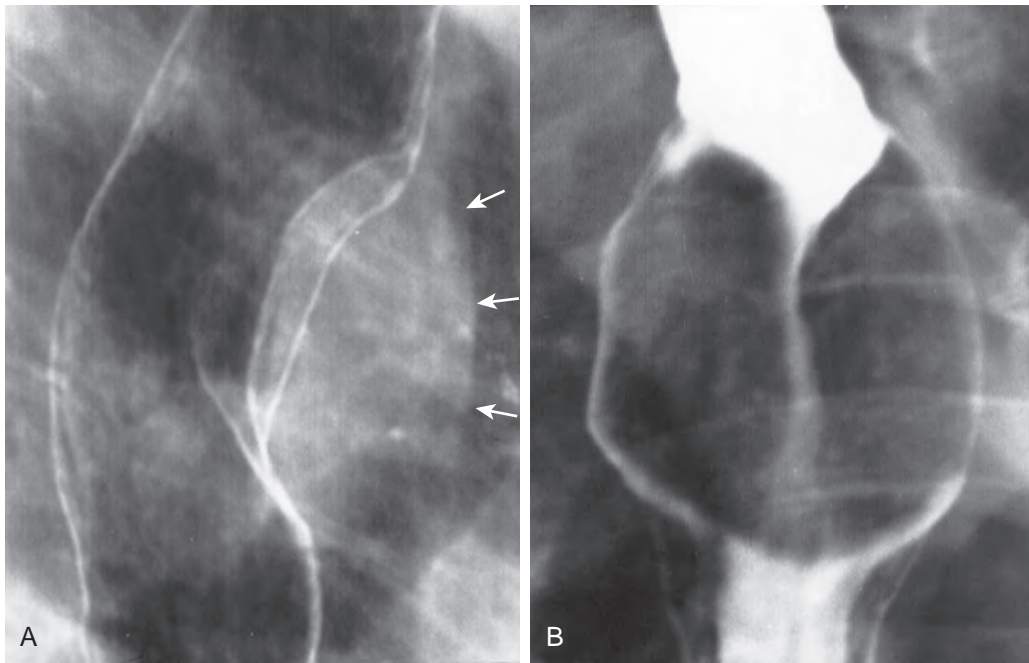


Figure 22-8 Esophageal leiomyoma. **A.** Tangential view reveals the characteristic features of a submucosal lesion. The outer margin of the leiomyoma is seen as a soft tissue shadow (arrows) abutting the lung. **B.** En face view shows a smooth, rounded filling defect in the esophagus, with splitting of barium around the lesion. The esophagus appears widened at this level. (Courtesy Marc P. Banner, MD, Philadelphia.)

GASTROINTESTINAL STROMAL TUMOR

In the past, almost all mesenchymal neoplasms in the esophagus were thought to be benign leiomyomas, but recent studies have shown that GISTs are more common in the esophagus than previously recognized.⁵⁸⁻⁶¹ Like leiomyomas, these tumors consist histologically of multiple spindle cells, but GISTs are characterized by their unique immunohistochemical expression of CD117, also known as C-KIT.⁶² Immunohistochemical testing is therefore extremely helpful for differentiating GISTs from leiomyomas because only GISTs are positive for CD117 and CD34.³⁹ Patients with esophageal GISTs may be asymptomatic, or they may present with dysphagia, depending on the size of the lesion and how much it encroaches on the lumen. Unlike leiomyomas, which are always benign, however, esophageal GISTs appear to have a malignant potential similar to that of GISTs elsewhere in the gastrointestinal tract (with the development of recurrent tumor after surgical resection), so more aggressive management of these tumors may be warranted.⁶¹ Patients with esophageal GISTs could also benefit from adjuvant treatment with imatinib (Gleevec), a tyrosine kinase inhibitor.⁶¹ Thus, differentiation of leiomyomas from GISTs in the esophagus has important ramifications for patient management.

Radiographic Findings

Esophageal GISTs typically appear on barium studies as discrete submucosal masses that are indistinguishable from leiomyomas or other mesenchymal tumors in the esophagus (Fig. 22-9).⁶¹ Like GISTs elsewhere in the gastrointestinal tract, however, esophageal GISTs tend to be larger, more heterogeneous (secondary to cystic changes and necrosis), and more enhancing lesions than esophageal leiomyomas on contrast-enhanced CT (Fig. 22-10A).⁶¹ Esophageal GISTs also have uniform and marked fluorine-18-deoxyglucose (FDG) avidity on positron emission tomography (PET)/CT scans (Fig. 22-10B), another



Figure 22-9 Esophageal GIST. The lesion appears as a discrete submucosal mass (arrow) that is indistinguishable from an esophageal leiomyoma on barium esophagography. (From Winant A, Gollub MJ, Shia J, et al: Imaging and clinicopathologic features of esophageal gastrointestinal stromal tumors. *AJR* 203:306-314, 2014.)

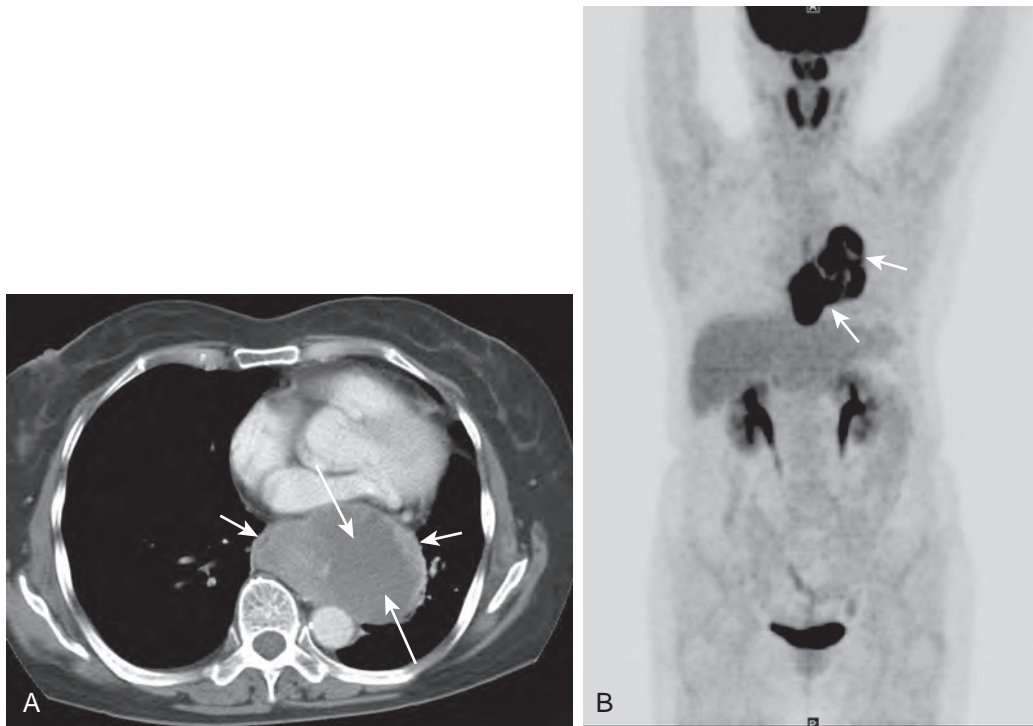


Figure 22-10 Esophageal GIST. **A.** Contrast-enhanced axial CT scan shows a large, heterogeneous, well-circumscribed mass that is inseparable from the left lateral wall of the distal esophagus. Note peripheral enhancing solid components (short arrows) and large internal cystic areas (long arrows). **B.** Coronal PET/CT scan (maximum intensity projection) shows uniform and marked FDG avidity of large left paraesophageal mass (arrows). The findings on CT and PET enable differentiation of GISTs from leiomyomas. (From Winant A, Gollub MJ, Shia J, et al: *Imaging and clinicopathologic features of esophageal gastrointestinal stromal tumors*. *AJR* 203:306–314, 2014.)

useful imaging feature for differentiating these tumors from leiomyomas.⁶¹ Radiologists should be familiar with the imaging and clinicopathologic features of esophageal GISTs and of the importance of differentiating these lesions from leiomyomas because of their apparent malignant potential.

LEIOMYOMATOSIS AND IDIOPATHIC MUSCULAR HYPERTROPHY

Esophageal leiomyomatosis is a rare benign condition in which neoplastic proliferation of smooth muscle causes marked circumferential thickening of the esophageal wall, usually in the distal esophagus.^{63–65} This condition is found predominantly in children and young adults who present with long-standing dysphagia.⁶⁵ Esophageal leiomyomatosis can occur sporadically or on a familial basis with autosomal dominant inheritance.^{66,67} In some cases, this condition is associated with widespread visceral leiomyomatosis^{68–70} or hereditary nephritis (Alport's syndrome).^{66,67,69,71} Depending on the extent of the lesion, an esophagectomy or esophagogastrectomy is almost always curative.^{63,67}

Idiopathic muscular hypertrophy of the esophagus is closely related to esophageal leiomyomatosis.^{72–75} This condition is characterized by non-neoplastic thickening of smooth muscle in the esophageal wall, possibly as a response to severe esophageal spasm. In contrast to patients with leiomyomatosis, these individuals usually remain asymptomatic or present with dysphagia during late adulthood.^{73,75} Occasionally, however, patients with idiopathic muscular hypertrophy of the esophagus may have such severe dysphagia that an esophagectomy is required.

Radiographic Findings

Esophageal leiomyomatosis may be manifested on barium studies by smooth, tapered narrowing of the distal esophagus with decreased or absent esophageal peristalsis, mimicking the appearance of primary achalasia (Fig. 22-11A).^{63,65,71} However, the narrowed segment tends to be longer than that in achalasia, and leiomyomatosis is sometimes associated with relatively symmetric paracardiac defects in the gastric fundus because of bulging of this thickened mass of muscle into the proximal stomach (see Fig. 22-11A).⁶⁵ CT may reveal marked circumferential thickening of the distal esophageal wall, resembling the findings of secondary achalasia caused by metastatic tumor at the gastroesophageal junction (Figs. 22-11B and C).⁶⁵ However, leiomyomatosis usually occurs in children or adolescents with long-standing dysphagia, whereas secondary achalasia occurs in older adults with recent onset of dysphagia and weight loss.⁷⁶ Thus, despite its rarity, the diagnosis of esophageal leiomyomatosis can usually be suggested on the basis of the clinical and radiographic findings.

Idiopathic muscular hypertrophy of the esophagus may be manifested on esophagography by a corkscrew appearance with multiple lumen-obliterating, nonperistaltic contractions.^{72–74} In other cases, this condition may produce an achalasia-like appearance, with tapered narrowing of the distal esophagus and proximal dilation on barium studies (Fig. 22-12A)^{73,75} and marked circumferential thickening of the distal esophageal wall on CT (Fig. 22-12B).^{73,75} The radiographic findings may therefore be indistinguishable from those of esophageal leiomyomatosis. However, patients with idiopathic muscular hypertrophy of the esophagus usually present later in life than those with

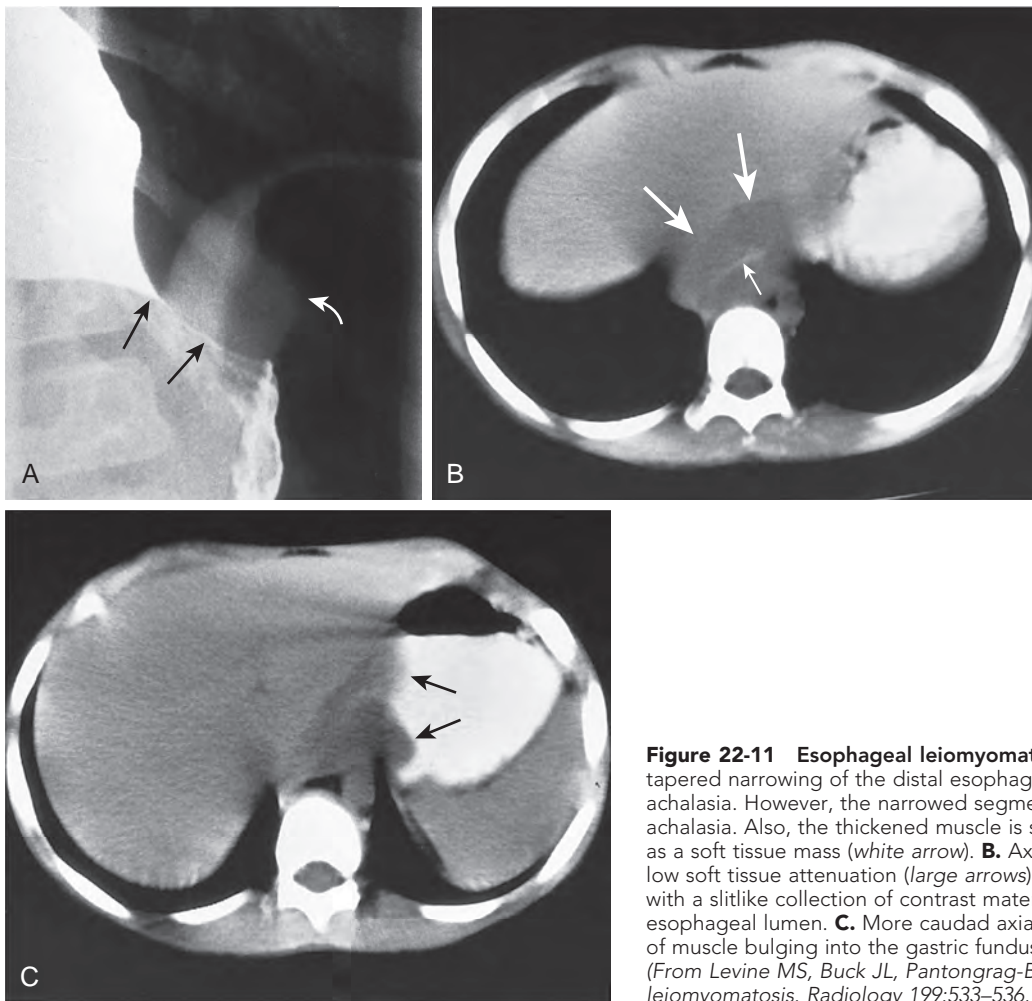


Figure 22-11 Esophageal leiomyomatosis. **A.** Barium study shows smooth, tapered narrowing of the distal esophagus (black arrows), resembling achalasia. However, the narrowed segment is longer than that typically seen in achalasia. Also, the thickened muscle is seen bulging into the gastric fundus as a soft tissue mass (white arrow). **B.** Axial CT scan shows a mass of relatively low soft tissue attenuation (large arrows) surrounding the distal esophagus with a slitlike collection of contrast material (small arrow) in the compressed esophageal lumen. **C.** More caudad axial CT scan shows this thickened mass of muscle bulging into the gastric fundus (arrows) on both sides of the cardia. (From Levine MS, Buck JL, Pantongrag-Brown L, et al: *Esophageal leiomyomatosis*. *Radiology* 199:533–536, 1996.)

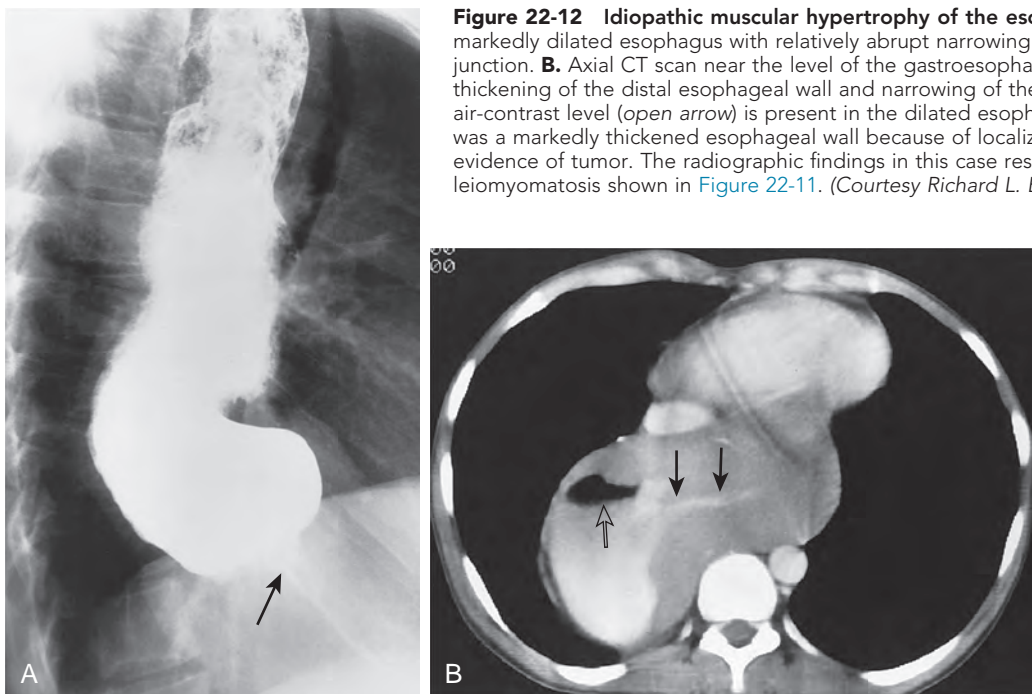


Figure 22-12 Idiopathic muscular hypertrophy of the esophagus. **A.** Barium study reveals a markedly dilated esophagus with relatively abrupt narrowing (arrow) near the gastroesophageal junction. **B.** Axial CT scan near the level of the gastroesophageal junction shows massive thickening of the distal esophageal wall and narrowing of the lumen (closed arrows). An air-contrast level (open arrow) is present in the dilated esophagus to the right. At surgery, there was a markedly thickened esophageal wall because of localized muscular hypertrophy without evidence of tumor. The radiographic findings in this case resemble those of esophageal leiomyomatosis shown in Figure 22-11. (Courtesy Richard L. Baron, MD, Pittsburgh, PA.)

leiomyomatosis, so the clinical history is helpful for differentiating these conditions.

FIBROVASCULAR POLYP

Fibrovascular polyps are rare, benign, tumor-like lesions characterized by the development of pedunculated intraluminal masses that can grow to gigantic sizes in the esophagus. The lesions consist histologically of varying amounts of fibrovascular and adipose tissue covered by normal squamous epithelium.⁷⁷⁻⁷⁹ Depending on the predominant mesenchymal components, these lesions have variously been called hamartomas, fibromas, lipomas, fibrolipomas, fibromyxomas, and fibroepithelial polyps.⁸⁰ However, they have all now been classified together as *fibrovascular polyps*,^{79,80} a term recommended by the World Health Organization in its histologic classification of tumors.⁸¹

Fibrovascular polyps almost always arise in the cervical esophagus near the level of the cricopharynx.⁷⁸⁻⁸⁰ They probably originate from loose submucosal tissue in the cervical esophagus, gradually elongating over a period of years as they are dragged inferiorly into the middle or distal third of the esophagus by esophageal peristalsis until the intraluminal portion of the mass has attained gigantic proportions.⁷⁶ Occasionally, fibrovascular polyps can even prolapse through the cardia into the gastric fundus.⁷⁷ Regardless of the size of the polyp, its proximal end is almost always attached to the cervical esophagus by a discrete pedicle.⁸²

Clinical Findings

Fibrovascular polyps usually occur in older men who present with long-standing dysphagia that slowly progresses over a

period of years as the intraluminal portion of the polyp gradually enlarges.⁸³ Other patients may develop wheezing or inspiratory stridor because of compression of the adjacent trachea by the distended esophagus.^{77,78,83} Occasionally, these individuals may have a spectacular clinical presentation with regurgitation of a fleshy mass into the pharynx or mouth.^{77,79,80,82} Some distraught patients have even tried to bite off the lesion with their teeth or remove it manually with their fingers. Apart from the bizarre clinical features of this entity, regurgitated fibrovascular polyps in the pharynx are potentially life-threatening because they have rarely been known to occlude the larynx, causing asphyxia and sudden death.⁸⁴

Malignant degeneration of fibrovascular polyps is thought to be extremely rare. Nevertheless, removal of these lesions is recommended because of the progressive and eventually debilitating nature of the symptoms and the theoretical risk of asphyxia and sudden death. Small fibrovascular polyps may be resected endoscopically, but large tumors should be removed surgically because significant bleeding may occur when the stalk is transected.⁸³

Radiographic Findings

Fibrovascular polyps can sometimes be recognized on chest radiographs by the presence of a right-sided superior mediastinal mass, anterior tracheal bowing, or both.⁸³ The polyps usually appear on esophagography as smooth, expansile, sausage-shaped intraluminal masses that arise in the cervical esophagus and extend into the upper or middle third of the thoracic esophagus (Fig. 22-13A).^{77,78,80,85} Occasionally, these lesions may show varying degrees of lobulation (Fig. 22-14A)⁷⁹ or may extend into the distal esophagus or even the gastric fundus.^{77,83} Although most fibrovascular polyps have a site of

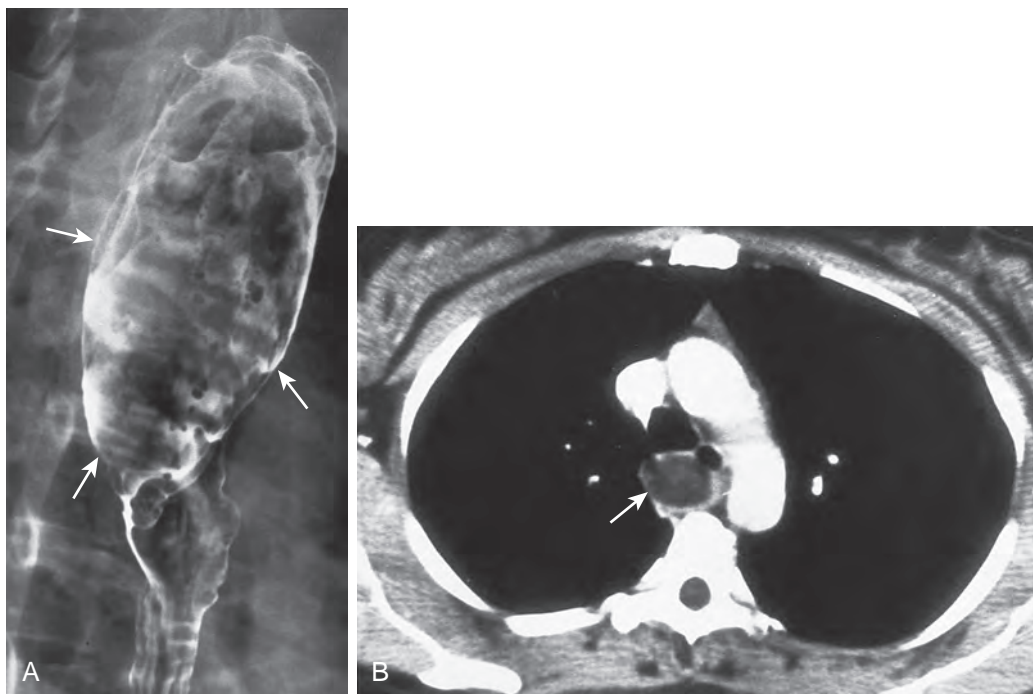


Figure 22-13 Fibrovascular polyp. **A.** Barium study shows a smooth, sausage-shaped mass (arrows) expanding the lumen of the upper thoracic esophagus. This lesion has the classic appearance of a fibrovascular polyp. **B.** Axial CT scan shows an expansile mass (arrow) in the thoracic esophagus with a thin rim of contrast material surrounding the lesion, confirming its intraluminal location. The fat density of the polyp is caused by an abundance of adipose tissue in this lesion. (From Levine MS, Buck JL, Pantongrag-Brown L, et al: Fibrovascular polyps of the esophagus: Clinical, radiographic, and pathologic findings in 16 patients. *AJR* 166:781-787, 1996.)

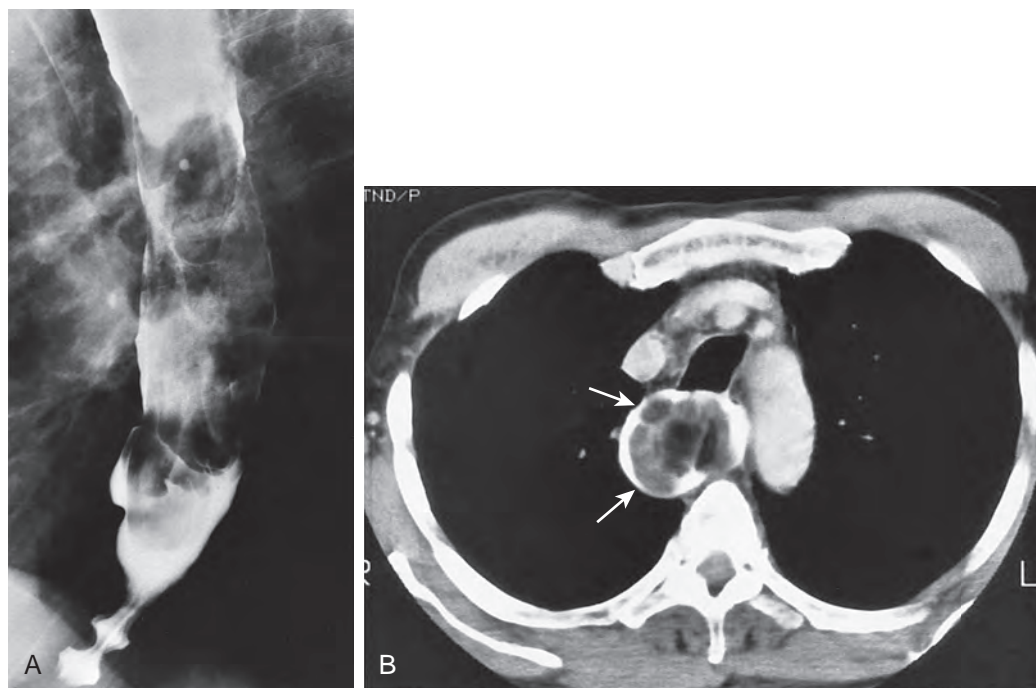


Figure 22-14 Fibrovascular polyp. **A.** Barium study shows an expansile mass extending into the distal thoracic esophagus. In contrast to the polyp in Figure 22-13A, this lesion has a lobulated contour, so it could be mistaken for a malignant esophageal tumor. **B.** Axial CT scan also shows an expansile mass (arrows) in the esophagus with intraluminal contrast material surrounding the lesion. In this case, note the heterogeneous appearance of the polyp with areas of fat juxtaposed with areas of soft tissue density. (From Levine MS, Buck JL, Pantongrag-Brown L, et al: Fibrovascular polyps of the esophagus: Clinical, radiographic, and pathologic findings in 16 patients. *AJR* 166:781–787, 1996.)

attachment in the cervical esophagus, it is often difficult to demonstrate the proximal pedicle on barium studies.⁸³

Fibrovascular polyps containing an abundance of adipose tissue may appear on CT as fat density lesions that expand the lumen of the esophagus, with a thin rim of contrast surrounding the polyp, confirming its intraluminal location (Fig. 22-13B).^{83,86–88} Polyps containing equal amounts of adipose and fibrovascular tissue may appear as heterogeneous lesions with focal areas of fat density juxtaposed with areas of soft tissue density (Fig. 22-14B), and polyps containing an abundance of fibrovascular tissue may appear as areas of soft tissue density with a paucity of fat.⁸³ Thus, fibrovascular polyps may be manifested by a spectrum of findings on CT, depending on the amount of adipose and fibrovascular tissue in these lesions. Occasionally, a centrally located feeding artery within the polyp may show contrast enhancement on CT.⁸⁹

Fibrovascular polyps containing an abundance of adipose tissue are characterized by high signal intensity on T1-weighted magnetic resonance imaging (MRI).⁸⁷ Such polyps may be manifested on endoscopic sonography by increased echogenicity because of their high fat content.^{79,90}

Differential Diagnosis

Despite their size, fibrovascular polyps are sometimes difficult to diagnose on barium studies. These lesions can be mistaken for giant, coalescent air bubbles, extrinsic masses compressing the esophagus, or other polypoid intraluminal tumors, such as spindle cell carcinomas or primary malignant melanomas of the esophagus, particularly if the polyps are lobulated (see Chapter 24). However, these malignant tumors are often confined to the mid or distal thoracic esophagus, whereas fibrovascular polyps always extend superiorly into the cervical

esophagus. When fibrovascular polyps contain an abundance of adipose tissue, the typical findings on CT or MRI should suggest the correct diagnosis.

GRANULAR CELL TUMOR

Since its original description by Abrikossoff in 1926, granular cell myoblastoma has been recognized as a rare benign tumor that predominantly involves the skin, tongue, breast, and subcutaneous tissues.^{91,92} Abrikossoff believed that these tumors had a myogenic origin, but pathologic data suggest that they have a neural derivation, arising from Schwann cells.⁹³ The term *granular cell myoblastoma* is therefore a misnomer, and the lesions have more correctly been described as *granular cell tumors*.^{94–96} Histologically, these lesions consist of sheets of polygonal tumor cells containing an eosinophilic-staining granular cytoplasm.^{94,96} The tumors are covered by hyperplastic but otherwise normal squamous epithelium. About 7% of granular cell tumors are located in the gastrointestinal tract, and one third of these lesions are located in the esophagus.^{92,95}

Most granular cell tumors in the esophagus occur as solitary lesions, ranging from 0.5 to 2.0 cm in size.⁹⁴ Some larger lesions may cause dysphagia.^{94,96,97} The treatment of choice for symptomatic patients with granular cell tumors is local excision because these tumors almost never recur after endoscopic or surgical removal.^{92,94–97} In contrast, asymptomatic patients with granular cell tumors found by endoscopic biopsy probably do not require surgery because of the negligible risk of malignant degeneration.^{97,98} Occasionally, the findings on endoscopic biopsy specimens can be mistaken for squamous cell carcinoma as a result of pseudoepitheliomatous hyperplasia of the overlying squamous mucosa.^{94,96,98}

Radiographic Findings

Granular cell tumors usually appear on esophagography as small, round or ovoid submucosal masses in the distal or, less commonly, middle third of the esophagus (Fig. 22-15).^{94,96} Because of their typical submucosal appearance, they are most often mistaken for leiomyomas.⁹⁴ Occasionally, granular cell tumors arising at the gastric cardia may be manifested by a polypoid or submucosal mass that distorts or obliterates the normal anatomic landmarks of this region.⁹⁶ Rarely, multiple granular cell tumors may be present in the esophagus or stomach (Fig. 22-16).^{97,99}

LIPOMA

The esophagus is the least common site of involvement by lipomas in the gastrointestinal tract. These tumors may appear on barium studies as discrete submucosal masses (Fig. 22-17) or, more commonly, as pedunculated, intraluminal masses.¹⁰⁰⁻¹⁰³ Rarely, pedunculated lipomas in the upper esophagus can be regurgitated into the pharynx, causing asphyxia and sudden death.¹⁰² Lipomas in the esophagus may be diagnosed preoperatively by their characteristic fat density on CT.¹⁰⁴



Figure 22-15 Granular cell tumor. A smooth submucosal mass (arrow) is seen in the midesophagus. This lesion cannot be differentiated from leiomyomas or other submucosal lesions in the esophagus. (From Levine MS: *Radiology of the Esophagus*. Philadelphia, WB Saunders, 1989.)

HEMANGIOMA

The esophagus is the least common site of involvement by vascular tumors in the gastrointestinal tract. Rarely, multiple esophageal hemangiomas may be found in patients with Osler-Weber-Rendu disease, a hereditary disorder characterized by telangiectasias of the face, lips, and mucous membranes.¹⁰⁵ However, most vascular tumors in the esophagus are solitary cavernous hemangiomas.¹⁰⁶ These highly vascular lesions may occasionally ulcerate, causing massive hematemesis and fatal exsanguination.¹⁰⁶ Esophageal hemangiomas usually appear on barium studies as smooth or slightly lobulated submucosal masses that are indistinguishable from other, more common benign intramural tumors.¹⁰⁷ Because of the risk of significant bleeding, the treatment of choice is surgical enucleation of the lesion.^{106,107}

HAMARTOMA

Esophageal hamartomas are rare benign tumors characterized histologically by metaplastic respiratory epithelium and islets of cartilage in a fibrous stroma.^{108,109} These tumors usually appear on esophagography as pedunculated intraluminal masses that are indistinguishable from fibrovascular polyps.¹⁰⁸ Rarely, multiple esophageal hamartomas may be found in



Figure 22-16 Multiple granular cell tumors. The lesions are seen as discrete submucosal masses (arrows) in the middle and distal thirds of the esophagus. This patient had additional granular cell tumors in the stomach. (From Levine MS: *Radiology of the Esophagus*. Philadelphia, WB Saunders, 1989.)

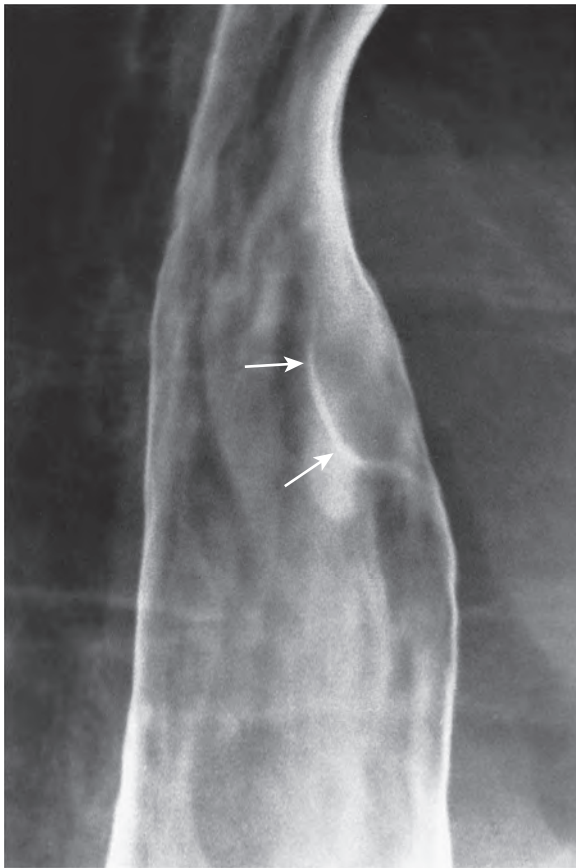


Figure 22-17 Esophageal lipoma. This patient had a discrete submucosal mass (arrows) indistinguishable from leiomyomas or other intramural tumors. (From Levine MS: *Radiology of the Esophagus*. Philadelphia, WB Saunders, 1989.)

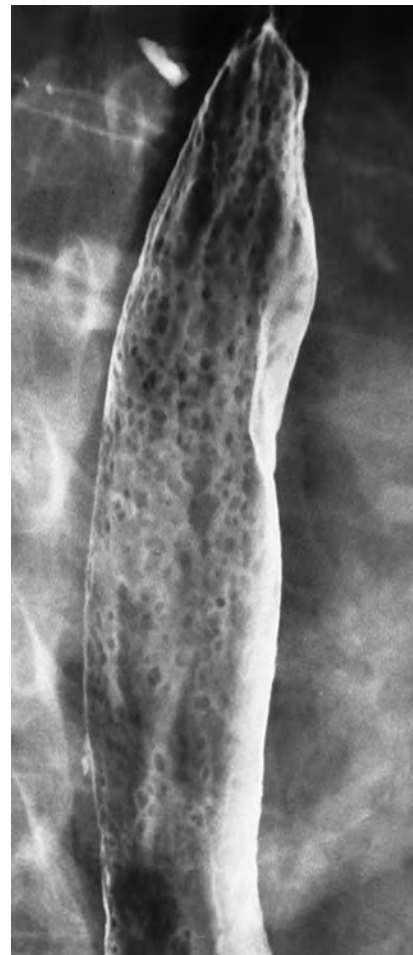


Figure 22-18 Cowden's disease with multiple hamartomatous polyps in the esophagus. The lesions appear as tiny nodular elevations on the mucosa. (Courtesy Stephen W. Trenkner, MD, Minneapolis.)

patients with Cowden's disease or multiple hamartoma syndrome, an autosomal dominant hereditary disorder characterized by multiple hamartomatous malformations of ectodermal, mesodermal, and endodermal layers as well as benign or malignant tumors of the skin, breast, gastrointestinal tract, and thyroid.^{110,111} Esophageal involvement may be manifested by innumerable tiny hamartomatous polyps in the esophagus, producing a diffusely nodular mucosa on double-contrast images (Fig. 22-18).^{110,111} When the esophagus is involved by this disease, widespread polyposis of the gastrointestinal tract is usually present. Cowden's disease should be distinguished from other polyposis syndromes, which almost never involve the esophagus.

OTHER MESENCHYMAL TUMORS

Other rare mesenchymal tumors in the esophagus include fibromas, neurofibromas, and myxofibromas.⁴⁷ These lesions usually appear on barium studies as discrete intramural masses that are indistinguishable from leiomyomas. When mesenchymal tumors contain a substantial amount of fibrovascular or adipose tissue, they can slowly elongate, forming pedunculated intraluminal masses. Because the latter tumors have characteristic clinical, radiographic, and pathologic findings, they have

been classified together as fibrovascular polyps (see earlier, "Fibrovascular Polyp").

CYSTS

Duplication Cyst

Esophageal duplication cysts constitute about 20% of all gastrointestinal tract duplications.¹¹² These cysts result from abnormal embryologic development in which nests of cells are sequestered from the primitive foregut.¹¹³ The lesions may be classified as cystic duplications or, less commonly, as tubular duplications. About 60% are located in the lower half of the posterior mediastinum, often projecting to the right of the distal esophagus.¹¹² Although most duplication cysts are noncommunicating, tubular duplications occasionally may communicate directly with the esophageal lumen. Histologically, duplication cysts contain a mucosa, submucosa, and muscularis propria and are lined by ciliated columnar or cuboidal epithelium.¹¹³ In about 40% of cases, ectopic gastric mucosa is found in the lining of the cyst wall.¹¹²

Esophageal duplication cysts may be detected as an isolated finding, but some lesions are associated with vertebral anomalies, esophageal atresia, or other congenital anomalies.¹¹²

Most adults with esophageal duplication cysts are asymptomatic, but symptoms may occasionally be caused by obstruction, bleeding, or infection of the cyst.^{114,115} Bleeding or perforation is more likely to occur when ectopic gastric mucosa is present in the cyst wall.¹⁰⁸

Radiographic Findings. Esophageal duplication cysts can sometimes be recognized on chest radiographs by the presence of a right lower mediastinal mass. Chest radiographs may occasionally reveal associated vertebral anomalies.¹¹² The cysts usually appear on esophagography as discrete submucosal masses that are indistinguishable from solid intramural tumors (Fig. 22-19). Rarely, communicating duplications may be manifested by tubular, branching outpouchings from the esophagus as a result of filling of these structures with barium (Fig. 22-20).¹¹⁶

Cross-sectional imaging studies can sometimes aid in the diagnosis of esophageal duplication cysts. Because these cysts are fluid-filled structures, they typically have homogeneous low attenuation on CT scans and high-signal intensity on T2-weighted MR images (Fig. 22-21).^{117,118} Endoscopic ultrasound may reveal a smooth, spherical or, less commonly, tubular

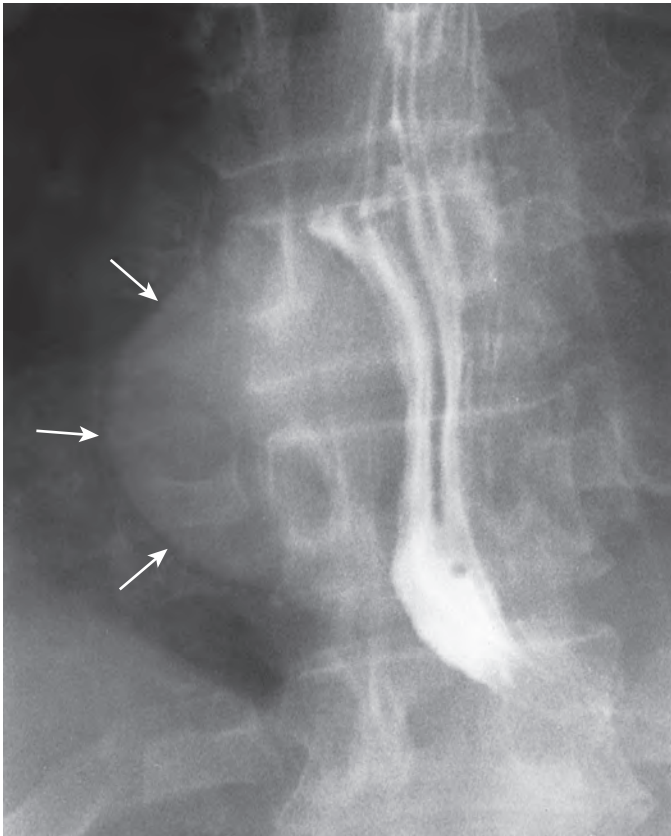


Figure 22-19 Duplication cyst. There is a large submucosal mass in the distal esophagus. The lateral border of the cyst (arrows) is readily visible where it abuts the right lung. Duplication cysts typically occur in this location. (From Levine MS: *Radiology of the Esophagus*. Philadelphia, WB Saunders, 1989.)

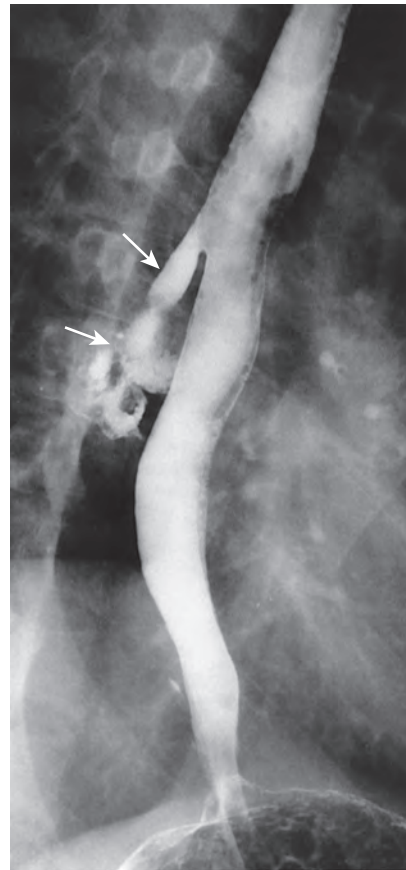


Figure 22-20 Duplication cyst. Barium study shows the rare communicating form of duplication cyst as a tubular, branching outpouching (arrows) from the midesophagus. (Courtesy Marie Latour, MD, Philadelphia.)

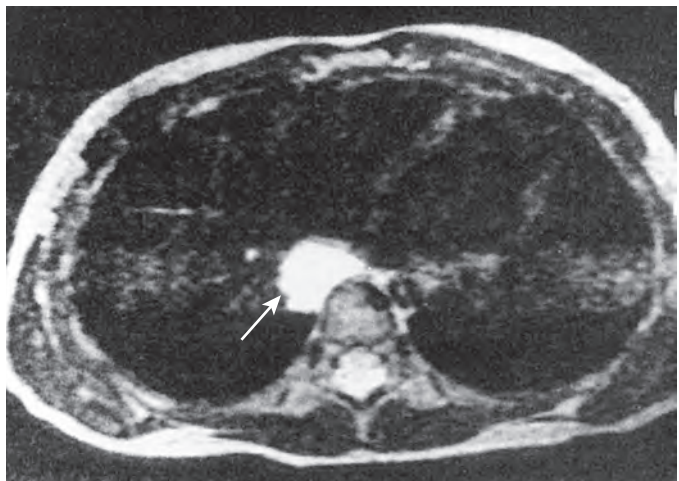


Figure 22-21 Duplication cyst. Axial T2-weighted MR image shows a fluid-filled, cystic mass (arrow) with high signal intensity in the right side of the mediastinum. (From Rafal RB, Markisz JA: *Magnetic resonance imaging of an esophageal duplication cyst*. *Am J Gastroenterol* 86:1809–1811, 1991.)

structure with a hyperechoic inner mucosa layer and a hypoechoic outer muscular layer.¹¹⁹ Technetium Tc 99m pertechnetate scintigraphy may help confirm the diagnosis of an esophageal duplication cyst containing ectopic gastric mucosa.¹¹²

Retention Cyst

Acquired esophageal cysts are much less common than congenital duplication cysts. They probably result from abnormal dilatation of columnar epithelial-lined mucous glands in the submucosa and are therefore called *esophageal retention cysts* or *mucocoeles*.¹²⁰⁻¹²³ Histologically, these cysts are lined by non-ciliated columnar or cuboidal epithelium.¹¹⁸ The pathogenesis of these lesions is uncertain, but it has been postulated that submucosal glands in the esophagus may become cystically dilated because of mechanical obstruction of the excretory ducts by mucus plugs or abnormally viscous mucus.^{120,121} This entity has sometimes been described as *esophagitis cystica*, but a more appropriate descriptive term is *esophageal retention cyst* because only minimal inflammatory change may be present in these lesions.^{120,121}

Esophageal retention cysts may appear on barium studies as solitary or, more commonly, multiple submucosal masses in the distal esophagus (Fig. 22-22).^{120,121,123} As a result, the lesions cannot be distinguished radiographically from other submucosal tumors. These patients are usually asymptomatic, however, so most esophageal retention cysts are discovered as incidental findings at autopsy.¹²⁰

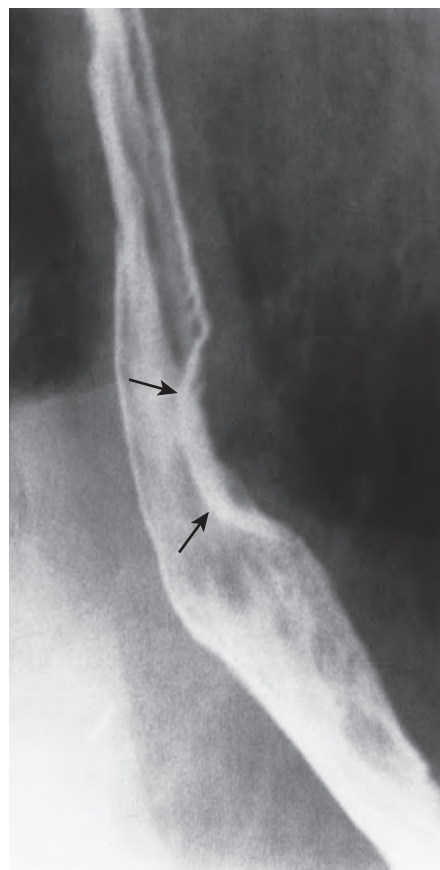


Figure 22-22 Esophageal retention cyst. The lesion is seen as a discrete submucosal mass (arrows) indistinguishable from leiomyomas or other intramural lesions. (From Levine MS: *Radiology of the Esophagus*. Philadelphia, WB Saunders, 1989.)

REFERENCES

- Ming SC: Tumors of the esophagus and stomach. In *Atlas of Tumor Pathology*, fascicle 7, Washington, DC, 1973, Armed Forces Institute of Pathology, pp 16–23.
- Plachta A: Benign tumors of the esophagus: Review of literature and report of 99 cases. *Am J Gastroenterol* 38:639–652, 1962.
- Miller BJ, Murphy F, Lukie BE: Squamous cell papilloma of esophagus. *Can J Surg* 21:538–540, 1978.
- Politoske EJ: Squamous papilloma of the esophagus associated with human papillomavirus. *Gastroenterology* 102:668–673, 1992.
- Carr NJ, Monihan JM, Sobin LH: Squamous cell papilloma of the esophagus: A clinicopathologic and follow-up study of 25 cases. *Am J Gastroenterol* 89:245–248, 1994.
- Napalkov NP, Pozharisski KM: Morphogenesis of experimental tumors of the esophagus. *J Natl Cancer Inst* 42:927–933, 1969.
- Samitz MH, Ackerman AB, Lantis LR: Squamous cell carcinoma arising at the site of oral florid papillomatosis. *Arch Dermatol* 96:286–290, 1967.
- Toso G: Epithelial papillomas—benign or malignant? *Laryngoscope* 81:1524–1531, 1971.
- Gilbert EF, Palladino A: Squamous papillomas of the uterine cervix: Review of the literature and report of a giant papillary carcinoma. *Am J Clin Pathol* 46:115–121, 1966.
- Minielly JA, Harrison EG, Fontana RS, et al: Verrucous squamous cell carcinoma of the esophagus. *Cancer* 20:2078–2087, 1967.
- Zeabart LE, Fabian J, Nord HJ: Squamous papilloma of the esophagus: A report of 3 cases. *Gastrointest Endosc* 25:18–20, 1979.
- Nuwayhid NS, Ballard ET, Cotton R: Esophageal papillomatosis. *Ann Otol Rhinol Laryngol* 86:623–625, 1977.
- Waterfall WE, Somers S, Desa DJ: Benign oesophageal papillomatosis. *J Clin Pathol* 31:111–115, 1978.
- Sandvik AK, Aase S, Kveberg KH, et al: Papillomatosis of the esophagus. *J Clin Gastroenterol* 22:35–37, 1996.
- Montesi A, Alessandro P, Graziani L, et al: Small benign tumors of the esophagus: Radiological diagnosis with double-contrast examination. *Gastrointest Radiol* 8:207–212, 1983.
- Walker JH: Giant papilloma of the thoracic esophagus. *AJR* 131:519–520, 1978.
- Spin FP: Adenomas of the esophagus: A case report and review of the literature. *Gastrointest Endosc* 20:26–27, 1973.
- McDonald GB, Brand DL, Thorning DR: Multiple adenomatous neoplasms arising in columnar-lined (Barrett's) esophagus. *Gastroenterology* 72:1317–1321, 1977.
- Levine MS, Caroline D, Thompson JJ, et al: Adenocarcinoma of the esophagus: Relationship to Barrett mucosa. *Radiology* 150:305–309, 1984.
- Bleshman MH, Banner MP, Johnson RC, et al: The inflammatory esophagogastric polyp and fold. *Radiology* 128:589–593, 1978.
- Staples DC, Knodell RG, Johnson LF: Inflammatory pseudotumor of the esophagus. *Gastrointest Endosc* 24:175–176, 1978.
- Jones TB, Heller RM, Kirchner SG, et al: Inflammatory esophagogastric polyp in children. *AJR* 133:314–316, 1979.
- Styles RA, Gibb SP, Tarshis A, et al: Esophagogastric polyps: Radiographic and endoscopic findings. *Radiology* 154:307–311, 1985.
- Ghahremani GG, Fisher MR, Rushovich AM: Prolapsing inflammatory pseudopolyp—fold complex of the oesophagogastric region. *Eur J Radiol* 4:47–51, 1984.
- Rywin AM, Ortega R: Glycogenic acanthosis of the esophagus. *Arch Pathol* 90:439–443, 1970.
- Rose D, Furth EE, Rubesin SE: Glycogenic acanthosis. *AJR* 164:96, 1995.
- Bender MD, Allison J, Cuartas F, et al: Glycogenic acanthosis of the esophagus: A form of benign epithelial hyperplasia. *Gastroenterology* 65:373–380, 1973.
- Stern Z, Sharon P, Ligumsky M, et al: Glycogenic acanthosis of the esophagus: A benign but confusing endoscopic lesion. *Am J Gastroenterol* 74:261–263, 1980.

29. Vadva MD, Triadafilopoulos G: Glycogenic acanthosis of the esophagus and gastroesophageal reflux. *J Clin Gastroenterol* 17:79–83, 1993.
30. Ghahremani GG, Rushovich AM: Glycogenic acanthosis of the esophagus: Radiographic and pathologic features. *Gastrointest Radiol* 9:93–98, 1984.
31. Glick SN, Teplick SK, Goldstein J, et al: Glycogenic acanthosis of the esophagus. *AJR* 139:683–688, 1982.
32. Berliner L, Redmond P, Horowitz L, et al: Glycogen plaques (glycogenic acanthosis) of the esophagus. *Radiology* 141:607–610, 1981.
33. Herschman BR, Uppaputhangkule V, Maas L, et al: Esophageal leukoplakia: A rare entity. *JAMA* 239:2021, 1978.
34. Graziani L, Bearzi I, Romagnoli A, et al: Significance of diffuse granularity and nodularity of the esophageal mucosa at double-contrast radiography. *Gastrointest Radiol* 10:1–6, 1985.
35. Itai Y, Kogure T, Okuyama Y, et al: Diffuse finely nodular lesions of the esophagus. *AJR* 128:563–566, 1977.
36. Itai Y, Kogure T, Okuyama Y, et al: Radiological manifestations of oesophageal involvement in acanthosis nigricans. *Br J Radiol* 49:592–593, 1976.
37. Attah EB, Hajdu SI: Benign and malignant tumors of the esophagus at autopsy. *J Thorac Cardiovasc Surg* 5:396–404, 1968.
38. Goldstein HM, Zornoza J, Hopens T: Intrinsic diseases of the adult esophagus: Benign and malignant tumors. *Semin Roentgenol* 16:183–197, 1981.
39. Lewis RB, Mehrotra AK, Rodriguez P, et al: Esophageal neoplasms: Radiologic-pathologic correlation. *Radiographics* 33:1083–1108, 2013.
40. Tsuzuki T, Kakegawa T, Arimori M, et al: Giant leiomyoma of the esophagus and cardia weighing more than 1,000 grams. *Chest* 60:396–399, 1971.
41. Barriero F, Seco JL, Molina J, et al: Giant esophageal leiomyoma with secondary megaesophagus. *Surgery* 7:436–439, 1976.
42. Godard JE, McCranie D: Multiple leiomyomas of the esophagus. *AJR* 117:259–262, 1973.
43. Shaffer HA: Multiple leiomyomas of the esophagus. *Radiology* 118:29–34, 1976.
44. Wahlen T, Astedt B: Familial occurrence of coexisting leiomyomas of vulva and oesophagus. *Acta Obstet Gynecol Scand* 44:197–203, 1965.
45. Schapiro RL, Sandrock AR: Esophagogastric and vulvar leiomyomatosis: A new radiologic syndrome. *J Can Assoc Radiol* 24:184–187, 1973.
46. Ullal SR: Hypertrophic osteoarthropathy and leiomyoma of the esophagus. *Am J Surg* 123:356–358, 1972.
47. Totten RS, Stout AP, Humphreys GH, et al: Benign tumors and cysts of the esophagus. *J Thorac Surg* 25:606–622, 1953.
48. Rubin RA, Lichtenstein GR, Morris JB: Acute esophageal obstruction: A unique presentation of a giant intramural esophageal leiomyoma. *Am J Gastroenterol* 87:1669–1671, 1992.
49. Glanz I, Grunbaum M: The radiological approach to leiomyoma of the oesophagus with a long-term follow-up. *Clin Radiol* 28:197–200, 1977.
50. Griff LC, Cooper J: Leiomyoma of the esophagus presenting as a mediastinal mass. *AJR* 101:472–481, 1967.
51. Gutman E: Posterior mediastinal calcification due to esophageal leiomyoma. *Gastroenterology* 63:665–666, 1972.
52. Ghahremani GG, Meyers MA, Port RB: Calcified primary tumors of the gastrointestinal tract. *Gastrointest Radiol* 2:331–339, 1978.
53. Itai Y, Shimazu H: Leiomyosarcoma of the oesophagus with dense calcification. *Br J Radiol* 51:469–471, 1978.
54. Megibow AJ, Balthazar EJ, Hulnick DH, et al: CT evaluation of gastrointestinal leiomyomas and leiomyosarcomas. *AJR* 144:727–731, 1985.
55. Orchard JL, Peternel WW, Arena S: Remarkably large, benign esophageal tumor: Difficulties in diagnosis. *Dig Dis* 22:266–269, 1977.
56. Schnug GE: Leiomyoma of the cardioesophageal junction. *Arch Surg* 65:342–346, 1952.
57. Stein LA, Margulis AR: The spheroid sign: A new sign for accurate differentiation of intramural from extramural masses. *AJR* 123:420–426, 1975.
58. Miettinen M, Sarlomo-Rikala M, Sobin LH, et al: Esophageal stromal tumors: A clinicopathologic, immunohistochemical, and molecular genetic study of 17 cases and comparison with esophageal leiomyomas and leiomyosarcomas. *Am J Surg Pathol* 24:211–222, 2000.
59. Shinagawa A, Zukotynski K, Krajewski K, et al: Esophageal gastrointestinal stromal tumor: Report of 7 patients. *Cancer Imaging* 12:100–108, 2012.
60. Iannicelli E, Saporì A, Panzuto F, et al: Oesophageal GIST: MDCT findings of two cases and review of the literature. *J Gastrointest Cancer* 43:481–485, 2012.
61. Winant A, Gollub MJ, Shia J, et al: Imaging and clinicopathologic features of esophageal gastrointestinal stromal tumors. *AJR* 203:306–314, 2014.
62. Sarloma-Rikala M, Kovatch AJ, Barusevicius A, et al: CD117: A sensitive marker for gastrointestinal stromal tumors that is more specific than CD34. *Mod Pathol* 11:728–734, 1998.
63. Fernandes JP, Mascarenhas MJ, daCosta JC, et al: Diffuse leiomyomatosis of the esophagus: A case report and review of the literature. *Am J Dig Dis* 20:684–690, 1975.
64. Kabuto T, Taniguchi K, Iwanaga T, et al: Diffuse leiomyomatosis of the esophagus. *Dig Dis Sci* 25:388–391, 1980.
65. Levine MS, Buck JL, Pantongrag-Brown L, et al: Esophageal leiomyomatosis. *Radiology* 199:533–536, 1996.
66. Cochat P, Guibaud P, Garcia Torres R, et al: Diffuse leiomyomatosis in Alport syndrome. *J Pediatr* 133:339–343, 1988.
67. Lonsdale RN, Roberts PF, Vaughan R, et al: Familial oesophageal leiomyomatosis and nephropathy. *Histopathology* 20:127–133, 1992.
68. Rosen RM: Familial multiple upper gastrointestinal leiomyoma. *Am J Gastroenterol* 85:303–305, 1990.
69. Lerone M, Dodero P, Romeo G, et al: Leiomyomatosis of oesophagus, congenital cataracts and hematuria: Report of a case with rectal involvement. *Pediatr Radiol* 21:578–579, 1991.
70. Faber K, Jones MA, Spratt D, et al: Vulvar leiomyomatosis in a patient with esophagogastric leiomyomatosis: Review of the syndrome. *Gynecol Oncol* 41:929–994, 1991.
71. Rabushka LS, Fishman EK, Kuhlman JE, et al: Diffuse esophageal leiomyomatosis in a patient with Alport syndrome: CT demonstration. *Radiology* 179:176–178, 1991.
72. Johnstone AS: Diffuse spasm and diffuse muscle hypertrophy of lower oesophagus. *Br J Radiol* 32:723–725, 1960.
73. Demian SD, Vargas-Cortes F: Idiopathic muscular hypertrophy of the esophagus: Postmortem incidental finding in six cases and review of the literature. *Chest* 73:288–292, 1978.
74. Zeller R, McLelland R, Meyers B, et al: Idiopathic muscular hypertrophy of the esophagus: A case report. *Gastrointest Radiol* 4:121–125, 1979.
75. Agostini S, Grimaud JC, Salducci J, et al: Idiopathic muscular hypertrophy of the esophagus: CT features. *J Comput Assist Tomogr* 12:1041–1043, 1988.
76. Tucker HJ, Snape WJ, Cohen SC: Achalasia secondary to carcinoma: Manometric and clinical features. *Ann Intern Med* 89:315–318, 1978.
77. Burrell M, Toffler R: Fibrovascular polyp of the esophagus. *Am J Dig Dis* 18:714–718, 1973.
78. Lolley D, Razzuk MA, Urschel HC: Giant fibrovascular polyp of the esophagus. *Ann Thorac Surg* 22:383–385, 1976.
79. Avezzano EA, Fleischer DE, Merida MA, et al: Giant fibrovascular polyps of the esophagus. *Am J Gastroenterol* 85:299–302, 1990.
80. Patel J, Kieffer RW, Martin M, et al: Giant fibrovascular polyp of the esophagus. *Gastroenterology* 87:953–956, 1984.
81. Watanabe H, Jass JR, Sobin LH: World Health Organization: Histological Typing of Oesophageal and Gastric Tumours, ed 2, Berlin, 1990, Springer-Verlag.
82. Timmons B, Sedwitz JL, Oller DW: Benign fibrovascular polyp of the esophagus. *South Med J* 84:1370–1372, 1991.
83. Levine MS, Buck JL, Pantongrag-Brown L, et al: Fibrovascular polyps of the esophagus: Clinical, radiographic, and pathologic findings in 16 patients. *AJR* 166:781–787, 1996.
84. Cochet B, Hohl P, Sans M, et al: Asphyxia caused by laryngeal impaction of an esophageal polyp. *Arch Otolaryngol* 106:176–178, 1980.
85. Carter MM, Kulkarni MV: Giant fibrovascular polyp of the esophagus. *Gastrointest Radiol* 9:301–303, 1984.
86. Walters NA, Coral A: Fibrovascular polyp of the oesophagus: The appearances on computed tomography. *Br J Radiol* 61:641–643, 1988.
87. Whitman GJ, Borkowski GP: Giant fibrovascular polyp of the esophagus: CT and MR findings. *AJR* 152:518–520, 1989.
88. LeBlanc J, Carrier G, Ferland S, et al: Fibrovascular polyp of the esophagus with computed tomographic and pathological correlation. *Can Assoc Radiol J* 41:87–89, 1990.
89. Kim TS, Song SY, Han J, et al: Giant fibrovascular polyp of the esophagus: CT findings. *Abdom Imaging* 20:653–655, 2005.
90. Lawrence SP, Larsen BR, Stacy CC, et al: Echoendosonographic and histologic correlation of a fibrovascular polyp of the esophagus. *Gastrointest Endosc* 40:81–84, 1994.
91. Paskin DL, Hall JD, Cookson PJ: Granular cell myoblastoma: A comprehensive review of 15 years experience. *Ann Surg* 175:501–504, 1972.
92. Lack EE, Worsham GF, Callihan MD, et al: Granular cell tumor: A clinicopathologic study of 110 patients. *J Surg Oncol* 13:301–306, 1980.
93. Fisher ER, Wechsler H: Granular cell myoblastoma—a misnomer: Electron microscopic and histochemical evidence concerning its Schwann cell derivation and nature (granular cell schwannoma). *Cancer* 15:936–954, 1962.

94. Gershwind ME, Chiat H, Addei KA, et al: Granular cell tumors of the esophagus. *Gastrointest Radiol* 2:327–330, 1978.
95. Johnston J, Helwig EB: Granular cell tumors of the gastrointestinal tract and perianal region: A study of 74 cases. *Dig Dis Sci* 26:807–816, 1981.
96. Rubesin SE, Herlinger H, Sigal H: Granular cell tumors of the esophagus. *Gastrointest Radiol* 10:11–15, 1985.
97. Orłowska J, Pachlewski J, Gugulski A, et al: A conservative approach to granular cell tumors of the esophagus: Four case reports and literature review. *Am J Gastroenterol* 88:311–315, 1993.
98. Subramanyam K, Shannon CR, Patterson M, et al: Granular cell myoblastoma of the esophagus. *J Clin Gastroenterol* 6:113–118, 1984.
99. Radin DR, Zelner R, Ray MJ, et al: Multiple granular cell tumors of the skin and gastrointestinal tract. *AJR* 147:1305–1307, 1986.
100. Kinnear JS: Report of case of intramural lipoma of the oesophagus. *Br J Surg* 42:439, 1955.
101. Nora PF: Lipoma of the esophagus. *Am J Surg* 108:353–356, 1964.
102. Allen MS, Talbot WH: Sudden death due to regurgitation of a pedunculated esophageal lipoma. *J Thorac Cardiovasc Surg* 54:756–758, 1967.
103. Liliequist B, Wiberg A: Pedunculated tumours of the oesophagus: Two cases of lipoma. *Acta Radiol Diagn (Stockh)* 15:383–392, 1974.
104. Gandini G, Andreis M, Avataneo T, et al: A case of esophageal lipoma diagnosed by computed tomography. *Diagn Radiol* 10:55–60, 1985.
105. Loughry RW: Hemangiomas of the esophagus. *Rocky Mt Med J* 68:37–39, 1971.
106. Grimes OF: Cavernous hemangioma of the esophagus. *Dis Chest* 48:384, 1965.
107. Govoni AF: Hemangiomas of the esophagus. *Gastrointest Radiol* 7:113–117, 1982.
108. Dieter RA, Riker WL, Holinger P: Pedunculated esophageal hamartoma in a child. *J Thorac Cardiovasc Surg* 59:851–854, 1970.
109. Shah B, Unger L, Heimlich HJ: Hamartomatous polyp of the esophagus. *Arch Surg* 110:326–328, 1975.
110. Hauser H, Ody B, Plojoux O, et al: Radiological findings in multiple hamartoma syndrome (Cowden disease): A report of three cases. *Radiology* 137:317–323, 1980.
111. Chen YM, Ott DJ, Wu WC, et al: Cowden's disease: A case report and literature review. *Gastrointest Radiol* 12:325–329, 1987.
112. Macpherson RI: Gastrointestinal tract duplications: Clinical, pathologic, etiologic, and radiologic considerations. *Radiographics* 13:1063–1080, 1993.
113. Vithespongse P, Blank S: Ciliated epithelial esophageal cyst. *Am J Gastroenterol* 56:436–440, 1971.
114. Gatzinsky P, Fasth S, Hansson G: Intramural oesophageal cyst with massive mediastinal bleeding. *Scand J Thorac Cardiovasc Surg* 12:143–145, 1978.
115. Whitaker JA, Deffenbaugh LD, Cooke AR: Esophageal duplication cyst. *Am J Gastroenterol* 73:329–332, 1980.
116. Erdozain JC, Lizasoain J, Martin-de-Argila C, et al: Esophagus duplication in a young adult. *Am J Gastroenterol* 90:663–665, 1995.
117. Bondestam S, Salo JA, Salonen OLM, et al: Imaging of congenital esophageal cysts in adults. *Gastrointest Radiol* 15:279–281, 1990.
118. Rafal RB, Markisz JA: Magnetic resonance imaging of an esophageal duplication cyst. *Am J Gastroenterol* 86:1809–1811, 1991.
119. Geller A, Wang KK, Dimagno EP: Diagnosis of foregut duplication cysts by endoscopic ultrasonography. *Gastroenterology* 109:838–842, 1995.
120. Voirol MW, Welsh RA, Genet EF: Esophagitis cystica. *Am J Gastroenterol* 59:446–453, 1973.
121. Farman J, Rosen Y, Dallemand S, et al: Esophagitis cystica: Lower esophageal retention cysts. *AJR* 128:495–496, 1977.
122. Edgin R, Mekhjian HS: Esophageal retention cyst: Unusual cause for dysphagia. *J Clin Gastroenterol* 3:57–59, 1981.
123. Hover AR, Brady CE, Williams JR, et al: Multiple retention cysts of the lower esophagus. *J Clin Gastroenterol* 4:209–212, 1982.

Carcinoma of the Esophagus

MARC S. LEVINE | ROBERT A. HALVORSEN

CHAPTER OUTLINE

Squamous Cell Carcinoma

Epidemiology
Predisposing Conditions
Pathology
Routes of Spread
Clinical Aspects
Endoscopic Findings
Radiographic Findings

Adenocarcinoma

Epidemiology and Pathogenesis
Pathology
Routes of Spread
Clinical Aspects
Radiographic Findings

Differential Diagnosis

Early Esophageal Cancer
Advanced Carcinoma

Staging

Computed Tomography
Endoscopic Ultrasound
Positron Emission Tomography
Ultrasonography of the Neck
Staging Algorithm

Treatment

Surgery
Radiation Therapy
Chemoradiation Therapy

Esophageal carcinoma constitutes only about 1% of all cancers and 7% of cancers in the gastrointestinal (GI) tract.¹ Nevertheless, it is a deadly disease, with an overall 5-year survival rate of only about 15%.² At one time, most malignant tumors of the esophagus were thought to be squamous cell carcinomas, but adenocarcinomas arising in Barrett's esophagus have increased dramatically in incidence since the 1970s. Because of important differences between these tumors, the chapter is divided into separate sections on squamous cell carcinoma and adenocarcinoma of the esophagus.

Squamous Cell Carcinoma

EPIDEMIOLOGY

Esophageal carcinoma is predominantly a disease of older men, with a male-to-female ratio of almost 4:1 and a peak incidence between 65 and 74 years of age.² The development of squamous cell carcinoma of the esophagus is a multifactorial

process associated with a variety of risk factors, including tobacco and alcohol consumption, obesity, nutritional deficiencies, exposure to various environmental carcinogens, and geographic location.

Two of the major risk factors for the development of esophageal cancer in the United States are tobacco and alcohol consumption.^{3,4} Tobacco and alcohol appear to have a synergistic effect, so people who smoke and drink have even higher rates of esophageal cancer.⁵ Although tobacco smoke is known to contain a variety of carcinogens, the development of esophageal carcinoma in alcoholics may be related to other factors such as poor health and nutritional deficiencies. Obesity also has been recognized as an important risk factor for the development of esophageal cancer.^{4,6}

Squamous cell carcinoma of the esophagus has striking geographic variations, with the highest incidences reported in an Asian esophageal cancer belt stretching from eastern Turkey and northern Iran to India and northern China.⁷ A high incidence has also been reported in South Africa and France. These regional variations in the frequency of esophageal cancer have been attributed primarily to environmental rather than hereditary factors. Dietary habits in particular have been implicated because people living in areas with a high incidence of esophageal cancer often have diets high in starch and low in fresh fruits and vegetables.⁷ Other environmental factors may also have a role in cancer pathogenesis. For example, nitrosamines and other nitroso compounds are potent carcinogens that occur in high concentrations in the food and water supply of parts of northern China.⁸ Epidemiologic studies in China and South Africa have shown that these areas also have unusually low levels of molybdenum in the soil.^{9,10} Because molybdenum is required for the metabolism of nitrite to ammonia, low levels of molybdenum in the soil could lead to the accumulation of nitrites and potentially carcinogenic nitrosamines in plants consumed by humans. The high prevalence of esophageal cancer in parts of Saudi Arabia has been attributed to contamination of drinking water by impurities such as petroleum oils.¹¹ Other substances such as tannin, betel leaves, and asbestos fibers have also been implicated in the development of esophageal cancer.¹²⁻¹⁴

Attention has also been focused on the potential role of human papillomavirus (HPV) in the pathogenesis of esophageal cancer, particularly in high-risk areas such as China and South Africa. In studies from China, HPV has been isolated by *in situ* hybridization techniques in 25% to 50% of esophageal cancer specimens.^{15,16} These data suggest that HPV may be an important contributing factor in the development of esophageal cancer.

PREDISPOSING CONDITIONS

Conditions that are thought to predispose patients to the development of squamous cell carcinoma of the esophagus include

achalasia, lye strictures, head and neck tumors, celiac disease, Plummer-Vinson syndrome, radiation, and tylosis. Because of the increased risk of developing esophageal cancer, periodic surveillance has often been advocated for patients with these conditions.

Achalasia

Achalasia is thought to be a premalignant condition associated with an increased risk of developing esophageal carcinoma. In various studies, the prevalence of esophageal cancer in patients with long-standing achalasia has ranged from 2% to 8%.¹⁷⁻¹⁹ Malignant degeneration presumably occurs as a result of chronic stasis esophagitis caused by retained food and debris in a dilated, obstructed esophagus.¹⁷⁻²⁰ Most patients have had achalasia for at least 20 years before the development of cancer.^{17,19,20} Unfortunately, a neoplastic lesion growing inside a massively dilated esophagus may not cause symptoms until it is an advanced, unresectable tumor.^{19,21} As a result, some authors believe that patients with long-standing achalasia should undergo annual surveillance with barium studies or endoscopy to detect developing cancers at the earliest possible stage.^{17,20,21} However, one study failed to show an increased cancer risk in these patients,²² so not all investigators accept the need for surveillance.

Lye Strictures

Patients with chronic lye strictures have an increased risk of developing esophageal carcinoma. In various studies, the prevalence of cancer has ranged from 2% to 16%.^{23,24} Although the pathogenesis is uncertain, it has been postulated that chronic inflammation and scarring from caustic esophagitis predispose these patients to the development of esophageal carcinoma. The average latent period between the ingestion of lye and development of cancer is 40 to 45 years.^{25,26} These patients usually seek medical attention for recurrent or suddenly worsening dysphagia many years after lye ingestion. Carcinomas arising in lye strictures have a better prognosis than most esophageal cancers, with 5-year survival rates of 8% to 33%.²⁵ This more favorable prognosis may be related to the presence of dense scar tissue surrounding the tumor, which prevents early invasion of adjacent mediastinal structures.^{25,26} Some investigators advocate periodic surveillance of patients with long-standing lye strictures, but these individuals are often in a socioeconomic group least likely to be compliant with surveillance programs.

Head and Neck Tumors

Patients with primary squamous cell carcinomas of the oral cavity, pharynx, and larynx have a substantially increased risk of developing separate primary esophageal carcinomas. In various studies, 2% to 8% of patients with head and neck tumors who underwent endoscopic surveillance were found to have synchronous esophageal cancers.²⁷⁻²⁹ This association has been attributed to common predisposing factors, primarily smoking and drinking because exposure to tobacco and alcohol considerably increases the risk of squamous cell carcinoma in both areas.³⁰ Radiologic or endoscopic evaluation of the esophagus has therefore been advocated in the initial work-up of all patients with head and neck tumors. Many of these synchronous esophageal cancers are small, asymptomatic lesions, so screening tests may detect such tumors at an early stage, when they are potentially curable.²⁹ Discovery of an advanced

lesion in the esophagus is also important because radical head and neck surgery may no longer be appropriate in these patients. The risk of developing subsequent metachronous esophageal carcinomas is also considerably increased in patients with head and neck tumors. Some form of ongoing surveillance is therefore required to detect metachronous esophageal lesions.

Celiac Disease

Celiac disease (nontropical sprue) is thought to be associated with an increased risk of developing esophageal carcinoma.^{31,32} The pathogenesis of cancer is uncertain, but it has been postulated that carcinogens are absorbed through an atrophic jejunal mucosa in patients with advanced celiac disease.³² Most patients have long-standing disease; malabsorption is present for an average of 35 years before the development of cancer.³¹ Some investigators therefore advocate radiologic or endoscopic surveillance of the esophagus in these patients.

Plummer-Vinson Syndrome

Plummer-Vinson, or Paterson-Kelly, syndrome is characterized by iron deficiency anemia, glossitis, postcricoid webs, and dysphagia.³³ This syndrome has been described primarily in women of Scandinavian origin. The prevalence of hypopharyngeal or esophageal carcinoma in Plummer-Vinson syndrome has ranged from 4% to 16%.^{33,34} Almost all such cancers are associated with postcricoid webs.³³ Radiologic or endoscopic examinations are therefore required to differentiate webs from superimposed hypopharyngeal or esophageal carcinomas in these patients.

Radiation

Esophageal cancer is a rare complication of chronic radiation injury to the esophagus. Most cases have occurred in the cervical or upper thoracic esophagus after radiation doses of 20 to 50 Gy to the mediastinum or neck.^{35,36} In one study, women who received radiation therapy for carcinoma of the breast were found to have an increased risk of esophageal carcinoma.³⁷ In general, however, the average latent period between radiation therapy and the development of cancer is about 30 years.³⁶ It is therefore difficult to prove that these lesions are not coincidental cancers arising in a previously irradiated area.

Tylosis

Tylosis (Howel-Evans syndrome) is an extremely rare, hereditary, autosomal dominant disorder characterized by hyperkeratosis of the palms and soles, with thickening and fissuring of the skin. This disorder is associated with an extraordinarily high risk of developing esophageal cancer.³⁸⁻⁴⁰ In one study, 95% of patients with tylosis had esophageal cancer by 65 years of age.³⁹ Most of these patients are found to have advanced, unresectable tumors at the time of clinical presentation. However, asymptomatic individuals with tylosis may have hyperkeratotic esophageal plaques containing foci of dysplasia, intramucosal carcinoma, or invasive carcinoma.⁴⁰ Thus, periodic surveillance of asymptomatic family members has been advocated to detect premalignant lesions before the development of overt carcinoma. Because of the high likelihood of developing esophageal cancer, a prophylactic esophagectomy is sometimes justified for these patients.

PATHOLOGY

Gross Features

Squamous cell carcinomas of the esophagus may appear grossly as infiltrating, polypoid, ulcerative, or superficial spreading lesions. Infiltrating lesions, the most common type, cause irregular narrowing and constriction of the lumen. Polypoid lesions are lobulated or fungating masses that protrude into the lumen. Primary ulcerative lesions are relatively flat masses in which the bulk of the tumor is necrotic and ulcerated. Less frequently, superficial spreading lesions may extend longitudinally in the wall, without invading beyond the mucosa or submucosa. Patients with superficial spreading carcinomas tend to have a better prognosis than those with more invasive forms of esophageal cancer.

Histologic Features

About 50% of esophageal cancers are squamous cell carcinomas, and the remaining 50% are adenocarcinomas arising in Barrett's mucosa.⁴¹ Other less common malignant tumors of the esophagus are discussed in Chapter 24.

At the time of clinical presentation, most squamous cell carcinomas of the esophagus are advanced lesions that have already invaded regional lymph nodes or other local or distant structures. As a result, affected individuals have a dismal prognosis, with overall 5-year survival rates of only about 15%.² In contrast, early esophageal cancers are relatively curable lesions, with 5-year survival rates of more than 90%.^{42,43} According to the Japanese Society for Esophageal Diseases, early esophageal cancer is defined histologically as cancer limited to the mucosa or submucosa without lymph node involvement.⁴⁴ Many of these cases have been reported in the Chinese literature as a result of mass screening of the adult population because of the high incidence of esophageal cancer in that country.^{8,45}

Considerable confusion exists in the literature regarding the terminology for "early" cancer. The terms *early esophageal cancer*, *superficial esophageal cancer*, and *small esophageal cancer* have been used interchangeably to describe malignant esophageal tumors diagnosed at an early stage. However, these lesions should not be considered synonymous because they have different histopathologic features that alter the prognosis of this disease. According to the Japanese Society for Esophageal Diseases, superficial esophageal cancer is confined to the mucosa or submucosa but, unlike patients with early esophageal cancer, patients with superficial cancers may have lymph node metastases.⁴⁴ *Small esophageal cancer* is another term used to describe tumors smaller than 3.5 cm, regardless of the depth of invasion or the presence or absence of lymph node metastases.^{46,47} Previous studies have shown that the 5-year survival for esophageal cancer decreases markedly when regional lymph nodes are involved by tumor.^{48,49} Thus, some superficial or small esophageal cancers may be early lesions histologically, whereas others may have already invaded regional lymph nodes, with a prognosis comparable to that of advanced esophageal cancer.^{47,49}

Distribution

Squamous cell carcinomas of the esophagus tend to be located in the upper, middle or, less commonly, distal third of the esophagus.^{48,50} Unlike adenocarcinomas arising in Barrett's mucosa, squamous cell carcinomas of the distal esophagus

almost never invade the stomach, and there is usually a discrete segment of normal esophagus between the tumor and gastric cardia.

ROUTES OF SPREAD

Esophageal carcinoma may invade local, regional, or distant structures by various pathways, including direct extension, lymphatic spread, and hematogenous metastases.

Direct Extension

Because the esophagus lacks a serosa and is attached to neighboring structures by only a loose adventitia, there is no anatomic barrier to prevent rapid spread of tumor into the adjacent mediastinum. As a result, esophageal cancer has a marked tendency to invade contiguous structures in the neck or chest, such as the thyroid, larynx, trachea, bronchi (usually the left main bronchus), aorta, thoracic duct, lung, pericardium, and diaphragm.^{48,50} The tracheobronchial tree is a particularly common site of involvement; tracheoesophageal or esophagobronchial fistulas develop in 5% to 10% of all patients with esophageal cancer.^{51,52} Rarely, aortoesophageal fistulas or even esophagopericardial fistulas may occur as a terminal complication of esophageal cancer caused by aortic or pericardial invasion by tumor.^{53,54}

Lymphatic Spread

Lymphatic metastases are found in up to 75% of patients with esophageal cancer.⁵⁵ Because the esophagus contains a rich network of interconnecting lymphatic channels, lymphatic spread from esophageal cancer is unpredictable, with jump metastases to lymph nodes in the neck or mediastinum often occurring in the absence of segmental lymph node involvement.^{55,56} Submucosal esophageal lymphatics also communicate subdiaphragmatically with paracardiac, lesser curvature, and celiac nodes in the upper abdomen; these nodal groups are involved by tumor in 25% to 50% of patients with esophageal cancer.^{55,56} Although tumors in the distal esophagus are more likely to metastasize to the abdomen, lymphatic spread of cancers in the upper or midesophagus can also result in metastases to celiac or other abdominal lymph nodes.⁵⁵

Discrete lymphatic metastases or satellite nodules are found in the esophagus at autopsy in about 50% of patients with esophageal cancer.⁵⁵ These lesions should be distinguished pathologically from rare double primary carcinomas of the esophagus.^{57,58} However, it may be impossible to determine whether two discrete lesions represent synchronous primary tumors or a single cancer with lymphatic dissemination.

Between 2% and 15% of patients dying of esophageal cancer have gastric metastases at autopsy.⁵⁹ These lesions probably result from tumor emboli that seed the gastric fundus via submucosal esophageal lymphatics extending subdiaphragmatically to the stomach.^{59,60} In such cases, the primary esophageal cancer may be located a considerable distance from the gastroesophageal junction, with a normal esophageal segment below the lesion.

Hematogenous Metastases

Hematogenous (bloodborne) metastases are often found in patients with advanced esophageal carcinoma. The most common sites of metastases are the lungs, liver, adrenals, kidneys, pancreas, peritoneum, and bones.

CLINICAL ASPECTS

Most patients with esophageal cancer develop dysphagia only when the lumen of the esophagus has been reduced by 50% to 75% of its normal size.^{48,50} By that time, malignant invasion of periesophageal lymph nodes or surrounding mediastinal structures has usually occurred.⁴⁸ As a result, most patients have advanced, unresectable tumors at the time of diagnosis. Occasionally, however, patients experience dysphagia while the tumor is at an early stage.^{46,61-63} It is therefore possible to detect early esophageal cancer in some patients who are symptomatic.

Dysphagia is the most common complaint in patients with advanced esophageal cancer.⁴⁸ Dysphagia is usually present for 2 to 4 months before these patients seek medical attention.⁴⁸ Some patients can accurately localize the level of obstruction, but others may have a sensation of blockage referred to the thoracic inlet or even the pharynx by a cancer arising in the middle or lower thoracic esophagus.⁵⁰ The esophagus should therefore be carefully evaluated in all patients with unexplained pharyngeal dysphagia to rule out an esophageal cancer below the subjective site of obstruction.

Patients with esophageal cancer may also present with odynophagia if the tumor is ulcerated or with substernal chest pain unrelated to swallowing if the tumor has invaded the mediastinum, so unremitting chest pain is an extremely poor prognostic sign.⁵⁰ Other common symptoms include anorexia and weight loss, which are present in up to 75% of cases.² Some patients may present with guaiac-positive stool or iron deficiency anemia as a result of occult bleeding from the friable surface of the tumor.⁴⁸ However, frank hematemesis is uncommon.^{64,65} Rarely, fatal hemorrhage may be caused by an aorto-esophageal fistula.^{66,67} The latter patients may have minimal hematemesis before the sudden development of massive hemorrhage, shock, and death.

Other patients with esophageal cancer may develop hoarseness because of direct extension of tumor into the larynx or involvement of the recurrent laryngeal nerve.⁴⁸ Recurrent aspiration may lead to a chronic cough. However, the presence of a paroxysmal cough on swallowing should suggest the development of a malignant tracheoesophageal or esophagobronchial fistula. Rarely, patients with esophageal cancer may have anorexia, weight loss, or other signs of widespread malignancy without experiencing dysphagia, so localizing esophageal symptoms are not always present.⁵⁰

ENDOSCOPIC FINDINGS

When multiple biopsy specimens are obtained, endoscopy has an overall sensitivity of almost 100% in the diagnosis of esophageal carcinoma.^{2,68,69} Brush cytology is also helpful when the esophageal lumen is so compromised by tumor that adequate biopsy specimens cannot be obtained. Detection of suspicious lesions on barium studies should therefore lead to early endoscopy and biopsy for a definitive diagnosis.

RADIOGRAPHIC FINDINGS

Early Esophageal Cancer

Double-contrast esophagography has been widely advocated as the best radiologic technique for diagnosing early esophageal cancer. Unfortunately, the increased sensitivity of this technique has resulted in a lower specificity because more

subtle abnormalities are suspected of representing cancer.⁴⁶ Nevertheless, it is probably best to accept a certain percentage of false-positive findings to avoid missing early tumors. When a lesion is detected on barium studies, endoscopy and biopsy should therefore be performed to confirm the presence of carcinoma.

Early esophageal cancers classically appear on double-contrast esophagograms as small protruded lesions less than 3.5 cm in diameter.^{46,61,63,70,71} They may be plaque-like lesions, often with central ulceration (Fig. 23-1), or small sessile polyps with a smooth or slightly lobulated contour (Fig. 23-2). Other early cancers may be superficial or depressed lesions, causing focal irregularity, nodularity, or ulceration of the mucosa (Fig. 23-3).⁷²⁻⁷⁴ When a lesion is detected on double-contrast studies, multiple projections should be obtained to determine its appearance en face and in profile (see Fig. 23-1).

Although most early esophageal cancers appear as focal lesions, superficial spreading carcinomas may be manifested by poorly defined nodules or plaques, producing a confluent area of mucosal nodularity or granularity (Fig. 23-4).^{63,72-75} Some superficial spreading carcinomas may be localized lesions, whereas others may involve a considerable segment of the esophagus.

Early esophageal cancers are generally thought to be small lesions, but some early cancers may appear on barium studies as relatively large intraluminal mass larger than 3.5 cm in diameter (Fig. 23-5).^{63,76} Such lesions may be indistinguishable from advanced carcinomas. Thus, early esophageal cancers are not

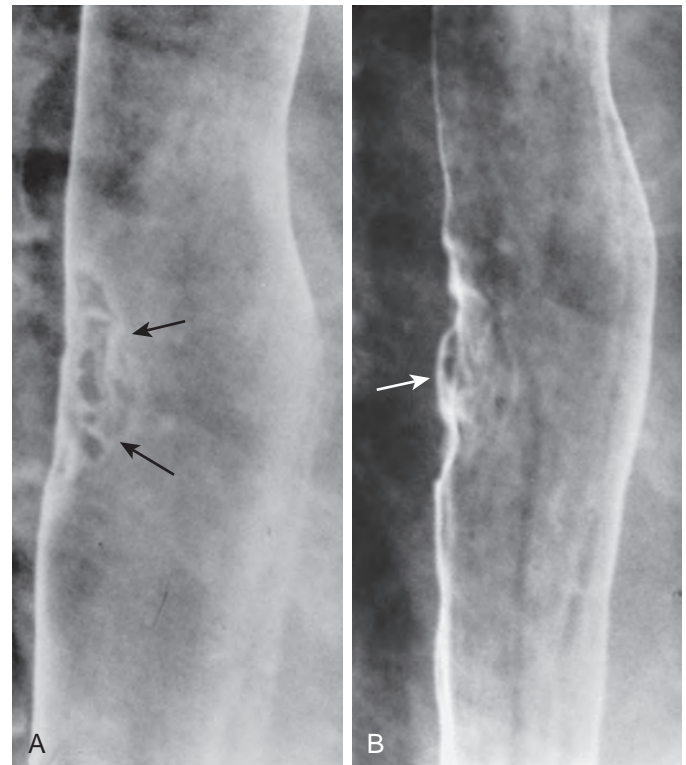


Figure 23-1 Early esophageal cancer. **A.** En face view from a double-contrast esophagogram shows a poorly defined lesion (arrows) in the midesophagus. **B.** However, a tangential view reveals a characteristic plaque-like lesion containing a flat area of central ulceration (arrow). (From Laufer I, Levine MS [eds]: *Double Contrast Gastrointestinal Radiology*, 2nd ed. Philadelphia, WB Saunders, 1992.)

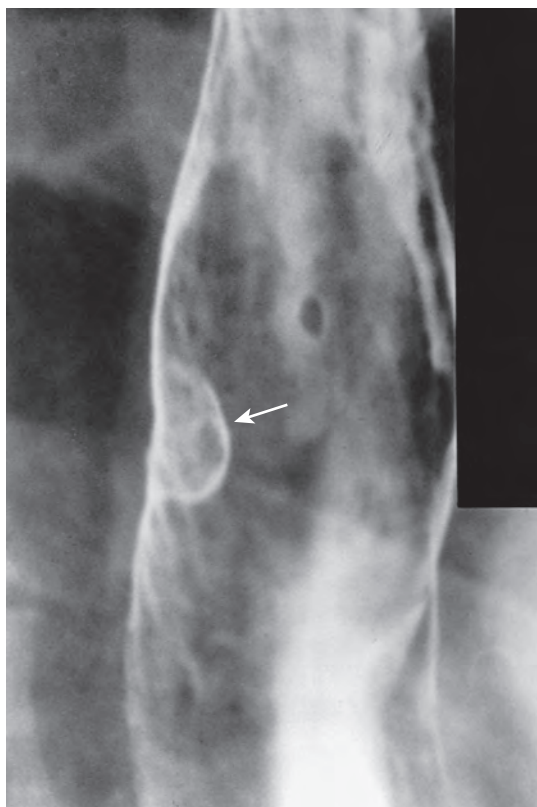


Figure 23-2 Early esophageal cancer. The lesion appears radiographically as a small sessile polyp (arrow) in the midesophagus. A benign squamous papilloma could produce a similar appearance. (Courtesy Seth N. Glick, MD, Philadelphia.)

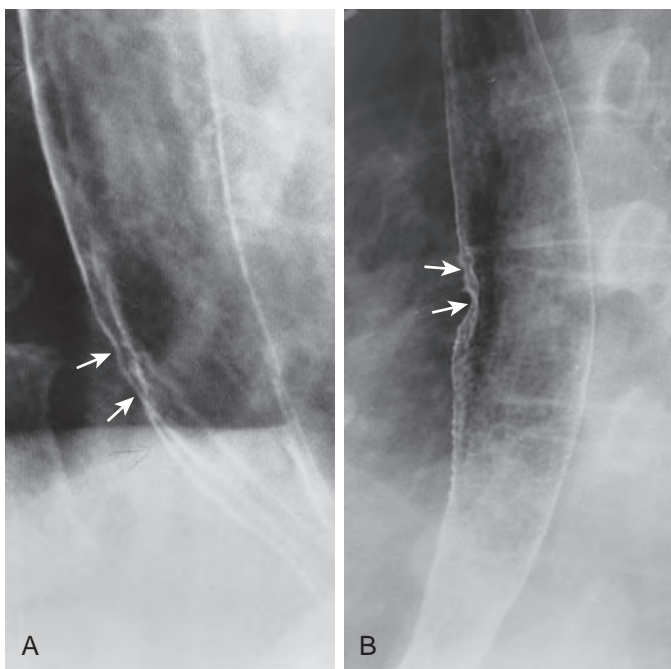


Figure 23-3 Two examples of early esophageal cancer. A, B. In both cases there is focal irregularity and puckering of one wall of the esophagus (arrows) without a discrete mass. (A courtesy Akiyoshi Yamada, MD, Tokyo.)

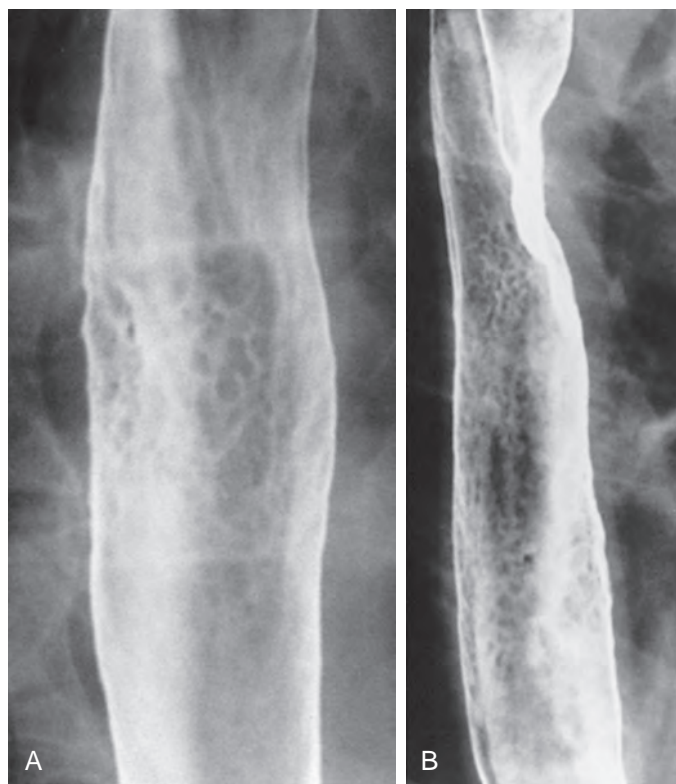


Figure 23-4 Superficial spreading carcinoma. A, B. There is focal nodularity in the midesophagus as a result of poorly defined nodules and plaques, producing a confluent area of disease. B. In another patient with a more extensive lesion, there is diffuse granularity of the mucosa. (A from Levine MS: *Radiology of the Esophagus*. Philadelphia, WB Saunders, 1989.)



Figure 23-5 Early esophageal cancer. This lesion appears as a relatively large polypoid mass indistinguishable from an advanced carcinoma. (From Levine MS: *Radiology of the Esophagus*. Philadelphia, WB Saunders, 1989.)

necessarily small cancers because they may undergo considerable intraluminal or intramural growth and still be classified histologically as early lesions.

Advanced Carcinoma

Chest Radiography. Almost 50% of patients with advanced esophageal cancers have abnormal chest radiographs.⁷⁷ The most common findings include mediastinal widening, a hilar, retrohilar, or retrocardiac mass, anterior tracheal bowing, a widened retrotracheal stripe, and an air-fluid level in the esophagus (Fig. 23-6).⁷⁷⁻⁷⁹ Anterior bowing of the trachea or thickening of the retrotracheal stripe beyond 3 mm in width may result from lymphatic infiltration or direct invasion of the retrotracheal area by tumor.^{78,79} Obstructing cancers may be recognized by an air-fluid level in the esophagus. However, esophageal obstruction from achalasia or other causes may also be manifested by anterior tracheal bowing or an esophageal air-fluid level.

Barium Studies. Double-contrast esophagography is often performed on patients with dysphagia to rule out carcinoma or other abnormalities in the esophagus. Some gastroenterologists believe that endoscopy is required for all patients with negative esophagograms to find tumors that are missed on barium studies. In a large series of patients with esophageal cancer, however, the lesion was detected on double-contrast esophagograms in 98% of cases, and malignant tumor was diagnosed or suspected on the basis of the radiographic findings in 96%.⁸⁰ An argument could be made that a high sensitivity is achieved in the radiographic diagnosis of esophageal cancer only by exposing an inordinate number of patients to unnecessary endoscopy. In the previous study, however, endoscopy was recommended to rule out malignant tumor in only about 1% of

all patients who underwent double-contrast examinations.⁸⁰ Similarly, in other series, endoscopy has failed to reveal any cases of esophageal carcinoma that were missed on double-contrast esophagograms.^{81,82} Thus, endoscopy is not routinely warranted for patients who have normal findings on barium studies.

Advanced esophageal carcinomas may appear on barium studies as infiltrating, polypoid, ulcerative, or varicoid lesions (Fig. 23-7).⁸³⁻⁸⁶ However, many esophageal cancers have mixed morphologic features, so there is considerable overlap in the classification of these tumors.

Infiltrating esophageal carcinomas are characterized by irregular narrowing and constriction of the lumen associated with a nodular or ulcerated mucosa and abrupt, well-defined proximal and distal margins (see Fig. 23-7A). Occasionally, these cancers have shelflike, overhanging margins, producing true annular lesions (Fig. 23-8A).⁸³ However, other infiltrating lesions have more gradual, tapered margins, occasionally mimicking the appearance of benign strictures (Fig. 23-8B).⁸⁴ Infiltrating lesions may eventually cause partial or even complete esophageal obstruction, with proximal dilation and minimal or no emptying of barium into the stomach.

Polypoid carcinomas appear as lobulated or fungating intraluminal masses, usually larger than 3.5 cm (see Fig. 23-7B).⁸³⁻⁸⁵ They often contain areas of ulceration caused by tumor necrosis. Bulky lesions may eventually cause luminal encroachment and obstruction. However, squamous cell carcinomas are not generally polypoid, so other malignant tumors such as spindle cell carcinoma should be considered in these patients (see Chapter 24).

Primary ulcerative carcinomas are those in which the bulk of the tumor mass is replaced by ulceration. When viewed in profile, these lesions appear as well-defined meniscoid ulcers,

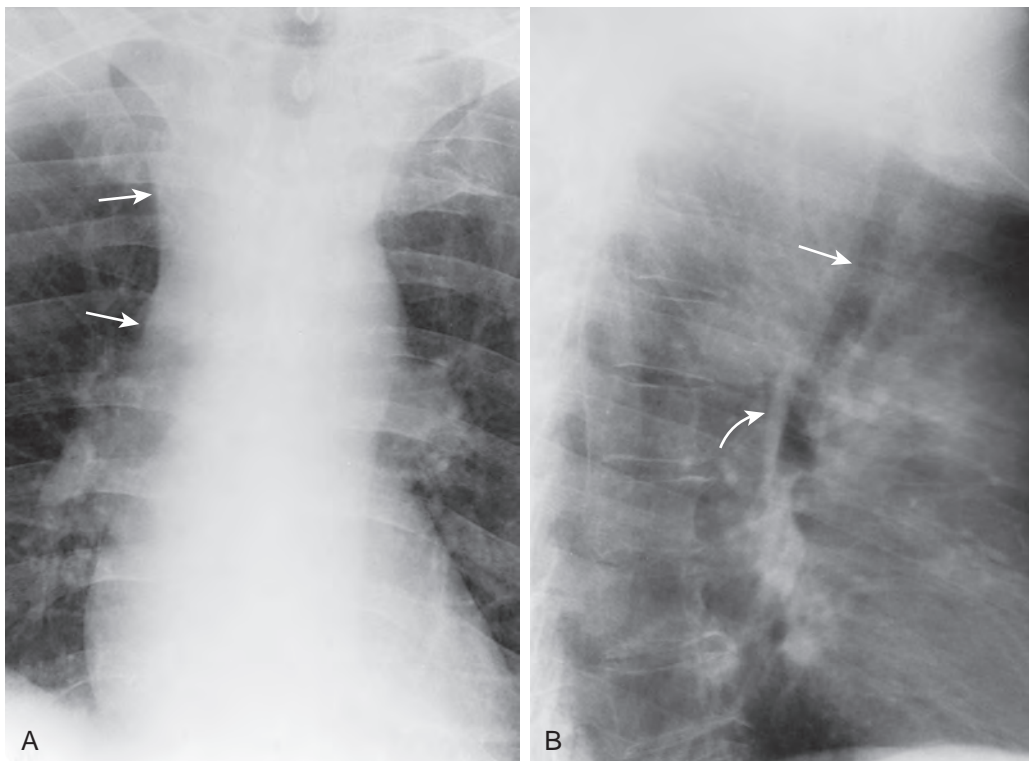


Figure 23-6 Advanced esophageal carcinoma with abnormal chest radiographs. **A.** Posteroanterior chest radiograph shows widening of the superior mediastinum on the right (arrows). **B.** Lateral radiograph shows increased soft-tissue density in the retrotracheal space with slight anterior bowing of the trachea (straight arrow) by an advanced esophageal cancer in this region. Also note thickening of the retrotracheal stripe inferiorly (curved arrow) caused by direct invasion of this area by tumor. (Courtesy Wallace T. Miller, MD, Philadelphia.)

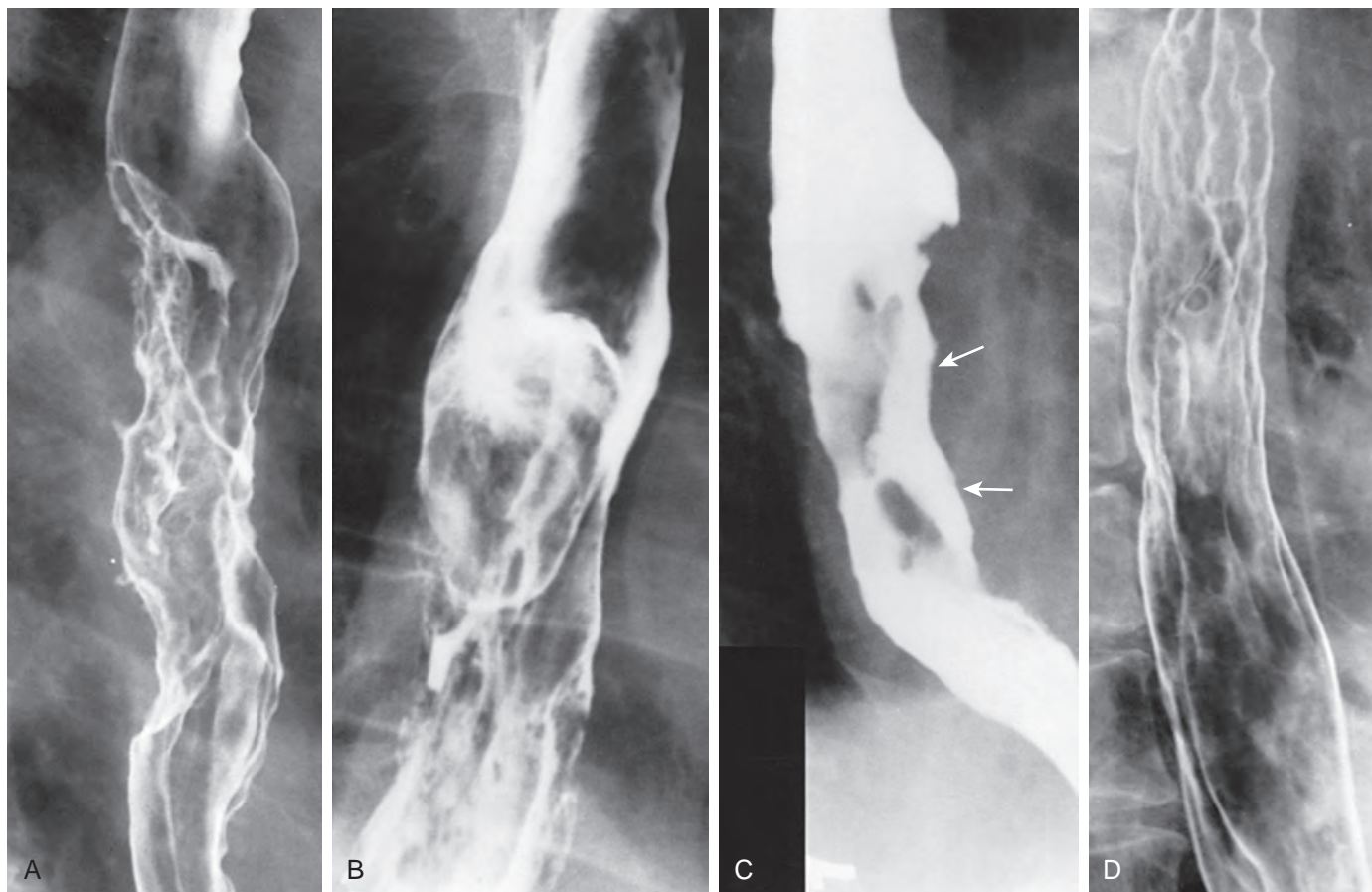


Figure 23-7 Advanced esophageal carcinoma: patterns of tumor. **A.** Infiltrating lesion. **B.** Polypoid lesion. **C.** Ulcerative lesion with a large, meniscoid ulcer (arrows) surrounded by a thick radiolucent rim of tumor. **D.** Varicoid lesion with thickened tortuous folds in the midesophagus caused by submucosal spread of tumor. (**A-C** from Levine MS: *Radiology of the Esophagus*. Philadelphia, WB Saunders, 1989; **D** courtesy Akiyoshi Yamada, MD, Tokyo.)

with a thick, irregular, radiolucent rim of tumor surrounding the ulcer (see Fig. 23-7C).^{85,87}

Varicoid carcinomas are those in which submucosal spread of tumor results in thickened, tortuous, or serpiginous longitudinal folds, mimicking the appearance of esophageal varices (see Fig. 23-7D).⁸⁸⁻⁹⁰ However, these entities can usually be differentiated at fluoroscopy (see later, “Differential Diagnosis”). Although varicoid carcinomas are uncommon, submucosal extension of tumor not infrequently produces a focal varicoid pattern adjacent to an obvious squamous cell carcinoma. In one study, a varicoid pattern was seen on esophagography in 40% of patients with esophageal cancer.⁹¹

Mediastinal involvement by advanced esophageal carcinoma can also be recognized on barium studies. Lymphatic spread of tumor to paratracheal, subcarinal, or paraesophageal lymph nodes may lead to extrinsic compression or displacement of the esophagus, often at a considerable distance from the primary lesion (Fig. 23-9). Mediastinal lymphadenopathy is usually characterized by a smooth, extrinsic esophageal impression with gently sloping, obtuse borders. This finding almost always indicates an advanced, unresectable lesion.

Lymphatic metastases from esophageal cancer may be manifested by discrete implants adjacent to or remote from the primary lesion. These metastases may appear on barium studies as small plaque-like, polypoid, submucosal, or ulcerated lesions

separated from the main tumor by normal intervening mucosa (Fig. 23-10).⁹² Although most of these satellite lesions represent lymphatic metastases from the original cancer, the possibility of two primary carcinomas (double primaries) should be considered when the lesions are separated by an unusually long segment of normal mucosa.⁵⁷

Squamous cell metastases to the stomach usually appear on barium studies as solitary, large submucosal masses in the gastric fundus.^{59,60} These lesions often contain areas of ulceration, so they may resemble ulcerated gastrointestinal stromal tumors (GISTs; Fig. 23-11). Less frequently, they can be mistaken for primary gastric carcinomas.⁹³ Because the appropriate treatment for esophageal cancer depends on the stage of the tumor, the gastric cardia and fundus should be carefully examined radiographically in all patients with esophageal cancer to rule out unsuspected metastases to the stomach.

Five percent to 10% of patients with esophageal cancer develop an esophageal-airway fistula (Fig. 23-12).^{51,52} This complication frequently occurs after radiation therapy, probably as a result of radiation-induced tumor necrosis. Most such fistulas involve the trachea or left main bronchus.⁵² Occasionally, however, a locally aggressive esophageal cancer may lead to the development of a necrotic, tumor-containing cavity in the mediastinum or lung that communicates directly with the

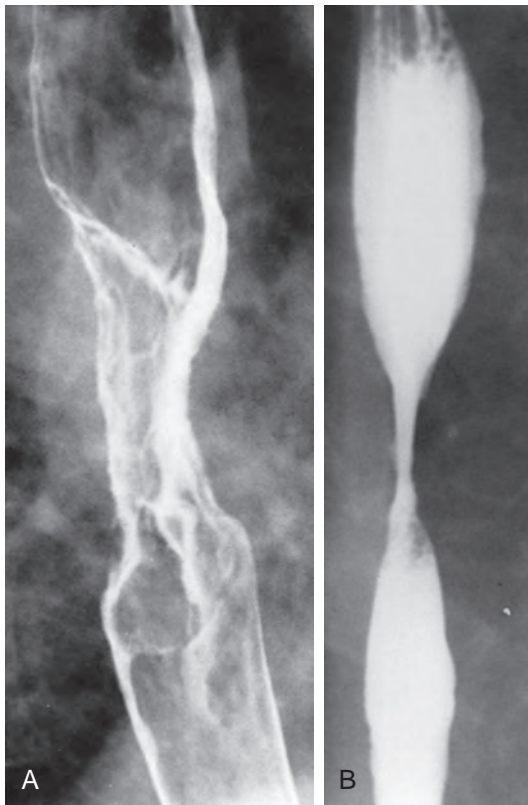


Figure 23-8 Other forms of infiltrative esophageal carcinoma.

A. This lesion has an annular appearance, with shelflike proximal and distal margins. **B.** In another patient, the cancer is manifested by a relatively smooth, tapered area of narrowing that could be mistaken for a benign stricture. (From Levine MS: *Radiology of the Esophagus*. Philadelphia, WB Saunders, 1989.)

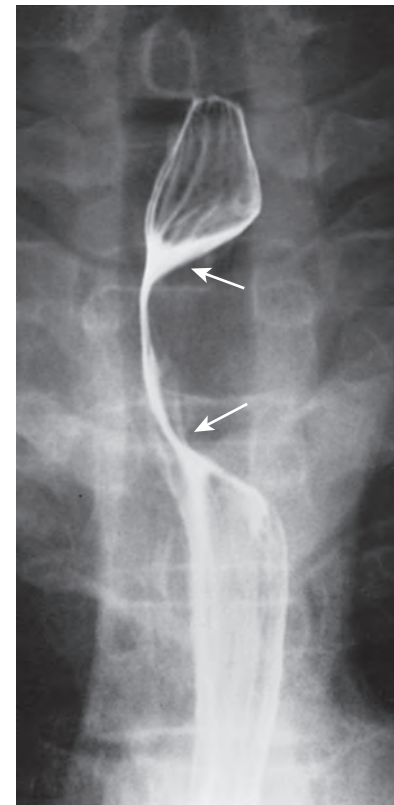


Figure 23-9 Advanced esophageal carcinoma with mediastinal adenopathy.

There is a smooth extrinsic area of mass effect on the left lateral wall of the upper thoracic esophagus (arrows) by mediastinal adenopathy from a distal esophageal cancer (not shown on this image). (From Levine MS: *Radiology of the Esophagus*. Philadelphia, WB Saunders, 1989.)

esophagus (Fig. 23-13). When an esophageal-airway fistula is suspected, the esophagogram should be performed with barium rather than water-soluble contrast agents because the latter agents are hyperosmolar and may draw fluid into the lungs if a fistula is present, causing severe pulmonary edema.

Esophageal-airway fistulas are usually recognized on esophagography by the presence of barium in the bronchi or distal trachea. In many cases, the origin of the fistulous track is identified within an obvious infiltrating carcinoma (see Fig. 23-12B). Once barium has entered the trachea or left main bronchus, however, it can be coughed up into the proximal trachea or larynx, so delayed overhead radiographs may erroneously suggest tracheobronchial aspiration. When an esophageal-airway fistula is suspected, the initial swallow should therefore be performed in a lateral projection with a video recording of the hypopharynx to differentiate a fistula from aspiration.

Rarely, patients with advanced esophageal cancer may develop esophagopericardial fistulas, manifested by pneumopericardium on chest radiographs or computed tomography (CT) scans.⁵⁴ In such cases, esophagography with water-soluble contrast agents may demonstrate esophageal perforation at the site of the tumor, with contrast material entering the pericardial sac.

Associated Conditions

Achalasia. Esophageal carcinomas arising in patients with achalasia usually appear on barium studies as polypoid masses

in the middle or, less commonly, distal third of the esophagus (Fig. 23-14).^{17,21} Because these lesions often develop in a massively dilated esophagus, they can reach an enormous size, producing bulky intraluminal masses that have a fungating or cauliflower appearance.²¹ Nevertheless, the lesions may be obscured by retained fluid and debris in a dilated, partially obstructed esophagus.¹⁹⁻²¹ Careful esophageal lavage with a soft rubber catheter may therefore be required to cleanse the esophagus before performing the radiologic examination.

Lye Strictures. The development of a lye-induced cancer may be manifested on barium studies by increasing stenosis, mass effect, nodularity, and/or ulceration within a preexisting lye stricture (Fig. 23-15). The underlying strictures are often located in the region of the tracheal bifurcation, so lye cancers may be complicated by the development of tracheoesophageal or esophagobronchial fistulas (see Fig. 23-15B).²⁵ Any change in the appearance of a chronic lye stricture should therefore be evaluated by endoscopy with multiple biopsy specimens and brushings to rule out a superimposed carcinoma.

Tylosis. When patients with tylosis develop esophageal symptoms, they usually have advanced esophageal carcinomas, manifested on barium studies by annular, infiltrating, or plaque-like lesions.⁴⁰ Occasionally, however, asymptomatic patients with tylosis may have discrete hyperkeratotic plaques containing one or more foci of dysplasia or intramucosal carcinoma. These

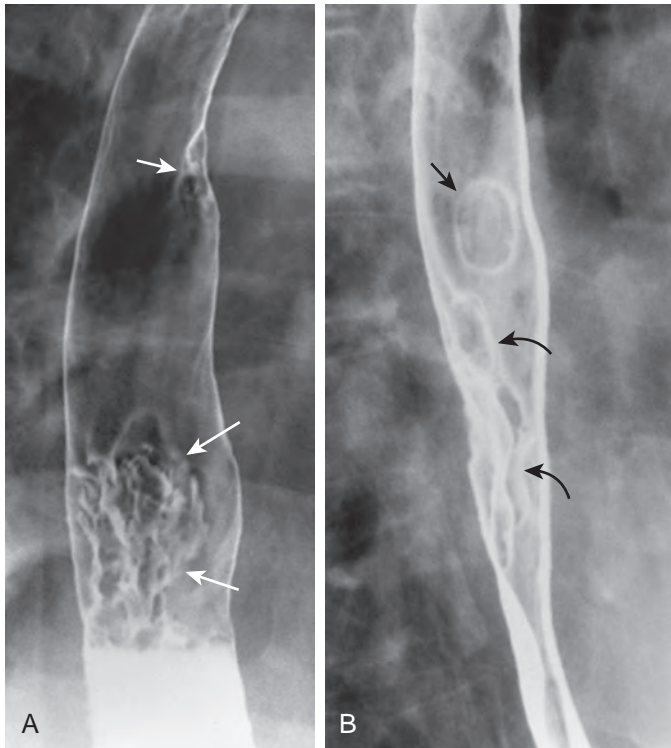


Figure 23-10 Two examples of advanced esophageal carcinoma with discrete lymphatic metastases. **A.** This patient has a large ulcerated cancer (*large arrows*) in the midesophagus with a discrete metastatic implant (*small arrow*) separated from the main lesion by normal intervening mucosa. The implant appears as a plaque-like lesion. **B.** In another patient, a polypoid carcinoma (*curved arrows*) is present in the midesophagus with a discrete submucosal implant (*straight arrow*) more proximally.

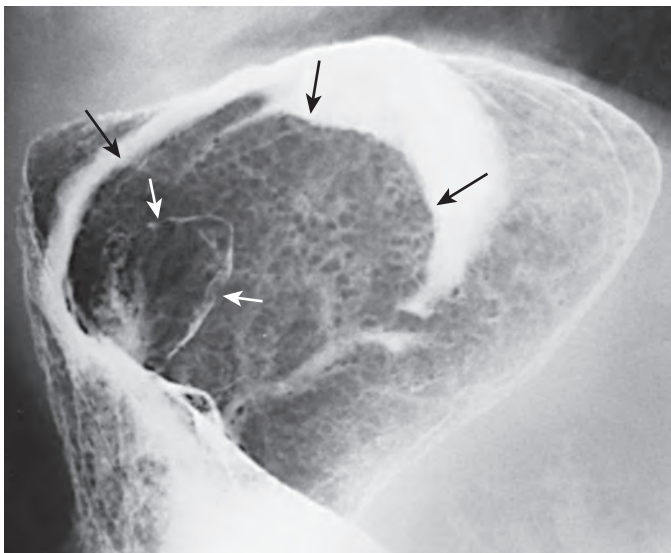


Figure 23-11 Advanced esophageal carcinoma with a squamous cell metastasis to the stomach. There is a giant submucosal mass (*black arrows*) in the gastric fundus, containing a triangular area of central ulceration (*white arrows*). A malignant gastrointestinal stromal tumor could produce similar findings. (From Glick SN, Teplick SK, Levine MS: *Squamous cell metastases to the gastric cardia*. *Gastrointest Radiol* 10:339–344, 1985.)

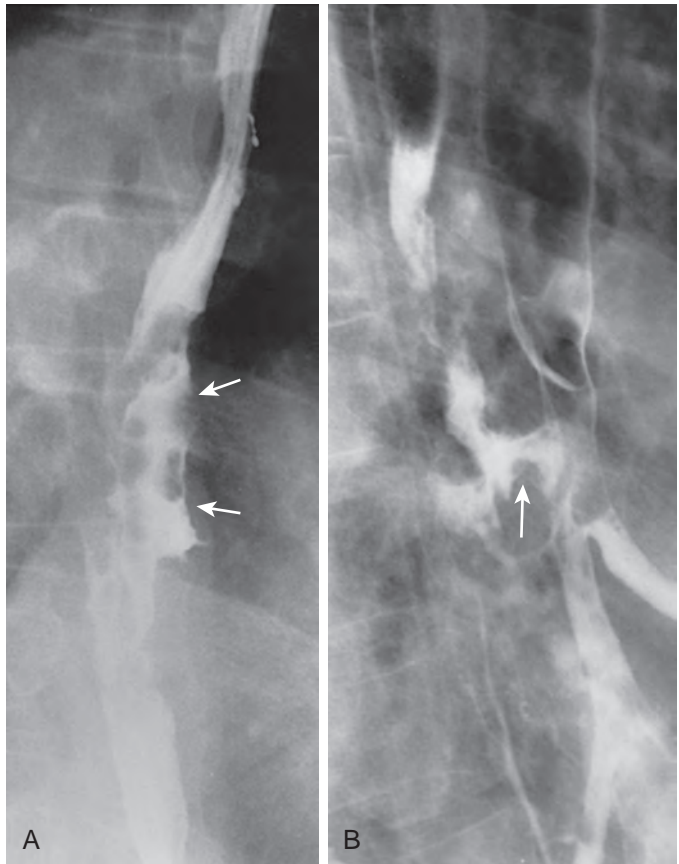


Figure 23-12 Advanced esophageal carcinoma with a tracheoesophageal fistula. **A.** An ulcerative esophageal carcinoma (*arrows*) is present in the midesophagus. **B.** A second esophagogram 4 months after radiation therapy shows partial regression of the tumor with the development of a tracheoesophageal fistula (*arrow*). (From Levine MS: *Radiology of the Esophagus*. Philadelphia, WB Saunders, 1989.)

lesions may appear on esophagograms as large, well-defined plaques, with normal intervening mucosa (Fig. 23-16).⁴⁰

Adenocarcinoma

Primary esophageal adenocarcinomas are almost always found to arise in the setting of Barrett's esophagus. In the past, such tumors were thought to be rare lesions, accounting for less than 5% of all esophageal cancers.⁹⁴⁻⁹⁶ However, many of these adenocarcinomas involving the gastroesophageal junction or gastric fundus were incorrectly classified as primary gastric carcinomas secondarily invading the lower end of the esophagus.^{94,95} Apart from difficulties in tumor classification, the incidence of esophageal adenocarcinoma in white men has increased by 300% to 500% in the past 30 years,^{41,97,98} and this tumor is the fastest growing cause of cancer mortality.⁹⁹ Currently, adenocarcinomas are thought to constitute at least 50% of all esophageal cancers.⁴¹ Nevertheless, many questions remain about the risk of malignant degeneration in Barrett's esophagus and the long-term management of patients with this condition.

EPIDEMIOLOGY AND PATHOGENESIS

Considerable attention has been focused on the relationship between esophageal adenocarcinoma and the columnar

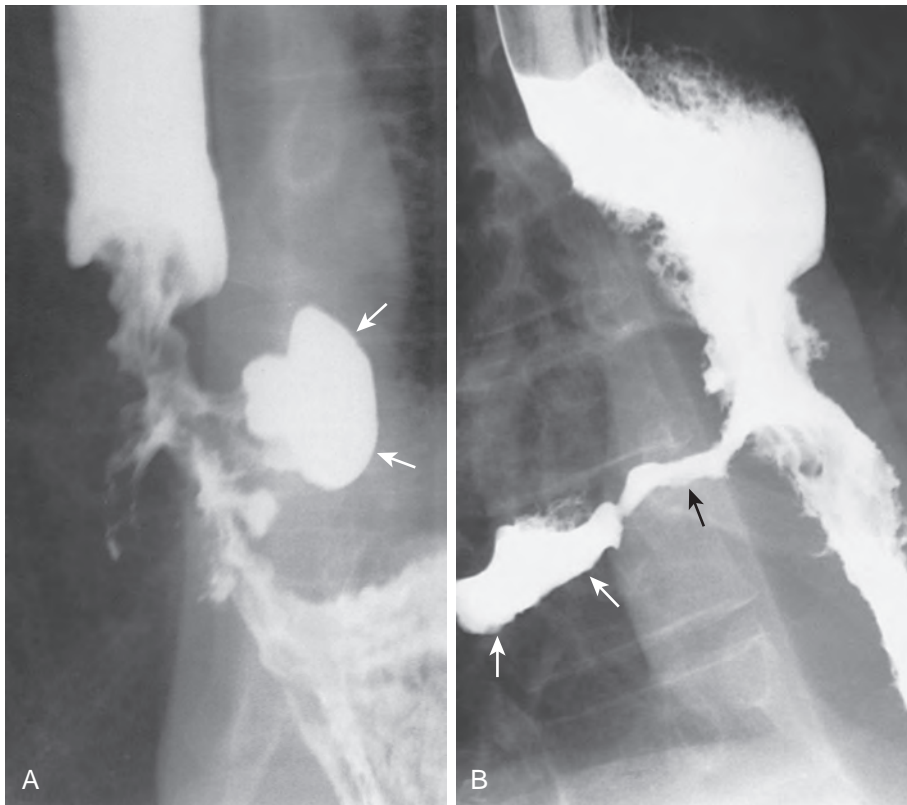


Figure 23-13 Two examples of advanced esophageal carcinoma with fistulas to the mediastinum and lung. In both cases, there is direct communication between the cancer and necrotic, tumor-containing cavities (arrows) in the mediastinum (**A**) and right lung (**B**). (From Levine MS: *Radiology of the Esophagus*. Philadelphia, WB Saunders, 1989.)

epithelium-lined esophagus, or Barrett's esophagus. In various studies, 90% to 100% of all primary esophageal adenocarcinomas have been found to arise on a background of Barrett's mucosa.¹⁰⁰⁻¹⁰² Thus, adenocarcinoma of the esophagus is not only more common than was previously recognized, but the vast majority of these tumors appear to result from malignant degeneration in Barrett's esophagus.

Barrett's Esophagus

Barrett's esophagus is a well-recognized condition in which there is progressive columnar metaplasia of the distal esophagus caused by long-standing gastroesophageal reflux and reflux esophagitis.¹⁰²⁻¹⁰⁶ In various studies, the prevalence of Barrett's esophagus in patients with reflux esophagitis has ranged from 5% to 15%, with an overall prevalence of about 10%.¹⁰⁷⁻¹⁰⁹ In a widely quoted study, Barrett's esophagus was found to occur in 4% of patients undergoing upper gastrointestinal endoscopy and in 9% of men older than 50 years.¹¹⁰ The clinical and radiologic aspects of Barrett's esophagus are presented in Chapter 19.

Various types of columnar epithelium have been described in Barrett's esophagus, including a junctional-type epithelium, a gastric fundus-type epithelium, and an intestinal-type or specialized columnar epithelium.^{111,112} It is believed, however, that intestinal metaplasia is the major prerequisite for a pathologic diagnosis of Barrett's esophagus.¹¹³ This intestinal metaplasia is characterized histologically by goblet cells with acidic mucin and, in some cases, enterocyte differentiation with brush border formation. The revised definition of Barrett's esophagus is based on an emerging consensus that intestinal metaplasia represents the type of epithelium that usually predisposes these patients to the development of esophageal adenocarcinoma.^{113,114}

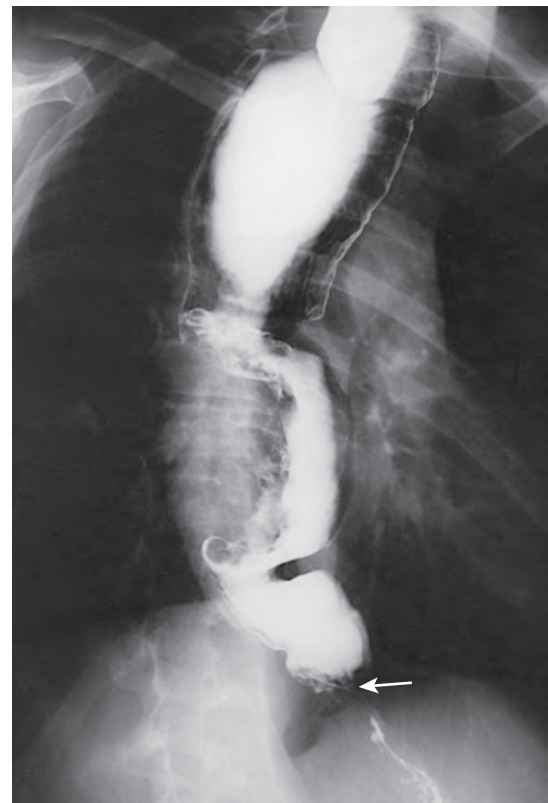


Figure 23-14 Advanced esophageal carcinoma associated with achalasia. There is a large, fungating mass in the lower esophagus in a patient with long-standing achalasia. Note beaklike narrowing (arrow) of the distal esophagus caused by incomplete opening of the lower esophageal sphincter. (From Levine MS: *Radiology of the Esophagus*. Philadelphia, WB Saunders, 1989.)

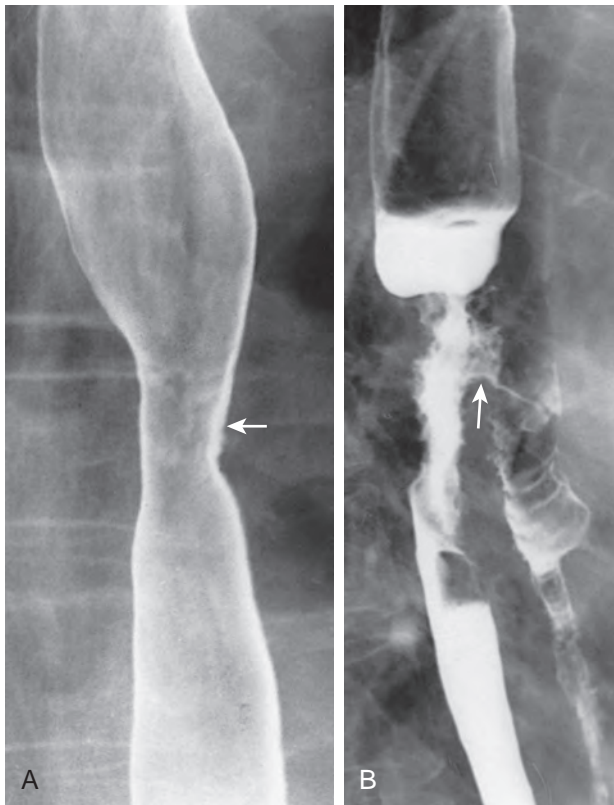


Figure 23-15 Advanced esophageal carcinoma arising in a lye stricture. **A.** Initial double-contrast esophagogram shows a focal stricture (arrow) in the midesophagus caused by previous lye ingestion. Note superficial ulceration and nodularity of the mucosa in the region of the stricture. These findings were worrisome for developing tumor, but the patient refused endoscopy. **B.** Another study 2 years later shows an advanced, infiltrating carcinoma at the site of the previous stricture, with an esophagobronchial fistula (arrow). (From Levine MS: *Radiology of the Esophagus*. Philadelphia, WB Saunders, 1989.)

Investigators have also developed histopathologic criteria for Barrett's esophagus in which patients are classified as having long-segment disease (i.e., extending more than 3 cm from the gastroesophageal junction) or short-segment disease (i.e., extending 3 cm or less from the gastroesophageal junction) based on the vertical extent of columnar metaplasia in the esophagus.¹¹⁵ Short-segment Barrett's esophagus is even more common than long-segment Barrett's esophagus, with a reported prevalence of 10% to 15% at endoscopy.¹¹⁴

Risk of Adenocarcinoma. In various series, the prevalence of adenocarcinoma in patients with Barrett's esophagus has ranged from 2% to 46%, with an overall prevalence of about 10%.^{*}

It should be recognized that prevalence data exaggerate the risk of cancer because many patients with Barrett's esophagus remain asymptomatic until the development of a superimposed carcinoma. Nevertheless, it has been estimated that patients with Barrett's esophagus have at least a 20-fold increased risk of developing esophageal adenocarcinoma.^{118,119} Current surveillance guidelines for Barrett's esophagus assume that the absolute annual risk of developing cancer is about 0.5%, but

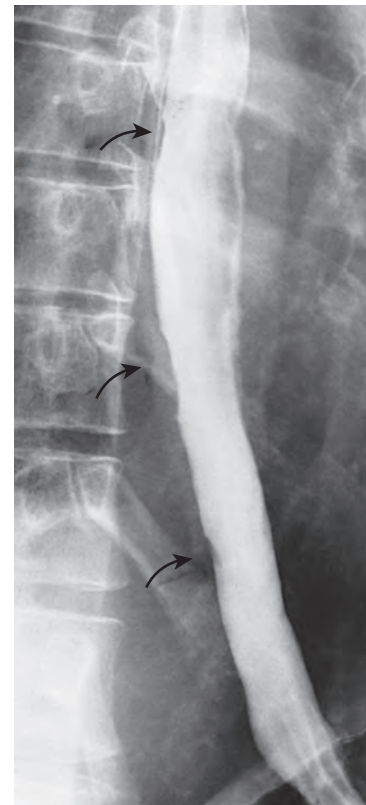


Figure 23-16 Tylosis with hyperkeratotic plaques. There are multiple discrete plaques (arrows) in the mid and distal esophagus. These lesions were found to be hyperkeratotic plaques in a patient with long-standing tylosis. (From Munyer TP, Margulis AR: Tylosis. *AJR* 136:1026–1027, 1981.)

one large study found that the actual risk was only 0.12%, calling into question the rationale for ongoing surveillance of asymptomatic patients who have Barrett's esophagus without associated dysplasia (see later, "Surveillance and Management of Barrett's Esophagus").¹²⁰

Dysplasia-Carcinoma Sequence. Pathologic data strongly suggest that esophageal adenocarcinoma in Barrett's esophagus evolves through a sequence of progressively severe epithelial dysplasia in areas of preexisting columnar metaplasia, usually intestinal metaplasia.^{121–124} These dysplastic changes can be detected on endoscopic biopsy specimens obtained from Barrett's esophagus. Dysplasia may occur in all types of Barrett's mucosa but is most likely to occur in areas of intestinal metaplasia.^{113,114} Dysplastic changes are classified as low grade or high grade on the basis of the histologic findings; high-grade dysplasia may subsequently progress to invasive adenocarcinoma. In various studies, the prevalence of high-grade dysplasia in patients with esophageal adenocarcinoma has ranged from 68% to 100%.^{105,116} Studies have also shown progression to cancer within 7 years in 22% of patients with high-grade dysplasia in Barrett's esophagus.²

When Barrett's esophagus is stratified into short-segment and long-segment disease, it has been found that patients with short-segment disease are more likely to develop dysplasia than the general population but are less likely to develop dysplasia than patients with long-segment disease.^{125,126} Esophageal adenocarcinoma has also been found to develop in patients with

*See references 101, 105, 107, 108, 116, and 117.

short-segment disease.^{125,127,128} Additional studies are needed, however, to further elucidate the cancer risk in these patients.

Surveillance and Management of Barrett's Esophagus.

Because of the increased cancer risk, many investigators advocate endoscopic surveillance of patients with known Barrett's esophagus to detect dysplastic changes, so these individuals can be treated before the development of overt carcinoma.^{2,100,103-105,121-123} Endoscopic biopsy specimens are generally recommended from all four quadrants of the lower esophagus at 1- to 2-cm intervals, starting at the gastroesophageal junction.² In patients with nondysplastic Barrett's esophagus, the American Gastroenterological Association recommends surveillance endoscopy at 2- to 5-year intervals, depending on the patient's age and health.¹²⁴ In patients with low-grade dysplasia, endoscopy is recommended at 1- to 2-year intervals because of an increased but uncertain risk of developing cancer.² If high-grade dysplasia or early cancer is detected, treatment should be undertaken to prevent the development of cancer or treat these cancers at a curable stage. In the past, a surgical esophagogastrectomy was the definitive treatment for high-grade dysplasia or early cancers in Barrett's esophagus. Currently, however, various forms of endoscopic therapy are recommended as less invasive alternatives associated with lower morbidity and mortality rates than surgery.⁹⁹ Radiofrequency ablation, photodynamic therapy, and endoscopic mucosal resection have all been shown to be effective and safe forms of therapy for treatment of high-grade dysplasia or early-stage cancer in Barrett's esophagus, with a high rate of dysplasia and tumor eradication and a reduced risk of disease progression in these patients.¹²⁹⁻¹³¹

Despite these recommendations, there is continued controversy about whether endoscopic surveillance of patients with Barrett's esophagus is a cost-effective approach for detecting esophageal adenocarcinoma because of the low incidence of neoplasia and the high cost of endoscopy.¹¹⁸ So far, endoscopic surveillance of patients with Barrett's esophagus has not been associated with a substantially decreased risk of death from esophageal adenocarcinoma.¹³² Thus, many questions remain about the role of endoscopic surveillance and its ultimate value in patients with Barrett's esophagus.

Attention has also been focused on the role of DNA flow cytometry and cellular genetics analysis to determine which patients with Barrett's esophagus are at greatest risk for the development of adenocarcinoma. Some investigators have shown that a subset of patients with Barrett's esophagus have genomic instability, with aneuploid populations of cells, predisposing to neoplastic transformation.¹³³ In various studies, the findings on DNA flow cytometry have correlated directly with the presence of high-grade dysplasia or invasive carcinoma on endoscopic biopsy specimens.^{133,134} Thus, flow cytometry represents another potential diagnostic tool for surveillance of Barrett's esophagus.

Much less frequently, the development of cancer in Barrett's esophagus may result from an adenoma-carcinoma sequence similar to that found in the colon. Benign adenomatous polyps have occasionally been documented in Barrett's mucosa, with or without focal areas of invasive adenocarcinoma.^{101,135,136} Because malignant degeneration of these adenomas represents another potential pathway for the development of adenocarcinoma, endoscopic resection of adenomatous polyps in Barrett's esophagus may decrease the risk of cancer.

Relationship Among Scleroderma, Barrett's Esophagus, and Adenocarcinoma.

Scleroderma, a connective tissue disease characterized by smooth muscle atrophy and fibrosis, affects the esophagus in about 75% of patients. Esophageal involvement is usually characterized by a patulous, incompetent lower esophageal sphincter and absent esophageal peristalsis, with poor clearance of refluxed peptic acid from the esophagus once reflux has occurred. As a result, patients with scleroderma often have reflux esophagitis. Because of the severity of esophagitis, these individuals have an even greater risk of developing Barrett's esophagus than other patients with reflux disease. In one study, 37% of those with scleroderma who underwent endoscopy for reflux symptoms had biopsy-proven Barrett's esophagus.¹³⁷ Because Barrett's esophagus predisposes to esophageal adenocarcinoma, patients with scleroderma also appear to have an increased risk of developing esophageal cancer.^{137,138} Thus, scleroderma should indirectly be considered to be a premalignant condition in the esophagus.

PATHOLOGY

Gross Features

Adenocarcinomas arising in Barrett's mucosa appear grossly as infiltrating, polypoid, ulcerative, or varicoid lesions. These tumors tend to be located in the distal or, less commonly, middle third of the esophagus.^{101,102,139} Unlike squamous cell carcinomas, adenocarcinomas of the distal esophagus frequently spread subdiaphragmatically to involve the gastric cardia or fundus.^{101,102,112,139} Studies have shown that adenocarcinomas arising in Barrett's esophagus account for up to 50% of all adenocarcinomas involving the gastroesophageal junction.^{101,102,139} The remaining lesions are primary carcinomas of the gastric cardia or fundus invading the esophagus. Whether they arise in the esophagus or in the stomach, these tumors have similar morphologic features in terms of pattern of growth, degree of differentiation, and depth of invasion.¹⁴⁰ Nevertheless, it is important to ascertain whether the cancer has arisen in Barrett's esophagus because it may be necessary to resect not only the primary tumor but all residual Barrett's mucosa in these patients. Detection of malignant tumor at the cardia should therefore lead to a careful search for Barrett's epithelium in the esophagus.

Histologic Features

At the time of diagnosis, most adenocarcinomas in Barrett's esophagus are advanced, unresectable tumors. Occasionally, however, early, potentially curable lesions may be detected by radiologic or endoscopic surveillance of patients with known Barrett's esophagus. Alternatively, early lesions may be detected fortuitously in patients who undergo barium studies or endoscopy because of their underlying reflux disease.^{63,123,141}

ROUTES OF SPREAD

Like squamous cell carcinomas, esophageal adenocarcinomas invade local, regional, or distant structures via direct extension, lymphatic spread, or hematogenous metastases. Unlike squamous cell carcinomas, however, adenocarcinomas in Barrett's esophagus have a marked tendency to invade the proximal stomach; involvement of the gastric cardia or fundus occurs in 35% to 50% of cases.^{101,102,139}

CLINICAL ASPECTS

Barrett's esophagus is predominantly a disease of older white men, with a male-to-female ratio of 3:1 and a mean age of about 65 years at the time of diagnosis. Nevertheless, there has been a significant increase in the incidence of these tumors in younger patients between 45 and 65 years of age.²

Patients with esophageal adenocarcinoma usually present with recent onset of dysphagia and weight loss.^{104,105,116,120} Other findings include upper GI bleeding, odynophagia, and chest pain.¹¹⁶ Because of their underlying reflux disease, some patients have long-standing reflux symptoms before the development of cancer.¹⁰⁴ By the time these individuals develop dysphagia, however, they almost always have advanced, unresectable tumors. Thus, patients with esophageal adenocarcinomas have a poor prognosis, with overall 5-year survival rates less than 20%.^{2,142}

Most patients with early adenocarcinomas in Barrett's esophagus are asymptomatic, but some may present with melena, guaiac-positive stool, or iron deficiency anemia as a result of low-grade bleeding from the friable surface of the tumor.⁶³ Others may seek medical attention because of their underlying reflux disease, so early cancers may be detected as fortuitous findings in patients presenting with reflux symptoms.⁶³

RADIOGRAPHIC FINDINGS

Early Adenocarcinoma

Like squamous cell carcinomas, early adenocarcinomas in Barrett's esophagus may appear on double-contrast esophagograms as plaquelike lesions or as flat sessile polyps.⁶³ Sessile or pedunculated polyps in the distal esophagus may also represent adenomatous polyps in Barrett's mucosa with or without foci of invasive carcinoma (Fig. 23-17).^{101,136} In patients with peptic strictures, the earliest manifestation of a developing adenocarcinoma may be a localized area of flattening, stiffening, or irregularity in one wall of the stricture (Fig. 23-18).^{63,101,102} Other patients may have superficial spreading carcinomas, manifested by confluent nodularity or granularity of the mucosa without a discrete lesion.⁶³ Although early adenocarcinomas are typically small lesions, some patients may have relatively larger polypoid masses that are indistinguishable radiographically from advanced cancers.⁶³

Advanced Adenocarcinoma

Advanced esophageal adenocarcinomas usually appear on barium studies as infiltrating lesions with irregular luminal narrowing, nodularity or ulceration of the mucosa, and abrupt, asymmetric margins (Fig. 23-19A).^{101,102,139} In general, these lesions cannot be distinguished radiographically from squamous cell carcinomas. In one study, however, esophageal adenocarcinomas were found to involve a longer vertical segment of the esophagus than squamous cell carcinomas.¹⁰² Adenocarcinomas are also more likely to involve the distal esophagus,¹⁰¹ so the presence of a long infiltrating lesion in the distal esophagus should suggest the possibility of adenocarcinoma.

Less frequently, these tumors may appear as polypoid intraluminal masses (Fig. 23-19B) or as primary ulcerative lesions, with a meniscoid ulcer surrounded by a thick rind of tumor (Fig. 23-19C).^{101,102} Occasionally, these lesions may have a varicoid appearance caused by submucosal spread of tumor

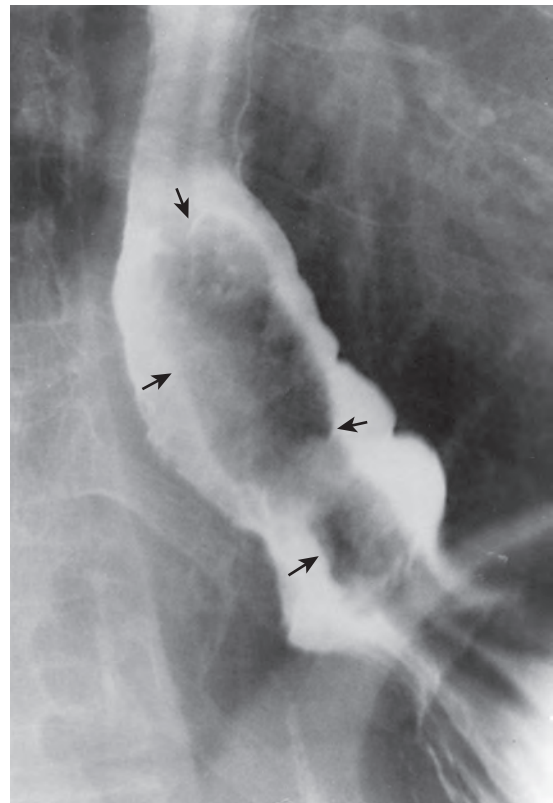


Figure 23-17 Early adenocarcinoma in Barrett's esophagus.

There is a large pedunculated polyp (arrows) in the distal esophagus. Pathologic examination of the resected specimen revealed an adenomatous polyp with a solitary focus of adenocarcinoma. (From Levine MS, Caroline D, Thompson JJ, et al: *Adenocarcinoma of the esophagus: Relationship to Barrett mucosa*. Radiology 150:305–309, 1984.)

(Fig. 23-19D).^{101,102,143} Similar findings may be present in patients with squamous cell carcinomas. However, many patients with adenocarcinomas arising in Barrett's esophagus have associated hiatal hernias, gastroesophageal reflux, reflux esophagitis, or peptic strictures.^{101,102} The possibility of adenocarcinoma should therefore be considered in any patient with esophageal cancer who has other clinical or radiologic signs of reflux disease.

When adenocarcinomas are located in the distal esophagus, they have a marked tendency to invade the gastric cardia or fundus.^{101,102,139} Gastric involvement may be manifested on barium studies by a polypoid or ulcerated mass in the fundus. In other patients, these tumors may cause distortion or obliteration of the normal anatomic landmarks at the cardia and irregular areas of ulceration without a discrete mass (Fig. 23-20).¹⁰¹ The findings may be quite subtle, so optimal double-contrast views of the gastric cardia and fundus are required to demonstrate these lesions. In general, esophageal adenocarcinomas invading the gastric cardia or fundus are difficult to differentiate radiographically from carcinomas of the cardia or fundus invading the distal esophagus. However, esophageal adenocarcinomas usually have a greater degree of esophageal involvement in relation to that of the stomach, whereas cardiac carcinomas have a greater degree of fundal involvement.



Figure 23-18 Early adenocarcinoma in Barrett's esophagus.

There is a relatively long peptic stricture in the distal esophagus with slight flattening and stiffening of one wall of the stricture (arrows). Surgery revealed an intramucosal adenocarcinoma arising in Barrett's esophagus. (From Levine MS, Caroline D, Thompson JJ, et al: Adenocarcinoma of the esophagus: Relationship to Barrett mucosa. *Radiology* 150:305–309, 1984.)

Differential Diagnosis

EARLY ESOPHAGEAL CANCER

Early squamous cell carcinomas and adenocarcinomas usually appear on double-contrast esophagograms as plaquelike lesions or as flat sessile polyps. However, squamous papillomas may also appear as small, sessile, slightly lobulated polyps that are indistinguishable from early esophageal cancers (see Chapter 22).¹⁴⁴ *Candida* esophagitis and glycogenic acanthosis usually produce multiple plaquelike defects in the esophagus, but a single large plaque can be mistaken for a plaquelike carcinoma. Occasionally, inflammatory exudates or pseudomembranes associated with severe reflux esophagitis may also appear radiographically as plaquelike defects indistinguishable from early adenocarcinomas (Fig. 23-21).¹⁴⁵ However, pseudomembrane formation may be suggested by the presence of other discrete satellite lesions or by a change in the size and appearance of the lesions at fluoroscopy. When the radiographic findings are equivocal, endoscopy and biopsy are required for a definitive diagnosis.

Because superficial spreading carcinomas are manifested on double-contrast esophagograms by tiny nodules or plaques, a localized area of *Candida* esophagitis could conceivably produce a similar appearance (Fig. 23-22).¹⁴⁶ However, the plaquelike

defects of candidiasis tend to be discrete lesions with well-defined borders and normal intervening mucosa, whereas the nodules or plaques of superficial spreading carcinoma tend to coalesce, producing a continuous area of disease. Superficial spreading carcinomas that are more extensive should be differentiated from other benign conditions causing a diffusely nodular mucosa, such as *Candida* esophagitis, glycogenic acanthosis or, rarely, leukoplakia, acanthosis nigricans, and squamous papillomatosis.^{146–150} However, the latter conditions also tend to produce discrete lesions rather than a continuous area of disease. Finally, superficial spreading carcinoma may produce a reticulonodular appearance that closely resembles the reticular pattern of Barrett's mucosa.¹⁵¹ However, this last finding is usually associated with a midesophageal stricture, with the reticular pattern extending distally a variable distance from the stricture (see Chapter 19).

ADVANCED CARCINOMA

Infiltrating esophageal carcinomas usually have an obvious malignant appearance. Occasionally, however, these lesions may resemble benign strictures with concentric narrowing and relatively smooth, tapered margins (see Fig. 23-8B).^{84,152} In such cases, an abrupt change in caliber and focal irregularity, nodularity, or stiffening of one or both walls of the stricture should raise the possibility of malignant tumor, particularly an adenocarcinoma in Barrett's esophagus.^{101,102} Rarely, esophageal cancer may cause beaklike narrowing of the distal esophagus, mimicking the appearance of primary achalasia.¹⁰² However, asymmetry, nodularity, or ulceration of the narrowed segment should suggest a malignant lesion.

When infiltrating cancers are detected in the esophagus, it may be difficult or impossible to differentiate squamous cell carcinomas from adenocarcinomas arising in Barrett's mucosa. However, adenocarcinomas tend to be located more distally in the esophagus and often invade the gastric cardia or fundus, whereas squamous cell carcinomas rarely extend subdiaphragmatically to involve the stomach.^{101,102,139} Other clinical or radiographic signs of reflux esophagitis should also favor adenocarcinoma. Nevertheless, endoscopy and biopsy are required for a definitive diagnosis.

Although squamous cell carcinomas and adenocarcinomas sometimes appear as polypoid masses in the esophagus, the presence of a bulky intraluminal mass (especially one that expands the esophagus without causing obstruction) should suggest the possibility of other rare malignant tumors such as spindle cell carcinoma and primary malignant melanoma of the esophagus (see Chapter 24).^{153,154} Rarely, benign tumors such as fibrovascular polyps may be manifested by polypoid lesions, but these tumors tend to appear as smooth, expansile, sausage-shaped masses in the upper thoracic esophagus (see Chapter 22).¹⁵⁵ Finally, impacted food in the esophagus may be confused radiographically with polypoid carcinomas. However, the presence of a stricture directly below the polypoid defect should suggest the possibility of a food impaction. Impacted debris may also obstruct the esophagus, whereas polypoid carcinomas rarely cause esophageal obstruction. Obviously, a history of sudden onset of dysphagia while eating meat or some other bulky food product should suggest this complication.

Primary ulcerative carcinomas usually appear as distinctive meniscoid ulcers surrounded by a thick, irregular rim of malignant tissue. However, the adjacent tumor mass is sometimes

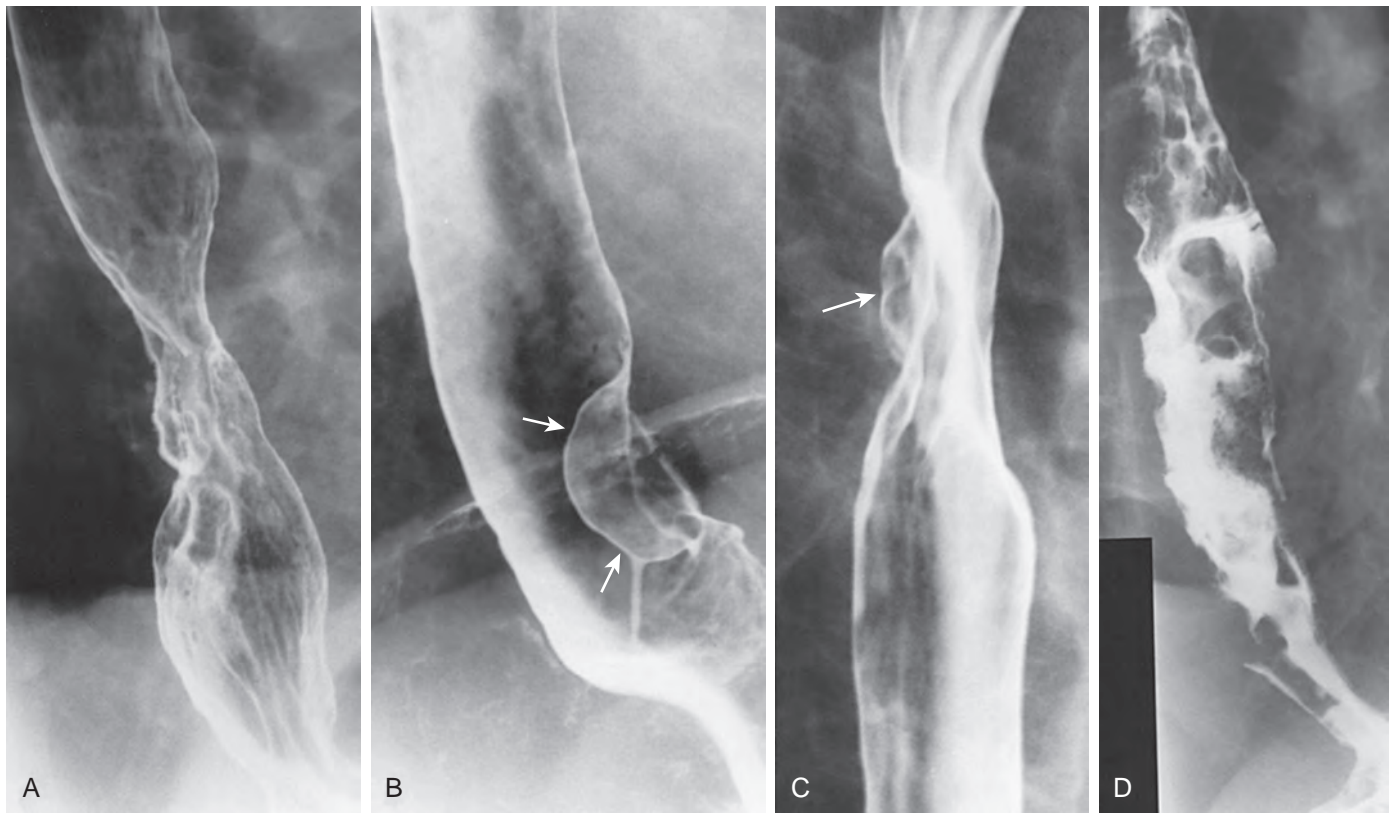


Figure 23-19 Advanced adenocarcinoma in Barrett's esophagus: patterns of tumor. **A.** Infiltrating lesion. **B.** Polypoid lesion (arrows). **C.** Ulcerative lesion (arrow). **D.** Varicoid lesion. (**B** from Levine MS: *Radiology of the Esophagus*. Philadelphia, WB Saunders, 1989; **C, D** from Levine MS, Caroline D, Thompson JJ, et al: *Adenocarcinoma of the esophagus: Relationship to Barrett mucosa*. *Radiology* 150:305–309, 1984.)

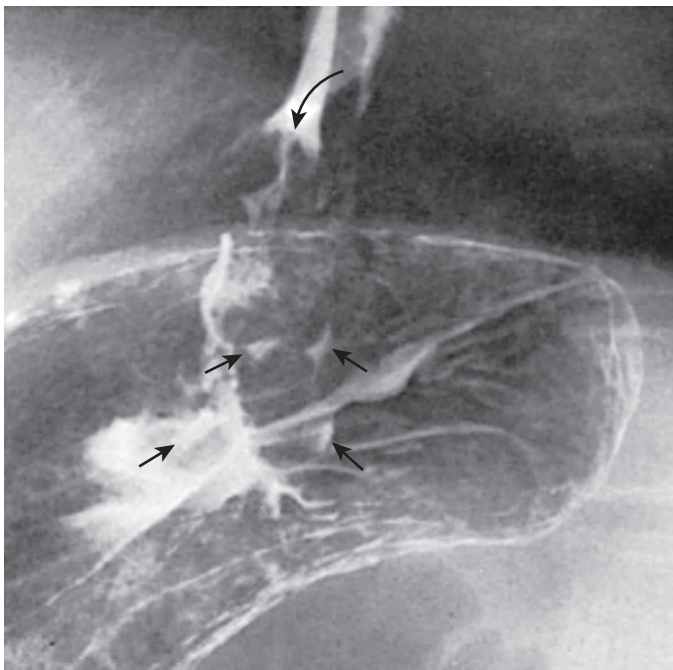


Figure 23-20 Adenocarcinoma in Barrett's esophagus invading the stomach. Double-contrast view of the gastric fundus shows obliteration of the normal anatomic landmarks at the cardia with irregular areas of ulceration (straight arrows). Also note tumor involving the distal esophagus (curved arrow). At surgery, this patient had a primary adenocarcinoma arising in Barrett's esophagus with associated gastric involvement. (From Levine MS, Caroline D, Thompson JJ, et al: *Adenocarcinoma of the esophagus: Relationship to Barrett mucosa*. *Radiology* 150:305–309, 1984.)

subtle, so these lesions can occasionally be mistaken for benign ulcers. Conversely, some patients with esophagitis may have large, flat ulcers with a surrounding mound of edema, erroneously suggesting an ulcerated carcinoma. Ulcers associated with potassium chloride or quinidine ingestion or nasogastric intubation can have a particularly ominous appearance (see Chapter 21). Endoscopy and biopsy may therefore be required to exclude a malignant lesion.

Although varicoid carcinomas can mimic the appearance of esophageal varices on a single radiograph, these entities can usually be differentiated at fluoroscopy.^{88–90,143} True varices tend to change in size and shape with peristalsis, respiration, and Valsalva maneuvers, whereas varicoid tumors have a rigid, fixed configuration, with an abrupt demarcation between the involved segment and adjacent normal mucosa. Most varicoid carcinomas are squamous cell carcinomas or adenocarcinomas, but other malignant tumors such as lymphoma may occasionally produce similar findings.¹⁵⁶

Rarely, localized submucosal extension of a squamous cell carcinoma or adenocarcinoma may produce a smooth submucosal mass, mimicking the appearance of a benign leiomyoma (Fig. 23-23).¹⁵⁷ However, a malignant tumor should be suspected if there is lobulation or ulceration of the lesion.

Staging

Most authors now recommend CT as the initial imaging test for staging esophageal cancer,^{158,159} and the Society of Thoracic Surgeons has issued guidelines recommending combined CT of the chest and abdomen for optimal staging.¹⁶⁰ Although CT has



Figure 23-21 Reflux esophagitis with a large pseudomembrane, mimicking a plaque-like adenocarcinoma. There is a longitudinally oriented, plaque-like lesion (arrows) on the anterolateral wall of the distal esophagus. The radiographic findings are worrisome for a plaque-like carcinoma, but endoscopy revealed pseudomembranes caused by severe reflux esophagitis without evidence of tumor. (From Levine MS, Cajade AG, Herlinger H, et al: Pseudomembranes in reflux esophagitis. *Radiology* 159:43–45, 1986.)



Figure 23-22 Localized area of *Candida* esophagitis. This appearance could be mistaken for a superficial spreading carcinoma. However, note how the plaques have discrete borders and are separated by short segments of normal mucosa. (From Levine MS: *Radiology of the Esophagus*. Philadelphia, WB Saunders, 1989.)

been the mainstay for staging esophageal carcinoma, the increasing use of endoscopic ultrasound (EUS) and positron emission tomography (PET) has altered the staging algorithm for patients with newly diagnosed esophageal cancer. Currently, a combination of CT, EUS, and PET is generally advocated to determine which patients should be treated with surgery versus chemotherapy, combination radiation and chemotherapy, or surgery with neoadjuvant therapy. As with any cancer, staging criteria for esophageal carcinoma include detection of local invasion, regional lymph node involvement, and distant metastases. The different imaging modalities have different strengths and weaknesses for staging esophageal cancer.

COMPUTED TOMOGRAPHY

Technique

When CT is performed for esophageal cancer staging, the scan should include the upper abdomen and thorax because of the high incidence of upper abdominal lymph node metastases at the time of diagnosis.¹⁶¹ Distal esophageal cancers are more likely to be associated with upper abdominal lymph node involvement (Fig. 23-24); the frequency of abdominal lymph node metastases is about 30% for thoracic esophageal cancers above the level of the carina but increases to 70% for cancers below the carina (Fig. 23-25).¹⁶² Because the lymphatic drainage

of the esophagus is longitudinal rather than circumferential (as in the remainder of the GI tract), lymph node metastases tend to occur above and below the site of the primary tumor, often at a considerable distance from the primary lesion rather than immediately adjacent to the tumor (Fig. 23-26). Intravenous contrast material is administered whenever possible to increase detectability of hepatic metastases and better differentiate lymph nodes from vascular structures in the mediastinum. It is controversial whether staging CT should also include the neck to assess for cervical lymph node metastases.

Staging Criteria

The major CT criteria for staging esophageal cancer include detection of (1) local mediastinal invasion, (2) regional lymph node involvement, and (3) distant metastases. CT is better at detecting local invasion of the mediastinum by esophageal cancer than it is at detecting local invasion by other GI cancers, presumably because the mediastinum is a contained space. Thus, direct invasion can be predicted by mass effect criteria that are not useful elsewhere in the GI tract.

The CT criteria for local invasion include the following: (1) loss of the fat plane between the tumor and adjacent structures in the mediastinum; and (2) displacement or indentation of other mediastinal structures. CT findings of displacement of the trachea or bronchus or indentation of the posterior wall of the trachea or bronchus by the tumor mass have been found to be highly accurate for predicting tracheal or bronchial invasion

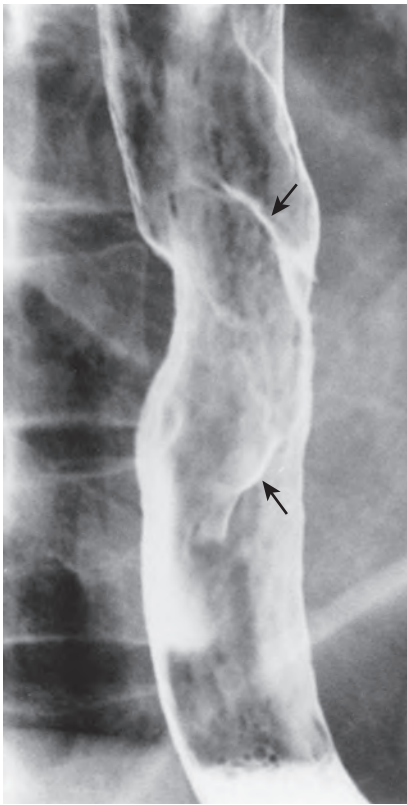


Figure 23-23 Esophageal carcinoma resembling a benign submucosal mass. However, this lesion (arrows) is larger and has a more irregular contour than most leiomyomas. (From Levine MS: *Radiology of the Esophagus*. Philadelphia, WB Saunders, 1989.)

(Figs. 23-27 and 23-28).¹⁶³⁻¹⁶⁵ The combined results from six studies with surgical confirmation revealed that CT had a sensitivity of 93%, specificity of 98%, and accuracy of 97% for predicting tracheobronchial invasion by esophageal cancer.¹⁶⁶

Mass effect criteria can also be used to predict pericardial invasion. If the tumor extends to the posterior surface of the heart with no intervening fat plane, and if the tumor bulges into the lumen of the left atrium on CT or magnetic resonance imaging (MRI), pericardial invasion can be predicted with a high level of confidence (Fig. 23-29). The combined results of those same six studies revealed that CT had a sensitivity, specificity, and accuracy of 94% for predicting pericardial invasion.¹⁶⁶

It is more difficult to predict aortic invasion because the esophagus normally contacts the aorta with no intervening fat plane (Fig. 23-30). Investigators have circumvented this problem by recognizing that the fat plane surrounding the aorta normally has a circumference of 360 degrees, similar to that of a compass. If an esophageal cancer obliterates the fat plane between the esophagus and aorta by more than 25% of the circumference (>90 degrees), tumor is considered to be invading the aorta (Fig. 23-31). If the tumor obliterates less than 45 degrees of the circumference, the aorta is not considered to be invaded by tumor (Fig. 23-32). Finally, if the tumor obliterates 45 to 90 degrees of the circumference, the CT findings are considered to be indeterminate for aortic invasion (Fig. 23-33). By using this criterion, the combined results of those same six

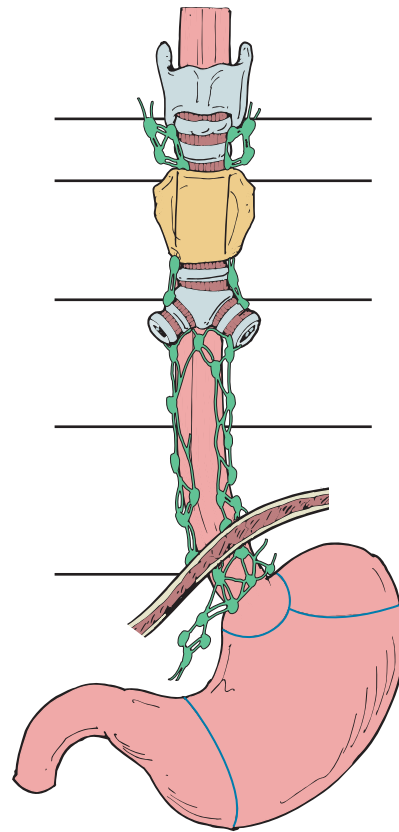


Figure 23-24 Longitudinal lymphatics of esophagus. Lymphatic channels surrounding the distal esophagus drain into paracardiac and lesser curvature lymph nodes in the upper abdomen, accounting for the high frequency of abdominal lymph node metastases in patients with distal esophageal cancers.

studies revealed that CT had a sensitivity of 88%, specificity of 96%, and accuracy of 94% for predicting aortic invasion.¹⁶⁶ CT is currently thought to have an overall accuracy of more than 90% in predicting local invasion and metastases from esophageal cancer.¹⁵⁹

Because lymph node enlargement is the CT criterion used to predict mediastinal or upper abdominal lymph node metastases, CT is limited by the fact that it cannot detect tumor in normal-sized lymph nodes. CT therefore fails to detect nodes that are involved by tumor in the absence of nodal enlargement. Enlarged lymph nodes adjacent to an esophageal cancer also may not be visualized if they are inseparable from the primary lesion. Conversely, when enlarged mediastinal lymph nodes are detected, CT cannot differentiate benign causes of lymph node enlargement from metastatic tumor. In one study, benign enlargement of lymph nodes occurred more frequently when the primary esophageal cancer was large and necrotic.¹⁶⁷ In general, CT has been found to be more accurate for predicting upper abdominal lymph node metastases than mediastinal lymph node metastases.¹⁶⁸

CT of the chest and upper abdomen also enables detection of distant metastases to the lungs, bones, liver, or other structures. These findings are useful for predicting long-term survival in patients with esophageal cancer. In one study, patients with CT findings of mediastinal or subdiaphragmatic invasion by tumor had a significantly shorter survival compared to patients without these findings.¹⁶⁸

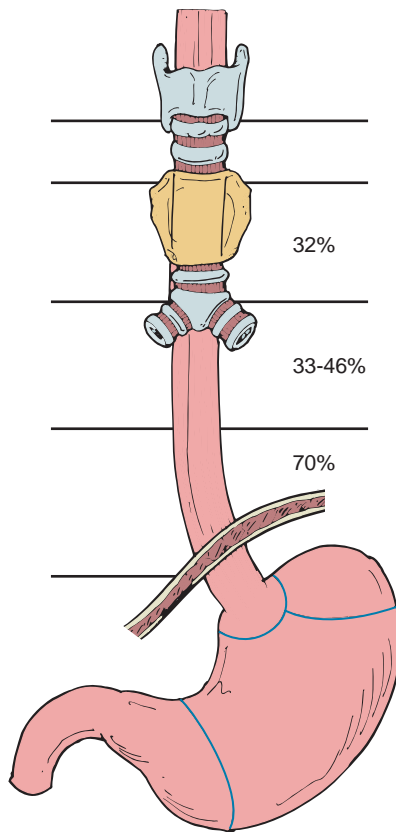


Figure 23-25 Relationship between frequency of subdiaphragmatic lymph node metastases and location of esophageal cancer. Distal esophageal cancers have a substantially higher frequency of subdiaphragmatic lymph node metastases than cancers located more proximally in the esophagus.

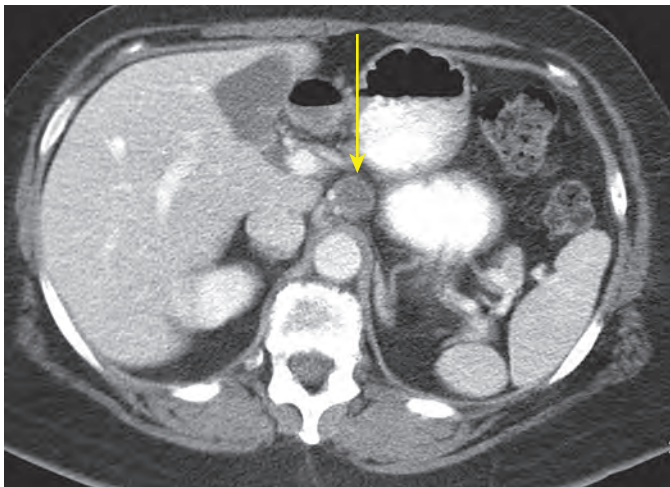


Figure 23-26 Enlarged subdiaphragmatic lymph node (arrow) as a result of lymphatic metastasis from esophageal carcinoma. Lymphatic metastases may occur at a considerable distance from the primary tumor because of the rich network of longitudinally oriented periesophageal lymphatics.

ENDOSCOPIC ULTRASOUND

Technique

The ultrasound probe is built into the tip of a fiberoptic endoscope designed specifically for EUS. The tip of the probe is covered by a distensible rubber balloon that can be filled with

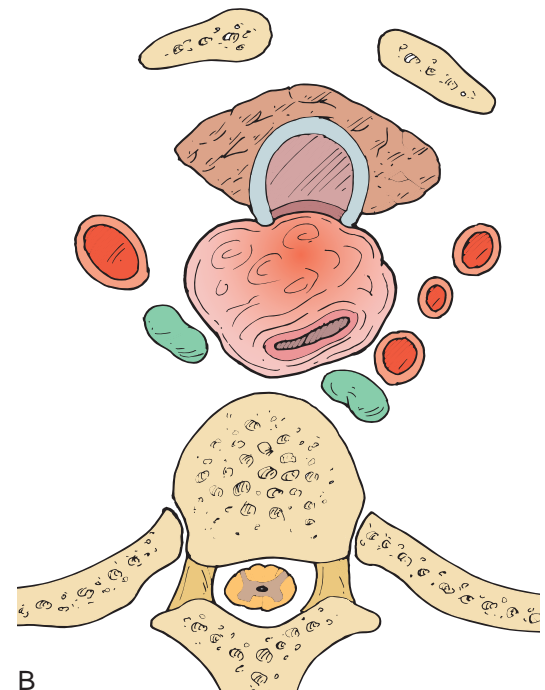
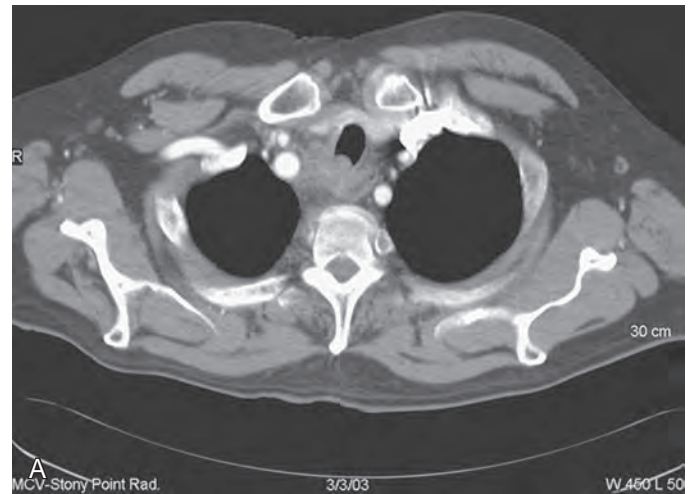


Figure 23-27 Tracheal invasion by esophageal carcinoma. **A.** CT scan shows esophageal tumor indenting the posterior wall of the trachea. This finding is indicative of tracheal invasion. **B.** Line drawing also shows tracheal invasion by esophageal tumor.

water to provide an acoustic interface between the transducer and esophageal wall. These ultrasound units are stand-alone devices that differ from the upper GI endoscope. The probes are similar in size to standard endoscopes, so they cannot pass through areas of marked luminal narrowing caused by advanced esophageal cancers, preventing adequate staging of these tumors. Reported rates of nontraversability of the tumor at EUS have ranged from 20% to 45%.^{169,170} To circumvent this problem, a tiny probe can be passed through the biopsy channel of a standard endoscope.^{171,172} These probes have the advantage of being able to traverse a greater percentage of esophageal cancers because of the smaller probe caliber. At the same time, these smaller probes use very high-frequency transducers, so they have a more limited field of view.

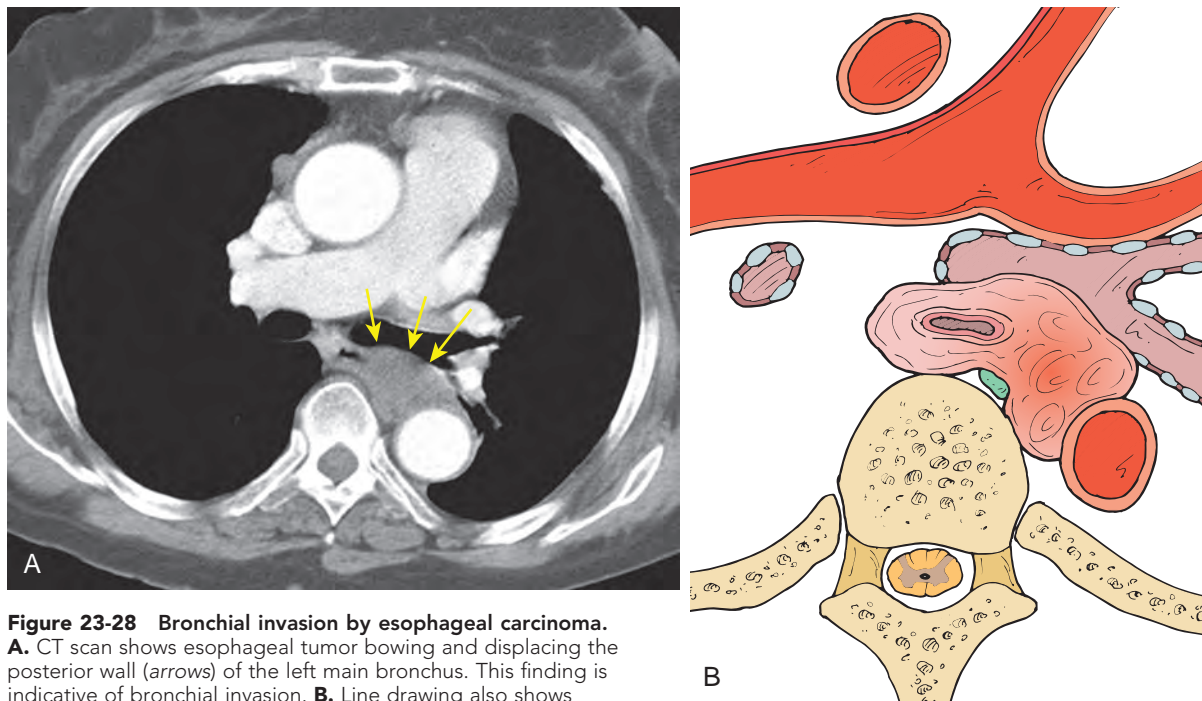


Figure 23-28 Bronchial invasion by esophageal carcinoma. **A.** CT scan shows esophageal tumor bowing and displacing the posterior wall (arrows) of the left main bronchus. This finding is indicative of bronchial invasion. **B.** Line drawing also shows bronchial invasion by tumor.

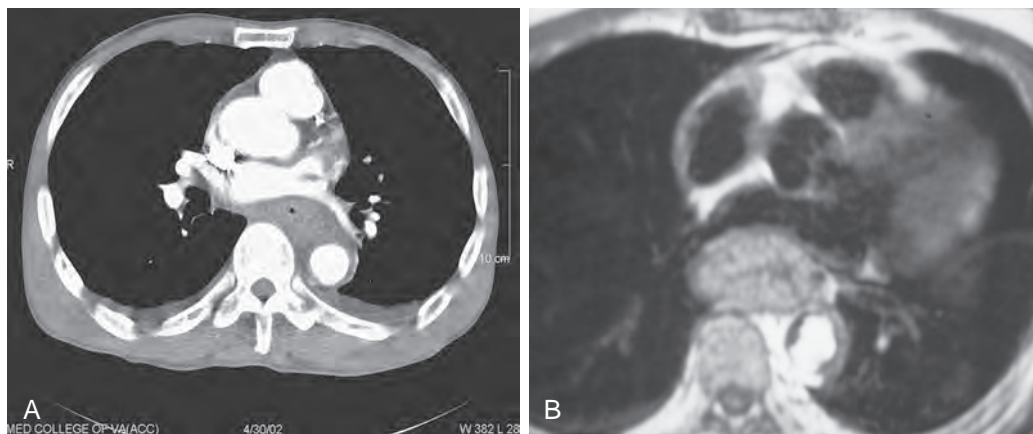


Figure 23-29 Pericardial invasion by esophageal carcinoma. **A.** CT scan shows esophageal tumor indenting the posterior wall of the left atrium. This finding is indicative of pericardial invasion. **B.** MRI scan also shows tumor indenting the posterior wall of the left atrium.

Staging Criteria

EUS provides excellent visualization of the five layers of the esophageal wall. These layers are recognized on EUS as alternating layers of increased and decreased echogenicity, producing five rings (Fig. 23-34). The inner echogenic line represents the mucosal interface with the transducer, the central echogenic line represents submucosal fat (fat is echogenic on ultrasound), and the outer echogenic line represents serosal fat. Tumors are usually manifested by hypoechoic masses causing disruption or widening of these esophageal rings (Fig. 23-35). EUS is excellent for detecting esophageal tumors and can often identify lesions that have spread beyond the wall, enabling differentiation of T2 tumors, which are confined to the esophageal wall, from T3 tumors, which extend beyond the esophageal wall into the periesophageal fat. The ability of EUS to detect T4 tumors, which are invading adjacent structures in the mediastinum, is limited by the inability to differentiate invasive tumors

from those that extend to adjacent structures without actual invasion.

A meta-analysis of 13 studies evaluating the accuracy of EUS for esophageal cancer staging has found that EUS has an overall accuracy of 89% for predicting the depth of tumor invasion in the esophageal wall and an accuracy of 79% for predicting mediastinal lymph node metastases (Fig. 23-36).¹⁷³ Many authors therefore believe that EUS should be complementary to helical CT for staging esophageal cancer. EUS is superior to CT for detecting the depth of invasion in the esophageal wall and mediastinal lymph node metastases, but CT is superior to EUS for detecting distant metastases. The ability of EUS to differentiate T2 from T3 tumors is particularly helpful for guiding treatment because patients with T2 tumors usually undergo primary surgical resection, whereas chemoradiation therapy is usually given to patients with T3 tumors. At institutions in which surgery is performed for both T2 and T3 tumors, however, this benefit of EUS is lost.

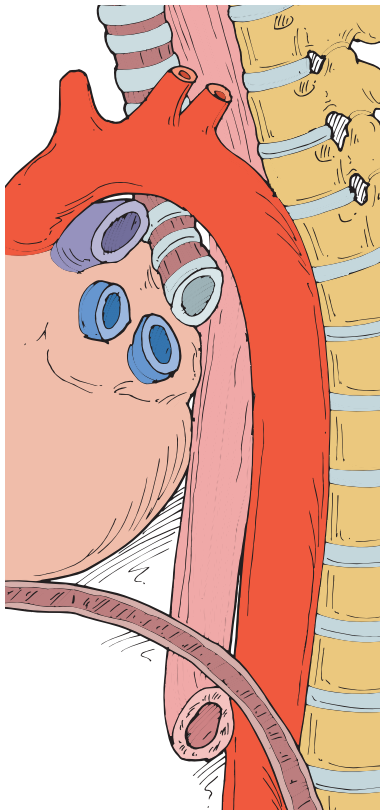


Figure 23-30 Normal contact between esophagus and descending thoracic aorta. There is direct contact between the esophagus and adjacent descending thoracic aorta.

The accuracy of EUS for nodal staging can be increased by transesophageal EUS-guided fine-needle aspiration (FNA) cytology of peritumoral lymph nodes in the mediastinum.¹⁷⁴ In one study, routine FNA of lymph nodes at EUS was found to have an accuracy of 93% for nodal staging versus an accuracy of 70% for EUS alone.¹⁷⁵ EUS with FNA can therefore improve local staging of esophageal cancer.

POSITRON EMISSION TOMOGRAPHY

PET using fluorine-18-deoxyglucose (FDG) is another useful test for staging esophageal cancer. Because these tumors and their metastases to the liver, lungs, cervical lymph nodes, and other sites are relatively FDG-avid (Figs. 23-37 and 23-38), PET or PET/CT can detect metastases that are not recognized on CT.¹⁷⁶ In one study, PET revealed metastases not visible on CT of the chest and upper abdomen in 17% of patients with esophageal cancer, including 38% of cervical lymph node metastases, 23% of bone metastases, and 15% of hepatic metastases.¹⁷⁷ PET is therefore particularly helpful when CT reveals no evidence of local invasion or distant metastases (Fig. 23-39). In another study, PET contributed important additional information for cancer staging in 14% of patients with esophageal cancer who underwent CT.¹⁷⁸

ULTRASONOGRAPHY OF THE NECK

Cervical lymph nodes appear to be of greater importance for esophageal cancer staging than has previously been recognized.

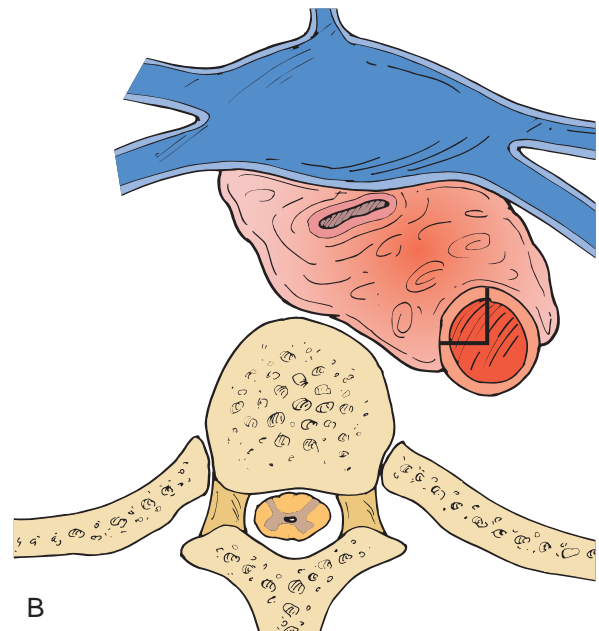
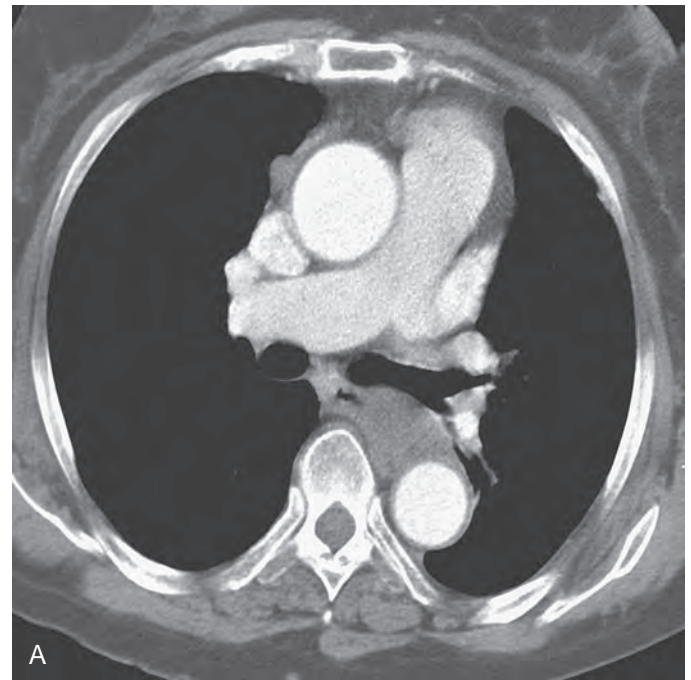


Figure 23-31 Aortic invasion by esophageal carcinoma. **A.** CT scan shows more than 90 degrees of contact between the esophageal tumor and aorta without intervening fat planes. This is a useful CT criterion for predicting aortic invasion. **B.** Line drawing also shows more than 90 degrees of contact between the tumor and aorta.

In one study, one third of patients who underwent esophagectomy for “curable” cancers of the thoracic esophagus were found to have cervical lymph node metastases when a lymph node dissection of the neck was performed at the time of esophagectomy.¹⁷⁹ Lymph node metastases were found to be as common in the neck as in the mediastinum. The frequency of cervical lymph node metastases directly correlates with the location of the tumor in the esophagus—80% of patients with tumors in the cervical esophagus have cervical lymph node metastases versus 52% with tumors in the proximal thoracic

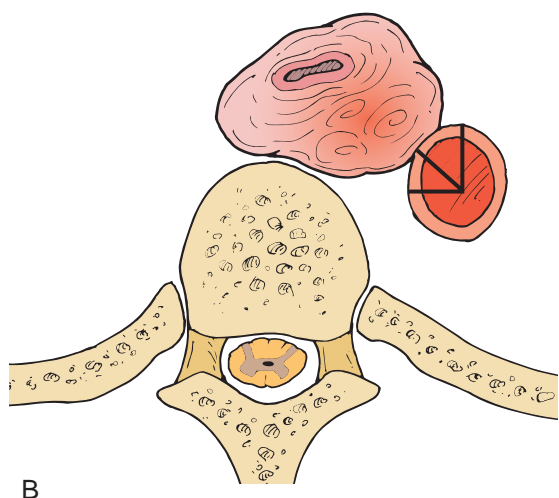
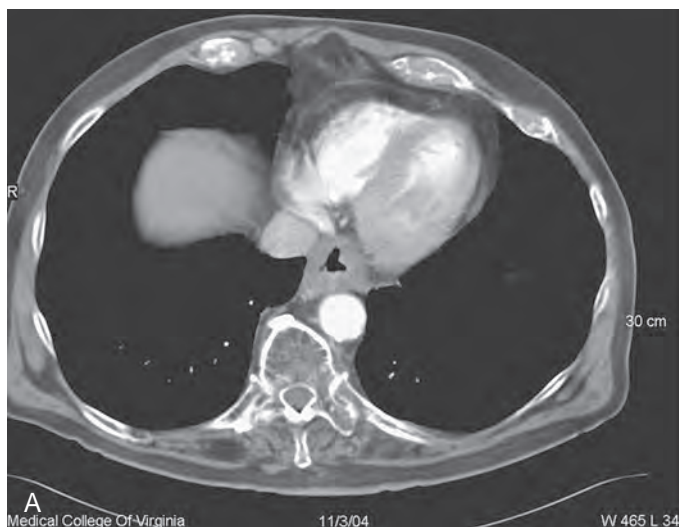


Figure 23-32 Esophageal carcinoma without evidence of aortic invasion. **A.** CT scan shows less than 45 degrees of contact between the esophageal tumor and aorta. This finding indicates that the aorta is not invaded by tumor. **B.** Line drawing also shows less than 45 degrees of contact between the esophageal tumor and aorta.

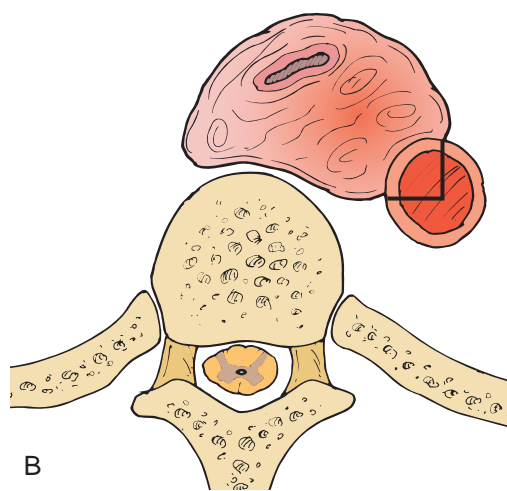
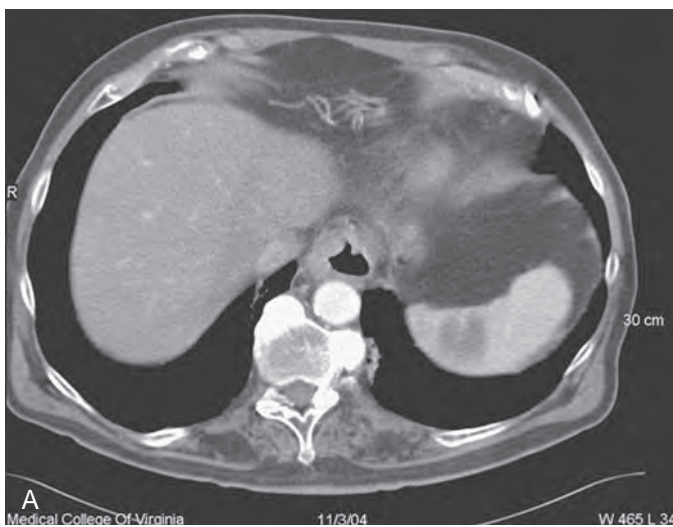


Figure 23-33 Indeterminate CT scan for aortic invasion by esophageal cancer. **A.** CT scan shows between 45 and 90 degrees of contact between the esophageal tumor and aorta. This finding is indeterminate for aortic invasion. **B.** Line drawing also shows between 45 and 90 degrees of contact between the esophageal tumor and aorta.

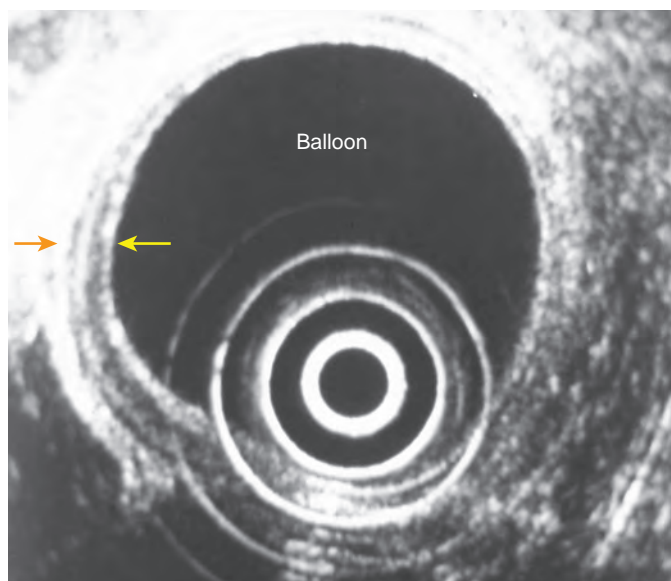


Figure 23-34 Normal endoscopic ultrasound. This image shows all five layers (arrows) of the esophageal wall.

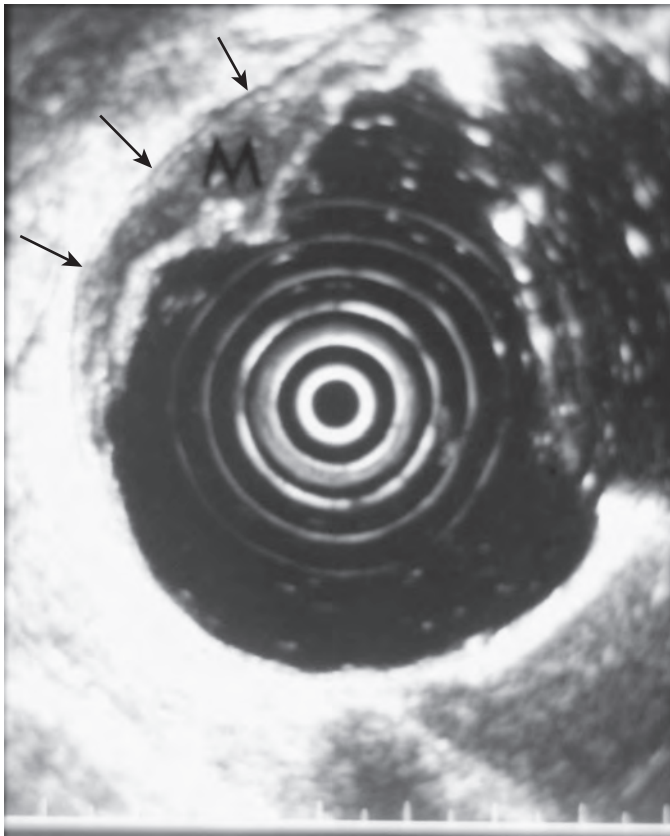


Figure 23-35 Endoscopic ultrasound of esophageal cancer. Endoscopic ultrasound shows a hypoechoic mass (M) causing focal widening of the esophageal wall. The thin black line peripherally (arrows) indicates that the tumor has not yet invaded the serosal fat.

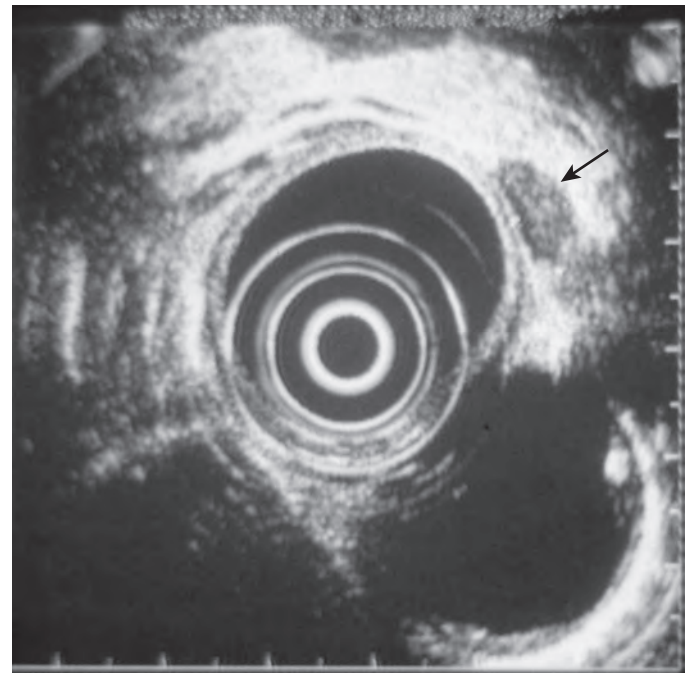


Figure 23-36 Endoscopic ultrasound of lymph node metastasis from esophageal carcinoma. The enlarged node is manifested by a hypoechoic focus (arrow).

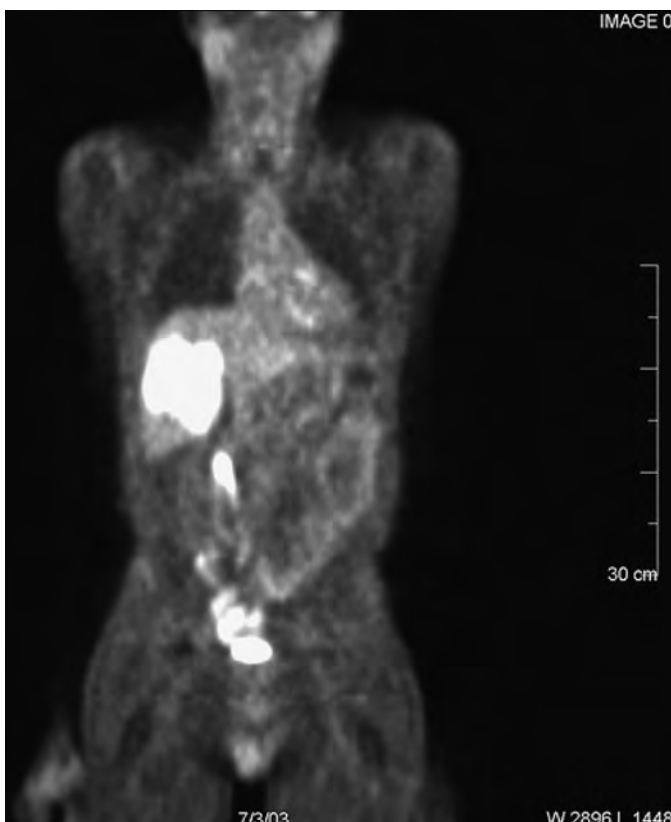


Figure 23-37 Liver metastasis from esophageal carcinoma on PET. This coronal PET image shows marked uptake of radionuclide in avid hepatic metastasis.

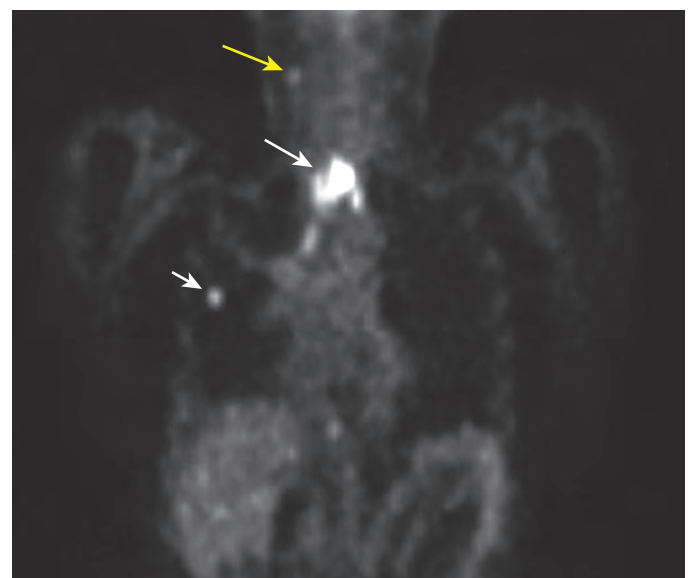


Figure 23-38 Cervical lymph node and pulmonary metastases from esophageal carcinoma on PET. This coronal PET image shows marked uptake of radionuclide (large white arrow) in a bulky esophageal tumor in the upper mediastinum. Also note uptake in metastases to a right cervical lymph node (yellow arrow) and right lung (small white arrow).

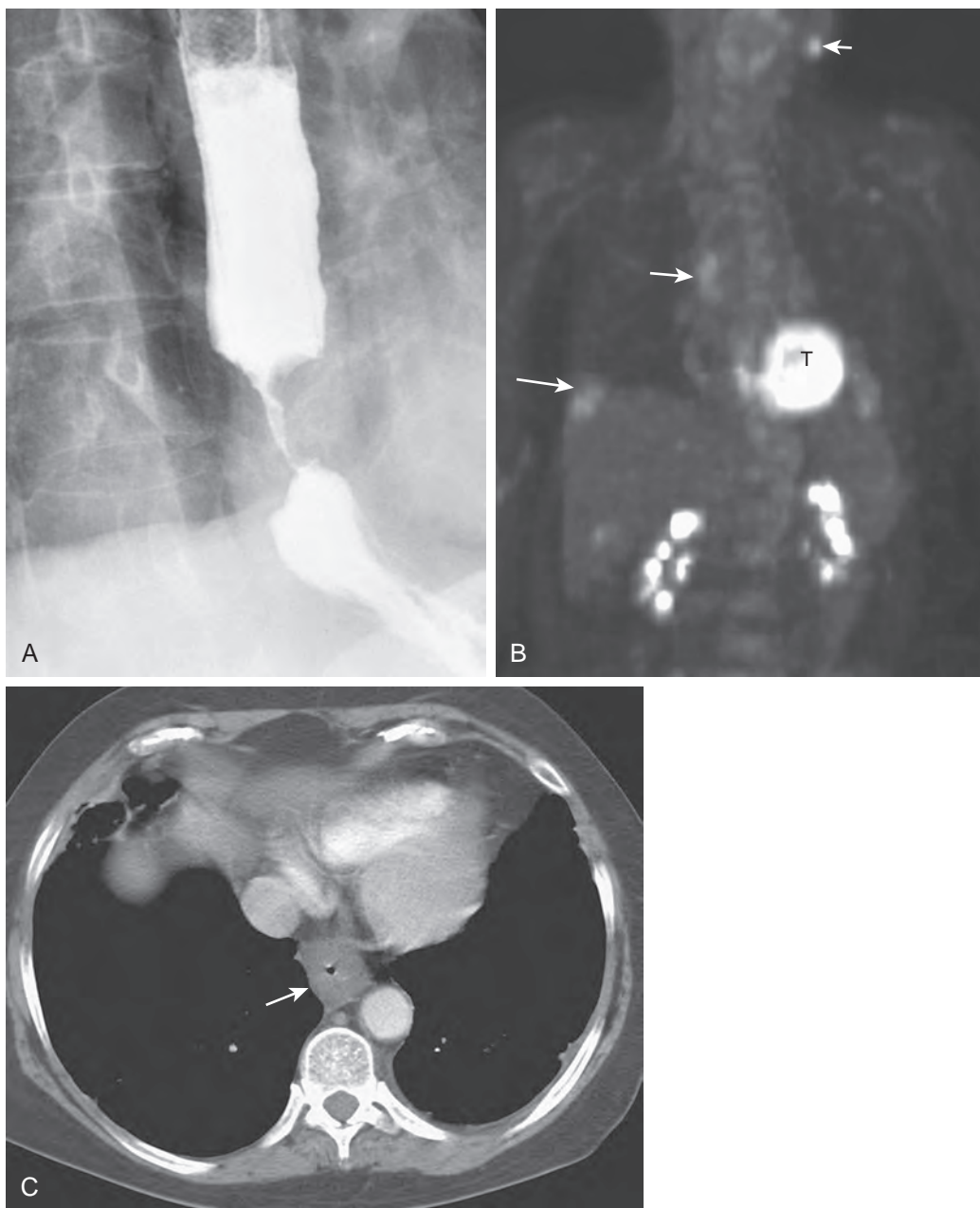


Figure 23-39 Value of PET for showing metastases not detected on CT scan. **A.** Barium study shows a circumferentially infiltrating carcinoma of the distal esophagus. **B.** Coronal PET image shows marked uptake of radionuclide in distal esophageal tumor (T). However, there is also uptake in metastases to the liver (*long arrow*), mediastinum (*medium arrow*), and a left cervical lymph node (*short arrow*). The PET scan has therefore dramatically altered the staging of this patient's disease. **C.** CT scan shows marked esophageal wall thickening by tumor (*arrow*). However, this lesion is potentially resectable without CT scan findings of local or distant metastases. (Note how there is less than 45 degrees of contact between the tumor and adjacent aorta.)

esophagus, 29% with tumors in the midthoracic esophagus, and 9% with tumors in the distal thoracic esophagus.¹⁸⁰

Because of the high frequency of cervical lymph node metastases from esophageal cancer, Asian and European authors have advocated ultrasonography of the neck with FNA for suspicious lymph nodes as another imaging test for staging esophageal cancer.^{181,182} Neck ultrasonography is performed with a high-frequency transducer in the range of 7.5 to 10 MHz. This examination is relatively easy to perform because the lymph nodes of interest in the neck are within 3 cm of the skin surface. Lymph nodes are considered to be abnormal if they have a diameter larger than 5 mm or a short-to-long ratio more than 50%.¹⁸³ In one study, ultrasonography of the neck with FNA of suspicious nodes had a sensitivity of 88%, specificity of 59%, and accuracy of 78% for detecting cervical lymph node metastases from esophageal cancer.¹⁸⁴

STAGING ALGORITHM

CT is usually recommended as the initial test for staging esophageal cancer. If CT reveals local invasion or distant metastases, no further imaging is warranted. If, however, CT is negative or indeterminate for local invasion or distant metastases, the patient can be referred for EUS. If the tumor still appears to be resectable on EUS, then PET or PET/CT can be performed to detect local invasion or distant metastases not recognized on CT or EUS. Further investigation is needed to determine whether ultrasonography or CT of the neck should be performed routinely to assess for cervical lymph node metastases in these patients.

Treatment

Depending on the stage of the tumor at the time of diagnosis, esophageal cancer may be treated by curative or palliative measures. Curative therapy includes surgery, radiation, and surgery combined with preoperative or postoperative radiation or chemotherapy. Palliative therapy includes surgery, radiation, chemotherapy, placement of an indwelling esophageal prosthesis, and laser treatment.

SURGERY

Curative resection of a carcinoma in the distal two thirds of the esophagus usually requires an esophagogastrectomy and gastric pull-through. Resection of a more proximal lesion may require a free jejunal graft for reconstruction of the pharyngoesophagus. Palliative surgery in patients with advanced esophageal cancer usually consists of an esophageal bypass procedure to control symptoms of obstruction or fistula formation. The most common bypass procedures include colonic interposition and creation of a gastric tube. Palliation may also be achieved by passage of an esophageal prosthesis (usually an expandable metallic stent) to bypass an obstruction or fistula. The normal and abnormal appearances after surgery or other palliative procedures for esophageal cancer are discussed in Chapter 27.

RADIATION THERAPY

Radiation therapy may be used for palliative or definitive treatment of esophageal cancer. Squamous cell carcinomas tend to

be more radiosensitive than adenocarcinomas.¹⁸⁵ Tumors in the cervical or upper thoracic esophagus also tend to be more radiosensitive than those in the middle or distal thoracic esophagus.¹⁸⁵ Partial or total regression of tumor occurs in most patients who undergo this form of treatment.¹⁸⁶⁻¹⁸⁸ Although they may have substantial amelioration of dysphagia in the initial months after therapy, tumor subsequently recurs locally in 30% to 85% of cases.^{185,188-190} Even when the cancer is eradicated from the esophagus, these patients often die as a result of widespread metastases to the liver, lungs, or mediastinum.^{185,188,191} Increased morbidity or mortality may also be attributed to complications of radiation therapy, such as esophageal ulceration, perforation, and fistula formation.^{190,192} As a result, the prognosis after radiation therapy is comparable to or slightly worse than that after surgery, with an average survival of only 9 to 10 months.

Partial regression of tumor after radiation therapy may be recognized on serial barium studies by a decrease in the size and bulk of the lesion. With total regression of tumor, esophagography may reveal a normal esophagus or a benign-appearing stricture at the site of the original lesion (Fig. 23-40).^{188,189,193,194} In most cases, these strictures appear as smooth, tapered areas of narrowing without evidence of nodularity, mass effect, or ulceration to suggest residual tumor. Even when there is total regression of tumor, however, these patients often die as a result of distant metastases, presumably because of unrecognized lymphatic involvement at the time of therapy.¹⁸⁸ Thus, disappearance of the cancer on radiologic or endoscopic studies does not necessarily indicate a cure.

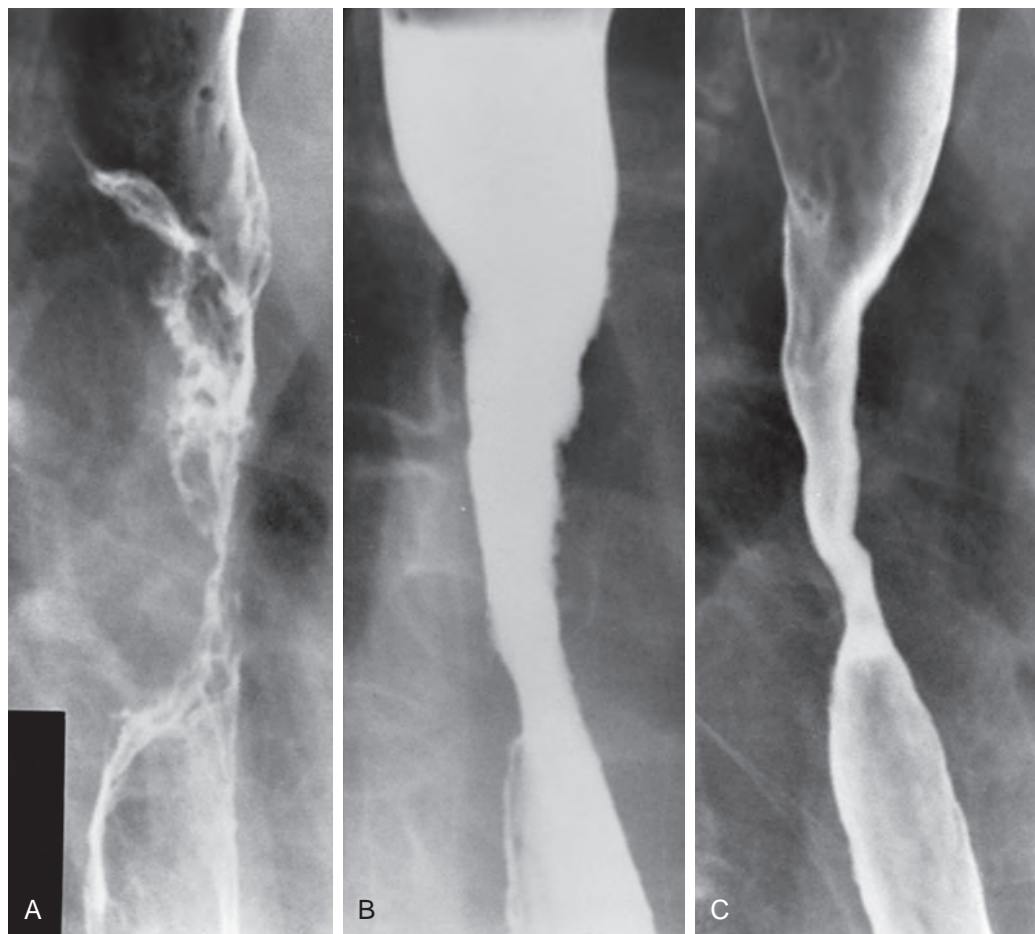
Although most patients have an initial clinical response to radiation therapy, recurrent dysphagia often occurs within 3 to 9 months after treatment because of local recurrence of tumor.^{185,188,189} Recurrent carcinoma may be recognized on barium studies by the development of a polypoid, ulcerative, or infiltrating lesion within or just beyond the margins of the original radiation portal.¹⁸⁸ However, an exacerbation of symptoms in these patients may be caused not only by recurrent tumor but also by benign radiation strictures, fistula formation, perforation, or opportunistic esophageal infections such as *Candida* and herpes esophagitis.¹⁸⁸ Thus, radiologic studies may differentiate recurrent carcinoma from other complications in these patients.

CHEMORADIATION THERAPY

Initial reports suggested that combined radiation and chemotherapy of patients with esophageal carcinoma produced an immediate and dramatic response, but that the long-term benefits of this approach were questionable. Preoperative chemoradiation therapy has also been advocated as an adjunct to surgery for patients with locally advanced tumors or regional lymphadenopathy.² Unfortunately, conflicting data have been reported about the value of multimodality therapy. In a study of patients with esophageal adenocarcinoma, preoperative chemoradiation therapy was found to be superior to surgery alone, with median survivals of 15 and 11 months, respectively.¹⁹⁵ In another study of patients with squamous cell carcinoma of the esophagus, however, preoperative chemoradiation therapy did not improve overall survival.¹⁹⁶ Nevertheless, chemoradiation therapy is a viable alternative to surgery in patients with advanced disease or medical conditions that preclude surgery.

Figure 23-40 Total regression of esophageal carcinoma with a benign-appearing residual stricture after radiation therapy.

A. Initial esophagogram shows an advanced, infiltrating carcinoma in the midesophagus. **B.** Second study 4 months after radiation therapy shows partial regression of the tumor, with residual areas of shallow ulceration. **C.** Third study 2 months later shows further regression of the lesion, with a smooth, tapered, benign-appearing radiation stricture in this location. (From Levine MS: *Radiology of the Esophagus*. Philadelphia, WB Saunders, 1989.)



REFERENCES

1. Livstone EM, Skinner DB: Tumors of the esophagus. In Berk JE, editor: *Gastroenterology*, Philadelphia, 1985, WB Saunders, pp 818–850.
2. Wang KK, Wongkeesong M, Buttar NS: American Gastroenterological Association technical review on the role of the gastroenterologist in the management of esophageal carcinoma. *Gastroenterology* 128:1471–1505, 2005.
3. Pottner LM, Morris LE, Blot WJ, et al: Esophageal cancer among black men in Washington, DC: Alcohol, tobacco, and other risk factors. *J Natl Cancer Inst* 67:777–783, 1981.
4. Engel LS, Chow WH, Vaughan TL, et al: Population-attributable risks of esophageal and gastric cancers. *J Natl Cancer Inst* 95:1404–1413, 2003.
5. Fielding JE: Smoking: Health effects and control. *N Engl J Med* 313:491–498, 1985.
6. Caygill CP, Johnston DA, Lopez M, et al: Lifestyle factors and Barrett's esophagus. *Am J Gastroenterol* 97:1328–1331, 2002.
7. Ribeiro U, Posner MC, Safatle-Ribeiro AV, et al: Risk factors for squamous cell carcinoma of the esophagus. *Br J Surg* 83:1174–1185, 1996.
8. Yang CS: Research on esophageal cancer in China: A review. *Cancer Res* 40:2633–2644, 1980.
9. Burrell RJW, Roach WA, Shadwell A: Esophageal cancer in the Bantu of the Transkei associated with mineral deficiency in garden plants. *J Natl Cancer Inst* 36:201–214, 1966.
10. Warwick GP, Harington JS: Some aspects of the epidemiology and etiology of esophageal cancer with particular emphasis on the Transkei, South Africa. *Adv Cancer Res* 17:81–229, 1973.
11. Amer MH, El-Yazigi A, Hannan MA, et al: Water contamination and esophageal cancer at Gassim Region, Saudi Arabia. *Gastroenterology* 98:1141–1147, 1990.
12. Stephen SJ, Urugoda CG: Some observations on oesophageal carcinoma in Ceylon, including its relationship to betel chewing. *Br J Cancer* 24:11–15, 1970.
13. Correa P: Precursors of gastric and esophageal cancer. *Cancer* 50:2554–2565, 1982.
14. Craighead JE, Mossman BT: The pathogenesis of asbestos-associated diseases. *N Engl J Med* 306:1446–1455, 1982.
15. Chang F, Shen Q, Zhou J, et al: Detection of human papillomavirus DNA in cytologic specimens derived from esophageal precancer lesions and cancer. *Scand J Gastroenterol* 25:383–388, 1990.
16. Chang F, Syrjanen S, Shen Q, et al: Screening for human papillomavirus infections in esophageal squamous cell carcinomas by in situ hybridization. *Cancer* 72:2525–2530, 1993.
17. Just-Viera JO, Haight C: Achalasia and carcinoma of the esophagus. *Surg Gynecol Obstet* 128:1081–1093, 1969.
18. Seliger G, Lee T, Schwartz S: Carcinoma of the proximal esophagus: A complication of long-standing achalasia. *Am J Gastroenterol* 57:20–25, 1972.
19. Carter R, Brewer LA: Achalasia and esophageal carcinoma. *Am J Surg* 130:114–118, 1975.
20. Wychulis AR, Woolam GL, Andersen HA, et al: Achalasia and carcinoma of the esophagus. *JAMA* 215:1638–1641, 1971.
21. Hankins JR, McLaughlin JS: The association of carcinoma of the esophagus with achalasia. *J Thorac Cardiovasc Surg* 69:355–360, 1975.
22. Chuong JJH, DuBovik S, McCallum RW: Achalasia as a risk factor for esophageal carcinoma: A reappraisal. *Dig Dis Sci* 29:1105–1108, 1984.
23. Bigger IA, Vinson PP: Carcinoma secondary to burn of the esophagus from ingestion of lye. *Surgery* 28:887–889, 1950.
24. Imre J, Kopp M: Arguments against long-term conservative treatment of oesophageal strictures due to corrosive burns. *Thorax* 27:594–598, 1972.
25. Appleqvist P, Salmo M: Lye corrosion carcinoma of the esophagus: A review of 63 cases. *Cancer* 45:2655–2658, 1980.
26. Hopkins RA, Postlethwait RW: Caustic burns and carcinoma of the esophagus. *Ann Surg* 194:146–148, 1981.
27. Weaver A, Fleming SM, Knechtges TC, et al: Triple endoscopy: A neglected essential in head and neck cancer. *Surgery* 86:493–496, 1979.
28. Atkinson D, Fleming S, Weaver A: Triple endoscopy: A valuable procedure in head

- and neck surgery. *Am J Surg* 144:416–419, 1982.
29. McGuirt WF: Panendoscopy as a screening examination for simultaneous primary tumors in head and neck cancer: A prospective sequential study and review of the literature. *Laryngoscope* 92:569–576, 1982.
 30. Wynder EL, Mushinski MH, Spivak JC: Tobacco and alcohol consumption in relation to the development of multiple primary cancers. *Cancer* 40:1872–1878, 1977.
 31. Harris OD, Cooke WT, Thompson H, et al: Malignancy in adult coeliac disease and idiopathic steatorrhea. *Am J Med* 42:899–912, 1967.
 32. Collins SM, Hamilton JD, Lewis TD, et al: Small bowel malabsorption and gastrointestinal malignancy. *Radiology* 126:603–609, 1978.
 33. Chisholm M: The association between webs, iron and postcricoid carcinoma. *Postgrad Med J* 50:215–219, 1974.
 34. Wynder EL, Hultberg S, Jacobsson F, et al: Environmental factors in cancer of the upper alimentary tract: A Swedish study with special reference to Plummer-Vinson (Paterson-Kelly) syndrome. *Cancer* 10:470–487, 1957.
 35. Chudecki B: Radiation cancer of the thoracic oesophagus. *Br J Radiol* 45:303–304, 1972.
 36. O'Connell EW, Seaman WB, Ghahremani GG: Radiation-induced esophageal carcinoma. *Gastrointest Radiol* 9:287–291, 1984.
 37. Ahsan H, Neugut AI: Radiation therapy for breast cancer and increased risk of esophageal carcinoma. *Ann Intern Med* 128:114–117, 1998.
 38. Shine I, Allison PR: Carcinoma of the oesophagus with tylosis. *Lancet* 1:951–953, 1966.
 39. Harper PS, Harper RMJ, Howel-Evans AW: Carcinoma of the oesophagus with tylosis. *Q J Med* 39:317–333, 1970.
 40. Munyer TP, Margulis AR: Tylosis. *AJR* 136:1026–1027, 1981.
 41. Blot W, Devesa S, Fraumeni J: Continued climb in rates of esophageal adenocarcinoma: An update. *JAMA* 270:1320, 1993.
 42. Froelicher P, Miller G: The European experience with esophageal cancer limited to the mucosa and submucosa. *Gastrointest Endosc* 32:88–90, 1986.
 43. Bonavina L: Early oesophageal cancer: Results of a European multicentre survey. *Group European pour l'Etude des Maladies de l'Oesophage. Br J Surg* 82:9–101, 1995.
 44. Japanese Society for Esophageal Diseases: Guide lines for the clinical and pathologic studies on carcinoma of the esophagus. *Jpn J Surg* 6:69–78, 1976.
 45. Roth MJ, Liu SF, Dawsey SM, et al: Cytologic detection of esophageal squamous cell carcinoma and precursor lesions using balloon and sponge samplers in asymptomatic adults in Linxian, China. *Cancer* 80:2047–2059, 1997.
 46. Moss AA, Koehler RE, Margulis AR: Initial accuracy of esophagograms in detection of small esophageal carcinoma. *AJR* 127:909–913, 1976.
 47. Zornoza J, Lindell MM: Radiologic evaluation of small esophageal carcinoma. *Gastrointest Radiol* 5:107–111, 1980.
 48. Mannell A: Carcinoma of the esophagus. *Curr Probl Surg* 19:553–647, 1982.
 49. Yamada A: Radiologic assessment of resectability and prognosis in esophageal carcinoma. *Gastrointest Radiol* 4:213–218, 1979.
 50. Postlethwait RW: Carcinoma of the esophagus. *Curr Probl Cancer* 2:1–44, 1978.
 51. Fitzgerald RH, Bartles DM, Parker EF: Tracheoesophageal fistulas secondary to carcinoma of the esophagus. *J Thorac Cardiovasc Surg* 82:194–197, 1981.
 52. Little AG, Ferguson MK, DeMeester TR, et al: Esophageal carcinoma with respiratory tract fistula. *Cancer* 53:1322–1328, 1984.
 53. Bottiglieri NG, Palmer ED, Briggs GW, et al: Aortoesophageal fistula complicating carcinoma of the esophagus. *Am J Dig Dis* 8:837–844, 1963.
 54. Vennos AD, Templeton PA: Pneumopericardium secondary to esophageal carcinoma. *Radiology* 182:131–132, 1992.
 55. Mandard AM, Chasle J, Marnay J, et al: Autopsy findings in 111 cases of esophageal cancer. *Cancer* 48:329–335, 1981.
 56. Sannohe Y, Hiratsuka R, Doki K: Lymph node metastases in cancer of the thoracic esophagus. *Am J Surg* 141:216–218, 1981.
 57. Rosengren JE, Goldstein HM: Radiologic demonstration of multiple foci of malignancy in the esophagus. *Gastrointest Radiol* 3:11–13, 1978.
 58. Davis M, Gogel H, McIntire C, et al: Esophageal carcinoma multiplex with gastric metastasis. *Gastrointest Radiol* 14:6–8, 1989.
 59. Glick SN, Teplick SK, Levine MS, et al: Gastric cardia metastasis in esophageal carcinoma. *Radiology* 160:627–630, 1986.
 60. Glick SN, Teplick SK, Levine MS: Squamous cell metastases to the gastric cardia. *Gastrointest Radiol* 10:339–344, 1985.
 61. Koehler RE, Moss AA, Margulis AR: Early radiographic manifestations of carcinoma of the esophagus. *Radiology* 119:1–5, 1976.
 62. Skinner DB: Surgical treatment for esophageal carcinoma. *Semin Oncol* 11:136–143, 1984.
 63. Levine MS, Dillon EC, Saul SH, et al: Early esophageal cancer. *AJR* 146:507–512, 1986.
 64. Carey LC, Darin JC, Worman LW, et al: Upper gastrointestinal hemorrhage from carcinoma of esophagus. *Arch Surg* 90:460–464, 1965.
 65. Barrie JR, Goodner JT: Hematemesis from cancer of the esophagus. *J Thorac Cardiovasc Surg* 56:289–292, 1968.
 66. Ghosh BC, Choudhry KU, Beattie EJ: Massive bleeding from esophageal cancer. *J Thorac Cardiovasc Surg* 63:977–979, 1972.
 67. Alrenga DP: Fatal hemorrhage complicating carcinoma of the esophagus: Report of four cases. *Am J Gastroenterol* 65:422–426, 1976.
 68. Graham DY, Schwartz JT, Cain GD, et al: Prospective evaluation of biopsy number in the diagnosis of esophageal and gastric carcinoma. *Gastroenterology* 82:228–231, 1982.
 69. Lal N, Bhasin DK, Malik AK, et al: Optimal number of biopsy specimens in the diagnosis of carcinoma of the oesophagus. *Gut* 33:724–726, 1992.
 70. Suzuki H, Kobayashi S, Endo M, et al: Diagnosis of early esophageal cancer. *Surgery* 71:99–103, 1971.
 71. Yamada A, Kobayashi S, Kawai B, et al: Study on x-ray findings of early oesophageal cancer. *Australas Radiol* 16:238–246, 1972.
 72. Itai Y, Kogure T, Okuyama Y, et al: Superficial esophageal carcinoma: Radiological findings in double-contrast studies. *Radiology* 126:597–601, 1978.
 73. Sato T, Sakai Y, Kajita A, et al: Radiographic microstructures of early esophageal carcinoma: Correlation of specimen radiography with pathologic findings and clinical radiography. *Gastrointest Radiol* 11:12–19, 1986.
 74. Lee SS, Ha HK, Byun JH, et al: Superficial esophageal cancer: Esophagographic findings correlated with histopathologic findings. *Radiology* 236:535–544, 2005.
 75. Itai Y, Kogure T, Okuyama Y, et al: Diffuse finely nodular lesions of the esophagus. *AJR* 128:563–566, 1977.
 76. Schmidt LW, Dean PJ, Wilson RT: Superficially invasive squamous cell carcinoma of the esophagus. *Gastroenterology* 91:1456–1461, 1986.
 77. Lindell MM, Hill CA, Libshitz HI: Esophageal cancer: Radiographic chest findings and their prognostic significance. *AJR* 133:461–465, 1979.
 78. Putman CE, Curtis A, Westfried M, et al: Thickening of the posterior tracheal stripe: A sign of squamous cell carcinoma of the esophagus. *Radiology* 121:533–536, 1976.
 79. Daffner RH, Postlethwait RW, Putman CE: Retrotracheal abnormalities in esophageal carcinoma: Prognostic implications. *AJR* 130:719–723, 1978.
 80. Levine MS, Chu P, Furth EE, et al: Carcinoma of the esophagus and esophagogastric junction: Sensitivity of radiographic diagnosis. *AJR* 168:1423–1426, 1997.
 81. DiPalma JA, Prechter GC, Brady CE: X-ray-negative dysphagia: Is endoscopy necessary? *J Clin Gastroenterol* 6:409–411, 1984.
 82. Halpert RD, Feczko PJ, Spickler EM, et al: Radiologic assessment of dysphagia with endoscopy. *Radiology* 157:599–602, 1985.
 83. Wiot JW, Felson B: Radiographic differential diagnosis of esophageal cancer. *JAMA* 226:1548–1552, 1973.
 84. Goldstein HM, Zornoza J, Hopens T: Intrinsic diseases of the adult esophagus: Benign and malignant tumors. *Semin Roentgenol* 16:183–197, 1981.
 85. Levine MS: Esophageal cancer: Radiologic diagnosis. *Radiol Clin North Am* 35:265–279, 1997.
 86. Iyer RB, Silverman PM, Tamm EP, et al: Diagnosis, staging, and follow-up of esophageal cancer. *AJR* 181:785–793, 2003.
 87. Gloyne RE, Zornoza J, Goldstein HM: Primary ulcerative carcinoma of the esophagus. *AJR* 129:599–600, 1977.
 88. Lawson TL, Dodds WJ, Sheft DJ: Carcinoma of the esophagus simulating varices. *AJR* 107:83–85, 1969.
 89. Yates CW, LeVine MA, Jensen KM: Varicoid carcinoma of the esophagus. *Radiology* 122:605–608, 1977.
 90. Sabetdotti G, Dreweck MO, Sabetdotti V, et al: Carcinoma of the esophagus: Varicoid pattern. *Radiographics* 26:271–274, 2006.
 91. Cho SR, Schneider V, Beachley MC, et al: Carcinoma of the esophagus: Assessment of submucosal extent. *J Can Assoc Radiol* 33:154–157, 1982.
 92. Steiner H, Lammer J, Hackl A: Lymphatic metastases to the esophagus. *Gastrointest Radiol* 9:1–4, 1984.
 93. Allen HA, Bush JE: Midesophageal carcinoma metastatic to the stomach: Its unusual appearance on an upper gastrointestinal series. *South Med J* 76:1049–1051, 1983.
 94. Raphael HA, Ellis FH, Dockerty MB: Primary adenocarcinoma of the esophagus: 18 year review and review of literature. *Ann Surg* 164:785–796, 1966.

95. Turnbull ADM, Goodner JT: Primary adenocarcinoma of the esophagus. *Cancer* 22:915–918, 1968.
96. Bosch A, Frias Z, Caldwell WL: Adenocarcinoma of the esophagus. *Cancer* 43:1557–1561, 1979.
97. Devesa SS, Blot WJ, Fraumeni JF: Changing patterns in the incidence of esophageal and gastric carcinoma in the United States. *Cancer* 83:2049–2053, 1998.
98. Bytzer P, Christensen PB, Damkier P, et al: Adenocarcinoma of the esophagus and Barrett's esophagus: A population-based study. *Am J Gastroenterol* 94:86–91, 1999.
99. Bennett C, Vakil N, Bergman J, et al: Consensus statements for management of Barrett's dysplasia and early-stage esophageal adenocarcinoma, based on a Delphi process. *Gastroenterology* 143:336–346, 2012.
100. Haggitt RC, Tryzelaar J, Ellis FH, et al: Adenocarcinoma complicating columnar epithelium-lined (Barrett's) esophagus. *Am J Clin Pathol* 70:1–5, 1978.
101. Levine MS, Caroline D, Thompson JJ, et al: Adenocarcinoma of the esophagus: Relationship to Barrett mucosa. *Radiology* 150:305–309, 1984.
102. Agha FP: Barrett carcinoma of the esophagus: Clinical and radiographic analysis of 34 cases. *AJR* 145:41–46, 1985.
103. Bozyski EM, Herlihy KJ, Orlando RC: Barrett's esophagus. *Ann Intern Med* 97:103–107, 1982.
104. Sjogren RW, Johnson LF: Barrett's esophagus: A review. *Am J Med* 74:313–321, 1983.
105. Spechler SJ, Goyal RK: Barrett's esophagus. *N Engl J Med* 315:362–371, 1986.
106. Levine MS, Herman JB, Furth EE: Barrett's esophagus and esophageal adenocarcinoma: The scope of the problem. *Abdom Imaging* 20:291–298, 1995.
107. Sarr MG, Hamilton SR, Marrone GC, et al: Barrett's esophagus: Its prevalence and association with adenocarcinoma in patients with symptoms of gastroesophageal reflux. *Am J Surg* 149:187–192, 1985.
108. Winters C, Spurling TJ, Chobanian SJ, et al: Barrett's esophagus: A prevalent, occult complication of gastroesophageal reflux disease. *Gastroenterology* 92:118–124, 1987.
109. Csendes A, Smok G, Burdiles P, et al: Prevalence of Barrett's esophagus by endoscopy and histologic studies: A prospective evaluation of 306 control subjects and 376 patients with symptoms of gastroesophageal reflux disease. *Dis Esophagus* 13:5–11, 2000.
110. Ford AC, Forman D, Reynolds PD, et al: Ethnicity, gender, and socioeconomic status as risk factors for esophagitis and Barrett's esophagus. *Am J Epidemiol* 162:454–460, 2005.
111. Paull A, Trier JS, Dalton MD, et al: The histologic spectrum of Barrett's esophagus. *N Engl J Med* 295:476–480, 1976.
112. Thompson JJ, Zinsser KR, Enterline HT: Barrett's metaplasia and adenocarcinoma of the esophagus and gastroesophageal junction. *Hum Pathol* 14:42–61, 1983.
113. Weinstein WM, Ippoliti AF: The diagnosis of Barrett's esophagus: Goblets, goblets, goblets. *Gastrointest Endosc* 44:91–95, 1996.
114. Hirota WK, Loughney N, Lazas DJ, et al: Specialized intestinal metaplasia, dysplasia, and cancer of the esophagus and esophagogastric junction: Prevalence and clinical data. *Gastroenterology* 116:277–285, 1999.
115. Sharma P, Morales TG, Sampliner RE: Short segment Barrett's esophagus—the need for standardization of the definition and of endoscopic criteria. *Am J Gastroenterol* 93:1033–1036, 1998.
116. Skinner DB, Walther BC, Riddell RH, et al: Barrett's esophagus: Comparison of benign and malignant cases. *Ann Surg* 198:554–565, 1983.
117. Reid BJ: Barrett's esophagus and esophageal adenocarcinoma. *Gastroenterol Clin North Am* 20:817–834, 1991.
118. Spechler SJ, Robbins AH, Rubins HB, et al: Adenocarcinoma and Barrett's esophagus: An overrated risk? *Gastroenterology* 87:927–933, 1984.
119. Solaymani-Dodaran M, Logan RF, West J, et al: Risk of oesophageal cancer in Barrett's oesophagus and gastro-oesophageal reflux. *Gut* 53:1070–1074, 2004.
120. Hvid-Jensen F, Pedersen L, Drewes AM, et al: Incidence of adenocarcinoma among patients with Barrett's esophagus. *N Engl J Med* 365:1375–1383, 2011.
121. Berenson MM, Riddell RH, Skinner DB, et al: Malignant transformation of esophageal columnar epithelium. *Cancer* 41:554–561, 1978.
122. Hamilton SR, Smith RRL: The relationship between columnar epithelial dysplasia and invasive adenocarcinoma arising in Barrett's esophagus. *Am J Clin Pathol* 87:301–312, 1987.
123. Reid BJ, Weinstein WM, Lewin KJ, et al: Endoscopic biopsy can detect high-grade dysplasia or early adenocarcinoma in Barrett's esophagus without grossly recognizable neoplastic lesions. *Gastroenterology* 94:81–90, 1988.
124. Spechler SJ, Sharma P, Souza RF, et al: American Gastroenterological Association medical position statement on the management of Barrett's esophagus. *Gastroenterology* 140:1084–1091, 2011.
125. Sharma P, Morales TH, Bhattacharyya A, et al: Dysplasia in short-segment Barrett's esophagus: A prospective 3-year follow-up. *Am J Gastroenterol* 92:2012–2016, 1997.
126. Weston AP, Krmpotich PT, Cherian R, et al: Prospective long-term endoscopic and histological follow-up of short-segment Barrett's esophagus: Comparison with traditional long-segment Barrett's esophagus. *Am J Gastroenterol* 92:407–413, 1997.
127. Schnell TG, Sontag SJ, Chejfec G: Adenocarcinoma arising in tongues or short-segments of Barrett's esophagus. *Dig Dis Sci* 37:137–143, 1992.
128. Nishimaki T, Watanabe K, Suzuki T, et al: Early esophageal adenocarcinoma arising in a short-segment of Barrett's mucosa after total gastrectomy. *Am J Gastroenterol* 91:1856–1857, 1996.
129. Prasad GA, Wang KK, Buttar NS, et al: Long-term survival following endoscopic and surgical treatment of high-grade dysplasia in Barrett's esophagus. *Gastroenterology* 132:1226–1233, 2007.
130. Shaheen NJ, Sharma P, Overholt BF, et al: Radiofrequency ablation in Barrett's esophagus with dysplasia. *N Engl J Med* 360:2277–2288, 2009.
131. Bulsiewicz WJ, Kim HP, Dellon ES, et al: Safety and efficacy of endoscopic mucosal therapy with radiofrequency ablation for patients with neoplastic Barrett's esophagus. *Clin Gastroenterol Hepatol* 11:636–642, 2013.
132. Corley DA, Mehtani K, Quesenberry C, et al: Impact of endoscopic surveillance on mortality from Barrett's esophagus-associated esophageal adenocarcinoma. *Gastroenterology* 145:312–319, 2013.
133. Reid BJ, Blount PL, Rubin CE, et al: Flow-cytometric and histological progression to malignancy in Barrett's esophagus: Prospective endoscopic surveillance of a cohort. *Gastroenterology* 102:1212–1219, 1992.
134. Robaszkiewicz M, Reid BJ, Volant A, et al: Flow-cytometric DNA content analysis of esophageal squamous cell carcinomas. *Gastroenterology* 101:1588–1593, 1991.
135. McDonald GB, Brand DL, Thorning DR: Multiple adenomatous neoplasms arising in columnar-lined (Barrett's) esophagus. *Gastroenterology* 72:1317–1321, 1977.
136. Keefe EB, Hiskin EC, Schubert F: Adenomatous polyp arising in Barrett's esophagus. *J Clin Gastroenterol* 8:271–274, 1986.
137. Recht MP, Levine MS, Katzka DA, et al: Barrett's esophagus in scleroderma: Increased prevalence and radiographic findings. *Gastrointest Radiol* 13:1–5, 1988.
138. Halpert RD, Laufer I, Thompson JJ, et al: Adenocarcinoma of the esophagus in patients with scleroderma. *AJR* 140:927–930, 1983.
139. Keen SJ, Dodd GD, Smith JL: Adenocarcinoma arising in Barrett's esophagus: Pathologic and radiologic features. *Mt Sinai J Med* 51:442–450, 1984.
140. Kalish RJ, Clancy PE, Orringer MB, et al: Clinical, epidemiologic, and morphologic comparison between adenocarcinomas arising in Barrett's esophageal mucosa and in the gastric cardia. *Gastroenterology* 86:461–467, 1984.
141. Dupas JL, Caproy JP, Loriaux A: Endoscopic diagnosis of early primary adenocarcinoma in Barrett's columnar-lined esophagus. *Endoscopy* 7:98–101, 1975.
142. Wong A, Fitzgerald RC: Epidemiologic risk factors for Barrett's esophagus and associated adenocarcinoma. *Clin Gastroenterol Hepatol* 3:1–10, 2005.
143. Odes HS, Maor E, Barki Y, et al: Varicoid carcinoma of the esophagus: Report of a patient with adenocarcinoma and review of the literature. *Am J Gastroenterol* 73:141–145, 1980.
144. Montesi A, Alessandro P, Graziani L, et al: Small benign tumors of the esophagus: Radiological diagnosis with double contrast examination. *Gastrointest Radiol* 8:207–212, 1983.
145. Levine MS, Cajade AG, Herlinger H, et al: Pseudomembranes in reflux esophagitis. *Radiology* 159:43–45, 1986.
146. Levine MS, Maccones AJ, Laufer I: *Candida* esophagitis: Accuracy of radiographic diagnosis. *Radiology* 154:581–587, 1985.
147. Glick SN, Teplick SK, Goldstein J, et al: Glycogenic acanthosis of the esophagus. *AJR* 139:683–688, 1982.
148. Itai Y, Kogure T, Okuyama Y, et al: Diffuse finely nodular lesions of the esophagus. *AJR* 128:563–566, 1977.
149. Itai Y, Kogure T, Okuyama Y, et al: Radiological manifestations of oesophageal involvement in acanthosis nigricans. *Br J Radiol* 49:592–593, 1976.
150. Nuwayhid NS, Ballard ET, Cotton R: Esophageal papillomatosis. *Ann Otol Rhinol Laryngol* 86:623–625, 1977.
151. Levine MS, Kressel HY, Caroline D, et al: Barrett esophagus: Reticular pattern of the mucosa. *Radiology* 147:663–667, 1983.

152. Agha FP, Whitehouse WM: Carcinoma of the esophagus: Its varied radiologic features. *Mt Sinai J Med* 51:430–441, 1984.
153. Agha FP, Keren DF: Spindle-cell squamous carcinoma of the esophagus: A tumor with biphasic morphology. *AJR* 145:541–545, 1985.
154. Yoo CC, Levine MS, McLarney JK, et al: Primary malignant melanoma of the esophagus: Radiographic findings in seven patients. *Radiology* 209:455–459, 1998.
155. Levine MS, Buck JL, Pantongrag-Brown L, et al: Fibrovascular polyps of the esophagus: Clinical, radiographic, and pathologic findings in 16 patients. *AJR* 166:781–787, 1996.
156. Caruso RD, Berk RN: Lymphoma of the esophagus. *Radiology* 95:381–382, 1970.
157. Engelman RM, Scialla AV: Carcinoma of the esophagus presenting radiologically as a benign lesion. *Dis Chest* 53:652–655, 1968.
158. Kim TJ, Kim HY, Lee KW, et al: Multimodality assessment of esophageal cancer: Preoperative staging and monitoring of response to therapy. *Radiographics* 29:403–421, 2009.
159. Absi A, Adelstein DJ, Rice T: Esophageal cancer. In Carey WD, editor: *Current Clinical Medicine*, ed 2. Philadelphia, 2010, WB Saunders/Elsevier, pp 643–648.
160. Varghese TK, Hofstetter WL, Rizk NP, et al: The Society of Thoracic Surgery guidelines on the diagnosis and staging of patients with esophageal cancer. *Ann Thorac Surg* 96:346–356, 2013.
161. Halvorsen RA, Thompson WM: CT of esophageal neoplasms. *Radiol Clin North Am* 27:667–685, 1989.
162. Akiyama H, Tsurumaru M, Kawamura T, et al: Principles of surgical treatment for carcinoma of the esophagus: Analysis of lymph node involvement. *Ann Surg* 194:438–445, 1981.
163. Thompson WM, Halvorsen RA, Foster WL, et al: Computed tomography for staging esophageal and gastroesophageal cancer: Reevaluation. *AJR* 141:951–958, 1983.
164. Coulomb M, Leas JF, Sarrazin R, et al: Computed tomography and esophageal carcinoma. *J Radiol* 62:475–487, 1981.
165. Picus D, Balfe DM, Koehler RE, et al: Computed tomography in the staging of esophageal carcinoma. *Radiology* 146:433–438, 1983.
166. Halvorsen RA, Thompson WM: CT of esophageal neoplasms. *Radiol Clin North Am* 27:667–685, 1989.
167. Lackner K, Weiland G, Koster O, et al: Computed tomography for tumors of the esophagus and stomach. *Fortschr Geb Rontgenstr Nuklearmed Ergänzungsband* 134:364–370, 1981.
168. Halvorsen RA, Magruder-Habib K, Foster W, et al: Esophageal cancer: Long-term follow-up of staging by computed tomography. *Radiology* 161:147–151, 1986.
169. Heidemann J, Schilling MK, Schmassmann A, et al: Accuracy of endoscopic ultrasonography in preoperative staging of esophageal carcinoma. *Dig Surg* 17:219–224, 2000.
170. Kelly S, Harris KM, Berry E, et al: A systematic review of the staging performance of endoscopic ultrasound in gastroesophageal carcinoma. *Gut* 49:534–539, 2001.
171. Koch J, Halvorsen RA, Thompson WM: Therapy hinges on staging in upper GI tract cancer. *Diagn Imaging* 15:74–81, 1993.
172. Menzel J, Domschke W: Gastrointestinal miniprobe sonography: The current status. *Am J Gastroenterol* 95:605–616, 2000.
173. Lightdale CJ, Kulkarni KG: Role of endoscopic ultrasonography in the staging and follow-up of esophageal cancer. *J Clin Oncol* 23:4483–4489, 2005.
174. Savides TJ: EUS FNA staging of esophageal cancer [editorial]. *Gastroenterology* 125:1883–1886, 2003.
175. Vasquez-Sequeiros E, Norton ID, Clain JE, et al: Impact of EUS-guided fine-needle aspiration on lymph node staging in patients with esophageal carcinoma. *Gastrointest Endosc* 53:751–757, 2001.
176. Kato H, Kuwano H, Nakajima M, et al: Comparison between positron emission tomography and computed tomography in the assessment of esophageal carcinoma. *Cancer* 94:921–928, 2002.
177. Imdahl A, Hentschel M, Kleimaier M, et al: Impact of FDG-PET for staging of esophageal cancer. *Langenbecks Arch Surg* 389:283–288, 2004.
178. Kato H, Miyazaki T, Nakajima M, et al: The incremental effect of positron emission tomography on diagnostic accuracy on the initial staging of esophageal cancer. *Cancer* 103:148–156, 2005.
179. Altorki NK, Skinner DB: Occult cervical nodal metastasis in esophageal cancer: Preliminary results of three-field lymphadenectomy. *J Thorac Cardiovasc Surg* 113:540–544, 1997.
180. Griffith JF, Chanc ACW, Ahuja AT, et al: Neck ultrasound in staging squamous oesophageal carcinoma—a high-yield technique. *Clin Radiol* 55:696–701, 2000.
181. Tachimori Y, Kato H, Watanabe H, et al: Neck ultrasonography for thoracic esophageal carcinoma. *Ann Thorac Surg* 57:1180–1183, 1994.
182. Van Overhagen H, Lameris JS, Berger MY, et al: Supraclavicular lymph node metastases in carcinoma of the esophagus and gastroesophageal junction: Assessment with CT, US, and US-guided fine-needle aspiration biopsy. *Radiology* 179:155–158, 1991.
183. Doldi SB, Lattuada E, Zappa MA, et al: Ultrasonographic evaluation of the cervical lymph nodes in preoperative staging of esophageal neoplasms. *Abdom Imaging* 23:275–277, 1998.
184. Natsugoe S, Yoshinaka H, Shimada M, et al: Assessment of cervical lymph node metastasis in esophageal carcinoma using ultrasonography. *Ann Surg* 229:62–66, 1999.
185. Beatty JD, DeBoer G, Rider WD: Carcinoma of the esophagus: Pre-treatment assessment, correlation of radiation treatment parameters with survival, and identification and management of radiation treatment failure. *Cancer* 43:2254–2267, 1979.
186. Parker EF, Gregorie HB: Carcinoma of the esophagus: Long-term results. *JAMA* 235:1018–1020, 1976.
187. Rosenberg JS, Franklin B, Steiger Z: Esophageal cancer: An inter-disciplinary approach. *Curr Probl Cancer* 11:1–52, 1981.
188. Levine MS, Langer J, Laufer I, et al: Radiation therapy of esophageal carcinoma: Correlation of clinical and radiographic findings. *Gastrointest Radiol* 12:99–105, 1987.
189. Pearson JG: The value of radiotherapy in the management of esophageal cancer. *AJR* 105:500–513, 1969.
190. Drucker MH, Mansour KA, Hatcher CR, et al: Esophageal carcinoma: An aggressive approach. *Ann Thorac Surg* 28:133–137, 1979.
191. Fraser RW, Wara WM, Thomas AN, et al: Combined treatment methods for carcinoma of the esophagus. *Radiology* 128:461–465, 1978.
192. Elkon D, Lee MS, Hendrickson FR: Carcinoma of the esophagus: Sites of recurrence and palliative benefits after definitive radiotherapy. *Int J Radiat Oncol Biol Phys* 4:615–620, 1978.
193. Leborgne R, Leborgne F, Barlocchi L: Cancer of the oesophagus: Results of radiotherapy. *Br J Radiol* 36:806–811, 1963.
194. Wara WM, Mauch PM, Thomas AN, et al: Palliation for carcinoma of the esophagus. *Radiology* 121:717–720, 1976.
195. Walsh TN, Noonan N, Hollywood D, et al: A comparison of multimodal therapy and surgery for esophageal adenocarcinoma. *N Engl J Med* 335:462–467, 1996.
196. Bosset JF, Gignoux M, Triboulet JP, et al: Chemoradiotherapy followed by surgery compared with surgery alone in squamous-cell cancer of the esophagus. *N Engl J Med* 337:161–167, 1997.

Other Malignant Tumors of the Esophagus

MARC S. LEVINE

CHAPTER OUTLINE

Metastases

Sites of Origin
Clinical Findings
Radiographic Findings
Differential Diagnosis

Secondary Achalasia

Pathogenesis
Clinical Findings
Radiographic Findings

Lymphoma

Clinical Findings
Radiographic Findings

Spindle Cell Carcinoma

Pathology
Clinical Findings
Radiographic Findings
Differential Diagnosis

Leiomyosarcoma

Clinical Findings
Radiographic Findings
Differential Diagnosis

Malignant Melanoma

Clinical Findings
Radiographic Findings
Differential Diagnosis

Kaposi's Sarcoma

Radiographic Findings

Small Cell Carcinoma

Radiographic Findings

Leukemia

Miscellaneous Tumors

Metastases

Esophageal metastases are found at autopsy in less than 5% of patients dying of carcinoma. Most cases result from direct invasion by primary malignant tumors of the stomach, lung, and neck or from contiguous involvement by tumor-containing lymph nodes in the mediastinum. These various forms of esophageal involvement by metastatic tumor produce characteristic radiographic findings that are discussed separately in later sections.

SITES OF ORIGIN

Carcinoma of the stomach accounts for about 50% of all esophageal metastases.¹ Tumors involving the gastric cardia or fundus may invade the distal esophagus by contiguous spread through the diaphragmatic hiatus. Carcinomas of the lung and breast are other less common causes of esophageal metastases.²⁻⁴ Most cases result from direct extension of tumor to the esophagus or from contiguous esophageal involvement by lymphadenopathy in the posterior mediastinum. The esophagus may also be involved by contiguous spread of malignant tumors in the neck, such as laryngeal, pharyngeal, and thyroid carcinomas. Rarely, the esophagus may be involved by hematogenous metastases from tumors arising in distant locations such as the kidney, liver, rectum, prostate, cervix, and skin.⁵⁻⁹ Thus, most malignant tumors are capable of metastasizing to the esophagus.

CLINICAL FINDINGS

Patients with esophageal metastases may present with dysphagia as a result of esophageal compression by enlarged mediastinal lymph nodes or actual invasion of the esophagus by tumor. Although the presence of esophageal metastases usually indicates a poor prognosis, some patients (particularly those with breast or lung cancer) may present with dysphagia as the initial manifestation of their disease.^{2,10} Also, patients with breast cancer often have late-onset metastases to the esophagus, with an average interval of approximately 8 years from the time of diagnosis to the development of dysphagia.^{4,11} When dysphagia occurs, these patients usually have widespread metastatic disease.^{3,11}

RADIOGRAPHIC FINDINGS

Direct Invasion

Direct invasion of the cervical or thoracic esophagus by carcinoma of the larynx, pharynx, thyroid, or lung produces characteristic findings on barium studies. Early invasion may be manifested by a smooth or slightly irregular indentation on the esophagus with gently sloping, obtuse borders and a contiguous soft tissue mass in the adjacent mediastinum or neck. The area of involvement may have a more serrated, scalloped, or nodular appearance as the esophageal wall is further infiltrated by tumor (Fig. 24-1). Eventually, there may be circumferential narrowing of the esophagus with mass effect, nodularity, ulceration, or obstruction (Fig. 24-2). Rarely, thyroid cancer invading the esophagus may be manifested by an expansile intraluminal mass, mimicking the appearance of a spindle cell carcinoma (see later, "Spindle Cell Carcinoma").¹²

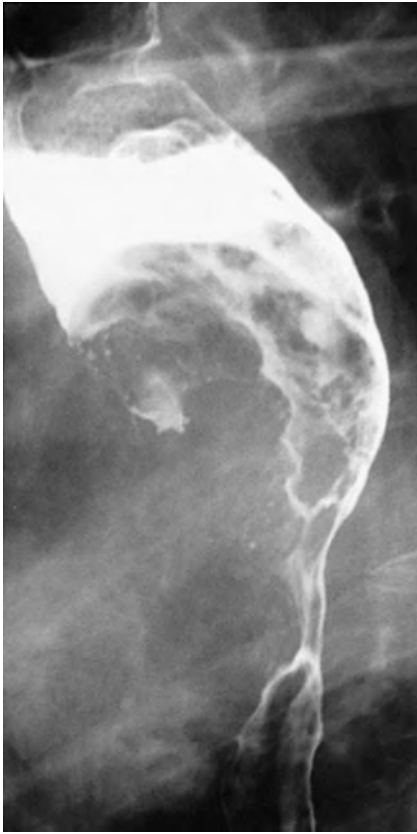


Figure 24-1 Direct esophageal invasion by carcinoma of the lung. There is eccentric mass effect and narrowing of the esophagus by tumor in the adjacent mediastinum. The scalloped contour of the esophagus in this region indicates direct invasion by tumor. (From Levine MS: *Radiology of the Esophagus*. Philadelphia, WB Saunders, 1989.)

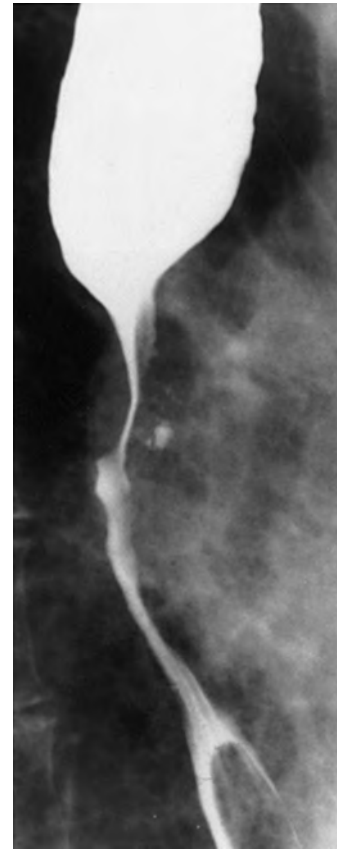


Figure 24-2 Direct esophageal invasion by carcinoma of the lung. This patient has a long segment of irregular narrowing in the midesophagus caused by circumferential involvement by metastatic tumor in the mediastinum. (Courtesy Robert A. Goren, MD, Philadelphia.)

Secondary esophageal involvement by carcinoma of the gastric cardia or fundus may be manifested radiographically by a polypoid mass extending from the fundus into the distal esophagus (Fig. 24-3) or by irregular narrowing of the distal esophagus without a discrete mass.^{13,14} Esophageal involvement is usually confined to a short segment of the distal esophagus but may extend as far proximally as the aortic arch.¹³ Occasionally, these tumors may cause smooth, tapered narrowing of the distal esophagus at or near the gastroesophageal junction, mimicking the appearance of achalasia (see later, “[Secondary Achalasia](#)”).

When the distal esophagus appears to be involved by tumor on barium studies, the gastric cardia and fundus should also be evaluated radiographically to determine whether there is associated gastric involvement. In some cases, barium studies may demonstrate an obvious malignant tumor in the stomach (see Fig. 24-3). In others, however, the presence of tumor in the gastric fundus may be recognized only by distortion or obliteration of the normal anatomic landmarks at the cardia associated with relatively subtle areas of nodularity, mass effect, or ulceration (Fig. 24-4).^{14,15} Thus, a meticulous double-contrast examination of the fundus is essential to rule out an underlying carcinoma of the cardia in these patients.

Contiguous Involvement by Mediastinal Lymph Nodes

Although any neoplasm that metastasizes to mediastinal lymph nodes may secondarily involve the esophagus, breast and lung cancer are the most common underlying malignant tumors in these patients.¹¹ Because of the proximity of the midesophagus to subcarinal lymph nodes, esophageal involvement by mediastinal lymphadenopathy usually occurs at this level.^{10,16} Barium studies typically reveal a smooth or slightly lobulated extrinsic indentation on the esophagus at or just below the carina (Fig. 24-5A).^{10,16} When tumor directly invades the esophagus, it may have a more irregular contour, often with areas of ulceration (Fig. 24-6).^{1,4,6} Eventually, the esophageal wall may be circumferentially infiltrated by tumor, producing an area of concentric narrowing with a surrounding soft tissue mass (Fig. 24-7).^{2,4,6} When esophageal involvement by mediastinal tumor is suspected on barium studies, CT should be performed to show the location and extent of lymphadenopathy in the mediastinum (Fig. 24-5B).

Hematogenous Metastases

True blood-borne or hematogenous metastases to the esophagus are extremely uncommon. Most cases are caused by

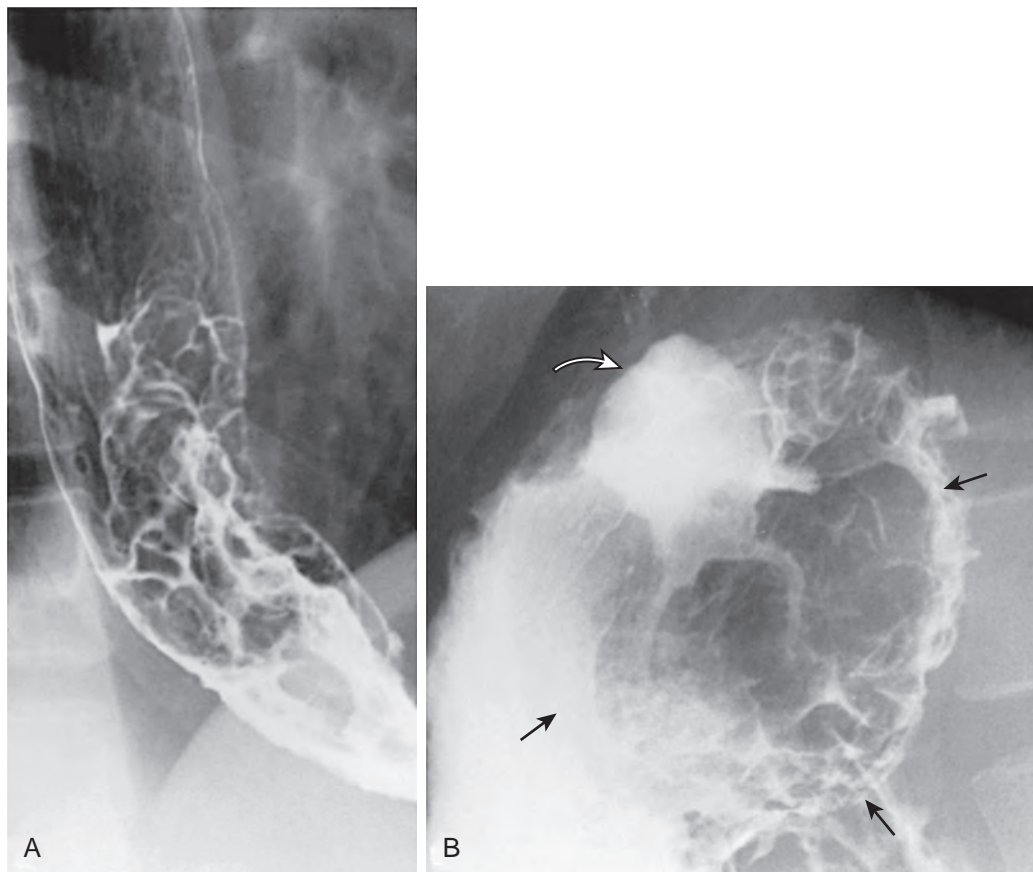


Figure 24-3 Direct esophageal invasion by gastric carcinoma. **A.** Double-contrast esophagogram shows a polypoid lesion in the distal esophagus that extends inferiorly to the gastroesophageal junction. **B.** Lateral view of the gastric fundus shows a large fundal mass (black arrows) containing an eccentric area of ulceration (white arrow). This patient had a primary gastric carcinoma invading the distal esophagus. (From Levine MS: *Radiology of the Esophagus*. Philadelphia, WB Saunders, 1989.)

carcinoma of the breast, but other distant tumors may also metastasize hematogenously to the esophagus. Surprisingly, however, malignant melanoma (which has the highest percentage of blood-borne metastases to the gastrointestinal tract) rarely involves the esophagus.^{5,9} Whatever the origin, blood-borne metastases to the esophagus usually appear on barium studies as short, eccentric strictures (usually in the middle third of the esophagus) with intact overlying mucosa and smooth, tapered margins (Fig. 24-8).^{1,4,6,17} Although blood-borne metastases to the esophagus tend to be infiltrating lesions, they occasionally may be manifested by one or more discrete submucosal masses or centrally ulcerated bull's-eye lesions.¹⁷

DIFFERENTIAL DIAGNOSIS

A smooth or slightly lobulated indentation on the esophagus may be caused by a variety of extrinsic mass lesions such as benign tumors and cysts in the mediastinum, aberrant vessels, and an ectatic aorta or aortic aneurysm compressing the esophagus. In contrast, esophageal invasion by metastatic tumor should be suspected when the area of mass effect has an irregular, serrated, or nodular contour or is associated with ulceration. As a result, malignant invasion of the esophagus usually can be

distinguished from benign lesions in the mediastinum that are compressing but not invading the esophagus.

The differential diagnosis for upper or midesophageal strictures caused by metastatic tumor includes Barrett's esophagus and scarring from mediastinal irradiation, caustic ingestion, eosinophilic esophagitis, or oral medications such as potassium chloride and quinidine. When these patients are known to have a previously irradiated malignant tumor in the thorax, the major diagnostic considerations include a benign radiation stricture and recurrent tumor. In such cases, computed tomography (CT) may be used to differentiate recurrent tumor from a radiation stricture by showing a mediastinal mass or lymphadenopathy in the region of the stricture.

Secondary Achalasia

The terms *secondary achalasia* and *pseudoachalasia* are used interchangeably to describe an entity in which the clinical, radiographic, endoscopic, and manometric features may be indistinguishable from those of primary, or idiopathic, achalasia. Malignancy-induced secondary achalasia is an uncommon condition, accounting for only 2% to 4% of patients with findings of achalasia at manometry.¹⁸ Almost 75% of

cases are caused by carcinoma of the gastric cardia or fundus directly invading the gastroesophageal junction or distal esophagus.^{19,20} Less frequently, hematogenous metastases from other malignant tumors such as breast, lung, pancreatic, uterine, and prostate cancer or even lymphoma involving the gastroesophageal junction may produce identical findings.^{8,19,21-23} Other benign causes of secondary achalasia include Chagas' disease, amyloidosis, and Nissen fundoplication.²⁴⁻²⁶ It is important to differentiate primary and secondary achalasia because primary achalasia may be treated by pneumatic dilation, botulinum toxin injection, or laparoscopic myotomy, whereas secondary achalasia often necessitates chemotherapy or other treatment for widespread metastatic disease.

PATHOGENESIS

Primary and secondary achalasia are characterized by absent esophageal peristalsis and a hypertensive lower esophageal sphincter that fails to relax normally in response to deglutition. In patients with primary achalasia, the motor disorder is thought to be caused by degeneration and loss of the ganglion cells of Auerbach's plexus in the esophagus. However, the precise mechanism whereby metastases produce this motility disorder is uncertain. Some patients have tumor directly invading the distal esophagus with actual destruction of myenteric ganglia.²⁷ However, others have tumor confined to the

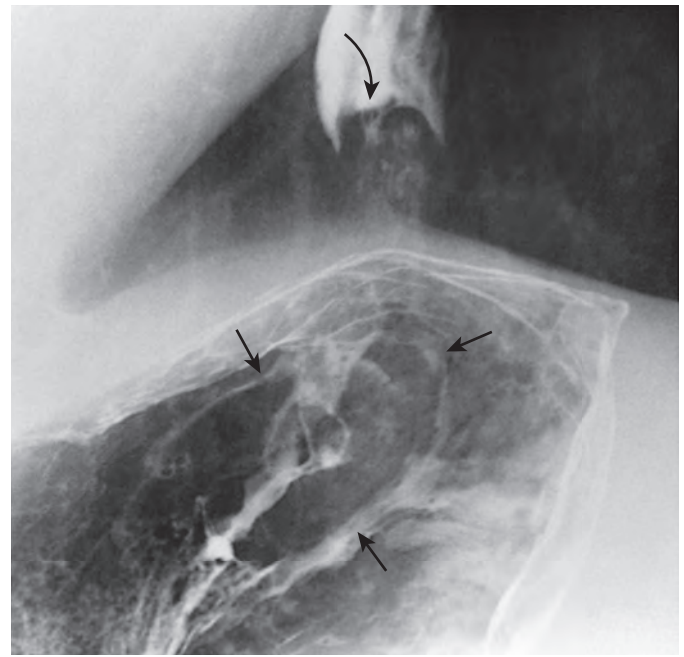


Figure 24-4 Direct esophageal invasion by carcinoma of the gastric cardia. Double-contrast view of the fundus shows obliteration of the normal anatomic landmarks at the cardia with a centrally ulcerated polypoid lesion (straight arrows) extending into the distal esophagus (curved arrow). (From Levine MS, Laufer I, Thompson JJ: Carcinoma of the gastric cardia in young people. *AJR* 140:69-72, 1983.)

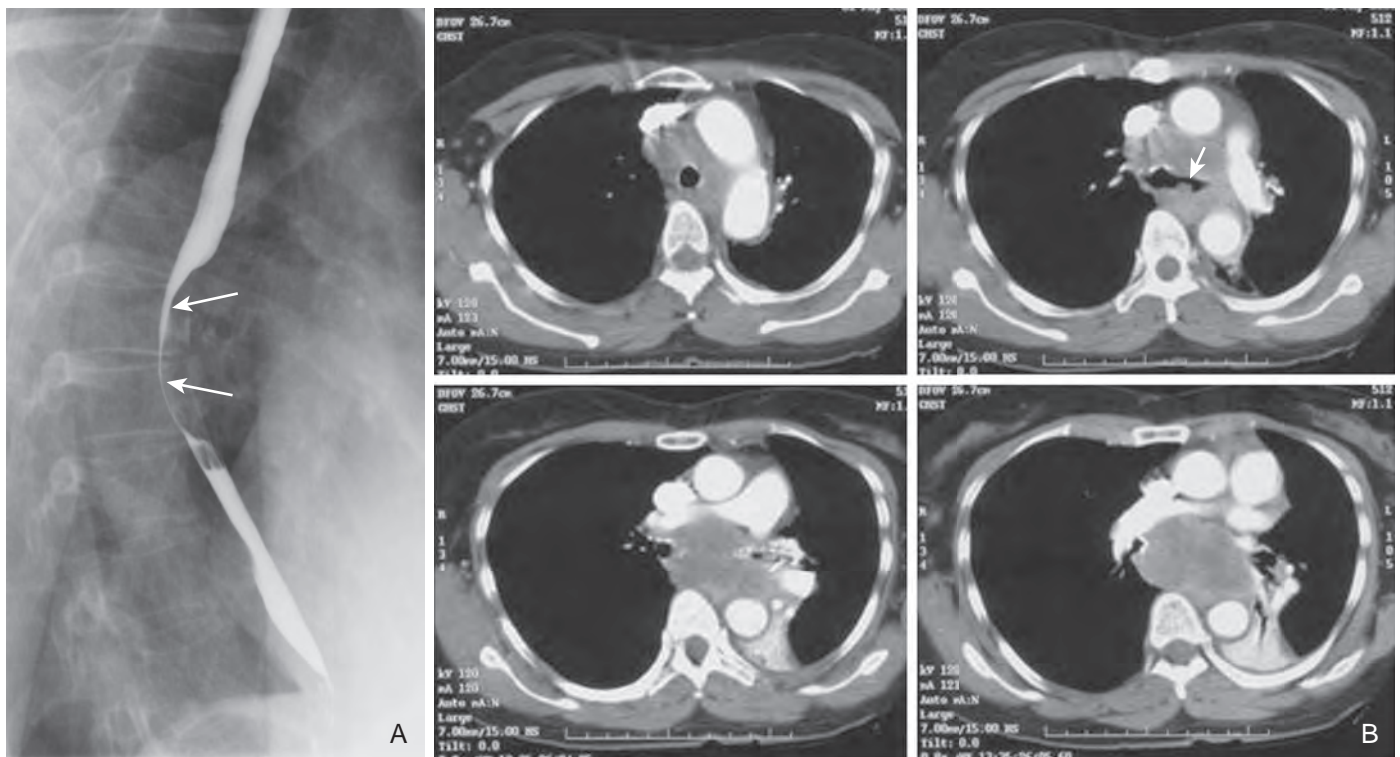


Figure 24-5 Esophageal compression by mediastinal lymphadenopathy from carcinoma of the lung. **A.** Barium study shows a large extrinsic indentation (arrows) on the anterolateral wall of the midesophagus just below the carina. **B.** CT scan shows bulky mediastinal and subcarinal adenopathy as the cause of this finding. An endobronchial lesion (arrow) is also seen in the left main bronchus near the carina. This patient was found to have a small cell carcinoma of the lung. (Courtesy Vincent Low, MD, Perth, Australia.)



Figure 24-6 Esophageal involvement by mediastinal lymphadenopathy from carcinoma of the cervix. There is eccentric mass effect on the midesophagus with an irregular contour and areas of ulceration caused by esophageal invasion by tumor in adjacent subcarinal nodes. (From Levine MS: *Radiology of the Esophagus*. Philadelphia, WB Saunders, 1989.)

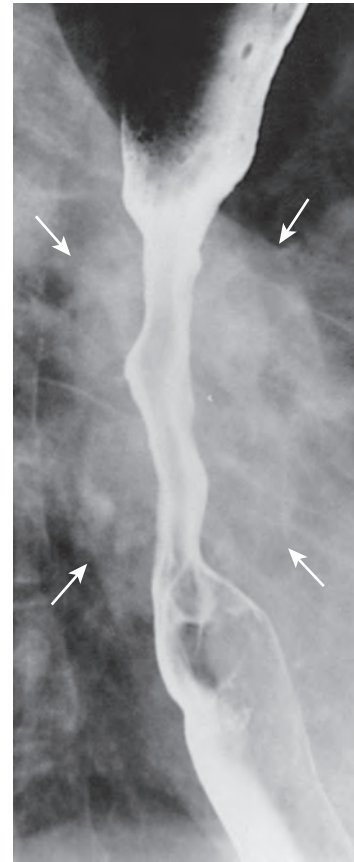


Figure 24-7 Circumferential esophageal involvement by metastatic breast cancer in the mediastinum. A relatively smooth, tapered area of narrowing is seen in the midesophagus. However, a surrounding soft tissue mass (arrows) in the mediastinum suggests esophageal encasement by lymphadenopathy. (From Levine MS: *Radiology of the Esophagus*. Philadelphia, WB Saunders, 1989.)

gastroesophageal junction without involvement of the neural plexus in the esophagus.²⁸ In such cases, the motor disorder may be caused by extraesophageal metastases to the vagus nerve or dorsal motor nucleus of the vagus nerve in the brain stem.^{20,28} Secondary achalasia may also occur as a paraneoplastic phenomenon caused by circulating tumor products that alter esophageal motor function.⁸ Finally, malignant neuroendocrine tumors (particularly small cell carcinoma of the lung) may express a variety of neural antigens that initiate an autoimmune response with circulating antibodies—known as anti-Hu antibodies—that cause neural degeneration and secondary achalasia.^{29,30}

CLINICAL FINDINGS

Although dysphagia occurs in primary and secondary achalasia, various clinical features are helpful for distinguishing these entities. Most patients with primary achalasia are between 20 and 50 years of age, and they have dysphagia for a mean duration of 4 to 6 years before seeking medical attention.^{18,31} In contrast, most patients with secondary achalasia are more than 60 years of age, and the duration of symptoms is usually less than 6 months.^{18,31} Secondary achalasia also is far more likely to

be associated with weight loss.³² An underlying malignant tumor should therefore be suspected whenever achalasia is diagnosed in older patients with recent onset of dysphagia and weight loss.^{18,31,32} Nevertheless, some patients with primary achalasia may be older than 60 years and others may have a relatively short duration of symptoms.^{31,33,34} Thus, it is not always possible to differentiate these conditions on clinical grounds.

RADIOGRAPHIC FINDINGS

Secondary achalasia is classically manifested on barium studies by absent esophageal peristalsis and smooth, tapered narrowing of the distal esophagus, producing a bird-beak configuration at or abutting the gastroesophageal junction (Fig. 24-9).^{8,19,31,35} Although the radiographic appearance may closely resemble that of primary achalasia, infiltration of the distal esophagus by tumor in secondary achalasia sometimes causes asymmetric or eccentric narrowing, abrupt transitions, rigidity, and mucosal nodularity or ulceration.^{31,35} Another important sign of malignancy is the length of the narrowed segment, which may extend 3.5 cm or more above the gastroesophageal junction in secondary achalasia (Fig. 24-10) but rarely extends this

far proximally in patients with primary achalasia.³¹ Finally, the degree of esophageal dilation is usually less in patients with secondary achalasia because of the rapid onset of disease.³¹ When findings of achalasia are present on barium studies, a narrowed distal esophageal segment longer than 3.5 cm with little or no proximal dilation in an older patient with recent onset of dysphagia should therefore be highly suggestive of secondary achalasia, even in the absence of other suspicious radiographic findings.³¹

Because secondary achalasia is usually caused by carcinoma of the gastric cardia or fundus invading the distal esophagus, careful radiologic evaluation of the fundus is essential in these patients. Not infrequently, an obvious polypoid, ulcerated, or infiltrating carcinoma may be demonstrated in the fundus (see Fig. 24-9B). With less advanced lesions, no gross abnormalities may be demonstrated in the gastric fundus on conventional single-contrast barium studies. However, double-contrast studies may reveal subtle evidence of tumor distorting or obliterating the normal anatomic landmarks at the gastric cardia (see Fig. 24-10).^{14,15} In contrast, the characteristic rosette that demarcates the gastric cardia on double-contrast studies should be normal in patients with primary achalasia.

CT is often helpful for differentiating primary and secondary achalasia. Patients with primary achalasia typically have little or no gastric esophageal wall thickening (Fig. 24-11A) and no evidence of mediastinal lymphadenopathy or a mass at the cardia on CT (Fig. 24-11B).^{36,37} In some cases, however, CT may reveal a pseudomass at the cardia because of inadequate distention of this region.³⁸ In contrast, patients with secondary achalasia often have a thickened wall in the distal esophagus on CT, and the thickened wall tends to be lobulated and asymmetric (Fig. 24-12A). CT may also reveal a soft tissue mass at the cardia (Fig. 24-12B), mediastinal lymphadenopathy, and the presence of pulmonary, pleural, or hepatic metastases.^{39,40} CT is also helpful for detecting the site of the primary tumor in patients with secondary achalasia caused by carcinoma of the gastric cardia or fundus, lung, or pancreas or other malignant neoplasms in the chest or abdomen.



Figure 24-8 Hematogenous metastasis to the esophagus from carcinoma of the breast. The lesion is manifested by a short, benign-appearing stricture (arrow) in the midesophagus. (From Levine MS: *Radiology of the Esophagus*. Philadelphia, WB Saunders, 1989.)

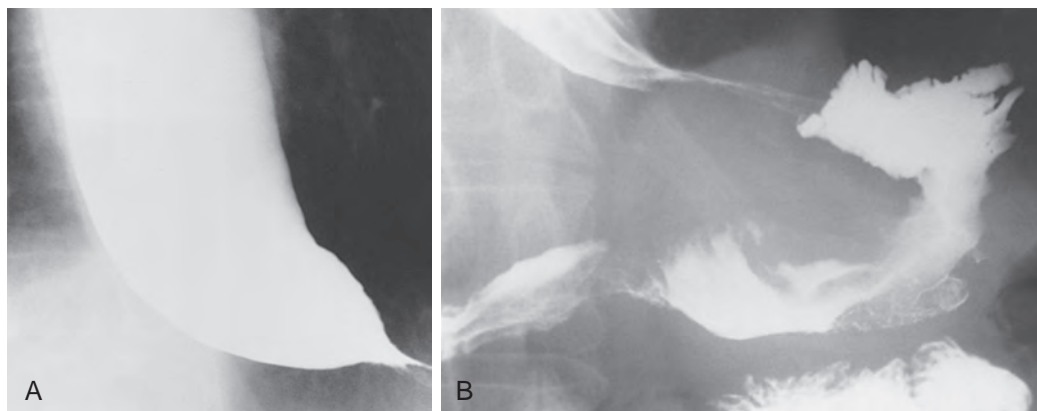


Figure 24-9 Secondary achalasia caused by gastric carcinoma. **A.** There is smooth, tapered narrowing of the distal esophagus, producing the characteristic bird-beak appearance of primary achalasia. **B.** However, a view of the stomach reveals a diffusely infiltrating carcinoma of the gastric body and fundus that has invaded the distal esophagus.



Figure 24-10 Secondary achalasia caused by carcinoma of the gastric cardia. There is smooth, tapered narrowing of the distal esophagus, but the narrowed segment extends a considerable distance from the gastroesophageal junction (a finding not often seen in patients with primary achalasia). Also note how the tumor causes marked nodularity of the gastric fundus with obliteration of the normal anatomic landmarks at the cardia. (From Levine MS: *Radiology of the Esophagus*. Philadelphia, WB Saunders, 1989.)

Lymphoma

The esophagus is the least common site of gastrointestinal involvement by lymphoma, accounting for only about 1% of cases.⁴¹ Both non-Hodgkin's and, less commonly, Hodgkin's lymphoma may involve the esophagus. These patients almost always have generalized lymphoma with direct invasion of the esophagus by lymphomatous nodes in the mediastinum, contiguous spread of lymphoma from the gastric fundus, or synchronous development of lymphoma in the esophagus.⁴²⁻⁴⁵ Rarely, primary esophageal lymphoma (usually Hodgkin's lymphoma) may occur without extraesophageal disease.⁴⁶⁻⁵¹ Cases of AIDS-related primary esophageal lymphoma have also been reported.^{52,53} When esophageal lymphoma is suspected, endoscopy should be performed with deep esophageal biopsy specimens to confirm the diagnosis. However, false-negative biopsy specimens have been reported in 25% to 35% of cases because of the patchy nature of the disease and sampling error.⁵¹ Thus, some patients may require surgery for a definitive diagnosis.

CLINICAL FINDINGS

Most patients with esophageal lymphoma have no esophageal symptoms, so the diagnosis is usually made at autopsy in patients with widespread disease.^{41,42} However, some patients may develop dysphagia as a result of esophageal narrowing or obstruction by tumor.^{42,43} Rarely, they may present with dysphagia as the initial manifestation of their disease.⁵⁴

RADIOGRAPHIC FINDINGS

Secondary involvement of the esophagus by gastric lymphoma may be manifested on barium studies by irregular narrowing of the distal esophagus caused by contiguous

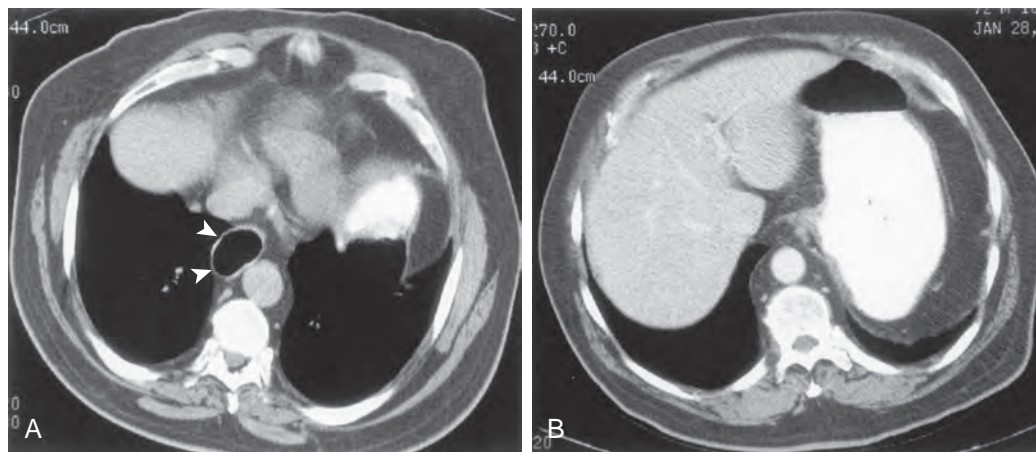


Figure 24-11 Primary achalasia on CT. A. CT scan shows a dilated esophagus (arrowheads) without esophageal wall thickening or mediastinal adenopathy. **B.** Another scan more caudally shows no evidence of a soft tissue mass at the gastroesophageal junction. (Note barium in the gastric fundus.) This patient had long-standing primary achalasia.

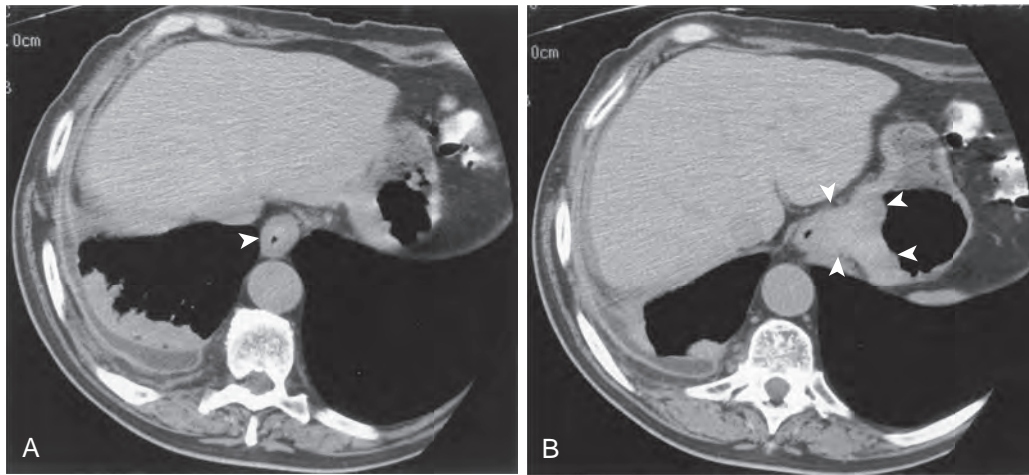


Figure 24-12 Secondary achalasia on CT. A. CT scan shows asymmetric thickening of the esophageal wall (arrowhead) in the distal esophagus at the level of beaklike narrowing seen on a prior barium study (not shown). **B.** Another CT image more caudally shows an asymmetric soft tissue mass (arrowheads) at the gastroesophageal junction protruding into the medial aspect of the gas-filled fundus. This patient had a carcinoma of the cardia causing secondary achalasia.

spread of tumor from the gastric fundus (Fig. 24-13).^{42-44,55} In such cases, careful radiologic examination of the gastric cardia and fundus may demonstrate a polypoid, ulcerated, or infiltrating lesion in the fundus secondary to the underlying gastric lymphoma. Transcardiac extension of gastric lymphoma is thought to occur in about 10% of patients.⁵⁵ However, these lesions cannot be distinguished radiographically from carcinoma of the gastric fundus invading the distal esophagus.

Mediastinal lymphoma may cause extrinsic compression of the esophagus, resulting in a smooth indentation with obtuse, gently sloping borders.⁴² Further esophageal involvement may be manifested by a more irregular or serrated contour abnormality secondary to invasion of the wall by tumor. Eventually, mediastinal lymphoma may cause diffuse esophageal narrowing (Fig. 24-14A). CT is particularly useful for determining the extent of disease in the mediastinum (Fig. 24-14B). Other patients may develop esophageal-airway fistulas, usually as a complication of radiation therapy.^{56,57}

Intrinsic esophageal lymphoma may be manifested by a spectrum of abnormalities, including submucosal nodules, enlarged folds, polypoid masses, and strictures. The most common finding is a polypoid or ulcerated mass or an infiltrating lesion indistinguishable from esophageal carcinoma (Fig. 24-15).^{42-44,48-52} Less frequently, lymphomatous infiltration of the submucosa may result in enlarged, tortuous longitudinal folds, mimicking the appearance of varices.⁴²⁻⁴⁵ Occasionally, discrete submucosal masses may be found in the esophagus, suggesting multiple leiomyomas.^{43,44} Other patients may have innumerable small submucosal nodules in the esophagus (Fig. 24-16).^{58,59} Although leukemic infiltrates, hematogenous metastases, and Kaposi's sarcoma have also been described as unusual causes of submucosal nodules, the lesions tend to be larger and less numerous in these patients. Rarely, esophageal lymphoma may cause aneurysmal dilation similar to that found in the small intestine.⁵¹

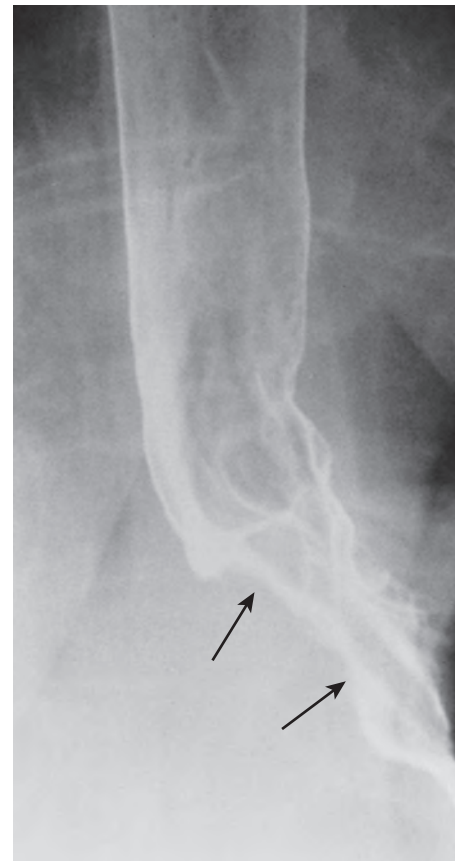


Figure 24-13 Esophageal involvement by gastric lymphoma. There is irregular narrowing (arrows) of the distal esophagus caused by contiguous spread of lymphoma from the gastric fundus. Carcinoma of the gastric cardia invading the distal esophagus could produce identical findings. (From Levine MS: *Radiology of the Esophagus*. Philadelphia, WB Saunders, 1989.)

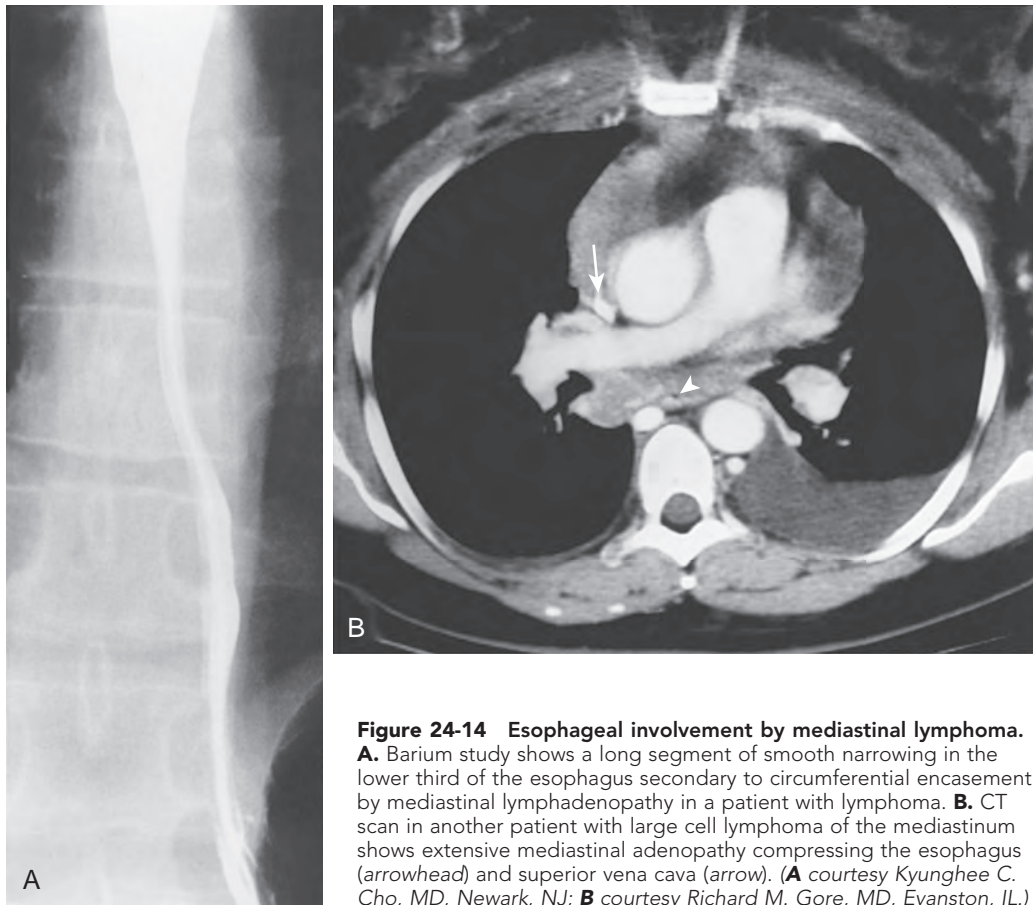


Figure 24-14 Esophageal involvement by mediastinal lymphoma. **A.** Barium study shows a long segment of smooth narrowing in the lower third of the esophagus secondary to circumferential encasement by mediastinal lymphadenopathy in a patient with lymphoma. **B.** CT scan in another patient with large cell lymphoma of the mediastinum shows extensive mediastinal adenopathy compressing the esophagus (arrowhead) and superior vena cava (arrow). (**A** courtesy Kyunghie C. Cho, MD, Newark, NJ; **B** courtesy Richard M. Gore, MD, Evanston, IL.)

Spindle Cell Carcinoma

Malignant polypoid epithelial tumors of the esophagus containing both carcinomatous and sarcomatous elements are exceedingly uncommon, accounting for only 0.5% to 1.5% of all esophageal neoplasms.⁶⁰ Terms formerly used to describe these lesions include *carcinosarcoma*, *pseudosarcoma*, *polypoid carcinoma*, and *spindle cell variant of squamous cell carcinoma*. However, many investigators believe that these lesions represent various expressions of a single malignant tumor, which has been designated *spindle cell squamous carcinoma* or, simply, *spindle cell carcinoma*.⁶¹⁻⁶³

PATHOLOGY

In the past, carcinosarcomas of the esophagus were thought to contain a mixture of carcinomatous and sarcomatous elements.^{64,65} In contrast, pseudosarcomas were thought to be composed primarily of sarcoma-like spindle cells with adjacent areas of squamous cell carcinoma.⁶⁶⁻⁶⁸ Because the sarcomatous portion of the tumor rarely metastasized to other structures, pseudosarcomas were thought to be less aggressive lesions that had a better prognosis than carcinosarcomas.⁶⁵ In subsequent studies, however, it was shown that metastases also occurred

from the sarcomatous portion of so-called pseudosarcomas and that these lesions behaved as aggressively as carcinosarcomas.^{61,69} Thus, carcinosarcoma and pseudosarcoma appear to be the same pathologic entity, with varying degrees of anaplastic spindle cell metaplasia of the carcinomatous portion of the tumor.^{61,63,70}

CLINICAL FINDINGS

Patients with spindle cell carcinoma almost always present with dysphagia and weight loss.⁷¹ Most patients are older men who often have a history of cigarette smoking or alcohol consumption.^{68,71} The clinical presentation is therefore indistinguishable from that of squamous cell carcinoma.

It has been suggested that spindle cell carcinoma has a better prognosis than squamous cell carcinoma because these tumors tend to remain superficial, with local invasion and regional or distant metastases occurring late in the course of the disease.^{64,72} However, other investigators have found that as many as 50% of patients with spindle cell carcinoma have metastatic disease at the time of diagnosis, and the overall 5-year survival rate is only 2% to 8%.^{65,71} Thus, the prognosis of this tumor is probably comparable to that of squamous cell carcinoma.



Figure 24-15 Primary AIDS-related non-Hodgkin's lymphoma of the esophagus. There is an irregular, ulcerated area of narrowing with a shelflike proximal border in the distal thoracic esophagus. This lesion is indistinguishable from an advanced esophageal carcinoma. (Courtesy Jackie Brown, MD, Vancouver, Canada.)

RADIOGRAPHIC FINDINGS

Spindle cell carcinomas tend to be located in the mid or lower esophagus, appearing on barium studies as large polypoid masses that expand or dilate the lumen without causing obstruction (Fig. 24-17).^{62,63,65,69,72} Similarly, CT may reveal a bulky mass expanding the lumen of the esophagus. In some cases, barium may form a dome over the intraluminal portion of the tumor, producing a cupola effect.^{62,63,65} Occasionally, a broad-based or narrow pedicle may be observed.^{62,63,68,69} Rarely, torsion of the pedicle results in spontaneous sloughing of the tumor.⁶⁸ Spindle cell carcinomas usually can be differentiated from squamous cell carcinomas and adenocarcinomas because the latter tumors tend to infiltrate and narrow the lumen, producing very different radiographic findings.⁷³ Rarely, however, spindle cell carcinomas may be infiltrating lesions indistinguishable from squamous cell carcinomas or adenocarcinomas.^{65,71}

DIFFERENTIAL DIAGNOSIS

The differential diagnosis for an expansile polypoid intraluminal mass includes other benign and malignant tumors of the esophagus. Benign lesions such as a giant fibrovascular polyp or leiomyoma may occasionally produce similar findings, but these

lesions tend to have a smoother contour and are less lobulated.⁷⁴ Primary malignant melanoma of the esophagus is another rare neoplasm characterized by an expansile intraluminal mass indistinguishable from spindle cell carcinoma (see later, “**Malignant Melanoma**”). Other unusual malignant tumors of the esophagus, such as lymphoma, leiomyosarcoma, and Kaposi's sarcoma, might also be considered. A definitive diagnosis of spindle cell carcinoma can therefore be made only on histologic grounds.

Leiomyosarcoma

Leiomyosarcomas of the esophagus are rare, low-grade, malignant tumors characterized by slow growth and late metastases.^{75,76} These tumors are almost always thought to arise de novo rather than from preexisting leiomyomas.^{77,78} They are usually located in the distal two thirds of the esophagus because this is the portion of the esophagus that is lined by smooth muscle.^{79,80} The lesions may eventually spread by direct extension to the pleura, pericardium, diaphragms, and stomach, or they may metastasize hematogenously to the liver, lungs, and bones.^{76,78,79} Because of their relatively slow growth rates, esophageal leiomyosarcomas have a better prognosis than squamous cell carcinomas, with 5-year survival rates approaching 35%.^{79,81} Nevertheless, rapid progression of esophageal leiomyosarcomas has occasionally been documented.⁸¹ Leiomyosarcomas involving the esophagus should be differentiated from gastrointestinal stromal tumors (GISTs), which also have malignant potential (see Chapter 22).

CLINICAL FINDINGS

Esophageal leiomyosarcomas are usually found in middle-aged or older patients^{76,82} and are slightly more common in men than in women.^{79,82} Dysphagia is the most common presenting clinical complaint, but dysphagia can be minimal or absent if the tumor has a predominantly exophytic pattern of growth with little encroachment on the lumen.⁸³ When dysphagia does occur, it is often present for a longer interval (6-12 months) than in patients with esophageal carcinoma because of slower growth of these tumors.⁷⁹ Although rare, gastrointestinal bleeding may occur if the lesion is ulcerated.⁷⁷

An esophagectomy or esophagogastrectomy is the treatment of choice for esophageal leiomyosarcomas.^{76,79,80,82} Even when metastases are present, resection of the primary tumor may lead to prolonged survival of these patients. Because leiomyosarcomas are radiosensitive, bulky lesions can be palliated by radiation therapy in nonsurgical candidates.^{76,79,80}

RADIOGRAPHIC FINDINGS

Esophageal leiomyosarcomas sometimes contain large exophytic components that can be recognized on chest radiographs by the presence of a mediastinal mass.^{76,83,84} Rarely, chest radiographs reveal dense calcification within the tumor.⁸⁵ Leiomyosarcomas typically appear on barium studies as large, lobulated intramural masses containing areas of ulceration or tracking (Fig. 24-18A).⁸³ These tumors therefore have the same radiographic features as malignant GISTs in the stomach and small bowel. Less commonly, they appear as polypoid, expansile intraluminal masses or as infiltrative lesions with irregular luminal narrowing.^{75,78,83,84,86}

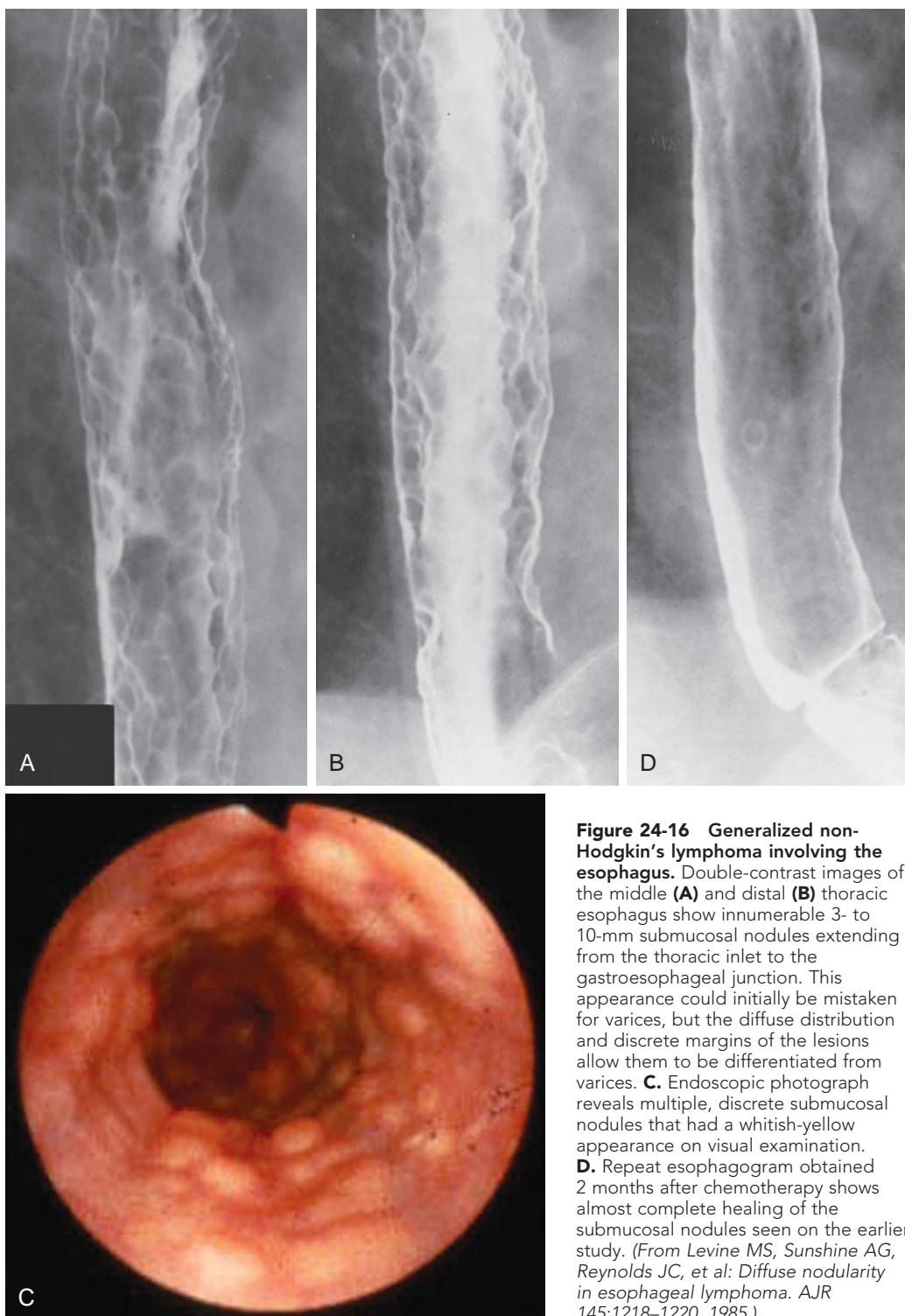


Figure 24-16 Generalized non-Hodgkin's lymphoma involving the esophagus. Double-contrast images of the middle (**A**) and distal (**B**) thoracic esophagus show innumerable 3- to 10-mm submucosal nodules extending from the thoracic inlet to the gastroesophageal junction. This appearance could initially be mistaken for varices, but the diffuse distribution and discrete margins of the lesions allow them to be differentiated from varices. **C.** Endoscopic photograph reveals multiple, discrete submucosal nodules that had a whitish-yellow appearance on visual examination. **D.** Repeat esophagogram obtained 2 months after chemotherapy shows almost complete healing of the submucosal nodules seen on the earlier study. (From Levine MS, Sunshine AG, Reynolds JC, et al: Diffuse nodularity in esophageal lymphoma. *AJR* 145:1218-1220, 1985.)



Figure 24-17 Spindle cell carcinoma of the esophagus. There is a large polypoid intraluminal mass in the midesophagus that expands the lumen without causing obstruction. This appearance is typical of spindle cell carcinoma but can also be seen with primary malignant melanoma of the esophagus (see Fig. 24-19). (From Laufer I, Levine MS [eds]: *Double Contrast Gastrointestinal Radiology*, 2nd ed. Philadelphia, WB Saunders, 1992.)

Esophageal leiomyosarcomas are characterized on CT by heterogeneous masses containing large exophytic components, central areas of low density, and extraluminal gas or contrast material within the tumor secondary to necrosis and cavitation (Fig. 24-18B).^{78,80,81,83} Similar CT findings have been reported for malignant GISTs involving the stomach and small bowel.

Esophageal leiomyosarcomas may be manifested on magnetic resonance imaging (MRI) scans by esophageal masses that are isointense with skeletal muscle on T1-weighted images (Fig. 24-18C) and hyperintense on T2-weighted images (Fig. 24-18D).^{83,87} MRI may also reveal a central signal void caused by extraluminal gas within the tumor (see Figs. 24-18C and D).⁸³

Esophageal leiomyosarcomas are characterized on endoscopic sonography by well-defined hyperechoic masses arising from the muscular layer of the esophageal wall.⁸¹ These tumors can also be recognized on angiography as hypervascular masses with tumor vessels, dilated vascular channels or venous lakes, and early venous drainage.⁷⁸

DIFFERENTIAL DIAGNOSIS

Esophageal leiomyosarcomas that appear on barium studies as intramural masses must be differentiated from leiomyomas and other benign mesenchymal tumors in the esophagus. However, these benign intramural lesions tend to be smaller and less lobulated and rarely contain areas of ulceration or tracking. Leiomyosarcomas that appear as polypoid masses must be differentiated from spindle cell sarcoma, malignant melanoma, lymphoma, Kaposi's sarcoma, and a giant fibrovascular polyp, but the latter neoplasm usually has a much smoother contour and almost always arises in the cervical esophagus near the cricopharynx.⁷⁴ Finally, leiomyosarcomas that appear as infiltrative lesions must be differentiated from a squamous cell carcinoma or adenocarcinoma arising in Barrett's mucosa.⁷³

Malignant Melanoma

Primary malignant melanoma of the esophagus is a rare but aggressive tumor that accounts for less than 1% of all malignant esophageal neoplasms.⁸⁸ In the past, these lesions were thought to represent metastases from occult melanomas of the eye, skin, or anus. However, esophageal metastases are rarely found in patients with documented melanomas elsewhere.^{5,9} The seeming paradox of developing melanoma in a structure such as the esophagus is explained by the fact that small numbers of melanocytes are present in the esophageal mucosa in 2% to 8% of patients.⁸⁹⁻⁹¹ As in the skin, esophageal melanoma presumably develops because of malignant degeneration of these preexisting melanocytes. A review of the literature suggests that primary malignant melanoma is at least 10 times more common than metastatic melanoma involving the esophagus.⁸⁸

CLINICAL FINDINGS

Primary esophageal melanoma is an extremely aggressive tumor that is usually diagnosed in older adults. Most patients present with dysphagia and weight loss,⁸⁸ but the diagnosis is rarely suggested on clinical grounds. These tumors can sometimes be recognized at endoscopy as darkly pigmented masses, but pigmentation is not always apparent on visual inspection.⁸⁸ The treatment of primary esophageal melanoma is surgical; an extensive esophageal resection is usually performed. However, these tumors tend to be advanced lesions at the time of diagnosis. As a result, affected individuals have a dismal prognosis, with 5-year survival rates of less than 5% and an average overall survival of only 10 to 13 months from the time of diagnosis.^{88,92}

RADIOGRAPHIC FINDINGS

Esophageal melanomas have strikingly similar findings on barium studies, appearing as bulky, polypoid intraluminal masses that expand the esophagus without causing obstruction (Fig. 24-19).⁹³⁻⁹⁶ CT may also reveal a large soft tissue mass expanding the esophagus.^{95,96} These findings occur because melanoma tends to grow intraluminally along the long axis of the esophagus, producing a polypoid mass that widens the lumen as it enlarges.⁹⁵ Most esophageal melanomas are located in the lower half of the esophagus,⁸⁸ probably because of the greater concentration of melanocytes in this region.⁸⁹⁻⁹¹

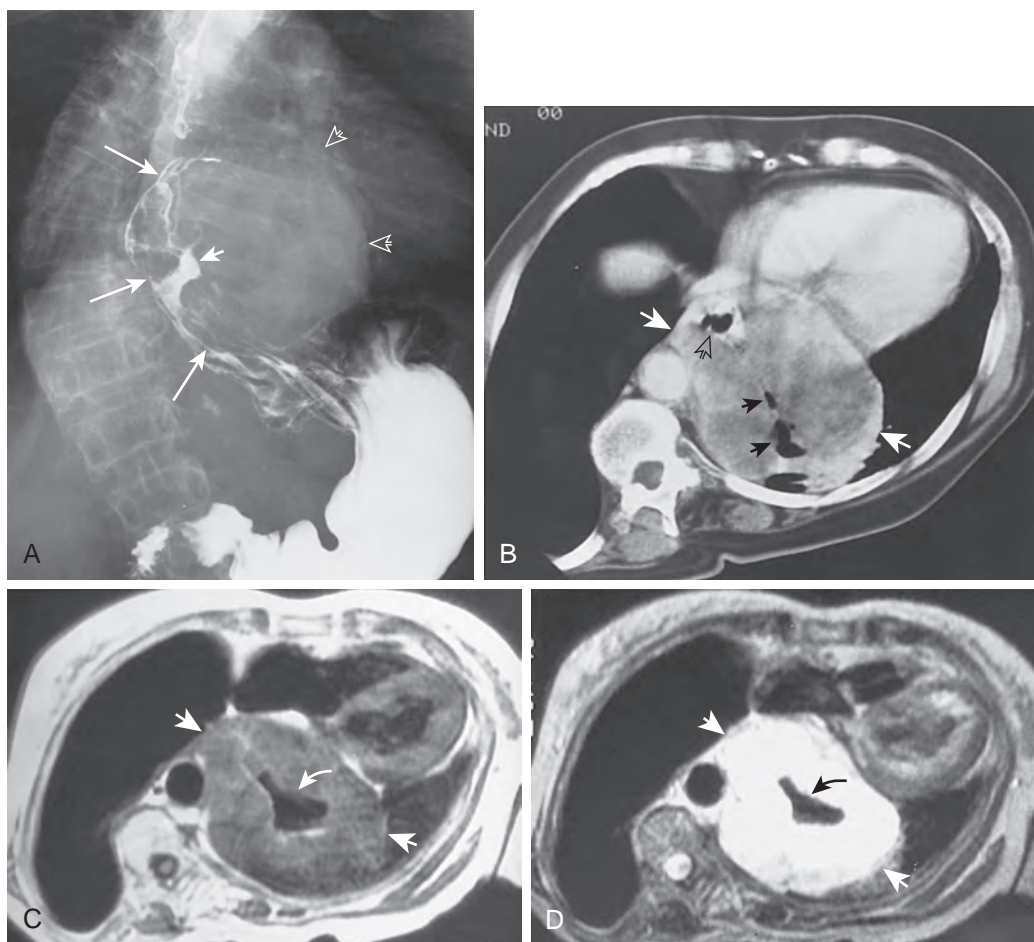


Figure 24-18 Esophageal leiomyosarcoma. **A.** Barium study shows a giant intramural mass (*large arrows*) with a bulky exophytic component in the mediastinum (*open arrows*). Note the relatively small central ulcer (*small arrow*) within the lesion. **B.** CT scan shows a heterogeneous mass (*white arrows*) in the left side of the mediastinum with central areas of low density. Note the extraluminal collections of gas (*solid black arrows*) within the lesion that are separate from the esophageal lumen (*open black arrow*). **C.** T1-weighted (TR/TE, 674/12) MRI scan also shows a mass (*straight arrows*) in the left side of the mediastinum. Note how the mass is isointense with skeletal muscle. **D.** T2-weighted (2697/80) MRI scan shows how the lesion (*straight arrows*) is markedly hyperintense relative to skeletal muscle. In both **C** and **D**, there is a focal area of signal void (*curved arrows*) caused by extraluminal gas within the tumor. (From Levine MS, Buck JL, Pantongrag-Brown L, et al: Leiomyosarcoma of the esophagus: Radiographic findings in 10 patients. *AJR* 167:27–32, 1996.)



Figure 24-19 Primary malignant melanoma of the esophagus. There is a polypoid mass expanding the lumen of the distal esophagus. This lesion cannot be distinguished from spindle cell carcinoma (see Fig. 24-17) or other rare malignant tumors of the esophagus. (From Yoo CC, Levine MS, McLarney JK, et al: *Primary malignant melanoma of the esophagus: Radiographic findings in seven patients. Radiology* 209:455–459, 1998.)

DIFFERENTIAL DIAGNOSIS

The major consideration in the differential diagnosis of a large polypoid intraluminal mass in the esophagus is spindle cell carcinoma.^{62,63,65} Other unusual tumors of the esophagus that may produce similar findings include leiomyosarcoma, lymphoma, and Kaposi's sarcoma. In contrast, squamous cell carcinoma and adenocarcinoma of the esophagus rarely appear as expansile esophageal masses because these tumors tend to infiltrate and narrow the lumen rather than expand it.

Kaposi's Sarcoma

Kaposi's sarcoma is a multifocal neoplasm of the reticuloendothelial system that is typically manifested by slow-growing cutaneous lesions on the lower extremities. However, a much more aggressive form of Kaposi's sarcoma has been found to develop in patients with AIDS. In studies from the 1980s, more than 30% of AIDS patients in the United States had Kaposi's sarcoma,⁹⁷ and about 50% of patients with Kaposi's sarcoma had gastrointestinal lesions, usually in the stomach or small bowel and occasionally in the esophagus.^{98–100} With the development of more effective medical therapy for the HIV virus to prevent the development of AIDs, however, gastrointestinal



Figure 24-20 Kaposi's sarcoma involving the esophagus. Multiple submucosal masses (arrows) are seen in the esophagus. This patient had additional submucosal lesions elsewhere in the gastrointestinal tract. (Courtesy Robert A. Goren, MD, Philadelphia.)

Kaposi's sarcoma is rarely encountered in modern medical practice.

RADIOGRAPHIC FINDINGS

Esophageal involvement by Kaposi's sarcoma may be manifested on barium studies by a single polypoid mass in the esophagus or by multiple submucosal lesions (Fig. 24-20).^{98,100} When multiple submucosal lesions are present, the differential diagnosis includes lymphoma and leukemia involving the esophagus. Kaposi's sarcoma should be suspected, however, when one or more discrete esophageal lesions are found in AIDS patients with associated skin lesions.

Small Cell Carcinoma

Primary small cell carcinoma of the esophagus is a rare but aggressive malignant tumor characterized by early metastases and a rapidly fatal course. The tumor may be derived from argyrophilic cells or Kulchitsky cells of neuroectodermal origin.^{90,101} Affected individuals typically present with rapidly progressive dysphagia and weight loss.^{102,103} These patients have a dismal prognosis, with an average survival of 6 months

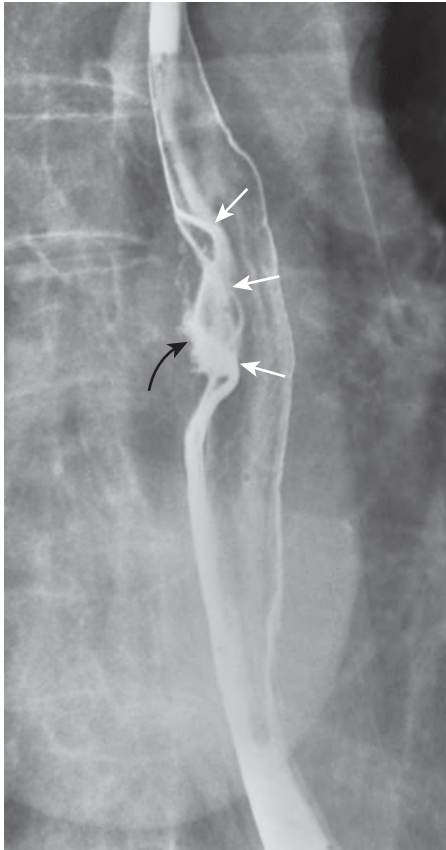


Figure 24-21 Small cell carcinoma of the esophagus. There is a smoothly margined, sessile mass (white arrows) containing a relatively flat central area of ulceration (black arrow) on the right posterolateral wall of the midesophagus below the level of the carina. Squamous cell carcinoma of the esophagus could produce identical findings. (From Levine MS, Pantongrag-Brown L, Buck JL, et al: *Small cell carcinoma of the esophagus: Radiographic findings*. Radiology 199:703–705, 1996.)

or less from the time of diagnosis.¹⁰¹⁻¹⁰³ Because of the likelihood of distant metastases, surgery has been recommended primarily for palliation, whereas combination radiation and chemotherapy has been advocated to improve patient survival.^{101,103,104}

RADIOGRAPHIC FINDINGS

Advanced small cell carcinomas of the esophagus may appear on barium studies as bulky polypoid or fungating masses, sometimes containing areas of ulceration or cavitation.^{62,105,106} Less advanced lesions may be characterized by strikingly similar radiographic findings, appearing as smoothly margined, sessile, centrally ulcerated masses, usually in the midesophagus near the level of the carina (Fig. 24-21).^{107,108} Although this appearance is more likely to be caused by squamous cell carcinoma, it is important to obtain endoscopic biopsy specimens because a preoperative histologic diagnosis of small cell carcinoma may dramatically alter the management of these patients. Rarely, regression of small cell carcinoma has been documented on follow-up barium studies after combination radiation and chemotherapy.¹⁰⁷

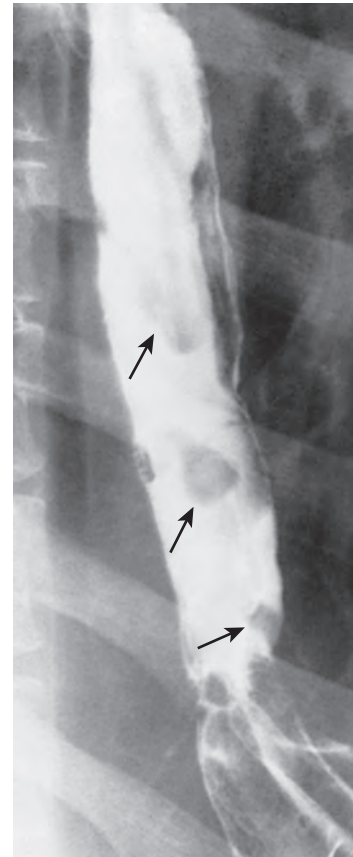


Figure 24-22 Leukemic infiltration of the esophagus. This patient has multiple submucosal masses (arrows) in the esophagus caused by leukemic deposits. (Courtesy Sadi R. Antonmattei, MD, Arecibo, Puerto Rico.)

Leukemia

Although rarely diagnosed before death, esophageal involvement by leukemia has been reported at autopsy in 2% to 13% of patients.^{109,110} These leukemic deposits may appear on barium studies as one or more discrete nodular elevations (Fig. 24-22).^{103,105} Coalescent intramural lesions may also be manifested by irregular areas of narrowing in the middle or distal third of the esophagus on barium studies (Fig. 24-23A) and by esophageal wall thickening on CT (Fig. 24-23B).¹¹¹ Rarely, bulky leukemic deposits may appear as polypoid lesions in the esophagus.¹¹² These leukemic implants may undergo marked regression after radiation therapy.¹¹¹ Esophageal symptoms may therefore be palliated by mediastinal irradiation, but the overall prognosis for this disease is unchanged.

Miscellaneous Tumors

Other rare malignant tumors in the esophagus include adenoid cystic carcinoma,^{113,114} chondrosarcoma,¹¹⁵ synovial sarcoma,¹¹⁶ and malignant carcinoid tumor.¹¹⁷ In general, sarcomas tend to be more polypoid than carcinomas, which are more infiltrating lesions. Nevertheless, a definitive diagnosis can be made only on histologic grounds.

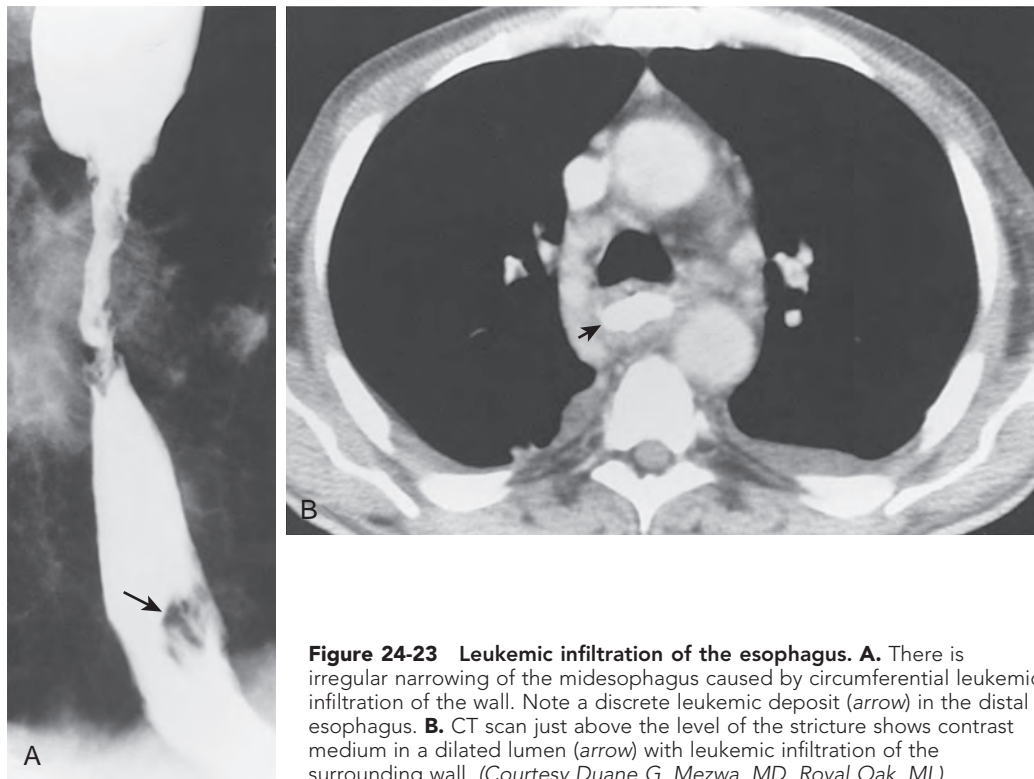


Figure 24-23 Leukemic infiltration of the esophagus. **A.** There is irregular narrowing of the midesophagus caused by circumferential leukemic infiltration of the wall. Note a discrete leukemic deposit (arrow) in the distal esophagus. **B.** CT scan just above the level of the stricture shows contrast medium in a dilated lumen (arrow) with leukemic infiltration of the surrounding wall. (Courtesy Duane G. Mezwa, MD, Royal Oak, MI.)

REFERENCES

1. Agha FP: Secondary neoplasms of the esophagus. *Gastrointest Radiol* 12:187–193, 1987.
2. Polk HC, Camp FA, Walker AW: Dysphagia and esophageal stenosis: Manifestation of metastatic mammary cancer. *Cancer* 20:2002–2007, 1967.
3. Holyoke ED, Nemoto T, Dao TL: Esophageal metastases and dysphagia in patients with carcinoma of the breast. *J Surg Oncol* 1:97–107, 1969.
4. Anderson MF, Harell GS: Secondary esophageal tumors. *AJR* 135:1243–1246, 1980.
5. Wood CB, Wood RAB: Metastatic malignant melanoma of the esophagus. *Am J Dig Dis* 20:786–789, 1975.
6. Fisher MS: Metastasis to the esophagus. *Gastrointest Radiol* 1:249–251, 1976.
7. Gore RM, Sparberg M: Metastatic carcinoma of the prostate to the esophagus. *Am J Gastroenterol* 77:358–359, 1982.
8. Feczko PJ, Halpert RD: Achalasia secondary to nongastrointestinal malignancies. *Gastrointest Radiol* 10:273–276, 1985.
9. Schneider A, Martini N, Burt ME: Malignant melanoma metastatic to the esophagus. *Ann Thorac Surg* 55:516–517, 1993.
10. Stankey RM, Roshe J, Sogocio RM: Carcinoma of the lung and dysphagia. *Dis Chest* 55:13–17, 1969.
11. Varanasi RV, Saltzman JR, Krims P, et al: Breast carcinoma metastatic to the esophagus: Clinicopathological and management features of four cases, and literature review. *Am J Gastroenterol* 90:1495–1499, 1995.
12. Cooney BS, Levine MS, Schnall MD: Metastatic thyroid carcinoma presenting as an expansile intraluminal esophageal mass. *Abdom Imaging* 20:20–22, 1995.
13. Balthazar EJ, Goldfine S, Davidian NM: Carcinoma of the esophagogastric junction. *Am J Gastroenterol* 74:237–243, 1980.
14. Freeny PC, Marks WM: Adenocarcinoma of the gastroesophageal junction: Barium and CT examination. *AJR* 138:1077–1084, 1982.
15. Levine MS, Laufer I, Thompson JJ: Carcinoma of the gastric cardia in young people. *AJR* 140:69–72, 1983.
16. Fleischner FG, Sachs E: Retrotracheal lymphadenopathy in bronchial carcinoma, revealed by the barium-filled esophagus. *AJR* 90:792–798, 1963.
17. Libshitz HI, Lindell MM, Dodd GD: Metastases to the hollow viscera. *Radiol Clin North Am* 20:487–499, 1982.
18. Parkman HP, Cohen S: Malignancy-induced secondary achalasia. *Dysphagia* 8:292–296, 1993.
19. Lawson TL, Dodds WJ: Infiltrating carcinoma simulating achalasia. *Gastrointest Radiol* 1:245–248, 1976.
20. McCallum RW: Esophageal achalasia secondary to gastric carcinoma: Report of a case and review of the literature. *Am J Gastroenterol* 71:24–29, 1979.
21. Joffe N: Right-angled narrowing of the distal oesophagus secondary to carcinoma of the tail of the pancreas. *Clin Radiol* 30:33–37, 1979.
22. Eaves R, Lambert J, Rees J, et al: Achalasia secondary to carcinoma of the prostate. *Dig Dis Sci* 28:278–284, 1983.
23. Davis JA, Kantrowitz PA, Chandler HL, et al: Reversible achalasia due to reticulum-cell sarcoma. *N Engl J Med* 293:130–132, 1975.
24. Ferreira-Santos R: Aperistalsis of the esophagus and colon (megaesophagus and megacolon) etiologically related to Chagas' disease. *Am J Dig Dis* 6:700–726, 1961.
25. Costigan DJ, Clouse RE: Achalasia-like esophagus from amyloidosis. *Dig Dis Sci* 28:763–765, 1983.
26. Wehrli NE, Levine MS, Rubesin SE, et al: Secondary achalasia and other esophageal motility disorders after laparoscopic Nissen fundoplication for gastroesophageal reflux disease. *AJR* 189:1464–1468, 2007.
27. Simeone J, Burrell M, Toffler R: Esophageal aperistalsis secondary to metastatic invasion of the myenteric plexus. *AJR* 127:862–864, 1976.
28. Shulze KS, Goresky CA, Jabbari M, et al: Esophageal achalasia associated with gastric carcinoma: Lack of evidence for widespread plexus destruction. *Can Med Assoc J* 112:857–864, 1975.
29. Lee HR, Lennon VA, Camilleri M, et al: Paraneoplastic gastrointestinal motor dysfunction: Clinical and laboratory characteristics. *Am J Gastroenterol* 96:373–379, 2001.
30. De Giorgio R, Bovara M, Barbara G, et al: Anti-HuD-induced neuronal apoptosis underlying paraneoplastic gut dysmotility. *Gastroenterology* 125:70–79, 2003.
31. Woodfield CA, Levine MS, Rubesin SE, et al: Diagnosis of primary versus secondary achalasia: Reassessment of clinical and radiographic criteria. *AJR* 175:727–731, 2000.
32. Tucker HJ, Snape WJ, Cohen SC: Achalasia secondary to carcinoma: Manometric and clinical features. *Ann Intern Med* 89:315–318, 1978.
33. Sandler RS, Bozymski EM, Orlando RC: Failure of clinical criteria to distinguish between primary achalasia and achalasia secondary to tumor. *Dig Dis Sci* 27:209–213, 1982.

34. Tracey JP, Traube M: Difficulties in the diagnosis of pseudoachalasia. *Am J Gastroenterol* 89:2014–2018, 1994.
35. Seaman WB, Wells J, Flood CA: Diagnostic problems of esophageal cancer: Relationship to achalasia and hiatus hernia. *AJR* 90:778–791, 1963.
36. Tishler JM, Shin MS, Stanley RJ, et al: CT of the thorax in patients with achalasia. *Dig Dis Sci* 28:692–697, 1983.
37. Rabushka LS, Fishman EK, Kuhlman JE: CT evaluation of achalasia. *J Comput Assist Tomogr* 15:434–439, 1991.
38. Marks WM, Callen PW, Moss AA: Gastroesophageal region: Source of confusion on CT. *AJR* 136:359–362, 1981.
39. Carter M, Deckmann RC, Smith RC, et al: Differentiation of achalasia from pseudoachalasia by computed tomography. *Am J Gastroenterol* 92:624–628, 1997.
40. Ba-Ssalamah A, Zacherl J, Noebauer-Huhmann IM, et al: Dedicated multi-detector CT of the esophagus: spectrum of diseases. *Abdom Imag* 34:3–18, 2009.
41. Rosenberg SA, Diamond HD, Jaslowitz B, et al: Lymphosarcoma: A review of 1,269 cases. *Medicine (Baltimore)* 40:31–84, 1961.
42. Caruso RD, Berk RN: Lymphoma of the esophagus. *Radiology* 95:381–382, 1970.
43. Carnovale RL, Goldstein HM, Zornoza J, et al: Radiologic manifestations of esophageal lymphoma. *AJR* 128:751–754, 1977.
44. Zornoza J, Dodd GD: Lymphoma of the gastrointestinal tract. *Semin Roentgenol* 15:272–287, 1980.
45. Levine MS, Rubesin SE, Pantongrag-Brown L, et al: Non-Hodgkin's lymphoma of the gastrointestinal tract: Radiographic findings. *AJR* 168:165–172, 1997.
46. Stein HA, Murray D, Warner HA: Primary Hodgkin's disease of the esophagus. *Dig Dis Sci* 26:457–461, 1981.
47. Doki T, Hamada S, Murayama H, et al: Primary malignant lymphoma of the esophagus. *Endoscopy* 16:189–192, 1984.
48. Taal BG, Van Heerde P, Somers R: Isolated primary oesophageal involvement by lymphoma: A rare cause of dysphagia: Two case histories and a review of other published data. *Gut* 34:994–998, 1993.
49. Oguzkurt L, Karabulut N, Cakmakci E, et al: Primary non-Hodgkin's lymphoma of the esophagus. *Abdom Imaging* 22:8–10, 1997.
50. Gaskin CM, Low VHS, Ho LM: Isolated primary non-Hodgkin's lymphoma of the esophagus. *AJR* 176:551–552, 2001.
51. Coppens E, Nakadi IE, Nagy N, et al: Primary Hodgkin's lymphoma of the esophagus. *AJR* 180:1135–1137, 2003.
52. Radin DR: Primary esophageal lymphoma in AIDS. *Abdom Imaging* 18:223–224, 1993.
53. Sabate JM, Franquet T, Palmer J, et al: AIDS-related primary esophageal lymphoma. *Abdom Imaging* 22:11–13, 1997.
54. Traube M, Waldron JA, McCallum RW: Systemic lymphoma initially presenting as an esophageal mass. *Am J Gastroenterol* 77:835–837, 1982.
55. Hricak H, Thoeni RF, Margulis AR, et al: Extension of gastric lymphoma into the esophagus and duodenum. *Radiology* 135:309–312, 1980.
56. Lambert A: Malignant tracheoesophageal fistula secondary to Hodgkin's disease. *J Thorac Cardiovasc Surg* 69:820–826, 1975.
57. Kirsch HL, Cronin DW, Stein GN, et al: Esophageal perforation: An unusual presentation of esophageal lymphoma. *Dig Dis Sci* 28:371–374, 1983.
58. Levine MS, Sunshine AG, Reynolds JC, et al: Diffuse nodularity in esophageal lymphoma. *AJR* 145:1218–1220, 1985.
59. Gedgaudas-McClees RK, Maglinte DD: Lymphomatous esophageal nodules: The difficulty in radiological differential diagnosis. *Am J Gastroenterol* 80:529–530, 1985.
60. Xu L, Sun C, Wu L, et al: Clinical and pathological characteristics of carcinosarcoma of the esophagus: Report of four cases. *Ann Thorac Surg* 37:197–203, 1984.
61. Martin MR, Kahn LB: So-called pseudosarcoma of the esophagus: Nodal metastases of the spindle cell element. *Arch Pathol Lab Med* 101:604–609, 1977.
62. Olmsted WW, Lichtenstein JE, Hyams VJ: Polypoid epithelial malignancies of the esophagus. *AJR* 140:921–925, 1983.
63. Agha FP, Keren DF: Spindle-cell squamous carcinoma of the esophagus: A tumor with biphasic morphology. *AJR* 145:541–545, 1985.
64. Talbert JL, Cantrell JR: Clinical and pathological characteristics of carcinosarcoma of the esophagus. *J Thorac Cardiovasc Surg* 45:1–12, 1963.
65. McCort JJ: Esophageal carcinosarcoma and pseudosarcoma. *Radiology* 102:519–524, 1972.
66. Razzuk MA, Urschel HC, Race GJ, et al: Pseudosarcoma of the esophagus. *J Thorac Cardiovasc Surg* 61:650–653, 1971.
67. Postlethwait RW, Wechsler AS, Shelburne JD: Pseudosarcoma of the esophagus. *Ann Thorac Surg* 19:198–205, 1975.
68. Nichols T, Yokoo H, Craig RM, et al: Pseudosarcoma of the esophagus. *Am J Gastroenterol* 72:615–622, 1979.
69. Halvorsen RA, Foster WL, Williford ME, et al: Pseudosarcoma of the esophagus: Barium swallow and CT findings. *J Can Assoc Radiol* 34:278–281, 1983.
70. Osamura RY, Shimamura K, Hata J: Polypoid carcinoma of the esophagus: A unifying term for carcinosarcoma and pseudosarcoma. *Am J Surg Pathol* 2:201–208, 1978.
71. Hinderleider CD, Aguam AS, Wilder JR: Carcinosarcoma of the esophagus: A case report and review of the literature. *Int Surg* 64:13–19, 1979.
72. Kenneweg DJ, Cimmino CV: Carcinosarcoma of the esophagus. *AJR* 101:482–484, 1967.
73. Levine MS: Esophageal cancer: Radiologic diagnosis. *Radiol Clin North Am* 35:265–279, 1997.
74. Levine MS, Buck JL, Pantongrag-Brown L, et al: Fibrovascular polyps of the esophagus: Clinical, radiographic, and pathologic findings in 16 patients. *AJR* 166:781–787, 1996.
75. Wolfel DA: Leiomyosarcoma of the esophagus. *AJR* 89:127–131, 1963.
76. Franklin GO, Antler AS, Thelmo WL, et al: Esophageal leiomyosarcoma. *N Y State J Med* 82:1100–1103, 1982.
77. Glanz I, Grunebaum M: The radiological approach to leiomyoma of the oesophagus with a long-term follow-up. *Clin Radiol* 28:197–200, 1977.
78. Balthazar EJ: Gastrointestinal leiomyosarcoma—unusual sites: Esophagus, colon, and porta hepatis. *Gastrointest Radiol* 6:295–301, 1981.
79. Weinstein EC, Kim YS, Young GJ, et al: Leiomyosarcoma of the esophagus. *Milit Med* 4:206–209, 1988.
80. Patel SR, Anandarao N: Leiomyosarcoma of the esophagus. *N Y State J Med* 90:371–372, 1990.
81. Koga H, Iida M, Suekane H, et al: Rapidly growing esophageal leiomyosarcoma: Case report and review of the literature. *Abdom Imaging* 20:15–19, 1995.
82. Choh JH, Khazei AH, Ihm HJ: Leiomyosarcoma of the esophagus: Report of a case and review of the literature. *J Surg Oncol* 32:223–226, 1986.
83. Levine MS, Buck JL, Pantongrag-Brown L, et al: Leiomyosarcoma of the esophagus: Radiographic findings in 10 patients. *AJR* 167:27–32, 1996.
84. Berk RN, Scher GS, Bode DF: Unusual tumors of the gastrointestinal tract. *AJR* 113:159–169, 1971.
85. Itai Y, Shimazu H: Leiomyosarcoma of the oesophagus with dense calcification. *Br J Radiol* 51:469–471, 1978.
86. Athanasoulis CA, Aral IM: Leiomyosarcoma of the esophagus. *Gastroenterology* 54:271–274, 1968.
87. Ohnishi T, Yoshioka H, Ishida O: MR imaging of gastrointestinal leiomyosarcoma. *Radiat Med* 9:114–117, 1991.
88. Sabanathan S, Eng J, Pradhan GN: Primary malignant melanoma of the esophagus. *Am J Gastroenterol* 84:1475–1481, 1989.
89. De la Pava S, Nigogosyan G, Pickren JW, et al: Melanosis of the esophagus. *Cancer* 16:48–50, 1963.
90. Tateishi R, Taniguchi H, Wada A, et al: Argrophil cells and melanocytes in esophageal mucosa. *Arch Pathol* 98:87–89, 1974.
91. Sharma SS, Venkateswaran A, Chacko A, et al: Melanosis of the esophagus: An endoscopic, histochemical, and ultrastructural study. *Gastroenterology* 100:13–16, 1991.
92. Chalkiadakis G, Wihlm JM, Morand G, et al: Primary malignant melanoma of the esophagus. *Ann Thorac Surg* 39:472–475, 1985.
93. Isaacs JL, Quirke P: Two cases of primary malignant melanoma of the oesophagus. *Clin Radiol* 39:455–457, 1988.
94. Brown JH, Chew FS: Primary esophageal melanoma. *AJR* 157:318, 1991.
95. Yoo CC, Levine MS, McLarney JK, et al: Primary malignant melanoma of the esophagus: Radiographic findings in seven patients. *Radiology* 209:455–459, 1998.
96. Gollub MJ, Prowda JC: Primary melanoma of the esophagus: Radiologic and clinical findings in six patients. *Radiology* 213:97–100, 1999.
97. Friedman SL, Wright TL, Altman DF: Gastrointestinal Kaposi's sarcoma in patients with acquired immunodeficiency syndrome: Endoscopic and autopsy findings. *Gastroenterology* 89:102–108, 1985.
98. Rose HS, Balthazar EJ, Megibow AJ, et al: Alimentary tract involvement in Kaposi sarcoma: Radiographic and endoscopic findings in 25 homosexual men. *AJR* 139:661–666, 1982.
99. Wall SD, Friedman SL, Margulis AR: Gastrointestinal Kaposi's sarcoma in AIDS: Radiographic manifestations. *J Clin Gastroenterol* 6:165–171, 1984.
100. Umerah BC: Kaposi sarcoma of the oesophagus. *Br J Radiol* 53:807–808, 1980.
101. Law SYK, Fok M, Lam KY, et al: Small cell carcinoma of the esophagus. *Cancer* 73:2894–2899, 1994.

102. Attar BM, Levendoglu HA, Rhee H: Small cell carcinoma of the esophagus. *Dig Dis Sci* 35:145–152, 1990.
103. Beyer KI, Marshall JB, Diaz-Arias AA, et al: Primary small-cell carcinoma of the esophagus: Report of 11 cases and review of the literature. *J Clin Gastroenterol* 13:135–141, 1995.
104. Hussein AM, Feun LG, Sridhar KS, et al: Combination chemotherapy and radiation therapy for small-cell carcinoma of the esophagus. *Am J Clin Oncol* 13:369–373, 1990.
105. Ignacio AG, Chintapalli K, Choi H: Primary oat cell carcinoma of the esophagus. *Am J Gastroenterol* 82:78–81, 1987.
106. Mulder LD, Gardiner GA, Weeks DA: Primary small cell carcinoma of the esophagus: Case presentation and review of the literature. *Gastrointest Radiol* 16:5–10, 1991.
107. Hirsch JA, Levine MS, Silberg DG, et al: Small-cell carcinoma of the esophagus with regression after combination chemotherapy and radiation therapy. *Can Assoc Radiol J* 46:45–47, 1995.
108. Levine MS, Pantongrag-Brown L, Buck JL, et al: Small-cell carcinoma of the esophagus: Radiographic findings. *Radiology* 199:703–705, 1996.
109. Prolla JC, Kirsner JB: The gastrointestinal lesions and complications of the leukemias. *Ann Intern Med* 61:1084–1103, 1964.
110. Givler RL: Esophageal lesions in leukemia and lymphoma. *Am J Dig Dis* 15:31–36, 1970.
111. Thompson BC, Feczko PJ, Mezwa DG: Dysphagia caused by acute leukemic infiltration of the esophagus [letter]. *AJR* 155:654, 1990.
112. Gildenhorn HL, Fahey JL, Solomon RD: Functional esophageal obstruction due to leukemic infiltration. *AJR* 88:736–740, 1962.
113. O'Sullivan JP, Cockburn JS, Drew CE: Adenoid cystic carcinoma of the esophagus. *Thorax* 30:476–480, 1975.
114. Kabuto T, Taniguchi K, Iwanaga T, et al: Primary adenoid cystic carcinoma of the esophagus. *Cancer* 43:2452–2456, 1979.
115. Yaghamai I, Ghahremani GG: Chondrosarcoma of the esophagus. *AJR* 126:1175–1177, 1976.
116. Block MJ, Iozzo RV, Edmunds LH, et al: Polypoid synovial sarcoma of the esophagus. *Gastroenterology* 92:229–233, 1987.
117. Brenner S, Heimlich H, Widman M: Carcinoid of esophagus. *N Y State J Med* 69:1337–1339, 1969.

Miscellaneous Abnormalities of the Esophagus

MARC S. LEVINE

CHAPTER OUTLINE

Mallory-Weiss Tear

Pathogenesis

Clinical Findings

Radiographic Findings

Esophageal Hematoma

Pathogenesis

Clinical Findings

Radiographic Findings

Esophageal Perforation

Pathogenesis

Clinical Findings

Radiographic Findings

Foreign Body Impaction

Clinical Findings

Radiographic Findings

Treatment

Fistulas

Esophageal-Airway Fistula

Esophagopleural Fistula

Aortoesophageal Fistula

Esophagopericardial Fistula

Diverticula

Pulsion and Traction Diverticula

Epiphrenic Diverticulum

Ectopic Gastric Mucosa

Congenital Esophageal Stenosis

Clinical Findings

Radiographic Findings

Differential Diagnosis

Extrinsic Impressions

Normal Impressions

Abnormal Impressions

Esophageal Retraction

Varices

Uphill Varices

Downhill Varices

Idiopathic Varices

Mallory-Weiss Tear

PATHOGENESIS

A Mallory-Weiss tear is recognized as a relatively common injury in which a sudden, rapid increase in intraesophageal pressure produces a linear mucosal laceration at or near the

gastric cardia. These tears are usually caused by violent retching or vomiting after an alcoholic binge or by protracted vomiting for any reason.¹⁻³ Less commonly, Mallory-Weiss tears may be caused by prolonged hiccuping or coughing, seizures, straining at stool, childbirth, or blunt abdominal trauma.⁴ Similar injuries may also result from direct laceration of the mucosa by an advancing endoscope or by a sharp foreign body in the esophagus, such as a taco.⁵⁻⁷

CLINICAL FINDINGS

Mallory-Weiss tears account for 5% to 10% of all cases of acute upper gastrointestinal (GI) bleeding.^{8,9} Some patients may have massive hematemesis, but most tears heal spontaneously within 48 to 72 hours, so bleeding is usually self-limited.^{1,4,9} These patients therefore have an excellent prognosis with an overall mortality rate of only about 3%.^{2,4} Although most patients can be managed conservatively, selective intra-arterial infusion of vasopressin, transcatheter embolization, endoscopic electrocoagulation, or surgical repair of the tear may occasionally be required to control bleeding.¹⁰⁻¹³

RADIOGRAPHIC FINDINGS

The vast majority of Mallory-Weiss tears are diagnosed at endoscopy.³ Nevertheless, these mucosal lacerations are occasionally recognized on double-contrast esophagograms as shallow, longitudinally oriented, linear collections of barium in the distal esophagus at or just above the gastroesophageal junction (Fig. 25-1). The radiographic appearance may be indistinguishable from that of a linear ulcer in the distal esophagus caused by reflux esophagitis, but a history of recent vomiting or hematemesis (particularly in alcoholics) should suggest the correct diagnosis.

Esophageal Hematoma

PATHOGENESIS

Most esophageal hematomas are caused by a mucosal laceration or tear in the distal esophagus. If the tear is partially or completely occluded by edema or blood clot, continued hemorrhage may lead to progressive submucosal dissection of blood, producing an intramural hematoma.¹⁴ As with Mallory-Weiss tears, the underlying laceration is usually caused by a sudden increase in intraesophageal pressure resulting from one or more episodes of violent retching or vomiting.^{14,15} Esophageal hematomas may also be caused by esophageal instrumentation or, rarely, by blunt trauma.¹⁶⁻¹⁸ Occasionally, spontaneous hematomas may develop in patients who have impaired hemostasis because of thrombocytopenia, bleeding disorders, or

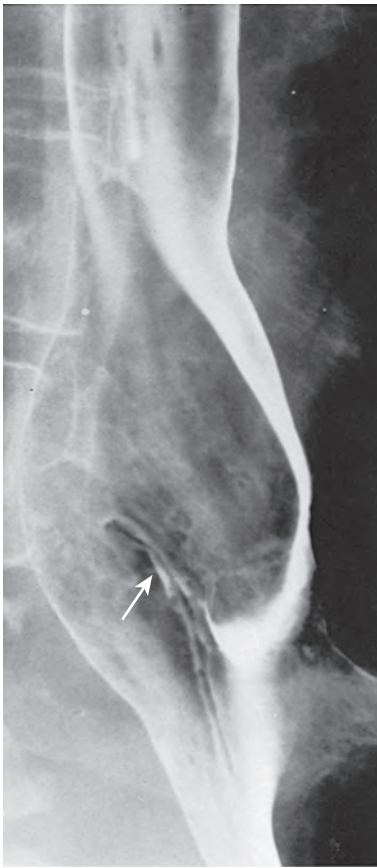


Figure 25-1 Mallory-Weiss tear. A linear collection of barium (arrow) is visible in the distal esophagus just above the gastroesophageal junction. Although a linear ulcer from reflux esophagitis could produce a similar appearance, the correct diagnosis was suggested by the clinical history. (Courtesy Harvey M. Goldstein, MD, San Antonio, TX.)

anticoagulation.^{19,20} In contrast to traumatic hematomas, which almost always occur as solitary lesions in the distal esophagus, spontaneous hematomas tend to spare the distal esophagus and are more likely to be multifocal.¹⁵

CLINICAL FINDINGS

Patients with esophageal hematomas usually present with severe chest pain, dysphagia, or hematemesis.^{14,20,21} Despite the dramatic clinical findings, most esophageal hematomas resolve in 1 to 2 weeks on conservative treatment without need for surgery.^{14,17,20,21} These lesions should therefore be considered self-limited because they almost never progress to complete transmural perforation.

RADIOGRAPHIC FINDINGS

Esophageal hematomas usually appear on barium studies as solitary submucosal masses in the distal esophagus that are indistinguishable from leiomyomas or other benign intramural lesions (Fig. 25-2).^{14,17-19,22} When a mucosal laceration is present, however, barium may dissect beneath the mucosa into the hematoma. This intramural dissection produces a characteristic double-barreled appearance caused by parallel collections of contrast material in true and false lumens separated by a thin, radiolucent stripe (Fig. 25-3).^{16,23-25} Rarely, a double-barreled

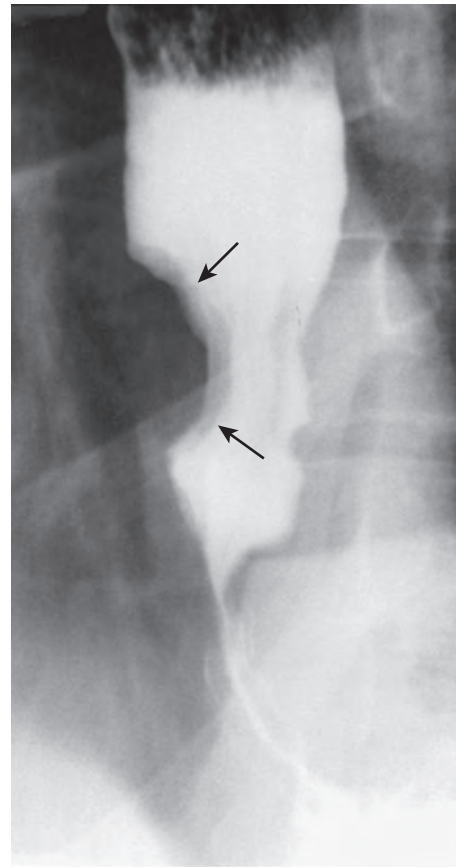


Figure 25-2 Esophageal hematoma. There is a smooth submucosal mass (arrows) in the distal esophagus. The hematoma was caused by a pneumatic dilation procedure for achalasia. The esophagus is narrowed below the hematoma because of the patient's underlying achalasia. (From Levine MS: *Radiology of the Esophagus*. Philadelphia, WB Saunders, 1989.)

appearance may also be caused by intramural tracking of barium secondary to Crohn's disease, *Candida* esophagitis, tuberculous esophagitis, or esophageal intramural pseudodiverticulosis.

Esophageal hematomas may be recognized on CT by the presence of a well-defined intramural mass, which sometimes has a tubular appearance, extending a considerable distance along the long axis of the esophagus.^{23,26,27} If the hematoma is acute or subacute, hyperdense areas may be present within the lesion.²⁶

Esophageal Perforation

Esophageal perforation is the most serious and rapidly fatal type of perforation in the GI tract. Untreated thoracic esophageal perforations have a mortality rate of almost 100% because of the fulminant mediastinitis that occurs after esophageal rupture.²⁸ Perforation of the cervical esophagus is a more common but less devastating injury. Early diagnosis of esophageal perforation is important because of the potential need for prompt surgical intervention.

PATHOGENESIS

Instrumentation

Endoscopic procedures are responsible for up to 75% of all esophageal perforations.^{29,30} This complication occurs in about

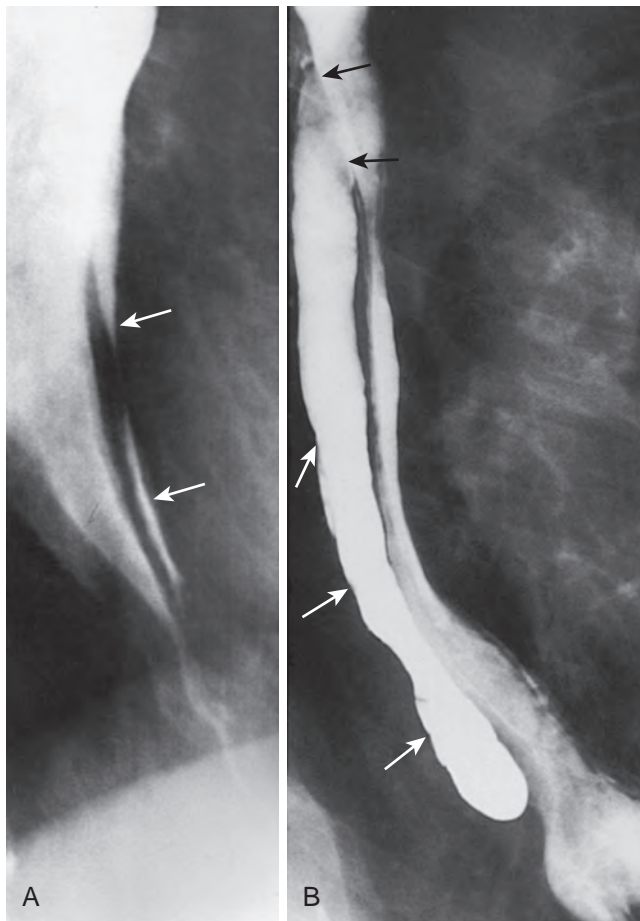


Figure 25-3 Two examples of intramural dissections with a double-barreled esophagus. **A, B.** The longitudinal intramural tracks (white arrows) are separated from the esophageal lumen by a radiolucent mucosal stripe. Both patients had traumatic dissections that occurred during esophageal instrumentation. The site of the laceration (black arrows) is well seen in **B**. (**A** courtesy Sang Y. Han, MD, Birmingham, AL; **B** courtesy Frank H. Miller, MD, Chicago.)

1 in 3000 patients who undergo endoscopic examinations with modern fiberoptic instruments.³⁰ Most endoscopic perforations involve the piriform sinus or cricopharyngeal region in which the posterior wall of the pharyngoesophageal junction is compressed by the advancing endoscope against the cervical spine.^{29,31} The presence of cervical osteophytes or a pharyngeal diverticulum increases the risk of perforation.³⁰ Unlike cervical esophageal perforations, which often occur in the absence of underlying disease, thoracic esophageal perforations usually result from endoscopic injury at or above esophageal strictures or from therapeutic maneuvers such as variceal sclerotherapy, balloon dilation, bougienage, stent or nasogastric tube placement, and foreign body removal.^{30,32,33} Perforation may also occur after esophageal surgery, usually at the site of a ruptured anastomosis (see Chapter 27).

Foreign Bodies

Most foreign body perforations in adults are caused by impacted animal or fish bones in the hypopharynx that erode through the piriform sinus or cricopharyngeal region. Rarely, foreign body obstructions in the thoracic esophagus also lead to perforation as a result of transmural inflammation and

pressure necrosis at the site of impaction (see later, “[Foreign Body Impaction](#)”). Esophageal perforation may also be caused by accidental or intentional ingestion of caustic agents (see Chapter 21).

Trauma

Penetrating injuries to the esophagus are usually caused by knife or bullet wounds. Because the neck lacks the bony protection afforded by the thorax, these injuries generally involve the cervical esophagus.²⁹ Rarely, blunt trauma to the neck, chest, or abdomen can also lead to pharyngeal or esophageal perforation or transection (see next section).³⁴

Spontaneous Esophageal Perforation (Boerhaave’s Syndrome)

In spontaneous esophageal perforation, a sudden, rapid increase in intraluminal esophageal pressure causes a full-thickness perforation of normal underlying esophageal tissue, with ensuing mediastinitis, sepsis, and shock. Most cases result from violent retching or vomiting, usually after an alcoholic binge.^{35,36} Occasionally, however, spontaneous rupture of the esophagus may result from other causes of increased intraesophageal pressure, such as coughing, weightlifting, childbirth, defecation, seizures, status asthmaticus, and blunt trauma to the chest or abdomen.³⁶

Spontaneous esophageal perforations usually occur as 1- to 4-cm long, vertically oriented, linear tears on the left lateral wall of the distal esophagus just above the gastroesophageal junction.^{35,36} The left side of the distal esophagus is more vulnerable to perforation because of the lack of supporting mediastinal structures in this region, whereas the right side of the distal esophagus is protected by the descending thoracic aorta.^{29,36} Rarely, spontaneous perforation of the upper thoracic esophagus or even the cervical esophagus has been reported.^{37,38}

CLINICAL FINDINGS

Cervical Esophageal Perforation

Most cervical esophageal perforations occur as direct complications of endoscopy. Affected individuals may develop neck pain, dysphagia, or fever. Physical examination often reveals subcutaneous emphysema in the neck as a result of gas escaping from the pharynx into the adjacent soft tissues. If untreated, these patients may develop a retropharyngeal abscess, occasionally leading to sepsis and shock.

Cervical esophageal perforations often heal on conservative management, so most small perforations can be treated nonoperatively. However, larger perforations may require a cervical mediastinotomy and open drainage to prevent abscess formation. These injuries have a much better prognosis than thoracic esophageal perforations, with an overall mortality rate of less than 15%.³⁰

Thoracic Esophageal Perforation

Patients with thoracic esophageal perforation may present with the classic triad of vomiting, substernal chest pain, and subcutaneous emphysema of the chest wall and neck.^{35,39} However, some patients have atypical chest pain referred to the left shoulder or back,³⁵ whereas others have epigastric pain, particularly if the perforation involves the intra-abdominal segment of the esophagus below the diaphragmatic hiatus.⁴⁰ Furthermore, subcutaneous emphysema is not always present on physical examination. As a result, thoracic esophageal perforation can be

mistaken for a variety of acute cardiothoracic or abdominal conditions.^{35,36,39} Signs or symptoms of esophageal perforation can also be masked by treatment with steroids.⁴¹ This clinical confusion sometimes leads to delayed diagnosis and treatment of a life-threatening condition. Unfortunately, the mortality rate for thoracic esophageal perforation approaches 70% by 24 hours.³⁵ Thus, early diagnosis is essential for improving patient survival.

Unlike cervical esophageal perforations, which are often treated conservatively, thoracic esophageal perforations may require an emergent thoracotomy (with surgical closure of the perforation and mediastinal drainage) to prevent the development of mediastinitis, sepsis, and death.⁴² More recently, thoracic esophageal perforations have also been treated successfully with occlusive, removable esophageal stents, obviating the need for surgery.^{43,44} Rarely, thoracic esophageal perforations associated with Boerhaave's syndrome may heal spontaneously without intervention.⁴⁵ Other small, self-contained perforations can sometimes be managed nonoperatively with broad-spectrum antibiotics.³⁰

RADIOGRAPHIC FINDINGS

Plain Radiographs

Cervical Esophageal Perforation. Subcutaneous emphysema or retropharyngeal gas may be visible on anteroposterior or lateral radiographs of the neck within 1 hour after a pharyngeal or cervical esophageal perforation (Fig. 25-4A).²⁹ Subsequently, air may dissect along fascial planes from the neck into the chest, producing pneumomediastinum (see Fig. 25-4A).²⁹ Lateral radiographs of the neck may also demonstrate widening of the prevertebral space, anterior deviation of the trachea and, eventually, a retropharyngeal abscess containing mottled gas or a single air-fluid level.

Thoracic Esophageal Perforation. About 90% of patients with thoracic esophageal perforations have abnormal chest radiographs. The earliest signs of perforation include mediastinal

widening and pneumomediastinum; the latter finding is usually recognized by the presence of radiolucent streaks of gas along the left lateral border of the aortic arch and descending thoracic aorta or along the right lateral border of the ascending aorta and heart (Fig. 25-5A).^{29,35,36} Subsequently, gas in the mediastinum may dissect along fascial planes superiorly to the supraclavicular area, producing subcutaneous emphysema in the neck within several hours of the perforation.³⁶

At least 75% of thoracic esophageal perforations are associated with a pleural effusion or hydropneumothorax.⁴⁶ Distal perforations often result in a sympathetic left pleural effusion or left basilar atelectasis because of irritation of the adjacent pleura and lung parenchyma (see Fig. 25-5A). Pleural effusions may be present within 12 hours of perforation and are occasionally detected before the development of mediastinal or cervical emphysema. If the mediastinal pleura ruptures, gas and fluid may enter the pleural space directly from the mediastinum, producing a hydropneumothorax. Because the distal esophagus directly abuts the mediastinal pleura on the left, 75% of hydropneumothoraces are on the left side, whereas 5% are on the right and 20% are bilateral.³⁵

Rarely, abdominal radiographs may reveal extraluminal collections of gas in the lesser sac or retroperitoneum when the intra-abdominal segment of the distal esophagus is perforated below the diaphragmatic hiatus.^{40,47} Affected individuals may have vague abdominal discomfort without chest pain or other classic signs of esophageal perforation, so the diagnosis is often delayed in these patients. On the other hand, intra-abdominal esophageal perforations have a more benign clinical course, sometimes healing spontaneously on conservative treatment.^{40,47}

Fluoroscopic Examinations

Fluoroscopic esophagography is an excellent study for patients with suspected esophageal perforation. The ideal contrast agent for this examination provides diagnostic information about the site and extent of perforation without posing a risk to the patient. It has been shown experimentally that barium in the

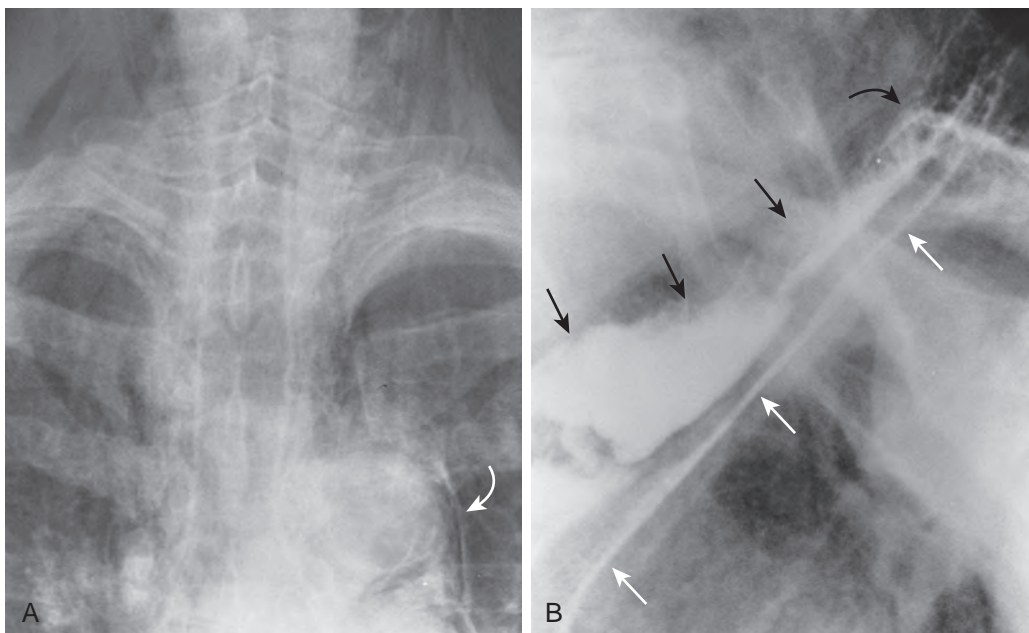


Figure 25-4 Cervical esophageal perforation by traumatic endoscopy.

A. Close-up view from a posteroanterior chest radiograph obtained several hours after the procedure shows extensive subcutaneous emphysema in the neck and associated pneumomediastinum (curved arrow). **B.** Study using water-soluble contrast medium in a steep oblique projection reveals a cervical esophageal perforation (curved black arrow) with contrast medium extending inferiorly in the mediastinum (straight black arrows) behind the esophagus (white arrows). (From Levine MS: *Radiology of the Esophagus*. Philadelphia, WB Saunders, 1989.)

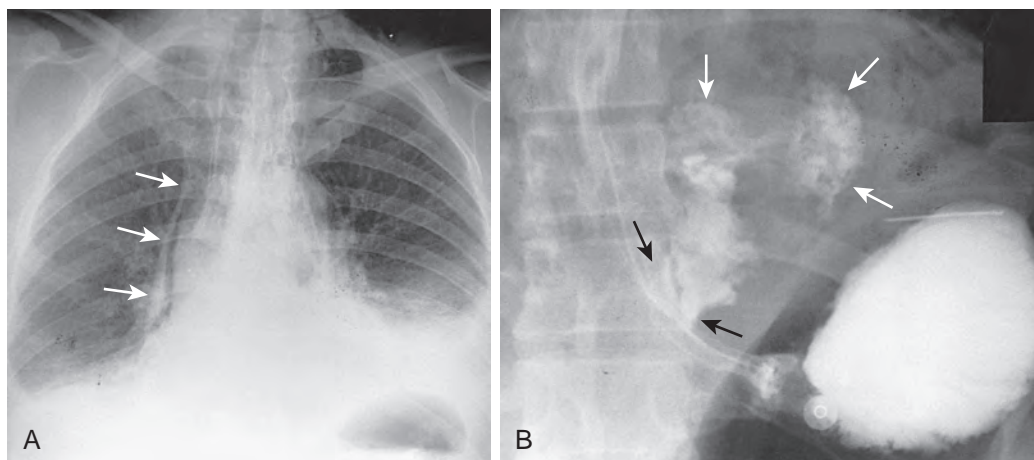


Figure 25-5 Spontaneous esophageal perforation (Boerhaave's syndrome). **A.** Posteroanterior chest radiograph shows a right-sided pneumomediastinum (arrows) and left pleural effusion. These findings are highly suggestive of spontaneous esophageal perforation in a patient (particularly an alcoholic) with severe retching or vomiting. **B.** Subsequent study using water-soluble contrast medium confirms the presence of a localized perforation of the left lateral wall of the distal esophagus (black arrows), with extension of the leak laterally and superiorly in the mediastinum (white arrows). (Courtesy Seth N. Glick, MD, Philadelphia.)

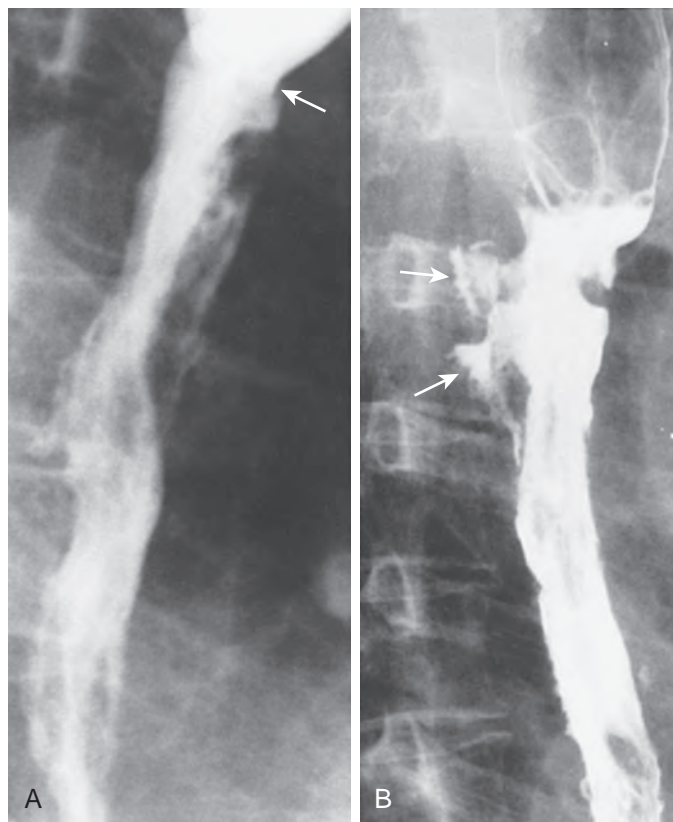


Figure 25-6 Importance of using high-density barium for the diagnosis of subtle perforations. **A.** Initial study using water-soluble contrast medium after an esophagogastric anastomosis (arrow), but no definite site of perforation is seen. **B.** Repeat examination performed moments later with high-density barium shows a sealed-off anastomotic perforation (arrows) that was not visible with a water-soluble contrast medium. This case dramatically illustrates how high-density barium should be given to all patients with suspected perforation if the initial study using water-soluble contrast medium fails to demonstrate a leak.

mediastinum is capable of inciting an inflammatory reaction with subsequent granuloma formation and fibrosis,^{48,49} but there is little or no evidence that mediastinal barium causes clinically significant mediastinitis. Although water-soluble contrast agents such as diatrizoate meglumine and diatrizoate sodium (Gastroview, Mallinckrodt, St. Louis) do not produce a detectable histologic response and have no known deleterious effects on the neck, mediastinum, and pleural or peritoneal cavities,^{48,49} water-soluble contrast media are hypertonic agents that are capable of causing severe pulmonary edema if aspirated into the lungs.⁵⁰ On the other hand, barium that extravasates from the esophagus can remain in the mediastinum indefinitely, limiting the radiologist's ability to assess healing on follow-up fluoroscopic examinations. In contrast, water-soluble contrast agents are rapidly absorbed from the mediastinum, so follow-up studies are not compromised by residual extraluminal contrast medium at or near the site of perforation. This is the major rationale for using water-soluble contrast agents as the initial contrast media for the fluoroscopic evaluation of patients with suspected esophageal perforation. Alternatively, some investigators advocate the use of low-osmolality, water-soluble contrast agents such as iohexol (Omnipaque, GE Healthcare, Princeton, NJ) to decrease the risks of aspirated contrast material in the lungs.⁵¹ Others favor the use of barium as the initial contrast agent for patients with suspected esophageal perforation, particularly in patients who are at high risk for aspiration.⁵² When water-soluble contrast agents are used, the pharynx should be carefully observed at fluoroscopy, and the examination should be aborted if significant aspiration is detected during the initial swallow.

A major disadvantage of water-soluble contrast agents is that they are less radiopaque than barium and less adherent to sites of leakage, limiting their ability to depict perforations, particularly small or subtle perforations.⁵³ In various studies, 50% of cervical esophageal perforations and up to 25% of thoracic esophageal perforations were missed on fluoroscopic examinations performed only with water-soluble contrast agents.⁵⁴⁻⁵⁶ When the initial study with water-soluble contrast medium fails to show a leak (Fig. 25-6A), the examination should therefore

immediately be repeated with barium to detect subtle leaks that are more likely to be visualized with a more radiopaque contrast agent (Fig. 25-6B).^{48,49,53,57-59} Although low-density barium is able to visualize 22% to 38% of leaks missed on esophagograms performed with water-soluble contrast agents,^{60,61} high-density barium (i.e., the 250% w/v barium suspension used for double-contrast upper GI examinations) is capable of detecting 50% of leaks that are not visualized with water-soluble contrast agents because of the greater opacity of high-density barium.⁶² Leaks detected only with high-density barium are more likely to be characterized by small, blind-ending tracks or tiny extraluminal collections than those visualized with a water-soluble contrast agent, but patient management is still affected in most cases.⁶² High-density barium should therefore be used to optimize detection of esophageal perforation on fluoroscopic examinations when no leak is initially detected with a water-soluble contrast agent (see Fig. 25-6). In these cases, the downside of retained barium in the mediastinum is more than offset by the earlier diagnosis and treatment of a potentially life-threatening condition.

Esophageal perforations are recognized on esophagography by extravasation of contrast medium from the esophagus into the neck or mediastinum. In patients with spontaneous perforation (Boerhaave's syndrome), contrast medium is usually seen extravasating from the left lateral wall of the distal esophagus into the adjacent mediastinum (see Fig. 25-5B).⁵³ Rarely, spontaneous perforation of the upper thoracic or even the cervical esophagus may also be demonstrated (Fig. 25-7).³⁸

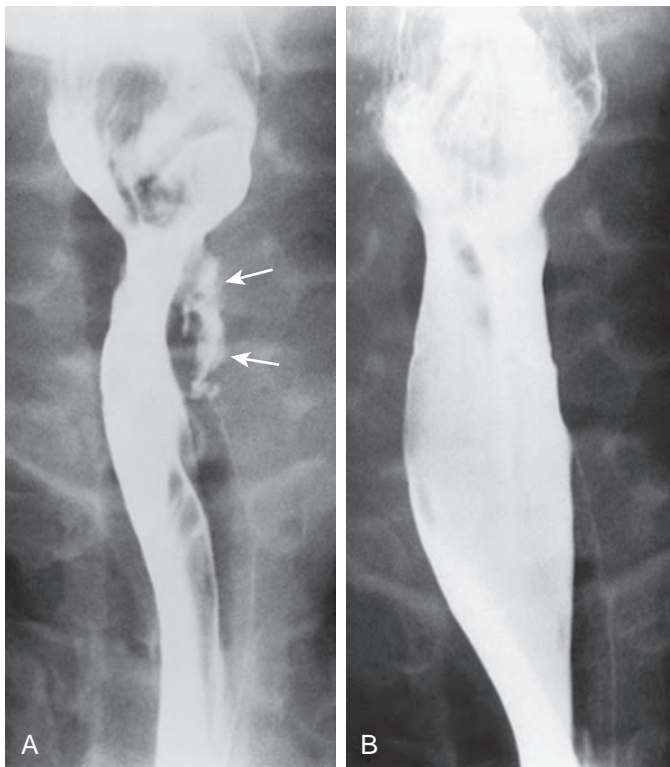


Figure 25-7 Spontaneous perforation of the cervical esophagus after an alcoholic binge. **A.** There is a small, sealed-off perforation (arrows) of the lower cervical esophagus. **B.** Follow-up esophagogram 6 weeks later shows complete healing of the perforation without evidence of a residual leak. (A and B from Isserow JA, Levine MS, Rubesin SE: Spontaneous perforation of the cervical esophagus after an alcoholic binge: Case report. *Can Assoc Radiol J* 49:241–243, 1998.)

Regardless of the site of perforation, a sealed-off leak is usually manifested by a contained extraluminal collection that communicates with the adjacent lumen (see Figs. 25-6B and 25-7A). In contrast, larger perforations may result in free extravasation of contrast medium into the mediastinum, with extension along fascial planes superiorly or inferiorly from the site of perforation (see Figs. 25-4B and 25-5B). In patients with contained perforations, follow-up esophagograms may be obtained to document healing of the leak prior to initiating oral feeding (see Fig. 25-7B).

Computed Tomography

Computed tomography (CT) may also be performed on patients in whom esophageal perforation is suspected on clinical grounds. In such cases, the finding of extraluminal gas, fluid, or contrast material in the mediastinum should be highly suggestive of esophageal perforation (Fig. 25-8).⁶³ Pleural and pericardial fluid collections are other less specific findings.⁶⁴ When a perforation is present, CT also is useful for determining the extent of extraluminal gas and fluid in the mediastinum and for monitoring patients who are treated nonoperatively.⁶³ CT has been shown to be a more sensitive technique than fluoroscopic esophagography for detecting esophageal perforation, most likely because of its ability to show indirect signs of a leak after the leak has sealed off.^{64,65} Conversely, esophagography has a higher specificity than CT, particularly in the setting of previous surgery, in which variable amounts of residual gas and fluid may be present in the mediastinum in the absence of an actual leak.⁶⁵ Another limitation of CT is its frequent inability to locate the exact site of perforation. At our institution, we generally perform fluoroscopic esophagography as the initial examination in patients with suspected esophageal perforation. If the findings on esophagography are equivocal or if esophagography fails to show a leak in patients with a high clinical suspicion for esophageal perforation, CT is performed to increase the sensitivity for detection of leaks.

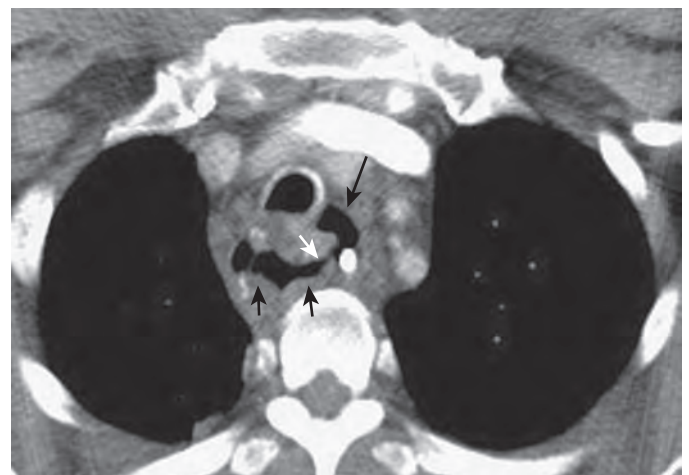


Figure 25-8 Postsurgical leak into mediastinum on CT. Axial contrast-enhanced CT scan 10 days after an esophagogastrectomy and gastric pull-through shows gas in the proximal end of the intrathoracic stomach (short black arrows) with a focal leak from the anastomotic region (white arrow) into the adjacent mediastinum (long black arrow). (From Lantos JE, Levine MS, Rubesin SE, et al: Comparison between esophagography and chest computed tomography for evaluation of leaks after esophagectomy and gastric pull-through. *J Thorac Imaging* 28:121–128, 2013.)

Foreign Body Impaction

Almost 80% of all pharyngeal or esophageal foreign body impactions occur in children who accidentally or intentionally ingest coins, toys, or other foreign objects.⁶⁶ Foreign body impactions in adults are usually caused by animal or fish bones or inadequately chewed boluses of meat, vegetables, or other bulky food items.^{66,67} Bones tend to lodge in the pharynx near the level of the cricopharyngeus, whereas food usually lodges in the distal esophagus near the gastroesophageal junction.⁶⁸ In contrast to impactions resulting from sharp foreign bodies, food impactions are often caused by underlying esophageal rings or strictures. Although 80% to 90% of foreign bodies in the esophagus pass spontaneously, the remaining 10% to 20% require some form of therapeutic intervention.^{66,69}

CLINICAL FINDINGS

Animal or fish bones tend to lodge in the pharynx, often near the level of the cricopharyngeus.⁶⁸ The patient may complain of pharyngeal dysphagia or of a sensation of a foreign body in the throat. In contrast, food impactions tend to occur in the distal esophagus and are manifested by the sudden onset of substernal chest pain, odynophagia, or dysphagia.⁶⁸ Some patients with distal foreign body impactions have dysphagia that is referred to the pharynx, however, so the subjective site of obstruction is unreliable in determining the level of impaction.

Esophageal perforation occurs in less than 1% of all patients with foreign body impactions.⁶⁷ However, the risk of perforation increases substantially if the impaction persists longer than 24 hours.^{67,70} Perforation results from transmural esophageal inflammation and subsequent pressure necrosis at the site of impaction. The development of mediastinitis may lead to sudden, rapid clinical deterioration, manifested by chest pain, sepsis, and shock.⁷⁰ Rarely, an impacted foreign body can erode through the wall of the esophagus, producing an aorto-esophageal, esophagobronchial, or esophagopericardial fistula (see later, “Fistulas”).

RADIOGRAPHIC FINDINGS

Plain Radiographs

Anteroposterior and lateral radiographs of the neck and chest may occasionally demonstrate bones or other radiopaque foreign bodies in the pharynx or esophagus. Lateral radiographs of the neck are usually more helpful than anteroposterior radiographs in identifying animal or fish bones lodged in the pharynx or cervical esophagus (Fig. 25-9) because these bones are easily obscured by the overlying cervical spine on anteroposterior radiographs. Nevertheless, considerable difficulty may be encountered in differentiating small bone fragments from calcified thyroid or cricoid cartilage.

Fluoroscopic Examinations

In patients with suspected foreign body impaction in the pharynx or cervical esophagus, an early barium swallow may be performed to determine whether a foreign body is present and whether it is causing obstruction. Animal or fish bones in the pharynx or cervical esophagus are easily obscured by intraluminal barium, so they may be difficult to detect on fluoroscopic examinations. However, these foreign bodies are sometimes recognized as linear filling defects in the vallecula,

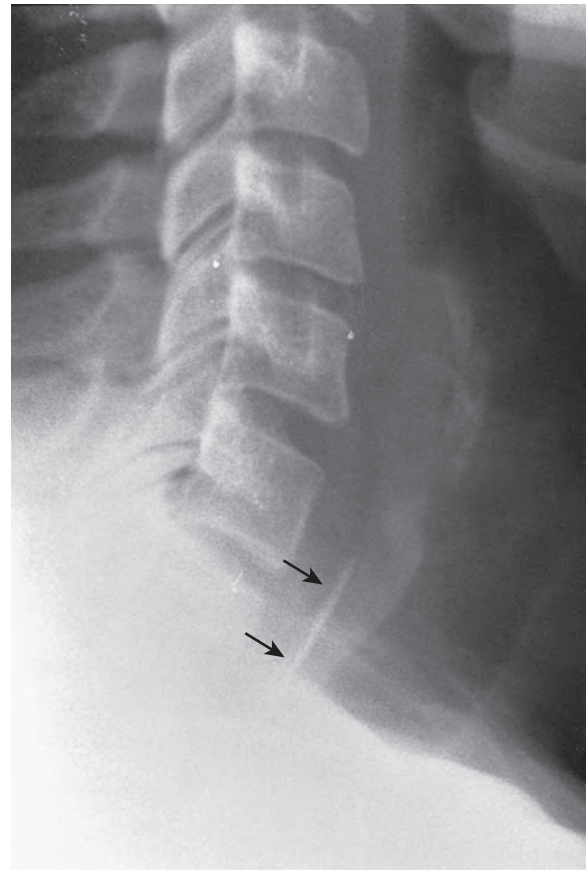


Figure 25-9 Swallowed pork bone in the neck near the pharyngo-esophageal junction. Note the faintly calcified density (arrows) in the region of the cricopharyngeus on a lateral view of the neck. (From Levine MS: *Radiology of the Esophagus*. Philadelphia, WB Saunders, 1989.)

piriform sinus, or cricopharyngeal region (Fig. 25-10). Cotton balls or marshmallows soaked in barium may occasionally be helpful for showing bones lodged in the pharynx or cervical esophagus.

Foreign body impactions in the thoracic esophagus usually result from a large bolus of meat or other food that has lodged above the gastroesophageal junction or above a pathologic area of narrowing, usually a Schatzki ring or peptic stricture.⁶⁶⁻⁶⁸ When an impacted food bolus causes esophageal obstruction, barium studies typically reveal a polypoid defect in the esophagus, with an irregular meniscus caused by barium outlining the superior border of the impacted bolus (Figs. 25-11A and 25-12A). Although the radiographic appearance could be mistaken for an obstructing esophageal carcinoma, the correct diagnosis is almost always apparent from the clinical history. The absence of proximal esophageal dilation in patients with an acute food impaction is also a helpful finding because the esophagus is often dilated in patients with obstructing tumors. In some cases, a small amount of barium may trickle around the impacted food bolus into the distal esophagus, erroneously suggesting a stricture (see Fig. 25-12A). Thus, it may be extremely difficult to ascertain whether the underlying esophagus is normal or abnormal at the time of impaction because the obstructing bolus prevents adequate visualization of the esophagus below this level.

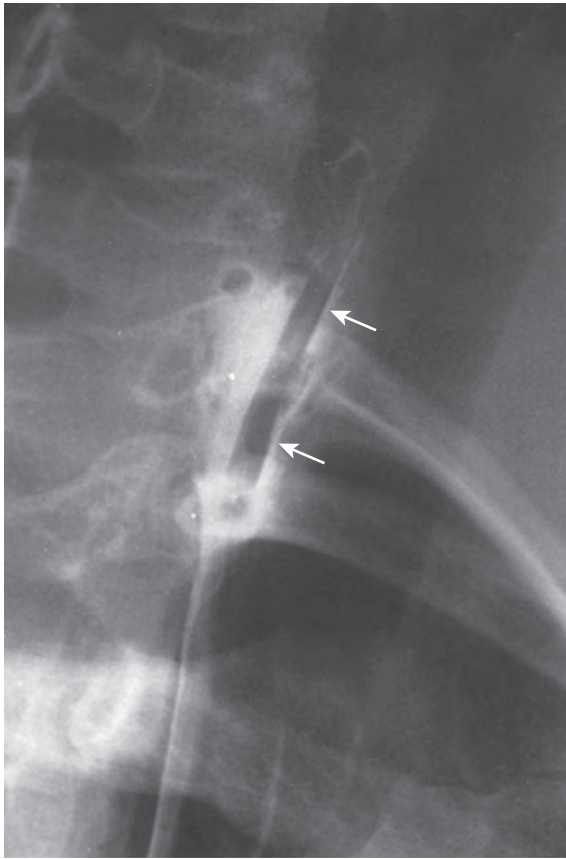


Figure 25-10 Turkey bone in the cervical esophagus. Barium swallow reveals a linear filling defect (arrows) resulting from a bone lodged in the cervical esophagus just below the cricopharynx. (From Levine MS: *Radiology of the Esophagus*. Philadelphia, WB Saunders, 1989.)

Esophageal perforation is a potential complication of food impaction that usually develops after the impacted bolus has been present longer than 24 hours,⁶⁷ but this complication has been reported as early as 6 hours after the onset of impaction.⁷¹ Esophageal perforation may be manifested by focal extravasation of contrast material into the mediastinum at the site of impaction (Fig. 25-13). Despite the risk of perforation, barium probably should be used as the initial contrast agent in patients with suspected food impaction because these individuals are also at higher risk for aspiration. Alternatively, endoscopy (rather than a barium study) may be performed as the first diagnostic test in this clinical setting because of potential difficulty visualizing and retrieving an impacted food bolus when retained barium is present above the impaction. The fluoroscopist should therefore consult with a gastroenterologist before performing a barium study on these patients.

After the food impaction has been relieved, a follow-up esophagogram may be performed several weeks later to rule out an underlying Schatzki ring or peptic stricture as the cause of the impaction (see Fig. 25-11B).⁶⁶⁻⁶⁸ Rarely, food impactions may be caused by malignant strictures or even by giant thoracic osteophytes or other structures impinging on the esophagus.^{66,72} In other patients, follow-up esophagography may reveal a normal underlying esophagus (see Fig. 25-12B).

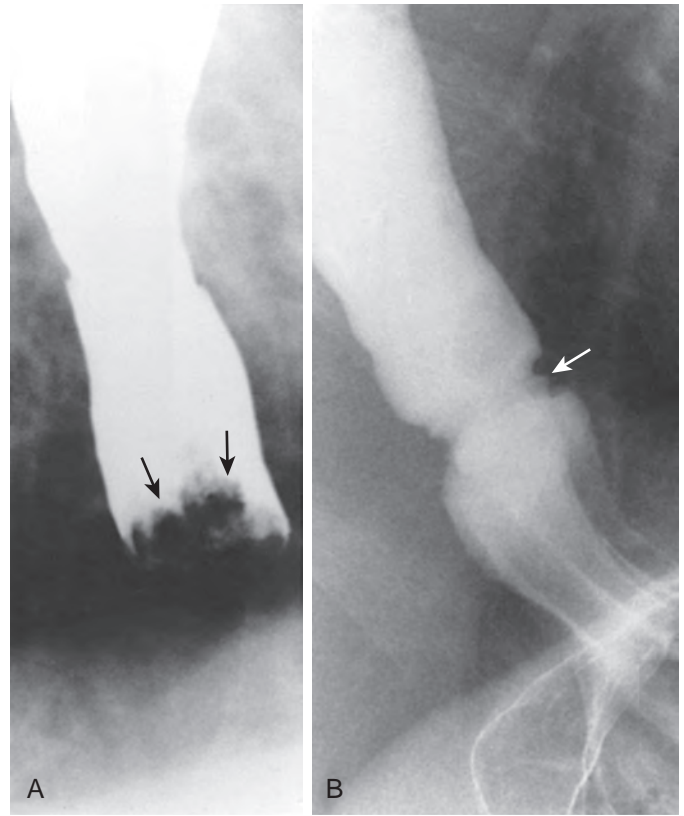


Figure 25-11 Distal foreign body obstruction caused by an underlying Schatzki ring. **A.** Initial esophagogram shows barium outlining the superior border of an impacted bolus of meat (arrows) in the distal esophagus with complete obstruction at this level. **B.** Second esophagogram after endoscopic removal of the foreign body shows an underlying Schatzki ring (arrow) as the cause of this impaction.

TREATMENT

When swallowed foreign bodies fail to pass spontaneously, some form of therapeutic intervention is required for their removal. Impacted foreign bodies in the pharynx or esophagus may be removed by endoscopy or the use of a wire basket or Foley catheter balloon under fluoroscopic guidance.^{66-69,73-75} These techniques appear to be safe and effective for extracting blunt foreign bodies from the esophagus. Alternatively, radiologists may attempt to relieve esophageal food impactions by a variety of noninvasive maneuvers. A single dose of 1 mg of intravenous (IV) glucagon sometimes facilitates passage of impacted food in the distal esophagus by relaxing the lower esophageal sphincter.⁷⁶⁻⁷⁸ Administration of gas-forming (i.e., effervescent) agents has also been advocated to distend the esophagus above an obstructing food bolus and facilitate passage of the bolus into the stomach.⁷⁹ Combination therapy with glucagon, an effervescent agent, and water has been shown to relieve esophageal food impactions in about 70% of patients.⁸⁰⁻⁸² Rarely, however, abrupt distention of the obstructed esophagus by a gas-forming agent may cause esophageal perforation,⁸⁰ particularly if the obstructing bolus has been present longer than 24 hours. Because of the potential risk of esophageal perforation, it may be prudent to avoid such maneuvers in all patients with food impactions, instead referring them to endoscopy for removal of the obstructing food bolus.

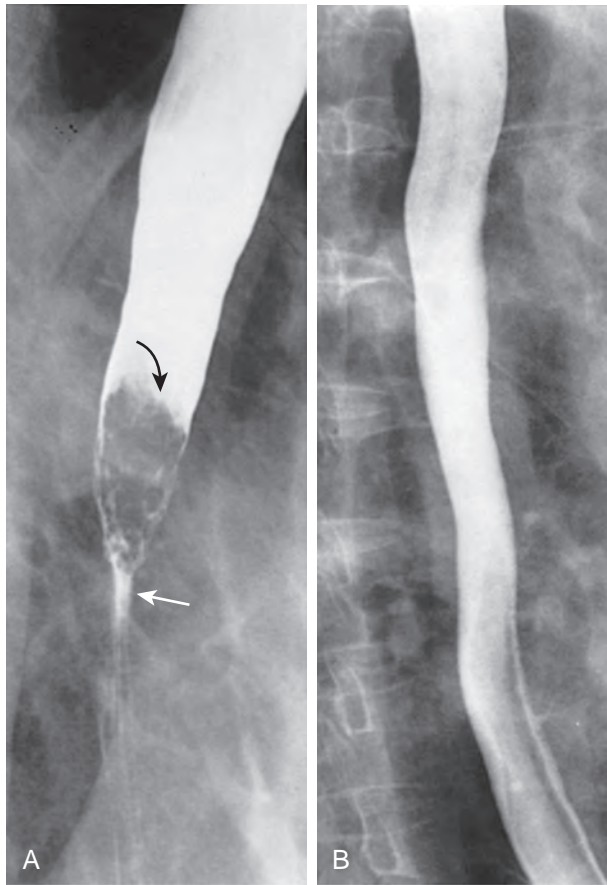


Figure 25-12 Foreign body obstruction in a normal esophagus. **A.** An impacted meat bolus in the midesophagus appears as a polypoid filling defect (curved black arrow). The incompletely distended esophagus below the impaction (white arrow) could be mistaken for a pathologic area of narrowing. **B.** Repeat esophagogram after removal of the foreign body shows a normal underlying esophagus. (From Levine MS: *Radiology of the Esophagus*. Philadelphia, WB Saunders, 1989.)



Figure 25-13 Foreign body obstruction with associated perforation. A polypoid defect (curved black arrow) is present in the distal esophagus as a result of an esophageal food impaction. In addition, there is extravasation of contrast medium into a focal collection (small white arrows) in the mediastinum, indicating perforation. Also note the large diverticulum (large white arrow) in the midesophagus. This perforation occurred within 6 hours of the onset of impaction. (From Gougoutas C, Levine MS, Laufer I: *Esophageal food impaction with early perforation*, AJR 171:427–428, 1998.)

Fistulas

ESOPHAGEAL-AIRWAY FISTULA

Most esophageal-airway fistulas result from direct invasion of the tracheobronchial tree by advanced esophageal carcinomas. Tracheoesophageal or esophagobronchial fistulas (usually involving the left main bronchus) have been reported in 5% to 10% of patients with esophageal cancer.^{83,84} They tend to occur after radiation therapy, presumably because radiation-induced tumor necrosis accelerates fistula formation. Other esophageal-airway fistulas may be caused by esophageal instrumentation, endobronchial stents eroding into the esophagus, foreign bodies, blunt or penetrating injuries to the chest or, rarely, perforation of an esophageal diverticulum.^{32,85} Esophagobronchial fistulas may also be caused by tuberculosis, histoplasmosis, or other granulomatous diseases in which necrotic, caseating mediastinal lymph nodes erode into the esophagus and bronchial tree.⁸⁶ Rarely, esophagobronchial fistulas may be congenital.⁸⁷

Patients with esophageal-airway fistulas often present with paroxysmal coughing after ingestion of liquids. Others develop recurrent aspiration pneumonia, hemoptysis, or a productive

cough with particles of food in the sputum. These fistulas may be difficult to differentiate from tracheobronchial aspiration on clinical grounds.

When an esophageal-airway fistula is suspected, the fluoroscopic examination should be performed with barium rather than water-soluble contrast agents because the latter agents are hypotonic and may draw fluid into the lungs, causing severe, potentially fatal pulmonary edema.⁵⁰ Most fistulas are readily demonstrated on barium studies and are found to arise within advanced, infiltrating esophageal carcinomas (Fig. 25-14). Once barium has entered the trachea or bronchi, however, it can be coughed up into the proximal trachea or larynx, so delayed overhead radiographs may erroneously suggest tracheobronchial aspiration. The initial swallow should therefore be performed in a lateral projection (with a video recording of the pharynx) to differentiate a fistula from aspiration.

ESOPHAGOPLEURAL FISTULA

Esophagopleural fistulas are usually caused by previous surgery, esophageal instrumentation, radiation, or advanced esophageal carcinoma directly invading the pleural space.⁸⁸ In contrast to

patients with esophageal-airway fistulas, these individuals may have nonspecific clinical findings such as chest pain, fever, dysphagia, or dyspnea.^{88,89} When an esophagopleural fistula is suspected, the diagnosis can be confirmed by recovery of ingested methylene blue in fluid aspirated during thoracentesis. Nonoperative management of esophagopleural fistulas is associated with mortality rates approaching 100%, whereas surgical repair is associated with mortality rates of about 50%.⁹⁰ Early diagnosis and surgical repair of these fistulas is therefore essential.

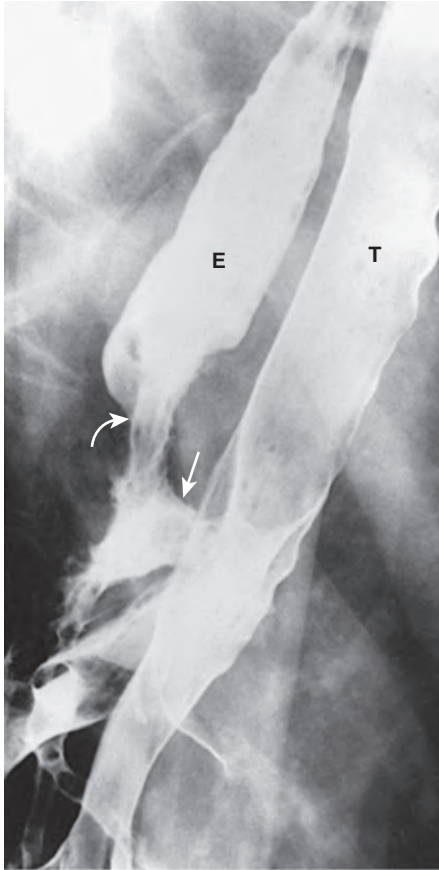


Figure 25-14 Esophagobronchial fistula. This fistula (straight arrow) was caused by an advanced, infiltrating esophageal carcinoma (curved arrow). E, Esophagus; T, trachea. (From Levine MS: *Radiology of the Esophagus*. Philadelphia, WB Saunders, 1989.)

Chest radiographs may reveal a pleural effusion, pneumothorax, or hydropneumothorax on the side of the fistula (Fig. 25-15A).⁸⁸ Pneumomediastinal or mediastinal widening is usually not present on chest radiographs because the mediastinum tends not to be directly involved by the fistula. When an esophagopleural fistula is suspected because of the clinical or plain film findings, a fluoroscopic examination using a water-soluble contrast agent should be performed to confirm the presence of a fistula and determine its precise location (Fig. 25-15B). CT may also be helpful for showing extraluminal collections of contrast medium, gas, or fluid in the pleural space from an esophagopleural fistula or even a gastropleural fistula after an esophagogastricomy and gastric pull-through (Fig. 25-16).⁹¹

Occasionally, surgical disruption of the muscularis propria during a myotomy for achalasia, resection of a leiomyoma, or dissection of malignant tumor adherent to the esophagus may cause eccentric ballooning and thinning of the esophageal wall, resulting in the development of an esophagopleural fistula.⁹² In such cases, CT or esophagography with water-soluble contrast agents may reveal an esophagopleural fistula at the site of esophageal ballooning or thinning (Fig. 25-17).⁹²

AORTOESOPHAGEAL FISTULA

Aortoesophageal fistulas are rare but highly lethal fistulas, usually caused by intraesophageal rupture of an atherosclerotic, syphilitic, or dissecting aneurysm of the descending thoracic aorta.⁹³⁻⁹⁵ Aortoesophageal fistulas may also be caused by a swallowed foreign body, esophageal carcinoma, infected aortic graft, or erosion of an endovascular stent into the esophagus.^{95,96}

Affected patients may initially present with several small sentinel episodes of arterial hematemesis, followed by a symptom-free latent period of hours to weeks and a sudden, final episode of massive hematemesis, exsanguination, and death.⁹³⁻⁹⁵ This latent period has been attributed to a blood clot occluding the fistula, hypotension, and vasoconstriction in response to severe hypovolemia.⁹³ As a result, early diagnosis of an impending aortoesophageal fistula provides the opportunity for definitive, potentially lifesaving surgery with placement of an aortic graft.

Aortoesophageal fistulas should be suspected in patients with arterial hematemesis who have a large atherosclerotic

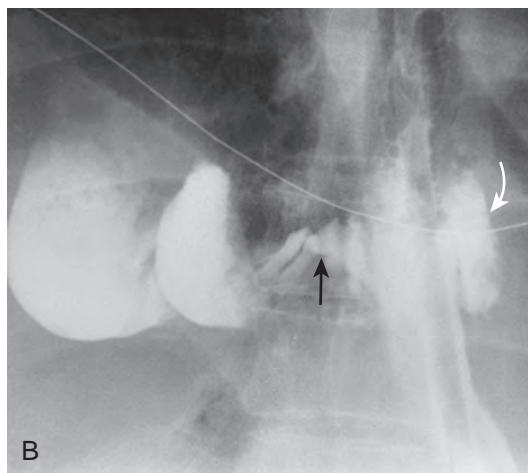
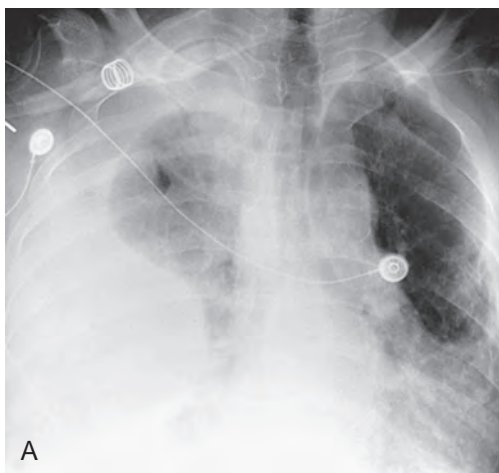


Figure 25-15 Esophagopleural fistula caused by endoscopic sclerotherapy of esophageal varices. A. Posteroanterior chest radiograph shows a large right pleural effusion. B. Study using water-soluble contrast medium reveals an esophagopleural fistula (black arrow), with contrast medium extending laterally in the right pleural space. There also is extravasated contrast medium in the mediastinum (curved white arrow). (From Levine MS: *Radiology of the Esophagus*. Philadelphia, WB Saunders, 1989.)

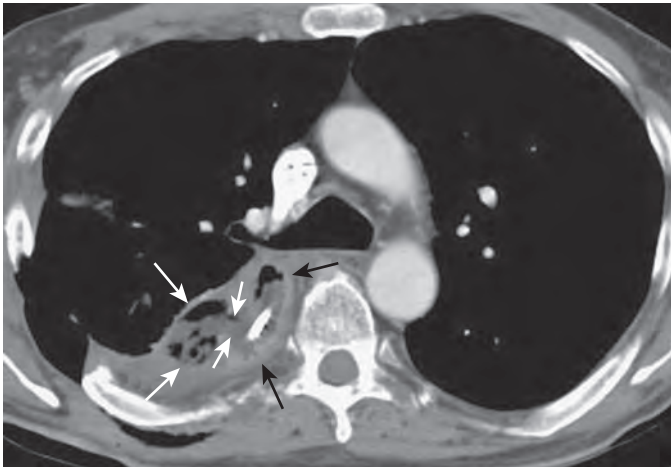
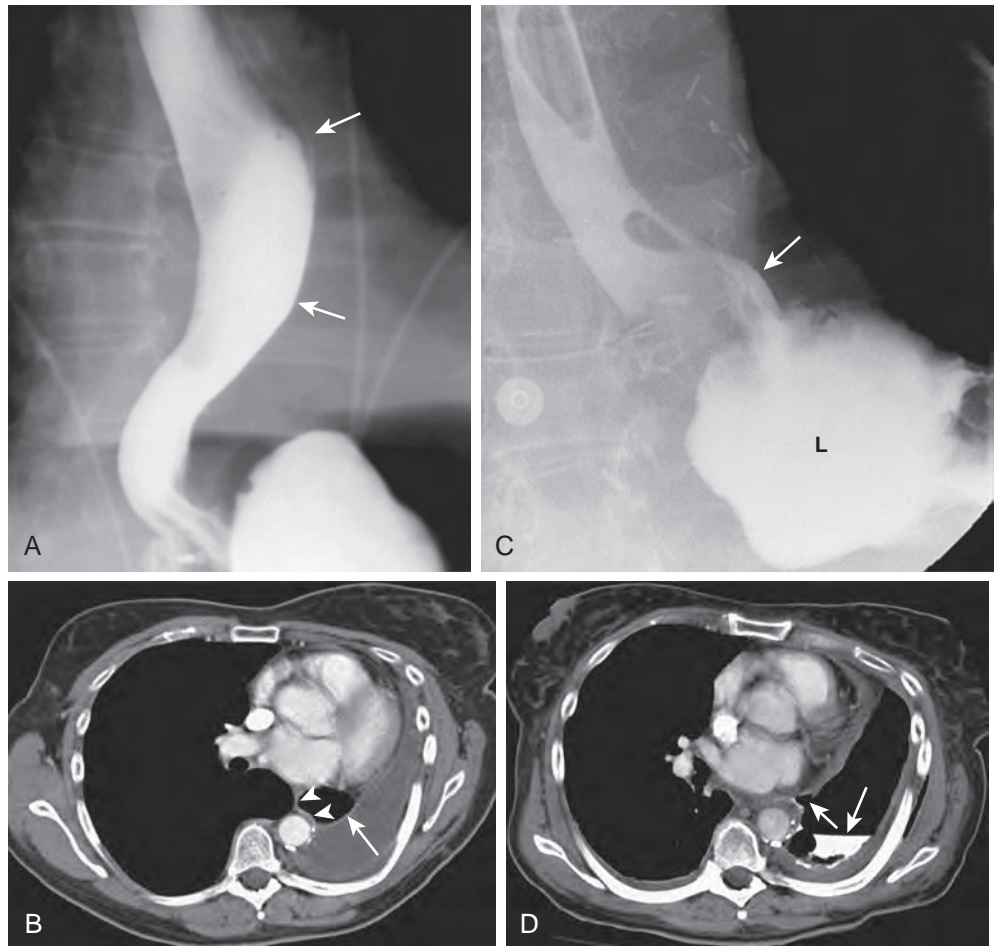


Figure 25-16 Gastropleural fistula after an esophagogastrectomy and gastric pull-through. Axial contrast-enhanced CT scan 4 days after surgery shows focal breakdown (small white arrows) of the right lateral wall of the intrathoracic stomach (black arrows), with fluid and gas entering a loculated collection (large white arrows) in the right pleural space, indicating the presence of a gastropleural fistula. Note a right-sided chest tube abutting the inferior aspect of this collection. (From Lantos JE, Levine MS, Rubesin SE, et al: Comparison between esophagography and chest computed tomography for evaluation of leaks after esophagectomy and gastric pull-through. *J Thorac Imaging* 28:121–128, 2013.)

Figure 25-17 Esophagopleural fistula secondary to esophageal wall ballooning and thinning after a pneumonectomy. **A.** Single-contrast esophagogram 5 months after a left pneumonectomy shows asymmetric ballooning (arrows) of the left lateral wall of the midesophagus. **B.** CT shows postsurgical changes from the left pneumonectomy with asymmetric ballooning and thinning (arrow) of the left lateral wall of the midesophagus. Note the normal thickness of the right posterolateral wall (arrowheads) of the midesophagus for comparison. **C.** Repeat esophagogram with water-soluble contrast medium 10 months after surgery shows leakage (L) of water-soluble contrast material from the left lateral wall (arrow) of the ballooned midesophagus into the left pleural space, indicating an esophagopleural fistula. **D.** CT also shows an esophagopleural fistula (short arrow) at the site of esophageal wall ballooning and thinning, with oral contrast medium (long arrow) and air in the left pleural space. (From Liu PS, Levine MS, Torigian DA: Esophagopleural fistula secondary to esophageal wall ballooning and thinning after pneumonectomy: Findings on chest CT and esophagography. *AJR* 186:1627–1629, 2006.)



aneurysm of the descending thoracic aorta on chest radiographs.⁹⁵ In such cases, studies using water-soluble contrast agents may reveal extrinsic compression or displacement of the esophagus by the aneurysm but rarely show leakage of contrast medium into the aorta because of the flow dynamics of these structures (Fig. 25-18A).⁹³ When an infected aortic graft has eroded into the esophagus, extravasated contrast medium from the esophagus may occasionally outline the coiled springs of the graft (Fig. 25-18C).^{93,96} The presence of an aorto-esophageal fistula may be confirmed by demonstrating extravasation of contrast medium from the aorta into the esophagus on aortography. The origin of the fistulous track is often occluded by thrombus, however, so aortography may also fail to delineate the actual fistula in these patients (Fig. 25-18B).⁹⁴

ESOPHAGOPERICARDIAL FISTULA

Esophagopericardial fistulas are rare fistulas caused by severe esophagitis, esophageal cancer, swallowed foreign bodies, or surgery.⁹⁷ These fistulas usually lead to the rapid development of severe pericarditis or cardiac tamponade caused by leakage of esophageal contents into the pericardial space. Chest radiographs reveal pneumopericardium or hydropneumopericardium in 25% to 50% of cases.⁹⁷ The diagnosis may be confirmed by having the patient swallow a water-soluble contrast agent to

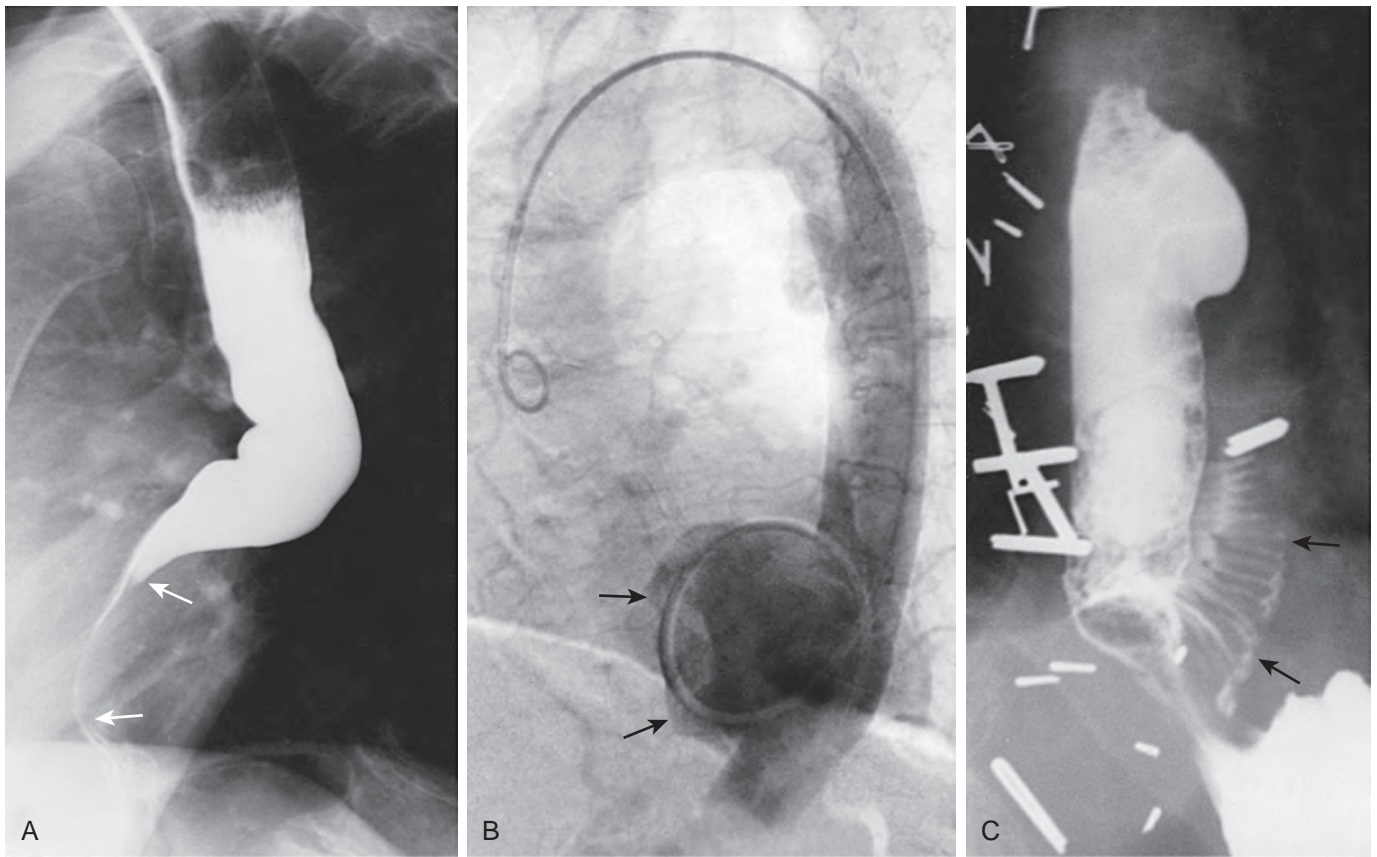


Figure 25-18 Aortoesophageal fistula caused by an aortic aneurysm. **A.** Initial esophagogram shows anterior displacement and narrowing of the distal esophagus (arrows) by an aneurysm of the descending thoracic aorta. **B.** Subsequent aortogram reveals a saccular aneurysm with intraluminal thrombus (arrows) occluding the origin of the fistula. Although radiographic studies failed to demonstrate the fistula, an aortoesophageal fistula was found at surgery. **C.** Another esophagogram after placement of a Dacron aortic graft shows a recurrent aortoesophageal fistula with extravasated contrast medium from the esophagus outlining the aortic graft (arrows). This fistula was caused by infection of the graft. (From Baron RL, Koehler RE, Gutierrez FR, et al: *Clinical and radiographic manifestations of aortoesophageal fistulas*. *Radiology* 141:599–605, 1981.)

demonstrate the fistulous track or gross filling of the pericardial sac with contrast medium (Fig. 25-19).

Diverticula

Esophageal diverticula may be classified by their location or by their mechanism of formation. The most common locations include the pharyngoesophageal junction (i.e., Zenker's diverticulum) (see Chapter 16), midesophagus, and distal esophagus just above the gastroesophageal junction (i.e., epiphrenic diverticulum). When classified by their mechanism of formation, a pulsion diverticulum develops because of increased intraluminal esophageal pressure from underlying esophageal dysmotility (especially diffuse esophageal spasm), whereas a traction diverticulum develops because of fibrosis in adjacent periesophageal tissues. In the past, many midesophageal diverticula were thought to be traction diverticula caused by scarring from tuberculosis or histoplasmosis in perihilar or subcarinal lymph nodes. This type of diverticulum has decreased considerably in frequency, however, so most midesophageal diverticula are now thought to be of the pulsion variety.⁹⁸

PULSION AND TRACTION DIVERTICULA

Pulsion and traction diverticula are usually incidental findings in the esophagus without clinical significance. When symptoms

are present in patients with one or more pulsion diverticula, they are typically related to the patient's underlying esophageal dysmotility,⁹⁹ but some diverticula that are extremely large may cause symptoms.

Radiographic Findings

Diverticula are readily detected on esophagograms as barium-filled outpouchings from the esophagus. They are best seen in profile, but they may be recognized en face as ring shadows on double-contrast studies. Once a diverticulum has been detected, it should be classified as a pulsion or traction diverticulum. Pulsion diverticula are much more common, usually located in the middle or distal thirds of the esophagus, and often associated with other radiographic evidence of motor dysfunction. They usually have a rounded contour and a wide neck and are frequently multiple (Fig. 25-20). Because they contain no muscle in their wall, they tend to remain filled after the esophagus has emptied of barium (see Fig. 25-20B).

Traction diverticula are usually located in the midesophagus and have a tented or triangular configuration as a result of scarring and retraction from surgery, radiation, or granulomatous disease in the adjacent mediastinum (Fig. 25-21). Traction diverticula typically occur as solitary outpouchings containing all layers of the esophageal wall, including the muscle propria, so they tend to empty when the esophagus collapses. Thus, it is

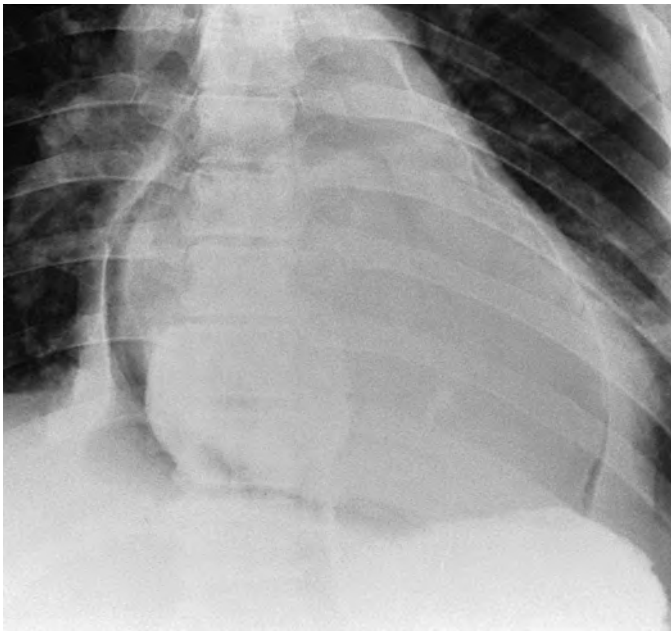
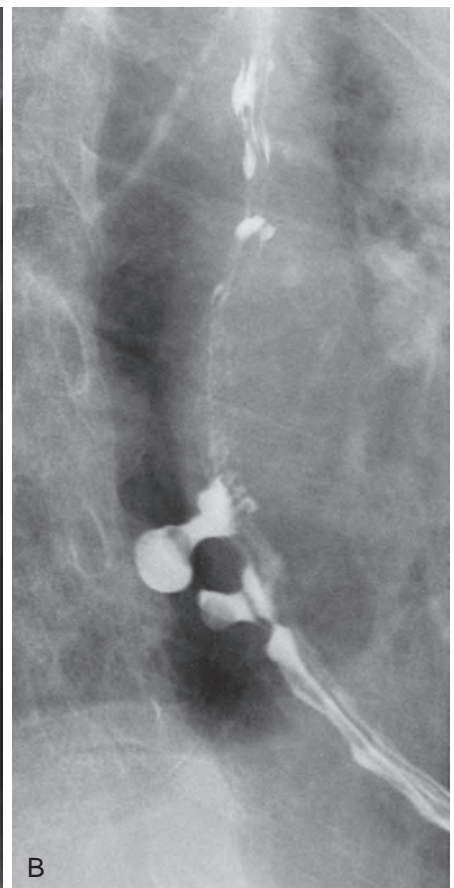
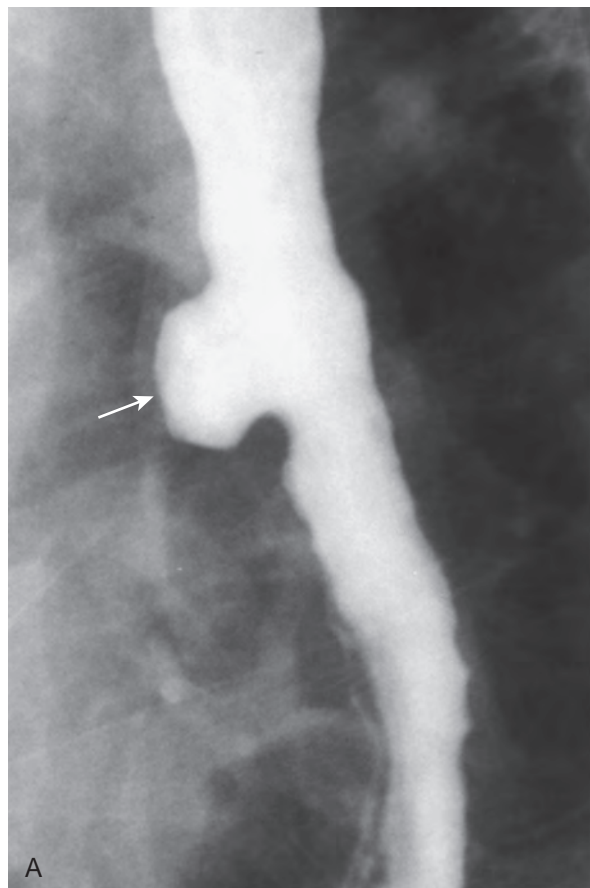


Figure 25-19 Esophagopericardial fistula caused by a perforated ulcer associated with severe reflux esophagitis. Posteroanterior chest radiograph after oral administration of water-soluble contrast medium reveals a pneumopericardium with free leakage of contrast medium into the pericardial space. Air and contrast medium outline the inner aspect of the pericardial sac. Contrast medium is also faintly seen in a hiatal hernia. (From Cyrlak D, Cohen AJ, Dana ER: Esophagopericardial fistula: Causes and radiographic features. *AJR* 141:177–179, 1983.)

Figure 25-20 Pulsion diverticula. A. Note the smooth contour and wide neck of this pulsion diverticulum (arrow) in the midesophagus. There also is evidence of esophageal dysmotility with weak nonperistaltic contractions more distally. Pulsion diverticula are often associated with esophageal motor dysfunction, particularly diffuse esophageal spasm. **B.** In another patient, the pulsion diverticula remain filled after most of the barium has emptied from the esophagus by peristalsis. Again, note the rounded contour and wide necks of the diverticula. (B from Levine MS: *Radiology of the Esophagus*. Philadelphia, WB Saunders, 1989.)



usually possible to distinguish pulsion and traction diverticula on radiologic criteria.

EPIPHRENIC DIVERTICULUM

An epiphrenic diverticulum is an uncommon form of esophageal diverticulum that arises in the distal esophagus, usually within 10 cm from the gastroesophageal junction. It is generally believed to be a pulsion diverticulum caused by diffuse esophageal spasm with markedly increased intraluminal esophageal pressures.^{99,100} In one study, however, diffuse esophageal spasm was found in less than 10% of patients with epiphrenic diverticula,¹⁰¹ so other, as yet undefined, factors may also contribute to the development of these structures. Investigators have also found a significant correlation between the size of the diverticulum and the presence of symptoms (i.e., epiphrenic diverticula >5 cm in diameter are more likely to cause symptoms).¹⁰¹ Thus, the development of symptoms appears to be related primarily to the size of the diverticulum rather than to underlying esophageal dysmotility in these patients.

When an epiphrenic diverticulum fills with food, it may compress the true lumen of the esophagus, causing dysphagia.^{101,102} Food or fluid that accumulates within an epiphrenic diverticulum may also be regurgitated into the esophagus with subsequent reflux symptoms, chest pain, or aspiration.¹⁰¹ Rarely, these diverticula may perforate into the mediastinum or form a fistula to the airway. When symptoms associated with an epiphrenic diverticulum are particularly severe or intractable,

they may necessitate surgical intervention, usually a diverticulectomy and esophagomyotomy.^{103,104}

Radiographic Findings

An epiphrenic diverticulum may be recognized on chest radiographs by the presence of a soft tissue mass (often containing

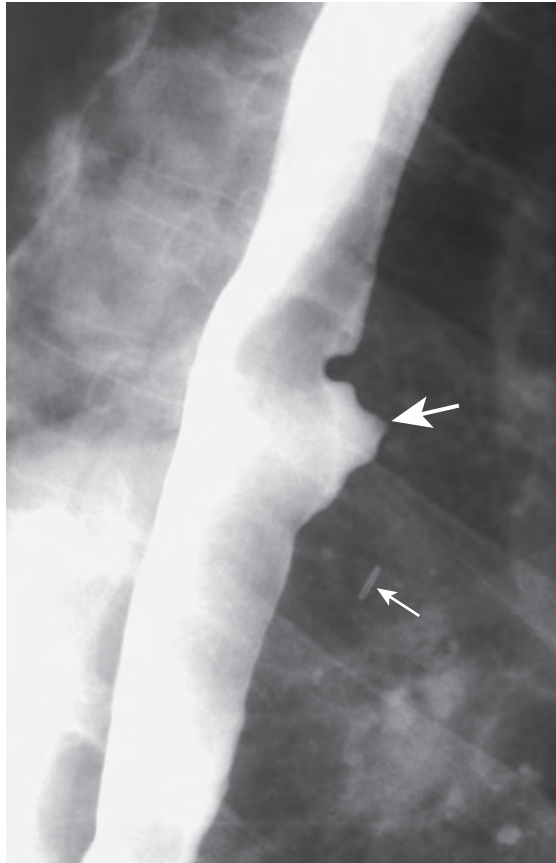


Figure 25-21 Traction diverticulum. The diverticulum has a pointed or triangular tip (large arrow) as a result of traction and volume loss in the adjacent mediastinum from prior surgery. A surgical clip (small arrow) is seen in the mediastinum. (From Levine MS: *Radiology of the Esophagus*. Philadelphia, WB Saunders, 1989.)

an air-fluid level) that mimics a hiatal hernia (Fig. 25-22A and B). Barium studies usually reveal a solitary diverticulum arising from the right side of the distal esophagus (Fig. 25-22C), but epiphrenic diverticula can occasionally be multiple or arise from the left side.¹⁰¹ These structures vary markedly in size, ranging from 1 to 12 cm in greatest diameter.¹⁰¹ When the diverticulum is large enough, barium studies may reveal preferential filling or prolonged retention of barium within the diverticulum, regurgitation of barium or debris from the diverticulum, or compression of the adjacent esophagus by the diverticulum.¹⁰¹

Ectopic Gastric Mucosa

Ectopic gastric mucosa in the esophagus is a common congenital anomaly, with a reported incidence of 4% to 10% at endoscopy.^{105,106} Unlike Barrett's mucosa, ectopic gastric mucosa is unrelated to gastroesophageal reflux disease, and most patients with this finding are asymptomatic. The ectopic patch of gastric mucosa is almost always located in the upper esophagus at or just above the thoracic inlet; hence, it has been called the *inlet patch*.¹⁰⁵

Ectopic gastric mucosa in the esophagus can sometimes be recognized on double-contrast esophagography by a shallow depression with small indentations at its superior and inferior borders (Fig. 25-23).¹⁰⁷⁻¹⁰⁹ These lesions are usually found on the right lateral wall of the upper thoracic esophagus at or near the thoracic inlet.¹⁰⁷⁻¹⁰⁹ Although this depression could be mistaken for ulceration or even an intramural dissection on barium studies,¹⁰⁹ the appearance and location of ectopic gastric mucosa are so characteristic that endoscopy is not warranted in asymptomatic patients. Rarely, affected individuals may develop dysphagia because of associated webs or strictures.^{110,111}

Congenital Esophageal Stenosis

Congenital esophageal stenosis is a rare developmental anomaly caused by defective embryologic separation of the primitive foregut from the respiratory tract, with sequestration of tracheobronchial precursor cells in the esophageal wall.^{112,113} Infants may have a severe form of congenital esophageal stenosis

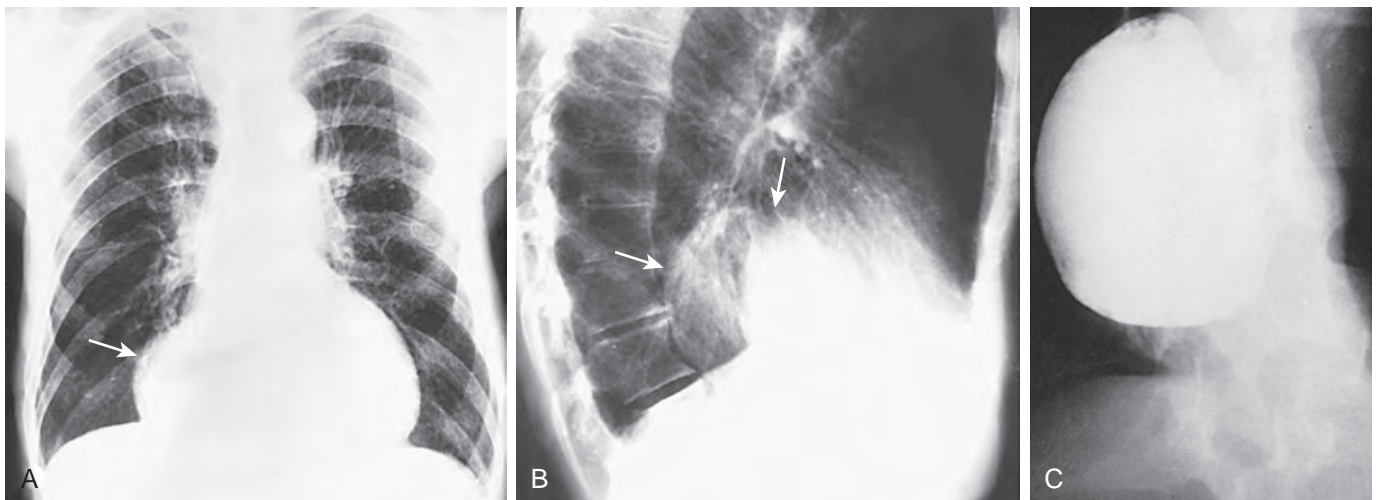


Figure 25-22 Large epiphrenic diverticulum. **A.** Posteroanterior chest radiograph shows a prominent bulge along the right border of the heart (arrow). **B.** Lateral chest radiograph shows a soft tissue mass (arrows), mimicking the appearance of a hiatal hernia. **C.** A barium study reveals a large epiphrenic diverticulum that remains filled with barium after the esophagus has emptied. (From Levine MS: *Radiology of the Esophagus*. Philadelphia, WB Saunders, 1989.)

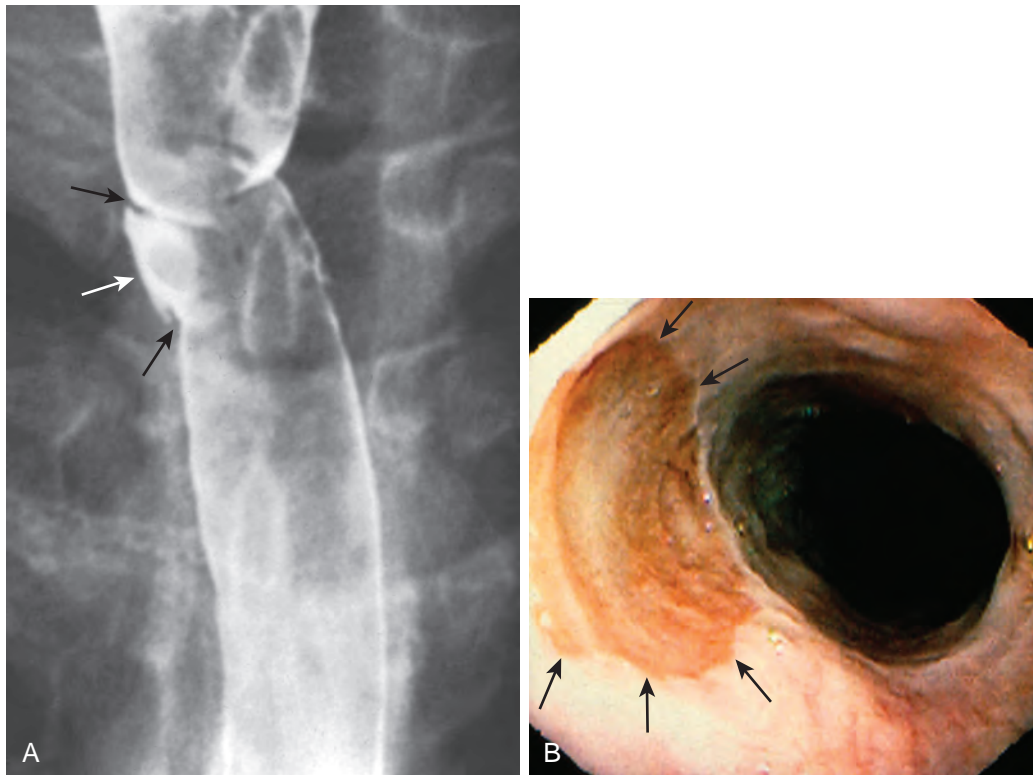


Figure 25-23 Ectopic gastric mucosa in the esophagus. **A.** There is a broad, flat depression (white arrow) on the right lateral wall of the upper esophagus near the thoracic inlet, with a pair of small indentations (black arrows) at both ends of the lesion. Although it could be mistaken for an ulcer, this lesion has the typical appearance and location of ectopic gastric mucosa in the esophagus. **B.** Endoscopy shows a reddish-brown, epithelium-lined depression (arrows) in the upper esophagus characteristic of ectopic gastric mucosa. (From Lee J, Levine MS, Shultz CF: Ectopic gastric mucosa in the oesophagus mimicking ulceration. *Eur J Radiol* 31:97–200, 1997.)

associated with esophageal atresia or tracheoesophageal fistulas,¹¹⁴ but adults may have a mild form of the disease manifested by esophageal strictures.^{115–117}

CLINICAL FINDINGS

Patients with severe forms of congenital esophageal stenosis typically present during infancy with marked dysphagia and vomiting,^{114,118} but patients with milder forms of stenosis may present during adolescence or early adulthood with a long-standing history of intermittent dysphagia, chest pain, and occasional food impactions.^{115–117} For reasons that are unclear, almost all reported cases in adults have been men.^{115–117} Dysphagia in these patients is usually alleviated by endoscopic dilation of the strictures.¹¹⁴

RADIOGRAPHIC FINDINGS

Congenital esophageal stenosis in adults is usually characterized on esophagography by the presence of smooth, tapered strictures in the upper or midesophagus.^{115,116,119,120} The strictures often contain multiple ringlike constrictions, producing a distinctive radiographic appearance on double-contrast esophagograms (Fig. 25-24).¹²⁰ The cause of these ringlike constrictions is uncertain, but they may represent cartilaginous rings similar to those found in the trachea.¹²⁰ Whatever the explanation, the presence of an esophageal stricture with distinctive ringlike constrictions should suggest the diagnosis of congenital esophageal stenosis in the proper clinical setting.

DIFFERENTIAL DIAGNOSIS

Eosinophilic esophagitis is another more common cause of esophageal strictures with distinctive ringlike indentations.¹²¹ The correct diagnosis is often suggested by a history of allergies or asthma or a peripheral eosinophilia in these patients (see Chapter 21). Fixed transverse folds in the distal esophagus associated with longitudinal scarring from reflux esophagitis may also resemble the ringlike indentations of congenital esophageal stenosis, but these transverse folds almost always occur in the distal esophagus in the region of a peptic stricture.¹²² Finally, fine transverse striations may be seen in patients with a so-called feline esophagus, but these transverse striations occur as a transient finding and are not associated with strictures.¹²³

Extrinsic Impressions

NORMAL IMPRESSIONS

A variety of normal structures in the mediastinum, including the heart, aortic arch, and left main bronchus, may cause extrinsic impressions on the esophagus (see Chapter 17). In about 10% of patients, a smooth, gently sloping indentation may also be seen on the right posterolateral wall of the upper thoracic esophagus between the thoracic inlet and aortic arch (Fig. 25-25A).¹²⁴ Correlation with CT has shown that this impression is caused by an unusually prominent right inferior supra-azygous recess of the lung indenting the upper esophagus (Fig. 25-25B).¹²⁴ In patients with this normal anatomic variant,

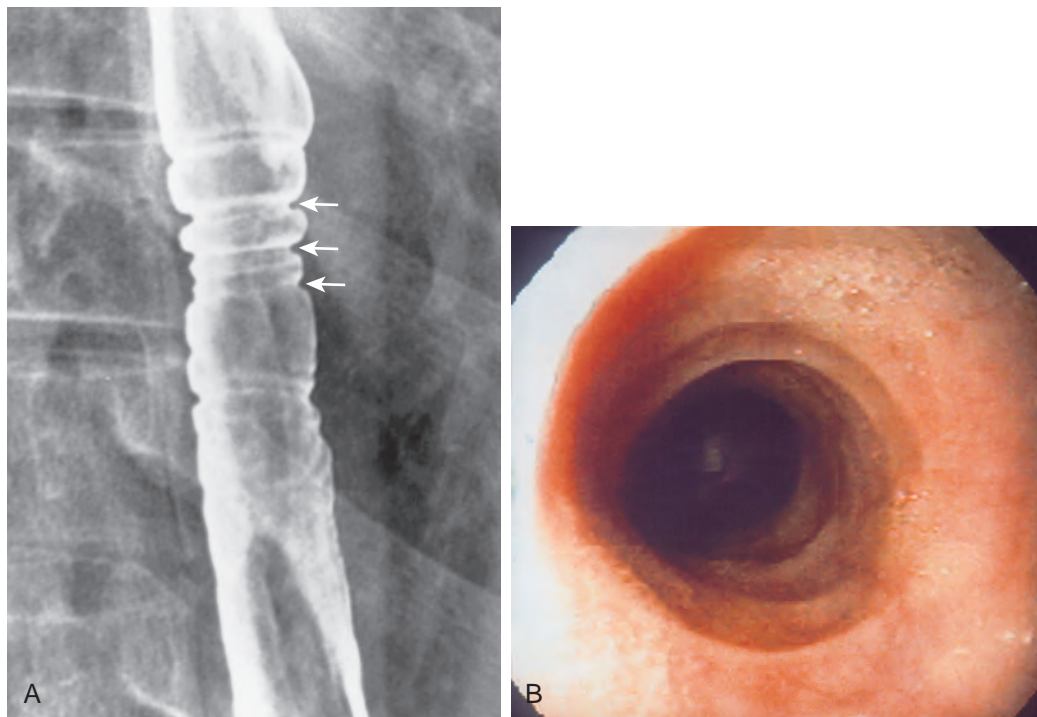


Figure 25-24 Congenital esophageal stenosis. **A.** There is a mild area of narrowing in the midesophagus with distinctive ringlike indentations (arrows) in the region of the stricture. **B.** Endoscopy also shows ringlike indentations that resemble tracheal rings. (**A** from Luedtke P, Levine MS, Rubesin SE, et al: Radiologic diagnosis of benign esophageal strictures: A pattern approach. *RadioGraphics* 23:897–909, 2003.)

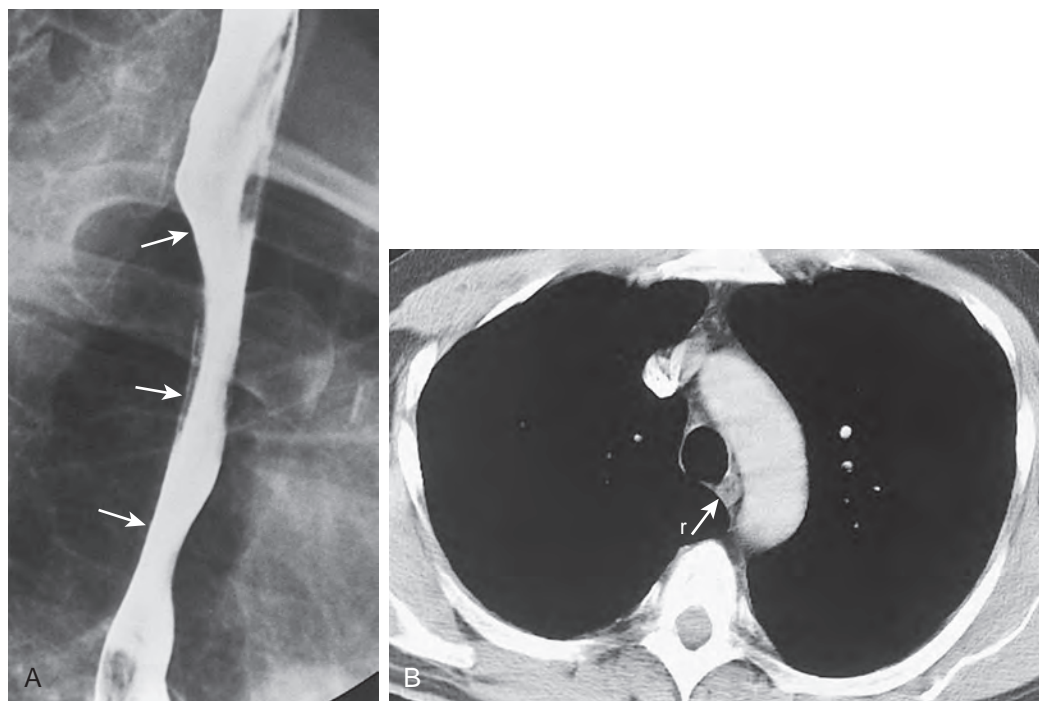


Figure 25-25 Extrinsic impression on the esophagus by a prominent right inferior supra-azygous recess. **A.** There is a smooth, gently sloping indentation (arrows) on the right posterolateral wall of the upper thoracic esophagus between the thoracic inlet and aortic arch. **B.** In the same patient, CT of the chest shows a prominent right inferior supra-azygous recess (r) impinging on the right posterolateral wall of the upper esophagus (arrow). (From Sam JW, Levine MS, Miller WT: The right inferior supra-azygous recess: A cause of upper esophageal pseudomass on double-contrast esophagography. *AJR* 171:1583–1586, 1998.)

the outer wall of the right upper thoracic esophagus is directly apposed to the adjacent lung, producing a smooth demarcation between the soft tissue density of the esophageal wall and the gaseous density of the lung, so the actual thickness of the esophageal wall can be visualized in this region. Because of its frequency, radiologists should be aware of this variant, so it is not mistaken for adenopathy or other masses in the mediastinum, and unnecessary cross-sectional imaging of the chest can be avoided. A narrowed thoracic inlet (in the sagittal dimension) is another anatomic variant that occasionally results in extrinsic compression of the right side of the barium-filled esophagus, erroneously suggesting a mass lesion in this region.¹²⁵ In such patients, however, CT will reveal a narrowed thoracic inlet without evidence of a mass.¹²⁵

ABNORMAL IMPRESSIONS

Abnormal impressions are usually caused by the heart and great vessels. An enlarged left atrium or ventricle may produce a broad impression on the anterior wall of the distal esophagus. In contrast, a tortuous or ectatic descending thoracic aorta may cause a prominent impression on the posterior wall of the distal esophagus near the esophageal hiatus of the diaphragm (Fig. 25-26). In some patients, compression of the distal esophagus by the aorta or an aortic aneurysm may cause dysphagia (i.e., dysphagia aortica).¹²⁶ Similarly, congenital abnormalities of the



Figure 25-26 Esophageal impression (arrow) by an ectatic descending thoracic aorta. The esophagus is narrowed at the level of deviation. (From Levine MS, Gilchrist AM: Esophageal deviation: Pushed or pulled? AJR 149:513–514, 1987.)

great vessels, such as an aberrant subclavian artery and double aortic arch, may compress the esophagus, causing dysphagia (i.e., dysphagia lusoria). The esophagus may also be compressed or displaced by masses in the mediastinum, including substernal thyroid goiters, mediastinal lymphadenopathy, and other benign or malignant neoplasms. CT or magnetic resonance imaging (MRI) of the chest may be performed to determine the cause of the underlying mediastinal mass in these patients.

ESOPHAGEAL RETRACTION

Esophageal deviation may be caused by pulmonary, pleural, or mediastinal scarring with retraction of the esophagus toward the diseased hemithorax (Fig. 25-27). It is usually possible to differentiate this retraction from esophageal displacement by a mediastinal mass, using the radiologic sign illustrated in Figure 25-28.¹²⁷ When the esophagus is displaced or pushed by an extrinsic mass in the mediastinum, it tends to be narrower at this level than above or below the deviated segment (see Figs. 25-26 and 25-28A), whereas the esophagus tends to be wider at this level when it is retracted or pulled by pleuropulmonary scarring (see Figs. 25-27 and 25-28B).¹²⁷ When esophageal retraction is suggested by barium studies, chest radiographs should be obtained to confirm the presence of tuberculosis,

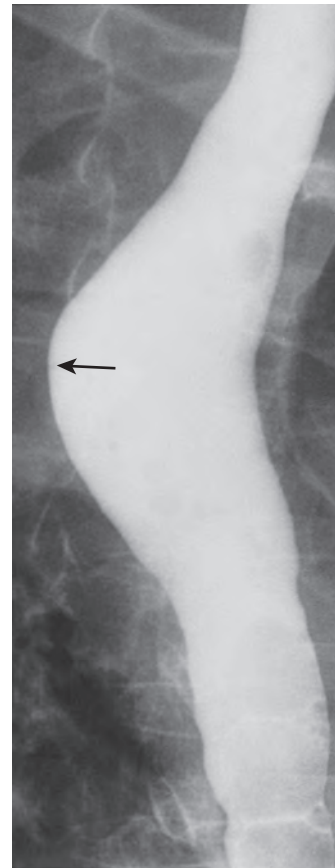


Figure 25-27 Esophageal retraction by pleuropulmonary scarring. The esophagus is deviated to the right (arrow) because of scarring and volume loss from right upper lobe tuberculosis. The esophagus is widened at the level of deviation. This characteristic widening indicates retraction of the esophagus toward the side of pleuropulmonary scarring rather than displacement by a mass on the opposite side.

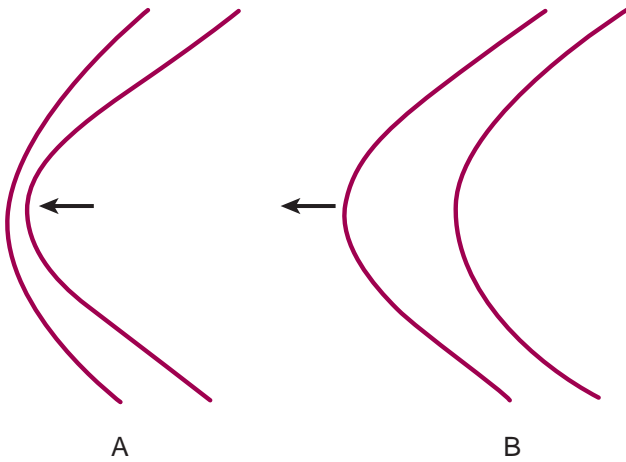


Figure 25-28 Pushed versus pulled esophagus. **A.** When the esophagus is displaced or pushed by an extrinsic mediastinal mass, it tends to be narrower at this level (arrow) than above or below the deviated segment. **B.** When the esophagus is retracted or pulled by pleuropulmonary scarring and volume loss, however, it tends to be wider at this level (arrow) than above or below the deviated segment. (From Levine MS, Gilchrist AM: *Esophageal deviation: Pushed or pulled?* AJR 149:513–514, 1987.)

radiation damage, postsurgical changes, or other causes of scarring and volume loss in the adjacent hemithorax. It is important to determine whether the esophagus has been pushed or pulled from its normal midline position because esophageal retraction from pleuropulmonary scarring usually occurs as an incidental finding, whereas esophageal displacement by a mediastinal mass may require further investigation with CT or MRI to determine the nature and extent of the mass.

Varices

UPHILL VARICES

Pathophysiology

Uphill varices develop as a result of changes in the venous drainage of the esophagus caused by altered flow dynamics in patients with portal hypertension. Normally, the cervical and upper thoracic esophagus are drained by the supreme intercostal vein, bronchial veins, inferior thyroid vein, and other mediastinal collaterals, the midthoracic esophagus is drained by the azygos and hemiazygos veins, and the distal thoracic esophagus is drained by a periesophageal plexus of veins that communicate distally with the coronary vein. In turn, the coronary vein drains into the splenic vein near its junction with the portal vein or directly into the portal vein. In portal hypertension, however, increased portal venous pressure leads to reversal of venous flow through the coronary vein into a plexus of dilated periesophageal veins that anastomose superiorly with collaterals from the azygos and hemiazygos venous systems. Because the azygos vein drains directly into the superior vena cava, portal venous blood returns to the right side of the heart via the superior vena cava rather than the inferior vena cava, thus bypassing the obstructed portal system.

Clinical Findings

Esophageal varices are important because of the potentially catastrophic consequences of variceal rupture and hemorrhage.

Variceal bleeding occurs in 25% to 35% of patients with cirrhosis, and as many as 30% of these bleeding events are fatal.^{128,129} Although some patients have a major variceal hemorrhage with one or more episodes of massive hematemesis, others have intermittent, low-grade bleeding with melena, guaiac-positive stool, or iron-deficiency anemia. Surprisingly, however, the size and extent of varices correlate poorly with the degree of bleeding.

Radiographic Findings

Chest Radiographs. Esophageal varices may occasionally be manifested on chest radiographs by a retrocardiac posterior mediastinal mass. This finding is caused by dilated periesophageal veins or, less commonly, by dilated azygos or hemiazygos veins.¹³⁰⁻¹³² The mass is usually more obvious on radiographs obtained with the patient in the recumbent position because hydrostatic pressure tends to overcome portal pressure in the upright position, shifting blood flow to more dependent collateral vessels.

Barium Studies. Esophagography has not traditionally been considered a reliable technique for detecting esophageal varices. Some authors have advocated the use of anticholinergic agents to improve visualization of varices by decreasing esophageal peristalsis,^{133,134} but such agents are contraindicated in patients with glaucoma, cardiac disease, or urinary retention.

Whether or not pharmacologic agents are used, optimal demonstration of varices requires meticulous attention to radiographic technique because varices can easily be obscured on overly distended or collapsed views of the esophagus (Fig. 25-29). The examination should be performed with the patient in a recumbent (usually prone right anterior oblique) position, using a high-density barium suspension or paste to increase adherence of barium to the esophageal mucosa. Mucosal relief views of the collapsed esophagus are particularly helpful for demonstrating varices (see Fig. 25-29D). However, peristalsis tends to squeeze blood from the thin-walled varices, rendering them invisible for as long as 15 to 30 seconds (see Fig. 25-29C). The fluoroscopist must therefore wait for the varices to refill before obtaining mucosal relief views. If necessary, the patient should be asked to spit his or her saliva into a basin to avoid initiating a new peristaltic sequence and collapsing the varices again. With optimal technique, esophagography has a sensitivity of almost 90% in detecting esophageal varices.¹³⁵

Because of the underlying venous anatomy, uphill varices tend to be most prominent in the distal third or half of the thoracic esophagus, fading gradually as they ascend to the level of entry of the azygos vein into the superior vena cava. Varices are usually best seen on mucosal relief views, appearing as tortuous or serpiginous longitudinal filling defects in the collapsed or partially collapsed esophagus (see Fig. 25-29D).¹³⁶ Varices may also be seen on double-contrast images when they are etched in white because of trapping of barium between the edge of the varices and adjacent esophageal wall (see Fig. 25-29A). Because varices alternately distend and collapse with peristalsis, respiration, and varying degrees of esophageal distention, they may be observed as a transient finding at fluoroscopy.

Computed Tomography. Esophageal varices may be recognized on CT by a thickened, lobulated esophageal wall

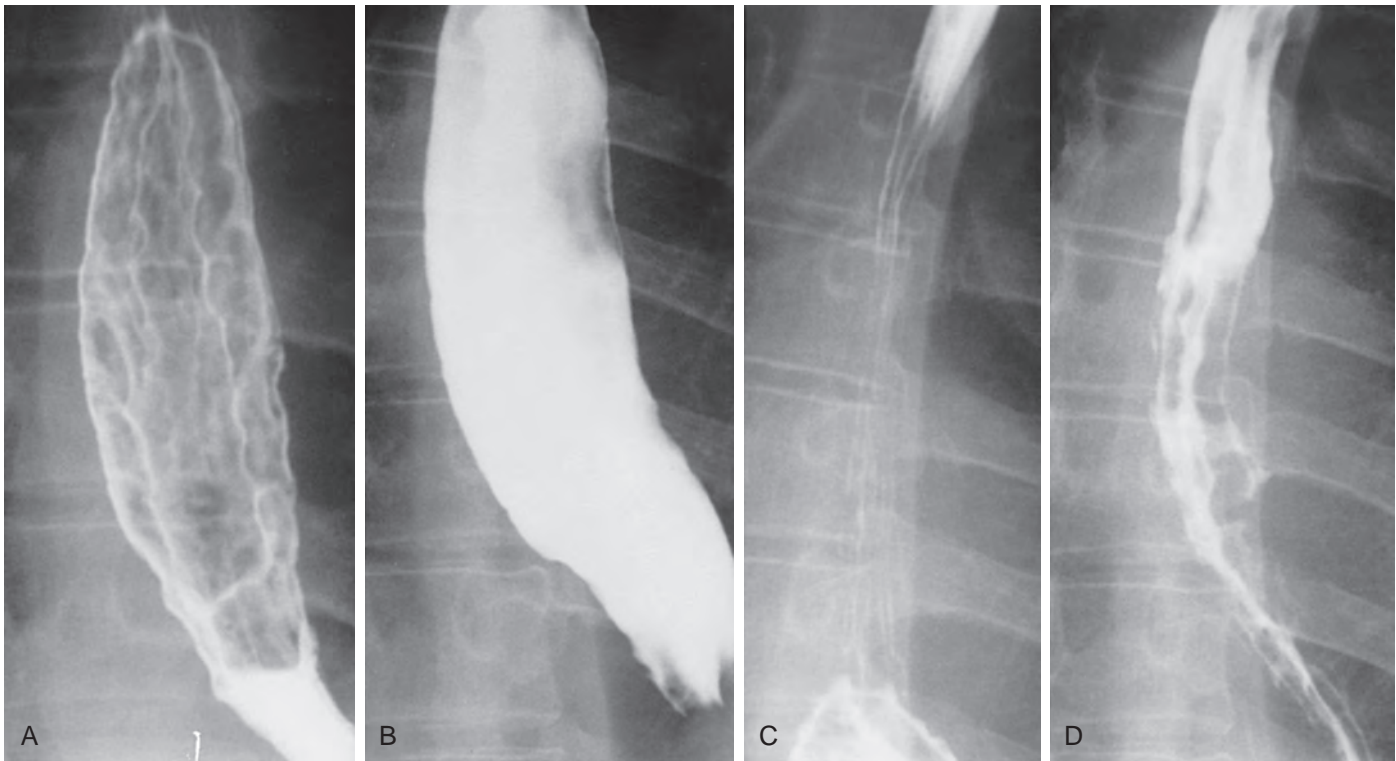


Figure 25-29 Uphill esophageal varices. **A.** Multiple varices are seen on a double-contrast esophagogram. Note how the varices are etched in white. **B.** The varices are obscured by intraluminal barium on a single-contrast image. **C.** The varices also are not visible on a mucosal relief view immediately after a peristaltic stripping wave that has squeezed blood from the dilated veins, causing them to collapse. **D.** However, the varices can be recognized as serpiginous filling defects on another view several seconds after passage of the peristaltic wave. (From Levine MS: *Radiology of the Esophagus*. Philadelphia, WB Saunders, 1989.)

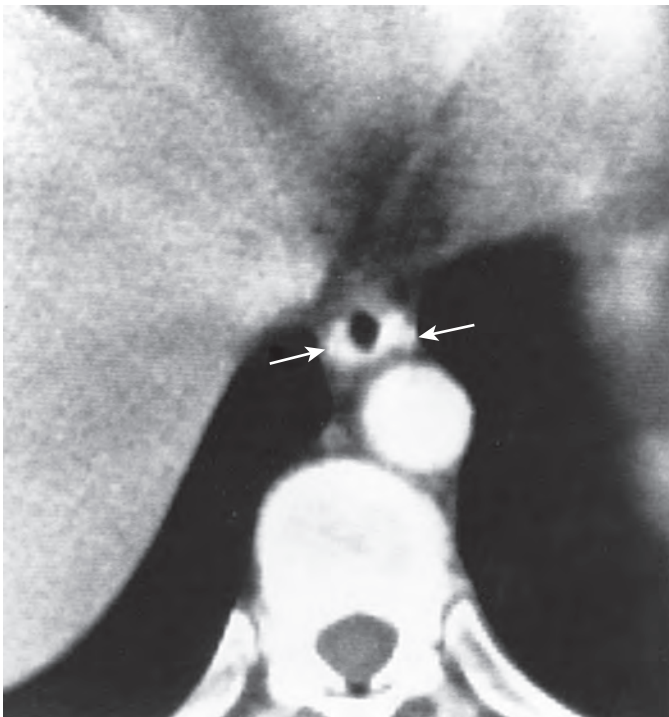


Figure 25-30 Esophageal varices on CT. Axial contrast-enhanced CT scan shows dense enhancement of the varices (arrows). (Courtesy Robert A. Halvorsen, MD, San Francisco.)

containing round, tubular, or serpentine structures that have homogeneous attenuation and enhance with the administration of IV contrast medium to the same degree as adjacent vessels (Fig. 25-30).¹³⁷⁻¹³⁹ CT may also reveal coronary, paraesophageal, retrogastric, paraumbilical, perisplenic, omental, mesenteric, and abdominal wall varices in patients with portal hypertension.¹³⁹ Occasionally, dilated azygos, hemiazygos, or paraesophageal veins can be mistaken for a posterior mediastinal mass on an unenhanced CT scan.^{132,140} However, the marked degree of enhancement that occurs within these dilated vascular structures after infusion of contrast medium should establish the correct diagnosis.^{132,140}

Angiography. Arteriograms of the celiac artery, selective arteriograms of the superior mesenteric or splenic artery, or, less frequently, portal venograms may be obtained to confirm the presence of uphill varices and determine the nature and extent of underlying venous abnormalities. With portal hypertension, images obtained during the venous phase of the examination usually fail to demonstrate the portal vein because of reversal of blood flow through numerous collateral vessels to bypass the obstructed venous system. In almost all cases, the coronary vein acts to shunt portal blood through a periesophageal plexus of veins, producing uphill varices, which communicate with the azygos venous system and superior vena cava (Fig. 25-31). Delineation of the angiographic anatomy is important when a surgical shunt is contemplated to control variceal bleeding.

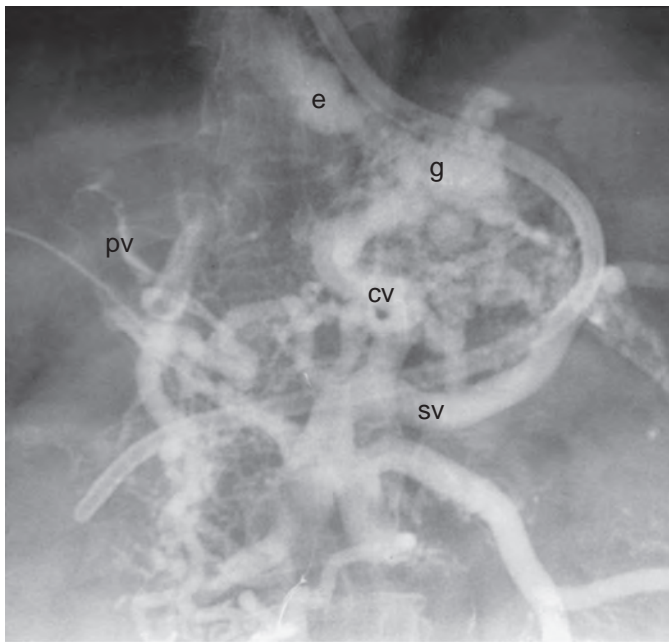


Figure 25-31 Angiographic demonstration of esophageal and gastric varices due to portal hypertension. This image from a portal venogram shows cavernous transformation of the portal vein (pv) with reversal of blood flow through the coronary vein (cv) and splenic vein (sv), producing gastric (g) and esophageal (e) varices. (Courtesy Dana R. Burke, MD, Bethesda, MD.)

Differential Diagnosis

A diagnosis of esophageal varices can usually be made on the basis of the radiologic findings. Occasionally, however, submucosal edema and inflammation associated with esophagitis may be manifested by thickened, tortuous longitudinal folds, mimicking the appearance of varices.¹⁴¹ Some esophageal carcinomas may also produce a varicoid appearance because of submucosal spread of tumor (Fig. 25-32).¹⁴²⁻¹⁴⁴ However, varices tend to change in size and shape at fluoroscopy with respiration, peristalsis, and other maneuvers, whereas varicoid tumors have a more fixed, rigid appearance.¹⁴²⁻¹⁴⁴ An abrupt demarcation between the involved segment and adjacent normal esophagus should also favor tumor because uphill varices tend to fade superiorly without an obvious demarcation. Finally, varicoid carcinomas may cause dysphagia, whereas this symptom rarely occurs in patients with varices. Thus, it is usually possible to differentiate these entities on clinical and radiologic grounds.

Treatment

The treatment of bleeding esophageal varices includes IV infusion of vasopressin or somatostatin analogues (e.g., octreotide), esophageal balloon tamponade, portosystemic shunt surgery, the Sugiura procedure, endoscopic sclerotherapy, endoscopic variceal ligation, and transjugular intrahepatic portosystemic shunt (TIPS).^{128,145} The primary aims of therapy are to control active bleeding and prevent rebleeding.

Endoscopic Sclerotherapy. Endoscopic sclerotherapy has emerged as a viable alternative to surgery for controlling variceal bleeding and decreasing the risk of recurrent bleeding with



Figure 25-32 Varicoid carcinoma. Thickened, tortuous folds in the mid-esophagus mimic the appearance of varices. This appearance is caused by submucosal spread of tumor. (Courtesy Akiyoshi Yamada, MD, Tokyo.)

fewer complications than surgery.¹⁴⁶⁻¹⁴⁸ This procedure is performed by paravariceal injection or direct intraluminal injection of varices with a sclerosing solution via a fiberoptic endoscope. The sclerosing agent causes a severe inflammatory reaction and intramural fibrosis with mechanical obliteration of the varices. However, as many as 30% of patients who undergo sclerotherapy develop complications, including mild chemical esophagitis, ulceration, strictures, and esophageal perforation.¹⁴⁹⁻¹⁵²

Contrast studies performed immediately after sclerotherapy may reveal esophageal dysmotility, esophagitis, irregular luminal narrowing, or, rarely, intramural hematomas.^{150,153,154} Mucosal sloughing at the sites of injection may cause ulceration (Fig. 25-33A),^{150,153} whereas transmural necrosis may lead to the development of transverse or longitudinal intramural tracks (Fig. 25-33B), esophagopleural fistulas, or localized esophageal perforation (Fig. 25-33C).^{153,155} Contrast studies performed 30 days or more after sclerotherapy may reveal esophageal strictures of varying length and caliber (Fig. 25-33D).¹⁵²

Sclerosed varices are usually manifested on CT by a thickened esophageal wall with outer high-attenuation and inner low-attenuation regions on contrast-enhanced scans, producing a characteristic laminated appearance.^{156,157} This finding may result from a sclerosant-induced inflammatory reaction, edema, or hemorrhage within the esophageal wall, so normal

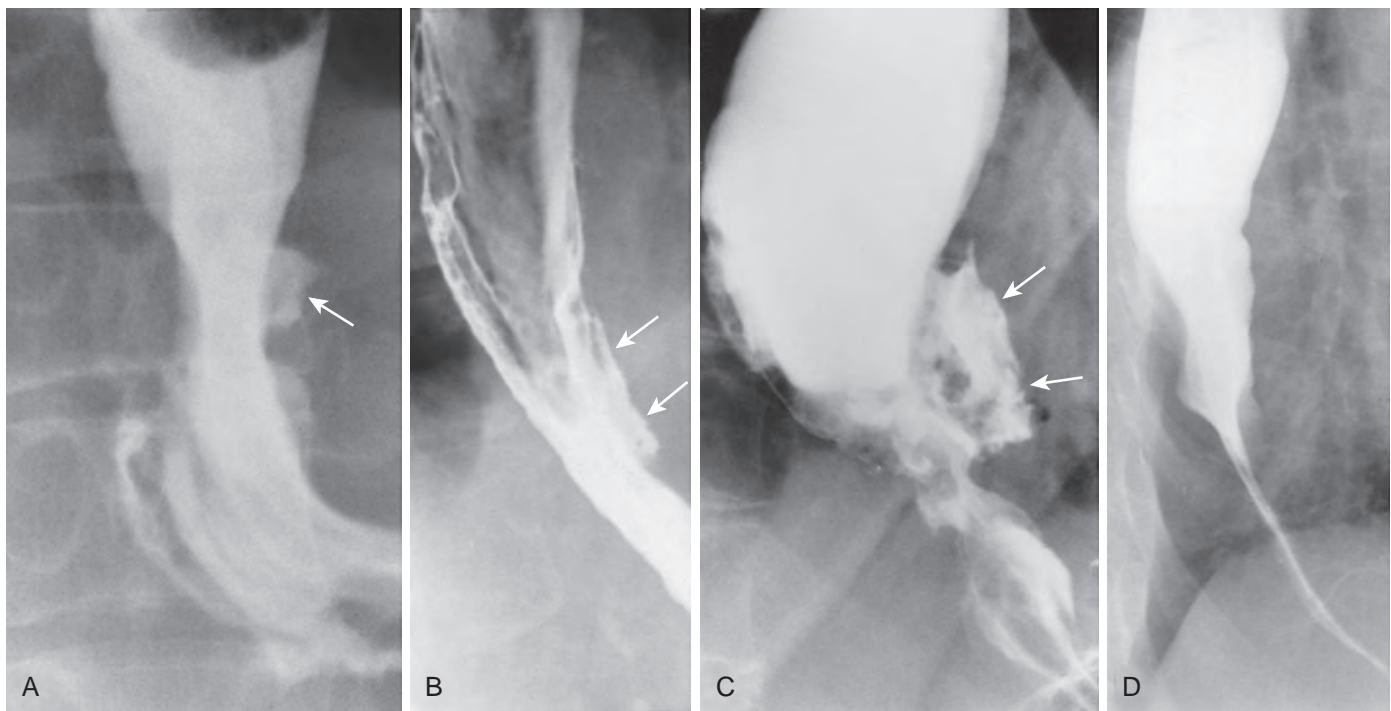


Figure 25-33 Complications of endoscopic sclerotherapy of varices. **A.** There is a relatively deep ulcer (arrow) with associated narrowing of the distal esophagus caused by edema and spasm. **B.** This patient has a longitudinal intramural track (arrows) in the distal esophagus. **C.** Another patient has a focal, sealed-off perforation of the distal esophagus with contrast medium entering an extraluminal collection (arrows). **D.** This patient has a long, tapered stricture in the distal esophagus several months after endoscopic sclerotherapy. (**A**, **B**, and **D** from Levine MS: *Radiology of the Esophagus*. Philadelphia, WB Saunders, 1989.)

enhancement of varices no longer occurs. CT may also demonstrate a predominantly low-attenuation mediastinal effusion and obliteration of mediastinal fat planes because of an acute paraesophageal reaction after sclerotherapy.¹⁵⁷ In contrast, a mediastinal abscess from esophageal perforation may be manifested on CT by a predominantly high-attenuation mediastinal fluid collection associated with mediastinal or pleural gas.¹⁵⁷ Thus, CT may be helpful in determining the nature and extent of postsclerotherapy complications in these patients.

Endoscopic Variceal Ligation. Endoscopic variceal ligation or banding is another technique for the treatment of bleeding esophageal varices in which the varices are ensnared and ligated with endoscopically placed rubber bands, causing strangulation, sloughing, fibrosis, and eventual obliteration of the varices.¹⁵⁸ It has been shown that variceal ligation is associated not only with lower rebleeding rates than endoscopic sclerotherapy but also with fewer complications.^{159,160} Contrast studies may occasionally be performed after variceal ligation to rule out esophageal perforation. In such cases, the ligated varices may be recognized on esophagography as smooth, rounded filling defects in the distal esophagus that are indistinguishable from small polyps (Fig. 25-34).¹⁶¹ However, the correct diagnosis should be apparent from the clinical history.

DOWNHILL VARICES

Pathophysiology

Because the venous structures draining the cervical and upper thoracic esophagus communicate with the supreme intercostal

vein, bronchial veins, inferior thyroid vein, and other mediastinal collaterals, obstruction of the superior vena cava may lead to reversal of flow through those vessels into esophageal and paraesophageal veins to bypass the obstruction. Because blood flows downward in the dilated esophageal veins, they are called *downhill varices*.¹⁶²

The location and extent of downhill varices depend pathophysiologically on whether the superior vena cava is obstructed above or below the site of entry of the azygos vein into the superior vena cava.^{162,163} If the obstruction occurs above the entry of the azygos vein, downhill varices can return blood from the head and upper extremities via the azygos vein to the superior vena cava below the level of obstruction. As a result, downhill varices are confined to the upper or midthoracic esophagus in these cases. If, however, the obstruction occurs at or below the site of entry of the azygos vein into the superior vena cava, the azygos venous system can no longer be used to bypass the obstruction. In such cases, venous flow continues via downhill varices to the distal esophagus, where the coronary vein diverts blood to the portal vein and inferior vena cava, bypassing the obstructed superior vena cava. Thus, downhill varices of this type may involve the entire thoracic esophagus.

Downhill varices are often caused by bronchogenic carcinoma or, less frequently, by other metastatic tumors or lymphoma in the mediastinum.¹⁶²⁻¹⁶⁴ When the superior vena cava is obstructed by malignant tumor, the patient rarely survives long enough for the varices to extend distally, so they are almost always confined to the upper thoracic esophagus, regardless of whether the obstruction occurs above or below the entry of the

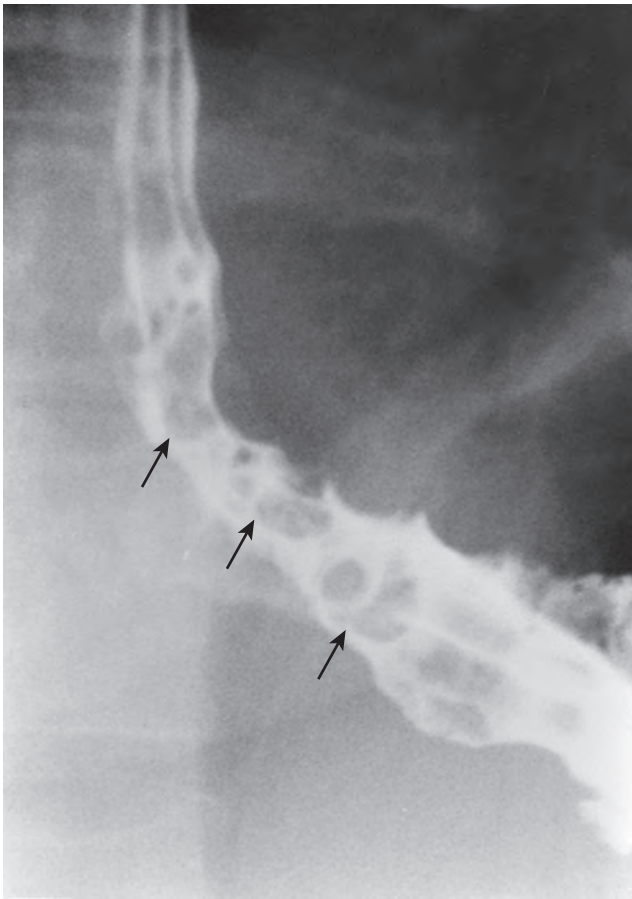


Figure 25-34 Appearance of ligated esophageal varices. A study with water-soluble contrast medium shows several smooth, rounded filling defects (arrows), which could be mistaken for neoplastic lesions in the distal esophagus. These represent banded varices 1 day after endoscopic variceal ligation.

azygos vein into the superior vena cava.¹⁶² Occasionally, however, obstruction of the superior vena cava may be caused by benign lesions such as a substernal goiter or mediastinal fibrosis caused by radiation or histoplasmosis (i.e., sclerosing mediastinitis).^{165,166} In such cases, long-standing obstruction of the superior vena cava at or below the level of entry of the azygos vein may lead to the development of extensive downhill varices involving the entire thoracic esophagus.^{162,166} With greater use of central venous catheters for hyperalimentation or chemotherapy, catheter-induced thrombosis has also been recognized as an increasingly common cause of superior vena cava obstruction.^{167,168} Regardless of the cause of the obstruction, catheter-directed thrombolysis and/or endovascular stents have been shown to be safe and effective alternatives to surgical bypass for treatment of these patients.^{168,169}

Clinical Findings

Obstruction of the superior vena cava results in the superior vena cava syndrome, characterized by facial, periorbital, neck, and bilateral arm swelling and dilated superficial veins over chest wall. Although most patients with downhill varices caused by the superior vena cava syndrome are asymptomatic, affected individuals may occasionally develop hematemesis or

low-grade GI bleeding with melena, guaiac-positive stool, or iron-deficiency anemia.¹⁷⁰ Downhill varices should therefore be suspected in any patient with superior vena cava obstruction who develops signs of upper GI bleeding.

Radiographic Findings

Like uphill varices, downhill varices appear on barium studies as serpiginous longitudinal filling defects in the esophagus (Fig. 25-35).¹⁶⁴ However, they can be differentiated from uphill varices by their location because they are almost always confined to the upper or middle third of the thoracic esophagus, whereas uphill varices are predominantly located in the distal third. As expected, downhill varices are best visualized on mucosal relief views of the collapsed or partially collapsed esophagus with the use of a high-density barium suspension.

When downhill varices are suspected on the basis of barium studies, the patient should be evaluated for other clinical or radiologic signs of superior vena cava obstruction. Chest radiography or CT may reveal obvious widening of the superior mediastinum caused by mediastinal lymphadenopathy (see Fig. 25-35A), tumor, substernal thyroid goiter, or, less commonly, mediastinal fibrosis. Venography may be required to confirm the diagnosis and determine the level and degree of stenosis or obstruction and extent of collateral circulation, particularly if a surgical shunt, catheter-directed thrombolysis, or endovascular stent is contemplated.

Differential Diagnosis

Downhill varices may be confused radiographically with varicoid carcinomas that produce thickened, tortuous folds in the upper or midesophagus as a result of submucosal spread of tumor (see Fig. 25-32).¹⁴²⁻¹⁴⁴ However, downhill varices tend to change in size and shape at fluoroscopy, whereas varicoid tumors have a more fixed appearance and more abrupt, well-defined borders.

IDIOPATHIC VARICES

Rarely, esophageal varices may occur in patients who have no other signs of hepatic cirrhosis, portal hypertension, or superior vena cava obstruction.^{171,172} Because the mechanism of variceal formation is unknown, they have been called *idiopathic varices*. It has been postulated that these varices develop as a result of a congenital weakness in the venous channels of the esophagus.¹⁷¹⁻¹⁷³ Although idiopathic varices are extremely uncommon, they are important because of the risk of variceal bleeding.¹⁷¹

Radiographic Findings

Uphill and downhill varices tend to occur as multiple lesions, but an idiopathic varix usually occurs as a solitary lesion, appearing as a smooth, slightly lobulated submucosal mass in the esophagus (Fig. 25-36A).¹⁷⁴ As a result, the radiographic findings may erroneously suggest a submucosal tumor such as a leiomyoma. However, an idiopathic varix can usually be effaced or even obliterated by esophageal distention (Fig. 25-36B), so images obtained with the patient in an upright or recumbent position with variable esophageal distention should suggest a vascular origin of the lesion.¹⁷⁴ It is important to be aware of this entity, so endoscopists do not inadvertently biopsy a varix without careful visual inspection.

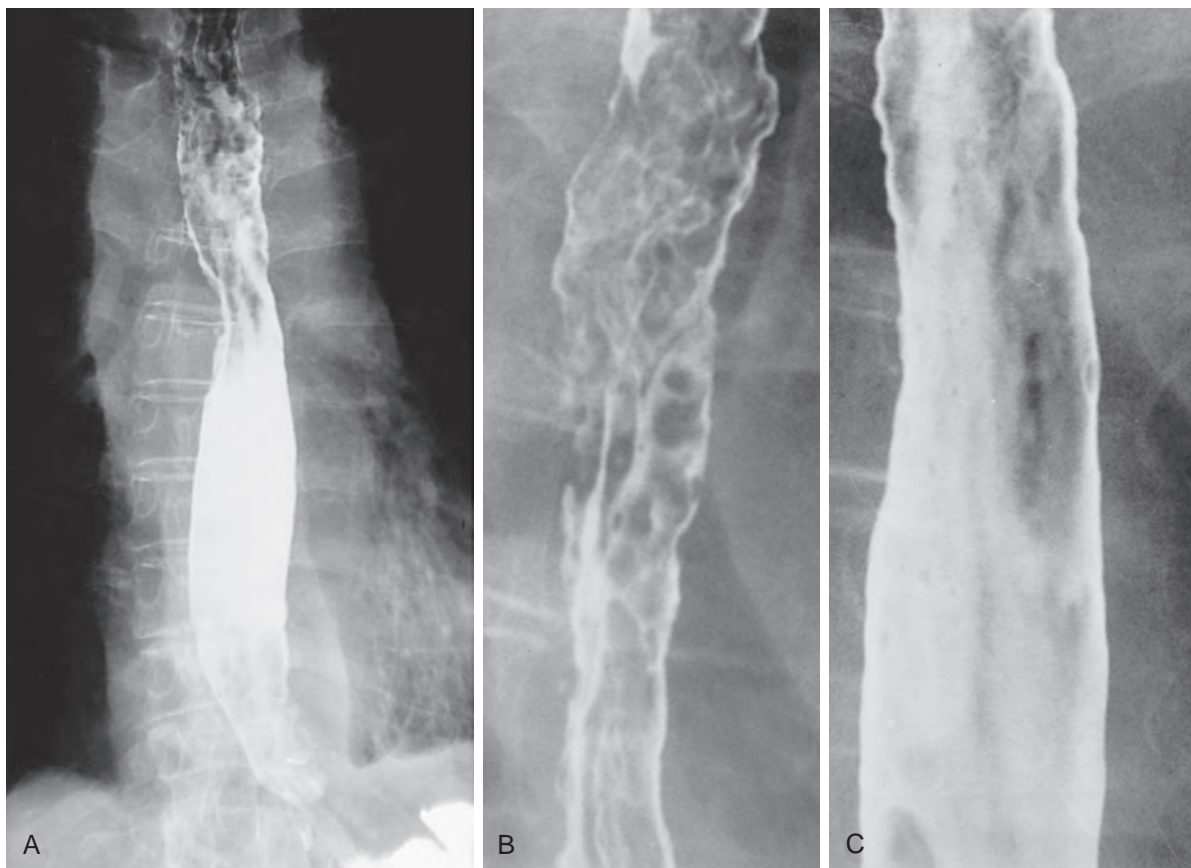


Figure 25-35 Downhill esophageal varices due to superior vena cava obstruction by bronchogenic carcinoma. **A.** Chest radiograph with barium in the esophagus shows thickened, nodular folds in the midesophagus with a normal-appearing esophagus below this level. Note how the superior mediastinum is widened because of adenopathy from metastatic lung cancer. **B.** Mucosal relief view of the esophagus shows prominent downhill varices. **C.** Another view moments later shows obliteration of the varices with greater esophageal distention. (From Levine MS: *Radiology of the Esophagus*. Philadelphia, WB Saunders, 1989.)

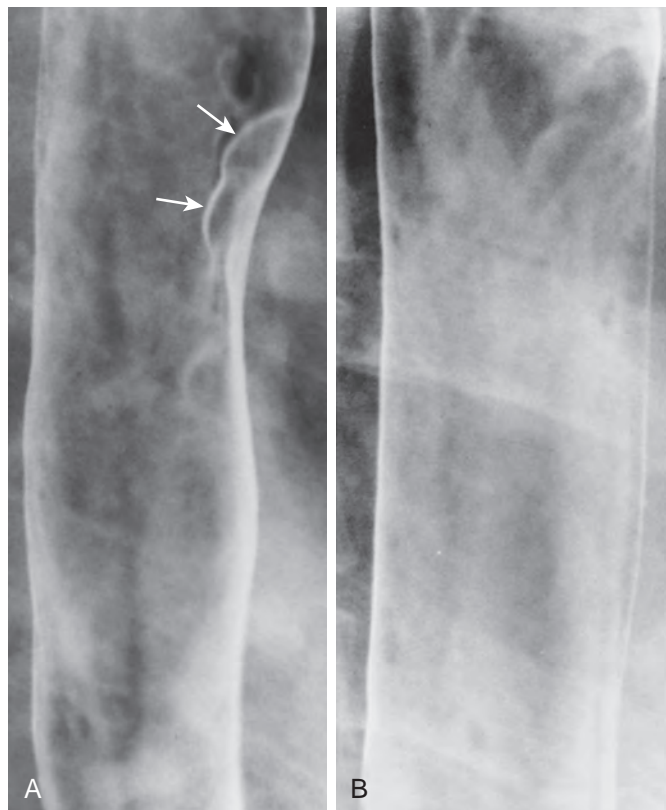


Figure 25-36 Idiopathic varix. **A.** There is a slightly lobulated submucosal mass (arrows) that is indistinguishable from a leiomyoma or other submucosal tumors. **B.** Another view moments later shows obliteration of the varix with greater esophageal distention. (Courtesy Seth N. Glick, MD, Philadelphia.)

REFERENCES

- Ansari A: Mallory-Weiss syndrome: Revisited. *Am J Gastroenterol* 64:460–466, 1975.
- Bubrick MP, Lundeen JW, Onstad GR, et al: Mallory-Weiss syndrome: Analysis of fifty-nine cases. *Surgery* 88:400–405, 1980.
- Hastings PR, Peters KW, Cohn I: Mallory-Weiss syndrome: Review of 69 cases. *Am J Surg* 142:560–562, 1981.
- Graham DV, Schwartz JT: The spectrum of the Mallory-Weiss tear. *Medicine (Baltimore)* 57:307–318, 1977.
- Baker RW, Spiro AH, Trnka YM: Mallory-Weiss tear complicating upper endoscopy. *Gastroenterology* 82:140–142, 1982.
- Hunter TB, Protell RL, Horsley WW: Food laceration of the esophagus: The taco tear. *AJR* 140:503–504, 1983.
- Penston JG, Boyd EJ, Wormsley KG: Mallory-Weiss tears occurring during endoscopy: Report of four cases. *Endoscopy* 24:262–265, 1992.
- Foster DN, Miloszewski K, Losowsky MS: Diagnosis of Mallory-Weiss lesions: A common cause of upper gastrointestinal bleeding. *Lancet* 2:483–485, 1976.
- Knave CM: Mallory-Weiss syndrome: Characterization of 75 Mallory-Weiss lacerations in 528 patients with upper gastrointestinal hemorrhage. *Gastroenterology* 71:5–8, 1976.
- Clark RA: Intraarterial vasopressin infusion for treatment of Mallory-Weiss tears of the esophagogastric junction. *AJR* 133:449–451, 1979.
- Carson GM, Casarella WJ, Spiegel RM: Transcatheter embolization for treatment of Mallory-Weiss tears of the esophagogastric junction. *Radiology* 128:309–313, 1978.
- Papp JP: Electrocoagulation of actively bleeding Mallory-Weiss tears. *Gastrointest Endosc* 26:128–130, 1980.
- Harris JM, DiPalma JA: Clinical significance of Mallory-Weiss tears. *Am J Gastroenterol* 88:2056–2058, 1993.
- Dallemand S, Amorosa JK, Morris DW, et al: Intramural hematomas of the esophagus. *Gastrointest Radiol* 8:7–9, 1983.
- Shay SS, Berendson RA, Johnson LF: Esophageal hematoma: Four new cases, a review, and proposed etiology. *Dig Dis Sci* 26:1019–1024, 1981.
- Bradley JL, Han SY: Intramural hematoma (incomplete perforation) of the esophagus associated with esophageal dilatation. *Radiology* 130:59–62, 1979.
- Steenbergen WV, Fevery J, Broeckaert L, et al: Intramural hematoma of the esophagus: Unusual complication of variceal sclerotherapy. *Gastrointest Radiol* 9:293–295, 1984.
- de Vries RA, Kremer-Schneider MME, Otten MH: Intramural hematoma of the esophagus caused by minor head injury 6 hours previously. *Gastrointest Radiol* 16:283–285, 1991.
- Andress M: Submucosal haematoma of the oesophagus due to anti-coagulant therapy. *Acta Radiol Diagn* 11:216–219, 1971.
- Ashman FC, Hill MC, Saba GP, et al: Esophageal hematoma associated with thrombocytopenia. *Gastrointest Radiol* 3:115–118, 1978.
- Meulman N, Evans J, Watson A: Spontaneous intramural haematoma of the oesophagus: A report of three cases and review of the literature. *Aust N Z J Surg* 64:190–193, 1994.
- Chen P, Lebowitz R, Lewicki AM: Spontaneous hematoma of the esophagus. *Radiology* 100:281–282, 1971.
- Lowman RM, Goldman R, Stern H: The roentgen aspects of intramural dissection of the esophagus. *Radiology* 93:1329–1331, 1969.
- Joffe N, Millan VG: Postemetic dissecting intramural hematoma of the esophagus. *Radiology* 95:379–380, 1970.
- Pellicano A, Watier A, Gentile J: Spontaneous double-barreled esophagus. *J Clin Gastroenterol* 9:149–154, 1987.
- Demos TC, Okrent DH, Studlo JD, et al: Spontaneous esophageal hematoma diagnosed by computed tomography. *J Comp Assist Tomogr* 10:133–135, 1986.
- Herbetko J, Delany D, Ogilvie BC, et al: Spontaneous intramural haematoma of the oesophagus: Appearance on computed tomography. *Clin Radiol* 44:327–328, 1991.
- Campbell TC, Andrews JL, Neptune WB: Spontaneous rupture of the esophagus (Boerhaave's syndrome). *JAMA* 235:526–528, 1976.
- Love L, Berkow AE: Trauma to the esophagus. *Gastrointest Radiol* 2:305–321, 1978.
- Pasricha PJ, Fleischer DE, Kalloo AN: Endoscopic perforations of the upper digestive tract: A review of their pathogenesis, prevention, and management. *Gastroenterology* 106:787–802, 1994.
- Meyers MA, Ghahremani GG: Complications of fiberoptic endoscopy: I. Esophagoscopy and gastroscopy. *Radiology* 115:293–300, 1975.
- Baron TH: Expandable metal stents for the treatment of cancerous obstruction of the gastrointestinal tract. *N Engl J Med* 344:1681–1687, 2001.
- Ghahremani GG, Turner MA, Port RB: Iatrogenic intubation injuries of the upper gastrointestinal tract in adults. *Gastrointest Radiol* 5:1–10, 1980.
- Polsky S, Kerstein MD: Pharyngo-esophageal perforation due to blunt trauma. *Am Surg* 61:994–996, 1995.
- O'Connell ND: Spontaneous rupture of the esophagus. *AJR* 99:186–203, 1967.
- Rogers LF, Puig W, Dooley BN, et al: Diagnostic considerations in mediastinal emphysema: A pathophysiologic approach to Boerhaave's syndrome and spontaneous pneumomediastinum. *AJR* 115:495–511, 1972.
- Bradham RR, deSaussure C, Lemel AL: Spontaneous perforation of the cervical esophagus. *Arch Surg* 111:284–285, 1976.
- Isserow JA, Levine MS, Rubesin SE: Spontaneous perforation of the cervical esophagus after an alcoholic binge. *Can Assoc Radiol J* 49:241–243, 1998.
- Janjua KJ: Boerhaave's syndrome. *Postgrad Med J* 73:265–270, 1997.
- Han SY, Tishler JM: Perforation of the abdominal segment of the esophagus. *AJR* 143:751–754, 1984.
- Klygis LM, Jutabha R, McCrohan MB, et al: Esophageal perforations masked by steroids. *Abdom Imaging* 18:10–12, 1993.
- Kaman L, Iqbal J, Kundil B, et al: Management of esophageal perforation in adults. *Gastroenterol Res* 3:235–244, 2010.
- Freeman RK, Van Woerkom JM, Ascoti JJ: Esophageal stent placement for the treatment of iatrogenic intrathoracic esophageal perforation. *Ann Thorac Surg* 83:2003–2007, 2007.
- D'Cunha J, Rueth NM, Groth SS, et al: Esophageal stents for anastomotic leaks and perforations. *J Thorac Cardiovasc Surg* 142:39–46, 2011.
- Maglinte DDT, Edwards MC: Spontaneous closure of esophageal tear in Boerhaave's syndrome. *Gastrointest Radiol* 4:223–225, 1979.
- Parkin GJS: The radiology of perforated esophagus. *Clin Radiol* 24:324–332, 1973.
- Healy ME, Mindelzun RE: Lesser sac pneumoperitoneum secondary to perforation of the intraabdominal esophagus. *AJR* 142:325–326, 1984.
- James AE, Montali RJ, Chaffee V, et al: Barium or Gastrografin: Which contrast media for diagnosis of esophageal tears? *Gastroenterology* 68:1103–1113, 1975.
- Vessal K, Montali RJ, Larson SM, et al: Evaluation of barium and Gastrografin as contrast media for the diagnosis of esophageal ruptures or complications. *AJR* 123:307–319, 1975.
- Chiu CL, Gambach RR: Hypaque pulmonary edema: A case report. *Radiology* 111:91–92, 1974.
- Brick SH, Caroline DF, Lev-Toaff AS, et al: Esophageal disruption: Evaluation with io-hexol esophagography. *Radiology* 169:141–143, 1988.
- Gollub MJ, Bains MS: Barium sulfate: A new (old) contrast agent for diagnosis of postoperative esophageal leaks. *Radiology* 202:360–362, 1997.
- Rubesin SE, Levine MS: Radiologic diagnosis of gastrointestinal perforation. *Radiol Clin North Am* 41:1095–1115, 2003.
- Foster JH, Jolly PC, Sawyers JL, et al: Esophageal perforation: Diagnosis and treatment. *Ann Surg* 161:701–709, 1965.
- Berry BE, Ochsner JL: Perforation of the esophagus: A 30 year review. *J Thorac Cardiovasc Surg* 65:1–7, 1973.
- Wychulis AR, Fontana RS, Payne WS: Instrumental perforations of the esophagus. *Dis Chest* 55:184–189, 1969.
- Dodds WJ, Stewart ET, Vlymen WJ: Appropriate contrast media for evaluation of esophageal disruption. *Radiology* 144:439–441, 1982.
- Foley MJ, Ghahremani GG, Rogers LF: Reappraisal of contrast media used to detect upper gastrointestinal perforations. *Radiology* 144:231–237, 1982.
- Levine MS: What is the best oral contrast material to use for the fluoroscopic diagnosis of esophageal rupture? *AJR* 162:1243, 1994.
- Tanomkiat W, Galassi W: Barium sulfate as contrast medium for evaluation of postoperative anastomotic leaks. *Acta Radiol* 41:482–485, 2000.
- Buecker A, Wein BB, Neuerburg JM, et al: Esophageal perforation: Comparison of use of aqueous and barium-containing contrast media. *Radiology* 202:683–686, 1997.
- Swanson JO, Levine MS, Redfern RO, et al: Usefulness of high-density barium for detection of leaks after esophagogastrectomy, total gastrectomy, and total laryngectomy. *AJR* 181:415–420, 2003.
- White CS, Templeton PA, Attar S: Esophageal perforation: CT findings. *AJR* 160:767–770, 1993.
- Wu CH, Chen CM, Chen CC, et al: Esophagography after pneumomediastinum without CT findings of esophageal perforation: Is it necessary? *AJR* 201:977–984, 2013.

65. Lantos JE, Levine MS, Rubesin SE, et al: Comparison between esophagography and chest computed tomography for evaluation of leaks after esophagectomy and gastric pull-through. *J Thorac Imaging* 28:121–128, 2013.
66. Webb WA: Management of foreign bodies of the upper gastrointestinal tract. *Gastroenterology* 94:204–216, 1988.
67. Nandi P, Ong GB: Foreign bodies in the oesophagus: Review of 2,394 cases. *Br J Surg* 65:5–9, 1978.
68. Giordano A, Adams G, Boies L, et al: Current management of esophageal foreign bodies. *Arch Otolaryngol* 107:249–251, 1981.
69. Ginsberg GG: Management of ingested foreign objects and food bolus impactions. *Gastrointest Endosc* 41:33–38, 1995.
70. Barber GB, Peppercorn MA, Ehrlich C, et al: Esophageal foreign body perforation. *Am J Gastroenterol* 79:509–511, 1984.
71. Gougoutas C, Levine MS, Laufer I: Esophageal food impaction with early perforation. *AJR* 171:427–428, 1998.
72. Underberg-Davis S, Levine MS: Giant thoracic osteophyte causing esophageal food impaction. *AJR* 157:319–320, 1991.
73. Shaffer HA, Alford BA, de Lange EE, et al: Basket extraction of esophageal foreign bodies. *AJR* 147:1010–1013, 1986.
74. Macpherson RI, Hill JG, Othersen HB, et al: Esophageal foreign bodies in children: Diagnosis, treatment, and complications. *AJR* 166:919–924, 1996.
75. Harned RK, Strain JD, Hay TC, et al: Esophageal foreign bodies: Safety and efficacy of Foley catheter extraction of coins. *AJR* 168:443–446, 1997.
76. Hogan WJ, Dodds WJ, Hoke SE, et al: Effect of glucagon on esophageal motor function. *Gastroenterology* 69:160–165, 1975.
77. Ferrucci JT, Long JA: Radiologic treatment of esophageal food impaction using intravenous glucagon. *Radiology* 125:25–28, 1977.
78. Trenkner SW, Maglinte DD, Lehman GA, et al: Esophageal food impaction: Treatment with glucagon. *Radiology* 149:401–403, 1983.
79. Rice BT, Spiegel PK, Dombrowski PJ: Acute esophageal food impaction treated by gas-forming agents. *Radiology* 146:299–301, 1983.
80. Smith JC, Janower ML, Geiger AH: Use of glucagon and gas-forming agents in acute esophageal food impaction. *Radiology* 159:567–568, 1986.
81. Kaszar-Seibert DJ, Korn WT, Bindman DJ, et al: Treatment of acute esophageal food impaction with a combination of glucagon, effervescent agent, and water. *AJR* 154:533–534, 1990.
82. Robbins MI, Shortlee MJ: Treatment of acute esophageal food impaction with glucagon, an effervescent agent, and water. *AJR* 162:325–328, 1994.
83. Fitzgerald RH, Bartles DM, Parker EF: Tracheoesophageal fistulas secondary to carcinoma of the esophagus. *J Thorac Cardiovasc Surg* 82:194–197, 1981.
84. Little AG, Ferguson MK, DeMeester TR, et al: Esophageal carcinoma with respiratory tract fistula. *Cancer* 53:1322–1328, 1984.
85. Spalding AR, Burney DP, Richie RE: Acquired benign bronchoesophageal fistulas in the adult. *Ann Thorac Surg* 28:378–383, 1979.
86. Vasquez RE, Landay M, Kilman WJ, et al: Benign esophagorespiratory fistulas in adults. *Radiology* 167:93–96, 1988.
87. Sheiner NM, LaChance C: Congenital esophagobronchial fistula in the adult. *Can J Surg* 23:489–491, 1980.
88. Weschler RJ, Steiner RM, Goodman LR, et al: Iatrogenic esophageal-pleural fistula: Subtlety of diagnosis in the absence of mediastinitis. *Radiology* 144:239–243, 1982.
89. Massard G, Wihlm JM: Early complications: Esophagopleural fistula. *Chest Surg Clin N Am* 9:617–631, 1999.
90. Massard G, Ducrocq X, Hentz JG, et al: Esophagopleural fistula: An early and long-term complication after pneumonectomy. *Ann Thorac Surg* 58:1437–1440, 1994.
91. Weschler RJ: CT of esophageal-pleural fistulae. *AJR* 147:907–909, 1986.
92. Liu PS, Levine MS, Torigian DA: Esophagopleural fistula secondary to esophageal wall ballooning and thinning after pneumonectomy: Findings on chest CT and esophagography. *AJR* 186:1627–1629, 2006.
93. Baron RL, Koehler RE, Gutierrez FR, et al: Clinical and radiographic manifestations of aortoesophageal fistulas. *Radiology* 141:599–605, 1981.
94. Khawaja FI, Varindani MK: Aortoesophageal fistula: Review of clinical, radiographic and endoscopic features. *J Clin Gastroenterol* 9:342–344, 1987.
95. Hollander JE, Quick G: Aortoesophageal fistula: A comprehensive review of the literature. *Am J Med* 91:279–287, 1991.
96. Seymour EQ: Aortoesophageal fistula as a complication of aortic prosthetic graft. *AJR* 131:160–161, 1978.
97. Cyrlak D, Cohen AJ, Dana ER: Esophagopericardial fistula: Causes and radiographic features. *AJR* 141:177–179, 1983.
98. Kaye MD: Oesophageal motor dysfunction in patients with diverticula of the mid-thoracic oesophagus. *Thorax* 29:666–672, 1974.
99. Debas HT, Payne WS, Cameron AJ, et al: Pathophysiology of lower esophageal diverticulum and its implications for treatment. *Surg Gynecol Obstet* 151:593–600, 1980.
100. Dodds WJ, Stef JJ, Hogan WJ, et al: Radial distribution of peristaltic pressure in normal subjects and patients with esophageal diverticulum. *Gastroenterology* 69:584–590, 1975.
101. Fasano NC, Levine MS, Rubesin SE, et al: Epiphrenic diverticulum: Clinical and radiographic findings in 27 patients. *Dysphagia* 18:9–15, 2003.
102. Niv Y, Fraser G, Krugliak P: Gastroesophageal obstruction from food in an epiphrenic esophageal diverticulum. *J Clin Gastroenterol* 16:314–316, 1993.
103. Altorki NK, Sunagawa M, Skinner DB: Thoracic esophageal diverticula: Why is operation necessary? *J Thorac Cardiovasc Surg* 105:260–264, 1993.
104. Benacci JC, Deschamps C, Trastek VF, et al: Epiphrenic diverticulum: Results of surgical treatment. *Ann Thorac Surg* 55:1109–1114, 1993.
105. Jabbari M, Goresky CA, Lough J, et al: The inlet patch: Heterotopic gastric mucosa in the upper esophagus. *Gastroenterology* 89:352–356, 1985.
106. Borhan-Manesh F, Farnum JB: Incidence of heterotopic gastric mucosa in the upper esophagus. *Gut* 32:968–972, 1991.
107. Ueno J, Davis SW, Tanakami A, et al: Ectopic gastric mucosa in the upper esophagus: Detection and radiographic findings. *Radiology* 191:751–753, 1994.
108. Takeji H, Ueno J, Nishitani H: Ectopic gastric mucosa in the upper esophagus: Prevalence and radiographic findings. *AJR* 164:901–904, 1995.
109. Lee J, Levine MS, Schultz CF: Ectopic gastric mucosa in the oesophagus mimicking ulceration. *Eur J Radiol* 31:197–200, 1997.
110. Buse PE, Zuckerman GR, Balfé DM: Cervical esophageal web associated with a patch of heterotopic gastric mucosa. *Abdom Imaging* 18:227–228, 1993.
111. Galan AR, Katzka DA, Castell DO: Acid secretion from an esophageal inlet patch demonstrated by ambulatory pH monitoring. *Gastroenterology* 115:1574–1576, 1998.
112. Anderson LS, Shackelford GD, Mancilla-Jimenez R, et al: Cartilaginous esophageal ring: A cause of esophageal stenosis in infants and children. *Radiology* 108:665–666, 1973.
113. Rose JS, Kassner EG, Jurgens KH, et al: Congenital esophageal strictures due to cartilaginous rings. *Br J Radiol* 48:16–18, 1975.
114. Yeung CK, Spitz L, Brereton RJ, et al: Congenital esophageal stenosis due to tracheobronchial remnants: A rare but important association with esophageal atresia. *J Pediatr Surg* 27:852–855, 1992.
115. McNally PR, Collier EH, Lopiano MC, et al: Congenital esophageal stenosis: A rare cause of food impaction in the adult. *Dig Dis Sci* 35:263–266, 1990.
116. McNally PR, Lemon JC, Goff JS, et al: Congenital esophageal stenosis presenting as non-cardiac, esophageal chest pain. *Dig Dis Sci* 38:369–373, 1993.
117. Katzka DA, Levine MS, Ginsberg GG, et al: Congenital esophageal stenosis in adults. *Am J Gastroenterol* 95:32–36, 2000.
118. Murphy SG, Yazbeck S, Russo P: Isolated congenital esophageal stenosis. *J Pediatr Surg* 30:1238–1241, 1995.
119. Pokieser P, Schima W, Schober E, et al: Congenital esophageal stenosis in a 21-year-old man: Clinical and radiographic findings. *AJR* 170:147–148, 1998.
120. Oh CH, Levine MS, Katzka DA, et al: Congenital esophageal stenosis in adults: Clinical and radiographic findings in seven patients. *AJR* 176:1179–1182, 2001.
121. Zimmerman SL, Levine MS, Rubesin SE, et al: Idiopathic eosinophilic esophagitis in adults: The ringed esophagus. *Radiology* 236:159–165, 2005.
122. Levine MS, Goldstein HM: Fixed transverse folds in the esophagus: A sign of reflux esophagitis. *AJR* 143:275–278, 1984.
123. Gohel VK, Edell SL, Laufer I, et al: Transverse folds in the human esophagus. *Radiology* 128:303–308, 1978.
124. Sam JW, Levine MS, Miller WT: The right inferior supraazygous recess: A cause of upper esophageal pseudomass on double-contrast esophagography. *AJR* 171:1583–1586, 1998.
125. McClure MJ, Ellis PK, Kelly IMG, et al: Esophageal pseudomass: Extrinsic compression of the esophagus due to a narrow thoracic inlet. *AJR* 174:1003–1004, 2000.
126. Birholz JC, Ferrucci JT, Wyman SM: Roentgen features of dysphagia aortica. *Radiology* 111:93–96, 1974.
127. Levine MS, Gilchrist AM: Esophageal deviation: Pushed or pulled? *AJR* 149:513–514, 1987.
128. Sharara AI, Rockey DC: Gastroesophageal variceal hemorrhage. *N Engl J Med* 345:669–681, 2001.

129. Graham DY, Smith JL: The course of patients after variceal hemorrhage. *Gastroenterology* 80:800–809, 1981.
130. Jonsson K, Rian RL: Pseudotumoral esophageal varices associated with portal hypertension. *Radiology* 97:593–597, 1970.
131. Ishikawa T, Saeki M, Tsukune Y, et al: Detection of paraesophageal varices by plain films. *AJR* 144:701–704, 1985.
132. Lau KK, Phillips G, McKenzie A: Pseudotumoral paraesophageal varices. *Gastrointest Radiol* 17:193–194, 1992.
133. Ghahremani GG, Port RB, Winans CS, et al: Esophageal varices: Enhanced radiologic visualization by anticholinergic drugs. *Am J Dig Dis* 17:703–712, 1972.
134. Liu CI: Enhanced visualization of esophageal varices by Buscopan. *AJR* 121:232–235, 1974.
135. Farber E, Fischer D, Eliakim R, et al: Esophageal varices: Evaluation with esophagography with barium versus endoscopic gastroduodenoscopy in patients with compensated cirrhosis-blinded prospective study. *Radiology* 237:535–540, 2005.
136. Cockerill EM, Miller RE, Chernish SM, et al: Optimal visualization of esophageal varices. *AJR* 126:512–523, 1976.
137. Clark KE, Foley WD, Berland LL, et al: CT evaluation of esophageal and upper abdominal varices. *J Comput Assist Tomogr* 4:510–515, 1980.
138. Balthazar EJ, Naidich DP, Megibow AJ, et al: CT evaluation of esophageal varices. *AJR* 148:131–135, 1987.
139. Cho KC, Patel YD, Wachsberg RH, Seeff J: Varices in portal hypertension: Evaluation with CT. *Radiographics* 15:609–622, 1995.
140. Ishikawa T, Tsukune Y, Ohyama Y, et al: Venous abnormalities in portal hypertension demonstrated by CT. *AJR* 134:271–276, 1980.
141. Rabin M, Schmaman IB: Reflux esophagitis resembling varices. *S Afr Med J* 55:293–295, 1979.
142. Lawson TL, Dodds WJ, Sheft DJ: Carcinoma of the esophagus simulating varices. *AJR* 107:83–85, 1969.
143. Silver TM, Goldstein HM: Varicoid carcinoma of the esophagus. *Dig Dis* 19:56–58, 1974.
144. Yates CW, LeVine MA, Jensen KM: Varicoid carcinoma of the esophagus. *Radiology* 122:605–608, 1977.
145. Garcia-Tsao G: Current management of the complications of cirrhosis and portal hypertension: Variceal hemorrhage, ascites, and spontaneous bacterial peritonitis. *Gastroenterology* 120:726–748, 2001.
146. Macdougall BRD, Westaby D, Theodossi A, et al: Increased long-term survival in variceal haemorrhage using injection sclerotherapy: Results of a controlled trial. *Lancet* 1:124–127, 1982.
147. Hootegem PV, Van Besien K, Broeckaert L, et al: Endoscopic sclerotherapy of esophageal varices: Long-term follow-up, recurrence, and survival. *J Clin Gastroenterol* 10:368–372, 1988.
148. Infante-Rivard C, Esnaola S, Villeneuve JP: Role of endoscopic variceal sclerotherapy in the long-term management of variceal bleeding: A meta-analysis. *Gastroenterology* 96:1087–1092, 1989.
149. Barsoum MS, Abdel-Wahab MH, Bollous F, et al: The complications of injection sclerotherapy of bleeding oesophageal varices. *Br J Surg* 69:79–81, 1982.
150. Tihansky DP, Reilly JJ, Schade RR, et al: The esophagus after injection sclerotherapy of varices: Immediate postoperative changes. *Radiology* 153:43–47, 1984.
151. Korula J, Pandya K, Yamada S: Perforation of esophagus after endoscopic variceal sclerotherapy. *Dig Dis Sci* 34:324–329, 1989.
152. Guynn TP, Eckhauser FE, Knol JA, et al: Injection sclerotherapy-induced esophageal strictures: Risk factors and prognosis. *Am Surg* 57:567–571, 1991.
153. Agha FP: The esophagus after endoscopic injection sclerotherapy: Acute and chronic changes. *Radiology* 153:37–42, 1984.
154. Steenbergen WV, Fevery J, Broeckaert L, et al: Intramural hematoma of the esophagus: Unusual complication of variceal sclerotherapy. *Gastrointest Radiol* 9:293–295, 1984.
155. Wilbom SL, Rector WG, Schaefer JW: An esophagobronchial fistula after endoscopic variceal sclerotherapy. *J Clin Gastroenterol* 10:81–83, 1988.
156. Halden WJ, Harnsberger HR, Mancuso AA: Computed tomography of esophageal varices after sclerotherapy. *AJR* 140:1195–1196, 1983.
157. Mauro MA, Jaques PF, Swankowski TM, et al: CT after uncomplicated esophageal sclerotherapy. *AJR* 147:57–60, 1986.
158. Stiegmann GV, Goff JS, Sun JH, et al: Endoscopic variceal ligation: An alternative to sclerotherapy. *Gastrointest Endosc* 35:431–434, 1989.
159. Stiegmann GV, Goff JS, Michaletz-Onody PA, et al: Endoscopic sclerotherapy as compared with endoscopic ligation for bleeding esophageal varices. *N Engl J Med* 326:1527–1532, 1992.
160. Laine L, el-Newihi HM, Migikovsky B, et al: Endoscopic ligation compared with sclerotherapy for the treatment of bleeding esophageal varices. *Ann Intern Med* 119:1–7, 1993.
161. Low VHS, Levine MS: Endoscopic banding of esophageal varices: Radiographic findings. *AJR* 172:941–942, 1999.
162. Felson B, Lessure AP: “Downhill” varices of the esophagus. *Dis Chest* 46:740–746, 1964.
163. Otto DL, Kurtzman RS: Esophageal varices in superior vena caval obstruction. *AJR* 92:1000–1012, 1964.
164. Mikkelsen WJ: Varices of the upper esophagus in superior vena caval obstruction. *Radiology* 81:945–948, 1963.
165. Salyer JM, Harrison HN, Winn DF, et al: Chronic fibrous mediastinitis and superior vena caval obstruction due to histoplasmosis. *Dis Chest* 35:364–377, 1959.
166. Sorokin JJ, Levine SM, Moss EG, et al: Downhill varices: Report of a case 29 years after resection of a substernal thyroid gland. *Gastroenterology* 73:345–348, 1977.
167. Chen JC, Bongard F, Klein SR: A contemporary perspective on superior vena cava syndrome. *Am J Surg* 160:207–211, 1990.
168. Kee ST, Kinoshita L, Razavi MK, et al: Superior vena cava syndrome: Treatment with catheter-directed thrombolysis and endovascular stent placement. *Radiology* 206:187–193, 1998.
169. Lanciego C, Chacon JL, Julian A, et al: Stenting as first option for endovascular treatment of malignant superior vena cava syndrome. *AJR* 177:585–593, 2001.
170. Fleig WE, Stange EF, Ditschuneit H: Upper gastrointestinal hemorrhage from downhill esophageal varices. *Dig Dis Sci* 27:23–27, 1982.
171. Schaefer J, Bramschreiber J, Mistilis S, et al: Gastroesophageal variceal bleeding in the absence of hepatic cirrhosis or portal hypertension. *Gastroenterology* 46:583–588, 1964.
172. Kelsen K, Burbige J: Idiopathic esophageal varices. *Am J Gastroenterol* 77:539–540, 1982.
173. Harinck E, Fernandes J, Vervat D: Congenital esophageal varices in identical twins without portal hypertension. *J Pediatr Surg* 6:488, 1971.
174. Trenkner SW, Levine MS, Laufer I, et al: Idiopathic esophageal varix. *AJR* 141:43–44, 1983.

Abnormalities of the Gastroesophageal Junction

MARC S. LEVINE

CHAPTER OUTLINE

Radiographic Technique

Normal Radiographic Appearances

Cardia
Z Line
Mucosal Ring
Muscular Ring

Schatzki Ring

Pathogenesis
Clinical Findings
Radiographic Findings
Differential Diagnosis

Hiatal Hernia

Axial Hiatal Hernia
Paraesophageal Hernia

Carcinoma of the Cardia

Prolapsed Esophagogastric Mucosa

Other Abnormalities

The gastroesophageal junction has traditionally been a difficult area to evaluate on barium studies because the physiologic events associated with swallowing produce a dynamic, constantly changing appearance. The use of complicated, often contradictory terminology to describe normal and abnormal findings at the cardia has also been a source of confusion. Evaluation of the cardia, perhaps more than of any other area in the upper gastrointestinal (GI) tract, requires meticulous attention to radiographic technique. Although rings, strictures, and hernias are best seen on conventional single-contrast barium studies, neoplastic lesions at the cardia are better delineated on double-contrast studies. Thus, radiologists must use different techniques during the fluoroscopic examination to optimally evaluate this area.

Radiographic Technique

The gastric cardia is a notoriously difficult area to examine on single-contrast barium studies. Because of the overlying rib cage, the fundus is not accessible to manual palpation or compression. If the fundus is not fully distended, crowded gastric folds may obscure surface detail in this region. If larger volumes of barium are used to distend the fundus, however, it becomes relatively opaque, so only contour abnormalities can be identified. Because of the inherent limitations of single-contrast barium studies in examining the cardia and fundus,

double-contrast techniques have been used to improve radiographic visualization of this area.

The routine double-contrast esophagogram should include a double-contrast examination of the gastric cardia and fundus.^{1,2} After upright double-contrast views of the esophagus have been obtained, the patient should be placed in the recumbent right lateral position (i.e., right side down) to visualize the gastric cardia directly en face. The cardia should be observed for several seconds and, if it appears normal, a single spot image should be obtained. If the cardia appears abnormal, however, additional spot images should be taken as the patient is rotated farther, so that questionable lesions can be demonstrated both en face and in profile.

After the double-contrast portion of the study has been completed, the patient should be placed in the prone, right anterior oblique position and instructed to rapidly gulp a thin, low-density barium suspension to achieve optimal distention of the distal esophagus. Single-contrast technique is particularly important for evaluating possible rings, strictures, or hernias in this region because upright double-contrast views often fail to produce the degree of distention needed to optimally demonstrate these abnormalities.³ If necessary, a bolster may be placed beneath the patient's upper abdomen to increase intra-abdominal pressure and improve esophageal distention. When a lower esophageal ring is detected, barium tablets or barium-impregnated marshmallows may also be used to help determine the caliber and obstructive potential of the ring and, if the tablet or marshmallow becomes impacted above the ring, to determine whether this impaction reproduces the patient's dysphagia.^{4,5}

Normal Radiographic Appearances

The esophagus is a relatively nondistensible tubular structure with a saccular distal segment that communicates with the stomach. The saccular segment has been termed the *phrenic ampulla* or *vestibule* because it is the "entrance hall" to the stomach.⁶ Manometric studies have shown that the esophageal vestibule corresponds to the location of the lower esophageal sphincter, a 2- to 4-cm in length high-pressure zone just above the gastroesophageal junction that prevents reflux of acid into the esophagus.^{7,8} The vestibule extends inferiorly through the esophageal hiatus of the diaphragm before joining the stomach several centimeters below the hiatus. The short intra-abdominal segment of the esophagus terminates at the gastroesophageal junction or gastric cardia. The left lateral aspect of the cardia is demarcated anatomically by sling fibers that hook around a notch formed between the distal esophagus and gastric fundus (the cardiac incisura). Important anatomic structures in this region that may be recognized on barium studies include the cardia, Z line, and lower esophageal mucosal and muscular

rings. These structures are discussed separately in the following sections.

CARDIA

The gastric cardia is often not visualized on single-contrast barium studies because this region is obscured by barium in the fundus or by overlying gastric rugae. However, the ability to recognize the normal appearances of the cardia has improved dramatically with the use of double-contrast technique. In one study, the normal anatomic landmarks at the cardia were seen on more than 95% of double-contrast examinations but on only 20% of single-contrast examinations.⁹ Thus, double-contrast technique is essential for evaluating this area.

The radiographic appearance of the cardia on double-contrast studies depends on how firmly it is anchored by the surrounding phrenoesophageal membrane to the esophageal hiatus of the diaphragm. When the cardia is well anchored, protrusion of the distal esophagus into the fundus produces a circular elevation containing three or four stellate folds that radiate to a central point at the gastroesophageal junction, also known as the cardiac rosette (Fig. 26-1A).^{9,10} This elevation is demarcated from the adjacent fundus by a curved hooding fold that surrounds it laterally and superiorly. Several longitudinal folds are usually seen extending inferiorly from the cardiac rosette along the posterior wall of the lesser curvature. However, it should be recognized that the cardiac rosette reflects the closed resting state of the lower esophageal sphincter, so this normal

anatomic landmark will be transiently obliterated by relaxation of the lower esophageal sphincter during deglutition.¹⁰

When the cardia is less firmly anchored to the surrounding phrenoesophageal membrane, the cardiac rosette may be visible without an associated protrusion or circular elevation (Fig. 26-1B).¹⁰ With further ligamentous laxity, the rosette itself may vanish and the cardia may be characterized by only a single undulant or crescentic line that traverses the region of the esophageal orifice (Fig. 26-1C).¹⁰ Finally, severe ligamentous laxity may lead to the formation of an axial hiatal hernia, so no cardiac structure is identified below the diaphragm. Instead, gastric folds may converge superiorly to a point several centimeters above the esophageal hiatus (Fig. 26-1D).¹⁰ This finding should therefore suggest an axial hiatal hernia, and a single-contrast esophagogram should be obtained with the patient in a prone position to confirm the presence of a hernia.

Radiologists should be familiar with the various radiographic appearances of the cardia, because malignant tumors involving the cardia may be recognized only by distortion or obliteration of these normal anatomic landmarks (see later, "Carcinoma of the Cardia").

Z LINE

The Z line is an irregular serrated line that demarcates the squamocolumnar mucosal junction.^{6,11} The Z line can sometimes be recognized on double-contrast esophagograms as a thin radiolucent stripe in the distal esophagus with a

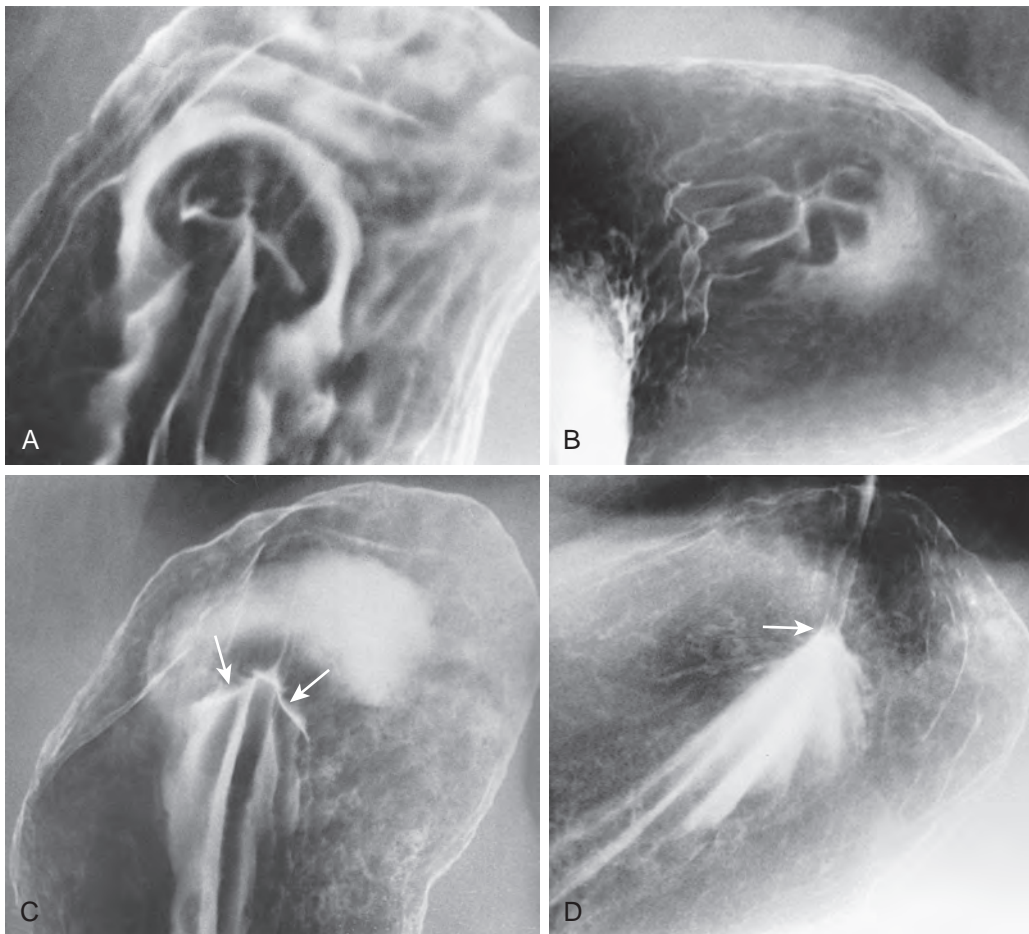


Figure 26-1 Normal appearances of the gastric cardia. **A.** This patient has a well-anchored cardia appearing as a circular protrusion with centrally radiating folds (the cardiac rosette). **B.** In another patient, there are stellate folds without a surrounding protrusion because of laxity of the ligaments surrounding the cardia. **C.** Further ligamentous laxity has resulted in obliteration of the cardiac rosette. Instead, this patient has a single crescentic line (arrows) at the cardia. **D.** In another patient with severe ligamentous laxity, gastric folds in a small hiatal hernia are seen converging superiorly toward a point (arrow) several centimeters above the esophageal hiatus of the diaphragm. (From Levine MS: *Radiology of the Esophagus*. Philadelphia: WB Saunders, 1989.)



Figure 26-2 Z line. The normal Z line is seen as a thin, zigzagging, radiolucent stripe (dots) in the distal esophagus near the gastroesophageal junction. (From Levine MS: *Radiology of the Esophagus*. Philadelphia: WB Saunders, 1989.)

characteristic zigzag appearance (Fig. 26-2). Occasionally, the Z line can be mistaken for superficial ulceration associated with reflux esophagitis, particularly if the esophagus is not completely distended. Because the Z line represents the histologic squamocolumnar junction, it is usually located at or near the gastroesophageal junction.

MUCOSAL RING

A lower esophageal mucosal ring is the most common ringlike narrowing found in the distal esophagus. The ring consists of a membranous ridge covered by squamous epithelium superiorly and columnar epithelium inferiorly, so it corresponds histologically to the squamocolumnar junction.^{12,13} This mucosal ring, also known as a B ring, is manifested on barium studies by a thin, weblike area of narrowing at the gastroesophageal junction (Fig. 26-3).^{11,13,14} The ring has smooth, symmetric margins and a height of 2 to 4 mm.^{11,13,14} Mucosal rings with a diameter more than 20 mm rarely cause symptoms.¹¹ If the diameter of the ring is less than 20 mm, however, it may cause dysphagia and might therefore represent a pathologic finding (see later, “Schatzki Ring”).

Lower esophageal mucosal rings are fixed, reproducible structures on barium studies, but the distal esophagus must be adequately distended to visualize these structures. Single-contrast technique with the patient in a prone, right anterior oblique position is particularly well suited for

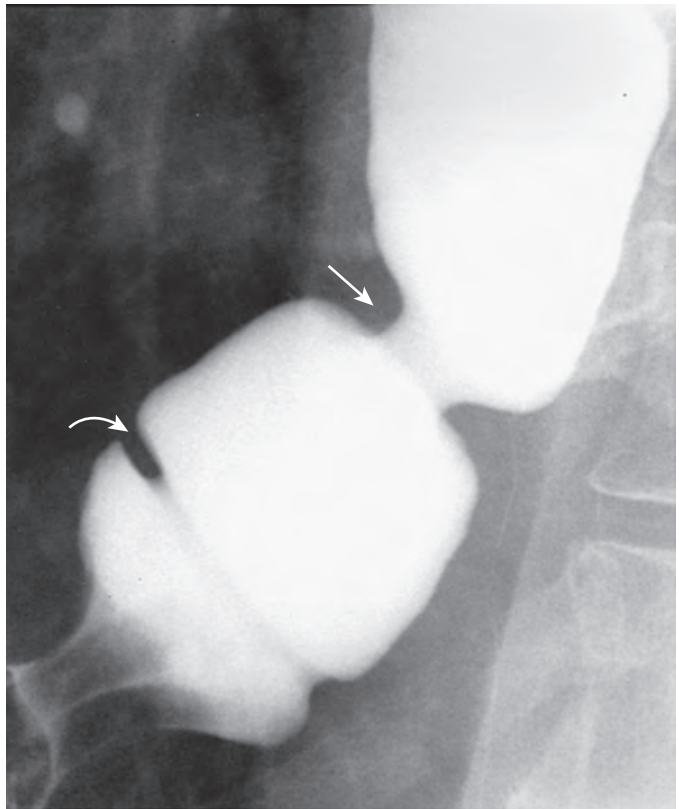


Figure 26-3 Lower esophageal rings. The mucosal ring appears on a prone single-contrast esophagogram as a thin, weblike constriction (curved arrow) at the gastroesophageal junction above a small hiatal hernia, whereas the muscular ring appears as a relatively broad area of narrowing (straight arrow) near the superior border of the esophageal vestibule. Unlike mucosal rings, muscular rings are often observed as a transient finding at fluoroscopy. (From Levine MS: *Radiology of the Esophagus*. Philadelphia: WB Saunders, 1989.)

demonstrating lower esophageal rings because it is the best technique for achieving optimal distention of the distal esophagus. It has been shown that more than 50% of lower esophageal rings seen on prone single-contrast views of the esophagus are not visualized on the double-contrast phase of the examination.^{3,15} Thus, biphasic studies are required to demonstrate these structures.

MUSCULAR RING

A muscular or contractile ring, also known as an A ring, is a much less common finding in the distal esophagus than a mucosal ring (B ring). Muscular rings are located at the proximal end of the esophageal vestibule near the tubulovesicular junction and are completely covered by squamous epithelium.⁸ Unlike a mucosal ring, which is a fixed anatomic structure, a muscular ring occurs as a transient physiologic phenomenon resulting from active muscular contraction in the distal esophagus in the region of the lower esophageal sphincter.

A muscular ring usually appears on esophagography as a relatively broad, smooth area of tapered narrowing that changes considerably in caliber and configuration during the fluoroscopic examination (see Fig. 26-3).^{7,11,13} Because a muscular ring is caused by active muscular contraction, it may vanish completely with esophageal distention, so it is observed as a

transient finding at fluoroscopy.^{7,11,13} Not infrequently, mucosal and muscular rings are visible during the same examination (see Fig. 26-3). In such cases, the fixed nature of the mucosal ring readily distinguishes this structure from the changing appearance of the muscular ring above.

Schatzki Ring

Although some investigators have used the terms *Schatzki ring* and *lower esophageal ring* interchangeably, Schatzki himself originally described this entity as a pathologically stenotic ring that caused dysphagia.¹⁶ Because most lower esophageal rings do not cause symptoms, they probably should not be called Schatzki rings. Instead, the term should be reserved for symptomatic patients with narrow-caliber rings at the gastroesophageal junction. Thus, the diagnosis of a Schatzki ring is made on the basis of the clinical and radiographic findings.

PATHOGENESIS

The pathogenesis of a Schatzki ring is uncertain. Some investigators favor a congenital origin, but the rarity of symptoms before 50 years of age tends to refute this theory.⁶ Other investigators believe that a Schatzki ring represents an annular, ring-like stricture caused by scarring from reflux esophagitis.^{6,13,17-19} This theory is supported by one study showing that Schatzki rings undergo transformation into true, reflux-induced (peptic) strictures on serial barium studies.¹⁸ Nevertheless, it is difficult to explain the frequent absence of reflux symptoms in these patients, so the data are inconclusive.

CLINICAL FINDINGS

Schatzki rings are typically manifested by episodic dysphagia for solids.^{15,16,20,21} In a study of 332 patients, Schatzki found that lower esophageal rings less than 13 mm in diameter almost always caused dysphagia, whereas rings more than 20 mm in diameter almost never caused dysphagia.²⁰ A statistical analysis of Schatzki's original data 40 years later showed that a 1-mm decrease in ring diameter corresponded to a 46% increase in the likelihood that a patient has dysphagia.²²

Patients with Schatzki rings typically present with episodic dysphagia for solids, sometimes remaining asymptomatic until a large bolus of food lodges above the ring. Because the most frequent offending agent is an inadequately chewed piece of meat, this condition has been described as the *steak house syndrome*.²³ The impacted bolus in the distal esophagus may cause severe chest pain or an uncomfortable sticking sensation behind the lower sternum.²⁴ Resolution of symptoms almost always occurs when the impacted bolus is passed, regurgitated, or removed. Rarely, a prolonged bolus obstruction may lead to esophageal perforation.¹³

Relief from symptoms is sometimes obtained by advising these individuals to eat more slowly and chew their food more carefully. However, some patients with recurrent dysphagia require mechanical disruption or dilation of the ring or, rarely, surgery.^{21,25,26}

RADIOGRAPHIC FINDINGS

A Schatzki ring usually appears on barium studies as a thin (2 to 4 mm in height), weblike constriction (<13 mm in diameter)

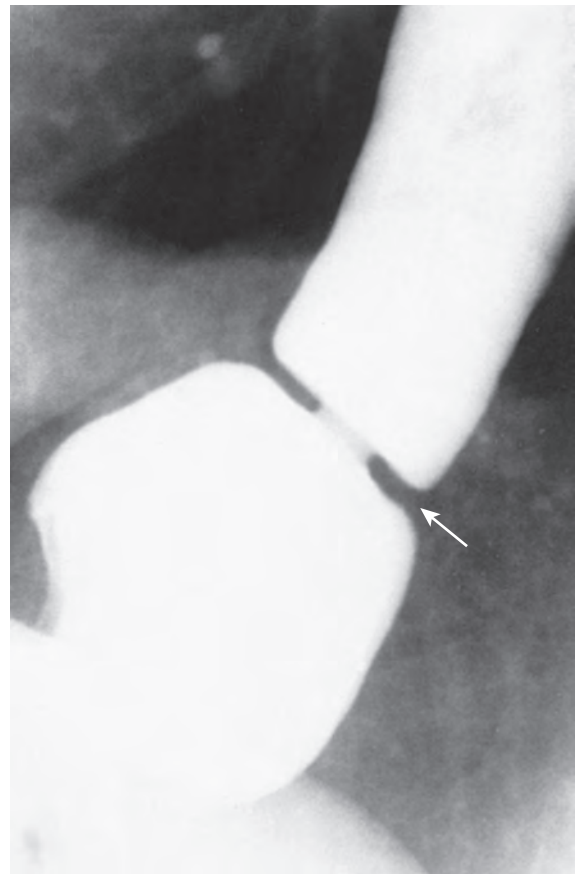


Figure 26-4 Schatzki ring. The ring appears on a prone single-contrast esophagogram as a thin, weblike (<13 mm in diameter) constriction (arrow) at the gastroesophageal junction above a hiatal hernia. Note that except for its smaller caliber, it has the same appearance and location as an asymptomatic mucosal ring. This patient presented with dysphagia.

at the gastroesophageal junction (Fig. 26-4).^{11,13-16,20} A hiatal hernia is almost always observed below the level of the ring. Except for its smaller caliber, a Schatzki ring therefore has the same appearance and location as an asymptomatic mucosal ring. Almost all rings less than 13 mm in diameter cause dysphagia,²⁰ so they may be classified as Schatzki rings on the basis of the radiographic findings. Occasionally, however, rings between 13 and 20 mm may also cause symptoms, so the diagnosis of a Schatzki ring in these patients requires some knowledge of the clinical history.

Like other rings in the lower esophagus, Schatzki rings are visualized on barium studies only if the lumen above and below the ring is distended beyond the caliber of the ring. As a result, single-contrast views of the distal esophagus with the patient prone (optimizing distention of the distal esophagus) may demonstrate Schatzki rings that are not visible, even in retrospect, on the double-contrast phase of the examination because of inadequate distention of this region (Fig. 26-5).^{3,15} Conversely, overdistention of a hiatal hernia on prone views can result in overlap of the distal end of the esophagus and proximal end of the hernia, producing a double density of two superimposed, convex collections of barium that obscures the region of the gastroesophageal junction and prevents visualization even of high-grade Schatzki rings (Fig. 26-6A).²⁷ When this overlap

Figure 26-5 Schatzki ring seen only on a prone single-contrast esophagogram.

A. Upright double-contrast view of the distal esophagus shows no evidence of a lower esophageal ring. **B.** However, a prone single-contrast view from the same examination shows a hiatal hernia with an unequivocal Schatzki ring (arrow) above the hernia. Note how the hernia was not visualized on the upright double-contrast image (**A**) because it had fallen below the diaphragm on this view.

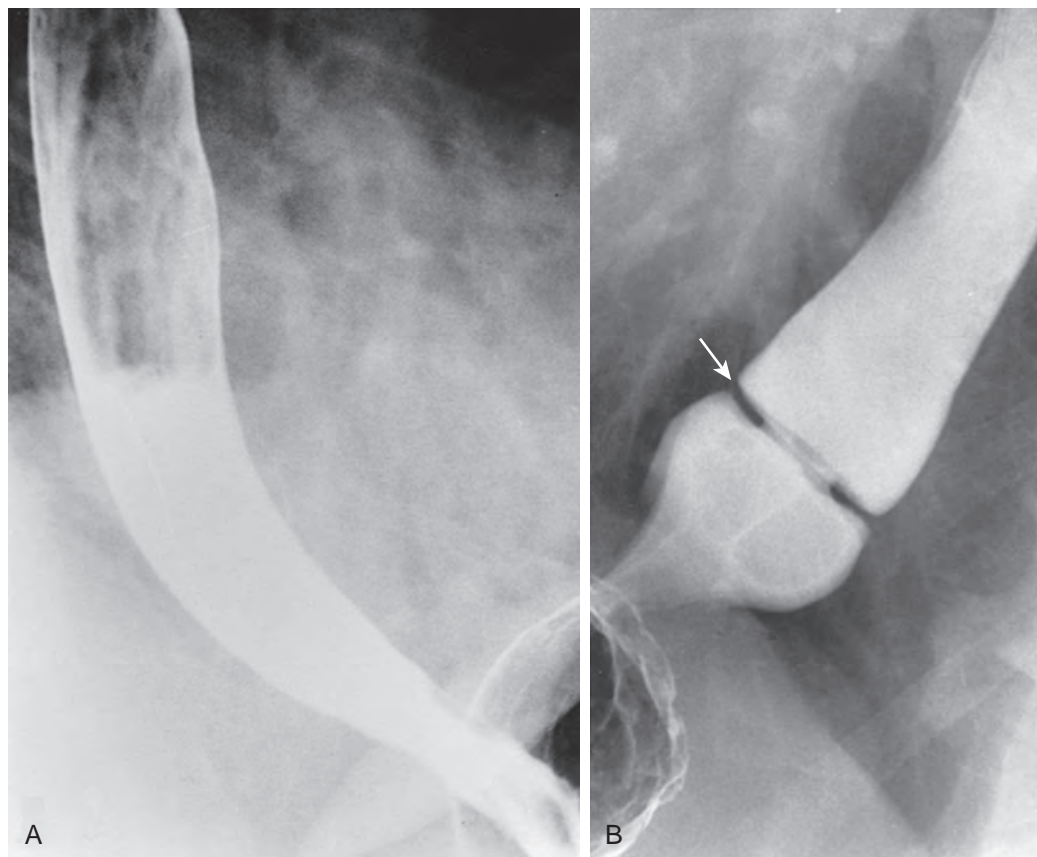
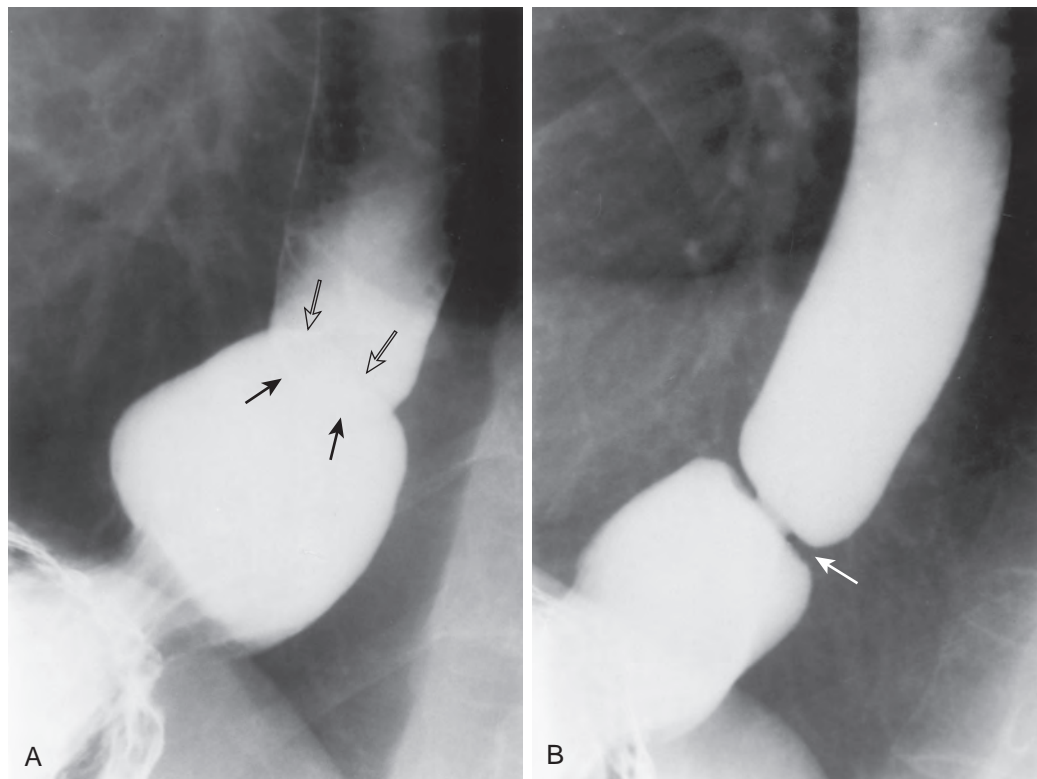


Figure 26-6 Overlap phenomenon obscuring Schatzki ring. **A.** Prone single-contrast view of the distal esophagus shows a hiatal hernia without evidence of a lower esophageal ring. However, there is a double density with two superimposed convex collections of barium caused by overlap of the distal end of the esophagus (solid arrows) and the proximal end of the hernia (open arrows). **B.** Repeat view with less distention of the hernia shows a tight Schatzki ring (arrow) when the distal esophagus and adjacent hiatal hernia no longer overlap. (From Hsu WC, MS Levine, Rubesin SE, Overlap phenomenon: A potential pitfall in the radiographic detection of lower esophageal rings, *AJR*, 180, 745-747, 2003.)



phenomenon occurs, additional prone views of the distal esophagus should be obtained when the hiatal hernia is less distended to avoid overlap of the hernia and adjacent distal esophagus, enabling visualization of these rings (Fig. 26-6B).²⁷ If a lower esophageal ring still cannot be detected because of persistent overlap in patients with clinical symptoms of a ring, the patient should be instructed to swallow a barium tablet; if the tablet lodges at the gastroesophageal junction, a Schatzki ring should be strongly suspected, and the patient should undergo endoscopy for further evaluation and a possible dilation procedure. With optimal technique, biphasic esophagography is thought to be even more sensitive than endoscopy for detecting Schatzki rings.¹⁵

DIFFERENTIAL DIAGNOSIS

A Schatzki ring has such a characteristic appearance that the radiographic findings are virtually diagnostic of this entity. Occasionally, however, other abnormalities may produce similar findings. Ringlike peptic strictures constitute as many as 40% of all peptic strictures in the distal esophagus (see Chapter 19).²⁸ These strictures often resemble Schatzki rings, but careful analysis generally shows that they have more tapered, asymmetric margins and are slightly longer (4 to 10 mm) than true Schatzki rings.²⁸ Despite these subtle distinctions, there is probably overlap between the findings of ringlike peptic strictures and Schatzki rings detected on barium studies or endoscopy. Nevertheless, the treatment is similar (a dilation procedure), so this differentiation may be of limited clinical importance.

Esophageal webs are occasionally found in the distal esophagus in the region of a peptic stricture (see Chapter 19).²⁹ These webs can resemble Schatzki rings but are located above the gastroesophageal junction and are almost always associated with peptic strictures, so they can be differentiated from lower esophageal rings on the basis of radiographic findings.²⁹ Rarely, a short, annular esophageal carcinoma can produce a localized constriction that superficially resembles a Schatzki ring. However, the presence of asymmetry, irregularity, and shelflike borders should indicate the need for early endoscopy to rule out a malignant lesion.

Hiatal Hernia

Hiatal hernias are classified as axial or paraesophageal, depending on the relationship of the cardia to the diaphragm and herniated portion of the stomach. The vast majority of hernias are axial, and only a tiny percentage are paraesophageal.³⁰ Despite its rarity, a paraesophageal hernia, unlike an axial hiatal hernia, is considered to be a potentially life-threatening condition because of the risk of volvulus, incarceration, or strangulation of the herniated portion of the stomach.

AXIAL HIATAL HERNIA

Pathogenesis

The phrenoesophageal membrane is a firm elastic structure surrounding the gastroesophageal junction that normally tethers the distal esophagus to the diaphragm and prevents the proximal portion of the stomach from herniating through the esophageal hiatus of the diaphragm into the chest. With aging, however, a lifetime of constant swallowing causes

progressive wear and tear on the phrenoesophageal membrane, with eventual stretching or rupture of the membrane and axial herniation of the proximal portion of the stomach into the chest.^{7,8,30,31} Not surprisingly, the prevalence of axial hiatal hernias increases with age; 60% of older adults in the United States are found to have such hernias on barium studies.³²

Clinical Significance

Considerable controversy exists about the relationship between an axial hiatal hernia and the subsequent development of gastroesophageal reflux and reflux esophagitis. Some investigators believe that the hernia predisposes to gastroesophageal reflux disease, but others believe that an axial hiatal hernia is of doubtful clinical significance when it occurs as an isolated finding without other clinical or radiologic signs of reflux disease.³³⁻³⁵ This subject is discussed in greater detail in Chapter 19.

Radiographic Diagnosis

An axial hiatal hernia may be recognized radiographically when the gastroesophageal junction is located above the esophageal hiatus of the diaphragm. Many of these hernias are sliding hernias that are only present when the patient is recumbent. Single-contrast barium studies with the patient prone are more likely to demonstrate a sliding hiatal hernia than double-contrast studies with the patient upright because the hernia is frequently reduced into the abdomen in the upright position and is more difficult to distend adequately when the patient is standing.³ The patient should therefore be instructed to drink a thin, low-density barium suspension continuously while in the prone, right anterior oblique position for optimal visualization of these structures. In contrast, fixed axial hernias are those in which the hernia persists, even when the patient is upright. This observation is clinically important because patients with a large fixed hernia may have a short esophagus, necessitating an esophageal lengthening procedure such as a Collis gastroplasty at the time of surgery if an antireflux operation is contemplated.

Because a lower esophageal mucosal ring demarcates the anatomic location of the gastroesophageal junction, an axial hiatal hernia may be diagnosed on barium studies obtained with the patient prone when a mucosal ring is observed 2 cm or more above the diaphragmatic hiatus (see Fig. 26-3).¹¹ Even in the absence of a definite mucosal ring, a hiatal hernia can often be recognized by the presence of gastric folds within the hernia (Fig. 26-7). These folds may continue inferiorly through the diaphragmatic hiatus into the abdominal portion of the stomach. Not infrequently, the hernia may be kinked or narrowed at the esophageal hiatus because of extrinsic compression by the surrounding diaphragm at this level. Occasionally, a prominent diagonal notch may also be seen on the left lateral and superior aspect of the hernia because of crossing gastric sling fibers at the cardiac incisura (Fig. 26-8).³⁰

When a moderate-sized or large axial hiatal hernia is present, double-contrast views of the stomach obtained with the patient in an upright or right lateral recumbent position also permit assessment of the mucosa within the hernia for ulcers, neoplasms, or other abnormalities not easily seen on single-contrast images. Ulcers are particularly likely to develop at the hiatal orifice (so-called riding ulcers), where the gastric mucosa is repeatedly exposed to trauma on the ridge riding over the hiatus (Fig. 26-9).³⁶ Occasionally, gastric carcinomas that develop within hiatal hernias may be manifested on double-contrast



Figure 26-7 Axial hiatal hernia. Gastric rugae are seen in the hernia on this prone single-contrast view of the esophagus. (From Levine MS: *Radiology of the Esophagus*. Philadelphia: WB Saunders, 1989.)

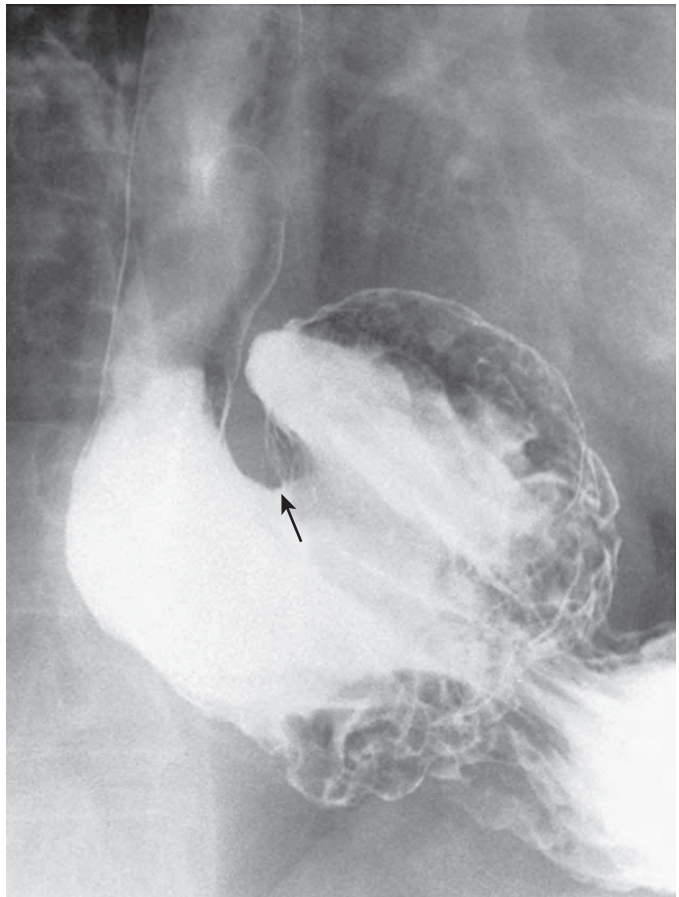


Figure 26-8 Large axial hiatal hernia. There is a prominent diagonal notch (arrow) on the superior aspect of the hernia caused by crossing gastric sling fibers at the cardiac incisura. This appearance may erroneously suggest a mixed axial-paraesophageal hernia. (From Levine MS: *Radiology of the Esophagus*. Philadelphia: WB Saunders, 1989.)

studies by polypoid masses or infiltrative lesions with thickened, distorted folds in the hernia.³⁷

When barium studies are performed on patients with giant hiatal hernias (i.e., hernias containing 50% or more of the stomach), the weight of the barium may cause the gastric fundus to droop inferiorly beneath the herniated gastric body, especially in the upright position, producing a distinctive radiographic appearance, also known as a floppy fundus (Fig. 26-10).³⁸ These patients may develop symptoms such as postprandial pain, early satiety, nausea, retching, and vomiting because of the mechanical effect of ingested food and liquids pooling in the floppy fundus or because of subsequent traction on the stomach, which impedes emptying of the hernia.³⁸ Because symptoms result from distortion of the gastric anatomy, these symptoms usually resolve only after surgical repair of the hernia.³⁸

A giant hiatal hernia associated with a floppy fundus can be mistaken on barium studies for an organoaxial gastric volvulus, a potentially life-threatening condition because of the risk of incarceration, strangulation, and infarction of the affected stomach (see Chapter 34).^{36,39,40} In organoaxial gastric volvulus, however, most or all of the stomach herniates above the diaphragm into the lower thorax, with the greater curvature of the stomach rotated above the lesser curvature, producing a so-called upside-down intrathoracic stomach.^{41,42} In contrast, normal anatomic relationships are preserved in patients with a floppy fundus.



Figure 26-9 Hiatal hernia with a riding ulcer. There is a hiatal hernia with a large ulcer (arrow) in the proximal stomach where it traverses the esophageal hiatus of the diaphragm, probably because of repeated trauma to the gastric mucosa at the level of the hiatus.

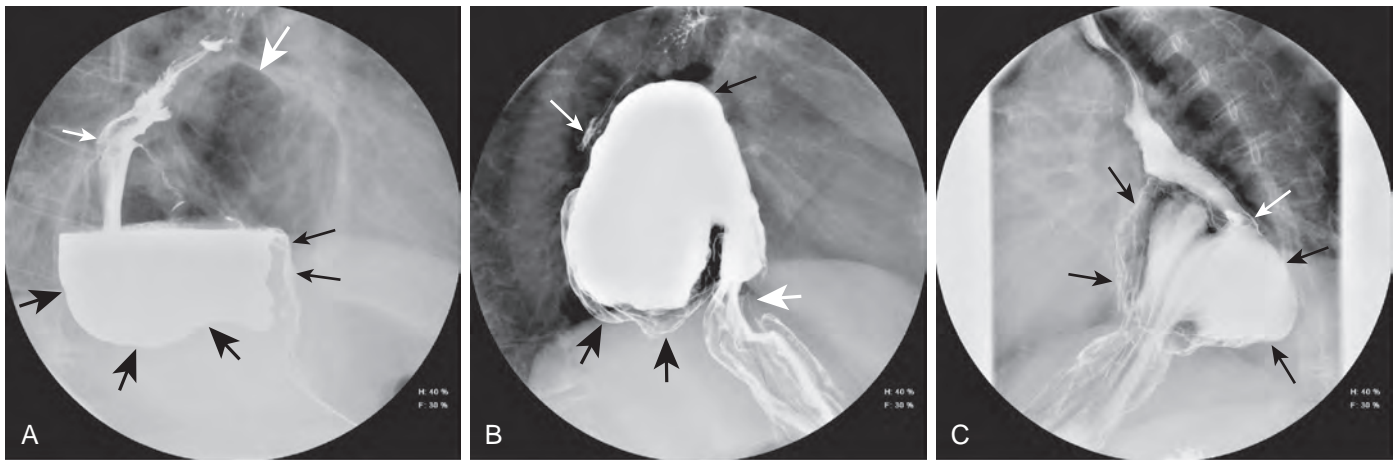


Figure 26-10 Large axial hiatal hernia with a floppy fundus. **A.** Upright double-contrast view shows a large hiatal hernia, with the gastric fundus (large black arrows) flopping inferiorly beneath the most superior portion of the gas-filled gastric body (large white arrow). Note how there is pooling of barium in the floppy fundus, with a small amount of barium spilling over into the portion of the stomach (small black arrows) that traverses the diaphragm. **B.** Supine oblique view also shows a floppy fundus (large black arrows) inferior to the most superior portion of the gastric body (small black arrow). Note how there is narrowing of the stomach (large white arrow) where it traverses the diaphragm. **C.** Prone oblique view now shows the gastric fundus (black arrows) in its expected location above the intrathoracic portion of the gastric body, so the fundus is no longer flopped inferiorly. In **A**, **B**, and **C**, the small white arrows denote the location of the gastroesophageal junction above the diaphragm. (From Huang SY, Levine MS, Rubesin SE, et al: Large hiatal hernias with a floppy fundus. *AJR* 188:960–964, 2007.)

PARAESOPHAGEAL HERNIA

Pathogenesis

In patients with a paraesophageal hernia, a variable portion of the stomach herniates through the esophageal hiatus of the diaphragm into the chest alongside the distal esophagus while the cardia retains its normal position below the diaphragm. This type of hernia is thought to occur through an unusually large defect in the phrenoesophageal membrane that progressively increases in size with age.³⁶ Paraesophageal hernias therefore develop primarily in older adults (i.e., patients > 70 years of age). Less frequently, these hernias may occur as a result of blunt trauma (e.g., automobile accidents) to the chest or abdomen in patients of any age. Affected individuals may eventually develop a mixed type of axial-paraesophageal hernia if the gastroesophageal junction also rises above the diaphragm.⁴³ Rarely, the entire stomach or a major portion of the stomach herniates through the esophageal hiatus, producing a gastric volvulus (see Chapter 34).

Clinical Significance

Many patients with paraesophageal hernias are asymptomatic, and the hernia is an incidental finding on barium studies performed for other reasons. Unlike axial hernias, paraesophageal hernias are rarely associated with gastroesophageal reflux or reflux esophagitis. As these hernias enlarge, however, twisting or torsion and obstruction at or near the esophageal hiatus of the diaphragm may lead to incarceration, strangulation, infarction, or perforation of the herniated portion of the stomach.^{43–47} Because of these potentially life-threatening complications, some authors believe that surgery is warranted in all patients with paraesophageal hernias (assuming that they are surgical candidates), even when these individuals are asymptomatic.^{48,49} However, conservative management may be appropriate for older patients with paraesophageal hernias who are asymptomatic because of the high risk of surgery in this group. Laparoscopic repair of paraesophageal hernias has also been advocated as a less invasive technique than traditional surgery.⁵⁰

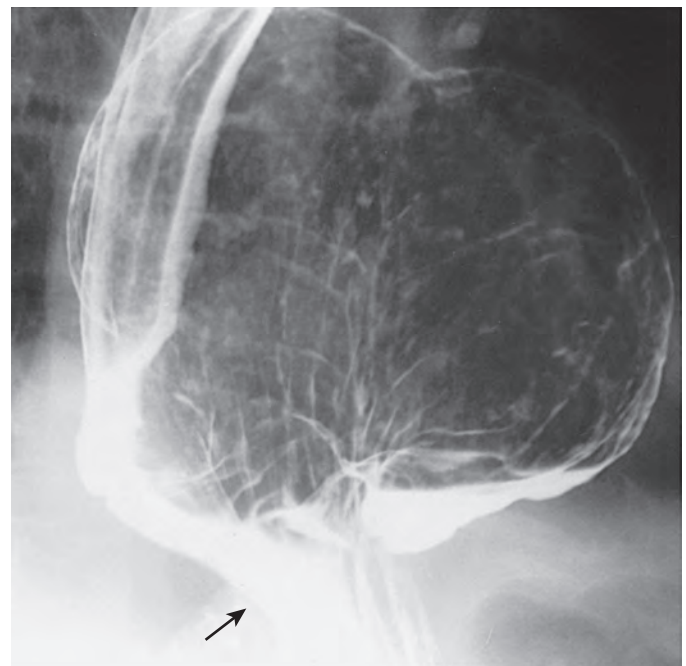


Figure 26-11 Paraesophageal hernia. The gastric fundus has herniated into the chest alongside the distal esophagus, but the gastric cardia (arrow) retains its normal position below the diaphragm. (From Levine MS: *Radiology of the Esophagus*. Philadelphia: WB Saunders, 1989.)

Radiographic Diagnosis

A paraesophageal hernia may be diagnosed on barium studies when the gastric fundus has herniated through the esophageal hiatus of the diaphragm alongside the distal esophagus while the cardia retains its normal position below the diaphragm (Fig. 26-11). In a mixed axial-paraesophageal hernia, however, the cardia has also herniated above the diaphragm into the chest (Fig. 26-12). Occasionally, an axial hiatal hernia can be



Figure 26-12 Mixed axial-paraesophageal hernia. The gastric fundus has herniated into the chest alongside the distal esophagus. In this patient, however, the cardia (arrow) has also herniated above the diaphragm. These are features of a mixed hernia.

mistaken radiographically for a mixed axial-paraesophageal hernia because of a prominent notch on the superior aspect of the hernia that erroneously suggests a paraesophageal component (see Fig. 26-8).³⁰

In patients with a gastric volvulus or upside-down intrathoracic stomach, almost the entire stomach has herniated through the esophageal hiatus into the chest and has assumed an inverted or upside-down configuration (see Chapter 34). Rarely, traction or torsion of the stomach at or near the level of the hiatus may lead to obstruction, strangulation, infarction, or perforation of the intrathoracic stomach.⁴¹ These patients may undergo surgery on an emergent basis without preoperative barium studies because of their rapidly deteriorating clinical condition.

Carcinoma of the Cardia

The clinical and radiographic aspects of carcinoma of the cardia are discussed in detail in Chapter 32. On barium studies, advanced lesions at the cardia may appear as obvious exophytic or infiltrating lesions in the gastric fundus. However, other lesions at the cardia may be recognized only by relatively subtle nodularity, mass effect, or ulceration in this region with distortion, effacement, or obliteration of the normal anatomic landmarks at the cardia (Fig. 26-13).^{9,10,51,52} Because these abnormalities at the cardia are extremely difficult to demonstrate on conventional single-contrast barium studies, double-contrast technique is essential for detecting these lesions at the earliest possible stage.

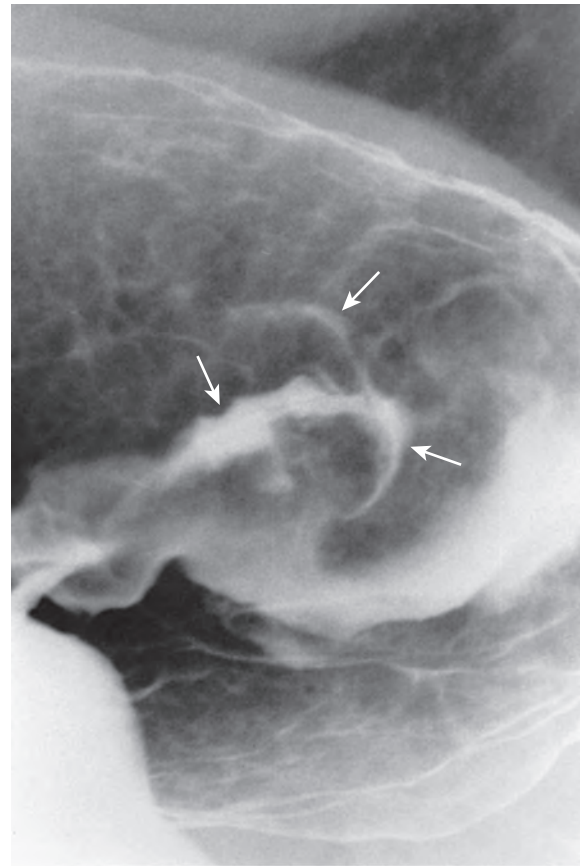


Figure 26-13 Carcinoma of the gastric cardia. The normal anatomic landmarks at the cardia have been obliterated and replaced by irregular areas of ulceration (arrows) caused by tumor in this region. (From Levine MS: *Radiology of the Esophagus*. Philadelphia, WB Saunders, 1989.)

Prolapsed Esophagogastric Mucosa

Retrograde or antegrade prolapse of mucosa in the esophago-gastric region may produce a polypoid filling defect in the distal esophagus or gastric fundus (Fig. 26-14A).^{53,54} However, mucosal prolapse usually occurs as a transient phenomenon, so the filling defect intermittently vanishes at fluoroscopy (Fig. 26-14B). The distal esophagus may also invaginate into a sliding hiatal hernia or a hiatal hernia may invaginate into the fundus, producing an apparent mass lesion in this region (Fig. 26-15A).⁵⁵ However, greater distention of the fundus with barium or gas usually displaces the invaginated hernia above the diaphragm and reduces the invaginated distal esophagus, so this lesion is also observed as a transient finding at fluoroscopy (Fig. 26-15B). Thus, it is usually possible to differentiate prolapsed esophagogastric mucosa or invaginated hernias from true polypoid lesions at the cardia.

Other Abnormalities

Other abnormalities occurring at or near the gastroesophageal junction include peptic strictures (see Chapter 19), inflammatory esophagogastric polyps (see Chapter 19), esophageal or gastric varices (see Chapters 25 and 34), primary or secondary achalasia (see Chapters 18 and 24), and squamous cell metastases to the cardia (see Chapter 23).

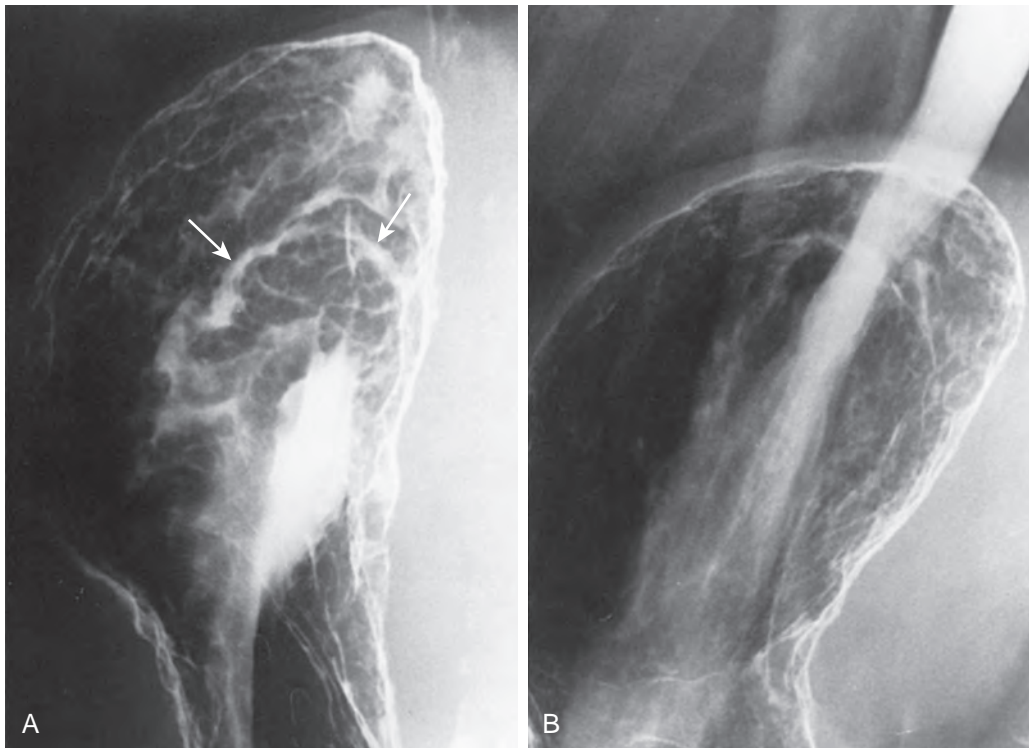


Figure 26-14 Pseudotumor in the gastric fundus caused by retrograde prolapse of esophagogastric mucosa. **A.** Initial double-contrast view of the stomach shows an apparent polypoid mass (arrows) in the fundus at the expected location of the cardia. **B.** Repeat view as the patient swallows additional barium shows a normal fundus. This pseudotumor was caused by intermittent retrograde prolapse of mucosa in the esophagogastric region.

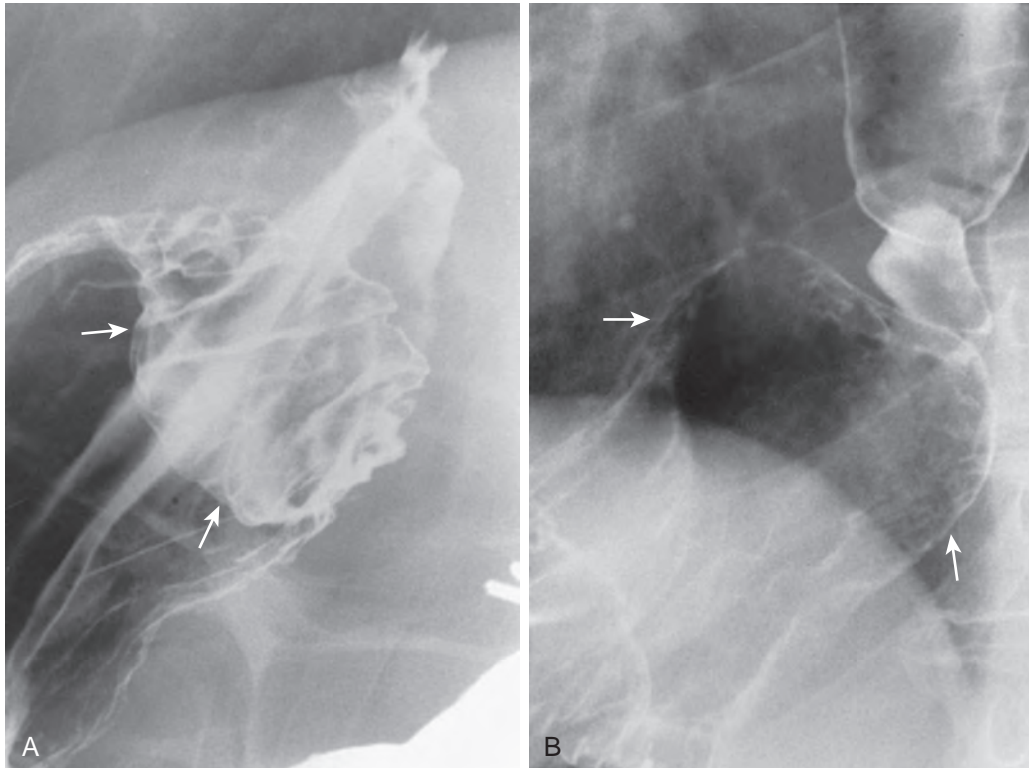


Figure 26-15 Pseudotumor in the gastric fundus caused by an invaginated hiatal hernia. **A.** An apparent mass lesion (arrows) is seen in the fundus on a double-contrast radiograph. **B.** Moments later, the invaginated hernia (arrows) has risen above the diaphragm, and the pseudotumor is no longer seen.

REFERENCES

- Levine MS, Rubesin SE, Herlinger H, et al: Double-contrast upper gastrointestinal examination: Technique and interpretation. *Radiology* 168:593–602, 1988.
- Levine MS, Rubesin SE: Radiologic investigation of dysphagia. *AJR* 154:1157–1163, 1990.
- Chen YM, Ott DJ, Gelfand DW, et al: Multiphasic examination of the esophagogastric region for strictures, rings, and hiatal hernia: Evaluation of the individual techniques. *Gastrointest Radiol* 10:311–316, 1985.
- Wolf BS: Use of a half-inch barium tablet to detect minimal esophageal strictures. *J Mt Sinai Hosp* 28:80–95, 1961.
- Ott DJ, Kelley TF, Chen YM, et al: Evaluation of the esophagus with a marshmallow bolus: Clarifying the cause of dysphagia. *Gastrointest Radiol* 16:1–4, 1991.
- Friedland GW: Historical review of the changing concepts of lower esophageal anatomy: 430 B.C.–1977. *AJR* 131:373–388, 1978.
- Wolf BS, Heitmann P, Cohen BR: The inferior esophageal sphincter, the manometric high pressure zone and hiatal incompetence. *AJR* 103:251–276, 1968.
- Dodds WJ: Current concepts of esophageal motor function: Clinical implications for radiology. *AJR* 128:549–561, 1977.
- Freeny PC: Double-contrast gastrography of the fundus and cardia: Normal landmarks and their pathologic changes. *AJR* 133:481–487, 1979.
- Herlinger H, Grossman R, Laufer I, et al: The gastric cardia in double-contrast study: Its dynamic image. *AJR* 135:21–29, 1980.
- Ott DJ, Gelfand DW, Wu WC, et al: Esophagogastric region and its rings. *AJR* 142:281–287, 1984.
- Johnston JR, Griffin JC: Anatomic location of the lower esophageal ring. *Surgery* 61:528–534, 1967.
- Goyal RK, Glancy JJ, Spiro HM: Lower esophageal ring. *N Engl J Med* 282:1298–1305, 1970.
- Schatzki R, Gary JE: The lower esophageal ring. *AJR* 75:246–261, 1956.
- Ott DJ, Chen YM, Wu WC, et al: Radiographic and endoscopic sensitivity in detecting lower esophageal mucosal ring. *AJR* 147:261–265, 1986.
- Schatzki R, Gary JE: Dysphagia due to a diaphragm-like localized narrowing in the lower esophagus (“lower esophageal ring”). *AJR* 70:911–922, 1953.
- Scharschmidt BF, Watts HD: The lower esophageal ring and esophageal reflux. *Am J Gastroenterol* 69:544–549, 1978.
- Chen YM, Gelfand DW, Ott DJ, et al: Natural progression of the lower esophageal mucosal ring. *Gastrointest Radiol* 12:93–98, 1987.
- Marshall JB, Kretschmar JM, Diaz-Arias AA: Gastroesophageal reflux as a pathogenic factor in the development of symptomatic lower esophageal rings. *Arch Intern Med* 150:1669–1672, 1990.
- Schatzki R: The lower esophageal ring: Long-term follow-up of symptomatic and asymptomatic rings. *AJR* 90:805–810, 1963.
- DeVault KR: Lower esophageal (Schatzki's) ring: Pathogenesis, diagnosis and therapy. *Dig Dis* 14:323–329, 1996.
- Pezzullo JC, Lewicki AM: Schatzki ring, statistically reexamined. *Radiology* 228:609–613, 2003.
- Norton RA, King GD: “Steak house syndrome”: The symptomatic lower esophageal ring. *Lahey Clin Found Bull* 13:55–59, 1963.
- Desai DC, Rider JA, Puletti EJ, et al: Lower esophageal ring. *Gastrointest Endosc* 15:100–105, 1968.
- Arvanitakis C: Lower esophageal ring: Endoscopic and therapeutic aspects. *Gastrointest Endosc* 24:17–18, 1977.
- Burdick JS, Venu RP, Hogan WJ: Cutting the defiant lower esophageal ring. *Gastrointest Endosc* 39:616–619, 1993.
- Hsu WC, Levine MS, Rubesin SE: Overlap phenomenon: A potential pitfall in the radiographic detection of lower esophageal rings. *AJR* 180:745–747, 2003.
- Gupta S, Levine MS, Rubesin SE, et al: Usefulness of barium studies for differentiating benign and malignant strictures of the esophagus. *AJR* 180:737–744, 2003.
- Weaver JW, Kaude JV, Hamlin DJ: Webs of the lower esophagus: A complication of gastroesophageal reflux? *AJR* 142:289–292, 1984.
- Dodds WJ: Esophagus and esophagogastric region. In Margulis AR, Burhenne HJ, editors: *Alimentary Tract Radiology*, ed 3, St. Louis, 1983, CV Mosby, pp 529–603.
- Wolf BS: Sliding hiatal hernia: The need for redefinition. *AJR* 117:231–247, 1973.
- Ellis H: Diaphragmatic hernia—a diagnostic challenge. *Postgrad Med J* 62:325–327, 1986.
- Cohen S, Harris LD: Does hiatus hernia affect competence of the gastroesophageal sphincter? *N Engl J Med* 284:1053–1056, 1971.
- Behar J: Reflux esophagitis: Pathogenesis, diagnosis, and management. *Arch Intern Med* 136:560–566, 1976.
- Wright RA, Hurwitz AL: Relationship of hiatal hernia to endoscopically proved reflux esophagitis. *Dig Dis Sci* 24:311–313, 1979.
- Skinner DB: Hernias (hiatal, traumatic, and congenital). In Berk JE, editor: *Bockus Gastroenterology*, ed 4, Philadelphia, 1985, WB Saunders, pp 705–716.
- Maglinte DDT, Ghahremani GG, Gin FM, et al: Radiologic features of carcinomas arising in hiatal hernias. *AJR* 166:789–794, 1996.
- Huang SY, Levine MS, Rubesin SE: Large hiatal hernias with a floppy fundus. *AJR* 188:960–964, 2007.
- Babb RR, Peck OC, Jamplis RW: Gastric volvulus and obstruction in paraesophageal hiatus hernia: A surgical emergency. *Am J Dig Dis* 17:119–128, 1972.
- McArthur KE: Hernias and volvulus of the gastrointestinal tract. In Feldman M, Scharschmidt BF, Sleisenger MH, editors: *Sleisenger & Fordtran's Gastrointestinal and Liver Disease*, ed 6, Philadelphia, 1998, WB Saunders, pp 317–331.
- Gerson DE, Lewicki AM: Intrathoracic stomach: When does it obstruct? *Radiology* 119:257–264, 1976.
- Abbara S, Kalan MMH, Lewicki AM: Intrathoracic stomach revisited. *AJR* 181:403–414, 2003.
- Wo JM, Branum GD, Hunter JG, et al: Clinical features of type III (mixed) paraesophageal hernia. *Am J Gastroenterol* 91:914–916, 1996.
- Shocket E, Neber J, Drosig RE: The acutely obstructed, incarcerated paraesophageal hiatal hernia. *Am J Surg* 108:805–810, 1964.
- Hill LD: Incarcerated paraesophageal hernia: A surgical emergency. *Am J Surg* 126:286–291, 1973.
- Dunn DB, Quick G: Incarcerated paraesophageal hernia. *Am J Emerg Med* 8:36–39, 1990.
- Landreneau RJ, Hazelrigg SR, Johnson JA, et al: The giant paraesophageal hernia: A particularly morbid condition of the esophageal hiatus. *Mo Med* 87:884–888, 1990.
- Vitelli CE, Jaffe BM, Kahng KU: Paraesophageal hernia. *N Y State J Med* 89:654–657, 1989.
- Landreneau RJ, Johnson JA, Marshall JB, et al: Clinical spectrum of paraesophageal herniation. *Dig Dis Sci* 37:537–544, 1992.
- Oddsottir M, Franco AL, Laycock WS, et al: Laparoscopic repair of paraesophageal hernia: New access, old technique. *Surg Endosc* 9:164–168, 1995.
- Freeny PC, Marks WM: Adenocarcinoma of the gastroesophageal junction: Barium and CT examination. *AJR* 138:1077–1084, 1982.
- Levine MS, Laufer I, Thompson JJ: Carcinoma of the gastric cardia in young people. *AJR* 140:69–72, 1983.
- Kaye JJ, Stassa G: Mimicry and deception in the diagnosis of tumors of the gastric cardia. *AJR* 110:295–303, 1970.
- Rudnick JP, Ferrucci JT, Eaton SB, et al: Esophageal pseudotumor: Retrograde prolapse of gastric mucosa into the esophagus. *AJR* 115:253–256, 1972.
- Ghahremani GG, Collins PA: Esophagogastric invagination in patients with sliding hiatus hernia. *Gastrointest Radiol* 1:253–261, 1976.

Postoperative Esophagus

STEPHEN E. RUBESIN

CHAPTER OUTLINE

General Principles

Gastroesophageal Reflux and Hiatal Hernia

Normal Postoperative Appearances

Complications

Benign Strictures

Carcinoma

Esophagogastrectomy

Colonic Interposition, Jejunal Interposition, and Free Jejunal Graft

Palliative Intubation

Achalasia

Pneumatic Dilation

Cardiomyotomy

Varices

General Principles

Radiologic evaluation of the postoperative esophagus requires an understanding of the operative procedures and of the normal postoperative radiologic appearances. The purpose of the radiologic examination is to do the following: (1) define the postoperative anatomy and establish a baseline; (2) assess the efficacy of the procedure; and (3) detect complications during the early (<4 weeks after surgery) or late (>4 weeks after surgery) postoperative periods.¹⁻⁵ During the early postoperative period, the most common complications include stasis resulting from adynamic ileus or vagotomy, obstruction resulting from anastomotic edema, and perforation resulting from anastomotic breakdown (Box 27-1).¹⁻⁵ During the late postoperative period, the most common complications include aspiration, gastroesophageal reflux, anastomotic strictures, and recurrent tumor (see Box 27-1).¹⁻⁵

An anastomotic or staple line leak is the most common serious complication of esophageal surgery (Fig. 27-1). Sutures and staples hold less well in the esophagus than elsewhere in the gastrointestinal tract because the esophagus lacks a serosa, esophageal muscle is stringy and soft, and mucosa retracts from the cut esophageal margin because of mobility between the squamous mucosa, fatty submucosa, and muscularis propria.² Leaks also occur at staple lines because of focal ischemia caused by the crush effect of the staple line on viable tissue. A delay in the diagnosis of postoperative perforation leads to increased morbidity and mortality resulting from mediastinitis, abscess formation, or sepsis.⁴ Postoperative patients complaining of cervical, thoracic, or epigastric pain, fever, dysphagia, or respiratory distress may therefore require an emergent esophagogram. At our institution, esophagograms are routinely performed

between the sixth and eighth postoperative days because some patients with esophageal perforation are asymptomatic and others have delayed leaks.⁶ Mildly delayed leaks (postoperative days 7-21) are often caused by ischemia at a staple line.

Edema, hemorrhage, and spasm at an anastomosis are the most common causes of obstruction in the early postoperative period. This obstruction usually resolves within 1 to 2 weeks after surgery. Obstruction may also occur when the viscus used as the esophageal substitute passes through the diaphragm (Fig. 27-2). In the late postoperative period, obstruction is usually caused by a benign stricture related to a healed anastomotic leak, ischemia at the anastomosis, or chronic gastroesophageal reflux. Other patients may have recurrent cancer or a tight diaphragmatic hiatus as the cause of a narrowing.

Esophageal dysmotility, delayed gastric emptying caused by pylorospasm or gastric atony, or diarrhea may be the result of manipulation, damage, or intentional surgical resection of the vagus nerve. Vocal cord paralysis or dysphagia with abnormal motility of the inferior constrictor muscles or proximal esophageal muscles may result from recurrent laryngeal injury.

Any form of esophageal surgery that disrupts the lower esophageal sphincter may result in gastroesophageal reflux. An antireflux procedure may be included as part of the esophago-gastric anastomosis to prevent postoperative gastroesophageal reflux. Complications of postoperative gastroesophageal reflux include aspiration, reflux esophagitis, stricture formation, Barrett's esophagus, and adenocarcinoma arising in Barrett's esophagus.

The thoracic duct may also be damaged during surgery. The thoracic duct passes superiorly, anterior to the spine, between the aorta and azygos vein. At the level of the T5 vertebral body, the thoracic duct crosses behind the esophagus and then continues cranially along the left side of the esophagus. Although uncommon, thoracic duct damage may result in chylothorax or chylous ascites.²

Early postoperative complications may be manifested by a variety of findings on chest and abdominal radiographs. A dilated viscus with air-fluid levels should suggest gastric outlet obstruction when the stomach is used to replace the esophagus. Pneumomediastinum, cervical or subcutaneous emphysema, a widened mediastinum, or a rapidly enlarging pleural effusion should suggest anastomotic breakdown and perforation.⁷ Nevertheless, chest and abdominal radiographs may be normal in patients with perforation.

Depending on the nature of the surgery and status of the patient, the postoperative radiologic examination should be tailored to demonstrate suspected complications. Barium and water-soluble contrast agents each have advantages and disadvantages in evaluating patients during the early postoperative period.⁸⁻¹⁸ This subject is discussed in detail in Chapters 1 and 17. Briefly, water-soluble contrast agents should be used during the early postoperative period to rule out a perforation or anastomotic leak into the mediastinum or pleural space. If no

BOX 27-1 COMPLICATIONS OF ESOPHAGEAL SURGERY**EARLY COMPLICATIONS****Common Complications**

- Anastomotic or staple line leak
- Anastomotic narrowing
- Gastric or duodenal atony
- Aspiration
- Gastroesophageal reflux
- Delayed bypass emptying
- Anastomotic edema
- Anastomotic narrowing
- Gastric or duodenal atony
- Obstruction at diaphragm—pyloric channel obstruction or spasm

Uncommon Complications

- Pneumothorax
- Pneumomediastinum
- Mediastinal hematoma
- Empyema
- Vocal cord paresis
- Chylothorax
- Ischemia of colonic or jejunal bypass
- Splenic injury
- Pancreatitis

LATE COMPLICATIONS**Common Complications**

- Anastomotic stricture
- Aspiration
- Recurrent carcinoma
- Gastroesophageal reflux and its sequelae

Uncommon Complications

- Delayed conduit emptying
- Tracheoesophageal fistula
- Anastomotic or staple line leak

water-soluble contrast medium is seen to extravasate from the esophagus on initial spot images, high-density barium should then be given for a more detailed examination.^{1,19,20} Barium or low-osmolality, water-soluble contrast agents such as iohexol (Omnipaque) may be used as the primary contrast agent if aspiration or an esophageal-airway fistula is suspected.

Gastroesophageal Reflux and Hiatal Hernia

Patients with gastroesophageal reflux may undergo surgery because of intractable reflux esophagitis, peptic strictures, or Barrett's esophagus. With most of these surgical procedures, the crura are dissected, the esophagus is mobilized, the vagus nerves are preserved, the hiatal hernia is reduced, the diaphragm is repaired, and the intra-abdominal esophagus is restored. A variable portion of gastric fundus is usually wrapped around the proximal stomach.^{4,21}

NORMAL POSTOPERATIVE APPEARANCES

In a Nissen fundoplication, the gastric fundus is loosely wrapped 360 degrees around the proximal stomach to create an antireflux valve.²² The Nissen fundoplication wrap normally appears

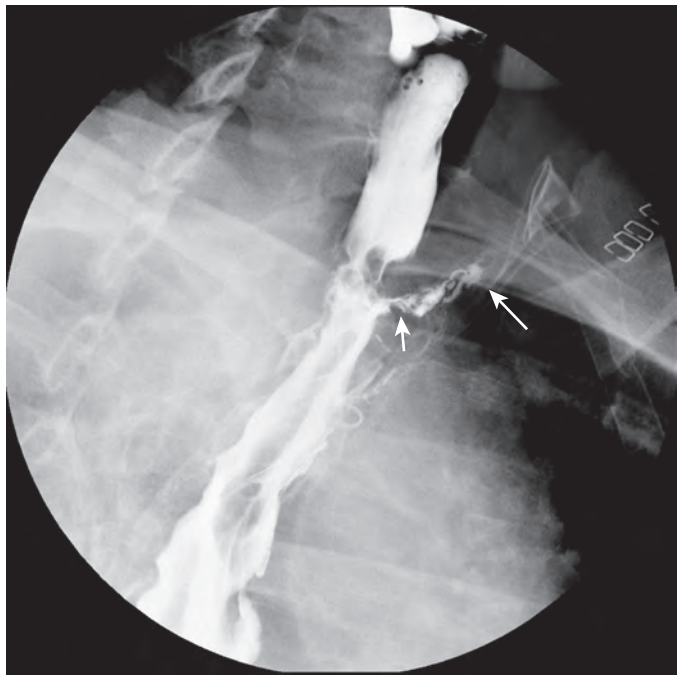


Figure 27-1 Esophagogastric anastomosis with leak near esophagogastric anastomosis. Spot radiograph centered at the esophagogastric anastomosis shows a 3-cm long track of barium arising from the left anterolateral wall of the anastomosis (*small arrow*). The track extends to the left and is just entering (*large arrow*) a mediastinal drain.

as a 2- to 3-cm fundal mass, with a smooth contour and surface (Fig. 27-3).^{23,24} If the patient drinks barium in a recumbent, steep oblique, or lateral position, the lumen is shown to pass through the center of the fundoplication wrap.²⁵ The smooth symmetric wrap and its consistent relationship with the lumen readily differentiates a fundoplication wrap from a true tumor in the fundus.

In a Belsey Mark IV repair, the gastric fundus is sutured to the intra-abdominal esophagus, creating an acute esophagogastric junction angle (angle of His); a 270-degree fundoplication wrap is then created.^{26,27} The gastric wrap of a Belsey Mark IV repair produces a smaller defect than a Nissen fundoplication.²⁸ Two distinct angles are formed passing through the 270-degree fundoplication.²⁹ The intra-abdominal esophagus has a shallow upper angle where the esophagus, fundus, and diaphragm are sutured together and a lower angle where the stomach is pulled upward toward the esophagus.²⁸

A less than circumferential wrap may be made anteriorly or posteriorly, especially in patients with esophageal dysmotility and poor esophageal clearance. Wraps may be made loosely (Fig. 27-4), especially if the surgery is performed laparoscopically. Knowledge of the exact surgical technique performed is helpful for radiologic interpretation.

COMPLICATIONS

Complications related directly to surgery include pneumothorax and pneumomediastinum. Acute hemorrhage usually arises from the short gastric vessels ligated at surgery or is related to operative injury of the spleen or liver. Instrumental perforation

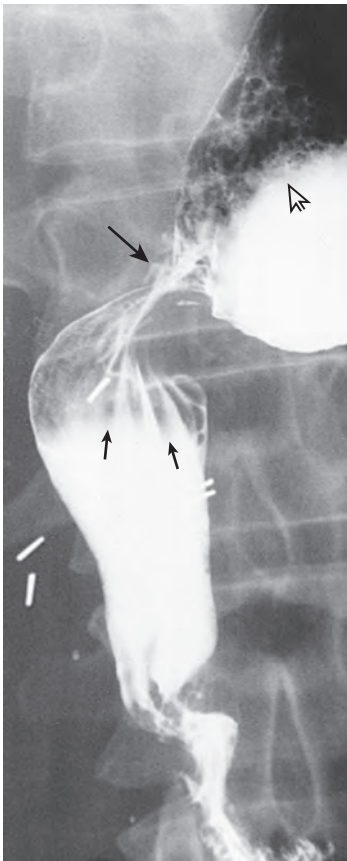


Figure 27-2 Postoperative obstruction after esophagogastrectomy. There is tapered narrowing of the stomach (large arrow) where it passes through the diaphragm. Below the diaphragm, twisting of the stomach is manifested radiographically by gastric folds (small arrows) radiating toward the area of narrowing. The stomach proximal to the obstruction shows dilation, delayed emptying of barium, and retained debris (open arrow). (From Rubesin SE, Beatty SM: *The postoperative esophagus*. *Semin Roentgenol* 39:401–410, 1994.)

of the esophagus or stomach may not be detected during surgery and may lead to a left upper quadrant abscess. Late esophageal perforation may be caused by ischemia or diathermy injury.^{2,4}

Obstruction

During the early postoperative period, edema of the fundoplication wrap may cause transient dysphagia. This complication may be manifested on esophagograms by a large, smooth fundal mass associated with smooth, tapered narrowing of the intra-abdominal esophagus and delayed emptying of contrast material (Fig. 27-5).²³ The edema usually subsides within 1 to 2 weeks; a follow-up esophagogram demonstrates a much smaller defect in this region because of the normal fundoplication wrap.

Some patients may have persistent narrowing at the fundoplication, causing dysphagia or the so-called gas bloat syndrome, with upper abdominal fullness and an inability to belch after meals.²¹ Patients may also complain of an inability to vomit and increased flatulence. In such cases, esophagograms may demonstrate fixed narrowing of the lumen as a result of a tight fundoplication wrap (Fig. 27-6) or excessive closure of the esophageal hiatus of the diaphragm.^{30,31} It is sometimes



Figure 27-3 Normal Nissen fundoplication. The fundoplication wrap is seen as a smooth-surfaced, well-defined mass (arrows) in the gastric fundus.

difficult to distinguish a persistent reflux-induced distal esophageal stricture from a tight wrap. Examination of the preoperative images is helpful.

Recurrent Hiatal Hernia and Gastroesophageal Reflux

Complete disruption of the fundoplication sutures and crural repair is manifested radiographically by a recurrent hiatal hernia and gastroesophageal reflux, without visualization of the fundoplication wrap (Fig. 27-7).^{32,33} Partial disruption of the fundoplication sutures may be manifested by a partially intact wrap associated with one or more outpouchings from the gastric fundus (Fig. 27-8) or by an hourglass appearance of the stomach as the fundus slips through the fundoplication.^{32,33} An hourglass stomach may also be caused by inappropriate placement of the fundoplication around the gastric body. Finally, disruption of the diaphragmatic sutures (but not the fundoplication sutures) may result in a recurrent hiatal hernia, with continued demonstration of an intact fundoplication wrap (Fig. 27-9).³² A paraesophageal hernia may occur at diaphragmatic repair breakdown (Fig. 27-10).

Benign Strictures

Benign esophageal strictures may be treated by various surgical and nonsurgical procedures, including esophageal bougienage, fluoroscopically controlled balloon dilation, endoscopically

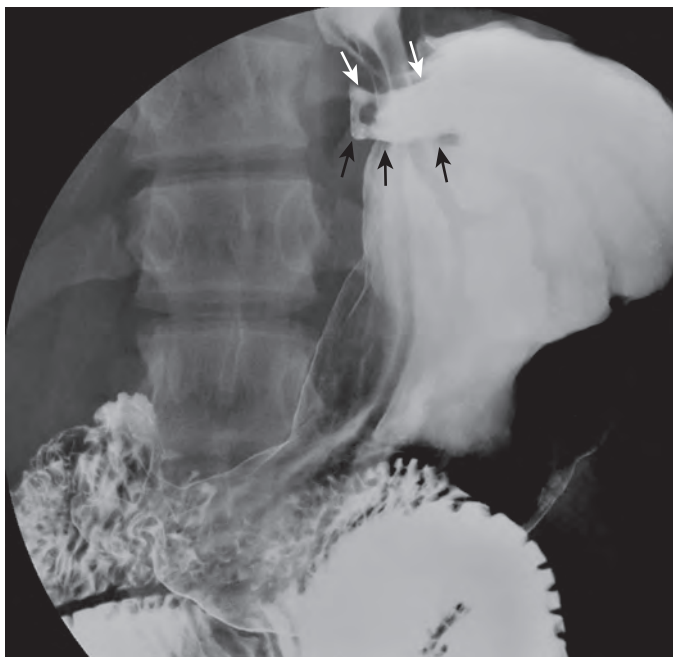


Figure 27-4 Loose fundoplication wrap. The loose fundoplication wrap is filled with barium and is manifested as a white/barium-filled rectangular structure crossing the gastric cardia (white arrows). The wall of the fundoplication wrap is seen as a thick, linear radiolucency (black arrows) adjacent to the rectangular barium collection. (From Rubesin SE, Levine MS: *Postoperative esophagus*. In Levine MS: *Radiology of the Esophagus*. Philadelphia, WB Saunders, 1989, pp 267–290.)

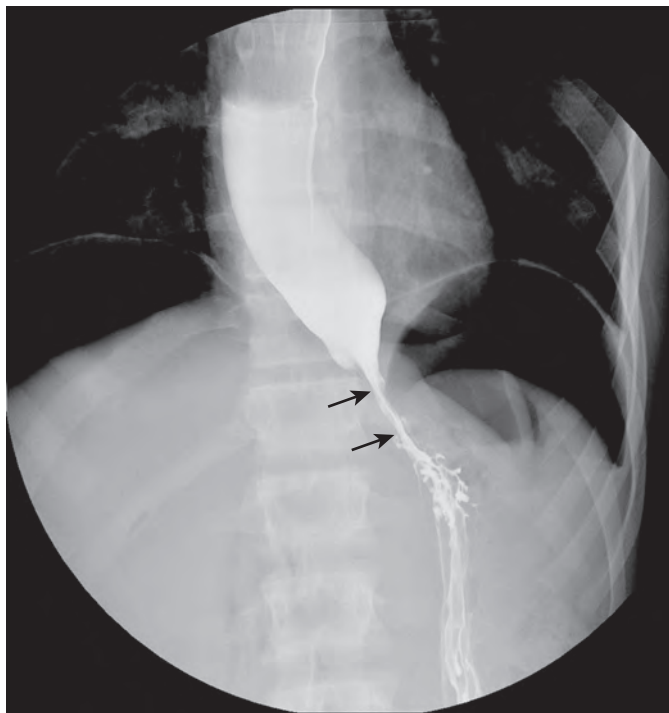


Figure 27-5 Postoperative wrap edema. One day after laparoscopic fundoplication wrap surgery, the patient had chest pain and difficulty handling her secretions. A low-magnification radiograph shows a large volume of gas (carbon dioxide) underneath the left and right hemidiaphragms. The esophagus just proximal to the fundoplication is a tight 3 mm in luminal diameter (arrows). The thoracic esophagus is dilated and showed delayed esophageal emptying. One week later, the esophageal obstruction caused by edema of the fundoplication wrap had resolved. The esophageal narrowing increased to about 8 mm.

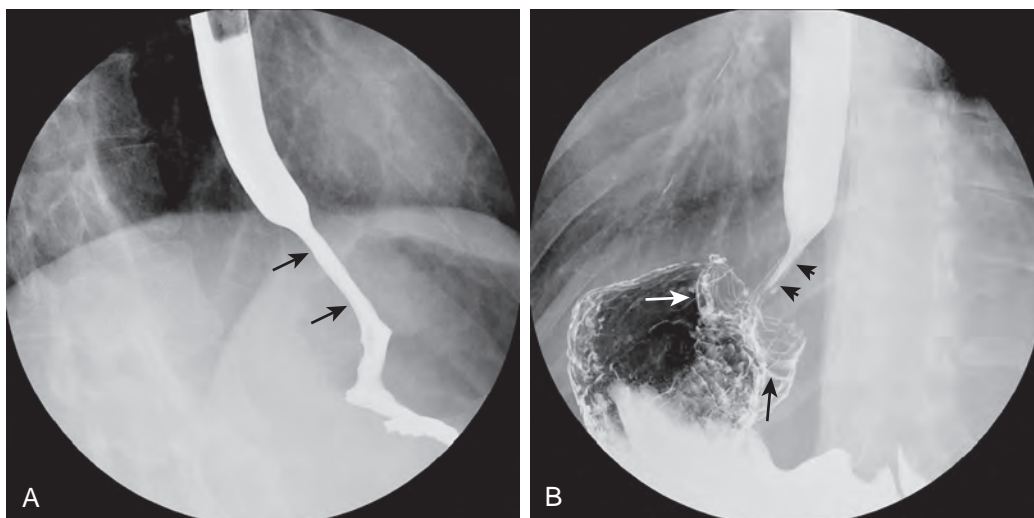


Figure 27-6 Persistent obstruction by a tight Nissen fundoplication wrap. **A.** Spot radiograph obtained with patient in an erect position shows that the lumen of the stomach is mildly narrowed (measuring ≈ 6 mm in luminal diameter; arrows) by a tight fundoplication wrap (arrows). **B.** Spot radiograph obtained while the patient is drinking in a right anterior oblique position shows a narrowed distal esophagus (thin arrows) and large fundoplication wrap (arrowheads).

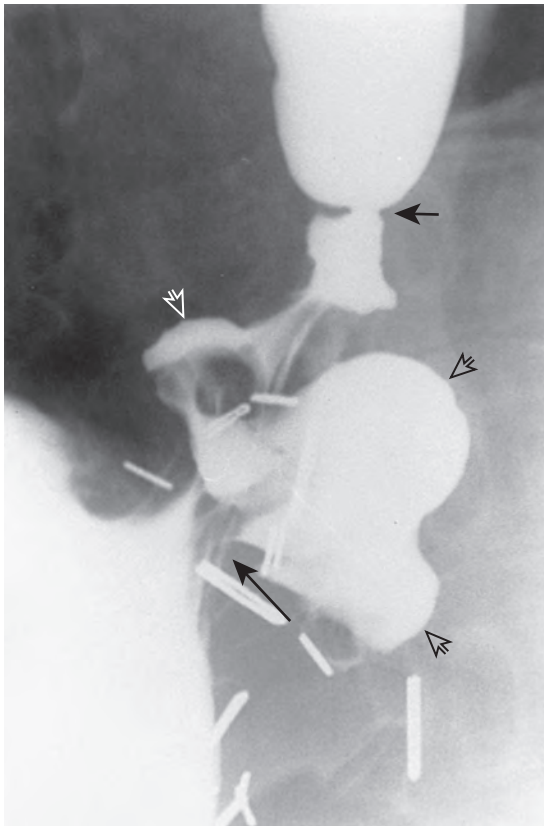


Figure 27-7 Breakdown of fundoplication wrap and recurrent hiatal hernia. Multiple gastric outpouchings (open arrows) are seen above the level of the diaphragm (large black arrow). The expected mass of the fundoplication wrap is not present in the gastric fundus. A focal peptic stricture is also seen at the gastroesophageal junction (small black arrow). (From Rubesin SE, Levine MS: *Postoperative esophagus*. In Levine MS: *Radiology of the Esophagus*. Philadelphia, WB Saunders, 1989, pp 267–290.)

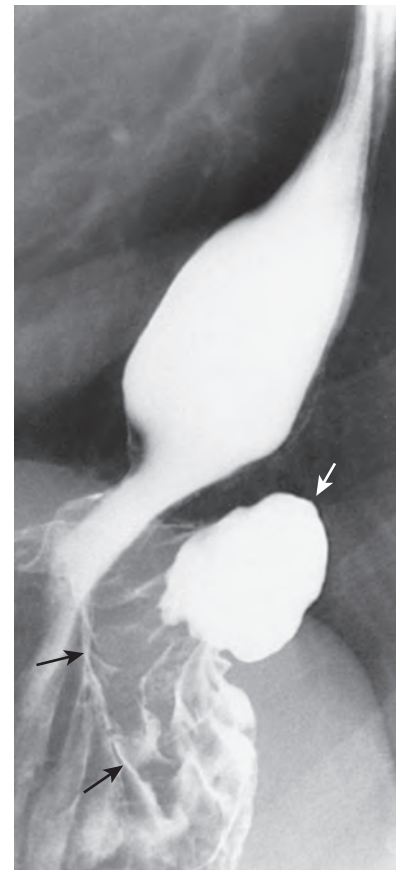


Figure 27-8 Partial breakdown of fundoplication wrap. The fundal wrap is partially intact (black arrows) but does not encircle the distal esophagus. A small fundal outpouching is present (white arrow). Barium is seen in the distal esophagus because of gastroesophageal reflux.

placed esophageal stents, and esophageal replacement with a gastric tube, jejunal graft, or colonic interposition. The site, extent, and cause of the stricture affect the therapeutic choice. Peroral balloon or endoscopic dilation of strictures under fluoroscopic guidance is an effective alternative to esophageal bougienage.^{34,35} This procedure has a lower risk of perforation and a longer symptom-free interval than esophageal bougienage.^{36–39}

Surgery is usually required for the treatment of lye strictures. Esophageal replacement surgery may also be performed on patients with intractable strictures caused by gastroesophageal reflux disease.

Carcinoma

Because they usually have advanced tumors at the time of diagnosis, patients with esophageal carcinoma continue to have 5-year survival rates of only 5% to 30%, despite advances in radiologic imaging, surgical technique, and treatment with radiation or chemotherapy. Treatment for esophageal carcinoma is primarily palliative, focused on reversing starvation and cachexia by relieving dysphagia and restoring the ability to swallow. Palliation of advanced esophageal cancers can be achieved not only by surgery but also by radiation therapy, esophageal stent placement, and endoscopic laser therapy.

ESOPHAGOGASTRECTOMY

The esophagus can be removed by a transthoracic or a combined transhiatal-cervical approach. Distant metastases and aortic or tracheobronchial invasion by tumor are relative contraindications to surgery, but local extension of tumor and mediastinal adenopathy are not.⁴⁰

Transthoracic Approach

A right-sided thoracotomy and abdominal incision (Ivor-Lewis operation) are performed on many patients with midthoracic esophageal cancers.⁵ A left-sided thoracoabdominal incision is performed on patients with cancers involving the distal esophagus and cardia or lesions that have extensive nodal metastases near the celiac axis or lesser curvature of the stomach. After resection of the diseased esophagus and cardia, the stomach is mobilized on its vascular pedicle and placed in the thorax, with the lesser curvature facing the mediastinum (Fig. 27-11). A vertically oriented portion of the stomach may be removed, so that the stomach becomes tubular and functions as a conduit. An antireflux procedure may also be performed by invaginating the distal esophagus into the stomach. A gastric drainage procedure such as a pyloroplasty or pyloromyotomy is usually performed because the vagus nerves are sacrificed at surgery.

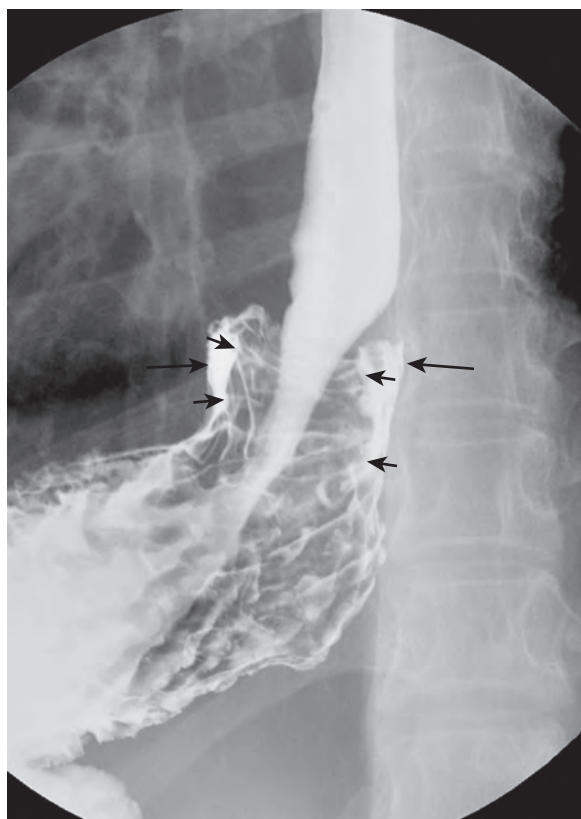


Figure 27-9 Recurrent hiatal hernia resulting from disruption of sutures closing the esophageal hiatus of the diaphragm. A small hiatal hernia (long arrows) lies above the diaphragm. An intact fundoplication wrap (short arrows) is manifest as a radiolucent filling defect in the barium pool within the hernia and as a “mass” surrounding the distal esophagus.

Transhiatal-Transcervical Approach

The stomach can also be used as a palliative bypass organ for advanced esophageal carcinoma, without resorting to a thoracotomy.^{41,42} In such cases, the stomach is brought superiorly through an anterior or posterior mediastinal tunnel into the neck via a combined transcervical-transhiatal approach. The fundus is then anastomosed to the cervical esophagus (and occasionally the pharynx) via a cervical approach. The diseased esophagus can be resected through the hiatal and cervical exposures, or it can be excluded. If the stomach has been placed substernally, the small opening of the thoracic inlet is widened by resecting the medial portion of the clavicle, sternoclavicular joint, and upper portion of the manubrium. A pyloromyotomy or pyloroplasty is performed to facilitate gastric emptying. A temporary feeding jejunostomy tube is usually inserted.

The transthoracic approach allows en bloc resection of the esophagus and local lymph nodes for complete staging and potential cure. Anastomotic or other staple line leaks in the middle mediastinum, however, are serious complications. The transhiatal approach allows removal of some, but not all cervical, intrathoracic, and intra-abdominal lymph nodes. A complete mediastinal lymph node exploration for staging or cure is not possible, but anastomotic leaks into the neck with the transhiatal approach are less serious than leaks into the mediastinum with the transthoracic approach. Neverthe-



Figure 27-10 Paraesophageal herniation of gastric fundus after breakdown of diaphragmatic repair. Low magnification image demonstrating a large paraesophageal herniation of the gastric fundus (PH) above the left hemidiaphragm (arrow). The hernia is next to the distal esophagus (E).

less, the two techniques have about the same success rate for cure.⁵

Complications

The most common complications during the early postoperative period include anastomotic leaks, obstruction, gastric atony and dilation, and aspiration into the larynx. A study using water-soluble contrast medium (followed by high-density barium if there is no evidence of a leak²⁰) is usually performed within 7 to 10 days after surgery to rule out a leak at the esophagogastric anastomosis (see Fig. 27-1), at the line of creation of the gastric tube, and at the pyloroplasty. Leaks along the vertical staple line of the gastric tube may be caused by ischemia. These leaks may appear more than 7 days after surgery. Surgical drains may migrate through leaks near the esophagogastric anastomosis or along the gastric staple line.⁴³ Surgical drains may also enter a viscus by pressure necrosis or be inappropriately placed in a viscus at surgery or at a later intervention. Mechanical obstruction may occur at the esophagogastric anastomosis or pylorus (Fig. 27-12) because of edema, hemorrhage, or leak. Mechanical obstruction may also occur at the distal end of the intrathoracic portion of the stomach because of gastric volvulus or extrinsic compression by the diaphragm. Pancreatitis may rarely develop because the duodenum is freed from the pancreatic head to allow the stomach to be pulled superiorly into the chest.²

The most common complications during the late postoperative period include gastroesophageal reflux and its sequelae,

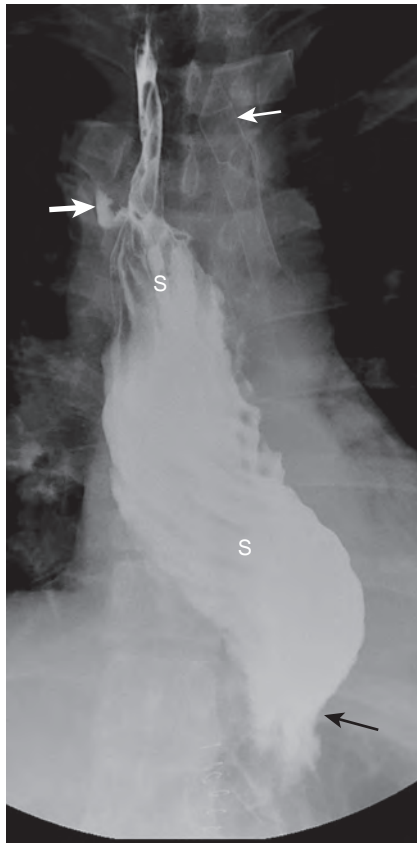


Figure 27-11 Transthoracic esophagogastrectomy. The stomach (S) has been pulled into the right hemithorax. There is a small contained leak (thick white arrow) at the esophagogastric anastomosis. There is no obstruction as the stomach passes through the diaphragm (black arrow). A mediastinal drain (thin white arrow) is present.

anastomotic strictures, fistulas, and recurrent tumor.⁴⁰ Acute gastroesophageal reflux may result in aspiration pneumonia. Chronic gastroesophageal reflux may lead to reflux esophagitis (Fig. 27-13), peptic strictures (Fig. 27-14), Barrett's esophagus and, eventually, esophageal adenocarcinoma. Healing of anastomotic leaks may result in benign anastomotic strictures. Long-standing anastomotic leaks may result in fistulas to the tracheobronchial tree, pleura, or directly into the lungs (Fig. 27-15). Although recurrent tumor in the mediastinum is best demonstrated by computed tomography (CT) or magnetic resonance imaging (MRI), barium studies may reveal a smooth or spiculated area of extrinsic mass effect on the mediastinal border of the stomach (Fig. 27-16).^{40,44} Recurrent esophageal carcinoma may also be demonstrated by barium studies as a focal mucosal nodularity, nodular mass, or nodular stricture in the distalmost remaining esophagus or at the esophagogastric anastomosis (Fig. 27-17). Any suspicious area should be further evaluated by endoscopy and biopsy. Delayed perforations may occasionally be caused by a recurrent mediastinal tumor or mediastinal irradiation.

Several complications may be related to esophageal exclusion if the diseased esophagus has been bypassed but not resected. If the native esophagus is disrupted, a left subphrenic abscess may develop. The excluded esophagus may also form a posterior mediastinal mucocele.⁴⁵ These mucocoeles may become infected or compress the tracheobronchial tree. Symptoms may also be

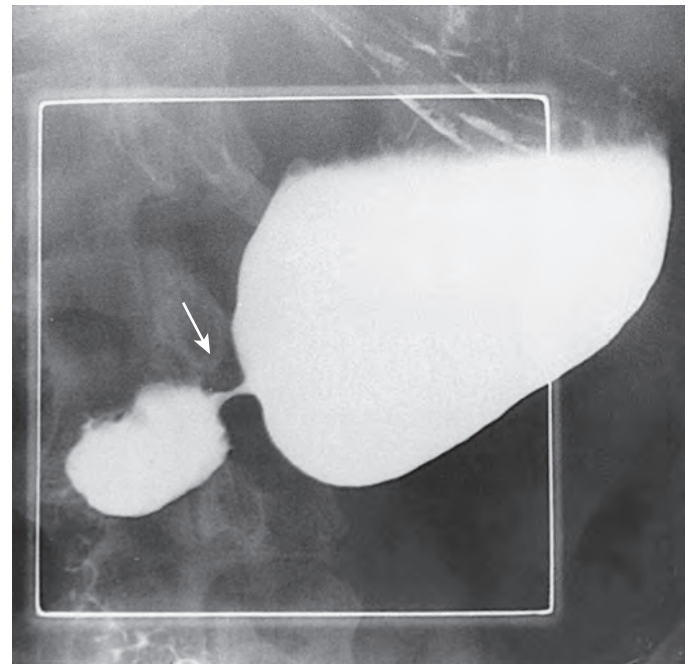


Figure 27-12 Obstruction at pylorus after pyloroplasty performed during esophagogastrectomy. There is smooth symmetric narrowing of the pylorus (arrow). Obstruction was manifested fluoroscopically by delayed gastric emptying and radiographically by a barium-fluid-air level in the stomach, indicating retained fluid, rather than the normally expected barium-air level. (From Rubesin SE, Beatty SM: *The postoperative esophagus*. *Semin Roentgenol* 39:401–410, 1994.)

caused by gastroesophageal reflux into the excluded esophagus. Carcinoma may develop in an esophagus bypassed for a lye stricture.⁴⁵

COLONIC INTERPOSITION, JEJUNAL INTERPOSITION, AND FREE JEJUNAL GRAFT

Various segments of the colon and jejunum may be used to bypass severe peptic strictures, caustic strictures, or inoperable esophageal cancers. When colonic interposition is performed, the right or transverse colon is placed in an isoperistaltic direction (Fig. 27-18), whereas the left colon is placed in an isoperistaltic or antiperistaltic direction.⁴⁶ If the colon is placed in the anterior mediastinum, the cologastric anastomosis is usually located on the anterior wall of the stomach.⁴⁶ If the colon is placed in the posterior mediastinum, however, the cologastric anastomosis is located on the posterior wall of the upper stomach.⁴⁶ A vagotomy and pyloroplasty are also performed. A preoperative barium enema may be done to rule out significant colonic disease before surgery. A preoperative angiogram may also be obtained to demonstrate the vascular anatomy of the colon and rule out vascular disease, particularly in patients with suspected atherosclerosis.⁴⁷

Colonic interposition is a procedure performed when the stomach cannot be used for esophageal replacement—for example, in patients with prior gastric surgery. Colonic interposition is associated with much higher morbidity and mortality rates than esophagogastrectomy. Anastomotic leaks occur in 25% to 40% of patients⁴⁰ and are usually located at the proximal anastomosis, leading to abscess and stricture formation

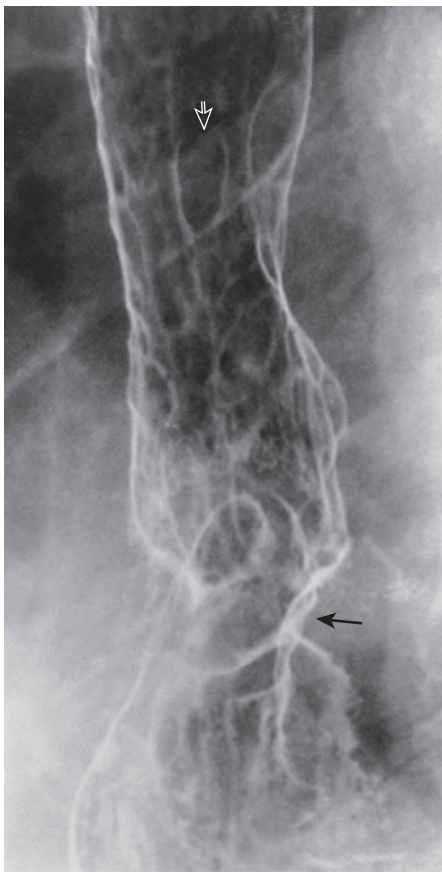


Figure 27-13 Esophagogastric anastomosis with reflux esophagitis. Numerous confluent plaques and pseudomembranes (*open arrow*) are seen on the esophageal mucosa above the esophagogastric junction (*solid arrow*). Free gastroesophageal reflux was seen at fluoroscopy.

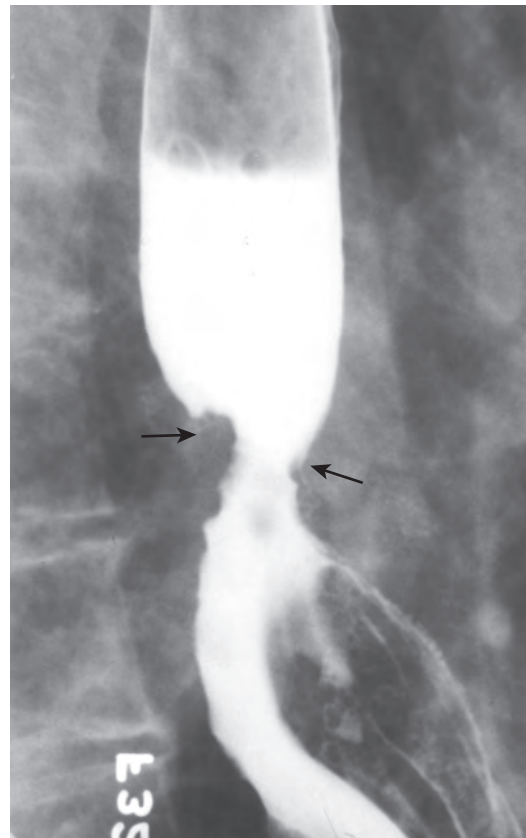


Figure 27-14 Esophagogastric anastomosis with peptic stricture. An 8 mm in luminal diameter, short, asymmetric narrowing (*arrows*) is seen at and just above the esophagogastric anastomosis. This region was wider on the immediate postoperative study.

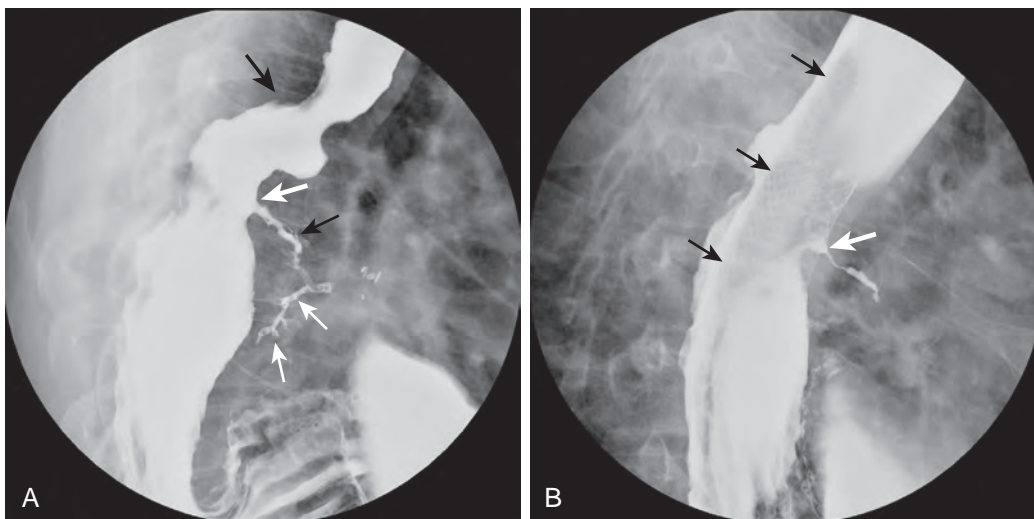


Figure 27-15 Fistula from postoperative stomach extending into the right lung. **A.** Spot radiograph centered near the esophagogastric anastomosis (*black arrows*) shows a fistula arising at a 3-mm diameter hole in the proximal stomach (*thick white arrow*) at its staple line. The leak fills subsegmental bronchi (*thin white arrows*). **B.** Spot radiograph obtained after a metallic stent (*black arrows*) was placed. Barium goes around and through the stent. Barium around the outside of the stent fills the fistula (*white arrow*).

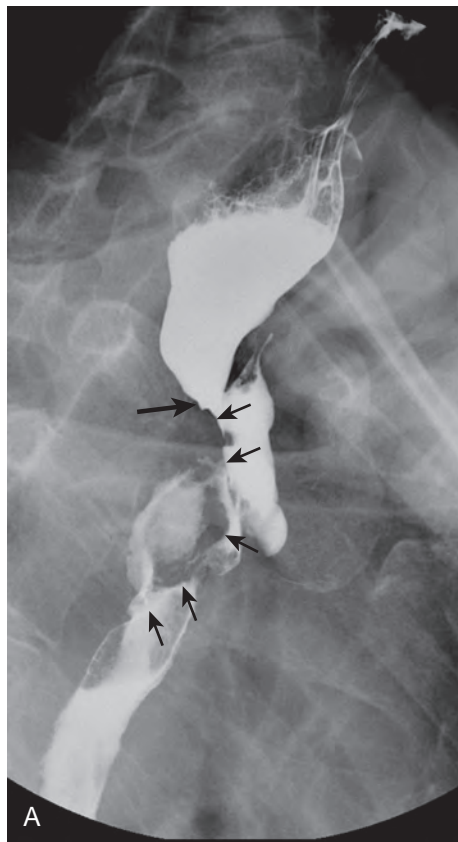


Figure 27-16 Recurrent mediastinal tumor after esophagogastrectomy. **A.** A large lobulated mass (short arrows) invades the postoperative stomach just below the esophagogastric anastomosis (long arrow). **B.** Axial image from an unenhanced CT scan shows a large mass (m) invading the posterior wall of the trachea (black arrows) and narrowing and compressing the pulled-through stomach (white arrow).

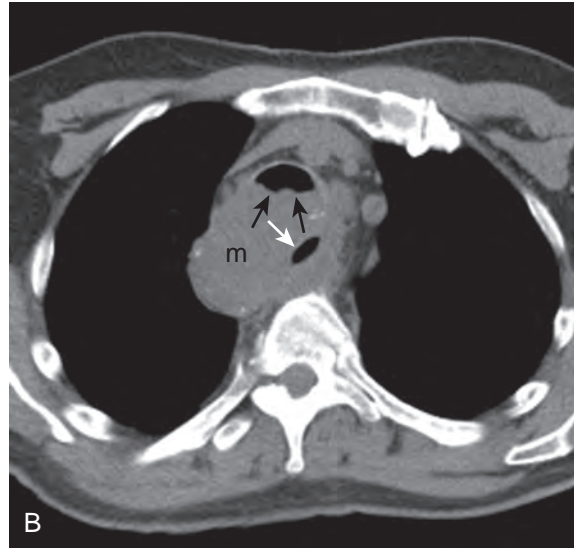


Figure 27-17 Recurrent esophageal cancer at esophagogastric anastomosis. Spot radiograph shows a plaquelike elevation (thin arrows) and two small submucosa-appearing masses (thick arrows) just above the narrowed esophagogastric anastomosis (open arrow).

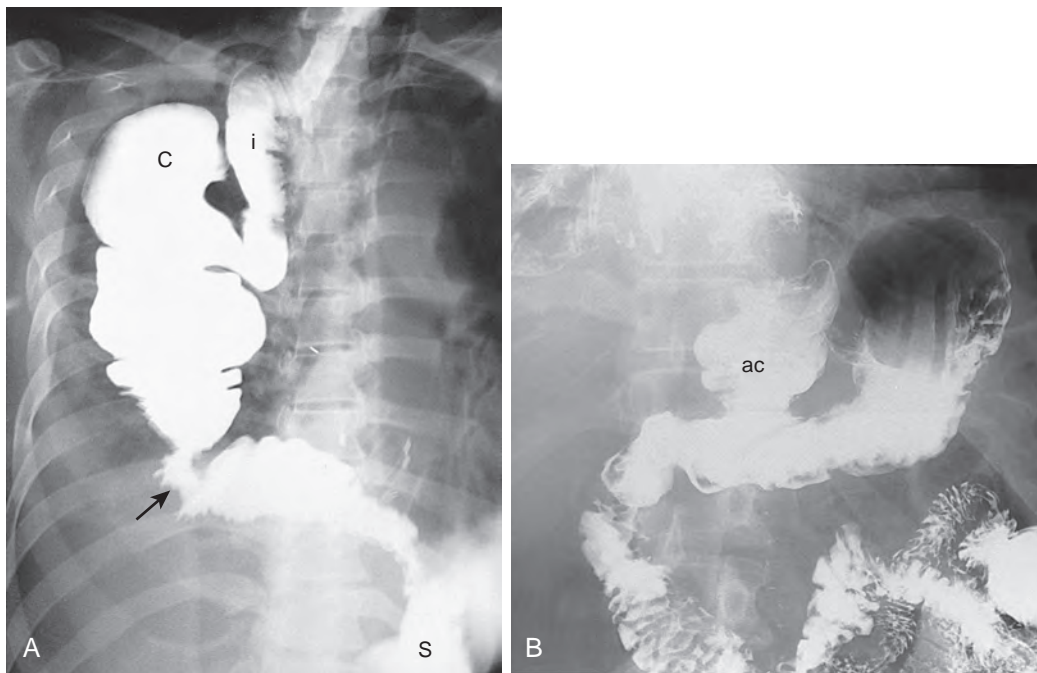


Figure 27-18 Normal colonic interposition. **A.** There is an isoperistaltic right colonic interposition with anastomosis of the terminal ileum (i) to the cervical esophagus. Mild narrowing of the colon is seen where it passes through the diaphragm (arrow). **B.** The ascending colon (ac) is anastomosed to the lesser curvature of the stomach. C, cecum; S, stomach. (From Rubesin SE, Levine MS: *Postoperative esophagus*. In Levine MS: *Radiology of the Esophagus*. Philadelphia, WB Saunders, 1989, pp 267–290.)

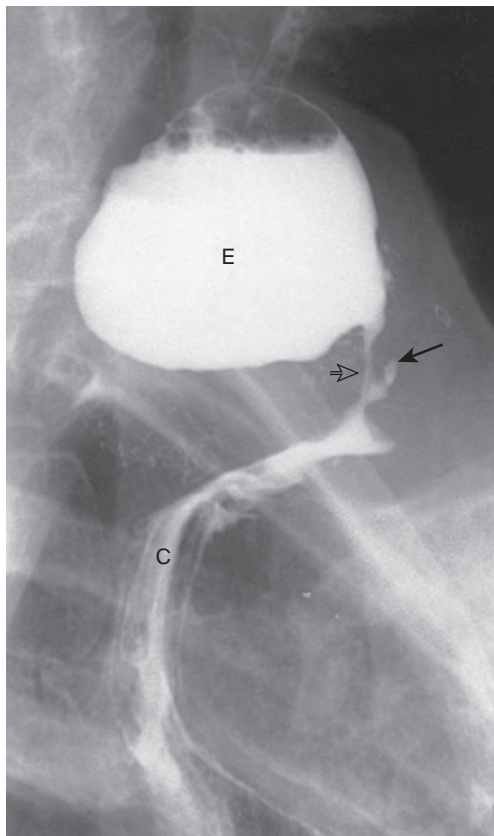


Figure 27-19 Colonic interposition with stricture formation after an anastomotic leak at the esophagocolonic anastomosis. A tight stricture (open arrow) is present at the anastomosis between the dilated esophagus (E) and collapsed colon (C). A short, blind-ending track (solid arrow) is seen at the site of a prior anastomotic leak. (From Rubesin SE, Levine MS: *Postoperative esophagus*. In Levine MS: *Radiology of the Esophagus*. Philadelphia, WB Saunders, 1989, pp 267–290.)

(Fig. 27-19).^{47,48} Other postoperative complications include anastomotic edema and obstruction, chylothorax, mediastinal hematoma or abscess, empyema, and intra-abdominal abscess.⁴⁷ Ischemia of the transposed colon may be manifested radiographically by spasm, ulceration, loss of haustration, or a nodular mucosa.⁴⁸ Occasionally, during the early postoperative period, the mucosal folds in the interposed transverse colon may resemble jejunal folds, but this finding disappears after 1 to 3 months.⁴⁶

Stricture formation at the proximal anastomosis is the most common late postoperative complication, occurring in 20% to 40% of patients (see Fig. 27-19).⁴⁶⁻⁴⁸ Chronic ischemia can result in short or long stricture in other segments of the colonic interposition.⁴⁹ The transposed colon may also become dilated and redundant, leading to the development of delayed graft emptying, with bloating, pain, and dysphagia. Other late complications include diverticulitis or carcinoma of the transposed colon, coloesophageal reflux, colobronchial fistulas, gastric outlet obstruction, and small bowel obstruction within the transverse mesocolon defect created at the time of surgery.⁵⁰

PALLIATIVE INTUBATION

Palliative placement of an esophageal stent may be performed to allow oral feeding through advanced obstructing esophageal cancers or to obturate malignant tracheoesophageal fistulas. The use of expandable intraesophageal metallic stents (Fig. 27-20) has replaced the use of plastic tubes (e.g., Celestin tubes).⁵⁰⁻⁵⁶ These metallic stents may be placed endoscopically, surgically, or fluoroscopically. A study using water-soluble contrast medium is performed after stent placement to evaluate stent position and patency and rule out esophageal perforation. The stent should be fixed in position, with its upper tip proximal to the tumor and its lower tip distal to the tumor.

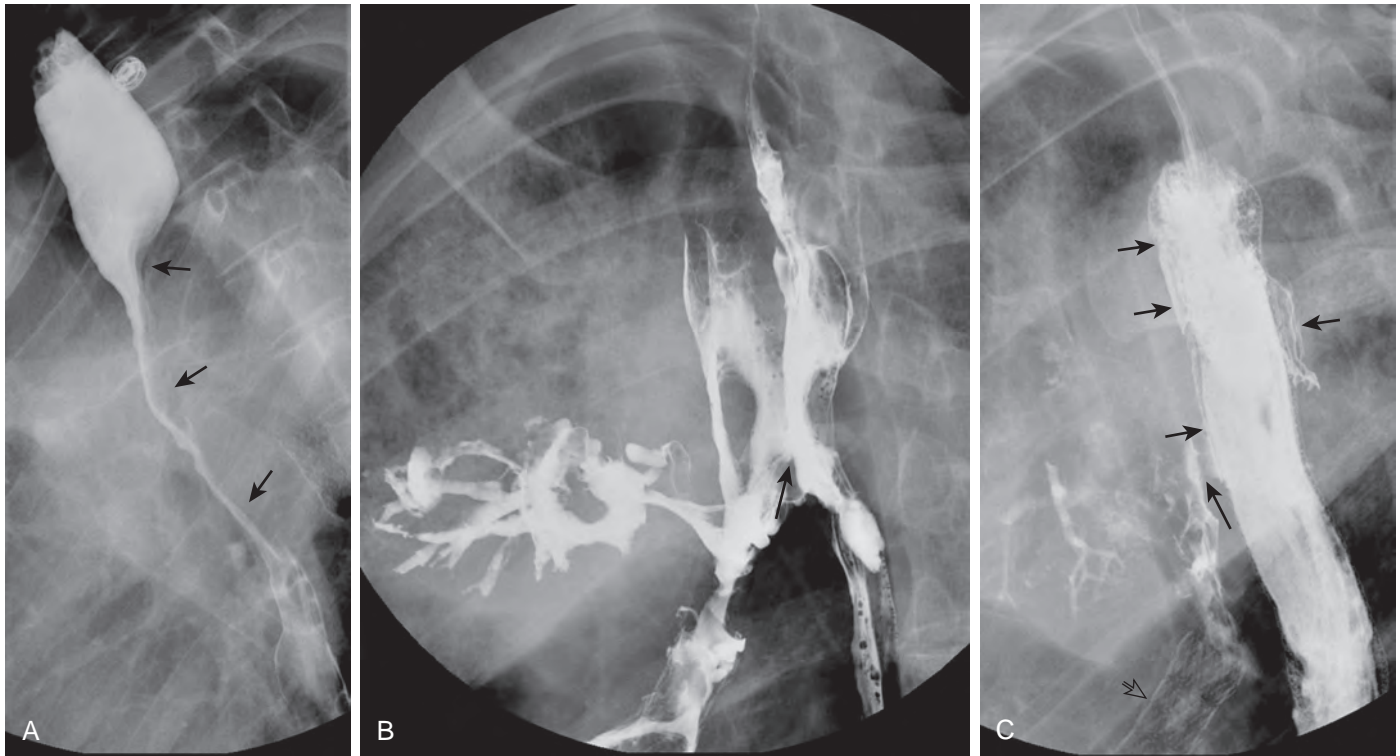


Figure 27-20 Stent placement for squamous cell carcinoma of the right lung invading the esophagus. **A.** Spot radiograph of the right upper mediastinum with the patient in a right posterior oblique position shows a 10-cm long, broad-based extrinsic mass impression on the posterior wall of the esophagus (arrows). **B.** Spot radiograph obtained 3 months later, after radiation therapy, shows less extrinsic mass impression. However, a fistula (arrow) from tumor at the carina invading the esophagus has now formed. Bronchi and the trachea are filled with barium. Presumptively, necrosis of the tumor after radiation therapy has contributed to the fistula formation. A stent is also present in the right mainstem bronchus. **C.** Spot radiograph obtained after esophageal stent placement shows barium going through the uncovered portion of the stent to surround the stent (short arrows). This barium eventually goes into the tracheoesophageal fistula (long arrow). The stent in the right mainstem bronchus is identified (open arrow).

Contrast medium should flow easily through the lumen of the stent.

Esophageal perforation is the most serious complication.^{51,54,57} Obstruction of the stent may be caused by kinking of the stent or luminal obstruction resulting from mucosal prolapse, epithelial hyperplasia, food impaction, or residual or recurrent tumor.^{51,57-59} Reflux of gastric contents through the stent may lead to reflux esophagitis or aspiration pneumonia.^{60,61} Reflux through a stent is such a common problem that stents with antireflux mechanisms have been designed.⁶² Passage of food or liquid around the outside of the stent's proximal margin or reflux of gastric contents around the stent's distal margin may fill a tracheoesophageal fistula (see Fig. 20C) or leak. Metallic stents may initially be malpositioned, or they can migrate.⁴⁵ Rarely, a stent may cause pressure necrosis of the esophageal wall, resulting in a mediastinal leak or aorto-esophageal fistula. Ulceration of the esophagus or stomach may also occur.

Achalasia

Neither medical therapy nor surgery can correct the abnormal esophageal motility and lower esophageal sphincter dysfunction that occur in patients with achalasia. The two major forms of therapy, pneumatic dilation and cardiomyotomy, are both

aimed at improving esophageal emptying by disrupting the high-pressure LES. Intramuscular injection of botulinum toxin has also been used for the treatment of achalasia.

PNEUMATIC DILATION

The most serious complication of pneumatic dilation is lower esophageal perforation, occurring in 1% to 4% of patients.⁶³ Although the presence of chest pain or fever after the procedure should suggest this complication, some patients may have clinically silent or delayed perforations.⁶⁴ A study using water-soluble contrast medium should therefore be performed after pneumatic dilation to rule out a perforation, regardless of the patient's symptoms.^{65,66} If no perforation is seen with water-soluble contrast medium, high-density barium should be given to demonstrate greater anatomic detail and subtle leaks. Perforations usually occur on the left posterolateral wall of the distal esophagus, just above the diaphragm. Some patients may have small, sealed-off perforations that resemble intramural dissections, whereas others may have free perforations into the mediastinum or pleural space.^{67,68} Increasing symptoms during the early postoperative period may necessitate a repeat esophagogram to demonstrate a delayed perforation or perforation that was not initially visualized because of edema and spasm at the dilation site. In addition, edema and

spasm at the gastroesophageal junction may lead to delayed esophageal emptying, despite adequate disruption of the lower esophageal sphincter fibers. Thus, the radiographic appearance immediately after dilation is a poor predictor of the efficacy of the procedure.⁶⁶

CARDIOMYOTOMY

A cardiomyotomy, or Heller myotomy, is an effective form of therapy for patients with untreated achalasia or achalasia that is unresponsive to bougienage, Botox therapy, or pneumatic dilation. The procedure is performed using an open or laparoscopic technique. During myotomy, the LES fibers are surgically divided, thereby disrupting the sphincter. Some surgeons perform a concomitant antireflux procedure. After cardiomyotomy, there should be free flow of contrast medium from the esophagus into the stomach, with decreased esophageal dilation and absence of the beaklike narrowing of the esophagogastric region associated with achalasia.⁶⁹ In about 50% of cases, there is eccentric ballooning of the esophagus at the site of Heller myotomy (Fig. 27-21).⁷⁰ The most common early postoperative complication is perforation of the distal esophagus.⁷¹ Persistent dysphagia during the late postoperative period may indicate an incomplete myotomy or tight fundoplication wrap. Conversely, postoperative gastroesophageal reflux, reflux esophagitis, and peptic strictures may indicate the need for an antireflux procedure.

Varices

Endoscopic sclerotherapy or variceal banding, transjugular intrahepatic portosystemic shunts, portosystemic shunt surgery, and esophageal devascularization procedures are the major forms of therapy for esophageal varices. Endoscopic sclerotherapy and variceal banding are discussed in Chapter 25.

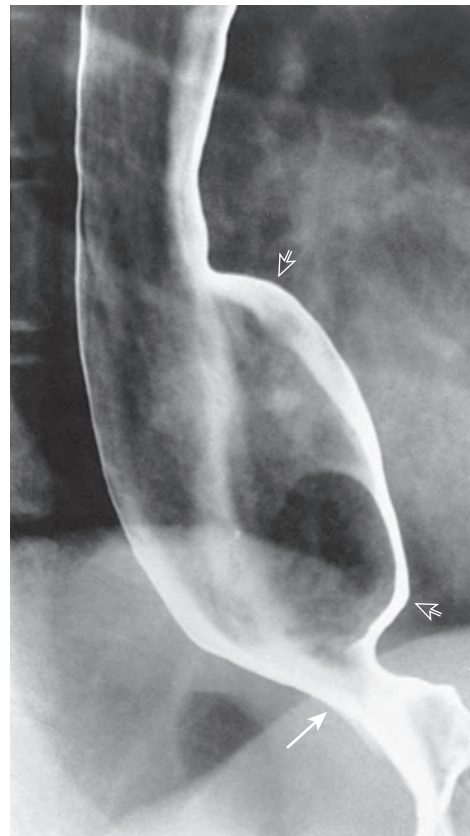


Figure 27-21 Ballooning of the distal esophagus after cardiomyotomy for achalasia. There is eccentric outpouching or ballooning of the distal esophageal wall at the cardiomyotomy site (open arrows). The gastroesophageal junction (solid arrow) is widely patent. (From Rubesin SE, Levine MS: *Postoperative esophagus*. In Levine MS: *Radiology of the Esophagus*. Philadelphia, WB Saunders, 1989, pp 267–290.)

REFERENCES

- Rubesin SE, Levine MS: Postoperative esophagus. In Levine MS, editor: *Radiology of the Esophagus*, Philadelphia, 1989, WB Saunders, pp 267–290.
- Orringer MB: Complications of esophageal surgery. In Zuidema GD, editor: *Shackelford's Surgery of the Alimentary Tract*, vol 1, Philadelphia, 1991, WB Saunders, pp 434–459.
- Rubesin SE, Beatty SM: The postoperative esophagus. *Semin Roentgenol* 29:401–418, 1994.
- Peters JH, DeMeester TR: Esophagus: Anatomy, physiology and gastroesophageal reflux disease. In Greenfield LJ, Mulholland MW, Oldham KT, et al, editors: *Surgery: Scientific Principles and Practice*, Philadelphia, 2001, Lippincott Williams & Wilkins, pp 659–692.
- Orringer MB: Tumors, injuries, and miscellaneous conditions of the esophagus. In Greenfield LJ, Mulholland MW, Oldham KT, et al, editors: *Surgery: Scientific Principles and Practice*, Philadelphia, 2001, Lippincott Williams & Wilkins, pp 692–735.
- Anbari M, Levine MS, Cohen R, et al: Delayed leaks and fistulas after esophagogastrectomy: Radiologic evaluation. *AJR* 160: 1217–1220, 1993.
- Dodds WJ, Stewart ET, Vlymen WJ: Appropriate contrast media for evaluation of esophageal disruption. *Radiology* 144:439–441, 1982.
- Ott DJ, Gelfand DW: Gastrointestinal contrast agents: Indications, uses and risks. *JAMA* 249: 2380–2384, 1984.
- James AE, Montali RJ, Chaffee V, et al: Barium or gastrografin: Which contrast media for diagnosis of esophageal tears? *Gastroenterology* 68:1103–1113, 1975.
- Foley MJ, Ghahremani GG, Rogers LF: Reappraisal of contrast media used to detect upper gastrointestinal perforations. *Radiology* 144: 231–237, 1982.
- Dunbar JS, Skinner GB, Wortzman G, et al: An investigation of effects of opaque media on the lungs with comparison of barium, Lipiodol and Dionosil. *AJR* 82:902–926, 1959.
- Reich SB: Production of pulmonary edema by aspiration of water-soluble nonabsorbable contrast media. *Radiology* 92:367–370, 1969.
- Chiu CL, Gambach RR: Hypaque pulmonary edema: A case report. *Radiology* 111:91–92, 1974.
- Ginai AZ, ten Kate FJW, ten Berg RGM, et al: Experimental evaluation of various contrast agents for use in the gastrointestinal tract in case of suspected leakage: Effects on the lungs. *Br J Radiol* 57:895–901, 1984.
- Ginai AZ, ten Kate FJW, ten Berg RGM, et al: Experimental evaluation of various contrast agents for use in the gastrointestinal tract in case of suspected leakage: Effects on the mediastinum. *Br J Radiol* 58:585–592, 1985.
- Ginai AZ: Clinical use of Hexabrix for radiological evaluation of leakage from the upper gastrointestinal tract based on experimental study. *Br J Radiol* 60:343–346, 1987.
- Brick SH, Caroline DF, Lev-Toaff AS, et al: Esophageal disruption: Evaluation with iohexol esophagography. *Radiology* 169:141–143, 1988.
- Gollub MJ, Bains MS: Barium sulfate: New (old) contrast agent for diagnosis of postoperative esophageal leaks. *Radiology* 202:360–362, 1997.
- Reichle RL, Fishman EK, Nixon MS, et al: Evaluation of the postsurgical esophagus after partial esophagogastrectomy for esophageal cancer. *Invest Radiol* 28:247–257, 1993.
- Swanson JO, Levine MS, Redfern RO, Rubesin SE: Usefulness of high-density barium for detection of leaks after esophagogastrectomy, total gastrectomy, and total laryngectomy. *AJR* 181: 415–420, 2003.

21. Bredenburg CE: Gastrointestinal reflux and hiatal hernia. In Fromm D, editor: *Gastrointestinal Surgery*, New York, 1985, Churchill Livingstone, pp 163–205.
22. Nissen R: Gastropepy and “fundoplication” in surgical treatment of hiatal hernia. *Am J Dig Dis* 6:954–961, 1961.
23. Skucas J, Mangla JC, Adams JT, et al: An evaluation of the Nissen fundoplication. *Radiology* 118:539–543, 1976.
24. Thoeni RF, Moss AA: The radiographic appearance of complications following Nissen fundoplication. *Radiology* 131:17–21, 1979.
25. Cohen WN: The fundoplication repair of sliding esophageal hiatus hernia: The roentgenographic appearance. *AJR* 104:625–631, 1968.
26. Skinner DB, Belsey RHR: Surgical management of esophageal reflux and hiatal hernia: Long-term results with 1030 patients. *J Thorac Cardiovasc Surg* 53:33–54, 1967.
27. Orringer MB, Skinner DB, Belsey RHR: Long-term results of the Mark IV operation for hiatal hernia and analyses of recurrence and their treatment. *J Thorac Cardiovasc Surg* 63:25–33, 1972.
28. Feigin DS, James AE, Stitik FP, et al: The radiological appearance of hiatal hernia repairs. *Radiology* 110:71–77, 1974.
29. Teixidor HS, Evans JA: Roentgenographic appearance of the distal esophagus and the stomach after hiatal hernia repair. *AJR* 119:245–258, 1973.
30. Demeester TR, Johnson LE, Kent AH: Evaluation of current operations for the prevention of gastroesophageal reflux. *Ann Surg* 180:511–525, 1974.
31. Polk HC: Fundoplication for reflux esophagitis: Misadventures with the operation of choice. *Ann Surg* 183:645–652, 1976.
32. Saik RP, Greenburg AG, Peskin GW: A study of fundoplication disruption and deformity. *Am J Surg* 134:19–24, 1977.
33. Hatfield M, Shapir J: The radiologic manifestations of failed antireflux procedures. *AJR* 144:1209–1214, 1985.
34. London RL, Trotman BW, DiMarino AJ, et al: Dilatation of severe esophageal strictures by inflatable balloon catheter. *Gastroenterology* 80: 173–175, 1981.
35. Owman T, Lunderquist A: Balloon catheter dilatation of esophageal strictures—a preliminary report. *Gastrointest Radiol* 7:301–305, 1982.
36. Goldthorn JF, Ball WS, Wilkinson LG, et al: Esophageal strictures in children: Treatment by serial balloon catheter dilatation. *Radiology* 153:655–658, 1984.
37. Starck E, Paolucci V, Herzer M, et al: Esophageal stenosis: Treatment with balloon catheters. *Radiology* 153:637–640, 1984.
38. Dawson SL, Mueller PR, Ferrucci JT, et al: Severe esophageal strictures: Indications for balloon catheter dilatation. *Radiology* 153:631–635, 1984.
39. McLean GK, Cooper GS, Hartz WH, et al: Radiologically-guided balloon dilatation of gastrointestinal strictures: I. Technique and factors influencing procedural success. *Radiology* 165: 35–40, 1987.
40. Owen JW, Balfe DM, Koehler RE, et al: Radiologic evaluation of complications after esophagogastric resection. *AJR* 140:1163–1169, 1983.
41. Gandi SK, Naunheim KS: Complications of transhiatal esophagectomy. *Chest Surg Clin North Am* 7:601–612, 1997.
42. Orringer MB, Marshall B, Stirling MC: Transhiatal esophagectomy: Clinical experience and refinements. *Ann Surg* 230:392–403, 1999.
43. Wilmot ASH, Levine MS, Rubesin SE, et al: Intraluminal migration of surgical drains after transhiatal esophagogastric resection. *AJR* 189:780–785, 2007.
44. Agha FP, Orringer MB, Amendola MA: Gastric interposition following transhiatal esophagectomy: Radiographic evaluation. *Gastrointest Radiol* 10:17–24, 1985.
45. Glickstein M, Gefter WB, Low D, et al: Esophageal mucocele after surgical isolation of the esophagus. *AJR* 149:729–730, 1987.
46. Agha FP, Orringer MB: Colonic interposition: Radiographic evaluation. *AJR* 142:703–708, 1984.
47. Christensen LR, Shapir J: Radiology of colonic interposition and its associated complications. *Gastrointest Radiol* 11:233–240, 1986.
48. Larson TC, Shuman LS, Libshitz HI, et al: Complications of colonic interposition. *Cancer* 56:681–690, 1985.
49. Li DX, Levine MS, Rubesin SE, Laufer I: Non-anastomotic strictures after colonic interposition. *AJR* 189:30–34, 2007.
50. Perlmutter DH, Tapper D, Teele RL, et al: Colobronchial fistula as a late complication of colo-esophageal interposition. *Gastroenterology* 86: 1570–1572, 1984.
51. Acunas B, Rozanes I, Akpınar S, et al: Palliation of malignant esophageal strictures with self-expanding nitinol stents: Drawbacks and complications. *Radiology* 199:648–652, 1996.
52. Han Y-M, Song H-Y, Lee J-M, et al: Esophago-respiratory fistulae due to esophageal carcinoma: Palliation with a covered Gianturco stent. *Radiology* 199:65–70, 1996.
53. Song H-Y, Park S-I, Do Y-S, et al: Expandable metallic stent placement in patients with benign esophageal strictures: Results of long-term follow-up. *Radiology* 203:131–136, 1997.
54. Gollub MJ, Gerdes H, Bains MS: Radiographic appearances of esophageal stents. *Radiographics* 17:1169–1182, 1997.
55. Song H-Y, Park S-I, Jung H-Y, et al: Benign and malignant esophageal strictures: Treatment with polyurethane-covered retrievable expandable metallic stent. *Radiology* 203:747–752, 1999.
56. Therasse E, Oliva VL, Lafontaine E, et al: Balloon dilation and stent placement for esophageal lesions: Indications, methods and results. *Radiographics* 23:89–115, 2003.
57. Lipinski JK, Conway SS, Kottler RE, et al: The radiology of oesophageal tubes for malignant strictures. *Clin Radiol* 33:453–459, 1982.
58. Giarardet RE, Ransdell HT, Wheat MW: Palliative intubation in the management of esophageal carcinoma. *Ann Thorac Surg* 18: 417–430, 1974.
59. Anderson GS, Levine MS, Rubesin SE, et al: Esophageal stents: Findings on esophagography in 46 patients. *AJR* 187:1274–1279, 2006.
60. Kairaluoma MI, Kalevi J, Karkola P, et al: Celestin tube palliation of unresectable esophageal carcinoma. *J Thorac Cardiovasc Surg* 73:783–786, 1977.
61. Haynes JW, Miller PR, Steiger Z, et al: Celestin tube use: Radiographic manifestations of associated complications. *Radiology* 150:41–44, 1984.
62. Hans-Ulrich L, Marriott A, Wilbraham L, et al: Effectiveness of open versus antireflux stents for palliation of distal esophageal carcinoma and prevention of symptomatic gastroesophageal reflux. *Radiology* 225:359–365, 2002.
63. Okike N, Payne WS, Neufeld DM, et al: Esophagomyotomy versus forceful dilatation for achalasia of the esophagus: Results in 899 patients. *Ann Thorac Surg* 28:119–125, 1979.
64. Zegel HG, Kressel HY, Levine GM, et al: Delayed perforation after pneumatic dilatation for the treatment of achalasia. *Gastrointest Radiol* 4:219–221, 1979.
65. Stewart ET, Miller WN, Hogan WJ, et al: Desirability of roentgen esophageal examination immediately after pneumatic dilatation for achalasia. *Radiology* 130:589–591, 1979.
66. Ott DJ, Wu WC, Gelfand DW, et al: Radiographic evaluation of the achalasic esophagus immediately following pneumatic dilatation. *Gastrointest Radiol* 9:185–191, 1984.
67. Bradley JL, Han SY: Intramural hematoma (incomplete perforation) of the esophagus associated with esophageal dilatation. *Radiology* 130:59–62, 1979.
68. Agha FP, Lee HH: The esophagus after endoscopic pneumatic balloon dilatation for achalasia. *AJR* 146:25–29, 1986.
69. Meyer JA: Nonmalignant disease of the esophagus. In Fromm D, editor: *Gastrointestinal Surgery*, New York, 1985, Churchill Livingstone, pp 113–162.
70. Rubesin SE, Kennedy M, Levine MS, et al: Distal esophageal ballooning following Heller myotomy. *Radiology* 167:345–347, 1988.
71. Yoo C, Levine MS, Redfern RO, et al: Laparoscopic Heller myotomy and fundoplication: Findings and predictive value of early postoperative radiographic studies. *Abdom Imaging* 29:643–647, 2004.

Esophagus: Differential Diagnosis

MARC S. LEVINE

CHAPTER OUTLINE

Table 28-1. Ulceration

Table 28-2. Mucosal Nodularity

Table 28-3. Solitary Mass Lesions

Table 28-4. Multiple Submucosal Masses

Table 28-5. Thickened Folds

Table 28-6. Strictures

TABLE
28-1

Ulceration

Cause	Radiographic Findings	Distribution	Comments
COMMON			
Reflux esophagitis	Shallow, punctate, or linear ulcers; deep ulcers less common	Distal	Reflux symptoms, hiatal hernia, and/or gastroesophageal reflux
<i>Candida</i> esophagitis	Ulcers associated with diffuse plaque formation ("shaggy" esophagus)	Variable	Odynophagia in immunocompromised (usually AIDS) patients
Herpes esophagitis	Discrete superficial ulcers	Middle or distal	Odynophagia in immunocompromised patients; occasionally in healthy patients
Drug-induced esophagitis	Discrete superficial ulcers; occasionally giant, flat ulcers	Midesophagus near aortic arch or left main bronchus	Odynophagia in patients taking oral medications (e.g., doxycycline or tetracycline)
UNCOMMON			
Radiation esophagitis	Superficial or deep ulcers	Conform to radiation portal	History of radiation therapy
Caustic esophagitis	Superficial or deep ulcers	Variable	History of caustic ingestion
Tuberculous esophagitis	Superficial or deep ulcers	Variable	History of pulmonary tuberculosis or AIDS
Cytomegalovirus esophagitis	One or more giant, flat ulcers	Variable	AIDS patients with odynophagia
HIV esophagitis	One or more giant, flat ulcers	Variable	HIV-positive or AIDS patients with odynophagia
Crohn's disease	Aphthoid ulcers	Variable	Advanced Crohn's disease in small bowel or colon
Nasogastric intubation	Shallow ulcers or giant, flat ulcers	Distal	History of intubation
Alkaline reflux esophagitis	Superficial or deep ulcers	Distal	Partial or total gastrectomy
Behçet's disease	Superficial ulcers	Variable	Oral and genital ulcers and ocular inflammation
Epidermolysis bullosa dystrophica	Superficial ulcers or bullae	Variable	Skin disease
Benign mucous membrane pemphigoid	Superficial ulcers or bullae	Variable	Skin disease

TABLE
28-2

Mucosal Nodularity

Cause	Radiographic Findings	Distribution	Comments
COMMON			
Reflux esophagitis	Nodular or granular mucosa (nodules poorly defined)	Distal third or half of thoracic esophagus	Reflux symptoms, hiatal hernia, and/or gastroesophageal reflux
<i>Candida</i> esophagitis	Discrete plaques	Localized or diffuse	Odynophagia in immunocompromised patients
Glycogenic acanthosis	Nodules or plaques	Localized or diffuse	Asymptomatic
UNCOMMON			
Barrett's esophagus	Reticular pattern	Localized	Often adjacent to distal aspect of midesophageal stricture
Radiation esophagitis	Granular mucosa and decreased distensibility	Conforms to radiation portal	Temporal relationship to radiation therapy
Superficial spreading carcinoma	Poorly defined, coalescent nodules or plaques	Localized or diffuse	May be asymptomatic
Esophageal papillomatosis	Multiple excrescences	Diffuse	Asymptomatic
Acanthosis nigricans	Tiny nodules	Diffuse	Skin disease
Cowden's disease	Tiny nodules (hamartomatous polyps)	Diffuse	Hereditary disorder with associated malignant tumors of skin, gastrointestinal tract, and thyroid
Leukoplakia	Tiny nodules	Localized or diffuse	Rare

TABLE
28-3

Solitary Mass Lesions

Cause	Radiographic Findings	Distribution	Comments
MUCOSAL LESIONS			
Papilloma	Sessile or slightly lobulated polyp	Variable	Asymptomatic
Adenoma	Sessile or pedunculated polyp	Distal	Arises in Barrett's mucosa
Inflammatory esophagogastric polyp	Polypoid protuberance with contiguous fold arising near cardia	Distal	Associated reflux esophagitis
Adenocarcinoma or squamous cell carcinoma	Plaquelike, sessile, or polypoid lesion	Variable	Small lesions may be early esophageal cancers
Spindle cell carcinoma	Bulky polypoid mass	Variable	Expands lumen without causing obstruction
Primary malignant melanoma	Bulky polypoid mass	Variable	Expands lumen without causing obstruction
SUBMUCOSAL LESIONS			
Leiomyoma	Smooth submucosal mass	Variable	Usually asymptomatic; rarely ulcerated
Fibrovascular polyp	Large pedunculated mass with sausage-shaped appearance	Arises in cervical esophagus but extends distally	May occlude larynx, causing asphyxia and sudden death
Granular cell tumor	Smooth submucosal mass	Usually distal	Associated lesions on skin or tongue
Lipoma	Sessile or pedunculated lesion	Variable	Fat density on computed tomography (CT)
Hemangioma	Smooth submucosal mass	Variable	Risk of exsanguination
Idiopathic varix	Smooth submucosal mass	Variable	Effaced or obliterated with esophageal distention (unless thrombosed)
Duplication cyst	Smooth submucosal mass	Right lateral wall of distal esophagus	Fluid density on CT

TABLE 28-4 Multiple Submucosal Masses

Cause	Distribution	Comments
BENIGN LESIONS		
Leiomyomas	Middle or distal	May be asymptomatic
Granular cell tumors	Middle or distal	Associated lesions on skin or tongue
Hemangioma	Diffuse	Osler-Weber-Rendu disease
Retention cysts (esophagitis cystica)	Distal	Asymptomatic
MALIGNANT LESIONS		
Hematogenous metastases	Middle or distal	Very rare in esophagus
Lymphoma	Diffuse	Usually non-Hodgkin's lymphoma
Leukemia	Diffuse	Usually asymptomatic
Kaposi's sarcoma	Diffuse	Patients with AIDS

TABLE 28-5 Thickened Folds

Cause	Radiographic Findings	Distribution	Comments
Varices	Tortuous or serpiginous folds	Uphill—distal Downhill—middle	Effaced or obliterated with esophageal distention; no dysphagia
Esophagitis	Smooth, nodular, or scalloped folds	Diffuse	Reflux symptoms or other findings of esophagitis
Varicoid carcinoma	Thickened, lobulated folds	Variable	Rigid, fixed appearance at fluoroscopy; dysphagia common
Lymphoma	Thickened, lobulated folds	Variable	Usually non-Hodgkin's lymphoma

TABLE 28-6 Strictures

Cause	Radiographic Findings	Comments
DISTAL ESOPHAGUS		
Peptic strictures	Symmetric or asymmetric; moderate length or ringlike	Associated hiatal hernia
Barrett's esophagus	Symmetric or asymmetric (i.e., peptic strictures)	Barrett's mucosa found in 40% of peptic strictures
Nasogastric intubation	Long area of narrowing	Rapidly progressive
Zollinger-Ellison syndrome	Long area of narrowing	May be initial manifestation of disease; hypergastrinemia
Crohn's disease	Short or long	Advanced Crohn's disease in small bowel or colon
Alkaline reflux strictures	Short or long	Rapidly progressive; seen after partial or total gastrectomy
Carcinoma (usually adenocarcinoma)	Irregular narrowing with nodularity or ulceration	Arises in Barrett's esophagus; often invades gastric cardia and fundus; recent onset of dysphagia and weight loss
UPPER OR MIDESOPHAGUS		
Barrett's esophagus	Tapered or ringlike	Hiatal hernia and/or gastroesophageal reflux; adjacent reticular pattern abutting distal aspect of stricture
Radiation	Usually tapered	History of radiation therapy (>50 Gy)
Eosinophilic esophagitis	Variable narrowing with concentric rings (ringed esophagus)	History of allergies, asthma, and peripheral eosinophilia; predominantly in men
Caustic ingestion	Single or multiple; long strictures common	History of caustic ingestion
Oral medications	Often near level of enlarged left atrium, left main bronchus, or aortic arch	Potassium chloride, quinidine, alendronate, nonsteroidal anti-inflammatory drugs, tetracycline, or doxycycline
Opportunistic infection (usually candidiasis)	Short or long	History of <i>Candida</i> esophagitis
Epidermolysis bullosa dystrophica	High strictures or webs	Skin disease
Benign mucous membrane pemphigoid	High strictures or webs	Skin disease
Chronic graft-versus-host disease	Relatively long	History of bone marrow transplantation
Glutaraldehyde-induced injury	Long and tapered	Rapidly progressive stricture within weeks of endoscopy
Congenital esophageal stenosis	Tapered narrowing with concentric rings	Long-standing dysphagia for solids; food impactions
Carcinoma (usually squamous cell carcinoma)	Irregular narrowing with nodularity or ulceration	History of smoking and/or alcohol consumption; recent onset of dysphagia and weight loss
Metastatic tumor	Tapered or irregular narrowing	Usually lung or breast cancer
SMALL-CALIBER ESOPHAGUS		
Eosinophilic esophagitis	Associated rings common	History of allergies, asthma, and peripheral eosinophilia; predominantly in men
Lichen planus	Sometimes have focal strictures	Skin lesions; predominantly in women
Caustic ingestion	Greater irregularity and narrowing than other causes of small-caliber esophagus	History of caustic ingestion

SECTION

V

Stomach and Duodenum

Peptic Ulcers

MARC S. LEVINE

CHAPTER OUTLINE

Epidemiology and Pathogenesis

Helicobacter pylori Gastritis

Nonsteroidal Anti-inflammatory Drugs

Steroids

Tobacco, Alcohol, and Coffee

Stress

Gastroduodenal Reflux of Bile and Delayed Gastric Emptying

Hereditary Factors

Clinical Findings

Treatment

Radiographic Findings

Gastric Ulcers

Duodenal Ulcers

Pyloric Channel Ulcers

Differential Diagnosis

Approach to Ulcers

Complications

Upper Gastrointestinal Bleeding

Obstruction

Perforation

Zollinger-Ellison Syndrome

Pathology

Clinical Aspects

Radiographic Findings

Differential Diagnosis

Gastric or duodenal ulcers (peptic ulcers) are thought to occur in about 10% of the adult population in the West.¹ Peptic ulcers are important not only because of the frequent occurrence of pain or other symptoms, but also because of the morbidity and mortality associated with complications such as bleeding and perforation. It has been well established that *Helicobacter pylori* and nonsteroidal anti-inflammatory drugs (NSAIDs) have a major role in ulcer development. Duodenal ulcers are almost always benign, but a small percentage of gastric ulcers are found to be malignant, so gastric ulcers require careful evaluation and follow-up to differentiate benign from malignant lesions.

Epidemiology and Pathogenesis

During the early 20th century, gastric ulcers were much more common than duodenal ulcers.² Since that time, there has been a dramatic reversal of this relationship, so duodenal ulcers are now more common than gastric ulcers.² Although duodenal ulcers occur in adults of all ages, gastric ulcers are found

predominantly in patients older than 40 years.^{1,2} Regardless of their site of origin, peptic ulcers have an equal gender distribution.³ Gastric and duodenal ulcers are characterized by seasonal variations, with a higher frequency in spring and autumn and a lower frequency in summer.⁴

A voluminous body of literature has shown convincingly that *H. pylori* and NSAIDs are responsible for the vast majority of gastric ulcers and that *H. pylori* is the causative agent for almost all duodenal ulcers. Nevertheless, *H. pylori*-negative ulcers may occasionally develop in the absence of NSAID use.⁵ Other possible causes of gastric ulcers include steroids, tobacco, alcohol, coffee, stress, duodenogastric reflux of bile, and delayed gastric emptying. Hereditary factors have also been implicated. These subjects are discussed separately in the following sections.

HELICOBACTER PYLORI GASTRITIS

H. pylori is a gram-negative, spiral bacillus that was first isolated on endoscopic biopsy specimens from the stomach by Warren and Marshall in 1983.⁶ Since then, *H. pylori* has been recognized as the major cause of gastric and duodenal ulcers.⁷⁻⁹ In various studies, the prevalence of *H. pylori* gastritis has ranged from 60% to 80% in patients with gastric ulcers and from 95% to 100% in patients with duodenal ulcers.^{7,10,11}

The mechanism whereby *H. pylori* predisposes to the development of ulcers remains uncertain. It has been shown that patients with *H. pylori* gastritis have increased secretion of gastrin, with high basal and peak acid outputs.¹² As a result, a gastrin-mediated increase in gastric acid secretion may be a key factor in the pathogenesis of ulcers. Although most people with *H. pylori* never develop ulcers, more virulent strains of the organism are more likely to be associated with ulcer formation.^{12,13} In particular, a *cagA*-positive strain of *H. pylori* has been implicated in patients with duodenal ulcers and, to a lesser degree, gastric ulcers.¹⁴ Many of these patients also have evidence of gastric metaplasia at the borders of the ulcers, with infection of the metaplastic epithelium by *H. pylori*.^{14,15} The infected mucosa may therefore be more susceptible to ulceration.

NONSTEROIDAL ANTI-INFLAMMATORY DRUGS

In various studies, the prevalence of gastric ulcers in patients treated with aspirin or other NSAIDs has ranged from 15% to 30%.¹⁶⁻¹⁸ It has been shown that NSAIDs inhibit prostaglandin production by blocking the formation of cyclooxygenase 1 (COX-1), a rate-limiting enzyme for the synthesis of prostaglandins.^{18,19} This phenomenon occurs even with aspirin doses as low as 10 mg daily (compared with a dose of 81 mg daily for cardiovascular prophylaxis).²⁰ Because prostaglandins have cytoprotective properties, inhibition of prostaglandin synthesis can lead to mucosal injury and ulceration.^{18,19,21,22}

The development of gastric ulcers in patients on NSAIDs is also related to a topical effect caused by breakdown of the mucosal barrier.^{19,22} It has been shown that aspirin disrupts the mucus gel layer in the stomach, allowing acid to damage the gastric mucosa, even in the presence of normal or decreased acid secretion.²³ Altered mucosal resistance is therefore thought to be a major factor in ulcer pathogenesis. Nevertheless, it has been shown that patients taking enteric-coated aspirin have the same risk of upper gastrointestinal (GI) bleeding as those taking non-enteric-coated aspirin.²⁴ Ulcers have also been induced in cats by intravenous (IV) infusion of aspirin.²⁵ Thus, the development of ulcers is ultimately mediated by a combination of the topical and systemic effects of NSAIDs.

Chronic NSAID use is associated not only with an increased frequency of ulcers but also an increased frequency of complications such as perforation, obstruction, and bleeding.^{26,27} Studies have shown that people taking NSAIDs have a twofold to sixfold higher risk of developing these complications than those not taking NSAIDs.¹⁸ The risk increases even further in people over 60 years of age.²¹ A careful NSAID history should therefore be obtained in all patients with *H. pylori*-negative ulcers because of the likelihood that these ulcers are NSAID-related.

STEROIDS

Some investigators believe that steroids predispose to the development of ulcers, particularly gastric ulcers. This concern often results in discontinuation of steroids in patients with ulcer symptoms or GI bleeding. In a large study, however, patients receiving steroids were found to have the same frequency of ulcers as the general population.²⁸ It is therefore questionable whether steroids have any role in ulcer pathogenesis. Nevertheless, steroids can mask the clinical findings associated with ulcers, so a large or even perforated ulcer may fail to produce symptoms in these patients.

TOBACCO, ALCOHOL, AND COFFEE

Some investigators have found that cigarette smokers are more likely to have ulcers than nonsmokers^{29,30} and that perforated ulcers are also more likely to occur in these individuals.³¹ Others have found no significant correlation between smoking and ulcers.³² Although alcohol and coffee may stimulate acid secretion, their role in ulcer pathogenesis remains uncertain.²⁹

STRESS

Some investigators believe that emotional stress contributes to the development of peptic ulcers by increasing peptic acid secretion.^{33,34} In one study, extreme emotional stress after a major earthquake in Japan resulted in an increased frequency of gastric ulcers, particularly bleeding ulcers.³⁵ Others have found that stressful life events are no more common in patients with ulcers than in the general population.³⁶ Thus, the role of stress in the development of ulcers remains uncertain.

GASTRODUODENAL REFLUX OF BILE AND DELAYED GASTRIC EMPTYING

Some patients with gastric ulcers have an unusually high concentration of bile acids in the stomach,³⁷ so duodenogastric

reflux of bile has been implicated in ulcer pathogenesis. Gastric stasis from gastric outlet obstruction or gastroparesis may also predispose to the development of gastric ulcers by prolonging exposure of the stomach to its own peptic secretions.³⁸ The latter ulcers have been called Dragstedt ulcers based on the name of the investigator who described them.³⁸

HEREDITARY FACTORS

A small percentage of patients with peptic ulcers have a family history of ulcers.^{39,40} This familial aggregation of ulcers is explained primarily by hereditary rather than environmental factors because studies have found a much greater concordance of ulcers in monozygotic twins than in dizygotic twins.³⁹ Patients with blood type O also have a higher incidence of ulcers than those with other blood types.³⁹ Finally, peptic ulcers are more common in patients with genetic syndromes such as multiple endocrine neoplasia type 1, systemic mastocytosis, and tremor-nystagmus-ulcer syndrome.³⁹ Thus, hereditary factors have clearly been implicated in the development of ulcers.

Clinical Findings

Patients with peptic ulcers often present with localized epigastric pain between the xiphoid cartilage and umbilicus.⁴¹ Ulcer pain tends to have a rhythmic nature; gastric ulcer pain typically occurs less than 2 hours after meals, whereas duodenal ulcer pain occurs 2 to 4 hours after meals and is more likely to wake the patient at night.⁴¹ Nevertheless, there is so much overlap in the timing of the pain that it is difficult to differentiate gastric and duodenal ulcers on clinical grounds.

Some patients with peptic ulcers may have right upper quadrant, back, or chest pain or other symptoms such as bloating, belching, nausea, vomiting, anorexia, and weight loss.⁴¹ Depending on the clinical findings, the differential diagnosis may include reflux esophagitis, gastritis, duodenitis, cholecystitis, irritable bowel syndrome, ischemic bowel disease, Crohn's disease, pancreatitis, and gastric or pancreatic carcinoma.⁴¹

The diagnosis of peptic ulcer disease is complicated by the fact that patients with classic ulcer symptoms are not always found to have ulcers.⁴² Conversely, 25% to 50% of patients with gastric or duodenal ulcers are asymptomatic.^{41,43} These individuals may not seek medical attention until the development of potentially catastrophic complications such as perforation, bleeding, or obstruction. When ulcers on the posterior wall of the stomach or duodenum penetrate into the pancreas, the normally rhythmic epigastric pain associated with ulcers is replaced by a more constant pain that radiates to the back. In contrast, free perforation of a gastric or duodenal ulcer causes peritonitis. The major factors contributing to mortality in patients with perforated peptic ulcers include age older than 60 years and a delay of more than 24 hours from the time of diagnosis to the time of surgery.⁴⁴

Patients with antral, pyloric channel, or duodenal ulcers associated with edema, spasm, or scarring may present with postprandial nausea and vomiting related to gastric outlet obstruction. Other patients with pyloric channel ulcers may develop the so-called pyloric channel syndrome with severe postprandial epigastric pain relieved by vomiting.^{45,46}

Peptic ulcers are the most common cause of acute upper GI bleeding, accounting for about 50% of cases.⁴⁷ Some patients have one or more episodes of massive hemorrhage, manifested

by hematemesis, melena, or rectal bleeding, whereas others have chronic, low-grade bleeding, manifested by guaiac-positive stool or iron-deficiency anemia.⁴¹ Gastric ulcers are more likely to bleed than duodenal ulcers, probably because of the greater size of the ulcer craters and older age of the patients.⁴¹ When ulcers are found in the duodenum, however, postbulbar duodenal ulcers are more likely to be associated with upper GI bleeding (particularly massive bleeding) than those in the duodenal bulb.⁴⁸ Bleeding from ulcers ceases spontaneously in about 80% of cases, but some form of therapy is required to control the bleeding in the remaining 20%.⁴³

Treatment

The treatment for peptic ulcers depends on the underlying cause. If *H. pylori* gastritis is confirmed by endoscopic biopsy specimens or by noninvasive tests such as a urea breath test, serologic test, or stool antigen test (see Chapter 30), there is strong evidence that eradication of *H. pylori* leads to more rapid healing of gastric and duodenal ulcers and a much lower rate of ulcer recurrence.⁴⁹⁻⁵¹ Expert panels convened by the National Institutes of Health and American Digestive Health Foundation therefore concluded that all patients with *H. pylori*-related gastric or duodenal ulcers should receive combination therapy with antimicrobial and antisecretory agents.^{52,53} Various combinations of antibiotics and antisecretory agents (proton pump inhibitors) have been shown to be highly effective in eradicating *H. pylori*.⁵⁴⁻⁵⁶ As a result, these patients can literally be cured of their ulcer disease without need for long-term maintenance therapy with antisecretory agents, unless they become infected by another strain of the organism.

In the absence of *H. pylori*, H₂ receptor antagonists have proved to be highly effective in accelerating healing of gastric and duodenal ulcers by suppressing acid secretion.⁵⁷ Proton pump inhibitors such as omeprazole are even more effective in suppressing acid secretion and accelerating ulcer healing by selectively inhibiting the gastric proton pump that controls the first step in the production of gastric acid.⁵⁸ Because NSAID-related ulcers are associated with decreased synthesis of prostaglandins (see earlier), misoprostol (a synthetic prostaglandin E analogue) has been used to accelerate ulcer healing in these patients.⁵⁹ Prostaglandins and prostaglandin analogues also decrease the risk of developing gastric ulcers in patients on

NSAIDs.⁶⁰ Sucralfate, colloidal bismuth, and carbenoxolone are other drugs that have been used to treat ulcers.

Surgery may be required for recurrent or intractable ulcers that fail to heal with medical therapy, for ulcer complications such as bleeding, obstruction, and perforation, and for ulcers that have equivocal or suspicious findings on barium studies or endoscopy. The most common operations include partial gastrectomy, vagotomy and pyloroplasty, and hyperselective vagotomy. These surgical procedures and their complications are discussed in Chapter 35. Because of better diagnosis and medical treatment of peptic ulcers, the need for surgery in these patients has decreased considerably since the late 1960s.^{61,62}

Radiographic Findings

GASTRIC ULCERS

Examination Technique

The double-contrast examination should be performed as a biphasic study that includes double-contrast views of the stomach with a high-density barium suspension and prone or upright compression views with a low-density barium suspension (see Chapter 17). Ulcer detection is facilitated by IV administration of 0.1 mg of glucagon to induce gastric hypotonia. Ulcers located on the posterior wall or on the lesser or greater curvature of the stomach are usually well seen on routine double-contrast views obtained with the patient in a supine or supine oblique position. Flow technique can be used to better delineate shallow ulcers on the posterior wall by slowly rotating the patient from side to side to manipulate a thin layer of high-density barium over the dependent surface (Fig. 29-1).⁶³ Upright compression views are also helpful for evaluating ulcers on the lesser curvature.⁶⁴

It is important to be aware of the limitations of double-contrast studies for detecting ulcers on the anterior (nondependent) wall of the stomach. Because of the effect of gravity, these ulcers may not fill with barium on double-contrast views with the patient in the usual supine or supine oblique position (Fig. 29-2A). Prone compression views of the gastric antrum and body should therefore be obtained routinely to demonstrate these anterior wall ulcers (Fig. 29-2B). Double-contrast views of the anterior wall can also be obtained by placing the patient in a prone Trendelenburg position.⁶⁵

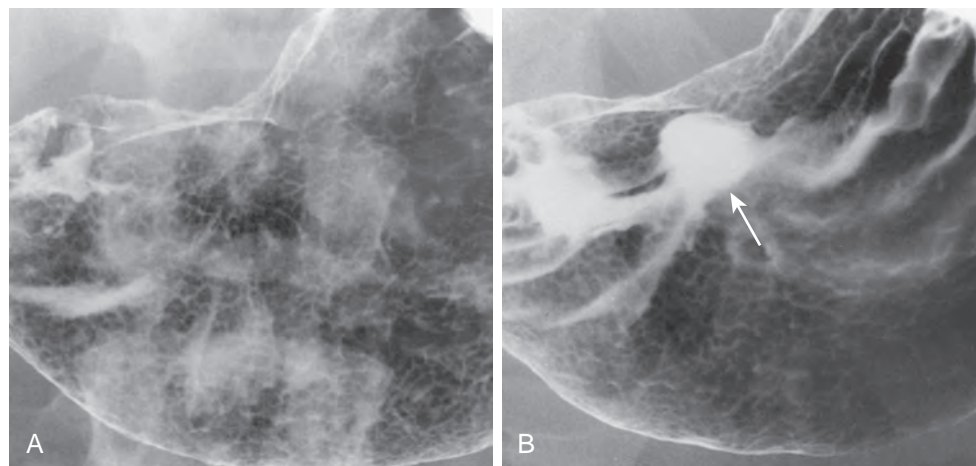


Figure 29-1 Importance of flow technique for posterior wall ulcers.

A. Supine double-contrast view shows no evidence of an ulcer, even in retrospect. **B.** With flow technique, an ulcer (arrow) is seen on the posterior wall of the antrum. Note how folds radiate to the edge of the ulcer crater. (From Laufer I, Levine MS [eds]: *Double Contrast Gastrointestinal Radiology*, 2nd ed. Philadelphia, WB Saunders, 1992.)

Shape

Gastric ulcers are typically seen as round or ovoid collections of barium (see Figs. 29-1B and 29-2B). Ulcer craters may have a variety of shapes and configurations, appearing as linear, rod-shaped, rectangular, serpiginous, or flame-shaped lesions (Fig. 29-3).⁶⁶⁻⁶⁹ Linear ulcers constitute about 5% of all gastric ulcers diagnosed on double-contrast studies.⁶⁸ These linear ulcers

probably represent a stage of ulcer healing in the stomach and duodenum.^{68,69}

Size

The radiographic sensitivity in detecting gastric ulcers is related primarily to ulcer size; ulcers larger than 5 mm are more likely to be detected on barium studies.⁷⁰ A major advantage of double-contrast technique is its ability to distend the stomach

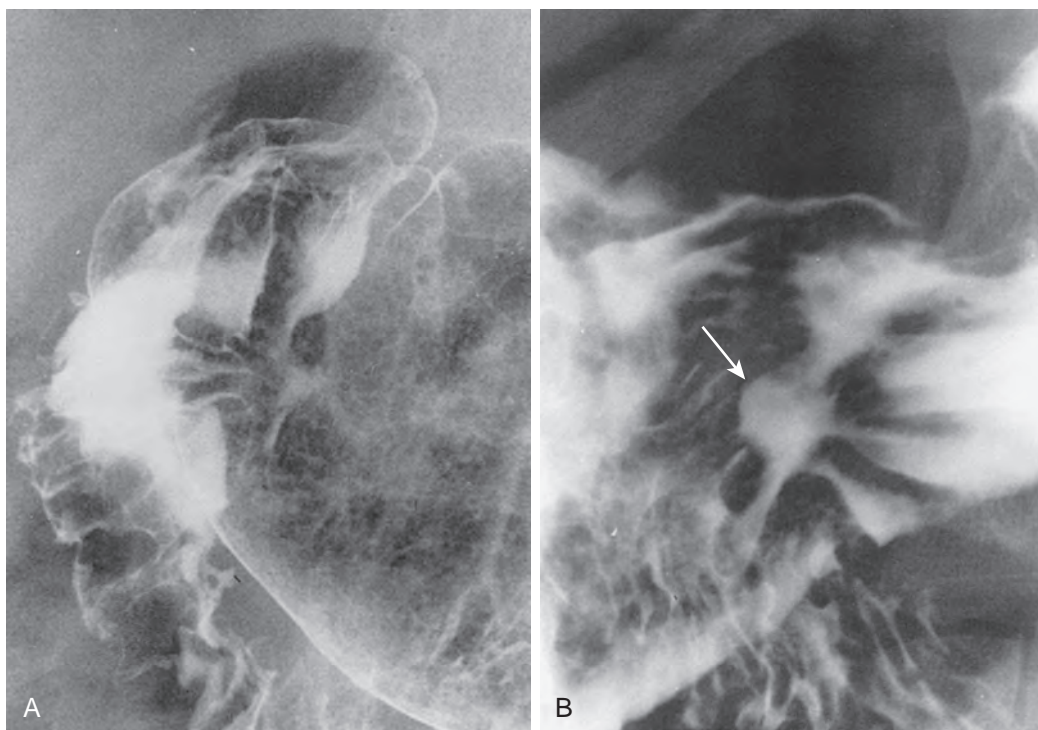
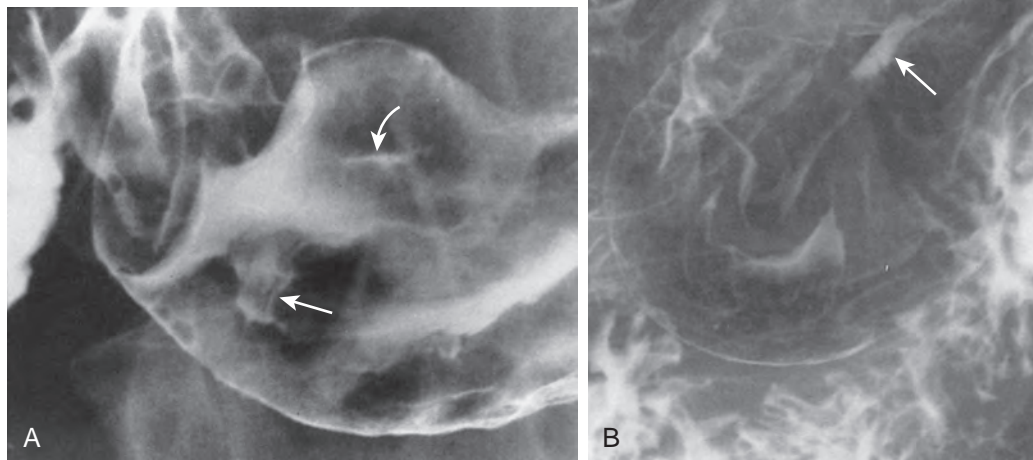


Figure 29-2 Importance of prone compression for anterior wall ulcers. **A.** Supine double-contrast view shows abnormal folds in the antrum without a definite ulcer. **B.** Prone compression view shows filling of an anterior wall ulcer (arrow). Note how folds radiate to the edge of the ulcer crater. (From Laufer I, Levine MS [eds]: *Double Contrast Gastrointestinal Radiology*, 2nd ed. Philadelphia, WB Saunders, 1992.)

Figure 29-3 Gastric ulcers of different shapes.

A. This patient has star-shaped (straight arrow) and linear (curved arrow) ulcers in the antrum. **B.** In another patient, a rod-shaped ulcer (arrow) is seen in the stomach.



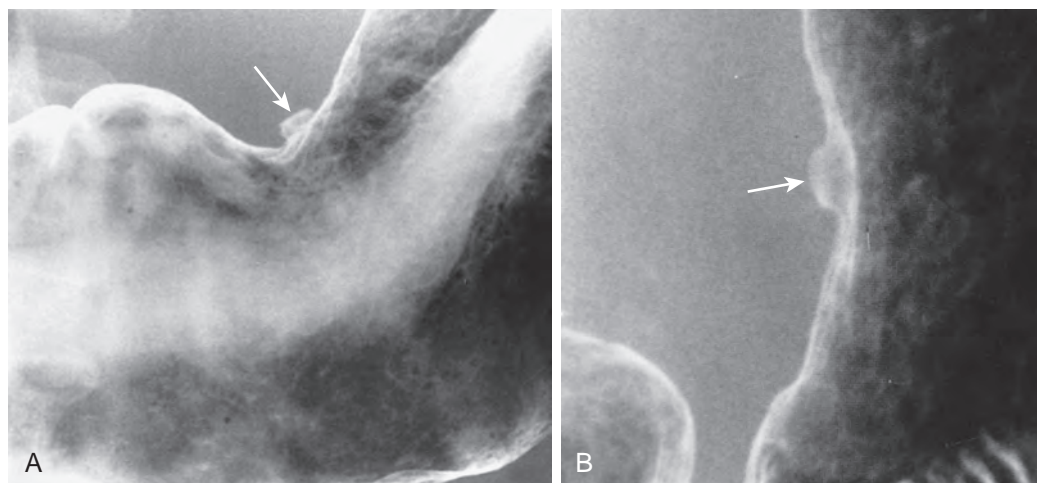


Figure 29-4 Small gastric ulcers. **A, B.** Despite their small size, these lesser curvature ulcers (arrows) are well seen on double-contrast radiographs.

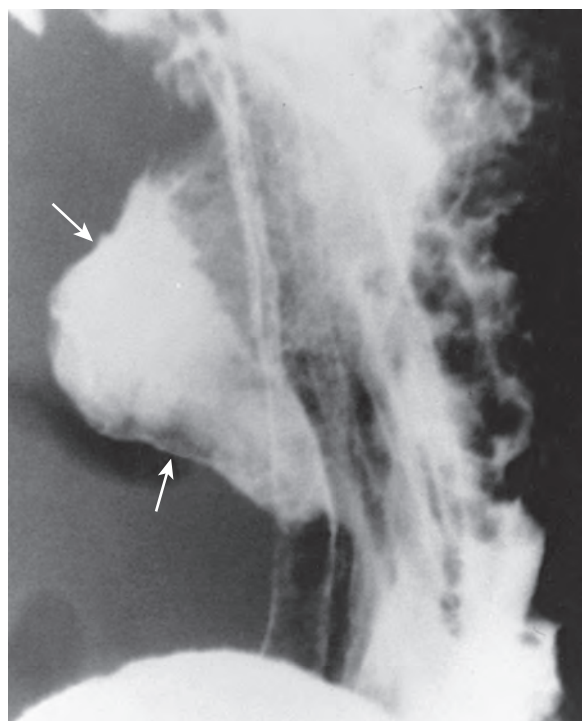


Figure 29-5 Giant gastric ulcer. A giant ulcer (arrows) is seen projecting from the lesser curvature of the upper gastric body. Large ulcers tend to be located more proximally in the stomach.

and efface normal folds, enabling visualization of small ulcers (Fig. 29-4). Most gastric ulcers diagnosed on double-contrast studies are smaller than 1 cm.⁶⁹ The high prevalence of small ulcers may also be related to the aggressive medical treatment that these patients often receive before undergoing radiologic investigations.

Large ulcers tend to be located more proximally in the stomach (Fig. 29-5).⁷¹ These ulcers may occasionally be recognized on abdominal radiographs by the presence of gas in the ulcer crater. Giant gastric ulcers (ulcers > 3 cm in size) are

associated with a higher risk of complications such as bleeding and perforation.⁷² However, most giant ulcers are found to be benign.⁷² Thus, the size of the ulcer crater has no relationship to the presence of carcinoma.

Location

Most benign gastric ulcers are located on the lesser curvature or posterior wall of the gastric antrum or body.^{69,71,73,74} In various studies, only 1% to 7% of benign ulcers were found to be located on the anterior wall and 3% to 11% on the greater curvature.^{69,71,73,75} In younger people, ulcers tend to be located in the antrum, whereas in older individuals, they are more likely to be located in the upper body, particularly on the lesser curvature.^{76,77} These high lesser curvature ulcers in older patients have been called *geriatric ulcers*.⁷¹

Benign greater curvature ulcers are almost always located in the distal half of the stomach; the vast majority are caused by ingestion of aspirin or other NSAIDs.^{69,78} Because these ulcers rarely occur on the proximal half of the greater curvature, any ulcers in this location should be considered worrisome for malignant tumor until proved otherwise. Except for these ulcers high on the greater curvature, the location of the ulcer has no relationship to the presence of carcinoma.

Gastric ulcers are occasionally found in hiatal hernias.⁷⁹ They tend to occur on the lesser curvature aspect of the hernia, where the hernia sac is compressed by the adjacent esophageal hiatus of the diaphragm (see Chapter 26).⁷⁴ Because the hernia is inaccessible to palpation, double-contrast technique is particularly helpful for showing these ulcers.

Morphologic Features

Ulcers on the lesser or greater curvature are readily visualized in profile on barium studies, permitting analysis of the size, shape, and depth of the ulcer crater as well as associated findings such as radiating folds, Hampton's line, or an ulcer mound or collar. Ulcers on the anterior or posterior wall may be difficult or impossible to visualize in profile, however, so these lesions must be evaluated on the basis of their appearance en face. In such cases, double-contrast technique is particularly helpful in assessing the surrounding mucosa for signs of benign or malignant disease.

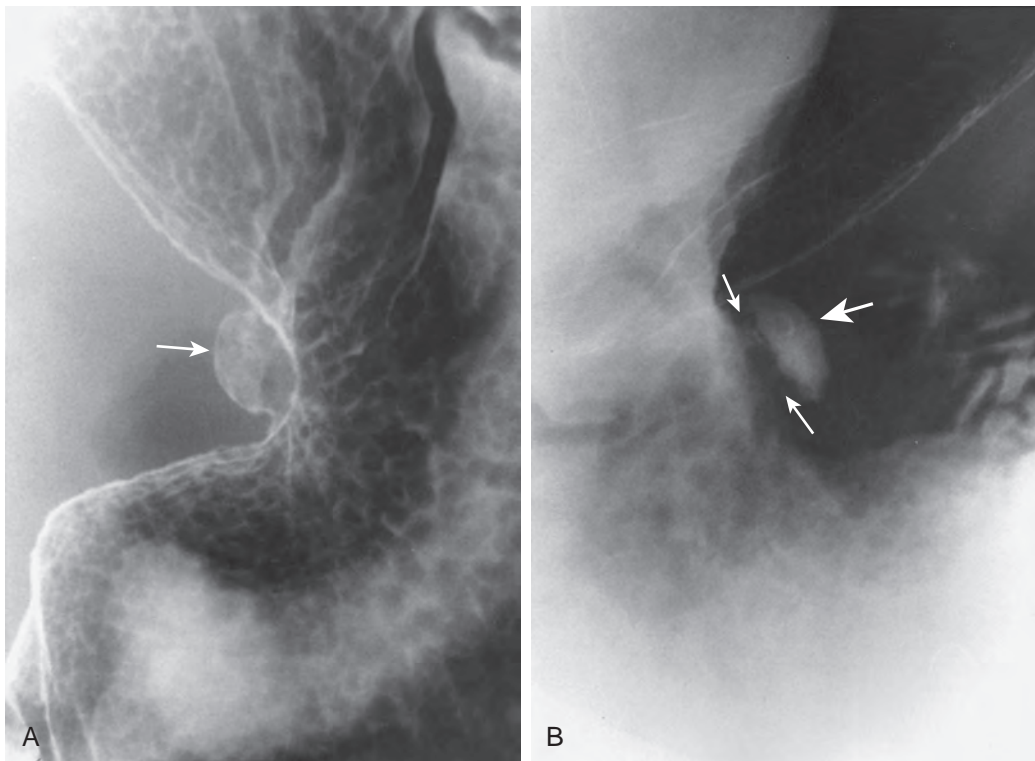


Figure 29-6 Lesser curvature ulcers. **A.** A smooth, round ulcer (arrow) is seen projecting beyond the lesser curvature. The radiating folds and enlarged areas gastricae in the adjacent mucosa are caused by surrounding edema and inflammation. **B.** In another patient, a lesser curvature ulcer (large arrow) is demonstrated on a prone compression view. Note the radiolucent band of edema or ulcer collar (small arrows) adjacent to the ulcer. Both these cases demonstrate classic features of benign gastric ulcers. (A from Levine MS, Creteur V, Kressel HY, et al: *Benign gastric ulcers: Diagnosis and follow-up with double contrast radiography*. *Radiology* 164:9–13, 1987.)

Lesser Curvature Ulcers. Ulcers on the lesser curvature typically appear as smooth, round or ovoid craters that project beyond the contour of the adjacent gastric wall (Fig. 29-6; see Fig. 29-4).^{64,69,80,81} In some patients with lesser curvature ulcers, upright compression views may reveal a thin radiolucent line that separates barium in the ulcer crater from barium in the gastric lumen.^{64,80} This so-called Hampton's line results from undermining of the mucosa surrounding the crater.⁶⁴ In other patients, the rim of undermined mucosa may become more edematous, producing a wide radiolucent band, or ulcer collar (see Fig. 29-6B).⁶⁴ Occasionally, edema and inflammation surrounding the ulcer produces an ulcer mound, seen in profile as a smooth, bilobed, hemispheric mass projecting into the lumen on both sides of the ulcer.⁶⁴ Ulcer mounds usually have poorly defined outer borders that form obtuse, gently sloping angles with the adjacent gastric wall.⁶⁴ Hampton's lines and ulcer mounds and collars are considered to be classic features of benign gastric ulcers, but these findings are present in only a small percentage of all patients with lesser curvature ulcers.

Retraction of the gastric wall adjacent to lesser curvature ulcers sometimes leads to the development of smooth, symmetric folds that radiate directly to the edge of the ulcer crater (see Fig. 29-6A).⁶⁹ Occasionally, these ulcers may be associated with retraction of the opposite wall, producing an incisura on the greater curvature. Other lesser curvature ulcers may be associated with focal enlargement of areas gastricae surrounding the ulcer because of edema and inflammation of the adjoining mucosa (see Fig. 29-6A).⁶⁹

Greater Curvature Ulcers. In the past, almost all ulcers on the greater curvature of the stomach were thought to be malignant.⁸² It is now recognized, however, that benign ulcers do occur on the distal half of the greater curvature in patients who are taking aspirin or other NSAIDs (Figs. 29-7 and 29-8).^{69,78} The location of these ulcers on the greater curvature is presumably related to the effect of gravity because the dissolving aspirin tablets collect in the most dependent portion of the stomach, causing localized mucosal injury. Such lesions have been called *sump ulcers* because of their typical location on the greater curvature.⁷⁸ A similar phenomenon may also account for the frequent finding of linear or serpiginous erosions in the body of the stomach, on or near the greater curvature in patients who are taking NSAIDs (see Chapter 30).⁸³ Because of their location, greater curvature ulcers have a tendency to penetrate inferiorly into the gastrocolic ligament, occasionally leading to the development of a gastrocolic fistula (see later, "Fistulas").

In contrast to ulcers on the lesser curvature, greater curvature ulcers may appear to have an intraluminal location because of circular muscle spasm and retraction of the adjacent gastric wall (see Fig. 29-8A).⁸⁴ Greater curvature ulcers may also be associated with considerable surrounding mass effect and thickened, irregular folds secondary to marked edema and inflammation accompanying the ulcers (see Fig. 29-8).^{69,84} Because of these morphologic features, benign greater curvature ulcers often have a suspicious radiographic appearance, so the usual radiographic criteria for differentiating benign and malignant ulcers elsewhere in the stomach are unreliable for ulcers in this location.^{69,84} Endoscopy and biopsy may therefore be required

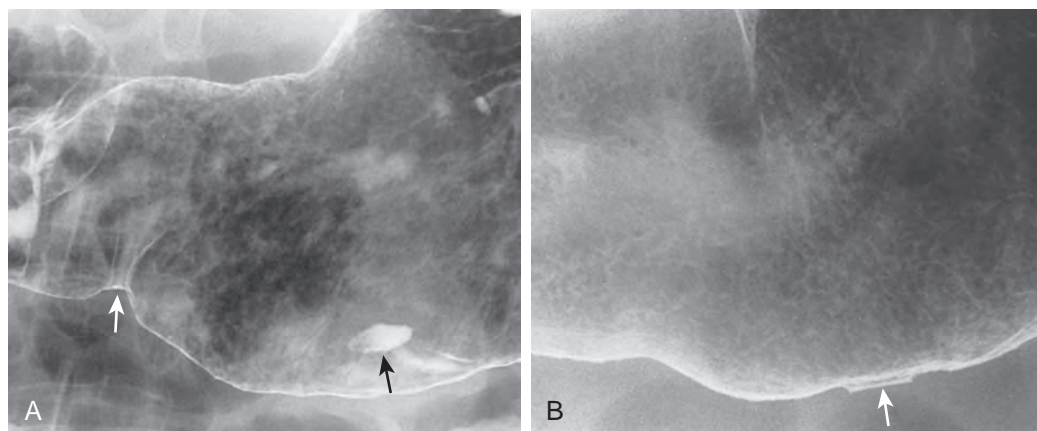


Figure 29-7 Greater curvature ulcers caused by aspirin and indomethacin. **A.** A small aspirin-induced ulcer (black arrow) is seen in the gastric body abutting the greater curvature. An area of scarring is also seen more distally on the greater curvature (white arrow) secondary to scarring from a previous ulcer in this location. **B.** In another patient, an extremely shallow indomethacin-induced ulcer (arrow) is seen on the greater curvature. Radiating folds and other signs of ulcer disease are absent. This ulcer could easily be missed without optimal technique. (From Laufer I, Levine MS [eds]: *Double Contrast Gastrointestinal Radiology*, 2nd ed. Philadelphia, WB Saunders, 1992.)

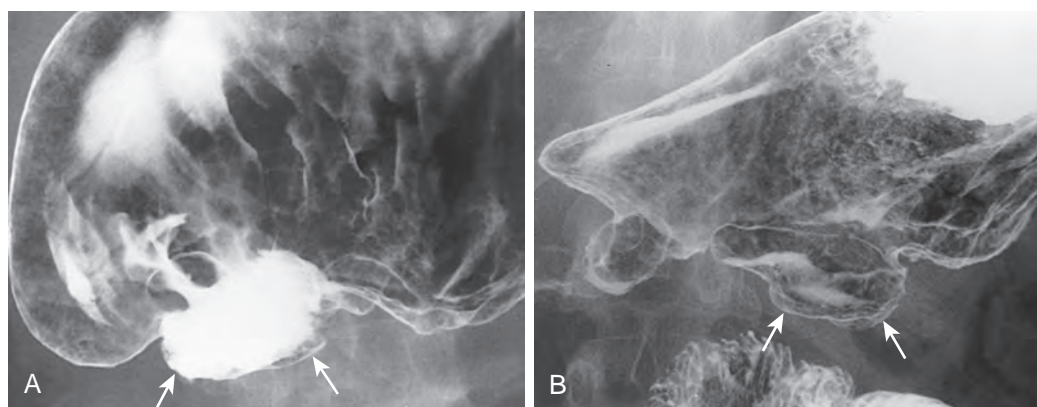


Figure 29-8 Giant greater curvature ulcers caused by aspirin. **A.** This large ulcer (arrows) on the greater curvature has an apparent intraluminal location and is associated with thickened, irregular folds and considerable mass effect from a surrounding mound of edema. **B.** In another patient, thickened, irregular folds are seen abutting a large greater curvature ulcer (arrows). In both cases, endoscopic biopsy specimens revealed no evidence of tumor, and follow-up studies after treatment with antisecretory agents showed complete healing of the ulcers. Both patients had been on high doses of aspirin. (A from Laufer I, Levine MS [eds]: *Double Contrast Gastrointestinal Radiology*, 2nd ed. Philadelphia, WB Saunders, 1992.)

for some greater curvature ulcers, despite a history of aspirin ingestion.

Posterior Wall Ulcers. Ulcers on the posterior (dependent) wall of the gastric antrum or body may fill with barium on routine double-contrast views, producing the conventional appearance of an ulcer crater (Fig. 29-9; see Fig. 29-1B). However, shallow ulcers on the posterior wall may appear as ring shadows on these views because of a thin layer of barium coating the rim of the unfilled crater (Fig. 29-10A). In such cases, flow technique can be used to manipulate the barium pool over the surface of the ulcer and demonstrate filling of the ulcer crater (Fig. 29-10B).⁶³ It is important not only to determine the size and shape of these posterior wall ulcers, but also to assess the appearance of the adjoining mucosa. Not infrequently, the areae gastricae are enlarged or distorted in the region of the ulcer because of surrounding edema and inflammation.⁶⁹ An ulcer collar or mound can sometimes be seen en face as a radiolucent halo of edematous tissue with poorly

defined outer borders that fade peripherally into the adjacent mucosa. Posterior wall ulcers may also be associated with a spectacular collection of folds that radiate directly to the edge of the ulcer crater.⁶⁹ Occasionally, the edema and spasm associated with antral ulcers may cause such severe narrowing and deformity of the distal stomach that it is difficult to evaluate these ulcers by the usual radiologic criteria (Fig. 29-11).

Anterior Wall Ulcers. Ulcers on the anterior (nondependent) wall of the gastric antrum or body may also appear as ring shadows on routine double-contrast views because of barium coating the rim of the unfilled ulcer crater tangential to the central beam of the x-ray (Fig. 29-12A).^{81,85} In such cases, the ulcer may be shown by turning the patient 180 degrees into the prone position, so the ulcer is located on the dependent wall and fills with barium (Fig. 29-12B). Prone compression views of the stomach with low-density barium should therefore be obtained routinely to demonstrate these anterior wall ulcers.

Multiplicity

With double-contrast technique, multiple ulcers have been detected in about 20% of patients with ulcers or ulcer scars,⁸⁶ a figure approximating the 20% to 30% prevalence of multiple ulcers at endoscopy, surgery, and autopsy.⁸⁷ The presence of multiple ulcers is often thought to favor benign disease. In one study, however, 20% of patients with multiple gastric ulcers had malignant lesions.⁸⁸ It is now recognized that patients may have coexisting benign and malignant ulcers, so each ulcer must be evaluated individually on barium studies.

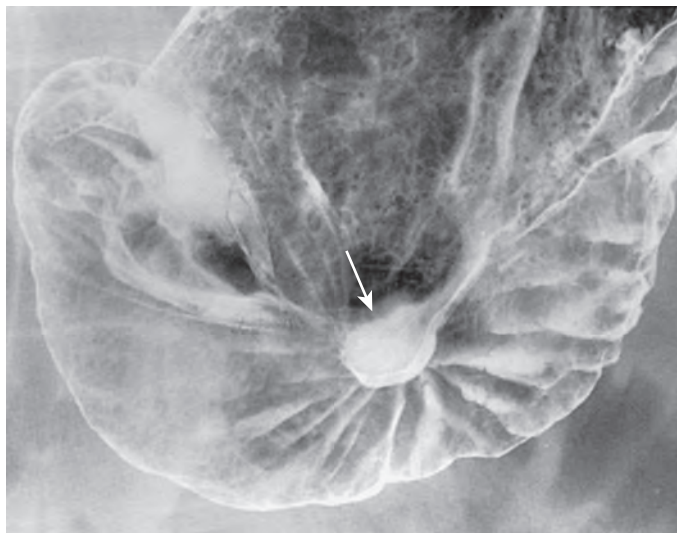
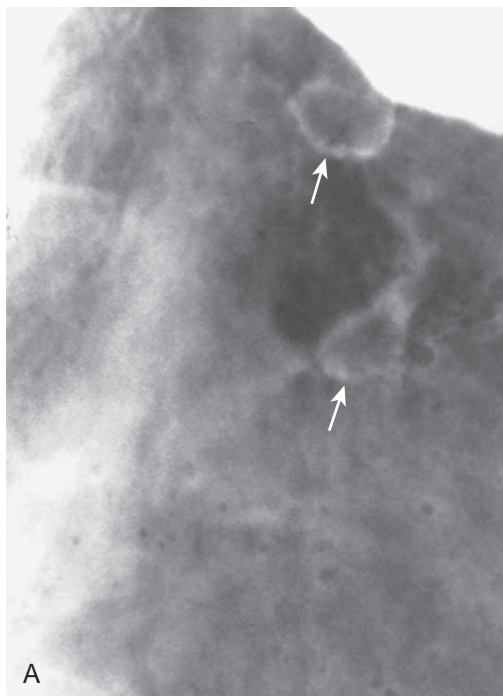


Figure 29-9 Posterior wall ulcer. A large ulcer (arrow) is present on the posterior wall of the stomach. Multiple folds are seen radiating to the edge of the ulcer crater. (From Laufer I, Levine MS [eds]: *Double Contrast Gastrointestinal Radiology*, 2nd ed. Philadelphia, WB Saunders, 1992.)

Figure 29-10 Ring shadows caused by shallow posterior wall ulcers. **A.** Supine double-contrast view shows two discrete ring shadows (arrows) in the upper body of the stomach secondary to barium coating the rim of shallow, unfilled ulcers on the posterior wall. **B.** The use of flow technique to manipulate the barium pool over the surface of the ulcers results in filling of the ulcer craters (arrows).



When multiple gastric ulcers are present, they tend to be located in the gastric antrum or body (see Fig. 29-3A). Multiple gastric ulcers are more likely to develop in patients who are taking aspirin or other NSAIDs (see Fig. 29-7A). In one study, 80% of patients with multiple ulcers had a history of aspirin use.⁸⁷ A careful drug history should therefore be obtained from these patients.

Ulcer Healing and Scarring

The radiologic assessment of ulcer healing is important for evaluating the success or failure of medical therapy and for

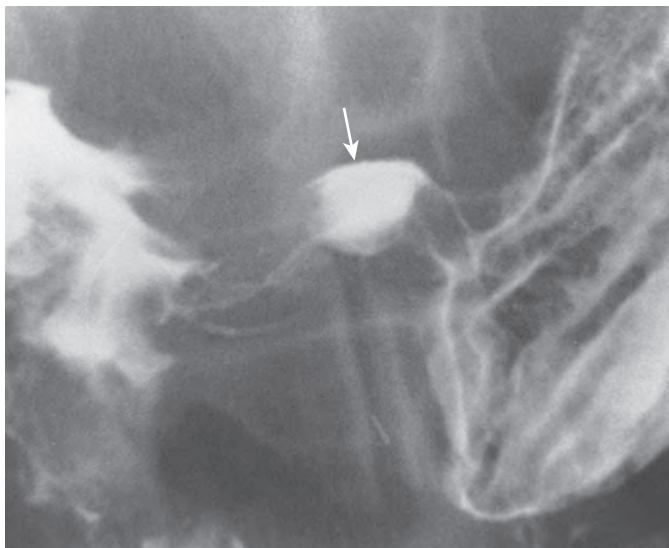


Figure 29-11 Antral ulcer associated with marked edema and spasm. A large ulcer (arrow) is seen in the gastric antrum. This ulcer is difficult to evaluate by the usual radiologic criteria because of antral narrowing and deformity secondary to marked edema and spasm accompanying the ulcer.

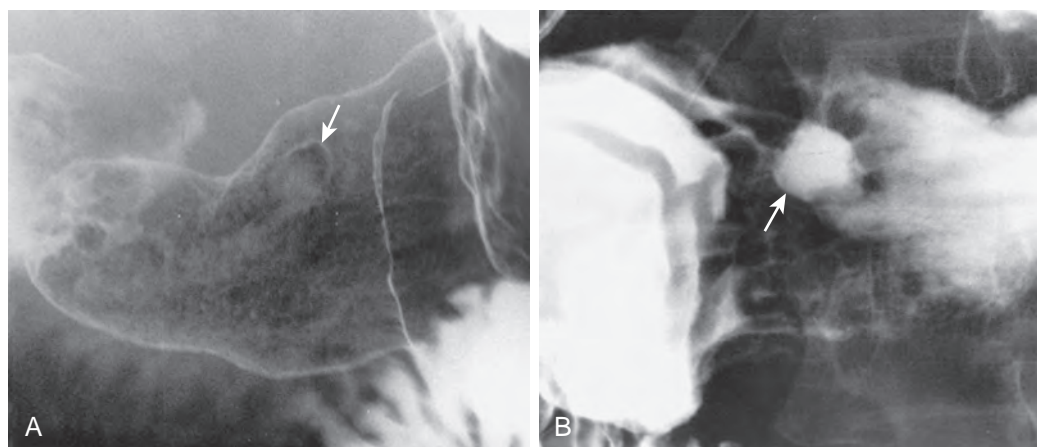


Figure 29-12 Partial ring shadow caused by an anterior wall ulcer. **A.** Supine double-contrast view shows a partial ring shadow (arrow) in the antrum. **B.** Prone compression view shows the anterior wall ulcer (arrow) filling with barium. (From Levine MS, Rubesin SE, Herlinger H, et al: *Double contrast upper gastrointestinal examination: Technique and interpretation*. Radiology 168:593–602, 1988.)

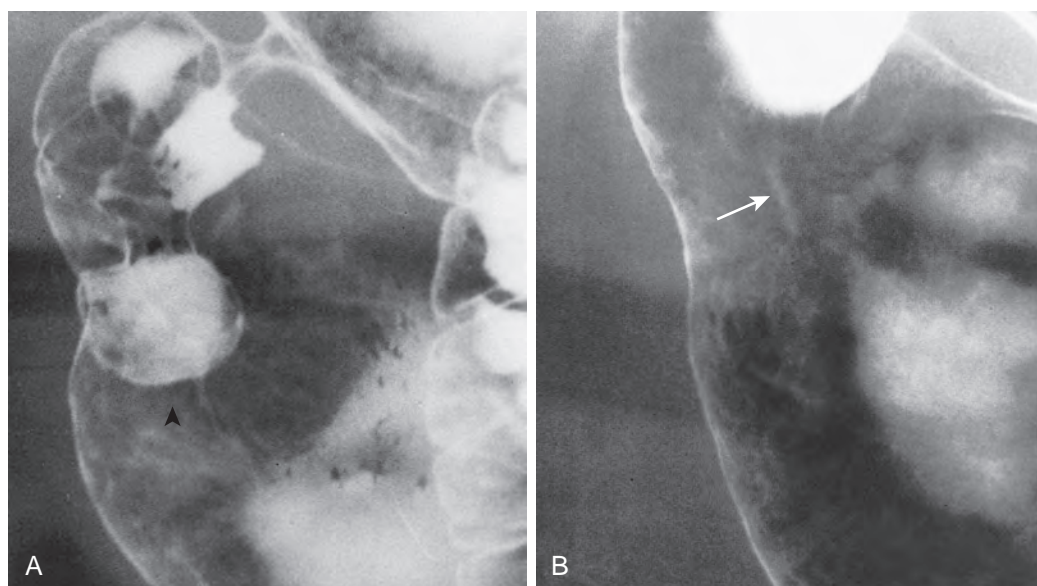


Figure 29-13 Development of a linear ulcer during healing. **A.** A large, round ulcer (arrowhead) is seen on the posterior wall of the antrum. **B.** Follow-up study 8 weeks later shows substantial ulcer healing with a residual linear ulcer (arrow) in this location. (From Levine MS, Creteur V, Kressel HY, et al: *Benign gastric ulcers: Diagnosis and follow-up with double-contrast radiography*. Radiology 164:9–13, 1987.)

confirming the presence of benign ulcer disease (see later, “Benign Versus Malignant Ulcers”). Ulcer healing may be manifested on barium studies not only by a decrease in the size of the ulcer crater but also by a change in its shape. Previously round or ovoid ulcers often have a linear appearance on follow-up studies, so linear ulcers presumably represent a stage of ulcer healing (Fig. 29-13).^{68,69} Other ulcers may undergo splitting, so the ulcer crater is replaced by two separate niches at the periphery of the original ulcer (Fig. 29-14).⁶⁹ This phenomenon most likely occurs because healing and re-epithelialization are more rapid in the central portion of the ulcer than in the periphery.

Benign gastric ulcers usually have a marked response to treatment with antisecretory agents. The average interval between the initial barium study showing the ulcer and the follow-up study showing complete healing is about 8 weeks.⁶⁹

Follow-up studies to demonstrate ulcer healing should therefore be performed after 6 to 8 weeks of medical treatment because studies performed sooner are unlikely to show complete healing.

In general, complete radiologic healing of a gastric ulcer has been considered a reliable sign that the ulcer is benign. Rarely, complete healing of malignant ulcers may occur with medical therapy.^{89,90} However, nodularity of the ulcer scar or irregularity, clubbing, or amputation of radiating folds should suggest the possibility of an underlying malignant tumor. The surrounding gastric mucosa must therefore be evaluated carefully after ulcer healing has occurred. If suspicious findings are present, endoscopy and biopsy are still required to rule out a malignant lesion.

Ulcer healing may lead to the development of ulcer scars, which are visible on double-contrast studies in 90% of patients with healed gastric ulcers.⁶⁹ These scars are usually manifested

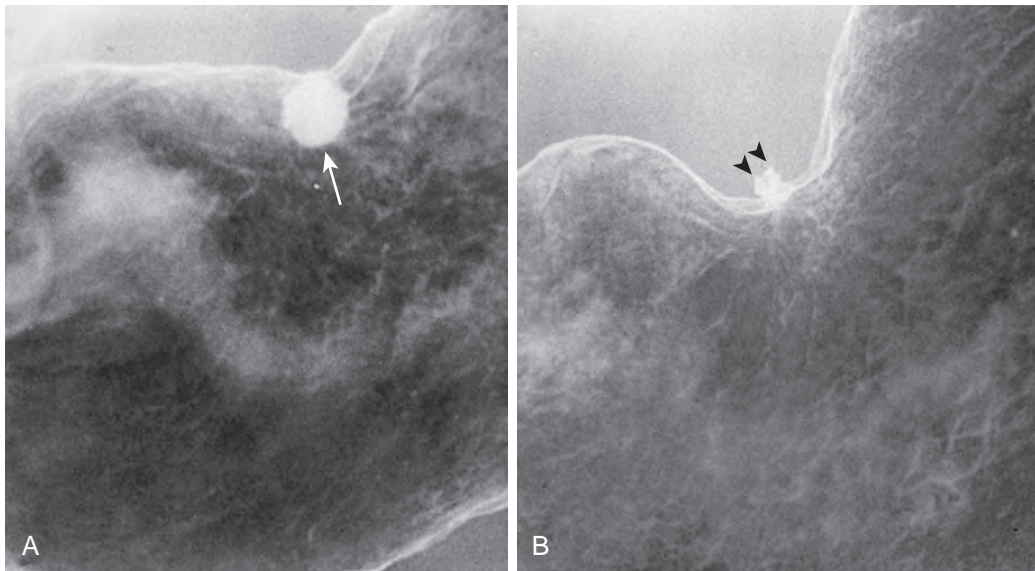


Figure 29-14 Splitting of an ulcer during healing. **A.** A round ulcer (arrow) is seen adjacent to the lesser curvature. **B.** Follow-up study several weeks later shows splitting of the ulcer with two closely spaced niches (arrowheads) at the site of the original crater.

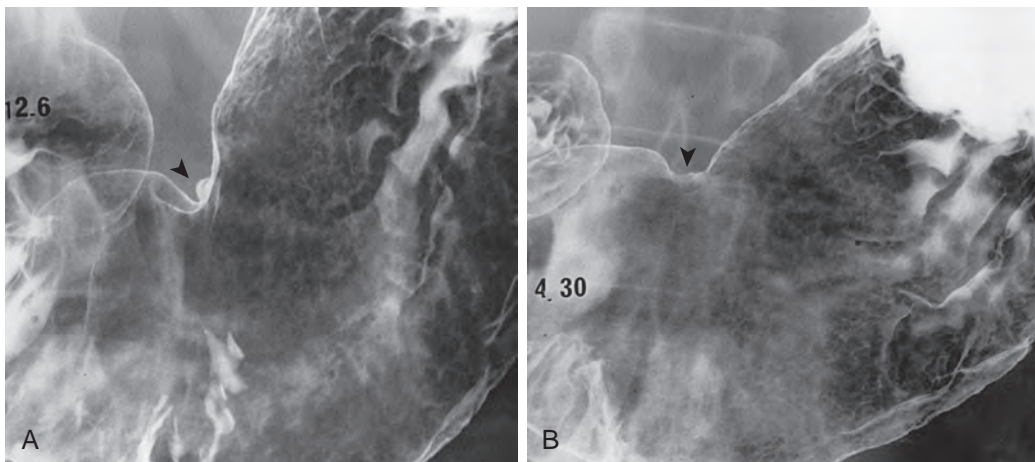


Figure 29-15 Healing of a lesser curvature ulcer with scarring. **A.** A small, benign-appearing ulcer (arrowhead) is seen on the lesser curvature. **B.** Follow-up study 5 months later shows complete healing of the ulcer with slight flattening and retraction of the adjacent gastric wall (arrowhead). (From Laufer I, Levine MS [eds]: *Double Contrast Gastrointestinal Radiology*, 2nd ed. Philadelphia, WB Saunders, 1992.)

by a central pit or depression, radiating folds, and/or retraction of the adjacent gastric wall.^{69,91,92} The location of the ulcer is a major determinant of the morphologic features of the scar. Healing of ulcers on the lesser curvature is often associated with the development of relatively innocuous scars, manifested by slight flattening or retraction of the adjacent gastric wall (Fig. 29-15).^{69,91} In contrast, healing of ulcers on the greater curvature or posterior wall is sometimes associated with the development of a spectacular collection of radiating folds (Fig. 29-16).^{69,81,91} The folds may converge to a central point or to a circular or linear pit or depression (Fig. 29-17).^{69,91,92} This central depression can be mistaken radiographically for a shallow, residual ulcer crater. However, the central depression of an ulcer scar tends to have more gradually sloping margins than an ulcer crater and should remain unchanged on sequential follow-up studies. A re-epithelialized ulcer scar can

also be differentiated from an active ulcer by the presence of normal *areae gastricae* within the central portion of the scar (Fig. 29-18).⁶⁹

Healing of antral ulcers may also lead to the development of a prominent transverse fold that can be mistaken for an antral web or diaphragm.⁹¹ In other patients, severe scar formation may be manifested by antral narrowing and deformity (Fig. 29-19A). The narrowed segment usually has a smooth, tapered appearance, but asymmetric scarring may result in flattening and shortening of the lesser or greater curvature, so the pylorus has an eccentric location in relation to the antrum and duodenal bulb (Fig. 29-19B). Occasionally, an ulcer scar may be associated with such irregular antral narrowing that it mimics the linitis plastica appearance of a primary scirrhous carcinoma of the stomach.⁹³ When antral scarring cannot be differentiated from a scirrhous carcinoma on radiologic criteria, endoscopy

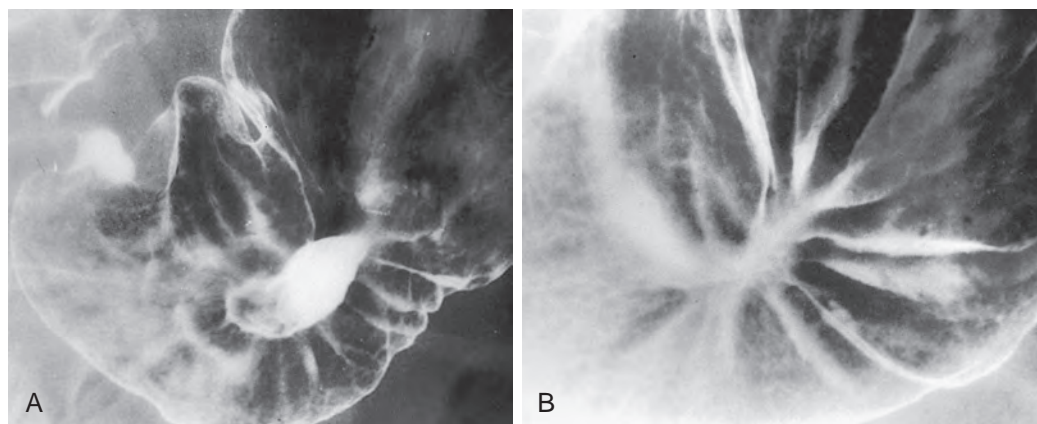


Figure 29-16 Healing of a posterior wall ulcer with scarring. **A.** There is a large posterior wall ulcer with multiple folds radiating to the edge of the ulcer crater. **B.** Follow-up study 8 weeks later shows complete healing of the ulcer with a spectacular collection of folds radiating to the site of the previous crater. (From Laufer I, Levine MS [eds]: *Double Contrast Gastrointestinal Radiology*, 2nd ed. Philadelphia, WB Saunders, 1992.)

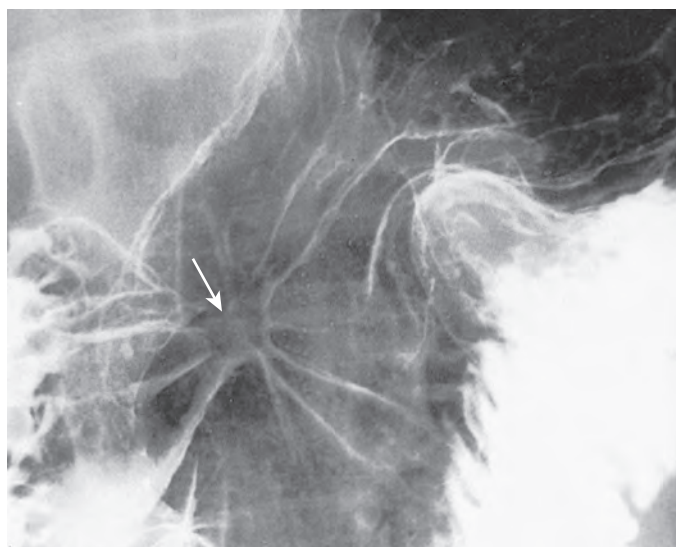


Figure 29-17 Ulcer scar with folds radiating to a central depression. Multiple folds are seen radiating to a central area (arrow) that could be mistaken for a shallow, residual ulcer crater. (From Levine MS, Creteur V, Kressel HY, et al: *Benign gastric ulcers: Diagnosis and follow-up with double-contrast radiography*. *Radiology* 164:9–13, 1987.)

and biopsy are required for a more definitive diagnosis. Healing of ulcers on the lesser curvature of the gastric body may also lead to marked retraction and deformity of the opposite wall, producing a deep incisura on the greater curvature.^{91,92} Rarely, scarring of the gastric body may result in the development of a so-called hourglass stomach with marked circumferential narrowing of the gastric body (Fig. 29-19C).

Benign Versus Malignant Ulcers

More than 95% of gastric ulcers diagnosed in the United States are found to be benign.^{64,94} Nevertheless, radiologic examinations are often thought to be unreliable in differentiating benign ulcers from ulcerated carcinomas. Early reports indicated that 6% to 16% of gastric ulcers that appeared benign on conventional single-contrast barium studies were malignant.⁹⁵⁻⁹⁸

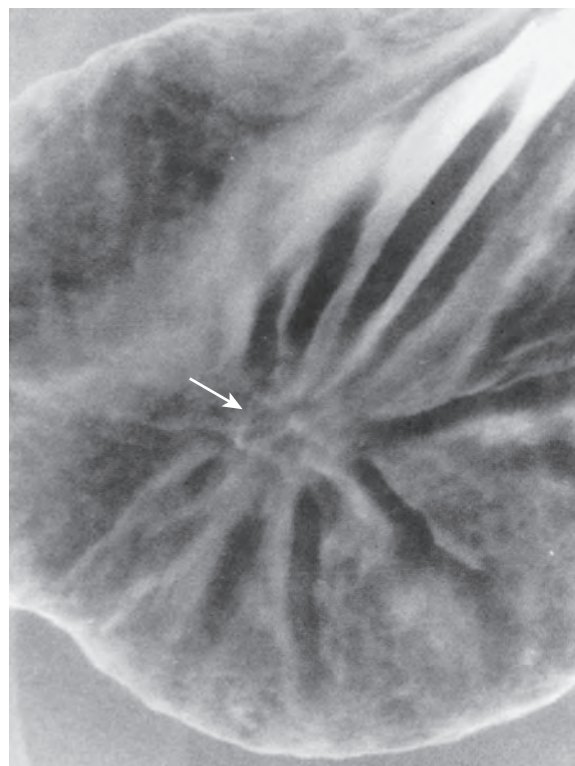


Figure 29-18 Re-epithelialized ulcer scar with centrally radiating folds. This scar can be differentiated from an active ulcer by the presence of normal areae gastricae within the central portion of the scar (arrow). (From Levine MS, Rubesin SE, Herlinger H, et al: *Double contrast upper gastrointestinal examination: Technique and interpretation*. *Radiology* 168:593–602, 1988.)

Although these studies were performed between 1955 and 1975, many gastroenterologists have used these data as the justification for performing endoscopy and biopsy on all patients with radiographically diagnosed gastric ulcers to rule out gastric carcinoma.

With double-contrast techniques, it is possible to obtain a far more detailed study of the mucosa surrounding the ulcer for signs of malignancy, such as irregular mass effect, nodularity,

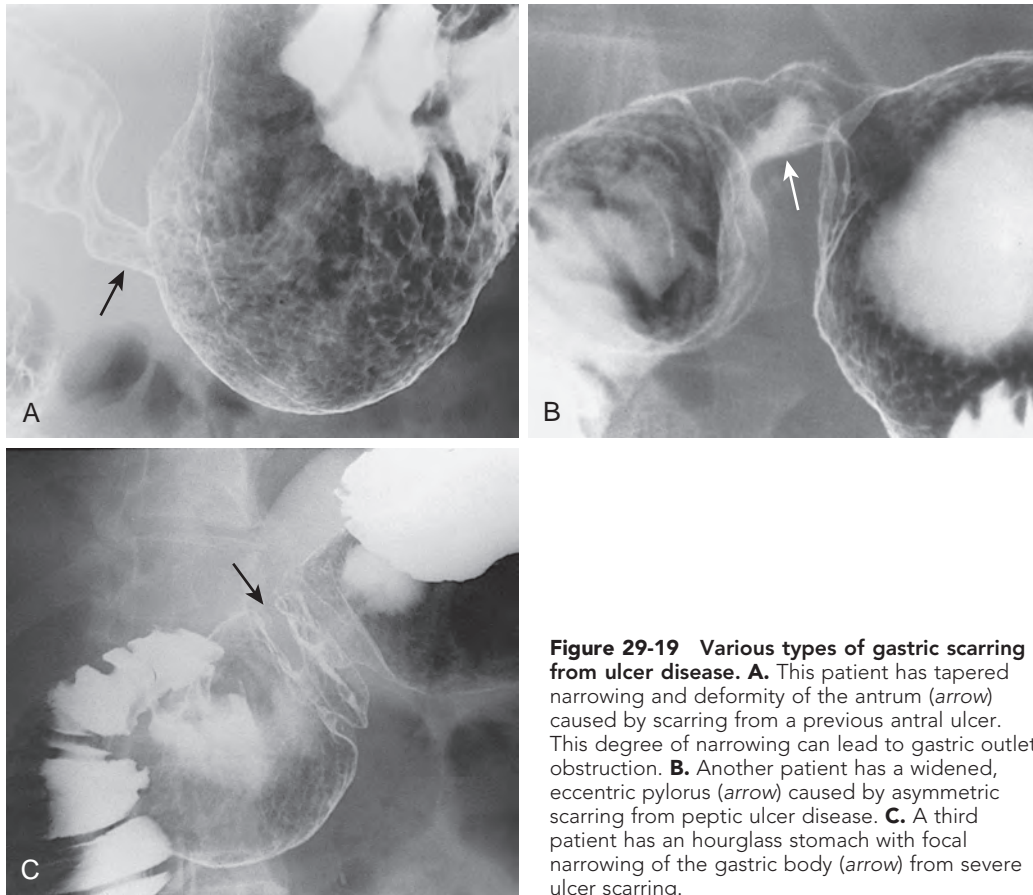


Figure 29-19 Various types of gastric scarring from ulcer disease. **A.** This patient has tapered narrowing and deformity of the antrum (arrow) caused by scarring from a previous antral ulcer. This degree of narrowing can lead to gastric outlet obstruction. **B.** Another patient has a widened, eccentric pylorus (arrow) caused by asymmetric scarring from peptic ulcer disease. **C.** A third patient has an hourglass stomach with focal narrowing of the gastric body (arrow) from severe ulcer scarring.

rigidity, and mucosal destruction. Several studies have found that almost all gastric ulcers with an unequivocally benign appearance on double-contrast examinations are benign lesions.^{69,99} In those studies, about two thirds of all benign ulcers had a benign radiographic appearance, so unnecessary endoscopy can be avoided in most patients with gastric ulcers diagnosed on double-contrast examinations. This finding has important implications for the evaluation of gastric ulcers because barium studies are safer and less expensive than endoscopy.

Unequivocally benign gastric ulcers are characterized en face by a round or ovoid ulcer crater surrounded by a smooth mound of edema or regular, symmetric folds that radiate directly to the edge of the crater (see Figs. 29-9, 29-13A, 29-14A, and 29-16A).^{69,99} The areae gastricae adjacent to the ulcer may be enlarged as a result of inflammation and edema of the surrounding mucosa (see Fig. 29-6A).⁶⁹ When viewed in profile, benign gastric ulcers project outside the gastric lumen and are sometimes associated with a smooth, symmetric ulcer mound or collar or with smooth, straight folds that radiate to the edge of the ulcer crater (see Figs. 29-4, 29-6, and 29-15A).

In contrast, malignant ulcers are characterized en face by an irregular ulcer crater eccentrically located within a discrete tumor mass.⁶⁹ There may be focal nodularity of the surrounding mucosa or distortion or obliteration of adjacent areae gastricae because of tumor infiltrating this region.⁶⁹ Although radiating folds may be present, they are often nodular, clubbed, fused, or amputated because of infiltration of the folds by tumor (Fig. 29-20).¹⁰⁰ When viewed in profile,

malignant ulcers do not project beyond the expected gastric contour, and there is often a discrete tumor mass that forms acute angles with the adjacent gastric wall rather than the obtuse, gently sloping angles expected for a benign mound of edema (Fig. 29-21).

Equivocal ulcers are those that have mixed features of benign and malignant disease, so a confident diagnosis cannot be made on radiologic criteria. For example, edema and inflammation surrounding a benign ulcer may result in enlarged, distorted areae gastricae, mass effect, or thickened, irregular folds, producing an indeterminate radiographic appearance (Fig. 29-22). Similarly, NSAID-induced greater curvature ulcers that have an apparent intraluminal location or substantial associated mass effect and shouldered edges may result in equivocal radiographic findings (see Fig. 29-8A). Most ulcers that have an equivocal appearance are ultimately found to be benign lesions. Nevertheless, it seems prudent to err on the side of caution by suggesting the possibility of malignant tumor for some benign lesions to avoid missing an early cancer.

Gastric ulcers that have an unequivocally benign appearance on double-contrast studies can be followed with serial double-contrast studies until complete healing without need for endoscopic evaluation.⁶⁹ However, ulcers that have an equivocal or suspicious appearance should be evaluated by endoscopy for a more definitive diagnosis. Although endoscopy is a sensitive technique for diagnosing gastric carcinoma, false-negative biopsy specimens and brushings have been reported in some patients with malignant lesions.¹⁰¹ If the radiographic findings are suggestive of malignant tumor, negative histologic or



Figure 29-20 Malignant gastric ulcer. This patient has an irregular ulcer on the posterior wall of the antrum with scalloped borders and nodular, clubbed folds surrounding the ulcer. These are classic features of a malignant gastric ulcer. (From Levine MS, Creteur V, Kressel HY, et al: *Benign gastric ulcers: Diagnosis and follow-up with double contrast radiography*. Radiology 164:9–13, 1987.)

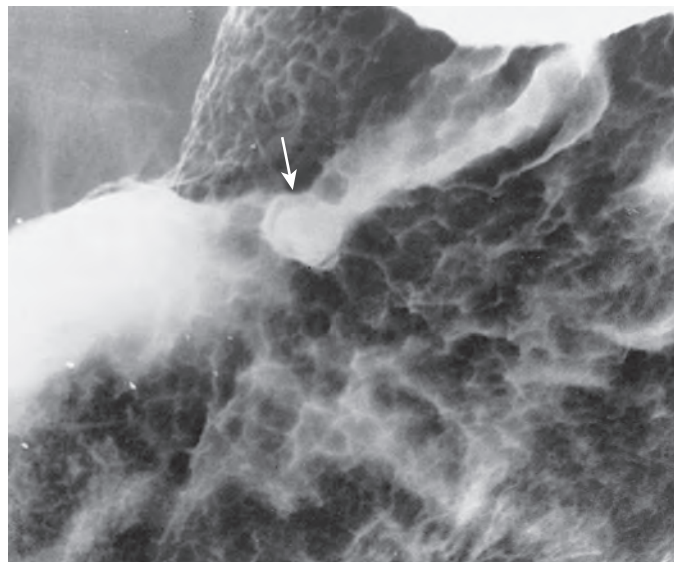


Figure 29-22 Benign gastric ulcer with an indeterminate radiographic appearance. A small ulcer (arrow) is seen near the lesser curvature with enlarged, nodular areae gastricae surrounding the ulcer because of edema and inflammation of the adjacent mucosa. Although the radiographic findings are equivocal, endoscopic biopsy specimens revealed no evidence of tumor, and a follow-up study after treatment showed complete healing of the ulcer.

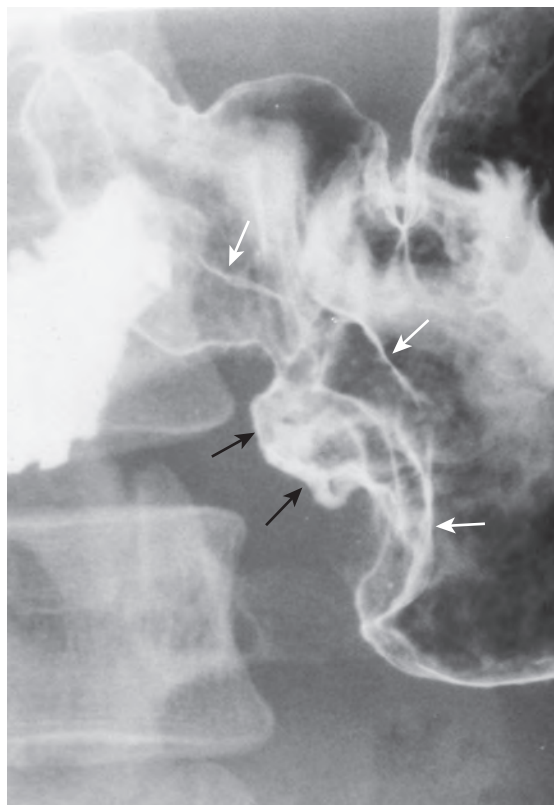


Figure 29-21 Malignant gastric ulcer. This patient has an ulcerated mass on the greater curvature of the antrum. Note how the ulcer (black arrows) projects inside the gastric lumen within a discrete tumor mass etched in white (white arrows) that forms acute angles with the adjacent gastric wall rather than the obtuse angles expected for a benign mound of edema. These are classic features of a malignant gastric ulcer.

cytologic findings therefore should not be taken as definitive evidence of a benign ulcer. Instead, follow-up barium studies should be performed until complete ulcer healing is documented. If the ulcer fails to heal with adequate medical treatment, or if it continues to have a suspicious radiographic appearance, repeat endoscopy and biopsy may be required. Even if endoscopic biopsy specimens and brushings remain negative, surgical resection should be considered for some patients with suspicious findings or intractable ulcers on serial barium studies.

DUODENAL ULCERS

In contrast to gastric ulcers, duodenal ulcers are almost always benign. When duodenal ulcers are detected on barium studies, these patients can therefore be treated medically without need for endoscopy. Unlike gastric ulcers, duodenal ulcers are often located on the anterior wall of the duodenal bulb, so prone compression views of the duodenum should be obtained routinely to detect these lesions. Duodenal ulcers may also be obscured by edema, spasm, or scarring of the bulb. Conversely, barium trapped in the crevices of a deformed bulb can mimic ulcer craters. Radiologists should therefore be aware of the limitations of barium studies in diagnosing duodenal ulcers and of the need to perform a biphasic examination in these patients.

Examination Technique

Double-contrast views of the duodenum must be complemented by prone compression views to demonstrate ulcers on the anterior wall of the bulb.¹⁰² These anterior wall ulcers may be hidden in the barium pool unless adequate compression of the bulb is obtained with an inflatable balloon or other prone compression device (Fig. 29-23). Other duodenal ulcers are best seen on upright compression views. Thus, optimal radiologic

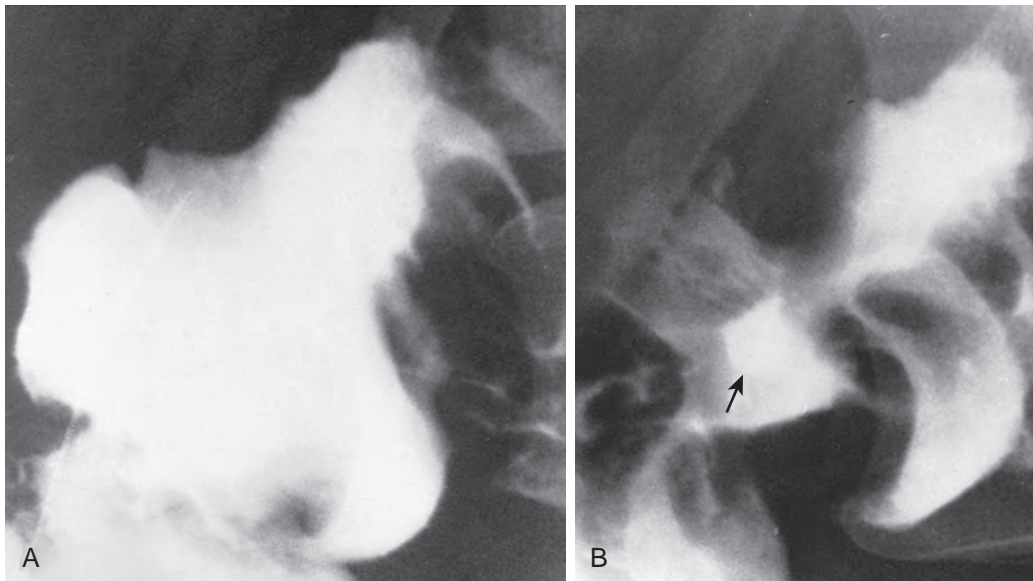


Figure 29-23 Importance of prone compression for anterior wall duodenal ulcers. **A.** Initial prone view shows no evidence of a duodenal ulcer. **B.** Prone compression of the bulb with an inflatable balloon clearly demonstrates an ulcer crater (arrow) on the anterior wall. This ulcer was hidden in the barium pool on the earlier radiograph.

evaluation of the duodenum requires a biphasic examination that includes double-contrast views of the duodenal bulb with a high-density barium suspension and prone or upright compression views with a low-density barium suspension.¹⁰³

Shape

Most duodenal ulcers appear as round or ovoid collections of barium (Fig. 29-24). About 5% of duodenal ulcers diagnosed on double-contrast studies have a linear configuration (Fig. 29-25).^{68,104} These linear ulcers tend to be located near the base of the duodenal bulb and often have a transverse orientation in relation to the bulb (see Fig. 29-25A).¹⁰⁴ As in the stomach, linear ulcers are thought to represent a stage of ulcer healing,^{66,104} and they may be indistinguishable from linear ulcer scars.

Size

Most duodenal ulcers diagnosed on double-contrast studies are smaller than 1 cm. A major advantage of double-contrast technique is its ability to demonstrate small ulcers, frequently no more than several millimeters in diameter (see Fig. 29-24B and C). Nevertheless, giant ulcers are occasionally detected in the duodenum (see later, “Giant Duodenal Ulcers”).

Location

About 90% of duodenal ulcers are located in the duodenal bulb and the remaining 10% in the postbulbar duodenum.^{46,105} Bulbar ulcers may involve the apex, central portion, or base of the bulb (see Fig. 29-24). Unlike gastric ulcers, which rarely develop on the anterior wall, as many as 50% of duodenal ulcers are located on the anterior wall of the bulb.^{77,106} Postbulbar ulcers are usually located in the proximal descending duodenum above the papilla of Vater (see later, “Postbulbar Ulcers”). Thus, the presence of one or more ulcers distal to the papilla should raise the possibility of Zollinger-Ellison syndrome (see later, “Zollinger-Ellison Syndrome”).

Morphologic Features

Bulbar Ulcers. Ulcers in the duodenal bulb usually appear as discrete niches that can be visualized en face or in profile (see Fig. 29-24). The ulcers are often surrounded by a smooth, radiolucent mound of edematous mucosa. Occasionally, the size of the ulcer mound may be quite striking in relation to the central crater (see Fig. 29-26B). Bulbar ulcers also tend to be associated with radiating folds that converge centrally at the edge of the crater (see Fig. 29-24B and C). In patients with shallow ulcers or small healing ulcers, the ulcer crater may be visible only with optimal radiographic technique. Thus, the presence of radiating folds should prompt a careful search for an active ulcer at the site of fold convergence before attributing these folds to an ulcer scar.

As in the stomach, ulcers on the anterior wall of the duodenal bulb may be difficult to detect on routine double-contrast views. Other anterior wall ulcers may be manifested by a ring shadow caused by barium coating the rim of the unfilled ulcer crater (Fig. 29-26A).⁸⁵ These anterior wall ulcers can be demonstrated by obtaining prone or upright compression views of the bulb to fill the crater with barium (Fig. 29-26B).

Duodenal ulcers are often associated with considerable deformity of the bulb secondary to edema and spasm accompanying the ulcer or scarring from a previous ulcer (see Fig. 29-24B).¹⁰² This deformity may obscure small ulcers in the bulb, resulting in a substantial number of false-negative examinations. It is therefore important to recognize the limitations of the radiologic diagnosis of duodenal ulcers in the presence of a deformed bulb. Nevertheless, symptomatic patients with a deformed bulb on barium studies should probably be treated for an active duodenal ulcer because of the high risk of ulcer disease, whether or not an ulcer is demonstrated with certainty.

Postbulbar Ulcers. Postbulbar ulcers are usually located on the medial wall of the proximal descending duodenum above the

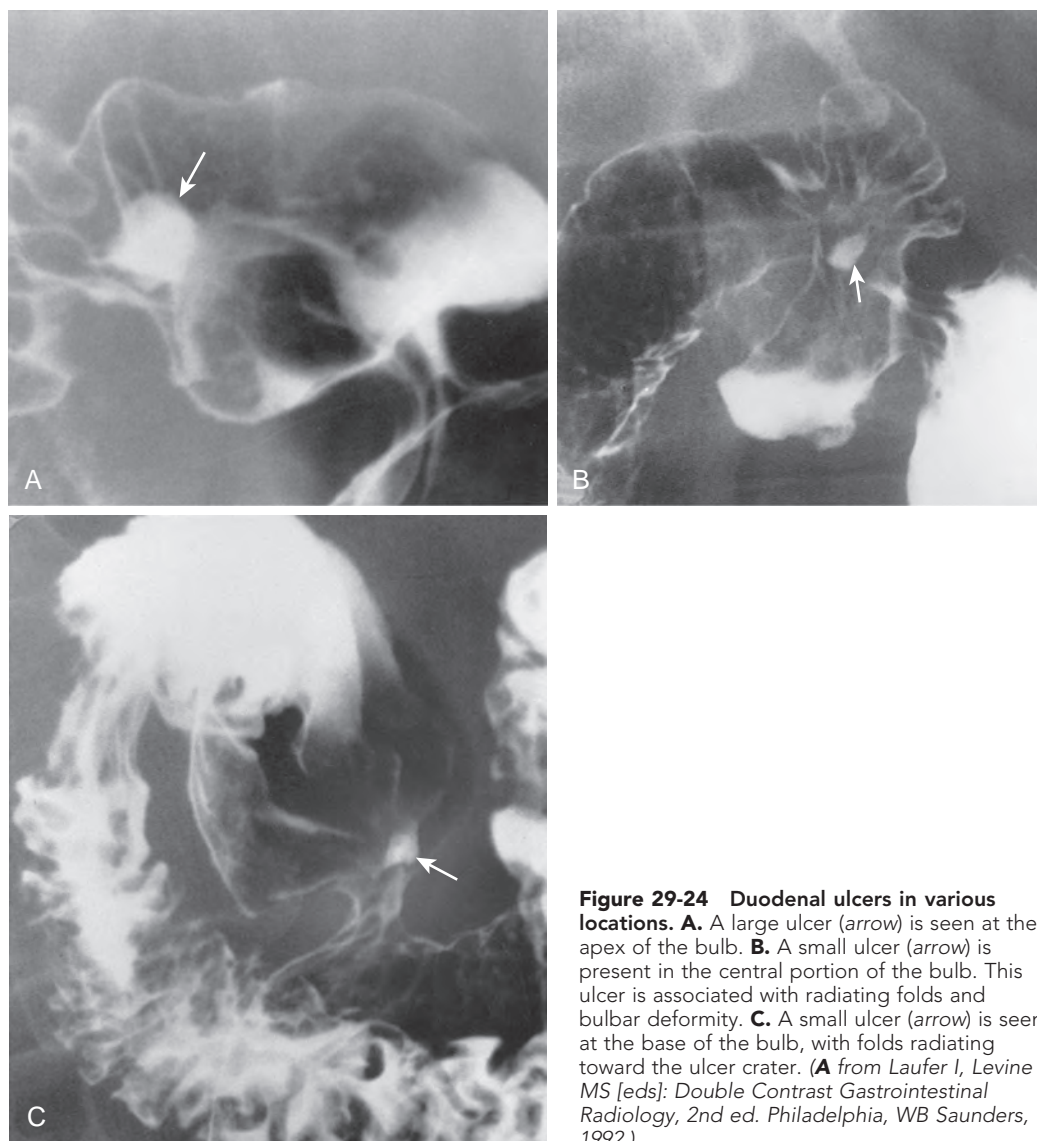


Figure 29-24 Duodenal ulcers in various locations. **A.** A large ulcer (arrow) is seen at the apex of the bulb. **B.** A small ulcer (arrow) is present in the central portion of the bulb. This ulcer is associated with radiating folds and bulbar deformity. **C.** A small ulcer (arrow) is seen at the base of the bulb, with folds radiating toward the ulcer crater. (**A** from Laufer I, Levine MS [eds]: *Double Contrast Gastrointestinal Radiology*, 2nd ed. Philadelphia, WB Saunders, 1992.)

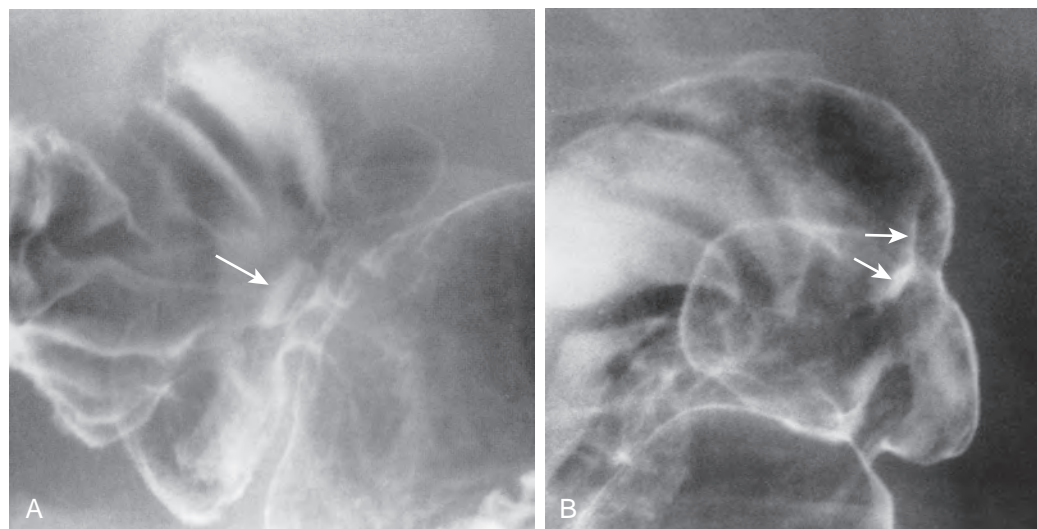


Figure 29-25 Linear duodenal ulcers. **A.** A linear ulcer (arrow) is seen at the base of the bulb. The ulcer has a transverse orientation in relation to the bulb. **B.** In another patient, a linear ulcer (arrows) is seen at the apex of the bulb. (From Laufer I, Levine MS [eds]: *Double Contrast Gastrointestinal Radiology*, 2nd ed. Philadelphia, WB Saunders, 1992.)

Figure 29-26 Ring shadow caused by an anterior wall duodenal ulcer. **A.** Supine oblique double-contrast view of the duodenum shows a ring shadow (arrow) in the bulb as a result of barium coating the rim of an unfilled ulcer crater on the nondependent surface. **B.** Prone compression view shows filling of the anterior wall ulcer (arrow). Note the large radiolucent mound of edema surrounding the ulcer. (From Laufer I, Levine MS [eds]: *Double Contrast Gastrointestinal Radiology*, 2nd ed. Philadelphia, WB Saunders, 1992.)

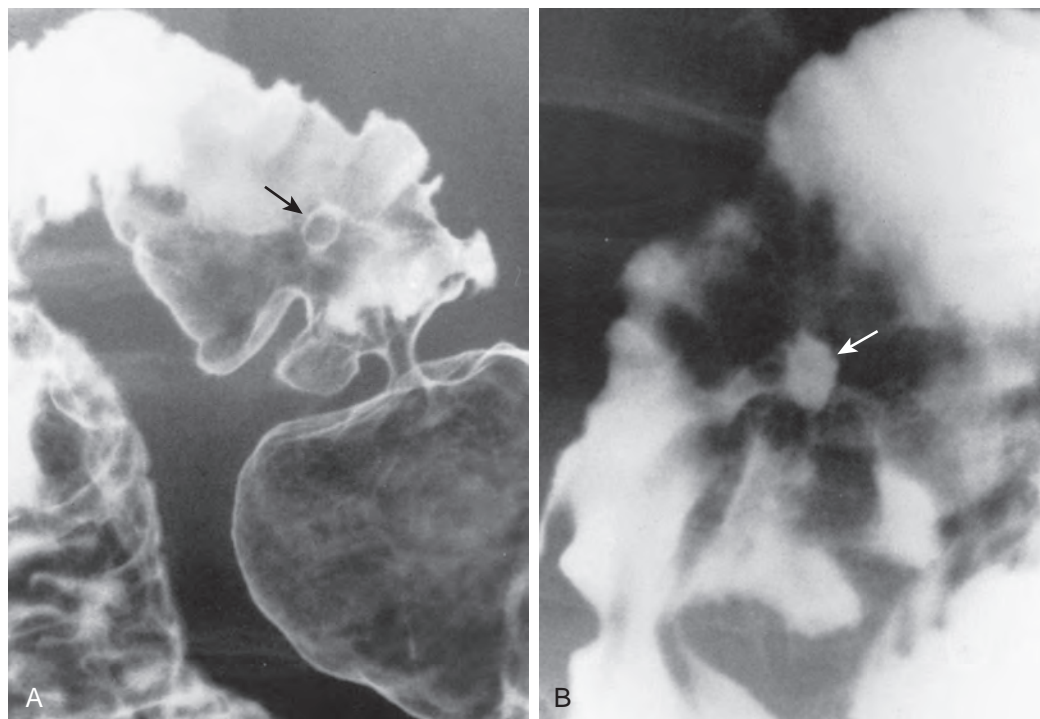
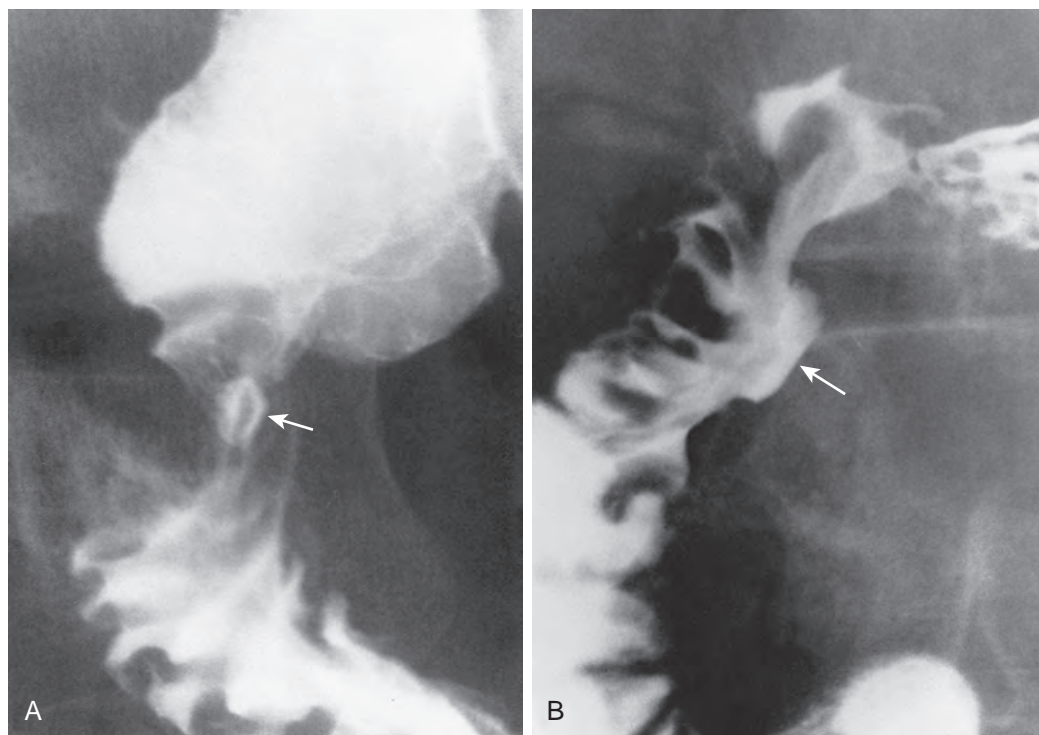


Figure 29-27 Postbulbar duodenal ulcers. **A.** An ulcer (arrow) is seen on the medial wall of the proximal descending duodenum. There is also a smooth, rounded indentation of the lateral wall caused by associated edema and spasm. **B.** Another patient has a large, relatively flat ulcer (arrow) on the medial wall of the postbulbar duodenum above the papilla of Vater. Folds radiate toward the ulcer crater.



papilla of Vater (Fig. 29-27).^{46,105,107} These ulcers are notoriously difficult to demonstrate on barium studies, presumably because severe edema and spasm accompanying the ulcer prevent visualization of the ulcer crater. This edema and spasm often result in circumferential narrowing of the adjacent lumen or eccentric narrowing with a smooth, rounded indentation on the lateral wall of the descending duodenum opposite the crater (see Fig.

29-27A).¹⁰⁷ If the ulcer crater itself is obscured by edema and spasm, this indentation may be the only radiologic sign of a postbulbar ulcer (Fig. 29-28).

Many postbulbar duodenal ulcers are larger than 1 cm, so they tend to be larger than bulbar ulcers, which are usually smaller than 1 cm.⁴⁶ Large postbulbar ulcers may cause marked narrowing of the adjacent duodenum proximally and distally,



Figure 29-28 Postbulbar duodenal ulcer not visualized on barium study. A prominent indentation is seen on the lateral aspect of the proximal descending duodenum (arrow) as a result of edema and spasm accompanying a postbulbar ulcer that was not visualized on this study. The ulcer was seen at subsequent endoscopy.

secondary to severe edema and spasm accompanying these ulcer craters (Fig. 29-29).⁴⁶ The larger size of the ulcers could help explain the higher prevalence of upper GI bleeding and the poorer response of postbulbar ulcers to medical therapy.⁴⁶ Healed postbulbar ulcers may occasionally be associated with focal scarring and fibrosis, resulting in the development of a so-called *ring stricture* with eccentric narrowing of the postbulbar duodenum (Fig. 29-30).¹⁰⁸ An annular pancreas constricting the postbulbar duodenum may produce similar findings.

Giant Duodenal Ulcers. Giant duodenal ulcers are defined as duodenal ulcers larger than 2 cm.¹⁰⁹ These ulcers are important because of a greater risk of complications such as perforation, obstruction, and upper GI bleeding.¹¹⁰ Nevertheless, treatment with antisecretory agents may lead to dramatic ulcer healing, so these patients can often be managed conservatively without need for surgery.¹¹¹ Giant duodenal ulcers are almost always located in the duodenal bulb and may be so large that they replace virtually the entire bulb (Figs. 29-31 and 29-32). Paradoxically, giant ulcers can be mistaken on barium studies for a scarred or even normal bulb. However, the duodenal bulb would be expected to change in size and shape at fluoroscopy, whereas these giant ulcers will have a fixed, unchanging configuration (see Fig. 29-32).^{109,111,112}

Giant duodenal ulcers may occasionally be recognized on ultrasound studies as discrete, hypoechoic cystic lesions anterolateral to the head of the pancreas.¹¹³ The differential diagnosis

for these lesions includes a duodenal diverticulum and pancreatic pseudocyst. In such cases, a barium study should be performed for a more definitive diagnosis.

Multiplicity

About 15% of patients with duodenal ulcers have multiple ulcers.¹¹⁴ Most of these are located in the duodenal bulb. The presence of multiple ulcers should raise the possibility of Zollinger-Ellison syndrome (see later, “[Zollinger-Ellison Syndrome](#)”).

Ulcer Healing and Scarring

Duodenal ulcers usually heal rapidly during treatment with antisecretory agents. As the ulcers decrease in size, they often have a linear configuration.^{66,104} Ulcer healing may lead to the development of an ulcer scar, manifested by radiating folds, bulbar deformity, or both. When radiating folds are present, they almost always converge at the site of the previous ulcer. In some patients, a residual depression in the central portion of the scar simulates an active ulcer crater. As a result, it is often difficult to differentiate small, healing ulcers from ulcer scars. Nevertheless, follow-up barium studies to demonstrate ulcer healing are probably unnecessary for patients with uncomplicated duodenal ulcers who have an adequate clinical response to medical therapy because these ulcers are almost always benign. Follow-up studies should therefore be reserved for patients with intractable ulcer symptoms or ulcer complications such as obstruction.

Bulbar deformity is caused by asymmetric scarring and retraction of the duodenal bulb during ulcer healing. Uninvolved segments of the bulb may balloon out between areas of fibrosis, producing one or more pseudodiverticula, which can usually be differentiated from ulcers by their tendency to change in size and shape at fluoroscopy. When multiple pseudodiverticula are present, the duodenal bulb may have a classic clover-leaf appearance (Fig. 29-33).

PYLORIC CHANNEL ULCERS

Pyloric channel ulcers should be treated as gastric ulcers rather than duodenal ulcers in terms of the need for aggressive evaluation and follow-up to differentiate these lesions from ulcerated carcinomas. Most pyloric channel ulcers are smaller than 1 cm and are located on the lesser curvature aspect of the pylorus. These ulcers tend to be located on the anterior wall of the pylorus, so they may appear as ring shadows on routine double-contrast views (Fig. 29-34A).¹¹⁵ In such cases, the ulcers should fill with barium on prone or upright compression views (Fig. 29-34B). Some pyloric channel ulcers may cause marked edema and spasm of the pylorus and distal antrum, so optimal radiologic evaluation of this area is not always possible.

Pyloric channel ulcers must be differentiated on barium studies from pseudodiverticula caused by scarring from previous ulcer disease or surgical pyloroplasty. However, ulcers usually have a fixed configuration, whereas pseudodiverticula are more likely to change in size and shape at fluoroscopy. The presence of folds in the region of the outpouching should also suggest a pseudodiverticulum rather than an ulcer. Occasionally, adult hypertrophic pyloric stenosis may be manifested by a narrowed, elongated pyloric channel with diamond-shaped outpouchings or dimples extending superiorly or inferiorly from this region, but these patients usually have a

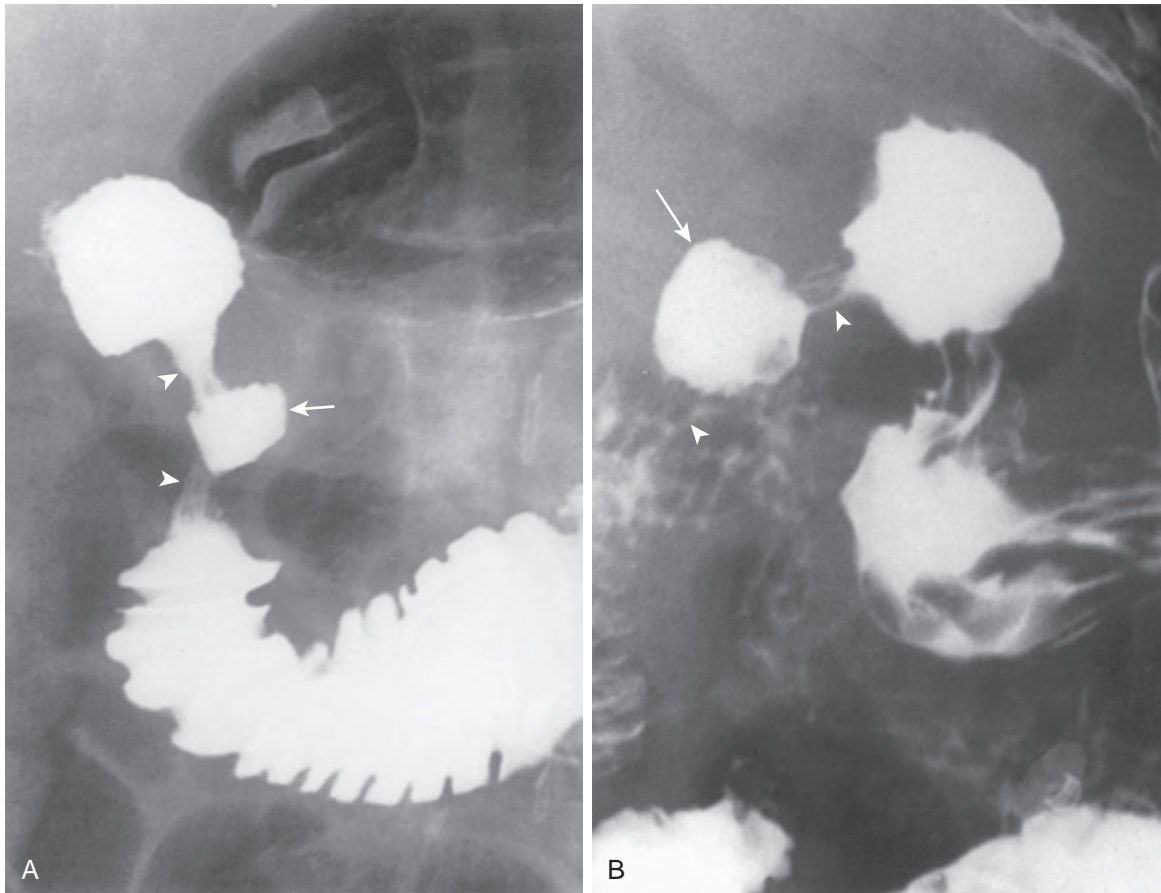


Figure 29-29 Large postbulbar duodenal ulcers. A, B. Two patients with large postbulbar ulcers (arrows) in the proximal descending duodenum. In both cases, note marked narrowing of the adjacent duodenum proximally and distally (arrowheads) as a result of severe edema and spasm accompanying these ulcer craters. (From Carucci LR, Levine MS, Rubesin SE, et al: Upper gastrointestinal tract barium examination of postbulbar duodenal ulcers. *AJR* 182:927–930, 2004.)

long-standing history of obstructive symptoms. Healing of pyloric channel ulcers may lead to narrowing, elongation, or angulation of the pylorus, sometimes associated with gastric outlet obstruction.

Differential Diagnosis

Gastric or duodenal ulcers may occasionally be simulated by various double-contrast artifacts.¹¹⁶ An inadequate or poorly prepared barium suspension may result in the development of barium precipitates that resemble tiny ulcers in the stomach or duodenum. However, these precipitates can be differentiated from ulcers by their failure to project beyond the contour of the stomach or duodenum in profile and by the absence of associated findings such as mucosal edema or radiating folds. Stalactites are hanging droplets of barium that are sometimes seen on the anterior (nondependent) gastric wall.¹¹⁷ Although a stalactite can be mistaken for a small ulcer on a single view, the transient nature of this finding at fluoroscopy differentiates a stalactite from a true ulcer. Finally, calcified densities (e.g., renal calculi or calcified splenic arteries) or contrast-containing structures (e.g., colonic diverticula) overlying the stomach or duodenum can be mistaken for ulcers on double-contrast images. These artifacts are easily recognized by obtaining multiple images in different projections.

The most important consideration in the differential diagnosis of a benign gastric ulcer is an ulcerated gastric carcinoma (see earlier, “[Benign Versus Malignant Ulcers](#)”). An ulcer that is surrounded by a discrete mound of edema can also be mistaken for an ulcerated submucosal mass such as a gastrointestinal stromal tumor (GIST).^{118,119} However, the edematous mass surrounding an ulcer usually has poorly defined borders that form obtuse angles with the adjacent gastric wall, whereas a submucosal mass has well-defined borders that form right angles with the adjacent gastric wall.¹¹⁹ When gastric ulcers are associated with massive edema, there may be such narrowing and deformity that the radiographic findings erroneously suggest an infiltrating carcinoma. This problem is more likely to occur with prepyloric ulcers that cause gastric outlet obstruction, so it is not possible to adequately assess the distal antrum. If a malignant lesion cannot be excluded on radiologic criteria, endoscopy and biopsy should be performed for a more definitive diagnosis.

Although multiple gastric or duodenal ulcers may be present in patients with uncomplicated peptic ulcer disease, this finding should raise the possibility of Zollinger-Ellison syndrome, cytomegalovirus infection, caustic ingestion, lymphoma, and other granulomatous conditions such as Crohn’s disease, tuberculosis, sarcoidosis, and syphilis (see Chapters 30 and 33). In many cases, the correct diagnosis is suggested by the clinical history.



Figure 29-30 Postbulbar ring stricture. There is eccentric narrowing (arrow) of the postbulbar duodenum secondary to scarring and fibrosis from a previous ulcer in this location. (From Laufer I, Levine MS [eds]: *Double Contrast Gastrointestinal Radiology*, 2nd ed. Philadelphia, WB Saunders, 1992.)

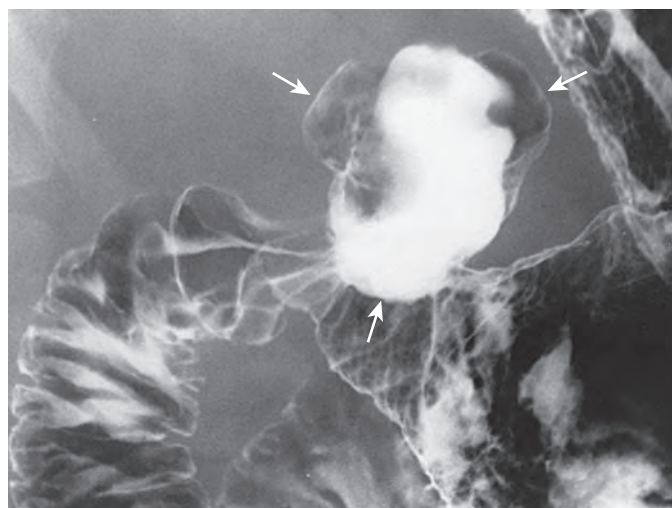


Figure 29-31 Giant duodenal ulcer. This giant ulcer (arrows) has replaced almost the entire duodenal bulb. Paradoxically, such ulcers can be mistaken for a scarred or even normal bulb.

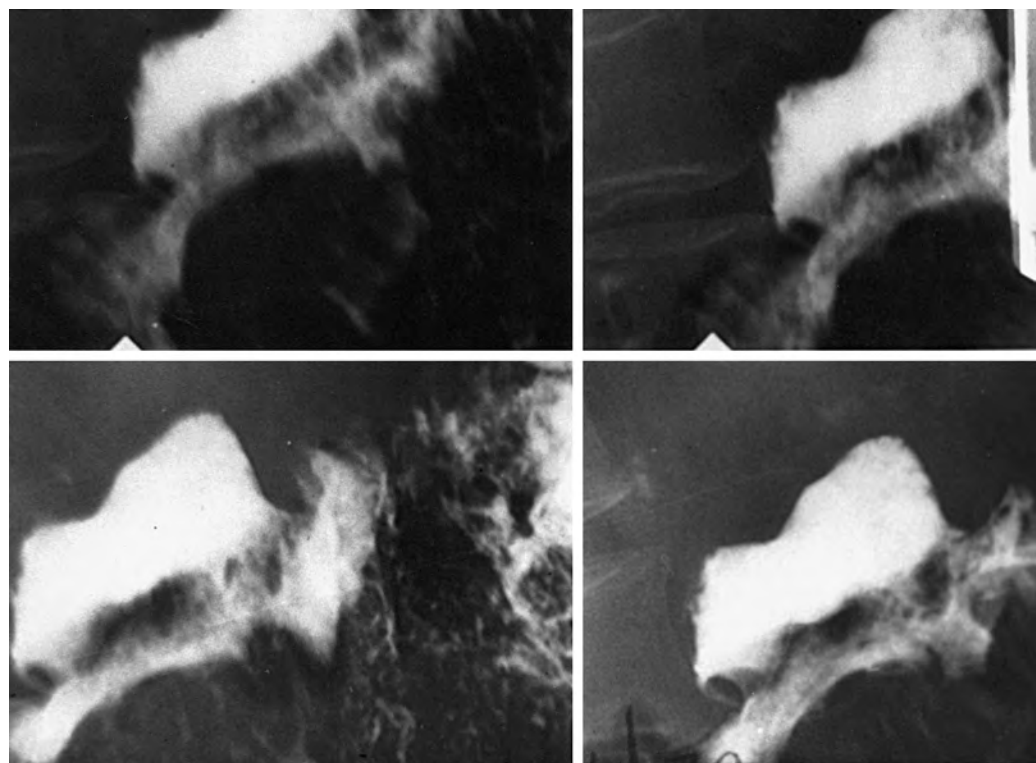


Figure 29-32 Giant duodenal ulcer. Four spot images of the bulb show a giant ulcer that has a constant size and shape. In contrast, the duodenal bulb usually has a changing appearance at fluoroscopy. Also note the large radiolucent band of edema adjacent to the ulcer.

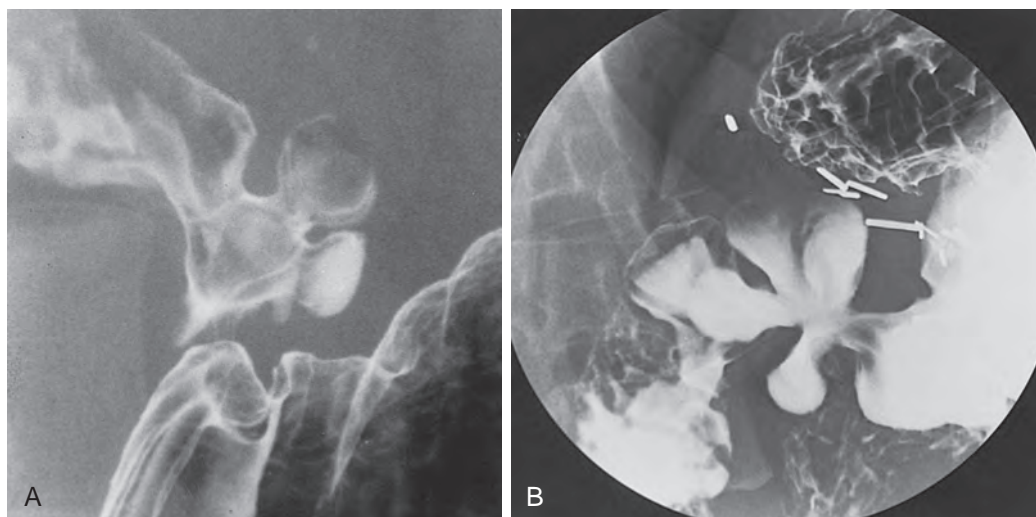


Figure 29-33 Scarred duodenal bulb. **A, B.** Two examples of marked bulbar deformity with multiple pseudodiverticula, producing a cloverleaf appearance.

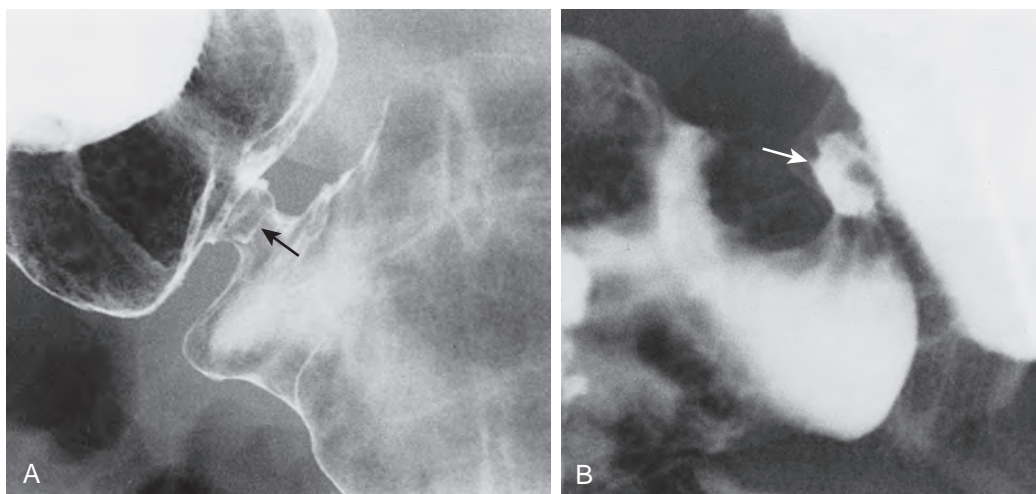


Figure 29-34 Pyloric channel ulcer. **A.** Initial double-contrast view with the patient in a supine position shows a partial ring shadow (arrow) in the region of the pylorus. **B.** Prone compression view shows barium filling an ulcer crater (arrow) on the anterior wall of the pyloric channel.

Gastric ulcer scars that are manifested by radiating folds must be differentiated from early gastric cancers in which the folds tend to have a more lobulated, nodular, or irregular appearance.¹⁰⁰ If the radiographic findings are equivocal, endoscopy and biopsy should be performed for a more certain diagnosis. Benign-appearing ulcer scars may also result from healing of lymphomatous gastric lesions treated with chemotherapy (see Chapter 33).¹²⁰ Finally, ulcer scars may resemble surgical scars resulting from prior gastrectomy, cystogastrectomy (internal drainage of a pancreatic pseudocyst into the stomach), or wedge resection of the stomach,⁹² but ulcer scars can usually be differentiated from surgical scars on the basis of the clinical history.

Approach to Ulcers

In view of current recommendations that all *H. pylori*-positive patients with gastric or duodenal ulcers be treated with

antimicrobial and antisecretory agents,^{52,53} it is important to determine whether patients with ulcers are infected with *H. pylori*. Although endoscopy and biopsy may be performed to document the presence of this infection, highly accurate noninvasive tests for *H. pylori*, such as a urea breath test and serologic test, are widely available (see Chapter 30). The combination of a double-contrast upper GI study and noninvasive testing for *H. pylori* could therefore replace endoscopy as a reasonable approach for evaluating patients with dyspepsia, epigastric pain, or other upper GI symptoms.⁸

Here is one scenario. Patients with persistent upper GI symptoms who fail to respond to an empiric trial of antisecretory agents could undergo a double-contrast barium study as the first diagnostic examination. If the barium study reveals a gastric or duodenal ulcer, a noninvasive test for *H. pylori* could be performed to determine whether the patient should receive antibiotics and conventional antisecretory agents. If the barium study reveals gastritis or duodenitis without an ulcer, however,

there is not yet enough evidence to justify treatment with antibiotics, even if these patients are infected with *H. pylori* (see Chapter 30). Thus, testing for *H. pylori* would not be required in most cases. Finally, if the barium study reveals a suspicious gastric ulcer or any abnormality that is equivocal or suspicious for malignant tumor, endoscopy should be performed for a more definitive diagnosis.

If randomized, controlled trials ultimately reveal that symptomatic patients with *H. pylori* gastritis should be treated with antimicrobial agents in the absence of ulcers, noninvasive tests for *H. pylori* could be performed routinely at the time of the initial barium study. Clinical decisions regarding treatment with antisecretory agents or antibiotics could then be made on the basis of the combined results of the barium study and noninvasive tests for *H. pylori*. Nevertheless, endoscopy would still be required for any patients with equivocal or suspicious radiographic findings.

Complications

The major complications of peptic ulcers include upper GI bleeding, obstruction, and perforation. Such events can be life-threatening, so early diagnosis and treatment of these complications are essential for decreasing the morbidity and mortality in patients with peptic ulcers.

UPPER GASTROINTESTINAL BLEEDING

Endoscopy has a sensitivity of more than 90% in detecting the site of hemorrhage in patients with bleeding peptic ulcers.¹²¹ Barium studies are less accurate because of the difficulty obtaining adequate mucosal coating in the presence of bleeding and the inability to determine whether a radiographically diagnosed lesion is the actual source of bleeding. Nevertheless, double-contrast studies can detect the bleeding site in 70% to 80% of patients with acute upper GI hemorrhage.^{121,122}

The most frequent radiologic sign of bleeding in a gastric or duodenal ulcer is a blood clot at the base of the ulcer, typically seen as a smooth or irregular filling defect in the barium-filled ulcer crater (Fig. 29-35).¹²² Although granulation tissue or debris in the ulcer may produce similar findings, the defect is likely to represent an adherent blood clot in patients with a history of recent upper GI bleeding. If the clot is dislodged, recurrent bleeding may result in potentially catastrophic consequences. These patients should therefore be observed carefully for 24 to 48 hours when a blood clot is detected on barium studies.

OBSTRUCTION

Although ulcers in the fundus, body, or proximal antrum of the stomach rarely cause gastric outlet obstruction, ulcers in the distal antrum, pyloric channel, or duodenum may cause obstruction secondary to edema and spasm associated with the ulcer crater or scarring and fibrosis associated with ulcer healing. In patients with severe gastric outlet obstruction, abdominal radiographs may reveal a dilated stomach containing food and debris (Fig. 29-36A). This food or fluid in the stomach may dilute ingested barium, compromising the radiographic examination (Fig. 29-36B). The stomach should therefore be decompressed with a nasogastric tube before performing barium studies on these patients.

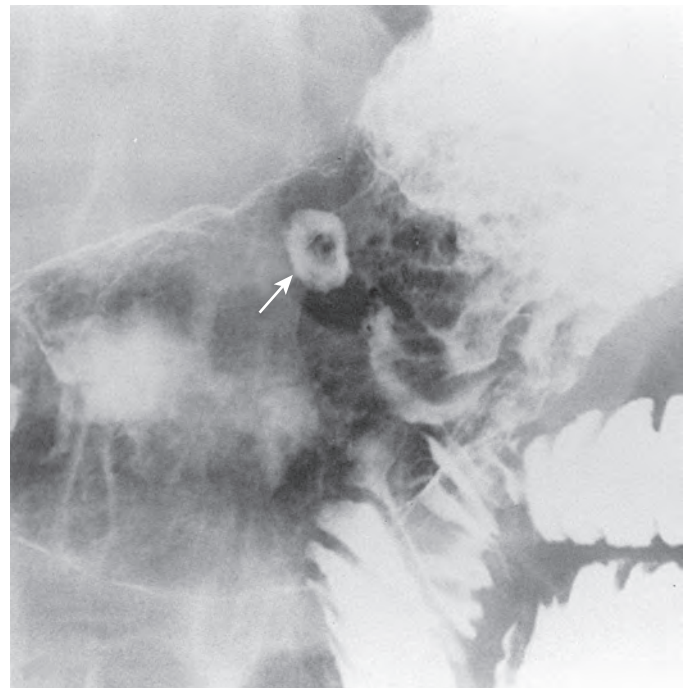


Figure 29-35 Ulcer with blood clot. A radiolucent filling defect is seen in the central portion of a barium-filled ulcer (arrow) on the posterior wall of the stomach. This patient presented with hematemesis 1 day earlier. (From Laufer I, Levine MS [eds]: *Double Contrast Gastrointestinal Radiology*, 2nd ed. Philadelphia, WB Saunders, 1992.)

Severe scarring from ulcers in the distal antrum or pyloric channel may be manifested on barium studies by a relatively short segment of narrowing with delayed emptying of barium from the stomach (see Fig. 29-19A). It is sometimes difficult to differentiate areas of scarring from a localized scirrhous carcinoma involving the prepyloric region of the antrum,¹²³ but irregular narrowing and abrupt, shelflike proximal borders should favor a malignant lesion (see Chapter 32). If the findings are equivocal or suspicious for tumor, endoscopy and biopsy should be performed for a more definitive diagnosis.

Although scarring from duodenal bulb ulcers rarely causes obstruction, postbulbar ulcers may lead to obstructing strictures in the proximal descending duodenum (see earlier, “**Postbulbar Ulcers**”). Other causes of duodenal narrowing and obstruction include Crohn’s disease, tuberculosis, tumors, hematomas, duplication cysts, and extrinsic compression of the duodenum by an annular pancreas, pancreatitis, pancreatic pseudocyst, or pancreatic carcinoma.

PERFORATION

Penetrating ulcers on the anterior wall of the stomach or duodenum may perforate directly into the peritoneal cavity, whereas penetrating ulcers on the posterior wall of the stomach or duodenum usually result in a walled-off or confined perforation. Some penetrating ulcers may also involve other hollow organs, producing a fistula. These various types of perforations are considered separately in the following sections.

Free Perforation

Ulcers on the anterior wall of the stomach or duodenum directly abut the peritoneal cavity, so perforation of a penetrating ulcer

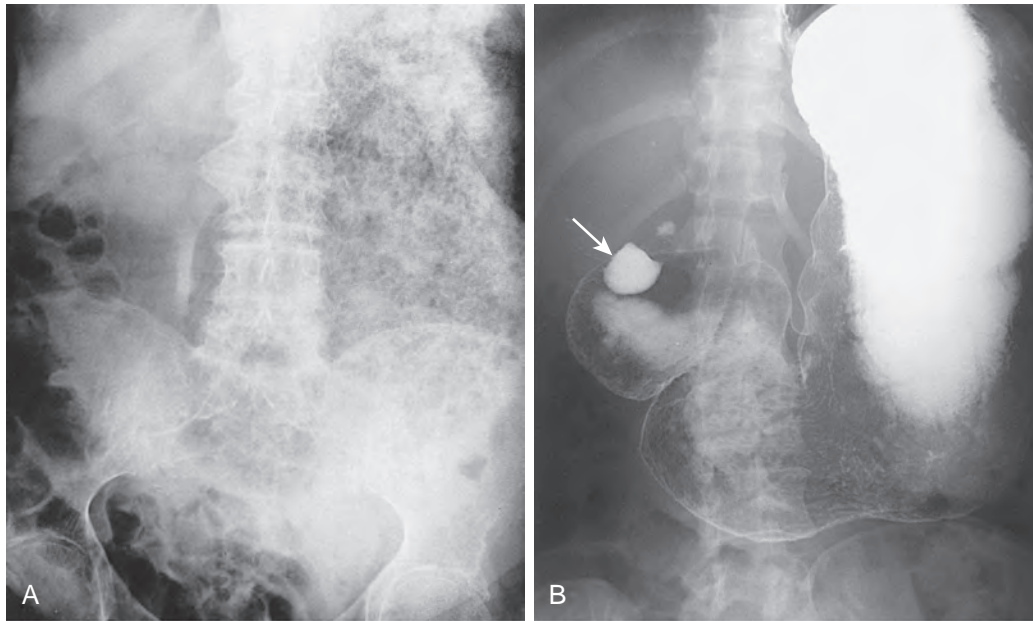


Figure 29-36 Gastric outlet obstruction caused by pyloric channel ulcers. **A.** Abdominal radiograph shows a markedly dilated stomach with retained food and debris caused by gastric outlet obstruction. After the stomach was decompressed, endoscopy revealed a pyloric channel ulcer causing the obstruction. **B.** In another patient, an overhead radiograph from a barium study shows a dilated stomach with retained fluid diluting the barium and no emptying into the duodenum. A large pyloric channel ulcer (arrow) is also seen.

in this location may result in acute peritonitis with free spillage of gastric and duodenal contents into the peritoneal cavity. Because duodenal ulcers are often located on the anterior wall of the bulb, a perforated duodenal ulcer is the most common cause of peritonitis in the adult population. The volume of gas that escapes into the peritoneal cavity from a perforated ulcer depends on how quickly the site of perforation seals off. In one study, free intraperitoneal air was detected on abdominal radiographs in only about two thirds of patients with perforated duodenal ulcers.¹²⁴ Thus, the presence of pneumoperitoneum in an acutely ill patient strongly supports the diagnosis of a perforated ulcer, but the absence of pneumoperitoneum in no way excludes this diagnosis.

If abdominal radiographs reveal pneumoperitoneum in patients with clinical signs of peritonitis, immediate surgery is warranted. If there is no evidence of pneumoperitoneum, studies with water-soluble contrast agents or computed tomography (CT) may be performed to determine whether a perforation has occurred. Only about 50% of patients with perforated duodenal ulcers are found to have extravasation of contrast medium from the duodenum, presumably because the perforation has sealed off by the time the examination is performed.¹²⁵ When extravasation of contrast medium does occur, about 50% of patients are found to have a generalized leak into the peritoneal cavity and 50% are found to have a walled-off leak (Fig. 29-37)¹²⁵ (see later, “[Confined Perforation](#)”).

When an ulcer causes free perforation, studies with water-soluble contrast agents may show contrast medium leaking from the stomach or duodenum into the subhepatic space or elsewhere into the peritoneal cavity. CT may reveal inflammatory changes in the soft tissues abutting the stomach and duodenum, extraluminal fluid or contrast material, and varying amounts of free intraperitoneal air.¹²⁶ The site of perforation

can sometimes be identified on CT by interruption of the enhanced gastroduodenal wall or by tiny extraluminal air bubbles in close proximity to the perforation.¹²⁷

Less frequently, ulcers on the posterior wall of the stomach may perforate into the lesser peritoneal cavity, or lesser sac, a potential space between the stomach and pancreas. An abscess in the lesser sac may be manifested by extraluminal gas collections in the left upper quadrant on abdominal radiographs (Fig. 29-38) or by extrinsic mass effect on the posterior wall of the stomach or actual leakage of contrast material into the lesser sac on studies with water-soluble contrast agents. CT is extremely useful for documenting these lesser sac collections or abscesses.¹²⁸

Confined Perforation

Penetrating ulcers on the posterior wall of the stomach or duodenum are often associated with the development of a walled-off or confined perforation secondary to an inflammatory reaction and fibrous adhesions that seal off the perforation site as the ulcer enters adjacent structures. The pancreas is involved in most patients with confined perforations. Other less common sites of involvement include the lesser omentum, transverse mesocolon, liver, spleen, biliary tract, and colon. If the affected structure is a hollow organ such as the colon or biliary tract, this process may lead to the development of a fistula (see later, “[Fistulas](#)”).

Less than 50% of patients with posterior penetrating ulcers and confined perforations have evidence of extraluminal gas or contrast medium collections on studies with water-soluble contrast agents. A posterior penetrating ulcer should be suspected, however, when an unusually deep ulcer crater is seen in profile on the posterior wall of the stomach or duodenum. In such cases, CT may be helpful for demonstrating signs of pancreatic penetration, including loss of fascial planes and the presence of

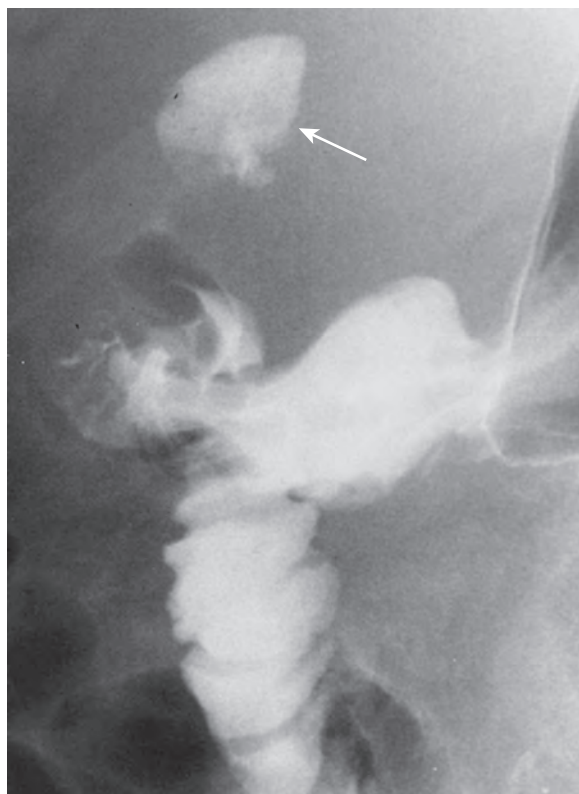


Figure 29-37 Perforated duodenal ulcer. Water-soluble contrast medium is seen tracking superiorly from the region of the duodenal bulb into a sealed-off collection (arrow). This patient presented with clinical signs of peritonitis.

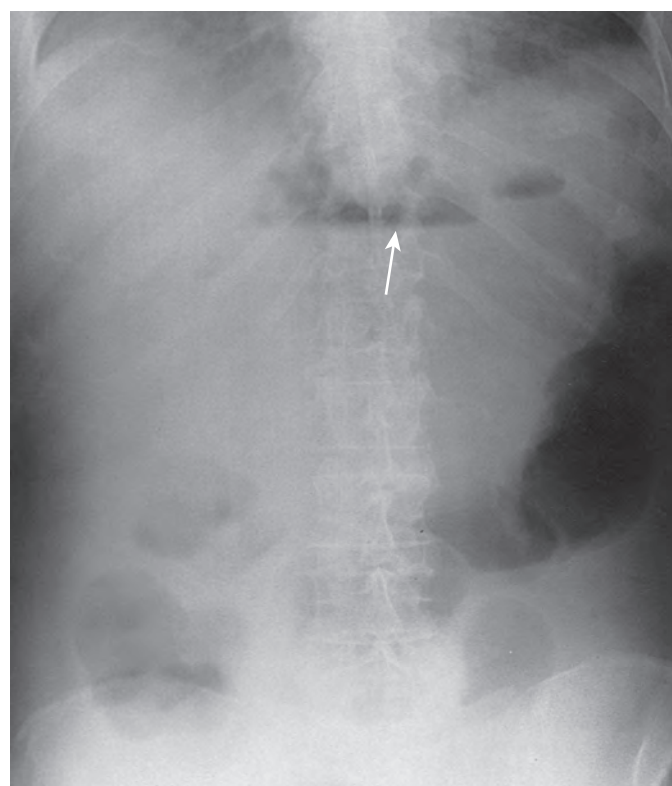


Figure 29-38 Lesser sac abscess caused by a perforated gastric ulcer. Upright abdominal radiograph shows an air-fluid level (arrow) in the lesser sac caused by a lesser sac abscess. Subsequent study with a water-soluble contrast agent revealed a perforated posterior wall gastric ulcer with leakage of the contrast agent directly into the lesser sac.

soft tissue bands or low-density sinus tracks between these structures.¹²⁹

Penetrating ulcers on the lesser curvature of the stomach may occasionally enter the adjacent hepatic parenchyma, resulting in the development of an abscess in the left lobe of the liver. This complication should be suspected when contrast studies demonstrate a deep ulcer on the lesser curvature associated with a large area of extrinsic mass effect on the adjacent gastric wall (Fig. 29-39A). In such cases, CT can be used to confirm the presence of a confined perforation involving the liver (Fig. 29-39B).

Splenic penetration by a gastric ulcer is extremely unusual because of the rarity of benign ulcers on the posterior wall or greater curvature of the gastric fundus. Although barium studies are usually nonspecific, transmural penetration by an ulcer high on the greater curvature or posterior wall of the stomach may be suspected if the ulcer extends well beyond the adjacent gastric contour.¹³⁰ In such cases, CT may demonstrate extension of the ulcer directly into the substance of the spleen.¹³¹ If CT confirms splenic penetration by a benign gastric ulcer, early surgery is required because of the risk of massive, potentially life-threatening GI bleeding if the ulcer ruptures into the spleen.¹³¹

Fistulas

Penetrating ulcers in the stomach or duodenum may occasionally erode through the wall of adjacent hollow organs, producing a variety of fistulas, including gastroduodenal, gastroduodenal, gastroduodenal, choledochoduodenal, duodenorenal,

and gastropericardial fistulas. These fistulas are considered separately in the following sections.

Gastroduodenal Fistulas (Double-Channel Pylorus). The double-channel pylorus is an acquired gastroduodenal fistula caused by a penetrating ulcer in the distal antrum that erodes directly into the base of the duodenal bulb.¹³²⁻¹³⁴ These ulcers are usually located on the lesser curvature of the prepyloric antrum but are occasionally located on the greater curvature.^{133,134} Paradoxically, the development of a double-channel pylorus may lead to improved ulcer symptoms, possibly because the fistula facilitates gastric emptying.¹³⁴

Although the double-channel pylorus is difficult to visualize on endoscopy, it is readily detected on barium studies.^{133,134} The double-channel pylorus is typically manifested by two discrete tracks extending from the distal antrum into the base of the duodenal bulb (Fig. 29-40). The track on the greater curvature side of the stomach usually represents the true pyloric channel, whereas the track on the lesser curvature side represents the fistula. The barium-filled tracks are often separated by a thin radiolucent bridge or septum that is best seen on prone compression views. Sequential barium studies may show progression from a penetrating prepyloric ulcer to a double-channel pylorus.

Gastrocolic Fistulas. In the past, most gastrocolic fistulas were thought to be caused by primary carcinoma of the stomach or transverse colon invading the gastrocolic ligament.¹³⁵ With the

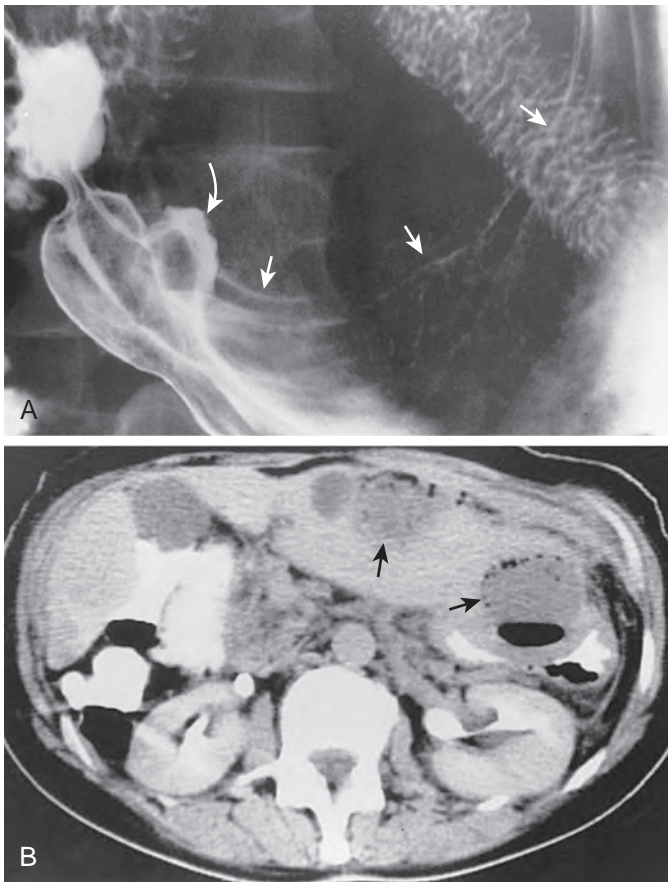


Figure 29-39 Penetrating lesser curvature ulcer with an associated hepatic abscess. **A.** Barium study shows a deep ulcer (curved arrow) on the lesser curvature of the distal antrum. Also note the large area of extrinsic mass effect (straight arrows) on the adjacent gastric wall. **B.** CT scan reveals several gas- and fluid-containing abscess cavities (arrows) in the left lobe of the liver. These abscesses were caused by penetration of the ulcer into the hepatic parenchyma.

increasing use of aspirin and other NSAIDs in today's pill-oriented society, however, benign NSAID-induced ulcers on the greater curvature of the stomach have become a more common cause of gastrocolic fistulas than carcinoma of the stomach or transverse colon.^{78,136-138} Affected individuals typically have a history of taking high doses of aspirin or other NSAIDs. As the ulcers enlarge, they penetrate inferiorly into the gastrocolic ligament, eventually producing a gastrocolic fistula. These fistulas are classically manifested by the triad of feculent vomiting, foul-smelling eructations, and diarrhea,¹³⁵ but some patients may present with abdominal pain or other nonspecific clinical findings.¹³⁷ When a gastrocolic fistula is suspected on clinical grounds, endoscopy is contraindicated because of the risk of perforation and peritonitis.¹³⁶ In contrast to gastrocolic fistulas caused by malignant tumors, fistulas complicating NSAID-induced greater curvature ulcers sometimes heal on medical therapy without need for surgery.^{137,139}

In patients with gastrocolic fistulas complicating NSAID-induced ulcers, barium studies may reveal giant ulcers on the greater curvature of the gastric antrum or body with early filling of the transverse colon via the fistula (Fig. 29-41).^{136,137} Because of the greater pressures generated during a barium enema examination, this technique can sometimes demonstrate fistulas that are not visualized on upper GI studies.¹³⁸ When fistulas are shown on barium studies, patients should be questioned about a possible history of NSAID use. Other causes of gastrocolic fistulas include gastric or colonic carcinoma, lymphoma, Crohn's disease, and tuberculosis.

Duodenocolic Fistulas. Duodenocolic fistulas are usually caused by carcinoma of the ascending colon or hepatic flexure invading the descending duodenum. Occasionally, these fistulas may result from penetrating ulcers in the duodenal bulb or postbulbar duodenum that have eroded into the hepatic flexure of the colon.^{140,141} Affected individuals may present with abdominal pain, diarrhea, feculent vomiting, foul-smelling

Figure 29-40 Double channel pylorus. **A.** Double-contrast view of the antrum shows a prepyloric lesser curvature ulcer (curved arrow) that communicates distally with the base of the duodenal bulb (straight arrow). **B.** Prone view of the antrum also delineates the lesser curvature ulcer (curved arrow) with a track (straight arrow) extending from the ulcer into the duodenum. Note the normal pyloric channel (open arrow) inferiorly.

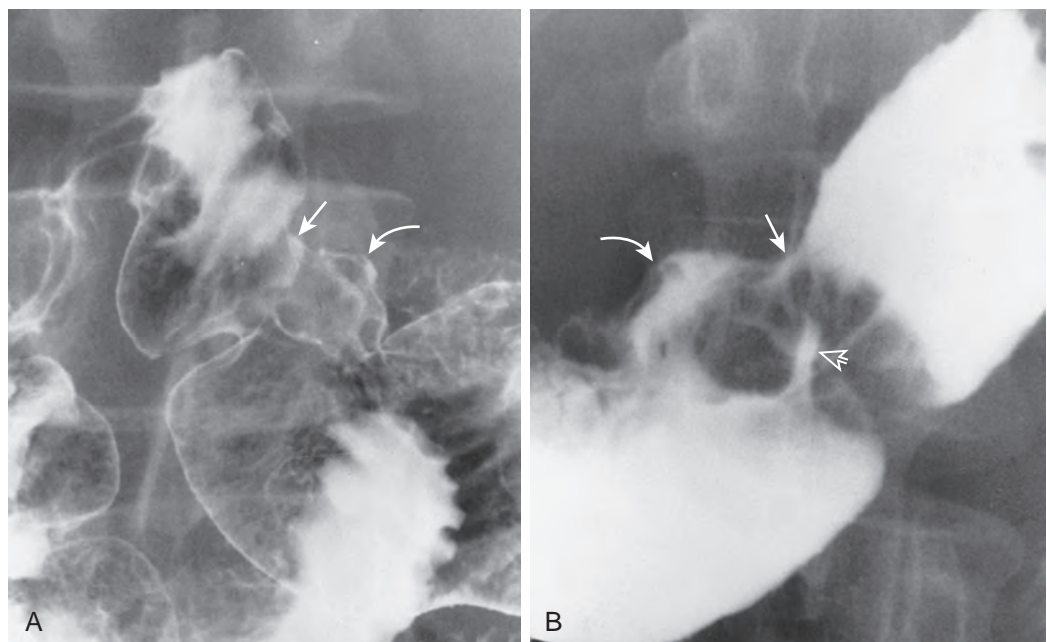




Figure 29-41 Gastrocolic fistula caused by an aspirin-induced greater curvature ulcer. Double-contrast upper GI study reveals a giant ulcer (large arrow) on the greater curvature of the stomach, with barium entering a wide fistulous track (small arrows) that communicates directly with the transverse colon. This patient had been on high doses of aspirin. (From Levine MS, Kelly MR, Laufer I, et al: *Gastrocolic fistulas: The increasing role of aspirin*. *Radiology* 187:359–361, 1993.)

eructations, or undigested food in the stool. Although upper GI studies may fail to demonstrate the fistula, barium enema examinations are often successful because of the greater pressures generated by this technique.¹⁴¹

Choledochoduodenal Fistulas. About 90% of enterobiliary fistulas occur as complications of stones in the biliary tract; only about 5% are caused by peptic ulcer disease.¹⁴² Most of the latter patients have penetrating duodenal ulcers that rupture into the common bile duct, producing a choledochoduodenal fistula.¹⁴² These patients usually have symptoms related to their underlying ulcers but occasionally present with abnormal liver function tests, jaundice, or ascending cholangitis.¹⁴³ Abdominal radiographs may reveal pneumobilia with gas in the gallbladder or bile ducts (Fig. 29-42), and barium studies may demonstrate a duodenal ulcer or duodenal scarring, sometimes associated with reflux of barium into the biliary tree.^{143–145} Rarely, these ulcers may lead to the development of cholecystoduodenal, cholecystogastric, or choledochogastric fistulas.¹⁴²

Duodenorenal Fistulas. Penetrating postbulbar duodenal ulcers rarely may rupture posteriorly into the pyelocalyceal system of the right kidney, producing a duodenorenal fistula. These fistulas may be demonstrated on barium studies or retrograde pyelography. Other rare causes of duodenorenal fistulas include malignant tumors, infection, and trauma.

Gastropericardial Fistulas. Ulcers in the intrathoracic portion of the stomach (a hiatal hernia or gastric pull-through after



Figure 29-42 Pneumobilia caused by a choledochoduodenal fistula. Close-up view from an abdominal radiograph shows gas in the gallbladder (straight arrow) and bile ducts (curved arrow) secondary to a choledochoduodenal fistula in a patient with a giant duodenal ulcer.

esophagogastrectomy) rarely may erode through the pericardium, producing a gastropericardial fistula.¹⁴⁶ This complication is catastrophic for the patient because it usually leads to the rapid development of purulent pericarditis, cardiac tamponade, and death. The sudden appearance of pneumopericardium on chest radiographs of an acutely ill patient with an intrathoracic stomach should raise the possibility of a gastropericardial fistula. Upper GI studies with water-soluble contrast agents may document the presence of a fistula by showing extravasation of contrast medium into the pericardial sac.¹⁴⁷ Because of the high mortality associated with this complication, the best hope for survival is early surgery with drainage of the pericardium and closure of the fistula.¹⁴⁶

Zollinger-Ellison Syndrome

Since its original description by Zollinger and Ellison in 1955,¹⁴⁸ Zollinger-Ellison syndrome has been recognized as a life-threatening condition characterized by marked hypersecretion of gastric acid and a severe form of peptic ulcer disease secondary to high levels of gastrin in patients with underlying gastrinomas. These tumors not only may cause a devastating ulcer diathesis but may also behave as malignant lesions, metastasizing to the liver or other structures (see Chapter 98). The development of potent antisecretory agents for controlling acid secretion and sophisticated techniques for localizing these islet

cell tumors have had a major impact on patient survival. Although barium studies may reveal typical findings of peptic ulcer disease, it is sometimes possible to suggest the diagnosis of Zollinger-Ellison syndrome on the basis of the radiographic findings.

PATHOLOGY

Zollinger-Ellison syndrome is caused by the uncontrolled release of gastrin from autonomously functioning non- β islet cell tumors, also known as gastrinomas (see Chapter 98). About 75% of these tumors are located in the pancreas, 15% in the duodenum, and 10% in other extraintestinal locations such as the liver, ovaries, and lymph nodes.^{149,150} Most gastrinomas are thought to be malignant; metastases are found at the time of diagnosis in 30% to 50% of patients.¹⁵⁰ The liver is the most frequent site of metastatic disease.

Most gastrinomas occur sporadically, but 25% of these tumors are transmitted as part of a hereditary syndrome (multiple endocrine neoplasia type 1).¹⁵¹ This syndrome is characterized not only by pancreatic tumors but also by parathyroid, pituitary, and adrenal tumors.

CLINICAL ASPECTS

More than 90% of patients with Zollinger-Ellison syndrome have upper GI ulcers caused by hypersecretion of gastric acid.¹⁵⁰ The presenting signs and symptoms may be indistinguishable from those associated with ordinary peptic ulcers. However, the possibility of Zollinger-Ellison syndrome should be considered in patients who have multiple ulcers, ulcers in unusual locations, ulcers that are resistant to medical therapy, or recurrent ulcers postoperatively.^{149,150}

The second most common clinical problem in Zollinger-Ellison syndrome is diarrhea, which occurs in up to 50% of patients and is the presenting symptom in 35%.^{149,150} This diarrhea is related primarily to the severe volume load caused by the secretion of several liters of acid into the intestines each day. The acidic pH of the small bowel may also damage the intestinal mucosa, resulting in a spruelike state with villous atrophy, malabsorption, and steatorrhea.¹⁵² Other patients may initially present with reflux symptoms or dysphagia secondary to the development of severe reflux esophagitis or peptic strictures.¹⁵³

The diagnosis of Zollinger-Ellison syndrome is established by the demonstration of hypergastrinemia and gastric acid hypersecretion in a patient with peptic ulcers, diarrhea, or other clinical features of a gastrinoma. In the appropriate clinical setting, fasting serum gastrin levels higher than 1000 pg/mL should be virtually diagnostic of Zollinger-Ellison syndrome.¹⁵⁰ However, not all patients have such high serum gastrin levels. Furthermore, hypergastrinemia may occur in patients with atrophic gastritis, gastric outlet obstruction, and G-cell hyperplasia.

In the past, total gastrectomy was the treatment of choice for preventing hypersecretion of acid and its complications in patients with Zollinger-Ellison syndrome. However, H₂ receptor antagonists (e.g., cimetidine, ranitidine) and proton pump inhibitors (e.g., omeprazole) have proved to be extremely effective in suppressing acid secretion and promoting ulcer healing without need for surgery.^{150,154,155} A total gastrectomy should therefore be reserved for noncompliant patients.

As fewer patients succumb to the ulcer diathesis in Zollinger-Ellison syndrome, malignant spread of gastrinomas has become a major cause of long-term morbidity and mortality in these individuals. Greater attention has therefore been focused on early detection and excision of the gastrinomas before the development of hepatic metastases.^{156,157} Although the primary tumors are often difficult to detect on preoperative imaging studies, successful localization of gastrinomas can be achieved by CT, angiography, or selective portal venous sampling for gastrin or by whole-body imaging with somatostatin scintigraphy.¹⁵⁸⁻¹⁶¹ The most important prognostic factor affecting survival is the extent of tumor at the time of surgery. Patients with no tumor or lesions that are resectable at laparotomy have 5-year survival rates higher than 90%, whereas patients with liver metastases have 5-year survival rates less than 20%.¹⁵⁰

RADIOGRAPHIC FINDINGS

Zollinger-Ellison syndrome may be manifested on barium studies by a characteristic constellation of findings.¹⁶²⁻¹⁶⁶ Hypersecretion of acid often results in a large volume of fluid in the stomach, duodenum, and proximal jejunum that dilutes ingested barium and compromises the mucosal coating. Many patients have markedly thickened gastric folds, particularly in the fundus and body of the stomach, not only because of edema and inflammation but also because of gastrin-induced parietal cell hyperplasia (Fig. 29-43A). Duodenal and jejunal folds may also have a grossly thickened, edematous appearance because of a severe inflammatory response to the enormous volume of gastric secretions entering the small bowel. Although thickened folds may be caused by a variety of conditions in the stomach and duodenum (see later, “Differential Diagnosis”), the combination of thickened folds and excessive fluid in the stomach, duodenum, and proximal jejunum should suggest the possibility of Zollinger-Ellison syndrome.

Approximately 75% of the ulcers in Zollinger-Ellison syndrome are located in the stomach or duodenal bulb, so they cannot be differentiated from uncomplicated peptic ulcers.¹⁶⁷ The remaining 25% are located in the postbulbar duodenum or proximal jejunum.¹⁶⁷ Because peptic ulcers rarely occur distal to the papilla of Vater, the presence of one or more ulcers in the third or fourth portion of the duodenum or even the proximal jejunum should be highly suggestive of Zollinger-Ellison syndrome (Fig. 29-43B). Patients with this syndrome are also more likely to have multiple ulcers than other patients with peptic ulcer disease.¹⁶⁷

DIFFERENTIAL DIAGNOSIS

Markedly thickened gastric folds may be present in a variety of conditions, including *H. pylori* gastritis, hypertrophic gastritis, Ménétrier's disease, and lymphoma. Similarly, thickened duodenal or jejunal folds may be caused by inflammatory or infectious processes. Although thickened folds are a nonspecific finding, the simultaneous presence of increased fluid in the upper GI tract and one or more ulcers in unusual locations should strongly suggest Zollinger-Ellison syndrome. If this syndrome is suspected on the basis of the radiographic findings, a fasting serum gastrin level should be obtained for a more definitive diagnosis.

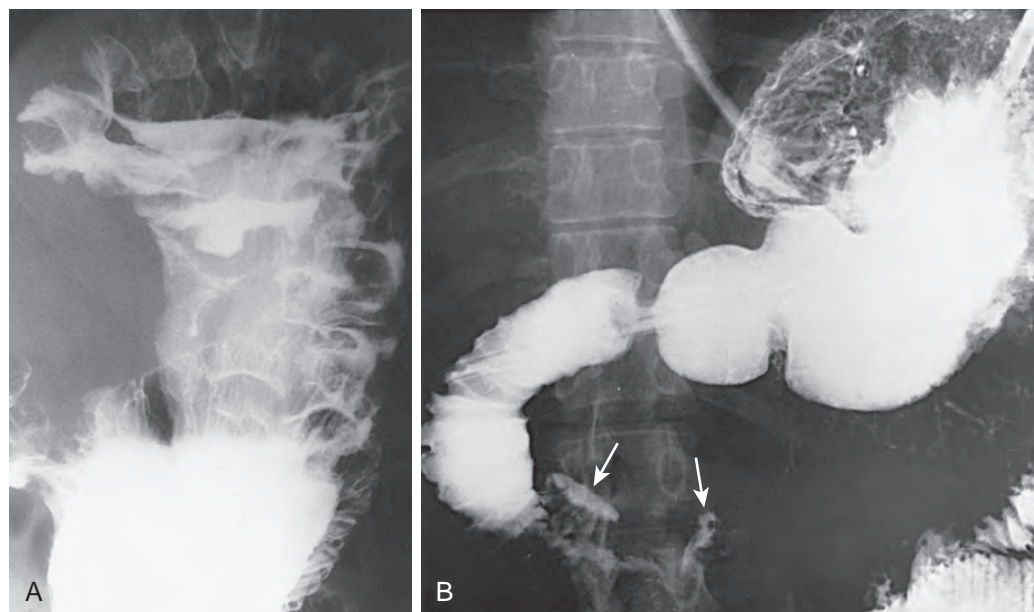


Figure 29-43 Zollinger-Ellison syndrome. **A.** There are markedly thickened folds in the gastric fundus and body. Also note how the barium is diluted by excessive fluid in the stomach. **B.** In another patient, two discrete ulcers (arrows) are seen in the third and fourth portions of the duodenum. Ordinary peptic ulcers rarely occur distal to the papilla of Vater, so ulcers in this location should suggest the possibility of Zollinger-Ellison syndrome. (**B** courtesy Stephen W. Trenkner, MD, Minneapolis.)

REFERENCES

- Boyd EJS, Wormsley KG: Etiology and pathogenesis of peptic ulcer. In Berk JE, Haubrich WS, Kalser MH, et al, editors: *Bockus Gastroenterology*, ed 4, Philadelphia, 1985, WB Saunders, pp 1013–1059.
- Bonnevie O: Changing demographics of peptic ulcer disease. *Dig Dis Sci* 30(Suppl 11):85–145, 1985.
- Kurata JH, Haile BM, Elashoff JD: Sex differences in peptic ulcer disease. *Gastroenterology* 88:96–100, 1985.
- Sonnenberg A, Wasserman IH, Jacobsen SJ: Monthly variation of hospital admission and mortality of peptic ulcer disease: A reappraisal of ulcer periodicity. *Gastroenterology* 103:1192–1198, 1992.
- Hung LCT, Ching JYL, Sung JYJ, et al: Long-term outcome of *Helicobacter pylori*-negative idiopathic bleeding ulcers: A prospective cohort study. *Gastroenterology* 128:1845–1850, 2005.
- Warren JR, Marshall BJ: Unidentified curved bacilli on gastric epithelium in active chronic gastritis. *Lancet* 2:1273–1275, 1983.
- Peterson WL: *Helicobacter pylori* and peptic ulcer disease. *N Engl J Med* 324:1043–1048, 1991.
- Levine MS, Rubesin SE: The *Helicobacter pylori* revolution: Radiologic perspective. *Radiology* 195:593–596, 1995.
- Pattison CP, Combs MK, Marshall BJ: *Helicobacter pylori* and peptic ulcer disease: Evolution to revolution to resolution. *AJR* 168:1415–1420, 1997.
- Yardley JH, Paull G: *Campylobacter pylori*: A newly recognized infectious agent in the gastrointestinal tract. *Am J Surg Pathol* 12(Suppl): 89–99, 1988.
- Chamberlain CE, Peura DA: *Campylobacter (Helicobacter) pylori*: Is peptic disease a bacterial infection? *Arch Intern Med* 150:951–955, 1990.
- Peek RM, Blaser MJ: Pathophysiology of *Helicobacter pylori*-induced gastritis and peptic ulcer disease. *Am J Med* 102:200–207, 1997.
- Graham DU: *Helicobacter pylori* infection in the pathogenesis of duodenal ulcer and gastric cancer: A model. *Gastroenterology* 113:1983–1991, 1997.
- Schottker B, Adamu MA, Weck MN, et al: *Helicobacter pylori* infection is strongly associated with gastric and duodenal ulcers in a large prospective study. *Clin Gastroenterol Hepatol* 10:487–493, 2012.
- Moss S, Calam J: *Helicobacter pylori* and peptic ulcers: The present position. *Gut* 33:289–292, 1992.
- Larkai EN, Smith JL, Lidsky MD, et al: Gastro-duodenal mucosa and dyspeptic symptoms in arthritic patients during chronic nonsteroidal anti-inflammatory drug use. *Am J Gastroenterol* 82:1153–1158, 1987.
- Bellary SV, Isaacs PET, Lee FI: Upper gastrointestinal lesions in elderly patients presenting for endoscopy: Relevance of NSAID usage. *Am J Gastroenterol* 86:961–964, 1991.
- Laine L: Approaches to nonsteroidal anti-inflammatory drug use in the high-risk patient. *Gastroenterology* 120:594–606, 2001.
- Hawkey CJ: Nonsteroidal anti-inflammatory drug gastropathy. *Gastroenterology* 119:521–535, 2000.
- Cryer B, Feldman M: Effects of very low dose daily, long-term aspirin therapy on gastric, duodenal, and rectal prostaglandin levels and on mucosal injury in healthy humans. *Gastroenterology* 117:17–25, 1999.
- Lanza FL: NSAIDs and the gastrointestinal tract. *Abdom Imaging* 22:1–4, 1997.
- Wallace JL: Nonsteroidal anti-inflammatory drugs and gastroenteropathy: The second hundred years. *Gastroenterology* 112:1000–1016, 1997.
- Davenport HW: Salicylate damage to the gastric mucosal barrier. *N Engl J Med* 276:1307–1312, 1967.
- Kelly JP, Kaufman DW, Jurgelon JM, et al: Risk of aspirin-associated major upper gastrointestinal bleeding with enteric-coated or buffered product. *Lancet* 348:1413–1416, 1996.
- Bugat R, Thompson MR, Aures D, et al: Gastric mucosal lesions produced by intravenous infusion of aspirin in cats. *Gastroenterology* 7:754–759, 1976.
- Lanas A, Serrano P, Bajador E, et al: Evidence of aspirin use in both upper and lower gastrointestinal perforation. *Gastroenterology* 112:683–689, 1997.
- Wilcox CM, Alexander LN, Cotsonis GA, et al: Nonsteroidal anti-inflammatory drugs are associated with both upper and lower gastrointestinal bleeding. *Dig Dis Sci* 42:990–997, 1997.
- Conn HO, Blitzer BL: Nonassociation of adrenocorticosteroid therapy and peptic ulcer. *N Engl J Med* 294:473–479, 1976.
- Friedman GD, Siegel AB, Seltzer CC: Cigarettes, alcohol, coffee, and peptic ulcer. *N Engl J Med* 290:469–473, 1974.
- Piper DW, Nasiry R, McIntosh J, et al: Smoking, alcohol, analgesics, and chronic duodenal ulcer. *Scand J Gastroenterol* 19:1015–1021, 1984.
- Svanes C, Soreide JA, Skarstein A, et al: Smoking and ulcer perforation. *Gut* 41:177–180, 1997.
- Wormsley KG: Smoking and duodenal ulcer. *Gastroenterology* 75:139–142, 1978.
- Peters MN, Richardson CT: Stressful life events, acid hypersecretion, and ulcer disease. *Gastroenterology* 84:114–119, 1983.
- Walker P, Luther J, Samloff IM, et al: Life events, stress and psychosocial factors in men with peptic ulcer disease. *Gastroenterology* 94:323–330, 1988.
- Aoyama N, Kinoshita Y, Fujimoto S, et al: Peptic ulcers after the Hanshin-Awaji

- earthquake: Increased incidence of bleeding ulcers. *Am J Gastroenterol* 93:311–316, 1998.
36. Thomas J, Greig M, Piper DW: Chronic gastric ulcer and life events. *Gastroenterology* 78:905–911, 1980.
 37. Rhodes J, Barnardo DE, Phillips SF, et al: Increased reflux of the bile into the stomach in patients with gastric ulcers. *Gastroenterology* 57:241–252, 1969.
 38. Dragstedt LR: A concept of the etiology of gastric and duodenal ulcers. *Gastroenterology* 30:208–220, 1956.
 39. Rotter JI: The genetics of peptic ulcers: More than one gene, more than one disease. *Prog Med Genet* 4:1–58, 1980.
 40. Tarpila S, Samloff IM, Pikkarainen P, et al: Endoscopic and clinical findings in first-degree relatives of duodenal ulcer patients and control subjects. *Scand J Gastroenterol* 17:503–506, 1982.
 41. Roth JLA, Stein GN, Morissey JR, et al: Diagnosis of peptic ulcer. In Berk JE, Haubrich WS, Kalser MH, et al, editors: *Bockus Gastroenterology*, ed 4, Philadelphia, 1985, WB Saunders, pp 1060–1115.
 42. Sharma MP, Choudhary G: Nocturnal pain and duodenal ulcer. *Br J Clin Pract* 42:198–199, 1967.
 43. Dunn JP, Etter LE: Inadequacy of the medical history in the diagnosis of duodenal ulcer. *N Engl J Med* 266:68–72, 1962.
 44. Krippaehne WW, Fletcher WS, Dunphy JE: Acute perforation of duodenal and gastric ulcer: Factors affecting mortality. *Arch Surg* 88:874–882, 1964.
 45. Burge H, Gill AM, Lewis RH: The pyloric-channel syndrome and gastric ulceration. *Lancet* 1:73–75, 1963.
 46. Glickman MG, Szemes G, Loeb P, et al: Peptic ulcer of the pyloric region. *AJR* 113:147–158, 1971.
 47. Laine L, Peterson WL: Bleeding peptic ulcer. *N Engl J Med* 331:717–727, 1994.
 48. Carucci LR, Levine MS, Rubesin SE, et al: Upper gastrointestinal tract barium examination of postbulbar duodenal ulcers. *AJR* 182: 927–930, 2004.
 49. Graham DY, Lew GM, Klein PD, et al: Effect of treatment of *Helicobacter pylori* infection on the long-term recurrence of gastric or duodenal ulcer. *Ann Intern Med* 116:705–708, 1992.
 50. Hentschel E, Brandstatter G, Dragosics B, et al: Effect of ranitidine and amoxicillin plus metronidazole on the eradication of *Helicobacter pylori* and the recurrence of duodenal ulcer. *N Engl J Med* 328:308–312, 1993.
 51. Van der Hulst RWM, Rauws EAJ, Koycu B, et al: Prevention of ulcer recurrence after eradication of *Helicobacter pylori*: A prospective long-term follow-up study. *Gastroenterology* 113:1082–1086, 1997.
 52. NIH Consensus Development Panel on *Helicobacter pylori* in Peptic Ulcer Disease: NIH Consensus Conference. *Helicobacter pylori* in peptic ulcer disease. *JAMA* 272:65–69, 1994.
 53. The report of the Digestive Health Initiative International Update Conference on *Helicobacter pylori*. *Gastroenterology* 113:S4–S8, 1997.
 54. Walsh JH, Peterson WL: The treatment of *Helicobacter pylori* infection in the management of peptic ulcer disease. *N Engl J Med* 333:984–991, 1995.
 55. Bayerdorffer E, Miehke S, Mannes GA, et al: Double-blind trial of omeprazole and amoxicillin to cure *Helicobacter pylori* infection in patients with duodenal ulcers. *Gastroenterology* 108:1412–1417, 1995.
 56. Vakil N, Megraud F: Eradication therapy for *Helicobacter pylori*. *Gastroenterology* 133:985–1001, 2007.
 57. Isenberg JI, McQuaid KR, Laine L, et al: Acid-peptic disorders. In Yamada T, editor: *Textbook of Gastroenterology*, Philadelphia, 1991, JB Lippincott, pp 1241–1339.
 58. McFarland RJ, Bateson MC, Green JRB, et al: Omeprazole provides quicker symptom relief and duodenal ulcer healing than ranitidine. *Gastroenterology* 98:278–283, 1990.
 59. Agrawal NM, Saffouri B, Kruss DM, et al: Healing of benign gastric ulcers: A placebo-controlled comparison of two dosage regimens of Misoprostol, a synthetic analog of prostaglandin E1. *Dig Dis Sci* 30(Suppl 11):164S–170S, 1985.
 60. Gilbert DA, Surawicz CM, Silverstein FE, et al: Prevention of acute, aspirin-induced gastric mucosal injury by 15-R-15 methyl prostaglandin E2: An endoscopic study. *Gastroenterology* 86:339–345, 1984.
 61. Penn I: The declining role of the surgeon in the treatment of acid-peptic disease. *Arch Surg* 115:134–135, 1980.
 62. Gustavsson S, Kelly KA, Melton LJ, et al: Trends in peptic ulcer surgery: A population-based study in Rochester, Minnesota, 1956–1985. *Gastroenterology* 94:688–694, 1988.
 63. Kikuchi Y, Levine MS, Laufer I, et al: Value of flow technique for double-contrast examination of the stomach. *AJR* 147:1183–1184, 1986.
 64. Nelson SW: The discovery of gastric ulcers and the differential diagnosis between benignancy and malignancy. *Radiol Clin North Am* 7:5–25, 1969.
 65. Goldsmith MR, Paul RE, Poplack WE, et al: Evaluation of routine double contrast views of the anterior wall of the stomach. *AJR* 126:1159–1163, 1976.
 66. Poplack WE, Paul RE, Goldsmith MR, et al: Linear and rod-shaped peptic ulcers. *Radiology* 122:317–321, 1977.
 67. Amaral NM: Radiographic diagnosis of shallow gastric ulcers: A comparative study of technique. *Radiology* 129:597–600, 1978.
 68. Braver JM, Paul RE, Philipps E, et al: Roentgen diagnosis of linear ulcers. *Radiology* 132:29–32, 1979.
 69. Levine MS, Creteur V, Kressel HY, et al: Benign gastric ulcers: Diagnosis and follow-up with double-contrast radiography. *Radiology* 164: 9–13, 1987.
 70. Ott DJ, Gelfand DW, Wu WC: Detection of gastric ulcer: Comparison of single- and double-contrast examination. *AJR* 139:93–97, 1982.
 71. Gelfand DW, Dale WJ, Ott DJ: The location and size of gastric ulcers: Radiologic and endoscopic evaluation. *AJR* 143:755–758, 1984.
 72. Barragry TP, Blatchford JW, Allen MO: Giant gastric ulcers: A review of 49 cases. *Ann Surg* 203:255–259, 1986.
 73. Sun DCH, Stempien SJ: The Veterans Administration Cooperative Study on Gastric Ulcer: Site and size of the ulcer as determinants of outcome. *Gastroenterology* 61:576–584, 1971.
 74. Thompson G, Stevenson GW, Somers S: Distribution of gastric ulcers by double-contrast barium meal with endoscopic correlation. *J Can Assoc Radiol* 34:296–297, 1983.
 75. Findley JW: Ulcers on the greater curvature of the stomach. *Gastroenterology* 40:183–187, 1961.
 76. Amberg JR, Zboralske FF: Gastric ulcers after 70. *AJR* 96:393–399, 1966.
 77. Sheppard MC, Holmes GKT, Cockel R: Clinical picture of peptic ulceration diagnosed endoscopically. *Gut* 18:524–530, 1977.
 78. Kottler RE, Tuft RJ: Benign greater curve gastric ulcer: The “sump-ulcer.” *Br J Radiol* 54:651–654, 1981.
 79. Hocking BV, Alp MH, Grant AK: Gastric ulceration within hiatus hernia. *Med J Aust* 2:207–208, 1976.
 80. Wolf BS: Observations on roentgen features of benign and malignant ulcers. *Semin Roentgenol* 6:140–150, 1971.
 81. Levine MS: Erosive gastritis and gastric ulcers. *Radiol Clin North Am* 32:1203–1214, 1994.
 82. Pack GT: The relationship of gastric ulcer to gastric cancer. *Cancer* 3:515–522, 1950.
 83. Levine MS, Verstandig A, Laufer I: Serpiginous gastric erosions caused by aspirin and other nonsteroidal antiinflammatory drugs. *AJR* 146:31–34, 1986.
 84. Zboralske FF, Stargardt FL, Harell GS: Profile roentgenographic features of benign greater curvature ulcers. *Radiology* 127:63–67, 1978.
 85. Linbert M, Krause GR: The “ring” shadow in the diagnosis of ulcer. *AJR* 90:767–773, 1963.
 86. Bloom SM, Paul RE, Matsue H, et al: Improved radiologic detection of multiple gastric ulcers. *AJR* 128:949–952, 1977.
 87. Dagradi AE, Falkner RE, Lee ER: Multiple benign gastric ulcers. *Am J Gastroenterol* 62:36–45, 1974.
 88. Taxin RN, Livingston PA, Seamon WB: Multiple gastric ulcers: A radiographic sign of benignity? *Radiology* 114:23–27, 1975.
 89. Sakita T, Ogura Y, Takasu S, et al: Observations on the healing of ulcerations in early gastric cancer. *Gastroenterology* 60:835–844, 1971.
 90. Kagan RA, Steckel RJ: Gastric ulcer in a young man with apparent healing. *AJR* 128:831–834, 1977.
 91. Keller RJ, Wolf BS, Khilnani MT: Roentgen features of healing and healed benign gastric ulcers. *Radiology* 97:353–359, 1970.
 92. Gelfand DW, Ott DJ: Gastric ulcer scars. *Radiology* 140:37–43, 1981.
 93. Levine MS, Kong V, Rubesin SE, et al: Scirrhous carcinoma of the stomach: Radiologic and endoscopic diagnosis. *Radiology* 175:151–154, 1990.
 94. Wenger J, Brandborg LL, Spellman FA: Cancer: I. Clinical aspects. *Gastroenterology* 61:598–605, 1971.
 95. Hayes MA: The gastric ulcer problem. *Gastroenterology* 29:609–620, 1955.
 96. Kirsch IE: Benign and malignant gastric ulcers: Roentgen differentiation. *Radiology* 64:357–365, 1955.
 97. Elliott GU, Wald SM, Benz RI: A roentgenologic study of ulcerating lesions of the stomach. *AJR* 77:612–622, 1957.
 98. Schulman A, Simpkins KC: The accuracy of radiological diagnosis of benign, primarily and secondarily malignant gastric ulcers and their correlation with three simplified radiological types. *Clin Radiol* 26:317–325, 1975.
 99. Thompson G, Somers S, Stevenson GW: Benign gastric ulcer: A reliable radiologic diagnosis? *AJR* 141:331–333, 1983.
 100. Ichikawa H: Differential diagnosis between benign and malignant ulcers of the stomach. *Clin Gastroenterol* 2:329–332, 1973.
 101. Segal AW, Healy MJR, Cox AG, et al: Diagnosis of gastric cancer. *BMJ* 2:669–672, 1975.

102. Stein GN, Martin RD, Roy RH, et al: Evaluation of conventional roentgenologic techniques for demonstration of duodenal ulcer craters. *AJR* 91:801-807, 1964.
103. Levine MS, Rubesin SE, Herlinger H, et al: Double contrast upper gastrointestinal examination: Technique and interpretation. *Radiology* 168:593-602, 1988.
104. de Roos A, Op den Orth JO: Linear niches in the duodenal bulb. *AJR* 140:941-944, 1983.
105. Rodriguez HP, Aston JK, Richardson CT: Ulcers in the descending duodenum: Postbulbar ulcers. *AJR* 119:316-322, 1973.
106. Classen M: Endoscopy in benign peptic ulcer. *Clin Gastroenterol* 2:315-318, 1973.
107. Ball RP, Segal AL, Golden R: Postbulbar ulcers of the duodenum. *AJR* 59:90-99, 1948.
108. Bilbao MK, Frische LH, Rosch J, et al: Postbulbar duodenal ulcer and ring-stricture. *Radiology* 100:27-35, 1971.
109. Mistilis SP, Wiot JF, Nedelman SH: Giant duodenal ulcer. *Ann Intern Med* 59:155-164, 1963.
110. Eisenberg RL, Margulis AR, Moss AA: Giant duodenal ulcers. *Gastrointest Radiol* 2:347-353, 1978.
111. Jazewski R, Crane SA, Cid AA: Giant duodenal ulcers: Successful healing with medical therapy. *Dig Dis Sci* 28:486-489, 1983.
112. Kirsh IE, Brendel T: The importance of giant duodenal ulcer. *Radiology* 91:14-19, 1968.
113. Parulekar SG, Lubert M: Ultrasound demonstration of giant duodenal ulcer. *Gastrointest Radiol* 8:29-31, 1983.
114. Kawai K, Ida K, Misaki F, et al: Comparative study for duodenal ulcer by radiology and endoscopy. *Endoscopy* 5:7-13, 1973.
115. Wills JS: Pyloric channel ulcers and the air-contrast examination. *Radiology* 130:250-252, 1979.
116. Gobel VK, Kressel HY, Laufer I: Double contrast artifacts. *Gastrointest Radiol* 3:139-146, 1978.
117. Op den Orth JO, Ploem S: The stalactite phenomenon on double contrast studies of the stomach. *Radiology* 117:523-525, 1975.
118. Linsman JR: Gastric ulcers simulating intramural, extramucosal tumors. *AJR* 101:421-424, 1967.
119. Bonfield RE, Mantel W: The problem of differentiating benign antral ulcers from intramural tumors. *Radiology* 106:25-27, 1973.
120. Fox ER, Laufer I, Levine MS: Radiographic response of gastric lymphoma to chemotherapy. *AJR* 142:711-714, 1984.
121. Thoeni RF, Cello JP: A critical look at the accuracy of endoscopy and double-contrast radiography of the upper gastrointestinal (UGI) tract in patients with substantial UGI hemorrhage. *Radiology* 135:305-308, 1980.
122. Fraser GM: The double contrast barium meal in patients with acute upper gastrointestinal bleeding. *Clin Radiol* 29:625-634, 1978.
123. Balthazar EJ, Rosenberg H, Davidian MM: Scirrhous carcinoma of the pyloric channel and distal antrum. *AJR* 134:669-673, 1980.
124. Edwards RH, Foster JH: Pneumoperitoneum in perforated duodenal ulcer. *Am J Surg* 104:551-554, 1962.
125. Jacobson G, Berne CJ, Meyers HI, et al: The examination of patients with suspected perforated ulcer using a water-soluble contrast medium. *AJR* 86:37-49, 1961.
126. Fultz PJ, Skucas J, Weiss SL: CT in upper gastrointestinal tract perforations secondary to peptic ulcer disease. *Gastrointest Radiol* 17:5-8, 1992.
127. Ongolo-Zogo P, Borson O, Garcia P, et al: Acute gastroduodenal peptic ulcer perforation: Contrast-enhanced and thin-section spiral CT findings in 10 patients. *Abdom Imaging* 24:329-332, 1999.
128. Jeffrey RB, Federle MP, Wall S: Value of computed tomography in detecting occult gastrointestinal perforation. *J Comput Assist Tomogr* 7:825-827, 1983.
129. Madrazo BL, Halpert RD, Sandler MA, et al: Computed tomographic findings in penetrating peptic ulcer. *Radiology* 153:751-754, 1984.
130. Joffe N, Antonioli DA: Penetration into spleen by benign gastric ulcers. *Clin Radiol* 32:177-181, 1981.
131. Glick SN, Levine MS, Teplitz SK, et al: Splenic penetration by benign gastric ulcer: Preoperative recognition with CT. *Radiology* 163:637-639, 1987.
132. Farack UM, Goresky CA, Jabbari M, et al: Double pylorus: A hypothesis concerning its pathogenesis. *Gastroenterology* 66:596-600, 1974.
133. Jamshidnejad J, Koehler RE, Narayan D: Double channel pylorus. *AJR* 130:1047-1050, 1978.
134. Hegedus V, Poulsen PE, Reichardt J: The natural history of the double pylorus. *Radiology* 126:29-34, 1978.
135. Smith DL, Dockerty MB, Black BM: Gastrocolic fistulas of malignant origin. *Surg Gynecol Obstet* 134:829-832, 1972.
136. Laufer I, Thornley GD, Stolberg H: Gastrocolic fistula as a complication of benign gastric ulcer. *Radiology* 119:7-11, 1976.
137. Levine MS, Kelly MR, Laufer I, et al: Gastrocolic fistulas: The increasing role of aspirin. *Radiology* 187:359-361, 1993.
138. Tavenor T, Smith S, Sullivan S: Gastrocolic fistula: A review of 15 cases and an update of the literature. *J Clin Gastroenterol* 16:189-191, 1993.
139. Thyssen EP, Weinstock LB, Balfe DM, et al: Medical treatment of benign gastrocolic fistula. *Ann Intern Med* 118:433-435, 1993.
140. Sasson L, Weiskopf S: Duodenocolic fistula as a complication of peptic ulcer. *Am J Gastroenterol* 29:51-58, 1958.
141. Starzl TE, Dorr TW, Meyer WH: Benign duodenocolic fistula. *Arch Surg* 78:611-619, 1959.
142. Berguer LH: Internal biliary fistulas. *Am J Gastroenterol* 43:11-22, 1965.
143. Constant E, Turcotte JG: Choledochoduodenal fistula: The natural history and management of an unusual complication of peptic ulcer disease. *Ann Surg* 167:221-228, 1968.
144. McEwan-Alvarada G, Dysart DN: Choledochoduodenal fistulas complicating duodenal ulcer. *Am J Dig Dis* 12:947-954, 1967.
145. Hoppenstein JM, Medoza CB, Watne AL: Choledochoduodenal fistula due to perforating duodenal ulcer disease. *Ann Surg* 173:145-147, 1971.
146. West AB, Nolan N, O'Brian DS: Benign peptic ulcers penetrating pericardium and heart: Clinicopathological features and factors favoring survival. *Gastroenterology* 94:1478-1487, 1988.
147. O'Driscoll J, Hourihane JB: Intrapericardial barium in a case of peptic ulceration. *Br J Radiol* 49:177-179, 1976.
148. Zollinger RM, Ellison EH: Primary peptic ulcerations of the jejunum associated with islet cell tumors of the pancreas. *Ann Surg* 142:709-728, 1955.
149. Wolfe MM, Jensen RT: Zollinger-Ellison syndrome: Current concepts in diagnosis and management. *N Engl J Med* 317:1200-1209, 1987.
150. Del Valle J, Yamada T: Zollinger-Ellison syndrome. In Yamada T, editor: *Textbook of Gastroenterology*, Philadelphia, 1991, JB Lippincott, pp 1340-1352.
151. Ballard HS, Frane B, Havtsock RJ: Familial multiple endocrine adenoma-peptic ulcer complex. *Medicine (Baltimore)* 43:481-516, 1964.
152. Mausbach CM, II, Wilkins RM, Dobbins WO, et al: Intestinal mucosal function and structure in the steatorrhea of Zollinger-Ellison syndrome. *Arch Intern Med* 121:487-494, 1968.
153. Miller LS, Vinayek R, Frucht H, et al: Reflux esophagitis in patients with Zollinger-Ellison syndrome. *Gastroenterology* 98:341-346, 1990.
154. Maton PN, Vinayek R, Frucht H, et al: Long-term efficacy and safety of omeprazole in patients with Zollinger-Ellison syndrome: A prospective study. *Gastroenterology* 97:827-836, 1989.
155. Lew EA, Pisegna JR, Starr JA, et al: Intravenous pantoprazole rapidly controls gastric acid hypersecretion in patients with Zollinger-Ellison syndrome. *Gastroenterology* 118:696-704, 2000.
156. Fraker DL, Norton JA, Alexander HR, et al: Zollinger-Ellison syndrome: Surgery should still play an important role in its management. *Ann Surg* 220:320-330, 1994.
157. Norton JA, Fraker DL, Alexander HR, et al: Surgery to cure the Zollinger-Ellison syndrome. *N Engl J Med* 341:635-644, 1999.
158. Wank SA, Doppman JL, Miller DL, et al: Prospective study of the ability of computerized axial tomography to localize gastrinomas in patients with Zollinger-Ellison syndrome. *Gastroenterology* 92:905-912, 1987.
159. Maton PN, Miller DL, Doppman JL, et al: The role of selective angiography in the management of patients with Zollinger-Ellison syndrome. *Gastroenterology* 92:913-918, 1987.
160. Cherner JA, Doppman JL, Norton JA, et al: Selective venous sampling for gastrin to localize gastrinomas: A prospective assessment. *Ann Intern Med* 105:841-847, 1986.
161. Gibril F, Reynolds JC, Doppman JL, et al: Somatostatin receptor scintigraphy: Its sensitivity compared with that of other imaging methods in detecting primary and metastatic gastrinomas: A prospective study. *Ann Intern Med* 125:26-34, 1996.
162. Amberg JR, Ellison EH, Wilson SD, et al: Roentgenographic observations in the Zollinger-Ellison syndrome. *JAMA* 190:185-187, 1964.
163. Missakian MM, Carlson HC, Huzenga KA: Roentgenographic findings in Zollinger-Ellison syndrome. *AJR* 94:429-437, 1965.
164. Nelson SW, Christoforidis AJ: Roentgenologic features of the Zollinger-Ellison syndrome: Ulcerogenic tumor of the pancreas. *Semin Roentgenol* 3:254-266, 1968.
165. Zboralske FF, Amberg JR: Detection of the Zollinger-Ellison syndrome: The radiologist's responsibility. *AJR* 104:529-543, 1968.
166. Nelson SW, Lichtenstein JE: The Zollinger-Ellison syndrome. In Marshak RH, editor: *Radiology of the Stomach*, Philadelphia, 1983, WB Saunders, pp 334-381.
167. Ellison EH, Wilson SD: The Zollinger-Ellison syndrome: Reappraisal and evaluation of 260 registered cases. *Ann Surg* 160:514-530, 1964.

Inflammatory Conditions of the Stomach and Duodenum

MARC S. LEVINE

CHAPTER OUTLINE

Erosive Gastritis

Pathogenesis
Clinical Findings
Radiographic Findings
Differential Diagnosis

Antral Gastritis

Radiographic Findings
Differential Diagnosis

Helicobacter pylori Gastritis

Clinical Findings
Radiographic Findings
Differential Diagnosis

Hypertrophic Gastritis

Radiographic Findings
Differential Diagnosis

Ménétrier's Disease

Pathology
Clinical Findings
Radiographic Findings
Differential Diagnosis

Atrophic Gastritis

Pathogenesis
Clinical Findings
Radiographic Findings
Differential Diagnosis

Granulomatous Conditions

Crohn's Disease
Sarcoidosis
Tuberculosis
Syphilis
Fungal Diseases

Other Infections

Cytomegalovirus Infection
Cryptosporidiosis
Toxoplasmosis
Strongyloidiasis

Eosinophilic Gastroenteritis

Radiographic Findings
Differential Diagnosis

Emphysematous Gastritis

Radiographic Findings
Differential Diagnosis

Caustic Ingestion

Radiographic Findings

Radiation

Radiographic Findings

Floxuridine Toxicity

Pathogenesis
Clinical Findings
Radiographic Findings

Duodenitis

Radiographic Findings

Erosive Gastritis

Erosions are defined histologically as epithelial defects that do not penetrate beyond the muscularis mucosae. Although erosive gastritis is rarely diagnosed on conventional single-contrast barium studies, it has become a relatively frequent finding on double-contrast studies, with an overall prevalence of 0.5% to 20% reported in the radiology literature.¹⁻⁶ However, not all patients with erosive gastritis are symptomatic. As a result, it is difficult to be certain of the clinical importance of gastric erosions demonstrated on radiologic or endoscopic examinations.

PATHOGENESIS

Aspirin or other nonsteroidal anti-inflammatory drugs (NSAIDs) are thought to be the most common cause of erosive

gastritis, accounting for about 50% of cases.⁷ Other causes include alcohol, stress, trauma, burns, Crohn's disease, viral or fungal infection, and endoscopic heater probe therapy or other iatrogenic trauma.⁸⁻¹³ Still other patients with erosive gastritis have no apparent predisposing factors for this condition.¹⁴ These cases presumably occur as a variant of peptic ulcer disease.

Considerable attention has been focused on the role of aspirin and other NSAIDs in the development of erosive gastritis. Clinical and laboratory investigations have shown that these agents are capable of disrupting the mucosal barrier in the stomach, causing erosive gastritis and gastric ulcers (see Chapter 29).^{8,15-18} In one study, 40% of patients receiving aspirin for 3 months or longer had endoscopic evidence of erosive gastritis.¹⁶ Other studies on healthy volunteers have shown that as few as two aspirin tablets may cause acute erosive gastritis that is recognized on endoscopy within 24 hours.^{17,18} Maximal damage

usually occurs within 1 to 3 days, and healing may be documented on endoscopy within 1 week.¹⁹ Thus, gastric erosions may form rapidly after ingestion of aspirin or other NSAIDs and may heal rapidly when these drugs are withdrawn.

CLINICAL FINDINGS

Patients with erosive gastritis may present with dyspepsia, epigastric pain, or signs of upper gastrointestinal (GI) bleeding.²⁰ However, other patients are asymptomatic. Gastric erosions can persist for years in the absence of clinical symptoms.²¹ Because erosions may be detected as an incidental finding on barium studies or endoscopy, it is important to rule out other abnormalities in the stomach before assuming that these erosions are the cause of the patient's symptoms.

RADIOGRAPHIC FINDINGS

Two types of erosions may be detected on double-contrast studies. The most common type is the complete or varioliform

erosion in which punctate or slitlike collections of barium representing the epithelial defects are surrounded by radiolucent halos of edematous, elevated mucosa (Fig. 30-1).^{3,5,14} Varioliform erosions typically occur in the gastric antrum and are often aligned on the crests of the rugal folds.^{3,5,20} Because they are shallow lesions, erosions on the posterior (dependent) wall may be better delineated by flow technique to manipulate a thin layer of barium over the dependent mucosal surface.²² The surrounding mounds of edema may prevent filling of the central pits or depressions, so these erosions sometimes appear as filling defects in the thin barium pool without central collections of barium. In other patients, erosive gastritis may be manifested only by scalloped antral folds (Fig. 30-2A). Depending on the quality of mucosal coating, erosions may be faintly seen on the crest of the folds (Fig. 30-2B). These scalloped antral folds often persist after the erosions have healed. Residual epithelial nodules or polyps may occasionally be detected at the site of the healed erosions. These hyperplastic polyps are thought to represent the sequelae of chronic erosive gastritis.²⁰

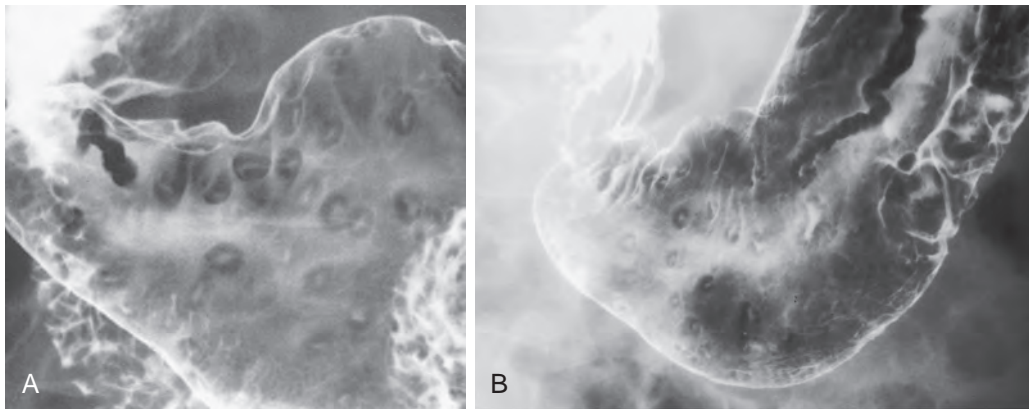


Figure 30-1 Erosive gastritis with varioliform erosions.
A, B. In both patients, multiple varioliform erosions are seen in the antrum as tiny barium collections with surrounding halos of edematous mucosa. (**A** from Laufer I, Levine MS [eds]: *Double Contrast Gastrointestinal Radiology*, 2nd ed. Philadelphia, WB Saunders, 1992.)

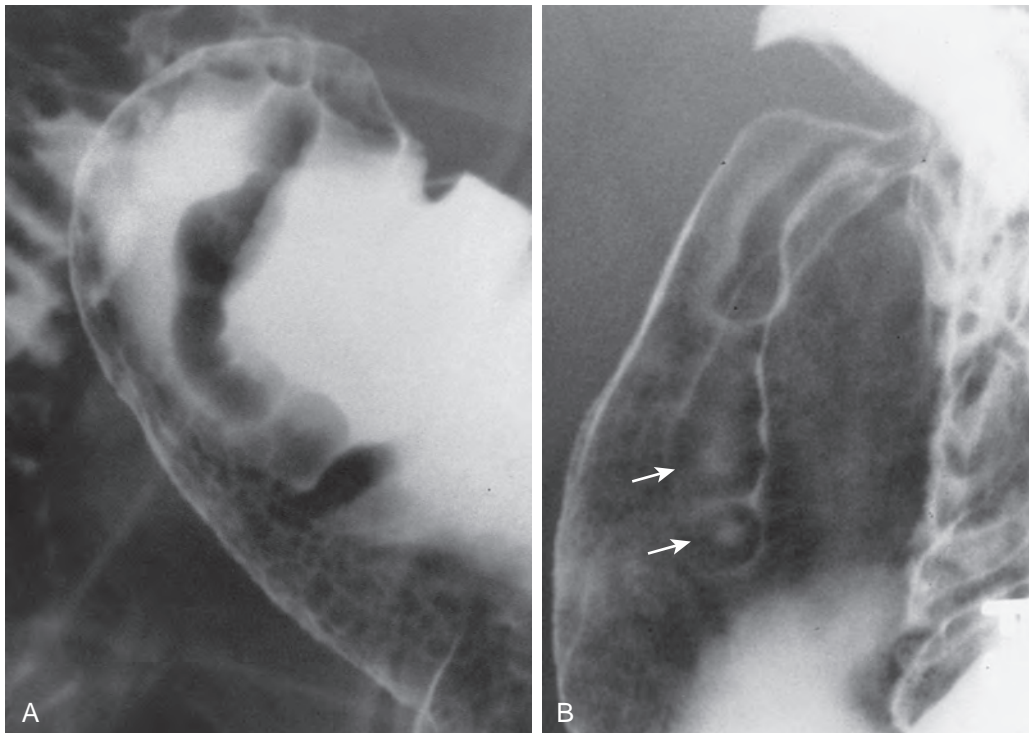


Figure 30-2 Erosive gastritis with scalloped antral folds.
A. A thickened, scalloped fold is present in the gastric antrum.
B. In another patient, several erosions (arrows) can be seen on the crest of a scalloped fold.



Figure 30-3 Erosive gastritis with incomplete erosions. Numerous linear and punctate erosions are seen in the gastric antrum and body. Many of the erosions are incomplete (i.e., they are not surrounded by radiolucent mounds of edema).

Incomplete or flat erosions are epithelial defects that are not associated with elevation of the surrounding mucosa. These erosions appear as linear streaks or dots of barium (Fig. 30-3).^{6,14} Because the surrounding mucosa is normal, incomplete erosions are much more difficult to detect than varioliform erosions, accounting for only 5% to 19% of all erosions found on double-contrast studies.^{6,7}

Although no causative significance is generally attributed to the shape or location of gastric erosions seen on double-contrast studies, aspirin and other NSAIDs may occasionally produce incomplete, linear or serpiginous erosions that tend to be clustered in the body of the stomach on or near the greater curvature (Fig. 30-4).²³ It has been postulated that these erosions result from localized mucosal injury as the dissolving capsules or tablets collect by gravity in the dependent portion of the stomach. Whatever the explanation, these distinctive linear or serpiginous erosions should be highly suggestive of recent aspirin or other NSAID use. Nevertheless, most patients with NSAID-induced erosive gastritis have typical varioliform erosions in the gastric antrum.^{7,23} Aspirin or other NSAIDs should therefore be considered the most likely cause of erosive gastritis, even when the erosions have a varioliform appearance.

Recurrent episodes of NSAID-induced erosion formation and healing may eventually lead to relatively subtle flattening and deformity of the greater curvature of the antrum, a radiologic sign of NSAID-related gastropathy (Fig. 30-5).^{24,25} Detection of gastric erosions or greater curvature flattening should therefore lead to careful questioning of the patient about a possible history of aspirin or other NSAID use. If recent ingestion of these drugs is confirmed in symptomatic patients,

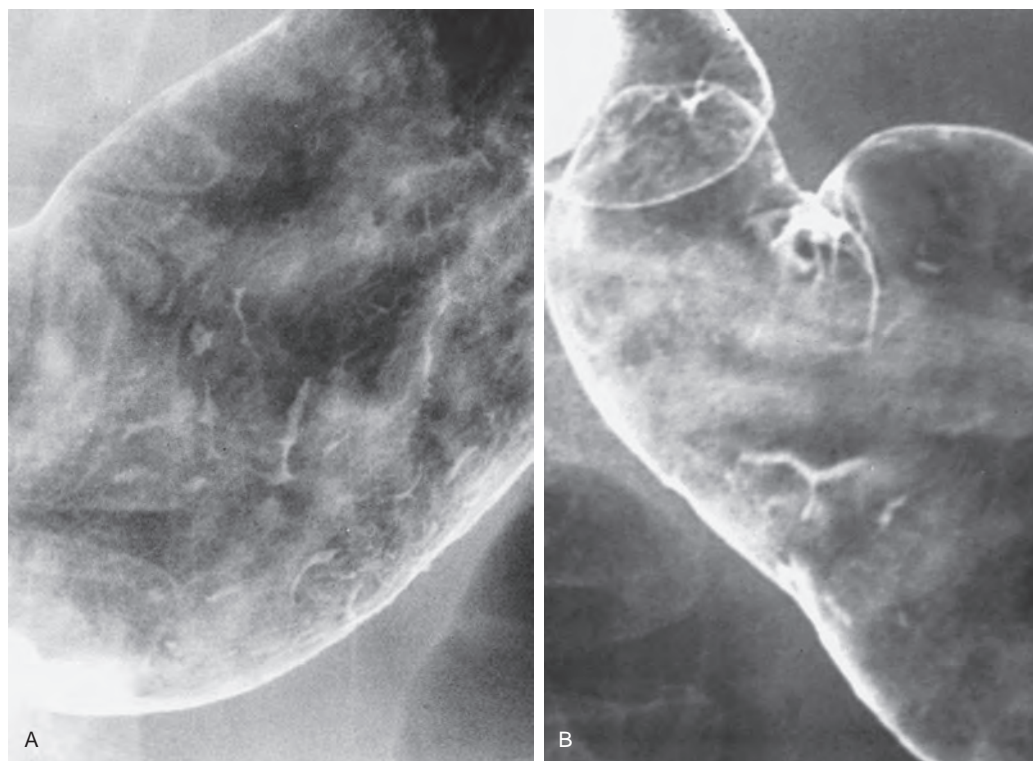


Figure 30-4 Erosive gastritis caused by nonsteroidal anti-inflammatory drugs. A, B. Distinctive linear and serpiginous erosions are clustered in the body (A) and antrum (B) of the stomach near the greater curvature as a result of NSAID ingestion. The patient in A was taking naproxen, and the patient in B was taking ibuprofen. (A from Levine MS, Verstandig A, Laufer I: *Serpiginous gastric erosions caused by aspirin and other nonsteroidal antiinflammatory drugs*. AJR 146:31–34, 1986.)

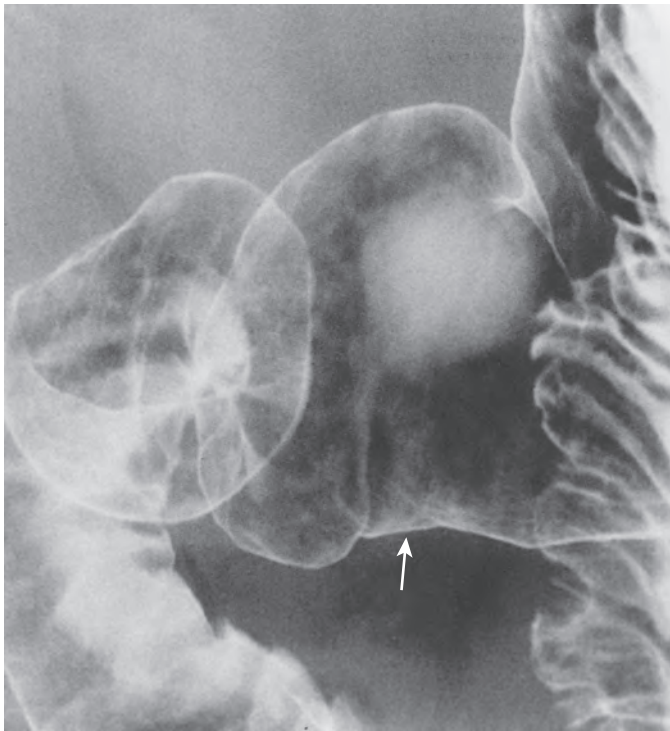


Figure 30-5 Antral flattening caused by NSAIDs. There is flattening and deformity of the greater curvature of the distal antrum (arrow) as a result of chronic aspirin therapy. This finding is characteristic of NSAID-related gastropathy.

withdrawal of the offending agent usually produces a marked clinical response.²³

Crohn's disease is another condition that can be manifested on double-contrast studies by multiple erosions or aphthoid ulcers in the stomach.^{10,11} However, these patients usually have associated Crohn's disease involving the small bowel or colon (see later, "[Crohn's Disease](#)"). Shallow ulcers or erosions may also result from opportunistic infection by cytomegalovirus (CMV) in patients with AIDS (see later, "[Cytomegalovirus](#)"),²⁶ or they may occur as a complication of endoscopic heater probe therapy or other iatrogenic trauma ([Fig. 30-6](#)).¹³

DIFFERENTIAL DIAGNOSIS

Gastric erosions can sometimes be mistaken on barium studies for ulcerated submucosal masses or bull's-eye lesions in the stomach. However, the central ulcer of a bull's-eye lesion is considerably larger than an erosion, and the surrounding mass tends to be larger than the radiolucent mound of edema surrounding an erosion (see Chapter 33). Bull's-eye lesions also tend to be more sporadic than erosions and are not typically aligned on the crests of the folds. As a result, it is almost always possible to distinguish these lesions by radiographic criteria.

Antral Gastritis

Some patients have a form of gastritis that is confined to the gastric antrum, an entity also known as *antral gastritis*. Alcohol, tobacco, coffee and, more recently, *Helicobacter pylori* have been implicated in the development of antral gastritis (see later, "[Helicobacter pylori Gastritis](#)"). Some patients with this



Figure 30-6 Heater probe ulcers and erosions. Shallow, irregular ulcers and linear erosions are seen en face (white arrows) and in profile (black arrow) on the greater curvature of the stomach. These ulcerations occurred as a direct complication of endoscopic heater probe therapy. (From Rummerman J, Rubesin SE, Levine MS, et al: *Gastric ulceration caused by heater probe coagulation*. *Gastrointest Radiol* 13:200–202, 1988.)

condition have increased secretion of peptic acid, but others have normal or even decreased acid secretion. Affected individuals may present with dyspepsia, epigastric pain, or other symptoms indistinguishable from those of peptic ulcer disease. Treatment is generally aimed at suppressing acid secretion in the stomach.

RADIOGRAPHIC FINDINGS

Antral gastritis may be manifested on barium studies by thickened folds, antral erosions (see earlier, "[Erosive Gastritis](#)"), crenulation of the lesser curvature, mucosal nodularity, transverse antral striae, a hypertrophied antral-pyloric fold, and antral narrowing. Some patients have thickened, scalloped, or lobulated folds that are oriented longitudinally in the antrum ([Fig. 30-7A](#)), whereas others have thickened transverse antral folds ([Fig. 30-7B](#)). Thickened folds, which are detected radiographically in about 75% of cases, should be recognized as the single most common sign of antral gastritis on barium studies.⁷ The vast majority of these patients are found to have *H. pylori* as the cause of their gastritis (see later, "[Helicobacter pylori Gastritis](#)").⁷

Crenulation or irregularity of the lesser curvature of the distal antrum may also be recognized as a sign of antral gastritis on barium studies (see [Fig. 30-7B](#)).²⁷ Other patients may have fine transverse striations, or antral striae, as a sign of chronic antral gastritis,²⁸ although this finding can also be seen as a normal variant.²⁹ Still other patients may have a single lobulated fold that arises on the lesser curvature of the prepyloric antrum and extends into the pylorus or base of the duodenal bulb ([Fig. 30-8](#)).^{30,31} This so-called hypertrophied

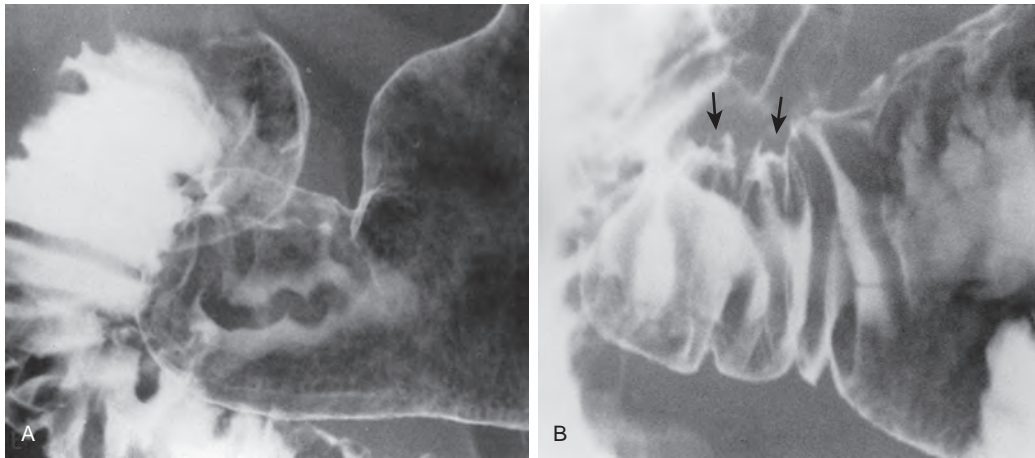
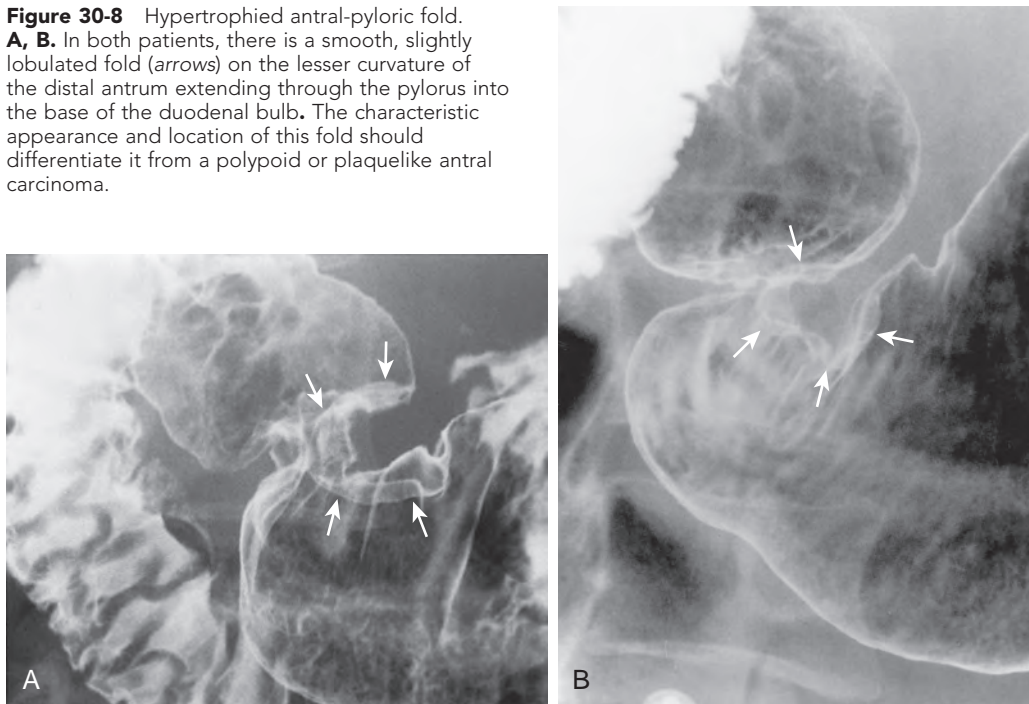


Figure 30-7 Antral gastritis. **A.** This patient has thickened scalloped folds that are oriented longitudinally in the antrum. **B.** In another patient, there are thickened transverse folds in the antrum with fine nodularity and crenulation of the adjacent lesser curvature (arrows).

Figure 30-8 Hypertrophied antral-pyloric fold. **A, B.** In both patients, there is a smooth, slightly lobulated fold (arrows) on the lesser curvature of the distal antrum extending through the pylorus into the base of the duodenal bulb. The characteristic appearance and location of this fold should differentiate it from a polypoid or plaque-like antral carcinoma.



antral-pyloric fold is thought to be a sequela of chronic antral gastritis and is often associated with other radiographic signs of gastritis. Endoscopy is not warranted when a characteristic antral-pyloric fold is seen on barium studies.³¹ If the fold is more lobulated and cannot be distinguished from a polypoid or plaque-like carcinoma on the lesser curvature, however, endoscopy and biopsy should be performed to rule out malignant tumor.

DIFFERENTIAL DIAGNOSIS

Severe antral gastritis associated with antral narrowing must be differentiated from gastric carcinoma. With malignant tumors, however, the narrowed antrum tends to have a more abrupt transition with the adjacent stomach and a more fixed, rigid contour. Thus, it is usually possible to differentiate these

conditions by radiographic criteria. When the folds are markedly thickened and lobulated, antral gastritis can also mimic the appearance of lymphoma or even a submucosally infiltrating carcinoma.³² In such cases, endoscopy may be required for a more definitive diagnosis.

Helicobacter pylori Gastritis

H. pylori (formerly known as *Campylobacter pylori*) is a gram-negative bacillus that was first isolated from the stomach by Warren and Marshall in 1983.³³ Since then, *H. pylori* has been recognized as the most common cause of chronic active gastritis.^{34,35} The organism is usually found in clusters or clumps beneath the mucous layer on surface epithelial cells or, less commonly, superficial foveolar cells in the stomach.³⁶ *H. pylori* gastritis is characterized pathologically by an acute inflammatory

reaction in the mucosa with accumulation of neutrophils, plasma cells and, eventually, lymphoid nodules.³⁶ The gastric antrum is the most common site of involvement, but the proximal half of the stomach or even the entire stomach may be involved by this disease.^{35,37} *H. pylori* gastritis is important not only because it may cause upper GI symptoms but also because it is associated with the development of gastric and duodenal ulcers (see Chapter 29), gastric carcinoma (see Chapter 32), and low-grade, B-cell, mucosa-associated lymphoid tissue (MALT) lymphoma (see Chapter 33).

CLINICAL FINDINGS

H. pylori infection is acquired by oral ingestion of the bacterium and is mainly transmitted within families during early childhood.³⁸ *H. pylori* is a worldwide pathogen, being most common in developing countries. In developed countries, *H. pylori* is more common in lower socioeconomic populations.^{35,38} The prevalence of *H. pylori* also increases with age; more than 50% of Americans over 60 years of age are infected by this organism.³⁹ Some people with *H. pylori* may present with dyspepsia, epigastric pain, or other upper GI symptoms,³⁵ but most are asymptomatic.³⁹ Even when symptoms are present, it is often difficult to prove that the symptoms are caused by *H. pylori* because of the high prevalence of this infection.

H. pylori gastritis can be eradicated from the stomach by treatment with a combination of antibiotics and antisecretory agents (proton pump inhibitors).⁴⁰ In a consensus development panel sponsored by the National Institutes of Health in 1994 and a subsequent update conference sponsored by the American Digestive Health Foundation in 1997, combination therapy with antibiotics and antisecretory agents was recommended for all *H. pylori*-positive patients with gastric or duodenal ulcers to accelerate ulcer healing and decrease the rate of ulcer recurrence.^{41,42} However, there are conflicting data about the value of *H. pylori* eradication therapy in patients with non-ulcer dyspepsia.⁴³⁻⁴⁵ As a result, the panels did not recommend treatment for this subset of patients.^{41,42} It therefore remains unclear whether combination therapy should be reserved for patients with *H. pylori* who have gastric or duodenal ulcers or whether patients with *H. pylori* who have nonulcer dyspepsia would also benefit from treatment.

H. pylori gastritis can be accurately diagnosed at endoscopy on the basis of histologic specimens, cultures, and the rapid urease test.^{46,47} However, noninvasive tests for *H. pylori*, such as the urea breath test (using orally administered ¹⁴C- or ¹³C-labeled urea) serologic tests, and stool antigen tests have reported sensitivities and specificities of greater than 90%.^{38,46,47} Highly accurate noninvasive tests are therefore available for detecting this infection.

RADIOGRAPHIC FINDINGS

H. pylori gastritis is the most common cause of thickened folds in the gastric antrum or body on double-contrast barium studies (Fig. 30-9).^{7,48-52} However, other patients may have diffusely thickened folds in the stomach or thickened folds that are confined to the fundus.⁴⁹ Still others with *H. pylori* gastritis may have markedly thickened, lobulated gastric folds (i.e., polypoid gastritis) in a diffuse (Fig. 30-10) or localized (Fig. 30-11) distribution.^{7,49} In such cases, it may be difficult or impossible to differentiate *H. pylori* gastritis from other infiltrative conditions or even malignant tumor involving the stomach (see later, "Differential Diagnosis").

H. pylori gastritis may also be manifested on double-contrast studies by enlarged areae gastricae (≥ 3 mm in diameter) in the stomach (see Fig. 30-9).^{7,49} In the past, enlarged areae gastricae were associated with hypersecretory states and duodenal ulcers.^{53,54} In retrospect, however, this association was probably related to underlying *H. pylori* gastritis in many of these patients. The presence of enlarged areae gastricae should therefore suggest the possibility of *H. pylori*, particularly if associated with thickened gastric folds.^{7,49}

Patients with chronic *H. pylori* gastritis may gradually acquire lymphoid tissue in the gastric mucosa, resulting in the development of intramucosal aggregates of lymphocytes or lymphoid follicles containing germinal centers.^{55,56} This phenomenon is thought to be mediated by a specific immune response to *H. pylori*.⁵⁷ In one study, more than 90% of patients with lymphoid hyperplasia of the stomach were found to have *H. pylori* gastritis.² Lymphoid hyperplasia is therefore a potential marker for *H. pylori* gastritis, even in the absence of other findings. These enlarged lymphoid follicles are manifested on double-contrast barium studies by innumerable tiny

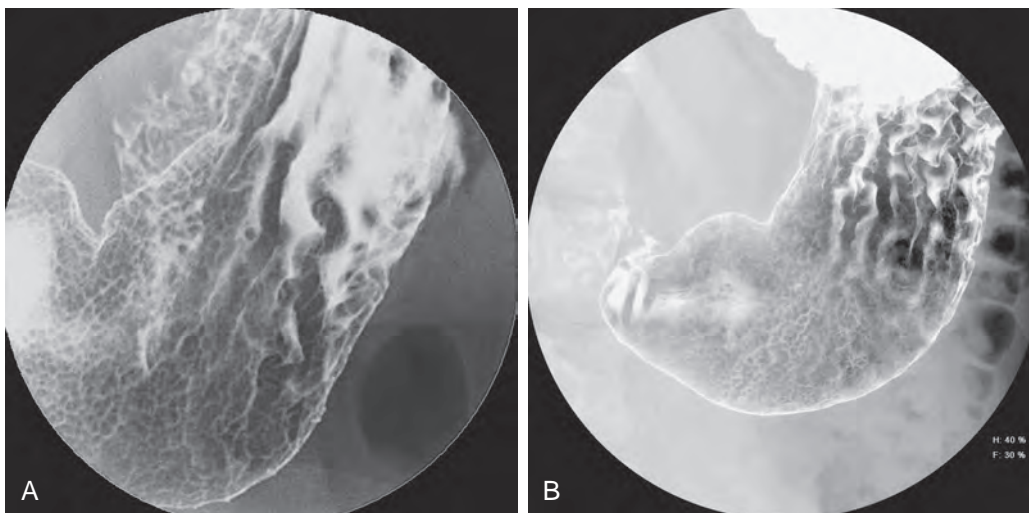


Figure 30-9 *H. pylori* gastritis. **A, B.** In both patients, thickened folds are seen in the body of the stomach and enlarged areae gastricae in the proximal antrum as a result of chronic infection by *H. pylori*. (**A** from Levine MS, Laufer I: *The gastrointestinal tract: Dos and don'ts of digital imaging*. Radiology 207:311-316, 1998.)

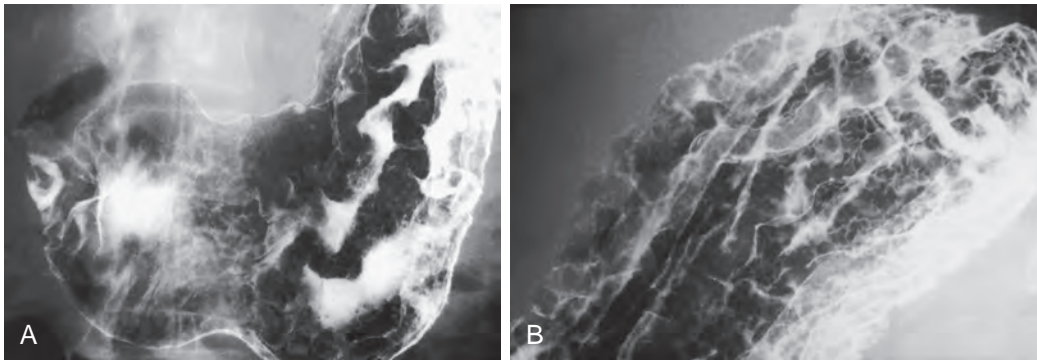


Figure 30-10 *H. pylori* causing diffuse polypoid gastritis. **A, B.** Markedly thickened, lobulated folds are seen in the gastric body (**A**) and fundus (**B**). This appearance could be mistaken for severe hypertrophic gastritis, Ménétrier's disease, or lymphoma, but endoscopic biopsy specimens revealed *H. pylori* gastritis without evidence of tumor. (From Sohn J, Levine MS, Furth EE, et al: *Helicobacter pylori* gastritis: Radiographic findings. Radiology 195:763-767, 1995.)

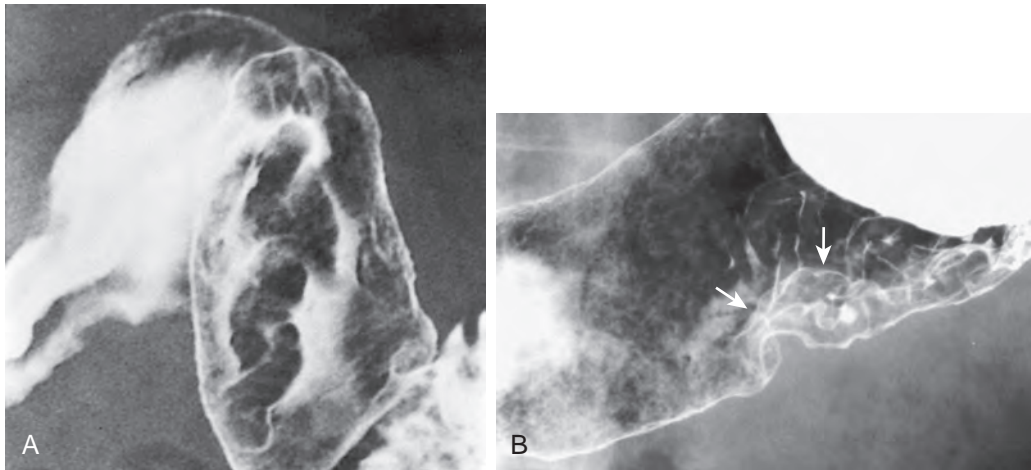


Figure 30-11 *H. pylori* causing localized polypoid gastritis. **A, B.** Focally thickened, lobulated folds are seen in the gastric antrum in **A** and in the gastric body (arrows) in **B**. These findings are worrisome for a localized lymphoma or submucosally infiltrating carcinoma. In both patients, however, endoscopic biopsy specimens revealed *H. pylori* gastritis without evidence of tumor.

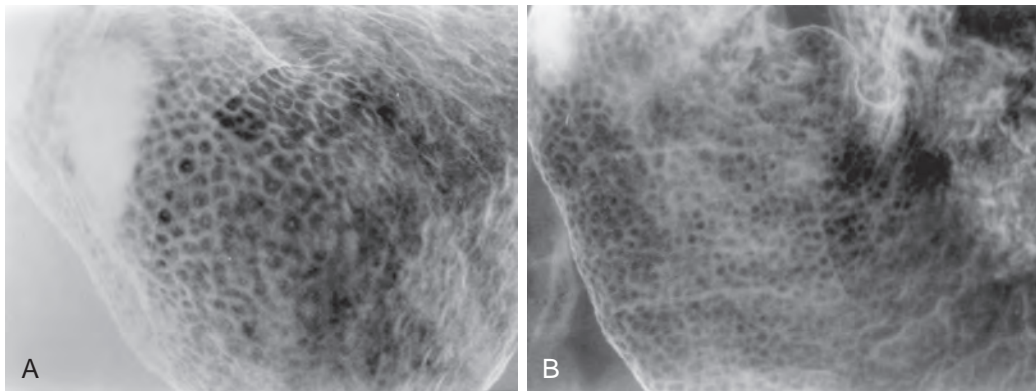


Figure 30-12 *H. pylori* gastritis with lymphoid hyperplasia. **A, B.** In both patients, enlarged lymphoid follicles are seen as innumerable tiny, round nodules that carpet the mucosa of the gastric antrum. In **A**, note how many of the nodules have central umbilications with punctate collections of barium seen en face in the lesions. (From Torigian DA, Levine MS, Gill NS, et al: *Lymphoid hyperplasia of the stomach: Radiographic findings in five adult patients. AJR 177:71-75, 2001.*)

(1-3 mm in diameter), round, frequently umbilicated nodules that carpet the mucosa of the gastric antrum or antrum and body (Fig. 30-12).⁵⁸ The radiographic findings are therefore similar to those of lymphoid hyperplasia in the small bowel or colon.

DIFFERENTIAL DIAGNOSIS

The radiographic findings of *H. pylori* gastritis may be indistinguishable from those of hypertrophic gastritis, Ménétrier's disease, or lymphoma when the thickened, lobulated folds have a diffuse distribution,⁵⁹ and the findings may be

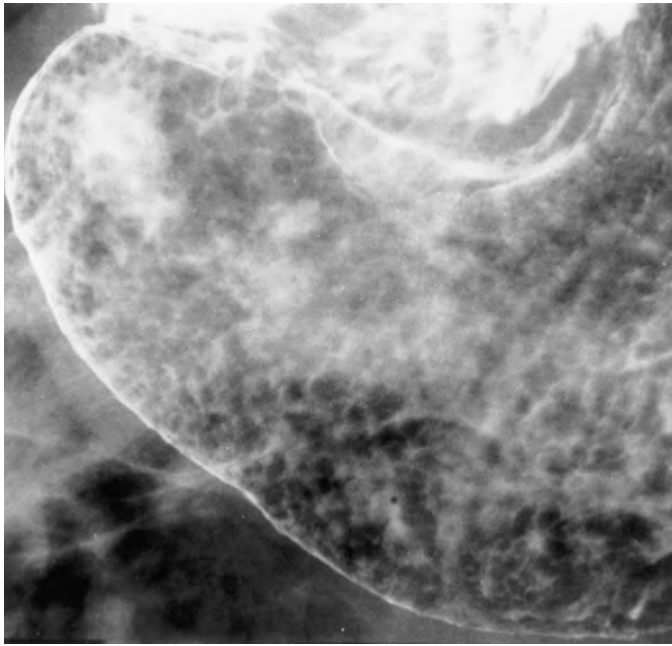


Figure 30-13 Low-grade gastric MALT lymphoma. There are multiple round, variably sized, confluent nodules with poorly defined borders in the gastric antrum. These findings are characteristic of gastric MALT lymphoma. In contrast, the nodules of lymphoid hyperplasia have more discrete borders and a more uniform size (see Fig. 30-12). (From Yoo CC, Levine MS, Furth EE, et al: *Gastric mucosa-associated lymphoid tissue lymphoma: Radiographic findings in six patients*. *Radiology* 208:239–243, 1998.)

indistinguishable from malignant tumors such as lymphoma or a submucosally infiltrating carcinoma when the enlarged, polypoid folds have a focal distribution.^{7,49} In other patients with *H. pylori* gastritis, computed tomography (CT) may reveal circumferential thickening of the antrum or focal thickening of the posterior gastric wall, occasionally simulating a gastric carcinoma.⁶⁰ Endoscopy and biopsy are required for a definitive diagnosis when malignant tumor is suspected on the basis of the radiographic findings. Nevertheless, it is important to be aware of the association between *H. pylori* and this polypoid form of gastritis, so careful testing for the organism is performed at the time of endoscopy.

When *H. pylori* gastritis is associated with lymphoid hyperplasia of the stomach, the major consideration in the differential diagnosis is low-grade gastric MALT lymphoma (see Chapter 33). However, gastric MALT lymphoma is manifested on double-contrast studies by multiple round, variably sized, often confluent nodules with poorly defined borders (Fig. 30-13).⁶¹ In contrast, the nodules of gastric lymphoid hyperplasia have more discrete borders, a more uniform size, and, not infrequently, central umbilications (see Fig. 30-12).⁵⁸ Lymphoid hyperplasia of the stomach should also be differentiated from enlarged areae gastricae, another finding associated with *H. pylori* gastritis.^{7,46} However, enlarged areae gastricae have a more polygonal or angulated configuration, producing a sharply margined reticular network (see Fig. 30-9), and they do not contain central umbilications. Other unusual neoplastic lesions such as leukemic infiltrates or even some of the polyposis syndromes may also be manifested on double-contrast studies by multiple small nodules, but the nodules tend to

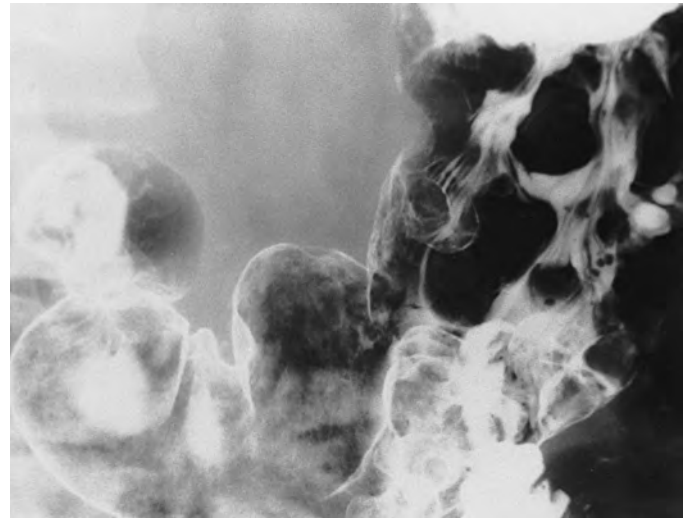


Figure 30-14 Hypertrophic gastritis. Markedly thickened, lobulated folds are seen in the body of the stomach. The antrum appears normal. (From Laufer I, Levine MS [eds]: *Double Contrast Gastrointestinal Radiology*. 2nd ed. Philadelphia, WB Saunders, 1992.)

have a more variable size and more sporadic distribution. Thus, it is usually possible to differentiate lymphoid hyperplasia in the stomach from other conditions on radiographic criteria. If the findings are equivocal, however, endoscopic biopsy specimens should be obtained for a more definitive diagnosis.

Hypertrophic Gastritis

Hypertrophic gastritis, also known as hypertrophic hypersecretory gastropathy, is characterized by marked glandular hyperplasia and increased secretion of acid in the stomach.^{62,63} Gastric folds may be thickened, not only because of glandular hyperplasia but also because of edema and inflammation. Although the pathogenesis of this condition is uncertain, glandular hyperplasia in the stomach may be caused by pituitary, hypothalamic, or vagal stimuli.⁶² These patients may present with epigastric pain, nausea and vomiting, or, less frequently, signs of upper GI bleeding.^{62,63} If the radiographic or endoscopic findings support the diagnosis of hypertrophic gastritis, treatment with antisecretory agents is usually recommended to suppress acid secretion in the stomach.

RADIOGRAPHIC FINDINGS

Hypertrophic gastritis is manifested on barium studies by thickened folds, predominantly in the gastric fundus and body, because the acid-secreting portion of the stomach is most affected by this condition (Fig. 30-14). Several studies have shown a significant correlation between the degree of fold thickening and the amount of acid secretion in the stomach.^{64,65} The presence of markedly thickened, lobulated folds in the stomach should therefore suggest the possibility of hypertrophic gastritis. In retrospect, however, many if not most cases of previously diagnosed hypertrophic gastritis probably resulted from infection by *H. pylori*, a much more common cause of thickened gastric folds (see earlier, “*Helicobacter pylori* Gastritis”).

DIFFERENTIAL DIAGNOSIS

H. pylori gastritis, Ménétrier's disease, and lymphoma are the major considerations in the differential diagnosis of thickened, lobulated gastric folds. *H. pylori* gastritis can usually be differentiated from hypertrophic gastritis by noninvasive tests for *H. pylori*, such as the urea breath test and serologic tests (see earlier, "*Helicobacter pylori* Gastritis"). Ménétrier's disease should be suspected in patients who have normal or decreased acid secretion and a protein-losing enteropathy (see later, "Ménétrier's Disease"), whereas lymphoma should be suspected when associated findings such as ulcers, masses, or bull's-eye lesions are present in the stomach (see Chapter 33). Gastric carcinoma is a less common cause of thickened folds and is usually associated with loss of distensibility and decreased or absent peristalsis in the involved portion of the stomach.⁶⁶ If the radiographic findings are equivocal, endoscopy and biopsy may be required to rule out malignant tumor. Rarely, other conditions such as Zollinger-Ellison syndrome, eosinophilic gastritis, and varices may be manifested by thickened folds in the stomach, but the correct diagnosis can usually be suggested on the basis of the clinical history and presentation.

Ménétrier's Disease

Since its original description by Ménétrier in 1898, Ménétrier's disease has been recognized as a rare condition of unknown etiology characterized by marked foveolar hyperplasia in the stomach, enlarged gastric rugae, hypochlorhydria, and hypoproteinemia. In the past, this condition was also called cystic gastritis, giant hypertrophic gastritis, giant mucosal hypertrophy, and hyperplastic gastropathy. Ménétrier's disease may cause chronic disabling symptoms, occasionally necessitating gastric resection. Despite its rarity, this entity has received considerable attention in the radiology literature because of its often dramatic appearance on barium studies.

PATHOLOGY

Ménétrier's disease is characterized histologically by thickening and hyperplasia of the mucosa as a result of cystic dilation and elongation of gastric mucous glands associated with deepening of the foveolar pits.⁶⁷ Despite these findings, gastric acid output is decreased or absent in about 75% of cases.⁶⁸ Some patients have a protein-losing enteropathy resulting from loss of protein from the hyperplastic mucosa into the gastric lumen.⁶⁹ Others have varying degrees of gastritis in a patchy or diffuse distribution.

CLINICAL FINDINGS

Ménétrier's disease tends to occur in older patients and is more common in men than in women.⁶⁸ Affected individuals often present with epigastric pain, nausea and vomiting, diarrhea, anorexia, weight loss, and/or peripheral edema.^{68,70} Laboratory studies may reveal hypoalbuminemia resulting from a protein-losing enteropathy, hypochlorhydria resulting from decreased acid secretion, or both. Rarely, the development of gastric carcinoma has been described in patients with preexisting Ménétrier's disease.^{71,72} However, it is unclear whether Ménétrier's disease is a premalignant condition or whether this association is coincidental.

Some patients with Ménétrier's disease have spontaneous remission of symptoms, whereas others respond to treatment with antisecretory agents, vagotomy, or antibiotics. However, most patients have a prolonged illness with intractable symptoms.⁷⁰ A total gastrectomy may be required for patients who are unresponsive to medical therapy.

RADIOGRAPHIC FINDINGS

Ménétrier's disease is typically manifested on barium studies by considerably thickened, lobulated folds in the gastric fundus and body, with relative sparing of the antrum (Fig. 30-15A).^{73,74} In one study, however, the antrum was involved in almost 50% of patients,⁷⁵ so diffuse thickening of gastric folds in no way precludes this diagnosis. The greatest degree of fold thickening usually occurs on or near the greater curvature.⁷³ When the disease is confined to one portion of the stomach, focally enlarged folds may erroneously suggest a polypoid carcinoma (Fig. 30-15B).⁷³

Ménétrier's disease is characterized on CT by a markedly thickened gastric wall, with masslike elevations representing giant, heaped-up folds protruding into the lumen (Fig. 30-15C).⁷⁴ When Ménétrier's disease is suspected on barium studies or CT, full-thickness endoscopic biopsy specimens should be obtained to confirm the diagnosis.

DIFFERENTIAL DIAGNOSIS

Although a variety of conditions may be manifested by thickened gastric folds, these conditions rarely produce the degree of fold thickening seen in Ménétrier's disease. When *H. pylori* gastritis is associated with markedly thickened, lobulated folds, the radiographic findings may be indistinguishable from those of Ménétrier's disease.⁴⁶ Gastric lymphoma is sometimes associated with enlarged folds, but neoplastic infiltration should be suggested by the presence of polypoid masses, ulcers, or bull's-eye lesions in these patients (see Chapter 33). Occasionally, gastric carcinoma may be manifested by thickened folds, but infiltrating cancers tend to narrow the lumen, whereas the stomach usually remains pliant and distensible in patients with Ménétrier's disease. Zollinger-Ellison syndrome may also be characterized by thickened folds, but the presence of increased secretions in the stomach or other associated abnormalities (e.g., ulcers, thickened folds) in the duodenum and proximal jejunum should suggest the correct diagnosis (see Chapter 29). Gastric varices should also be included in the differential diagnosis, but varices tend to have a more serpiginous appearance and are usually confined to the region of the gastric cardia or fundus (see Chapter 34). Other conditions involving the stomach, such as Crohn's disease, eosinophilic gastritis, sarcoidosis, tuberculosis, and syphilis, may also be manifested by thickened folds. In these cases, however, the correct diagnosis is usually suggested by the clinical history and presentation.

Atrophic Gastritis

Atrophic gastritis is important because of its association with pernicious anemia, a megaloblastic anemia caused by decreased synthesis of intrinsic factor and subsequent malabsorption of vitamin B₁₂. Pernicious anemia is a disease of older adults; it accounts for 50 of 100,000 hospital admissions in the United States.⁷⁶ Although the pathogenesis of this disease is uncertain,

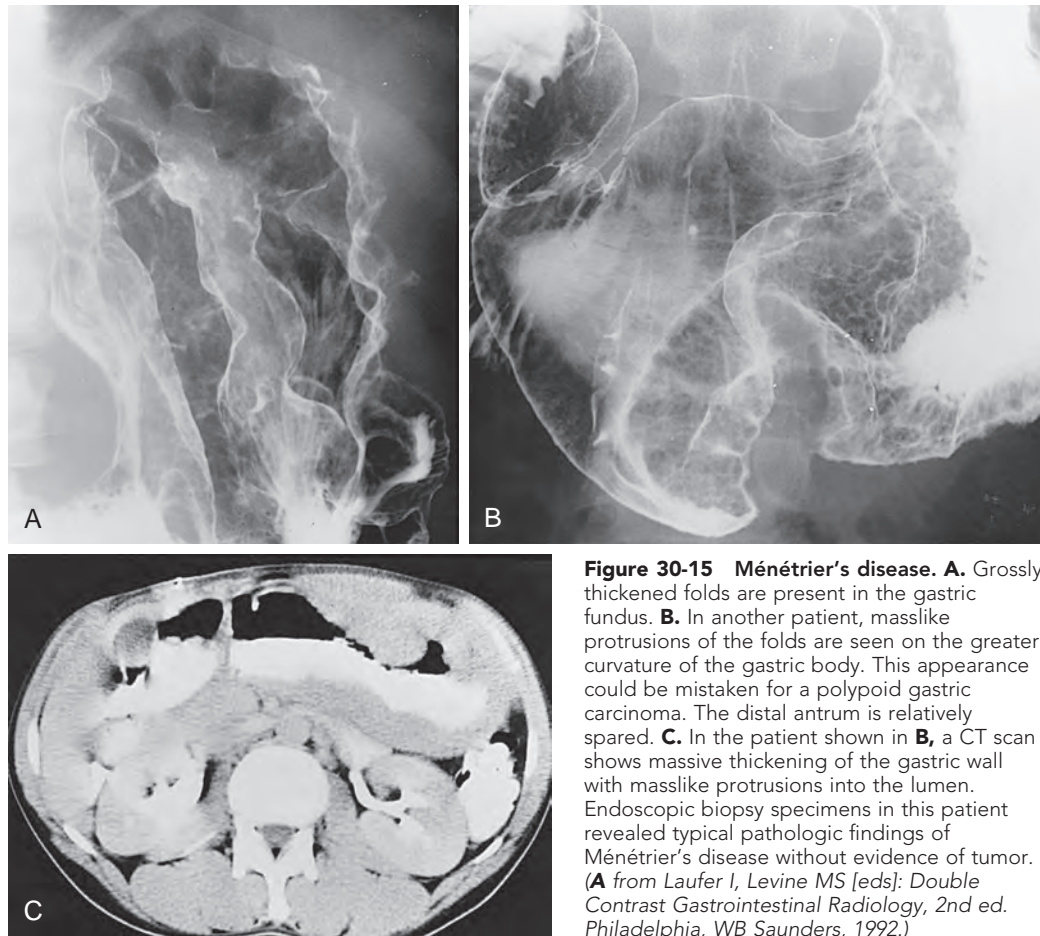


Figure 30-15 Ménétrier's disease. **A.** Grossly thickened folds are present in the gastric fundus. **B.** In another patient, masslike protrusions of the folds are seen on the greater curvature of the gastric body. This appearance could be mistaken for a polypoid gastric carcinoma. The distal antrum is relatively spared. **C.** In the patient shown in **B**, a CT scan shows massive thickening of the gastric wall with masslike protrusions into the lumen. Endoscopic biopsy specimens in this patient revealed typical pathologic findings of Ménétrier's disease without evidence of tumor. (**A** from Laufer I, Levine MS [eds]: *Double Contrast Gastrointestinal Radiology*, 2nd ed. Philadelphia, WB Saunders, 1992.)

an autoimmune mechanism has been postulated because of the frequent finding of parietal cell or intrinsic factor antibodies in these individuals.⁷⁷

More than 90% of patients with pernicious anemia have underlying atrophic gastritis, characterized pathologically by atrophy of mucosal glands, loss of parietal and chief cells, thinning of the mucosa and, eventually, intestinal metaplasia.⁷⁸ The finding of intestinal metaplasia is particularly worrisome because it is widely believed to be the precursor lesion of the intestinal type of gastric cancer. The literature has also implicated chronic *H. pylori* infection as a major cause of atrophic gastritis, intestinal metaplasia, and gastric carcinoma (see Chapter 32).

PATHOGENESIS

Atrophic gastritis may be classified into two types—type A and type B—which have different histologic, immunologic, and secretory characteristics.^{36,79,80} In type A gastritis, mucosal atrophy is confined to the gastric fundus and body with antral sparing. This type of atrophic gastritis is thought to result from immunologic injury (i.e., antiparietal cell antibodies) and is usually associated with pernicious anemia.⁷⁹

In contrast, type B gastritis is characterized predominantly by antral disease with limited involvement of the fundus and body. This form of atrophic gastritis is more common and usually results from mucosal injury by *H. pylori* or, less

commonly, by other endogenous or exogenous agents such as bile acids or alcohol.^{36,79,80} In patients with *H. pylori*, it has been postulated that the organism progressively damages the gastric mucous layer, causing chronic atrophic gastritis and gastric atrophy.^{34,81} A particular strain of *H. pylori* known as *cagA* (cytotoxin-associated gene A) has been associated with an increased prevalence and degree of atrophic gastritis, predisposing these patients to the development of gastric carcinoma,⁸² so the risk of malignant degeneration may not be the same for all patients with this infection.

CLINICAL FINDINGS

Although atrophic gastritis rarely causes symptoms, some patients with pernicious anemia initially present with neurologic symptoms as a result of long-standing vitamin B₁₂ deficiency. Early diagnosis of pernicious anemia is therefore important, so vitamin B₁₂ replacement therapy can be initiated before the development of irreversible neurologic sequelae. Because the average adult has a 3- to 6-year body store of vitamin B₁₂, the gastric abnormalities in pernicious anemia may predate the hematologic and neurologic abnormalities in this condition by several years. The diagnosis of atrophic gastritis on upper GI studies might therefore permit these patients to be treated with vitamin B₁₂ supplements before the full-blown clinical entity of pernicious anemia has developed.

Relationship to Gastric Carcinoma

Patients with atrophic gastritis and pernicious anemia are at increased risk for the development of gastric carcinoma. In one study, the risk of developing gastric cancer in these patients was found to be about three times greater than that in the general population.⁸³ Although some investigators advocate endoscopic or radiologic surveillance of patients with known pernicious anemia, others believe that the risk of cancer is not high enough to warrant routine screening.⁸⁴⁻⁸⁶ Nevertheless, any patient with pernicious anemia who has occult GI bleeding should be evaluated aggressively to rule out a superimposed gastric carcinoma.

The literature suggests that patients with *H. pylori*-associated atrophic gastritis have a substantially increased risk of developing gastric carcinoma (see Chapter 32). Evidence from several studies has shown that the risk of gastric cancer in *H. pylori*-positive patients is about four times greater than that in patients without this infection.⁸⁷ Because of the high prevalence of *H. pylori* in the population, however, it remains unclear whether widespread eradication of *H. pylori* is justified from a societal perspective to prevent the development of cancer.

RADIOGRAPHIC FINDINGS

The diagnosis of atrophic gastritis may be suggested on single-contrast studies by the presence of a narrowed, tubular stomach with decreased or absent mucosal folds, predominantly in the body and fundus, also known as a bald fundus (Fig. 30-16).⁸⁸ In one study, 80% of patients with atrophic gastritis and pernicious anemia had a fundal diameter of 8 cm or less, absent folds in the fundus and body, and small (1-2 mm in diameter) or absent areae gastricae in the stomach; however, this combination of findings was also present in about 10% of age-matched controls.⁸⁹ The radiologic diagnosis of atrophic gastritis in patients with pernicious anemia has therefore been limited by a lack of criteria that are sensitive and specific for this condition.

When atrophic gastritis is suspected on double-contrast studies, serum vitamin B₁₂ levels should be obtained to determine whether vitamin B₁₂ replacement therapy is indicated.

Many questions remain about the appearance of the areae gastricae in patients with atrophic gastritis. It was previously postulated that variations in the size of the areae gastricae depend on parietal cell mass.⁹⁰ Thus, the small size and frequent absence of areae gastricae in patients with atrophic gastritis may be explained by the loss of parietal cells in these individuals. In contrast, focal enlargement of the areae gastricae should raise the possibility of intestinal metaplasia or even a superficial spreading carcinoma, so this finding should be evaluated by endoscopy and biopsy.

DIFFERENTIAL DIAGNOSIS

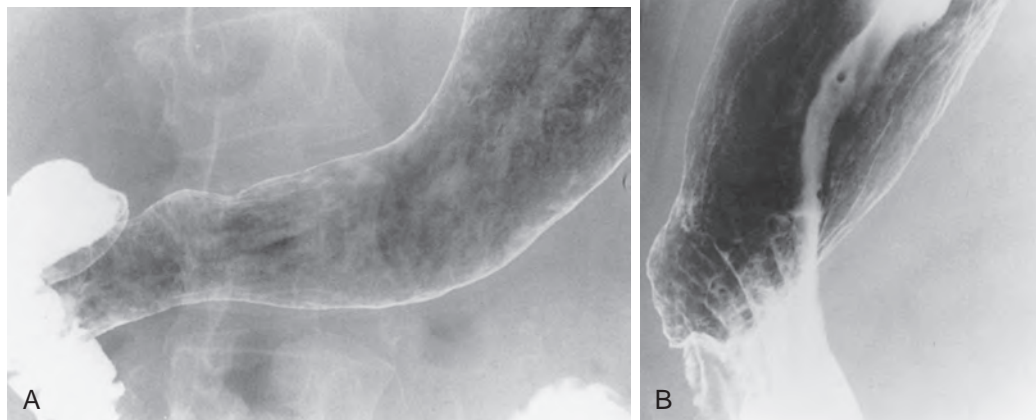
Scirrhou carcinoma of the stomach (i.e., linitis plastica) is the most important consideration in the differential diagnosis of atrophic gastritis. However, scirrhou tumors are usually characterized by a nodular, distorted mucosa and thickened, irregular folds,⁹¹ whereas atrophic gastritis is characterized by a smooth, featureless mucosa and decreased or absent folds. Thus, scirrhou carcinomas can almost always be differentiated from atrophic gastritis by radiologic criteria. Scarring from peptic ulcer disease or other conditions may also be characterized by gastric narrowing, but the antrum and body tend to be involved, rather than the fundus.

Granulomatous Conditions

CROHN'S DISEASE

Although Crohn's disease primarily affects the small bowel and colon, early signs of upper GI involvement may be detected on double-contrast barium studies in more than 20% of patients with granulomatous ileocolitis.⁹² Occasionally, the onset of upper GI disease coincides with or even precedes the onset of

Figure 30-16 Atrophic gastritis. A, B. The stomach has a tubular configuration with decreased distensibility, a paucity of mucosal folds, and absence of discernible areae gastricae. These findings are characteristic of atrophic gastritis.



ileal or colonic disease, so these patients do not necessarily have known Crohn's disease when they seek medical attention. Endoscopic biopsy specimens from the stomach or duodenum may fail to reveal granulomas because of the superficial nature of the biopsy specimens and patchy distribution of the disease.⁹³ Thus, the absence of definitive histologic findings should not discourage a diagnosis of gastroduodenal Crohn's disease if the clinical and radiographic findings suggest this condition.

Clinical Findings

Patients with early gastroduodenal involvement by Crohn's disease are often asymptomatic, but those with more advanced disease may present with pain, vomiting, weight loss, or signs of upper GI bleeding.^{94,95} Others may have diarrhea because of associated ileocolic Crohn's disease. The development of a gastroduodenal or duodenocolic fistula is classically manifested by feculent vomiting, diarrhea, and weight loss,⁹⁶ but this triad of findings is present in only about 30% of patients, so gastroduodenal fistulas are not often suspected on clinical grounds.⁹⁷

Asymptomatic patients with early gastroduodenal Crohn's disease require no specific treatment. In patients with more advanced disease, medical treatment for Crohn's disease may relieve epigastric pain or other upper GI complaints.⁹⁴ In contrast, a surgical bypass procedure such as a gastrojejunostomy or duodenojejunostomy may be required to alleviate symptoms of gastric outlet obstruction.⁹⁴

Radiographic Findings

As in the ileum or colon, gastroduodenal Crohn's disease is characterized by nonstenotic and stenotic phases of involvement. The initial nonstenotic phase is manifested by a spectrum of findings, including aphthoid ulcers, larger ulcers, thickened folds, and distorted, effaced or, rarely, cobblestoned mucosa. Subsequent scarring and fibrosis may cause antral, pyloric, or duodenal narrowing with progressive gastric outlet obstruction. Thus, the radiologic features of gastroduodenal Crohn's disease are similar to those in the small bowel and colon.

Gastric Involvement. Gastric Crohn's disease almost always involves the antrum or antrum and body of the stomach.⁹⁸ More proximal extension of Crohn's disease is unusual, and isolated fundal involvement rarely occurs.⁹⁹ When the stomach is affected by Crohn's disease, the duodenum also tends to be involved.^{98,100,101} Most patients have associated granulomatous ileocolitis, but the diagnosis of Crohn's disease may not be known at the time of clinical presentation. When gastric involvement is suggested by upper GI studies, a small bowel follow-through or barium enema should be performed to determine whether there is concomitant ileocolic disease.

Aphthoid ulcers, the earliest histologic lesions of Crohn's disease, are detected in the stomach on double-contrast studies in more than 20% of patients with granulomatous ileocolitis.⁹² These aphthoid ulcers tend to be located in the gastric antrum or in the antrum and body, appearing as punctate or slitlike collections of barium surrounded by radiolucent mounds of edema (Fig. 30-17).^{11,92,102} As a result, these lesions may be indistinguishable from varioliform gastric erosions (see earlier, "Erosive Gastritis").

More advanced gastroduodenal Crohn's disease may be manifested by one or more larger ulcers, thickened folds (Fig. 30-18), or a nodular or cobblestoned mucosa in the gastric antrum or body.^{98,100} Subsequent scarring may lead

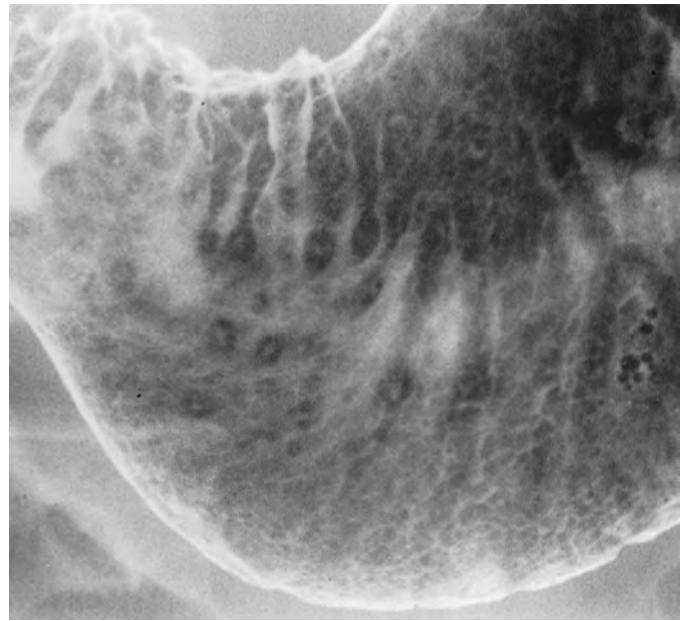


Figure 30-17 Early gastric Crohn's disease with aphthoid ulcers. These lesions are indistinguishable from varioliform erosions in the stomach, but the patient had typical findings of Crohn's disease in the terminal ileum. (Courtesy Robert A. Goren, MD, Philadelphia.)

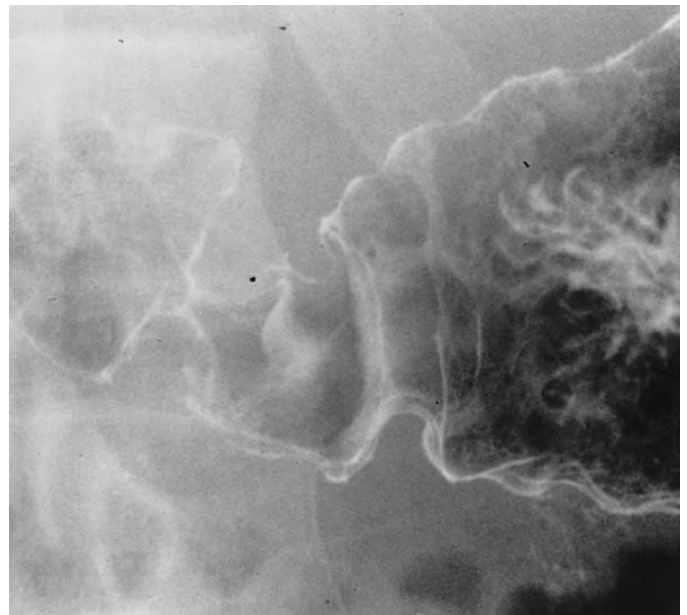


Figure 30-18 Gastric Crohn's disease. Thickened, nodular folds are seen in the antrum of the stomach. (From Levine MS: *Crohn's disease of the upper gastrointestinal tract*. *Radiol Clin North Am* 25:79-91, 1987.)

to the development of a narrowed, tubular, funnel-shaped antrum that has been likened to the appearance of the sacramental ram's horn, or shofar, used to sound the advent of the Jewish New Year (Fig. 30-19).¹⁰³ In other patients, combined gastroduodenal scarring may produce a single, continuous tubular structure involving the antrum and duodenum with obliteration of the normal anatomic landmarks at the pylorus (Fig. 30-20).^{94,100} Because of its resemblance

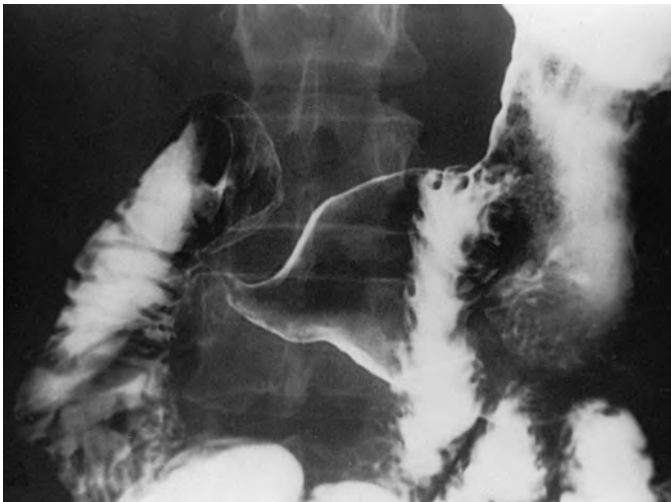


Figure 30-19 Gastric Crohn's disease with antral narrowing. There is smooth, funnel-shaped narrowing of the antrum, resulting in the classic ram's horn sign of gastric Crohn's disease. (From Levine MS: *Crohn's disease of the upper gastrointestinal tract*. Radiol Clin North Am 25:79–91, 1987.)



Figure 30-20 Gastroduodenal Crohn's disease. There is contiguous narrowing of the antrum and duodenum with obliteration of the normal anatomic landmarks at the pylorus. Because the antrum and duodenum merge together as a single tubular structure, this finding has been described as the pseudo-Billroth I sign of gastroduodenal Crohn's disease. (From Levine MS: *Crohn's disease of the upper gastrointestinal tract*. Radiol Clin North Am 25:79–91, 1987.)

to a postsurgical stomach after a Billroth I partial gastrectomy, this finding has been described as the pseudo-Billroth I sign of gastroduodenal Crohn's disease.¹⁰⁴ Rarely, filiform polyps may be found in the stomach as a sequela of granulomatous gastritis (Fig. 30-21).¹⁰⁵

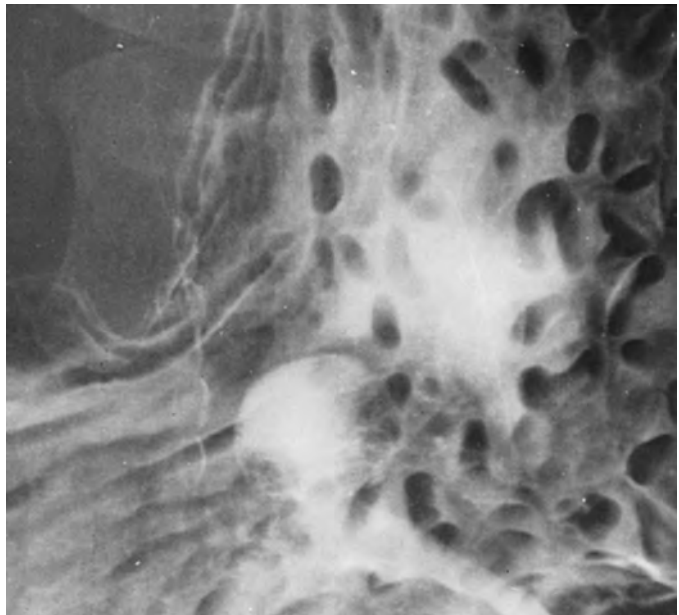


Figure 30-21 Gastric Crohn's disease with filiform polyps. Multiple linear and ovoid filling defects are seen in the stomach of a patient with long-standing Crohn's disease. (From Levine MS: *Crohn's disease of the upper gastrointestinal tract*. Radiol Clin North Am 25:79–91, 1987.)

Patients with Crohn's disease may occasionally develop gastroduodenal fistulas.^{96,97,106} These individuals usually have underlying Crohn's disease of the transverse colon with extension of a fistula via the gastocolic ligament to the greater curvature of the stomach. On barium studies, the greater curvature may have a nodular or spiculated appearance with thickened, distorted folds in the region of the fistula. These findings probably represent a nonspecific inflammatory response to the adjoining fistula rather than actual extension of Crohn's disease to the stomach. Gastroduodenal fistulas are demonstrated on only about one third of upper GI examinations, so barium enemas are often required for diagnosis of these fistulas.⁹⁷

Although patients with ileocolic Crohn's disease are thought to be at increased risk for developing carcinoma of the small bowel and colon, the relationship between gastric Crohn's disease and gastric carcinoma remains controversial. Anecdotal cases of gastric cancer have been reported in patients with long-standing gastric Crohn's disease,¹⁰⁷ but it is uncertain whether this association is coincidental.

Duodenal Involvement. Although duodenal involvement by Crohn's disease is usually associated with antral involvement, isolated duodenal Crohn's disease occurs more frequently than isolated Crohn's disease of the stomach.¹⁰⁰ As elsewhere in the GI tract, aphthoid ulcers represent the earliest morphologic abnormality on double-contrast studies of the duodenum (Fig. 30-22).^{11,102} With progression, duodenal Crohn's disease may be manifested by thickened, nodular folds (Fig. 30-23), ulcers, or even a cobblestoned appearance because of intersecting linear ulcers similar to those found in advanced ileocolitis.¹⁰⁸

Subsequent scarring may lead to the development of one or more areas of asymmetric duodenal narrowing with outward ballooning or sacculization of the duodenal wall between areas of fibrosis.¹⁰⁸ These strictures typically involve the postbulbar

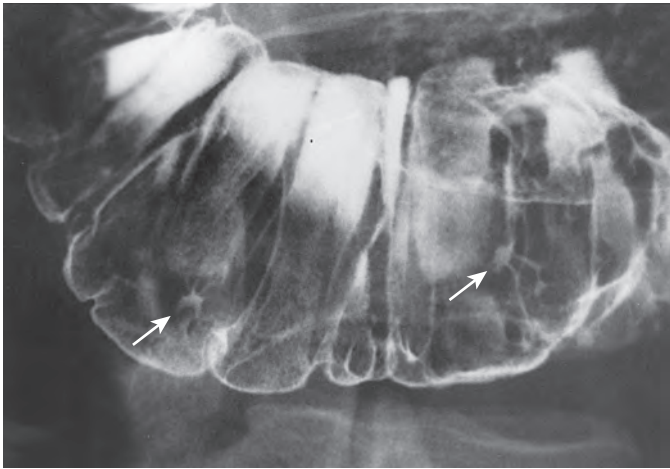


Figure 30-22 Duodenal Crohn's disease with aphthoid ulcers. Several discrete aphthoid ulcers (arrows) are seen in the distal duodenum near the ligament of Treitz. Note the stellate configuration of the ulcers. (Courtesy Louis Engelhom, MD, Brussels.)



Figure 30-23 Duodenal Crohn's disease with thickened folds. The folds have a thickened, nodular appearance in the proximal duodenum. Peptic duodenitis could produce similar findings.

duodenum, appearing as smooth, tapered areas of narrowing that extend from the apical portion of the duodenal bulb into the descending duodenum (Fig. 30-24).^{104,108} As a result, scarring from duodenal Crohn's disease can usually be differentiated on barium studies from the cloverleaf bulbar deformity associated with scarring from peptic ulcer disease.¹⁰⁴ Other patients may have one or more strictures in the second or third portions of the duodenum that cause marked obstruction and proximal dilation, resulting in a so-called megaduodenum (Fig. 30-25).¹⁰⁸

Primary duodenal Crohn's disease is rarely associated with the development of fistulas. However, duodenocolic fistulas may occasionally result from advanced Crohn's disease



Figure 30-24 Duodenal Crohn's disease with stricture formation. There is smooth, tapered narrowing of the apical portion of the bulb and adjacent segment of the descending duodenum. This appearance is characteristic of Crohn's disease.



Figure 30-25 Duodenal Crohn's disease with a megaduodenum. There is high-grade obstruction (arrow) of the distal duodenum with marked duodenal dilation above this level. (From Levine MS: Crohn's disease of the upper gastrointestinal tract. *Radiol Clin North Am* 25:79-91, 1987.)

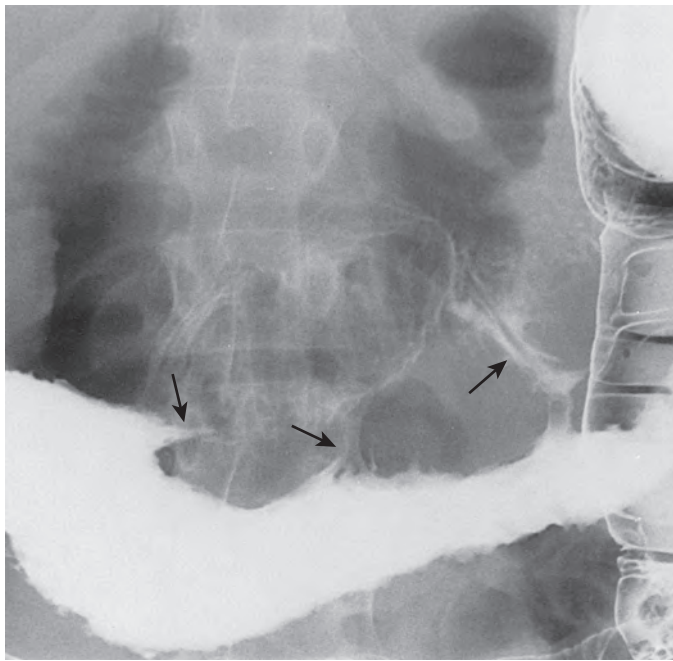


Figure 30-26 Crohn's disease with duodenocolic fistulas. Barium enema shows three separate fistulas (arrows) extending from the superior border of the transverse colon to the third and fourth portions of the duodenum. The tubular, severely ulcerated appearance of the transverse colon is secondary to advanced granulomatous colitis. Duodenocolic fistulas almost always result from primary Crohn's disease of the colon with nonspecific inflammatory changes in the duodenum adjoining the fistula. (From Levine MS: *Crohn's disease of the upper gastrointestinal tract*. *Radiol Clin North Am* 25:79-91, 1987.)

involving the transverse colon with subsequent fistulization to the third or fourth portions of the duodenum (Fig. 30-26).^{104,109} Thickened, spiculated folds may be demonstrated in the affected duodenum, but the fistula itself is more likely to be visualized on barium enema than on upper gastrointestinal examination because of the higher pressures generated with this technique. Because these duodenal changes represent a nonspecific inflammatory response rather than actual involvement of the duodenum by Crohn's disease, follow-up barium studies after resection of the fistula may show a completely normal duodenum.¹⁰⁹

Differential Diagnosis

Stomach. Aphthoid ulcers in the stomach may be indistinguishable on double-contrast studies from gastric erosions resulting from NSAIDs or other causes. Although gastric involvement by Crohn's disease is much less common than erosive gastritis, the possibility of Crohn's disease should be suspected when gastric erosions are present in patients with crampy abdominal pain and diarrhea. A small bowel follow-through should therefore be performed to evaluate the terminal ileum in these individuals.

The funnel-shaped antral narrowing associated with more advanced gastroduodenal Crohn's disease must be differentiated from other conditions, particularly a scirrhous gastric carcinoma. In one study, about one third of patients with antral narrowing caused by Crohn's disease underwent surgery because the radiographic findings simulated those of a scirrhous carcinoma.¹⁰³ However, the narrowed antrum of Crohn's disease tends to have a smooth, tubular configuration, whereas

scirrhous carcinoma produces a linitis plastica appearance with a distorted, more irregular mucosal contour.⁹¹ Antral narrowing may also be caused by a variety of other conditions, including scarring from peptic ulcer disease, sarcoidosis, tuberculosis, syphilis, eosinophilic gastritis, caustic ingestion, and radiation. In such cases, the correct diagnosis is often suggested by the clinical history and presentation.

Gastrocolic fistulas may be caused not only by Crohn's disease but also by benign penetrating ulcers on the greater curvature of the stomach in patients who are taking aspirin or other NSAIDs (see Chapter 29).¹¹⁰ Occasionally, these fistulas may also be caused by carcinoma of the stomach or transverse colon invading the gastrocolic ligament.¹⁰⁶ When Crohn's disease is responsible for the fistula, a barium enema examination usually reveals findings of advanced granulomatous colitis in the transverse colon.

Duodenum. Aphthoid ulcers in the duodenum may be indistinguishable on double-contrast studies from varioliform duodenal erosions (see later, "Duodenitis"). However, erosive duodenitis usually involves the duodenal bulb, whereas the aphthoid ulcers of Crohn's disease may be located anywhere in the duodenum from the bulb to the ligament of Treitz. The presence of one or more ulcers in the duodenal bulb or postbulbar duodenum should raise the possibility of Zollinger-Ellison syndrome, but these patients usually have markedly thickened folds and increased secretions in the stomach (see Chapter 29). Thickened, nodular folds in the descending duodenum may be caused not only by Crohn's disease but also by duodenitis, pancreatitis, or other conditions.

Although a smooth segment of tapered narrowing in the postbulbar duodenum is characteristic of the stenotic phase of Crohn's disease, scarring from uncomplicated postbulbar duodenal ulcers may produce a similar appearance.¹¹¹ In contrast, annular duodenal carcinomas can usually be differentiated from benign strictures by their shelflike, overhanging borders. When duodenal involvement by Crohn's disease is suspected on an upper GI examination, a small bowel follow-through or barium enema should be performed to search for associated Crohn's disease in the small bowel or colon.

SARCOIDOSIS

Sarcoidosis is a systemic granulomatous disease of unknown origin, characterized pathologically by the presence of noncaseating granulomas. Most patients have thoracic sarcoidosis, with bilateral hilar lymphadenopathy or fibronodular pulmonary infiltrates on chest radiographs. About 40% of patients have extrathoracic disease involving the eye, skin, lymph nodes, liver, spleen, heart, and musculoskeletal or nervous system. Although sarcoidosis is rarely thought to affect the GI tract, one study found noncaseating granulomas on mucosal biopsy specimens from the stomach in 10% of patients with known sarcoidosis.¹¹² Thus, GI involvement by sarcoidosis may be more common than is generally recognized.

Clinical Findings

Sarcoidosis involves the stomach more frequently than any other portion of the GI tract. Most patients with gastric sarcoidosis are asymptomatic,¹¹² but some may present with nausea, vomiting, bloating, or weight loss because of gastric outlet obstruction.¹¹³ Others may present with epigastric pain or signs

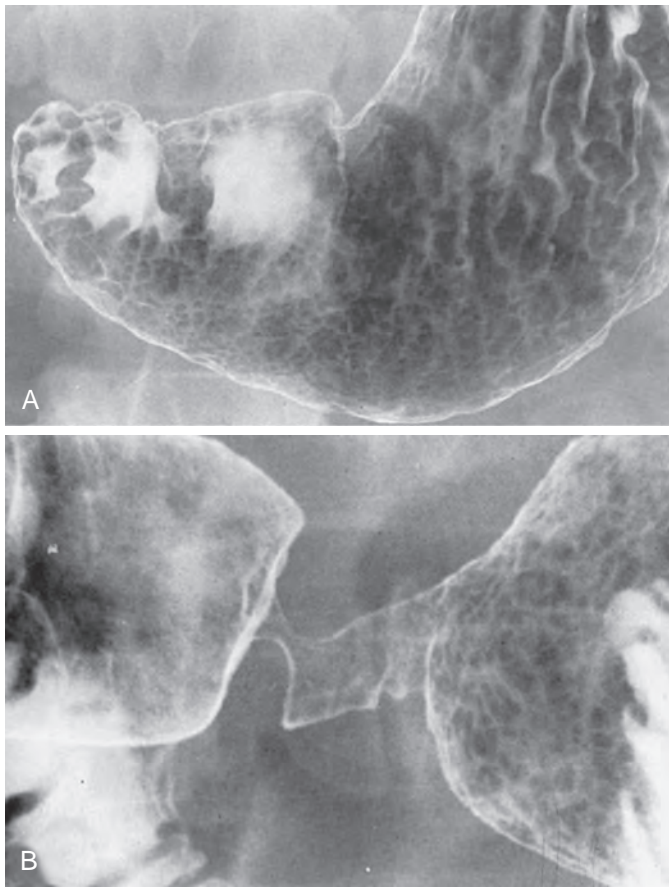


Figure 30-27 Gastric sarcoidosis. **A.** Double-contrast study shows considerable nodularity of the mucosa in the gastric antrum. This patient had pulmonary sarcoidosis, and endoscopic biopsy specimens revealed noncaseating granulomas in the stomach. **B.** In another patient, more advanced gastric sarcoidosis is manifested by marked antral narrowing and deformity. (**B** courtesy Seth N. Glick, MD, Philadelphia.)

of upper GI bleeding resulting from ulceration of the overlying mucosa.¹¹⁴ Treatment with steroids produces a dramatic clinical response in about two thirds of symptomatic patients.¹¹³ Surgical intervention may occasionally be required for patients who have persistent gastric outlet obstruction, massive bleeding, or radiographic or endoscopic findings suggestive of malignant tumor.

Radiographic Findings

Gastric sarcoidosis may be manifested by a spectrum of radiographic findings. In patients with superficial disease, double-contrast studies may reveal a localized area of mucosal nodularity or thickened, irregular folds (Fig. 30-27A).^{115,116} Other patients may have benign- or malignant-appearing ulcers in the stomach.^{114,116} More advanced sarcoidosis may result in smooth, cone-shaped antral narrowing and deformity (Fig. 30-27B).¹¹⁴ Similar findings may be caused by scarring from peptic ulcer disease, caustic ingestion, radiation, and other granulomatous conditions, including Crohn's disease, tuberculosis, and syphilis. Rarely, sarcoidosis may produce more irregular gastric narrowing, mimicking the linitis plastica appearance of an advanced scirrhous carcinoma of the stomach.¹¹⁷ The possibility of gastric sarcoidosis should be suspected, however,

when chest radiographs reveal characteristic findings of sarcoidosis in the thorax.

TUBERCULOSIS

Gastroduodenal involvement occurs in less than 0.5% of all patients with tuberculosis.¹¹⁸ The stomach and duodenum are rarely involved because of the paucity of lymphoid tissue in the upper GI tract, high acidity of peptic secretions, and rapid passage of ingested organisms into the small bowel. Most patients with gastric or duodenal tuberculosis are found to have generalized tuberculosis. Gastroduodenal infection is presumably caused by ingestion of the bacillus or by hematogenous spread to lymphatics in the wall of the stomach or duodenum.¹¹⁹ Although routine pasteurization of milk has dramatically decreased the incidence of GI tuberculosis in the United States, some patients may travel to the United States from other countries such as South Africa or India, where tuberculosis is endemic. Gastric and duodenal tuberculosis have also been encountered in patients with AIDS, particularly those of Haitian origin.¹²⁰

Clinical Findings

Patients with gastroduodenal tuberculosis may present with epigastric pain or signs of upper GI bleeding.¹²¹⁻¹²³ Subsequently, they may develop nausea and vomiting because of progressive scarring and gastric outlet obstruction.¹²³ Although the clinical findings are nonspecific, the possibility of gastroduodenal tuberculosis should be considered in patients who have known pulmonary tuberculosis or who have migrated from areas in which tuberculosis is endemic.

Stool cultures for tuberculosis are unreliable; some patients with pulmonary tuberculosis have positive cultures in the absence of GI infection, whereas others have negative cultures despite GI infection.¹¹⁹ A definitive diagnosis of gastroduodenal tuberculosis can be made when endoscopic biopsy specimens reveal caseating granulomas in the stomach or duodenum, but granulomas may not be found because of their submucosal location and the small size of the specimen samples.¹²³ Depending on the severity of disease, gastroduodenal tuberculosis may be treated by antituberculous drug therapy or, if necessary, gastric resection or bypass.

Radiographic Findings

Gastric tuberculosis may be manifested on barium studies by one or more areas of ulceration, usually on the lesser curvature of the antrum or in the region of the pylorus.^{120,124} Subsequent scarring may cause marked antral narrowing, eventually leading to the development of gastric outlet obstruction.^{124,125} Occasionally, the narrowed antrum may have an irregular contour, simulating the linitis plastica appearance of a primary scirrhous carcinoma of the stomach.¹²⁴ As in the ileocecal region, advanced gastric tuberculosis may be associated with the development of multiple tracks and fistulas.¹²⁴

Duodenal tuberculosis may also be manifested on barium studies by ulcers, thickened folds, narrowing, or fistulas.¹²⁶⁻¹²⁸ As in Crohn's disease, duodenal tuberculosis is often associated with contiguous involvement of the distal antrum. Enlarged tuberculous lymph nodes adjacent to the duodenum may cause widening, narrowing, or obstruction of the duodenal sweep.¹²⁸ Rarely, duodenorenal fistulas may result from spread of tuberculosis from the right kidney to the duodenum.¹²⁹

SYPHILIS

Gastric syphilis is a rare disease, occurring in less than 1% of all patients with secondary or tertiary syphilis.¹³⁰ Nevertheless, gastric involvement should be suspected in young patients with untreated lues who develop epigastric pain, nausea, vomiting, or signs of upper GI bleeding.¹³¹ The diagnosis of gastric syphilis can be confirmed by isolating *Treponema pallidum* on endoscopic biopsy specimens or by demonstrating the typical spirochetes with dark-field microscopy.¹³² Affected individuals usually have a marked clinical response to antiluetic therapy if they are treated before substantial gastric scarring has occurred.

Radiographic Findings

Secondary syphilis involving the stomach is sometimes associated with a severe form of gastritis. In such cases, barium studies may reveal nodules, erosions, shallow or deep ulcers, and thickened folds, predominantly in the antrum (Fig. 30-28).^{130,131,133} In contrast, tertiary syphilis involving the stomach is characterized by progressive scarring and fibrosis, eventually producing a tubular, funnel-shaped antrum.^{130,133} This appearance may be indistinguishable from antral narrowing caused by Crohn's disease, caustic ingestion, radiation, or other granulomatous conditions such as tuberculosis and sarcoidosis. Other patients with tertiary syphilis may have focal narrowing of the gastric body, producing an hourglass- or dumbbell-shaped stomach.¹³³ Rarely, the narrowed stomach may have a more irregular contour, mimicking the linitis plastica appearance of a scirrhous carcinoma of the stomach.¹³⁴ When gastric syphilis is suspected on the basis of the clinical and radiographic findings, endoscopic biopsy specimens are required for a definitive diagnosis.

FUNGAL DISEASES

A variety of fungal diseases may rarely involve the stomach. Gastric histoplasmosis may be manifested by thickened folds, ulceration, or narrowing of the stomach.¹³⁵ Gastric candidiasis may be associated with the development of large aphthoid ulcers or even centrally ulcerated bull's-eye lesions.^{12,136} Other

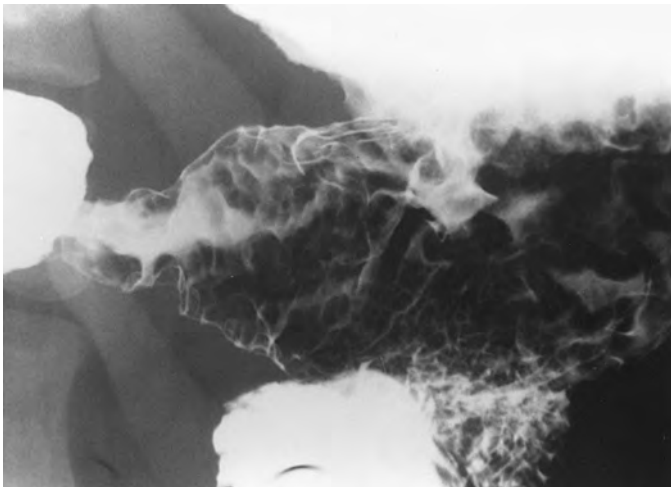


Figure 30-28 Gastric syphilis. Mucosal nodularity and thickened folds are seen in the antrum in a patient with proven gastric syphilis.

rare fungal infections of the stomach include actinomycosis and mucormycosis.^{137,138}

Other Infections

CYTOMEGALOVIRUS INFECTION

Cytomegalovirus (CMV), a member of the herpesvirus group, is the most common viral pathogen affecting the GI tract in patients with AIDS.¹³⁹ Although the esophagus and colon are more frequent sites of involvement (see Chapters 20 and 58), patients infected with the human immunodeficiency virus (HIV) may occasionally develop CMV gastritis and duodenitis.^{26,140-144} Affected individuals may present with severe abdominal pain or signs of upper GI bleeding.¹⁴³ The treatment of CMV gastritis or duodenitis includes relatively toxic antiviral agents such as ganciclovir, which is associated with bone marrow suppression.¹⁴⁵ Thus, endoscopic biopsy specimens, brushings, or cultures are required for a definitive diagnosis before treating these patients.

Radiographic Findings

CMV gastritis may be manifested on barium studies by mucosal nodularity, erosions, ulcers, thickened folds and, in severe cases, irregular antral narrowing (Fig. 30-29).^{26,140,141} Other opportunistic infections such as cryptosporidiosis and toxoplasmosis may occasionally produce similar findings in patients with AIDS (see later, "Cryptosporidiosis" and "Toxoplasmosis"). Rarely, deep ulcers can result in the development of fistulas to adjacent structures such as the colon.¹⁴² When CMV gastritis is suspected, the diagnosis may be confirmed by demonstrating characteristic inclusion bodies on endoscopic biopsy specimens or brushings or by obtaining positive cultures for CMV.

CMV duodenitis may be manifested on barium studies by luminal narrowing with thickened or effaced folds in the proximal duodenum (Fig. 30-30).^{143,144} The differential diagnosis includes other opportunistic infections in the duodenum in patients with AIDS, such as cryptosporidiosis, strongyloidiasis,

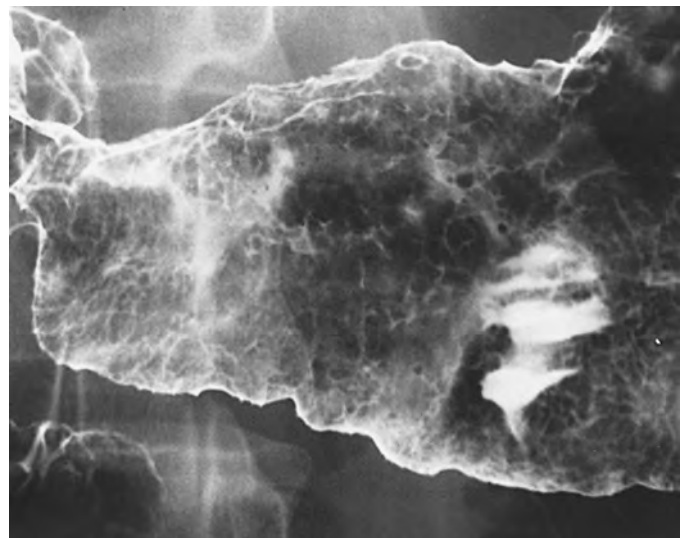


Figure 30-29 Cytomegalovirus gastritis. Mucosal nodularity and tiny ulcerations are seen in the gastric antrum. Note the irregular contour of the stomach. This patient had AIDS.

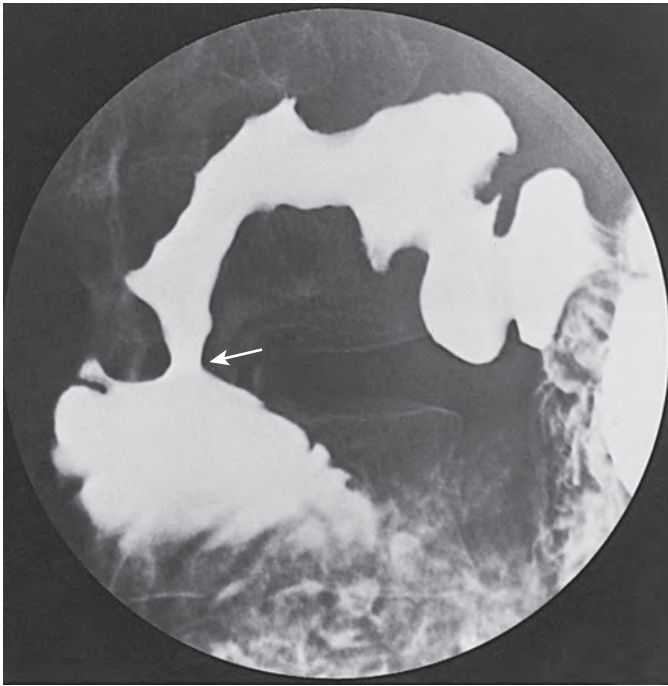


Figure 30-30 Cytomegalovirus duodenitis. There is marked narrowing and effacement of folds in the proximal descending duodenum and a relatively abrupt transition (arrow) to a normal-appearing duodenum more distally. This patient had AIDS. (From Mong A, Levine MS, Furth EE, et al: Cytomegalovirus duodenitis in an AIDS patient. *AJR* 172:939–940, 1999.)

and tuberculosis. Endoscopic biopsy specimens, brushings, or viral cultures for CMV are therefore required for a definitive diagnosis.

CRYPTOSPORIDIOSIS

Cryptosporidium, a protozoan, may infect the small bowel in patients with AIDS, causing a profuse secretory diarrhea (see Chapter 42). Much less frequently, cryptosporidiosis may involve the stomach; in these cases, barium studies may reveal antral narrowing and rigidity, occasionally associated with one or more deep ulcers.^{140,146,147} CT may also reveal a narrowed antrum with marked thickening of the gastric wall.¹⁴⁸ CMV gastritis should be the major consideration in the differential diagnosis of antral narrowing and ulceration in patients with AIDS (see earlier, “Cytomegalovirus Infection”). When infectious gastritis is suspected on the basis of the radiographic findings, biopsy specimens, brushings, or viral cultures should be obtained from the stomach for a more definitive diagnosis.

TOXOPLASMOSIS

Opportunistic infection of the stomach by toxoplasmosis is a rare cause of antral narrowing on barium studies or of a thickened gastric wall on CT in patients with AIDS.^{149,150} The diagnosis may be confirmed by demonstration of the teardrop-shaped trophozoites in histologic specimens from the stomach.^{149,150} Toxoplasmosis should therefore be included in the differential diagnosis of gastric narrowing or wall thickening in HIV-positive patients.

STRONGYLOIDIASIS

Strongyloides stercoralis is a parasite of worldwide distribution that causes infection of the stomach, duodenum, and proximal small bowel.^{151–153} Cases are occasionally encountered in metropolitan areas of the United States in patients who have emigrated from areas of endemic infection, such as Africa, Asia, and South America.¹⁵³ Strongyloidiasis also occurs as an opportunistic infection in patients with AIDS. Affected individuals may present with abdominal pain, nausea and vomiting, diarrhea, malabsorption, or hypoalbuminemia as a result of a protein-losing enteropathy.¹⁵² A peripheral eosinophilia is present in 25% to 35% of cases.¹⁵²

Radiographic Findings

Gastric involvement by strongyloidiasis may occasionally be manifested on barium studies by antral gastritis or narrowing.^{151,153} However, the duodenum and proximal jejunum are more common sites of involvement. Barium studies may reveal thickened or effaced folds, ulceration, and narrowing or dilation of the affected bowel (Fig. 30-31A).^{151–153} As the disease progresses, there may be tubular narrowing of the lumen and obliteration of the normal fold pattern in the duodenum, producing a classic lead pipe appearance (Fig. 30-31B). Some patients may eventually develop a massively dilated duodenum, or megaduodenum (see Fig. 30-31B). Other conditions associated with a megaduodenum include Zollinger-Ellison syndrome, scleroderma, Crohn's disease, and celiac disease. Scarring of the duodenal wall may occasionally permit reflux of barium into the biliary tree via an incompetent sphincter of Oddi.^{152,153} Although strongyloidiasis is rarely found in the United States, this diagnosis should be considered when barium studies reveal characteristic findings in patients with AIDS or in patients who have a recent history of travel to endemic areas.

Eosinophilic Gastroenteritis

Eosinophilic gastroenteritis is an unusual condition characterized by eosinophilic infiltration of the gastrointestinal tract, primarily the stomach and small bowel.¹⁵⁴ This condition should be differentiated from eosinophilic esophagitis (see Chapter 21). Most patients with eosinophilic gastroenteritis have a peripheral eosinophilia ranging from 10% to 80%,¹⁵⁴ and about 50% of patients have a history of allergic diseases. The clinical symptoms are related to the site and extent of GI disease. Gastric involvement may be manifested by epigastric pain, nausea and vomiting, or, less frequently, signs of upper GI bleeding, whereas small bowel involvement may be manifested by diarrhea, malabsorption, or a protein-losing enteropathy.¹⁵⁴ Some patients have self-limited disease that resolves spontaneously without relapse, but others have chronic relapsing disease, requiring treatment with steroids.^{154,155}

RADIOGRAPHIC FINDINGS

Eosinophilic gastritis usually involves the antrum or antrum and body of the stomach.¹⁵⁶ Rarely, however, disease may be confined to the proximal portion of the stomach with antral sparing.¹⁵⁷ Barium studies may reveal mucosal nodularity, thickened folds, or narrowing and rigidity of the distal half of

Figure 30-31 Duodenal strongyloidiasis. **A.** Markedly thickened, edematous folds are present in the duodenum. This patient had AIDS. **B.** In another patient with more advanced disease, there is a markedly dilated duodenum (a megaduodenum) with obliteration of folds. Also note the smooth, tubular appearance of the proximal jejunum, producing a lead pipe appearance. This patient had recently immigrated to the United States from an area in which strongyloidiasis was endemic. (**B** courtesy Murray K. Dalinka, MD, Philadelphia.)

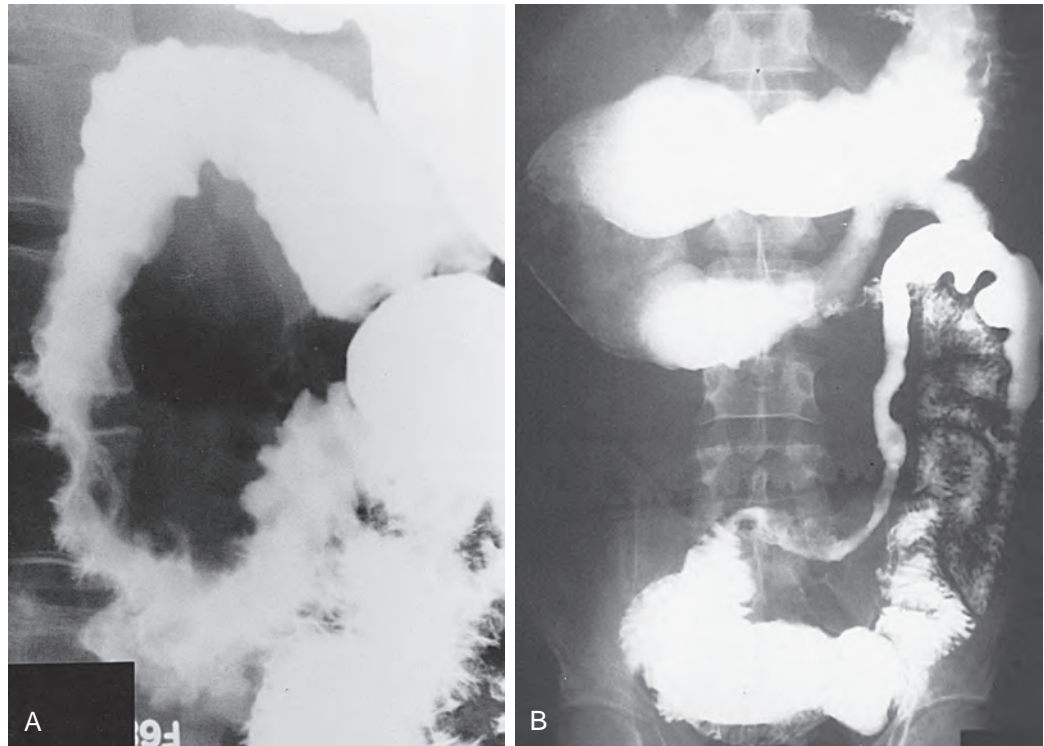


Figure 30-32 Eosinophilic gastritis. Thickened, nodular folds are seen in the gastric antrum. Other causes of antral gastritis could produce identical findings. (From Herlinger H, Maglinte D [eds]: *Clinical Radiology of the Small Intestine*. Philadelphia, WB Saunders, 1989.)

the stomach (Fig. 30-32).¹⁵⁸ Occasionally, severe antral narrowing may cause gastric outlet obstruction.¹⁵⁹ About 50% of patients with eosinophilic gastritis have concomitant involvement of the small bowel, manifested by diffuse thickening and nodularity of small bowel folds (see Chapter 43).¹⁵⁸

DIFFERENTIAL DIAGNOSIS

When eosinophilic gastritis is manifested by thickened folds, the differential diagnosis includes antral gastritis, *H. pylori* gastritis, hypertrophic gastritis, Ménétrier's disease, Zollinger-Ellison syndrome, lymphoma, and other conditions associated with thickened folds. Despite its rarity, eosinophilic gastritis should be considered in patients who have a peripheral eosinophilia or history of allergic diseases. When eosinophilic gastritis causes antral narrowing, the differential diagnosis includes scirrhous gastric carcinoma, caustic ingestion, radiation, Crohn's disease, and other granulomatous conditions involving the stomach, such as sarcoidosis, tuberculosis, and syphilis. In such cases, the correct diagnosis may be suggested by the clinical history and presentation. When eosinophilic gastritis is suspected on the basis of the upper GI examination, a small bowel follow-through should be performed to determine whether the small bowel is also involved by this disease.

Emphysematous Gastritis

Emphysematous gastritis is a rare type of phlegmonous gastritis in which gas is found in the gastric wall because of infection by gas-forming organisms such as *Escherichia coli*, *Proteus vulgaris*, *Clostridium perfringens*, and *Staphylococcus aureus*.^{160,161} This condition is usually caused by profound insults to the stomach, such as caustic ingestion, gastroduodenal surgery, or gastric volvulus.¹⁶⁰ Subsequent ischemia or necrosis permits gas-forming organisms to enter the gastric wall. Affected individuals may present with an acute fulminating illness characterized by severe abdominal pain, hematemesis, tachycardia, fever, and shock.¹⁶⁰ Supportive therapy with parenteral fluids and antibiotics should be initiated, but a nasogastric tube should not be placed in the stomach because of the high risk of



Figure 30-33 Emphysematous gastritis. Close-up view from an abdominal radiograph shows numerous mottled and bubbly collections of gas in the wall of the stomach. An attempted embolization of a gastric carcinoma led to gastric necrosis and subsequent infection by gas-forming organisms.

perforation. Despite intensive treatment, mortality rates as high as 60% have been reported.¹⁶⁰

RADIOGRAPHIC FINDINGS

Emphysematous gastritis is characterized on abdominal radiographs by multiple streaks, bubbles, or mottled collections of gas in the wall of the stomach, silhouetting the gastric shadow (Fig. 30-33).^{160,161} These intramural gas collections have a constant relationship to the stomach with changes in the patient's position, so they can be differentiated from residue or food, which shifts to the dependent portion of the stomach on upright or decubitus views.¹⁶⁰ Studies with water-soluble contrast agents may confirm the extraluminal location of these gas collections. In other patients, intramural dissection or actual extravasation of contrast medium may be demonstrated. Occasionally, CT may reveal small collections of gas in the gastric wall that are not recognized on abdominal radiographs.¹⁶²

DIFFERENTIAL DIAGNOSIS

Emphysematous gastritis must be differentiated from other rare conditions known as gastric emphysema and gastric pneumatosis. In contrast to emphysematous gastritis, gastric emphysema is characterized by long, linear collections of intramural gas that extend circumferentially around the stomach (see Chapter 34).^{161,163} In gastric emphysema, gas is thought to enter the wall of the stomach via mucosal rents caused by increased

intraluminal pressure associated with gastric outlet obstruction or by iatrogenic trauma resulting from endoscopy or other gastric instrumentation. Despite the dramatic radiographic findings, affected individuals are often asymptomatic. Thus, gastric emphysema can usually be differentiated from emphysematous gastritis on the basis of the clinical and radiographic findings.

Gastric pneumatosis is an extremely rare form of pneumatosis intestinalis in which multiple gas-filled cysts or blebs are found in the wall of the stomach.¹⁶¹ This condition much more commonly involves the small bowel or colon (see Chapter 12). When present in the stomach, the gas-filled intramural cysts may be indistinguishable from the bubbly gas collections associated with emphysematous gastritis. However, patients with gastric pneumatosis are usually asymptomatic, whereas patients with emphysematous gastritis are acutely ill. Thus, these conditions can be differentiated on the basis of the clinical history and presentation.

Caustic Ingestion

Accidental or intentional ingestion of caustic agents may lead to severe injury of the upper GI tract. Although the esophagus is more commonly involved (see Chapter 21), gastroduodenal injury may also occur. The esophagus is typically damaged by strong alkaline agents such as liquid lye (concentrated sodium hydroxide), whereas the stomach and duodenum are more likely to be damaged by strong acids such as hydrochloric, sulfuric, acetic, oxalic, carbolic, and nitric acids. Nevertheless, esophageal injury often occurs in patients who ingest strong acids, and gastroduodenal injury occurs in 5% to 10% of patients who ingest strong alkali.¹⁶⁴ Pathologically, injury to the stomach and duodenum occurs in three phases: (1) an acute necrotic phase 1 to 4 days after caustic ingestion; (2) an ulceration-granulation phase 5 to 28 days after caustic ingestion; and (3) a final phase of cicatrization and scarring 3 to 4 weeks after caustic ingestion.^{164,165}

Patients with gastroduodenal injury by caustic agents may present with severe abdominal pain, nausea, vomiting, hematemesis, fever, and shock.^{165,166} Studies with water-soluble contrast agents are sometimes performed to assess the extent and severity of injury to the upper GI tract. In patients who are stable and have no evidence of perforation, conservative treatment can be initiated with antibiotics, steroids, and parenteral feedings.¹⁶⁶ After a latent period of 3 to 4 weeks, however, many patients develop rapidly progressive gastric outlet obstruction because of antral scarring and fibrosis.¹⁶⁶ As a result, a gastrojejunostomy or partial gastrectomy is sometimes required in these individuals.¹⁶⁵

RADIOGRAPHIC FINDINGS

Ingested caustic agents tend to flow down the lesser curvature of the stomach into the antrum, causing severe pylorospasm that delays emptying into the duodenum.¹⁶⁷ As a result, the lesser curvature and distal antrum of the stomach sustain the greatest degree of damage, whereas the duodenum is relatively spared.¹⁶⁷ During the acute phase of injury, studies with water-soluble contrast agents may reveal thickened folds, ulceration, gastric atony, or mural defects resulting from edema and hemorrhage.¹⁶⁷ In fulminating cases, gastric necrosis may be manifested on abdominal radiographs or CT by streaky, bubbly,

or mottled collections of intramural gas that are unaffected by changes in the patient's position.¹⁶⁸ These intramural collections may result from mechanical disruption of the wall or from secondary infection by gas-forming organisms.¹⁶⁸ In such cases, studies with water-soluble contrast agents may reveal a confined perforation with intramural dissection of contrast medium or loculated perigastric collections (Fig. 30-34). Rarely, these studies may reveal free perforation into

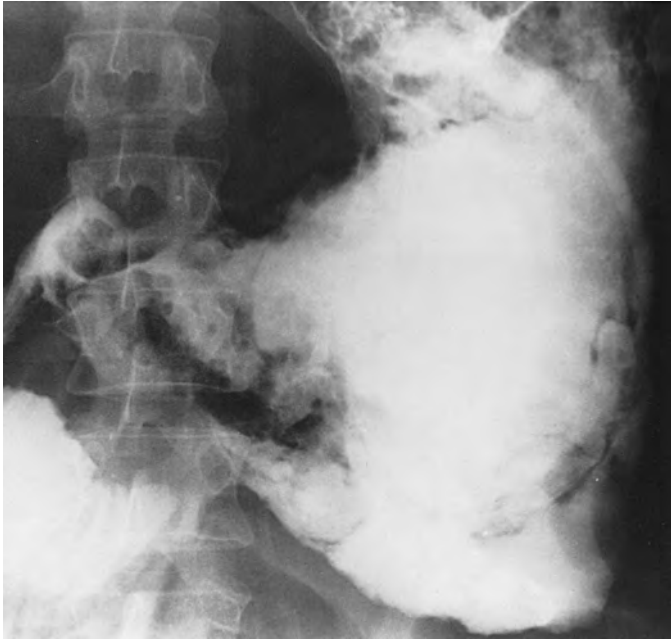
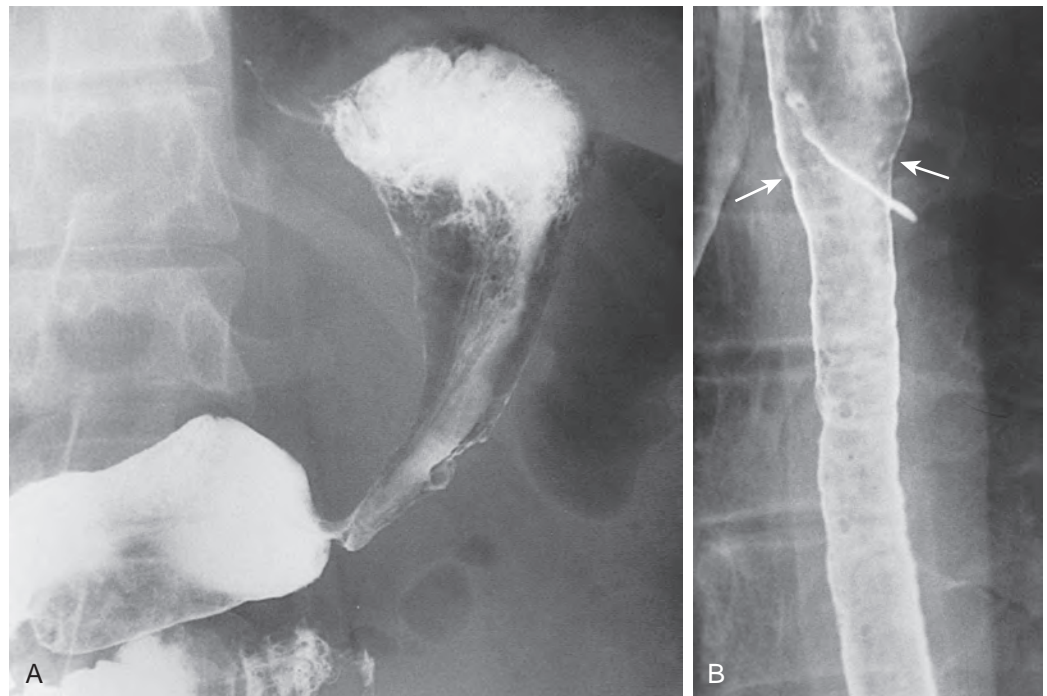


Figure 30-34 Severe gastric injury caused by caustic ingestion. This study with a water-soluble contrast medium shows a grossly abnormal stomach with intramural dissection of contrast medium and numerous mural defects resulting from edema and hemorrhage after acid ingestion.

Figure 30-35 Caustic scarring of the stomach and esophagus.

A. Double-contrast study of the stomach shows marked antral narrowing and deformity as a result of scarring from previous lye ingestion. **B.** Esophagogram shows an associated stricture in the esophagus, extending distally from the carina (arrows) to the gastroesophageal junction. Aspirated barium is also present in both main bronchi. (From Levine MS: *Radiology of the Esophagus*. Philadelphia, WB Saunders, 1989.)



the peritoneal cavity. A case of delayed gastric perforation 2 days after ingestion of hydrochloric acid has been reported in which necrosis of the gastric wall was recognized on CT by the absence of the normally enhancing mucosa and remaining gastric wall.¹⁶⁹

If patients survive the acute illness, barium studies performed 4 weeks or more after caustic ingestion may reveal progressive narrowing and deformity of the antrum or antrum and body of the stomach.^{167,170} In some patients, the narrowed antrum may have a smooth, tubular configuration (Fig. 30-35A), whereas in others, it may have a more irregular contour, mimicking the appearance of a primary scirrhous carcinoma of the stomach (Fig. 30-36).^{167,171} Other conditions in the differential diagnosis of antral narrowing include Crohn's disease, sarcoidosis, tuberculosis, syphilis, radiation, and severe scarring from peptic ulcer disease. However, the diagnosis of caustic injury is usually apparent from the clinical history. About 20% of patients with antral scarring from caustic ingestion have associated esophageal scarring (Fig. 30-35B).¹⁷⁰

Because caustic agents cause intense pylorospasm, which has a protective effect on the duodenum, the duodenal bulb and sweep may appear normal in patients with marked antral scarring (see Fig. 30-36). Occasionally, however, duodenal injury may be manifested on barium studies by thickened folds, spasm, ulceration and, eventually, strictures in the duodenum anywhere from the bulb to the ligament of Treitz.¹⁶⁷ These patients almost always have evidence of associated gastric injury.

Radiation

Radiation doses of 50 Gy or more to the upper abdomen may cause substantial injury to the stomach and duodenum when these structures are included in the radiation portal.¹⁷²⁻¹⁷⁴ The distal antrum and pyloric region are usually affected, but the duodenal sweep may also be involved in patients who have

received radiation to the right upper quadrant. Inflammatory changes in the stomach and duodenum typically occur 1 to 6 months after radiation therapy, whereas scarring and fibrosis occur 6 months or more after treatment.^{172,173} Affected individuals may present with dyspepsia, epigastric pain, nausea, vomiting, or signs of upper GI bleeding.^{172,173} Although the symptoms may suggest peptic ulcer disease, the possibility of radiation injury should be considered in any patient who has received radiation therapy to the upper abdomen during the previous 12 months.

RADIOGRAPHIC FINDINGS

The acute phase of radiation injury may be manifested on barium studies by gastroparesis, spasm, thickened folds, or ulceration, predominantly involving the distal gastric antrum and pyloric region and, occasionally, the duodenum.¹⁷²⁻¹⁷⁴ Rarely, perforation of deep ulcers may result in acute peritonitis.¹⁷² Subsequent scarring can lead to the development of antral narrowing 6 months or more after completion of radiation therapy.^{172,174} In such cases, CT may reveal luminal narrowing with nonspecific gastric wall thickening and stranding in the perigastric fat.¹⁷⁴ Rarely, the narrowed antrum may have an irregular contour, simulating a scirrhou carcinoma of the stomach.¹⁷⁵

Floxuridine Toxicity

Because floxuridine (5-FUDR) is taken up almost completely by the liver after infusion into the hepatic artery, it is the agent of choice for hepatic artery infusion chemotherapy in patients with unresectable liver metastases. In the past, 5-FUDR was administered via catheters placed percutaneously into the hepatic artery, but surgically implantable infusion pumps have replaced external catheter systems at many hospitals as the primary means of delivering 5-FUDR into the liver in patients with liver metastases.¹⁷⁶ Although uncommon, gastroduodenal inflammation, ulceration, and bleeding may occur as a direct complication of this form of chemotherapy.

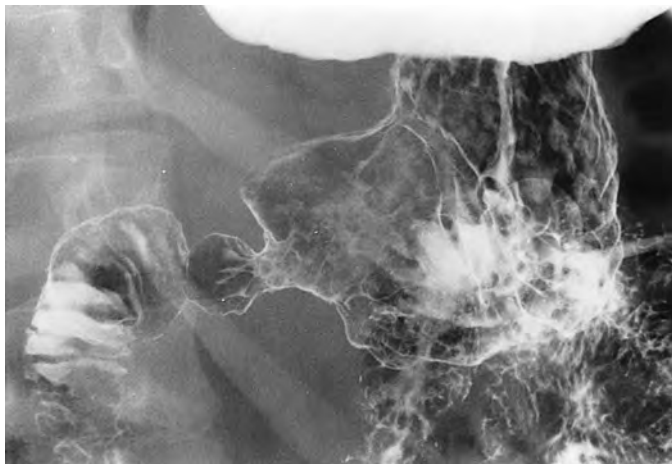


Figure 30-36 Caustic scarring of the stomach. There is asymmetric narrowing and deformity of the distal antrum secondary to scarring from previous acid ingestion. This appearance could be mistaken for a scirrhou carcinoma of the antrum. The duodenum appears normal.

PATHOGENESIS

In patients who are receiving 5-FUDR via percutaneous catheters in the hepatic artery, gastroduodenal toxicity occurs because the drug is infused directly into vessels supplying the stomach and duodenum, such as the gastroduodenal and right gastric arteries. In patients who have hepatic artery infusion pumps, the gastroduodenal and right gastric arteries are surgically ligated at the time of pump placement to prevent overflow of the drug into these vessels. Despite such precautions, gastroduodenal toxicity has been reported as a complication of 5-FUDR therapy via a hepatic artery infusion pump,¹⁷⁷⁻¹⁷⁹ presumably because of the development of small collateral channels between the hepatic artery and gastroduodenal or right gastric arteries after these vessels have been ligated. Whatever the explanation, it is important to recognize that severe gastroduodenal toxicity may occur as a complication of hepatic artery infusion of 5-FUDR, not only via an external catheter system but also via an implantable pump.

CLINICAL FINDINGS

Gastroduodenal toxicity should be suspected when patients who are receiving hepatic artery infusion of 5-FUDR develop intractable nausea, vomiting, epigastric pain, or sign of upper GI bleeding.¹⁷⁹ Although the possibility of metastatic tumor may be considered in these patients, the temporal relationship between 5-FUDR therapy and the onset of symptoms should suggest the correct diagnosis. In most cases, cessation of chemotherapy produces rapid clinical improvement.

RADIOGRAPHIC FINDINGS

Gastroduodenal toxicity resulting from 5-FUDR may be manifested on barium studies by gastroduodenal ulceration or by severe gastritis or duodenitis with markedly thickened, edematous folds in the stomach or duodenum (Fig. 30-37).¹⁷⁹⁻¹⁸²



Figure 30-37 Severe duodenitis caused by 5-floxuridine toxicity. A barium study shows markedly thickened, edematous folds in the duodenum to the level of the ligament of Treitz. This patient was receiving 5-FUDR via a hepatic artery infusion pump. (From Hiehle JF, Levine MS: Gastrointestinal toxicity of 5-FU and 5-FUDR: Radiographic findings. *Can Assoc Radiol J* 42:109-112, 1991.)

Ischemia, bleeding, vasculitis, or other inflammatory or infectious conditions may produce similar findings. However, the temporal relationship between 5-FUDR therapy and the onset of symptoms should suggest the correct diagnosis.

Duodenitis

The pathophysiology of duodenitis is controversial. Because this condition is often associated with gastric hyperacidity, it has been postulated that duodenitis represents part of the spectrum of peptic ulcer disease.¹⁸³⁻¹⁸⁵ However, some patients with duodenitis have normal or even decreased gastric acid secretion, so it may be a distinct clinical entity unrelated to peptic ulcer disease.¹⁸⁶⁻¹⁸⁸ Other data suggest that *H. pylori* may also have a role in the development of this condition.¹⁸⁹

Whatever the pathophysiology, duodenitis is thought to be an important cause of upper GI symptoms, including dyspepsia, epigastric pain, nausea, fatty food intolerance, and early satiety.^{183,184,187,190} Less frequently, erosive duodenitis may be associated with signs of upper GI bleeding, such as hematemesis, melena, and guaiac-positive stool.¹⁸⁷

RADIOGRAPHIC FINDINGS

The diagnosis of duodenitis may be suggested on barium studies in patients who have a spastic, irritable duodenal bulb or thickened, nodular folds in the proximal duodenum (Fig. 30-38).¹⁹¹ For reasons that are unclear, patients with chronic renal failure who are undergoing dialysis often have enlarged duodenal folds to a degree rarely encountered in other patients with duodenitis (Fig. 30-39).^{192,193} However, thickened folds are sometimes present on barium studies in patients in whom there is no endoscopic or histologic evidence of inflammation, so duodenitis has not generally been considered to be a reliable radiologic diagnosis.¹⁹⁴

With double-contrast technique, it is possible to demonstrate more subtle signs of inflammatory disease in the duodenum. This inflammation may be manifested by mucosal

nodules or nodular folds or by diffuse coarsening of the mucosal surface pattern of the bulb, with lucent areas surrounded by barium-filled grooves that resemble the *areae gastricae* in the stomach.¹⁹⁴⁻¹⁹⁶ With double-contrast technique, it also is possible to diagnose erosive duodenitis, a condition previously

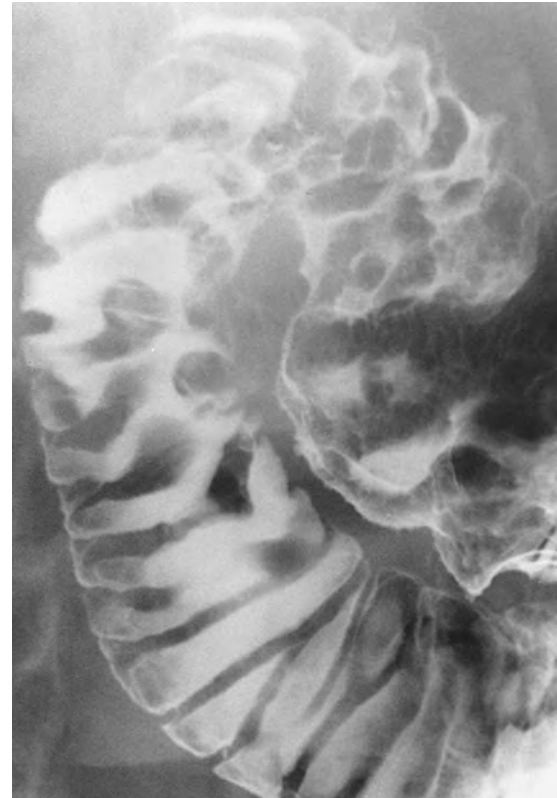


Figure 30-39 Severe duodenitis associated with chronic renal failure. Grossly thickened, polypoid folds are seen in the proximal duodenum. This patient was undergoing dialysis for chronic renal failure. (From Laufer I, Levine MS [eds]: *Double Contrast Gastrointestinal Radiology*, 2nd ed. Philadelphia, WB Saunders, 1992.)

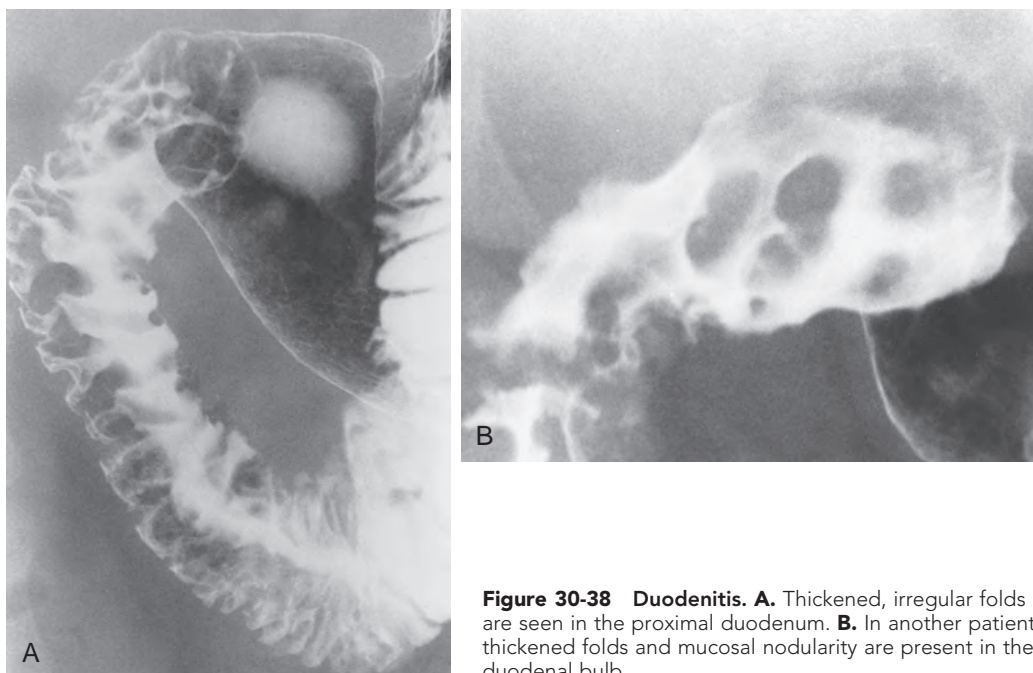


Figure 30-38 Duodenitis. **A.** Thickened, irregular folds are seen in the proximal duodenum. **B.** In another patient, thickened folds and mucosal nodularity are present in the duodenal bulb.

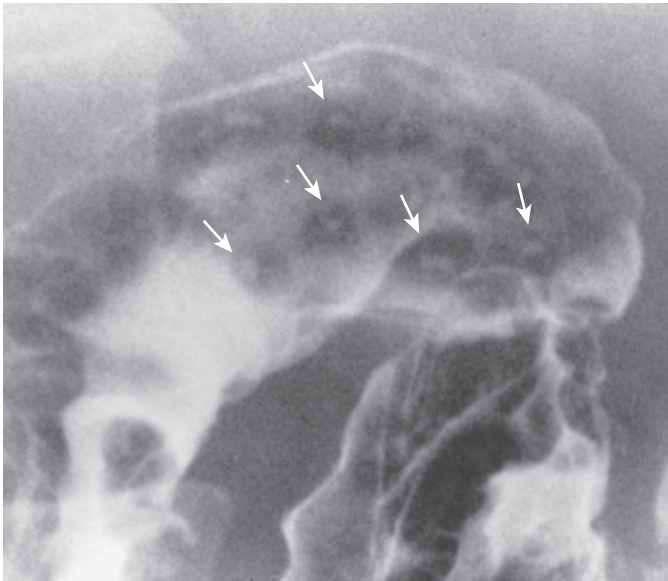


Figure 30-40 Erosive duodenitis. Varioliform erosions are seen in the duodenum as tiny flecks of barium surrounded by radiolucent mounds of edematous mucosa (arrows). (From Levine MS, Rubesin SE, Herlinger H, et al: *Double-contrast upper gastrointestinal examination: technique and interpretation*. Radiology 168:593–602, 1988.)

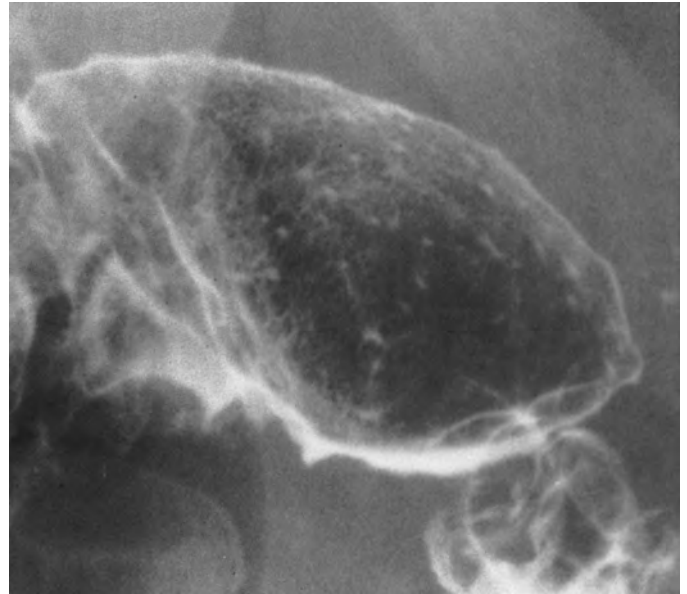


Figure 30-41 Mucosal pits simulating erosive duodenitis. Punctate collections of barium trapped in tiny epithelial pits can be mistaken for duodenal erosions. However, these collections are not surrounded by radiolucent mounds of edema. (From Bova JG, Kamath V, Tio FO, et al: *The normal mucosal surface pattern of the duodenal bulb: Radiologic-histologic correlation*. AJR 145:735–738, 1985.)

thought to be solely in the domain of the endoscopist.^{6,194,196} These erosions may be found in the duodenal bulb or, less commonly, in the descending duodenum. As in the stomach, incomplete erosions appear as tiny flecks of barium in the duodenum, whereas complete or varioliform erosions appear as central barium collections surrounded by radiolucent halos of edematous mucosa (Fig. 30-40).^{6,194,196} False-positive radiologic diagnoses may occasionally be made because of normal mucosal pits in the duodenum that are mistaken for incomplete erosions on double-contrast studies (Fig. 30-41).¹⁹⁷ Thus, a confident diagnosis of erosive duodenitis can be made only when true varioliform erosions are demonstrated.

Some patients with celiac disease (nontropical sprue) may have severe duodenitis with thickened folds, nodular mucosa, ulcers, or strictures in the descending duodenum.^{198,199} Others may have small (1–4 mm) hexagonal filling defects in the duodenal bulb, producing a distinctive mosaic pattern, or so-called bubbly bulb (Fig. 30-42).²⁰⁰ In contrast to heterotopic gastric mucosa, which predominantly involves the juxtapyloric region of the bulb (see Chapter 31), these nodules tend to be distributed more diffusely throughout the bulb. The presence of a bubbly bulb or thickened duodenal folds should therefore suggest the possibility of celiac disease in patients with malabsorption. A small bowel enema or small bowel biopsy may be required for a definitive diagnosis (see Chapter 43).

Duodenitis may also be caused by Crohn's disease, caustic ingestion, radiation, 5-FUDR toxicity, and infectious processes such as tuberculosis and strongyloidiasis. These conditions and their radiographic findings are discussed elsewhere in this chapter. Finally, duodenitis may occur in patients with underlying pancreatitis involving the head of the pancreas. In such cases, the correct diagnosis is suggested by thickened, spiculated

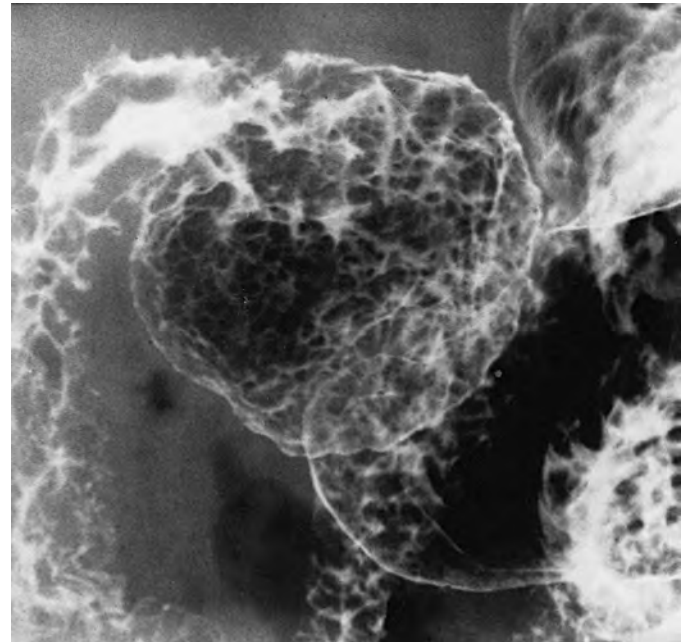


Figure 30-42 Celiac disease with a bubbly bulb. There are multiple hexagonal filling defects in the duodenal bulb and thickened, irregular folds in the descending duodenum caused by severe duodenitis in a patient with celiac disease. (From Jones B, Bayless TM, Hamilton SR, et al: *"Bubbly" duodenal bulb in celiac disease: Radiologic-pathologic correlation*. AJR 142:119–122, 1984.)

duodenal folds associated with widening of the duodenal sweep or compression of the medial aspect of the descending duodenum (see Chapter 34). When underlying pancreatitis is suspected as the cause of these findings, CT should be performed for a more definitive diagnosis.

REFERENCES

1. Poplack W, Paul RE, Goldsmith M, et al: Demonstration of erosive gastritis by the double-contrast technique. *Radiology* 117:519–521, 1975.
2. Laufer I: An assessment of the accuracy of double contrast gastro-duodenal radiology. *Gastroenterology* 71:874–878, 1976.
3. Op den Orth JO, Dekker W: Gastric erosions: Radiological and endoscopic aspects. *Radiol Clin (Belg)* 45:88–89, 1976.
4. Op den Orth JO, Dekker W: Gastric polyps or erosions. *AJR* 129:357–358, 1977.
5. Tragardh B, Wehlin L, Ohashi K: Radiologic appearance of complete gastric erosions. *Acta Radiol Diagn (Stockh)* 19:634–642, 1978.
6. Catalano D, Pagliari U: Gastroduodenal erosions: Radiological findings. *Gastrointest Radiol* 7:235–240, 1982.
7. Dheer S, Levine MS, Redfern RO, et al: Radiographically diagnosed antral gastritis: Findings in patients with and without *Helicobacter pylori* infection. *Br J Radiol* 75:805–811, 2002.
8. Lanza F, Royer G, Nelson R: An endoscopic evaluation of the effects of non-steroidal anti-inflammatory drugs on the gastric mucosa. *Gastrointest Endosc* 21:103–105, 1975.
9. Roberts DM: Chronic gastritis, alcohol, and non-ulcer dyspepsia. *Gut* 13:768–774, 1972.
10. Laufer I, Trueman T: Multiple superficial gastric erosions due to Crohn's disease of the stomach: Radiologic and endoscopic diagnosis. *Br J Radiol* 49:726–728, 1976.
11. Ariyama J, Wehlin L, Lindstrom CG, et al: Gastroduodenal erosions in Crohn's disease. *Gastrointest Radiol* 5:121–125, 1980.
12. Cronan J, Burrell M, Trepeta R: Aphthoid ulcerations in gastric candidiasis. *Radiology* 134:607–611, 1980.
13. Rumberman J, Rubesin SE, Levine MS, et al: Gastric ulceration caused by heater probe coagulation. *Gastrointest Radiol* 13:200–202, 1988.
14. Laufer I, Hamilton J, Mullens JE: Demonstration of superficial gastric erosions by double contrast radiography. *Gastroenterology* 68:387–391, 1975.
15. MacDonald WC: Correlation of mucosal histology and aspirin intake in chronic gastric ulcer. *Gastroenterology* 65:381–389, 1973.
16. Silvano GR, Ivey KJ, Butt JH, et al: Incidence of gastric lesions in patients with rheumatic disease on chronic aspirin therapy. *Ann Intern Med* 91:517–520, 1979.
17. O'Laughlin JC, Hoftiezer JW, Ivey KJ: Effect of aspirin on the human stomach in normals: Endoscopic comparison of damage produced one hour, 24 hours, and 2 weeks after administration. *Scand J Gastroenterol* 16:211–214, 1981.
18. Lanza FL, Nelson RS, Rack MF: A controlled endoscopic study comparing the toxic effects of sulindac, naproxen, aspirin, and placebo on the gastric mucosa of healthy volunteers. *J Clin Pharmacol* 24:89–95, 1984.
19. Graham DY, Smith JL, Dobbs SM: Gastric adaptation occurs with aspirin administration in man. *Dig Dis Sci* 28:1–6, 1983.
20. McLean AM, Paul RE, Philipps E, et al: Chronic erosive gastritis—clinical and radiological features. *J Can Assoc Radiol* 33:158–162, 1982.
21. McAdam WAF, Morgan AG, Jackson A, et al: Multiple persisting idiopathic gastric erosions. *Gut* 16:410, 1975.
22. Kikuchi Y, Levine MS, Laufer I, et al: Value of flow technique for double contrast examination of the stomach. *AJR* 147:1183–1184, 1986.
23. Levine MS, Verstandig A, Laufer I: Serpiginous gastric erosions caused by aspirin and other nonsteroidal anti-inflammatory drugs. *AJR* 146:31–34, 1986.
24. Laveran-Stiebar RL, Laufer I, Levine MS: Greater curvature antral flattening: A radiologic sign of NSAID-related gastropathy. *Abdom Imaging* 19:295–297, 1994.
25. Catalano O: Greater curvature antral flattening due to nonsteroidal antiinflammatory drugs. *Fortschr Röntgenstr* 167:122–124, 1997.
26. Balthazar EJ, Megibow AJ, Hulnick DH: Cytomegalovirus esophagitis and gastritis in AIDS. *AJR* 144:1201–1204, 1985.
27. Turner CJ, Lipitz LR, Pastore RA: Antral gastritis. *Radiology* 113:305–312, 1974.
28. Cho KC, Gold BM, Printz DA: Multiple transverse folds in the gastric antrum. *Radiology* 164:339–341, 1987.
29. Seymour EQ, Meredith HC: Antral and esophageal rimple: A normal variation. *Gastrointest Radiol* 3:147–149, 1978.
30. Glick SN, Cavanaugh B, Teplick SK: The hypertrophied antral-pyloric fold. *AJR* 145:547–549, 1985.
31. Arora R, Levine MS, Harvey RT, et al: Hypertrophied antral-pyloric fold: Reassessment of radiographic findings in 40 patients. *Radiology* 213:347–351, 1999.
32. Lewis TD, Laufer I, Goodacre RL: Arteriovenous malformation of the stomach: Radiologic and endoscopic features. *Am J Dig Dis* 23:467–470, 1978.
33. Warren JR, Marshall BJ: Unidentified curved bacilli on gastric epithelium in active chronic gastritis. *Lancet* 2:1273–1275, 1983.
34. Kuipers EJ, Uytterlinde AM, Pena AS, et al: Long-term sequelae of *Helicobacter pylori* gastritis. *Lancet* 345:1525–1528, 1995.
35. Pattison CP, Combs MJ, Marshall BJ: *Helicobacter pylori* and peptic ulcer disease: Evolution to revolution to resolution. *AJR* 168:1415–1420, 1997.
36. Appelman HD: Gastritis: Terminology, etiology, and clinicopathological correlations: Another biased view. *Hum Pathol* 25:1006–1019, 1994.
37. Bayerdorffer E, Lehn N, Hatz R, et al: Difference in expression of *Helicobacter pylori* gastritis in antrum and body. *Gastroenterology* 102:1575–1582, 1992.
38. Suerbaum S, Michetti P: *Helicobacter pylori* infection. *N Engl J Med* 347:1175–1186, 2002.
39. Dooley CP, Cohen H, Fitzgibbons PL, et al: Prevalence of *Helicobacter pylori* infection and histologic gastritis in asymptomatic patients. *N Engl J Med* 321:1562–1566, 1989.
40. Vakil N, Megraud F: Eradication therapy for *Helicobacter pylori*. *Gastroenterology* 133:985–1001, 2007.
41. NIH Consensus Development Panel on *Helicobacter pylori* in Peptic Ulcer Disease: NIH Consensus Conference. *Helicobacter pylori* in peptic ulcer disease. *JAMA* 272:65–69, 1994.
42. International Update Conference on *Helicobacter pylori*: The report of the Digestive Health Initiative International Update Conference on *Helicobacter pylori*. *Gastroenterology* 113:S4–S8, 1997.
43. McColl K, Murray L, El-Omar E, et al: Symptomatic benefit from eradicating *Helicobacter pylori* infection in patients with nonulcer dyspepsia. *N Engl J Med* 339:1869–1874, 1998.
44. Blum AL, Talley NJ, O'Morain C, et al: Lack of effect of treating *Helicobacter pylori* infection in patients with nonulcer dyspepsia. *N Engl J Med* 339:1875–1881, 1998.
45. Talley NJ, Vakil N, Ballard ED, et al: Absence of benefit of eradicating *Helicobacter pylori* in patients with nonulcer dyspepsia. *N Engl J Med* 341:1106–1111, 1999.
46. Cutler AF, Havstad S, Ma CK, et al: Accuracy of invasive and noninvasive tests to diagnose *Helicobacter pylori* infection. *Gastroenterology* 109:136–141, 1995.
47. Choi J, Kim CH, Kim D, et al: Prospective evaluation of a new stool antigen test for the detection of *Helicobacter pylori*, in comparison with histology, rapid urease test, ¹³C-urea breath test, and serology. *J Gastroenterol Hepatol* 26:1053–1059, 2011.
48. Morrison S, Dahms BB, Hoffenberg E, et al: Enlarged gastric folds in association with *Campylobacter pylori* gastritis. *Radiology* 171:819–821, 1989.
49. Sohn J, Levine MS, Furth EE, et al: *Helicobacter pylori* gastritis: Radiographic findings. *Radiology* 195:763–767, 1995.
50. Mond DJ, Pochaczewsky R, Vernace F, et al: Can the radiologist recognize *Helicobacter pylori* gastritis? *J Clin Gastroenterol* 20:199–202, 1995.
51. Crocker JD, Bender GN: Antral nodularity, fold thickness, and narrowing: Signs on the upper gastrointestinal series that may indicate chronic active gastritis secondary to *Helicobacter pylori*. *Invest Radiol* 30:480–483, 1995.
52. Rubesin SE, Furth EE, Levine MS: Gastritis from NSAIDs to *Helicobacter pylori*. *Abdom Imaging* 30:142–159, 2005.
53. Rose C, Stevenson GW: Correlation between visualization and size of the areae gastricae and duodenal ulcer. *Radiology* 139:371–374, 1981.
54. Watanabe H, Magota S, Shiiba S, et al: Coarse areae gastricae in the proximal body and fundus: A sign of gastric hypersecretion. *Radiology* 146:303–306, 1983.
55. Genta RM, Hamner HW, Graham DY: Gastric lymphoid follicles in *Helicobacter pylori* infection: Frequency, distribution, and response to triple therapy. *Hum Pathol* 24:577–583, 1993.
56. Genta RM, Hamner HW: The significance of lymphoid follicles in the interpretation of gastric biopsy specimens. *Arch Pathol Lab Med* 118:740–743, 1994.
57. Wyatt JL, Rathbone BJ: Immune response of the gastric mucosa to *Campylobacter pylori*. *Scand J Gastroenterol Suppl* 142:44–49, 1988.
58. Torigian DA, Levine MS, Gill NS, et al: Lymphoid hyperplasia of the stomach: Radiographic findings in five adult patients. *AJR* 177:71–75, 2001.
59. Chaloupka JC, Gay BB, Caplan D: *Campylobacter* gastritis simulating Ménétrier's disease by upper gastrointestinal radiography. *Pediatr Radiol* 20:200–201, 1990.
60. Urban BA, Fishman EK, Hruban RH: *Helicobacter pylori* gastritis mimicking gastric carcinoma at CT evaluation. *Radiology* 179:689–691, 1991.
61. Yoo CC, Levine MS, Furth EE, et al: Gastric mucosa-associated lymphoid tissue lymphoma: Radiographic findings in six patients. *Radiology* 208:239–243, 1998.

62. Stempien SJ, Dagradi AE, Reingold IM, et al: Hypertrophic hypersecretory gastropathy. *Am J Dig Dis* 9:471–493, 1964.
63. Tan DTD, Stempien SJ, Dagradi AE: The clinical spectrum of hypertrophic hypersecretory gastropathy. *Gastrointest Endosc* 18:69–73, 1971.
64. Moghadam M, Gluckmann R, Eyler WR: The radiological assessment of gastric acid output. *Radiology* 89:888–895, 1967.
65. Press AJ: Practical significance of gastric rugal folds. *AJR* 125:172–183, 1975.
66. Balthazar EJ, Davidian MM: Hyperrugosity in gastric carcinoma: Radiographic, endoscopic, and pathologic features. *AJR* 136:531–535, 1981.
67. Wolfsen HC, Carpenter HA, Talley NJ: Ménétrier's disease: A form of hypertrophic gastropathy or gastritis? *Gastroenterology* 104:1310–1319, 1993.
68. Scharschmidt BF: The natural history of hypertrophic gastropathy (Ménétrier's disease). *Am J Med* 63:644–652, 1977.
69. Jarnum S, Jensen KB: Plasma protein turnover (albumin, transferrin, IgG, IgM) in Ménétrier's disease (giant hypertrophic gastritis): Evidence of non-selective protein loss. *Gut* 13:128–137, 1972.
70. Searcy RM, Malagelada JR: Ménétrier's disease and idiopathic hypertrophic gastropathy. *Ann Intern Med* 100:560–565, 1984.
71. Rubin RG, Fink H: Giant hypertrophy of the gastric mucosa associated with carcinoma of the stomach. *Am J Gastroenterol* 47:379–388, 1967.
72. Williams SM, Harned RK, Settles RH: Adenocarcinoma of the stomach in association with Ménétrier's disease. *Gastrointest Radiol* 3:387–390, 1978.
73. Reese DE, Hodgson JR, Dockerty MB: Giant hypertrophy of the gastric mucosa (Ménétrier's disease): A correlation of the roentgenographic, pathologic, and clinical findings. *AJR* 88:619–626, 1962.
74. Friedman J, Platnick J, Farruggia S, et al: Ménétrier's disease. *Radiographics* 29:297–301, 2009.
75. Olmsted WW, Cooper PH, Madewell JE: Involvement of the gastric antrum in Ménétrier's disease. *AJR* 126:524–529, 1976.
76. Maxfield DL, Boyd WC: Pernicious anemia: A review, an update, and an illustrative case. *J Am Osteopath Assoc* 8:133–142, 1983.
77. Jeffries GH, Slesinger MH: Studies of parietal cell antibody in pernicious anemia. *J Clin Invest* 44:2021–2038, 1965.
78. Joske RA, Finckh ES, Wood IJ: Gastric biopsy: A study of 1,000 consecutive successful gastric biopsies. *Q J Med* 24:269–294, 1955.
79. Strickland RG, Mackay IR: A reappraisal of the nature and significance of chronic atrophic gastritis. *Am J Dig Dis* 18:426–440, 1973.
80. Furth EE, Rubesin SE, Levine MS: Pathologic primer on gastritis: An illustrated sum and substance. *Radiology* 197:693–698, 1995.
81. Kuipers EJ, Klinkenberg-Knol EC, Vandenbroucke-Grauls JE, et al: Role of *Helicobacter pylori* in the pathogenesis of atrophic gastritis. *Scand J Gastroenterol* 32(Suppl 223):28–34, 1997.
82. Sozzi M, Valentini M, Figura N, et al: Atrophic gastritis and intestinal metaplasia in *Helicobacter pylori* infection: The role of CagA status. *Am J Gastroenterol* 93:375–379, 1998.
83. Elsborg L, Mosbech J: Pernicious anaemia as a risk factor in gastric cancer. *Acta Med Scand* 206:315–318, 1979.
84. Cheli R, Santi L, Ciancamerla G, et al: A clinical and statistical follow-up study of atrophic gastritis. *Am J Dig Dis* 18:1061–1066, 1973.
85. Siurala M, Lehtola J, Ihamakki T: Atrophic gastritis and its sequelae: Results of 19–23 years follow-up examinations. *Scand J Gastroenterol* 9:441–446, 1974.
86. Borch K: Epidemiologic, clinicopathologic, and economic aspects of gastroscopic screening of patients with pernicious anemia. *Scand J Gastroenterol* 21:21–30, 1986.
87. Asaka M, Takeda H, Sugiyama T, et al: What role does *Helicobacter pylori* play in gastric cancer? *Gastroenterology* 113:S56–S60, 1997.
88. Laws JW, Pitman RG: The radiological features of pernicious anaemia. *Br J Radiol* 33:229–237, 1960.
89. Levine MS, Palman CL, Rubesin SE, et al: Atrophic gastritis in pernicious anemia: Diagnosis by double-contrast radiography. *Gastrointest Radiol* 14:215–219, 1989.
90. Mackintosh CE, Kree L: Anatomy and radiology of the areae gastricae. *Gut* 18:855–864, 1977.
91. Levine MS, Kong V, Rubesin SE, et al: Scirrhous carcinoma of the stomach: Radiologic and endoscopic diagnosis. *Radiology* 175:151–154, 1990.
92. Levine MS: Crohn's disease of the upper gastrointestinal tract. *Radiol Clin North Am* 25:79–91, 1987.
93. Danzi JT, Farmer RG, Sullivan BH, et al: Endoscopic features of gastro-duodenal Crohn's disease. *Gastroenterology* 70:9–13, 1976.
94. Nugent FW, Richmond M, Park SK: Crohn's disease of the duodenum. *Gut* 18:115–120, 1977.
95. Wagtmans MJ, Verspaget HW, Lamers CB, et al: Clinical aspects of Crohn's disease of the upper gastrointestinal tract: A comparison with distal Crohn's disease. *Am J Gastroenterol* 92:1467–1470, 1997.
96. Metzger WH, Ranganath KA: Crohn's disease presenting as a gastrocolic fistula. *Am J Gastroenterol* 65:258–261, 1976.
97. Kokal W, Pickleman J, Steinberg JJ, et al: Gastrocolic fistula in Crohn's disease. *Surg Gynecol Obstet* 146:701–704, 1978.
98. Marshak RH, Maklansky D, Kurzbarn JD, et al: Crohn's disease of the stomach and duodenum. *Am J Gastroenterol* 77:340–343, 1982.
99. Gray RR, Grosman H: Crohn's disease involving the proximal stomach. *Gastrointest Radiol* 10:43–45, 1985.
100. Legge DA, Carlson HC, Judd ES: Roentgenologic features of regional enteritis of the upper gastrointestinal tract. *AJR* 110:355–360, 1970.
101. Beaudin D, DaCosta LR, Prentice RSA, et al: Crohn's disease of the stomach. *Am J Dig Dis* 18:623–629, 1973.
102. Kelvin FM, Gedgaudas RK: Radiologic diagnosis of Crohn's disease (with emphasis on its early manifestations). *Crit Rev Diagn Imaging* 16:43–91, 1981.
103. Farman J, Faegenburg D, Dallemann S, et al: Crohn's disease of the stomach: The "ram's horn" sign. *AJR* 123:242–251, 1975.
104. Nelson SW: Some interesting and unusual manifestations of Crohn's disease ("regional enteritis") of the stomach, duodenum, and small intestine. *AJR* 107:86–101, 1969.
105. Zegel HG, Laufer I: Filiform polyposis. *Radiology* 127:615–619, 1978.
106. Laufer I, Joffe N, Stolberg H: Unusual causes of gastrocolic fistula. *Gastrointest Radiol* 2:21–25, 1977.
107. Patel M, Banerjee B, Block JG, et al: Gastric Crohn's disease complicated by adenocarcinoma of the stomach: Case report and review of the literature. *Am J Gastroenterol* 92:1368–1371, 1997.
108. Thompson WM, Cockrill H, Rice RP: Regional enteritis of the duodenum. *AJR* 123:252–261, 1975.
109. Herlinger H, O'Riordan D, Saul S, et al: Non-specific involvement of bowel adjoining Crohn's disease. *Radiology* 159:47–51, 1986.
110. Laufer I, Thornley GD, Stolberg H: Gastrocolic fistula as a complication of benign gastric ulcer. *Radiology* 119:7–11, 1976.
111. Bilbao MK, Frische LH, Rosch J, et al: Postbulbar duodenal ulcer and ring-stricture. *Radiology* 100:27–35, 1971.
112. Palmer ED: Note on silent sarcoidosis of the gastric mucosa. *J Lab Clin Med* 52:231–234, 1958.
113. Chinitz MA, Brandt LJ, Frank MS, et al: Symptomatic sarcoidosis of the stomach. *Dig Dis Sci* 30:682–688, 1985.
114. Dunbar RD: Sarcoidosis and its radiologic manifestations. *Crit Rev Diagn Imaging* 28:185–220, 1978.
115. Levine MS, Ekberg O, Rubesin SE, et al: Gastrointestinal sarcoidosis: Radiographic findings. *AJR* 153:293–295, 1989.
116. Farman J, Ramirez G, Rybak B, et al: Gastric sarcoidosis. *Abdom Imaging* 22:248–252, 1997.
117. Bellan L, Semelka R, Warren CPW: Sarcoidosis as a cause of linitis plastica. *J Can Assoc Radiol* 39:72–74, 1988.
118. Chazan BI, Aitchison JD: Gastric tuberculosis. *BMJ* 2:1288–1290, 1960.
119. Thoeni RF, Margulis AR: Gastrointestinal tuberculosis. *Semin Roentgenol* 14:283–294, 1979.
120. Brody JM, Miller DK, Zeman RK, et al: Gastric tuberculosis: A manifestation of acquired immunodeficiency syndrome. *Radiology* 159:342–348, 1986.
121. Subei I, Attar B, Schmitt G, et al: Primary gastric tuberculosis. *Am J Gastroenterol* 82:769–772, 1987.
122. Misra D, Rai RR, Nundy S, et al: Duodenal tuberculosis presenting as bleeding peptic ulcer. *Am J Gastroenterol* 83:203–204, 1988.
123. Nair KV, Pai CG, Rajogopal KP, et al: Unusual presentations of duodenal tuberculosis. *Am J Gastroenterol* 86:756–760, 1991.
124. Pinto RS, Zausner J, Beranbaum ER: Gastric tuberculosis. *AJR* 110:808–812, 1970.
125. Jadvar H, Mindelzun RE, Olcott EW, et al: Still the great mimicker: Abdominal tuberculosis. *AJR* 168:1455–1460, 1997.
126. Black GA, Carsky EW: Duodenal tuberculosis. *AJR* 131:329–330, 1978.
127. Tishler JMA: Duodenal tuberculosis. *Radiology* 130:593–595, 1979.
128. Gupta SK, Jain AK, Gupta JP, et al: Duodenal tuberculosis. *Clin Radiol* 39:159–161, 1988.
129. Schwartz DT, Barnes HA, Lattimer JK, et al: Pyeloduodenal fistula due to tuberculosis. *J Urol* 104:373–375, 1970.
130. Cooley RN, Childers JH: Acquired syphilis of the stomach. *Gastroenterology* 39:201–207, 1960.
131. Reisman TN, Leverett FL, Hudson JR, et al: Syphilitic gastropathy. *Am J Dig Dis* 20:588–593, 1975.
132. Sachar DB, Klein RS, Swerdlow F, et al: Erosive syphilitic gastritis: Dark-field and immunofluorescent diagnosis from biopsy specimen. *Ann Intern Med* 80:512–515, 1974.

133. Jones BV, Lichtenstein JE: Gastric syphilis: Radiologic findings. *AJR* 160:59–61, 1993.
134. Anai H, Okada Y, Okubo K, et al: Gastric syphilis simulating linitis plastica type of gastric cancer. *Gastrointest Endosc* 36:624–626, 1990.
135. Fisher JR, Sanowski RA: Disseminated histoplasmosis producing hypertrophic gastric folds. *Am J Dig Dis* 23:282–285, 1978.
136. Nelson RS, Bruni HC, Goldstein HM: Primary gastric candidiasis in uncompromised subjects. *Gastrointest Endosc* 22:92–94, 1975.
137. Van Olmen G, Larmuseau ME, Geboes K, et al: Primary gastric actinomycosis. *Am J Gastroenterol* 79:512–516, 1984.
138. Lawson H, Schman A: Gastric phycomycosis. *Br J Surg* 61:743–746, 1974.
139. Rotterdam H, Tsang P: Gastrointestinal disease in the immunocompromised patient. *Hum Pathol* 25:1123–1140, 1994.
140. Falcone S, Murphy BJ, Weinfeld A: Gastric manifestations of AIDS: Radiographic findings on upper gastrointestinal examination. *Gastrointest Radiol* 16:95–98, 1991.
141. Farman J, Lerner ME, Ng C, et al: Cytomegalovirus gastritis: Protean radiologic manifestations. *Gastrointest Radiol* 17:202–206, 1992.
142. Agel NM, Tanner P, Drury A, et al: Cytomegalovirus gastritis with perforation and gastroduodenal fistula formation. *Histopathology* 18:165–168, 1991.
143. Wilcox CM, Schwartz DA: Symptomatic CMV duodenitis. *J Clin Gastroenterol* 14:293–297, 1992.
144. Mong A, Levine MS, Furth EE, et al: Cytomegalovirus duodenitis in an AIDS patient. *AJR* 172:939–940, 1999.
145. Buhles WC, Mastro BJ, Tinker AJ, et al: Ganciclovir treatment of life- or sight-threatening cytomegalovirus infection: Experience in 314 immunocompromised patients. *Rev Infect Dis* 10(Suppl 3):S495–S506, 1988.
146. Berk RN, Wall SD, McArdle CB, et al: Cryptosporidiosis of the stomach and small intestine in patients with AIDS. *AJR* 143:549–554, 1984.
147. Ventura G, Cauda R, Larocca LM, et al: Gastric cryptosporidiosis complicating HIV infection: Case report and review of the literature. *Eur J Gastroenterol Hepatol* 9:307–310, 1997.
148. Soulen MC, Fishman EK, Scatarige JC, et al: Cryptosporidiosis of the gastric antrum: Detection using CT. *Radiology* 159:705–706, 1986.
149. Smart PE, Weinfeld A, Thompson NE, et al: Toxoplasmosis of the stomach: A cause of antral narrowing. *Radiology* 174:369–370, 1990.
150. Alpert L, Miller M, Alpert E, et al: Gastric toxoplasmosis in acquired immunodeficiency syndrome: Antemortem diagnosis with histopathologic characterization. *Gastroenterology* 110:258–264, 1996.
151. Louisy CL, Barton CJ: The radiological diagnosis of *Strongyloides stercoralis* enteritis. *Radiology* 98:535–541, 1971.
152. Berkman YM, Rabinowitz J: Gastrointestinal manifestations of strongyloidiasis. *AJR* 115:306–311, 1972.
153. Dallemand S, Waxman M, Farman J: Radiological manifestations of *Strongyloides stercoralis*. *Gastrointest Radiol* 8:45–51, 1983.
154. Vitellas KM, Bennett WF, Bova JG, et al: Radiographic manifestations of eosinophilic gastroenteritis. *Abdom Imaging* 20:406–413, 1995.
155. De Chambrun GP, Gonzalez F, Canva JY, et al: Natural history of eosinophilic gastroenteritis. *Clin Gastroenterol Hepatol* 9:950–956, 2011.
156. Burhenne HJ, Carbone JV: Eosinophilic (allergic) gastroenteritis. *AJR* 96:332–338, 1966.
157. Balfe DM: Eosinophilic gastritis. *AJR* 152:1322, 1989.
158. Wehnt WD, Olmsted WW, Neiman HL, et al: Eosinophilic gastritis. *Radiology* 120:85–89, 1976.
159. Freundlich IM, Schaupp R, Lehman JS: Eosinophilic gastroenteritis: A case report with extensive jejunal involvement. *Radiology* 86:493–495, 1966.
160. Meyers HJ, Parker JJ: Emphysematous gastritis. *Radiology* 89:426–431, 1967.
161. Nelson SW: Extraluminal gas collections due to diseases of the gastrointestinal tract. *AJR* 115:225–248, 1972.
162. Monteferrante M, Shimkin P: CT diagnosis of emphysematous gastritis. *AJR* 153:191–192, 1989.
163. Schorr S, Marcus M: Intramural gastric emphysema. *Br J Radiol* 35:641–644, 1962.
164. Franken EA: Caustic damage of the gastrointestinal tract: Roentgen features. *AJR* 118:77–85, 1973.
165. Citron BP, Pincus JJ, Geokas MC, et al: Chemical trauma of the esophagus and stomach. *Surg Clin North Am* 48:1303–1311, 1968.
166. Goldman LP, Weigert JM: Corrosive substance ingestion: A review. *Am J Gastroenterol* 79:85–90, 1984.
167. Muhletaler CA, Gerlock AJ, de Soto L, et al: Gastroduodenal lesions of ingested acids: Radiographic findings. *AJR* 135:1247–1252, 1980.
168. Levitt R, Stanley RJ, Wise L: Gastric bullae: An early roentgen finding in corrosive gastritis following alkali ingestion. *Radiology* 115:597–598, 1975.
169. Kanne JP, Gunn M, Blackmore CC: Delayed gastric perforation resulting from hydrochloric acid ingestion. *AJR* 185:682–683, 2005.
170. Potesman NL: Corrosive gastritis due to hydrochloric acid ingestion. *AJR* 99:182–185, 1967.
171. Kleinhaus U, Rosenberger A, Adler O: Early and late radiological features of damage to the stomach caused by acid ingestion. *Radiol Clin (Belg)* 46:26–37, 1977.
172. Roswit B, Malsky SJ, Reid CB: Severe radiation injuries of the stomach, small intestine, colon, and rectum. *AJR* 114:460–475, 1972.
173. Goldstein HM, Rogers LF, Fletcher GH, et al: Radiological manifestations of radiation-induced injury to the normal upper gastrointestinal tract. *Radiology* 117:135–140, 1975.
174. Capps GW, Fulcer AS, Szucs RA, et al: Imaging features of radiation-induced changes in the abdomen. *Radiographics* 17:1455–1473, 1997.
175. Lane D: Irradiation gastritis simulating carcinoma. *Med J Aust* 2:576–577, 1970.
176. Williams NN, Daly JM: Infusional versus systemic chemotherapy for liver metastases from colorectal cancer. *Surg Clin North Am* 69:401–410, 1989.
177. Wells JJ, Nostrant TT, Wilson JAP, et al: Gastroduodenal ulcerations in patients receiving selective hepatic artery infusion chemotherapy. *Am J Gastroenterol* 80:425–429, 1985.
178. Shike M, Gillin JS, Kemeny N, et al: Severe gastroduodenal ulcerations complicating hepatic artery infusion chemotherapy for metastatic colon cancer. *Am J Gastroenterol* 81:176–179, 1986.
179. Hiehle JF, Levine MS: Gastrointestinal toxicity of 5-FU and 5-FUDR: Radiographic findings. *J Can Assoc Radiol* 42:109–112, 1991.
180. Hall DA, Clouse ME, Gramm HF: Gastroduodenal ulceration after hepatic arterial infusion chemotherapy. *AJR* 136:1216–1218, 1981.
181. Chuang VP, Wallace S, Stroehlein J, et al: Hepatic artery infusion chemotherapy: Gastroduodenal complications. *AJR* 137:347–350, 1981.
182. Mann FA, Kubal WS, Ruzicka FF: Radiographic manifestations of gastrointestinal toxicity associated with intra-arterial 5-fluorouracil infusion. *Radiographics* 2:329–339, 1982.
183. Thomson WO, Robertson AG, Imrie CW, et al: Is duodenitis a dyspeptic myth? *Lancet* 1:1197–1198, 1977.
184. Greenlaw R, Sheehan DG, DeLuca V, et al: Gastroduodenitis: A broader concept of peptic ulcer disease. *Dig Dis Sci* 25:660–662, 1980.
185. Sircus W: Duodenitis: A clinical, endoscopic, and histopathologic study. *Q J Med* 56:593–600, 1985.
186. Gelzayd EA, Gelfand DW, Rinaldo JA: Nonspecific duodenitis: A distinct clinical entity? *Gastrointest Endosc* 19:131–133, 1973.
187. Gelzayd EA, Biederman MA, Gelfand DW: Changing concepts of duodenitis. *Am J Gastroenterol* 64:213–216, 1975.
188. Collen MJ, Loeberberg MJ: Basal gastric acid secretion in nonulcer dyspepsia with or without duodenitis. *Dig Dis Sci* 34:246–250, 1989.
189. Wyatt JL, Rathbone BJ, Dixon ME, et al: *Campylobacter pyloridis* and acid-induced gastric metaplasia in the pathogenesis of duodenitis. *J Clin Pathol* 40:841–848, 1987.
190. Cheli R: Symptoms in chronic nonspecific duodenitis. *Scand J Gastroenterol* 17(Suppl):84–86, 1982.
191. Fraser GM, Pitman RG, Lawrie JH, et al: The significance of the radiological finding of coarse mucosal folds in the duodenum. *Lancet* 2:979–982, 1964.
192. Wiener SN, Vertes V, Shapiro H: The upper gastrointestinal tract in patients undergoing chronic dialysis. *Radiology* 92:110–114, 1969.
193. Zukerman GR, Mills BA, Koehler RE, et al: Nodular duodenitis: Pathologic and clinical characteristics in patients with end-stage renal disease. *Dig Dis Sci* 11:1018–1024, 1983.
194. Levine MS, Turner D, Ekberg O, et al: Duodenitis: A reliable radiologic diagnosis? *Gastrointest Radiol* 16:99–103, 1991.
195. Glick SN, Gohel VK, Laufer I: Mucosal surface patterns of the duodenal bulb. *Radiology* 150:317–322, 1984.
196. Gelfand DW, Dale WJ, Ott DJ, et al: Duodenitis: Endoscopic-radiologic correlation in 272 patients. *Radiology* 157:577–581, 1985.
197. Bova JG, Kamath V, Tio FO, et al: The normal mucosal surface pattern of the duodenal bulb: radiologic-histologic correlation. *AJR* 145:735–738, 1985.
198. Marn CS, Gore RM, Ghahremani GG: Duodenal manifestations of nontropical sprue. *Gastrointest Radiol* 11:30–35, 1986.
199. Schweiger GD, Murray JA: Postbulbar duodenal ulceration and stenosis associated with celiac disease. *Abdom Imaging* 23:347–349, 1998.
200. Jones B, Bayless TM, Hamilton SR, et al: “Bubbly” duodenal bulb in celiac disease: Radiologic-pathologic correlation. *AJR* 142:119–122, 1984.

Benign Tumors of the Stomach and Duodenum

MARC S. LEVINE

CHAPTER OUTLINE

Mucosal Lesions

Hyperplastic Polyp
Adenomatous Polyp
Duodenal Polyp
Villous Tumor
Polyposis Syndromes

Submucosal Lesions

Gastrointestinal Stromal Tumor
Leiomyoblastoma
Lipoma
Hemangioma
Lymphangioma
Glomus Tumor
Neural Tumor
Granular Cell Tumor
Inflammatory Fibroid Polyp
Ectopic Pancreatic Rest
Brunner Gland Hyperplasia (Brunner Gland Hamartoma)
Duplication Cyst

Between 85% and 90% of all neoplasms in the stomach and duodenum are benign.¹ About 50% are mucosal lesions and 50% are submucosal. Most of these benign neoplasms are discovered fortuitously on radiologic or endoscopic studies performed for other reasons. Occasionally, however, tumors that are large or ulcerated may cause abdominal pain or upper gastrointestinal (GI) bleeding. Depending on their histologic features, some benign tumors are also important because of an associated risk of malignancy. Although gastric and duodenal polyps are rarely diagnosed on single-contrast barium studies, the use of double-contrast technique has led to greater detection of these lesions.

Mucosal Lesions

Gastric polyps comprise about 50% of all benign neoplasms in the stomach.² Polyps are much less common in the duodenum. In the past, gastric polyps were rarely detected on single-contrast barium studies, with a reported incidence of only 0.01% to 0.05%.³ However, the routine use of double-contrast technique has dramatically improved our ability to detect gastric polyps, with a reported incidence of 1% to 2% on double-contrast studies.^{4,5} Most are small, innocuous hyperplastic polyps, but some larger lesions are adenomatous polyps capable of undergoing malignant degeneration via an adenoma-carcinoma sequence similar to that in the colon. The need for endoscopic

biopsy and removal of these polyps is directly related to their size and appearance. Radiologists therefore have an important role in the detection of gastric polyps and in subsequent decisions about patient management.

HYPERPLASTIC POLYP

Hyperplastic polyps are the most common benign epithelial neoplasms in the stomach, comprising 75% to 90% of all gastric polyps.⁶ Because hyperplastic polyps are not premalignant, they must be differentiated from adenomatous polyps, which have a known risk of malignant degeneration. Although histologic specimens are required for a definitive diagnosis, hyperplastic polyps have such a characteristic appearance on double-contrast barium studies that they can usually be differentiated from adenomatous polyps without need for endoscopy.

Pathology

Hyperplastic polyps consist histologically of elongated, branching, cystically dilated glandular structures.^{7,8} They usually appear grossly as small, sessile nodules with a smooth, dome-shaped contour. Because these polyps have a self-limited growth pattern, most are smaller than 1 cm.^{4,8} Hyperplastic polyps almost never undergo malignant degeneration.^{8,9} Nevertheless, affected individuals are at increased risk for harboring separate, coexisting gastric carcinomas. In various series, 8% to 28% of patients with hyperplastic polyps in the stomach have been found to have synchronous gastric carcinomas.^{7,9} This association is probably related to the presence of underlying atrophic gastritis, which predisposes to the development of polyps and cancer.⁸ Hyperplastic polyps are therefore important because of the increased risk of these patients developing gastric carcinoma.

Fundic gland polyps appear to be a variant of hyperplastic polyps arising within fundic gland mucosa in the fundus and body of the stomach.¹⁰ They consist histologically of cystically dilated, hyperplastic fundic glands that have no malignant potential.¹¹ Because affected individuals almost always have multiple (up to 50) gastric polyps, this entity has been called *fundic gland polyposis*.¹¹ Fundic gland polyps are typically found in middle-aged women.¹² Fundic gland polyposis can occur as an isolated condition in the stomach but also develops in about 40% of patients with familial adenomatous polyposis syndrome (FAPS; see Chapter 61).¹³ Thus, colonoscopy is often recommended for patients with fundic gland polyposis to determine whether they have FAPS and whether colonic surveillance is warranted.

Clinical Findings

Most hyperplastic polyps are small (<1 cm in diameter), innocuous lesions detected as incidental findings on radiologic or

endoscopic examinations.⁴ Rarely, polyps that have a friable or ulcerated surface may cause low-grade upper GI bleeding, and pedunculated polyps in the gastric antrum may prolapse through the pylorus, causing intermittent symptoms of gastric outlet obstruction.¹⁴

Radiographic Findings

Most hyperplastic polyps in the stomach appear on double-contrast studies as smooth, sessile, round or ovoid nodules, ranging from 5 to 10 mm in diameter.^{4,8} They tend to occur as multiple lesions in the gastric fundus or body (Fig. 31-1).⁴ When multiple polyps are present, they also tend to be similar in size.⁸

Hyperplastic polyps on the dependent surface of the stomach (i.e., the posterior wall) typically appear on double-contrast studies as smooth, round filling defects in the barium pool, whereas polyps on the nondependent surface (i.e., the anterior wall) appear as ring shadows that are etched in white because of trapping of barium between the edge of the polyp and adjacent mucosa (see Fig. 31-1A). A small hanging droplet of barium, or stalactite, on a nondependent or anterior wall polyp can be mistaken en face for a central area of ulceration (see Fig. 31-1B),¹⁵ but this droplet of barium is seen as a transient finding at fluoroscopy. Occasionally, one or more stalactites may be present as the only sign of hyperplastic polyps on the anterior wall.¹⁶ In such cases, careful examination of the area with prone compression views should demonstrate the underlying polyps responsible for this phenomenon.

Although most hyperplastic polyps are smaller than 1 cm, some atypical polyps can be as large as 2 to 6 cm, appearing as lobulated or pedunculated lesions (Fig. 31-2).^{14,17} A giant

hyperplastic polyp or conglomerate mass of hyperplastic polyps can occasionally be mistaken for a polypoid gastric carcinoma (see Fig. 31-2B).^{14,17} Rarely, pedunculated hyperplastic polyps in the antrum may prolapse through the pylorus into the duodenum, causing gastric outlet obstruction (Fig. 31-3).¹⁴

Fundic gland polyps appear on double-contrast examinations as multiple small (<1 cm in diameter), rounded nodules in the gastric fundus or body that are indistinguishable from hyperplastic polyps (Fig. 31-4).^{11,12,18} In some patients, spontaneous regression of fundic gland polyps has been reported.^{12,13,18}

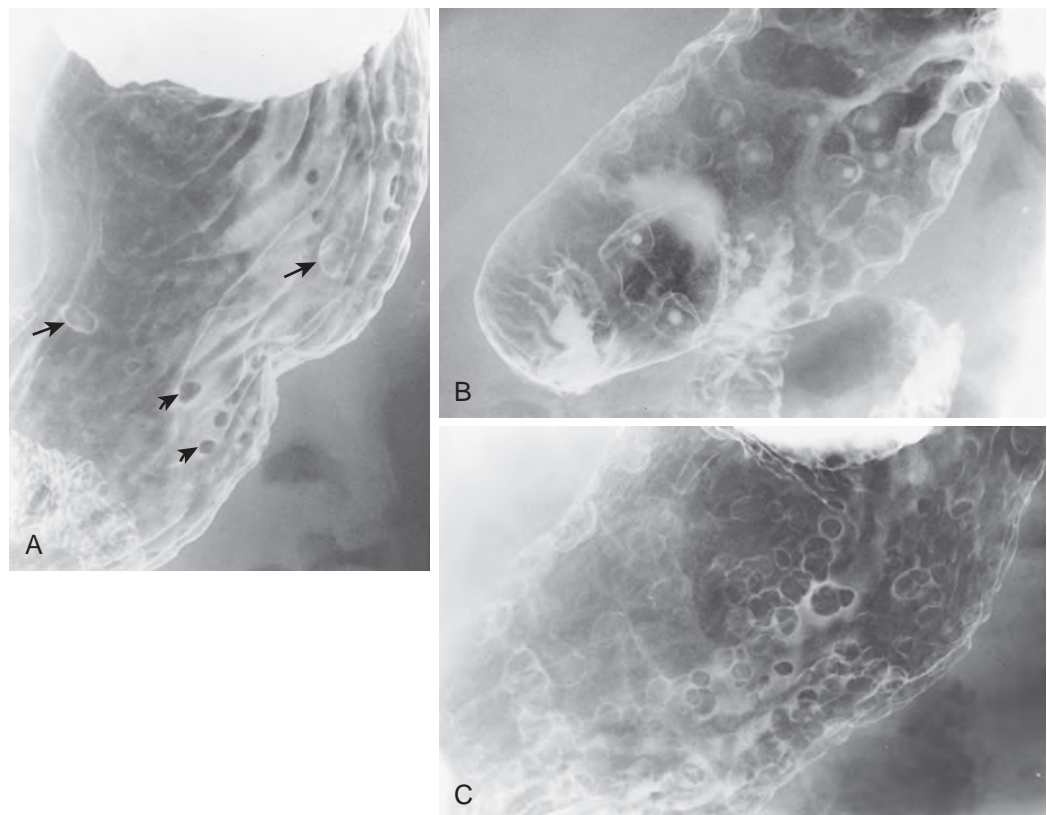
Differential Diagnosis

Hyperplastic polyps that appear as ring shadows on double-contrast studies must be differentiated from shallow ulcers on the dependent or posterior gastric wall and from unfilled ulcers on the nondependent or anterior wall. With flow technique, however, shallow ulcers on the dependent wall should fill with barium,¹⁹ whereas ulcers on the nondependent wall should fill with barium on prone compression views. Thus, it is usually possible to differentiate these lesions with a biphasic examination, which includes flow technique and prone compression.

Polyps that appear as ring shadows must also be distinguished from see-through artifacts caused by overlying structures that are calcified (e.g., phleboliths) or partially filled with contrast material (e.g., barium-containing colonic diverticula). Such structures can mimic the appearance of anterior wall polyps on a single view (Fig. 31-5A), but their location outside the stomach is readily apparent on images obtained in other projections (Fig. 31-5B).

Hyperplastic polyps that are lobulated or are larger than 1 cm in size cannot be distinguished from adenomatous polyps

Figure 31-1 Multiple hyperplastic polyps. A. Polyps on the dependent surface or posterior wall appear as filling defects in the barium pool (small curved arrows), whereas polyps on the nondependent surface or anterior wall are etched in white (straight arrows). **B.** This patient has multiple anterior wall polyps containing hanging droplets of barium, or stalactites, which could be mistaken for central areas of ulceration. **C.** Innumerable hyperplastic polyps are present in the gastric body. (**B** from Laufer I, Levine MS [eds]: *Double Contrast Gastrointestinal Radiology*, 2nd ed. Philadelphia, WB Saunders, 1992.)



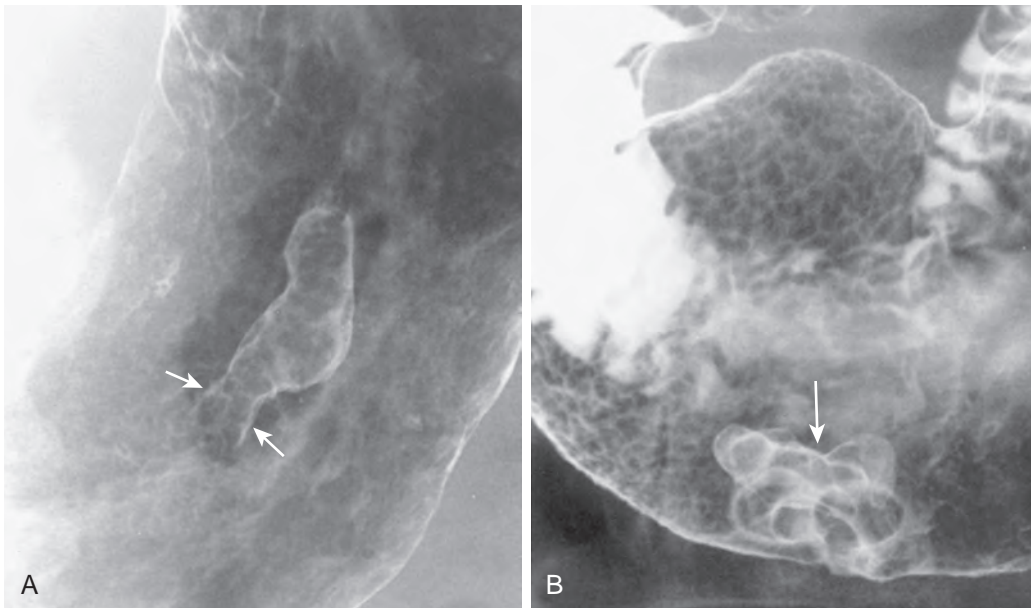


Figure 31-2 Atypical hyperplastic polyps. **A.** A long, pedunculated polyp is present in the gastric body. The polyp has a discrete stalk (arrows). This patient had pernicious anemia. **B.** A conglomerate mass of hyperplastic polyps (arrow) is seen in the antrum in another patient. This lesion is quite lobulated and could be mistaken for a polypoid carcinoma.

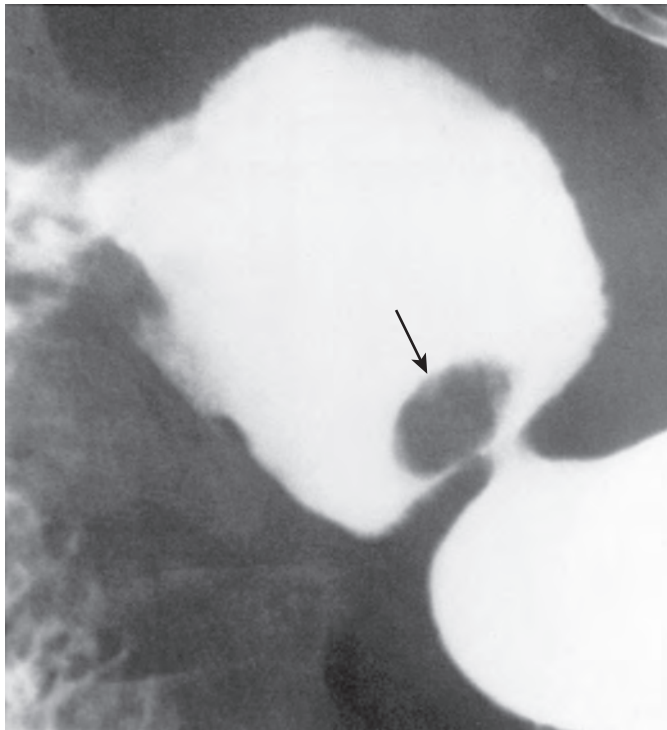


Figure 31-3 Prolapsed hyperplastic polyp. This patient has a pedunculated polyp (arrow) that has prolapsed from the antrum into the base of the duodenal bulb.

in the stomach. Rarely, giant hyperplastic polyps or a conglomerate mass of hyperplastic polyps can mimic a polypoid gastric carcinoma (see Fig. 31-2B).^{14,17} Thus, polyps that are unusually large or lobulated should be evaluated by endoscopy and biopsy and, if necessary, resected for a definitive diagnosis.

The differential diagnosis for multiple hyperplastic polyps in the stomach includes multiple adenomatous polyps and gastric involvement by one of the polyposis syndromes. However,

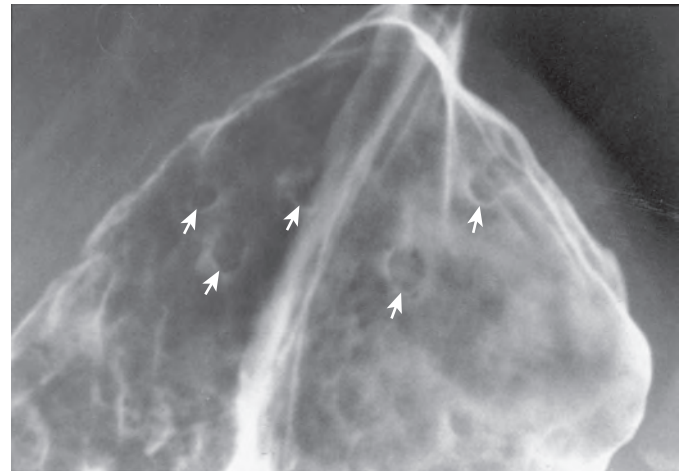


Figure 31-4 Fundic gland polyposis. Multiple tiny polyps (arrows) are present in the gastric fundus. These lesions have no malignant potential and are indistinguishable radiographically from hyperplastic polyps.

adenomatous polyps tend to be larger and less numerous and are more lobulated than most hyperplastic polyps. Both types of polyps can occur simultaneously in some patients,¹⁴ but an adenomatous polyp should be suspected if one lesion is disproportionately larger than the others.⁴ A generalized polyposis syndrome should be suspected if multiple polyps are also present in the small bowel or colon (see Chapter 61).

Treatment

Almost all smooth, sessile polyps smaller than 1 cm are hyperplastic polyps that have no malignant potential. Small, round, or ovoid gastric polyps detected on double-contrast studies should therefore be considered innocuous lesions without need for further investigation or treatment. Endoscopic biopsy or polypectomy should be performed, however, if the polyp is lobulated or pedunculated, larger than 1 cm, or enlarges on follow-up barium studies.

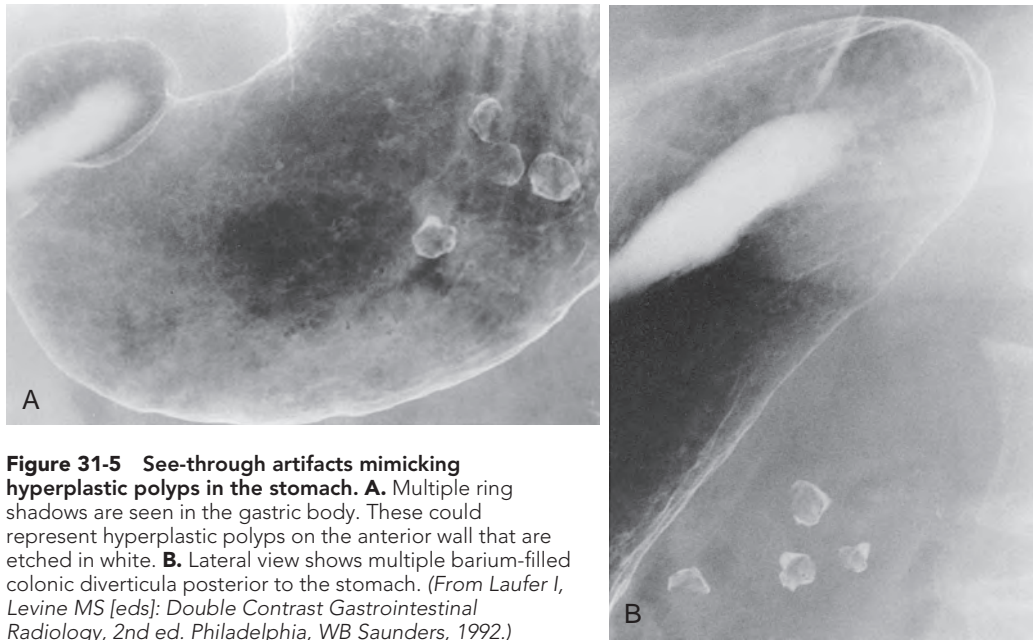


Figure 31-5 See-through artifacts mimicking hyperplastic polyps in the stomach. **A.** Multiple ring shadows are seen in the gastric body. These could represent hyperplastic polyps on the anterior wall that are etched in white. **B.** Lateral view shows multiple barium-filled colonic diverticula posterior to the stomach. (From Laufer I, Levine MS [eds]: *Double Contrast Gastrointestinal Radiology*, 2nd ed. Philadelphia, WB Saunders, 1992.)

ADENOMATOUS POLYP

Adenomatous polyps constitute less than 20% of all gastric polyps.^{4,5,9} Nevertheless, these polyps are important because they are capable of undergoing malignant degeneration. Thus, they must be treated more aggressively than hyperplastic polyps in the stomach.

Pathology

Adenomatous polyps are composed of dysplastic epithelium. Depending on the predominant glandular architecture, they may be classified as tubular, villous, or tubulovillous adenomas; the vast majority are tubular or mixed tubulovillous adenomas.⁷ Malignant degeneration of these lesions occurs via an adenoma-carcinoma sequence similar to that in the colon. Foci of carcinoma in situ or invasive carcinoma are present in almost 50% of resected adenomatous polyps larger than 2 cm, but malignant changes are rarely found in smaller lesions.^{7,20} As in the colon, the risk of malignant tumor therefore depends primarily on polyp size. Nevertheless, adenocarcinoma is 30 times more common than adenomatous polyps in the stomach, so most gastric cancers are thought to originate de novo and not from preexisting polyps.^{8,9}

Adenomatous polyps are often found in the stomach in patients with chronic atrophic gastritis.^{21,22} Because of the association between atrophic gastritis and gastric carcinoma (see Chapter 32), the risk of developing a separate gastric cancer may be greater than the risk of malignant degeneration in an adenomatous polyp.⁸ As many as 30% to 40% of patients with adenomatous polyps in the stomach have been found to have gastric carcinomas.^{8,9} Thus, detection of an adenomatous polyp in the stomach should lead to a careful search for other lesions.

Clinical Findings

Because of their larger size, adenomatous polyps in the stomach produce symptoms more frequently than hyperplastic polyps. These patients may present with epigastric pain,

bloating, upper GI bleeding or, rarely, symptoms of gastric outlet obstruction.^{23,24}

Radiographic Findings

Most adenomatous polyps diagnosed in the stomach on barium studies are larger than 1 cm.^{5,9,22} They usually occur as solitary lesions, most frequently in the antrum (Fig. 31-6),^{8,20} but multiple adenomatous polyps are sometimes found (Fig. 31-7). The polyps may be sessile or pedunculated, and they tend to be more lobulated than hyperplastic polyps (see Figs. 31-6 and 31-7). When the lesions are pedunculated, the stalk may be seen en face as an inner ring shadow overlying the head of the polyp, producing the Mexican hat sign, which is typically found with pedunculated polyps in the colon (see Fig. 31-6B). Rarely, pedunculated antral polyps may prolapse through the pylorus, causing intermittent gastric outlet obstruction.³

As with hyperplastic polyps, lesions on the nondependent or anterior wall may be etched in white on double-contrast views. Occasionally, a hanging droplet of barium (i.e., stalactite) on these nondependent lesions can mimic the appearance of ulceration.¹⁵ However, adenomatous polyps are rarely ulcerated.

Differential Diagnosis

Adenomatous polyps in the stomach that appear as smooth, sessile lesions may be difficult to distinguish on barium studies from hyperplastic polyps. However, most adenomatous polyps are larger than 1 cm and usually occur as solitary lesions, whereas hyperplastic polyps are almost always smaller than 1 cm and are often multiple.⁴ Adenomatous polyps that are sessile and have a smooth contour can also be mistaken for benign gastrointestinal stromal tumors (GISTs) or other submucosal lesions. Finally, adenomatous polyps that are larger and more lobulated may be indistinguishable from polypoid gastric carcinomas (see Fig. 31-7). Adenomatous polyps often harbor one or more foci of carcinoma in situ or invasive carcinoma, so aggressive management of these lesions is required.

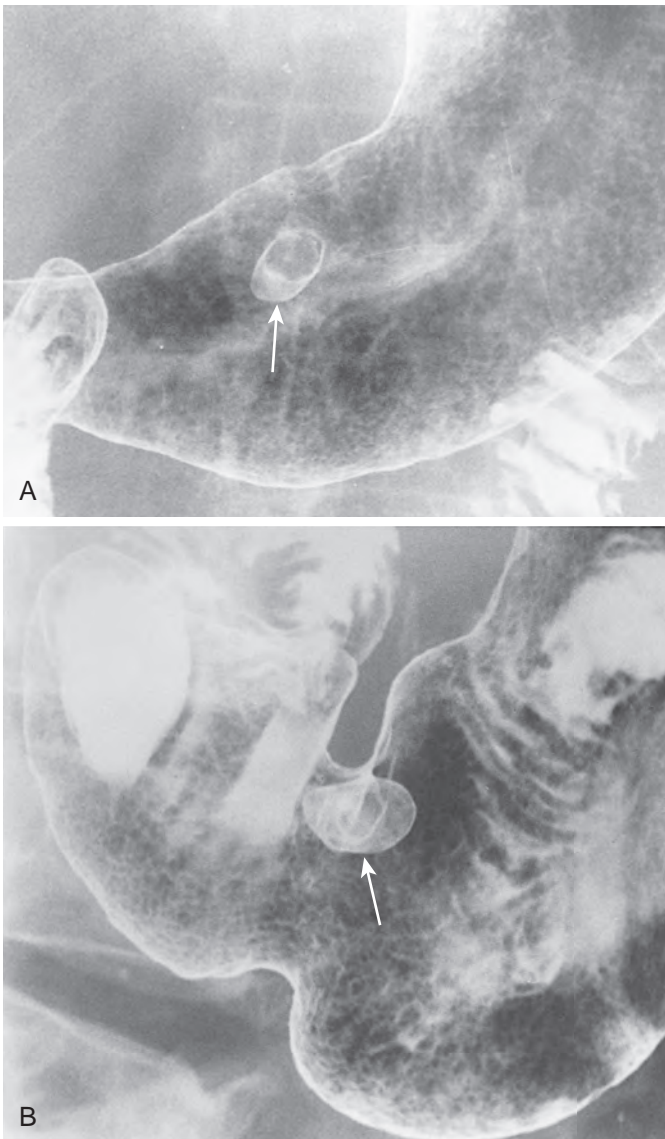


Figure 31-6 Adenomatous polyps. **A.** A sessile polyp (arrow) is present in the antrum. **B.** A pedunculated antral polyp (arrow) is seen in another patient. The stalk appears as an inner ring shadow overlying the head of the polyp, producing the Mexican hat sign. (B courtesy Dean D. Maglinte, MD, Indianapolis.)

Treatment

When a gastric polyp is detected on barium studies, endoscopic biopsy specimens should be obtained if the lesion has features of an adenomatous polyp (i.e., >1 cm, is lobulated or pedunculated, or enlarges on follow-up barium studies). If biopsy specimens confirm the presence of an adenomatous polyp, it should be resected because of the risk of malignant degeneration.²⁵ Regardless of the endoscopic findings, polyps larger than 2 cm should always be resected because of the even greater likelihood that they are adenomatous and the high risk of malignant tumor in adenomatous polyps of this size.^{3,5,9} If invasive carcinoma is present in the resected specimen, a wedge resection of the stomach or partial gastrectomy may be required.²⁶ As in the colon, a much more aggressive approach is therefore warranted in the management of adenomatous

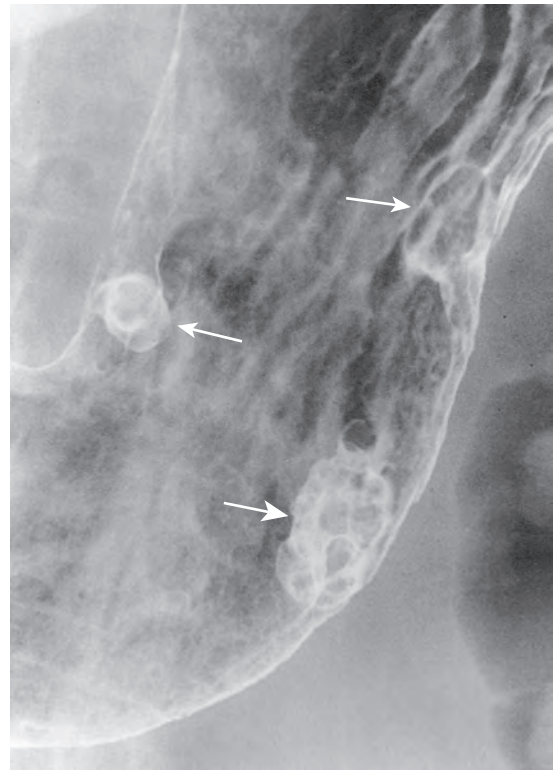


Figure 31-7 Multiple adenomatous polyps. The polyps (arrows) are larger and more lobulated than most hyperplastic polyps in the stomach. The most distal lesion on the greater curvature is indistinguishable from a polypoid carcinoma. (From Laufer I, Levine MS [eds]: *Double Contrast Gastrointestinal Radiology*, 2nd ed. Philadelphia, WB Saunders, 1992.)

polyps than hyperplastic polyps because of the increased cancer risk in these patients.

DUODENAL POLYP

Duodenal polyps are much less common than gastric polyps. Hyperplastic polyps, which constitute most gastric polyps, are rarely found in the duodenum. Instead, most duodenal polyps are adenomatous.²⁷ Because these polyps rarely cause symptoms, they are usually detected as incidental findings on radiologic or endoscopic examinations. Occasionally, however, duodenal polyps may cause low-grade upper GI bleeding or obstructive jaundice.²⁸

Radiographic Findings

Duodenal polyps usually appear on barium studies as smooth, sessile lesions in the first or second portion of the duodenum (Fig. 31-8). They tend to be smaller than 2 cm, but giant duodenal polyps have occasionally been described.²⁹ Most duodenal polyps occur as solitary lesions, but multiple adenomatous, hamartomatous, or inflammatory polyps may be found in the duodenum as part of a diffuse polyposis syndrome (see Chapter 61).

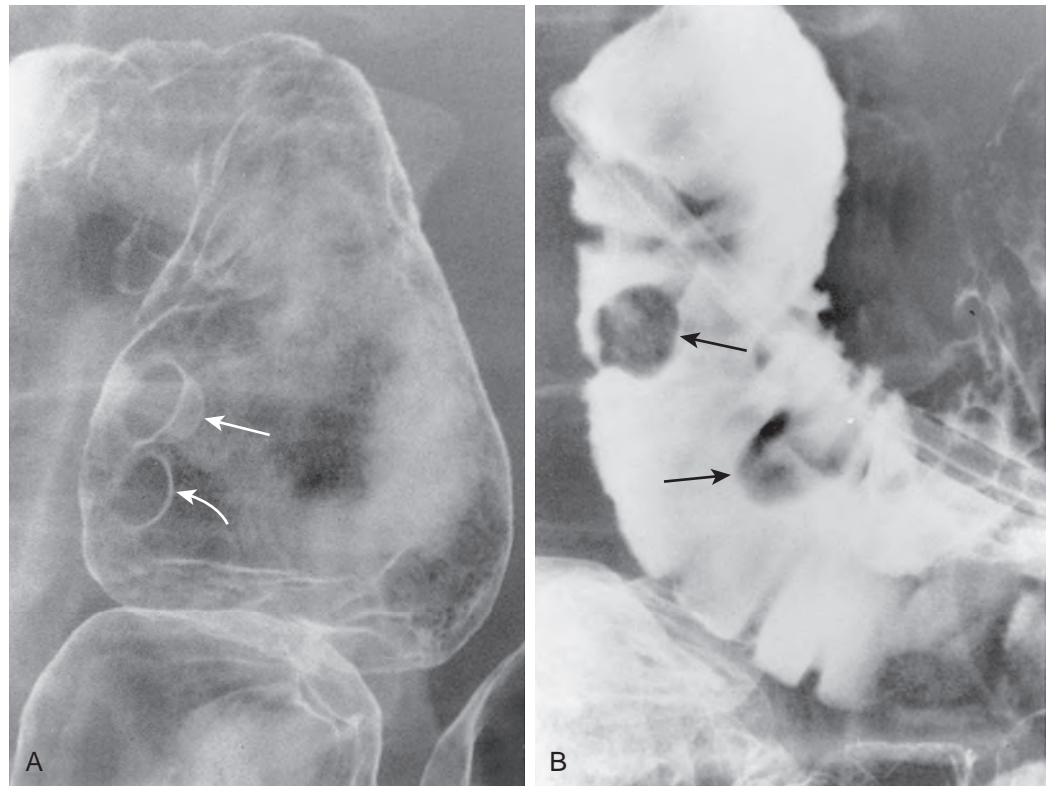
Differential Diagnosis

Sessile polyps in the duodenum may be difficult to distinguish on barium studies from benign GISTs, Brunner gland hamartomas, or other submucosal masses, so endoscopy may be

Figure 31-8 Duodenal polyps.

A. Two polyps are present in the duodenal bulb. The lower polyp is seen as a ring shadow (curved arrow) and the higher polyp as a bowler hat (straight arrow).

B. Several adenomatous polyps (arrows) are seen in the descending duodenum in another patient. This study was performed by injecting barium through a tube in the proximal duodenum. (A from Laufer I, Levine MS [eds]: *Double Contrast Gastrointestinal Radiology*, 2nd ed. Philadelphia, WB Saunders, 1992.)



required for a definitive diagnosis. Occasionally, antral mucosa or even pedunculated antral polyps that prolapse through the pylorus can be mistaken for polypoid lesions in the duodenum (Fig. 31-9; see also Fig. 31-3). However, prolapsed antral mucosa is usually manifested by a characteristic mushroom-shaped defect at the base of the bulb. In other patients, apparent polypoid lesions may result from heaped-up areas of redundant mucosa on the inner aspect of the superior duodenal flexure between the first and second portions of the duodenum (Fig. 31-10). However, these flexural pseudolesions can usually be differentiated from true polyps by their characteristic location and changeable appearance at fluoroscopy.^{30,31}

VILLOUS TUMOR

Adenomatous polyps in the stomach and duodenum that contain predominantly villous elements have been called villous adenomas, papillary adenomas, papillomas, or adenomatous papillomas.³² Because of their high malignant potential, however, the term *villous tumors* is probably best, because it avoids the erroneous impression that these lesions are always benign.^{33,34}

Pathology

Villous tumors in the stomach and duodenum closely resemble those in the colon, appearing grossly as polypoid masses with numerous frondlike projections. They usually occur as solitary lesions, ranging from 3 to 9 cm in size, but giant villous tumors as large as 15 cm have been reported.^{34,35} Villous tumors rarely cause gastric outlet obstruction because of the soft consistency



Figure 31-9 Prolapsed antral mucosa. The prolapsed mucosa produces a mushroom-shaped defect (arrows) at the base of the duodenal bulb. The characteristic appearance and location of prolapsed antral mucosa should differentiate this finding from a true polypoid lesion. (From Laufer I, Levine MS [eds]: *Double Contrast Gastrointestinal Radiology*, 2nd ed. Philadelphia, WB Saunders, 1992.)

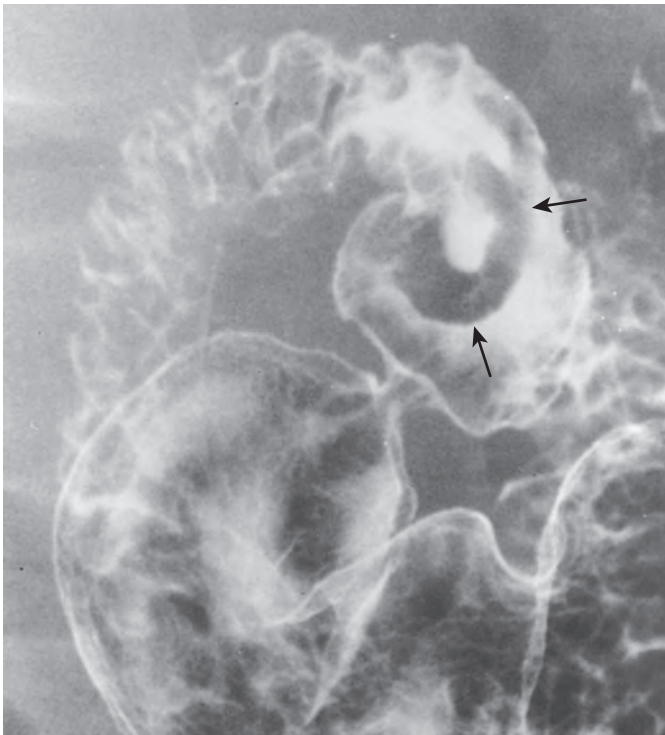


Figure 31-10 Duodenal pseudolesion. Redundant mucosa at the superior duodenal flexure simulates an ulcerated mass (arrows) at the apex of the duodenal bulb. However, the characteristic appearance and location of this finding should suggest a flexural pseudolesion.

of these lesions. They are equally distributed in the stomach, but duodenal lesions tend to be located in the descending duodenum near the papilla of Vater.^{33,35}

Villous tumors in the stomach and duodenum are associated with an even higher risk of malignant change than villous tumors in the colon. The risk of malignant tumor is directly related to the size of the lesion. In the stomach, malignant changes are found in 50% of lesions 2 to 4 cm in size and in 80% of lesions larger than 4 cm. Similarly, malignant changes are found in 30% to 60% of villous tumors in the duodenum, with the highest cancer risk in lesions larger than 4 cm.^{32,33} Although villous tumors in the stomach and duodenum have been classified as benign neoplasms in this chapter, for all practical purposes they should be treated as malignant lesions.

Clinical Findings

Most patients with villous tumors in the stomach and duodenum are over 50 years of age. They may present with signs or symptoms of upper GI bleeding, such as melena, guaiac-positive stool, and iron deficiency anemia.^{33,34} Because villous tumors in the duodenum are often located near the papilla of Vater, some patients may develop obstructive jaundice.^{33,34} In contrast to villous tumors in the colon, however, villous tumors in the stomach and duodenum rarely cause diarrhea or electrolyte depletion.^{33,34} Although gastric and duodenal lesions have the same secretory capabilities as those in the colon, reabsorption of fluid and electrolytes in the small and large bowel apparently prevents the development of a diarrheal syndrome.

Villous tumors in the stomach and duodenum should be resected because of the high risk of malignant degeneration.

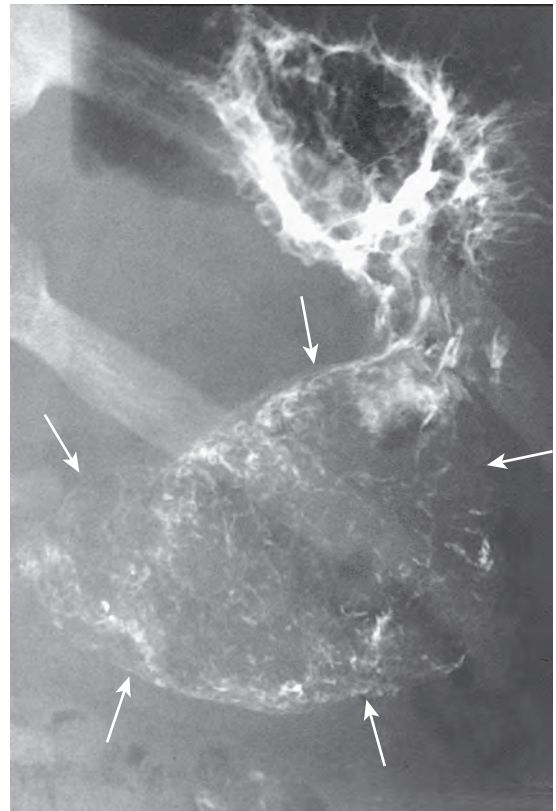


Figure 31-11 Villous tumor in the stomach. A giant villous tumor (arrows) in the gastric antrum has a characteristic soap bubble appearance because of trapping of barium between the frondlike projections of the tumor. This lesion could be mistaken for a bezoar but, in contrast to bezoars, it did not move with changes in the patient's position. (Courtesy Abraham Ghiatis, MD, San Antonio, TX.)

Some benign lesions can be removed by endoscopy, but those harboring invasive cancer usually require surgery.^{32,33,35}

Radiographic Findings

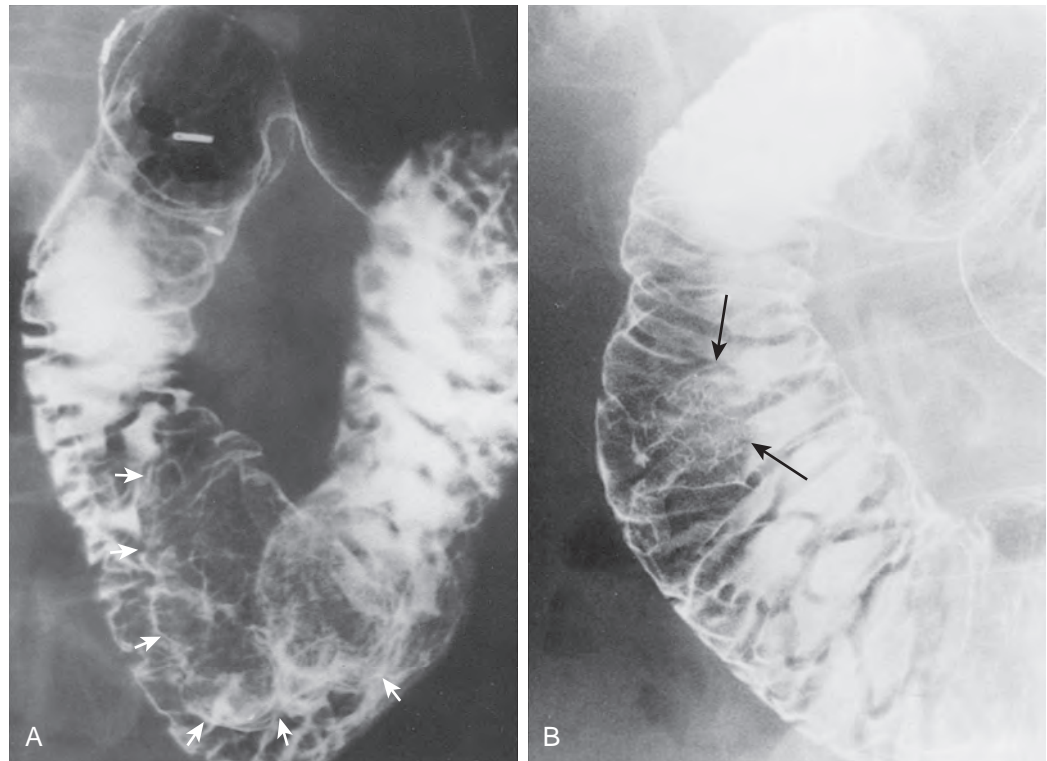
Villous tumors in the stomach and duodenum usually appear on barium studies as polypoid masses, ranging from 2 to 9 cm in size.³⁴⁻³⁶ The lesions often have a reticular or soap bubble appearance with serrated, feathery margins caused by trapping of barium in multiple clefts between the frondlike projections of the tumor (Figs. 31-11 and 31-12).^{30,36,37} Thus, villous tumors in the stomach and duodenum have the same radiographic features as those in the colon.

Villous tumors in the duodenum tend to be located near the papilla of Vater (see Fig. 31-12),³³⁻³⁵ but occasionally are found as far proximally as the duodenal bulb.³⁸ Because these lesions are easily obscured by superimposed mucosal folds, they are best visualized on double-contrast studies with optimal distention of the duodenum. Hypotonic duodenography (after intravenous [IV] administration of 1 mg of glucagon) is a particularly effective technique for effacing the overlying folds, so subtle lesions in the peripapillary duodenum are better seen (see Fig. 31-12B).^{35,37}

Differential Diagnosis

A large gastric bezoar may occasionally produce a soap bubble appearance, mimicking that of a villous tumor in the stomach

Figure 31-12 Villous tumors in the duodenum. **A.** This villous tumor appears as a polypoid mass (arrows) just below the level of the papilla. Note the characteristic reticular surface of the lesion. **B.** In another patient, a more subtle villous tumor (arrows) is seen with optimal distention of the descending duodenum. Again, note the reticular surface of the lesion. (A from Laufer I, Levine MS [eds]: *Double Contrast Gastrointestinal Radiology*, 2nd ed. Philadelphia, WB Saunders, 1992.)



as a result of barium trapped in the interstices of the bezoar. However, the freely mobile nature of the bezoar with changes in the patient's position should suggest the correct diagnosis. Carcinoma or lymphoma of the stomach or duodenum may also be manifested by a bulky intraluminal mass, but these lesions rarely produce a soap bubble appearance.

POLYPOSIS SYNDROMES

With the widespread use of double-contrast radiography and endoscopy, gastroduodenal involvement by the polyposis syndromes has proved to be far more common than previously recognized (see Chapter 61). In patients with FAPS, detection of adenomatous polyps in the stomach or duodenum is particularly important because of the malignant potential of these lesions and the increased risk of developing gastric or duodenal carcinoma. Some investigators therefore believe that periodic surveillance of the upper GI tract should be performed on all patients with FAPS. Other polyposis syndromes involving the stomach and duodenum include Peutz-Jeghers syndrome, Cronkhite-Canada syndrome, juvenile polyposis, and Cowden's disease (see Chapter 61). In patients with Cronkhite-Canada syndrome, barium studies may reveal distinctive whiskering along the margins of the stomach because of trapping of barium between tiny mucosal excrescences (Fig. 31-13).³⁹ When accompanied by characteristic ectodermal findings, this appearance should be highly suggestive of Cronkhite-Canada syndrome.

Submucosal Lesions

The terms *submucosal* and *intramural* are used interchangeably in this chapter. Nevertheless, it should be recognized that all submucosal lesions are intramural, but not all intramural

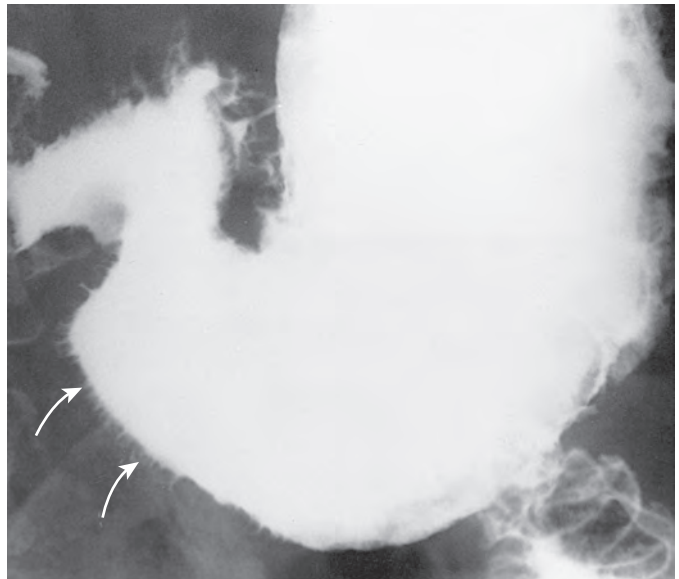


Figure 31-13 Cronkhite-Canada syndrome involving the stomach. A single-contrast view shows whiskering (arrows) of the greater curvature because of trapping of barium between tiny mucosal excrescences. This finding is characteristic of gastric involvement by Cronkhite-Canada syndrome.

lesions are submucosal because they can also arise from the muscularis propria or even the subserosa. These mesenchymal lesions constitute about 50% of all benign neoplasms in the stomach or duodenum.² Almost 90% are GISTs.⁴⁰ Other submucosal lesions include leiomyoblastomas, lipomas, hemangiomas, lymphangiomas, glomus tumors, neural tumors, granular cell tumors, inflammatory fibroid polyps, ectopic pancreatic

rests, Brunner gland hamartomas, and duplication cysts. Most benign submucosal tumors are discovered as incidental findings at surgery or autopsy, but lesions that are large or ulcerated may cause abdominal pain or upper GI bleeding. Some mesenchymal tumors are important because of an increased risk of malignancy. Submucosal masses may be difficult to visualize at endoscopy because the overlying mucosa appears normal. As a result, barium studies are particularly helpful for detecting these lesions.

GASTROINTESTINAL STROMAL TUMOR

Although GISTs were once thought to represent smooth muscle tumors (leiomyomas and leiomyosarcomas), they are now believed to arise from the interstitial cells of Cajal and are characterized by their unique immunohistochemical expression of CD-117, also known as c-kit, a cell surface membrane receptor with tyrosine kinase activity.^{41,42} In one study, almost all submucosal masses previously classified as smooth muscle tumors were found to be GISTs, with the exception of submucosal masses in the esophagus, in which true leiomyomas were far more common.⁴² GISTs constitute about 90% of mesenchymal tumors and 40% of all benign tumors in the stomach and duodenum.^{1,40,43} These lesions are important, not only because they may cause symptoms, but also because a small percentage are found to be malignant.

Pathology

GISTs consist histologically of intersecting bundles of spindle-shaped cells in a characteristic whorling pattern that distinguishes these tumors from normal smooth muscle.^{40,44} Depending on their growth pattern, GISTs may appear grossly as endogastric, exogastric, or so-called dumbbell lesions.¹ About 80% are endogastric lesions that remain intramural but grow toward the lumen. Another 15% are exogastric lesions that grow outward from the stomach toward the peritoneal cavity. The remaining 5% are dumbbell-shaped lesions that have endogastric and exogastric components.

Almost all benign gastric and duodenal GISTs occur as solitary lesions, but multiple tumors are found in 1% to 2% of patients.¹ Most benign GISTs in the stomach and duodenum are smaller than 3 cm, but some patients may have giant lesions as large as 25 cm.⁴⁴ As these tumors enlarge, they often outgrow their blood supply, causing central necrosis and ulceration.⁴⁵ In various series, ulceration has been documented in 50% to 70% of all gastric GISTs larger than 2 cm.^{1,45}

About 90% of GISTs in the stomach are found to be benign lesions.¹ However, it is often difficult to differentiate benign from malignant GISTs by histopathologic criteria.^{46,47} The most commonly accepted microscopic index of malignancy is the degree of mitotic activity in the tumor.⁴⁴ Nevertheless, mitotic activity may be increased in only a portion of a malignant GIST, so random biopsy specimens or frozen sections may erroneously suggest a benign lesion. Thus, a definitive diagnosis of malignant tumor ultimately depends on the tumor's biologic behavior and the demonstration of invasive growth beyond the stomach via direct extension, lymphatic spread, or hematogenous metastases (see Chapter 33).⁴³

Clinical Findings

Benign gastric and duodenal GISTs occur with about equal frequency in men and women. Affected individuals are usually

over 50 years of age.⁴⁴ Most patients with lesions smaller than 3 cm are asymptomatic. As these tumors enlarge, ulceration of the lesion may cause epigastric pain or upper GI bleeding, manifested by hematemesis, melena, guaiac-positive stool, or iron deficiency anemia.^{43,44} Occasionally, pedunculated GISTs in the gastric antrum may cause nausea and vomiting because of intermittent gastric outlet obstruction.^{48,49}

Radiographic Findings

Most benign GISTs are not diagnosed on abdominal radiographs, but a large tumor in the stomach can occasionally be recognized as a soft tissue mass indenting the gastric air shadow.² Rarely, benign GISTs in the stomach contain irregular streaks or clumps of mottled calcification that are visible on abdominal radiographs, barium studies, or computed tomography (CT) (Fig. 31-14).^{50,51} Mucinous adenocarcinomas of the stomach may also calcify, but the calcification in these lesions tends to have a punctate, granular, or finely stippled appearance (see Chapter 32).⁵² The differential diagnosis for left upper quadrant calcification also includes calcified adrenal, renal, or splenic lesions.

Benign GISTs typically appear on barium studies as discrete submucosal masses (Figs. 31-15 and 31-16). These tumors have the same radiographic features as intramural, extramucosal lesions elsewhere in the GI tract. When viewed in profile, the lesions have a smooth surface that is etched in white on double-contrast images, and their borders form right angles or slightly obtuse angles with the adjacent gastric or duodenal wall (see Fig. 31-15A). When viewed en face, the intraluminal surface of these tumors has abrupt, well-defined borders (see Fig. 31-15B). Because the overlying mucosa is usually intact, a normal *areae gastricae* pattern can sometimes be seen overlying these lesions.

Gastric GISTs vary in size from tiny lesions of several millimeters to enormous masses that encroach substantially on the lumen.⁴⁴ Tumors larger than 2 cm frequently contain areas of ulceration, manifested by a central barium-filled crater within the surrounding submucosal mass (see Fig. 31-16A). Because of their characteristic appearance, centrally ulcerated GISTs viewed en face have been described as bull's-eye or target lesions. Occasionally, a hanging droplet of barium (i.e., stalactite) on an anterior wall GIST can mimic the appearance of ulceration (see Fig. 31-15B), but the stalactite can usually be recognized as a transient finding at fluoroscopy.¹⁵

Because ulcerated GISTs may cause major upper GI bleeding, ulceration is generally considered an indication for surgery. Rarely, however, complete healing of ulceration in benign gastric GISTs can occur in patients treated conservatively with antisecretory agents (see Fig. 31-16B), so medical treatment may lead to cessation of bleeding when surgery is contraindicated.⁵³ If necessary, bleeding can also be controlled angiographically by selective embolization of feeding vessels.⁵⁴

Although most benign GISTs in the stomach have a typical submucosal appearance, exogastric tumors that grow outward from the stomach may be difficult to differentiate from extrinsic mass lesions. However, the presence of a central dimple or spicule at the apex of the mass should suggest an intramural rather than an extrinsic lesion.⁵⁵ This area of tenting probably results from traction on the gastric wall by the base or pedicle of the mass as it enlarges. Other GISTs that grow intraluminally may develop pseudopedicles. Rarely, pedunculated antral GISTs may prolapse into the duodenum or act as the lead

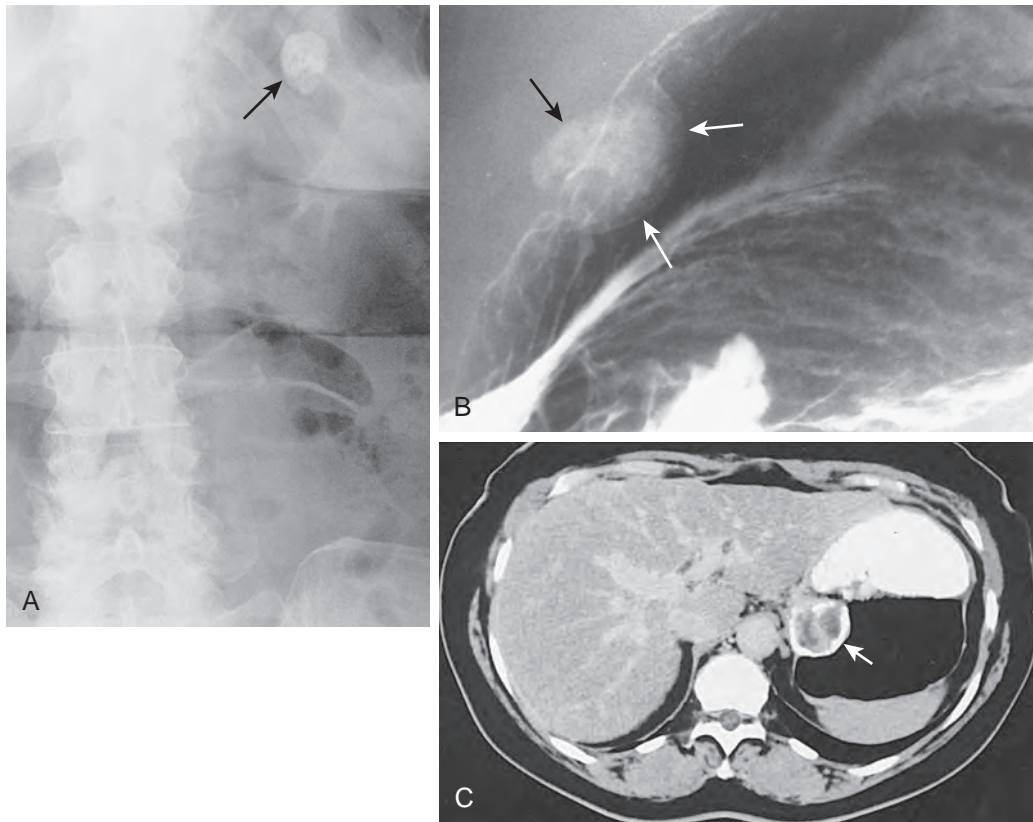


Figure 31-14 Benign GISTs with calcification. **A.** Close-up view of an abdominal radiograph reveals a dense clump of calcification (arrow) in the left upper quadrant. **B.** Barium study shows that this calcification (black arrow) is located within a discrete submucosal mass (white arrows) in the stomach. At surgery, the lesion was found to be a benign GIST. **C.** In another patient, a peripherally calcified benign gastric GIST (arrow) is shown on a CT scan. (C courtesy Alec J. Megibow, MD, New York.)

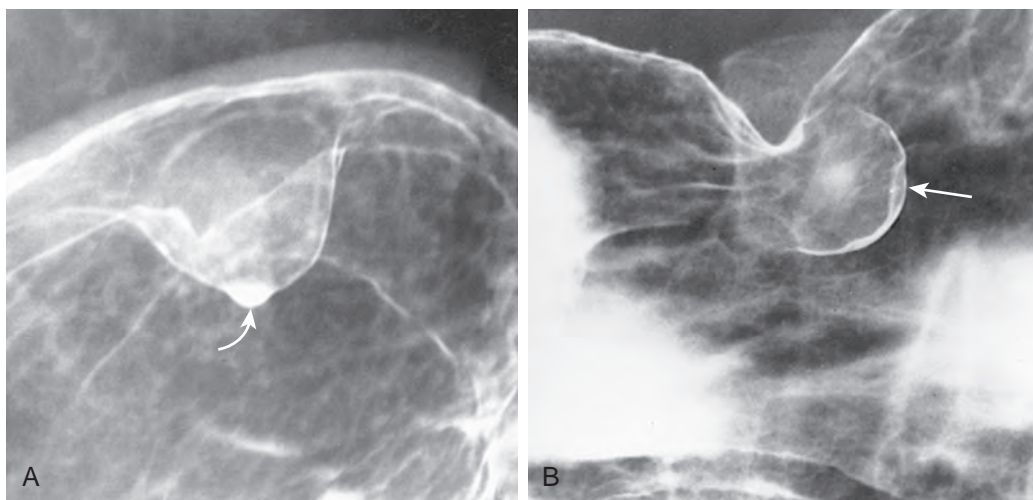


Figure 31-15 Benign GISTs. **A.** A submucosal mass is seen in profile in the gastric fundus. The lesion has smooth borders that form slightly obtuse angles with the adjacent gastric wall. This view was taken with the patient upright, and a barium stalactite (arrow) is seen hanging down from the inferior surface of the lesion. **B.** In another patient, a small GIST is seen en face (arrow) in the gastric body. This lesion also has typical features of a submucosal mass with smooth, well-defined borders. A hanging droplet of barium or stalactite is visible on the surface of this anterior wall lesion. (From Laufer I, Levine MS [eds]: *Double Contrast Gastrointestinal Radiology*, 2nd ed. Philadelphia, WB Saunders, 1992.)

point for a gastrogastic or gastroduodenal intussusception (Fig. 31-17).^{48,49}

Differential Diagnosis

GISTs are the most common benign submucosal tumors in the stomach and duodenum. However, other intramural lesions

may also be manifested by discrete submucosal masses. Occasionally, lipomas may be recognized by their tendency to change in size and shape at fluoroscopy (see later, “**Lipoma**”), whereas ectopic pancreatic rests may be suggested by their characteristic location on the greater curvature of the distal antrum (see later, “**Ectopic Pancreatic Rest**”). In most cases, however, these

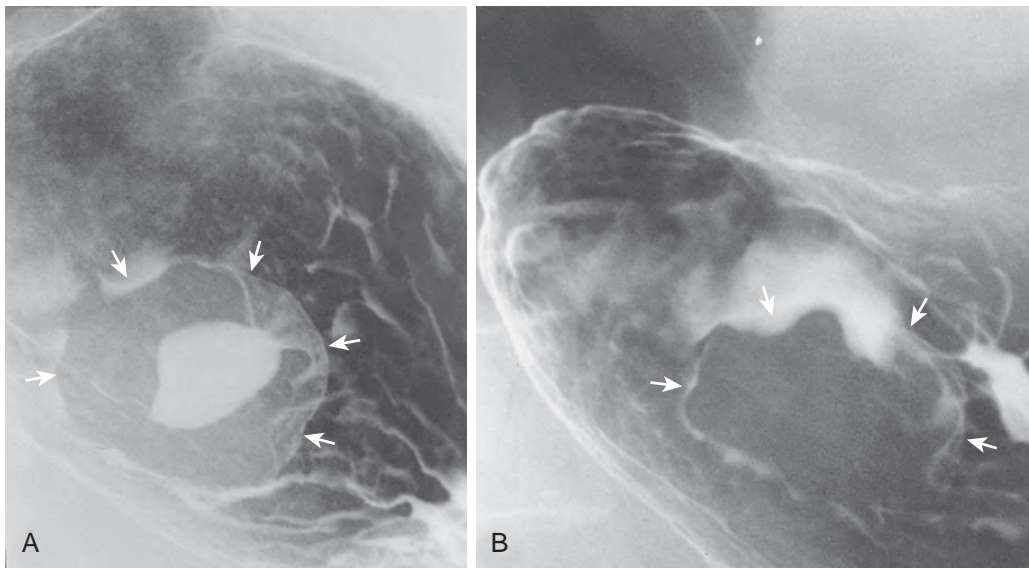


Figure 31-16 Ulcerated GIST with complete healing of the ulcer. **A.** Initial study reveals a relatively large benign GIST (arrows) in the fundus with a central area of ulceration, producing a bull's-eye lesion. **B.** Follow-up study 3 years later shows complete healing of the ulcer within the tumor (arrows). (From O'Riordan D, Levine MS, Yeager BA: Complete healing of ulceration within a gastric leiomyoma. *Gastrointest Radiol* 10:47-49, 1985.)

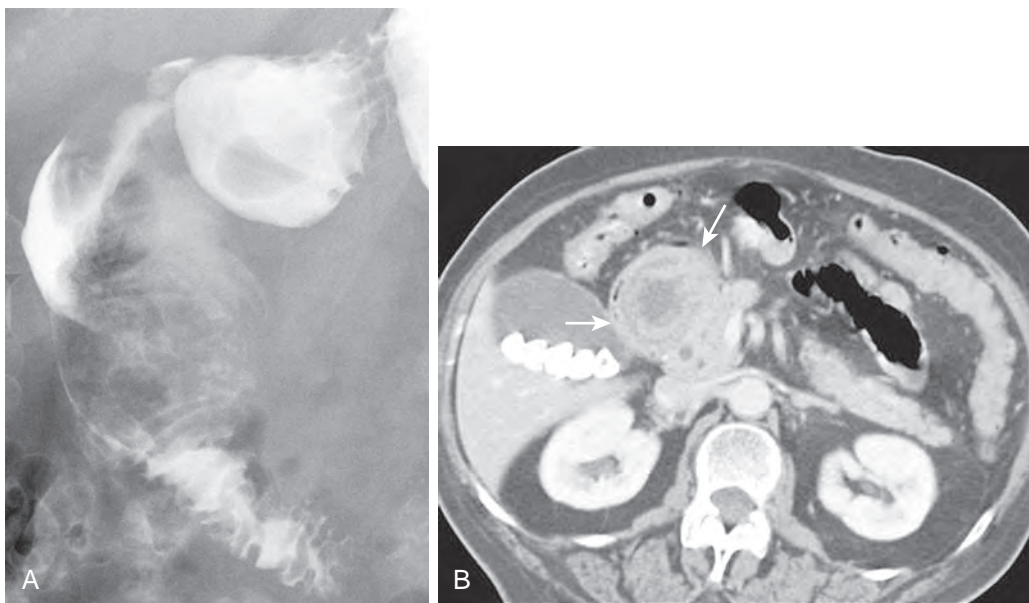


Figure 31-17 Benign GIST with gastroduodenal intussusception. **A.** A large, smooth mass extends from the duodenal bulb into the descending duodenum. Note the characteristic coiled spring appearance of an intussusception and foreshortening of the distal antrum. This patient had a benign GIST in the stomach that prolapsed through the pylorus, acting as the lead point for this gastroduodenal intussusception. **B.** CT scan shows the target sign of an intussusception with concentric rings (arrows) in the descending duodenum.

submucosal lesions cannot be differentiated by radiologic criteria.

Centrally ulcerated GISTs that are viewed en face appear as typical bull's-eye or target lesions. Although a solitary bull's-eye lesion in the stomach or duodenum is most likely to represent an ulcerated GIST on empiric grounds, other benign mesenchymal tumors that are ulcerated can produce identical findings. In contrast, the presence of multiple bull's-eye lesions should suggest a malignant tumor such as metastatic disease or lymphoma because GISTs in the stomach or duodenum are rarely multiple.¹

An antral or duodenal ulcer surrounded by a radiolucent mound of edema may simulate an ulcerated GIST. Conversely, an ulcerated GIST may erroneously suggest an ulcer in the stomach or duodenum. However, a benign GIST usually has discrete borders, whereas the edematous mound surrounding a gastric or duodenal ulcer tends to have a more gradual transition.

Exogastric GISTs are often difficult to distinguish on barium studies from extrinsic masses involving the stomach, particularly pancreatic pseudocysts or other pancreatic lesions compressing the stomach. Gastric compression by an enlarged liver, spleen, kidney, or other abdominal mass may produce similar findings. As noted, however, the presence of a central dimple or spicule at the apex of the mass should suggest an exogastric intramural lesion such as a GIST.⁵⁵ When extrinsic mass lesions are suspected, ultrasound, CT, and magnetic resonance imaging (MRI) may be helpful for establishing the correct diagnosis.

Treatment

Small, asymptomatic submucosal masses detected in the stomach or duodenum on barium studies can probably be followed conservatively without need for endoscopic or surgical intervention, because most of these lesions are found to be benign GISTs. In such cases, follow-up barium studies or endoscopy may be performed at yearly intervals to be certain that the

tumor is not enlarging. However, ulcerated lesions or lesions larger than 2 cm should probably be resected because of the increased risk of malignancy and the difficulty distinguishing benign and malignant GISTs by histopathologic criteria.^{1,41,43} Depending on the size of the lesion, it can be enucleated, locally excised or, if necessary, removed by partial gastrectomy or duodenectomy.^{43,44} Patients who have more worrisome lesions may benefit from adjuvant therapy with imatinib (Gleevec), a tyrosine kinase inhibitor, to decrease the risk of developing recurrent tumor.⁵⁶

LEIOMYOBLASTOMA

Leiomyoblastomas are unusual smooth muscle tumors that occur predominantly in the stomach. However, these tumors have also been reported in the small bowel, retroperitoneum, and uterus.⁵⁷ Leiomyoblastomas differ histologically from GISTs, but the gross morphologic findings are almost identical.⁴⁴ As with GISTs, leiomyoblastomas are important because of the risk of malignancy in these lesions.

Pathology

Leiomyoblastomas consist histologically of round, polygonal, or epithelioid cells with eccentric nuclei, perinuclear vacuolization, and a clear or acidophilic cytoplasm.⁵⁷⁻⁵⁹ Because of the histologic findings, these tumors have also been called *epithelioid leiomyomas*.^{58,59} Most leiomyoblastomas are benign lesions, but metastases to the liver or other structures occur in about 10% of patients.⁶⁰ As with GISTs, malignant lesions usually have increased mitotic activity on microscopic examination.⁵⁸ Size is also an important factor in predicting biologic behavior because metastases rarely occur with lesions smaller than 6 cm.⁵⁸ Nevertheless, some authors believe that all leiomyoblastomas should be resected because of the difficulty in distinguishing benign and malignant lesions by histopathologic criteria.^{57,59}

Leiomyoblastomas tend to occur as solitary lesions in the stomach, usually in the antrum, but multiple tumors have been reported.^{58,61} As with GISTs, most lesions appear as submucosal masses, often with central necrosis and ulceration.^{60,61} Occasionally, they may have an exogastric pattern of growth.⁶¹

Clinical Findings

In contrast to leiomyomas, leiomyoblastomas are more common in men than in women.^{60,61} These patients may be asymptomatic or may present with pain, vomiting, upper GI bleeding, or

a palpable abdominal mass.^{57,60,61} Rarely, giant exogastric leiomyoblastomas may rupture suddenly into the peritoneal cavity, causing catastrophic intraperitoneal bleeding.⁶²

Radiographic Findings

Gastric leiomyoblastomas are indistinguishable on barium studies from GISTs (see earlier, “Gastrointestinal Stromal Tumor”). Most appear as smooth submucosal masses, often containing central areas of ulceration (Fig. 31-18).⁶¹ Some endogastric lesions can become pedunculated, whereas exogastric lesions can be mistaken for extrinsic masses involving the stomach (Fig. 31-19A).⁶¹ Cystic degeneration of these exogastric

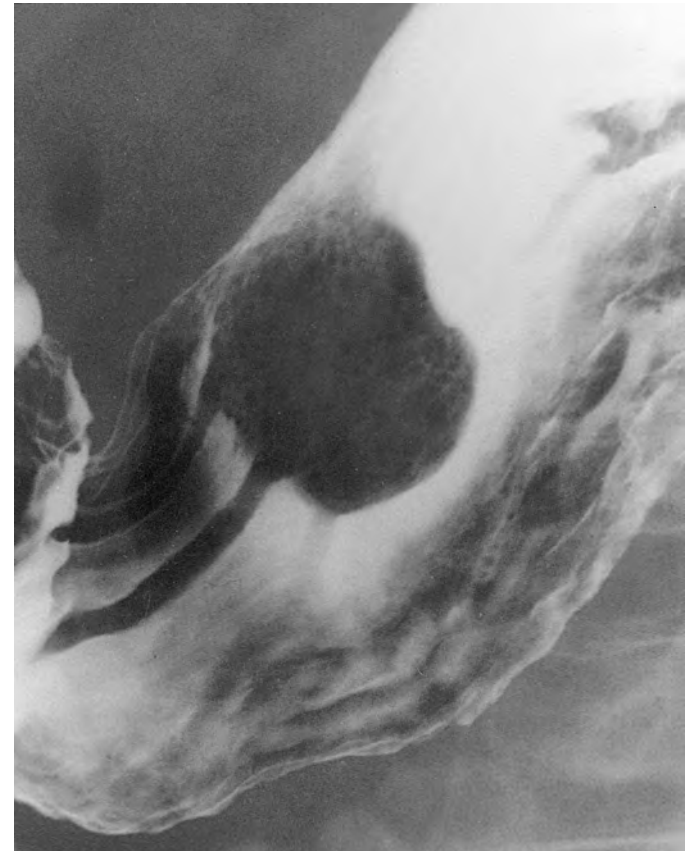
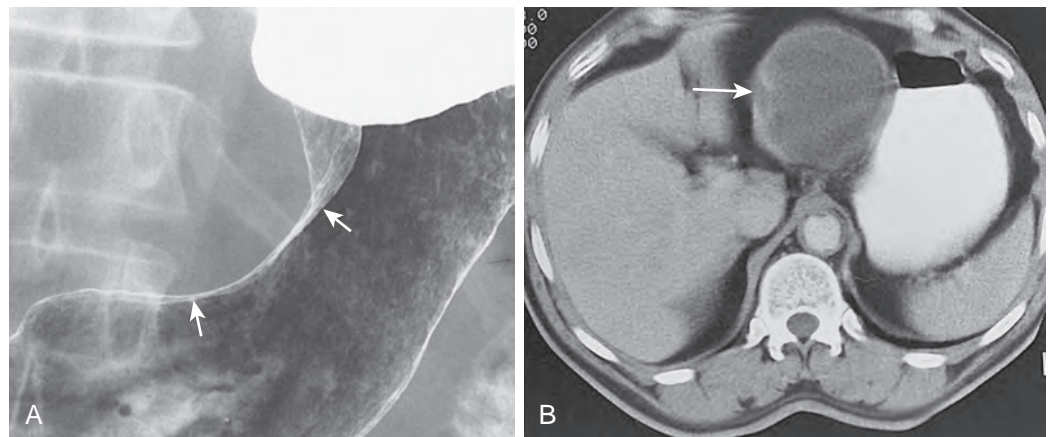


Figure 31-18 Gastric leiomyoblastoma. A large submucosal mass is present in the gastric body. This lesion is indistinguishable from a benign GIST.

Figure 31-19 Exogastric leiomyoblastoma. **A.** Barium study shows a smooth extrinsic impression (arrows) on the lesser curvature of the gastric body. **B.** CT scan shows a smooth, well-defined cystic mass (arrow) abutting the stomach. At surgery, this patient was found to have an exogastric leiomyoblastoma with cystic degeneration of the tumor. (Courtesy Kyunghee C. Cho, MD, Newark, NJ.)



leiomyoblastomas is occasionally manifested on CT by a cystic mass abutting the stomach (see Fig. 31-19B).^{63,64} Rarely, CT may show areas of calcification within the tumor.⁶⁴ The differential diagnosis for these lesions is discussed in detail in the previous section on GISTs.

LIPOMA

Gastric lipomas are rare tumors, accounting for only about 5% of GI tract lipomas and less than 1% of all gastric neoplasms.⁶⁵ Duodenal lipomas are even rarer. Most of these lesions are detected as incidental findings on barium study, endoscopy, or autopsy. Thus far, no cases of malignant degeneration of GI lipomas have been reported. Occasionally, however, lesions that are large or ulcerated may cause obstruction or bleeding. Although lipomas are difficult to differentiate on barium studies from other submucosal masses in the stomach or duodenum, CT has proved to be a valuable technique for diagnosing these lesions.

Pathology

Lipomas are composed of mature fat cells surrounded by a fibrous capsule. They tend to occur as solitary lesions, usually in the gastric antrum.⁶⁶⁻⁶⁸ About 95% are endogastric lesions

that arise in the submucosa and grow toward the lumen, whereas the remaining 5% are exogastric lesions that arise in the subserosa and grow outward from the stomach.⁶⁶ As lipomas enlarge, they may develop central ulcers caused by pressure necrosis of the overlying mucosa.⁶⁷

Clinical Findings

Small lipomas usually cause no symptoms, but larger lesions may undergo ulceration, causing abdominal pain or upper GI bleeding.^{66,67,69} Rarely, pedunculated antral lipomas that prolapse through the pylorus may cause intermittent gastric outlet obstruction with recurrent nausea and vomiting.⁶⁶ Small lipomas in asymptomatic patients can be followed without need for surgery. However, larger lesions that cause symptoms should be resected.⁶⁷

Radiographic Findings

Barium studies typically reveal a smooth submucosal mass or centrally ulcerated bull's-eye lesion indistinguishable from a benign GIST or other mesenchymal tumor (Fig. 31-20A).⁶⁸ Most gastric lipomas occur as isolated lesions in the antrum,⁶⁶⁻⁶⁸ but multiple lipomas are occasionally present in the stomach or duodenum.⁷⁰ Because lipomas have a soft consistency, the correct diagnosis can be suggested if the lesions change in size

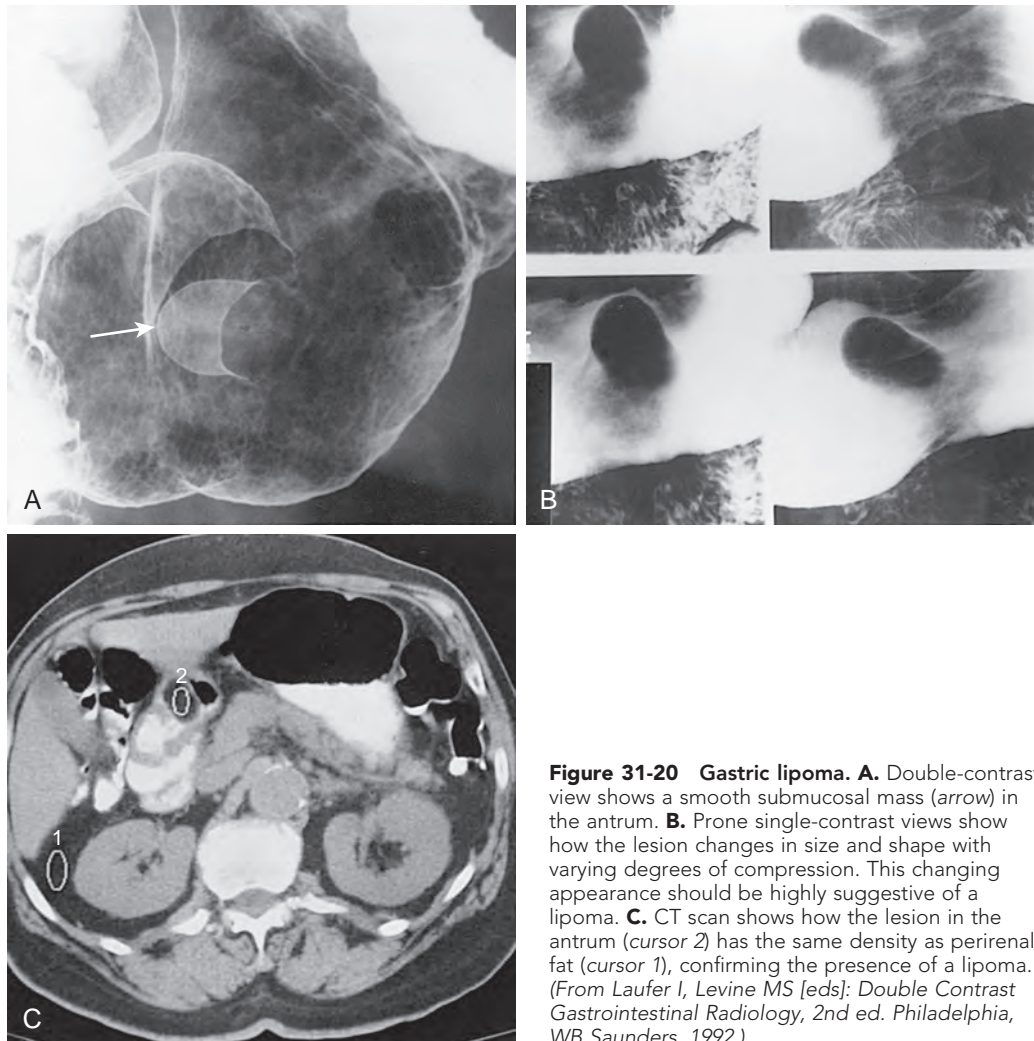


Figure 31-20 Gastric lipoma. **A.** Double-contrast view shows a smooth submucosal mass (arrow) in the antrum. **B.** Prone single-contrast views show how the lesion changes in size and shape with varying degrees of compression. This changing appearance should be highly suggestive of a lipoma. **C.** CT scan shows how the lesion in the antrum (cursor 2) has the same density as perirenal fat (cursor 1), confirming the presence of a lipoma. (From Laufer I, Levine MS [eds]: *Double Contrast Gastrointestinal Radiology*, 2nd ed. Philadelphia, WB Saunders, 1992.)

and shape at fluoroscopy (Fig. 31-20B).⁷⁰ Rarely, pedunculated antral lipomas may prolapse through the pylorus into the duodenum, acting as the lead point for a gastroduodenal intussusception.⁶⁸

CT has proved to be of considerable value for diagnosing GI lipomas.⁷¹⁻⁷⁵ These lesions typically appear on CT as well-circumscribed lesions of uniform fatty density with an attenuation of 70 to 120 HU (Fig. 31-20C).^{71,74} Occasionally, CT may reveal linear strands of soft tissue density or ulceration within the tumor.^{68,74} It should therefore be recognized that these findings can occur in a benign lipoma and are not signs of a liposarcoma, which is extremely rare in the GI tract. When a gastric or duodenal lipoma is definitively diagnosed by CT, unnecessary endoscopy or surgery can be avoided.

HEMANGIOMA

Hemangiomas constitute less than 2% of all benign tumors in the stomach. They are even rarer in the duodenum. The lesions may be classified as capillary hemangiomas composed of numerous tiny vascular structures or, less commonly, as cavernous hemangiomas composed of large blood spaces or sinusoids lined by endothelial tissue. It is uncertain whether these lesions are congenital malformations or true neoplasms capable of autonomous growth. They tend to occur as solitary lesions, but multiple hemangiomas may be present in the stomach, small bowel, and colon in patients with hemangiomatosis. Occasionally, GI hemangiomas are associated with telangiectasia of the skin.⁷⁶

Although sarcomatous changes are rarely found in GI hemangiomas, these highly vascular lesions are dangerous because of the risk of massive upper GI bleeding. Endoscopy typically reveals a bluish black submucosal lesion. Surgical resection is usually curative.

Radiographic Findings

Hemangiomas in the stomach typically appear on barium studies as smooth submucosal masses indistinguishable from GISTs or other mesenchymal tumors.⁷⁶ However, the presence of phleboliths within the lesion should be virtually pathognomonic of a hemangioma.⁷⁷ Such phleboliths are occasionally visible on abdominal radiographs, and their intimate relationship to the stomach may be confirmed on barium studies or CT.⁷⁷ The presence of other hemangiomas on the skin should also suggest the correct diagnosis.

LYMPHANGIOMA

Lymphangiomas are rare benign tumors of the stomach and duodenum.⁷⁸ These lesions consist histologically of irregularly dilated lymphatic channels lined by benign-appearing endothelial cells. Lymphangiomas are thought to be developmental malformations arising from sequestered lymphatic tissue.⁷⁸ They often have a cystic appearance because of progressive accumulation of fluid.

Although they may occur anywhere in the body, lymphangiomas rarely affect the GI tract. These lesions are usually detected as incidental findings in asymptomatic patients. Occasionally, however, they are large enough to cause obstruction or intussusception.⁷⁸ Gastric or duodenal lymphangiomas that cause symptoms should be resected.

Radiographic Findings

Lymphangiomas may appear on barium studies as smooth intramural masses indistinguishable from benign GISTs or other mesenchymal tumors in the stomach and duodenum.⁷⁸ Because of their cystic nature, these lesions may be pliable at fluoroscopy and are occasionally seen to change in shape with manual compression.⁷⁸ However, gastric and duodenal lipomas may produce identical findings.

GLOMUS TUMOR

Glomus tumors are derived from glomus bodies, specialized arteriovenous communications that regulate temperature in the skin.⁷⁹ Because glomus bodies are particularly abundant in the nail beds and pads of the finger tips and toes, glomus tumors are typically subungual in location. Rarely, glomus tumors are found in the stomach.⁷⁹⁻⁸¹

Most patients with glomus tumors in the stomach are asymptomatic. However, ulcerated tumors may cause upper GI bleeding.^{79,81} Local excision is usually curative, but these highly cellular lesions can appear malignant on frozen sections at the time of surgery, so an unnecessarily extensive resection is sometimes performed.^{79,80}

Radiographic Findings

Glomus tumors in the stomach usually occur as solitary lesions in the antrum, ranging from 1 to 4 cm in size.⁸⁰ These tumors appear on barium studies as smooth submucosal masses (with or without ulceration) that are indistinguishable from benign GISTs or other more common mesenchymal tumors in the stomach (Fig. 31-21).⁸² Occasionally, glomus

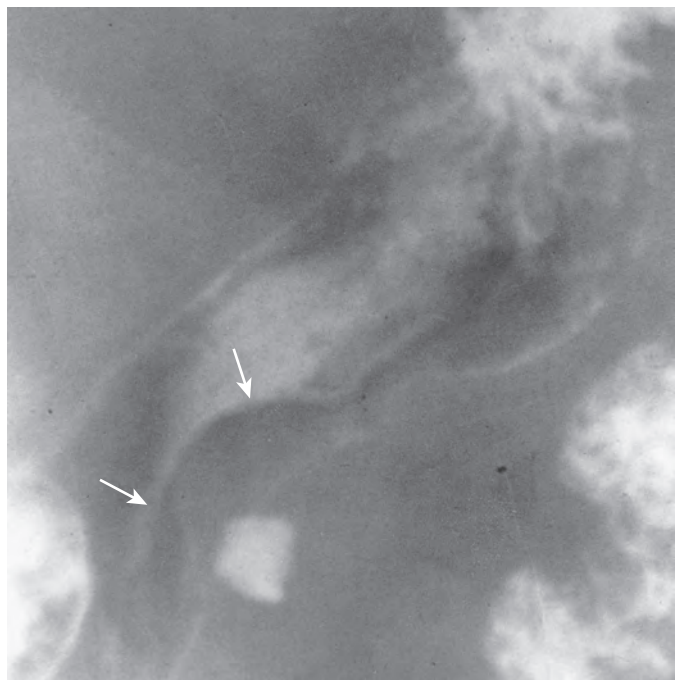


Figure 31-21 Glomus tumor. An ulcerated submucosal mass (arrows) is seen on the greater curvature of the antrum. This lesion cannot be distinguished from other more common mesenchymal tumors in the stomach. (Courtesy Bruce Knox, MD, Norfolk, VA.)

tumors contain tiny flecks of calcification.⁷⁹ These tumors also have a soft consistency, so they can be mistaken for lipomas because of their tendency to change in size and shape at fluoroscopy.⁸²

NEURAL TUMOR

Neural tumors constitute 5% to 10% of benign gastric neoplasms.¹ Most are nerve sheath tumors (schwannomas, neuromas, or neurilemmomas). The tumors are composed histologically of Schwann cells with elongated nuclei that have a palisade arrangement. As they outgrow their blood supply, these tumors may undergo central necrosis and ulceration, causing GI bleeding. Most nerve sheath tumors are benign, but sarcomatous changes have occasionally been reported.¹

Neurofibromas are other less common neural tumors in the stomach. These tumors arise from sympathetic nerves of the Auerbach myenteric plexus or, less frequently, the Meissner plexus.⁸³ Gastric neurofibromas are usually small lesions detected as incidental findings at surgery or autopsy. Occasionally, however, these tumors may cause epigastric pain, nausea, vomiting, or upper GI bleeding.⁸³ They tend to be isolated lesions, but multiple neurofibromas may be present in the stomach and duodenum in patients with generalized neurofibromatosis (von Recklinghausen's disease).^{84,85} This condition is characterized by cutaneous, intracranial, or intraspinal neurofibromas, skin pigmentation, bone abnormalities, and other congenital malformations. About 10% of neurofibromas in the stomach eventually undergo malignant degeneration.⁸³ The risk of malignancy seems to be greatest in lesions associated with generalized neurofibromatosis.

Radiographic Findings

Neural tumors in the stomach usually appear on barium studies as discrete submucosal masses (with or without ulceration) that are indistinguishable from benign GISTs or other mesenchymal tumors (Fig. 31-22). However, some exogastric lesions may grow outward from the stomach, projecting as lobulated masses into the peritoneal cavity.⁸³ Others may have an hourglass or dumbbell configuration.⁸³ Although they are rare lesions, gastric and duodenal neurofibromas should be suspected when multiple submucosal masses are found in the stomach and duodenum in patients with cutaneous neurofibromas or other stigmata of neurofibromatosis (Fig. 31-23).

GRANULAR CELL TUMOR

Granular cell tumors are rare benign tumors that occur predominantly in the skin, tongue, breast, and subcutaneous tissues.⁸⁶ These tumors originally were called granular cell myoblastomas, but subsequent histochemical and electron microscopic data have indicated that they have a neural derivation, arising from Schwann cells.⁸⁷ The lesions consist histologically of sheets of polygonal tumor cells containing an eosinophilic-staining granular cytoplasm.⁸⁷ About 7% of granular cell tumors are located in the GI tract, including the esophagus, stomach, colon, appendix, and biliary tree.⁸⁸ Granular cell tumors in the stomach are usually found unexpectedly at surgery or autopsy.⁸⁹ Occasionally, however, ulcerated lesions may cause epigastric pain or upper GI bleeding.⁸⁹ Surgical resection is almost always curative.

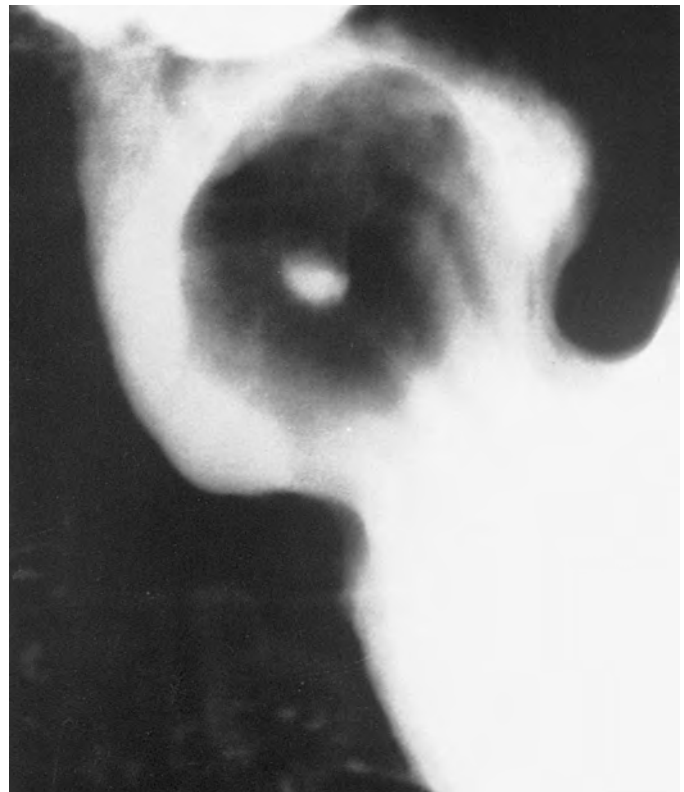


Figure 31-22 Gastric neurofibroma. An ulcerated submucosal mass is seen en face in the antrum. This lesion cannot be distinguished from an ulcerated GIST. (Courtesy Sat Somers, MD, Ontario, Canada.)



Figure 31-23 Duodenal neurofibromas in a patient with neurofibromatosis. Multiple submucosal masses are present in the first and second portions of the duodenum. This patient also had cutaneous neurofibromas and other stigmata of neurofibromatosis. (Courtesy Seth N. Glick, MD, Philadelphia.)

Radiographic Findings

Granular cell tumors in the stomach usually appear on barium studies as discrete submucosal masses, ranging from 0.5 to 2.5 cm in size.⁸⁹ Occasionally, multiple granular cell tumors are present in the stomach (Fig. 31-24).⁹⁰ Despite their rarity, granular cell tumors should be suspected when one or more submucosal lesions are found in the stomach in patients who have additional lesions involving the skin, tongue, or breast.

INFLAMMATORY FIBROID POLYP

Inflammatory fibroid polyps are uncommon submucosal lesions characterized histologically by whorls of fibrous tissue and blood vessels associated with an inflammatory infiltrate containing a high percentage of eosinophils.⁹¹ These lesions tend to occur in the stomach but are also found in the small bowel and colon. Because of the histologic findings, inflammatory fibroid polyps have also been called eosinophilic granulomas and fibromas with eosinophilic infiltration.⁹² However, inflammatory fibroid polyps are unrelated to eosinophilic granulomas of the lung or bone, which are composed primarily of histiocytes rather than fibroblasts. These lesions are not associated with a peripheral eosinophilia, as is eosinophilic gastroenteritis, a separate and more diffuse condition.

Although the pathogenesis is uncertain, it has been postulated that inflammatory fibroid polyps have an allergic or inflammatory origin and are therefore not true neoplasms. One theory is that a localized break in the mucosa incites an inflammatory response in the adjacent submucosa, with connective tissue proliferation in the form of a polypoid mass. Whatever their origin, inflammatory fibroid polyps are benign lesions without any known risk of malignant degeneration.

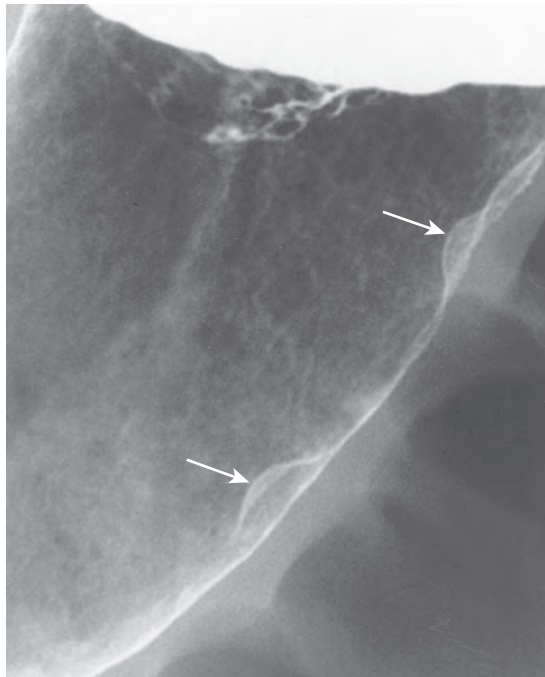


Figure 31-24 Granular cell tumors. Several small submucosal masses (arrows) are present on the greater curvature of the stomach. This patient had additional granular cell tumors on the tongue.

Clinical Findings

Most patients with inflammatory fibroid polyps are asymptomatic, but some may present with epigastric pain or upper GI bleeding because of superficial ulceration of these lesions.⁹¹ Rarely, pedunculated polyps in the distal antrum may cause intermittent gastric outlet obstruction.⁹¹

Radiographic Findings

Inflammatory fibroid polyps in the stomach are usually located in the antrum, occurring as solitary lesions that range from 1 to 5 cm in size.^{93,94} The lesions may appear on barium studies as sessile or, less frequently, pedunculated polyps with a smooth or slightly lobulated contour (Fig. 31-25).^{93,94} As a result, they may be indistinguishable from adenomatous polyps in the stomach. Other inflammatory fibroid polyps that have a submucosal appearance may be indistinguishable from benign GISTs.⁹⁴ When these lesions are pedunculated, they may occasionally prolapse through the pylorus, causing gastric outlet obstruction. Rarely, inflammatory fibroid polyps are larger or more lobulated, mimicking the appearance of polypoid gastric carcinomas.⁹¹

ECTOPIC PANCREATIC REST

Although they are not true neoplasms, ectopic pancreatic rests are included in this chapter because they are submucosal lesions that are difficult to distinguish from GISTs or other mesenchymal tumors in the stomach and duodenum. Most ectopic pancreatic rests are discovered as incidental findings in patients seeking medical attention for other reasons. It may be necessary to resect these lesions, however, if they cause symptoms or if a neoplastic condition cannot be excluded on radiologic or endoscopic examinations.

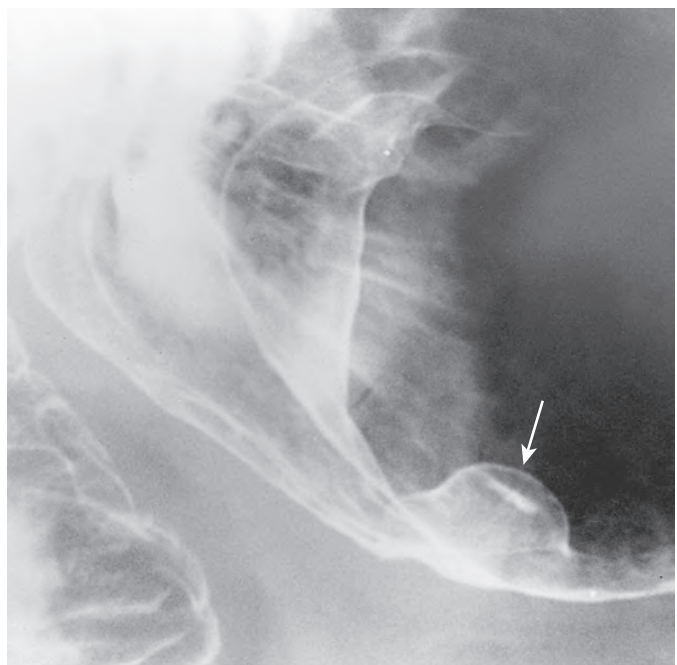


Figure 31-25 Inflammatory fibroid polyp. A sessile, slightly lobulated polyp (arrow) is seen on the greater curvature of the gastric antrum. This lesion is indistinguishable from an adenomatous polyp in the stomach.

Pathology

Ectopic pancreatic rests consist histologically of all pancreatic elements, including acini, ducts, and islet cells, but ductal structures tend to be arranged more haphazardly in these lesions than in normal pancreatic tissue. Ectopic pancreatic rests are thought to result from abnormal embryologic development in which fragments of the ventral or dorsal pancreatic anlage are implanted in the intestinal wall.⁹⁵ These primitive epithelial buds may undergo varying degrees of differentiation toward mature glandular tissue. The term *adenomyosis* has been used to encompass a histologic spectrum of lesions, ranging from undifferentiated glandular epithelium to well-differentiated pancreatic tissue.⁹⁶ Lesions consisting of poorly differentiated acinar and ductal structures have been called adenomyomas, whereas well-differentiated nodules of pancreatic tissue have been called ectopic, heterotopic, or aberrant pancreatic rests.⁹⁶

Ectopic pancreatic rests occur throughout the GI tract, but about 80% are located in the stomach, duodenum, or proximal jejunum.⁹⁷ Occasionally, this anomaly is found in the gallbladder, biliary tree, liver, spleen, omentum, mesentery, appendix, or mediastinum, or even in a Meckel's diverticulum.⁹⁸

Clinical Findings

Most patients with ectopic pancreatic rests in the stomach or duodenum are asymptomatic, but some may present with epigastric pain or upper GI bleeding.^{99,100} It has been postulated that complications result from irritation or ulceration of the adjacent gastric or duodenal mucosa by pancreatic secretions.⁹⁵ Occasionally, lesions arising near the pylorus may cause gastric outlet obstruction.¹⁰¹ Rarely, ectopic pancreatic rests develop the same diseases that affect normal pancreatic tissue, including pancreatitis, pseudocysts, and benign or malignant pancreatic tumors.¹⁰² Because upper GI symptoms are more likely to be caused by peptic ulcer disease or other unrelated disorders, this anomaly should not be accepted as the source of the patient's symptoms without careful radiographic or endoscopic evaluation of the entire stomach and duodenum. Ectopic pancreatic rests should be resected only if the patient is symptomatic or if a significant neoplasm cannot be excluded nonoperatively.

Radiographic Findings

Ectopic pancreatic rests in the stomach and duodenum usually appear on barium studies as smooth, broad-based submucosal masses, closely resembling benign GISTs or other mesenchymal tumors (Fig. 31-26).^{95,97,103,104} They almost always occur as solitary lesions, ranging from 1 to 3 cm in size.¹⁰⁴ Ectopic pancreatic rests in the stomach tend to be located on the greater curvature of the distal antrum within 1 to 6 cm from the pylorus (see Fig. 31-26),^{103,104} whereas duodenal lesions are most frequently found in the proximal duodenum between the duodenal bulb and papilla of Vater.

Ectopic pancreatic rests in the stomach and duodenum often contain a central umbilication or dimple, representing the orifice of a primitive ductal system.^{103,104} In about 50% of patients, this orifice is manifested by a central collection of barium, ranging from 1 to 5 mm in diameter and 5 to 10 mm in depth.¹⁰³ When viewed en face, these umbilicated lesions have the typical bull's-eye appearance of ulcerated GISTs or other mesenchymal tumors. Rarely, barium may reflux into rudimentary ductal structures that terminate in tiny club-shaped



Figure 31-26 Ectopic pancreatic rest. The lesion appears as a discrete submucosal mass (arrows) on the greater curvature of the distal antrum. This is a characteristic location for ectopic pancreatic rests. (From Laufer I, Levine MS [eds]: *Double Contrast Gastrointestinal Radiology*, 2nd ed. Philadelphia, WB Saunders, 1992.)

pouches, a finding that is almost pathognomonic of ectopic pancreatic rests.⁹⁵

Differential Diagnosis

The presence of a centrally umbilicated submucosal mass on the greater curvature of the distal gastric antrum within 1 to 6 cm from the pylorus should be highly suggestive of an ectopic pancreatic rest. Benign GISTs on the greater curvature may produce similar findings, but these lesions often contain areas of ulceration, and their location in the stomach is more variable. Other conditions such as metastatic disease and lymphoma may also be manifested by bull's-eye lesions, but these patients usually have multiple lesions in the stomach and duodenum, whereas ectopic pancreatic rests almost always occur as solitary lesions. Rarely, ectopic pancreatic rests that are found elsewhere in the stomach and are larger or more lobulated may be indistinguishable from benign or malignant gastric tumors.¹⁰⁵ If the radiographic findings are equivocal, endoscopy and biopsy should be performed for a more definitive diagnosis.

BRUNNER GLAND HYPERPLASIA (BRUNNER GLAND HAMARTOMA)

Brunner glands in the duodenum normally secrete an alkaline mucus that protects the mucosa from the damaging effects of acidic gastric juices entering the duodenum. Brunner gland hyperplasia is therefore thought to occur as a response to hypersecretion of acid in the stomach.¹⁰⁶ However, hyperchlorhydria has been documented by gastric analysis in less than 50% of patients with this condition,¹⁰⁷ so a causal relationship between gastric hyperacidity and Brunner gland hyperplasia has not been proved.

Pathology

Hyperplastic Brunner glands may be manifested grossly by diffuse enlargement of Brunner glands throughout the proximal duodenum or by massive enlargement of a single gland. In

the past, solitary lesions were called Brunner gland adenomas.^{108,109} However, pathologic examination of these lesions has revealed an intimate admixture of ducts, acini, smooth muscle, and adipose tissue without evidence of cellular atypia, so many investigators now believe that these lesions should be classified as hamartomas rather than as true neoplasms.^{110,111} Their hamartomatous origin is supported by the absence of malignant degeneration in these enlarged glands. Nevertheless, Brunner gland hamartomas are important because they can be mistaken for neoplastic lesions on radiologic or endoscopic examination and because they may occasionally cause symptoms.

Clinical Findings

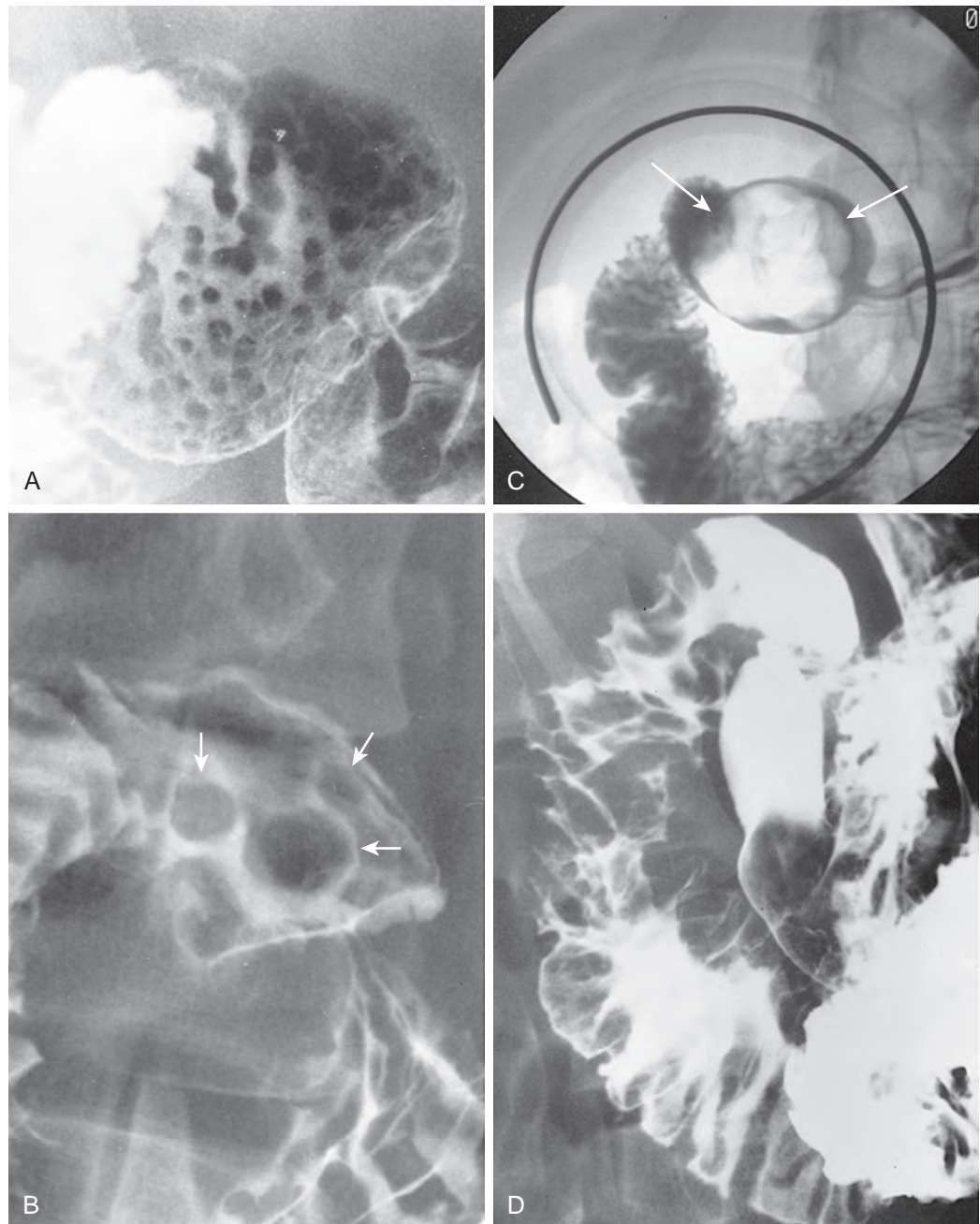
Except for its association with duodenal ulcers and gastric hypersecretory states,¹⁰⁶ the diffuse form of Brunner gland

hyperplasia has no clinical significance. In contrast, solitary Brunner gland hamartomas may occasionally cause obstructive symptoms, epigastric pain, or upper GI bleeding because of ulceration of the overlying mucosa.^{108,111,112} Although the diffuse form of Brunner gland hyperplasia requires no specific treatment, solitary lesions should be resected if they cause symptoms or if the pathologic diagnosis is in doubt.¹¹¹ An endoscopic polypectomy may be feasible if the lesion is small or pedunculated, but surgery may be required for larger lesions.^{111,112}

Radiographic Findings

The diffuse form of Brunner gland hyperplasia is manifested on barium studies by multiple small, rounded nodules in the proximal duodenum, producing a characteristic cobblestone or Swiss cheese appearance (Fig. 31-27A).^{113,114} The nodules

Figure 31-27 Brunner gland hyperplasia: spectrum of findings. **A.** Multiple tiny, rounded nodules are present in the duodenal bulb in a patient with diffuse Brunner gland hyperplasia. **B.** This patient has several Brunner gland hamartomas in the duodenum, manifested by submucosal masses (arrows) in the bulb. **C.** A large polypoid defect (arrows) is seen in the duodenal bulb in another patient with a giant Brunner gland hamartoma. **D.** A fourth patient with enlarged Brunner glands has markedly thickened, disorganized folds in the descending duodenum because of concomitant duodenitis. (**A** from Laufer I, Levine MS [eds]: *Double Contrast Gastrointestinal Radiology*, 2nd ed. Philadelphia, WB Saunders, 1992; **C** courtesy Jackie Brown, MD, Vancouver, Canada; **D** courtesy Dean D. T. Maglinte, MD, Indianapolis.)



tend to be most abundant in the duodenal bulb, with fewer nodules in the descending duodenum, so the lesions correspond to the normal anatomic distribution of Brunner glands.¹¹³ Occasionally, central flecks of barium may be identified in the nodules. In these cases, it has been postulated that these lesions represent chronic duodenal erosions in various stages of reepithelialization.¹¹⁵

Brunner gland hamartomas may appear as one or more submucosal or sessile lesions, ranging from several millimeters to several centimeters in size (Fig. 31-27B).^{109,111,113,114,116,117} Some patients with giant Brunner gland hamartomas may have large polypoid defects in the duodenum (Fig. 31-27C).¹¹⁸ Other patients with enlarged Brunner glands may have markedly thickened, irregular folds in the proximal duodenum because of concomitant duodenitis (Fig. 31-27D).¹¹⁷ Rarely, large intramural masses may cause mechanical obstruction of the duodenum or act as the lead point for a duodenojejunal intussusception.^{111,116,119}

Differential Diagnosis

The differential diagnosis for the diffuse form of Brunner gland hyperplasia includes the various polyposis syndromes, benign lymphoid hyperplasia, heterotopic gastric mucosa, and nodular duodenitis. Although the polyposis syndromes may be manifested by multiple rounded nodules in the duodenum, these patients almost always have a generalized intestinal polyposis, whereas Brunner gland hyperplasia is confined to the duodenum. Similarly, benign lymphoid hyperplasia is characterized by multiple small nodules in the duodenal bulb and proximal duodenum (Fig. 31-28).¹²⁰ However, these patients often have generalized lymphoid hyperplasia of the small bowel or colon. Unlike Brunner's glands, heterotopic gastric mucosa in the duodenum is characterized by angulated or polygonal 1- to 5-mm nodules or plaques that tend to be clustered near the base of the duodenal bulb (Fig. 31-29).^{121,122} Finally, nodular duodenitis may be manifested by thickened nodular folds that can resemble hyperplastic Brunner glands. However, the nodular folds tend to coalesce in the inflamed duodenum, whereas enlarged Brunner glands have more discrete borders.

Solitary Brunner gland hamartomas are difficult to distinguish from other polypoid lesions in the duodenum. Depending on their appearance, they can resemble mucosal lesions such as adenomatous polyps or submucosal lesions such as benign GISTs. Occasionally, prolapsed gastric mucosa in the duodenal bulb may produce a similar appearance. However, prolapsed mucosa is usually recognized as a mushroom-shaped defect at the base of the bulb that occurs as a transient finding at fluoroscopy (see Fig. 31-9). Rarely, a pedunculated polyp in the gastric antrum that has prolapsed into the duodenum can also be mistaken for a Brunner gland hamartoma.³

DUPLICATION CYST

Duplication cysts are hollow, epithelium-lined, spherical or tubular structures that are directly attached to some portion of the GI tract, usually the distal ileum.^{123,124} They tend to occur on the mesenteric border of the bowel, often sharing a common blood supply and muscular coat with the adjacent bowel wall. Most duplication cysts are spherical duplications that have no direct communication with the normal GI



Figure 31-28 Benign lymphoid hyperplasia. Innumerable tiny nodules are present in the duodenal bulb. This patient had hypogammaglobulinemia. (From Laufer I, Levine MS [eds]: *Double Contrast Gastrointestinal Radiology*, 2nd ed. Philadelphia, WB Saunders, 1992.)

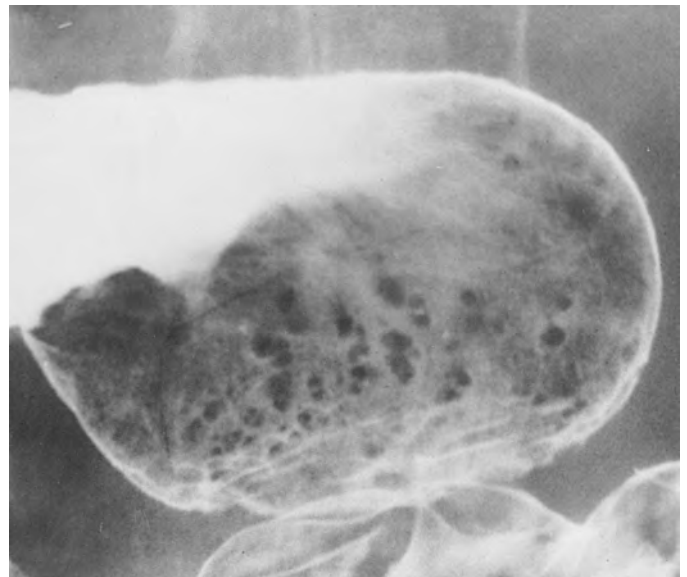


Figure 31-29 Heterotopic gastric mucosa in the duodenum. There are discrete, angulated filling defects near the base of the duodenal bulb. This appearance is so characteristic of heterotopic gastric mucosa that a confident diagnosis can be made on the basis of double-contrast studies without need for endoscopy. (From Laufer I, Levine MS [eds]: *Double Contrast Gastrointestinal Radiology*, 2nd ed. Philadelphia, WB Saunders, 1992.)

tract.^{124,125} However, the rare tubular form of duplication cyst may communicate with the GI lumen at its proximal or distal end.^{124,125}

Duplication cysts of the stomach and duodenum are uncommon lesions, comprising only 4% to 5% of all intestinal duplications.^{125,126} However, they may be associated with a variety of

complications such as bleeding, obstruction, or perforation. These lesions should therefore be surgically repaired or removed whenever feasible.

Pathology

GI duplication cysts are congenital malformations, probably resulting from faulty embryologic budding or defective recanalization of the alimentary tube during early fetal life.^{124,127,128} Histologically, they are fluid-filled cysts containing a well-developed smooth muscle layer and mucous membrane lining. This mucous membrane is usually identical to that of the parent bowel, but duplication cysts may occasionally contain gastric, intestinal, pancreatic, or even respiratory epithelium.^{124,129} When ectopic gastric mucosa is present in the cyst, secretion of peptic acid may cause ulceration or bleeding.¹²⁹ Depending on the volume of secretions within the cysts, they may vary from 1 to 25 cm in size.¹²⁹ Gastric duplication cysts usually arise from the greater curvature of the antrum or body,^{123,126} whereas duodenal duplication cysts usually arise from the medial aspect of the first or second portion of the duodenum.^{125,127,129}

Duplication cysts of the stomach and duodenum may be associated with a variety of other congenital anomalies, including intestinal or biliary atresia, malrotation, imperforate anus, double gallbladder, and double uterus. These patients also tend to have duplication cysts elsewhere in the GI tract.¹³⁰ Unlike mediastinal duplication cysts, those in the stomach and duodenum are rarely associated with hemivertebrae or other vertebral anomalies.^{126,129}

Clinical Findings

Gastric duplication cysts are twice as common in women as in men,¹³⁰ whereas duodenal duplication cysts have an approximately equal gender distribution.¹²⁷ Because most gastric duplication cysts cause symptoms during the first year of life, they are almost always diagnosed during early childhood.^{126,130} In contrast, 35% to 40% of duodenal duplication cysts are discovered in patients over 20 years of age.^{129,131}

Children or adults with duplication cysts of the stomach or duodenum typically present with a palpable abdominal mass and vomiting as the enlarging cyst encroaches on the adjacent stomach or duodenum.^{126,127,129,130} In infants with gastric duplication cysts, nonbilious vomiting may erroneously suggest hypertrophic pyloric stenosis.¹³² In contrast, duodenal duplication cysts tend to be associated with bilious vomiting.¹²⁵ Less frequently, older children or adults may present with abdominal pain, weight loss, fever, or upper GI bleeding.^{125-127,129,130} Abdominal pain most likely results from progressive distention of the cyst by its own secretions. Fever occurs if the cyst becomes infected. Upper GI bleeding is caused by localized pressure necrosis of the adjacent gastric or duodenal wall or by ulceration of a cyst that communicates directly with the stomach or duodenum.^{125,127} Occasionally, duodenal duplication cysts may compress the ampulla of Vater or the pancreatic or common bile ducts, causing acute pancreatitis or obstructive jaundice.^{127,129} Rarely, duplication cysts may present as surgical emergencies because of torsion or perforation of the cyst with associated peritonitis.^{129,133}

Because of these complications, duplication cysts of the stomach and duodenum should be treated surgically. Gastric duplication cysts can often be excised without difficulty from their attachment to the greater curvature of the stomach.¹³⁰

Because of their proximity to the ampulla of Vater, however, duodenal duplication cysts frequently cannot be resected without performing a pancreaticoduodenectomy and reconstructive biliary surgery. Alternatively, some surgeons prefer to create a window between the cyst and duodenum by excising a portion of the common wall between these structures to permit internal drainage and decompression of the cyst.^{125,129}

Radiographic Findings

Duplication cysts of the stomach and duodenum may occasionally be recognized on abdominal radiographs by curvilinear calcification in the cyst wall.^{134,135} However, calcification is more commonly seen in mesenteric, renal, or adrenal cysts.

Gastric duplication cysts typically appear on barium studies as intramural or extrinsic mass lesions involving the greater curvature or, less commonly, the posterior wall or lesser curvature of the gastric antrum (Fig. 31-30A).^{123,136} Similarly, duodenal duplication cysts may be recognized as smooth intramural or extrinsic masses involving the medial wall of the descending duodenum (Fig. 31-31).^{125,129,131} As gastric and duodenal duplication cysts enlarge, they may encroach considerably on the lumen of the stomach and duodenum, causing progressive obstruction. Rarely, communicating duplication cysts can be recognized as ovoid or tubular barium-filled structures adjacent to the stomach or duodenum because of opacification of the cyst lumen (Fig. 31-32).^{137,138}

Both ultrasonography and CT may be helpful in confirming the cystic nature of gastric and duodenal duplication cysts that are visualized indirectly on barium studies. These structures usually appear on ultrasound examination as sonolucent masses with strong posterior wall echoes and through-transmission.^{138,139} In some patients, the mucosal lining of the cyst is manifested by an echogenic inner ring surrounded by a relatively hypoechoic muscle layer.^{138,139} Echogenic internal components may occasionally be seen in cysts that are infected or hemorrhagic.¹³⁹ Duplication cysts can also be recognized by CT as thin-walled, fluid-filled structures abutting the greater curvature of the stomach or medial wall of the descending duodenum (see Fig. 31-30B).^{135,137,140} Rarely, CT may demonstrate cyst wall calcification or enteroliths within the cyst.¹⁴⁰

Differential Diagnosis

The finding on barium studies of a smooth intramural lesion on the greater curvature of the gastric antrum or medial wall of the descending duodenum should suggest the possibility of a duplication cyst, particularly in children. Other intramural lesions (e.g., benign GISTs, lipomas, or hematomas) or extrinsic lesions (e.g., pancreatic tumors or pseudocysts or choledochal cysts) involving the stomach or duodenum may produce similar findings. When duplication cysts are suspected on barium studies, ultrasonography or CT may be helpful for documenting the cystic nature of these structures. Other cystic lesions in the upper abdomen, such as choledochal cysts, mesenteric cysts, omental cysts, and pancreatic pseudocysts, may resemble duplication cysts on ultrasound or CT studies.^{139,140} Nevertheless, the finding of a cystic mass contiguous with the greater curvature of the stomach or medial wall of the duodenum, but separable from the gallbladder, extrahepatic biliary tree, and pancreas, should be highly suggestive of a duplication cyst.

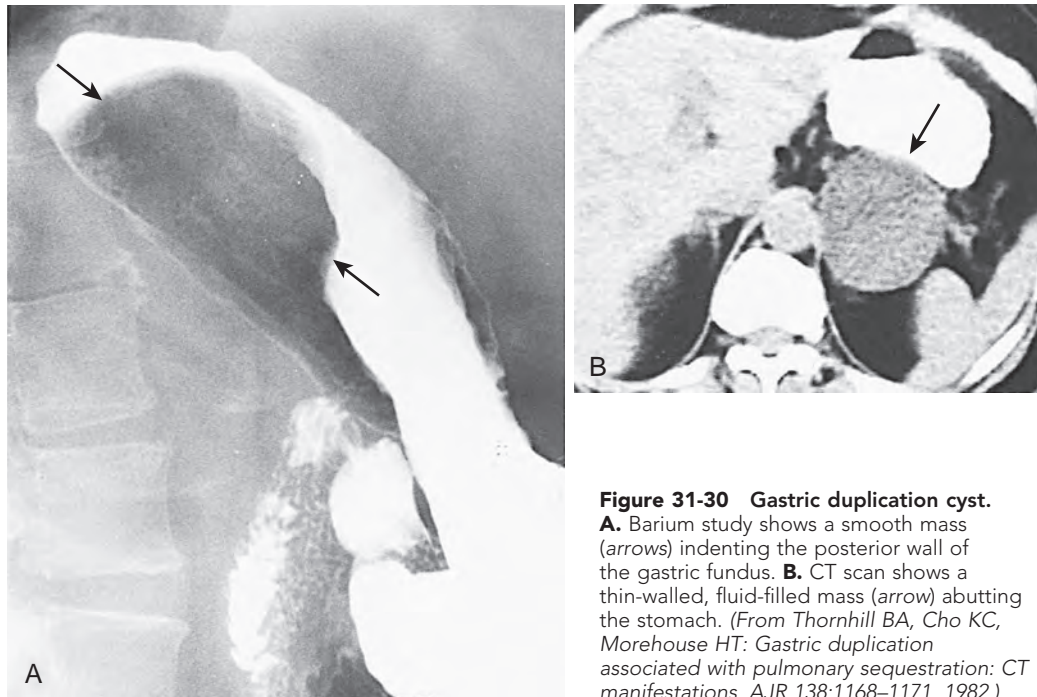


Figure 31-30 Gastric duplication cyst. **A.** Barium study shows a smooth mass (arrows) indenting the posterior wall of the gastric fundus. **B.** CT scan shows a thin-walled, fluid-filled mass (arrow) abutting the stomach. (From Thornhill BA, Cho KC, Morehouse HT: Gastric duplication associated with pulmonary sequestration: CT manifestations. *AJR* 138:1168–1171, 1982.)

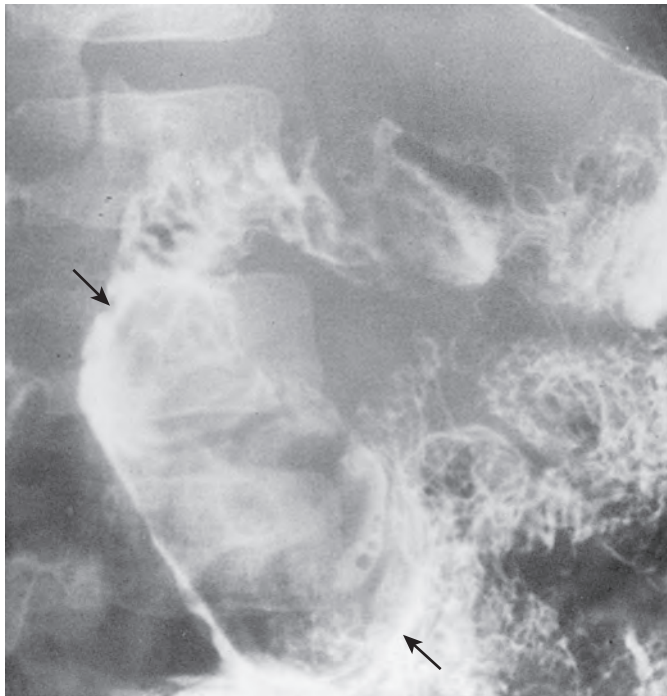


Figure 31-31 Duodenal duplication cyst. There is a large intramural mass (arrows) in the descending duodenum. Note the smooth contour of the lesion. An intramural hematoma or choledochal cyst could produce similar findings.

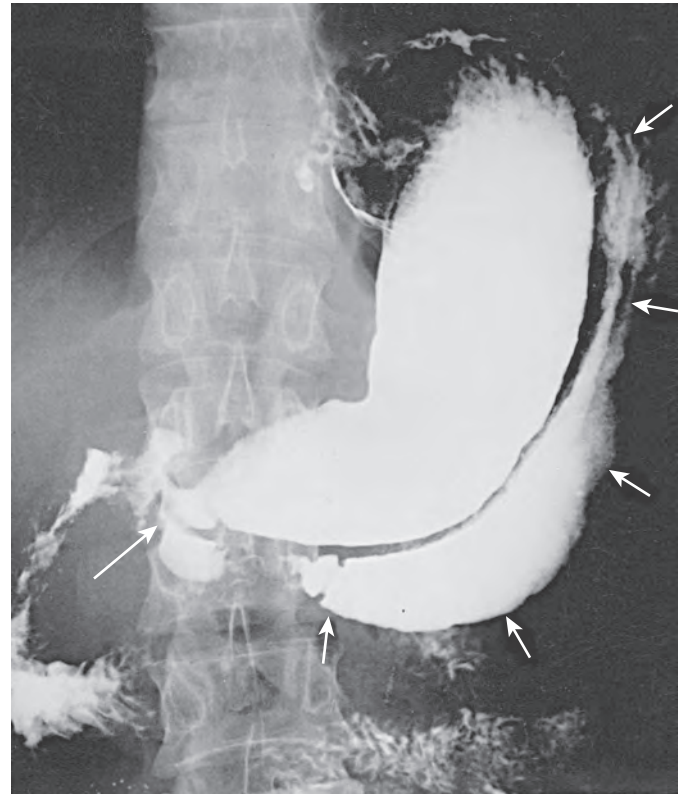


Figure 31-32 Communicating gastric duplication. Barium has entered a long, tubular duplication cyst (short arrows) on the greater curvature of the stomach. The duplication extends from the fundus to the pylorus, where it communicates with the lumen (long arrow). This form of duplication is extremely uncommon. (From Marshak RH, Lindner AE, Maklansky D [eds]: *Radiology of the Stomach*. Philadelphia, WB Saunders, 1983.)

REFERENCES

- Good CA: Benign tumors of the stomach and duodenal bulb. *J Can Assoc Radiol* 16:92-104, 1965.
- Ochsner SF, Janetos GP: Benign tumors of the stomach. *JAMA* 191:881-887, 1965.
- Marshak RH, Feldman F: Gastric polyps. *Am J Dig Dis* 10:909-935, 1965.
- Gordon R, Laufer I, Kressel HY: Gastric polyps found on routine double-contrast examination of the stomach. *Radiology* 134:27-30, 1980.
- Feczko PJ, Halpert RD, Ackerman LV: Gastric polyps: Radiological evaluation and clinical significance. *Radiology* 155:581-584, 1985.
- Ming S-C: The classification and significance of gastric polyps. In Yardly JH, Morson BC, Abell M, editors: *The Gastrointestinal Tract*, Baltimore, 1977, Williams & Wilkins, pp 149-175.
- Tomosulo J: Gastric polyps: Histologic types and their relationship to gastric carcinoma. *Cancer* 27:1346-1355, 1971.
- Ming S-C: The adenoma-carcinoma sequence in the stomach and colon: II. Malignant potential of gastric polyps. *Gastrointest Radiol* 1: 121-125, 1976.
- Ming S-C, Goldman H: Gastric polyps: A histogenetic classification and its relation to carcinoma. *Cancer* 18:721-726, 1965.
- Burt RW: Gastric fundic gland polyps. *Gastroenterology* 125:1462-1469, 2003.
- Iida M, Yao T, Watanabe H, et al: Fundic gland polyposis in patients without familial adenomatosis coli: Its incidence and clinical features. *Gastroenterology* 86:1437-1442, 1984.
- Tsuchigame T, Saito R, Ogata Y, et al: Clinical evaluation of gastric fundic gland polyps without familial polyposis coli. *Abdom Imaging* 20: 101-105, 1995.
- Iida M, Yao T, Itoh H, et al: Natural history of fundic gland polyposis in patients with familial adenomatosis coli/Gardner's syndrome. *Gastroenterology* 89:1021-1025, 1985.
- Joffe N, Antonioli DA: Atypical appearances of benign hyperplastic polyps. *AJR* 131:147-152, 1978.
- Op den Orth JO, Ploem S: The stalactite phenomenon on double contrast studies of the stomach. *Radiology* 117:523-525, 1975.
- Aronchick J, Laufer I, Glick SN: Barium stalactites: Observations on their nature and significance. *Radiology* 149:588-591, 1983.
- Smith HJ, Lee EL: Large hyperplastic polyps of the stomach. *Gastrointest Radiol* 8:19-23, 1983.
- Hizawa K, Iida M, Matsumoto T, et al: Natural history of fundic gland polyposis without familial adenomatosis coli: Follow-up observations in 31 patients. *Radiology* 189:429-432, 1993.
- Kikuchi Y, Levine MS, Laufer I, et al: Value of flow technique for double-contrast examination of the stomach. *AJR* 147:1183-1184, 1986.
- Op den Orth JO, Dekker W: Gastric adenomas. *Radiology* 141:289-293, 1981.
- Laxen F: Gastric carcinoma and pernicious anaemia in long-term endoscopic follow-up of subjects with gastric polyps. *Scand J Gastroenterol* 19:535-540, 1984.
- Borch K: Epidemiologic, clinicopathologic, and economic aspects of gastroscopic screening of patients with pernicious anemia. *Scand J Gastroenterol* 21:21-30, 1986.
- Bone GE, McClelland RN: Management of gastric polyps. *Surg Gynecol Obstet* 142:933-938, 1976.
- Kumar A, Quick CRG, Carr-Locke DL: Prolapsing gastric polyp, an unusual cause of gastric outlet obstruction: A review of the pathology and management of gastric polyps. *Endoscopy* 28:452-455, 1996.
- Lanza FL, Graham DY, Nelson RS, et al: Endoscopic upper gastrointestinal polypectomy: Report of 73 polypectomies in 63 patients. *Am J Gastroenterol* 75:345-348, 1981.
- ReMine SG, Hughes RW, Jr, Weiland LH: Endoscopic gastric polypectomies. *Mayo Clin Proc* 56:371-375, 1981.
- Hancock RJ: An 11-year review of primary tumours of the small bowel including the duodenum. *Can Med Assoc J* 103:1177-1179, 1970.
- Griffen WO, Schaefer JW, Schindler S, et al: Ampullary obstruction by benign duodenal polyps. *Arch Surg* 97:444-449, 1968.
- Deutschberger O, Tchertkoff V, Daino J, et al: Benign duodenal polyp: Review of the literature and report of a giant adenomatous polyp of the duodenal bulb. *Am J Gastroenterol* 38:75-84, 1962.
- Nelson JA, Sheft DJ, Minagi H, et al: Duodenal pseudopolyp: The flexural fallacy. *AJR* 123: 262-267, 1975.
- Burrell M, Toffler R: Flexural pseudolesions of the duodenum. *Radiology* 120:313-315, 1976.
- Schulten ME, Dyas R, Beal JM: Villous adenoma of the duodenum: A case report and review of the literature. *Am J Surg* 132:90-96, 1976.
- Mir-Madjlessi S-H, Farmer RG, Hawk WA: Villous tumors of the duodenum and jejunum: Report of four cases and review of the literature. *Am J Dig Dis* 18:467-476, 1973.
- Miller JH, Givsvold JJ, Weiland LH, et al: Upper gastrointestinal tract: Villous tumors. *AJR* 134:933-936, 1980.
- Kutim ND, Ranson JHC, Gouge TH, et al: Villous tumors of the duodenum. *Ann Surg* 181:164-168, 1975.
- Gaitini O, Kleinhaus U, Munichor M, et al: Villous tumors of the stomach. *Gastrointest Radiol* 13:105-108, 1988.
- Ring EJ, Ferucci JT, Eaton SB, et al: Villous adenoma of the duodenum. *Radiology* 104:45-48, 1972.
- Boyer CW: Adenoma of the duodenal bulb: A case report. *AJR* 90:753-755, 1963.
- Kilcheski T, Kressel HY, Laufer I, et al: The radiographic appearance of the stomach in Cronkhite-Canada syndrome. *Radiology* 141: 57-60, 1981.
- Salmela H: Smooth muscle tumors of the stomach. *Acta Chir Scand* 134:384-391, 1968.
- Kindblom LG, Remotti HE, Aldenborg F, et al: Gastrointestinal pacemaker cell tumor (GIPACT): Gastrointestinal stromal tumors show phenotypic characteristics of the interstitial cells of Cajal. *Am J Pathol* 152:1259-1269, 1998.
- Miettinen M, Sobin LH, Sarlomo-Rikala M: Immunohistochemical spectrum of GISTs at different sites and their differential diagnosis with a reference to CD117 (KIT). *Mod Pathol* 13:1134-1142, 2000.
- Delikaris P, Golematis B, Missitzis G, et al: Smooth muscle neoplasms of the stomach. *South Med J* 76:440-442, 1983.
- Morrissey K, Cho ES, Gray GE, et al: Muscular tumors of the stomach: Clinical and pathological study of 113 cases. *Ann Surg* 178:148-155, 1973.
- Tayiem AK: Recurrent massive gastrointestinal bleeding due to gastric leiomyoma. *J Kans Med Soc* 81:460-461, 1980.
- Suster S: Gastrointestinal stromal tumors. *Semin Diagn Pathol* 13:297-313, 1996.
- Sanders L, Silverman M, Rossi R, et al: Gastric smooth muscle tumors: Diagnostic dilemmas and factors affecting outcome. *World J Surg* 20:992-995, 1996.
- Grundy A, Rayter Z, Shorthouse AJ: Gastrogastric intussuscepting leiomyomas. *Gastrointest Radiol* 9:319-321, 1984.
- Crowther KS, Wyld L, Yamani Q, Jacob G: Gastroduodenal intussusception of a gastrointestinal stromal tumour. *Br J Radiol* 75:987-989, 2002.
- Crummey AB, Juhl JH: Calcified gastric leiomyoma. *AJR* 87:727-728, 1962.
- Graham JC, Blanchard IT, Scatliff JH: Calcified gastric leiomyoma presenting as a mediastinal mass. *AJR* 114:529-531, 1972.
- McGinnis GO: Adenocarcinoma of the stomach with calcification: A case report. *Gastroenterology* 39:90-93, 1960.
- O'Riordan D, Levine MS, Yeager BA: Complete healing of ulceration within a gastric leiomyoma. *Gastrointest Radiol* 10:47-49, 1985.
- Cho KJ, Reuter SR: Angiography of duodenal leiomyomas and leiomyosarcomas. *AJR* 135: 31-35, 1980.
- Herlinger H: The recognition of exogastric tumours: Report of six cases. *Br J Radiol* 39: 25-36, 1966.
- Reichardt P, Boukovinas I, Brodowicz T, et al: Adjuvant therapy in primary GIST: State-of-the-art. *Ann Oncol* 23:2776-2781, 2012.
- Lavin P, Hajdu SI, Foote FW: Gastric and extra-gastric leiomyoblastomas: Clinicopathologic study of 44 cases. *Cancer* 29:305-311, 1972.
- Appelman HD, Helwig EB: Gastric epithelioid leiomyoma and leiomyosarcoma (leiomyoblastoma). *Cancer* 38:708-728, 1976.
- Dalaker K, Harket R: Leiomyoblastoma (epithelioid leiomyoma) of the stomach. *Acta Chir Scand* 146:141-144, 1980.
- van Steenberg W, Kojima T, Geboes K, et al: Gastric leiomyoblastoma with metastases to the liver: A 36-year follow-up study. *Gastroenterology* 89:875-881, 1985.
- Faegenburg D, Farman J, Dallemard S: Leiomyoblastoma of the stomach. *Radiology* 117: 297-300, 1975.
- Kelsey JR: Leiomyoblastoma of the stomach presenting as acute intraperitoneal hemorrhage. *Gastroenterology* 51:539-541, 1966.
- Choi BI, Ok ID, Im JG, et al: Exogastric cystic leiomyoblastoma with unusual CT appearance. *Gastrointest Radiol* 13:109-111, 1988.
- Lerner ME, Farman J, Cho K, et al: Leiomyoblastoma: Varied CT appearance. *Clin Imaging* 16:194-197, 1992.
- Fernandez MJ, Davis RP, Nora PF: Gastrointestinal lipomas. *Arch Surg* 118:1081-1083, 1983.
- Turkington RW: Gastric lipoma: Report of a case and review of the literature. *Am J Dig Dis* 10:719-726, 1965.
- Maderal F, Hunter F, Fuselier G, et al: Gastric lipomas: An update of clinical presentation, diagnosis, and treatment. *Am J Gastroenterol* 79:964-967, 1984.

68. Taylor AJ, Stewart ET, Dodds WJ: Gastrointestinal lipomas: A radiologic and pathologic review. *AJR* 155:1205–1210, 1990.
69. Chu AG, Clifton JA: Gastric lipoma presenting as peptic ulcer: Case report and review of the literature. *Am J Gastroenterol* 78:615–618, 1983.
70. Deeths TM, Madden PN, Dodds WJ: Multiple lipomas of the stomach and duodenum. *Dig Dis* 20:771–774, 1975.
71. Megibow AJ, Redmond PE, Bosniak MA, et al: Diagnosis of gastrointestinal lipomas by CT. *AJR* 133:743–745, 1979.
72. Heiken JP, Forde KA, Gold RP: Computed tomography as a definitive method for diagnosing gastrointestinal lipomas. *Radiology* 142:409–414, 1982.
73. Imoto T, Nobe T, Koga M, et al: Computed tomography of gastric lipomas. *Gastrointest Radiol* 8:129–131, 1983.
74. Thompson WM, Keened AI, Levy AD: Imaging characteristics of gastric lipomas in 16 adult and pediatric patients. *AJR* 181:981–985, 2003.
75. Mendez-Uriburu L, Ahualli J, Mendez-Uriburu J, et al: CT appearances of intraabdominal and intrapelvic fatty lesions. *AJR* 183:933–943, 2004.
76. Kerekes ES: Gastric hemangiomas. *Radiology* 82:468–469, 1964.
77. Simms SM: Gastric hemangioma associated with phleboliths. *Gastrointest Radiol* 10:51–53, 1985.
78. Davis M, Fenoglio-Preiser C, Haque AK: Cavernous lymphangioma of the duodenum. *Gastrointest Radiol* 12:10–12, 1987.
79. Harig BM, Rosen Y, Dallemand S, et al: Glomus tumor of the stomach. *Am J Gastroenterol* 63:423–428, 1975.
80. Appelman HD, Helwig EB: Glomus tumors of the stomach. *Cancer* 23:203–213, 1969.
81. Weitzner S: Glomus tumor of the stomach: Report of a case and review of the literature. *Am J Gastroenterol* 51:322–328, 1969.
82. Schneider HJ: Glomus tumor of the stomach. *AJR* 92:1026–1028, 1964.
83. Banks BM: Neurofibroma of the stomach. *Gastroenterology* 41:158–167, 1950.
84. Perea VD, Gregory LJ: Neurofibromatosis of the stomach: Report of a case associated with von Recklinghausen's disease and review of the literature. *JAMA* 182:259–263, 1962.
85. Hoare AM, Elkington SG: Gastric lesions in generalized neurofibromatosis. *Br J Surg* 63:449–451, 1976.
86. Lack EE, Worsham GF, Callihan MD, et al: Granular cell tumor: A clinicopathologic study of 110 patients. *J Surg Oncol* 13:301–306, 1980.
87. Fisher ER, Wechsler H: Granular cell myoblastoma—a misnomer: Electron microscopic and histochemical evidence concerning its Schwann cell derivation and nature (granular cell schwannoma). *Cancer* 15:936–954, 1962.
88. Johnston J, Helwig EB: Granular cell tumors of the gastrointestinal tract and perianal region: A study of 74 cases. *Dig Dis Sci* 26:807–816, 1981.
89. Naidech HJ, Axelrod RS, Seliger G: Granular cell tumor (myoblastoma) of the stomach. *AJR* 113:245–247, 1971.
90. Schwartz DT, Gaetz HP: Multiple granular cell myoblastomas of the stomach. *Am J Clin Pathol* 44:453–457, 1965.
91. Carlson E, Ward JG: Inflammatory gastric polyps (eosinophilic granulomas of the stomach). *Am J Surg* 99:352–357, 1960.
92. Salm R: Gastric fibroma with eosinophilic infiltration. *Gut* 6:85–91, 1965.
93. Allman RN, Cavanagh RC, Helwig EB, et al: Inflammatory fibroid polyp. *Radiology* 127:69–73, 1978.
94. Harned RK, Buck JL, Shekitka KM: Inflammatory fibroid polyps of the gastrointestinal tract: Radiologic evaluation. *Radiology* 182:863–866, 1992.
95. Besemann EF, Auerbach SH, Wolfe WW: The importance of roentgenologic diagnosis of aberrant pancreatic tissue in the gastrointestinal tract. *AJR* 107:71–76, 1969.
96. Bush WH, Hall DG, Ward BH: Adenomyosis of the gastric antrum in children. *Radiology* 111:179–181, 1974.
97. Copleman B: Aberrant pancreas in the gastric wall. *Radiology* 81:107–111, 1963.
98. Martinez LO, Gregg M: Aberrant pancreas in the gallbladder. *J Can Assoc Radiol* 24:234–235, 1973.
99. Tonkin RD, Field TE, Wykes PR: Pancreatic heterotopia as a cause of dyspepsia. *Gut* 3:135–139, 1962.
100. Clark RE, Teplick SK: Ectopic pancreas causing massive gastrointestinal hemorrhage: Report of a case diagnosed angiographically. *Gastroenterology* 69:1331–1333, 1975.
101. Matsumoto Y, Kawai Y, Kimura K: Aberrant pancreas causing pyloric obstruction. *Surgery* 76:827–829, 1974.
102. Green PHR, Barratt PJ, Percy JB, et al: Acute pancreatitis occurring in gastric aberrant pancreatic tissue. *Am J Dig Dis* 22:734–740, 1977.
103. Kilman WJ, Berk RN: The spectrum of radiographic features of aberrant pancreatic rests involving the stomach. *Radiology* 123:291–296, 1977.
104. Thoeni RF, Gedgudas RK: Ectopic pancreas: Usual and unusual features. *Gastrointest Radiol* 5:37–42, 1980.
105. Shah A, Gordon AR, Ginsberg GG, et al: Ectopic pancreatic rest in the proximal stomach mimicking gastric neoplasms. *Clin Radiol* 62:600–602, 2007.
106. Franzin G, Musola R, Ghidini O, et al: Nodular hyperplasia of Brunner's glands. *Gastrointest Endosc* 31:374–378, 1985.
107. Kaplan EL, Dyson WL, Fitts WT: The relationship of gastric hyperacidity to hyperplasia of Brunner's glands. *Arch Surg* 98:636–639, 1969.
108. Nelson OE, Whitaker EG, Roberts FM: Adenoma of Brunner's glands. *Am J Surg* 110:977–980, 1965.
109. Osborne R, Toffler R, Lowman RM: Brunner's gland adenoma of the duodenum. *Am J Dig Dis* 18:689–694, 1973.
110. ReMine WH, Brown PW, Gomes MMR, et al: Polypoid hamartomas of Brunner's glands. *Arch Surg* 100:313–316, 1970.
111. Strutynsky N, Posniak R, Mori K: Obstructing hamartoma of Brunner's glands of the duodenum. *Dig Dis Sci* 27:279–282, 1982.
112. Ponka JL, Shaalan AK: Massive gastrointestinal hemorrhage secondary to tumors of Brunner's glands. *Am J Surg* 108:51–56, 1964.
113. Dodd GD, Fishler JS, Park OK: Hyperplasia of Brunner's glands: Report of two cases with review of the literature. *Radiology* 60:814–823, 1953.
114. Weinberg PE, Levin B: Hyperplasia of Brunner's glands. *Radiology* 84:259–262, 1965.
115. Walk L: Nodular hyperplasia of duodenal Brunner's glands—does it exist? *Endoscopy* 14:162–165, 1982.
116. Maglinte DD, Mayes SL, Ng AC, et al: Brunner's gland adenoma: Diagnostic considerations. *J Clin Gastroenterol* 4:127–131, 1982.
117. Merine D, Jones B, Ghahremani GG, et al: Hyperplasia of Brunner glands: The spectrum of its radiographic manifestations. *Gastrointest Radiol* 16:104–108, 1991.
118. van Rooij WJJ, van der Horst JJ, Stuijbergen WNHM, et al: Extreme diffuse adenomatous hyperplasia of Brunner's glands: Case report. *Gastrointest Radiol* 15:285–287, 1990.
119. Lempke RE: Intussusception of the duodenum: Report of a case due to Brunner's gland hyperplasia. *Ann Surg* 150:160–166, 1959.
120. Govoni AF: Benign lymphoid hyperplasia of the duodenal bulb. *Gastrointest Radiol* 1:267–269, 1976.
121. Langkemper R, Hoek AC, Dekker W, et al: Elevated lesions in the duodenal bulb caused by heterotopic gastric mucosa. *Radiology* 137:621–624, 1980.
122. Agha FP, Ghahremani GG, Tsang TK, et al: Heterotopic gastric mucosa in the duodenum: Radiographic findings. *AJR* 150:291–294, 1988.
123. Kremer RM, Lepoff RB, Izant RJ: Duplication of the stomach. *J Pediatr Surg* 5:360–364, 1970.
124. Taft DA, Hairston JT: Duplication of the alimentary tract. *Am Surg* 42:455–462, 1976.
125. Soper RT, Selke AC: Duplication cyst of the duodenum: Case report and discussion. *Surgery* 68:562–566, 1970.
126. Pruksapong C, Donovan RJ, Pinit A, et al: Gastric duplication. *J Pediatr Surg* 14:83–85, 1979.
127. Inouye WY, Farrell C, Fitts WT, et al: Duodenal duplication: Case report and literature review. *Ann Surg* 162:910–916, 1965.
128. Agha FP, Gabriele OF, Abdulla FH: Complete gastric duplication. *AJR* 137:406–407, 1981.
129. Thompson NW, Labow SS: Duplication of the duodenum in the adult. *Arch Surg* 94:301–306, 1967.
130. Bartels RJ: Duplication of the stomach. *Am Surg* 33:747–752, 1967.
131. Faegenburg D, Bosniak M: Duodenal anomalies in the adult. *AJR* 88:642–657, 1962.
132. Kammerer M: Duplication of the stomach resembling hypertrophic pyloric stenosis. *JAMA* 207:2101–2102, 1969.
133. Kleinhaus S, Boley SJ, Winslow P: Occult bleeding from a perforated gastric duplication in an infant. *Arch Surg* 116:122, 1981.
134. Alford BA, Armstrong P, Franken EA, et al: Calcification associated with duodenal duplications in children. *Radiology* 134:647–648, 1980.
135. Omojola MF, Hood IC, Stevenson GW: Calcified gastric duplication. *Gastrointest Radiol* 5:235, 1980.
136. Bower RJ, Sieber WK, Kiesewetter WB: Alimentary tract duplications in children. *Ann Surg* 188:669–674, 1978.
137. McAlister WH, Siegel MJ: Duodenal duplication. *AJR* 152:1328–1329, 1989.
138. Hulnick DH, Balthazar EJ: Gastric duplication cyst: GI series and CT correlation. *Gastrointest Radiol* 12:106–108, 1987.
139. Kangaroo H, Sample WF, Hansen G, et al: Ultrasonic evaluation of abdominal gastrointestinal tract duplication in children. *Radiology* 131:191–194, 1979.
140. Bar-Ziv J, Katz R, Nobel M, et al: Duodenal duplication cyst with enteroliths: Computed tomography and ultrasound diagnosis. *Gastrointest Radiol* 14:220–222, 1989.

Carcinoma of the Stomach and Duodenum

MARC S. LEVINE | ALEC J. MEGIBOW | MICHAEL L. KOCHMAN

CHAPTER OUTLINE

Gastric Carcinoma

Epidemiology

Dietary Factors

Pathology

Routes of Spread

Clinical Findings

Endoscopic Findings

Radiographic Findings

Carcinoma of the Cardia

Computed Tomographic Findings

Differential Diagnosis

Staging

Treatment and Prognosis

Duodenal Carcinoma

Gastric Carcinoma

There has been a dramatic decline in the incidence of gastric carcinoma since the late 1940s.¹⁻⁴ Nevertheless, it remains a deadly disease, with overall 5-year survival rates of less than 20%.⁴⁻⁸ Since the 1980s, attention has been focused on the role of double-contrast barium studies and endoscopy for the early diagnosis of gastric cancer. The Japanese have had tremendous success in detecting early gastric cancer by mass screening of the adult population with these techniques. However, it is difficult to justify such screening programs outside Japan because of the lower incidence of this malignancy. Thus, the prognosis for gastric carcinoma remains dismal in most parts of the world.

EPIDEMIOLOGY

Gastric carcinoma has striking geographic variations, with the highest incidences reported in Japan, Chile, Finland, Poland, and Iceland.^{3,8} However, Japanese immigrants and their offspring living in the United States have a significantly lower incidence of gastric cancer than those living in Japan.^{8,9} Such epidemiologic data suggest that environmental factors have a major role in the development of gastric carcinoma. Dietary habits may be particularly important in explaining the observed geographic differences in cancer risk. *Helicobacter pylori* infection of the stomach has also increasingly been implicated as a major risk factor in the development of gastric carcinoma in various parts of the world. Other predisposing conditions include atrophic gastritis, pernicious anemia, gastric polyps, partial gastrectomy, Ménétrier's disease, and hereditary factors. These risk factors for gastric cancer are discussed separately in the following sections.

DIETARY FACTORS

Studies have shown that diets rich in salted, smoked, or poorly preserved foods are associated with an increased risk of gastric cancer,^{4,10,11} whereas diets rich in fruits and vegetables are associated with a decreased risk.^{4,12} Foods containing nitrates or nitrites have also been implicated in the development of gastric cancer.^{4,9} These compounds are converted by bacteria to nitrosamines, which are thought to have a carcinogenic effect on the stomach.¹³ Thus, populations with a higher average intake of nitrates and nitrites probably have a higher gastric cancer risk. Conversely, vitamin C (ascorbic acid) appears to have a protective effect by reducing nitrites to nitric oxide and preventing the formation of nitrosamine compounds.¹⁴ This could explain why the consumption of fruit and vegetables is associated with a lower risk of developing gastric cancer. One study also found that a high intake of cereal fiber is associated with a significantly lower risk of carcinoma of the cardia,¹⁵ possibly because of the nitrite-scavenging properties of cereal fiber.

Helicobacter pylori Gastritis

H. pylori has increasingly been implicated as a major risk factor in the pathogenesis of gastric carcinoma; *H. pylori* is thought to be the leading cause of gastric cancer worldwide.¹⁶ Various studies have found that people with *H. pylori* gastritis have a two to six times greater risk of developing gastric cancer than those without this infection.¹⁷⁻¹⁹ It has been well documented that people with long-standing *H. pylori* gastritis are more likely to develop atrophic gastritis.^{16,20,21} Over a period of years, chronic atrophic gastritis may progress to gastric atrophy, intestinal metaplasia, dysplasia, and, eventually, gastric carcinoma.^{4,22-24} Other studies have found that people with *H. pylori* gastritis are more likely to develop the intestinal type of gastric carcinoma than people without this infection (see later, "Gastric Carcinoma: Pathology").^{25,26} It has also been shown that certain strains of *H. pylori*, which produce a vacuolating cytotoxin, cytotoxin-associated gene A (*cagA*), are associated with a higher prevalence of atrophic gastritis and gastric carcinoma.^{27,28} A meta-analysis of 16 studies from the literature found that infection with *cagA*-positive strains of *H. pylori* substantially increased the risk of gastric cancer compared to the risk associated with *H. pylori* infection irrespective of *cagA* status.²⁹

Nevertheless, gastric cancer develops in only a tiny percentage of all people with *H. pylori* gastritis, so other genetic or environmental factors presumably have a role in cancer pathogenesis. In a cost-effectiveness model, Parsonnet and colleagues found that widespread screening and treatment of adults for *H. pylori* is a potentially cost-effective strategy for the prevention of gastric cancer, particularly in high-risk populations.³⁰

However, further investigation is needed to determine whether such an approach is justified.

Atrophic Gastritis

Atrophic gastritis has been classified into two types, which have different histologic, immunologic, and secretory characteristics. Type A gastritis is usually associated with pernicious anemia (see next section). In contrast, type B gastritis (which is more common) predominantly involves the antrum and usually results from mucosal injury by *H. pylori* or, less commonly, by other toxic agents (see Chapter 30).³¹ Long-term studies indicate that about 10% of patients with type B gastritis develop gastric carcinoma within 10 to 20 years.^{32,33} It has been postulated that chronic atrophic gastritis leads to the development of intestinal metaplasia, dysplasia, and, eventually, adenocarcinoma.^{4,22,23} This pathologic sequence of events is supported by the frequent association of gastric carcinoma and intestinal metaplasia on surgical specimens.^{22,23} Thus, chronic atrophic gastritis and intestinal metaplasia are thought to be important precursor conditions for the development of gastric carcinoma.

Pernicious Anemia

Type A gastritis predominantly involves the gastric fundus and body and is usually thought to result from immunologic injury by antiparietal cell antibodies in patients with pernicious anemia.³¹ This type of gastritis may also be associated with an increased risk of gastric cancer. In various studies, the incidence of gastric cancer in patients with pernicious anemia has been two to three times greater than that expected for the general population.^{34,35} Most such tumors involve the gastric fundus or body. Although some investigators advocate radiologic or endoscopic surveillance of patients with known pernicious anemia, others believe that the cancer risk is not high enough to warrant routine surveillance.³⁶ Nevertheless, any patient with pernicious anemia who has guaiac-positive stool or other upper gastrointestinal (GI) complaints should be aggressively evaluated for possible gastric carcinoma.

Gastric Polyps

Adenomatous polyps account for less than 20% of all gastric polyps.³⁷ Despite their rarity, these polyps are premalignant lesions that are capable of undergoing malignant degeneration via an adenoma-carcinoma sequence similar to that found in the colon.³⁸ Nearly 50% of gastric adenomas larger than 2 cm are found to harbor carcinomatous foci.^{39,40} All adenomatous polyps should therefore be resected because of the risk of malignant transformation. Nevertheless, adenocarcinoma is about 30 times more common than adenomatous polyps in the stomach, so most gastric cancers are thought to originate *de novo* and not from preexisting polyps.³⁸

Partial Gastrectomy

Patients who undergo partial gastrectomy appear to be at increased risk for the development of gastric carcinoma. A gastric stump cancer is defined as a primary carcinoma of the gastric remnant occurring a minimum of 5 years after partial gastrectomy for gastric ulcers or other benign disease.⁴¹ Affected individuals have usually undergone a Billroth II rather than a Billroth I procedure.^{42,43} These tumors tend to be located in the distal portion of the gastric remnant near the gastrojejunal anastomosis. It has been postulated that recurrent bile reflux

above the anastomosis causes chronic gastritis, intestinal metaplasia, and, eventually, gastric carcinoma. In various studies, the mortality from gastric cancer 15 years or more after partial gastrectomy has been three to seven times greater than that expected for the general population.⁴³⁻⁴⁵ Some authors therefore advocate routine endoscopic surveillance of the gastric remnant starting 15 years after surgery.⁴⁵ However, other investigators have found no greater incidence of gastric carcinoma than that expected for the general population as long as 25 years after surgery.⁴⁶ Thus, the need for surveillance in these patients remains controversial.

Gastric carcinoma has also been reported as a late complication of gastrojejunostomy for benign disease in the absence of partial gastrectomy.^{47,48} As in patients who have undergone a Billroth II procedure, bile reflux gastritis and intestinal metaplasia are thought to be predisposing factors. Whatever the explanation, the risk of developing gastric carcinoma also appears to be increased in patients who undergo a gastrojejunostomy without a gastric resection.

Ménétrier's Disease

Ménétrier's disease is a rare disorder of unknown etiology characterized by a hypertrophic gastropathy associated with decreased gastric acid secretion and a protein-losing enteropathy (see Chapter 30). Anecdotal cases of gastric carcinoma have been described in patients with Ménétrier's disease.⁴⁹ However, it is unclear whether this association is coincidental or whether Ménétrier's disease is a premalignant condition.

Hereditary Factors

Hereditary factors have also been implicated in the development of gastric cancer because a positive family history has been associated with an increased risk of this malignancy.⁵⁰ In one study, the prevalence of *H. pylori* gastritis was significantly higher in subjects who had parents with gastric cancer than in other subjects.⁵¹ Such findings suggest that familial aggregation of gastric cancer may be explained at least partly by familial clustering of *H. pylori* gastritis. Patients with gastric cancer also have been found to have a higher frequency of blood type A and a lower frequency of blood type O than the general population.⁵²

PATHOLOGY

Gross Features

Most gastric carcinomas are polypoid or ulcerated lesions.⁵³⁻⁵⁵ Polypoid carcinomas have a plaque-like, lobulated, or fungating appearance. Ulcerated carcinomas may contain deep, irregular or broad, shallow areas of ulceration caused by necrosis and excavation of the tumor.⁵³ The ulcer may be surrounded by a thin rind of malignant tissue or by an obvious mass lesion, so many polypoid tumors have ulcerated components. Less commonly, gastric carcinomas may be diffusely infiltrative lesions that spread along the gastric wall with relatively little intraluminal growth.⁵³ These scirrhous tumors may produce a classic linitis plastica appearance because of submucosal thickening and fibrosis incited by the tumor. Other gastric carcinomas may be superficial spreading lesions that are confined to the mucosa or submucosa without invading the deep muscle layers of the gastric wall.⁵³

Rarely, patients with gastric carcinoma have multiple primary lesions separated by normal intervening mucosa. In various

series, two or more synchronous tumors have been found in 2% to 8% of all patients with gastric cancer.^{56,57} In such cases, individual lesions may have different morphologic features.

Histologic Features

More than 95% of malignant neoplasms in the stomach are adenocarcinomas.³ The remaining lesions consist of lymphoma, gastrointestinal stromal tumors (GISTs), Kaposi's sarcoma, carcinoid, and other rare malignant tumors (see Chapter 33). Gastric carcinomas may be classified into two types: (1) an intestinal type characterized by well-formed glandular structures that tend to grow in a fungating manner; and (2) a diffuse type characterized by poorly cohesive cells that tend to infiltrate and thicken the gastric wall without producing a discrete mass.⁵⁸ Intestinal-type lesions are more likely to involve the distal stomach and are often associated with underlying atrophic gastritis. In contrast, diffuse-type lesions are more likely to involve the entire stomach (especially the gastric cardia) and tend to have a worse prognosis.⁵⁹

Gastric carcinomas have been further classified by the World Health Organization into the following subtypes—papillary, tubular, mucinous, and signet ring cell.⁶⁰ Most tumors that are capable of forming glandular structures secrete mucinous substances and, occasionally, excessive mucin accumulates extracellularly in colloid or mucinous adenocarcinomas.⁵³ Other adenocarcinomas are composed of distinctive signet ring cells containing large amounts of intracytoplasmic mucin and compressed, eccentric nuclei.⁵³ As they infiltrate the gastric wall, these signet ring cells often incite a desmoplastic response in the submucosa and muscularis propria, producing the classic pathologic features of a primary scirrhous carcinoma. In various series, scirrhous tumors have been found to account for 5% to 15% of all gastric cancers.^{5,7}

Most adenocarcinomas of the stomach are diagnosed at an advanced stage. By definition, advanced gastric cancers have already invaded the muscularis propria. These tumors are usually associated with metastases to regional lymph nodes or other local or distant structures. In contrast, early gastric cancers are defined histologically as cancers in which malignant invasion is limited to the mucosa or submucosa, regardless of the presence or absence of lymph node metastases.^{61,62} The largest number of early gastric cancers has been reported in Japan as a result of mass screening of the adult population. Unlike advanced carcinomas, which have a dismal prognosis, early gastric cancers are curable lesions with 5-year survival rates greater than 90% (see later, “[Treatment and Prognosis](#)”).

Distribution

At one time, most gastric carcinomas were located in the antrum.⁶³ Since the late 1940s, however, there has been a gradual shift in the distribution of gastric cancer from the antrum proximally to the body and fundus.^{1,63,64} This changing distribution has been attributed primarily to a rising incidence of carcinoma of the gastric cardia, which has increased at a rate exceeding that of any other cancer.^{4,65-67} As a result, these tumors now have a relatively even distribution in the stomach, with about 30% located in the antrum, 30% in the body, and 40% in the fundus or cardiac region.^{1,6,7,64} This changing pattern of disease has important implications for cancer detection because the gastric cardia and fundus must be carefully evaluated for signs of malignancy in all patients who undergo barium studies or endoscopy to rule out gastric carcinoma.

ROUTES OF SPREAD

Gastric carcinoma may invade local, regional, or distant structures by four pathways—direct extension, lymphatic spread, intraperitoneal seeding, and hematogenous metastases. The various pathways of spread are discussed separately in the following sections.

Direct Extension

Gastric carcinoma has a tendency to invade adjacent structures such as the liver, pancreas, and spleen.^{55,68} Longitudinal spread of tumor along the GI tract is also relatively common. The distal esophagus is directly involved by carcinoma of the cardia in about 60% of patients,⁶⁹ whereas the duodenum is involved by carcinoma of the antrum in 5% to 25% of patients.⁷⁰⁻⁷² Tumor involving the greater curvature of the stomach may also spread inferiorly via the gastrocolic ligament to the transverse colon, occasionally resulting in the development of a gastrocolic fistula.⁷³

Lymphatic Spread

Because of the abundant lymphatics in the stomach, lymph node metastases are found in 74% to 88% of patients with gastric carcinoma.⁵³ These patients may initially have involvement of local (perigastric) nodes and, subsequently, regional (celiac, hepatic, left gastric, and splenic) or distant (left supraclavicular and left axillary) nodes.⁸ The frequency of lymphatic metastases is related to the size and depth of penetration of the tumor. Nevertheless, lesions are still classified histologically as early gastric cancers, regardless of the presence of local lymph node metastases, if malignant invasion is confined to the mucosa or submucosa.⁶¹

Intraperitoneal Seeding

Patients with advanced gastric carcinoma may develop malignant ascites, resulting in intraperitoneal-seeded or omental metastases.⁶⁸ Diffuse carcinomatosis may also lead to the development of small bowel obstruction. Some patients with signet ring cell adenocarcinomas have bilateral “drop” metastases to the ovaries, known as Krukenberg tumors.⁷⁴ Although other malignant tumors can also have drop metastases to the ovaries, gastric carcinoma is responsible for most cases.⁷⁴ Some patients with gastric carcinoma may present with bilateral ovarian masses as the initial manifestation of their disease.

Hematogenous Metastases

Because the stomach is drained by the portal vein, the liver is the most common site of hematogenous (blood-borne) metastases from gastric carcinoma.⁵⁵ Other less common sites of hematogenous spread include the lungs, adrenals, kidneys, bones, and brain.

CLINICAL FINDINGS

Gastric carcinoma is usually considered a disease of middle and late life, with a peak incidence between 50 and 70 years of age.^{8,54,75} However, 3% to 5% of patients with gastric cancer are less than 35 years of age and 1% are less than 30 years of age.⁷⁶⁻⁷⁸ The percentage of young patients with gastric cancer has more than doubled since 1970.⁷⁷ For reasons that are unclear, these young people tend to have more aggressive lesions that are associated with a worse prognosis than most gastric cancers.^{77,78}

Gastric carcinoma is twice as common in men as in women.^{2,8,11} The male predilection of these tumors is even greater for carcinoma of the cardia, which is seven times more likely to occur in men than in women.^{79,80} This explanation for this discrepancy is unclear.

Most patients with gastric carcinoma are symptomatic only when they have advanced tumors with local or distant metastases.^{8,9} The most common presenting findings include epigastric pain, bloating, early satiety, nausea, vomiting, dysphagia, anorexia, weight loss, and signs or symptoms of upper GI bleeding, such as hematemesis, melena, guaiac-positive stool, and iron deficiency anemia.^{8,9,54} However, similar findings may be caused by ulcers, gastritis, or other benign conditions. As a result, there is often a considerable lag between the onset of symptoms and the diagnosis of gastric cancer.

The clinical presentation is also affected by the location and morphologic features of the tumor. For example, nausea and vomiting are common findings in patients with obstructing lesions involving the distal antrum or pyloric region.⁴ In contrast, patients with scirrhous carcinomas may develop early satiety because of the decreased compliance of a stomach that is diffusely infiltrated by tumor.⁸¹ Other patients with carcinoma of the cardia may present with recent onset of dysphagia caused by tumor obstructing the cardia.^{82,83} Some individuals with dysphagia may complain of food sticking behind the sternum, whereas others may have a sensation of blockage referred upward to the thoracic inlet or even the pharynx. The gastric cardia and fundus should therefore be carefully evaluated in all patients with dysphagia, regardless of the subjective site of obstruction, to rule out a carcinoma of the cardia masquerading as an esophageal or pharyngeal disorder.

Some patients with advanced gastric cancer may initially present with signs or symptoms of metastatic disease, such as anorexia, weight loss, abdominal masses, hepatic enlargement, jaundice, ascites, back pain, or neurologic findings. Patients with ovarian metastases may have bilateral pelvic masses (so-called Krukenberg tumors), and patients with drop metastases to the rectosigmoid colon may have a palpable Blumer's shelf on rectal examination.

ENDOSCOPIC FINDINGS

When brushings and biopsy specimens are obtained, endoscopy has a reported overall sensitivity of 94% to 98% in the diagnosis of gastric carcinoma.⁸⁴⁻⁸⁷ However, multiple biopsy specimens should be taken from suspicious lesions to decrease the risk of sampling error. It should also be recognized that endoscopy is a much less reliable technique for diagnosing scirrhous tumors than other gastric carcinomas. In various series, the sensitivity of endoscopic brushings and biopsy specimens in detecting these lesions has ranged from only 33% to 70%.⁸⁸⁻⁹⁰ False-negative histologic findings may occur not only because these scirrhous carcinomas are located predominantly in the submucosa, but also because the tumor cells are often separated by sheets of fibrosis. In some cases, multiple endoscopic examinations may be required for a definitive histologic diagnosis.⁹⁰ Thus, excessive reliance on negative endoscopic biopsy specimens may cause inordinate delays in the treatment of these patients. Finally, the presence and extent of tumor is often underestimated on the basis of the gross endoscopic findings because the mucosa overlying these lesions usually appears normal.⁹¹

RADIOGRAPHIC FINDINGS

Early Gastric Cancer

The double-contrast upper GI examination has been widely recognized as the best radiologic technique for the diagnosis of early gastric cancer.⁹²⁻⁹⁵ The Japanese Endoscopic Society has divided these lesions into three basic types.⁹⁶ Type I lesions are elevated lesions that protrude more than 5 mm into the lumen. Type II lesions are superficial lesions that are further subdivided into three groups—types IIa, IIb, and IIc—depending on their morphologic features. Type IIa lesions are elevated but protrude less than 5 mm into the lumen. Type IIb lesions are essentially flat. Type IIc lesions are slightly depressed but do not penetrate beyond the muscularis mucosae. Type III lesions are true mucosal ulcerations, with the ulcer penetrating the muscularis mucosae but not the muscularis propria. When early gastric cancers exhibit more than one of these morphologic features, they may have a dual classification, with the most predominant pattern listed first (e.g., type III + IIc).

Type I early gastric cancers typically appear as small, elevated lesions in the stomach.^{93,94} Because adenomatous polyps may undergo malignant degeneration (see earlier, "Gastric Polyps"), the possibility of early gastric cancer should be suspected for any sessile or pedunculated polyps larger than 1 cm. Other type I lesions may protrude considerably into the lumen and still be classified histologically as early gastric cancers (Fig. 32-1A).⁹⁴ Thus, polypoid carcinomas cannot be diagnosed definitively as early or advanced lesions on the basis of the radiographic findings.

Type II early gastric cancers are superficial lesions with elevated (IIa), flat (IIb), or depressed (IIc) components. These lesions may be manifested by plaque-like elevations, mucosal nodularity, shallow areas of ulceration, or some combination of these findings (Fig. 32-1B and C).⁹²⁻⁹⁵ Occasionally, type II lesions may be quite extensive and involve a considerable surface area of the stomach.

Type III early gastric cancers are characterized by shallow, irregular ulcer craters with nodularity of the adjacent mucosa and clubbing, fusion, or amputation of radiating folds (Fig. 32-1D).^{93,94} Careful analysis of the radiographic findings usually allows these lesions to be distinguished from benign gastric ulcers, which have different radiographic features (see Chapter 29). Although some lesions with an equivocal or suspicious appearance are found to be benign ulcers, endoscopy and biopsy should be performed for all lesions with suspicious radiographic findings to avoid missing early cancers.

About 70% of the ulcers in type IIc or III early gastric cancers are reported to undergo substantial healing on medical treatment.⁹⁷ It has been postulated that these cancers are characterized by a cycle of ulceration, healing, and recurrent ulceration. Rarely, complete healing of malignant ulcers has also been described.⁹⁷ However, malignant tumors should still be suspected on follow-up barium studies if mucosal nodularity or other abnormalities are detected at the site of the previous ulcer.

Japanese researchers have reported an incidence of early gastric cancer (i.e., the percentage of all gastric cancers detected as early lesions) of 25% to 46%⁹⁸⁻¹⁰¹ compared with an incidence of only 5% to 24% in Western countries.^{93-95,102-108} This discrepancy can be attributed to mass screening of the adult population in Japan because of the unusually high prevalence of gastric carcinoma in that country. Occasionally, early gastric cancers

Figure 32-1 Early gastric cancers. **A.** A type I lesion is seen as a polypoid mass (arrow) on the greater curvature of the gastric body. Despite its size, this lesion was found to be an early cancer. **B.** A type IIa lesion is manifested by a focal cluster of shallow elevations and nodules (arrows) in the gastric body. **C.** A type IIc lesion is manifested by shallow, irregular areas of ulceration and nodularity (arrows) in the gastric antrum. **D.** A type III lesion is seen as a scalloped, irregular antral ulcer with nodular, clubbed folds surrounding the ulcer crater. (A courtesy Kyunghee C. Cho, MD, Newark, NJ; B from Laufer I, Levine MS [eds]: *Double Contrast Gastrointestinal Radiology*, 2nd ed. Philadelphia, WB Saunders, 1992; D from Levine MS, Creteur V, Kressel HY, et al: *Benign gastric ulcers: diagnosis and follow-up with double-contrast radiography. Radiology* 164:9–13, 1987.)

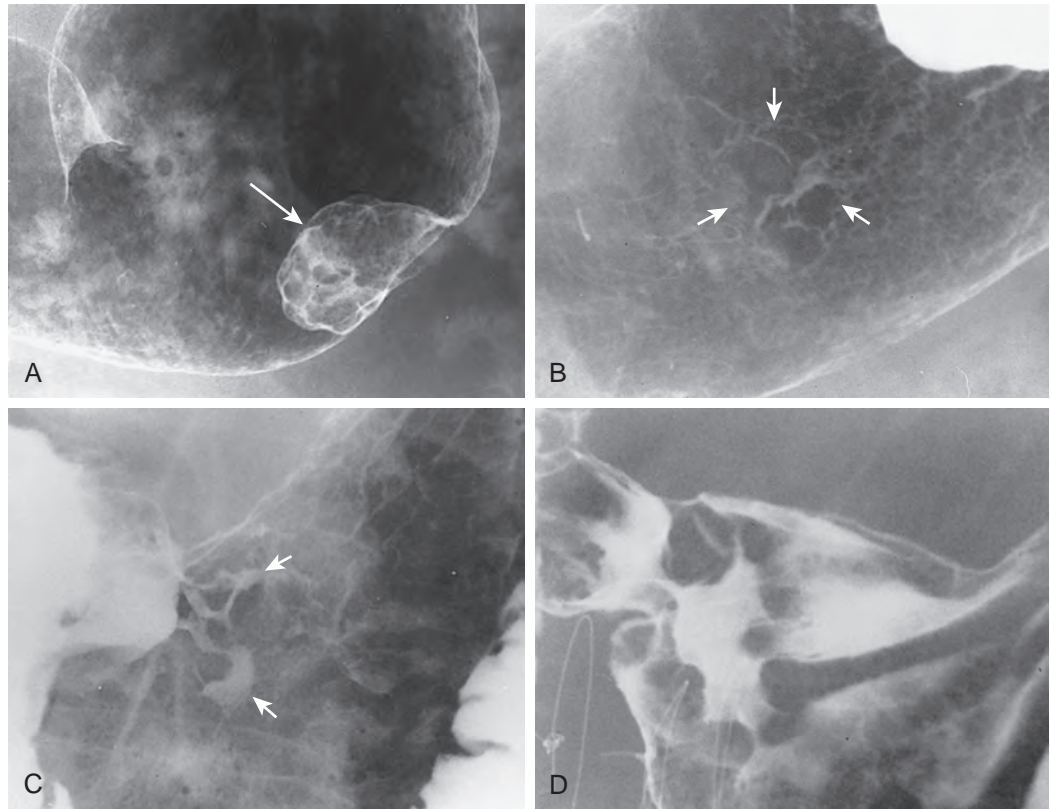
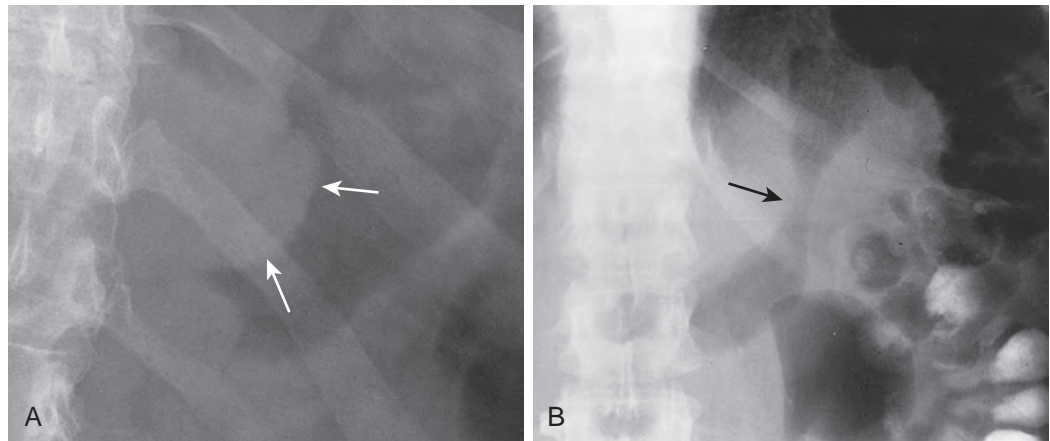


Figure 32-2 Findings of gastric carcinoma on abdominal radiographs. **A.** Close-up view from an abdominal radiograph shows a soft tissue mass (arrows) indenting the lesser curvature of the gas-filled stomach. This was a polypoid gastric carcinoma. **B.** In another patient, the gas-filled stomach has a narrowed, tubular appearance (arrow) caused by a scirrhous carcinoma (linitis plastica).



may be detected in symptomatic patients with epigastric pain, upper GI bleeding, or other complaints.⁹⁵ Early gastric cancers may also be discovered fortuitously in patients who undergo radiologic or endoscopic examinations for other reasons. Nevertheless, radiologists and endoscopists in the West are unlikely to detect a substantial number of early gastric cancers as long as these examinations are performed predominantly on symptomatic patients.⁹⁵

Advanced Carcinoma

Abdominal Radiographs. Polypoid gastric carcinomas are occasionally recognized on abdominal radiographs by the presence of a soft tissue mass indenting the gastric air shadow (Fig.

32-2A). Primary scirrhous carcinomas can also be recognized by a narrowed, tubular configuration of the gas-filled stomach (Fig. 32-2B). Rarely, mucin-producing scirrhous carcinomas may contain gross areas of calcification that have a stippled, punctate, or sandlike appearance (Fig. 32-3A).^{109–111} When abdominal radiographs are worrisome for gastric carcinoma, barium studies or computed tomography (CT) should be performed for a more definitive diagnosis (Fig. 32-3B). CT is a particularly sensitive technique for demonstrating the calcification in mucin-producing scirrhous tumors (Fig. 32-3C).

Barium Studies. Accurate diagnosis of gastric cancer has always been an important goal of barium studies of the upper

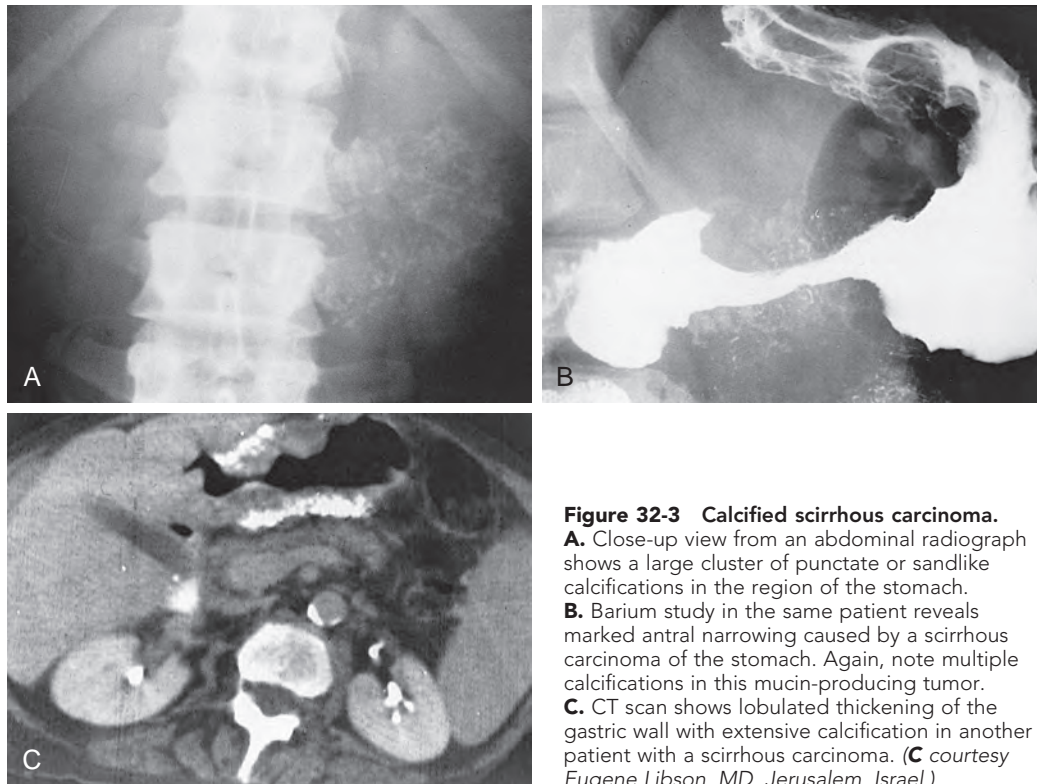


Figure 32-3 Calcified scirrhous carcinoma.

A. Close-up view from an abdominal radiograph shows a large cluster of punctate or sandlike calcifications in the region of the stomach.

B. Barium study in the same patient reveals marked antral narrowing caused by a scirrhous carcinoma of the stomach. Again, note multiple calcifications in this mucin-producing tumor.

C. CT scan shows lobulated thickening of the gastric wall with extensive calcification in another patient with a scirrhous carcinoma. (**C** courtesy Eugene Libson, MD, Jerusalem, Israel.)

GI tract. Unfortunately, single-contrast examinations have an overall sensitivity of only 75% in diagnosing these tumors.¹¹² In one study of 80 patients with gastric carcinoma, however, the lesion was detected on double-contrast examinations in 99% of cases, and malignant tumor was diagnosed or suspected on the basis of the radiographic findings in 96%.¹¹² In the same study, it was found that endoscopy had been recommended because of radiographic findings that were equivocal or suggestive of tumor in only 4% of all patients who underwent double-contrast examinations during this period. Thus, a high sensitivity can be achieved in the diagnosis of gastric carcinoma on double-contrast studies without exposing an inordinate number of patients to unnecessary endoscopy. In another study, missed gastric cancers usually resulted from perceptual errors related to depressed lesions overlooked in the thin barium pool with compression or flow technique.¹¹³

Advanced gastric carcinomas may appear as polypoid, ulcerative, or infiltrating lesions. However, many tumors have mixed morphologic features, so there is considerable overlap in the classification of these lesions. Because scirrhous carcinomas and cardiac carcinomas produce distinctive radiographic findings, these lesions are considered separately in later sections.

Polypoid carcinomas are lobulated or fungating masses that protrude into the lumen (Figs. 32-4 and 32-5). On double-contrast studies, lesions on the dependent or posterior wall are seen as filling defects in the barium pool, whereas lesions on the nondependent or anterior wall are etched in white by a thin layer of barium trapped between the edge of the mass and adjacent mucosa. These tumors often contain one or more irregular areas of ulceration. Occasionally, polypoid antral carcinomas may prolapse through the pylorus into the duodenum,

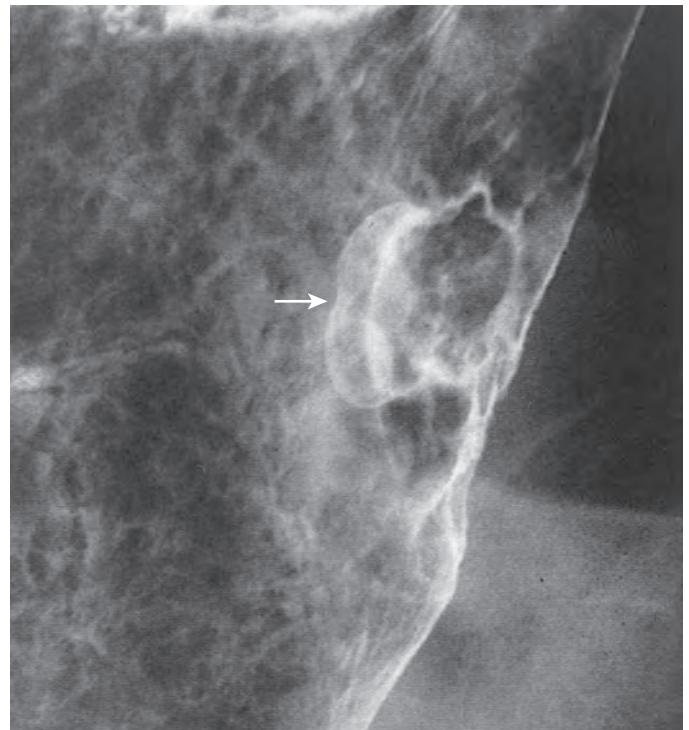


Figure 32-4 Polypoid gastric carcinoma. A polypoid mass (arrow) is seen on the greater curvature of the stomach.

appearing as mass lesions at the base of the bulb (Fig. 32-6). Rarely, two or more synchronous carcinomas may be present in the stomach (see Fig. 32-5).^{56,57,114}

Ulcerated carcinomas are those in which the bulk of the tumor mass has been replaced by ulceration (Figs. 32-7 and

32-8). Although these lesions are often called *malignant ulcers*, the term is a misnomer, because it is not the ulcer but the surrounding tumor that is malignant. In general, malignant ulcers are characterized en face by an irregular ulcer crater eccentrically located within a ring of malignant tissue.^{115,116} The ulcers may have scalloped, angular, or stellate borders. Discrete tumor nodules are often seen in the adjacent mucosa. Folds converging to the edge of the ulcer may be blunted, nodular, clubbed, or fused as a result of tumor infiltration.^{115,116} On double-contrast studies, malignant ulcers on the nondependent or anterior wall

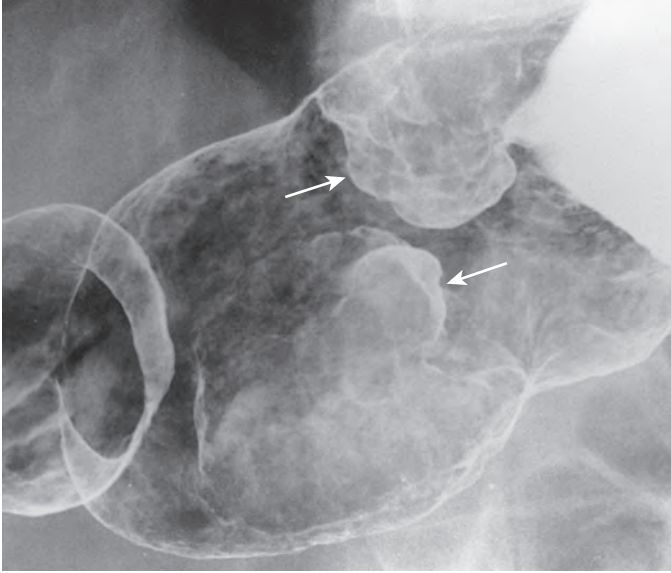


Figure 32-5 Synchronous gastric carcinomas. Two discrete polypoid masses (arrows) are seen in the stomach as a result of separate, primary gastric carcinomas.

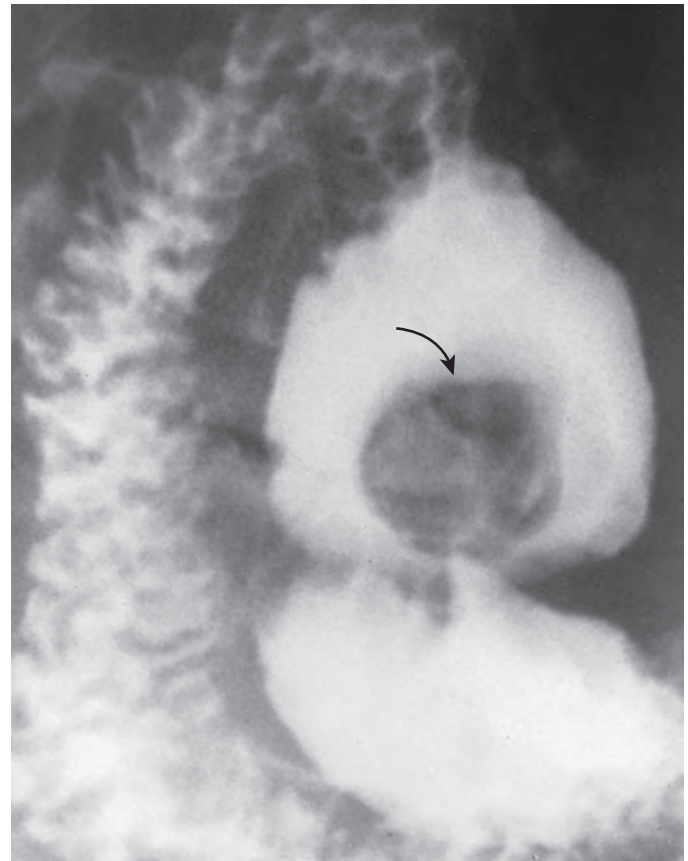


Figure 32-6 Prolapsed antral carcinoma. A polypoid mass (arrow) is seen at the base of the duodenal bulb. This patient had an antral carcinoma that had prolapsed into the duodenum.

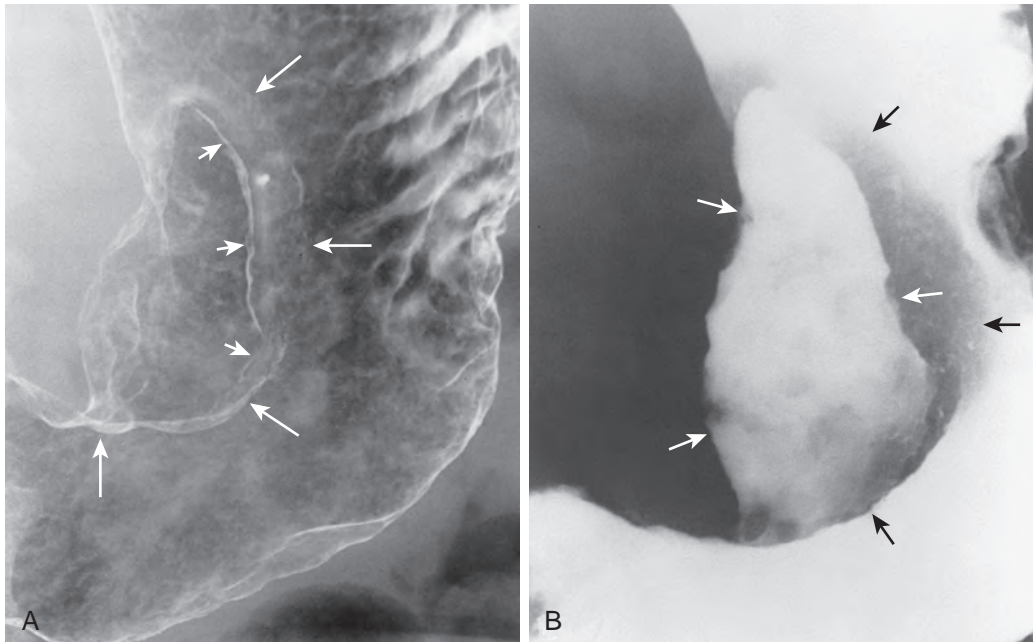


Figure 32-7 Ulcerated gastric carcinoma. A. Double-contrast view of the stomach shows a relatively large mass that is etched in white (large arrows) near the lesser curvature of the gastric body. Also note a second curvilinear density (small arrows) secondary to barium coating the rim of an unfilled central ulcer. **B.** Prone compression view shows the mass as a radiolucent filling defect (black arrows) on the anterior wall of the stomach. Note how the central ulcer (white arrows) fills with barium when the patient is in the prone position. The ulcer has a convex inner border and an intraluminal location, demonstrating the features of a Carman-Kirklin meniscus complex. (From Laufer I, Levine MS [eds]: *Double Contrast Gastrointestinal Radiology*, 2nd ed. Philadelphia, WB Saunders, 1992.)

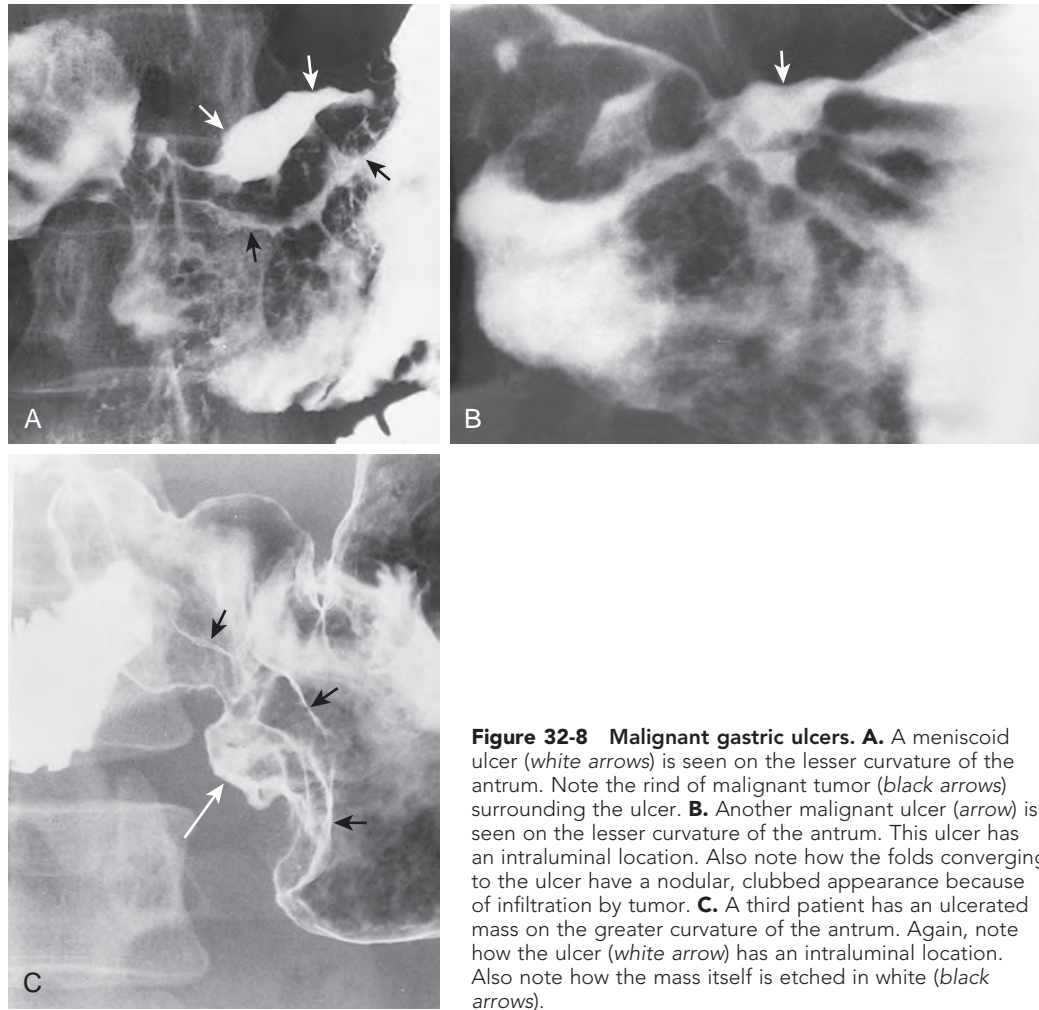


Figure 32-8 Malignant gastric ulcers. **A.** A meniscoid ulcer (white arrows) is seen on the lesser curvature of the antrum. Note the rind of malignant tumor (black arrows) surrounding the ulcer. **B.** Another malignant ulcer (arrow) is seen on the lesser curvature of the antrum. This ulcer has an intraluminal location. Also note how the folds converging to the ulcer have a nodular, clubbed appearance because of infiltration by tumor. **C.** A third patient has an ulcerated mass on the greater curvature of the antrum. Again, note how the ulcer (white arrow) has an intraluminal location. Also note how the mass itself is etched in white (black arrows).

may be etched in white, so a double ring shadow is observed in the stomach, with the outer ring representing the edge of the tumor and the inner ring representing the edge of the ulcer (see Fig. 32-7A). In such cases, prone compression views should demonstrate filling of the ulcer crater within a discrete tumor mass on the anterior wall (see Fig. 32-7B). A biphasic examination is therefore essential for proper interpretation of these lesions.

When viewed in profile, malignant ulcers usually have an intraluminal location, often within a discrete tumor mass (see Figs. 32-8B and C), whereas benign ulcers project beyond the adjacent contour of the stomach.^{115,116} However, this criterion can be used only for ulcers on or near the lesser or greater curvature. The tumor mass surrounding malignant ulcers usually forms acute angles with the adjacent gastric wall rather than the obtuse, gently sloping angles expected for a benign mound of edema.^{115,116} Clubbed or nodular folds may also be seen radiating to the edge of the ulcer crater or to the edge of the surrounding mass as a result of tumor infiltrating these folds (see Fig. 32-8B).

No sign in GI radiology has generated more confusion than the meniscus sign of a malignant ulcer, which was originally described by Carman in 1921¹¹⁷ and refined by Kirklin in

1934.¹¹⁸ The Carman-Kirklin meniscus complex is caused by a cancer straddling the lesser curvature of the gastric antrum or body, in which the tumor is a broad, flat lesion with central ulceration and elevated margins. Careful compression of the lesion may reveal a meniscoid ulcer with a convex inner border and a concave outer border that does not project beyond the expected gastric contour (see Figs. 32-7B and 32-8A).^{115,116} A radiolucent halo may be seen abutting the meniscus because of apposition of the elevated edges of the tumor on the anterior and posterior walls. Although the Carman-Kirklin meniscus complex is a reliable radiologic sign of malignancy, it can be demonstrated in only a small percentage of all patients with malignant ulcers.

Infiltrating carcinomas are manifested by irregular narrowing of the stomach with nodularity and spiculation of the mucosa (Fig. 32-9). Some infiltrating lesions may have polypoid or ulcerated components. In advanced cases, these lesions may cause gastric outlet obstruction.

Transpyloric spread of antral carcinoma into the duodenum can be demonstrated on barium studies in 5% to 25% of patients.⁷⁰⁻⁷² Duodenal involvement is manifested by mass effect, nodularity, ulceration, or irregular narrowing of the proximal duodenum. Although transpyloric spread of tumor

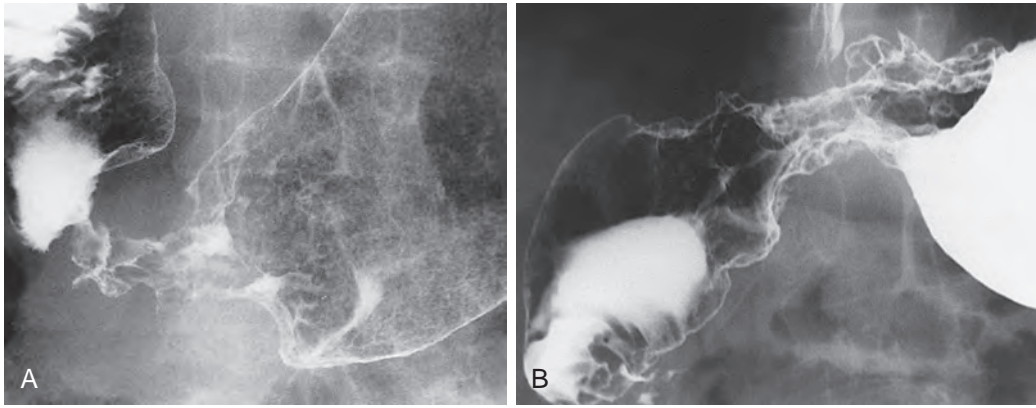
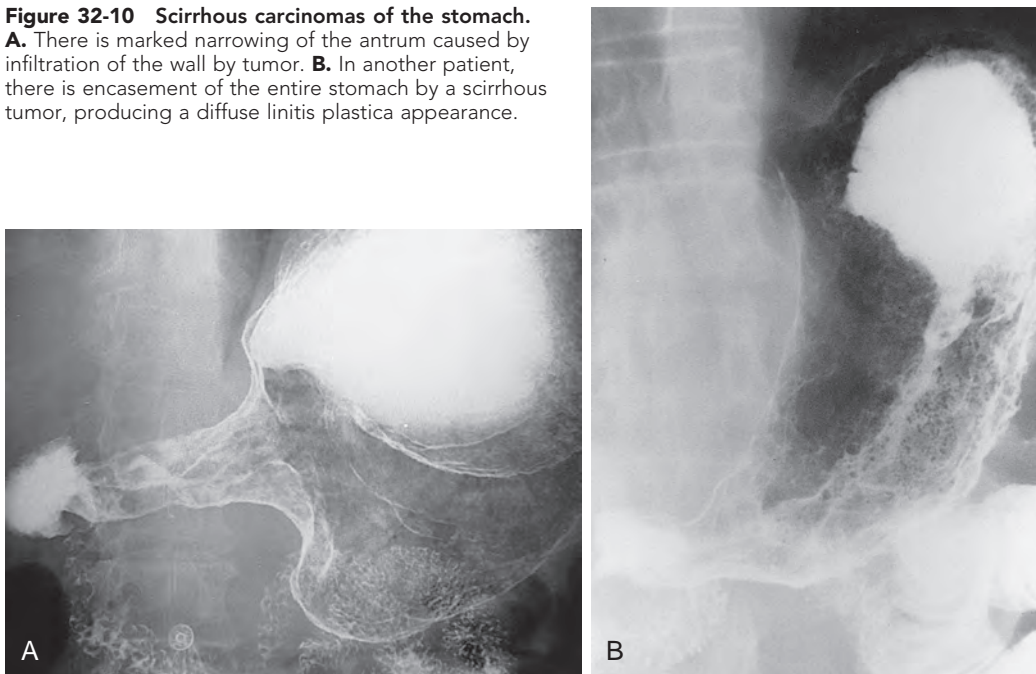


Figure 32-9 Infiltrating gastric carcinomas. **A.** Irregular narrowing and ulceration are seen in the antrum because of an advanced, infiltrating carcinoma. **B.** In another patient, an infiltrating carcinoma of the proximal stomach causes marked narrowing and spiculation of the upper gastric body.

Figure 32-10 Scirrhou carcinomas of the stomach. **A.** There is marked narrowing of the antrum caused by infiltration of the wall by tumor. **B.** In another patient, there is encasement of the entire stomach by a scirrhou tumor, producing a diffuse linitis plastica appearance.



occurs in a higher percentage of patients with gastric lymphoma, gastric carcinoma is more likely to produce this finding because of its higher incidence.⁷²

Rarely, advanced gastric carcinomas on the greater curvature of the stomach may spread inferiorly via the gastrocolic ligament to the superior border of the transverse colon, resulting in the development of a gastrocolic fistula.⁷³ Although these fistulas may occasionally be shown on an upper GI study, they are more likely to be demonstrated on a barium enema because of the higher pressures generated during this examination.

Scirrhou Carcinoma

Scirrhou gastric carcinomas are traditionally thought to involve the distal half of the stomach, arising near the pylorus and gradually extending upward from the antrum into the body and fundus.^{81,119} These tumors are classically manifested on barium studies by irregular narrowing and rigidity of the stomach,

producing a linitis plastica (“leather bottle”) appearance (Fig. 32-10).^{81,119} In advanced cases, the stomach may be diffusely infiltrated by tumor (see Fig. 32-10B). Other patients may have localized scirrhou tumors confined to the prepyloric region of the antrum, appearing as short, annular lesions with shelflike proximal margins (Fig. 32-11).¹²⁰ With double-contrast technique, however, 20% to 40% of patients with scirrhou tumors are found to have localized lesions involving the gastric fundus or body with sparing of the antrum (Figs. 32-12 and 32-13).^{90,91} Detection of these lesions has presumably improved because of better gaseous distention of the proximal stomach on double-contrast studies. Whatever the explanation, radiologists should be aware that a large percentage of scirrhou carcinomas are localized lesions involving the gastric fundus or body rather than the classic form of linitis plastica involving the distal stomach.

Because of intense fibrosis incited by scirrhou gastric carcinomas, these tumors may convert the stomach into a narrowed,

rigid tube that loses its normal compliance and distensibility. As a result, barium paradoxically may empty from the stomach more rapidly than normal, so all the ingested barium enters the duodenum and proximal small bowel within minutes of starting the examination. This same phenomenon accounts for the early satiety that develops in some patients because the narrowed, rigid stomach is incapable of expanding to accommodate ingested food.

Although scirrhous carcinomas are often manifested by relatively marked gastric narrowing, some tumors cause only mild loss of distensibility. Instead, these lesions may be recognized on double-contrast studies primarily by distortion of the normal surface pattern of the stomach with mucosal nodularity, spiculation, ulceration, or thickened, irregular folds (see



Figure 32-11 Localized scirrhous carcinoma of the distal antrum. A short, annular lesion is seen in the prepyloric region of the antrum. Note how the lesion has an abrupt, shelflike proximal border. (From Laufer I, Levine MS [eds]: *Double Contrast Gastrointestinal Radiology*, 2nd ed. Philadelphia, WB Saunders, 1992.)

Fig. 32-13).⁹⁰ Thus, some lesions are likely to be missed if the radiologist relies too heavily on gastric narrowing as the major criterion for diagnosing these tumors.

CARCINOMA OF THE CARDIA

Tumors arising at the cardia are notoriously difficult to detect on conventional single-contrast barium studies. Because the overlying rib cage precludes manual palpation or compression of the fundus, even large lesions at the cardia may be obscured by crowded folds or relatively opaque barium, which prevents adequate visualization of this region. With double-contrast technique, however, it is possible to evaluate the normal anatomic landmarks at the cardia and surrounding gastric mucosa for signs of malignancy. As a result, double-contrast barium studies may detect lesions at the cardia that are missed on conventional single-contrast examinations.¹²¹⁻¹²⁵

When viewed en face, the normal cardia often appears on double-contrast studies as a circular elevation containing four or five stellate folds that radiate to a central point at the gastroesophageal junction, also known as the *cardiac rosette* (see Chapter 26).^{122,123} Some lesions at the cardia may be recognized only by subtle nodularity, mass effect, or ulceration in this region with distortion, effacement, or obliteration of the rosette (Fig. 32-14).¹²²⁻¹²⁵ Enlargement or lobulation of the surrounding elevation should also suggest a neoplastic lesion. Finally, an abnormal protrusion at the cardia should persist when additional barium is swallowed, whereas an apparent abnormality at the cardia must be an artifact if it vanishes as the lower esophageal sphincter relaxes and the cardia opens.¹²³

Advanced carcinomas of the gastric cardia or fundus may be polypoid or infiltrating lesions. Polypoid tumors usually appear as lobulated intraluminal masses in the gastric fundus, often containing irregular areas of ulceration.^{125,126} In contrast, infiltrating lesions are manifested by thickened, nodular folds and decreased distensibility of the fundus.^{125,126} Advanced tumors may completely encase the fundus, producing a linitis plastica appearance (Fig. 32-15).

When an equivocal or suspicious lesion is detected in the region of the gastric cardia or fundus, endoscopy should be

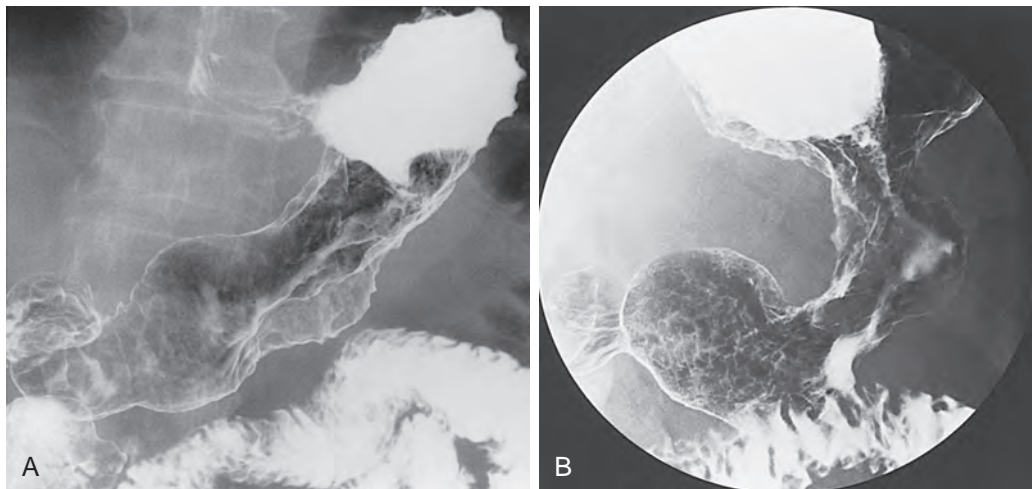


Figure 32-12 Localized scirrhous carcinomas of the proximal stomach. A. Irregular narrowing is seen in the gastric fundus and body with sparing of the antrum. **B.** Another patient has a scirrhous carcinoma of the gastric body with sparing of the fundus and antrum. (A from Laufer I, Levine MS [eds]: *Double Contrast Gastrointestinal Radiology*, 2nd ed. Philadelphia, WB Saunders, 1992.)

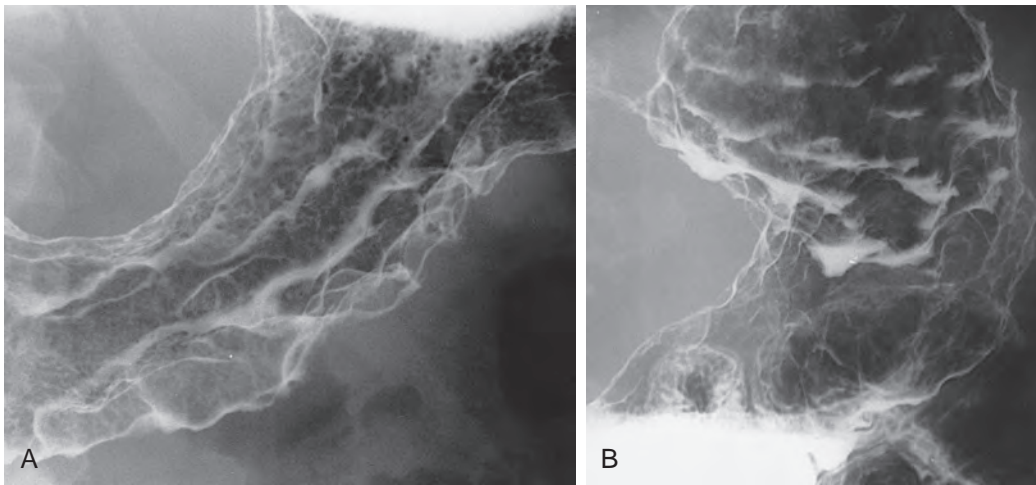


Figure 32-13 Scirrhous carcinomas of the proximal stomach with thickened folds. **A.** This patient has a localized scirrhous carcinoma of the gastric body. The tumor has caused only mild loss of distensibility. However, there is distortion of the normal surface pattern of the stomach with thickened, irregular folds and mucosal nodularity. **B.** In another patient, a scirrhous carcinoma of the fundus and body is manifested by thickened, lobulated folds without significant narrowing. (**A** from Levine MS, Kong V, Rubesin SE, et al: *Scirrhous carcinoma of the stomach: Radiologic and endoscopic diagnosis. Radiology 175:151–154, 1990.*)

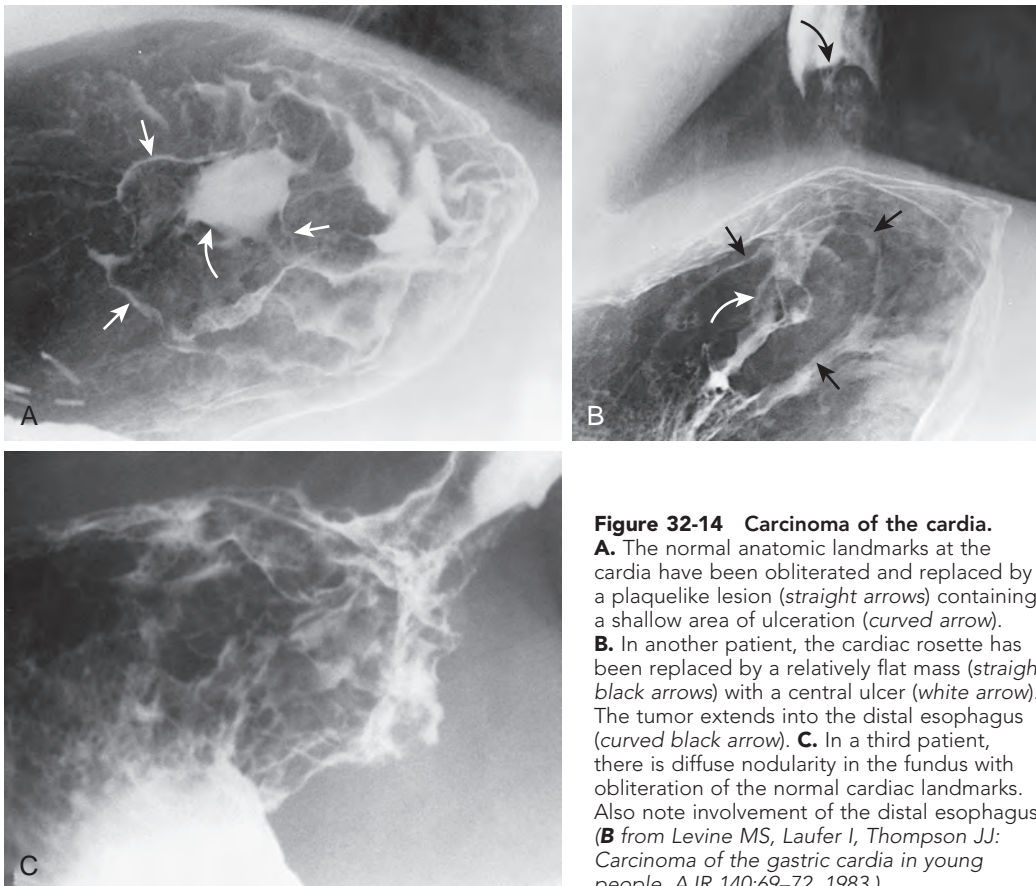


Figure 32-14 Carcinoma of the cardia.

A. The normal anatomic landmarks at the cardia have been obliterated and replaced by a plaque-like lesion (straight arrows) containing a shallow area of ulceration (curved arrow).

B. In another patient, the cardiac rosette has been replaced by a relatively flat mass (straight black arrows) with a central ulcer (white arrow). The tumor extends into the distal esophagus (curved black arrow).

C. In a third patient, there is diffuse nodularity in the fundus with obliteration of the normal cardiac landmarks. Also note involvement of the distal esophagus.

(**B** from Levine MS, Laufer I, Thompson JJ: *Carcinoma of the gastric cardia in young people. AJR 140:69–72, 1983.*)

performed for a more definitive diagnosis. Nevertheless, radiographically demonstrated lesions at the cardia may occasionally be missed at endoscopy.¹²⁷ The barium study should therefore be repeated, despite a negative endoscopic examination, if the initial barium study suggests a malignant lesion. Rarely, some patients with continuing radiologic evidence of

malignancy may require surgery without preoperative histologic confirmation.

Secondary esophageal involvement by advanced lesions may be manifested on barium studies by a polypoid or fungating mass extending from the gastric fundus into the distal esophagus or by thickened folds or irregular narrowing of the distal

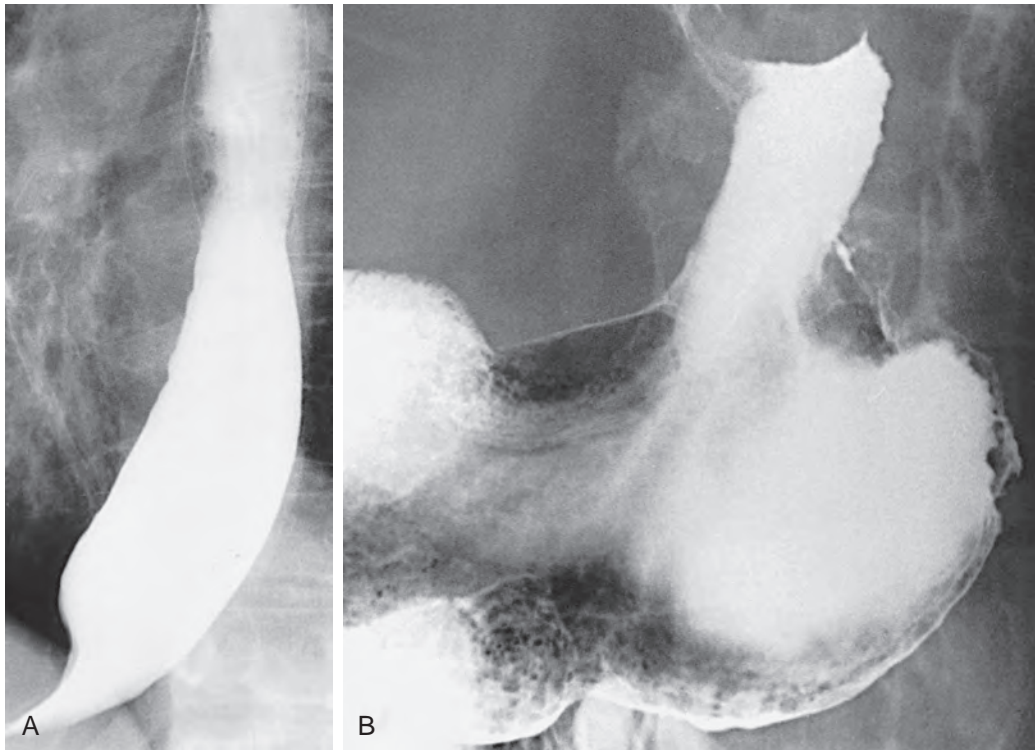


Figure 32-15 Secondary achalasia caused by gastric carcinoma. **A.** There is smooth, tapered narrowing of the distal esophagus, producing the classic beaklike appearance of achalasia. **B.** A radiograph of the stomach reveals an advanced scirrhous carcinoma of the gastric fundus that has invaded the distal esophagus. (From Levine MS: *Radiology of the Esophagus*. Philadelphia, WB Saunders, 1989.)

esophagus without a discrete lesion (see Fig. 32-14B and C).^{125,126} Esophageal involvement is usually confined to a 4- to 5-cm segment above the gastroesophageal junction but may occasionally extend as far proximally as the aortic arch.¹²⁶ Submucosal spread of tumor can also result in secondary achalasia with tapered, beaklike narrowing of the distal esophagus at or just above the gastroesophageal junction (see Fig. 32-15A and Chapter 24).^{126,128} However, certain morphologic features such as asymmetry, abrupt transitions, and mucosal nodularity or ulceration should suggest an underlying malignancy.¹²⁸ Secondary achalasia should also be suspected when the narrowed segment extends proximally a discrete distance from the gastroesophageal junction.¹²⁹ In such cases, careful radiologic evaluation of the gastric fundus is essential to rule out a carcinoma of the cardia as the cause of these findings.

COMPUTED TOMOGRAPHIC FINDINGS

The widespread availability of multidetector CT (MDCT) scanners has improved the diagnosis of gastric carcinoma on CT because of its ability to create high-quality images in any conceivable view plane (Fig. 32-16). Detection of these lesions requires optimal gastric distention to efface the overlying rugal folds and accentuate areas of asymmetry along the contour of the stomach. Some authors recommend oral administration of a neutral (water-attenuation) contrast agent,¹³⁰⁻¹³³ whereas others recommend the use of an oral effervescent agent (as is used for double-contrast barium studies of the stomach) to optimize gastric distention.^{134,135}

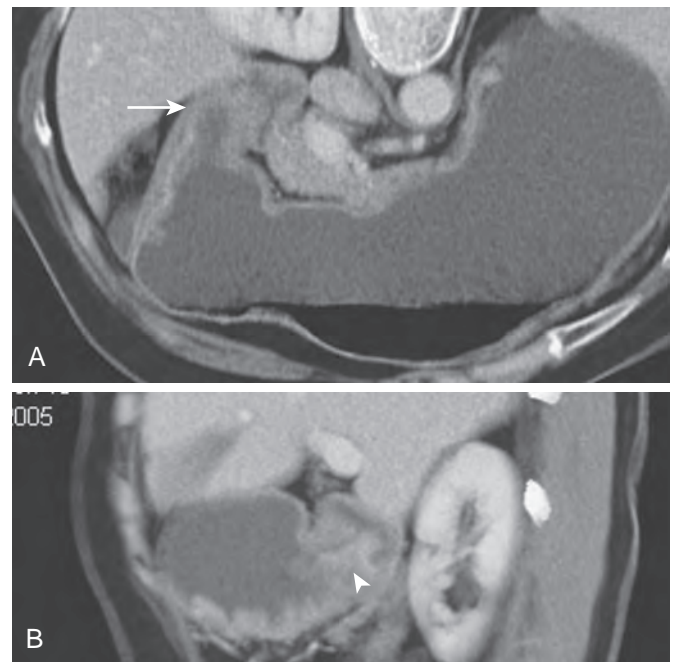


Figure 32-16 MDCT evaluation of gastric carcinoma. **A, B.** Two 3D volume-rendered images in a patient with antral carcinoma show localized wall thickening in the antropylic region of the stomach. **A** shows the lesion (arrow) in a rendering that simulates a left posterior oblique view from an upper GI barium study, whereas **B** shows the lesion (arrowhead) in an orientation that simulates a right anterior oblique view from a barium study. Note the importance of adequately distending the stomach to demonstrate this finding.

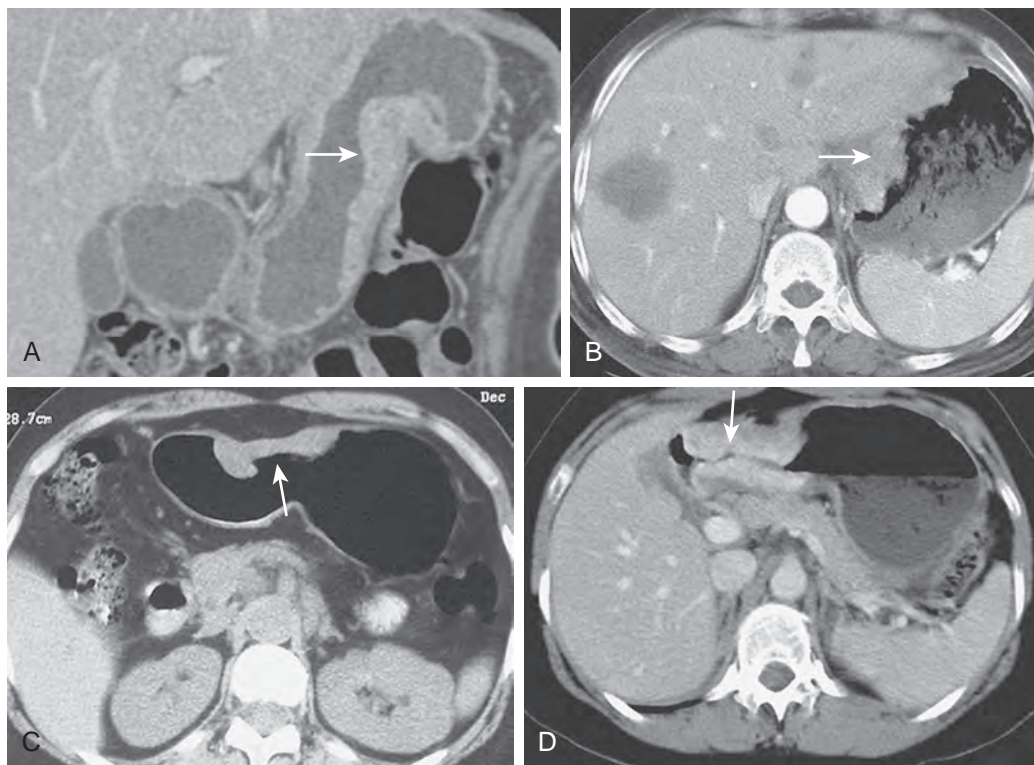


Figure 32-17 MDCT of gastric carcinoma correlated with Borrmann classification. Images from four different patients show the various CT appearances of gastric carcinoma (arrows). **A.** Type I polypoid neoplasm. **B.** Type II fungating neoplasm. Also note the presence of multiple hepatic metastases in this patient. **C.** Type III ulcerated neoplasm. **D.** Type IV infiltrating neoplasm.

Optimal MDCT detection of gastric cancer requires that imaging data be collected with the thinnest possible detector configuration (0.6–0.75 mm). Overlapping reconstructions enable the creation of 3D data sets with near-isotropic voxels. Display images are created at 3- to 4-mm intervals and are transmitted directly to the picture archiving and communications system (PACS). Thin slices are simultaneously transmitted to a workstation or thin client server, enabling the creation of 3D images. Clinically useful 3D images displaying the gastric tumor and extragastric extension can be created and selected for the patient's electronic imaging database. The thin sections are not permanently archived, although 3D renderings created from these sections are archived. Intravenous administration of iodinated contrast material is critical, not only for assessing the primary tumor but also for local staging and detection of distant metastases. The images should include the abdomen and pelvis because of the tendency for gastric carcinoma to disseminate widely in the peritoneal cavity.

The Borrmann classification of gastric carcinoma includes four morphologic types of gastric cancer—type I (polypoid), type II (fungating), type III (ulcerated), and type IV (infiltrating). Each of these four types can be visualized on MDCT (Fig. 32-17).¹³⁶ This classification encompasses the spectrum of radiographic findings expected for gastric carcinoma. Although the infiltrating and ulcerated types of cancer are readily recognized as distinct imaging entities,^{137,138} the polypoid and fungating types may be difficult to differentiate. MDCT is not generally used to predict the histology of the tumor, but calcification and/or areas of low attenuation within a thickened gastric wall should suggest the presence of a mucinous carcinoma (Fig. 32-18).¹³⁹

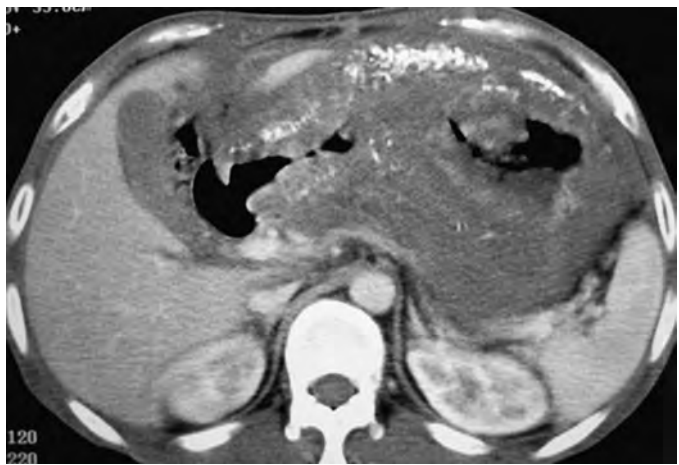


Figure 32-18 Mucinous adenocarcinoma of the stomach. This MDCT scan shows massive thickening of the gastric wall and marked luminal narrowing by an advanced, infiltrating carcinoma. Also note extensive calcification within the tumor. This type of calcification is characteristic of mucinous tumors of the stomach.

Gastric carcinoma is often manifested on MDCT by focal thickening of the gastric wall. In one study, wall thickening greater than 1 cm on CT had a sensitivity of 100% for detecting gastric cancer, but a specificity of less than 50%.¹⁴⁰ Localized wall thickening is a particularly frequent finding in the gastric antrum¹⁴¹ and at the gastroesophageal junction,¹⁴² leading to false-positive diagnoses of tumor. Smooth antral wall thickening (≤ 12 mm), with or without submucosal low attenuation, is

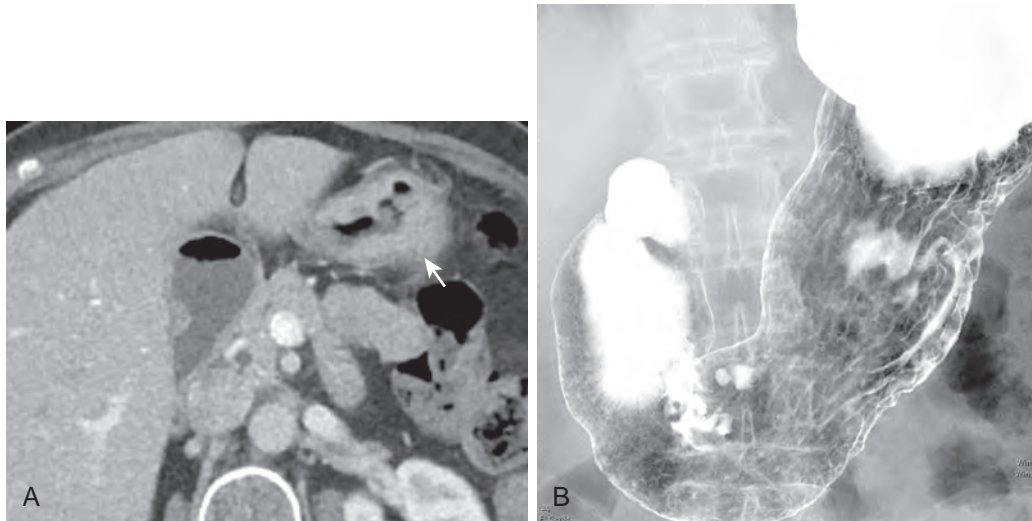


Figure 32-19 False-positive MDCT for gastric carcinoma. **A.** Representative axial MDCT scan shows a focal area of apparent wall thickening (arrow) on the greater curvature of the gastric body that is worrisome for an infiltrating tumor. **B.** A frontal view of the stomach from a subsequent double-contrast upper GI examination shows a normal-appearing stomach without any findings to suggest tumor in the gastric body. In patients with known gastric cancer, the accuracy of MDCT can be improved by using appropriate technique to ensure that the stomach is maximally distended. Nevertheless, it is not always possible to achieve optimal gastric distention on routine abdominal CT.

often seen as a normal finding.¹⁴¹ When a mass is suspected at the gastroesophageal junction, repeat scanning with oral effervescent agent in the prone or left-side down decubitus position should distend the normal stomach and efface the wall, accentuating the presence of tumor.¹⁴¹ If there is still a high index of suspicion for malignant tumor, endoscopic ultrasound (EUS) and biopsy are recommended for a more definitive diagnosis. If, however, the index of suspicion for tumor is low, a double-contrast barium study may be performed to confirm that the stomach is normal. A similar approach may be used to exclude malignant tumor in patients with apparent wall thickening elsewhere in the stomach on MDCT (Fig. 32-19). The symmetry of wall thickening and uniformity of contrast enhancement are also features that help differentiate benign from malignant causes of wall thickening.

Gastric carcinomas often enhance on MDCT after intravenous (IV) administration of iodinated contrast material at rates of 3 mL/s or greater (Fig. 32-20). Some of these tumors may have stratified wall enhancement characterized by brightly enhancing mucosal and serosal layers with less enhancement of the submucosal and muscular layers (Fig. 32-21).^{131,143} Radiologic-pathologic correlation has shown that the degree of enhancement depends on differences in proliferation of cancer cells; more tightly aggregated cells tend to enhance more brightly, whereas more scattered cells result in lower regions of attenuation.¹⁴⁴ MDCT with IV contrast enhancement therefore improves tumor detection and can also be used to produce high-quality CT angiograms that serve as roadmaps for surgeons.¹⁴⁵

DIFFERENTIAL DIAGNOSIS

Early Gastric Cancer

Early gastric cancers may appear on barium studies as depressed (ulcerated), elevated (polypoid), or superficial lesions. Ulcerated cancers must be distinguished from benign gastric ulcers (see earlier, “Early Gastric Cancer”). Occasionally, early gastric



Figure 32-20 Gastric carcinoma with differential wall enhancement on MDCT. This 3D MDCT scan shows wall thickening and hyperdense attenuation in the distal esophagus and region of the gastroesophageal junction (straight arrow) caused by a biopsy-proven adenocarcinoma. The gastric wall is diffusely abnormal, with a thin, uniformly enhancing mucosal layer and a thickened, hypodense submucosal layer (curved arrow), possibly from edema. A focal area of increased mural density (arrowhead) is seen extending from the greater curvature of the distal antrum into the adjacent perigastric fat, suggesting tumor extension.

lymphomas may also appear as ulcerated lesions (see Chapter 33). Polypoid cancers must be distinguished from adenomatous or hyperplastic polyps or other benign or malignant tumors in the stomach. Finally, superficial cancers must be distinguished from a focal area of gastritis or intestinal metaplasia. When early gastric cancer is suspected on barium studies, endoscopy and biopsy are required for a definitive diagnosis.

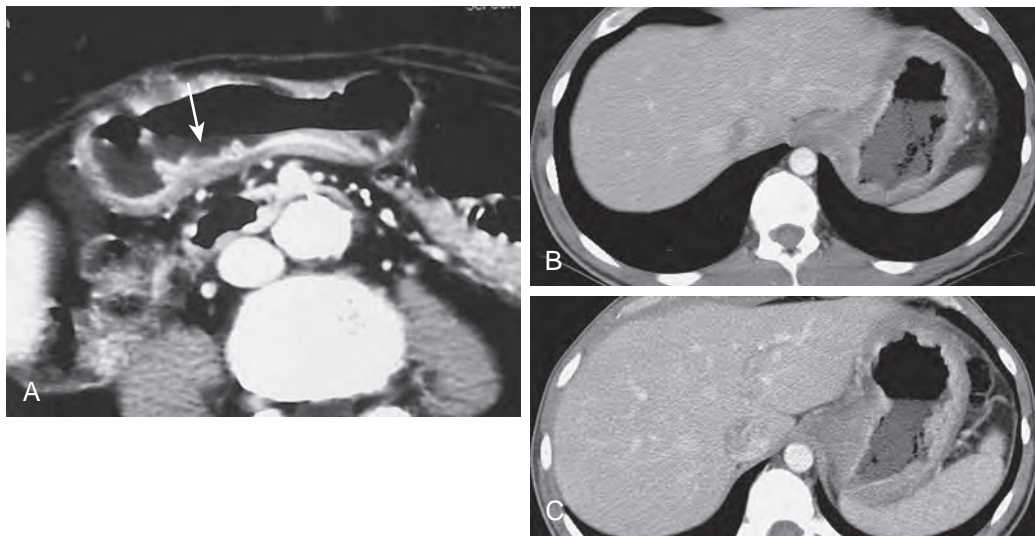


Figure 32-21 Gastric carcinoma with stratified enhancement patterns on MDCT. **A.** Contrast-enhanced MDCT scan shows a malignant posterior wall ulcer (arrow) with irregular margins. Note decreased enhancement of the adjacent mucosa and a relatively hypodense submucosa. **B, C.** Contrast-enhanced MDCT scans through the proximal stomach in a 35-year-old man show an irregularly thickened gastric wall extending to the gastroesophageal junction secondary to a primary scirrhous carcinoma with linitis plastica. Note the variable enhancement of the mucosa, prominent hyperdensity interspersed throughout the submucosa, and poor margination at the serosa.

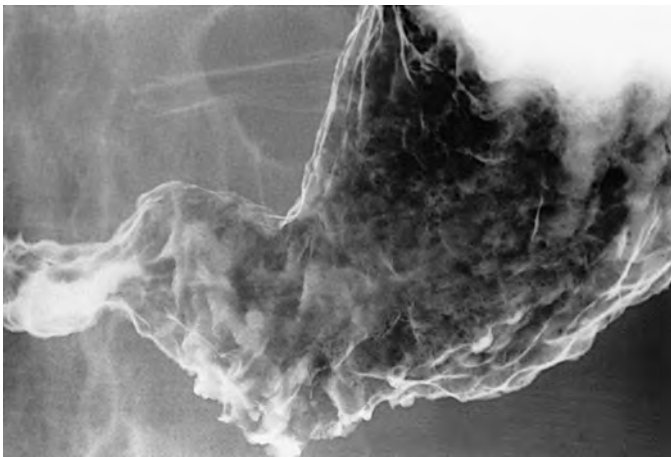


Figure 32-22 Metastatic breast cancer involving the stomach. There is antral narrowing with distortion of the normal surface pattern and a nodular, irregular mucosa in this region. A primary scirrhous carcinoma of the stomach could produce identical findings. (From Levine MS, Kong V, Rubesin SE, et al: *Scirrhous carcinoma of the stomach: Radiologic and endoscopic diagnosis*. *Radiology* 175:151–154, 1990.)

Advanced Carcinoma

The major consideration in the differential diagnosis of an ulcerated gastric carcinoma is a benign gastric ulcer with a surrounding mound of edema (see Chapter 29). Polypoid or ulcerated carcinomas must also be distinguished from other polypoid or ulcerated malignant tumors such as lymphoma and malignant GISTs (see Chapter 33). Although the presence of a large, lobulated submucosal mass should favor the diagnosis of lymphoma or a malignant GIST, histologic specimens are required to differentiate these lesions.

Most cases of linitis plastica are caused by gastric carcinoma, but metastatic breast cancer (Fig. 32-22), omental metastases, and non-Hodgkin's lymphoma involving the stomach may

produce similar radiographic findings (see Chapter 33).^{90,146,147} Cone-shaped antral narrowing and deformity may also be caused by scarring from peptic ulcer disease, caustic ingestion, radiation, or a variety of granulomatous diseases, including Crohn's disease, tuberculosis, sarcoidosis, and syphilis (see Chapter 30).¹⁴⁸ Antral narrowing may also occur in older patients who have a so-called senile antrum secondary to gastric atrophy.¹⁴⁹ In general, a smooth antral contour and lack of nodularity, spiculation, or ulceration should suggest benign disease. Rarely, however, these conditions may produce more irregular gastric narrowing, mimicking the appearance of malignant linitis plastica.

Carcinoma of the cardia invading the distal esophagus may be indistinguishable from a primary adenocarcinoma in Barrett's esophagus invading the stomach (see Chapter 23).¹⁵⁰ However, carcinoma of the cardia tends to have a greater degree of gastric involvement in relation to that of the esophagus, whereas primary adenocarcinoma of the esophagus usually has a greater degree of esophageal involvement. Squamous cell carcinoma of the esophagus may also spread distally via submucosal esophageal lymphatics to the gastric cardia or fundus, producing a polypoid lesion in the fundus (see Chapter 23).^{151,152} Occasionally, a conglomerate mass of varices in the fundus may be manifested by a single lobulated lesion that closely resembles a polypoid fundal or cardiac carcinoma (see Chapter 34).^{153,154} Inadequate gaseous distention of the fundus can also mimic the appearance of an infiltrating fundal tumor on double-contrast studies (Fig. 32-23A). However, additional views of the stomach after administration of an additional dose of effervescent agent should show that the fundus is normal in these patients (Fig. 32-23B).

STAGING

CT, EUS, magnetic resonance imaging (MRI), and ¹⁸F-fluorodeoxyglucose (FDG)-positron emission tomography (18-FDG-PET)/CT have important roles in staging patients with

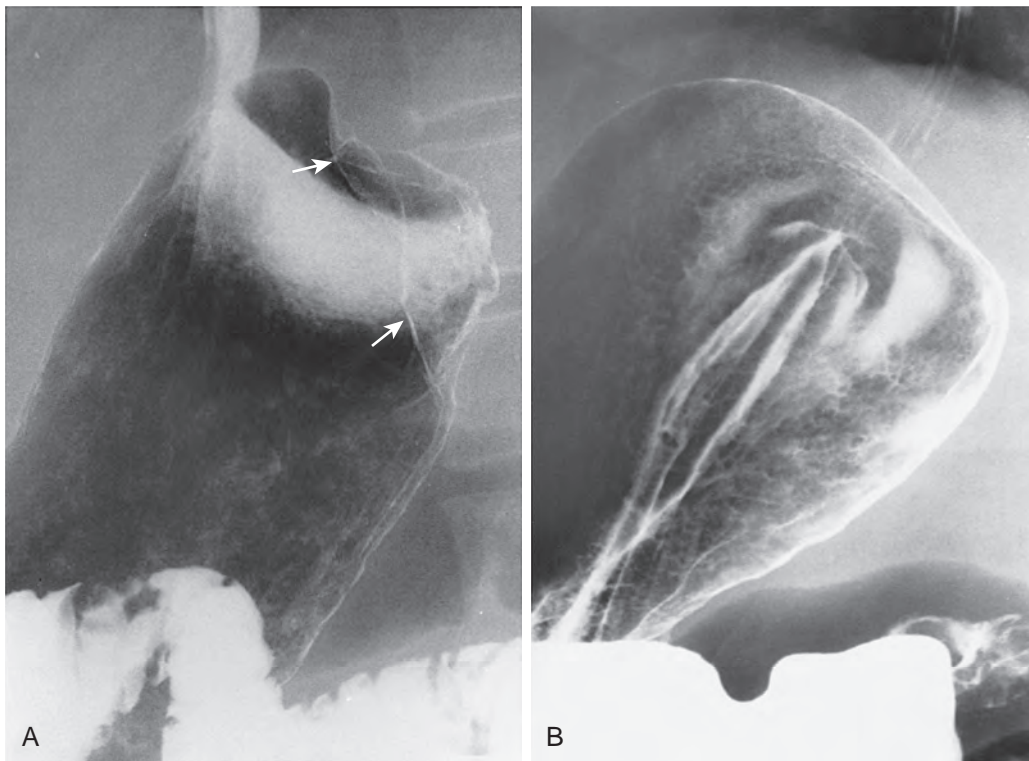


Figure 32-23 Inadequate gaseous distention mimicking a fundal tumor. **A.** Double-contrast radiograph of the stomach shows a possible infiltrating lesion (arrows) on the posterior wall of the fundus. **B.** After administration of additional effervescent agent, there is better distention of the fundus, eliminating the possibility of tumor. Note how the normal cardiac rosette is now visible.

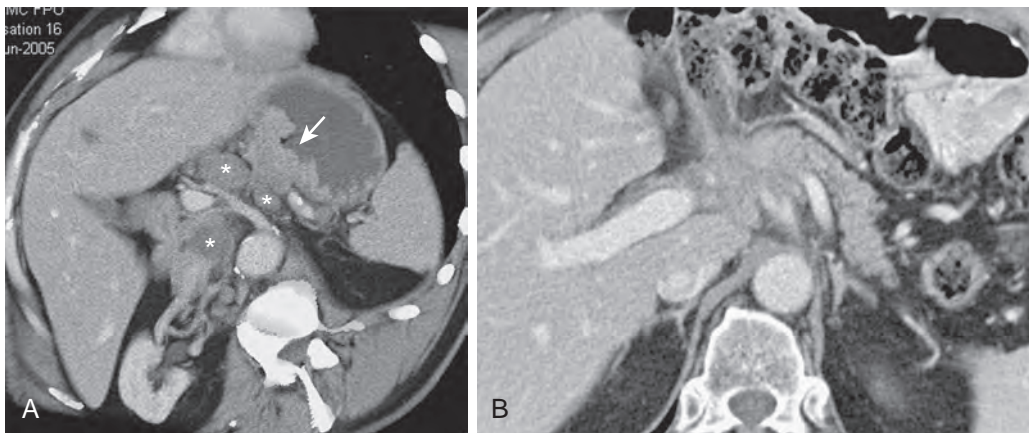


Figure 32-24 Perigastric lymph node metastases from gastric carcinoma. **A.** 3D MDCT scan shows an ulcerated carcinoma of the gastroesophageal junction manifested by an irregular mass with central ulceration (arrow). Enlarged perigastric lymph nodes (asterisks) are present in a periceliac distribution. **B.** In another patient who underwent a previous gastrectomy for gastric carcinoma, an MDCT scan shows peripancreatic lymphadenopathy simulating a carcinoma of the head of the pancreas.

gastric carcinoma. These techniques are therefore discussed separately in the following sections.

Computed Tomography

MDCT is a useful imaging test for staging gastric carcinoma, not only to assess disease spread beyond the gastric wall, but also intraperitoneal seeding and blood-borne metastases. At the same time, MDCT does not always permit accurate depiction of local tumor extension or lymph node involvement. When the diagnosis of gastric carcinoma is already known, MDCT is facilitated by the use of oral effervescent or water-attenuation agents to distend the stomach maximally.

Studies have indicated that MDCT has an increasing role in gastric cancer staging. In a study of 106 patients with gastric carcinoma, T-stage accuracy improved from 77% on axial images to 84% on volumetric images.¹⁵⁵ In another study of 65

patients with gastric cancer, MDCT enabled detection of 96% of advanced gastric cancers and 41% of early gastric cancers, with an overall T-stage accuracy of 85%.¹⁴⁴ By using an effervescent agent to maximize gastric distention and create a 3D volume-rendered “luminal cast” (CT gastroscopy) with multiplanar reformatted images and IV contrast enhancement, other investigators have been able to achieve high accuracy in differentiating T1a from T1b tumors.¹⁵⁶ In one study of 41 patients with gastric cancer, the accuracy of MDCT for serosal invasion was 93%,¹³¹ so MDCT is better for staging patients who have more advanced disease.

Multiple lymphatic channels freely communicate within the gastric wall, providing collateral pathways that facilitate the spread of tumor into regional and distant lymph nodes (Fig. 32-24). Despite numerous technologic advances, MDCT is less useful for detecting lymphatic metastases from gastric

carcinoma, with an overall N-stage accuracy of only 60% to 80%. CT is limited by its inability to identify lymphatic metastases in lymph nodes that are not enlarged. The detection of such metastases could potentially be improved by using monoenergetic, low-keV images derived from dual-energy CT acquisitions.

Gastric carcinoma can metastasize by various routes, including direct extension, spread of tumor via ligamentous and mesenteric structures, intraperitoneal seeding, lymphatic extension, and hematogenous metastases. Each of these modes of spread may be recognized on MDCT. For example, carcinoma of the cardia may extend via the gastrohepatic ligament into the liver; this pathway of spread is particularly well shown on MDCT.¹⁵⁷ Similarly, carcinoma of the gastric antrum or body may extend via the gastrocolic ligament to invade the transverse colon (Fig. 32-25).

In patients with advanced gastric carcinoma, peritoneal carcinomatosis may be manifested on MDCT by characteristic findings, including soft tissue masses and nodules in peritoneal reflections, retraction of the mesenteric root, omental caking, and loculated ascites. Once tumor enters the peritoneal cavity, the tumor cells gravitate to its most dependent portion (the pouch of Douglas in a woman and rectovesical space in a man). The ovaries are another frequent site of intraperitoneal seeding (Fig. 32-26).¹⁵⁸ Krukenberg tumors were originally described as solid ovarian metastases from signet ring cell gastric adenocarcinomas, but the term is now used to refer to any metastases to the ovaries, regardless of the primary source. Despite

widespread knowledge of the varied radiologic appearances of peritoneal carcinomatosis, detection of intraperitoneal metastases by MDCT remains poor.^{159,160} In one study, 18-FDG-PET/CT was found to have an even lower sensitivity than MDCT for detecting these intraperitoneal implants.¹⁶¹

Gastric cancers can also extend through regional lymphatics in a sheetlike fashion into the retroperitoneum, causing ureteral obstruction. Hematogenous metastases from gastric carcinoma are usually found in the liver, but these tumors can metastasize via the blood to a variety of sites.

Endoscopic Ultrasonography

The introduction and dissemination of EUS has substantially improved the accuracy of local staging for gastric cancer.¹⁶² A major advantage of EUS is its ability to visualize the various layers of the gastric wall, perigastric lymph nodes, and relationship of the tumor to the surrounding tissues, enabling determination of the depth of wall invasion and extent of regional lymph node involvement by tumor. Nevertheless, EUS is best performed as a complementary test to cross-sectional imaging studies such as CT for local tumor staging.

Technique. EUS uses high-frequency transducers, typically in the frequency range of 5 to 12 MHz, yielding an effective usable clinical resolution of 200 μ m. There are two basic types of endosonographic equipment available for clinical use—a dedicated EUS endoscope with maneuvering and biopsy capabilities and a standard endoscope in which the EUS equipment is fitted onto catheters and passed through the endoscope. The vast majority of published literature in the United States is based on data obtained with dedicated EUS endoscopes.

EUS requires a trained examiner and is therefore operator dependent.¹⁶³ The examination is usually performed under conscious sedation in an outpatient setting. Dedicated echoendoscopes have a suction capability, so air can be removed from the stomach and deaerated water instilled to allow for better acoustic coupling. An inflatable balloon surrounds the transducer and is filled with deaerated water to increase the surface contact area and improve the imaging window.

With standard technique, EUS visualizes the stomach as a five-layered structure; each individual layer corresponds to a histologically defined layer of the gastric wall (Fig. 32-27).¹⁶⁴ The first hyperechoic layer represents the balloon-mucosal interface, the second hypoechoic layer represents the deep mucosa, the third hyperechoic layer represents the submucosa, the fourth hypoechoic layer represents the muscularis propria, and the fifth hyperechoic layer represents the subserosa and serosa. With proper sonographic technique, EUS may visualize these gastric wall layers and surrounding tissues without air-induced artifacts or interference from gastric contents.

EUS is performed from the transgastric position, allowing visualization of the gastric wall, adjacent lymph nodes, and nearby organs, including the pancreas, spleen, left kidney, and, to a limited degree, the liver. However, EUS is limited by its inability to assess for metastases in the right lobe of the liver or more remote sites because of a limited depth of penetration and imaging window.

If the diagnosis of gastric cancer has not been established before EUS, the examination can be combined with a standard upper endoscopy, so biopsy specimens of the primary tumor can be obtained.¹⁶⁵ As on CT, it may be difficult on EUS to differentiate neoplastic involvement of the stomach from

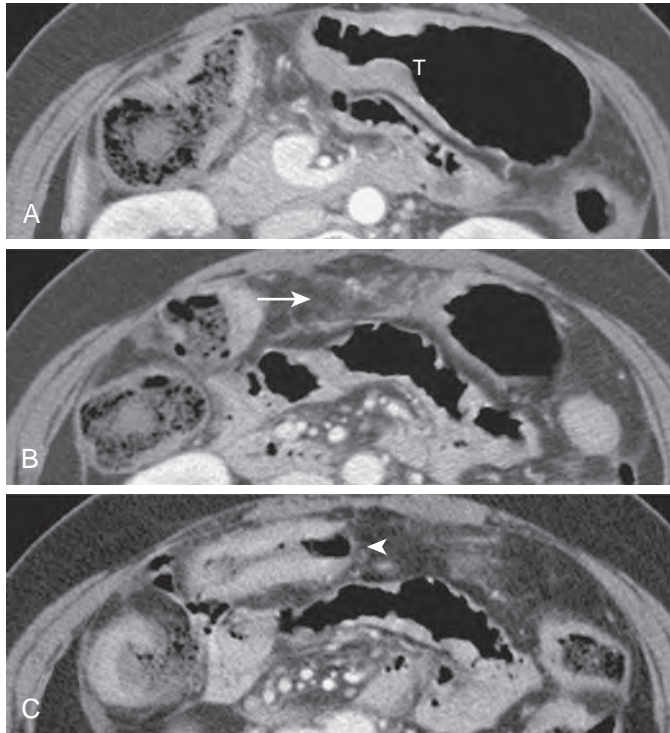


Figure 32-25 Gastric carcinoma invading the transverse colon via the gastrocolic ligament on sequential axial MDCT scans. **A.** The gastric tumor (T) is manifested by localized wall thickening in the midportion of the stomach. **B.** Nodular densities are present in the gastrocolic ligament (arrow). **C.** Another segment of localized wall thickening (arrowhead) is seen in the transverse colon secondary to invasion by tumor.

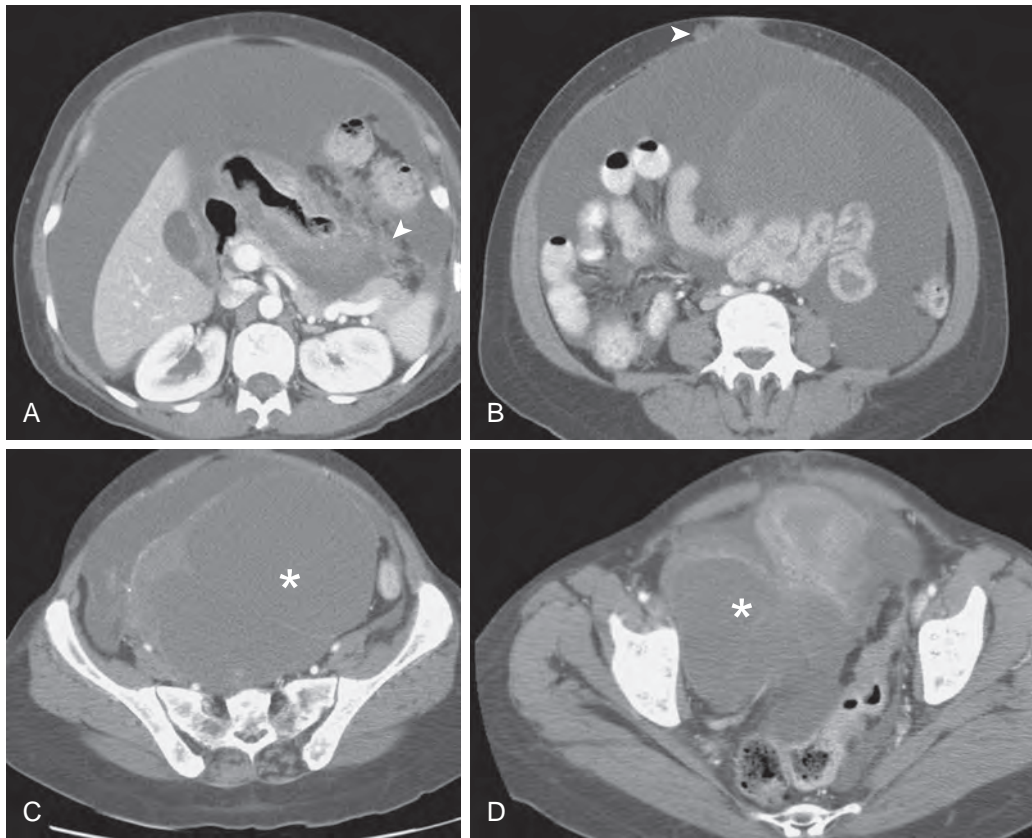


Figure 32-26 Gastric carcinoma with peritoneal and ovarian metastases. **A.** MDCT scan shows a linitis plastica type neoplasm infiltrating the gastric wall. Multiple nodules are seen in the gastrocolic ligament (arrowhead) associated with large-volume ascites. **B.** A so-called Sister Mary Joseph nodule is seen to the right of the umbilicus (arrowhead). **C, D.** Left and right adnexal masses (asterisks) are present. The morphology is similar to that of epithelial ovarian neoplasms. Although the term *Krukenberg tumor* classically applies only to solid ovarian masses arising from signet ring cell carcinomas of the stomach, it is now generally used for ovarian metastases from any primary source.

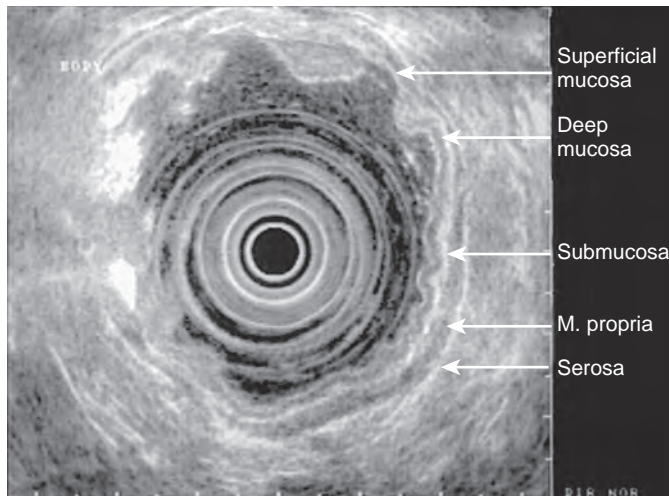


Figure 32-27 Endoscopic ultrasound appearance of the normal gastric wall. Note the typical five-layer wall pattern with a total wall thickness of only several millimeters. (Arrows denote the corresponding wall layers.)

inflammatory processes or fibrosis. EUS also cannot differentiate an early gastric cancer from an adenoma based on echogenicity alone, but evidence of disruption of the normal layers of the gastric wall, local invasion, or suspicious lymph nodes should strongly suggest malignant tumor.

Results. EUS has been shown to be a highly accurate technique for assessing the depth of tumor invasion and presence or absence of regional lymph node involvement in patients with gastric carcinoma.¹⁶⁶⁻¹⁶⁸ In most studies, the overall accuracy of EUS for T staging has ranged from 85% to 88%.¹⁶⁹⁻¹⁷¹ Nevertheless, EUS does have limitations in staging by T classification of gastric cancer because differentiation of subserosal (T2) from serosal (T3) invasion can be extremely difficult. EUS may also overestimate the depth of tumor invasion because of peritumoral inflammation and fibrosis or may underestimate the extent of tumor because of microscopic tumor infiltration of deeper layers of the gastric wall or microscopic nodal metastases.¹⁷² In one study, over staging of the depth of invasion of tumor in the gastric wall led to inappropriate neoadjuvant therapy in 50% of patients.¹⁷³

The finding of a thickened muscularis propria is almost pathognomonic of a malignant gastric tumor, usually gastric carcinoma and, less frequently, lymphoma (Fig. 32-28).^{174,175} EUS is also the most sensitivity imaging technique for detecting perigastric lymph nodes. Unlike CT, in which the detection of abnormal lymph nodes depends entirely on size, the EUS criteria for involved lymph nodes include roundness and hypoechogenicity.^{176,177} Malignant lymph nodes can be detected on EUS with a specificity of almost 90%, but the sensitivity is lower, ranging from 55% to 80%.^{166,170,178,179}

The overall diagnostic accuracy of EUS for determining nodal status (N classification) has ranged from 70% to 90%. A

major limitation of EUS is its inability to detect unenlarged nodes more than 3 cm from the gastric wall. Thus, unless the nodes are enlarged and within range of the transducer, EUS may have limited value in planning the extent of lymphadenectomy. The development of real-time guided, fine-needle aspiration technique increases the accuracy of lymph node assessment because individual lymph nodes can be sampled for tumor.¹⁸⁰

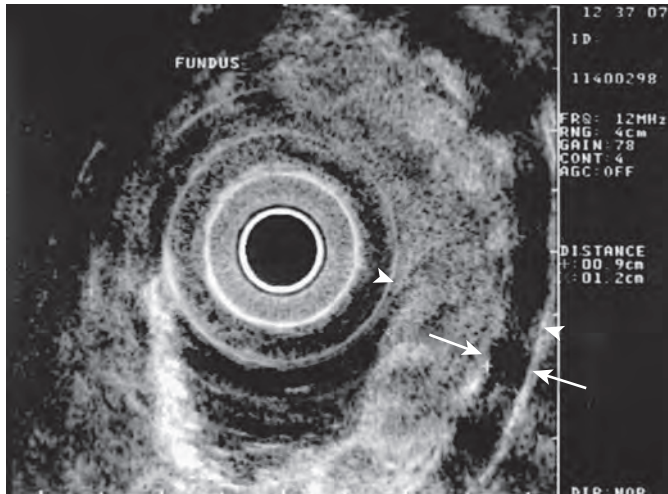


Figure 32-28 Endoscopic ultrasound appearance of linitis plastica. There is marked thickening of the entire gastric wall (arrowheads) with associated thickening of the muscularis propria (arrows).

Nevertheless, some studies have found no significant difference in the overall accuracy of EUS and MDCT for detecting lymph node metastases from gastric cancer,^{181,182} so the ultimate role of EUS remains uncertain.

Other Imaging Modalities. MRI has emerged as another clinically useful imaging test for staging gastric cancer. Diffusion-weighted imaging (DWI) has been shown to be comparable to MDCT for local staging but is more sensitive than MDCT for detecting lymph node metastases.¹⁸³ 18-FDG-PET/CT is also a useful test for whole-body imaging of distant metastases from gastric cancer and for detecting recurrent tumor after treatment.¹⁸⁴ However, 18-FDG-PET/CT has been shown to be inferior to MDCT and diffusion-weighted MRI for detecting regional lymph node metastases (Fig. 32-29).

Summary. The approach to the preoperative staging of patients with gastric carcinoma remains controversial and depends to a major degree on the available imaging, oncologic, and surgical expertise.¹⁶⁵ After the histologic diagnosis of gastric cancer has been made, a cross-sectional imaging study (usually MDCT) is performed to exclude liver metastases or direct extension of tumor into adjacent organs. In patients without metastases or disseminated tumor, EUS can then be performed for local staging of tumor. In such cases, EUS may help select patients with advanced carcinoma for whom neoadjuvant radiation or chemotherapy should be administered before surgery. Patients with T1 to T3 tumors will most likely undergo attempts for curative resection and possibly multimodality therapy, whereas

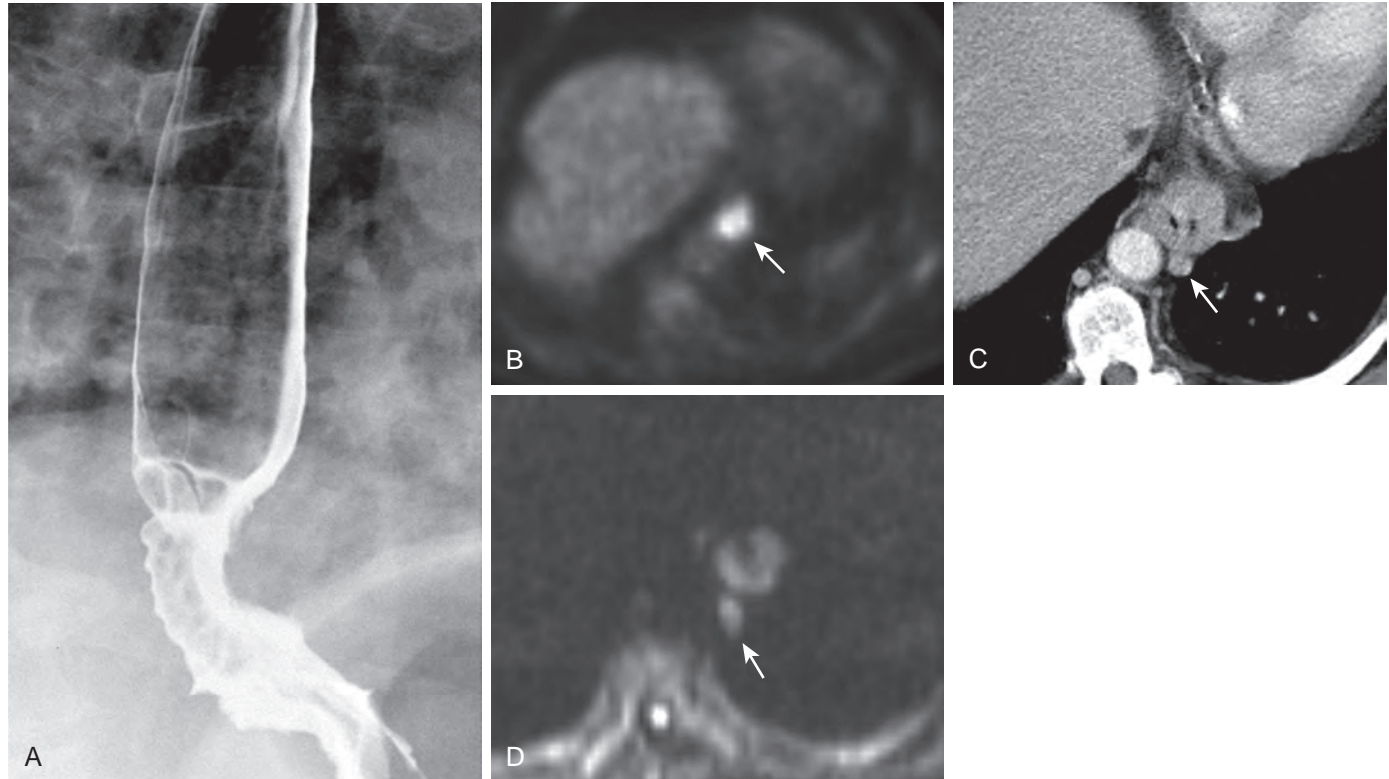


Figure 32-29 Comparison of MDCT, 18-FDG-PET/CT, and the diffusion-weighted MRI for detecting lymphatic metastasis from esophageal cancer. **A.** Barium study shows an infiltrating adenocarcinoma of the distal esophagus extending distally into the gastroesophageal junction. **B.** 18-FDG-PET/CT image shows marked FDG activity (arrow) in the region of the distal esophageal tumor. **C.** MDCT scan shows an enlarged lymph node (arrow) adjacent to the tumor that was not seen on the PET scan. **D.** Diffusion-weighted MRI scan shows two areas of increased signal secondary to restricted diffusion on this high B value image. Note how the tumor and adjacent lymph node (arrow) are both clearly visible.

patients with T4 tumors may undergo a palliative bypass procedure or endoscopic palliation. Occasional patients with T1 N0 M0 lesions may also undergo endoscopic therapy for attempts at cure if they are not reasonable candidates for surgery.¹⁸⁵ Thus, MDCT and EUS should be considered complementary tests for the preoperative evaluation of patients with gastric carcinoma and selection of optimal treatment regimens.¹⁸⁶

TREATMENT AND PROGNOSIS

Surgery is the only curative form of therapy in patients with gastric carcinoma. Depending on the location of the tumor, a subtotal or total gastrectomy or esophagogastrectomy may be performed. Unfortunately, about 60% of patients who undergo surgery are found to have unresectable tumors.⁸ Nevertheless, a palliative resection or bypass procedure may still be performed on these patients to prevent complications such as bleeding or obstruction. Radiation therapy has also been advocated for palliation of inoperable lesions. Adjuvant chemotherapy has been used in some patients, but the benefits of this treatment remain uncertain. Laser therapy and intraluminal stents have sometimes been used for treatment of patients with obstructing tumors. A detailed discussion of the various operations and postoperative complications is presented in Chapter 35.

Patients with advanced gastric carcinoma have a dismal prognosis, with 5-year survival rates of only 3% to 21%.⁴⁻⁷ In contrast, patients with early gastric cancer have 5-year survival rates of 85% to 100%.^{99,100,107,108,187} Early detection of these lesions is therefore essential for improving patient survival. Thus far, most early gastric cancers have been detected in Japan as a result of mass screening of the adult population in that country. However, some symptomatic patients with gastric cancer in the West are also found to have early lesions. Because it frequently is not possible to distinguish early gastric cancer from advanced carcinoma on preoperative studies, an aggressive surgical approach is justified for all patients with resectable lesions.

Duodenal Carcinoma

Duodenal carcinoma is a rare malignant tumor, accounting for less than 1% of all gastrointestinal neoplasms.¹⁸⁸ Almost all these lesions are located in the second, third, or fourth portions of the duodenum at or distal to the ampulla of Vater.^{189,190} Patients with advanced duodenal cancer usually present with nausea, vomiting, abdominal pain, weight loss, or signs or symptoms of upper GI bleeding. Rarely, however, early duodenal cancer may be detected on double-contrast barium studies or endoscopy in symptomatic patients.¹⁹¹ An increased incidence of duodenal carcinoma has been reported in patients with Gardner's syndrome (see Chapter 61) and celiac disease (see Chapter 43), so some form of radiologic or endoscopic surveillance may be warranted for these patients.^{192,193} Duodenal carcinoma has also been associated with Crohn's disease and neurofibromatosis.¹⁹⁴⁻¹⁹⁶

Duodenal carcinomas usually appear on barium studies as polypoid, ulcerated, or annular lesions at or, more commonly, distal to the ampulla of Vater (Fig. 32-30). Some polypoid carcinomas may arise in preexisting villous tumors (see Chapter 31). Occasionally, duodenal carcinomas have a more proximal location, appearing as ulcerated masses in the proximal descending duodenum or even the duodenal bulb.¹⁹⁷

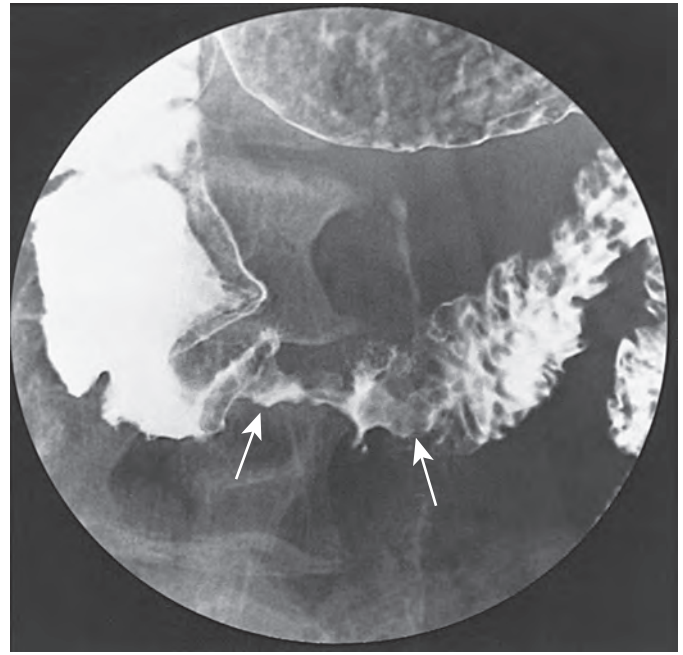


Figure 32-30 Duodenal carcinoma. An annular, ulcerated lesion (arrows) is seen in the third portion of the duodenum.

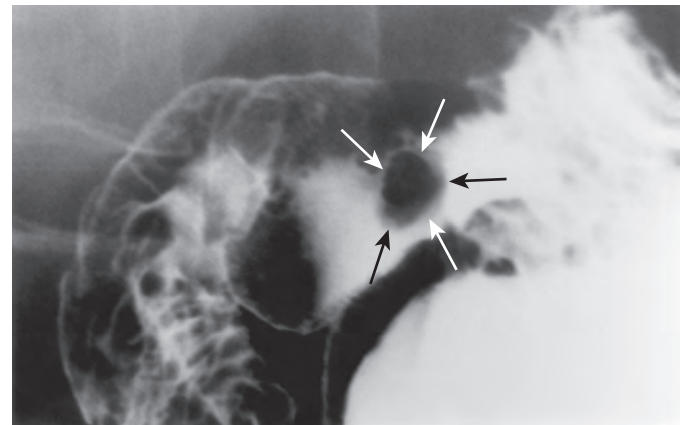


Figure 32-31 Early duodenal cancer. Double-contrast spot image of the duodenum shows a sessile, slightly lobulated, 1.3-cm polypoid lesion (arrows) in the duodenal bulb. This was an early cancer that was confined to the mucosa. (From Bradford D, Levine MS, Hoang D, et al: Early duodenal cancer: Detection on double-contrast upper gastrointestinal radiography. *AJR* 174:1564-1566, 2000.)

Nevertheless, the vast majority of duodenal ulcers are benign, so endoscopy should be considered only for lesions that have suspicious radiographic features. Rarely, early duodenal cancers may appear on double-contrast barium studies as small (<2 cm), sessile, polypoid or ulcerated lesions in the duodenum (Fig. 32-31).¹⁹¹

Duodenal carcinoma is usually manifested on CT by a localized area of wall thickening, producing a soft tissue mass (Fig. 32-32). Features such as tumor necrosis and ulceration are readily identified.¹⁹⁸ When CT reveals an exophytic or intramural mass containing central necrosis and ulceration, this combination of findings is reported to have a sensitivity of 100% and accuracy of 86% for the detection of malignant tumor.¹⁹⁹

Figure 32-32 Duodenal carcinoma. **A.** 3D volume-rendered MDCT scan shows narrowing of the postbulbar duodenum by an eccentric soft tissue mass arising in the wall (arrow). **B.** A barium study from the same patient shows an advanced, infiltrating carcinoma of the descending duodenum.

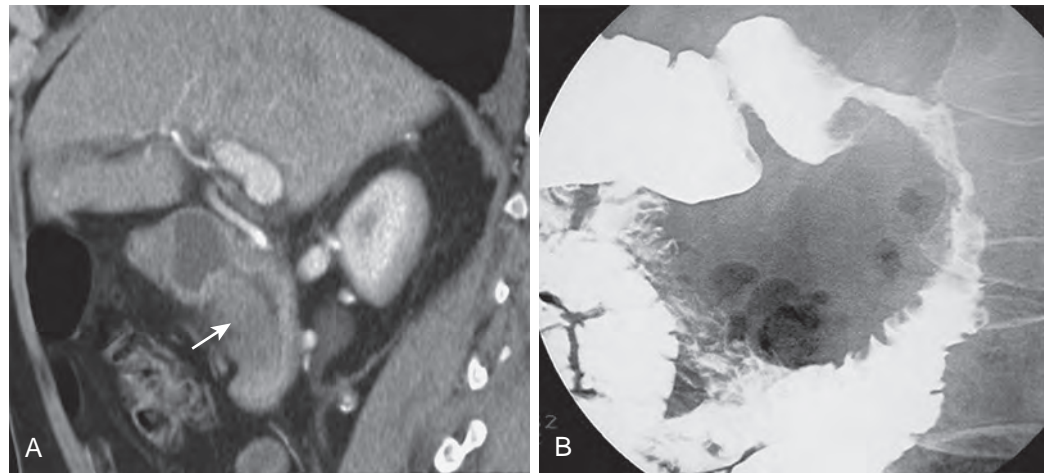
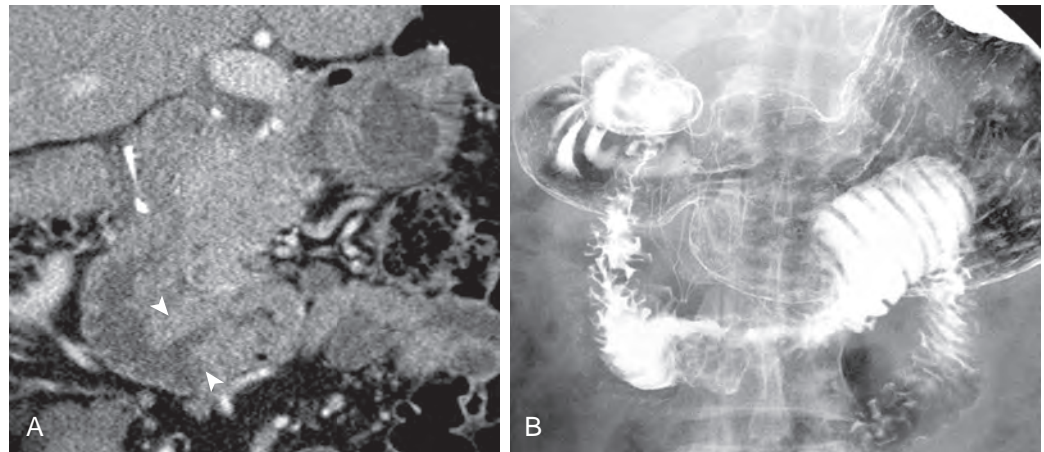


Figure 32-33 Duodenal carcinoma. **A.** Image from 3D MDCT enterography shows an annular lesion (arrowheads) in the third portion of the duodenum. **B.** Barium study confirms presence of this lesion in the distal duodenum.



CT is also useful for differentiating primary duodenal carcinoma from extrinsic tumors involving the duodenum, usually from the pancreas.²⁰⁰ Studies have shown that 3D MDCT is particularly helpful for localizing neoplasms to the duodenum and for accurately defining tumor extent (Fig. 32-33 and 34).²⁰¹ MDCT can also be helpful for detecting periampullary duodenal neoplasms. The differential diagnosis of duodenal wall thickening on CT includes lymphoma, Crohn's disease, hematomas, and duodenitis from a wide variety of causes. However, it is usually possible to suggest the correct diagnosis on the basis of the clinical history and findings on barium studies and CT.

Although ampullary and periampullary carcinomas may be confused with primary pancreatic carcinomas, it is important to distinguish these lesions because ampullary tumors have a much better prognosis. Hypotonic CT duodenography may be useful for differentiating these tumors. The examination is facilitated by placing the patient in the left side down decubitus position after administration of an effervescent agent and 1.0 mg of IV glucagon to obtain scans of the gas-filled duodenal sweep. Ampullary and periampullary lesions may be well demonstrated with this technique (Fig. 32-35).²⁰² CT and MRI scans may also suggest the diagnosis of an ampullary or periampullary tumor when these studies show an ampullary mass, papillary bulging, and irregular narrowing of the distal common bile duct.²⁰³

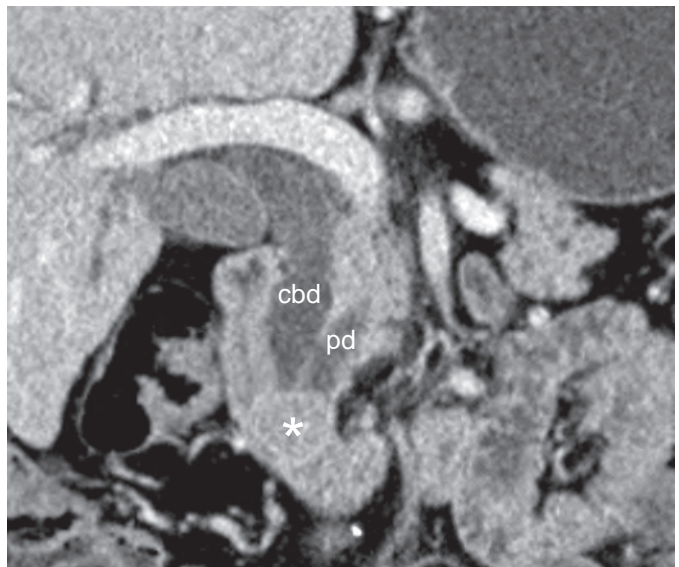


Figure 32-34 Periampullary duodenal carcinoma. This volume-rendered MDCT scan shows a mass (asterisk) in the periampullary duodenum obstructing the common bile duct with associated dilation of the common bile duct (cbd) and pancreatic duct (pd). MDCT is helpful for determining the cause of periampullary biliary obstruction.

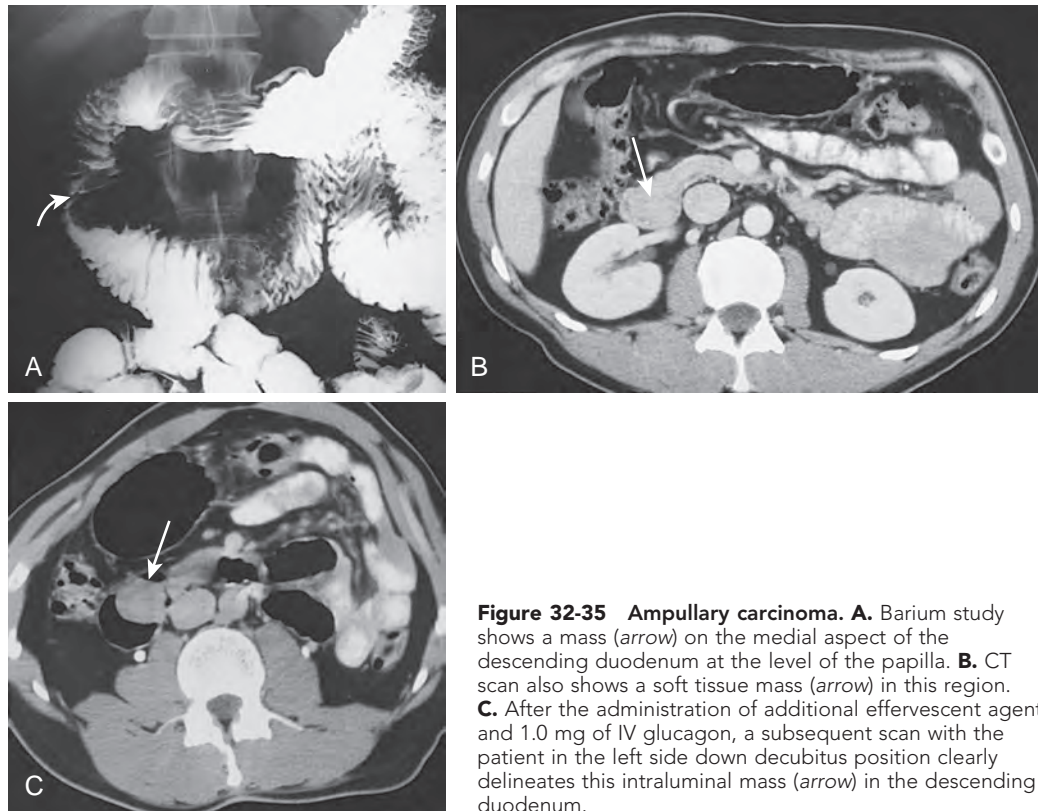


Figure 32-35 Ampullary carcinoma. **A.** Barium study shows a mass (arrow) on the medial aspect of the descending duodenum at the level of the papilla. **B.** CT scan also shows a soft tissue mass (arrow) in this region. **C.** After the administration of additional effervescent agent and 1.0 mg of IV glucagon, a subsequent scan with the patient in the left side down decubitus position clearly delineates this intraluminal mass (arrow) in the descending duodenum.

REFERENCES

1. Cady B, Ramsden DA, Stein A, et al: Gastric cancer: Contemporary aspects. *Am J Surg* 133: 423–429, 1977.
2. Devesa SS, Silverman DT: Cancer incidence and mortality trends in the United States: 1935–74. *J Natl Cancer Inst* 60:545–571, 1978.
3. Howson CP, Hiyama T, Wynder EL: The decline in gastric cancer: Epidemiology of an unplanned triumph. *Epidemiol Rev* 8:1–27, 1986.
4. Fuchs CS, Mayer RJ: Gastric carcinoma. *N Engl J Med* 333:32–41, 1995.
5. Moore JR: Gastric carcinoma: 30-year review. *Can J Surg* 29:25–28, 1986.
6. McBride CM, Boddie AW: Adenocarcinoma of the stomach: Are we making any progress? *South Med J* 80:283–286, 1987.
7. Cady B, Rossi RL, Silverman ML, et al: Gastric adenocarcinoma: A disease in transition. *Arch Surg* 124:303–308, 1989.
8. Boland CR, Scheiman JM: Tumors of the stomach. In Yamada T, editor: *Textbook of Gastroenterology*, Philadelphia, 1991, JB Lippincott, pp 1353–1379.
9. Kurtz RC, Sherlock P: Carcinoma of the stomach. In Berk JE, editor: *Bockus Gastroenterology*, Philadelphia, 1985, WB Saunders, pp 1278–1304.
10. Oiso T: Incidence of stomach cancer and its relation to dietary habits and nutrition in Japan between 1900 and 1975. *Cancer Res* 35: 3254–3258, 1975.
11. Neugut AI, Hayek M, Howe G: Epidemiology of gastric cancer. *Semin Oncol* 23:281–291, 1996.
12. Harrison LE, Zhang ZF, Karpeh MS, et al: The role of dietary factors in the intestinal and diffuse histologic subtypes of gastric adenocarcinoma. *Cancer* 80:1021–1028, 1997.
13. Mirvish SS: The etiology of gastric cancer: Intragastric nitrosamide formation and other theories. *J Natl Cancer Inst* 71:629–647, 1983.
14. Mirvish SS: Effects of vitamins C and E on *N*-nitroso compound formation, carcinogenesis, and cancer. *Cancer* 58:1842–1850, 1986.
15. Terry P, Lagergren J, Ye W, et al: Inverse association between intake of cereal fiber and risk of gastric cardia cancer. *Gastroenterology* 120: 387–391, 2001.
16. Correa P, Houghton JM: Carcinogenesis of *Helicobacter pylori*. *Gastroenterology* 133:659–672, 2007.
17. Parsonnet J, Friedman GD, Vandersteen DP, et al: *Helicobacter pylori* infection and the risk of gastric carcinoma. *N Engl J Med* 325:1127–1131, 1991.
18. Forman D, Newell DG, Fullerton F, et al: Association between infection with *Helicobacter pylori* and risk of gastric cancer: Evidence from a prospective investigation. *BMJ* 302:1302–1305, 1991.
19. Nomura A, Stemmermann GN, Chyou PH, et al: *Helicobacter pylori* infection and gastric carcinoma among Japanese Americans in Hawaii. *N Engl J Med* 325:1132–1136, 1991.
20. Asaka M, Takeda H, Sugiyama T, et al: What role does *Helicobacter pylori* play in gastric cancer? *Gastroenterology* 113(Suppl):S56–S60, 1997.
21. McFarlane GA, Munro A: *Helicobacter pylori* and gastric cancer. *Br J Surg* 84:1190–1199, 1997.
22. Morson BC: Carcinoma arising from areas of intestinal metaplasia in the gastric mucosa. *Br J Cancer* 9:377–385, 1955.
23. Correa P, Haenszel W, Cuello C, et al: Gastric precancerous process in a high-risk population: Cross-sectional studies. *Cancer Res* 50: 4731–4736, 1990.
24. Craanen ME, Dekker W, Blok P, et al: Intestinal metaplasia and *Helicobacter pylori*: An endoscopic bioptic study of the gastric antrum. *Gut* 33:16–20, 1992.
25. Hansson LE, Engstrand L, Nyren O, et al: Prevalence of *Helicobacter pylori* infection in subtypes of gastric cancer. *Gastroenterology* 109:885–888, 1995.
26. Martin-de-Argila C, Boixeda D, Redondo C, et al: Relation between histologic subtypes and location of gastric cancer and *Helicobacter pylori*. *Scand J Gastroenterol* 32:303–307, 1997.
27. Sozzi M, Valentini M, Figura N, et al: Atrophic gastritis and intestinal metaplasia in *Helicobacter pylori* infection: The role of *CagA* status. *Am J Gastroenterol* 93:375–379, 1998.
28. Blaser MJ, Perez-Perez GI, Klebanoff H, et al: Infection with *Helicobacter pylori* strains possessing *cagA* is associated with an increased risk of developing adenocarcinoma of the stomach. *Cancer Res* 55:2111–2115, 1995.
29. Huang JQ, Zheng GF, Sumanac K, et al: Meta-analysis of the relationship between *cagA* seropositivity and gastric cancer. *Gastroenterology* 125:1636–1644, 2003.

30. Parsonnet J, Harris RA, Hack HM, et al: Modelling cost-effectiveness of *Helicobacter pylori* screening to prevent gastric cancer: A mandate for clinical trials. *Lancet* 348:150–154, 1996.
31. Strickland RG, Mackay IR: A reappraisal of the nature and significance of chronic atrophic gastritis. *Am J Dig Dis* 18:426–440, 1973.
32. Walker IR, Strickland RG, Ungar B, et al: Simple atrophic gastritis and gastric carcinoma. *Gut* 12:906–911, 1971.
33. Cheli R, Santi L, Ciancamerla G, et al: A clinical and statistical follow-up study of atrophic gastritis. *Am J Dig Dis* 18:1061–1066, 1973.
34. Elsborg L, Mosbech J: Pernicious anaemia as a risk factor in gastric cancer. *Acta Med Scand* 206:315–318, 1979.
35. Brinton L, Gridley G, Hrubec Z, et al: Cancer risk following pernicious anaemia. *Br J Cancer* 59:810–813, 1989.
36. Schafer LW, Larson DE, Metton LJ, et al: Risk of development of gastric carcinoma in patients with pernicious anemia: A population-based study in Rochester, Minnesota. *Mayo Clin Proc* 60:444–448, 1985.
37. Ming S-C: The classification and significance of gastric polyps. In Yardley JH, Morson BC, Abell M, editors: *The Gastrointestinal Tract*, Baltimore, 1977, Williams & Wilkins, pp 149–175.
38. Ming S-C: The adenoma-carcinoma sequence in the stomach and colon: II. Malignant potential of gastric polyps. *Gastrointest Radiol* 1: 121–125, 1976.
39. Tomosulo J: Gastric polyps. Histologic types and their relationship to gastric carcinoma. *Cancer* 27:1346–1355, 1971.
40. Op den Orth JO, Dekker W: Gastric adenomas. *Radiology* 141:289–293, 1981.
41. Feldman F, Seaman WB: Primary gastric stump carcinoma. *AJR* 115:257–267, 1972.
42. Morgenstein L, Yamakawa T, Seltzer D: Carcinoma of the gastric stump. *Am J Surg* 125:29–38, 1973.
43. Caygill CPJ, Hill MJ, Kirkham JS, et al: Mortality from gastric cancer following gastric surgery for peptic ulcer. *Lancet* 1:929–931, 1986.
44. Offerhaus GJA, Tersmette AC, Huijbregtse K: Mortality caused by stomach cancer after remote partial gastrectomy for benign conditions: 40 years of follow-up of an Amsterdam cohort of 2633 postgastrectomy patients. *Gut* 29:1588–1590, 1980.
45. Viste A, Opheim P, Thunold J, et al: Risk of carcinoma following gastric operations for benign disease. *Lancet* 2:502–504, 1986.
46. Schafer LW, Larson DE, Melton LJ, et al: The risk of gastric carcinoma after surgical treatment for benign ulcer disease: A population-based study in Olmsted County, Minnesota. *N Engl J Med* 309:1210–1213, 1983.
47. Dougherty SH, Foster CA, Eisenberg MM: Stomach cancer following gastric surgery for benign disease. *Arch Surg* 117:294–297, 1982.
48. Goodman P, Levine MS, Gohil MN: Gastric carcinoma after gastrojejunostomy for benign disease: Radiographic findings. *Gastrointest Radiol* 17:211–213, 1992.
49. Williams SM, Harned RK, Settles RH: Adenocarcinoma of the stomach in association with Menetrier's disease. *Gastrointest Radiol* 3:387–390, 1978.
50. La Vecchia C, Negri E, Franceschi S, et al: Family history and the risk of stomach and colorectal cancer. *Cancer* 70:50–55, 1992.
51. Brenner H, Bode G, Boeing H: *Helicobacter pylori* infection among offspring of patients with stomach cancer. *Gastroenterology* 118: 31–35, 2000.
52. Bental HH, Aird I: A relationship between cancer of stomach and the ABO blood groups. *BMJ* 1:799–801, 1953.
53. Ming S-C: Atlas of Tumor Pathology, Fascicle 7, Tumors of the Esophagus and Stomach, Washington, DC, 1973, Armed Forces Institute of Pathology, pp 144–205.
54. Olearchyk AS: Gastric carcinoma: A critical review of 243 cases. *Am J Gastroenterol* 70:25–45, 1978.
55. Wanke M, Schwan H: Pathology of gastric cancer. *World J Surg* 3:675–684, 1979.
56. Moertel CG, Borgen JA, Soule EH: Multiple gastric cancers. *Gastroenterology* 32:1095–1103, 1957.
57. Mitsudomi T, Watanabe A, Matsusake T, et al: A clinicopathological study of synchronous multiple gastric cancers. *Br J Surg* 76:237–240, 1989.
58. Lauren P: The two histological main types of gastric carcinoma: Diffuse and so-called intestinal-type carcinoma. *Acta Pathol Microbiol Scand* 64:31–49, 1965.
59. Lauren PA, Nevalainen JT: Epidemiology of intestinal and diffuse types of gastric carcinoma: A time-trend study in Finland with comparison between studies from high- and low-risk areas. *Cancer* 71:2926–2933, 1993.
60. Watanabe H, Jass JR, Sobin LH: Histologic Typing of Oesophageal and Gastric Tumors, ed 2, Berlin, 1990, Springer-Verlag.
61. Shirakabe H, Nishizawa M, Maruyama M, et al: Atlas of X-Ray Diagnosis of Early Gastric Cancer, New York, 1982, Igaku-Shoin, pp 1–18.
62. Antonioli DA: Precursors of gastric carcinoma: A critical review with a brief description of early (curable) gastric cancer. *Hum Pathol* 25:994–1005, 1994.
63. Meyers WC, Damiano RJ, Rotolo FS, et al: Adenocarcinoma of the stomach: Changing patterns over the last 4 decades. *Ann Surg* 205:1–8, 1987.
64. Antonioli DA, Goldman H: Changes in the location and type of gastric adenocarcinoma. *Cancer* 50:775–781, 1982.
65. Powell J, McConkey CC: Increasing incidence of adenocarcinoma of the gastric cardia and adjacent sites. *Br J Cancer* 62:440–443, 1990.
66. Blot WJ, Devesa SS, Kneller RW, et al: Rising incidence of adenocarcinoma of the esophagus and gastric cardia. *JAMA* 265:1287–1289, 1991.
67. Pera M, Cameron AJ, Trastek VF, et al: Increasing incidence of adenocarcinoma of the esophagus and esophagogastric junction. *Gastroenterology* 104:510–513, 1993.
68. Fenoglio-Preiser CM, Noffsinger AE, Belli J, et al: Pathologic and phenotypic features of gastric cancer. *Semin Oncol* 23:292–306, 1996.
69. Dodge OG: The surgical pathway of gastroesophageal carcinoma. *Br J Surg* 49:121–125, 1961.
70. Koehler RE, Hanelin LG, Laing FC, et al: Invasion of the duodenum by carcinoma of the stomach. *Am J Surg* 128:201–205, 1977.
71. Menuck L: Transpyloric extension of gastric carcinoma. *Am J Dig Dis* 23:269–274, 1978.
72. Cho KC, Baker SR, Alterman DD, et al: Transpyloric spread of gastric tumors: Comparison of adenocarcinoma and lymphoma. *AJR* 167: 467–469, 1996.
73. Smith DL, Dockerty MB, Black BM: Gastrocolic fistulas of malignant origin. *Surg Gynecol Obstet* 134:829–834, 1972.
74. Holtz F, Hart WR: Krukenberg tumors of the ovary: A clinicopathologic analysis of 27 cases. *Cancer* 50:2438–2447, 1982.
75. Hansen RM, Hanson GA: Gastric carcinoma. *Am J Gastroenterol* 74:497–503, 1980.
76. Bloss RS, Miller TA, Copeland EM: Carcinoma of the stomach in the young adult. *Surg Gynecol Obstet* 150:883–886, 1980.
77. Holburt E, Freedman SI: Gastric carcinoma in patients younger than 36 years. *Cancer* 60: 1395–1399, 1987.
78. Grabiec J, Owen DA: Carcinoma of the stomach in young persons. *Cancer* 56:388–396, 1985.
79. MacDonald WC: Clinical and pathologic features of adenocarcinoma of the gastric cardia. *Cancer* 29:724–731, 1972.
80. Morales TG: Adenocarcinoma of the gastric cardia. *Dig Dis* 15:346–356, 1997.
81. Raskin MM: Some specific radiological findings and consideration of linitis plastica of the gastrointestinal tract. *Crit Rev Diagn Imaging* 8:87–105, 1976.
82. Fierst SM: Carcinoma of the cardia and fundus of the stomach. *Am J Gastroenterol* 57:403–409, 1972.
83. Webb JN, Busuttill A: Adenocarcinoma of the oesophagus and of the oesophagogastric junction. *Br J Surg* 65:475–479, 1978.
84. Qizilbash AH, Castelli M, Kowalski MA, et al: Endoscopic brush cytology and biopsy in the diagnosis of cancer of the upper gastrointestinal tract. *Acta Cytol* 24:313–318, 1980.
85. Llanos O, Guzman S, Duarte I: Accuracy of the first endoscopic procedure in the differential diagnosis of gastric lesions. *Ann Surg* 195:224–226, 1982.
86. Graham DY, Schwartz JT, Cain GD, et al: Prospective evaluation of biopsy number in the diagnosis of esophageal and gastric cancer. *Gastroenterology* 82:228–231, 1982.
87. Tatsuta M, Iishi H, Okuda S, et al: Prospective evaluation of diagnostic accuracy of gastrofibroscopic biopsy in diagnosis of gastric cancer. *Cancer* 63:1415–1420, 1989.
88. Winawer SJ, Posner G, Lightdale CJ, et al: Endoscopic diagnosis of advanced gastric cancer: Factors influencing yield. *Gastroenterology* 69:1183–1187, 1975.
89. Evans E, Harris O, Dickey D, et al: Difficulties in the endoscopic diagnosis of gastric and oesophageal cancer. *Aust N Z J Surg* 55:541–544, 1985.
90. Levine MS, Kong V, Rubesin SE, et al: Scirrhous carcinoma of the stomach: Radiologic and endoscopic diagnosis. *Radiology* 175:151–154, 1990.
91. Park MS, Ha HK, Choi BS, et al: Scirrhous gastric carcinoma: Endoscopy versus upper gastrointestinal radiography. *Radiology* 231: 421–426, 2004.
92. Koga M, Nakata H, Kiyonari H, et al: Roentgen features of the superficial depressed type of early gastric carcinoma. *Radiology* 15:289–292, 1975.
93. Montesi A, Graziani L, Pesaresi A, et al: Radiologic diagnosis of early gastric cancer by routine double-contrast examination. *Gastrointest Radiol* 7:205–215, 1982.
94. Gold RP, Green PH, O'Toole KM, et al: Early gastric cancer: Radiographic experience. *Radiology* 152:283–290, 1984.

95. White RM, Levine MS, Enterline HT, et al: Early gastric cancer: Recent experience. *Radiology* 155:25–27, 1985.
96. Murakami T: Pathomorphological diagnosis. In Murakami T, editor: *Early Gastric Cancer*, Tokyo, 1971, University of Tokyo Press, pp 53–55.
97. Sakita T, Ogura Y, Takasu S, et al: Observations on the healing of ulcerations in early gastric cancer: The life cycle of the malignant ulcer. *Gastroenterology* 60:835–844, 1971.
98. Kawai K: Diagnosis of early gastric cancer. *Endoscopy* 1:23–28, 1971.
99. Kaneko E, Nakamura T, Umeda N, et al: Outcome of gastric carcinoma detected by gastric mass survey in Japan. *Gut* 18:626–630, 1977.
100. Okui K, Tejima H: Evaluation of gastric mass survey. *Acta Chir Scand* 146:185–187, 1980.
101. Kaibara N, Kawaguchi H, Nishidoi H, et al: Significance of mass survey for gastric cancer from the standpoint of surgery. *Am J Surg* 142:543–545, 1981.
102. Evans DMD, Craven JL, Murphy F, et al: Comparison of early gastric cancer in Britain and Japan. *Gut* 19:1–9, 1978.
103. Seifert E, Butke H, Gail K, et al: Diagnosis of early gastric cancer. *Am J Gastroenterol* 71: 563–567, 1979.
104. Ohman U, Emas S, Rubio C: Relation between early and advanced gastric cancer. *Am J Surg* 140:351–355, 1980.
105. Green PH, O'Toole KM, Weinberg LM, et al: Early gastric cancer. *Gastroenterology* 81:247–256, 1981.
106. Busuttill A, Webb JN: Early carcinoma of the stomach: A ten-year survey. *J R Coll Surg Edinb* 26:322–327, 1981.
107. Carter KJ, Schaffer HA, Ritchie WP: Early gastric cancer. *Ann Surg* 199:604–609, 1984.
108. Green PHR, O'Toole KM, Slonim D, et al: Increasing incidence and excellent survival of patients with early gastric cancer: Experience in a United States medical center. *Am J Med* 85:658–661, 1988.
109. Thomas RL, Rice RP: Calcifying mucinous adenocarcinoma of the stomach. *Radiology* 88:1002–1003, 1967.
110. Balthazar E, Rosenthal N: Calcifying mucin-producing adenocarcinoma of stomach. *N Y State J Med* 73:2704–2706, 1973.
111. Lwin TOM, Soodeen TH: A case report on calcified mucinous adenocarcinoma of the stomach. *J Can Assoc Radiol* 24:370–373, 1973.
112. Low VHS, Levine MS, Rubesin SE, et al: Diagnosis of gastric carcinoma: Sensitivity of double-contrast barium studies. *AJR* 162:329–334, 1994.
113. Shindoh N, Nakagawa T, Ozaki Y, et al: Overlooked gastric carcinoma: Pitfalls in upper gastrointestinal radiology. *Radiology* 217:409–414, 2000.
114. Brandt D, Muramatsu Y, Ushio K, et al: Synchronous early gastric cancer. *Radiology* 173: 649–652, 1989.
115. Nelson SW: The discovery of gastric ulcers and the differential diagnosis between benignancy and malignancy. *Radiol Clin North Am* 7:5–25, 1969.
116. Wolf BS: Observations on roentgen features of benign and malignant gastric ulcers. *Semin Roentgenol* 6:140–150, 1971.
117. Carman RD: A new roentgen-ray sign of ulcerating gastric cancer. *JAMA* 77:990–992, 1921.
118. Kirklin BR: The value of the meniscus sign in the roentgenologic diagnosis of ulcerating gastric carcinoma. *Radiology* 22:131–135, 1934.
119. Marshak RH, Lindner AE, Maklansky D: Carcinoma of the stomach. In Marshak RH, Lindner AE, Maklansky D, editors: *Radiology of the Stomach*, Philadelphia, 1983, WB Saunders, pp 108–146.
120. Balthazar EJ, Rosenberg H, Davidian MM: Scirrhus carcinoma of the pyloric channel and distal antrum. *AJR* 134:669–673, 1980.
121. Kobayashi S, Yamada A, Kawai B, et al: Study on early cancer of the cardiac region: X-ray findings of the surrounding area of the oesophagogastric junction. *Australas Radiol* 16:258–270, 1972.
122. Freeny PC: Double-contrast gastrography of the fundus and cardia: Normal landmarks and their pathologic changes. *AJR* 133:481–487, 1979.
123. Herlinger H, Grossman R, Laufer I, et al: The gastric cardia in double-contrast study: Its dynamic image. *AJR* 135:21–29, 1980.
124. Levine MS, Laufer I, Thompson JJ: Carcinoma of the gastric cardia in young people. *AJR* 140:69–72, 1983.
125. Freeny PC, Marks WM: Adenocarcinoma of the gastroesophageal junction: Barium and CT examination. *AJR* 138:1077–1084, 1982.
126. Balthazar EJ, Goldfine S, Davidian NM: Carcinoma of the esophagogastric junction. *Am J Gastroenterol* 74:237–243, 1980.
127. Milnes JP, Hine KR, Holmes GKT, et al: Limitations of endoscopy in the diagnosis of carcinoma of the cardia of the stomach. *Br J Radiol* 55:593–595, 1982.
128. Lawson TL, Dodds WJ: Infiltrating carcinoma simulating achalasia. *Gastrointest Radiol* 1: 245–248, 1976.
129. Woodfield CA, Levine MS, Rubesin SE, et al: Diagnosis of primary versus secondary achalasia: Reassessment of clinical and radiographic criteria. *AJR* 175:727–731, 2000.
130. Ba-Ssalamah A, Prokop M, Uffmann M, et al: Dedicated multidetector CT of the stomach: Spectrum of diseases. *Radiographics* 23:625–644, 2003.
131. Kumano S, Murakami T, Kim T, et al: T staging of gastric cancer: Role of multi-detector row CT. *Radiology* 237:961–966, 2005.
132. Vorbeck F, Osterreicher C, Puspok A, et al: Comparison of spiral-computed tomography with water-filling of the stomach and endosonography for gastric lymphoma of mucosa-associated lymphoid tissue-type. *Digestion* 65:196–199, 2002.
133. Mani NB, Suri S, Gupta S, et al: Two-phase dynamic contrast-enhanced computed tomography with water-filling method for staging of gastric carcinoma. *Clin Imaging* 25:38–43, 2001.
134. Kim JH, Park SH, Hong HS, et al: CT gastrography. *Abdom Imaging* 30:509–517, 2005.
135. Inamoto K, Kouzai K, Ueda T, et al: CT virtual endoscopy of the stomach: Comparison study with gastric fiberoscopy. *Abdom Imaging* 30:473–479, 2005.
136. Kim JP, Lee JH, Kim SJ, et al: Clinicopathologic characteristics and prognostic factors in 10783 patients with gastric cancer. *Gastric Cancer* 1:125–133, 1998.
137. Balthazar EJ, Siegel SE, Megibow AJ, et al: CT in patients with scirrhus carcinoma of the GI tract: imaging findings and value for tumor detection and staging. *AJR* 165:839–845, 1995.
138. Kim JI, Kim YH, Lee KH, et al: Type-specific diagnosis and evaluation of longitudinal tumor extent of Borrmann type IV gastric cancer: CT versus gastroscopy. *Korean J Radiol* 14:597–606, 2013.
139. Park MS, Yu JS, Kim MJ, et al: Mucinous versus nonmucinous gastric carcinoma: Differentiation with helical CT. *Radiology* 223:540–546, 2002.
140. Insko EK, Levine MS, Birnbaum BA, et al: Benign and malignant lesions of the stomach: Evaluation of CT criteria for differentiation. *Radiology* 228:166–171, 2003.
141. Pickhardt PJ, Asher DB: Wall thickening of the gastric antrum as a normal finding: Multidetector CT with cadaveric comparison. *AJR* 181: 973–979, 2003.
142. Thompson WM, Halvorsen RA, Foster W, et al: Computed tomography of the gastroesophageal junction: Value of the left lateral decubitus view. *J Comput Assist Tomogr* 8:346–349, 1984.
143. Lee DH, Seo TS, Ko YT: Spiral CT of gastric carcinoma: Staging and enhancement pattern. *Clin Imaging* 25:32–37, 2001.
144. Shimizu K, Ito K, Matsunaga N, et al: Diagnosis of gastric cancer with MDCT using the water-filling method and multiplanar reconstruction: CT-histologic correlation. *AJR* 185: 1152–1158, 2005.
145. Usui S, Hiranuma S, Ichikawa T, et al: Preoperative imaging of surrounding arteries by three-dimensional CT: Is it useful for laparoscopic gastrectomy? *Surg Laparosc Endosc Percutan Tech* 15:61–65, 2005.
146. Cormier WJ, Gaffey TA, Welch JM, et al: Linitis plastica caused by metastatic lobular carcinoma of the breast. *Mayo Clin Proc* 55:747–753, 1980.
147. Levine MS, Pantongrag-Brown L, Aguilera NS, et al: Non-Hodgkin lymphoma of the stomach: A cause of linitis plastica. *Radiology* 201:375–378, 1996.
148. Eisenberg RL: *Gastrointestinal Radiology: A Pattern Approach*, ed 2, Philadelphia, 1990, JB Lippincott, pp 205–222.
149. Bryk D, Elguezal A: Roentgen problems in evaluating the atrophic stomach of the elderly. *AJR* 123:236–241, 1975.
150. Levine MS, Caroline D, Thompson JJ, et al: Adenocarcinoma of the esophagus: Relationship to Barrett mucosa. *Radiology* 150:305–309, 1984.
151. Allen HA, Bush JE: Midesophageal carcinoma metastatic to the stomach: Its unusual appearance on an upper gastrointestinal series. *South Med J* 76:1049–1051, 1983.
152. Glick SN, Teplick SK, Levine MS, et al: Gastric cardia metastasis in esophageal carcinoma. *Radiology* 160:627–630, 1986.
153. Anderson MF, Dunnick NR: Pseudotumor caused by gastric varices. *Am J Dig Dis* 22:929–932, 1977.
154. Carucci LR, Levine MS, Rubesin SE, et al: Tumorous gastric varices: Radiographic findings in 10 patients. *Radiology* 212:861–865, 1999.
155. Kim HJ, Kim AY, Oh ST, et al: Gastric cancer staging at multi-detector row CT gastrography: Comparison of transverse and volumetric CT scanning. *Radiology* 236:879–885, 2005.
156. Hwang SW, Lee DH, Lee SH, et al: Preoperative staging of gastric cancer by endoscopic ultrasonography and multidetector-row computed tomography. *J Gastroenterol Hepatol* 25:512–518, 2010.

157. Ge MY, Yin HB, Wan KM, et al: Computed tomography of gastrohepatic ligament Involvement by gastric carcinoma. *Abdom Imaging* 38:697–704, 2013.
158. Kim SH, Kim WH, Park KJ, et al: CT and MR findings of Krukenberg tumors: Comparison with primary ovarian tumors. *J Comput Assist Tomogr* 20:393–398, 1996.
159. Sotiropoulos GC, Kaiser GM, Lang H, et al: Staging laparoscopy in gastric cancer. *Eur J Med Res* 10:88–91, 2005.
160. Burbidge S, Mahady K, Naik K: The role of CT and staging laparoscopy in the staging of gastric cancer. *Clin Radiol* 68:251–255, 2013.
161. Lim JS, Kim MJ, Yun MJ, et al: Comparison of CT and ¹⁸F-FDG pet for detecting peritoneal metastasis on the preoperative evaluation for gastric carcinoma. *Korean J Radiol* 7:249–256, 2006.
162. Rosch T: Endoscopic ultrasonography. *Endoscopy* 26:148–168, 1994.
163. Kochman ML, Scheiman JM: Endosonography—is it sound for the masses? *J Clin Gastroenterol* 19:2–5, 1994.
164. Kimmey MB, Martin RW, Haggitt RC, et al: Histological correlates of gastrointestinal endoscopic ultrasound images. *Gastroenterology* 96:433–441, 1989.
165. Kadish S, Kochman ML: Applications of gastrointestinal endoscopy in oncology. *Oncology* 9:967–980, 1995.
166. Botet JF, Lightdale CJ, Zauber AG: Preoperative staging of gastric cancer: Comparison of endoscopic US and dynamic CT. *Radiology* 181:426–432, 1991.
167. Abe S, Lightdale CJ, Brennan MF: The Japanese experience with endoscopic ultrasonography in the staging of gastric cancer. *Gastrointest Endosc* 39:586–591, 1993.
168. Rosch T: Endosonographic staging of gastric cancer: A review of literature results. *Gastrointest Endosc Clin N Am* 5:549–557, 1995.
169. Murata Y, Suzuki S, Hashimoto H: Endoscopic ultrasonography of the upper gastrointestinal tract. *Surg Endosc* 2:180–183, 1988.
170. Dittler JH, Siewert JR: Role of endoscopic ultrasonography in gastric carcinoma. *Endoscopy* 25:162–166, 1993.
171. Colin Jones DG, Rosch T, Dittler HL: Staging of gastric cancer by endoscopy. *Endoscopy* 25:34–38, 1993.
172. Tio TL, Coene PPLO, Schouwink MH, et al: Esophagogastric carcinoma. Preoperative TNM classification with endosonography. *Radiology* 173:411–417, 1989.
173. Kutup A, Vashist YK, Groth S, et al: Endoscopic ultrasound staging in gastric cancer: Does it help management decisions in the era of neoadjuvant treatment? *Endoscopy* 44:572–576, 2012.
174. Andriulli A, Recchia S, De Angelis C, et al: Endoscopic ultrasonographic evaluation of patients with biopsy negative gastric linitis plastica. *Gastrointest Endosc* 36:611–615, 1990.
175. Mendis RE, Gerdes H, Lightdale CJ, et al: Large gastric folds: A diagnostic approach using endoscopic ultrasonography. *Gastrointest Endosc* 40:437–441, 1994.
176. Hildebrandt U, Feifel G: Endosonography in the diagnosis of lymph nodes. *Endoscopy* 25:243–245, 1993.
177. Faigel DO, Ginsberg GG, Furth EE, et al: Endosonography for malignant lymphadenopathy: Caveats and pitfalls. *Gastrointest Endosc* 43:294, 1996.
178. Akahoshi K, Misawa T, Fujishima H, et al: Regional lymph node metastasis in gastric cancer: Evaluation with endoscopic US. *Radiology* 182:559–564, 1992.
179. Tio TL, Kallimanis GE: Endoscopic ultrasonography of perigastric lymph nodes. *Endoscopy* 26:776–779, 1994.
180. Wiersema MJ, Kochman ML, Cramer HM, et al: Endosonography-guided real-time fine-needle aspiration biopsy. *Gastrointest Endosc* 40:700–707, 1994.
181. Polkowski M, Palucki J, Wronska E, et al: Endosonography versus helical computed tomography for locoregional staging of gastric cancer. *Endoscopy* 36:617–623, 2004.
182. Habermann CR, Weiss F, Riecken R, et al: Preoperative staging of gastric adenocarcinoma: Comparison of helical CT and endoscopic US. *Radiology* 230:465–471, 2004.
183. Joo I, Lee JM, Kim JH, et al: Prospective comparison of 3T MRI with diffusion-weighted imaging and MDCT for the preoperative TNM staging of gastric cancer. *J Magn Reson Imaging* 2014. <http://dx.doi.org/10.1002/jmri.24586>.
184. Ozkan E, Araz M, Soydal C, et al: The role of ¹⁸F-FDG-PET/CT in the preoperative staging and posttherapy follow up of gastric cancer: Comparison with spiral CT. *World J Surg Oncol* 9:75, 2011.
185. Akahoshi K, Chijiwa Y, Hamada S, et al: Endoscopic ultrasonography: A promising method for assessing the prospects of endoscopic mucosal resection in early gastric cancer. *Endoscopy* 29:614–619, 1997.
186. Gore RM: Upper gastrointestinal tract tumours: Diagnosis and staging strategies. *Cancer Imaging* 5:95–98, 2005.
187. Everett SM, Axon ATR: Early gastric cancer in Europe. *Gut* 41:142–150, 1997.
188. Spira IH, Ghazi A, Wolff WI: Primary adenocarcinoma of the duodenum. *Cancer* 39:1721–1726, 1977.
189. Cortese AF, Cornell GN: Carcinoma of the duodenum. *Cancer* 29:1010–1015, 1972.
190. Joesting DR, Beart RW, Jr, van Heerden JA, et al: Improving survival in adenocarcinoma of the duodenum. *Am J Surg* 141:228–231, 1981.
191. Bradford D, Levine MS, Hoang D, et al: Early duodenal cancer: Detection on double-contrast upper gastrointestinal radiography. *AJR* 174:1564–1566, 2000.
192. Itoh H, Iida M, Kuroiwa S, et al: Gardner's syndrome associated with carcinoma of the duodenal bulb: Report of a case. *Am J Gastroenterol* 80:248–250, 1985.
193. Levine ML, Dorf BS, Bank S: Adenocarcinoma of the duodenum in a patient with nontropical sprue. *Am J Gastroenterol* 81:800–802, 1986.
194. Meiselman MS, Ghahremani GG, Kaufman MW: Crohn's disease of the duodenum complicated by adenocarcinoma. *Gastrointest Radiol* 12:333–336, 1987.
195. Slezak P, Rubio C, Blomqvist L, et al: Duodenal adenocarcinoma in Crohn's disease of the small bowel: A case report. *Gastrointest Radiol* 16:15–17, 1991.
196. McGlinchey JJ, Santer GJ, Haggani MT: Primary adenocarcinoma of the duodenum associated with cutaneous neurofibromatosis. *Postgrad Med J* 58:115–116, 1982.
197. Barloon TJ, Lu CH, Honda H, et al: Primary adenocarcinoma of the duodenal bulb: Radiographic and pathologic findings in two cases. *Gastrointest Radiol* 14:223–225, 1989.
198. Farah MC, Jafri SZ, Schwab RE, et al: Duodenal neoplasms: Role of CT. *Radiology* 162:839–843, 1987.
199. Kazerooni EA, Quint LE, Francis IR: Duodenal neoplasms: Predictive value of CT for determining malignancy and tumor resectability. *AJR* 159:303–309, 1992.
200. Jayaraman MV, Mayo-Smith WW, Movson JS, et al: CT of the duodenum: An overlooked segment gets its due. *Radiographics* 21:S147–S160, 2001.
201. House MG, Yeo CJ, Cameron JL, et al: Predicting resectability of periampullary cancer with three-dimensional computed tomography. *J Gastrointest Surg* 8:280–288, 2004.
202. Bree RL, Megibow AJ: Hypotonic CT duodenography in the evaluation of periampullary neoplasms. *Radiology* 177:251, 1990.
203. Chung YE, Kim MJ, Kim HM, et al: Differentiation of benign and malignant ampullary obstructions on MR imaging. *Eur J Radiol* 80:198–203, 2011.

Other Malignant Tumors of the Stomach and Duodenum

MARC S. LEVINE | ALEC J. MEGIBOW

CHAPTER OUTLINE

Metastases

Clinical Findings
Radiographic Findings
Differential Diagnosis

Lymphoma

Pathology
Clinical Findings
Endoscopic Findings
Treatment and Prognosis
Radiographic Findings
Differential Diagnosis
Duodenal Lymphoma

Malignant Gastrointestinal Stromal Tumor

Pathology
Clinical Findings
Radiographic Findings
Differential Diagnosis
Malignant Duodenal Gastrointestinal Stromal Tumor

Kaposi's Sarcoma

Clinical Findings
Pathologic and Endoscopic Findings
Radiographic Findings
Differential Diagnosis

Carcinoid Tumors

Pathology
Clinical Findings
Radiographic Findings

Miscellaneous Tumors

Metastases

Gastric metastases are found at autopsy in less than 2% of patients who die of carcinoma.¹ Duodenal metastases are even rarer. Nevertheless, metastases to the stomach and duodenum have been encountered more frequently as combined treatment with surgery, radiation, and/or chemotherapy has led to prolonged survival of patients with widespread metastatic disease. Most lesions are hematogenous metastases from malignant melanoma or carcinoma of the breast or lung. Less frequently, the stomach or duodenum may be involved by lymphatic spread of tumor or by direct extension of tumor from neighboring structures or mesenteric reflections such as the gastocolic ligament, transverse mesocolon, and greater omentum. These various forms of spread produce characteristic

radiographic findings that are considered separately in the following sections.

CLINICAL FINDINGS

Most gastroduodenal metastases are discovered unexpectedly at surgery or autopsy.² However, some patients with ulcerated metastases may develop signs or symptoms of upper gastrointestinal (GI) bleeding, such as hematemesis, melena, and guaiac-positive stool.^{3,4} Others may present with epigastric pain, nausea, vomiting, early satiety, anorexia, or weight loss. One or more of these findings are sometimes caused by systemic chemotherapy or the hypercalcemia associated with widespread metastatic disease.⁵ As a result, gastroduodenal metastases may not be suspected, even if symptoms are present.

Most patients with gastroduodenal metastases have a known underlying malignancy. Occasionally, however, metastases to the stomach or duodenum may occur as the initial manifestation of an occult primary tumor.⁴ Certain malignancies such as carcinoma of the breast and kidney can also metastasize to the stomach or duodenum many years after treatment of the original lesion.^{5,6} It is therefore important to obtain a detailed clinical history in these patients.

RADIOGRAPHIC FINDINGS

Hematogenous Metastases

True hematogenous or blood-borne metastases to the stomach or duodenum may be caused by a variety of malignant tumors. Although malignant melanoma has the highest percentage of hematogenous metastases to the GI tract,⁷ breast cancer is such a common disease that it rivals melanoma as the most common cause of metastases to the bowel.⁵ Much less frequently, the stomach or duodenum may be involved by hematogenous metastases from thyroid or testicular carcinoma or from other remote tumors.¹

Hematogenous metastases usually appear on barium studies as one or more discrete submucosal masses in the stomach, duodenum, or small intestine (Fig. 33-1).^{5,8-11} When multiple lesions are present, they tend to be of varying sizes because of periodic showers of tumor emboli into the arterial supply of the bowel.^{8,12} As these submucosal masses outgrow their blood supply, they may undergo central necrosis and ulceration, resulting in the development of classic “bull’s-eye” or “target” lesions (Fig. 33-2).^{8,10-13} In general, bull’s-eye lesions have large central ulcers in relation to the size of the surrounding mass.^{8,12} Superficial fissures may occasionally radiate toward the central ulcer crater, producing a characteristic spoke wheel pattern (see Fig. 33-2B).⁸

Hematogenous metastases to the stomach or duodenum are sometimes manifested by larger, more lobulated masses that can be mistaken radiographically for malignant gastrointestinal

Figure 33-1 Gastric metastases from malignant melanoma. **A.** A discrete submucosal mass (arrow) is seen in the gastric fundus. **B.** In another patient, a large submucosal mass (arrow) is present in the duodenal bulb.

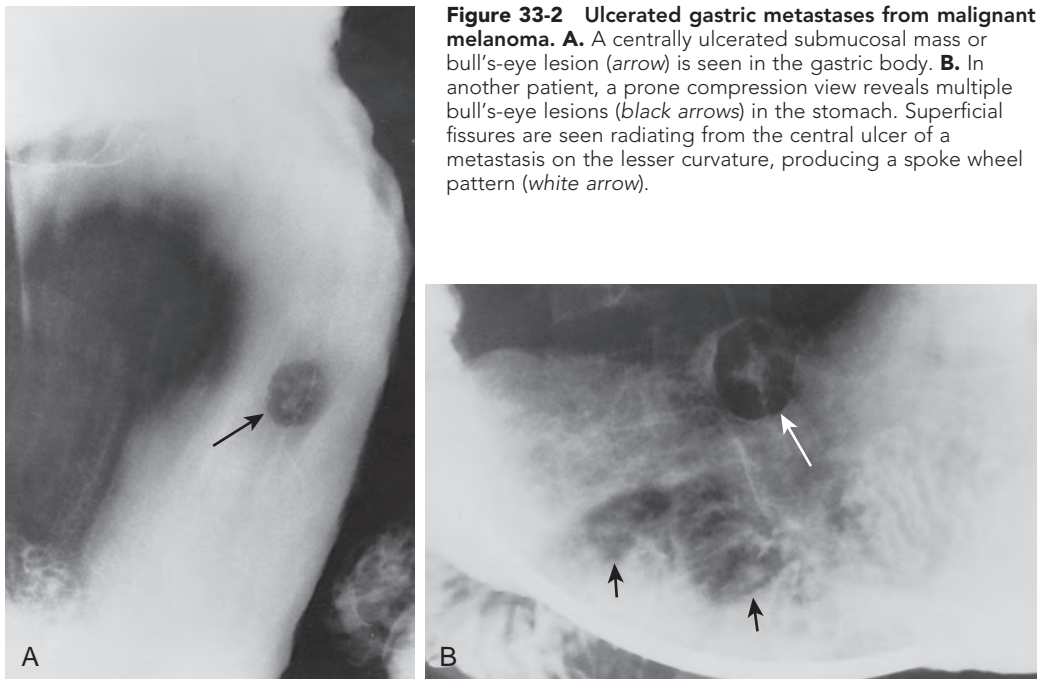
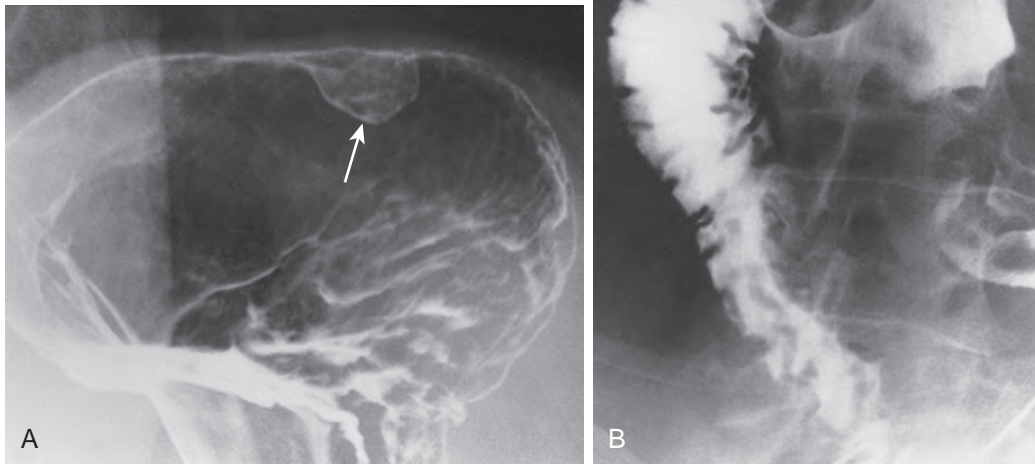


Figure 33-2 Ulcerated gastric metastases from malignant melanoma. **A.** A centrally ulcerated submucosal mass or bull's-eye lesion (arrow) is seen in the gastric body. **B.** In another patient, a prone compression view reveals multiple bull's-eye lesions (black arrows) in the stomach. Superficial fissures are seen radiating from the central ulcer of a metastasis on the lesser curvature, producing a spoke wheel pattern (white arrow).

stromal tumors (GISTs) or even polypoid carcinomas (Fig. 33-3).¹³ Other metastases, particularly those from malignant melanoma, may become necrotic, resulting in the development of giant cavitated lesions. These cavitated metastases can be recognized on barium studies as amorphous collections of barium (usually ranging from 5-15 cm in size) that communicate with the lumen (Fig. 33-4).^{11,14} Computed tomography (CT) is particularly well suited for demonstrating these giant cavitated lesions.¹⁵

Hematogenous metastases to the stomach from breast cancer may produce a linitis plastica or "leather bottle" appearance indistinguishable from that of a primary scirrhous carcinoma of the stomach (Fig. 33-5).^{5,8,9,11} This linitis plastica appearance is caused not by fibrosis (as in patients with scirrhous carcinoma) but by highly cellular infiltrates of metastatic tumor in the gastric wall.⁸ Although the degree of luminal narrowing is variable, these lesions can still be recognized on double-contrast studies by distortion of the normal surface pattern of the

stomach with mucosal nodularity, spiculation, ulceration, or thickened, irregular folds (see Fig. 33-5).¹⁶ Some of these tumors may involve the proximal portion of the stomach with sparing of the antrum (see Fig. 33-5B).¹⁶ The possibility of metastatic disease should therefore be considered in any patient with linitis plastica who has a history of breast carcinoma.

Metastatic disease to the stomach is usually found on CT studies performed as part of the routine work-up of patients with known malignant tumors. Although many extragastric tumors can metastasize to the stomach, careful evaluation of

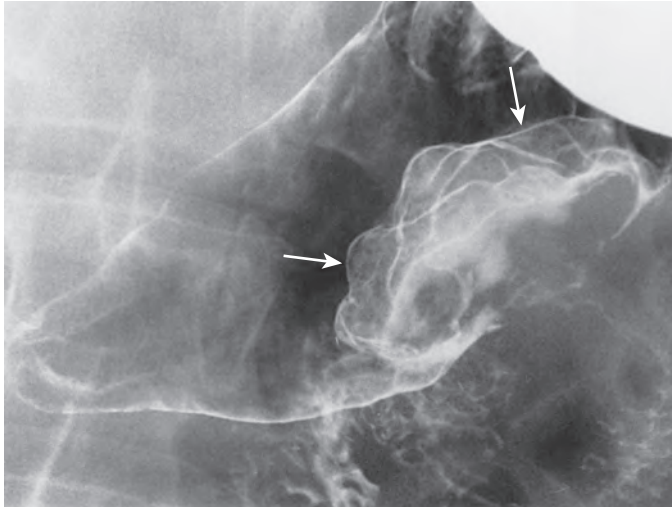


Figure 33-3 Gastric metastasis from malignant melanoma. There is a large lobulated mass (arrows) on the greater curvature of the stomach. This lesion could be mistaken for a malignant GI stromal tumor or even an adenocarcinoma.

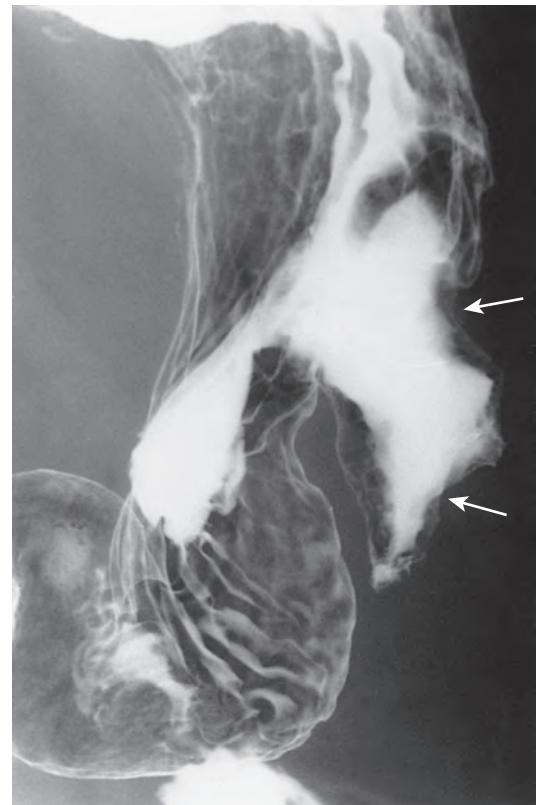


Figure 33-4 Cavitated metastasis from malignant melanoma. A giant cavitated lesion (arrows) is seen on the greater curvature of the stomach. A malignant GI stromal tumor or lymphoma could produce similar findings. (From Laufer I, Levine MS [eds]: *Double Contrast Gastrointestinal Radiology*, 2nd ed. Philadelphia, WB Saunders, 1992.)

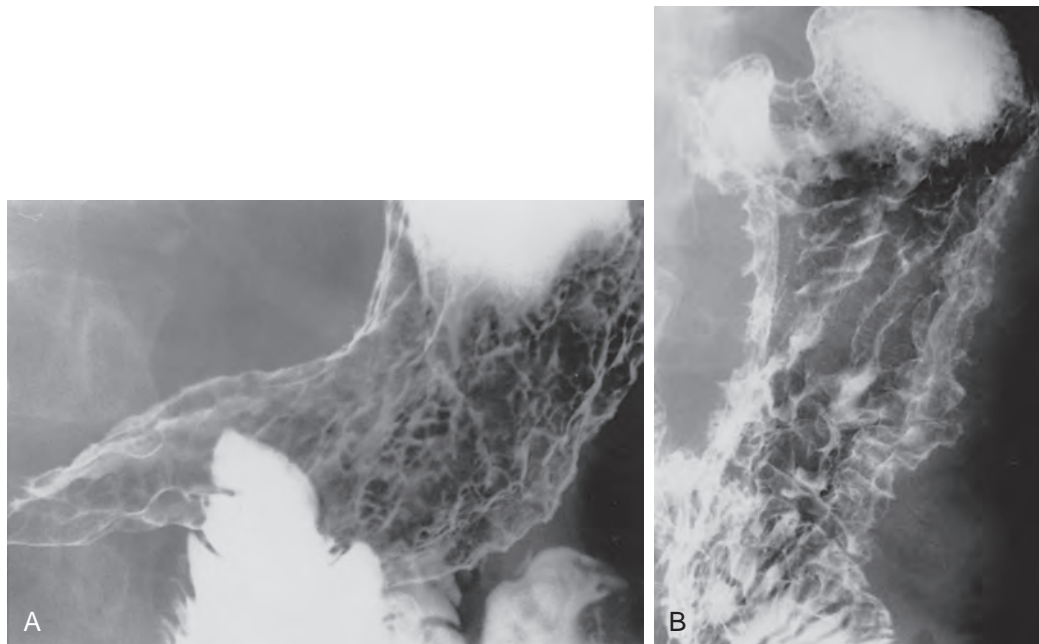


Figure 33-5 Metastatic breast cancer involving the stomach with a linitis plastica appearance. **A.** There is only mild loss of distensibility of the gastric antrum and body, but the mucosa has a nodular, irregular appearance because of infiltration by metastatic tumor. **B.** In another patient, the area of involvement is confined to the proximal half of the stomach. The fundus and body have an irregular contour with thickened, spiculated folds. (From Levine MS, Kong V, Rubesin SE, et al: *Scirrhus carcinoma of the stomach: Radiologic and endoscopic diagnosis. Radiology* 175:151–154, 1990.)

the stomach is particularly important in patients with known malignant melanoma or breast or lung cancer. It has been found that metastatic breast cancer involves the stomach in 5% to 27% of patients, often causing extensive gastric wall thickening (sometimes associated with increased attenuation of the wall after intravenous [IV] contrast enhancement) that simulates the linitis plastica appearance of a scirrhous gastric cancer (Fig. 33-6).^{17,18} In other patients, CT may demonstrate more focal wall thickening (Fig. 33-7). Because these tumors often reside deeply within the gastric wall, it can be difficult to obtain a definitive pathologic diagnosis from endoscopic biopsy specimens. Nevertheless, in the proper clinical setting, CT findings should be highly suggestive of metastatic breast cancer involving the stomach.¹⁹

Hematogenous metastases to the stomach from malignant melanoma, bronchogenic carcinoma, and Kaposi's sarcoma may also be detected on CT.

Lymphatic Spread

Gastric metastases are found at autopsy in 2% to 15% of patients who die of squamous cell carcinoma of the esophagus.²⁰ These metastases are thought to be caused by tumor emboli that seed the gastric cardia or fundus via submucosal esophageal lymphatics extending subdiaphragmatically to paracardiac, lesser curvature, and celiac nodes. Squamous cell metastases to the gastric fundus may appear on barium studies as giant submucosal masses, often containing central areas of ulceration (Fig. 33-8).^{20,21} As a result, these lesions can be mistaken for benign or malignant GISTs or even adenocarcinomas.²² Squamous cell metastases to paracardiac or other lymph nodes in the upper abdomen are sometimes recognized on CT scans as low-attenuation masses relative to skeletal muscle (Fig. 33-9).

The duodenum is occasionally involved by peripancreatic lymphadenopathy from pancreatic carcinoma, lymphoma, or

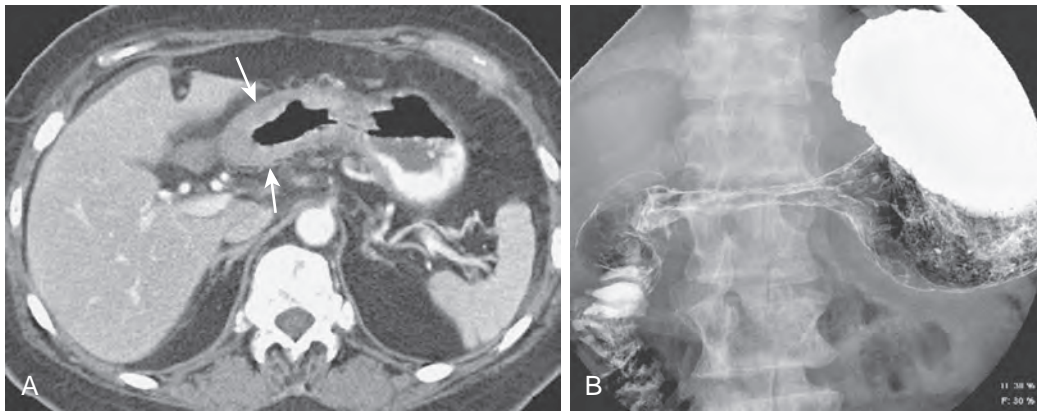
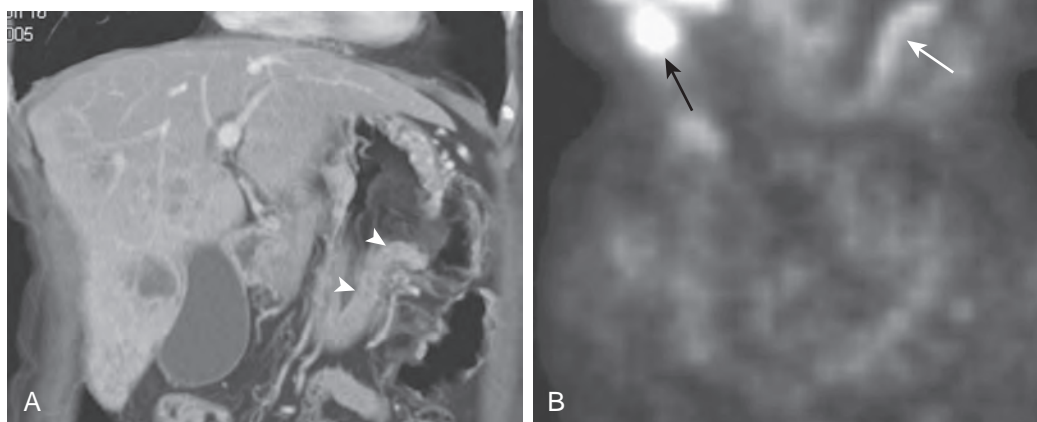


Figure 33-6 Metastatic breast cancer to the stomach with a linitis plastica appearance on CT. A. Multidetector CT (MDCT) scan of an older woman with metastatic breast carcinoma and early satiety shows marked thickening of the wall of the gastric antrum (arrows). The radiographic findings are indistinguishable from those of a primary scirrhous carcinoma of the stomach. **B.** Barium study in the same patient shows marked narrowing of the antrum, producing a classic linitis plastica appearance.

Figure 33-7 Metastatic breast cancer to the gastric wall on CT. A. MDCT scan of a middle-aged woman with metastatic breast carcinoma shows localized thickening of the greater curvature of the stomach (arrowheads). **B.** ¹⁸F-FDG-PET/CT image in the same patient shows increased activity in the gastric wall (white arrow) and liver (black arrows).



other malignant tumors. In such cases, barium studies may reveal nodular indentations on the medial border of the descending duodenum or widening of the duodenal sweep. However, pancreatic carcinoma, pancreatic pseudocysts, and pancreatitis can produce identical radiographic findings. CT is

extremely helpful for determining the cause of a widened duodenal sweep and for differentiating a pancreatic mass from adjacent lymphadenopathy.

Malignant tumors that metastasize to retroperitoneal lymph nodes near the superior mesenteric root may be manifested on barium studies by extrinsic mass effect, nodular indentations, ulceration, or, in advanced cases, obstruction of the distal duodenum near the ligament of Treitz (Fig. 33-10A).²³ CT is ideally suited for demonstrating retroperitoneal adenopathy as the cause of these abnormalities (Fig. 33-10B). Occasionally, retroperitoneal tumor involving the duodenum may cause delayed



Figure 33-8 Squamous cell metastasis to the gastric cardia. A giant submucosal mass (arrow) in the fundus could be mistaken for a benign or malignant gastrointestinal stromal tumor. (From Glick SN, Teplick SK, Levine MS: *Squamous cell metastases to the gastric cardia*. *Gastrointest Radiol* 10:339–344, 1985.)



Figure 33-9 Metastatic adenopathy from squamous cell carcinoma of the esophagus. A bulky mass of adenopathy is seen in the region of the lesser sac. The low attenuation of the enlarged nodes is characteristic of squamous cell metastases.

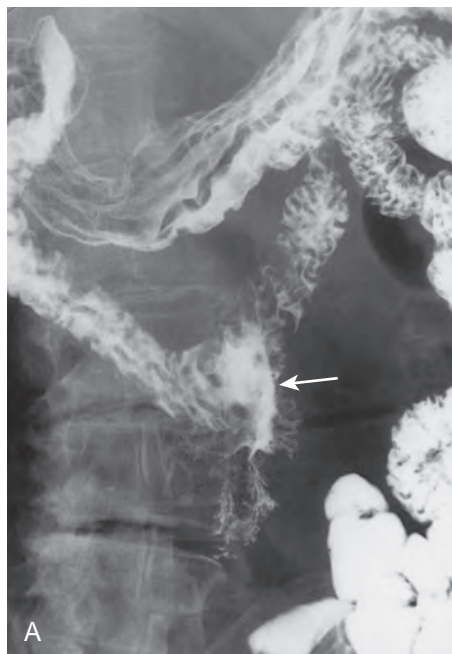
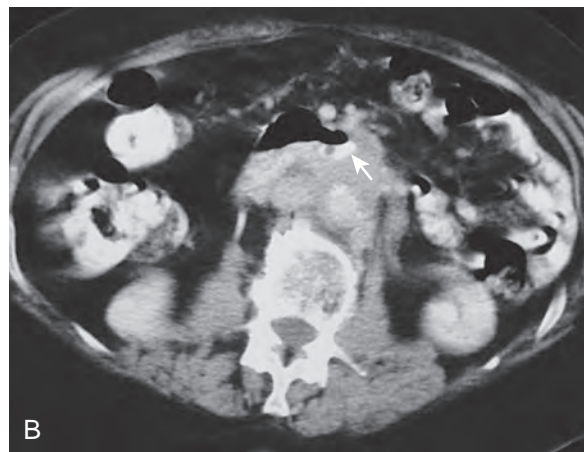


Figure 33-10 Duodenal invasion by retroperitoneal adenopathy. **A.** Barium study shows an ulcerated lesion (arrow) at the junction of the third and fourth portions of the duodenum. **B.** CT scan reveals a conglomerate mass of para-aortic adenopathy encasing the distal duodenum with associated ulceration (arrow).



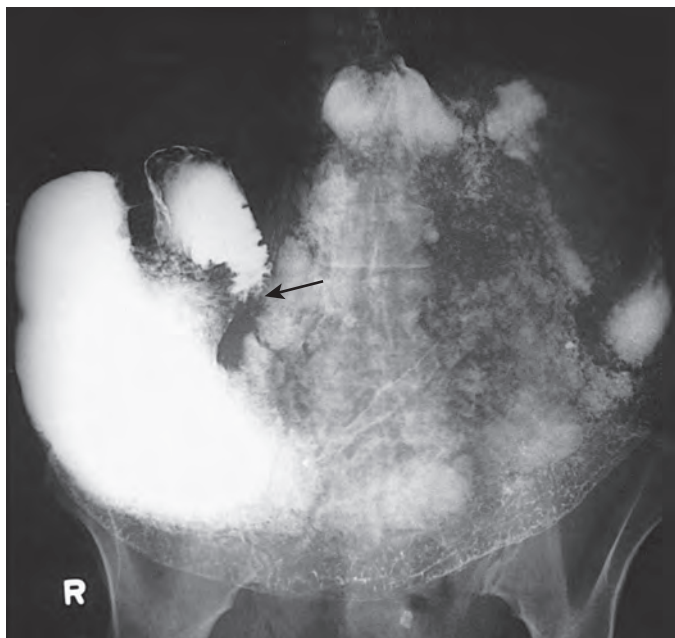


Figure 33-11 Duodenal obstruction by retroperitoneal metastases. Delayed overhead radiograph from an upper gastrointestinal study shows abrupt narrowing of the descending duodenum (arrow) with massive gastric dilation out of proportion to the degree of duodenal dilation. The dilated stomach extends inferiorly into the pelvis. (From Shammash JB, Rubesin SE, Levine MS: Massive gastric distention due to duodenal involvement by retroperitoneal tumors. *Gastrointest Radiol* 17:214–216, 1992.)

gastric emptying and massive gastric dilation out of proportion to the degree of duodenal dilation (Fig. 33-11).²⁴ This disproportionate gastric dilation is probably related to vagal destruction by retroperitoneal tumor, which decreases gastric peristalsis and exacerbates gastric distention.

Direct Invasion

The stomach and duodenum may be directly invaded by malignant tumors arising in neighboring structures such as the esophagus, pancreas, and kidney. The stomach and duodenum may also be involved by direct extension of colonic carcinoma along mesenteric reflections (including the gastrocolic ligament and transverse mesocolon) or by contiguous spread of tumor from the greater omentum. Because the radiographic findings depend on the pathways of spread, the various primary malignant tumors are discussed separately in the following sections.

Esophageal Carcinoma. In contrast to squamous cell carcinomas of the esophagus, adenocarcinomas arising in Barrett's mucosa have a marked tendency to invade the gastric cardia or fundus.^{25,26} Gastric involvement may be manifested on barium studies by a large polypoid or ulcerated mass in the gastric fundus. In other cases, however, double-contrast views of the fundus may reveal more subtle findings, with distortion or obliteration of the normal anatomic landmarks at the cardia (the cardiac rosette) and irregular areas of ulceration or nodularity (see Chapter 23).²⁵ It is sometimes difficult to determine whether these tumors at the gastroesophageal junction have arisen in the esophagus or stomach. In general, however, esophageal adenocarcinomas have a disproportionate degree of

esophageal involvement in relation to that of the stomach, whereas gastric or cardiac carcinomas have a greater degree of fundal involvement.

Pancreatic Carcinoma. The radiographic manifestations of gastroduodenal involvement by pancreatic carcinoma depend on whether the underlying tumor is located in the head, body, or tail of the pancreas. Carcinoma of the pancreatic head may cause widening of the duodenal sweep or extrinsic compression of the medial border of the descending duodenum or greater curvature of the gastric antrum, whereas carcinoma of the pancreatic body or tail may cause extrinsic compression of the posterior wall of the gastric fundus and body or the superior border of the distal duodenum near the ligament of Treitz.²⁷ Invasion of the stomach or duodenum may be manifested on barium studies by spiculated mucosal folds, nodularity, mass effect, ulceration, obstruction or, rarely, fistula formation (Figs. 33-12 to 33-14).²⁷

Many patients with suspected pancreatic neoplasms undergo CT as the initial diagnostic examination. Although CT is of limited value in predicting minimal duodenal invasion by pancreatic carcinoma, distention of the duodenum with gas or water can facilitate detection of subtle findings of invasion. CT is of greater value in determining the cause of an abnormal retrogastric impression because it can differentiate pancreatic carcinoma from pancreatic pseudocysts (Fig. 33-15), retrogastric varices, or other abnormalities in the retroperitoneum compressing the stomach.^{28,29}

Renal Cell Carcinoma. Direct invasion of the duodenum by right-sided renal cell carcinoma may be manifested on barium studies by mass effect, nodularity, or ulceration of the right posterolateral border of the descending duodenum. However, renal cell carcinoma tends not to elicit a desmoplastic response in the wall of the bowel, so duodenal involvement is sometimes manifested by a polypoid intraluminal mass, mimicking the appearance of a primary duodenal carcinoma.^{6,8} In patients with advanced renal cell carcinoma, CT is useful for determining the extent of tumor and its proximity to the duodenum. When a contiguous lesion is identified, however, CT is not reliable for determining whether tumor is invading the duodenum.

Colonic Carcinoma. Colonic carcinoma may involve the stomach or duodenum by direct extension along mesenteric reflections such as the gastrocolic ligament or transverse mesocolon. The gastrocolic ligament is the proximal portion of the greater omentum that extends superiorly from the anterosuperior border of the transverse colon to the greater curvature of the stomach (Fig. 33-16). Because of this anatomic relationship, carcinoma of the transverse colon may invade the stomach via the gastrocolic ligament, producing mass effect, nodularity, and spiculated tethered folds on the greater curvature of the gastric antrum or body.⁸ In other patients, carcinoma of the ascending colon or hepatic flexure may invade the duodenum via the lateral reflection of the transverse mesocolon, producing mass effect, nodularity, ulceration, or spiculated folds on the lateral border of the descending duodenum (Fig. 33-17A).^{30,31} In such cases, a barium enema examination may show the underlying colonic neoplasm responsible for these findings, and CT may show the mode of spread to the stomach or duodenum (Fig. 33-17B).

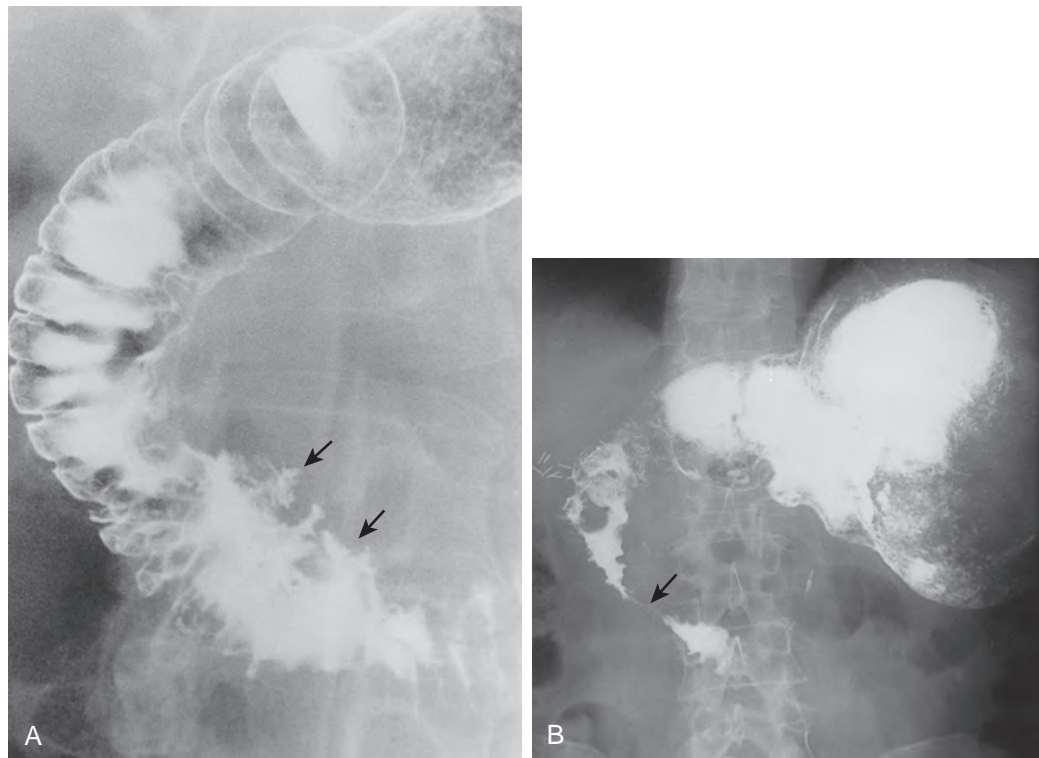


Figure 33-12 Duodenal invasion by pancreatic carcinoma. **A.** Irregular ulceration (arrows) is seen on the medial border of the descending duodenum, secondary to invasion by pancreatic carcinoma. **B.** In another patient, there is narrowing and obstruction of the descending duodenum (arrow) by an advanced pancreatic carcinoma. This patient has gastric outlet obstruction with a dilated, fluid-filled stomach diluting the ingested barium. (**A** from Laufer I, Levine MS [eds]: *Double Contrast Gastrointestinal Radiology*, 2nd ed. Philadelphia, WB Saunders, 1992.)

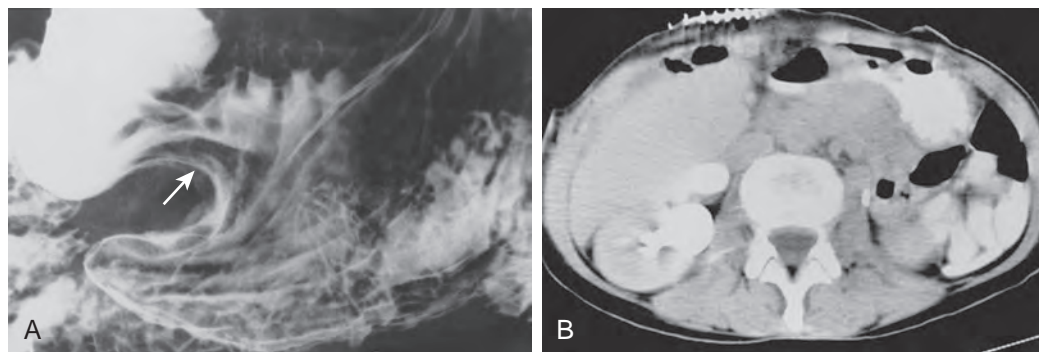


Figure 33-13 Gastric invasion by pancreatic carcinoma. **A.** Barium study shows a focal area of mass effect (arrow) on the greater curvature of the stomach. **B.** CT scan reveals an advanced pancreatic carcinoma invading the stomach.

Carcinoma of the transverse colon invading the stomach or carcinoma of the hepatic flexure invading the duodenum may occasionally lead to the development of a gastrocolic or duodenocolic fistula (see Chapter 34).³² In today's pill-oriented society, however, most such fistulas are caused by aspirin-induced or other nonsteroidal anti-inflammatory drug (NSAID)-induced greater curvature ulcers that penetrate via the gastrocolic ligament into the transverse colon (see Chapter 29).

Gallbladder Carcinoma. Advanced carcinoma of the gallbladder may directly invade adjacent structures such as the liver, duodenum, and hepatic flexure of the colon. Duodenal

involvement by tumor has been reported in about 20% of patients.³³ CT is particularly useful for showing gastric and duodenal invasion by tumor (Fig. 33-18).

Omental Metastases. Bulky metastatic deposits in the greater omentum, or so-called omental cakes, usually result from widespread intraperitoneal dissemination of ovarian carcinoma or, less frequently, cervical, uterine, bladder, gastric, colonic, pancreatic, or breast carcinoma.³⁴ These omental deposits may spread superiorly to the stomach via the proximal portion of the greater omentum, also known as the gastrocolic ligament (see Fig. 33-16). Gastric involvement by omental metastases is characterized on barium studies by mass effect, nodularity,

flattening, or spiculated, tethered folds on the greater curvature of the gastric antrum or body (Fig. 33-19A).³⁵ These changes reflect serosal involvement by tumor and a desmoplastic response that occurs along the insertion of the gastrocolic ligament on the greater curvature. In advanced cases, there may be circumferential narrowing of the gastric antrum resulting from encasement by metastatic tumor.³⁵

Carcinoma of the transverse colon invading the stomach via the gastrocolic ligament may produce identical radiographic findings (see earlier, "Colonic Carcinoma").⁸ In such cases, however, a barium enema examination should demonstrate the primary colonic carcinoma responsible for these findings. In contrast, patients with omental metastases involving the stomach almost always have associated colonic involvement by omental tumor, with mass effect, nodularity, and spiculated folds on the superior border of the transverse colon (Fig. 33-19B) or, in advanced cases, circumferential narrowing of the bowel.³⁶ In our experience, gastric involvement by omental metastases is far more common than gastric invasion by colonic carcinoma via the gastrocolic ligament.

When gastric involvement by omental metastases is suspected on barium studies, CT is extremely helpful for



Figure 33-14 Gastric invasion by pancreatic carcinoma. There is extrinsic mass effect (black arrows) on the posterior wall of the gastric fundus from an adjacent carcinoma of the pancreatic tail. The spiculated contour of the stomach (white arrows) indicates gastric invasion by tumor. (From Laufer I, Levine MS [eds]: *Double Contrast Gastrointestinal Radiology*, 2nd ed. Philadelphia, WB Saunders, 1992.)

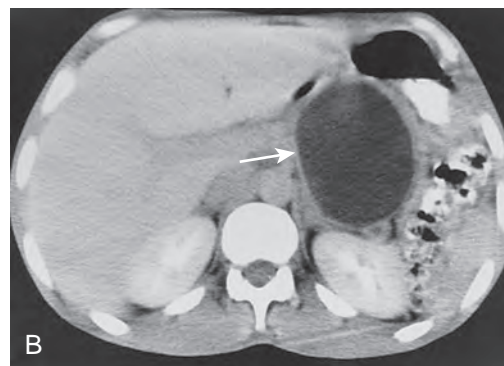
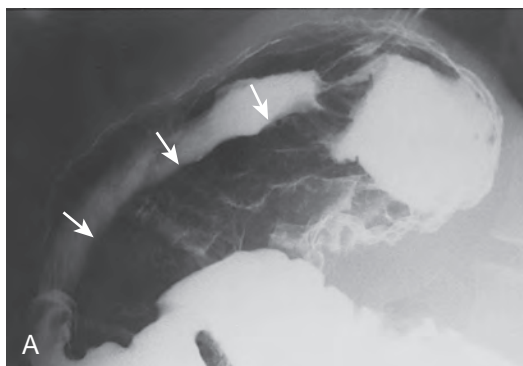


Figure 33-15 Gastric involvement by a pancreatic pseudocyst. **A.** Barium study shows smooth extrinsic compression (arrows) of the posterior wall of the gastric fundus. **B.** CT scan reveals a large pancreatic pseudocyst (arrow) as the cause of this finding.

delineating the extent of metastatic tumor. Although barium studies provide indirect evidence of omental tumor, CT can reveal omental masses as small as 1 cm in diameter.³⁷ More extensive omental metastases may be manifested on CT by a spectrum of findings, ranging from a lacy reticular appearance to bulky masses.³⁷ Non-neoplastic processes involving the omentum (notably tuberculous peritonitis) can simulate omental tumor. When the greater omentum is diffusely infiltrated by tumor, an omental cake may displace the colon or small bowel from the anterior abdominal wall (Fig. 33-19C).^{34,38} Unless the lumen of the bowel is distended with contrast medium or gas, however, it is difficult to determine whether tumor is invading the stomach or transverse colon.

DIFFERENTIAL DIAGNOSIS

Hematogenous metastases that appear as small nodular lesions in the stomach or duodenum may be difficult to differentiate

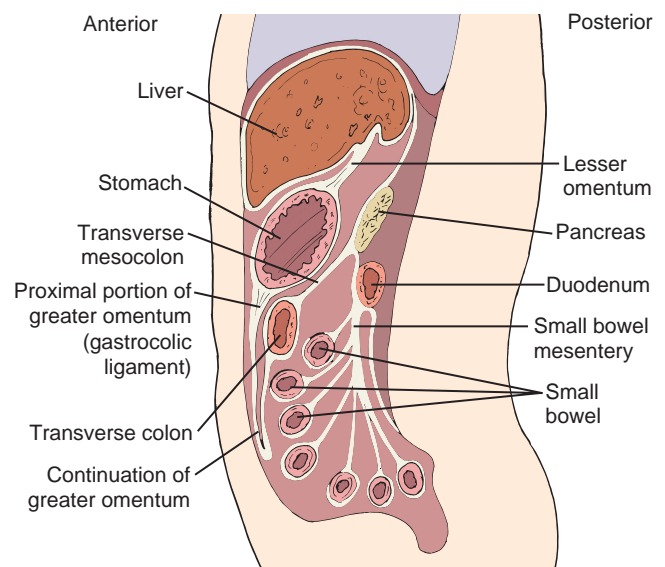


Figure 33-16 Sagittal diagram shows the mesenteric attachments of the stomach, small bowel, and colon. Because the proximal portion of the greater omentum (the gastrocolic ligament) inserts along the greater curvature of the stomach, contiguous spread of tumor from the transverse colon or greater omentum primarily affects this region. (From Rubesin SE, Levine MS: *Omental cakes: colonic involvement by omental metastases*. *Radiology* 154:593–596, 1985.)

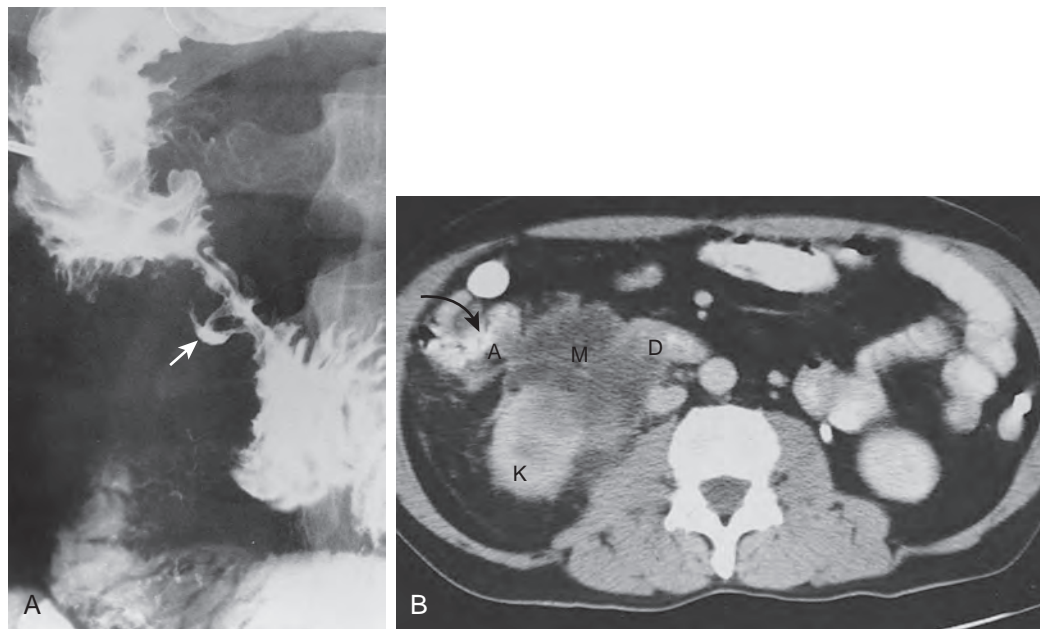


Figure 33-17 Duodenal invasion by colonic carcinoma. **A.** A large area of mass effect is seen on the lateral border of the descending duodenum with associated ulceration (*white arrow*). This finding was caused by carcinoma of the hepatic flexure invading the duodenum. **B.** In another patient, CT scan shows invasion of the duodenum by recurrent carcinoma arising from the region of an ileotransverse colonic anastomosis (A). A heterogeneous mass (M) is seen invading the duodenum (D) and right kidney (K). Contrast medium is present in the bowel (*black arrow*) adjacent to the anastomosis.

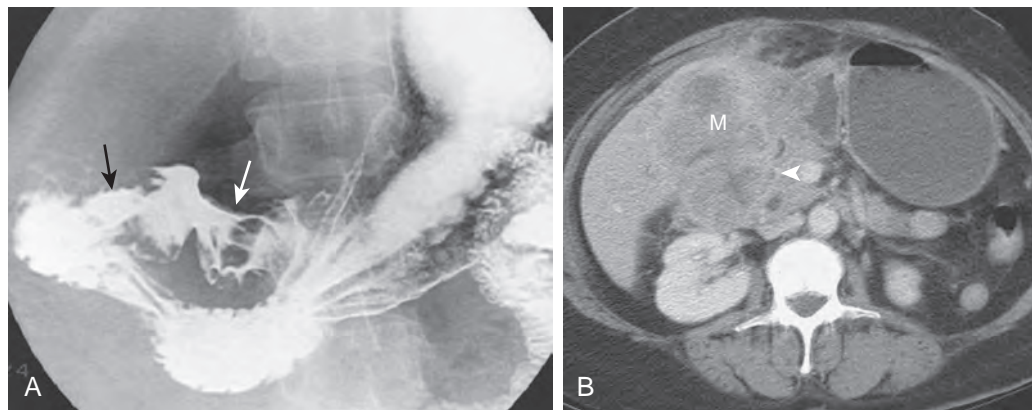


Figure 33-18 Gallbladder carcinoma invading the stomach and duodenum. **A.** Barium study shows narrowing and ulceration of the postbulbar duodenum (*black arrow*) and distortion of the distal gastric antrum (*white arrow*) because of invasion by tumor. **B.** CT scan in the same patient shows an advanced carcinoma of the gallbladder (M) directly encasing and narrowing the descending duodenum (*arrowhead*). Also note tumor invading the distal stomach and infiltrating the peritoneal cavity.

on barium studies from multiple hyperplastic or adenomatous polyps. Metastases that have a more typical submucosal appearance can be mistaken for benign intramural lesions such as GISTs, lipomas, or ectopic pancreatic rests. However, these benign mesenchymal tumors tend to occur as solitary lesions, whereas metastases are usually multiple. Centrally ulcerated bull's-eye lesions may be caused not only by hematogenous metastases but also by lymphoma, Kaposi's sarcoma, or carcinoid tumors. Occasionally, varioliform erosions surrounded by unusually prominent mounds of edema can be mistaken for bull's-eye lesions. However, varioliform erosions are rarely larger than 1 cm, and the central barium collections are considerably smaller than those seen in ulcerated submucosal masses.

Giant cavitated lesions in the stomach and duodenum may be caused not only by metastatic disease (particularly malignant melanoma) but also by lymphoma or malignant GISTs. However, malignant GISTs tend to occur as solitary lesions, so the presence of multiple cavitated masses in the stomach, duodenum, or small bowel should favor a diagnosis of metastatic disease or lymphoma.

The linitis plastica appearance caused by metastatic breast cancer may be indistinguishable on barium studies from that of a primary scirrhous carcinoma of the stomach. Circumferential gastric involvement by pancreatitis, pancreatic carcinoma, colonic carcinoma, omental metastases, lymphoma, or Crohn's disease and scarring from various types of severe gastritis may

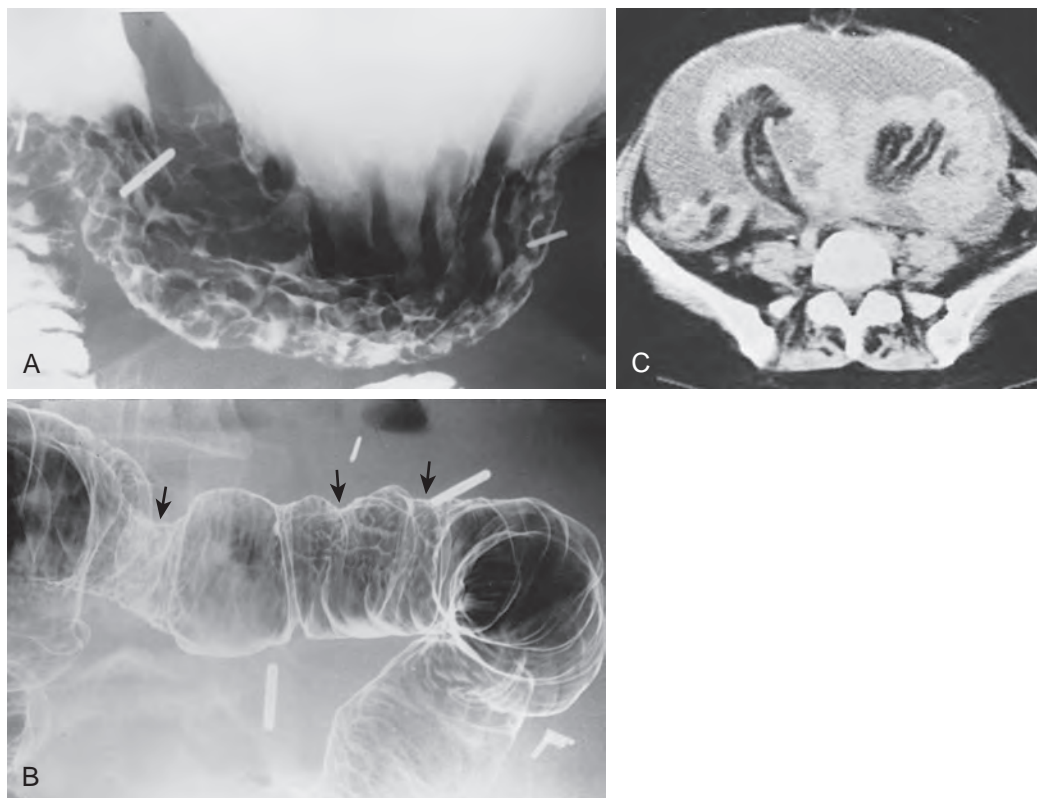


Figure 33-19 Gastric and colonic involvement by omental metastases from ovarian carcinoma. **A.** Upper GI study shows spiculated folds and nodularity on the greater curvature of the gastric antrum and body as a result of direct extension of tumor from the greater omentum. **B.** Barium enema shows spiculation and tethering of the superior border of the transverse colon (arrows) as a result of simultaneous colonic involvement by omental tumor. **C.** In another patient, CT scan reveals ascites with a bulky omental cake separating the small bowel from the anterior abdominal wall. (**C** from Laufer I, Levine MS [eds]: *Double Contrast Gastrointestinal Radiology*, 2nd ed. Philadelphia, WB Saunders, 1992.)

produce similar findings. Nevertheless, the possibility of metastatic disease should be considered when a linitis plastica appearance is detected in patients who were previously treated for breast cancer.

Direct invasion of the stomach and duodenum by metastatic tumor may be simulated by various benign and malignant conditions in the upper abdomen. Compression or displacement of the greater curvature or posterior wall of the stomach or of the medial border of the descending duodenum may be caused not only by pancreatic carcinoma but also by pancreatitis, pancreatic pseudocysts (see Fig. 33-15), peripancreatic lymphadenopathy, abdominal aortic aneurysms, or other retroperitoneal processes. Various signs of bowel wall invasion (e.g., mass effect, nodularity, and spiculated, tethered folds) may also result from a nonspecific desmoplastic response to inflammatory conditions involving the stomach. Thus, pancreatitis may produce changes on the greater curvature that are impossible to distinguish from pancreatic or colonic carcinoma or omental metastases involving the stomach. Other imaging techniques such as CT are usually helpful for differentiating these conditions.

Lymphoma

Lymphoma involves the stomach more frequently than any other portion of the gastrointestinal tract. Gastric lymphoma accounts for 50% of all GI lymphomas, 25% of all extranodal lymphomas, and 3% to 5% of all malignant tumors in the

stomach.³⁹⁻⁴¹ More than 50% of patients with gastric lymphoma have localized disease that is confined to the stomach and regional lymph nodes (primary gastric lymphoma); the remainder have generalized lymphoma with associated gastric involvement (secondary gastric lymphoma).⁴¹ When it occurs, duodenal lymphoma usually results from contiguous transpyloric spread of lymphoma from the stomach. Because of its rarity, duodenal lymphoma is considered separately in a later section.

The vast majority of gastric lymphomas are non-Hodgkin's lymphomas of B-cell origin.⁴² There is considerable evidence that these lymphomas arise from mucosa-associated lymphoid tissue (MALT) occurring in patients with chronic *Helicobacter pylori* gastritis.⁴³ It has therefore been postulated that most primary non-Hodgkin's gastric lymphomas originate as low-grade MALT lymphomas, which, if untreated, eventually progress to more high-grade lymphomas. In the past, low-grade proliferation of lymphoid tissue in the stomach was sometimes known as pseudolymphoma.⁴⁴ However, these pseudolymphomas are currently thought to represent monoclonal B-cell proliferations or true B-cell MALT lymphomas.^{45,46} As a result, the term *pseudolymphoma* has largely been abandoned.

Because the gross pathologic findings are nonspecific, gastric lymphoma is often difficult to differentiate from gastric carcinoma on radiologic or endoscopic examination. However, gastric lymphoma has a much better prognosis than gastric carcinoma, with overall 5-year survival rates of 50% to 60%.⁴⁷⁻⁴⁹

Thus, failure to obtain biopsy specimens from an advanced lesion that is assumed to be inoperable gastric cancer may deprive the patient of the opportunity for cure or long-term palliation. Proper staging of the tumor is also important, so a rational decision can be made about treatment options such as surgery, radiation, and chemotherapy.

PATHOLOGY

The vast majority of gastric lymphomas are non-Hodgkin's lymphomas. Only rarely are these patients found to have Hodgkin's lymphoma. Because of confusion with prior classification systems, pathologists at the National Cancer Institute have developed a working formulation that recognizes three prognostic categories of non-Hodgkin's lymphoma—low grade, intermediate grade, and high grade.⁵⁰ Advanced lesions are usually classified as high-grade lymphomas of the large cell or immunoblastic type.⁵¹

The literature suggests that most primary non-Hodgkin's gastric lymphomas are low-grade B-cell lymphomas that arise from MALT.^{52,53} These lesions have been classified as marginal zone B-cell MALT lymphomas by the International Lymphoma Study Group.⁵⁴ Paradoxically, these low-grade MALT lymphomas often occur in the stomach, which normally contains no organized lymphoid tissue.^{52,53} However, it has been well documented that chronic *H. pylori* gastritis leads to the acquisition of lymphoid follicles and aggregates in the lamina propria (MALT)⁵⁵⁻⁵⁷ and the subsequent development of low-grade, B-cell MALT lymphomas.^{52,53,58} Studies have also suggested that almost all patients with low-grade MALT lymphomas have particular strains of *H. pylori* containing the cytotoxin-associated gene A (*cagA*),⁵⁹ so these strains may have an important role in the pathogenesis of gastric MALT lymphoma.

Gastric MALT lymphomas are manifested pathologically by infiltration of the epithelium with small centrocyte-like cells, giving rise to the lymphoepithelial lesions characteristic of these tumors.⁵⁴ In various series, MALT lymphomas have been found to constitute as many as 50% to 72% of all primary gastric lymphomas,^{60,61} so this is a more common tumor than was previously recognized.

It has been shown that regions of low-grade MALT lymphoma are present on histopathologic examination in approximately 30% of patients with high-grade gastric lymphoma.^{60,62} The findings from these studies support the concept that most non-Hodgkin's gastric lymphomas originate as low-grade gastric MALT lymphomas, which subsequently undergo transformation to intermediate- or high-grade lymphomas. These low-grade MALT lymphomas could therefore be considered to be a form of early gastric lymphoma, defined as lymphoma limited to the mucosa or submucosa of the gastric wall, regardless of the presence or absence of lymph node metastases.⁴⁶

Primary gastric lymphoma is usually confined to the stomach or regional lymph nodes at the time of diagnosis. In the Ann Arbor staging system,⁴¹ stage IE lesions involve the gastric wall, stage IIE lesions involve regional lymph nodes in the abdomen, stage III lesions involve lymph nodes above and below the diaphragm, and stage IV lesions are widely disseminated lymphomas that involve extra-abdominal lymph nodes and the omentum, mesentery, peritoneum, liver, spleen, lungs, or brain. The major factors affecting survival of patients with primary gastric lymphoma are the depth of invasion of the gastric wall and presence or absence of nodal disease.

CLINICAL FINDINGS

Gastric lymphoma occurs more frequently in men than in women, and the average age at the time of diagnosis is 55 to 60 years.⁶³ Patients with advanced lesions may present with abdominal pain, nausea, vomiting, anorexia, weight loss, a palpable epigastric mass, or signs of upper GI bleeding.⁶³ Occasionally, these patients may develop an acute abdomen because of spontaneous perforation of an ulcerated gastric lymphoma or perforation complicating systemic chemotherapy.⁶⁴ Patients with generalized lymphoma may also present with a fever or other signs of systemic disease. Whether or not affected individuals have primary gastric lymphoma or generalized lymphoma with gastric involvement, these lesions are often quite extensive in relation to the clinical presentation. Gastric lymphoma should therefore be suspected when a relatively advanced lesion in the stomach is associated with a paucity of clinical complaints.

In contrast to patients with early gastric cancer, who are usually asymptomatic (see Chapter 32), patients with early gastric lymphoma (particularly those with low-grade B-cell MALT lymphoma) may present with epigastric pain, dyspepsia, bloating, nausea, and/or vomiting.⁶⁵⁻⁶⁷ The symptoms at presentation are therefore indistinguishable from those caused by gastric or duodenal ulcers, gastritis, or duodenitis. Some patients may have underlying *H. pylori* gastritis as the cause of their symptoms. Whatever the explanation, the development of symptoms provides an opportunity to diagnose these low-grade gastric MALT lymphomas before they progress to more advanced lesions.

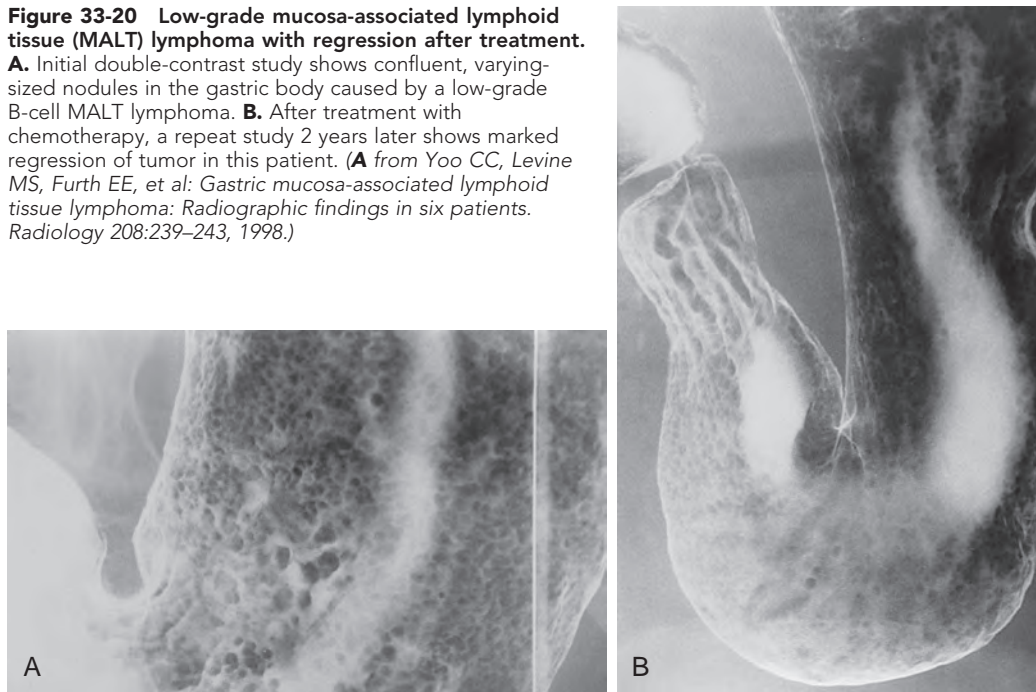
ENDOSCOPIC FINDINGS

Low-grade gastric MALT lymphomas may be manifested at endoscopy by shallow ulcers, polypoid lesions, or erythematous, nodular mucosa.^{65,67} In contrast, high-grade lymphomas may be manifested by enlarged rugal folds, infiltrative masses, or nodular, polypoid, or ulcerated lesions in the stomach.^{68,69} Occasionally, endoscopy may reveal a characteristic volcano crater, with a discrete ulcer surrounded by a narrow ridge of tumor.⁶⁹ Depending on the endoscopic findings, gastric lymphomas may be difficult to differentiate from carcinomas, benign GISTs, metastatic tumor, Ménétrier's disease, hypertrophic gastritis, or even benign gastric ulcers. Endoscopic biopsy specimens are therefore required for a definitive diagnosis. Superficial biopsy specimens may be nondiagnostic because lymphomas often infiltrate the gastric wall beneath an intact mucosa. Whenever possible, multiple brushings and biopsy specimens should therefore be obtained from ulcerated or polypoid areas in which tumor is more likely to be present. Deep biopsy specimens should also be obtained when the overlying mucosa appears normal. With adequate cytologic and biopsy specimens, endoscopy has a reported sensitivity of 85% to 95% in diagnosing gastric lymphoma.⁷⁰⁻⁷²

TREATMENT AND PROGNOSIS

When the diagnosis of gastric lymphoma has been established, proper staging of the tumor is needed to determine the appropriate treatment and assess prognosis. Additional diagnostic examinations include chest radiography, chest and abdominal CT scans, and ¹⁸F-fluorodeoxyglucose (¹⁸F-FDG)-labeled

Figure 33-20 Low-grade mucosa-associated lymphoid tissue (MALT) lymphoma with regression after treatment. **A.** Initial double-contrast study shows confluent, varying-sized nodules in the gastric body caused by a low-grade B-cell MALT lymphoma. **B.** After treatment with chemotherapy, a repeat study 2 years later shows marked regression of tumor in this patient. (**A** from Yoo CC, Levine MS, Furth EE, et al: *Gastric mucosa-associated lymphoid tissue lymphoma: Radiographic findings in six patients.* *Radiology* 208:239–243, 1998.)



PET/CT imaging. When CT and ^{18}F -FDG-PET/CT scans are normal, routine staging laparotomy is probably unnecessary.⁷³

Many investigators think that the best treatment for early or localized gastric lymphoma with or without regional lymph node involvement (stage IE or IIE lesions) is a subtotal gastrectomy with postoperative radiation or chemotherapy.*

Although the role of systemic chemotherapy for localized gastric lymphoma remains controversial, advanced gastric lymphoma (stage III or IV lesions) is sometimes treated by radiation therapy, chemotherapy, or both, without a gastric resection.⁶³ Massive upper GI bleeding or even gastric perforation may occur as a complication of systemic chemotherapy, resulting in treatment failures.⁶⁴

In contrast to high-grade gastric lymphomas, low-grade MALT lymphomas can often be treated successfully by combination therapy with proton pump inhibitors. In various studies, complete or partial regression of tumor has been reported in 60% to 80% of patients after eradication of *H. pylori* from the stomach.^{66,76} One theory is that *H. pylori* evokes an immunologic response that stimulates growth of the tumor. Whatever the explanation, eradication of *H. pylori* from the stomach with antibiotics appears to be a viable alternative to surgery, radiation, or chemotherapy as a first-line treatment for low-grade gastric MALT lymphomas.

Long-term survival depends primarily on the stage of the tumor at the time of diagnosis. In various studies, reported 5-year survival rates have ranged from 62% to 90% for stage IE lesions and from 29% to 50% for stage IIE lesions, but substantially lower rates are reported for stages III and IV lesions.^{47,49,72,77} Patients with low-grade gastric MALT lymphomas have a much better prognosis than patients with high-grade lymphomas; low-grade lymphomas are associated with 5-year survival rates

of 75% to 91%,^{60,67} whereas high-grade MALT lymphomas are associated with 5-year survival rates of less than 60%.⁶⁷

After treatment, some patients may develop recurrent gastric lymphoma, whereas others are found to have recurrent tumor in distal nodal groups without evidence of gastric disease. Patients with recurrent lymphoma almost always become symptomatic within 2 years of treatment, so the prognosis is excellent for patients who remain asymptomatic for more than 5 years.⁷⁸ Gastric lymphoma has a better prognosis than gastric carcinoma because of its inherent growth characteristics and its tendency to remain in the gastric wall for prolonged periods.

RADIOGRAPHIC FINDINGS

Low-Grade Mucosa-Associated Lymphoid Tissue Lymphoma

Low-grade gastric MALT lymphomas may be manifested on double-contrast studies by variably sized, rounded, often confluent nodules involving a focal or, less frequently, diffuse segment of the stomach (Fig. 33-20).⁷⁹⁻⁸² Other MALT lymphomas may appear as small polypoid or ulcerated lesions, as shallow, irregular ulcers with nodular surrounding mucosa, or as focally distorted, enlarged rugal folds.⁸⁰⁻⁸² These early lymphomas may be indistinguishable from early gastric cancer on the basis of the radiographic findings.

Endoscopic biopsy specimens should be obtained for a definitive diagnosis when low-grade MALT lymphomas are suspected on the basis of the radiographic findings. Although some patients may be found to have other conditions such as *H. pylori* gastritis without evidence of tumor (see later, “Differential Diagnosis”), it seems reasonable to accept a certain percentage of false-positive diagnoses because of the importance of detecting gastric MALT lymphomas at an early, curable stage.

*See references 41, 49, 63, 72, 74, and 75.

Advanced Gastric Lymphoma

Advanced gastric lymphomas have an average diameter of 10 cm or more at the time of diagnosis.⁴⁰ Although the entire stomach may be infiltrated by tumor, most cases involve the antrum and body.⁸³ Depending on the gross pathologic features, gastric lymphomas may be classified radiographically as infiltrative, ulcerative, polypoid, or nodular lesions.^{40,83-86} There is considerable overlap between these types, however, with many lesions having combined radiographic features.

Infiltrative gastric lymphomas are characterized by focal or diffuse enlargement of rugal folds caused by submucosal spread of tumor (Fig. 33-21A).^{40,83-86} The folds can be massively enlarged and often have a distorted, nodular contour, so they

can be mistaken for polypoid masses. Even with extensive lymphomatous infiltration, the stomach typically remains pliable and distensible because of the absence of associated fibrosis.^{40,83} However, some non-Hodgkin's lymphomas may produce a linitis plastica appearance indistinguishable from that of a primary scirrhous carcinoma of the stomach.⁸⁷ These lesions are characterized by varying degrees of narrowing of the gastric antrum, body, or fundus with nodularity, ulceration, and thickened or effaced mucosal folds (Fig. 33-21B). This linitis plastica appearance is caused by dense infiltrates of lymphomatous tissue in the gastric wall without associated fibrosis.⁸⁷ The histopathologic findings are therefore similar to those of metastatic breast cancer in which gastric narrowing is caused by highly cellular deposits of metastatic tumor.⁸⁸ Conversely,

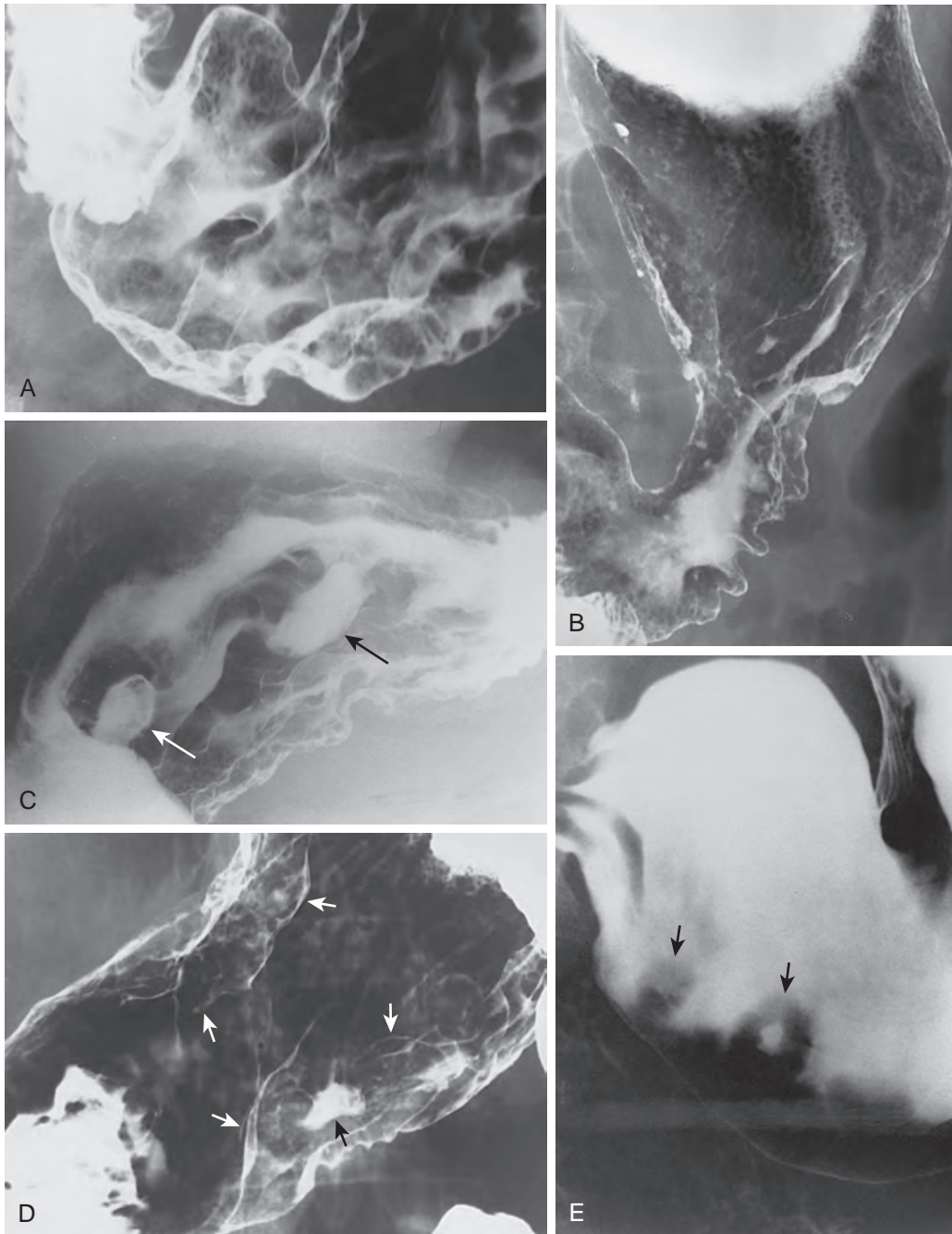


Figure 33-21 Various forms of gastric lymphoma. **A.** Diffusely thickened, irregular folds are present in the stomach because of lymphomatous infiltration of the gastric wall. **B.** This patient has linitis plastica, manifested by focal narrowing of the gastric body with nodularity and sacculation of the adjacent greater curvature. **C.** Several discrete ulcers (arrows) and thickened, lobulated folds are seen in the gastric fundus and body. **D.** Two separate polypoid masses (white arrows) are seen on the lesser and greater curvature of the stomach. The greater curvature mass is ulcerated (black arrow). **E.** Two centrally ulcerated submucosal masses, or bull's-eye lesions (arrows), are present in the gastric antrum. (**A** and **E** from Laufer I, Levine MS [eds]: *Double Contrast Gastrointestinal Radiology*, 2nd ed. Philadelphia, WB Saunders, 1992; **B** from Levine MS, Pantongrag-Brown L, Aguilera NS, et al: *Non-Hodgkin lymphoma of the stomach: A cause of linitis plastica*. *Radiology* 201:375-378, 1996; **D** courtesy Duane G. Mezwa, MD, Royal Oak, MI.)

Hodgkin's lymphoma involving the stomach produces a linitis plastica appearance by inciting a marked desmoplastic response similar to that of a primary scirrhous carcinoma.⁸⁹

Ulcerative lymphomas are characterized by one or more ulcerated lesions in the stomach (Fig. 33-21C).^{40,83-86} Occasionally, the ulcers may be surrounded by a smooth mound of tumor or symmetric radiating folds, mimicking the appearance of benign gastric ulcers.⁸⁴ Usually, however, these ulcers have an irregular configuration associated with nodular surrounding mucosa or thickened, irregular folds resulting from lymphomatous infiltration of the gastric wall (see Fig. 33-21C).^{40,84-86} Other gastric lymphomas may appear as giant cavitated lesions as a result of necrosis and excavation of the tumor.^{84,86}

Polypoid gastric lymphomas are characterized by one or more lobulated intraluminal masses indistinguishable from those of polypoid carcinomas (Fig. 33-21D).^{40,83,84} Finally, the nodular form of gastric lymphoma is characterized by multiple submucosal nodules or masses, ranging from several millimeters to several centimeters in size.^{84,85} These submucosal masses often ulcerate, producing typical bull's-eye or target lesions (Fig. 33-21E).⁹⁰ In such cases, the central barium collections tend to be relatively large in relation to the surrounding elevations. Other patients may have multiple polyps indistinguishable from those associated with the various polyposis syndromes.

About 10% of patients with gastric lymphoma have contiguous transcardiac spread of tumor from the gastric fundus into the distal esophagus.⁹¹ Esophageal involvement is usually manifested by thickened, irregular folds, luminal narrowing or, less frequently, a polypoid mass in the distal esophagus.⁹¹ Because

adenocarcinoma is a much more common malignant tumor in the stomach, these findings are more likely to result from distal esophageal involvement by a fundal or cardiac carcinoma.

Gastric lymphoma may also extend into the duodenum by contiguous transpyloric spread. In various series, 30% to 40% of patients with gastric lymphoma have associated duodenal involvement on barium studies (see later, "Duodenal Lymphoma").^{91,92} Because gastric carcinoma invades the duodenum in only 5% to 25% of patients,^{92,93} it has been suggested that concomitant involvement of the stomach and duodenum by tumor should favor a diagnosis of lymphoma. However, adenocarcinoma is so much more common than lymphoma that it is still the most likely diagnosis on empirical grounds.⁹²

Patients with advanced gastric lymphoma are sometimes treated exclusively with radiation or chemotherapy. Follow-up barium studies or CT scans are useful in these patients for documenting the response to treatment and for evaluating GI bleeding or other symptoms that develop after the initiation of radiation or chemotherapy (Figs. 33-22 and 33-23).^{94,95} Follow-up studies may show dramatic regression or resolution of the lymphomatous lesions, often associated with narrowing and deformity of the stomach at the site of the previous lesion as a result of residual scarring and fibrosis.⁹⁵ In other patients, chemotherapy may lead to marked regression of ulcerated mass lesions with the development of benign-appearing ulcers or ulcer scars at the site of the previous lesions (see Fig. 33-22C).⁹⁴ Chemotherapy may also lead to further ulceration, a confined perforation or, rarely, free perforation of these lymphomatous lesions with the development of massive upper GI bleeding or peritonitis (see Figs. 33-22B and 33-23B).⁹⁴

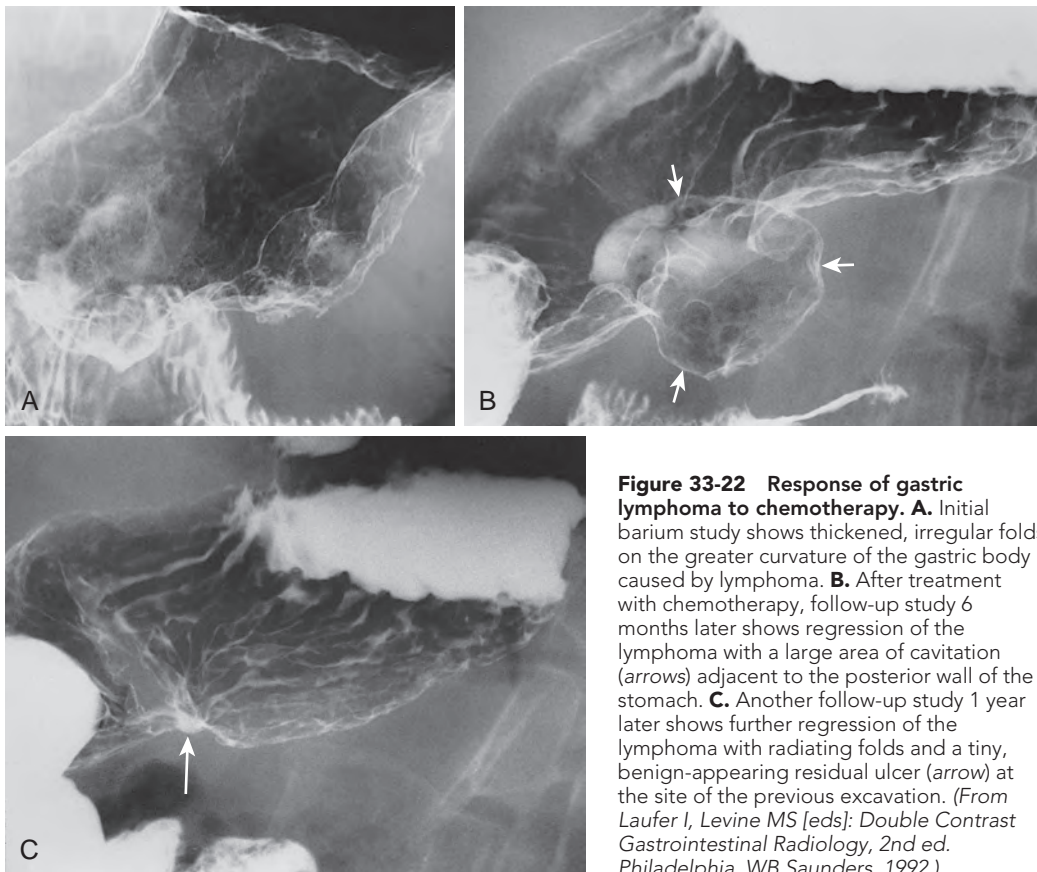


Figure 33-22 Response of gastric lymphoma to chemotherapy. **A.** Initial barium study shows thickened, irregular folds on the greater curvature of the gastric body caused by lymphoma. **B.** After treatment with chemotherapy, follow-up study 6 months later shows regression of the lymphoma with a large area of cavitation (arrows) adjacent to the posterior wall of the stomach. **C.** Another follow-up study 1 year later shows further regression of the lymphoma with radiating folds and a tiny, benign-appearing residual ulcer (arrow) at the site of the previous excavation. (From Laufer I, Levine MS [eds]: *Double Contrast Gastrointestinal Radiology*, 2nd ed. Philadelphia, WB Saunders, 1992.)

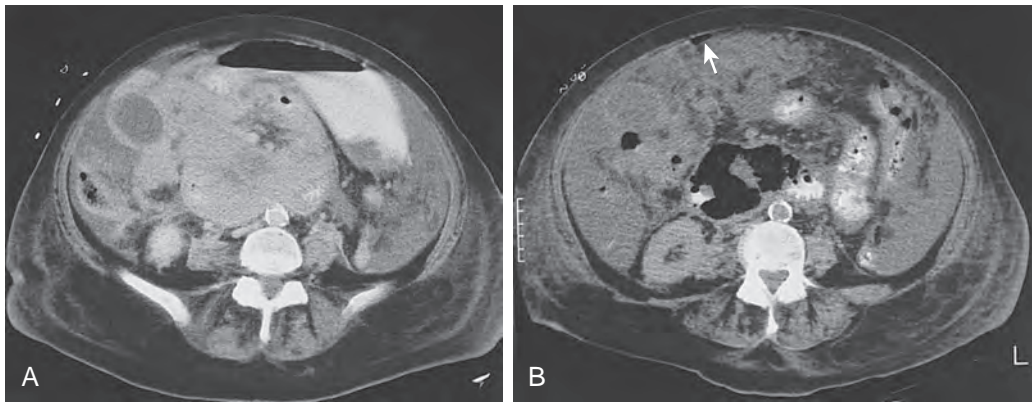


Figure 33-23 Response of duodenal lymphoma to chemotherapy. **A.** CT scan shows a conglomerate mass of adenopathy surrounding the mesenteric vessels. The duodenum is encased by this mass. **B.** Repeat CT scan after two cycles of chemotherapy shows multiple tiny collections of gas in the duodenal wall as a result of rapid tumor lysis and mural necrosis. A tiny amount of free air (arrow) is seen in the peritoneal cavity. This patient had developed clinical signs of peritonitis.

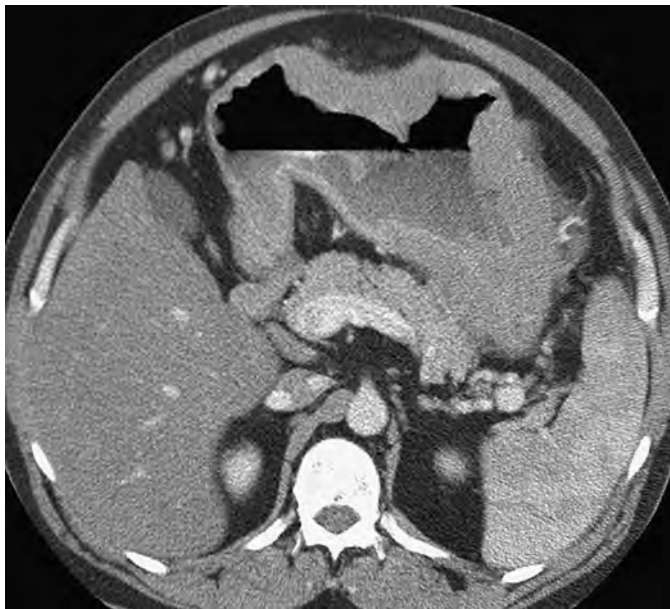


Figure 33-24 Gastric lymphoma on CT. CT scan shows marked thickening of the gastric wall with homogeneous enhancement caused by the infiltrative form of gastric lymphoma. Small perigastric lymph nodes are present in the adjacent fat.

Imaging Modalities

Computed Tomography. CT is the primary imaging modality for the pretreatment evaluation of abdominal lymphoma. It is important to recognize gastric involvement at the time of the initial study. As on barium studies, advanced gastric lymphoma is characterized on CT by infiltrating, polypoid, or ulcerated lesions.^{96,97} In contrast, low-grade gastric MALT lymphomas infrequently produce any abnormalities on CT and, when abnormalities such as wall thickening or masses are detected, endoscopic biopsy specimens almost always reveal high-grade lymphoma.⁹⁸ With more advanced lesions, the most common CT finding is marked thickening of the gastric wall caused by infiltration by tumor (Fig. 33-24). The wall thickening is usually greater and displays a more uniform enhancement pattern than in patients with gastric cancer, unless cavitation is present (see

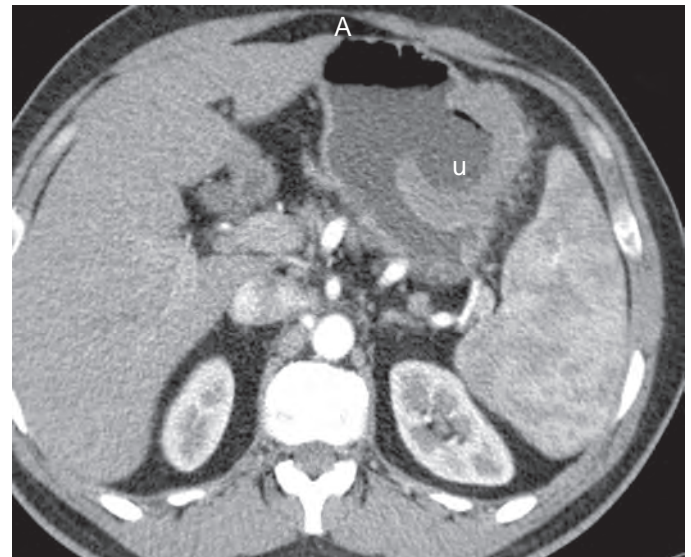


Figure 33-25 Ulcerated gastric lymphoma on CT. A large ulcer crater (u) is present within a soft tissue mass in the stomach. A, gastric antrum.

Fig. 33-24). Although the gastric contour is usually preserved, the mural stratification seen in the normal stomach and accentuated in hypertrophic gastritis is lost.^{96,97} Other patients may have polypoid or ulcerated masses on CT (Fig. 33-25). Growth into and away from the gastric lumen (endogastric and exogastric growth patterns) are common, and some lesions can directly invade adjacent organs (Fig. 33-26). Any portion of the stomach may be involved by tumor, and transpyloric spread of lymphoma into the duodenum is often detected on CT (Fig. 33-27). The development of lymphadenopathy beyond the expected drainage pathways of primary gastric carcinoma should also favor a diagnosis of gastric lymphoma, but a histologic diagnosis is required before initiating therapy.

Endoscopic Ultrasonography. Endoscopic ultrasonography (EUS) has been shown to be a valuable technique for staging patients with non-Hodgkin's gastric lymphoma, with an overall accuracy of approximately 90%.^{99,100} The findings on EUS may

be highly suggestive of lymphoma, but histologic specimens are required for a definitive diagnosis. Non-Hodgkin's gastric lymphoma may be manifested on EUS by a spectrum of findings, ranging from a hypoechoic mass that disrupts the normal wall layer pattern to selective thickening of the second and third echogenic layers or diffuse thickening of all five wall layers.¹⁰⁰ In patients who are treated nonoperatively, EUS is also useful for documenting the response to therapy.

DIFFERENTIAL DIAGNOSIS

Gastric MALT lymphomas that appear as small polypoid or ulcerated lesions in the stomach may be indistinguishable on barium studies from early gastric cancer. When MALT lymphomas are manifested by multiple, confluent, rounded nodules in the stomach, the differential diagnosis includes severe gastritis, lymphoid hyperplasia, or even a polyposis syndrome involving the stomach. In some cases, this mucosal nodularity may be difficult to differentiate from enlarged areae gastricae, a finding

often associated with *H. pylori* gastritis.¹⁰¹ However, areae gastricae tend to be more uniform in size, producing a sharply margined reticular network. Lymphoid hyperplasia associated with chronic *H. pylori* gastritis may also be manifested by innumerable nodules in the stomach (see Chapter 30).¹⁰² However, the nodules of lymphoid hyperplasia appear as innumerable, tiny, rounded lesions carpeting the antrum or antrum and body of the stomach. Unlike the poorly defined, confluent nodules in low-grade MALT lymphoma, the nodules of lymphoid hyperplasia also tend to have more discrete borders, a more uniform size, and, not infrequently, central umbilications.¹⁰²

Advanced infiltrative gastric lymphomas may be difficult to distinguish radiographically from other causes of thickened gastric folds, such as *H. pylori* gastritis, hypertrophic gastritis, Ménétrier's disease, and gastric carcinoma. Other infiltrative lymphomas may produce a linitis plastica appearance indistinguishable from that of a primary scirrhous carcinoma.¹⁶ Deep endoscopic biopsy specimens are therefore required for a definitive diagnosis.

Ulcerated gastric lymphomas may be impossible to distinguish radiographically from ulcerated carcinomas. Much less frequently, ulcerated lymphomas that have a relatively innocuous appearance can be mistaken for benign gastric ulcers.⁸⁴ When lymphoma is characterized by multiple areas of ulceration, the differential diagnosis includes various inflammatory or infectious conditions involving the stomach, such as Zollinger-Ellison syndrome, Crohn's disease, tuberculosis, syphilis, and cytomegalovirus (see Chapters 29 and 30). However, the correct diagnosis is often suggested by the clinical history.

Polypoid gastric lymphomas may be indistinguishable from polypoid gastric carcinomas. Other lymphomas that appear as submucosal masses can be mistaken for malignant GISTs. Although uncommon, giant cavitated lymphomas may be impossible to differentiate from cavitated GISTs or cavitated metastases. However, malignant GISTs tend to occur as solitary lesions in the stomach, whereas lymphoma and metastatic disease are often manifested by multiple lesions in the stomach, duodenum, and small bowel. In patients with gastric lymphoma, exophytic masses typically demonstrate homogeneous attenuation on CT,^{96,97} whereas malignant GISTs often



Figure 33-26 Gastric lymphoma invading the spleen on CT. The gastric wall is eccentrically thickened (asterisk) by tumor directly invading the splenic parenchyma (arrow).

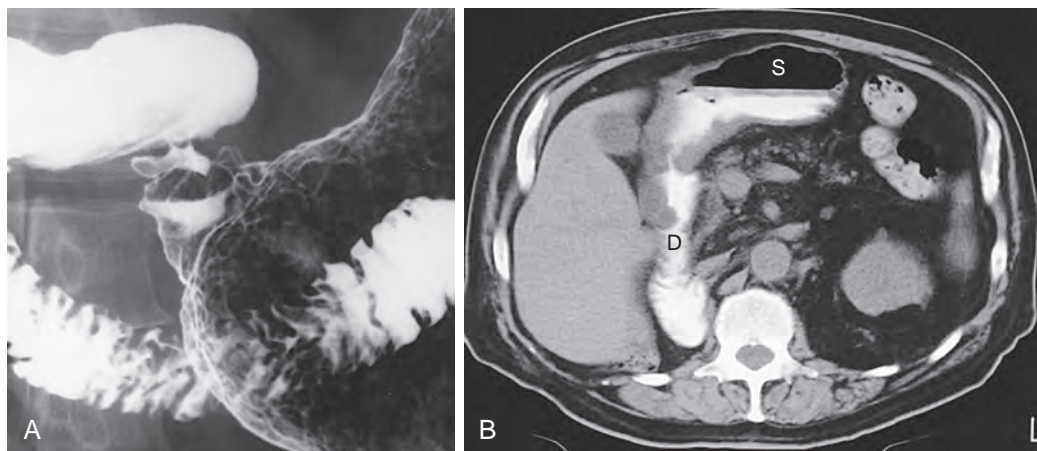


Figure 33-27 Transpyloric spread of lymphoma into the duodenum. **A.** Barium study shows nodularity and deformity of the distal antrum and pyloric region caused by gastric lymphoma. The duodenal bulb appears normal. **B.** CT scan reveals a lymphomatous mass extending from the distal antrum into the proximal duodenum. Even in retrospect, duodenal involvement is not seen on the barium study. D, duodenum; S, stomach. (Courtesy Edward Lubat, MD, Ridgewood, NJ.)

have a heterogeneous appearance because of areas of liquefactive necrosis (see later, “Malignant Gastrointestinal Stromal Tumor”).

Bull’s-eye lesions in the stomach may be caused not only by lymphoma but also by Kaposi’s sarcoma, carcinoid tumors, or metastases (particularly those from malignant melanoma). However, lymphomatous lesions tend to be of relatively uniform size, whereas metastases are often of variable size as a result of periodic showers of tumor emboli into the bowel.^{8,12} Benign GISTs that are ulcerated may also have a bull’s-eye appearance, but they usually occur as solitary lesions in the stomach or duodenum.

DUODENAL LYMPHOMA

Duodenal involvement by lymphoma usually results from contiguous spread of tumor from the distal stomach or proximal jejunum (see Fig. 33-27) or from encasement of the duodenum by a conglomerate mass of lymphomatous nodes in the retroperitoneum (see Fig. 33-23A).¹⁰⁵ Because of the paucity of lymphoid tissue in the duodenum, primary duodenal lymphomas are rare lesions, constituting less than 5% of all small bowel lymphomas.¹⁰⁴ As in the stomach, duodenal lymphoma is characterized radiographically by infiltrative, ulcerative, polypoid, and nodular forms.

Duodenal lymphoma may be manifested by a variety of appearances on CT. These include marked and uniform soft tissue attenuation thickening of the duodenal wall (Fig. 33-28), an ulcerated mass (Fig. 33-29), or thickened, exaggerated duodenal folds (Fig. 33-30).

Occasionally, duodenal or small bowel lymphoma may occur as a complication of long-standing celiac disease.^{105,106} Treatment with a gluten-free diet has not been effective in preventing this complication. Thus, periodic radiologic surveillance of the duodenum and small bowel has been advocated to detect developing lymphomas at the earliest possible stage.¹⁰⁶

Malignant Gastrointestinal Stromal Tumor

GISTs are uncommon tumors that constitute only 1% to 3% of all malignant neoplasms in the stomach.^{63,107} These tumors are

often confined to the wall of the stomach for prolonged periods before invading adjacent structures, so they have a better prognosis than gastric adenocarcinomas. Because of their rarity, malignant GISTs in the duodenum are considered separately in a later section.

PATHOLOGY

GISTs are the most common mesenchymal tumors in the GI tract. Most of these tumors are incompletely differentiated or undifferentiated and do not fulfill modern pathologic criteria for classification as leiomyomas or leiomyosarcomas. As a result, the generic designation of gastrointestinal stromal tumors has been widely adopted.¹⁰⁸ GISTs are characterized by positive immunoreactivity for KIT (CD117), a tyrosine kinase growth factor receptor, allowing differentiation from true leiomyomas or leiomyosarcomas.¹⁰⁹ Pharmacologic targeting of these receptors with KIT-tyrosine kinase inhibitors has been shown to be useful for treating patients with GISTs.¹¹⁰

GISTs have been classified pathologically into three categories—spindle cell type (70%), epithelioid type (20%),



Figure 33-28 Duodenal lymphoma on CT. CT scan in an HIV-positive patient shows a large soft tissue mass encasing the third and fourth portions of the duodenum.

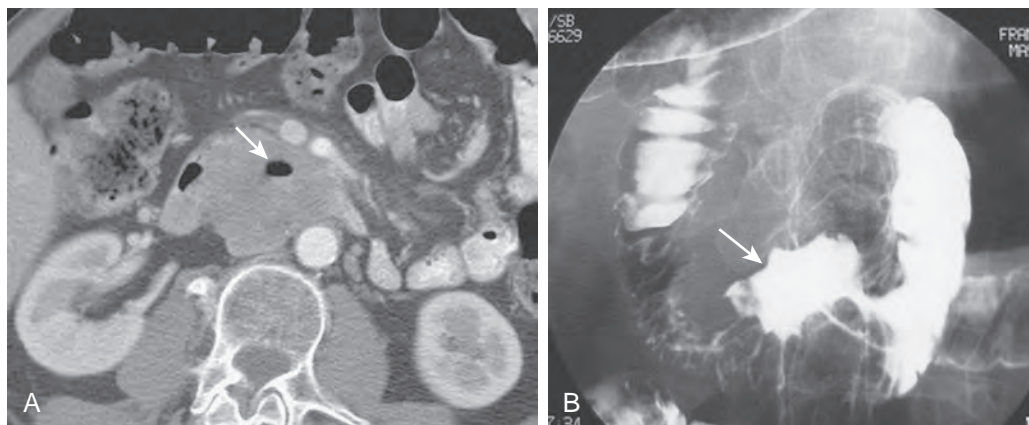


Figure 33-29 Ulcerated duodenal lymphoma on CT. **A.** CT scan from a 6-year-old boy shows a soft tissue mass in the duodenum with an air-filled central ulcer crater (arrow). Endoscopic biopsy specimens revealed non-Hodgkin’s lymphoma. **B.** Barium study shows a mass lesion with thickened, irregular folds and a large area of ulceration (arrow) in the third portion of the duodenum.

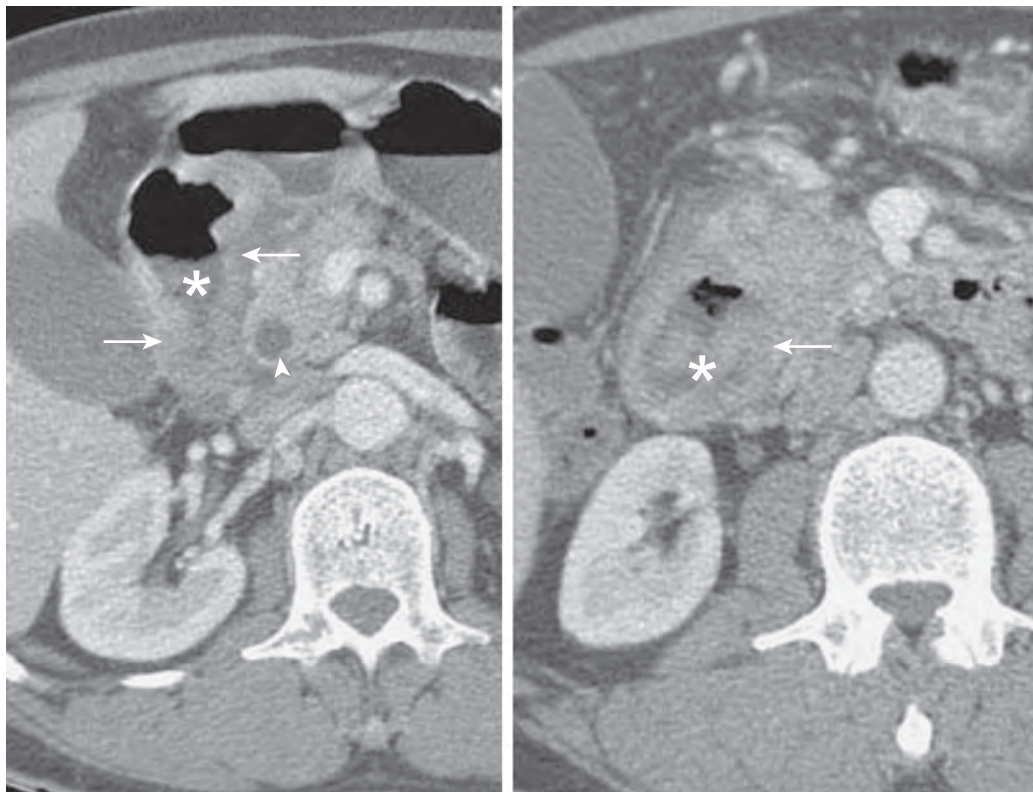


Figure 33-30 Duodenal lymphoma with exaggerated duodenal folds on CT. Sequential CT images in a patient with jaundice show deformity of the descending duodenum with a homogeneously thickened wall and thickened, exaggerated folds (arrows) caused by biopsy-proven non-Hodgkin's lymphoma. The duodenal lumen contains air and fluid (asterisks). Also note dilation of the common bile duct (arrowhead).

and mixed type (10%).¹¹⁰ The spindle cell type consists histologically of interlacing whorls of spindle-shaped cells with eosinophilic cytoplasm and elongated nuclei.¹¹¹ The less common epithelioid type contains distinctive epithelioid cells with eccentric nuclei and perinuclear vacuolization. In the past, GISTs with an epithelioid morphology were termed *epithelioid leiomyosarcomas* or *leiomyoblastomas*.¹¹²

The stomach is the most common site of GI involvement by malignant GISTs. About 90% involve the fundus and body, and the remaining 10% involve the antrum.¹⁰⁷ These tumors are mesenchymal lesions that usually originate from the outer layer of the muscularis propria. Malignant stromal tumors involving the stomach tend to be large lesions with an average diameter of 10 cm at the time of diagnosis.¹⁰⁷ They often contain large cystic cavities or ulcers because of hemorrhage or necrosis within the tumor.¹¹¹

Malignant GISTs of the stomach may have endogastric or exogastric patterns of growth. Because of their origin in the outer muscular layer, exogastric growth into the abdominal cavity is particularly common.¹¹¹ As they enlarge, exogastric lesions may invade adjacent structures such as the pancreas, colon, or diaphragm. Patients with advanced lesions often have widespread intraperitoneal seeding or hematogenous metastases to the liver.¹¹³ Unlike gastric carcinomas, however, malignant GISTs rarely metastasize to regional lymph nodes, so lymphadenopathy is quite uncommon.¹¹³

The most commonly accepted index of malignancy is the degree of mitotic activity in the tumor. Gastric GISTs smaller than 5 cm and with five or fewer mitoses/50 consecutive

high-power fields (HPF) are most likely benign; GISTs larger than 10 cm and with more than five mitoses/50 HPF are considered malignant; and GISTs that fall between these categories are considered indeterminate lesions with uncertain malignant potential.¹¹⁴ Finally, GISTs with more than 50 mitoses/50 HPF are considered high-grade malignancies that behave in an extremely aggressive fashion.¹¹⁴ However, the degree of mitotic activity, cellular atypia, and nuclear pleomorphism may vary markedly within an individual lesion, so histopathologic criteria are not always reliable for differentiating benign and malignant GISTs.

CLINICAL FINDINGS

Malignant GISTs of the stomach are more common in men,¹¹⁵ usually over 50 years of age.¹¹⁶ The average duration of symptoms at the time of diagnosis is 4 to 6 months.¹⁰⁷ Because malignant GISTs frequently ulcerate, affected individuals often present with signs of upper GI bleeding, including hematemesis, melena, guaiac-positive stool, and iron deficiency anemia.^{109,111} Other common presenting findings include early satiety, bloating, vomiting, abdominal pain, weight loss, and a palpable abdominal mass.^{110,111} However, some patients with exogastric tumors may remain asymptomatic until the lesions have reached enormous sizes.

It is important to be aware of the limitations of endoscopy in diagnosing malignant GISTs because positive endoscopic biopsy specimens may not be obtained unless the overlying mucosa is ulcerated. CT may be performed to determine the

relationship of suspicious lesions to the gastric wall and guide needle aspiration biopsies of endoscopically inaccessible lesions.

Patients with malignant GISTs of the stomach generally have a better prognosis than patients with gastric carcinomas; reported 5-year survival rates range from 20% to 55%.¹¹⁷ Tumors smaller than 5 cm have the best possibility for cure, although it is questionable whether these lesions are all malignant. In contrast, tumors larger than 8 cm are often found to be advanced, unresectable lesions at the time of diagnosis.¹¹⁸ Surgery is the only curative form of therapy. Depending on the extent of tumor, a wedge resection or a subtotal or total gastrectomy may be required. However, malignant GISTs rarely metastasize to regional lymph nodes, so a lymph node dissection is of little therapeutic benefit to these patients. Chemotherapy also is highly ineffective, with a response rate of less than 10%.¹¹⁰ In contrast, imatinib, a tyrosine kinase inhibitor, has been shown to be an effective therapeutic agent for prolonging survival in patients with unresectable lesions or metastatic disease.¹¹⁰

RADIOGRAPHIC FINDINGS

Abdominal radiographs generally have limited value for diagnosing malignant GISTs involving the stomach. Occasionally, however, these tumors may be recognized by the presence of a soft tissue mass indenting the gastric bubble.¹¹⁹ One or more extraluminal gas collections may also be seen in the left upper quadrant as a result of necrosis and cavitation of the tumor.¹²⁰ Rarely, abdominal radiographs may reveal mottled areas of calcification (see Fig. 33-33), but CT is a more sensitive technique for demonstrating this finding (see Fig. 33-35A).¹²¹

More than 90% of patients with malignant GISTs of the stomach have abnormal barium studies,¹⁰⁷ but the correct diagnosis is suggested in only about 50% of cases because of difficulty distinguishing these lesions from benign GISTs or other benign or malignant lesions in the stomach. Intramural lesions typically appear as large, lobulated submucosal masses in the gastric fundus or body (Fig. 33-31).¹⁰⁷ Malignant GISTs may contain one or more ulcers or, not infrequently, large areas of

cavitation (Fig. 33-32).¹⁰⁷ Exogastric lesions may be manifested by giant soft tissue masses that cause extrinsic compression of the adjacent gastric wall (Figs. 33-33 and 33-34).^{107,122} An important clue to the diagnosis of an exogastric tumor is the presence of a central dimple or spicule at the site of attachment or pedicle of the mass (see Fig. 33-34A).¹²³ Rarely, endogastric tumors may appear as polypoid intraluminal masses indistinguishable from primary gastric carcinomas.¹¹¹

The diagnosis of a GIST should be suggested on CT or magnetic resonance imaging (MRI) by the presence of an enhancing mass in the wall of the stomach (Fig. 33-35).^{124,125} Size has been shown to an important predictive feature of malignancy because lesions smaller than 5 cm are more likely to be low-grade tumors (see Fig. 33-35), whereas lesions larger than 5 cm are more likely to be high-grade or frankly malignant tumors (Fig. 33-36).¹²⁶ Large GISTs often have a more exogastric growth pattern and tend to be more heterogeneous and have a greater



Figure 33-31 Malignant gastrointestinal stromal tumor. A large, lobulated submucosal mass is seen in the gastric fundus.

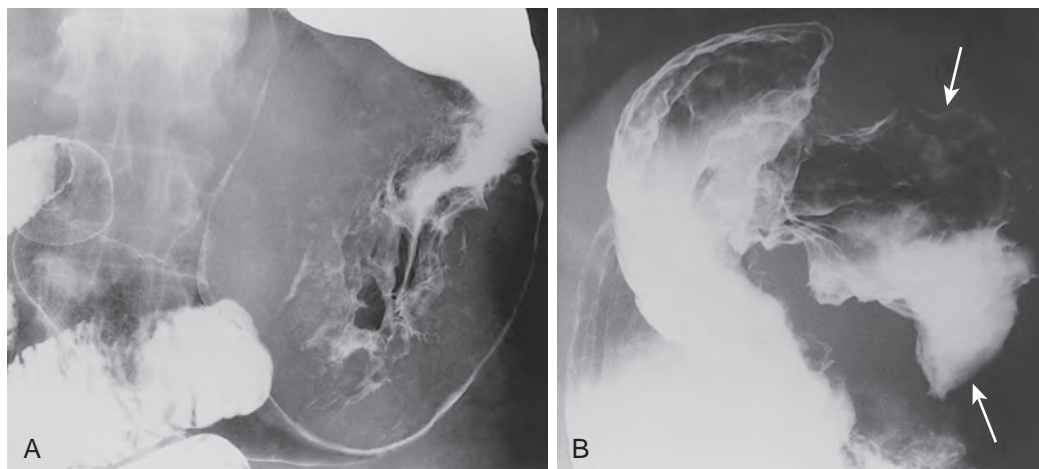


Figure 33-32 Malignant gastrointestinal stromal tumor with cavitation. **A.** A giant mass is present in the stomach. Barium is trapped within irregular cavities in the mass. **B.** Another cavitated lesion is manifested by a giant extraluminal collection of barium (arrows). (A courtesy Hans Herlinger, MD, Philadelphia.)

degree of necrosis than higher grade tumors (Fig. 33-37).¹¹¹ Ulceration or cavitation within malignant GISTs is easily recognized on CT (see Fig. 33-37). CT is particularly helpful for demonstrating the extent of the mass and invasion of adjacent structures (Fig. 33-38).¹²⁷⁻¹²⁹ Rarely, malignant GISTs may be so necrotic that they appear as water-density lesions (Fig. 33-39).

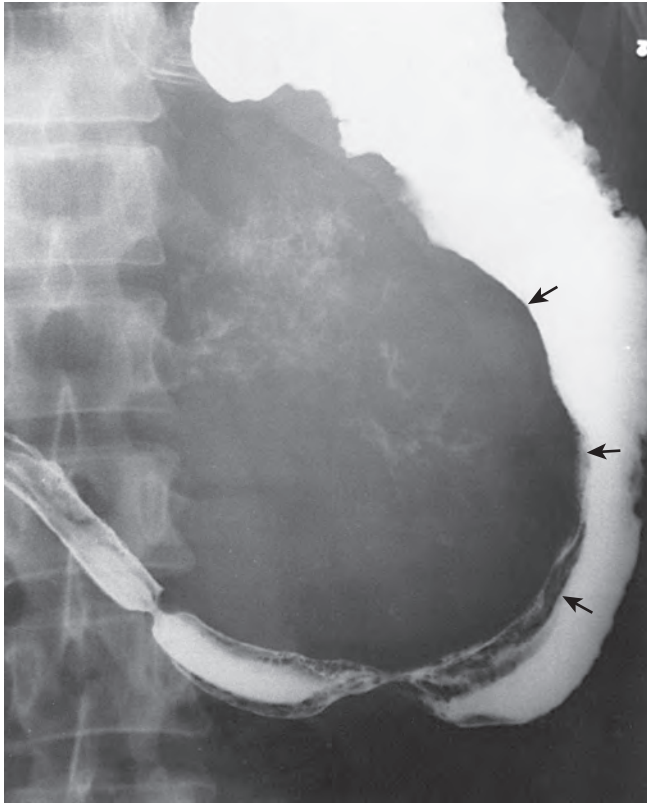


Figure 33-33 Exogastric malignant gastrointestinal stromal tumor with calcification. A giant exogastric mass causes displacement and compression (arrows) of the lesser curvature of the stomach. Mottled areas of calcification are seen in the tumor.

Malignant GISTs in the stomach usually metastasize to the liver and peritoneal cavity (Fig. 33-40); 15% to 47% of patients present with overt metastatic disease to the liver and peritoneum.¹¹⁰ Metastases are usually large heterogeneous lesions. Like the primary tumor, metastases may be multilocular lesions containing fluid-fluid levels and are usually positive on ¹⁸F-FDG-PET/CT. After treatment, liquefied lesions should be carefully inspected to exclude mural nodules, a sign of incomplete response to therapy (see Fig. 33-40). Necrosis and cavitation are particularly common after treatment with tyrosine kinase inhibitors such as imatinib (see Fig. 33-40). Peritoneal involvement by tumor is indistinguishable on CT from other intraperitoneal-seeded metastases.¹³⁰

Malignant GISTs of the stomach are characterized on angiography by relatively well-circumscribed, hypervascular masses with huge feeding arteries and draining veins and intense tumor staining.¹³¹ It is not possible, however, to differentiate benign and malignant GISTs by angiographic criteria. Angiography also is unable to distinguish malignant GISTs from other hypervascular lesions such as carcinoids, neurogenic tumors, and vascular metastases.

DIFFERENTIAL DIAGNOSIS

Because some malignant GISTs may be as small as 2 cm, it is not always possible to distinguish benign and malignant GISTs by radiographic criteria.¹⁰⁸ In general, however, submucosal masses that are larger and more lobulated or contain areas of necrosis or ulceration are more likely to be malignant. The major considerations in the differential diagnosis include lymphoma and other benign or malignant tumors of mesenchymal origin. Cavitated GISTs may be impossible to distinguish radiographically from lymphoma or metastases from malignant melanoma or other tumors. However, patients with lymphoma or metastatic melanoma often have multiple lesions in the stomach and small bowel, whereas cavitory GISTs almost always occur as solitary lesions.

Malignant GISTs that have an exogastric growth pattern can mimic the appearance of extrinsic mass lesions arising in the liver, pancreas, kidney, or mesentery. In such cases, the typical

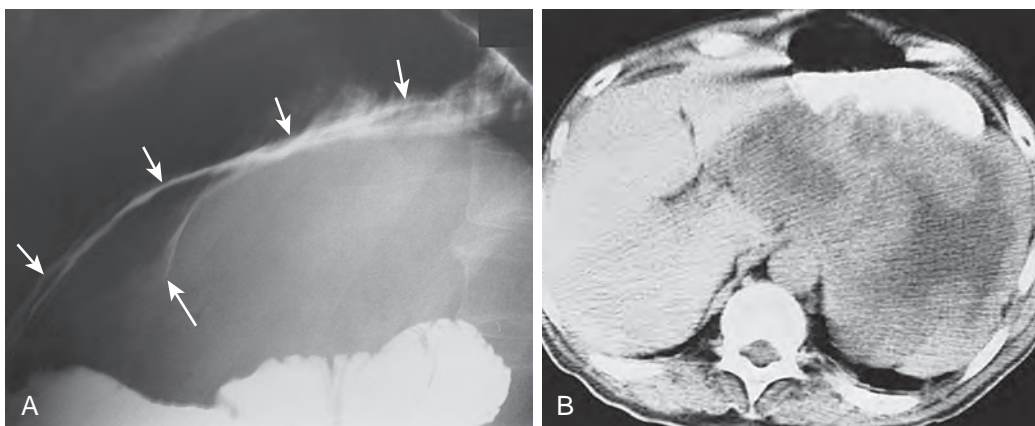


Figure 33-34 Exogastric malignant gastrointestinal stromal tumor. A. Lateral radiograph of the stomach shows a giant exogastric mass compressing the posterior wall of the gastric fundus (short arrows). A central dimple or spicule (long arrow) is seen at the site of attachment of the mass. This finding should suggest the possibility of an exogastric GIST. **B.** CT scan reveals a giant heterogeneous mass with multiple low-density areas caused by necrosis of tumor. This heterogeneous appearance is characteristic of malignant GISTs on CT. (Courtesy Hans Herlinger, MD, Philadelphia.)

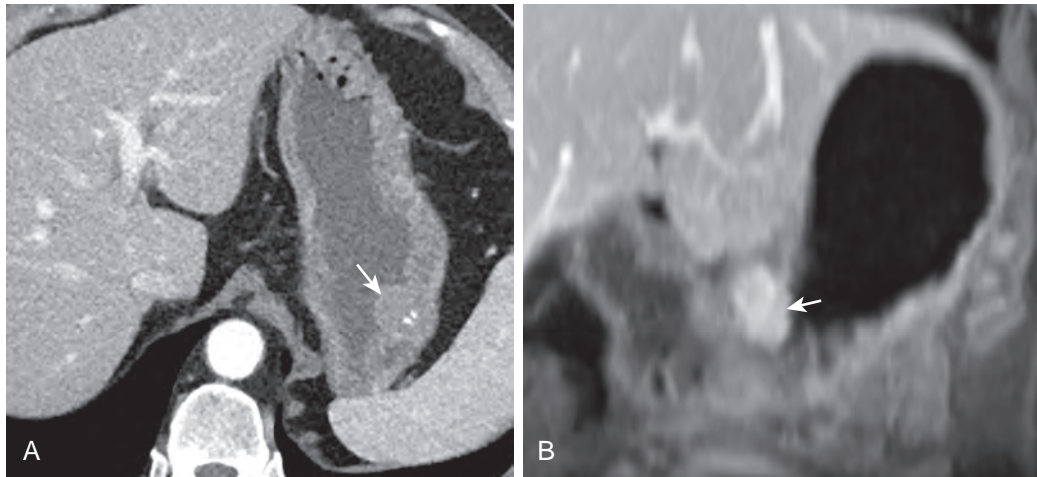


Figure 33-35 Small, low-grade gastrointestinal stromal tumors on CT and MRI. **A.** A low-grade epithelioid lesion is seen on CT as a small (2 cm), well-defined mass (arrow) on the posterior wall of the gastric fundus. Note discrete areas of punctate calcification, an occasional finding in these tumors. **B.** Another low-grade lesion is seen on a 3D gadolinium radial VIBE (volumetric interpolated breath-hold examination) image at MRI as a small (3 cm), homogeneous intramural mass (arrow) at the level of the gastric incisura.

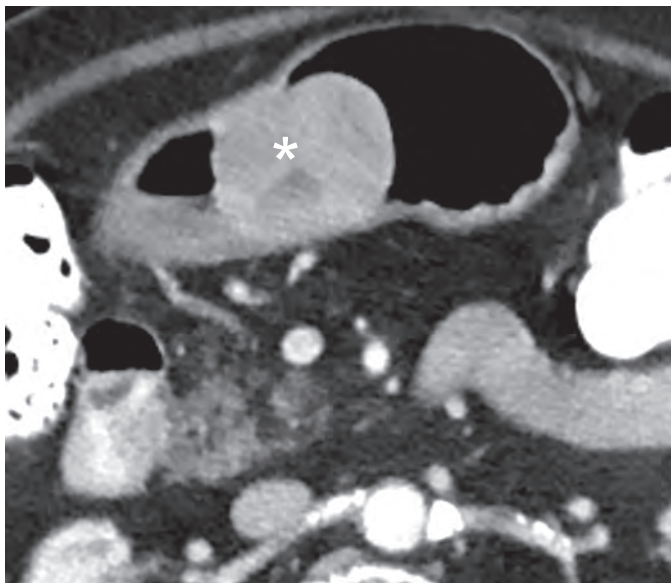


Fig. 33-36 Gastrointestinal stromal tumor with high mitotic activity on CT. Axial CT scan shows a sharply circumscribed heterogeneous mass (asterisk) in the gastric antrum. This heterogeneity on CT should suggest a more high-grade lesion with areas of necrosis.

CT finding of a bulky, heterogeneous mass involving the gastric wall should suggest the correct diagnosis (see Fig. 33-37). Exophytic adenocarcinomas have also been reported, but these lesions are extremely rare.¹³² Occasionally, water-density GISTs may be difficult to distinguish from cystic pancreatic neoplasms or pancreatic pseudocysts. Angiography may be helpful in determining the origin of the mass in these patients. Duplication cysts may also appear on CT as water-density lesions involving the greater curvature of the stomach. However, duplication cysts tend to be smaller and may occasionally communicate with the gastric lumen.^{133,134}

MALIGNANT DUODENAL GASTROINTESTINAL STROMAL TUMOR

Malignant GISTs constitute only 10% of all malignant tumors in the duodenum.¹³⁵ Unlike malignant GISTs of the stomach, the gender distribution is approximately equal.^{135,136} These patients may present with signs of upper GI bleeding, weight loss, abdominal pain, a palpable mass, or obstructive jaundice.^{135,137} Many patients remain asymptomatic until they have advanced lesions. Aggressive surgical treatment (e.g., duodenectomy or pancreaticoduodenectomy) is often advocated.^{135,137} Because malignant duodenal GISTs often invade adjacent structures or metastasize to the liver, these patients have a relatively poor prognosis.¹³⁷

About 80% of malignant duodenal GISTs are located in the second or third portion of the duodenum.¹³⁵ Intramural lesions may appear on barium studies as submucosal masses, often containing areas of ulceration or cavitation (Fig. 33-41).^{135,137} Despite their large size, they rarely cause duodenal obstruction. Other tumors that have an exoenteric growth pattern may be indistinguishable on barium studies from pancreatic neoplasms, pancreatic pseudocysts, or other extrinsic mass lesions involving the duodenum. Like GISTs elsewhere in the GI tract, smaller (<5 cm), more homogeneous duodenal GISTs on CT tend to be low-grade tumors (Fig. 33-42A), whereas GISTs larger than 5cm are more high grade or frankly malignant (Fig. 33-42B). Malignant GISTs usually appear on CT as bulky exophytic masses that enhance heterogeneously because of variable necrosis, ulceration, and cavitation (see Fig. 33-42B).¹³⁸

Kaposi's Sarcoma

The classic form of Kaposi's sarcoma occurs primarily in older men and is manifested by slow-growing violaceous or hemorrhagic lesions on the lower extremities. With the AIDS epidemic that began in the 1980s, patients with this disease were found to develop a much more aggressive form of Kaposi's sarcoma characterized by widespread visceral lesions, particularly in the

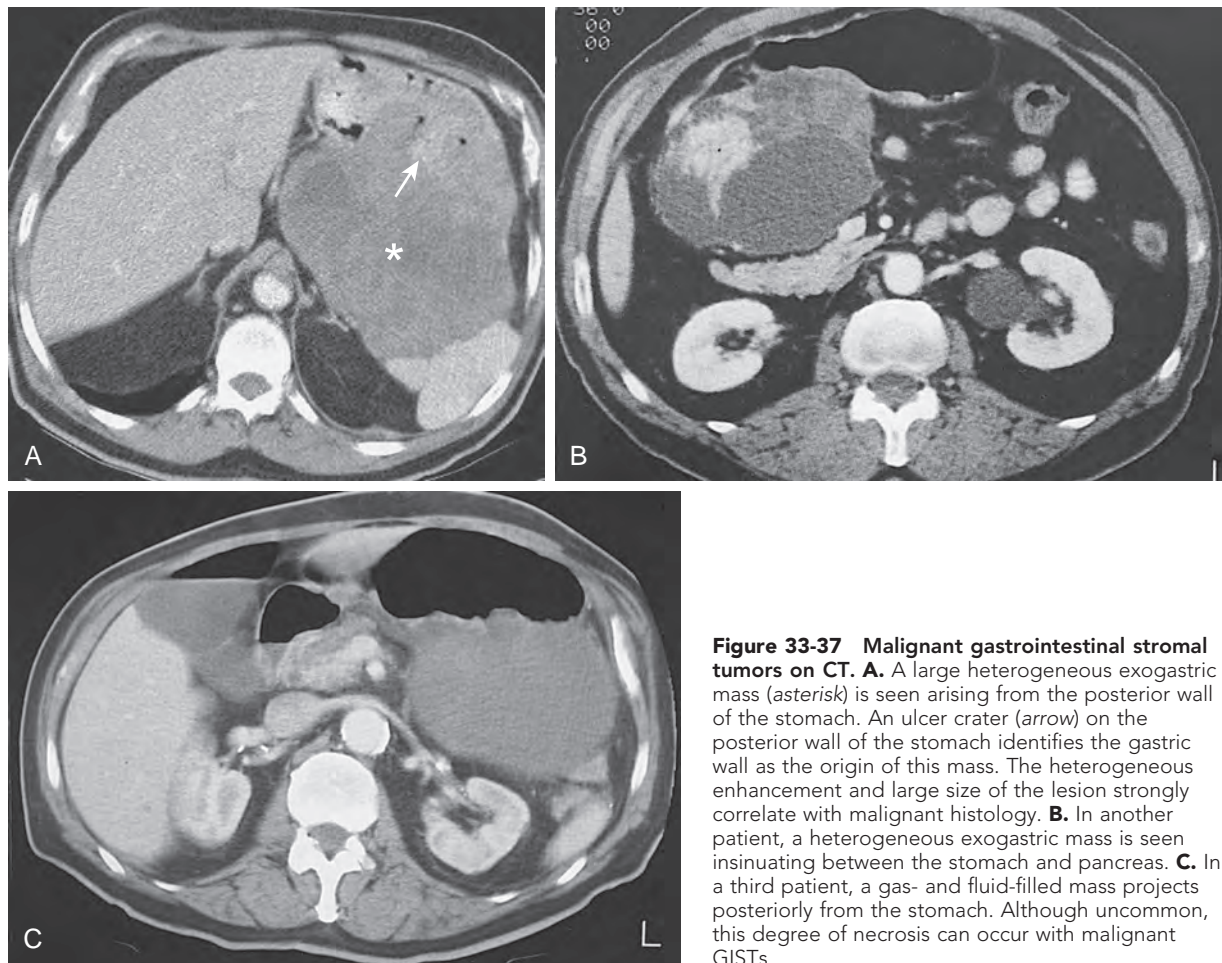


Figure 33-37 Malignant gastrointestinal stromal tumors on CT. **A.** A large heterogeneous exogastric mass (asterisk) is seen arising from the posterior wall of the stomach. An ulcer crater (arrow) on the posterior wall of the stomach identifies the gastric wall as the origin of this mass. The heterogeneous enhancement and large size of the lesion strongly correlate with malignant histology. **B.** In another patient, a heterogeneous exogastric mass is seen insinuating between the stomach and pancreas. **C.** In a third patient, a gas- and fluid-filled mass projects posteriorly from the stomach. Although uncommon, this degree of necrosis can occur with malignant GISTs.

GI tract. In various studies, about 35% of patients with AIDS had Kaposi's sarcoma,¹³⁹⁻¹⁴² and about 50% with Kaposi's sarcoma had GI tract involvement.^{140,143-145} The stomach, duodenum, and small bowel were the most common sites of involvement.^{143,146} The colon was affected less frequently, and the esophagus was rarely involved by Kaposi's sarcoma.^{143,146} Demonstration of these lesions has important prognostic implications, so optimal radiographic technique is required when barium studies are performed on patients with AIDS. During the past two decades, however, the development of effective antiviral therapy for human immunodeficiency virus (HIV)-positive patients has markedly decreased the prevalence of AIDS and AIDS-associated conditions such as Kaposi's sarcoma, so this malignancy is not often encountered in modern medical practice.

CLINICAL FINDINGS

For reasons that are unclear, most AIDS patients with Kaposi's sarcoma are homosexuals rather than IV drug abusers or transfusion recipients.^{142,147,148} GI tract involvement by Kaposi's sarcoma is almost always associated with cutaneous disease, but occasional cases have been reported in the absence of skin lesions.^{145,148} Although some patients may present with abdominal pain or upper GI bleeding, Kaposi's sarcoma involving the stomach or duodenum rarely causes symptoms, even if multiple

lesions are present.¹⁴⁸ Instead, GI symptoms usually result from recurrent opportunistic infections in these patients. In fact, patients with Kaposi's sarcoma have a worse prognosis than other patients with AIDS because they are even more likely to develop opportunistic infections.^{141,142,148} In general, GI involvement by Kaposi's sarcoma requires treatment only if it causes symptoms because these lesions rarely affect the progression of AIDS or contribute directly to the patient's death.¹⁴⁸ Radiation or chemotherapy are occasionally used to treat GI Kaposi's sarcoma, but these forms of therapy pose substantial risks in patients who are already immunocompromised.¹⁴⁸

PATHOLOGIC AND ENDOSCOPIC FINDINGS

Kaposi's sarcoma is probably a lesion of vascular origin, consisting histologically of whorled bundles of spindle-shaped cells in a matrix of vascular clefts containing red blood cells and hemosiderin.^{146,149} Gastroduodenal involvement by Kaposi's sarcoma may be manifested on endoscopy by a variety of findings, including flat hemorrhagic patches or macular discolorations, raised, reddish purple nodules, often containing central areas of ulceration (volcano lesions), and coalescent plaques or masses.^{143,144,146,148} Although the gross appearance at endoscopy is characteristic, false-negative biopsy specimens are often obtained because of the submucosal origin of the lesions.^{140,141,143,144,148}

RADIOGRAPHIC FINDINGS

Small macular discolorations of the mucosa cannot be shown on barium studies, so endoscopy is a much more sensitive technique for detecting the earliest GI lesions of Kaposi's sarcoma.^{143,144,146} However, elevated lesions can be shown on barium studies, particularly if double-contrast technique is used.¹⁴⁰ Gastroduodenal involvement may be manifested on barium studies by one or more submucosal defects ranging from 0.5 to 3.0 cm (Fig. 33-43).^{140,146,150,151} As these nodules

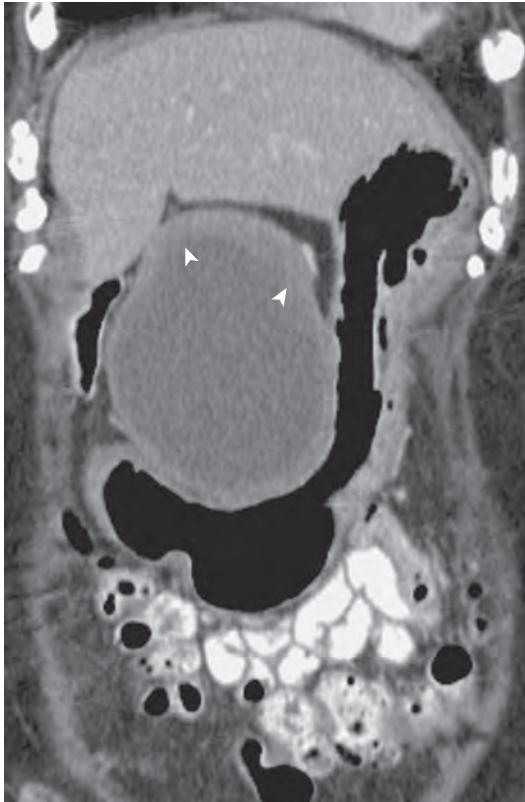


Figure 33-38 Malignant gastrointestinal stromal tumor on CT. Off-axis, coronal, volume-rendered MDCT scan shows a large mass arising from the lesser curvature of the stomach. The wall of the lesion (arrowheads) is irregularly thickened.

enlarge, they often ulcerate, producing one or more bull's-eye or target lesions (Fig. 33-44).^{143,146,151} Other patients may have thickened, nodular folds or polypoid masses in the stomach or duodenum (Fig. 33-45).^{140,146} Rarely, an infiltrating form of Kaposi's sarcoma involving the stomach may produce a linitis plastica appearance indistinguishable from that of a primary scirrhous carcinoma (Fig. 33-46).¹⁵² When suspicious lesions are detected in the stomach or duodenum, a small bowel follow-through may be performed to determine whether additional lesions are present in the small bowel.

CT may occasionally demonstrate tumor nodules in the stomach or duodenum caused by Kaposi's sarcoma in AIDS patients who are being evaluated for opportunistic infection (see Fig. 33-44C).^{153,154} CT can also be used to determine whether retroperitoneal adenopathy, splenomegaly, or other evidence of Kaposi's sarcoma is present in the abdomen.^{155,156}

DIFFERENTIAL DIAGNOSIS

Kaposi's sarcoma and non-Hodgkin's lymphoma are the major considerations in the differential diagnosis of multiple, small nodular elevations or bull's-eye lesions in the stomach or duodenum in patients with AIDS.^{140,146} In such cases, the presence of skin lesions should strongly favor Kaposi's sarcoma, whereas the absence of skin lesions should favor lymphoma. Metastases, leukemic infiltrates, or a polyposis syndrome may produce similar findings, but the correct diagnosis is usually suggested on the basis of the clinical history. When ulceration, narrowing, or thickened folds are demonstrated in the stomach, the possibility of opportunistic infections such as cryptosporidiosis, cytomegalovirus, and tuberculosis should also be considered.¹⁵¹ Endoscopic biopsy specimens, brushings, and cultures are therefore required to differentiate Kaposi's sarcoma or other infiltrative lesions from the various opportunistic infections that occur in these patients.

Carcinoid Tumors

Carcinoids are neuroendocrine tumors that are capable of producing a variety of vasoactive substances. Only 2% to 3% of all GI carcinoids are located in the stomach or duodenum.^{157,158} Nevertheless, these lesions are important because they are slow-growing tumors with a well-recognized malignant potential.

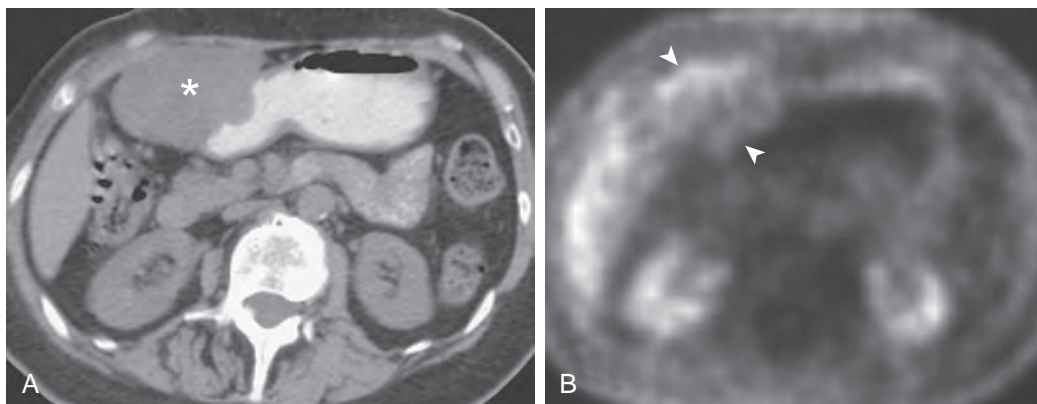


Figure 33-39 Malignant gastrointestinal stromal tumor with necrosis on CT. A. Non-contrast-enhanced CT scan shows a water-attenuation mass (asterisk) arising from the anterolateral wall of the stomach. **B.** ¹⁸F-FDG-PET/CT image shows increased activity (arrowheads) in the periphery of the mass. Viable tissue is typically located in the periphery of malignant GISTs that are highly necrotic.



Figure 33-40 High-grade malignant gastrointestinal stromal tumor with intra-abdominal metastases on CT. Coronal CT scan shows metastatic tumor (asterisk) in the liver. Also note malignant ascites and multiple intraperitoneal masses, including a perihepatic diaphragmatic implant (uppermost arrowhead), a subhepatic necrotic peritoneal implant with tumor nodules along its periphery (central arrowheads), and a thick-walled, necrotic pelvic floor implant (lowermost arrowhead). The fluid attenuation of these lesions reflects their response to imatinib, whereas a more homogeneous soft tissue lesion (arrow) in the left abdomen is likely to be a more recent implant.

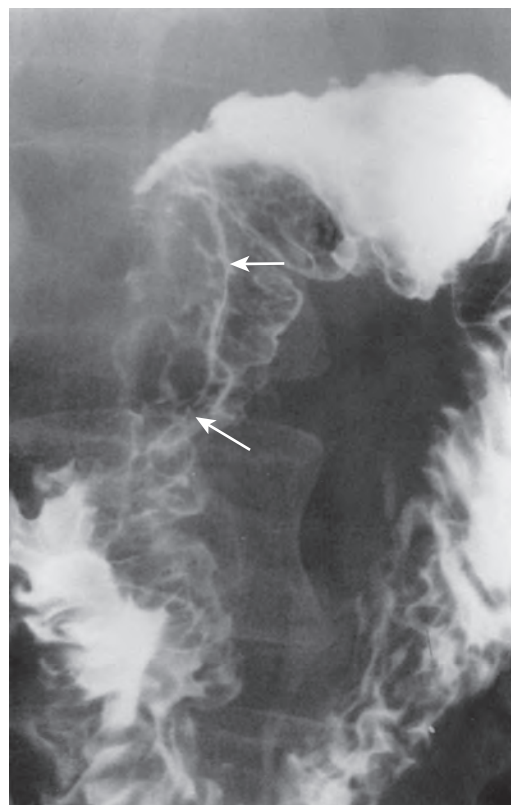


Figure 33-41 Malignant gastrointestinal stromal tumor of the duodenum. Barium study shows a large intramural mass (arrows) on the lateral border of the descending duodenum.

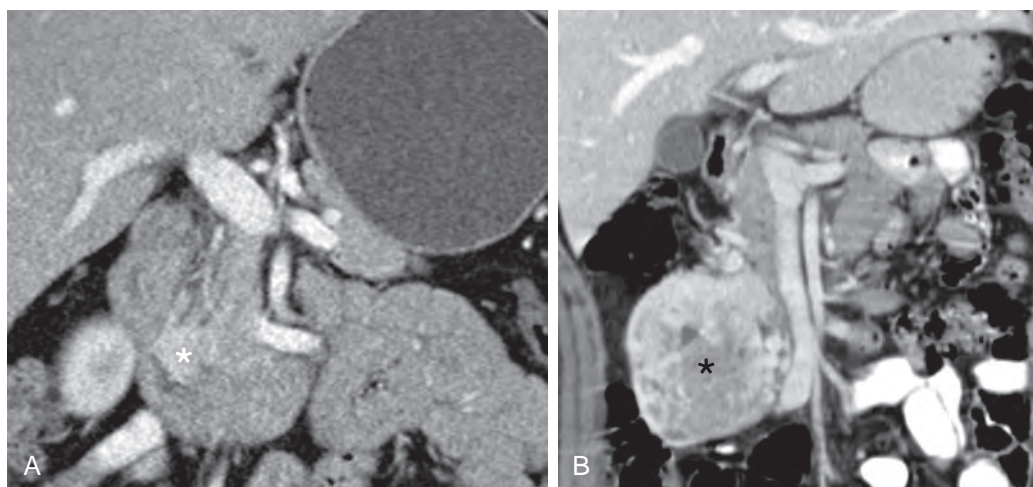


Figure 33-42 Gastrointestinal stromal tumors of the duodenum on CT. **A.** Coronal MDCT scan shows a small, round, uniformly hyperdense mass (asterisk) in the periampullary region of the duodenum. After the lesion was resected, pathologic specimens revealed a low-grade GIST. **B.** In a different patient, MDCT scan shows a high-grade malignant GIST as a large (>5 cm), heterogeneously enhancing lesion (asterisk) projecting from the lateral wall of the descending duodenum.

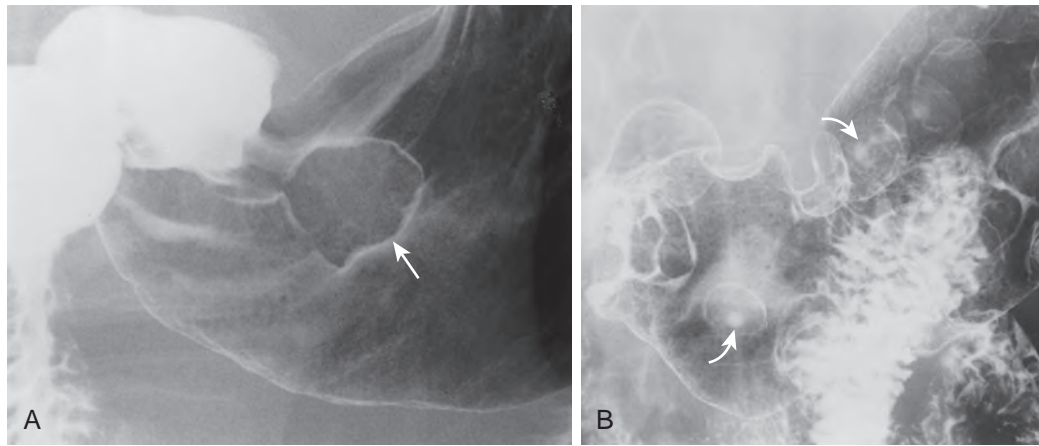


Figure 33-43 Kaposi's sarcoma with submucosal masses in AIDS patients. **A.** A solitary submucosal mass (arrow) is seen in the gastric antrum. **B.** In another patient, multiple submucosal masses are present in the stomach. The tiny collections of barium (arrows) seen overlying several anterior wall lesions represent hanging droplets of barium (stalactites) rather than ulcers.

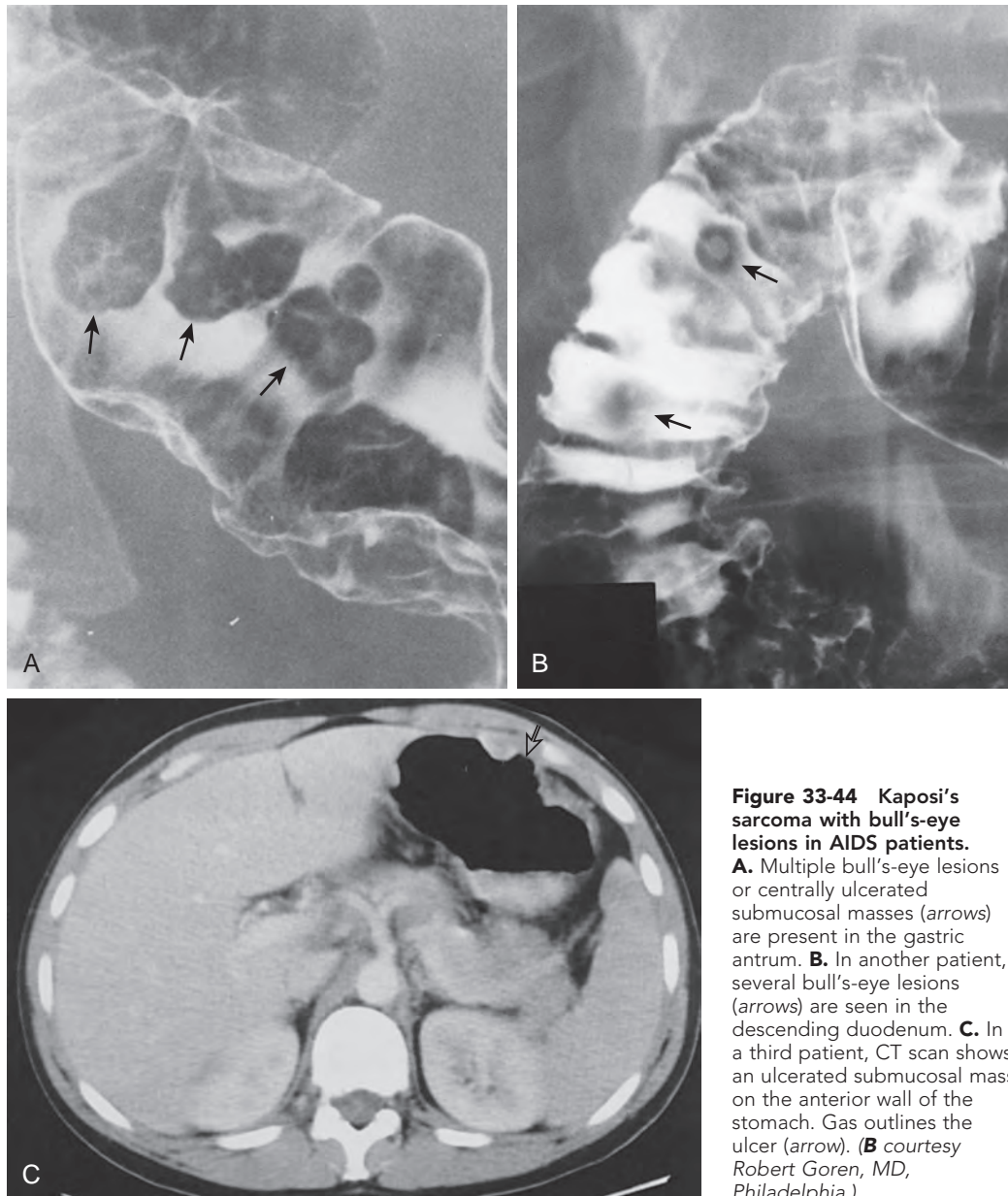


Figure 33-44 Kaposi's sarcoma with bull's-eye lesions in AIDS patients.

A. Multiple bull's-eye lesions or centrally ulcerated submucosal masses (arrows) are present in the gastric antrum. **B.** In another patient, several bull's-eye lesions (arrows) are seen in the descending duodenum. **C.** In a third patient, CT scan shows an ulcerated submucosal mass on the anterior wall of the stomach. Gas outlines the ulcer (arrow). (**B** courtesy Robert Goren, MD, Philadelphia.)



Figure 33-45 Kaposi's sarcoma in an AIDS patient. Multiple polypoid masses are seen on the posterior wall of the fundus.



Figure 33-46 Kaposi's sarcoma with a linitis plastica appearance in an AIDS patient. The stomach has a markedly narrowed, irregular appearance caused by the infiltrating form of Kaposi's sarcoma.

PATHOLOGY

Carcinoid tumors of the stomach usually originate from enterochromaffin-like cells (Kulchitsky cells) arising in the gastric mucosa.^{159,160} These tumors are argyrophilic but argentaffin-negative and lack the enzyme required for the synthesis of 5-hydroxytryptamine (serotonin), so they rarely show

evidence of endocrine function.¹⁶¹ As a result, patients with gastric carcinoids almost never exhibit symptoms of the carcinoid syndrome.

There are three major types of carcinoid tumors. Type I tumors are most common, accounting for 70% to 80% of gastric carcinoids.¹⁵⁸ This type is associated with chronic atrophic gastritis and is usually characterized by one or more small (<1 cm) submucosal masses in the gastric fundus or body with infrequent metastases.¹⁵⁸ In contrast, type II tumors are least common, accounting for only 5% to 10% of gastric carcinoids.¹⁵⁸ Patients with Zollinger-Ellison syndrome (especially those with hypergastrinemia and multiple endocrine neoplasia type 1 [MEN-1 syndrome]) are at high risk for developing type II carcinoid tumors.^{158, 159,160,162-164} It has been shown that hypergastrinemia in these patients causes proliferation of enterochromaffin-like cells responsible for the development of gastric carcinoids. Such carcinoids usually appear as multiple small polyps in the gastric fundus with little, if any malignant potential, so affected individuals have an excellent prognosis.^{159,162} Finally, type III tumors account for 15% to 25% of gastric carcinoids.¹⁵⁸ These lesions usually occur as solitary masses larger than 2 cm and are sporadic tumors that are not associated with atrophic gastritis, Zollinger-Ellison syndrome, or hypergastrinemia.^{159,162} Type III carcinoids are more aggressive lesions, with metastases in 75% of cases.¹⁵⁸

Duodenal carcinoids rarely arise from enterochromaffin cells or produce detectable serotonin levels, so these lesions almost never result in the development of the carcinoid syndrome.¹⁶⁵ Duodenal carcinoids may be associated with Zollinger-Ellison syndrome or neurofibromatosis type 1.¹⁶⁵

CLINICAL FINDINGS

Gastric carcinoids have an equal gender distribution and usually occur in patients over 40 years of age.¹⁶¹ Many patients are asymptomatic, but some may present with abdominal pain, nausea, vomiting, weight loss, anorexia, or signs of upper GI bleeding.^{161,165-168} Although larger lesions are more likely to bleed, massive bleeding of ulcerated carcinoids as small as 1 cm has been described.¹⁶⁹ Gastric carcinoids may be associated with primary hypergastrinemia in patients with Zollinger-Ellison syndrome or with secondary hypergastrinemia in patients with chronic atrophic gastritis.^{159,162,163}

Most gastric carcinoids are low-grade malignant tumors that can eventually metastasize to the liver or other structures. Metastases are found in 20% to 30% of all patients with gastric carcinoids at the time of diagnosis,¹⁵⁸ but long-term survival has been reported, even when regional or hepatic metastases are present. Five-year survival rates approaching 95% have been reported for localized gastric carcinoids versus 5-year survival rates of about 50% for gastric carcinoids of all stages.¹⁶⁰ These patients therefore have a better overall prognosis than those with gastric carcinoma.

RADIOGRAPHIC FINDINGS

Gastric carcinoid tumors associated with hypergastrinemia usually appear on barium studies as multiple small polyps in the gastric fundus or body.¹⁶³ In contrast, sporadic carcinoids may be manifested on barium studies or CT by one or more polypoid or submucosal masses in the stomach (Figs. 33-47 and 33-48).¹⁶¹ Some of the masses may ulcerate,

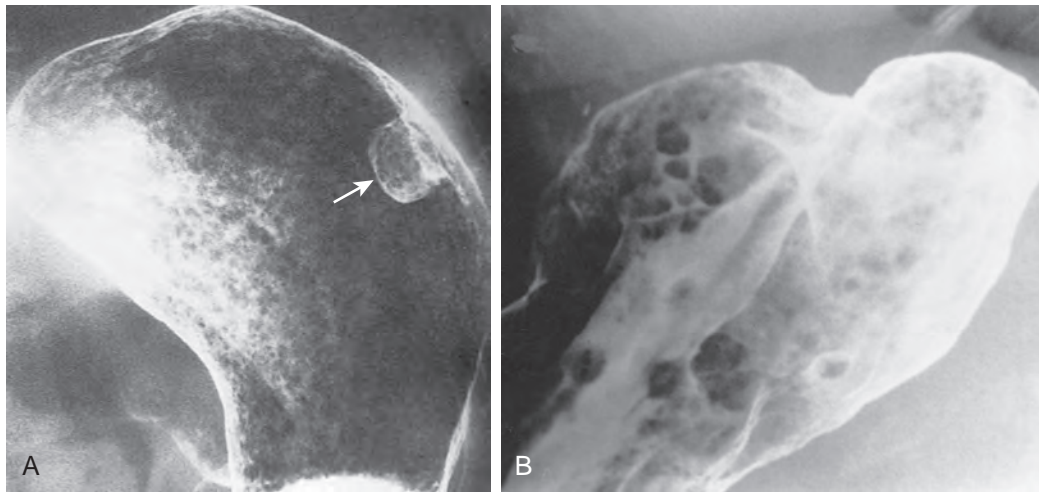


Figure 33-47 Gastric carcinoid tumors. **A.** A solitary submucosal mass (arrow) is seen in the gastric fundus. **B.** In another patient, multiple submucosal nodules are present in the fundus.

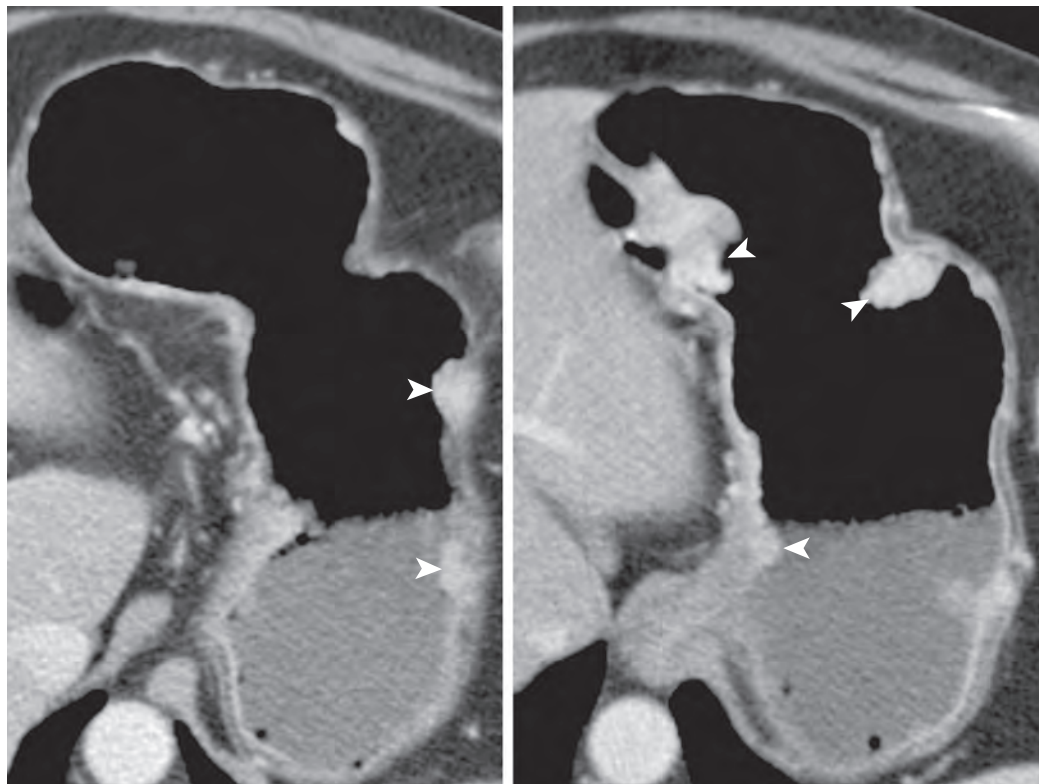


Figure 33-48 Gastric carcinoid tumors on CT. Sequential CT scans show multiple carcinoid tumors as enhancing polypoid masses (arrowheads) in the proximal stomach.

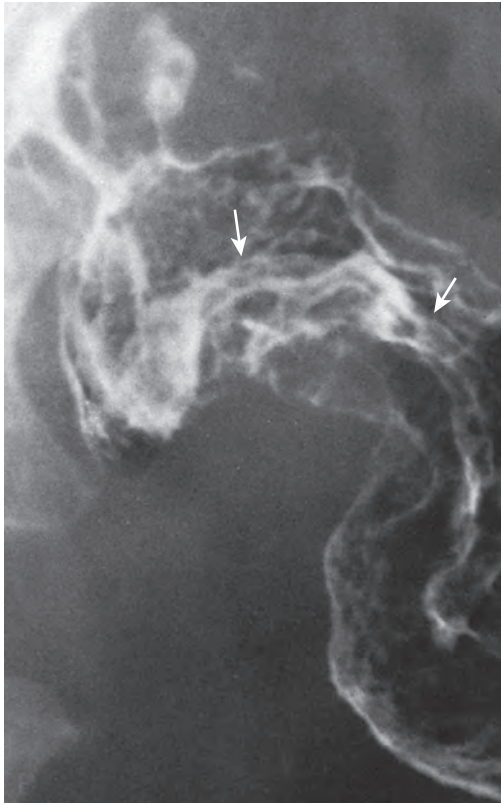


Figure 33-49 Gastric carcinoid tumor. A polypoid mass (arrows) is present on the greater curvature of the gastric antrum. This lesion is indistinguishable from other polypoid tumors in the stomach.



Figure 33-50 Duodenal carcinoid. Barium study shows a smooth, round submucosal mass (arrow) in the duodenal bulb. At surgery, this patient was found to have a malignant duodenal carcinoid tumor involving periduodenal lymph nodes.

producing typical bull's-eye lesions.¹⁶¹ The differential diagnosis for solitary, submucosal-appearing gastric carcinoids includes benign GISTs, ectopic pancreatic rests, and other mesenchymal tumors, whereas the differential diagnosis for multiple gastric carcinoids includes metastases, lymphoma, Kaposi's sarcoma, and gastric involvement by one of the polyposis syndromes. Other patients may have sessile or pedunculated lesions indistinguishable from hyperplastic or adenomatous polyps.^{170,171} Still other patients may have benign-appearing or malignant-appearing gastric ulcers.¹⁶³ Occasionally, advanced carcinoid tumors may appear as large polypoid masses indistinguishable from polypoid carcinomas (Fig. 33-49).^{161,172}

Duodenal carcinoids may be manifested by one or more polypoid defects in the duodenal bulb or proximal descending duodenum.^{165,173-175} These tumors may appear as discrete submucosal masses or intraluminal polyps (Fig. 33-50) or, less frequently, as polypoid or ulcerated lesions on barium studies or CT (Fig. 33-51).^{165,173-175} When gastric or duodenal carcinoids are detected radiographically, endoscopic biopsy specimens are required for a definitive diagnosis.

Miscellaneous Tumors

Other rare malignant tumors that may occur in the stomach or duodenum include liposarcomas, fibrosarcomas, neurofibrosarcomas, plasmacytomas, hemangioendotheliomas, hemangiopericytomas, choriocarcinomas, and malignant autonomic nerve tumors.¹⁷⁶⁻¹⁸¹ Rarely, the stomach may be involved by



Figure 33-51 Duodenal carcinoids on CT. Arterial phase 3D volume-rendered MDCT scan shows two hyperdense masses (arrows) in the duodenal bulb. The larger mass contains a central area of ulceration. Endoscopic biopsy specimens revealed duodenal carcinoid tumors.

leukemia or multiple myeloma (Fig. 33-52).^{182,183} Squamous cell carcinomas and adenosquamous carcinomas have also been described as rare malignant tumors in the stomach arising from congenital rests of squamous epithelium or from preexisting areas of squamous metaplasia.^{184,185}

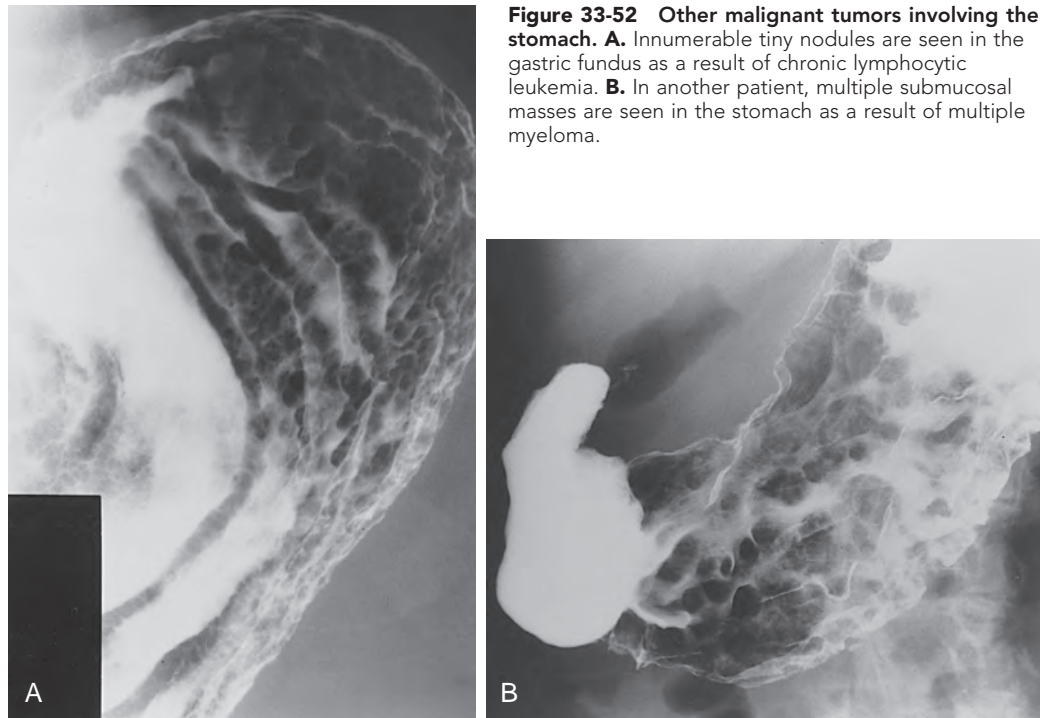


Figure 33-52 Other malignant tumors involving the stomach. **A.** Innumerable tiny nodules are seen in the gastric fundus as a result of chronic lymphocytic leukemia. **B.** In another patient, multiple submucosal masses are seen in the stomach as a result of multiple myeloma.

REFERENCES

- Menuck LS, Amberg JR: Metastatic disease involving the stomach. *Am J Dig Dis* 20:903-913, 1975.
- Asch MJ, Wiedel PD, Habif DV: Gastrointestinal metastases from carcinoma of the breast: Autopsy study and 18 cases requiring operative intervention. *Arch Surg* 96:840-843, 1968.
- Klein MS, Sherlock P: Gastric and colonic metastases from breast carcinoma. *Am J Dig Dis* 17:881-886, 1972.
- Hsu CC, Chen JJ, Changchien CS: Endoscopic features of metastatic tumors in the upper gastrointestinal tract. *Endoscopy* 28:249-253, 1996.
- Chang SF, Burrell MI, Brand MH, et al: The protean gastrointestinal manifestations of metastatic breast carcinoma. *Radiology* 126:611-617, 1978.
- Khilnani MT, Wolf BS: Late involvement of the alimentary tract by carcinoma of the kidney. *Am J Dig Dis* 5:529-540, 1960.
- Das Gupta TK, Brasfield RD: Metastatic melanoma of the gastrointestinal tract. *Arch Surg* 88:969-973, 1964.
- Meyers MA, McSweeney J: Secondary neoplasms of the bowel. *Radiology* 105:1-11, 1972.
- Joffe N: Metastatic involvement of the stomach secondary to breast carcinoma. *AJR* 123:512-521, 1975.
- Goldstein HM, Beydonn MT, Dodd GD: Radiologic spectrum of metastatic melanoma to the gastrointestinal tract. *AJR* 129:605-612, 1977.
- Lipshutz HI, Lindell MM, Dodd GD: Metastases to the hollow viscera. *Radiol Clin North Am* 20:487-499, 1982.
- Felson B: "Bull's eye" lesions: Solitary or multiple nodules in the gastrointestinal tract with large central ulceration. *JAMA* 229:825-826, 1974.
- McDermott VG, Low VHS, Keogan MT, et al: Malignant melanoma metastatic to the gastrointestinal tract. *AJR* 166:809-813, 1996.
- Zornoza J, Goldstein HM: Cavitating metastases of the small intestine. *AJR* 129:613-615, 1977.
- Radin DR, Halls JM: Cavitating metastases of the stomach and duodenum. *J Comput Assist Tomogr* 11:283-287, 1987.
- Levine MS, Kong V, Rubesin SE, et al: Scirrhous carcinoma of the stomach: Radiologic and endoscopic diagnosis. *Radiology* 175:151-154, 1990.
- Caskey CI, Scatarige JC, Fishman EK: Distribution of metastases in breast carcinoma: CT evaluation of the abdomen. *Clin Imaging* 15:166-171, 1991.
- Taal BG, Peterse H, Boot H: Clinical presentation, endoscopic features, and treatment of gastric metastases from breast carcinoma. *Cancer* 89:2214-2221, 2000.
- Winston CB, Hadar O, Teitcher JB, et al: Metastatic lobular carcinoma of the breast: Patterns of spread in the chest, abdomen, and pelvis on CT. *AJR* 175:795-800, 2000.
- Glick SN, Teplick SK, Levine MS, et al: Gastric cardia metastasis in esophageal carcinoma. *Radiology* 160:622-630, 1986.
- Glick SN, Teplick SK, Levine MS: Squamous cell metastases to the gastric cardia. *Gastrointest Radiol* 10:339-344, 1985.
- Allen HA, Bush JE: Midesophageal carcinoma metastatic to the stomach: Its unusual appearance on an upper gastrointestinal series. *South Med J* 76:1049-1051, 1983.
- Smith SJ, Carlson HC, Gisvold JJ: Secondary neoplasms of the small bowel. *Radiology* 125:29-33, 1977.
- Shammash JB, Rubesin SE, Levine MS: Massive gastric distention due to duodenal involvement by retroperitoneal tumors. *Gastrointest Radiol* 17:214-216, 1992.
- Levine MS, Caroline D, Thompson JJ, et al: Adenocarcinoma of the esophagus: Relationship to Barrett mucosa. *Radiology* 150:305-309, 1984.
- Keen SJ, Dodd GD, Smith JL: Adenocarcinoma arising in Barrett's esophagus: Pathologic and radiologic features. *Mt Sinai J Med* 51:442-450, 1984.
- Mani JR, Zboralske F, Margulis AR: Carcinoma of the body and tail of the pancreas. *AJR* 96:429-446, 1966.
- Balthazar EJ, Megibow AJ, Naidich DP, et al: Computed tomographic recognition of gastric varices. *AJR* 142:1121-1125, 1984.
- Marn CS, Glazer GM, Williams DM, et al: CT-angiographic correlation of collateral venous pathways in isolated splenic vein occlusion: New observations. *Radiology* 175:375-380, 1990.
- Treitel H, Meyers MA, Maza V: Changes in the duodenal loop secondary to carcinoma of the hepatic flexure of the colon. *Br J Radiol* 43:209-213, 1970.
- Meyers MA, Whalen JP: Roentgen significance of the duodenocolic relationships: An anatomic approach. *AJR* 117:263-274, 1973.
- Vieta JO, Blanco R, Valentine GR: Malignant duodenocolic fistula: Report of two cases with one or more synchronous gastrointestinal cancers. *Dis Colon Rectum* 19:542-552, 1976.
- Yamaguchi K, Enjoji M: Carcinoma of the gallbladder: A clinicopathology of 103 patients and a newly proposed staging. *Cancer* 62:1425-1432, 1988.
- Levitt RG, Koehler RE, Sagel SS, et al: Metastatic disease of the mesentery and omentum. *Radiol Clin North Am* 20:501-510, 1982.

35. Rubesin SE, Levine MS, Glick SN: Gastric involvement by omental cakes: Radiologic findings. *Gastrointest Radiol* 11:223-228, 1986.
36. Rubesin SE, Levine MS: Omental cakes: Colonic involvement by omental metastases. *Radiology* 154:593-596, 1985.
37. Walkey MM, Friedman AC, Radecki PD: Computed tomography of peritoneal carcinomatosis. *Radiology* 171:152-170, 1989.
38. Levitt RG, Sagel SS, Stanley RJ: Detection of neoplastic involvement of the mesentery and omentum by computed tomography. *AJR* 131:835-838, 1978.
39. Freeman C, Berg JW, Cutler SJ: Occurrence and prognosis of extranodal lymphomas. *Cancer* 29:252-260, 1972.
40. Menuck LS: Gastric lymphoma: A radiologic diagnosis. *Gastrointest Radiol* 1:157-161, 1976.
41. Brady LW: Malignant lymphoma of the gastrointestinal tract. *Radiology* 137:291-298, 1980.
42. Papadimitriou CS, Papacharalampous NX, Kittas C: Primary gastrointestinal lymphoma: A morphologic and immunohistochemical study. *Cancer* 55:870-879, 1985.
43. Farinha P, Gascoyne RD: *Helicobacter pylori* and MALT lymphoma. *Gastroenterology* 128:1579-1605, 2005.
44. Orr RK, Lininger JR, Lawrence W: Gastric pseudolymphoma: A challenging clinical problem. *Ann Surg* 200:185-194, 1984.
45. Harris NL: Extranodal lymphoid infiltrates and mucosa-associated lymphoid tissue (MALT): A unifying concept. *Am J Surg Pathol* 15:879-884, 1991.
46. Kitamura K, Yamaguchi T, Okamoto K, et al: Early gastric lymphoma. *Cancer* 77:850-857, 1996.
47. Dworkin B, Lightdale CJ, Weingrad DN, et al: Primary gastric lymphoma: A review of 50 cases. *Dig Dis Sci* 27:986-992, 1982.
48. Brooks JJ, Enterline HT: Primary gastric lymphomas: A clinicopathologic study of 58 cases with long-term follow-up and literature review. *Cancer* 51:701-711, 1983.
49. Brands F, Monig SP, Raab M: Treatment and prognosis of gastric lymphoma. *Eur J Surg* 163:803-813, 1997.
50. National Cancer Institute: National Cancer Institute sponsored study of classifications of non-Hodgkin's lymphomas: Summary and description of a working formulation for clinical usage. The Non-Hodgkin's Lymphoma Pathologic Classification Project. *Cancer* 48:2112-2135, 1982.
51. Lewin KJ, Ranchod M, Dorfman RF: Lymphomas of the gastrointestinal tract. *Cancer* 42:693-707, 1978.
52. Wotherspoon AC, Ortiz-Hidalgo C, Falzon MR, et al: *Helicobacter pylori*-associated gastritis and primary B-cell gastric lymphoma. *Lancet* 338:1175-1176, 1991.
53. Eidt S, Stolte M, Fischer R: *Helicobacter pylori* gastritis and primary gastric non-Hodgkin's lymphomas. *J Clin Pathol* 47:436-439, 1994.
54. Harris NL, Jaffe ES, Stern H, et al: A revised European-American classification of lymphoid neoplasms: A proposal from the International Lymphoma Study Group. *Blood* 84:1361-1392, 1994.
55. Stolte M, Eidt S: Lymphoid follicles in antral mucosa: Immune response to *Campylobacter pylori*? *J Clin Pathol* 42:1269-1271, 1989.
56. Eidt S, Stolte M: Prevalence of lymphoid follicles and aggregates in *Helicobacter pylori* gastritis in antral and body mucosa. *J Clin Pathol* 46:832-835, 1993.
57. Genta RM, Hamner HW, Graham DY: Gastric lymphoid follicles in *Helicobacter pylori* infection: Frequency, distribution, and response to triple therapy. *Hum Pathol* 24:577-583, 1993.
58. Isaacson P, Wright DH: Extranodal malignant lymphoma arising from mucosa-associated lymphoid tissue. *Cancer* 53:2515-2524, 1984.
59. Eck M, Schmauber B, Haas R, et al: MALT-type lymphoma of the stomach is associated with *Helicobacter pylori* strains expressing the CagA protein. *Gastroenterology* 112:1482-1486, 1997.
60. Cogliatti SB, Schmid U, Schumacher U, et al: Primary B-cell gastric lymphoma: A clinicopathological study of 145 patients. *Gastroenterology* 101:1159-1170, 1991.
61. Akaza K, Motoori T, Nakamura S, et al: Clinicopathologic study of primary gastric lymphoma of B cell phenotype with special reference to low-grade B cell lymphoma of mucosa-associated lymphoid tissue among the Japanese. *Pathol Int* 45:832-845, 1995.
62. Chan JKC, Ng CS, Isaacson PG: Relationship between high-grade lymphoma and low-grade B-cell mucosa-associated lymphoid tissue lymphoma (MALToma) of the stomach. *Am J Pathol* 136:1153-1164, 1990.
63. Nelson RS, Lanza FL: Malignant tumors of the stomach. In Berk JE, Haubrich WS, Kalser MH, et al, editors: *Bockus Gastroenterology*, ed 4, Philadelphia, 1985, WB Saunders, pp 1267-1277.
64. Sandler RS: Primary gastric lymphoma. *Am J Gastroenterol* 79:21-25, 1984.
65. Seifert E, Schulte F, Weismuller J, et al: Endoscopic and biopsic diagnosis of malignant non-Hodgkin's lymphoma of the stomach. *Endoscopy* 25:497-501, 1993.
66. Roggero E, Zucca E, Pinotti G, et al: Eradication of *Helicobacter pylori* infection in primary low-grade gastric lymphoma of mucosa-associated lymphoid tissue. *Ann Intern Med* 122:767-769, 1995.
67. Taal BG, Boot H, van Heerde P, et al: Primary non-Hodgkin lymphoma of the stomach: Endoscopic pattern and prognosis in low versus high grade malignancy in relation to the MALT concept. *Gut* 39:556-561, 1996.
68. Grossman E, Winawer SJ: Diffuse gastrointestinal lymphosarcoma: Gastroscopic and proctoscopic observations. *Gastrointest Endosc* 16:202-204, 1970.
69. Nelson RS, Lanza FL: The endoscopic diagnosis of gastric lymphoma: Gross characteristics and histology. *Gastrointest Endosc* 20:183-184, 1974.
70. Cabre-Fiol V, Vilardell F: Progress in the cytological diagnosis of the gastric lymphoma. *Cancer* 41:1456-1461, 1978.
71. Spinelli P, Gullo CL, Pizzetti P: Endoscopic diagnosis of gastric lymphomas. *Endoscopy* 12:211-214, 1980.
72. Shin MH, Karas M, Nisce L, et al: Management of primary gastric lymphoma. *Ann Surg* 195:196-202, 1982.
73. Shen YY, Kao A, Yen FR: Comparison of ¹⁸F-fluoro-2-deoxyglucose positron emission tomography and gallium-67 citrate scintigraphy for detecting malignant lymphoma. *Oncol Rep* 9:321-325, 2002.
74. Mittal B, Wasserman TH, Griffith RC: Non-Hodgkin's lymphoma of the stomach. *Am J Gastroenterol* 78:780-787, 1983.
75. Amer MH, El-Akkad S: Gastrointestinal lymphoma in adults: Clinical features and management of 300 cases. *Gastroenterology* 106:846-858, 1994.
76. Bayerdorffer E, Neubauer A, Rudolph B, et al: Regression of primary gastric lymphoma of mucosa-associated lymphoid tissue after cure of *Helicobacter pylori* infection. *Lancet* 345:1591-1594, 1995.
77. Lim FE, Hartman AS, Tan EGC, et al: Factors in the prognosis of gastric lymphoma. *Cancer* 39:1715-1720, 1977.
78. Loehr WJ, Mujahed Z, Zahn RD, et al: Primary lymphoma of the gastrointestinal tract: A review of 100 cases. *Ann Surg* 170:232-238, 1969.
79. Levine MS, Elmas N, Furth EE, et al: *Helicobacter pylori* and gastric MALT lymphoma. *AJR* 166:85-86, 1996.
80. Yoo CC, Levine MS, Furth EE, et al: Gastric mucosa-associated lymphoid tissue lymphoma: Radiographic findings in six patients. *Radiology* 208:239-243, 1998.
81. Kim YH, Lim HK, Han JK, et al: Low-grade gastric mucosa-associated lymphoid tissue lymphoma: Correlation of radiographic and pathologic findings. *Radiology* 212:241-248, 1999.
82. Park MS, Kim KW, Yu JS, et al: Radiographic findings of primary B-cell lymphoma of the stomach: Low-grade versus high-grade malignancy in relation to the mucosa-associated lymphoid tissue concept. *AJR* 179:1297-1304, 2002.
83. Sherrick DW, Hodgson JR, Dockerty MB: The roentgenologic diagnosis of primary gastric lymphoma. *Radiology* 84:925-932, 1965.
84. Zornoza J, Dodd GD: Lymphoma of the gastrointestinal tract. *Semin Roentgenol* 15:272-287, 1980.
85. Fork FT, Ekberg O, Haglund U: Radiology in primary gastric lymphoma. *Acta Radiol Diagn* 25:481-488, 1984.
86. Levine MS, Rubesin SE, Pantongrag-Brown L, et al: Non-Hodgkin's lymphoma of the gastrointestinal tract: Radiographic findings. *AJR* 168:165-172, 1997.
87. Levine MS, Pantongrag-Brown L, Aguilera NS, et al: Non-Hodgkin lymphoma of the stomach: A cause of linitis plastica. *Radiology* 201:375-378, 1996.
88. Joffe N: Metastatic involvement of the stomach secondary to breast carcinoma. *AJR* 123:512-521, 1975.
89. Bloch C: Roentgen features of Hodgkin's disease of the stomach. *AJR* 99:175-181, 1967.
90. Ounnick NR, Harell GS, Parker BR: Multiple "bull's-eye" lesions in gastric lymphoma. *AJR* 126:965-969, 1976.
91. Hricak H, Thoeni RJ, Margulis AR, et al: Extension of gastric lymphoma into the esophagus and duodenum. *Radiology* 135:309-312, 1980.
92. Cho KC, Baker SR, Alterman DD, et al: Transpyloric spread of gastric tumors: Comparison of adenocarcinoma and lymphoma. *AJR* 167:467-469, 1996.
93. Koehler RE, Hanelin LG, Laing FC, et al: Invasion of the duodenum by carcinoma of the stomach. *AJR* 128:201-205, 1977.
94. Fox ER, Laufer I, Levine MS: Response of gastric lymphoma to chemotherapy: Radiographic appearance. *AJR* 142:711-714, 1984.
95. Libshitz HI, Lindell MM, Maor MH, et al: Appearance of the intact lymphomatous

- stomach following radiotherapy and chemotherapy. *Gastrointest Radiol* 10:25–29, 1985.
96. Buy JN, Moss AA: Computed tomography of gastric lymphoma. *AJR* 138:859–865, 1982.
 97. Megibow AJ, Balthazar EJ, Naidich DP, et al: Computed tomography of gastrointestinal lymphoma. *AJR* 141:541–547, 1983.
 98. Choi D, Lim HK, Lee SJ, et al: Gastric mucosa-associated lymphoid tissue lymphoma: Helical CT findings and pathologic correlation. *AJR* 178:1117–1122, 2002.
 99. Tio TL, den Hartog-Jager FC, Tytgat GN: Endoscopic ultrasonography of non-Hodgkin lymphoma of the stomach. *Gastroenterology* 91:401–408, 1986.
 100. Caletti G, Ferrari A, Brocchi E, et al: Accuracy of endoscopic ultrasonography in the diagnosis and staging of gastric cancer and lymphoma. *Surgery* 113:14–27, 1993.
 101. Dheer S, Levine MS, Redfern RO, et al: Radiographically diagnosed antral gastritis: Findings in patients with and without *Helicobacter pylori* infection. *Br J Radiol* 75:805–811, 2002.
 102. Torigian DA, Levine MS, Gill NS, et al: Lymphoid hyperplasia of the stomach: Radiographic findings in five adult patients. *AJR* 177:71–75, 2001.
 103. Meyers MA, Katzen B, Alonso DR: Transpyloric extension to duodenal bulb in gastric lymphoma. *Radiology* 115:575–580, 1975.
 104. Balikian JP, Nassar NT, Shamma'a MH, et al: Primary lymphomas of the small intestine including the duodenum: A Roentgen analysis of twenty-nine cases. *AJR* 107:131–141, 1969.
 105. Holmes GKT, Stokes PL, Sorahan TM, et al: Coeliac disease, gluten-free diet, and malignancy. *Gut* 17:612–619, 1976.
 106. Collins SM, Hamilton JD, Lewis TD, et al: Small-bowel malabsorption and gastrointestinal malignancy. *Radiology* 126:603–609, 1978.
 107. Nauert TC, Zornoza J, Ordonez N: Gastric leiomyosarcomas. *AJR* 139:291–297, 1982.
 108. Suster S: Gastrointestinal stromal tumors. *Semin Diagn Pathol* 13:297–313, 1996.
 109. Sarlomo-Rikala M, Kovatch AJ, Barusevicius A, et al: CD117: A sensitive marker for gastrointestinal stromal tumors that is more specific than CD34. *Mod Pathol* 11:728–734, 1998.
 110. Ho MY, Blanke CD: Gastrointestinal stromal tumors: Disease and treatment update. *Gastroenterology* 140:1372–1376, 2011.
 111. Levy AD, Remotti HE, Thompson WM, et al: Gastrointestinal stromal tumors: Radiologic features with pathologic correlation. *Radiographics* 23:283–304, 2003.
 112. Appelman HD, Helwig EB: Gastric epithelioid leiomyoma and leiomyosarcoma (leiomyoblastoma). *Cancer* 38:708–728, 1976.
 113. Burkill GJC, Badran M, Al-Muderis O, et al: Malignant gastrointestinal stromal tumor: Distribution, imaging features, and pattern of metastatic spread. *Radiology* 226:527–532, 2003.
 114. Franquemont DW: Differentiation and risk assessment of gastrointestinal stromal tumors. *Am J Clin Pathol* 103:41–47, 1995.
 115. Miettinen M, Sarlomo-Rikala M, Lasota J: Gastrointestinal stromal tumors: Recent advances in understanding of their biology. *Hum Pathol* 30:1213–1220, 1999.
 116. Ludwig DJ, Traverso LW: Gut stromal tumors and their clinical behavior. *Am J Surg* 173:390–394, 1997.
 117. Ranchod M, Kempson RL: Smooth muscle tumors of the gastrointestinal tract and retroperitoneum. *Cancer* 39:255–262, 1977.
 118. Bedikian AY, Khankhanian N, Heilbrun LK, et al: Primary lymphomas and sarcomas of the stomach. *South Med J* 73:21–24, 1980.
 119. Stauber SL, Messer J, Berger HW: Gastric leiomyosarcoma diagnosed on chest roentgenogram: Importance of the stomach bubble. *Mt Sinai J Med* 50:514–516, 1983.
 120. Phillips JC, Lindsay JW, Kendall JA: Gastric leiomyosarcoma: Roentgenologic and clinical findings. *Am J Dig Dis* 15:239–246, 1970.
 121. Scatarige JC, Fishman EK, Jones B, et al: Gastric leiomyosarcoma; CT observations. *J Comput Assist Tomogr* 9:320–327, 1985.
 122. Train JS, Hertz I, Keller RJ: Exogastric smooth muscle tumors. *Am J Gastroenterol* 76:544–550, 1981.
 123. Herlinger H: The recognition of exogastric tumors: Report of six cases. *Br J Radiol* 39:25–34, 1966.
 124. Sharp RM, Ansel HJ, Keel SB: Best cases from the AFIP: Gastrointestinal stromal tumor. *Radiographics* 21:1557–1560, 2001.
 125. Horton KM, Juluru K, Montgomery E, et al: Computed tomography imaging of gastrointestinal stromal tumors with pathologic correlation. *J Comput Assist Tomogr* 28:811–817, 2004.
 126. Kim HC, Lee JM, Kim KW, et al: Gastrointestinal stromal tumors of the stomach: CT findings and prediction of malignancy. *AJR* 183:893–898, 2004.
 127. McLeod AJ, Zornoza J, Shirkhoda A: Leiomyosarcoma: Computed tomographic findings. *Radiology* 52:133–136, 1984.
 128. Megibow AJ, Balthazar EJ, Hulnick DH, et al: CT evaluation of gastrointestinal leiomyomas and leiomyosarcomas. *AJR* 144:727–733, 1985.
 129. Disler DG, Chew FS: Gastric leiomyosarcoma. *AJR* 159:58, 1992.
 130. Villanueva A, Perez C, Sabate JM, et al: CT manifestations of peritoneal leiomyosarcomatosis. *Eur J Radiol* 17:166–169, 1993.
 131. Granmayeh M, Jonsson K, McFarland W, et al: Angiography of abdominal leiomyosarcoma. *AJR* 130:725–730, 1978.
 132. Lee DH, Choi BI, Lee MG, et al: Exophytic adenocarcinoma of the stomach: CT findings. *AJR* 163:77–80, 1994.
 133. Lo J, Sage MR, Paterson HS, et al: Gastric duplication in an adult. *J Comput Assist Tomogr* 7:328–330, 1983.
 134. Hulnick DH, Balthazar EJ: Gastric duplication cyst: GI series and CT correlation. *Gastrointest Radiol* 12:106–108, 1987.
 135. Pujari BD, Deadhare SG: Leiomyosarcoma of the duodenum. *Int Surg* 61:237–238, 1976.
 136. McBrien MP, Garrett PEM: Leiomyosarcoma of the duodenum. *Br J Surg* 58:685–689, 1971.
 137. Kanematsu M, Imaeda T, Iianuma G, et al: Leiomyosarcoma of the duodenum. *Gastrointest Radiol* 16:109–112, 1991.
 138. Kim HC, Lee JM, Son KR, et al: Gastrointestinal stromal tumors of the duodenum: CT and barium study findings. *AJR* 183:415–419, 2004.
 139. Hill CA, Harle TS, Mansell PWA: The prodrome, Kaposi sarcoma, and infections associated with acquired immunodeficiency syndrome: Radiologic findings in 39 patients. *Radiology* 149:393–399, 1983.
 140. Wall SD, Friedman SL, Margulis AR: Gastrointestinal Kaposi's sarcoma in AIDS: Radiographic manifestations. *J Clin Gastroenterol* 6:165–171, 1984.
 141. Friedman SL, Wright TL, Altman DF: Gastroenterology Kaposi's sarcoma with acquired immunodeficiency syndrome. *Gastroenterology* 89:102–108, 1985.
 142. Henderson RG, Rahmatulla TD: An epidemic tumour. *Br J Radiol* 60:511–512, 1987.
 143. Saltz RK, Kurtz RC, Lightdale CJ, et al: Kaposi's sarcoma: Gastrointestinal involvement correlation with skin findings and immunologic function. *Dig Dis Sci* 29:817–823, 1984.
 144. Ell C, Matek W, Gramatzki M, et al: Endoscopic findings in a case of Kaposi's sarcoma with involvement of the large and small bowel. *Endoscopy* 17:161–164, 1985.
 145. Lustbader I, Sherman A: Primary gastrointestinal Kaposi's sarcoma in a patient with acquired immune deficiency syndrome. *Am J Gastroenterol* 82:894–895, 1987.
 146. Rose HS, Balthazar EJ, Megibow AJ, et al: Alimentary tract involvement in Kaposi sarcoma: Radiographic and endoscopic findings in 25 homosexual men. *AJR* 139:661–666, 1982.
 147. Jaffe HW, Bregman DJ, Selik RM: Acquired immune deficiency syndrome in the United States: The first 1,000 cases. *J Infect Dis* 148:339–345, 1983.
 148. Friedman SL: Gastrointestinal and hepatobiliary neoplasms in AIDS. *Gastroenterol Clin North Am* 17:465–486, 1988.
 149. Balthazar EJ, Richman A: Kaposi's sarcoma of the stomach. *Am J Gastroenterol* 67:375–379, 1977.
 150. Frager DH, Frager JD, Brandt LJ, et al: Gastrointestinal complications of AIDS: Radiologic features. *Radiology* 158:597–603, 1986.
 151. Falcone S, Murphy BJ, Weinfeld A: Gastric manifestations of AIDS: Radiographic findings on upper gastrointestinal examination. *Gastrointest Radiol* 16:95–98, 1991.
 152. Hadjiyane C, Lee YH, Stein L, et al: Kaposi's sarcoma presenting as linitis plastica. *Am J Gastroenterol* 86:1823–1825, 1991.
 153. Leibman AJ, Gold BM: Gastric manifestations of autoimmune deficiency syndrome-related Kaposi's sarcoma on computed tomography. *J Comput Tomogr* 10:85–88, 1986.
 154. Jeffrey RB, Jr, Goodman PC, Olsen WL, et al: Radiologic imaging of AIDS. *Curr Probl Diagn Radiol* 17:73–117, 1988.
 155. Jeffrey RB, Nyberg DA, Bottles K, et al: Abdominal CT in acquired immunodeficiency syndrome. *AJR* 146:7–13, 1986.
 156. Herts BR, Megibow AJ, Birnbaum BA, et al: High attenuation lymphadenopathy in AIDS patients: Significance of findings on CT. *Radiology* 185:777–781, 1992.
 157. Hwang EG, Sagel SS, Brunt EM: Multiple gastric carcinoids. *Radiographics* 29:1206–1209, 2009.
 158. Ganeshan D, Bhosale P, Yang T, et al: Imaging features of carcinoid tumors of the gastrointestinal tract. *AJR* 201:773–786, 2013.
 159. Modlin IM, Tang LH: The gastric enterochromaffin-like cell: An enigmatic cellular link. *Gastroenterology* 111:783–810, 1996.
 160. Modlin IM, Sandor A, Tang LH, et al: A 40-year analysis of 265 gastric carcinoids. *Am J Gastroenterol* 92:633–638, 1997.
 161. Balthazar EJ, Megibow A, Bryk D: Gastric carcinoid tumors: Radiographic features in eight cases. *AJR* 139:1123–1127, 1982.
 162. Rindi G, Luinetti O, Cornaggia M, et al: Three subtypes of gastric argyrophil carcinoid and the gastric neuroendocrine carcinoma: A clinicopathologic study. *Gastroenterology* 104:994–1006, 1993.

163. Berger MW, Stephens DH: Gastric carcinoid tumors associated with chronic hypergastrinemia in a patient with Zollinger-Ellison syndrome. *Radiology* 201:371–373, 1996.
164. Sculco D, Bilgrami S: Pernicious anemia and gastric carcinoid tumor: Case report and review. *Am J Gastroenterol* 92:1378–1380, 1997.
165. Levy AD, Taylor LD, Abbott RM, et al: Duodenal carcinoids: Imaging features with clinical-pathologic comparison. *Radiology* 237:967–972, 2005.
166. DeLuca RF, Ferrer JP, Gambescia RA, et al: Gastric carcinoid endoscopically simulating leiomyoma. *Am J Gastroenterol* 70:163–166, 1978.
167. Wengrower D, Fich A: Primary duodenal carcinoid. *Am J Gastroenterol* 82:1069–1070, 1987.
168. Abrams JS: Multiple malignant carcinoids of the stomach. *Arch Surg* 115:1219–1221, 1980.
169. Honig LJ, Weingarten G: A gastric carcinoid tumor with massive bleeding. *Am J Gastroenterol* 61:40–44, 1974.
170. Gueller R, Haddad JK: Gastric carcinoids simulating benign polyps. *Gastrointest Endosc* 21:153–155, 1975.
171. Syre-Smith G: Polypoid carcinoid tumor of the stomach. *J Can Assoc Radiol* 28:217–218, 1977.
172. Okeon MM, Bieber WP: Carcinoid tumor of the stomach resembling carcinoma. *AJR* 103:314–316, 1968.
173. Seymour EQ, Griffin CN, Kurtz SM: Carcinoid tumors of the duodenal cap presenting as multiple polypoid defects. *Gastrointest Radiol* 7:19–21, 1982.
174. Clements JL, Roche RR: Carcinoid of the duodenum: A report of six cases. *Gastrointest Radiol* 9:17–21, 1984.
175. Eschelmann DJ, Duva-Frissora AD, Martin LC, et al: Metastatic carcinoid presenting as a duodenal mass. *AJR* 156:1301–1302, 1991.
176. Lopez-Negrete L, Luyando L, Sala J, et al: Liposarcoma of the stomach. *Abdom Imaging* 22:373–375, 1997.
177. Godard JE, Fox JE, Levinson MJ: Primary gastric plasmacytoma. *Am J Dig Dis* 18:508–512, 1973.
178. Yoon SE, Ha HK, Lee YS, et al: Upper gastrointestinal series and CT findings of primary gastric plasmacytoma: Report of two cases. *AJR* 173:1266–1268, 1999.
179. Pentimone F, Camici M, Cini G, et al: Duodenal plasmacytoma: A rare extramedullary location simulating a carcinoma. *Acta Haematol* 61:155–160, 1979.
180. Jindrak K, Bochetto JF, Alpert LI: Primary gastric choriocarcinoma. *Hum Pathol* 7:595–604, 1976.
181. Jain KA, Gerscovich EO, Goodnight JJ: Malignant autonomic nerve tumor of the duodenum. *AJR* 168:1461–1463, 1997.
182. Feingold ML, Goldstein MJ, Lieberman PH: Multiple myeloma involving the stomach: Report of a case with gastroscopic observations. *Gastrointest Endosc* 16:107–110, 1969.
183. Kwak HS, Jin GY, Lee JM: Radiologic findings of multiple myeloma with gastric involvement: A case report. *Korean J Radiol* 3:133–135, 2002.
184. Won OH, Farman J, Krishnan MN, et al: Squamous cell carcinoma of the stomach. *Am J Gastroenterol* 69:594–598, 1978.
185. Straus R, Heschel S, Fortmann DJ: Primary adenosquamous carcinoma of the stomach. *Cancer* 24:985–995, 1969.

Miscellaneous Abnormalities of the Stomach and Duodenum

RONALD L. EISENBERG | MARC S. LEVINE

CHAPTER OUTLINE

Varices

Gastric Varices
Duodenal Varices

Portal Hypertensive Gastropathy

Radiographic Findings

Diverticula

Gastric Diverticula
Duodenal Diverticula

Webs and Diaphragms

Antral Webs and Diaphragms
Duodenal Webs and Diaphragms

Adult Hypertrophic Pyloric Stenosis

Gastric Outlet Obstruction

Duodenal Obstruction

Superior Mesenteric Root Syndrome
Other Causes

Gastric Dilation Without Gastric Outlet Obstruction

Acute Gastric Dilation
Chronic Gastric Dilation and Gastroparesis

Abnormal Extrinsic Masses

Stomach
Duodenum

Widening of the Duodenal Sweep

Pancreatic Diseases Affecting the Stomach and Duodenum

Unusual Filling Defects

Bezoars
Foreign Bodies
Hematomas
Intragastric and Intraduodenal Gallstones

Gastric Volvulus

Gastroduodenal and Duodenojejunal Intussusceptions

Fistulas

Gastrocolic and Duodenocolic Fistulas
Cholecystoduodenal Fistulas
Other Fistulas

Gastric and Duodenal Perforation

Benign Gastric Emphysema

Amyloidosis

Cystic Fibrosis

Varices

GASTRIC VARICES

Pathophysiology

Portal Hypertension. The gastric fundus contains a venous plexus that is normally drained by numerous short gastric veins anastomosing distally with the splenic vein and proximally with branches of the coronary vein as well as venous channels surrounding the distal esophagus. Blood in the short gastric veins normally empties via the splenic vein into the portal venous system. In patients with portal hypertension, however, increased pressure in the portal and splenic veins leads to reversal of blood flow through the short gastric veins into the fundal venous plexus, producing fundal varices. As a result, gastric varices develop in 20% of patients with portal hypertension.¹ Because elevated portal pressure also causes reversal of flow through the coronary vein (producing uphill esophageal varices), some patients with portal hypertension have combined gastric and esophageal varices. However, others with portal hypertension have isolated gastric varices, and an

even greater number have isolated esophageal varices (see Chapter 25).

One explanation for the frequent failure to visualize gastric varices in patients with portal hypertension is that the venous channels in the gastric fundus have thicker, better connective tissue support than the thin-walled, loosely supported veins in the distal esophagus. As a result, varices may be more likely to form in the esophagus than in the stomach, despite comparable elevations in pressure. Even when gastric varices are present, they may be obscured on barium studies or endoscopy by overlying gastric rugae.

Splenic Vein Obstruction. In patients with splenic vein obstruction, increased pressure in the splenic vein beyond the obstruction leads to reversal of flow through the short gastric veins to the fundal plexus of veins, producing gastric varices. Because these patients have normal portal pressure, however, venous blood from the dilated fundal plexus can enter the portal venous system via the coronary vein without producing uphill esophageal varices. As a result, splenic vein obstruction is characterized by isolated varices

in the gastric fundus without associated varices in the esophagus.

Splenic vein obstruction may result from intrinsic thrombosis or, more commonly, from extrinsic compression of the splenic vein by a variety of benign or malignant conditions, including pancreatitis, pancreatic pseudocysts, pancreatic carcinoma, metastatic disease, lymphoma, and retroperitoneal fibrosis or bleeding.²⁻⁵ Intrinsic thrombosis of the splenic vein may be idiopathic or may result from polycythemia or other myeloproliferative disorders.³

Clinical Findings

Gastric varices are important because of the risk of gastrointestinal (GI) bleeding, which can range from low-grade, intermittent bleeding to massive hematemesis.^{6,7} Gastric varices are less likely to bleed than esophageal varices because of their subserosal location and the greater thickness of overlying gastric tissue.⁸ When gastric variceal bleeding occurs, however, it tends to be more severe than esophageal variceal bleeding and is associated with a higher mortality rate.¹ When gastric varices are associated with esophageal varices, affected individuals usually have the stigmata of portal hypertension. In contrast, patients with isolated gastric varices caused by splenic vein obstruction may present with abdominal pain and weight loss from underlying pancreatitis or pancreatic carcinoma.³ Splenomegaly is also a frequent finding in splenic vein obstruction, but a normal-sized spleen does not exclude this condition.⁹

Radiographic Findings

Abdominal Radiographs. Large gastric varices may occasionally be recognized on chest or abdominal radiographs as one or more lobulated soft tissue densities in the gas-filled fundus. Depending on the cause of the varices (portal hypertension or splenic vein obstruction), abdominal radiographs may also reveal splenomegaly, ascites, or pancreatic calcification. When gastric varices are suspected on the basis of abdominal radiographs other imaging tests such as barium studies, endoscopy, or computed tomography (CT) should be performed for a more definitive diagnosis.

Barium Studies. Conventional single-contrast barium studies are thought to be unreliable for detecting gastric varices. Double-contrast technique has therefore been advocated to improve visualization of these structures.^{5,10} Gastric varices may appear as thickened, tortuous folds or as round submucosal filling defects in the gastric fundus, resembling the appearance of a bunch of grapes (Fig. 34-1).^{3,5} Less frequently, a conglomerate mass of fundal varices, also known as tumorous gastric varices, may be manifested by a large polypoid mass that can be mistaken on barium studies for a polypoid carcinoma or even a malignant gastrointestinal stromal tumor (GIST) (Figs. 34-2 and 34-3).^{3,10-13} Tumorous varices have characteristic features, however, appearing in profile as smooth submucosal masses with an undulating contour and discrete borders on the posteromedial wall of the gastric fundus (see Figs. 34-2 and 34-3) and en face as thickened, tortuous folds that fade peripherally into the adjacent mucosa.¹³ These radiographic features should allow differentiation from polypoid gastric neoplasms in most cases. Rarely, dilated gastroepiploic veins may be manifested by varices in the antrum or body of the stomach (Fig. 34-4).¹⁴

When gastric varices are detected on barium studies, it is important to determine whether uphill esophageal varices are

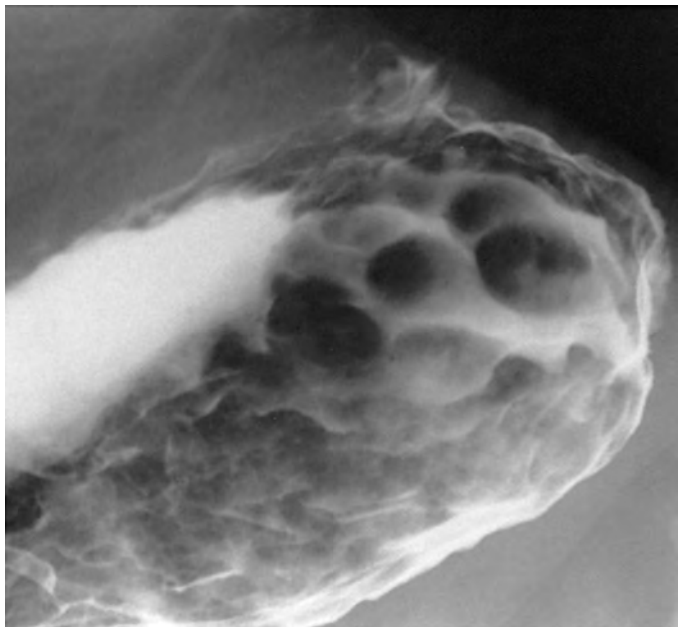


Figure 34-1 Gastric varices. Multiple rounded submucosal filling defects are seen in the gastric fundus, resembling the appearance of a bunch of grapes. (From Levine MS, Kieu K, Rubesin SE, et al: Isolated gastric varices: Splenic vein obstruction or portal hypertension? *Gastrointest Radiol* 15:188-192, 1990.)

also present in these patients. The presence of combined esophageal and gastric varices almost always indicates portal hypertension as the underlying cause. In contrast, isolated gastric varices should raise the possibility of splenic vein obstruction with a patent portal vein (see Fig. 34-3).^{3,5} Nevertheless, portal hypertension is much more common than splenic vein obstruction, so most patients with gastric varices, even in the absence of esophageal varices, are found to have portal hypertension as the underlying cause (see Fig. 34-2).¹⁵ If necessary, CT or angiography may be performed to document the presence of varices and elucidate their pathophysiology.

Computed Tomography. Gastric varices are usually recognized on CT as enhancing, well-defined, round or tubular densities on the posterior or posteromedial wall of the gastric fundus (Fig. 34-5).¹⁶ CT is more sensitive than conventional radiologic examinations in detecting these lesions because barium studies can only demonstrate varices that protrude into the lumen, whereas CT can delineate deeper intramural and perigastric varices.¹⁶ CT may also reveal cirrhotic liver disease, splenomegaly, or ascites in patients with portal hypertension (see Fig. 34-5) and splenomegaly or pancreatic disease in patients with splenic vein obstruction.

Angiography. Angiography may be performed to confirm the presence of gastric varices and determine the nature of the underlying venous abnormality. With portal hypertension, reversal of flow through the coronary and short gastric veins leads to the formation of esophageal and gastric varices, with absent visualization of the portal and splenic veins. With splenic vein obstruction, however, delayed images reveal normal filling of a patent portal vein without evidence of esophageal varices, as blood is diverted from the fundal plexus of veins via the coronary vein to the portal venous system, bypassing the

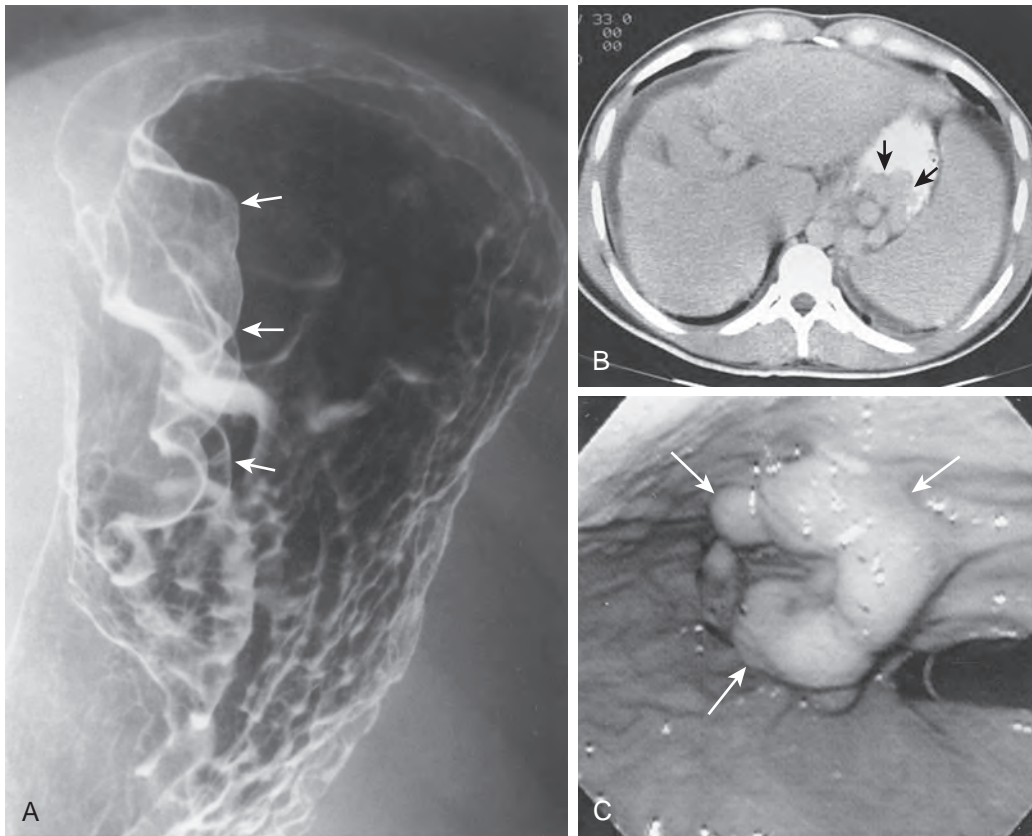


Figure 34-2 Conglomerate mass of gastric varices (also known as tumorous varices). **A.** Barium study shows a large, lobulated submucosal mass (arrows) on the medial aspect of the gastric fundus. Although this lesion could be mistaken for a malignant GI stromal tumor or even a polypoid carcinoma, note its smooth undulating contour. **B.** Unenhanced CT scan shows a lobulated soft tissue mass (arrows) on the posteromedial wall of the fundus. **C.** Endoscopic photograph shows a conglomerate mass of varices (arrows) in the gastric fundus adjacent to the cardia. This patient had underlying portal hypertension. (B and C from Levine MS, Kieu K, Rubesin SE, et al: Isolated gastric varices: Splenic vein obstruction or portal hypertension? *Gastrointest Radiol* 15:188–192, 1990.)

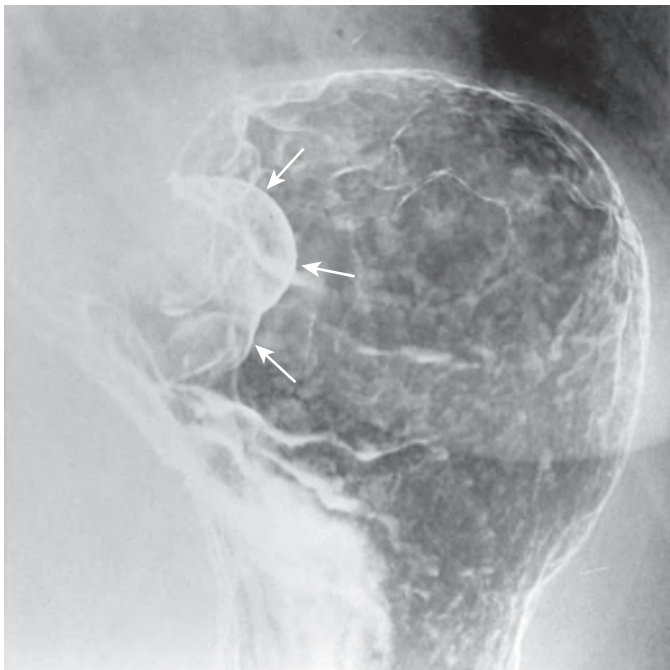


Figure 34-3 Conglomerate mass of isolated gastric varices caused by splenic vein obstruction. A smooth, undulating mass (arrows) is seen on the posteromedial wall of the gastric fundus. Note the resemblance to the gastric varices in Figure 34-2. This patient had underlying pancreatitis causing splenic vein obstruction. (Courtesy William M. Thompson, MD, Minneapolis.)

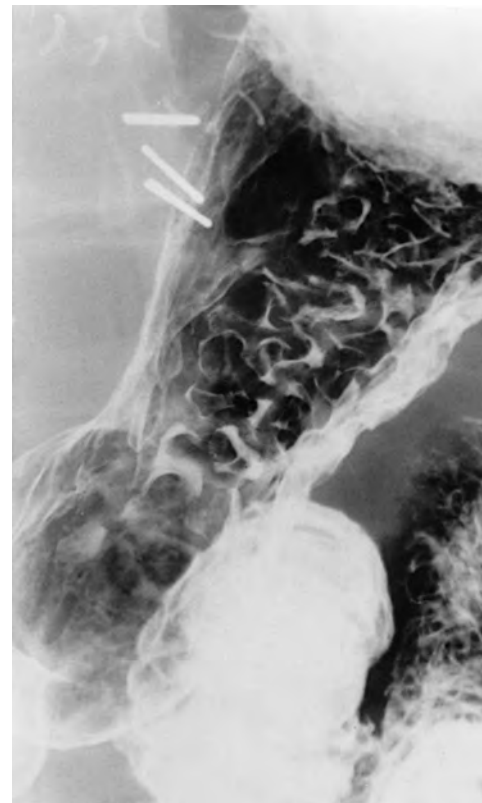


Figure 34-4 Nonfundal gastric varices. Thickened, tortuous folds are seen in the body of the stomach caused by markedly dilated gastroepiploic veins. This patient had severe portal hypertension. (From Levine MS: *Radiology of the Esophagus*. Philadelphia, WB Saunders, 1989.)

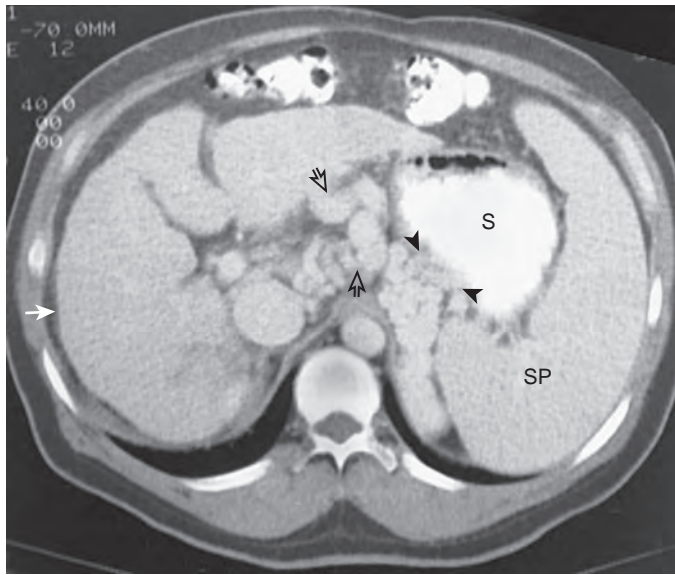


Figure 34-5 Gastric varices on CT. Enhancing collaterals are seen in the gastric wall (arrowheads), gastrohepatic ligament (open arrows), and left retroperitoneal space. This patient also has cirrhosis with splenomegaly and minimal ascites (solid arrow) caused by portal hypertension. S, stomach; SP, spleen. (Courtesy Richard M. Gore, MD, Evanston, IL.)

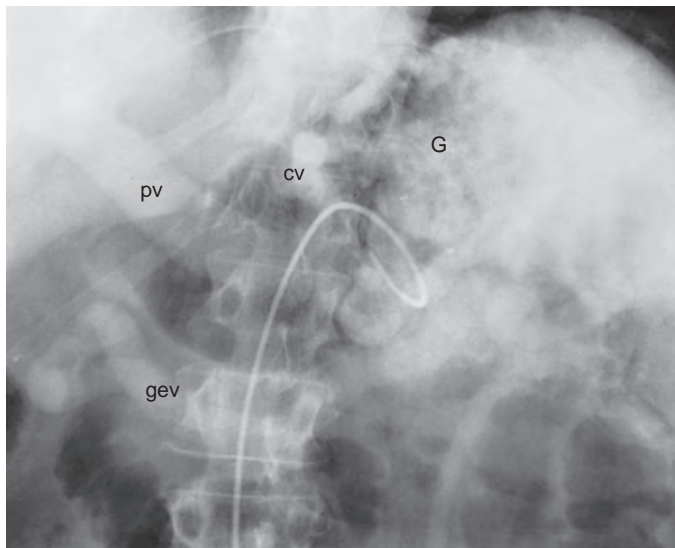


Figure 34-6 Angiographic demonstration of gastric varices due to splenic vein obstruction. Image from the venous phase of a splenic arteriogram shows a densely opacified spleen with absent visualization of the splenic vein, extensive gastric varices (G), and a dilated coronary vein (cv) diverting blood from the fundal plexus of veins to the portal vein (pv). Note the presence of a dilated gastroepiploic vein (gev). (Courtesy Dana R. Burke, MD, Bethesda, MD.)

obstructed splenic vein (Fig. 34-6). Thus, portal hypertension can usually be differentiated from splenic vein obstruction by angiography, so appropriate therapy can be instituted in these patients.

Differential Diagnosis

When gastric varices are manifested on barium studies by thickened, nodular folds in the fundus, the differential diagnosis

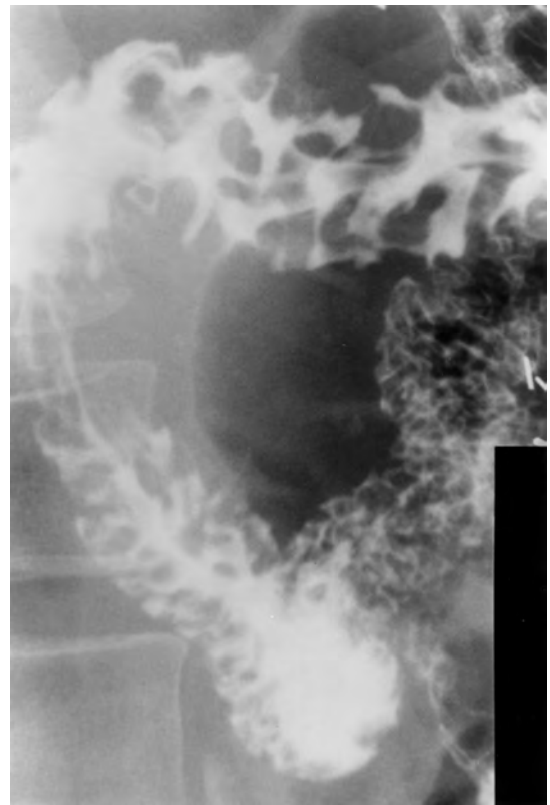


Figure 34-7 Duodenal varices. Thickened, serpiginous folds are seen in the proximal descending duodenum.

includes *Helicobacter pylori* gastritis, Ménétrier's disease, Zollinger-Ellison syndrome, pancreatitis, and lymphoma.¹⁷ However, gastric varices tend to be more tortuous or lobulated than these other conditions and are often associated with esophageal varices. Occasionally, a conglomerate mass of fundal varices may resemble a polypoid carcinoma or even a malignant GIST (see Figs. 34-2 and 34-3).^{3,10-13} However, the vascular origin of these lesions is suggested by their smooth undulating contour and typical location on the posteromedial wall of the gastric fundus. CT or angiography may be required for a definitive diagnosis. It is particularly important to differentiate gastric varices from other lesions before performing endoscopic biopsy or surgery because inadvertent perforation of a varix may lead to catastrophic GI bleeding.

Treatment

Emergent treatment for bleeding gastric varices is rarely necessary. When major bleeding does occur in patients with splenic vein obstruction, the patients are almost always cured by simple splenectomy because portal venous pressure is normal in these individuals.¹⁸ In contrast, some form of portosystemic shunt may be required for gastric varices caused by portal hypertension, as splenectomy alone has no effect on portal venous pressure in these patients. Thus, the choice of treatment for gastric varices depends on the underlying cause.

DUODENAL VARICES

Duodenal varices typically appear on barium studies as thickened, serpiginous folds in the proximal duodenum (Fig. 34-7).

They are almost always associated with esophageal varices and may be complicated by GI bleeding. Occasionally, an isolated duodenal varix can present as a solitary filling defect.¹⁹

Portal Hypertensive Gastropathy

Portal hypertensive gastropathy is a distinct pathologic entity caused by chronic portal hypertension.²⁰ Chronic venous congestion in the stomach results in mucosal hyperemia, capillary ectasia, and increased numbers of submucosal arteriovenous communications with dilated arterioles, capillaries, and veins in the gastric wall.²¹ For reasons that are unclear, portal hypertensive gastropathy occurs more frequently in patients with cirrhosis than in other patients with portal hypertension. This condition is a cause of acute and chronic upper GI bleeding, even in the absence of esophageal or gastric varices. It has been estimated that nonvariceal bleeding from portal hypertensive gastropathy is responsible for up to 30% of all cases of upper GI bleeding in patients with portal hypertension.²²

RADIOGRAPHIC FINDINGS

Portal hypertensive gastropathy predominantly involves the gastric fundus and is manifested on barium studies by thickened, nodular folds with undulating contours and indistinct borders (Fig. 34-8).²³ Although the pathophysiologic basis for this fold thickening is uncertain, it could result from a combination of mucosal hyperemia and dilated submucosal vessels. Gastric varices may also appear as thickened folds on barium studies, but the folds tend to have a more serpentine configuration and are often associated with discrete submucosal masses (see Fig. 34-1). The differential diagnosis also includes various forms of gastritis (especially *H. pylori* gastritis), lymphoma, and, rarely, Ménétrier's disease.

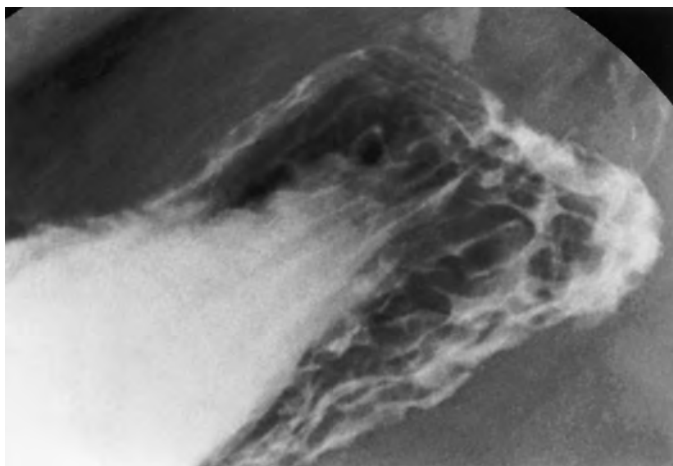


Figure 34-8 Portal hypertensive gastropathy. Thickened, nodular folds are seen in the gastric fundus. Note how the folds have an undulating contour and indistinct borders. Although gastric varices could produce a similar appearance, they tend to have a more serpentine configuration and are often manifested by discrete submucosal masses (see Fig. 34-1). (From Chang D, Levine MS, Ginsberg GG, et al: Portal hypertensive gastropathy: Radiographic findings in eight patients. *AJR* 175:1609–1612, 2000.)

Diverticula

GASTRIC DIVERTICULA

Gastric diverticula almost always arise on a discrete neck from the posterior wall of the fundus and usually cause no symptoms. Barium studies best show a gastric fundal diverticulum in profile on lateral views of the fundus, but a collection of barium pooling within the diverticulum can occasionally mimic an area of ulceration (Fig. 34-9).

Intramural or partial gastric diverticulum is a rare anomaly of no clinical importance that is characterized by focal invagination of the mucosa into the muscular layer of the gastric wall.²⁴ These structures are almost always located on the greater curvature of the distal antrum. The diverticulum may be manifested on barium studies by a tiny collection of barium extending outside the contour of the adjacent gastric wall (Fig. 34-10). Although these structures can be mistaken for ulcers or even ectopic pancreatic rests on the greater curvature, they tend to have a changeable configuration at fluoroscopy, whereas true ulcers have a fixed appearance.

DUODENAL DIVERTICULA

True Diverticula

Duodenal diverticula are detected as incidental findings on upper GI barium studies in up to 15% of patients. The diverticula are acquired lesions, consisting of a sac of mucosal and submucosal layers herniating through a muscular defect. These diverticula often fill and empty by gravity as a result of pressure generated by duodenal peristalsis. Most duodenal diverticula are located on the medial border of the descending duodenum in the periampullary region (Fig. 34-11), but they not infrequently are found in the third or fourth portion of the duodenum and can occasionally be located on the lateral border of the descending duodenum (Fig. 34-12).

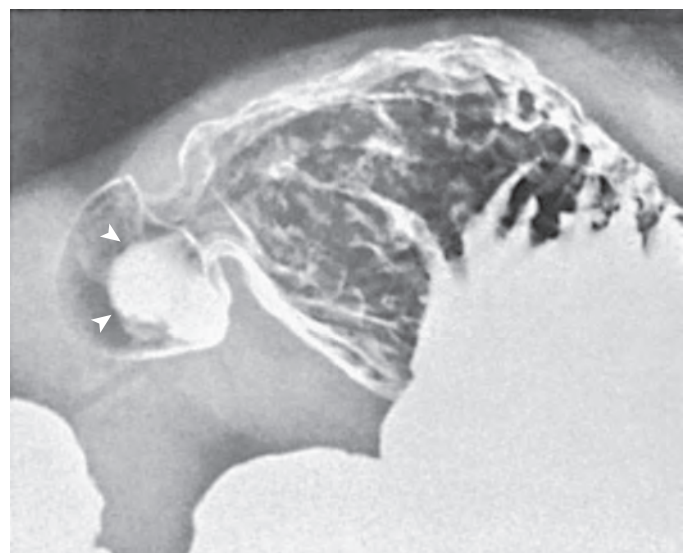


Figure 34-9 Gastric diverticulum. A large diverticulum is seen arising from the posterior wall of the fundus. Pooling of barium (arrowheads) in the diverticulum could be mistaken for an area of ulceration. (From Eisenberg RL: *Gastrointestinal Radiology: A Pattern Approach*, 3rd ed. Philadelphia, JB Lippincott, 1996.)

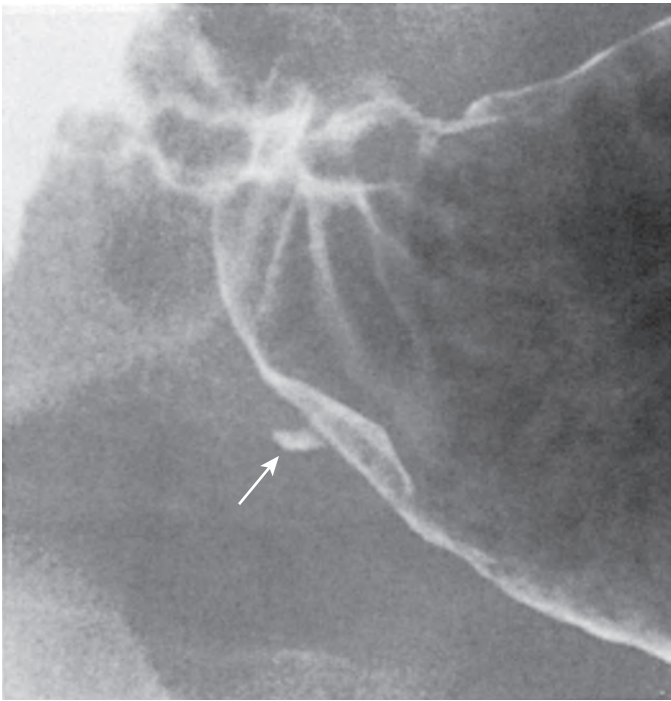


Figure 34-10 Intramural or partial gastric diverticulum. A tiny barium-filled outpouching (arrow) is seen on the greater curvature of the distal antrum. There is a heaped-up area overlying the diverticulum that could be mistaken for an ectopic pancreatic rest.

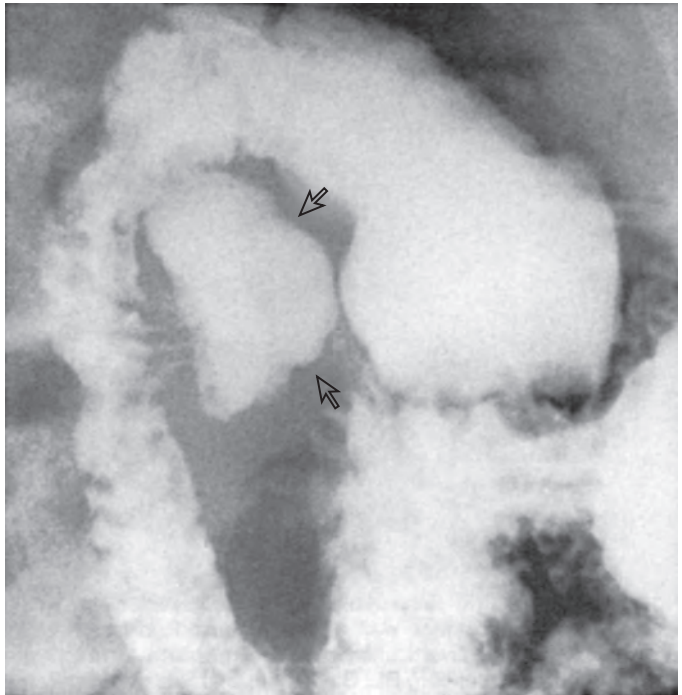


Figure 34-11 Duodenal diverticulum. A typical diverticulum (arrows) is seen arising from the medial border of the descending duodenum. (From Eisenberg RL: *Gastrointestinal Radiology: A Pattern Approach*, 3rd ed. Philadelphia, JB Lippincott, 1996.)

Duodenal diverticula typically appear on barium studies as smooth, round or ovoid outpouchings arising on a discrete neck from the medial border of the descending duodenum (see Fig. 34-11). They are often multiple and may change in size and shape at fluoroscopy. The lack of inflammatory reaction (spasm or edema) allows a duodenal diverticulum to be differentiated from a postbulbar ulcer. Bizarre multilobulated or giant diverticula are occasionally seen.²⁵ Filling defects representing inspissated food particles or blood clots can sometimes be found within the diverticulum (Fig. 34-13).

When duodenal diverticula contain gas or a combination of fluid and gas, they are readily visible on CT. However, a diverticulum that is predominantly fluid-filled can occasionally mimic the CT findings of a cystic neoplasm in the head of the pancreas (Fig. 34-14A).²⁶ The correct diagnosis can still be established, however, if intradiverticular gas is identified (Fig. 34-14B).²⁶

More than 90% of patients with duodenal diverticula are asymptomatic.²⁷ Occasionally, however, these patients may develop serious complications such as duodenal diverticulitis, upper GI bleeding, gastric outlet obstruction, and pancreatobiliary disease. Because duodenal diverticula are retroperitoneal structures, duodenal diverticulitis and perforation can occur without clinical signs of peritonitis or radiographic signs of free intraperitoneal air. Instead, abdominal radiographs may reveal localized retroperitoneal gas adjacent to the duodenum and upper pole of the right kidney.²⁸ Studies with barium or water-soluble contrast agents may demonstrate localized extravasation of contrast material from the perforated diverticulum into a contained extraluminal collection or a deformed diverticulum secondary to a previous perforation that subsequently sealed off.²⁹ CT is particularly helpful for showing a

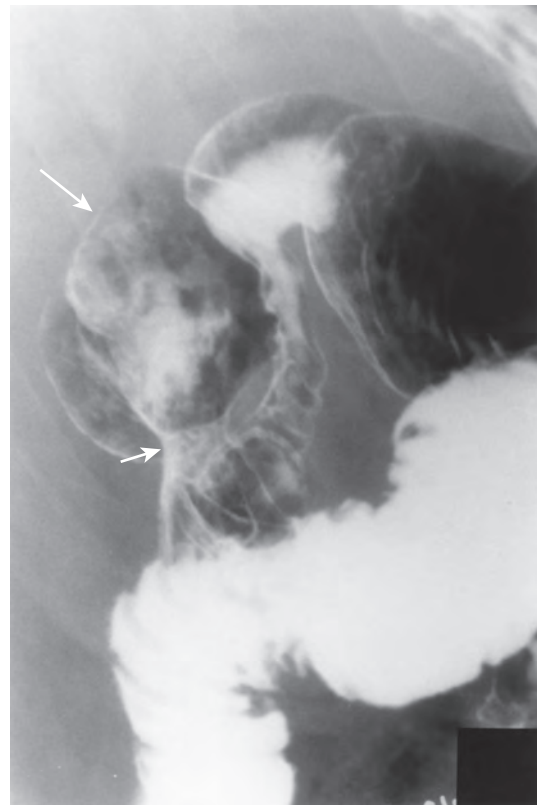


Figure 34-12 Lateral duodenal diverticulum. A diverticulum (long arrow) is seen arising from the lateral border of the descending duodenum. Note how the diverticulum has a discrete neck (short arrow). Also note how the diverticulum is compressing the adjacent duodenum.

contained perforation or inflammatory changes involving adjacent structures.³⁰

Rarely, duodenal diverticula may cause massive upper GI bleeding.³¹ In such cases, scanning with ^{99m}Tc-labeled red blood cells or angiography may be required to localize the site of bleeding.³¹ Duodenal diverticula have also been described as a rare cause of duodenal or even biliary obstruction. Anomalous insertion of the common bile duct and pancreatic duct into a duodenal diverticulum can be demonstrated in about 3% of carefully performed T-tube cholangiograms.³² This anatomic

variation can impair drainage of bile into the duodenum, predisposing these patients to biliary obstruction, bile duct stones, and pancreatitis.

Pseudodiverticula

Pseudodiverticula are exaggerated outpouchings or sacculations of the inferior and superior recesses of the duodenal bulb related to acute or chronic duodenal ulcer disease (Fig. 34-15).



Figure 34-13 Duodenal diverticulum with a blood clot. This diverticulum contains a large, irregular filling defect representing a blood clot in a patient with recent upper GI bleeding. (From Eisenberg RL: *Gastrointestinal Radiology: A Pattern Approach*, 3rd ed. Philadelphia, JB Lippincott, 1996.)



Figure 34-15 Duodenal pseudodiverticula. Two exaggerated outpouchings or pseudodiverticula (arrows) are seen at the base of the bulb caused by scarring from previous peptic ulcer disease.

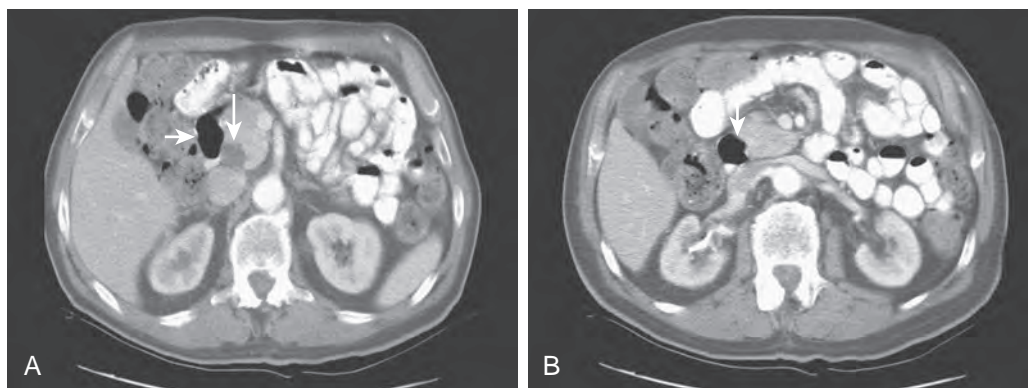


Figure 34-14 Duodenal diverticulum mimicking a cystic pancreatic neoplasm on CT. **A.** CT scan with oral and intravenous contrast material at the level of the pancreatic head shows a fluid-filled cystic lesion (long arrow) that was initially thought to represent a cystic pancreatic tumor. Note air and contrast material in the duodenum (short arrow). **B.** A follow-up CT scan at a similar level 6 months later shows filling of the diverticulum with gas (arrow), confirming the diagnosis of a duodenal diverticulum. (From Macari M, Lazarus D, Israel G, et al: *Duodenal diverticula mimicking cystic neoplasms of the pancreas: CT and MR imaging findings in seven patients*. *AJR* 180:195-199, 2003.)

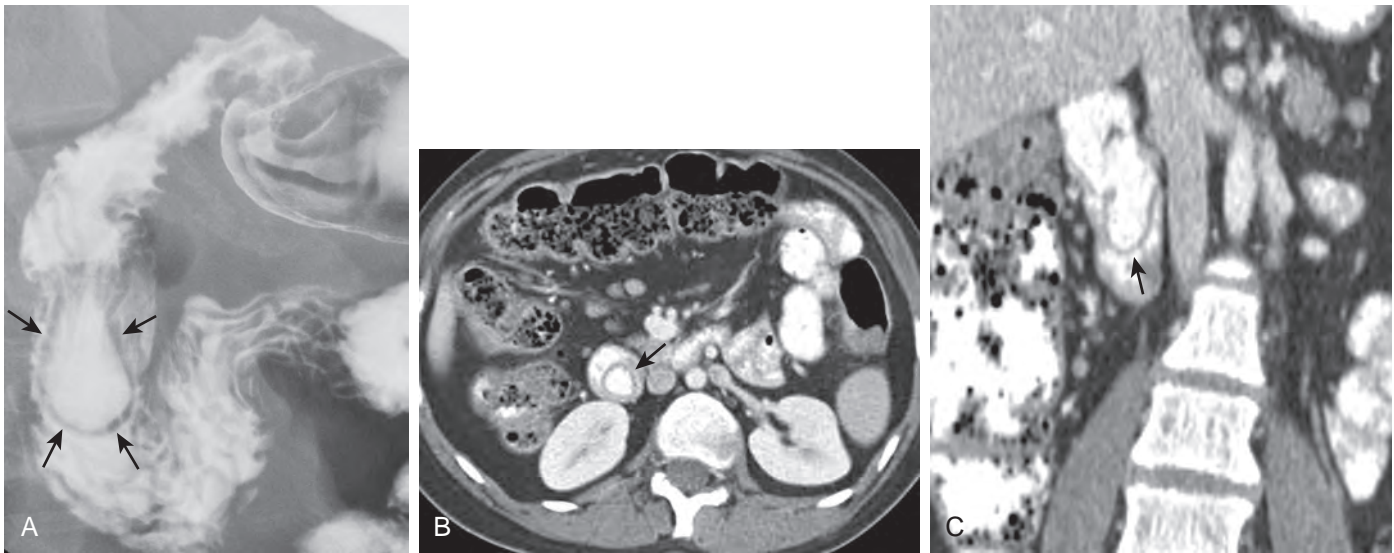


Figure 34-16 Intraluminal duodenal diverticulum. **A.** The finger-like, barium-filled sac in the descending duodenum is separated from barium in the adjacent lumen by a radiolucent band (arrows) representing the wall of the diverticulum. **B** and **C.** Axial (**B**) and coronal (**C**) CT scans also show the barium-filled intraluminal sac separated from barium in the adjacent duodenal lumen by a thin lower density web (arrows).

The sacculations may be caused by edema and spasm associated with an active ulcer or by asymmetric fibrosis and retraction associated with scarring from a healed ulcer. However, the degree of deformity is not directly related to the size of the ulcer because some small duodenal ulcers may produce large sacculations, whereas other large ulcers may have little or no effect on the contour of the bulb.

Intraluminal Diverticula

An intraluminal duodenal diverticulum is a sac of duodenal mucosa originating from the second portion of the duodenum near the papilla of Vater. The term *intraluminal diverticulum* is actually a misnomer because this structure is not a diverticulum, but begins as a congenital duodenal web or diaphragm containing a small central aperture; the web gradually elongates over time because of forward pressure by food and duodenal peristalsis.³³ As a result, the diverticulum usually extends antegrade into the distal descending duodenum or, occasionally, the third or fourth portion of the duodenum. When filled with barium, this structure has a characteristic radiographic appearance on barium studies and abdominal CT, with a finger-like intraluminal sac separated from barium in the adjacent lumen by a thin radiolucent stripe representing the elongated web, or “wall,” of the diverticulum (Fig. 34-16).^{33,34} Because of the resemblance to a wind sock at small airports, this structure has also been called a “wind sock” diverticulum.

Both an intraluminal duodenal diverticulum and congenital duodenal diaphragm can be associated with a variety of other anomalies, including annular pancreas, midgut volvulus, situs inversus, choledochoceles, congenital heart disease, Down syndrome, imperforate anus, Hirschsprung’s disease, omphalocele, and exstrophy of the bladder.

Patients with an intraluminal duodenal diverticulum may present with nausea and vomiting from associated duodenal obstruction.³³ The usual treatment is surgery, but some patients may benefit from endoscopic disruption of the underlying duodenal web responsible for their symptoms, avoiding the need for surgery.³³

Webs and Diaphragms

ANTRAL WEBS AND DIAPHRAGMS

Antral webs and diaphragms are thin membranous septa that are usually located within 3 cm of the pyloric canal and are oriented perpendicular to the long axis of the stomach.³⁵ Clinical symptoms of partial gastric outlet obstruction correlate with the size of the central aperture of the web or diaphragm; obstructive symptoms do not occur if the diameter of the aperture is greater than 1 cm. Even with minute central orifices as small as 2 mm, these diaphragms may not cause obstructive symptoms until adult life.

Nonobstructive antral webs and diaphragms appear on barium studies as persistent, sharply defined, 2- to 3-cm-wide, band like defects in the barium column occurring at right angles to the gastric wall (Fig. 34-17).³⁵ A similar appearance may be produced by a prominent transverse antral fold, but transverse folds do not generally extend across the gastric lumen, and they are not perfectly straight. Antral webs and diaphragms are best visualized when the antrum is adequately distended proximal and distal to this structure. Occasionally, the antrum distal to the web can be mistaken radiographically for the duodenal bulb (Fig. 34-18) or, less frequently, for a gastric diverticulum or ulcer. With severe obstruction, gastric emptying is greatly delayed, and barium can be seen to pass in a thin stream (jet phenomenon) through the central orifice of the web.³⁶

DUODENAL WEBS AND DIAPHRAGMS

Duodenal webs and diaphragms are weblike projections in the duodenal lumen that cause varying degrees of obstruction. Most reported cases have involved the second portion of the duodenum near the ampulla of Vater. A congenital duodenal web usually appears on barium studies as a thin radiolucent line extending across the lumen, often associated with proximal duodenal dilation (Fig. 34-19). Because the obstruction is

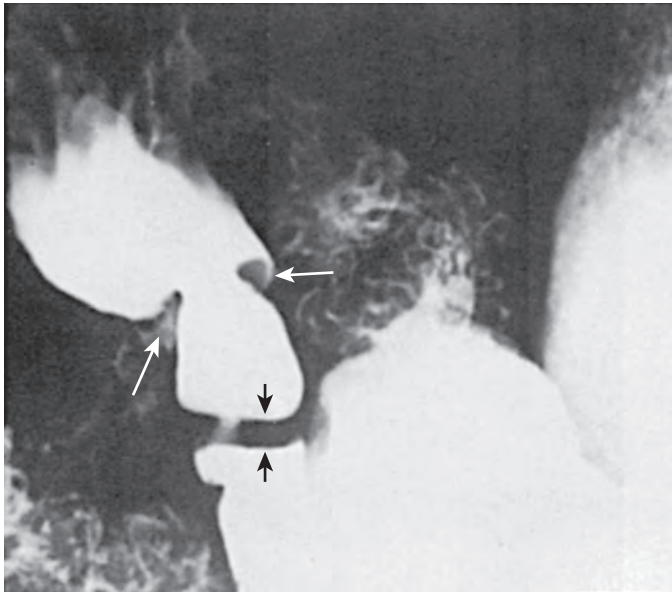


Figure 34-17 Antral mucosal diaphragm. A bandlike defect (black arrows) is seen arising at right angles to the gastric wall. The web is approximately 5 mm in thickness. The pyloric channel is denoted by white arrows. (From Bjorgvinsson E, Rudzki C, Lewicki AM: Antral web. *Am J Gastroenterol* 79:663–665, 1984.)

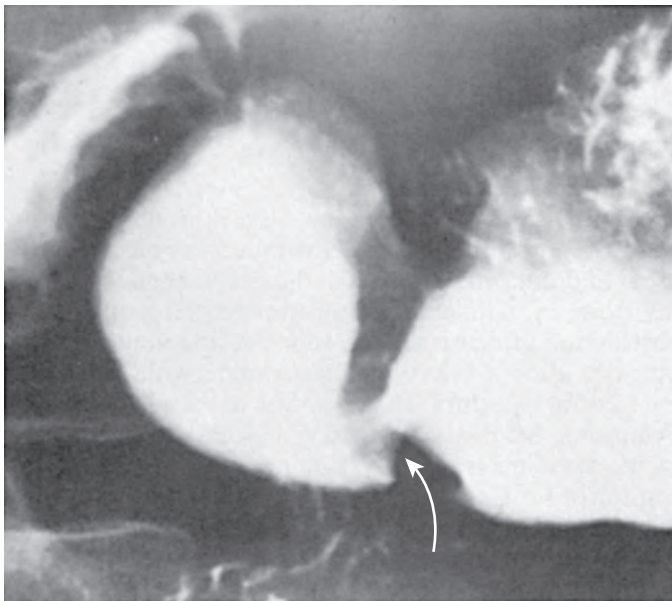


Figure 34-18 Antral mucosal diaphragm. The lumen is so narrowed by the diaphragm (arrow) that the antrum distal to the diaphragm could be mistaken for the duodenal bulb. (From Eisenberg RL: *Gastrointestinal Radiology: A Pattern Approach*, 3rd ed. Philadelphia, JB Lippincott, 1996.)

incomplete, small amounts of gas may be present in more distal portions of the bowel.³⁷ Rarely, a web may balloon distally, forming an intraluminal duodenal diverticulum (see earlier, “[Intraluminal Diverticula](#)”). Although the vast majority of duodenal webs and diaphragms are thought to be congenital, acquired duodenal diaphragms similar to those in the small bowel have been described as a rare complication of long-term use of nonsteroidal anti-inflammatory drugs (NSAIDs).³⁸

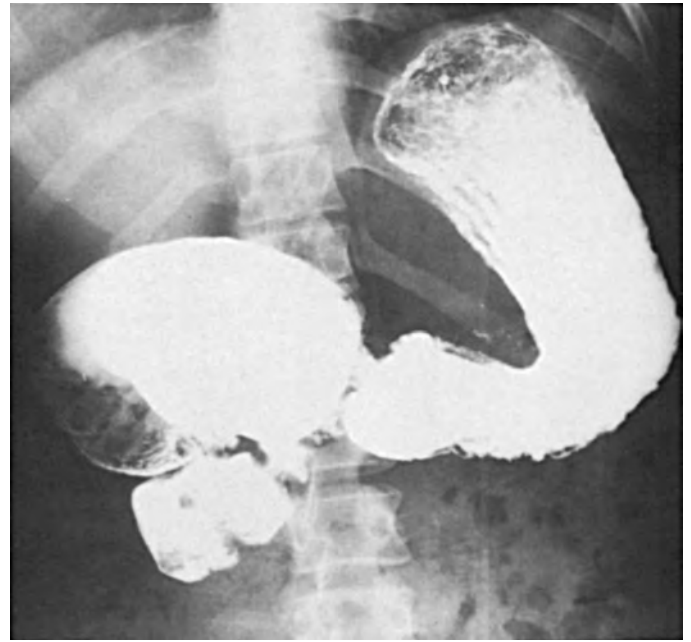


Figure 34-19 Duodenal web. There is high-grade stenosis of the second portion of the duodenum. The presence of gas in the bowel distal to the web indicates that the obstruction is incomplete. (From Eisenberg RL: *Gastrointestinal Radiology: A Pattern Approach*, 3rd ed. Philadelphia, JB Lippincott, 1996.)

Adult Hypertrophic Pyloric Stenosis

The histologic, anatomic, and radiographic abnormalities in adult hypertrophic pyloric stenosis are indistinguishable from those in the infantile form.³⁹ The disease in adults may represent a milder form of the same entity observed in infants and children. Most cases of adult hypertrophic pyloric stenosis go unrecognized because these individuals are asymptomatic. However, some patients complain of nausea and vomiting, epigastric pain, weight loss, or anorexia, and approximately 50% of patients with adult hypertrophic pyloric stenosis have associated gastric ulcers. These ulcers probably develop as a result of delayed gastric emptying with increased gastrin production and hyperacidity. In contrast to children, adults with this condition rarely develop high-grade gastric outlet obstruction.

Adult hypertrophic pyloric stenosis is typically manifested on barium studies by elongation and narrowing of the pyloric canal as a result of a hypertrophied pyloric muscle ([Fig. 34-20](#)).³⁹ The pylorus can be as long as 2 to 4 cm in these patients (the normal length is <1 cm in adults). The proximal end of the narrowed pylorus merges gradually with the adjacent antrum, producing a smooth, tapered juncture without the shoulders expected for a malignant neoplasm. In contrast, the distal end of the hypertrophied pyloric muscle may bulge into the duodenum, producing a distinctive concave indentation on the base of the duodenal bulb (see [Fig. 34-20](#)).³⁹ Some patients may have findings of gastric outlet obstruction.

Gastric Outlet Obstruction

Peptic ulcer disease is the most common cause of gastric outlet obstruction in adults, accounting for about two thirds of cases

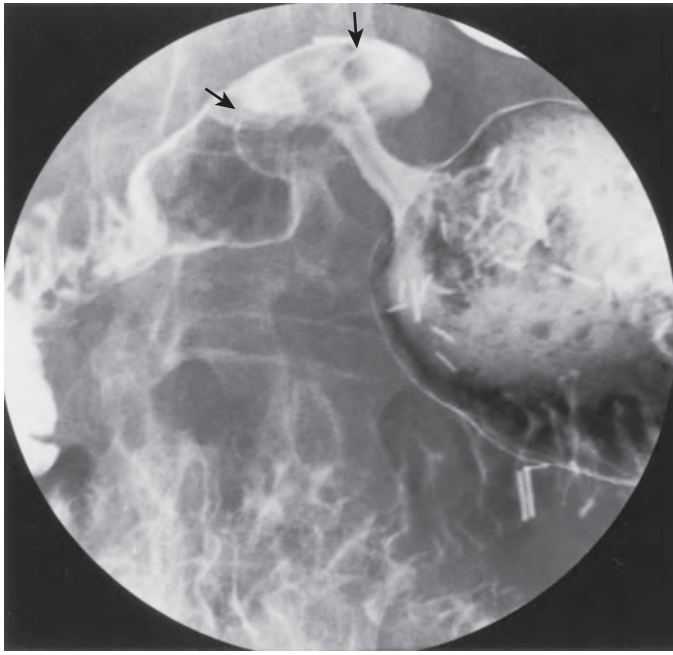


Figure 34-20 Adult hypertrophic pyloric stenosis. The pyloric canal is narrowed and elongated, with a characteristic concave indentation (arrows) on the base of the duodenal bulb caused by bulging of the pyloric muscle mass into the duodenum.

(Fig. 34-21). The ulcers are usually located in the duodenal bulb, but may also be located in the pyloric channel or gastric antrum or, rarely, in the gastric body. Narrowing of the lumen in peptic ulcer disease can result from acute inflammation, edema and spasm, muscular hypertrophy, or fibrosis and scarring. In many cases, more than one of these factors contributes to the development of gastric outlet obstruction. Most patients with peptic ulcer disease causing pyloric obstruction have a long-standing history of ulcer symptoms. A gastric carcinoma should therefore be suspected when gastric outlet obstruction develops in previously asymptomatic patients.

An annular carcinoma of the distal antrum or pylorus is the second most common cause of gastric outlet obstruction, accounting for nearly one third of cases (Fig. 34-22). Occasionally, metastases to the stomach or other malignant tumors may also produce obstructive symptoms. In contrast to patients with peptic ulcer disease, patients with gastric outlet obstruction caused by malignant tumors often have recent onset of abdominal pain and weight loss.⁴⁰

Abdominal radiographs in patients with gastric outlet obstruction often demonstrate the outline of the dilated, gas-filled stomach. Barium studies may reveal mottled, nonopaque material representing retained food and debris in the stomach. Depending on the degree of obstruction, there can be a marked delay in gastric emptying, with barium sometimes retained in the stomach for 24 hours or longer. Over time, the stomach may become enormously dilated, extending inferiorly into the lower abdomen or even the pelvis. In patients with gastric outlet obstruction, the radiologist must always attempt to differentiate a benign lesion (e.g., peptic ulcer disease) from a malignant lesion (e.g., gastric carcinoma) as the cause of obstruction on barium studies. The presence of a persistent collection of barium within the duodenal bulb, pyloric channel, or prepyloric gastric antrum should suggest peptic ulcer disease as the

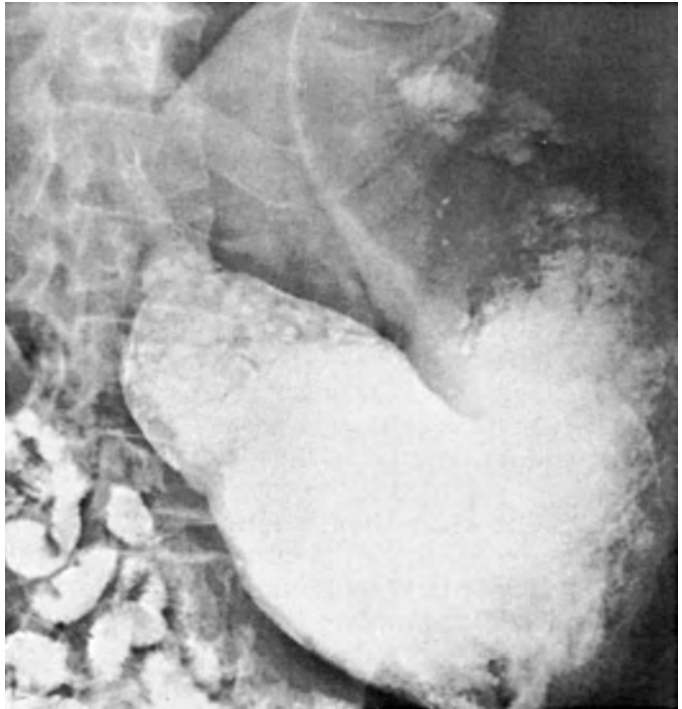


Figure 34-21 Gastric outlet obstruction caused by peptic ulcer disease. Note gastric distention and dilution of ingested barium by retained fluid in the stomach. (From Eisenberg RL: *Gastrointestinal Radiology: A Pattern Approach*, 3rd ed. Philadelphia, JB Lippincott, 1996.)

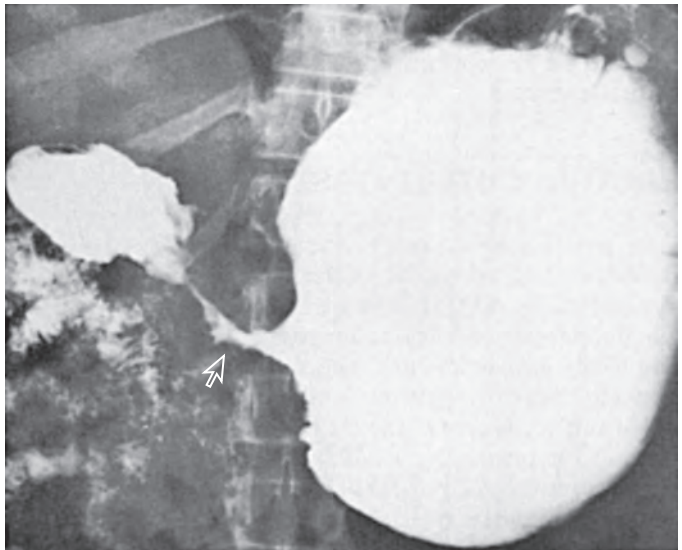


Figure 34-22 Gastric outlet obstruction caused by an annular carcinoma of the antrum. There is irregular narrowing of the distal antrum (arrow) with proximal dilation of the stomach. (From Eisenberg RL: *Gastrointestinal Radiology: A Pattern Approach*, 3rd ed. Philadelphia, JB Lippincott, 1996.)

likely cause of obstruction. Distortion and scarring of the bulb, with associated pseudodiverticula, should also suggest ulcer disease as the likely cause of obstruction. Conversely, the presence of a discrete mass, nodularity, or irregularity in the adjacent antrum should suggest a malignant tumor. Nevertheless, it is not always possible to differentiate benign and

malignant cases of gastric outlet obstruction on radiographic criteria. When gastric carcinoma cannot be excluded, endoscopy or even surgical exploration may be required for a definitive diagnosis.

Gastric outlet obstruction may occasionally be caused by other conditions involving the stomach and duodenum. Granulomatous diseases such as Crohn's disease, sarcoidosis, syphilis, and tuberculosis may cause marked antral narrowing and obstruction (Fig. 34-23). Severe pancreatitis or cholecystitis

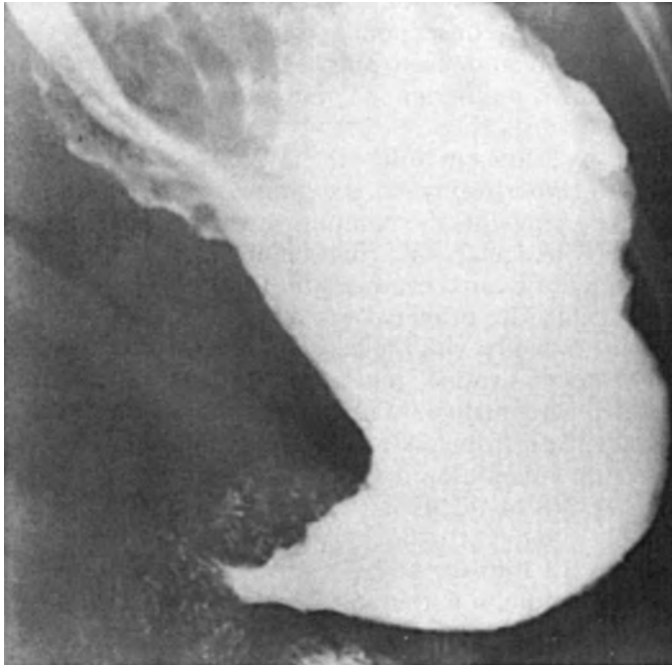


Figure 34-23 Gastric outlet obstruction caused by Crohn's disease. There is tapered narrowing of the distal antrum caused by Crohn's disease involving the stomach. (From Eisenberg RL: *Gastrointestinal Radiology: A Pattern Approach*, 3rd ed. Philadelphia, JB Lippincott, 1996.)

may cause intense spasm and edema of the adjacent duodenum with associated gastric outlet obstruction.⁴¹ Antral narrowing and obstruction may also be caused by other rare conditions such as amyloidosis (see later, "Amyloidosis") and scarring from previous ingestion of corrosive substances.

Prolapse of a benign antral polyp into the duodenum may occasionally produce intermittent gastric outlet obstruction, with an intraluminal filling defect seen at the base of the duodenal bulb. Other conditions causing gastric outlet obstruction include antral mucosal webs and diaphragms, adult hypertrophic pyloric stenosis, and gastric volvulus (these conditions are discussed elsewhere in the chapter).

Duodenal Obstruction

A variety of congenital anomalies, inflammatory disorders, and malignant tumors may cause duodenal obstruction. Many of these conditions are discussed elsewhere in the text.

SUPERIOR MESENTERIC ROOT SYNDROME

The transverse portion of the duodenum has a fixed position in the retroperitoneum. As a result, this portion of the duodenum is in a closed compartment bounded anteriorly by the root of the mesentery, which carries the superior mesenteric vessel sheath (artery, vein, and nerve), and posteriorly by the aorta and lumbar spine (at the L2-3 level), where the lumbar lordosis is most pronounced. Even in asymptomatic people, there is often a transient delay of barium where the transverse duodenum crosses the spine. This delay can be associated with mild, inconstant dilation of the proximal duodenum (Fig. 34-24).

Any process that tends to close the nutcracker-like jaws of the aortomesenteric angle results in some degree of compression of the transverse portion of the duodenum. This phenomenon is most likely to occur in asthenic persons, particularly those who rapidly lose weight and retroperitoneal fat because of debilitating illness; the increased dragging effect of the mesenteric root in these patients narrows the aortomesenteric

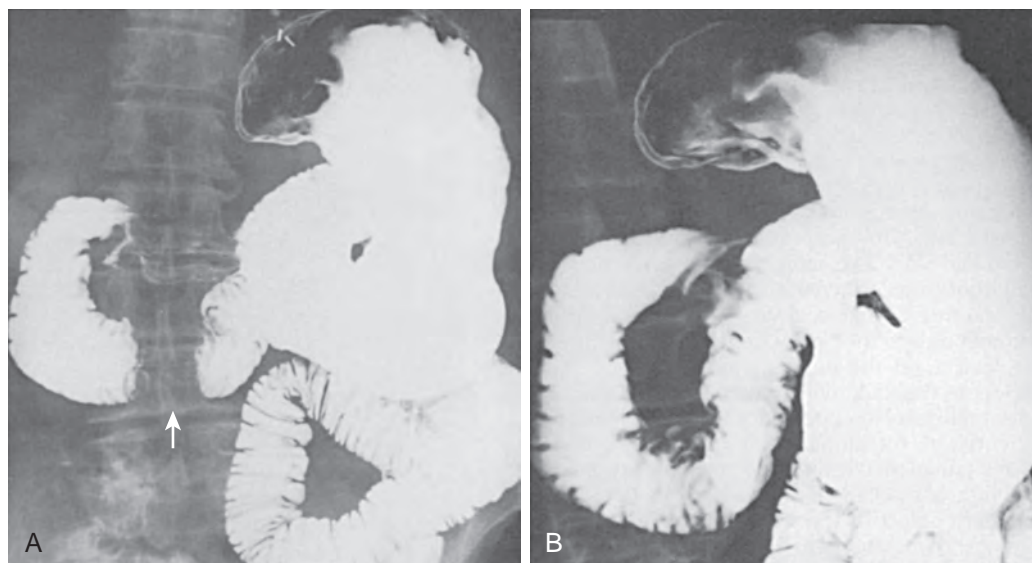


Figure 34-24 Asymptomatic patient with findings mimicking those of superior mesenteric root syndrome. **A.** Frontal view shows an extrinsic, vertically oriented, bandlike defect (arrow) and apparent obstruction of the third portion of the duodenum by the superior mesenteric root. **B.** Prone, right anterior oblique view obtained moments later shows a normal duodenal sweep without evidence of obstruction.

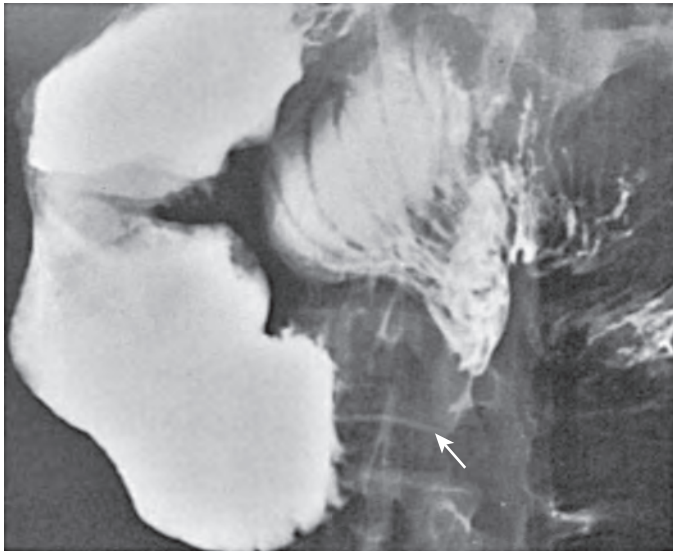


Figure 34-25 Superior mesenteric root syndrome caused by scleroderma. The duodenum is markedly dilated and atonic proximal to an extrinsic, vertically oriented, bandlike defect (arrow) at the aortomesenteric angle. (From Eisenberg RL: *Gastrointestinal Radiology: A Pattern Approach*, 3rd ed. Philadelphia, JB Lippincott, 1996.)

angle. Prolonged bed rest or immobilization in the supine position (e.g., patients with body casts or whole-body burns or patients fixed in a position of hyperextension after spinal injury or surgery) also causes the mesenteric root to compress the anterior aspect of the transverse duodenum, resulting in varying degrees of duodenal obstruction.^{42,43}

In patients with scleroderma or other causes of decreased duodenal peristalsis, the combination of the lumbar spine, aorta, and mesenteric root may constitute enough of a barrier to cause substantial obstruction of the transverse duodenum. As a result, the superior mesenteric root syndrome sometimes occurs in patients with scleroderma, who have a dilated atonic duodenum proximal to the level of the superior mesenteric root (Fig. 34-25). Other collagen diseases such as dermatomyositis and systemic lupus erythematosus may produce similar radiographic findings. In Chagas' disease, inflammatory destruction of intramural autonomic plexuses by *Trypanosoma cruzi* can lead to generalized GI aperistalsis and dilation that usually involve the esophagus and colon but can also affect the duodenum. Disordered duodenal motility and dilation can also result from neuropathies associated with diabetes, porphyria, and thiamine deficiency or from surgical vagotomy for peptic ulcer disease or chemical vagotomy from drugs such as atropine, morphine, and diphenoxylate (Lomotil).

Any space-occupying process within the aortomesenteric angle can also compress the transverse duodenum, causing the superior mesenteric root syndrome. As a result, inflammatory thickening of the bowel wall or mesenteric root by pancreatitis, Crohn's disease, and peptic ulcer disease or neoplastic thickening of the mesenteric root by metastases to the mesentery or mesenteric lymph nodes can lead to duodenal obstruction.⁴⁴ Occasionally, a metastatic tumor involving the duodenum may cause delayed gastric emptying and massive gastric dilation out of proportion to the degree of duodenal obstruction, possibly because of injury to the vagal nerve by retroperitoneal tumor.⁴⁵

Regardless of the underlying pathophysiology, the superior mesenteric root syndrome is associated with characteristic radiographic findings. Barium studies usually reveal marked dilation of the first and second portions of the duodenum associated with an extrinsic, vertically oriented, bandlike defect in the transverse portion of the duodenum overlying the spine (see Fig. 34-25). In some cases, obstruction may be partially relieved by placing the patient in the prone position. CT may demonstrate beaklike compression of the third portion of the duodenum between the superior mesenteric vessels and aorta, thereby confirming the diagnosis of the superior mesenteric root syndrome.⁴⁶

OTHER CAUSES

Intramural hematoma, intraluminal duodenal diverticulum, and aortoduodenal fistula (discussed elsewhere in this chapter) are other causes of duodenal obstruction. Ulceration with stricture formation can also be a complication of radiation therapy to the upper abdomen.⁴⁷ A rare cause of duodenal obstruction is the preduodenal portal vein, which crosses in front of the duodenum, rather than behind it. This anomaly is associated with other malformations such as duodenal bands and annular pancreas, which are more likely to be the cause of obstruction than the anomalous crossing vessel. The major reason to be aware of the preduodenal portal vein is so it is not injured at the time of surgery for these other malformations.⁴⁸

Gastric Dilation Without Gastric Outlet Obstruction

Acute or chronic dilation of the stomach with prolonged retention of food or barium can occur in the absence of gastric outlet obstruction. Gastric retention is defined as vomiting of food eaten more than 6 hours earlier or the presence of food in the stomach at the time of an upper GI series (assuming that the patient has not eaten for 8 to 10 hours). However, gastric retention is not synonymous with gastric outlet obstruction, and corrective surgery is not always indicated for these patients.⁴⁹

The appearance of nonobstructive gastric dilation is indistinguishable from that of organic gastric outlet obstruction. Abdominal radiographs may reveal a massively dilated, gas- and fluid-containing stomach extending inferiorly into the lower abdomen or pelvis (Fig. 34-26). Administration of barium confirms the presence of a dilated stomach with decreased or absent gastric peristalsis and a large amount of retained food and debris in the lumen.

ACUTE GASTRIC DILATION

Acute gastric dilation is characterized by sudden, severe distention of the stomach, usually occurring within several days after abdominal surgery (Fig. 34-27). In affected individuals, a normal stomach can expand rapidly into a hyperemic, cyanotic, atonic sac that fills the abdomen. This postoperative complication has become much less common as a result of improved operative and postoperative care, including meticulous handling of tissues at surgery, better anesthetics, nasogastric suction, and careful monitoring of acid-base and electrolyte balances. Acute gastric dilation may also occur as a complication of other

medical or surgical conditions, including abdominal trauma and peritoneal inflammatory processes.

Appropriate therapy usually produces a rapid clinical response but, if untreated, acute gastric dilation may be a life-threatening condition. Pain is seldom severe until these patients have marked gastric dilation. Aerophagia (air swallowing) in some patients may also contribute to rapid gaseous distention of the stomach. In fulminant cases, acute gastric dilation may cause severe vomiting, aspiration, fluid and electrolyte disturbances, dehydration, perforation, peritonitis, and shock.⁵⁰

CHRONIC GASTRIC DILATION AND GASTROPARESIS

The two most common causes of chronic gastric dilation and gastroparesis are diabetes and narcotics. Some patients are asymptomatic, but others develop chronic nausea, vomiting, bloating, early satiety, and postprandial abdominal fullness.⁵¹⁻⁵³ About 40% of patients with diabetes have a dilated stomach with decreased or absent gastric peristalsis and delayed gastric emptying (diabetic gastropathy).⁵² Most of these patients have long-standing, poorly controlled diabetes associated with a peripheral neuropathy or other complications.⁵¹ Narcotic medications may also cause marked gastroparesis that gradually resolves after withdrawal of the offending agent. Other patients with neurologic abnormalities (e.g., brain tumors, bulbar poliomyelitis, tabes dorsalis) may develop chronic gastric retention, although these patients are more likely to develop esophageal dysmotility. Marked gastric dilation may also develop in patients with scleroderma, polymyositis, dermatomyositis, myotonic muscular dystrophy, electrolyte and acid-base imbalances, lead poisoning, and porphyria (Fig. 34-28).^{54,55}

The radiologic diagnosis of gastroparesis is typically made on the basis of an endoscopic examination showing no evidence of gastric outlet obstruction combined with a nuclear medicine solid emptying scan showing delayed emptying of solids from the stomach.⁵² In patients with nausea and vomiting or other related symptoms, however, the diagnosis of gastroparesis can also be established on barium studies showing decreased or absent gastric peristalsis at fluoroscopy, with varying degrees of gastric dilation and delayed emptying of barium from the stomach in the absence of findings of mechanical gastric outlet obstruction.⁵³ Barium studies are therefore extremely helpful for differentiating gastroparesis from gastric outlet obstruction in patients with nausea and vomiting.

Abnormal Extrinsic Masses

STOMACH

Extrinsic impressions on the stomach may be caused by a prominent left lobe of the liver, aberrant position of the spleen or left kidney, or pathologic enlargement of any of these structures (Fig. 34-29). CT can aid in differentiating these extrinsic defects from true gastric lesions.

DUODENUM

A variety of abnormalities involving organs in the right upper quadrant may cause displacement of or extrinsic impressions on the duodenal bulb and sweep. A dilated common bile duct typically produces an obliquely oriented, tubular indentation



Figure 34-26 Massive gastric dilation. Abdominal radiograph shows an enormous amount of gas filling a markedly dilated stomach that extends inferiorly into the pelvis. (From Eisenberg RL: *Gastrointestinal Radiology: A Pattern Approach*, 3rd ed. Philadelphia, JB Lippincott, 1996.)



Figure 34-27 Acute gastric dilation from recent abdominal surgery. (From Eisenberg RL: *Gastrointestinal Radiology: A Pattern Approach*, 3rd ed. Philadelphia, JB Lippincott, 1996.)

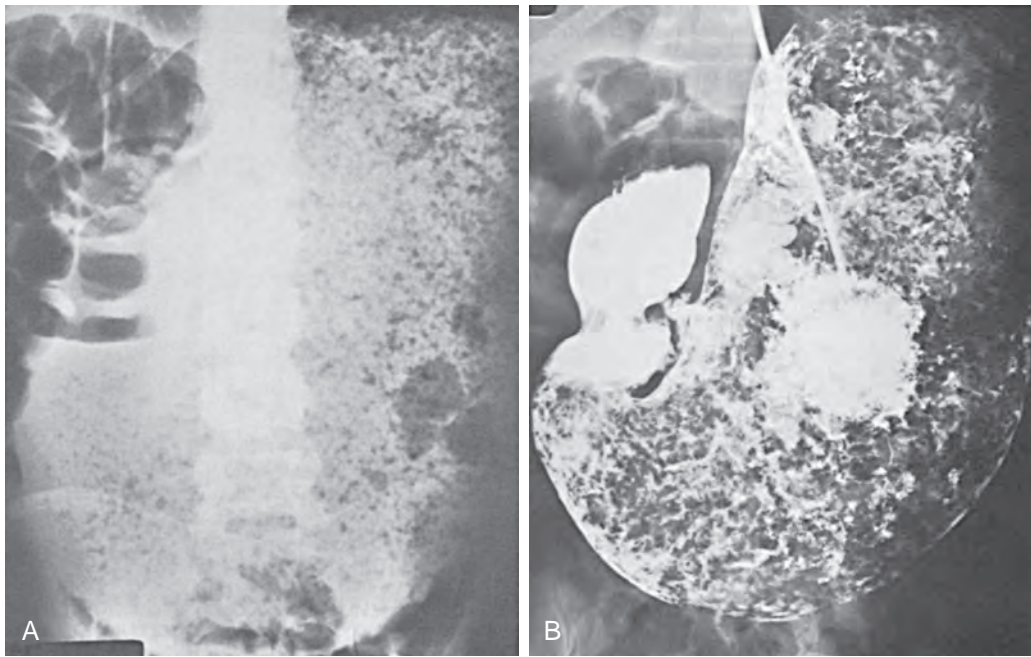


Figure 34-28 Chronic gastric dilation caused by severe electrolyte and acid-base imbalances. **A.** Abdominal radiograph shows a marked amount of particulate material in a massively dilated stomach extending inferiorly into the pelvis. **B.** Barium study confirms the presence of marked gastric dilation.

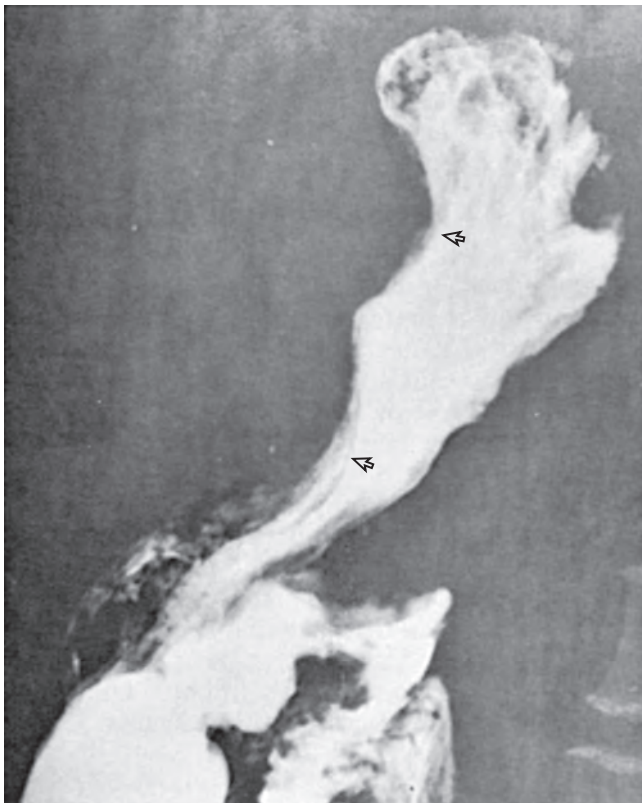


Figure 34-29 Gastric impressions by a polycystic liver. Two large extrinsic impressions (arrows) on the anterior aspect of the stomach could be mistaken for intramural lesions. (From Eisenberg RL: *Gastrointestinal Radiology: A Pattern Approach*, 3rd ed. Philadelphia, JB Lippincott, 1996.)

on the duodenal bulb (Fig. 34-30), but even a normal common bile duct may occasionally produce a linear impression on the bulb. Extrinsic compression of the duodenum may also result from an enlarged gallbladder secondary to hydrops of the gallbladder, tumor, a pericholecystic abscess or other causes.

Hepatomegaly or anomalous lobes of the liver may cause leftward displacement of the duodenal bulb and sweep.⁵⁶ Duodenal displacement may be particularly marked when there is hypertrophy of the caudate lobe. Hepatic cysts and tumors and metastatic lymphadenopathy in the periportal region may also produce one or more extrinsic impressions on the duodenal bulb and sweep.

Masses in the right kidney or adrenal may cause an extrinsic indentation on the right posterolateral aspect of the descending duodenum.⁵⁷ Generalized renal enlargement secondary to hydronephrosis, multiple cysts, polycystic kidney disease, or renal cell carcinoma may also compress and displace the duodenum (Fig. 34-31). In other patients, anterior displacement of the duodenum may be caused by an enlarged right adrenal gland from Addison's disease or adrenal carcinoma.

The midportion of the descending duodenum is crossed anteriorly by the transverse colon. In approximately 3% of patients, there is an abnormally close positional relationship between these two structures, resulting in a mutual indentation.⁵⁸ Carcinoma of the right side of the colon, especially the hepatic flexure, can result in an extrinsic impression on the outer border of the descending duodenum.⁵⁹ This finding may be caused by adjacent adenopathy or by direct extension of tumor across the short fascial plane of the lateral reflection of the transverse mesocolon, which attaches the hepatic flexure of the colon to the lower portion of the descending duodenum.

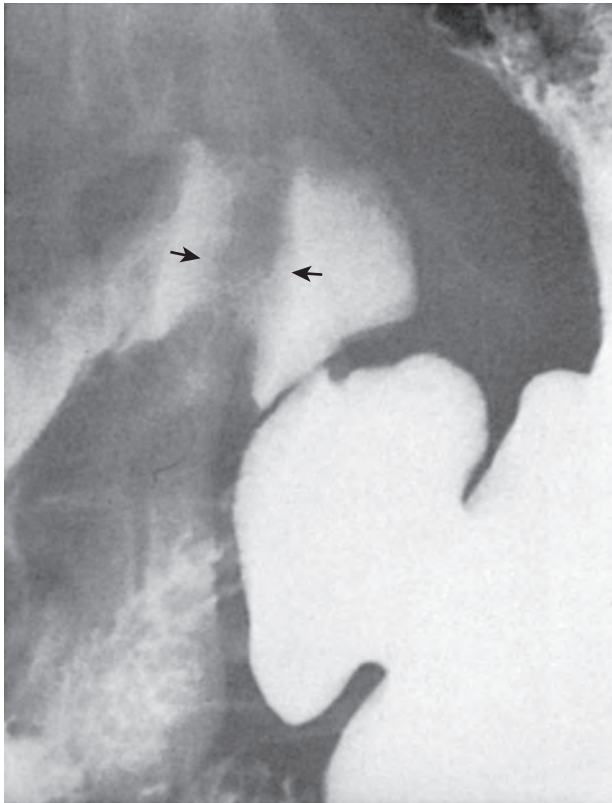


Figure 34-30 Duodenal impression by a dilated common bile duct. The dilated duct produces a characteristic tubular impression (arrows) on the duodenum near the apex of the bulb. (From Eisenberg RL: *Gastrointestinal Radiology: A Pattern Approach*, 3rd ed. Philadelphia, JB Lippincott, 1996.)

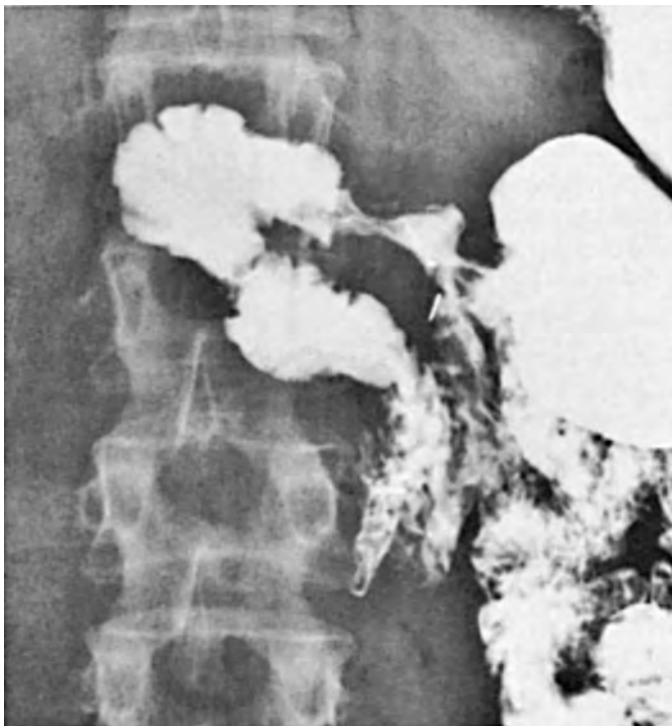


Figure 34-31 Duodenal impression by a polycystic right kidney. The duodenum is displaced to the left of the spine by the polycystic kidney. (From Eisenberg RL: *Gastrointestinal Radiology: A Pattern Approach*, 3rd ed. Philadelphia, JB Lippincott, 1996.)

Dilated vessels can also produce one or more extrinsic impressions on the outer wall of the duodenal bulb and sweep. These impressions may be caused by duodenal varices resulting from portal hypertension or by dilated arterial collateral pathways resulting from occlusion of the celiac axis or superior mesenteric artery.⁶⁰

Widening of the Duodenal Sweep

Although widening of the duodenal sweep on barium studies is often considered to be synonymous with an enlarged head of the pancreas, this finding is not always caused by pancreatic disease, so it must be interpreted with caution. There is great variation in the configuration of the duodenal sweep among normal patients, and slight degrees of widening are difficult to recognize with confidence. In heavy patients, the combination of a high transverse stomach and long vertical course of the descending duodenum can also create the erroneous impression of a widened sweep.

True widening of the duodenal sweep may be caused by pancreatic neoplasms or by benign pancreatic disease (e.g., pancreatitis, pancreatic pseudocysts; Figs. 34-32 and 34-33; see next section). There are numerous radiographic criteria for distinguishing benign and malignant pancreatic disease involving the duodenum, but this differentiation is often difficult on barium studies. When pancreatic abnormalities are suspected, CT or other cross-sectional imaging studies should therefore be performed for a more definitive diagnosis.

Widening of the duodenal sweep may also be caused by enlarged peripancreatic lymph nodes secondary to lymphoma, metastases, or various inflammatory conditions (Fig. 34-34).⁶¹ Depending on their location, mesenteric cysts or tumors may

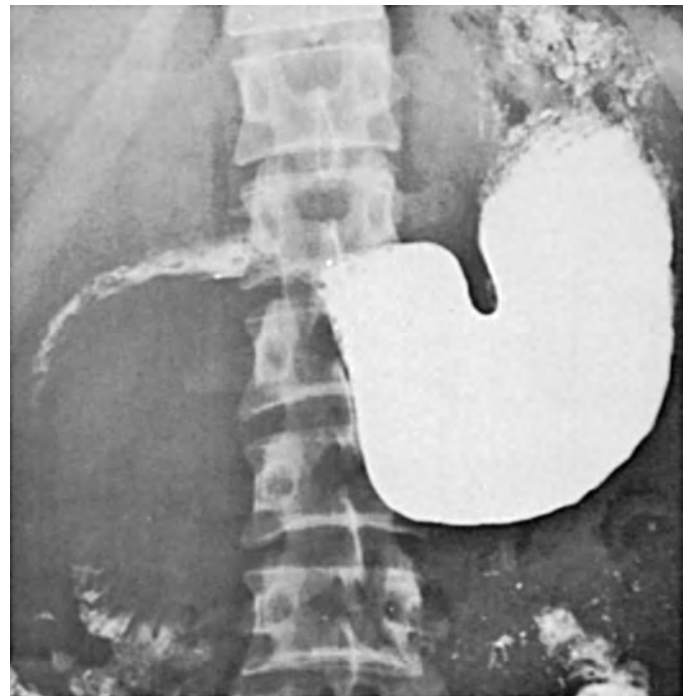


Figure 34-32 Widening of the duodenal sweep by acute pancreatitis. (From Eisenberg RL: *Gastrointestinal Radiology: A Pattern Approach*, 3rd ed. Philadelphia, JB Lippincott, 1996.)



Figure 34-33 Widening of the duodenal sweep by a pancreatic pseudocyst. Pancreatitis or pancreatic carcinoma could produce similar findings (see Fig. 34-32). (From Eisenberg RL: *Gastrointestinal Radiology: A Pattern Approach*, 3rd ed. Philadelphia, JB Lippincott, 1996.)



Figure 34-35 Widening of the duodenal sweep by a choledochal cyst. (From Eisenberg RL: *Gastrointestinal Radiology: A Pattern Approach*, 3rd ed. Philadelphia, JB Lippincott, 1996.)

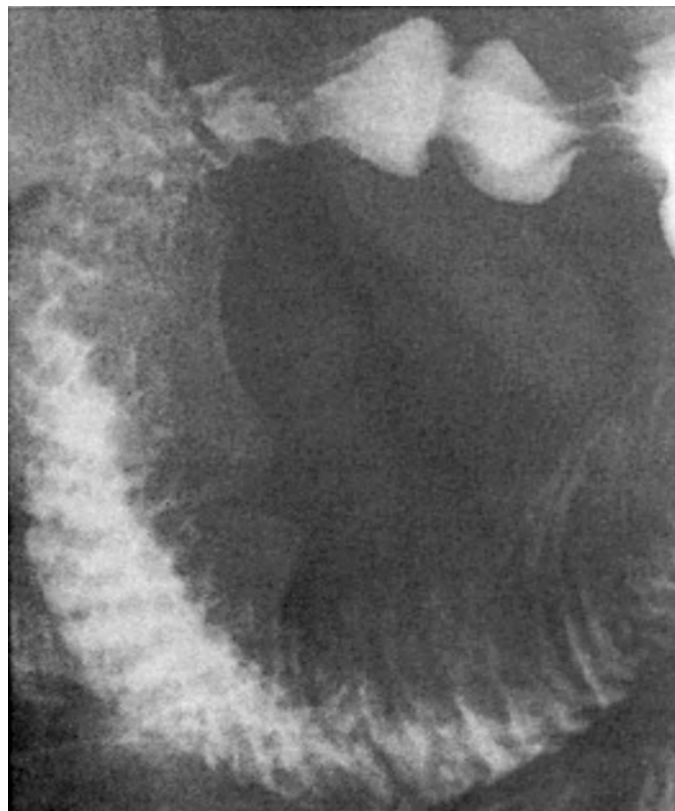


Figure 34-34 Widening of the duodenal sweep by peripancreatic lymphoma. Enlarged peripancreatic lymph nodes have produced a double contour on the medial border of the duodenum with associated spiculation. Pancreatitis or pancreatic carcinoma could produce similar findings (see Fig. 34-36). (From Eisenberg RL: *Gastrointestinal Radiology: A Pattern Approach*, 3rd ed. Philadelphia, JB Lippincott, 1996.)

produce similar findings. Rarely, dilated pancreaticoduodenal collateral vessels in patients with an occluded celiac axis or superior mesenteric artery can produce a smooth, concave impression on the medial aspect of the descending duodenum that simulates a mass in the head of the pancreas.

Retroperitoneal masses (primary or metastatic neoplasms or cysts) can also widen the duodenal sweep. Downward displacement of the third portion of the duodenum by an aortic aneurysm can produce a similar radiographic appearance. A choledochal cyst near the ampulla of Vater can result in generalized widening of the duodenal sweep (Fig. 34-35) or a localized impression near the papilla.

Pancreatic Diseases Affecting the Stomach and Duodenum

Before the advent of ultrasound, CT, and magnetic resonance imaging (MRI), alterations in the configuration and mucosal pattern of the antrum and duodenal sweep were carefully evaluated on barium studies as indirect signs of inflammatory or neoplastic disease involving the head of the pancreas. Although primarily of historical interest, the findings on upper GI barium studies may occasionally suggest otherwise unexpected pancreatic disease.

Enlargement of the head of the pancreas can produce a mass impression on the inner aspect of the duodenal sweep that

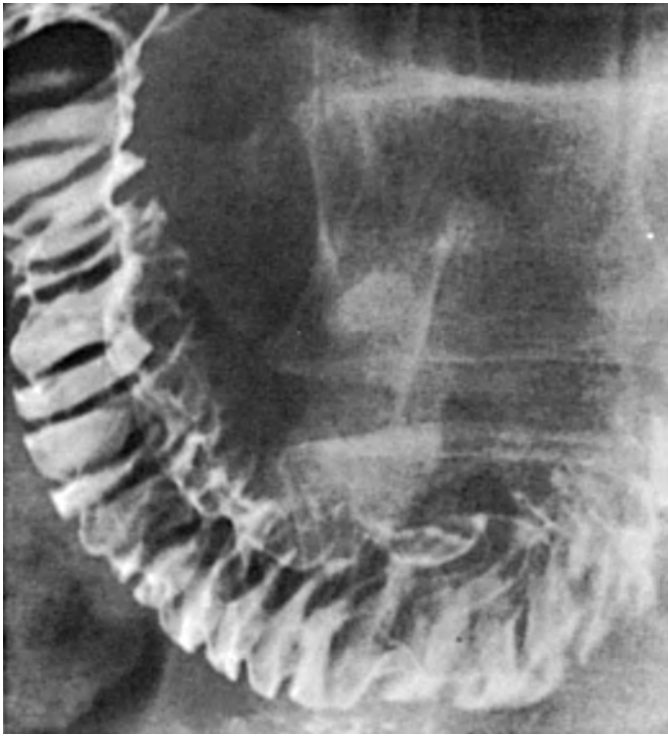


Figure 34-36 Duodenal involvement by pancreatic carcinoma. An enlarged pancreatic head produces a double contour on the medial border of the duodenal sweep. (From Eisenberg RL: *Gastrointestinal Radiology: A Pattern Approach*, 3rd ed. Philadelphia, JB Lippincott, 1996.)

creates a double contour effect (Fig. 34-36). Another nonspecific sign, originally attributed to malignant disease, but probably more common in inflammatory disorders, is the so-called inverted 3 sign of Frostberg (Fig. 34-37). The central limb of the inverted 3 represents the point of fixation of the duodenal wall, where the pancreatic and common bile ducts insert into the papilla. The impressions above and below this point reflect tumor mass, edema of the major and minor papillae, or edema of the duodenal wall from adjacent pancreatitis. Pancreatitis or pancreatic tumor invading the duodenum may also be manifested by spiculation and tethering of the medial wall of the duodenum because of a desmoplastic reaction in the serosa (Fig. 34-38).

In advanced disease, duodenal involvement by pancreatitis, pancreatic pseudocysts, or pancreatic carcinoma may be manifested by the development of ulcers, cavities, or even pancreaticoduodenal fistulas. Pancreatitis, pseudocysts, or neoplasms involving the head of the pancreas may also produce a smooth area of extrinsic mass effect on the greater curvature of the gastric antrum, also known as the antral pad sign.⁶² Further infiltration of the stomach by the inflammatory process or tumor may result in an irregular gastric contour with spiculated, tethered mucosal folds on the greater curvature (Fig. 34-39). Similarly, disease involving the body or tail of the pancreas may be manifested by extrinsic compression, flattening, or spiculation of the posterior wall of the gastric fundus or body (Fig. 34-40A and B). When gastric involvement by pancreatic disease is suspected on barium studies, other imaging tests such as CT, MRI, or ultrasound should be performed for a more definitive diagnosis (Fig. 34-40C).

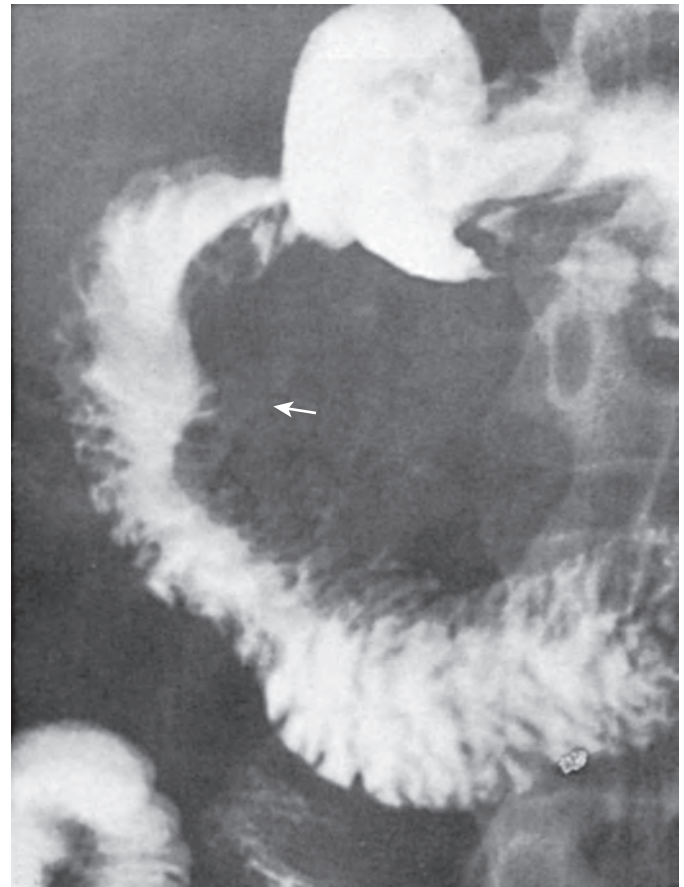


Figure 34-37 Inverted 3 sign of Frostberg. There is a widened duodenal sweep, with fixation of the duodenal wall at the papilla (arrow), producing the inverted 3 sign. This patient had acute pancreatitis, so the inverted 3 sign is not specific for pancreatic carcinoma.

Unusual Filling Defects

BEZOARS

A bezoar consists of an accumulated mass of ingested food within the gastric lumen. Phytobezoars (composed of undigested vegetable matter) have typically been associated with the eating of unripe persimmons, a fruit containing substances that coagulate on contact with gastric acid to produce a sticky, gelatinous material, which traps seeds, skin, and other foodstuffs, acting as the nidus for developing bezoars. Trichobezoars (composed of hair) occur predominantly in women who swallow their own hair, usually because of schizophrenia or other mental illness. The accumulated mass of hair can enlarge until it occupies the lumen of the entire stomach, often assuming the shape of that organ. A small percentage of bezoars, also known as trichophytobezoars, are composed of a combination of hair and vegetable matter.

Despite the classic association of gastric bezoars with vegetable matter and hair, the most common cause of this finding in modern radiology practice is gastroparesis in patients who have diabetes or are taking narcotic medications.⁶³ Because of the important role of gastric peristalsis in the mechanical breakdown of ingested food, patients with decreased or absent gastric peristalsis are at increased risk for developing bezoars. Less



Figure 34-38 Duodenal involvement by pancreatitis. There is an extrinsic impression on the medial border of the descending duodenum, with spiculated mucosal folds. (From Eisenberg RL: *Gastrointestinal Radiology: A Pattern Approach*, 3rd ed. Philadelphia, JB Lippincott, 1996.)

frequently, gastric bezoars may also be found in patients with chronic gastric outlet obstruction secondary to scarring from peptic ulcer disease or other causes. Finally, bezoars may develop after partial gastrectomy or bariatric surgery in which the antrum and body of the stomach (the portions of the stomach responsible for gastric peristalsis) have been resected (Billroth I or II) or bypassed (Roux-en-Y gastric bypass).⁶³ Because there is little or no gastric peristalsis in the remaining gastric remnant or pouch, bezoars are more likely to develop in these patients. If a postoperative stricture develops at the gastroduodenal or gastrojejunal anastomosis, the risk of bezoar formation increases even further.⁶³

Symptoms of gastric bezoars, which result from the mechanical effects of the foreign body in the stomach, include crampy epigastric pain and a sense of fullness or heaviness in the upper abdomen.⁶³ Large bezoars may also cause symptoms of gastric outlet obstruction. Some bezoars may be chronic findings, necessitating endoscopy for mechanical breakdown of the mass of food matter in the stomach, but others may resolve rapidly (in <2 weeks) on conservative medical treatment.⁶³

A bezoar is sometimes visible on abdominal radiographs as a soft tissue mass floating in the stomach at the air-fluid interface (Fig. 34-41). Barium studies may show a conglomerate mass of debris with barium trapped in the interstices of the bezoar, producing a characteristic mottled appearance (Fig. 34-42).⁶³ With changes in patient position, many bezoars are freely movable within the gastric lumen.⁶³ Bezoars can also develop in the gastric remnant after a partial gastrectomy (Billroth I and II) or in the gastric pouch

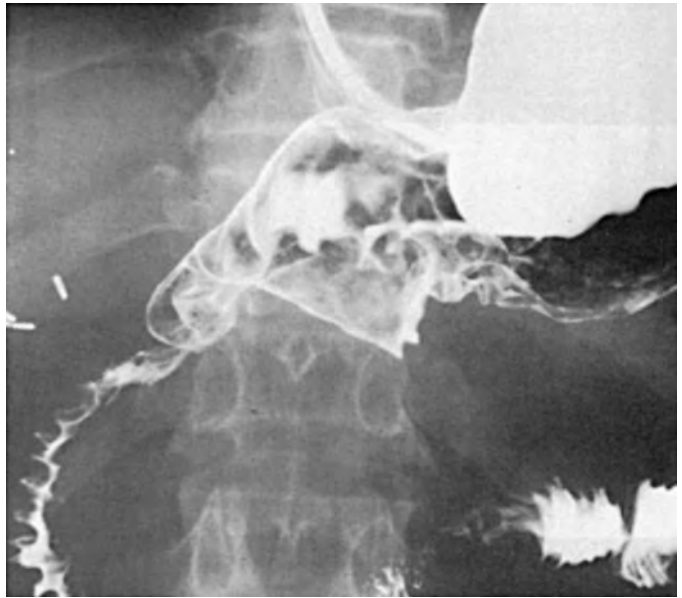


Figure 34-39 Gastric involvement by pancreatitis. There is flattening, irregularity, and spiculation of the greater curvature of the antrum caused by extension of the inflammatory process to the stomach. Also note involvement of the proximal descending duodenum.

after gastric bypass (Roux-en-Y gastric bypass), especially when strictures develop at the gastroduodenal or gastrojejunal anastomosis, delaying emptying of ingested food. Occasionally, a bezoar may be unusually smooth, simulating an enormous gas bubble (Fig. 34-43). Bezoars are usually characterized on CT by inhomogeneous intraluminal masses that have a mottled appearance and are often seen floating at the air-fluid interface (Fig. 34-44).⁶⁴

FOREIGN BODIES

Foreign bodies may appear as radiolucent filling defects in the barium-filled stomach or duodenum. This appearance is produced by a variety of ingested substances, including food, pills, and nondigestible material.

HEMATOMAS

In patients with upper GI bleeding, blood clots may appear as one or more filling defects in the stomach or duodenum. Hemorrhage into the wall of the stomach secondary to a bleeding diathesis, anticoagulant therapy, or trauma can lead to the development of a large intramural gastric mass, usually involving the fundus.

Intramural duodenal hematomas are a recognized complication of blunt trauma to the abdomen. More than 80% of reported cases have occurred in children or young adults; child abuse is a major cause in infants and young children.⁶⁵ It is believed that the hematoma results from the duodenum being crushed between the anterior abdominal wall and vertebral column. Because the second and third portions of the duodenum are fixed in a retroperitoneal position, they are prone to this type of injury if enough force is applied to the anterior abdominal wall. When the mucosa is separated from the

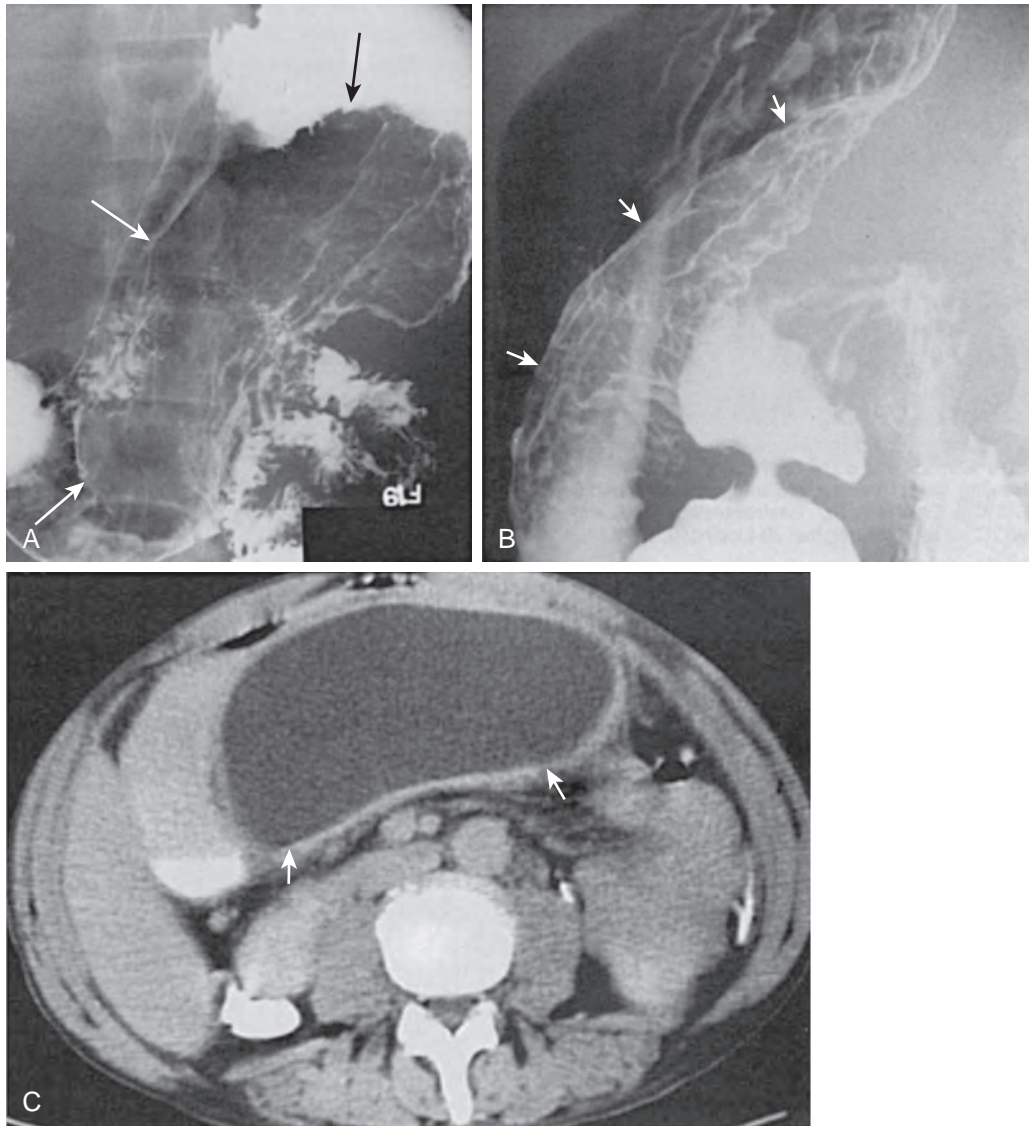


Figure 34-40 Gastric involvement by a pancreatic pseudocyst. **A.** Supine view of the stomach shows a large area of extrinsic mass effect (arrows) on the upper gastric body. **B.** Lateral view shows the retrogastric mass (arrows) in profile. **C.** CT scan reveals a large pancreatic pseudocyst (arrows) compressing and displacing the stomach. (From Laufer I, Levine MS [eds]: *Double Contrast Gastrointestinal Radiology*, 2nd ed. Philadelphia, WB Saunders, 1992.)

loose submucosa, blood may dissect along submucosal compartments. Intramural duodenal hematomas may also be caused by a bleeding diathesis, anticoagulation, or endoscopic trauma.⁶⁶

Intramural duodenal hematomas may appear on barium studies as well-circumscribed intramural masses with discrete margins. Some degree of stenosis and obstruction is usually present (Fig. 34-45A). CT may reveal marked thickening of the duodenal wall in these patients.⁶⁷ CT is also helpful for differentiating duodenal perforation from a hematoma without perforation. The presence of perforation is indicated by extraluminal gas or extravasated contrast material in the right anterior pararenal space.⁶⁷ The right psoas margin may be obliterated because of associated retroperitoneal bleeding. A coil spring appearance has been described and, rarely, delayed rupture into the peritoneal or retroperitoneal space may occur. Although some patients

have discrete hematomas, others have diffuse bleeding in the duodenal wall, manifested by thickened, spiculated folds or thumbprinting (Fig. 34-45B).

INTRAGASTRIC AND INTRADUODENAL GALLSTONES

An intragastric gallstone is an extremely rare cause of a filling defect in the stomach. Gallstones may enter the stomach or duodenum in patients with cholecystogastric or cholecystoduodenal fistulas. Similar to other foreign bodies in the stomach, intragastric gallstones may cause mucosal irritation, ulceration, bleeding, perforation, and even obstruction. Erosion of a gallstone into the duodenal bulb may also cause gastric outlet obstruction (Bouveret's syndrome), a rare but life-threatening condition.^{68,69}

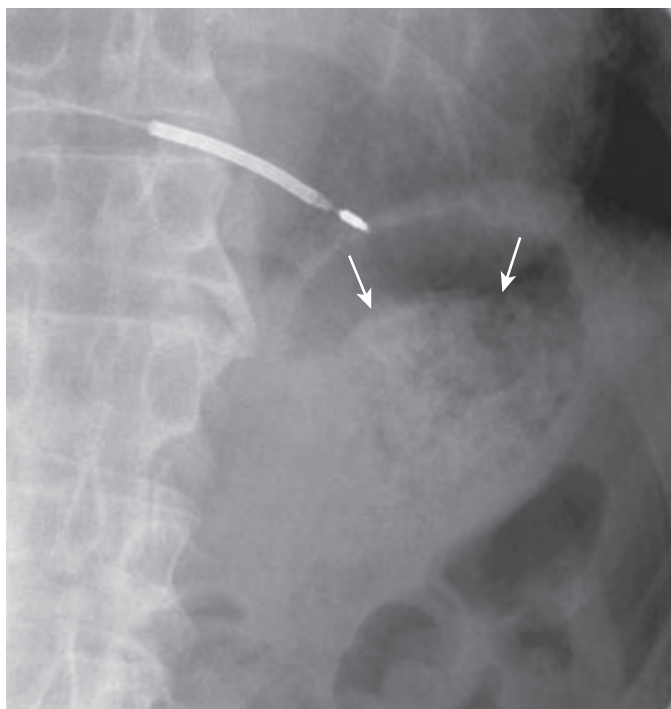


Figure 34-41 Gastric bezoar. Supine abdominal radiograph shows a gastric bezoar as a mottled soft tissue mass (arrows) floating in the stomach at the air-fluid interface.

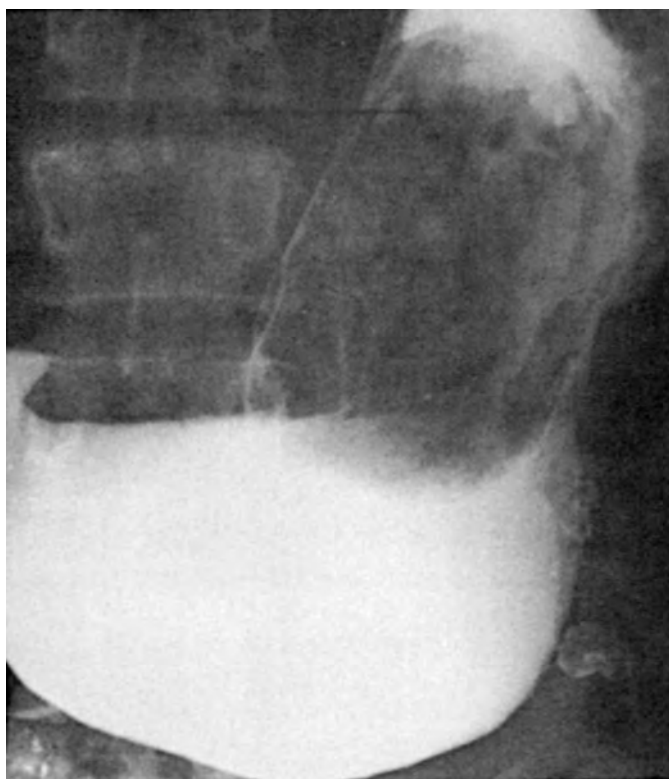


Figure 34-43 Gastric bezoar. The bezoar appears as a smooth filling defect in the stomach that could be mistaken for an enormous gas bubble. This patient was a model airplane builder who had been ingesting glue. (From Eisenberg RL: *Gastrointestinal Radiology: A Pattern Approach*, 3rd ed. Philadelphia, JB Lippincott, 1996.)

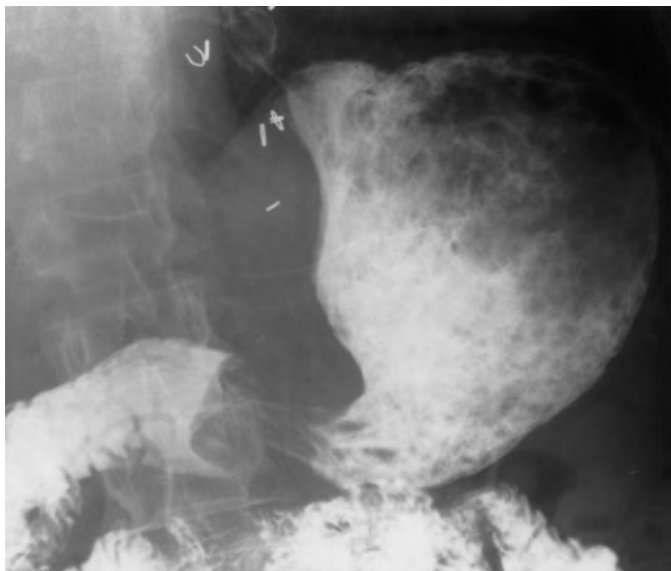


Figure 34-42 Gastric bezoar. The bezoar is manifested by a conglomerate mass of debris with barium trapped in its interstices, producing a characteristic mottled appearance.

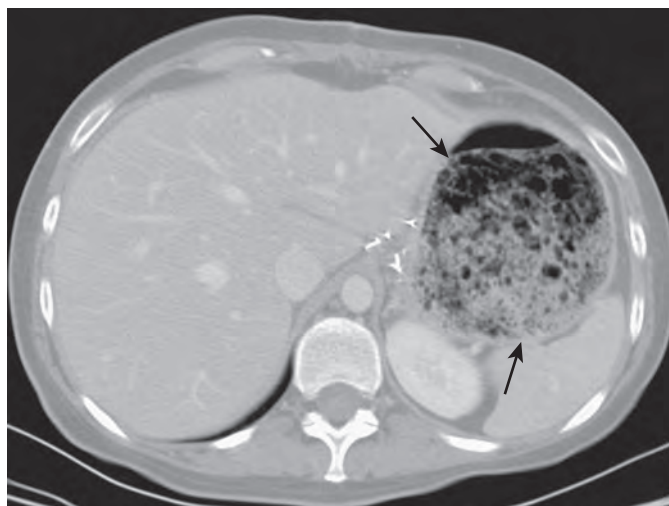


Figure 34-44 Gastric bezoar on CT. The bezoar is characterized on CT by an inhomogeneous intraluminal mass with a mottled gas pattern (arrows). This patient underwent a partial gastrectomy and now has a bezoar in the gastric remnant because of a stricture at the gastrojejunal anastomosis (not visualized on this image). (From Woodfield CA, Levine MS: *The postoperative stomach*. *Eur J Radiol* 53:341–352, 2005.)

Gastric Volvulus

Gastric volvulus is an uncommon acquired twist of the stomach on itself that can lead to obstruction or strangulation with potentially life-threatening gastric infarction. It is usually associated with a large defect in the diaphragm that allows all or part of the stomach to herniate into the thorax. Free upward movement of the stomach into the chest is normally limited by

various ligaments, which anchor the stomach within the abdomen. The most rigid point of attachment is the site at which the second portion of the duodenum assumes a retroperitoneal position, thus becoming fixed to the posterior abdominal wall. The gastrocolic and gastrolenal ligaments also

contribute to fixation of the stomach. Because of these points of anatomic fixation, torsion of the stomach may occur, with significant degrees of gastric herniation. Less frequently, gastric volvulus may be associated with eventration or paralysis of the diaphragm in the absence of a true hernia. Cases of idiopathic gastric volvulus without apparent cause have also been reported.

With small herniations, the proximal portion of the stomach enters the hernial sac first. Obstruction or strangulation almost

never occurs at this stage. As herniation progresses, the body and a variable portion of the antrum come to lie above the diaphragm, so the stomach can eventually become an entirely intrathoracic organ that is prone to a volvulus. The term *organo-axial volvulus* refers to rotation of the stomach upward around its long axis—a line connecting the cardia with the pylorus. In this condition, the antrum moves from an inferior to superior position, with the intrathoracic stomach located in the right hemithorax. In *mesenteroaxial volvulus*, however, the stomach rotates from right to left or left to right about the long axis of the gastrohepatic omentum (a line connecting the middle of the lesser curvature with the middle of the greater curvature), with the intrathoracic stomach usually located in the left hemithorax.⁷⁰

Patients with chronic gastric volvulus may be asymptomatic if there is no gastric outlet obstruction or vascular compromise. Other patients may develop postprandial pain or vomiting if there is partial gastric outlet obstruction.⁷¹ In contrast, an acute gastric volvulus may present as a surgical emergency if the vascular supply to the stomach is compromised. An acute volvulus should be suggested by the classic triad of violent retching with production of little vomitus, constant severe epigastric pain, and an inability to advance a nasogastric tube beyond the distal esophagus. Vascular occlusion causes gastric necrosis, perforation, and shock, with a mortality rate of approximately 30%.

The radiographic signs of gastric volvulus are characteristic. Chest radiographs may reveal an intrathoracic stomach with a double air-fluid level in the chest when the patient is upright. Barium studies may reveal inversion of the intrathoracic stomach, with the greater curvature above the lesser curvature, the cardia and pylorus positioned in close proximity, and downward pointing of the pylorus and duodenum (also described as an upside-down intrathoracic stomach; Fig. 34-46).⁷² Gastric volvulus may also be recognized on CT by the presence of an enlarged, twisted stomach in the thorax with identification of one or more sites of torsion.⁷³ Barium studies are useful for showing gastric outlet obstruction, whereas CT is useful for showing signs of ischemia.

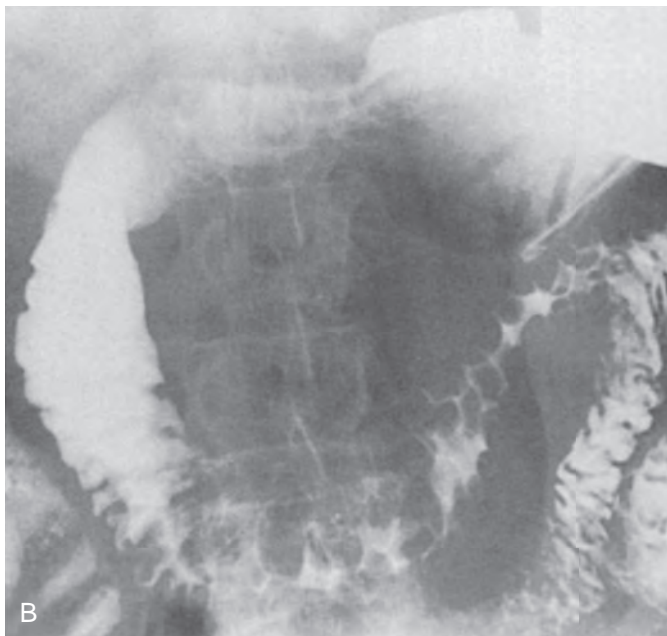
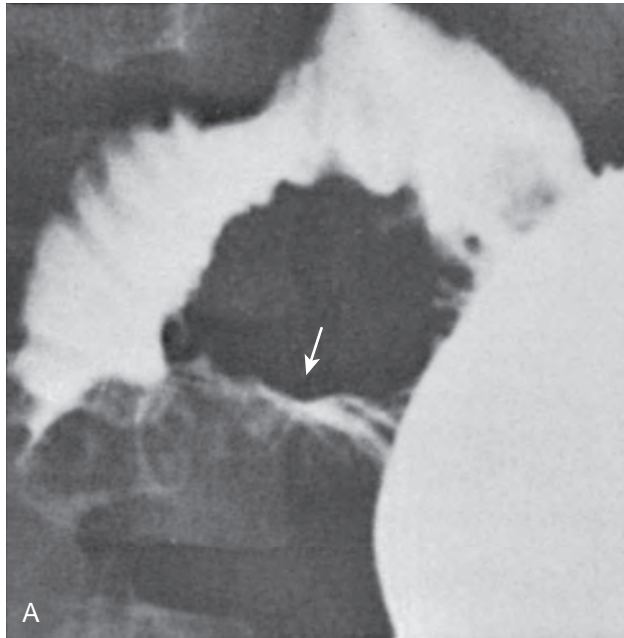


Figure 34-45 Intramural duodenal bleeding. **A.** There is marked narrowing and compression of the distal descending duodenum (arrow) by a large hematoma in a young child who had been kicked in the abdomen by his father. **B.** In another patient who had been undergoing anticoagulant therapy for a prosthetic heart valve, there is thumbprinting of the distal duodenum due to extensive intramural hemorrhage. (**A** from Eisenberg RL: *Gastrointestinal Radiology: A Pattern Approach*, 3rd ed. Philadelphia, JB Lippincott, 1996; **B** courtesy Richard L. Baron, MD, Pittsburgh.)

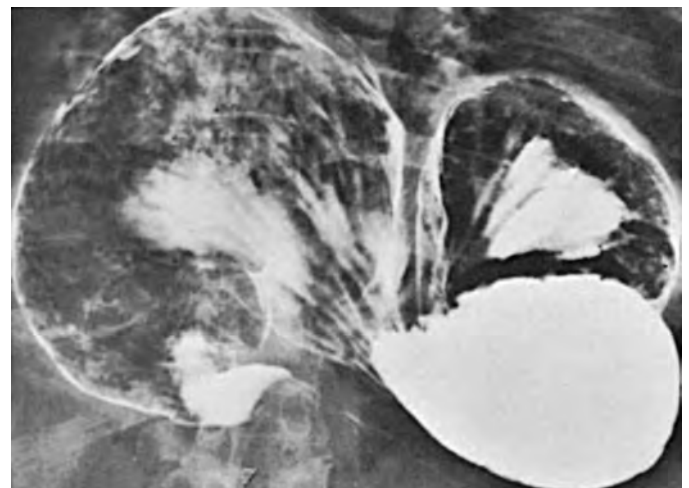


Figure 34-46 Gastric volvulus. This patient has an organoaxial volvulus of the stomach causing gastric outlet obstruction. The stomach is located above the diaphragm, with inversion of the greater curvature above the lesser curvature and downward pointing of the pylorus. (From Eisenberg RL: *Gastrointestinal Radiology: A Pattern Approach*, 3rd ed. Philadelphia, JB Lippincott, 1996.)

Gastroduodenal and Duodenojejunal Intussusceptions

Gastroduodenal and duodenojejunal intussusceptions are rare entities, usually associated with gastric or duodenal tumors that serve as the lead point for the intussusception. In gastroduodenal intussusception, characteristic radiographic signs include foreshortening and narrowing of the gastric antrum, converging or telescoping mucosal folds in the antrum or duodenum, prepyloric collar-shaped outpouchings, widening of the pyloric channel, a coil spring appearance of duodenal mucosal folds, and widening of the duodenum with an associated intraluminal mass.^{74,75} Similarly, duodenojejunal intussusception produces an intraluminal mass associated with a characteristic coil spring pattern.⁷⁶

Fistulas

GASTROCOLIC AND DUODENOCOLIC FISTULAS

Fistulous communications between the stomach and duodenum and other abdominal organs may occur as a complication of benign or malignant disease. In the past, gastrocolic fistulas usually resulted from primary carcinomas of the colon or stomach.⁷⁷ In today's pill-oriented society, however, benign greater curvature gastric ulcers caused by aspirin or other NSAIDs have become a more common cause of gastrocolic fistulas than malignant tumors.⁷⁸ Occasionally, these greater curvature ulcers may penetrate inferiorly via the gastrocolic ligament to the superior border of the transverse colon, which is almost always the site of the colonic end of the fistula (Fig. 34-47).

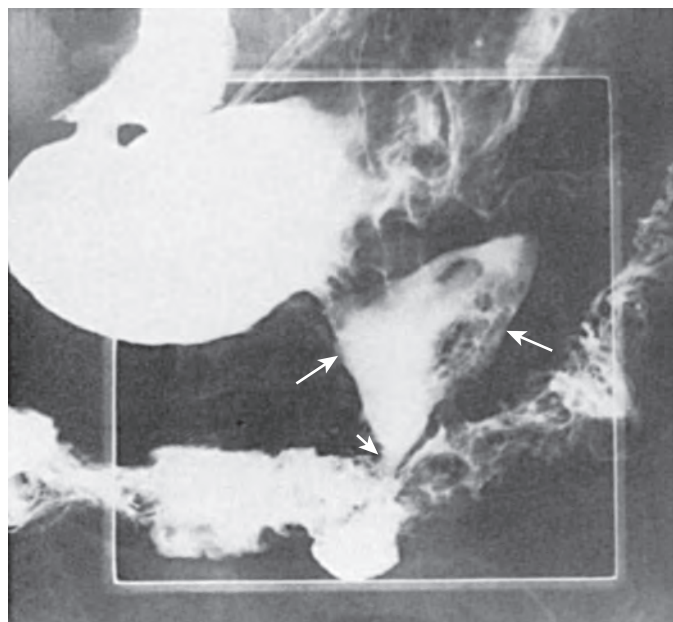


Figure 34-47 Gastrocolic fistula caused by a benign greater curvature ulcer. Upper GI study shows a giant ulcer (long arrows) on the greater curvature of the stomach, with barium entering a fistula (short arrow) that communicates with the superior border of the transverse colon. This patient had an aspirin-induced ulcer as the cause of the gastrocolic fistula. (From Levine MS, Kelly MR, Laufer I, et al: *Gastrocolic fistulae: The increasing role of aspirin*. Radiology 187:359–361, 1993.)

Malignant tumors causing gastrocolic (Fig. 34-48) or duodenocolic (Fig. 34-49) fistulas tend to be bulky, infiltrating lesions associated with a marked inflammatory reaction. These tumors apparently extend from the serosa of one viscus into the wall of another, followed by lumen to lumen necrosis. The presence of a fibrous stroma within the wall of a malignant fistula accounts for the length of these tracks and the relative separation of bowel loops.⁷⁷

Malignant gastrocolic fistulas are frequently demonstrated on barium enema examinations but are rarely detected on upper GI barium studies. Increased intraluminal pressure in the colon at the time of a barium enema examination may overcome the resistance of a rigid, nondistensible fistula, allowing passage of barium into the stomach. In contrast, intraluminal pressure in the stomach during an upper GI barium study may not be sufficient to overcome this resistance.⁷⁹

A fistulous communication between the stomach, jejunum, and colon (gastrojejunocolic fistula) or directly between the stomach and colon represents a serious complication of marginal ulceration after gastric surgery for peptic ulcer disease (Fig. 34-50).⁸⁰ Most patients with this condition have diarrhea and weight loss; pain, vomiting, and bleeding occur in one third to one half of cases. These patients have a high mortality rate, especially if diagnosis of the fistula is delayed.

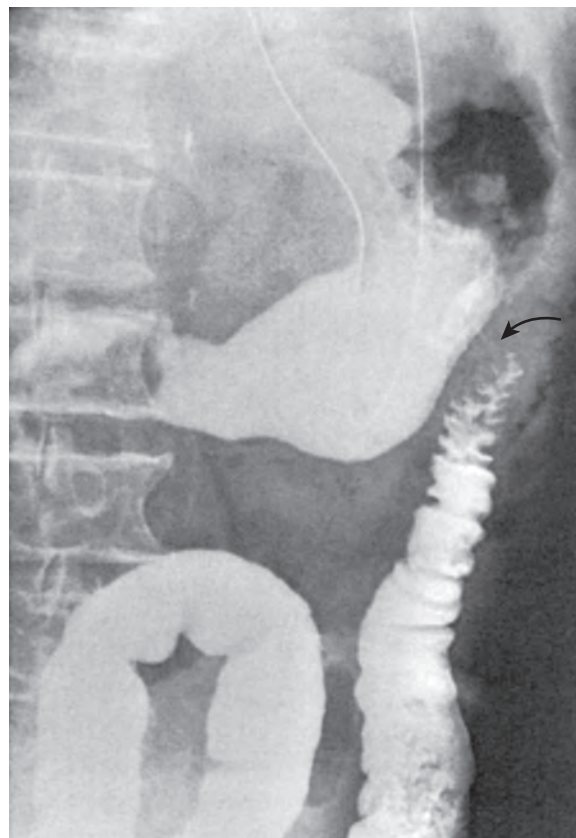


Figure 34-48 Gastrocolic fistula caused by carcinoma of the splenic flexure. Barium enema shows an annular carcinoma of the splenic flexure, with barium entering the stomach via a gastrocolic fistula (arrow). (From Eisenberg RL: *Gastrointestinal Radiology: A Pattern Approach*. 3rd ed. Philadelphia, JB Lippincott, 1996.)

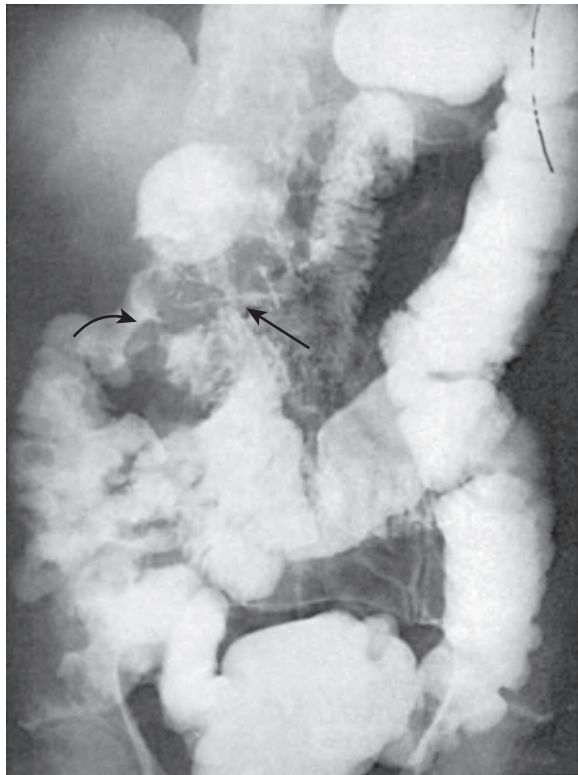


Figure 34-49 Duodenocolic fistula caused by carcinoma of the proximal transverse colon. Barium enema shows an annular carcinoma (curved arrow) of the proximal transverse colon, with barium entering the duodenum via a duodenocolic fistula (straight arrow). (From Vieta JO, Blanco R, Valentini GR: Malignant duodenocolic fistula: Report of two cases, each with one or more synchronous gastrointestinal cancers. *Dis Colon Rectum* 19:542–552, 1976.)



Figure 34-50 Gastrojejunal fistula. This patient had undergone a partial gastrectomy and gastrojejunostomy. There is a large anastomotic ulcer (arrow) at the gastrojejunostomy with filling of the jejunum and transverse colon via a gastrojejunal fistula. (From Thoeni RH, Hodgson JR, Scudamore HH: The roentgenologic diagnosis of gastrocolic and gastrojejunal fistulae. *AJR* 83:876–881, 1960.)

CHOLECYSTODUODENAL FISTULAS

Fistulas between the gallbladder and duodenum may be caused by acute cholecystitis (90%) or by severe peptic ulcer disease (6%). The remaining cases are caused by trauma or tumor. Acute cholecystitis usually results in the development of a cholecystoduodenal fistula, but the inflamed gallbladder can also perforate into the stomach, jejunum, or hepatic flexure of the colon. In patients with severe peptic ulcer disease, a penetrating duodenal or gastric ulcer can perforate into the gallbladder or bile duct.⁸¹ Regardless of the cause, abdominal radiographs often show gas in the biliary tree. On upper GI barium studies, barium may fill the cholecystoduodenal fistula (Fig. 34-51).

OTHER FISTULAS

Aortoduodenal fistulas can occur as a complication of abdominal aortic aneurysms or prosthetic vascular grafts. Pressure necrosis of the third portion of the duodenum, which is fixed and apposed to the anterior wall of an aortic aneurysm, can lead to digestion of the aortic wall by enteric secretions, with the development of an aortoduodenal fistula. Secondary fistulas result from pseudoaneurysm formation with erosion into the adherent duodenum or dehiscence of the suture line associated with leakage of intestinal contents through the duodenum, whose blood supply has been compromised at surgery. An

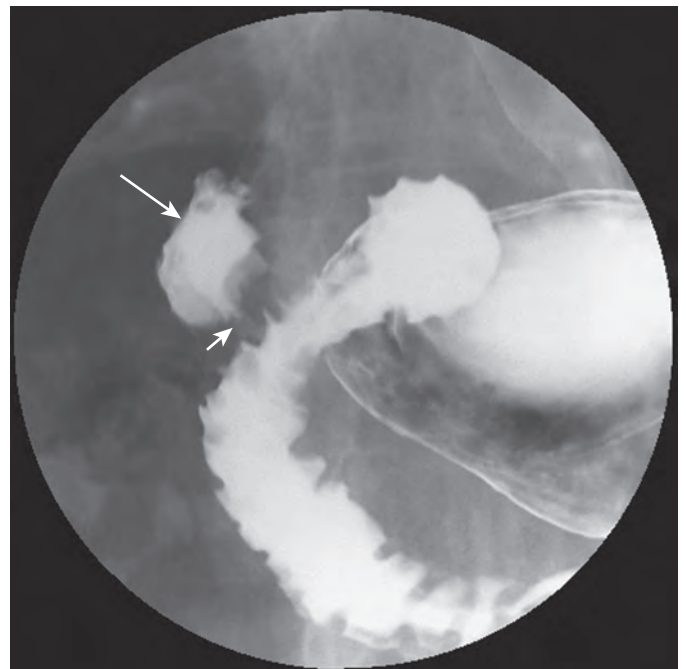


Figure 34-51 Cholecystoduodenal fistula. Barium study shows barium filling the gallbladder (long arrow) via a fistula (short arrow) from the descending duodenum. Also note thickened folds and decreased distensibility of the duodenum in this patient with a long-standing history of ulcer disease. The fistula presumably developed as a complication of a penetrating postbulbar duodenal ulcer.

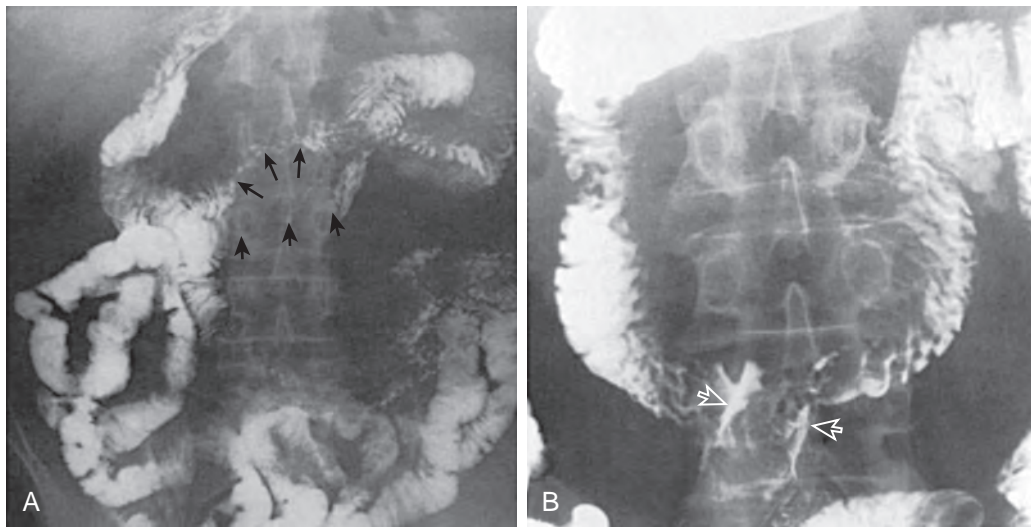


Figure 34-52 Aortoduodenal fistulas. **A.** The fistula causes extrinsic compression of the third portion of the duodenum (*thin arrows*) and displacement of an adjacent loop of jejunum (*thick arrows*). No contrast medium is seen entering the fistula. **B.** In another patient with an aortic graft, extravasated water-soluble contrast medium from the distal duodenum is seen tracking between the graft and aorta (*arrows*). (**A** from Wyatt GM, Rauchway MI, Spitz HB: Roentgen findings in aortoenteric fistulae. *AJR* 126:714–722, 1976.)

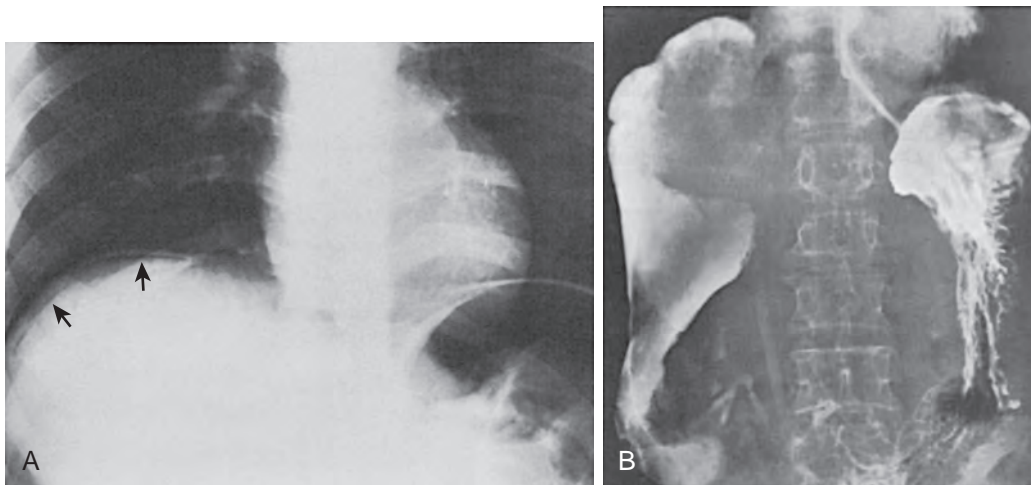


Figure 34-53 Pneumoperitoneum caused by a perforated duodenal ulcer. **A.** Free intraperitoneal air is seen beneath the right hemidiaphragm (*arrows*). **B.** Study using a water-soluble contrast agent shows free extravasation of contrast agent from the duodenum into the right side of the peritoneal cavity. (From Eisenberg RL: *Gastrointestinal Radiology: A Pattern Approach*, 3rd ed. Philadelphia, JB Lippincott, 1996.)

aortoduodenal fistula is often a fatal condition, characterized by abdominal pain, GI bleeding, and a palpable, pulsatile mass. Barium studies may demonstrate compression or displacement of the third portion of the duodenum by an extrinsic mass (Fig. 34-52A). Rarely, in patients with aortic grafts, the wall of the abdominal aorta may be outlined by extraluminal contrast medium tracking along the graft into the paraprosthesis space (Fig. 34-52B).⁸²

Fistulas between the duodenum and right kidney may occasionally develop as a complication of pyelonephritis, particularly tuberculous pyelonephritis. The pathologic mechanism is usually rupture of a perirenal abscess into the duodenum, which is best demonstrated on retrograde pyelography. Rarely,

a duodenal ulcer may penetrate into the right kidney, producing a duodenorenal fistula.

Gastric and Duodenal Perforation

The most frequent cause of pneumoperitoneum in patients with peritonitis is a perforated peptic ulcer, either a gastric ulcer or, more commonly, a duodenal ulcer (Fig. 34-53A). In approximately 30% of patients with perforated ulcers, however, there is no evidence of free intraperitoneal air on abdominal radiographs. The failure to demonstrate pneumoperitoneum is therefore of little value in excluding the possibility of a perforated ulcer. In general, the absence of gas in the stomach and

presence of gas in the small and large bowel should suggest a gastric perforation as the cause of pneumoperitoneum. Conversely, the absence of colonic gas and presence of a gastric air-fluid level and small bowel distention make a colonic perforation more likely. The findings on abdominal radiographs can be misleading, however, so a firm diagnosis of the site of perforation requires study with a water-soluble contrast agent (Fig. 34-53B).⁸³

Benign Gastric Emphysema

Gas in the wall of the stomach can be a sign of infection, ischemia, or increased intraluminal pressure, but benign gastric emphysema may occasionally be demonstrated in the absence of underlying disease.⁸⁴ Although pneumatosis cystoides intestinalis may also affect the wall of the stomach, this condition usually involves the small bowel or colon (see Chapter 12). Gastric emphysema is most commonly caused by severe vomiting or by endoscopy or other iatrogenic injury that allows gas in the lumen to dissect via mucosal rents into the wall of the stomach. Gastric emphysema is typically manifested on abdominal radiographs by linear collections of gas in the gastric wall (Fig. 34-54).

Benign gastric emphysema should be differentiated from a life-threatening condition, emphysematous gastritis, a rare fulminant form of gastritis associated with gas-forming infection. This condition is usually caused by ischemia, severe gastroenteritis, ingestions of caustic substances, and gastroduodenal surgery that compromises the vascular supply of the stomach. Emphysematous gastritis is characterized by cystic, bubbly collections of gas in the gastric wall that have a very different appearance than the linear intramural collections seen in gastric emphysema (see Chapter 12).

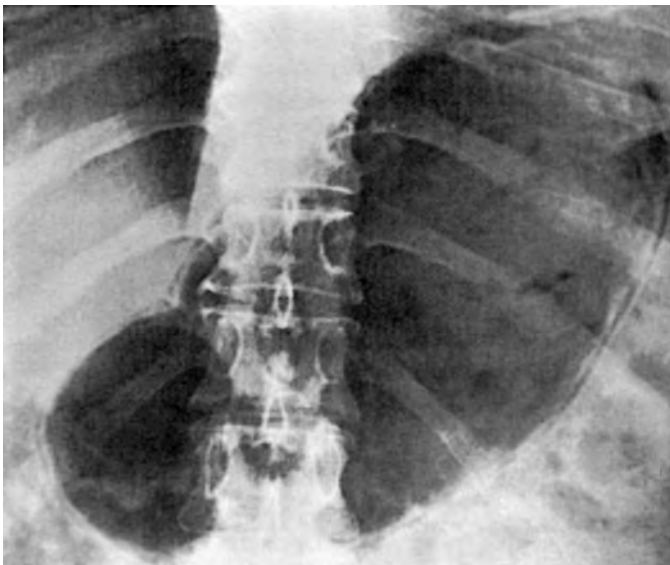


Figure 34-54 Benign gastric emphysema. Linear collections of gas are seen in the gastric wall as a complication of endoscopy. (From Eisenberg RL: *Gastrointestinal Radiology: A Pattern Approach*, 3rd ed. Philadelphia, JB Lippincott, 1996.)

Amyloidosis

Deposition of an amorphous, eosinophilic, extracellular, protein-polysaccharide complex of amyloid in the stomach can produce a broad spectrum of radiographic findings. Amyloid infiltration is sometimes associated with marked narrowing and rigidity of the wall of the stomach (especially the antrum), producing a linitis plastica appearance.⁸⁵ Generalized thickening of gastric folds can also occur (Fig. 34-55).

Cystic Fibrosis

Cystic fibrosis is sometimes manifested on barium studies by a thickened, coarse fold pattern in the duodenum (Fig. 34-56). Associated findings include nodular indentations on the duodenal wall, smudging or poor definition of the mucosal fold pattern, and redundancy, distortion, and kinking of the duodenal contour.^{86,87} These changes are usually confined to the first and second portions of the duodenum, but occasionally extend into the proximal jejunum. The cause of duodenal fold thickening in cystic fibrosis is uncertain. It has been postulated that lack of secretion of pancreatic bicarbonate results in inadequate buffering of gastric acid, causing irritation and inflammation of the duodenum in these patients.⁸⁷



Figure 34-55 Gastric involvement by amyloidosis. There are thickened, nodular folds in the stomach secondary to infiltration of the gastric wall by amyloidosis. (From Eisenberg RL: *Gastrointestinal Radiology: A Pattern Approach*, 3rd ed. Philadelphia, JB Lippincott, 1996.)

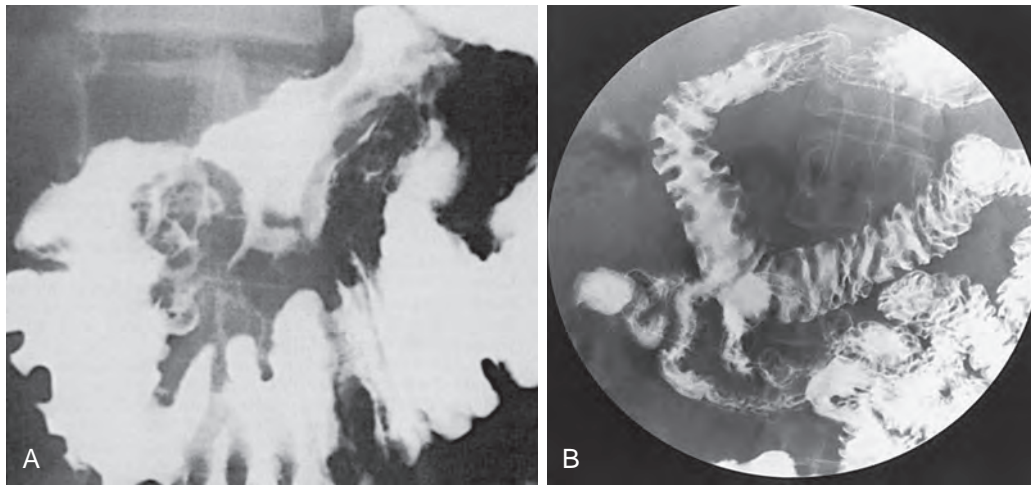


Figure 34-56 Duodenal involvement by cystic fibrosis. A and B. In both cases, a thickened, coarse fold pattern is seen in the duodenum. (A from Eisenberg RL: *Gastrointestinal Radiology: A Pattern Approach*, 3rd ed. Philadelphia, JB Lippincott, 1996.)

REFERENCES

- Ryan BM, Stockbrugger RW, Ryan JM: A pathophysiologic, gastroenterologic, and radiologic approach to the management of gastric varices. *Gastroenterology* 126:1175–1189, 2004.
- Sutton JP, Yarrowborough DY, Richards JT: Isolated splenic vein occlusion. *Arch Surg* 100:623–626, 1970.
- Muhletaler C, Gerlock J, Goncharenko V, et al: Gastric varices secondary to splenic vein occlusion: Radiographic diagnosis and clinical significance. *Radiology* 132:593–598, 1979.
- Lavender S, Lloyd-Davies RW, Thomas ML: Retroperitoneal fibrosis causing localized portal hypertension. *BMJ* 3:627–628, 1970.
- Cho KJ, Martel W: Recognition of splenic vein occlusion. *AJR* 131:439–443, 1978.
- Hershfield NB, Morrow I: Gastric bleeding due to splenic vein thrombosis. *Can Med Assoc J* 98:649–652, 1968.
- Goldstein GB: Splenic vein thrombosis causing gastric varices and bleeding. *Am J Gastroenterol* 58:319–325, 1972.
- Okuda K, Yasumoto M, Goto A, et al: Endoscopic observations of gastric varices. *Am J Gastroenterol* 60:357–365, 1973.
- Itzhak Y, Glickman MG: Splenic vein thrombosis in patients with a normal size spleen. *Invest Radiol* 12:158–163, 1977.
- Rice RP, Thompson WM, Kelvin FM, et al: Gastric varices without esophageal varices: An important pre-endoscopic diagnosis. *JAMA* 237:1976–1979, 1977.
- Belgrad R, Carlson HC, Payne WS, et al: Pseudotumoral gastric varices. *AJR* 91:751–756, 1964.
- Kaye JJ, Stassa G: Mimicry and deception in the diagnosis of tumors of the gastric cardia. *AJR* 110:295–303, 1970.
- Carucci LR, Levine MS, Rubesin SE, et al: Tumorous gastric varices: Radiographic findings in 10 patients. *Radiology* 212:861–865, 1999.
- Sos T, Meyers MA, Baltaxe HA: Nonfundic gastric varices. *Radiology* 105:579–580, 1972.
- Levine MS, Kieu K, Rubesin SE, et al: Isolated gastric varices: Splenic vein obstruction or portal hypertension? *Gastrointest Radiol* 15: 188–192, 1990.
- Balthazar EJ, Megibow A, Naidich D, et al: Computed tomographic recognition of gastric varices. *AJR* 142:1121–1125, 1984.
- Marshall JP, Smith PD, Hoyumpa AM: Gastric varices: Problems in diagnosis. *Am J Dig Dis* 22:947–955, 1977.
- Babb RR: Splenic vein obstruction: A curable cause of variceal bleeding. *Am J Dig Dis* 21:512–513, 1976.
- Bateson EM: Duodenal and antral varices. *Br J Radiol* 42:744–747, 1969.
- Smart HL, Triger DR: Clinical features, pathophysiology, and relevance of portal hypertensive gastropathy. *Endoscopy* 23:224–228, 1991.
- Panes J, Bordas JM, Pique JM, et al: Increased gastric mucosal perfusion in cirrhotic patients with portal hypertensive gastropathy. *Gastroenterology* 103:1875–1882, 1992.
- Balan KK, Grime JS, Sutton R, et al: Do alterations in the rate of gastric emptying after injection sclerotherapy for esophageal varices play any role in the development of portal hypertensive gastropathy? *HPB Surg* 11:141–148, 1999.
- Chang D, Levine MS, Ginsberg GG, et al: Portal hypertensive gastropathy: Radiographic findings in eight patients. *AJR* 175:1609–1612, 2000.
- Treichel J, Gerstenberg E, Palme G, et al: Diagnosis of partial gastric diverticula. *Radiology* 119:13–18, 1976.
- Millard JR, Ziter FMH, Slover WP: Giant duodenal diverticula. *AJR* 121:334–337, 1974.
- Macari M, Lazarus D, Israel G, et al: Duodenal diverticula mimicking cystic neoplasms of the pancreas: CT and MR imaging findings in seven patients. *AJR* 180:195–199, 2003.
- Afridi SA, Fichtenbaum CJ, Taubin H: Review of duodenal diverticula. *Am J Gastroenterol* 86:935–938, 1991.
- Wolfe RD, Pearl MJ: Acute perforation of duodenal diverticulum with roentgenographic demonstration of localized retroperitoneal emphysema. *Radiology* 104:301–302, 1972.
- Pugash RA, O'Brien SE, Stevenson GW: Perforating duodenal diverticulitis. *Gastrointest Radiol* 15:156–158, 1990.
- Gore RM, Ghahremani GG, Kirsch MD, et al: Diverticulitis of the duodenum: Clinical and radiological manifestations of seven cases. *Am J Gastroenterol* 86:981–985, 1991.
- Rioux L, Des Groseilliers S, Fortin M, et al: Massive upper gastrointestinal bleeding originating from a fourth-stage duodenal diverticulum. *Can J Surg* 39:510–512, 1996.
- Nelson JA, Burhenne HJ: Anomalous biliary and pancreatic duct insertion into duodenal diverticula. *Radiology* 120:49–52, 1976.
- Materne R: The duodenal wind sock sign. *Radiology* 218:749–750, 2001.
- Johnston P, Dessler TS: MDCT of intraluminal “windsock” duodenal diverticulum with surgical correlation and multiplanar reconstruction. *AJR* 183:249–250, 2004.
- Clements JL, Jinkins JR, Torres WE, et al: Antral mucosal diaphragms in adults. *AJR* 133:1105–1111, 1979.
- Bjorgvinsson E, Rudzki C, Lewicki AM: Antral web. *Am J Gastroenterol* 79:663–665, 1984.
- Pratt AD: Current concepts of the obstructing duodenal diaphragm. *Radiology* 100:637–643, 1971.
- Rha SE, Lee JH, Lee SY, et al: Duodenal diaphragm associated with long-term use of nonsteroidal anti-inflammatory drugs: A rare cause of duodenal obstruction in an adult. *AJR* 175: 920–921, 2000.
- Balthazar EJ: Hypertrophic pyloric stenosis in adults: Radiographic features. *Am J Gastroenterol* 78:449–453, 1983.
- Balthazar EJ, Rosenberg H, Davidian MM: Scirrhous carcinoma of the pyloric channel and distal antrum. *AJR* 134:669–674, 1980.
- Aranha GV, Prinz RA, Greenlee HB, et al: Gastric outlet and duodenal obstruction from inflammatory pancreatic disease. *Arch Surg* 119: 833–835, 1984.
- Berk RN, Coulson DB: The body cast syndrome. *Radiology* 94:303–305, 1970.
- Wallace RG, Howard WB: Acute superior mesenteric artery syndrome in the severely burned patient. *Radiology* 94:307–310, 1970.
- Simon M, Lerner MA: Duodenal compression by the mesenteric root in acute pancreatitis and in inflammatory conditions of the bowel. *Radiology* 79:75–81, 1962.

45. Shammash JB, Rubesin SE, Levine MS: Massive gastric distention due to duodenal involvement by retroperitoneal tumors. *Gastrointest Radiol* 17:214–216, 1992.
46. Ooi GC, Chan KL, Ko KF, et al: Computed tomography of the superior mesenteric artery syndrome. *Clin Imaging* 21:210–212, 1997.
47. Rogers LF, Goldstein HM: Roentgen manifestations of radiation injury to the gastrointestinal tract. *Gastrointest Radiol* 2:281–291, 1977.
48. Braun P, Collins PP, Ducharme JC: Preduodenal portal vein: A significant entity? Report of two cases and a review of the literature. *Can J Surg* 17:316–322, 1974.
49. Rimer DG: Gastric retention without mechanical obstruction. *Arch Intern Med* 117:287–299, 1966.
50. Horowitz M, Fraser RJL: Gastroparesis: Diagnosis and management. *Scand J Gastroenterol* 30(Suppl 213):7–16, 1995.
51. Gramm HF, Reuter K, Costello P: The radiologic manifestations of diabetic gastric neuropathy and its differential diagnosis. *Gastrointest Radiol* 3:151–155, 1978.
52. Parkman HP, Hasler WL, Fisher RS: American Gastroenterological Association medical position statement: Diagnosis and treatment of gastroparesis. *Gastroenterology* 127:1589–1591, 2004.
53. Levin AA, Levine MS, Rubesin SE, et al: An 8-year review of barium studies in the diagnosis of gastroparesis. *Clin Radiol* 63:407–414, 2008.
54. Horowitz M, McNeil JD, Maddern GJ, et al: Abnormalities of gastric and esophageal emptying in polymyositis and dermatomyositis. *Gastroenterology* 90:434–439, 1986.
55. Nowak TV, Ionasescu V, Anuras S: Gastrointestinal manifestations of the muscular dystrophies. *Gastroenterology* 82:800–810, 1982.
56. Chon H, Arger PH, Miller WT: Displacement of duodenum by an enlarged liver. *AJR* 119:85–88, 1973.
57. Bluth I, Vitale P: Right renal enlargement causing alterations in the descending duodenum: A radiographic demonstration. *Radiology* 76:777–784, 1961.
58. Poppel MH: Duodenocolic apposition. *AJR* 83:851–856, 1960.
59. Treitel H, Meyers MA, Maza V: Changes in the duodenal loop secondary to carcinoma of the hepatic flexure of the colon. *Br J Radiol* 43:209–213, 1970.
60. Shimkin PM, Pearson KD: Unusual arterial impressions upon the duodenum. *Radiology* 103:295–297, 1972.
61. Zeman RK, Schiebeler M, Clark LR, et al: The clinical and imaging spectrum of pancreaticoduodenal lymph node enlargement. *AJR* 144:1223–1227, 1985.
62. Asrani AV: The antral pad sign. *Radiology* 229:421–422, 2003.
63. Hewitt AN, Levine MS, Rubesin SE, et al: Gastric bezoars: Reassessment of clinical and radiographic findings in 19 patients. *Br J Radiol* 82:901–907, 2009.
64. Ripolles T, Garcia-Aguayo G, Martinez MJ, et al: Gastrointestinal bezoars: Sonographic and CT characteristics. *AJR* 177:65–69, 2001.
65. Kleinman PK, Brill PW, Winchester P: Resolving duodenal-jejunal hematoma in abused children. *Radiology* 160:747–750, 1986.
66. Ghishan FK, Werner M, Vieira P, et al: Intramural duodenal hematoma: An unusual complication of endoscopic small bowel biopsy. *Am J Gastroenterol* 82:368–370, 1987.
67. Kunin JR, Korobkin M, Ellis JH, et al: Duodenal injuries caused by blunt abdominal trauma: Value of CT in differentiating perforation from hematoma. *AJR* 160:221–223, 1993.
68. Singh AK, Shirkhoda A, Lal N, et al: Bouveret's syndrome: Appearance on CT and upper gastrointestinal radiography before and after stone obturation. *AJR* 181:828–830, 2003.
69. Brennan GB, Rosenberg RD, Arora S: Bouveret syndrome. *Radiographics* 24:1171–1175, 2004.
70. Gerson DE, Lewicki AM: Intrathoracic stomach: When does it obstruct? *Radiology* 119:257–264, 1976.
71. Allen MS, Trastek VF, Deschamps C, et al: Intrathoracic stomach: Presentation and results of operation. *J Thorac Cardiovasc Surg* 105:253–258, 1993.
72. Scott RL, Felker R, Winer-Muram H, et al: The differential retrocardiac air-fluid level: A sign of intrathoracic gastric volvulus. *J Can Assoc Radiol* 37:119–121, 1986.
73. Chiechi MV, Hamrick-Turner J, Abbitt PL: Gastric herniation and volvulus: CT and MR appearance. *Gastrointest Radiol* 17:99–101, 1992.
74. Meyers MA: Gastroduodenal intussusception. *Am J Med Sci* 254:347–355, 1967.
75. Choi SH, Han JK, Kim SH, et al: Intussusception in adults: From stomach to rectum. *AJR* 183:691–698, 2004.
76. Van Beers B, Trigau JP, Pringot J: Duodenojejunal intussusception secondary to duodenal tumors. *Gastrointest Radiol* 13:24–26, 1988.
77. Smith DL, Dockerty MD, Black BM: Gastrocolic fistulas of malignant origin. *Surg Gynecol Obstet* 134:829–832, 1972.
78. Levine MS, Kelly MR, Laufer I, et al: Gastrocolic fistulas: The increasing role of aspirin. *Radiology* 187:359–361, 1993.
79. Martinez LO, Manheimer LH, Casal GL, et al: Malignant fistulas of the gastrointestinal tract. *AJR* 131:215–218, 1978.
80. Swartz MJ, Paustian FF, Chleborad WJ: Recurrent gastric ulcer with spontaneous gastrojejunal and gastrocolic fistulas. *Gastroenterology* 44:527–531, 1963.
81. Haff RC, Wise L, Ballinger WF: Biliary-enteric fistulas. *Surg Gynecol Obstet* 133:84–88, 1971.
82. Wyatt GM, Rauchway MI, Spitz HB: Roentgen findings in aortoenteric fistulas. *AJR* 126:714–722, 1976.
83. Miller RE: The radiological evaluation of intraperitoneal gas (pneumoperitoneum). *Crit Rev Diagn Imaging* 4:61–85, 1973.
84. Lee S, Rutledge JN: Gastric emphysema. *Am J Gastroenterol* 79:899–904, 1984.
85. Carlson HC, Breen JF: Amyloidosis and plasma cell dyscrasias: Gastrointestinal involvement. *Semin Roentgenol* 21:128–138, 1986.
86. Phelan MS, Fine DR, Zentler-Munro L, et al: Radiographic abnormalities of the duodenum in cystic fibrosis. *Clin Radiol* 34:573–577, 1983.
87. Agrons GA, Corse WR, Markowitz RI, et al: Gastrointestinal manifestations of cystic fibrosis: Radiologic-pathologic correlation. *Radiographics* 16:871–893, 1996.

Postoperative Stomach and Duodenum

LAURA R. CARUCCI

CHAPTER OUTLINE

Diagnostic Evaluation Following Gastric and Duodenal Surgery

Surgical Considerations for Peptic Ulcer Disease

Indications for Surgery

Surgical Procedures for Peptic Ulcer Disease

Surgical Procedures for Gastric Resection

Billroth I Procedure

Billroth II Procedure

Roux-en-Y Gastrojejunostomy

Identification of Postsurgical Anatomy on Imaging Studies

Complications After Gastric Resection

Surgical Considerations for Gastric and Duodenal Neoplasms

Surgery for Gastric Masses

Surgery for Duodenal Masses

Complications Following Gastric and Duodenal Surgery for Neoplasm

Surgery for Weight Loss

Roux-en-Y Gastric Bypass

Laparoscopic Adjustable Gastric Banding

Sleeve Gastrectomy

Biliopancreatic Diversion with Duodenal Switch

Gastric and duodenal operations are usually performed for peptic ulcer disease (PUD), benign or malignant gastric or duodenum masses, and the treatment of obesity. Imaging studies are often an integral part of the evaluation of patients following gastric or duodenal surgery. Radiologic evaluation of postoperative patients requires understanding of the operative procedures, appreciation of the expected postoperative appearance, and knowledge of potential complications. In the early postoperative setting, the radiologist is often asked to assess the postsurgical anatomy and evaluate for possible early postoperative complications such as leakage. In the late postoperative course, radiologic evaluation may be undertaken to evaluate for more delayed complications or symptoms of abdominal pain, nausea and vomiting, weight loss, and weight gain.

Gastroduodenal surgical procedures may include resection and/or bypass of portions of the intestinal tract. Treatment of PUD may involve some form of vagotomy, often in conjunction with a procedure to improve gastric emptying (pyloroplasty or antrectomy). Following distal gastric resection,

continuity of the gastrointestinal (GI) tract may be reestablished via a Billroth I gastroduodenostomy or gastrojejunostomy (Billroth II or Roux-en-Y gastrojejunostomy). For treatment of gastric neoplasms, gastrojejunostomy is favored over gastroduodenostomy because this allows for wider surgical margins. The most common bariatric procedures currently performed in the United States include Roux-en-Y gastric bypass, laparoscopic adjustable gastric banding, and sleeve gastrectomy (gastric sleeve).

This chapter provides an overview of the more common surgical procedures performed on the stomach and duodenum as well as the indications for surgery, approaches to the radiologic evaluation, expected postsurgical appearance, and possible complications. Radiologists need to have an understanding of the expected postoperative anatomy to assess for possible complications and diagnose recurrent disease.

Diagnostic Evaluation Following Gastric and Duodenal Surgery

The imaging approach in patients following gastric and duodenal surgery depends on the type of surgical procedure performed, postoperative time course, patient's clinical status, and patient's presenting symptoms. Fluoroscopic and computed tomography (CT) studies are usually performed to evaluate postoperative patients; both may occasionally be necessary to establish the most accurate diagnosis.

Fluoroscopic Studies and Upper Gastrointestinal Examinations. Following abdominal surgery, an overhead scout radiograph should be obtained prior to administration of contrast to assess for postoperative clips, a staples and/or suture lines. The pattern of sutures and staples may help determine the surgical procedure performed if the patient history is unreliable. Also, surgical material should be identified prior to the administration of oral contrast so that radiopaque surgical material is not later mistaken for a small leak. In the early postoperative course, drains and abnormal gas collections may be assessed. Any expected or inadvertent indwelling surgical foreign body (e.g., gastric band device) should also be assessed on the scout radiograph.

In patients following gastric and/or duodenal surgery, the postoperative anatomy should be evaluated at the onset of the fluoroscopic procedure. Because each patient has unique surgical variations, a detailed, cookbook-style upper gastrointestinal examination (UGI) protocol for position changes during the study and required exposures does not tend to apply. Studies must be modified based on the surgical anatomy. Optimal patient positioning to evaluate an anastomosis is variable, depending on the type of surgical procedure

performed. The postoperative anatomy involving the stomach or duodenum should be evaluated prior to proceeding to other portions of the planned examination (e.g., assessment of esophageal motility or esophageal pathology). The initial contrast bolus should be observed fluoroscopically through the resected, oversewn, banded, sutured, or stapled sites and promptly imaged before there is contrast opacification of overlapping structures.

In the early postoperative setting, a UGI should be performed initially using water-soluble contrast agents to assess for possible postoperative leak because water-soluble contrast agents have no known damaging effects when extravasated into the peritoneal cavity or mediastinum.^{1,2} If no leak is identified with water-soluble contrast, barium should be administered. Barium may detect more subtle leaks and other complications.^{1,2} If the study is performed in the late postoperative course and a leak is not suspected, barium may be initially administered.

Single-contrast technique may be preferable to assess the postoperative anatomy, including any surgical anastomosis, and to evaluate for possible fistulas or staple line dehiscence following gastric surgery. In addition, supine patient positioning may be necessary and preferable in the debilitated or early postoperative patient. Double-contrast studies may provide more optimal assessment of mucosal detail, but may be difficult to perform in the postoperative patient because of diminished patient mobility or cooperation.³ Also, a patulous gastrojejunal or gastroduodenal anastomosis (gastric outlet) may preclude optimal gaseous distention of a gastric pouch or remnant. Intravenous (IV) glucagon administration may help slow the passage of barium and air through the gastric remnant and therefore allow for more optimal distention.⁴

Computed Tomography. Computed tomography (CT) may also be performed to assess for postoperative complications. CT can provide detail about the overall anatomy in the abdomen and pelvis, evaluate the bowel in its entirety, and assess the extent of any postoperative fluid collections.

Abdominopelvic CT following gastric and duodenal surgery is ideally performed following the administration of positive oral and IV contrast. Positive oral contrast helps depict the proximal GI anatomy on CT. As with fluoroscopic studies, water-soluble oral contrast should be administered rather than barium in the early postoperative course or if perforation is a consideration. Oral contrast may be administered at intervals prior to the CT study; however, it should also be administered immediately prior to image acquisition to opacify the residual stomach.

Nuclear Medicine. Scintigraphic studies may be of benefit for patients following gastric and/or duodenal surgery to assess for possible motility problems or postgastrectomy syndromes, including GI stasis and dumping syndrome. Radiolabeled solids or liquids can be used to evaluate gastric emptying.⁵ A time-activity curve can be applied to determine the emptying time of the stomach.

Endoscopy. Endoscopy may be useful to assess a surgical anastomosis and evaluate for possible complications such as marginal ulcer disease. Endoscopy may be of particular benefit for diagnosing inflammatory conditions such

as bile reflux gastritis and for diagnosing early tumor recurrence.^{6,7}

Surgical Considerations for Peptic Ulcer Disease

There has been a decline in the number of operative procedures performed for peptic ulcer disease over the last 3 decades.⁸ This is partly because of increased use of medications such as histamine-2 blockers (H2 blockers), proton pump inhibitors (PPIs), and agents to protect the gastric mucosa, including sucralfate and prostaglandin analogues. Identification and treatment of *Helicobacter pylori* infection has been overwhelmingly beneficial, as has the understanding of the role of nonsteroidal anti-inflammatory drugs (NSAIDs) in peptic ulcer disease.⁹ Surgical therapy is usually reserved for patients with severe and emergent complications of ulcer disease. The most common complications of peptic disease, in decreasing order of frequency, are bleeding, perforation, and obstruction. Most peptic ulcer related deaths in the United States are caused by bleeding,^{8,10} which may include melena and/or hematemesis. Patients with perforation may present with an acute abdomen.⁸ A detailed discussion of peptic ulcer disease and its manifestations may be found elsewhere (see Chapter 29).

INDICATIONS FOR SURGERY

Indications for surgery in the setting of peptic ulcer disease may include perforation, bleeding, gastric or duodenal obstruction, intractability, and nonhealing ulcers.^{8,11-14}

Perforation. In patients with acute ulcer perforation, the ulcer may simply be oversewn. In younger patients in particular, simple closure is often successful, with less than 20% chance of recurrence. However, a simple patch may be inadequate for older patients, and more definitive therapy may entail resection.¹⁵

Bleeding. In approximately 70% of cases of major bleeding from PUD, the bleeding stops spontaneously.¹⁵ Surgery may be necessary because of shock or continued bleeding, despite optimal medical management and endoscopic therapy. Surgical management may consist of vagotomy with pyloroplasty or vagotomy with antrectomy (see later).¹⁴

Obstruction. Gastric outlet or duodenal obstruction occurs in less than 10% of patients with PUD.¹⁴ This typically requires resection, usually with a gastrojejunostomy.

Nonhealing Ulcers. Patients with ulcers that fail to heal despite 12 to 15 weeks of optimal medication may be surgical candidates. As many as 10% to 15% of duodenal ulcers do not heal after a 6-week course of high-dose H2 blockers and PPIs, and in 15% to 30% of ulcers that initially heal with medical treatment, relapse occurs.^{14,16} In the case of refractory gastric ulcers, underlying gastric cancer must always be a consideration. In patients with intractable ulcers, elective surgical intervention is preferable, with a lower recurrence rate as compared with more urgent or emergent surgical management.

SURGICAL PROCEDURES FOR PEPTIC ULCER DISEASE

The physiologic basis of surgery for PUD includes methods to decrease secretion of hydrochloric acid from parietal cells located in the body and fundus of the stomach and to remove the portion of the gastric mucosa that is most predisposed to ulcers. Typically, surgical management of peptic ulcer disease includes truncal vagotomy with pyloroplasty, vagotomy with distal gastrectomy, or a highly selective vagotomy (HSV). Overall, vagotomy with distal gastrectomy results in the lowest ulcer recurrence rates; however, this has increased morbidity as compared with other treatment options.^{12,14}

Patients undergoing surgery for peptic ulcer disease may alternatively undergo simple oversewing of a bleeding ulcer or a simple patch of a perforated ulcer.^{8,9} UGI may be performed following this surgery to assess for leaks. A simple patch of a perforated ulcer may appear as a localized filling defect or may simulate an ulcer on UGI.¹⁷

Vagotomy

Vagotomy decreases total acid secretion. Also, parietal cell response to gastrin and other stimulants decreases after vagotomy.

Truncal vagotomy requires complete transection of the anterior and posterior vagus nerve trunk and results in denervation of the stomach, liver, gallbladder, pancreas, small intestines, and proximal large intestine. Loss of the antropyloric mechanism results in gastric stasis, and a pyloroplasty, gastroduodenostomy, or gastrojejunostomy must be performed to improve gastric drainage.⁸ Gastrojejunostomy is the preferred choice for patients with gastric outlet obstruction or a severely diseased duodenum. Truncal vagotomy has the side effects of dumping or diarrhea in 10% of patients.⁸

Highly selective vagotomy (HSV),¹ also called parietal cell vagotomy or proximal gastric vagotomy, is a relatively safe procedure with minimal side effects that decreases total acid secretion by 75%.⁸ With HSV, the vagal nerve supply to the proximal 2/3 to 3/4 of the stomach (parietal cell location) is severed with preservation of the distal branches to the antrum and pylorus. The antropyloric mechanism remains intact and the innervation to remaining abdominal viscera is preserved, minimizing gastrointestinal side effects.⁸ This operation does not alter gastric emptying and therefore does not require a drainage procedure, gastric resection, or an anastomosis. Elective HSV may be a preferred treatment for refractory PUD in the absence of gastric outlet obstruction.¹⁸ However, overall elective HSV for treatment of PUD has largely been replaced by long-term PPI treatment.⁸ Also, patients with pyloric and prepyloric ulcers have higher ulcer recurrence rates after HSV than those with duodenal ulcers alone. In this setting, a truncal vagotomy with antrectomy may be preferable.

Radiography or CT studies following vagotomy may reveal multiple clips in the expected distribution of the vagus nerve and/or its branches.

Pyloroplasty

Pyloroplasty consists of reconstructing the pyloric channel to increase its diameter and improve gastric emptying.

Following truncal vagotomy, impairment of gastric tone and interruption of the antropyloric mechanism result in gastric stasis, and a gastric drainage procedure is required. Pyloroplasty is relatively easy for the surgeon to perform, with less necessary dissection as compared with antrectomy. It also avoids surgical difficulties that may arise with a duodenal stump following antrectomy, and continuity of the GI tract is not altered.⁹

Heineke-Mikulicz Pyloroplasty. A Heineke-Mikulicz pyloroplasty consists of a longitudinal incision from the distal antrum to the proximal duodenum through the pylorus, followed by a transverse closure (essentially parallel to the base of the duodenal bulb) to increase the diameter of the pyloric channel.

Finney Pyloroplasty. A Finney pyloroplasty may be preferred when a longer incision of the duodenum is required to control bleeding or with scarring of the pylorus and duodenal bulb. A Finney pyloroplasty is essentially a side-to-side gastroduodenostomy. An incision is made along the greater curvature of the distal stomach, extending through the pylorus along the medial aspect of the duodenum. An inverted U-shaped incision is made, opening the pyloric channel.

Jaboulay Pyloroplasty. A Jaboulay pyloroplasty is actually a gastroduodenostomy between the antrum and duodenum. The pylorus is not technically incised. This results in a large opening between the distal stomach and duodenum and avoids any inflammatory process in the pyloric area.

Antrectomy

An antrectomy will remove the source of gastrin and prevent gastric stasis. When performed in combination with truncal vagotomy, antrectomy is the gold standard for reducing acid secretion, with the lowest recurrence rates when compared to vagotomy with pyloroplasty and HSV alone. Antral resection with vagotomy is the most definitive operation for treating ulcer disease. Ulcer recurrence following antrectomy is less than 1%, whereas following vagotomy and pyloroplasty, recurrence rates range from 4% to 27%, and recurrence rates following HSV range from 4% to 11%.¹⁹⁻²³ However, low recurrence rates must be weighed against postgastrectomy and postvagotomy complications that occur in up to 20% of patients; these may include diarrhea, dumping, bile reflux gastritis, weight loss, and metabolic consequences.^{9,23,24} Also, there is increased morbidity and mortality risk with gastric resection as compared with HSV alone or vagotomy with pyloroplasty. Antrectomy with vagotomy may be most beneficial for patients with complicated PUD (e.g., patients with bleeding, obstruction, nonhealing, and/or recurrent ulcers).

Antrectomy typically leaves enough of a gastric remnant to allow for maintenance of adequate nutrition, but a bowel anastomosis is necessary. Antrectomy with Billroth I reconstruction (gastroduodenostomy) is the most physiologic anastomosis because it restores normal bowel continuity. Alternatively, a Billroth II reconstruction (gastrojejunostomy) may be performed. A loop of jejunum is brought up to the greater curvature side of the gastric remnant. The duodenal stump must be closed, and this may be technically challenging, especially if the duodenum is diseased.⁹

Surgical Procedures for Gastric Resection

Partial gastrectomy may consist of resection of the antrum, distal two thirds of the stomach, distal 60% of the stomach, or high subtotal gastrectomy, depending on the type of disease (e.g., ulcer, cancer) and its location. Following gastric surgery, GI tract continuity requires an anastomosis and distal partial gastrectomy, and the distal partial gastrectomy procedure is named according to the type of anastomosis between the gastric remnant and small intestine, regardless of the extent of gastric resection. Surgical procedures to restore continuity following distal gastric resection include Billroth I and II procedures and Roux-en-Y gastrojejunostomy.

Following antrectomy for peptic ulcer disease, GI continuity is reestablished with a Billroth I gastroduodenostomy or Billroth II gastrojejunostomy. An additional choice for the gastrojejunostomy may be a Roux-en-Y gastrojejunostomy. However, when antrectomy is performed for ulcer disease, there is typically a large gastric remnant (60% to 70% of the stomach); Roux-en-Y gastrojejunostomy should be avoided in this setting. In the presence of a large gastric remnant, Roux-en-Y construction will predispose to gastric stasis and marginal ulcers.⁸ Distal gastrectomy for gastric neoplasm typically results in a smaller gastric remnant, and Roux-en-Y gastrojejunostomy may be preferable to prevent biliopancreatic secretions and duodenal contents from entering the gastric remnant and esophagus.

BILLROTH I PROCEDURE

The Billroth I procedure consists of antrectomy with a gastroduodenal anastomosis (Fig. 35-1). The distal gastric remnant is anastomosed to the end of the proximal duodenum. GI tract continuity is restored with preservation of the duodenal passage. Constructing the gastroduodenal anastomosis to approximate the size of the pylorus helps delay gastric emptying and reduce problems with postgastrectomy dumping. Because of anastomotic requirements, gastroduodenostomy may only be performed following antrectomy. For more significant gastric resections, a gastrojejunostomy is necessary. Also, in patients with gastric outlet obstruction caused by PUD, gastrojejunostomy is preferable to gastroduodenostomy.

BILLROTH II PROCEDURE

The classic Billroth II procedure is a distal gastrectomy with a loop-type gastrojejunostomy (Fig. 35-2). The gastric remnant is anastomosed to the side of the proximal jejunum. An area of the jejunum approximately 12 to 15 cm distal to the ligament of Treitz (the first or second loop of jejunum) is typically chosen and is brought to the greater curvature of the gastric remnant. The anastomosis may involve the entire end or a portion of the gastric remnant; an anastomosis along the dependent greater curvature of the gastric remnant facilitates gastric emptying.²⁵ This then creates a proximal or afferent loop consisting of the oversewn duodenal stump and the most proximal jejunum, which carry the biliopancreatic secretions. There is then a distal or efferent loop extending downstream, carrying gastric contents distally. The gastrojejunostomy may be anterior to the transverse colon (antecolic) or posterior to the transverse colon (retrocolic). A retrocolic configuration

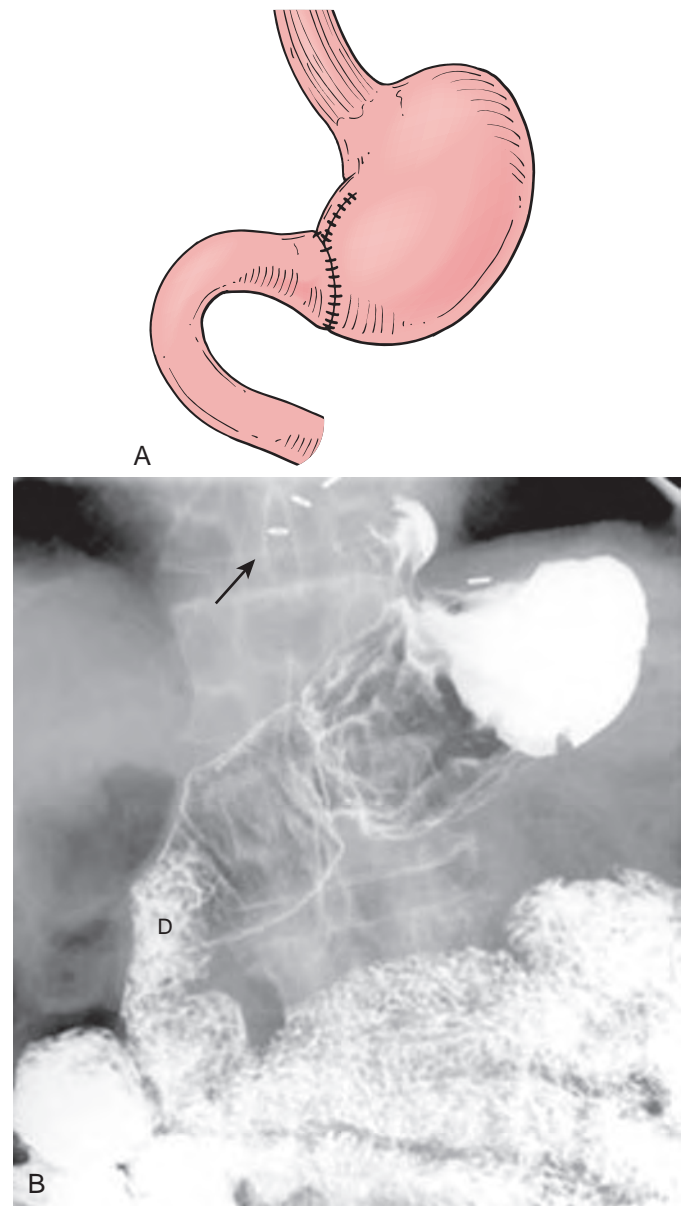


Figure 35-1 Billroth I. **A.** There is an antrectomy with an end-to-end gastroduodenostomy. **B.** UGI image shows slight foreshortening of the stomach following antrectomy. No normal pylorus is seen, and there has been a gastroduodenostomy. Also note surgical clips from truncal vagotomy (arrow). **D**, duodenum.

allows for a shorter afferent loop, which may result in fewer postoperative complications.⁴

ROUX-EN-Y GASTROJEJUNOSTOMY

With a Roux-en-Y gastrojejunostomy, the jejunum is transected, and the proximal end of the jejunum (the Roux limb) is anastomosed to the gastric remnant, usually end-to-side (Fig. 35-3). The small bowel may be brought up anterior or posterior to the transverse colon (antecolic or retrocolic, respectively). When the small bowel is brought up posterior to the transverse colon, an opening is made in the transverse mesocolon, which must be repaired. For malignancy, an antecolic location may be

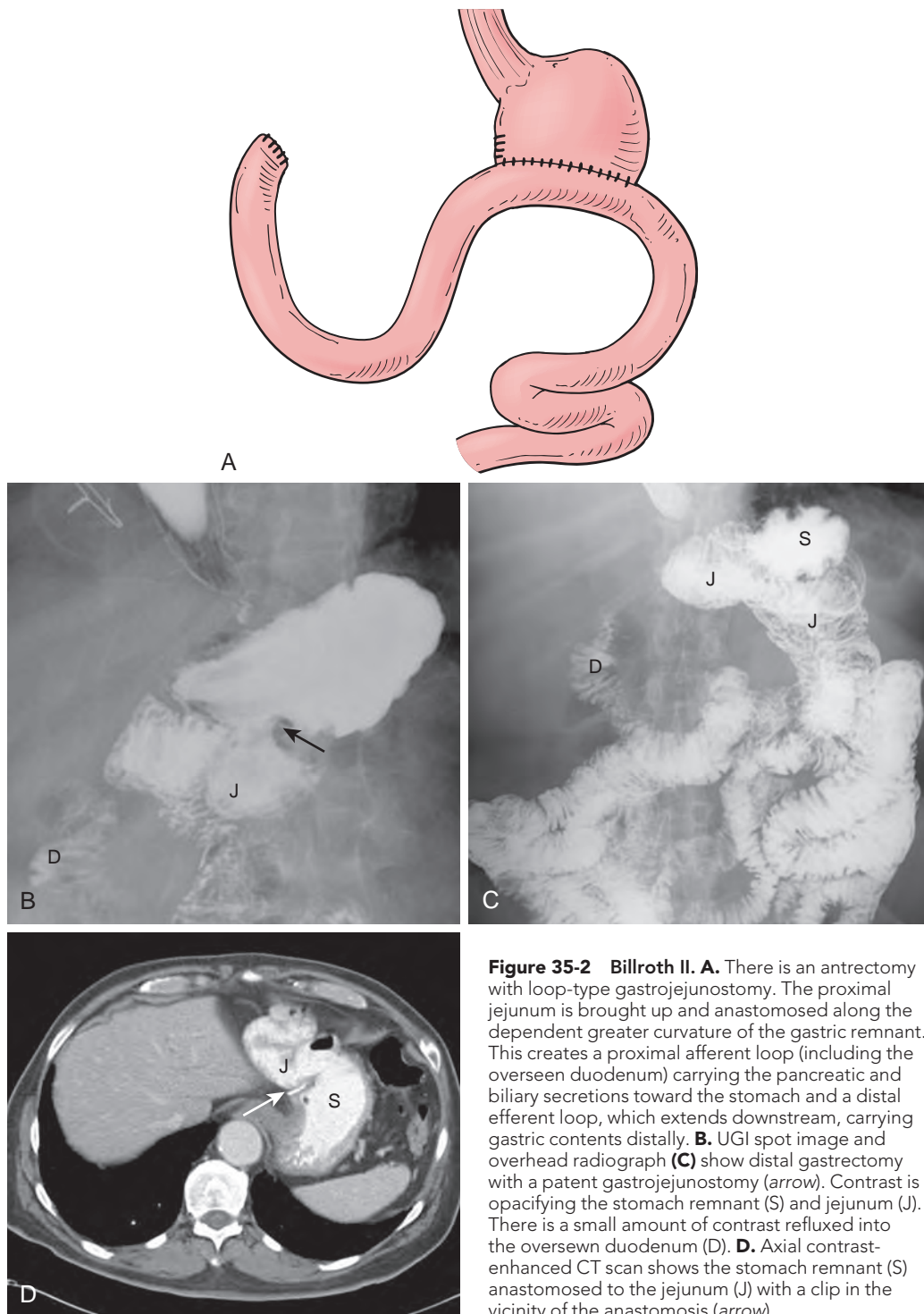


Figure 35-2 Billroth II. **A.** There is an antrectomy with loop-type gastrojejunostomy. The proximal jejunum is brought up and anastomosed along the dependent greater curvature of the gastric remnant. This creates a proximal afferent loop (including the oversewn duodenum) carrying the pancreatic and biliary secretions toward the stomach and a distal efferent loop, which extends downstream, carrying gastric contents distally. **B.** UGI spot image and overhead radiograph (**C**) show distal gastrectomy with a patent gastrojejunostomy (arrow). Contrast is opacifying the stomach remnant (S) and jejunum (J). There is a small amount of contrast refluxed into the oversewn duodenum (D). **D.** Axial contrast-enhanced CT scan shows the stomach remnant (S) anastomosed to the jejunum (J) with a clip in the vicinity of the anastomosis (arrow).

preferable to minimize obstruction caused by tumor recurrence in the lesser sac.²⁶ The end of the proximal jejunal segment is then anastomosed to the more distal jejunum at least 40 to 60 cm from the gastrojejunal anastomosis. This procedure diverts duodenal contents and biliopancreatic secretions away from the stomach and prevents bile reflux into the stomach, which may help minimize bile reflux gastritis.²⁷ However, transection of the small bowel alters intestinal motility, and there may be impaired emptying of the Roux limb as a consequence. A Roux-en-Y gastrojejunostomy should ideally be performed

in the setting of a small gastric remnant to minimize marginal ulcer disease and problems with gastric stasis.

IDENTIFICATION OF POSTSURGICAL ANATOMY ON IMAGING STUDIES

The postoperative anatomy following gastroduodenostomy or gastrojejunostomy may be evaluated with UGI or CT. Procedures for distal gastrectomy should be readily identified on UGI. Along with foreshortening of the stomach caused by

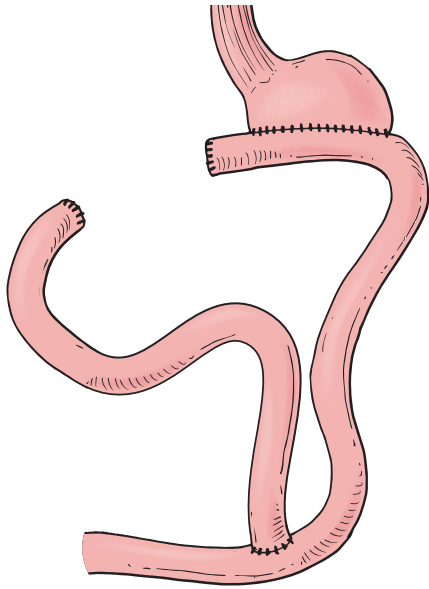


Figure 35-3 Roux-en-Y gastrojejunostomy. There is a distal gastrectomy with gastrojejunostomy. The jejunum is transected and anastomosed to the gastric remnant with an additional left midabdominal jejunostomy.

distal resection, there is absence of a normal pylorus in a gastroduodenostomy, typically with an end-to-end anastomosis (see Fig. 35-1). This may be difficult or impossible to identify on CT if the gastric remnant consists of most of the stomach, and surgical clips or sutures are not present. In the setting of a gastrojejunostomy, jejunal loops will be contiguous with the gastric remnant. On CT, a jejunal limb will be contiguous with the gastric remnant and can be followed through its antecolic or retrocolic course. Sutures or staples may be seen along the proximal duodenal stump. On UGI, the gastrojejunal anastomosis should appear widely patent (see Fig. 35-2). A portion of the cut end of the stomach may be oversewn or inverted to restrict the size of the stoma, which can produce deformity and plication defects around the margins of the anastomosis.¹⁷ Plication defects can be mistaken for leaks, ulcers, or recurrent tumor if not appreciated.⁴ Unlike a plication defect, there will be persistent contrast in a leak following passage of the bolus. The adjacent gastric folds will appear thickened and lobulated in the case of recurrent ulcer or tumor as compared with postoperative deformity. Comparison with a baseline postoperative UGI may help clarify the process. Alternatively, endoscopy may be necessary.

COMPLICATIONS AFTER GASTRIC RESECTION

Metabolic Problems

Anemia may be a consequence of gastric resection. Iron deficiency is the most common cause, but vitamin B₁₂ or folate deficiency may also occur. Contributing factors may include malabsorption, inadequate oral intake, and chronic bleeding. Iron deficiency anemia may be related to rapid passage through the proximal jejunum, with resultant decreased iron absorption. Also, decreased acid and pepsin may limit the conversion of organic iron to inorganic iron (absorbable by the GI tract).²⁸ Loss of intrinsic factor production in the stomach can lead to vitamin B₁₂ deficiency.

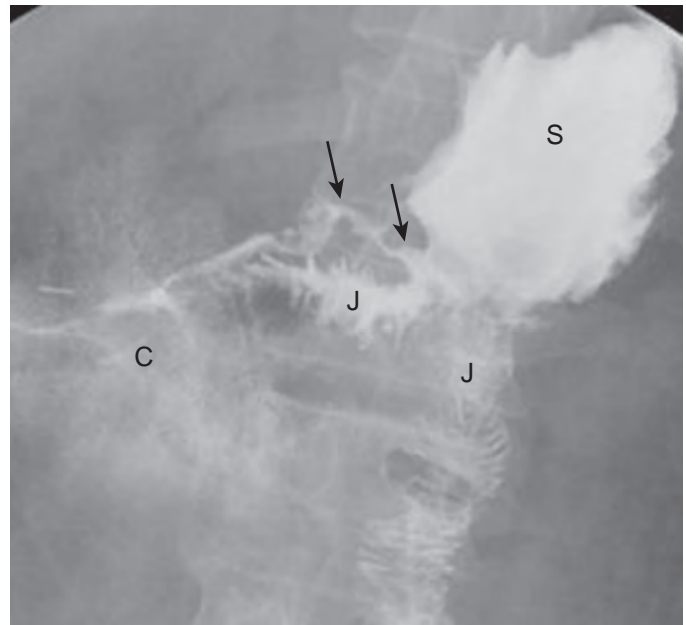


Figure 35-4 Anastomotic leak following Billroth II gastrojejunostomy. This UGI image shows Billroth II anatomy. There are thickened folds in the anastomotic region secondary to postoperative edema in this recent postoperative patient. There is extravasation of contrast material from the gastrojejunal anastomosis, with the leak (arrows) extending toward an amorphous extraluminal contrast collection (C). J, jejunum; S, stomach remnant.

Gastric surgery may also disturb calcium and vitamin D metabolism, resulting in metabolic bone disease. Calcium is absorbed in the duodenum, which is bypassed in a gastrojejunostomy. Also, fat malabsorption can occur because of bacterial overgrowth, insufficient mixing of food with digestive enzymes, or afferent loop syndrome. This can result in decreased absorption of fat-soluble vitamin D.⁸

Postoperative Leak

Anastomotic leak or breakdown of a suture line can occur at any anastomosis in up to 5% of patients.²⁹ Following a Billroth I procedure, leaks may occur at the gastroduodenal anastomosis. With a Billroth II, leaks may occur at the gastrojejunostomy or from the oversewn duodenal stump. With a Roux-en-Y reconstruction, leakage may also occur at these sites or, rarely, at the jejunojejunal anastomosis.

Water-soluble contrast should be used on UGIs if leakage is a concern. Extravasation of contrast material may be seen, with contrast opacifying a track or collection or coursing freely in the peritoneal cavity (Fig. 35-4). A fistula may be seen with contrast opacifying another structure. Any postoperative drain should be carefully evaluated because opacification of a drain may be the only manifestation of a leak on UGI. CT may be necessary to determine the extent and location of collections and abscesses more definitively and to assess for leakage from the oversewn duodenum (Fig. 35-5). Dehiscence of the duodenal stump suture line may be difficult to diagnose with imaging studies and can be a serious complication, resulting in leakage of bile and pancreatic sections into the peritoneal cavity.²⁶ The duodenal stump may be difficult to opacify in retrograde fashion (antepertaltic) on UGI. As a result, a fluoroscopic study that does not demonstrate an anastomotic leak following gastrojejunostomy does not exclude the presence of leakage,

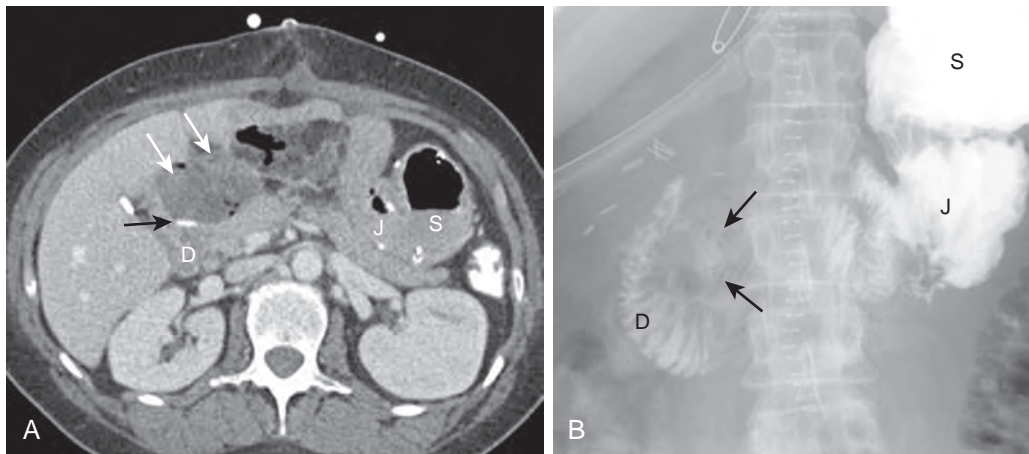


Figure 35-5 Duodenal stump leak after Billroth II. **A.** Axial contrast-enhanced CT scan shows the stomach remnant (S) anastomosed to the jejunum (J) with a clip (black arrow) in the vicinity of the oversewn duodenal stump (D). There is a fluid collection containing gas anterior to the duodenal stump (white arrows). Also note foci of adjacent extraluminal gas. **B.** Supine UGI image shows the Billroth II anatomy with a small amount of reflux in the afferent limb opacifying the duodenal stump (D). There is an amorphous collection (arrows) of contrast, confirming a duodenal stump leak.

particularly from the oversewn duodenal stump.³⁰ CT may reveal complex fluid or gas collections in the vicinity of the duodenal stump (see Fig. 35-5), in the subhepatic or peripancreatic space, or findings of peritonitis.²⁶

Gastric Stasis

Stasis in a gastric remnant can result in postprandial bloating, vomiting, abdominal pain, and weight loss. Gastric stasis occurs without evidence of mechanical intestinal obstruction or anastomotic narrowing in up to 25% of patients, depending on the type of reconstruction that was performed.³¹ Ineffective gastric emptying, impaired bowel motility, and alkaline reflux gastritis can contribute to gastric stasis.³² UGI should reveal a patent anastomosis without obstruction. Nuclear medicine studies may be of benefit to assess gastric emptying.⁵ Severe gastric stasis may require surgical revision with repositioning of the anastomosis or total gastrectomy.

Roux Syndrome

Roux syndrome, or Roux stasis syndrome, may occur following distal gastrectomy with a Roux-en-Y gastrojejunostomy. With this syndrome, patients have an atonic stomach with delayed emptying of the gastric remnant and Roux limb without evidence of obstruction.^{8,32} This represents a motility abnormality rather than a mechanical problem. Patients may present with vomiting, epigastric pain, and weight loss.

On UGI, there is dilation of the gastric remnant with delayed emptying. The efferent limb is typically dilated, without evidence of mechanical obstruction. It is important to assess the anastomosis to make sure that an anastomotic stricture is not a contributing factor. A gastric emptying nuclear medicine scan may also show delayed solid and/or liquid emptying. GI motility testing shows abnormal motility in the Roux limb, with propulsive activity toward the stomach rather than away from the stomach.⁸ Promotility medications may be beneficial.

Obstruction

Gastric outlet or small bowel obstruction can be an early or late postoperative complication following ulcer surgery. Obstruction may be caused by postoperative edema or hematoma in the

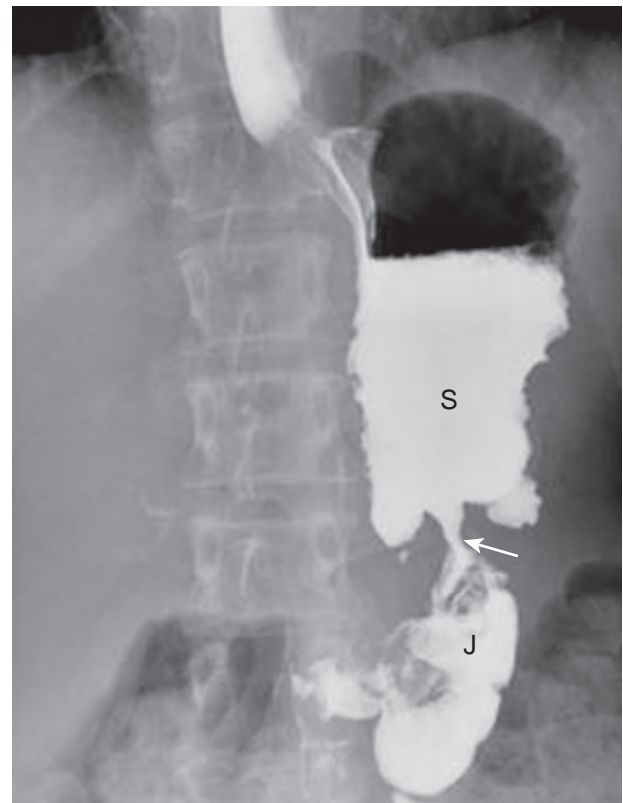


Figure 35-6 Stomal stenosis following Billroth II. This UGI image obtained with the patient drinking in the upright position shows stenosis of the gastrojejunal anastomosis (arrow). Also note the outpouchings adjacent to the anastomosis caused by postsurgical deformity and redundancy. There are no thickened, lobulated folds to suggest ulcers. J, jejunum; S, stomach remnant.

early postoperative course. In contrast, late postoperative obstruction can be caused by anastomotic strictures, with or without stomal ulcers, adhesive disease, or internal hernias.³⁰ UGI may reveal an anastomotic stricture with gastric outlet obstruction (Fig. 35-6). The patient should be positioned at

fluoroscopy so that the anastomosis is viewed in profile, without overlapping structures, to optimally assess anastomotic width and height. Endoscopic treatment and balloon dilation of strictures may be beneficial in some patients.³³

Bezoar Formation

A bezoar is a potential complication of subtotal gastrectomy. A bezoar may form in a gastric remnant as a result of decreased peristalsis and absence of gastric acid, especially when a vagotomy has been performed. Retained ingested material can coalesce to become a large masslike conglomerate. On UGI and CT, this appears as a large mottled mass within the gastric remnant. Contrast material and gas trapped within the interstices of the mass may help establish the correct diagnosis (Fig. 35-7). Also, bezoars are usually mobile, allowing for distinction from a gastric tumor. A bezoar can lead to gastric outlet obstruction and occasionally small bowel obstruction if the bezoar passes into the jejunum. Bezoars may be successfully treated endoscopically, but surgical intervention may be necessary, especially with an associated obstruction.

Dumping Syndrome

Dumping is a phenomenon caused by destruction or bypass of the pyloric sphincter (as with pyloroplasty or antrectomy) with rapid gastric emptying; however, other factors likely play a role.⁸ Patients with early dumping syndrome experience vasomotor

and cardiovascular symptoms, including tachycardia, dizziness, diaphoresis, weakness, nausea, abdominal cramping, diarrhea, and the need to lie down after eating.^{18,32,34} Postprandial symptoms may be severe and disabling. High-carbohydrate food may precipitate the worst attacks. A rapid influx of sugars into the proximal jejunum may cause a strong osmotic effect, drawing fluid into the bowel.

Crampy abdominal pain and distention are not uncommon, and diarrhea often follows. Early dumping occurs 15 to 20 minutes after a meal in 5% to 50% of patients, depending on the specific operation.³⁵ Clinically significant dumping occurs in 5% to 10% of patients after pyloroplasty or distal gastrectomy.⁸ Because of the abdominal pain associated with eating, patients tend to lose weight and become malnourished.³⁶

UGI in early dumping syndrome may reveal very rapid transit time with rapid opacification of the colon. Conservative therapy for dumping syndrome consists of dietary management; most patients improve with dietary changes over time.⁸ A somatostatin analogue may be beneficial.³⁶ Surgical management may be necessary in a small percentage of patients, but the results of surgery for dumping symptoms are variable and unpredictable.^{8,35}

Late dumping, also called postprandial (reactive) hypoglycemia, occurs 2 to 4 hours after a meal and may have similar vasomotor symptoms, but does not typically have the associated GI symptoms.³⁶ This can be alleviated by the administration of carbohydrates.⁸

Stomal and Anastomotic Ulceration

Recurrent ulcers following gastric surgery for PUD occur at or near the anastomosis, usually on the duodenal or jejunal side of the anastomosis for a Billroth I or II procedure, respectively.³⁷ In a Billroth II, the efferent loop is more commonly involved than the afferent loop.¹⁷ These ulcers are referred to as stomal, marginal, or postanastomotic ulcers; they occur primarily following inadequate gastric resection with a retained segment of antrum or because of a hypersecretory state or gastrinoma. In the setting of a Roux-en-Y gastrojejunostomy for PUD, a large gastric remnant predisposes to marginal ulcers.

UGI may reveal an ulcer crater with surrounding edema (Fig. 35-8). Stomal ulcers may be difficult to diagnose on UGI studies because of opacification of overlapping structures, and it may be difficult to distinguish barium trapping in distorted folds and plication defects from an ulcer.⁴ A baseline postoperative comparison study may be most beneficial to make this distinction. Secondary signs of ulcers may include narrowing at the anastomosis with thickened, edematous, and masslike folds. UGI findings may be less reliable compared with endoscopy,^{6,38} but contrast studies are increasingly necessary when endoscopy is limited or difficult.³⁰ If recurrent ulcers fail to respond to medical management, total gastrectomy may be necessary.

Jejunogastric Intussusception

Intussusception may occur in the vicinity of any anastomosis. Jejunogastric intussusception is a rare complication following gastrojejunostomy, with a reported incidence of 0.1%; the efferent loop intussuscepts into the stomach more often than the afferent loop.³⁹ Prolapse may occur in an antegrade or retrograde direction. Retrograde migration of the jejunal segment into the gastric remnant can be acute, chronic, or



Figure 35-7 Bezoar following Billroth I. This supine UGI image shows a gastroduodenostomy. Also note clips from a prior vagotomy (arrow). There is a conglomerate mass in the gastric remnant, with contrast in the interstices consistent with a bezoar. Gastric atony and diminished gastric drainage contribute to bezoar formation. D, duodenum.



Figure 35-8 Billroth II with a recurrent ulcer. This upright UGI image shows a gastrojejunostomy with edema in the vicinity of the anastomosis. The gastric remnant is dilated and contains a large amount of fluid and debris. There is a focal ulcer crater in the jejunum adjacent to the anastomosis (arrows) with surrounding edema and fold thickening. J, jejunum.



Figure 35-9 Jejuno-gastric intussusception following Billroth II. A right lateral UGI image shows a dilated gastric remnant with a filling defect in the gastric remnant near the gastrojejunal anastomosis caused by retrograde migration of the jejunum into the stomach. Jejunal folds are seen within the gastric remnant (arrows). J, jejunum.

intermittent and can result in partial or complete gastric outlet obstruction.^{30,40} On CT, the proximal jejunum, along with the adjacent mesenteric fat and vessels, can be seen within the lumen of the gastric remnant.⁴¹ On UGI, contrast can be seen outlining the jejunal folds within the gastric remnant, producing a coil spring appearance (Fig. 35-9). A gastrojejunal intussusception may be manifested by narrowing of the distal gastric remnant with a coil spring filling defect in the adjacent proximal jejunum.

Afferent Loop Syndrome

Following gastrojejunostomy, the afferent loop (duodenal stump containing biliopancreatic secretions) may become dilated, which can lead to abdominal pain, nausea, vomiting, postprandial fullness, and, rarely, obstructive jaundice. This has been called *afferent loop syndrome*; it occurs in less than 1% of patients.⁴ Afferent loop syndrome may be caused by blockage of this limb and may occur with adhesions, kinking or fibrosis near the anastomosis, internal hernias, or volvulus.⁴² Partial obstruction of the afferent loop results in luminal dilation with accumulation of biliary, pancreatic, and duodenal secretions. Acute complete obstruction may also occur. Afferent loop syndrome can also be due to preferential flow of ingested contents into the afferent limb (retrograde) rather than into the efferent limb.

Diagnosis of afferent loop syndrome caused by obstruction may be best made on CT. CT reveals a dilated, fluid-filled afferent loop (Fig. 35-10) and may also reveal the cause of

obstruction.^{42,43} On UGI, the obstructed afferent loop may not be opacified. The diagnosis may be inferred by the absence of opacification of the afferent limb and mass effect on the opacified efferent limb by the fluid-filled, unopacified afferent segment. However, lack of opacification of the afferent limb occurs in up to 20% of all patients following gastrojejunostomy, so lack of opacification by itself is not a reliable indicator of afferent loop syndrome.⁴⁴ Afferent loop syndrome can also be due to preferential flow of ingested contents into a dilated afferent limb rather than the efferent limb, and this can be readily identified with UGI (see Fig. 35-10C). In afferent loop syndrome, hepatobiliary scintigraphy reveals retention in the dilated biliopancreatic segment.

Bile Reflux Gastritis, Chronic Remnant Gastritis

A common complication following gastric surgery is chronic gastritis. Bile reflux gastritis occurs in 5% to 15% of patients following partial gastrectomy.^{36,45} Without an intact pylorus, chronic reflux of bile and pancreatic secretions into the gastric remnant can result in inflammatory change in the residual stomach. Following resection of the pylorus, most patients have bile in the stomach, with some degree of inflammation on endoscopic examination, and therefore many patients remain asymptomatic in the setting of bile reflux.⁸ However, a subset of patients will have bile reflux gastritis and present with nausea, bilious vomiting, and epigastric pain, possibly with excessive enterogastric reflux.⁸ There does not appear to

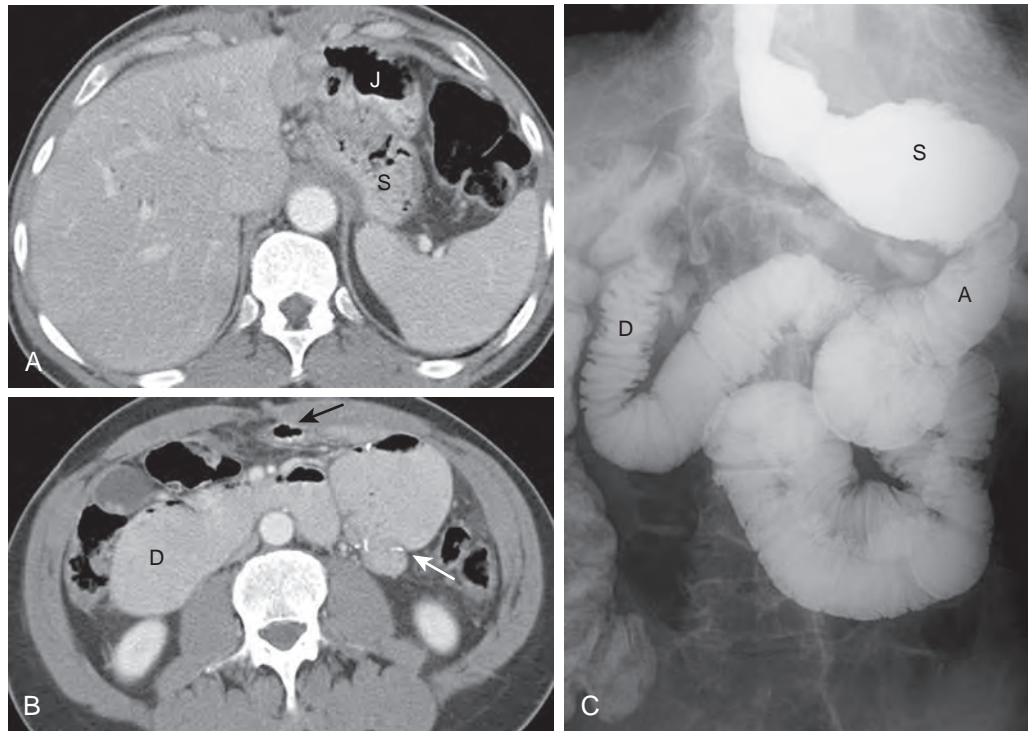


Figure 35-10 Afferent loop syndrome following Roux-en-Y gastrojejunostomy. **A, B.** Axial-contrast enhanced CT images **A.** A small gastric remnant (S) is anastomosed to a jejunal Roux limb (J). **B.** There is a small bowel anastomosis in the left midabdomen (white arrow). The afferent limb is markedly dilated and fluid-filled, with distention of the duodenum (D). The efferent jejunal limb is decompressed (black arrow). **C.** Overhead radiograph following UGI shows a dilated gastric remnant (S) with reflux into the esophagus. There is preferential filling of a dilated afferent limb (A) and duodenum (D). Note contrast in the right colon from a prior study.

be a strong correlation between the degree of inflammation and the degree of symptoms. The onset of pain is not associated with meals. The differential diagnosis may include afferent loop syndrome, obstruction, and gastric stasis, and UGI may help establish the diagnosis. UGI may reveal thickened gastric folds without associated obstruction (Fig. 35-11). Ulcers may or may not be present in the perianastomotic region of the gastric remnant.⁴

Conversion to Roux-en-Y gastrojejunostomy with at least 45 cm of isoperistaltic jejunal loop between the gastric remnant and duodenum may help alleviate bile reflux gastritis by diverting bile and pancreatic secretions away from the gastric remnant.^{8,32}

Neoplasms After Surgery for Benign Ulcer Disease

Following partial gastrectomy for benign disorders, especially PUD, there is an increased risk of gastric remnant neoplasms.^{30,46} This occurs in the late postoperative course, with a 15- to 20-year latent period, at which point the relative risk increases twofold to fourfold.⁴⁷ Malignant tumors most likely develop as a result of gradual progression from normal mucosa to intestinal metaplasia to dysplasia, and, subsequently, to cancer over time, presumably as a consequence of prolonged achlorhydria and chronic enterogastric reflux of bile and pancreatic secretions.⁴⁸ Truncal vagotomy reduces gastric acid and may contribute to this process. Stump tumors involve the distal gastric remnant at or near the anastomosis.⁴⁶ On UGI, stump tumors appear as infiltrating, plaquelike, polypoid, or ulcerative lesions in the gastric remnant near the anastomosis.

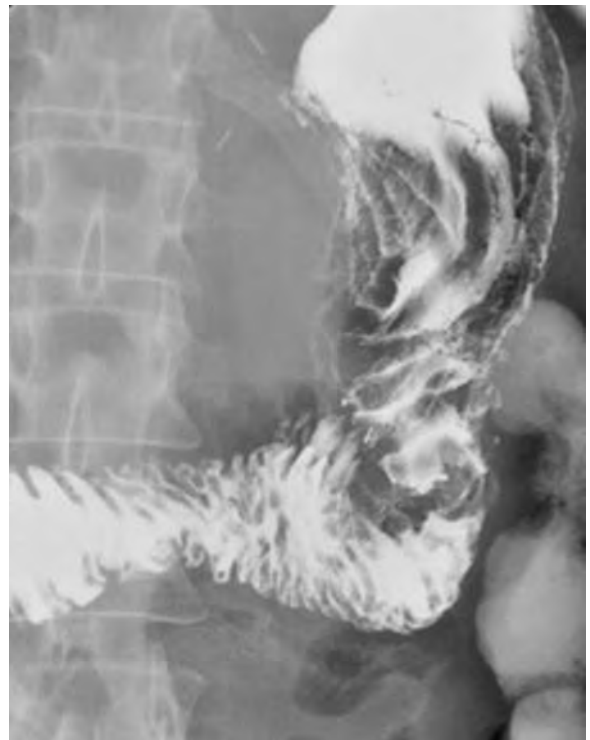


Figure 35-11 Bile reflux gastritis following Billroth II. A supine double-contrast UGI image shows distal gastrectomy with gastrojejunostomy. There are thickening and lobulated folds in the gastric remnant caused by bile reflux gastritis.

Surgical Considerations for Gastric and Duodenal Neoplasms

Gastric and duodenal neoplasms are discussed in detail elsewhere in this textbook. Neoplasms of the stomach and duodenum require resection, with the extent and location of resection dependent on the benign or malignant nature of the lesion, lesion location, extent of disease, and underlying physiologic status of the patient.

SURGERY FOR GASTRIC MASSES

The goal of surgical treatment for gastric tumor is to remove the grossly visible tumor completely and obtain histologically free surgical margins. The extent of the procedure depends on the degree of tumor infiltration in and through the gastric wall, extension into adjacent organs, and lymph node involvement. Upper endoscopy and endoscopic ultrasound (EUS) can be useful to determine the location and extent of disease spread within the gastric wall.⁹ It is essential to properly stage any patient who is being considered for subtotal gastrectomy for cancer prior to operative intervention. For example, when a total gastrectomy is planned, the proximal extent of disease should be determined preoperatively to determine whether a distal esophagectomy is also necessary.

There are several different surgical procedures that may be performed to treat gastric masses. The size and location of the tumor, in conjunction with the surgeon's experience and preference, help determine the exact surgical procedure performed. Malignant gastric lesions usually require distal or total gastrectomy.⁴⁹ Surgical procedures for gastric cancer may include a Billroth II, Roux-en-Y gastrojejunostomy, Roux-en-Y esophagojejunostomy, or primary esophagogastric anastomosis. Omentectomy and/or splenectomy may be performed simultaneously, if necessary.

The location of the primary tumor determines the type of resection performed.⁵⁰ For a lesion located in the mid to distal stomach, particularly along the greater curvature, subtotal gastric resection may be performed, ideally with margins of 5 to 6 cm around the lesion. A gastroenterostomy is performed to restore continuity of the GI tract. The need for wide margins usually requires a gastrojejunostomy rather than gastroduodenostomy, and a Billroth I is not typically performed for malignant disease. Gastrojejunostomy may be a loop-type or Roux-en-Y configuration.

Larger and more proximal tumors may require total gastrectomy with an esophagojejunal anastomosis, typically a Roux-en-Y esophagojejunostomy. The distal esophagus may also be resected with a more cephalad esophagojejunal anastomosis.⁹ For lesions in the proximal stomach, particularly within 5 cm of the gastroesophageal junction, proximal gastric resection may be possible with a primary esophagogastric anastomosis. However, proximal subtotal gastrectomy with esophagogastric anastomosis is not commonly performed because of problems with gastroesophageal reflux, and the anastomosis between the esophagus and distal stomach may be less secure, resulting in an increased risk of anastomotic leaks. Total gastrectomy with esophagojejunostomy may be preferable. However, anastomotic leaks are of particular concern following esophagojejunostomy, occurring in up to 12% of patients and with a mortality of approximately 33% (Fig. 35-12).⁵¹

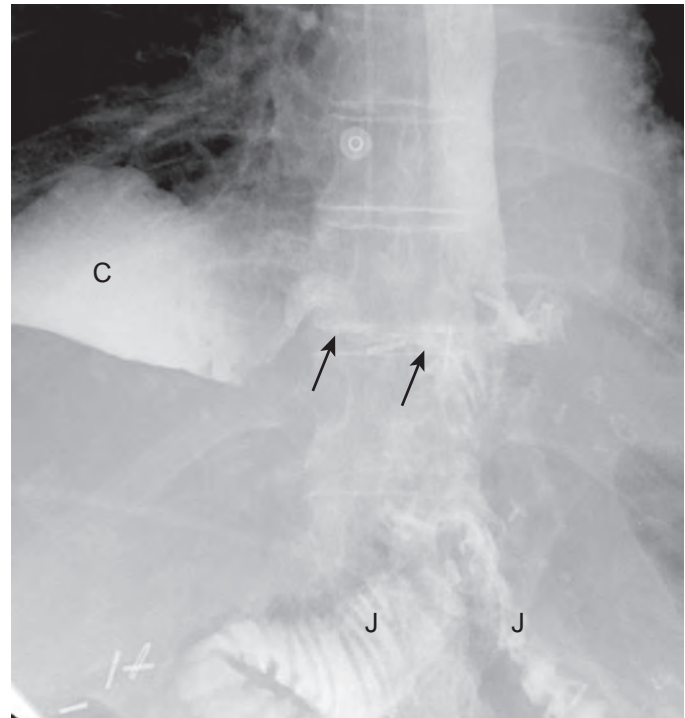


Figure 35-12 Leak following total gastrectomy and esophagojejunostomy. A supine UGI image using water-soluble contrasts shows a Roux-en-Y esophagojejunostomy. There is a leak (arrows) from the anastomotic area with contrast opacifying a large collection (C) in the right upper abdomen. J, jejunum.

SURGERY FOR DUODENAL MASSES

Resection of duodenal malignancies typically requires pancreaticoduodenectomy. This entails reanastomosis of the GI tract, bile duct, and pancreatic remnant. Distal gastrectomy may be performed with a gastrojejunostomy. Alternatively, the stomach and pylorus may be preserved with an end-to-side proximal duodenojejunostomy just distal to the pylorus, also known as a pyloric-sparing Whipple procedure. The bile duct and residual pancreas may be anastomosed separately to the jejunum with a pancreaticojejunostomy and choledochojejunostomy.

COMPLICATIONS FOLLOWING GASTRIC AND DUODENAL SURGERY FOR NEOPLASM

In general, perioperative and postoperative morbidity is relatively common following surgery for gastric cancer. Resections may be extensive, and patients tend to be relatively debilitated. The complications of diarrhea, dumping syndrome, malnutrition, and weight loss increase postoperative difficulties. Following gastric resection and with denervation of the stomach, there may be alterations to intestinal motility, absorption, and biliary kinetics.

A variety of physiologic and metabolic problems may arise, and these problems may be increased with a larger gastric resection.³⁰ Chronic nutritional problems can be serious, outweighing other complications and concerns. Potential metabolic problems following gastrectomy include iron or vitamin B₁₂ deficiency, anemia, malnutrition, weight loss, and bone disease (e.g., osteomalacia, osteoporosis). Anemia may occur following

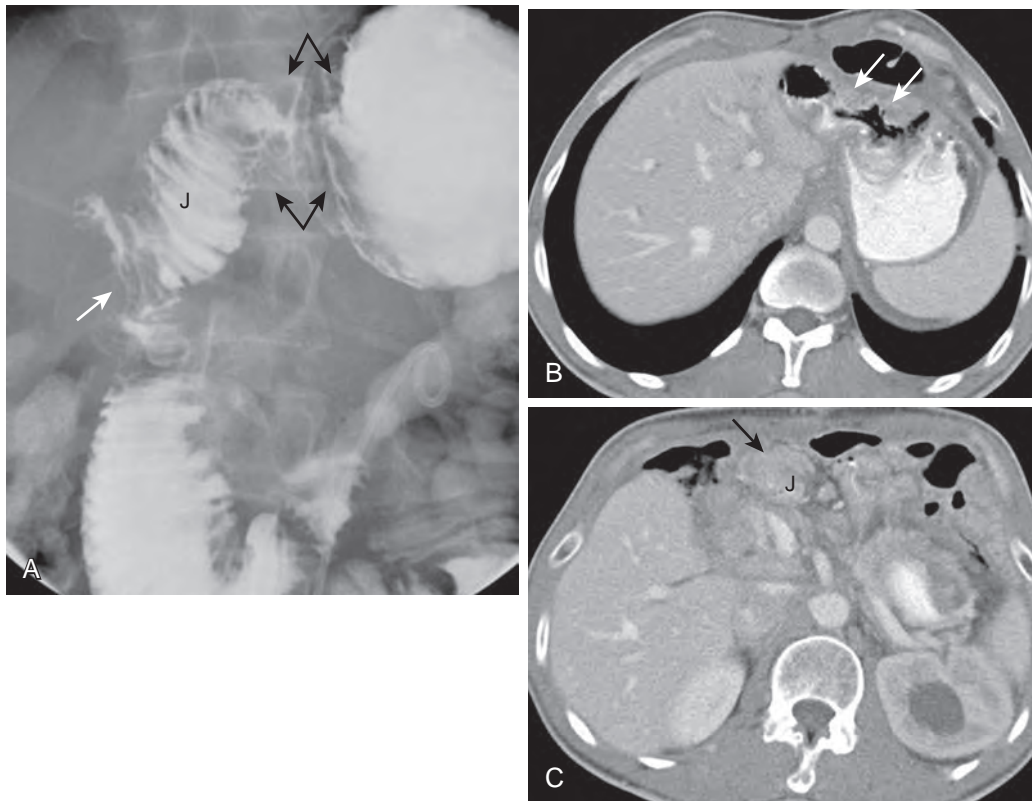


Figure 35-13 Recurrent tumor following distal gastrectomy for gastric cancer. **A.** Supine UGI image shows thickened, lobulated folds along the distal gastric remnant and gastrojejunal anastomosis (*black arrows*). There are also tumor implants (*white arrow*) along the jejunal limb (J). **B, C.** Axial contrast-enhanced CT scans show lobulated soft tissue along the distal gastric remnant (*white arrows*) caused by tumor recurrence. Also note a tumor implant (*black arrow*) along the jejunal limb (J).

gastric surgery because of malabsorption, inadequate oral intake, and/or chronic blood loss. If a partial pancreatic resection has been performed, there may also be a deficiency of digestive enzymes, resulting in malabsorption.

Gastric resection for neoplasm can result in many of the same complications as gastric resection for PUD, including leaks, obstruction, stomal ulcers, and other mechanical problems. In addition to the many benign causes of obstruction that are seen following surgery for PUD, obstruction following surgery for gastric or duodenal neoplasm can be caused by local tumor recurrence, metastatic nodal masses, or peritoneal carcinomatosis.⁴²

Recurrent Carcinoma

Patients who have undergone partial gastrectomy for gastric cancer are at continued risk of developing tumor recurrence. Recurrence in the surgical bed can be in the form of local bowel tumor recurrence, regional adenopathy, or tumor implants from carcinomatosis.

On UGI following partial gastrectomy for a localized gastric carcinoma, tumor recurrence may appear infiltrating, plaque-like, polypoid, and/or ulcerative. There may be narrowing and decreased distensibility of the gastric remnant, with straightened and irregular contours.⁴ Comparison with a baseline postoperative study may be helpful for differentiating recurrent tumor from postsurgical plication defects and suture-related changes. There may be mass effect on the bowel, with spiculated, tethered folds caused by tumor implants (*Fig. 35-13*).

CT may detect local tumor recurrence, regional adenopathy, and tumor implants. Recurrent tumor at the anastomosis may be manifested by focal irregular bowel wall thickening, often with soft tissue density in the bowel wall (see *Fig. 35-13*). CT can also readily identify distant nodal metastases and hematogenous metastases to solid organs and osseous structures.²⁶

Surgery for Weight Loss

Obesity is an epidemic in the United States and the Western world that has had an increasing impact on radiology. Obesity is typically defined in terms of body mass index (BMI), which provides a standard definition for national surveillance and takes into account patient weight and height. BMI is expressed as kg/m^2 . Overweight is defined as a BMI of greater than 25 kg/m^2 , obese as greater than 30 kg/m^2 , morbidly obese as greater than 40 kg/m^2 , and superobese as greater than 50 kg/m^2 .^{52,53} Weight concerns have been increasingly prevalent in the United States. There has been a 74% increase in obesity between 1991 and 2001 and, from 1960 to 2000, the prevalence of obesity has more than doubled and the prevalence of morbid obesity has quadrupled.⁵³⁻⁵⁵ Currently, more than 65% of U.S. adults are considered overweight or obese, with more than 30% of the population considered obese and 5% to 7% considered morbidly obese.^{53,56}

Bariatric surgery is a successful treatment option for morbid obesity with regard to long-term weight loss, decreased morbidity, and improved life expectancy.^{55,57,58} Bariatric procedures

have increased by more than 800% in the United States between 1998 and 2004, and more than 220,000 procedures are performed annually.^{54,59} Bariatric surgery is typically reserved for patients who fail to lose weight with conservative measures, including diet, exercise, and behavior modification. Surgical techniques for weight loss include malabsorptive, restrictive, or combination (restrictive and malabsorptive) procedures.

Malabsorptive procedures bypass a segment of small bowel to decrease the length of the absorptive surface. The classic malabsorptive procedure is the jejunioileal bypass.

Restrictive procedures combine a small gastric pouch with a narrow outlet to induce early and prolonged satiety. A small gastric pouch is created to limit food intake and create early satiety. This is combined with a narrow outlet or stoma to delay emptying and prolong satiety. Examples of restrictive procedures include laparoscopic adjustable gastric banding, horizontal and vertical gastropasty, and sleeve gastrectomy.

Combination procedures use both restrictive (small gastric pouch, narrow outlet) and malabsorptive (bypass of a small bowel segment) components. These include the Roux-en-Y gastric bypass and biliopancreatic diversion.

The original bariatric procedure was a malabsorptive procedure, known as the jejunioileal bypass. This was developed in the 1950s and involved joining the proximal small intestine to the distal small intestine, bypassing a large segment of small bowel. The stomach and duodenum were left intact. This procedure resulted in successful weight loss, but was associated with significant complications from malabsorption. Malabsorption can cause mineral and electrolyte imbalances, vitamin depletion, protein calorie malnutrition, anemia, and peripheral neuropathy. The jejunioileal bypass resulted in liver disease in up to 30% of patients, liver failure in up to 10% of patients, and renal failure in up to 37% of patients. This procedure is no longer performed because of the severity of complications.⁶⁰

Subsequently, restrictive bariatric procedures were developed. Restrictive procedures have been a popular treatment option for bariatric surgeons and include gastropasties, gastric band placements, and sleeve gastrectomies. Gastropasty is a purely restrictive procedure in which a small gastric pouch is created with a narrow stoma to communicate with the remainder of the stomach. The remainder of the GI tract is left intact. In a horizontal gastropasty, there is a staple line along the proximal stomach, with a central or greater curvature stoma. This procedure had limited long-term success because of gastric wall stretching, with pouch and stomal enlargement. There were also problems with frequent staple line disruptions. Following initial success, many patients stopped losing weight or actually gained weight.

The vertical banded gastropasty (VBG) creates a small gastric pouch along the proximal lesser curvature of the stomach, with a vertical staple line along the proximal stomach. The lesser curvature of the stomach is thicker and stretches less as compared with the greater curvature. A polypropylene band is placed around the stoma to prevent stretching. Circular staples create a window for the band, and identification of the circular staples on a radiograph indicates that a VBG was performed. VBG has resulted in adequate weight loss and remains popular outside the United States. However, VBG requires patient compliance and will fail with maladaptive eating. Complications include pouch dilation, stomal stenosis, staple line dehiscence, gastroesophageal reflux, and vomiting. In the

United States, the VBG has been replaced by other bariatric procedures.

Currently, the most common bariatric procedures performed in the United States are the Roux-en-Y gastric bypass, laparoscopic adjustable gastric banding, and the gastric sleeve procedure (sleeve gastrectomy). Certain challenges may arise when imaging bariatric patients because of body habitus, specifically with regard to patient weight and abdominal girth. Imaging equipment capacity may be a concern, and procedural modifications are often necessary for radiography, UGI, and CT studies in this setting.^{54,59}

ROUX-EN-Y GASTRIC BYPASS

The Roux-en-Y gastric bypass (RYGB) is a proven bariatric procedure with the highest long-term success rates and the most sustained weight loss compared with other bariatric procedures.^{55,57,58,61,62} RYGB has been the most common bariatric procedure performed in the United States in recent years.⁶³

RYGB is a combined procedure that is predominately restrictive, but also has a malabsorptive component. In this procedure, a small gastric pouch is created to exclude the remainder of the stomach and duodenum (biliopancreatic limb) from the path of food. A jejunal Roux limb is brought up to the gastric pouch in antecolic or retrocolic fashion (retrocolic through a defect in the transverse mesocolon). A narrow gastrojejunal anastomosis or stoma is created between the gastric pouch and Roux limb. The small gastric pouch and narrow stoma comprise the restrictive component of the procedure (Fig. 35-14A). The length of the bypassed small bowel can be varied to increase or decrease the amount of the malabsorptive component. The Roux limb typically has a short, oversewn or blind-ending component and an antegrade-flowing component or alimentary limb (because of an end-to-side anastomosis). The alimentary limb is anastomosed downstream to the biliopancreatic limb with a side-to-side jejunojejunal (JJ) anastomosis, usually in the left midabdomen. This procedure therefore creates an alimentary limb, biliopancreatic or excluded limb, and distal common channel downstream from the JJ anastomosis (see Fig. 35-14A).

Assessing Postoperative Complications

Despite the success of RYGB, many complications can occur. Knowledge of the expected postsurgical anatomy is essential to assess for postoperative complications following RYGB.

Upper Gastrointestinal Examination. Following RYGB, a UGI may be performed early postoperatively to assess for complications, including leak or obstruction. In the late postoperative course, patients may undergo evaluation because of epigastric pain, dysphagia, failed weight loss, excessive weight loss, or symptoms of obstruction. As with patients following gastric or duodenal surgery for PUD or neoplasm, in the early postoperative course, water-soluble contrast should be administered initially to assess for leakage. If no leak is seen with water-soluble contrast, barium may be administered. In the late postoperative course, barium may be administered initially.

Initial fluoroscopic evaluation should be performed with the patient in the left posterior oblique (LPO) position. This is the ideal position to assess the proximal postsurgical anatomy, including the gastrojejunal (GJ) anastomosis. Rapid sequence imaging may help acquire images with optimal distention of the

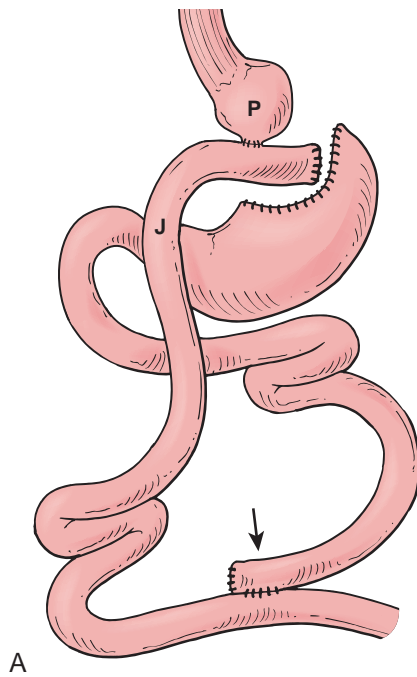
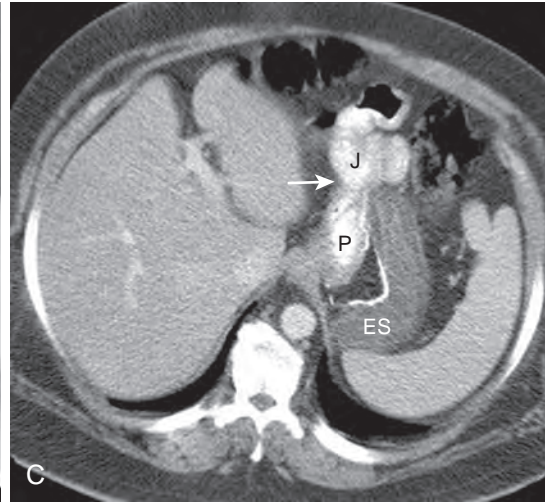
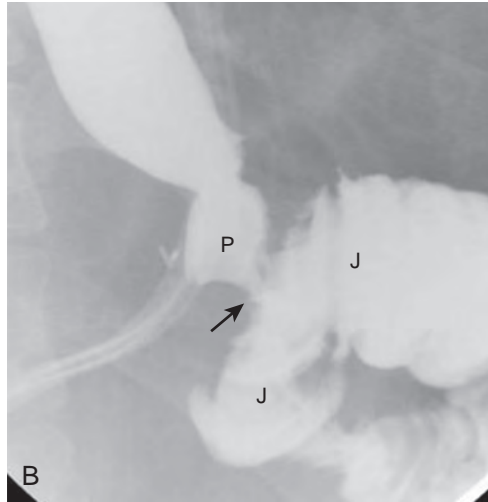


Figure 35-14 Roux-en-Y Gastric Bypass **A.** RYGB anatomy. A small gastric pouch (P) is created to exclude the remainder of the stomach and the duodenum from the path of food. There is a gastrojejunostomy with a jejunal Roux limb (J) anastomosed to the pouch via a narrow stoma and a more downstream jejunojejunostomy (arrow). This creates an alimentary limb (pouch, Roux limb), biliopancreatic limb (including the excluded stomach and duodenum), and downstream common channel. **B.** UGI image in the LPO position shows a small gastric pouch (P) with a narrow anastomosis (arrow) to the jejunal Roux limb (J). Note the surgical drain. **C.** Axial contrast-enhanced CT scan with oral and IV contrast shows an opacified small gastric pouch (P) anastomosed (arrow) to the jejunal Roux limb (J). There is a small amount of fluid in the excluded stomach (ES).



pouch, stoma, and adjacent Roux limb (Fig. 35-14B). Additional fluoroscopic views may be obtained as necessary. Overhead radiographs should be obtained serially until contrast passes the JJ anastomosis in the early postoperative course, because leak or obstruction may rarely occur at this site. In the late postoperative course, the study should be continued until the terminal ileum is opacified because complications of obstruction or internal hernia may not become apparent until the terminal ileum is opacified.

Computed Tomography. RYGB patients are ideally imaged following administration of positive oral contrast and IV contrast. Positive oral contrast administered just prior to the study should opacify the gastric pouch and alimentary limb. This should help distinguish the alimentary limb from the excluded biliopancreatic limb (Fig. 35-14C). Again, water-soluble contrast is administered in the early postoperative course or if perforation is a concern. On CT, the gastric pouch, GJ anastomosis, Roux limb, excluded stomach, biliopancreatic limb, and JJ anastomosis

should be visualized and evaluated. The JJ anastomosis is usually found in the left midabdomen.

Complications

Extraluminal Leak. The most common serious complication in the early postoperative course following RYGB is a postoperative leak, occurring in up to 6% of patients and usually diagnosed within 10 days of surgery.^{61,62,64} Postoperative leaks are associated with increased postoperative morbidity and mortality, and additional surgery may be required in up to 80% of patients.⁶⁴ To decrease morbidity following a leak, early diagnosis and treatment are essential.

On UGI following RYGB, leakage usually extends to the left of the GJ anastomosis into the left upper quadrant of the abdomen.^{64,65} The majority of leaks (more than 75%) arise from the GJ anastomosis. Leaks may also arise from the distal esophagus, gastric pouch, blind-ending jejunal limb and, rarely, the JJ anastomosis.⁶⁴ A UGI can demonstrate the origin and extent of leak with opacification of an extraluminal collection or tract,

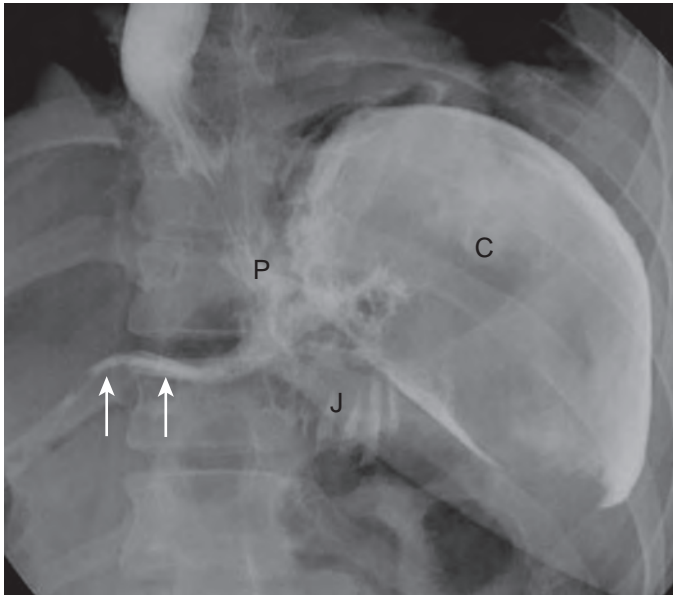


Figure 35-15 Leak following RYGB. A supine UGI image shows an edematous gastric pouch (P) and jejunal limb (J). There is as large leak from the gastrojejunal anastomosis opacifying a large left upper quadrant collection (C) as well as the surgical drain (arrows).

usually in the left upper quadrant (Fig. 35-15). On occasion, the sole manifestation of leak may be contrast opacification of an indwelling surgical draining. This may be best identified on a postprocedural radiograph.

It is important to assess for leakage at the outset of the fluoroscopic study. Later on during the procedure, the excluded stomach may become opacified via retrograde flow. This can appear as a collection of contrast in the left upper quadrant of the abdomen. The intragastric location may be confirmed by rotating the patient to the right to opacify the more distal excluded stomach and duodenum.⁶⁵ An anastomotic leak must also be distinguished from a postsurgical plication defect on UGI. A plication defect is a focal outpouching along the suture line that will readily fill and empty with contrast material during the study and will have well-defined margins. A leak typically appears more ill-defined, with stasis of contrast.

Communication with the Excluded Stomach. During the RYGB procedure, the gastric pouch is separated from the remainder of the stomach by a staple line or by complete transection. Staple line dehiscence or disruption allows communication between the gastric pouch and remainder of the stomach. This may be caused by overdistention of the pouch with food or inadequate initial surgical division. In the case of complete transection, communication with the excluded stomach can occur via a gastrogastic fistula. Overall, communication between the pouch and excluded stomach occurs in up to 4% of patients, and this complication allows ingested material to enter the excluded stomach. As a result, there may be inadequate weight loss or actual weight gain, and elective surgical revision may be necessary for a more optimal clinical outcome.⁶⁶

In the acute postoperative course, leakage into the excluded stomach may be a consequence of a free leak. An early postoperative leak into the excluded stomach is associated with

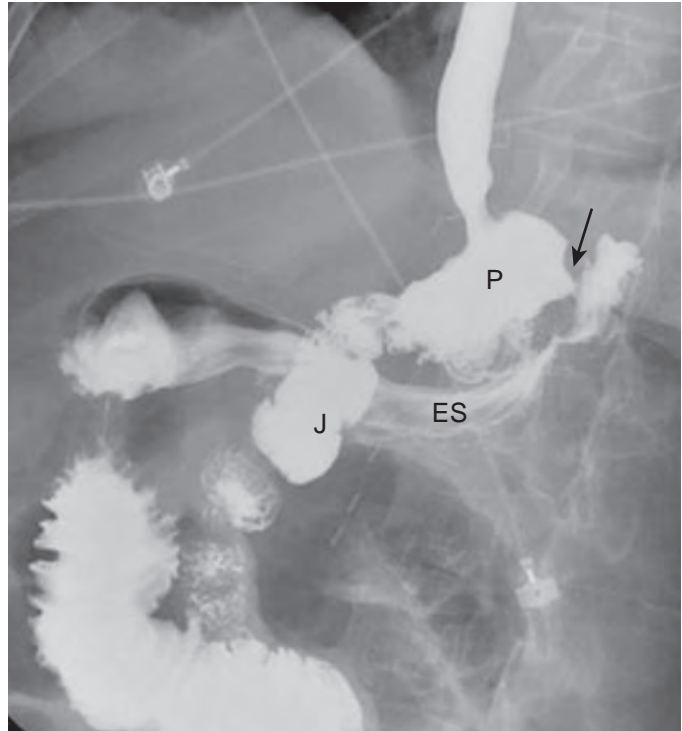


Figure 35-16 Staple line dehiscence following RYGB. A right lateral UGI image shows opacification of the gastric pouch (P) and the jejunal limb (J) following RYGB. Contrast material is also seen crossing the gastric staple line (arrow) to opacify the excluded stomach (ES).

an extraluminal leak in as many as 88% of patients.⁶⁶ In the remote postoperative course, communication with the excluded stomach will usually result in failure of the procedure, with failure of weight loss or recurrent weight gain in up to 61% of patients.⁶⁶

On UGI, the gastric pouch will be opacified along with the excluded stomach, with contrast crossing the gastric staple line (Fig. 35-16) or entering the excluded stomach via a gastrogastic fistula. Depending on the significance of the communication, contrast may preferentially enter the excluded stomach or jejunal Roux limb. This diagnosis should be made at initial fluoroscopy, because later on during the study contrast may enter the excluded stomach via retrograde flow. In the early postoperative course, it also is important to assess for an associated free leak.

Communication between the gastric pouch and excluded stomach may be difficult to diagnose accurately on CT. It may not be possible to distinguish contrast material in the excluded stomach because of staple line dehiscence from retrograde flow. The presence of contrast material in the excluded stomach but not in the duodenum on CT may suggest communication with the excluded stomach; however, UGI may be necessary for a more definitive diagnosis.⁶⁶

Marginal Ulcers. Marginal ulcers following RYGB occur near the GJ anastomosis in up to 3% of patients because of exposure of the jejunal mucosa to gastric secretions.⁶⁷ On UGI, a marginal ulcer appears as a focal outpouching near the GJ anastomosis, with stasis of contrast material in the crater and associated fold thickening and edema. Marginal ulcers decrease in

incidence with smaller pouch size and tend to respond well to medical management. Occasionally however, surgical treatment may be required.

Obstruction

Acute Obstruction. Obstruction in the early postoperative course is most often caused by postoperative edema and/or hematoma, typically involving the GJ or JJ anastomosis. In addition, in the setting of a retrocolic Roux limb, edema or a hematoma may occur where the Roux limb crosses the transverse mesocolon. Narrowing in any of these locations can cause obstruction.

Acute obstruction caused by edema or a hematoma usually resolves spontaneously with delayed initiation of diet. However, significant narrowing of the JJ anastomosis may require surgical intervention. Edema at the JJ anastomosis can result in acute distention of the excluded stomach. This can exert pressure on the gastric staple line and result in perforation if not promptly treated. Acute gastric distention may be temporarily relieved by percutaneous gastrostomy catheter placement until the edema resolves.

Late Obstruction. Small bowel obstruction following RYGB occurs in approximately 5% of patients, with a similar incidence following open and laparoscopic technique.^{68,69} Obstruction in the late postoperative course may be caused by adhesive disease, internal hernias, stomal stenosis, abdominal wall hernias, and, rarely, intussusception.⁶⁸ Following open surgery, adhesions are the usual cause of obstruction. Alternatively, after laparoscopic RYGB, internal hernias are a more common cause. Presumably, a lack of adhesions following laparoscopic surgery allows for increased bowel mobility and an increased potential for internal hernias.^{68,70,71}

Patterns of Small Bowel Obstruction. Because of the alterations made to the GI tract following RYGB, there are three patterns of obstruction that can occur relative to the JJ anastomosis. The pattern of obstruction can be classified according to an ABC taxonomic system.^{65,72}

Type A obstruction occurs with dilation of the alimentary limb only. The biliopancreatic limb is decompressed. This should be readily diagnosed on UGI with a dilated Roux limb extending toward the JJ anastomosis (Fig. 35-17). On CT, the diagnosis may be difficult because the excluded stomach and duodenum will be decompressed, and identification of the RYGB anatomy and dilated Roux limb are necessary to make the diagnosis.

In type B obstruction, there is dilation of the biliopancreatic, or excluded, limb only. On UGI, diagnosis may be difficult because the biliopancreatic limb is not routinely opacified. It may be possible to infer the diagnosis from displacement of the Roux limb by a fluid-filled, dilated biliopancreatic limb. On CT, the excluded stomach and duodenum will be dilated and fluid-filled, but it is essential to recognize the RYGB anatomy and identify a decompressed Roux limb to make this diagnosis. This represents a type of closed loop obstruction, with no natural means to decompress the excluded stomach. Percutaneous gastric decompression may therefore be necessary to alleviate the pressure and prevent perforation and additional complications.

In type C obstruction, there is obstruction at the level of the common channel, with dilated alimentary and biliopancreatic limbs (via retrograde flow; Fig. 35-18).

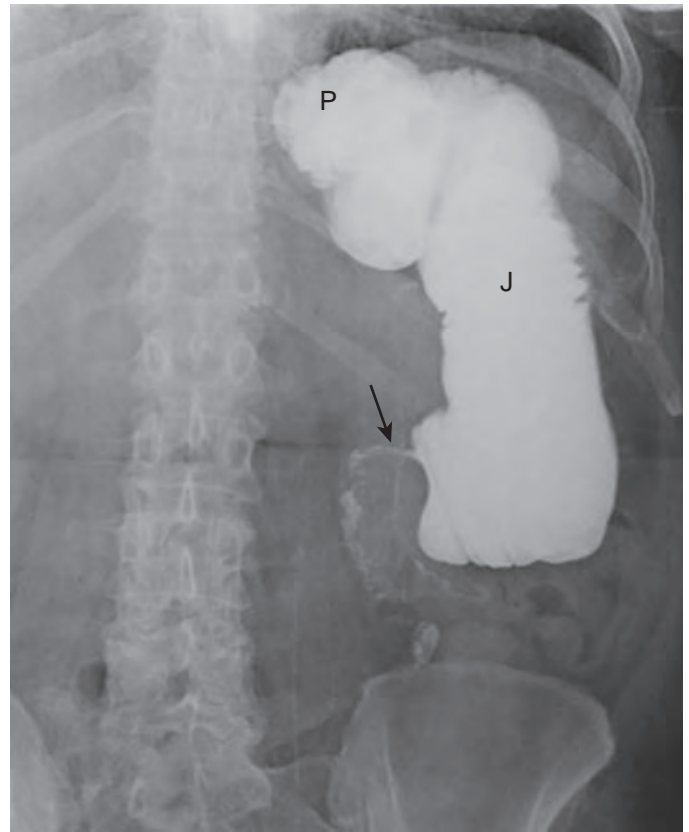


Figure 35-17 Obstruction of the alimentary limb following RYGB caused by JJ stomal stenosis. An overhead radiograph from UGI shows a dilated gastric pouch (P) and jejunal Roux limb (J) (alimentary limb) extending toward an abrupt transition at the JJ anastomosis (arrow) caused by stomal stenosis and fibrosis.

Internal Hernia. Internal hernia (IH) occurs in approximately 3% of RYGB patients and is more common following laparoscopic than open surgery.^{61,67,73} This is considered a late postoperative complication; however, IH can occur at any time following RYGB and can occur on multiple occasions.

With an IH, bowel herniates through a mesenteric defect, usually a surgically created defect. The most common defects following RYGB include a defect in the transverse mesocolon for a retrocolic Roux limb, mesenteric defect for the JJ anastomosis, and defect posterior to the Roux limb (Petersen's defect).^{67,71,73,74} IH can result in obstruction, ischemia, infarction, and bowel perforation and can be a life-threatening complication of RYGB, especially if diagnosis and treatment are delayed. However, the diagnosis of IH can be problematic clinically and with imaging studies. Symptoms may be nonspecific or intermittent, and a high index of suspicion is necessary. On UGI and CT, knowledge of the postoperative anatomy and changes to the expected course of the bowel are essential to make the diagnosis.⁷³

UGI findings of IH may include an abnormal bowel configuration with clustered, displaced small bowel loops. Clustered small bowel is usually found in the left abdomen (90%), but clustered small bowel can be located anywhere in the abdomen and pelvis (Fig. 35-19). Clustered bowel may be seen displacing other bowel. A small bowel limb may be seen entering and exiting the clustered segment, and stasis of contrast tends to

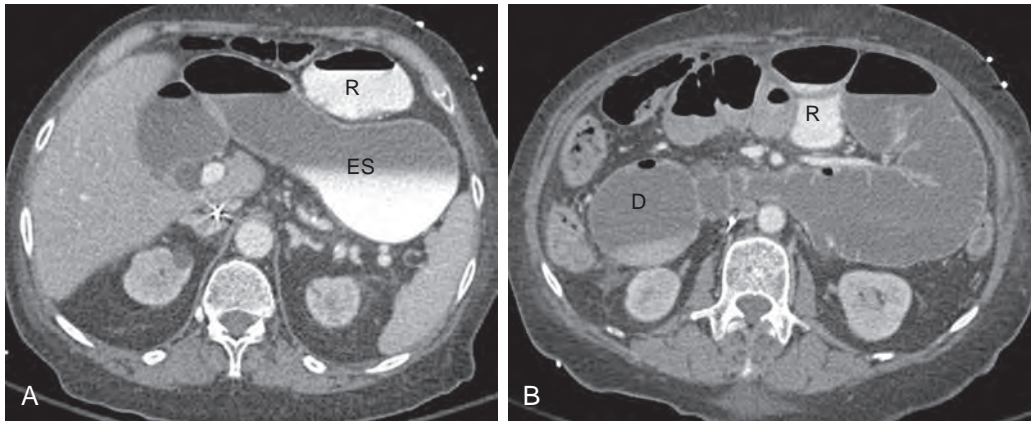


Figure 35-18 Small bowel obstruction following RYGB with obstruction of the common channel. A, B. Axial CT images following positive oral and IV contrast show marked dilation of the excluded stomach (ES) and duodenum (D) as well as the opacified Roux limb (R) caused by downstream obstruction of the common channel. Also note that oral contrast is present in the excluded stomach but not the duodenum because of staple line dehiscence more cephalad (not shown).

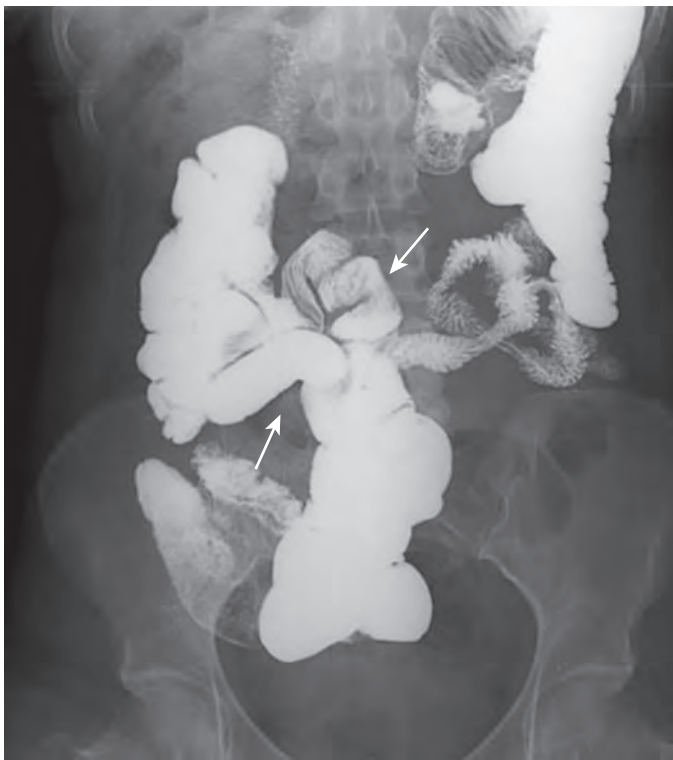


Figure 35-19 Internal hernia following RYGB. An overhead radiograph during UGI with small bowel follow-through on an RYGB patient shows an atypical bowel configuration, with clustered, displaced small bowel loops in the right midabdomen. A small bowel limb can be seen entering and exiting the clustered segment (arrows).

occur in clustered bowel.⁷³ A change in bowel configuration as compared with a prior study may be seen with displacement of a JJ suture line, usually into the left upper quadrant.⁷³

CT in the setting of internal hernia will also show clustered small bowel in an atypical location (Fig. 35-20). Associated mesenteric findings can be identified, including swirling and stretching of the mesenteric vessels. Findings of IH on CT include small bowel in the left upper quadrant above the transverse mesocolon, cephalad displacement of the JJ anastomosis,

clustered blood vessels in the left upper quadrant, and a swirling appearance of mesenteric fat or vessels.^{75,76} Comparison with a prior postoperative study is helpful to identify a change in the bowel configuration.

Stomal Stenosis. Stomal stenosis may occur at the GJ or JJ anastomosis, typically in the late postoperative course. GJ stomal stenosis occurs in up to 10% of patients, results in a dilated gastric pouch and esophagus with delayed emptying, and tends to respond well to endoscopic dilation. JJ stomal stenosis is less common, occurring in less than 1% of patients, but is less often successfully treated with endoscopic dilation and may require surgical revision (see Fig. 35-17).^{65,77}

Abdominal Wall Hernias. Abdominal wall hernias are much less common following laparoscopic RYGB as compared with open technique, but can occur at any incision or port site and can cause obstruction. Obstruction is more commonly caused by hernias with a small neck as compared with larger hernias.^{61,65}

Intussusception. Intussusception following RYGB is usually associated with the JJ anastomosis. The suture line may in some way act as a lead point. Also, there is altered motility in the vicinity of the anastomosis. Intussusception is often transient, but may be a fixed finding, rarely resulting in obstruction and incarceration (Fig. 35-21).^{65,78}

LAPAROSCOPIC ADJUSTABLE GASTRIC BANDING

Gastric band placement is a restrictive procedure that limits the volume of food that can be consumed. The first gastric band was introduced in 1986 and was made available laparoscopically in the early 1990s. The first *adjustable* gastric band device was approved for use in the United States by the U.S. Food and Drug Administration (FDA) in 2001. Since then, additional versions of the band have been approved, and the concept of a reversible, adjustable gastric band has become an increasingly popular treatment option for morbid obesity in the United States.⁷⁹

Laparoscopic adjustable gastric band placement (LAGB) is the least invasive bariatric procedure to date; it involves no cutting, stapling, or bypassing of portions of the GI tract. The

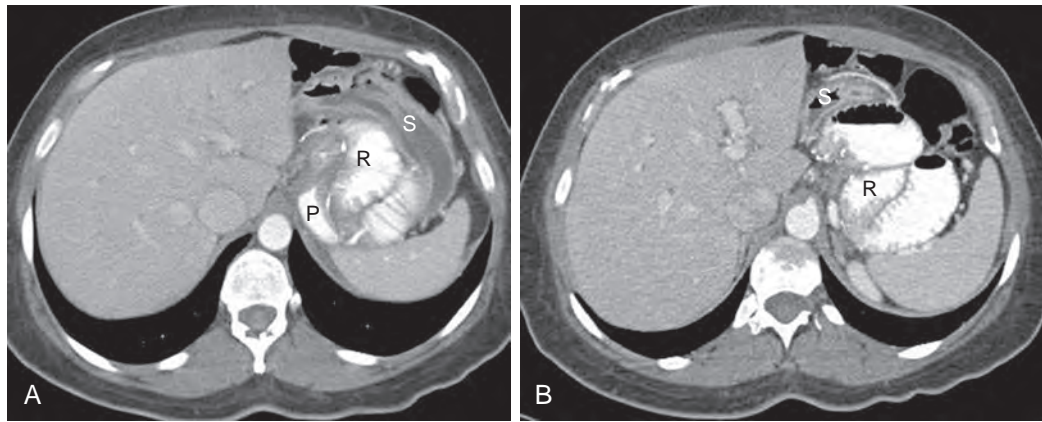


Figure 35-20 Internal hernia following RYGB on CT. A, B. Axial CT images following positive oral and IV contrast show RYGB anatomy with the Roux limb (R) clustered, dilated, and displaced cephalad to the pouch (P) and compressing the excluded stomach (S) secondary to an internal hernia. The JJ suture line was also displaced cephalad (not shown).

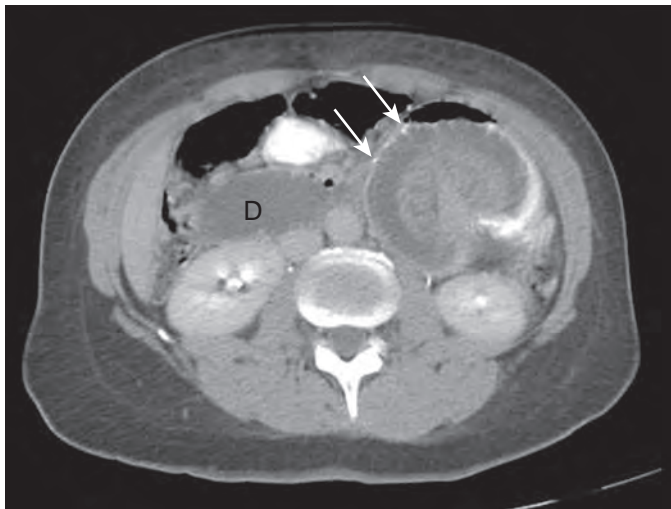


Figure 35-21 Intussusception following RYGB on CT. Axial CT scan following positive oral and IV contrast shows a fixed intussusception about the JJ anastomosis, with focal bowel dilation and dilation of the fluid-filled duodenum (D) caused by associated obstruction of the biliopancreatic limb (type B obstruction). Note anastomotic suture (arrows).

procedure is reversible, and the band can be adjusted according to the patient's weight loss curve and/or symptoms. Weight loss results with LAGB are similar to those of other restrictive procedures, but overall weight reduction may be less than RYGB in the long term, particularly in superobese patients (BMI > 50 kg/m²).⁸⁰⁻⁸³ Nevertheless, LAGB is an effective weight loss procedure, with improved obesity-related comorbidities, and has less overall morbidity as compared with RYGB.^{80,81,83}

The LAGB procedure consists of placing a silicone band around the upper stomach to create a small gastric pouch and a narrow stoma through the band that communicates with the remainder of the stomach (Fig. 35-22A).^{79,80} The small pouch and narrow stoma limit food intake and delay emptying. The band is sutured to the adjacent stomach wall to help hold it in place and decrease the chance of band slippage. The band has an inflatable inner balloon cuff connected via tubing to a subcutaneous port in the anterior abdominal wall, usually along

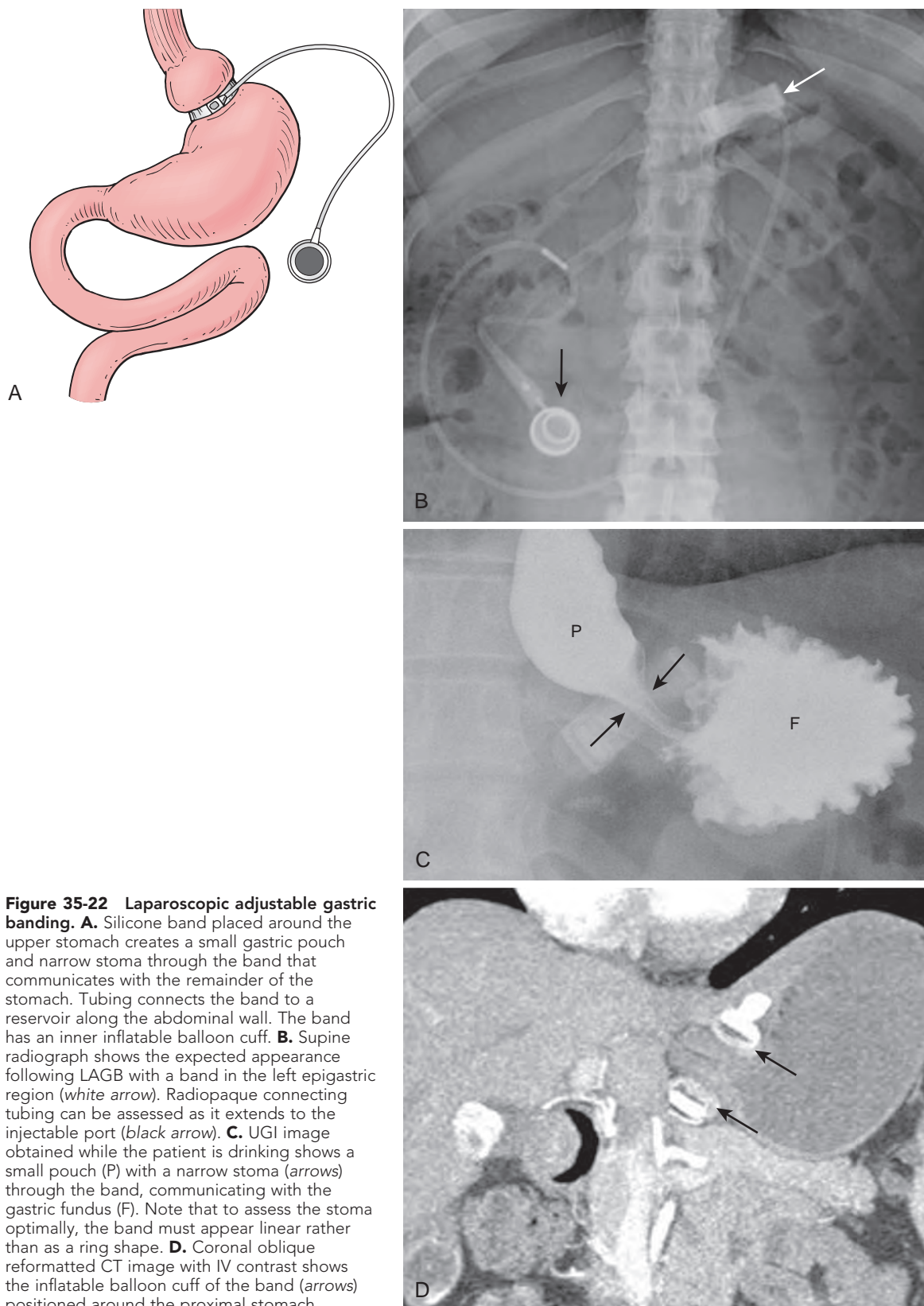
the right anterior rectus sheath. The port may be accessed percutaneously to inflate or deflate the balloon cuff of the band and adjust the size of the stoma. The stomal diameter may be narrowed by injecting the port with fluid to inflate the cuff or widened by aspirating fluid from the port to deflate the cuff. Inflation of the band can be performed in small increments to avoid complications from obstruction. Also, fluid can be removed from the band if the patient is experiencing obstructive symptoms.

Imaging Following Laparoscopic Adjustable Gastric Banding

Radiography. The radiopaque band should be located in the left epigastric region (Fig. 35-22B). The angle of the long axis of the band with the vertical (along the patient's spine) should be 4 to 58 degrees in the anteroposterior projection. This is called the phi angle. The device, connecting tubing, and port should be assessed to ensure that the device is intact, without kinking or discontinuity.

Upper Gastrointestinal Examination. Early postoperative UGI is useful to evaluate band position and assess for possible leakage or obstruction. On a scout radiograph, the location and angle of the band should be assessed, as well as the continuity of the connecting tubing and position of the reservoir. Before administering oral contrast, the patient should be positioned at fluoroscopy so the band is visualized in profile, usually with the patient in the supine anteroposterior or slight right posterior oblique position. In this position, the ring should appear as a straight line rather than having an O shape configuration (Fig. 35-22C). This allows for optimal evaluation of the pouch and stoma through the band and helps ensure that opacification of the fundus does not obscure the stoma. During the early postoperative course, water-soluble contrast should be administered followed by barium if no leak is detected. In the late postoperative course, and if there is no concern for perforation, barium may be administered initially.

As for all patients following gastric surgery, initial attention should be directed toward the postoperative anatomy, in this case, the gastric pouch and stoma. Ingested contrast should be followed fluoroscopically from the esophagus into the pouch, through the stoma created by the band, and into the remainder



of the stomach (see Fig. 35-22C). The distal esophagus, pouch size and configuration, and stomal diameter should be evaluated. The ideal stoma size has been reported to be 3 to 5 mm.⁸⁴ Fluoroscopy also allows for assessment of esophageal motility, esophageal and pouch dilation, and changes over time during the study.

Computed Tomography. Following LAGB, CT may be helpful to assess for a source of infection and evaluate soft tissue changes related to the device components. CT studies should include the abdominal wall soft tissues in the field of view because soft tissue processes related to the tubing or port might otherwise be missed. The radiopaque band should be identified along the proximal stomach (Fig. 35-22D); the tubing can be followed along its intraperitoneal course and in the overlying soft tissues as it connects to the port in the abdominal wall.

Band Adjustment

Periodic band adjustments following LAGB are typically necessary to achieve optimal weight loss and minimize symptoms of obstruction. Band adjustments may be performed at fluoroscopy. Ideally, the patient is administered oral contrast before and after adjustment to evaluate for adequate change in stomal caliber and prevent obstruction caused by an overinflated band. The use of fluoroscopy allows for an accurate adjustment of stomal size and also decreases potential complications from an excessively narrowed stoma, including obstruction, motility disorders, pouch dilation, band slippage, and band migration. Several band adjustments may be necessary to achieve an optimal result in terms of weight reduction, with an average of three adjustments necessary per patient.⁸⁵⁻⁸⁷

The degree of adjustment is best determined in conjunction with the surgeon and is based on the patient's weight loss curve and symptomatology. At fluoroscopy, the subcutaneous port is localized, and a noncoring, deflected-tip, 20- to 22-gauge needle with an attached, saline-filled syringe is inserted and advanced until it hits the back wall of the reservoir. Saline should be easily injected and withdrawn to confirm appropriate position. The amount of saline instilled or removed should be documented. After adjustment, oral contrast is administered to confirm adequate narrowing of the stoma without obstruction.

Complications

Overall, LAGB is a relatively safe surgical procedure, with minimal perioperative mortality, but some degree of morbidity occurs in up to 35% of patients and additional surgery may be necessary in as many as 11% of patients.^{80,81,88} Additional surgical procedures are often performed laparoscopically and may be relatively minor in nature (such as involving the port or tubing).

Following LAGB, early complications are rare and may include gastric perforation in less than 0.5% of patients, improper band positioning in less than 0.1% of patients, early postoperative band slippage in less than 0.1% of patients, and acute stomal obstruction in less than 1.4% of patients.^{80,81,83-85,88} Early dysphagia and pouch esophageal reflux are common until dietary habits change.

Complications following LAGB are much more common in the late postoperative course; these may include pouch dilation, band slippage, band erosion, obstruction, and device-related complications, including device failure. The most common late complications are pouch dilation and band

slippage, and early diagnosis is important to prevent further complications.^{85,86,88} Gastric necrosis is rare, occurring in less than 0.3% of patients, and is most often caused by band slippage with strangulation.^{80,81,83}

Pouch Dilation. Pouch dilation may occur in as many as 25% of patients following LAGB, but the incidence has decreased over time with surgical modifications of the gastric band procedure.⁸⁹ As in all bariatric procedures, dilation of the pouch can result in failed weight loss. Also, pouch dilation may necessitate removal of the device.

Upper Gastrointestinal Examination. Pouch dilation following LAGB can be seen with a normal or widened stoma, narrow stoma, or band slippage. In the case of a normal or widened stoma, pouch dilation is usually caused by dietary noncompliance and chronic overfilling of the pouch. The pouch is dilated and has a concentric appearance, and the stoma is widely patent (Fig. 35-23). This may require nutritional counseling.^{79,84,90} In the case of pouch dilation with a narrow stoma, pouch configuration should be evaluated (concentric or eccentric dilation). Concentric pouch dilation with a narrow stoma may occur in the acute setting, with vomiting, dysphagia, esophageal dysmotility, and obstruction (Fig. 35-24). This is usually caused by band overinflation at adjustment. Rarely, focal weakness in the balloon cuff can result in eccentric stomal narrowing, with concentric pouch dilation. When pouch dilation caused by a tight stoma is identified, the band should be deflated immediately to prevent further complications.^{79,85} Eccentric pouch dilation with a tight stoma is caused by band slippage (Fig. 35-25; see later).

Computed Tomography. Pouch dilation may be recognized on CT, especially with coronal and sagittal images, but the caliber of the stoma is not well assessed on CT. If pouch dilation is noted on CT, UGI may be of benefit to determine if there is obstruction caused by the band.

Pouch Dilation with Band Slippage. Pouch dilation may be a consequence of band slippage. In this case, the band becomes

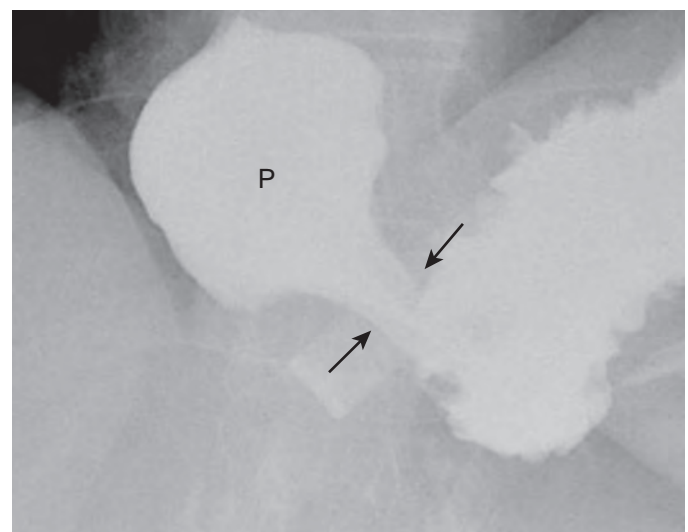


Figure 35-23 Concentric pouch dilation following LAGB with a widened stoma. Supine UGI image obtained during drinking shows a concentrically dilated pouch (P) with a widened stoma (arrows) through the band. This is typically caused by chronic overdistention and may require nutritional counseling.

dislodged from its original position, with herniation of a portion of the stomach above the band. This results in an eccentrically dilated pouch, with a tight stoma. Band slippage may occur in as many as 24% of patients, but the incidence varies with the surgical technique used.^{80,84,89-91} Surgical procedural modifications and patient training in regard to modification of

eating habits have resulted in a decreased incidence of band slippage over time.⁸⁹ Risk factors for band slippage include overeating with overdistention of the pouch, band overinflation, and excessive vomiting.

Band slippage is considered a late complication of LAGB. Patients may present with acute food intolerance, pain, vomiting, progressive gastroesophageal reflux, esophageal motility disorders, early satiety, and aspiration pneumonia. Rarely, band slippage may result in sudden complete dysphagia, severe abdominal pain, and acute gastric obstruction. Three types of band slippage have been described—anterior, posterior, and concentric slippage, with complete displacement of the band distally. In all types of band slippage, similar consequences are possible. Progressive eccentric pouch dilation with progressive herniation of the stomach above the band may occur if untreated. Band slippage can lead to acute obstruction, gastric volvulus, ischemia, infarction, perforation, and hemorrhage. The most serious complication is necrosis of the gastric pouch. Early detection and treatment of band slippage are essential to prevent further complications. Once diagnosed, the band should be deflated immediately.⁹²

Radiography. On abdominal radiography, there is increased separation between the gastric band and medial aspect of the left hemidiaphragm. As the stomach herniates superiorly through a slipped gastric band, the band may tilt along its horizontal axis so that the anterior and posterior sides of the band are no longer superimposed. This can produce an O shape configuration, termed the *O sign*.⁹³ A more vertical or horizontal configuration of the band will result in an abnormal phi angle. An air-fluid level may also be seen within a dilated gastric pouch above the band (see Fig. 35-25A).

Upper Gastrointestinal Examination. On a preliminary radiograph, an abnormal band position is noted, with a change in configuration of the band as compared with a prior

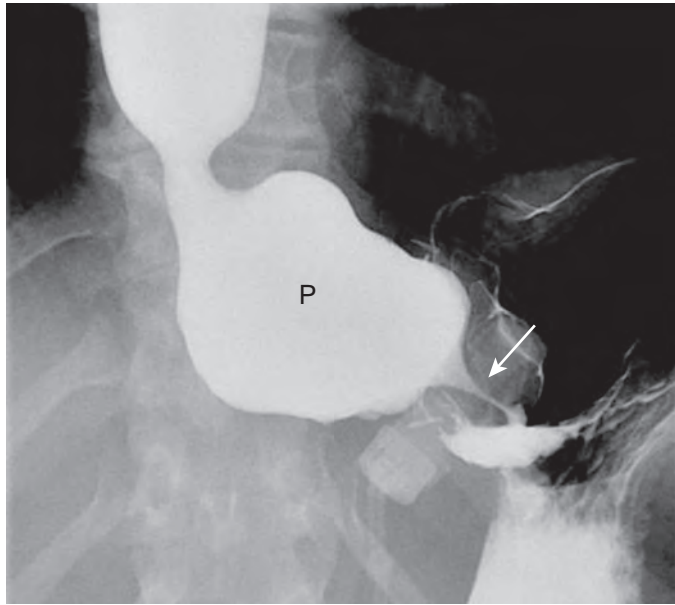


Figure 35-24 Concentric pouch dilation following LAGB with a narrow stoma. Upright UGI image obtained during drinking shows a concentrically dilated pouch (P) with a tight stoma (arrow) through the band. The band is causing obstruction, and the upright position is necessary to empty the pouch. In this case, the band should be deflated to prevent further complications.

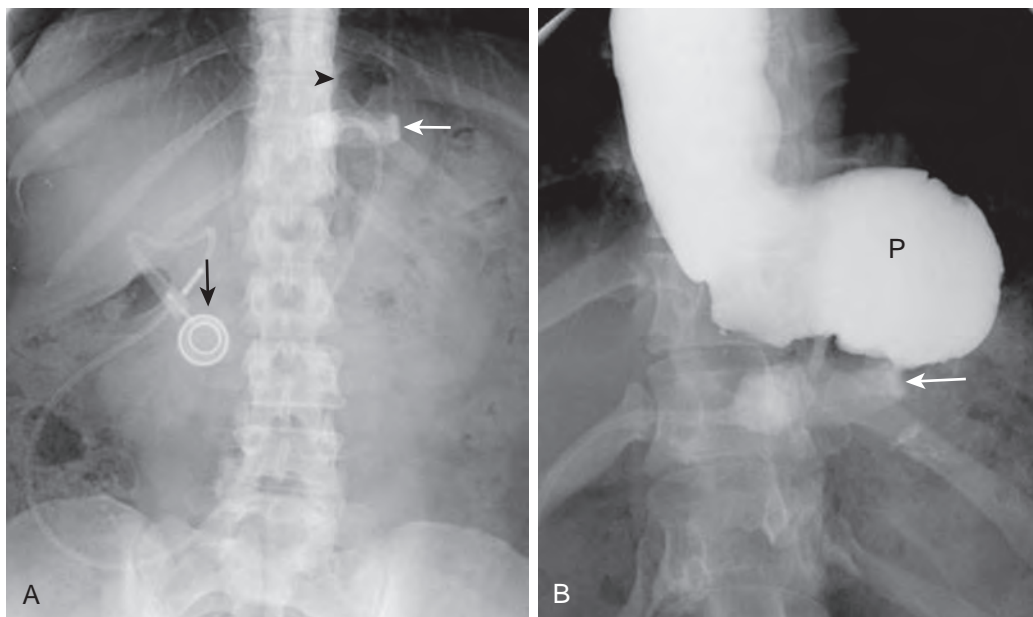


Figure 35-25 Band slippage following LAGB. **A.** Supine radiograph in the same patient as in Figure 35-22 1 year later shows a change in the configuration of the band (white arrow) (see Fig. 35-22B). It is now inferiorly located and horizontal in configuration. There is a dilated, gas-filled stomach bubble superior to the band (arrowhead). The port (black arrow) is relatively unchanged. **B.** UGI image shows an eccentrically dilated gastric pouch (P) above the horizontal band (arrow), with obstruction at the level of the band caused by band slippage. The esophagus is also dilated.

postoperative study. The band may be displaced inferiorly in a more vertical or horizontal configuration with an abnormal phi angle (see Fig. 35-25A). Following ingestion of contrast, eccentric pouch dilation is seen with a tight stoma at the level of the band (see Fig. 35-25B). Band slippage results in luminal obstruction by the band, and slippage may become more apparent with increased luminal distention during the study. Posterior slippage is associated with upward herniation of the posterior gastric wall through the band, and anterior slippage is associated with downward displacement of the band over the anterior wall of the stomach.^{79,85}

Intragastric Erosion and Migration of the Band. The gastric band can erode into the lumen of the stomach in approximately 2% of patients following LAGB, with a higher incidence reported with longer follow-up. With this complication, the band gradually erodes into the gastric wall, enters the lumen, and may even migrate distally, resulting in downstream obstruction. Band erosion may be a consequence of NSAID use, excessive vomiting, or increased pressure within the band itself from overinflation. Patients may present with nonspecific pain, GI bleeding, abdominal and/or port abscess, peritonitis, perforation, and, rarely, pneumoperitoneum. Patients with band erosion may also present with weight gain, despite seemingly adequate band adjustments, because the band is no longer creating a narrow stoma. Band migration requires removal of the band and repair of the stomach because this could lead to fatal hemorrhage.⁹⁴

On UGI, contrast material is seen surrounding the intragastric portion of the band, so that the band appears as an intraluminal filling defect within the stomach (Fig. 35-26). Contrast may or may not be seen within the stoma, depending on the

degree of erosion. Band erosion may be suspected on CT when contrast is seen within and surrounding the band or if the band is completely intraluminal. There may be associated inflammatory change, abscess formation, or peritonitis.

Device-Related Complications. Following LAGB, there may be problems related to indwelling foreign bodies, including the band, connecting tubing, and reservoir. Device-related complications have been reported in up to 26% of patients, and these complications tend to require surgical repair.^{88,95}

Infection of the port, connecting tubing, or band occurs in as many as 6% of patients. The abdominal wall port may migrate through the soft tissues or become inverted in as many as 3% of patients, precluding band adjustments. Leakage of contents from the band system results in spontaneous band deflation, occurring in up to 5% of patients. Fluid loss can occur from a defect in the port, tubing, or inflatable balloon cuff, and leakage from the system can result from the use of an inappropriate needle for port access. Acute band deflation widens the stoma, so these patients experience a sudden change in dietary habits and poor weight loss, despite seemingly appropriate band adjustments. If leakage from the system is suspected, a radiograph should be obtained to look for discontinuity or kinking of the connecting tubing or device. In addition, inserting a designated volume of saline into the port and measuring for a discrepancy on return may be helpful. Injection of the port with water-soluble contrast at fluoroscopy can diagnose a leak from the system and can determine the origin of the leak to help direct surgical intervention.^{85,86,88}

SLEEVE GASTRECTOMY

The laparoscopic sleeve gastrectomy (or gastric sleeve) was first introduced in 1999; it is a restrictive procedure that limits the volume of food that can be consumed. Initially, sleeve gastrectomy was performed as the first part of a planned, staged bariatric procedure for treatment of very high-risk or superobese (BMI > 50 kg/m²) patients to decrease perioperative morbidity and mortality. The first stage consisted of the sleeve gastrectomy. Following initial weight loss and clinical improvement, a second operation was performed at a later date. The second procedure could be a biliopancreatic diversion or Roux-en-Y gastric bypass. However, the success of the sleeve gastrectomy alone in some patients eliminated the necessity of the second operation, so sleeve gastrectomy is now increasingly used as a stand-alone procedure.⁹⁶ This procedure constituted approximately 5% of all bariatric surgeries in 2008.⁹⁷

The sleeve gastrectomy consists of resection of 70% to 85% of the stomach along the greater curvature. The remaining stomach has a tubular configuration, and the pylorus and duodenum are left intact (Fig. 35-27A). This restricts the gastric capacity while maintaining the normal pathway of food. Also, the tubular stomach, in conjunction with an intact pylorus, creates a high-pressure restrictive system. Unlike restrictive gastric banding, there is no need for periodic band adjustments or intervention, and there is no indwelling foreign body. Absence of an indwelling foreign body reduces the risk of infection, and there are no problems with slippage, erosion, or device malfunction. As compared with RYGB, there is no major alteration made to the course of the GI tract, and there is no risk of

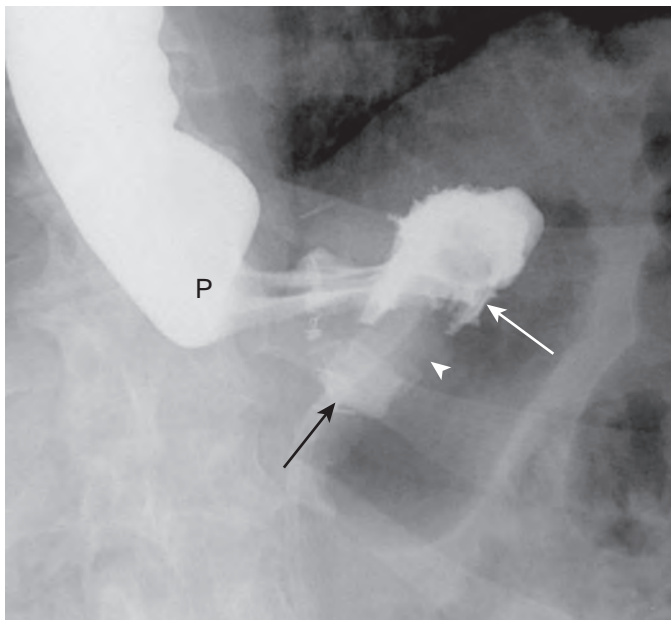


Figure 35-26 Band erosion following LAGB. UGI image following LAGB obtained with the patient drinking shows a small gastric pouch (P). The band is in an appropriate linear position (black arrow) for UGI. Rather than opacifying a stoma through the band, contrast is seen surrounding the left aspect of the band so that this portion of the band appears as a filling defect (white arrow). This is caused by intragastric erosion of the band. The expected location of the stoma is denoted with an arrowhead.

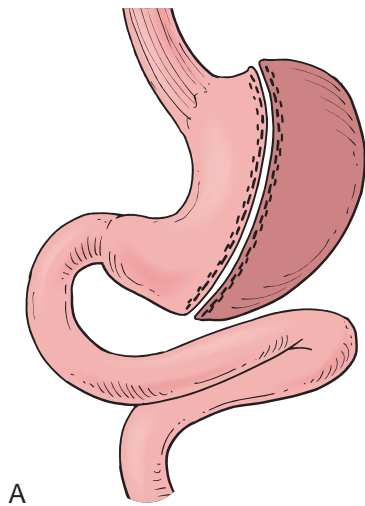
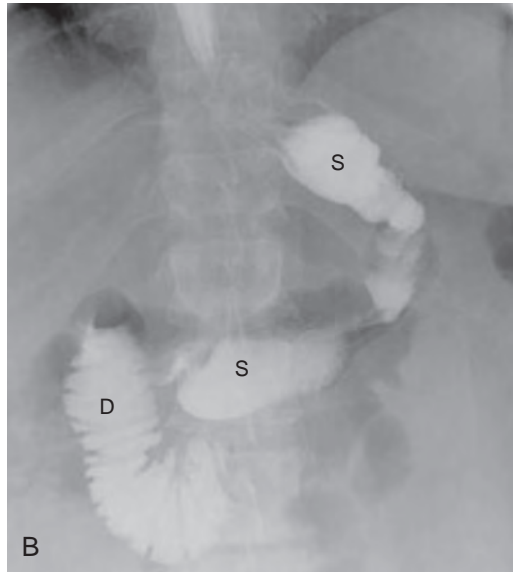


Figure 35-27 Sleeve gastrectomy. **A.** Gastric sleeve, with approximately 70% of the stomach resected (*shaded area*) along the greater curvature and with relative sparing of the antrum. The pylorus and duodenum are left intact. **B.** Supine UGI image shows the narrowed, tubular configuration of the gastric sleeve (S) in a recently postoperative patient with an intact pylorus and duodenum (D). **C.** Axial contrast-enhanced CT scan shows a narrowed stomach, with sutures along the resected greater curvature (*arrows*) and prominence of mesenteric fat in the expected location of the remainder of the stomach. Also note evidence of surgical injury to the left lobe of the liver.



malabsorption. However, the sleeve gastrectomy procedure is not reversible.⁹⁸

Imaging Following Sleeve Gastrectomy

Upper Gastrointestinal Examination. As for all early postoperative patients, water-soluble contrast is first used to assess for possible leakage. Barium is administered if there is no leak identified or initially in the late postoperative course. Administration of oral contrast reveals a long narrowed, tubular gastric pouch. Narrowing of the stomach is seen along the greater curvature. The distal gastric antrum and pylorus are preserved (Fig. 35-27B). Gastric peristalsis may be significantly diminished or absent.⁹⁸

Computed Tomography. CT may be of benefit following sleeve gastrectomy to assess the postoperative anatomy and evaluate the surrounding structures. The gastric sleeve appears as a narrowed, tubular stomach, often with a staple line along the greater curvature. Prominence of the mesenteric fat may be seen in the expected location of the resected portion of the stomach (Fig. 35-27C). With a stand-alone sleeve gastrectomy,

no additional bowel suture line or anastomosis is seen, and no Roux limb should be seen extending toward the stomach. The duodenum and small bowel should have a normal course. However, a jejunal limb may be seen anastomosed to the gastric sleeve when sleeve gastrectomy is performed in conjunction with RYGB.

Complications

The overall complication rate following sleeve gastrectomy is approximately 5%. Potential complications include leakage, strictures, hemorrhage, and infection.⁹⁸

Postoperative leaks have been reported following sleeve gastrectomy in as many as 5% of patients. Leaks usually arise from the proximal end of the greater curvature staple line near the gastroesophageal junction and extend laterally (Fig. 35-28). Proximal gastric leaks may be difficult to treat, with prolonged associated morbidity.⁹⁹

Late complications include stricture, pouch dilation, gastric outlet obstruction, hiatal hernia, and gastroesophageal reflux. Postoperative strictures and fibrosis can occur at the upper, mid, or distal end of the staple line (Fig. 35-29). Strictures

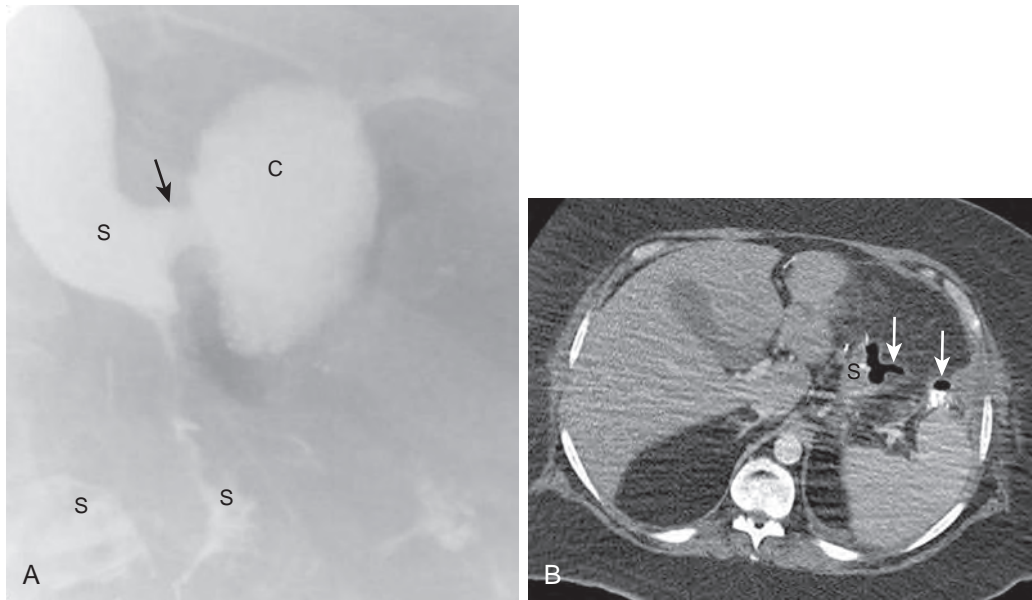


Figure 35-28 Leak following sleeve gastrectomy. **A.** UGI image following sleeve gastrectomy shows contrast opacifying an edematous, narrowed, and irregular gastric sleeve (S), with leakage from the proximal sleeve (arrow) into an extraluminal collection (C) extending to the left. Additional amorphous extraluminal contrast is seen more inferiorly. **B.** Axial CT scan with IV and positive oral contrast shows the leak (arrows) from the gastric sleeve (S) with extraluminal contrast and gas laterally in the left upper quadrant.

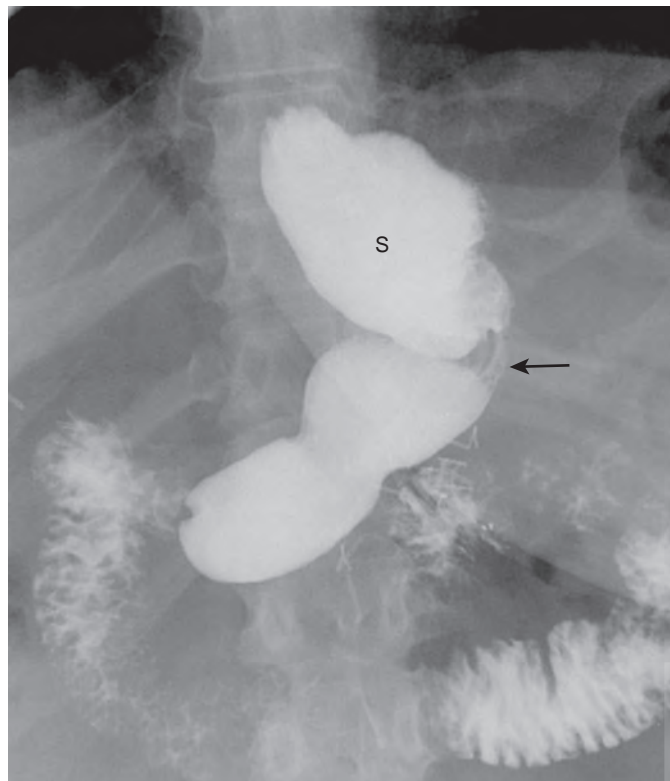


Figure 35-29 Gastric sleeve with stricture and proximal pouch dilation. Supine UGI image in a patient following sleeve gastrectomy shows a focal stricture in the midsleeve (arrow) with proximal dilation of the sleeve (S).

may also involve the gastric pouch diffusely. Gastric dilation can occur because of underlying fibrosis and strictures or because of overdistention and stretching of the remaining stomach. As in all bariatric procedures, pouch dilation can result in failure to lose weight or weight gain. Focal strictures may respond to endoscopic dilation, but longer segments of narrowing may necessitate surgical revision or resection of portions of the pouch with a subsequent gastrojejunostomy. Postoperative gastroesophageal reflux is not uncommon, having been reported in as many as 21% of patients. Hiatal hernias and severe gastroesophageal reflux may necessitate conversion to RYGB.⁹⁸

BILIOPANCREATIC DIVERSION WITH DUODENAL SWITCH

Biliopancreatic diversion with duodenal switch (BPD-DS) includes restrictive and malabsorptive mechanisms of weight loss. A sleeve gastrectomy is performed to limit the size of the stomach (restrictive). The duodenum is transected at the level of the duodenal bulb, and the proximal ileum is brought up and anastomosed to the duodenal bulb. The pylorus remains intact. This creates an alimentary limb consisting of the gastric sleeve, pylorus, duodenal bulb, and proximal ileum (Fig. 35-30). The biliopancreatic limb consists of the more downstream duodenum and jejunum and is anastomosed to the distal ileum approximately 75 to 100 cm proximal to the ileocecal valve. The malabsorptive component is created by rearranging the small intestine to bypass the small bowel and separate the flow of food from bile and pancreatic juices, limiting the absorption of calories and resulting in weight loss.¹⁰⁰

BPD-DS is effective in terms of weight loss, and less patient compliance is necessary as compared with restrictive procedures alone. However, because of complications, including those from malabsorption, this procedure tends to be reserved for superobese patients. It remains less widely performed overall as compared with RYGB. There is an increased risk of nutritional deficiencies, osteoporosis, protein loss and malnutrition, anemia, chronic diarrhea, and dumping syndrome. Also, the risks and surgical complications are increased with multiple

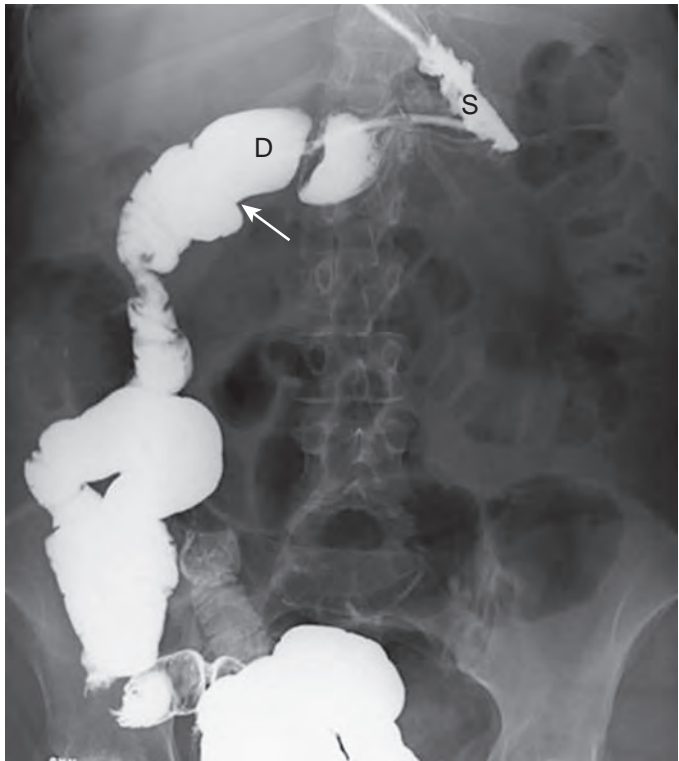


Figure 35-30 Biliopancreatic diversion with duodenal switch. Overhead radiograph during UGI with small bowel follow-through shows a gastric sleeve (S) as the restrictive component of the procedure. There is an intact duodenal bulb (D) with a duodenal to proximal ileal anastomosis (arrow). This bypasses a long segment of small bowel and separates the biliopancreatic contents from the ingested material, resulting in malabsorption. There is a nasogastric tube in place.

anastomotic suture lines. Mechanical complications following BPD-DS occur in approximately 20% of patients and may include obstruction, abdominal wall hernia, and anastomotic leaks. Bowel obstruction is identified in as many as 16% of patients.¹⁰¹

REFERENCES

1. Dodds WJ, Stewart ET, Vlymen WJ: Appropriate contrast media for evaluation of esophageal disruption. *Radiology* 144:439–441, 1982.
2. Foley MJ, Ghahremani GG, Rogers LF: Reappraisal of contrast media used to detect upper gastrointestinal perforations: Comparison of ionic water-soluble media with barium sulfate. *Radiology* 144:231–237, 1982.
3. Gohel VK, Laufer I: Double-contrast examination of the postoperative stomach. *Radiology* 129:601–607, 1978.
4. Woodfield CA, Levine MS: The postoperative stomach. *Eur J Radiol* 53:341–352, 2005.
5. Malmud LS, Fisher RS, Knight LC, Rock E: Scintigraphic evaluation of gastric emptying. *Semin Nucl Med* 12:116–125, 1982.
6. Max MH, West B, Knutson CO: Evaluation of postoperative gastroduodenal symptoms: Endoscopy or upper gastrointestinal roentgenography? *Surgery* 86:578–582, 1979.
7. Cotton PB, Shorvon PJ: Analysis of endoscopy and radiography in the diagnosis, follow-up and treatment of peptic ulcer disease. *Clin Gastroenterol* 13:383–403, 1984.
8. Dempsey DT: Stomach. In Brunnicardi F, Andersen D, Billiar T, et al, editors: *Schwartz's Principles of Surgery*, ed 9, New York, 2009, McGraw-Hill, pp 889–948.
9. Rosen MJ, d Ponsky J: *Atlas of Surgical Techniques for the Upper Gastrointestinal Tract and Small Bowel*, Philadelphia, 2010, Saunders.
10. Dallal HJ, Palmer KR: ABC of the upper gastrointestinal tract: Upper gastrointestinal haemorrhage. *BMJ* 323:1115–1117, 2001.
11. Blatchford O, Murray WR, Blatchford M: A risk score to predict need for treatment for upper-gastrointestinal haemorrhage. *Lancet* 356:1318–1321, 2000.
12. Harbison SP, Dempsey DT: Peptic ulcer disease. *Curr Probl Surg* 42:346–454, 2005.
13. Mulholland MW, Debas HT: Recent advances in the treatment of duodenal ulcer disease. A surgical perspective. *West J Med* 147:301–308, 1987.
14. Mulholland MW, Debas HT: Chronic duodenal and gastric ulcer. *Surg Clin North Am* 67:489–507, 1987.
15. Jordan PH, Jr, Morrow C: Perforated peptic ulcer. *Surg Clin North Am* 68:315–329, 1988.
16. Boyd EJ, Penston JG, Johnston DA, Wormsley KG: Does maintenance therapy keep duodenal ulcers healed? *Lancet* 1:1324–1327, 1988.
17. Shaw PC, Op den Orth JO: Postoperative stomach and duodenum. *Radiol Clin North Am* 32:1275–1291, 1994.
18. Carbonell A: Highly selective vagotomy. In Ponsky J, Michael J, Rosen MJ, editors: *Atlas of Surgical Techniques for the Upper GI Tract and Small Bowel*, Philadelphia, 2010, Saunders, pp 105–112.

19. Bardhan KD, Cust G, Hinchliffe RF, et al: Changing pattern of admissions and operations for duodenal ulcer. *Br J Surg* 76:230–236, 1989.
20. Elashoff JD, Grossman MI: Trends in hospital admissions and death rates for peptic ulcer in the United States from 1970 to 1978. *Gastroenterology* 78:280–285, 1980.
21. Kurata JH, Honda GD, Frankl H: Hospitalization and mortality rates for peptic ulcers: A comparison of a large health maintenance organization and United States data. *Gastroenterology* 83:1008–1016, 1982.
22. McConnell DB, Baba GC, Deveney CW: Changes in surgical treatment of peptic ulcer disease within a veterans hospital in the 1970s and the 1980s. *Arch Surg* 124:1164–1167, 1989.
23. Kocer B, Surmeli S, Solak C, et al: Factors affecting mortality and morbidity in patients with peptic ulcer perforation. *J Gastroenterol Hepatol* 22:565–570, 2007.
24. Jordan PH, Jr, Thornby J: Should it be parietal cell vagotomy or selective vagotomy-antrectomy for treatment of duodenal ulcer? A progress report. *Ann Surg* 205:572–590, 1987.
25. Burhenne HJ: Roentgen anatomy and terminology of gastric surgery. *Am J Roentgenol Radium Ther Nucl Med* 91:731–743, 1964.
26. Kim KW, Choi BI, Han JK, et al: Postoperative anatomic and pathologic findings at CT following gastrectomy. *Radiographics* 22:323–336, 2002.
27. Osugi H, Fukuhara K, Takada N, et al: Reconstructive procedure after distal gastrectomy to prevent remnant gastritis. *Hepatogastroenterology* 51:1215–1218, 2004.
28. Schrock TR, Way LW: Total gastrectomy. *Am J Surg* 135:348–355, 1978.
29. Burrell M, Curtis AM: Sequelae of stomach surgery. *CRC Crit Rev Diagn Imaging* 10:17–97, 1977.
30. Smith C, Deziel DJ, Kubicka RA: Evaluation of the postoperative stomach and duodenum. *Radiographics* 14:67–86, 1994.
31. Fich A, Neri M, Camilleri M, et al: Stasis syndromes following gastric surgery: clinical and motility features of 60 symptomatic patients. *J Clin Gastroenterol* 12:505–512, 1990.
32. Carbonell A: Surgical treatment of postgastrectomy syndromes. In Ponsky J, Rosen MJ, editors: *Atlas of Surgical Techniques for the Upper GI Tract and Small Bowel*, Philadelphia, 2010, Saunders, pp 169–176.
33. de Lange EE, Shaffer HA, Jr: Anastomotic strictures of the upper gastrointestinal tract: Results of balloon dilation. *Radiology* 167:45–50, 1988.
34. Woodward ER, Hocking MP: Postgastrectomy syndromes. *Surg Clin North Am* 67:509–520, 1987.
35. Alexander-Williams J, Hoare AM: The stomach. Part II: Partial gastric resection. *Clin Gastroenterol* 8:321–353, 1979.
36. Eagon JC, Miedema BW, Kelly KA: Postgastrectomy syndromes. *Surg Clin North Am* 72:445–465, 1992.
37. Schirmer BD, Meyers WC, Hanks JB, et al: Marginal ulcer. A difficult surgical problem. *Ann Surg* 195:653–661, 1982.
38. Ott DJ, Munitz HA, Gelfand DW, et al: The sensitivity of radiography of the postoperative stomach. *Radiology* 144:741–743, 1982.
39. Wheatley MJ: Jejunogastric intussusception diagnosis and management. *J Clin Gastroenterol* 11:452–454, 1989.
40. Poppel MH: Gastric intussusceptions. *Radiology* 78:602–608, 1962.
41. Hammond N, Miller FH, Dynes M: Intussusception into the enteroanastomosis after Billroth II gastrectomy and Roux-en-Y jejunostomy: Sonographic and CT findings. *AJR* 177:624–626, 2001.
42. Kim HC, Han JK, Kim KW, et al: Afferent loop obstruction after gastric cancer surgery: Helical CT findings. *Abdom Imaging* 28:624–630, 2003.
43. Gale ME, Gerzof SG, Kiser LC, et al: CT appearance of afferent loop obstruction. *AJR* 138:1085–1088, 1982.
44. Op den Orth JO: Tubeless hypotonic examination of the afferent loop of the Billroth II stomach. *Gastrointest Radiol* 2:1–5, 1977.
45. Delcore R, Cheung LY: Surgical options in postgastrectomy syndromes. *Surg Clin North Am* 71:57–75, 1991.
46. Goodman P, Levine MS, Gohil MN: Gastric carcinoma after gastrojejunostomy for benign disease: radiographic findings. *Gastrointest Radiol* 17:211–213, 1992.
47. Stalnikowicz R, Benbassat J: Risk of gastric cancer after gastric surgery for benign disorders. *Arch Intern Med* 150:2022–2026, 1990.
48. Kodera Y, Yamamura Y, Torii A, et al: Gastric remnant carcinoma after partial gastrectomy for benign and malignant gastric lesions. *J Am Coll Surg* 182:1–6, 1996.
49. Welch CE, Malt RA: Surgery of the stomach, duodenum, gallbladder, and bile ducts. *N Engl J Med* 316:999–1008, 1987.
50. Fuchs CS, Mayer RJ: Gastric carcinoma. *N Engl J Med* 333:32–41, 1995.
51. Levine MS, Fisher AR, Rubesin SE, et al: Complications after total gastrectomy and esophagojejunostomy: radiologic evaluation. *AJR* 157:1189–1194, 1991.
52. Buckley O, Ward E, Ryan A, et al: European obesity and the radiology department. What can we do to help? *Eur Radiol* 19:298–309, 2009.
53. Flegal KM, Carroll MD, Ogden CL, Curtin LR: Prevalence and trends in obesity among US adults, 1999–2008. *JAMA* 303:235–241, 2010.
54. Carucci LR: Imaging obese patients: problems and solutions. *Abdom Imaging* 38:630–646, 2013.
55. Brolin RE: Update: NIH consensus conference. *Gastrointestinal surgery for severe obesity. Nutrition* 12:403–404, 1996.
56. Buchwald H: Consensus conference statement bariatric surgery for morbid obesity: Health implications for patients, health professionals, and third-party payers. *Surg Obes Relat Dis* 1:371–381, 2005.
57. Fisher BL, Schauer P: Medical and surgical options in the treatment of severe obesity. *Am J Surg* 184:9S–16S, 2002.
58. National Institutes of Health Consensus Development Conference on Gastrointestinal Surgery for Severe Obesity: *Gastrointestinal surgery for severe obesity: National Institutes of Health Consensus Development Conference Statement. Am J Clin Nutr* 55:615S–619S, 1992.
59. Zhao Y, Encinosa W: Bariatric Surgery Utilization and Outcomes in 1998 and 2004, Rockville, MD, 2007, Agency for Healthcare Research and Quality.
60. Singh D, Laya AS, Clarkston WK, Allen MJ: Jejunioileal bypass: A surgery of the past and a review of its complications. *World J Gastroenterol* 15:2277–2279, 2009.
61. DeMaria EJ, Sugerman HJ, Kellum JM, et al: Results of 281 consecutive total laparoscopic Roux-en-Y gastric bypasses to treat morbid obesity. *Ann Surg* 235:640–645, 2002.
62. Schauer PR, Ikramuddin S, Gourash W, et al: Outcomes after laparoscopic Roux-en-Y gastric bypass for morbid obesity. *Ann Surg* 232:515–529, 2000.
63. Santry HP, Gillen DL, Lauderdale DS: Trends in bariatric surgical procedures. *JAMA* 294:1909–1917, 2005.
64. Carucci LR, Turner MA, Conklin RC, et al: Roux-en-Y gastric bypass surgery for morbid obesity: Evaluation of postoperative extraluminal leaks with upper gastrointestinal series. *Radiology* 238:119–127, 2006.
65. Carucci LR, Turner MA, Yu J: Imaging evaluation following Roux-en-Y gastric bypass surgery for morbid obesity. *Radiol Clin North Am* 45:247–260, 2007.
66. Carucci LR, Conklin RC, Turner MA: Roux-en-Y gastric bypass surgery for morbid obesity: Evaluation of leak into excluded stomach with upper gastrointestinal examination. *Radiology* 248:504–510, 2008.
67. Higa KD, Ho T, Boone KB: Internal hernias after laparoscopic Roux-en-Y gastric bypass: Incidence, treatment and prevention. *Obes Surg* 13:350–354, 2003.
68. Champion JK, Williams M: Small bowel obstruction and internal hernias after laparoscopic Roux-en-Y gastric bypass. *Obes Surg* 13:596–600, 2003.
69. Filip JE, Mattar SG, Bowers SP, Smith CD: Internal hernia formation after laparoscopic Roux-en-Y gastric bypass for morbid obesity. *Am Surg* 68:640–643, 2002.
70. Higa KD, Boone KB, Ho T: Complications of the laparoscopic Roux-en-Y gastric bypass: 1,040 patients—what have we learned? *Obes Surg* 10:509–513, 2000.
71. Iannelli A, Buratti MS, Novellas S, et al: Internal hernia as a complication of laparoscopic Roux-en-Y gastric bypass. *Obes Surg* 17:1283–1286, 2007.
72. Tucker ON, Escalante-Tattersfield T, Szomstein S, Rosenthal RJ: The ABC System: A simplified classification system for small bowel obstruction after laparoscopic Roux-en-Y gastric bypass. *Obes Surg* 17:1549–1554, 2007.
73. Carucci LR, Turner MA, Shaylor SD: Internal hernia following Roux-en-Y gastric bypass surgery for morbid obesity: Evaluation of radiographic findings at small-bowel examination. *Radiology* 251:762–770, 2009.
74. Blachar A, Federle MP, Dodson SF: Internal hernia: Clinical and imaging findings in 17 patients with emphasis on CT criteria. *Radiology* 218:68–74, 2001.
75. Lockhart ME, Tessler FN, Canon CL, et al: Internal hernia after gastric bypass: Sensitivity and specificity of seven CT signs with surgical correlation and controls. *AJR* 188:745–750, 2007.
76. Reddy SA, Yang C, McGinnis LA, et al: Diagnosis of transmesocolic internal hernia as a complication of retrocolic gastric bypass: CT imaging criteria. *AJR* 189:52–55, 2007.
77. Blachar A, Federle MP, Pealer KM, et al: Gastrointestinal complications of laparoscopic Roux-en-Y gastric bypass surgery: Clinical and imaging findings. *Radiology* 223:625–632, 2002.
78. Carucci LR, Turner MA: Radiologic evaluation following Roux-en-Y gastric bypass surgery for morbid obesity. *Eur J Radiol* 53:353–365, 2005.
79. Carucci LR, Turner MA, Szucs RA: Adjustable laparoscopic gastric banding for morbid

- obesity: Imaging assessment and complications. *Radiol Clin North Am* 45:261–274, 2007.
80. Chevallier JM, Zinzindohoué F, Douard R, et al: Complications after laparoscopic adjustable gastric banding for morbid obesity: Experience with 1,000 patients over 7 years. *Obes Surg* 14:407–414, 2004.
81. DeMaria EJ, Jamal MK: Laparoscopic adjustable gastric banding: Evolving clinical experience. *Surg Clin North Am* 85:773–787, vii, 2005.
82. Mogdol P, Chosidow D, Marmuse JP: Laparoscopic gastric bypass versus laparoscopic adjustable gastric banding in the super-obese: A comparative study of 290 patients. *Obes Surg* 15:76–81, 2005.
83. Zinzindohoué F, Chevallier JM, Douard R, et al: Laparoscopic gastric banding: A minimally invasive surgical treatment for morbid obesity: prospective study of 500 consecutive patients. *Ann Surg* 237:1–9, 2003.
84. Wiesner W, Schob O, Hauser RS, Hauser M: Adjustable laparoscopic gastric banding in patients with morbid obesity: Radiographic management, results, and postoperative complications. *Radiology* 216:389–394, 2000.
85. Carucci LR, Turner MA: Imaging after bariatric surgery for morbid obesity: Roux-en-Y gastric bypass and laparoscopic adjustable gastric banding. *Semin Roentgenol* 44:283–296, 2009.
86. Favretti F, Cadière GB, Segato G, et al: Laparoscopic banding: selection and technique in 830 patients. *Obes Surg* 12:385–390, 2002.
87. Frigg A, Peterli R, Zynamon A, et al: Radiologic and endoscopic evaluation for laparoscopic adjustable gastric banding: preoperative and follow-up. *Obes Surg* 11:594–599, 2001.
88. Suter M, Giusti V, Worreth M, et al: Laparoscopic gastric banding: a prospective, randomized study comparing the Lapband and the SAGB: Early results. *Ann Surg* 241:55–62, 2005.
89. Zappa MA, Micheletto G, Lattuada E, et al: Prevention of pouch dilatation after laparoscopic adjustable gastric banding. *Obes Surg* 16:132–136, 2006.
90. Zacharoulis D, Roy-Chadhury SH, Dobbins B, et al: Laparoscopic adjustable gastric banding: Surgical and radiological approach. *Obes Surg* 12:280–284, 2002.
91. Weiner R, Blanco-Engert R, Weiner S, et al: Outcome after laparoscopic adjustable gastric banding—8 years experience. *Obes Surg* 13: 427–434, 2003.
92. Kriwanek S, Schermann M, Ali Abdullah S, Roka R: Band slippage—a potentially life-threatening complication after laparoscopic adjustable gastric banding. *Obes Surg* 15:133–136, 2005.
93. Pieroni S, Sommer EA, Hito R, et al: The “O” sign, a simple and helpful tool in the diagnosis of laparoscopic adjustable gastric band slippage. *AJR* 195:137–141, 2010.
94. Hainaux B, Agneessens E, Rubesova E, et al: Intra-gastric band erosion after laparoscopic adjustable gastric banding for morbid obesity: Imaging characteristics of an underreported complication. *AJR* 184:109–112, 2005.
95. Keidar A, Carmon E, Szold A, Abu-Abeid S: Port complications following laparoscopic adjustable gastric banding for morbid obesity. *Obes Surg* 15:361–365, 2005.
96. Gluck B, Movitz B, Jansma S, et al: Laparoscopic sleeve gastrectomy is a safe and effective bariatric procedure for the lower BMI (35.0–43.0 kg/m²) population. *Obes Surg* 21:1168–1171, 2011.
97. Buchwald H, Oien DM: Metabolic/bariatric surgery worldwide 2008. *Obes Surg* 19:1605–1611, 2009.
98. Carucci LR, Turner MA: Imaging following bariatric procedures: Roux-en-Y gastric bypass, gastric sleeve, and biliopancreatic diversion. *Abdom Imaging* 37:697–711, 2012.
99. Jurovich C, Thalheimer A, Seyfried F, et al: Gastric leakage after sleeve gastrectomy—clinical presentation and therapeutic options. *Langenbecks Arch Surg* 396:981–987, 2011.
100. Hess DS, Hess DW: Biliopancreatic diversion with a duodenal switch. *Obes Surg* 8:267–282, 1998.
101. Mitchell MT, Carabetta JM, Shah RN, et al: Duodenal switch gastric bypass surgery for morbid obesity: imaging of postsurgical anatomy and postoperative gastrointestinal complications. *AJR* 193:1576–1580, 2009.

Stomach and Duodenum: Differential Diagnosis

MARC S. LEVINE

CHAPTER OUTLINE

Table 36-1. **Gastric Ulcers (No Mass)**

Table 36-2. **Gastric Mass Lesions**

Table 36-3. **Thickened Gastric Folds**

Table 36-4. **Gastric Narrowing**

Table 36-5. **Gastric Outlet Obstruction**

Table 36-6. **Duodenal Filling Defects**

Table 36-7. **Thickened Duodenal Folds**

Table 36-8. **Dilated Duodenum (Megaduodenum)**

Table 36-9. **Extrinsic Impressions On the Duodenum**

TABLE
36-1

Gastric Ulcers (No Mass)

Cause	Location	Comments
EROSIONS		
Idiopathic	Antrum or body; often aligned on rugal folds	Varioliform erosions
Aspirin or other nonsteroidal anti-inflammatory drugs	Antrum or body; may be on or near greater curvature	Varioliform, linear, or serpiginous erosions
Crohn's disease	Antrum or body	Associated Crohn's disease in small bowel or colon
ULCERS		
<i>Helicobacter pylori</i>	Usually on lesser curvature or posterior wall of antrum or body	Accounts for 70%-80% of gastric ulcers
Aspirin or other nonsteroidal anti-inflammatory drugs	Distal half of greater curvature	May simulate malignant ulcer
Gastritis	Variable	Hypertrophic gastritis, granulomatous conditions, radiation, caustic ingestion, infections
Zollinger-Ellison syndrome	Variable	Associated ulcers in atypical locations; hypergastrinemia
Early gastric cancer	Variable	Nodular or deformed folds surrounding ulcer

TABLE 36-2
Gastric Mass Lesions

Cause	Radiographic Findings	Comments
BENIGN MUCOSAL LESIONS		
Hyperplastic polyps	Round sessile polyps in fundus or body; usually multiple	Not premalignant
Adenomatous polyps	Lobulated or pedunculated polyps in antrum; often solitary	Premalignant
Polyposis syndromes	Multiple polyps in stomach (also in small bowel or colon)	Familial adenomatosis polyposis, Peutz-Jeghers syndrome, Cronkhite-Canada syndrome, juvenile polyposis, Cowden's disease
Villous tumor	Giant mass with soap bubble appearance	Premalignant; rare in stomach
Bezoar	Giant masslike filling defect; freely movable	Unusual eating habits; gastroparesis or gastric outlet obstruction
MALIGNANT MUCOSAL LESIONS		
Carcinoma	Polypoid mass; ulceration common	Usually advanced gastric cancer but may occasionally be early cancer
BENIGN SUBMUCOSAL LESIONS		
Benign gastrointestinal stromal tumor	Smooth submucosal mass; ulceration common; rarely multiple	May be difficult to differentiate from malignant gastrointestinal stromal tumor
Leiomyoblastoma	Smooth submucosal mass; ulceration common	Risk of malignancy
Lipoma	Submucosal mass with changeable shape at fluoroscopy; fat density on CT	Usually asymptomatic
Hemangioma	Submucosal mass with phleboliths	Risk of massive gastrointestinal bleeding
Lymphangioma	Submucosal mass	Rare
Glomus tumor	Submucosal mass	Usually asymptomatic
Neurofibroma	Solitary or multiple submucosal masses	Von Recklinghausen's disease
Granular cell tumor	Solitary or multiple submucosal masses	Associated lesions on skin or tongue
Inflammatory fibroid polyp	Sessile or pedunculated polyp in antrum; usually solitary	Usually asymptomatic
Ectopic pancreatic rest	Submucosal mass with central umbilication; usually on greater curvature of distal antrum	Usually asymptomatic
Duplication cyst	Submucosal mass on greater curvature of antrum or body; rarely communicates with lumen	Usually asymptomatic during first year of life
Varices	Multiple submucosal masses in fundus (likened to a bunch of grapes)	Portal hypertension or splenic vein obstruction
MALIGNANT SUBMUCOSAL LESIONS		
Malignant gastrointestinal stromal tumor	Solitary, lobulated submucosal mass; ulceration or cavitation common	Better prognosis than carcinoma
Metastases	One or more submucosal masses; ulceration or cavitation common; bull's-eye lesions of varying sizes	Most commonly malignant melanoma or metastatic breast cancer
Lymphoma	One or more submucosal masses; ulceration or cavitation common; bull's-eye lesions of varying sizes	Usually non-Hodgkin's lymphoma
Kaposi's sarcoma	Multiple submucosal masses or bull's-eye lesions	Homosexuals with AIDS; usually have Kaposi's sarcoma on skin
Carcinoid	Multiple submucosal masses or bull's-eye lesions	Carcinoid syndrome uncommon
Leukemia	Multiple submucosal masses or polyps	Rare
Multiple myeloma	Multiple submucosal masses	Rare

TABLE
36-3

Thickened Gastric Folds

Cause	Distribution	Comments
BENIGN CONDITIONS		
Antral gastritis	Antrum	Epigastric pain or dyspepsia
<i>Helicobacter pylori</i> gastritis	Usually antrum or antrum and body; sometimes diffuse	Associated with peptic ulcer disease
Hypertrophic gastritis	Fundus and body	Increased acid secretion; frequent duodenal ulcers
Ménétrier's disease	Fundus and body (massive folds)	Hypochlorhydria and hypoproteinemia
Zollinger-Ellison syndrome	Fundus and body (increased secretions; ulcers common)	Hypergastrinemia resulting from non-beta islet cell tumors
Varices	Fundus and cardia (serpentine folds)	Portal hypertension or splenic vein obstruction
Eosinophilic gastritis	Antrum	Peripheral eosinophilia; history of allergic diseases
Crohn's disease	Antrum and body	Associated Crohn's disease in small bowel or colon
Sarcoidosis	Antrum	Pulmonary sarcoidosis
Tuberculosis	Antrum	History of AIDS or travel to endemic areas
Caustic ingestion	Antrum	History of caustic ingestion
Radiation	Antrum	History of radiation therapy (>50 Gy)
Floxuridine toxicity	Antrum and body	Hepatic artery infusion chemotherapy
Amyloidosis	Antrum	Systemic amyloidosis
MALIGNANT CONDITIONS		
Lymphoma	Localized or diffuse	May have generalized lymphoma
Carcinoma	Localized or diffuse	Associated narrowing and rigidity of stomach

TABLE
36-4

Gastric Narrowing

Cause	Radiographic Findings	Comments
BENIGN CONDITIONS		
Scarring from peptic ulcer disease	Smooth or asymmetric antral narrowing	History of ulcers
Atrophic gastritis	Diffusely narrowed, tubular stomach with decreased or absent folds	Pernicious anemia
Eosinophilic gastritis	Antral narrowing	Peripheral eosinophilia; history of allergic diseases
Crohn's disease	Funnel-shaped antral narrowing (ram's horn or shofar sign)	Associated Crohn's disease in small bowel or colon
Sarcoidosis	Cone-shaped antral narrowing	Pulmonary sarcoidosis
Tuberculosis	Antral narrowing; fistulas common	History of AIDS or travel to endemic areas
Syphilis	Funnel-shaped antral narrowing	Occurs in <1% of patients with syphilis
Caustic ingestion	Narrowing of antrum or antrum and body	History of caustic ingestion; esophageal scarring in 20%
Radiation	Antral narrowing	History of radiation therapy (>50 Gy)
Cytomegalovirus infection	Antral narrowing and ulceration	History of AIDS
Amyloidosis	Antral narrowing	Systemic amyloidosis
Antral diaphragm or web	Transverse weblike area of antral narrowing	May be asymptomatic
MALIGNANT CONDITIONS		
Scirrhous carcinoma	Linitis plastica	Antral narrowing classic, but isolated involvement of proximal stomach in 40%
Metastatic breast cancer	Linitis plastica	Recent or remote history of breast cancer
Omental cake	Mass effect and spiculated folds on greater curvature; occasionally circumferential	Omental metastases from ovarian carcinoma or other malignant neoplasms
Non-Hodgkin's lymphoma	Linitis plastica	May have generalized non-Hodgkin's lymphoma
Hodgkin's lymphoma	Linitis plastica	May have generalized Hodgkin's lymphoma
Kaposi's sarcoma	Linitis plastica	Homosexuals with AIDS; usually have Kaposi's sarcoma on skin

TABLE 36-5 Gastric Outlet Obstruction

Cause	Radiographic Findings	Comments
Peptic ulcer disease	Antral, pyloric, or duodenal ulcer with spasm, edema, or scarring	Difficult to differentiate from tumor if high-grade obstruction
Antral scarring	Antral narrowing	Crohn's disease, sarcoidosis, tuberculosis, syphilis, caustic ingestion, radiation
Carcinoma	Infiltrating antral or pyloric channel tumor	Usually advanced lesions
Other malignant tumors	Irregular narrowing or extrinsic compression of antrum or duodenum	Pancreatic carcinoma, lymphoma, retroperitoneal metastases
Hypertrophic pyloric stenosis	Elongated, narrowed pylorus	Uncommon cause of obstruction in adults
Antral diaphragm or web	Transverse, weblike area of antral narrowing	Degree of obstruction depends on size of central aperture of web
Gastric volvulus	Dilated, upside-down intrathoracic stomach	Surgical emergency if incarcerated or strangulated
Gastroparesis	Flaccid stomach with decreased or absent peristalsis but no gastric outlet obstruction	History of diabetes, narcotic use, or other conditions associated with gastroparesis

TABLE 36-6 Duodenal Filling Defects

Cause	Radiographic Findings	Comments
NON-NEOPLASTIC CONDITIONS		
Prolapsed antral mucosa	Mushroom-shaped defect at base of bulb	Usually asymptomatic
Flexural pseudotumor	Filling defect at superior duodenal flexure resulting from redundant mucosa	May simulate mass
Heterotropic gastric mucosa	Tiny, polygonal, or angulated nodules at base of bulb	No clinical significance
Brunner gland hyperplasia	Multiple rounded nodules in proximal duodenum (Swiss cheese appearance)	Associated with duodenitis
Benign lymphoid hyperplasia	Multiple tiny, rounded nodules in proximal duodenum	Associated with immunologic disorders
Choledochocoele	Submucosal mass in region of ampulla	Congenital anomaly
Duplication cyst	Submucosal mass on medial wall of descending duodenum	Congenital anomaly
Intramural hematoma	Submucosal mass on medial wall of duodenum	Bleeding diathesis, anticoagulation, or trauma
BENIGN TUMORS		
Polyps	Smooth, sessile elevations; usually solitary	Hyperplastic or adenomatous
Polypoid syndromes	Multiple polypoid lesions	Familial adenomatous polyposis, Peutz-Jeghers syndrome, Cronkhite-Canada syndrome, juvenile polyposis
Villous adenoma	Polypoid mass with frondlike projections; usually near ampulla	High malignant potential
Mesenchymal lesions	Submucosal mass, often with central ulceration or umbilication	Leiomyoma, lipoma, neurogenic tumor, Brunner gland hamartoma, ectopic pancreatic rest
MALIGNANT TUMORS		
Duodenal carcinoma	Polypoid mass at or distal to papilla of Vater	Gastrointestinal bleeding or obstruction
Ampullary carcinoma	Polypoid mass in region of ampulla	Jaundice common
Malignant gastrointestinal stromal tumor	Lobulated submucosal mass; ulceration or cavitation common	Better prognosis than carcinoma
Metastases	Multiple submucosal masses or bull's-eye lesions	Most commonly malignant melanoma or metastatic breast cancer
Lymphoma	Multiple submucosal masses or bull's-eye lesions	Usually non-Hodgkin's lymphoma
Kaposi's sarcoma	Multiple submucosal masses or bull's-eye lesions	Homosexuals with AIDS; usually have Kaposi's sarcoma on skin
Carcinoid	Multiple submucosal masses or bull's-eye lesions	Carcinoid syndrome uncommon

**TABLE
36-7****Thickened Duodenal Folds**

Cause	Radiographic Findings	Comments
Duodenitis	Thickened, nodular folds in proximal duodenum; occasionally associated with erosions	Not a reliable diagnosis unless folds grossly thickened
Brunner gland hyperplasia	Thickened, nodular folds in proximal duodenum	Usually associated with duodenitis
Chronic renal failure	Markedly thickened, nodular folds, particularly in bulb	Usually on dialysis
Pancreatitis	Thickened folds associated with medial compression or widening of duodenal sweep	Elevated serum amylase level; CT, MRI, or ultrasound for confirmation
Zollinger-Ellison syndrome	Thickened folds in stomach, duodenum, and proximal jejunum	Ulcers in atypical locations
Crohn's disease	Thickened folds, ulceration, or strictures	Associated Crohn's disease in small bowel or colon
Parasitic infection (giardiasis, strongyloidiasis)	Thickened or effaced folds, irritability, and spasm in duodenum and proximal jejunum	Stool cultures or small bowel brushings and biopsy specimens for diagnosis
Cryptosporidiosis	Thickened folds in duodenum and small bowel	History of AIDS; profuse secretory diarrhea
Celiac disease	Thickened folds in proximal duodenum	Often associated with bubbly bulb
Intramural hemorrhage	Thickened, spiculated folds or thumbprinting	History of bleeding diathesis, anticoagulation, or trauma
Varices	Serpentine folds in proximal duodenum	Portal hypertension
Lymphoma	Thickened folds or thumbprinting	Usually non-Hodgkin's lymphoma

**TABLE
36-8****Dilated Duodenum (Megaduodenum)**

Cause	Associated Radiographic Findings	Comments
Scleroderma	Dilated small bowel with hide-bound appearance	Systemic signs of scleroderma
Celiac disease	Dilated small bowel with decreased number of folds in jejunum	Malabsorption
Zollinger-Ellison syndrome	Thickened folds and increased secretions in stomach and duodenum; one or more ulcers	Hypergastrinemia
Strongyloidiasis	Thickened or effaced folds, ulceration, or lead pipe appearance in duodenum and jejunum	History of AIDS or travel to endemic areas
Superior mesenteric root syndrome	Broad, linear crossing defect on distal duodenum by mesenteric root	Thin or bedridden patients
Vagotomy	Dilated small bowel	Appropriate surgical history
Obstruction	Benign or malignant narrowing or extrinsic compression of duodenum	Postbulbar ulcer, Crohn's disease, pancreatitis, metastatic disease
Ileus	Dilated duodenum without mechanical obstruction	Postoperative ileus, metabolic imbalance, pancreatitis

**TABLE
36-9****Extrinsic Impressions on the Duodenum**

Cause	Location	Radiographic Findings	Comments
Pancreatic disease	Medial	Widened duodenal sweep	Pancreatitis, pancreatic pseudocyst, or pancreatic carcinoma
Peripancreatic adenopathy	Medial	Widened duodenal sweep	Peripancreatic metastases or lymphoma
Aortic aneurysm	Medial	Widened duodenal sweep	Aortoduodenal fistula is a rare complication
Gallbladder disease	Superior	Extrinsic compression of bulb or proximal duodenum	Acute or chronic cholecystitis or hydrops of the gallbladder
Liver disease	Superior	Extrinsic compression of bulb or proximal duodenum	Hepatomegaly of any cause
Renal disease	Posterolateral	Extrinsic compression of descending duodenum	Polycystic kidneys, renal cell carcinoma
Colonic disease	Anterolateral	Extrinsic compression of descending duodenum	Carcinoma of the hepatic flexure

SECTION

VI

Small Bowel

Barium Examinations of the Small Intestine

STEPHEN E. RUBESIN

CHAPTER OUTLINE

Normal Small Intestine

Principles for Performing and Interpreting Small Bowel Examinations

Small Bowel Follow-Through

Peroral Pneumocolon

Enteroclysis

Preparation

Metoclopramide

Anesthesia

Intubation

Single-Contrast Enteroclysis

Air-Contrast Enteroclysis

Methylcellulose-Contrast Enteroclysis

Hypotonic Duodenography

Small Bowel Studies Using Water-Soluble Contrast Agents

Retrograde Examinations of the Small Intestine

Barium Enema

Ileostomy Enema

Choice of Fluoroscopic Examination

Chronic Diarrhea

Small Bowel Obstruction

Abdominal Pain

Suspected Perforation

Malabsorption

Unexplained Gastrointestinal Bleeding

The focus of this chapter is on barium examinations of the mesenteric small intestine. Normal anatomy pertinent to understanding barium examinations is presented. The variety of contrast examinations for studying the small intestine is then described. Finally, a symptom-based approach to contrast imaging of the small intestine is presented.

Normal Small Intestine

The small intestine is extremely tortuous, beginning at the pylorus and extending about 11 feet in the living human from the pylorus to the ileocecal valve. Intestinal length is extremely variable, depending on neuromuscular tone and vascular flow. For example, the denervated, bloodless intestine stretched at autopsy varies from 10 to 30 feet.¹ A patient with a small bowel obstruction will have a tortuous, long, and wide small intestine in which the jejunum may fall deep into the pelvis.

The mesenteric portion of the small intestine is suspended from the retroperitoneum by the relatively short root of the small bowel mesentery, extending about 15 cm from the duodenojejunal junction to the right iliac fossa.² The mesenteric small intestine is divided into the jejunum and ileum. The jejunum arbitrarily comprises the proximal 40% of the mesenteric small intestine and the ileum makes up the distal 60% (Fig. 37-1). The jejunum typically occupies the left upper quadrant, and the ileum occupies the pelvis and right lower quadrant. The location of the jejunum and ileum is often variable, however, given the mobility of the intestine on the root of the mesentery. Not infrequently, the jejunum flops into the right upper quadrant or changes position during fluoroscopic examination of the small bowel.

The small intestine has a smooth curvilinear contour, as readily seen on abdominal radiographs or cross-sectional imaging studies in patients with free intraperitoneal air. The inner contour of the intestine is characterized by folds that encircle the lumen, known as the folds of Kerckring, valvulae conniventes, or plicae circulares (Fig. 37-2). These folds are composed of mucosa and submucosa (Fig. 37-3) and increase the surface area of the small intestine by 300%.¹ The small bowel folds lie perpendicular to the longitudinal axis of the intestine and are thicker, taller, and more numerous in the jejunum than in the ileum (Table 37-1).^{2,3} Villi are leaf- or finger-shaped protrusions of epithelium and lamina propria (see Fig. 37-3) that stud the surface of the folds. Each villus has a core of lamina propria containing a cellular stroma, capillaries, a lacteal, and nerves. Villi are tall and thin in the jejunum and shorter and broader in the ileum.¹ Duodenal villi are more variable and can be short and broad, leaf-shaped, or branched.¹ The villi are about 1 mm in cross section and are just at the limits of fluoroscopic resolution (Fig. 37-4). In contrast, the microvillous brush border of the small intestine is invisible on all radiographic examinations.

The small intestine is one of the largest immunologic organs of the body and a major site of interaction with foreign food antigens, pathogens, and toxins.⁴ The host defenses begin at the epithelial surface with a mucus layer containing immunoglobulins (especially secretory IgA) and enzymes. This mucus prevents microbes from adhering to the epithelium and acts as a buffer and lubricant.¹ A variety of other defenses also protect the host from these food antigens, including intraluminal gastric acid, bile salts, and pancreatic enzymes, and small bowel peristalsis.

The small bowel epithelium is composed of a single layer of cells bound by tight junctions impermeable to large molecules and pathogens. Intramucosal phagocytes include granulocytes, macrophages, and Paneth cells. Three distinct lymphocyte populations are present in the intestine within the epithelium, lamina propria, and Peyer's patches. Intraepithelial lymphocytes



Figure 37-1 Normal small intestine. Overhead radiograph from enteroclysis (small bowel enema) shows the jejunum (J) in the left upper quadrant and the ileum (I) in the right lower quadrant. The transverse colon is also seen (T). The folds are more numerous, taller, and slightly thicker in the jejunum than in the ileum. The jejunum can be up to 4 cm in diameter and the ileum up to 3 cm in diameter.

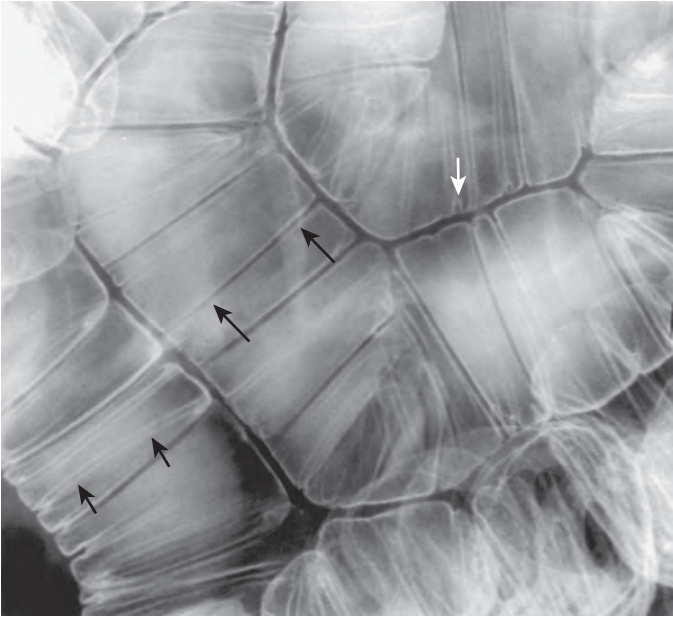


Figure 37-2 Normal small bowel folds. Spot image of the mid-small intestine from enteroclysis shows the folds as linear radiolucent filling defects (long black arrows) in the shallow barium pool. In contrast, nondependent folds are etched in white (short black arrows). The height of the folds (white arrow) indicates that this image was obtained from the distal jejunum–proximal ileum. The mucosal surface is smooth.

are located in the basal portion of the epithelium and comprise up to 30% of the cell population in the mucosa. Immunocytes in the lamina propria are composed mainly of IgA-secreting plasma cells and lymphocytes. T lymphocytes of helper-inducer and suppressor-cytotoxic types are present. Lymphoid



Figure 37-3 Portions of two small bowel folds are present on this histologic photomicrograph. Each fold (plica) is composed of a mucosal layer (M) (epithelium, lamina propria, and muscularis mucosae) covering a submucosal core (S). Each villus (arrow) is composed of a single layer of epithelial cells covering a core of lamina propria. The muscularis propria is composed of an inner circular muscle layer (C) and outer longitudinal muscle layer (L).

TABLE 37-1 Normal Parameters for Enteroclysis and Small Bowel Follow-Through		
Parameter	Enteroclysis	Small Bowel Follow-Through
NUMBER OF FOLDS PER INCH		
Jejunum	Four to seven	Difficult to count
Ileum	Two to four (or less)	Difficult to count
FOLD THICKNESS (MM)		
Jejunum	1-2	2-3
Ileum	1-1.5	1-2
FOLD HEIGHT (MM)		
Jejunum	3-7	Difficult to assess
Ileum	1-3	Difficult to assess
LUMEN WIDTH (CM)		
Jejunum	<4 cm	<3
Ileum	<3	<2

aggregates span the muscularis mucosae, with portions of these aggregates in the lamina propria and submucosa. These lymphoid aggregates increase in size and number in the distal ileum (Fig. 37-5), forming confluent Peyer’s patches in the lower ileum. A specialized epithelium that is one cell layer in thickness separates these lymphoid aggregates from the lumen, facilitating antigen processing. The lymphoid aggregates do not have a capsule, defined borders, a medulla, or afferent lymphatics that are present in lymph nodes.¹ The follicular areas are composed of B cells, and the parafollicular regions are composed of T cells.

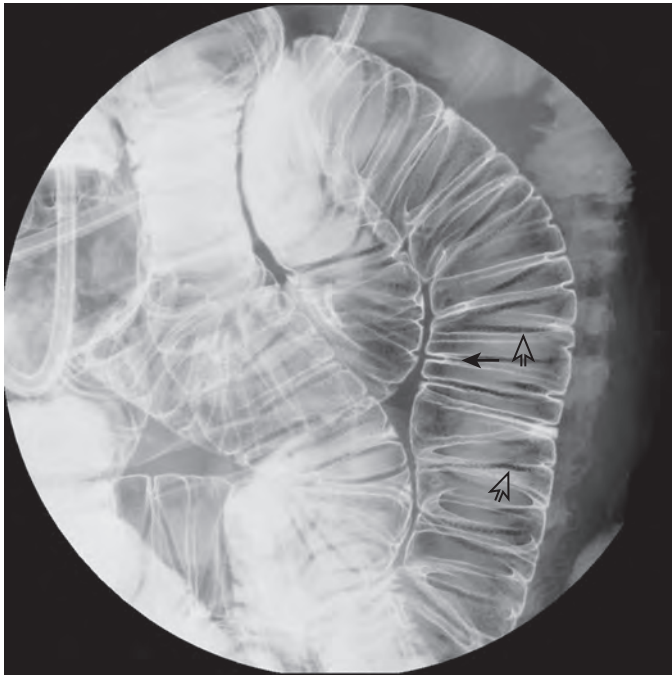


Figure 37-4 Normal villi demonstrated by enteroclysis. Spot image of the jejunum shows villi in one loop as tiny, submillimeter, round radiolucent filling defects (*open arrows*). This loop can be identified as jejunum by the relatively tall height of the folds (*thin arrow*).



Figure 37-5 Lymphoid hyperplasia of the distal ileum caused by common variable immunodeficiency. Spot image of the distal ileum shows numerous 1- to 2-mm round or ovoid radiolucent filling defects in the shallow barium pool (*arrow*). These lymphoid follicles are more numerous and extend more proximally than usual. The ileal side of the ileocecal valve is identified (*I*).

Principles for Performing and Interpreting Small Bowel Examinations

The small intestine is a difficult structure to image. The intraluminal environment is hostile to barium preparations. A large amount of fluid (≈ 9 L) enters the small intestine each day, with only 1.5 to 1.9 L entering the colon.⁵ Bile acids, gastric acids, pancreatic secretions, and the epithelial mucus layer interact with barium in the small intestine. Fortunately, most modern barium suspensions no longer suffer from flocculation and clumping, as often occurred in the past.

Because of the inherent length and motility of the small intestine, imaging of this structure can take a long time. Intestinal loops overlap and change in size, shape, and position with peristalsis. Normal small bowel transit ranges from 30 to 120 minutes. The transit time can be lengthened dramatically in patients with obstruction or adynamic ileus from various causes.

The radiologist evaluates the overall location, course, and size of various portions of the small intestine.⁶ For example, the radiologist determines the location of the duodenojejunal junction and the location of the first loops of jejunum. The radiologist also evaluates the luminal contour and searches for abnormalities that extend beyond the small intestine (e.g., diverticula [Fig. 37-6], sacculations, ulcers, exoenteric masses) or lesions that protrude into the lumen (e.g., polyps [Fig. 37-7], abnormal folds). The small bowel folds are best evaluated when the lumen is fully distended, and the folds lie perpendicular to



Figure 37-6 Jejunal diverticula. Spot image from enteroclysis shows at least 10 small diverticula extending from the mesenteric border of a jejunal loop. Some diverticula are etched in white by barium (*white arrows*), and others are filled with barium (*black arrow*).

the longitudinal axis of the bowel. Fold width also depends on the degree of luminal distention; the greater the distention, the thinner the folds appear (Fig. 37-8). The folds are best shown after mucus has been washed off the luminal surface by the barium column. If folds are evaluated long after the barium column has passed, intestinal secretions can lift barium away

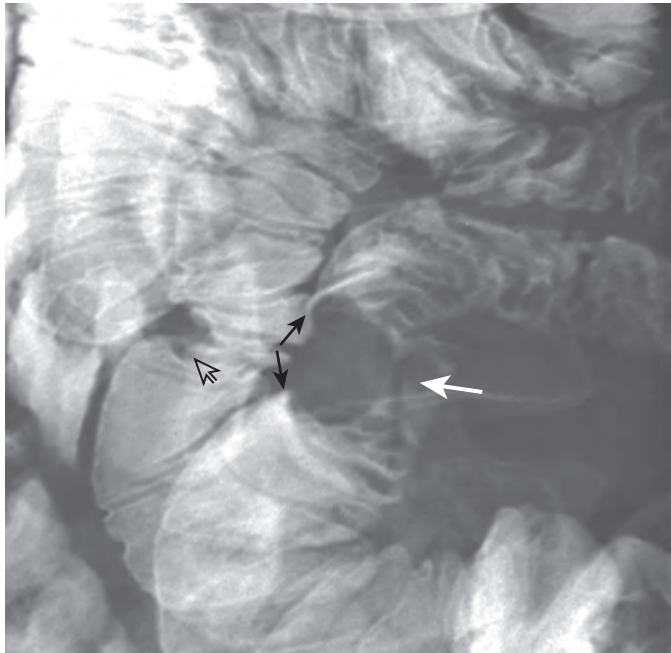


Figure 37-7 Carcinoid tumor in the ileum. Spot image of the distal ileum shows a 1.5-cm ovoid radiolucent filling defect (white arrow) protruding into the barium column. Note how the folds (black arrows) are pulled toward the tumor by a desmoplastic reaction at the base of the lesion. A second small carcinoid tumor is seen (open arrow). This desmoplastic reaction is typical of carcinoid tumors or intraperitoneal metastases.

from the mucosal surface so that the folds may erroneously appear thickened. En face mucosal detail is seen during compression of the barium column or with double-contrast technique. Visualization of this mucosal detail is necessary for detecting mucosal granularity or nodularity or small ulcers, such as aphthoid ulcers (Fig. 37-9).

Fluoroscopy is a key component of any small bowel examination. The radiologist examines the head of the barium column to understand the course of the small intestine and to detect contour abnormalities or filling defects in the barium column. The radiologist also assesses bowel motility, distensibility, and pliability during the fluoroscopic examination. Fixation of intestinal loops can also be recognized by manual palpation of the bowel.

Small Bowel Follow-Through

There are many ways to perform a small bowel follow-through examination. In this chapter, I discuss the technique that I use. A small bowel follow-through is a single-contrast examination of the esophagus, stomach, and small intestine that uses barium most appropriate for the small bowel. For this examination, the patient drinks a large volume (500-1000 mL) of low-density (30%-50% w/v) barium specifically designed for evaluating the small intestine.

The patient should not eat or drink after 9 to 11 PM the day before the examination. If a peroral pneumocolon is to be performed, the patient should receive a barium enema preparation to cleanse the terminal ileum and right side of the colon.

A single-contrast upper gastrointestinal (GI) series is often performed (using 1-2 cups of low-density barium) as a prelude to examining the small bowel. The purpose of the upper GI series is to show gross upper GI involvement by diseases that affect the small bowel, such as Crohn's disease and scleroderma. Esophageal or gastric abnormalities may also be detected as incidental findings, given the high frequency of upper GI

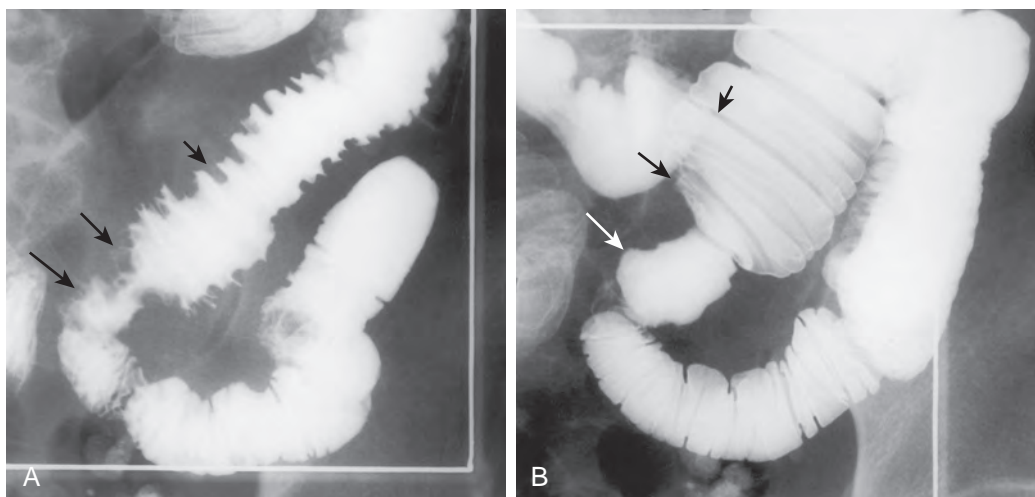


Figure 37-8 Variation in the width of small bowel folds with luminal distention. **A.** Spot image obtained during early single-contrast phase of enteroclysis shows a focal area of tapered narrowing (medium-sized arrow) containing an irregular collection of barium (long arrow). Note apparent widening of the small bowel folds (short arrow) when the lumen is incompletely distended. **B.** Spot image obtained during early phase of methylcellulose filling (the loop is still visualized mainly in single contrast before a transradiant methylcellulose effect has been achieved) shows how the narrowed segment has a more abrupt proximal margin (long black arrow). An amorphous collection of barium (white arrow) disrupts the normal luminal contour and fold pattern. This was an ulcerated adenocarcinoma of the distal jejunum causing low-grade small bowel obstruction. Note the normal width of the small bowel folds (short black arrow) in the distended jejunum proximal to the tumor.

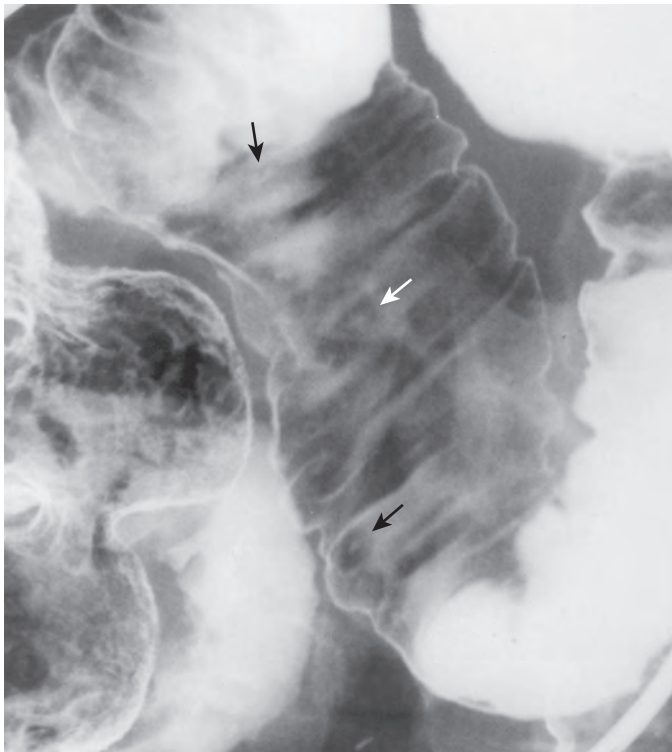


Figure 37-9 Aphthoid ulcers in Crohn's disease. Spot image of the terminal ileum from a peroral pneumocolon shows aphthoid ulcers (arrows) as punctate barium collections surrounded by radiolucent halos of edema.

disorders such as gastroesophageal reflux disease. However, a double-contrast upper GI examination using high-density barium is not performed, because this barium is not designed for evaluating the small intestine and, if used, high-density barium often prevents adequate visualization of pelvic small bowel loops. The radiologist therefore sacrifices double-contrast evaluation of the upper GI tract to ensure a more optimal examination of the small intestine. After the esophagus, stomach, and duodenum are evaluated, the patient leaves the fluoroscopic suite and slowly sips an additional 1 to 2 cups of low-density barium.

In some practices, a technologist obtains overhead radiographs and a radiologist evaluates the overheads views, only fluoroscopy and palpating the small bowel when an abnormality is suspected or when barium has reached the terminal ileum. Such an approach is strongly discouraged. A small bowel follow-through relies on fluoroscopic detection and spot image documentation of all abnormalities. Each loop of small bowel is palpated when it is optimally distended by low-density barium (Fig. 37-10). The radiologist should therefore evaluate the patient at least several times—about 15 to 30 minutes after the single contrast upper GI series is performed and then at 15- to 45-minute intervals, depending on how fast the barium column is progressing through the small intestine. The patient is turned into various positions, and manual palpation (including supine, lateral, and prone compression views) is used to splay out individual small bowel loops. In my practice, I no longer obtain overhead radiographs. If the big picture is required, a digital spot radiograph obtained at the lowest magnification is usually adequate for this purpose.

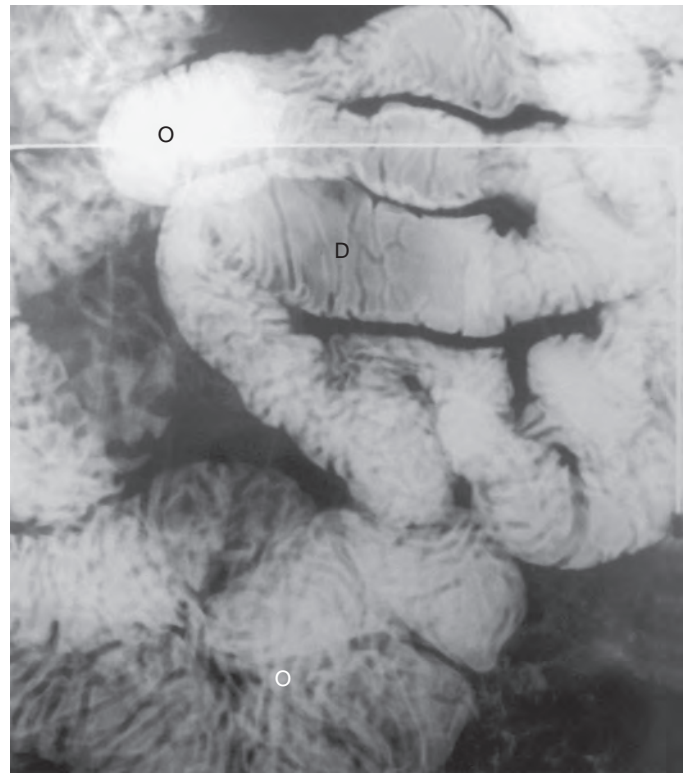


Figure 37-10 Normal small bowel follow-through. Spot radiograph with compression shows the distal jejunum. When the loops are well distended (D) and separated from each other, an image from a small bowel follow-through is comparable to that from enteroclysis. When loops are overlapping (black O), however, the density of the barium may obscure anatomic detail. When loops are overlapping and partially collapsed, the overlapping folds may form a feathery pattern (white O).

The length of the examination can be shortened by administering a standard dose of 20 mg of metoclopramide (Reglan) orally 20 to 30 minutes before the study or 10 mg intravenously at the beginning of the examination.⁷⁻⁹ Metoclopramide accelerates gastric emptying and small bowel transit. Unfortunately, metoclopramide also increases resting muscle tone, resulting in incomplete small bowel distention.¹⁰ The result is a faster but less optimal examination.

Some radiologists administer two to three doses of effervescent agent (600-900 mL of CO₂) when the barium column reaches pelvic loops of ileum or the terminal ileum. This technique shortens the examination and demonstrates small bowel loops on an air-contrast study. Nevertheless, administration of an effervescent agent can be uncomfortable because large volumes of gas can incite intestinal cramping. It also results in decreased luminal distention in comparison to enteroclysis, and only one third to one half of the small bowel is shown on the air-contrast study.¹¹

Some radiologists use a premade mixture of 24% w/v barium suspended in methylcellulose. This barium suspension produces greater luminal distention than a routine small bowel follow-through, as well as a transradiant effect that mimics enteroclysis.¹² However, the barium is not as dense as that used for a routine small bowel follow-through so it can be more difficult to detect filling defects in the barium column. Luminal distention is also less than that in

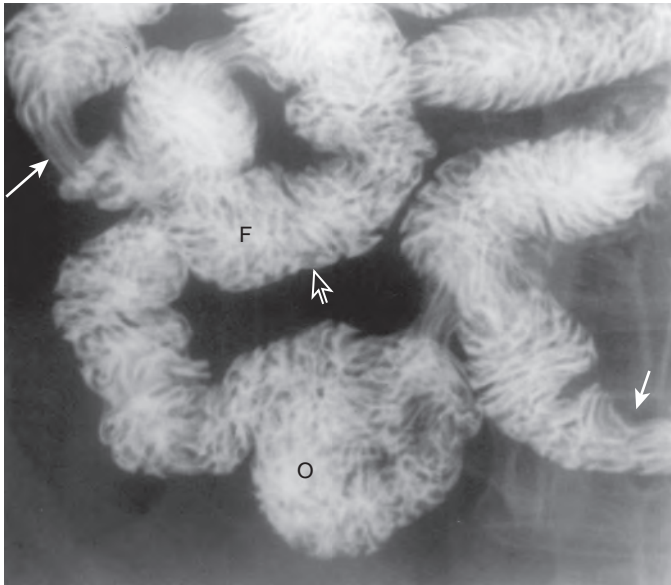


Figure 37-11 Partially distended small bowel during small bowel follow-through. Folds (F) in a partly distended proximal ileal loop have a feathery pattern. The contour is well visualized (open arrow) when a loop is isolated. When loops are contracting (short arrow), a smooth impression is seen on the mesenteric border, mimicking an extrinsic lesion indenting the small bowel. When a loop is collapsed or contracting, folds lie parallel to the longitudinal axis of the small bowel (long arrow). Dense areas of barium may result from overlapping loops (black O) that can be separated by compression.

enteroclysis, because it is limited by the rate of gastric emptying at the pylorus.

The small bowel follow-through has two important limitations. Even with the use of metoclopramide, the pylorus delays emptying of barium from the stomach so the small bowel may be incompletely distended. As a result, it can be difficult to evaluate luminal contour (Fig. 37-11) or detect filling defects in the barium column. Because normal transit time for the small bowel is 30 to 120 minutes, it also is not feasible for the radiologist to remain in the fluoroscopy suite for the entire examination. As a result, the small bowel can only be evaluated intermittently, and lesions can be missed, depending on the degree of filling and distention of individual small bowel loops at the time of fluoroscopy.

PERORAL PNEUMOCOLON

A peroral pneumocolon may be performed in conjunction with a small bowel follow-through.¹³⁻¹⁶ This is a double-contrast examination, primarily used to evaluate patients with suspected Crohn's disease in the terminal ileum or evaluate the right side of the colon in patients in whom a barium enema or colonoscopy failed to visualize this portion of the bowel adequately.

The patient undergoes a barium enema preparation to clear feces from the terminal ileum and right side of the colon. After a routine small bowel follow-through has been performed, 1 mg of glucagon is administered intravenously, and air is insufflated into the rectum via a Foley catheter. The colon is slowly distended with air as the patient is turned into various positions to manipulate air into the cecum and terminal ileum. Air can be refluxed successfully into the terminal ileum in 85% to 90%

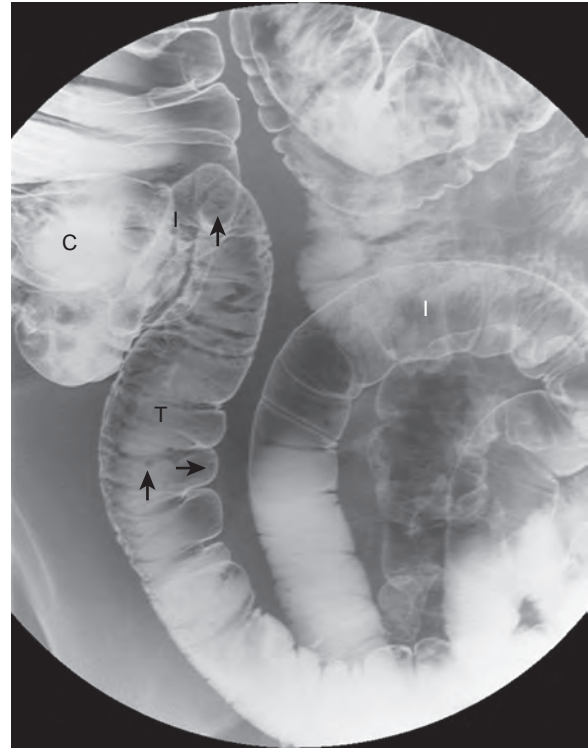


Figure 37-12 Normal distal ileum demonstrated during peroral pneumocolon (arrows). Spot radiograph shows the terminal ileum (T) and distal ileum (white I) in an air-contrast study. The mucosa is smooth and featureless. The ileal folds (arrows) are of normal thickness. The cecum (C) and ileal side of the ileocecal valve (black I) are also identified.

of patients. Double-contrast spot images of the pelvic ileum, terminal ileum, and right side of the colon are then obtained (Fig. 37-12).

Enteroclysis

The small intestine has been examined via intubation techniques since the 1920s.¹⁷⁻²⁰ All these techniques entail positioning a tube beyond the pylorus, overdistending the small bowel with various contrast agents, and detecting abnormalities at fluoroscopy. The multiplicity of techniques for performing enteroclysis reflects the imperfections of each individual technique. Lack of universal acceptance of this procedure by the radiologic community is related to the relatively high level of expertise needed to perform enteroclysis and to patient discomfort during the intubation procedure.

PREPARATION

An unprepped patient often has feces in the terminal ileum and right side of the colon. This fecal matter obscures mucosal detail, mimics polyps, and impedes passage of contrast material through the distal ileum.²¹ A preparation is therefore given to clear feces from the terminal ileum and right colon before the examination. This can be a full barium enema-type preparation, including osmotic cathartics such as magnesium citrate and colonic stimulants such as bisacodyl. At my institution, I have achieved successful cleansing of the right side of the colon with a clear liquid diet the day before the examination

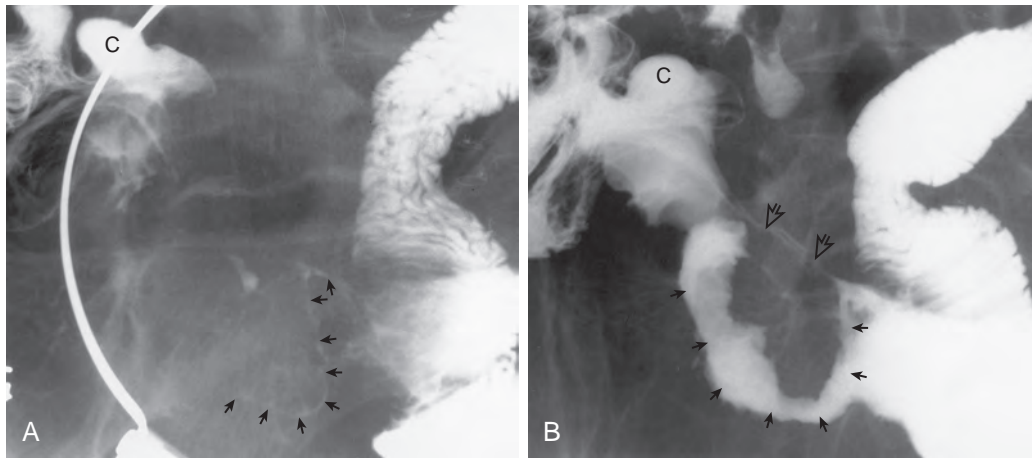


Figure 37-13 Value of metoclopramide for evaluating narrowing of the terminal ileum in a patient with Crohn's disease. **A.** Spot radiograph from a small bowel follow-through shows a stringlike segment of narrowing (arrows) in the terminal ileum inferior to the cecum (C). **B.** After metoclopramide has been administered, the narrowed segment (short arrows) distends considerably but is still abnormal, with effaced folds and nodular mucosa caused by Crohn's disease. An ileoileal fistula (open arrows) is also visualized. These images show how narrowing in Crohn's disease may be caused by a combination of spasm, edema, inflammatory change, and fibrosis.

combined with four 5-mg tablets of bisacodyl given the evening before the examination. The patient does not eat or drink after midnight. On the day of the examination, the patient should temporarily discontinue medications such as narcotics that decrease small bowel peristalsis.

METOCLOPRAMIDE

Metoclopramide is administered orally or intravenously before the examination.^{21,22} Metoclopramide begins to take effect 1 to 3 minutes after intravenous (IV) injection of a 10-mg dose or 30 to 60 minutes after ingestion of two 10-mg tablets.²³ This drug facilitates passage of the enteroclysis catheter by relaxing the pyloric sphincter and duodenal bulb and by increasing gastric antral contractions.^{24,25} Passage of barium through the small bowel is accelerated because metoclopramide increases peristalsis in the duodenum and jejunum. Metoclopramide may also improve visualization of strictures in Crohn's disease (Fig. 37-13). However, its use is contraindicated in patients with known pheochromocytomas because it may stimulate catecholamine release from these lesions, precipitating a hypertensive crisis.²⁶ It is also contraindicated in patients with epilepsy or patients receiving drugs that may cause extrapyramidal reactions because it increases the frequency and severity of seizures associated with these reactions.

ANESTHESIA

The major complaint that patients have about enteroclysis is intubation. Patients can be made more comfortable by the use of conscious sedation.²⁷ One protocol for conscious sedation includes a combination of fentanyl or diazepam for analgesia and midazolam for an amnesic effect.²¹ Oral diazepam alone can be used as an alternative.²⁴

INTUBATION

A variety of enteroclysis catheters are available from several manufacturers.²⁸⁻³⁰ The catheters have a diameter of 8 to 13 F, an end hole or side holes, and a balloon attached to their tips.

One manufacturer has a multiple-lumen catheter capable of a diagnostic study and therapeutic decompression.³¹

I suggest having the patient ingest a small amount (15-30 mL) of enteroclysis barium orally before intubation. This barium coats the antrum, pylorus, and duodenal bulb, which are important landmarks that guide the radiologist in passing the enteroclysis catheter.

A complete description of intubation techniques is beyond the scope of this chapter, but is described in several references.^{6,21,22,24} The enteroclysis catheter can be passed into the oropharynx via an oral or nasal route. The oral route has the advantage of allowing visualization of catheter passage into the throat but the disadvantage of causing more gagging. Oral intubation is made easier by the use of a topical anesthetic spray. In contrast, the nasal route causes less gagging because there is less contact of the catheter with the base of the tongue and posterior pharyngeal wall. However, nasal intubation may cause nasal bleeding and may result in prolonged nasal discomfort as the catheter is manipulated during the examination. Nasal intubation is made easier with the use of topical lidocaine jelly in the intubated naris.

The major purpose of the catheter guidewire is to torque or guide the tip of the catheter along the longitudinal axis of the bowel. The guidewire is sometimes placed at the tip of the catheter, with appropriate torquing to guide the catheter in the proper direction. At other times, the guidewire is retracted, allowing the soft tip of the catheter to pass through sensitive regions, such as the pylorus, or to curve around tight bends, such as the apex of the duodenal bulb (Fig. 37-14). Passage of the catheter into the duodenum is also facilitated by changing the configuration of the bowel with manual compression (Fig. 37-15) or by turning the patient on the fluoroscopic table. The tip of the catheter can be left in the second portion of the duodenum for single-contrast or air-contrast enteroclysis. When methylcellulose is used, however, the tip of the catheter should ideally be placed in the first loop of jejunum to limit reflux of methylcellulose into the stomach. Inflation of the balloon on the catheter also helps prevent methylcellulose from refluxing into the stomach. If the patient complains of discomfort during inflation of the balloon, it should immediately be deflated until

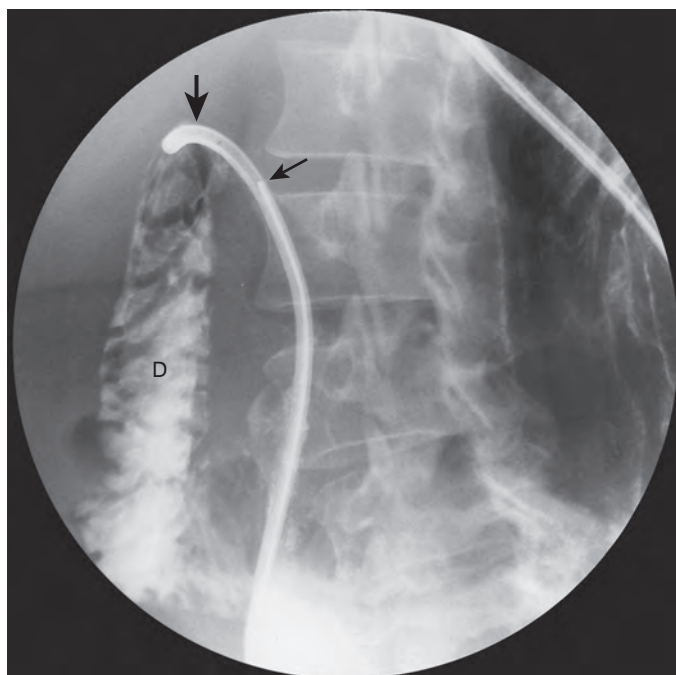


Figure 37-14 Enteroclysis catheter directed around the apex of the duodenal bulb. The soft tip of the enteroclysis catheter is bending around the 180-degree turn (thick arrow) between the duodenal bulb and proximal descending duodenum. The wire (thin arrow) has been retracted, allowing the catheter tip to be more pliable so that it can bend around this curve. Contrast in the duodenum (D) is the residue of 30 mL of barium swallowed at the outset of the study to outline the anatomy of the pyloric region and facilitate passage of the catheter.

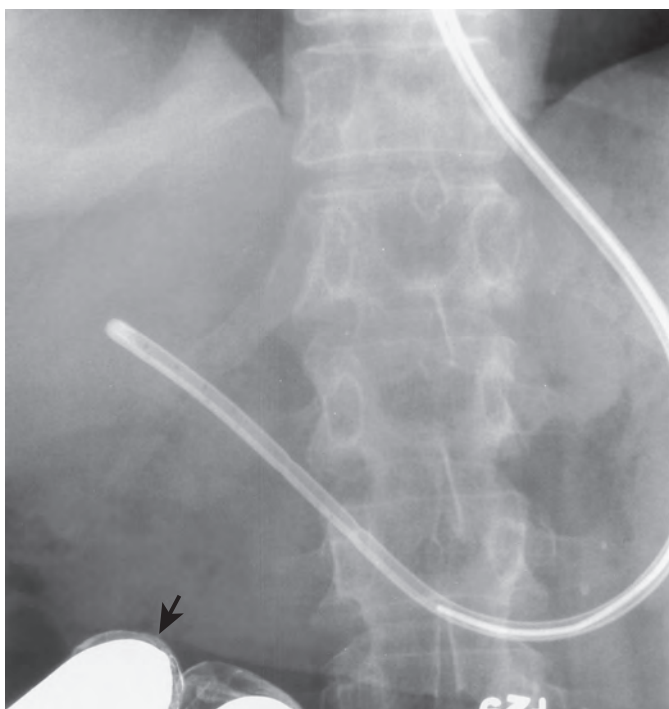


Figure 37-15 Compression by examiner to guide the enteroclysis catheter. The hand of the examiner covered by a lead glove (arrow) pushes on the greater curvature of the stomach. This directs the enteroclysis catheter toward the pylorus. Note how the guidewire is retracted from the tip of the catheter.

the discomfort subsides. Duodenal perforation was reported in one patient during intubation for enteroclysis.³²

Successful intubation during enteroclysis depends on the skill and experience of the examining radiologist, whether or not sedation is used, and the patient's anatomy. Intubation is more difficult in patients with a prominent cricopharyngeus, hiatal hernia, and transversely oriented stomach. Intubation is also potentially more difficult in patients with a dilated atonic stomach resulting from diabetes or other causes.

Contrast material can be infused through the enteroclysis catheter with syringes or a variety of pumps. The use of an electric pump (e.g., a minidialysis pump, RS-7800; Renal Systems, Minneapolis) enables the radiologist to control the infusion rate accurately, which can be adjusted during the examination.³³ If the infusion rate is too fast, overdistention of the jejunum may cause hypotonia of the bowel. If the infusion rate is too slow, however, the lumen may be suboptimally distended, prolonging the examination time. Flow rates are generally between 50 and 150 mL/min.

The following descriptions of the various types of enteroclysis reflect my experiences with these techniques. Each radiologist should carefully evaluate the advantages and disadvantages of each before choosing a particular method for performing enteroclysis.

SINGLE-CONTRAST ENTEROCLYSIS

A low-density (20%-40% w/v) barium is the usual contrast agent for single-contrast enteroclysis.^{25,34} In rare cases of

suspected perforation, water-soluble contrast agents (e.g., meglumine diatrizoate, diatrizoate sodium) can be used. The enteroclysis catheter is passed into the proximal duodenum. Contrast is instilled via a syringe, pump, or gravity feed bag. Between 600 and 1200 mL of barium are injected at an initial rate of about 75 mL/min. After administering a large volume of barium, water may be instilled into the catheter to push barium into the distal ileum and obtain a moderate double-contrast effect.

Single-contrast studies are simpler to perform than other types of enteroclysis because only one contrast agent is used. Reflux of barium into the stomach rarely induces vomiting, as sometimes occurs with methylcellulose. With an air- or methylcellulose-contrast technique, the mucosal surface of the small bowel is readily demonstrated en face. With single-contrast technique, however, evaluation of mucosal detail en face depends on compression and analysis of fold morphology. Although single-contrast technique is inferior to double-contrast techniques for visualizing mucosal detail, the diagnosis of many small bowel abnormalities (e.g., adhesions, tumors, hernias) does not require subtle demonstration of surface detail. In patients with known or suspected malabsorption, however, double-contrast enteroclysis techniques are recommended.

AIR-CONTRAST ENTEROCLYSIS

Air contrast is the standard form of enteroclysis in Japan and has become a favorite technique of Dr. Dean Maglinte, one of the leading proponents of enteroclysis.^{21,35-37} I have used the technique at one of my institutions, where an electric pump was

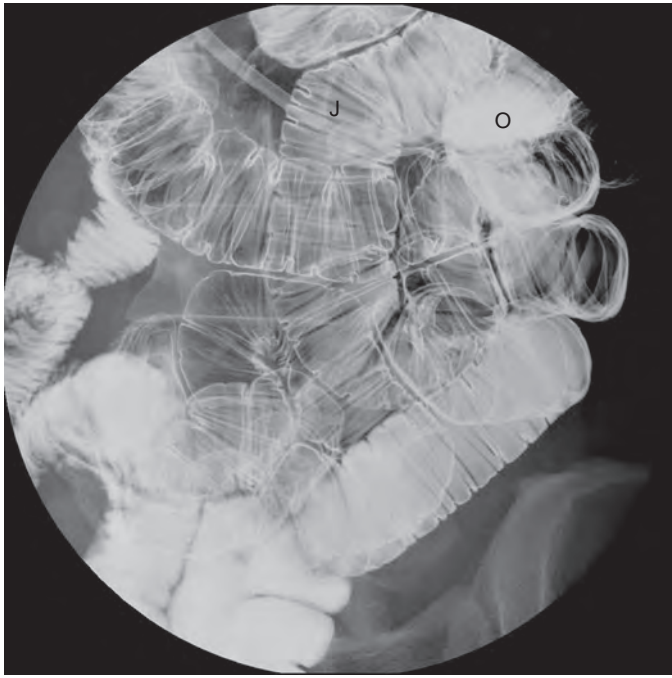


Figure 37-16 Jejunum during air-contrast enteroclysis. Coned-down view from an overhead radiograph demonstrates the small intestine in an air-contrast study. The jejunum (J) is well shown where loops are seen without overlap. When loops overlap (O), however, the small bowel is not optimally visualized.

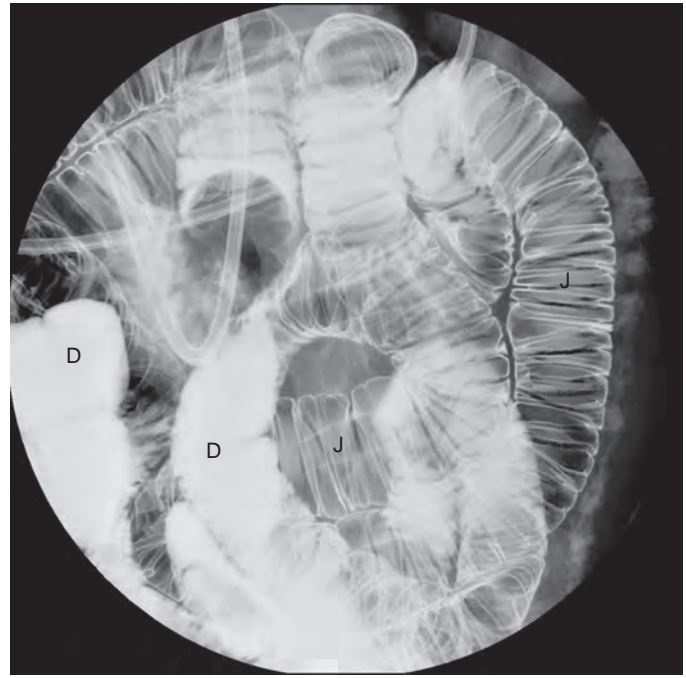


Figure 37-17 Too much barium on air-contrast enteroclysis. Mid-small bowel loops are well visualized (J) in some areas. In other areas, however, dense barium (D) obscures folds and mucosal detail. It is sometimes difficult to titrate the appropriate volume of barium for air-contrast enteroclysis.

not available for methylcellulose infusion. After intubation of the proximal duodenum, between 300 and 600 mL of barium varying from 40% to 80% w/v is instilled by gravity, syringe, or pump. The infusion rate of barium is altered to preserve peristalsis and for uniform distention of the proximal and mid-small bowel. Room air or carbon dioxide is administered when barium reaches the pelvic small bowel²¹ or terminal ileum.³⁷ Small bowel hypotonia may be induced by IV injection of 1 mg of glucagon after barium has reached the right side of the colon.⁶

Air-contrast enteroclysis produces spectacular mucosal detail in loops coated by barium and distended by gas (Fig. 37-16). However, I have found it difficult to titrate the amount of barium necessary to coat the bowel without having too much barium in the lumen. Unlike double-contrast studies of the stomach and colon, it is more difficult to manipulate the barium pool so some loops are visualized only with dense barium, despite using various patient positions and compression (Fig. 37-17). Overlap of barium-filled loops with air-filled loops also results in radiographic overexposure of the loops demonstrated in air contrast. Distention of pelvic loops with air is sometimes incomplete.

Another disadvantage of air-contrast enteroclysis is that injection of large volumes of air into the small intestine may cause considerable discomfort. Sedation of these patients is therefore strongly recommended by some authors.²¹

In summary, I have achieved beautiful demonstration of the jejunum but suboptimal demonstration of pelvic ileal loops with air-contrast enteroclysis. Air-contrast techniques are more likely to be of value for patients with intestinal disease involving long segments of small bowel (e.g., malabsorptive state, Crohn's disease). Methylcellulose-contrast enteroclysis is more effective,

however, for patients with adhesions or other lesions involving shorter segments of bowel.

METHYLCELLULOSE-CONTRAST ENTEROCLYSIS

During methylcellulose-contrast enteroclysis, a small volume of barium is propelled through the small intestine by a large volume of radiolucent liquid (the methylcellulose; Fig. 37-18).^{22,38} Medium-density (40% to 80% w/v) barium coats the intestinal mucosa, and methylcellulose distends the lumen. This is a biphasic examination. The radiologist follows the column of barium, looking for obstructing lesions (see Fig. 37-8) or lesions in the barium pool (Fig. 37-19). The small bowel folds and en face mucosal detail are then evaluated when the lumen is distended by methylcellulose. Full luminal distention by methylcellulose straightens the valvulae conniventes, better delineates en face mucosal detail, and overdistends the lumen, increasing conspicuity of low-grade obstructing lesions.

Varying amounts and densities of barium have been used for methylcellulose-contrast enteroclysis. I routinely use 220 to 300 mL of 80% w/v barium, infusing barium at 60 to 80 mL/min via a syringe until about half of the expected intestinal loops are visualized. Herlinger and associates use 180 to 220 mL of 80% w/v barium.²⁴ Maglinte and colleagues recommend infusing 300 to 600 mL of 50% w/v barium until pelvic loops of the ileum are filled.³⁹ The amount of barium infused for this examination ultimately depends on the perceived length and diameter of the small intestine and on the presence or absence of obstruction or increased intraluminal fluid.

The use of methylcellulose enables the radiologist to see through overlapping small bowel loops to a greater degree than that allowed with single-contrast or air-contrast enteroclysis.

However, methylcellulose-contrast enteroclysis also has several disadvantages. Methylcellulose is a thick sticky substance that may require dilution in the “barium kitchen.” Bubbles will form if methylcellulose is shaken, not stirred. Unless an electric pump is used, methylcellulose is messy and difficult to instill. The enteroclysis catheter tip should be placed in the jejunum because reflux of methylcellulose into the stomach may induce projectile vomiting. If the radiologist needs to visualize the duodenum, the catheter should therefore be retracted to the proximal duodenum at the end of the examination and additional barium infused (Fig. 37-20). Once methylcellulose has reached the

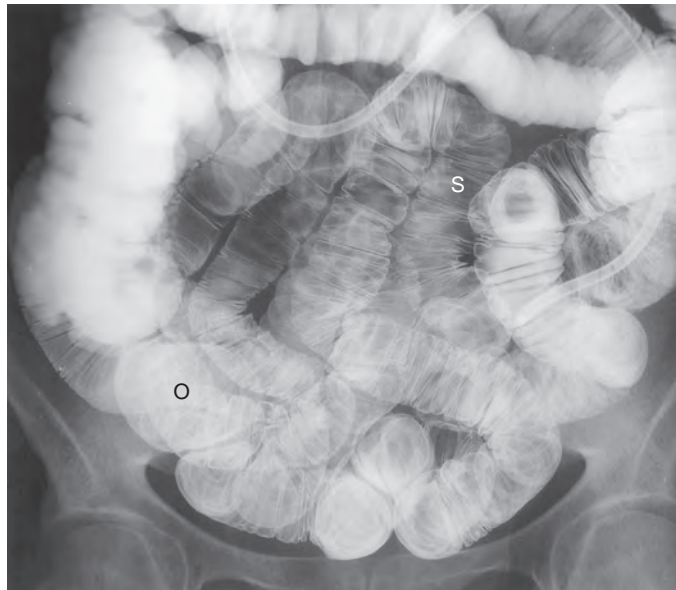


Figure 37-18 Methylcellulose-contrast enteroclysis. Overhead radiograph obtained at the end of the enteroclysis examination shows exquisite anatomic detail in nonoverlapping loops (S). Anatomic detail may be difficult to visualize, however, when loops overlap (O), even though the methylcellulose allows partial visualization of these overlapping loops, termed a *transradiant effect*.

colon, uncontrollable diarrhea may ensue, requiring placement of an enema tip in the rectum to allow rectal drainage and alleviate patient discomfort and embarrassment.

Methylcellulose-contrast enteroclysis almost always results in excellent double contrast in the jejunum. With infusion of enough methylcellulose, a double-contrast examination of the terminal ileum may also be achieved (Fig. 37-21). However, barium diffusion into the methylcellulose may result in a poor double-contrast effect in the ileum, resulting in only a single-contrast examination of the distal ileum (Fig. 37-22). To prevent diffusion of barium into the methylcellulose, the radiologist limits compression, especially in pelvic loops of the ileum. Thus, the double-contrast barium enema and peroral pneumocolon are more reliable techniques if a detailed double-contrast examination of the terminal ileum is required.

HYPOTONIC DUODENOGRAPHY

Hypotonic duodenography is a detailed examination of the duodenum and, in some patients, the first two loops of jejunum.⁶ This examination is used to elucidate confusing radiographic, computed tomography (CT), or endoscopic findings in the duodenum and first loop of the jejunum. High-density barium is administered via an enteroclysis catheter placed in the proximal descending duodenum. After high-density barium has entered the duodenum and first jejunal loop, the patient is rotated on the fluoroscopic table to coat the mucosa. A standard dose of 1 mg of glucagon is administered intravenously to induce intestinal hypotonia. Air is then injected into the catheter to distend the duodenal lumen, and spot images are obtained (Fig. 37-23).

A similar examination can be performed less invasively by having the patient swallow an effervescent agent and high-density barium. The patient is then placed with the right side down. When the duodenum has adequately filled with barium, 1 mg of glucagon is injected IV to induce intestinal hypotonia. The patient is then rotated on the table to coat the mucosa, and spot images are obtained. This technique is limited, however, because there is less control over the volume of barium and air

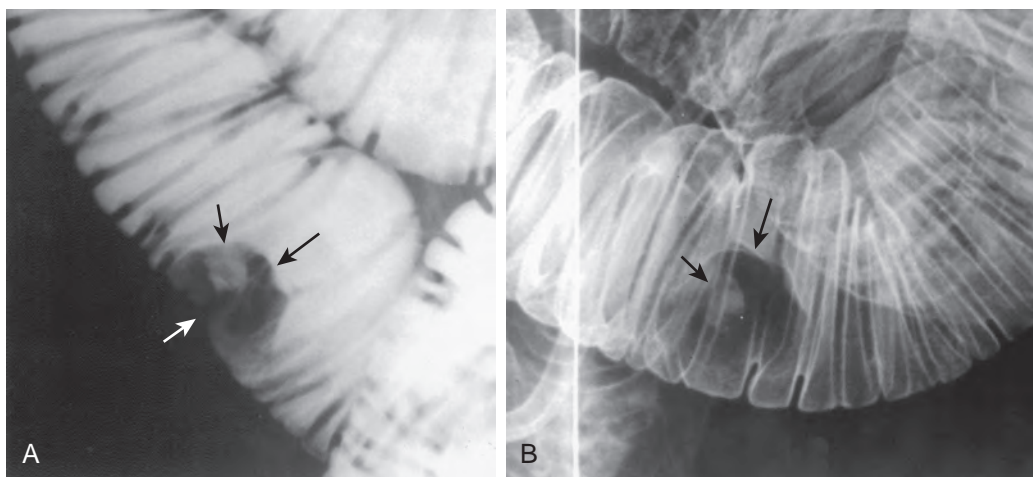


Figure 37-19 Metastatic melanoma demonstrated during enteroclysis. **A.** Spot image obtained during the single-contrast phase of enteroclysis shows a polypoid mass as a lobulated radiolucent filling defect (long black arrow) in the barium column. The normal luminal contour is disrupted (white arrow). A central barium collection is seen (short black arrow). **B.** Spot radiograph obtained during the methylcellulose phase again shows a slightly lobulated radiolucent filling defect (long arrow), with a central barium collection (short arrow), representing an ulcer. Apart from the ulceration, the surface of the polyp is smooth, indicating the submucosal origin of the lesion.

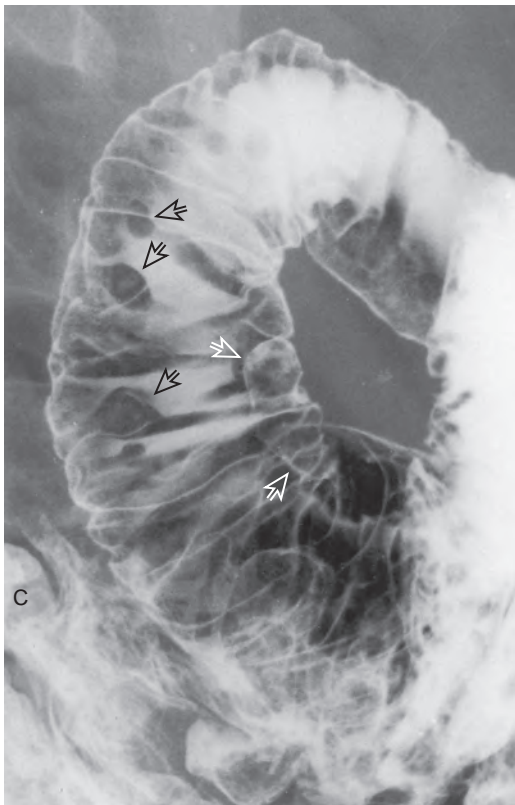


Figure 37-20 Air-contrast examination of duodenum after enteroclysis. Spot radiograph shows multiple small polyps (several identified by open black arrows) as radiolucent filling defects in the shallow barium pool on the posterior wall of the descending duodenum. The papilla of Vater is enlarged (open white arrows). Contrast in the colon (C) partly obscures the third portion of the duodenum. This patient had familial adenomatous polyposis syndrome. The polyps were tubular adenomas; the enlarged papilla of Vater resulted from an adenocarcinoma arising in a tubulovillous adenoma.

in the duodenum with the oral route than with the intubation technique.

Small Bowel Studies Using Water-Soluble Contrast Agents

The small intestine is a hostile environment for imaging with water-soluble contrast agents. These hyperosmolar agents draw fluid into the intestinal lumen and are further diluted by excess fluid in the lumen in patients with hypotonia or obstruction. As a result, the radiographic density of water-soluble contrast agents is generally inadequate for diagnostic purposes in patients with small bowel obstruction. These contrast agents are therefore not indicated for examining the small bowel, except in patients with suspected leaks.

In general, leaks arising in the duodenum or first several loops of jejunum can be demonstrated by water-soluble contrast studies. Leaks in the mid- or distal small bowel, however, are often missed because of dilution of the water-soluble contrast agent with fluid. When a leak is suspected in the distal small bowel (particularly at an ileocolic anastomosis), it may therefore be preferable to perform a water-soluble



Figure 37-21 Crohn's disease demonstrated by enteroclysis. Spot image shows thickened nodular folds (arrows) in the terminal ileum.

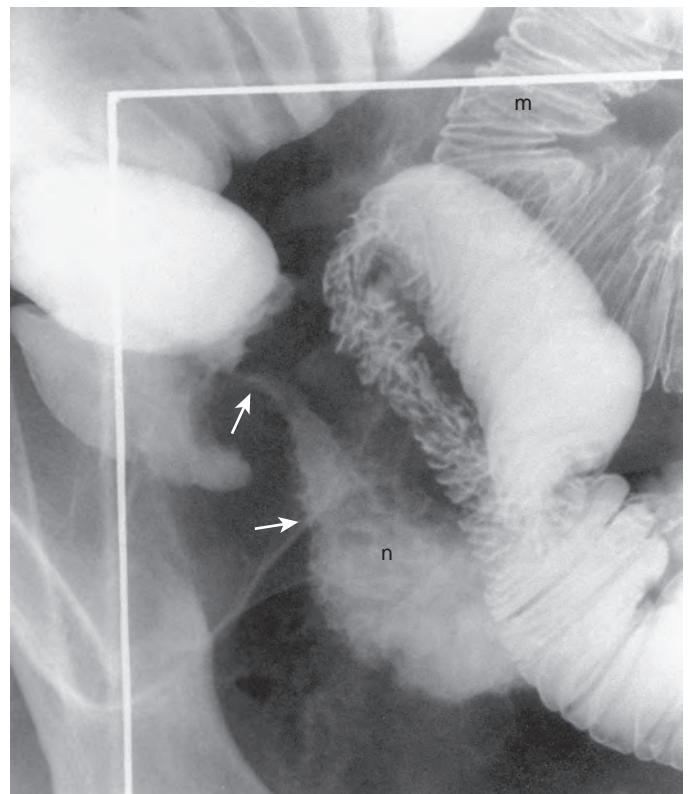


Figure 37-22 Diffusion of barium into methylcellulose column in neoterminal ileum in Crohn's disease. Spot image shows tapered narrowing of the neoterminal ileum (arrows), with minimal nodularity of the mucosa (n). The neoterminal ileum is seen only in single contrast, whereas a double-contrast effect (m) is seen more proximally. This patient underwent prior resection of the terminal ileum, cecum, and proximal ascending colon for Crohn's disease. This image shows recurrent Crohn's disease in the neoterminal ileum.

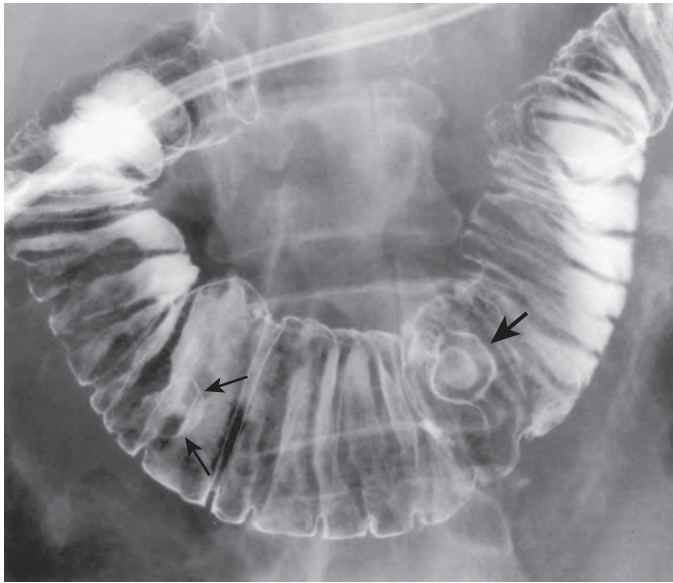


Figure 37-23 Hypotonic duodenogram. Upper endoscopy revealed a polypoid lesion in the duodenum. A radiographic study was requested for clarification. Spot image of the distal duodenum in air-contrast study shows a 1.8-cm polypoid lesion (*thin arrows*) etched in white in the second portion of the duodenum. A 2-cm polypoid lesion (*thick arrow*) is also seen at the junction of the third and fourth portions of the duodenum. Repeat endoscopy with biopsy and subsequent surgery revealed an adenocarcinoma of the second portion of the duodenum and a hemangioma of the fourth portion.

contrast enema with reflux of contrast medium into the distal ileum.

Suspected leaks in the mid–small bowel initially may be evaluated by CT. If the small bowel is not dilated, enteroclysis using water-soluble contrast may then be performed (Fig. 37-24).⁶

Retrograde Examinations of the Small Intestine

BARIUM ENEMA

The barium enema is an underused but powerful examination for imaging the terminal ileum and distal small bowel.⁴⁰ If plain abdominal radiographs or CT cannot differentiate a distal small bowel obstruction from an adynamic ileus, a single-contrast barium enema may be extremely helpful in these patients. The study can be used not only to rule out an obstructing lesion in the colon as a cause of dilated small bowel but also to evaluate the distal ileum by refluxing barium through the ileocecal valve. Reflux of barium into a dilated terminal ileum indicates the presence of an adynamic ileus, whereas reflux of barium into a narrowed terminal ileum (with dilated, gas-filled ileal loops more proximally) indicates the presence of a small bowel obstruction. In many cases, barium can be refluxed in a retrograde fashion to the site of transition, enabling the radiologist to determine the site and cause of obstruction (see Chapter 46). In patients with high-grade small bowel obstruction, a barium enema is faster and easier on the patient than an enteroclysis examination or small bowel follow-through.

A single-contrast or double-contrast barium enema may be performed in patients with suspected Crohn's disease.

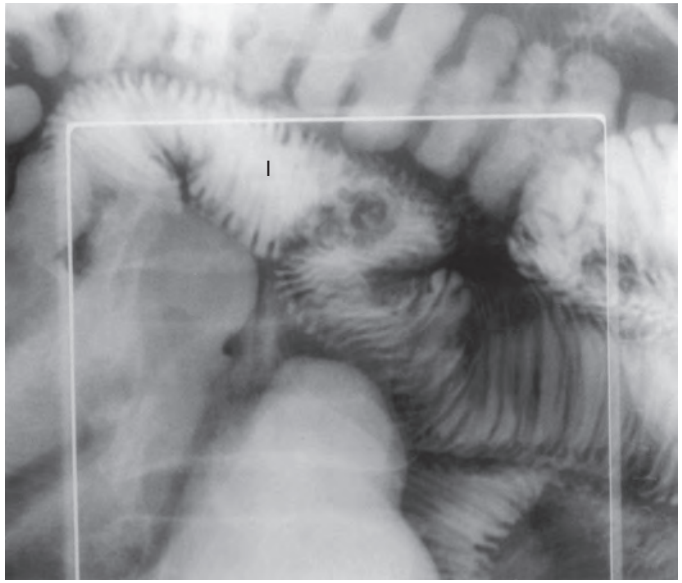


Figure 37-24 Enteroclysis using water-soluble contrast. Spot image from water-soluble contrast enteroclysis shows a normal proximal fold pattern (l). When the small bowel is not distended, a study using water-soluble contrast can demonstrate anatomic detail. When the small bowel is hypomotile or distended, however, intraluminal fluid dilutes the water-soluble contrast, limiting visualization of the bowel.

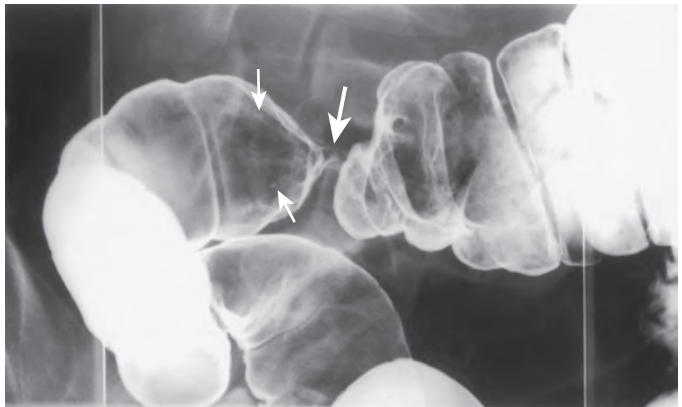


Figure 37-25 Barium enema demonstrating recurrent Crohn's disease. On previous endoscopy, it was not possible to pass the endoscope through the ileocolic anastomosis into the neoterminal ileum in a patient who had prior surgery for Crohn's disease. A double-contrast barium enema shows a short stricture (*large arrow*) at the ileocolic anastomosis. Aphthoid ulcers (*small arrows*) are also seen in the adjacent neoterminal ileum.

Double-contrast studies have the advantage of being able to diagnose early inflammatory lesions of Crohn's disease, such as aphthoid ulcers (Fig. 37-25). However, single-contrast studies are more reliable for refluxing large volumes of barium into the distal small bowel when it is important to assess the terminal ileum and distal ileum for radiographic signs of Crohn's disease.

In patients who are not obstructed, a standard barium enema preparation may be helpful. However, in patients with high-grade small bowel obstruction, an oral preparation is contraindicated. Such studies should be performed without any preparation or after gentle cleansing enemas.

A standard dose of 1 mg of glucagon is administered IV to relax the colon and ileocecal valve. Up to 2.5 L of 20% to 30% w/v barium is instilled via an enema bag or tip. Reflux of barium through the ileocecal valve is possible in about 85% of patients. If a distal small bowel obstruction is present, an attempt should be made to reflux barium directly to the site of obstruction. In some cases, water can be added to the enema bag to propel the barium retrograde through the distal ileum.

ILEOSTOMY ENEMA

The small bowel proximal to an ileostomy can easily be evaluated by a retrograde examination through the ileostomy stoma. If there is clinical suspicion of a leak or obstruction, no preparation is used. If there is clinical suspicion of recurrent Crohn's disease, however, an oral preparation (e.g., magnesium citrate, Phospho-Soda) may be helpful for eliminating debris from the small bowel before performing the examination. The patient is also instructed not to eat solids the day before the procedure.

A soft catheter (e.g., Foley catheter) is inserted into the ileostomy. If disease is suggested at the ileostomy or near the peritoneal reflection (e.g., Crohn's disease, stricture, leak), the balloon of the catheter should not be inflated. If injection of barium shows no evidence of disease in the distal ileum at or near the peritoneal reflection, the catheter balloon may be inflated with 3 to 5 mL of air or saline, and the catheter is retracted to the peritoneal reflection. If there is doubt about disease at the ileostomy, the opening can be explored with a small finger. If inflation of the balloon is contraindicated, and barium leaks out from the ileostomy stoma, the radiologist can withdraw the catheter, distend the balloon outside the ostomy, and push the distended balloon against the outside of the ileostomy to seal the ileostomy opening.

A wide variety of contrast agents can be injected via the catheter. If a leak from the distal small bowel is suspected, water-soluble contrast agents may be used. If a distal small bowel obstruction is suspected, a single-contrast ileostomy enema can be performed with 30% to 50% w/v barium. Thin barium is injected via a syringe until the site of obstruction is reached and characterized. If Crohn's disease or tumor is suspected, a double-contrast ileostomy enema can be performed by first injecting 40% to 80% w/v barium into the proximal ileum, followed by air or methylcellulose to visualize mucosal detail (Fig. 37-26). As with all small bowel studies, fluoroscopy and spot images are the mainstays of diagnosis. The ileostomy and small bowel adjacent to the anterior abdominal wall are best visualized with the patient in a lateral position. The ileostomy is best filled after the catheter is removed, the ostomy bag is replaced, and the patient is turned to an orthogonal position (usually a steep oblique or lateral position).

Choice of Fluoroscopic Examination

Zealots of enteroclysis, small bowel follow-through, CT, CT enteroclysis, magnetic resonance (MR) enteroclysis, and capsule enteroscopy abound. This section attempts to provide a rational approach to fluoroscopic imaging of the small bowel.

The unifying feature of all forms of barium diagnosis is palpation of each loop of small intestine when the loop is optimally distended. This necessitates that the radiologist remain with the patient during enteroclysis or return to the fluoroscopic suite at 15- to 30-minute intervals for small bowel

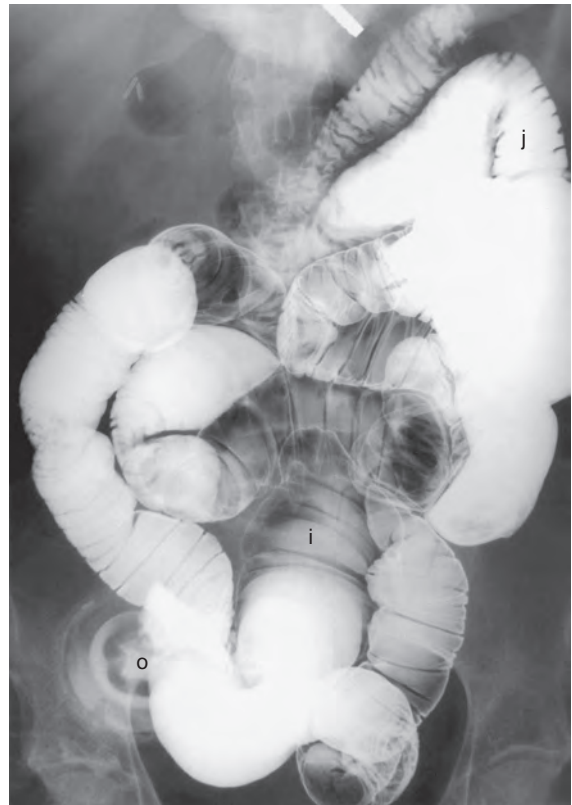


Figure 37-26 Ileostomy enema. This patient complained of abdominal pain and distention. A total colectomy had previously been performed. CT revealed a dilated small bowel. An overhead radiograph obtained at the end of a retrograde ileostomy enema shows diffuse dilation of small bowel to the level of the proximal jejunum (j). No site of narrowing or obstruction is identified in this patient with an intestinal adynamic ileus. Air-contrast effect in the ileum (i) results from air present in the small bowel before barium was instilled via the ostomy (o).

follow-through studies, depending on the rate of progression of barium through the small intestine. Because of emphasis on fluoroscopic and spot image diagnosis, enteroclysis is associated with only a slightly higher radiation dose to the patient than small bowel follow-through.⁴¹ A single-contrast examination evaluates the luminal contour and filling defects in the barium column. A double-contrast examination evaluates the luminal contour, filling defects in the barium column or pool, and mucosal detail en face. The small bowel folds are well evaluated by either technique only when the lumen is fully distended.

The major advantage of the small bowel follow-through over enteroclysis is that it is easier on the patient and avoids the need for intubation of the small intestine, so that sedation is unnecessary. Long segments of abnormal bowel are easy to visualize (Fig. 37-27) as long as frequent fluoroscopy is performed. As a result, diseases involving long segments of small bowel, such as Crohn's disease, ischemia, and radiation changes, are readily detected on small bowel follow-through. However, enteroclysis has a number of important advantages over the small bowel follow-through. Because the radiologist is at the patient's side for the entire examination, fluoroscopy can be performed whenever needed. During enteroclysis, the pylorus also is bypassed, so that radiographic contrast agents can be instilled at an optimal rate for obtaining luminal distention. Short

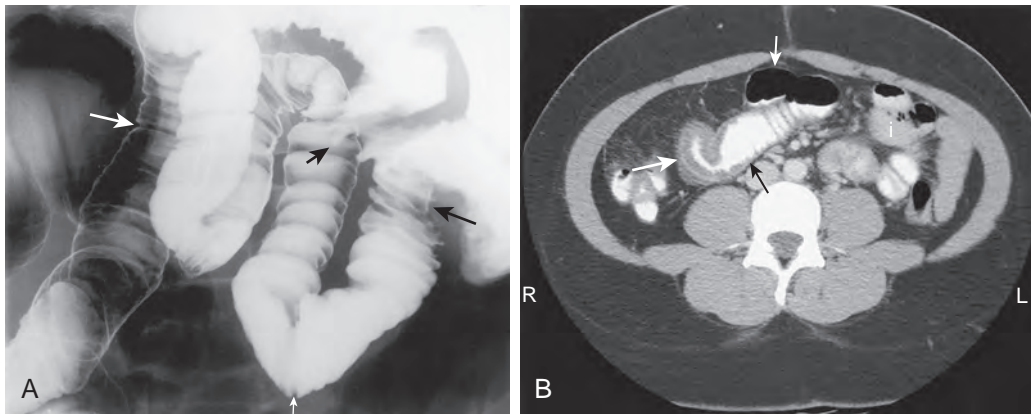


Figure 37-27 Long segment of radiation enteropathy demonstrated by small bowel follow-through. **A.** Spot image shows abnormal loops of ileum (between *long arrows*). The folds are thickened but retain their normal orientation perpendicular to the longitudinal axis of the small bowel. Two areas of angulation (*short arrow*) are identified as a result of radiation serositis. No obstruction was seen. **B.** CT scan shows marked wall thickening (*long white arrow*) in a loop of ileum. Mild fold thickening is seen more proximally (*black arrow*). Note the normal wall thickness (*short white arrow*) in small bowel proximal to the diseased segment. Little anatomic detail is available in some loops (i).

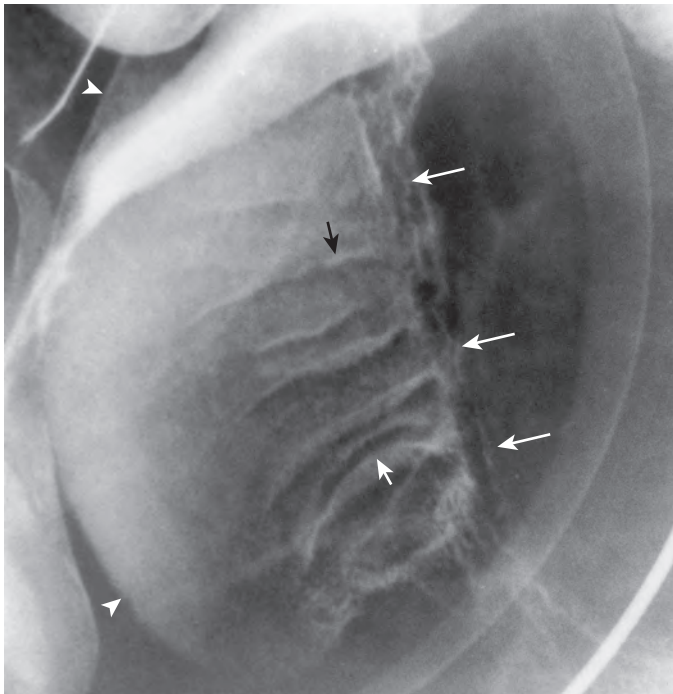


Figure 37-28 Mesenteric border ulcer demonstrated on enteroclysis in patient with Crohn's disease. Spot image shows a thin linear collection of barium (*long arrows*) along the mesenteric border of the distal ileum. Folds (*short arrow*) are pulled toward the site of ulceration, leading to sacculization (*arrowheads*) of the relatively uninvolved antimesenteric border.

lesions such as tumors or skip lesions in Crohn's disease are better demonstrated by enteroclysis because the lumen is over-distended, making subtle areas of focal narrowing more conspicuous (see Fig. 37-7). The small bowel folds are also better evaluated by enteroclysis because the lumen is distended, and the folds are straightened.⁴² Major mucosal abnormalities such as cobblestoning can be demonstrated on single-contrast small bowel follow-throughs with compression, but demonstration of subtle mucosal abnormalities requires double-contrast technique (Fig. 37-28).

The choice of which radiographic study to perform (small bowel follow-through vs. enteroclysis) depends primarily on the indication for the examination. Various clinical settings for evaluating the small bowel are discussed in the following sections.

CHRONIC DIARRHEA

Small bowel follow-through is an adequate examination for the diagnosis of Crohn's disease or other inflammatory diseases involving long segments of bowel.²⁴ In general, a small bowel follow-through can demonstrate cobblestoning, mesenteric border ulcers, fissures, fistulas (Fig. 37-29), and long segments of narrowing. However, the small bowel follow-through can miss short skip lesions in Crohn's disease, as well as the aphthoid ulcers of early Crohn's disease. If a surgeon desires a full evaluation of disease extent and possible skip lesions before surgery in a patient with known Crohn's disease, enteroclysis is a better preoperative examination. If a patient has a normal-appearing terminal ileum during a small bowel follow-through but there is a strong clinical suspicion of Crohn's disease, a peroral pneumocolon can be obtained for air-contrast views of the terminal ileum. Ideally, this study should be performed after the patient has received a barium enema preparation to eliminate debris from the distal ileum and right side of the colon. A peroral pneumocolon or double-contrast barium enema with reflux of barium into the terminal ileum enables much better detection of mucosal nodularity and aphthoid ulcers (Fig. 37-30) than a conventional small bowel follow-through.

Enteroclysis may not visualize the terminal ileum any better than a small bowel follow-through (see Fig. 37-22). Over-distention of ileal loops in the pelvis during enteroclysis may cause so much overlap of loops that it is difficult to demonstrate the terminal ileum in isolation. The double-contrast effect of enteroclysis using methylcellulose is often lost before barium has reached the terminal ileum because of progressive mixing of barium and methylcellulose. An air-contrast enteroclysis may be performed, but a peroral pneumocolon or double-contrast barium enema is easier on the patient and will enable air-contrast images of the terminal ileum to be obtained in the 85% of patients in whom air or barium can be refluxed into the terminal ileum.

SMALL BOWEL OBSTRUCTION

As described in Chapter 46, the sun never sets on patients with suspected small bowel obstruction without these patients undergoing abdominal CT (unless they go directly to surgery). CT has a major advantage over barium studies in that it does not rely on barium reaching the site of obstruction but uses intraluminal fluid to outline the transition zone. CT also is a considerably shorter procedure than an antegrade barium study in patients with high-grade obstruction. A small bowel follow-through and enteroclysis are therefore discouraged in patients with high-grade small bowel obstruction shown by plain abdominal radiography or CT. Retrograde examination of the small bowel by barium enema (Fig. 37-31) or colostomy enema is the preferred examination in the setting of high-grade distal small bowel obstruction or if there is a question of whether the patient has an adynamic ileus, proximal colonic lesion, or distal small bowel obstruction. An antegrade study can be performed after decompression by a nasogastric tube or long tube (Kantor or Miller-Abbott tube; Fig. 37-32) or via a combination enteroclysis-decompression catheter.

Vomiting is more a symptom of gastroduodenal or proximal small bowel disease than of distal small bowel disease. In patients with vomiting and no evidence of plain radiographic or CT findings of distal small bowel obstruction, a single- or double-contrast upper GI series with evaluation of the proximal small bowel may be performed. Alternatively, if an upper endoscopy has cleared the stomach and proximal duodenum, enteroclysis or hypotonic duodenography extending into the first several small bowel loops may be considered.

ABDOMINAL PAIN

Unexplained abdominal pain can be evaluated by a small bowel follow-through or enteroclysis. The small bowel follow-through is superior to enteroclysis for evaluation of small bowel transit time and the motility component of motor disorders. In contrast, enteroclysis is superior for showing the structural

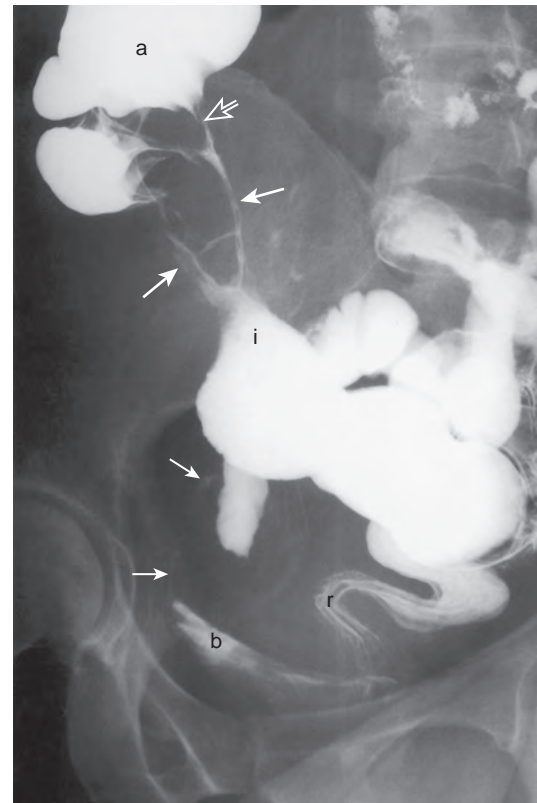


Figure 37-29 Multiple fistulas demonstrated on small bowel follow-through in a patient with Crohn's disease. An overhead radiograph obtained after barium reached the colon shows several tracks (*thick arrows*) coursing from the dilated distal ileum (*i*) to the ascending colon (*a*). One of these is a diseased terminal ileum and the other is an ileocolic fistula. Another fistula (*open arrow*) enters the medial wall of the ascending colon above the ileocecal valve. A thin, barium-etched fistula (*thin arrows*) courses from the ileum to the barium-filled urinary bladder (*b*). *r*, rectum.

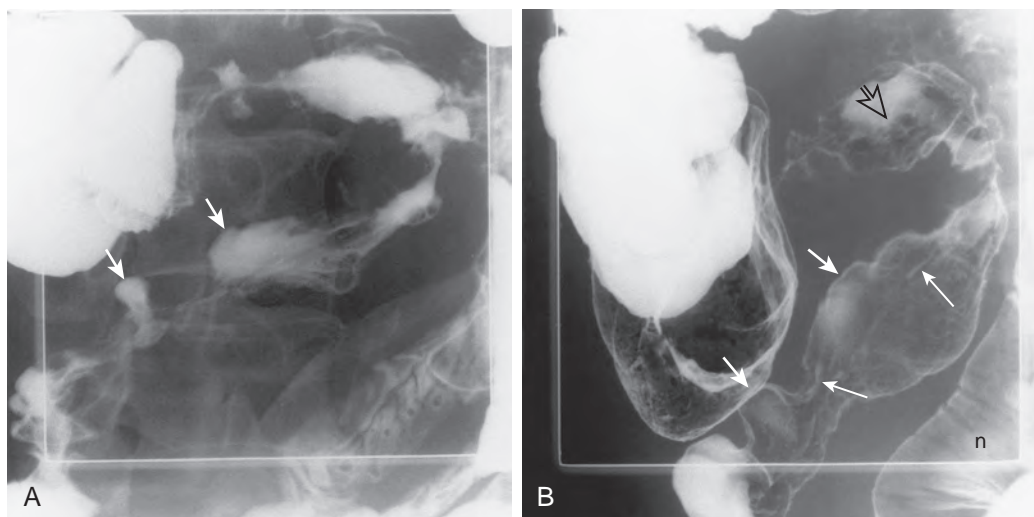


Figure 37-30 Peroral pneumocolon in a patient with suspected Crohn's disease. **A.** Spot radiograph from small bowel follow-through shows an abnormal terminal ileum, manifested by sacculations (*arrows*) alternating with areas of narrowing. **B.** Spot image from peroral pneumocolon shows that most of the areas of narrowing are more distensible than shown in **A**. Several mesenteric border ulcers (*long arrows*) and sacculations (*short arrows*) characteristic of Crohn's disease are now visualized. The mucosa is focally nodular (*open arrow*). Compare and contrast the appearance of the mucosa in the terminal ileum with that in an adjacent loop of normal ileum (*n*).

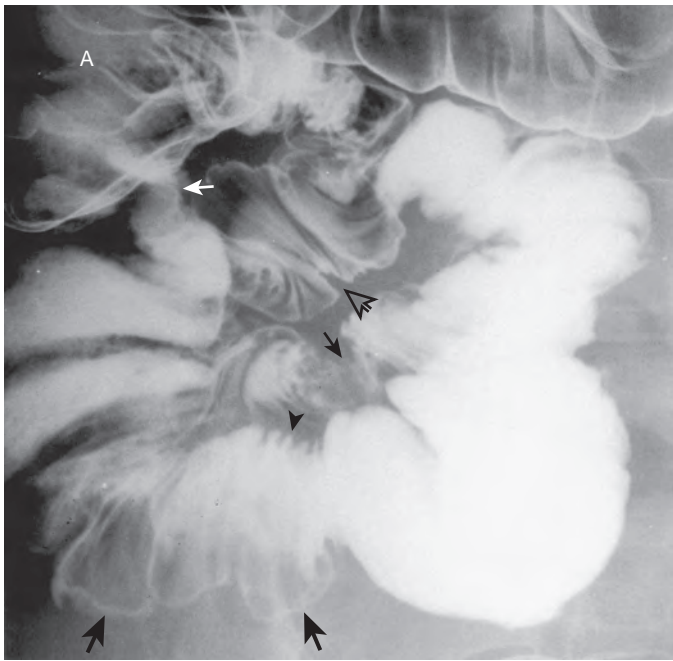


Figure 37-31 Recurrent carcinoid tumor with small bowel obstruction on barium enema. The distal ileum is dilated, and small bowel folds are tethered (*open arrow*). In one loop, folds are bunched together (*arrowhead*) by the mesenteric desmoplastic process, and the opposite walls are sacculated (*large arrows*). Several short segments of narrowing (*short arrows*) are also seen. The ascending colon is identified (A).

components of motor disorders (e.g., diverticula in jejunoileal diverticulosis, sacculations or an increased number of small bowel folds in scleroderma). Enteroclysis is also superior for showing short lesions such as isolated adhesions (*Fig. 37-33*) or tumors that may account for abdominal pain.

Transient intussusceptions usually occur as normal variants or are associated with motor disorders. When a transient intussusception shown on CT is associated with signs of obstruction or tumor, the radiologist should perform enteroclysis because this technique is superior for excluding short lesions, such as tumors and adhesions, which may cause intussusception. However, most transient intussusceptions are not associated with signs of obstruction or tumor. In this scenario, it is unclear whether a small bowel follow-through is sufficient for excluding a structural abnormality. Clearly, enteroclysis will provide a more confident diagnosis of normality for ruling out tumor or an adhesion in this setting.

SUSPECTED PERFORATION

As noted, suspected perforation of the duodenum and proximal jejunum can be adequately evaluated with a water-soluble, small bowel follow-through. Diagnosis of perforation in the presence of dilated small intestine from obstruction or adynamic ileus is difficult, however, because water-soluble contrast agents provide inadequate density when diluted by intraluminal fluid. Water-soluble contrast agents are further diluted because of their hyperosmolar nature, which causes more fluid to be drawn into the small bowel lumen. In the presence of dilated distal small intestine, retrograde examination of the small bowel with water-soluble contrast agents is therefore preferable for excluding a



Figure 37-32 Complete small bowel obstruction demonstrated on enteroclysis after decompression of the small bowel by a Miller-Abbott tube. There is an abrupt, beaklike cutoff in the ileum (*long white arrow*) with complete small bowel obstruction caused by an adhesion. The proximal small intestine has been decompressed by a Miller-Abbott tube (the tip of the tube is denoted by a *short white arrow*) and is only mildly dilated. The mercury-filled bag (M) has flipped in a retrograde fashion. Note how the tube is seen as a filling defect (*black arrow*) in the barium column.

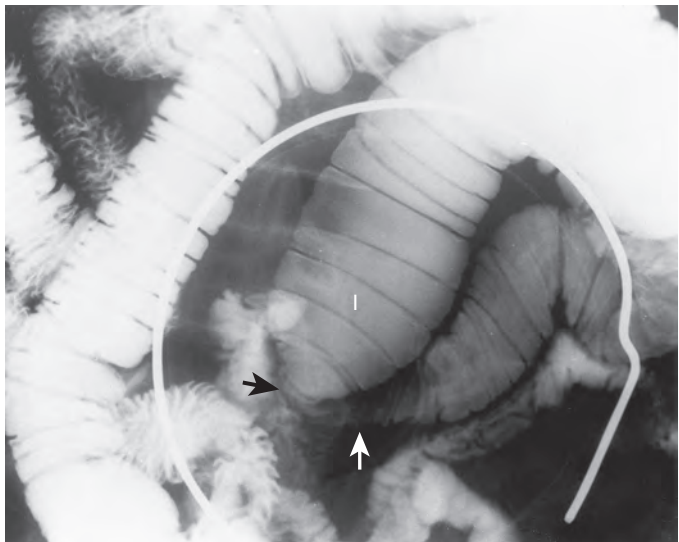


Figure 37-33 Adhesions and low-grade small bowel obstruction demonstrated on enteroclysis. This patient had intermittent abdominal pain and distention and a history of prior abdominal surgery. There is abrupt angulation (*black arrow*) of the ileum, with narrowing (*white arrow*) distal to the site of angulation. The folds in the transition zone are preserved, and the mucosa is smooth. The ileum (I) proximal to the adhesion is mildly dilated.

distal small bowel leak, particularly a leak at an ileocolic anastomosis. Water-soluble enteroclysis (see Fig. 37-24) should be performed after intestinal decompression in patients with suspected perforation of the mid- or distal small bowel.

MALABSORPTION

A classification and discussion of malabsorption is presented in Chapter 43. A small bowel follow-through is adequate for detecting large structural lesions that cause bacterial overgrowth (e.g., jejunoileal diverticulosis, Crohn's disease with obstruction). However, enteroclysis is the procedure of choice for showing malabsorptive disorders involving the mucosa and submucosa of the bowel (e.g., celiac disease [Fig. 37-34], Whipple's disease, amyloidosis). A strong argument can therefore be made for air-contrast enteroclysis in the setting of malabsorption because the mucosal surface of the jejunum, the most common site of disorders causing malabsorption, can be exquisitely shown. CT is also a helpful adjunct for diagnosing disorders primarily or secondarily involving lymph nodes.

UNEXPLAINED GASTROINTESTINAL BLEEDING

A small bowel follow-through is limited for detecting causes of small intestinal bleeding.^{39,43-48} Small tumors are easily missed.⁴⁵ In one study comparing expertly performed enteroclysis with non-expertly performed small bowel follow-through procedures, enteroclysis detected 90% of tumors diagnosed at surgery,

whereas small bowel follow-through detected only 33%.⁴⁵ It is therefore difficult to establish a confident diagnosis of normalcy on a small bowel follow-through. A combination of a small bowel follow-through (to exclude obstruction or stricture) and capsule endoscopy may be an acceptable alternative for evaluating patients with GI bleeding. However, capsule endoscopy also has its limitations. Because normal small bowel transit time varies from 30 to 120 minutes, the gastroenterologist or physician's assistant will spend an inordinate amount of time at a computer workstation evaluating the images. Capsule endoscopy also has limited ability to localize lesions. Finally, capsule endoscopy is not infallible, because a considerable portion of the intestine is not examined by the video capsule.

Methylcellulose-contrast enteroclysis is adequate for the demonstration of most small bowel tumors (see Fig. 37-7). However, it usually will not detect varices, arteriovenous malformations, or nonsteroidal anti-inflammatory drug (NSAID)-induced erosions or potassium chloride-induced erosions as well as capsule endoscopy. Air-contrast enteroclysis may allow diagnosis of subtle ulcerative lesions in the proximal small intestine with greater sensitivity than methylcellulose-contrast enteroclysis. Although I have not had great success with air-contrast enteroclysis in the pelvic ileum, this is the standard enteroclysis technique performed in Japan.

In summary, a small bowel follow-through is indicated only when assessing for large structural causes of GI bleeding (Fig. 37-35). This test is probably indicated only if there is low



Figure 37-34 Celiac disease demonstrated on enteroclysis. Spot image shows a decreased number of folds per inch in the jejunum.

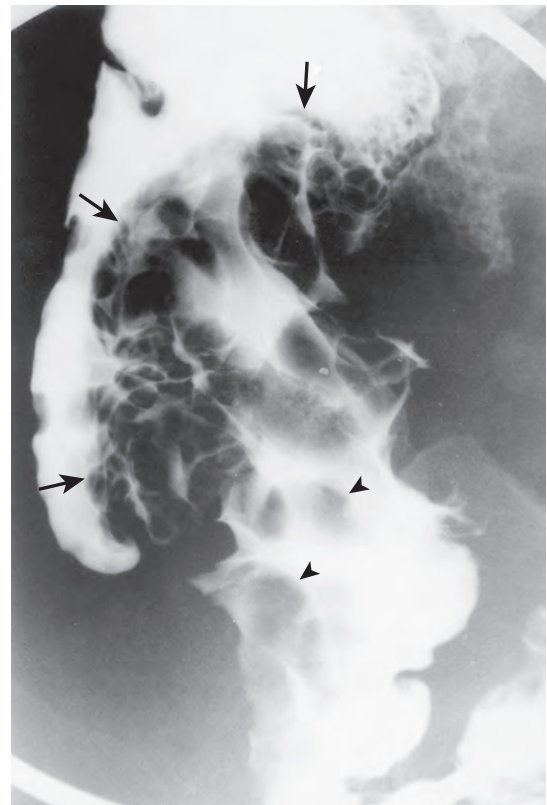


Figure 37-35 Ileocecal lymphoma demonstrated on small bowel follow-through. Spot image of the ileocecal region shows marked lobulation and enlargement of the ileocecal valve (arrows), with spread of tumor into the medial wall of the cecum and ascending colon. The folds of the distal ileum also are marked enlargement and lobulated (arrowheads). This patient with mantle cell lymphoma presented with GI bleeding.

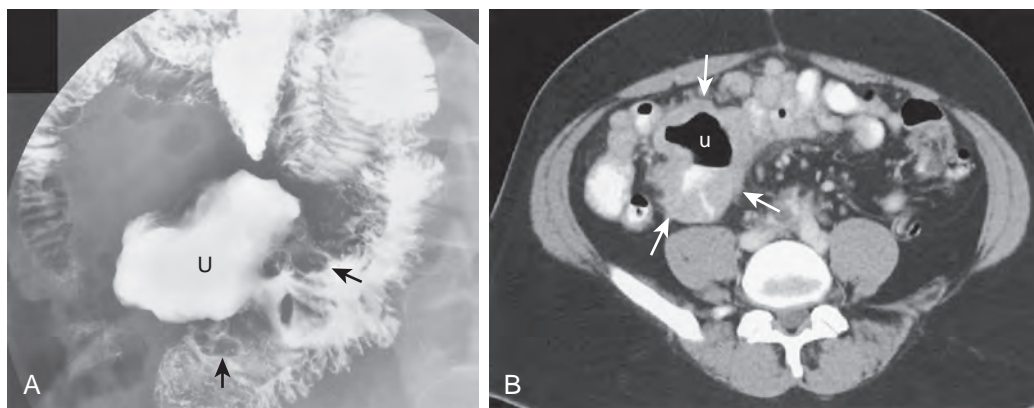


Figure 37-36 Gastrointestinal stromal tumor demonstrated on small bowel follow-through. A. Spot image shows a large, irregular, barium-filled cavity (U) on the mesenteric border of the mid-small bowel. Coarse, lobulated tumor nodules (arrows) are present adjacent to the cavity. **B.** Axial CT scan shows the bulk of the tumor (arrows) surrounding the cavity (u). The mucosal changes are not apparent. This patient presented with GI bleeding.

TABLE
37-2

Choice of Barium Studies for Evaluating Small Bowel in Various Clinical Settings

Clinical Scenario	Initial Study
Chronic diarrhea (excluding Crohn's disease)	Small bowel follow-through
Known Crohn's disease	
Acute abdominal pain	CT to exclude abscess
Anastomotic recurrence	Barium enema
Exclude skip lesion before surgery	Enteroclysis
Acute abdominal pain	CT (ultrasound if gynecologic disease suspected)
Chronic abdominal pain	Small bowel follow-through followed by enteroclysis if small bowel disease is still suspected
Small bowel obstruction	CT followed by barium enema as problem-solving tools for high-grade distal small bowel or proximal colonic obstruction
Low-grade obstruction	Small bowel follow-through or enteroclysis
Vomiting	Upper GI series with evaluation of proximal small bowel
Malabsorption	Enteroclysis (consider air-contrast)
Unexplained GI bleeding	Small bowel follow-through, capsule endoscopy
	Methylcellulose enteroclysis
	Air-contrast enteroclysis if NSAID erosions must be excluded
	CT angiography—role to be determined
Suspected hematogenous metastases	Enteroclysis
Suspected perforation	CT can suggest presence of perforation; suboptimal for evaluating site and cause of perforation
Upper GI tract	Water-soluble contrast upper GI series
Bypassed duodenum	HIDA scan or injection of water-soluble contrast agent into indwelling duodenal-biliary tube
Proximal jejunum	Small bowel follow-through with water-soluble contrast
Mid-small bowel	Water-soluble contrast enema or water-soluble contrast enteroclysis
Distal small bowel, ileocolic anastomosis	Water-soluble contrast enema

HIDA, Hepato-iminodiacetic acid; NSAID, nonsteroidal anti-inflammatory drug.

suspicion of an abnormality, if a large lesion such as lymphoma, GI stromal tumor (Fig. 37-36), ischemia, or hematoma is suspected, or if capsule endoscopy is planned as a follow-up.

Air-contrast enteroclysis is indicated when looking for subtle erosions in patients taking NSAIDs. Methylcellulose-contrast enteroclysis and air-contrast enteroclysis are satisfactory when searching for subtle lesions or small tumors. In patients with known malignant tumors, enteroclysis will permit a more confident diagnosis of normalcy or of metastatic disease than will a small bowel follow-through.

The role of CT or MR angiography for bleeding tumors has yet to be established. CT and MR enterography are

inferior to enteroclysis because they do not assess en face mucosal detail and they have lower resolution than enteroclysis. As a result, barium enteroclysis should be superior to CT or MR enteroclysis for the diagnosis of Crohn's disease, diseases causing malabsorption, or primary tumors. I believe that if a patient is to undergo intubation, a barium enteroclysis study should be performed (rather than CT or MR enteroclysis), except perhaps when searching for a cause of GI bleeding.

A summary of the choice of examinations for evaluating the small bowel in various clinical settings is presented in Table 37-2.

REFERENCES

- Fenolgio-Preiser CM, Hoffsinger AE, Stemmermann GN, et al: Normal anatomy of the small intestine. In Fenolgio-Preiser CM, Hoffsinger AE, Stemmermann GN, et al, editors: *Gastrointestinal Pathology: An Atlas and Text*, ed 2, Philadelphia, 1999, Lippincott-Raven, pp 275–309.
- Herlinger H: Anatomy of the small intestine. In Herlinger H, Maglinte DDT, Birnbaum BA, editors: *Clinical Imaging of the Small Intestine*, ed 2, New York, 1999, Springer-Verlag, pp 3–12.
- Rubessin SE, Furth EE: Differential diagnosis of small intestinal abnormalities with radiologic-pathologic correlation. In Herlinger H, Maglinte DDT, Birnbaum BA, editors: *Clinical Imaging of the Small Intestine*, ed 2, New York, 1999, Springer, pp 527–566.
- Taskalova-Hogenova H, Farre-Castany MA, Stapankova R, et al: The gut as a lymphoepithelial organ: The role of intestinal epithelial cells in mucosal immunity. *Folia Microbiol (Praha)* 40:385–391, 1995.
- Montrose MH, Keely SJ, Barrett KE: Electrolyte secretion and absorption: Small intestine and colon. In Yamada T, Alpers DH, Kaplowitz N, et al, editors: *Textbook of Gastroenterology*, ed 4, Philadelphia, 2003, Lippincott Williams & Wilkins, pp 308–340.
- Rubessin SE, Levine MS: Principles of Performing a Small Bowel Examination, Westbury, NY, 2005, E-Z-EM.
- Grivaux M, Cornet A, Wattez E: Le metoclopramide en radiologie digestive. *Semin Hosp Paris* 44:2338–2345, 1964.
- Howarth FH, Cockell R, Roper BW, et al: The effect of metoclopramide upon gastric motility and its value in barium progress meals. *Clin Radiol* 20:294–300, 1969.
- Kreel L: The use of oral metoclopramide in the barium meal and follow-through examination. *Br J Radiol* 43:31–35, 1970.
- Grumbach K, Herlinger H, Laufer I, et al: Metoclopramide-ceruletide-assisted small bowel examination. *Rofo* 149:47–51, 1988.
- Fraser GM, Preston PG: The small bowel follow-through enhanced with an oral effervescent agent. *Clin Radiol* 34:673–679, 1983.
- Fitch D: The small-bowel see-through: An improved method of radiographic small-bowel visualization. *Can J Med Radiat Tech* 26:167–171, 1995.
- Kressel HY, Evers KA, Glick SN, et al: The peroral pneumocolon examination: Technique and indications. *Radiology* 144:414–416, 1982.
- Kellett MJ, Zboralske FF, Margulis AR: Peroral pneumocolon examination of the ileocecal region. *Gastrointest Radiol* 1:361–365, 1977.
- Kelvin FM, Gedgaudas RK, Thompson WM, et al: The peroral pneumocolon examination: Its role in evaluating the terminal ileum. *AJR* 139:115–121, 1982.
- Fitzgerald EJ, Thompson GT, Somers SS, et al: Pneumocolon as an aid to small bowel studies. *Clin Radiol* 36:633–637, 1985.
- Einhorn M: *The Duodenal Tube and Its Possibilities*, ed 2, Philadelphia, 1926, FA Davis.
- Pesquera GS: Method for direct visualization of lesions in the small intestine. *AJR* 22:254–257, 1929.
- Gershon-Cohen J, Shay H: Barium enteroclysis method for direct immediate examination of the small intestine by single and double contrast technique. *AJR* 42:456–458, 1939.
- Schatzki R: Small bowel enema. *AJR* 50:743–751, 1943.
- Maglinte DDT, Lappas JC, Heitkamp DE, et al: Technical refinements in enteroclysis. *Radiol Clin North Am* 41:213–229, 2003.
- Herlinger H: A modified technique for the double contrast small bowel enema. *Gastrointest Radiol* 3:201–207, 1978.
- Schulze-Delrieu K: Metoclopramide drug therapy. *N Engl J Med* 305:28–33, 1981.
- Herlinger H, Maglinte DD, Tsuneyoshi Y: Enteroclysis: Technique and variations. In Herlinger H, Maglinte DD, Birnbaum BA, editors: *Clinical Imaging of the Small Intestine*, ed 2, New York, 1999, Springer-Verlag, pp 95–124.
- Nolan DJ, Cadman PJ: The small bowel enema made easy. *Clin Radiol* 38:295–301, 1987.
- Plovin PF, Mennard J, Corrol P: Hypertensive crisis in patients with pheochromocytoma given metoclopramide. *Lancet* 2:1357–1358, 1976.
- Maglinte DDT, Lappas JC, Chernish SM, et al: Improved tolerance of enteroclysis by use of sedation. *AJR* 151:951–952, 1988.
- Maglinte DDT: Balloon enteroclysis catheter. *AJR* 143:761–762, 1984.
- Taverner DS, Odurny A: Enteroclysis—the influence of tube design. *Clin Radiol* 49:176–178, 1994.
- Traill ZC, Nolan DL: Technical report: Intubation fluoroscopy times using new enteroclysis tube. *Clin Radiol* 50:339–340, 1994.
- Maglinte DDT, Stevens LH, Hall RC, et al: Dual purpose tube for enteroclysis and nasogastric-nasoenteric decompression. *Radiology* 185:281–282, 1992.
- Diner WC: Duodenal perforation during intubation for small bowel enema study. *Radiology* 168:39–41, 1988.
- Maglinte DDT, Miller RE: A comparison of pumps used for enteroclysis. *Radiology* 152:815, 1984.
- Sellink JL, Miller RE: *Radiology of the Small Bowel: Modern Enteroclysis Technique and Atlas*, The Hague, 1982, Martinus Nijhoff.
- Kobayashi S, Nishizawa M, Mizuno K, et al: X-ray examination of the small intestine: I. Double contrast method as a routine examination [in Japanese]. *Jpn J Clin Radiol* 19:619–625, 1974.
- Kobayashi S, Nishizawa M: X-ray examination of small intestine—double contrast method by duodenal intubation. *Stomach Intest* 11:157–165, 1976.
- Shirakabe H, Kobayashi S: Air double contrast barium study of the small bowel. In Herlinger H, Maglinte D, editors: *Clinical Radiology of the Small Intestine*, Philadelphia, 1989, WB Saunders, pp 139–145.
- Trickey SE, Halls J, Hodson CJ: A further development of the small bowel enema. *J R Soc Med* 56:1070–1073, 1963.
- Maglinte DDT, Lappas JC, Kelvin FM, et al: Small bowel radiography: How, when and why? *Radiology* 163:297–305, 1987.
- Miller RE: Complete reflux examination of the small bowel. *Radiology* 84:457–462, 1986.
- Salomonowitz E: Radiation dose of double contrast and single contrast examinations. In Herlinger H, Maglinte D, editors: *Clinical Radiology of the Small Intestine*, Philadelphia, 1989, WB Saunders, pp 147–150.
- Taverne PP, van der Jagt EJ: Small bowel radiography: A prospective comparative study of three techniques in 200 patients. *Rofo* 143:293–297, 1985.
- Maglinte DDT, Elmore MF, Eisenberg M, et al: Meckel diverticulum: Radiologic demonstration by enteroclysis. *AJR* 134:925–932, 1980.
- Maglinte DDT, Burney BT, Miller RE: Lesions missed on small bowel follow-through: Analysis and recommendations. *Radiology* 144:737–739, 1982.
- Bessette JR, Maglinte DDT, Kelvin FM, et al: Primary malignant tumors in the small bowel: A comparison of the small-bowel enema and conventional follow-through examination. *AJR* 153:741–744, 1989.
- Hara AK, Leighton JA, Sharma UK, Fleischer DE: Small bowel: Preliminary comparison of capsule endoscopy with barium study and CT. *Radiology* 230:260–265, 2004.
- Artigas JM, Martí M, Soto JA, et al: Multidetector CT angiography for acute gastrointestinal bleeding: technique and findings. *Radiographics* 33:1453–1470, 2013.
- Bentley BS, Tulchinsky M: SPECT/CT helps in localization and guiding management of small bowel gastrointestinal hemorrhage. *Clin Nucl Med* 39:94–96, 2014.

Computed Tomography Enterography

JOEL G. FLETCHER | DAVID H. BRUINING

CHAPTER OUTLINE

Computed Tomography Enterography: How It Differs From Routine Abdominal Computed Tomography

Indications

Technique

Interpretation of Computed Tomography Enterography Images

Suspected Crohn's Disease

Gastrointestinal Bleeding

Low-Grade Obstruction

Radiation Dose and Computed Tomography Enterography

Integration with Other Tests

Computed Tomography Enterography: How It Differs From Routine Abdominal Computed Tomography

Computed tomography enterography (CTE) reflects individualization of the abdominal pelvic CT technique for patients with small bowel disorders. CTE provides visualization of the small bowel lumen, wall, and perienteric tissues by distending the small bowel with large volumes of oral contrast and obtaining multiplanar, high-resolution images of the bowel during appropriate phase(s) of enhancement. It differs from routine abdominal pelvic CT in the amount and type of oral contrast given to the patient prior to scanning, timing of image acquisition with respect to the intravenous (IV) contrast bolus, routine reconstruction of thin multiplanar images, and other factors related to patient-specific indications (e.g., Crohn's disease or obscure gastrointestinal [GI] bleeding). CT acquisition for CT enteroclysis is similar, but the luminal small bowel distention is achieved by infusion of enteric contrast via a nasojejunum tube.

Indications

CTE is performed in patients with known or suspected Crohn's disease, patients with obscure GI bleeding, diarrhea of unknown cause (often in association with imaging of the pancreas), and in patients with abdominal pain of unknown cause in an outpatient setting. Multiphase CTE is often used as a complementary technique with capsule endoscopy in patients with obscure GI bleeding, and its complementarity with other tests is reviewed later in this chapter. CTE may also be used to evaluate for the presence and cause of low-grade obstruction (when an enteroclysis cannot be performed), and to examine for findings or

complications of other small bowel disorders (e.g., small bowel diverticulosis, celiac disease, polyposis syndromes).

Technique

The CTE technique is adapted to the indication for the examination. Table 38-1 describes common variations of CTE technique, linking them to clinical indications. All types of CTE require the ingestion of large amounts of oral contrast and adaptation of the CT x-ray tube potential and tube current to adjust for patient size and diagnostic task to minimize radiation dose appropriately, yet provide an accurate diagnosis.¹

For CTE, 1300 to 2000 mL of oral contrast is typically administered to the patient over an hour in divided increments (e.g., 450 mL at 60, 45, and 15 minutes prior to the examination).²⁻⁵ Contrast agents are generally divided into neutral enteric agents that demonstrate CT number attenuation similar to that of water and positive enteric contrast agents containing barium or iodine, which have CT numbers much greater than those of enhancing structures. Neutral agents are preferred for most small bowel indications because they allow greater conspicuity of many small bowel pathologies, such as segmental inflammation or masses, which usually are hyperenhancing compared with the adjacent small bowel wall. Positive agents are useful when the suspected pathology is known to be an intraluminal filling defect (e.g., polyposis syndromes), serosal metastases are suspected, or IV iodinated dye is contraindicated. Although a variety of neutral enteric contrast agents are available, many centers use commercially available products, which often contain sorbitol, which retards absorption of water across the small bowel wall, improves small bowel distention compared with water alone, and provides an expanded time window during which small bowel imaging can be achieved with a high degree of reproducibility.³ Alternatively, locust bean gum or polyethylene glycol may also be used.^{2,6} If patients have difficulty with oral ingestion of these neutral agents, they can complete ingestion of the recommended volume with water. Patients need to be informed that enteric agents using sorbitol or polyethylene glycol may cause loose bowel movements as the agent is expelled shortly after the test. Because of the requirement for the ingestion of large volumes, CTE using non-water agents is an outpatient procedure, and radiologists and referring clinicians should consider alternatives for hospitalized patients (for whom routine abdominal-pelvic CT or CTE with water may be preferred). Also, approximately 30% of jejunal loops will be collapsed using the peroral CTE technique⁷; therefore, so in the presence of known or suspected jejunal pathology, CT enteroclysis or magnetic resonance (MR) enterography, in which the jejunum is imaged repeatedly with different pulse sequences, may be preferred.

IV contrast is typically delivered at a rate of 3 to 5 mL/s, with imaging during the enteric or portal phase of enhancement. The enteric phase of enhancement refers to imaging during

TABLE
38-1

Common Types of Computed Tomography Enterography Examinations by Patient Indication

Indication	Phase(s) of Enhancement	Dose Level	Comments
R/O small bowel disease	Enteric or portal	Routine abdominopelvic CT	Neutral oral contrast, high resolution*
R/O or FU Crohn's disease	Enteric or portal	Less than for routine abdominopelvic CT	Neutral oral contrast, high resolution*
Active GI bleed	Arterial and portal or delayed	Routine abdominopelvic CT	Neutral oral contrast, high resolution*
Obscure GI bleed	Arterial, enteric and delayed	More than for routine abdominopelvic CT (because of more than one phase of enhancement)	Neutral oral contrast, high resolution*
Polyposis syndrome	Noncontrast	Less than for routine abdominopelvic CT	Enteroclysis preferred, positive oral contrast, high resolution
Low-grade obstruction	Enteric or portal	Routine abdominopelvic CT	Enteroclysis preferred, neutral oral contrast, high resolution

*Axial slice thickness is ≤ 3 mm, with routine coronal \pm sagittal multiplanar reconstructions or interactive 3D viewing of volumetric CT data at a computer workstation.

CT, computed tomography; FU, follow-up; GI, gastrointestinal; R/O, rule out.

peak enhancement of the small bowel wall, which is generally regarded as 50 seconds after the initiation of IV contrast material.⁸ The enteric phase demonstrates findings of Crohn's disease, hyperenhancing polyps, and most small bowel vascular lesions. The timing of the enteric phase is similar to that of the pancreatic phase because the superior mesenteric and portal veins are opacified with IV contrast media and the hepatic veins have not yet filled with contrast; thus, synchronous evaluation of the pancreas can often be performed with a single acquisition. In the hepatic or portal phase of enhancement, hepatic veins are filled with contrast; this may be a more appropriate phase of enhancement if correlative imaging of the liver is also needed. For the most common indication of imaging Crohn's disease, active Crohn's disease is adequately demonstrated in the enteric and portal phases.⁹

Because one of the goals of CTE is to display small fistulas and intramural or intraluminal masses, high-resolution CT imaging is required, with the axial slice thickness generally reconstructed on the order of 3 mm or less. Multiplanar coronal reformatted images are required, and sagittal reformatted images are also generally obtained to aid in the evaluation of suspected small bowel segments and the mesenteric vasculature. The pitch or CT scanner table speed is adjusted so that the abdomen and pelvis can be imaged within a single breath-hold (i.e., 6 to 15 seconds). For most clinical indications (e.g., to rule out small bowel disease, evaluate Crohn's disease), only a single phase of contrast enhancement is required.⁹

Irrespective of the indication, the CTE acquisition technique should be adapted to patient size and diagnostic goal.^{1,10} One of the best radiation dose-saving techniques is for the radiologist to limit the number of phases acquired to those that are necessary for the suspected diagnosis. Multiple phases of enhancement are reserved for the investigation of obscure GI bleeding¹¹ or situations in which multiphasic imaging of solid organs is required. Tube current adaptation can be carried out through the use of technique charts or automatic exposure control.^{12,13} The routine use of automatic exposure control will lower radiation dose by approximately 30% in large CT practices.¹² Additionally, tube energy selection (kV) can be performed using technique charts or vendor-supplied kV selection programs, which take into account patient size, iodine contrast-to-noise ratio (CNR), and CT system limitations.¹⁴ Selection of kV and technique charts generally reduce radiation dose by an

additional 20% to 30%. One of the advantages of lower kV is that it not only reduces radiation dose, but increases the iodine signal and iodine-related CNR, which can be used to increase the conspicuity of hyperenhancing bowel segments and masses or lower the radiation dose.

The dose level chosen for different types of enterography examinations depends on the image contrast between the suspected small bowel pathology and normal, enhancing bowel wall, as well as other pathology, which may be suspected in the solid organs (see Table 38-1). In Crohn's disease, the diagnostic task requires differentiating relatively large differences in CT number between normal and hyperenhancing bowel segments, so routine abdominal pelvic CT dose levels can be lowered by 30% to 50% without sacrificing diagnostic performance.^{13,15,16} Similarly, if using positive enteric contrast to evaluate for filling defects such as polyps in polyposis syndromes, the CT number differences between the suspected pathology and adjacent bright lumen are large, and the radiation dose can be substantially reduced (analogous to CT colonography). In contrast, CTE performed to evaluate synchronously for pancreatic or small bowel masses or hepatic metastases will require routine abdominal pelvic dose level settings so that important low-contrast structures and masses can be visualized adequately.

The lower radiation dose levels frequently used in CTE, along with the thinner slices, often result in noisier images, which can be accurately interpreted without diagnostic compromise in the setting of Crohn's disease.^{13,15,17} A variety of CT image noise reduction methods can be used (e.g., iterative reconstruction) to improve the image quality of the lower dose CTE images so that they resemble those obtained with a routine dose.¹⁸ CT noise reduction is especially useful when reducing radiation dose with low-kV techniques to improve disease conspicuity and compensate for the increased image noise associated with low-kV imaging.^{1,19}

Interpretation of Computed Tomography Enterography Images

Routine CT enterography performed for general indications of Crohn's disease requires only the review of axial and coronal images, although interactive viewing with a volume viewer or

in other planes is often helpful. Similar to fluoroscopy, a systematic approach to view the bowel is required to maximize disease detection. Because Crohn's disease, GI bleeding, and small bowel tumor exclusion are frequent indications for CTE, CT findings in these entities will first be considered, with emphasis on the differential diagnosis. Appropriate diagnosis relies on combining knowledge of the intraluminal morphology seen at fluoroscopy with the mural and intraluminal enhancement seen at cross-sectional imaging.

Normal small bowel findings at CTE are similar to those observed fluoroscopically. The jejunal caliber is slightly larger than the ileum, and the jejunal valvulae conniventes are slightly thicker and more closely spaced than in the ileum.²⁰ Approximately 30% of jejunal folds will be collapsed and should not be confused with small bowel masses.⁷ In the enteric phase of enhancement, the jejunum enhances to a significantly greater degree than the ileum, with the attenuation difference normalizing in later phases²¹ (Fig. 38-1).

SUSPECTED CROHN'S DISEASE

CTE images in patients with known or suspected Crohn's disease should be scrutinized for CT findings of mural inflammation anywhere along the GI tract, penetrating disease (e.g., sinus tracts, fistulas, phlegmon, and abscesses), bowel obstruction, and inflammatory bowel disease (IBD)-related extraenteric findings, including mesenteric venous thromboses, sacroiliitis, and primary sclerosing cholangitis. Chapters 40 and 54 describe the imaging features of Crohn's disease in greater detail.

CT findings of mural inflammation include segmental mural hyperenhancement, mural thickening, mural stratification, abnormal mural or perienteric fat, and the comb sign.⁵ Mural hyperenhancement refers to segmental attenuation (or enhancement) greater than that of adjacent small bowel loops.²² Although not specific, it is generally considered to be the most sensitive findings for Crohn's disease-related inflammation,¹⁶ and it is highly correlated with endoscopic and histologic findings of inflammation.²² Because the jejunum

enhances more avidly than the ileum, comparison to only nearby loops is important in this evaluation. Jejunal hyperenhancement associated with jejunal Crohn's disease is often more difficult for radiologists to appreciate because of the prominence of the valvulae conniventes, or jejunal folds (Fig. 38-2). Other imaging features such as penetrating ulcers, mural thickening, and disruption of the fold pattern are often seen in jejunal Crohn's disease, which frequently involves a longer length and multiple segments compared with ileal Crohn's disease.

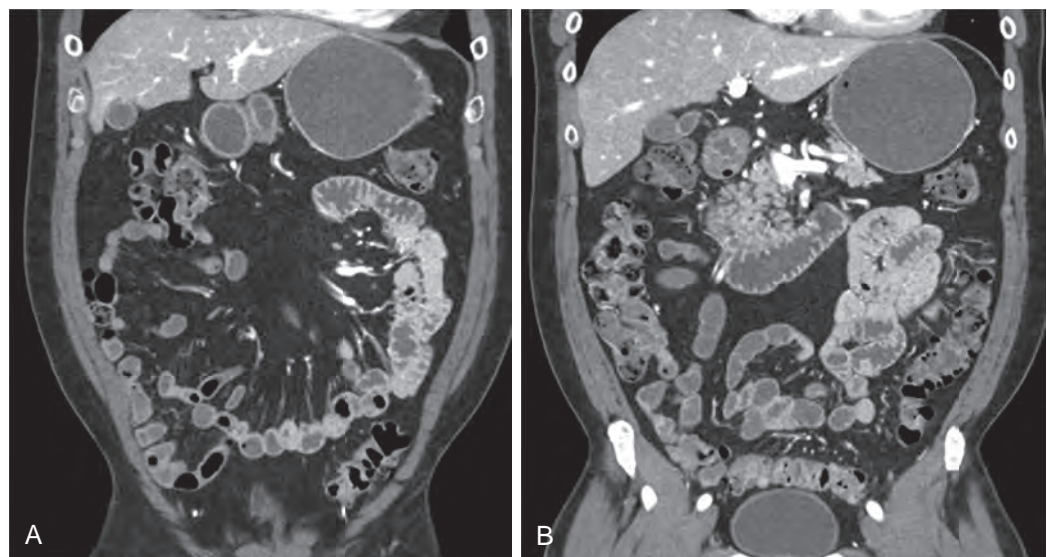
A wide variety of diseases can also cause mural hyperenhancement; however, patchy and asymmetric hyperenhancement or continuous hyperenhancement along the mesenteric border are pathognomonic for Crohn's disease (Video 38-1; Table 38-2). Contraction of small bowel loops can cause increased attenuation of a small bowel loop,²¹ but is usually readily distinguished by smooth tapering of the adjacent distended segments on either end. Infection, backwash ileitis, angioedema (often from angiotensin-converting enzyme [ACE] inhibitors), vasculitis, and bowel ischemia can all cause segmental hyperenhancement of bowel loops. However, these entities are not usually associated with asymmetric enhancement or penetrating complications. When faced with equivocal hyperenhancement, comparing two nearby distended bowel loops and taking into account secondary signs of Crohn's disease (e.g., mural stratification, perienteric edema, and the comb sign) are often helpful. Radiation enteritis can also produce narrowed and hyperenhancing bowel loops, but it is easily distinguished from Crohn's disease because of the history of radiation and symmetric hyperenhancement.²³

An additional video for this topic is available online.



Mural thickening greater than 3 mm is also considered abnormal in small bowel loops in which the lumen is distended. Collapsed bowel loops, especially in the jejunum, can sometimes be mistaken for small bowel wall thickening because of the valvulae conniventes, which can become confluent when the

Figure 38-1 Normal CTE images. A, B. Coronal images demonstrate a normal small bowel appearance with CTE performed in the enteric phase in a 46-year-old man with negative capsule endoscopy. Note the increased number of folds and increased enhancement in the jejunum, in addition to the collapse of several jejunal loops, all of which are normal findings.



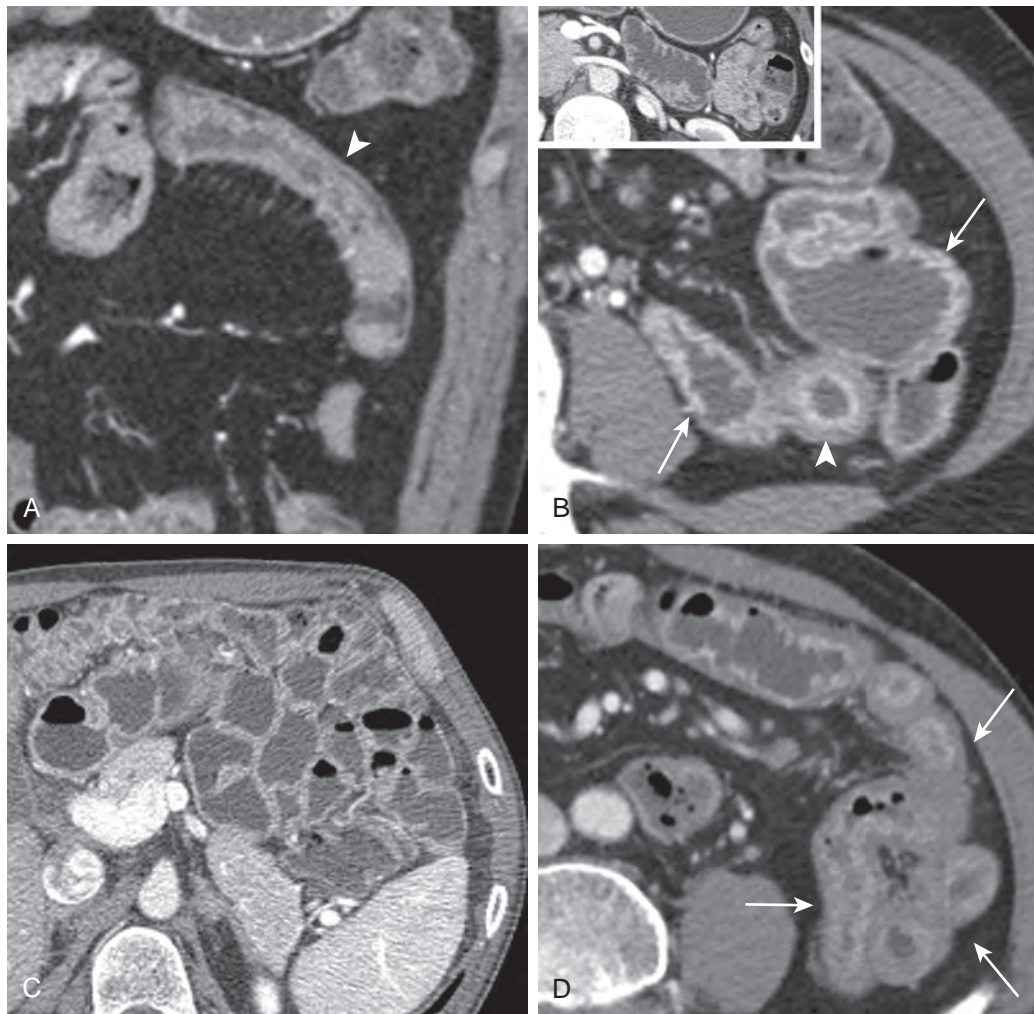


Figure 38-2 CTE images of inflammatory and infectious jejunal Crohn's disease. **A, B.** Jejunal Crohn's disease is manifested by disruption of the normal fold pattern, asymmetric involvement (**A**, arrowhead), segmental hyperenhancement compared with normal jejunal loops (**B**, inset and arrows), and mural stratification (**A, B**, arrowheads). **C.** Celiac sprue demonstrates a diffuse loss of jejunal folds. **D.** Neutropenic enterocolitis (arrows) appears similar to Crohn's disease but involves long bowel segments and symmetric mural stratification; it is seen in immunocompromised patients.

TABLE 38-2

Differential Diagnosis of Segmental Small Bowel Mural Hyperenhancement

Disease Entity	Comments	Differential Imaging Features
Crohn's disease	Jejunal involvement frequently overlooked	Asymmetric, patchy or mesenteric border hyperenhancement; multifocality; perianal disease or other penetrating complications
Backwash ileitis		Symmetric involvement; continuous with pancolonic involvement, patulous ileocecal valve
Angioedema	Often associated with abdominal pain and use of ACE inhibitors	Symmetric involvement, dilated loop, ascites
Contraction, peristalsis	Delayed images often help	Smooth tapering on proximal and distal ends; compare with other phases of enhancement
Radiation enteritis	History of pelvic radiation	Long-segment hyperenhancement without asymmetry
NSAID enteropathy	History of NSAID ingestion	Focal 1- to 2-cm lesion, often multiple, with intervening normal-appearing bowel
Ischemia	Patient often older or had recent cardiac event	Symmetric involvement; concurrent closed loop obstruction, venous or arterial occlusion or thrombosis
Infection or neutropenic enteritis	Clinical history often suggestive	Symmetric involvement
Vasculitis		Symmetric involvement; vessel and solid organ involvement

lumen is collapsed. Similar to hyperenhancement, mural thickening in Crohn's disease is frequently asymmetric and located along the mesenteric border. Focal or segmental wall thickening can be seen in hemorrhage and intestinal edema, as well as the spectrum of entities causing mural enhancement (see earlier).

Other imaging findings can be seen in Crohn's disease-related enteric inflammation. Mural stratification (also called the target sign) refers to a laminated appearance (two or three layers) to the bowel wall and is often seen in IBD (Crohn's disease, ulcerative colitis) and other benign small bowel

diseases.^{4,23,24} It is usually related to inflammation (Crohn's disease, nonsteroidal anti-inflammatory drug (NSAID) enteropathy), infection, or a vascular cause (e.g., ischemia, hemorrhage, vasculitis, radiation enteritis). Fibrofatty proliferation of the mesentery is a pathognomonic finding in Crohn's disease.⁴ Similar to mesenteric border linear ulcers seen at small bowel fluoroscopy, fibrofatty proliferation appears on the CT examination as a large amount of fat along the mesenteric border of small bowel loops or circumferentially about the rectum. The comb sign is not pathognomonic but is frequently seen in IBD; it refers to engorged vasa recta,²⁵ which enter the bowel at angles and become enlarged in active inflammation.

Penetrating Crohn's complications such as fistulas, sinus tracts, phlegmons, and abscesses frequently are seen in approximately 25% of Crohn's patients, and their detection frequently leads to changes in medical management or radiologic or surgical intervention.^{26,27} Fistulas appear as extraenteric tracts on CTE, generally arise from inflamed small bowel loops, and may be clinically unsuspected in up to 50% of cases.²⁸ Crohn's fistulas often cause tethering of affected small bowel loops, and asterisk-shaped fistulas complexes are often seen between distal ileal loops, sigmoid or ascending colon, and the bladder (Fig. 38-3). Fistulas are named by the structures to which they connect (e.g., enteroenteric, enterocutaneous, enterovesical, perianal). Fistulas can arise from other causes, usually as a result of surgery, infection, or pancreatitis. Rarely, pelvic infection with actinomycosis can mimic fistulizing Crohn's disease with

bowel wall thickening, with diffuse inflammatory changes in the mesentery, fistulas, (including perianal fistulas), or masslike phlegmonous change, often in women with an IUD.²⁹

Neoplasms can be confused with small bowel Crohn's disease. Primary GI lymphoma can cause asymmetric segmental wall thickening, but it is generally distinguished by lack of hyperenhancing bowel loops. Carcinoid small bowel disease will occasionally be mistaken for Crohn's disease. The clue to this diagnosis is the multifocality of the masses and characteristic appearance of the mesenteric metastasis. The imaging differentiation of these entities from Crohn's disease can sometimes be difficult and require biopsy because both tumors can arise in the setting of chronic Crohn's inflammation in addition to adenocarcinoma.

GASTROINTESTINAL BLEEDING

CTE for gastrointestinal bleeding is generally performed for obscure GI bleeding, with endoscopy, CT angiography, or abdominal and pelvic CT performed in the acute setting. CTE for obscure GI bleeding is performed after upper and lower endoscopy and is included in the 2011 American Society for Gastrointestinal Endoscopy (ASGE) practice guidelines for overt and obscure GI bleeding.³⁰ Obscure GI bleeding is recurrent or persistent bleeding with no source found at initial upper and lower endoscopy. Overt obscure GI bleeding means that bleeding is visible as melena, hematemesis, or hematochezia,

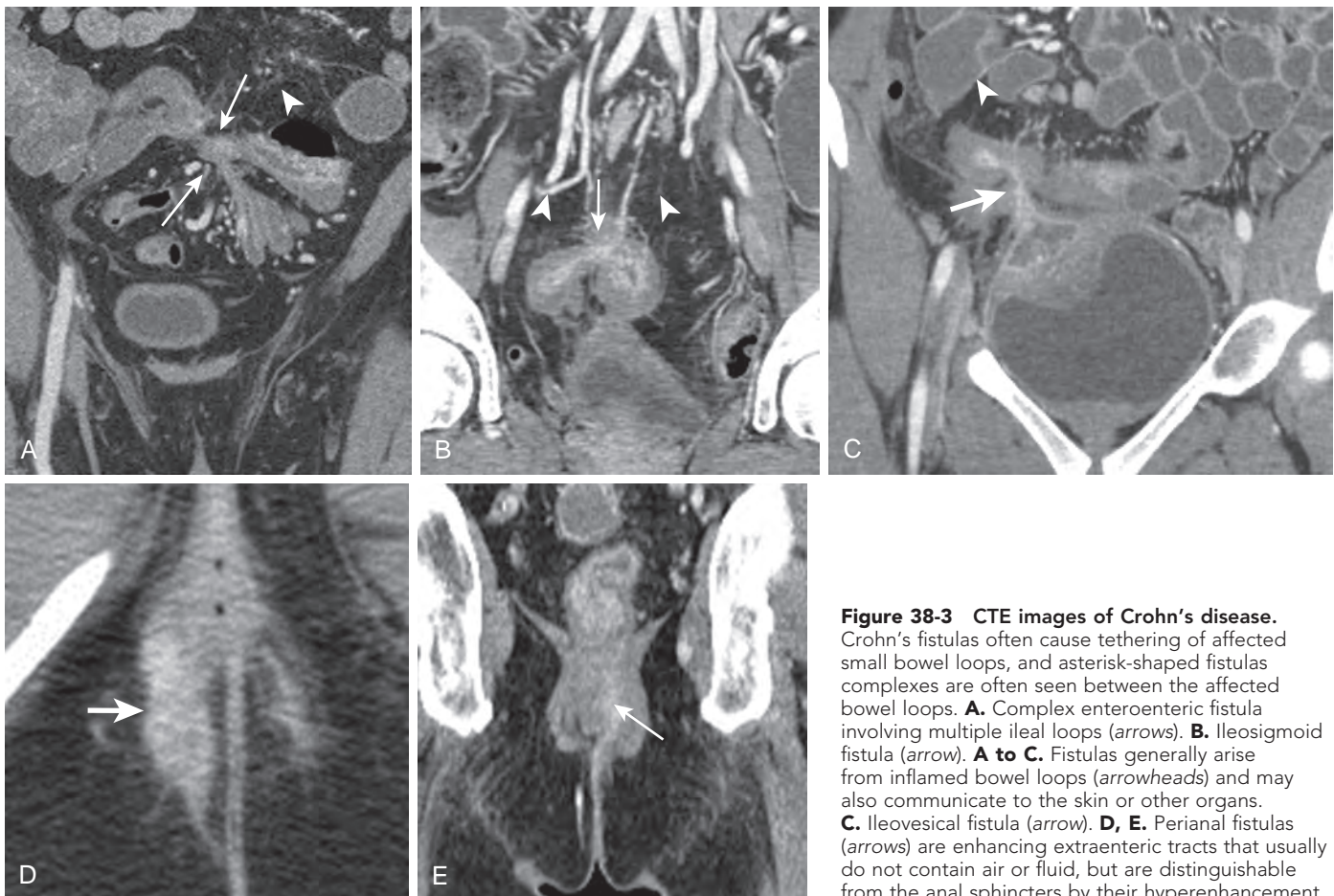


Figure 38-3 CTE images of Crohn's disease. Crohn's fistulas often cause tethering of affected small bowel loops, and asterisk-shaped fistulas complexes are often seen between the affected bowel loops. **A.** Complex enteroenteric fistula involving multiple ileal loops (arrows). **B.** Ileosigmoid fistula (arrow). **A to C.** Fistulas generally arise from inflamed bowel loops (arrowheads) and may also communicate to the skin or other organs. **C.** Ileovesical fistula (arrow). **D, E.** Perianal fistulas (arrows) are enhancing extraenteric tracts that usually do not contain air or fluid, but are distinguishable from the anal sphincters by their hyperenhancement.

whereas occult, obscure GI bleeding occurs in those with iron deficiency anemia.³¹ Common causes of GI bleeding in younger patients include small bowel tumors, Meckel's diverticula, Crohn's or celiac disease, Dieulafoy lesions, and varices; angioectasias, NSAID enteropathy, and celiac disease are more common in older individuals.³¹

Interpretation of multiphasic CTE in obscure GI bleeding is challenging and requires a systematic approach because of the variety of potential bleeding sources. The role of the radiologist is to identify any active bleeding in addition to any underlying causes, such as a tumor or vascular lesion. An initial search is performed of images obtained during the arterial phase of enhancement for high-attenuation structures that may indicate intraluminal debris, active bleeding, neoplasm, or vascular lesions, with findings correlated on the subsequent phase of enhancement to distinguish small bowel lesions from intraluminal debris and bleeding. Debris often possesses sharp edges and appears unchanged over multiple phases. A progressive accumulation of intraluminal contrast signals active bleeding (Fig. 38-4). The morphology of the small bowel lesions (e.g., intraluminal filling defects or focal regions of bowel thickening) will aid in narrowing of the differential diagnosis. Intraluminal filling defects that are not debris generally represent a neoplasm, arise from the bowel wall, and will change in enhancement over time. Focal regions of bowel thickening, such as Crohn's disease, lymphoma, and metastases, will also have an enhancement that evolves progressively.

Small bowel tumors are frequently identified at multiphase CTE in patients with obscure GI bleeding. Tumors in these patients tend to be smaller and at an earlier stage than symptomatic patients. Several studies have suggested that small bowel neoplasms may be more readily identified at CTE than capsule endoscopy because of their exoenteric or submucosal origin.^{11,32,33} Carcinoid (neuroendocrine) tumors are generally hyperenhancing tumors and may appear as an enhancing polyp, often with a shoulder-like morphology, with slight puckering or retraction along the serosal surface, or as multifocal enhancing tumors over a distance of 20 to 30 cm³⁴ (Fig. 38-5). The involvement of mesenteric vessels by tumors can simulate the segmental wall thickening seen in Crohn's disease, but will also cause retraction of the affected bowel loops. In obscure GI bleeding, focal small bowel lesions with classic mesenteric metastases with soft tissue, radiating strands of desmoplasia adjacent to the primary tumor, or liver metastases are infrequently seen.³⁴

GI stromal tumors are known to hemorrhage and ulcerate frequently and are generally hyperenhancing, but may be isoenhancing. They may appear as round or intraluminal filling defects, but often have an exoenteric component.³⁵ Small bowel lymphomas demonstrate an appearance similar to that seen on routine abdominal CT (isointense enhancement, adjacent lymphadenopathy with or without aneurysmal ulceration), but are frequently smaller. Melanoma metastases are often seen as intramural lesions because of their hematogenous spread;

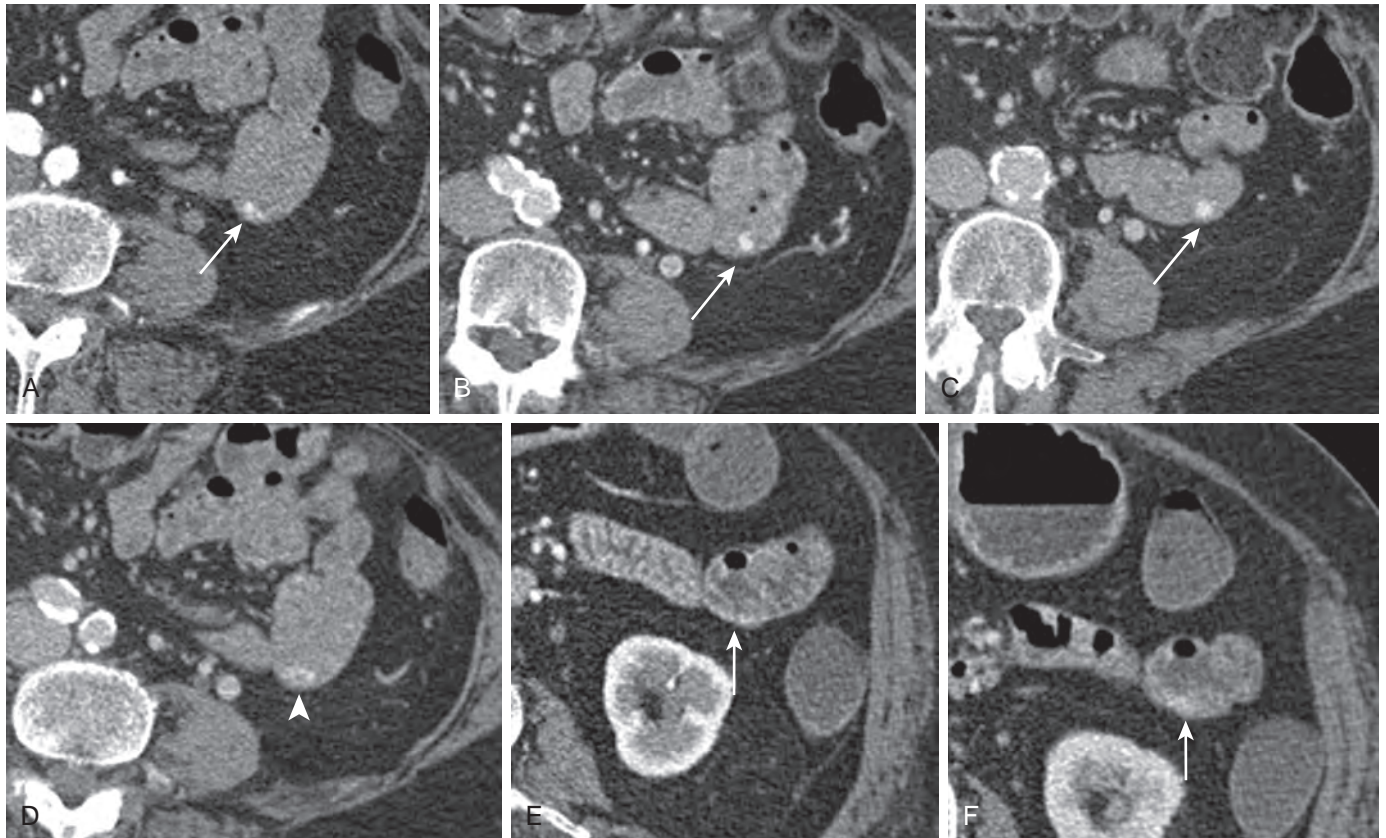


Figure 38-4 Two patients with active jejunal bleeding. **A to C.** These images demonstrate a jejunal angioectasia as displayed during arterial, enteric, and delayed phases, respectively (arrows). **D.** An image at a slightly inferior level shows layering of extravasated contrast in the distal jejunal lumen (arrowhead). **E, F.** Images in another patient poorly demonstrate the patient's jejunal vascular malformation (not shown), but indicate active jejunal bleeding in the enteric and delayed phases, respectively, with progressive accumulation of contrast within the jejunal lumen (arrows).

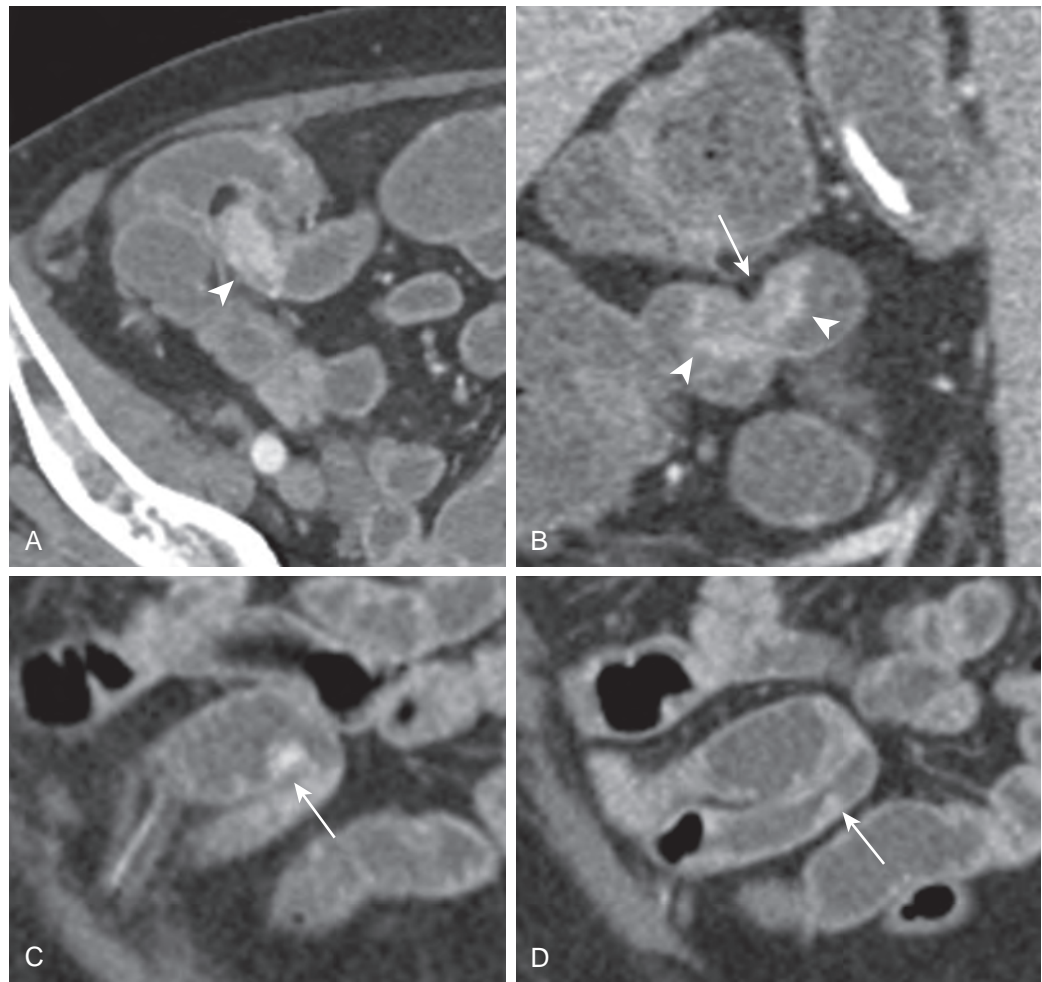


Figure 38-5 Neuroendocrine tumors demonstrated by CTE.

A. Small bowel carcinoid (neuroendocrine) tumors (arrowhead) can be seen as hyperenhancing polyps or mural masses, which are nonspecific in appearance. **B.** However, flat or sessile polyps with luminal shouldering (arrowheads) with retraction along the serosal surface (arrow) are characteristic for small bowel neuroendocrine tumors. **C.** Ileal carcinoids are often multiple (arrow). **D.** The tumors cause narrowing of the lumen (arrow).

however, in this clinical setting, they have a nonspecific appearance and are frequently not hypervascular.

Vascular lesions are often detected at capsule endoscopy and are increasingly being detected with multiphase CTE (Fig. 38-6). Huprich and colleagues have proposed a classification for vascular lesions at multiphase enterography that is analogous to the endoscopic classification of vascular lesions.^{36,37} They have classified vascular lesions at enterography into angiodysplasias, arterial lesions, and venous lesions. Angioectasias are the most common vascular small bowel lesions and are thin, tortuous veins that lack an internal elastic layer and possess arterial-venous communication. They are frequently multifocal and seen in older individuals. At CTE, they are rounded structures that are generally best seen in the enteric phase using multiplanar images or 3D workstations, with washout on delayed-phase images. In older individuals, it is common to see prominent jejunal veins, so identification of round morphology or active bleeding is imperative prior to referral to balloon endoscopy for ablation. Arterial lesions include Dieulafoy lesions, arteriovenous fistulas, and arteriovenous malformations. A Dieulafoy lesion is an artery in the submucosa that does not undergo normal branching and bleeds through a small mucosal defect. It manifests as an arterially enhancing lesion, often with active bleeding and extravasation of IV contrast into the bowel lumen; it is not associated with mucosal pathology. Because arterial lesions can be intramural,

arteriovenous malformations (AVMs) may be missed at prior colonoscopy and are not infrequently seen in the cecum and rectum. These lesions are often heralded by the presence of a dilated right ileocolic or superior hemorrhoidal vein in the arterial phase, whereas AVMs in the small bowel wall will also possess large draining veins.³⁸ Venous lesions include small bowel varices (congenital or caused by chronic mesenteric vein thrombosis in Crohn's disease), venous hemangiomas, and other venous lesions.

Meckel's diverticula are also a commonly identified source of GI bleeding, particularly in young patients, may have an internal ulcer, gastric mucosa, or tumor, and may intussuscept, with a classic appearance of fat within the intussusceptum surrounded by a collar of soft tissue.³⁹ NSAID enteropathy is a source of GI bleeding in older patients and is seen as a short segment of circumferential narrowing or luminal diaphragm, often causing a partial obstruction or capsule retention. The diaphragms are often multifocal and may demonstrate focal hyperenhancement.

LOW-GRADE OBSTRUCTION

Patients with high-grade small bowel obstruction present symptomatically to the emergency room and generally undergo routine abdominal CT, which can detect findings leading to surgical management.⁴⁰ CT and MR enteroclysis are more

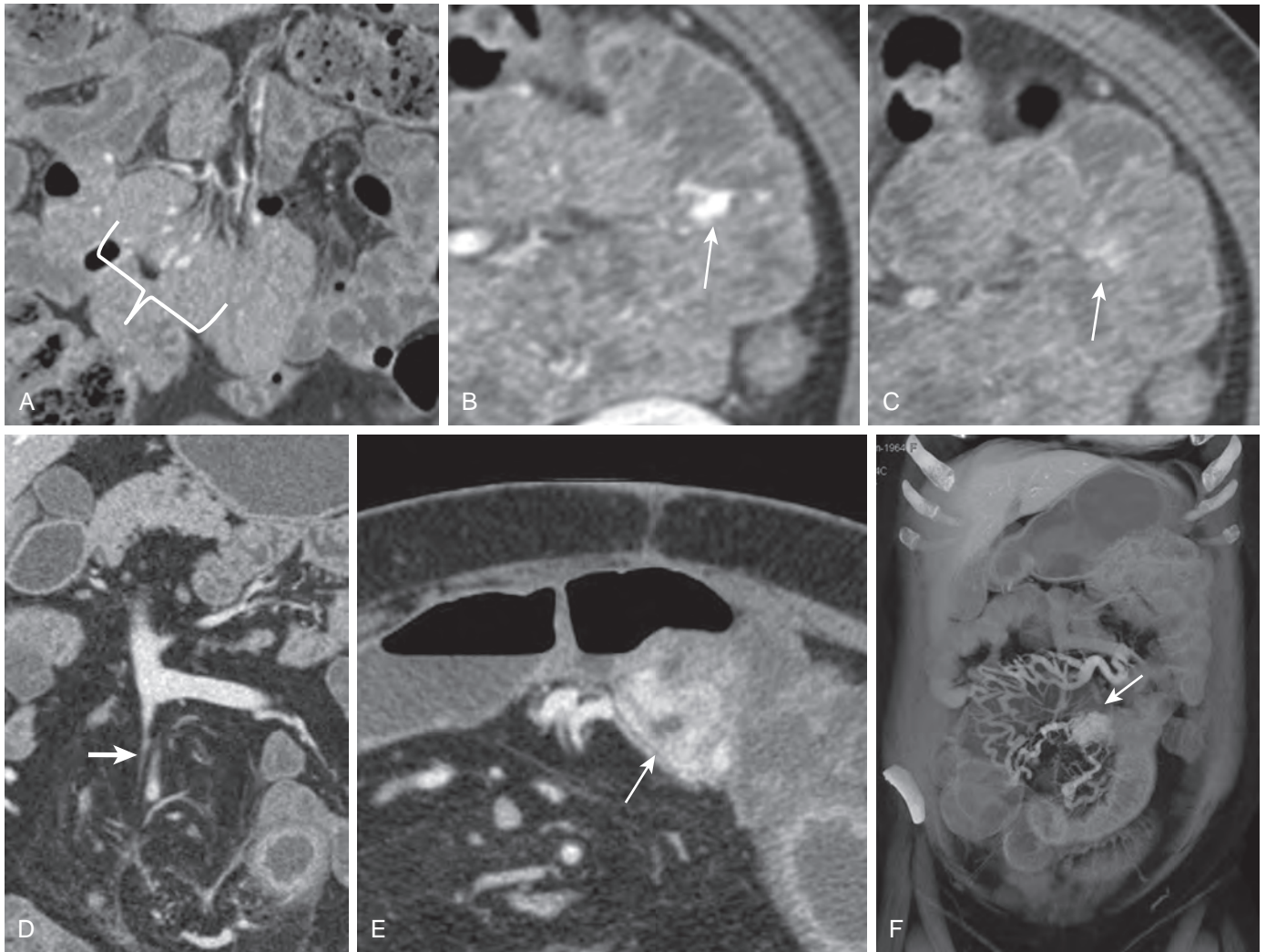


Figure 38-6 CTE images of gastrointestinal vascular lesions. Vascular lesions can be classified as angioectasias, arterial lesions, and venous lesions (usually varices). **A.** Angioectasias (bracket) occur in older individuals, are most prominent in the enteric phase, and are distinguished from prominent penetrating veins by a lobulated or rounded shape, best seen on multiplanar or 3D reformations. **B.** Dieulafoy lesions are one type of arterial lesions and exhibit bright arterial enhancement (arrow), often with extravasation of IV contrast into the small bowel lumen (**C**, arrow), and can be treated endoscopically, as in this case. Venous lesions can be congenital or acquired. **D.** Crohn's disease patients often have chronic occlusion of the proximal superior mesenteric vein (arrow) or mesenteric venous branches, with collateral flow forming varices (**E**, **F**, arrows) over time.

sensitive for low-grade small bowel obstruction compared with CTE, but require nasojejunal intubation.^{41,42} CTE is often performed when the patient is unwilling to undergo enteroclysis or as a general imaging test to exclude small bowel pathology. The criteria for partial obstruction are identical to those for routine CT (zone of transition from dilated to decompressed bowel [see Chapter 46]); frequently seen causes include adhesions, tumors, Crohn's disease, hernia, radiation enteritis, intussuscepting Meckel's diverticulum, and diaphragm disease.

Patients with structuring Crohn's disease represent an important subpopulation of patients with partial obstruction at enterography. Approximately 20% of asymptomatic patients with strictures and partial small bowel obstruction at enterography will not have any symptoms.^{6,29} The term *strictures* is reserved for narrowed small bowel segments that cause proximal dilation and partial small bowel obstruction. Crohn's strictures generally have inflammatory and fibrotic components, with decreasing hyperenhancement and proximal dilation

correlating with the increased levels of fibrosis.⁴³ CTE is highly accurate for the detection of Crohn's strictures,⁴⁴ and detection of multifocal strictures can be especially important for guiding surgical management, such as stricturoplasty.⁴⁵

Radiation Dose and Computed Tomography Enterography

An understanding of anticipated benefits and risks is needed to inform patients and clinicians about the medical justification for a CTE examination.^{46,47} In terms of benefit, one large prospective study of over 250 patients with known or suspected Crohn's disease found that approximately 50% of patients with known Crohn's disease and 50% of patients with suspected Crohn's disease had management decisions changed as a result of CTE findings.²⁷ In patients with Crohn's disease, small bowel disease was excluded in approximately 12%, medication changes

were made in another 15%, and anticipated surgical management was altered in approximately 7%.²⁷ In another study of 152 IBD patients presenting to the emergency room of a tertiary care hospital, CTE changed management in 81% and 69% of Crohn's and ulcerative colitis patients, respectively, with urgent non-IBD diagnoses identified in 13% and 28% of patients, respectively.⁴⁸ In another study of approximately 150 Crohn's patients, about 50% of Crohn's patients with a normal-appearing ileum on ileoscopy had other objective evidence of mural or proximal small bowel inflammation.⁴⁹ Also, penetrating complications, which often prompt medical or surgical management, are unsuspected in up to 50% of Crohn's patients with fistulas or abscesses.²⁸ In obscure GI bleeding, the benefit of CTE is that it may detect small bowel tumors, which are difficult to find using optical methods alone. An additional benefit is that CTE can be performed and interpreted immediately on presentation in the case of overt, obscure GI bleeding, whereas capsule endoscopy requires 1 day to acquire and interpret data.

Nevertheless, Crohn's disease patients have higher cumulative radiation doses,⁵⁰ and an increased dose may be harmful for pediatric patients, particularly young females.⁵¹ The National Academies of Sciences BEIR VII report stated that "at statistical doses of 100 mSv or less, statistical limitations make it difficult to evaluate cancers in humans," but they concluded that "...the preponderance of information indicates that there will be some risk, even at low doses, although the risk is small."⁵² The radiation dose imparted by a single CTE examination is over an order of magnitude smaller than that cited in the BEIR VII report, and state of the art dose reduction techniques often result in examinations performed at dose levels similar to annual background radiation levels. Because of these concerns, however, MR enterography may be a more appropriate test in young individuals, especially those undergoing repeated outpatient examinations.⁵³ Both radiology and gastroenterology societies have considered the benefits and risks of CTE and recommend it as an appropriate test in the correct clinical setting.^{30,54}

Integration with Other Tests

Ileocolonoscopy is frequently performed synchronously with CTE because the two tests are considered complementary. Optical colonoscopy can detect and stage colonic inflammation better compared with CTE,⁵⁵ and it can also detect colonic neoplasia and perform surveillance biopsies for risk assessment. Enterography, on the other hand, can identify mural

and proximal disease in the ileum, particularly in the setting of terminal ileum skipping.⁴⁹ In the setting of obscure GI bleeding, all patients should undergo upper and lower endoscopy to detect treatable causes of GI bleeding originating from esophageal, gastric, duodenal, and colonic sources prior to small bowel imaging.

Capsule endoscopy is a very sensitive tool for mucosal inflammation in Crohn's disease but the capsule can be retained, necessitating endoscopic or surgical removal in patients with strictures. This may be a particularly significant problem in Crohn's disease, in which asymptomatic strictures may be present. Conversely, one of the limitations of CTE is the limited visualization of jejunal loops, and capsule endoscopy is likely to be complementary with CTE in detecting jejunal disease and early mucosal disease in the ileum.^{6,56} Capsule endoscopy is a first-line test in obscure GI bleeding after consideration has been given to repeat upper and lower endoscopy, and it provides complementary information compared with CTE.³⁰ Balloon-assisted endoscopy is used in many centers to investigate the cause of obscure overt GI bleeding and can be used to biopsy or treat small bowel lesions detected by capsule endoscopy or CTE.

MR enterography is also routinely used to detect small bowel Crohn's disease. Several prospective studies have shown that the performance of CTE and MR enterography is similar for identifying mural inflammation in small numbers of patients.^{57,58} CTE is easier to accomplish in a practice setting and may be less prone to interobserver variability.⁵⁹ MR enterography is often preferred for younger patients because of the lack of ionizing radiation and necessity for CT imaging in acute flares.⁵³ CTE may be especially useful when MR expertise and experience are not available, there is a clinical concern for sepsis, the patient is having her or his first CTE examination, or suspected, complex intra-abdominal penetrating disease is present, which may prompt further surgical or interventional therapy, or in older patients. In these situations, the clinical benefit of CTE will far outweigh potential risks. MR enterography, given limited resources, may be more useful in asymptomatic patients, when obstruction is suspected, or when patients are younger or have known perianal disease.

Fluoroscopic small bowel examination is useful, particularly in patients with colonic resections or resections of the ileocecal valve, so the functional importance of narrowed and dilated segments can be ascertained. Moreover, fluoroscopic examination also provides a single view of complex small bowel disease in the presence of prior surgical changes.

REFERENCES

- Del Gaizo AJ, Fletcher JG, Yu L, et al: Reducing radiation dose in CT enterography. *Radiographics* 33:1109–1124, 2013.
- Ajay W, Goehde S, Schneemann H, et al: Oral contrast agents for small bowel MRI: Comparison of different additives to optimize bowel distension. *Eur Radiol* 14:458–464, 2004.
- Young BM, Fletcher JG, Booya F, et al: Head-to-head comparison of oral contrast agents for cross-sectional enterography: Small bowel distention, timing, and side effects. *J Comput Assist Tomogr* 32:32–38, 2008.
- Paulsen SR, Huprich JE, Fletcher JG, et al: CT enterography as a diagnostic tool in evaluating small bowel disorders: Review of clinical experience with over 700 cases. *Radiographics* 26:641–657, 2006.
- Elsayes KM, Al-Hawary MM, Jagdish J, et al: CT enterography: Principles, trends, and interpretation of findings. *Radiographics* 30:1955–1970, 2010.
- Solem CA, Loftus EV, Jr, Fletcher JG, et al: Small-bowel imaging in Crohn's disease: A prospective, blinded, 4-way comparison trial. *Gastrointest Endosc* 68:255–266, 2008.
- Wold PB, Fletcher JG, Johnson CD, Sandborn WJ: Assessment of small bowel Crohn disease: Noninvasive peroral CT enterography compared with other imaging methods and endoscopy—feasibility study. *Radiology* 229:275–281, 2003.
- Schindera ST, Nelson RC, DeLong DM, et al: Multi-detector row CT of the small bowel: Peak enhancement temporal window—initial experience. *Radiology* 243:438–444, 2007.
- Vandenbroucke F, Mortelet KJ, Tatli S, et al: Noninvasive multidetector computed tomography enterography in patients with small-bowel Crohn's disease: Is a 40-second delay better than 70 seconds? *Acta Radiol* 48:1052–1060, 2007.
- Yu L, Liu X, Leng S, et al: Radiation dose reduction in CT: Techniques and future perspective (PMC3271708). *Imaging Med* 1:65–84, 2009.
- Huprich JE, Fletcher JG, Fidler JL, et al: Prospective blinded comparison of wireless capsule endoscopy and multiphase CT enterography in

- obscure gastrointestinal bleeding. *Radiology* 260:744–751, 2011.
12. McCollough CH, Bruesewitz MR, Kofler JM, Jr: CT dose reduction and dose management tools: Overview of available options. *Radiographics* 26:503–512, 2006.
 13. Allen BC, Baker ME, Einstein DM, et al: Effect of altering automatic exposure control settings and quality reference mAs on radiation dose, image quality, and diagnostic efficacy in MDCT enterography of active inflammatory Crohn's disease. *AJR* 195:89–100, 2010.
 14. Hough D, Fletcher J, Grant K, et al: Lowering kV to reduce radiation dose in contrast-enhanced abdominal CT: Initial assessment of a prototype automatic kV selection tool. *AJR* 199:1070–1077, 2012.
 15. Kambadakone AR, Prakash P, Hahn PF, Sahani DV: Low-dose CT examinations in Crohn's disease: Impact on image quality, diagnostic performance, and radiation dose. *AJR* 195:78–88, 2010.
 16. Siddiki H, Fletcher JG, Hara AK, et al: Validation of a lower radiation computed tomography enterography imaging protocol to detect Crohn's disease in the small bowel. *Inflamm Bowel Dis* 17:778–786, 2011.
 17. Lee SJ, Park SH, Kim AY, et al: A prospective comparison of standard-dose CT enterography and 50% reduced-dose CT enterography with and without noise reduction for evaluating Crohn disease. *AJR* 197:50–57, 2011.
 18. Sagara Y, Hara AK, Pavlicek W, et al: Abdominal CT: Comparison of low-dose CT with adaptive statistical iterative reconstruction and routine-dose CT with filtered back projection in 53 patients. *AJR* 195:713–719, 2010.
 19. Kaza RK, Platt JF, Al-Hawary MM, et al: CT enterography at 80 kVp with adaptive statistical iterative reconstruction versus at 120 kVp with standard reconstruction: Image quality, diagnostic adequacy, and dose reduction. *AJR* 198:1084–1092, 2012.
 20. Levine MS, Rubesin SE, Laufer I: Pattern approach for diseases of mesenteric small bowel on barium studies. *Radiology* 249:445–460, 2008.
 21. Booya F, Fletcher JG, Huprich JE, et al: Active Crohn disease: CT findings and interobserver agreement for enteric phase CT enterography. *Radiology* 241:787–795, 2006.
 22. Bodily KD, Fletcher JG, Solem CA, et al: Crohn disease: Mural attenuation and thickness at contrast-enhanced CT enterography—correlation with endoscopic and histologic findings of inflammation. *Radiology* 238:505–516, 2006.
 23. Macari M, Megibow AJ, Balthazar EJ: A pattern approach to the abnormal small bowel: Observations at MDCT and CT enterography. *AJR* 188:1344–1355, 2007.
 24. Gore RM, Balthazar EJ, Ghahremani GG, Miller FH: CT features of ulcerative colitis and Crohn's disease. *AJR* 167:3–15, 1996.
 25. Meyers MA, McGuire PV: Spiral CT demonstration of hypervascularity in Crohn disease: "Vascular jejunitization of the ileum" or the "comb sign". *Abdom Imaging* 20:327–332, 1995.
 26. Bruining DH, Loftus EV, Jr, Ehman EC, et al: Computed tomography enterography detects intestinal wall changes and effects of treatment in patients with Crohn's disease. *Clin Gastroenterol Hepatol* 9:679–683, 2011.
 27. Bruining DH, Siddiki HA, Fletcher JG, et al: Benefit of computed tomography enterography in Crohn's disease: Effects on patient management and physician level of confidence. *Inflamm Bowel Dis* 18:219–225, 2012.
 28. Booya F, Akram S, Fletcher JG, et al: CT enterography and fistulizing Crohn's disease: Clinical benefit and radiographic findings. *Abdom Imaging* 34:467–475, 2009.
 29. Lee JJ, Ha HK, Park CM, et al: Abdominopelvic actinomycosis involving the gastrointestinal tract: CT features. *Radiology* 220:76–80, 2001.
 30. ASGE Standards of Practice Committee, Fisher L, Lee Krinsky M, Anderson MA, et al: The role of endoscopy in the management of obscure GI bleeding. *Gastrointest Endosc* 72:471–479, 2010.
 31. Raju GS, Gerson L, Das A, Lewis B: American Gastroenterological Association (AGA) Institute technical review on obscure gastrointestinal bleeding. *Gastroenterology* 133:1697–1717, 2007.
 32. Hakim FA, Alexander JA, Huprich JE, et al: CT-enterography may identify small bowel tumors not detected by capsule endoscopy: Eight years experience at Mayo Clinic Rochester. *Dig Dis Sci* 56:2914–2919, 2011.
 33. Ross A, Mehdizadeh S, Tokar J, et al: Double balloon enteroscopy detects small bowel mass lesions missed by capsule endoscopy. *Dig Dis Sci* 53:2140–2143, 2008.
 34. Levy AD, Sobin LH: From the archives of the AFIP: Gastrointestinal carcinoids: Imaging features with clinicopathologic comparison. *Radiographics* 27:237–257, 2007.
 35. Sandrasegaran K, Rajesh A, Rydberg J, et al: Gastrointestinal stromal tumors: Clinical, radiologic, and pathologic features. *AJR* 184:803–811, 2005.
 36. Yano T, Yamamoto H, Sunada K, et al: Endoscopic classification of vascular lesions of the small intestine (with videos). *Gastrointest Endosc* 67:169–172, 2008.
 37. Huprich J, Barlow J, Hansel S, et al: Multi-phase CT enterography evaluation of small-bowel vascular lesions. *AJR* 201:65–72, 2013.
 38. Murphy KP, McLaughlin PD, O'Connor OJ, Maher MM: Imaging the small bowel. *Curr Opin Gastroenterol* 30:134–140, 2014.
 39. Pantongrag-Brown L, Levine MS, Elsayed AM, et al: Inverted Meckel diverticulum: Clinical, radiologic, and pathologic findings. *Radiology* 199:693–696, 1996.
 40. Balthazar EJ, Liebeskind ME, Macari M: Intestinal ischemia in patients in whom small bowel obstruction is suspected: Evaluation of accuracy, limitations, and clinical implications of CT in diagnosis. *Radiology* 205:519–522, 1997.
 41. Walsh DW, Bender GN, Timmons JH: Comparison of computed tomography-enteroclysis and traditional computed tomography in the setting of suspected small bowel obstruction. *Emerg Radiol* 5:29–37, 1998.
 42. Maglinte DD, Kelvin FM, Rowe MG, et al: Small-bowel obstruction: Optimizing radiologic investigation and nonsurgical management. *Radiology* 218:39–46, 2001.
 43. Chiorean MV, Sandrasegaran K, Saxena R, et al: Correlation of CT enteroclysis with surgical pathology in Crohn's disease. *Am J Gastroenterol* 102:2541–2550, 2007.
 44. Vogel J, da Luz Moreira A, Baker M, et al: CT enterography for Crohn's disease: Accurate pre-operative diagnostic imaging. *Dis Colon Rectum* 50:1761–1769, 2007.
 45. Lewis RT, Maron DJ: Efficacy and complications of surgery for Crohn's disease. *Gastroenterol Hepatol* (NY) 6:587–596, 2010.
 46. McCollough CH, Guimaraes L, Fletcher JG: In defense of body CT. *AJR* 193:28–39, 2009.
 47. Fletcher JG, Kofler JM, Coburn JA, et al: Perspective on radiation risk in CT imaging. *Abdom Imaging* 38:22–31, 2013.
 48. Israeli E, Ying S, Henderson B, et al: The impact of abdominal computed tomography in a tertiary referral centre emergency department on the management of patients with inflammatory bowel disease. *Aliment Pharmacol Ther* 38:513–521, 2013.
 49. Samuel S, Bruining DH, Loftus EV, Jr, et al: Endoscopic skipping of the distal terminal ileum in Crohn's disease can lead to negative results from ileocolonoscopy. *Clin Gastroenterol Hepatol* 10:1253–1259, 2012.
 50. Pelloquin JM, Pardi DS, Sandborn WJ, et al: Diagnostic ionizing radiation exposure in a population-based cohort of patients with inflammatory bowel disease. *Am J Gastroenterol* 103:2015–2022, 2008.
 51. Linet MS, Kim KP, Rajaraman P: Children's exposure to diagnostic medical radiation and cancer risk: Epidemiologic and dosimetric considerations. *Pediatr Radiol* 39(Suppl 1):S4–S26, 2009.
 52. Committee to Assess Health Risks from Exposure to Low Levels of Ionizing Radiation: Health Risks From Exposure to Low Levels of Ionizing Radiation, BEIR VII Phase 2, Washington DC, 2006, National Academies Press.
 53. Guimaraes LS, Fidler JL, Fletcher JG, et al: Assessment of appropriateness of indications for CT enterography in younger patients. *Inflamm Bowel Dis* 16:226–232, 2010.
 54. Huprich JE, Rosen MP, Fidler JL, et al: ACR appropriateness criteria on Crohn's disease. *J Am Coll Radiol* 7:94–102, 2010.
 55. Johnson KT, Hara AK, Johnson CD: Evaluation of colitis: Usefulness of CT enterography technique. *Emerg Radiol* 16:277–282, 2009.
 56. Voderholzer WA, Beinhörl J, Rogalla P, et al: Small bowel involvement in Crohn's disease: A prospective comparison of wireless capsule endoscopy and computed tomography enteroclysis. *Gut* 54:369–373, 2005.
 57. Lee SS, Kim AY, Yang SK, et al: Crohn disease of the small bowel: Comparison of CT enterography, MR enterography, and small-bowel follow-through as diagnostic techniques. *Radiology* 251:751–761, 2009.
 58. Siddiki HA, Fidler JL, Fletcher JG, et al: Prospective comparison of state-of-the-art MR enterography and CT enterography in small-bowel Crohn's disease. *AJR* 193:113–121, 2009.
 59. Schmidt S, Lepori D, Meuwly JY, et al: Prospective comparison of MR enteroclysis with multi-detector spiral-CT enteroclysis: Interobserver agreement and sensitivity by means of "sign-by-sign" correlation. *Eur Radiol* 13:1303–1311, 2003.

Computed Tomography Enteroclysis

ANA CATARINA SILVA | DEAN D. T. MAGLINTE

CHAPTER OUTLINE

Historical Background

Clinical Indications and Comparison With Other Imaging Methods

Small Bowel Crohn's Disease

Small Bowel Neoplasms

Small Bowel Obstruction

Miscellaneous Indications

Technical Pitfalls and Limitations

Comments

Summary

"As the number of imaging examinations and radiologic procedures continues to rise, so do radiologists' opportunities to improve their roles as consultants and clinical team members."¹ The mesenteric small intestine is the most challenging segment of the gastrointestinal (GI) tract to examine. It is the longest segment of the alimentary tube and has the widest mucosal surface, yet the incidence of disease is low and the clinical presentations are mimicked by diseases of adjacent visceral organs, with a higher incidence of abnormalities. The significant role of imaging, therefore, is to exclude small bowel (SB) disease reliably or diagnose early, small, or localized disease with confidence.²⁻¹⁷

Methods of imaging that do not distend the SB lumen have historically been shown not to allow reliable exclusion of SB disease or early demonstration of small or early mucosal or submucosal abnormalities. In addition, these examinations do not give the radiologist and clinician the confidence to exclude small neoplasms and low-grade SB occlusion (SBO) or depict early mucosal SB Crohn's disease (aphthae) or nonsteroidal anti-inflammatory drug (NSAID) enteropathy. SB imaging reports are therefore not infrequently equivocal or noninformative, and repeated imaging examinations or performance of more expensive and invasive endoscopic methods are done before a definitive diagnosis or confident exclusion of SB disease is made.

The investigation of SB diseases requires methods of examination that have a high negative predictive value and high sensitivity. Intubation infusion examinations (enteroclysis and its modifications) have been shown to overcome most of the inherent limitations of conventional examinations (peroral ingested or nonenteral volume-challenged) but have inherent limitations.¹⁸ Decades of experience have shown that only examinations that distend the lumen and coat the mucosa fulfill these roles.^{2-17,19} Several of these reports were not generated from well-controlled clinical trials; many are experience-based. The enteroclysis technique and its modifications have remained the most accurate methods that reliably exclude SB abnormalities and allow early diagnosis of disease.

Progress in imaging of the SB during the past few decades has largely occurred because of refinements in the application of various modalities. These include orally ingested conventional abdominal and pelvic computed tomography (CT) or magnetic resonance imaging (MRI) with intravenous (IV) contrast (CT enterography and MR enterography), conventional barium enteroclysis methods (computed tomography enteroclysis [CTE] and magnetic resonance enteroclysis [MRE]), and technical refinements in performing double-contrast (DC) barium enteroclysis.^{7,20-82}

Some updates on how to perform CTE, its modifications, and DC barium enteroclysis, as well as its clinical applications, have been recently described but are beyond the scope of this chapter. Interested readers are referred to these articles.^{51,83-85}

This chapter presents an update of the current role of CTE modifications in the diagnosis and management of SB diseases from evidence- and experience-based analyses. We examine why enteral volume-challenged examinations, despite their reported higher accuracy and reliability in ruling out SB disease, are infrequently performed in clinical practice. The roles of the different modifications of CTE are discussed. Evidence- and experience-based recommendations are made to improve early diagnosis and influence prognosis, decrease irradiation of the patient, and lower the costs of investigation. An overview of clinical indications, comparison with other cross-sectional imaging techniques, common technical pitfalls, and limitations are briefly presented.

Historical Background

Enteroclysis was first described by Pesquera in 1929.⁸⁶ Several investigators have modified his technique,⁸⁷⁻⁹³ but the method did not gain popularity because of technical problems, including issues with enteric tubes and inadequacy of fluoroscopic units. It was not until 1971 that Johan Sellink⁹⁴ rejuvenated the technique in Europe and received attention in North America through additional publications by several investigators in the late 1970s and early 1980s.^{12,93,95} His technique was tried by interested radiologists in North America but was not adopted by most of them because of discomfort to patients and the time requirement. Klöppel modified the Sellink method using a lower density, water-soluble enteral contrast and adapted it to monoslice CT.²¹ With the development of multislice CT technology, this method was subsequently modified by Maglinte and colleagues^{52,84,96,97} into a positive enteral contrast CTE and a neutral enteral contrast with IV contrast CTE in several newer studies.

Each modification has distinct strengths and limitations for different clinical indications. An 11% dilution of water-soluble contrast was used for the positive enteral contrast CTE after trials of multiple dilutions of iodinated contrast, and water was used for the neutral enteral contrast with IV contrast CTE.

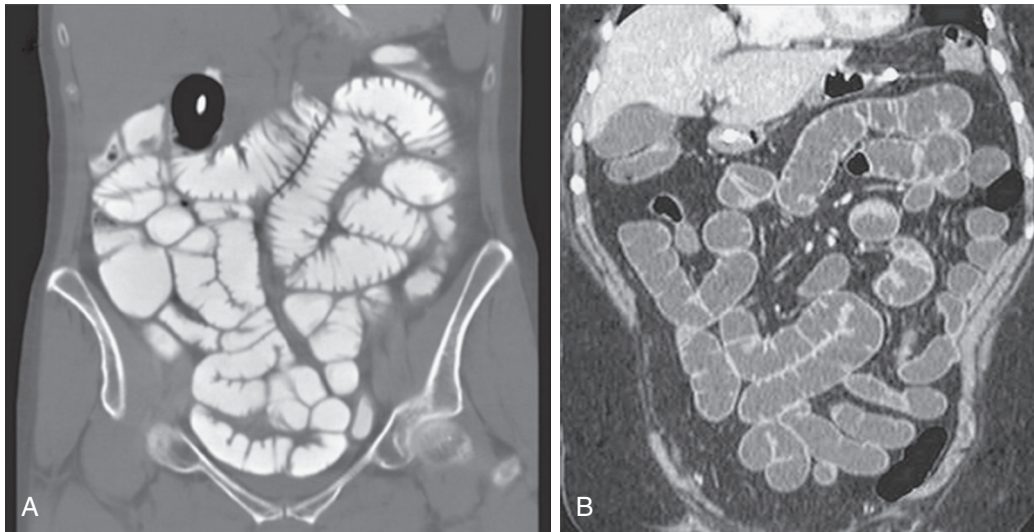


Figure 39-1 CTE modifications—normal examinations. **A.** Positive enteral contrast CTE. The 11% dilution of water-soluble iodinated contrast with the wide window settings used optimizes visualization of the valvulae conniventes. **B.** Neutral enteral contrast CTE with IV contrast using water. Soft tissue window settings optimize the evaluation of the intestinal wall, mesentery, and solid abdominal organs, a global abdominal examination. Volume (3.5 mL) of neutral enteral contrast used in our protocol includes filling of the colon needed for appropriate staging of Crohn's disease, which includes assessment of the perianal region according to the report of the working party of the 2005 Montreal World Congress of Gastroenterology for inflammatory bowel disease.

Using a wide window CT setting for the positive enteral contrast optimizes visualization of the valvulae conniventes from several dilutions that we have tried in the past.^{51,84,85,98} The use of methylcellulose suspension, which has been withdrawn from commercial distribution in the United States because of contamination as a neutral enteral contrast, was abandoned and replaced with plain tap water for the neutral CTE with IV contrast modification. Absorption is not an issue with CTE compared with CT enterography because of the volume used, the use of a hypotonic agent (glucagon), and continued infusion during CT acquisition (Fig. 39-1). Biscaldi and associates^{27,99-101} have applied the enteroclysis technique using retrograde infusion for selected indications.

Enteroclysis and its cross-sectional modifications, despite their reported accuracy, are mostly performed as a problem-solving tool in tertiary medical centers at present. This method usually follows an orally ingested SB examination (conventional abdominal-pelvic CT with oral and IV contrast, CT enterography, or MR enterography) in patients with negative or equivocal findings or with persistent symptoms despite negative findings. In a minority of specialist centers, in which the various enteroclysis modifications are done regularly, the method is used as a primary diagnostic investigation to exclude or diagnose early SB disease confidently. It is also used in patients with high clinical suspicion of SB disease to decrease radiation burden, decrease cost of work-up,^{22,83-85,102,104,105} and minimize delays in the diagnosis of SB diseases.

Clinical Indications and Comparison with Other Imaging Methods

The lack of a current evidence-based guideline results in inappropriate use and overuse in clinical practice, wasting expenditures by inappropriate referrals, incorrect interpretation, and

duplicative use¹⁰⁵ and resulting in increased cost of investigation, increased radiation burden to patient, and delays in diagnosis, which influence prognosis. Evidence- and experience-based comparisons provide insights on the clinical performance of the different methods of investigation of SB diseases and a rational basis for making recommendations. Although there are limitations in the appraisal of these research studies, they can provide useful guidelines for optimal use of current imaging studies.

SMALL BOWEL CROHN'S DISEASE

In the United States, CT enterography has recently replaced small bowel follow-through (SBFT) as the most frequently used method of SB imaging, particularly for SB Crohn's disease in most practices.^{18,19,26,81,106} With advances in multidetector CT technology, there is validity in this shift.^{19,107} Multidetector CT has simplified evaluation of the small intestine and mesentery compared with the SBFT. The term *CT enterography* was first introduced by Zamboni and Raptopoulos^{11,19,107} in 1997 in reference to a modified abdominal CT technique to address SB Crohn's disease. A large volume of a 2% barium-based or 2% to 5% water-soluble, iodine-based, oral contrast material was administered 1 to 2 hours before scanning. A high dose of IV contrast material and biphasic injection rate regimen of IV contrast were used.

Another orally ingested SB-focused CT method was subsequently described, in which a neutral enteric contrast material (polyethylene glycol [PEG] solution and whole milk) and isotonic oral solution were used.^{108,109} It was not until 2006, when the Mayo Clinic Rochester group reported their experience initially using water and a water-methylcellulose solution, which was replaced by a PEG electrolyte solution and subsequently by low-concentration barium (0.1% w/v ultra-low-dose barium with sorbitol [VoLumen, Bracco Diagnostics, Princeton, NJ]), that CT enterography caught the attention of the radiology

and gastroenterology community.^{110,111} Invited commentaries, which accompanied the reports by Bodily,¹¹² Paulsen,¹¹³ and Maglinte¹⁹ and their colleagues predicted that CT enterography would replace the traditional SBFT as the initial radiologic method of investigation for SB Crohn's and other SB diseases if expertise in DC barium enteroclysis or CTE were not available. Enteroclysis is used as a problem-solving tool in referral centers when questions relevant to management are not fully answered by CT enterography.

The optimal radiologic approach to the patient with suspected, early SB Crohn's disease, or when the clinical indication is to rule out SB Crohn's disease compared with the patient with established SB Crohn's disease, is poorly understood. Although phenotype classification is required when disease is diagnosed, the latter requires staging details for therapeutic decision making, whereas the former requires reliable exclusion of disease. The lag time from the onset of symptoms to confirmation of the diagnosis of SB Crohn's disease has been approximately 36 months.¹¹⁴ Transmural and penetrating phenotypes are usually manifest at the time of diagnosis; it is no longer early SB disease. There has been no recent update on this information because of the more common use of CT enterography, capsule endoscopy (CE), and recent modifications of barium and cross-sectional enteroclysis hybrids. It is likely that the lag time will shorten with these newer, albeit more expensive, techniques.

The use of conventional SBFT as the initial method of examination because of its low cost seems misguided because this likely contributes to the long lag time; it does not reliably exclude early disease and, when an abnormality is suspected, requires additional imaging to confirm the finding.^{15,103} This is one of the reasons for repeated SB imaging with orally ingested methods of investigation before a diagnosis is made. Evidence-based analysis has shown that the negative predictive value of CT enterography is 67% (compared with 48% for SBFT or 63% for MR enterography); these were in patients with aphthoid manifestations of the disease.¹¹⁵ In a report comparing CT enterography with CTE, the conclusion was made that CT enterography "compared favorably" with CTE in the diagnosis of SB Crohn's disease.¹⁰⁷ An invited commentary on the report concluded that the comparison was flawed. The research actually compared two forms of CT enterography, one with enteral

contrast orally ingested (enterography) and the other with enteral contrast hand-injected through a tube (labeled as CTE). Contrast was not continuously infused during CT scan acquisition, as it should be in a technically satisfactory CTE. Distention of the SB was similar, as expected. The disease phenotype was not categorized.¹⁰⁷

An evaluation of published reports does not indicate aphthoid lesions as the only manifestation of SB Crohn's disease with cross-sectional imaging as the method of examination. Radiologists must understand that when reporting the SB examination of patients with Crohn's disease, the disease phenotype, sites of involvement, and severity are categorized. Phenotype classification of SB Crohn's disease using all imaging modalities has been previously reported.¹¹⁶ This is central information for referring clinicians when formulating a course of management. It is no longer enough to state that the findings are consistent with SB Crohn's disease. CTE and MRE have been compared with biphasic barium enteroclysis. CTE has been proven to be significantly superior to enteroclysis in depicting Crohn's disease-associated intramural and extramural abnormalities.^{117,118} The best current evidence-based analysis shows that CTE is a good test for the diagnosis of SB Crohn's disease but barium enteroclysis is required in patients with high clinical suspicion of disease and with a negative CTE.⁶⁰ In the clinical scenario in which there is a high pretest probability (e.g., 85%), a positive CTE result confirms the presence of disease (0.99) but a negative test result is equivocal (0.5). Further investigation with barium enteroclysis was recommended.^{60,119}

A similar conclusion was made in a report comparing MRE with barium enteroclysis and CTE.¹²⁰ In another report, it was concluded that MRE does not perform as well as barium enteroclysis but the additional extraluminal details and absence of ionizing radiation enhances its overall performance.¹²¹ MR imaging is able to depict morphologic changes in the assessment of SB Crohn's disease.¹²²

In another evidence-based comparison between CTE and barium enteroclysis, Minordi and co-workers⁶⁰ concluded that CTE is a good test for the diagnosis of SB Crohn's disease but barium enteroclysis is required in patients with a high clinical suspicion of disease and a negative result on CTE. Further investigation with barium enteroclysis was also recommended (Fig. 39-2).



Figure 39-2 Limitations of cross-sectional imaging in the diagnosis of aphthoid lesions of early SB Crohn's disease. **A, B.** Images show no evidence of hyperenhancement, transmural edema, or wall thickening on CTE done to rule out SB Crohn's disease. Upper and lower endoscopies were not informative. **C.** DC barium enteroclysis shows diffuse aphthoid ileitis with tiny ulcers and beginning submucosal edema evidenced by mild thickening of the plicae circulares (curved arrow). Inflammatory disease markers were abnormal. Patient also had an unexplained lower GI bleed.

Aphthoid lesions are below the spatial resolution of currently used cross-sectional imaging (CT or MR). These abnormalities become perceptible with cross-sectional imaging when submucosal and transmural abnormalities become manifest. They are subtle with DC barium enteroclysis and are easier to diagnose when accompanied by submucosal edema.¹²³⁻¹²⁵ In the symptomatic patient, however, with mucosal hyperenhancement by cross-sectional imaging in an adequately distended segment, particularly when accompanied by submucosal edema, early SB Crohn's disease should be considered, but further confirmation should be recommended.

A false-positive diagnosis of SB Crohn's disease has significant ramifications for patients. The Minordi report⁶⁰ used the biphasic enteroclysis method with methylcellulose, which has been shown to efface surface markings of the SB.^{67,105,126} An insight into the problem of the diagnosis of early SB Crohn's disease was also provided in another evidence-based analysis comparing CT enterography, MR enterography, and the SBFT.¹¹⁵ Phenotype classification using an endoscopic grading of disease severity¹¹⁰ was used as the reference standard. All three methods of investigation showed similar high sensitivity and specificity, but the SBFT was only 76% effective compared with 87% for CT and MR enterographies. The SBFT had the worst interobserver agreement (35%). The negative predictive values (CT enterography 67%, MR enterography 63%, and SBFT 35%) allow an understanding of the problems in the diagnosis of early SB Crohn's disease using nonenteral, volume-challenged examinations and examinations in which mucosal coating is not optimized and abnormalities are smaller than the spatial resolution of the modality. The use of CE early in the investigation may be a rational approach compared with cross-sectional imaging in practices with no expertise in performing DC barium enteroclysis, despite its shortcomings.¹⁰⁴

A comparison between CE and the various modifications of enteroclysis^{46,67,104,127} has further shown that cross-sectional imaging (CT or MRI) does not reveal the aphthae of early SB Crohn's disease when it is the only manifestation of the disease. Several of these evidence-based comparisons predated CE or newer methods of enteroscopy. Most patients had known disease or were highly suspected of having SB Crohn's disease, and the phenotype of SB Crohn's disease was not categorized. In addition, there were heterogeneous tests used as reference standards, including the SBFT, biphasic methylcellulose enteroclysis, and subjective indices. In another meta-analysis, CE was shown to have an incremental yield of 31% more than CT enterography.^{128,129}

In other reports, DC barium enteroclysis and both modifications of CTE compared favorably with CE in the evaluation of suspected Crohn's disease and obscure GI bleeding.^{67,104}

SMALL BOWEL NEOPLASMS

Although the small intestine represents almost 75% of the total length of the GI tract and almost 90% of its mucosal surface, SB neoplasms remain rare; they account for less than 5% of all GI tumors.¹³⁰ Colon cancer is 50 times more common than SB cancer.¹³¹ Adenocarcinoma, mostly located in the duodenum and proximal jejunum, makes up 30% to 40% of cancers. Carcinoid, mostly in the ileum and uncommon in the proximal SB, makes up 35% to 42%; lymphomas, mostly in the ileum and jejunum, approximately 15% to 20%; and sarcomas, which are evenly distributed, approximately 10% to 15%.¹³²

The incidence of SB cancer has increased during the past several decades—fourfold for carcinoid, less dramatic for adenocarcinoma and lymphoma, and stable for lymphoma. The incidence is higher in North America, Western Europe, and Oceania than in Asia.¹³³ An increase in the 5-year relative survival (U.S. SEER data, 1992-2005), particularly for carcinoid (80.7%), has been noted.¹³⁴ This is secondary to novel adjuvant therapies and not to imaging. The relative contribution of imaging to this improvement has not been evaluated. The relative survival is 64.1% for lymphoma, 57.9% for sarcomas, and 28.0% for adenocarcinoma. There is, however, no significant change in the long-term survival for any of the histologic types.¹³⁴ This has been attributed to most patients being diagnosed late, with local extension or distant tumor spread at the time of surgery and the long interval between the onset of symptoms and time of diagnosis. Reports have shown 40% local spread and 30% distant spread (Fig. 39-3).^{135,136} A prior analysis of why these delays occur showed that the major delay was after medical help was sought, longest after a false-negative result of radiologic examination.¹³⁶ In this report, the delay because of the patient failing to report symptoms was less than 2 months, the physician not ordering an appropriate diagnostic test about 8 months, and the radiologist failing to make the diagnosis approximately 12 months. This is a lag time of approximately 2 years, longest after a false-negative result of a radiologic examination.¹³⁶

The vague clinical presentation of these tumors, usually abdominal pain and less often GI bleeding, is also contributory.

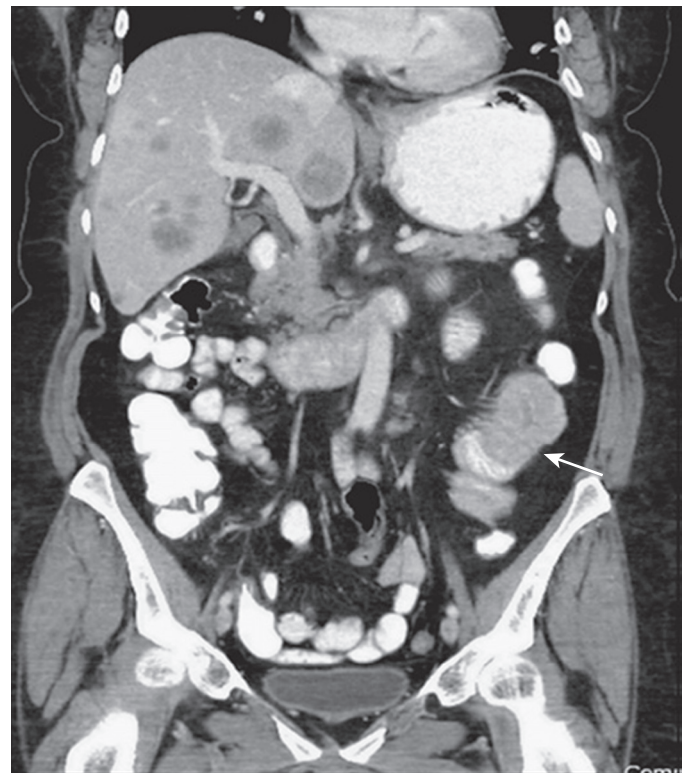


Figure 39-3 Late diagnosis of SB malignancies. Shown is a CT scan of the abdomen and pelvis with IV contrast in a patient with chronic recurrent nausea and vomiting. Coronal images show a mass in the proximal jejunum (arrow) consistent with proximal SB malignancy; also note liver metastases. Surgical pathologic findings showed adenocarcinoma.

These data underlie the need for a reliable method of examination when there is a possibility of SB neoplasm or unexplained abdominal symptoms and upper and lower GI evaluations are unrevealing. The role of imaging in these patients is to rule out or confirm early SB tumor reliably. SB tumors are rare and frequently underdiagnosed or diagnosed late (see Fig. 39-3). Curative resection remains the only curative therapy for SB malignancies.¹³⁷ There is no rigorous imaging comparison evaluating multiple peroral SB examinations and intubation-infusion distended SB modifications. A prior comparison of orally ingested SB barium examination with enteral volume-challenged examinations showed the sensitivity of orally ingested SB examination to be 61%, whereas that of enteroclysis was 95%.¹³⁸ This result highlights the difference in diagnosing filling defects when the SB is distended.

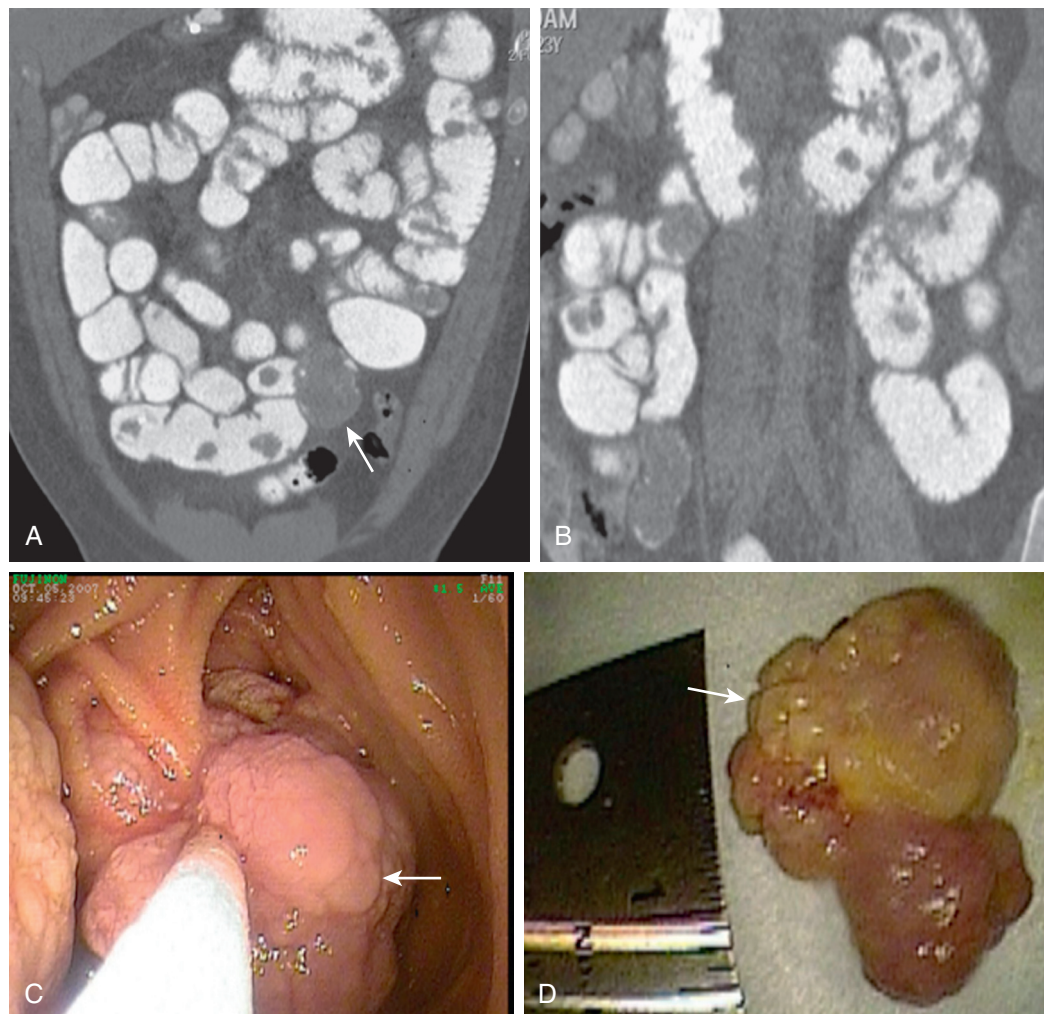
There have been no rigorous head to head comparisons between CTE and MRE or between CT enterography and MR enterography. MR imaging is frequently recommended because of the lack of ionizing radiation.¹²⁰ Both CTE and MRE have been shown to have high accuracies, more than 90%, but the discomfort of intubation has been a deterrent, and hence the rationale for recommending MR enterography.^{28,57,97,139-141}

However, this deterrent is not an issue when appropriate conscious sedation is administered and may even be preferred by patients who do not want to drink the large amount of

oral contrast and want to have no recall of their experience.¹⁴² There is an important factor for radiologists to consider—a lack of knowledge on the part of ordering physicians who want to do what is best for their patients but do not understand which imaging study is the most reliable to answer questions relevant to patient work-up and management in the evaluation of SB diseases, particularly when the possibility of SB neoplasm is concerned. Radiologists must function as consultants, so that when orally ingested SB examination results are not informative and unexplained abdominal symptoms persist, recommendation should be made to refer these patients to centers in which enteral, volume-challenged examinations are routinely performed.

An added role of CTE in the work-up of SB neoplasms is to guide the enteroscopist about which route to take in the evaluation of patients who may require biopsy or endoscopic removal of SB lesions. When multiple defects are present, the precise location of the largest lesion is readily estimated by CTE using currently available software. Although this can be done with neutral enteral CTE, the positive enteral CTE modification is simpler to use with vessel analysis software when required, although localization can be frequently estimated (Fig. 39-4). Changes in the practice of radiology in the past 3 decades and knowledge of the long-term survival of patients with malignant SB tumors are reminders to referring physicians

Figure 39-4 Use of CTE to guide enteroscopic approach in a patient with multiple SB abnormalities. A. Coronal image of a positive enteral contrast CTE on a patient with Peutz-Jeghers syndrome done because of symptoms of mechanical SBO. Multiple filling defects are seen throughout the mesenteric SB and duodenum. The largest (arrow) showed intermittent intussusception on real-time (fluoroscopic) phase of the examination. **B.** Multiple small polyps in the duodenum, proximal jejunum, and midileum. **C.** Enteroscopic image shows the largest polypoid mass (arrow). **D.** Hamartomatous mass (arrow) removed during double-balloon enteroscopy done using the oral approach. The use of vessel analysis software allows determination of the distance of an abnormality from the ligament of Treitz or ileocecal valve. (From Maglinte DD: Fluoroscopic and CT enteroclysis: Evidence-based clinical update. *Radiol Clin North Am* 51:149–176, 2013.



and radiologists of the important role of imaging in the evaluation of SB tumors.¹⁴¹

SMALL BOWEL OBSTRUCTION

SB obstruction is a common clinical condition, often presenting with signs and symptoms similar to those seen in other acute abdominal disorders. Once suspected based on the patient's clinical history and physical examination, radiologists must verify or exclude the presence of obstruction and provide cogent information on the site, severity, and probable cause of the obstruction and presence of strangulation.¹⁴³⁻¹⁴⁷ Although initial reports showed high accuracy of CT of the abdomen and pelvis with oral and IV contrasts in the diagnosis of SBO,^{148,149} a subsequent evidence-based comparison showed an overall accuracy of 65%.¹⁵⁰⁻¹⁵² In this analysis, however, the accuracy of conventional CT increased to 81% for high-grade and complete obstruction. With low-grade obstruction, accuracy was 48%, statistically similar to the sensitivity of abdominal radiography for SBO.¹⁵³

These patients have recurrent symptoms, and additional conventional CT examinations are often obtained until the obstruction becomes severe enough to be diagnosed. In patients with symptoms of recurrent low-grade adhesive obstruction, following an initial negative orally ingested CT examination usually done in the emergency department, a recommendation should be made to the referring physician that if a further investigation is needed, these patients should be referred for enteral volume-challenged examinations. In this subset of patients, similar to patients with suspected SB Crohn's disease or tumor, repeated examinations that are unable to rule out obstruction reliably are done before appropriate imaging is

requested. Findings of adhesions are often present in retrospect but are not confidently diagnosed because of the lack of an appreciable transition point; the latter is exaggerated with enteral, volume-challenged examinations. This diagnosis should be made even when nonobstructive, because these are known to cause symptoms of recurrent or chronic abdominal pain in patients with prior abdominal surgery (Figs. 39-5 and 39-6).

Dense, anterior, parietal peritoneal adhesions increase the risk of bowel injury during laparoscopy and may require alternative trocar insertion sites.¹⁵⁴ The number and sites of SBO and length of the SB proximal to the first point of obstruction assist the surgeon in deciding whether an adequate absorptive surface is available for the formation of an ostomy or bypass (generally, 125 cm).^{143,145,146} Conventional CT and other nonenteral, volume-challenged examinations are not sensitive for lower grades of SBO that present usually in the subacute phase.^{103,150-152,155} CTE is the most accurate method for the further investigation of these patients and in those with SBO diagnosed by conventional CT, in whom additional, management-relevant questions are not answered.^{145-147,150} In the former group of patients, symptoms frequently subside with nonsurgical management.

Confirmation of the diagnosis by CTE prevents the repeated performance of orally ingested enteral contrast SB CT or MR examinations. These examinations neither confidently diagnose nor exclude low-grade obstruction in the appropriate clinical setting. A larger volume of neutral oral contrast may minimize this disadvantage, but patients with this condition experience nausea and sometimes vomit with the volumes given for CT enterography. Not infrequently, they are unable to finish ingesting the optimal volume required. By directly infusing contrast into the SB and providing a fluid volume challenge, the presence

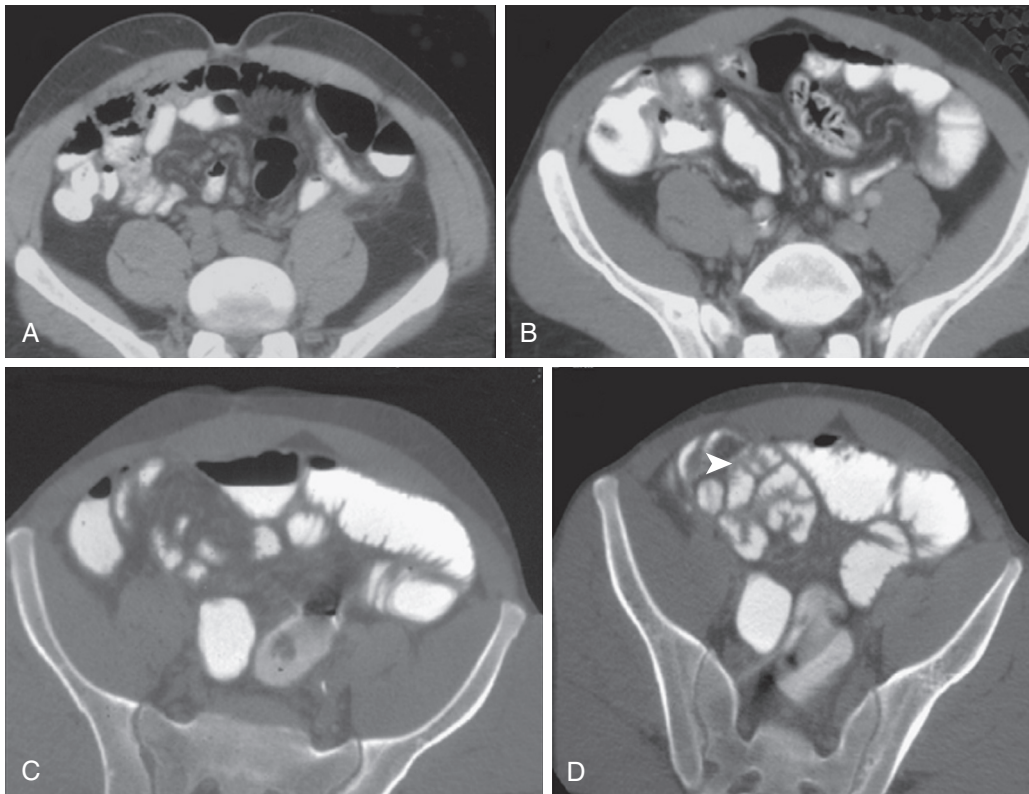


Figure 39-5 Conventional CT and CTE in low-grade small bowel obstruction. A, B. There is no evidence of a gradient or transition point to suggest mechanical obstruction in a patient with symptoms of recurrent SBO. **C, D.** CTE of the same patient demonstrates the transition point and prestenotic dilation from an anterior parietal adhesive obstruction posterior to the right rectus muscle. Interloop (visceral) adhesions (arrowhead) are noted in segments posterior to the parietal adhesive obstruction.

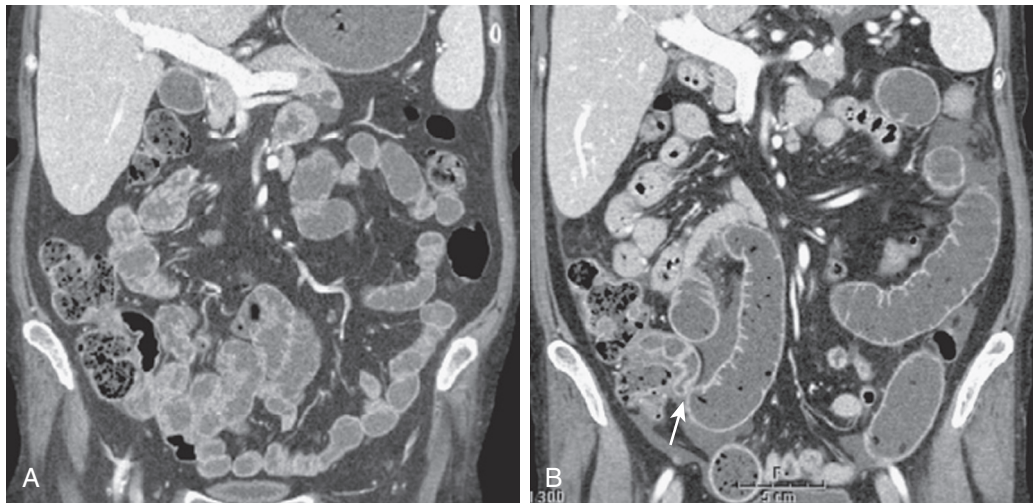


Figure 39-6 Demonstration of transition point and prestenotic dilation. A. Coronal image of CT abdomen and pelvis with orally ingested neutral contrast shows filling loops of the SB, including distal loops, but no evidence of mechanical obstruction seen in patient with tuberculous stricture (same patient as in Fig. 39-1). **B.** Stricture now apparent (arrow) with prestenotic dilation during enteral volume challenge. Note the so-called dirty feces sign from inspissated debris. (From Gollub MJ, Maglinte DD: *CT enterography and CT enteroclysis*. In Shirkhoda A [ed]: *Variants and Pitfalls in Body Imaging*, 2nd ed. Philadelphia, Lippincott Williams & Wilkins, 2011, pp 328–362.)

of an existing low-grade obstruction, gradient, or prestenotic dilation is exaggerated and reliably diagnosed; vomiting is avoided by controlling infusion rates fluoroscopically and understanding several variables involved in enteroclysis that require fluoroscopic guidance (see Fig. 39-6).^{143,146} Even when no gradient is observed, demonstration of subtle deformities such as luminal narrowing and fixations are easier to appreciate. Real-time (fluoroscopic) observations add to the confidence in making or excluding the diagnosis.

This observation adds to the morphologic details provided by multiplanar CT. Cross-referenced assessment provides more precise assessment of the location and characterization of the cause. The positive enteral CTE modification is preferred for this subset of patients, although this condition can be diagnosed also with neutral enteral CTE with IV contrast. The lack of real-time control by the radiologist on the rate of infusion and volume needed for neutral enteral CTE add to the possibility of vomiting in this group of patients, which makes this modification less ideal. The method can be modified, particularly in patients with inflammatory SB disease with low-grade obstructive symptoms, with indirect monitoring of the infusion rates; this requires fluoroscopic guidance. Determining the optimal infusion rates on either modification is difficult and requires experience because there are several variables that influence it, and each patient is different.⁸⁵ In the subset of patients with recurrent symptoms, a subtle gradient or transient stasis may be observed fluoroscopically and may not be depicted on the CT image.

Correlating the fluoroscopic observation and the anatomic information depicted by multiplanar CT allows a confident report of low-grade adhesive obstruction from a parietal or visceral adhesion or both. Neutral enteral with IV contrast CTE excels in evaluating mural abnormalities in addition to the mesentery and solid viscera. In patients in whom the obstruction has resolved, adhesions are still reliably visualized on CTE. When patients with a history of malignant neoplasm and prior abdominal surgery present with an SBO, radiologists are often faced with the difficult task of determining the exact cause of

the obstruction. CTE provides the necessary intraluminal and extraluminal information to help differentiate SBO caused by seeded or hematogenous metastases from that caused by radiation exposure or postsurgical adhesions.^{6,96,156,157} Thus, in addition to anatomic information regarding tumor size and location, CTE can reliably assess for the presence of associated low-grade obstruction.¹⁵⁸

There is a subset of patients with SBO for whom surgeons prefer initial conservative management (i.e., tube decompression of the distended SB) over surgery.^{159,160} These are patients with the following: (1) SBO in the immediate postoperative period; (2) a history of prior abdominal surgery for a malignant tumor; (3) a prior history of radiation therapy; or (4) Crohn's disease with prior surgery. Further characterization of the severity and nature of the obstruction are of value for management. The use of the triple-lumen, long decompression-enteroclysis (Maglinte Long Tube; MDEC, Cook, Bloomington, IN) has allowed us to participate in the management of these patients by preliminary decompression of the distended SB, performance of a diagnostic CTE, and further long-tube decompression after the examination.^{84,85,143,145,146,161-163}

The use of positive enteral CTE allows assessment of the cause and severity of the obstruction in addition to more efficient, long-tube suction (Fig. 39-7).^{143,146,164} Participation in the care and management of this subset of patients is important for radiologists to consider; it could help change the low prestige and perception of mediocrity of radiology as a specialty by other physicians.^{165,166}

Our technique of examination is modified in patients with a prior history of pancreatoduodenectomy (Whipple procedure). They may present with symptoms in the subacute or chronic setting unexplained by cross-sectional imaging, which is now the routine examination of the postoperative pancreas,^{167,168} and questions relevant to management require evaluation of hepaticojejunal, pancreatojejunal, gastrojejunal, and pylorojejunal anastomoses.¹⁶⁹⁻¹⁷⁵ The catheter tip and balloon are positioned immediately distal to the gastroesophageal junction and retracted until mild resistance is met to

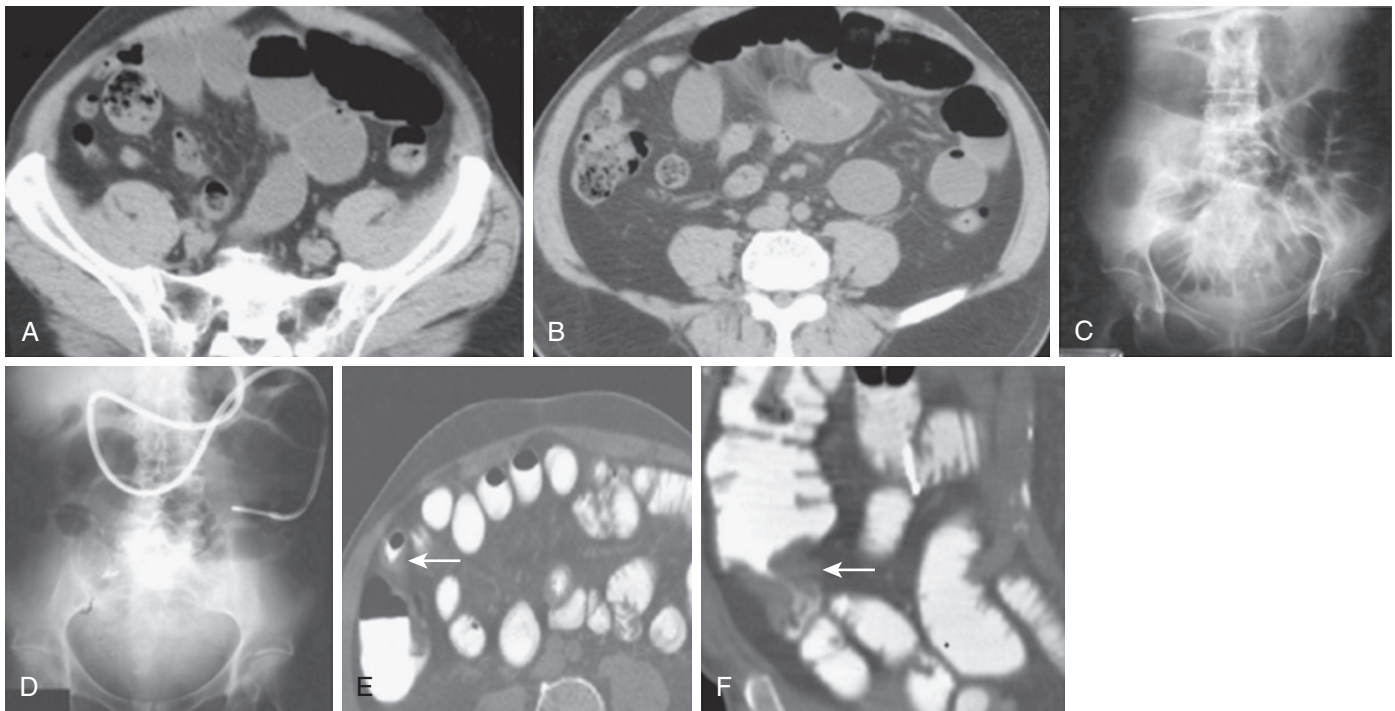


Figure 39-7 Use of long tube decompression in postoperative examinations. **A, B.** Axial images of CT of the abdomen and pelvis in a patient with symptoms of SBO, taken in an outside institution, show findings consistent with mechanical SBO. Laparoscopic exploration did not show a point of mechanical obstruction. **C.** Abdominal radiograph obtained following initial nasogastric suction with long tube (note catheter tip in the gastric antrum) at the Indiana University Hospital. **D.** Overnight suction after long tube advanced to proximal jejunum shows decrease in distention of SB loops. **E.** Axial CT section of positive enteral CTE shows mural thickening and narrowed lumen at the level of the proximal ascending colon (arrow). **F.** Coronal image of CTE shows an annular lesion, raising the possibility of carcinoma (arrow). Colonoscopy and biopsy showed tuberculous colitis simulating malignancy (patient had a false-negative result from an incomplete colonoscopy at the outside institution).

prevent gastroesophageal reflux during controlled infusion. This modification allows for the evaluation of the pylorojejunal anastomosis and hepaticojejunal and pancreatojejunal anastomoses, as well as distal segments of the SB in real-time and cross-sectional images. This modification has been termed the *CT Whipplegram* for lack of a better name (Fig. 39-8). It simplifies the evaluation of all the anastomoses and the distal SB when partial obstruction enters the differential diagnosis to explain postoperative symptoms in those with prior lower abdominal surgical procedures. We also use this modification in patients with prior Billroth procedures or prior partial or total removal of the upper GI tract and a Roux-en-Y anastomosis (Fig. 39-9). The balloon and catheter tip are positioned immediately distal to the anastomosis. The esophageal anastomosis is evaluated initially using enteral contrast with the catheter tip above it before advancement of the catheter. This simplifies the examination of this subset of postsurgical patients, in whom examination is difficult with orally ingested contrast with conventional fluoroscopic or cross-sectional imaging. The timing of surgical intervention, as well as the optimal method of radiologic investigation in patients with incomplete, open loop SBO, has changed during the past 2 decades.^{47,146,176}

Evidence-based analysis has shown the added value of CTE over other methods of examination.^{104,150-152,155} Reliable exclusion or confirmation of the diagnosis, detection of multiple levels of obstruction, and objective classification of severity and cause are useful information provided by CTE in the evaluation of these patients. Advances in imaging techniques have changed how work-ups are planned for patients with suspected SBO.

Conventional CT has high sensitivity in diagnosing high-grade obstruction and is helpful in confirming the presence or absence of strangulation; several reports have confirmed the value of CT for this indication (Fig. 39-10).^{143,144-152,164,177-181}

Although the specificity of contrast-enhanced CT for intestinal ischemia has been reported to be as low as 44%, its high sensitivity (90%) and negative predictive value (89%) are helpful in making decisions concerning continued nonoperative management versus surgery.^{177,182-187} The dictum, “Never let the sun rise or set on small bowel obstruction,” once popular among general surgeons because of the feared complication of strangulation and the clinical difficulty associated with its preoperative recognition, is now outdated.^{188,189}

MISCELLANEOUS INDICATIONS

When the cause of blood loss from the GI tract is still not clear after upper and lower endoscopies (obscure GI bleed), studies have recommended several options, each with their own proponents, which may present as a long-term and difficult management problem. Angioectasias are the most common cause of obscure GI bleeding and are only visible on endoscopy or potentially on arterial phase, catheter-based or CT angiography. Imaging studies are insensitive to these small, flat, vascular lesions. A three-phase CT enterography has been described, with the goal of detecting angioectasias and other arterial phase-dominant lesions.¹⁹⁰⁻¹⁹² The radiation burden (effective dose, 59 mSv/examination) and the relative risks should be considered in young patients. Unless the patient is slowly or actively

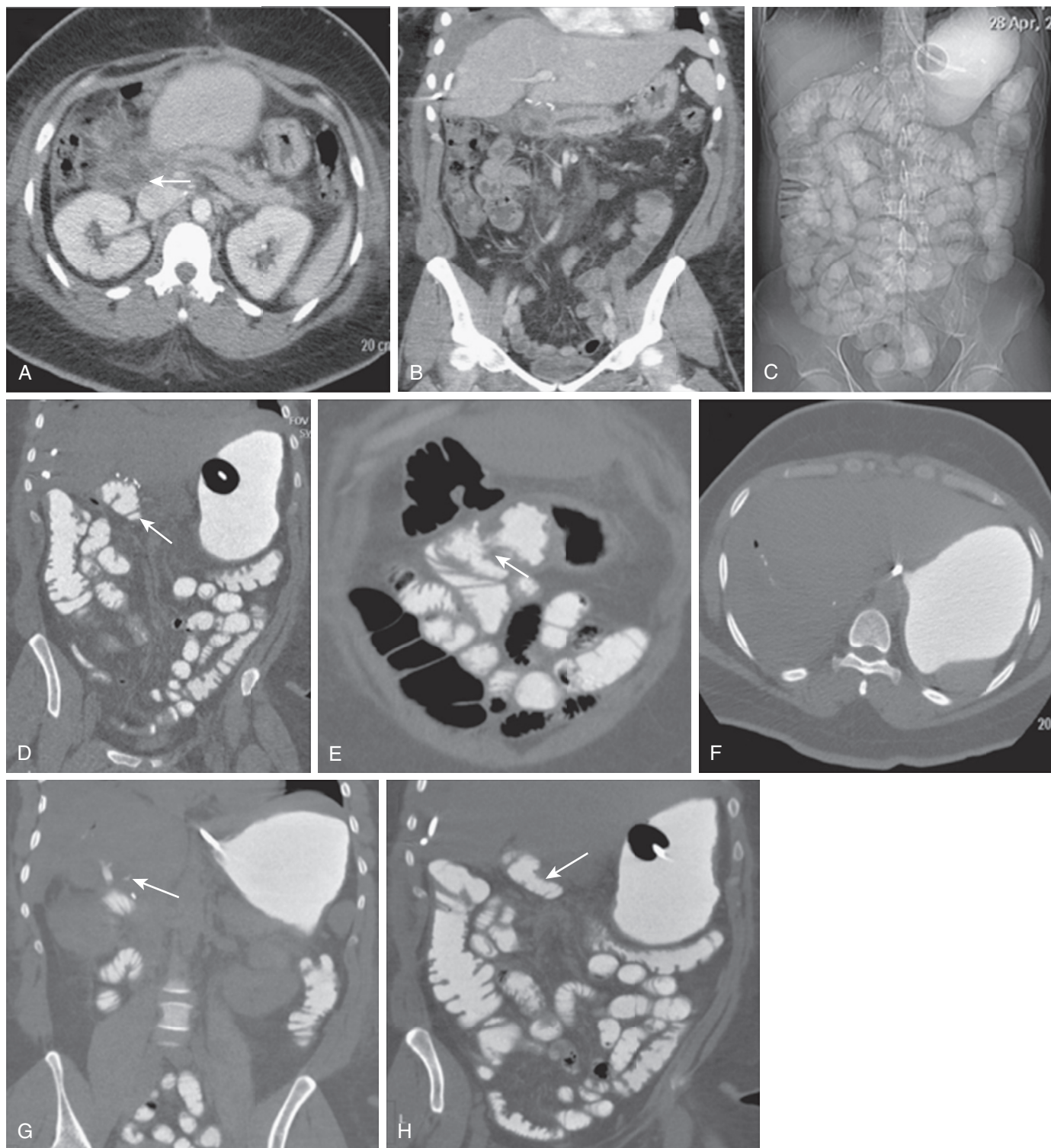


Figure 39-8 CT Whipplegram. **A.** Axial CT of a patient after recent Whipple procedure. This was done for a neuroendocrine tumor with persistent vomiting and nonresolving fluid collection in the perihepatic space that was referred for CTE to exclude distal SBO and leak at the level of a pancreaticojejunostomy. Note reactive inflammatory changes to the right of the dilated pancreatic duct (*arrow*). **B.** Coronal image shows fluid collection and drainage catheter in the right perihepatic space. **C.** Scanogram showing uniform distention of the SB with antireflux balloon of enteroclysis catheter immediately distal to the gastroesophageal junction. **D.** Coronal CTE image shows normal caliber of biliopancreatic limb (*arrow*). **E.** Coronal image shows a patent pyloroduodenal anastomosis (*arrow*) without evidence of a leak. **F.** Axial image shows small amount of pneumobilia and contrast in the intrahepatic tributary. **G.** Coronal image of CTE shows small amount of leak to the left of the hepaticojejunostomy (*arrow*). **H.** Coronal image of CTE shows no evidence of distal mechanical SBO. The *arrow* points to a well-delineated biliopancreatic limb.

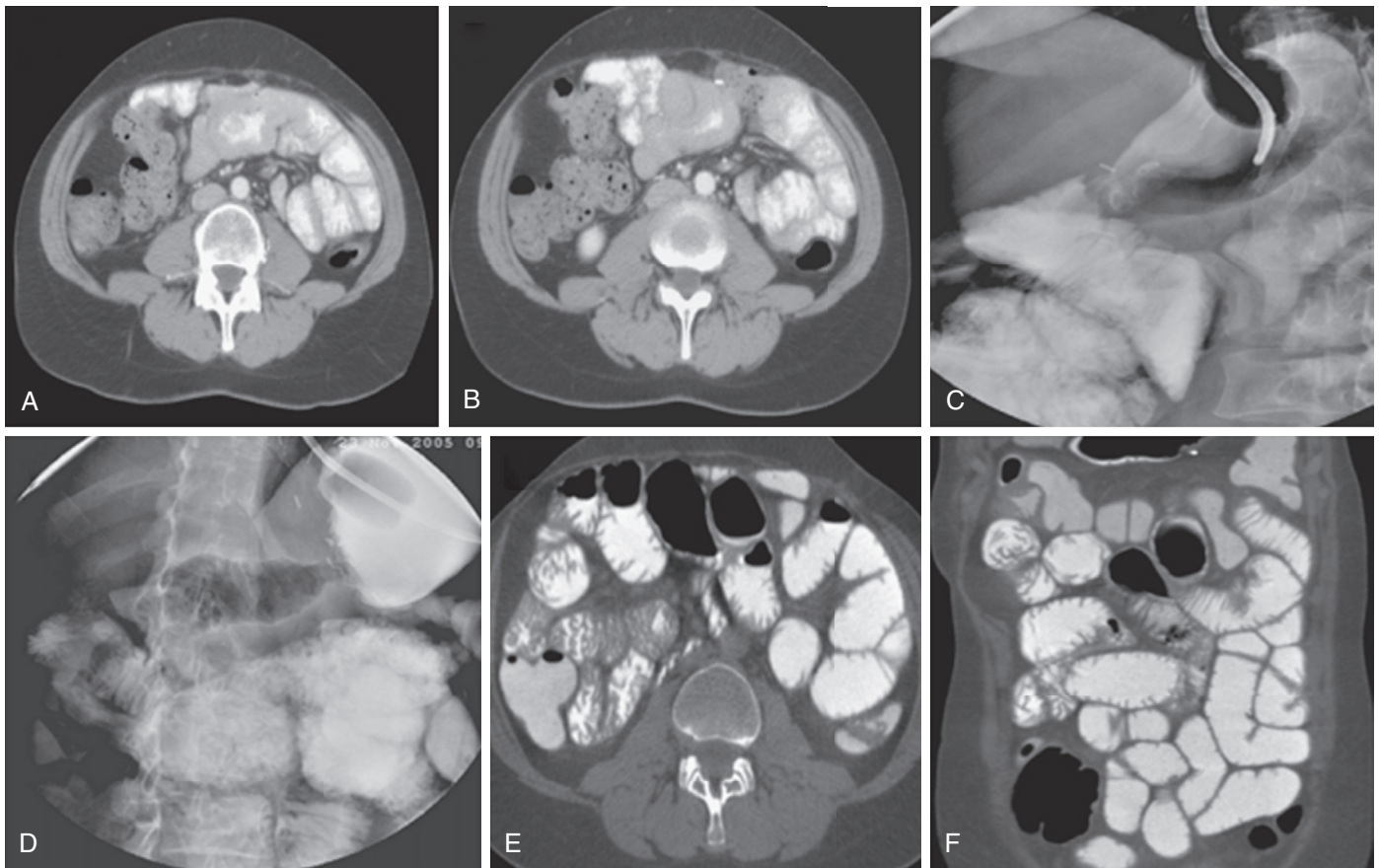


Figure 39-9 CTE in the evaluation of late postsurgical complications. **A, B.** Axial CT images with oral and IV contrast in a patient with abdominal distention, nausea, and vomiting and a history of prior ulcer surgery. An apparent abnormality is seen in the proximal SB. The possibility of intussusception and a mass were reported. **C.** Image during fluoroscopic phase of positive enteral CTE shows the balloon distal to the gastroesophageal junction. **D.** Frontal radiograph shows dilated gas and fluid-filled proximal SB, without evidence of a mass or intussusception. Stasis was seen at fluoroscopy at this level, suggesting postsurgical dysmotility. **E, F.** Axial and coronal images of CTE show dilated proximal SB loop compatible with dysmotility noted on real-time (fluoroscopic) evaluation, without evidence of a mass or intussusception. An abnormality noted is secondary to admixture defects secondary to stasis related to dysmotility from a prior Billroth 1 procedure done with vagotomy. (Data from Gollub MJ, Maglinte DD: CT enterography and CT enteroclysis. In Shirkhoda A [ed]: *Variants and Pitfalls in Body Imaging*, 2nd ed. Philadelphia, Lippincott Williams & Wilkins, 2011, pp 328–362).

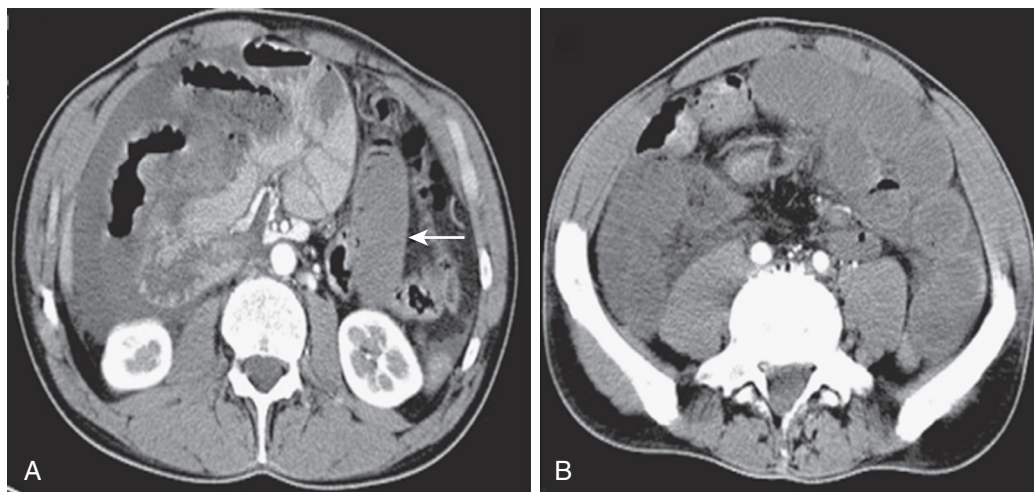


Figure 39-10 Strangulation in intestinal obstruction. **A.** Axial image of CT in a patient with abdominal pain, nausea, and vomiting. The arrow shows a nonperfused segment of the proximal jejunum in late arterial phase CT acquisition. Note the abnormal superior mesenteric vascular course, which suggests midgut volvulus. **B.** Axial at the level of the superior aspect of the pelvis shows the absence of perfusion of mesenteric SB, consistent with infarction confirmed at surgery.

bleeding at the time of acquisition, CT enterography or CTE will not demonstrate the angioectasias that can be seen on endoscopy or SB enteroscopy. CTE has the advantage of reliably excluding small SB neoplasms because it examines the entire small intestine and mesentery. In centers in which expertise in performing DC barium air enteroclysis is available, it should be performed when NSAID enteropathy is a clinical possibility and cross-sectional imaging is not informative. A history of heme-positive stools or hematochezia indicates that mucosal abrasion or ulceration is present, and examinations that depict the mucosa should be considered (e.g., DC barium enteroclysis in the nonemergent setting).

The need to perform an SB examination in the emergent setting on a bleeding patient after endoscopic examinations with negative results make CT enterography a practical approach after the patient is stabilized following a negative endoscopic examination. DC barium enteroclysis should be recommended for patients with equivocal or noninformative cross-sectional imaging studies or CE with a heme-positive stool examination. This method allows for the exclusion of SB neoplasm, early Crohn's disease, NSAID enteropathy, and other SB abnormalities (Fig. 39-11).

Another observation obtained during fluoroscopy in the subset of patients with recurrent abdominal pain is that in some patients with visceral hypersensitivity or irritable bowel syndrome (IBS), the abdominal symptoms are reproduced during contrast infusion and distention of the SB. This confirms the clinical suspicion.^{2,193} Lack of reproduction of abdominal symptoms, however, does not exclude the diagnosis, because no

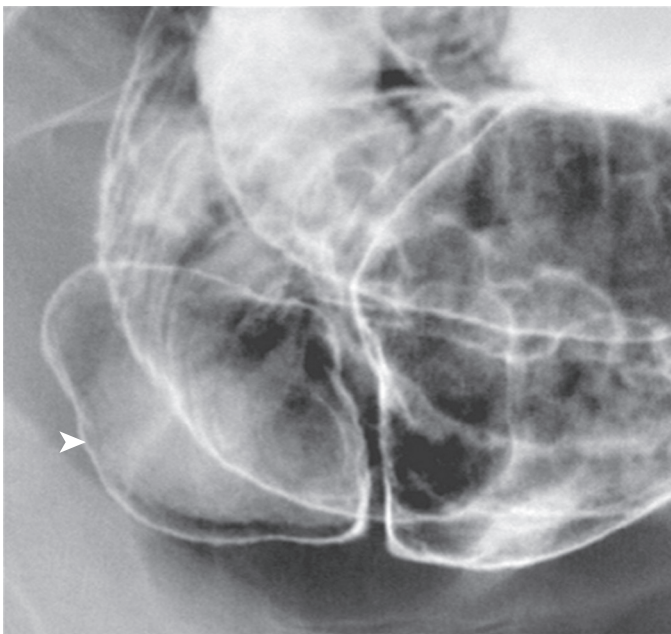


Figure 39-11 Role of imaging in occult GI bleeding. Teenage patient with heme-positive stools with negative results by upper and lower endoscopies, CT enterography, and Meckel scan and CE. DC barium enteroclysis shows a small Meckel diverticulum (arrowhead). Small ulcerations were seen in the surgical specimen. Enteroclysis with careful fluoroscopic evaluation is the most accurate method of diagnosing Meckel diverticulum. (Data from Maglinte DD, Elmore MF, Isenberg M, Dolan PA: Meckel diverticulum: Radiologic demonstration by enteroclysis. *AJR* 134:925-932, 1980.)

scientific validation of this fluoroscopic observation during enteroclysis has been reported; the predictive values are therefore difficult to evaluate scientifically. In our experience, it may coexist with an SB anatomic abnormality and may be important information for management. The primary role of imaging in the investigation of patients suspected of IBS is to exclude morphologic SB abnormality. No guidelines exist for imaging IBS; this awaits further research.¹⁹⁴

Technical Pitfalls and Limitations

The discomfort and pain associated with nasoenteric intubation is the most significant factor that has limited the implementation of enteroclysis and its cross-sectional modifications in clinical practice, despite its diagnostic accuracy.¹⁹⁵ The fact that patients have been able to undergo enteroclysis without conscious sedation does not indicate that it is a well-tolerated procedure. A stoic patient can undergo the examination but cannot forget the discomfort and pain endured during the procedure. Several studies have shown that physicians underestimate discomfort during intubation procedures and, like their patient, are unwilling to undergo intubation procedures on themselves without sedation or analgesia.¹⁹⁶⁻²⁰¹ This basic pitfall, seemingly forgotten by most radiologists, is obviated by the use of conscious sedation, which allows patients to tolerate unpleasant procedures while maintaining adequate cardiopulmonary function and their ability to respond purposefully to verbal commands.²⁰² In practices which conscious sedation is not practical and expertise in intubation is available, the use of a parenteral sedative (e.g., diazepam [Valium]) and a local intranasal anesthetic gel (a 3-mL combination of tetrahydrozoline 0.1% and tetracaine 2%) makes enteroclysis intubation acceptable.

Many patients tolerate enteroclysis with the use of only a sedative as initially reported²⁰³; however, their recall of nasal pain, gagging, and occasional vomiting are good. A recent survey of the safety and patient-reported effectiveness compared using only a sedative and intranasal gel with a regimen combining an amnesic, analgesic, and local nasal anesthetic and intranasal gel showed that the latter is better tolerated; when an adequate amnesic dose is administered, patients forget the discomfort.¹⁴² The addition of a local nasal anesthetic to the amnesic-analgesic medication likely explains the success of our busy, patient-friendly enteroclysis practice.¹⁴² Unless contraindicated, our conscious sedation protocol uses a combination of midazolam (2 to 7 mg) given in 1-mg increments. An analgesic (fentanyl, 50 to 150 µg), given IV in 25-µg increments and carefully monitored by a radiology sedation nurse, may be administered selectively if needed for severe pain because it decreases gastric and small bowel motility. This regimen is safe and effective. In most patients, all that is required is the nasal numbing spray and amnesic. Radiologists who want to start a conscious sedation protocol for enteroclysis should make arrangements with interventional radiology sections who have used dedicated radiology nurses for their procedures.²⁰⁴ Smaller catheters also decrease discomfort, but currently available small catheters do not have the balloon attachment to prevent reflux; the use of 13-Fr enteroclysis catheters with a balloon attachment (Maglinte enteroclysis catheter; Cook) is therefore preferred.

Performance pitfalls of enteroclysis relate more to experience and familiarity with catheters, balloons, pumps, and

various oral contrast agents, which have all been described.¹⁸ Nuances related to catheterization, rates of infusion, and type of modification to be used, depending on the clinical indication, have also been described.^{52,83-85,205,206} It would be helpful if 2 to 3 days are spent observing a practice that performs these procedures daily. There has been a prevalent misconception that enteroclysis is simply positioning a nasoenteric catheter and infusing contrast, which is the recipe for an “enterocrisis!” All patients are different, and optimizing the protocol for every modification of enteroclysis, depending on the clinical indication and addressing multiple technical variables, requires an understanding of basic principles; unfortunately, this is not intuitive. Understanding the various pitfalls and limitations in the evaluation of SB disease and optimizing SB imaging techniques decrease errors in the performance of these procedures.

Comments

CTE is a hybrid technique that combines the methods of fluoroscopic, intubation-infusion SB examinations with those of abdominal CT. The use of multidetector CT technology has made this a versatile examination that has evolved into two distinct technical modifications, with their specific clinical applications.

The efficacy of imaging procedures in confirming or confidently excluding SB disease is not frequently considered in the investigation of SB diseases by radiologists and referring physicians. The influence on the referring physician’s diagnostic confidence when formulating a course of management by using an SB examination and how it is reported is also infrequently considered by radiologists, which may involve looking beyond reported statistical accuracy.²⁰⁷ Hence, it is not uncommon to see patients with several imaging examinations previously done before a diagnostic examination is performed or its confident exclusion is established. This situation also explains requests for a second reading or opinion on examinations already reported. Imaging is a rapidly growing part of health care spending, and an overall consideration of costs when looking at the effectiveness of SB diagnostic procedures is not given serious thought; what is convenient and revenue-producing currently seem to be the primary considerations.

Not infrequently, peroral ingested SB examinations that do not involve direct participation by radiologists are done several times before a diagnosis is made. Available guidelines do not include assessment of the evidence of efficacy of diagnostic imaging on diagnostic confidence and patient management.²⁰⁷

When ordering SB imaging procedures, unlike for other abdominal organs, it should be realized that the incidence of SB diseases is low and the clinical presentation not specific. Thus, examination methods with a high negative predictive value

and high sensitivity should be performed first if expertise is available.*

In SB imaging, the examination that reliably excludes SB disease or confirms early or small abnormalities and gives the referring physician confidence in formulating a treatment should be given primary consideration. Procedures that provide equivocal or inconclusive information and do not provide clinicians the confidence to formulate a management plan should not be repeatedly used. Enteroclysis and its modifications, when done appropriately, with due consideration for patient comfort, fulfills this role. Few reports that show the superiority of enteroclysis and its modifications have been based on well-controlled trials.

Only rather recently have clinically important advances been based predominantly on evidence generated from well-controlled trials, which may not be possible with SB imaging.^{165,207-218} The number of well-controlled trials in SB imaging is few and will likely remain this way. Referring physicians and radiologists must rely on the art of medicine to fill in the gaps.²⁰⁹ In the literature, there is enough clinical evidence to show the superiority of enteroclysis and its modifications over orally ingested enteral SB examinations.

Summary

The diagnostic evaluation of SB diseases has changed profoundly during the past few decades.¹⁰² The important role of radiology in the investigation of SB diseases remains poorly understood by referring physicians who treat the patients and radiologists who perform the examinations. An important factor for radiologists to consider is that there is a lack of knowledge on the part of ordering physicians, who want to do what is best for their patients but do not understand which imaging study is the most reliable to answer questions relevant to patients’ work-up and management in the evaluation of SB diseases. This is particularly true when the possibility of an SB neoplasm is concerned or there is a recurrent, low-grade adhesive obstruction.

Radiologists must function as consultants so that when orally ingested SB examination results are not informative, and unexplained abdominal symptoms persist, these patients should be referred to centers in which enteral, volume-challenged examinations are routinely performed. Evidence- and experience-based analyses have shown that there are no shortcuts to reliable SB imaging. When properly performed, the added value of the different modifications of CTE to patient care is not difficult to understand. Examinations that distend the SB diagnose smaller and early lesions and allow confident exclusion of SB disease, an important factor to consider when imaging the patient for possible SB disease.

*References 2, 3, 6, 12, 14, 15, 103, 125, 138, 155.

REFERENCES

1. Lee CI, Forman HP: Radiology health services research: From imperative to legislative mandate. *AJR* 196:1111–1114, 2011.
2. Antes G: Why not enteroclysis? *N Engl J Med* 303:1420, 1980.
3. Barloon TJ, Lu CC, Honda H, et al: Does a normal small-bowel enteroclysis exclude small-bowel disease? A long-term follow-up of consecutive normal studies. *Abdom Imaging* 19:113–115, 1994.
4. Bartram CI: Small bowel enteroclysis: Cons. *Abdom Imaging* 21:245–246, 1996.
5. Bender GN: Radiographic examination of the small bowel. An application of odds ratio analysis to help attain an appropriate mix of small bowel follow-through and enteroclysis in a working-clinical environment. *Invest Radiol* 32:357–362, 1997.
6. Bender GN, Maglinte DD, Klöppel VR, Timmons JH: CT enteroclysis: A superfluous diagnostic procedure or valuable when investigating small-bowel disease? *AJR* 172:373–378, 1999.
7. Bender GN, Timmons JH, Williard WC, Carter J: Computed tomographic enteroclysis: One methodology. *Invest Radiol* 31:43–49, 1996.
8. Chernish SM, Maglinte DD, O’Connor K: Evaluation of the small intestine by enteroclysis for Crohn’s disease. *Am J Gastroenterol* 87: 696–701, 1992.

9. Diner WC, Hoskins EO, Navab F: Radiologic examination of the small intestine: Review of 402 cases and discussion of indications and methods. *South Med J* 77:68–74, 1984.
10. Dixon PM, Roulston ME, Nolan DJ: The small bowel enema: A ten-year review. *Clin Radiol* 47:46–48, 1993.
11. Halpert RD, Feczko PJ, Keller CE, Iorio J: Enteroclysis for the examination of the small bowel. *Henry Ford Hosp Med J* 33:116–121, 1985.
12. Herlinger H: Why not enteroclysis? *J Clin Gastroenterol* 4:277–283, 1982.
13. Lappas JC: Small bowel imaging. *Curr Opin Radiol* 4:32–38, 1992.
14. Maglinte DD, Kelvin FM, O'Connor K, et al: Current status of small bowel radiography. *Abdom Imaging* 21:247–257, 1996.
15. Maglinte DD, Lappas JC, Kelvin FM, et al: Small bowel radiography: How, when, and why? *Radiology* 163:297–305, 1987.
16. Nolan DJ: Small bowel enteroclysis: Pros. *Abdom Imaging* 21:243–244, 1996.
17. Nolan DJ: The true yield of the small-intestinal barium study. *Endoscopy* 29:447–453, 1997.
18. Gollub MJ, Maglinte CT: CT enterography and CT enteroclysis. In Shirkhoda A, editor: *Variants and Pitfalls in Imaging*, Philadelphia, 2011, Lippincott, pp 328–362.
19. Maglinte D: Invited commentary. *Radiographics* 26:657–662, 2006.
20. Gourtsoyiannis N, Papanikolaou N, Grammatikakis J, et al: MR imaging of the small bowel with a true-FISP sequence after enteroclysis with water solution. *Invest Radiol* 35:707–711, 2000.
21. Klöppel R, Thiele J, Bosse J: The Sellink CT method. *Rofo* 156:291–292, 1992.
22. Maglinte DD, Siegelman ES, Kelvin FM: MR enteroclysis: The future of small-bowel imaging? *Radiology* 215:639–641, 2000.
23. Umschaden HW, Szolar D, Gasser J, et al: Small-bowel disease: Comparison of MR enteroclysis images with conventional enteroclysis and surgical findings. *Radiology* 215:717–725, 2000.
24. Adamek HE, Schantzen W, Rinas U, et al: Ultra-high-field magnetic resonance enterography in the diagnosis of ileitis (neo-)terminalis: A prospective study. *J Clin Gastroenterol* 46:311–316, 2012.
25. Apostolopoulos P, Liatsos C, Gralnek IM, et al: The role of wireless capsule endoscopy in investigating unexplained iron deficiency anemia after negative endoscopic evaluation of the upper and lower gastrointestinal tract. *Endoscopy* 38:1127–1132, 2006.
26. Baker ME, Einstein DM, Veniero JC: Computed tomography enterography and magnetic resonance enterography: The future of small bowel imaging. *Clin Colon Rectal Surg* 21:193–212, 2008.
27. Biscaldi E, Ferrero S, Remorgida V, Rollandi GA: Bowel endometriosis: CT-enteroclysis. *Abdom Imaging* 32:441–450, 2007.
28. Boudiaf M, Jaff A, Soyer P, et al: Small-bowel diseases: Prospective evaluation of multidetector row helical CT enteroclysis in 107 consecutive patients. *Radiology* 233:338–344, 2004.
29. Broglia L, Gigante P, Papi C, et al: Magnetic resonance enteroclysis imaging in Crohn's disease. *Radiol Med* 106:28–35, 2003.
30. Cappabianca S, Granata V, Di Grezia G, et al: The role of nasoenteric intubation in the MR study of patients with Crohn's disease: Our experience and literature review. *Radiol Med* 116:389–406, 2011.
31. Cohen ME, Barkin JS: Enteroscopy and enteroclysis: The combined procedure. *Am J Gastroenterol* 84:1413–1415, 1989.
32. Dave-Verma H, Moore S, Singh A, et al: Computed tomographic enterography and enteroclysis: Pearls and pitfalls. *Curr Probl Diagn Radiol* 37:279–287, 2008.
33. Di Mizio R, Rollandi GA, Bellomi M, et al: Multidetector-row helical CT enteroclysis. *Radiol Med* 111:1–10, 2006.
34. Doerfler OC, Ruppert-Kohlmaier AJ, Reittner P, et al: Helical CT of the small bowel with an alternative oral contrast material in patients with Crohn disease. *Abdom Imaging* 28:313–318, 2003.
35. Feuerbach S: MRI enterography: The future of small bowel diagnostics? *Dig Dis* 28:433–438, 2010.
36. Fidler J: MR imaging of the small bowel. *Radiol Clin North Am* 45:317–331, 2007.
37. Fidler JL, Guimaraes L, Einstein DM: MR imaging of the small bowel. *Radiographics* 29:1811–1825, 2009.
38. Finke M: Enteroclysis: Double contrast examination of the small bowel. *Radiol Technol* 59:143–149, 1987.
39. Furukawa A, Yamasaki M, Furuichi K, et al: Helical CT in the diagnosis of small bowel obstruction. *Radiographics* 21:341–355, 2001.
40. Gasparaitis AE, MacEneaney P: Enteroclysis and computed tomography enteroclysis. *Gastroenterol Clin North Am* 31:715–730, 2002.
41. Gerson LB, Van Dam J: Wireless capsule endoscopy and double-balloon enteroscopy for the diagnosis of obscure gastrointestinal bleeding. *Tech Vasc Interv Radiol* 7:130–135, 2004.
42. Gollub MJ: Multidetector computed tomography enteroclysis of patients with small bowel obstruction: A volume-rendered "surgical perspective." *J Comput Assist Tomogr* 29:401–407, 2005.
43. Gollub MJ, DeCorato D, Schwartz LH: MR enteroclysis: Evaluation of small-bowel obstruction in a patient with pseudomyxoma peritonei. *AJR* 174:688–690, 2000.
44. Jain TP, Gulati MS, Makharia GK, et al: CT enteroclysis in the diagnosis of obscure gastrointestinal bleeding: Initial results. *Clin Radiol* 62:660–667, 2007.
45. Kerr JM: Small bowel imaging: CT enteroclysis or barium enteroclysis? Critically appraised topic. *Abdom Imaging* 33:31–33, 2008.
46. Kohli MD, Maglinte DD: CT enteroclysis in small bowel Crohn's disease. *Eur J Radiol* 69:398–403, 2009.
47. Kohli MD, Maglinte DD: CT enteroclysis in incomplete small bowel obstruction. *Abdom Imaging* 34:321–327, 2009.
48. Korman U, Kurugoglu S, Ogut G: Conventional enteroclysis with complementary MR enteroclysis: A combination of small bowel imaging. *Abdom Imaging* 30:564–575, 2005.
49. La Seta F, Buccellato A, Tesè L, et al: Multidetector-row CT enteroclysis: Indications and clinical applications. *Radiol Med* 111:141–158, 2006.
50. Lalitha P, Reddy MCh, Reddy KJ, Kumari MV: Computed tomography enteroclysis: A review. *Jpn J Radiol* 29:673–681, 2011.
51. Maglinte DD, Bender GN, Heitkamp DE, et al: Multidetector-row helical CT enteroclysis. *Radiol Clin North Am* 41:249–262, 2003.
52. Maglinte DD, Lappas JC, Heitkamp DE, et al: Technical refinements in enteroclysis. *Radiol Clin North Am* 41:213–229, 2003.
53. Masselli G, Brizi GM, Parrella A, et al: Crohn disease: Magnetic resonance enteroclysis. *Abdom Imaging* 29:326–334, 2004.
54. Masselli G, Brizi MG, Menchini L, et al: Magnetic resonance enteroclysis imaging of Crohn's. *Radiol Med* 110:221–233, 2005.
55. Masselli G, Casciani E, Poletti E, Gualdi G: Comparison of MR enteroclysis with MR enterography and conventional enteroclysis in patients with Crohn's disease. *Eur Radiol* 18:438–447, 2008.
56. Masselli G, Casciani E, Poletti E, et al: Assessment of Crohn's disease in the small bowel: Prospective comparison of magnetic resonance enteroclysis with conventional enteroclysis. *Eur Radiol* 16:2817–2827, 2006.
57. Masselli G, Gualdi G: Evaluation of small bowel tumors: MR enteroclysis. *Abdom Imaging* 35:23–30, 2010.
58. Matsumoto T, Esaki M, Kurahara K, et al: Double-contrast barium enteroclysis as a patency tool for nonsteroidal anti-inflammatory drug-induced enteropathy. *Dig Dis Sci* 56:3247–3253, 2011.
59. McGovern R, Barkin JS: Enteroscopy and enteroclysis: An improved method for combined procedure. *Gastrointest Radiol* 15:327–328, 1990.
60. Minordi LM, Vecchioli A, Guidi L, et al: Multidetector CT enteroclysis versus barium enteroclysis with methylcellulose in patients with suspected small bowel disease. *Eur Radiol* 16:1527–1536, 2006.
61. Minordi LM, Vecchioli A, Poloni G, Bonomo L: CT enteroclysis: Multidetector technique (MDCT) versus single-detector technique (SDCT) in patients with suspected small-bowel Crohn's disease. *Radiol Med* 112:1188–1200, 2007.
62. Nygaard A, Sandvik L, Mulahasanovic A, et al: Magnetic resonance enteroclysis in the diagnosis of small-intestinal Crohn's disease: Diagnostic accuracy and inter- and intra-observer agreement. *Acta Radiol* 47:1008–1016, 2006.
63. Neu B, Ell C, May A, et al: Capsule endoscopy versus standard tests in influencing management of obscure digestive bleeding: Results from a German multicenter trial. *Am J Gastroenterol* 100:1736–1742, 2005.
64. Parrish FJ: Small bowel CT-enteroclysis: Technique, pitfalls and pictorial review. *Australas Radiol* 50:289–297, 2006.
65. Patak MA, Froehlich JM, von Weymarn C, et al: Non-invasive distension of the small bowel for magnetic-resonance imaging. *Lancet* 358:987–988, 2001.
66. Prassopoulos P, Papanikolaou N, Grammatikakis J, et al: MR enteroclysis imaging of Crohn disease. *Radiographics* 21(Spec. No.):S161–S172, 2001.
67. Rajesh A, Sandrasegaran K, Jennings SG, et al: Comparison of capsule endoscopy with enteroclysis in the investigation of small bowel disease. *Abdom Imaging* 34:459–466, 2009.
68. Schmidt S, Chevallier P, Chalaron M, et al: Multidetector CT enteroclysis: Comparison of the reading performance for axial and coronal views. *Eur Radiol* 15:238–246, 2005.
69. Schmidt S, Felley C, Meuwly JY, et al: CT enteroclysis: Technique and clinical applications. *Eur Radiol* 16:648–660, 2006.
70. Schmidt S, Lepori D, Meuwly JY, et al: Prospective comparison of MR enteroclysis with

- multidetector spiral-CT enteroclysis: Interobserver agreement and sensitivity by means of "sign-by-sign" correlation. *Eur Radiol* 13: 1303–1311, 2003.
71. Suzuki T, Matsushima M, Okita I, et al: Clinical utility of double-balloon enteroscopy for small intestinal bleeding. *Dig Dis Sci* 52:1914–1918, 2007.
72. Torregrosa A, Pallardó Y, Hinojosa J, et al: Magnetic resonance enterography: Technique and indications. Findings in Crohn's disease. *Radiologia* 55:422–430, 2013.
73. Turetschek K, Schober E, Wunderbaldinger P, et al: Findings at helical CT enteroclysis in symptomatic patients with Crohn disease: Correlation with endoscopic and surgical findings. *J Comput Assist Tomogr* 26:488–492, 2002.
74. Umschaden HW, Gasser J: MR enteroclysis. *Radiol Clin North Am* 41:231–248, 2003.
75. Valek V, Kysela P, Vavrikova M: Crohn's disease at the small bowel imaging by the ultrasound-enteroclysis. *Eur J Radiol* 62:153–159, 2007.
76. Van Weyenberg SJ, Meijerink MR, Jacobs MA, et al: MR enteroclysis in the diagnosis of small-bowel neoplasms. *Radiology* 254:765–773, 2010.
77. Wiarda BM, Heine DG, Rombouts MC, et al: Jejunal abnormalities at MR enteroclysis. *Eur J Radiol* 67:125–132, 2008.
78. Wiarda BM, Kuipers EJ, Heitbrink MA, et al: MR enteroclysis of inflammatory small-bowel diseases. *AJR* 187:522–531, 2006.
79. Wiarda BM, Kuipers EJ, Houdijk LP, Tuynman HA: MR enteroclysis: Imaging technique of choice in diagnosis of small bowel diseases. *Dig Dis Sci* 50:1036–1040, 2005.
80. Willis JR, Chokshi HR, Zuckerman GR, Ali-perti G: Enteroscopy-enteroclysis: Experience with a combined endoscopic-radiographic technique. *Gastrointest Endosc* 45:163–167, 1997.
81. Wold PB, Fletcher JG, Johnson CD, Sandborn WJ: Assessment of small bowel Crohn disease: Noninvasive peroral CT enterography compared with other imaging methods and endoscopy—feasibility study. *Radiology* 229: 275–281, 2003.
82. Masselli G, Gualdi G: MR imaging of the small bowel. *Radiology* 264:333–348, 2012.
83. Maglinte DD, Kohli MD, Romano S, Lappas JC: Air (CO₂) double-contrast barium enteroclysis. *Radiology* 252:633–641, 2009.
84. Maglinte DD, Sandrasegaran K, Lappas JC: CT enteroclysis: Techniques and applications. *Radiol Clin North Am* 45:289–301, 2007.
85. Maglinte DD, Sandrasegaran K, Lappas JC, Chiorean M: CT enteroclysis. *Radiology* 245: 661–671, 2007.
86. Pesquera GS: Method for direct visualization of lesions in the small intestine. *AJR* 22:254–257, 1929.
87. Ghelew B, Mengis O: Mise en évidence de l'intestin grele par une nouvelle technique radiologique. *Presse Med* 46:444–445, 1938.
88. Schatzki R: Small bowel enema. *AJR* 50:743–751, 1943.
89. Lura A: Radiology of the small intestine. IV. Enema of the small intestine with special emphasis on the diagnosis of tumors. *Br J Radiol* 24:264–270, 1951.
90. Herlinger H, Maglinte D: Historical aspects. In Herlinger H, Maglinte D, editors: *Clinical Radiology of the Small Intestine*, Philadelphia, 1989, WB Saunders, pp 41–44.
91. Scott-Harden W: Examination of the small bowel. In McLaren J, editor: *Modern Trends in Diagnostic Radiology*, London, 1960, Butterworth, pp 84–87.
92. Pygott F, Street DF, Shellshear MF, et al: Radiological investigation of the small intestine by small bowel enema technique. *Gut* 1:366–370, 1960.
93. Herlinger H: A modified technique for the double contrast small bowel enema. *Gastrointest Radiol* 3:201–207, 1978.
94. Sellink JL: Examination of the small intestine by means of duodenal intubation. *Ned Tijdschr Geneesk* 115:743–778, 1971.
95. Sellink JL: Proceedings: Why enteroclysis of the small intestine? *Br J Radiol* 49:288–289, 1976.
96. Rajesh A, Maglinte DD: Multislice CT enteroclysis: Technique and clinical applications. *Clin Radiol* 61:31–39, 2006.
97. Romano S, De Lutio E, Rollandi GA, et al: Multidetector computed tomography enteroclysis (MDCT-E) with neutral enteral and IV contrast enhancement in tumor detection. *Eur Radiol* 15:1178–1183, 2005.
98. Maglinte D, Bender GN, Heitkamp DE, et al: Multidetector-row helical CT enteroclysis. *Radiol Clin North Am* 41:249–262, 2003.
99. Biscaldi E, Ferrero S, Fulcheri E, et al: Multislice CT enteroclysis in the diagnosis of bowel endometriosis. *Eur Radiol* 17:211–219, 2007.
100. Biscaldi E, Ferrero S, Remorgida V, Rollandi G: MDCT enteroclysis urography with split-bolus technique provides information on ureteral involvement in patients with suspected bowel endometriosis. *AJR* 196:W635–W640, 2011.
101. Rollandi G, Curone PF, Biscaldi E, et al: Spiral CT of the abdomen after distention of small bowel loops with transparent enema in patients with Crohn's disease. *Abdom Imaging* 24:544–549, 1999.
102. Maglinte DD: Small bowel imaging—a rapidly changing field and a challenge to radiology. *Eur Radiol* 16:967–971, 2006.
103. Maglinte DD, Burney BT, Miller RE: Lesions missed on small-bowel follow-through: Analysis and recommendations. *Radiology* 144:737–739, 1982.
104. Maglinte DD, Sandrasegaran K, Chiorean M, et al: Radiologic investigations complement and add diagnostic information to capsule endoscopy of small-bowel diseases. *AJR* 189: 306–312, 2007.
105. Hillman BJ: The irresistible march of technology. *J Am Coll Radiol* 6:823, 2009.
106. Zamboni GA, Raptopoulos V: CT enterography. *Gastrointest Endosc Clin N Am* 20:347–366, 2010.
107. Paulsen SR, Huprich JE, Fletcher JG, et al: CT enterography as a diagnostic tool in evaluating small bowel disorders: Review of clinical experience with over 700 cases. *Radiographics* 26:641–657, 2006.
108. Rosen MP, Siewert B, Sands DZ, et al: Value of abdominal CT in the emergency department for patients with abdominal pain. *Eur Radiol* 13:418–424, 2003.
109. Thompson SE, Raptopoulos V, Sheiman RL, et al: Abdominal helical CT: Milk as a low-attenuation oral contrast agent. *Radiology* 211:870–875, 1999.
110. Colombel JF, Solem CA, Sandborn WJ, et al: Quantitative measurement and visual assessment of ileal Crohn's disease activity by computed tomography enterography: Correlation with endoscopic severity and C-reactive protein. *Gut* 55:1561–1567, 2006.
111. Hara AK, Leighton JA, Sharma VK, Fleischer DE: Small bowel: Preliminary comparison of capsule endoscopy with barium study and CT. *Radiology* 230:260–265, 2004.
112. Bodily KD, Fletcher JG, Solem CA, et al: Crohn disease: Mural attenuation and thickness at contrast-enhanced CT enterography—correlation with endoscopic and histologic findings of inflammation. *Radiology* 238:505–516, 2006.
113. Paulsen SR, Huprich JE, Hara AK: CT enterography: Noninvasive evaluation of Crohn's disease and obscure gastrointestinal bleed. *Radiol Clin North Am* 45:303–315, 2007.
114. Goldberg HI, Caruthers SB, Jr, Nelson JA, Singleton JW: Radiographic findings of the National Cooperative Crohn's Disease Study. *Gastroenterology* 77(Pt 2):925–937, 1979.
115. Lee SS, Kim AY, Yang SK, et al: Crohn disease of the small bowel: Comparison of CT enterography, MR enterography, and small-bowel follow-through as diagnostic techniques. *Radiology* 251:751–761, 2009.
116. Maglinte DD, Gourtsoyiannis N, Rex D, et al: Classification of small bowel Crohn's subtypes based on multimodality imaging. *Radiol Clin North Am* 41:285–303, 2003.
117. Sailer J, Peloschek P, Schober E, et al: Diagnostic value of CT enteroclysis compared with conventional enteroclysis in patients with Crohn's disease. *AJR* 185:1575–1581, 2005.
118. Maglinte DD: Fluoroscopic and CT enteroclysis: Evidence-based clinical update. *Radiol Clin North Am* 51:149–176, 2013.
119. Minordi LM, Vecchioli A, Guidi L, et al: CT findings and clinical activity in Crohn's disease. *Clin Imaging* 33:123–129, 2009.
120. Ryan ER, Heaslip IS: Magnetic resonance enteroclysis compared with conventional enteroclysis and computed tomography enteroclysis: A critically appraised topic. *Abdom Imaging* 33:34–37, 2008.
121. Gourtsoyiannis N, Grammatikakis J, Papamastorakis G, et al: Imaging of small intestinal Crohn's disease: Comparison of MR enteroclysis and conventional examination. *Eur Radiol* 16:1915–1925, 2006.
122. Malago R, Manfredi R, Benini L, et al: Assessment of Crohn's disease activity in the small bowel with MR-enteroclysis: Clinicoradiological correlations. *Abdom Imaging* 33: 669–675, 2008.
123. Ekberg O: Crohn's disease of the small bowel examined by double contrast technique: A comparison with oral technique. *Gastrointest Radiol* 1:355–359, 1977.
124. Ekberg O: Double contrast examination of the small bowel. *Gastrointest Radiol* 1:349–353, 1977.
125. Ekberg O, Fork FT, Hildell J: Predictive value of small bowel radiography for recurrent Crohn disease. *AJR* 135:1051–1055, 1980.
126. Liangpunsakul S, Chadawada V, Rex DK, et al: Wireless capsule endoscopy detects small bowel ulcers in patients with normal results from state of the art enteroclysis. *Am J Gastroenterol* 98:1295–1298, 2003.
127. Sandrasegaran K, Maglinte DD, Jennings SG, Chiorean MV: Capsule endoscopy and imaging tests in the elective investigation of small bowel disease. *Clin Radiol* 63:712–723, 2008.
128. Triester SL, Leighton JA, Leontiadis GI, et al: A meta-analysis of the yield of capsule endoscopy compared to other diagnostic modalities in patients with obscure gastrointestinal bleeding. *Am J Gastroenterol* 100:2407–2418, 2005.

129. Triester SL, Leighton JA, Leontiadis GI, et al: A meta-analysis of the yield of capsule endoscopy compared to other diagnostic modalities in patients with non-stricturing small bowel Crohn's disease. *Am J Gastroenterol* 101:954-964, 2006.
130. Schottenfield J, Beebe-Dimmer JL, Vigneau FD: Histological subtypes of small intestinal cancers. *Ann Epidemiol* 19:439-522, 2009.
131. Wheeler JM, Warren BF, Mortensen NJ, et al: An insight into the genetic pathway of adenocarcinoma of the small intestine. *Gut* 50:218-223, 2002.
132. Schottenfield J, Beebe-Dimmer JL, Vigneau FD: The epidemiology and pathogenesis of neoplasia in the small intestine. *Ann Epidemiol* 19:58-69, 2009.
133. Haselkorn T, Whittemore AS, Lilienfeld DE: Incidence of small bowel cancer in the United States and worldwide: Geographic, temporal, and racial differences. *Cancer Causes Control* 16:781-787, 2005.
134. Pan SY, Morrison H: Epidemiology of cancer of the small intestine. *World J Gastrointest Oncol* 3:33-42, 2011.
135. Bilimoria KY, Bentrem DJ, Wayne JD: Small bowel cancer in the United States: Changes in survival over the last 20 years. *Ann Surg* 249: 63-71, 2009.
136. Maglinte DD, O'Connor K, Bessette J, et al: The role of the physician in the late diagnosis of primary malignant tumors of the small intestine. *Am J Gastroenterol* 86:304-308, 1991.
137. Talamonti S, Goetz LH, Rao S, Joehl RJ: Primary cancers of the small bowel: Analysis of prognostic factors and results of surgical management. *Arch Surg* 137:564-570, 2002.
138. Bessette JR, Maglinte DD, Kelvin FM, Chernish SM: Primary malignant tumors in the small bowel: A comparison of the small-bowel enema and conventional follow-through examination. *AJR* 153:741-744, 1989.
139. Gourtsoyiannis NC, Bays D, Papaioannou N, et al: Benign tumors of the small intestine: Pre-operative evaluation with a barium infusion technique. *Eur J Radiol* 16:115-125, 1993.
140. Masselli G, Poletti E, Casciani E, et al: Small-bowel neoplasms: Prospective evaluation of MR enteroclysis. *Radiology* 251:743-750, 2009.
141. Soyer P, Mounir A, Hoeffel C, et al: Helical CT-enteroclysis in the detection of small-bowel tumours: A meta-analysis. *Eur Radiol* 23:388-399, 2013.
142. Maglinte DD, Applegate KE, Rajesh A, et al: Conscious sedation for patients undergoing enteroclysis: Comparing the safety and patient-reported effectiveness of two protocols. *Eur J Radiol* 70:512-516, 2009.
143. Maglinte D, Kelvin FM, Rowe M, et al: Small-bowel obstruction: Optimizing radiologic investigation and nonsurgical management. *Radiology* 218:39-46, 2001.
144. Herlinger H, Maglinte D: Small bowel obstruction. In Herlinger H, Maglinte D, editors: *Clinical Radiology of the Small Intestine*, Philadelphia, 1989, WB Saunders, pp 467-506.
145. Maglinte D, Balthazar EJ, Kelvin FM, Megibow AJ: The role of radiology in the diagnosis of small-bowel obstruction. *AJR* 168:1171-1180, 1997.
146. Maglinte D, Howard TJ, Lillemoe K, et al: Small bowel obstruction: State-of-the-art imaging and its role in clinical management. *Clin Gastroenterol Hepatol* 6:130-139, 2008.
147. Maglinte D, Kelvin FM, Sandrasegaran K, et al: Radiology of small-bowel obstruction: Contemporary approach and controversies. *Abdom Imaging* 30:160-178, 2005.
148. Fukuya T, Hawes DR, Lu C, et al: CT diagnosis of small-bowel obstruction: Efficacy in 60 patients. *AJR* 158:765-769, 1992.
149. Megibow A, Balthazar EJ, Cho K: Bowel obstruction: Evaluation with CT. *Radiology* 180:313-318, 1991.
150. Maglinte DD, Gage SN, Harmon BH, et al: Obstruction of the small intestine: Accuracy and role of CT in diagnosis. *Radiology* 188:61-64, 1993.
151. Maglinte DD, Peterson LA, Vahey TN, et al: Enteroclysis in partial small bowel obstruction. *Am J Surg* 147:325-329, 1984.
152. Maglinte DD, Reyes BL, Harmon BH, et al: Reliability and role of plain film radiography and CT in the diagnosis of small-bowel obstruction. *AJR* 167:1451-1455, 1996.
153. Shrake PD, Rex DK, Lappas JC, Maglinte DD: Radiographic evaluation of suspected small bowel obstruction. *Am J Gastroenterol* 86:175-178, 1991.
154. Maglinte D, Reyes B: Computed tomographic diagnosis of partial small-bowel obstruction secondary to anterior peritoneal adhesions: Relevance to laparoscopic cholecystectomy. *Emerg Radiol* 3:84-86, 1996.
155. Maglinte DD, Hall R, Miller RE, et al: Detection of surgical lesions of the small bowel by enteroclysis. *Am J Surg* 147:225-229, 1984.
156. Walsh D, Bender G, Timmons J: Comparison of computed tomography-enteroclysis and traditional computed tomography in the setting of suspected partial small-bowel obstruction. *Emerg Radiol* 5:29-37, 1998.
157. Caroline D, Herlinger H, Laufer I, et al: Small-bowel enema in the diagnosis of adhesive obstruction. *AJR* 143:1133-1139, 1984.
158. Bender GN, Maglinte DD, McLarny JH, et al: Malignant melanoma: Patterns of metastasis to the small bowel, reliability of imaging studies, and clinical relevance. *Am J Gastroenterol* 96:2392-2400, 2001.
159. Bass KN, Jones B, Bulkley GB: Current management of small-bowel obstruction. *Adv Surg* 31:1-34, 1997.
160. Hayanga AJ, Bass-Wilkins K, Bulkley GB: Current management of small-bowel obstruction. *Adv Surg* 39:1-33, 2005.
161. Maglinte DD, Kelvin FM, Micon LT, et al: Nasointestinal tube for decompression or enteroclysis: Experience with 150 patients. *Abdom Imaging* 19:108-112, 1994.
162. Maglinte DD, Stevens LH, Hall RC, et al: Dual-purpose tube for enteroclysis and nasogastric-nasointestinal decompression. *Radiology* 185: 281-282, 1992.
163. Bender G, Maglinte DD: Small bowel obstruction: The need for greater radiologist involvement. *Appl Radiol* 28:7-9, 1999.
164. Staunton M, Malone DE: Can diagnostic imaging reliably predict the need for surgery in small bowel obstruction? Critically appraised topic. *Can Assoc Radiol J* 56:79-81, 2005.
165. Glazer GM, Ruiz-Wibbelsmann JA: Decades of perceived mediocrity: Prestige and radiology. *Radiology* 260:311-316, 2011.
166. Bender GN, Maglinte D: Small-bowel obstruction: The need for greater radiologist involvement [editorial]. *Emerg Radiol* 4:337-339, 1997.
167. Yamauchi FI, Ortega CD, Blasbalg R, et al: Multidetector CT evaluation of the postoperative pancreas. *Radiographics* 32:743-764, 2012.
168. Scialpi M, Scaglione M, Volterrani L, et al: Imaging evaluation of post pancreatic surgery. *Eur J Radiol* 53:417-424, 2005.
169. Agarwal A, Maglinte DD, Goggins WC, et al: Internal hernia after pancreas transplantation with enteric drainage: An unusual cause of small bowel obstruction. *Transplantation* 80: 149-252, 2005.
170. Sandrasegaran K, Maglinte DD: Imaging of small bowel-related complications following major abdominal surgery. *Eur J Radiol* 53:374-386, 2005.
171. Sandrasegaran K, Maglinte DD, Howard TJ, Lappas JC: Surgery for chronic pancreatitis: Cross-sectional imaging of postoperative anatomy and complications. *AJR* 184:1118-1127, 2005.
172. Sandrasegaran K, Maglinte DD, Lappas JC, et al: Small-bowel complications of major gastrointestinal tract surgery. *AJR* 185:671-681, 2005.
173. Sandrasegaran K, Maglinte DD, Rajesh A, et al: CT of acute biliopancreatic limb obstruction. *AJR* 186:104-109, 2006.
174. Lall CG, Sandrasegaran K, Maglinte DT, Fridell JA: Bowel complications seen on CT after pancreas transplantation with enteric drainage. *AJR* 187:1288-1295, 2006.
175. Sandrasegaran K, Lall C, Berry WA, et al: Enteric drainage pancreatic transplantation. *Abdom Imaging* 31:588-595, 2006.
176. Maglinte DD, Heitkamp DE, Howard TJ, et al: Current concepts in imaging of small bowel obstruction. *Radiol Clin North Am* 41:263-283, 2003.
177. Frager D, Medwid SW, Baer JW, et al: CT of small-bowel obstruction: Value in establishing the diagnosis and determining the degree and cause. *AJR* 162:37-41, 1994.
178. Frager DH, Baer JW, Rothpearl A, Bossart PA: Distinction between postoperative ileus and mechanical small-bowel obstruction: Value of CT compared with clinical and other radiographic findings. *AJR* 164:891-894, 1995.
179. Romano S, Bartone G, Romano L: Ischemia and infarction of the intestine related to obstruction. *Radiol Clin North Am* 46:925-942, 2008.
180. Romano S, Lassandro F, Scaglione M, et al: Ischemia and infarction of the small bowel and colon: Spectrum of imaging findings. *Abdom Imaging* 31:277-292, 2006.
181. Staunton M, Malone DE: Can acute mesenteric ischemia be ruled out using computed tomography? Critically appraised topic. *Can Assoc Radiol J* 56:9-12, 2005.
182. Seror D, Feigin E, Szold A, et al: How conservatively can postoperative small-bowel obstruction be treated? *Am J Surg* 165:121-126, 1993.
183. Ha H, Rha S, Kim J, et al: CT diagnosis of strangulation in patients with small-bowel obstruction: Current status and future direction. *Emerg Radiol* 7:47-55, 2000.
184. Gazelle G, Goldberg MA, Wittenberg J, et al: Efficacy of CT in distinguishing small-bowel obstruction from other causes of small-bowel dilatation. *AJR* 162:43-47, 1994.
185. Frager D, Baer JW, Medwid S: Detection of intestinal ischemia in patients with acute small-bowel obstruction due to adhesions or hernia: Efficacy of CT. *AJR* 166:67-71, 1996.

186. Balthazar E, Bauman JS, Megibow A: CT diagnosis of closed-loop obstruction. *J Comput Assist Tomogr* 9:953–955, 1985.
187. Balthazar E, Birnbaum BA, Megibow A, et al: Closed-loop and strangulating intestinal obstruction: CT signs. *Radiology* 185:769–775, 1992.
188. Barnett WO, Petro AB, Williamson JW: A current appraisal of problems with gangrenous bowel. *Ann Surg* 183:653–659, 1976.
189. Otamiri T, Sjodahl R, Ihse I: Intestinal obstruction with strangulation of the small bowel. *Acta Chir Scand* 153:307–310, 1987.
190. Huprich JE, Fletcher JG, Fidler JL, et al: Prospective blinded comparison of wireless capsule endoscopy and multiphase CT enterography in obscure gastrointestinal bleeding. *Radiology* 260:744–751, 2011.
191. Huprich JE: Multi-phase CT enterography in obscure GI bleeding. *Abdom Imaging* 34:303–309, 2009.
192. Huprich JE, Fletcher JG, Alexander JA, et al: Obscure gastrointestinal bleeding: Evaluation with 64-section multiphase CT enterography—initial experience. *Radiology* 246:562–571, 2008.
193. Antes G: Radiology of small-bowel motility disorders. In Gourtsoyiannis NC, editor: *Radiological Imaging of the Small Intestine*, Berlin, 2002, Springer-Verlag, pp 235–246.
194. O'Connor OJ, McSweeney SE, McWilliams S, et al: Role of radiologic imaging in irritable bowel syndrome: Evidence-based review. *Radiology* 262:485–494, 2012.
195. Barloon TJ, Lu CC, Franken EA, Jr, et al: Small bowel enteroclysis survey. *Gastrointest Radiol* 13:203–206, 1988.
196. Redmond PL, Kumpe DA: Fentanyl and diazepam for analgesia and sedation during radiologic special procedures. *Radiology* 164:284, 1987.
197. Trevisani L, Sartori S, Gaudenzi P, et al: Upper gastrointestinal endoscopy: Are preparatory interventions or conscious sedation effective? A randomized trial. *World J Gastroenterol* 10:564–570, 2004.
198. Zaman A, Hahn M, Hapke R, et al: A randomized trial of peroral versus transnasal unsedated endoscopy using an ultrathin videoendoscope. *Gastrointest Endosc* 49 (Pt 1):279–284, 1999.
199. Madan A, Minocha A: Who is willing to undergo endoscopy without sedation: Patients, nurses or the physicians? *South Med J* 97:800–805, 2004.
200. Singer AJ, Richman PB, Kowalska A, Thode HC, Jr: Comparison of patient and practitioner assessments of pain from commonly performed emergency department procedures. *Ann Emerg Med* 33:652–658, 1999.
201. Maglinte DD, Cordell WH: Strategies for reducing the pain and discomfort of nasogastric intubation. *Acad Emerg Med* 6:166–169, 1999.
202. American Society of Anesthesiologists Task Force on Sedation and Analgesia by Non-Anesthesiologists: Practice guidelines for sedation and analgesia by non-anesthesiologists. *Anesthesiology* 96:1004–1017, 2002.
203. Maglinte DD, Lappas JC, Chernish SM, et al: Improved tolerance of enteroclysis by use of sedation. *AJR* 151:951–952, 1988.
204. Muller P, Wittenberg KH, Kaufman J: Patterns of analgesia and nursing care for interventional radiology procedures: A national survey of physician practices and preferences. *Radiology* 202:339–343, 1997.
205. Maglinte DD, Lappas JC, Chernish SM, Sellink JL: Intubation routes for enteroclysis. *Radiology* 158:553–554, 1986.
206. Maglinte DD, Miller RE: A comparison of pumps used for enteroclysis. *Radiology* 152: 815, 1984.
207. Reed MH: Evidence in diagnostic imaging: Going beyond accuracy. *J Am Coll Radiol* 9:90–92, 2012.
208. Brink JA, Amis ES, Jr: Image wisely: A campaign to increase awareness about adult radiation protection. *Radiology* 257:601–602, 2010.
209. Brink JA: The art and science of medical guidelines: What we know and what we believe. *Radiology* 254:20–21, 2010.
210. Huprich JE, Fletcher JG: CT enterography: Principles, technique and utility in Crohn's disease. *Eur J Radiol* 69:393–397, 2009.
211. Elsayes KM, Al-Hawary MM, Jagdish J, et al: CT enterography: Principles, trends, and interpretation of findings. *Radiographics* 30:1955–1970, 2010.
212. Megibow AJ, Babb JS, Hecht EM, et al: Evaluation of bowel distention and bowel wall appearance by using neutral oral contrast agent for multi-detector row CT. *Radiology* 238:87–95, 2006.
213. Oliva M, Erturk S, Ichikawa T, et al: Abdominal MDCT with neutral oral contrast media (VoLumen): Comparison with positive oral contrast media and water (abstract no. SSJ06-03). Presented at the 92nd Scientific Assembly and Annual Meeting of the Radiological Society of North America, Chicago, Nov. 26–Dec. 1, 2005.
214. Arslan H, Etlik O, Kayan M, et al: Peroral CT enterography with lactulose solution: Preliminary observations. *AJR* 185:1173–1179, 2005.
215. Bilimoria KY, Bentrem DJ, Wayne JD, et al: Small bowel cancer in the United States: Changes in epidemiology, treatment, and survival over the last 20 years. *Ann Surg* 249:63–71, 2009.
216. Krishnaraj A: Standing our ground. *J Am Coll Radiol* 7:8–9, 2010.
217. Lee CI, Forman HP: Radiology health services research: From imperative to legislative mandate. *AJR* 196:1111–1114, 2011.
218. Gunderman RB, Chou HY: Effective argumentation. *AJR* 196:1345–1349, 2011.

Magnetic Resonance Enterography

GABRIELE MASSELLI | GIANFRANCO GUALDI

CHAPTER OUTLINE

Technical Considerations

Enteral Contrast Agents for Magnetic Resonance Imaging
Technique
Magnetic Resonance Imaging Protocol and Pulse Sequences

Image Interpretation

Clinical Applications

Crohn's Disease
Small Bowel Neoplasms
Celiac Disease
Bowel Ischemia and Vasculitis
Infections
Small Bowel Obstruction

Summary

Small bowel radiology has undergone dramatic changes in the past 2 decades. Despite recent advances in small bowel endoscopy and video capsule technology, radiologic imaging remains an important means of evaluating patients with suspected or established small bowel disease.¹⁻⁵ Cross-sectional imaging techniques are used to investigate extraluminal abnormalities and intraluminal changes and have gradually replaced barium contrast examinations for many indications.⁶⁻¹³

Magnetic resonance imaging (MRI) has many properties that make it well suited to imaging of the small bowel, such as the lack of ionizing radiation, improved tissue contrast that can be achieved by using a variety of pulse sequences, and the ability to perform real-time functional imaging.¹⁴⁻¹⁸ Moreover, MR modalities allow visualization of the entire bowel without overlapping bowel loops as well as the detection of intra- and extraluminal abnormalities. These morphologic MR findings, combined with contrast enhancement features and functional information, help make an accurate diagnosis and consequently characterize small bowel diseases. These features dramatically change the image interpretation process.¹⁸ Radiologists must focus on morphologic findings and functional data of small bowel motility to exploit MR capabilities fully. Optimal distention of the small bowel loops is crucial for the correct evaluation of the bowel wall because collapsed bowel loops may hide lesions or mimic disease by mistakenly suggesting that the collapsed segments are actually an abnormality-related thickened bowel wall.¹⁹⁻²¹

Two main techniques have been used to achieve small bowel distention, MR enteroclysis with infusion of the contrast material through a nasojejunal tube and MR enterography with

oral administration of contrast material.¹⁸ There is a general preference among radiologists for performing enterography over enteroclysis; however, this preference is controversial.^{18,21-23} MR enteroclysis is known to provide better depiction of endoluminal lesions in the small intestine than that achieved at MR enterography performed with an oral contrast agent.²¹ It is also generally acknowledged that MR enteroclysis provides optimal small bowel distention and allows more accurate detection of strictures.²¹⁻²³ However, nasointestinal intubation for MR enteroclysis may cause patient discomfort, and it involves various technical and logistical difficulties, as well as exposure to radiation. MR enteroclysis performed with the continuous administration of an enteric contrast agent is not possible at all facilities.

Although Crohn's disease is the primary indication for MR enterography because many patients require multiple follow-up imaging examinations, MR enterography is performed with increasing frequency for the evaluation of other small bowel diseases. MR imaging offers detailed morphologic information and functional data of small bowel disease, thereby allowing the diagnosis of early or subtle structural abnormalities and guiding patient therapy.

Technical Considerations

ENTERAL CONTRAST AGENTS FOR MAGNETIC RESONANCE IMAGING

A number of enteral agents have been proposed for use in small bowel MR imaging. The most important features of enteral contrast agents include uniform and homogeneous opacification, adequate distention of the small bowel lumen, high contrast between the lumen and small bowel, low cost, and absence of serious adverse side-effects.

There are three main groups of enteral agents. The signal intensity that results from their use varies according to the pulse sequence used.^{24,25} Positive contrast enteral agents, which yield high signal intensity on T1-weighted images, include gadolinium chelates,²⁵ manganese ions,²⁶ ferrous ions,²⁷ and foods such as blueberry juice.²⁸ Although these enteral agents can show mural thickening on T1-weighted images,²⁹ they inevitably are limited regarding the detection of more subtle mucosal or wall hyperenhancement after the intravenous injection of gadolinium-based contrast material. Consequently, their routine use is not recommended.

Negative contrast enteral agents, which yield low signal intensity on T2-weighted and especially T2*-weighted images, constitute solutions with superparamagnetic iron oxides (SPIOs), including nanoparticles of maghemite in bentonite matrix, and ultrasmall SPIOs (USPIOs).³⁰ Currently, the only negative contrast agent commercially available in the United States is ferumoxsil oral suspension, which is used in MR cholangiopancreatography to reduce the signal from

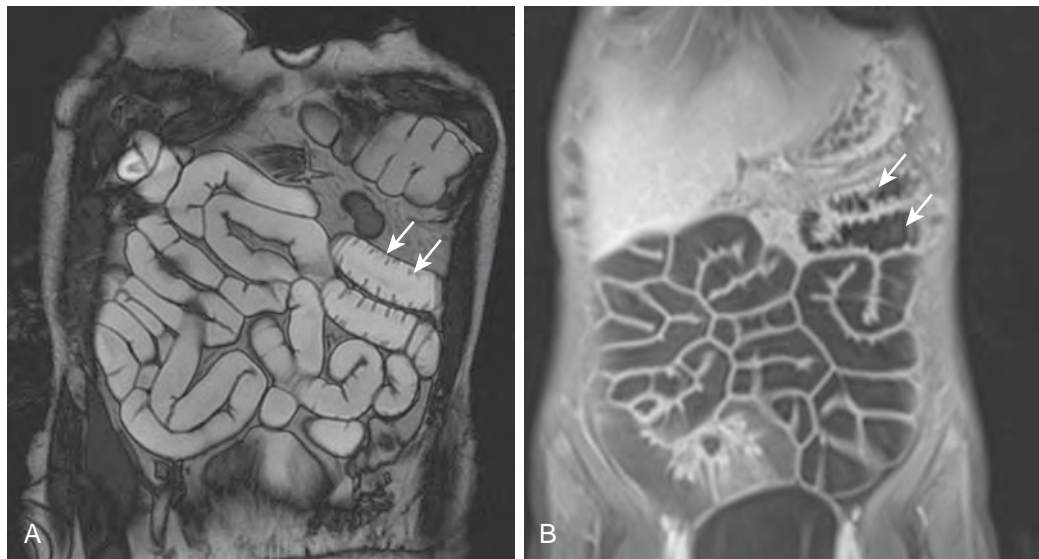


Figure 40-1 Normal MR enterography findings. Iso-osmotic polyethylene glycol–water solution (biphasic contrast agent) acts as a positive intraluminal contrast agent (bright lumen) on (A) true FISP as a negative agent (black lumen) on a 3D T1-weighted fat-saturated VIBE image (B). Normal valvulae conniventes (arrows) in a well-distended jejunum are visible.

surrounding bowel. The high signal intensity of inflammation in the bowel wall and in the surrounding fat may be more conspicuous on T2-weighted images obtained with a negative contrast agent because of the greater contrast achieved between the high signal intensity of inflammation and the low signal intensity of the lumen. Side effects (observed in 5% to 15% of cases) associated with these enteral agents include poor palatability of the agent, nausea, vomiting, and rectal leakage.²⁴ Moreover, the low signal intensity of intraluminal contrast on T2-weighted images and associated susceptibility effects may reduce the conspicuity of the normal small bowel wall, low signal intensity lesions, such as carcinoid tumors, and intraluminal abnormalities.

The third group of agents are biphasic enteral contrast agents, which have been most widely tested and are most commonly used for MR enteroclysis and MR enterography.³¹⁻³³ They produce low signal intensity on T1-weighted images and high signal intensity on T2-weighted images. The low signal intensity of these agents on T1-weighted images improves the contrast between the bowel lumen and hyperenhancing mural inflammation or masses after intravenous administration of contrast material (Fig. 40-1). The marked contrast between the lumen and dark bowel wall on T2-weighted images improves the detection of endoluminal abnormalities and more effectively highlights transmural ulcers.^{34,35} Commercially available biphasic enteral agents include water, polyethylene glycol, barium sulfate (VoLumen; E-Z-Em/Bracco, Lake Success, NY), and nonosmotic agents such as locust bean gum and methylcellulose.^{36,37} Polyethylene glycol is a high-osmolar, nonabsorbed, nonfermented contrast medium that has been shown to provide excellent intraluminal contrast and luminal distention,³⁸⁻⁴⁰ although this enteral agent may cause mild diarrhea. Barium sulfate, an enteral contrast agent that contains sorbitol, whose osmotic properties cause it to retain water, has also proved to be effective.⁴¹ Barium sulfate and water–polyethylene glycol solution are both superior to plain water

and water–methylcellulose solution for achieving optimal small bowel distention.⁴¹

TECHNIQUE

Optimal distention of the small bowel loops is crucial for the correct evaluation of the bowel wall. This is because collapsed bowel loops may obscure lesions or mimic disease by mistakenly suggesting that the collapsed segments are actually an abnormality-related thickened bowel wall.⁴²

MR enteroclysis has been shown to depict early disease and the number of involved segments more accurately,¹⁸⁻²² whereas enterography is more time-efficient for radiologists and other staff because nasojejunal tube placement is not required. Although jejunal distention is frequently suboptimal,¹⁸⁻²² the ileum, which is the most common site of small bowel involvement in Crohn's disease and the region of most interest to clinicians, is usually well depicted. Enterography also eliminates radiation exposure and the technical and logistical difficulties of nasojejunal tube insertion, and it removes a potential barrier to patient compliance with future examinations.

Enterography techniques require the ingestion of a large amount of fluid that fills the stomach and small bowel. Patient tolerance is the current limitation. As yet, there is no consensus on the optimal volume of oral contrast medium needed for an enterographic examination⁴⁰⁻⁴⁵; a volume of 1350 to 1500 mL is adequate in most cases.

Although rapid transit (<20 minutes) to the right colon has been observed, there is a delay of at least 40 to 60 minutes from contrast material ingestion to imaging in most patients.⁴⁶ Although some authors⁴⁶⁻⁴⁸ advocate imaging the patient twice (e.g., after 20 minutes for optimal visualization of the distended jejunum and after 45 minutes for the ileum), a single acquisition performed 40 minutes after the ingestion of oral contrast material is effective and practical in terms of patient compliance and efficient time use of the MR imager.^{7,18}

MAGNETIC RESONANCE IMAGING PROTOCOL AND PULSE SEQUENCES

A preprocedural fast of 4 hours is recommended³⁶ because fasting reduces the amount of food residue and debris in the intestinal lumen, which may mimic mass lesions or polyps. Patients are imaged in the supine or prone position. The prone position helps separate bowel loops, provide maximal bowel coverage on coronal images, and decrease the imaging volume.^{41,48} Although the prone position does offer better distention, it does not translate to better lesion detection.⁴⁸ The supine position affords greater patient comfort and is indicated for patients with abdominal pain, stomas, and/or abdominal wall fistulas.

For the MR enterography protocol, an initial thick slab T2-weighted MR cholangiopancreatographic study helps assess small bowel distention. If there is inadequate distention of the ileum, the patient can return to the waiting room to drink more oral contrast material. The MR technical protocol is shown in Table 40-1.

Antiperistaltic agents such as hyoscine butylbromide (Buscopan; Boehringer Ingelheim, Ingelheim, Germany) or glucagon (Glucagen; Novo Nordisk, Bagsvaerd, Denmark) are used intravenously to eliminate peristalsis and reduce motion artifact.¹⁸ Achieving reduced peristalsis is of considerable importance for the T1-weighted 3D sequences performed after the administration of intravenous contrast material and may help limit intraluminal flow artifacts on images obtained with the half-Fourier acquisition. I administer an initial 10 mg of hyoscine butylbromide or 0.2 mg of glucagon immediately before the examination starts to reduce intraluminal flow voids. The patient receives an additional dose of the same strength prior to gadolinium-based contrast material injection.

The T2-weighted sequence based on the half-Fourier reconstruction technique, termed *half-Fourier RARE* (rapid acquisition and relaxation enhancement) or *single-shot fast spin-echo*, allows each image to be obtained in less than 1 second, minimizing artifacts caused by small bowel peristalsis.¹⁴ They produce high contrast between the lumen and bowel wall, providing excellent depiction of wall thickening and changes in the fold pattern.

Limitations of half-Fourier RARE include its sensitivity to intraluminal flow voids and the fact that it poorly depicts the mesentery because of k space filtering effects,^{10,14} which are related to the combination of a single-shot acquisition and

partial Fourier technique. The latter results in selective spatial filtering, leading to the loss of fine details of tissues that exhibit low to moderate T2 relaxation times. The coronal and axial balanced gradient-echo MR images that are obtained yield contrast that is intermediate relative to contrast on T1- and T2-weighted images.

Various acronyms are used to describe the balanced gradient-echo sequences, including fast imaging employing steady-state acquisition (FIESTA), true fast imaging with steady-state precession (FISP), and balanced steady-state free precession, depending on the manufacturer. These pulse sequences are particularly effective as a means of obtaining information about mural and extraintestinal abnormalities. The black boundary artifact encountered at fat-water interfaces with the balanced gradient-echo sequence can be clearly differentiated from abnormal bowel wall thickening because the fat-water interface is of low signal intensity, which contrasts with the moderate signal intensity of the thickened small bowel wall.

Two- or three-dimensional spoiled gradient-echo fat-saturated T1-weighted sequences can be used to acquire contrast-enhanced images. Because contrast-enhanced images acquired with 3D volumetric sequences provide better spatial resolution and allow multiplanar reconstruction, they are preferred with fully cooperative patients. When patients have difficulty in breath holding and remaining still, a 2D T1-weighted sequence, which is less susceptible to motion artifacts but has reduced spatial resolution, may be used instead of the 3D volumetric sequences. Gadolinium-based contrast material is administered by injecting 0.2 mmol/kg of body weight at a rate of 2 mL/sec, followed by a bolus injection of 20 mL of isotonic saline. Coronal gradient-echo fat-saturated T1-weighted sequences are obtained before and 30 and 70 seconds after the injection, followed by an axial sequence beginning 90 seconds after the injection, which covers the entire abdomen. The entire protocol for MR enterography takes 20 to 25 minutes.

Few studies have investigated the role of diffusion-weighted imaging for the detection of bowel inflammation in Crohn's disease. The apparent diffusion coefficient may facilitate quantitative analysis of disease activity. Visual assessment of diffusion-weighted images may provide greater accuracy, whereas calculation of the apparent diffusion coefficient may facilitate a quantitative analysis of disease activity.⁴⁹⁻⁵¹

Some authors have demonstrated that inflamed bowel segments have more restricted diffusion compared with normal

TABLE 40-1 Parameters for 1.5-T MR Small Bowel Imaging

Parameter	True FISP		T2-Weighted Half-Fourier RARE		T1-Weighted 3D Vibe	2D True FISP
	Axial	Coronal	Axial/Axial Fat-Saturated	Coronal	Coronal/Axial	Coronal and Axial
Repetition time/echo time (msec)	4.3/2.2	4.3/2.2	1000/90	1000/90	4.1/1.1	500/75
Flip angle (degrees)	50	50	150	150	10	50
Field of view (mm)	320-400	320-400	320-400	320-400	320-400	400
Matrix	256 × 224	256 × 224	256 × 224	256 × 224	256 × 224	256 × 256
Parallel imaging factor	2	2	2	2	3	2
Section thickness (mm)*	5	3	4	3	2.5	10
No. of signals acquired	1	1	1	1	1	6
Receiver bandwidth (Hz)	125	125	62.5	62.5	62.50	1930
Acquisition time (sec)	19	21	15-20	15-20	15-20	25

*Intersection gap is 0 mm for all sequences.

VIBE, volumetric interpolated breath-hold examination.

bowel segments, and have further shown that diffusion-weighted imaging (DWI) is more sensitive than dynamic contrast-enhanced (DCE) MRI for actively inflamed terminal ileum; combining both techniques can potentially improve diagnostic specificity.⁴⁹ Other authors have reported a sensitivity, specificity, and accuracy of 86.0%, 81.4%, and 82.4%, respectively, for the detection of disease-active segments.⁵⁰ Another study demonstrated restricted diffusion in inflamed portions of the colon in patients with ulcerative colitis,⁵¹ one of which also showed that DWI had similar accuracy to contrast-enhanced sequences for detecting inflamed bowel. The outcomes of these studies suggest an evolving role for DWI in inflammatory bowel disease.

The ultrafast acquisition of the balanced steady-state free precession (SSFP) technique described earlier allows high temporal resolution imaging of the whole length and width of the abdomen in a coronal slice with subsecond repetition times during a single breath-hold. The resulting cine sequence can be used to evaluate small bowel peristalsis visually, and identify areas of altered motility, specifically focal areas of paralysis or hypomotility. Cine MR sequences have been found to detect more specific findings for Crohn's disease than standard MR enterography and identified significantly more patients with Crohn's disease than those identified on MR enterography alone.⁵² Moreover, cine MRI was a feasible approach for detecting a longitudinal ulcer in small bowel Crohn's disease, which appeared as asymmetric involvement or mesenteric rigidity with antimesenteric flexibility.⁵³ More recently, software methods have been developed to assess small bowel motility in an automated manner as well as analyzing the motility quantitatively,^{54,55} suggesting a role for quantified motility in assessing disease activity.

MRI of the small bowel can be performed with a 3-T system,⁵⁶ but the higher field strength requires modifications of the pulse sequences that are used at 1.5 T. Higher specific absorption rates because of the long acquisition time needed to obtain axial sections of the entire abdomen with a half-Fourier RARE sequence at 3 T are often a limiting factor. The use of parallel imaging techniques may help reduce the acquisition time and decrease the specific absorption rate, but such reductions are achieved at the expense of the signal-to-noise ratio. The use of FISP sequences is not always feasible at 3 T because of distortion artifacts. However, it is possible to obtain dynamic T1-weighted images at 3 T that have spatial resolution commensurate with that of T1-weighted images obtained at 1.5 T.

Image Interpretation

Initially, MR fluoroscopic sequences are used to assess the grade of distention of the small bowel and provide a panoramic view of the caliber and location of the jejunal and ileal loops. The images are displayed in the cine loop mode to visualize small bowel mobility.

The transit of the polyethylene glycol solution through the small bowel is considered normal when unimpeded flow of intraluminal solution from the duodenojejunal junction to the ascending colon is observed, with no evidence of transit delay or stenosis. Low-grade stenosis is diagnosed when contrast material reaches the site of obstruction without any delay and flows into the loop below the obstruction. In patients with a high-grade partial small bowel obstruction, the arrival of contrast material at the site of obstruction is delayed, and only a minimal amount flows into the collapsed loop beyond the

obstruction, thus making it difficult to define the fold pattern. A transition zone between the dilated bowel above and the narrowed bowel below marks the site of any obstruction. MR fluoroscopic pulse sequences yield useful information concerning the distensibility of narrowed areas, facilitate the differentiation of contractions from strictures in the evaluation of prestenotic dilation, evaluate small bowel mobility, and demonstrate findings similar to those seen at barium enema examinations, such as the morphology of the stenosis, which help differentiate among mucosal, submucosal, and extraparietal origins of disease.¹⁸

Balanced gradient-echo and T2-weighted images are examined to detect the presence of bowel wall thickening. Multiplanar projections can be obtained by alternating between axial and coronal acquisitions.

The main challenge in MR image interpretation is bowel underdistention, which may mimic or mask disease. When mural thickening is consistently observed on images from different sequences and planes, the likelihood of a correct diagnosis increases. A wall thickness more than 3 mm in a properly distended small bowel loop should be regarded as abnormal. The presence of perienteric or mesenteric abnormalities is evaluated; a fat-saturated T2-weighted study can help detect perienteric inflammation and penetration. Gadolinium-enhanced images are obtained to enable detection of any hyperenhancement of the bowel wall. In a narrowed segment, hyperenhancement can be used to differentiate contraction from mural disease. If the enhancement is identical to that of adjacent bowel loops in the same segment, it most likely represents underdistended contracted normal bowel. If there is more mucosal enhancement (mucosal hyperemia) or notably less submucosal enhancement (bowel wall edema), true disease should be suspected. Delayed images may also help distinguish transient contractions from wall thickening.

If hyperenhancement is seen in a bowel wall of normal thickness, it is necessary to differentiate between true disease and artifact. In these cases, it is important to compare the enhancement with that of other loops that are similarly distended, and with that of bowel loops within the same segment, because normal jejunum enhances more robustly than normal ileum.

The enhancement pattern of bowel loops can help differentiate between small bowel diseases. Homogeneous hyperenhancement (white) can be seen in ischemia, inflammatory bowel disease, adhesions, and occasionally in tumors. A hypoenhancing (gray) wall may be seen in inflammatory bowel disease and tumors. Mural stratification (the target pattern) is typically seen in active Crohn's disease.^{14,18}

Clinical Applications

CROHN'S DISEASE

The evaluation of chronic inflammatory bowel disease presents several problems. First, it is important to identify the presence of Crohn's disease and differentiate it from other small bowel diseases. Second, the number, length, and locations of the segments involved in each patient need to be determined. Third, if a stenosis is present, it needs to be classified as inflammatory or fibrous so that the patient can receive appropriate medical or surgical therapy.

Furthermore, if inflammatory activity is present, it is important to distinguish among mild, moderate, and severe disease

because medical management differs depending on the disease stage. Fourth, the presence of mesenteric complications, such as abscesses and fistulas, need to be assessed because their presence influences the choice of therapy.⁵⁷⁻⁵⁹

The visualization of early changes of Crohn's disease, such as ulcerations and subtle wall thickening, is highly dependent on the quality of luminal distention.^{1,2,18} High-resolution (thin section) true FISP and half-Fourier RARE images can depict early Crohn's disease changes; for example, an aphthous ulcer appears as a nidus of high signal intensity surrounded by a halo of moderate signal intensity (Fig. 40-2).^{35,58}

Barium contrast enteroclysis and capsule endoscopy are more accurate than MRI as a means of detecting subtle mucosal abnormalities.^{1,3,18} However, the clinical importance of a mucosal break or a few superficial aphthous lesions is not clear. There is evidence that suggests that up to 13% of healthy asymptomatic individuals may have mucosal breaks and other minor lesions of the small bowel at capsule endoscopy.¹³

Two types of ulcers are seen in Crohn's disease, superficial aphthoid ulcers and deep fissuring ulcers. Deep fissuring ulcers are more clinically significant. They penetrate the mucosa into the deeper layers of the bowel wall, resulting in submucosal inflammation and edema. On MRI, they appear as thin lines of

high signal intensity oriented longitudinally or transversally (fissure ulcers) within a thickened bowel wall (Fig. 40-3).

Sensitivity values for the detection of bowel ulceration in the literature range from 75% to 90%.^{17,21,42} MRI can also be used to detect minimal disease on the basis of mucosal enhancement of the bowel wall after intravenous injection of contrast medium¹⁸ (Fig. 40-4).

Segmental mural hyperenhancement is a nonspecific finding of early disease, whereas the presence of asymmetric mural enhancement and thickening is pathognomonic for Crohn's disease. The sensitivity and specificity values of MRI for the detection of Crohn's disease in the literature range from 88% to 98% and from 78% to 100%, respectively.^{16,17,19,21-23}

Cine sequences more accurately demonstrate the number of abnormal bowel segments than static MRI scans. Altered bowel motility is an early imaging sign of Crohn's disease and helps identify abnormal bowel segments with subtle signs of inflammation on static images.⁶⁰

The management of Crohn's disease continues to evolve medically and surgically, and MR enterography has the potential to affect diagnosis and management.⁶¹⁻⁷⁰ Classification of disease activity in Crohn's disease based solely on clinical and laboratory parameters has not been clinically reproducible.^{69,71}

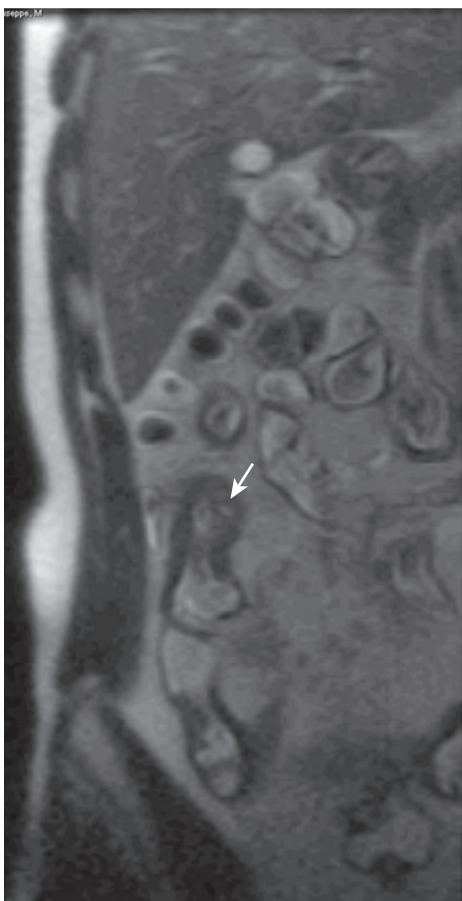


Figure 40-2 MR enterography in 22-year-old patient with Crohn's disease. Coronal half-Fourier RARE sequence shows aphthoid ulcerations (arrow), each of which is seen as a nidus of high signal intensity (an ulcer crater) surrounded by a rim of moderate signal intensity. Capsule endoscopy and colonoscopy were used to confirm these findings.

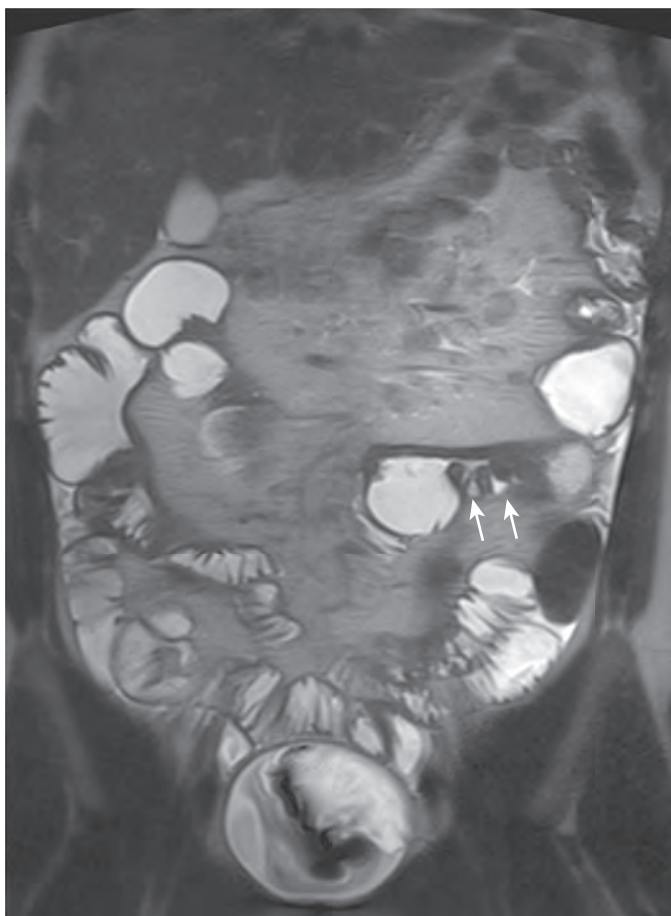


Figure 40-3 MR enterography in 25-year-old patient with Crohn's disease. Coronal half-Fourier RARE sequence shows mucosal irregularity (arrows) as thin lines of high signal intensity oriented longitudinally or transversally (fissure ulcers) within a thickened ileal wall, which is consistent with diffuse ulcerations in Crohn's ileitis.

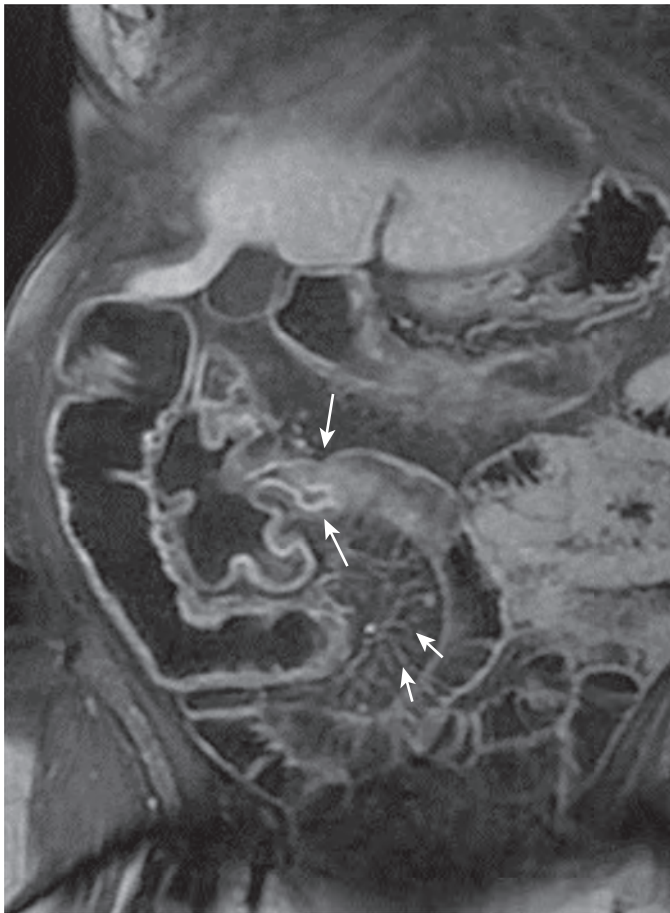


Figure 40-4 MR enterography in 36-year-old man with suspected Crohn's disease. Coronal contrast-enhanced T1-weighted fat-saturated VIBE image of terminal ileum shows uniform wall enhancement of terminal ileum with normal thickness (*long arrows*), a finding that indicates mild inflammatory changes. Note increased vascularity in the adjacent small bowel mesentery (*short arrows*).

Behavior of disease first referred to the indication for surgery—perforating or nonperforating disease.⁵⁹ These definitions have been expanded to nonsurgical situations, and disease activity has been categorized as primarily inflammatory, primarily fibrostenotic, or primarily penetrating, depending on the dominating feature at a given point in time.

To overcome the limitations of the subjective nature and poor reproducibility of the clinical inflammatory index,⁷¹ an imaging-based classification was proposed.⁶¹ Crohn's disease was classified into four broad groups: active inflammatory; perforating and fistulating; fibrostenotic; and reparative and regenerative subtypes. The subtype classification requires accurate information concerning the presence of ulceration, edema, spasm, stricture, fistula formation, and associated inflammatory mesenteric mass. Given its high accuracy for the detection of morphologic and functional abnormalities, MRI has the potential to offer reproducible and objective data to classify the patient's subtype of Crohn's disease correctly and plan and monitor patient therapy (Table 40-2).

Bowel wall thickening (usually ranging from 1 to 2 cm), is the most consistent feature of Crohn's disease on cross-sectional imaging.²³⁻²⁴ It can be found in the acute and chronic phases of disease.

TABLE
40-2

Correlation Between Typical Findings of Crohn's Disease Stages and Magnetic Resonance Pulse Sequences

Disease Stage	Balanced Gradient-Recalled Echo	Half-Fourier RARE	Contrast-Enhanced T1-Weighted
Active	Fold thickening, mural ulcers, mural thickening, comb sign, mesenteric lymph nodes	Fold thickening, mural ulcers, mural thickening, mural edema	Mucosal hyperemia, mural thickening, mural edema, comb sign, mesenteric lymph nodes
Fibrostenotic	Stricture	Stricture, mural fibrosis	Stricture, mural fibrosis
Penetrating	Deep fissuring ulcers, fistulas, abscesses	Deep fissuring ulcers, fistulas, abscess	Fistulas, abscess
Regenerative	Regenerative polyps, decreased luminal diameter	Regenerative polyps, decreased luminal diameter	Decreased luminal diameter

MR signs that indicate active Crohn's disease include mucosal hyperenhancement, mural stratification with a prominent vasa recta (comb sign), and mesenteric fat stranding (Fig. 40-5). Mural hyperenhancement correlates with inflammation at histologic examination and is the most sensitive imaging finding of active disease.⁷² Mucosal and serosal enhancement, combined with intervening submucosal edema, contribute to a stratified or layered appearance on contrast-enhanced fat-suppressed T1-weighted images. A blurred wall enhancement pattern on delayed phase images is strongly correlated with high-grade disease and is observed, above all, in patients with extremely active inflammation.⁶² Mucosal hyperenhancement on MR enterography has demonstrated good correlation with the Crohn's disease activity index and is the most sensitive finding in active disease, which significantly correlates with histologic findings. Several studies have reported MR enterography sensitivities for the detection of active inflammatory disease ranging from 73% to 90%.⁶²⁻⁶⁶

Submucosal edema in the small bowel produces increased signal intensity on T2-weighted images and is seen with active inflammation.⁶⁶ DWI can be useful to detect inflammation in small bowel Crohn's disease (Fig. 40-6).^{50,51}

Linear ulcers along the mesenteric border constitute one of the most important signs of small bowel Crohn's disease. The ulcers run parallel to the shortened, concave, or straightened and somewhat rigid mesenteric border. The adjacent mesentery is thickened and retracted, especially at its junction with the affected bowel segment. The rigidity of the mesenteric border is caused by transmural inflammation that extends from the linear ulcer into the mesentery. Another highly characteristic feature is the sparing of the relatively redundant antimesenteric border, which retains pliability and forms folds and sacculations. Deformity of bowel loops such as

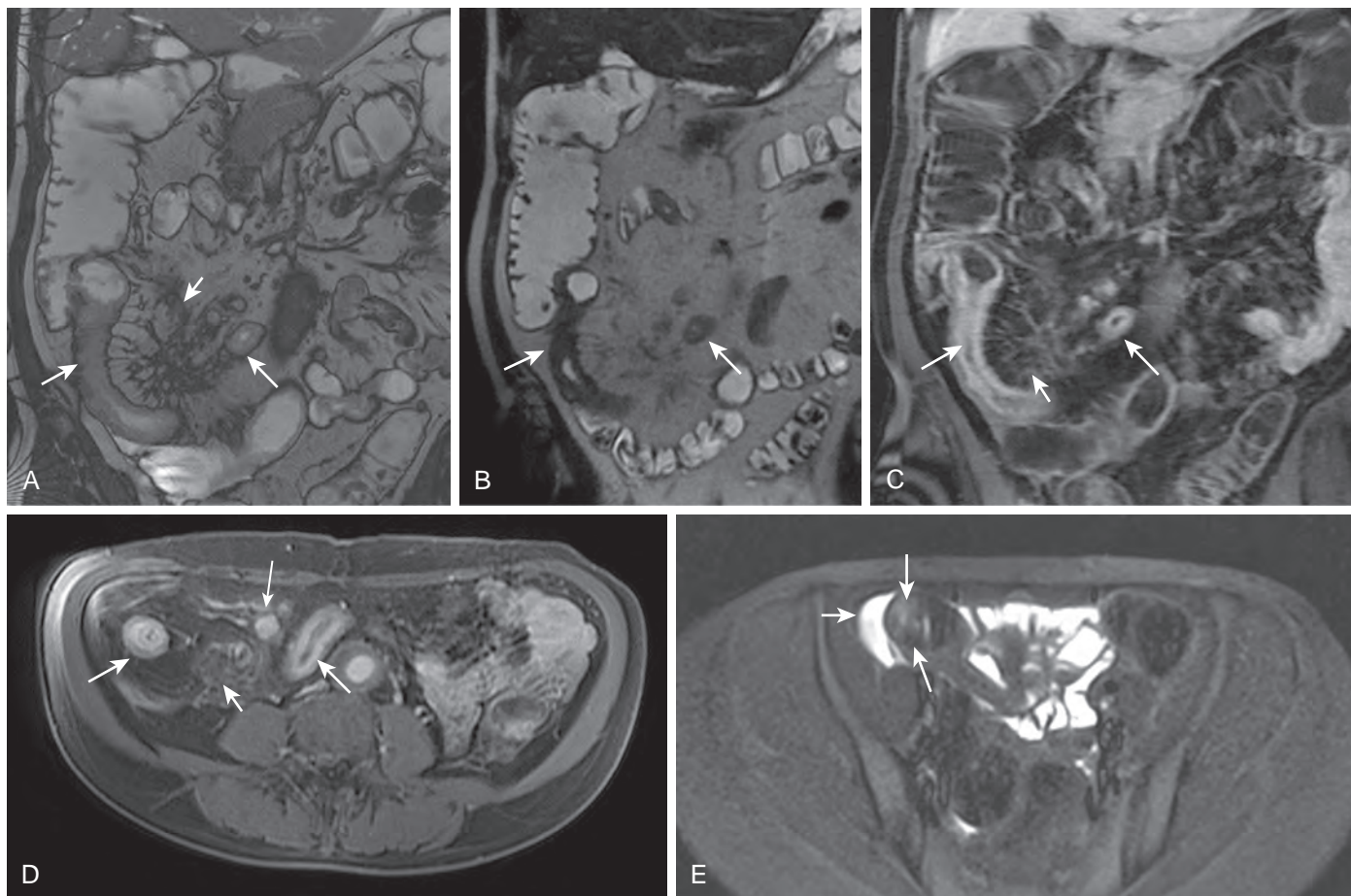


Figure 40-5 MR enterography in 48-year-old man with active Crohn's disease. **A.** Coronal true FISP image shows extensive fibrofatty proliferation of mesentery (*short arrow*) associated with diseased ileal loops (*long arrows*). **B.** Coronal half-Fourier RARE sequence shows diseased ileal loops (*arrows*) but provides poor information concerning the mesentery. Coronal (**C**) and axial (**D**) contrast-enhanced fat-saturated T1-weighted VIBE images show stratified contrast enhancement with avid enhancement of mucosa relative to submucosal and muscular layers (*long arrow*) and layered appearance. Note the high signal intensity linear structure caused by increased vascularity (*short arrows*) close to the mesenteric border of the small bowel segment involved, the so-called comb sign and inflamed mesenteric nodes (*small arrow* in **D**). **E.** T2-weighted fat sat image shows increased signal intensity of the thickened wall, indicative of submucosal edema (*arrows*) with small fluid collection.

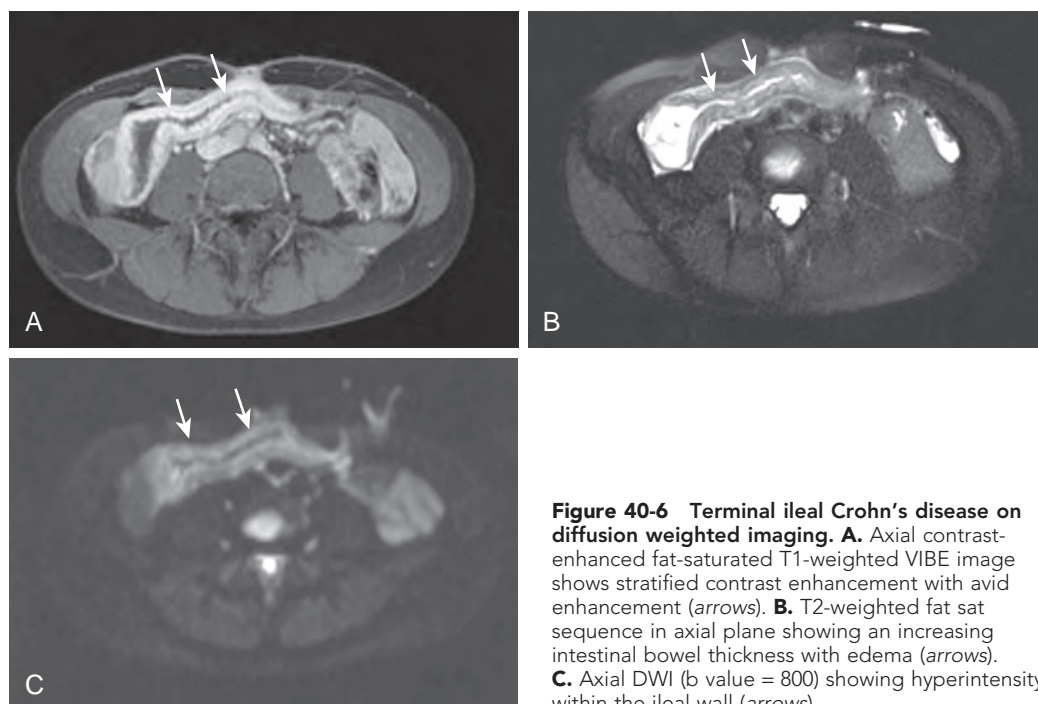


Figure 40-6 Terminal ileal Crohn's disease on diffusion weighted imaging. **A.** Axial contrast-enhanced fat-saturated T1-weighted VIBE image shows stratified contrast enhancement with avid enhancement (*arrows*). **B.** T2-weighted fat sat sequence in axial plane showing an increasing intestinal bowel thickness with edema (*arrows*). **C.** Axial DWI (*b* value = 800) showing hyperintensity within the ileal wall (*arrows*).

pseudodiverticulum formation caused by asymmetric involvement by longitudinal ulcers and ulcer scars is well demonstrated on axial and coronal images.

The fibrostenotic disease subtype is characterized by the presence of strictures that may progress to bowel obstruction. The stricture can be classified as functionally significant if the upstream bowel dilation is more than 3 cm in diameter. In the fibrostenotic subtype of the disease, low-level inhomogeneous mural enhancement is demonstrated, with no evidence of associated edema (Fig. 40-7).

On cine images, fibrotic strictures appear as aperistaltic bowel segments that often demonstrate fixed mural thickening and luminal narrowing. The thickened submucosa of a strictured, fibrotic bowel segment does not typically display increased signal intensity on T2-weighted images in the absence of active disease because of the lack of mural inflammation and edema.

Reparative or regenerative disease subtype reflects inactive Crohn's disease and may be associated with other subtypes of disease located in different bowel loops. It is characterized by mucosal atrophy and presence of regenerative polyps. A minimal decrease in luminal diameter can be seen but there is no mural edema or evidence of active inflammation (Fig. 40-8).

The MR enterography features of the fistula-forming and perforating disease subtype include the demonstration of deep fissuring ulcers and sinus tracts, fistulas, to adjacent bowel loops or other organs, the demonstration of an associated abscess, and extraintestinal involvement.

Adhesions are frequent in Crohn's disease findings and usually are considered as prefistulous lesions. They are

manifestations of serosal involvement and a clear sign of the transmural extension of the disease.

Sinus tracts and fistulas are demonstrated by the high signal intensity of their fluid content on true FISP and half-Fourier acquisition single-shot turbo spin-echo (HASTE) images (Fig. 40-9). The cumulative risk of developing fistulas, for patients with Crohn's disease is 33% after 10 years and 50% after 20 years, with perianal fistulas being the most common type.^{69,73,74} The imaging findings related to fistulas include bowel angulation associated with bowel wall contiguity and linear tracts between these bowel loops.

Multiplanar MR enterography is useful for the complete evaluation of sinus tracts (Fig. 40-10). Desmoplastic and/or fibrotic reactions in the mesentery around the fistula create a star appearance of the fistula. Inflamed fistulas can demonstrate intense contrast enhancement because of their hypervascularity and hyperemia.

Extraintestinal complications, such as mesenteric inflammation, abscesses, and involvement of adjacent viscera, can also be well depicted by MR enterography in patients with fistula-forming and perforating subtypes of Crohn's disease. These findings are of clinical importance and can be observed (using cross-sectional imaging techniques) in up to 50% of patients (fibrofatty proliferation) and 35% of patients (abscesses), respectively.^{10,11} Fibrofatty proliferation of the mesentery is the most common cause of bowel loop separation seen on small bowel studies in patients with Crohn's disease.^{2,3}

The fibrofatty proliferation is the results of perivascular inflammation with fibrosis and muscularis propria contraction.²⁷ The extent of fibrofatty proliferation and its

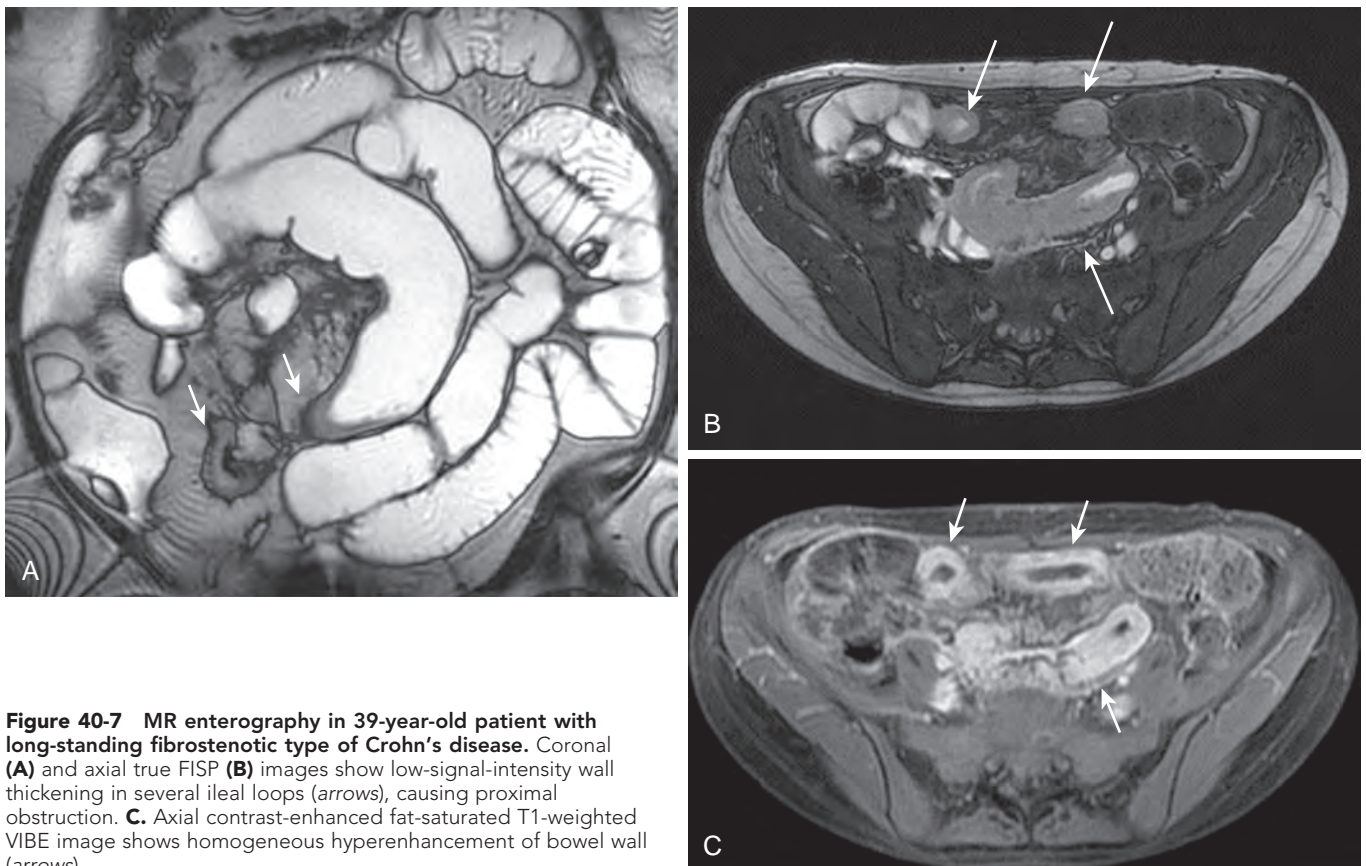


Figure 40-7 MR enterography in 39-year-old patient with long-standing fibrostenotic type of Crohn's disease. Coronal (A) and axial true FISP (B) images show low-signal-intensity wall thickening in several ileal loops (arrows), causing proximal obstruction. C. Axial contrast-enhanced fat-saturated T1-weighted VIBE image shows homogeneous hyperenhancement of bowel wall (arrows).

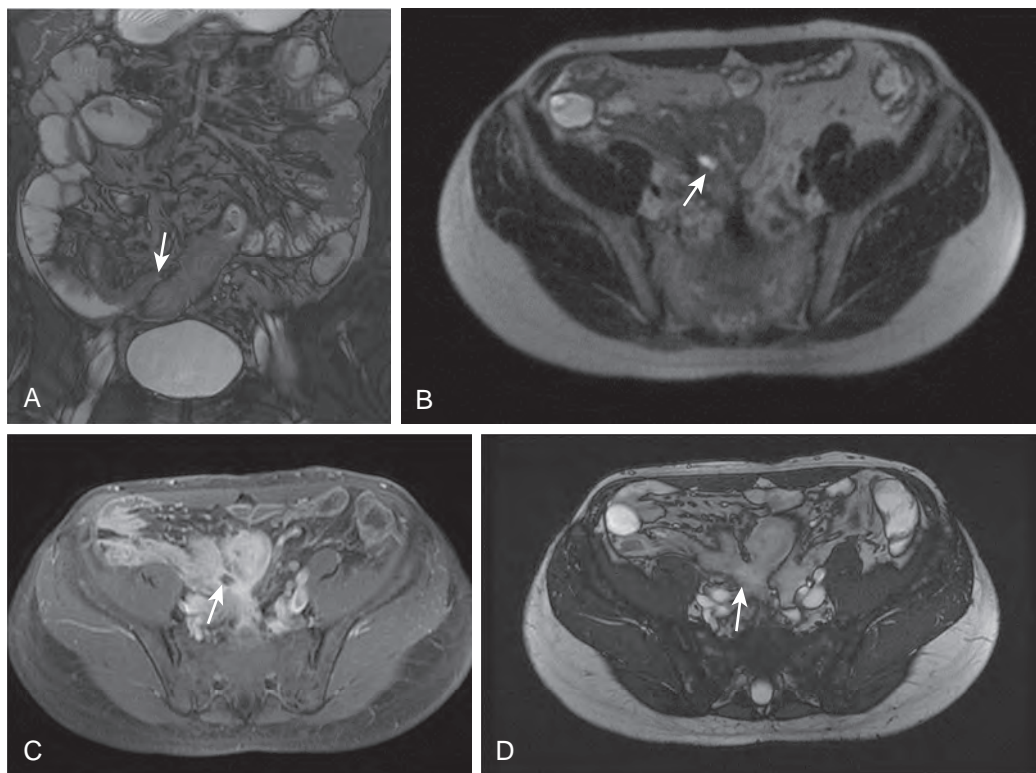


Figure 40-8 31-year-old man with fistulizing Crohn's disease subtype. **A.** Coronal true FISP image shows adherence between diseased distal ileal loops (arrow). **B.** Axial half-Fourier RARE image and axial contrast-enhanced, fat-saturated T1-weighted VIBE image (**C**) sequences showing a ileoileal fistula (arrow), with intense contrast enhancement because of their higher vascular flow and hyperemia, indicative of active inflammation. **D.** Axial true FISP image shows also desmoplastic and inflammatory reactions in the mesentery around the fistula, creating a stellar appearance (arrow). Multipplanar MR enterography is useful for a complete evaluation of the fistular tracts.

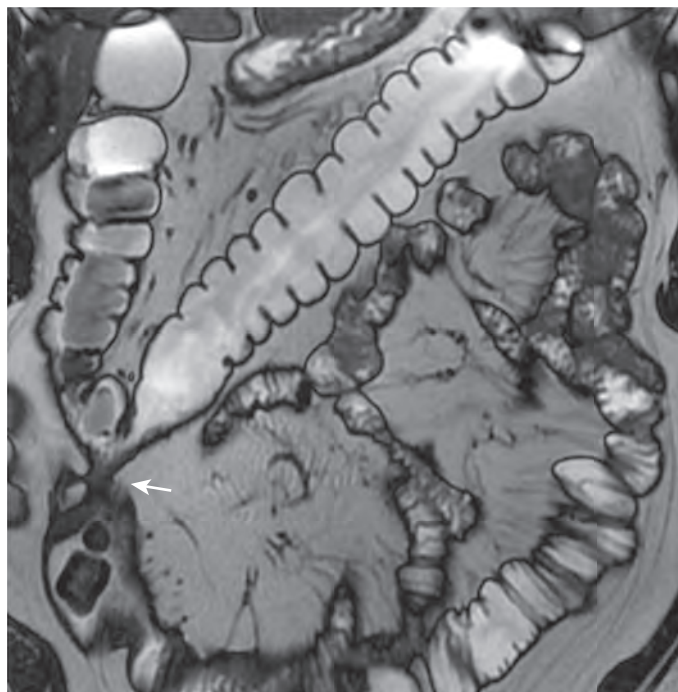


Figure 40-9 Crohn's disease fistula. Coronal true FISP sequence shows fistula tract between the terminal ileal and transverse colon (arrow).

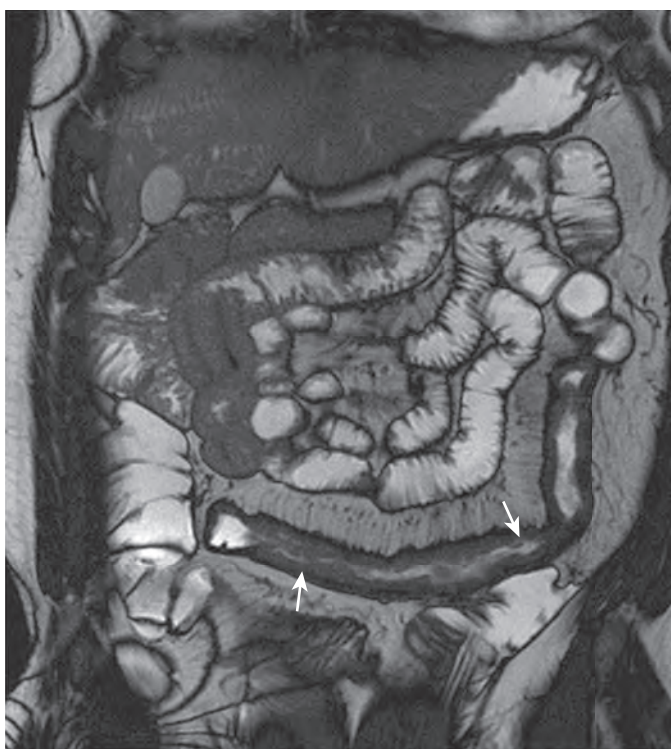


Figure 40-10 Regenerative polyps on MR enterography. Coronal true FISP image shows mucosal atrophy and presence of regenerative polyps (arrows). A minimal decrease in luminal diameter can be seen, but there is no mural edema.

composition—mostly fatty or fibrotic—is best assessed with MR enterography using true FISP sequences.

Abscesses can be recognized by their fluid content and mural hypervascularity, and MR enterography can detect, localize, and indicate the cause of fluid collections (Fig. 40-11). Phlegmons show increased signal intensity as the thickened bowel wall on T2-weighted images. Sinus tracts are often associated with a phlegmon in the adjacent tissue.

SMALL BOWEL NEOPLASMS

The diagnosis of small bowel tumors, particularly early detection and differential diagnosis, is challenging.^{18,75} Although the spatial resolution of MRI is inferior to that of multidetector

computed tomography (MDCT), the main advantages of the former are the combination of good soft tissue contrast, detection of extraenteric abnormalities, and lack of radiation exposure, which allows repeated data acquisition for functional bowel evaluation (Fig. 40-12).⁷⁶⁻⁸³

Enteroclysis provides greater distention of the entire small bowel than enterography in patients suspected of having small bowel neoplasms because small polypoid masses that do not produce obstruction are more difficult to detect using oral contrast material distention.¹⁸

Moreover, MR enteroclysis delineates superficial changes more accurately than MR enterography,^{21,67} and the evaluation of endoluminal abnormalities is particularly important in the detection of early-stage small bowel neoplasms. MR enteroclysis

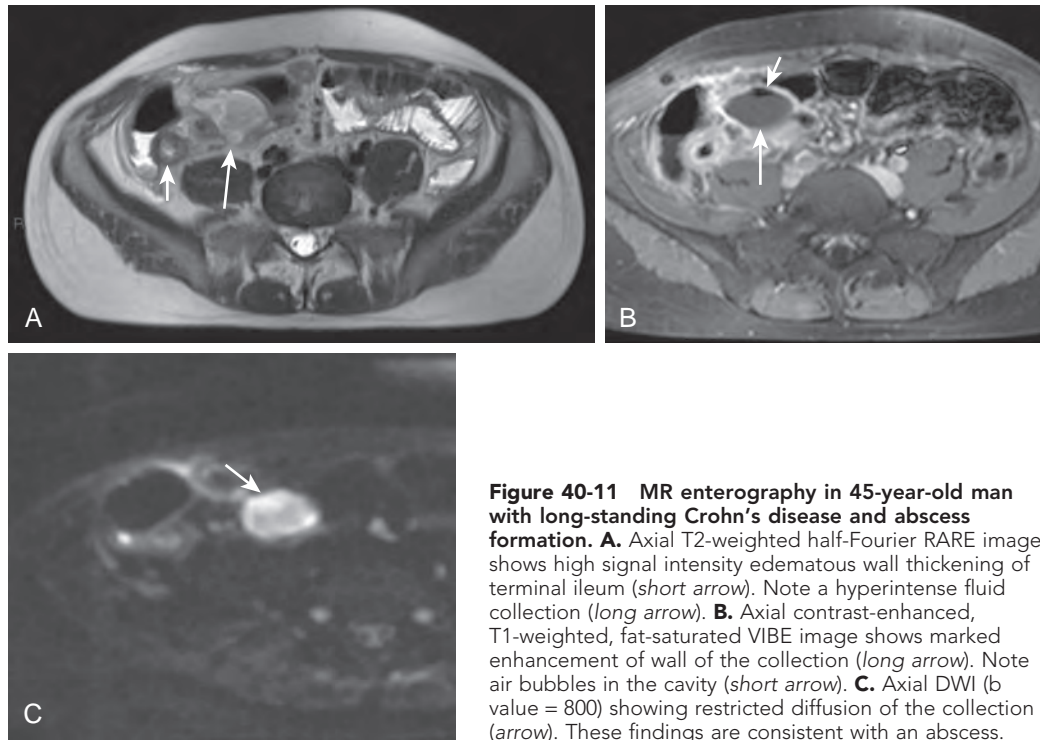


Figure 40-11 MR enterography in 45-year-old man with long-standing Crohn's disease and abscess formation. **A.** Axial T2-weighted half-Fourier RARE image shows high signal intensity edematous wall thickening of terminal ileum (*short arrow*). Note a hyperintense fluid collection (*long arrow*). **B.** Axial contrast-enhanced, T1-weighted, fat-saturated VIBE image shows marked enhancement of wall of the collection (*long arrow*). Note air bubbles in the cavity (*short arrow*). **C.** Axial DWI (b value = 800) showing restricted diffusion of the collection (*arrow*). These findings are consistent with an abscess.

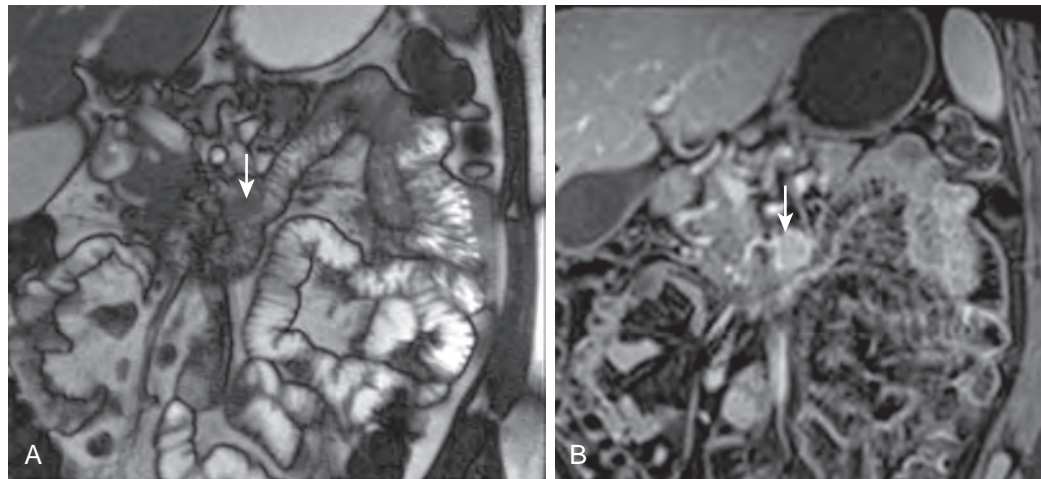


Figure 40-12 MR enterography of jejunal gastrointestinal stromal tumor in 55-year-old patient with unexplained gastrointestinal bleeding. **A.** Coronal true FISP image shows lobulated mass that arises from a jejunal loop, with smooth borders and extraluminal growth (*arrow*), suggesting submucosal origin of the neoplasm. **B.** Coronal contrast-enhanced, fat-saturated, T1-weighted VIBE image shows homogeneous enhancement of the mass (*arrow*).

has yielded a 96.6% accuracy in the detection of small bowel neoplasms.^{67,75}

A recent study has shown that MR enterography is an accurate, well-tolerated, promising imaging modality to diagnose or exclude small bowel tumors in symptomatic patients with negative upper and lower endoscopy findings.⁷⁹ MR enterography can help triage patients to more invasive diagnostic methods.⁸²

MR enterography, which allows improved localization of small bowel polyps in patients with Peutz-Jeghers syndrome, is performed to identify larger lesions that should be resected at double-balloon enteroscopy or surgery.⁸³ It may also be helpful for excluding the presence of lesions in bowel segments not examined at endoscopy or surgery.

MR enteroclysis has proved to be more sensitive than CT enteroclysis for the detection of mucosal lesions of the small bowel⁷⁸ because of improved detection of segments with subtle abnormalities. These findings may be the result of the better soft tissue contrast afforded by MRI, which is required for tissue characterization and the detection of subtle areas of abnormality,⁷⁹⁻⁸¹ and of its functional capabilities. Another advantage of MRI over CT is that the enhanced soft tissue contrast produced by MRI may provide more information regarding the nature of mesenteric small bowel tumors, thereby allowing better characterization of small bowel tumors. In this regard, benign tumors such as hemangiomas are typically strongly hyperintense on T2-weighted MR images, whereas lipomas or tumors with a marked fat content are spontaneously hyperintense on T1-weighted MR scans.⁸¹ With few exceptions (e.g., lymphoma), thickening of a long segment of the small bowel is indicative of a benign condition. When perienteric fat stranding is seen adjacent to the thickened bowel segment, an inflammatory process should be suspected; when the perienteric fat adjacent to the thickened bowel segment has a normal appearance, an acute inflammatory condition is less likely.⁸⁰

CELIAC DISEASE

The sensitivity and specificity of serologic tests (e.g., transtissue glutaminase, antiendomysial antibodies) and of the histologic examination of biopsy specimens from the duodenum are high.

Therefore, MRI is not performed to help detect celiac disease. MRI can, however, provide morphologic information obtained noninvasively, such as fold pattern abnormalities and bowel dilation, as well as extraintestinal findings, such as mesenteric vascular congestion, lymphadenopathy, hyposplenism, and intussusception.⁸⁴

Small bowel MR findings in celiac disease reflect the underlying villous atrophy. A decrease in the number of jejunal folds and an increase in the number of ileal folds results in a jejuno-ileal fold pattern reversal, which is observed in 63% to 68% of patients with untreated celiac disease and may, consequently, be considered to be highly suggestive of celiac disease (Fig. 40-13).^{85,86} By demonstrating intraintestinal and extraintestinal features, MRI may lead to the diagnosis of celiac disease in adults with nonspecific gastrointestinal (GI) symptoms, which may subsequently be confirmed with the aid of jejunal biopsy and serologic tests.⁸⁶

Furthermore, MRI may be used for follow-up and detection of the complications of celiac disease, such as adenocarcinoma and lymphoma. Refractory celiac disease should be suspected in patients who do not respond well to a gluten-free diet. This condition warrants a more aggressive diagnostic pathway because the type II subtype is associated with high mortality caused, above all, by its association with ulcerative jejunitis and enteropathy-associated T-cell lymphoma (EATL).

Transient intussusception is more frequently found in patients with severe celiac disease (i.e., type 2 refractory celiac disease). When the intussusception is less than 3 cm long, occurs in the absence of a lead point tumor, and is not responsible for small bowel obstruction at MR enterography, the findings are consistent with transient, self-limiting small bowel intussusception.

MR enterography can effectively be used to detect lymphoma associated with celiac disease. An association has also been observed between certain mural characteristics and the presence of celiac disease, most notably that of a smooth marginal component, which is commonly observed in diseased segments in patients with celiac disease.⁸⁷ Because the expected findings are unlikely to emerge from within the bowel lumen, MR enterography, as opposed to enteroclysis, should be performed

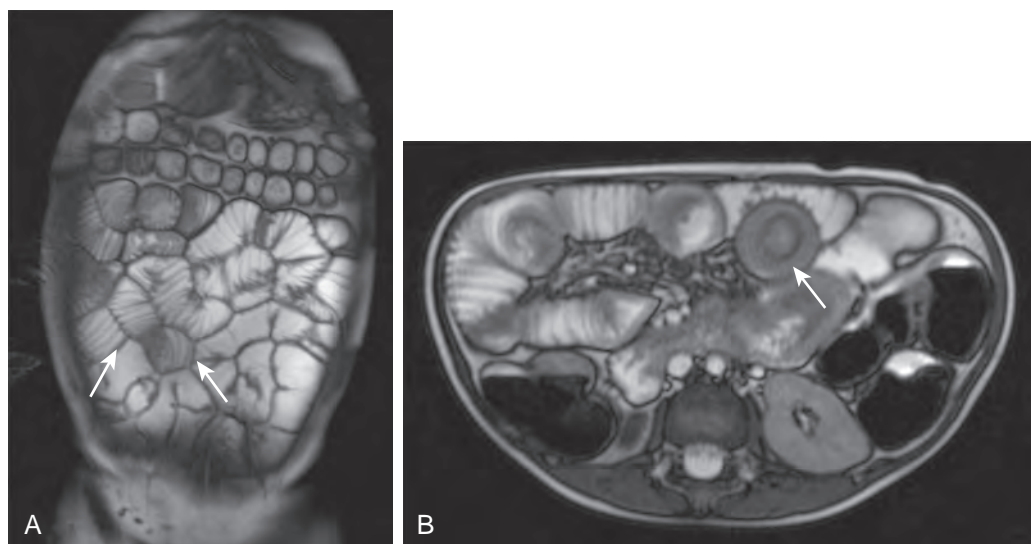


Figure 40-13 MR enterography of celiac disease in 25-year-old woman. **A.** T2-weighted coronal HASTE image shows increased number of folds along ileal loops (arrows), with normal fold pattern in the jejunum. **B.** T2-weighted HASTE axial image shows jejunojejunal intussusception (arrow).

to detect complications in patients with known celiac disease and a poor response to medical therapy, as well as in those with recurrent or persistent symptoms despite gluten withdrawal.

BOWEL ISCHEMIA AND VASCULITIS

Bowel ischemia is a common but complex disorder with various primary causes and diverse clinical and imaging manifestations. Primary causes of insufficient blood flow to the intestine are numerous; these include thromboembolism, non-occlusive conditions (e.g., hypovolemia, hypotension, low cardiac output status, therapy with digoxin, α -adrenergic agonists, or β -receptor blocking agents), bowel obstructions, neoplasms, abdominal inflammatory conditions, chemotherapy- and radiation-induced enteropathies, and vasculitides. Regardless of the primary cause, the imaging findings of bowel ischemia are similar. MR enterography can depict the ischemic bowel segment and may also be helpful in determining the primary cause.⁸³

MR enterographic features of ischemia include thickening of the bowel wall, with or without the target sign, poor contrast enhancement of the bowel wall, and low-grade obstruction. Absence of enhancement or poor enhancement of the bowel wall appears to be the most specific finding. However, in some cases, the ischemic segment shows prolonged enhancement⁸³ because of abnormal perfusion (e.g., delayed return of venous blood with resultant slowing of the arterial supply or arteriospasm). Ischemia appears as marked enhancement of the bowel wall on gadolinium-enhanced T1-weighted fat-suppressed MRI scans, with persistent enhancement in the same region on late venous phase images obtained after gadolinium chelate injection.

INFECTIONS

Infectious processes are rarely detected initially at MR enterography. However, MRI may be useful for visualizing small bowel abnormalities that occur in the setting of chronic infectious diseases such as tuberculosis, as well as for monitoring such abnormalities during treatment.

Infectious diseases often cause a diffuse involvement of the jejunum and ileum, characterized by thickening of all jejunal wall layers with wall edema. The findings resolve completely after therapy (Fig. 40-14). Less common small bowel infections include giardiasis, tuberculosis, nontuberculous mycobacterial infection, and histoplasmosis. Such infections are more commonly seen in the setting of acquired immunodeficiency syndrome (AIDS). The associated MRI findings tend to be non-specific, such as bowel wall thickening, a stratified pattern of bowel enhancement, and enlargement of adjacent lymph nodes. GI tract tuberculosis tends to involve the ileocecal region; the cecum and ascending colon are usually involved to a greater degree than the terminal ileum. Characteristic MRI features of tuberculous enteritis include asymmetric thickening of the ileocecal valve and medial wall of the cecum, with deformation and contraction of the cecum and extension to the terminal ileum. Markedly enlarged adjacent lymph nodes with central areas of necrosis are often seen.^{80,83}

SMALL BOWEL OBSTRUCTION

MRI not only yields anatomic and functional information identical to that provided by conventional enteroclysis in cases of small bowel obstruction (SBO), but it also illustrates extraluminal features more clearly.^{88,89} MRI can also be used to

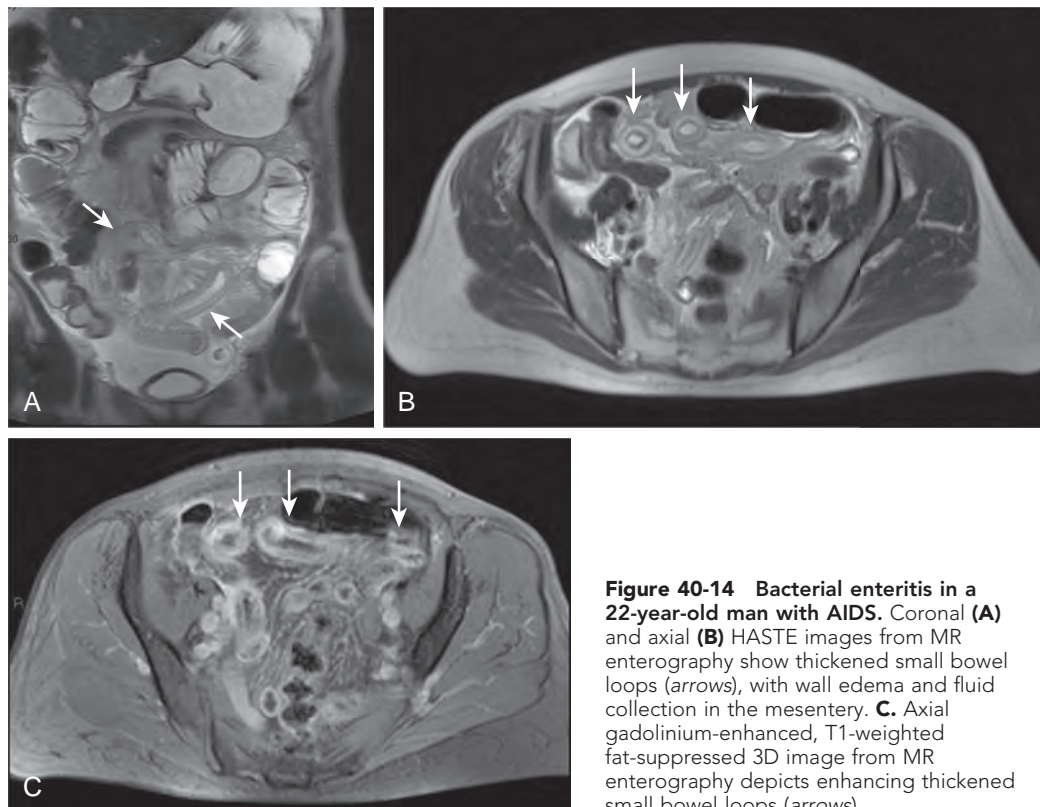


Figure 40-14 Bacterial enteritis in a 22-year-old man with AIDS. Coronal (A) and axial (B) HASTE images from MR enterography show thickened small bowel loops (arrows), with wall edema and fluid collection in the mesentery. C. Axial gadolinium-enhanced, T1-weighted fat-suppressed 3D image from MR enterography depicts enhancing thickened small bowel loops (arrows).

help detect bowel obstructions in the acute setting and differentiate malignant from benign forms in 92% of cases.⁸⁹ The use of MRI to evaluate possible high-grade SBO is useful in children and pregnant patients.

Features indicative of a malignant cause of obstruction include the presence of a mass, localized segmental mural thickening, and moderate or marked peritoneal thickening and enhancement. Benign intestinal obstruction is characterized by more generalized mural thickening and the absence of a true mass (Fig. 40-15).⁹⁰ Low-grade SBO may have numerous causes, although the most common are adhesions. Because MR enteroclysis can be used to monitor small bowel filling in real time without exposing the patient to ionizing radiation, it should be preferred over CT enteroclysis as a means of evaluating a low-grade obstruction.^{91,92}

Summary

MR enterography plays a pivotal role in the evaluation of the small bowel. MR enterography is rapidly becoming a first-line imaging modality for the diagnosis of inflammatory diseases and is gaining clinical acceptance for evaluation of small bowel disorders beyond Crohn's disease.

MR enterography allows evaluation of each bowel segment at multiple time points, which may facilitate differentiation of stricture from peristalsis as well as small bowel function.

MR enterography can be used to monitor response to powerful biologic therapies without the patient incurring

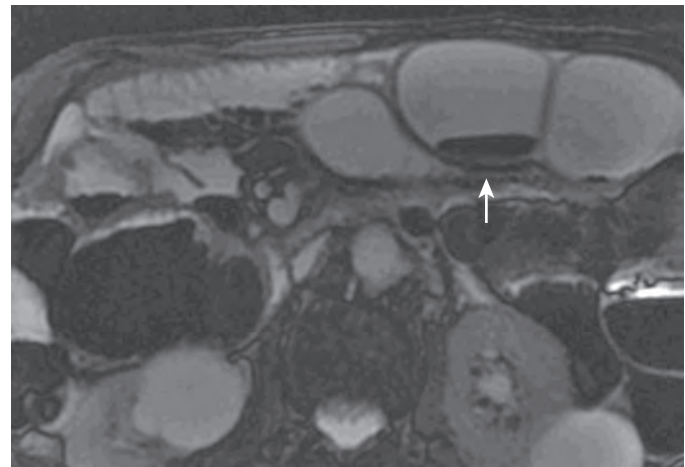


Figure 40-15 MR enterography of small bowel obstruction in 59-year-old patient. Axial half-Fourier RARE image shows a focal transition point at level, a jejunal loop with a so-called beak pattern (arrow), indicative of closed loop obstruction.

additional risk and may be a useful, noninvasive, radiation-free method of screening high-risk patients for subclinical intestinal inflammation. MR modalities, which help detect intraluminal and extraluminal morphologic and functional abnormalities without ionizing radiation, will keep radiology competitive in this era of improving endoscopic technology.

REFERENCES

- Maglinte DD, Sandrasegaran K, Chiorean M, et al: Radiologic investigations complement and add diagnostic information to capsule endoscopy of small bowel diseases. *AJR* 189:306–312, 2007.
- Kelvin FM, Maglinte DD: Enteroclysis or small bowel follow-through in Crohn's diseases? *Gastroenterology* 114:1349–1351, 1998.
- Maglinte DD, Kohli MD, Romano S, Lappas JC: Air (CO₂) double-contrast barium enteroclysis. *Radiology* 252:633–641, 2009.
- Fraquelli M, Colli A, Casazza G, et al: Role of US in detection of Crohn's disease: Meta-analysis. *Radiology* 236:95–101, 2005.
- Fukumoto A, Tanaka S, Imagawa H, et al: Usefulness and limitations of transabdominal ultrasonography for detecting small bowel tumors. *Scand J Gastroenterol* 44:332–338, 2009.
- Martínez MJ, Ripollés T, Paredes JM, et al: Assessment of the extension and the inflammatory activity in Crohn's disease: Comparison of ultrasound and MRI. *Abdom Imaging* 34:141–148, 2009.
- Cronin CG, DeLappe E, Lohan DG, et al: Normal small bowel wall characteristics on MR enterography. *Eur J Radiol* 75:207–211, 2010.
- Elsayes KM, Al-Hawary MM, Jagdish J, et al: CT enterography: Principles, trends, and interpretation of findings. *Radiographics* 30:1955–1970, 2010.
- Horsthuis K, Stokkers PC, Stoker J: Detection of inflammatory bowel disease: Diagnostic performance of cross-sectional imaging modalities. *Abdom Imaging* 33:407–416, 2008.
- Furukawa A, Saotome T, Yamasaki M, et al: Cross-sectional imaging in Crohn's disease. *Radiographics* 24:689–702, 2004.
- Schreyer AG, Seitz J, Feuerbach S, et al: Modern imaging using computer tomography and magnetic resonance imaging for inflammatory bowel disease (IBD). *Inflamm Bowel Dis* 10:45–54, 2004.
- Maglinte DD, Bender GN, Heitkamp DE, et al: Multidetector-row helical CT enteroclysis. *Radiol Clin North Am* 41:249–262, 2003.
- Maglinte DD: Capsule imaging and the role of radiology in the investigation of diseases of the small bowel. *Radiology* 236:763–767, 2005.
- Fidler JL, Guimaraes L, Einstein DM: MR imaging of the small bowel. *Radiographics* 29:1811–1825, 2009.
- Wiarda BM, Kuipers EJ, Heitbrink MA, et al: MR Enteroclysis of inflammatory small bowel diseases. *AJR* 187:522–531, 2006.
- Umschaden HW, Szolar D, Gasser J, et al: Small-bowel disease: Comparison of MR enteroclysis images with conventional enteroclysis and surgical findings. *Radiology* 215:717–725, 2000.
- Gourtsoyiannis NC, Grammatikakis J, Papamastorakis G, et al: Imaging of small intestinal Crohn's disease: Comparison between MR enteroclysis and conventional enteroclysis. *Eur Radiol* 16:1915–1925, 2006.
- Masselli G, Gualdi G: MR imaging of the small bowel. *Radiology* 264:333–348, 2012.
- Prassopoulos P, Papanikolaou N, Grammatikakis J, et al: MR enteroclysis imaging of Crohn's disease. *Radiographics* 21(Spec No):S161–S172, 2001.
- Maglinte DD, Siegelman ES, Kelvin FM: MR enteroclysis: The future of small bowel imaging? *Radiology* 215:639–641, 2000.
- Masselli G, Casciani E, Poletti E, Gualdi G: Comparison of MR enteroclysis with MR enterography and conventional enteroclysis in patients with Crohn's disease. *Eur Radiol* 18:438–447, 2008.
- Negaard A, Paulsen V, Sandvik L, et al: A prospective randomized comparison between two MRI studies of the small bowel in Crohn's disease, the oral contrast method and MR enteroclysis. *Eur Radiol* 17:2294–2301, 2007.
- Schreyer AG, Geissler A, Albrich H, et al: Abdominal MRI after enteroclysis or with oral contrast in patients with suspected or proven Crohn's disease. *Clin Gastroenterol Hepatol* 2:491–497, 2004.
- Laghi A, Paolantonio P, Iafrate F, et al: Oral contrast agents for magnetic resonance imaging of the bowel. *Top Magn Reson Imaging* 13:389–396, 2002.
- Rieber A, Aschoff A, Nüssle K, et al: MRI in the diagnosis of small bowel disease: Use of positive and negative oral contrast media in combination with enteroclysis. *Eur Radiol* 10:1377–1382, 2000.
- Small WC, DeSimone-Macchi D, Parker JR, et al: A multisite phase III study of the safety and efficacy of a new manganese chloride-based gastrointestinal contrast agent for MRI of the abdomen and pelvis. *J Magn Reson Imaging* 10:15–24, 1999.
- Kivelitz D, Gehl HB, Heuck A, et al: Ferric ammonium citrate as a positive bowel contrast agent for MR imaging of the upper abdomen. Safety and diagnostic efficacy. *Acta Radiol* 40:429–435, 1999.
- Karantanas AH, Papanikolaou N, Kalef-Ezra J, et al: Blueberry juice used per os in upper abdominal MR imaging: Composition and initial clinical data. *Eur Radiol* 10:909–913, 2000.

29. Rieber A, Nüssle K, Reinshagen M, et al: MRI of the abdomen with positive oral contrast agents for the diagnosis of inflammatory small bowel disease. *Abdom Imaging* 27:394–399, 2002.
30. Schreyer AG, Gölder S, Scheibl K, et al: Dark lumen magnetic resonance enteroclysis in combination with MRI colonography for whole bowel assessment in patients with Crohn's disease: First clinical experience. *Inflamm Bowel Dis* 11:388–394, 2005.
31. Fidler J: MR imaging of the small bowel. *Radiol Clin North Am* 45:317–331, 2007.
32. Sood RR, Joubert I, Franklin H, et al: Small bowel MRI: Comparison of a polyethylene glycol preparation and water as oral contrast media. *J Magn Reson Imaging* 15:401–408, 2002.
33. Laghi A, Carbone I, Catalano C, et al: Polyethylene glycol solution as an oral contrast agent for MR imaging of the small bowel. *AJR* 177:1333–1334, 2001.
34. Lin ME, Narra V: Developing role of magnetic resonance imaging in Crohn's disease. *Curr Opin Gastroenterol* 24:135–140, 2008.
35. Gore R, Masselli G, Caroline D: Crohn's disease of the small bowel. In Gore R, Levine M, editors: *Textbook of Gastrointestinal Radiology*, ed 3, Philadelphia, 2008, Saunders Elsevier, pp 781–806.
36. Umschaden HW, Gasser J: MR enteroclysis. *Radiol Clin North Am* 41:231–248, 2003.
37. Lauenstein TC, Schneemann H, Vogt FM, et al: Optimization of oral contrast agents for MR imaging of the small bowel. *Radiology* 228:279–283, 2003.
38. Ajaj W, Goyen M, Schneemann H, et al: Oral contrast agents for small bowel distension in MRI: Influence of the osmolarity for small bowel distention. *Eur Radiol* 15:1400–1406, 2005.
39. McKenna DA, Roche CJ, Murphy JMP, McCarthy PA: Polyethylene glycol solution as an oral contrast agent for MRI of the small bowel in a patient population. *Clin Radiol* 61:966–970, 2006.
40. Kuehle CA, Ajaj W, Ladd SC, et al: Hydro-MRI of the small bowel: Effect of contrast volume, timing of contrast administration, and data acquisition on bowel distention. *AJR* 187:W375–W385, 2006.
41. Gourtsoyiannis NC, Papanikolaou N: Magnetic resonance enteroclysis. *Semin Ultrasound CT MR* 26:237–246, 2005.
42. Masselli G, Casciani E, Poletti E, et al: Assessment of Crohn's disease in the small bowel: Prospective comparison of magnetic resonance enteroclysis with conventional enteroclysis. *Eur Radiol* 16:2817–2827, 2006.
43. Zhu J, Xu JR, Gong HX, Zhou Y: Updating magnetic resonance imaging of small bowel: Imaging protocols and clinical indications. *World J Gastroenterol* 14:3403–3409, 2008.
44. Cronin CG, Lohan DG, Browne AM, et al: Magnetic resonance enterography in the evaluation of the small bowel. *Semin Roentgenol* 44:237–243, 2009.
45. Lohan D, Cronin C, Meehan C, et al: MR small bowel enterography: Optimization of imaging timing. *Clin Radiol* 62:804–807, 2007.
46. Korman U, Kurugoglu S, Ogut G: Conventional enteroclysis with complementary MR enteroclysis: A combination of small bowel imaging. *Abdom Imaging* 30:564–575, 2005.
47. Tolan DJ, Greenhalgh R, Zealley IA, et al: MR enterographic manifestations of small bowel Crohn's disease. *Radiographics* 30:367–384, 2010.
48. Cronin CG, Lohan DG, Mhuirheartaigh JN, et al: MRI small bowel follow-through: Prone versus supine patient positioning for best small bowel distention and lesion detection. *AJR* 191:502–506, 2008.
49. Oto A, Kayhan A, Williams JTB, et al: Active Crohn's disease in the small bowel: Evaluation by diffusion weighted imaging and quantitative dynamic contrast enhanced MR imaging. *J Magn Reson Imaging* 33:615–624, 2011.
50. Kiryu S, Dodanuki K, Takao H, et al: Free-breathing diffusion weighted imaging for the assessment of inflammatory activity in Crohn's disease. *J Magn Reson Imaging* 29:880–886, 2009.
51. Oussalah A, Laurent V, Bruot O, et al: Diffusion-weighted magnetic resonance without bowel preparation for detecting colonic inflammation in inflammatory bowel disease. *Gut* 59:1056–1065, 2010.
52. Kitazume Y, Satoh S, Hosoi H, et al: Cine magnetic resonance imaging evaluation of peristalsis of small bowel with longitudinal ulcer in Crohn's disease: Preliminary results. *J Comput Assist Tomogr* 31:876–883, 2007.
53. Odille F, Menys A, Ahmed A, et al: Quantitative assessment of small bowel motility by nonrigid registration of dynamic MR images. *Magn Reson Med* 68:783–793, 2012.
54. Menys A, Atkinson D, Odille F, et al: Quantified terminal ileal motility during MR enterography as a potential biomarker of Crohn's disease activity: A preliminary study. *Eur Radiol* 22:2494–2501, 2012.
55. Lauenstein TC, Ajaj W, Narin B, et al: MR imaging of apparent small bowel perfusion for diagnosing mesenteric ischemia: Feasibility study. *Radiology* 234:569–575, 2005.
56. Patak MA, von Weymarn C, Froehlich JM: Small bowel MR imaging: 1.5T versus 3T. *Magn Reson Imaging Clin N Am* 15:383–393, 2007.
57. Masselli G, Gualdi G: CT and MR enterography in evaluating small bowel diseases: When to use which modality? *Abdom Imaging* 38:249–259, 2013.
58. Wiarda BM, Horsthuis K, Dobben AC, et al: Magnetic resonance imaging of the small bowel with the true FISP sequence: Intra- and interobserver agreement of enteroclysis and imaging without contrast material. *Clin Imaging* 33:267–273, 2009.
59. Leyendecker JR, Bloomfield RS, DiSantis DJ, et al: MR enterography in the management of patients with Crohn's disease. *Radiographics* 29:1827–1846, 2009.
60. Froehlich JM, Waldherr C, Stoupis C, et al: MR motility imaging in Crohn's disease improves lesion detection compared with standard MR imaging. *Eur Radiol* 20:1945–1951, 2010.
61. Maglinte DD, Gourtsoyiannis N, Rex D, et al: Classification of small bowel Crohn's subtypes based on multimodality imaging. *Radiol Clin North Am* 41:285–303, 2003.
62. Zappa M, Stefanescu C, Cazals-Hatem D, et al: Which magnetic resonance imaging findings accurately evaluate inflammation in small bowel Crohn's disease? A retrospective comparison with surgical pathologic analysis. *Inflamm Bowel Dis* 17:984–993, 2011.
63. Rimola J, Rodriguez S, Garcia-Bosch O, et al: Magnetic resonance for assessment of disease activity and severity in ileocolonic Crohn's disease. *Gut* 58:1113–1120, 2009.
64. Sinha R, Murphy P, Sanders S, et al: Diagnostic accuracy of high-resolution MR enterography in Crohn's disease: Comparison with surgical and pathological specimen. *Clin Radiol* 68:917–927, 2013.
65. Gee MS, Harisinghani MG: MRI in patients with inflammatory bowel disease. *J Magn Reson Imaging* 33:527–534, 2011.
66. Maccioni F, Bruni A, Viscido A, et al: MR imaging in patients with Crohn's disease: Value of T2- versus T1-weighted gadolinium enhanced MR sequences with use of an oral superparamagnetic contrast agent. *Radiology* 238:517–530, 2006.
67. Masselli G, Poletti E, Casciani E, et al: Small bowel neoplasms: Prospective evaluation of MR enteroclysis. *Radiology* 251:743–750, 2009.
68. Sharman A, Zealley IA, Greenhalgh R, et al: MRI of small bowel Crohn's disease: Determining the reproducibility of bowel wall gadolinium enhancement measurements. *Eur Radiol* 19:1960–1967, 2009.
69. Fletcher JG, Fidler JL, Bruining DH, Huprich JE: New concepts in intestinal imaging for inflammatory bowel diseases. *Gastroenterology* 140:1795–1806, 2011.
70. Horsthuis K, Bipat S, Bennink RJ, Stoker J: Inflammatory bowel disease diagnosed with US, MR, scintigraphy, and CT: Meta-analysis of prospective studies. *Radiology* 247:64–79, 2008.
71. Harvey RF, Bradshaw JM: A simple index of Crohn's-disease activity. *Lancet* 1:514, 1980.
72. Koh DM, Miao Y, Chinn RJ, et al: MR imaging evaluation of the activity of Crohn's disease. *AJR* 177:1325–1332, 2001.
73. Lee SS, Kim AY, Yang SK, et al: Crohn's disease of the small bowel: Comparison of CT enterography, MR enterography, and small bowel follow-through as diagnostic techniques. *Radiology* 251:751–761, 2009.
74. Siddiki HA, Fidler JL, Fletcher JG, et al: Prospective comparison of state-of-the-art MR enterography and CT enterography in small bowel Crohn's disease. *AJR* 193:113–121, 2009.
75. Van Weyenberg SJ, Meijerink MR, Jacobs MA, et al: MR enteroclysis in the diagnosis of small bowel neoplasms. *Radiology* 254:765–773, 2010.
76. Maglinte DD, Lappas JC, Sandrasegaran K: Malignant tumors of the small bowel. In Gore R, Levine M, editors: *Textbook of Gastrointestinal Radiology*, ed 3, Philadelphia, 2008, Saunders Elsevier, pp 853–869.
77. Masselli G, Casciani E, Poletti E, et al: Magnetic resonance imaging of small bowel neoplasms. *Cancer Imaging* 13:92–99, 2013.
78. Albert JG, Martiny F, Krummnerl A, et al: Diagnosis of small bowel Crohn's disease: A prospective comparison of capsule endoscopy with magnetic resonance imaging and fluoroscopic enteroclysis. *Gut* 54:1721–1727, 2005.
79. Amzallag-Bellenger E, Soyer P, Barbe C, et al: Prospective evaluation of magnetic resonance enterography for the detection of mesenteric small bowel tumours. *Eur Radiol* 23:1901–1910, 2013.
80. Masselli G, Colaiacomo MC, Marcelli G, et al: MRI of the small-bowel: How to differentiate primary neoplasms and mimickers. *Br J Radiol* 85:824–837, 2012.
81. Soyer P, Boudiaf M, Fishman EK, et al: Imaging of malignant neoplasms of the mesenteric small bowel: New trends and perspectives. *Crit Rev Oncol Hematol* 80:10–30, 2011.
82. Amzallag-Bellenger E, Oudjit A, Ruiz A, et al: Effectiveness of MR enterography for the assessment of small bowel diseases beyond Crohn's disease. *Radiographics* 32:1423–1444, 2012.

83. Caspari R, von Falkenhausen M, Krautmacher C, et al: Comparison of capsule endoscopy and magnetic resonance imaging for the detection of polyps of the small intestine in patients with familial adenomatous polyposis or with Peutz-Jeghers' syndrome. *Endoscopy* 36:1054–1059, 2004.
84. Masselli G, Picarelli A, Di Tola M, et al: Celiac disease: Evaluation with dynamic contrast-enhanced MR imaging. *Radiology* 256:783–790, 2010.
85. Van Weyenberg SJ, Meijerink MR, Jacobs MA, et al: MR enteroclysis in refractory celiac disease: Proposal and validation of a severity scoring system. *Radiology* 259:151–161, 2011.
86. Tomei E, Semelka RC, Braga L, et al: Adult celiac disease: What is the role of MRI? *J Magn Reson Imaging* 24:625–629, 2006.
87. Lohan DG, Alhajeri AN, Cronin CG, et al: MR enterography of small bowel lymphoma: Potential for suggestion of histologic subtype and the presence of underlying celiac disease. *AJR* 190: 287–293, 2008.
88. Van Weyenberg SJ, Van Waesberghe JH, Ell C, Pohl J: Enteroscopy and its relationship to radiological small bowel imaging. *Gastrointest Endosc Clin N Am* 19:389–407, 2009.
89. Beall DP, Fortman BJ, Lawler BC, Regan F: Imaging bowel obstruction: A comparison between fast magnetic resonance imaging and helical computed tomography. *Clin Radiol* 57: 719–724, 2002.
90. Low RN, Chen SC, Barone R: Distinguishing benign from malignant bowel obstruction in patients with malignancy: Findings at MR imaging. *Radiology* 228:157–165, 2003.
91. Lienemann A, Sprenger D, Steitz HO, et al: Detection and mapping of intraabdominal adhesions by using functional cine MR imaging: Preliminary results. *Radiology* 217:421–425, 2000.
92. Costa-Silva L, Brandão AC: MR enterography for the assessment of small bowel diseases. *Magn Reson Imaging Clin N Am* 21:365–383, 2013.

Crohn's Disease of the Small Bowel

MARK E. BAKER | RICHARD M. GORE

CHAPTER OUTLINE

Clinical Considerations

Classification and Therapy

Diagnostic Tools

Ileocolonoscopy and Video Capsule Endoscopy

Barium Contrast Examinations

Ultrasound

Magnetic Resonance Imaging

Computed Tomography

Nomenclature for CT and MR Enterography Findings

Computed Tomography and Magnetic Resonance

Enterography Findings of Small Bowel Crohn's Disease

Assessment of Disease Activity

Additional Imaging Considerations

Positron Emission Tomography, Positron Emission

Tomography/Computed Tomography, and Positron

Emission Tomography/Magnetic Resonance Imaging

Crohn's Jejunoileitis

Crohn's Associated Adenocarcinoma, Neuroendocrine Tumor, and Lymphoma

Clinical Considerations

Crohn's disease is an idiopathic inflammatory disease that can affect any part of the gastrointestinal (GI) tract from the mouth to the anus. Patients with this disease have a genetic predilection to an abnormal immunologic response to environmental factors, including food, and gut flora leading to a chronic inflammatory response. The small bowel is the major site of involvement. With the exception of malignant neoplasms, Crohn's disease can be the most devastating disease to involve the GI tract. Its prevalence has increased, mostly in younger age groups, with a peak age between 15 and 25 years.¹⁻³ It has a worldwide distribution but is most common in northern Europe, North America, and Japan.⁴ Four studies have shown a bimodal distribution, with the first peak in the second or third decade of life and the second, smaller peak in the sixth or seventh decade. However, four other studies have shown a unimodal distribution, peaking in the second or third decade, and decreasing thereafter.⁵ The colonic predominance in older adults has led some to speculate that the second peak incidence in this cohort is caused by ischemia or diverticulitis. Both genders are equally affected, although some studies have shown a slight female predominance.⁵ A familial tendency has frequently been described.¹⁻³

The small bowel is commonly involved by Crohn's disease, with the terminal ileum the most common location. In a review

combining multiple population-based studies on the natural history of adult Crohn's disease, approximately one third of patients had ileitis, one third had colitis, and one third had ileocolitis.⁶ Isolated perianal disease occurs in 2% to 3%,⁷ but perianal or rectal fistulae are common in colonic or rectal disease (10% to 37%).⁶ Upper GI tract involvement is being recognized with increasing frequency but almost invariably occurs with small bowel or colonic disease. The gastric and duodenal manifestations of Crohn's disease are discussed in Chapter 30, and the colonic features of this disease are discussed in Chapter 58. Although the focus of this chapter is on Crohn's disease of the small bowel, there are differences in presentation from colonic disease. Patients with colonic Crohn's disease are more likely to present with blood loss, perianal disease, toxic colitis, and extraintestinal complications. Crohn's disease in the small bowel has a slightly better prognosis, although there are more likely to be complications such as abscesses, fistulae, and obstruction. Abdominal pain, mild diarrhea, weight loss, and pyrexia are common clinical findings. Other patients may present with a right lower quadrant mass, representing the diseased ileum or cecum. Delays of 3 to 4 years have been reported between the onset of often subtle symptoms and the diagnosis of Crohn's disease in the small bowel.⁷

Many factors contribute to the development of diarrhea in patients with Crohn's disease. An inflamed bowel mucosa causes increased secretion of fluid and electrolytes. Extensive terminal ileal disease or resection impairs bile salt reabsorption, leading to the malabsorption of fat and fat-soluble vitamins. Bacterial overgrowth secondary to strictures, fistulae to the colon, adhesions, aneurysmal dilation, or bypassed loops can also cause diarrhea. The combination of decreased food absorption and intermittent obstruction may lead to significant weight loss in these patients.^{7,8}

Classification and Therapy

Over the years, attempts have been made to classify Crohn's disease anatomically, clinically, and operatively. This has evolved from the International Working Party in 1991 to the Vienna classification in 1998, and finally to the Montreal revision of the Vienna classification in 2005.⁹

The Montreal revision classifies the disease into age of diagnosis, location, and disease behavior. Disease behavior is classified into nonstricturing, nonpenetrating (uncomplicated, active inflammatory alone), stricturing, and penetrating, with the addition of perianal disease as a modifier. It is the behavior subcategory that is of interest in regard to the radiographic manifestations. As a result of these morphologic subtypes, radiologists and even gastroenterologists have concluded that they are separate entities. The problem with this discrete approach is that the complex relationship between active inflammatory and stricturing disease and stricturing and penetrating disease has been forgotten or avoided. Crohn's disease

is a progressive process, starting with acute inflammation. It may be stopped or retarded with therapy; there may be mucosal healing. However, when it progresses, it often progresses to the fibrostenotic phase, with stricture formation. Active inflammation commonly coexists in the presence of stricture formation.^{10,11} There is also strong pathologic and clinical evidence that fistulae form in the face of fibrostenosis. Two pathologic series have shown that fistula formation without stricturing disease is uncommon to rare (4% to 7% of the time).^{12,13} Thus, if there is no stricture, penetrating disease (sinus tracts, fistulae, abscess, or free perforation) will be very unlikely. Because of the potential progression of disease from acute inflammation to fibrostenosis and then fistulization, it is important for the radiologist to think more broadly than using the Montreal and Vienna classifications, especially with computed tomography (CT) and magnetic resonance (MR) enterography. We are thus beginning to use the following terms—*active inflammatory disease, mixed active inflammatory and fibrostenotic disease, fibrostenotic disease, and inactive or quiescent disease with the addition of penetrating disease* (generally in the presence of mixed disease) based on radiographic findings (see later, “[Nomenclature for Computed Tomography and Magnetic Resonance Enterography Findings](#)”).

Medications useful for the active inflammatory subtype of Crohn's disease include 5-aminosalicylate-based drugs, corticosteroid-based drugs, and antibiotics (e.g., metronidazole, ciprofloxacin). Second-line medications are immunosuppressive agents such as azathioprine, 6-mercaptopurine, and methotrexate.^{14,15} Targeted monoclonal antibodies such as infliximab, which targets human tumor necrosis factor- β , and natalizumab, which targets β_4 integrin, a leukocyte adhesion molecule, have become available.¹⁵ These drugs are very expensive and have complications. This arsenal of medications has prompted the need for noninvasive, reproducible, and objective measurements of Crohn's disease activity, especially the distinction between active inflammatory disease from mixed fibrostenotic and active inflammatory disease with or without penetrating disease. Some centers of excellence would argue that penetrating disease can only be treated with surgery rather than medical therapy.

The fistulizing-perforating type requires antibiotics initially to treat the active infection. Monoclonal antibodies have proven effective in patients with perianal disease and enterocutaneous fistulae. However, internal fistulae (enteroenteric, enterocolic, enterovesicular, and complex internal fistulae) are much more difficult to treat medically.¹⁶ Percutaneous abscess drainage is a suitable means of treating Crohn's disease-related abscesses. The fibrostenotic subtype of Crohn's disease may need strictureplasty or bowel resection because small bowel obstruction is the major clinical manifestation of this type. The quiescent or reparative type of Crohn's disease may require maintenance medication.¹⁷

Diagnostic Tools

There are many examinations available for diagnosing, staging, and following Crohn's disease of the small bowel. These include ileocolonoscopy with direct inspection and biopsy of the terminal ileum, push enteroscopy to examine the proximal and mid small bowel, video capsule endoscopy, conventional small bowel follow-through, conventional enteroclysis, CT with (CTE) or without enterography or enteroclysis, MR enterography (MRE)

or enteroclysis, ultrasonography, and lately positron emission tomography (PET), PET/CT, and PET/MRI.^{18,19} These studies are used to do the following:

- Demonstrate the early changes of Crohn's disease.
- Depict the full extent of involvement and the possible presence of skip lesions if surgery is contemplated.
- Determine the cause of any clinical deterioration in previously stable patients with Crohn's disease.
- Distinguish between spasm (active inflammatory disease), mixed active and fibrostenotic disease, and fibrostenotic disease (stricture formation); increasingly used to dictate medical versus surgical therapy, especially with MR enterography.
- Investigate postoperative complications of Crohn's disease.
- Definitively rule out the presence of Crohn's disease in the small bowel, especially in patients with an indeterminate colitis.

ILEOCOLONOSCOPY AND VIDEO CAPSULE ENDOSCOPY

Ileocolonoscopy (Figs. 41-1 and 41-2) allows the accurate diagnosis of Crohn's disease of the colon and terminal ileum. It provides assessment of disease activity and consequences of inflammation visually and with guided biopsy, including strictures, mass lesions, bleeding, and the development of dysplasia or malignancy. In general, this examination is considered the gold standard for diagnosis.

Video capsule endoscopy is a new means of directly inspecting the entire length of the small bowel. It uses an ingested sealed capsule that measures 27 mm in length and 11 mm in width. The camera within the capsule, which also contains a light source, takes two photographs at eight times magnification every second and runs on electricity supplied by onboard batteries. During the typical small bowel examination, an average of about 55,000 photographs are taken. The capsule is propelled through the GI tract by peristalsis. The images are transmitted in radiofrequency signals to and stored on a recorder device placed in a belt worn by the patient throughout the day of the procedure. The capsule is disposable and is not recovered after the test. At the end of the study, the recorder device is retrieved and the images obtained are downloaded onto a computer. The computer generates a video that is then reviewed for relevant pathology.²⁰

Early studies have shown video capsule endoscopy (see Fig. 41-2B) to be the most sensitive means of diagnosing nonstricturing Crohn's disease.²¹⁻²⁶ However, the presence of a potentially obstructing stricture is a major contraindication for the use of capsule. Furthermore, many if not most of the studies that have shown the high sensitivity have not had corroborating reference standards. The studies that compared capsule with CT enterography-enteroclysis and/or MR enterography-enteroclysis have only shown that capsule is superior for disease more proximal to the terminal ileum, with no significant difference between the imaging studies and capsule in the terminal ileum.²⁷⁻²⁹ The only reference standard used to demonstrate the increased diagnostic efficacy of capsule over imaging has been the capsule findings. Even a recent four-center Danish trial, which showed that capsule is superior to CTE or MRE, only had the terminal ileum as a reference standard (5 of 93 had surgery); also, in this trial, a capsule examination was only performed after the enterography showed no stricture.³⁰ In this study, the

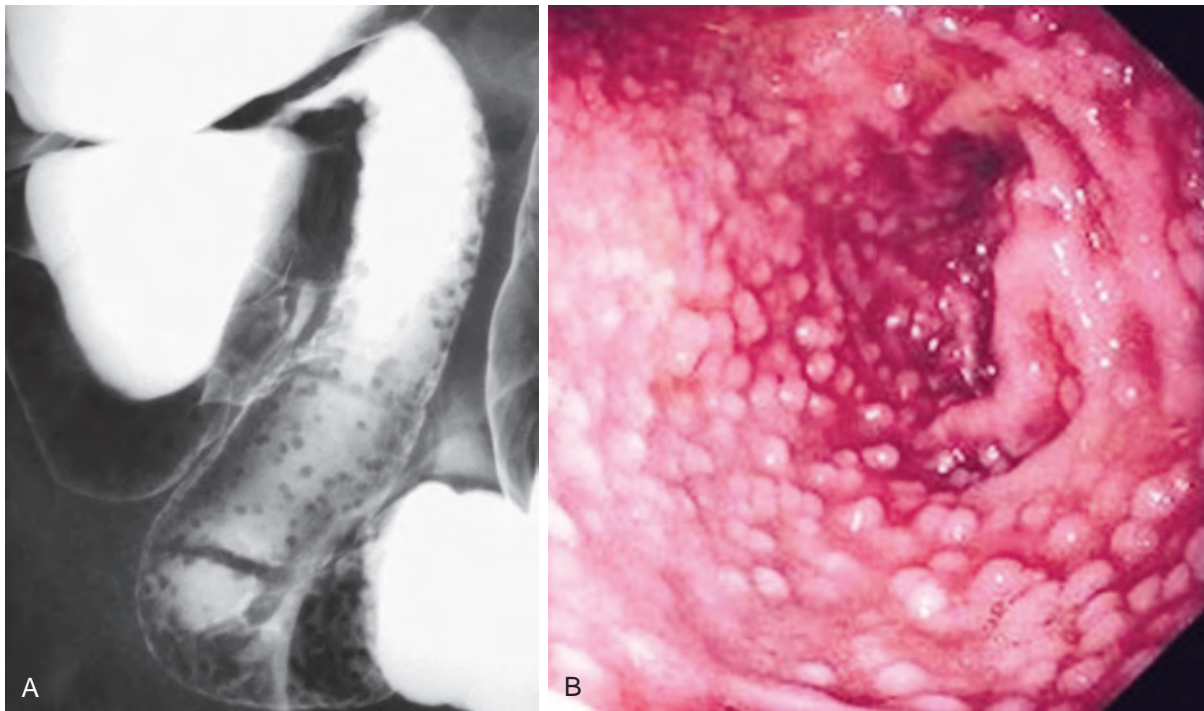


Figure 41-1 Early active inflammatory Crohn's diseases: Enlarged lymphoid follicles. **A.** Double-contrast barium enema examination with reflux into the terminal ileum shows prominent lymphoid follicles. This is a nonspecific finding that can be found in a variety of forms of infectious, inflammatory, immunologic, and neoplastic disease. **B.** Image from an ileocolonoscopy study shows multiple lymphoid follicles in this patient with early Crohn's disease.

superiority of capsule was for proximal disease, not the terminal ileum.

Capsule is well known to be highly sensitive but relatively low in specificity. In a comparison of standard small bowel examination, ileocolonoscopy, CTE, and capsule performed in Crohn's patients at the Mayo Clinic, the specificity of capsule was only 53% (sensitivity, 83%). In this study, the sensitivity and specificity of CTE and ileocolonoscopy were 82% and 89% and 74% and 100%, respectively.³¹

BARIUM CONTRAST EXAMINATIONS

In this new millennium, the barium–fluoroscopic barium examination of the small bowel for Crohn's disease has been largely supplanted by CTE and MRE. However, there are patients who have medical conditions that preclude the use of CTE or MRE with contrast enhancement (e.g., severe chronic kidney disease) who have known or suspected Crohn's disease. These patients must be evaluated with a barium examination using fluoroscopy.

There are two methods of examining the small bowel with barium using fluoroscopy—the standard small bowel series and enteroclysis. For accuracy, both require meticulous fluoroscopic technique using patient rotation and graded compression with a lead glove, inflatable paddle, or wooden spoon. Enteroclysis is available only in certain centers and requires intubation of the proximal small bowel via the nose or mouth. This is uncomfortable for most patients, and conscious sedation is used in some centers to improve patient tolerance.³²

As a general rule, the key radiographic finding in Crohn's disease is asymmetry. Radiologists usually think of asymmetry as skip disease in the z direction (see Figs. 41-1A, Fig. 41-2C,

and Fig. 41-6). However, the asymmetry of Crohn's is also in the xy direction (see Fig 41-2C). Crohn's disease always affects the mesenteric more than the antimesenteric border. The normal undulating fold pattern on the mesenteric border will become ulcerated, effaced, flattened, and foreshortened, whereas there is relative sparing of the antimesenteric border, giving rise to the pseudodiverticulosis sometimes associated with the disease (see Fig. 41-5). This classic feature is better portrayed with barium examinations, but can be seen with CT or MR enterography.

Marshak's ten principles of Crohn's disease are worth remembering because they assist the radiologist in detecting and characterizing disease.³³ Initially presented in 1973, these principles have generally held very true. The principles most helpful for the radiologist include principle 3 (the string sign is the most pathognomonic barium manifestation and does not represent fibrosis but spasm secondary to ulceration), principle 8 (following surgery, recurrence is common), and principle 9 (look for recurrence at anastomotic and stricture-plasty sites).

Early Active Radiographic Inflammatory Disease

The pathologic and radiologic findings correlate well in early Crohn's disease.³⁴⁻⁴⁰ The earliest histologic changes consist of hyperplasia of lymphoid tissue (see Fig. 41-1A) and obstructive lymphedema in the submucosa. Because the submucosa extends into the core of mucosal folds, the folds may thicken at this stage in a smooth, symmetric manner. However, in general, symmetric fold thickening in Crohn's disease is an uncommon finding, and is identified only early in the disease. When the disease advances, the folds become much more asymmetrically thickened, giving a macronodular polygonal appearance; the

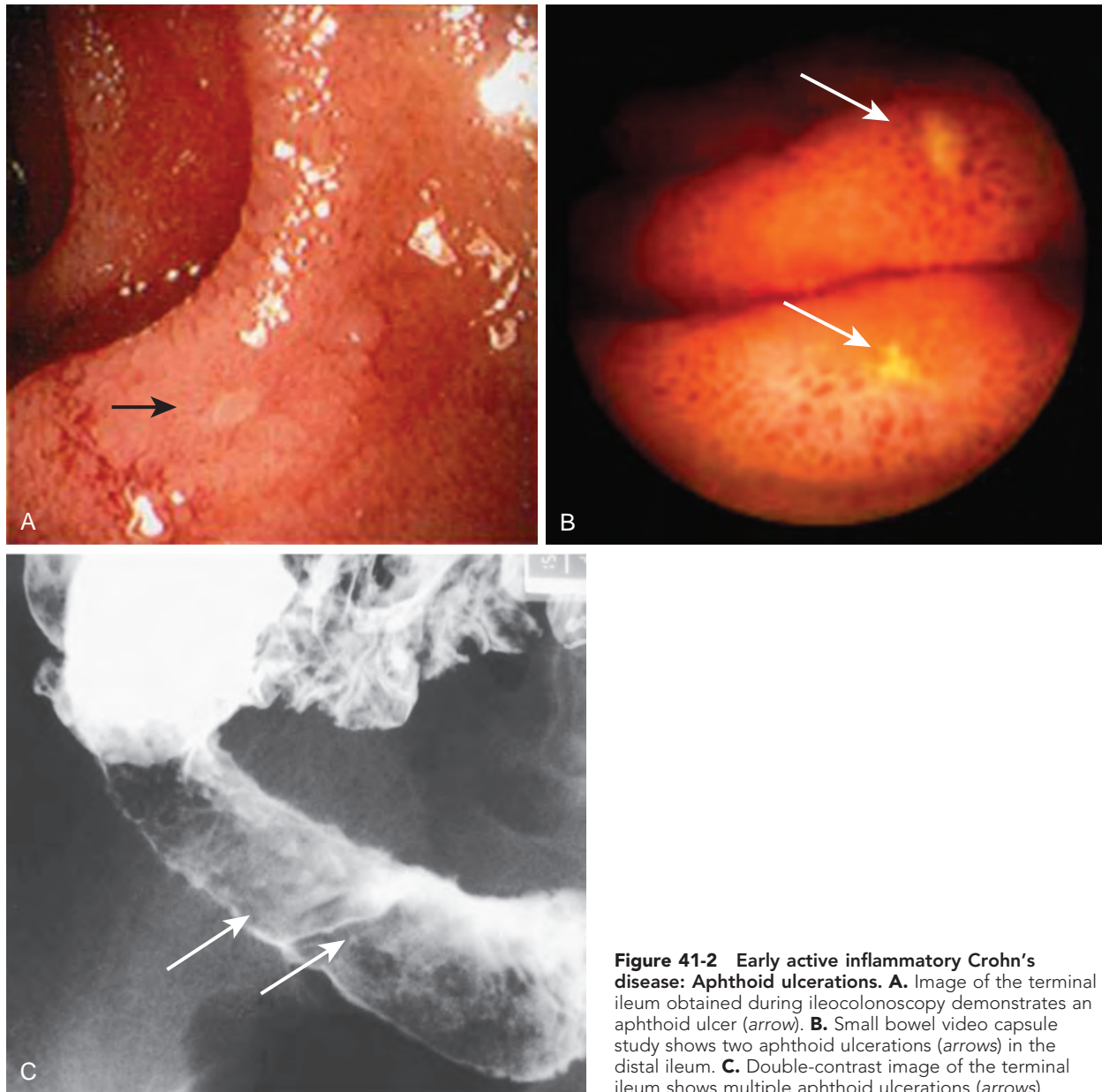


Figure 41-2 Early active inflammatory Crohn's disease: Aphthoid ulcerations. **A.** Image of the terminal ileum obtained during ileocolonoscopy demonstrates an aphthoid ulcer (arrow). **B.** Small bowel video capsule study shows two aphthoid ulcerations (arrows) in the distal ileum. **C.** Double-contrast image of the terminal ileum shows multiple aphthoid ulcerations (arrows).

macronodules vary in size (at this point, the main differential is lymphoma; see later).

Hyperplasia of lymphoid follicles (see Fig. 41-1) in the lamina propria can be associated with shallow, 1- to 3-mm mucosal erosions surrounded by a small halo of edema, also known as aphthoid ulcers (see Fig. 41-2).⁴¹⁻⁴⁴

Intermediate Radiographic Active Inflammatory Disease

As the disease gradually extends transmurally, further changes take place in the mucosa and submucosa. Progressive submucosal edema may cause the base of the folds to widen until some folds are partially or completely obliterated or effaced, especially on the mesenteric side. This process is similar to the thumbprinting that occurs in patients with bowel ischemia. In patients with ischemia, however, the fold abnormalities change

over a period of days to weeks, whereas in patients with Crohn's disease, the fold abnormalities persist and are usually associated with changes of more advanced Crohn's disease elsewhere in the small bowel. The mucosal inflammatory infiltrate tends to vary focally in intensity. This infiltrate, together with patchy submucosal fibrosis, leads to a distortion and interruption of folds.⁴¹⁻⁴⁵ The fold pattern in this stage can be described as macronodular (>1 cm), with the nodules asymmetric in size, location, and appearance.

Some aphthoid ulcers may enlarge and deepen, producing a stellate or rose thorn appearance. Other aphthoid ulcers may fuse with adjacent ulcers, producing crescentic or linear shapes. A typical finding is that of a long linear ulcer on the mesenteric border, which may be accentuated by a parallel radiolucency caused by fusion of thickened, transaxially oriented folds. The mesenteric border ulcer is associated with thickening, sclerosis,

and retraction of the adjacent mesentery and of the straightened mesenteric border of the involved bowel. At the same time, the unaffected, or relatively unaffected, redundant antimesenteric border becomes pleated, scalloped, or sacculated, giving a pseudodiverticular-like pattern (distinct from the pseudodiverticular pattern present in scleroderma, in which the outpouchings are much closer together because of the foreshortening of the bowel).

An inflammatory cellular infiltrate with focally pronounced edema and granulation tissue can give rise to localized mucosal elevations or inflammatory polyps. These lesions are common in the colon but infrequent in the small bowel. Inflammatory pseudopolyps usually occur in small numbers in an area of mucosa that is denuded of folds. Occasionally, a bowel segment contains many inflammatory pseudopolyps (≤ 1 cm in

diameter), separated from one another by curving lines of barium occupying the crevices between the elevations. When seen in profile, the polyps appear as notches demarcated by protrusions of barium. The diameter of these bowel segments is not reduced. This is called the nodular pattern of Crohn's disease to underscore its essential difference from the ulceronodular, or cobblestone, pattern of advanced, fissuring, ulcer-related Crohn's disease (Fig. 41-3).⁴¹⁻⁴⁵

Advanced Radiographic Active Inflammatory Disease

In advanced Crohn's disease, the process has extended transmurally to the serosa and beyond. Deep linear clefts of ulceration, or fissures, are typical of this stage of the disease (Fig. 41-4). Islands of surviving mucosa surrounded by extensive ulceration

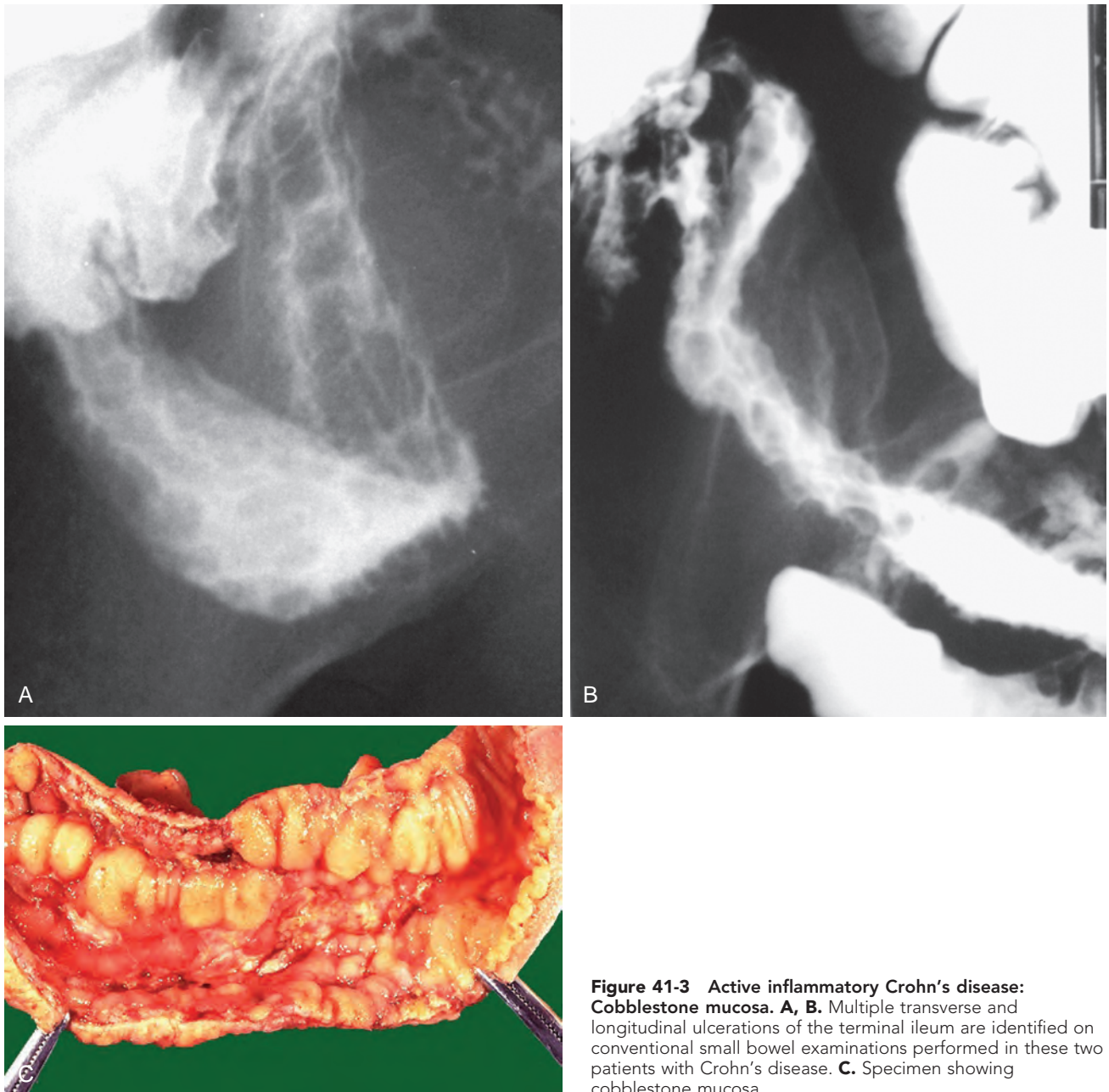


Figure 41-3 Active inflammatory Crohn's disease: Cobblestone mucosa. A, B. Multiple transverse and longitudinal ulcerations of the terminal ileum are identified on conventional small bowel examinations performed in these two patients with Crohn's disease. C. Specimen showing cobblestone mucosa.

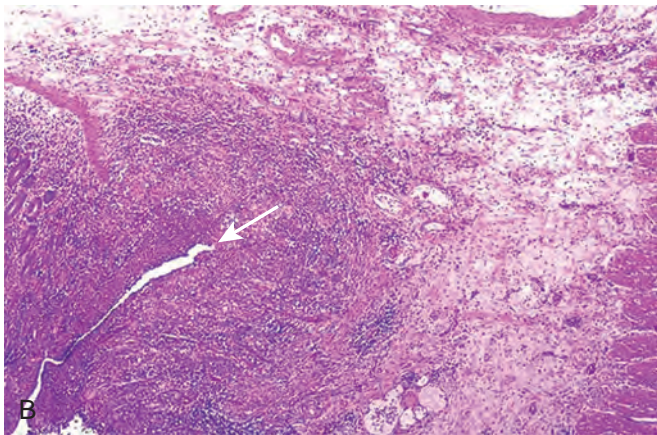
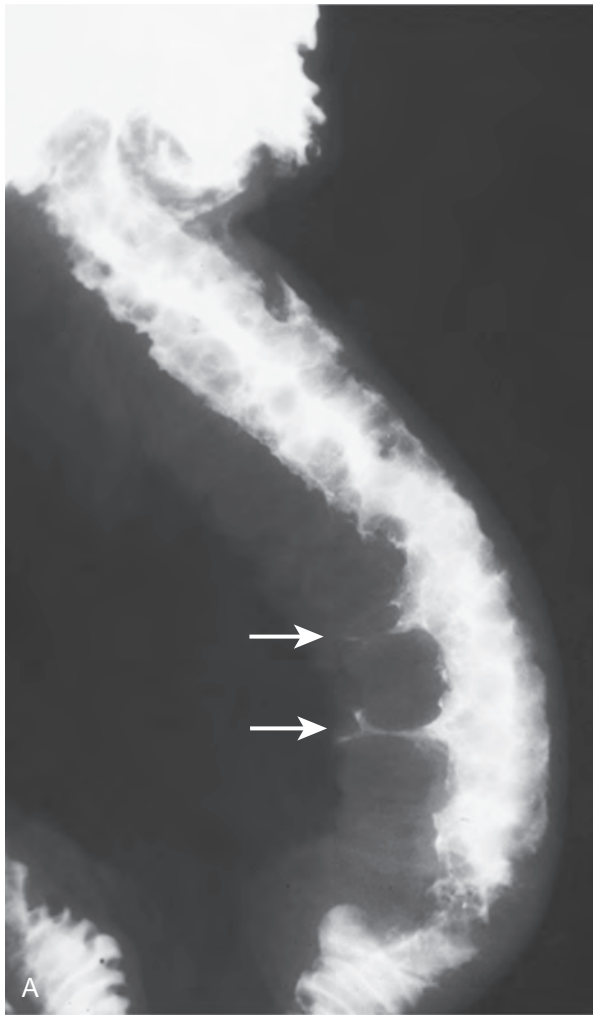


Figure 41-4 Deep ulcerations of fistulizing-perforating Crohn's disease. **A.** Specimen radiograph shows two deep ulcerations (arrows) penetrating into the fat of the small bowel mesentery. **B.** A fissuring ulcer (arrow) is identified on this pathologic image.

give the appearance of elevations above the ulcerated background. These islands of mucosa are therefore known as pseudopolyps. The deep fissures characteristic of this advanced stage may be manifested by a combination of axial and transaxial fissuring, which separates the pseudopolyps from one another. This finding is always associated with luminal narrowing; it is

referred to as the ulceronodular or cobblestone pattern of advanced Crohn's disease (see Fig. 41-3).⁴¹⁻⁴⁵ This pattern should not be confused with the nodular pattern of less advanced Crohn's disease.

Changes associated with linear mesenteric ulceration advance in a caudad direction as the disease progresses. Antimesenteric redundancy of the opposite bowel wall gradually disappears as it is incorporated in the transaxial extension of ulcerated Crohn's disease (Fig. 41-5). The bowel wall is now thickened by a combination of fibrosis and inflammatory infiltrate. Another feature of transmural disease is the so-called fat wrapping that occurs as the hypertrophied subperitoneum is tethered toward the bowel wall by mesenteric perivascular fibrosis.⁴⁵

Quiescent or Inactive Disease

Very little has been written about the barium findings of quiescent disease. Presumably, the mucosa is normal in these patients. Thus, the fold pattern should be normal.

Fibrostenotic Disease

The strictures of small bowel Crohn's disease (Figs. 41-6 and 41-7) are caused by collagen deposition, predominantly in the submucosa. It is important to differentiate fibrostenotic strictures from the luminal narrowing that can result from spasm. The classic string sign of Crohn's is primarily caused by spasm in segments of active inflammatory disease. Fluoroscopically, the lumen, coated with barium, appears initially narrowed, with no or only mild upstream dilation. Then, when a peristaltic wave propels the barium through the lumen, the lumen expands to a near-normal caliber. A fibrostenotic predominant stricture will not change its caliber with peristalsis, and the upstream, nonaffected lumen will be dilated, regardless of the state of peristalsis. It should be noted that in many if not most cases of the string sign, the lumen of the affected bowel never fully distends, and there is often some degree of upstream ballooning or dilation during peristalsis. This suggests that more than spasm is occurring in the affected segment (Crohn's is a progressive process; at sites of active disease, there is often active proliferation of smooth muscle and collagen that restricts compliance).

These strictures are an important cause of small bowel obstruction, often necessitating surgery. Strictures or stricture-like findings are reported in 21% of patients with small bowel Crohn's disease.^{7,44} MDCT, magnetic resonance imaging (MRI), CT enterography, CT enteroclysis, and MR enteroclysis are valuable techniques for differentiating fibrotic strictures from lumen narrowing by spasm or active ulcerated stenotic disease. It is important to note that active inflammation is present in many, if not most, fibrostenotic strictures (see later). Obstruction by a fibrous stricture may require surgery; whenever possible, it should consist of strictureplasty to avoid bowel resection.⁴⁵ Some patients with Crohn's disease may develop high-grade small bowel obstruction; this complication is reliably documented by CT and MR.

Other patients with Crohn's disease may have multiple strictures, representing advanced skip lesions. Stasis related to strictures can be associated with bacterial overgrowth. This is especially true in patients who develop aneurysmal dilation of the small bowel (see Fig. 41-7), usually between two strictures. Strictures are generally well shown by barium study.

Resection of bowel in patients with Crohn's disease is followed by a high frequency (85%) of disease recurrence.

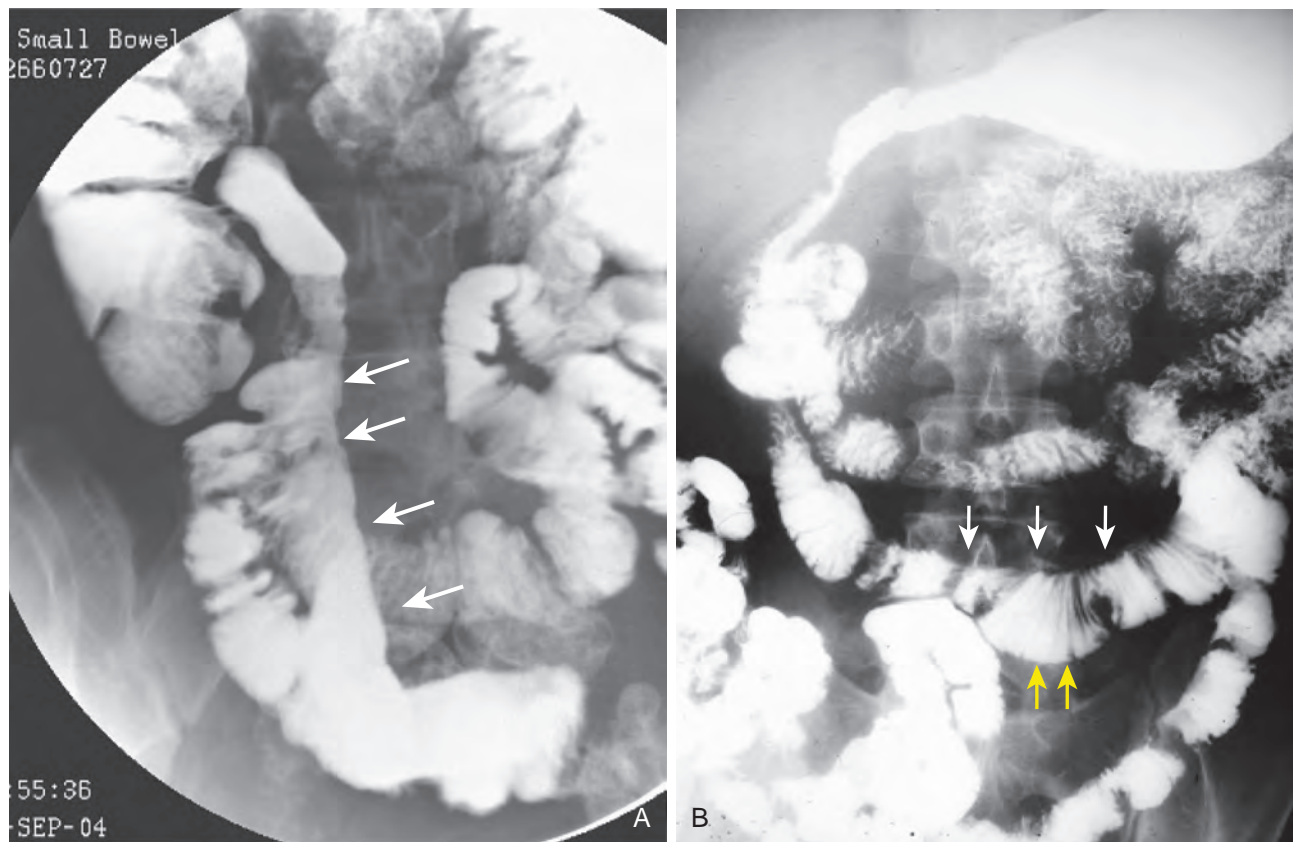


Figure 41-5 Sacculations in Crohn's disease. **A.** There is straightening of the mesenteric border (arrows) of the terminal ileum because of fibrofatty proliferation of the mesentery. **B.** Multiple segments of small bowel show straightening and shortening of the mesenteric border (white arrows) with a redundant antimesenteric border forming sacculations (yellow arrows).

Recurrent inflammation has been detected within 8 days of surgery, provided that exposure to the fecal stream had been reestablished. Multiple resections have made Crohn's disease of the small bowel a major cause of the short bowel syndrome.^{7,44}

Fistulizing or Penetrating Disease

Fistulizing or penetrating disease is manifest by sinus tracts, fistulae, abscess, and uncommonly free perforation. Abscesses develop in some 20% of patients with Crohn's disease, and most can be treated with percutaneous drainage.⁴ Inflammatory lesions may remain closely related to a diseased segment of bowel or may extend beyond the bowel, occasionally into the psoas muscle. In some cases, barium may enter an abscess cavity, a collection of tracts, or multiple small spaces within an inflammatory mass. However, CT, ultrasonography, and MRI are preferred diagnostic methods for evaluating abscesses in patients with Crohn's disease.

Fistulae are abnormal communications between two epithelial surfaces or an epithelial surface and the skin, which occur in 6% to 33% of patients with Crohn's disease.⁷ Fistulae occur in the presence of, and likely as a result of, stricture formation (fistulae are only rarely found in isolation, only 4% to 7% of the time; Fig. 41-8). Ileocecal, ileosigmoid, and enteroenteric fistulae are the most common and are often multiple. An enterocolic fistula may lead to bacterial overgrowth and is one of the causes of malabsorption associated with Crohn's disease.

Enterocutaneous fistulae can be well shown by barium studies, CT, and MRI.

Because the attachment of the transverse mesocolon crosses the mid-descending duodenum, Crohn's-related fistulae between the transverse colon and duodenum are not unusual. Recurrent Crohn's disease in the neoterminal ileum after ileotransverse colonic anastomosis may be associated with such a fistula. Ileosigmoid fistulae are encountered more often. These may serve a useful purpose by bypassing strictures in the ileocecal area. In most cases, the entry site of these fistulae into the sigmoid colon shows only nonspecific inflammatory changes. If surgery is contemplated, it is usually adequate to resect the diseased ileum and stricture, leaving the sigmoid colon intact.⁷

Disease Activity as Assessed by Barium

In the 1970s, the National Cooperative Crohn's Disease Study attempted to determine whether barium examinations could accurately assess response to therapy and whether barium findings correlated with clinical response, as judged by the Crohn's Disease Activity Index (CDAI).⁴⁶ Patients were divided into those with active, symptomatic disease (CDAI > 150; $n = 295$) and patients with disease that had been active, but was now quiescent (CDAI < 150; $n = 274$). The investigators concluded that the findings on barium examination did not correlate with clinical symptoms or response. In general, there was little improvement of barium findings during the study; only patients

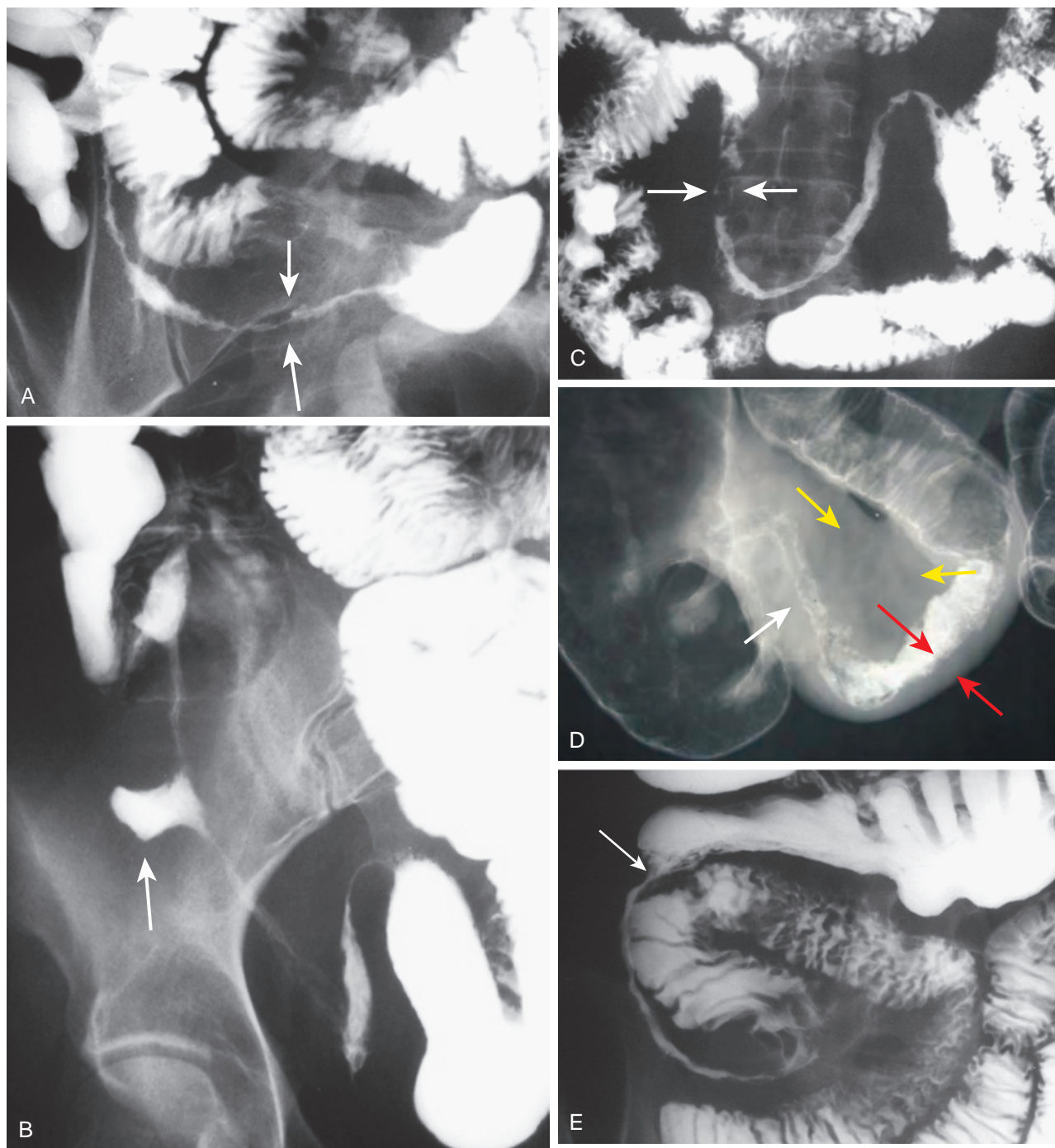


Figure 41-6 Fibrostenotic Crohn's disease. These four patients demonstrate the string sign of Crohn's disease with narrowing and rigidity of the involved segments because of cicatrizing Crohn's disease. **A.** The terminal ileum is narrowed (arrows) and there is minimal proximal dilation. **B.** There is a sacculum (arrow) identified along the antimesenteric border of this very narrowed ileum. **C.** A segment of marked luminal narrowing (arrows) is identified in the distal jejunum. **D.** Specimen radiograph shows narrowing of the lumen of the terminal ileum (white arrow) associated with mural thickening (red arrows). Note the creeping fat (yellow arrows) on the mesenteric side of the distal ileum. **E.** Recurrent, stricturing Crohn's disease is evident on both sides of the ileocolic anastomosis (arrow).

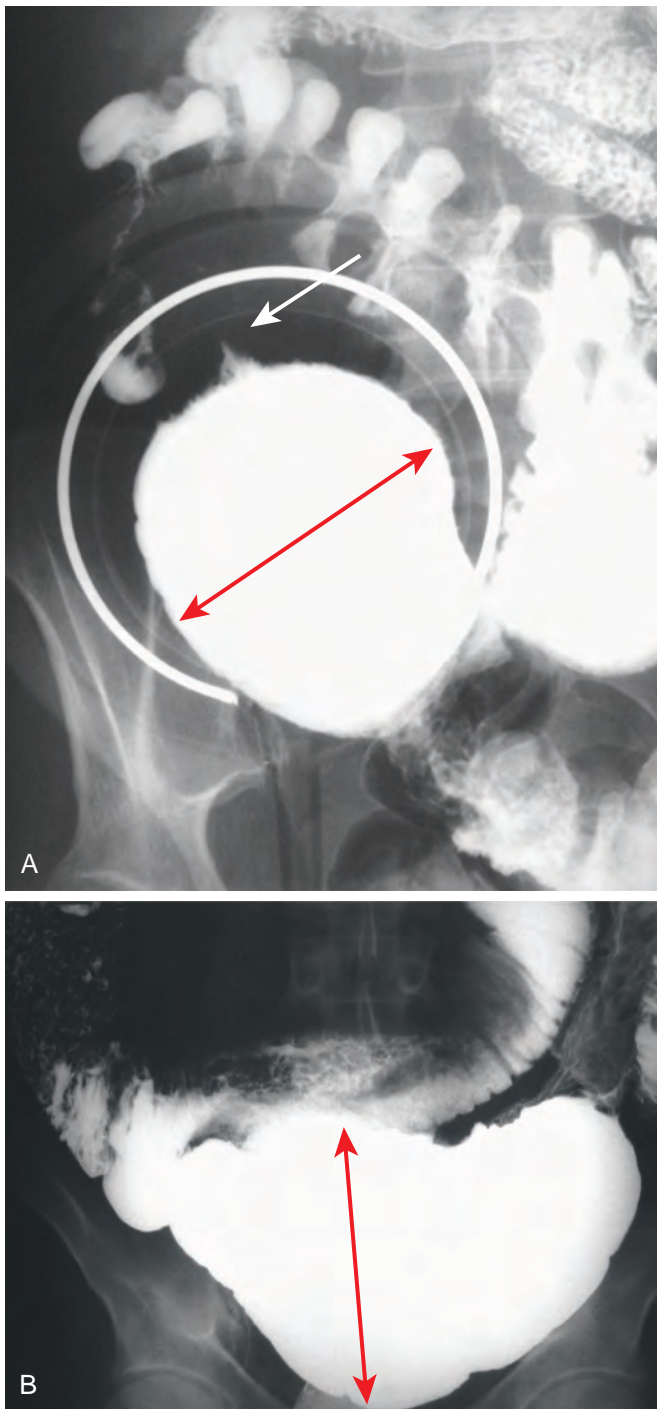


Figure 41-7 Aneurysmal dilation of fibrostenotic small bowel in Crohn's disease. **A.** There is segmental marked dilation (red arrow) of a segment of the terminal ileum caused by a distal stricture (white arrow). **B.** There is a long segment of aneurysmal dilation (red arrow) of distal ileum located between two strictures.

treated for longer than 6 months with prednisone showed a statistically significant improvement in findings.

ULTRASOUND

Ultrasound has been increasingly used to assess Crohn's disease, especially in the pediatric population.⁴⁷ The examination

requires meticulous, systematic scanning of all parts of the bowel, using graded compression and a high-frequency transducer after the administration of oral contrast. Recently, investigations have shown the added benefit of contrast-enhanced ultrasound in assessing Crohn's disease, especially in differentiating fibrosis from active inflammation.⁴⁸ Mural thickening (Fig. 41-9) is the most common abnormality seen in patients with Crohn's disease of the small bowel.⁴⁹⁻⁶⁷ It is typically concentric, and the mural echogenicity depends on the degree of inflammatory infiltration and fibrosis. In early acute disease, mural stratification is retained. With long-standing disease, a target or pseudokidney appearance may be identified. In patients with burned out, long-standing disease, fat deposition in the submucosa may be present.

Actively inflamed gut appears rigid and fixed, with decreased or absent peristalsis.⁴⁹⁻⁶⁷ Color Doppler imaging typically shows hyperemia. Findings on spectral Doppler analysis include increased superior mesenteric and/or inferior mesenteric artery blood flow, increased pulsatility index, decreased resistive index, and increased portal vein velocity.⁴⁹⁻⁶⁷ Increased systolic and diastolic flow through the superior mesenteric artery may also be seen, attesting to disease activity. Creeping fat of the mesentery manifests as a uniform echogenic halo around the mesenteric border of the encased gut. As with barium study, MDCT, and MRI, this abnormal fat causes separation of bowel loops.

Prominent lymph nodes are seen in most patients with the active inflammatory phase of Crohn's disease. These perienteric lymph nodes, which are located in the subperitoneal space of the small bowel mesentery, present as focal hypoechoic masses that are spherical and have lost their normal echogenic streak emanating from the nodal hilum. These nodes are typically hyperemic, moderate in size, and tender. Abnormal lymph nodes are not commonly seen in quiescent Crohn's disease.⁴⁹⁻⁶⁷

Crohn's disease strictures show mural thickening of the gut, with the luminal surfaces of the involved segments in apposition (Fig. 41-10). The lumen may appear as a narrow, linear, echogenic central region within the thickened segment of small bowel. Dilated hyperperistaltic segments can be seen proximal to the strictured segments. Aneurysmal dilation and sacculation may be seen proximal to the involved segments.

Fistula appear as linear bands of varying echogenicity (Fig. 41-11), extending from the gut to the bladder, another segment of bowel, or bladder. Gas within the fistula will appear echogenic and may show the so-called ring-down artifact. An empty or partially closed tract will appear as a hypoechoic segment of bowel or bladder. Abscesses on ultrasound manifest as a fluid-filled or complex mass, which may contain gas.⁴⁹⁻⁶⁷

Recently, in an animal model, ultrasound elastography-derived shear wave velocity was found to help distinguish acutely inflamed from fibrotic bowel.⁶⁸ Much work needs to be performed to determine whether this technique can distinguish mixed fibrostenotic and active inflammatory disease from pure active inflammatory disease or fibrostenotic disease.

MAGNETIC RESONANCE IMAGING

Magnetic resonance imaging (see Chapter 40) has become a well-established technique in evaluating patients with known or suspected Crohn's disease by virtue of its ability to help confirm the diagnosis; localize lesions; assess their severity, extent, and inflammatory activity; and identify extraintestinal

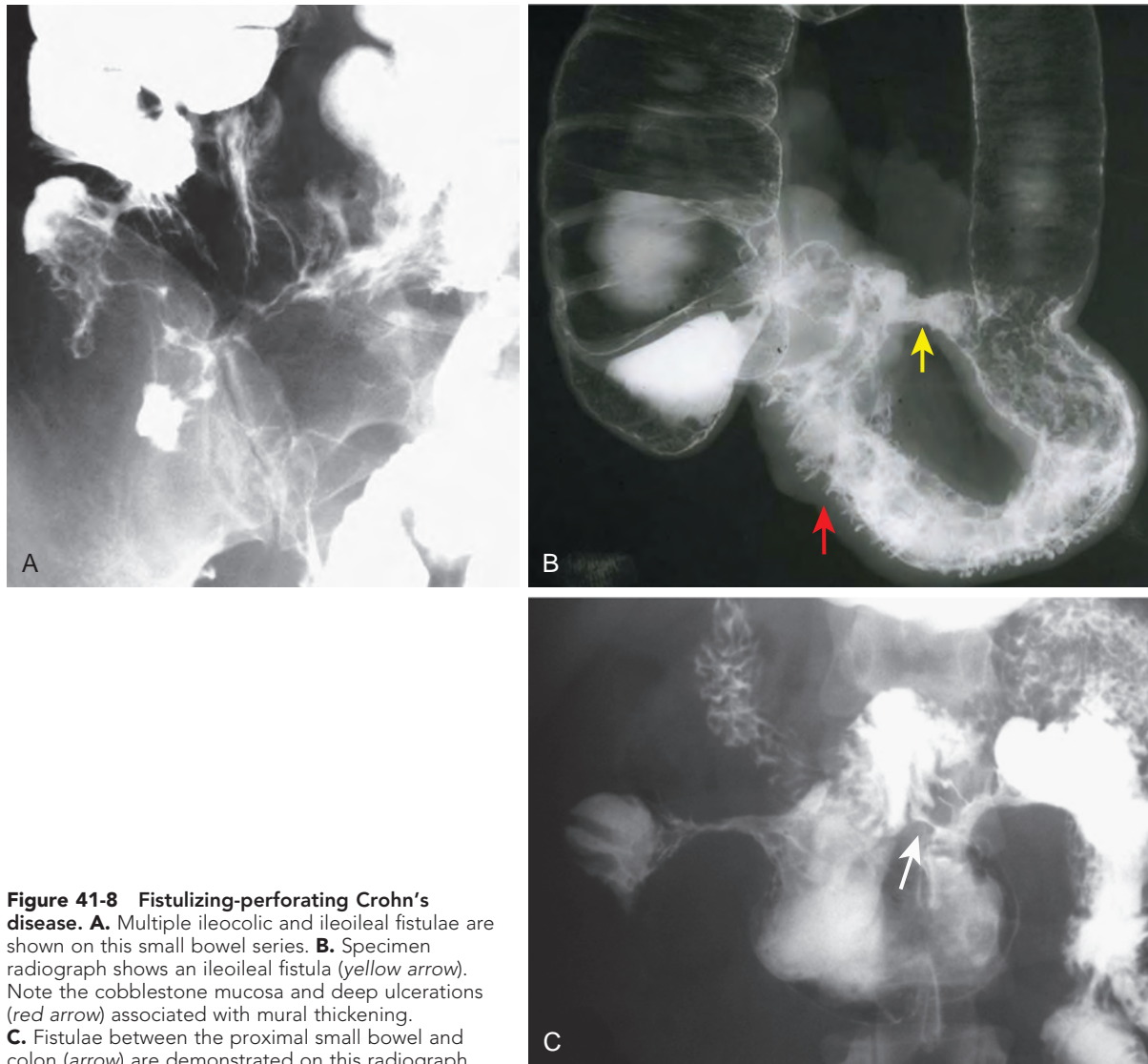


Figure 41-8 Fistulizing-perforating Crohn's disease. **A.** Multiple ileocolic and ileoileal fistulae are shown on this small bowel series. **B.** Specimen radiograph shows an ileoileal fistula (yellow arrow). Note the cobblestone mucosa and deep ulcerations (red arrow) associated with mural thickening. **C.** Fistulae between the proximal small bowel and colon (arrow) are demonstrated on this radiograph.

complications that may require surgical intervention.⁶⁹⁻⁸⁸ MR enteroclysis is an emerging diagnostic tool that combines the advantages of conventional enteroclysis and MRI. However, MR enterography (MRE) is the most practical method of evaluating patients with Crohn's disease.

MRE has two major advantages over CTE. No ionizing radiation is used and, as a result, multiple pulse sequences with and without contrast enhancement can be performed. Static imaging can help identify wall edema and lymphatic distention, and contrast-enhanced imaging can be performed long after the injection has been given, potentially allowing for further characterization. The major disadvantage is a long examination time, requiring relatively long breath holding. Furthermore, magnet time is at a premium in many institutions and is used for many other disease states. Bowel motion remains a problem; glucagon and hyoscyamine (Levsin) are the only antiperistaltic agents approved in the United States (Buscopan or hyoscine butylbromide is an excellent agent but only approved in countries other than the United States). Finally, spatial resolution, even with 3-T magnets, does not approach the resolution of

MDCT with its near-isotropic imaging. Nevertheless, MRE is equivalent to CTE for the evaluation of Crohn's disease.⁸⁹⁻⁹²

Adequate distention of the bowel lumen is ideal in MRE because collapsed bowel loops can potentially hide lesions or mimic pathology. However, in general, the small bowel affected by Crohn's disease can almost always be detected unless there is significant bowel motion or no distention of a large amount of small bowel. Different methods have been used to achieve adequate distention. MR enteroclysis provides distention of the entire small bowel, visualizes mucosal abnormalities, and can show functional information about small bowel mobility.

Regardless of the pulse sequence, it is important to obtain imaging in orthogonal planes, often axial and coronal. These planes should be obtained in all patients on static and post-contrast scans. As with CTE, disease presence, strictures, and especially fistulae and sinus tracts are best elucidated with orthogonal imaging.

Many T2-weighted pulse sequences are available on modern scanners. New, fast, T2-weighted spin-echo sequences can be obtained in a single breath-hold. These include T2-weighted,

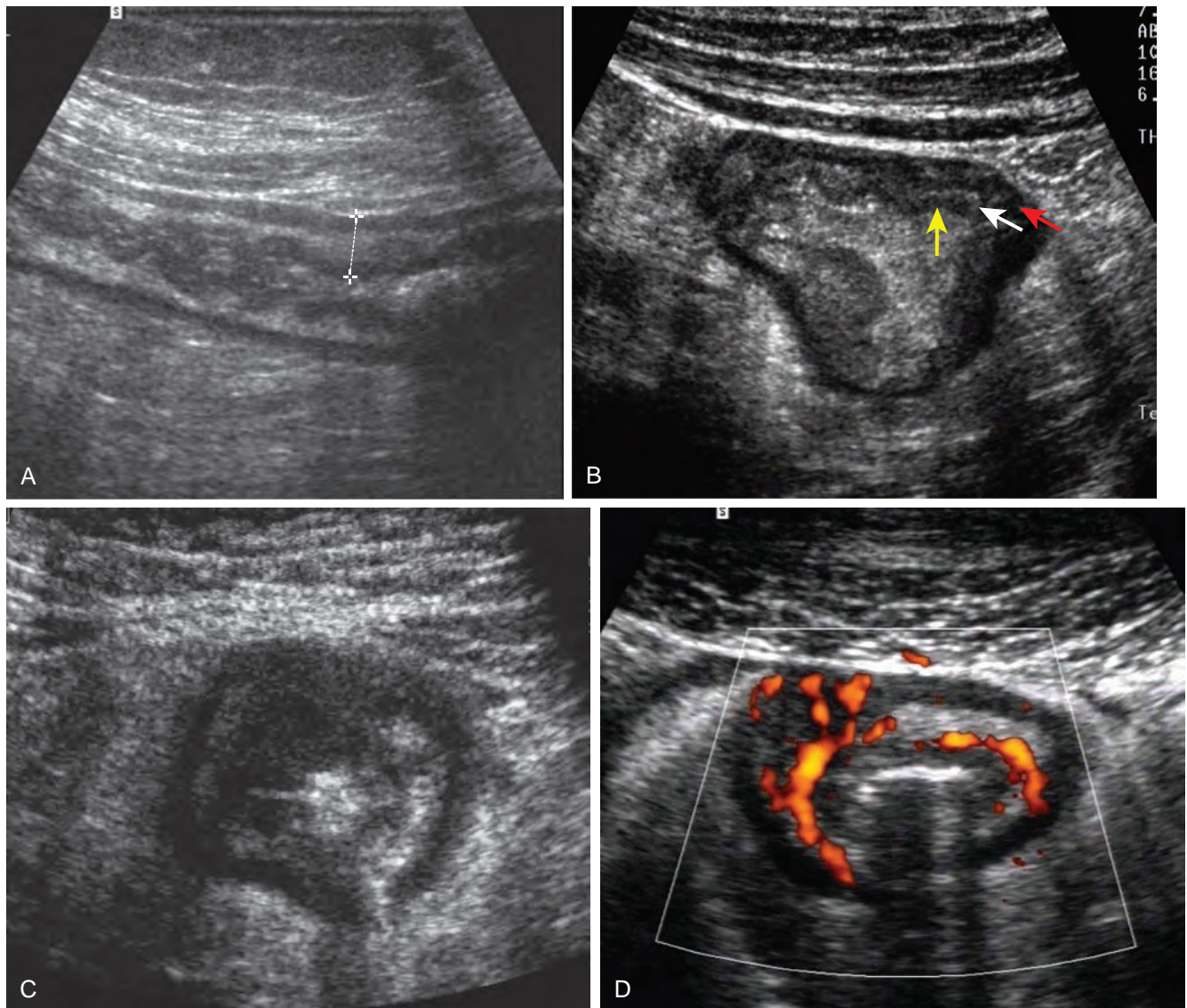


Figure 41-9 Crohn's disease: Sonographic features. **A.** Mural thickening is the sonographic hallmark of Crohn's disease. **B.** In acute disease, mural stratification is maintained. Yellow arrow, mucosa-muscularis mucosae; white arrow, submucosa; red arrow, muscularis mucosae. **C.** In chronic Crohn's disease, mural stratification is lost. **D.** The density of vessels seen on color flow Doppler ultrasound correlates with the degree of disease activity. (Courtesy Dr. Pierre-Jean Valette, Lyons, France.)

half-Fourier rapid acquisition with relaxation enhancement (RARE), turbo spin-echo (TSE), fast spin-echo (FSE), half-Fourier acquisition single-shot turbo spin-echo (HASTE), single-shot turbo spin-echo (SSTSE), EXPRESS, and the newest sequence, called BLADE, which uses periodically rotated overlapping parallel lines with enhanced reconstruction (PROPELLER). These T2-weighted sequences are obtained with and without fat saturation. Fat saturation helps identify and characterize increased T2 signal in abnormal loops of bowel (increased T2 signal in the wall can result from increased fluid from edema or lymphatic distention or from fat deposition). T1-weighted, gadolinium-enhanced, spoiled gradient-echo (SGE) sequences are also important in evaluating the location, extent, and severity of Crohn's disease.⁶⁹⁻⁸⁸ T1-weighted gadolinium-enhanced MRI has been the most investigated pulse sequence in Crohn's disease. A variety of 2D and 3D techniques are available; the most common use a fast, 3D, fat

saturated gradient-echo sequence acquired in a single breath-hold lasting 15 to 20 seconds. These sequences have a variety of names, such as VIBE, FAME, THRIVE, and 3D QUICK.⁶⁹⁻⁸⁸ T1 acquisition in regard to contrast enhancement varies, with acquisition commonly at 30, 60, and 90 seconds postinjection start. More delayed imaging of up to 8 minutes postcontrast may be helpful.¹⁰

Multiple coronal, true fast imaging with steady-state precession (FISP), cine motility sequences have been reported to differentiate between a high-grade and low-grade partial small bowel obstruction. These sequences give an MR "fluoroscopic" depiction of peristalsis above a stricture, showing the progressive dilation of bowel proximal to the stricture. Some believe that static imaging may not be able to make this distinction. However, in our experience, most significant strictures (predominantly fibrostenotic) demonstrated dilated loops of small bowel (>3 cm) proximally.

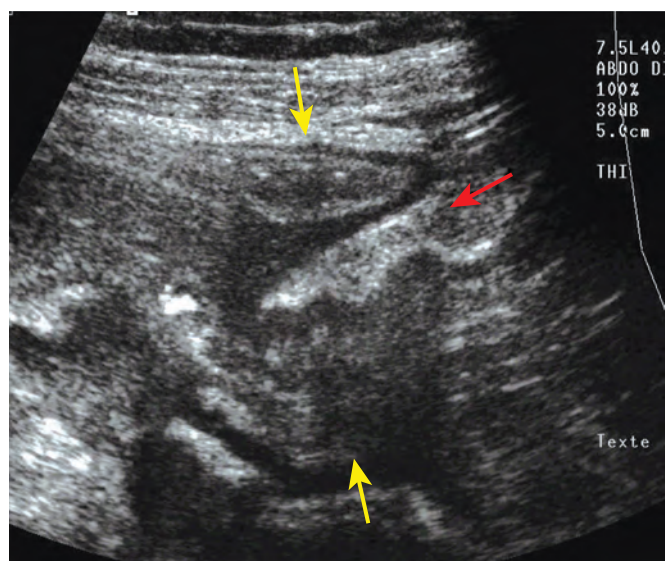


Figure 41-10 Fibrostenosing Crohn's disease: Sonographic features. Marked thickening of a segment of ileum (yellow arrows) is identified, causing dilation of the proximal small bowel (red arrow). (Courtesy of Dr. Pierre-Jean Valette, Lyons, France.)

Recently, in an animal model of Crohn's disease, magnetization transfer helped detect fibrosis.⁹³

COMPUTED TOMOGRAPHY

There are three major CT techniques (see Chapter 38) used for the evaluation of Crohn's disease of the small bowel—conventional positive intraluminal contrast studies, CT enterography (CTE), and CT enteroclysis.⁹⁴⁻¹⁰⁶ Conventional CT using positive intraluminal contrast agents is generally reserved for postoperative patients in whom a bowel leak is suspected. In a patient with an acute exacerbation of symptoms, one might argue that identifying an abscess is the most important question. Thus, conventional CT with positive oral agents should be used. However, many patients with acute symptoms do not have an abscess but have exacerbation of the disease, obstruction or progressive stricture formation with or without fistulization. We have found that CT enterography, even in these acutely ill patients, can confidently distinguish an abscess using neutral oral contrast agents. CT enteroclysis is a rarely used technique and is reserved for those institutions in which it is performed routinely. Finally, the assessment of mural enhancement is hindered by the presence of positive

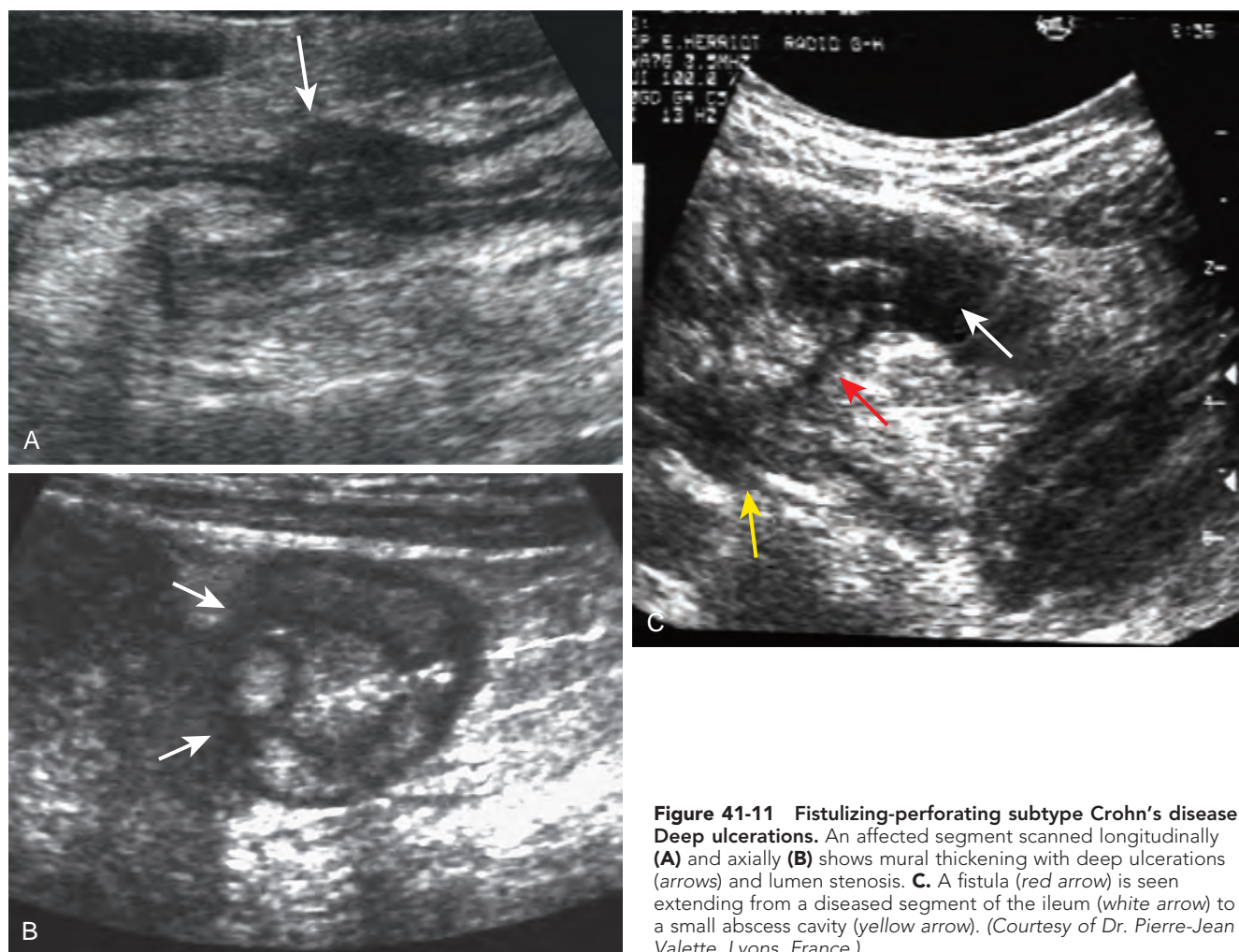


Figure 41-11 Fistulizing-perforating subtype Crohn's disease: Deep ulcerations. An affected segment scanned longitudinally (A) and axially (B) shows mural thickening with deep ulcerations (arrows) and lumen stenosis. C. A fistula (red arrow) is seen extending from a diseased segment of the ileum (white arrow) to a small abscess cavity (yellow arrow). (Courtesy of Dr. Pierre-Jean Valette, Lyons, France.)

intraluminal contrast because this contrast obscures inner wall hyperenhancement.

CT enterography uses MDCT with a narrow section thickness and reconstruction interval, vis-à-vis (IV) contrast material, and large volumes of neutral contrast agent to distend the lumen in an effort to improve the detection of small bowel inflammation and extracolonic complications. CT can be performed during the enteric phase (45 seconds after injection) and portal venous phase (70 seconds after injection). Regardless of the technique used, there is no significant difference in detecting Crohn's disease.¹⁰⁷ Jejunal attenuation is greater than ileal attenuation, and collapsed bowel loops demonstrate greater attenuation than distended bowel loops.¹⁰⁸ CT enteroclysis uses contrast material infused through a nasojejunal tube. Both positive (dilute barium) and neutral contrast (water, methylcellulose, VoLumen) agents may be administered. CT enteroclysis uses the same technique as standard fluoroscopic enteroclysis, except that imaging is performed with contrast-enhanced MDCT, as in CT enterography.³² All MDCT datasets should be reconstructed in at least two planes, typically axial and coronal. Occasionally, sagittal or oblique planes are helpful in identifying fistulae.

Every effort should be made to limit radiation exposure in patients, especially if they have had multiple CT scans in the past. Several studies have shown that some Crohn's patients can receive large cumulative doses (>100 mSv) over the course of their disease, and often are examined with CT two to three times a year.¹⁰⁹⁻¹¹² In one series, encompassing a 15-year period, the mean ionizing radiation dose was 36.1 mSv. Over the entire study period, there was an increasing use of CT, and although CT accounted for only 16.2% of all imaging studies, it accounted for 77.2% of the radiation dose. Also, in this study, the total ionizing radiation exceeded 75 mSv in 15.5% of patients. Patients who receive higher doses have onset of disease before 17 years of age, have upper GI tract or penetrating disease, require IV steroids or infliximab, or have had multiple surgeries.¹⁰⁹ There is recent evidence that radiation exposure from CT scans in children results in an increased risk of brain tumors and leukemia.^{113,114} Most pediatric centers almost exclusively use MRE or ultrasound as a means of evaluating their patients.

Efforts to reduce the dose from MDCT are ongoing and include alterations in kVp and mAs in relation to body habitus, weight, body mass index (BMI), and altering the scan pitch, as well as applying new reconstruction techniques, generally termed *iterative reconstruction*, to initial lower dose images. Dose reductions from a CT scan are typically 15 to 20 mGy but can successfully be reduced to less than 10 mGy, and even below 5 mGy, have been achieved. However, the most substantial reductions in dose have been in patients who weigh less than 160 pounds. It remains to be seen whether sub-mSv imaging is possible without data loss. Crohn's disease identification is a high-contrast issue with CT (i.e., identifying a process with a higher attenuation compared with background). To date, low-contrast objects (an object of lower attenuation compared with background) are lost with lower dose MDCT,¹¹⁵ even with any of the known iterative reconstruction techniques, including model-based iterative reconstruction.¹¹⁶⁻¹¹⁸ To achieve a substantial reduction in dose from CT, radiologists may have to accept a lower sensitivity in detecting low-attenuation lesions in the liver, which are the low-contrast entities that occur most frequently in a patient population.

The most effective strategy for reducing ionizing radiation exposure in patients with Crohn's disease is to shift imaging to

MRE from CTE. Our strategy is first to perform CTE on all patients with Crohn's disease if they have not had one performed. This serves as the baseline examination, establishing the location and extent of disease. The study is fast, the spatial resolution is superb, and there is little to no bowel motion artifact. We favor CTE or MRE as the initial study because bowel motion remains a problem for MRE in the United States. Furthermore, the spatial resolution of MRE is still not equivalent to that of CTE. As a result, the risk of missing disease on an initial MRE image is relatively high. However, every other examination, except for patients who are acutely ill or perioperative, should be MRE. Acutely ill patients should be examined with CTE, especially if abscess detection and potential drainage is relatively likely. Once detected, the abscess can be rapidly drained using CT guidance. Postoperative patients should be examined after the ingestion of positive oral contrast medium and the administration of rectal contrast medium if there is a colonic anastomosis, because a leak may be present.

Nomenclature for CT and MR Enterography Findings

In an effort to measure the impact of CTE and MRE in the care of Crohn's patients, interested radiologists in the Abdominal Radiology Society (ARS), Crohn's Disease-Focused Panel are in the process of developing a nomenclature to describe the findings of Crohn's disease and how to interpret those findings. Tables 41-1 and 41-2 summarize this work, which should be considered a work in progress. The ultimate goal is to have international input and approval from radiologic, gastroenterologic and surgical societies. The purpose of a common nomenclature is to define and standardize the terms used to describe the findings and the conclusions that can be drawn from those findings. Ultimately, these terms and conclusions will be essential in measuring outcomes in regard to treatment and the impact of imaging on predicting treatment. These terms will be used here in the subsequent discussion of the findings of MRE and CTE.

COMPUTED TOMOGRAPHY AND MAGNETIC RESONANCE ENTEROGRAPHY FINDINGS OF SMALL BOWEL CROHN'S DISEASE

Both CTE and MRE identify the transmural, extramural, and mesenteric manifestations of small bowel Crohn's disease.^{119,120} Historically, investigators have described findings as mucosal, submucosal, serosal, or extramural-mesenteric. However, in many cases, the mucosa may be entirely destroyed, replaced by acute and chronic inflammatory cells. Furthermore, the precise anatomic location of the finding may not actually be known. Therefore, we think it best to avoid the use of these specific terms and prefer to use terms that are more generic and descriptive, rather than anatomic (see Table 41-1). Finally, because the findings on CTE and MRE are similar or identical, we will combine the discussion into one section.

Wall Findings

Hyperenhancement. One of the most consistent MRE/CTE findings is wall hyperenhancement. This is defined as increased signal intensity or attenuation on contrast-enhanced scans in a noncontracted segment of bowel. Comparison with adjacent or nearby small bowel segments is helpful in making this

TABLE
41-1

Abdominal Radiology Society Nomenclature for Computed Tomography and Magnetic Resonance Enterography Findings in Small Bowel Crohn's Disease (Work in Progress)

Findings	Description
WALL FINDINGS	
WALL HYPERENHANCEMENT	Increased attenuation and signal intensity on contrast-enhanced scan in noncontracted segment; compare with nearby small bowel segments.
Stratified (bilaminar or trilaminar)	Inner wall hyperenhancement or halo; no clinically significant difference between the two patterns
Homogeneous	Transmural hyperenhancement
Normal	
Asymmetric	Asymmetric or patchy hyperenhancement, often along mesenteric border with relative sparing along the antimesenteric border
WALL THICKENING	
• Mild	3-4 mm
• Moderate	5-7 mm
• Severe	>7 mm
Intramural edema	Hyperintense T2 signal; only on MRE (preferably fat suppressed); cannot comment on CTE
LUMINAL NARROWING	
STRICTURE	Narrowed diameter in a noncollapsed loop, with or without mural hyperenhancement
UPSTREAM DILATION	Luminal narrowing + upstream dilation (see below)
	Bowel lumen >3 cm, unequivocal segmental dilation of small bowel proximal to narrowed segment or small bowel feces sign above narrowed segment
• Mild	<4 cm
• Moderate	4-5.9 cm
• Severe	>6 cm
Ulcer	Wall defect that does not extend outside bowel wall in a thickened wall
Sinus tract	Wall defect that extends outside lumen but not to adjacent organs (usually accompanied by angulation and fixation of adjacent bowel and/or tethering of bowel or urinary bladder)
Simple fistula	Single tract; affected loops often angulated and tethered; describe origin and termination location
Complex fistula	Multiple tracts; asterisk appearance; +/-interloop abscess or inflammatory mass (phlegmon)
MESENTERIC FINDINGS	
Vasa recta distention	Also known as the comb sign in the literature; inflamed bowel loop with dilation of mesenteric vessels larger than adjacent to bowel loops
Fibrofatty proliferation	Increased fat adjacent to abnormal bowel, displacing bowel loops; usually along mesenteric border, unless perirectal; often associated with mesenteric border inflammation; if perirectal, then circumferential
Perienteric edema, inflammation	Increased attenuation (CT) or high T2 signal (MR) in mesenteric fat adjacent to abnormal bowel loops
Inflammatory mass	Ill-defined, masslike process of soft tissue attenuation and signal intensity (not water attenuation and signal intensity; also known as a phlegmon) usually associated with penetrating disease, such as complex fistula and inflammatory stranding in the mesenteric fat
Abscess	Mesenteric or peritoneal fluid collection with rim enhancement or internal gas
Amenable to percutaneous drainage	Well-formed collection >3 cm, accessible to intervention
Not amenable to percutaneous drainage	Not well formed, or <3 cm, or not accessible to intervention because of bowel, bony, or vascular structures
Adenopathy	>1.5 cm in short axis
Likely inflammatory	If <2 cm in short axis
EXTRAINTESTINAL FINDINGS	
Sacroiliitis	
PSC	Discontinuous, intrahepatic bile duct visualization and/or extrahepatic ductal wall thickening without significant upstream dilation
Venous thrombus, thrombosis (occlusive)	Mesenteric, portal, IVC, iliac, femoral, gonadal
Nephrolithiasis and cholelithiasis	
Avascular necrosis	Femoral head most common; if present, describe articular collapse

Baker ME, Fidler JL, Fletcher JG, Bruining DH, and other members of the SAR Crohn's Disease Focused Panel: Unpublished work in progress, 2014.

TABLE
41-2

Abdominal Radiology Society Nomenclature for Computed Tomography and Magnetic Resonance Enterography Dictation Impressions in Small Bowel Crohn's Disease

Findings	Description
Active inflammatory small bowel Crohn's disease (luminal narrowing present or absent)	Wall hyperenhancement in noncontracted small bowel segment; wall thickening, mesenteric changes are variable but often present
Quiescent or inactive small bowel Crohn's disease	Absent wall hyperenhancement, ± wall thickening, no mesenteric changes except fatty proliferation
Mixed fibrostenotic and active inflammatory small bowel Crohn's disease (a controversial classification to some; see text)	Stricture, wall thickening, wall hyperenhancement, luminal narrowing with upstream dilation; most strictures have inflammatory and fibrotic components
Penetrating Crohn's disease (added in addition to determination of active or mixed Crohn's disease)	Sinus tract and/or fistula; inflammatory mass; abscess; free perforation; associated with mixed fibrostenotic and active inflammatory small bowel Crohn's disease or active inflammatory small bowel Crohn's disease
Fibrostenotic small bowel Crohn's disease	Wall thickening, no wall hyperenhancement, absent mural edema (MRE only), no mesenteric changes, lumen narrowed, with upstream dilation

Baker ME, Fidler JL, Fletcher JG, Bruining DH, and other members of the SAR Crohn's Disease Focused Panel: Unpublished work in progress, 2014.

differentiation. Furthermore, accompanying mesenteric findings, such as vasa recta distention or fibrofatty proliferation, are almost always present. Hyperenhancement may be layered or stratified into two patterns, bilaminar and trilaminar. In the bilaminar pattern, only the inner wall hyperenhances (Figs. 41-12 and 41-13). This is often referred to in the literature as mucosal hyperenhancement. Because the mucosa may be destroyed, we prefer to describe rather than conclude that the mucosa is present. In the trilaminar pattern, there is inner and outer wall (sometimes referred to as serosal) hyperenhancement, with the intervening wall relatively hypoenhancing, giving a halo effect (Fig. 41-14). This pattern is much more commonly seen in MRE; it may very well be present in CTE but

is not as well identified because of poorer contrast resolution compared with MRE. There is likely no clinically significant difference between bilaminar and trilaminar hyperenhancement. Both are present with active inflammation. Hyperenhancement may be homogeneously transmural (Figs. 41-15 and 41-16), asymmetric, or patchy (Figs. 41-17 and 41-18). The hyperenhancement may at times be very subtle; viewing with narrow windows facilitates identification (see Fig. 41-18). When asymmetric, the pseudosacculation of the nonaffected segment is sometimes present (see Fig. 41-17).

Thickening. Bowel wall thickening, usually more than 1.5 to 2 cm, is another consistent feature of Crohn's disease. Although

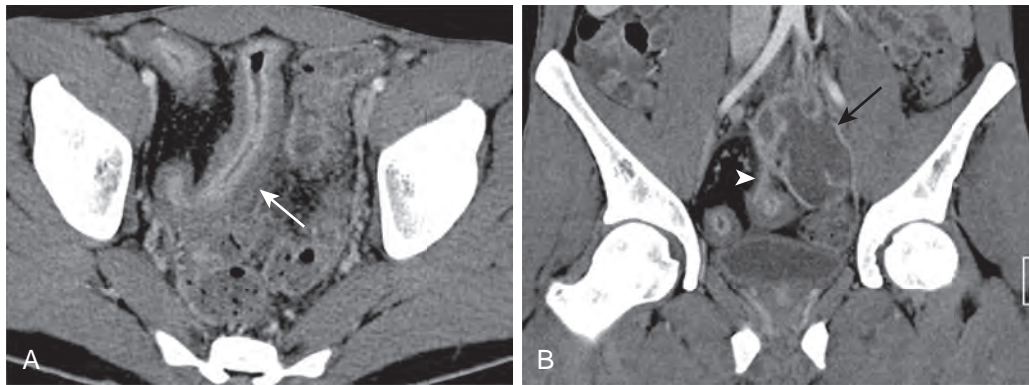


Figure 41-12 Mixed fibrostenotic and active inflammatory small bowel Crohn's disease of the distal ileum with penetrating disease: Bilaminar hyperenhancement. CT enterography in axial (A) and coronal (B) reconstructions show bilaminar hyperenhancement, severe wall thickening (>1 cm) (white arrow), and a fistulous tract extending cephalad (arrowhead) toward an abscess (black arrow).

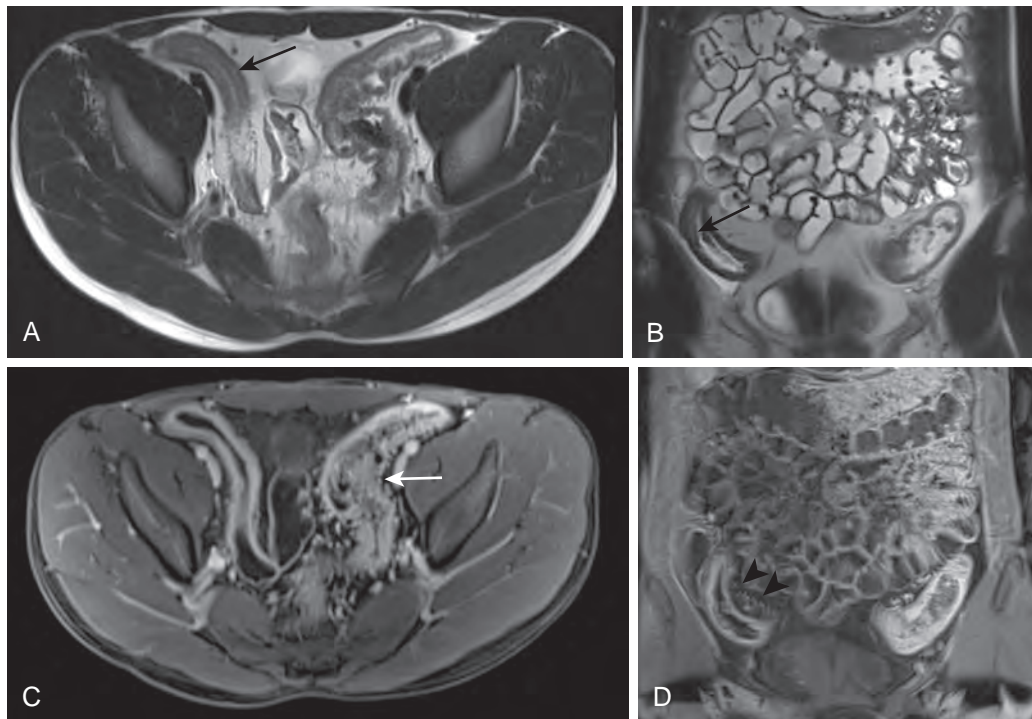
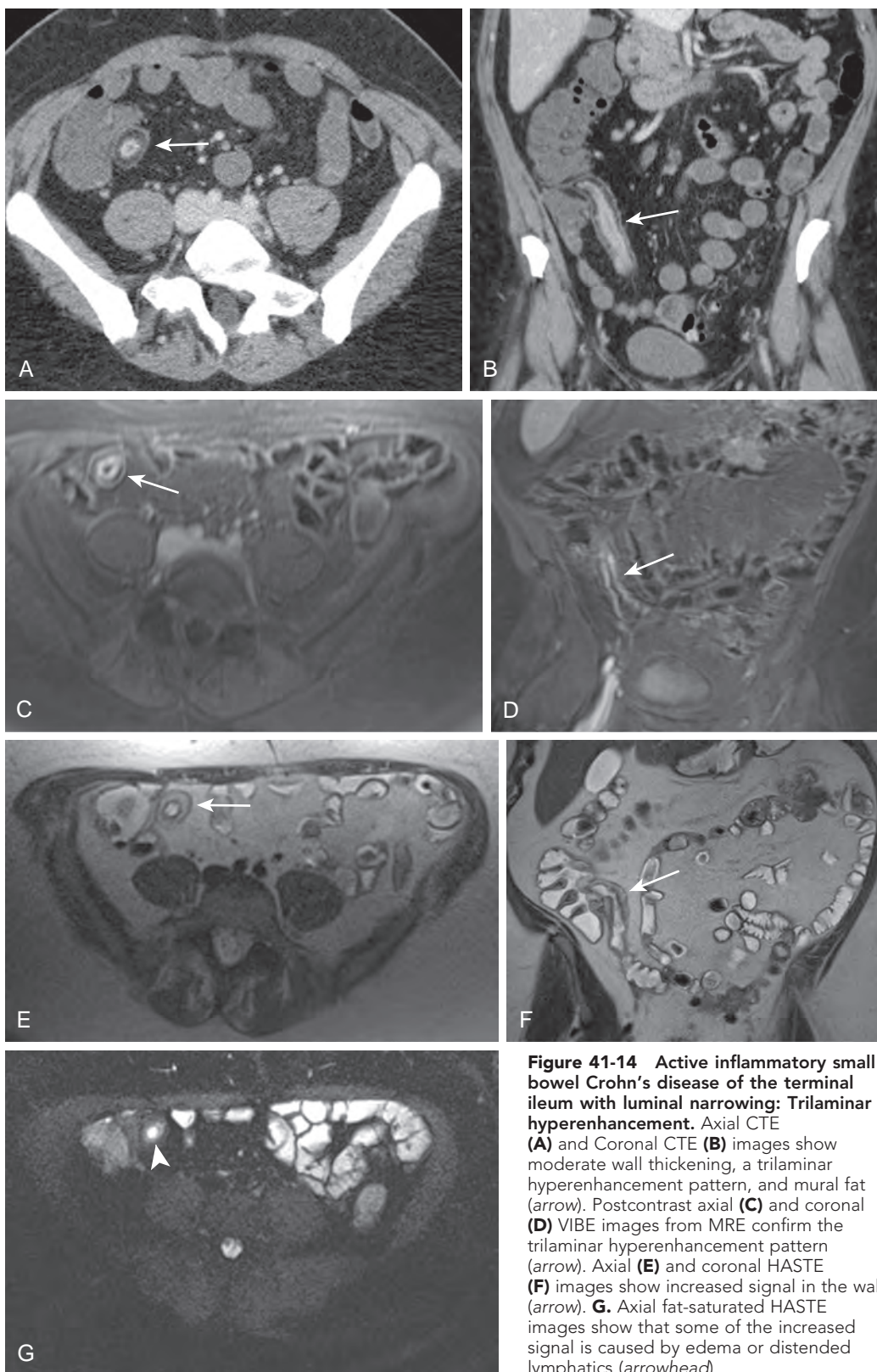


Figure 41-13 Active inflammatory small bowel Crohn's disease of the distal ileum with mild luminal narrowing: Bilaminar hyperenhancement. MRE using HASTE (A, B) and postcontrast VIBE (C, D). A, B. HASTE images show increased signal because of edema and/or lymphatic distention (black arrow). C, D. Postcontrast VIBE images show a bilaminar hyperenhancement pattern, moderate wall thickening (5-10 mm), and vasa recta distention (arrowheads). There is also colitis (white arrow).



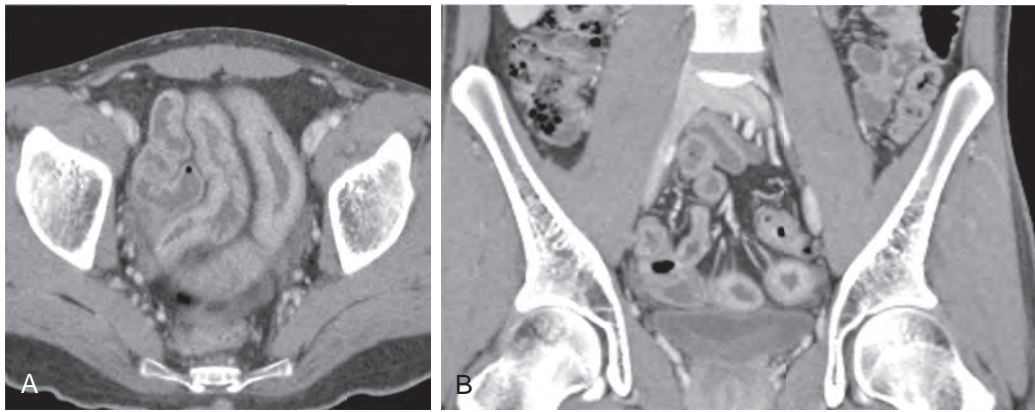


Figure 41-15 Active inflammatory small bowel Crohn's disease of the distal ileum with segments of normal lumen and mild luminal narrowing: Homogeneous enhancement pattern. Axial (A) and Coronal (B) CTE images show a long length of diseased ileum with homogeneous hyperenhancement and moderate wall thickening.

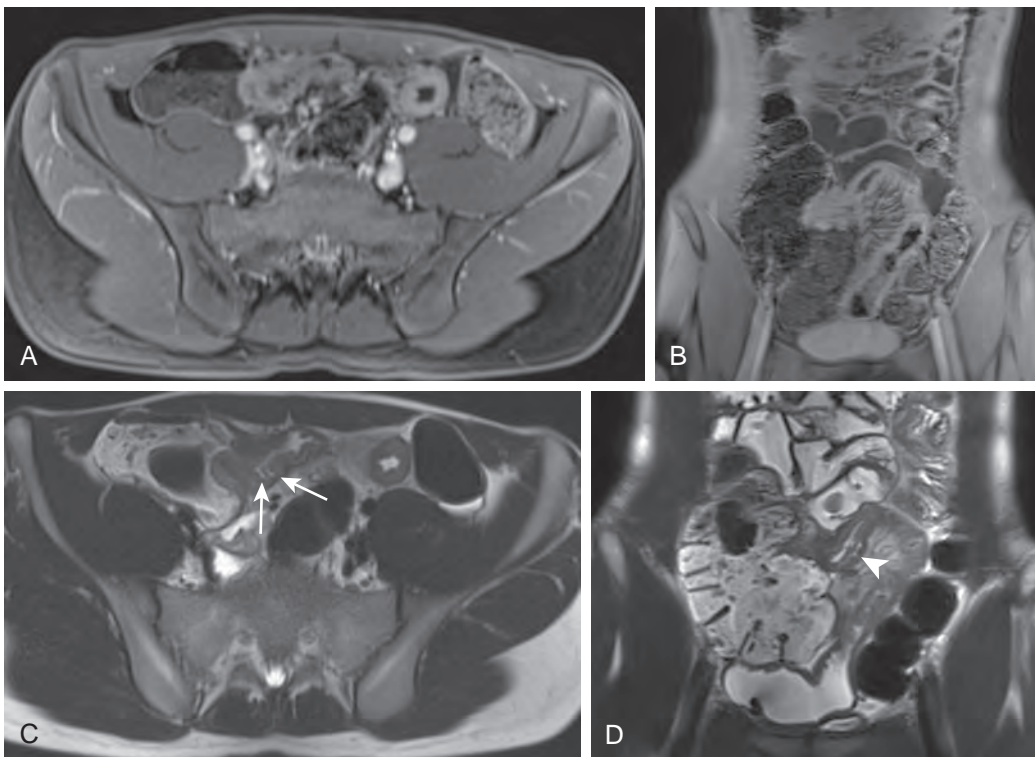


Figure 41-16 Mixed fibrostenotic and active inflammatory small bowel Crohn's disease of the distal ileum: Homogeneous and trilaminar hyperenhancement, deep ulcers, and an intramural sinus tract. Postcontrast axial (A) and coronal (B) VIBE images from MRE show segments of trilaminar and homogeneous hyperenhancement. Axial (C) and coronal HASTE (D) images show deep ulcers (arrows) and an intramural sinus tract (arrowhead). There is moderate upstream dilation (4-5.9 cm). The vasa recta are also dilated.

wall thickening is most often symmetric (see Fig. 41-16), as with hyperenhancement, it may also be asymmetric (see Figs. 41-17 and 41-18). It is important that the bowel be distended when assessing bowel wall thickening. Thickening may be mild (3-4 mm), moderate (5-10 mm) or severe (>10 mm). When severe, especially when focal and short segment, causing obstruction, one may suspect that a complicating tumor is present (see later).

On MRE thickened, cobblestoning or pseudopolyposis may be present. These are patchy, sharply demarcated areas of high signal intensity along affected small bowel segments (Fig.

41-19). Additionally, pseudopolyposis may be identified as a papillary, endoluminal nodule that generally uniformly hyperenhances (Fig. 41-20).

On MRE there may be intramural edema in the thickened wall. This is identified on fat-saturated, T2-weighted images as a high signal (must be fat-saturated imaging because intramural fat may also cause an increased T2 signal; see Fig. 41-13).

Luminal Narrowing, Stricture Formation, and Upstream Dilation. Initially, when the disease is present, the bowel lumen is not significantly narrowed (see Fig. 41-18). However, as the

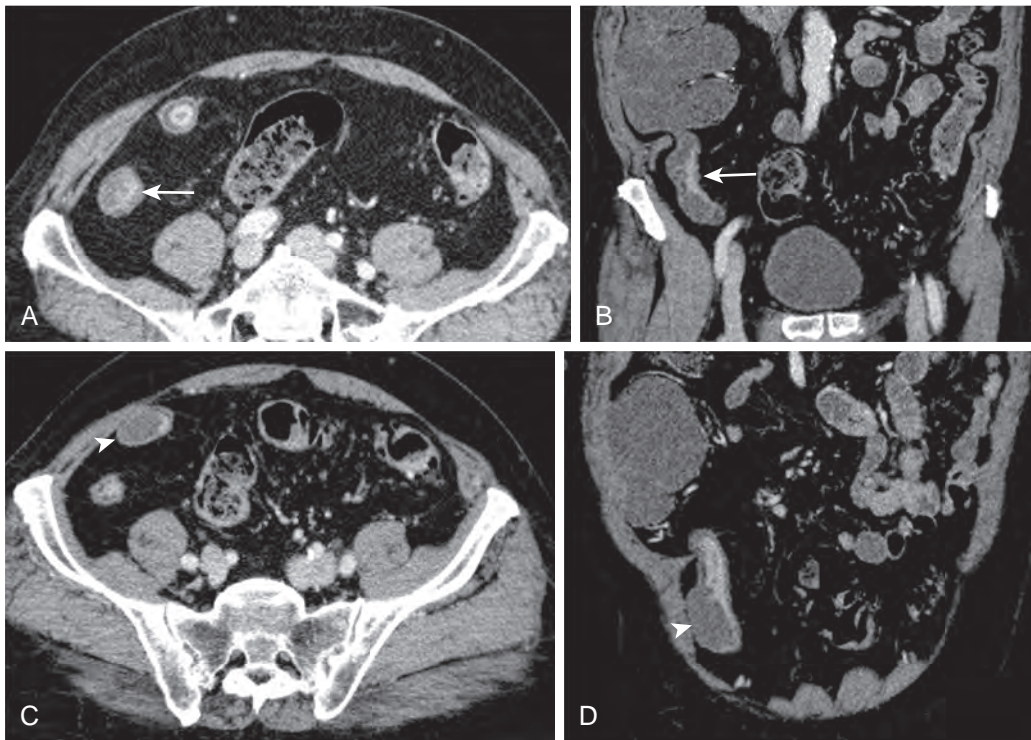


Figure 41-17 Active inflammatory small bowel Crohn's disease with and without luminal narrowing: Asymmetric changes. Axial (A) and Coronal (B) CTE images at one level show wall thickening along the mesenteric border, with a normal antimesenteric border (arrow). At this site of disease, the lumen is not narrowed. On the same images, there is another anterior, small bowel loop with trilaminar hyperenhancement, moderate wall thickening, and luminal narrowing. Just upstream, in the distal ileum, axial (C) and coronal (D) images show pseudosacculation (arrowhead).

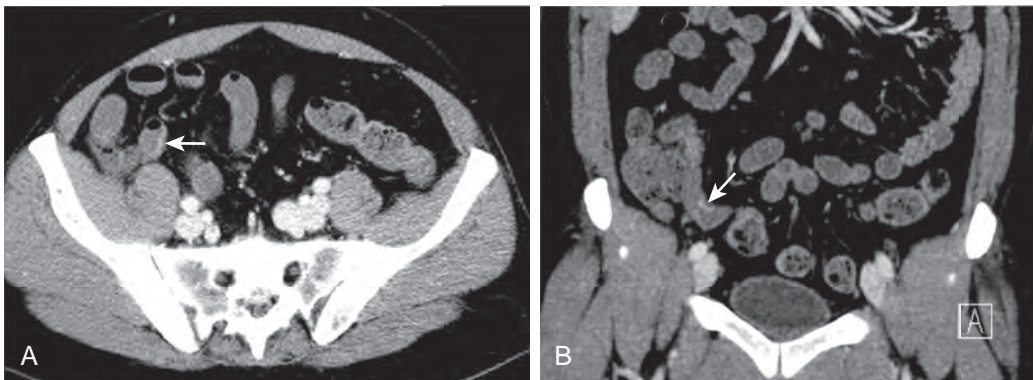


Figure 41-18 Active inflammatory small bowel Crohn's disease without luminal narrowing: Subtle asymmetric changes. Axial (A) and Coronal (B) CTE images of the distal ileum show very subtle bilaminar hyperenhancement and mild wall thickening (arrow).

disease progresses, the affected bowel lumen narrows (see Figs. 41-14 and 41-15). As noted, luminal narrowing in Crohn's can be caused by spasm or the proliferation of smooth muscle and/or fibrous tissue. The two can be differentiated with MRE/CTE by the presence or absence of upstream dilation. Using dynamic, fluoroscopic MR techniques, one can also identify ballooning, upstream dilation caused by a fixed stricture. We define a stricture as an area of luminal narrowing associated with upstream dilation more than 3 cm (see later, "Mixed Fibrostenotic and Active Inflammatory Small Bowel Crohn's Disease"). When the upstream segment is less than 4 cm, it is considered mild, 4 to 5.9 cm is moderate, and more than 6 cm is severe.

Ulcer and Sinus Tract. Ulcerations can be identified on cross-sectional enterography, much more commonly with MRE. Images achieved with MR enteroclysis, with consistent and continuous luminal dilation, can provide sufficient resolution to detect early lesions of Crohn's disease, such as blunting, flattening, thickening, distortion of small bowel folds, nodularity, and aphthous-type ulcers. Differentiating an ulcer from a sinus tract and an ulcer from pseudopolypoidosis can be difficult. We have arbitrarily defined an ulcer as a wall defect that does not extend outside the bowel wall (Figs. 41-21 to 41-23). A sinus tract extends outside the lumen, but does not extend to adjacent organs. When a sinus tract is present, there is almost always

some degree of bowel angulation, loop separation, and/or tethering of the bowel or urinary bladder. Furthermore, there is almost always stricture formation. Pseudopolypoidosis has an intraluminal-endoluminal component. Aphthoid ulcerations may enlarge and coalesce to form deeper, usually linear, ulcerations, which frequently assume a longitudinal and transverse orientation. When longitudinal, these are called intramural sinus tracts. On T2-weighted images, they appear as thin lines of high signal intensity within the thickened bowel wall (see Figs. 41-16 and 41-23).

Simple and Complex Fistulae. A simple fistula is a single, soft tissue tract that extends from one loop of bowel to another or to another adjacent organ or structure, such as the urinary bladder or psoas muscle (Fig. 41-24). A complex fistula contains multiple tracts that extend to several loops of bowel and/or other organs or structures (Figs. 41-25 and 41-26). These can take on an asterisk appearance (see Fig. 41-26) and can be associated with an inflammatory mass or interloop abscess. As with sinus tracts, all small bowel fistulae from Crohn's disease are associated with stricture formation. On true FISP and HASTE sequences, sinus tracts and fistulae can present as higher signal linear- to tubular-shaped structures, often containing

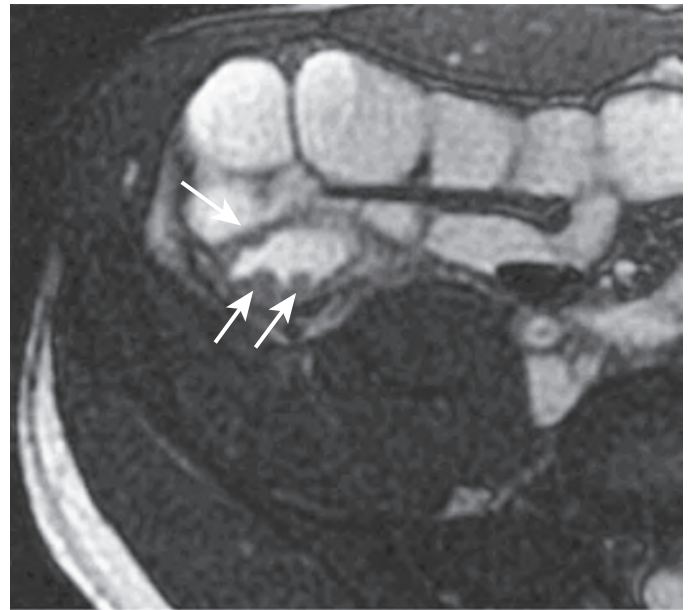


Figure 41-19 Inflammatory pseudopolyps: MRI features. Axial true FISP scan of the distal ileum shows pseudopolyps as small nodular defects protruding through the thickened bowel wall (arrows).

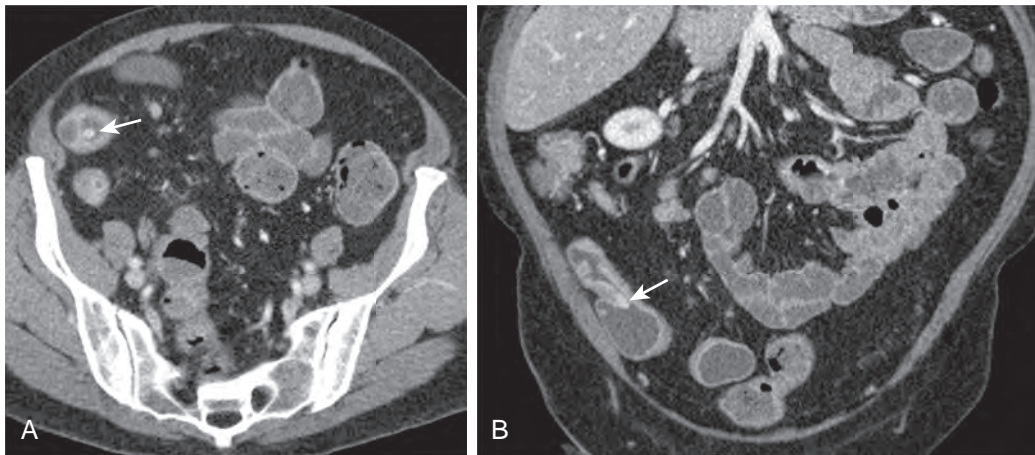


Figure 41-20 Mixed fibrostenotic and active inflammatory small bowel Crohn's disease: Inflammatory polyp at a stricture site. Axial (A) and Coronal (B) CTE images show a hyperenhancing polypoid filling defect representing an inflammatory polyp (arrow).

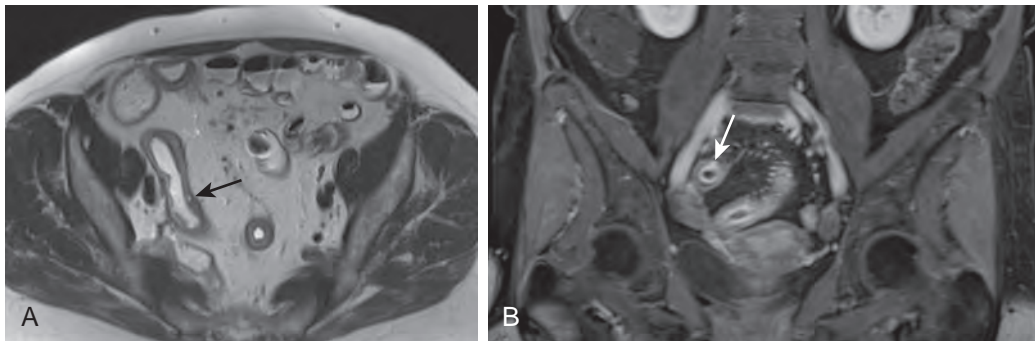


Figure 41-21 Active inflammatory small bowel Crohn's disease without luminal narrowing: Focal ulcer. A. Axial HASTE sequence shows subtle increased signal in the wall (arrow) from edema and lymphatic distention. There is a focal, very high-signal area representing an ulcer. B. On the coronal postcontrast-enhanced VIBE image, the ulcer enhances (arrow). There is also trilaminar hyperenhancement and distention of the vasa recta.

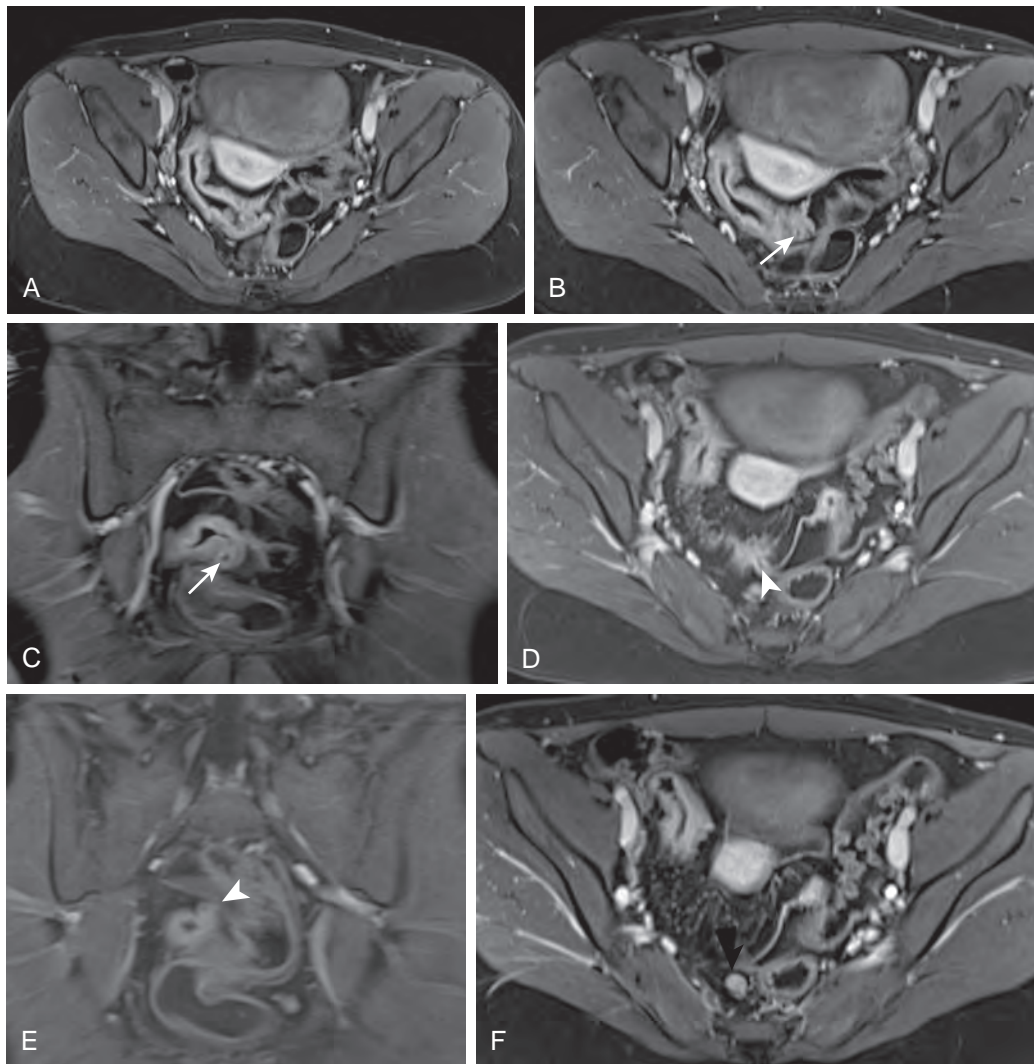


Figure 41-22 Mixed fibrostenotic and active inflammatory small bowel Crohn's disease: Ulcer and sinus tract. **A.** Axial postcontrast VIBE image from MRE shows a bilaminar hyperenhancement and moderate wall thickening. Axial **(B)** and coronal **(C)** postcontrast VIBE images show an ulcer contained within the wall (arrow). Axial **(D)** and coronal **(E)** postcontrast VIBE images show a sinus tract extending outside the wall toward a tethered loop of small bowel (white arrowhead). **F.** Axial postcontrast-enhanced VIBE image shows an intermediate-sized, homogeneously enhancing lymph node (black arrowhead)

central high signal intensity because of their fluid content. However, these tracts may not contain fluid and may present on these T2-weighted pulse sequences as linear, low-signal tracts that hyperenhance on postcontrast-enhanced T1-weighted sequences.

Mesenteric Findings

Vasa Recta Distention. In most cases of active inflammatory Crohn's disease, the straight arteries or vasa recta arising from the mesenteric arcades and extending toward the small bowel are dilated. This has been described in the literature as the comb sign. Vasa recta distention is identified with CTE and MRE as short, parallel, low-attenuation or signal intensity linear structures perpendicular to the intestinal long axis of the diseased bowel. They are best demonstrated on contrast-enhanced CTE or T1-weighted

images as hyperenhancing linear structures (Fig. 41-27; also see Fig. 41-13).

Fibrofatty Proliferation. In many cases of Crohn's disease, there is increased fat adjacent to the affected bowel, displacing the small bowel loops, generally along the mesenteric border. This leads to loop separation. Fibrofatty proliferation of the mesentery develops in nearly 50% of patients with Crohn's disease and is the most common cause of bowel loop separation. The fibrofatty proliferation is the result of perivascular inflammation (Fig. 41-28).

Perienteric Edema and Inflammation. Perienteric edema or inflammation is identified as increased attenuation (CT) or high T2 signal (MR) in the mesenteric fat adjacent to affected segments of small bowel. The finding is much easier to identify

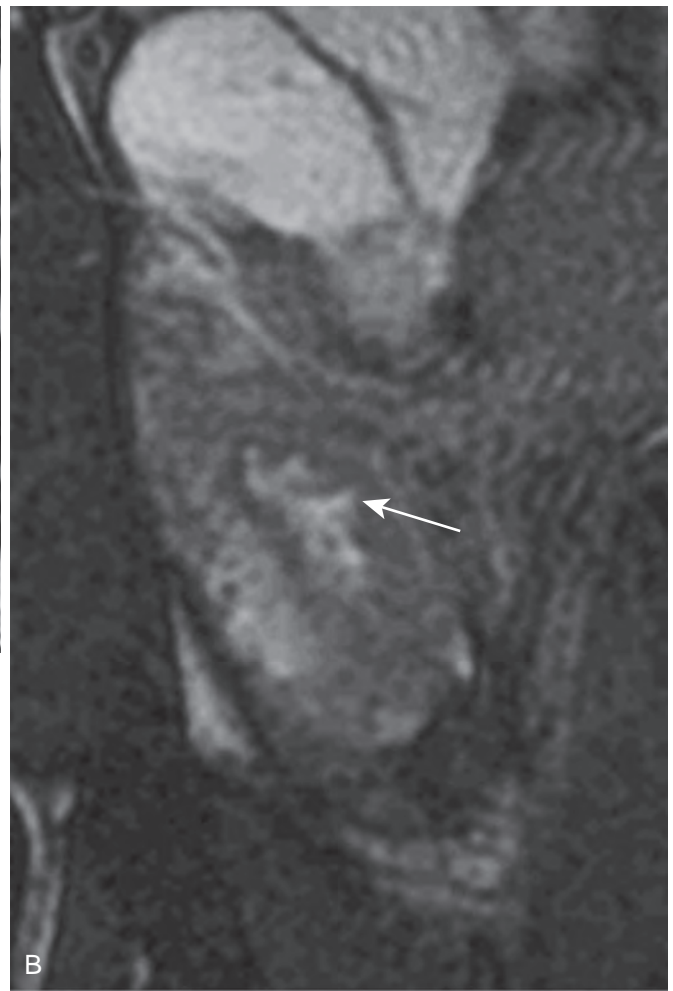
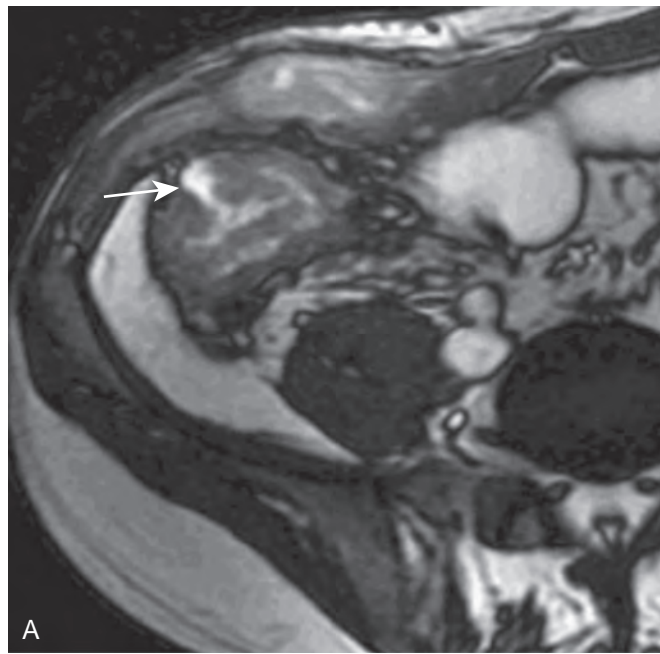


Figure 41-23 Deep ulceration. Axial (**A**) and coronal (**B**) true FISP MR images of the terminal ileum. Ulcers are visualized as thin lines of high signal intensity, longitudinally or transversely (fissure ulcers; arrows) oriented within the thickened bowel wall.

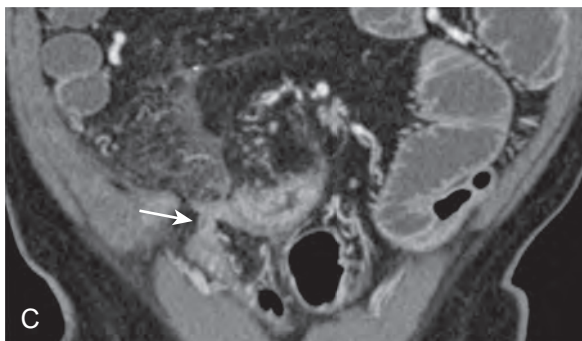


Figure 41-24 Mixed fibrostenotic and active inflammatory small bowel Crohn's disease: Simple fistula, inflammatory mass and abscess.

A. Postcontrast-enhanced, axial CTE shows bilaminar hyperenhancement and moderate wall thickening of a loop of distal ileum. **B.** Just inferior to this, there is a small abscess laterally (white arrowhead), and the start of a single fistula is identified (arrow). **C.** The fistula is best identified in the coronal plane (arrow). **D.** More inferiorly in the pelvis, on the axial view, there is an inflammatory mass (black arrowhead).

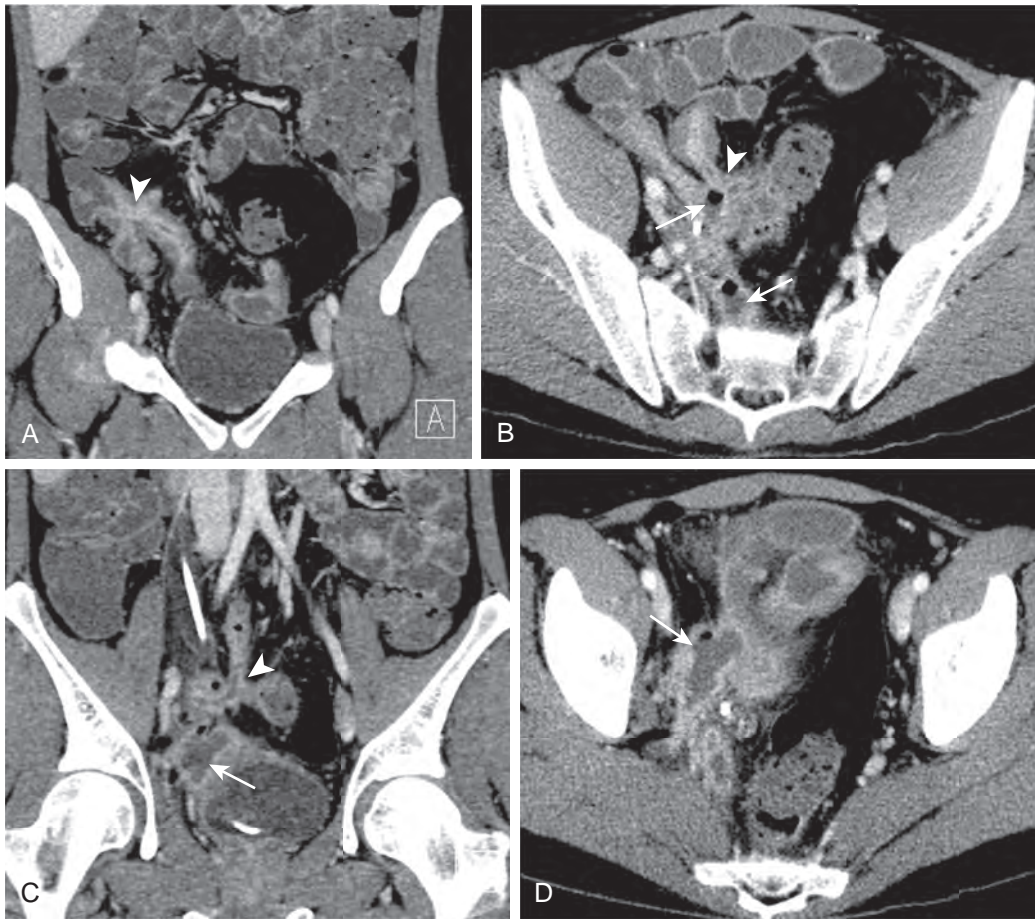


Figure 41-25 Mixed fibrostenotic and active inflammatory small bowel Crohn's disease with penetrating disease: Complex enterocecal, enteroenteric, enterosigmoid, enterovesicular fistula involving the right ureter, with abscesses. **A.** Postcontrast-enhanced, coronal CTE image shows bilaminar hyperenhancement and wall thickening of the terminal ileum and an enteroenteric, enterocecal fistula (arrowhead). **B.** Axial CTE image shows the enteroenteric and enterosigmoid fistula (arrowhead), an inflammatory mass surrounding the right ureter (filled with a stent), and two small abscesses (arrows). **C.** Coronal CTE image shows the fluid-filled enteroenteric and enterosigmoid fistula tract (arrowhead), as well as an abscess (arrow) between the fistula and urinary bladder dome. **D.** Axial CTE image shows the abscess (arrow) adjacent to the dome of the urinary bladder. At surgery, the bladder dome was involved.

on MRE as fat suppressed, T2-weighted pulse sequences (see Fig. 41-26).

Inflammatory Mass and Abscess

An inflammatory mass is defined as an ill-defined, masslike process of soft tissue attenuation or increased signal intensity (but not water attenuation–signal intensity) in the mesenteric fat, almost always associated with penetrating disease, which arises from mixed disease (fibrostenotic and acute inflammatory disease; see Fig. 41-24). An abscess is a well-formed, thick-walled, near-water to water attenuation collection in the mesenteric fat. An abscess should be described as amenable or not amenable to percutaneous drainage (see Figs. 41-12, 41-24, 41-25, and 41-27). This should be determined on the basis of size (>3 cm; generally, the size above which a pigtail catheter can be deployed) and whether the collection can be entered without traversing bowel, vessels, or bony structures. When using neutral oral contrast agents, it is very important to scrutinize the images carefully using scrolling techniques in the axial and coronal planes to differentiate an abscess from

a dilated loop of bowel, because both will contain near-water to water attenuation contents.

Adenopathy. Enlarged mesenteric lymph nodes are commonly present in patients with active inflammatory Crohn's disease. Enlargement is defined as more than 1.5 cm in the short axis. These are likely inflammatory if less than 2 cm. If more than 2 cm, especially if multiple, one should carefully scrutinize the adjacent, affected bowel for the presence of a tumor (see Fig. 41-22).

Extraintestinal Findings

Extraintestinal findings on MRE/CTE are relatively common. These include sacroiliitis (Fig. 41-29), primary sclerosing cholangitis (PSC), venous thrombosis, cholelithiasis, nephrolithiasis, and avascular necrosis, usually of the femoral head. PSC is identified as discontinuous, intrahepatic, biliary ductal visualization and/or extrahepatic ductal wall thickening without significant upstream biliary dilation. Common veins thrombosed in Crohn's include the superior mesenteric and portal veins,

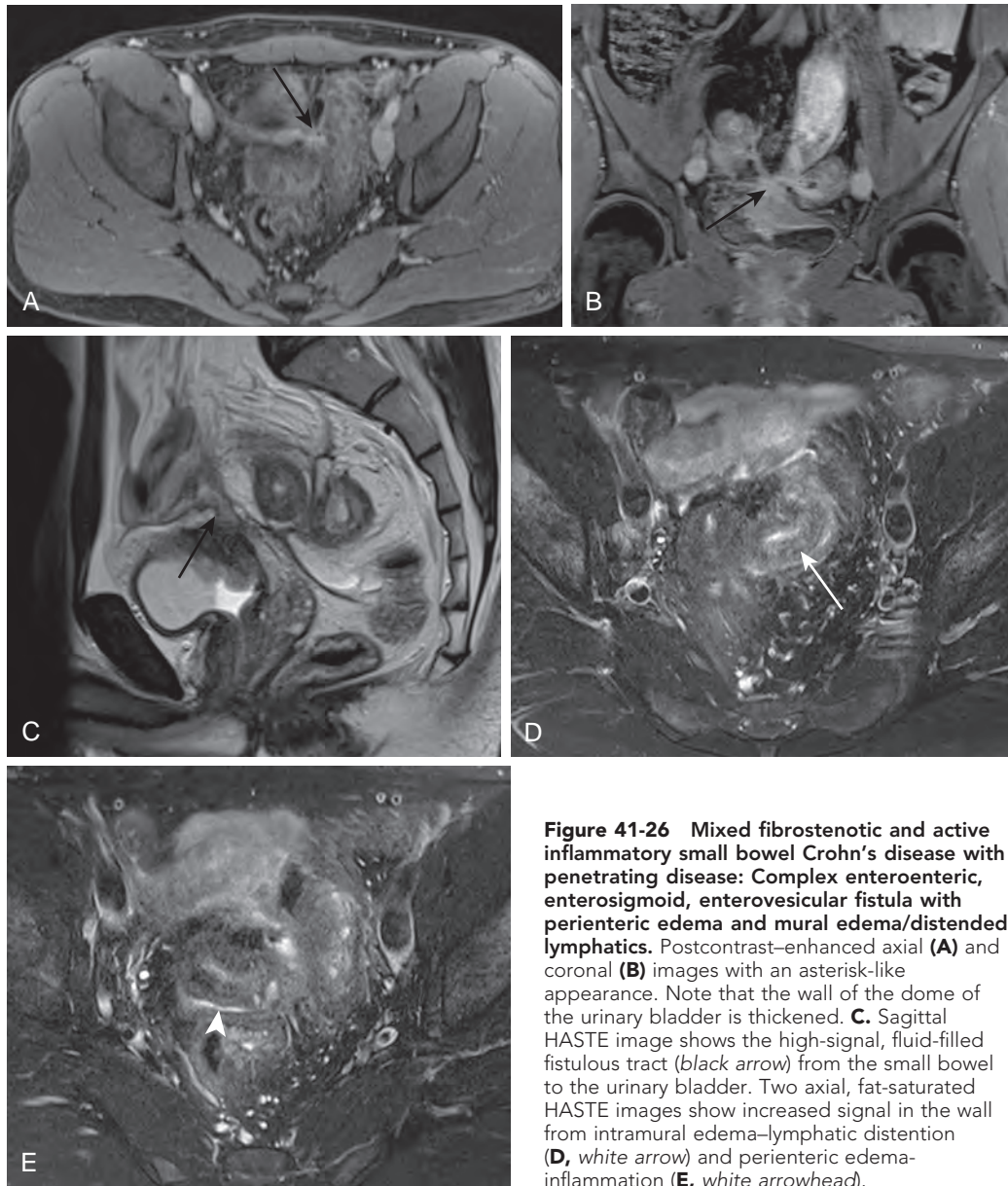


Figure 41-26 Mixed fibrostenotic and active inflammatory small bowel Crohn's disease with penetrating disease: Complex enteroenteric, enterosigmoid, enterovesicular fistula with perienteric edema and mural edema/distended lymphatics. Postcontrast-enhanced axial (A) and coronal (B) images with an asterisk-like appearance. Note that the wall of the dome of the urinary bladder is thickened. C. Sagittal HASTE image shows the high-signal, fluid-filled fistulous tract (black arrow) from the small bowel to the urinary bladder. Two axial, fat-saturated HASTE images show increased signal in the wall from intramural edema-lymphatic distention (D, white arrow) and perienteric edema-inflammation (E, white arrowhead).



Figure 41-27 Mixed fibrostenotic and active inflammatory small bowel Crohn's disease with penetrating disease: Vasa recta distention, multifocal disease, sinus tracts, and abscesses. A. Coronal postcontrast-enhanced CTE image shows multifocal disease with bilaminar to homogeneous hyperenhancement and moderate wall thickening. Axial (B) and coronal (C) images through the terminal ileum show small interloop abscesses (arrowheads) and sinus tracts (arrows). The vasa recta are also distended.

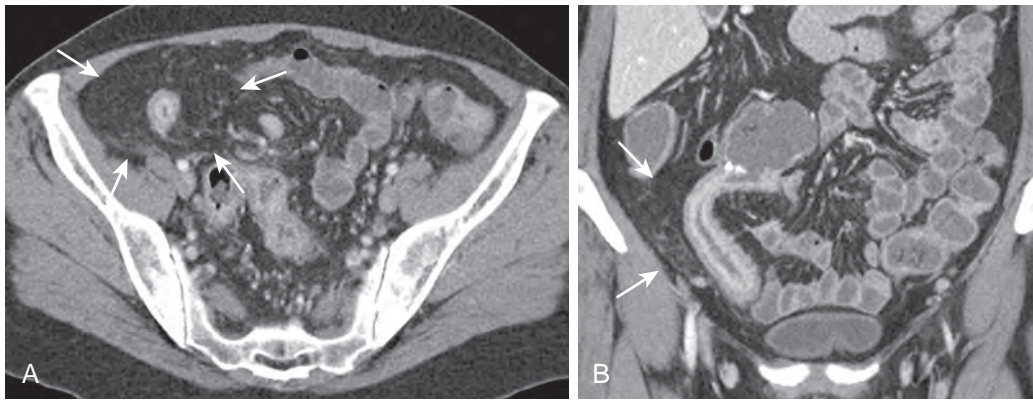


Figure 41-28 Active inflammatory small bowel Crohn's disease with luminal narrowing: Fibrofatty proliferation. Axial (A) and Coronal (B) CTE images show bilaminar hyperenhancement, moderate wall thickening, and luminal narrowing of the neoterminal ileum. The affected loop is surrounded by excess fat (arrows).

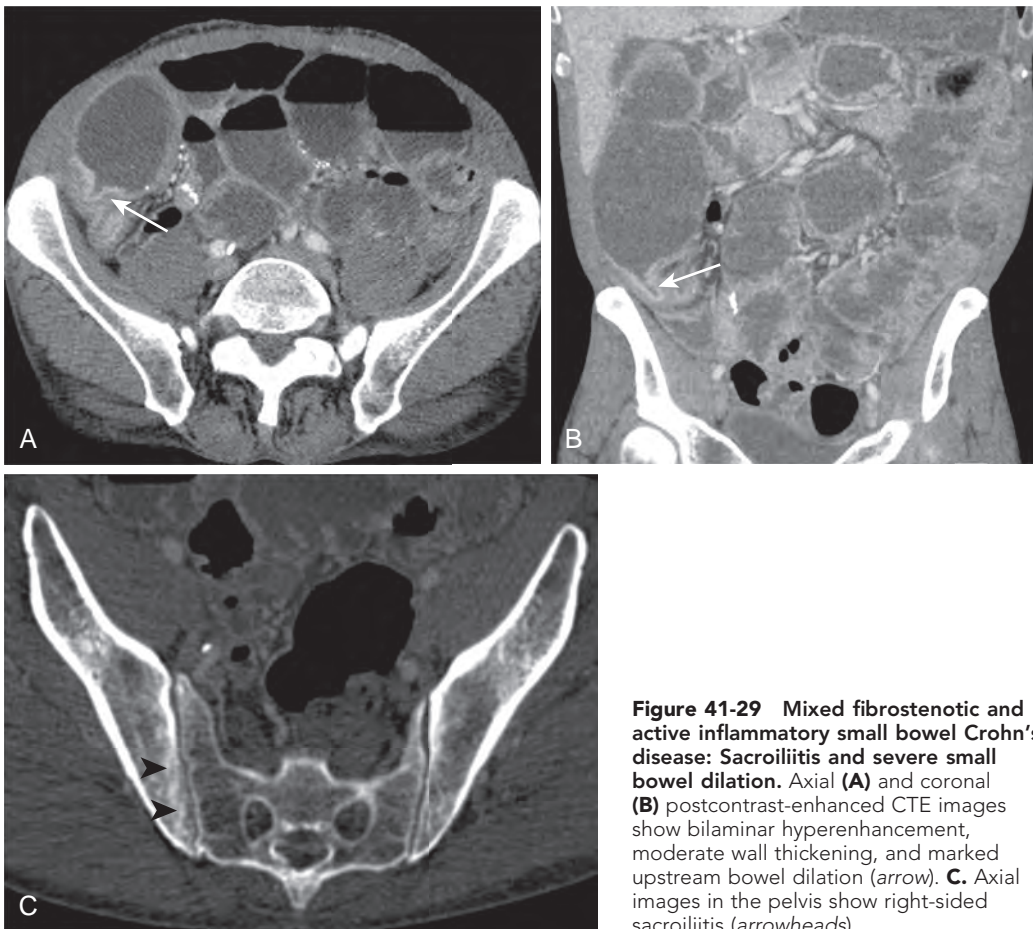


Figure 41-29 Mixed fibrostenotic and active inflammatory small bowel Crohn's disease: Sacroiliitis and severe small bowel dilation. Axial (A) and coronal (B) postcontrast-enhanced CTE images show bilaminar hyperenhancement, moderate wall thickening, and marked upstream bowel dilation (arrow). C. Axial images in the pelvis show right-sided sacroiliitis (arrowheads).

gonadal vein, iliac and femoral veins, and inferior vena cava (IVC).

Active Inflammatory Small Bowel Crohn's Disease

One of the major problems with the current literature concerning assessing active inflammation is that multiple reference standards are used as a surrogate for truth.⁸⁷ However, there is general consensus amongst investigators that active inflammatory disease is present when there is wall hyperenhancement in a thickened (>3 mm), noncontracted, small bowel segment. In

addition to this constellation of findings, there are almost always adjacent mesenteric changes, such as vasa recta distention. In acute inflammatory disease, the lumen can narrow but there should be no upstream bowel dilation. When assessed as such, the dictation should add the absence or presence of luminal narrowing (see Figs. 41-13 to 41-15, 41-17 to 41-19, 41-21, and 41-28).

In CTE and MRE, layered enhancement, or mural stratification, is thought to be highly specific for active inflammation.^{87,121} The degree of enhancement of these various layers

may reflect the underlying disease activity. However, it is not clear if bilaminar and trilaminar hyperenhancement indicate different processes. Most studies only describe layered enhancement or a striated pattern and do not distinguish between the two types of enhancement. Furthermore, it is likely that MRE more commonly identifies the trilaminar pattern than CTE simply because it is more sensitive to enhancement. The peripheral layer of hyperenhancement in the trilaminar pattern is generally much more subtle on CTE than the inner layer of hyperenhancement.

In studies that have relied on endoscopy as the reference standard, the level of enhancement follows the level of disease activity. However, when other standards are used, such as CDAI or blood markers, the correlation is less evident. It is important to note that the presence of acute inflammation does not exclude fibrosis.^{10,11,121} Further, enhancement can be secondary to factors other than acute inflammation, such as micro-vascular density and disease chronicity.¹²² Enhancing mesenteric lymph nodes and vasa recta distention are also highly suggestive of active inflammatory Crohn's disease.

The use of T2-weighted pulse sequences to predict disease activity has been less extensively investigated.^{88,121} On fat saturated sequences, increased T2 signal in the bowel wall indicates edema and is likely also predictive of the level of acute inflammation. Conversely, if there is no increased mural T2 signal, it is likely that a thickened loop of bowel is fibrotic (fibrostenosis alone without inflammation). However, as with T1 enhancement, fibrotic strictures can and often do occur concurrently with acute inflammation (fibrostenotic predominant with active inflammation).

Quiescent or Inactive Small Bowel Crohn's Disease

Quiescent disease is defined as absent or only minimal wall hyperenhancement with either a normal or thickened bowel wall (Fig. 41-30). Mesenteric changes should be absent, except for fibrofatty proliferation.

Inactive Crohn's disease can be associated with other phases of Crohn's disease in other portions of the gut. There may be a decrease in the lumen diameter and wall thickening but not active inflammation as identified in the "burned out" segment.

Mixed Fibrostenotic and Active Inflammatory Small Bowel Crohn's Disease

Mixed disease is defined as wall hyperenhancement, wall thickening and stricture formation (i.e., luminal narrowing with upstream dilation >3 cm in diameter) (Figs 41-31 to 41-33; also see Figs. 41-12, 41-16, 41-20, 41-22, 41-24 to 41-27, and 41-29). In this disease category, there are findings of both acute inflammation and of a fixed stricture causing some element of obstruction. Obstruction may be long standing and cause either marked bowel dilation or a stool sign (see Figs. 41-29, 41-31, and 41-32). The term *mixed* is controversial, especially with gastroenterologists. They are concerned that when fibrostenosis is added to the diagnosis, patients will not be treated medically. It remains to be seen if this group of patients are best treated with medical or surgical therapy. Another important aspect in patients with mixed disease is that penetrating disease may also be present (see Figs. 41-12, 41-24 to 41-27, and 41-33). In our experience, penetrating disease is never identified without mixed disease being present.

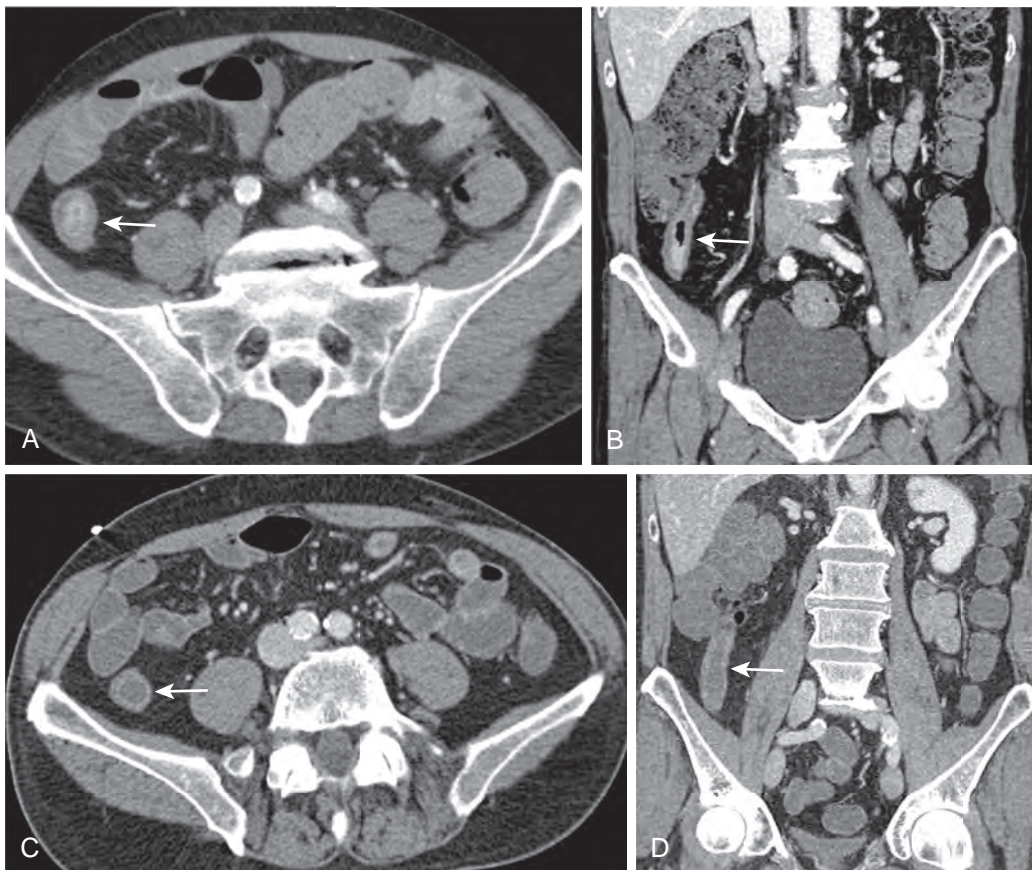


Figure 41-30 Quiescent disease. Axial (A) and coronal (B) CTE images are obtained before starting 6-mercaptopurine and show active, inflammatory, small bowel Crohn's disease of the terminal ileum with luminal narrowing, trilaminar hyperenhancement, and moderate wall thickening (arrows). Axial (C) and coronal (D) CTE images obtained 3 months later show a normal caliber lumen, minimal bilaminar to trilaminar hyperenhancement, and only mild wall thickening (arrows). The mucosa was normal at endoscopy.

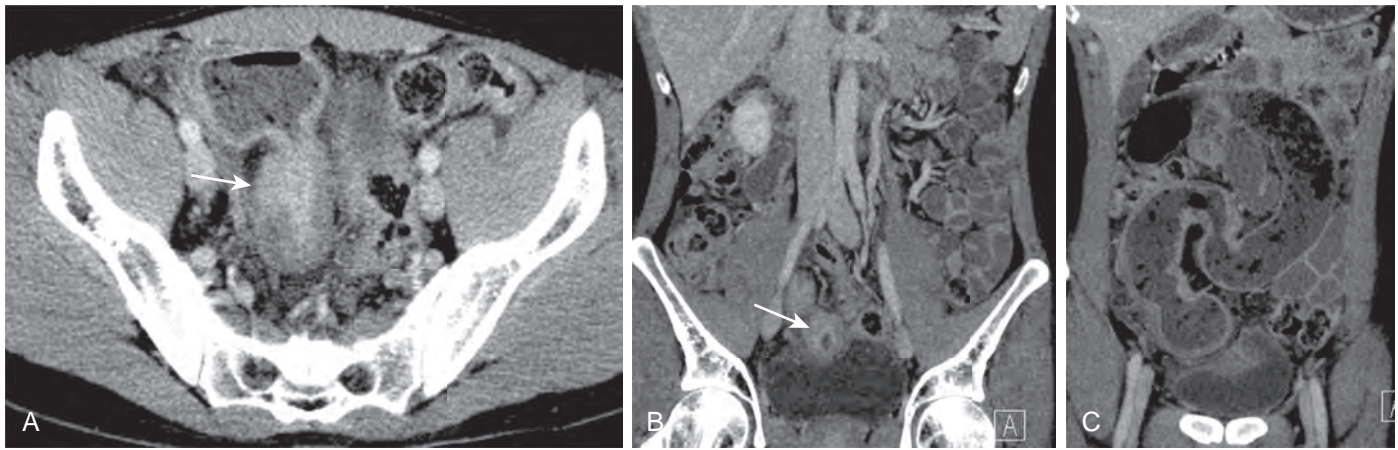


Figure 41-31 Mixed fibrostenotic and active inflammatory small bowel Crohn's disease: Moderate small bowel dilation with a stool sign. Postcontrast-enhanced axial (A) and coronal (B) CTE images show bilaminar to homogenous hyperenhancement, with marked bowel wall thickening in the distal ileum (arrows). C. Upstream to the stricture, there is a small bowel stool.

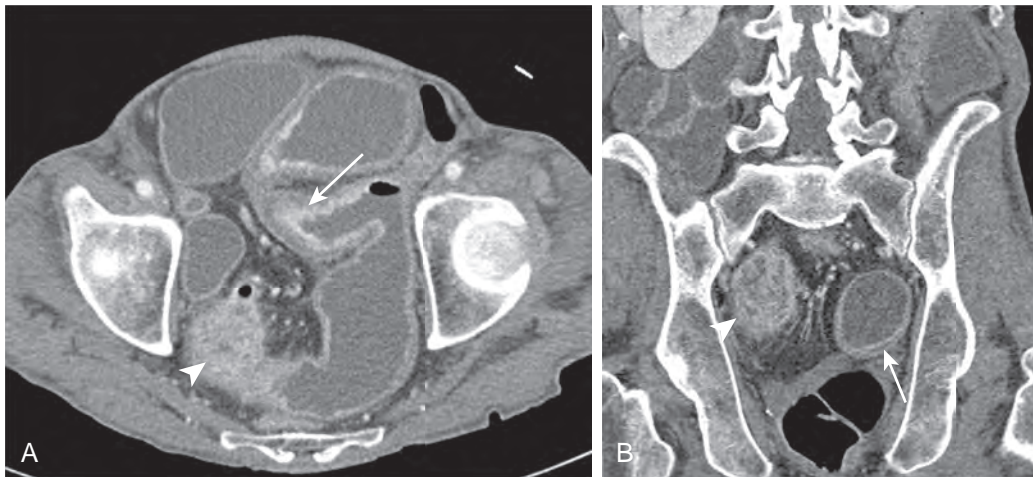


Figure 41-32 Mixed fibrostenotic and active inflammatory small bowel Crohn's disease with an adenocarcinoma. Postcontrast-enhanced axial (A) and coronal (B) CTE images show bilaminar hyperenhancement and moderate wall thickening associated with marked upstream dilation (arrows). Distal to the disease, there is a soft tissue mass (arrowheads) representing an obstructing adenocarcinoma. The patient had long-standing Crohn's disease.

Penetrating Crohn's Disease

Penetrating disease is present when there is sinus tract or fistula formation, an inflammatory mass or abscess, or free perforation (see Figs. 41-12, 41-24 to 41-27, 41-30, and 41-33). This can be in addition to the determination of active inflammatory or mixed disease. However, in almost all cases, penetrating disease occurs when there is mixed disease present. This Crohn's subtype is characterized by transmural extension of the inflammatory process, with resultant fistula formation or perforation. Deep ulcers precede sinus and fistula formation to adjacent organs and the development of abscesses. On CTE, sinus tracts are small, linear- to tubular-shaped densities extending into the mesenteric fat, outside the wall of the bowel. On MRE, sinus tracts and fistulae are demonstrated by the high signal intensity of their fluid content on true FISP and HASTE images. When present, fistulae extend from the proximal aspect of strictured, active disease or just upstream to the

disease. Furthermore, the bowel affected by the fistulae are angulated and tethered and appeared fixed. There is loss of the normal undulating, curved contour of the small bowel. Interestingly, in cases of an enterovesicular fistula, urinary bladder gas is often absent. In these cases, there is a tethered loop of bowel, angulated toward the urinary bladder, with a linear strand of tissue extending toward the bladder and thickening of the wall of the bladder. There may be interloop inflammatory masses or abscesses. The multiplanar imaging capabilities of CTE and MRE are particularly useful in depicting complex fistulae and sinus tracts. Abscesses also occur in penetrating disease.

Fibrostenotic Small Bowel Crohn's Disease

Fibrostenotic disease is present when there is wall thickening, luminal narrowing, and significant upstream dilation (>3 cm), but no wall hyperenhancement. Furthermore, there is no mural edema (MRE) or mesenteric changes. In these cases, there is no

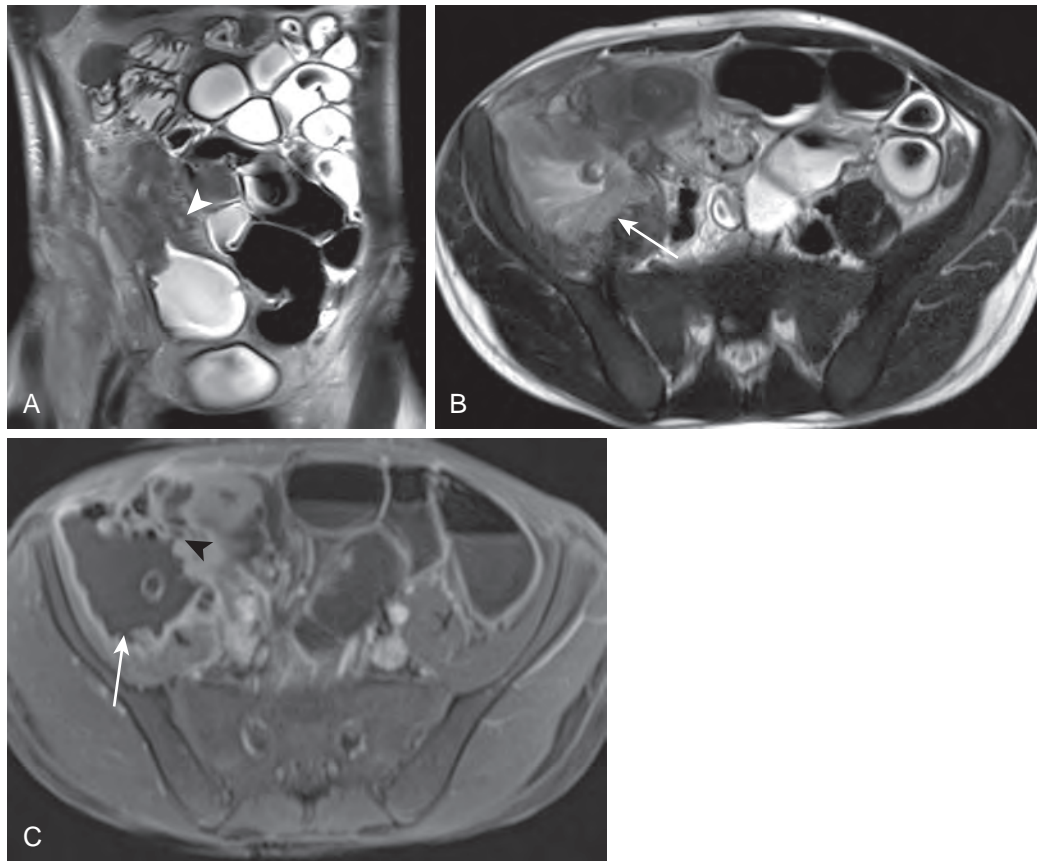


Figure 41-33 Mixed fibrostenotic and active inflammatory small bowel Crohn's disease with penetrating disease. **A.** Coronal HASTE image from MRE shows marked wall thickening of the terminal ileum with increased signal in the wall indicating mural edema–lymphatic dilation. There is also a sinus tract (white arrowhead) with increased signal in the tract. The upstream lumen is markedly dilated. **B.** Axial HASTE images show the terminal ileal wall thickening as well as an iliopsoas abscess (arrow) with heterogeneous signal. **C.** Postcontrast–enhanced axial VIBE image shows homogeneous hyperenhancement of the wall, moderate wall thickening, and the tract (black arrowhead) from the bowel to the abscess (arrow).

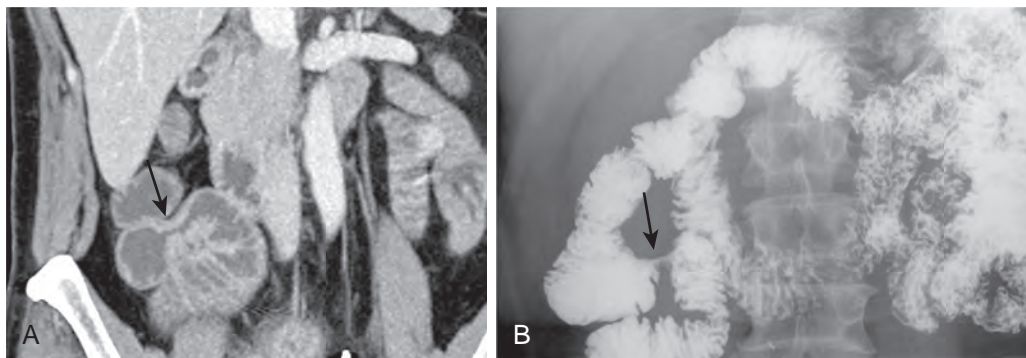


Figure 41-34 Fibrostenotic disease. **A.** Postcontrast-enhanced coronal CTE image shows mild wall thickening without hyperenhancement in the distal ileum (arrow). There is moderate upstream dilation. **B.** Small bowel series performed 3 months earlier shows the fixed stricture (arrow), with upstream dilation.

active inflammatory component. Small bowel obstruction is the predominant clinical manifestation of this disease subtype. CTE and MRE demonstrate a fixed narrowing of the involved bowel, with associated wall thickening. There is moderate to marked prestenotic dilation (Fig. 41-34).

ASSESSMENT OF DISEASE ACTIVITY

MRI and, to a lesser extent MDCT, have the potential to make the classification system of subtypes of Crohn's disease

more objective and reproducible and can help the clinician plan appropriate therapy. Differentiation between fibrotic and inflammatory stenosis is useful for selecting patients for medical (inflammatory) versus surgical (fibrotic) treatment. However, what has been published so far is based on different reference standards, including clinical indices, endoscopic scoring, biopsies, and surgical specimens.^{87,88} The problem of differentiating active inflammatory disease from fibrostenotic disease is further compounded by the fact that there is no accepted pathologic definition of these entities. Furthermore,

active inflammation and fibrostenosis coexist. Finally, patients who undergo surgical resection are distinctly different from those undergoing endoscopic biopsy because they have more severe disease.

Magnetic Resonance Imaging–Derived Disease Activity Indices

Although investigatory, several centers have compared MRE findings with endoscopic findings and have derived MRI scores (magnetic resonance index of activity [MaRIA] and activity index score [AIS]) to assess activity.^{123,124} The MaRIA is derived predominantly from findings in Crohn's colitis, whereas the AIS is derived from terminal ileal Crohn's disease based on initial histologic correlation and subsequently validated with endoscopy and endoscopic biopsies. The MaRIA is derived as follows:

$$\text{MaRIA} = (1.5 \times \text{wall thickness [in mm]}) + (0.02 \times \text{relative contrast enhancement of the bowel wall}) + (5 \times \text{the presence of edema}) + (10 \times \text{ulceration})$$

where relative contrast enhancement of the bowel wall is defined as the wall signal intensity postenhancement minus the wall signal intensity pre-enhancement divided by the wall signal intensity pre-enhancement; the presence of edema is based on hyperintensity on T2-weighted pulse sequences relative to the psoas muscle signal; and ulceration refers to deep depressions in the mucosal surface.

The AIS is derived as follows:

$$\text{AIS} = 1.79 + (1.34 \times \text{mural thickness [in mm]}) + 0.94 \times \text{mural T2 score}$$

where the mural T2 score is a qualitative score from 0 to 3, ranging from equivalent to adjacent, normal bowel wall signal to marked increased signal, nearly equivalent to the lumen.

Although these scores have been validated in small numbers of patients in two separate centers, more studies are necessary to determine their broad applicability.

Additional Imaging Considerations

POSITRON EMISSION TOMOGRAPHY, POSITRON EMISSION TOMOGRAPHY/COMPUTED TOMOGRAPHY, AND POSITRON EMISSION TOMOGRAPHY/MAGNETIC RESONANCE IMAGING

PET and PET/CT have been used recently to assess the level of inflammation in patients with Crohn's disease.¹²⁵⁻¹²⁸ The studies are preliminary but show that the addition of PET may assist in characterizing the disease further. The recent addition of PET

to MR (PET/MR hybrid imaging, or molecular MR) is an exciting new area of research.¹²⁹ As with other imaging investigations of small bowel Crohn's disease, accepted, validated surrogates of disease activity, supported by pathology, will be necessary to show efficacy.

CROHN'S JEJUNOILEITIS

Diffuse jejunoileitis forms a subset of Crohn's enteritis in which the distal ileum may be spared and disease progression may be craniad. It affects less than 10% of patients with Crohn's disease of the small bowel.⁷ Jejunoileitis affects younger patients, has a more acute onset, and requires more extensive bowel resections than distal Crohn's disease. In some cases, proximal progression with involvement of the duodenum has been noted.

CROHN'S ASSOCIATED ADENOCARCINOMA, NEUROENDOCRINE TUMOR, AND LYMPHOMA

An increased prevalence of small bowel carcinoma has been reported in patients with Crohn's disease involving the small bowel.^{130,131} Most investigators agree that Crohn's cancers exhibit special features—younger persons are more likely to be affected; the distal ileum is the usual site of involvement (most adenocarcinomas of the small bowel are proximal, centered around the ligament of Treitz); and areas of long-standing disease are more likely to undergo malignant change, rendering a radiologic diagnosis more difficult. Surgically bypassed bowel is another site more likely to be involved by tumor when radiologic diagnosis is extremely difficult, but this form of surgery is no longer performed. Carcinoma may also arise at the site of fistulae, so that any bleeding from these fistulae should be viewed with suspicion. A preoperative radiologic diagnosis is almost always impossible because of the absence of characteristic features; this is also usually the case at laparotomy. However, careful scrutiny of an obstructive site is essential to identify a mass (see Fig. 41-32). It is not surprising that patients with Crohn's carcinoma have a dismal prognosis, with an overall survival from the time of diagnosis measured in months.

Studies have shown an association between neuroendocrine tumors and Crohn's disease, with the tumor present in the face of disease.¹³² Although there has been some concern that lymphoma may develop in patients with Crohn's disease, evidence to date does not confirm the association of Crohn's disease and lymphoma.¹³³ However, with the increasing use of long-term immunomodulators and anti-tumor necrosis factor therapy, the risk of lymphoma may increase in Crohn's patients.

Acknowledgment

To Reed P. Rice, MD, a valued friend, colleague, mentor, and teacher, who taught me (MEB) all I know about Crohn's disease.

REFERENCES

1. Nguyen GC, Chong CA, Chong RY: National estimates of the burden of inflammatory bowel disease among racial and ethnic groups in the United States. *J Crohns Colitis* 18:288–295, 2014.
2. Ponder A, Long MD: A clinical review of recent findings in the epidemiology of inflammatory bowel disease. *Clin Epidemiol* 5:237–247, 2013.
3. Ng SC: Epidemiology of inflammatory bowel disease: Focus on Asia. *Best Pract Res Clin Gastroenterol* 28:363–372, 2014.
4. Molodecky NA, Soon IS, Rabi DM, et al: Increasing incidence and prevalence of the inflammatory bowel diseases with time, based on systematic review. *Gastroenterology* 142: 46–54, 2012.
5. Rungoe C, Langholz E, Andersson M, et al: Changes in medical treatment and surgery rates in inflammatory bowel disease: a nationwide cohort study 1979–2011. *Gut* 2013. doi: 10.1136/gutjnl-2013-305607. [Epub ahead of print.]
6. Peyrin-Biroulet L, Loftus EV, Jr, Colombel JF, Sandborn WJ: The natural history of

- adult Crohn's disease in population-based cohorts. *Am J Gastroenterol* 105:289–297, 2010.
7. Malaty HM, Mehta S, Abraham B, et al: The natural course of inflammatory bowel disease-indeterminate from childhood to adulthood: within a 25 year period. *Clin Exp Gastroenterol* 6:115–121, 2013.
 8. Riddell RH: Pathology of idiopathic inflammatory bowel disease. In Sartor RB, Sandborn WJ, editors: *Kirsner's Inflammatory Bowel Diseases*, ed 6, Edinburgh, 2004, Saunders, pp 399–424.
 9. Satsangi J, Silverberg MS, Vermeire S, Colombi JF: The Montreal classification of inflammatory bowel disease: Controversies, consensus and implications. *Gut* 55:749–753, 2006.
 10. Zappa M, Stefanescu C, Cazals-Hamtem D, et al: Which magnetic resonance imaging findings accurately evaluate inflammation in small bowel Crohn's disease? A retrospective comparison with surgical pathologic analysis. *Inflamm Bowel Dis* 17:984–993, 2011.
 11. Adler J, Pungalia DR, Dillman JR, et al: Computed tomography enterography findings correlate with tissue inflammation, not fibrosis in resected small bowel Crohn's disease. *Inflamm Bowel Dis* 18:849–856, 2012.
 12. Kelly JK, Preshaw RM: Origin of fistulae in Crohn's disease. *J Clin Gastroenterol* 11:193–196, 1989.
 13. Oberhuber G, Stangl PC, Vogelsang H, et al: Significant association of strictures and internal fistula formation in Crohn's disease. *Virchows Arch* 437:293–297, 2000.
 14. van Assche G: Emerging drugs to treat Crohn's disease. *Expert Opin Emerg Drugs* 12:49–59, 2007.
 15. Creed TJ, Probert CS: Review article: Steroid resistance in inflammatory bowel disease—mechanisms and therapeutic strategies. *Aliment Pharmacol Ther* 25:111–122, 2007.
 16. Parsi MA, Lashner BA, Achkar JP, et al: Type of fistula determines response to infliximab in patients with fistulous Crohn's disease. *Am J of Gastroenterol* 99:445–449, 2004.
 17. Teitelbaum JE, Saeed S, Triantafyllopoulou M, et al: Infliximab in pediatric Crohn disease patients with enterovesicular fistulae. *J Pediatr Gastroenterol Nutr* 44:279–282, 2007.
 18. Panes J, Bouhnik Y, Reinisch W, et al: Imaging techniques for assessment of inflammatory bowel disease: Joint ECCO and ESGAR evidence-based consensus guidelines. *J Crohn's Colitis* 7:556–585, 2013.
 19. Ueno F, Matsui T, Matsumoto T, et al: Evidence-based clinical practice guidelines for Crohn's disease, integrated with formal consensus of experts in Japan. *J Gastroenterol* 48:31–72, 2013.
 20. Valle J, Alcantara M, Perez-Gruesso MJ, et al: Clinical features of patients with negative results from traditional diagnostic work-up and Crohn's disease findings from capsule endoscopy. *J Clin Gastroenterol* 40:692–696, 2006.
 21. Marmo R, Rotondano G, Piscopo R, et al: Capsule endoscopy versus enteroclysis in the detection of small-bowel involvement in Crohn's disease: A prospective trial. *Clin Gastroenterol Hepatol* 3:772–776, 2005.
 22. Triester SL, Leighton JA, Leontiadis GI, et al: A meta-analysis of the yield of capsule endoscopy compared to other diagnostic modalities in patients with non-stricturing small bowel Crohn's disease. *Am J Gastroenterol* 101:954–964, 2006.
 23. Bruining DH, Loftus EV: Evolving diagnostic strategies for inflammatory bowel disease. *Curr Gastroenterol Rep* 8:478–485, 2006.
 24. Hara AK, Leighton JA, Sharma VK, et al: Imaging of small bowel disease: Comparison of capsule endoscopy, standard endoscopy, barium examination, and CT. *Radiographics* 25:697–711, 2005.
 25. Hara AK, Leighton JA, Heigh RI, et al: Crohn disease of the small bowel: Preliminary comparison among CT enterography, capsule endoscopy, small-bowel follow-through, and ileoscopy. *Radiology* 238:128–134, 2006.
 26. Hara AK, Leighton JA, Sharma VK, et al: Small bowel: Preliminary comparison of capsule endoscopy with barium study and CT. *Radiology* 230:260–265, 2004.
 27. Voderholzer WA, Beinhöelz J, Rogalla P, et al: Small bowel involvement in Crohn's disease: A prospective comparison of wireless capsule endoscopy and computed tomography enteroclysis. *Gut* 54:369–373, 2005.
 28. Erber WF, Erber JA: Meta-analysis of the yield of capsule endoscopy in patients with Crohn's Disease. *Am J of Gastroenterol* 101:954–964, 2006.
 29. Golder SK, Schreyer AG, Endlicher E, et al: Comparison of capsule endoscopy and magnetic resonance (MR) enteroclysis in suspected small bowel disease. *Int J Colorectal Dis* 2:97–104, 2006.
 30. Jensen DM, Nathan T, Rafaelsen SR, Kjeldsen J: Diagnostic accuracy of capsule endoscopy for small bowel Crohn's disease is superior to that of MR enterography or CT enterography. *Clin Gastroenterol Hepatol* 9:124–129, 2011.
 31. Solem CA, Loftus EV, Fletcher JG, et al: Small-bowel imaging in Crohn's disease: A prospective, blinded, 4-way comparison trial. *Gastrointest Endosc* 68:255–286, 2008.
 32. Maglinte DD: Fluoroscopic and CT enteroclysis: Evidence-based clinical update. *Radio Clin North Am* 51:149–176, 2013.
 33. Marshak RH: Granulomatous disease of the intestinal tract (Crohn's disease). *Radiology* 114:3–22, 1975.
 34. Goldberg HI, Caruthers SB, Nelson JA, et al: Radiographic findings of the National Cooperative Crohn's Disease Study. *Gastroenterology* 77:925–937, 1979.
 35. Maglinte DDT, Chernish SM, Kelvin FM, et al: Crohn disease of the small intestine: Accuracy and relevance of enteroclysis. *Radiology* 184:1–6, 1992.
 36. Glick SN: Crohn's disease of the small intestine. *Radiol Clin North Am* 25:25–45, 1987.
 37. Rubesin SE, Bronner M: Radiologic-pathologic concepts in Crohn's disease. *Adv Gastrointest Radiol* 1:27–55, 1991.
 38. Ekberg O, Lindstrom C: Superficial lesions in Crohn's disease of the small bowel. *Gastrointest Radiol* 4:389–393, 1979.
 39. Jones B, Hamilton SR, Rubesin SE, et al: Granular small bowel mucosa: A reflection of villous abnormality. *Gastrointest Radiol* 12: 219–225, 1987.
 40. Nolan DJ, Gourtsoyannis NC: Crohn's disease of the small intestine: A review of the radiological appearances in 100 consecutive patients examined by a barium infusion technique. *Gastrointest Radiol* 31:597–603, 1980.
 41. Marshak RH, Wolf BS: Roentgen findings in regional enteritis. *AJR* 74:1000–1014, 1955.
 42. Herlinger H, Rubesin SE, Furth EE: Mesenteric border linear ulcer in Crohn's disease: Historical, radiologic and pathologic perspectives. *Abdom Imaging* 23:122–126, 1998.
 43. Buck JL, Dachman AH, Sobin LH: Polypoid and pseudopolypoid manifestations of inflammatory bowel disease. *Radiographics* 11:293–304, 1991.
 44. Nolan DJ, Piris J: Crohn's disease of the small intestine: A comparative study of the radiological and pathological appearances. *Clin Radiol* 31:591–596, 1980.
 45. Herlinger H, Furth EE, Rubesin SE: Fibrofatty proliferation of the mesentery in Crohn's disease: The query corner. *Abdom Imaging* 23:1–3, 1998.
 46. Goldberg HI, Caruthers SB, Nelson JA, Singleton JW: Radiographic findings of the national cooperative Crohn's disease study. *Gastroenterology* 77:925–937, 1979.
 47. Strobel D, Goertz RS, Bernatik T: Diagnostics in inflammatory bowel disease: Ultrasound. *World J Gastroenterol* 17:3192–3197, 2011.
 48. Quaiia E: Contrast-enhanced ultrasound of the small bowel in Crohn's disease. *Abdom Imaging* 38:1005–1013, 2013.
 49. Tarjan Z, Toth G, Gyorko T, et al: Ultrasound in Crohn's disease of the small bowel. *Eur J Radiol* 35:176–182, 2000.
 50. Maconi G, Sampietro GM, Parente F, et al: Contrast radiology, computed tomography and ultrasonography in detecting internal fistulae and intra-abdominal abscesses in Crohn's disease: A prospective comparative study. *Am J Gastroenterol* 98:1545–1555, 2003.
 51. Parente F, Maconi G, Bollani S, et al: Bowel ultrasound in assessment of Crohn's disease and detection of related small bowel strictures: A prospective comparative study versus x ray and intraoperative findings. *Gut* 50:490–495, 2002.
 52. Bru C, Sans M, Defelitto MM, et al: Hydrocolonoscopy for evaluating inflammatory bowel disease. *AJR* 177:99–105, 2001.
 53. Byrne MF, Farrell MA, Abass S, et al: Assessment of Crohn's disease activity by Doppler sonography of the superior mesenteric artery, clinical evaluation and the Crohn's disease activity index: A prospective study. *Clin Radiol* 56:973–978, 2001.
 54. Maconi G, Radice E, Greco S, et al: Bowel ultrasound in Crohn's disease. *Best Pract Res Clin Gastroenterol* 20:93–112, 2006.
 55. Fraquelli M, Colli A, Casazza C, et al: Role of US in detection of Crohn disease: Meta-analysis. *Radiology* 236:95–101, 2005.
 56. Spalinger J, Patriquin H, Miron M-C, et al: Doppler US in patients with Crohn disease: Vessel density in the diseased bowel reflects disease activity. *Radiology* 217:787–793, 2000.
 57. De Pascale A, Garofalo G, Perna M, et al: Contrast-enhanced ultrasonography in Crohn's disease. *Radiol Med (Torino)* 111:539–550, 2006.
 58. Calabrese E, La Seta F, Buccellato A, et al: Crohn's disease: A comparative prospective study of transabdominal ultrasonography, small intestine contrast ultrasonography, and small bowel enema. *Inflamm Bowel Dis* 11:139–145, 2005.
 59. Yekeler E, Danalioglu A, Movasseghi B, et al: Crohn disease activity evaluated by Doppler ultrasonography of the superior mesenteric artery and the affected small-bowel segments. *J Ultrasound Med* 24:59–65, 2005.

60. Parente F, Greco S, Molteni M, et al: Modern imaging of Crohn's disease using bowel ultrasound. *Inflamm Bowel Dis* 10:452–461, 2004.
61. Miao YM, Koh DM, Amin Z, et al: Ultrasound and magnetic resonance imaging assessment of active bowel segments in Crohn's disease. *Clin Radiol* 57:913–918, 2002.
62. Potthast S, Rieber A, Von Tirpitz C, et al: Ultrasound and magnetic resonance imaging in Crohn's disease: A comparison. *Eur Radiol* 12:1416–1422, 2002.
63. Rispo A, Imbriaco M, Celentano L, et al: Non-invasive diagnosis of small bowel Crohn's disease: Combined use of bowel sonography and Tc-99m-HMPAO leukocyte scintigraphy. *Inflamm Bowel Dis* 11:376–382, 2005.
64. Ruess L, Blask ARN, Bulas DI, et al: Inflammatory bowel disease in children and young adults: Correlation of sonographic and clinical parameters during treatment. *AJR* 175:79–84, 2000.
65. Maconi G, Di Sabatino A, Ardizzone S, et al: Prevalence and clinical significance of sonographic detection of enlarged regional lymph nodes in Crohn's disease. *Scand J Gastroenterol* 40:1328–1333, 2005.
66. Bremner AR, Pridgeon J, Fairhurst J, et al: Ultrasound scanning may reduce the need for barium radiology in the assessment of small-bowel Crohn's disease. *Acta Paediatr* 93:479–481, 2004.
67. Valette PJ, Rioux M, Pilleul F, et al: Ultrasonography of chronic inflammatory bowel diseases. *Eur Radiol* 11:1859–1866, 2001.
68. Dillman JR, Stidham RW, Higgins PDR, et al: US elastography-derived shear wave velocity helps distinguish acutely inflamed from fibrotic bowel in a Crohn disease animal model. *Radiology* 267:757–766, 2013.
69. Wiarda BM, Kuipers EJ, Heitbrink MA, et al: MR enteroclysis of inflammatory small-bowel diseases. *AJR* 187:522–531, 2006.
70. Masselli G, Casciani E, Poletti E, et al: Assessment of Crohn's disease in the small bowel: Prospective comparison of magnetic resonance enteroclysis with conventional enteroclysis. *Eur Radiol* 16:2817–2827, 2006.
71. Pauls S, Gabelmann A, Schmidt SA, et al: Evaluating bowel wall vascularity in Crohn's disease: A comparison of dynamic MRI and wideband harmonic imaging contrast-enhanced low MI ultrasound. *Eur Radiol* 16:2410–2417, 2006.
72. Gourtsoyiannis NC, Grammatikakis J, Papanastorakis G, et al: Imaging of small intestinal Crohn's disease: Comparison between MR enteroclysis and conventional enteroclysis. *Eur Radiol* 16:1915–1925, 2006.
73. Rottgen R, Herzog H, Lopez-Hanin E, et al: Bowel wall enhancement in magnetic resonance colonography for assessing activity in Crohn's disease. *Clin Imaging* 30:27–31, 2006.
74. Maccioni F, Bruni A, Viscido A, et al: MR imaging in patients with Crohn disease: Value of T2- versus T1-weighted gadolinium-enhanced MR sequences with use of an oral superparamagnetic contrast agent. *Radiology* 238:517–530, 2006.
75. Koh M, Miao Y, Chinn RJS, et al: MR imaging evaluation of the activity of Crohn's disease. *AJR* 177:1325–1332, 2001.
76. Gourtsoyiannis NC, Papanikolaou N: Magnetic resonance enteroclysis. *Semin Ultrasound CT MRI* 26:237–246, 2005.
77. Wiarda BM, Kuipers EJ, Houdijk LP, et al: MR enteroclysis: Imaging technique of choice in diagnosis of small bowel diseases. *Dig Dis Sci* 50:1036–1040, 2005.
78. Horsthuis K, Lavini Mphil C, Stoker J: MRI in Crohn's disease. *J Magn Reson Imaging* 22:1–12, 2005.
79. Laghi A, Paolantonio P, Passariello R: Small bowel. *Magn Reson Imaging Clin North Am* 13:331–348, 2005.
80. Zalis M, Singh AK: Imaging of inflammatory bowel disease: CT and MR. *Dig Dis* 22:56–62, 2004.
81. Narin B, Ajaj W, Gohde S, et al: Combined small and large bowel MR imaging in patients with Crohn's disease: A feasibility study. *Eur Radiol* 14:1535–1542, 2004.
82. Gourtsoyiannis N, Papanikolaou N, Grammatikakis J, et al: Assessment of Crohn's disease activity in the small bowel with MR and conventional enteroclysis: Preliminary results. *Eur Radiol* 14:1017–1024, 2004.
83. Low RN, Sebrechts CP, Politske DA, et al: Crohn disease with endoscopic correlation: Single-shot fast spin-echo and gadolinium-enhanced fat-suppressed spoiled gradient-echo MR imaging. *Radiology* 222:652–660, 2002.
84. Sempere GAJ, Sanjuan VM, Chulia EM, et al: MRI evaluation of inflammatory activity in Crohn's disease. *AJR* 184:1829–1835, 2005.
85. Schunk K: Small bowel magnetic resonance imaging for inflammatory bowel disease. *Top Magn Reson Imaging* 13:409–425, 2002.
86. Maccioni F, Bruni A, Viscido A, et al: MR imaging in patients with Crohn disease: Value of T2- versus T1-weighted gadolinium-enhanced MR sequences with use of an oral superparamagnetic contrast agent. *Radiology* 238:517–530, 2006.
87. Makanyanga J, Punwani S, Taylor SA: Assessment of wall inflammation and fibrosis in Crohn's disease: Value of T1-weighted gadolinium-enhanced MR imaging. *Abdom Imaging* 37:933–943, 2012.
88. Maccioni F, Staltari I, Pino AR, Tiberti A: Value of T2-weighted magnetic resonance imaging in the assessment of wall inflammation and fibrosis in Crohn's disease. *Abdom Imaging* 37:944–957, 2012.
89. Lee SS, Kim AY, Yang SK, et al: Crohn disease of the small bowel: Comparison of CT enterography, MR enterography, and small-bowel follow-through as diagnostic techniques. *Radiology* 251:751–761, 2009.
90. Siddiki HA, Fidler JL, Fletcher JG, et al: Prospective comparison of state-of-the-art MR enterography and CT enterography in small-bowel Crohn's disease. *AJR Am J Roentgenol* 193:113–121, 2009.
91. Jensen MD, Ormstrup T, Vagn-Hansen C, et al: Interobserver and intermodality agreement for detection of small bowel Crohn's disease with MR enterography and CT enterography. *Inflamm Bowel Dis* 17:1081–1088, 2011.
92. Fiorino G, Bonifacio C, Peyrin-Biroulet L, et al: Prospective comparison of computed tomography enterography and magnetic resonance enterography for assessment of disease activity and complications in ileocolonic Crohn's disease. *Inflamm Bowel Dis* 17:1073–1080, 2011.
93. Swanson AJ, Schmiedlin-Ren P, Higgins PD, et al: Magnetization transfer helps detect intestinal fibrosis in an animal model of Crohn disease. *Radiology* 259:127–135, 2011.
94. Booya F, Fletcher JG, Huprich JE, et al: Active Crohn disease: CT findings and interobserver agreement for enteric phase CT enterography. *Radiology* 241:787–795, 2006.
95. Bodily KD, Fletcher JG, Solem CA, et al: Crohn disease: Mural attenuation and thickness at contrast-enhanced CT enterography—correlation with endoscopic and histologic findings of inflammation. *Radiology* 238:505–516, 2006.
96. Colombel JF, Solem CA, Sandborn WJ, et al: Quantitative measurement and visual assessment of ileal Crohn's disease activity by computed tomography enterography: Correlation with endoscopic severity and C-reactive protein. *Gut* 55:1561–1567, 2006.
97. Wold PB, Fletcher JG, Johnson CD, et al: Assessment of small bowel Crohn disease: Non-invasive peroral CT enterography compared with other imaging methods and endoscopy—feasibility study. *Radiology* 229:275–281, 2003.
98. Maglinte DD: Science to practice: Do mural attenuation and thickness at contrast-enhanced CT enterography correlate with endoscopic and histologic findings of inflammation in Crohn disease? *Radiology* 238:381–382, 2006.
99. Sailer S, Peloschek P, Schobe E, et al: Diagnostic value of CT enteroclysis compared with conventional enteroclysis in patients with Crohn's disease. *AJR* 185:1575–1581, 2005.
100. Hara AK, Leighton JA, Heigh RI, et al: Crohn disease of the small bowel: Preliminary comparison among CT enterography, capsule endoscopy, small-bowel follow-through, and ileoscopy. *Radiology* 238:128–134, 2005.
101. Paulsen SR, Huprich JE, Fletcher JG, et al: CT enterography as a diagnostic tool in evaluating small bowel disorders: Review of clinical experience with over 700 cases. *Radiographics* 26:641–657, 2006.
102. Liu YB, Liang CH, Zhang ZL, et al: Crohn disease of small bowel: Multidetector row CT with CT enteroclysis, dynamic contrast enhancement, CT angiography, and 3D imaging. *Abdom Imaging* 31:668–674, 2006.
103. Zissin R, Hertz M, Paran H, et al: Small bowel obstruction secondary to Crohn disease: CT findings. *Abdom Imaging* 29:320–325, 2004.
104. Lee SS, Ha HK, Yang S-K, et al: CT of prominent pericolic or perienteric vasculature in patients with Crohn's disease: Correlation with clinical disease activity and findings on barium studies. *AJR* 179:1029–1036, 2002.
105. Choi D, Jin Lee S, Ah Cho Y, et al: Bowel wall thickening in patients with Crohn's disease: CT patterns and correlation with inflammatory activity. *Clin Radiol* 58:68–74, 2001.
106. Furukawa A, Saotome T, Yamasaki M, et al: Cross-sectional imaging in Crohn disease. *Radiographics* 24:689–702, 2004.
107. Vandenbroucke F, Mortelet KJ, Tatli S, et al: Noninvasive multidetector computed tomography enterography in patients with small-bowel Crohn's disease: Is a 40-second delay better than 70 seconds? *Acta Radiol* 48:1052–1060, 2007.
108. Baker ME, Walter J, Obuchowski NA, et al: Mural attenuation in normal small bowel and active inflammatory Crohn's disease on CT enterography: Location, absolute attenuation, relative attenuation, and the effect of wall thickness. *AJR* 192:417–423, 2009.
109. Desmond AN, O'Regan K, Curran C, et al: Crohn's disease: Factors associated with exposure to high levels of diagnostic radiation. *Gut* 57:1524–1529, 2008.

110. Peloquin JM, Pardi DS, Sandborn WJ, et al: Diagnostic ionizing radiation exposure in a population-based cohort of patients with inflammatory bowel disease. *Am J Gastroenterol* 103:2015–2022, 2008.
111. Kroeker KI, Lam S, Birchall I, Fedorak RN: Patients with IBD are exposed to high levels of ionizing radiation through CT scan diagnostic imaging: A five-year study. *J Clin Gastroenterol* 45:34–39, 2011.
112. Chatu S, Subramanian V, Pollok RC: Meta-analysis: Diagnostic medical radiation exposure in inflammatory bowel disease. *Aliment Pharmacol Ther* 35:529–539, 2012.
113. Pearce MS, Salotti JA, Little MP, et al: Radiation exposure from CT scans in childhood and subsequent risk of leukaemia and brain tumors: A retrospective cohort study. *Lancet* 380:499–505, 2012.
114. Brenner DJ, Hall EJ: Cancer risks from CT scans: Now we have data, what next? *Radiology* 265:330–331, 2012.
115. Kanal KM, Chung JH, Wang J, et al: Image noise and liver lesion detection with MDCT: A phantom study. *AJR* 197:437–441, 2011.
116. Hernandez-Giron I, Geleijns J, Calzado A, Veldkamp WJH: Automated assessment of low contrast sensitivity for CT systems using a model observer. *Med Phys* 38(Suppl 1):S25, 2011.
117. Baker ME, Dong F, Primak A, et al: Contrast-to-noise ratio and low-contrast object resolution on full-and low-dose MDCT: SAFIRE versus filtered back projection in a low-contrast object phantom and in the liver. *AJR* 199:8–18, 2012.
118. Pickhardt PJ, Lubner MG, Kim DH, et al: Abdominal CT with model-based iterative reconstruction (MBIR): Initial results of a prospective trial comparing ultralow-dose with standard-dose imaging. *AJR* 199:1266–1274, 2012.
119. Elsayes KM, Al-Hawary MM, Jagdish J, et al: CT enterography: Principles, trends, and interpretation of findings. *Radiographics* 30:1955–1974, 2010.
120. Ziech M, Bossuyt PM, Laghi A, et al: Grading luminal Crohn's disease: Which MRI features are considered as important? *Eur J Radiol* 81:e467–e472, 2012.
121. Punwani S, Rodriguez-Justo M, Bainbridge A, et al: Mural inflammation in Crohn disease: Location-matched histologic validation of MR imaging features. *Radiology* 252:712–720, 2009.
122. Taylor SA, Punwani S, Rodriguez-Justo M, et al: Mural Crohn disease: Correlation of dynamic contrast-enhanced MR imaging findings with angiogenesis and inflammation at histologic examination—pilot study. *Radiology* 251:369–379, 2009.
123. Rimola J, Ordas I, Rodriguez S, et al: Magnetic resonance imaging for evaluation of Crohn's disease: Validation of parameters of severity and quantitative index of activity. *Inflamm Bowel Dis* 17:1759–1768, 2011.
124. Steward MJ, Punwani S, Proctor I, et al: Non-performing small bowel Crohn's disease assessed by MRI enterography: Derivation and histopathological validation of an MR-based activity index. *Eur J Radiol* 81:2080–2088, 2012.
125. Louis E, Ancion G, Colard A, et al: Non-invasive assessment of Crohn's disease intestinal lesions with (18)F-FDG PET/CT. *J Nucl Med* 48:1053–1059, 2007.
126. Groshar D, Bernstein H, Stern D, et al: PET/CT enterography in Crohn disease: Correlation of disease activity on CT enterography with 18F-FDG uptake. *J Nucl Med* 51:1009–1014, 2010.
127. Syn PB, Morteale KJ, Britz-Cunningham S, et al: Low-dose 18F-FDG PET/CT enterography: Improving on CT enterography assessment of patients with Crohn disease. *J Nucl Med* 51:1841–1848, 2010.
128. Lenze F, Wessling J, Bremer J, et al: Detection and differentiation of inflammatory versus fibromatous Crohn's disease strictures: Prospective comparison of 18F-FDG-PET/CT, MR-enteroclysis, and transabdominal ultrasound versus endoscopic/histologic evaluation. *Inflamm Bowel Dis* 18:2252–2260, 2012.
129. Maccioni F, Patak M, Signore A, Laghi A: New frontiers of MRI in Crohn's disease: Motility imaging, diffusion-weighted imaging, perfusion MRI, MR spectroscopy, molecular imaging, and hybrid imaging (PET/MRI). *Abdom Imaging* 37:974–982, 2012.
130. Friedman S: Cancer in Crohn's disease. *Gastroenterol Clin North Am* 35:621–639, 2006.
131. Shaukat A, Virnig DJ, Howard D, et al: Crohn's disease and small bowel adenocarcinoma: A population-based case-control study. *Cancer Epidemiol Biomarkers Prev* 20:1120–1123, 2011.
132. Sigel JE, Goldblum JR: Neuroendocrine neoplasms arising in inflammatory bowel disease: A report of 14 cases. *Mod Pathol* 11:537–542, 1998.
133. Dulai PS, Siegel CA: The risk of malignancy associated with the use of biological agents in patients with inflammatory bowel disease. *Gastroenterol Clin North Am* 43:525–541, 2014.

Inflammatory Disorders of the Small Bowel Other Than Crohn's Disease

STEPHEN E. RUBESIN

CHAPTER OUTLINE

Small Intestine as an Immunologic Organ

Parasitic Infestations

Ascariasis
Hookworm Infestation (Ancylostomiasis)
Strongyloidiasis
Anisakiasis
Tapeworm (Cestode) Infestation
Trematode (Flukes) Infestation
Giardiasis
Trypanosomiasis

Bacterial Infections

Tuberculosis
Yersiniosis
Salmonellosis
Campylobacteriosis

Fungal Infections

Histoplasmosis

Viral Infections

Drug-Induced Disorders

Ulcers and Stenoses Related to Nonsteroidal Anti-Inflammatory Drugs
Fluorinated Antipyrinidines

Inflammatory Disease in Immunodeficiency

Selective Immunoglobulin A and Common Variable Immunodeficiency
Graft-Versus-Host Disease
Typhlitis
Gastrointestinal Infections in AIDS
Human Immunodeficiency Virus Enteritis
Cytomegalovirus Infection
Cryptosporidiosis
Isosporiasis and Other Intracellular Protozoans
Mycobacterium Avium-Intracellulare Complex
Actinomycosis
Candidiasis

Differential Diagnosis

With increasing immigration, tourism, and globalization of the economy, infectious conditions of the small bowel are more likely to be encountered. Some of these patients with acute infectious diseases may undergo imaging studies for symptoms such as diarrhea or right lower quadrant pain (Figs. 42-1 and 42-2). This chapter presents a review of the wide spectrum of inflammatory and infectious disorders involving the small bowel other than Crohn's disease. Inflammatory disorders that

cause malabsorption are discussed in Chapter 43, and Crohn's disease is given special treatment in Chapter 41.

Small Intestine as an Immunologic Organ

The microflora of the upper gastrointestinal (GI) tract originates from swallowed food and from the oral cavity. Small amounts of bacteria and yeasts are present in the esophagus, stomach, and duodenum—about 10^6 bacteria/mL compared with 10^{11} to 10^{12} bacteria/mL in the distal small bowel and colon.¹

A variety of mechanisms prevent bacterial colonization of the small intestine. Secretion of water, electrolytes, and mucus by epithelial cells is an important component of host protection. Mucous secretions help prevent adherence of infectious agents to epithelial cells or penetration of toxins into these cells. Intestinal motility and fluid flow also impede bacterial colonization of the small bowel. Diarrhea caused by increased secretion of fluid and electrolytes also facilitates the passage of infectious agents out of the small intestine. Bacterial colonization may occur if there is small bowel stasis because of a motor disorder, diverticulosis, or strictures.

The small intestine is one of the largest immunologic organs in the body because it has an enormous surface area that is constantly exposed to foreign antigens. In healthy individuals, the small intestine is in a chronic state of low-grade inflammation and immune activity.² In most people, foreign antigens are eliminated without producing clinical symptoms. The small intestine can exclude foreign antigens without inducing autoimmune intestinal disease caused by cross-reactivity of foreign and host antigens.

The immune system includes intraepithelial lymphocytes, lymphoid tissue in Peyer's patches in the lamina propria, neutrophils, macrophages, and mast cells. Peyer's patches are unencapsulated lymphoid clusters spanning the lamina propria.² A specialized epithelium overlies the Peyer's patches; M cells in this specialized epithelium transport antigens to the underlying lymphoid tissue.

B cells in the lamina propria synthesize immunoglobulin A (IgA) and, to a lesser degree, IgM, IgG, and IgE. Intraluminal secretion of IgA inhibits bacterial adherence to the epithelium, preventing bacterial colonization. IgA also neutralizes bacterial toxins, minimizing any deleterious effects on epithelial cell function. IgA also blocks absorption of intraluminal antigens. IgA helps neutralize intracellular pathogens but does not cause their destruction.

Intraepithelial lymphocytes are primarily T cells. These cells lie in the basal epithelium, secrete cytokines, and are involved with antigen recognition and tolerance to oral antigens. They also perform immunosurveillance against abnormal epithelial



Figure 42-1 Acute infectious enteritis. An oncologist presented with 7 days of diarrhea and right lower quadrant pain after returning from a conference in the Caribbean. CT through the pelvis shows a thickened bowel wall (arrows) in the distal ileum with a mural stratification pattern of enhancing mucosa, thickened but low-attenuation submucosa, and enhancing muscularis propria. The patient's symptoms resolved within 3 weeks. A follow-up CT was normal. Although stool cultures were negative, the presumptive diagnosis was acute infectious enteritis.

cells. T cells are markedly increased in number in graft-versus-host disease, celiac disease, and protozoan infections.

Polymorphonuclear neutrophils differentiate in the bone marrow, leave the peripheral circulation, enter the lamina propria, and traverse the epithelium to enter the intestinal lumen. Neutrophils recognize and phagocytize antibody-coated bacteria. Macrophages in the lamina propria are derived from monocytes produced in the bone marrow. They also pass through the epithelium into the lumen and are important in bacterial phagocytosis and killing. Mast cells are found in all layers of the bowel wall. They contain granules with preformed mediators of inflammation such as histamine and 5-hydroxytryptamine and are important in the defense against intestinal parasites and food antigens.

Parasitic Infestations

Worms and protozoa infect more than 25% of the world's population. Helminths (worms) are divided into roundworms (nematodes), tapeworms (cestodes), and flukes (trematodes). Nematodes are round and unsegmented. They have a body cavity and are divided into separate sexes.² Cestodes are tapelike and segmented and are hermaphrodites. Trematodes are leaf-shaped and unsegmented and are also hermaphrodites.

ASCARIASIS

Ascaris lumbricoides is the most common intestinal worm, infecting about 25% of the world's population, most frequently people living in the tropics and subtropics.³ Ascariasis is acquired by ingesting mature eggs from contaminated soil, food, or water. Two to 3 weeks after ingestion of eggs, larvae develop in the small intestine. The larvae penetrate the mucosa, enter vessels in the bowel wall to reach the portal venous system, and migrate through the liver and heart to the lungs. The larvae then



Figure 42-2 Acute infectious ileitis. A young man presented with 2 weeks of right lower quadrant pain and mild diarrhea. This spot image from a peroral pneumocolon shows numerous smooth, ovoid, 3- to 5-mm nodules in the terminal ileum. Endoscopic follow-up was recommended because of the degree of nodularity and the confluent appearance of the nodules (arrow). Endoscopic biopsy specimens obtained several days later showed acute inflammatory changes in the terminal ileum. A follow-up barium study was normal. Although no stool cultures were obtained, the presumptive diagnosis was acute infectious ileitis.

penetrate the alveoli, enter the tracheobronchial tree, and are swallowed. Development is completed in the small intestine, where the worms attach to the mucosal surface of the midjejunum. Worms may grow up to 40 cm in length.

Symptoms include abdominal pain and malabsorption. If the worms are present in large numbers, ascariasis can cause small bowel obstruction resulting from luminal obstruction or intussusception.^{4,5} Mature worms that migrate into the bile or pancreatic ducts may cause cholangitis or pancreatitis.

Ascaris can be identified on plain abdominal radiographs, barium studies, and computed tomography (CT) scans. Long, smooth, convoluted tubular filling defects are seen in the intestinal lumen on barium studies (Fig. 42-3) or CT.⁶ If barium enters the worm's intestinal tract, a long, thin line of barium will be present within the tubular radiolucent filling defect caused by the worm (see Fig. 42-3). Small bowel folds are usually of normal size but may be enlarged. Small nodules reflect submucosal cysts surrounded by fibrotic tissue. The radiographic diagnosis can be confirmed by detection of ova in stool specimens.

HOOKWORM INFESTATION (ANCYLOSTOMIASIS)

Hookworms are small (8-10 mm) nematodes that infect almost 1 billion people worldwide.² The incidence of hookworm



Figure 42-3 Ascariasis. A young man presented with crampy abdominal pain and mild diarrhea 1 month after returning from a vacation in Central America. This spot image of the ileum from a small bowel follow-through shows numerous smooth, tubular filling defects in the barium column (representative ascarids identified by thick arrows). Barium faintly stains the body cavity of one worm (thin arrow). (From Forbes A, Misiewicz JJ, Compton CC, et al: *Atlas of Clinical Gastroenterology*, 3rd ed. Edinburgh, Elsevier-Mosby, 2005.)

disease has decreased markedly in the southern United States with improved sanitation. *Ancylostoma duodenale* is found in southern Europe, the Mediterranean region, and the western coast of South America. *Necator americanus* causes hookworm infestation in the southern United States, the Caribbean, and South America. Both species are found in India and southeast Asia.⁷ Near adult stage larvae and adult worms attach to the small intestinal mucosa. Ova are secreted into the feces. Infection results primarily from filarial invasion of the feet (in people who walk barefoot) or hands.

Although hookworm infestation can cause abdominal pain, diarrhea, or acute GI bleeding, iron-deficiency anemia is the most common clinical presentation. Peripheral eosinophilia is present in most patients.

The jejunal mucosa is edematous and hemorrhagic at sites of intestinal attachment. Hookworms have not been demonstrated on barium studies. Jejunal fold thickening and irritability may be present.⁸ Ileal strictures have also been reported.² Regional lymphadenopathy may be present. A definitive diagnosis requires the GI demonstration of ova in stool specimens or worms in jejunal aspirates or biopsy specimens.

STRONGYLOIDIASIS

Strongyloides stercoralis is a nematode usually found in the tropics and subtropics and in areas of poor sanitation or areas in which human waste is used as fertilizer. In the United States, strongyloidiasis is found in people living in Appalachia,⁹ military personnel returning from endemic regions, and patients who are immunocompromised because of malnutrition, steroid use, AIDS, or other causes.

Filariform larvae about 0.5 mm long penetrate the skin, migrate through the venous system to the lungs, penetrate the

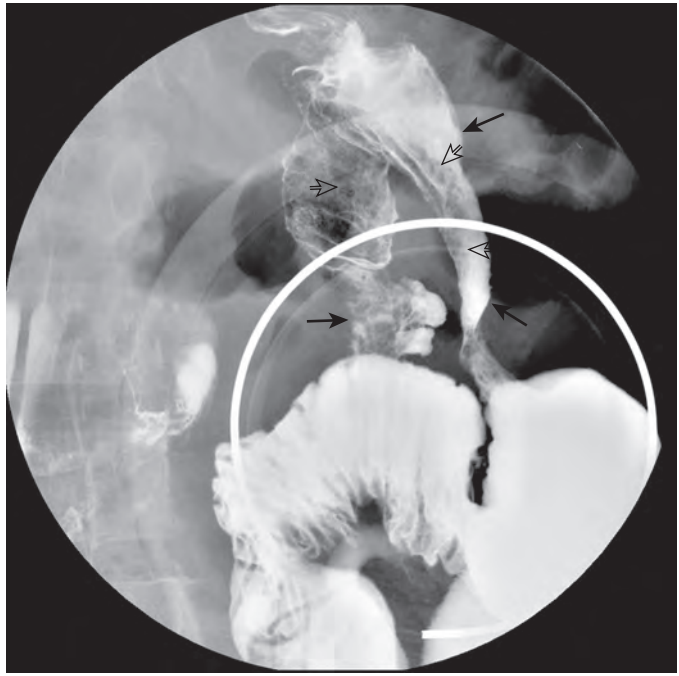


Figure 42-4 Strongyloidiasis. This spot radiograph from a small bowel follow-through in a patient with a history of partial gastrectomy shows a tubular configuration of the pancreaticobiliary and alimentary limbs (long arrows). Moderate mucosal nodularity is present (open arrows). Saccululation and fold thickening are present in the pancreaticobiliary limb.

alveoli, enter the tracheobronchial tree, and are swallowed. The larvae are transformed into adult worms in the small intestine. The females penetrate the mucosa of the duodenum and proximal jejunum and live in the superficial layers of the proximal small bowel. Male worms are expelled. Female worms are about 2 mm in length.

Strongyloidiasis differs from other nematode diseases because autoinfection may occur; these infections may be life-threatening in an immunocompromised host. Eggs released into the intestinal lumen form rhabditiform larvae that develop into infective filariform larvae in the intestinal lumen or in the soil. The filariform larvae may reinvade intestinal mucosa or perianal skin. Most larvae die in lymphatics in the wall of the small bowel or in the mesentery.

Strongyloidiasis may cause a wide variety of clinical symptoms. These include abdominal pain, diarrhea, weight loss, and malabsorption.

Mild infestation by strongyloidiasis cannot be detected on imaging studies. With chronic infection, thickened folds are seen in the duodenum and jejunum on barium studies.¹⁰ With severe infection, the small bowel folds are effaced or obliterated, and the jejunum can assume a narrowed, tubular configuration (Fig. 42-4).¹¹⁻¹³ Strongyloidiasis is also a cause of papillary stenosis and small intestinal dilation. A definitive diagnosis can be made by duodenal aspiration or biopsy.

ANISAKIASIS

Members of the Anisakidae family are nematode parasites of marine mammals. *Anisakis* larvae are found in intermediate hosts such as squid and fish (e.g., salmon, cod, anchovy, tuna,

mackerel, Pacific pollock, Pacific red snapper, herring).¹⁴ Human infection is acquired by eating raw, inadequately cooked, or pickled fish. Anisakiasis is most common in areas in which raw fish such as sushi or sashimi is frequently eaten. Ingested larvae usually attach and invade the stomach, but small or large bowel involvement may occur. Edema and inflammation develop at the site of attempted larval penetration. Ulceration and perforation with the formation of inflammatory masses have been reported. Symptoms of small bowel involvement can mimic those of acute appendicitis, Crohn's disease, or small bowel obstruction.

Anisakis larvae have been detected on double-contrast studies of the stomach and colon as thin, curved, 5-mm filling defects in the shallow barium pool.¹⁵ Focal, irregular fold thickening may be seen in the small bowel. Strictures and short, ulcerated lesions have also been described.⁸ Perforation with mesenteric abscess formation may lead to a mesenteric mass or abscess detected on cross-sectional imaging studies.¹⁶

TAPEWORM (CESTODE) INFESTATION

Cestodes live as adults in the GI tract of definitive hosts and as cysticerci in the tissue of intermediate hosts. Humans are the definitive hosts for *Taenia saginata* (beef tapeworm), *Taenia solium* (pork tapeworm), *Hymenolepis nana* (dwarf tapeworm), and *Diphyllobothrium latum* (fish tapeworm). Humans are intermediate hosts for *Echinococcus granulosus*, *Echinococcus multilocularis*, and *Taenia solium*. These worms attach to the intestinal mucosa by a scolex. A connecting region is followed by the strobila and a ribbon-like chain of developing segments (the proglottids). The number of proglottids varies from 3 to 4000, and the length of the cestode varies from several millimeters to several meters.¹⁷

Humans are infected by eating inadequately cooked beef, pork, or fish (e.g., pike, salmon, trout, whitefish, turbot). After infected flesh is ingested, the cysticercus breaks down, releasing a scolex that attaches in the upper jejunum. The adult worm develops, and proglottids and ova are released into the lumen. Tapeworm infection usually causes no symptoms. Because of its long length (up to 4–6 m), *T. saginata* may cause obstructive symptoms. In contrast, *D. latum* may cause vitamin B₁₂ deficiency and macrocytic anemia.

TREMATODE (FLUKES) INFESTATION

A variety of flukes may involve the liver, biliary tract, and intestines. The genus *Schistosoma* infects more than 150 million people worldwide.² *S. mansoni* is endemic in Africa, the Middle East, and Latin America, *S. japonicum* is endemic primarily in Asia, and *S. haematobium* is endemic in the Middle East and Africa. *S. haematobium* mainly causes genitourinary disease but is occasionally found in the appendix. Because colonic infection by schistosomiasis is more common than small bowel infection, this disease is discussed in Chapter 58.

GIARDIASIS

Giardiasis is the most common parasitic disease worldwide. In the United States, giardiasis is usually found in the Rocky Mountain states.^{18,19} Surface water contaminated by feces

from wild animals is the principal source of infection. Cysts remain viable in cold water for 1 to 3 months² and can also survive the chlorine levels of many municipal water systems. Giardiasis is transmitted primarily by fecal-oral transmission from contaminated food and pets and occasionally by oral-anal contact. The risk of infection is greater in patients with immunodeficiency states and hypochlorhydria.

After cyst ingestion, trophozoites emerge in the duodenum and proximal jejunum. The trophozoites remain in the intestinal lumen or penetrate the mucus gel layer of the proximal intestine to attach to the glycocalyx of the enterocytes. The trophozoites do not invade the epithelium. Mature cysts are excreted in the stool.

The infection varies from the asymptomatic carrier state to self-limited diarrhea or chronic, watery diarrhea. Because the infection is patchy, biopsy specimens may be normal in infected patients. Some patients may have villous atrophy with crypt hyperplasia and variable inflammation, and others may have lymphoid hyperplasia.

The small intestine frequently appears normal on small bowel follow-through studies. In about 50% of patients, there is increased intraluminal fluid and rapid small bowel transit. Some reports have described thickened folds and irritability in the duodenum and jejunum (Fig. 42-5).^{20,21} Because barium studies are abnormal in fewer than 50% of infected patients and radiographic findings are nonspecific, the diagnosis depends on the detection of cysts and trophozoites on stool examinations, detection of trophozoites on duodenal biopsies or aspirates, or positive fluorescent antibody test.²²

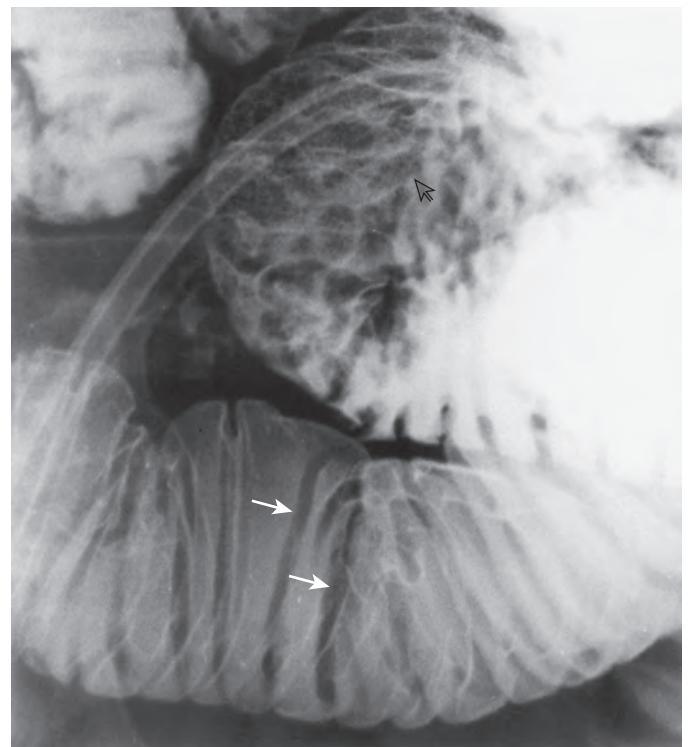


Figure 42-5 Giardiasis. Spot image of the jejunum from an enteroclysis examination shows mildly thickened folds (arrows). Tiny mucosal nodules (open arrow) reflect enlargement of villi. (Courtesy Hans Herlinger, MD.)

TRYPANOSOMIASIS

Chagas' disease is caused by the protozoan *Trypanosoma cruzi*, spread by the bite of the reduviid bug. Chagas' disease is endemic in central Brazil, northern Argentina, and Venezuela but has also been reported in southern areas of the United States. It is estimated that 350,000 people in the United States are seropositive for this infection.²³ *T. cruzi* produces a neurotoxin that attacks autonomic ganglion cells throughout the body, including those in the heart, GI tract, urinary tract, and respiratory tract.²⁴ The esophagus, duodenum, and colon are the GI organs most commonly affected, resulting in secondary achalasia, megaduodenum, and megacolon. Involvement of the mesenteric small bowel leads to dilation of the small bowel, with delayed transit.

Bacterial Infections

Traveler's diarrhea and foodborne diseases are common problems related to tainted water supplies and improperly prepared or stored food. Bacteria are the organisms usually responsible for traveler's diarrhea, which explains why prophylactic use of antibiotics decreases the incidence of traveler's diarrhea.²⁵ Chemicals, viruses, and parasites are less frequent causes of traveler's diarrhea. Enterotoxigenic *Escherichia coli* is the most common cause of traveler's diarrhea. Enteroadherent and enteropathogenic *E. coli* are less frequent causes. *Shigella* and *Campylobacter jejuni* are the next most common pathogens, but these bacteria usually involve the colon. This infection is rarely diagnosed on imaging studies, because acute watery diarrhea develops during or shortly after a period of travel.

TUBERCULOSIS

Tuberculosis is endemic in Asia. Intestinal tuberculosis is uncommon in the West, usually occurring in the homeless, alcoholics, inmates, farm workers, immigrants, or people infected with human immunodeficiency virus (HIV). With the rise of AIDS and immigration, intestinal tuberculosis has become more common in developed countries. In one hospital in London with an extensive population of Asian immigrants, new diagnoses of tuberculosis were almost as common as new diagnoses of Crohn's disease.²⁶ The proposed mechanisms of infection of the GI tract include the ingestion of infected sputum or milk and hematogenous spread to submucosal lymphatics.²⁷ Intestinal tuberculosis frequently occurs without radiographic evidence of pulmonary disease.^{26,27}

Intestinal tuberculosis primarily occurs in the ileocecal region. The distribution of tuberculosis parallels the distribution of the lymphatics. In one autopsy series of over 1000 cases, 90% of patients had ileal disease and 75% had cecal disease. Other sites were not infrequently involved, however, including the ascending colon in 51%, transverse colon in 33%, descending colon in 23%, and appendix in 33%.²⁸ Skip lesions may be present.

The three classic forms of GI tuberculosis are the ulcerative, hypertrophic, and ulcerohypertrophic forms.²⁹ Sloughing of mucosa overlying submucosal tubercles results in ulceration. These ulcers usually appear as short (3–6 mm in length) collections perpendicular to the longitudinal axis of the bowel. The ulcers may be stellate or longitudinal. Extensive inflammation and fibrosis of the bowel wall result in the hypertrophic form

of tuberculosis associated with extensive mesenteric lymphadenopathy and adhesions. Bacilli are found primarily in necrotic mesenteric lymph nodes rather than the intestinal wall. Endoscopic biopsy specimens and tissue cultures are frequently negative.^{30,31} In one study, acid-fast bacilli and caseating necrosis were found in only 32% and 50% of patients with GI tuberculosis, respectively.³² In some cases, laparoscopic diagnosis with cultures and histologic examination of ascitic fluid may be helpful. Not infrequently, however, the diagnosis of tuberculosis is made only by pathologic examination of resected surgical specimens.

Complications of small bowel tuberculosis include strictures and obstruction, fistulas, enteroliths, and chronic appendicitis.

Barium studies may reveal perpendicular, stellate, or longitudinal ulcers of varying size with heaped-up margins in the colon or ileum (usually the terminal ileum).³³ Short or long strictures may be associated with nodular mucosa. A narrow, contracted cecum associated with a gaping ileocecal valve and disproportionate inflammation of the ascending colon are findings that help distinguish ileocecal tuberculosis from Crohn's disease (Fig. 42-6).³⁴ However, longitudinal ulceration, sinus

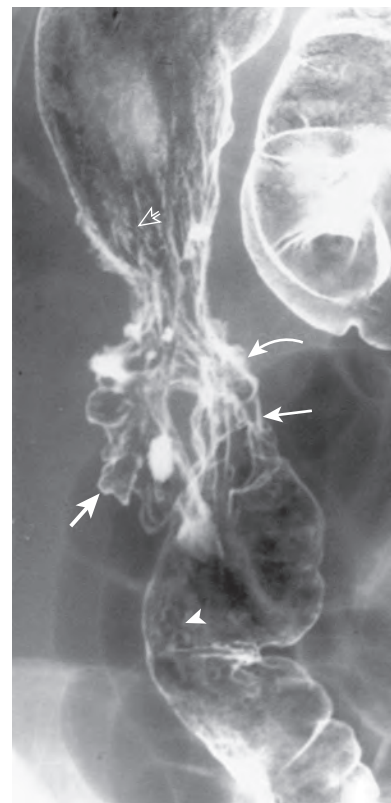


Figure 42-6 Ileocecal tuberculosis. This spot image of the ascending colon from a double-contrast barium enema shows disproportionately severe disease in the cecum versus the terminal ileum. The cecum is contracted and sacculated (*large arrow*). Granular and nodular mucosa (*open arrow*) is present in the cecum and ascending colon. The ileocecal valve is gaping (*curved arrow*). Only the distal 2 cm of the terminal ileum is narrowed (*thin arrow*). The remainder of the terminal ileum has a finely nodular mucosa (*arrowhead*). (From Rubesin SE, Bartram CI, Laufer I: *Inflammatory bowel disease*. In Levine MS, Rubesin SE, Laufer I [eds]: *Double Contrast Gastrointestinal Radiology*, 3rd ed. Philadelphia, WB Saunders, 2000, pp 417–470.)

tracts, and fistulas in the terminal ileum may be indistinguishable from those in Crohn's disease on barium studies.

CT often reveals thickening of the ileocecal valve. The medial wall of the cecum is disproportionately thickened and is often associated with a soft tissue mass that engulfs the terminal ileum.³⁵ Wall thickening may be uniform or heterogeneous. Lymphadenopathy predominates in the pericecal region but may extend into the mesentery.

Historically, radiologic differentiation of tuberculosis from Crohn's disease was facilitated by predominance of the tuberculous inflammatory process in the cecum and ascending colon, with a patulous ileocecal valve lumen and thickened ileocecal valve lips in patients with tuberculosis.³⁶ Barium studies showing disease predominantly in the cecum and ascending colon with cecal contraction and CT showing low-attenuation lymph nodes indicative of caseous necrosis should suggest tuberculosis rather than Crohn's disease as the diagnosis in these patients.³⁷ However, tuberculosis and Crohn's disease may have a similar lymphatic distribution and overlapping radiographic findings.³⁶ The clinical history and patient demographics should therefore be considered before suggesting the diagnosis of Crohn's disease.

YERSINIOSIS

Yersinia are gram-negative cocci acquired after the ingestion of contaminated food or water. *Yersinia enterocolitica* is more frequently encountered than *Yersinia pseudotuberculosis* in the United States. *Yersinia* invades epithelial cells, enters Peyer's patches in the lamina propria and submucosa, and spreads to mesenteric lymph nodes.³⁸ Ileitis, colitis, mesenteric adenitis, periappendicitis, and hemolytic uremic syndrome have been reported.³⁹ Bacterial multiplication in Peyer's patches and regional lymph nodes can result in distant infections, including chronic hepatitis, ankylosing spondylitis, and lung and kidney infections.⁴⁰

Yersinia infection leads to the development of aphthoid ulcers overlying hyperplastic lymph follicles in the bowel. Hyperplasia of follicular and interfollicular regions results in massive lymphadenopathy.⁴¹ Acute vasculitis may cause ischemia.

The radiographic appearance in *Yersinia* enterocolitis depends on the course of infection. Early in the disease, aphthoid ulcers and thickened folds may be the predominant findings in the terminal ileum.⁴² Later in the disease, the ulcers disappear but thickened undulating folds persist (Fig. 42-7). The inflammatory process is distinguished from Crohn's disease by the absence of luminal narrowing, fissures, or fistulas. The inflammatory process usually resolves in 4 to 6 weeks.

SALMONELLOSIS

Salmonella infections in the GI tract may have distinct clinical forms, including gastroenteritis, typhoid fever, and an asymptomatic carrier state. Foodborne outbreaks resulting in diarrhea are usually caused by *Salmonella enteritidis* and *Salmonella typhimurium*, found in a wide variety of sources, including eggs, poultry, and livestock. Diarrheal outbreaks caused by fecal-oral spread from human reservoirs are less common.¹ *Salmonella* enter and multiply in M cells and enterocytes and then disseminate to lymphoid tissue and macrophages in the submucosa and mesenteric lymph nodes. The diarrheal form of salmonellosis varies from a few loose stools to a severe, watery,

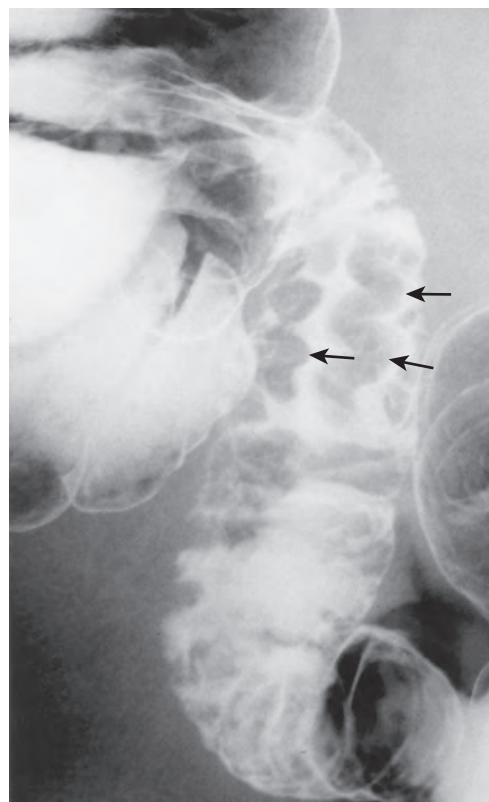


Figure 42-7 *Yersinia* ileitis. This spot image of the terminal ileum from a double-contrast barium enema shows thickened, undulating folds (arrows) in the terminal ileum. No ileal narrowing is seen.

diarrheal state. The diarrhea usually lasts from 3 to 7 days. Bacteremia is uncommon, occurring in 6% to 8% of patients.¹

Typhoid fever is usually caused by *Salmonella typhi* and *Salmonella paratyphi*. Humans are the reservoir for *S. typhi*. The organism is transmitted by the fecal-oral route, so this disease is usually found in regions with contaminated water and poor waste treatment. In most patients, a brief episode of diarrhea precedes the febrile illness. A systemic, acute febrile illness then lasts for 3 to 5 weeks, accompanied by nonspecific symptoms such as headaches, malaise, abdominal discomfort, and arthralgia. Complications of *Salmonella* include GI bleeding and perforation related to a lymphoid reaction in the ileocecal region. Bacteremia can lead to other infections, including meningitis, pericarditis, orchitis, and splenic or liver abscesses. Hepatosplenomegaly may be present. Perforation or peritonitis may cause an adynamic ileus.

Salmonella may be manifested on barium studies by longitudinally oriented ulcers in the distal ileum overlying Peyer's patches.² Prominent lymphoid hyperplasia may be present, and vascular thrombosis may be seen. The disease is sometimes detected on CT performed to evaluate hepatosplenomegaly, right lower quadrant pain, and fever. CT may reveal circumferential thickening of the terminal ileum.⁴³ Barium studies may demonstrate nonspecific fold thickening in the terminal ileum.

CAMPYLOBACTERIOSIS

Campylobacter comprises a group of gram-negative rods, including *Campylobacter jejuni*, *Campylobacter fetus*, and *Campylobacter coli*. These organisms may cause an acute enteritis or

colitis, or affected individuals may remain in an asymptomatic carrier state.⁴⁴ Colonic infections may be severe, resulting in fulminant colitis with GI bleeding or toxic megacolon.⁴⁴ Systemic manifestations (e.g., arthritis, endocarditis, genital infections, urinary infections) may occur. Cross-reactivity of *C. jejuni* and neural antigens may result in Guillain-Barré syndrome.²

When the small intestine is involved, multiple superficial ulcers may develop in the distal ileum and region of the ileocecal valve. Barium studies may reveal thickened folds and aphthoid ulcers in the distal ileum and terminal ileum.^{45,46} The radiographic findings are indistinguishable from those of yersiniosis or early Crohn's disease.

Fungal Infections

HISTOPLASMOSIS

Histoplasma capsulatum is a dimorphic fungus commonly found in the Mississippi and Ohio River valleys. This fungus occurs in a mycelial form at ambient temperature and in a yeast form at body temperature.⁴⁷ The fungus usually infects older patients or immunocompromised hosts. Small bowel infection is common in patients with disseminated disease, but clinical symptoms are usually minimal. Ileocecal disease is characterized by ulceration, mucosal nodularity, strictures, and lymphadenopathy.⁴⁷ Intestinal perforation and peritonitis may also be seen.^{48,49}

Viral Infections

Numerous viruses may infect the small intestine, resulting in an acute diarrheal state. Radiologic studies are rarely performed in this clinical setting. The diagnosis can be made by viral cultures or by enzyme-linked immunosorbent assay (ELISA) or electron microscopy of stool specimens. Cytomegalovirus involving the small bowel is described later (see “Cytomegalovirus Infection”).

Drug-Induced Disorders

Drugs may cause a variety of abnormalities in the small intestine. Ischemia can result from systemic hypotension and hypovolemia, mesenteric arterial vasoconstriction, and slow mesenteric flow with venous thrombosis (Box 42-1).⁵⁰ Ischemia is discussed in Chapter 47. Anticoagulants may cause GI bleeding. Small bowel hypomotility can be caused by narcotics, drugs with anticholinergic properties, or neurotoxic side effects (Box 42-2). Drugs may cause malabsorption by a number of mechanisms, including interference with fat digestion and absorption; decreased gastric, pancreatic, and biliary secretions; increased intestinal transit; and small bowel mucosal injury (Box 42-3). Alcohol may also cause malabsorption by damage to intestinal crypts and villi. Metals such as aluminum, lead, gold, cadmium, mercury, zirconium, and iron may also damage small bowel epithelium.

ULCERS AND STENOSES RELATED TO NONSTEROIDAL ANTI-INFLAMMATORY DRUGS

The small bowel is probably the most frequent site of gastrointestinal blood loss caused by nonsteroidal anti-inflammatory

BOX 42-1 DRUGS CAUSING SMALL BOWEL ISCHEMIA

Antihypertensive drugs and diuretics
Norepinephrine
Dopamine
Vasopressin
Digoxin
Cocaine
Ergotamines
Ergotamine
Methysergide
Oral contraceptives

BOX 42-2 DRUGS ASSOCIATED WITH SMALL BOWEL HYPOMOTILITY

Anticholinergic drugs
Phenothiazines
Tricyclic antidepressants
Verapamil
Clonidine
Vincristine
Narcotics

BOX 42-3 DRUGS ASSOCIATED WITH VARIOUS FORMS OF MALABSORPTION

Tetracycline
Cholestyramine
Colchicine
Neomycin
Methotrexate
Methylodopa
Allopurinol
Thiazide diuretics
Clofazimine

drug (NSAID) use. NSAID-related lesions have been detected with increased frequency by capsule endoscopy, enteroscopy, and enteroclysis. Small bowel ulcers are found at autopsy in approximately 8% of people who take NSAIDs.^{51,52} The mechanism of injury is unknown.

NSAID-related injury is found primarily in the ileum. Punctate, linear, or circumferential ulcers secondary to NSAIDs may cause GI bleeding or perforation. Chronic inflammation and scarring lead to the formation of characteristic weblike diaphragms and ringlike strictures in the small bowel.⁵³⁻⁵⁵ The mucosal diaphragms vary from slightly enlarged valvulae conniventes to thick, rigid, ringlike areas of narrowing. Pathologically, thick layers of hyalinized collagen are found to interdigitate with the muscularis mucosae.^{2,56}

NSAID-induced ulcers may be detected on air contrast enteroclysis. Any form of enteroclysis can detect small bowel strictures, but thin webs may be difficult to differentiate from prominent small bowel folds. Thicker webs may be seen as 2- to 5-mm thick rings encircling the bowel, associated with a tapered contour (see Chapter 46).⁵⁴

FLUORINATED ANTIPYRIMIDINES

Cells in the small bowel crypts have a high turnover rate and are particularly susceptible to chemotherapeutic drugs

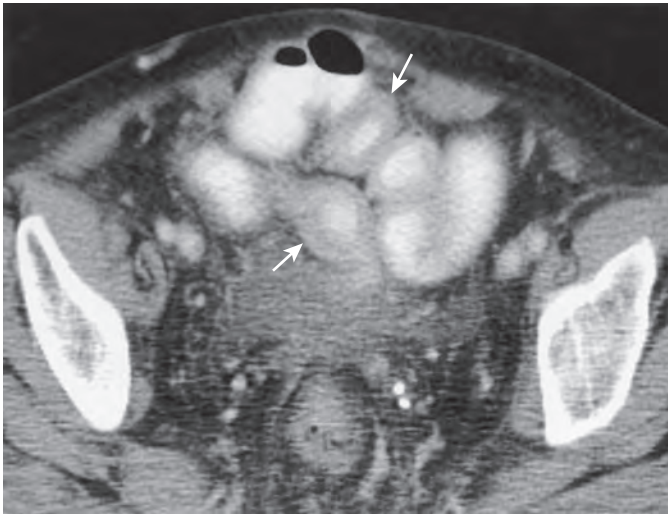


Figure 42-8 5-FUDR chemotoxicity. CT through the upper pelvis shows homogeneous thickening of the wall of several small bowel loops (arrows).

that inhibit cell proliferation. Mucosal damage occurs within the first 3 days of chemotherapy. Mucosal regeneration occurs within several weeks after cessation of chemotherapy.⁵⁰ Enteritis may be caused by chemotherapeutic agents such as dactinomycin, bleomycin, cytarabine, doxorubicin, methotrexate, 5-fluorouracil, and vincristine.⁵⁰

Enteritis related to chemotherapy can sometimes be detected on CT performed in patients with known metastatic disease who have abdominal pain and diarrhea.

Two antipyrimidines, 5-fluorouracil (5-FU) and floxuridine (5-FUDR), are used for the treatment of colonic carcinoma metastatic to the liver. Direct infusion of these agents into the hepatic artery may cause severe gastroduodenal inflammation and ulceration.⁵⁷ Intravenous (IV) infusion may also produce a severe form of gastroduodenitis and associated enteropathy, manifested by nausea, vomiting, and diarrhea. CT (usually performed for follow-up of liver metastases) may reveal marked wall thickening in the distal ileum (Fig. 42-8).⁵⁸ Barium studies may show smooth, thickened, or effaced ileal folds (Fig. 42-9).⁵⁹ The diagnosis is suggested based on the clinical history of recent chemotherapy with 5-FU or 5-FUDR. The diagnosis is confirmed if there is improvement or resolution of clinical symptoms after cessation of chemotherapy and regression of radiologic abnormalities on follow-up imaging studies.

Inflammatory Disease in Immunodeficiency

SELECTIVE IMMUNOGLOBULIN A AND COMMON VARIABLE IMMUNODEFICIENCY

Selective IgA and common variable immunodeficiency are the most common primary immune deficiency states in adults.⁶⁰ In selective IgA deficiency, there are a decreased number of IgA-producing plasma cells in the lamina propria and submucosa.² GI tract infections are uncommon, however, because there is a compensatory increase in IgM-producing plasma cells. Bacterial and viral infections of the sinonasal regions cause most clinical complaints. There is a questionable increase in giardial

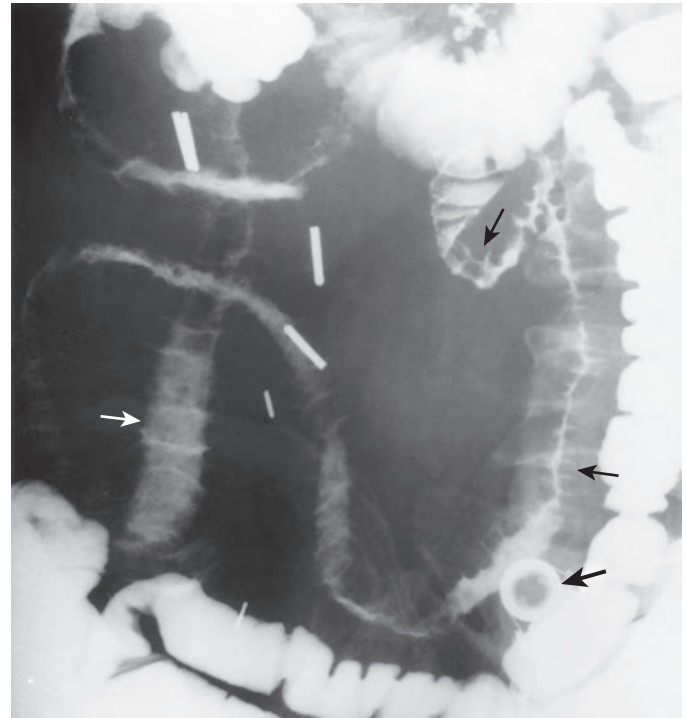


Figure 42-9 5-FUDR chemotoxicity. This spot image of the right lower quadrant shows three loops of neoterminal ileum with markedly thickened, relatively smooth folds (thin arrows) perpendicular to the longitudinal axis of the bowel. A portion of the infusion pump is identified (thick arrow). The ascending colon and cecum are surgically absent after a right hemicolectomy for colonic cancer.

infections. On barium studies, nodular lymphoid hyperplasia of the ileum is often present.

Common variable immunodeficiency is a heterogeneous group of varying B- and T-cell abnormalities that result in decreased production of IgG, IgM, and IgA, with an abnormal response to antigens and increased susceptibility to GI and respiratory infections. This heterogeneous disorder is associated with autoimmune diseases such as autoimmune hepatitis and sclerosing cholangitis. About one third of patients have the autoimmune form of atrophic gastritis with pernicious anemia and its increased risk of gastric carcinoma. Splenomegaly is frequently found. There may also be an increased risk of small bowel lymphoma in these patients.^{61,62}

Polyclonal B-cell lymphoid hyperplasia is present in the small intestine.² Lymphoid aggregates of T cells are present in the epithelium and lamina propria. A varying amount of villous atrophy is seen. Unlike gluten-sensitive enteropathy, however, a paucity of inflammatory cells is present in the lamina propria. A granulomatous reaction may also be present.

Barium studies may reveal extensive nodular lymphoid hyperplasia in the ileum (Fig. 42-10).^{63,64} The nodules are slightly larger and are more numerous and more widely distributed than the usual lymphoid follicles seen in the terminal ileum in children and young adults.

Giardiasis is common in patients with common variable immunodeficiency. Unlike disease in immunocompetent individuals, giardiasis in common variable immunodeficiency may cause severe mucosal damage and malabsorption. There is also an increased risk of colonic infections (e.g., salmonellosis) that can mimic ulcerative colitis.⁶⁰

GRAFT-VERSUS-HOST DISEASE

GI epithelium is damaged during the induction protocols for bone marrow transplantation. Anorexia, cramping, abdominal pain, and watery diarrhea occur immediately after induction by chemotherapy or radiation. Within 3 weeks, the enterocyte population is restored and symptoms subside. However, acute graft-versus-host disease (GVHD) develops in 30% to 50% of patients 3 to 11 weeks after allogeneic bone marrow transplantation. Acute GI symptoms include diarrhea, anorexia, vomiting, abdominal pain, and GI bleeding. A protein-losing enteropathy and secondary infections may occur.^{2,60} In patients with this disease, CD4⁺ T lymphocytes from the donor graft recognize host histocompatibility antigens as foreign, leading to a T cell–mediated attack on various tissues of the host. Tissue damage is most clinically evident in the skin, liver, mucous membranes, eyes, and GI tract. A maculopapular rash may be present on the palms, soles, and trunk. Acute watery diarrhea results from denudation of the intestinal epithelium. Biopsy findings vary from individual crypt cell death to total necrosis of the epithelium.⁶⁵ Submucosal edema is present. Acute GVHD is often complicated by cytomegalovirus, astrovirus, adenovirus, and *Clostridium difficile* infections.⁶⁶ Cholestasis and mild hepatocellular necrosis are reflected by abnormal liver function test results.

Chronic GVHD develops 3 to 13 months after transplantation and occurs without prior acute GVHD in 25% of patients. Esophageal changes are seen in 15% of patients, as described in Chapter 21.⁶⁷ Unlike acute GVHD, which is characterized by enterocyte necrosis, chronic GVHD is characterized by patchy fibrosis of the lamina propria and submucosa, with bacterial overgrowth.

Barium studies may confirm the diagnosis of acute or chronic GVHD and show the extent of disease. Thickened

folds and nodular mucosa may be seen (Fig. 42-11). A tubular (ribbon-like or so-called toothpaste) bowel may result from sloughing of the epithelium or such rapid transit that barium fails to coat the surface of the small bowel (Fig. 42-12).⁶⁸⁻⁷⁰ Barium may also adhere to the necrotic bowel surface, so that it is sometimes detected on abdominal radiographs or CT scans obtained after the initial barium study.^{71,72} CT may reveal a diffusely thickened small bowel wall (Fig. 42-13) with extensive submucosal edema (i.e., a target sign) or pneumatosis.⁷³ The mesentery may also be engorged, and ascites may be present.

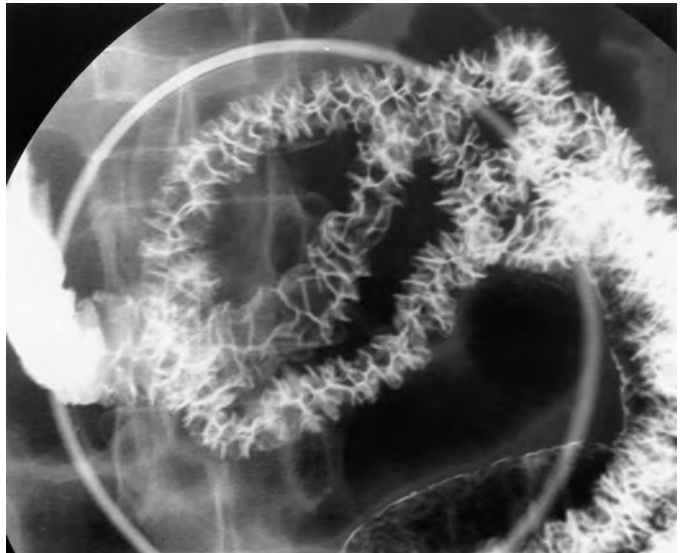


Figure 42-11 Graft-versus-host disease. This spot image from a small bowel follow-through shows diffuse fold thickening in the jejunum.

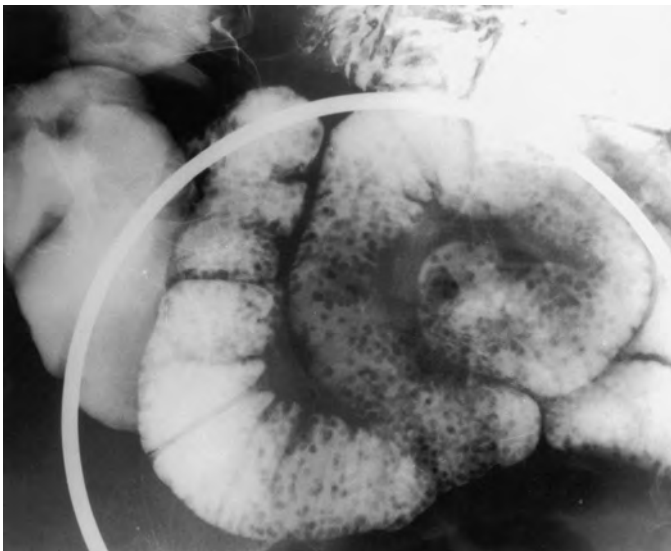


Figure 42-10 Marked lymphoid hyperplasia in a patient with common variable immunodeficiency. This spot image from a small bowel follow-through shows innumerable 1- to 2-mm, round nodules in the distal ileum and terminal ileum. These lymphoid follicles are increased in number and extent in comparison to the usual lymphoid pattern confined primarily to the terminal ileum. The lymphoid follicles are not enlarged or confluent.

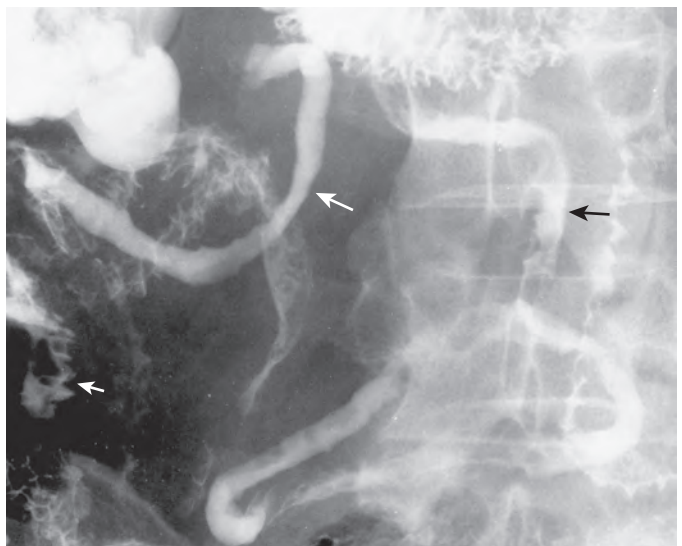


Figure 42-12 Graft-versus-host disease. This spot image from a small bowel follow-through shows that the jejunum and upper ileum have a diffusely narrowed, tubular appearance. In some loops the folds are markedly thickened (small arrow), whereas in other loops the folds are completely effaced (large arrows).

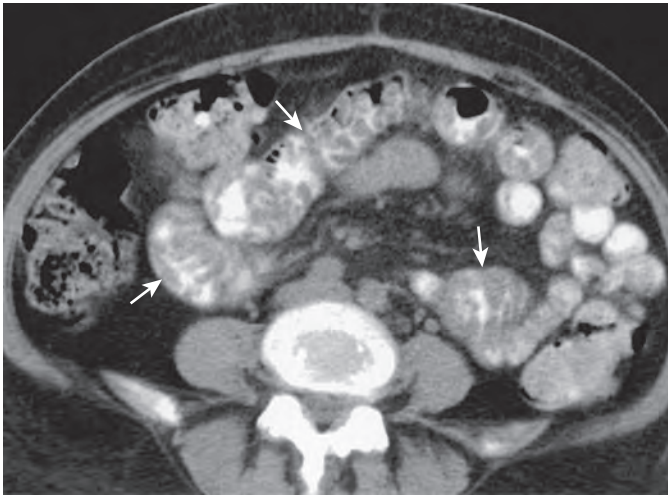


Figure 42-13 Graft-versus-host disease. CT through the top of the iliac crest shows extensive fold thickening (arrows) in mid small bowel loops.

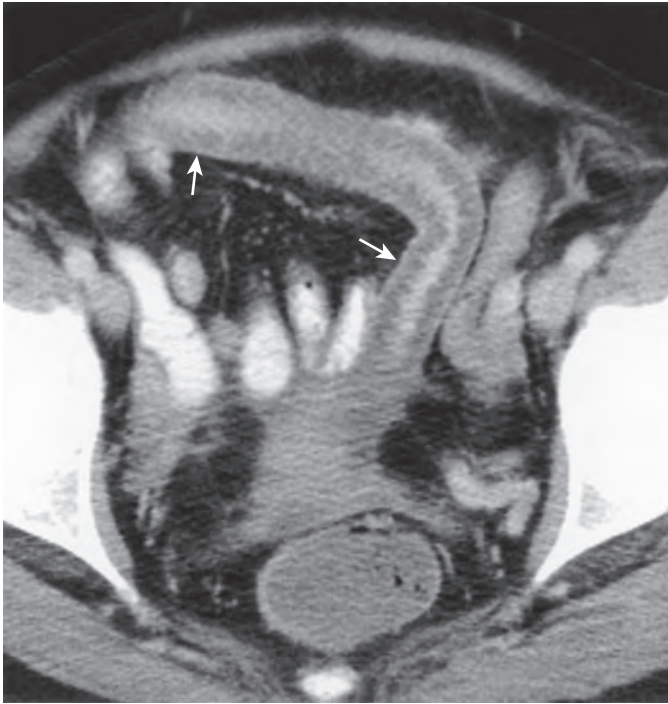


Figure 42-14 Neutropenic enteritis. CT through the pelvis shows marked thickening of an ileal loop (arrows) with a mural stratification pattern because of low-attenuation submucosal edema and inflammation. Other images revealed marked cecal inflammation compatible with typhlitis.

TYPHLITIS

Neutropenic enterocolitis primarily affects the cecum and, to a lesser degree, the terminal ileum and appendix. Neutropenic enterocolitis is sometimes detected on CT scans to evaluate abdominal pain or fever in patients with various forms of leukemia (Fig. 42-14). This entity is discussed in detail in Chapter 58.

GASTROINTESTINAL INFECTIONS IN AIDS

About 50% of patients infected with HIV have chronic diarrhea.^{74,75} This can be related to AIDS enteropathy, infectious enteritis or colitis, motility disturbances, or drug-induced side effects of antiretroviral and antimicrobial agents.⁷⁶ A wide variety of viruses, bacteria, protozoa, and fungi can infect the small bowel in patients with AIDS. Some pathogens, such as *Mycobacterium avium-intracellulare*, are unique to AIDS. Other pathogens such as *Salmonella* have an increased incidence in patients with AIDS compared with immunocompetent patients. Patients with AIDS often have several concurrent infections, resulting in chronic diarrhea, malabsorption, protein-calorie malnutrition, and weight loss.

HUMAN IMMUNODEFICIENCY VIRUS ENTERITIS

The GI tract can be a portal of entry for HIV through tears in the rectal mucosa or even intact intestinal epithelium. HIV adheres to M cells in the intestinal epithelium.⁷⁷ The virus is subsequently delivered to intraepithelial lymphocytes, to lymphocytes in lymphoid follicles, and to macrophages in the lamina propria.⁷⁸ HIV infection results in near-complete destruction of CD4⁺ intraepithelial lymphocytes, leading to abnormal differentiation of IgA-secreting B cells and decreased numbers of mucosal IgA plasma cells. HIV also alters enterocyte differentiation.⁷⁹ As a result, HIV infection causes villous atrophy, crypt hyperplasia, edema, and chronic inflammation.⁸⁰ Nutrient absorption is impaired because of the loss of mature enterocytes.

An acute self-limited diarrhea lasting 1 to 3 weeks occurs in approximately one third of patients with acute HIV infection. The radiologist is not usually involved at this stage. AIDS enteropathy is defined as osmotic diarrhea and malabsorption occurring without evidence of other enteric infections. The radiologist may be asked to perform imaging studies on patients with chronic diarrhea, however, because endoscopy can establish the diagnosis in only about 40% of patients with suspected small bowel infection, and stool analysis can establish the diagnosis in only about 60% of patients.⁸¹⁻⁸³ Imaging studies are used to show the presence of small bowel disease and can sometimes aid in the differential diagnosis of these conditions.

CYTOMEGALOVIRUS INFECTION

Cytomegalovirus (CMV) is a double-stranded DNA virus in the herpesvirus group. A self-limited diarrheal infection can be seen in immunocompetent individuals.⁸⁴ After the initial infection, the virus enters a latent phase in circulating mononuclear cells throughout the GI tract.⁸⁵ The virus is usually reactivated when the host becomes immunocompromised. CMV accumulates in nuclear and cytoplasmic inclusions in epithelial cells, mononuclear cells, endothelial cells, fibroblasts, histiocytes, and smooth muscle cells of the GI tract. The infection results in varying degrees of inflammation and necrosis. Endothelial cell damage causes submucosal ischemia, with secondary epithelial ulceration. Ulceration leads to pseudomembrane formation and perforation.

In the small intestine, discrete erosions and penetrating ulcers are separated by normal mucosa.⁸⁶ Barium studies and CT usually show ulceration in the distal small bowel and terminal

ileum (Figs. 42-15 and 42-16) and in the cecum and ascending colon.^{86,87} However, some patients primarily have duodenal or jejunal disease or even diffuse small bowel disease.⁸⁸⁻⁹⁰ Intestinal perforation and ileocolic intussusceptions associated with lymphoid hyperplasia have also been described.⁹¹

CRYPTOSPORIDIOSIS

Cryptosporidium parvum is a unicellular, spore-forming coccidial protozoan that causes an acute self-limited diarrhea in immunocompetent patients. In patients with CD4⁺ counts less than 200 cells/mm³, however, *C. parvum* may cause a diffuse mucosal enteropathy, resulting in chronic, voluminous, watery diarrhea and malabsorption.⁹² This parasite is transmitted by the fecal-oral route via contaminated water or by person-to-person or pet-to-person contact.⁹³ Cryptosporidia are present in vacuoles beneath the membrane of epithelial cells at the villous tips but outside the epithelial cell cytoplasm. Infection results in a spectrum of findings, ranging from a normal histologic appearance to villous atrophy with severe inflammation.

Barium studies may reveal a variable degree of fold thickening in the duodenum and mesenteric small bowel (Fig. 42-17).^{94,95} One series reported proximal small bowel predominance with cryptosporidial enteritis.⁹⁶

ISOSPORIASIS AND OTHER INTRACELLULAR PROTOZOANS

Iso sporidia belli is an obligate intracellular protozoan acquired by ingestion of contaminated food or water or by homosexual

transmission.⁹⁷ Invasion of villous enterocytes results in villous atrophy and inflammation, often associated with extensive eosinophilic infiltration of the small bowel wall. Profuse watery diarrhea and malabsorption may ensue. Barium studies may reveal thickened small bowel folds, primarily in the duodenum and proximal small intestine.⁹⁸

Cyclospora cayetanensis is an obligate intracellular protozoan that also causes villous atrophy and acute and chronic

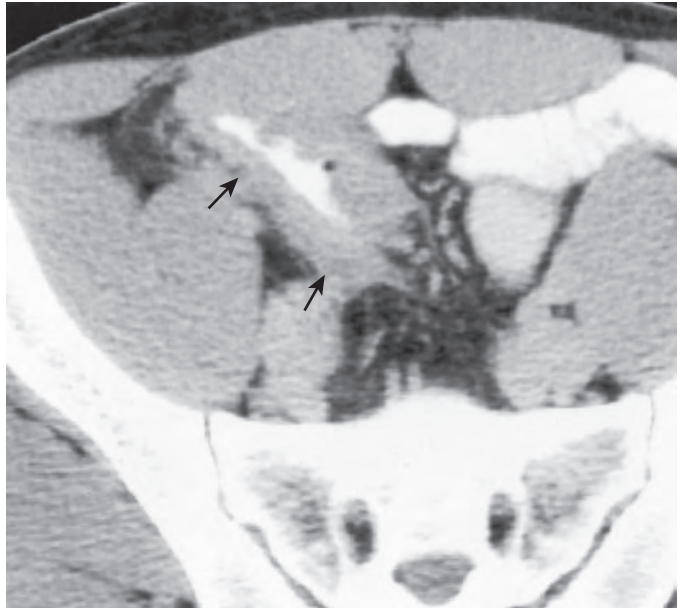


Figure 42-16 Cytomegalovirus infection in a patient with AIDS. CT through the pelvis shows marked wall thickening of the distal ileum (arrows). There also is irregularity of the mucosal surface caused by ulceration. (Courtesy Emil J. Balthazar, MD, and Hans Herlinger, MD.)

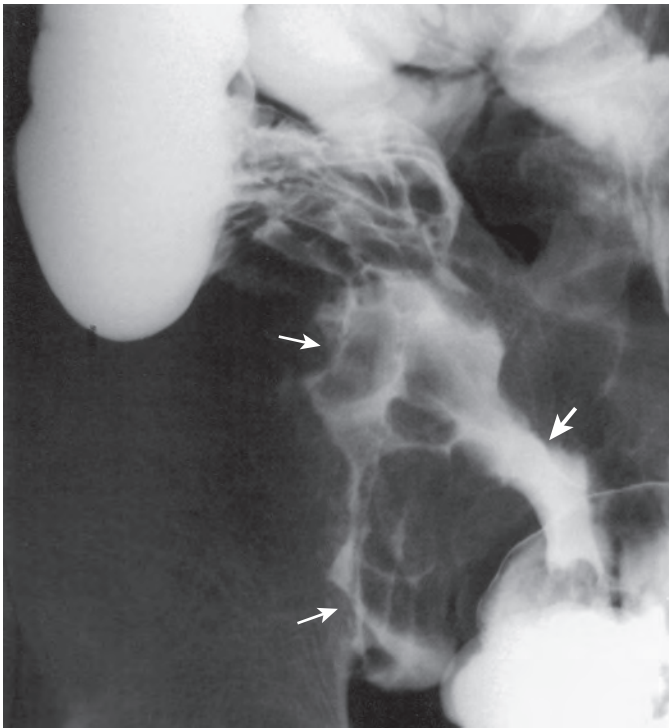


Figure 42-15 Cytomegalovirus infection in a patient with AIDS. This spot image of the terminal ileum from a small bowel follow-through shows large, lobulated folds (thin arrows) and barium-filled grooves caused by ulceration. Localized perforation is manifested by a barium-filled track (thick arrow) extending into the mesentery. (Courtesy Emil J. Balthazar, MD, and Hans Herlinger, MD.)

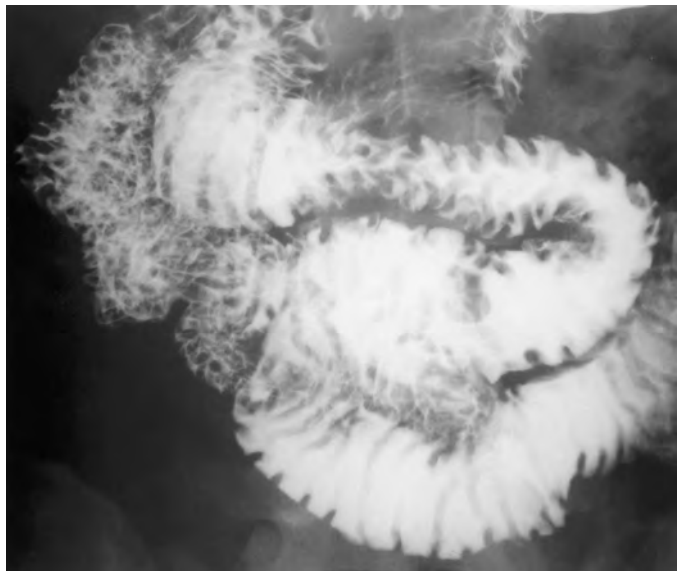


Figure 42-17 Cryptosporidiosis. This spot image of the mid small bowel shows mild, diffuse thickening of the folds. (Courtesy Hans Herlinger, MD.)

inflammation in normal or immunocompromised individuals. A chronic or relapsing watery diarrhea is usually present.

Microsporidia are a group of spore-forming, obligate, intracellular protozoans that infect the small intestine or disseminate to other organs, depending on the species.^{99,100} A chronic watery diarrhea is usually present.

Enterocytozoon bienersi infects 10% to 34% of patients with HIV infection and CD4⁺ counts of less than 50 cells/mm³. This protozoan infects enterocytes in the jejunum, resulting in villous atrophy and inflammation.¹⁰¹

MYCOBACTERIUM AVIUM-INTRACELLULARE COMPLEX

Two acid-fast obligate intracellular mycobacteria, *Mycobacterium avium* and *Mycobacterium intracellulare*, form the *Mycobacterium avium-intracellulare* (MAI) complex. These organisms are ubiquitous in the environment and are not enteric pathogens in immunocompetent patients. However, immunosuppressed patients exposed to aerosols, soil, or food containing MAI may develop disseminated infection. Genetic analysis of MAI isolated from AIDS patients has shown that most of these infections are caused by *M. avium*, so the term *M. avium* complex (MAC) is currently favored.¹⁰² HIV-infected patients with CD4⁺ counts less than 100 cell/mm³ may have disseminated MAC infection involving the liver, spleen, bone marrow, lymph nodes, and gastrointestinal tract. GI involvement may cause chronic diarrhea, abdominal pain, malabsorption, weight loss, hepatosplenomegaly, and lymphadenopathy.

The small intestine is the most severely infected portion of the GI tract. Jejunal and ileal predominance have been described.^{85,103,104} Barium studies may reveal thickened small bowel folds caused by infiltration of the lamina propria and submucosa by macrophages packed with acid-fast organisms (Fig. 42-18). Fine mucosal nodularity may also be seen as a result of villous blunting from diffuse infiltration of the lamina

propria. Aphthoid ulcers have also been described.¹⁰⁵ CT may reveal mesenteric lymphadenopathy, which is often more prominent than the retroperitoneal lymphadenopathy in these patients. Enlarged lymph nodes may have normal or low attenuation (Fig. 42-19). Hepatomegaly, splenomegaly, and ascites may also be detected in patients with disseminated infection.¹⁰⁶

Small bowel infection by *Mycobacterium tuberculosis* in patients with AIDS produces radiographic findings similar to those in immunocompetent patients with *M. tuberculosis*.¹⁰⁷ However, disseminated tuberculosis involving the peritoneum (Fig. 42-20), liver, spleen, and pancreas is more common in patients with AIDS.¹⁰⁸ The findings of tuberculous peritonitis include high-attenuation ascites, peritoneal



Figure 42-19 Mesenteric and retroperitoneal lymphadenopathy in a patient with *Mycobacterium avium* complex enteritis. CT through the tip of the liver shows a large left para-aortic nodal mass with a low-attenuation center (black arrow). Masslike infiltration of the small bowel mesentery (white arrow) is also present.

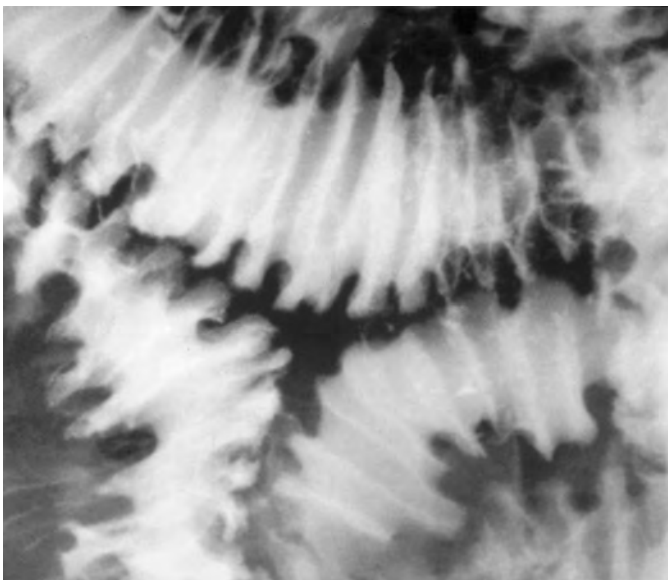


Figure 42-18 *Mycobacterium avium* complex enteritis. This spot image from a small bowel follow-through shows moderately thickened, smooth folds in the affected small bowel.

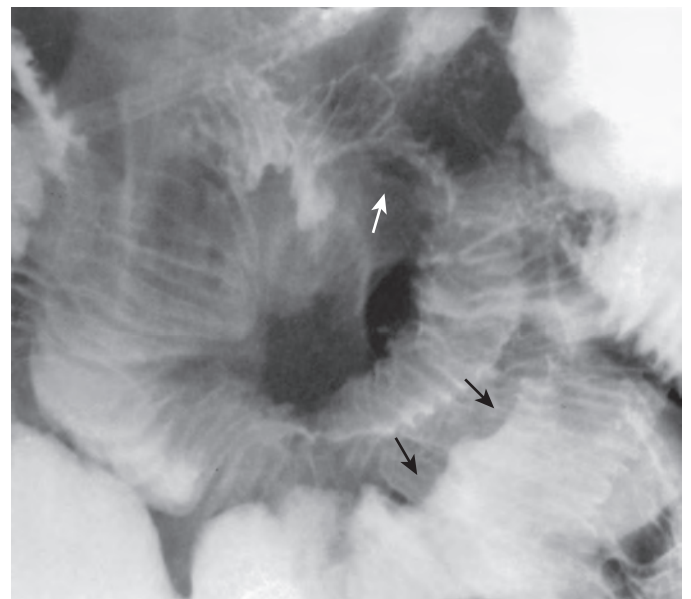


Figure 42-20 Tuberculous peritonitis in a patient with AIDS. This spot image from an enteroclysis examination shows extrinsic mass impressions (arrows) on the mesenteric border of midjejunal loops. Small bowel folds are also mildly enlarged.

and omental nodules, and low-attenuation lymphadenopathy (see Chapter 110).

ACTINOMYCOSIS

Actinomyces israelii is a filamentous bacterium that is part of the normal oral flora. GI actinomycosis usually involves the terminal ileum (Fig. 42-21) and appendix. A transmural infection mimicking Crohn's disease may be seen.¹⁰⁹ Fistulas are often present.

CANDIDIASIS

Fungal spores or hyphae of *Candida* may be found as a result of noninvasive colonization of blind loops or necrotic tissue. In contrast, invasive candidiasis may occur in the small intestine in patients with disseminated candidal infections, including patients with AIDS.^{110,111} Mucosal invasion causes ulceration and even perforation. Barium studies may reveal thickened small bowel folds.

Differential Diagnosis

The radiologist usually encounters infectious disease of the small intestine during the work-up of patients with acute right lower quadrant pain or during the work-up of patients with chronic diarrhea, malabsorption, and weight loss.¹¹² Acute

enteritis that causes abdominal pain rather than diarrhea can mimic appendicitis on clinical grounds. If CT performed to rule out acute appendicitis shows thickened ileal folds (Fig. 42-22) or regional mesenteric lymphadenopathy, various infectious pathogens (e.g., *Yersinia*) must be considered. However, a CT diagnosis of mesenteric adenitis is not indicative of a specific cause. A definitive diagnosis therefore requires stool cultures and biopsy specimens. Unfortunately, these cultures and biopsies are often negative or nonspecific in patients with acute infections. In such cases, follow-up CT or endoscopy may be needed to rule out small bowel lymphoma.

The inflammatory response to a variety of damaging agents such as chemical toxins, radiation, and infection is often similar. As a result, the CT or radiographic findings of thickened folds or villous enlargement are often nonspecific in patients with chronic diarrhea. When small bowel folds are thickened, the radiologist should therefore consider the age, travel history, and immune status of the patient. Proximal or diffuse small bowel fold thickening in patients with AIDS is caused by a variety of infections, including MAC, cryptosporidiosis (see Fig. 42-22), and isosporiasis. Patients receiving 5-FU or 5-FUDR may have intestinal chemotoxicity (see Figs. 42-8 and 42-9). Patients who have undergone allogeneic bone marrow transplantation may have GVHD (see Figs. 42-11 to 42-13) or CMV infection. Patients with proximal or diffuse small bowel fold thickening and a clinical history of malabsorption may have other types of disorders (see Chapter 43).

Disease involving the distal ileum usually indicates a disorder that has an affinity for lymphatic tissue in the small intestine, including Crohn's disease, *Yersinia* enterocolitis (see



Figure 42-21 Actinomycosis in a patient with AIDS. This spot image from a double-contrast barium enema shows mucosal nodularity (arrows) and irregular fold thickening in the terminal ileum.

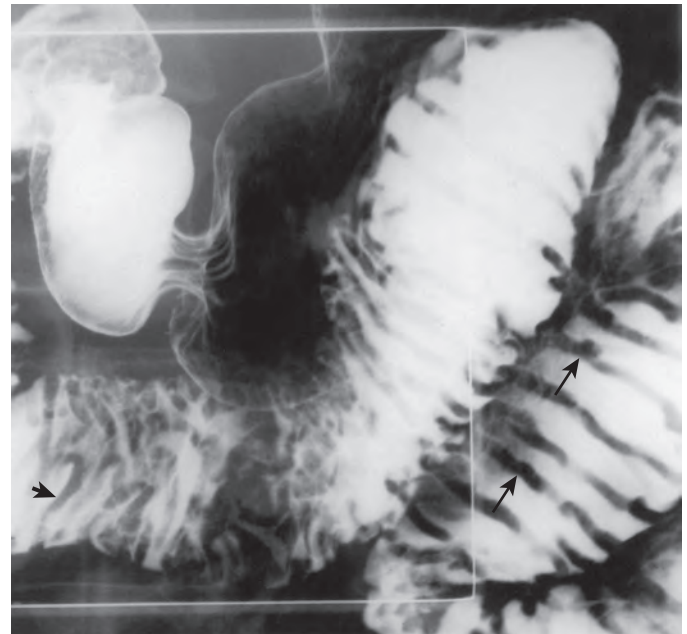


Figure 42-22 Proximal small bowel fold thickening in a patient with AIDS. This spot image from a small bowel follow-through shows mildly thickened undulating folds (thin arrows) in a proximal loop of jejunum. Compare these jejunal folds with folds in the third portion of the duodenum (thick arrow). Normal duodenal folds should be slightly thicker than jejunal folds. Enteroscopic biopsy specimens revealed cryptosporidiosis.

Fig. 42-7), tuberculosis (see Fig. 42-6), and lymphoma. In patients with acute diarrhea, aphthoid ulcers are not specific for Crohn's disease because they reflect nonspecific inflammation of lymphoid tissue with erosion of the overlying mucosa. Any acute infection or inflammatory process can therefore lead to the development of aphthoid ulcers or thickened folds in the terminal ileum. In patients with thickened folds in the terminal ileum, an acute infection such as yersiniosis should be favored. Unfortunately, it may be difficult to obtain a definitive diagnosis in these patients because cultures and biopsy specimens are often negative for a specific pathogen.

Aphthoid ulcers, mesenteric border ulcers, cobblestoning, strictures, and fistulas should be highly suggestive of Crohn's disease in patients with chronic diarrhea (see Chapter 41). However, these findings are not always specific for Crohn's disease. If, for example, there is a clinical history of an immunodeficiency state or if the patient has lived in a region of the world in which tuberculosis is endemic, then tuberculosis (see Fig. 42-6), actinomycosis (see Fig. 42-21), Behçet's disease, and cytomegalovirus (see Figs. 42-15 and 42-16) should be considered, depending on the clinical history. The CT findings of bowel wall thickening, mesenteric lymphadenopathy, and mesenteric infiltration or abscess formation also are not specific for Crohn's disease, so further work-up is required.

Florid lymphoid reactions in the terminal ileum may result from prior enteric infection, immunodeficiency states

(in particular, common variable immunodeficiency), and lymphoma. Small (1-2 mm), round, uniform nodules separated by normal mucosa are indicative of lymphoid hyperplasia (see Fig. 42-23), which can probably be followed without further diagnostic testing. However, lymphoid nodules that are larger (>2 mm), more confluent, and not round, smooth, and uniform should be investigated for lymphoma (Fig. 42-24).

Small bowel wall thickening on CT is not a specific finding. However, a mural stratification pattern with a low-attenuation submucosa suggests a vascular or inflammatory process (see Fig. 42-1), but not a malignant tumor. Lack of contrast enhancement should suggest necrosis and a possible vascular component to the disease. Fat deposition in the small bowel submucosa should suggest Crohn's disease. Ileal wall thickening in patients with AIDS may be caused by inflammatory conditions or AIDS-related lymphoma (Fig. 42-25).

Lymphadenopathy adjacent to abnormal small bowel loops is not a particularly helpful finding because it can be seen with infectious disorders, Crohn's disease, carcinoid tumor, intraperitoneal metastases, and lymphoma. Extensive mesenteric lymphadenopathy in patients with chronic diarrhea or malabsorption is typically seen in patients with gluten-sensitive enteropathy, Whipple's disease (Fig. 42-26), and MAI infections. Lymphadenopathy in celiac disease is usually reactive, but lymphoma cannot be excluded.

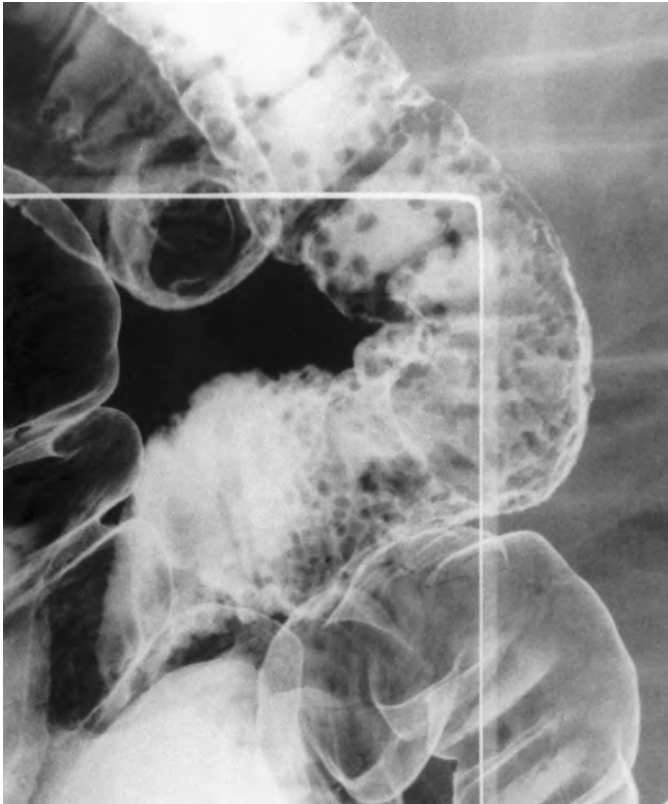


Figure 42-23 Lymphoid hyperplasia in the terminal ileum. This spot image from a double-contrast barium enema shows discrete, round, uniformly sized, one to two radiolucent filling defects in the terminal ileum separated by normal mucosa.



Figure 42-24 Mantle cell lymphoma in the terminal ileum. This spot image from a small bowel follow-through shows small, round, ovoid or polygonal nodules ranging from 1 to 4 mm. The nodules are confluent in some areas (arrows). This type of mucosal nodularity requires endoscopic biopsies to rule out lymphoma. The nodularity does not resemble cobblestoning because transversely and longitudinally oriented barium-filled clefts are not seen.

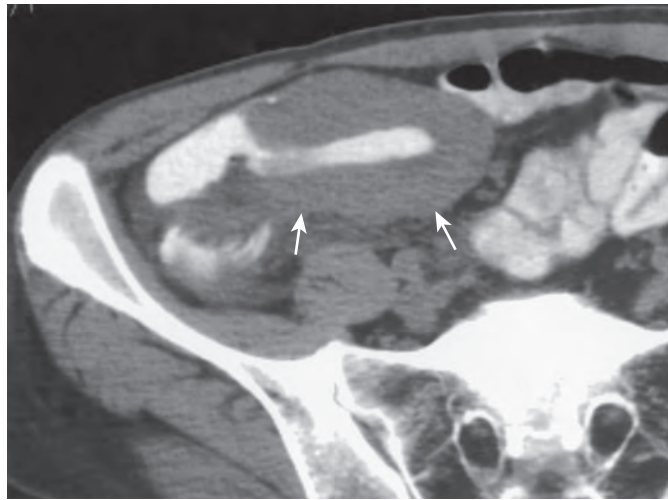


Figure 42-25 Ileal wall thickening in a patient with AIDS. CT through the pelvis shows marked (1.5–2 cm) wall thickening (arrows) of uniform attenuation in the terminal ileum. The medial wall of the cecum is also thickened. Biopsy specimens revealed lymphoma. Marked wall thickening of uniform attenuation should be considered highly worrisome for small bowel lymphoma.

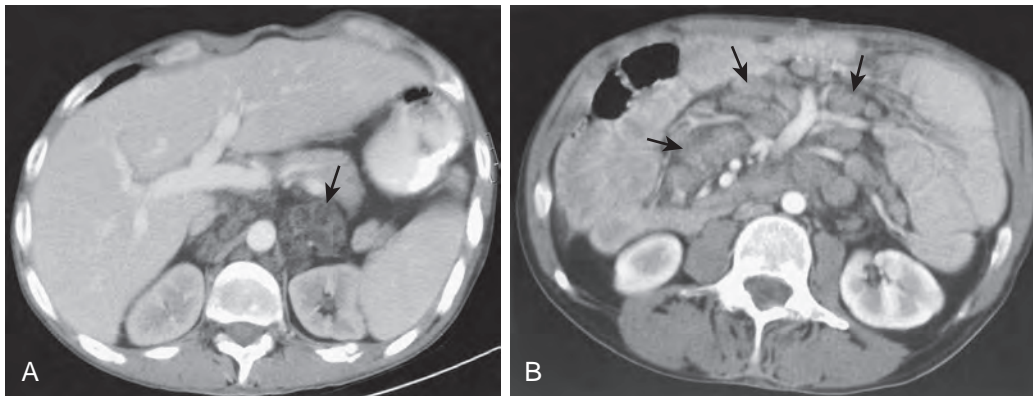


Figure 42-26 Lymphadenopathy in Whipple's disease. **A.** CT through the liver shows low-attenuation lymphadenopathy in the retrocaval, retrocrural and left para-aortic (arrow) regions. **B.** An image caudal to **A** shows marked mesenteric lymphadenopathy (arrows) of more uniform and higher attenuation.

REFERENCES

- Geboes K: Inflammatory disorders of the small intestine. In Morson and Dawson's Gastrointestinal Pathology, ed 5, Chichester, England, 2013, Wiley-Blackwell, pp 315–372.
- Fenoglio-Preiser CM, Noffsinger AE, Stemmermann GN, et al: Non-neoplastic lesions of the small intestine. In Fenoglio-Preiser CM, Lantz P, Listrom M, et al, editors: Gastrointestinal Pathology: An Atlas and Text, ed 2, Philadelphia, 1999, Lippincott-Raven, pp 309–358.
- Pawloski ZS: Ascariasis: Host-pathogen biology. *Rev Infect Dis* 4:806–814, 1982.
- Hesse AA, Nouri A, Hassan HS, Hashish AA: Parasitic infestations requiring surgical interventions. *Semin Pediatr Surg* 21:142–150, 2012.
- Blumenthal DS, Schultz MG: Incidence of intestinal obstruction in children infected with *Ascaris lumbricoides*. *Am J Trop Med Hyg* 24:801–804, 1975.
- Hommeyer SC, Hamill GS, Johnson JA: CT diagnosis of intestinal ascariasis. *Abdom Imaging* 20:315–316, 1995.
- Markell EK, Voge M: Medical Parasitology, ed 4, Philadelphia, 1976, WB Saunders.
- Herlinger H: Parasitic and bacterial inflammatory diseases. In Herlinger H, Maglinte DD, Birnbaum BA, editors: Clinical Imaging of the Small Intestine, ed 2, New York, 1999, Springer, pp 291–309.
- Ramírez-Olivencia G, Espinosa MÁ, Martín AB, et al: Imported strongyloidiasis in Spain. *Int J Infect Dis* 18:32–37, 2014.
- Drasin GF, Moss JPO, Cheng SH: *Strongyloides stercoralis* colitis: Findings in four cases. *Radiology* 126:619–621, 1978.
- Medina LS, Heiken JP, Gold RP: Pipestem appearance of small bowel in strongyloidiasis is not pathognomonic of fibrosis and irreversibility. *AJR* 159:543–544, 1992.
- Dallemand S, Waxman M, Farman J: Radiological manifestations of *Strongyloides stercoralis*. *Gastrointest Radiol* 8:45–51, 1983.
- Hamilton KW, Abt PL, Rosenbach MA: Donor-derived strongyloides stercoralis infections in renal transplant patients. *Transplantation* 91:1019–1024, 2011.
- Muraoka A, Suehiro I, Fuigii M, et al: Acute gastric anisakiasis: 28 cases during the last 10 years. *Dig Dis Sci* 41:2362–2365, 1996.
- Matsui T, Iida M, Murakami M, et al: Intestinal anisakiasis: Clinical and radiologic features. *Radiology* 157:299–302, 1985.
- Céspedes M, Saez A, Rodríguez I, et al: Chronic anisakiasis presenting as a mesenteric mass. *Abdom Imaging* 25:548–550, 2000.
- Pearson RD: Parasitic diseases: Helminths. In Yamada T, Alpers DH, Kaplowitz N, et al, editors: Textbook of Gastroenterology, ed 4, Philadelphia, 2003, Lippincott Williams & Wilkins, pp 2608–2625.
- Kapus KD, Lundgren RG, Jr, Juranek DD, et al: Intestinal parasitism in the United States: Update on a continuing problem. *Am J Trop Med Hyg* 50:705, 1994.

19. Katelaris PH, Farthing MJG: Diarrhea and malabsorption in giardiasis: A multifactorial process? *Gut* 33:295–297, 1992.
20. Barry MA, Weatherhead JE, Hotez PJ, Woc-Colburn L: Childhood parasitic infections endemic to the United States. *Pediatr Clin North Am* 60:471–485, 2013.
21. Brandon J, Glick SN, Teplick SK: Intestinal giardiasis: Importance of serial filming. *AJR* 144:581–584, 1985.
22. Li E, Stanley SL: Parasitic diseases: Protozoa. In Yamada T, Alpers DH, Kaplowitz N, et al, editors: *Textbook of Gastroenterology*, ed 4, Philadelphia, 2003, Lippincott Williams & Wilkins, pp 2588–2607.
23. Holbert RD, Margiros E, Hirsch CP, Nunenmacher SJ: Chagas disease: A case in south Mississippi. *J Miss State Med Assoc* 36:1–5, 1995.
24. Smith B: The myenteric plexus in Chagas disease. *J Pathol Bacteriol* 94:462–463, 1967.
25. Olsen SJ, MacKinnon LC, Goudling JS, et al: Surveillance for foodborne-disease outbreaks—United States, 1993–1997. *MMWR Morb Mortal Wkly Rep* 49(SS-1):1–62, 2000.
26. Yönel O, Hamzaoglu HO: What is the most accurate method for the diagnosis of intestinal tuberculosis? *Turk J Gastroenterol* 21:91–96, 2010.
27. Carreira GF, Young S, Lewicki AM: Intestinal tuberculosis. *Gastrointest Radiol* 1:147–155, 1976.
28. Cullen JH: Intestinal tuberculosis: Clinical pathological study. *Q Bull Sea View Hosp* 5:143–160, 1940.
29. Thoeni RF, Margulis AR: Gastrointestinal tuberculosis. *Semin Roentgenol* 14:283–294, 1979.
30. Ferentzi CV, Sieck JO, Ali MA: Colonoscopic diagnosis and medical treatment of ten patients with colonic tuberculosis. *Endoscopy* 20:62–65, 1988.
31. Hoshino M, Shibata M, Goto N, et al: A clinical study of tuberculous colitis. *Gastroenterol Jpn* 14:299–305, 1979.
32. Kim KM, Lee A, Choi KY: Intestinal tuberculosis: Clinicopathologic analysis and diagnosis by endoscopic biopsy. *Am J Gastroenterol* 93:606–609, 1998.
33. Nakano H, Jaramillo E, Watanabe M, et al: Intestinal tuberculosis: Findings on double-contrast barium enema. *Gastrointest Radiol* 17:108–114, 1992.
34. Vaidya MG, Sodhi JS: Gastrointestinal tract tuberculosis: A study of 102 cases including 55 hemicolectomies. *Clin Radiol* 29:189–195, 1978.
35. Balthazar EJ, Gordon R, Hulnick D: Ileocecal tuberculosis: CT and radiologic evaluation. *AJR* 154:499–503, 1990.
36. Almadi MJ, Ghosh S, Aljebreen AM: Differentiating intestinal tuberculosis from Crohn's disease: A diagnostic challenge. *Am J Gastroenterol* 104:1003–1012, 2009.
37. Park SJ, Han JK, Kim TK, et al: Tuberculous colitis: Radiologic-colonoscopy correlation. *AJR* 175:121–128, 2000.
38. Hanski C, Autschka U, Schmoranz HP, et al: Immunohistochemical and electron microscopic study of interaction of *Yersinia enterocolitica* serotype 08 with intestinal mucosa during experimental enteritis. *Infect Immun* 57:673–678, 1989.
39. VanTrappen G, Agg HO, Ponette E, et al: *Yersinia* enteritis and enterocolitis: Gastroenterological aspects. *Gastroenterology* 72:220–227, 1977.
40. Saebø A, Lasser J: *Yersinia enterocolitica*, an inducer of chronic inflammations. *Int J Tissue React* 16:51–57, 1994.
41. Case records of the Massachusetts General Hospital: Weekly clinicopathological exercises. Case 28-1990. A 72-year-old woman with abdominal pain and an ileocecal radiographic abnormality. *N Engl J Med* 323:113–123, 1990.
42. Ekberg O, Sjöström B, Brahme F: Radiological findings in *Yersinia* ileitis. *Radiology* 123:15–19, 1977.
43. Balthazar EJ, Charles HW, Megibow AJ: *Salmonella* and *Shigella*-induced ileitis. CT findings in four patients. *J Comput Assist Tomogr* 20:375–378, 1996.
44. Zilbauer M, Dorrell N, Wren BW, Bajaj-Elliott M: *Campylobacter jejuni*-mediated disease pathogenesis: An update. *Trans R Soc Trop Med Hyg* 102:123–129, 2008.
45. Brodey PA, Fertig S, Aron JM: *Campylobacter* enterocolitis: Radiographic feature. *AJR* 139:1199–1201, 1982.
46. Herlinger H: Parasitic and bacterial inflammatory diseases. In Herlinger H, Maglinte DD, Birnbaum BA, editors: *Clinical Imaging of the Small Intestine*, ed 2, New York, 1999, Springer, pp 291–308.
47. Fantry GT, Fantry LE, James SP: Chronic infections of the small intestine. In Yamada T, Alpers DH, Kaplowitz N, et al, editors: *Textbook of Gastroenterology*, ed 4, Philadelphia, 2003, Lippincott Williams & Wilkins, pp 1561–1579.
48. Alterman DD, Cho KC: Histoplasmosis involving the omentum in an AIDS patient: CT demonstration. *J Comput Assist Tomogr* 12:664–665, 1988.
49. Heneghan SJ, Li J, Petrossian E, Bizer LS: Intestinal perforation from gastrointestinal histoplasmosis in acquired immunodeficiency syndrome: Case report and review of the literature. *Arch Surg* 128:464–466, 1993.
50. Levin MS: Miscellaneous diseases of the small intestine. In Yamada T, Alpers DH, Kaplowitz N, et al, editors: *Textbook of Gastroenterology*, ed 4, Philadelphia, 2003, Lippincott Williams & Wilkins, pp 1663–1684.
51. Allison MC, Howatson AG, Torrance CJ, et al: Gastrointestinal damage associated with the use of non-steroidal anti-inflammatory drugs. *N Engl J Med* 327:749–754, 1992.
52. Handa O, Naito Y, Fukui A, et al: The impact of non-steroidal anti-inflammatory drugs on the small intestinal epithelium. *J Clin Biochem Nutr* 54:2–6, 2014.
53. Bjarnason I, Price AB, Zanelli G, et al: Clinicopathological features of nonsteroidal antiinflammatory drug-induced small intestinal strictures. *Gastroenterology* 94:1070–1074, 1988.
54. Levi S, deLacey G, Price AB, et al: "Diaphragm-like" strictures of the small bowel in patients treated with non-steroidal anti-inflammatory drugs. *Br J Radiol* 63:186–189, 1990.
55. Wilson IH, Cooley NV, Luibel FJ: Nonspecific stenosing small bowel ulcers. *Am J Gastroenterol* 50:449–455, 1968.
56. Lang J, Price AB, Levi AJ, et al: Diaphragm disease: Pathology of disease of the small intestine induced by non-steroidal anti-inflammatory drugs. *J Clin Pathol* 41:516–526, 1988.
57. Hiehle JF, Levine MS: Gastrointestinal toxicity of 5-FU and 5-FUDR: Radiographic findings. *Can Assoc Rad J* 42:109–112, 1991.
58. Carucci LR, Jacobs R, Levine JE, et al: Toxic effects of fluorouracil on the small bowel. *RSNA Gastrointestinal Cases of the Day*. 2002. Available at: RSNA.org.
59. Kelvin FM, Gramm HF, Gluck WL, et al: Radiologic manifestations of small bowel toxicity due to floxuridine therapy. *AJR* 146:39–43, 1977.
60. Shanahan F: Gastrointestinal manifestations of immunologic disorders. In Yamada T, Alpers DH, Kaplowitz N, et al, editors: *Textbook of Gastroenterology*, ed 4, Philadelphia, 2003, Lippincott Williams & Wilkins, pp 2705–2722.
61. Sander CA, Medeiros LJ, Weiss LM, et al: Lymphoproliferative lesions in patients with common variable immunodeficiency syndrome. *Am J Surg Pathol* 16:1170–1183, 1992.
62. Chiamonte C, Glick SN: Nodular lymphoid hyperplasia of the small bowel complicated by jejunal lymphoma in a patient with common variable immunodeficiency syndrome. *AJR* 163:1118–1119, 1994.
63. Crooks DJM, Brown WR: The distribution of intestinal nodular lymphoid hyperplasia in immunoglobulin deficiency. *Clin Radiol* 31:701–706, 1980.
64. Herlinger H: Immune deficiency diseases. In Herlinger H, Maglinte DDT, Birnbaum BA, editors: *Clinical Imaging of the Small Intestine*, ed 2, New York, 1999, Springer, pp 309–330.
65. Washington J, Jagasia M: Pathology of graft-versus-host disease in the gastrointestinal tract. *Hum Pathol* 40:909–917, 2009.
66. Jones B, Kramer SS, Saral R, et al: Gastrointestinal inflammation after bone marrow transplantation: Graft-versus-host disease or opportunistic infection. *AJR* 150:277–281, 1988.
67. McDonald GB, Sullivan KM, Plumley TF: Radiographic features of esophageal involvement in chronic graft-versus-host disease in humans. *AJR* 142:501–506, 1984.
68. Fisk JD, Shulman HM, Greening RR, et al: Gastrointestinal radiographic features of human graft-vs.-host disease. *AJR* 136:329–336, 1981.
69. Rosenberg HK, Serota FT, Koch P, et al: Radiographic features of gastrointestinal graft-versus-host disease. *Radiology* 38:371–374, 1981.
70. Gramm HF, Vincent ME, Braver JM: Differential diagnosis of tubular small bowel. *Curr Imaging* 2:62–70, 1990.
71. Ma LD, Jones B, Lazenby AJ, et al: Persistent oral contrast lining the intestine in severe mucosal disease: Elucidation of radiographic appearance. *Radiology* 191:747–749, 1981.
72. Jones B, Fishman EK, Kramer S, et al: Computed tomography of gastrointestinal inflammation after bone marrow transplantation. *AJR* 146:691–695, 1986.
73. Navari RM, Sharma P, Deeg HJ, et al: Pneumatosis cystoides intestinalis following allogeneic marrow transplantation. *Transplant Proc* 15:1720–1724, 1983.
74. Smith PD, Janoff EN: Gastrointestinal complications of the acquired immunodeficiency syndrome. In Yamada T, Alpers DH, Kaplowitz N, et al, editors: *Textbook of Gastroenterology*, ed 4, Philadelphia, 2003, Lippincott Williams & Wilkins, pp 2567–2589.
75. Dworkin B, Wormser GP, Rosenthal WS, et al: Gastrointestinal manifestations of the acquired immunodeficiency syndrome: A review of 22 cases. *Am J Gastroenterol* 80:774–778, 1985.

76. Poles M, Fuerst M, McGowan I, et al: HIV-related diarrhea is multifactorial and fat malabsorption is commonly present, independent of HAART. *Am J Gastroenterol* 96:1831–1837, 2001.
77. Fenoglio-Prieser CM, Noffsinger AE, Stemmermann GN, et al: AIDS-related diseases. In Fenoglio-Prieser CM, Lantz P, Listrom M, et al, editors: *Gastrointestinal Pathology: An Atlas and Text*, ed 2, Philadelphia, 1999, Lippincott-Raven, pp 563–595.
78. Amerongen HM, Weltzin R, Farnet CM, et al: Transepithelial transport of HIV-1 by intestinal M cells: A mechanism for transmission of AIDS. *J AIDS* 4:760–765, 1991.
79. Heise C, Dandekar S, Kumar P, et al: Human immunodeficiency virus infection of enterocytes and mononuclear cells in human jejunal mucosa. *Gastroenterology* 100:1521–1527, 1991.
80. Kotler DP, Reka S, Clayton F: Intestinal mucosal inflammation associated with human immunodeficiency virus infection. *Dig Dis Sci* 38:1119–1126, 1993.
81. Greenson JK, Belitsos PC, Yardley JH, et al: AIDS enteropathy: Occult enteric infections and duodenal mucosal alterations in chronic diarrhea. *Ann Intern Med* 114:366–372, 1991.
82. Wilcox CM, Schwartz DA, Cotsonis G, Thompson SE: Chronic unexplained diarrhea in human immunodeficiency virus infection: Determination of the best diagnostic approach. *Gastroenterology* 110:30–37, 1996.
83. Rene E, Marche C, Regnier B, et al: Intestinal infections in patients with acquired immunodeficiency syndrome: A prospective study in 132 patients. *Dig Dis Sci* 34:773–780, 1989.
84. Surawicz C, Myerson D: Self-limited cytomegalovirus colitis in immunocompetent individuals. *Gastroenterology* 94:194–199, 1988.
85. Pantongrag-Brown L, Nelson AM, Brown AE, et al: Gastrointestinal manifestations of acquired immunodeficiency syndrome: Radiologic-pathologic correlation. *Radiographics* 15:1155–1178, 1995.
86. Balthazar EJ, Martino JM: Giant ulcers of the ileum and colon caused by cytomegalovirus in patients with AIDS. *AJR* 166:1275–1276, 1996.
87. Balthazar EJ, Megibow AJ, Fazzini E, et al: Cytomegalovirus virus colitis in AIDS: Radiographic findings in 11 patients. *Radiology* 155:585–589, 1985.
88. Teixidor HS, Honig CL, Norsoph E, et al: Cytomegalovirus infection of the alimentary canal: Radiologic findings with pathologic correlation. *Radiology* 163:317–323, 1987.
89. DeRiso A, Kemeny MM, Torres RA, Oliver JML: Multiple jejunal perforations second to cytomegalovirus in a patient with acquired immune deficiency syndrome. *Dig Dis Sci* 34:623–629, 1989.
90. Williams CM, Schwartz DA: Symptomatic CMV duodenitis: An important clinical problem in AIDS. *J Clin Gastroenterol* 14:293–297, 1992.
91. Kram HB, Shoemaker WC: Intestinal perforation due to cytomegalovirus infection. *Dis Colon Rectum* 33:1037–1040, 1990.
92. Marcos LA, Gotuzzo E: Intestinal protozoan infections in the immunocompromised host. *Curr Opin Infect Dis* 26:295–301, 2013.
93. DuPont HL, Chappell CL, Sterling CR, et al: The infectivity of cryptosporidium parvum in healthy volunteers. *N Engl J Med* 332:855–859, 1995.
94. Wall S, Ominsky S, Altman DF, et al: Multifocal abnormalities of the gastrointestinal tract in AIDS. *AJR* 146:1–5, 1986.
95. Megibow AJ, Balthazar EJ, Hulnick DH: Radiology of non-neoplastic gastrointestinal disorders in acquired immune deficiency syndrome. *Semin Roentgenol* 22:31–41, 1987.
96. Berk RN, Wall SD, McCardle CB, et al: Cryptosporidiosis of the stomach and small intestine in patients with the acquired immunodeficiency syndrome. *AJR* 143:549–554, 1984.
97. DeHovitz JA, Pape JW, Boncy M, Johnson WD: Clinical manifestations and therapy of *Isospora belli* infections in patients with acquired immunodeficiency syndrome. *N Engl J Med* 315:87–90, 1986.
98. Shein R, Gleb A: *Isospora belli* in a patient with acquired immunodeficiency syndrome. *J Clin Gastroenterol* 6:525–528, 1984.
99. Leder K, Ryan N, Spelman D, Crowe SM: Microsporidial disease in HIV-infected patients: A report of 42 patients and review of the literature. *Scand J Infect Dis* 30:331–338, 1998.
100. Case records of the Massachusetts General Hospital: Weekly clinicopathological exercises. Case 51-1993. A 36-year-old man with AIDS, increase in chronic diarrhea, and intermittent fever and chills. *N Engl J Med* 329:1946–1954, 1993.
101. Slavik T: Human immunodeficiency virus-related gastrointestinal pathology: A southern Africa perspective with review of the literature. Part 1: Infections. *Arch Pathol Lab Med* 136:305–315, 2012.
102. Yakus MA, Good RCL: Geographic distribution, frequency, and specimen source of *Mycobacterium avium* complex serotypes isolated from patients with acquired immunodeficiency syndrome. *J Clin Microbiol* 28:926–929, 1990.
103. Vincent ME, Robbins AR: *Mycobacterium avium-intracellulare* complex enteritis: Pseudo-Whipple's disease in acquired immunodeficiency. *AJR* 144:921–922, 1985.
104. Schneebaum GW, Novick DM, Chabon AB, et al: Terminal ileitis associated with *Mycobacterium avium-intracellulare* infection in a homosexual man with acquired immune deficiency syndrome. *Gastroenterology* 92:1127–1132, 1987.
105. Frager DH, Frager JD, Brandt LJ, et al: Gastrointestinal complications of AIDS: Radiologic features. *Radiology* 158:597–605, 1986.
106. Nyberg DA, Federle MP, Jeffrey RB, et al: Abdominal CT findings of disseminated *Mycobacterium avium-intracellulare* in AIDS. *AJR* 145:297–299, 1985.
107. Jadvar H, Mindelzun RE, Olcott EW, Levitt DB: Still the great mimicker: Abdominal tuberculosis. *AJR* 168:1455–1460, 1997.
108. Radin DR: Intraabdominal *Mycobacterium tuberculosis* vs. *Mycobacterium avium-intracellulare* infections in patients with AIDS: Distinction based on CT findings. *AJR* 156:487–491, 1991.
109. Litt HI, Levine MS, Maki DD, et al: Ileal actinomycosis in a patient with AIDS. *AJR* 172:1297–1299, 1999.
110. Yan L, Yang C, Tang J: Disruption of the intestinal mucosal barrier in *Candida albicans* infections. *Microbiol Res* 168:389–395, 2013.
111. Radin DR, Fong T, Halls JM, Pontrelli GN: Monilial enteritis in acquired immunodeficiency syndrome. *AJR* 141:1289–1290, 1983.
112. Rubesin SE, Furth EE: Differential diagnosis of small intestinal abnormalities with radiologic-pathologic explanation. In Herlinger H, Maglinte DD, Birnbaum BA, editors: *Clinical Imaging of the Small Intestine*, ed 2, New York, 1999, Springer, pp 527–566.

CHAPTER OUTLINE

Digestion and Absorption

Carbohydrate Digestion and Absorption
Protein Digestion and Absorption
Fat Digestion and Absorption
Fluids and Electrolytes

Anatomic Classification of Malabsorption

Hepatobiliary and Pancreatic Disorders
Gastric Disorders
Small Bowel Disorders

Diagnosis of Malabsorption: Clinical Perspective**Bacterial Overgrowth**

Jejunioileal Diverticulosis
Progressive Systemic Sclerosis, Visceral Neuropathies,
and Myopathies

Epithelial Cell Damage

Celiac Disease
Tropical Sprue
Giardiasis
Whipple's Disease
Eosinophilic Gastroenteritis
Amyloidosis
Short Gut Syndrome

Nonformation of Chylomicrons

Abetalipoproteinemia

Lymphatic Obstruction and Lymphangiectasia**Multifactorial Diseases**

Diabetes Mellitus
Cystic Fibrosis

Differential Diagnosis of Fold Enlargement in Malabsorption

Malabsorption is caused by a variety of diseases originating in the liver and biliary tree, pancreas, and small intestine.¹⁻³ Normal digestion and absorption are presented as a background for understanding intestinal malfunction. A description of diseases of the small intestine that result in malabsorption is then presented.

Digestion and Absorption

The components of most foods (carbohydrates, proteins, and fats) cannot be used in their natural state. Foods must first be digested and then absorbed by the gastrointestinal (GI) tract. Proper functioning of the stomach, liver and biliary tree, pancreas, and small bowel and, to a lesser degree, salivary glands

and colon, is required for normal digestion and absorption of food.

CARBOHYDRATE DIGESTION AND ABSORPTION

Carbohydrates account for 40% to 50% of daily caloric intake.⁴ Ingested carbohydrates are derived from plants, except for lactose, which originates in dairy products. Simple sugars include the monosaccharides, fructose and glucose, and the disaccharides, sucrose and lactose. Starches are soluble polymers of glucose found in the cell walls of plants. The starches are α -amylose, a linear polymer of glucose, and amylopectin, a branched form of glucose. Dietary fibers are nondigestible carbohydrates (nonstarch polysaccharides) that are structural components of plant cell walls.

The GI tract is adapted for digesting carbohydrates to a monosaccharide form that can be transported across the epithelium of the small intestine. Luminal digestion of starches is accomplished by amylase secreted by the parotid gland and pancreas. Salivary amylase is of minor importance because this enzyme is deactivated in the acidic environment of the stomach. Amylase digestion of starches is so efficient that starch digestion is more dependent on the form of the starch than on the availability of luminal amylase.⁴ Amylase deficiency is present only in cases of severe pancreatic insufficiency.

Enzymes on the apical membrane of the enterocytes are responsible for further digestion of the products of luminal digestion and breakdown of disaccharides. For example, sucrose isomaltase is an enzyme that cleaves sucrose into glucose and fructose. Brush border lactase cleaves lactose into glucose and galactose. This enzyme is critical for mammalian survival because early nutrition is provided by the mother's milk.⁴ The monosaccharides are then brought across the epithelium by passive diffusion, facilitative transport of proteins, or sodium-coupled active transport.

Colonic bacteria digest dietary fiber that reaches the colon, producing a variety of products, including short-chain fatty acids, methane, and hydrogen. Short-chain fatty acids are rapidly absorbed in the colon, providing energy for colonic epithelial cells.

Digestion of lactose, sucrose, and starches is incomplete because digestion depends on the type of food and contact time with the brush border. Between 2% and 20% of starch is not digested.⁴ Most small bowel diseases result in global dysfunction of the intestinal mucosa, leading to carbohydrate malabsorption, with subsequent diarrhea, flatulence, and weight loss. Specific disaccharidase deficiencies result in similar symptoms. For example, trehalose is a disaccharide of glucose found in insects, yeasts, and mushrooms. As a result, people who are trehalase-deficient have severe diarrhea after ingestion of mushrooms.

PROTEIN DIGESTION AND ABSORPTION

Proteins in the lumen of the GI tract derive from the diet (70-100 g/day), from salivary, gastric, pancreatic, and biliary secretions (30 g/day), and from sloughed epithelial cells (30 g/day).⁵ Protein digestion begins in the stomach. Inactive precursors (pepsinogens) are secreted from chief cells and are activated to pepsins in the acidic environment of the stomach. Proteins in the gastric lumen are digested to a mixture of large polypeptides, smaller oligopeptides, and free amino acids.

The exocrine pancreas secretes five inactive precursor zymogens into the duodenal lumen. Enteropeptidase (enterokinase) on the brush border of the duodenal enterocytes converts trypsinogen into trypsin. Trypsin then activates the remainder of the pancreatic zymogens—chymotrypsinogen, proelastase, and procarboxypeptidases A and B.⁵ These pancreatic enzymes break proteins into oligopeptides (60%-70%) and free amino acids (30%-40%).⁵ Peptidases on the brush border of the enterocytes further degrade the intraluminal oligopeptides, resulting in a mixture of tripeptides, dipeptides, and free amino acids. Distinct transport systems separately transport free amino acids and peptides of two to three amino acids into the epithelial cells. Various peptidases within the enterocytes further digest the small polypeptides. Amino acids leave the enterocytes via transport mechanisms across the basal membrane, passing into the portal circulation.

FAT DIGESTION AND ABSORPTION

The sources of fat include diet (120-150 g), biliary secretions (40-50 g), and sloughed intestinal cells and bacteria.⁶ Most dietary fat is composed of neutral fats, long-chain triglycerides. Phospholipids and sterols (including cholesterol) comprise only a small percentage of dietary fat.⁶

Lipid digestion begins in the stomach with the hydrolysis of triglycerides by gastric and salivary lipase; 20% to 30% of intraluminal fat digestion occurs in the stomach. The grinding action of the antrum helps reduce triglycerides into smaller particles. The fat globules are dispersed in a stable form with a large surface area, termed *emulsification*. Gastric lipid digestion has an increased role in patients with cystic fibrosis or a partial gastrectomy.⁶

After chyme reaches the small intestine, bile salts and lecithin secreted by the liver solubilize the fat, allowing the fat to be broken into smaller droplets by the agitating action of the small bowel. Lipolytic enzymes secreted by the pancreas break triglycerides, phospholipids, and sterol esters into their component monoglycerides and free fatty acids. Bile salts combine with the monoglycerides and free fatty acids to form micelles. The micelles deliver the breakdown products of fat to the microvilli of the epithelial cell brush border.

After brush border uptake, long-chain fatty acids and monoglycerides are delivered to smooth endoplasmic reticulum in the cytoplasm for resynthesis into complex lipids.⁶ Phospholipids, an important component of cell membranes, are synthesized in the rough endoplasmic reticulum. Triglycerides resynthesized in the endoplasmic reticulum of enterocytes are secreted by enterocytes as lipoproteins. These lipoproteins are multimolecular aggregates of lipid and protein, with a configuration that allows transport through aqueous intracellular fluid or plasma. Lecithin is the primary phospholipid in lipoproteins

and is derived primarily from bile salts (10-20 g/day) or diet (5-10 g/day). Cholesterol is primarily derived from biliary secretions (1-2 g/day), with a minor component (0.2-0.5 g/day) from the diet.

Most dietary fat enters the lymphatic circulation through lacteals located in each villus and is then passed via mesenteric lymphatics to the thoracic duct and superior vena cava. About 25% of triglycerides are transported to the liver bound to albumin.

Digestion of fat is very efficient. Almost all dietary triglyceride is absorbed by enterocytes. No ingested triglyceride is found in the colon. The small amount of fecal fat (<7 g/day) is derived from phospholipids in sloughed intestinal membranes or intestinal bacteria. After micelle delivery, bile salts return to the small bowel lumen to solubilize more free fatty acids and monoglycerides. Eventually, conjugated bile salts (95%) are resorbed in the ileum via an active sodium-coupled process. Some bile salts are passively absorbed in the proximal small intestine. Fecal loss of bile salts is balanced by synthesis of bile in the liver.

FLUIDS AND ELECTROLYTES

Diarrhea and malabsorption are not synonymous. Malabsorption may occur in some diarrheal states. A large volume of fluid (8-10 L) enters the GI lumen each day, but only 100 mL of fluid is normally excreted in the feces.⁷ The daily fluid load includes about 2 L of oral intake, 0.5 to 1.5 L of saliva, 2.5 L of gastric juice, 0.5 L of bile, 1.5 L of pancreatic secretions, and 1 L of intestinal secretions. The small bowel absorbs about 7 L of fluid daily, with 1.5 to 1.9 L of fluid reaching the colon. The colon is capable of resorbing up to 4 L of fluid on a daily basis. Diarrhea therefore occurs if more than 4 L of fluid reaches the colon or if abnormally functioning colonic mucosa cannot resorb the 1.9 L of fluid that normally enters the colon each day.

Anatomic Classification of Malabsorption

In summary, carbohydrate digestion requires a functioning pancreas and small bowel brush border enzymes. Normal protein digestion requires adequate gastric and pancreatic function and small bowel brush border enzymes. Fat digestion requires normal hepatic, biliary, exocrine, pancreatic, and small bowel function. An anatomic classification of malabsorption by abnormalities of the liver, biliary tree, stomach, and small intestine aids the radiologist in understanding malabsorption (Table 43-1).³

HEPATOBIILIARY AND PANCREATIC DISORDERS

Bile salt insufficiency caused by biliary obstruction or decreased hepatic synthesis leads to mild malabsorption. Any disease that destroys pancreatic exocrine tissue decreases bicarbonate and pancreatic enzyme secretion. Maldigestion does not occur until 90% of the pancreatic exocrine tissue has been destroyed.⁴ The most common cause of pancreas-related maldigestion is alcohol-related pancreatitis. Patients with cystic fibrosis have malabsorption, but this is a less common disease.

TABLE 43-1 Anatomically Oriented Classification of Malabsorption

Organ	Disease or Condition	Pathophysiology
Stomach	Zollinger-Ellison syndrome Postgastrectomy	Pancreatic enzyme inactivation by acid Rapid transit of nutrients, dilution of pancreatic enzymes
	Pernicious anemia	Intrinsic factor deficiency (vitamin B ₁₂ malabsorption)
Pancreas	Chronic pancreatitis, cystic fibrosis, pancreatic cancer	Decreased pancreatic enzyme and bicarbonate secretion
Liver, biliary tree	Severe parenchymal liver disease	Decreased bile salt formation
	Cholestatic liver disease (primary biliary cirrhosis, drug-induced cholestasis), bile duct obstruction (bile duct carcinoma, pancreatic cancer, gallstones, sclerosing cholangitis)	Decreased bile salt delivery to duodenum
Small intestine	Jejunal diverticulosis, scleroderma, small intestinal fistulas, stricture in Crohn's disease, diabetes, pseudo-obstruction	Stasis with bacterial overgrowth, bile salt deconjugation
	Crohn's disease, small intestinal resection, cholecystocolonic fistula	Increased bile salt loss
	Lactase deficiency, Crohn's disease	Disaccharidase deficiency
	Celiac disease, tropical sprue, Whipple's disease, eosinophilic gastroenteritis, radiation enteropathy, Crohn's disease, intestinal ischemia, ileal resection	Loss of normal epithelial cells
	Abetalipoproteinemia	Nonformation of chylomicrons
	Lymphangiectasia, lymphoma, tuberculosis, carcinoid	Lymphatic obstruction
	Diabetes mellitus, giardiasis, adrenal insufficiency, hyperthyroidism, hypogammaglobulinemia, amyloidosis, AIDS	Multiple causes

From Rubesin SE, Rubin RA, Herlinger H: Small bowel malabsorption: Clinical and radiological perspectives. *Radiology* 184:297–305, 1992.

GASTRIC DISORDERS

Diseases of the stomach may cause mild malabsorptive states. Patients with pernicious anemia have decreased production of intrinsic factor, leading to vitamin B₁₂ deficiency. In patients with Zollinger-Ellison syndrome, inflammation and ulceration in the duodenum and first several loops of jejunum cause diarrhea, not malabsorption. About one third of patients with Zollinger-Ellison syndrome have diarrhea related to gastric hypersecretion and intestinal mucosal damage. Mild malabsorption results from excess acid entering the duodenum, which inactivates pancreatic enzymes.

SMALL BOWEL DISORDERS

Malabsorption can result from a wide variety of mechanisms beginning in the intestinal lumen and extending deep to the small mesentery (see Table 43-1).

Bacterial Overgrowth (Intraluminal Stasis)

Any disease that causes stasis in the lumen of the small intestine can lead to bacterial overgrowth and small bowel dysfunction (Box 43-1).³ Disorders that cause chronic small bowel obstruction (e.g., Crohn's disease, adhesions) may result in stagnation and bacterial overgrowth. Diseases with intrinsic small bowel hypomotility (e.g., diabetes, scleroderma, jejunal diverticulosis) can also lead to stasis and bacterial overgrowth. Stasis in surgical blind loops or the afferent loop of a gastrojejunostomy can also result in bacterial overgrowth.

In patients with bacterial overgrowth, malabsorption is related to several mechanisms, including intraluminal bacterial deconjugation of bile salts and fermentation of carbohydrates. Concomitant epithelial cell dysfunction may be present. Bacterial digestion of malabsorbed fat forms compounds that

can stimulate small bowel or colonic secretion. Solutes of malabsorbed carbohydrates and deconjugated bile salts are also osmotically active, resulting in water and electrolyte loss.

Brush Border Disease

Brush border enzyme deficiencies or transport mechanism deficiencies may cause osmotic diarrhea, malabsorption, or both. The most common example of osmotic diarrhea caused by brush border disaccharidase deficiency is so-called lactase deficiency (lactose-phlorizin hydrolase deficiency) with lactose intolerance.⁴ The norm for most people is for brush border lactose-phlorizin hydrolase levels to decline in older children and adolescents to 5% to 10% of early childhood levels. As a result, lactase-phlorizin hydrolase deficiency is the norm, and the ingestion of dairy products can lead to diarrhea, flatulence, and cramps in most adults. Preservation of lactose-phlorizin hydrolase is an autosomally recessive trait, found typically in northern Europeans. Intermediate activity of this enzyme is found in heterozygotes.

Mucosal Damage

Inflammation or necrosis of crypt cells and immature villous cells causes secretory diarrhea. Blood, pus, and mucus in the intestinal lumen lead to osmotic diarrhea. Widespread epithelial damage is therefore characterized by a combination of osmotic and secretory diarrhea and nutrient malabsorption. Diseases that destroy proximal small bowel epithelium cause generalized malabsorption of fats, proteins, carbohydrates, iron, and folate, whereas diseases that damage distal ileal mucosa primarily cause malabsorption of fat because of bile salt loss and vitamin B₁₂ deficiency. Mucosal diseases causing malabsorption typically involve relatively long segments of small bowel. These diseases are relatively uncommon, however; they

BOX 43-1 DISEASES CAUSING SMALL BOWEL HYPOMOTILITY AND MALABSORPTION***GENETIC DISORDERS**

Familial visceral neuropathies
Familial visceral myopathies
 Muscular dystrophy

COLLAGEN-VASCULAR DISORDERS

Progressive systemic sclerosis
 Dermatomyositis, polymyositis
 Periarthritis nodosa
 Systemic lupus erythematosus

ENDOCRINE DISORDERS

Diabetes mellitus
 Hypothyroidism
 Hypoparathyroidism

NEUROLOGIC DISEASES

Parkinson's disease
 Multiple sclerosis
 Chagas' disease
Spinal cord injury

DRUGS

Narcotics
 Phenothiazines
 Antiparkinson medications
 Ganglionic blockers
 Tricyclic antidepressants

OTHER

Celiac disease
Radiation enteritis
Jejunal diverticulosis
Amyloidosis
 Lead poisoning

Data from Rubesin SE: Diseases of the small bowel causing malabsorption. In Taveras JM, Ferrucci JT (eds): Radiology: Diagnosis, Imaging, Intervention. Philadelphia, JB Lippincott, 1993, pp 1–17.

*Disorders typically having a malabsorptive state are highlighted in bold.

include celiac disease, tropical sprue, Whipple's disease, and eosinophilic enteritis.

Postmucosal Disease

Any disorder that obstructs lacteals in the villi or lymphatics in the small bowel mesentery may cause fat malabsorption. In primary lymphangiectasia, for example, abnormal formation of lymphatics results in impaired absorption of chylomicrons and fat-soluble vitamins and loss of lymph into the intestinal lumen from lymphoenteric fistulas.

Diseases with Multifactorial Causes

Malabsorption is caused by several mechanisms in many diseases. In amyloidosis, for example, malabsorption can be attributed to stasis with bacterial overgrowth, mucosal destruction caused by ischemia, and disruption of nutrient absorption by amyloid deposition in the lamina propria. Fat malabsorption in hyperthyroidism is attributed to rapid small bowel transit.

Diagnosis of Malabsorption: Clinical Perspective

Malabsorption is characterized by diarrhea, steatorrhea, excessive gas, abdominal pain, and weight loss. Diarrhea is caused by decreased intestinal absorption, colonic secretion of fluid induced by hydroxy fatty acids, and osmotic overload of bile salts and fatty acids. *Steatorrhea* is the term used for the bulky, foul-smelling, greasy stools caused by the malabsorption of fat. Excessive gas production is related to fermentation of carbohydrates by intestinal bacteria and results in borborygmi, flatulence, and abdominal distention. Abdominal pain has a variety of causes, including pancreatic inflammation, biliary disease, small bowel obstruction, and ischemia.

Unfortunately, adults with malabsorption often have an insidious presentation. Steatorrhea may be so mild that it is unrecognized by the patient. Mild steatorrhea is typical of low-grade bile duct obstruction, chronic hepatic disease, mild to moderate pancreatic insufficiency, and even mild celiac disease. Many patients with malabsorption present with symptoms related to a specific vitamin or nutrient deficiency. For example, vitamin A deficiency may cause night blindness, vitamin K deficiency results in easy bruisability, petechiae, or hematuria, vitamin D or calcium malabsorption results in paresthesias, tetany, or bone pain, and decreased absorption of folate, vitamin B, or iron may cause pallor, glossitis, stomatitis, and cheilosis.

The clinician has a broad array of laboratory tests and biopsies to make a diagnosis of malabsorption. The reader is referred to textbooks of gastroenterology for further description of these tests. Radiologic imaging in patients with a clinical diagnosis of malabsorption is performed as an adjunct to help identify diseases (e.g., jejunoileal diverticulosis) that cause malabsorption. Radiologic imaging is also used to detect complications of diseases that cause malabsorption (e.g., T-cell lymphoma arising in celiac disease).

Bacterial Overgrowth

A wide variety of disorders may cause small bowel hypomotility with resulting stasis and bacterial overgrowth (see Box 43-1) or intestinal pseudo-obstruction.

JEJUNOILEAL DIVERTICULOSIS

Small bowel diverticula are acquired protrusions of mucosa and submucosa on the mesenteric border of the small bowel, where the vasa recta pierce the muscularis propria. The diverticula are larger and more numerous in the jejunum, decreasing in size and number as they progress into the ileum.^{8,9} Jejunoileal diverticula develop in a heterogeneous group of disorders associated with abnormalities of smooth muscle or the myenteric plexus. Small bowel dysmotility is frequent. Some cases of jejunoileal diverticulosis may be a manifestation of systemic sclerosis or a forme fruste of isolated scleroderma.¹⁰

Jejunoileal diverticulosis is not uncommon, occurring in about 2% of the population,⁸ but most people with jejunal diverticulosis are asymptomatic. In patients with numerous diverticula, stasis with bacterial overgrowth and malabsorptive symptoms may occur. Complications of jejunal diverticula, including GI obstruction or perforation, may cause abdominal symptoms.

Diverticula are readily identified on barium studies as 1- to 7-cm round, barium-filled sacs on the mesenteric border of the small bowel (Fig. 43-1). The mouths of the diverticula are broad-based and the necks are variable in length. Air-fluid levels may be present on upright or cross-table lateral radiographs. If there are numerous diverticula, the course of the small bowel may be obscured by the numerous sacs. On computed tomography (CT) scans, large diverticula are easily mistaken for small intestinal loops. The best way that diverticula are detected by CT is visualization of an air-fluid level in a focal sacculation.¹¹ The motor disorder seen in jejunoileal diverticulosis is manifested by decreased peristalsis, increased intraluminal fluid and gas, luminal dilation, and prolonged transit time.

Although other small bowel disorders may be associated with sacculations or diverticula, jejunoileal diverticulosis is easily differentiated from the sacculations in Crohn's disease, scleroderma, or prior surgery, a solitary Meckel's diverticulum, or diverticula confined to the terminal ileum.^{1,10}

Jejunoileal diverticulosis may be complicated by pneumatosis cystoides intestinalis or free intraperitoneal air caused by perforation or benign pneumatosis.¹² Jejunal diverticulitis may cause abdominal pain, free perforation obstruction or abscess formation, or GI bleeding.¹²⁻¹⁶ Jejunal diverticulitis is manifested on CT as a stranding or mass in the small bowel mesentery adjacent to a diverticulum or true abscess formation. Mechanical obstruction may result from volvulus, enterolith impaction, or diverticulitis. Heterotopic tissue or neoplasms are rare complications.



Figure 43-1 Jejunoileal diverticulosis causing malabsorption. This overhead radiograph from a small bowel follow-through shows multiple large diverticula on the mesenteric border of jejunum and ileum. The sacs are smooth, but many have a lobulated contour.

PROGRESSIVE SYSTEMIC SCLEROSIS, VISCERAL NEUROPATHIES, AND MYOPATHIES

The small intestine is clinically involved in about 40% of patients with progressive systemic sclerosis (scleroderma).¹⁷ The smooth muscle, especially that of the circular muscle layer, degenerates and is replaced by collagen.¹⁸ The muscular abnormalities result in duodenal and jejunal dilation (Fig. 43-2) and hypomotility, with prolonged small bowel transit time and increased intraluminal fluid. Patchy and predominant fibrosis of the circular muscle layer leads to bunching of small bowel folds, producing the so-called hidebound bowel (see Fig. 43-2).¹⁹ Despite luminal dilation, an increased number of small bowel folds per inch is usually seen. Asymmetric scarring leads to wide-mouthed sacculations, usually on the mesenteric border of the small bowel.^{20,21} As with any small bowel disorder characterized by hypomotility, transient intussusceptions and pneumatosis intestinalis may occur, with or without pneumoperitoneum.

Several forms of visceral myopathies and neuropathies present with malabsorption or intestinal pseudo-obstruction. These include autosomal dominant and recessive conditions or isolated cases.²² Other isolated cases have been caused by Epstein-Barr virus infection or abnormalities of cytoskeleton filament proteins.²³ Visceral myopathies are characterized histologically by degeneration and fibrosis of the inner circular and outer longitudinal smooth muscle layers.²⁴ Congenital neuropathies are characterized by degeneration of the myenteric plexus

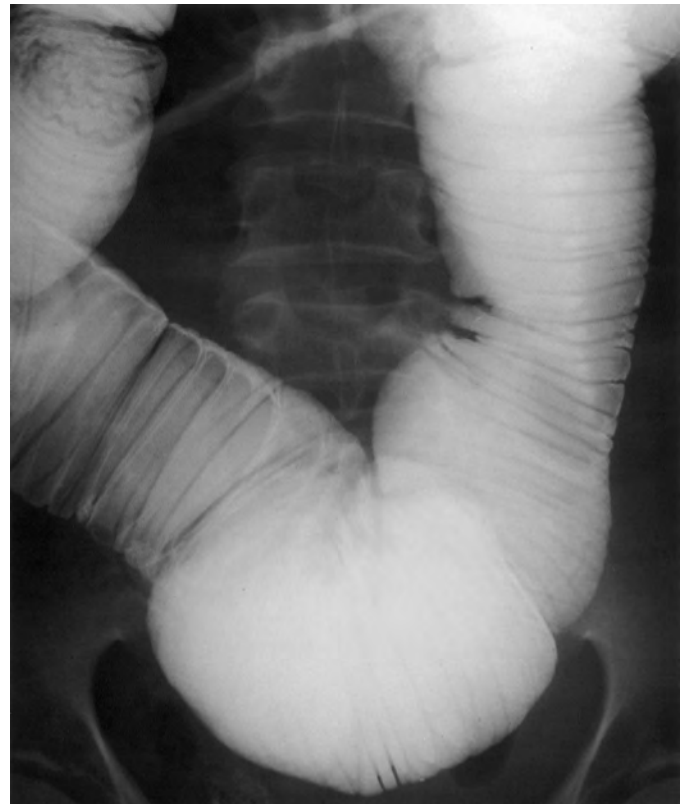


Figure 43-2 Scleroderma. This spot radiograph from enteroclysis shows a massively dilated small bowel. (Compare the diameter of the lumen with the size of a lumbar vertebral body.) There is also an increased number of folds per inch, producing the hidebound sign.

of the bowel. Decreased or absent peristalsis is seen in visceral myopathies and scleroderma, but large-amplitude, nonpropulsive contractions are seen in visceral neuropathies.²⁴ Marked duodenal enlargement typically occurs in visceral myopathies, whereas small bowel dilation may be present in visceral myopathies and neuropathies. The increased number of folds and sacculations typical of scleroderma are not found. The colon demonstrates hypercontractility in visceral neuropathy and dilation and lack of haustration in visceral myopathy.²⁴

Epithelial Cell Damage

CELIAC DISEASE

Celiac disease (gluten-sensitive enteropathy, or celiac sprue) is a chronic immunologic inflammatory disease in which the gliadin fraction of wheat, barley, or rye gluten incites damage to the small bowel mucosa. Removal of wheat products from the diet reverses this mucosal damage. Although the mechanism of celiac disease is not completely understood, it is postulated that there is suspension of normal immune tolerance to foreign food antigens.^{25,26} The gliadin fraction of ingested wheat products stimulates an immune response in the epithelium of the small intestine, leading to mucosal inflammation and destruction. Lymphocytic infiltration may also occur in the stomach (as lymphocytic gastritis) or colon.

Celiac disease occurs in about 1 in 200 whites.²⁵ Most people with celiac disease ignore minor symptoms or are asymptomatic. Celiac disease resulting in severe clinical symptoms is uncommon and is usually encountered in whites, particularly northern Europeans and people from Ireland.²⁶ Children may present with diarrhea, abdominal distention, weight loss, and failure to thrive. Young adults may present with diarrhea, steatorrhea, or infertility. Older adults may present with steatorrhea, anemia, weight loss, or other symptoms. Patients who develop symptoms in adulthood or who develop celiac disease *de novo* in adulthood may present with symptoms related to the malabsorption of specific nutrients such as vitamin A or B₁₂. Bleeding or purpura related to vitamin K deficiency may be present. Aphthous stomatitis, cheilosis, and glossitis are not infrequent. In adults, symptoms in celiac disease may be precipitated by

pregnancy, respiratory therapy, and gastric surgery.²⁷ Gluten-sensitive enteropathy is seen in patients with dermatitis herpetiformis.²⁸ Celiac disease has also been associated with other skin diseases, such as psoriasis, eczema, cutaneous amyloid, and mycosis fungoides.²⁴

The diagnosis of celiac disease can be made when physicians test for serum antibodies associated with celiac disease in patients with minimal GI complaints or indicators of malabsorption, such as vitamin deficiencies. Immunoglobulin A (IgA) and IgG antibodies to gliadin are elevated in 75% to 85% of patients with celiac disease.²⁹ These antibodies may also be elevated in some patients with inflammatory bowel disease or liver disease. Endomysial antibody is also elevated in a large percentage of patients with celiac disease.^{30,31}

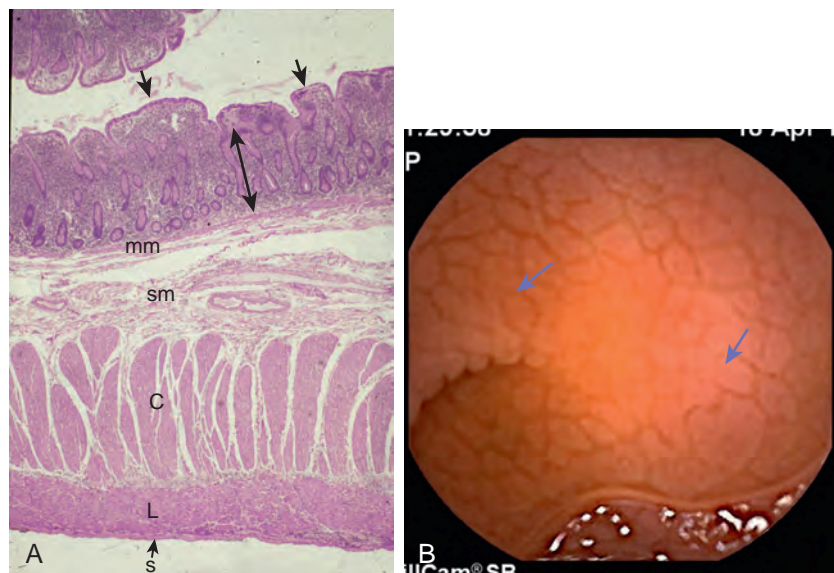
The antigen for antiendomysial antibody is tissue transglutaminase (tTG). An enzyme-linked immunosorbent assay (ELISA) test for IgA anti-tTG is reported to have a sensitivity of 90% to 95% for the diagnosis of celiac disease. Other studies have shown less favorable results for antiendomysial antibody.³¹ Some patients with celiac disease have IgA deficiency, so this test will have false-negative results in these patients. Small bowel biopsies and follow-up biopsies after gluten withdrawal are usually required for a definitive diagnosis.³²

Biopsy specimens in celiac disease typically reveal a loss of intestinal villi associated with crypt hyperplasia and infiltration of the lamina propria by plasma cells and lymphocytes (Fig. 43-3).³³ Lesser degrees of villous atrophy may be present, however, ranging from mild villous flattening to partial villous atrophy or a flat mucosa. Because other diseases may cause loss of intestinal villi, biopsy-proven reversal of mucosal changes after gluten withdrawal is essential for confirming this diagnosis. Nevertheless, some patients may develop disease that is refractory to gluten withdrawal.

Radiographic Findings

Although endoscopic or capsular biopsy is required for a definitive diagnosis of celiac disease, enteroclysis may help establish the diagnosis in patients with atypical symptoms.³⁴ Enteroclysis is particularly of value for detecting complications in patients with known celiac disease and a poor response to medical

Figure 43-3 Celiac disease. A. A jejunal resection specimen demonstrates marked flattening and loss of villi (short arrows). The crypts are elongated relative to the height of the villi ("crypt hyperplasia") (double arrow). There is an increased inflammatory infiltrate expanding the lamina propria. The muscularis mucosa (mm), submucosa (sm), circular muscle layer of the muscularis propria (C), longitudinal muscle layer of the muscularis propria (L), and serosa (s-tiny arrow) are identified. (H & E, 40×). **B.** Capsule endoscopy shows villous atrophy of the jejunum.



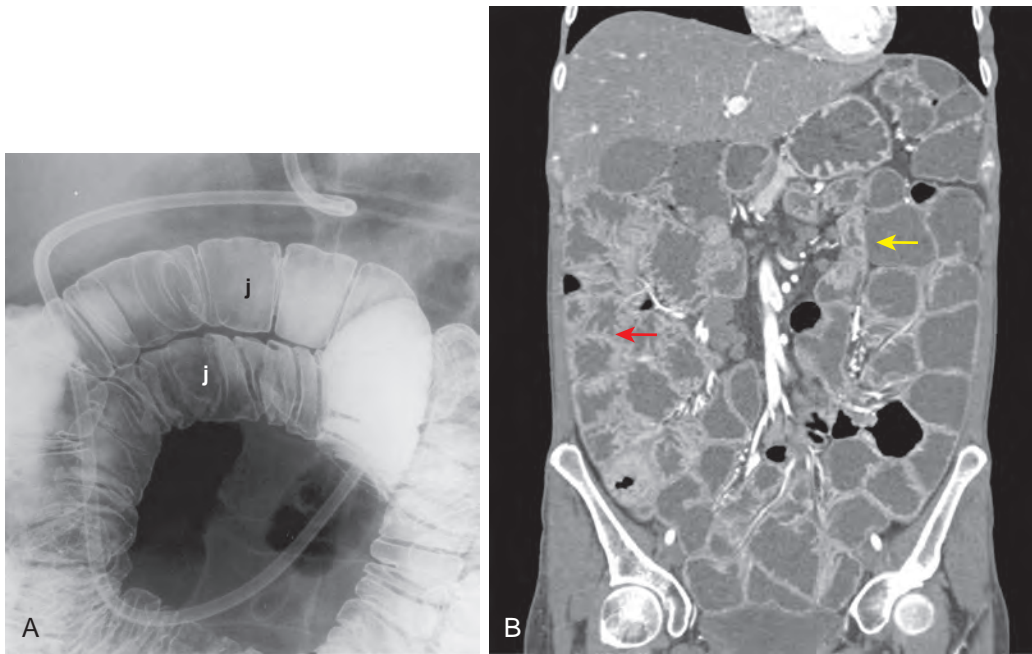


Figure 43-4 Celiac disease. **A.** This spot radiograph from enteroclysis shows a paucity of folds (two to three folds/inch) in two loops of jejunum (j). However, the folds are of normal thickness. **B.** Coronal reformatted CT scan in another patient show markedly increased small bowel secretions. Note that the ileal folds (red arrow) are larger than jejunal folds (yellow arrow).

therapy or patients with recurrent symptoms despite gluten withdrawal.³⁴⁻³⁶

The radiographic findings in celiac disease reflect the villous atrophy that results in loss of mucosal surface area. This mucosal atrophy is manifested as a decreased number of folds in the proximal jejunum (Fig. 43-4), the portion of the small bowel that is most severely atrophic. Three or fewer folds per inch are present in 75% of adult patients with known or suspected celiac disease.³⁴ Four folds per inch in the proximal jejunum is indeterminate for celiac disease, because the proximal jejunum normally has four to seven folds per inch. The mucosal surface pattern may appear finely reticular in uncomplicated celiac disease, with polygonal radiolucent islands of mucosa surrounded by barium-filled grooves.^{34,35} This radiographic pattern reflects the “mosaic” pattern visualized when celiac mucosa is examined under a dissecting microscope.³⁷ Villous atrophy reveals the underlying groove pattern of the mucosa and crypt openings.

In contrast, ileal folds may be increased in number and thicker than normal in celiac disease, an adaptive response to increase the mucosal surface area of the small bowel.³⁸ This phenomenon has been termed *jejunization of the ileum*. If jejunal or proximal ileal folds are enlarged or nodular, complications such as ulcerative jejunoileitis, lymphoma, or edema related to hypoproteinemia should be suspected.³⁵ Nevertheless, thickened nodular folds and discrete mucosal nodules can be seen in the duodenum in patients with uncomplicated celiac disease (Fig. 43-5), reflecting the effect of gastric acid on atrophic duodenal mucosa, in association with inflammation, Brunner’s gland hyperplasia, and gastric metaplasia.³⁹⁻⁴¹

Enteroclysis is much more accurate than small bowel follow-through studies for evaluating fold patterns and establishing the diagnosis of celiac disease or one of its complications. However, transient intussusceptions occur in 25% of patients with celiac disease, and these intussusceptions are better shown on small bowel follow-throughs.^{42,43} Diffuse hypomotility in celiac disease may also be better shown on small bowel follow-through studies.



Figure 43-5 Duodenitis in celiac disease. This spot radiograph centered on the second and third parts of the duodenum shows thick, nodular folds.

Complications

The major complications of celiac disease include malabsorption refractory to gluten withdrawal, hyposplenism, neuropathy, intestinal ulceration and pneumatosis, lymphadenopathy, the cavitory mesenteric lymph node syndrome, and malignancy.^{35,37,44,45} In patients with known celiac disease, complications are frequently heralded by development of fever, acute

abdominal pain, abdominal distention, weight loss, or steatorrhea, despite adherence to a gluten-free diet. CT and enteroclysis are complementary radiologic tests for the diagnosis of these complications.⁴⁶

Splenic atrophy occurs in one third to one half of patients with celiac disease.⁴⁷⁻⁴⁹ Decreased splenic size correlates with decreased splenic function.⁴⁹ A small spleen may be shown on any radiologic test capable of visualizing the spleen.

Mesenteric and retroperitoneal lymphadenopathy are not uncommon in celiac disease and are usually caused by reactive lymphoid hyperplasia.^{50,51} Mesenteric or retroperitoneal lymphadenopathy can be of low attenuation (Fig. 43-6), reflecting fat deposition in lymph nodes, or of normal attenuation. The cavitary mesenteric lymph node syndrome is a rare, usually fatal disorder, typically occurring in patients with celiac disease or patients with small bowel villous atrophy refractory to a gluten-free diet.⁵²⁻⁵⁴ This condition is characterized by markedly enlarged, cavitary lymph nodes filled with lipid-rich hyaline material. CT may reveal mesenteric or retroperitoneal masses of low attenuation, with or without fat-fluid levels (Fig. 43-7).³⁵

Although numerous malignant tumors have been described in patients with celiac disease, there is definitely an increased incidence of squamous cell carcinoma of the pharynx and esophagus and of adenocarcinoma and lymphoma of the small bowel in these patients.^{24,55-62} Malignant tumors are the most common cause of death in adults with celiac disease.⁵⁹⁻⁶³

Small bowel lymphomas are T-cell lymphomas in patients with celiac disease. These tumors have a 300-fold higher incidence in celiac disease than in the general population and are the most common malignant tumors complicating celiac disease.^{24,57,58} T-cell lymphomas in celiac disease are distinct from typical B-cell small bowel lymphomas. T-cell lymphomas usually involve long segments of bowel. Both T- and B-cell lymphomas may have a multifocal distribution. Unlike most small bowel lymphomas, T-cell lymphoma tumors tend to be located in the jejunum rather than in the ileum.³⁵ T-cell lymphomas are usually manifested on barium studies, and CT and magnetic resonance imaging (MRI) scans (Fig. 43-8) by thickened, nodular folds in long segments of jejunum.³⁵ In some

patients, however, radiographic studies may reveal a cavitary or annular lesion (Fig. 43-9).

Radiologic differentiation of T-cell lymphoma from ulcerative jejunoileitis is not possible. Ulcerative jejunoileitis is an entity in which multiple ulcers develop in the small bowel during the fifth or sixth decade of life.^{64,65} About 75% of these patients have celiac disease or villous atrophy unresponsive to gluten withdrawal.⁴⁶ Patients usually present with fever, abdominal pain, weight loss, or abdominal distention. This entity is complicated by GI bleeding, perforation, or obstruction. Ulceration is most prominent in the jejunum but is also seen in the ileum or colon. Thickened, nodular folds may be present in the

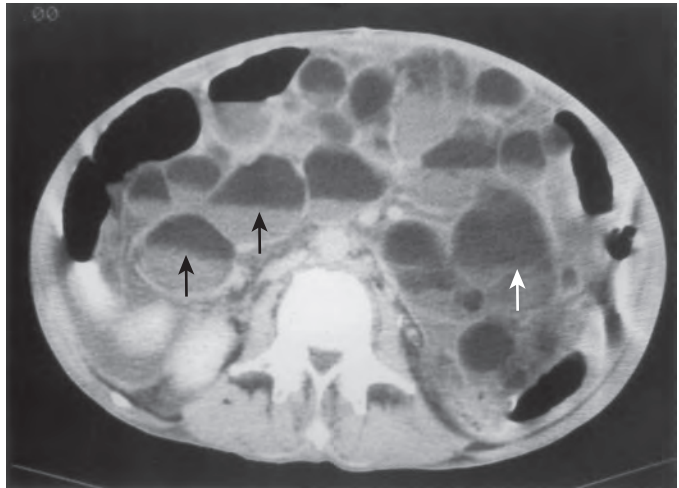


Figure 43-7 Cavitary mesenteric lymph node syndrome. This CT scan shows numerous ovoid masses in the abdomen. The masses have fat and debris levels (arrows). These represent enlarged, cavitary lymph nodes that could be mistaken for loops of small bowel with air-fluid levels. However, the fat and fluid attenuation of the nodes and the lack of opacification by positive oral contrast should suggest the correct diagnosis. (From Rubesin SE, Herlinger H, Saul SH, et al: Adult celiac disease and its complications. *RadioGraphics* 9:1045-1066, 1989.)

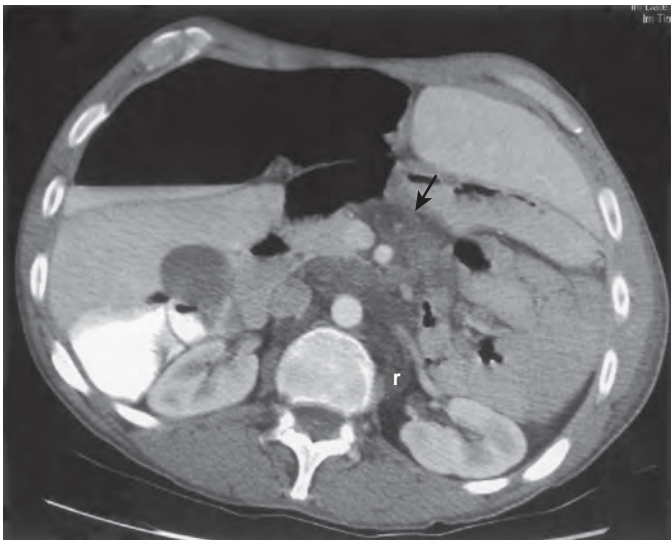


Figure 43-6 Lymphadenopathy in celiac disease. This CT scan shows numerous low-attenuation lymph nodes (arrow) in the root of the small bowel mesentery and in the retroperitoneum (r).

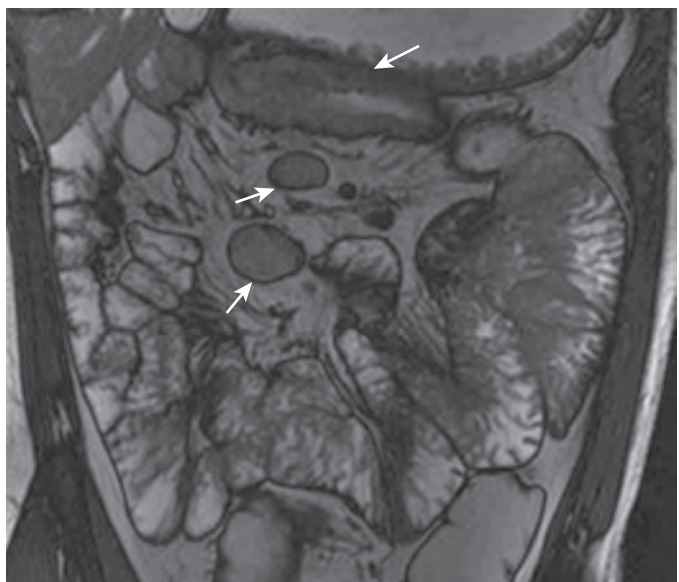


Figure 43-8 T-cell lymphoma complicating celiac disease. This coronal MRI scan shows mural thickening of the jejunum (long arrow) and enlarged lymph nodes (arrows) in the adjacent mesentery. (Courtesy Gabriele Masselli, MD, Rome, Italy.)



Figure 43-9 T-cell lymphoma complicating celiac disease. This spot radiograph from enteroclysis shows a short annular lesion (large arrow) with central ulceration (small arrows) in the jejunum. Note the decreased number of jejunal folds proximal to the lesion because of underlying celiac disease.

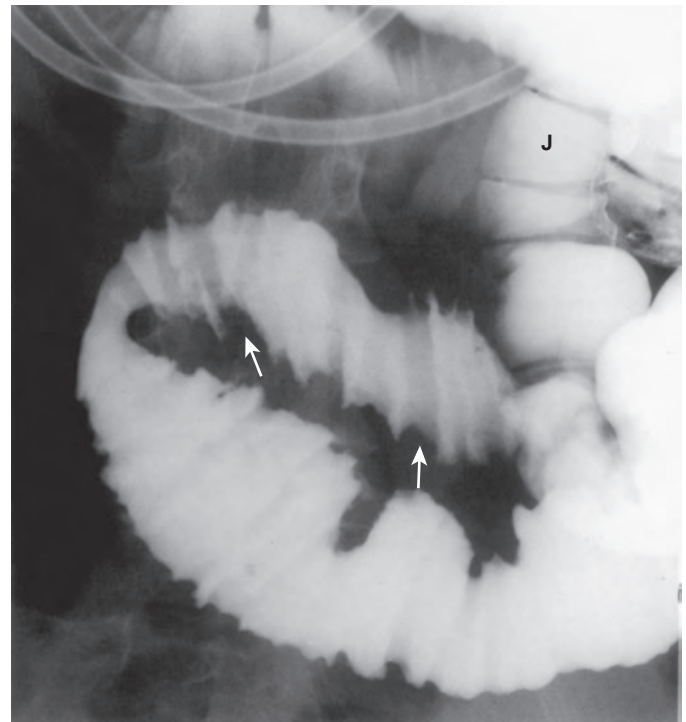


Figure 43-10 Ulcerative jejunoileitis complicating celiac disease. This spot radiograph during the early phase of enteroclysis shows a loop of jejunum with moderately thickened, irregular folds (arrows) caused by ulcerative jejunoileitis. Also note a decreased number of normal-sized folds more proximally in the jejunum (J) because of underlying celiac disease. (From Rubesin SE, Herlinger H, Saul SH, et al: *Adult celiac disease and its complications*. RadioGraphics 9:1045–1066, 1989.)

jejunum, mimicking the radiographic appearance of lymphoma (Fig. 43-10). Some cases of ulcerative jejunoileitis may progress to stricture formation (Fig. 43-11).

Small bowel adenocarcinomas are usually annular infiltrating lesions involving the duodenum or jejunum.³⁵ These tumors have a threefold higher incidence in celiac disease than in the general population. They are usually advanced tumors at the time of diagnosis.⁵³

TROPICAL SPRUE

Tropical sprue is a persistent contamination of the small bowel by enteric pathogens that occurs in residents of endemic tropical or subtropical areas such as the Caribbean, southeast Asia, and India. Travelers to endemic areas usually develop tropical sprue only after prolonged visits. The disease is uncommon in children. Patients initially suffer a watery diarrheal illness that may remit or progress to chronic malabsorption. Although unproven, it has been postulated that colonization of the small intestine by toxigenic strains of coliform bacteria causes tropical sprue.⁶⁶ Combined folate and vitamin B₁₂ deficiency in tropical sprue can lead to megaloblastic anemia. In tropical sprue, villous atrophy is partial and crypt hyperplasia is not severe. The histologic changes of tropical sprue are found in the duodenum, jejunum, and ileum, unlike the duodenal and jejunal

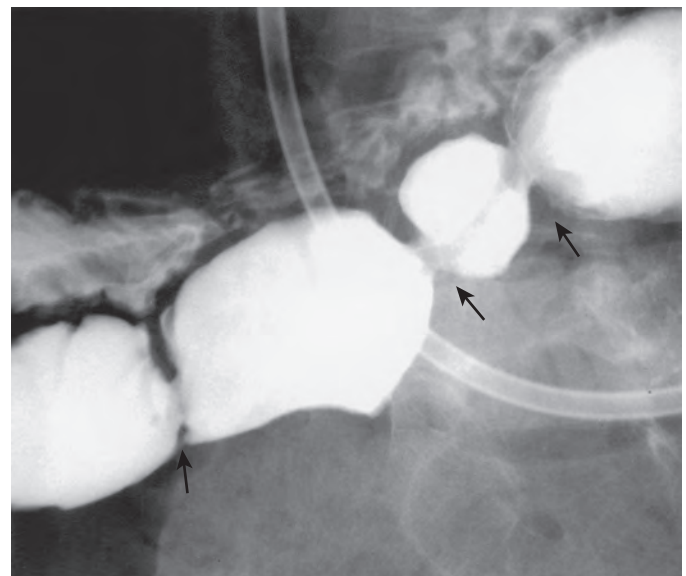


Figure 43-11 Strictures in ulcerative jejunoileitis complicating celiac disease. This spot radiograph from enteroclysis shows three short segments of ringlike narrowing (arrows) in the jejunum. (From Rubesin SE, Herlinger H, Saul SH, et al: *Adult celiac disease and its complications*. RadioGraphics 9:1045–1066, 1989.)

changes in celiac disease. Tropical sprue responds to antibiotic and folate therapy.²⁴

Tropical sprue is radiographically distinct from celiac disease. Thickened folds are seen in the jejunum (Fig. 43-12) and even the ileum, in contrast to the normal-sized folds (although decreased in number) in uncomplicated celiac disease.

GIARDIASIS

The protozoan *Giardia lamblia* is a frequent cause of endemic and epidemic diarrhea worldwide. Outbreaks of diarrhea are less frequent in the United States. Rarely, giardiasis is heralded by malabsorptive symptoms.⁶⁷ The protozoan attaches to the mucosal surface of the intestine, causing little damage to the underlying small bowel.³³ Barium studies in patients with giardiasis usually show no abnormalities. In severe cases, thickened folds may be seen in the distal duodenum and proximal jejunum.^{68,69} There may be rapid transit of barium and spasm in the proximal small bowel.^{70,71}

WHIPPLE'S DISEASE

Tropheryma whipplei (formerly called *Tropheryma whippelii*) is a gram-positive bacillus with a thick wall and trilaminar membrane.⁷² This recently cultured (1991) bacterium is responsible for the rare systemic bacterial disease first described by George Whipple in 1907.⁷³ It has been postulated that a defect in monocyte-macrophage function prevents affected individuals from eliminating the Whipple's bacillus.



Figure 43-12 Tropical sprue. This spot radiograph from a small bowel follow-through shows moderately thickened, slightly undulating folds in the jejunum. Unlike celiac disease, the number of folds per inch in the jejunum is normal.

Whipple's disease usually occurs in whites, particularly men, with a male predominance of 6:1.⁷⁴ GI symptoms include bloating, weight loss, and steatorrhea. Extraintestinal manifestations include arthritis, arthralgias, cardiac disease, fever, and multiple central nervous system findings, including dementia and myoclonus. Arthritis is the most common extraintestinal manifestation. These patients typically have a migratory arthritis involving large and small joints. Cardiac involvement is characterized by pericarditis, valvular defects, and congestive heart failure. Peripheral lymphadenopathy is not uncommon.

Whipple's disease is typically manifested on barium studies by thickened, nodular folds, primarily in the distal duodenum and jejunum (Fig. 43-13).⁷⁵ Fine mucosal nodularity is sometimes demonstrated as a result of villous blunting caused by expansion of the lamina propria by lacteals distended with fat and by innumerable macrophages containing digested bacilli.³³

CT may reveal enlarged, low-attenuation lymph nodes in the mesentery and retroperitoneum (see Fig. 43-22).⁷⁶ Fat accumulation in obstructed lymph nodes accounts for this low-attenuation lymphadenopathy. Other causes of low-attenuation mesenteric and retroperitoneal lymphadenopathy include *Mycobacterium avium-intracellulare* infection in patients with AIDS, celiac disease, and metastatic testicular carcinoma.^{35,77,78}

The diagnosis of Whipple's disease is confirmed on biopsy specimens showing a lamina propria packed with periodic acid–Schiff (PAS)-positive macrophages containing gram-positive, acid-fast, negative bacilli.³³ Electron micrography may be performed to verify the diagnosis.

EOSINOPHILIC GASTROENTERITIS

Eosinophilic enteritis is a rare heterogeneous group of disorders characterized by an eosinophilic infiltrate in various organs and various layers of the GI tract. Symptoms depend on the distribution and location of the eosinophilic infiltrate. If the small bowel mucosa and submucosa are infiltrated by eosinophils, mild steatorrhea, protein loss, weight loss, and iron deficiency



Figure 43-13 Whipple's disease. This overhead radiograph from a small bowel follow-through shows thickened, nodular folds in the proximal and mid small bowel.

may occur. Eosinophilic infiltration of the muscularis propria results in gastric outlet obstruction or small bowel obstruction.⁷⁹ Eosinophilic infiltration involving primarily the serosa of the small bowel is rare but can result in eosinophilic ascites.⁸⁰ Eosinophilic enteritis usually develops during the third to sixth decades of life. About 50% of patients have a peripheral eosinophilia or an allergic history (including asthma, hay fever, drug sensitivity, or urticaria). The diagnosis of eosinophilic enteritis requires biopsy confirmation of eosinophilic infiltration of the small bowel wall in the absence of extraintestinal disease or parasitic infection.

Eosinophilic infiltration of the small bowel can involve the jejunum or entire small bowel, is typically patchy, and can be unifocal or multifocal. With the mucosal form of eosinophilic enteritis, barium studies may reveal smooth or nodular, thickened folds perpendicular to the longitudinal axis of the small bowel (Fig. 43-14).^{81,82} Spasm is a frequent finding. Eosinophilic enteritis can mimic the radiographic findings of other diseases causing submucosal bleeding in the small bowel (e.g., ischemia). Concomitant gastric disease is found in about 50% of patients. In these patients, barium studies may reveal antral polyps or thickened, nodular antral folds. Thus, clues to the diagnosis of eosinophilic enteritis include simultaneous involvement of the gastric antrum and small bowel, peripheral eosinophilia, and history of allergic diseases.

AMYLOIDOSIS

Amyloidosis is a group of diseases characterized by the extracellular deposition of insoluble fibrillar proteins with specific histologic staining and characteristic features on electron microscopy. In primary amyloidosis and amyloidosis associated with multiple myeloma, a variable portion of an immunoglobulin light chain is deposited predominantly in the muscular layers of the small bowel. This results in small bowel hypomotility. Primary amyloidosis also affects the tongue, heart, kidneys, blood vessels, nerves, and muscles. In secondary and hereditary forms of amyloidosis, amyloid is primarily deposited in the

mucosa, resulting in malabsorption. Secondary amyloidosis is associated with chronic GI diseases such as Crohn's disease and schistosomiasis and chronic systemic inflammatory diseases such as tuberculosis, rheumatoid arthritis, leprosy, chronic osteomyelitis, and familial Mediterranean fever. Ischemia and infarction can result from amyloid deposition in blood vessels.

Barium studies reveal abnormalities in the small bowel in about 40% of patients with primary amyloidosis, including decreased small bowel motility; transient intussusceptions; thickened, nodular folds; focal ulceration; and, rarely, acute perforation.⁸³⁻⁸⁵ Enteroclysis may reveal a finely granular mucosal surface pattern, reflecting blunting of villi and deposition of amyloid in the lamina propria.^{85,86} Large amyloid deposits in the lamina propria may be manifest by 4- to 10-mm, smooth-surfaced, nodular elevations (Fig. 43-15).⁸⁵ Chronic ischemia and infarction may also be manifested by numerous 3- to 4-mm nodules and by erosions and thickened mucosal folds.⁸⁵ Although ischemic changes are reversible, the fine granularity and submucosal nodules do not respond to therapy.⁸⁵

SHORT GUT SYNDROME

Resection of large lengths of the small intestine results in an acute diarrheal illness and long-term malabsorptive state.⁸⁷ Disease states that lead to extensive small bowel resections include vascular damage from volvulus, superior mesenteric artery embolus, superior mesenteric vein thrombosis, and strangulated hernia, Crohn's disease, radiation enteropathy, and abdominal trauma.⁸⁷ Barium studies are of value for documenting the amount of small intestine remaining (Fig. 43-16) and the presence of residual or recurrent small bowel disease—usually the same disease that necessitated small bowel resection. Barium studies may also reveal postsurgical complications such as adhesions and anastomotic strictures. Other complications include gastric hypersecretion with ulcer formation and renal calculi caused by hyperoxaluria after ileal resection. Ileal resection can also lead to cholelithiasis.

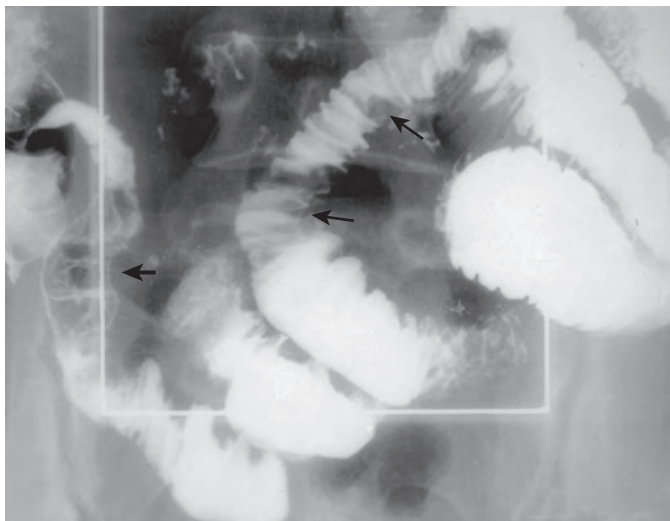


Figure 43-14 Eosinophilic enteritis. This spot radiograph from a small bowel follow-through shows thickened, straight folds (small arrows) in several loops of distal small bowel and an abnormal surface pattern (thick arrow) in the terminal ileum.

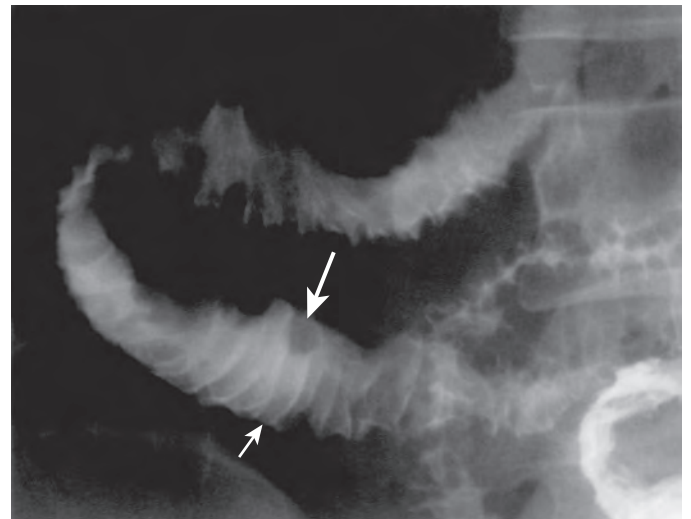


Figure 43-15 Amyloidosis involving the small bowel. This spot radiograph from a small bowel follow-through shows smooth, thickened folds (small arrow) caused by edema from low-grade ischemia and focal nodularity (large arrow) caused by amyloid deposits in the submucosa.

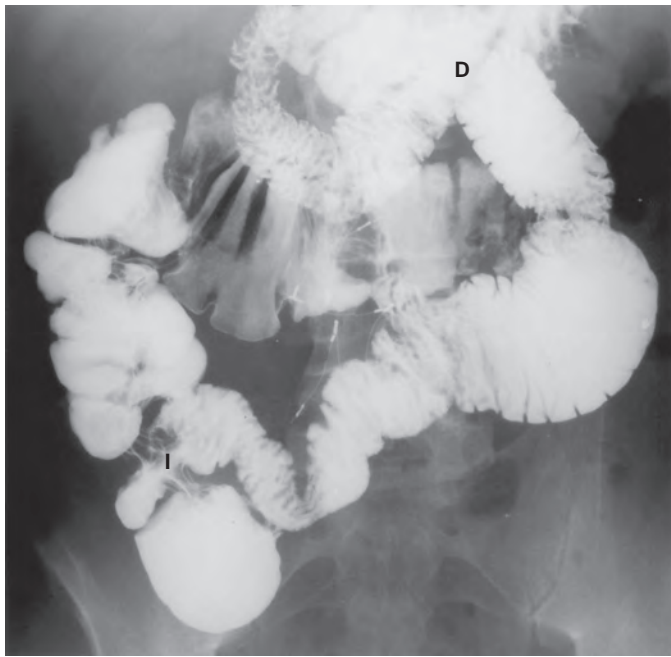


Figure 43-16 Short gut syndrome. This overhead radiograph shows a total of only three loops of small bowel from the duodenojejunal junction (D) to the ileocecal valve (I). The small bowel is dilated but not obstructed.

In some patients, portions of the remaining small intestine compensate for the loss of bowel by increasing the thickness and number of folds to increase the absorptive capability of the small bowel.⁸⁸ As a result, barium studies may reveal an increased number of ileal folds and increased fold height and thickness.

Nonformation of Chylomicrons

ABETALIPOPROTEINEMIA

Abetalipoproteinemia is a rare, autosomally transmitted disorder that is heterogeneous at the molecular level.⁸⁹ This disorder is linked to a defect in the microsomal triglyceride transport protein (MTTP).⁸⁹ Triglycerides and cholesterol esters are normally secreted from cells in association with the large, hydrophobic, apolipoprotein B (apoB). MTTP is an enzyme found in the endoplasmic reticulum necessary for the assembly of apoB-containing lipoproteins.⁸⁹ Without functioning MTTP, fats cannot be transported out from the basal membrane of enterocytes. This results in the accumulation of absorbed fats and fat-soluble vitamins within enterocytes. Triglycerides also accumulate in hepatocytes.

Symptoms and age at onset vary, depending on the specific defect in apoB-lipoprotein synthesis. Clinically apparent malabsorption may develop at any time, from infancy to early adulthood. Vitamin E deficiency results in spinocerebellar degeneration and acanthocytosis. Vitamin A deficiency results in retinitis pigmentosa, which typically develops during the second decade of life. Mental retardation may also be present.

Barium studies may reveal moderately thickened, nodular folds in the duodenum and proximal jejunum (Fig. 43-17).⁹⁰ It is difficult to explain the radiographic findings on the basis of the underlying pathology. There is no villous distortion or infiltration of the submucosa in abetalipoproteinemia, only



Figure 43-17 Abetalipoproteinemia. This spot radiograph of small bowel shows mildly thickened, irregular folds, possibly caused by intestinal secretions that prevent barium from adequately coating the mucosal surface because the microscopic pathology does not explain the apparent fold thickening in this condition (Courtesy Hans Herlinger, MD.)

accumulation of fat in enterocytes near the tips of the villi. No fat droplets are seen in the intercellular spaces or lymphatics. It has therefore been postulated that these “thickened folds” on barium studies are an artifact of malabsorption, in which increased secretions prevent barium from adequately coating the mucosa.⁹¹

Lymphatic Obstruction and Lymphangiectasia

Primary intestinal lymphangiectasia results from a congenital abnormality of lymphatic development. Secondary lymphangiectasia results from lymphatic obstruction in the small bowel wall and mesentery because of cardiac failure, retroperitoneal fibrosis, radiation therapy, or mesenteric lymph node involvement by Whipple’s disease, tuberculosis, sarcoidosis, lymphoma, or carcinoid tumor.

Lymphatic obstruction results in abnormal absorption of chylomicrons and fat-soluble vitamins, excessive leakage of lymph into the intestinal lumen, and impaired circulation of enteric lymphocytes. Chylous ascites results from serosal and mesenteric lymphatic obstruction. Blockage of the thoracic duct causes chylous pleural effusions.

In patients with primary lymphangiectasia, symptoms usually develop in older children and young adults. Diarrhea is present in 80% of patients. Steatorrhea is less common, occurring in 20% of patients.⁹² Edema of the extremities and chylous pleural effusions are common. Patients may develop hypogammaglobulinemia, lymphocytopenia (particularly of T lymphocytes), and hypoproteinemia.

Barium studies typically reveal thickened, straight, parallel, relatively smooth folds in the jejunum and ileum (Fig. 43-18).⁹² Disproportionate involvement of the duodenum and jejunum occurs in some patients.⁹³ Dilated lymphatic lacteals may cause villous distention and blunting, manifested radiographically by sharply defined 1-mm nodular radiolucencies in the small bowel (Fig. 43-19). Luminal distention is uncommon. CT may reveal a thickened small bowel wall (Fig. 43-20). In patients with secondary lymphangiectasia, CT may also reveal lymphadenopathy of normal or low attenuation.

Multifactorial Diseases

DIABETES MELLITUS

From 10% to 20% of patients with severe diabetes mellitus have diarrhea without malabsorption.⁹⁴ Steatorrhea, if present, is usually mild. Steatorrhea in patients with diabetes mellitus has a variety of causes, including hypomotility with bacterial overgrowth, pancreatic exocrine insufficiency, malabsorption of bile salts, and abnormal small bowel absorption or secretion. About 4% to 9% of patients with type 1 diabetes have clinical celiac disease related to the HLA-DR31-DQ2 haplotype.³³ The pathogenesis of diabetic malabsorption is uncertain. The proximal vagus nerves and sympathetic nerves of the small bowel show varying demyelination, but the myenteric and submucosal plexi are histologically normal.⁹⁵ As a result, diabetics with symptoms related to the small bowel usually have a severe neuropathy and often also have a nephropathy and retinopathy. Barium studies may reveal small bowel transit that is normal, slow, or rapid. Some patients may have accompanying gastroparesis.

CYSTIC FIBROSIS

Cystic fibrosis is an autosomal recessive disorder caused by a variety of defects in the cystic fibrosis transmembrane conductance regulator gene (*CFTR*) on chromosome 7q32.⁹⁶ At least 1000 mutations have been discovered in this gene, accounting for the wide variation in the severity and presentation of cystic fibrosis. Abnormalities in the *CFTR* gene in epithelial cells

result in abnormal duodenal bicarbonate secretion,⁹⁷ abnormal activity of peptide hydrolases, and abnormal chloride secretion. Loss of pancreatic enzyme secretion and subsequent maldigestion further compound small bowel problems. Malabsorption, if present, is related to bile acid and pancreatic exocrine abnormalities.^{96,98}

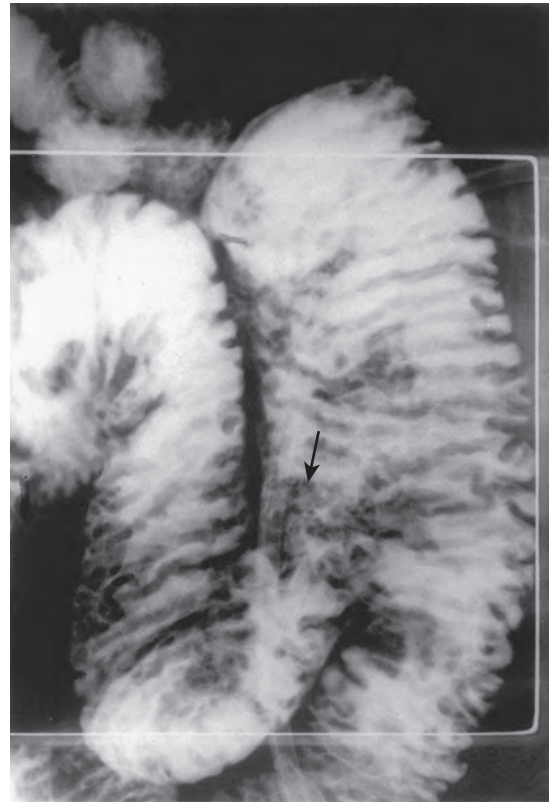


Figure 43-19 Lymphangiectasia. This spot radiograph from enteroclysis shows mildly thickened, irregular folds. Tiny mucosal nodules (arrow) are seen in one region because of enlarged, bulbous villi.

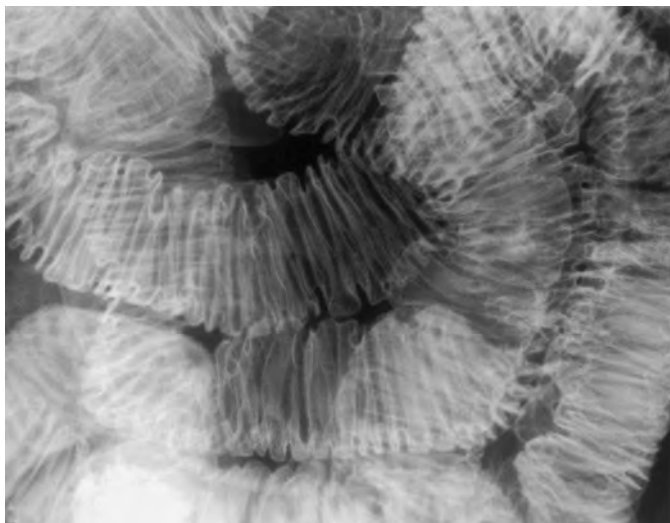


Figure 43-18 Lymphangiectasia. This spot radiograph of jejunum from enteroclysis shows smooth, mildly thickened, slightly undulating folds.



Figure 43-20 Lymphangiectasia. This CT scan through the upper pelvis shows diffuse thickening of the small bowel wall in profile (open arrow) and en face (large arrow). Stranding of the small bowel mesentery reflects dilated lymphatics and mild mesenteric lymph node enlargement (small arrows).



Figure 43-21 Cystic fibrosis. This spot radiograph from a small bowel follow-through shows luminal dilation and moderately thickened, straight folds.

Although cystic fibrosis does not cause a small bowel–related malabsorptive syndrome, it does lead to a meconium ileus equivalent, often resulting in a functional distal small bowel obstruction or even intussusception of the distal ileum.^{99,100} The proximal colon and distal small bowel are filled with thick, viscous fecal material. Cystic fibrosis is included in this chapter because folds in the duodenum and mesenteric small bowel may appear thickened (Fig. 43-21).¹⁰¹ The cause of these thickened folds is uncertain. It has been postulated that thick secretions coating the mucosa prevent barium from approaching the epithelial layer, leading to the erroneous impression of thickened folds. Whatever the explanation for thick folds, the possibility of ischemia or another malabsorptive state may erroneously be considered in patients with cystic fibrosis.

Differential Diagnosis of Fold Enlargement in Malabsorption

Small bowel folds are composed of mucosa and submucosa and are therefore enlarged by diseases involving the mucosa and submucosa.⁹¹ Smooth enlargement of folds usually indicates edema, hemorrhage, or inflammation in the lamina propria and submucosa. Tiny nodules (0.5–2 mm) usually indicate villous enlargement by mucosal inflammation, amyloid infiltration, or lacteal obstruction. Gross nodularity of folds usually indicates focal deposition of inflammatory cells, amyloid, or tumor.

Malabsorptive diseases manifested by thickened, smooth folds include giardiasis, lymphangiectasia, tropical sprue, and celiac disease complicated by severe hypoproteinemia. Fold changes in giardiasis and celiac disease occur in the proximal jejunum, whereas lymphangiectasia is more evenly distributed throughout the small bowel. Giardiasis is further characterized

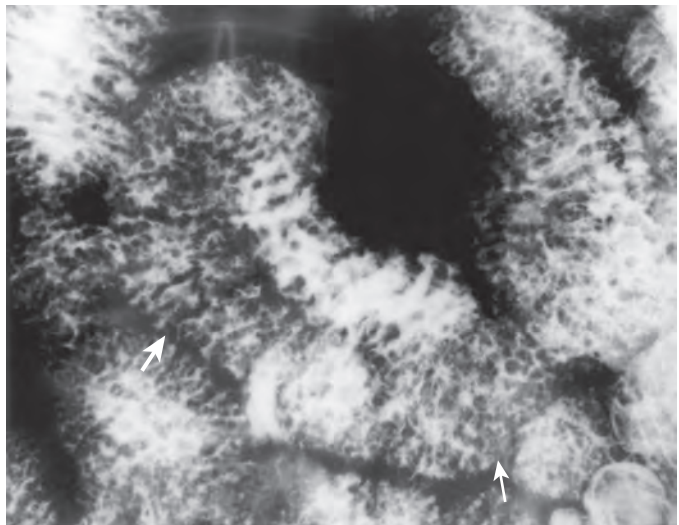


Figure 43-22 Lymphoma as a cause of diffuse nodular fold thickening. This spot radiograph from a small bowel follow-through shows moderately thickened, nodular small bowel folds (thick arrow). Tiny nodules reflect villous enlargement (thin arrow). This radiographic appearance is unusual for non-Hodgkin's lymphoma involving the small bowel but can be seen in T-cell lymphoma complicating celiac disease, Mediterranean lymphoma associated with immunoproliferative small intestinal disease, and lymphoma in patients with AIDS. (Courtesy K. Cho, MD.)

by rapid small bowel transit and spasm. Celiac disease is usually associated with a decreased number of folds per inch.

Malabsorptive diseases manifested by thickened, nodular folds include celiac disease complicated by lymphoma or ulcerative jejunoileitis, Whipple's disease, amyloidosis, eosinophilic enteritis, abetalipoproteinemia, and mastocytosis. Thickened, nodular folds in celiac-related lymphoma or ulcerative jejunoileitis are usually focal and located in the jejunum. There also is a decreased number of folds per inch in 75% of patients with celiac disease. In Whipple's disease and abetalipoproteinemia, the folds are more diffusely abnormal, although jejunal predominance occurs in some patients. Whipple's disease is typically a disease of middle-aged white men, whereas abetalipoproteinemia is a disease with retinitis pigmentosa and spinocerebellar degeneration that develops during the second and third decades of life. Eosinophilic gastroenteritis typically has a multifocal distribution, often associated with ileal predominance and skip areas. About 50% of patients with eosinophilic enteritis have a peripheral eosinophilia or allergic history. Amyloidosis is more diffusely distributed throughout the small bowel. Coarse mucosal deposits (nodules >5 mm) of amyloid may be present. Fine mucosal nodules (enlarged villi caused by dilated lacteals) may also be seen in patients with lymphangiectasia if an optimal radiographic technique is used.

Other diseases of the small bowel may produce thickened, finely nodular folds, but malabsorption is not present. About 50% of patients with mastocytosis have flushing, tachycardia, headaches, and urticaria pigmentosa. Mucosal nodularity is usually multifocal. However, malabsorption is rare in patients with mastocytosis. Some patients with diffuse lymphoma have diffusely thickened, nodular folds in large segments of the small intestine (Fig. 43-22). This radiographic pattern is present in patients with mantle cell lymphoma and Mediterranean lymphoma associated with immunoproliferative small intestinal disease (IPSID).

REFERENCES

- Rubenstein SE: Diseases of small bowel causing malabsorption. In Taveras JM, Ferrucci JT, editors: *Radiology: Diagnosis, Imaging, Intervention*, Philadelphia, 1993, JB Lippincott, pp 1–17.
- Powell DW: Approach to the patient with diarrhea. In Yamada T, Alpers DH, Kaplowitz N, et al, editors: *Handbook of Gastroenterology*, ed 4, Philadelphia, 2003, Lippincott Williams & Wilkins, pp 99–111.
- Rubenstein SE, Rubin RA, Herlinger H: Small bowel malabsorption: Clinical perspectives. *Radiology* 184:297–305, 1992.
- Traber P: Carbohydrate assimilation. In Yamada T, Alpers DH, Kaplowitz N, et al, editors: *Textbook of Gastroenterology*, ed 4, Philadelphia, 2003, Lippincott Williams & Wilkins, pp 389–413.
- Ganapathy V, Ganapathy ME, Leibach FH: Protein digestion and assimilation. In Yamada T, Alpers DH, Kaplowitz N, et al, editors: *Textbook of Gastroenterology*, ed 4, Philadelphia, 2003, Lippincott Williams & Wilkins, pp 438–449.
- Davidson NO: Intestinal lipid absorption. In Yamada T, Alpers DH, Kaplowitz N, et al, editors: *Textbook of Gastroenterology*, ed 4, Philadelphia, 2003, Lippincott Williams & Wilkins, pp 413–437.
- Devroede GJ, Philips SF: Conservation of sodium, chloride and water by the human colon. *Gastroenterology* 56:125–142, 1969.
- Maglinte DDT, Chernish SM, D'Weese R, et al: Acquired jejunoileal diverticular disease: Subject review. *Radiology* 158:577–580, 1986.
- Salmonowitz E, Wittich G, Hajek P, et al: Detection of intestinal diverticula by double-contrast small bowel enema: Differentiation from other intestinal diverticula. *Gastrointest Radiol* 8:271–278, 1983.
- Krishnamurthy S, Kelly MM, Rohrman CA, et al: Jejunal diverticulosis: A heterogeneous disorder caused by a variety of abnormalities of smooth muscle and myenteric plexus. *Gastroenterology* 85:538–547, 1983.
- Fintelmann F, Levine MS, Rubenstein SE: Jejunal diverticulosis: Findings on CT in 28 patients. *AJR* 190:1286–1290, 2008.
- Dunn V, Nelson JA: Jejunal diverticulosis and chronic pneumoperitoneum. *Gastrointest Radiol* 4:165–168, 1979.
- Ross CB, Richards WO, Sharp KW, et al: Diverticular disease of the jejunum and its complications. *Am Surg* 56:319–324, 1990.
- Benya EC, Ghahremani GG, Brosnan JJ: Diverticulitis of the jejunum: Clinical and radiological features. *Gastrointest Radiol* 16:24–28, 1991.
- Hines J, Rosenblatt J, Duncan DR, et al: Perforation of the mesenteric small bowel: Etiologies and CT findings. *Emerg Radiol* 20:155–161, 2013.
- Baskin RH, Mayo CW: Jejunal diverticulosis: A clinical study of 87 cases. *Surg Clin North Am* 32:1185–1196, 1952.
- Schuffler MD: Neuromuscular abnormalities of the small and large intestine. In White R, editor: *Gastrointestinal and Oesophageal Pathology*, Edinburgh, 1995, Churchill-Livingstone, pp 407–430.
- D'Angelo WA, Fries JF, Msai AST, et al: Pathologic observations in systemic sclerosis (scleroderma): A study of fifty-eight matched controls. *Am J Med* 46:428–440, 1969.
- Horowitz AL, Meyers MA: The “hide-bound” small bowel of scleroderma: Characteristic mucosal fold pattern. *AJR* 119:332–334, 1973.
- Queloz JM, Woloshin HJ: Sacculization of the small intestine in scleroderma. *Radiology* 105:513–515, 1972.
- Olmsted WW, Madewell JE: The esophageal and small bowel manifestations of progressive systemic sclerosis. *Gastrointest Radiol* 1:33–36, 1976.
- Camilleri M: Dysmotility of the small intestine. In Yamada T, Alpers DH, Kaplowitz N, et al, editors: *Textbook of Gastroenterology*, ed 4, Philadelphia, 2003, Lippincott Williams & Wilkins, pp 1486–1529.
- Domizio P, Martin JE: Muscular and mechanical disorders of the small intestine. In Shepherd NA, Warren BF, Williams GT, et al, editors: *Morson and Dawson's Gastrointestinal Pathology*, ed 5, Chichester, England, 2013, Wiley-Blackwell, pp 305–314.
- Rohrmann CA, Ricci MT, Krishnamurthy S, et al: Radiologic and histologic differentiation of neuromuscular disorders of the gastrointestinal tract: Visceral myopathies, visceral neuropathies, and progressive systemic sclerosis. *AJR* 143:933–941, 1981.
- Green PH, Cellier C: Celiac disease. *N Engl J Med* 357:1731–1743, 2007.
- DiSabatino A, Corazz GR: Coeliac disease. *Lancet* 373:1480–1493, 2009.
- Bai J, Moran C, Martinez C, et al: Celiac sprue after surgery of the upper gastrointestinal tract. *J Clin Gastroenterol* 13:521–524, 1991.
- Brow JR, Parker F, Weinstein WM, et al: The small intestinal mucosa in dermatitis herpetiformis: I. Severity and distribution of the small intestinal lesions and associated malabsorption. *Gastroenterology* 60:355–361, 1971.
- Hill ID: What are the sensitivity and specificity of serologic tests for celiac disease? Do sensitivity and specificity vary in different populations? *Gastroenterology* 128:S25–S32, 2005.
- Samaşca G, Sur G, Lupan I: Current trends and investigative developments in celiac disease. *Immunol Invest* 42:273–284, 2013.
- Rostami K, Kerckhaert J, Tiemessen R, et al: Sensitivity of antiendomysium and antigliadin antibodies in untreated celiac disease: Disappointing in clinical practice. *Am J Gastroenterol* 94:888–894, 1999.
- Savarymurtu SH, Sabbat J, Burke M, et al: Impact of endoscopic duodenal biopsy on the detection of small intestinal villous atrophy. *Postgrad Med J* 67:47–49, 1991.
- Brown I: The pathology of malnutrition and malabsorption. In Shepherd NA, Warren BF, Williams GT, et al, editors: *Morson and Dawson's Gastrointestinal Pathology*, ed 5, Chichester, England, 2013, Wiley-Blackwell, pp 373–396.
- Herlinger H, Maglinte DDT: Jejunal fold separation in adult celiac disease: Relevance of enteroclysis. *Radiology* 158:605–611, 1986.
- Rubenstein SE, Herlinger H, Saul SH, et al: Adult celiac disease and its complications. *Radiographics* 9:1045–1065, 1989.
- La Seta F, Salerno G, Brucellato A, et al: Radiologic indicators of adult coeliac disease assessed by double contrast enteroclysis. *Eur J Radiol* 15:157–162, 1992.
- Cooke WT, Holmes GKT: Coeliac Disease, Edinburgh, 1984, Churchill Livingstone.
- Bova JG, Friedman AC, Weser E, et al: Adaptation of the ileum in non-tropical sprue: Reversal of the jejunoileal fold pattern. *AJR* 144:299–302, 1985.
- Knauer CM, Monroe LS: The roentgenographic abnormalities of the duodenum in celiac sprue. *Digestion* 101:129–136, 1964.
- Jones B, Bayless TM, Hamilton SR, et al: “Bubbly” duodenal bulb in celiac disease: Radiologic-pathologic correlation. *AJR* 142:119–122, 1984.
- Marm CS, Gore RM, Ghahremani GG: Duodenal manifestations of nontropical sprue. *Gastrointest Radiol* 1:30–35, 1986.
- Ruoff M, Lindner AE, Marshak RH: Intussusception in sprue. *AJR* 104:525–528, 1968.
- Cohen MD, Lintott DJ: Transient small bowel intussusceptions in adult coeliac disease. *Clin Radiol* 29:529–534, 1978.
- Trier JS: Celiac sprue. *N Engl J Med* 325:1709–1719, 1991.
- Case records of the Massachusetts General Hospital: Weekly clinicopathological exercises. Case 15-1990. A 78-year-old woman from the Dominican Republic with chronic diarrhea. *N Engl J Med* 322:1067–1075, 1990.
- Baer AN, Bayless TM, Yardley JH: Intestinal ulceration and malabsorption syndromes. *Gastroenterology* 79:754–765, 1980.
- Robertson DAF, Swinson CN, Hall R, et al: Coeliac disease, splenic function and malignancy. *Gut* 23:666–669, 1982.
- O'Grady JG, Stevens FM, Harding B, et al: Hyposplenism and gluten-sensitive enteropathy. *Gastroenterology* 87:1326–1331, 1984.
- Robinson PJ, Bullen AW, Hall R, et al: Splenic size and function in adult coeliac disease. *Br J Radiol* 53:532–537, 1980.
- Simmonds JP, Rosenthal FD: Lymphadenopathy in coeliac disease. *Gut* 22:756–758, 1981.
- Jones B, Bayless TM, Fishman EK, et al: Lymphadenopathy in celiac disease: Computed tomographic observations. *AJR* 142:1127–1132, 1984.
- Matuchansky C, Colin R, Hemet J: Cavitation of mesenteric lymph nodes, splenic atrophy and a flat small intestinal mucosa: Report of 6 cases. *Gastroenterology* 87:606–614, 1984.
- Holmes GKT: Mesenteric lymph node cavitation in coeliac disease. *Gut* 27:728–733, 1986.
- Howat AJ, McPhie JL, Smith DA, et al: Cavitation of mesenteric lymph nodes: A rare complication of coeliac disease associated with poor outcome. *Histopathology* 27:349–354, 1995.
- Brunton FJ, Guyer PB: Malignant histiocytosis and ulcerative jejunitis of the small intestine. *Clin Radiol* 34:291–295, 1983.
- Wright BH, Jones DB, Clark H, et al: Is adult-onset coeliac disease due to a low-grade lymphoma of intraepithelial lymphocytes? *Lancet* 337:1373–1374, 1991.
- D'Souza PM, Girgis S, Teshima CW: Challenges in the diagnosis of enteropathy-associated T cell lymphoma. *Can J Gastroenterol* 27:255–256, 2013.
- Swinson CM, Salvin G, Coles EC, et al: Coeliac disease and malignancy. *Lancet* i:111–115, 1983.
- Holmes GKT, Dunn GI, Cockell R, et al: Adenocarcinoma of the upper small bowel complicating coeliac disease. *Gut* 21:1010–1016, 1980.
- O'Brien CJ, Savarymurtu S, Hodgson HJF, et al: Coeliac disease, adenocarcinoma of jejunum

- and in situ squamous carcinoma of oesophagus. *J Clin Pathol* 36:62–67, 1983.
61. Straker RJ, Gunasekaran S, Brady PG: Adenocarcinoma of the jejunum in association with celiac sprue. *J Clin Gastroenterol* 11:320–323, 1989.
 62. Dannenberg A, Godwin T, Raybourn J, et al: Multifocal adenocarcinoma of the small intestine in a patient with celiac sprue. *J Clin Gastroenterol* 11:73–76, 1989.
 63. Ludvigsson JF: Mortality and malignancy in celiac disease. *Gastrointest Endosc Clin N Am* 22:705–722, 2012.
 64. Lamont CM, Adams FG, Mills PR: Radiology in idiopathic chronic ulcerative enteritis. *Clin Radiol* 3:283–287, 1982.
 65. Zaplosky JH, Janower ML: Idiopathic chronic ulcerative enteritis: A report of two cases. *Radiology* 155:39–40, 1985.
 66. Fantry GT, Fantry LE, James SP: Chronic infections of the small intestine. In Yamada T, Alpers DH, Kaplowitz N, et al, editors: *Textbook of Gastroenterology*, ed 4, Philadelphia, 2003, Lippincott Williams & Wilkins, pp 1561–1579.
 67. Yardley JH, Bayless TM: Giardiasis. *Gastroenterology* 52:301–304, 1967.
 68. Peterson GM: Intestinal changes in *Giardia lamblia* infestation. *AJR* 77:670–677, 1957.
 69. Marshak RH, Ruoff M, Lindner AE: Roentgen manifestations of giardiasis. *AJR* 104:557–560, 1968.
 70. Fisher CH, Oh KS, Bayless TM, et al: Current perspectives on giardiasis. *AJR* 125:207–217, 1975.
 71. Brandon J, Glick SN, Teplick SK: Intestinal giardiasis: The importance of serial filming. *AJR* 144:581–584, 1985.
 72. Relman DA, Schmidt TM, MacDermott RP, et al: Identification of the uncultured bacillus of Whipple's disease. *N Engl J Med* 327:293–301, 1993.
 73. Whipple GH: A hitherto undescribed disease characterized anatomically by deposits of fat and fatty acids in the intestinal and mesenteric lymphatic tissues. *Bull Johns Hopkins Hosp* 18:382, 1907.
 74. Schwartzman S, Schwartzman M: Whipple's disease. *Rheum Dis Clin North Am* 39(2):313–321, 2013.
 75. Philips RL, Carson HC: The roentgenographic and clinical findings in Whipple's disease: A review of 8 patients. *AJR* 123:268–273, 1975.
 76. Davis SJ, Patel A: Case report: Distinctive echogenic lymphadenopathy in Whipple's disease. *Clin Radiol* 42:60–62, 1990.
 77. Jeffrey RB, Jr, Nyberg DA, Bottles K, et al: Abdominal CT in acquired immunodeficiency syndrome. *AJR* 146:7–13, 1986.
 78. Radin DR: Intraabdominal mycobacterium tuberculosis vs. mycobacterium avium intracellulare infections in patients with AIDS: Distinction based on CT findings. *AJR* 156:487–491, 1991.
 79. Marshak RH, Linder A, Maklansky D, et al: Eosinophilic gastroenteritis. *JAMA* 245:1677–1680, 1981.
 80. Smith TR, Schmiedeberg P, Flax H, et al: Non-mucosal predominantly serosal eosinophilic enteritis: A case report. *Clin Imaging* 14:235–238, 1990.
 81. MacCarty RL, Talley NJ: Barium studies in diffuse eosinophilic gastroenteritis. *Gastrointest Radiol* 15:183–187, 1990.
 82. Schulman A, Morton PCG, Dietrich BE: Eosinophilic gastroenteritis. *Clin Radiol* 31:101–104, 1980.
 83. Legge DA, Wollaeger AE, Carlson HC: Intestinal pseudo-obstruction in systemic amyloidosis. *Gut* 11:764–767, 1970.
 84. Yamada M, Hatakeyama S, Tsukagoshi H: Gastrointestinal amyloid deposition in AL (primary or myeloma associated) and AA (secondary) amyloidosis: Diagnostic value of gastric biopsy. *Hum Pathol* 16:1206–1211, 1985.
 85. Tada S, Iida M, Matsui T, et al: Amyloidosis of the small intestine: Findings on double-contrast radiographs. *AJR* 156:741–744, 1991.
 86. Smith TR, Cho KC: Small intestine amyloidosis producing a stippled punctate mucosal pattern: Radiological-pathological correlation. *Am J Gastroenterol* 81:477–479, 1986.
 87. Tappenden KA: Pathophysiology of short bowel syndrome: Considerations of resected and residual anatomy. *JPEN J Parenter Enteral Nutr* 38(1 Suppl):14S–22S, 2014.
 88. Gouttebel MC, Saint Aubert B, Colette C, et al: Intestinal adaptation in patients with short bowel syndrome. *Dig Dis Sci* 34:709–715, 1989.
 89. Zamel R, Khan R, Pollex RL, Hegele RA: Abetalipoproteinemia: Two case reports and literature review. *Orphanet J Rare Dis* 3:19, 2008.
 90. Weinstein MA, Pearson KD, Agus SG: Abetalipoproteinemia. *Radiology* 108:269–273, 1973.
 91. Rubesin SE, Furth EE: Differential diagnosis of small intestinal abnormalities with radiologic-pathologic explanation. In Herlinger H, Maglinte DD, Birnbaum BA, editors: *Clinical Imaging of the Small Intestine*, ed 2, New York, 1999, Springer, pp 527–566.
 92. Shimkin P, Waldman T, Krugman R: Intestinal lymphangiectasia. *AJR* 110:827–841, 1970.
 93. Kingham JGC, Moriarty KJ, Furness M, et al: Lymphangiectasia of the colon and small intestine. *Br J Radiol* 55:774–777, 1982.
 94. Valdovinos MA, Camilleri M, Zimmerman BR: Chronic diarrhea in diabetes mellitus: Mechanisms and an approach to diagnosis and treatment. *Mayo Clin Proc* 68:691, 1993.
 95. Yoshida MM, Schuffler MD, Sumi SM: There are no morphologic abnormalities of the gastric wall or abdominal vagus in patients with diabetic gastroparesis. *Gastroenterology* 94:907–914, 1988.
 96. Whitcomb DC: Hereditary diseases of the pancreas. In Yamada T, Alpers DH, Kaplowitz N, et al, editors: *Textbook of Gastroenterology*, ed 5, Philadelphia, 2003, Lippincott Williams & Wilkins, pp 2147–2165.
 97. Robinson PJ, Smith AL, Sly PD: Duodenal pH in cystic fibrosis and its relationship to fat malabsorption. *Dig Dis Sci* 35:1299–1304, 1990.
 98. Gaskin KJ, Waters DLM, Howman-Giles R, et al: Liver disease and common bile duct stenosis in cystic fibrosis. *N Engl J Med* 318:340–346, 1988.
 99. Park RW, Grand RJ: Gastrointestinal manifestations of cystic fibrosis: A review. *Gastroenterology* 81:1143–1161, 1981.
 100. Johansson ME, Sjövall H, Hansson GC: The gastrointestinal mucus system in health and disease. *Nat Rev Gastroenterol Hepatol* 10:352–361, 2013.
 101. Taussig L, Saldino R, di Sant'Agnese P: Radiographic abnormalities of the duodenum and small bowel in cystic fibrosis of the pancreas (mucoviscidosis). *Radiology* 106:369–376, 1973.

Benign Tumors of the Small Bowel

TEMEL TIRKES | JOHN C. LAPPAS

CHAPTER OUTLINE

Clinical Considerations

Imaging Considerations

Specific Tumors

Adenoma

Gastrointestinal Stromal Tumor

Lipoma

Hemangioma

Uncommon Tumors

Polyposis Syndromes

Familial Adenomatous Polyposis Syndrome

Peutz-Jeghers Syndrome

Cowden's Disease

Cronkhite-Canada Syndrome

Clinical Considerations

Primary neoplasms of the small bowel are uncommon and, although about 40 different histologic types of benign and malignant tumors have been identified, they constitute only 1% to 5% of all gastrointestinal neoplasms.^{1,2} Almost 75% of the tumors found at autopsy are benign, whereas most of the symptomatic tumors and tumors detected at surgery are malignant.¹ Regardless of the relative incidence of benign and malignant small bowel tumors, the low susceptibility of the small bowel to neoplastic transformation is remarkable when one considers its length, total mucosal surface area, and diversity of structural elements.

Benign small bowel tumors are usually discovered in patients between 50 and 80 years of age and occur with equal frequency in men and women. Symptomatic patients may present with abdominal pain and other clinical features of partial or intermittent small bowel obstruction.³ Intussuscepting neoplasms may cause significant intestinal obstruction and benign tumors are involved in most adult cases. Bleeding from benign tumors occurs in 40% to 50% of symptomatic patients.³⁻⁵ Anemia, occult bleeding, or intermittent gastrointestinal (GI) hemorrhage may be caused by ulceration of an epithelial adenoma or the mucosa overlying an intramural tumor. In clinical investigations in which enteroclysis was used to evaluate GI bleeding, small bowel neoplasms accounted for 50% of the diagnostic findings, with an almost equal detection of benign and malignant tumors.^{6,7} Constitutional symptoms such as malaise, anorexia, and weight loss are uncommon in patients with benign small bowel neoplasms, as is the ability to palpate the tumor on clinical examination.

Imaging Considerations

Diagnosis of benign small bowel neoplasms remains a dilemma because of the vagueness and paucity of symptoms as well as the difficulty in detecting these lesions on conventional radiologic studies. Because benign small bowel neoplasms are relatively uncommon, most radiologists do not have adequate experience with these tumors, so delayed or inaccurate diagnosis is common.¹⁻⁵ More sophisticated diagnostic methods of intestinal evaluation in patients suspected of small bowel neoplastic disease have been advocated.⁸

Barium-based methods of enteroclysis have been shown to be a reliable technique for the demonstration of small bowel tumors and the evaluation of occult GI bleeding and intestinal obstruction.⁸⁻¹⁰ Enteroclysis may also allow for accurate differentiation of detected benign small bowel tumors.⁹⁻¹¹ Computed tomography (CT) has now become the most readily available and commonly used imaging modality for the evaluation of patients with nonspecific abdominal symptoms. CT has the advantage of demonstrating intraluminal, mural, and extraintestinal abnormalities simultaneously. Certain CT findings can differentiate benign and malignant small bowel tumors and, for some benign tumors such as lipomas and leiomyomas, may allow for a specific diagnosis.¹¹⁻¹³ CT enteroclysis further improves the advantages inherent in multidetector CT (MDCT) scanners by using techniques of small bowel infusion via an enteric tube.^{14,15} Whether performed with positive enteral contrast media (e.g., iodinated, water-soluble) or preferably with neutral enteral contrast media (e.g., water) with intravenous (IV) contrast enhancement, CT enteroclysis has been shown to be an accurate method for the diagnosis of small bowel neoplasms, with a reported sensitivity and specificity of 85% and 97%, respectively.¹⁶ CT enterography, an enteric CT study without intubated intestinal infusion, is an alternative to CT enteroclysis for the investigation of small bowel neoplasms.¹⁷

CT enterography is dependent on the patient's ability to ingest a sufficient volume of oral contrast over a short period of time and interindividual variation in bowel transit time. The choice between the intubation-infusion method (enteroclysis) and oral approach (enterography) is one of preference and may also depend on the clinical indications, patient population, radiology practice, and diagnostic algorithms used by different centers.¹⁸ Magnetic resonance imaging (MRI) of the small bowel has been advocated because of its superior soft tissue contrast resolution, which allows for the differentiation of various pathologic changes in the bowel wall, multiplanar imaging capability, lack of associated exposure to ionizing radiation, possibility of repeated serial acquisitions, and elimination of the need for an iodinated contrast medium.¹⁹ Small bowel capsule endoscopy, although a sensitive technique for the detection of mucosal disease, including intestinal polyposis, has been shown to have limitations in the diagnosis of small bowel tumors.²⁰⁻²²

Specific Tumors

Although numerous benign tumors can be found in the small bowel, approximately 90% are adenomas, GI stromal tumors, lipomas, or hemangiomas. Reports of benign tumors arising from almost all mesenchymal cell types have appeared sporadically in the literature.²³ Benign small bowel tumors often display similar morphologic features on imaging studies. Although a specific histologic diagnosis may be difficult, useful diagnostic observations can be made based on the number and location of tumors and on certain radiologic features that differentiate these lesions.

ADENOMA

Adenomas found within the small bowel are benign glandular epithelial neoplasms that are classified similarly to colonic adenomas and may exhibit a malignant predisposition. Approximately 40% are villous adenomas, and the remainder show a tubular or tubulovillous morphology. As with colonic adenomas, the finding of cellular atypia, a villous component, or large size increases the risk for malignancy. Most patients with adenomas are asymptomatic, but they may occasionally present with GI bleeding or intestinal obstruction secondary to intussusception.

Most adenomas are small (1-2 cm) and have smooth or slightly lobulated contours. They may appear on barium studies as sessile or pedunculated intraluminal polyps or as small mural nodules on enteroclysis (Fig. 44-1). Radiologic differentiation from other polypoid lesions, such as polypoid carcinoma, hamartomatous or inflammatory polyp, or other small submucosal neoplasms, is difficult.

Although small bowel adenomas usually occur as solitary lesions, multiple lesions may be found as a manifestation of hereditary multiple polyposis syndromes (e.g., familial adenomatous polyposis syndrome, Gardner's syndrome).¹ Villous

adenomas are sessile and lobulated, usually larger than most adenomatous polyps, have a strong predilection for the duodenum, and carry a higher risk for malignant transformation (Fig. 44-2).²⁴

GASTROINTESTINAL STROMAL TUMOR

Gastrointestinal stromal tumors (GISTs) constitute a major subset of GI mesenchymal neoplasms and are characterized immunohistologically by the expression of c-kit protein (CD117).^{25,26} These are typically single, firm, circumscribed neoplasms, usually found in the stomach and small bowel.^{2,3,26} GI bleeding, obstruction from intraluminal growth and compression or intussusception are common clinical manifestations.

In reported preoperative series of patients with small bowel tumors, features on barium enteroclysis allowed for the accurate preoperative diagnosis of GISTs in 83% to 100% of patients.^{10,27} Submucosal tumors appear as smooth, round, or semilunar mural defects that are demarcated by sharp angles with the intestinal wall (Fig. 44-3).

CT is particularly useful in depicting the nature and extent of small bowel GISTs.²⁸ These tumors appear on CT as sharply defined masses that display a homogeneous soft tissue density and uniform contrast enhancement. It is difficult to predict the malignant potential of these tumors by imaging alone; however, experience with CT suggests that malignant GISTs are larger than benign tumors, less uniform in shape, and of heterogeneous tissue attenuation.²⁸ A more detailed discussion of GISTs can be found in Chapter 45.

LIPOMA

Lipomas of the small bowel account for 20% to 25% of all GI lipomas, and the small bowel represents the second most

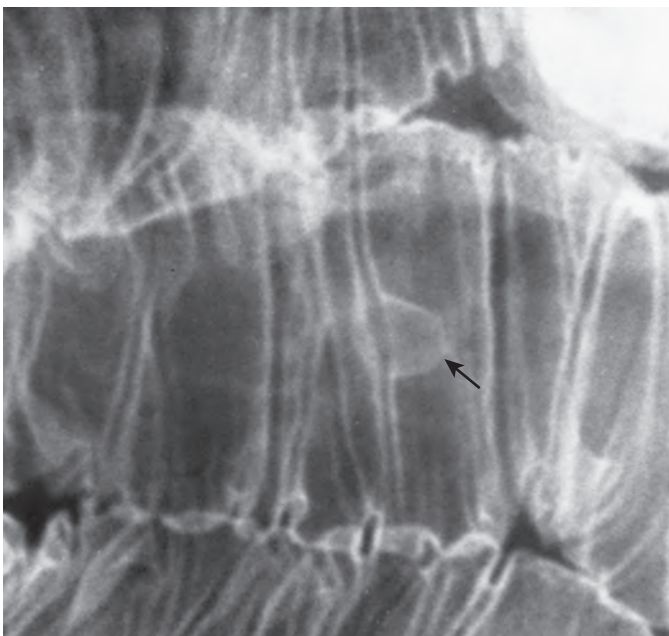


Figure 44-1 Adenoma. Enteroclysis shows a small (8-mm) jejunal adenoma appearing as a smooth, sessile mucosal nodule (arrow).

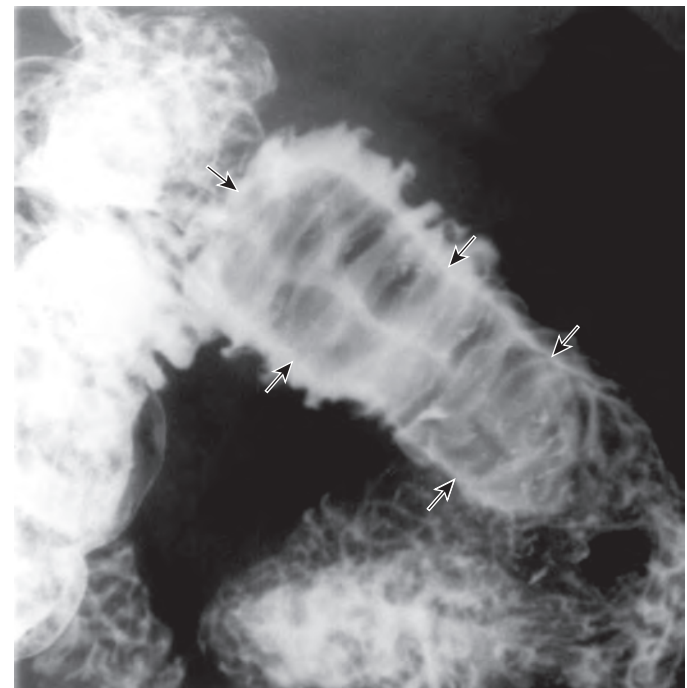


Figure 44-2 Tubulovillous adenoma. Enteroclysis shows an elongated jejunal tubulovillous adenoma (arrows).

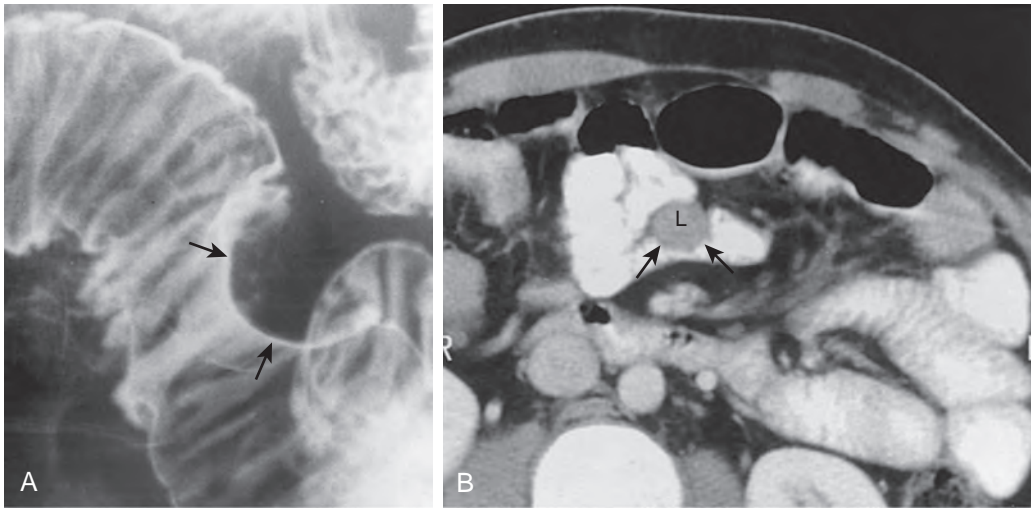


Figure 44-3 Gastrointestinal stromal tumor (GIST). **A.** The submucosal nature of the tumor is recognized on barium study by an area of semicircular mass effect on the lumen (arrows). The smooth surface results from stretching of the normal overlying mucosa. **B.** CT scan of the GIST (L) shows a smooth submucosal mass of homogeneous soft tissue (muscle) attenuation compressing the lumen (arrows).



Figure 44-4 Intussusception of a lipoma. A dilated small bowel loop shows an abrupt narrowing of its lumen at the entry into the intussusception (black arrow). Also note the stretched coil spring pattern of folds typical of intussusception. The contour of the lipoma is visible at the apex of the intussusception (white arrows).

common site for the occurrence of GI lipomas.²⁹ These benign neoplasms arise as a well-circumscribed submucosal proliferation of fat that usually grows intraluminally; outward extension tends to be impeded by the firmness of the muscularis propria. Small bowel lipomas are usually solitary, relatively avascular lesions of variable size (1-6 cm). Most of these tumors occur in the ileum. Although most patients with lipomas are asymptomatic, some may present with intermittent intestinal obstruction, possibly secondary to intussusception (Fig. 44-4).

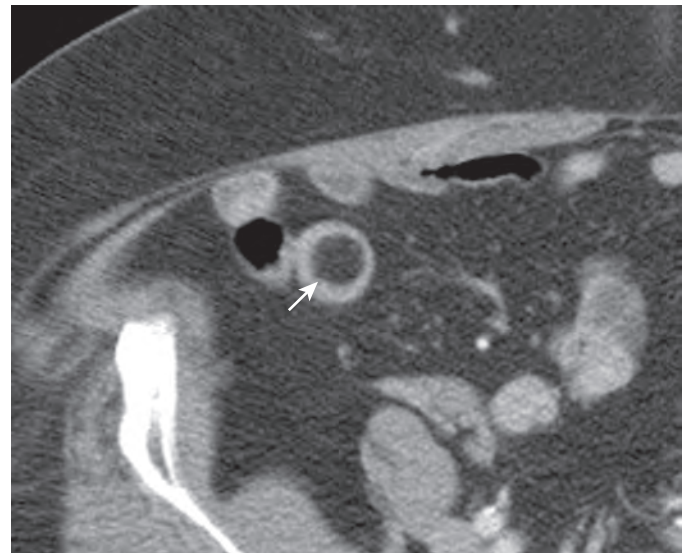


Figure 44-5 Lipoma. This CT scan shows a lipoma protruding into the bowel lumen (arrow). A well-circumscribed, intraluminal homogenous mass of negative attenuation consistent with fat is characteristic of an enteric lipoma on CT.

Barium studies demonstrate a sharply demarcated, often pedunculated tumor that tends to conform to the contour of the small bowel lumen.^{29,30} The configuration of the tumor may change during fluoroscopy with compression or peristalsis of the small bowel. CT can be diagnostic of small bowel lipoma by showing that the lesion has attenuation values consistent with those of fat³⁰ (Fig. 44-5). The presence of soft tissue stranding within an otherwise uniform lipoma on CT has been attributed to fibrovascular changes associated with ulceration of the tumor.³⁰

HEMANGIOMA

Benign angiomatous tumors are hamartomatous vascular growths, which are most likely congenital. Two principal forms are described—papillary (capillary) hemangiomas and cavernous hemangiomas. Cavernous hemangiomas predominate in the small bowel, occurring as simple polypoid tumors or, rarely,

as diffusely expansile lesions.³¹ Microscopically, these submucosal neoplasms consist of enlarged vascular channels or sinuses lined by endothelium and surrounded by minimal stromal tissue. Hemangiomas may be single or multiple. Although most hemangiomas are only millimeters in size, some may enlarge and protrude into the lumen. Direct invasion of the mucosa or penetration beyond the serosa is uncommon.

In contrast to other small bowel tumors, which are less likely to cause symptoms, 80% of patients with hemangiomas are symptomatic. Most of these patients present with GI bleeding that is often acute, severe, and intermittent. Anemia and occult fecal blood loss are also common clinical findings.

Hemangiomas must be of sufficient size to produce an intraluminal or intramural nodular defect on barium studies (Fig. 44-6). Although a rare occurrence, the finding of calcified phleboliths on abdominal radiographs can suggest the diagnosis. When discovered in patients with vascular cutaneous lesions or tuberous sclerosis, Turner's syndrome, or Osler-Weber-Rendu disease, such radiographic findings should increase suspicion for intestinal hemangiomas. Mesenteric arteriography may be performed to demonstrate an intestinal vascular abnormality, but differentiation between small vascular tumors and other vascular malformations is difficult. In one reported case, CT demonstrated a large jejunal hemangioma that appeared as a heterogeneous mass with prominent mesenteric vasculature.³² CT enteroclysis and CT enterography performed with neutral enteral and IV contrast media have the potential to demonstrate a vascular hemangioma, provided that the tumor is of sufficient size and the intestinal lumen is distended enough for optimal mural visualization (Fig. 44-7).¹⁴

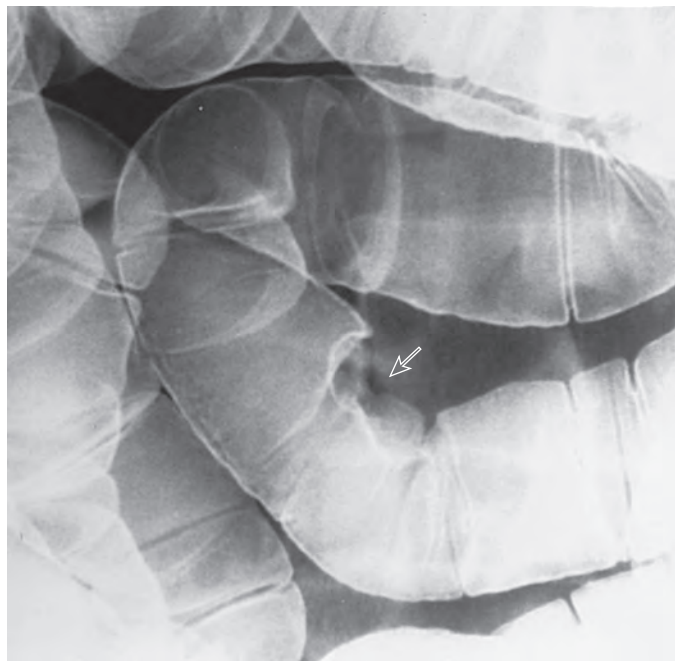


Figure 44-6 Hemangioma. Double-contrast enteroclysis demonstrates a 1.5-cm, slightly lobulated mural nodule (arrow) in a patient with occult gastrointestinal bleeding. A hemangioma was confirmed at surgery. (From Maglinte DD, Lappas JC, Kelvin FM, et al: *Small bowel radiography: How, when, and why?* Radiology 163:297–305, 1987.)

UNCOMMON TUMORS

Neurogenic tumors arise from the intramural neural plexus of the small bowel. Neurofibromas are the nerve tumors most frequently encountered and are composed of nerve sheath elements, notably Schwann cells and fibroblasts. Neurofibromas may occur as single tumors or, more commonly, as multiple lesions, with or without systemic neurofibromatosis type 1 (NF1). Although rare in the general population, neural tumors of the small bowel have been reported in 10% to 25% of patients with neurofibromatosis.³³ Symptomatic neurofibromas in NF1 are most common in the jejunum; clinical manifestations vary depending on tumor extent. Mucosal involvement may lead to GI bleeding or obstruction from intussusception or volvulus. Neurofibromas may originate within the intestinal wall, appearing as solitary or discrete multifocal intraluminal or intramural masses. Multiple or diffusely elongated tumors are evident as mural thickening on CT, whereas on barium studies, these tumors create scalloping of the intestinal wall from the intramural and intraluminal components of the neurofibromas.³³ Neurofibromas of mesenteric origin may encroach on adjacent small bowel, producing mass effect on the serosal surface, or may directly infiltrate the intestinal wall, producing focal or diffuse mural thickening and rigidity or submucosal or mucosal masses (Fig. 44-8).

Ganglioneuromas arise from sympathetic ganglia and manifest as focal polypoid lesions, multifocal polyps (ganglioneuromatous polyposis), or diffuse infiltrating lesions (ganglioneuromatosis). Imaging characteristics of these tumors are similar to those seen in the many forms of neurofibromas.³³

Inflammatory fibroid polyps, also referred to as inflammatory pseudotumors, are encountered almost exclusively in the ileum. They are usually solitary and are composed of a vascular fibrous stroma with a diffuse inflammatory infiltrate. Their



Figure 44-7 Cavernous hemangioma by CT. This is a coronal contrast-enhanced CT enteroclysis image of a patient with anemia requiring blood transfusions. There is a 1.3-cm polypoid mass (arrow) in the proximal jejunum that shows brisk enhancement.

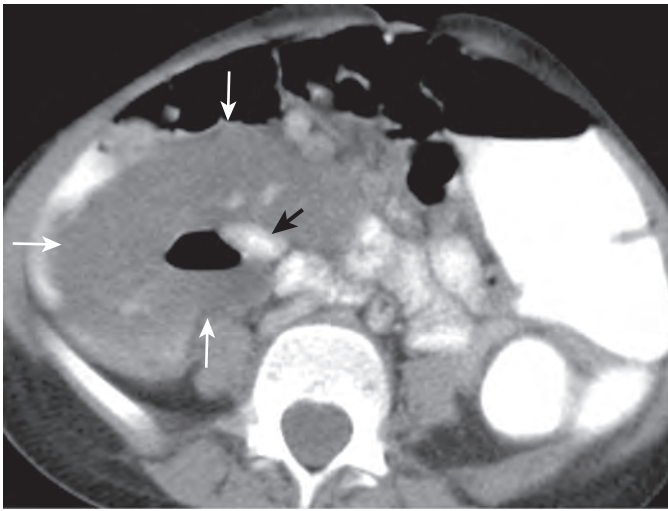


Figure 44-8 Plexiform neurofibroma. This CT scan in a 6-year-old boy with neurofibromatosis type 1 shows an elongated soft tissue mass in the right lower quadrant (white arrows) contiguous with multiple segments of small bowel (black arrow). Surgical pathology confirmed infiltration of the small bowel wall into the intermyenteric plexus.

exact cause remains uncertain, but they likely develop as an exuberant response to local intestinal injury.^{10,34} Barium studies demonstrate a nonspecific smooth, rounded mass in the distal small bowel. Affected individuals may occasionally present with obstructive symptoms caused by intussusception of the polyps.³⁴

Myoepithelial hamartoma is a rare developmental tumor consisting of varying amounts of pancreatic tissue, smooth muscle, and epithelial structures. The term *ectopic pancreatic rest* is used to describe these lesions when there is a predominance of pancreatic acinar tissue. Most myoepithelial hamartomas occur in the gastric antrum or duodenum, but some have been reported in the mesenteric small bowel.²³ Myoepithelial hamartomas are small, solitary lesions that appear on barium studies as smooth mural masses with occasional umbilication.

Heterotopic gastric mucosa may occur as an isolated lesion in the mesenteric small bowel or may be associated with malformations such as Meckel's diverticulum or an enteric duplication. Occasionally, barium studies may demonstrate a polypoid (sessile or pedunculated) lesion in the small bowel.

Polyposis Syndromes

FAMILIAL ADENOMATOUS POLYPOSIS SYNDROME

Familial adenomatous polyposis syndrome (FAPS) and its variants (Gardner's syndrome and Turcot's syndrome) are different manifestations of a hereditary disorder caused by a germline mutation of the adenomatous polyposis coli gene.³⁵ Adenomatous polyps in FAPS typically involve the colon but, to a lesser degree, the small bowel may manifest duodenal and jejunoileal adenomas and ileal lymphoid polyps. Of patients with FAPS and duodenal adenomas, 76% were found to have additional adenomas in the proximal jejunum, and 24% had distal jejunal and ileal polyps visualized by capsule endoscopy.³⁶ Isolated adenomas of the distal jejunum or ileum are rare, occurring in

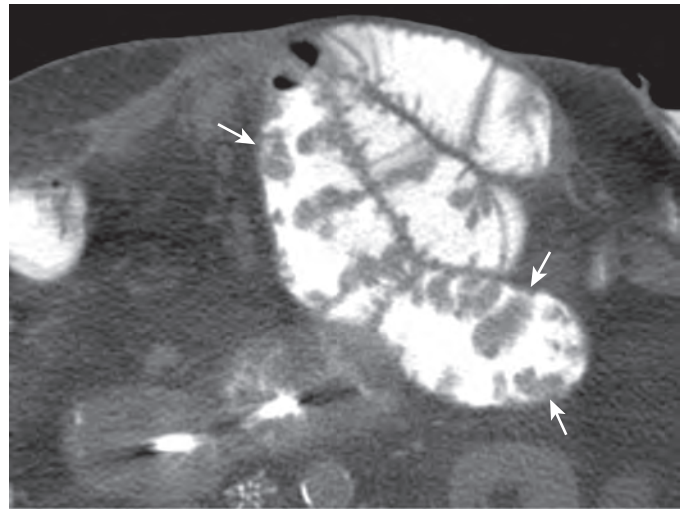


Figure 44-9 Familial adenomatous polyposis syndrome (FAPS). This CT scan from an enteroclysis performed with water-soluble contrast shows multiple polyps (arrows) within the jejunum.

only 3% of FAPS patients.³⁶ Because small bowel polyps in FAPS occur more frequently in those patients with sentinel duodenal adenomas, CT enteroclysis and capsule endoscopy may have an important role for the diagnosis of small bowel disease (Fig. 44-9).^{20,22,36}

Desmoid tumors are benign proliferations of musculoaponeurotic fibrous tissue that are locally aggressive and tend to recur without distant metastasis. Desmoid tumors are reported in 10% of patients with FAPS, with 50% of the tumors being intra-abdominal—85% to 100% of these tumors are confined to the mesentery.³⁷ CT is an ideal imaging method for the demonstration of desmoids, because it can show the extent of tumor invasion within the mesentery and affected small bowel.^{38,39}

PEUTZ-JEGHERS SYNDROME

Peutz-Jeghers syndrome (PJS) is an unusual autosomal dominant disorder with variable penetrance; about 50% of cases are familial and 50% are new mutations. PJS is characterized by GI hamartomatous polyps, mucocutaneous melanotic pigmentation, and a significant risk for developing a variety of malignancies.^{40,41} Patients with PJS present in early life with pigmented macules on the lips, buccal mucosa, and volar surfaces of the hands and feet. Cutaneous lesions often predate the formation of GI polyps, but typically fade during adolescence, with only the buccal lesions persisting into adulthood. Signs of GI polyps may be evident during the second or third decade of life, with GI bleeding or abdominal pain caused by transient small bowel intussusceptions.

Histologically, the polyps in PJS are benign hamartomas containing a proliferative smooth muscle core and lined by normal intestinal epithelium. These polyps are more commonly found in the jejunum than in the ileum, but may also occur in the stomach or colon. Patients with PJS are at increased risk for intestinal and extraintestinal malignancies, including esophageal, gastric, small bowel, colorectal, breast, ovarian, and pancreatic cancers.^{40,41} Most of the reported carcinomas of the GI tract in PJS patients appear to develop from coexisting adenomas rather than from the hamartomas, but a hamartoma-adenoma-carcinoma sequence is suspected in some cases.⁴⁰

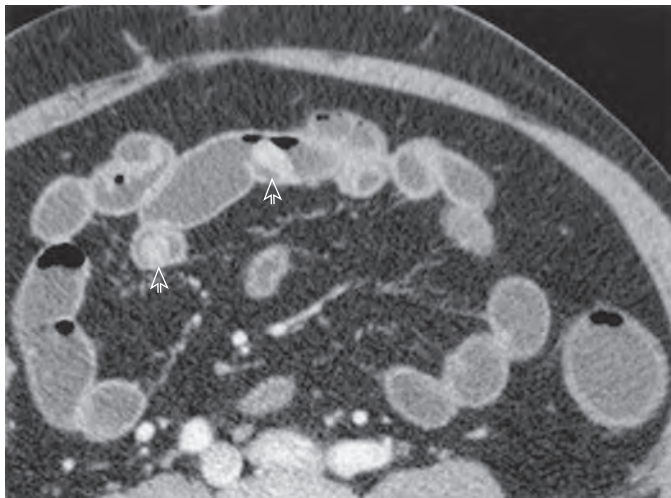


Figure 44-10 Peutz-Jeghers syndrome. CT enteroclysis performed with enteral water infusion and IV contrast enhancement shows multiple intraluminal polyps within the jejunum (arrows). The fluid density of the neutral enteral contrast medium is juxtaposed with the enhancing bowel wall, increasing the conspicuity of the tumor.

Barium studies may demonstrate luminal polyps of variable size in the small bowel. Larger polyps (2–3 cm) typically have a lobulated contour. Pedunculated lesions with broad-based attachments may also be found.^{42,43} Diffuse proliferation of intestinal polyps is not typical for PJS because uninvolved small bowel segments usually alternate with other segments containing several hamartomas. PJS polyps may be detected on CT as soft tissue masses within the contrast medium–filled intestinal loops and are exquisitely displayed by CT enteroclysis (Fig. 44-10).⁴⁴

COWDEN'S DISEASE

Cowden's disease, or multiple hamartoma-neoplasia syndrome, is an inherited condition characterized by hamartomas and

other abnormalities of the skin, breast, thyroid gland, and intestinal tract.⁴¹ Of patients with this disease, 80% present with benign dermatologic manifestations that serve as markers, with the most common being facial trichilemmomas, lipomas, and mucocutaneous keratoses. Patients with Cowden's syndrome are at a particularly high risk for developing breast and thyroid cancers.⁴¹ GI polyposis has been reported in 30% to 60% of patients and includes hamartomas indistinguishable from the polyps seen in juvenile polyposis syndrome, lipomatous polyps, and inflammatory polyps.^{41,43} One or more segments of the GI tract, especially the colon, or the entire GI tract may be involved.

In a review of Cowden's disease, the small bowel was found to be involved in 14 of 32 patients.⁴⁵ Enteroclysis may demonstrate multiple polyps that produce a nodular mucosal surface pattern in patients with diffuse involvement of the small bowel.⁴⁵

CRONKHITE-CANADA SYNDROME

Cronkhite-Canada syndrome is characterized by diffuse GI polyposis associated with distinctive clinical findings. Symptoms of abdominal pain, diarrhea, and anorexia precede or occur together with the development of ectodermal changes, including alopecia, hyperpigmentation, and dystrophy of nails. Disease onset is usually gradual, and older adults are primarily affected. Intestinal malabsorption and protein loss can be severe, and the clinical course is potentially fatal. Polyps occur in the stomach and colon in almost all patients, with the small bowel involved in more than 50% of cases. Cronkhite-Canada polyps are inflammatory in nature and consist of dilated cystic interstitial glands, closely resembling the hamartomas of juvenile polyps. Certain patterns of GI involvement have been described on barium studies: (1) diffuse involvement with innumerable small polyps (most common); (2) scattered polyps of various sizes; and (3) sparse involvement with few small polyps.^{46,47} Barium studies may also demonstrate thickened folds and increased luminal secretions in the small bowel because of hypoproteinemia and malabsorption.

REFERENCES

- McLaughlin PD, Maher MM: Primary malignant diseases of the small intestine. *AJR* 201; W9–W14, 2013.
- O'Riordan BG, Vilor M, Herrera L: Small bowel tumors: An overview. *Dig Dis* 14:245–257, 1996.
- Rangiah DS, Cox M, Richardson M, et al: Small bowel tumours: A 10-year experience in four Sydney teaching hospitals. *ANZ J Surg* 74:788–792, 2004.
- Ciresi DL, Scholten DJ: The continuing clinical dilemma of primary tumors of the small intestine. *Am Surg* 61:698–702, 1995.
- Minardi AJ, Jr, Zibari GB, Aultman DE, et al: Small-bowel tumors. *J Am Coll Surg* 186:664–668, 1998.
- Moch A, Herlinger H, Kochman ML, et al: Enteroclysis in the evaluation of obscure gastrointestinal bleeding. *AJR* 163:1381–1384, 1994.
- Rex DK, Lappas JC, Maglinte DD, et al: Enteroclysis in the evaluation of suspected small intestinal bleeding. *Gastroenterology* 97:60, 1989.
- Lappas JC, Maglinte DD: Radiological approach to investigation of the small intestine. In Gourtsoyiannis NC, editor: *Radiological Imaging of the Small Intestine*, New York, 2002, Springer, pp 447–463.
- Gourtsoyiannis NC, Bays D, Papaioannou N, et al: Benign tumors of the small intestine: Pre-operative evaluation with a barium infusion technique. *Eur J Radiol* 16:115–125, 1993.
- Nagi B, Verma V, Vaiphei K, et al: Primary small bowel tumors: A radiologic-pathologic correlation. *Abdom Imaging* 26:474–480, 2001.
- Gourtsoyiannis N, Mako E: Imaging of primary small intestinal tumours by enteroclysis and CT with pathological correlation. *Eur Radiol* 7:625–642, 1997.
- Buckley JA, Fishman EK: CT evaluation of small bowel neoplasms: Spectrum of disease. *Radiographics* 18:379–392, 1998.
- Laurent F, Raynaud M, Biset JM, et al: Diagnosis and categorization of small bowel neoplasms: Role of computed tomography. *Gastrointest Radiol* 16:115–119, 1991.
- Maglinte DD, Bender GN, Heitkamp DE, et al: Multidetector-row helical CT enteroclysis. *Radiol Clin North Am* 41:249–262, 2003.
- Maglinte DD, Lappas JC, Heitkamp DE, et al: Technical refinements in enteroclysis. *Radiol Clin North Am* 41:213–229, 2003.
- Pilleul F, Penigaud M, Milot L, et al: Possible small-bowel neoplasms: Contrast-enhanced and water-enhanced multidetector CT enteroclysis. *Radiology* 241:796–801, 2006.
- Horton KM, Fishman EK: The current status of multidetector row CT and three-dimensional imaging of the small bowel. *Radiol Clin North Am* 41:199–212, 2003.
- Masselli G, Gualdi G: CT and MR enterography in evaluating small bowel diseases: When to use which modality? *Abdom Imaging* 38:249–259, 2013.
- Amzallag-Bellenger E, Oudjit A, Ruiz A, et al: Effectiveness of MR enterography for the assessment of small-bowel diseases beyond Crohn disease. *Radiographics* 32:1423–1444, 2012.
- Hara AK, Leighton JA, Virender K, et al: Imaging of small bowel disease: Comparison of capsule endoscopy, standard endoscopy, barium examination, and CT. *Radiographics* 25:697–711, 2005.

21. Maglinte DD: Capsule imaging and the role of radiology in the investigation of diseases of the small bowel. *Radiology* 236:763–767, 2005.
22. Sandrasegaran K, Maglinte DD, Jennings SG, Chiorean MV: Capsule endoscopy and imaging tests in the elective investigation of small bowel disease. *Clin Radiol* 63:712–723, 2008.
23. Olmsted WW, Ros PR, Hjermstad BM, et al: Tumors of the small intestine with little or no malignant predisposition: A review of the literature and report of 56 cases. *Gastrointest Radiol* 12:231–239, 1987.
24. Witteman BJ, Janssens AR, Griffioen G, et al: Villous tumours of the duodenum. An analysis of the literature with emphasis on malignant transformation. *Neth J Med* 42:5–11, 1993.
25. Miettinen M, Lasota J: Gastrointestinal stromal tumors—definition, clinical, histological, immunohistochemical, and molecular genetic features and differential diagnosis. *Virchows Arch* 438:1–12, 2001.
26. Betz M, Kopp HG, Spira D, et al: The benefit of using CT-perfusion imaging for reliable response monitoring in patients with gastrointestinal stromal tumor (GIST) undergoing treatment with novel targeted agents. *Acta Radiol* 54:711–721, 2013.
27. Tirumani SH, Jagannathan JP, Krajewski KM, et al: Imatinib and beyond in gastrointestinal stromal tumors: A radiologist's perspective. *AJR* 201:801–810, 2013.
28. Sandrasegaran K, Rajesh A, Rydberg J, et al: Gastrointestinal stromal tumors: Clinical, radiologic, and pathologic features. *AJR* 184:803–811, 2005.
29. Taylor AJ, Stewart ET, Dodds WJ: Gastrointestinal lipomas: A radiologic and pathologic review. *AJR* 155:1205–1210, 1990.
30. Thompson WM: Imaging and findings of lipomas of the gastrointestinal tract. *AJR* 184:1163–1171, 2005.
31. Lightdale CJ, Hornsby-Lewis L: Tumors of the small intestine. In Haughbrich WS, Schaffner F, editors: *Bockus Gastroenterology*, ed 5, Philadelphia, 1995, WB Saunders, pp 1274–1290.
32. Varma JD, Hill MC, Harvey LA: Hemangioma of the small intestine manifesting as gastrointestinal bleeding. *Radiographics* 18:1029–1033, 1998.
33. Levy AD, Patel N, Dow N, et al: From the archives of the AFIP: Abdominal neoplasms in patients with neurofibromatosis type 1: Radiologic-pathologic correlation. *Radiographics* 25:455–480, 2005.
34. Harned RK, Buck JL, Shekitka KM: Inflammatory fibroid polyps of the gastrointestinal tract: Radiologic evaluation. *Radiology* 182:863–866, 1992.
35. Bronner MP: Gastrointestinal inherited polyposis syndromes. *Mod Pathol* 16:359–365, 2003.
36. Schulmann K, Hollerbach S, Kraus K, et al: Feasibility and diagnostic utility of video capsule endoscopy for the detection of small bowel polyps in patients with hereditary polyposis syndromes. *Am J Gastroenterol* 100:27–37, 2005.
37. Knudsen AL, Bulow S: Desmoid tumour in familial adenomatous polyposis. A review of literature. *Fam Cancer* 1:111–119, 2001.
38. Casillas J, Sais GJ, Greve JL, et al: Imaging of intra- and extraabdominal desmoid tumors. *Radiographics* 11:959–968, 1991.
39. Einstein DM, Tagliabue JR, Desai RK: Abdominal desmoids: CT findings in 25 patients. *AJR* 157:275–279, 1991.
40. McGarrity TJ, Kulin HE, Zaino RJ: Peutz-Jeghers syndrome. *Am J Gastroenterol* 95:596–604, 2000.
41. Schreiber IR, Baker M, Amos C, McGarrity TJ: The hamartomatous polyposis syndromes: A clinical and molecular review. *Am J Gastroenterol* 100:476–490, 2005.
42. Buck JL, Harned RK, Lichtenstein JE, Sobin LH: Peutz-Jeghers syndrome. *Radiographics* 12:365–378, 1992.
43. Cho GJ, Bergquist K, Schwartz AM: Peutz-Jeghers syndrome and the hamartomatous polyposis syndromes: Radiologic-pathologic correlation. *Radiographics* 17:785–791, 1997.
44. Sener RN, Kumcuoglu Z, Elmas N, et al: Peutz-Jeghers syndrome: CT and US demonstration of small bowel polyps. *Gastrointest Radiol* 16:21–23, 1991.
45. Chen YM, Ott DJ, Wu WC, et al: Cowden's disease: A case report and literature review. *Gastrointest Radiol* 12:325–329, 1987.
46. Dachman AH, Buck JL, Burke AP, et al: Cronkhite-Canada syndrome: Radiologic features. *Gastrointest Radiol* 14:285–290, 1989.
47. Kopáčová M, Urban O, Cyrany J, et al: Cronkhite-Canada syndrome: Review of the literature. *Gastroenterol Res Pract* 2013:856–873, 2013.

Malignant Tumors of the Small Bowel

KUMAR SANDRASEGARAN | CHRISTINE O. MENIAS

CHAPTER OUTLINE

Imaging Small Bowel Neoplasms

Adenocarcinoma

Carcinoid Tumors

Gastrointestinal Stromal Tumors

Lymphoma

Small Bowel Metastases

Summary

Malignant tumors of the small bowel are rare and account for only 3% to 6% of gastrointestinal (GI) tract malignancies. The most common malignancies include adenocarcinomas, carcinoid tumors, GI stromal tumors, lymphomas, and metastases. The diagnosis of a small bowel neoplasm has been an ongoing challenge for radiologists. Despite almost four decades of surgical and technologic advances in diagnostic modalities, the survival of these patients has not changed, largely as a result of delays in clinical diagnosis. In this chapter, we examine the common small bowel malignancies and evaluate how the radiologist may better diagnose these lesions.

The small intestine represents 75% of the length and 90% of the mucosal surface of the GI tract. Despite this large area of exposure to carcinogens, small bowel neoplasm are uncommon and account for only 3% to 6% of GI neoplasms.¹ Possible reasons for the low prevalence of small bowel cancers include rapid transit time reducing mucosal exposure to carcinogens, a high volume of fluid diluting carcinogens, the absence of bacterial degradation of bile salts, a high proliferation rate and apoptosis of mucosal cells, and immunomodulation by high levels of immunoglobulin A produced by the abundant ileal lymphoid tissue.²

Despite advances in diagnostic imaging and operative techniques, the survival of patients with primary malignant tumors has not changed in the last two decades.³ The main reasons for the absence of survival benefit are delayed diagnosis⁴ and lack of novel adjuvant therapies.³ Patients with small bowel neoplasms often present with nonspecific symptoms such as abdominal pain or GI bleeding.¹ Given the relative rarity of small bowel tumors, physicians have a low index of suspicion. The imaging tests ordered initially, such as fluoroscopic studies and routine abdominopelvic CT, have low sensitivity for small bowel neoplasms, which leads to further diagnostic delay. We will discuss general considerations for the imaging of suspected small bowel neoplasms and then examine the five most common small bowel malignancies—adenocarcinoma, carcinoid tumor, GI stromal tumor, lymphoma, and metastatic tumor (Table 45-1). In diagnosing small bowel malignancies,

location in the proximal or distal small bowel is an important differentiating factor.

The growth pattern of small bowel malignancies may be exoenteric or endoenteric. An exoenteric growth pattern is characterized by extension of tumor into the outer layers of the small bowel wall and mesentery without growth into the lumen, although an extrinsic luminal indentation may be seen. In contrast, an endoenteric growth pattern is characterized by tumor confined to the lumen and bowel wall without extension into the adjacent mesentery. Occasionally, a mixed pattern, with a dumbbell appearance, may be seen. Other imaging features such as the presence or absence of adenopathy, mesenteric masses, or bowel obstruction and the vascularity of liver metastases (if any) help narrow the differential diagnosis.

Imaging Small Bowel Neoplasms

When a small bowel neoplasm is suspected, small bowel enteroclysis or small bowel follow-through has traditionally been performed. These studies are relatively insensitive for the diagnosis of malignant small bowel tumors. In various series, abnormalities were present on small bowel follow-through in 53% to 83% of patients with primary malignant small bowel tumors, but direct evidence of tumor was found in only 30% to 44% of patients.⁵ In general, enteroclysis has better accuracy than small bowel follow-through.^{4,6} Nevertheless, a major limitation of enteroclysis is the lack of demonstration of extraintestinal abnormalities.

Techniques that allow for optical visualization of tumors include video capsule endoscopy and double-balloon endoscopy. These techniques are usually performed by GI physicians. Detailed discussions of these techniques have been published.⁷⁻⁹ Capsule endoscopy is now routinely performed for unexplained GI bleeding or suspected small bowel disease. It depicts small bowel mucosa very well (Fig. 45-1) but has many limitations, including lack of visualization of submucosal lesions (Fig. 45-2), limited angle of view, susceptibility to becoming lodged at the site of a stricture, incorrect triangulation of the site of disease, and the need to view several thousand images.⁹ Double-balloon endoscopy allows for sampling of the lesion but is time-consuming and often requires two procedures to evaluate the entire small bowel.^{10,11} This technique has a complication rate of approximately 1.2% to 3.6%, including bowel perforation,¹² has limited availability, and is only used in select cases.

Cross-sectional imaging examinations are not only able to view the mucosa, but also the bowel wall and adjacent mesentery. Dedicated small bowel computed tomography (CT) or magnetic resonance imaging (MRI) techniques may be divided into enteroclysis or enterography procedures. CT enterography has been increasingly used as the first-line investigation in small bowel disease, including Crohn's disease and small bowel neoplasm.¹³ In enterography, 1350 to 2000 mL of enteral contrast is ingested over a period of about 1 hour. In enteroclysis, a tube



Figure 45-1 Capsule endoscopy of proximal jejunum. This shows exquisite anatomic detail with depiction of individual villi. This degree of spatial resolution is not possible with imaging techniques. However, there are multiple pitfalls of capsule endoscopy.



Figure 45-2 Typical findings of gastrointestinal stromal tumor. This 65-year-old man presented with obscure gastrointestinal bleeding. Coronal reformation of CT shows a mildly hypervascular, 4-cm exoenteric mass (arrowhead) in the mid small bowel. This lesion was missed on prior capsule endoscopy (not shown).

TABLE
45-1

Typical Imaging Features of the Four Major Malignant Small Bowel Neoplasms

Neoplasm	Location	Growth Pattern*	Contrast Enhancement	Obstruction†	Other features
Cancer‡	Periampullary, prox. jejunum	Endoenteric	Variable, usually less than mucosa	Common	Apple core, constricting.
Carcinoid	Distal ileum	Endoenteric	Usually intense and homogenous	Rare	Small: often have spiculated mesenteric mass. Hypervascular liver metastases.
NHL	Ileum	Exoenteric	Usually = or > than mucosa	Rare	Often large; may show aneurysmal dilation, often with adenopathy.
GIST	Jejunum	Exoenteric	Usually intense and homogeneous	Rare	Usually no adenopathy. May show liver or mesenteric metastases.

*Endoenteric growth is into lumen of bowel, while exoenteric growth is outward into adjacent mesentery.

†Frequency of small bowel obstruction.

‡Small bowel adenocarcinoma.

GIST, Gastrointestinal stromal tumor; NHL, non-Hodgkin lymphoma; prox., proximal.

is placed in the distal duodenum or proximal jejunum and enteral contrast is mechanically pumped into the small bowel using a dedicated hydraulic pump (preferably) or by hand. In CT enteroclysis and enterography, the optimal enteral contrast is neutral contrast—with a Hounsfield density similar to that of water. Water, methylcellulose, mannitol, polyethylene glycol, and a proprietary preparation of 0.1% barium sulfate suspension (VoLumen, E-Z-EM, New York) are used. It is vital to administer an adequate bolus of intravenous (IV) contrast at a rate of 3 to 5 mL/s. Ideally, scanning should be done in at least two phases to include a late arterial phase (scan time to start, ≈35–50 seconds) and venous phase (70- to 80-second delay from contrast injection). Additional delayed phases may help demonstrate that the high density in the lumen is extravasated blood.

MRI enteroclysis or enterography has different types of enteral contrast; the most commonly used contrast in the United States is 0.1% barium sulfate solution. Antiperistaltic agents are commonly administered. If glucagon is used, it is advisable to give 0.5 mg intramuscularly or subcutaneously at the start of the study and then the same dose again before the GI postcontrast phases.^{14,15} The typical MRI enterography-enteroclysis protocol includes coronal T2-weighted, single-shot fast spin-echo (SSFSE) or coronal half-Fourier acquisition single-shot turbo spin-echo (HASTE), and coronal single-shot free precession sequences (e.g., fast imaging with steady-state precession [FIESTA], fast imaging with steady-state precession [FISP], fast field echo [FFE]). Postcontrast coronal, 3D fat-suppressed gradient echo sequences (e.g., volumetric interpolated breath-hold examination [VIBE], liver acquisition

with volume acceleration [LAVA], T1-weighted high-resolution isotropic volume examination [THRIVE]) need to be acquired in multiple phases, typically starting 35 seconds after gadolinium injection.¹⁵⁻¹⁷

A study of CT enteroclysis reported a sensitivity of 100% for diagnosing small bowel neoplasms ($N=21$).¹⁸ However, because this study did not have a reference standard, such as capsule endoscopy or long-term clinical and radiologic follow-up, it was not possible to ascertain its true sensitivity. A larger study of 219 patients with suspected small bowel neoplasms reported a sensitivity of 85% and specificity of 97% with CT enteroclysis. A prospective MRI enteroclysis study of 150 patients (including 19 with small bowel neoplasms) reported an overall sensitivity and specificity of 86% and 98%, respectively.¹⁹ Another MRI enteroclysis study of 91 patients with suspected small bowel neoplasms found a sensitivity of 91% and 94% for the two blinded reviewers and a specificity of 95% to 97%.¹⁷ It is likely that CT and MRI enteroclysis have a similar accuracy for diagnosing small bowel neoplasms, which is considerably better than that of fluoroscopic studies. CT is faster and better tolerated by ill patients compared with MRI, but has the disadvantage of using ionizing radiation. To our knowledge, there are no prospective or large studies comparing the sensitivity of enteroclysis versus enterography for the diagnosis of small bowel neoplasms. In general, enterography is easier to perform than enteroclysis and is the preferred diagnostic option in most centers.

Adenocarcinoma

The incidence of small bowel adenocarcinoma increased from 5.7/million in 1974 to 7.3/million in 2004.²⁰ Excluding periampullary tumors, the distribution is approximately 55% in the duodenum, 15% in the jejunum, and 13% in the ileum. There is a distal ileal preference in patients with Crohn's disease. Tumors in the jejunum have a significantly better survival than those in the ileum.³

Adenocarcinoma of the small bowel has risk factors similar to those of colon cancer. Small bowel adenocarcinoma is associated with familial adenomatous polyposis (FAP) and hereditary nonpolyposis colorectal cancer (HNPCC). The

generally accepted hypothesis is that adenocarcinoma occurs via an adenoma-carcinoma sequence and that there are mutations in key regulatory genes, such as *p53* and *k-ras*, in a manner similar to that for colon cancer.²⁰ Other risk factors include Crohn's disease and celiac disease.

Small bowel adenocarcinoma typically presents as an annular, constricting mass (Fig. 45-3). Less common radiographic features of small bowel adenocarcinoma include a polypoid or ulcerated mass or multiple filling defects. The tumors show heterogeneous enhancement on CT and MRI. Differentiation from active inflammation is important in diagnosing adenocarcinoma in the setting of Crohn's disease. Features that support the presence of malignancy include lack of mural stratification, asymmetric wall thickening, and a lobulated outer wall surface (Fig. 45-4). Mesenteric vascular congestion is unlikely to be seen in malignancy, unless there is coexisting inflammation. Surgery is the mainstay of treatment for small bowel adenocarcinoma. Adjuvant chemotherapy has been used

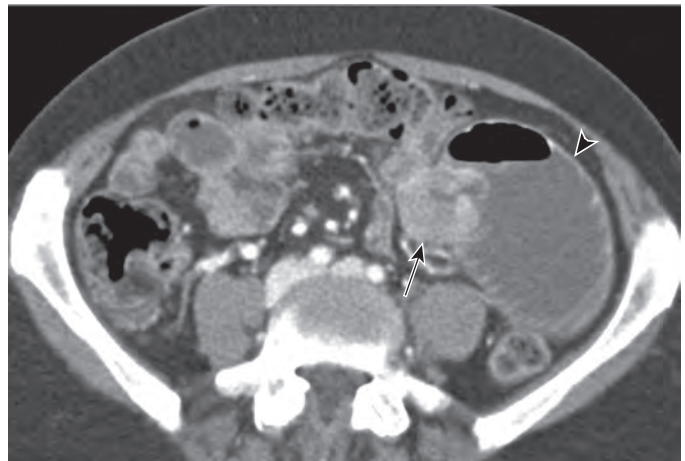


Figure 45-3 Typical findings of small bowel adenocarcinoma. Axial CT on a 67-year-old presenting with small bowel obstruction. There is an annular, constricting mass (arrow) in the proximal jejunum, with upstream bowel dilation (arrowhead). The location of this tumor and its imaging findings are characteristic of adenocarcinoma.

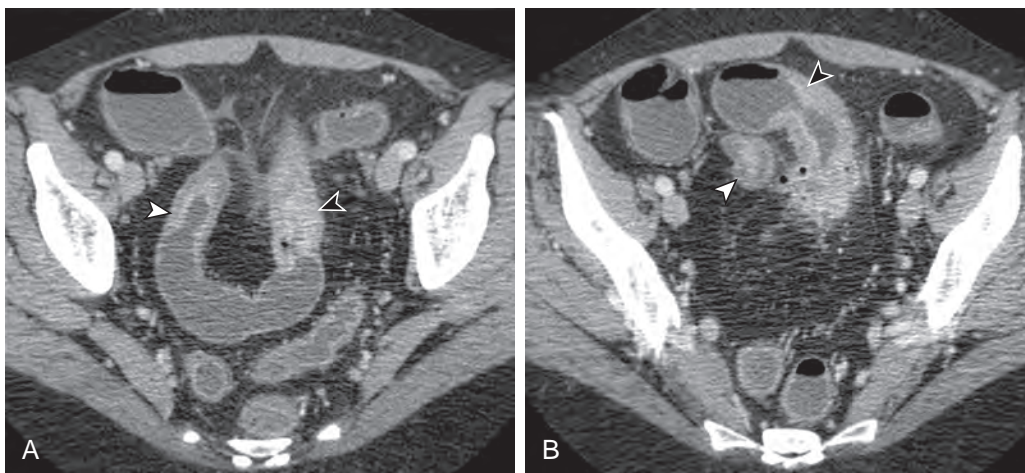


Figure 45-4 Diagnosing cancer in Crohn's disease. A, B. Axial CT scans in 41-year-old woman show mild wall thickening in the terminal ileum (white arrowhead). There is mural heterogeneity, with enhancement of the mucosa and edema in the submucosa. More proximally, an 8-cm segment of substantial wall thickening with homogeneous enhancement is seen (black arrowhead). **B.** There is proximal shouldering (black arrowhead). At surgery, Crohn's disease was found in the terminal ileum. The more proximal lesion was an adenocarcinoma. Good bowel distention and an IV contrast bolus are required to diagnose cancer in the presence of inflammatory bowel disease (white arrowhead).

increasingly, although there are no conclusive data that support its benefit²⁰

Carcinoid Tumors

The current term for all carcinoid tumors is *gastroenteropancreatic neuroendocrine tumors*. Surveillance, Epidemiology, and End Results (SEER) database findings on over 67,000 small bowel tumors, recorded over 30 years, have been published. These data show that the incidence of carcinoid tumor increased by 350% from 1974 to 2004.³ Carcinoid tumor is now considered to be the most common primary malignant lesion of the small bowel, with a slightly higher incidence (37.4% of all cases) than small bowel adenocarcinoma (36.9%). The incidence trajectory of carcinoid tumors, most likely the result of improved imaging technique, may widen this gap in the future.

Carcinoid tumors originate from the ectodermal cells of the neural crest and therefore may occur at any site in which these cells are present, including the GI, pancreatic, biliary, respiratory, and genitourinary tracts and the thymus. Approximately 95% of GI carcinoid tumors occur in the appendix, rectum, and small intestine. About 60% of small bowel carcinoid tumors occur within 40 cm of the ileocecal junction. There are no clear histologic differences between benign and malignant carcinoid tumors. All carcinoid tumors are potentially malignant, with the most important factor being the depth of invasion. Small bowel carcinoid tumors are more aggressive than appendiceal or colonic carcinoid tumors, and may show metastases even when small. Generally, tumors smaller than 1 cm are found to have metastasized 50% of the time, whereas tumors larger than 2 cm are found to have metastasized 95% of the time (Fig. 45-5).²¹ Ileal carcinoid tumors usually metastasize to peritoneal surfaces, omentum, lymph nodes, liver, and lungs.

The carcinoid syndrome consists of periodic cutaneous flushing, diarrhea, bronchospasm and, less commonly, valvular stenosis in the right heart. Only 20% of small bowel carcinoid tumors give rise to this syndrome. The liver deaminates serotonin secreted by the tumor into biologically inert 5-hydroxyindoleacetic acid (5-HIAA). Thus, in 85% of patients with carcinoid syndrome, there are hepatic metastases, the secretions from which enter the systemic circulation directly. In some cases, the syndrome may occur in the absence of hepatic metastases if there is liver dysfunction, high tumor load, or retroperitoneal metastases with venous outflow that bypasses the liver.

Small bowel follow-through studies are only about 25% sensitive for carcinoid tumors. Somatostatin receptor nuclear scintigraphy is 70% to 80% sensitive. If a CT examination is also performed, the two techniques have a combined sensitivity of more than 90%. When a tumor is incidentally found in the distal ileum, carcinoid tumor should be the leading consideration. When visible on CT, the primary tumor typically has a smooth, rounded, and intensely enhancing appearance (Figs. 45-5 and 45-6). The desmoplastic reaction caused by the release of vasoactive amines typically causes a spiculated mesenteric mass (see Fig. 45-6). This mass may be calcified in up to 70% of cases.²² Depending on the severity of the desmoplastic reaction, there may be indrawing or fixation of adjacent bowel loops. Liver lesions are best demonstrated on dual-phase CT. Small metastases are typically hypervascular (see Fig. 45-5), whereas larger lesions are heterogeneous, with peripheral hyperdensity. On MRI, carcinoid tumors are isointense to



Figure 45-5 Small bowel carcinoid. Coronal CT reformation in a 59-year-old woman with carcinoid presenting with diarrhea and wheezing shows a 3-cm hypervascular mass in the distal ileum (arrowhead). Despite the small size of the primary lesion, there are multiple hypervascular liver metastases (arrows).

muscle on T1-weighted images and isointense to mildly hyperintense to muscle on T2-weighted images. As with CT, intense enhancement may be seen. Positron emission tomography (PET) using ¹⁸F-fluorodeoxyglucose (FDG) is only 25% to 40% sensitive because well-differentiated carcinoids are hypometabolic. FDG avidity correlates with malignant potential and has prognostic significance. PET with ¹⁸fluorodopa is considered to be more sensitive than FDG PET, but this radiopharmaceutical has not yet been approved by the U.S. Food and Drug Administration (FDA).

Gastrointestinal Stromal Tumors

A gastrointestinal stromal tumor (GIST) is the most common mesenchymal tumor arising from the GI tract. It is characterized by the expression of a tyrosine kinase growth factor receptor and a gain-of-function mutation at the KIT receptor.²³ This is significant because the mutation allows for unchecked growth of the tumor and resistance to apoptosis. Like other small bowel tumors, the clinical presentation of GISTs is often nonspecific. Like GI lymphoma, the most common site of GISTs is the stomach (70%), followed by the small bowel (20%). Within the small bowel, GISTs are usually located in the jejunum,²⁴ and 20% to 30% of GISTs are malignant at presentation.^{25,26} Features associated with a poor prognosis include ileal location, tumor

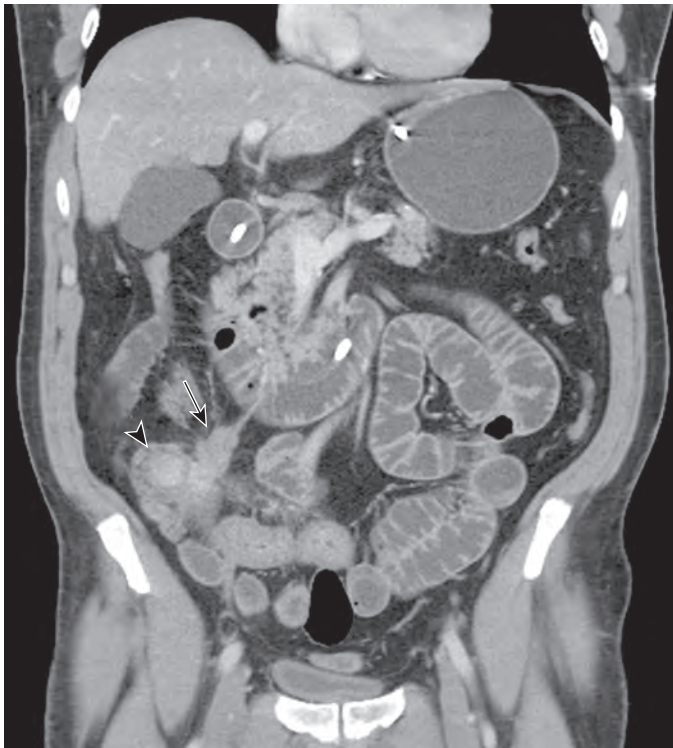


Figure 45-6 Mesenteric mass of small bowel carcinoid. Coronal CT reformation in a 68-year old man with carcinoid syndrome shows a hypervascular terminal ileal endoenteric mass (arrowhead), with an adjacent spiculated mass (arrow) in the mesentery. Spiculated mesenteric masses occur because of a desmoplastic reaction and need not contain tumor cells. Unlike this case, most mesenteric carcinoid lesions show calcification.



Figure 45-7 Ileal gastrointestinal stromal tumor. Coronal CT reformation in 54-year-old woman with obscure GI bleeding shows a 3-cm, intensely enhancing exoenteric mass (arrow) in the distal ileum. Its exoenteric nature made this mass more likely to be a gastrointestinal stromal tumor (GIST) than a carcinoid. Lymphoma is another possibility, but tends to be larger and has more heterogeneous enhancement. A GIST was diagnosed at surgery.

size, and high mitotic activity.²⁵ Tumors smaller than 2 cm are typically confined to the bowel, whereas those larger than 5 cm are usually malignant and have associated metastases.²⁷

Small GISTs (<5 cm) may show intense homogenous enhancement (Fig. 45-7; see Fig. 45-2). Larger GISTs show heterogeneous enhancement with exoenteric growth¹³ containing areas of low attenuation because of central necrosis or high attenuation because of hemorrhage or calcification (Fig. 45-8).^{28,29} Some GISTs may show a mixed growth pattern with endoluminal and exophytic components and a dumbbell shape. GISTs may be missed by techniques that only assess the mucosa, such as barium studies and capsule endoscopy (see Fig. 45-2). Findings that suggest a poor prognosis on CT include size larger than 5 cm, lobulated outline, heterogeneous enhancement, ulceration of tumor, and mesenteric fat infiltration (Fig. 45-9).²⁸⁻³¹

MRI often reveals a heterogeneous signal caused by internal hemorrhage and necrosis. On T1-weighted imaging, GISTs have low or intermediate signal, whereas on T2-weighted sequences, they exhibit heterogeneously high signal intensity. The most common metastases are to the mesentery and liver. Mesenteric metastases often show low density despite the primary tumor being hypervascular (see Fig. 45-9). Liver metastases are typically hypervascular on CT or MRI prior to chemotherapy.²⁹ Unlike adenocarcinoma and lymphoma, lymphatic spread is uncommon with GISTs.^{29,32} If significant adenopathy or lung metastases are present, an alternative diagnosis should be considered.

GISTs are relatively refractory to conventional chemotherapy and to radiotherapy. Surgical resection offers the best hope of cure. In the last 10 years, molecular therapy using tyrosine kinase inhibitors, has been developed. The first such drug was imatinib (Gleevec, Novartis, East Hanover, NJ). Sunitinib (Sutent, Pfizer, New York) and sorafenib (Nexavar, Bayer HealthCare, Wayne, NJ) are now also used as second- and third-line agents. Tyrosine kinase inhibitor drugs induce apoptosis of the tumor and are administered for metastatic disease and for large nonmetastatic primary tumors after surgical resection. Even when the resected specimen has clear margins, between 40% and 90% of patients develop hepatic or mesenteric recurrence, possibly because of microscopic spillage of tumor at the time of surgery.²⁷

After chemotherapy, mesenteric and liver metastases become hypovascular and often completely cystic on CT (Fig. 45-10).³³ As a result, treated metastases may be mistaken for benign liver cysts on CT. Such cystic lesions should not be considered non-viable. One of the first signs of relapse may be a new enhancing focus within a stable-sized cystic metastasis (see Fig. 45-10).³⁴ Given that size changes are not a significant feature of response or relapse of liver metastases being treated with tyrosine kinase inhibitors, Response Evaluation Criteria in Solid Tumors (RECIST) criteria are not predictive of medium-term response. Other response criteria have been suggested that take into account changes in the enhancement pattern of metastases as a guide to therapy response (Table 45-2).³⁵ As yet, these criteria have not been validated in multiple institutions. Radiologists

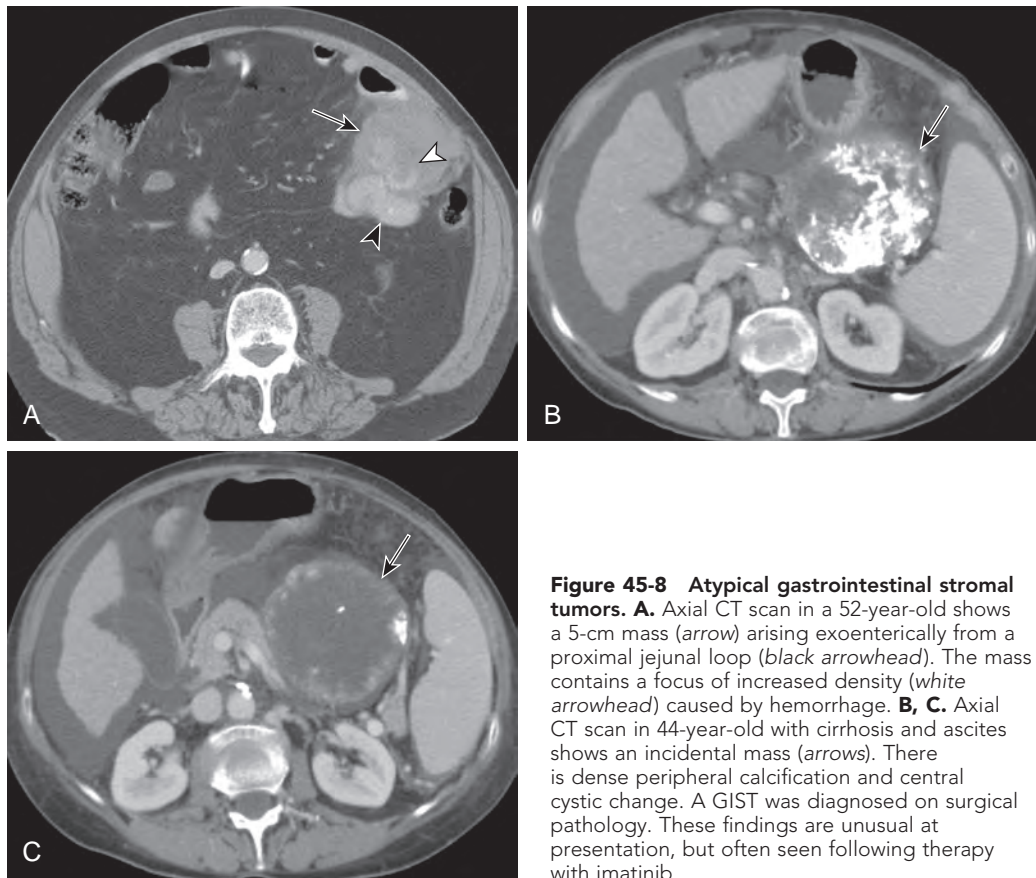


Figure 45-8 Atypical gastrointestinal stromal tumors. **A.** Axial CT scan in a 52-year-old shows a 5-cm mass (arrow) arising exoenterically from a proximal jejunal loop (black arrowhead). The mass contains a focus of increased density (white arrowhead) caused by hemorrhage. **B, C.** Axial CT scan in 44-year-old with cirrhosis and ascites shows an incidental mass (arrows). There is dense peripheral calcification and central cystic change. A GIST was diagnosed on surgical pathology. These findings are unusual at presentation, but often seen following therapy with imatinib.

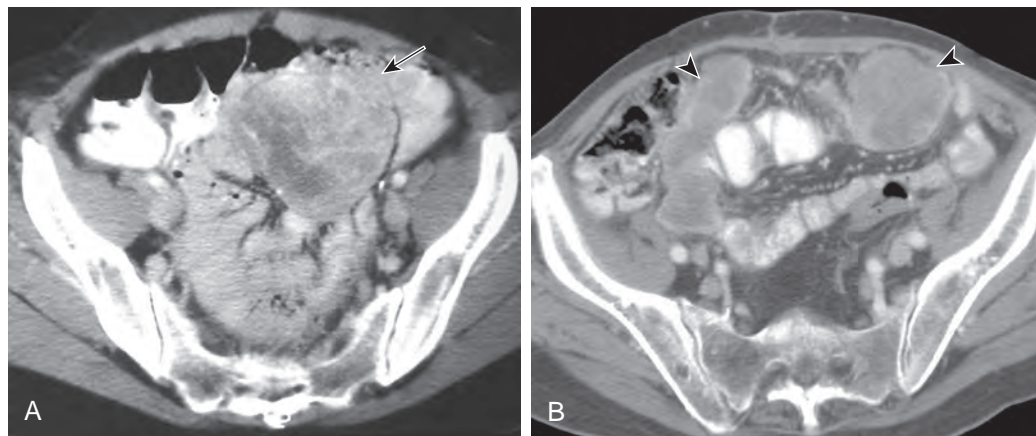


Figure 45-9 Assessing prognosis of GIST on CT. This 48-year-old woman had a GIST. **A.** At presentation, axial CT shows an 8-cm heterogeneously enhancing exoenteric mass (arrow) in the mid small bowel. The tumor was resected, and surgical pathology revealed a GIST with a high mitotic rate. **B.** Axial CT performed 4 months later shows interval growth of low-density mesenteric masses (arrowheads).

should also be aware that imatinib causes hypoalbuminemia and ascites, which may be mistaken for tumor progression (see Fig. 45-10).

Lymphoma

GI lymphoma may be primary or secondary. Primary GI lymphoma is diagnosed when the lymphadenopathy is confined to the region of the bowel mass, the peripheral white cell count and bone marrow aspirate are normal, and there is no evidence

of disease in the liver or spleen, mediastinal adenopathy on chest radiographs, and palpable adenopathy. Secondary lymphoma is diagnosed when multiple sites are affected.

In the West, the most common site of primary GI lymphoma is the stomach (40%-75%), followed by the small bowel (20%-30%), ileocecal region (10%-20%), colon (10%), and esophagus (<1%).³⁶ In some parts of the world, such as the Middle East, small bowel lymphoma secondary to immunoproliferative disorder accounts for 70% of GI lymphomas. In the small bowel, the ileum is the most common site (60%-65%) of involvement.

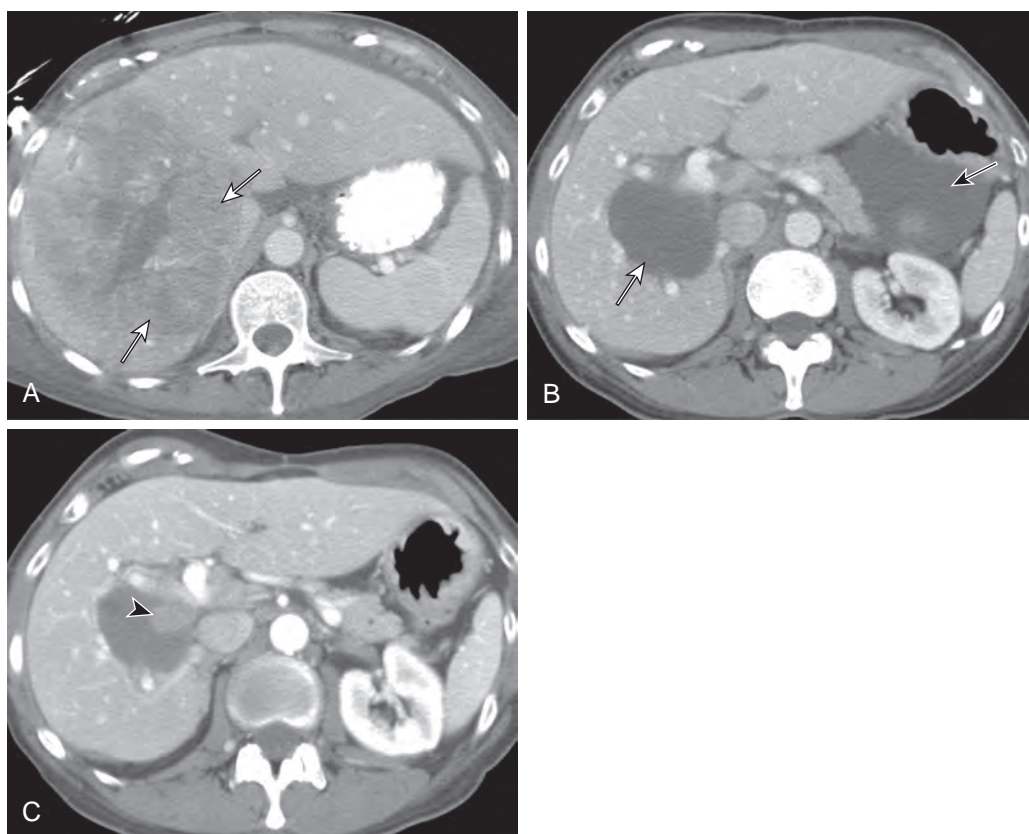


Figure 45-10 Treatment-related changes of GIST metastasis. This 69-year-old woman had a GIST and liver metastasis. **A.** Axial CT shows a metastasis of 10+ cm in the right lobe of the liver (arrows). **B.** Nine months after therapy with imatinib, the liver metastasis (white arrow) is smaller and completely cystic-appearing, without solid elements. It could be mistaken for a benign cyst if the prior examinations are not available. New-onset ascites (black arrow) is present and was misinterpreted by the radiologist as heralding peritoneal metastases. Ascites may be drug-induced and should not be reported as indicating tumor progression in the absence of solid mesenteric nodules. Imatinib is known to cause hypoalbuminemia, and albumin levels are used to determine the efficacy of therapy. The dose of imatinib was reduced because of the presence of moderate hypoalbuminemia. **C.** Axial CT performed 4 months later shows a mural nodule (arrowhead), a finding that indicates recurrent tumor. A new-onset mural nodule may be the only feature of tumor recurrence.

TABLE 45-2 Comparison of RECIST 1.1 and Choi Criteria in Assessing Response of GIST to Chemotherapy

Parameter	RECIST 1.1 Criteria	Choi Criteria
Complete response (CR)	Disappearance of all lesions and no new lesions	
Partial response (PR)	30+% decrease in size from baseline	10+% decrease in size or 15+% decrease in Hounsfield density
Stable disease (SD)	Not CR, PR, PD	
Progressive disease (PD)	20+% increase in size from prior minimum	10+% increase in size New or enlarging tumor nodules

The Choi criteria were developed at the MD Anderson Hospital in Houston. They allow easier diagnosis of partial response because most GISTs show reduction in enhancement prior to reduction in size.

An ileal predominance is also seen with carcinoid tumors, whereas a jejunal predilection is seen with adenocarcinomas and GISTs. Acquired immunodeficiency syndrome (AIDS) is associated with high-grade B-cell lymphoma, and celiac disease is associated with T-cell lymphoma. There is also a slightly increased risk of lymphoma in Crohn's patients following therapy with antitumor necrosis factor.^{37,38} Predictors of a poor

prognosis include T-cell type, high-grade histology, tumor size larger than 10 cm (Fig. 45-11), and tumor perforation.^{39,40}

As with other small bowel malignancies, small bowel lymphoma presents with nonspecific symptoms. Several imaging patterns of small bowel lymphoma have been described. The most common finding is a predominantly homogeneously enhancing exoenteric mass measuring at least 2 cm in diameter (see Fig. 45-11). This is in contrast to carcinoid tumors, in which the primary tumor is endoenteric and usually smaller than 2 cm. Unlike adenocarcinomas, luminal narrowing or bowel obstruction is not a key feature of lymphoma. Unlike GISTs, adjacent moderate- to large-volume lymphadenopathy is often found with lymphoma. Less common findings of small bowel lymphoma include an exophytic mass with ulceration and central necrosis. Luminal enlargement may occur because of infiltration of the myenteric plexus. This finding is called *aneurysmal dilation of bowel* (Fig. 45-12) and may be found in other submucosal neoplasms, including GISTs and melanoma metastases. Lymphomas show a homogeneously low signal on T1-weighted images and heterogeneously high signal on T2-weighted images.

Small bowel lymphoma that is limited to bowel or associated with adjacent adenopathy (stages IE and IIE, respectively) is often treated surgically because of the risk of perforation with chemotherapy (Fig. 45-13). The treatment of widespread

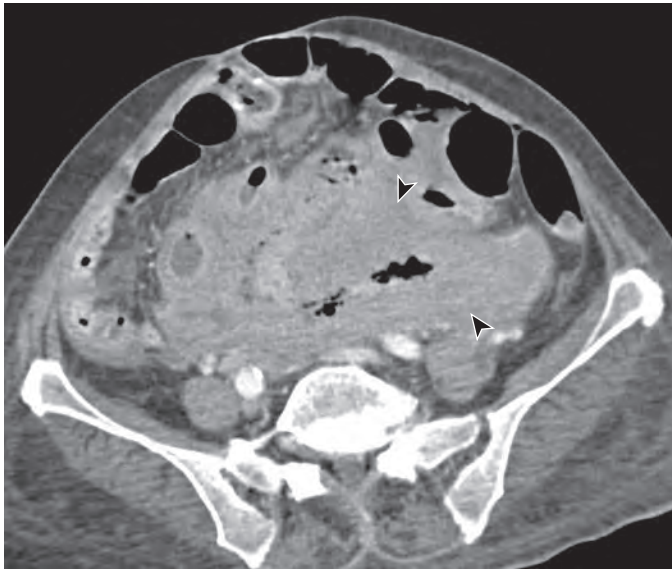


Figure 45-11 Typical primary lymphoma of the small bowel. A 43-year-old with celiac disease presented with abdominal pain and unexplained weight loss. Axial CT shows a large mass (arrowheads) involving a long segment of mid small bowel. This exoenteric mass enhances homogeneously and does not cause proximal obstruction. The history raised suspicion of T-cell non-Hodgkin lymphoma (NHL) of small bowel. The exoenteric growth, long segment involvement, and lack of proximal bowel obstruction are also features of small bowel NHL. The T-cell histology and large tumor size are poor prognostic features.

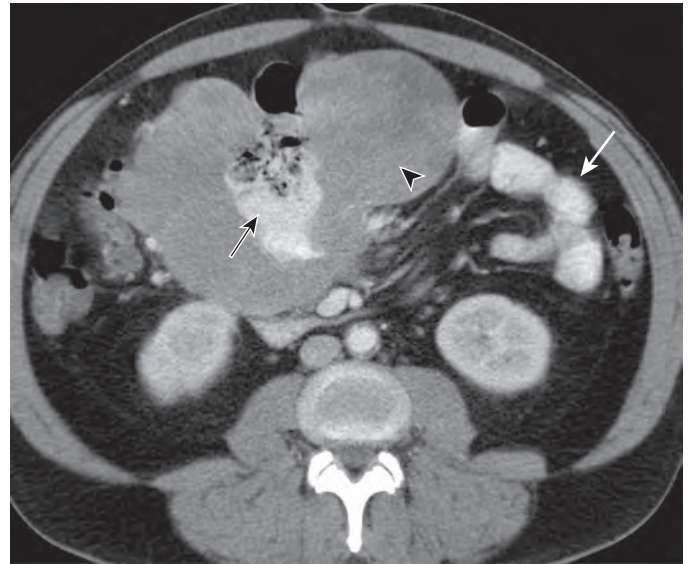


Figure 45-12 Aneurysmal bowel dilation in lymphoma. This 48-year-old man presented with abdominal pain and anemia. Axial CT shows a 12-cm small bowel mass (arrowhead) with a distended lumen containing oral contrast and gas (black arrow), a finding known as *aneurysmal bowel dilation*. The proximal bowel (white arrow) was unobstructed. This patient had B-cell non-Hodgkin lymphoma.

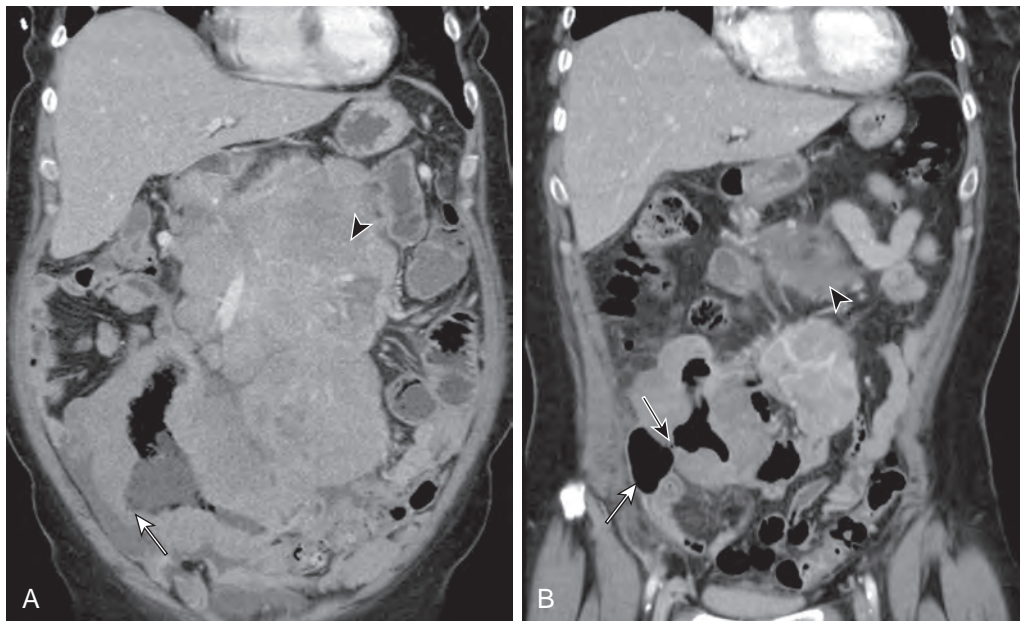


Figure 45-13 Risk of perforation of small bowel lymphoma with chemotherapy. This 57-year-old woman had anemia. **A.** Coronal reformation at presentation shows extensive mesenteric adenopathy (arrowhead) and a large mass involving the terminal ileum (arrow). The involved bowel showed eccentric wall thickening. The lumen is distended as a result of aneurysmal dilation. The patient was treated with chemotherapy. **B.** Coronal reformation obtained 3 months later because of an acute abdomen shows an extraluminal gas pocket (white arrow). The lateral wall of the ileum was almost nonexistent (black arrow) and had perforated as a result of rapid tumor lysis. Note the marked regression of mesenteric adenopathy (arrowhead).

lymphoma is not standardized. Management decisions may range from “watch and see” for asymptomatic, low-grade follicular lymphoma to combined chemotherapy and rituximab. Rituximab is a chimeric, monoclonal, anti-CD20 antibody that has been shown to be successful against B-cell lymphomas that express CD20 receptors in over 90% of cases. Rituximab may rarely cause an interstitial pneumonitis that can be mistaken on CT for tumor progression or a chest infection.

Small Bowel Metastases

Metastases to the small bowel often occur as an incidental finding in patients with known abdominal carcinomatosis. Metastatic tumor can involve the small bowel via intraperitoneal spread (the most common route of spread), hematogenous dissemination, or lymphatic channels. Hematogenous spread to the small bowel is usually from malignant melanoma or breast or lung cancer. Postmortem studies show that up to 70% of patients with metastatic melanoma have small bowel metastases. As a general rule, cross-sectional imaging studies have a low sensitivity for detecting these metastases.

In patients with known malignancy and small bowel obstruction, the main considerations are adhesions, radiation-induced strictures, and metastases. Adhesions show sharp zones of transitions, usually adjacent to the anterior parietal peritoneum. The presence of nodular defects or focal enhancement favors metastases (Fig. 45-14). Irregular bowel wall thickening of pelvic small bowel loops with a normal thickness of the proximal jejunum favors radiotherapy. However, all these entities have overlapping imaging appearances.

Summary

The diagnosis of small bowel tumors has not significantly improved over the last several years, despite advances in medical and surgical management, the introduction of capsule endoscopy, and refinements in diagnostic imaging. In most cases, capsule endoscopy is superior to imaging techniques for the diagnosis of small bowel mucosal lesions. However, imaging



Figure 45-14 Small bowel metastases causing obstruction.

This 81-year-old man with known malignant melanoma presented with bowel obstruction. Axial CT shows a serosal mass (arrow) in the distal small bowel with upstream bowel dilation (arrowhead). Multiple melanoma metastases were found at surgery.

tests have a complimentary role in diagnosis, primarily by better demonstration of the bowel wall and adjacent mesentery. Dedicated CT and MRI techniques such as enterography or enteroclysis should be used for the diagnosis of suspected small bowel neoplasms rather than small bowel follow-through or barium enteroclysis. Optimal technique requires adequate small bowel distention, multiphasic IV contrast sequences, and multiplanar reformations. Using the location of tumor, size, exoenteric or endoenteric growth pattern, enhancement pattern, and presence or absence of bowel obstruction (see Table 45-1), it is often possible to determine the type of small bowel neoplasm on imaging studies.

REFERENCES

- North JH, Pack MS: Malignant tumors of the small intestine: A review of 144 cases. *Am Surg* 66:46–51, 2000.
- Delaunoy T, Neczyporenko F, Limburg PJ, Erlichman C: Pathogenesis and risk factors of small bowel adenocarcinoma: A colorectal cancer sibling? *Am J Gastroenterol* 100:703–710, 2005.
- Bilimoria KY, Bentrem DJ, Wayne JD, et al: Small bowel cancer in the United States: Changes in epidemiology, treatment, and survival over the last 20 years. *Ann Surg* 249:63–71, 2009.
- Maglinte DD, O'Connor K, Bessette J, et al: The role of the physician in the late diagnosis of primary malignant tumors of the small intestine. *Am J Gastroenterol* 86:304–308, 1991.
- Zollinger RM, Jr: Primary neoplasms of the small intestine. *Am J Surg* 151:654–658, 1986.
- Bessette JR, Maglinte DD, Kelvin FM, Chernish SM: Primary malignant tumors in the small bowel: A comparison of the small-bowel enema and conventional follow-through examination. *AJR* 153:741–744, 1989.
- Yano T, Yamamoto H: Current state of double balloon endoscopy: The latest approach to small intestinal diseases. *J Gastroenterol Hepatol* 24:185–192, 2009.
- Boriskin HS, Devito BS, Hines JJ, et al: CT enterography vs. capsule endoscopy. *Abdom Imaging* 34:149–155, 2009.
- Sandrasegaran K, Maglinte DD, Jennings SG, Chiorean MV: Capsule endoscopy and imaging tests in the elective investigation of small bowel disease. *Clin Radiol* 63:712–723, 2008.
- Monkemuller K, Fry LC, Ebert M, et al: Feasibility of double-balloon enteroscopy-assisted chromoendoscopy of the small bowel in patients with familial adenomatous polyposis. *Endoscopy* 39:52–57, 2007.
- Scherubl H, Faiss S, Tschöpe R, Zeitz M: Double-balloon enteroscopy for the detection of midgut carcinoids. *Gastrointest Endosc* 62:994, 2005.
- Jarbandhan SV, van Weyenberg SJ, van der Veer WM, et al: Double balloon endoscopy associated pancreatitis: A description of six cases. *World J Gastroenterol* 14:720–724, 2008.
- Paulsen SR, Huprich JE, Fletcher JG, et al: CT enterography as a diagnostic tool in evaluating small bowel disorders: Review of clinical experience with over 700 cases. *Radiographics* 26:641–657, 2006.
- Fidler JL, Guimaraes L, Einstein DM: MR imaging of the small bowel. *Radiographics* 29:1811–1825, 2009.
- Leyendecker JR, Bloomfield RS, DiSantis DJ, et al: MR enterography in the management of patients with Crohn disease. *Radiographics* 29:1827–1846, 2009.
- Fidler J: MR imaging of the small bowel. *Radiol Clin North Am* 45:317–331, 2007.
- Van Weyenberg SJ, Meijerink MR, Jacobs MA, et al: MR enteroclysis in the diagnosis of small-bowel neoplasms. *Radiology* 254:765–773, 2010.
- Boudiaf M, Jaff A, Soyer P, et al: Small-bowel diseases: Prospective evaluation of

- multi-detector row helical CT enteroclysis in 107 consecutive patients. *Radiology* 233:338–344, 2004.
19. Masselli G, Poletti E, Casciani E, et al: Small-bowel neoplasms: Prospective evaluation of MR enteroclysis. *Radiology* 251:743–750, 2009.
 20. Speranza G, Doroshow JH, Kummar S: Adenocarcinoma of the small bowel: Changes in the landscape? *Curr Opin Oncol* 22:387–393, 2010.
 21. Gore RM, Berlin JW, Mehta UK, et al: GI carcinoid tumours: Appearance of the primary and detecting metastases. *Best Pract Res Clin Endocrinol Metab* 19:245–263, 2005.
 22. Pelage JP, Soyer P, Boudiaf M, et al: Carcinoid tumors of the abdomen: CT features. *Abdom Imaging* 24:240–245, 1999.
 23. Jeffree MA, Nolan DJ: Multiple ileal carcinoid tumours. *Br J Radiol* 60:402–403, 1987.
 24. Shinomura Y, Kinoshita K, Tsutsui S, Hirota S: Pathophysiology, diagnosis, and treatment of gastrointestinal stromal tumors. *J Gastroenterol* 40:775–780, 2005.
 25. Joensuu H, Fletcher C, Dimitrijevic S, et al: Management of malignant gastrointestinal stromal tumours. *Lancet Oncol* 3:655–664, 2002.
 26. Miettinen M, Lasota J: Gastrointestinal stromal tumors—definition, clinical, histological, immunohistochemical, and molecular genetic features and differential diagnosis. *Virchows Arch* 438:1–12, 2001.
 27. Dematteo RP, Lewis JJ, Leung D, et al: Two hundred gastrointestinal stromal tumors: Recurrence patterns and prognostic factors for survival. *Ann Surg* 231:51–58, 2000.
 28. Burkill GJ, Badran M, Al-Muderis O, et al: Malignant gastrointestinal stromal tumor: Distribution, imaging features, and pattern of metastatic spread. *Radiology* 226:527–532, 2003.
 29. Sandrasegaran K, Rajesh A, Rydberg J, et al: Gastrointestinal stromal tumors: Clinical, radiologic, and pathologic features. *AJR* 184: 803–811, 2005.
 30. Levy AD, Remotti HE, Thompson WM, et al: Gastrointestinal stromal tumors: Radiologic features with pathologic correlation. *Radiographics* 23:283–304, 2003.
 31. Ghanem N, Altehoefer C, Furtwangler A, et al: Computed tomography in gastrointestinal stromal tumors. *Eur Radiol* 13:1669–1678, 2003.
 32. Sandrasegaran K, Rajesh A, Rushing DA, et al: Gastrointestinal stromal tumors: CT and MRI findings. *Eur Radiol* 15:1407–1414, 2005.
 33. Chen MY, Bechtold RE, Savage PD: Cystic changes in hepatic metastases from gastrointestinal stromal tumors (GISTs) treated with Gleevec (imatinib mesylate). *AJR* 179:1059–1062, 2002.
 34. Shankar S, vanSonnenberg E, Desai J, et al: Gastrointestinal stromal tumor: New nodule-within-a-mass pattern of recurrence after partial response to imatinib mesylate. *Radiology* 235:892–898, 2005.
 35. Choi H, Charnsangavej C, Faria SC, et al: Correlation of computed tomography and positron emission tomography in patients with metastatic gastrointestinal stromal tumor treated at a single institution with imatinib mesylate: Proposal of new computed tomography response criteria. *J Clin Oncol* 25:1753–1759, 2007.
 36. d'Amore F, Brincker H, Gronbaek K, et al: Non-Hodgkin's lymphoma of the gastrointestinal tract: A population-based analysis of incidence, geographic distribution, clinicopathologic presentation features, and prognosis. Danish Lymphoma Study Group. *J Clin Oncol* 12:1673–1684, 1994.
 37. Ashworth LA, Billett A, Mitchell P, et al: Lymphoma risk in children and young adults with inflammatory bowel disease: Analysis of a large single-center cohort. *Inflamm Bowel Dis* 18: 838–843, 2012.
 38. Siegel CA, Marden SM, Persing SM, et al: Risk of lymphoma associated with combination anti-tumor necrosis factor and immunomodulator therapy for the treatment of Crohn's disease: A meta-analysis. *Clin Gastroenterol Hepatol* 7:874–881, 2009.
 39. Gill SS, Heuman DM, Mihos AA: Small intestinal neoplasms. *J Clin Gastroenterol* 33:267–282, 2001.
 40. Gou HF, Zang J, Jiang M, et al: Clinical prognostic analysis of 116 patients with primary intestinal non-Hodgkin lymphoma. *Med Oncol* 29:227–234, 2012.

Small Bowel Obstruction

STEPHEN E. RUBESIN | RICHARD M. GORE

CHAPTER OUTLINE

Terms Used in Describing Small Bowel Obstruction and Adynamic Ileus

Pathophysiology

Symptoms

Radiologic Imaging

Plain Radiography of the Abdomen

Computed Tomography

Barium Studies

Other Studies

Classification of Small Bowel Obstruction

Extrinsic Lesions

Intramural Lesions

Intraluminal Causes

Intussusception

In patients with known or suspected small bowel obstruction, the radiologist is called on to answer the following questions:

- Is the bowel obstructed?
- If so, what is the level of the obstruction?
- What is the cause of the obstruction?
- What is the severity of obstruction?
- Does the patient have a closed loop or simple obstruction (Fig. 46-1)?
- Is the bowel strangulated?
- Are ischemic changes present?
- Is immediate surgery needed, or should a trial of conservative therapy be used?

These questions are very important to answer because clinical findings may be misleading: approximately 88% of patients with partial small bowel obstruction resolve with conservative management within 48 hours; 37% of patients admitted with ischemic small bowel obstruction have a different clinical diagnosis. The preoperative diagnosis of strangulation is made on clinical grounds alone in 48% of patients. The purpose of this chapter is to provide a working classification for radiologic thinking about small bowel obstruction. After a description of the causes of small bowel obstruction, this chapter will present a radiologic approach to suspected small bowel obstruction (Box 46-1).

Terms Used in Describing Small Bowel Obstruction and Adynamic Ileus

Small bowel obstruction is a condition, not a disease. The term *small bowel obstruction* does not indicate the cause, severity, or

prognosis of the obstruction. The term *ileus* comes from the Greek variably meaning “to twist up,” “to wrap,” or “to roll up,”¹ implying that a patient is rolled up in discomfort. The term *ileus* means that the bowel lumen is dilated, but must have a qualifier before it that indicates neuromuscular-based dilation or mechanical obstruction. *Functional ileus*, *paralytic ileus*, *functional obstruction*, and *adynamic ileus* are equivalent terms indicating that the bowel is dilated because there is abnormal intestinal motility that prevents succus entericus from progressing down the gastrointestinal (GI) tract. Common causes of adynamic ileus include drugs that alter bowel motility (e.g., narcotics), recent abdominal surgery, intestinal ischemia, peritonitis, neuromuscular disorders (e.g., scleroderma), and endocrine disturbances (e.g., diabetes, hypothyroidism). If succus entericus cannot progress down the small bowel because the lumen is mechanically obstructed, the terms *small bowel obstruction*, *mechanical ileus*, or *mechanical obstruction* can be used. To avoid confusion, we will only use two distinct terms—*adynamic ileus* and *small bowel obstruction*.

Simple obstruction implies that the lumen is partially or completely occluded, but that blood flow is preserved. Strangulation or strangulated obstruction means that blood flow is compromised, leading to bowel wall edema, intestinal ischemia and, eventually, necrosis to perforation. A simple obstruction can be complete (i.e., no fluid or gas passes beyond the site of obstruction) or incomplete (i.e., some fluid and gas does pass beyond the site of obstruction). In open loop obstruction, intestinal flow is blocked distally, but the proximal loops are open and can be decompressed by vomiting or nasogastric intubation. In closed loop obstruction, both flow into and flow out of the closed loop are blocked, resulting in progressive accumulation of fluid in the closed loop (see Fig. 46-1).

Pathophysiology

After food has been digested in the stomach and duodenum, most of the contents entering the jejunum are in fluid state. If the neuromuscular function of the bowel is preserved, a large degree of luminal narrowing is needed to cause obstruction. Narrowing can be caused by abrupt angulation, kinking, or compression of the lumen by extrinsic disease; circumferential compromise of the lumen by intrinsic disease, intussusception, and/or obturation by intraluminal contents.

A series of physiologic factors leads to progressive accumulation of fluid in obstructed small bowel loops. Elevated intraluminal pressures stimulate secretion of water and electrolytes into the lumen.² Release of hormones such as vasoactive intestinal polypeptide (VIP) and various prostaglandins stimulates epithelial secretion and inhibits fluid resorption.³⁻⁵ Enzymatic breakdown of intraluminal contents increases the osmolality of intraluminal contents, also drawing more fluid into the lumen.

Intraluminal pressures are higher with closed loop than with open loop obstruction,² which leads to even further secretion

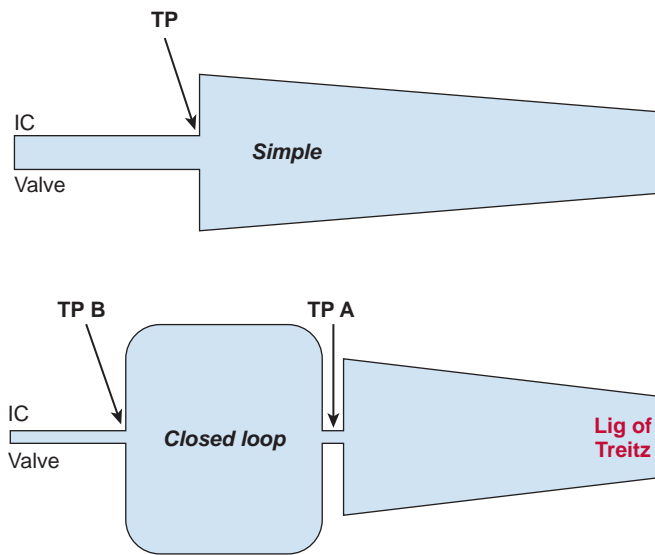


Figure 46-1 Simple versus closed loop small bowel obstruction.

In simple small bowel obstruction (**Simple**), there is a single discordance of small bowel caliber at the transition point (TP). There is tapering of the distention back to the ligament of Treitz (Lig of Treitz). In closed loop obstruction (**Closed loop**), the obstructed segment of bowel between the first transition point (TP A) and second transition point (TP B) becomes markedly dilated and is at risk for ischemia. There is tapering of the distention back to the ligament of Treitz proximal to TP A. The bowel is collapsed beyond the level of TP B. The degree of bowel caliber is triply discordant, most dilated between TP A and TP B, less dilated proximal to TP A, and collapsed beyond TP B. IC valve, ileocecal valve.

of fluid into the closed loop. High intraluminal pressures eventually exceed venous pressures and then capillary pressures. Loss of blood flow leads to the potential cascade of edema, small bowel ischemia, necrosis, and perforation. Stasis in a closed loop obstruction also leads to bacterial overgrowth. Subsequent bacterial invasion of the bowel leads to further edema and inflammation. Release of bacterial toxins into the circulation causes shock.²

In simple (open loop obstruction) of the proximal small intestine, vomiting or intubation leads to the loss of gastric, pancreatic, and biliary secretions. Loss of electrolytes in these secretions results in dehydration, metabolic alkalosis, hyponatremia, hypokalemia, and hyponatremia. Only minor changes in fluids and electrolytes are seen with open loop obstruction involving the distal small intestine because less fluid is lost.

Symptoms

Open loop (simple) obstruction of the proximal small bowel is characterized by frequent, large-volume, often bilious vomiting.² Abdominal pain is intense, but is often relieved by vomiting. Abdominal distention and tenderness are minimal because the small bowel is decompressed by vomiting.

In open loop (simple) obstruction of the distal small bowel, fluid fills the distensible small bowel loops. As a result, vomiting is infrequent and of low volume. Abdominal distention is of moderate to marked degree.

In closed loop obstructions, reflex vomiting may be present, even if the obstruction is distal. Abdominal distention may be absent. Abdominal pain is progressive and may rapidly worsen if ischemia progresses to infarction and perforation.

BOX 46-1 CAUSES OF SMALL BOWEL OBSTRUCTION IN ADULTS

EXTRINSIC LESIONS

- Adhesions
- Hernias
 - External
 - Inguinal
 - Femoral
 - Obturator
 - Sciatic
 - Perineal
 - Supravesical
 - Spigelian
 - Lumbar
 - Incisional
 - Umbilical
 - Internal
 - Paraduodenal
 - Epiploic foramen
 - Diaphragmatic (traumatic)
 - Transomental
 - Transmesenteric
 - Iliac fossa
- Extrinsic tumors in mesentery
 - Lymphoma
 - Peritoneal metastasis
 - Carcinoid
 - Desmoid
- Abscess
 - Diverticulitis
 - Pelvic inflammatory disease
 - Crohn's disease
- Aneurysm
- Hematoma
- Endometriosis
- Congenital
 - Annular pancreas
 - Ladd's bands

INTRAMURAL LESIONS

- Tumors infiltrating wall of small intestine
 - Adenocarcinoma
 - Carcinoid tumor
 - Lymphoma (rare)
 - GI stromal tumors (rare)
- Inflammatory conditions
 - Crohn's disease
 - Tuberculosis
 - Potassium chloride or NSAID-induced stricture
 - Eosinophilic gastroenteritis
- Vascular
 - Radiation enteropathy
 - Ischemia
- Hematoma
 - Post-traumatic hematoma
 - Thrombocytopenia
 - Anticoagulants
 - Henoch-Schönlein purpura
- Congenital
 - Atresia, stricture, stenosis
 - Duplication
 - Meckel's diverticulum

INTRALUMINAL CAUSES

- Obturation
- Gallstone
- Bezoar
- Foreign body
- Ascaris
- Meconium (cystic fibrosis)
- Intussuscepting tumor
- Inverted Meckel's diverticulum

Radiologic Imaging

This section discusses the role of a variety of imaging modalities in patients with small bowel obstruction.

PLAIN RADIOGRAPHY OF THE ABDOMEN

The plain radiograph of the abdomen has traditionally been used as the first radiologic study in the work-up of acute abdominal pain and suspected small bowel obstruction.^{5,6} Many adults admitted with clinical suspicion of acute small bowel obstruction undergo surgery on the basis of clinical, physical, and laboratory findings in conjunction with plain abdominal radiographs. The diagnosis of small bowel obstruction on abdominal radiographs relies on the demonstration of dilated loops of small bowel (**Fig. 46-2**), identified by their smooth luminal contour, valvulae conniventes, and central location in the abdomen. Air-fluid levels may traverse the entire lumen loop of the loop) or be trapped as bubbles between folds at the top of a fluid-filled bowel loop, resulting in a string of pearls sign. Fluid-filled loops may not be seen on supine radiographs but may be recognized on erect or cross-table lateral decubitus radiographs.

Plain abdominal radiographs have only moderate accuracy for the diagnosis of small bowel obstruction. In one series, abdominal radiographs had a sensitivity of 86% for the diagnosis of high grade obstruction, but a sensitivity of only 56% for the diagnosis of low-grade obstruction.⁷ In another series, abdominal radiographs revealed small bowel obstruction in 78% of patients with this condition.⁸ Obstructions can be missed by abdominal radiographs if vomiting or nasogastric intubation leads to decompression of small bowel loops. Fluid-filled loops (**Fig. 46-3**) may not be visible, leading to a false-negative diagnosis or erroneous interpretation of the level of obstruction. In a few patients, abdominal radiographs may be obtained before fluid and air accumulates in the lumen and dilates the small intestine. A false-positive diagnosis of obstruction occurs in up to 44% of patients, mistaking adynamic ileus

or aerophagia for obstruction. The level of obstruction can be accurately predicted in about 75% of patients.⁸

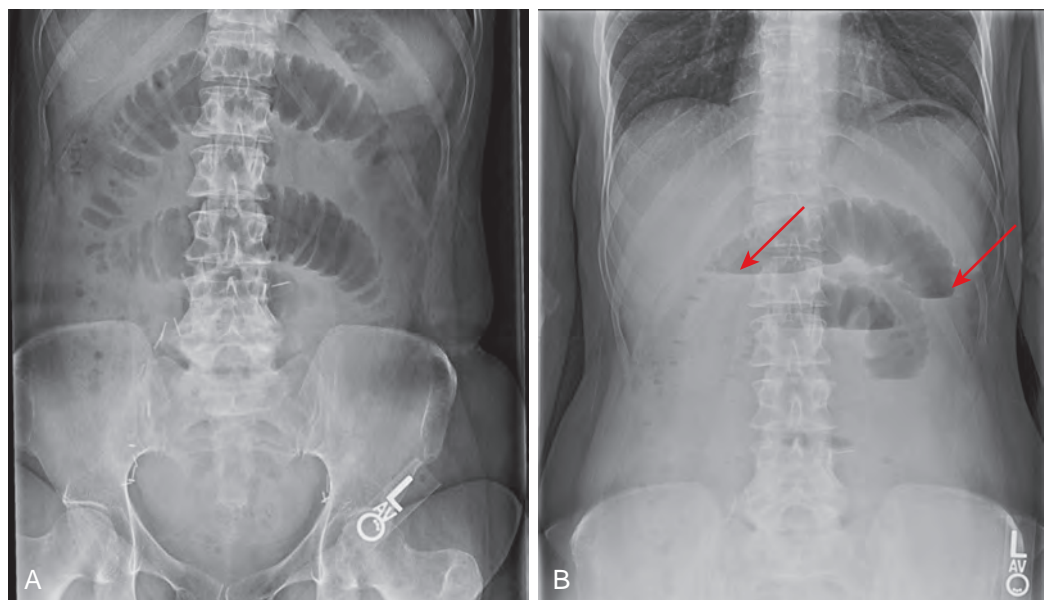
Unfortunately, plain abdominal radiographs are poor at suggesting the diagnosis of strangulation.^{9,10} In patients with strangulating obstruction, the underlying small bowel obstruction is diagnosed in only 50% of patients.^{9,10} Strangulation is suggested on abdominal radiographs by the demonstration of smooth, thick valvulae conniventes in a dilated loop or loops of small intestine. Linear pneumatosis paralleling in the wall of the small bowel or portal venous gas strongly suggests superimposed ischemia and infarction. Closed loop obstructions are often not visible because they are fluid-filled. However, a dilated, fluid-filled loop that does not change location or configuration on serial abdominal radiographs suggests a closed loop obstruction.

COMPUTED TOMOGRAPHY

Given the limitations of plain abdominal radiographs, computed tomography (CT) has become the premier imaging technique for the diagnosis of small bowel obstruction.¹¹ CT has a vital role in these patients because it is readily available, fast, and offers a comprehensive, noninvasive means of assessing the bowel lumen, bowel wall, and adjacent mesentery and vascularity. In comparison to barium studies, CT does not rely on oral contrast reaching the site of obstruction, but uses intestinal fluid proximal to the obstruction to outline the transition zone (see **Fig. 46-3**).¹² As a result, CT has become the imaging modality of choice for diagnosing a variety of conditions, including adynamic ileus, acute or prolonged high grade small bowel obstruction, suspected strangulation or perforation, and acute inflammatory processes such as appendicitis, Crohn's disease, or diverticulitis causing small bowel obstruction. CT is also the best examination for evaluating patients with a known primary tumor and suspected metastatic disease causing small bowel obstruction (**Fig. 46-4**).

CT has an accuracy of almost 90% for the diagnosis high-grade obstructions versus an accuracy of only 50% for low-grade

Figure 46-2 Plain radiographs demonstrating small bowel obstruction. **A.** Plain radiograph obtained with patient in supine position demonstrates diffuse small bowel dilation. **B.** Radiograph obtained with patient standing demonstrates numerous air-fluid levels (arrows).



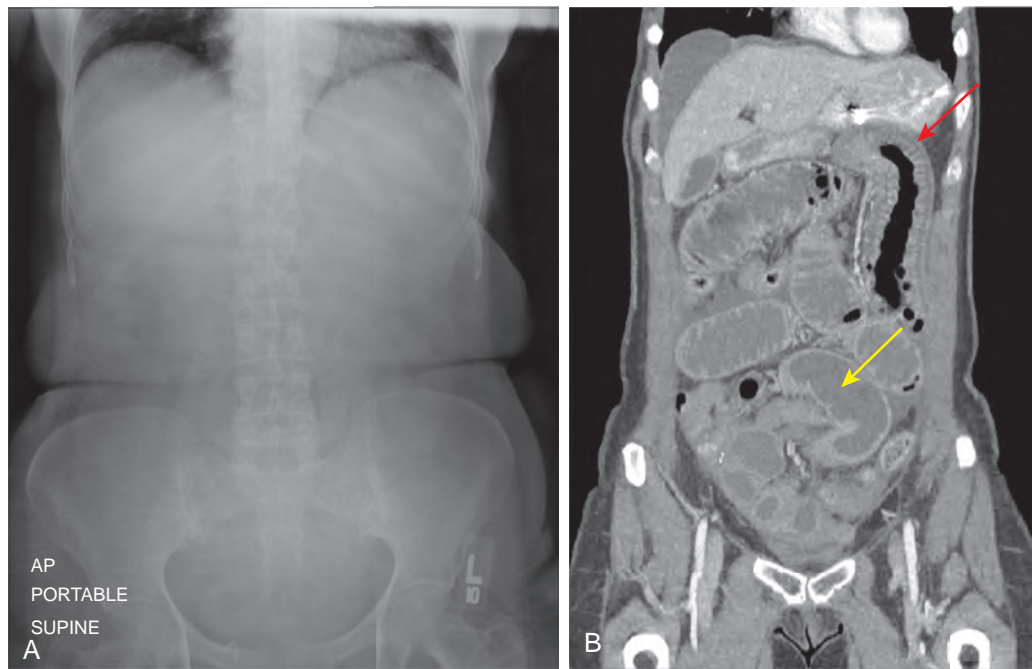


Figure 46-3 Plain abdominal radiography limitations. **A.** Supine radiograph of the abdomen shows a gasless abdomen. **B.** Coronal reformatted CT scan performed several hours later shows a distal small bowel obstruction with fluid-filled small bowel loops (yellow arrow) and an ischemic jejunal loop (red arrow) with mural thickening. If the bowel is completely filled with fluid, plain abdominal radiographs will misjudge the presence and level of small bowel obstruction.

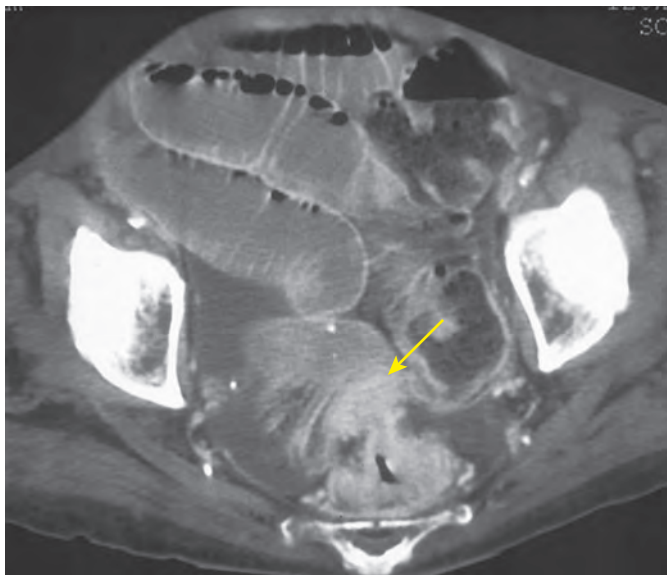


Figure 46-4 Transition zone with mass demonstrated at CT. Axial CT image through pelvis shows a dilated ileum. There is invasion of the distal ileum by a carcinoma (arrow) of the rectosigmoid junction.

obstructions.⁷ CT can accurately predict the cause of obstruction in 70% to 95% of patients¹²⁻¹⁶ and can often suggest superimposed ischemia and intestinal perforation. The entire abdomen is evaluated by CT, providing a vast array of information not demonstrated by an abdominal radiograph. For example, CT can identify a variety of causes of small bowel obstruction, such as carcinoid tumor, intraperitoneal or hematogenous metastasis, Crohn's disease, appendicitis, and diverticulitis.¹⁷

Although CT is the premier means of evaluating patients with small bowel obstruction, it does have limitations. It is difficult to distinguish an adynamic ileus of the small bowel from a distal small bowel obstruction if a transition zone is not identified.¹⁷ It can also be difficult to determine the location of the transition zone along the course of dilated small bowel, even with the ability to scroll through a scan on a picture archiving and communications system (PACS) workstation or visualize the intestine in any plane. The localization of the transition zone to an abdominal quadrant is not accurate in diagnosing the distance of the obstruction from the duodenal-jejunal junction because a markedly dilated jejunum may fall into the pelvis and an obstructed distal ileum may rotate into the left upper quadrant. Finally, although CT is an excellent technique for suggesting strangulation, it can usually but not always predict whether a bowel loop has reversible or irreversible ischemia or whether the affected small bowel will be viable at surgery.^{18,19} Abnormal bowel wall thickening or mesenteric engorgement also cannot always predict surgical viability of the bowel. In the setting of ischemia, a CT finding of pneumatosis indicates breakdown in the mucosal integrity of the bowel wall and is strongly suggestive of ischemia. The CT finding of pneumatosis can usually but not always predict irreversible ischemia at surgery. Patients with CT findings of free intraperitoneal gas or portomesenteric gas have a greater likelihood of irreversible transmural necrosis than patients with pneumatosis alone. Nevertheless, CT is currently the modality of choice for acutely ill patients with suspected high-grade or complete small bowel obstruction, suspected strangulation, or suspicion of an inflammatory process (e.g., appendicitis, Crohn's disease) or a hernia as the cause of small bowel obstruction.^{20,21}

BARIUM STUDIES

Various barium studies may be performed on patients with suspected small bowel obstruction, including small bowel follow-through, enteroclysis (small bowel enema), barium enema, and studies performed via indwelling nasogastric, nasojejunal, or jejunostomy tubes.

The use of barium is safe in patients with suspected small bowel obstruction because barium does not form concretions in the small bowel lumen proximal to an obstructing lesion. In obstructed patients, the residual fluid in dilated small bowel loops prevents barium from dehydrating and agglomerating. Barium also does not form concretions in the proximal ascending colon. However, concretions may form in the remainder of the colon because water is resorbed from the barium sulfate suspension. Therefore, barium sulfate should not be administered orally or via a proximal bowel tube in a patient with an obstructing lesion distal to the hepatic flexure of the colon because dense barium concretions can form, with the possibility of stercoral ulceration and perforation. If there is any doubt about the location of bowel obstruction, CT or barium enema should be performed before barium is administered proximal to the site of a colonic obstruction.

The presence of barium proximal to a small bowel obstruction makes surgery more hazardous because barium that spills into the peritoneal cavity may result in a form of granulomatous peritonitis. Some surgeons therefore request that small bowel examinations be performed with water-soluble contrast material rather than barium. Small bowel follow-through examinations using water-soluble contrast have even been advocated as a therapeutic technique to improve small bowel obstruction.²²

The use of hypertonic water-soluble contrast in small bowel obstruction can be problematic. This draws fluid into the lumen, whereas the aim of therapy is to decompress the small bowel. Dilution of water-soluble contrast material by retained fluid also may result in very poor radiologic detail, compromising the ability to diagnose small bowel obstruction or demonstrate the site and cause of obstruction. These limitations are partially obviated by the use of iso-osmolar iodinated oral contrast agents.

Small bowel follow-through and enteroclysis studies are not recommended to be performed in patients with high-grade distal small bowel obstruction. Because of small bowel dilation and diminished small bowel peristalsis, it may take an inordinate period of time for barium to reach the site of obstruction. Not infrequently, 24-hour follow-up radiographs must be obtained to visualize the site of a high-grade distal small bowel obstruction. By this time, the barium suspension is diluted and there is poor anatomic detail of the transition zone (Fig. 46-5). The transition zone may even be obscured by dilated-barium filled loops.

If a study must be performed from above in a patient with a high-grade small bowel obstruction, prior passage of a Miller-Abbot tube, Cantor tube, or enteroclysis catheter with a built-in suction port^{23,24} is helpful. The small bowel is first decompressed and then an antegrade barium study is performed.

If more information is needed after CT, a single-contrast barium enema with reflux of barium to the site of small bowel obstruction is often better than an antegrade study in patients with high-grade distal small bowel obstruction (Fig. 46-6). After the administration of 1 mg of intravenous (IV) glucagon to relax the ileocecal valve, barium can be refluxed into the distal ileum in 85% of patients. Barium is then pushed retrogradely by the addition of water to the enema bag. This is an excellent technique that can easily visualize pelvic loops of ileum and even the proximal ileum or distal jejunum. A barium enema is also an excellent technique in patients with an ileocolic anastomosis. A long length of small intestine can be visualized by retrograde flow of barium through the ileocolic anastomosis, resulting in the excellent demonstration of a transition zone. In patients with an ileostomy or colostomy, a retrograde ileostomy or colostomy study can also be performed to diagnose a distal small bowel obstruction.

Enteroclysis and small bowel follow-through examinations are reserved for patients with known or suspected low-grade small bowel obstruction. Enteroclysis should not be performed in patients with high-grade small bowel obstruction, suspected strangulation, suspected perforation, or adynamic ileus. Enteroclysis is superior to small bowel follow-through for the demonstration of short lesions such as strictures or tumors. By overdistending the small bowel lumen, enteroclysis

Figure 46-5 Small bowel follow-through poorly demonstrating transition zone.

A 24-year-old woman had acute abdominal pain and distention.

A. Barium had not reached the colon after 10 hours. An overhead radiograph obtained 24 hours after the ingestion of barium reveals diffuse small bowel dilation. The cecum (c) and ascending colon are relatively collapsed. A gap between the ileum (i) and cecum is minimally filled with barium (arrow). **B.** Axial CT scan through the pelvis demonstrates dilated ileum (l) and thick-walled distal ileum (arrows). Inflammatory stranding surrounds the contrast-filled right external iliac artery. This patient had Crohn's disease.

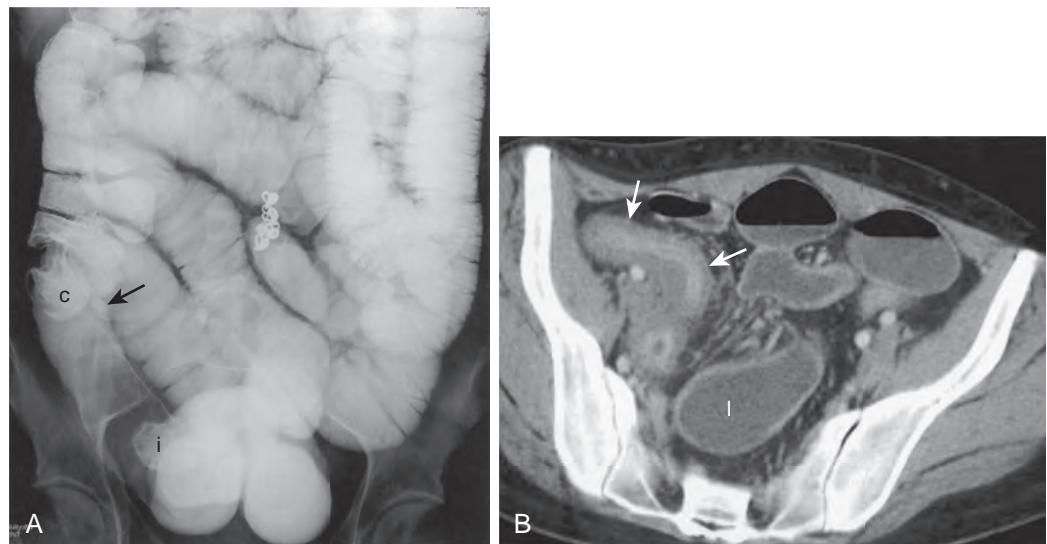




Figure 46-6 Barium enema demonstrating inguinal hernia as cause of high-grade, small bowel obstruction. The jejunum (J) is dilated. Barium refluxes into the distal ileum (I) and stops at the internal ring of the right inguinal canal (arrow).

can demonstrate subtle adhesions. Obstruction is implied by distention of the jejunal diameter to more than 4 cm and ileal diameter to more than 3 cm. A high-grade obstruction is implied by delayed passage of contrast to the transition zone, dilution of contrast material, and minimal passage of contrast material through the transition zone. A low-grade obstruction is diagnosed if there is delayed passage of contrast at the transition zone itself. Small bowel follow-through examinations are more physiologic, however, with inherent small bowel motility propelling the barium down the intestinal tract, allowing a more accurate estimate of transit time. Small bowel follow-through examinations are also much easier on the patient and examiner, but only in the setting of low-grade or absent small bowel obstruction. Long lesions such as Crohn's disease and ischemia (Fig. 46-7) can be easily demonstrated on small bowel follow-through in patients with low-grade obstruction. Small bowel follow-through examinations (especially with a peroral pneumocolon) are probably superior for the demonstration of the terminal ileum in comparison to enteroclysis.

OTHER STUDIES

CT and magnetic resonance (MR) enteroclysis are intubation techniques discussed in earlier chapters.²⁵ Similar to enteroclysis, these techniques have no role in patients with suspected high-grade small bowel obstruction. These techniques may be of value for patients with carcinoid tumor, radiation therapy,

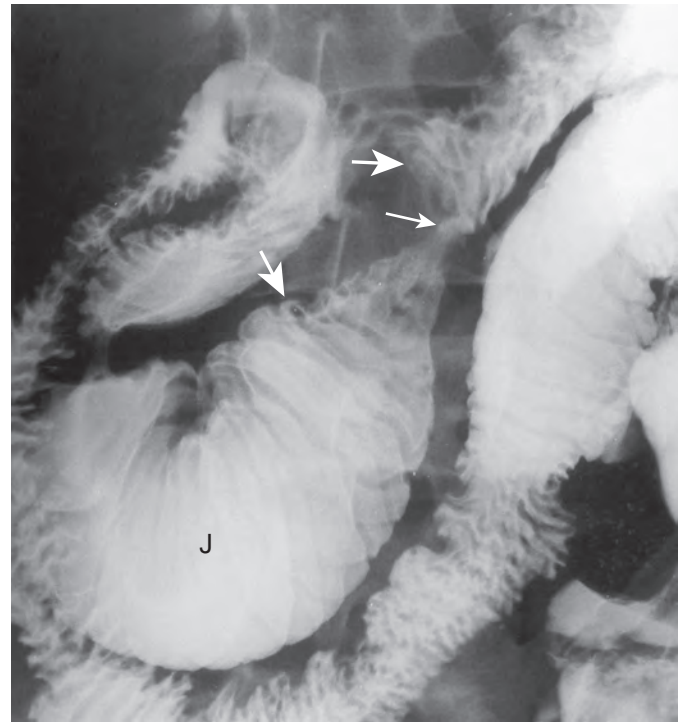


Figure 46-7 Small bowel follow-through demonstrates low-grade obstruction by ischemic stricture. A 3-cm tapered narrowing (thick arrows) has a small central ulcer (thin arrow) and preserved folds. The jejunum (J) is dilated proximal to the stricture. (From Rubesin SE, Furth EE: *Differential diagnosis of small intestinal abnormalities with radiologic-pathologic explanation*. In Herlinger H, Maglinte DD, Birnbaum BA (eds): *Clinical Imaging of the Small Intestine*, 2nd ed. New York, Springer, 1999, pp 527–566.)

and peritoneal metastasis. Transabdominal ultrasound and conventional MR imaging should be considered as primary imaging modalities for evaluating bowel obstruction only in the pediatric and pregnant population.^{26,27}

Classification of Small Bowel Obstruction

EXTRINSIC LESIONS

Adhesions

Adhesions are the most common cause of small bowel obstruction, accounting for about two thirds of cases.^{28,29} Most adhesions form after abdominal surgery; 10% to 15% of adhesions are attributed to prior or concurrent inflammation.²⁹ A small fraction of adhesions are thought to be congenital in origin. Although adhesions form in more than 90% of patients who have undergone laparotomy, only 5% of patients who have undergone laparotomy will develop an adhesive obstruction.³⁰

About 1% of patients will develop a small bowel obstruction in the immediate postoperative period. About 90% of these early postoperative obstructions are caused by adhesions (Fig. 46-8) and 7% by hernias, with the remainder related to abscess formation, intussusception, or technical factors.^{31,32}

The most important radiographic finding in the diagnosis of small bowel obstruction is the abrupt transition from a

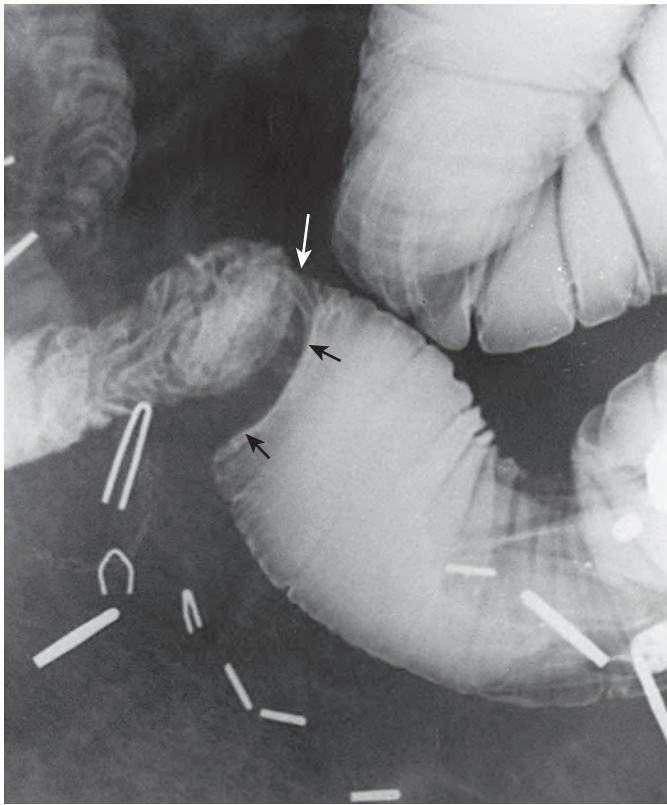


Figure 46-8 Partial small bowel obstruction by an adhesive band. Spot radiograph from an enteroclysis shows a long linear lucency (black arrows), which represents an adhesive band crossing the ileum. The ileum is focally narrowed (white arrow) by the band. Note preservation of small bowel folds (white arrow) in the area of narrowing and dilation of the bowel proximal to the band with collapse of bowel distal to the band.

dilated to nondilated small intestine at the site of obstruction. On barium studies, a sharp, straight, or curved edge (Fig. 46-9) is seen where the adhesive band crosses the bowel lumen. The adhesion itself may be manifest as a narrow, bandlike radiolucency crossing the bowel lumen between dilated proximal and collapsed distal loops. The bowel may be angulated toward the adhesion. Smooth, thin mucosal folds will be tethered toward the extraluminal adhesive process. The bowel may be completely cut off, with a rounded, beaklike, or sharp edge. Mucosal folds are preserved and no mucosal nodularity or mass is present. Several loops may be pulled together at the site of adhesions. Multiple bands or extensive adhesions may be present. Multiple bands are often associated with scar formation along the anterior abdominal wall at prior incision sites. Extensive adhesions are often caused by prior extensive intra-abdominal inflammatory processes, such as traumatic perforation, peritonitis, and postoperative abscesses.

Adhesions are not usually seen on CT. The CT diagnosis of adhesions is a diagnosis of exclusion: there is an abrupt transition from a dilated to collapsed small intestine without apparent cause (Fig. 46-10).³³ The transition zone may appear rounded or beaklike.^{13,34} Other abnormalities can cause a transition zone without apparent cause on CT, including small primary tumors, such as carcinoid tumor, small intraperitoneal metastases, and short inflammatory, ischemic, or drug-related strictures.³³ The CT diagnosis of adhesion is supported by a

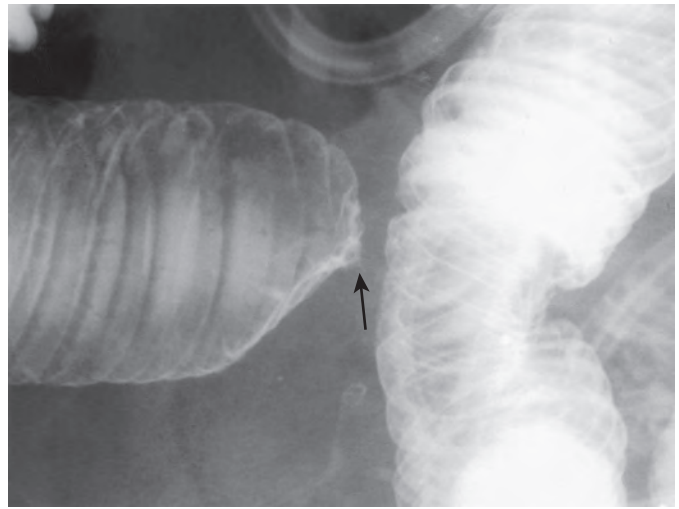


Figure 46-9 Adhesion causing complete small bowel obstruction. Abrupt beaklike narrowing (arrow) represents the site of adhesion obstructing the mid small bowel. (Courtesy Hans Herlinger, MD.)

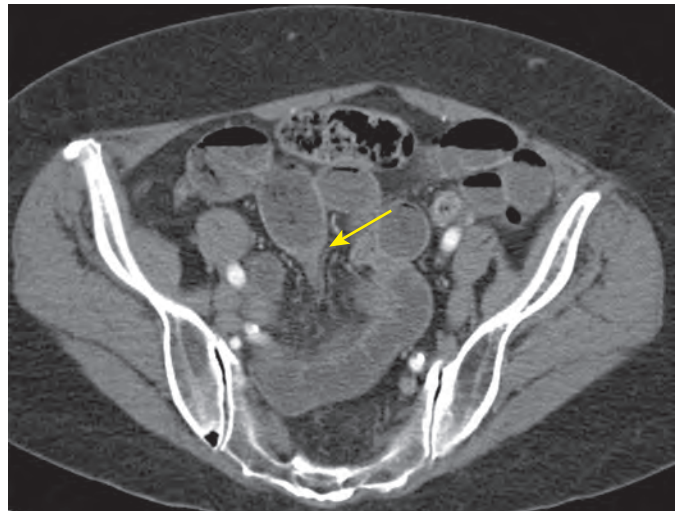


Figure 46-10 Narrowing at site of transition zone. Axial CT scan through the lower abdomen demonstrates dilated small intestine. There is an abrupt transition (arrow) between the collapsed and obstructed small bowel. The small bowel feces sign is present proximal to the obstruction.

history of prior laparotomy in the absence of a history of a tumor with a predilection for peritoneal spread (e.g., ovarian carcinoma) or a known history of inflammatory bowel disease. The CT diagnosis of adhesions is accurate in 70% to 95% of patients.^{7,13-16,35}

Closed Loop Obstruction and Strangulation

The most common causes of closed loop obstruction are single adhesive bands, internal or external hernias, or rents in the mesentery.^{36,37} The trapped loop or loops become progressively dilated and fluid-filled. The vessels feeding the trapped intestine may be compressed by the band or hernia orifice or occluded by twisting of the mesentery; either process results in strangulation. Both dilation and the risk of strangulation of the trapped loops depend on the stage and degree of compression or twisting.

The radiographic findings of strangulation vary, depending on the level of trapping and twisting. Initially, the closed loop may not be dilated. In the usual patient, however, the closed loop is dilated and fluid-filled, with little or no intraluminal gas. If the closed loop(s) are parallel to the plane of reconstruction on CT, they appear as a C- or U-shaped configuration.^{38,39} If the loops are imaged perpendicular to the plane of reconstruction, they appear in a radial configuration, with the trapped mesentery pointing toward the band or hernia orifice (Fig. 46-11). The loops that enter and exit the closed loop lay side by side and are narrowed or tapered at the level of the band or mesenteric rent.⁴⁰ The entry or exit site may have a beaklike appearance when imaged in cross section. The small intestine proximal to the closed loop may be dilated and fluid-filled, whereas the small intestine distal to the closed loop is collapsed. The mesenteric vessels radiate to the point of obstruction.

With a strangulated obstruction, there is a continuum from bowel wall edema to mild to moderate ischemia to transmural infarction and, finally, to perforation. CT has a sensitivity of approximately 90% in the diagnosis of strangulation in a closed loop obstruction.³⁸ CT may reveal circumferential bowel wall thickening of low, normal, or high attenuation. With the use of IV contrast material, wall thickening may show enhancement, delayed enhancement,⁴¹ or no enhancement.⁴² On unenhanced

CT scans, high-attenuation bowel wall thickening implies hemorrhage with ischemia. The lack of contrast enhancement is clear evidence of vascular obstruction.⁴² A mural stratification pattern (target sign), with low attenuation of the submucosa reflecting submucosal edema, may indicate a spectrum of pathology ranging from bowel wall edema to full-thickness infarction. Pneumatosis in the wall of the closed loop indicates a rent in the mucosa and strangulation. A sloughed mucosa or debris in a lumen may have the appearance of feces. CT cannot fully predict viability of the bowel, even if pneumatosis is present.⁴² Air in the mesenteric veins or portal venous system is highly suggestive of nonviable bowel.

If the closed loop is twisted, its mesentery appears twisted or whirled.⁴³ Fluid in the leaves of the small bowel mesentery is not specific for ischemia because intraperitoneal fluid is commonly seen in simple small bowel obstructions. However, strangulation is implied by haziness of the mesenteric fat and large mesenteric vessels, findings reflecting mesenteric edema and venous engorgement, respectively, related to compression or twisting of mesenteric vessels.

Enteroclysis or small bowel follow-through should not be performed in patients with high-grade small bowel obstruction and suspected closed loop obstruction. However, low-grade, potentially partial closed loop obstructions may occasionally be found on barium studies in less symptomatic patients (Fig. 46-12).^{44,45} There is adjacent smooth-surfaced compression of the inflow and outflow limbs as the trapped loops course under the band or through the hernia.^{44,45} Volvulus is implied by twisting of the folds at the point of obstruction. Smooth, thick valvulae conniventes in a partially closed loop imply edema with possible ischemia.

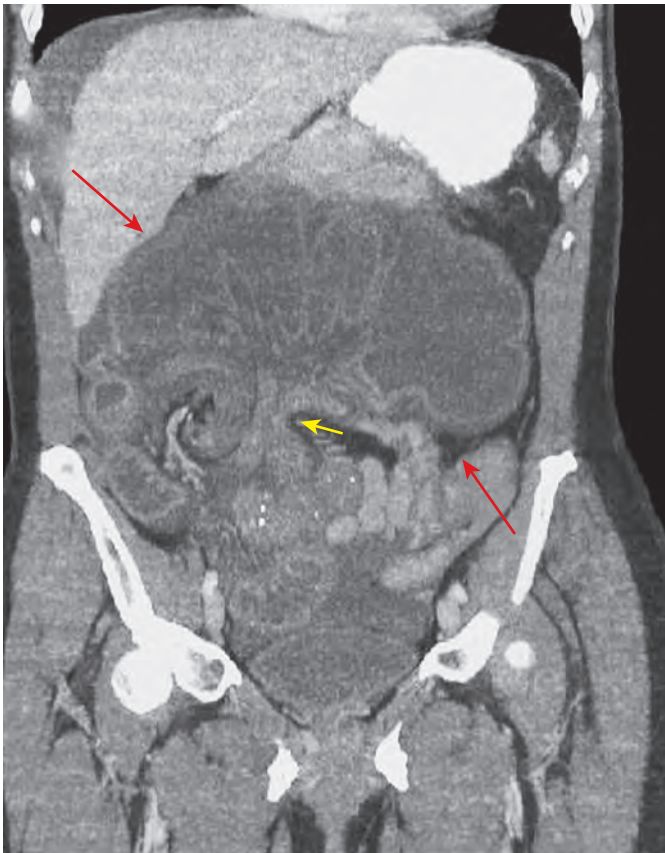


Figure 46-11 Closed loop obstruction caused by transmesenteric internal hernia in a patient with prior Roux-en-Y gastric bypass surgery. Note the markedly distended jejunal segments (red arrows) within the hernia sac, which converge at its orifice (yellow arrow). Ascites is also present.

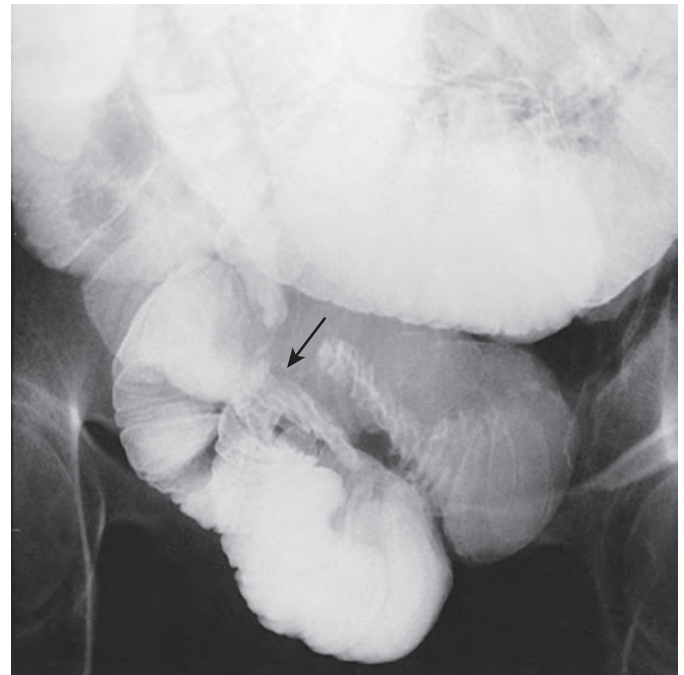


Figure 46-12 Partial closed loop obstruction demonstrated at enteroclysis. A loop of small bowel is focally dilated. As it enters and exits below an adhesive band, the loop is abruptly angulated and narrowed (arrow), and the folds are pulled toward the small bowel mesentery.

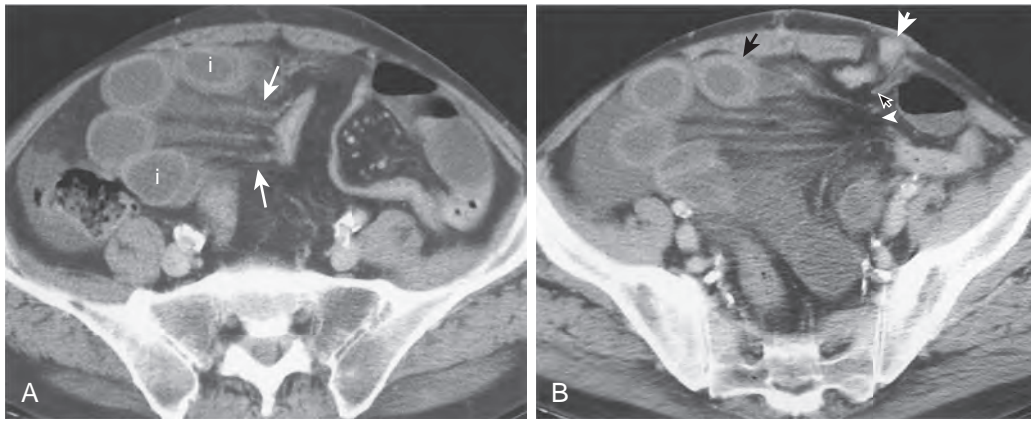


Figure 46-13 CT scan demonstrating Spigelian hernia resulting in closed loop obstruction with strangulation. **A.** Axial image through pelvis demonstrates four loops of intestine (between the *i*), with their mesentery (arrows) radiating toward the midline. Haziness of the small bowel mesentery results from vascular engorgement. **B.** Axial image just caudal to **A** demonstrates the mesentery radiating toward the left anterior abdominal wall (arrowhead). The radially arranged bowel has a thick wall with a mural stratification pattern (black arrow), indicative of minimum submucosal edema caused by ischemia. A loop of intestine is trapped in a Spigelian hernia (large white arrow). The loop exiting the hernia is abruptly angulated (open arrow). The site of volvulus is indicated by the open arrow and arrowhead. At surgery, a twist at the loop exiting the Spigelian hernia resulted in irreversible small bowel ischemia.

Hernias

Hernias occur at predictable sites of weakness in the abdominal wall where there is only fascia and peritoneum between the viscera and skin (Fig. 46-13). A wide variety of internal hernias (Fig. 46-14) occur at sites of mesenteric and omental weakness, normal openings of the peritoneal surface, or under adhesive or congenital bands.⁴⁶⁻⁴⁹ Prior to the era of laparotomy, hernias were the most common cause of small bowel obstruction.

Complications of hernias include incarceration, obstruction, and strangulation. Incarcerated hernias are not reducible, usually because of adhesions in the hernial sac. Urgent treatment is not always required because incarceration is not equivalent to obstruction or strangulation. Incarceration is not a radiologic diagnosis unless the fluoroscopist manually reduces the hernia (indicating that is not incarcerated) or the hernia retracts with change in the patient's position. When incarcerated hernias cause small bowel obstruction, the obstruction is usually high grade or complete.² Strangulation is a serious and life-threatening complication. Strangulated hernias are tense and irreducible.

Inguinal hernias comprise about 80% of anterior abdominal wall hernias; femoral hernias comprise only about 5%.² Inguinal hernias are more common in men than women (7:1), whereas femoral hernias are more common in women than men (1.8:1).² Most patients with an inguinal hernia have a patent processus vaginalis as the cause of the inguinal hernia. These hernias usually result from elevated abdominal pressure related to pregnancy, coughing, constipation, obesity, prostatic, or physical exertion. Inguinal hernias may be caused by weakening of the muscular aponeurosis and fascia because of age, cigarette smoking, or collagen deficiency (e.g., Marfan's, Ehlers-Danlos, and Hunter-Hurler syndromes).²

Direct inguinal hernias occur at Hesselbach's triangle, bounded anterosuperiorly by the inguinal ligament, medially by the rectus abdominis, and laterally by the inferior epigastric vessels that form the lateral umbilical fold. Herniations occur

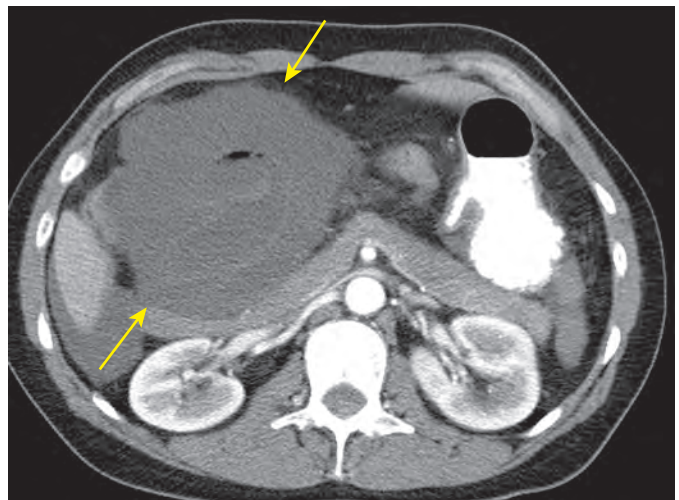


Figure 46-14 CT scan demonstrating a right paraduodenal internal hernia. There is a cluster of jejunal loops in the hernia sac (arrows) in the right upper quadrant. These loops are poorly perfused, and at surgery irreversible ischemia of the herniated intestine was found.

inferiorly where this region is covered only by peritoneum and the transversalis fascia. Indirect inguinal hernias (Fig. 46-15) occur in the deep inguinal ring in a fossa bounded medially by the inferior epigastric vessels. Because of this anatomy, indirect inguinal hernias are lateral to the inferior epigastric vessels and direct inguinal hernias are medial to the inferior epigastric vessels. Congenital indirect inguinal hernias enter a patent tunica vaginalis. The risk of a major complication in a patient with an inguinal hernia is low.

Weakness in the linea alba at the umbilicus leads to a umbilical or paraumbilical hernia (Fig. 46-16). Most pediatric umbilical hernias close spontaneously, but persistent umbilical hernias require surgery.²

Epigastric hernias also occur in defects in the linea alba. These hernias are more frequent in men. Multiple hernias are seen in 20% of patients. Epigastric hernias usually contain incarcerated preperitoneal fat and do not contain a peritoneal sac. Gastric herniation is uncommon.

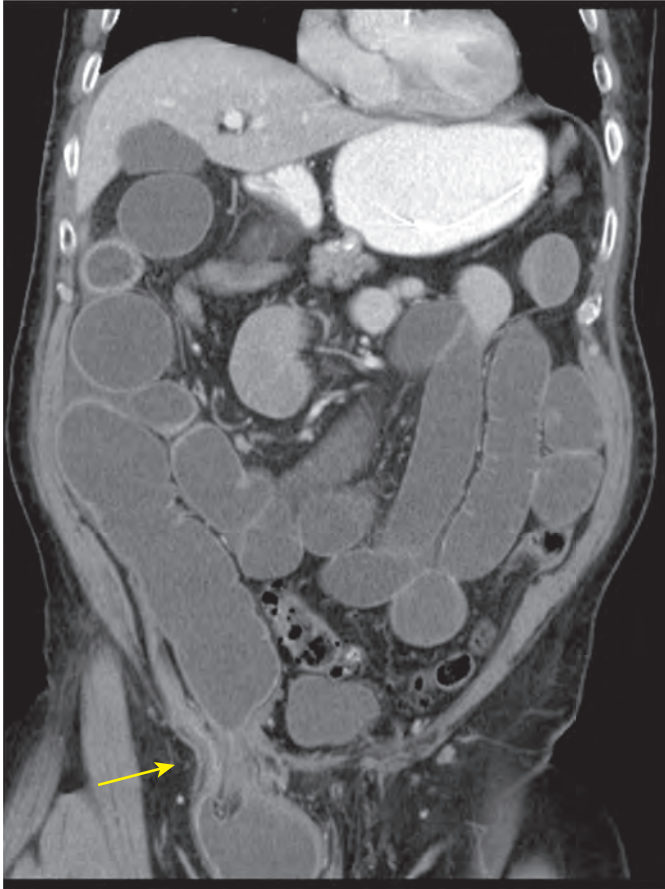


Figure 46-15 CT scan demonstrating inguinal hernia. Coronal reformatted image shows a right inguinal hernia (arrow) causing distal ileal obstruction.

Complications in parastomal hernias are uncommon. However, peritoneal herniation develops in more than 50% of patients who have had a colostomy for at least 5 years.

Above the semilunar line (the line of Spiegel), the aponeurosis of each internal oblique muscle splits to surround the rectus abdominis, with its posterior half joining the aponeurosis of the transversus abdominis posterior to the ipsilateral rectus. Below the semilunar line of Spigelius, the aponeuroses of the external and internal oblique muscles and the transversus abdominis pass anterior to the rectus. Spigelian hernias occur below the line of Spiegel, because the junction of the rectus abdominis and lateral flank muscles is weak owing to the lateral abdominal wall muscle aponeurosis passing only anterior to the rectus. A Spigelian hernia is usually small (1 to 2 cm) and intraparietal, rarely penetrating the fascia of the external oblique muscle (Fig. 46-17). Spigelian hernias contain omentum, small bowel, or colon. Incarceration and strangulation are common complications.

A Richter's hernia is a hernia in which only one wall of a bowel loop enters the hernia. The involved wall bowel wall may become ischemic or gangrenous.

The obturator foramen is covered by the obturator internus and externus muscles. The small superolateral corner of the obturator fossa is weakened at the site of penetration by the obturator nerve and vessel. Obturator hernias occur at this superolateral site (Fig. 46-18).

CT and barium studies may reveal smooth, tapered compression of the bowel loops entering and exiting the hernia, with the degree of narrowing determined by the width of the luminal opening (Fig. 46-19).⁵⁰ Dilation of the small bowel proximal to the hernia indicates obstruction at the entry site caused by compression or twisting. Dilation of loops with the hernia itself suggests obstruction at the outflow loop. The radiographic findings of strangulation are similar to those of adhesive obstruction. The sigmoid colon is usually found in a left inguinal hernia and the distal ileum usually enters a right inguinal hernia, although the cecum and appendix can also be pulled into a right inguinal hernia. On barium studies, lateral or steep oblique views are extremely helpful to show midline (Fig. 46-20) or obturator hernias. Upright views or views performed during the Valsalva maneuver are helpful for demonstrating pelvic hernias at fluoroscopy. Similarly, lateral views

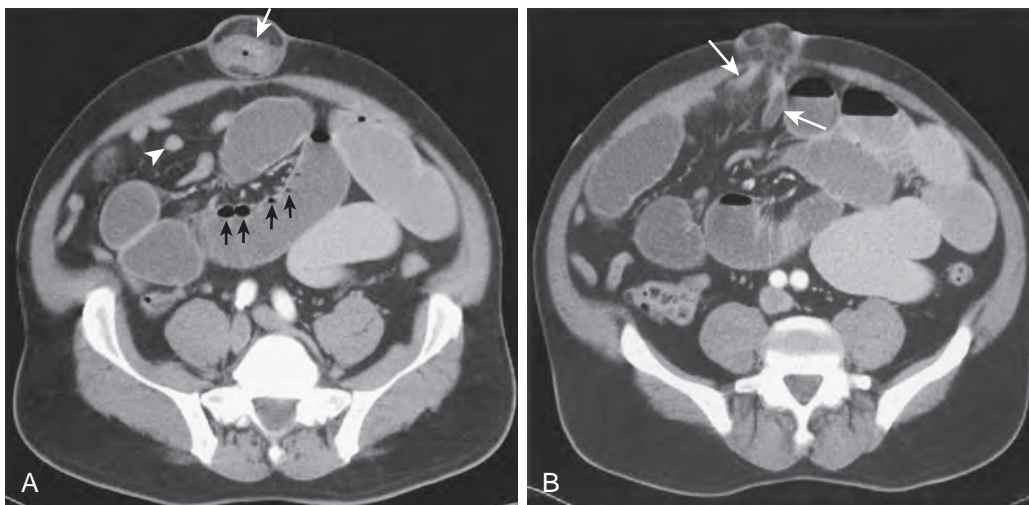


Figure 46-16 CT scan demonstrating umbilical hernia resulting in small bowel obstruction and strangulation.

A. Within the umbilical hernia, a loop of small intestine has a thick wall (white arrow). The small bowel is dilated and fluid-filled. The CT equivalent of a string of pearls sign is present (black arrows). The small bowel distal to the obstruction is collapsed (arrowhead). **B.** Axial image just caudal to **A** demonstrates collapsed loops (arrows) entering and exiting the hernia. The fat of the umbilical hernia is engorged. At surgery, the ileum within the hernia sac showed irreversible ischemia.



Figure 46-17 Intraparietal Spigelian hernia. A loop of ileum (large arrow) protrudes just lateral to the left rectus sheath (r). The hernia is intraparietal, covered by the fascia of the external oblique muscle (small arrows).

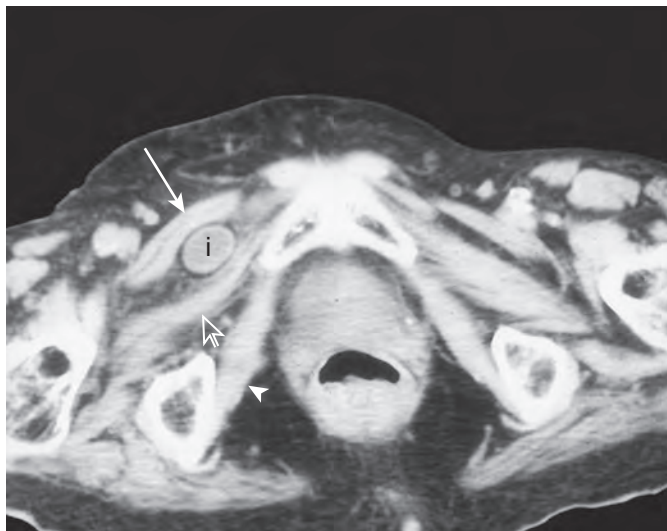


Figure 46-18 Obturator hernia. Axial CT scan through the pelvis shows a loop of ileum (i) between the pectineus muscle (large arrow) and the external obturator muscle (short arrow). The internal obturator muscle is identified by the arrowhead.

while the patient performs a Valsalva maneuver may enable visualization of anterior abdominal hernias on CT.⁵¹

Extrinsic Tumors in Mesentery or Retroperitoneum

A variety of neoplastic, inflammatory or vascular masses extrinsic to bowel may cause small bowel obstruction. These masses compress the bowel lumen and distort the lumen by a desmoplastic reaction involving the mesentery and peritoneal surfaces of the bowel.

Spread of inflammation from diverticulitis, most frequently sigmoid diverticulitis, can secondarily affect the small bowel. The inflammatory process may cause an adynamic ileus or small bowel obstruction.

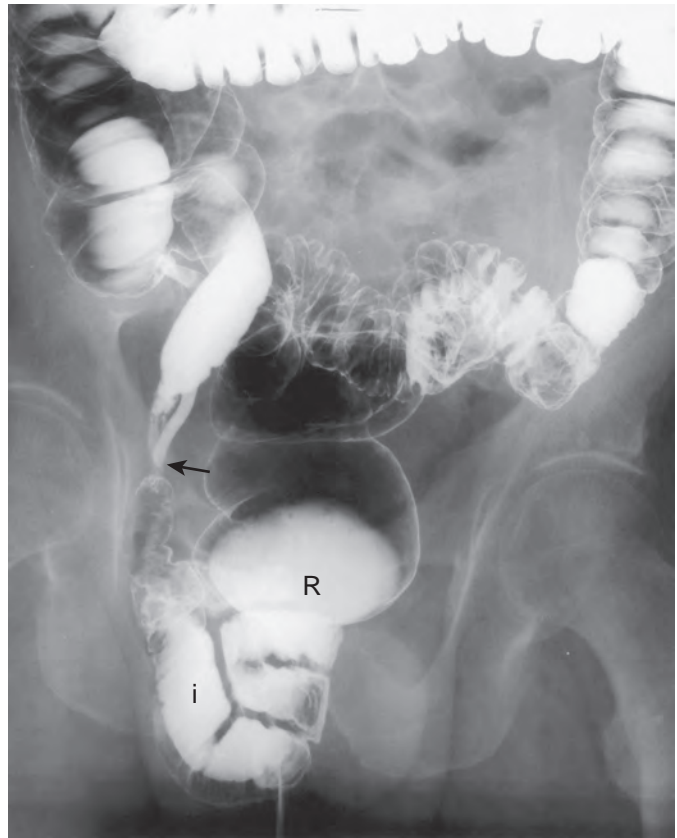


Figure 46-19 Right inguinal hernia containing ileum and appendix. Overhead view from barium enema, centered lower than usual, demonstrates ileum (i) below and to the right of the rectal ampulla (R). The tip of the appendix (arrow) enters the right inguinal canal. (From Forbes A, Misiewicz JJ, Compton CC, et al: *Atlas of Clinical Gastroenterology*, 3rd ed. Edinburgh, Elsevier Mosby, 2005.)

Carcinomatosis involving the small bowel mesentery is usually caused by ovarian carcinoma in women and by carcinomas arising from organs adjacent to the peritoneum (including stomach, pancreas, colon, and liver) in men and women. Carcinomatosis is frequently multifocal, occurring at dependent sites in the peritoneal cavity in which ascitic fluid accumulates (including the mesenteric border of the distal ileum, medial base of the cecum, sigmoid mesentery, pararectal fossae, and rectovesical or rectouterine space).⁵² Carcinomatosis produces an extensive desmoplastic reaction, manifested by extrinsic mass effect (Fig. 46-21), angulation of small bowel loops, luminal narrowing, and tethering of folds on both CT or barium studies.^{53,54} CT may demonstrate ascites or peritoneal implants on the surface of the liver, peritoneum, omentum, or mesentery. CT may also reveal the underlying malignant tumor responsible for the ascites. Carcinoid tumors, mycobacterial infection, and desmoid tumors may mimic intraperitoneal metastases. Metastases or lymphoma in retroperitoneal lymph nodes may secondarily infiltrate the small bowel mesentery, causing small bowel obstruction. Retroperitoneal nodal invasion may also resemble intraperitoneal metastases, with mass effect and desmoplastic tethering of the adjacent bowel.

Small carcinoid tumors typically appear as smooth-surfaced, submucosal masses 1 to 2 cm in diameter.⁵³ Once carcinoid tumors infiltrate the deep layers of the small bowel wall or

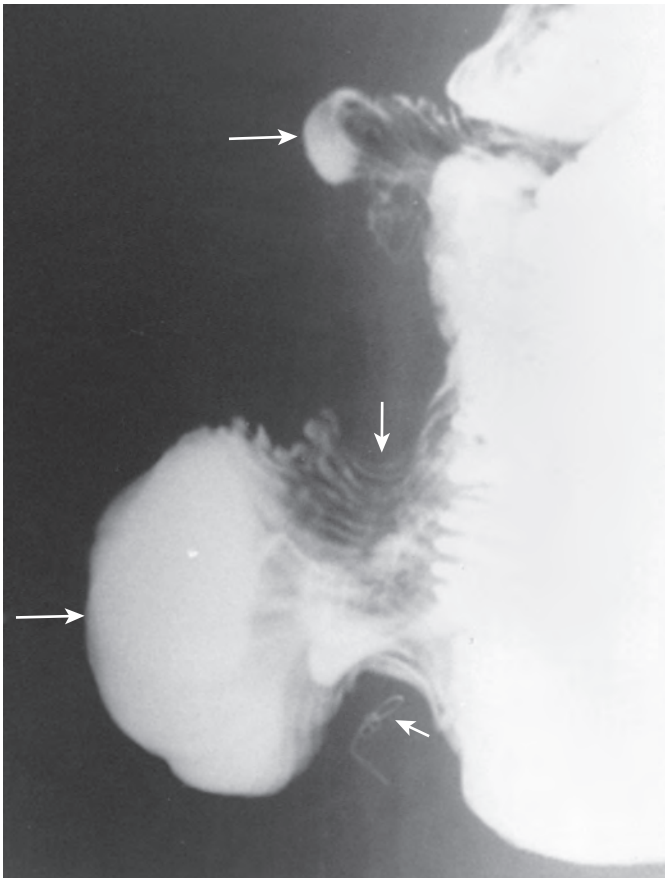


Figure 46-20 Incisional hernias detected on lateral view. Spot radiograph from small bowel follow-through shows intestinal loops (*large arrows*) protruding through the expected location of the anterior abdominal wall (identified by wire sutures, *small arrow*). Mild, smooth compression of the lower loop with preservation of normal folds (*mid-sized arrow*) is present at the neck of the lower hernia sac.

adjacent mesentery, however, they may be indistinguishable from intraperitoneal metastases on imaging studies. An intense desmoplastic reaction causes focal or multifocal angulation of the bowel wall, luminal narrowing, and tethering of mucosal folds toward the side of mass effect.⁵³ Invasive carcinoid tumors cannot be differentiated on barium studies from intraperitoneal metastases because both disorders are located in the distal ileum and can be multifocal. However, CT demonstration of a large central mesenteric nodal metastasis (with calcification in 50%) is almost diagnostic of carcinoid tumor (Fig. 46-22).⁵⁵

Primary non-Hodgkin's lymphoma of the small bowel does not usually cause obstruction because it is a soft tumor that only narrows the lumen.⁵⁶ However, non-Hodgkin's lymphoma arising in mesenteric lymph nodes or extending from the retroperitoneum into the small bowel mesentery may cause small bowel obstruction because of tumor infiltration and luminal narrowing (Fig. 46-23).⁵⁶

Enteric duplications may compress the small bowel loop and result in obstruction. Duplications typically are located on the mesenteric border of the distal ileum. As a result, barium studies may reveal an extrinsic mass impression on the mesenteric border of the distal ileum. Communication with the lumen of the adjacent small bowel is uncommon. CT typically demon-



Figure 46-21 Intraperitoneal metastases from carcinoid tumor. Spot radiograph of the right lower quadrant from small bowel follow-through demonstrates several areas of extrinsic mass impression and tethering of folds.

strates a mass of soft tissue or fluid attenuation on the mesenteric border of the affected bowel loop.

Slowly leaking aneurysms of the abdominal aorta or iliac vessels or surgery for these aneurysms may also cause a desmoplastic reaction. This can lead to distortion and narrowing of small bowel loops, causing partial or even high-grade small bowel obstruction.

INTRAMURAL LESIONS

Intrinsic tumors or inflammatory processes that infiltrate the submucosa and muscularis propria may cause obstruction by narrowing the lumen of the affected small bowel. A marked amount of circumferential luminal narrowing is necessary to obstruct small bowel because its contents are liquid. Constricting lesions include primary adenocarcinoma, Crohn's disease, and radiation enteropathy. Polypoid lesions of the small intestine may also cause obstruction by intussusception.

Primary Tumors

Adenocarcinoma of the small intestine has a predilection for the second to fourth portions of the duodenum and proximal jejunum. When patients with small bowel adenocarcinoma present with clinical signs of obstruction, these tumors are almost always at an advanced stage. Barium studies may reveal a short annular narrowing, with abrupt, nodular shelflike

margins (Fig. 46-24).⁵³ Nodularity or ulceration may be seen in the center of the lesion. The tumor is rigid and does not change shape with manual compression or peristalsis. A primary tumor may be confused with an annular intraperitoneal metastasis or adhesive band. However, intraperitoneal metastases are located primarily in the distal small bowel, the bowel wall is angulated,

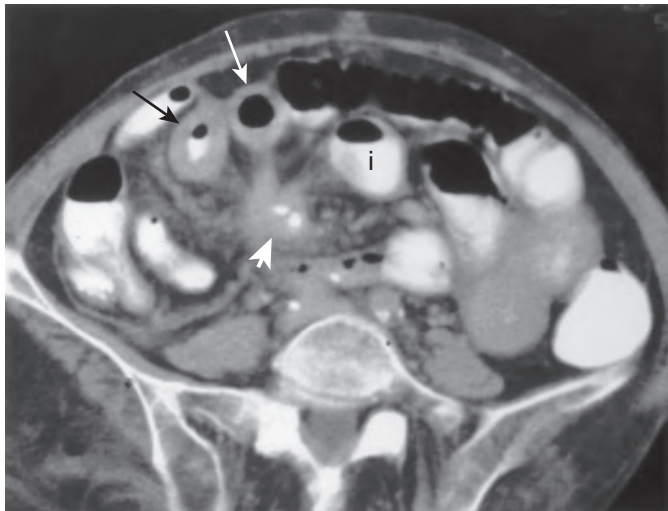


Figure 46-22 Carcinoid tumor causing partial obstruction and ischemia of the ileum. Axial CT scan through the pelvis demonstrates dilated ileum (i) but contrast in the colon, indicative of partial small bowel obstruction. A 2-cm centrally calcified mass (thick arrow) is seen in the root of the small bowel mesentery. Thick strands of tumor radiate from the ileum toward the mass. Two ileal loops (thin arrows) have uniformly thickened walls. At surgery, ischemic changes in the ileum were associated with the carcinoid tumor, which had spread to the root of the small bowel mesentery. (From Rubesin SE: Small bowel tumors. *Contemp Diagnost Radiol* 27:1-6, 2004.)

and the mucosal folds are preserved though spiculated and tethered, rather than nodular (Fig. 46-25).⁵⁷ An adhesive band may circumferentially narrow the lumen, but the mucosa is smooth, and the folds are tethered, not nodular (Fig. 46-26).⁵⁸

Primary lymphoma of small bowel rarely causes obstruction because it is an infiltrative tumor that destroys the muscular wall but does not cause a desmoplastic reaction. Primary lymphoma usually causes focal dilation or cavitation of the small bowel.⁵⁶ Even when primary lymphomas are circumferential and narrow the lumen, high-grade obstruction is unusual because of the soft cellular nature of these tumors.

Inflammatory Conditions

The advanced stenotic phase of Crohn's disease may cause recurrent episodes of partial small bowel obstruction. Although high-grade obstructions are uncommon, small bowel obstruction is the most frequent indication for surgery in patients with Crohn's disease.⁵⁹ When luminal narrowing is seen during barium studies (Fig. 46-27) or CT (Fig. 46-28), the narrowing may be caused by edema, spasm, inflammation, fibrosis or, rarely, a carcinoma. The diameter of the stricture may change during the course of the examination or on delayed images. Severe luminal narrowing has been termed the *string sign*. In such cases, the use of metoclopramide or the high-volume administration of contrast pressure of enteroclysis may distend the lumen to varying degrees, revealing an ulceronodular pattern. Obstruction is diagnosed on barium studies or CT by delayed passage of contrast medium through the diseased segment, with proximal small bowel dilation.⁶⁰⁻⁶² Bowel wall thickening or local mesenteric infiltration do not aid in the CT diagnosis of obstruction. Stenoses that resist the pressure of enteroclysis may require surgery.

Other primary inflammatory causes of small bowel obstruction are rare. Acute infections such as yersiniosis rarely cause

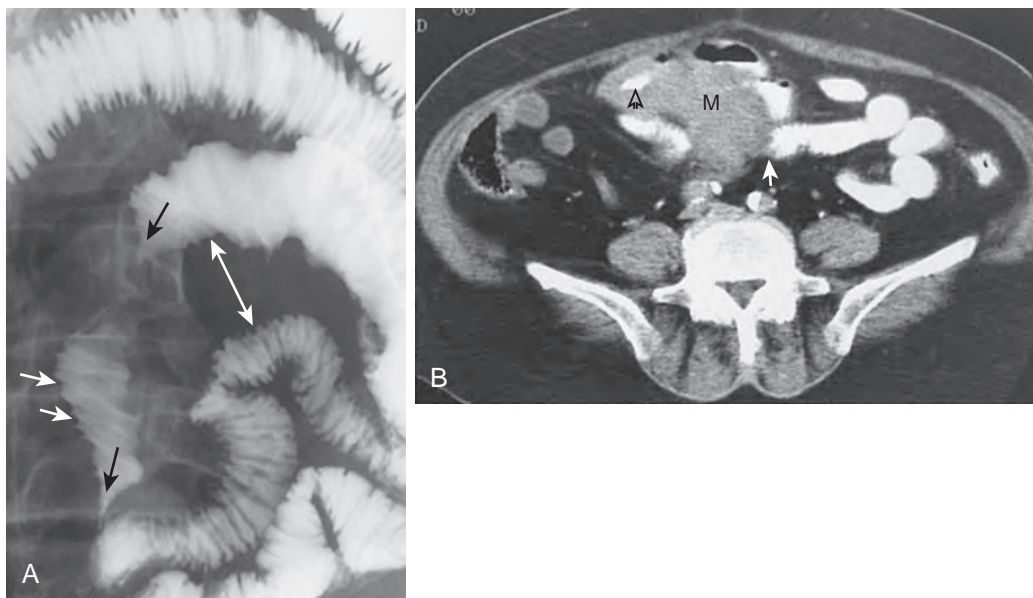


Figure 46-23 Non-Hodgkin's lymphoma secondarily arising in the small bowel mesenteric lymph nodes, partially obstructing the small intestine. **A.** Overhead image from enteroclysis shows that pelvic ileal loops are separated (double arrow) by a presumptive mass in the small bowel mesentery. The small bowel is narrowed, tapered, and partially obstructed at several sites (black arrows). Thick small bowel folds (white arrows) could be the result of ischemia caused by venous or lymphatic obstruction in the mesentery or direct tumor invasion. **B.** CT clarifies the radiographic findings. Separation of bowel loops is caused by a large, homogeneous mesenteric mass (M). A loop of intestine is tapered and partially obstructed (arrow). The tumor circumferentially infiltrates one intestinal loop (open arrow), accounting for the thick folds seen on the enteroclysis. (A from Rubesin SE, Gilchrist AM, Bronner M, et al: Non-Hodgkin lymphoma of the small intestine. *RadioGraphics* 10:985-998, 1990.)

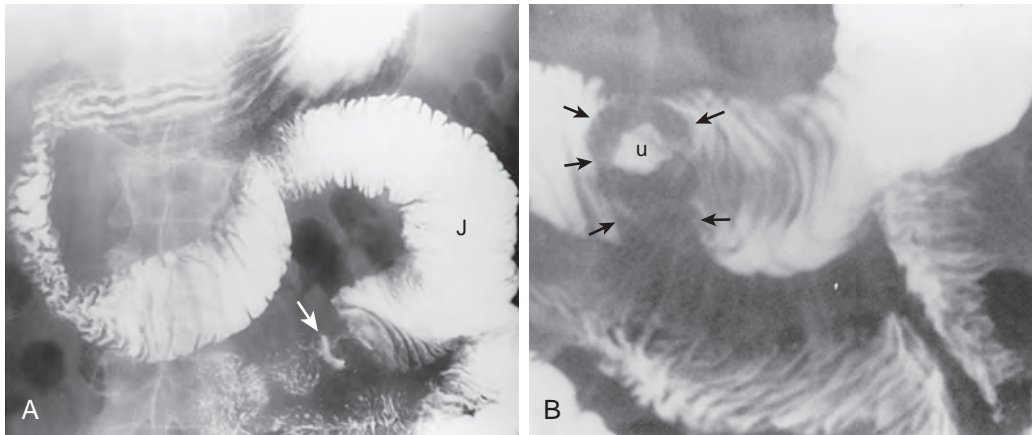


Figure 46-24 Adenocarcinoma of jejunum causing partial small bowel obstruction. **A.** Overhead image from an upper GI series shows a dilated distal duodenum and jejunum (J) proximal to a 3-cm focally ulcerated lesion (arrow). **B.** Spot radiograph shows a circumferential mass (black arrows) with central ulceration (u). This case is an example of how an upper GI series can be converted to a small bowel study when the distal duodenum is dilated.



Figure 46-25 Annular metastasis from colonic carcinoma. Spot radiograph from enteroclysis demonstrates a short annular lesion with a thin lumen (arrowheads). Although the proximal margin is abrupt, the folds are preserved and tethered (arrow).

small bowel obstruction because the acute inflammatory process heals without fibrosis. Tuberculosis is unusual in Western countries but may be seen in returning visitors or immigrants from Asia.⁶³ Tuberculosis may produce radiographic features identical to those of Crohn's disease, but the cecum and ascending colon tend to be more severely involved than the terminal ileum. Patients with tuberculosis may also have a patulous ileocecal valve, rather than the narrowed ileocecal valve typically seen in Crohn's disease. A definitive diagnosis of ileocecal tuberculosis requires culture and biopsy specimens.

Behçet's disease mimics Crohn's disease, but the ulcers are often larger and deeper in Behçet's disease. Focal perforation

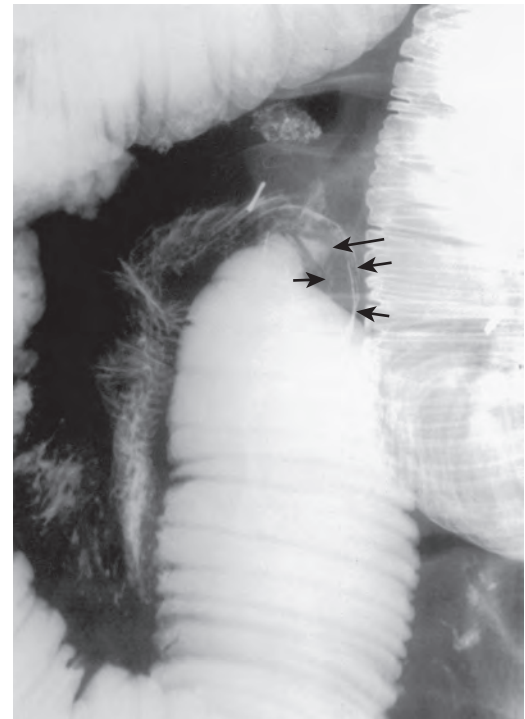


Figure 46-26 Circumferential adhesive band. Spot radiograph from enteroclysis shows abrupt angulation (long arrow) at the transition zone. The bowel just distal to the angulation is tight (short arrows), but folds are preserved throughout the region. (Courtesy Hans Herlinger, MD.)

with peritoneal reaction is not uncommon in Behçet's disease. Carcinoma of the cecum and lymphoma of the ileocecal valve invading the terminal ileum may also mimic Crohn's disease.⁵³

Vascular Diseases

Radiation Enteropathy. Radiation enteropathy may cause mild to moderate small bowel obstruction because of a combination of serositis and adhesions, wall fibrosis, and dysmotility. The changes are localized to the preexisting radiation portal, usually

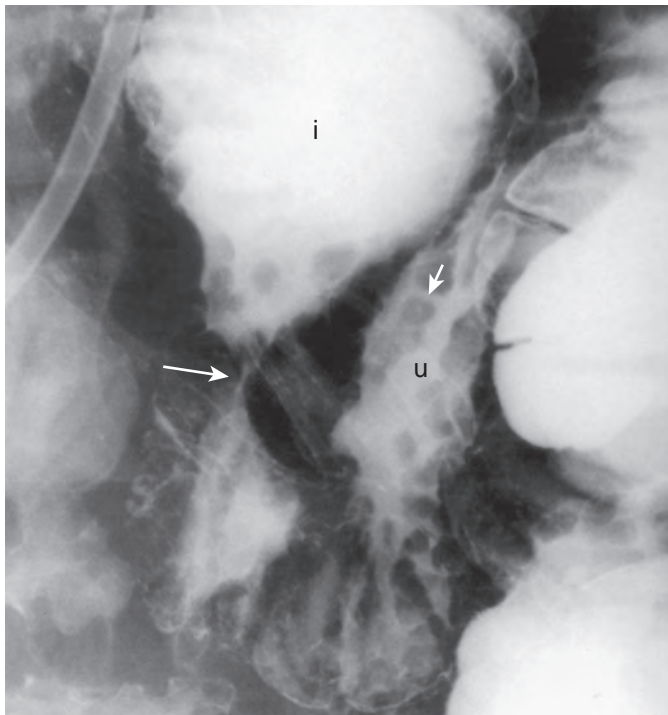


Figure 46-27 Crohn's disease causing partial small bowel obstruction. Spot radiograph from enteroclysis demonstrates a dilated ileum (i) proximal to a 1 cm in length by 1 mm in luminal diameter stricture (long arrow). An ulceronodular pattern (cobblestoning; u) is seen in the ileum distal to the stricture, manifested as transverse and longitudinal barium-filled, knifelike clefts or ulcers (short arrow) separating polygonal islands of relatively spared mucosa. (Courtesy Hans Herlinger, MD.)

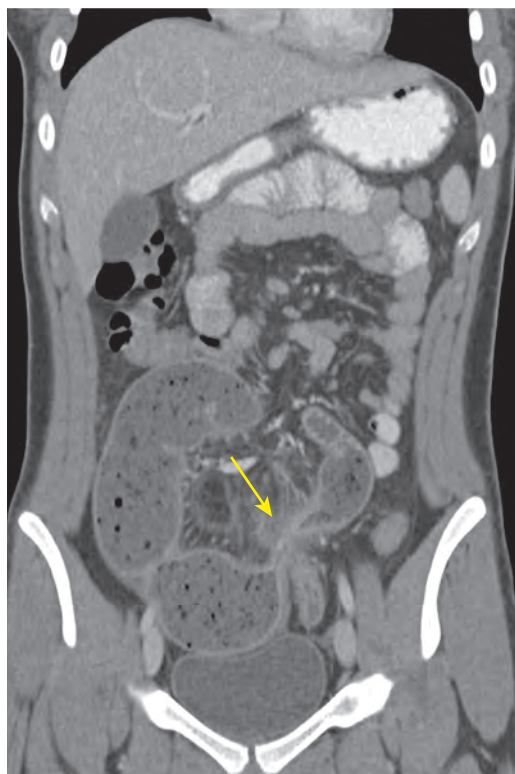


Figure 46-28 Crohn's disease causing partial small bowel obstruction. A. Coronal reformatted CT image shows a stricture (arrow) of the midileum, with proximal dilation and the small bowel feces sign.

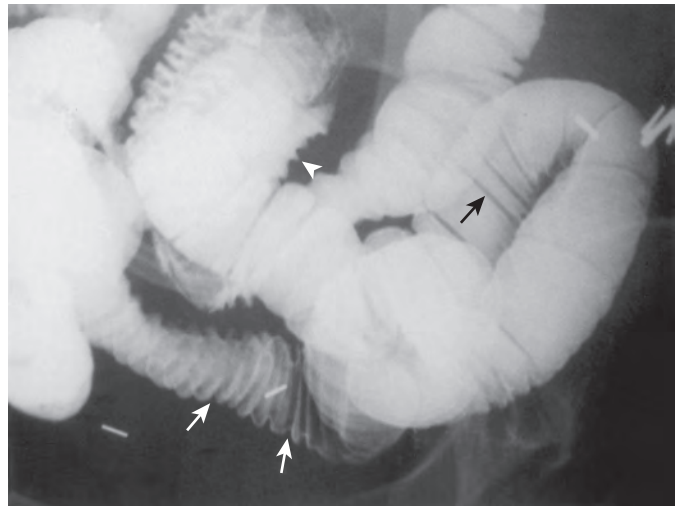


Figure 46-29 Radiation enteropathy causing low-grade small bowel obstruction. Spot radiograph from enteroclysis shows smooth, thick folds (white arrows) in a deep pelvic ileal loop. The folds are slightly angled, indicating radiation serositis. In profile, the spaces between thick loops have a spikelike appearance (arrowhead), so-called interspace spikes. A nearby loop has top normal-sized folds (black arrow) for comparison.

in the pelvic area. Submucosal edema and fibrosis are manifested on barium studies as smooth, straight, parallel thick folds that cross the small bowel lumen (Fig. 46-29).⁵³ Barium filling compressed interstices between the folds may result in interspace spikes. The lumen of the affected bowel may also be narrowed by submucosal fibrosis. Radiation-induced serositis and adhesions result in fixation and angulation of bowel loops and tethering of folds, similar to any extrinsic adhesive process.⁶⁴ CT may also reveal bowel wall and fold thickening, with submucosal edema demonstrated as a target sign (Fig. 46-30).⁶⁵ Small bowel obstruction caused by radiation serositis is suggested by proximal small bowel dilation associated with angulated loops (see Fig. 46-30B). Adhesive bands may form where the small bowel enters the radiation portal. Smooth, tapered strictures may develop 6 months or more after radiation therapy (Fig. 46-31). Surgery in patients with radiation enteropathy is not without risk because these patients may develop postoperative fistulas and interloop abscesses.²

Blunt abdominal trauma (often a seat belt injury) may result in stricture formation after healing of a bowel wall hematoma or ischemia. However, most hematomas resolve without sequelae after conservative treatment.⁶⁶ Strictures developing at enteroenterostomy sites (Fig. 46-32) may be the sequelae of ischemia, prior leak with fibrotic healing, or surgical technique.

Acute inflammation, ischemia, and ulceration related to the use of nonsteroidal anti-inflammatory drugs (NSAIDs) or potassium chloride tablets may also result in stricture formation.⁶⁷ In these cases, barium studies may reveal ringlike strictures (Fig. 46-33) with tiny central openings.

INTRALUMINAL CAUSES

Gallstones, bezoars, foreign bodies, meconium, and tangles of *Ascaris* worms may obturate the small bowel lumen, causing obstruction.

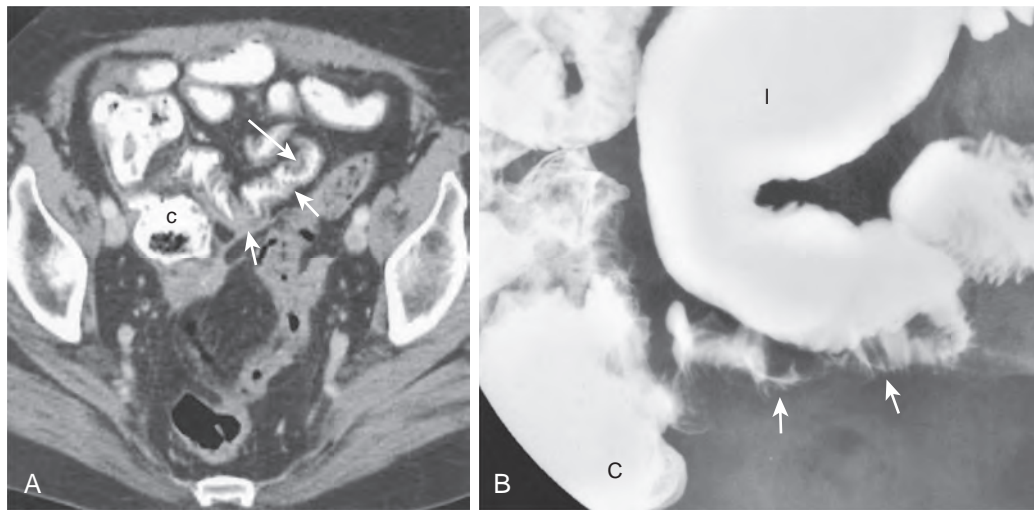


Figure 46-30 Radiation enteropathy causing low-grade small bowel obstruction. **A.** Axial CT through pelvis shows angulation and wall-thickening (short arrows) of the terminal ileum. In some areas, a mural stratification pattern caused by submucosal edema is evident (long arrow). The cecum (c) is identified. **B.** Spot radiograph from a small bowel follow-through shows angulation of the terminal ileum and smooth thick folds (arrows). The ileum (i) proximal to the radiation change is dilated. .

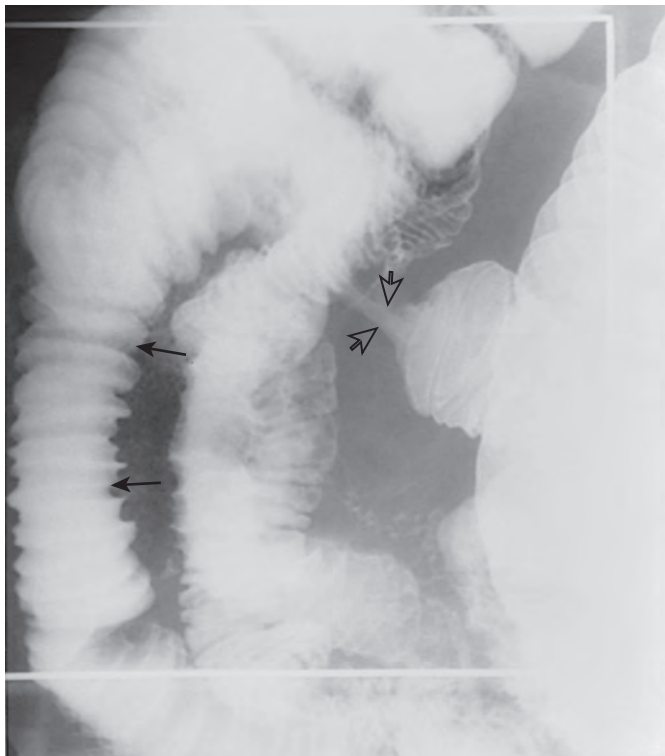


Figure 46-31 Radiation stricture. A 2-cm long smooth narrowing (open arrows) is present at the edge of the radiation portal. Smooth thick straight folds perpendicular to the longitudinal axis of the bowel (arrows) are typical of radiation change caused by submucosal edema or fibrosis.

Gallstone-induced small bowel obstruction (also known as gallstone ileus) usually occurs in older patients, especially women. A gallstone can erode through the wall of the gallbladder or bile duct into the small bowel or colon. Most fistulas extend from the gallbladder fossa to the duodenum. Passage of



Figure 46-32 High-grade obstruction at enteroenterostomy site. There is a 1- to 2-mm wide, barium-filled, side to side enteroenterostomy (arrows). The jejunum proximal to the obstruction is dilated.

gallstones through the GI tract may result in large gallstones becoming trapped in the narrowest segments of bowel, the terminal ileum and sigmoid colon. Calcified ectopic gallstones are visible on plain radiographs of the abdomen in only approximately 15% of patients. CT is superior for the demonstration of calcified gallstones (Fig. 46-34) as the cause of a small bowel or colonic obstruction.⁶⁸ The classic Rigler's triad of a calcified gallstone, gas in a shrunken gallbladder or biliary tree, and small bowel obstruction is seen in only a minority of patients on plain radiographs,⁶⁹ but is better detected on CT. In some patients, a gallstone may be detected on a small bowel follow-through examination as a calcified or noncalcified intraluminal radiolucent filling defect at the site of transition between dilated and nondilated small bowel.

Foreign body impactions in the small bowel are much less common than foreign body impactions in the pharynx or esophagus.⁷⁰ Small bowel obstruction by foreign bodies usually occurs in psychiatric or mentally challenged patients or in drug smugglers. Some people who eat indigestible food substances, such as persimmons, can develop small bowel bezoars.⁷¹ These patients often have a partial gastrectomy or gastroenterostomy

and may have an underlying obstructive lesion. Cameras used during capsule endoscopy may become stuck behind an obstructing small bowel lesion.

In adults with cystic fibrosis, inspissation of bowel contents may cause small bowel obstruction (meconium ileus equivalent). These patients may have a history of decreased intake of pancreatic enzyme supplements or narcotic use.

INTUSSUSCEPTION

Various extrinsic, intrinsic, and intraluminal processes result in small bowel intussusception. A loop of small intestine with part of its mesentery invaginates into the lumen of the bowel segment distal to it. The inner, advancing segment is termed the *intussusceptum* and the outer receiving segment the *intussusciens*. Most intussusceptions are nonobstructive, transient intussusceptions without a lead point that are detected on abdominal CT performed for other reasons.^{72,73} Nonobstructive transient intussusceptions are also seen in small bowel disorders associated with dysmotility, such as scleroderma or celiac disease. Benign or malignant polypoid tumors are the most common causes of small bowel intussusception in adults presenting with small bowel obstruction.⁷⁴ In postoperative patients, intussusceptions may be related to suture lines, adhesions, or intestinal tubes.⁷⁵

Barium studies typically reveal a narrow, tapered, barium-filled channel outlining the lumen of the intussusceptum (Fig. 46-35).⁵³ If barium refluxes between the outer wall of the

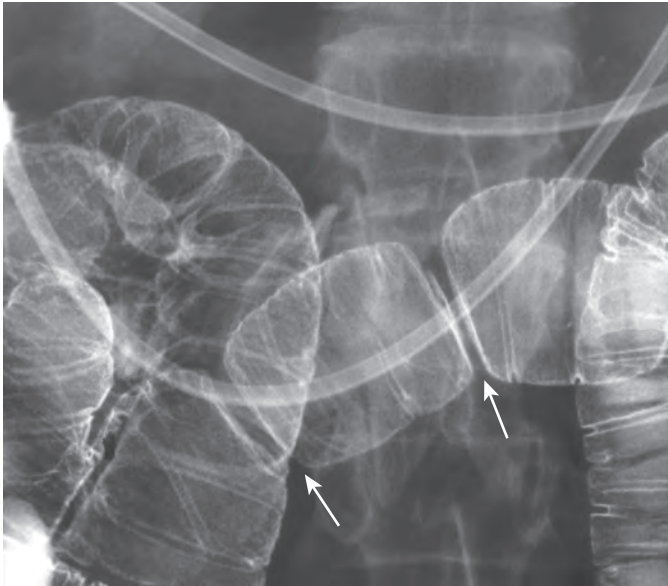


Figure 46-33 Ringlike strictures related to NSAID use. A spot radiograph from enteroclysis demonstrates two ringlike narrowings (arrows) in the jejunum. (Courtesy Arunas Gasparitis, MD, Chicago.)



Figure 46-34 Gallstone ileus. Coronal reformatted CT scan shows an obstructing calcified intraluminal gallstone (arrow).

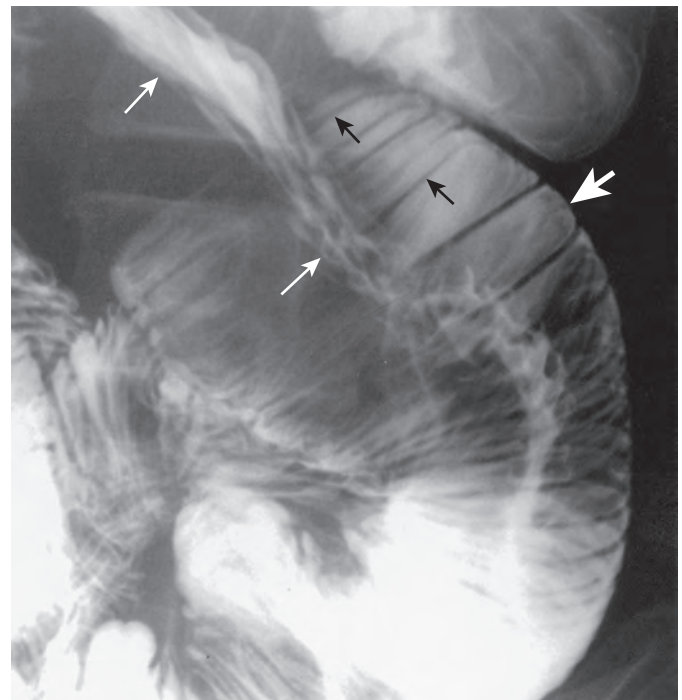


Figure 46-35 Jejunal intussusception caused by adhesion. The lumen of the intussusceptum is narrow and outlined by barium (long white arrows). Barium refluxes retrogradely between the serosal surface of the intussusceptum and mucosal surface of the intussusciens (thick white arrow). Barium coating the mucosal surface of the intussusciens reveals mucosal folds (short black arrows), the so-called coil spring. At surgery, the intussusception occurred at a site of adhesions.

intussusceptum and mucosal surface of the intussusciens, the mucosal folds of the intussusciens will be demonstrated as parallel folds perpendicular to the longitudinal axis of the bowel. This is the so-called coil spring sign. Coil spring folds that appear thicker than normal small bowel folds indicate that there is mucosal and submucosal edema because of lymphatic or venous congestion. If the intussusception is caused by an underlying tumor, a polypoid lead point may be identified. Barium filling the interstices of the lead point implies that the tumor is a mucosal lesion such as an adenoma or hamartoma. In contrast, a round, smooth-surfaced polypoid lead point suggests a submucosal lesion such as a lipoma or metastatic melanoma.

Small bowel intussusception may be manifested on CT by a pair of concentric rings of soft tissue, with an eccentrically located area of fat attenuation inside the outer ring.^{76,77} The outer ring of soft tissue represents the intussusciens, whereas the inner ring of soft tissue represents the wall of the intussusceptum. The eccentrically located fat represents the mesentery of the intussusceptum (Fig. 46-36). Vessels in the invaginating mesentery may be visible as punctate dots or thin, undulating strands of soft tissue or IV contrast attenuation. If the wall of the intussusciens is thickened, the possibility of bowel wall edema and ischemia should be considered.⁷⁸ Obstruction is implied by dilation of the small bowel proximal to the intussusception associated with collapsed small bowel distally.

The clinical history is helpful for evaluating patients with small bowel intussusception. Most patients with metastatic melanoma as the lead point have a history of prior surgical removal of melanoma from the skin. Some patients with a metastatic, melanoma-related intussusception present with symptoms from the intussusception as the initial manifestation of their disease.⁷⁸ Most patients with Peutz-Jeghers syndrome, an autosomal dominant disorder, have a family history of this syndrome. However, 45% of cases of Peutz-Jeghers syndrome occur as spontaneous mutations, so these patients may initially present with symptoms related to small bowel hamartomas. Most patients with Peutz-Jeghers syndrome have pigmented lesions on the lips, oral mucosa, face, or extremities.⁷⁹ However, pigmented lesions may be overlooked in patients of African or Asian origin; they may present with bleeding or abdominal pain caused by an intussuscepting hamartoma.

The location of the intussusception is of little value in distinguishing between polyps of different histologic types. Peutz-Jeghers polyps and adenomas are usually located in the proximal jejunum, whereas stromal tumors, metastatic melanoma, and lipomas have a relatively uniform distribution in the small bowel.

When small bowel intussusception occurs, barium filling the interstices of a lead point lesion should suggest a tumor of mucosal origin, such as a Peutz-Jeghers polyp or adenoma. Smooth and round but centrally umbilicated or ulcerated

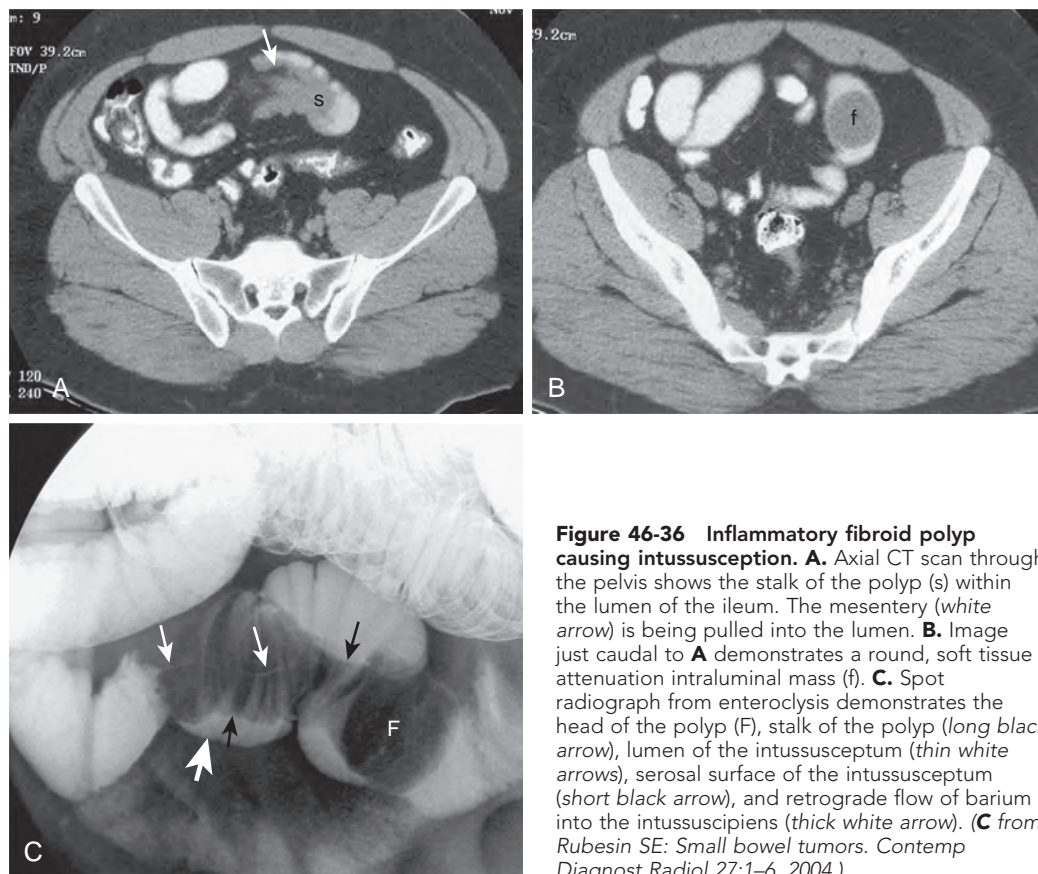


Figure 46-36 Inflammatory fibroid polyp causing intussusception. **A.** Axial CT scan through the pelvis shows the stalk of the polyp (s) within the lumen of the ileum. The mesentery (white arrow) is being pulled into the lumen. **B.** Image just caudal to **A** demonstrates a round, soft tissue attenuation intraluminal mass (f). **C.** Spot radiograph from enteroclysis demonstrates the head of the polyp (F), stalk of the polyp (long black arrow), lumen of the intussusceptum (thin white arrows), serosal surface of the intussusceptum (short black arrow), and retrograde flow of barium into the intussusciens (thick white arrow). (**C** from Rubesin SE: Small bowel tumors. *Contemp Diagnost Radiol* 27:1–6, 2004.)

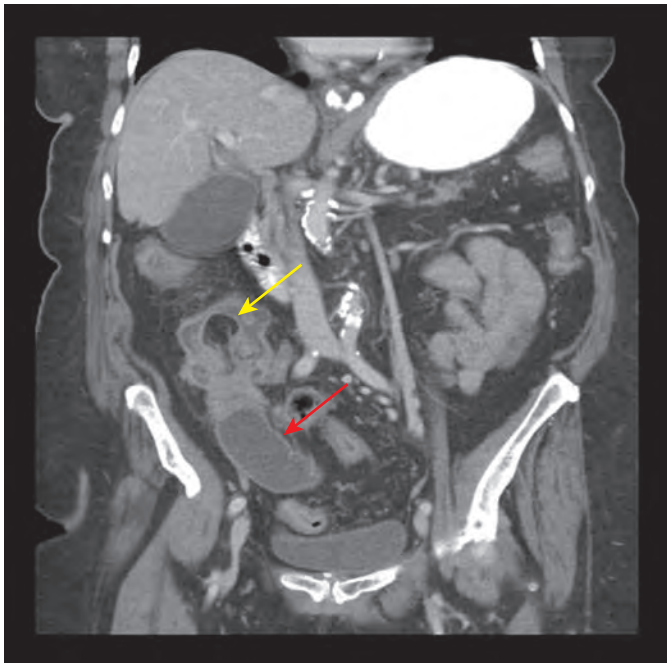


Figure 46-37 Ileal lipoma causing ileocolic intussusception. Coronal reformatted image shows an intussuscepted fat density lipoma (yellow arrow) causing dilation of the distal ileum (red arrow).

polypoid lead point lesions are usually submucosal tumors, such as stromal tumors or metastatic melanoma. Melanoma metastases have central umbilication or ulceration in more than 50% of patients.⁸⁰ Intussusception by soft melanoma metastases may be intermittent and may not cause obstruction. Multiple polypoid tumors in the jejunum or mid small intestine should suggest a diagnosis of Peutz-Jeghers syndrome or metastases, especially from malignant melanoma. Lipomas are smooth-surfaced, pliable, and often pedunculated lesions that have fat attenuation on CT (Fig. 46-37). The fat of a lipoma should be distinguished from the invaginating mesentery of an intussuscepting polyp. Inflammatory fibroid polyps are typically located in the distal ileum. Pedunculated polyps with long stalks that intussuscept are usually inflammatory fibroid polyps, lipomas, or inverted Meckel's diverticulum (Fig. 46-38).^{81,82} Other causes of intussusception include Henoch-Schönlein purpura, lymphoma, hematomas, and mesenteric lymphadenopathy. Causes of intussusception in patients with AIDS include B-cell lymphoma, Kaposi's sarcoma, mesenteric lymphadenopathy, lymphoid hyperplasia, and intestinal dysmotility.⁸³⁻⁸⁵

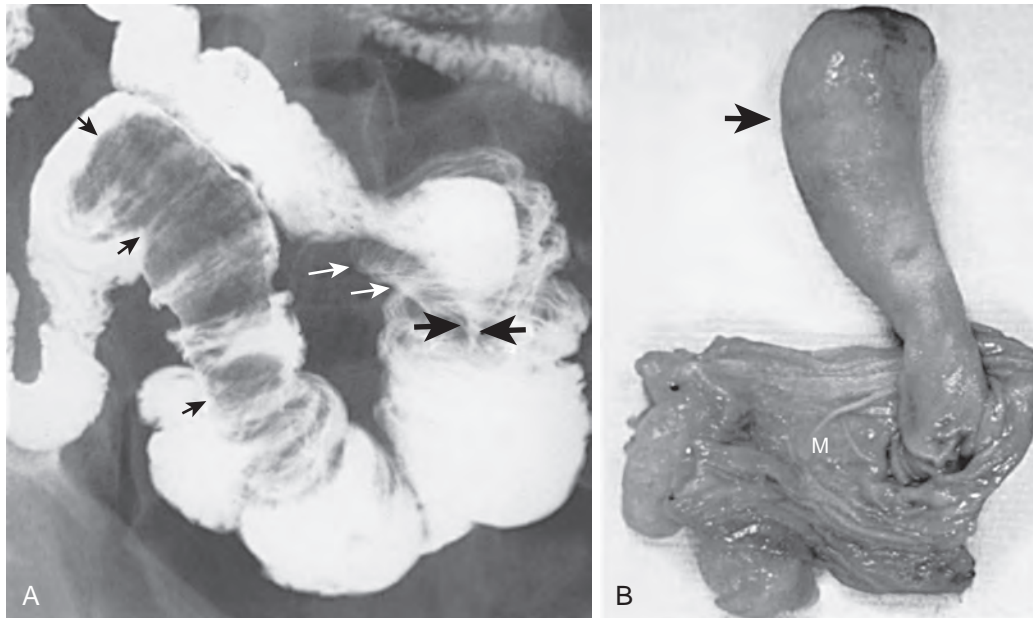


Figure 46-38 Inverted Meckel's diverticulum causing intussusception. **A.** Spot radiograph from a small bowel follow-through shows a tapered narrowing of the ileum (large black arrows) at the narrowest point of the intussusceptum. The mucosa of the intussusciens is outlined by refluxed barium (white arrows). **B.** Specimen photograph of the Meckel's diverticulum. There is a long polypoid intraluminal filling defect, which is the invaginated Meckel's diverticulum (M). (From Rubesin SE, Herlinger H, DeGaeta L: *Interlude: Test your skills*. Radiology 176:636, 644, 1990.)

REFERENCES

1. Haubrich WS: Medical Meanings. A Glossary of Word Origins, ed 2, Philadelphia, 2003, College of Physicians.
2. Soybel DI: Ileus and bowel obstruction. In Greenfield LJ, Mulholland MW, Oldham DT, et al, editors: *Surgery: Scientific Principles and Practice*, Philadelphia, 2001, Lippincott Williams & Wilkins, pp 798–812.
3. Taylor MR, Lalani N: Adult small bowel obstruction. *Acad Emerg Med* 20:528–544, 2013.
4. Ohman U: Studies on small intestinal obstruction. I. Intraluminal pressure in experiment low obstruction in the cat. *Acta Chir Scand* 141:413, 1975.
5. Rubesin SE, Herlinger H: CT evaluation of bowel obstruction: A landmark article [editorial]. *Radiology* 180:307–308, 1991.
6. Santillan CS: Computed tomography of small bowel obstruction. *Radiol Clin North Am* 51:17–27, 2013.
7. Maglinte DD, Gage S, Harmon B, et al: Obstruction of the small intestine: Accuracy and role of CT in diagnosis. *Radiology* 186:61–64, 1993.
8. Shrake PD, Rex DK, Lappas JC, et al: Radiographic evaluation of suspected small bowel obstruction. *Am J Gastroenterol* 86:175–178, 1991.
9. Hayakawa K, Tanikake M, Yoshida S, et al: CT findings of small bowel strangulation: The importance of contrast enhancement. *Emerg Radiol* 20:3–9, 2013.
10. Wiesner W, Mortelet K: Small bowel ischemia caused by strangulation in complicated small bowel obstruction. CT findings in 20 cases with histopathological correlation. *JBR-BTR* 94:309–314, 2011.
11. Mindelzun RE, Jeffrey RB: Unenhanced helical CT for evaluating acute abdominal pain: A little more cost, a lot more information. *Radiology* 205:43–45, 1997.
12. Maglinte DD, Balthazar EJ, Kelvin FM, Megibow AJ: The role of radiology in the diagnosis of small bowel obstruction. *AJR* 168:1171–1180, 1997.
13. Fukuya T, Hawes DR, Lu CC, et al: CT diagnosis of small bowel obstruction: Efficacy in 60 patients. *AJR* 158:765–769, 1992.
14. Gazelle GS, Goldberg MA, Wittenberg J, et al: Efficacy of CT in distinguishing small-bowel obstruction from other causes of small bowel dilatation. *AJR* 162:43–47, 1994.
15. Balthazar EJ: CT of small-bowel obstruction. *AJR* 162:255–261, 1994.
16. Taourel PG, Fabre JM, Pradel JA, et al: Value of CT in diagnosis and management of patients with suspected acute small-bowel obstruction. *AJR* 165:1187–1192, 1995.
17. Balthazar EJ: CT of the gastrointestinal tract. Principles and interpretation. *AJR* 156:23–32, 1991.
18. Balthazar EJ, Liebeskind ME, Macari M: Intestinal ischemia in patients in whom small bowel obstruction is suspected: Evaluation of accuracy, limitation and clinical implications of CT in diagnosis. *Radiology* 205:510–522, 1997.
19. Kernagis LY, Levine MS, Jacobs JE: Pneumatosis intestinalis in patients with ischemia: Correlation of CT findings with viability of the bowel. *AJR* 180:733–736, 2003.
20. Furukawa A, Yamasaki M, Takahashi M, et al: CT diagnosis of small bowel obstruction: Scanning technique, interpretation and role in the diagnosis. *Semin Ultrasound CT MRI* 24:336–352, 2003.
21. Obuz F, Terzi C, Sokmen S, et al: The efficacy of helical CT in the diagnosis of small bowel obstruction. *Eur J Radiol* 48:299–304, 2003.
22. Assalia A, Shein M, Kopelman D, et al: Therapeutic effect of oral Gastrografin in adhesive, partial small bowel obstruction: A prospective randomized trial. *Surgery* 115:433, 1994.
23. Maglinte DD, Steven LH, Hall RC, et al: Dual purpose tube for enteroclysis and nasogastric/nasoenteric decompression. *Radiology* 185:281–282, 1992.
24. Maglinte DD, Kelvin FM, Milcon LT, et al: Nasointestinal tube for decompression or enteroclysis: Experience with 150 patients. *Abdom Imaging* 19:108–112, 1994.
25. Bender GN, Maglinte DD, von Kloeppel R, et al: CT enteroclysis: A superfluous diagnostic procedure or valuable when investigating small-bowel disease? *AJR* 172:373–378, 1999.
26. Noone TC, Semelka RC, Chaney DM, et al: Abdominal imaging studies: Comparison of diagnostic accuracies resulting from ultrasound, computed tomography, and magnetic resonance imaging in the same individual. *Magn Reson Imaging* 22:19–24, 2004.
27. O'Malley ME, Wilson SR: US of gastrointestinal tract abnormalities with CT correlation. *Radiographics* 23:59–72, 2003.
28. Ellis H, Moran BJ, Thompson JN, et al: Adhesion-related hospital readmissions after abdominal and pelvic surgery: A retrospective cohort study. *Lancet* 353:1476–1480, 1999.
29. Menzies D, Ellis H: Intra-abdominal adhesions and their prevention by topical tissue plasminogen activator. *J R Soc Med* 82:534–535, 1989.
30. Ellis H: The causes and prevention of intestinal adhesions. *Br J Surg* 69:241–243, 1982.
31. Coletti L, Bossart PA: Intestinal obstruction during the early postoperative period. *Arch Surg* 88:774–778, 1964.
32. Stewart RM, Page CP, Bender J, et al: The incidence and risk of early postoperative obstruction: A cohort study. *Am J Surg* 154:643, 1987.
33. Birnbaum BA, Maglinte DDT: Small bowel obstruction. In Herlinger H, Maglinte DDT, Birnbaum BA, editors: *Clinical Imaging of the Small Intestine*, New York, 1999, Springer, pp 467–506.
34. Megibow AJ, Balthazar EJ, Cho KC, et al: Bowel obstruction: Evaluation with CT. *Radiology* 180:313–318, 1991.
35. Maglinte DD, Reyes BL, Harmon BH, et al: Reliability and role of plain film radiography and CT in the diagnosis of small-bowel obstruction. *AJR* 167:1451–1455, 1996.
36. Maglinte DD, Nolan DJ, Herlinger H: Preoperative diagnosis by enteroclysis of unsuspected closed-loop obstruction in medically managed patients. *J Clin Gastroenterol* 13:308–312, 1991.
37. Maglinte DD, Herlinger H, Nolan DJ: Radiologic features of closed loop obstruction: Analysis of 25 confirmed cases. *Radiology* 179:383–387, 1991.
38. Balthazar EJ, Birnbaum BA, Megibow AJ, et al: Closed-loop and strangulating intestinal obstruction: CT signs. *Radiology* 185:769–775, 1992.
39. Cho KC, Hoffman-Tretin JC, Alterman DD: Closed-loop obstruction of the small bowel: CT and sonographic appearance. *J Comput Assist Tomogr* 13:256–257, 1989.
40. Frager D, Baer JW, Medwid SW, et al: Detection of intestinal ischemia in patients with acute small-bowel obstruction due to adhesions or hernia: Efficacy of CT. *AJR* 166:67–71, 1996.
41. Zaleman M, van Gansbeke D, Lalmand B, et al: Delayed enhancement of the bowel wall: A new CT sign of small bowel strangulation. *J Comput Assist Tomogr* 20:379–381, 1996.
42. Ha HK, Kim JS, Lee MS, et al: Differentiation of simple and strangulated small-bowel obstruction: Usefulness of known CT criteria. *Radiology* 204:507–512, 1997.
43. Shaff MI, Himmelfarb E, Sacks GA, et al: The whirl sign: A CT finding in volvulus of the large bowel. *J Comput Assist Tomogr* 9:410, 1985.
44. Price J, Nolan DJ: Closed-loop obstruction: Diagnosis by enteroclysis. *Gastrointest Radiol* 14:251–254, 1989.
45. Maglinte DD, Herlinger H, Nolan DJ: Radiologic features of closed loop obstruction: Analysis of 25 confirmed cases. *Radiology* 179:383–387, 1991.
46. Hongo N, Mori H, Matsumoto S, et al: Internal hernias after abdominal surgeries: MDCT features. *Abdom Imaging* 36:349–362, 2011.
47. Martin LC, Merkle EM, Thompson WM: Review of internal hernias: Radiographic and clinical findings. *AJR* 186:703–717, 2006.
48. Haku T, Daidougi K, Kawamura H, Matsuzaki M: Internal herniation through a defect of the broad ligament of the uterus. *Abdom Imaging* 29:161–163, 2004.
49. Catqalano OA, Bencivenga A, Abbate M, et al: Internal hernia with volvulus and intussusception: Case report. *Abdom Imaging* 29:164–165, 2004.
50. Aguirre DDA, Casola G, Sirlin C: Abdominal wall hernias: MDCT findings. *AJR* 183:681–690, 2004.
51. Trainer V, Leung C, Owen RE, et al: External anterior abdominal wall and pelvic hernias with emphasis on the key diagnostic features on MDCT. *Clin Radiol* 68:388–396, 2013.
52. Meyers MA: Intraperitoneal spread of malignancies. In Meyers MA, Charnsangvee C, Oliphant M, editors: *Dynamic Radiology of the Abdomen*, ed 6, New York, 2011, Springer, pp 69–107.
53. Rubesin SE, Furth EE: Differential diagnosis of small intestinal abnormalities with radiologic-pathologic explanation. In Herlinger H, Maglinte DD, Birnbaum BA, editors: *Clinical Imaging of the Small Intestine*, ed 2, New York, 1999, Springer-Verlag, pp 527–566.
54. Zboralske FF, Bessolo RJ: Metastatic carcinoma to the mesentery and gut. *Radiology* 88:302–310, 1967.
55. Horton KM, Kamel I, Hofmann L, Fishman EK: Carcinoid tumors of the small bowel: A multi-technique imaging approach. *AKR* 182:559–567, 2004.
56. Rubesin SE, Gilchrist AM, Bronner M, et al: Non-Hodgkin lymphoma of the small intestine. *Radiographics* 10:985–998, 1990.
57. Levine MS, Drooz AT, Herlinger H: Annular malignancies of the small bowel. *Gastrointest Radiol* 12:53–58, 1987.
58. Caroline DF, Herlinger H, Laufer I, et al: Small-bowel enema in the diagnosis of adhesive obstruction. *AJR* 142:1133–1139, 1984.
59. De Cruz P, Kamm MA, Prideaux L, et al: Post-operative recurrent luminal Crohn's disease: A systematic review. *Inflamm Bowel Dis* 18:758–777, 2012.

60. Zissin R, Hertz M, Paran H, et al: Small bowel obstruction secondary to Crohn disease: CT findings. *Abdom Imaging* 29:320–325, 2003.
61. Gore RM, Balthazar EJ, Ghahremani GG, Miller FH: CT features of ulcerative colitis and Crohn's disease. *AJR* 167:3–15, 1996.
62. Greenstein-Orel S, Rubesin SE, Jones B, et al: Computed tomography vs barium studies in the acutely symptomatic patient with Crohn's disease. *J Comput Assist Tomogr* 11:1009–1016, 1987.
63. Lee WK, Van Tonder F, Tartaglia CJ, et al: CT appearances of abdominal tuberculosis. *Clin Radiol* 67:596–604, 2012.
64. Mendelsohn RM, Nolan DJ: The radiological features of radiation enteritis. *Clin Radiol* 36: 141–148, 1985.
65. Fishman EK, Zinreich JS, Jones B, et al: Computed tomographic diagnosis of radiation ileitis. *Gastrointest Radiol* 9:149–152, 1984.
66. Czyrko C, Weltz CR, Markowitz RI, et al: Blunt abdominal trauma resulting in intestinal obstruction: When to operate? *J Trauma* 30: 1567–1571, 1990.
67. Lim YJ, Chun HJ: Recent advances in NSAIDs-induced enteropathy therapeutics: New options, new challenges. *Gastroenterol Res Pract* 2013: 761060, 2013.
68. Grumbach K, Levine MS, Wexler JA: Gallstone ileus diagnosed by computed tomography. *J Comput Assist Tomogr* 10:146–148, 1986.
69. Balthazar EJ, Schechter LS: Gallstone ileus: The importance of contrast examinations in the roentgenographic diagnosis. *AJR* 125:374–378, 1975.
70. Wright CC, Closson FT: Updates in pediatric gastrointestinal foreign bodies. *Pediatr Clin North Am* 60:1221–1239, 2013.
71. Pice JE, Michaw SL, Morgenstein L: Fruit pit obstruction: The propitious pit. *Arch Surg* 111:773, 1976.
72. Sandrasegaran K, Kopecky KK, Rajesh A, Lappas J: Proximal small bowel intussusceptions in adults: CT appearance and clinical significance. *Abdom Imaging* 29:653–657, 2004.
73. Lvoff N, Breiman RS, Coakley FV, et al: Distinguishing features of self-limiting adult small bowel intussusception identified at CT. *Radiology* 227:68–72, 2003.
74. Warshauer DM, Lee JK: Adult intussusception detected at CT or MR imaging: Clinical imaging correlation. *Radiology* 212:853–860, 1999.
75. Sarr MG, Nagorney DM, McIlrath DC: Post-operative intussusception in the adult. *Arch Surg* 116:144, 1981.
76. Curcio CM, Feinstein RS, Humphrey RL, et al: Computed tomography of enteroenteric intussusception. *J Comput Assist Tomogr* 6:969–974, 1982.
77. Balthazar EJ: CT of the gastrointestinal tract: Principles and interpretation. *AJR* 156:23–32, 1991.
78. Shenoy S, Cassim R: Metastatic melanoma to the gastrointestinal tract: Role of surgery as palliative treatment. *W V Med J* 109:30–33, 2013.
79. Pannala R, Ross AS: Small bowel polyps, arteriovenous malformations, strictures, and miscellaneous lesions. *Gastrointest Endosc Clin N Am* 23:111–121, 2013.
80. Goldstein HM, Beydoon MT, Dodd GD: Radiologic spectrum of melanoma metastatic to the gastrointestinal tract. *AJR* 129:605–612, 1977.
81. Rubesin SE, Herlinger H, DeGaeta L: Interlude: Test your skills. Inverted Meckel's diverticulum. *Radiology* 178:636–644, 1990.
82. Ghahremani GG: Radiology of Meckel's diverticulum. *Crit Rev Diagn Imaging* 26:1–43, 1986.
83. Baleato-González S, Vilanova JC, García-Figueiras R, et al: Intussusception in adults: What radiologists should know. *Emerg Radiol* 19:89–101, 2012.
84. Stabile Ianora AA, Telegrafo M, Lorusso V, et al: Adult transient intestinal intussusception: Can abdominal CT guide resolution? *Recenti Prog Med* 104:376–380, 2013.
85. Tirumani H, Vassa R, Fasih, Ojili V: Small bowel obstruction in the emergency department: MDCT features of common and uncommon causes. *Clin Imag* 38:580–588, 2014.

Vascular Disorders of the Small Intestine

SIVA P. RAMAN | KAREN M. HORTON | ELLIOT K. FISHMAN

CHAPTER OUTLINE

Computed Tomography Imaging

Mesenteric Ischemia

Acute Mesenteric Ischemia

Chronic Mesenteric Ischemia

Vasculitis

Large Vessel Vasculitis

Medium Vessel Vasculitis

Small Vessel Vasculitis

Miscellaneous Disorders

Superior Mesenteric Artery Dissection

Trauma

Radiation Enteritis

Splanchnic Artery Aneurysms

Drug-Induced Small Bowel Angioedema

Median Arcuate Ligament Syndrome

Hemangiomas

Summary

Small bowel abnormalities continue to be a significant diagnostic challenge for clinicians and radiologists. Clinicians have historically struggled to diagnose many small bowel diseases because patients typically present with only nonspecific complaints such as abdominal pain, weight loss, or anemia. Therefore, in most cases, the diagnosis of small bowel pathology is highly dependent on the radiologist. Although fluoroscopic barium studies have traditionally been the mainstay in the diagnosis of many small bowel diseases, they have proven to be inherently limited because they image only the lumen of the bowel and provide very little information regarding extraluminal disease. Since its introduction in the late 1970's, computed tomography (CT) has proven to be extremely useful for the evaluation of the small intestine and has been used for the evaluation of such routine conditions as small bowel obstruction and Crohn's disease. However, over the last decade, CT has taken on a larger role in diagnosing a variety of more subtle bowel diseases, including vascular disorders of the small intestine.

Vascular disorders of the small bowel encompass a wide variety of conditions, which primarily affect the mesenteric vasculature. These conditions have traditionally proven very difficult to diagnose radiographically, and ultimately angiography or surgery is relied on to make the correct diagnosis. With the introduction of multidetector CT (MDCT), along with the development of sophisticated three-dimensional imaging tools, it is now possible to image the small bowel

vasculature, as well as the small intestine, in a single examination, offering a thorough evaluation in patients with a wide variety of suspected small bowel vascular disorders.

This chapter will review the current status of imaging regarding a variety of vascular disorders of the small intestine, including mesenteric ischemia and infarction, vasculitis, aneurysms, acute small bowel bleeding, and radiation enteritis. Although a variety of imaging modalities will be discussed, this chapter will concentrate on the use of MDCT and 3D imaging for the diagnosis of these conditions.

Computed Tomography Imaging

The last decade has brought significant improvements in CT technology with the development of 64-, 128-, and 256-slice and, most recently, dual-source scanners. These latest scanners have allowed markedly improved spatial and temporal resolutions, enabled the reliable acquisition of angiographic images at peak arterial enhancement, and reduced motion related artifacts.¹ In addition to improving the image quality of conventional axial images and multiplanar reformats, these technologic advances have improved our ability to create truly isotropic data sets, and have greatly facilitated the creation of 3D reconstructions. These technologic improvements, along with the latest 3D software packages and CT protocol refinements, allow high-resolution images of the small bowel, small bowel mesentery, and mesenteric vasculature to be obtained, largely obviating the need for any other imaging modality.

When a vascular disorder of the small bowel is suspected, the CT examination must be specifically focused to optimize evaluation of the bowel. Prior to the injection of intravenous (IV) contrast, most patients are given a neutral oral contrast agent (e.g., barium sulfate [VoLumen, E-Z-EM, New York]) to distend the small bowel maximally, although in a few select cases (e.g., when acute gastrointestinal hemorrhage is suspected) no oral contrast agent is given. Notably, positive contrast agents are never given because a beam-hardening artifact from the contrast can obscure subtle bowel wall thickening or enhancement abnormalities and can also interfere with 3D postprocessing. An injection of roughly 120 mL of nonionic IV contrast is then administered at a relatively high rate of 3 to 5 mL/s to maximize arterial enhancement. Arterial phase images are acquired at 30 seconds after the injection of contrast, followed by the acquisition of venous phase images at 60 to 70 seconds. The arterial phase images are important in the evaluation of the arterial mesenteric vasculature, small bowel hypoenhancement or hyperemia, vascular malformations, and hypervascular small bowel tumors. The venous phase images are critical for evaluating the mesenteric venous vasculature, identifying subtle areas of bowel wall thickening or hypovascular small bowel tumors,

and complete evaluation of the remainder of the abdomen and pelvis.

Images are acquired with thin collimation, with acquisition of 0.625- to 0.75-mm slices, which are then reconstructed into 3- to 5-mm axial slices for routine interpretation. Coronal and sagittal multiplanar reformations are created directly at most CT scanners immediately after acquisition of the axial source images. Simultaneously, a set of 0.5- to 0.75-mm isotropic² images are used to create 3D reconstructions.

Two primary 3D reconstruction methods, which are typically created interactively by a radiologist at an independent workstation, are the most useful for the evaluation of small bowel vascular disorders:

1. Maximum intensity projection (MIP) imaging involves the acquisition of the highest attenuation voxels in a dataset and the projection of these voxels into a 3D display. These images are most useful for complete visualization of the mesenteric vasculature and for better visualization of abnormalities in the small bowel mesentery by accentuating soft tissue structures and vessels in the midst of mesenteric fat.
2. Volume rendering (VR) is based on a complex algorithm that assigns a specific color and transparency to each voxel in a dataset based on its underlying attenuation and then presenting this data in a 3D display. This technique is the most useful for depicting abnormalities of the bowel wall itself and can accentuate subtle areas of bowel wall thickening or hyperemia.²

Because small bowel loops and the mesenteric vasculature are anatomically complex, and the relationships between different bowel loops and vascular structures are not easy to visualize using any single imaging plane, it is necessary to use a variety of imaging planes during 3D evaluation. To visualize the proximal portion of the celiac axis, superior mesenteric artery (SMA), and inferior mesenteric artery (IMA), the sagittal projection is often the most helpful (Fig. 47-1). However, to visualize the complicated vascular branching of the arterial vessels adequately as they extend distally, coronal or coronal oblique planes are necessary (Fig. 47-2). Similarly, the mesenteric veins are best seen in a coronal projection (Fig. 47-3).

After adequate evaluation of the mesenteric vessels, it is also important to image the bowel (Fig. 47-4) comprehensively. However, visualizing the small bowel in its entirety on the axial images can be difficult and time-consuming, and the full extent and distribution of bowel abnormalities can be difficult to appreciate. Moreover, in our experience, subtle abnormalities in the fold pattern of the small bowel are difficult to appreciate in the axial plane, and the terminal ileum and ileocecal valve tend not to be well visualized. Instead, the small bowel is best visualized in the coronal plane, using cut planes to remove overlapping bowel loops while performing 3D analysis.

Mesenteric Ischemia

ACUTE MESENTERIC ISCHEMIA

Accounting for roughly 5% of all hospital admissions, acute mesenteric ischemia (AMI) is a severe, life-threatening disorder, with mortality rates ranging from 60% to 80%.³⁻⁵ Unfortunately, AMI can be extremely difficult to diagnose clinically. Although patients complain of intense abdominal pain, their physical examination can be misleadingly unremarkable.

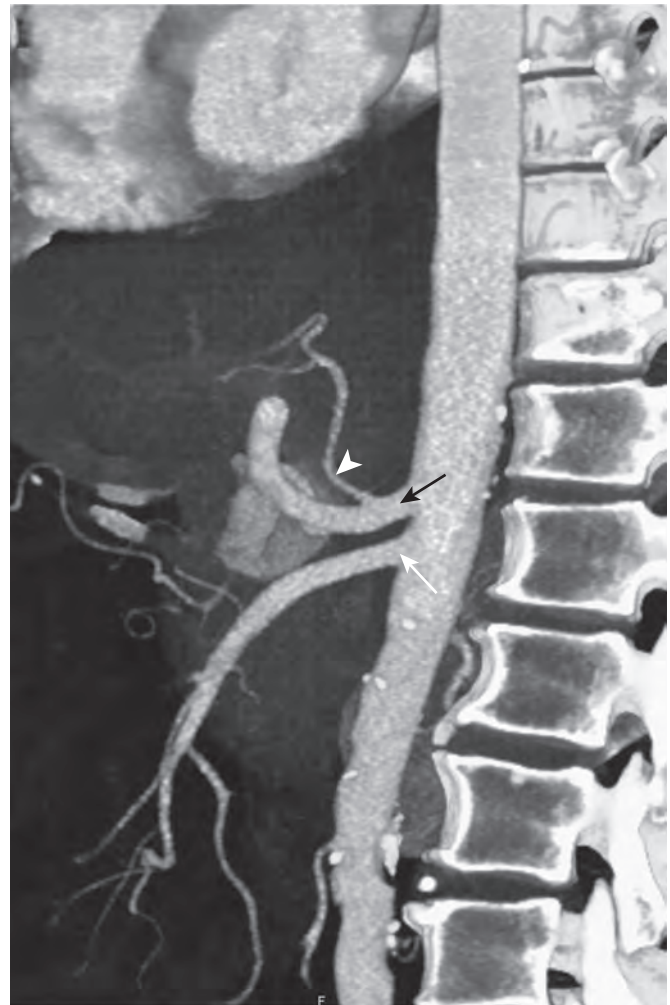


Figure 47-1 Normal celiac and superior mesenteric artery anatomy. Sagittal volume-rendered CT angiogram demonstrates normal anatomy of the celiac axis (black arrow) and superior mesenteric artery (white arrow). The left gastric artery (arrowhead) can also be seen arising from the celiac artery.

Laboratory markers are rarely suggestive, although lactate levels can be elevated, and no single laboratory marker is absolutely specific. Ultimately, given the nonspecific presentation of most patients, the diagnosis is contingent on radiology.

A relatively large proportion of cardiac output is routed to the small bowel in the resting state and after a meal, making the small bowel extremely sensitive to decreases in blood flow. Acute mesenteric ischemia can be broadly divided into three major categories: (1) arterial occlusion; (2) venous occlusion; and (3) nonocclusive mesenteric ischemia.

The most common cause is arterial occlusion, which accounts for 60% to 70% of all cases. Arterial occlusion can result from emboli to the SMA, usually in the setting of atrial fibrillation, but also secondary to recent myocardial infarction, mycotic aneurysms, and severe ulcerated plaque in the thoracic or abdominal aorta.⁶ The SMA is considered particularly vulnerable to emboli, given its wide caliber and narrow angle at takeoff, and a large embolus lodged at its origin can occlude blood flow to almost the entire small bowel and right colon. Most emboli lodge in the most proximal aspect of the SMA

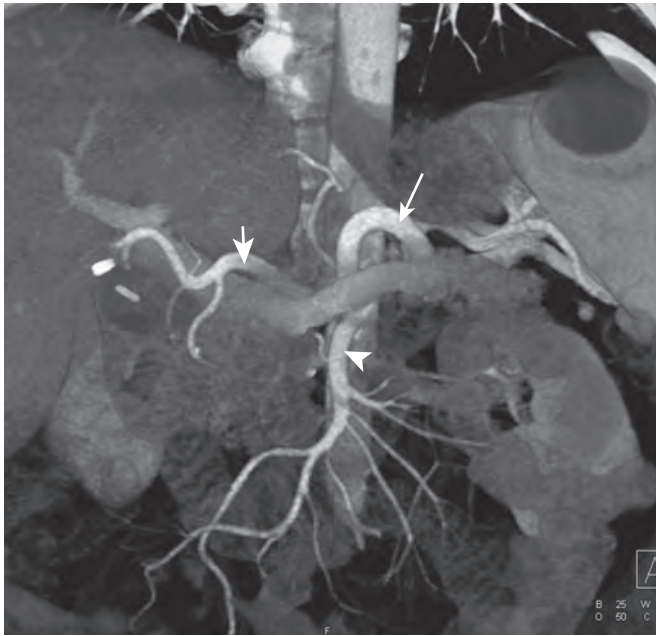


Figure 47-2 Coronal volume-rendered CT angiogram. This demonstrates the normal anatomy of the celiac axis (splenic artery, long arrow; common hepatic artery, short arrow) and superior mesenteric artery (arrowhead). The coronal projection allows easy identification of the branches arising from the SMA.

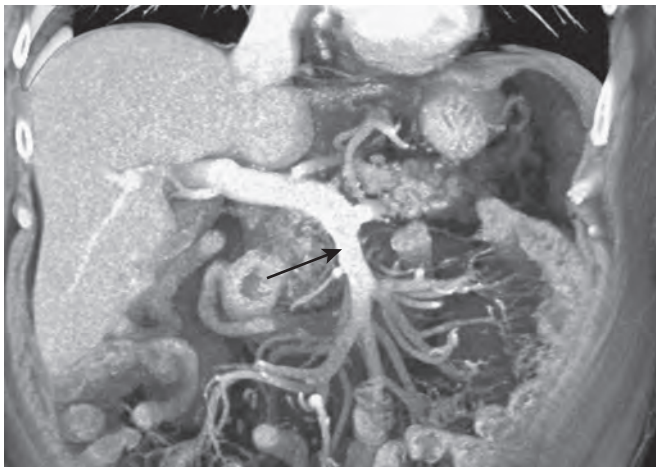


Figure 47-3 Coronal volume-rendered CT image in the venous phase. This demonstrates the normal appearance of the superior mesenteric vein (arrow) and its branches as they join the splenic vein and portal vein at the confluence.

(usually 3 to 10 cm from the origin), although smaller emboli can travel distally and occlude blood flow to a smaller segment of the small bowel or right colon⁷ (Figs. 47-5 to 47-8). Therefore, acute mesenteric ischemia should not be discounted when a relatively short segment of small bowel is involved, rather than the entire SMA territory.

Although most arterial occlusive ischemia of the small bowel is embolic in nature, there are several other causes. Thrombosis of the SMA can occur as a result of severe atherosclerotic disease or in patients with underlying hypercoagulability syndromes. When thrombosis occurs in the setting of underlying

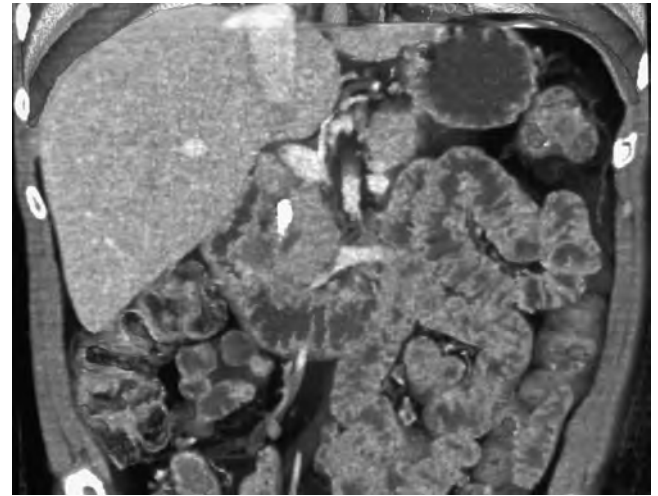


Figure 47-4 Coronal volume-rendered image. This shows the normal appearance of the small bowel.

atherosclerosis, the most common sites of occlusion are at the origins of the SMA and celiac artery. This particular subgroup of patients often has a history of chronic mesenteric ischemia, with development of AMI after superimposed thrombosis of a chronically narrowed and diseased vessel^{5,8} (Fig. 47-9). Notably, although arterial collaterals are not usually found in patients with acute occlusive AMI, patients with a history of chronic mesenteric ischemia and superimposed arterial thrombosis can have evidence of arterial collaterals, a sometimes confusing feature.⁹ More rarely, acute mesenteric ischemia can be seen in the setting of vasculitis, aortic dissection (with extension of an occluding dissection flap into the SMA), occlusion of the SMA by surrounding tumor, or thrombosis of an SMA aneurysm (Fig. 47-10).⁵

Venous occlusion (thrombosis of the superior mesenteric vein [SMV]) accounts for roughly 10% of all cases of AMI. A sizeable percentage of these patients are ultimately found to have a history of a specific hypercoagulability syndrome, personal or family history of unexplained thrombotic episodes, underlying malignancy, or oral contraceptive use, although a discrete cause for the venous occlusion is not found in at least one third of patients (Figs. 47-11 to 47-13).¹⁰ Unfortunately, although the acute symptoms of venous occlusive AMI are usually much less severe compared to those of arterial occlusion, this can lead to considerable delay in presentation and diagnosis, resulting in a mortality rate as high as 40%.⁵

Complicated small bowel obstructions are also a cause of occlusive ischemia because strangulation of the bowel results in occlusion of the vasculature leading to the involved bowel segment. This type of bowel ischemia typically involves a combination of arterial and venous occlusion (Fig. 47-14).

The final major category of acute mesenteric ischemia is nonocclusive ischemia, typically caused by hypotension and diminished blood flow to the small bowel resulting from underlying conditions such as cardiogenic shock, cardiac failure, acute myocardial infarction, severe hypovolemia, trauma, renal failure with overly aggressive dialysis, or severe vasoconstriction from drugs (e.g., digitalis, cocaine). Nonocclusive AMI accounts for roughly 30% of all cases of bowel ischemia and is associated with a 70% mortality rate.¹¹ The odds of acute mesenteric

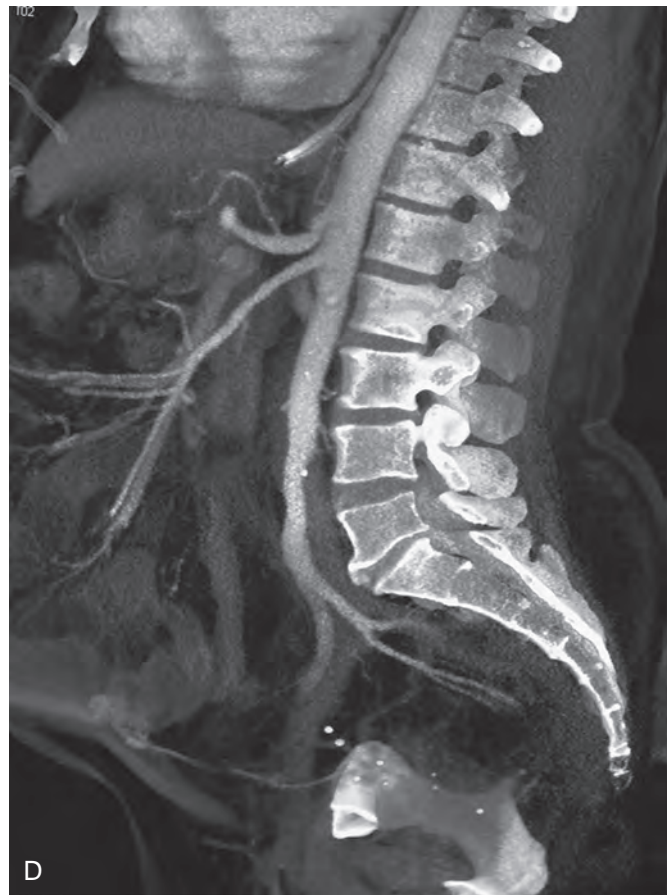
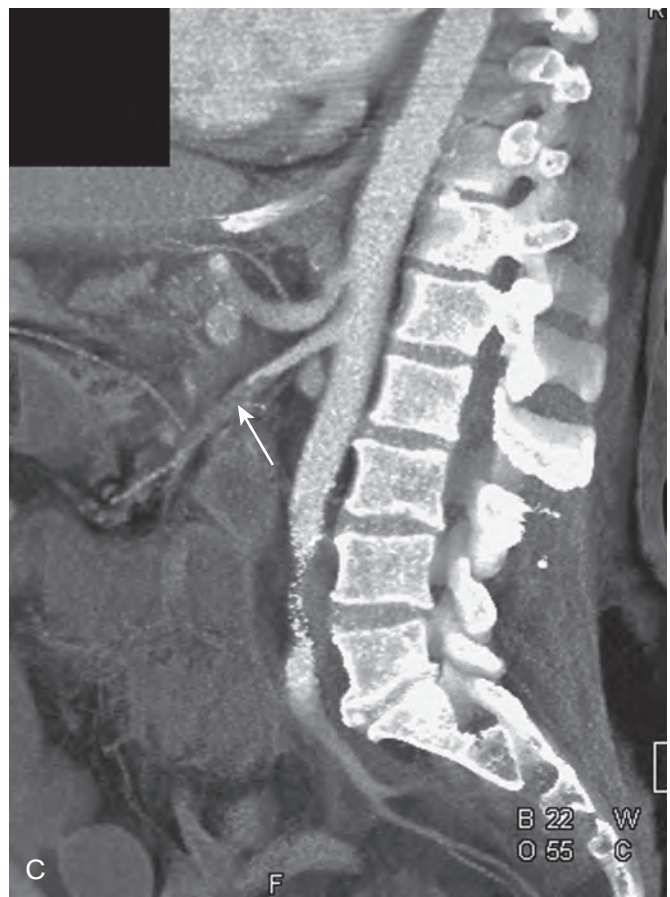
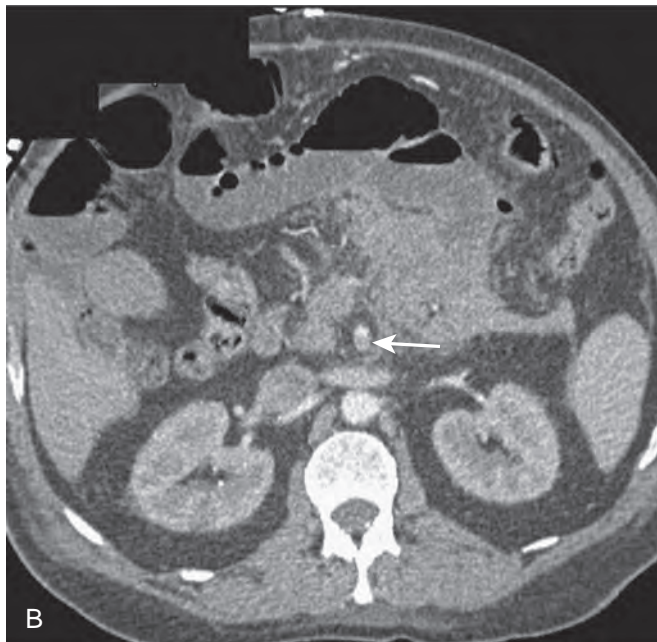
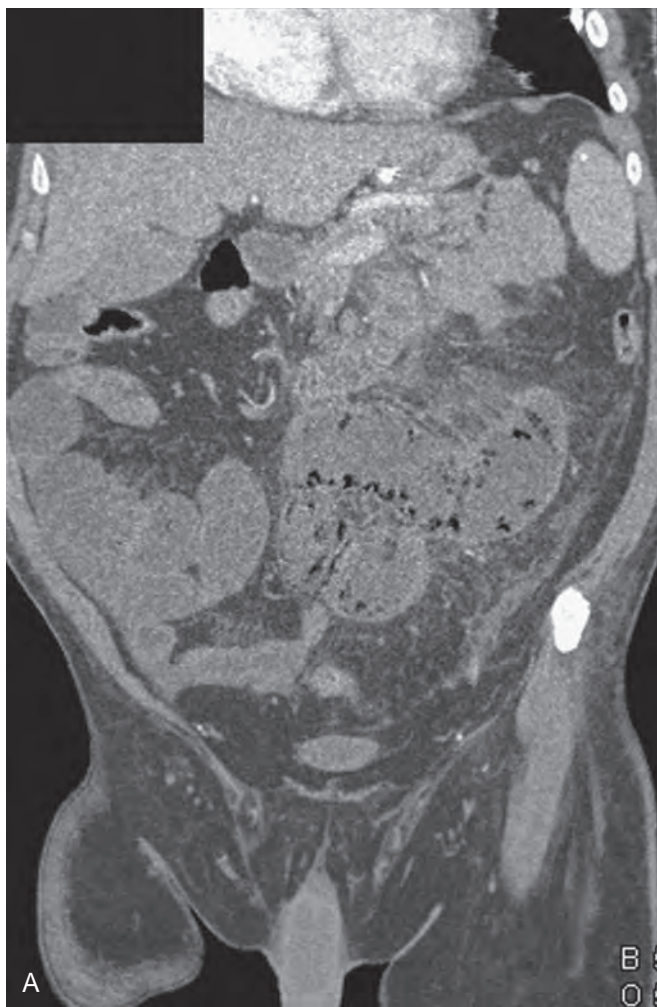


Figure 47-5 Superior mesenteric artery thrombosis: contrast-enhanced CT images in a patient with acute abdominal pain. **A.** Coronal contrast-enhanced CT image demonstrates dilated small bowel loops in the mid and right abdomen, with pneumatosis identified within several small bowel loops, predominantly in the central abdomen. **B.** Axial contrast-enhanced CT image demonstrates subtle thrombus (arrow) in the superior mesenteric artery. Multiple small bowel loops are dilated with thin walls (no appreciable bowel wall thickening) and a small amount of adjacent ascites, findings that raise concern for bowel ischemia. **C.** Volume-rendered contrast-enhanced image in the sagittal projection demonstrates a large thrombus (arrow) in the superior mesenteric artery, the full extent of which was not appreciated on the axial image. **D.** Volume-rendered contrast-enhanced CT image in the sagittal plane after surgical embolectomy demonstrates a patent superior mesenteric artery.

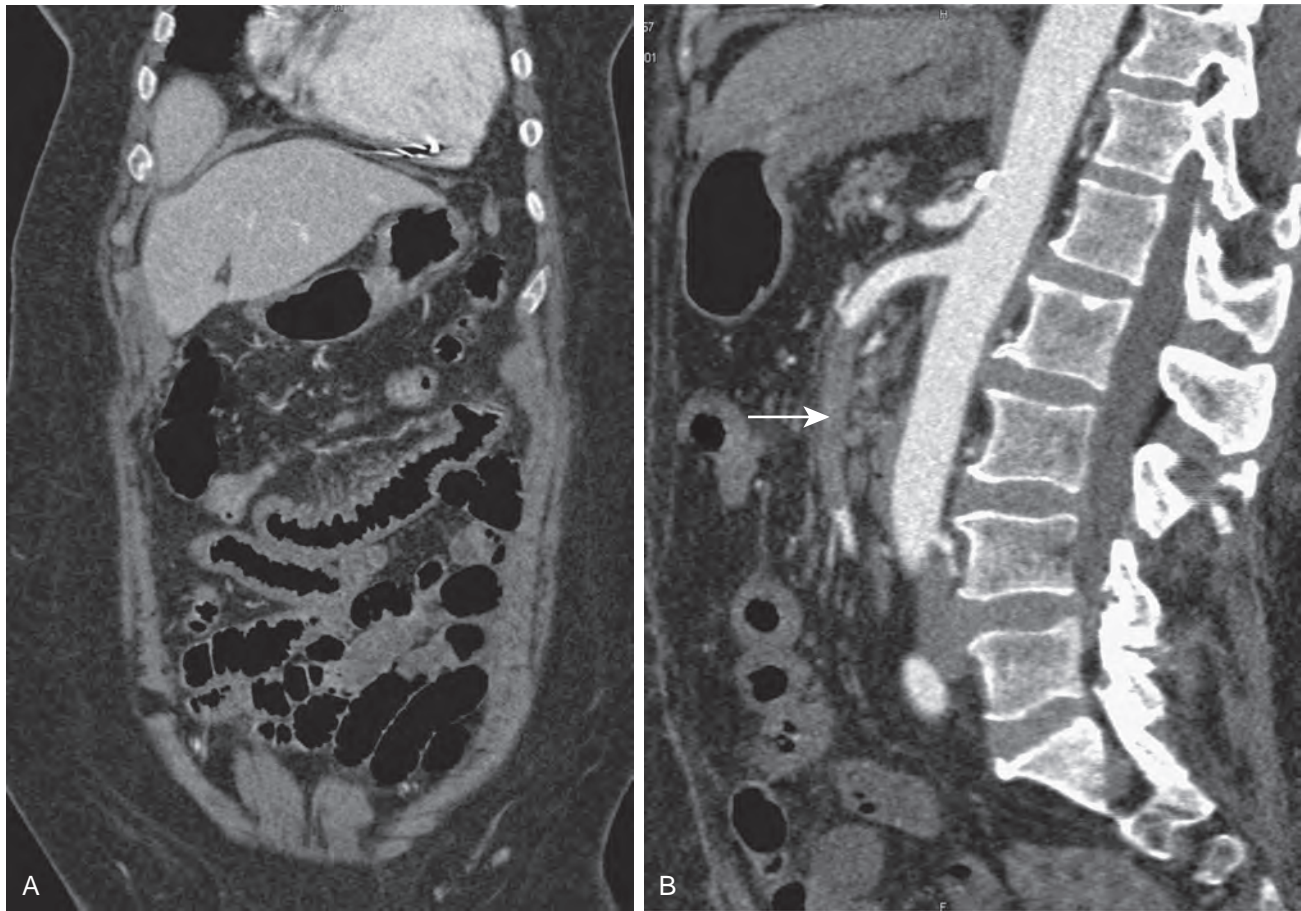


Figure 47-6 Superior mesenteric artery thrombus in patient with acute abdominal pain. **A.** Coronal contrast-enhanced multiplanar reconstruction demonstrates moderate wall thickening of multiple small bowel loops in the mid abdomen. **B.** Sagittal multiplanar reconstruction demonstrates occlusive thrombus (arrow) in the superior mesenteric artery. There is also calcification and narrowing of the origin of the celiac artery related to chronic atherosclerotic disease.

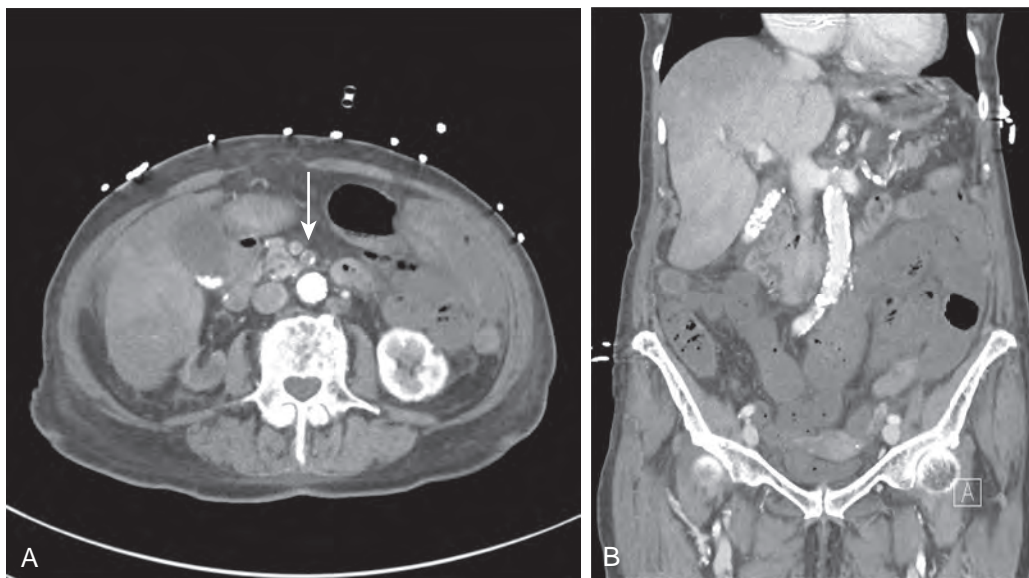


Figure 47-7 SMA embolism. **A.** Axial contrast-enhanced image demonstrates an acute embolism (arrow) in the SMA. **B.** Coronal contrast-enhanced image demonstrates diffusely hypoenhancing bowel with a relative paucity of bowel wall thickening, a common appearance for acute mesenteric ischemia caused by arterial occlusion.

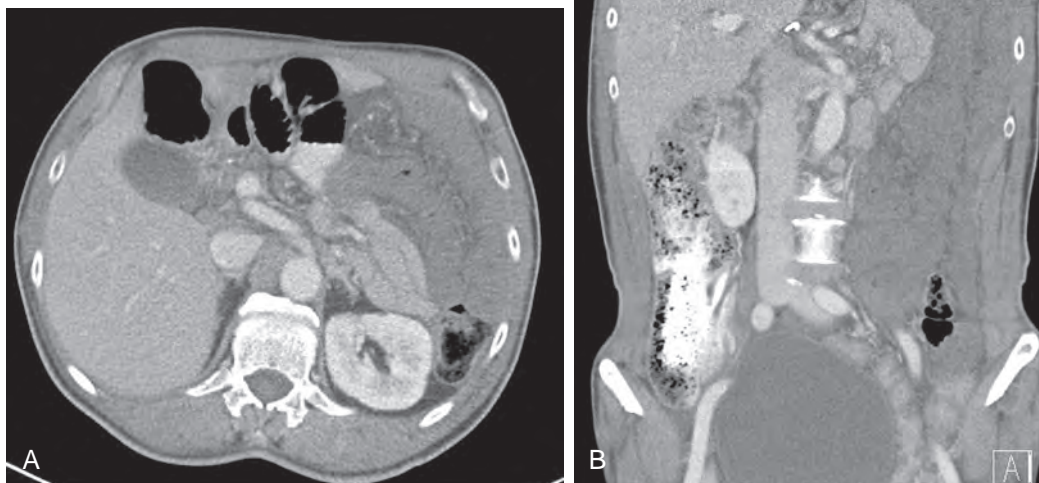


Figure 47-8 SMA embolism. Axial (A) and coronal (B) contrast-enhanced images demonstrate diffuse hypoenhancement (as a result of acute mesenteric ischemia) of the small bowel in the left hemiabdomen in a patient with subtle SMA embolism.

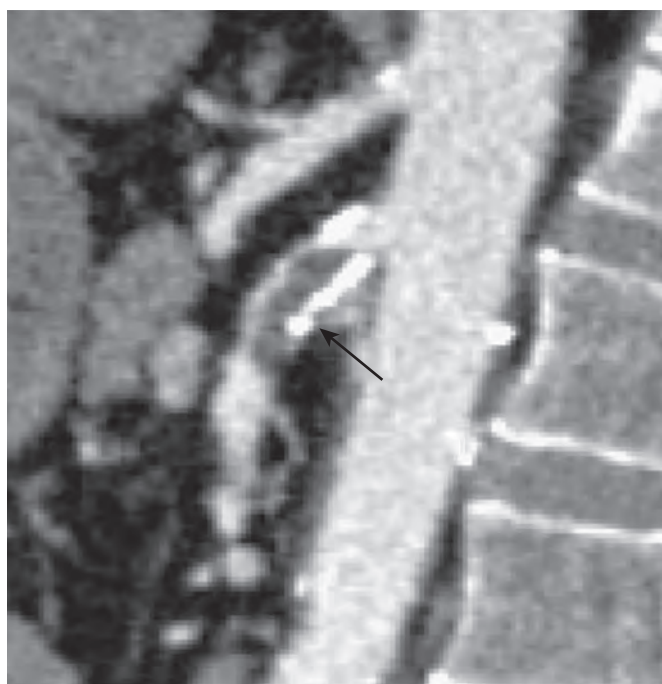


Figure 47-9 SMA thrombosis. Sagittal volume-rendered CT image demonstrates thrombus (arrow) formation at the origin of the SMA in a region of calcified atherosclerotic plaque.

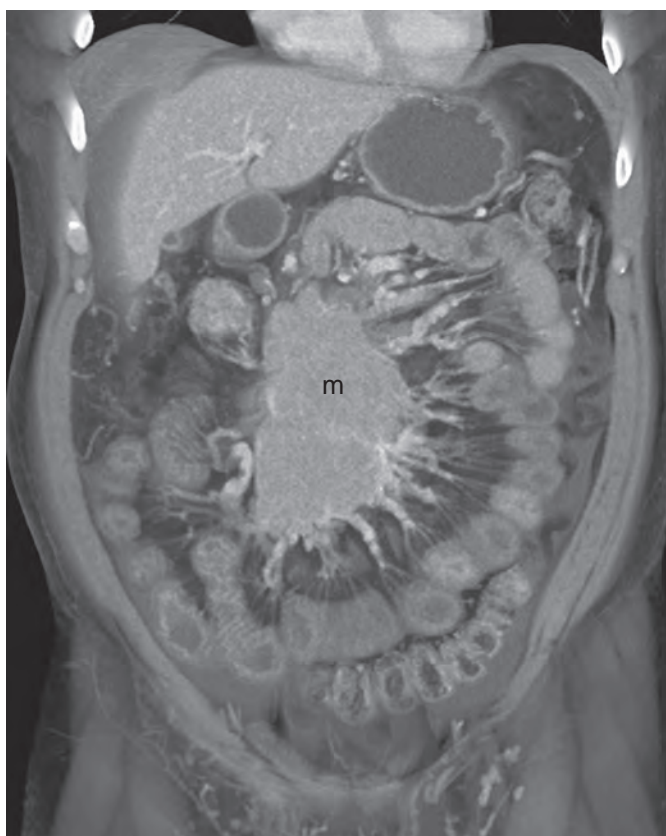


Figure 47-10 Carcinoid tumor causing mesenteric ischemia. Coronal volume-rendered contrast-enhanced CT image demonstrates a large mesenteric carcinoid tumor (m) encasing the mesenteric vessels, resulting in diffuse small bowel wall thickening related to ischemia.

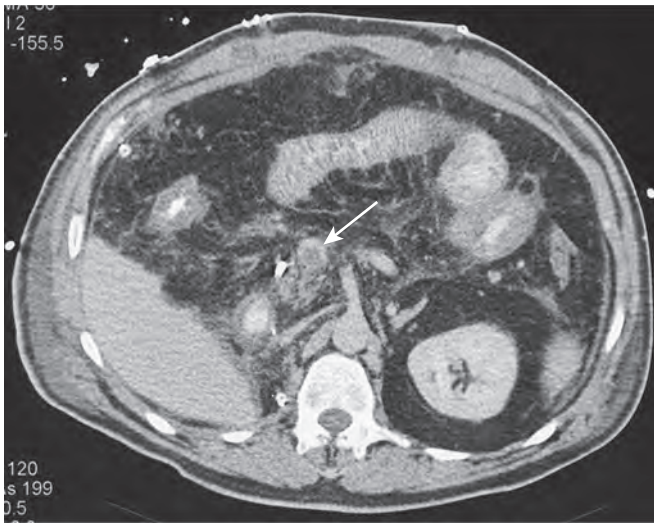


Figure 47-11 SMV thrombosis. Contrast-enhanced CT image in a patient with acute abdominal pain demonstrates thrombus in the SMV (arrow), with moderate thickening of the small bowel and right colon, which is concerning for bowel ischemia.

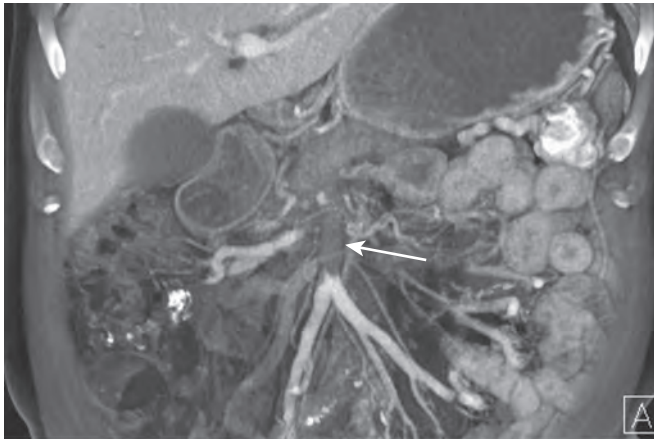


Figure 47-12 SMV thrombosis. Coronal volume-rendered contrast-enhanced CT demonstrates moderate thickening of the small bowel (predominantly in the left abdomen), with a large thrombus (arrow) in the SMV.

ischemia in the setting of a low-flow state are increased when the patient has underlying atherosclerotic disease or some other abnormality of the mesenteric vasculature. In younger patients, nonocclusive mesenteric ischemia has been reported with cocaine use, which results in splanchnic vasoconstriction to preserve blood flow to the heart and brain (Fig. 47-15).¹²

Although the diagnosis of AMI was once dependent on angiography, CT has now assumed a primary role in the diagnosis and has proven to be highly effective. Several studies have shown CT to be extremely accurate, with sensitivities greater than 90%.¹³⁻¹⁹ A large meta-analysis studying the accuracy of CT in AMI found a pooled sensitivity of 93.3% and specificity of 95.9%.¹⁸ There is little doubt that CT should be considered the first-line radiologic examination when AMI is suspected.

Computed Tomography Findings

Bowel Dilation. Small bowel dilation is common, although completely nonspecific. In a series of nine patients by Lee and

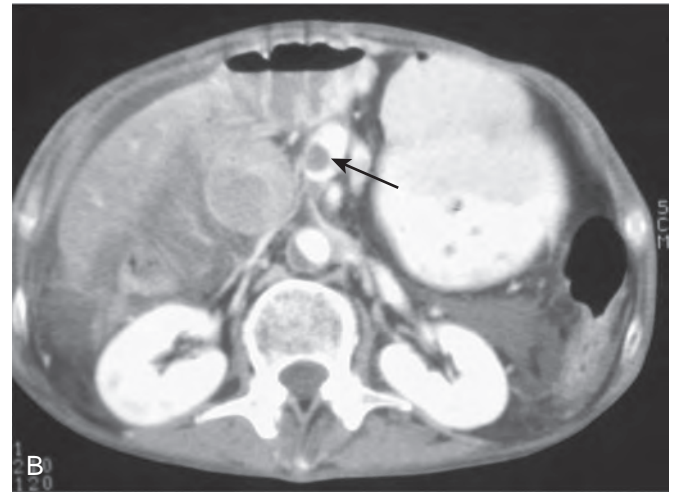
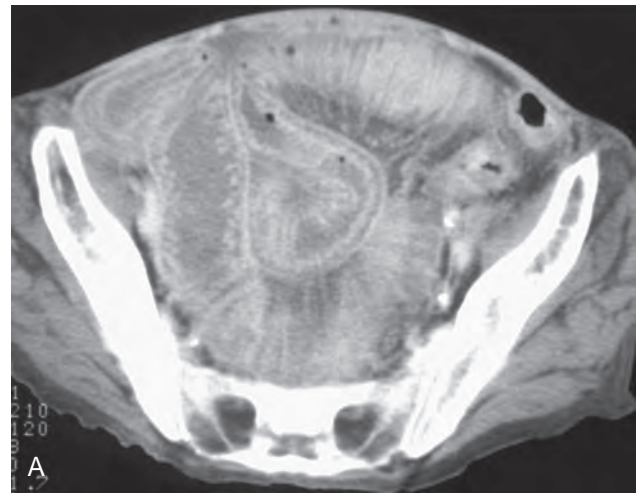


Figure 47-13 SMV thrombosis. **A.** Axial contrast-enhanced CT demonstrates severe thickening of the small bowel and right colon as a result of venous occlusive ischemia. The intense mucosal enhancement with submucosal hypodensity and edema represents an example of the target or halo appearance. **B.** Axial contrast-enhanced image demonstrates thrombus (arrow) within the SMV, representing the cause of the patient's bowel ischemia.

colleagues, eight of nine patients demonstrated bowel dilation.²⁰ In some cases, dilated bowel can be seen on the basis of an adynamic ileus and interruption of normal bowel peristalsis after an ischemic event and, in other cases, severe bowel dilation can be seen with irreversible transmural bowel infarction.^{21,22} In general, small bowel dilation is more common after venous occlusion than with arterial occlusion.²³

Bowel Wall Thickening. Although not completely specific, bowel wall thickening is the most common CT finding in bowel ischemia, likely on the basis of edema and hemorrhage within the bowel wall. The normal small bowel wall is usually from 3 to 5 mm thick. In the study by Lee and associates,²⁰ bowel wall thickening up to 1.5 cm was noted in patients with mesenteric vein thrombosis. However, it is important to remember that this finding is relatively nonspecific and can be seen in a great variety of other conditions.

Despite being a common finding in AMI, bowel wall thickening is usually seen after venous occlusion or thrombosis and is not a characteristic feature of AMI caused by arterial

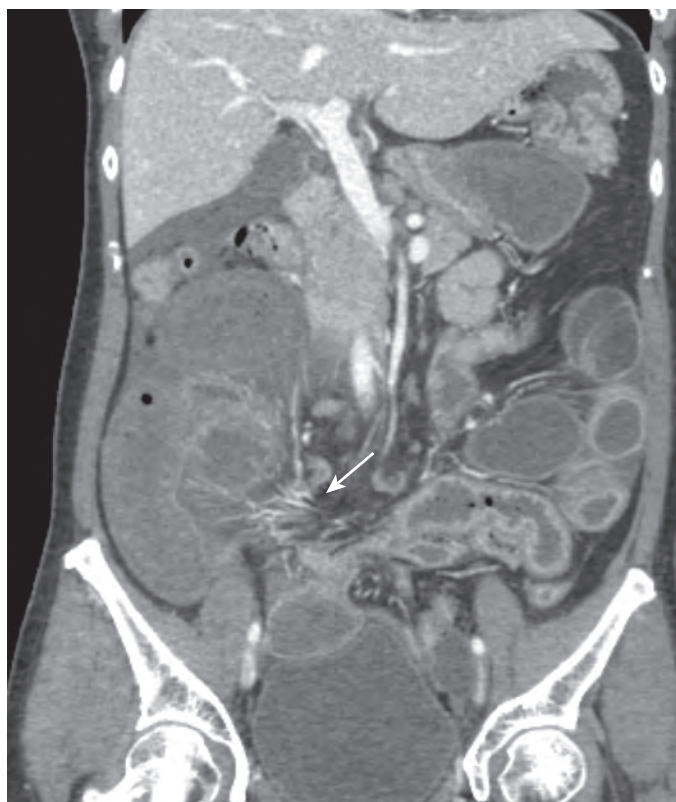


Figure 47-14 Closed loop obstruction leading to small bowel strangulation. Coronal contrast-enhanced CT image demonstrates multiple dilated loops of small bowel, many of which appear tethered and radiating toward a central point (arrow) indicating closed loop obstruction. In addition to several markedly thickened, hyperemic loops of small bowel, several loops of bowel in the right abdomen are poorly enhancing. There is also a small amount of interloop ascites. A strangulated ischemic small bowel was found at surgery.

occlusion.²⁴ In patients with AMI on the basis of arterial occlusion, the bowel wall is usually thinned, rather than thickened.^{14,15,20,25} Moreover, although small bowel wall thickening is a common finding in AMI, the presence and degree of bowel wall thickening do not usually correlate with the severity of ischemic damage.²⁵

Bowel Wall Attenuation and Abnormal Enhancement. The appearance of the bowel wall can vary dramatically in cases of bowel ischemia, with a low-density wall usually reflecting submucosal edema; high density within the wall is usually secondary to intramural hemorrhage.^{26,27} Notably, intramural hemorrhage can be a very difficult finding to identify without the aid of noncontrast images because hemorrhage within the bowel wall can be confused with normal enhancement of the wall. Bowel wall edema and hemorrhage are most common after venous thrombosis, although they can also be seen in the setting of reperfusion after arterial occlusion or a nonocclusive AMI.²²

Small bowel ischemia can result in diffuse hypoenhancement of the bowel wall and mucosa, a halo or target appearance, or diffuse hyperenhancement. Diffuse hypoenhancement of the bowel wall is the most specific finding and is usually seen in the setting of acute arterial occlusion or diffuse transmural infarction, regardless of any cause.¹⁵ Diffuse hyperenhancement of the

bowel wall or a halo appearance (with hyperenhancement of the bowel mucosa and diffuse, low-density edema of the submucosal layer) can also be seen with ischemia.²⁶ This mucosal hyperenhancement is usually seen after venous occlusion but can also occur secondary to reperfusion after arterial occlusion or nonocclusive ischemia.

Rarely seen in some patients with ischemia, there can be delayed enhancement of affected loops, likely on the basis of delayed delivery of contrast, as well as contrast persisting in the ischemic segment because of delayed washout.

Stranding and Ascites. Ascites and mesenteric stranding are nonspecific findings in patients with bowel ischemia. Their presence depends on the cause, duration, severity, and site of involvement of the bowel ischemia.²⁵ In general, the presence of mesenteric inflammation and edema is not synonymous with bowel infarction and can be seen with venous occlusion and strangulated bowel obstructions without evidence of frank infarction. Moreover, hemorrhage in the mesentery is a very common finding in cases of venous thrombosis. However, in patients with arterial occlusion, infiltration and edema of the mesentery is a much more ominous finding, often seen in the setting of bowel infarction.²²

Pneumatosis and Portomesenteric Venous Air. Pneumatosis and portomesenteric venous gas are relatively specific signs for transmural bowel infarction, although both are relatively rare (Fig. 47-16). When the mucosal layer of the bowel is disrupted after an infarction, air can extend directly into the bowel wall, producing pneumatosis, seen in 6% to 30% of cases of acute mesenteric ischemia.^{14,15,20,28} This gas can then extend further into the mesenteric veins and portal veins (portomesenteric venous air), a finding that is only seen in 3% to 14% of cases.

The specificity of pneumatosis and portomesenteric venous gas for ischemia and infarction approaches 100%. However, these two findings must be interpreted with a great deal of caution, because, rarely, they can be seen in a few nonischemic conditions as well, including iatrogenic mucosal injury (e.g., after the placement of a gastrostomy tube or jejunostomy tube), infections, bowel trauma, and inflammatory diseases (Fig. 47-17).²⁵ In addition, the radiologist must be careful not to confuse gas tracking along a bowel fold or gas immediately adjacent to the bowel wall with pneumatosis.

Patterns of Ischemia: Arterial Occlusive Ischemia Versus Venous Occlusive Ischemia. Although there can often be a great deal of overlap, the pattern of abnormalities seen on CT secondary to arterial occlusion and venous occlusion can vary. Although bowel wall thickening is commonly thought to represent a critical imaging finding in bowel ischemia, this finding is less commonly seen in cases of arterial occlusion. Rather, the bowel actually tends to become thinned (paper thin bowel) because there is a lack of arterial flow but no appreciable mural edema or intramural hemorrhage. This thinning can also be attributed to loss of intestinal muscular tone after the ischemic event. In most cases of arterial occlusion, hypoenhancement of the small bowel wall and mucosa is present, although hyperemia of the mucosa can rarely be seen in cases of reperfusion after an embolic event. Acutely, the bowel is not usually dilated unless there is evidence of infarction. Finally, there is generally a relative paucity of mesenteric fluid, hemorrhage, and fat stranding,

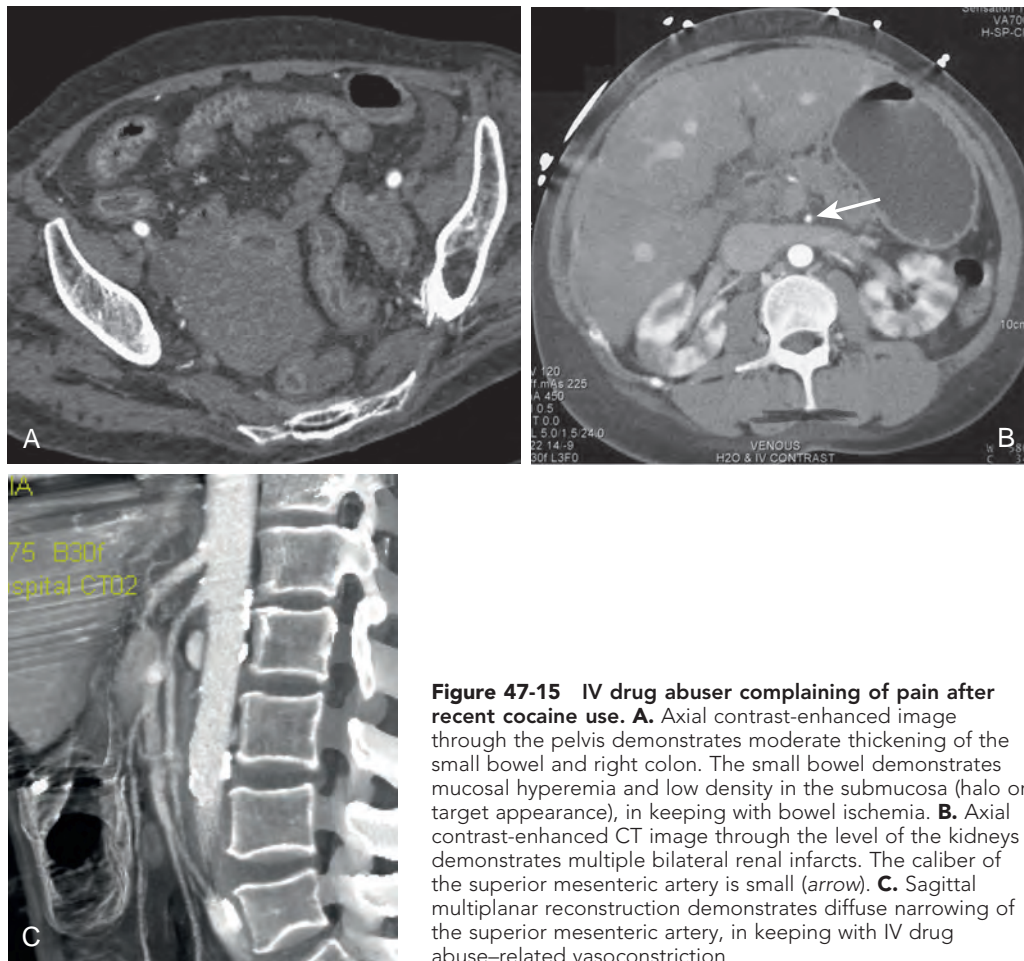


Figure 47-15 IV drug abuser complaining of pain after recent cocaine use. **A.** Axial contrast-enhanced image through the pelvis demonstrates moderate thickening of the small bowel and right colon. The small bowel demonstrates mucosal hyperemia and low density in the submucosa (halo or target appearance), in keeping with bowel ischemia. **B.** Axial contrast-enhanced CT image through the level of the kidneys demonstrates multiple bilateral renal infarcts. The caliber of the superior mesenteric artery is small (arrow). **C.** Sagittal multiplanar reconstruction demonstrates diffuse narrowing of the superior mesenteric artery, in keeping with IV drug abuse-related vasoconstriction.



Figure 47-16 Bowel infarction with pneumatosis. Contrast-enhanced axial CT image in a patient with mesenteric ischemia and infarcted bowel shows ascites, extensive pneumatosis, and air within the mesenteric veins. Despite emergent surgery, the patient died.

although these three features can be seen when there has been progression to frank bowel infarction. Given these findings, the CT appearance of acute AMI in the setting of arterial occlusion can be relatively difficult to identify; careful attention must be paid to subtle changes in bowel enhancement when an embolus is identified in the SMA.²²

The CT appearance after venous thrombosis is generally much more impressive, as the bowel wall is usually markedly thickened, the wall can be diffusely hypointense because of edema or hyperintense because of intramural hemorrhage, and the mucosa is often avidly hyperemic. The bowel can sometimes be moderately dilated, and there is typically significant mesenteric hemorrhage, edema, fluid, and fat-stranding, even in the absence of true bowel infarction.²²

As one would expect, complicated bowel obstructions demonstrate elements of venous and arterial occlusion, depending on the degree of strangulation, and can have a variable appearance on CT, depending on which vessels are compromised. Nonocclusive mesenteric ischemia does not have a characteristic pattern and can be the most difficult of the three types of AMI to diagnose (Figs. 47-18 and 47-19).

CHRONIC MESENTERIC ISCHEMIA

Chronic mesenteric ischemia (CMI), relatively uncommon (only 5% of all ischemic intestinal diseases) compared with AMI, is most common in older patients with widespread atherosclerotic disease and tends to be most prevalent in women, smokers, and those with diabetes and hypertension.²⁹ Patients usually complain of repeated bouts of abdominal pain, typically occurring immediately after a meal, and often develop fear of food, anorexia, and severe chronic weight loss. Notably, these symptoms do not arise acutely, but develop slowly over many

Figure 47-17 Benign pneumatosis intestinalis.

A, B. Axial noncontrast images demonstrate diffuse pneumatosis in multiple fluid-filled, mildly dilated small bowel loops. The patient was completely asymptomatic, and the pneumatosis was thought to be secondary to recent placement of a jejunostomy tube (arrow in **A**).

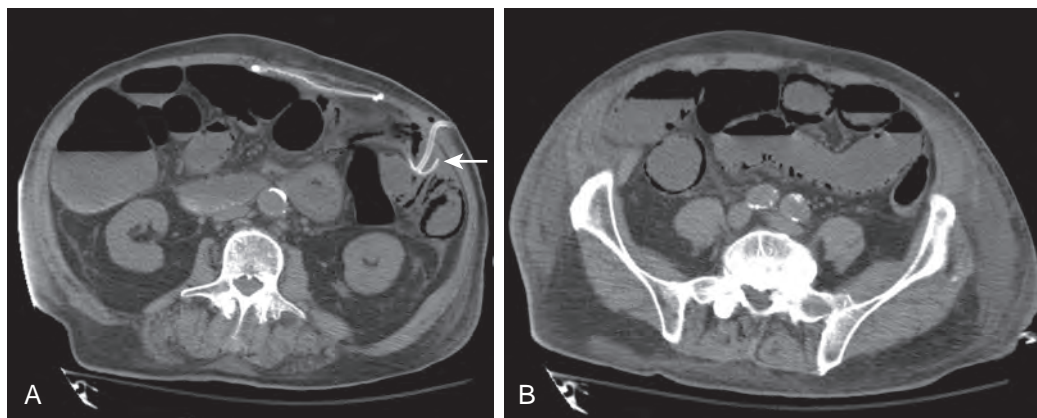


Figure 47-18 Nonocclusive mesenteric ischemia.

A, B. Axial contrast-enhanced images in a patient with septic shock demonstrate diffusely thickened, hypoenhancing loops of small bowel. The arterial and venous vasculature (not shown) was widely patent.

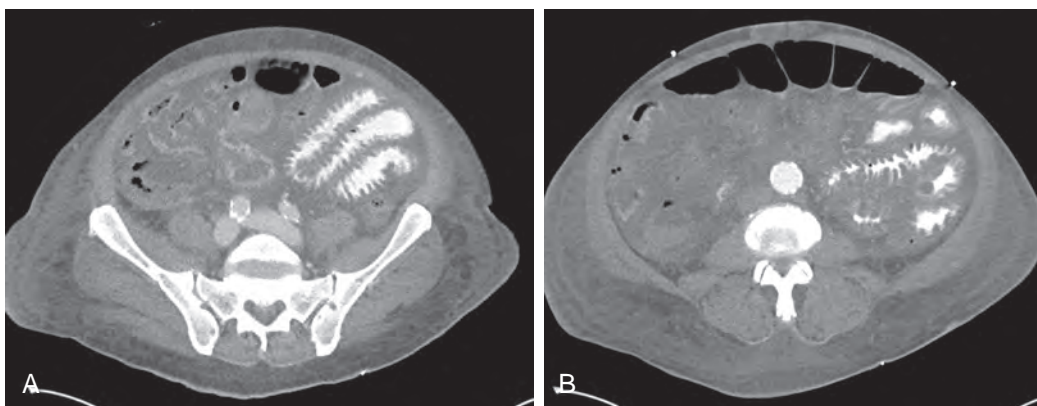
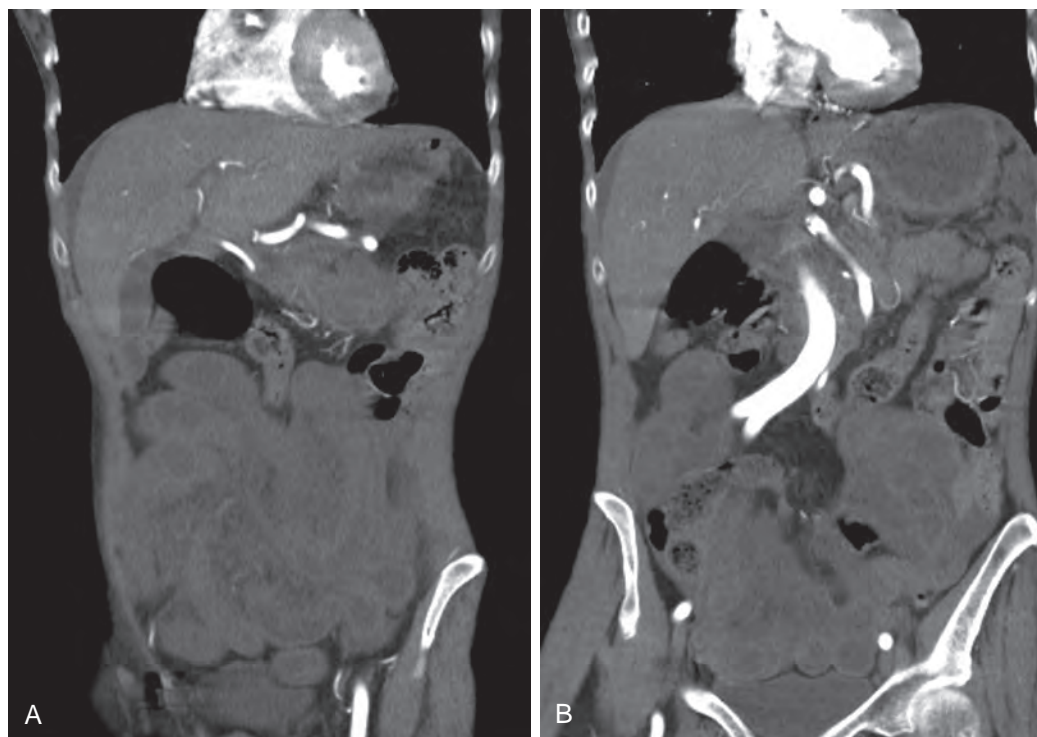


Figure 47-19 Nonocclusive mesenteric ischemia.

A, B. Coronal contrast-enhanced images demonstrate diffusely thickened, hypodense bowel in a patient with nonocclusive mesenteric ischemia. The arterial and venous vasculature was widely patent.



years; given the relatively nonspecific nature of the symptoms, the diagnosis is extremely difficult to make clinically.^{5,30}

Atherosclerotic disease of the mesenteric vessels is the primary cause of chronic mesenteric ischemia. However, the presence of atherosclerotic plaque and calcification alone does not automatically suggest that a patient suffers from CMI. Mesenteric atherosclerosis is a relatively common incidental finding and close to 20% of all patients older than 65 years will demonstrate more than 50% narrowing of a mesenteric vessel, without clinical symptoms in all but a few patients. Ultrasound and autopsy studies have confirmed this and have demonstrated that significant atherosclerotic disease can be present in multiple mesenteric arteries without symptoms of ischemia.^{5,31-33} Although rare, nonatherosclerotic diseases can also produce CMI, including such entities as vasculitis, median arcuate ligament syndrome, radiation vasculopathy, and fibromuscular dysplasia.^{5,34}

Most patients will remain asymptomatic unless there is significant disease in at least two of the three major mesenteric arteries (celiac axis, SMA, and IMA; Fig. 47-20). In most cases, atheroma involves the proximal segments of the mesenteric arteries, although more diffuse irregularity and narrowing of a vessel (with associated pruning of smaller branch vessels) can be present in patients with underlying diabetes.³⁰ In patients with more diffuse narrowing, ischemic symptoms can develop, even without a single discrete stenosis reaching the 50% threshold. The ultimate key to the diagnosis of CMI is not the presence of mesenteric vascular narrowing alone, but the simultaneous presence of collateral pathways, because symptoms usually develop when collateral pathways are no longer

sufficient to deliver blood supply to the bowel: Two major collateral pathways are the most common:

1. The pancreaticoduodenal arteries connect the celiac axis and SMA and can flow in either direction, depending on the site of occlusion.³⁰ The presence of large arterial collaterals surrounding the head of the pancreas is often the most important clue to the presence of a hemodynamically significant stenosis of the mesenteric vasculature, and should prompt a close examination of the mesenteric arteries on a sagittal reconstruction (Fig. 47-21).
2. The arc of Riordan and marginal artery of Drummond allow communication between the SMA and IMA (Fig. 47-22). In addition, in severe cases, when the celiac artery, SMA, and IMA are all compromised, pelvic, lumbar, or phrenic collateral vessels can develop.^{5,30,35-38}

Although catheter angiography was once the primary means of establishing the diagnosis of CMI, a number of other cross-sectional imaging modalities are now first-line options when trying to make this diagnosis. Duplex ultrasound has proven to be accurate as a screening test for the proximal mesenteric arteries, based on peak systolic and end-diastolic velocities measured while fasting and in the postprandial state.³⁹⁻⁴¹ The diagnosis of a critical stenosis on ultrasound is based primarily on velocity criteria, with a velocity of more than 275 cm/s in the proximal SMA or more than 200 cm/s in the proximal celiac artery in a fasting patient suggestive of a 70% or greater stenosis.⁴² Magnetic resonance angiography (MRA) has also been shown to correlate accurately with conventional angiography and can be a valuable option in patients for whom iodinated contrast agents are contraindicated.^{43,44} Recent MR imaging (MRI)

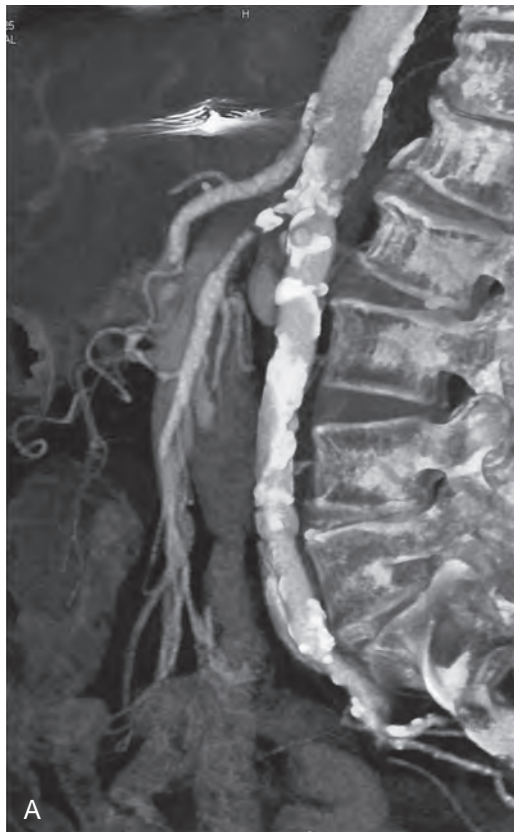
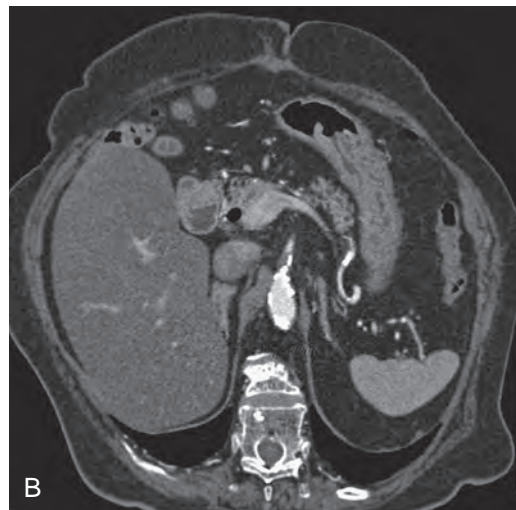


Figure 47-20 Chronic mesenteric ischemia.

A. Sagittal 3D CT angiogram demonstrates calcified atherosclerotic plaque at the origins of the celiac artery and SMA. **B.** Axial oblique multiplanar reformat (MPR) demonstrates calcified and soft plaque at the origin of the SMA.



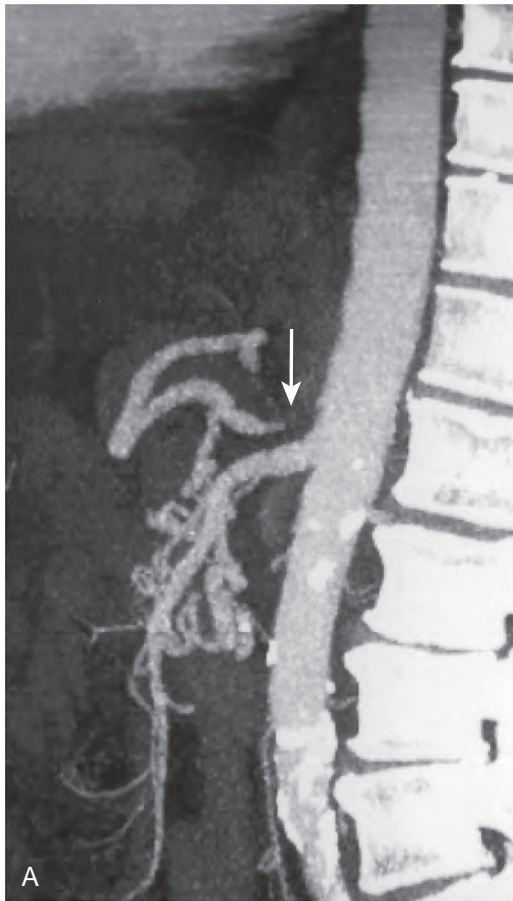


Figure 47-21 CT angiogram in a patient with celiac artery stenosis. **A.** Sagittal volume-rendered CT image shows marked narrowing (arrow) at the origin of the celiac artery. **B.** Coronal MIP image shows the pancreaticoduodenal collateral pathways (arrow) that have developed between the SMA and celiac axis.

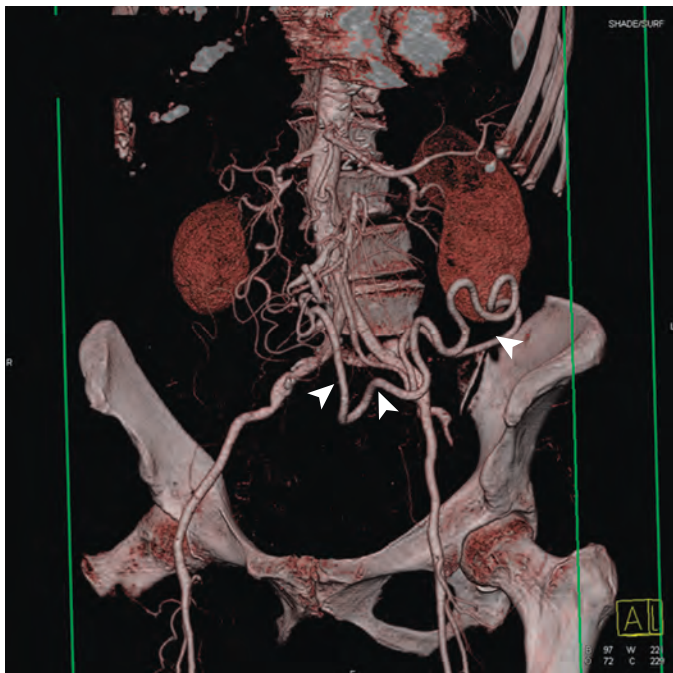
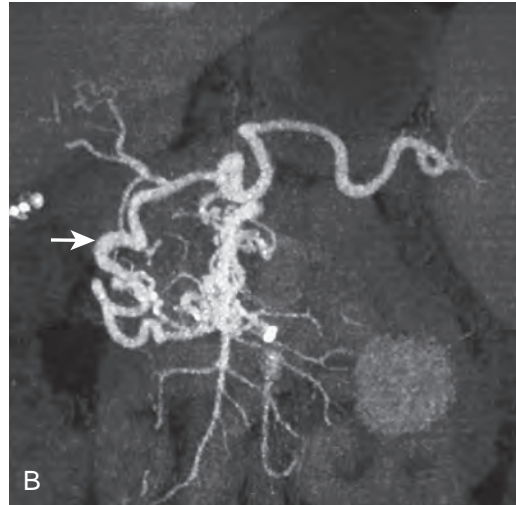


Figure 47-22 Marginal artery of Drummond. This coronal volume-rendered image demonstrate several large collateral vessels, including a large marginal artery of Drummond (arrowheads), in a patient with superior mesenteric artery stenosis. This is an important collateral pathway between the IMA and SMA.

protocols have also incorporated imaging of patients before and after a meal. Regardless, CT is the primary modality whereby the diagnosis of CMI is made. CT offers optimal visualization of the involved vascular segments, the ability to rotate and view the involved segments from any perspective using 3D techniques, and the ability to view calcification and soft plaque rather than the vessel lumen alone and, perhaps most importantly, it provides the added advantage of evaluating the bowel and nonvascular portions of the abdomen and pelvis.

Vasculitis

A general term encompassing a wide variety of diseases that result in inflammation and necrosis of blood vessels, vasculitis is often classified based on the size of the affected vasculature. Three primary categories of vasculitis have been described: (1) large vessel vasculitis affects the aorta and its major branches (the two most common types are Takayasu's arteritis and giant cell arteritis); (2) medium vessel vasculitis affects the visceral arteries and their branches, with classic examples in this category including polyarteritis nodosa, Kawasaki disease, and primary granulomatous central nervous system vasculitis; and (3) small vessel vasculitis affects arterioles, venules, and capillaries. This category includes the largest number of discrete entities; the most common are lupus vasculitis, Henoch-Schönlein purpura, Wegener's granulomatosis, and Churg-Strauss syndrome.^{45,46} Furthermore, some forms of vasculitis (usually small vessel vasculitis) have been termed *secondary vasculitis*

when caused by an underlying collagen vascular disease (e.g., lupus vasculitis, Behçet's disease), infection, malignancy, or drug reaction.⁴⁶

Each of these entities affects a characteristic distribution of blood vessels. The involvement of the small bowel can vary greatly, depending on the type of vasculitis and the vessels involved.

LARGE VESSEL VASCULITIS

Of the large vessel vasculitides, Takayasu's arteritis is the most likely to involve the mesenteric vessels. Takayasu's arteritis is a chronic granulomatous inflammatory disease of the large arteries, usually affecting the aorta and its main branches.⁴⁵ Women are affected about 10 times more often than men, and there appears to be a unique predilection for Asian patients. Takayasu's arteritis classically involves the aortic arch, but can also affect the abdominal aorta and mesenteric branches, resulting in abdominal pain, ischemia (acute or chronic), hemorrhage, or strictures.⁴⁵

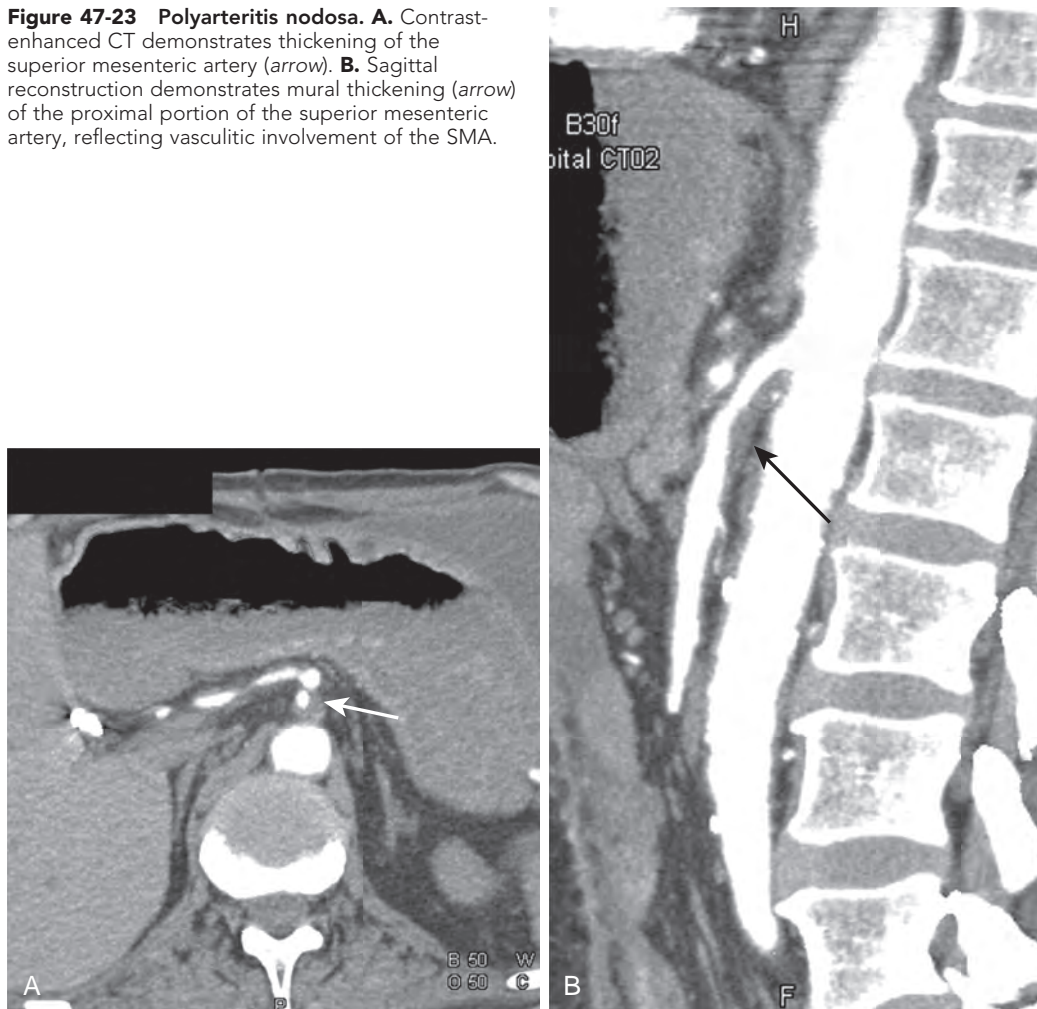
The radiographic diagnosis of mesenteric involvement by Takayasu's arteritis was once typically made using conventional angiography. However, these findings can now be well depicted with MDCT of the mesenteric vessels, with 3D reconstructions

depicting the full extent of the patient's disease. Particularly in the acute phase, the walls of the superior mesenteric artery can appear thickened, usually more regular and extensive than in atherosclerotic disease, and typically encompassing a much longer segment. As the involvement becomes more chronic, long-segment strictures and stenoses of the SMA can develop, along with poststenotic dilation, aneurysms and, in severe cases, occlusion, with collateral vessel formation. Unlike conventional angiography, CT also has the advantage of being able to visualize changes in the small bowel as a result of compromised blood flow, including increased or decreased wall enhancement, wall thickening, mesenteric stranding, and ascites and, in cases of frank infarction, pneumatosis and mesenteric venous gas.

MEDIUM VESSEL VASCULITIS

Of the medium vessel vasculitides, polyarteritis nodosa (PAN) is the most likely to affect the mesenteric arteries (Fig. 47-23). PAN is a fibrinoid necrotizing vasculitis that weakens the arterial wall of small and medium-sized vessels, leading to the formation of aneurysms, typically at branch points. The kidneys and renal arteries are the most commonly involved, with abnormalities present in up to 80% to 90% of patients. However, the small intestine and mesenteric vessels are also involved in over

Figure 47-23 Polyarteritis nodosa. A. Contrast-enhanced CT demonstrates thickening of the superior mesenteric artery (arrow). **B.** Sagittal reconstruction demonstrates mural thickening (arrow) of the proximal portion of the superior mesenteric artery, reflecting vasculitic involvement of the SMA.



50% of cases, with the small bowel being the most commonly involved portion of the gastrointestinal (GI) tract. Bowel involvement by PAN is thought to portend a particularly poor prognosis.⁴⁷ Abdominal pain is reported in up to two thirds of patients with this disorder, usually from ischemia, and GI hemorrhage and bowel perforation are common complications.^{45,46,48} In a series of 24 patients with polyarteritis nodosa and GI tract involvement, 54% developed a surgical abdomen, of whom 3 subsequently died.⁴⁵

Radiologic diagnosis is best made with high-quality CT angiographic images, which demonstrate aneurysms involving the renal, mesenteric, hepatic, splenic, or peripancreatic arteries.⁴⁹ Although this pattern of aneurysm formation is highly suggestive of PAN, patients with necrotizing angitis secondary to IV drug use, lupus vasculitis, and Wegener's granulomatosis can also have a similar distribution and appearance.

SMALL VESSEL VASCULITIS

Of the small vessel vasculitides, those most likely to involve the small bowel include Henoch-Schönlein purpura, systemic lupus erythematosus (SLE), and Behçet's disease.

Henoch-Schönlein Purpura

A small vessel vasculitis of unknown cause, Henoch-Schönlein purpura is the most common vasculitis of childhood.^{50,51} Although generally thought of as a purely pediatric condition, up to 30% of patients may be older than 20 years.⁴⁵ The disorder is characterized by the deposition of IgA-predominant complexes in the skin, joints, kidneys, and GI tract. The skin disease is typically the first manifestation, appearing as a petechial rash with purpura, often on the lower extremities.⁵¹

GI tract involvement can occur in up to 60% of patients, most often resulting in abdominal pain related to ischemia.⁵² Occult or overt GI bleeding is a very common feature, seen in up to 52% of patients, and intramural hematoma within the bowel wall is not uncommon.⁵⁰ Any part of the GI tract can be involved, but the small bowel is the most frequently involved site. Although certainly not specific for the disease, common CT findings include bowel wall thickening, bowel wall dilation, luminal narrowing, fold thickening, and ulceration (Fig. 47-24).⁵³ Multiple different bowel loops can be involved, and areas of intervening normal bowel can be seen. There are typically multiple stigmata of intense abdominal

inflammation, including enlarged mesenteric lymph nodes, engorged mesenteric vasculature, ascites, and mesenteric stranding.⁵² Particularly when presenting in the pediatric population, intussusception is a common surgical complication, occurring in up to 13.6% of patients, with the most common sites being ileoileal and ileocolic.⁵⁰ It is thought that this unique predisposition toward intussusception, particularly in locations within the small bowel, which are uncommon in normal children, is related to hemorrhage and edema within the bowel wall serving as a pathologic lead point.⁵⁰ Although the CT appearance of the bowel can be dramatic, less than 5% develop true bowel infarction or perforation, and the vast majority of cases will resolve without sequelae.⁴⁵

Systemic Lupus Erythematosus

SLE is a complex autoimmune disease with multisystem involvement that can affect any portion of the GI tract as a result of immune complex deposition in the wall of small arterioles feeding the bowel.^{45,54,55} Moreover, patients with SLE are further at risk for bowel complications, given that 27% to 42% of SLE patients are hypercoagulable because of underlying antiphospholipid syndrome, placing them at high risk for the development of mesenteric arterial or venous thrombosis.^{56,57} These two features (arteriolar vasculitis and central mesenteric thrombosis) place these patients at unique risk of bowel ischemia.

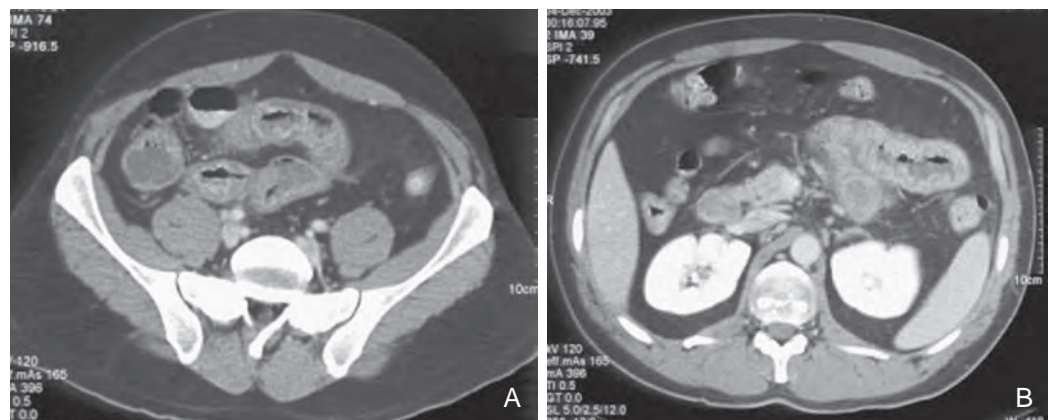
Abnormal CT findings in the bowel are usually reflective of bowel ischemia (see Fig. 47-20), including bowel wall thickening, edema, intramural hemorrhage, altered mucosal enhancement or, in more advanced cases, pneumatosis or mesenteric venous gas (Fig. 47-25).⁵⁴ 3D and multiplanar imaging of the mesenteric vessels are critical to avoid missing subtle cases of arterial or venous thrombosis. Particularly in those patients in whom the amount of thrombus is small and involves only a short segment, the abnormality can be easy to miss on conventional axial images. In patients in whom the bowel ischemia is secondary to the vasculitis itself (rather than thrombosis), subtle beading or pruning of the mesenteric artery branches may be most apparent on 3D MIP images.

Behçet's Disease

A small vessel vasculitis usually affecting young males (age 11 to 30 years), Behçet's disease is classically characterized by oral and genital ulcers, ocular inflammation, arthritis, and skin

Figure 47-24 Henoch-Schönlein purpura.

A, B. Contrast-enhanced CT image demonstrates moderate small bowel thickening. The small bowel is thickened with mucosal hyperemia and has a target appearance. This was ultimately proven to be a case of bowel ischemia secondary to Henoch-Schönlein purpura.



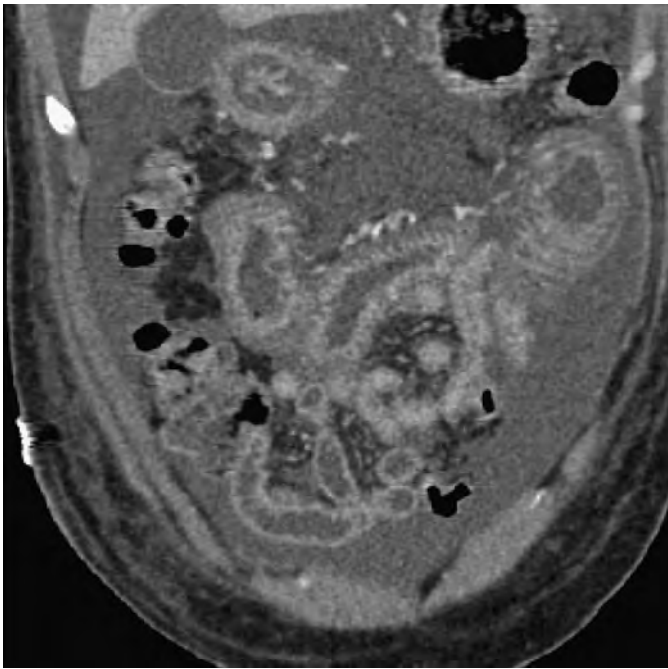


Figure 47-25 Lupus vasculitis in a 32-year old woman with lupus, abdominal pain, and elevated lactic acid level. This coronal contrast-enhanced image shows moderate ascites, marked thickening of the small bowel in the mid abdomen and left upper quadrant, and mucosal hyperemia and low density in the submucosal layer of the bowel wall. These findings reflect bowel ischemia secondary to lupus vasculitis.

lesions.⁴⁶ It is an uncommon necrotizing vasculitis of unknown cause that may involve multiple organs, including the GI tract in up to 50% of cases. The two most common locations in the GI tract are the distal ileum (including the ileocecal region) and esophagus, with involvement of the bowel characterized by severe ulceration. Typically, the diagnosis is made through biopsy of the mucosal ulcers, and patients are subsequently treated with steroids.

Given that the most common site of involvement in the small bowel is the distal ileum, Behçet's involvement in this location can very much mimic Crohn's disease. Severe ulcerations in the bowel wall place the patient at high risk of developing fistulas, sinus tracts, abscesses, and other complications, all of which can misleadingly suggest Crohn's disease (particularly given the patient population). Bowel wall thickening on CT can be severe and even masslike in appearance, asymmetrically involving the bowel wall, and can be confused with malignancy, particularly lymphoma (Fig. 47-26). The presence of large asymmetric ulcerations is a feature most often appreciated on fluoroscopic studies, and barium studies also demonstrate marked fold thickening of the involved bowel, often appearing focal and masslike and sometimes mimicking a small bowel lymphoma or neoplasm. In a series of 28 patients by Ha and co-workers with intestinal Behçet's, it was suggested that discrete, masslike, polypoid lesions in the bowel were more common in patients without complications, whereas bowel wall thickening was more common in patients with complications.⁵⁸ Similarly, most patients without complications had very little inflammatory change or fluid adjacent to the involved bowel segments, whereas severe mesenteric infiltration was more

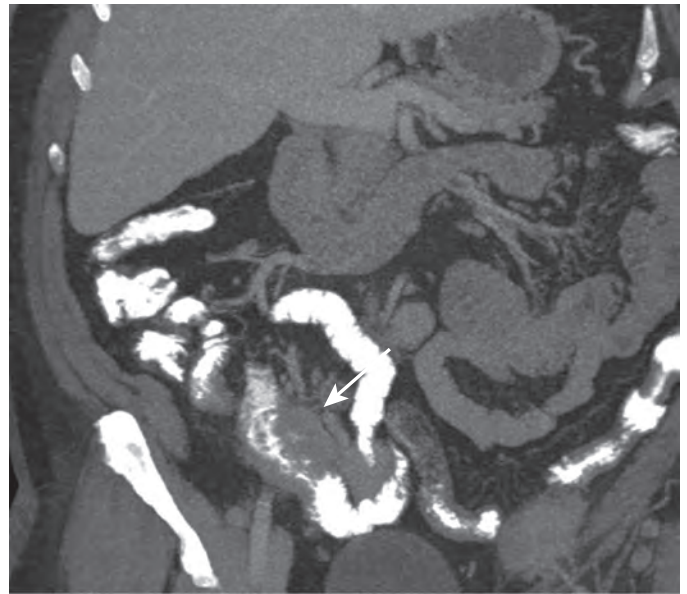


Figure 47-26 Behçet's disease. Coronal contrast-enhanced CT demonstrates marked thickening of the distal ileum (arrow), somewhat masslike in appearance. This was originally thought that it might represent lymphoma, but was found to be manifestation of Behçet's disease.

common in patients with complications such as peritonitis or perforation.

Acute Small Bowel Bleeding

Although much less common than the colon, the small bowel is an important site of GI bleeding, perhaps accounting for 3% to 5% of all cases.⁵⁹ The most frequent causes of small bowel bleeding include ulcerations, tumors, Crohn's disease, angiodysplasia, and vascular malformations.⁶⁰ Usually suspected after negative upper and lower endoscopy, small bowel bleeding is notoriously difficult to diagnose. Although some endoscopic procedures have been developed to evaluate the small bowel, these have not proven especially efficacious in identifying sources of bleeding. For example, push enteroscopy involves the use of a long endoscope to visualize the small bowel beyond the reach of a conventional endoscope. However, this technique is naturally limited by its ability to reach only 80 to 120 cm beyond the ligament of Treitz (thus not evaluating the distal small bowel), is time-consuming, and can miss small bowel bleeding that is intermittent in nature.^{59,61} Capsule endoscopy, which involves the evaluation of the small bowel with a wireless video capsule, has become an option for evaluating the entire small bowel. However, this technique is expensive, time-consuming, can be problematic in patients with bowel strictures and narrowing, and can also miss those with intermittent bleeding. Moreover, this technique is limited to the evaluation of the mucosal layer of the bowel and will miss bleeding from submucosal lesions.⁵⁹ Most importantly, given its time-consuming nature, capsule endoscopy is best reserved for cases of chronic bleeding rather than for the acute setting.

Although the two most common radiologic studies used in the setting of GI bleeding have traditionally been technetium 99m-labeled red blood cell (RBC) scans and catheter angiography, both these modalities have significant limitations in the

small bowel. Although tagged RBC scans can detect low rates of bleeding (>0.2 mL/min), are noninvasive, and can detect intermittent bleeding over long periods of time, this modality is limited by its poor spatial resolution and inability to localize sites of bleeding accurately. Catheter angiography is limited by its ability to only detect relatively rapid rates of bleeding (at least 1 mL/min) and by its difficulty in detecting intermittent hemorrhage. Moreover, it is an invasive modality with associated risks to patient safety and also suffers from poor contrast resolution, which can limit its ability to characterize the true site of bleeding accurately.⁶²

Computed Tomography in the Diagnosis of Gastrointestinal Bleeding. Computed tomography has taken on a growing role in the evaluation of small bowel bleeding in the acute setting, with its ability to identify extraluminal sources of bleeding (e.g., submucosal tumors, vascular malformations) and precisely localize the anatomic site of bleeding. Although the data regarding the use of CT in the acute setting is still relatively sparse, studies performed in animal models suggest that bleeding may be detectable at 0.35 mL/min, better than catheter angiography, and only slightly above the rate detected by tagged RBC studies. In the acute setting, the sensitivity of CT for acute GI hemorrhage has reported to be as high as 92%.^{59,63} Moreover, CT may be a better option than capsule endoscopy, even in the subacute or chronic setting. In a study by Huprich and colleagues, CT enterography (with arterial and venous phase imaging and the use of a neutral oral contrast agent to distend the small bowel) was more sensitive for the source of small bowel bleeding than capsule endoscopy (88% vs. 38%); CT's primary advantage was in cases of bleeding caused by small bowel masses.⁶⁴

Technique. Like other modalities, CT is somewhat limited when bleeding is intermittent, and it is critical that the study be performed when the patient is actively bleeding. In the acute setting, no oral contrast should be administered; positive oral contrast agents can mask sites of active bleeding, whereas neutral contrast agents (e.g., water, VoLumen) can potentially dilute sites of bleeding.^{62,65} Moreover, the potential need for intervention in the acute setting makes any oral ingestion contraindicated. However, neutral contrast agents may be of use in the chronic setting because there is less focus on identifying active bleeding and more focus on identifying an occult small bowel mass, ulcer, or vascular malformation.

Brisk injections (4 to 6 mL/s) of IV contrast are generally necessary because acquiring images at peak arterial enhancement improves the chances of visualizing active contrast extravasation or subtle vascular malformations. Portal venous phase images are also an important part of a GI bleeding protocol because they facilitate the visualization of hypovascular small bowel tumors and subtle bowel wall thickening. Some institutions use a noncontrast phase prior to the administration of contrast to avoid mistaking radiodense ingested materials, medications, sutures, or surgical clips for sites of bleeding. However, we do not routinely acquire noncontrast images at our institution because any active site of bleeding should change in configuration over the arterial and venous phases and ingested foreign material should remain identical in appearance.

Findings. In the acute setting, extravasated contrast material within the bowel is the most critical sign of active bleeding. This extravasation can be quite subtle in the most difficult cases,

although in the most obvious situations, an entire small bowel loop can be filled with extravasated contrast (Figs. 47-27 and 47-28). Importantly, normal mucosal enhancement when the bowel is not particularly well distended can be mistaken for active extravasation, as can hyperdense older clotted blood. In both these situations, it is important to note that active extravasation will typically have much higher Hounsfield attenuations (usually >90 HU) compared with older clotted blood or mucosal enhancement (usually <90 HU).⁶⁵ This is discussed more fully in Chapter 125.

Miscellaneous Disorders

SUPERIOR MESENTERIC ARTERY DISSECTION

Most cases of SMA dissection reflect extension of an aortic dissection into the SMA (Fig. 47-29). The dissection flap can extend a variable length into the SMA and, in some cases, can result in complete occlusion of the vessel, with resulting bowel ischemia. However, isolated visceral artery dissection (without an associated aortic dissection) is a rare phenomenon, usually involving the SMA, with the celiac and common hepatic arteries involved less often (Figs. 47-30 and 47-31). When this occurs, it is thought that the most likely causes are an intrinsic abnormality of the vessel wall, such as underlying vasculitis, cystic medial necrosis, fibromuscular dysplasia (FMD), aneurysm, or collagen vascular disease.⁶⁶⁻⁶⁹

Although rare, the identification of visceral artery dissections is becoming more common with improved CT scanner technology, multiplanar reformats, and 3D reconstructions. In particular, the orientation of the dissection flap, which can have a helical configuration, as well as a volume-averaging artifact, can make it difficult to identify an SMA dissection on axial images, and evaluation of the artery in multiple planes is mandatory. The dissection flap should thereby be easily visualized

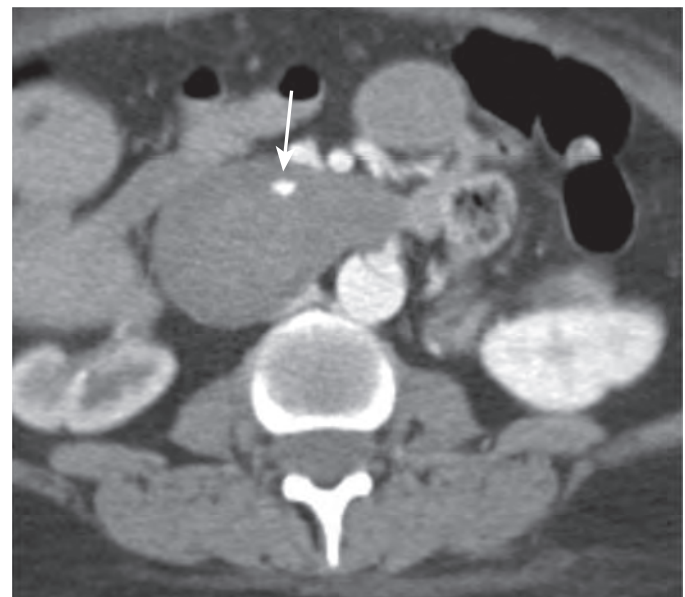


Figure 47-27 Acute gastrointestinal bleeding on CT. Contrast-enhanced arterial phase CT image demonstrates active extravasation within the duodenum (arrow), which is distended with hematoma. This was found to represent a bleeding duodenal ulcer when further evaluated with endoscopy.

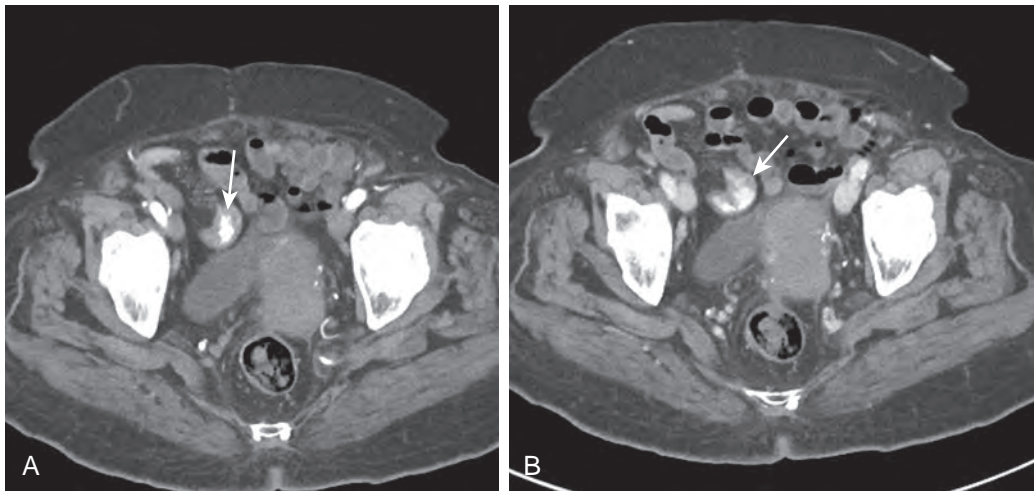


Figure 47-28 Acute small bowel hemorrhage on CT. Contrast-enhanced arterial (A) and venous (B) phase images demonstrate active extravasation of contrast material (arrow) into the right lower quadrant small bowel. The extravasated contrast changes in configuration and enlarges over the two phases, allowing it to be differentiated from ingested hyperdense material, even without noncontrast images.

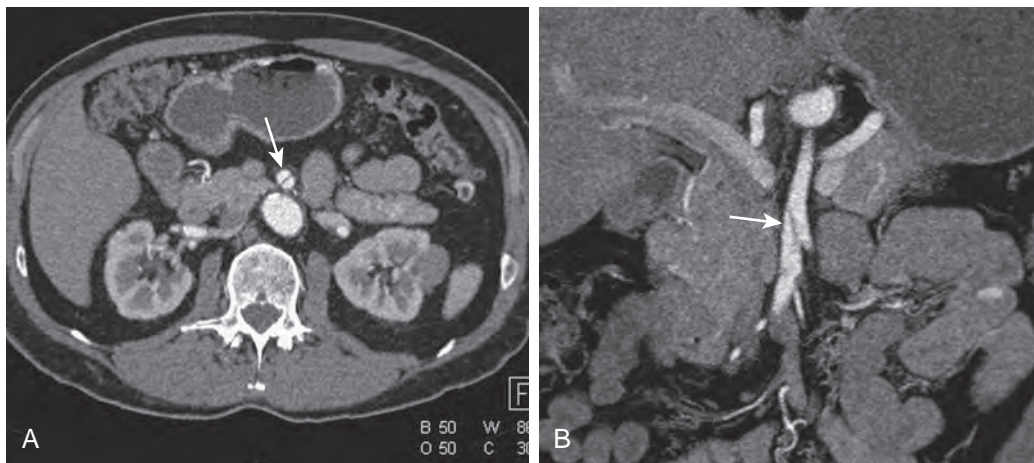


Figure 47-29 Dissection involving the superior mesenteric artery. Axial contrast-enhanced CT (A) and coronal volume-rendered (B) images demonstrate a dissection (arrows) involving the superior mesenteric artery

on CTA, and is typically located a few centimeters distal to the SMA origin, sometimes resulting in narrowing or occlusion of the lumen.⁷⁰ Patients can present with clinical symptoms related to intestinal ischemia or hemorrhage, and the decision to undergo operative repair, endovascular intervention, or conservative therapy is largely contingent on patient symptoms and the presence of bowel ischemia.⁶⁹

TRAUMA

Bowel and mesenteric injury is found in 5% of patients undergoing laparotomy after significant blunt abdominal trauma.⁷⁰ The mesenteric side of the small intestine is more vulnerable to vascular tears, resulting in mesenteric blood or hematoma. The antimesenteric border of the bowel, on the other hand, is more likely to perforate.⁷¹ The radiologist must have a high index of suspicion for mesenteric injury or bowel injury in trauma patients with fluid or increased density in the mesentery, whether or not pneumoperitoneum is present.

Another finding that can be seen in the setting of trauma and hypovolemic shock is the so-called shock bowel complex, in which there is severe submucosal edema and intense mucosal enhancement of the small bowel (Fig. 47-32). This appearance, which is often associated with other evidence of hypovolemic shock (including a flattened inferior vena cava [IVC], narrow aorta, peripancreatic fluid, diminished enhancement of the spleen and liver, and intense enhancement of the adrenal glands) should not be confused with bowel ischemia or bowel injury, because the abnormal appearance of the bowel should resolve with supportive therapy and volume resuscitation.⁷²

RADIATION ENTERITIS

The small intestine is the most common site of injury in patients undergoing radiation therapy, particularly in patients receiving high doses of radiation over a relatively short period of time. Patients with a history of previous intra-abdominal surgery or peritonitis are particularly susceptible to radiation enteritis

Figure 47-30 Dissection of the superior mesenteric artery. Contrast-enhanced axial CT image (A) and coronal volume-rendered reconstruction (B) demonstrate a dissection flap (arrows) in the superior mesenteric artery.

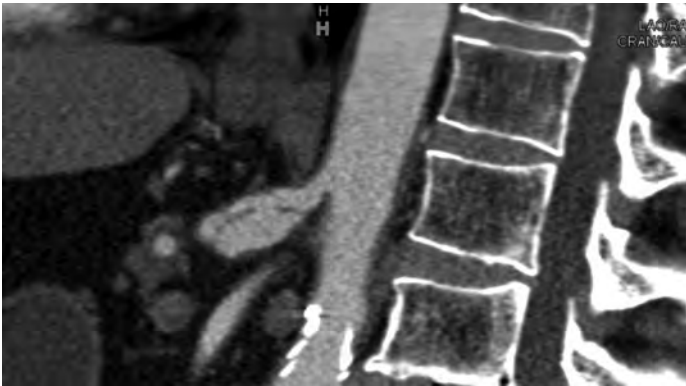
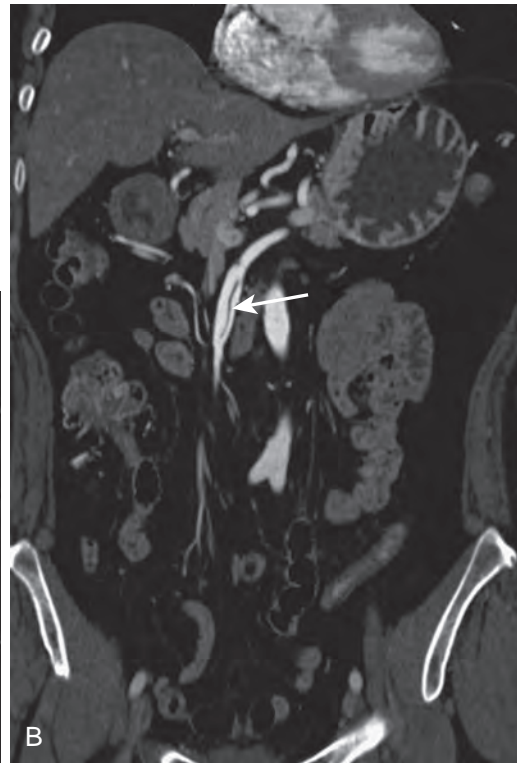
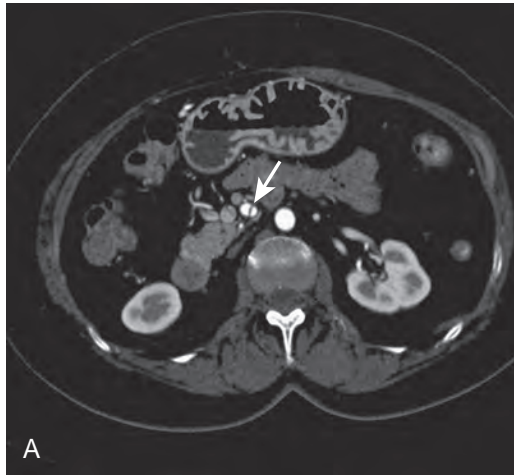


Figure 47-31 Sagittal contrast-enhanced CT. This demonstrates mild aneurysmal dilation of the celiac artery, with a dissection flap. No dissection was identified within the aorta itself.

because of the immobility of the intestine as a result of adhesions. Patients with diabetes or atherosclerotic disease are also at additional risk because the radiation is more likely to result in endarteritis and, ultimately, fibrosis. Patients can present with acute symptoms of radiation enteritis (pain, diarrhea, bleeding) during the radiation therapy, or symptoms of chronic radiation injury (pain, obstruction, malabsorption) can occur at any time point after the therapy (including decades later).

The diagnosis of radiation enteritis is usually made clinically based on the patient's history and presentation. However, CT can be helpful to confirm the suspected diagnosis and determine the severity and extent of involvement. In patients with acute radiation enteritis, CT will typically demonstrate thickening and edema of the small bowel wall, often with mucosal hyperemia, with associated mucosal ulceration generally best

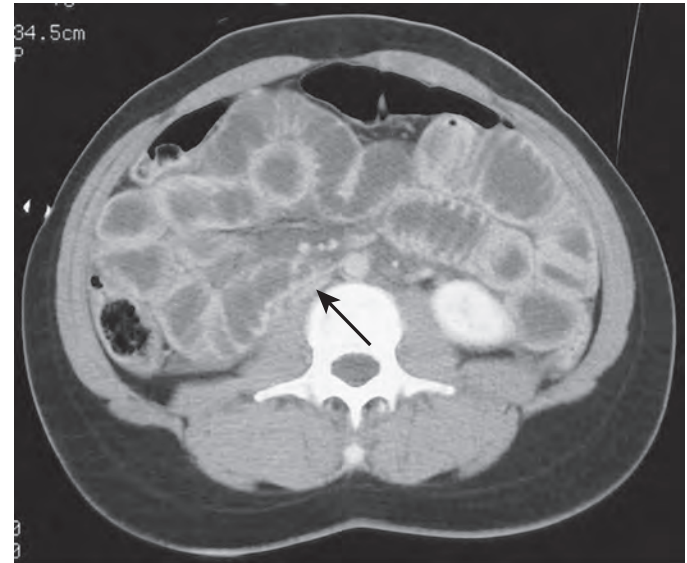


Figure 47-32 Shock bowel in a 23-year-old woman immediately after a motor vehicle accident. Contrast-enhanced CT demonstrates pneumoperitoneum, a flattened IVC (arrow) suggestive of hypovolemia, and a diffusely thickened, avidly enhancing small bowel. This constellation of findings represents the shock bowel complex.

appreciated on fluoroscopic barium studies (Fig. 47-33). Intramural hemorrhage can often be present in the acute stage. Over time, patients with chronic radiation injury can demonstrate stenoses, adhesions, strictures, small bowel obstruction, and fistulas. In the most obvious cases of chronic radiation injury, the small bowel mucosa will appear completely effaced, resulting in a smooth featureless appearance of the small bowel on

CT and fluoroscopic studies, often referred to as ribbon or toothpaste bowel.

SPLANCHNIC ARTERY ANEURYSMS

Splanchnic artery aneurysms are rare, with an incidence of 0.01% to 0.25% in autopsy series.⁷³ Most patients with splanchnic artery aneurysms are asymptomatic, and the diagnosis is most often made incidentally.⁷⁴ However, in some cases, these aneurysms can rupture, and patients can then present with abdominal pain and mesenteric hemorrhage.



Figure 47-33 Radiation enteritis. Axial contrast-enhanced CT image in a patient after radiation therapy for lymphoma demonstrates moderate thickening of several small bowel loops in the right abdomen, thought to be secondary to radiation enteritis. There is also minimal mesenteric stranding and ascites.

The splenic artery is the most commonly involved (60%), followed by the hepatic artery (20%), SMA (5.5%), celiac artery (4%), pancreatic arteries (2%), and gastroduodenal artery (1.5%).⁷⁵ The diagnosis can be made using any modality, including CT, MRI, ultrasound (US), or angiography, although MDCT is the easiest procedure for making the diagnosis, and 3D reconstructions can nicely illustrate the 3D shape and morphology of the aneurysm, providing a roadmap for surgical or endovascular repair. Although the treatment of these aneurysms has traditionally been surgical, endovascular repair has become increasingly common.⁷⁵

The most common location for an SMA aneurysm is within the first 5 cm of the vessel; the most common causes for an aneurysm in this location include endocarditis, atherosclerosis, and pancreatitis. Complications can include thrombosis and rupture, each of which carries a high mortality rate, because complications involving SMA aneurysms place the patient at great danger of small bowel ischemia. Celiac artery aneurysms are more frequent in men than women, and 75% of patients present with clinical symptoms, typically pain (Figs. 47-34 and 47-35).⁷⁶ The risk of rupture is 13%, with an almost 100% mortality rate when rupture occurs.⁷⁷ The most common cause of a celiac artery aneurysm is atherosclerotic disease, and most aneurysms occur either at or near the origin of the vessel.

DRUG-INDUCED SMALL BOWEL ANGIOEDEMA

A self-limited process characterized by the vascular leakage of serum from small vessels, angioedema is likely related to the abnormal release of bradykinin, resulting in severe vasodilation. Although in rare cases hereditary caused by a C1q esterase deficiency, angioedema is usually drug-related. Angiotensin-converting enzyme (ACE) inhibitors are the drugs most commonly known to cause angioedema, and most clinicians are familiar with the swelling, flushing, and facial edema that can characterize this drug reaction. Other drugs, however, including IV contrast itself, can also produce angioedema.^{78,79}

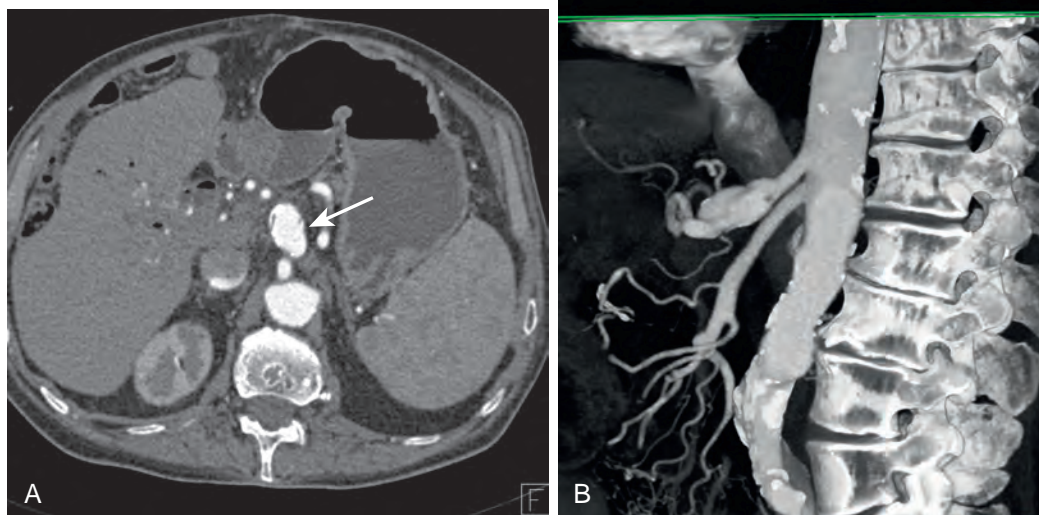


Figure 47-34 Celiac artery aneurysm. **A.** Axial contrast-enhanced CT image in the arterial phase demonstrates an aneurysm (arrow) of the celiac artery. **B.** Volume-rendered (VR) projection nicely demonstrates the complex shape of the celiac artery aneurysm, which begins approximately 1.5 cm distal to the origin of the celiac artery.

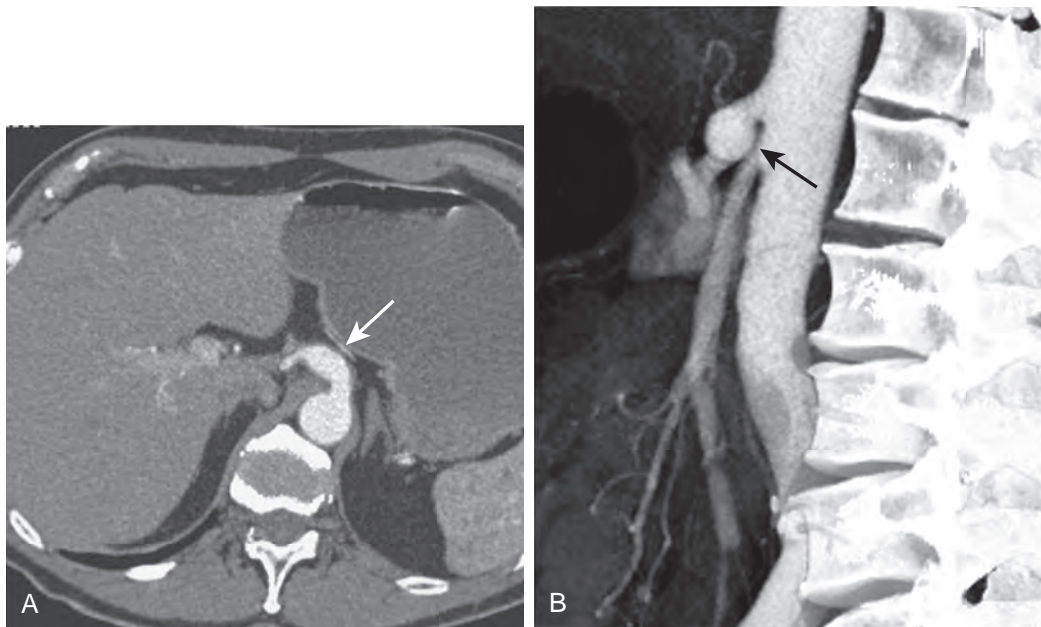


Figure 47-35 Celiac artery aneurysm. Axial (A) and sagittal (B) contrast-enhanced CT images demonstrate aneurysmal dilation of the celiac axis (arrows).

Although classically associated with the oral and respiratory mucosa, angioedema can also be seen in the small bowel, and has been increasingly reported in association with ACE inhibitor usage. The appearance on CT can be very striking, with marked segmental thickening of small bowel loops and intense mucosal enhancement, often resulting in a mistaken diagnosis of bowel ischemia or vasculitis.⁷⁸ Notably, however, this bowel abnormality should be relatively short-lived and transient if the offending drug is discontinued.

MEDIAN ARCUATE LIGAMENT SYNDROME

The median arcuate ligament is a fibrous arch that unites the right and left crura on either side of the aortic hiatus. Although there is a great deal of variation in the shape and orientation of the median arcuate ligament, in most individuals the ligament crosses above the celiac origin and anterior to the aorta. However, in 10% to 24% of individuals, the median arcuate ligament has a low insertion across the origin of the celiac axis, an anatomic abnormality that can be exacerbated in patients with an abnormally high takeoff of the celiac artery.^{80,81} This abnormal positioning of the median arcuate ligament can result in varying degrees of celiac artery compression.

In rare cases, the compression can be hemodynamically significant, resulting in collateral flow to the celiac artery from the SMA (Figs. 47-36 and 47-37). A small subset of individuals with this low insertion will be symptomatic, presenting with symptoms similar to those of CMI. In particular, most patients with clinical symptoms tend to be young women, and there is a tendency to develop symptoms after meals or exercise, or with inspiration. The cause of pain in patients with median arcuate ligament syndrome is controversial; some believe that the pain is a result of compromised blood flow and shunting of blood away from the SMA, but others think that the pain is a result of compression or chronic irritation of the celiac plexus.^{30,81-84} Because of controversy about the true cause of pain, there is a

great deal of disagreement about the best management strategy. There have been arguments in favor of open surgical release of the median arcuate ligament and endovascular angioplasty with stenting.

Although the diagnosis was once typically made with catheter angiography, CT with 3D reconstructions is now clearly the best means of evaluation. Sagittal reconstructions are of the utmost importance because the abnormally low insertion of the median arcuate ligament, compression of the celiac artery, and a characteristic-shaped indentation on the proximal celiac artery can all be optimally illustrated (see Figs. 47-31 and 47-32). Moreover, when the compression is hemodynamically significant, poststenotic dilation of the celiac artery can be seen, and prominent collaterals surrounding the pancreatic head from the SMA through the gastroduodenal and peripancreatic arteries can be present.⁸⁵ Also, given that median arcuate ligament compression is almost certainly a dynamic process, inspiratory and expiratory scans can be performed to evaluate for worsening compression on inspiration (Fig. 47-38).

HEMANGIOMAS

GI hemangiomas are rare benign vascular tumors that can occur anywhere in the GI tract, but are most frequently located in the small intestine (usually the jejunum).⁸⁶ Hemangiomas account for 7% to 10% of all benign small bowel tumors.⁸⁷ Histologically, hemangiomas are classified according to their major component. Capillary hemangiomas are composed of small capillaries with thin walls and blood-filled spaces lined by endothelial cells. Cavernous hemangiomas consist of larger blood-filled sinuses lined by single or multiple layers of endothelial cells.⁸⁸

Small bowel hemangiomas can be single or multiple and can be associated with hemangiomas or vascular malformations in other organs, such as the liver and skin. Accordingly, there have been reported associations between GI hemangiomas and

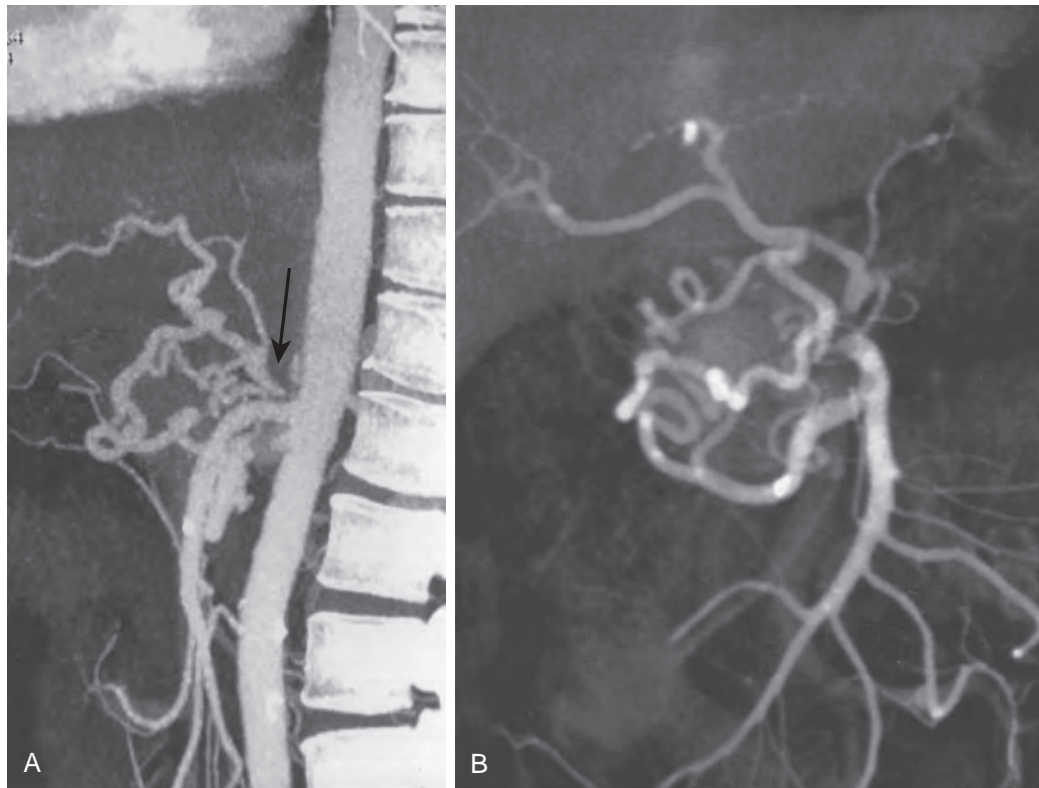


Figure 47-36 Median arcuate ligament syndrome. **A.** Sagittal contrast-enhanced image demonstrates a hooklike or J-shaped appearance of the proximal celiac axis, which is narrowed (arrow). **B.** Coronal MIP image shows enlarged and dilated pancreaticoduodenal collaterals supplying the celiac from the SMA.

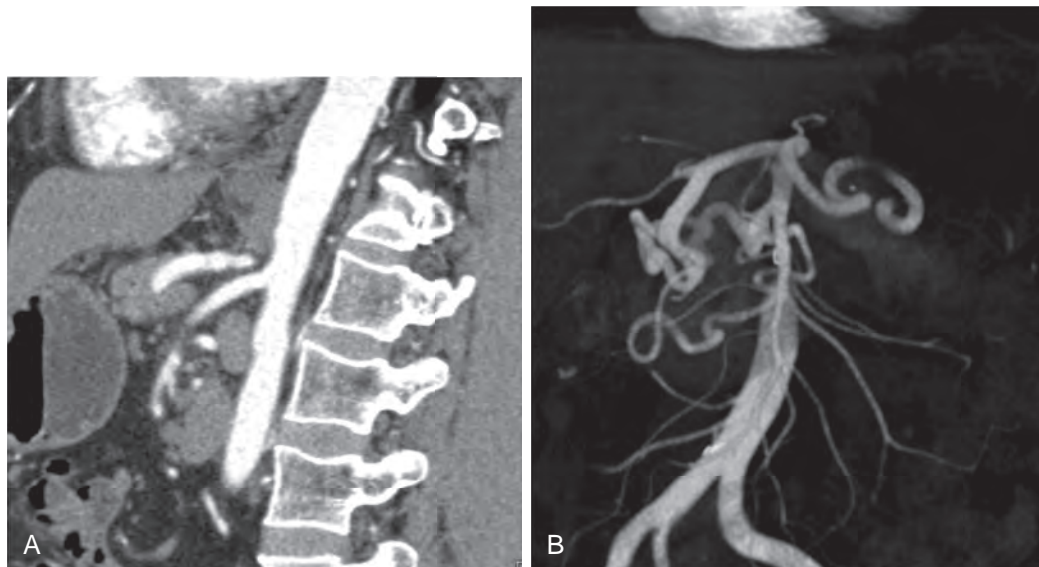


Figure 47-37 Median arcuate ligament syndrome. **A.** Sagittal contrast-enhanced image shows severe narrowing of the proximal celiac artery by a prominent median arcuate ligament. **B.** Coronal CTA with MIP shows enlarged and dilated pancreaticoduodenal collaterals supplying the celiac from the SMA.

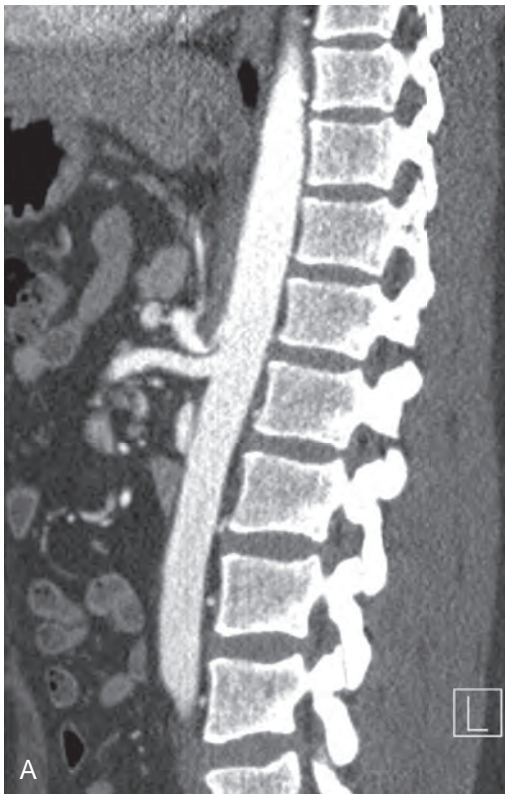
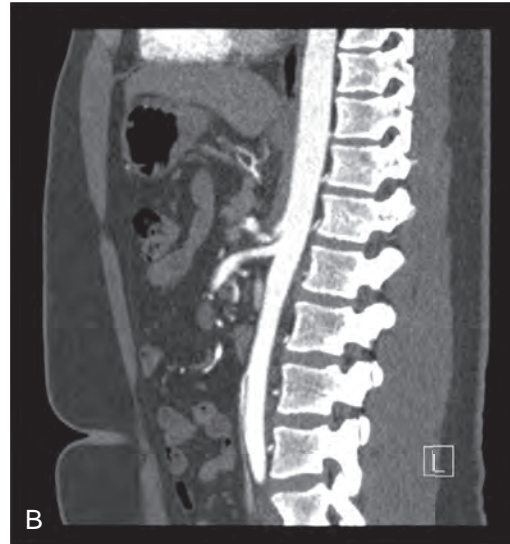


Figure 47-38 Median arcuate ligament syndrome. Expiratory (A) and inspiratory (B) contrast-enhanced sagittal CT images in a patient with median arcuate ligament syndrome. A. The expiratory image demonstrates a characteristic J-shaped indentation on the proximal celiac artery, with resultant compression. B. The degree of celiac artery compression increases on the inspiratory image.



Osler-Weber-Rendu syndrome, Maffucci's syndrome, Klippel-Trenaunay-Weber syndrome, and congenital blue rubber bleb nevus syndrome.⁸⁸

With hemangiomas, 90% eventually present with clinical symptoms, usually acute or chronic GI hemorrhage. Moreover, particularly when large, these lesions can result in small bowel obstruction, intussusception, or perforation. Nevertheless, small bowel hemangiomas have proven extremely difficult to diagnose radiographically, particularly prior to the CT era. In a review of the Japanese literature by Akamatsu and associates, a preoperative diagnosis was possible in only 24% of patients using small bowel series, angiography, or scintigraphy.^{88a} Although some of these lesions are undoubtedly now being diagnosed with capsule endoscopy, CT has emerged as a very good option for diagnosing these masses. Although there have been few reports in the literature, the appearance can vary greatly. In some cases, mural thickening of the involved bowel segment is seen, with intense associated enhancement on arterial phase images, whereas in other cases, a distinct hypervascular mass or a tangle of abnormal serpiginous vessels may be identified (Fig. 47-39). The presence of phleboliths within the lesions is readily apparent on CT and can strongly suggest the diagnosis.⁸⁸⁻⁹⁰

Summary

Advances in CT technology—the refinement of CT protocols to study the small bowel and mesenteric vasculature specifically and the development of modern 3D reconstruction software—over the last few years have markedly improved our ability to diagnose diseases of the small bowel. Whereas CT was once

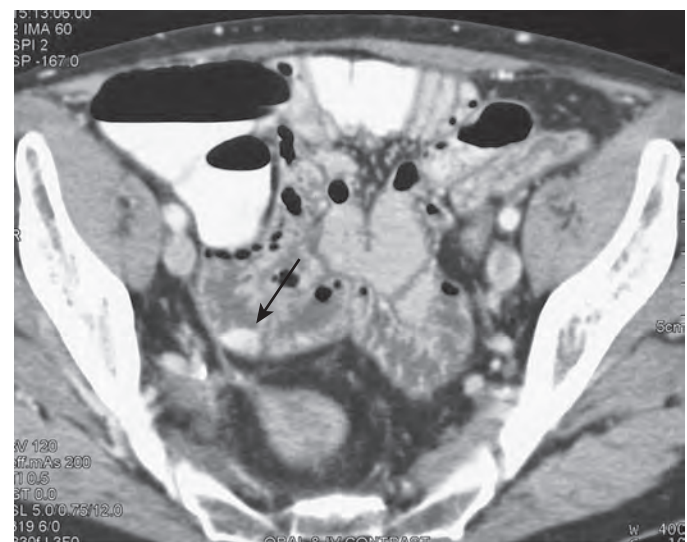


Figure 47-39 Contrast-enhanced axial CT image. This demonstrates a 9-mm enhancing lesion in the distal small bowel (arrow) ultimately proven to represent a hemangioma.

limited to only the most basic diagnoses in the small bowel, and fluoroscopic studies were used to make more subtle determinations and diagnoses, CT should now be considered as the first-line imaging study in patients with suspected vascular disorders of the small bowel. CT can accurately image the small bowel and mesenteric vasculature with a high degree of detail and subtlety and can identify a wide range of pathologies.

REFERENCES

1. Fishman EK, Ney DR, Heath DG, et al: Volume rendering versus maximum intensity projection in CT angiography: What works best, when, and why. *Radiographics* 26:905–922, 2006.
2. Johnson PT, Horton KM, Fishman EK: Nonvascular mesenteric disease: Utility of multidetector CT with 3D volume rendering. *Radiographics* 29:721–740, 2009.
3. Greenwald D, Brandt L, Reinus J: Ischemic bowel disease in the elderly. *Gastroenterol Clin North Am* 30:445–465, 2004.
4. Freeman A, Graham J: Damage control surgery and angiography in cases of acute mesenteric ischemia. *ANZ J Surg* 75:308–317, 2005.
5. Horton KM, Fishman EK: Multidetector CT angiography in the diagnosis of mesenteric ischemia. *Radiol Clin North Am* 45:275–288, 2007.
6. Batellier J, Kierny R: Superior mesenteric artery embolism: Eighty-two cases. *Ann Vasc Surg* 4: 112–116, 1990.
7. Tendler D: Acute intestinal ischemia and infarction. *Semin Gastroenterol Dis* 11:66–76, 2003.
8. McKinsey J, Gerwurtz B: Acute mesenteric ischemia. *Surg Clin North Am* 77:307–318, 1997.
9. Turkbey B, Akpinar E, Cil B, et al: Utility of multidetector CT in an emergency setting in acute mesenteric ischemia. *Diagn Interv Radiol* 15:256–261, 2009.
10. Rhee R, Gloviczki P, Mendonea C, et al: Mesenteric venous thrombosis: Still a lethal disease in the 1990's. *J Vasc Surg* 20:688–697, 1994.
11. Bassiouny H: Nonocclusive mesenteric ischemia. *Surg Clin North Am* 77:319–326, 1997.
12. Suhaker C, Al-Hakeem M, MacAurthur J, et al: Mesenteric ischemia secondary to cocaine abuse: Case reports and literature review. *Am J Gastroenterol* 92:1053–1054, 1997.
13. Smerud M, Johnson C, Stephens D: Diagnosis of bowel infarction: A comparison of plain films and CT scans in 23 patients. *AJR* 154:99–103, 1990.
14. Klein H, Lensing R, Klosterhalfen B, et al: Diagnostic imaging of mesenteric infarction. *Radiology* 197:79–82, 1995.
15. Taourel P, Deneuville M, Pradel J, et al: Acute mesenteric ischemia: Diagnosis with contrast-enhanced CT. *Radiology* 199:632–636, 1996.
16. Barmase M, Kang M, Wig J, et al: Role of multidetector CT angiography in the evaluation of suspected mesenteric ischemia. *Eur J Radiol* 80: e582–e587, 2011.
17. Ofer A, Abadi S, Nitecki S, et al: Multidetector CT angiography in the evaluation of acute mesenteric ischemia. *Eur Radiol* 19:24–30, 2009.
18. Meneke J: Diagnostic accuracy of multidetector CT in acute mesenteric ischemia: Systematic review and meta-analysis. *Radiology* 256:93–101, 2010.
19. Aschoff AJ, Stuber G, Becker BW, et al: Evaluation of acute mesenteric ischemia: Accuracy of biphasic mesenteric multidetector CT angiography. *Abdom Imaging* 34:345–357, 2009.
20. Lee R, Tung H, Tung PHM, et al: CT in acute mesenteric ischemia. *Clin Radiol* 58:279–287, 2002.
21. Alpen M, Glazer G, Francis I: Ischemia of infarcted bowel's findings. *Radiology* 166:149–152, 1988.
22. Clark R: Computed tomography of bowel infarction. *J Comput Assist Tomogr* 11:757–762, 1987.
23. Furukawa A, Kanasaki S, Kono N, et al: CT diagnosis of acute mesenteric ischemia from various causes. *AJR* 192:408–416, 2009.
24. Kim J, Ha H, Byun J: Intestinal infarction secondary to mesenteric venous thrombosis. *J Comput Assist Tomogr* 17:382–385, 1993.
25. Wiesner W, Khurana B, Hoon J, Ros P: CT of acute bowel ischemia. *Radiology* 226:635–650, 2003.
26. Bartnicke B, Balfe D: CT appearance of intestinal ischemia and intramural hemorrhage. *Radiol Clin North Am* 32:845–860, 1994.
27. Horton K, Corl F, Fishman E: CT of nonneoplastic diseases of the small bowel: Spectrum of disease. *J Comput Assist Tomogr* 23:417–428, 1999.
28. Salzano A, De Rosa A, Carbone M, et al: Computerized tomography features of intestinal infarction: 56 surgically treated patients of which 5 with reversible mesenteric ischemia. *Radiol Med (Torino)* 97:246–250, 1999.
29. Moawad J, Gewertz B: Chronic mesenteric ischemia. *Surg Clin North Am* 77:357–369, 1997.
30. Cognet F, Salem D, Dransart M, et al: Chronic mesenteric ischemia: Imaging and percutaneous treatment. *Radiographics* 22:863–879, 2002.
31. Jarvinen O, Laurikka J, Sisto T, et al: Atherosclerosis of visceral arteries. *Vasa* 24:9–14, 1995.
32. Croft R, Menon G, Marston A: Does intestinal angina exist? A critical study of obstructed visceral arteries. *Br J Surg* 68:316–318, 1981.
33. Roobottom C, Dubbins P: Significant disease of the celiac and superior mesenteric arteries in asymptomatic patients: Predictive value of Doppler sonography. *AJR* 161:985–988, 1993.
34. Shih MP, Hagspiel KD: CTA and MRA in mesenteric ischemia: Part I. Role in diagnosis and differential diagnosis. *AJR* 188:452–461, 2007.
35. Horton K, Fishman E: 3D CT angiography of the celiac and superior mesenteric arteries with multidetector CT data sets: Preliminary observations. *Abdom Imaging* 25:523–525, 2000.
36. Horton K, Fishman E: Multidetector row and 3D CT of the mesenteric vasculature: Normal anatomy and pathology. *Semin Ultrasound CT MR* 24:353–363, 2003.
37. Horton K, Fishman E: Volume-rendered 3D CT of the mesenteric vasculature: Normal anatomy, anatomic variants, and pathologic conditions. *Radiographics* 22:161–172, 2002.
38. Horton K, Fishman E: Multi-detector row CT of mesenteric ischemia: Can it be done? *Radiographics* 21:1463–1473, 2001.
39. Moneta G, Lee RW, Yeager R, et al: Mesenteric duplex scanning: A blinding prospective study. *J Vasc Surg* 17:79–84, 1993.
40. Perko M: Duplex ultrasound for assessment of superior mesenteric artery blood flow. *Eur J Vasc Endovasc Surg* 21:106–117, 2001.
41. Zwolak R, Fillinger M, Walsh D, et al: Mesenteric and celiac duplex scanning: A validation study. *J Vasc Surg* 27:1078–1087, 1998.
42. Hohenweller EJ: Chronic mesenteric ischemia: Diagnosis and treatment. *Semin Intervent Radiol* 26:346–351, 2009.
43. Meany J, Prince M, Nostrant T, Stanley J: Gadolinium-enhanced MR angiography of visceral arteries in patients with suspected chronic mesenteric ischemia. *J Magn Reson Imaging* 7:171–176, 1997.
44. Ernst O, Asnar V, Sergeant G, et al: Comparing contrast-enhanced breath hold MR angiography and conventional angiography in the evaluation of the mesenteric circulation. *AJR* 174: 433–439, 2000.
45. Ha H, Lee S, Rha S, et al: Radiologic features of vasculitis involving the gastrointestinal tract. *Radiographics* 20:779–794, 2000.
46. Hokama A, Kishimoto K, Ihama Y, et al: Endoscopic and radiographic features of gastrointestinal involvement in vasculitis. *World J Gastrointest Endosc* 4:50–56, 2012.
47. Levine S, Hellman D, Stone J: Gastrointestinal involvement in polyarteritis nodosa (1986–2000): Presentation and outcomes in 24 patients. *Am J Med* 112:386–391, 2002.
48. Bassel K, Harford W: Gastrointestinal manifestation of collagen vascular disease. *Semin Gastrointest Dis* 6:228–240, 1995.
49. Kato T, Fujii K, Wada R, Hidaka Y: A case of polyarteritis nodosa with lesions of the superior mesenteric artery illustrating the diagnostic usefulness of three-dimensional computed tomographic angiography. *Clin Rheumatol* 24:628–631, 2005.
50. Ebert EC: Gastrointestinal manifestations of Henoch-Schönlein purpura. *Dig Dis Sci* 53: 2011–2019, 2008.
51. Mills J, Michel B, Bloch D, et al: The American College of Rheumatology 1990 criteria for the classification of Henoch-Schönlein purpura. *Arthritis Rheum* 33:1114–1121, 1990.
52. Jeong Y, Ha H, Yoon C, et al: Gastrointestinal involvement in Henoch-Schönlein syndrome. *AJR* 168:965–968, 1997.
53. Siskind B, Burrell M, Pun H, et al: CT demonstration of gastrointestinal involvement in Henoch-Schönlein syndrome. *Gastrointest Radiol* 10:352–354, 1985.
54. Lalani T, Kanne J, Hatfield G, Chen P: Imaging findings in systemic lupus erythematosus. *Radiographics* 24:1069–1086, 2004.
55. Assimakopoulos SF, Dimitropoulou D, Lioussis SN: Education and imaging. Gastrointestinal: Intestinal vasculitis associated with systemic lupus erythematosus. *J Gastroenterol Hepatol* 23:992, 2008.
56. Espinosa G, Cervera R, Font J, Shoenfeld Y: Antiphospholipid syndrome: Pathogenic mechanisms. *Autoimmune Rev* 2:677–696, 2003.
57. Andrews P, Frampton G, Cameron J: Antiphospholipid syndrome and systemic lupus erythematosus. *Lancet* 342:988–989, 1993.
58. Ha H, Lee H, Yang S, et al: Intestinal Behçet syndrome: CT features of patients with and without complications. *Radiology* 209:449–454, 1998.
59. Buckley OSH, Lyburn ID, McGann G, et al: The role of computerized tomography in the evaluation of gastrointestinal bleeding following negative or failed endoscopy: A review of current status. *J Postgrad Med* 54:126–134, 2008.
60. Duchat F, Soyer P, Boudiag M, et al: Multi-detector row CT of patients with acute intestinal bleeding: A new perspective using multiplanar and MIP reformations from submillimeter isotropic voxels. *Abdominal Imaging* 35:296–305, 2010.
61. Fillipone A, Cianci R, Milano A, et al: Obscure and occult gastrointestinal bleeding: Comparison of different imaging modalities. *Abdominal Imaging* 37:41–52, 2012.
62. Geffroy Y, Rodallec MH, Boulay-Coletta I, et al: Multidetector CT angiography in acute gastrointestinal bleeding: Why, when, and how. *Radiographics* 31:E35–E47, 2011.

63. Scheffel H, Pfammatter T, Wildi S, et al: Acute gastrointestinal bleeding: Detection of source and etiology with multi-detector-row CT. *Eur Radiol* 17:1555–1565, 2007.
64. Huprich JE, Fletcher JG, Fidler JL, et al: Prospective blinded comparison of wireless capsule endoscopy and multiphase CT enterography in obscure gastrointestinal bleeding. *Radiology* 260:744–751, 2011.
65. Horton KM, Jeffrey RB, Federle MP, Fishman EK: Acute gastrointestinal bleeding: The potential role of 74 MDCT and 3D imaging in the diagnosis. *Emerg Radiol* 16:349–356, 2009.
66. Okino Y, Kiyosue H, Mori H, et al: Root of the small-bowel mesentery: Correlative anatomy and CT features of pathologic conditions. *Radiographics* 21:1475–1490, 2001.
67. Tokue H, Tsushima Y, Endo K: Imaging findings and management of isolated dissection of the visceral arteries. *Jpn J Radiol* 27:430–437, 2009.
68. Tameo MN, Dougherty MJ, Calligaro KD: Spontaneous dissection with rupture of the superior mesenteric artery from segmental arterial mediolysis. *J Vasc Surg* 53:1107–1112, 2011.
69. Lim E, Jung SW, Lee SH, et al: Endovascular management for isolated spontaneous dissection of the superior mesenteric artery: Report of two cases and literature review. *J Vasc Interv Radiol* 22:1206–1211, 2011.
70. Corbetti F, Vigo M, Bulzacchi A, et al: CT diagnosis of spontaneous dissection of the superior mesenteric artery. *J Comput Assist Tomogr* 13:965–967, 1989.
71. Nghiem H, Jeffrey R, Mindelzun R: CT of blunt trauma to the bowel and mesentery. *AJR* 160: 53–58, 1993.
72. Ames JT, Federle MP: CT hypotension complex (shock bowel) is not always due to traumatic hypovolemic shock. *AJR* 192:W230–W235, 2009.
73. Stanley J, Thompson N, Fry W: Splanchnic artery aneurysms. *Arch Surg* 101:689–697, 1970.
74. Pilleul F, Beuf O: Diagnosis of splanchnic artery aneurysms and pseudoaneurysms, with special reference to contrast-enhanced 3D magnetic angiography: A review. *Acta Radiol* 45:702–708, 2004.
75. Horton KM, Fishman EK: CT angiography of the mesenteric circulation. *Radiol Clin North Am* 48:331–345, 2010.
76. Messina L, Shanley C: Visceral artery aneurysms. *Surg Clin North Am* 77:425–442, 1997.
77. Shanley C, Shah N: Uncommon splanchnic artery aneurysms: Splenic, hepatic and celiac. *Annu Rev Surg* 10:506–515, 1996.
78. Park SW, Bae IY, Eun HW, et al: Small-bowel angioedema during screening computed tomography due to intravenous contrast material. *J Comput Assist Tomogr* 35:549–552, 2011.
79. Scheirey CD, Scholz FJ, Shortsleeve MJ, Katz DS: Angiotensin-converting enzyme-induced small bowel angioedema: Clinical and imaging findings in 20 patients. *AJR* 197:393–398, 2011.
80. Linder H, Kemprud E: A clinicoanatomic study of the arcuate ligament of the diaphragm. *Arch Surg* 103:600–605, 1971.
81. Duffy AJ, Panait LM, Eisenberg D, et al: Management of median arcuate ligament syndrome: A new paradigm. *Ann Vasc Surg* 23:778–784, 2009.
82. Nyman O, Ivancey K, Lindle M, Uher P: Endovascular treatment of chronic mesenteric ischemia: Report of five cases. *Cardiovasc Interv Radiol* 31:305–313, 1998.
83. Matsumoto A, Tegtmeyer C, Fitzcharles E, et al: Percutaneous transluminal angioplasty of visceral arterial stenosis: Results and long term clinical follow-up. *J Vasc Interv Radiol* 6:165–174, 1995.
84. Roayaie S, Jossart G, Gitlitz D, et al: Laparoscopic release of celiac artery compression syndrome facilitated by laparoscopic ultrasound scanning to confirm restoration of blood flow. *J Vasc Surg* 32:814–817, 2000.
85. Horton K, Talamini M, Fishman E: Median arcuate ligament syndrome: Evaluation with CT angiography. *Radiographics* 25:1177–1182, 2005.
86. Elias G, Toubia N: Hemangioma of the small intestine presenting with recurrent overt, obscure gastrointestinal bleeding. *Clin Gastroenterol Hepatol* 8:A18, 2010.
87. Sorbi D, Conio M, Gostout C: Vascular disorders of the small bowel. *Gastrointest Endosc Clin North Am* 9:71–92, 1999.
88. Corsi A, Ingegnoli AM, Abelli P, et al: Imaging of small bowel cavernous hemangioma: Report of a case with emphasis on the use of computed tomography and enteroclysis. *Acta Biomed* 78:139–143, 2007.
- 88a. Akamatsu T, Matsuda Y, et al: A case of multiple cavernous hemangioma of the small intestine and clinical review of the Japanese literature. *Gastroenterol Jpn* 25:494–498, 1990.
89. Ramanujam P, Venkatesh K, Bettinger L, et al: Hemangioma of the small intestine: Case report and literature review. *Am J Gastroenterol* 90: 2063–2064, 1995.
90. Fernandes D, Dionisio I, Neves S, et al: Cavernous hemangioma of small bowel: A rare cause of digestive hemorrhage. *Rev Esp Enferm Dig* 106:214–215, 2014.

Postoperative Small Bowel

TEMEL TIRKES | JOHN C. LAPPAS

CHAPTER OUTLINE

Small Bowel After Gastric Surgery

Afferent Loop Obstruction

Enterectomy and Anastomosis

Postoperative Blind Pouch and Loop

Enterostomy

Jejunostomy

Ileostomy

Ileal Reservoirs

Continent Ileostomy Reservoir

Ileoanal Pouches

Small Bowel Transplantation

Surgical treatment of disease of the small bowel requires the use of relatively few operative techniques, and most of these surgical interventions are applicable to any segment of the jejunum and ileum. Primarily, they include enterotomy for removal of polyps or foreign bodies, enteroplasty for treatment of strictures, enterectomy for resection of obstructed, traumatized, neoplastic, or necrotic segments, plication to prevent intestinal obstruction, and creation of ostomies or mucous fistulas for feeding or drainage purposes.¹ In addition, the small bowel is used for the surgical construction of reservoirs after gastrectomy and proctocolectomy and for the reconstitution of biliary and pancreatic flow into the gastrointestinal (GI) tract. Another development is the surgical option of small bowel transplantation for the treatment of select patients with short bowel syndrome and intestinal failure.

Radiologic studies are seldom performed as routine follow-up of the surgical procedure, but are done to assess the integrity of the small bowel or investigate postoperative complications. Appreciation of postoperative anatomy and associated intestinal alterations can be especially important because the pertinent surgical history may be incomplete or even unknown at the time of diagnostic imaging. In patients with a history of small bowel surgery who present with GI symptoms, the postoperative anatomy and site of any anastomosis can be evaluated by small bowel enteroclysis techniques.^{2,3} However, experience with CT enteroclysis is limited to a few institutions. An alternative technique for achieving adequate bowel distention is CT enterography, which does not require intubation but the patient must drink large quantities of oral contrast in a short period of time. Considering many factors specific to the patient and institution, the radiologist would make a choice between the intubation-infusion method (enteroclysis) and the oral approach (enterography).

Small Bowel After Gastric Surgery

Important although uncommon alterations in small intestinal physiology or anatomy may occur after certain operations on the stomach. In the postgastrectomy syndrome, various pathophysiologic disorders result from interruption of the pyloric sphincter mechanism or from the sequelae of a vagotomy. Rapid influx of hyperosmotic gastric contents into the small bowel may manifest clinically as the dumping syndrome, with symptoms of postprandial cramping and urgent diarrhea. Mild luminal dilation and hypermotility of the efferent jejunum can be observed on small bowel studies. Serotonin, enteroglucagon, and vasoactive intestinal polypeptide are also released systemically by the small intestine in response to luminal distention and are partly responsible for the vasomotor component of dumping.⁴ Small bowel dysmotility with bacterial colonization, intestinal malabsorption, and impaired pancreatic and biliary function may also contribute to postvagotomy diarrhea.⁵

AFFERENT LOOP OBSTRUCTION

An afferent loop may be created with an esophagoenterostomy, gastroenterostomy, or enteroenterostomy that results from various gastric or pancreaticogastric operations. In Billroth II gastroduodenostomy, the afferent loop is the duodenum, in Whipple's procedure it is the Roux jejunal limb, and in Roux-en-Y gastric bypass the afferent loop is the duodenum and proximal jejunum. Afferent loop obstruction, also referred to as biliopancreatic limb obstruction, is an uncommon complication of these surgical procedures and occurs with variable clinical severity, acuteness, and chronicity.⁶ Afferent loop syndrome refers to chronic partial obstruction of an afferent loop. Causes include stenosis of the anastomosis, adhesions, retrograde intussusception, volvulus, internal hernia, recurrent neoplasm, and inflammatory disease.^{6,7} The clinical diagnosis of afferent loop obstruction can be difficult because patients may have vague symptoms or the classic finding of bilious vomiting with relief of abdominal pain. Acute obstruction can result in pancreatitis, whereas chronic progression of the syndrome can result in malabsorption, intestinal bleeding, or perforation.⁸

Abdominal radiographs are often normal because the obstructed afferent loop is fluid-filled because of ongoing accumulation of biliary, pancreatic, and intestinal secretions. GI barium studies may suggest the diagnosis if there is nonfilling of the afferent loop or preferential filling of a dilated afferent loop associated with stasis (Fig. 48-1). However, the efficacy of barium studies is questionable because the afferent loop fails to opacify in 20% of normal patients.⁹

Computed tomography (CT) is helpful in visualization of the obstructed afferent loop.⁹⁻¹¹ A characteristic finding on the CT is a dilated, U-shaped afferent loop that traverses the midline (Fig. 48-2). Nonopacification of the afferent loop is usual after oral contrast administration. Transmitted pressure from the obstruction may be sufficient to distend the gallbladder and bile

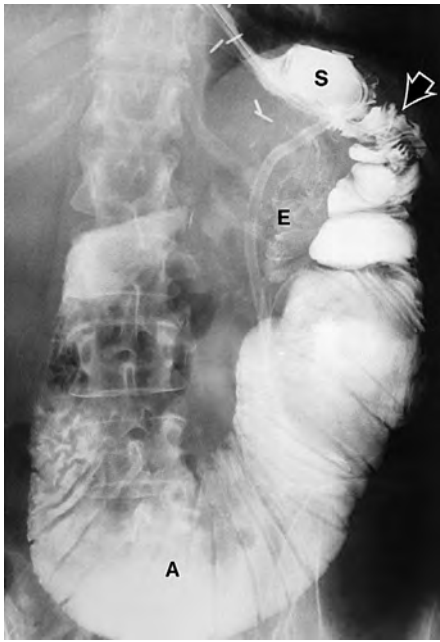


Figure 48-1 Afferent loop obstruction. Barium injection into small gastric remnant (S) results in preferential filling of a distended afferent loop (A). Only minimal contrast material enters the efferent (E) intestine. Distorted bowel margins are caused by kinking and tethering from adhesions (arrow).



Figure 48-3 Afferent loop obstruction after Roux-en-Y esophagojejunostomy. Coronal CT image displays obstructive distention of the afferent biliopancreatic limb (A) and common bile duct (arrow). The scan was performed with IV but without oral contrast media.

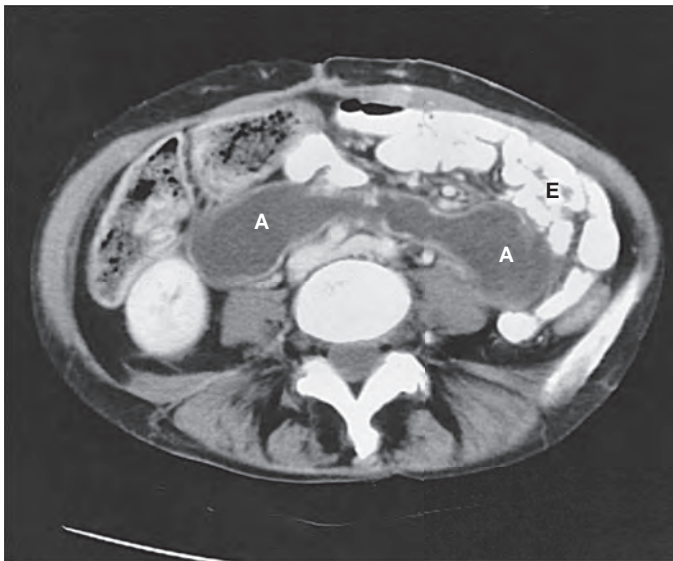


Figure 48-2 CT image of afferent loop obstruction. Oral contrast medium opacifies the normal efferent small bowel loops (E); the abnormal uniformly dilated afferent loop (A) remains nonopacified.

ducts.^{10,11} Coronal CT images aid in identifying the course of the obstructed loop and differentiating the intestine from other fluid collections (Fig. 48-3).⁶

Enterectomy and Anastomosis

Enterectomy refers to surgical excision of the intestine and its corresponding mesentery, as indicated by a wide variety of clinical conditions. Primary anastomosis generally follows

segmental resection of the small bowel, although in some patients an external ostomy is created in conjunction with closure or formation of a mucous fistula of the distal bowel segment.

Anastomosis of the small bowel is one of the most commonly performed GI surgical procedures because it is required for reconstituting continuity of the intestine after resection, bypassing an obstructed intestinal segment, and forming an enteric reservoir. Mechanical sutures and staples are established forms of instrumentation equal to the use of manual suturing techniques for all types of intestinal operations.¹²

Intestinal anastomoses can be constructed as an end-to-end, functional end-to-end (anatomic side-to-side), end-to-side, or side-to-side anastomosis (Fig. 48-4). An end-to-end anastomosis is preferred to reestablish continuity of the small bowel, provided there is minimal disparity in luminal size. An end-to-end anastomosis ideally serves to avoid small bowel stasis syndromes. Closing the two ends of an excised bowel segment and performing a side-to-side anastomosis in close proximity to the closed ends creates a functional end-to-end anastomosis that provides an increased anastomotic surface. An end-to-side anastomosis is used to compensate for disproportionate proximal and distal luminal sizes, and a side-to-side anastomosis is indicated in unusual clinical situations that require expeditious bypass of an intestinal obstruction (e.g., as with extensive neoplastic disease of the small bowel). When an end-to-side anastomosis is performed, the end of the proximal lumen is anastomosed to the side of the distal intestinal segment. This arrangement ensures that peristalsis within the blind (distal) segment is directed antegrade toward

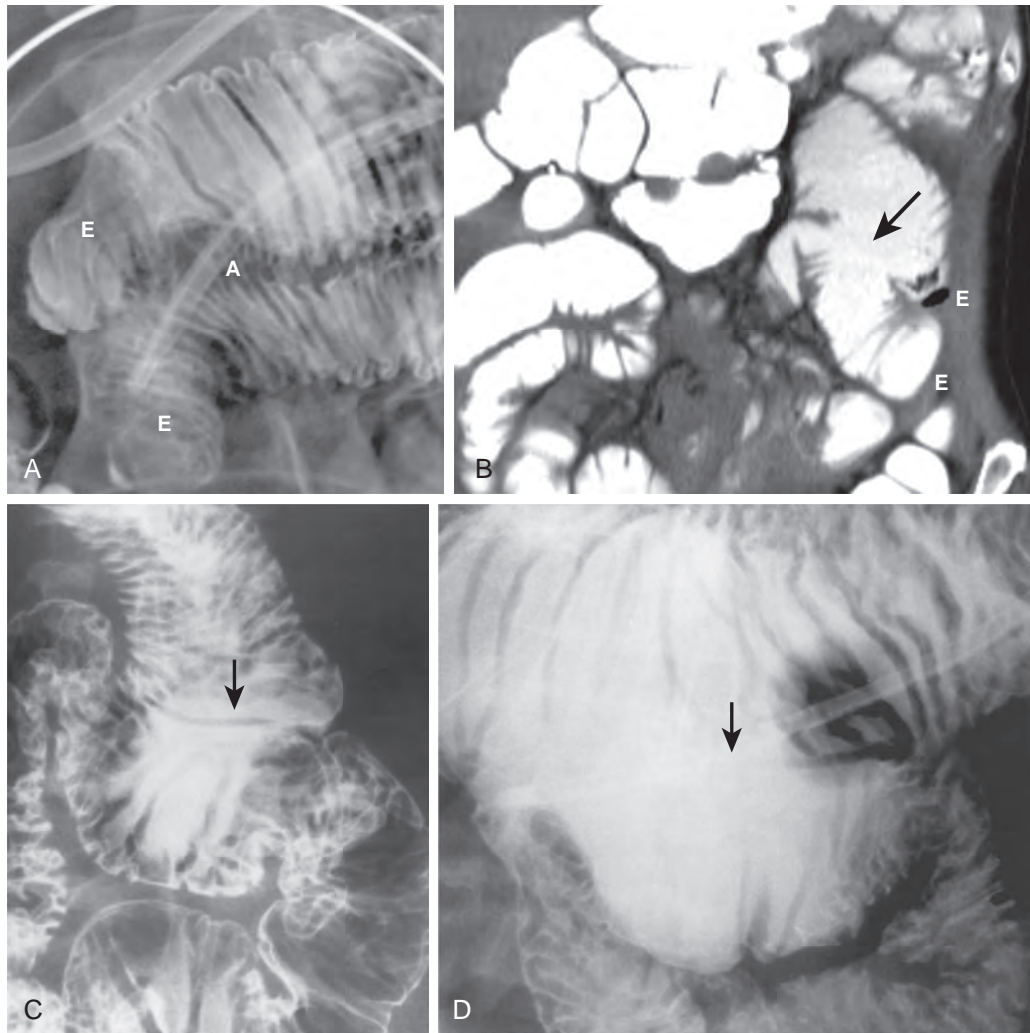


Figure 48-4 Intestinal anastomoses. **A.** Functional end-to-end jejunal anastomosis, created by an anatomic side-to-side technique, is evident on enteroclysis with characteristic short oversewn ends (E) in close proximity to a broad anastomotic lumen (A) traversed by the catheter. **B.** Functional end-to-end anastomosis (arrow) demonstrated on a coronal CT enteroclysis image with similar anatomic features. E indicates oversewn ends of the proximal and distal loops. **C.** End-to-side anastomosis (arrow). **D.** Side-to-side anastomosis (arrow). (From Lappas JC, Maglinte DD: Imaging of the postsurgical small bowel. *Radiol Clin North Am* 41:305–326, 2003.)

and beyond the anastomotic opening, thereby preventing stasis (Fig. 48-5).¹

Despite careful preoperative patient preparation and meticulous surgical technique, dehiscence of small bowel anastomoses can occur. Aside from technical considerations, several factors may adversely affect the success of an anastomosis, including sepsis, tissue hypoxia, malignancy, and advanced patient age. Intestinal perforation from an anastomotic dehiscence may be detected by the presence of free intraperitoneal air on abdominal radiographs. Contrast studies performed with water-soluble contrast media may demonstrate an intestinal leak, although similar findings are detectable on CT, which also provides the advantage of localizing contaminated peritoneal fluid and imaging the complication of abscess formation. Extraintestinal fluid collections, which progressively increase in volume in the postoperative period, are suggestive of an anastomotic disruption, and evidence of enteric contrast media extravasation is diagnostic. Suture dehiscence with a small or contained intestinal leak can also result in a localized

perianastomotic inflammatory process or phlegmon, which may result in partial intestinal obstruction (Fig. 48-6).

POSTOPERATIVE BLIND POUCH AND LOOP

Although the anatomic end-to-end and functional end-to-end surgical anastomoses have essentially replaced the side-to-side anastomosis to restore bowel continuity, the latter procedure is occasionally performed, and a postoperative blind pouch may develop. It should be appreciated that a blind pouch is not intentionally created, unlike a postoperative blind loop. During side-to-side anastomosis, division of the circular muscle can result in local dysmotility with stasis that leads to progressive dilation of the proximal anastomotic segment and formation of a blind intestinal pouch. An incorrectly performed end-to-side anastomosis (side of the proximal segment of intestine sutured to the end of the distal intestine) creates a similar anatomic abnormality. Occasionally, blind pouches may be encountered in association with a prior functional end-to-end (anatomic

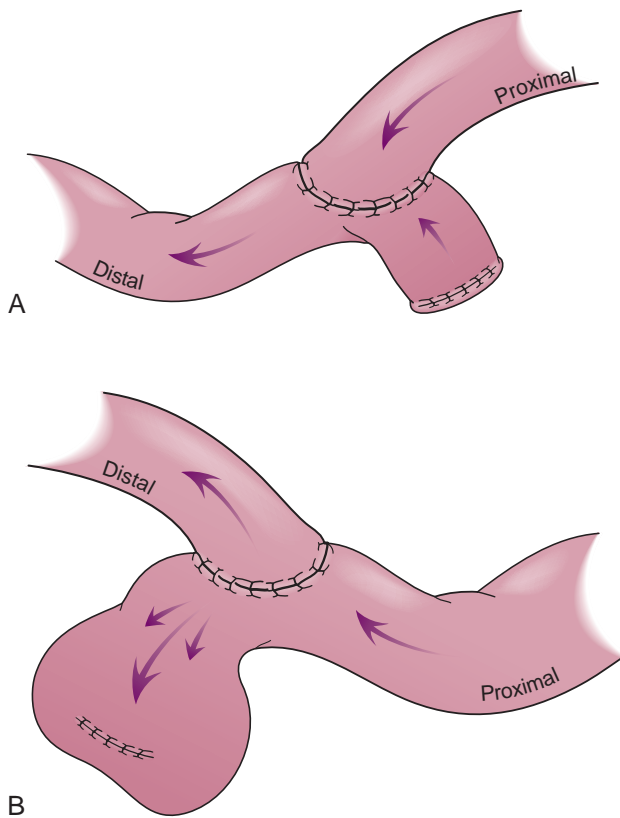


Figure 48-5 End-to-side anastomosis. A. Using correct surgical technique, the end of the proximal small bowel segment is anastomosed to the side of the distal small bowel segment, allowing intestinal contents to flow in a normal peristaltic direction (arrows) through a patent bowel lumen. **B.** An improper anastomosis, with the side of the proximal bowel segment sutured to the end of the distal bowel segment, allows intestinal peristalsis (arrows) to be directed into the blind segment and contributes to the complication of lumen dilation (pouch formation) and intestinal stasis.

side-to-side) surgical anastomosis because of abnormal local peristalsis and stasis.

In addition to intestinal stasis with potential for bacterial overgrowth, a postoperative blind pouch can be associated with inflammation, ulceration, and intestinal bleeding.¹³ Symptoms of abdominal pain and distention, episodic diarrhea, and a history of previous intestinal anastomosis suggest the clinical syndrome and its underlying abnormality, but diagnostic confirmation requires radiologic imaging. Segmental pouch resection and a restorative end-to-end anastomosis are corrective and eliminate the associated complications.

On CT, an intestinal blind pouch is recognized as a distinct saccular enteric structure, with surgical clips visible in the adjacent region.¹⁴ Small bowel contrast studies, particularly enteroclysis and CT enteroclysis, demonstrate the pouch and its anastomotic relationships (Fig. 48-7).

Although some clinical features are in common with the blind pouch syndrome, the anatomic abnormality associated with the blind loop syndrome is different. In blind loop syndrome, a segment of small intestine has been completely bypassed from the enteric stream by an enteroanastomosis. Stagnation of small bowel contents within the blind loop leads to bacterial overgrowth, which, in the most severely affected patients, can approximate the composition of normal colonic

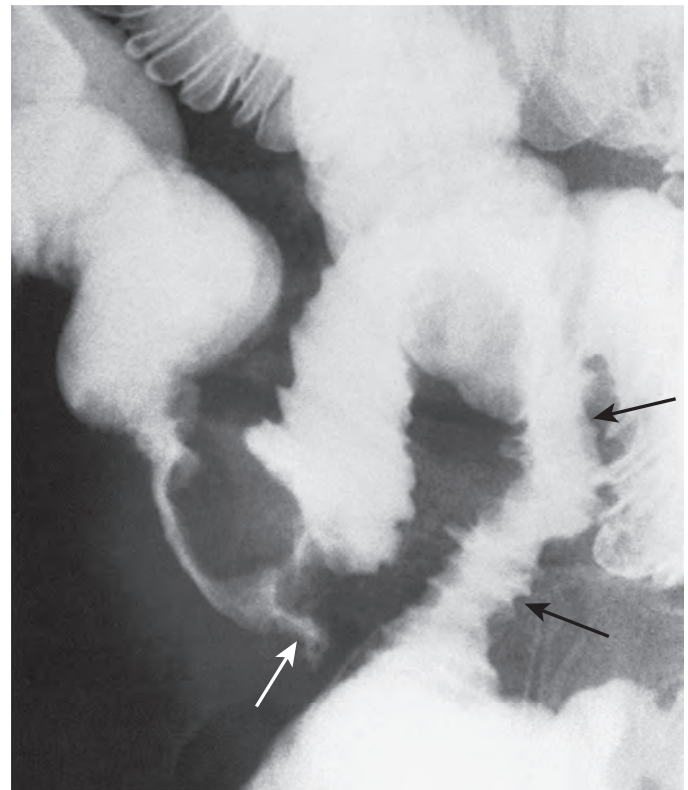


Figure 48-6 Perianastomotic phlegmon with intestinal narrowing. Symptoms of obstruction developed in this patient shortly after a segmental ileal resection with end-to-end anastomosis was performed for benign disease. Enteroclysis shows a short segment of luminal narrowing with a small leak (white arrow) and thickened folds (black arrows) of the adjacent ileal loop. At surgery, ischemic dehiscence of the anastomosis was associated with a localized inflammatory reaction and mural edema of the proximal bowel segment.

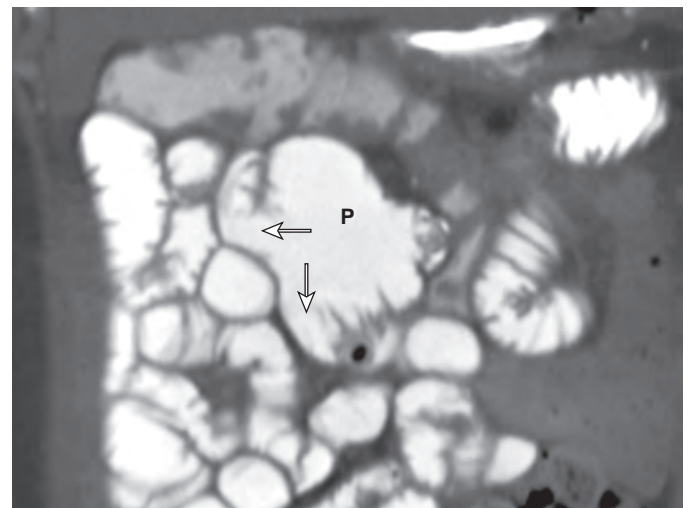


Figure 48-7 Blind pouch. CT enteroclysis shows formation of a sacular blind pouch (P) associated with a prior side-to-side jejunal anastomosis. Arrows point to the afferent and efferent limbs.

flora in quantity and complexity of organisms. Bacterial overgrowth in the small intestine may result in profound disturbances of absorptive function, with malabsorption of lipids and vitamin B₁₂ being most notable.¹⁵ Symptoms and clinical signs of the syndrome are those of malabsorption and include

diarrhea, steatorrhea, anemia, and nutritional deficiencies. As in the diagnosis of blind pouch, dedicated small bowel enteroclysis studies can accurately demonstrate the postoperative anatomic abnormality.

Enterostomy

Enterostomy refers to an intestinal opening that is surgically designed to communicate with the skin and function on a temporary or permanent basis. To prevent an intra-abdominal leak from the intestinal lumen, an enterostomy is made in small bowel segments that are sufficiently mobile to be brought into contact with the anterior abdominal wall.

JEJUNOSTOMY

Jejunostomy is an ideal route for administering nutritional support.¹ Advantages of a feeding jejunostomy over gastrostomy include reduced nausea, vomiting, and risk of pulmonary aspiration via gastroesophageal reflux. Surgical feeding jejunostomies are performed in malnourished patients with an anticipated lengthy postoperative course, in patients with pathology of the upper GI tract, including gastroparesis, malignancy, fistula, and anastomotic leaks proximal to the potential jejunostomy site, and in patients who are not candidates for endoscopic, fluoroscopic, or laparoscopic insertion of feeding jejunostomies or who have failed these approaches. Direct intubated jejunostomies satisfy temporary nutritional requirements, whereas long-term jejunal feeding is best accomplished by a Roux-en-Y type jejunostomy. Surgical placement of the jejunostomy, at least 70 cm distal from the duodenojejunal junction and fixation of the jejunal loop to the peritoneum, are common precautions used during jejunostomy construction. Some surgeons prefer injection of the jejunostomy catheter with a water-soluble contrast medium before initiating enteric feeding to ascertain proper catheter position and thus avoid a misdirected infusion.

Various complications can be associated with any of the surgical jejunostomy methods.^{1,16} In a series of patients with jejunostomy tubes, radiologic studies demonstrated complications related to catheter placement in 14% of cases; in 19% of cases, various mechanical problems were attributed to the location or function of the catheter.¹⁷ Abnormalities included enterogastric reflux of the alimentary fluid, malposition of the catheter, and dislodgment, with an intra-abdominal leak and small bowel obstruction at or near the jejunostomy site.

ILEOSTOMY

A distal enterostomy or ileostomy is primarily used for evacuation of intestinal contents in clinical situations that preclude normal use of the colon or require its surgical removal. A conventional (end) ileostomy, with total proctocolectomy, provides a relatively simple and often curative surgical approach that mitigates the future risks of malignancy or recurrent inflammation with these diseases. The loss of fecal continence and its attendant physical and psychological effects remain significant drawbacks of ileostomy surgery. Since the development of the ileoanal reservoir procedures, the use of conventional ileostomy has been restricted to patients with extensive Crohn's proctocolitis, anal sphincter dysfunction, reservoir failure, and older

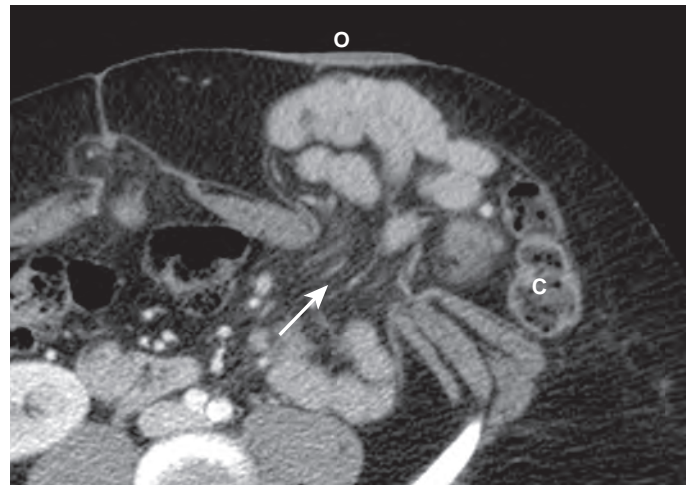


Figure 48-8 Parastomal hernia. This 51-year-old woman had a history of pelvis leiomyosarcoma requiring distal colonic resection and left lower quadrant colostomy. The CT image shows a large anterior abdominal wall defect with herniation of multiple small bowel loops and mesentery (arrow). The colon (c) proximal to the ostomy (o) is displaced to the side. This diagnosis requires careful review of several scan slices because the herniated loops and stoma are often in different axial scan planes.

patients.¹⁸ Another form of distal enterostomy, the loop (double-barrel) ileostomy, is performed in some situations to permit temporary intestinal diversion. Circumstances include Crohn's disease complicated by abscess or extensive fistulas and emergency intervention for intestinal obstruction, or as an adjunct to complex operations that require the protection of a distal enteric anastomosis to promote healing.

Creation of a conventional Brooke or everted end-ileostomy involves transection of the ileum with mobilization of a 5-cm ileal segment through an abdominal wall defect and a specific suturing technique to allow for ileostomy maturation.¹⁸ Malfunction of an ileostomy may result from adhesions, prestomal narrowing of the ileal lumen, paraileostomy herniation, and recurrent disease. These abnormalities can present early or late after operation and usually occur at or near the ileostomy site, producing symptoms of diarrhea or intestinal obstruction.

CT accurately detects parastomal hernias because it is the most commonly performed examination in patients with unexplained stoma-related abdominal symptoms. Herniation is often associated with large (>3-cm) defects in the anterior abdominal wall at the stomal site and is common lateral to the stoma (Fig. 48-8).¹⁹ Evaluation of patients with an ileostomy and suspected ileostomy dysfunction or other complication can also be safely performed by retrograde contrast media examinations, including enteroclysis.

Ileal Reservoirs

Ileal reservoirs are continence-preserving surgical procedures that offer patients the advantage of an improved body image and active lifestyle. Many surgeons consider the presence of Crohn's disease a contraindication for these procedures because of the increased risk for recurrent inflammatory disease and the potential for additional small bowel resection in these patients.¹⁸

CONTINENT ILEOSTOMY RESERVOIR

Kock introduced the concept of an internal reservoir associated with a postcolectomy ileostomy in 1969 and demonstrated that the terminal ileum could function as a low-pressure, highly compliant reservoir.²⁰ The complexity of Kock pouch construction and function now limits the application of the procedure to select patients with prior colectomy and conventional ileostomy or failed or contraindicated ileoanal pouch surgery.^{18,21}

Creation of a continent ileostomy involves the use of the distal 45 cm of ileum, with the most proximal ileal segment fashioned into a spherical reservoir by complex suturing techniques. By design, opposing directions of peristalsis prevent propulsive activity from emptying the pouch. Continence is further maintained by intussusception of the efferent ileal segment into the pouch to form the valve mechanism; the end of the ileum creates the abdominal wall stoma. Suturing of the pouch to the anterior abdominal wall provides stability and prevents volvulus of the pouch and peripouch herniation. Successful Kock pouch construction obviates the use of an external ileostomy appliance because the contents of the ileal reservoir are evacuated by stomal intubation.

Complications of the Kock pouch usually occur months after surgery and include various forms of valve dysfunction, non-specific inflammation of the reservoir or the afferent ileal segment (pouch ileitis), and fistulas. Although reasonable functional results, including long-term continence, are achieved, the incidence of surgical revision in patients with a continent ileostomy remains high.²²

Retrograde double-contrast barium examination following cleansing irrigation of the reservoir is the recommended method for evaluation of the Kock pouch.²³ Radiography in an oblique or lateral view is required to visualize the efferent ileal segment and ileostomy stoma adequately. Suspicion of suture dehiscence in the immediate postoperative period or pouch perforation, after intubation, should be evaluated using water-soluble rather than barium contrast media.

Barium studies of the normal reservoir show typical small bowel fold patterns interrupted by a linear mucosal ridge that represents the suture line between the two anastomosed ileal segments.²³ Surface granularity is seen with mild pouchitis, whereas ulceration and mucosal fold distortion occur with more severe pouch inflammation.²⁴ The intact continence valve appears as a tubular or round, lobular structure invaginated within the reservoir and associated with an array of stabilizing surgical clips. Sliding and eversion of the valve from the pouch results in valve shortening, with progressive lengthening and tortuosity of the efferent ileal segment to the stoma.²⁴ Difficulty in pouch intubation, chronic outflow obstruction, and incontinence ensue. Adenomas may occur in the continent ileostomy, and surveillance of the reservoir is required for patients who have undergone surgery for familial polyposis syndromes (Fig. 48-9).

ILEOANAL POUCHES

Creation of an ileal reservoir with an ileoanal anastomosis following colectomy and rectal mucosectomy has become an important surgical alternative for patients requiring total proctocolectomy. In patients with primary colonic mucosal disease, including chronic ulcerative colitis and adenomatous polyposis, this innovative operation removes potential disease-bearing

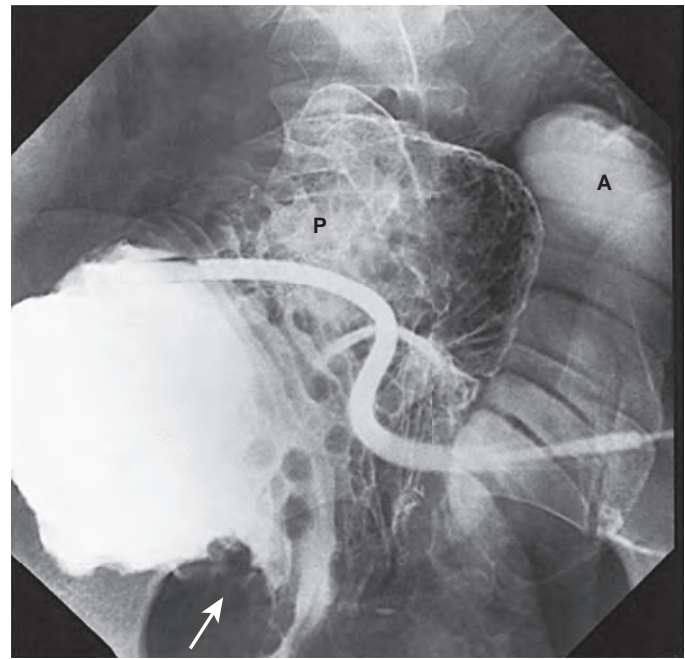


Figure 48-9 Kock pouch in a patient with familial adenomatous polyposis. Contrast medium injection of the pouch (P) after catheterization of the efferent limb shows multiple round mucosal defects representing recurrent adenomas. An irregular mass (arrow) suggests malignancy. A, afferent limb.

mucosa while preserving anal continence and the normal defecatory pathway.

Several forms of ileoanal pouch have been described, but the J pouch configuration is preferred because of the simplicity of its construction, adequate reservoir capacity, ease of emptying, and absence of a potentially obstructing efferent limb.^{18,25} An ileoanal J pouch is constructed from the distal 25 cm of ileum, fashioned into a J shape, and secured by side-to-side anastomosis of the two adjacent loops (Fig. 48-10A). After anorectal mucosectomy and rectal transection that spares the integrity of the anal sphincter, the constructed ileal pouch is anastomosed to the dentate line of the rectal cuff. A proximal diverting ileostomy is often established for 8 to 12 weeks to allow for healing of the extensive anastomoses, and eventual closure of the protective ileostomy renders the ileoanal pouch functional.

Although excellent functional results can be achieved in patients with an ileoanal reservoir, the procedure may be associated with significant complications.^{26,27} Common problems include pouchitis, small bowel obstruction, anastomosis dehiscence or stricture, fistula, and pelvic abscess. Most complications are adequately managed, but ileoanal pouch failure can occur in up to 10% of patients.²⁶ Radiologic evaluation of the ileoanal reservoir is required to assess its function and exclude anastomotic leakage from the reservoir and other postoperative complications.²⁸⁻³¹

Postoperative imaging of the ileoanal pouch is not routinely performed but reserved for clinically suspected complications.³² Contrast ileography or pouchography can be performed antegrade through the ileostomy stoma or preferably retrograde via a soft rectal catheter to visualize the ileoanal pouch and anastomosis. Water-soluble contrast media is used for early

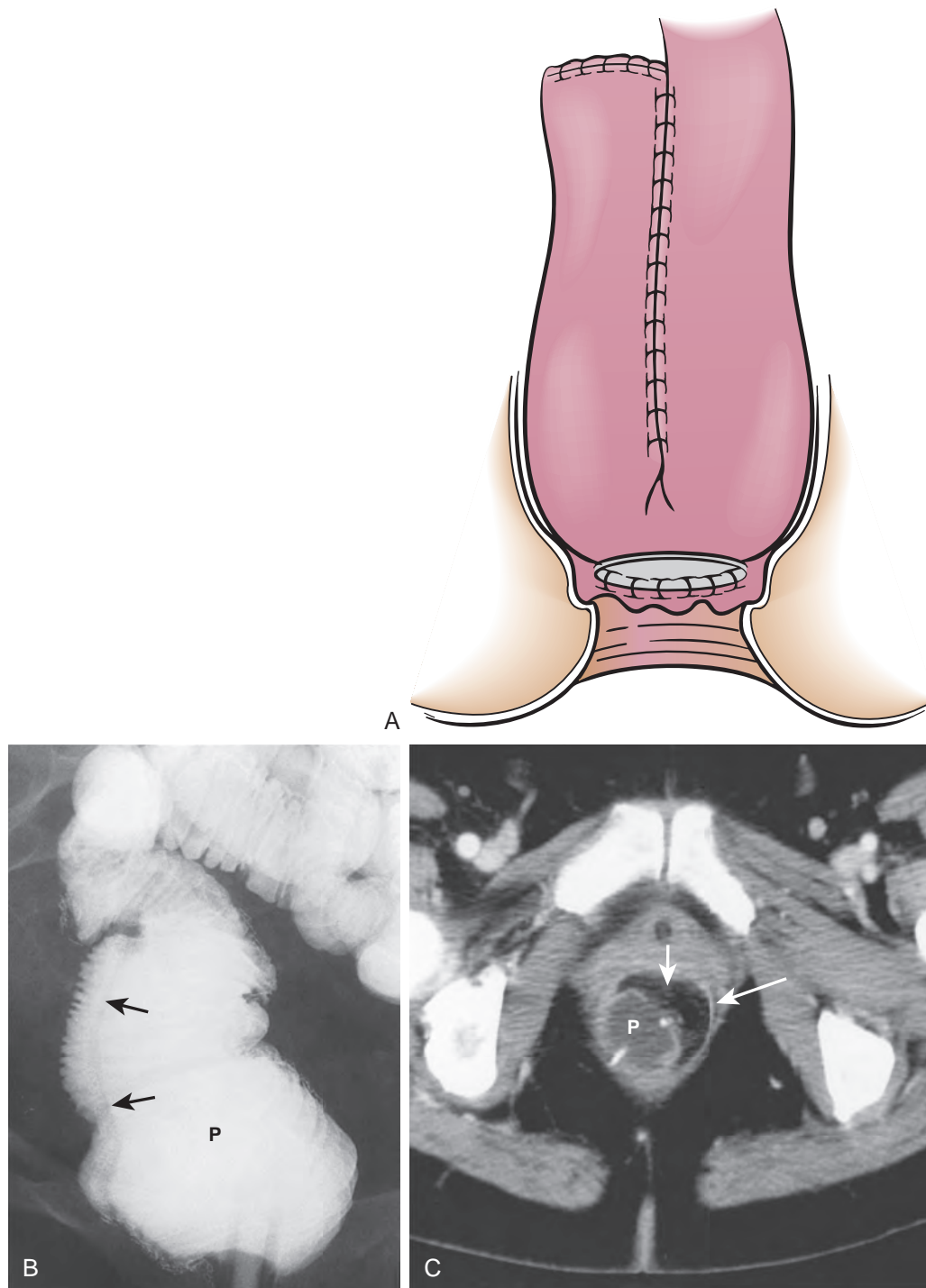


Figure 48-10 Ileoanal-J pouch. **A.** Schematic representation showing side-to-side anastomosis of the adjacent ileal loop and direct anastomosis of the inferior apex of the reservoir to the dentate line. **B.** Normal pouchogram with characteristic vertical raphe (arrows) created by the anastomotic line. **C.** CT image of normal pouch (P) with surrounding ileal mesentery (short arrow) and thin muscular anorectal wall (long arrow). (From Lappas JC, Maglinte DD: *Imaging of the postsurgical small bowel*. *Radiol Clin North Am* 41:305–326, 2003.)

postoperative examinations or if there is an abnormal clinical examination of the pouch; otherwise, barium is used for routine evaluations. On contrast studies, the normal J pouch is depicted as an ovoid intestinal structure with distinctive vertical raphes that correspond to the line of anastomosis, whereas on CT, a thin surgically stapled pouch wall is demonstrated, with adjacent normal fat (Fig. 48-10B and C).^{28,29}

Pouchitis or mucosal inflammation of the ileoanal pouch occurs in almost 50% of patients undergoing the procedure and presents as a clinically evident syndrome of fever, abdominal cramping, and diarrhea. Contrast pouchograms are non-specific but may demonstrate spasm and thickened ileal pouch folds. In patients with anastomotic dehiscence and pelvic sepsis, pouchograms may demonstrate abnormal findings, such as contrast extravasation, extraluminal gas, thickening and spiculation of pouch folds, and mass effect. On CT, patients with postoperative pelvic infections demonstrate abnormal pouch and rectal wall thickness in addition to inflammatory infiltration of the peripouch and perirectal fat. Abscesses typically occur in the peripouch region between the ileal mesenteric fat and adjacent rectal muscularis (Fig. 48-11). In patients with infectious complications after ileoanal pouch surgery, the findings on ileography are often nonspecific, whereas CT more accurately delineates the inflammatory process and can also direct therapeutic intervention.^{29,31} Later complications of intestinal obstruction manifest after closure of the ileostomy and commonly involve the closure site or distal small bowel. Adhesions, volvulus, and anastomotic stricture are often problematic because of the extensive surgical resection and bowel manipulations.^{25,26}

Small Bowel Transplantation

Intestinal transplantation has come of age for the past 3 decades and now offers hope of long-term survival in patients with life-threatening complications of intestinal failure and parenteral nutrition. Success rates have greatly improved, largely through advances in immunosuppression protocols,

improved surgical technique, postoperative care, and accumulated experience. Approximately 2500 intestinal transplantations have been performed worldwide at over 75 centers, and graft survival rates are reaching 80% at 1 year and 50% at 5 years at experienced centers.³³ More than 80% of all current survivors have stopped parenteral nutrition and resumed normal daily activities.

Intestinal failure may result from surgical or anatomic loss of intestine (short bowel syndrome) or from a significant functional abnormality. Conditions treated by small bowel transplantation include volvulus, necrotizing enterocolitis, and intestinal atresia in children and vascular disorders, Crohn's disease, and intestinal trauma in adults. Total parenteral nutrition (TPN), the primary treatment for most patients with intestinal failure, can also lead to life-threatening hepatic failure. These factors also influence the decision to transplant and the specific transplantation procedure used.³⁴

Three types of transplantation operations are performed.^{34,35} Isolated intestinal transplantation is performed in patients who maintain good hepatic function (Fig. 48-12). Combined intestinal and liver transplantation is done in those with TPN-related or inborn hepatic dysfunction. Multivisceral transplantations (intestine, liver, stomach, duodenum, and pancreas) comprise approximately 24% of adult transplantation procedures and are reserved for patients with extensive GI tract abnormalities caused by vascular, absorptive, or motility disorders.³⁴ In small bowel transplantation, a donor intestine is anastomosed to the recipient colon, with the creation of a diverting ileostomy; this can be closed a few months after transplantation following stabilization of the patient and the absence of graft rejection or infection. Current surgical practice usually excludes the colon from intestinal allografts.

Prior to intestinal transplantation, prospective candidates undergo a series of radiologic examinations to address a variety of clinical issues.^{36,37} GI contrast examinations are used to assess the nature and extent of bowel abnormality

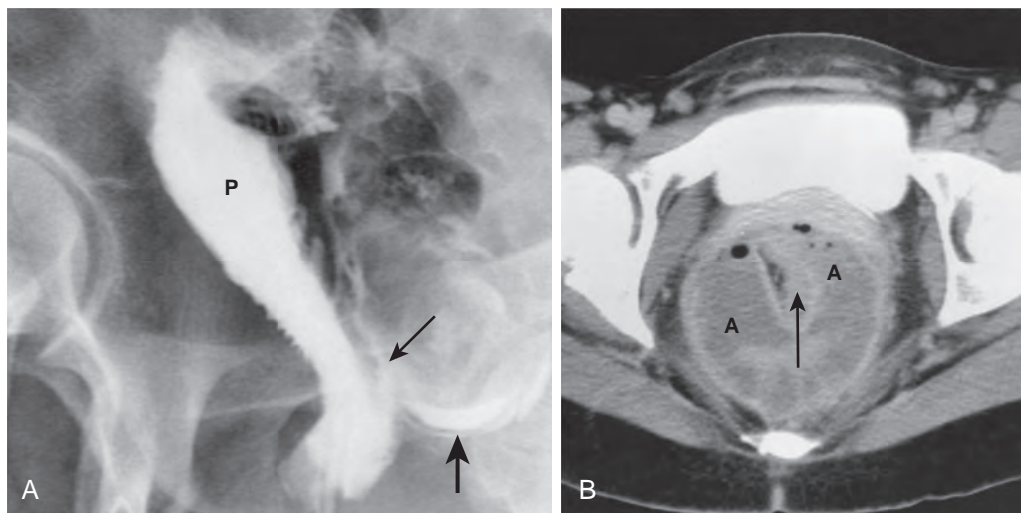


Figure 48-11 Peripouch abscess. A. J pouch ileogram demonstrates an anastomotic breakdown (thin arrow) with extravasation of water-soluble contrast media (thick arrow). Adjacent pelvic inflammation results in lumen narrowing and irregularity of the pouch (P). **B.** CT image defines a large multilocular abscess (A) that encircles the collapsed pouch and its fat density mesentery (arrow). Inflammation creates rectal wall thickening and stranding into the perirectal fat. (From Lappas JC, Maglinte DD: *Imaging of the postsurgical small bowel*. *Radiol Clin North Am* 41:305–326, 2003.)

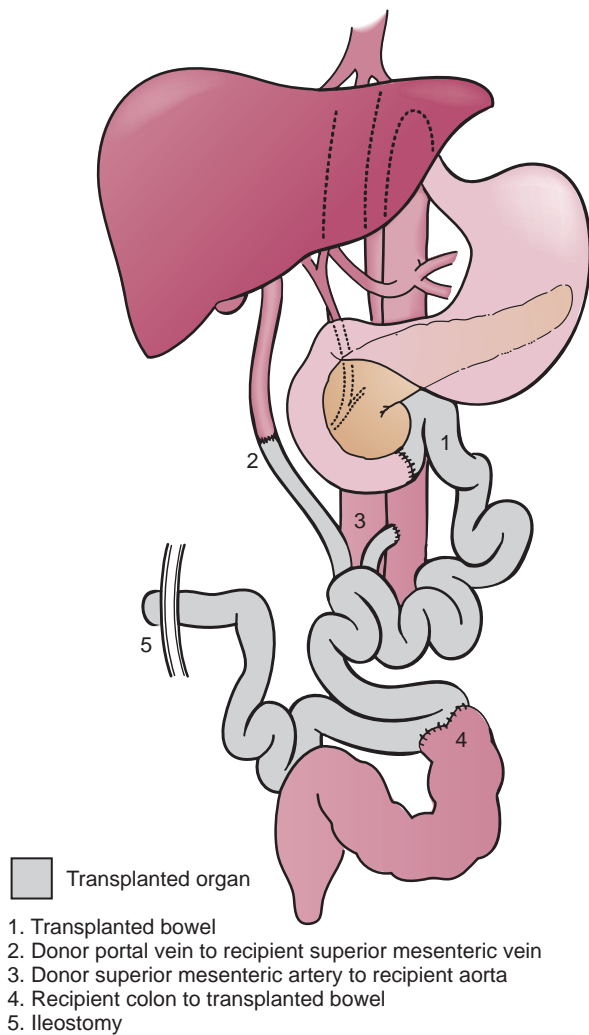


Figure 48-12 Schematic representation of isolated small bowel transplantation (donor intestine shaded). After critical donor-recipient arterial and venous anastomoses are established, the intestinal graft is anastomosed to the recipient colon with a temporary ileostomy.

and, in patients with short bowel syndrome, to map the amount of remaining intestine. After transplantation, contrast studies can be used to evaluate anastomoses, obstruction, fistulas, gastric emptying, intestinal transit, and small bowel mucosal patterns. Postsurgical anatomy includes a native to donor jejunojejunal, duodenojejunal, or gastrogastrostomy and a donor to native ileocolic anastomosis with an end-ileostomy. Healthy allografts show normal bowel caliber and mucosal patterns, active peristalsis, and normal transit times.

Abnormalities on early postoperative GI contrast studies include gastric atony and slow small bowel transit, with varying degrees of lumen dilation.³⁶ Edematous thickening of graft mucosal folds may be present early after operation because of harvesting injury. Fold thickening seen later in the postoperative period raises the suspicion of infection, rejection, or ischemia.³⁶ Loss of the normal fold pattern, resulting in a tubular appearance of the intestinal graft, may be caused by acute and chronic rejection and infection with cytomegalovirus (Figs. 48-13 and 48-14). However, radiologic studies are insensitive

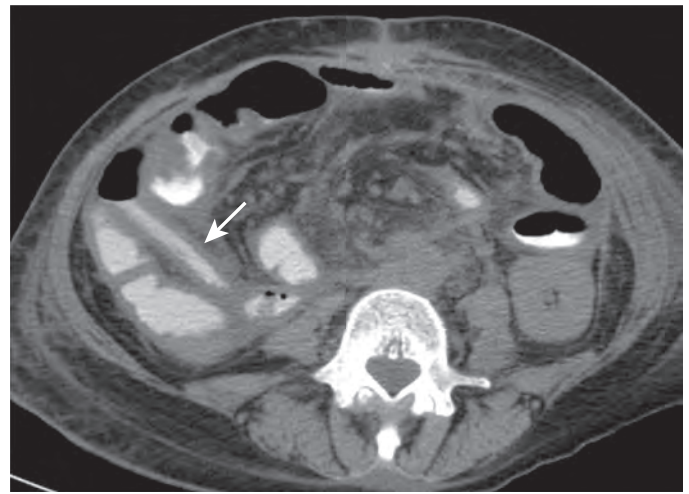


Figure 48-13 Small bowel transplant rejection. Unenhanced CT image in a 60-year-old woman with a history of small bowel transplantation. Small bowel loops within the right lower quadrant showing loss of bowel fold pattern and diffuse thickening (arrow). There is also mesenteric edema and a small amount of free fluid. The patient had a small bowel biopsy, and acute rejection was diagnosed.

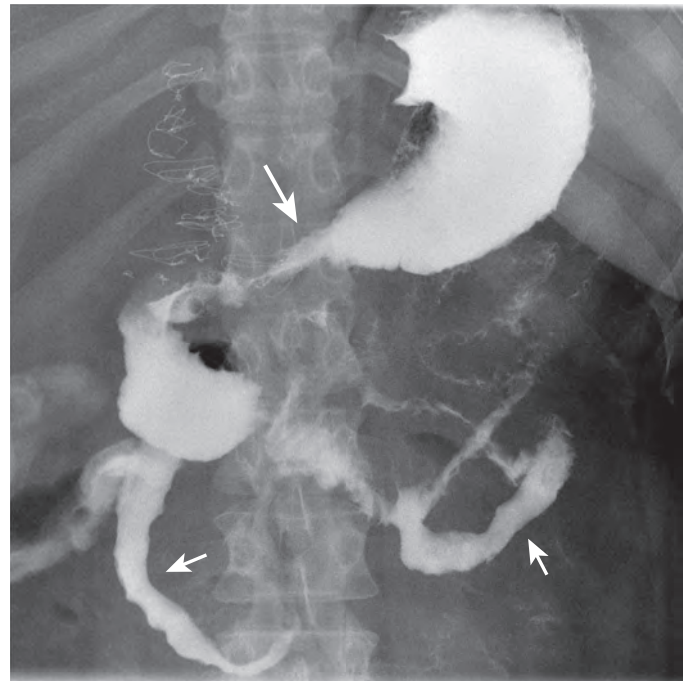


Figure 48-14 Small bowel transplant rejection. Patient who is status post-multivisceral transplantation presented with persistent nausea and vomiting. Image from an upper GI examination shows loss of mucosal folds in the proximal jejunum (short arrows). The pylorus shows luminal narrowing (long arrow), resulting in partial gastric outlet obstruction.

for the detection of acute graft rejection or infection, which are diagnosed using frequent surveillance ileoscopy with mucosal biopsy and zoom video endoscopy.³⁵

Indications for post-transplantation CT imaging are suspected abdominal infection, hemorrhage, hepatic abnormality, or post-transplantation lymphoproliferative disorder (PTLD).

On CT, uncomplicated small bowel grafts demonstrate non-dilated intestinal loops with normal wall thickness and patency of the critical vasculature.³⁸ Varying degrees of intra-abdominal fluid are common in the early postoperative period and consist of interloop ascites or loculated fluid collections, with or without infection. Abnormalities on CT may include intestinal dilation associated with ileus or obstruction and nonspecific bowel wall thickening caused by preservation injury, graft

rejection, infection, and ischemia. CT can delineate the spectrum of findings related to anastomotic leaks, thrombosis of arterial or venous grafts, PTLD, and complications specific to liver transplantation.^{36,38} PTLD is more common in intestinal transplantation than in other organ transplantations because of the degree of immunosuppression. Manifestations of PTLD include abdominal lymphadenopathy and solid masses of the intestinal tract and solid organs.

REFERENCES

- Abbott AM, Armstrong L, Jensen EH: Small intestine. In Yeo CJ, Matthews JB, editors: *Shackelford's Surgery of the Alimentary Tract*, ed 7, Philadelphia, 2013, Saunders, pp 835–863.
- Lappas JC, Maglinte DD: Radiological approach to investigation of the small intestine. In Gourtsiannis N, editor: *Medical Radiology—Diagnostic Imaging: Radiological Imaging of the Small Intestine*, New York, 2002, Springer-Verlag, pp 447–463.
- Maglinte DD, Lappas JC: Heitkamp: Technical refinements in enteroclysis. *Radiol Clin North Am* 41:213–229, 2003.
- Abumrad NN, Sawyers JL, Richards WO: Dumping syndrome and other early postgastroectomy sequelae. In Scott HJ, Sawyers JL, editors: *Surgery of the Stomach, Duodenum, and Small Intestine*, ed 2, Boston, 1992, BlackwellScientific, pp 620–631.
- Eagon JC, Miedema BW, Kelly KA: Postgastroectomy syndromes. *Surg Clin North Am* 72:445–465, 1992.
- Sandrasegaran K, Maglinte DD, Rajesh A, et al: CT of acute biliopancreatic limb obstruction. *AJR* 186:104–109, 2006.
- Jones KB: Biliopancreatic limb obstruction in gastric bypass at or proximal to the jejunojejunostomy: A potentially deadly, catastrophic event. *Obes Surg* 6:485–493, 1996.
- Conter RL, Converse JO, McGarrity TJ, Koch KL: Afferent loop obstruction presenting as acute pancreatitis and pseudocyst: Case reports and review of the literature. *Surgery* 108:22–27, 1990.
- Wise SW: Case 24: Afferent loop syndrome. *Radiology* 216:142–145, 2000.
- Gayer G, Barsuk D, Hertz M, et al: CT diagnosis of afferent loop syndrome. *Clin Radiol* 57:835–839, 2002.
- Hasuda K, Makino Y, Arata T, Yamada T: Afferent loop obstruction diagnosed by sonography and computed tomography. *Br J Radiol* 64:1156–1158, 1991.
- Steichen FM, Galibert LA, Wolsch RA, et al: Stapling techniques in operations on the gastrointestinal tract. In Baker RJ, Fischer JE, editors: *Mastery of Surgery*, ed 4, Philadelphia, 2001, Lippincott Williams & Wilkins, pp 201–225.
- Lappas JC: Imaging of the postsurgical small bowel. *Radiol Clin North Am* 41:305–41326, 2003.
- Sandrasegaran K, Maglinte DD, Rajesh A, et al: CT findings for postsurgical blind pouch of small bowel. *AJR* 186:110–113, 2006.
- Keusch GT, Gorbach SL: Enteric microbial ecology and infection. In Haubrich WS, Schaffner F, editors: *Bockus Gastroenterology*, ed 5, Philadelphia, 1995, Saunders, pp 1115–1145.
- McGonigal MD, Lucas CE, Ledgerwood AM: Feeding jejunostomy in patients who are critically ill. *Surg Gynecol Obstet* 168:275–277, 1989.
- Carucci LR, Levine MS, Rubesin SE, et al: Evaluation of patients with jejunostomy tubes: Imaging findings. *Radiology* 223:241–247, 2002.
- Becker JM: Surgical therapy for ulcerative colitis and Crohn's disease. *Gastroenterol Clin North Am* 28:371–390, 1999.
- Etherington RJ, Williams JG, Hayward MWJ, et al: Demonstration of para-ileostomy herniation using computed tomography. *Clin Radiol* 41:333–336, 1990.
- Kock NG: Continent ileostomy. *Prog Surg* 12:180–201, 1973.
- Peiser JG, Cohen Z, McLeod RS: Surgical treatment of ulcerative colitis—continent ileostomy. In Allan RN, Rhodes JM, Hanauer SB, et al, editors: *Inflammatory Bowel Diseases*, New York, 1997, Churchill Livingstone, p 753.
- Castillo E, Thomassie LM, Whitlow CB, et al: Continent ileostomy: Current experience. *Dis Colon Rectum* 48:1263–1268, 2005.
- Lycke KG, Gothlin JH, Jensen JK, et al: Radiology of the continent ileostomy reservoir: I. Method of examination and normal findings. *Abdom Imaging* 19:116–123, 1994.
- Lycke KG, Gothlin JH, Jensen JK, et al: Radiology of the continent ileostomy reservoir: II. Findings in patients with late complications. *Abdom Imaging* 19:124–131, 1994.
- Cima RR, Young-Fadok T, Pemberton JH: Procedures for ulcerative colitis. In Souba WW, Fink MP, Jurkovich GJ, et al, editors: *ACS Surgery, Principles and Practice*, New York, 2005, Web MD, pp 674–684.
- Marcello PW, Roberts PL, Schoetz DJ, Jr, et al: Long-term results of the ileoanal pouch procedure. *Arch Surg* 128:500–503, 1993.
- Meagher AP, Farouk R, Dozios RR, et al: J ileal pouch–anal anastomosis for chronic ulcerative colitis: Complications and long-term outcome in 1310 patients. *Br J Surg* 85:800–803, 1998.
- Alfisher MM, Scholz FJ, Roberts PL, Counihan T: Radiology of ileal pouch–anal anastomosis: Normal findings, examination pitfalls, and complications. *Radiographics* 17:81–98, 1997.
- Brown JJ, Balfe DM, Heiken JP, et al: Ileal J pouch: Radiologic evaluation in patients with and without postoperative infectious complications. *Radiology* 174:115–120, 1990.
- Hrung JM, Levine MS, Rombeau JL, et al: Total proctocolectomy and ileoanal pouch: The role of contrast studies for evaluating postoperative leaks. *Abdom Imaging* 23:375–379, 1998.
- Thoeni RF, Fell SC, Engelstad B, et al: Ileoanal pouches: Comparison of CT, scintigraphy, and contrast enemas for diagnosing postsurgical complications. *AJR* 154:73–78, 1990.
- Mowschenson PM, Critchlow JF: Outcome of early surgical complications following ileoanal pouch operation without diverting ileostomy. *Am J Surg* 169:143–145, 1995.
- Abu-Elmagd KM, Costa G, Bond GJ, et al: Five hundred intestinal and multivisceral transplantations at a single center: major advances with new challenges. *Ann Surg* 250:567–581, 2009.
- Abu-Elmagd KM: Intestinal transplantation for short bowel syndrome and gastrointestinal failure: Current consensus, rewarding outcomes, and practical guidelines. *Gastroenterology* 130 (Suppl 1):S132–S137, 2006.
- Abu-Elmagd KM: The small bowel contained allografts: Existing and proposed nomenclature. *Am J Transplant* 11:184–185, 2011.
- Campbell WL, Abu-Elmagd K, Furukawa H, et al: Intestinal and multivisceral transplantation. *Radiol Clin North Am* 33:595–614, 1995.
- Swerdlow DR, Trotter A, Girlanda R, et al: Computed tomography (CT) colonography with CT arteriography and venography for the workup of intestinal transplant candidates. *Clin Transplant* 27:126–131, 2013.
- Bach DB, Levin MF, Vellet AD, et al: CT findings in patients with small-bowel transplants. *AJR* 159:311–315, 1992.

Miscellaneous Abnormalities of the Small Bowel

STEPHEN E. RUBESIN

CHAPTER OUTLINE

Abnormalities of Small Bowel Development in Adults

Meckel's Diverticulum

Midgut Duplications

Heterotopic Tissue

Segmental Dilation

Intestinal Malrotation

Paraduodenal (Mesocolic) Hernias

Endometriosis

Intestinal Edema

Enteroliths and Bezoars

Abnormalities of Small Bowel Development in Adults

MECKEL'S DIVERTICULUM

The yolk sac provides nutrition to the fetus before the placenta develops. The yolk sac is connected to the midgut by the omphalomesenteric duct (vitellointestinal duct). This duct is obliterated during the seventh to eighth weeks of embryogenesis as the placenta assumes the nutritional feeding of the fetus.¹ Persistence of various portions of the omphalomesenteric duct leads to a variety of anomalies. Failure of the entire omphalomesenteric duct to atrophy leads to an enteroumbilical fistula. Failure of one portion of the duct to atrophy may result in a fusiform area of dilation, termed an *omphalomesenteric cyst*. Persistence of the vitellointestinal duct as a fibrous cord can lead to volvulus or compressive obstruction.

Meckel's diverticulum results from persistence of the omphalomesenteric duct at its attachment to the ileum. It is the most common congenital abnormality of the gastrointestinal (GI) tract; the prevalence of Meckel's diverticulum at autopsy is 1% to 4%.^{2,3} However, most people with this congenital anomaly never develop symptoms.

Meckel's diverticulum arises from the antimesenteric border of the ileum, usually within 100 cm of the ileocecal valve. It may be connected to the umbilicus by a fibrous band or to other intestinal loops by congenital bands or adhesions. The diverticulum usually varies from 2 to 15 cm in length and is about 2 cm in width.¹ Meckel's diverticulum contains all layers of the intestinal wall. The diverticulum is lined by small bowel epithelium and often contains heterotopic gastric or pancreatic tissue or Brunner's glands.¹

Infants (<2 years) with Meckel's diverticulum may present with GI bleeding caused by secretion of acid by ectopic gastric

mucosa and subsequent ulceration. Adults may present with GI bleeding, obstruction, or perforation.⁴⁻⁷ Diverticulitis results from ulceration and focal perforation of the diverticulum caused by ectopic gastric mucosa or an enterolith or foreign body impaction.⁸ Obstruction results from a variety of mechanisms, including intussusception, volvulus around a persistent fibrous or adhesive band, and ileal narrowing related to ulceration. The diverticulum may become incarcerated in an inguinal, femoral, or umbilical hernia, also known as a Littre hernia.⁹ A variety of tumors may arise in Meckel's diverticulum, including carcinoid tumors, adenocarcinomas, and benign or malignant mesenchymal tumors.¹⁰

Technetium pertechnetate scintigraphy can detect ectopic gastric mucosa in more than 85% of infants, children, and adults with Meckel's diverticulum who have acute or chronic GI bleeding.^{5,11-13} However, most adults are asymptomatic or develop symptoms related to obstruction. All imaging modalities (except enteroclysis) have poor sensitivity for the detection of Meckel's diverticulum. In a small percentage of cases, plain abdominal radiographs may reveal radiopaque enteroliths in a Meckel diverticulum^{14,15} or a dilated, gas-filled diverticulum in the right lower quadrant. Meckel's diverticulum is rarely diagnosed on small bowel follow-throughs, except in patients with excessive mesenteric fat related to obesity or Crohn's disease.^{16,17} Computed tomography (CT) or ultrasound may demonstrate a cystic or tubular structure attached to bowel in the right lower quadrant.

In adults without GI bleeding, enteroclysis is the best radiologic test for Meckel's diverticulum. A Meckel's diverticulum is detected in 2% to 3% of all patients undergoing enteroclysis, approaching the incidence at autopsy.¹⁸⁻²⁰ A blind-ending tubular or cystic sac (Fig. 49-1) is usually seen to communicate with the antimesenteric border of the distal ileum.²¹ One clue to the presence of the diverticulum is a triradiate fold pattern at the junction of the sac with the intestinal lumen. Folds in the diverticulum will be perpendicular to folds in the adjacent ileum. The surface of the diverticulum may be abnormal, containing a granular mucosa, focal ulceration, or focal polypoid mound of ectopic gastric mucosa or tumor. In other patients, an inverted Meckel diverticulum may appear as a polypoid intraluminal lesion (Fig. 49-2), which sometimes acts as lead point for a small bowel intussusception.²¹⁻²⁴

MIDGUT DUPLICATIONS

Small bowel duplication is a congenital incomplete or complete doubling of a variably long segment of bowel.² The duplication may be served by an independent mesentery or by the same mesentery as the adjacent bowel. Midgut duplication cysts contain all layers of the bowel wall, including a mucosa, submucosa, and inner circular muscle layer, with its

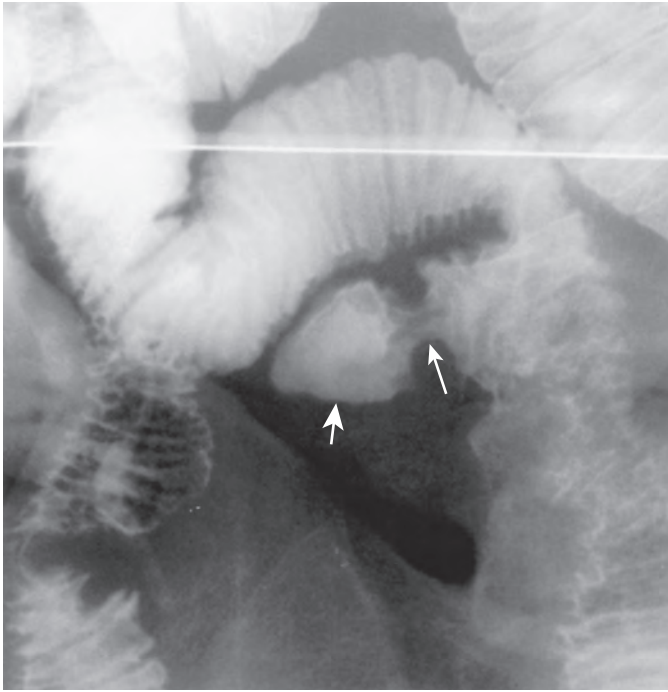


Figure 49-1 Meckel's diverticulum. A spot image when the diverticulum was incompletely distended shows a triangular sac (*thick arrow*) arising from the distal ileum. Smooth folds (*thin arrow*) radiate to the origin of the diverticulum. Note how this Meckel's diverticulum appears to arise from the concave border of the bowel. This image demonstrates how the concave border of a small bowel loop is not always its true mesenteric border because Meckel's diverticulum arises from the antimesenteric border of the ileum.

associated myenteric plexus.¹ Some duplications have a full longitudinal muscle layer, and others have no longitudinal muscle.² The mucosal lining of these cysts is usually intestinal. Duplication cysts may also contain gastric mucosa, pancreatic tissue, thyroid stroma, ciliated bronchial epithelium, lung, and cartilage.¹

Most midgut duplications involve the ileum, particularly the region of the ileocecal valve, and the duodenum. These are usually elongated lesions attached to the muscular layer of the adjacent small bowel. If secretions accumulate, the duplication may become a cystic mass protruding into the small bowel mesentery. Multiple duplications are found in about 5% of patients.^{25,26} Approximately 20% of these duplications communicate with the bowel lumen at the proximal or distal end of the cyst or at both ends.²⁷

Ectopic gastric epithelium lining a duplication cyst may cause peptic ulceration, with subsequent GI bleeding or perforation.²⁸ Obstruction may result from volvulus, intussusception, or compression of the adjacent bowel by the cyst. Rarely, duplication cysts are complicated by tumor.

Duplication cysts may be manifested on barium studies by an extrinsic mass indenting and compressing the mesenteric border of the adjacent bowel.²⁹ Barium enters the cyst in only a small percentage of cases (*Fig. 49-3*). CT or ultrasound may show a cystic mass embedded in the small bowel wall.^{29,30} If there is concern about GI ulceration or bleeding, a ^{99m}Tc-pertechnetate scan usually reveals heterotopic gastric mucosa in the cyst.



Figure 49-2 Inverted Meckel's diverticulum. Enteroclysis shows a long, smooth-surfaced, polypoid intraluminal filling defect (*closed arrow*) in the distal ileum. A tubular radiolucent filling defect (*open arrow*) resembles a stalk. This inverted Meckel's diverticulum could be mistaken for a pedunculated ileal polyp, such as a lipoma or inflammatory fibroid polyp. (From Rubesin SE, Herlinger H, DeGaeta L: *Test your skills. Inverted Meckel's diverticulum. Radiology 176:636, 644, 1990.*)

HETEROTOPIC TISSUE

Ectopic gastric mucosa is present in a wide variety of locations in the GI tract, including the esophagus, duodenum, and mesenteric small intestine, as well as in congenital abnormalities such as duplication cysts and Meckel's diverticulum. Congenital ectopic mucosa contains an orderly arrangement of superficial foveolar epithelium and underlying fundic glands partially lined by parietal and chief cells.³¹ Ectopic mucosa should be distinguished from the more common foveolar metaplasia found in the duodenal bulb in patients with peptic duodenitis.³² However, foveolar metaplasia in peptic duodenitis lacks organized gastric pits and glands.¹

Ectopic pancreas is most frequently encountered in the duodenum (28%), stomach (26%), or jejunum (16%).³³ The ectopic tissue may arise in various levels of the bowel wall, including the mucosa, submucosa, and serosa.³¹ Ectopic pancreatic tissue is composed of varying numbers of acini, ducts, and islet cells. Ectopic pancreas has also been reported in jejunal and ileal diverticula and Meckel's diverticulum, as well as in the gallbladder, bile ducts, umbilicus, and fallopian tubes.

Ectopic pancreas in the mesenteric small bowel is usually discovered incidentally as a nodule or mass of lobulated solid or cystic tissue abutting the bowel in patients operated on for other reasons. Although microscopic pancreatitis is not uncommon, clinical pancreatitis is very unusual. One case of ectopic pancreas in the jejunum has been reported in which the patient developed pancreatitis and pseudocyst formation.³⁴ In this patient, a cystic lesion abutted a jejunal loop, mimicking jejunal diverticulitis or a small perforated tumor (Fig. 49-4).

SEGMENTAL DILATION

The small intestine may have a focally dilated, aperistaltic segment, termed *segmental dilation*.^{35,36} In most cases, the

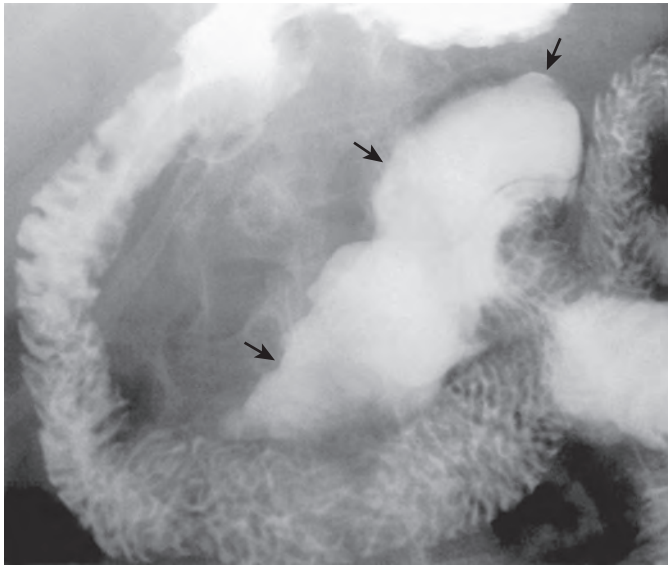


Figure 49-3 Duodenal duplication. Barium fills a 10-cm cavitory lesion that parallels the inner border of the third and fourth portions of the duodenum. The adjacent duodenum has normal folds. It is difficult to distinguish this duplication from an exophytic cavitory mass, such as a gastrointestinal stromal tumor (arrows). (Courtesy Hans Herlinger, MD.)

isolated atonic loop is in the ileum, giving rise to the term *ileal dysgenesis*. The cause of this condition is uncertain, but it has been postulated that it results from congenital neuromuscular dysfunction. Ganglion cells are present.² In children, ileal dysgenesis is associated with Meckel's diverticulum and omphaloceles.^{37,38} Ectopic mucosa (especially gastric mucosa) may be found in the dilated segment and may cause ulceration.

Segmental dilation may be manifested on barium studies by a focally dilated spherical or tubular segment of ileum (Fig. 49-5) in direct contiguity with the adjacent inflow and outflow loops of ileum.³⁹ The aperistaltic segment functions as a barrier to intestinal flow, resulting in partial small bowel obstruction. Ulcerated mucosa may be present in some patients. This condition can be distinguished from Meckel's diverticulum by its direct continuity with adjacent ileal loops. Ileal dysgenesis can also be distinguished from primary small bowel lymphoma with aneurysmal dilation by the normal mucosal surface of the dilated ileal loop.

INTESTINAL MALROTATION

Symptomatic patients with intestinal malrotation are usually infants and children with high-grade obstruction caused by midgut volvulus or Ladd's bands. The embryologic, clinical, and radiographic aspects of intestinal malrotation in infants and children are described in detail in Chapters 113 and 116. Adults with intestinal malrotation are usually asymptomatic or have vague abdominal complaints.⁴⁰⁻⁴²

The midgut is that portion of bowel related to the superior mesentery artery and vein axis; it is composed of the third and fourth portions of the duodenum, jejunum, ileum, cecum, appendix, ascending colon and transverse colon. Intestinal malrotation encompasses a number of variations based on the degree of rotation of the midgut in the umbilical cord and degree of rotation when and after it returns to the coelomic cavity. The variations include nonrotation, malrotation, hyperrotation, and reversed rotation.

During the eighth fetal week, the midgut loop rotates 90 degrees counterclockwise while it is within the umbilical cord, so that the cecum lies on the left side of the fetus and the

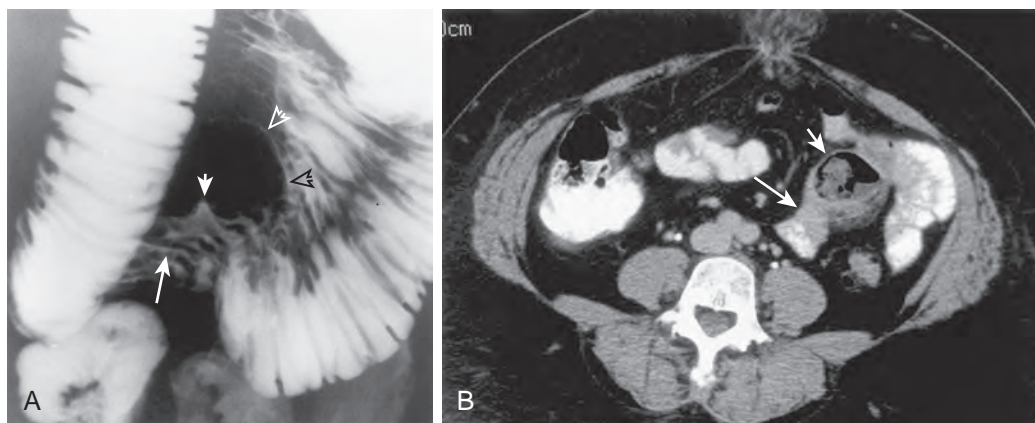


Figure 49-4 Ectopic pancreas in the jejunum complicated by pancreatitis and pseudocyst formation. **A.** Enteroclysis shows a tiny barium collection (short arrow) in the jejunum. Small bowel folds in this region are mildly thickened and undulating (long arrow) and are parallel to the longitudinal axis of the bowel rather than straight and perpendicular to the bowel, as seen in the normal adjacent jejunum. Mass effect (open arrows) is also seen at the edge of the lesion. **B.** CT scan shows a soft tissue mass (long arrow) replacing the contrast-filled lumen of the bowel. A central cavity (short arrow) contains air and soft tissue. At pathology, the soft tissue mass was ectopic pancreatic tissue with associated pancreatitis, and the cavity was a pseudocyst that communicated with the lumen. This lesion could easily be confused with jejunal diverticulitis or a cavitory mass, such as lymphoma.

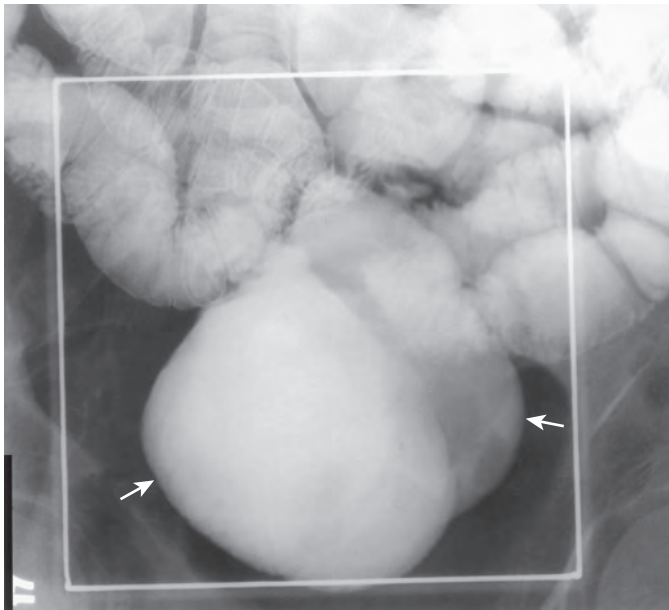


Figure 49-5 Ileal dysgenesis. Enteroclysis shows a large bilobed ileal segment (arrows). Normal entry and exit loops of pelvic ileum were seen on other views.

jejunum on the right.¹ If the midgut returns to the abdomen without further rotation, it maintains this orientation. Although this variation represents a 90-degree rotation, it has been confusingly termed *nonrotation* because the small bowel is not rotating within the coelomic cavity. Nonrotation actually represents small bowel rotation that stopped at 90 degrees of counterclockwise rotation within the umbilical cord. The third and fourth portions of the duodenum and duodenojejunal flexure are absent. Instead, the jejunum is in direct continuation with the second portion of the duodenum (Fig. 49-6). The jejunum and ileum lie in the right side of the abdomen, whereas the colon lies on the left side. The cecum is in the midline, with the terminal ileum entering the cecum from its right side. The appendix originates from a midline position, often low in the midline of the abdomen.⁴³

During the 10th fetal week, the midgut normally rotates another 90 degrees counterclockwise within the umbilical cord, so that the cecum lies superiorly on the right and the jejunum inferiorly on the left.⁴³

The jejunum is then the first midgut section to reenter the coelomic cavity, passing behind the superior mesenteric artery. During this part of rotation in the coelomic cavity, the jejunum comes to lie between the posteriorly located duodenum and anteriorly positioned colon. During the 11th week, the cecum rotates still another 90 degrees into the right lower quadrant, completing a 270-degree counterclockwise rotation.

Intestinal malrotation occurs when the midgut fails to complete its 180-degree counterclockwise rotation after the initial 90-degree rotation in the umbilical cord. The duodenojejunal junction is not fixed in its normal location to the left of the spine but instead lies inferiorly and to the right of the spine. The small bowel lies predominantly in the right or midabdomen. Mesenteric bands from the liver and posterior abdominal wall cross the second portion of the duodenum and extend to the cecum (Ladd's bands).

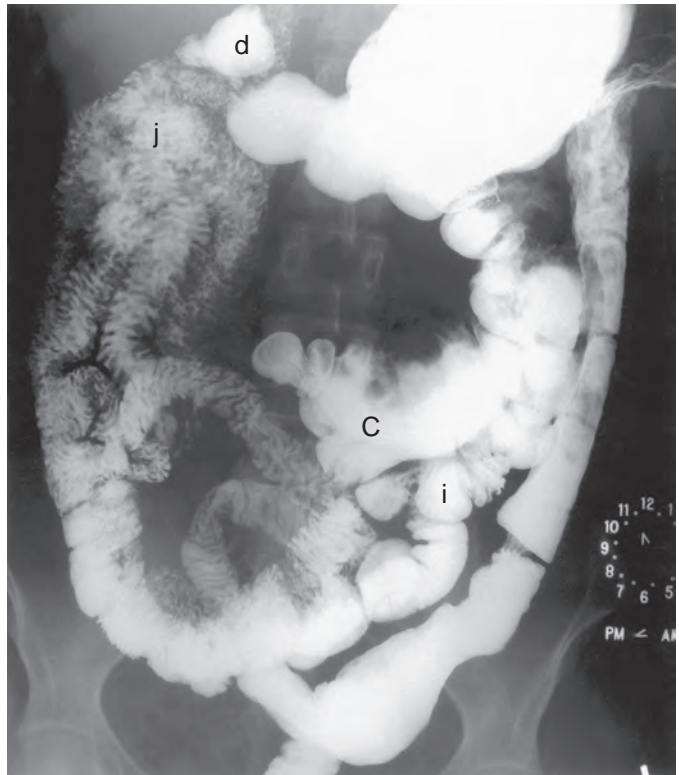


Figure 49-6 Intestinal nonrotation. This overhead radiograph from small bowel follow-through shows the duodenal bulb (d) in a normal location, with lack of the third and fourth portions of the duodenum and lack of a duodenojejunal junction to the left of the spine. The jejunum (j) is in the right upper quadrant, and most of the ileum is also in the right abdomen, with the distal ileum (i) crossing to the left to join a midline cecum (C). The colon lies in the left abdomen.

Intestinal hyperrotation occurs when the small intestine has rotated more than the usual 180 degrees, resulting in a long ascending colon, with the cecum located in the left upper quadrant. In a reversed rotation, the bowel enters the abdomen with a clockwise rotation, so the transverse colon lies posterior to the duodenum in the right upper quadrant.

Rather than being confused by the series of somewhat misnamed rotational terms, the radiologist can focus on the following: (1) how much duodenum is present; (2) the location of the duodenal-jejunal junction; (3) the anterior-posterior relationship of the jejunum and ileum to the transverse colon and duodenum; (4) the location of the cecum and the relationship of the appendix and ileocecal valve to the cecum; (5) the location and length of the ascending colon; and (6) the relationship of the superior mesenteric artery (SMA) to the superior mesenteric vein (SMV).

The location of the duodenojejunal junction should be ascertained in any adult with vomiting or abdominal pain. The normal duodenojejunal junction lies to the left of the spine, at about the level of the duodenal bulb. When the ligament of Treitz is in its normal position, the first loops of the jejunum may cross to the right of the spine as a normal variant—as long as the jejunum is not entering a posteriorly located right paraduodenal hernia. On the other hand, the duodenojejunal junction not infrequently has an abnormal location. An abnormally positioned duodenojejunal junction is important because it may cause twisting and obstruction of the proximal small

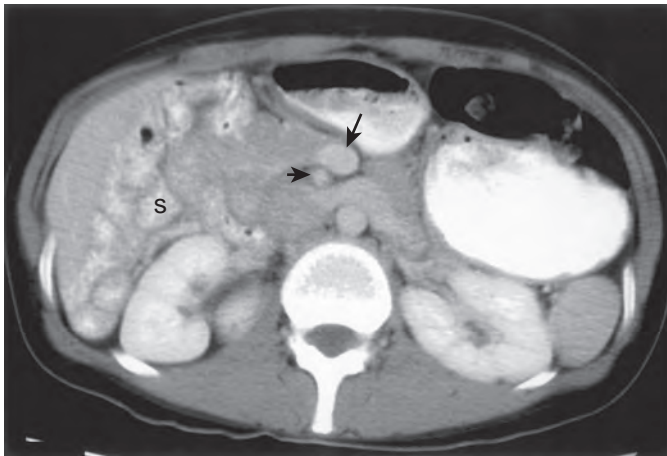


Figure 49-7 Intestinal malrotation. Axial CT through the tip of the liver shows that the superior mesenteric vein (*long arrow*) lies anterior and to the left of the superior mesenteric artery (*short arrow*). The jejunum (s) lies in the right upper quadrant.

bowel, manifested by duodenal dilation and slow transit of contrast material on barium studies. However, the typical corkscrew sign of intestinal malrotation and midgut volvulus in infants (see Chapter 113) is rarely found in adults.⁴⁴ Intestinal malrotation in adults is often recognized on CT, magnetic resonance imaging (MRI), or ultrasound by an abnormal relationship between the SMA and SMV, so that the vein lies anterior and to the left of the artery (Fig. 49-7).

PARADUODENAL (MESOCOLIC) HERNIAS

Paraduodenal hernias are the most common internal abdominal hernias, accounting for about 50% of all such hernias. Although abdominal hernias are discussed in detail in Chapter 112, paraduodenal hernias are discussed here because these hernias relate to abnormal rotation and fixation of the colonic mesentery to the retroperitoneum.^{45,46}

A left paraduodenal hernia represents a hernia of the proximal jejunum into the mesentery of the descending colon. The opening of a left paraduodenal hernia is just lateral to the fourth portion of the duodenum at the fossa of Landzert, an anatomic fossa found at autopsy in 2% of patients.⁴⁷ This fossa is present when the inferior mesenteric vein and ascending left colon artery are incompletely fixed to the retroperitoneum. Loops of jejunum can herniate beneath the mesentery of the descending colon, potentially causing small bowel obstruction or ischemia.

A left paraduodenal hernia may be manifested on barium studies by a variable number of jejunal loops clumped together in the left upper quadrant lateral to the fourth portion of the duodenum (Fig. 49-8). The inlet and outlet loops may be focally narrowed where they are compressed at the hernia orifice (see Fig. 49-8). The loops do not change position with time or palpation because they are fixed within the hernia sac. Barium may be retained in these loops on delayed images because of obstruction. Abdominal CT may reveal a cluster of small bowel loops lateral to the duodenum, between the adrenal gland and transverse or descending colon.⁴⁸ The proximal jejunum lies posterior to the inferior mesenteric vein (IMV) vessels and behind and lateral to the descending colon.

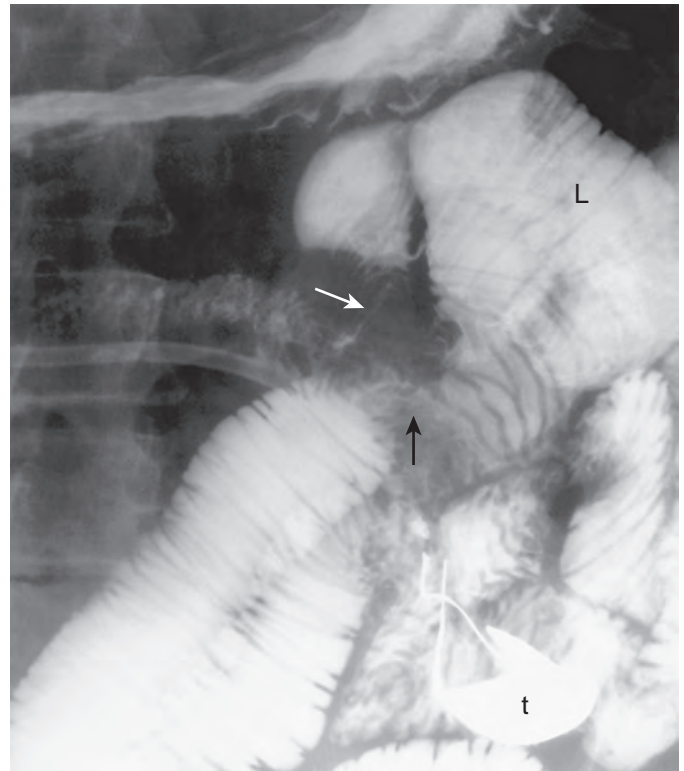


Figure 49-8 Left paraduodenal hernia. This coned-down image from overhead radiograph on enteroclysis performed via a Kantor tube (t) shows a cluster of jejunal loops (L) in the left upper quadrant. These loops are extrinsically compressed (*arrows*) at the entry site to the fossa of Landzert. (Courtesy Hans Herlinger, MD.)

A right paraduodenal hernia is a hernia of the jejunum into the mesentery of the ascending colon or right transverse mesocolon.⁴⁵ A right paraduodenal hernia occurs at the mesentericoparietal fossa (the fossa of Waldeyer), which is found in about 1% of autopsies.⁴⁷ This fossa lies in the upper portion of the jejunal mesentery, behind the superior mesenteric artery and just inferior to the third portion of the duodenum. The orifice of the hernia is bounded superiorly by the superior mesenteric artery and vein (small bowel mesentery). Once the proximal jejunum enters the orifice, it herniates to the right beneath the mesenteries of the transverse and/or ascending colon.

A right paraduodenal hernia may be manifested on barium studies by a variable number of jejunal loops clumped together in the right abdomen inferior to the third portion of the duodenum (Fig. 49-9). The herniated loops may be dilated and may show delayed emptying of barium. The inlet and outlet loops are closely apposed and narrowed because of extrinsic compression at the hernia orifice. CT or MRI may also reveal a focal cluster of jejunal loops in the right side of the abdomen inferior to the duodenum.⁴⁹ The branches of the superior mesenteric artery and vein are whirled posteriorly and to the right behind these vessels (Fig. 49-10), extending toward the right-sided jejunal loops.

Endometriosis

Endometrial tissue found outside the uterus is termed *endometriosis*. Diagnosis requires demonstration of at least two of the

following: glands, stroma, and hemosiderin related to bleeding.² This ectopic endometrial tissue primarily involves the peritoneal surfaces of the pelvis and pelvic organs, including the ovaries, fallopian tubes, and pouch of Douglas. Colonic involvement is found in 15% to 37% of women who undergo surgery for endometriosis.^{50,51} Ileal involvement is much less frequent,

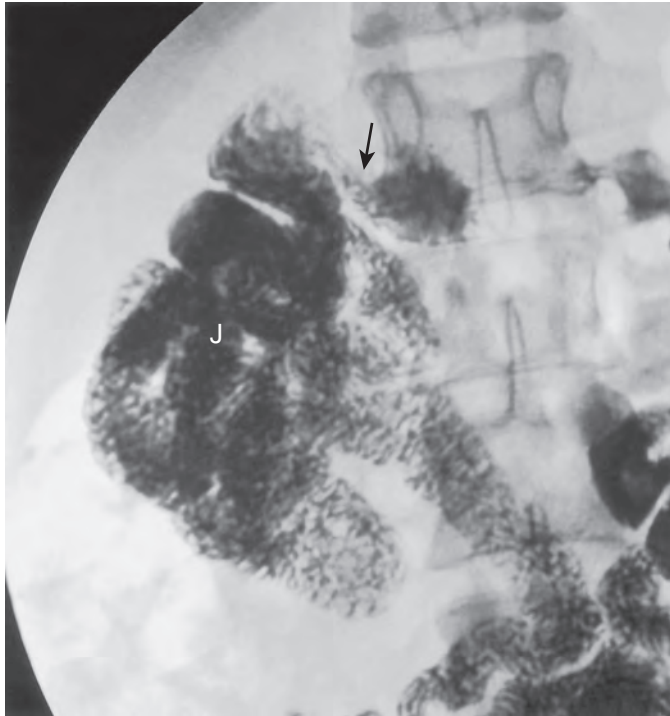


Figure 49-9 Right paraduodenal hernia. This low-power spot image from a small bowel follow-through shows a large cluster of jejunal loops (J) clumped together in the right upper quadrant. Note how there is compression of one loop (arrow) at the inlet to the fossa of Waldeyer.



Figure 49-10 Right paraduodenal hernia. Axial CT through the tip of the liver shows collapsed bowel (S) in the right upper quadrant. A tributary (arrow) of the superior mesenteric vein is looping behind this vein (v). (From Herlinger H, Jones B, Jacobs JE: *Miscellaneous abnormalities of the small bowel*. In Gore RM, Levine MS [eds]: *Textbook of Gastrointestinal Radiology*. Philadelphia, WB Saunders, 2000, pp 865–883.)

found in only 1% to 7% of surgical cases.^{52,53} Ectopic endometrial tissue usually has a serosal or subserosal location, but endometrial tissue may burrow into the muscularis propria, submucosa, or even mucosa. The endometrial tissue goes through the proliferative and secretory phases of the menstrual cycle, with sloughing and bleeding, leading to regeneration of endometrial tissue and fibrosis.¹ Bowel involvement is primarily characterized by extensive subserosal fibrosis and serosal puckering. Endometrial tissue burrowing into the muscularis propria may result in increased muscle thickness. Small bowel involvement results in crampy abdominal or pelvic pain or symptoms of intestinal obstruction.^{54–57} Cyclic pain associated with menses is found in a minority (14%–40%) of patients.^{57,58}

Endometriosis may be manifested radiographically by findings similar to those found with intraperitoneal spread of malignant tumor or inflammatory diseases. Barium studies may reveal focal or multifocal areas of extrinsic mass effect on ileal loops associated with spiculation of the bowel contour and tethering of mucosal folds (Fig. 49-11).^{59,60} Circumferential narrowing may be present, but mucosal folds are preserved. The radiographic or CT findings can mimic those of intraperitoneal metastases to the bowel (Fig. 49-12) or of a carcinoid tumor with intraperitoneal spread. Rarely, a solitary deposit of ileal endometriosis can mimic a primary carcinoid tumor or appendicitis, secondarily involving the adjacent ileum.⁶⁰

Intestinal Edema

The small bowel has a limited number of ways to react to various insults. Bowel wall edema is one component of this reaction to a wide variety of inflammatory or ischemic

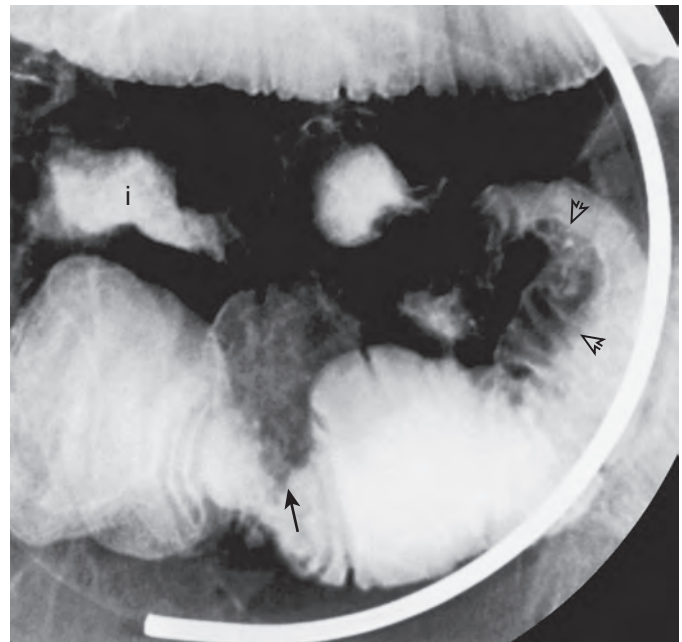


Figure 49-11 Ileal endometriosis. This spot image obtained during enteroclysis shows a focal, smooth, extrinsic mass impression (open arrows) on the mesenteric border of a pelvic loop of ileum. At a second site, there is another focal extrinsic mass impression (arrow) and tethering of folds toward the mesenteric border. The ileal mucosa is preserved. The distal ileum (i) is collapsed. These endometriosis implants in the ileum are indistinguishable from intraperitoneal metastases to the small bowel.

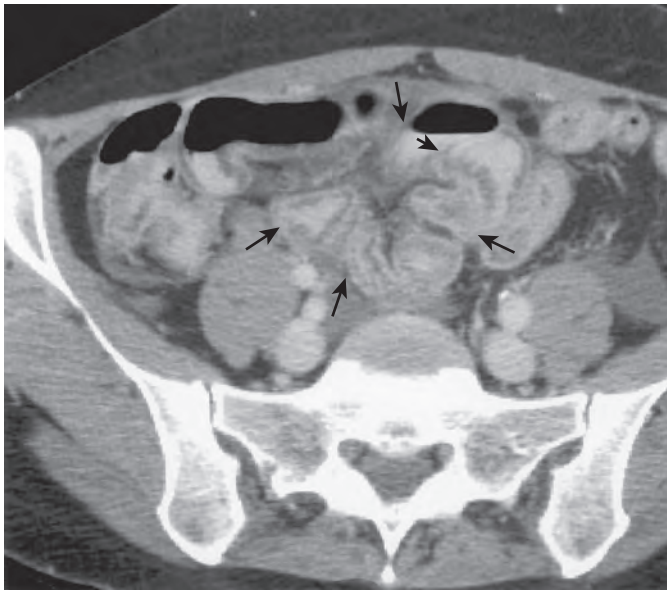


Figure 49-12 Ileal endometriosis. Axial CT through the pelvis shows ileal loops (long arrows) pulled toward the mesentery with associated tethering of folds (small arrow). The submucosa has slightly low attenuation.

conditions. This discussion focuses on bowel wall edema as the predominant component of this reaction.

Edema of the small intestine occurs primarily in the lamina propria and submucosa. This process is characterized by dilation of mucosal and submucosal lymphatics and increased interstitial fluid. Isolated bowel wall edema is usually associated with diseases that cause hypoalbuminemia (with a serum albumen level <2 g/dL).^{61,62} The two most common causes of small bowel edema are cirrhosis and the nephrotic syndrome. However, any intestinal disease associated with hypoalbuminemia related to malabsorption can cause bowel wall edema. For example, patients with gluten-sensitive enteropathy and hypoalbuminemia can have diffuse fold enlargement because of small bowel edema. Any intestinal disease that causes intraluminal protein loss can also result in hypoalbuminemia, including the enteropathy associated with congestive heart failure, constrictive pericarditis, and burns, Ménétrier's disease, lymphangiectasia, and Crohn's disease.^{61,63}

Several factors account for small bowel edema in patients with cirrhosis. Oncotic pressure is low as a result of hypoalbuminemia and hypovolemia. Small intestinal capillary pressure may also be elevated because of portal hypertension, congestive heart failure, and water and salt retention caused by decreased aldosterone catabolism and associated renal dysfunction.⁶¹⁻⁶⁴ In cirrhotics, congestive changes in the jejunum are similar to those of portal hypertensive gastropathy in the stomach, with an increased size and number of capillaries and venules in the lamina propria and submucosa.^{1,64}

Barium studies of the small bowel in patients with hypoalbuminemia may show smooth, straight, or slightly undulating, mildly thickened folds that are diffusely distributed throughout the small intestine (Fig. 49-13), although generally best visualized in the jejunum.⁶³ The luminal diameter of the jejunum is slightly increased.⁶² CT can also show edema of the small bowel

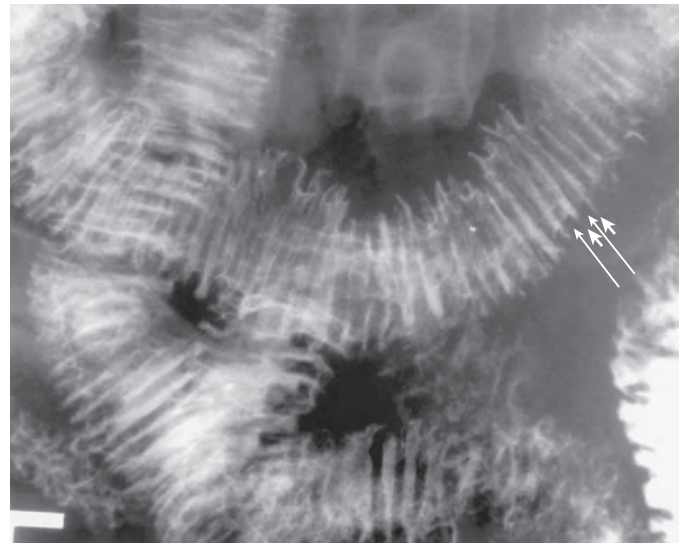


Figure 49-13 Small bowel edema in a patient with cirrhosis and hypoalbuminemia. This spot image from a small bowel follow-through shows diffusely thickened, smooth, straight folds (long arrows) perpendicular to the longitudinal axis of the bowel. Barium trapped between the folds forms the so-called interspace spikes (short arrows).

mesentery in 86% of patients. Omental and retroperitoneal edema is seen less frequently (56%).⁶⁵

Enteroliths and Bezoars

Bezoar derives from the Persian root *-padzahr*, meaning antidote.⁶⁶ A bezoar was a calculus found in the stomach or gallbladder of wild goats that lived in northeastern Persia. Bezoars were believed to have a variety of medicinal properties, especially as antidotes for poisoning. In humans, most bezoars are found in the stomach and are composed of indigestible organic substances such as hair (trichobezoars) or fruit (phytobezoars). Any vegetable or fruit with high fiber content can result in bezoar formation.

Bezoars and enteroliths are uncommon in the small intestine.⁶⁷ Bezoars form in areas of stasis such as the jejunal diverticula, Meckel's diverticulum, and bypassed small bowel loops after surgery for Crohn's disease. Bezoars also form proximally to strictures related to Crohn's disease, tuberculosis, or other causes. Small intestinal bezoars are composed of hair, undigested food, or medications such as nonabsorbable antacids. In areas of the world in which persimmons are eaten, most phytobezoars are related to the ingestion of unripe persimmons.^{68,69}

Small intestinal bezoars or enteroliths are intraluminal masses of mixed density and attenuation on CT (Fig. 49-14). These intraluminal masses may contain air, soft tissue, or calcium,^{70,71} and peripheral or laminated calcification may be present (see Fig. 49-14). Small intestinal bezoars are typically found in the distal ileum—the narrowest portion of the small bowel—or just proximal to pathologic areas of narrowing, such as strictures, anastomoses, or tumors. Bezoars can be confused with intraluminal gallstones associated with gallstone ileus. However, no air is identified in the biliary tree in patients with bezoars.

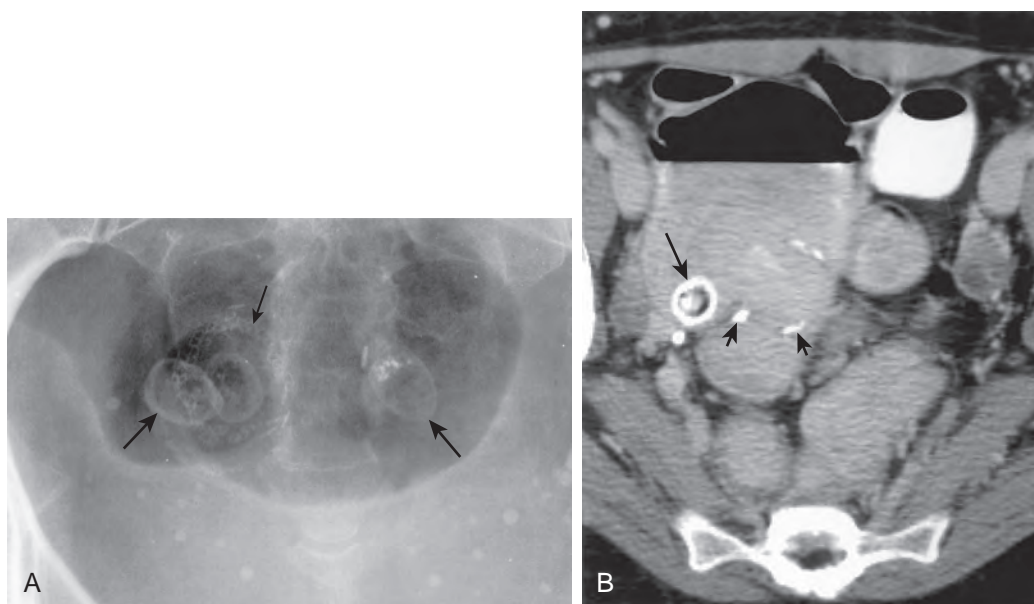


Figure 49-14 Enteroliths proximal to a stricture at the ileorectal anastomosis. A. Coned-down view from a plain abdominal radiograph shows three peripherally calcified ovoid structures (*large arrows*) near an anastomotic staple line (*small arrow*). **B.** Axial CT scan through the pelvis shows one of the enteroliths as a peripherally calcified structure (*large arrow*) containing central bubbles of air and soft tissue attenuation. Part of the staple line (*small arrows*) is identified.

REFERENCES

- Fenoglio-Preiser CM, Noffsinger AE, Stemmermann GN, et al (eds): Nonneoplastic lesions of the small intestine. In *Gastrointestinal Pathology, An Atlas and Text*, ed 2, Philadelphia, 1999, Lippincott-Raven, pp 309–458.
- Cuvellier C: Congenital abnormalities of the small intestine. In Shepherd NA, Warren BF, Williams GT, et al, editors: *Morson and Dawson's Gastrointestinal Pathology*, ed 5, Chichester, England, 2013, Wiley-Blackwell, pp 293–304.
- Levy A, Hobbs CM: Meckel diverticulum: Radiologic features with pathologic correlation. *Radiographics* 24:565–587, 2004.
- Yamaguchi M, Takeuchi S, Awazu S: Meckel's diverticulum: Investigation of 600 patients in the Japanese literature. *Am J Surg* 136:247–249, 1978.
- Maglinte DD, Jordan LG, Van Hove ED, et al: Chronic gastrointestinal bleeding from Meckel's diverticulum: Radiologic considerations. *J Clin Gastroenterol* 3:47–52, 1981.
- Leijonmarck CE, Bonman-Sandelin K, Frisell J, et al: Meckel's diverticulum in the adult. *Br J Surg* 73:146–149, 1986.
- Sagar J, Kumar V, Shah DK: Meckel's diverticulum: A systematic review. *J Roy Soc Med* 99:501–505, 2006.
- Bennet GL, Birnbaum BA, Balthazar EJ: CT of Meckel diverticulitis in 11 patients. *AJR* 182:625–629, 2004.
- Perlman JA, Hoover HC, Safer PK: Femoral hernia with strangulated Meckel's diverticulum (Littre's hernia). *Am J Surg* 139:286–289, 1980.
- Dixon AY, McAnaw M, McGregor DH, et al: Dual carcinoid tumors of Meckel's diverticulum presenting as metastasis in an inguinal hernia sac: Case report with literature review. *Am J Gastroenterol* 83:1283–1288, 1988.
- Chandramohan K, Agarwal M, Gurjar G, et al: Gastrointestinal tumor in Meckel's diverticulum. *World J Surg Oncol* 5:50, 2007.
- Sfakianakis GN, Conway JJ: Detection of ectopic gastric mucosa in Meckel's diverticulum and in other aberrations by scintigraphy: Indications and methods—a 10-year experience. Parts I and II. *J Nucl Med* 22:647–654, 732–738, 1981.
- Fries M, Mortensen W, Robertson B: Technetium pertechnetate scintigraphy to detect ectopic gastric mucosa in Meckel's diverticulum. *Acta Radiol Diagn* 25:417–422, 1984.
- Benahmou G: Small intestinal obstruction by an enterolith from a Meckel's diverticulum. *Int Surg* 64:43–45, 1979.
- Pantongrag-Brown J, Levine MS, Buetow PC, et al: Meckel's enteroliths: Clinical, radiologic and pathologic findings. *AJR* 167:1447–1450, 1996.
- Ekman CN: Regional enteritis associated with Meckel's diverticulum: A report of five cases. *Gastroenterology* 13:130–134, 1958.
- Glick SN, Maglinte DDT, Herlinger H: Association of Meckel's diverticulum and Crohn's disease. *Gastrointest Radiol* 13:67–71, 1988.
- Maglinte DDT, Elmore MF, Isenberg M, et al: Meckel diverticulum: Radiologic demonstration by enteroclysis. *AJR* 134:925–932, 1980.
- Maglinte DDT, Burney BT, Miller RE: Lesions missed on small bowel follow-through: Analysis and recommendations. *Radiology* 144:737–739, 1982.
- Salomonowitz E, Wittich G, Hajek P, et al: Detection of intestinal diverticula by double-contrast small bowel enema: Differentiation from other intestinal diverticula. *Gastrointest Radiol* 8:271–278, 1983.
- Ghahremani GG: Radiology of Meckel's diverticulum. *Crit Rev Diagn Imaging* 26:1–43, 1986.
- Freeny PC, Walker JH: Inverted diverticula of the gastrointestinal tract. *Gastrointest Radiol* 4:57–59, 1979.
- Rubenstein SE, Herlinger H: Test your skills: Inverted Meckel's diverticulum. *Radiology* 176:636, 644, 1990.
- Hamada T, Ishida O, Yasutomi M: Inverted Meckel diverticulum with intussusception. CT findings. *J Comput Assist Tomogr* 19:808–810, 1995.
- Bower RJ, Sieber WK, Kiesewetter WB: Alimentary duplications in children. *Ann Surg* 188:669–674, 1978.
- Buras RR, Guzzetta PC, Majd M: Multiple duplications of the small intestine. *J Pediatr Surg* 21:957–959, 1986.
- Case records of the Massachusetts General Hospital. Weekly clinicopathological exercises. Case 16-1980. *N Engl J Med* 302:958–962, 1980.
- Gilchrist AM, Sloan JM, Logan CJH, Mils JOM: Case report: Gastrointestinal bleeding due to multiple ileal duplications diagnosed by scintigraphy and barium studies. *Clin Radiol* 41:134–136, 1990.
- Ros PR, Olmsted WW, Moser RP, Jr, et al: Mesenteric and omental cysts: Histologic classification with imaging correlation. *Radiology* 164:327–332, 1987.
- Kelly RB, Mahoney PD, Johnson JF: CT demonstration of an unusual enteric duplication cyst. *J Comput Assist Tomogr* 10:506–507, 1986.
- Fenoglio-Preiser CM, Pascal RR, Perzin KH: *Tumors of the Intestines, Atlas of Tumor Pathology*, 2nd series, fascicle 27, Washington, DC, 1980, Armed Forces Institute of Pathology, pp 405–411.
- Rubenstein SE, Furth EE, Herlinger H: "Bubbly" duodenal bulb in clinically unsuspected or refractory adult celiac disease. *Abdom Imaging* 23:449–452, 1988.

33. Lai EC, Tompkins RK: Heterotopic pancreas: Review of a 26-year experience. *Am J Surg* 151:697–700, 1985.
34. Rubesin SE, Furth EE, Birnbaum BA, et al: Ectopic pancreas complicated by pancreatitis and pseudocyst formation mimicking jejunal diverticulitis. *Br J Radiol* 70:311–313, 1997.
35. Musselman JA, Ghahremai GG, Bordin GM, et al: Idiopathic localized dilatation of the ileum in adults. *Gastrointest Radiol* 6:313–317, 1981.
36. Ratcliffe J, Tait J, Lisle D, et al: Segmental dilatation of the small bowel: Report of three cases and literature review. *Radiology* 171:827–830, 1989.
37. Bell BR, Ternberg JL, Bower RJ: Ileal dysgenesis in infants and children. *J Pediatr Surg* 17:395–399, 1982.
38. Morewood DJ, Cunningham ME: Case report: Segmental dilation of the ileum presenting with anemia. *Clin Radiol* 36:267–268, 1985.
39. Javors BR, Gold RP, Ghahremani GG, et al: Idiopathic localized dilation of the ileum in adults: Findings on barium studies. *AJR* 164:87–90, 1994.
40. Balthazar EJ: Intestinal malrotation in adults: Roentgenographic assessment with emphasis on isolated complete and partial nonrotations. *AJR* 126:358–367, 1976.
41. Berardi RS: Anomalies of midgut rotation in the adult. *Surg Gynecol Obstet* 151:113–124, 1980.
42. Kern IB, Curie BG: The presentation of malrotation of the intestine in adults. *Ann R Coll Surg Engl* 72:239–242, 1990.
43. Strouse PJ: Disorders of intestinal rotation and fixation ('malrotation'). *Pediatr Radiol* 34:837–851, 2004.
44. Fukuya T, Brown BP, Lu CC: Midgut volvulus as a complication of intestinal malrotation in adults. *Dig Dis Sci* 38:438–444, 1993.
45. Meyers MA: Internal abdominal hernias. In Meyers MA, editor: *Dynamic Radiology of the Abdomen*, ed 5, New York, 2000, Springer, pp 712–728.
46. Suchato C, Peksan P, Panjapiyakul C: CT findings in symptomatic left paraduodenal hernia. *Abdom Imaging* 21:148–149, 1996.
47. Parsons PB: Paraduodenal hernia. *AJR* 69:563–589, 1953.
48. Olazabal A, Guasch I, Casas D: Case report: CT diagnosis of nonobstructive left paraduodenal hernia. *Clin Radiol* 46:288–289, 1992.
49. Warshauer DM, Mauro MA: CT diagnosis of paraduodenal hernia. *Gastrointest Radiol* 17:13–15, 1992.
50. Aronchick CA, Brooks FP, Dyson WL, et al: Ileocecal endometriosis presenting with abdominal pain and gastrointestinal bleeding. *Dig Dis Sci* 28:566–572, 1983.
51. Brosens JA: Endometriosis: Current issues in diagnosis and medical management. *J Reprod Med* 43:281–286, 1998.
52. McAfee CH, Greer HL: Intestinal endometriosis: A report of 29 cases with a review of the literature. *J Obstet Gynecol* 67:539–555, 1960.
53. Martinbeau PW, Pratt JH, Gaffey TA: Small bowel obstruction secondary to endometriosis. *Mayo Clin Proc* 50:239–243, 1975.
54. LiVolsi VA, Perzin KH: Endometriosis of the small intestine producing intestinal obstruction or simulating neoplasm. *Am J Dig Dis* 19:100–107, 1974.
55. Croom RD, Donovan ML, Schweisinger WH: Intestinal endometriosis. *Am J Surg* 148:660–667, 1984.
56. Gindoff PR, Jewelewicz R: Ileal resection in the operative treatment of endometriosis. *Obstet Gynecol* 69:511–513, 1987.
57. Minocha A, Davis MS, Wright RA: Small bowel endometriosis masquerading as regional enteritis. *Dig Dis Sci* 39:1126–1133, 1994.
58. Badawy SZY, Freedman L, Numann P, et al: Diagnosis and management of intestinal endometriosis: A report of five cases. *J Reprod Med* 33:851–855, 1988.
59. Nitsch B, Ho C-S, Cullen J: Barium study of small bowel endometriosis. *Gastrointest Radiol* 13:361–363, 1988.
60. Scarmato V, Levine MS, Herlinger HH, et al: Ileal endometriosis: Radiographic findings in five cases. *Radiology* 214:509–512, 2000.
61. Marshak RH, Khilnani M, Eliasoph J, Wolf BS: Intestinal edema. *AJR* 101:379–387, 1967.
62. Farthing MJG, Madewell JE, Bartram CI, et al: Radiologic features of the jejunum in hypoalbuminemia. *AJR* 136:883–886, 1981.
63. Balthazar EJ, Gade MF: Gastrointestinal edema in cirrhotics: Radiographic manifestations with emphasis on colonic involvement. *Gastrointest Radiol* 1:215–223, 1976.
64. Nagral AS, Joshi AS, Bhatia P, et al: Congestive jejunopathy in portal hypertension. *Gut* 34:694–697, 1993.
65. Chopra S, Dodd GD, Chintapalli KN, et al: Mesenteric, omental and retroperitoneal edema in cirrhosis: Frequency and spectrum of CT findings. *Radiology* 211:737–742, 1999.
66. Elgood C (trans): A treatise on the bezoar stone. By the late Mahmud bin Masud, the imad-uddin, physician of Ispahan. *Ann Med History* 7:73–80, 1935.
67. Javors BR, Bryk D: Enterolithiasis: Report of four cases. *Gastrointest Radiol* 8:359–362, 1983.
68. Kaplan O, Klausner JM, Lelcuk S, et al: Persimmon bezoars as a cause of intestinal obstruction: Pitfalls in their surgical management. *Br J Surg* 72:242–243, 1985.
69. Verstandig AG, Klin B, Bloom RA, et al: Small bowel phytobezoars: Detection with radiography. *Radiology* 172:705–707, 1989.
70. Ripolles T, Garcia-Aguayo J, Martinez M-J, Gil P: Gastrointestinal bezoars: Sonographic and CT characteristics. *AJR* 177:65–69, 2001.
71. Quirogoga S, Alvarez-Castells AA, Sebastia MC, et al: Small bowel obstruction secondary to bezoar: CT diagnosis. *Abdom Imaging* 22:315–317, 1997.

Small Intestine: Differential Diagnosis

STEPHEN E. RUBESIN

CHAPTER OUTLINE

Small Bowel Folds and Mucosal Changes

- Table 50-1. Normal Small Bowel Parameters**
- Table 50-2. Small Bowel Lumen Dilated, Normal Fold Thickness**
- Table 50-3. Smooth, Straight, Thickened Folds**
- Table 50-4. Micronodularity**
- Table 50-5. Irregular Fold Thickening, Diffuse**
- Table 50-6. Irregular Fold Thickening, Proximal Small Bowel**
- Table 50-7. Irregular Fold Thickening, Distal Ileum**
- Table 50-8. Tubular Bowel with Luminal Narrowing**
- Table 50-9. Tubular Bowel without Luminal Narrowing**
- Table 50-10. Solitary Polyp**
- Table 50-11. Multiple Polyps and Polyposis Syndromes**
- Table 50-12. Multiple Target Lesions**
- Table 50-13. Annular Lesion with Shelflike Margins**
- Table 50-14. Annular Lesion with Tapered Edges**
- Table 50-15. Exoenteric Cavitory Lesions**
- Table 50-16. Separation of Bowel Loops without Tethering**
- Table 50-17. Mass Effect with Tethering of Mucosal Folds**
- Table 50-18. Site Predilection of Diseases**

The tables in this chapter (Tables 50-1 to 50-18) concerning the differential diagnosis of small bowel diseases are not meant to be exhaustive. Instead, these tables present an approach for classifying the most common causes of various radiographic abnormalities in the small bowel in relation to the size, location, distribution, and radiographic characteristics of these abnormalities. A list of references is included for further reading.¹⁻⁴⁰

Small Bowel Folds and Mucosal Changes

Small bowel villi are formed by a single-cell epithelial surface covering a lamina propria filled with fat, vessels, inflammatory cells, and a central lacteal. Fine nodularity of the mucosal surface (also termed *micronodularity* or a *sandlike pattern*) therefore reflects enlargement of villi, usually by an abnormality in the lamina propria, such as edema, inflammation, or infiltration by amyloid or other substances. Small bowel folds are composed of mucosa and submucosa. Enlarged or effaced small bowel folds therefore reflect edema, hemorrhage, inflammation, or tumor in the lamina propria and submucosa.

Tables 50-3 through 50-7 classify small intestinal diseases by their location in the small bowel and whether the folds are smoothly enlarged or are enlarged and nodular. Many diseases have abnormal villi and enlarged folds because the pathologic process involves the lamina propria and submucosa. Smooth fold thickening usually implies edema related to hypoalbuminemia or to edema or hemorrhage related to vascular causes. Nodular fold thickening implies inflammation or infiltration by tumor, amyloid, or other substances. It is often difficult to distinguish smooth fold enlargement from mildly nodular folds. The radiographic findings of diseases associated with edema or hemorrhage can therefore overlap with those of inflammatory and infiltrative diseases.

TABLE
50-1

Normal Small Bowel Parameters

Parameter	Jejunum	Ileum
NORMAL PARAMETERS FOR ENTEROCLYSIS		
Folds per inch length	4-7	2-4
Thickness of folds (mm)	1-2	1.0-1.5
Diameter of lumen (cm)	≤4	≤3
Wall thickness (mm)	1.0-1.5	1.0-1.5
NORMAL PARAMETERS FOR SMALL BOWEL FOLLOW-THROUGH		
Thickness of folds (mm)	2-3	1-2
Diameter of lumen (cm)	≤3	≤2

Data from references 1 and 2.

TABLE 50-2 Small Bowel Lumen Dilated, Normal Fold Thickness

Parameter	Cause	Comments
Diffuse small bowel dilation	Mechanical obstruction, small bowel or colon	Air-fluid levels on abdominal radiographs. CT if high grade obstruction suspected, barium studies for partial or intermittent obstruction Common causes—adhesions, hernias, metastases, radiation enteropathy, colonic carcinoma with backup into dilated small bowel
	Adynamic ileus	Air-fluid levels to distal small bowel and in colon Common causes—postoperative, medications, ischemia, vagotomy Less common causes—systemic sclerosis (dilated duodenum, hidebound small bowel), amyloidosis, peritonitis, electrolyte imbalances (hypokalemia, uremia), blunt trauma, diabetes, hypothyroidism
Focal small bowel dilation	Proximal obstruction	Fluid levels in few small bowel loops in upper abdomen—primary adenocarcinoma, postoperative strictures, adhesions
	Focal adynamic ileus	Pancreatitis, postoperative manipulation or leak, pelvic irradiation
	Closed-loop obstruction	Group of air-fluid levels unchanging in position CT for diagnosis and evaluation of possible strangulation
	Adhesions Internal hernia	Focal region of dilated loops with air-fluid levels

Data from references 1 to 5.

TABLE 50-3 Smooth, Straight, Thickened Folds

Parameter	Cause	Comments
Diffusely distributed	Edema	Hypoalbuminemia—cirrhosis, nephrotic syndrome Protein-losing enteropathy Congestive heart failure Portal hypertension
Focal smooth fold thickening	Intramural hemorrhage	Segmental stack of coins appearance; interspace spikes; thumbprinting on mesenteric border Most patients return to normal within 2-3 wk
	Ischemia	
	Anticoagulants	
	Coagulopathies	
	Superior mesenteric vein thrombosis	
	Vasculitides	Ischemic changes, hemorrhage, ulceration or necrosis with small vessel disease (lupus, Henoch-Schönlein purpura)
	Blunt trauma	CT—look for possible perforation (e.g., mesenteric haziness or fluid, thickened bowel wall, lack of bowel contrast enhancement, focal pneumatosis, free intraperitoneal gas)
	Radiation enteropathy	Thickened folds, narrow interfold spaces (interspace spikes); barium changes resemble picket fence Changes confined to radiation portal

Data from references 1, 6 to 10, and 40.

TABLE 50-4 Micronodularity

Cause	Comments
Whipple's disease	White males with arthralgias, cardiovascular and neurologic symptoms CT—low-attenuation mesenteric lymph node mass
<i>Mycobacterium avium-intracellulare</i> (MAI) complex enteritis	AIDS MAI-laden macrophages in lamina propria CT—shows necrosis in enlarged lymph nodes
Abetalipoproteinemia	Adolescent with retinitis pigmentosa, acanthocytosis, spinocerebellar degeneration Retained fat globules in villous enterocytes
Histoplasmosis	<i>Histoplasma</i> -laden macrophages in lamina propria
Lymphangiectasia	Villi enlarged by dilated lacteals in primary form Edema in submucosa Mesenteric adenopathy causes secondary form
Macroglobulinemia	Lymphoma—may occur IgM macroglobulin in lamina propria
Radiation therapy	Associated with smooth, thickened, straight folds
Crohn's disease	Distal, terminal ileum Aphthoid ulcers, mesenteric border ulcers; cobblestoning; strictures, fissures, fistulae

*1- to 2-mm mucosal nodules. Micronodularity implies villous enlargement caused by an infiltrative process in lamina propria. This table lists diseases that often involve the mucosa and submucosa and also produce abnormal folds.

Data from references 1 to 9 and 11 to 16.

TABLE 50-5 Irregular Fold Thickening, Diffuse

Cause	Comments
Lymphangiectasia, primary	Submucosal edema plus micronodularity Congenital hypoplasia of lymphatics
Lymphangiectasia, secondary	Small bowel changes (as above) Obstruction of lymph drainage by retroperitoneal fibrosis, radiation, mesenteric lymphadenopathy (Whipple's, lymphoma)
Amyloidosis, types AA and AL	Fold thickening if deposits in vessels cause ischemia. Micronodularity in secondary amyloidosis—reflects amyloid deposits in lamina propria
Mastocytosis	4- to 10-mm nodules in submucosa (AL) Histamine release—associated headaches, flushing, diarrhea; urticaria pigmentosa (50%), bone lesions (20%) Stomach, duodenum—ulcers Small bowel—multiple urticaria-like nodules Thickened folds often segmental
Immunoproliferative small intestinal disease (IPSID)	Relates to multiple parasitic and/or bacterial infections Patient from Mediterranean region Extensive lymphoid hyperplasia Responds to treatment
Mediterranean lymphoma	Young patient with progression of IPSID to monoclonal lymphomatous infiltrate Lymphoid nodules enlarged, nonuniform, confluent Lymph node masses
AIDS	Associated with a heavy-chain disease
Graft-versus-host disease	Large variety of infections cause diffuse thickened folds. Often with cytomegalovirus infection (see Table 50-8)

Data from references 1 and 15 to 17.

TABLE 50-6 Irregular Fold Thickening, Proximal Small Bowel

Cause	Comments
T-cell lymphoma complicating celiac disease	Diarrhea recurs despite gluten-free diet Nodular fold thickening in long segments May have annular lesions
Ulcerative jejunoileitis	Complicates celiac disease Before inflammatory infiltrate changes to monoclonal lymphoma Radiographically indistinguishable from T-cell lymphoma
Tropical sprue	History of sojourn in tropics Unlike celiac disease, folds are thickened, no separation of jejunal folds
Zollinger-Ellison syndrome	Gastric and duodenal ulcers Increased intraluminal fluid
Strongyloidiasis	Effaced folds, tubular bowel contour with severe disease
AIDS-related infections	<i>Mycobacterium avium-intracellulare</i> (MAI) complex, isosporiasis, cryptosporidiosis
Gastrojejunostomy	Thick folds in efferent loop just distal to gastrojejunal anastomosis
Jejunostomy tube	Reaction to tube feeds

Data from references 1, 2, 5, and 18.

TABLE 50-7 Irregular Fold Thickening, Distal Ileum

Parameter	Cause	Comments
Minimal luminal narrowing	Crohn's disease, early	Coarse villous pattern, aphthoid ulcers Uncommon pattern if no associated colonic disease Not an unusual pattern in neoterminal ileum
	<i>Yersinia</i> enterocolitis	Early—thickened, nodular folds, ulcers 5-8 wk—lymphoid hyperplasia 8-12 wk—normal terminal ileum
	Salmonellosis, campylobacteriosis Mantle cell lymphoma	Similar to <i>Yersinia</i> but more ulceration Part of systemic disease Multiple nodules, mesenteric masses Prognosis poor
Moderate to marked luminal narrowing	Crohn's disease	Narrowing may change in diameter if caused by spasm, edema, or inflammation rather than fibrosis Mild—mesenteric border ulceration and antimesenteric sacculation Moderate—transmural extension with luminal narrowing and ulceronodular pattern Severe—strictures, fissures, fistulae CT best to determine presence of mesenteric abscesses
	Tuberculosis	Patient from endemic area or immunodeficient More pronounced in cecum, right colon Ulcers, transverse folds, patulous ileocecal valve, retracted cecum May be indistinguishable from Crohn's disease
	Behçet's disease	Associated with uveitis, genital ulcers, arthritis Penetrating ulcers, especially in colon
	AIDS-related infections	Cytomegalovirus, actinomycosis
	Cecal carcinoma, lymphoma	Cecal mass associated with retrograde extension of tumor via lymphatics into terminal ileum Thickened nodular folds

Data from references 1 and 19 to 24.

TABLE 50-8 Tubular Bowel with Luminal Narrowing

Cause	Comments
Graft-versus-host disease	Often complicated by cytomegalovirus infection Diffuse small bowel involvement "Toothpaste" appearance is function of rapid transit
Chronic ischemic changes	Prolonged adherence of barium Radiation or amyloidosis
Burnt-out Crohn's disease	Hypoperistaltic or aperistaltic loops Distal ileum
Strongyloidiasis	Active disease may be present nearby Jejunum Severe disease, but reversible

Data from references 1, 7, 10, 16, 17, 24, and 25.

TABLE 50-9 Tubular Bowel without Luminal Narrowing

Cause	Comments
Primary lymphoma	Segmental infiltrate effaces fold pattern 5-15 cm in length
Celiac disease, long-standing	Near-absence of folds in proximal jejunum Associated with a mosaic pattern

Data from references 1 to 3, 5, and 18.

TABLE 50-10 Solitary Polyp

Cause	Comments
Carcinoid, early	80% of carcinoid tumors in distal ileum Polyp in ileum—exclude carcinoid 30% multiple Early form of tumor (0.5-2.0 cm) before invasion and desmoplastic effect
Lipoma	Elongated lesions with pseudopedicle May ulcerate, change in shape CT—fat attenuation
Adenoma	85% of adenomas in duodenum 10% of adenomas in jejunum
Brunner gland polyp	First or second portions of duodenum
Hemangioma	Sessile polyp or carpet lesion May contain phleboliths
Gastrointestinal stromal tumor	Sessile polyp or target lesion Cavitary mass when large
Neurofibroma	Association with neurofibromatosis
Gangliocytic paraganglioma	Near papilla of Vater
Inverted Meckel's diverticulum	Elongated intraluminal "polyp" in distal ileum Associated with intussusception
Inflammatory fibroid polyp	Usually in ileum Elongated polyp composed of granulation tissue, with eosinophils

Data from references 1 and 26 to 28.

TABLE 50-11 Multiple Polyps and Polyposis Syndromes

Parameter	Cause	Comments
Multiple polyps	Hematogenous metastases	Most commonly metastatic melanoma
	Kaposi's sarcoma	Submucosal mass Known AIDS Plaque, submucosal mass, or target lesion
Polyposis syndromes	Carcinoid tumor	Multiple in 30% (see Table 50-10)
	Disseminated lymphoma	Multiple submucosal masses or target lesions
	Mantle cell lymphoma	Lymphomatous polyposis
	Peutz-Jeghers syndrome	Autosomal dominant, but 40% of patients are spontaneous mutants Sessile or pedunculated polyp with lobulated or villous surface Jejunum Young patients with bleeding or pain; pigmented lesions on mouth, lips, palms
	Cowden's disease	Autosomal dominant Polyps of varying histologies but hamartomatous polyps more often in colon than in small bowel Facial papillomas Associated thyroid disease (66%) and breast carcinoma (33%-50%)
	Cronkhite-Canada syndrome	Nonhereditary; mean age of 60 yr Diarrhea, ectodermal changes, protein loss Inflammatory polyps more frequent in stomach and in colon than in duodenum or small bowel
	Familial adenomatous polyposis syndrome	Autosomal dominant; 10%-30% of patients are spontaneous mutants Mutations in various portions of APC gene produce various clinical syndromes (e.g., Gardner's, Turcot's) Small bowel adenomas primarily in duodenum 12% develop periampullary carcinomas Desmoid tumors in root of small bowel mesentery
	Neurofibromatosis	Known clinical diagnosis

Data from reference 1.

TABLE 50-12 Multiple Target Lesions

Cause	Comments
Melanoma metastases	Hematogenous spread Submucosal lesions, often on antimesenteric border Large ulcer with spoke wheel radiating folds
Other hematogenous metastases	Breast and lung cancer
Lymphoma, disseminated	Involves stomach more frequently than small bowel
Kaposi's sarcoma	Involves stomach and duodenum more frequently than small bowel Plaquelike lesion or thickened folds more common morphologic forms Homosexuals with AIDS

Data from references 1 and 13.

TABLE 50-13 Annular Lesion with Shelflike Margins

Cause	Comments
Small bowel obstruction by adhesive band	Transition zone with sharply demarcated band compressing against distended proximal and collapsed distal small bowel Shelflike or beaklike narrowing Adjacent folds are normal; no mucosal nodularity
Adenocarcinoma, primary	Proximal jejunum Short lesion with shouldering Central ulceration; folds destroyed or nodular Obstruction not severe, unless late diagnosis
Metastases	Colon cancer most frequent primary tumor Mid to distal small bowel Desmoplasia with angulation causing obstruction Folds relatively preserved but may be tethered
Primary small bowel lymphoma	Long lesion without obstruction Nodular folds and effaced mucosa Center bulges aneurysmally Multiple in up to 25% of patients
Carcinoid	Misleading en face appearance of saddle lesion (polypoid lesion spreading circumferentially)
Anastomotic stricture	Clinical history; staple line
NSAID stricture	Multiple, ringlike thickened webs causing low-grade obstruction

Data from references 1, 18, and 29 to 35.

TABLE 50-14 Annular Lesion with Tapered Edges

Cause	Comments
Adhesion	Beaklike tapering with smooth folds
Crohn's disease	Stricture caused by primary disease or skip lesion Associated cobblestoning or mesenteric border ulcers
Radiation enteropathy	Strictures within area of severe damage or at entry site into radiation field Bowel loops often angulated; folds tethered because of serositis or fibrosis
Ischemia	Usually low-grade obstruction May be related to trauma

Data from references 1, 10, 23, and 24.

TABLE 50-15 Exoenteric Cavitary Lesions

Parameter	Comments
COMMON CAUSES	
Primary non-Hodgkin's lymphoma	Transmural ulceration with perforation into mesentery or cavitation of tumor that has invaded mesentery
Metastatic melanoma	Large, deeply ulcerated metastases
Malignant gastrointestinal stromal tumor	Cavity caused by central necrosis in tumor that subsequently communicates with bowel lumen or by ischemic necrosis of epithelium overlying tumor, with secondary ulceration
UNCOMMON CAUSES	
Adenocarcinoma	Deeply ulcerated tumor perforates
Jejunal diverticulitis with abscess cavity	
Ectopic pancreas with pancreatitis and pseudocyst formation	
Hematogenous metastasis from pulmonary carcinoma	
Crohn's disease	Fistula or perforation forms abscess cavity Other findings of Crohn's disease

Data from references 1, 13, 18, 37, and 38.

TABLE 50-16 Separation of Bowel Loops without Tethering

Cause	Comments
Prominent fat within small bowel mesentery	Most common of cause of separated loops More pronounced in ileum
Ascites	Loops retain normal pliability and mobility Small bowel loops centrally located CT for cause
Mesenteric masses	Lymphoma of mesenteric nodal origin — enlarges and displaces bowel; may surround it without obstruction (sandwich sign); later infiltrates intestinal wall causing obstruction Desmoid tumor related to familial adenomatous polyposis syndrome
Crohn's disease	CT distinguishes bunching of fat caused by mesenteric inflammation and scarring (fibrofatty proliferation) from abscess

Data from references 1 and 18.

TABLE 50-17 Mass Effect with Tethering of Mucosal Folds

Causes	Comments
Intraperitoneal metastases	Right lower quadrant, pelvis Multiple hemispheric masses on mesenteric border of distal ileum with crowded, tethered folds
Carcinoid tumor, early	Hemispheric sessile polyp, with adjacent desmoplastic crowding of folds Multiple in 30%
Carcinoid tumor, advanced	Intense desmoplastic effect on adjacent bowel loops Mesenteric metastases grow larger than primary tumor CT—central mesenteric mass (calcified in 50%), mesenteric stranding Associated with ascites, small bowel ischemia
Interloop or omental abscess	Extrinsic mass with mildly edematous folds radiating toward abscess
Retractile mesenteritis	Intestinal loops separated and pulled toward mesentery CT shows soft tissue mesenteric masses
Endometriosis	Sharply demarcated plaques invade serosa causing pleating of underlying mucosa Pelvic and terminal ileum; more often involves rectosigmoid colon
Pancreatitis	Desmoplastic changes in left upper quadrant: jejunum and splenic flexure
Root of mesentery nodal metastasis	At or left of duodenojejunal junction—left-sided colon cancer, transitional cell carcinoma of bladder Near second portion of duodenum—right-sided colon cancer
Cecal or appendiceal process involving terminal ileum	Cecal lymphoma, carcinoma Appendicitis Appendiceal tumors
Crohn's disease	Abscess, inflammatory process in mesentery Other findings of Crohn's disease

Data from references 1 and 38.

TABLE 50-18 Site Predilection of Diseases

Site	Disease
Proximal jejunum	Adenocarcinoma Jejunal diverticulosis Infections: giardiasis, Whipple's disease, cryptosporidiosis, isosporiasis Celiac disease Zollinger-Ellison–related pathology Polyps in Peutz-Jeghers syndrome
Distal ileum	Crohn's disease Carcinoid tumors Ileitis caused by <i>Yersinia</i> , <i>Campylobacter</i> , cytomegalovirus, Behçet's disease Intraperitoneal metastases Secondary involvement by inflammatory or neoplastic disease of cecum or appendix
Antimesenteric border	Radiation enteropathy Tuberculosis (right-sided colonic predominance) Meckel's diverticulum Hematogenous metastases
Mesenteric border	Sacculation in Crohn's disease Linear ulcers in Crohn's disease Peritoneally seeded metastases Jejunal diverticula Thumbprinting caused by intramural bleeding Mesenteric hematoma Intestinal duplication Cavitation in primary intestinal lymphoma

Data from references 1 to 5, 9 to 11, 13, 18, 21 to 24, 30, 39, and 40.

REFERENCES

- Herlinger H, Maglinte DDT, Birnbaum BB: Clinical radiology of the small intestine, New York, 1999, Springer-Verlag.
- Herlinger H, Maglinte DDT: Jejunal fold separation in adult celiac disease: Relevance of enteroclysis. *Radiology* 158:605–611, 1986.
- Rubenstein SE, Rubin RA, Herlinger H: Small bowel malabsorption: Clinical and radiologic perspectives. How we see it. *Radiology* 184:297–305, 1992.
- Horowitz AL, Meyers MA: The “hide-bound” small bowel of scleroderma: Characteristic mucosal fold pattern. *AJR* 119:332–334, 1973.
- Rubenstein SE, Grumbach K, Herlinger H, et al: Adult celiac disease and its complications. *Radiographics* 9:1045–1066, 1989.
- Marshak RH, Ruoff M, Lindner AE: Roentgen manifestations of giardiasis. *AJR* 104:557–560, 1968.
- Dallemand S, Waxman M, Farman J: Radiologic manifestations of *Strongyloides stercoralis*. *Gastrointest Radiol* 8:45–51, 1983.
- Schulman A, Morton PCG, Dietrich BE: Eosinophilic gastroenteritis. *Clin Radiol* 31:101–104, 1980.
- Khilnani MT, Marshak RH, Eliasoph J, Wolf BS: Intramural intestinal hemorrhage. *Am J Roentgenol Radium Ther Nucl Med* 92:1061–1071, 1964.
- Mendelson RM, Nolan DJ: The radiological features of radiation enteritis. *Clin Radiol* 36:141–148, 1985.
- Philips RL, Carlson HC: The roentgenographic and clinical findings in Whipple’s disease: A review of 8 patients. *AJR* 123:268–273, 1975.
- Vincent ME, Robbins AH: *Mycobacterium avium-intracellulare* complex enteritis: Pseudo-Whipple’s disease in AIDS. *AJR* 144:921–922, 1985.
- Berk RN, Wall SD, McArdle CT, et al: Cryptosporidiosis of the stomach and small intestine in patients with AIDS. *AJR* 143:549–554, 1984.
- Jones B, Hamilton SR, Rubenstein SE, et al: Granular small bowel mucosa: A reflection of villous abnormality. *Gastrointest Radiol* 12:219–225, 1987.
- Olmsted WW, Madewell JE: Lymphangiectasia of the small intestine. *Gastrointest Radiol* 1: 241–243, 1976.
- Kingham JGC, Moriarty KJ, Furness M, et al: Lymphangiectasia of the colon and small intestine. *Br J Radiol* 55:774–777, 1982.
- Tada S, Iida M, Matsui T, et al: Amyloidosis of the small intestine: Findings on double contrast radiographs. *AJR* 156:741–744, 1991.
- Rubenstein SE, Gilchrist AM, Bronner M, et al: Non-Hodgkin lymphoma of the small intestine. *Radiographics* 10:985–998, 1990.
- Glick SN, Teplick SK: Crohn’s disease of the small intestine: Diffuse mucosal granularity. *Radiology* 154:313–317, 1985.
- Ekberg O, Lindstrom C: Superficial lesions in Crohn’s disease of the small bowel. *Gastrointest Radiol* 4:389–393, 1979.
- Ekberg O, Sjöström B, Brahme F: Radiological findings in *Yersinia* ileitis. *Radiology* 123:15–19, 1977.
- Goldberg HI, Caruthers SB, Nelson JA, Singleton JW: Radiographic findings of the National Cooperative Crohn’s Disease Study. *Gastroenterology* 77:925–937, 1979.
- Herlinger H, Rubenstein SE, Furth EE: Mesenteric border ulcers in Crohn’s disease: Historical, radiologic and pathologic perspectives. *Abdom Imaging* 23:122–126, 1998.
- Rubenstein SE, Bronner M: Radiologic-pathologic concepts in Crohn’s disease. *Adv Gastrointest Radiol* 1:27–55, 1991.
- Jones B, Kramer S, Saral R, et al: Gastrointestinal inflammation after bone marrow transplantation: Graft-versus-host disease or opportunistic infection? *AJR* 150:277–281, 1988.
- Fenoglio-Preiser CM, Pascal RR, Perzin KH: Tumors of the intestines. *Atlas of Tumor Pathology*, series 2, fascicle 27, Washington, DC, 1990, Armed Forces Institute of Pathology.
- Hoffman JW, Fox PS, Wilson SD: Duodenal wall tumors and the Zollinger-Ellison syndrome. *Arch Surg* 107:334–339, 1973.
- Shimer GR, Helwig EB: Inflammatory fibroid polyps of the intestine. *Am J Clin Pathol* 81: 708–714, 1984.
- Collier PE, Turowski P, Diamond DL: Small intestinal adenocarcinoma complicating regional enteritis. *Cancer* 55:516–521, 1985.
- Bridge MF, Perzin KH: Primary adenocarcinoma of the jejunum and ileum: A clinicopathologic study. *Cancer* 36:1876–1887, 1975.
- Levine MS, Drooz AT, Herlinger H: Annular malignancies of the small bowel. *Gastrointest Radiol* 12:53–58, 1987.
- Issacson P: B cell lymphomas of the gastrointestinal tract. *Am J Surg Pathol* 9:117–128, 1985.
- Ranchod M, Kempson RL: Smooth muscle tumors of the gastrointestinal tract and retroperitoneum. *Cancer* 39:255–262, 1977.
- Wilson IH, Cooley NV, Luibel FJ: Nonspecific stenosing small bowel ulcers. *Am J Gastroenterol* 50:449–455, 1968.
- Lang J, Price AB, Levi AJ, et al: Diaphragm disease: Pathology of disease of the small intestine induced by nonsteroidal anti-inflammatory drugs. *J Clin Pathol* 41:516–526, 1988.
- Greenstein S, Jones B, Fishman EK, et al: Small bowel diverticulitis: CT findings. *AJR* 147:271–274, 1986.
- Rubenstein SE, Furth EE, Birnbaum BA, et al: Ectopic pancreas complicated by pancreatitis and pseudocyst formation mimicking jejunal diverticulitis. *Br J Radiol* 70:311–313, 1997.
- Meyers MM: Clinical involvement of mesenteric and antimesenteric borders of small bowel loops: II. Radiologic interpretation of pathologic alterations. *Gastrointest Radiol* 1:49–58, 1976.
- Vaidya MG, Sodhi JS: Gastrointestinal tract tuberculosis: A study of 102 cases including 55 hemicolectomies. *Clin Radiol* 29:189–195, 1978.
- Rubenstein SE: The simplified approach to differential diagnosis of small bowel abnormalities. *Radiol Clin North Am* 41:343–364, 2003.

SECTION
VII

Colon

Barium Studies of the Colon

MARC S. LEVINE | IGOR LAUFER

CHAPTER OUTLINE

Single- Versus Double-Contrast Technique

Double-Contrast Barium Enema

Preparation of the Patient

Materials and Equipment

Single-Contrast Barium Enema

Technical Problems

Poor Preparation

Diverticulosis

Incontinence

Filling of Entire Colon

Complications

Variations in Technique

Suspected Perforation

Peroral Pneumocolon

Colostomy Enema

The overall volume of barium enemas has decreased considerably in modern medical practice because of greater use of other diagnostic tests such as colonoscopy, computed tomography (CT) and, most recently, CT colonography. Nevertheless, the barium enema remains a valuable technique for evaluating patients with a variety of colorectal diseases. The double-contrast barium enema, in particular, has been shown to be a viable alternative to colonoscopy for colorectal cancer screening¹ and for detecting polyps and cancers in the proximal colon in patients with incomplete colonoscopy.² Both single- and double-contrast barium enemas also have the ability to demonstrate a variety of intramural and extrinsic abnormalities involving the colon that are more difficult to recognize at colonoscopy. In such cases, the full extent of disease may then be assessed by cross-sectional imaging studies such as CT.

Depending on the clinical indications for the barium enema and the patient's overall condition, single- or double-contrast techniques may be used to evaluate the colon. We believe that a double-contrast barium enema is generally the preferred examination because of its greater diagnostic capabilities, so it has received more emphasis in this chapter.

Single- Versus Double-Contrast Technique

Double-contrast technique is generally thought to be superior to single-contrast technique for detecting small polypoid lesions or flat carpet lesions (villous tumors) in the colon and for visualizing the early inflammatory changes of inflammatory

bowel disease (Crohn's disease and ulcerative colitis).^{3,4} This advantage of double-contrast technique is related to its ability to visualize the mucosal surface en face on double-contrast images. There are also specific signs such as the mucosal spiculation of endometriosis or metastatic disease that are better demonstrated on double-contrast studies (see Chapter 3).^{5,6} Finally, double-contrast technique enables evaluation of the rectum, which is not accessible to manual palpation on single-contrast studies.⁷

In contrast, single-contrast technique entails filling of each colonic loop with a continuous column of barium, enabling visualization of contour abnormalities such as polyps or ulcers in profile and circumferential areas of narrowing such as annular carcinomas. Polyps and polypoid masses can also be visualized en face by thinning the barium column with graded compression to delineate these lesions as filling defects within the barium pool. Despite the limitations of single-contrast technique in detecting polyps, it is the preferred examination for patients with suspected fistulas, obstruction, or intussusception, in whom careful control of the barium column is required. Single-contrast technique is also useful for showing ischemic colitis associated with thumbprinting that can be effaced by gaseous distention of the colon on double-contrast studies.⁸ Finally, single-contrast technique is used for patients who are too old or too debilitated to perform the various maneuvers required for a double-contrast study or in patients with poor sphincter tone who may be unable to retain rectally administered air, even with inflation of a rectal balloon.

Double-Contrast Barium Enema

PREPARATION OF THE PATIENT

A variety of regimens may be used for cleansing the colon, but most include the following basic components⁹:

- A clear liquid diet for 24 hours
- One or preferably two sets of laxatives on the afternoon and evening before the examination (e.g., one 16-ounce bottle of magnesium sulfate at 4 PM and four Dulcolax [bisacodyl] tablets at 10 PM)
- A suppository (e.g., a Dulcolax suppository) on the morning of the examination

If followed properly, this basic preparation is usually effective in cleansing the colon, but noncompliance can be a problem. When patients arrive in the department, they should be asked whether they have taken the preparation and whether it has been effective in producing clear, watery bowel movements. If there is any doubt about the adequacy of the preparation, a preliminary abdominal radiograph should be obtained. If this radiograph shows definite fecal residue in the colon, the examination should be postponed for 24 hours while the patient repeats the preparation.

Cleansing enemas may improve the cleanliness of the colon but are not generally recommended because residual fluid in the colon may dilute administered barium and limit mucosal coating, compromising the examination. For similar reasons, oral lavage regimens with solutions used to prepare patients for colonoscopy, such as GoLYTELY (polyethylene glycol electrolyte solution), should be avoided.¹⁰

MATERIALS AND EQUIPMENT

The choice of barium suspension is critical. A medium barium suspension of approximately 100% w/v is generally preferred for double-contrast barium enemas. Barium of this viscosity optimally coats the mucosa for a relatively prolonged period without precipitating or causing other artifacts. A Miller air enema tip is ideal for instilling barium and air into the colon.¹¹ The retention balloon attached to the enema tip is inflated only if the patient is unable to retain the barium or air because of inadequate anal sphincter tone (see later, “Insertion of Enema Tip”).

In modern radiology departments, barium enema examinations are almost always performed on digital fluoroscopic equipment. For double-contrast studies, the radiologist relies on fluoroscopy to position the patient for a series of digital spot images, followed by a routine sequence of overhead radiographs (see next section, “Routine Examination”).¹² Careful evaluation of the frozen image on the fluoroscopic monitor after each digital exposure enables the radiologist to better delineate subtle colonic abnormalities and differentiate spurious findings from true lesions at the time of fluoroscopy. The study is later reviewed at a computer workstation that allows routine postprocessing of the images for optimal interpretation.¹³ Subtle mucosal abnormalities and differences in density (e.g., as in patients with pneumatosis coli) may be apparent only after adjustment of the images.¹⁴

Administration of Glucagon

A standard dose of 1 mg of glucagon should be administered intravenously to improve the quality of the examination and decrease patient discomfort by producing a relaxant effect on the colon and eliminating or minimizing colonic spasm.^{15,16} The glucagon should be injected slowly to avoid nausea and vomiting, a frequent but transient side effect. Glucagon can be given to almost all patients, but this agent is contraindicated in patients with pheochromocytomas or poorly controlled, insulin-dependent diabetes.

Insertion of Enema Tip

Before inserting the lubricated enema tip, a brief digital rectal examination should be performed to assess anal sphincter tone and recognize anatomic variations that could interfere with insertion of the tip. In patients with an enlarged prostate, for example, the enema tip should be directed more posteriorly than usual to facilitate passage into the rectum. In patients with large external hemorrhoids or anal fissures, a topical anesthetic may be applied to the anus and enema tip to minimize discomfort during insertion. Patients who experience unusual discomfort when the tip is inserted should be reassured that the rectum quickly accommodates to the tip, so any discomfort they experience will be transient.

Routine Examination

A routine series of fluoroscopic spot images for double-contrast barium enemas is presented in Table 51-1, and selected views are illustrated in Figure 51-1. When the fluoroscopic portion of the study has been completed, a standard sequence of overhead radiographs is also obtained (see Fig. 51-1 and Table 51-1). The overhead radiographs include horizontal beam views—left and right lateral decubitus radiographs and a prone cross-table lateral radiograph—that are especially useful for differentiating retained stool from true polypoid lesions in the colon (Fig. 51-2).

Barium is usually administered into the colon under fluoroscopic guidance with the patient in a prone or left lateral position to facilitate passage of barium into the dependent sigmoid and descending colon. It is important to be certain that barium has passed around the splenic flexure into the transverse colon before draining barium and insufflating air because it can be difficult to propel the barium into the ascending colon and cecum if not enough barium has been administered. This problem is more likely to occur in patients with a long, redundant, barium-filled sigmoid colon extending into the left upper quadrant that is inadvertently mistaken for the splenic flexure (see later, “Filling of Entire Colon”).

As soon as enough air has been insufflated to distend the colon, double-contrast spot images should be obtained, starting with the sigmoid colon and continuing proximally in a systematic fashion. Early imaging of the sigmoid colon is particularly important because this portion of the colon may be obscured by opacified small bowel if barium refluxes via an incompetent ileocecal valve into pelvic loops of ileum. After all the loops in the sigmoid colon have been visualized with appropriate spot images, additional images of looping segments of the descending, transverse, and ascending colon should also be obtained. The patient should be rotated as needed under fluoroscopic guidance to visualize individual loops of colon in double contrast and avoid overlap with other loops, which could obscure polypoid or even annular lesions. With careful technique and attention to detail, even small subtle polyps can be detected.

As the patient turns, it is useful to watch the flow of barium across the mucosal surface because flow technique can be extremely helpful for delineating flat protruded lesions, shallow ulcerated lesions, and other subtle abnormalities in the colon. If a particular loop of colon is filled with barium because of its dependent location when the patient is in a supine position, she

TABLE 51-1 Routine Double-Contrast Barium Enema	
Position	Views
SPOT RADIOGRAPHS	
Prone	Rectum
Left posterior oblique	Sigmoid colon
Left lateral	Rectum
Supine	Rectum and cecum
Upright	Hepatic and splenic flexures
Supine, supine obliques	All remaining colonic segments
OVERHEAD RADIOGRAPHS	
Vertical beam	Posteroanterior
Angled (prone)	Rectosigmoid
Horizontal beam	Left and right lateral decubitus views
	Prone cross-table lateral view

or he should be turned into a prone position to visualize the same loop in double contrast by placing it in a nondependent location. Routine upright positioning of the patient is also important for obtaining optimal double-contrast views of the hepatic and splenic flexures. In patients with inguinal hernias, upright views may also be helpful for showing one or more loops of sigmoid colon or distal ileum within the hernias.

When the table is returned to a recumbent position, barium in the hepatic flexure falls by gravity into the ascending colon and cecum, so spot images of the cecum can be obtained. If too much barium is present in the cecum to visualize this structure adequately in double contrast, the patient should be slowly

rotated into a steep right posterior oblique or right lateral position, causing barium to flow from the cecum along the right lateral wall of the ascending colon toward the hepatic flexure and, simultaneously, air to rise into the cecum. The patient can then be returned to a supine position for adequate double-contrast views of the cecum.

Because the enema tip itself may obscure lesions in the distal rectum, the tip should be removed before obtaining spot images of this structure. The patient is usually placed in a left lateral position and asked to bear down to drain barium from the rectum before insufflating additional air to redistend the rectum. After the tip has been removed, spot images of the

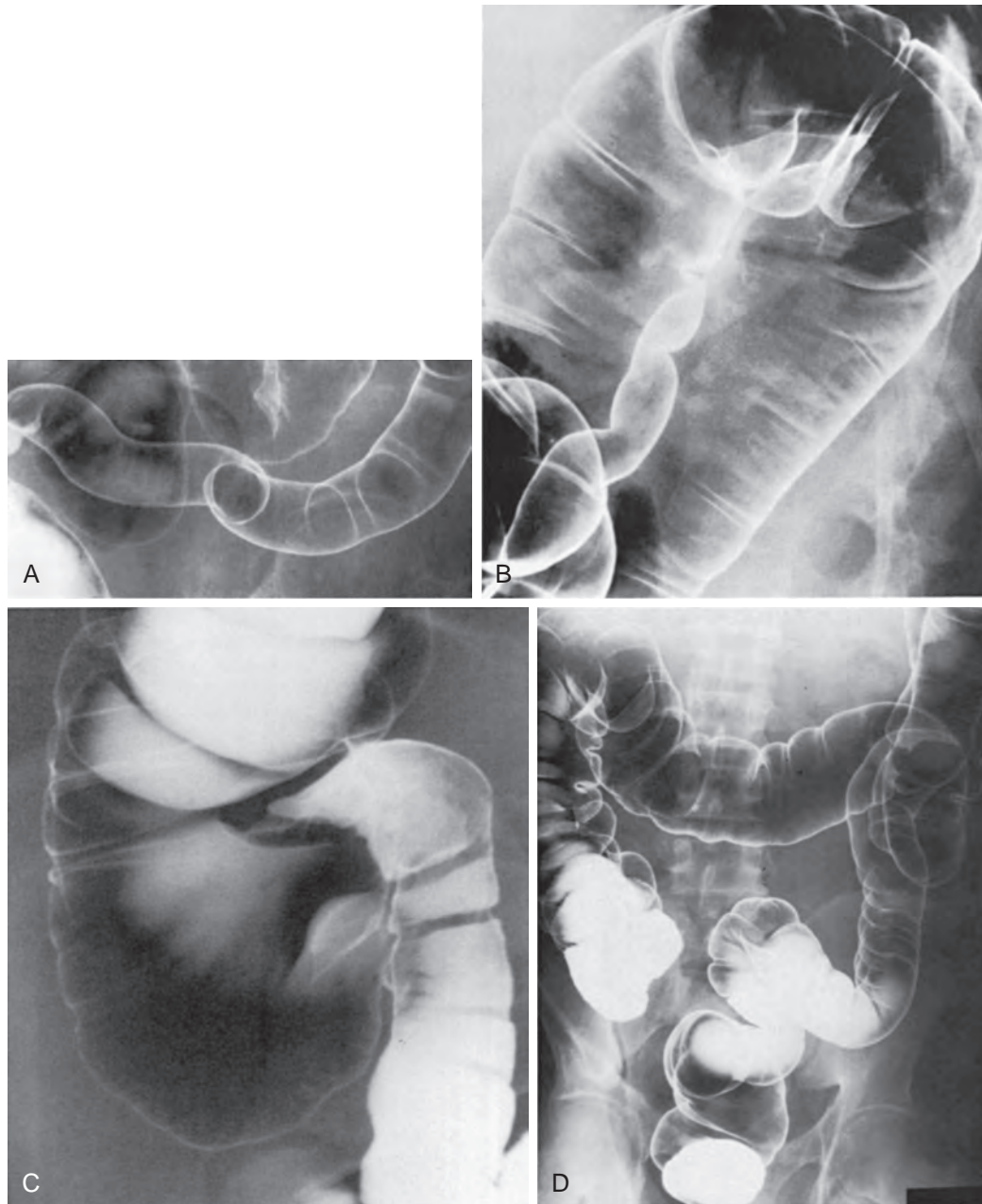


Figure 51-1 Selected radiographs from normal examinations. **A.** Spot radiograph of the sigmoid colon in the left posterior oblique position. **B.** Upright spot radiograph of the splenic flexure in the right posterior oblique position. **C.** Spot radiograph of the cecum and terminal ileum in the supine position. **D.** Overhead radiograph in the prone position.

Continued

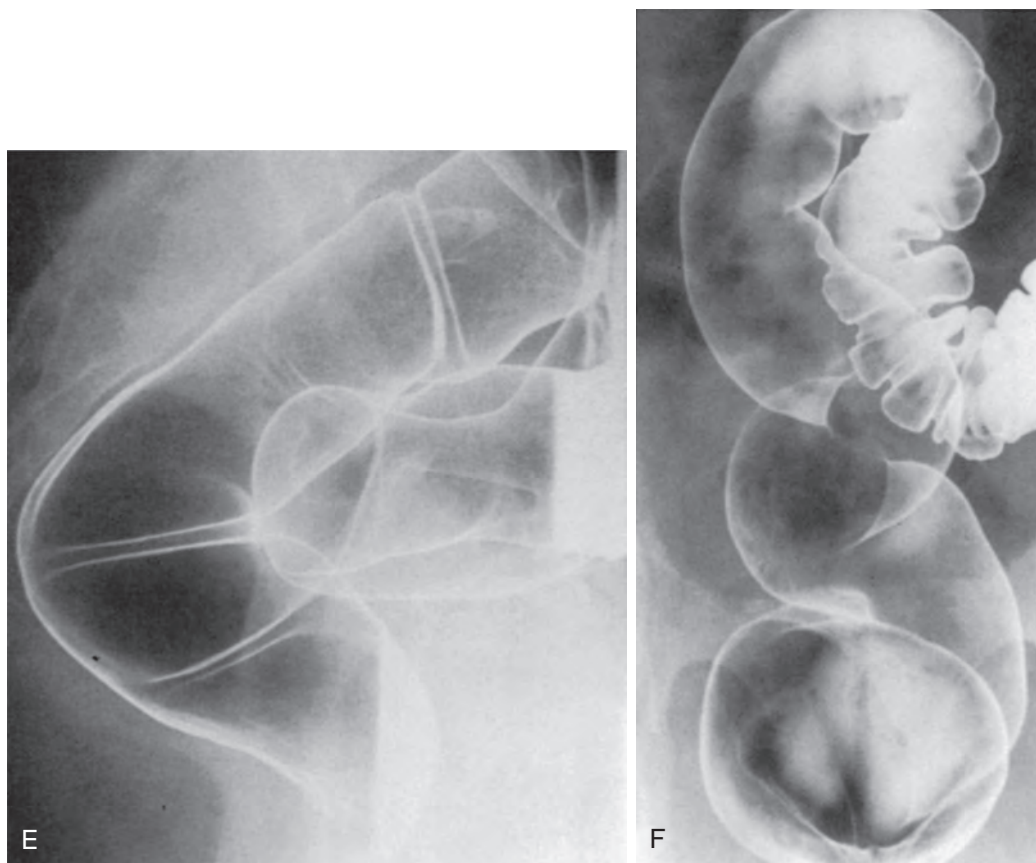


Figure 51-1, cont'd **E.** Prone, cross-table lateral overhead radiograph of the rectum. **F.** Coned-down view of prone angled radiograph of the rectosigmoid colon. (**B** and **D** from Laufer I, Levine MS [eds]: *Double Contrast Gastrointestinal Radiology*, 2nd ed. Philadelphia, WB Saunders, 1992.)

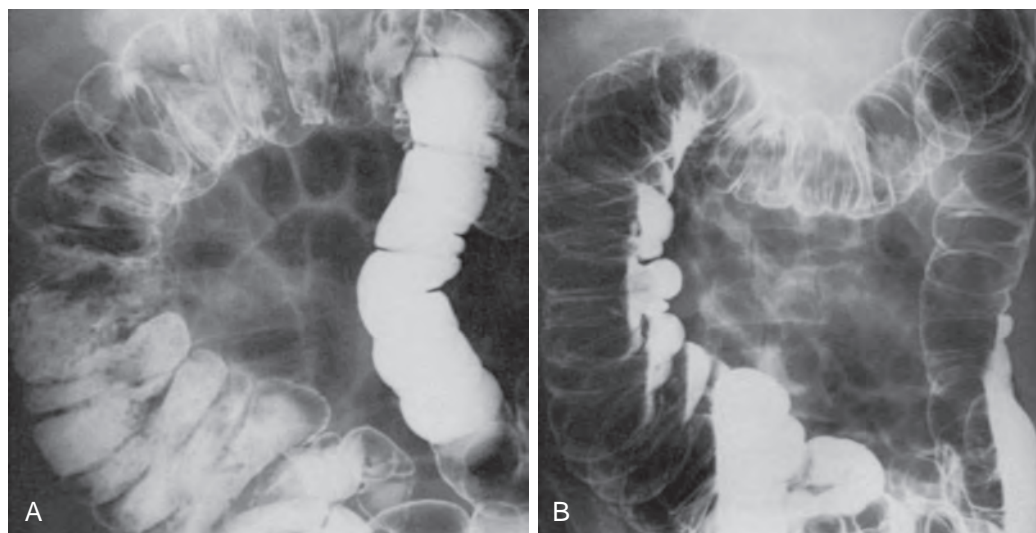


Figure 51-2 Importance of the decubitus view with imperfect bowel preparation. **A.** Oblique view shows considerable fecal residue in the right colon. **B.** Left lateral decubitus overhead radiograph shows fecal debris layering out in the barium, enabling a clear view of most of the right colon.

rectum are routinely obtained with the patient in left lateral, prone, and supine positions, respectively, to complete the fluoroscopic examination.

If barium accumulates in the rectum during the procedure, some patients may experience discomfort as they resist the natural urge to expel this barium from the rectum. Such

discomfort can be avoided by checking the rectum periodically at fluoroscopy and, if necessary, dropping the enema bag to the floor and having the patient gently bear down to eliminate excess barium from the rectum.

The digital spot images should be carefully reviewed at the control station adjoining the fluoroscopy room while the

overhead radiographs are being taken. Any questionable abnormalities should prompt further evaluation of the colon under fluoroscopic guidance after the overheads have been obtained to eliminate uncertainty and permit a more definitive radiologic diagnosis. When the examination has been completed, the patient should be granted immediate access to a conveniently located bathroom to evacuate administered barium and air from the colon.

Normal Appearances

The mucosal surface of the colon usually has a smooth, featureless appearance (Fig. 51-3A). In some patients, a fine network,

also known as innominate grooves or lines, may be seen on the mucosa (Fig. 51-3B).¹⁷ These grooves can be visualized en face with double-contrast technique or in profile in the barium-filled colon when it is partially collapsed (Fig. 51-3C).¹⁸ Occasionally, double-contrast views may reveal innominate pits rather than grooves (Fig. 51-3D).¹⁹ This normal finding should not be mistaken for superficial ulceration. In other patients, transverse striations are observed as a transient phenomenon caused by contraction of the muscularis mucosae (Fig. 51-3E). Still other patients have tiny (1- to 3-mm) nodules in the colon caused by prominent lymphoid follicles, which are observed most often in children but can also be seen as a normal finding

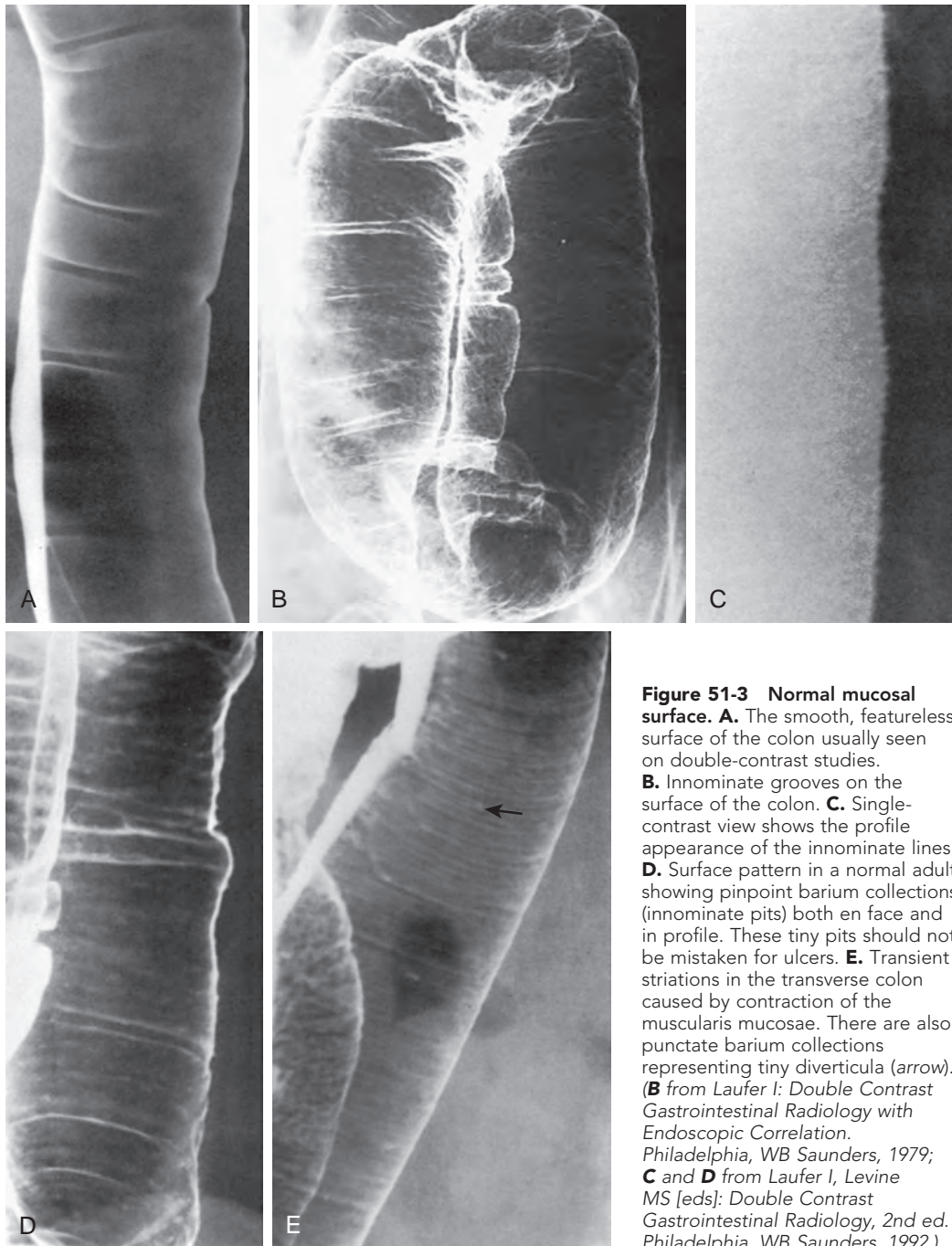


Figure 51-3 Normal mucosal surface. **A.** The smooth, featureless surface of the colon usually seen on double-contrast studies. **B.** Innominate grooves on the surface of the colon. **C.** Single-contrast view shows the profile appearance of the innominate lines. **D.** Surface pattern in a normal adult showing pinpoint barium collections (innominate pits) both en face and in profile. These tiny pits should not be mistaken for ulcers. **E.** Transient striations in the transverse colon caused by contraction of the muscularis mucosae. There are also punctate barium collections representing tiny diverticula (arrow). (B from Laufer I: *Double Contrast Gastrointestinal Radiology with Endoscopic Correlation*. Philadelphia, WB Saunders, 1979; C and D from Laufer I, Levine MS [eds]: *Double Contrast Gastrointestinal Radiology*, 2nd ed. Philadelphia, WB Saunders, 1992.)

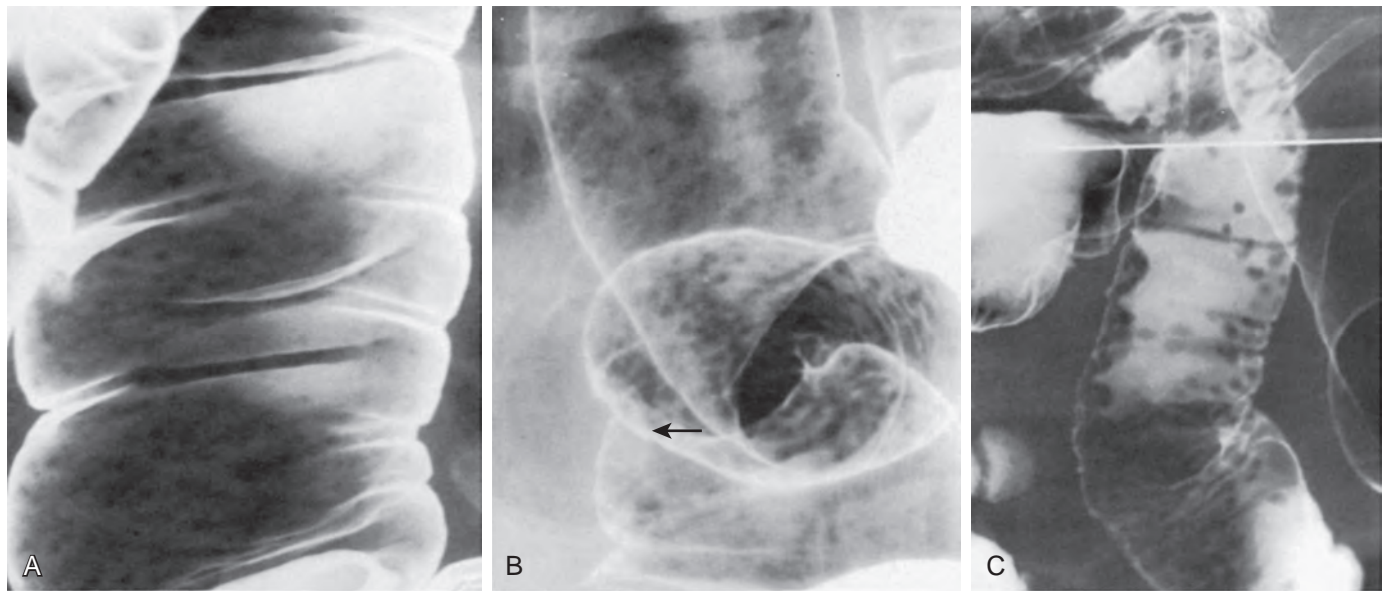


Figure 51-4 Lymphoid follicular pattern. **A.** Tiny rounded filling defects in the transverse colon constitute the normal lymphoid follicular pattern. **B.** Prominent lymphoid follicular pattern in another patient with a small polypoid colonic carcinoma (arrow). **C.** Normal lymphoid follicles in the terminal ileum.

in adults (Fig. 51-4A).^{20,21} Enlarged lymphoid follicles may be associated with a variety of conditions, including Crohn's disease, lymphoma, and immune deficiency states.²² Unusually prominent lymphoid follicles have also been reported in patients with colonic carcinoma (Fig. 51-4B),²³ so this observation should prompt a careful search for underlying malignant tumors in the colon. Enlarged lymphoid follicles may also be seen as a normal finding in the terminal ileum in young people (Fig. 51-4C) and in patients with conditions such as *Yersinia* enteritis and lymphoma.

Single-Contrast Barium Enema

Single-contrast barium enemas entail filling the entire colon with a solid column of barium of relatively low viscosity. Patient preparation, administration of glucagon, and insertion of the enema tip are the same as for double-contrast barium enemas (see earlier). Barium is usually introduced with the patient in a left lateral position. For patients with decreased or absent anal sphincter tone, the retention balloon on the enema tip should be inflated to facilitate retention of barium (see later, "Incontinence").

After the rectum has been evaluated, and as the remaining colon is filled with barium, the patient should be turned from the left lateral position into supine and supine oblique positions, and digital spot images of each colonic loop and flexure should be obtained. The patient should be rotated into different degrees of obliquity as needed to avoid or minimize overlapping bowel. The examination is not completed until the entire colon, including the cecum, has been visualized.

A critical component of the single-contrast enema is graded manual compression of the colon under fluoroscopic guidance to thin out the administered barium and visualize protruded lesions (e.g., polyps and polypoid carcinomas) en face as filling defects in the barium pool. Manual compression may be applied

with a leaded glove, balsam paddle, or the compression cone on the fluoroscopy tower. The ability to demonstrate polyps (especially small polyps) with graded compression requires some skill because these lesions can be missed if the colon is under-compressed or overcompressed at fluoroscopy. With practice and experience, even subtle protruded lesions can be visualized. Nevertheless, the hepatic and splenic flexures and rectum are often difficult to evaluate because of overlying bony structures (the rib cage and pelvic bones) that preclude manual palpation of these areas.

The single-contrast barium enema relies primarily on fluoroscopic evaluation of the colon (with appropriate spot images) to demonstrate abnormalities in the colon, so overhead radiographs are not routinely obtained. However, postevacuation radiographs may be helpful for showing protruded lesions on mucosal relief views of the collapsed colon. Postevacuation radiographs are also useful for assessing colonic emptying in patients with possible colonic motility disorders.

Technical Problems

POOR PREPARATION

Poor colonic preparation is a major limiting factor with barium enemas because of difficulty detecting polypoid lesions in the presence of retained stool. Poor preparation can also simulate pathologic conditions such as inflammatory bowel disease (Fig. 51-5). Similarly, retained fecal debris can mimic the appearance of polypoid tumors. Nevertheless, fecal debris can be differentiated from true polypoid lesions on double-contrast studies when retained stool falls into the barium pool on horizontal beam radiographs because of the effect of gravity. In general, fecal debris will be seen on the dependent surface, whereas true polypoid lesions on the nondependent surface will be etched in white (Fig. 51-6; see Chapter 2).

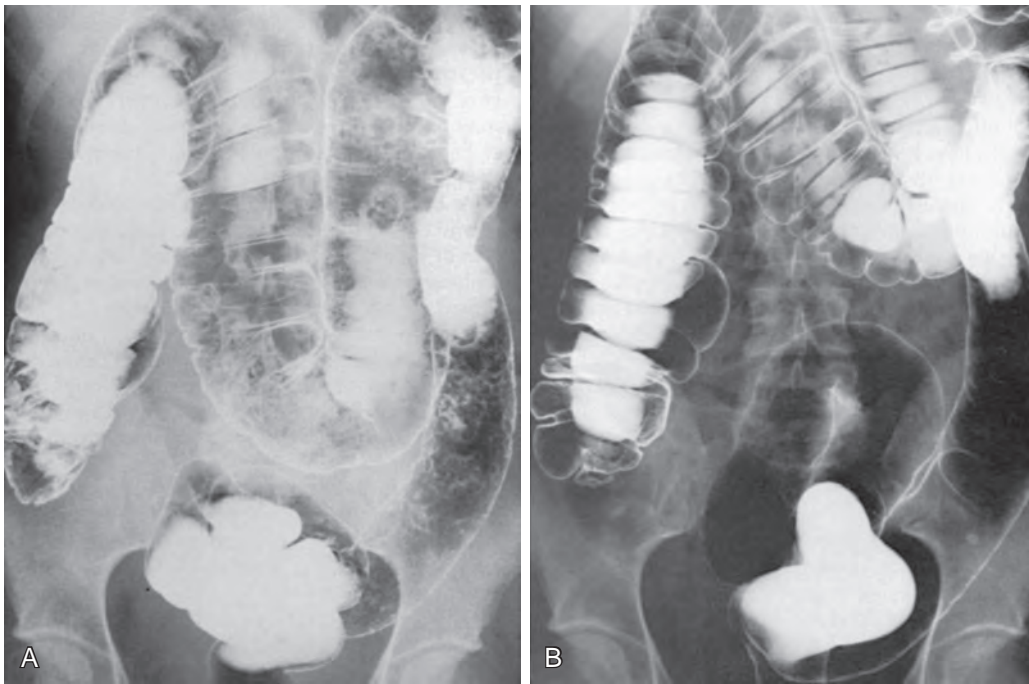


Figure 51-5 Poor preparation simulating inflammatory bowel disease. **A.** Initial study suggests that the mucosa is abnormal throughout the colon. **B.** Another examination with adequate colonic preparation shows that the mucosal surface is normal.

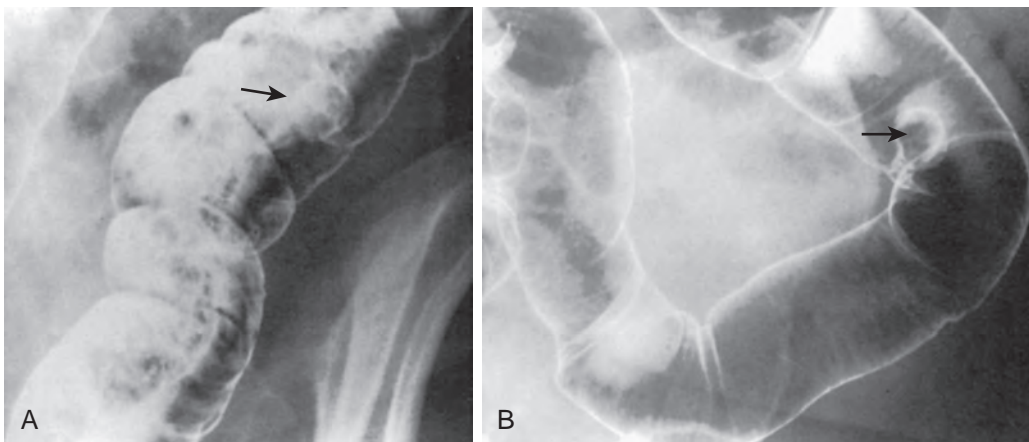


Figure 51-6 Detection of a polyp despite fecal debris. **A.** There is considerable fecal debris in the left side of the colon. Nevertheless, a polyp can be recognized as a lesion that is etched in white (arrow). **B.** After the fecal material has been cleared away, a repeat spot radiograph shows the pedunculated polyp (arrow) more clearly.

DIVERTICULOSIS

The presence of marked sigmoid diverticulosis poses a serious diagnostic dilemma for detecting polypoid lesions on double-contrast barium enemas because of frequent difficulty detecting protruded lesions in the presence of numerous diverticula. When filled with air, these diverticula may simulate polyps on the nondependent surface. In such cases, the sigmoid colon may be reexamined by single-contrast technique (also known as a sigmoid flush) to better visualize protruded lesions (Fig. 51-7).²⁴ Alternatively, sigmoidoscopy may be performed to exclude neoplastic lesions in the sigmoid colon more confidently.

INCONTINENCE

Incontinence is another factor that may preclude performing a complete or technically adequate single- or double-contrast barium enema examination. When patients are incontinent

because of decreased or absent anal sphincter tone, the retention balloon on the enema tip may be inflated with air to prevent loss of barium from the rectum. Although inflation of the balloon often salvages the study in incontinent individuals, it places the patient at risk for rectal perforation. The best way to minimize that risk is to follow basic guidelines for inflating the balloon.

Most importantly, the retention balloon should be inflated only in patients in whom a diagnostic barium enema otherwise would not be possible because of inadequate anal sphincter tone. Before the balloon is inflated, a careful history should be obtained for any risk factors for rectal perforation (including rectal neoplasms, severe proctitis, pelvic irradiation, and rectal surgery) because these are contraindications for inflating the balloon. If no such risk factors are present, barium should be administered into the rectum under fluoroscopic guidance before inflating the balloon. If the rectum distends normally, the retention balloon should be inflated with no more than

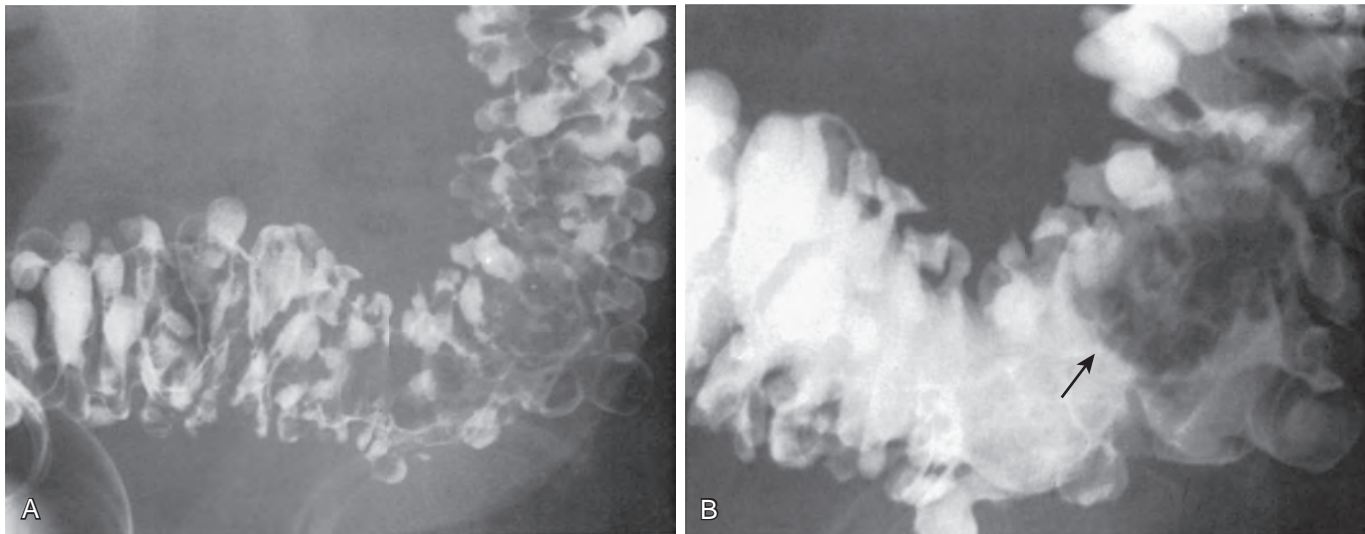


Figure 51-7 Diverticulosis with sigmoid flush. **A.** The diverticula are obvious on the double-contrast study, but a polypoid cancer cannot be identified. **B.** After refilling the colon with single-contrast barium, a polypoid cancer (arrow) is seen. (From Laufer I, Levine MS [eds]: *Double Contrast Gastrointestinal Radiology*, 2nd ed. Philadelphia, WB Saunders, 1992.)

100 mL of air by the radiologist (not the technologist) under fluoroscopic guidance to be certain that the balloon does not encounter resistance and is not overinflated. The balloon should be retracted distally against the anal verge to produce a tight seal, which prevents leakage of barium or air from the rectum during the examination.

FILLING OF ENTIRE COLON

Unless there is an obstructing lesion, the colon should be filled in its entirety from the rectum to the cecum. The fluoroscopist can be certain the cecum has filled when there is reflux of barium into the terminal ileum or appendix. Even in the absence of reflux into these structures, one can be confident of cecal filling when the ileocecal valve is identified. It is occasionally difficult to fill the right side of the colon on double-contrast barium enemas in patients with an unusually tortuous or redundant colon or in patients with a mobile, anteriorly rotated cecum caused by embryologic absence of fixation of the ascending colon in the right paracolic gutter. In such cases, an incompletely filled ascending colon should not be mistaken for the cecum, and the patient should be rotated additional times, as needed, until the cecum is definitively visualized. Rarely, it may be necessary to convert a double-contrast barium enema to a single-contrast study to obtain adequate filling of the ascending colon and cecum in patients with glucagon-resistant spasm.²⁵

Complications

Some patients experience abdominal discomfort or gas pains during and after barium enema examinations.²⁶ This discomfort can be minimized by using carbon dioxide instead of air to distend the colon.²⁷ The most serious complication is colonic perforation.²⁸ Although extremely uncommon, the usual site of perforation is the rectum; most cases result from inflation of a rectal balloon in a diseased rectum (see earlier, “*Incontinence*”). When rectal injury occurs, barium may be seen dissecting into the wall of the rectum (Fig. 51-8A) or extravasating into the pelvis or retroperitoneum. Much less frequently, there is

perforation of the intraperitoneal portion of the colon, almost always at the site of diseased bowel, with barium entering the peritoneal cavity (Fig. 51-8B). In patients with diverticulosis, administered air may extravasate from the diverticula during the double-contrast barium enema, resulting in the development of retroperitoneal or intraperitoneal air, or even pneumomediastinum (Fig. 51-8C).

A barium enema examination should not be performed immediately after endoscopic biopsy of normal or inflamed rectal mucosa with a large biopsy forceps because such patients are at risk for rectal perforation.^{29,30} If a deep rectal biopsy specimen has been obtained, the barium enema should therefore be postponed for at least 5 days. In contrast, more superficial biopsies performed with a small forceps through flexible endoscopes need not necessitate such lengthy delays.

Allergic complications are rare, but have been reported.³¹ Such patients may have reactions to the barium itself or to various additives, latex rectal catheters, or even glucagon. Latex enema tips have been replaced by silicone tips because the latex was thought to be the source of rare but severe allergic reactions.³²

Transient bacteremia has been documented after barium enemas,³³ but no clinical problems have been reported. In patients with high-risk cardiac lesions such as prosthetic heart valves, it may be prudent to use antibiotic prophylaxis, as recommended by the American Heart Association.³⁴ This prophylaxis consists of 3 g of amoxicillin by mouth 1 hour before the study and 1.5 g by mouth 6 hours after the study.

In patients with severe ulcerative colitis, air and contrast medium rarely may enter the perirectal veins, and gas may even be seen in the portal vein.³⁵ This complication can occur as a fatal event.

Variations in Technique

SUSPECTED PERFORATION

When colonic perforation is suspected, the study should be performed with a water-soluble contrast agent such as

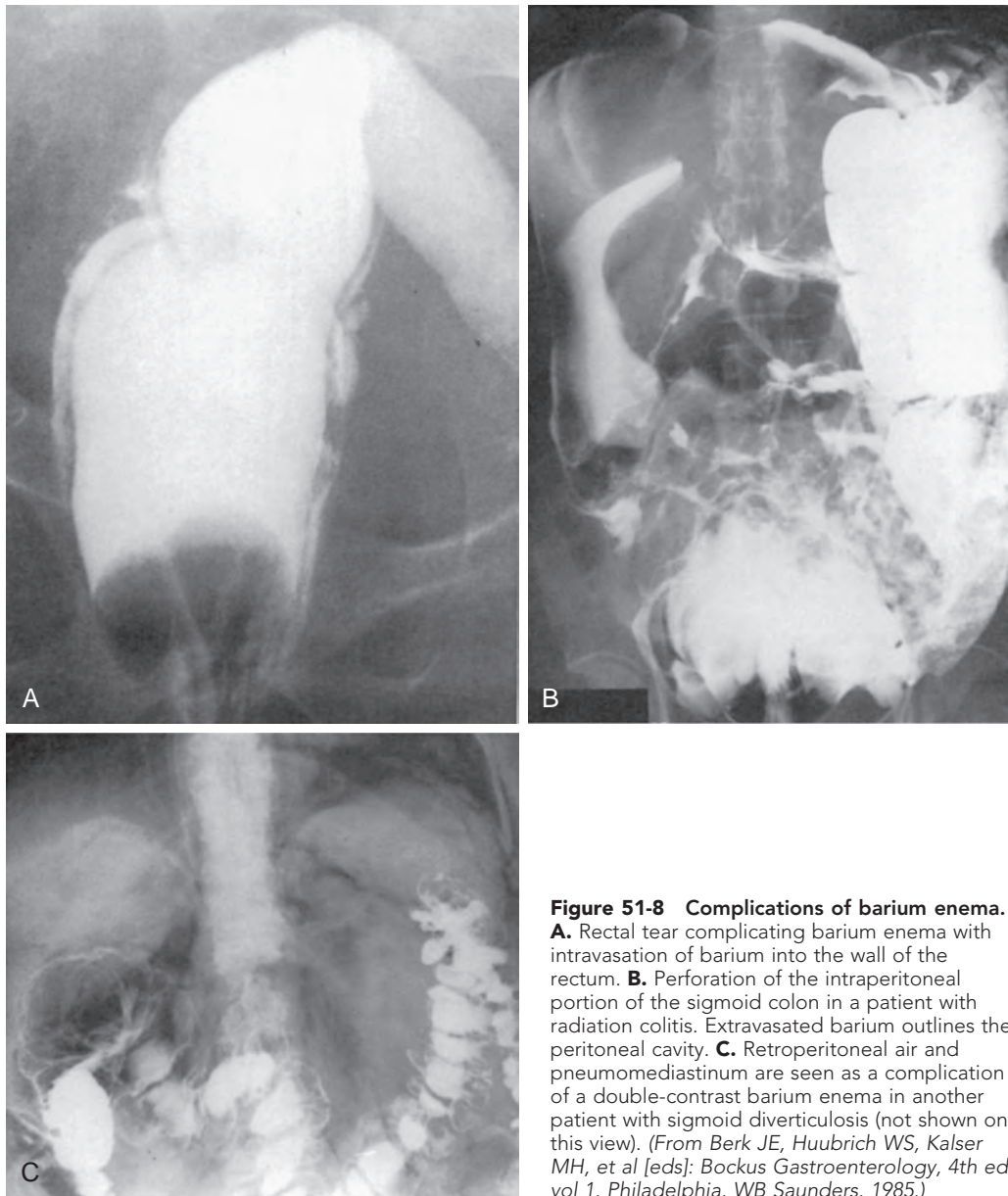


Figure 51-8 Complications of barium enema.

A. Rectal tear complicating barium enema with intravasation of barium into the wall of the rectum. **B.** Perforation of the intraperitoneal portion of the sigmoid colon in a patient with radiation colitis. Extravasated barium outlines the peritoneal cavity. **C.** Retroperitoneal air and pneumomediastinum are seen as a complication of a double-contrast barium enema in another patient with sigmoid diverticulosis (not shown on this view). (From Berk JE, Huubrich WS, Kalser MH, et al [eds]: *Bockus Gastroenterology*, 4th ed, vol 1. Philadelphia, WB Saunders, 1985.)

diatrizoate meglumine and diatrizoate sodium (Gastroview). If extravasation is not demonstrated, it may be prudent to repeat the examination with barium for better definition and detail. In patients with cystic fibrosis, a water-soluble enema can be administered for diagnostic or therapeutic purposes.³⁶ In such patients, the hyperosmolar agent draws fluid into the bowel that can liquefy viscous stool, sometimes with therapeutic results.

PERORAL PNEUMOCOLON

A peroral pneumocolon is sometimes performed in patients for whom the primary diagnostic interest is in the terminal ileum and cecum.³⁷ For this procedure, the patient undergoes preparation of the colon as for a barium enema. After orally administered barium has reached the right side of the colon, 1 mg of glucagon is administered intravenously and air is insufflated via a rectal catheter into the colon and refluxed into the

terminal ileum. This maneuver often provides excellent double-contrast views of the cecum and terminal ileum for better visualization of aphthoid ulcers and other abnormalities in these areas (Fig. 51-9).

COLOSTOMY ENEMA

Single- or double-contrast studies of satisfactory quality can be performed through a colostomy (Fig. 51-10).³⁸ This is particularly important for patients being followed after resection of a previous rectal carcinoma because of the increased risk of developing metachronous colon cancers at a later point in time. Barium may be administered through the colostomy stoma via a Foley catheter connected to an enema bag.

Contrast enemas after other types of colon surgery are discussed in Chapter 63.



Figure 51-9 Peroral pneumocolon. Excellent double-contrast visualization of the right colon and distal small bowel is obtained. (From Laufer I, Levine MS [eds]: *Double Contrast Gastrointestinal Radiology*, 2nd ed. Philadelphia, WB Saunders, 1992.)



Figure 51-10 Double-contrast colostomy enema. Satisfactory visualization of the residual colon is obtained after a colostomy. (From Laufer I, Levine MS [eds]: *Double Contrast Gastrointestinal Radiology*, 2nd ed. Philadelphia, WB Saunders, 1992.)

REFERENCES

1. Kung JW, Levine MS, Glick SN, et al: Colorectal cancer: Screening double-contrast barium enema examination in average-risk adults older than 50 years. *Radiology* 240:725–735, 2006.
2. Chong A, Shah JN, Levine MS, et al: Diagnostic yield of barium enema examinations after incomplete colonoscopy. *Radiology* 223:620–624, 2002.
3. Ott DJ, Chen YM, Gelfand DW, et al: Single-contrast vs double-contrast barium enema in the detection of colonic polyps. *AJR* 146:993–996, 1986.
4. Kelvin FM, Oddson TA, Rice RP, et al: Double contrast barium enema in Crohn's disease and ulcerative colitis. *AJR* 131:207–213, 1978.
5. Faccioli N, Manfredi R, Mainardi P, et al: Barium enema evaluation of colonic involvement in endometriosis. *AJR* 190:1050–1054, 2008.
6. Ginaldi S, Lindell MM, Zornoza J: The striped colon: A new radiographic observation in metastatic serosal implants. *AJR* 134:453–455, 1980.
7. Evers K, Laufer I, Gordon RL, et al: Double-contrast enema examination for detection of rectal carcinoma. *Radiology* 140:635–639, 1981.
8. Bartram CI: Obliteration of thumbprinting with double contrast enemas in acute ischemic colitis. *Gastrointest Radiol* 4:85–88, 1979.
9. Fork ET, Ekberg O, Nilsson G, et al: Colon cleansing regimens. *Gastrointest Radiol* 7:383–389, 1982.
10. Bakran A, Bradley JA, Breshnihan E, et al: Whole gut irrigation: An inadequate preparation for double contrast barium enema examination. *Gastroenterology* 73:28–30, 1977.
11. Miller RE: A new enema tip. *Radiology* 92:1492, 1969.
12. Rubesin SE: Examination of the colon: Techniques and normal anatomy. In Levine MS, Ramchandani P, Rubesin SE, editors: *Practical Fluoroscopy of the GI and GU Tracts*, Cambridge, 2013, Cambridge University Press, pp 156–168.
13. Levine MS, Laufer I: The gastrointestinal tract: Dos and don'ts of digital imaging (state of the art). *Radiology* 207:311–316, 1998.
14. Kaiser JS, Levine MS, Laufer I, et al: Value of digital fluoroscopy for the diagnosis of pneumatosis coli. *Eur J Radiol* 29:21–24, 1998.
15. Meeroff JC, Jorgens J, Eisenberg JJ: The effect of glucagon on barium-enema examination. *Radiology* 115:5–7, 1975.
16. Lappas JC, Maglinte DD, Chernish SM, et al: Discomfort during double-contrast barium enema examination: A placebo-controlled double-blind evaluation of the effect of glucagon and diazepam. *Radiology* 197:95–99, 1995.
17. Matsuura K, Nakata H, Takeda N, et al: Innominate lines of the colon. *Radiology* 123:581–584, 1977.
18. Williams I: Innominate grooves in the surface of the mucosa. *Radiology* 84:877–880, 1965.
19. Frank DF, Berk RN, Goldstein HM: Pseudoulcerations of the colon on barium enema examination. *Gastrointest Radiol* 2:129–131, 1977.
20. Laufer I, deSa D: The lymphoid follicular pattern: A normal feature of the pediatric colon. *AJR* 130:51–55, 1978.
21. Kelvin FM, Max RJ, Norton GA, et al: Lymphoid follicular pattern of the colon in adults. *AJR* 133:821–825, 1979.
22. Glick SN, Teplick SK, Goren RA: Small colonic nodularity and the double contrast barium enema. *Radiographics* 1:73–86, 1981.
23. Bronen RA, Glick SN, Teplick SK: Diffuse lymphoid follicles of the colon associated with colonic carcinoma. *AJR* 142:105–109, 1984.
24. Lappas JC, Maglinte DDT, Kopecky KK, et al: Diverticular disease: Imaging with post-double-contrast sigmoid flush. *Radiology* 168:35–37, 1988.

25. Levine MS, Gasparaitis AE: Barium filling for glucagon-resistant spasm on double-contrast barium enema examinations. *Radiology* 160: 264–265, 1986.
26. Gelfand DW: Complications of gastrointestinal radiologic procedures: I. Complications of routine fluoroscopic studies. *Gastrointest Radiol* 5:293–315, 1980.
27. Bessette JR, Maglinte DD: Double-contrast barium enema study: Simple conversion to CO₂. *Radiology* 162:274–275, 1987.
28. Gelfand DW, Ott DJ, Ramquist NA: Pneumoperitoneum occurring during double-contrast enema. *Gastrointest Radiol* 4:307–308, 1979.
29. Maglinte DDT, Strong RC, Strate RW, et al: Barium enema after colorectal biopsies: Experimental data. *AJR* 139:693–697, 1982.
30. Harned RK, Consigny PM, Cooper NB: Barium enema examination following biopsy of the rectum or colon. *Radiology* 145:11–16, 1982.
31. Schwartz EE, Glick SN, Foggs MB, et al: Hypersensitivity reactions after barium enema examination. *AJR* 143:103–104, 1984.
32. Gelfand DW: Barium enemas, latex balloons and anaphylactic reactions. *AJR* 156:1–2, 1991.
33. Butt J, Hentges D, Pelican G, et al: Bacteremia during barium enema study. *AJR* 130:715–718, 1978.
34. Dajani AS, Bisno AL, Kyung J, et al: Prevention of bacterial endocarditis: Recommendations by the American Heart Association. *JAMA* 264: 2919–2922, 1990.
35. Stein MG, Crues JV, III, Hamlin JA: Portal venous air associated with barium enema. *AJR* 140:1171–1172, 1983.
36. Glick SN, Kressel HY, Laufer I, et al: Meconium ileus equivalent: Treatment with Hypaque enema. *Diagn Imaging* 49:149–152, 1980.
37. Kressel HY, Evers KA, Glick SN, et al: The peroral pneumocolon examination: Technique and indication. *Radiology* 144:414–416, 1982.
38. Goldstein HM, Miller RH: Air contrast colon examination in patients with colostomies. *AJR* 127:607–610, 1976.

Functional Imaging of Anorectal and Pelvic Floor Dysfunction

SAT SOMERS | DEAN D. T. MAGLINTE

CHAPTER OUTLINE

Normal Anatomy

Assessment of Pelvic Floor

Preprocedure Preparation

Imaging Technique

Measurements

Anorectal Angle

Anal Canal Length

Level of Anorectal Junction

Pathology

Enterocoele and Sigmoidocele

Anterior Mucosal Wall Prolapse and Rectocele

Rectal Intussusception

Posterior-Lateral Rectal Pouches

Pelvic Floor Dyssynergy (Anismus)

Descending Perineum Syndrome

Anterior Mucosal Prolapse

Uterine and Vaginal Vault Prolapse

Cystocele

Constipation and Incontinence

Comparison with Other Methods of Examining the Pelvic Floor

Normal Variations

Summary

Pelvic floor disorders are an underdiagnosed source of morbidity and significantly diminish the quality of life. Most patients are women.¹ In any clinic that deals with pelvic floor disorders, about 80% of patients will be women between the ages of 35 and 50 years. Pelvic floor disorders are seen less frequently in men.

The demand for pelvic floor imaging is increasing. There are several factors that account for this, such as more patients seeking assistance, more physicians interested in this area, and more experience in the therapeutic options. Almost 24% of U.S. women complain of at least one pelvic disorder. The number of patients seeking assistance also increases with age, parity, and obesity.^{2,3} As the population ages, the need for pelvic floor imaging is expected to increase.⁴

The presenting symptoms of patients with pelvic floor disorders are variable. They can have anal incontinence, urinary incontinence and constipation. There may be prolapse of the rectum or vagina with a cystocele associated with any of these.

Anal incontinence ranges from constant soiling as a result of slow leakage, to the total inability to hold on to any stool in the rectosigmoid area. This latter group copes by emptying their

bowel at the faintest desire to defecate. They are therefore constantly emptying their bowel to avoid accidents. Overall, about 9% of women have fecal incontinence and 3% experience pelvic floor prolapse.² These signs and symptoms appear to be unrelated to the mode of delivery.⁵⁻⁸ However, parous women are not immune to functional pelvic floor disorders either.⁹⁻¹²

The presenting symptoms of constipation are also variable. This may be described as difficulty in initiating defecation, incomplete defecation, and considerable straining with defecation. Some patients may also complain that the stool is of inadequate size, weight, or water content. Patients who have difficulty in evacuation may use digital or positional maneuvers to assist in emptying the rectum. If this is not volunteered by the patient, it is useful to ask when taking a history prior to the examination because this information could be used to enhance the study.

Seemingly unrelated symptoms, such as bloating and abdominal pain, may also be related to pelvic floor disorders.¹³ Other apparently unrelated symptoms include dyspareunia, painful defecation, perineal pain, and rectal bleeding. Solitary rectal ulcer syndrome is often suspected when there is rectal bleeding.¹⁴⁻¹⁶

Preoperative identification of abnormalities causing pelvic floor disorder symptoms is important so that the appropriate surgery can be performed.¹⁷ This is especially true because one study has shown that there is a lifetime risk of 11% of at least one surgical procedure for pelvic organ prolapse and urinary incontinence and that the repeat surgery for recurrence is 29%.¹⁸

There is often a multispecialty involvement in the management of pelvic floor disorders. Radiologists, colorectal surgeons, gynecologists, and urologists may be involved. This chapter will only deal with the radiologic aspects.

Normal Anatomy

The pelvic floor is made up of the levator ani, urinary and anal sphincter mechanisms, and fascial supports of the pelvic viscera. The pelvic viscera include the rectum, vagina, bladder, and urethra (Fig. 52-1). An understanding of the structure and levels of pelvic floor support is important for the evaluation of pelvic floor dysfunction because this forms the basis of reconstructive surgery.¹⁹

There is an interaction between the colon and rectum in normal defecation. High-amplitude propagating waves that move fecal contents into the rectum stimulate the urge to defecate. As a result, the distention that this produces relaxes the internal sphincter through the anorectal inhibitory reflex in preparation for defecation. Defecation is then initiated by abdominal straining and voluntary pelvic floor relaxation whenever desired. Once the anal canal is open, the rectum is squeezed by abdominal contraction. About one third of the left colon and rectum is emptied in normal physiologic defecation.

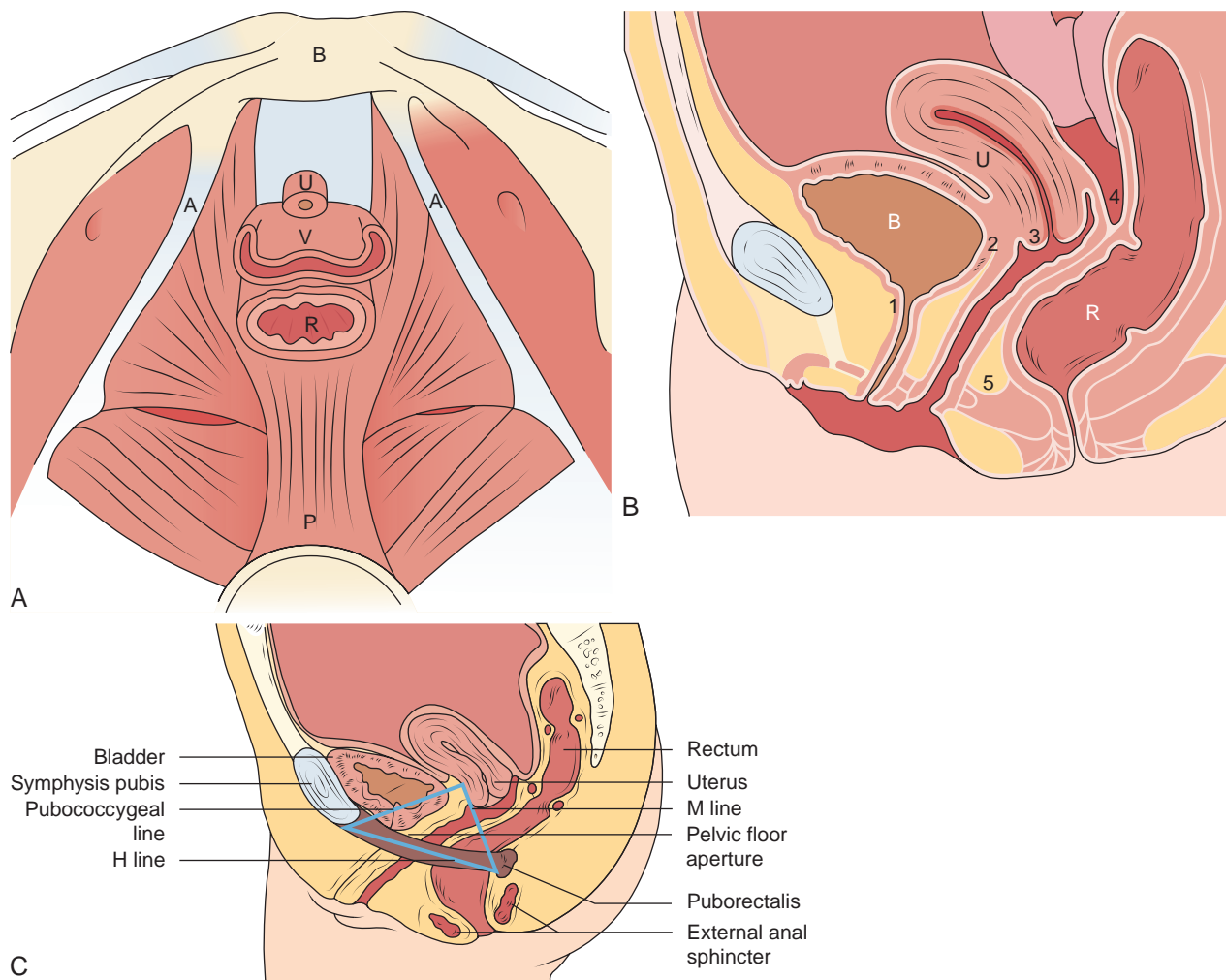


Figure 52-1 Schematic depiction of normal pelvic anatomy. **A.** Axial schematic drawing shows the anatomic structures that provide pelvic floor support. A, Arcus tendineus fascia pelvis (white line). B, pubic bone; P, puborectalis; R, rectum; U, urethra; V, vagina. **B.** Sagittal schematic of the pelvis demonstrates various sites of prolapse, including the bladder neck and urethra (1), bladder base (2), cervicovaginal vault (3), cul-de-sac (4), and rectum (5). B, bladder; R, rectum; U, uterus. **C.** Drawing of the sagittal midline view of the female pelvis shows bony landmarks and the puborectalis muscle, also called the levator sling. The pubococcygeal, H, and M lines and levator plate are delineated in blue. (A and B from Pannu HK, Kaufman HS, Cundiff GW, et al: *Dynamic MR imaging of pelvic organ prolapse: Spectrum of abnormalities*. *RadioGraphics* 20:1567–1582, 2000; C from Fielding JR: *Practical MR imaging of pelvic floor weakness*. *RadioGraphics* 22:295–304, 2002.)

This is secondary to continued mass colonic contractions and likely additional proximal rectal contractions.²⁰

Pelvic floor anatomy is complex, and dynamic cystocolpoproctography (DCP) does not show the anatomic details that pelvic magnetic resonance imaging (MRI) provides. This consideration, predictions of a hypothetical increase in cancer incidence, and deaths in patients exposed to radiation and questions relating to the clinical significance of DCP findings have made pelvic floor MRI an important preoperative tool.

Several studies have compared CP and dynamic pelvic floor MRI.^{21–23} A recent evidence-based comparison has shown that DCP is the functional imaging study for anorectal dysfunction and pelvic floor prolapse evaluation.²⁴ This is because, in most existing MR units, the patient is imaged supine rather than upright, a deficiency negated by open architecture MR magnets.²⁵ This is an embarrassing examination and is made less acceptable when the patient is asked to defecate in an artificial environment and in an unnatural (supine) position where the patient is usually asymptomatic. Evacuation is pivotal

for the functional evaluation of the pelvic floor. Additional important factors are economics and practicality in everyday practice. In most institutions, the additional expense incurred with MRI compared with DCP and relative lack of accessible time on an MRI unit that is subject to heavy demand by other clinical specialties are important considerations. The logistics of performing a tailored examination (drainage of an undrained bladder and emptying of rectoceles) are important practical considerations when evaluating for the full extent of pelvic organ prolapse.

The use of an open MRI system with patients defecating makes it functional. With an open architecture magnet, however, one must contend with images of a lower signal-to-noise ratio and soft tissue resolution.²⁶ To make it a single noninvasive functional study to look at specific organ prolapses, specialized coils are needed to improve soft tissue resolution and visualize the pelvic supporting structures and fascial condensations directly. Specialized coils make dynamic pelvic MRI more intrusive. Dynamic pelvic floor MRI is an evolving technology, and

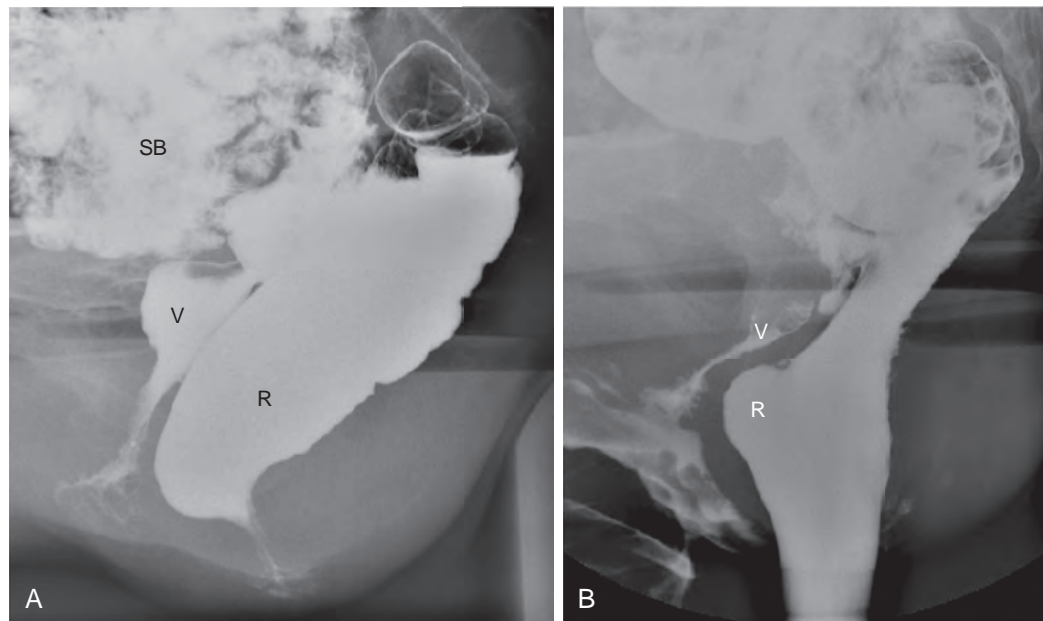


Figure 52-2 Normal rectum.

A. The normal rectum at rest. The anal canal is closed and there is a normal puborectalis angle. **B.** The rectum at defecation showing the anal canal totally open. A small rectocele is also present. This is normal during defecation as long as it totally empties at the end. R, rectocele; SB, small bowel; V, vagina with contrast.

its precise role in functional imaging of the pelvic floor still remains to be determined. It is likely that pelvic MRI with increased soft tissue resolution with endoluminal coils will complement the use of DCP when it is necessary to see structural details of the pelvic supportive tissues and endopelvic fascia for surgical management.²⁷ A static, high-definition MRI scan gives added information about muscle and/or ligamentous tears that may alter management, information that can only be inferred with DCP.

Defecation is initiated by descent of the pelvic floor. This can be seen on proctography as the anorectal junction descending from the resting position. As descent continues, the anal canal opens in the final moments. All this happens within seconds. Rapid emptying occurs when the anal canal is completely open. With the cessation of straining, tone returns to the anal sphincter and levator ani and the canal closes. The anorectal angle becomes more acute and the pelvic floor and anorectal junction return to their normal elevated resting position (postdefecation reflex; Fig. 52-2).

The pelvic floor is unlike other skeletal muscles. As a result of the continuous firing of motor units, even during rest, the pelvic floor has constant tone. This tone is only interrupted during defecation or urination. Therefore, a dynamic functional examination of the pelvic floor, especially to show the degree of prolapse, has to include defecation.²⁸

Assessment of Pelvic Floor

PREPROCEDURE PREPARATION

As with any procedure, it is extremely important to obtain a history of the patient's symptoms. Specific questions may have to be asked, such as the use of any maneuvers that may assist the patient. This is not always volunteered because the patient may be too embarrassed to disclose them.²⁹ Also, this is very intrusive, so the examination must be thoroughly explained prior to anything being done. This ensures that the patient understands the instructions given during the procedure.

Getting the patient to practice some of the maneuvers, such as squeezing the buttocks while sitting on the side of a stretcher prior to instillation of any contrast, is also useful. The patient should have maximum privacy and be comfortable as possible in the examination room. One way to achieve this is to use a remote control fluoroscopy unit, turning the lights down low and ensuring that the patient is the only person in the examination room.²⁰ In our unit, we also have blinds so that the patient cannot see the radiologist operating the remote fluoroscopy unit. Generally, if the patient is comfortable with the environment, the greater the likelihood of an accurate assessment of defecation.

IMAGING TECHNIQUE

Imaging of defecation was described as early as the 1950s.³⁰ It was not until the 1980s that Mahieu and colleagues described a technique that interested more radiologists.^{31,32} This technique has since been further modified with the addition of opacification of the small bowel, urinary bladder, and vagina.³³⁻⁴⁰ The opacification of these structures makes recognition of cystoceles, enteroceles, and sigmoidoceles easier. Preparation of the bowel with laxatives or enemas is not necessary, although some authors believe that a limited bowel preparation will be more comfortable for the patient and also provide a more standardized examination.⁴¹ The order of opacification is to give oral contrast first to opacify the small bowel. Usually, about 400 mL of contrast used for small bowel studies is sufficient. This is given about 45 to 60 minutes before the dynamic part of the examination. Some authors suggest waiting for up to 3 hours.³³ How long you have to wait depends on how long it takes for the small bowel contrast being used to opacify the pelvic loops of the small bowel.

Opacification of the urinary bladder is next, with water-soluble contrast normally used for cystography. About 150 to 200 mL of contrast is enough to make the bladder recognizable. Care must be taken not to overdistend or it could mask enteroceles. Overdistention is also uncomfortable for the patient.

The vagina is then opacified. This can be done with barium paste, high-density barium, or a thick solution of 50% contraceptive gel and 50% of water-soluble contrast with the highest concentration of iodide.⁴² The vaginal contrast is introduced with a bladder irrigation syringe connected to a soft catheter. A pediatric enema catheter works well. The catheter is inserted deep into the vagina and the contrast introduced as the syringe is slowly withdrawn. Care must be taken to ensure that there is sufficient contrast opacifying the whole vagina. In the past, a contrast-soaked tampon was used. However, it was noted that the tampon acted as a strut and did not allow any enteroceles, rectoceles, or sigmoidoceles to become apparent.

Finally, the rectum has to be opacified. It helps to have contrast material that has the consistency of stool or at least close to it. If it is too liquid, even normal patients will find it difficult to hold in the rectum.³⁴ Currently, there are no commercially made preparations available. The options are to use a thick esophageal paste such as Esobar (Bracco Diagnostics Inc., Monroe Township, New Jersey) or the thick paste, as suggested by Mahieu and associates.^{30,32} Three 50-mL syringes (150 mL total) of Esobar introduced into the rectum are usually enough to perform the procedure. When the syringes are filled, care should be taken to eliminate air bubbles because trapped air under pressure can cause discomfort to the patient (Fig. 52-3). The syringes are easier to fill if the paste is first warmed by holding the contrast tube under hot water. If the Mahieu preparation is used, it is useful to opacify the rectal wall first with contrast used for barium enemas. The doughy paste, if prepared as suggested, provides bulk but does not opacify the wall. Therefore, intussusceptions could be missed. The other disadvantage is that because of the consistency, it is difficult to introduce into the rectum. An orthopedic glue gun that is geared makes this thicker paste easier to introduce. To coat the rectal wall and fill the rectum with the Mahieu paste, attach a 50-cm length of 0.5-inch tube filled with high-density liquid barium to the glue gun, with a wide-bore enema tip at the end, so that both contrast agents can be introduced in one maneuver. The rectum is filled until the patient reports a sensation of fullness and a desire to defecate.

Finally, if you wish to measure the anal canal or determine the location of the anus, the surface around the anus should be opacified. This can be done with petroleum jelly opacified with barium. Petroleum jelly, 50 g, with 50 g of barium works well. This is smeared around the anus and along the natal cleft.

When the patient is ready for the study after all the contrast has been introduced, the patient is asked to sit on the defecography commode. The commode design should allow filming in lateral and frontal projections. A sturdy commode also dispels any fears that the patient may have about sitting on it. There are commercially available commodes but you can build one to your own design. A commode designed by Bernier and colleagues has a ruler in the midline so that direct measurements of the midline structures can be done if necessary.⁴⁰⁻⁴⁵ If a remote control fluoroscopy unit is used, the commode can be attached to the table top (Fig. 52-4). Positional changes of the commode can then be easily made by moving the tabletop. A remote control fluoroscopy unit is certainly preferable for this study.

The x-ray beam is aimed at the region of the reproductive organs. Therefore, keeping the radiation dose as low as possible is paramount. To keep the dose low, several investigators use only videofluoroscopy. Although the dose is low, the resolution is not adequate to record subtle radiographic changes. Therefore, it is recommended that videofluoroscopy be performed during the entire examination, with spot films being taken at key events. The key spot images are lateral views of the rectum at rest, lift (squeeze), cough, strain, defecation, and postdefecation. Other ways of reducing radiation dose include digital serial acquisition with one image/s for 30 seconds or using digital equipment with a low-dose program. Major reductions in radiation dose can also be achieved by slow pulsed fluoroscopy. Additional beam filtration can reduce radiation without impairing image quality.⁴⁴

The images at rest are taken without any conscious contraction of the pelvic muscles (Fig. 52-5A). On lifting (squeezing), there is maximal contraction of the pelvic floor musculature. This results in elevation of the entire pelvic floor (see Fig. 52-5B).⁴⁶ The muscles responsible for elevation of the pelvic floor are the puborectalis and levator ani. The anorectal angle

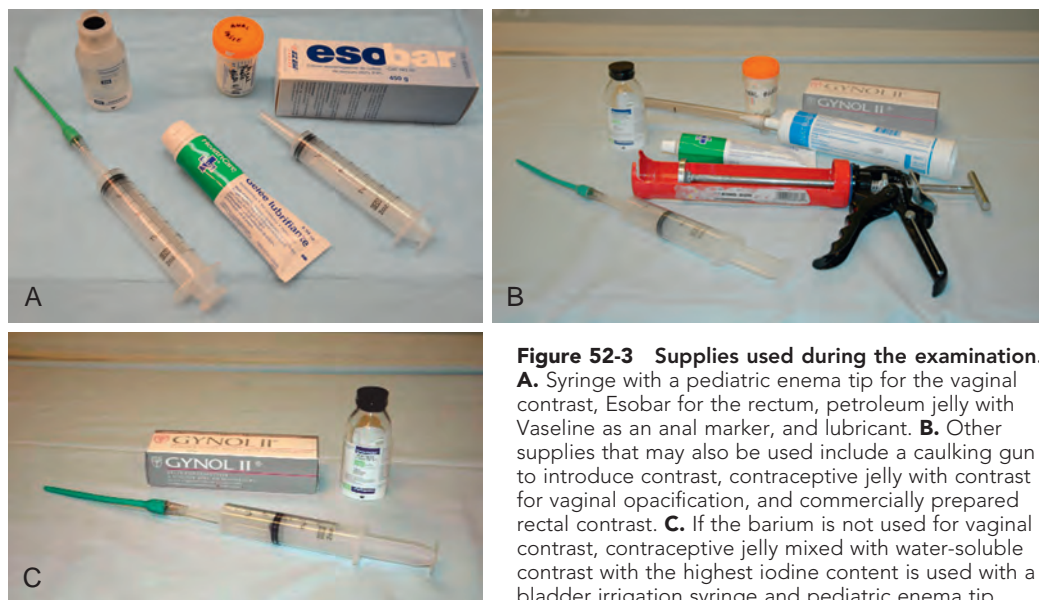


Figure 52-3 Supplies used during the examination. **A.** Syringe with a pediatric enema tip for the vaginal contrast, Esobar for the rectum, petroleum jelly with Vaseline as an anal marker, and lubricant. **B.** Other supplies that may also be used include a caulk gun to introduce contrast, contraceptive jelly with contrast for vaginal opacification, and commercially prepared rectal contrast. **C.** If the barium is not used for vaginal contrast, contraceptive jelly mixed with water-soluble contrast with the highest iodine content is used with a bladder irrigation syringe and pediatric enema tip.



Figure 52-4 Defecography commode. A. The commode for the procedure is attached to a remote fluoroscopy table so that the patient can be positioned using the tabletop movement. These steps make it easier for the patient to get to the seat. **B.** The dish in the commode has a radiopaque ruler (in centimeters) so that direct measurements can be made from the images. The dish is also covered with a plastic bag so that after each patient, all that needs to be done is to replace the bag. R, ruler.

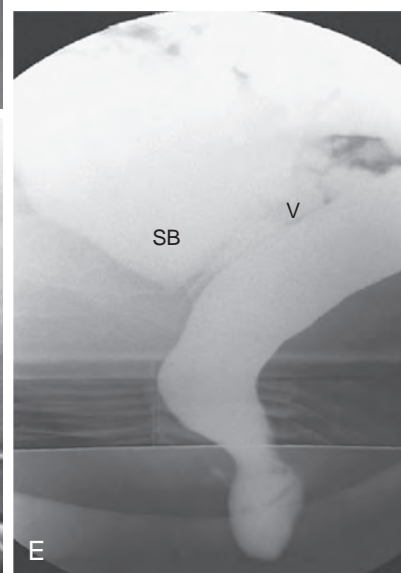
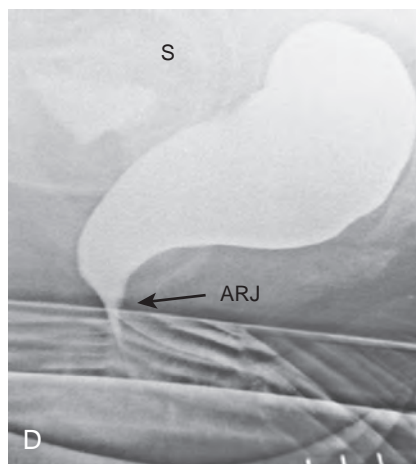
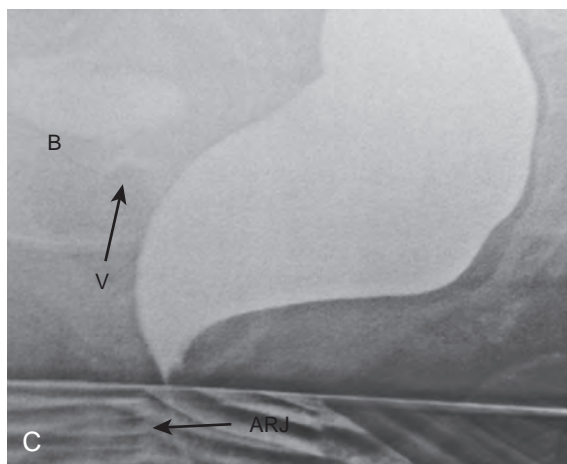
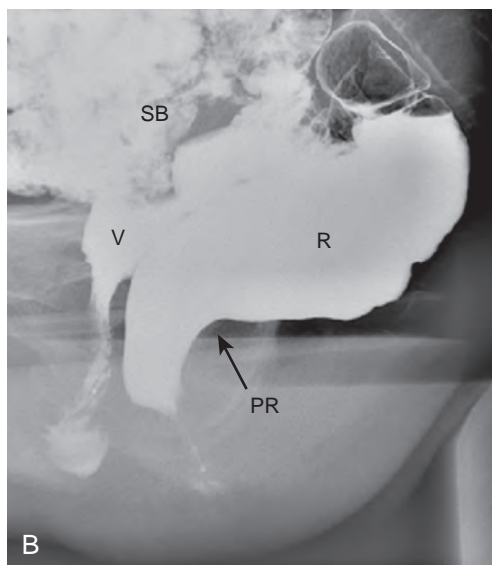
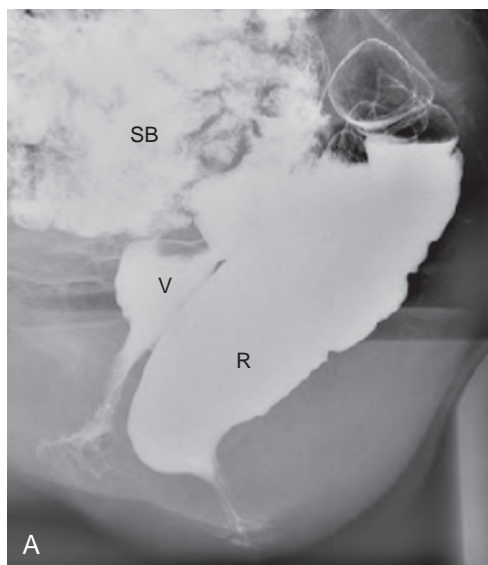
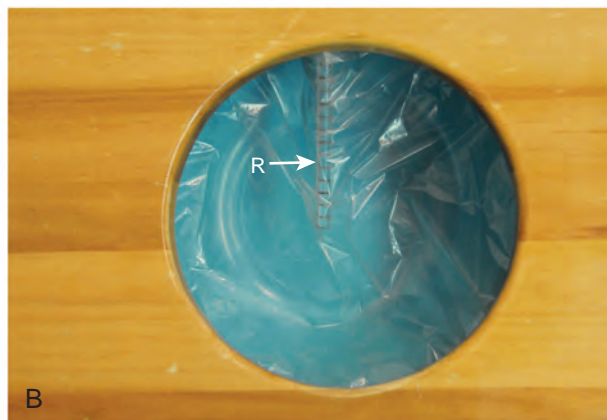


Figure 52-5 Normal examination. A. Normal, at rest. The vagina (V) has a close relationship to the anterior wall of the rectum (R). The small bowel (SB) has been opacified. **B.** Normal with lift (squeeze). The anorectal junction is above the level of the ischial tuberosities and there is good contraction of the puborectalis (PR). **C.** Normal, with coughing. There is virtual no movement of the anorectal junction (ARJ). The bladder (B) and vagina (V) have been opacified. **D.** Normal, with straining (S). Again, the ARJ maintains a normal position and there is no incontinence. **E.** Normal beginning of defecation. The anal canal is open and there is good emptying. At the end, the rectum is almost totally empty, with some stray contrast remaining.

becomes acute with maximum elevation. The squeeze image demonstrates pelvic floor strength, and impaired movement may reflect puborectalis atrophy.⁴⁷ The anal canal simultaneously lengthens. These changes can be measured and are indicators of the continence mechanism. When asked to cough, the patient should produce a powerful cough in the rest position. This action simultaneously increases intra-abdominal pressure and contraction of the anal and pelvic floor muscles. In normal individuals, there is minimal or no descent of the pelvic floor and total continence (see Fig. 52-5C). When asked to strain, the patient should strain downward maximally, without evacuating (see Fig. 52-5D). This maneuver stresses the continence mechanism and provides a measure of pelvic floor descent. The anal canal shortens during straining in most women (mean change, 2 mm).⁴⁶ Almost all patients demonstrate some perineal descent, but this is the least reliable portion of the examination because some patients paradoxically contract the pelvic floor muscles, perhaps for fear of incontinence. Straining is supposed to demonstrate the competence of the external anal sphincter.

Finally, spot films are obtained during defecation and post-defecation straining (see Fig. 52-5E). These films give a measurement of pelvic floor descent and an estimate of the completeness of emptying. Morphologic abnormalities such as intussusception and rectoceles are often visualized at this time, and the changes contributing to difficulty in defecation can be analyzed. Rectoceles are outpouchings of the rectum beyond the expected contour of the rectal wall (Fig. 52-6). They are often normal and are more common in women.⁴⁶ If a rectocele

does not empty completely during defecation, it may produce a feeling of incomplete evacuation of the rectum.

Measurements

Measurements taken from spot films include the anorectal angle, anal canal length, level of the anorectal junction, and descent and elevation of the anorectal junction (see Fig. 52-10).

ANORECTAL ANGLE

The anorectal angle (Fig. 52-7) is measured between the axis of the anal canal and the tangent to the posterior wall of the rectum. It can be difficult to measure because the posterior wall of the rectum is often not clearly delineated, and the angle becomes highly subjective.⁴⁷ Caution should therefore be exercised when assessing its significance. At rest, this angle is usually no greater than 120 degrees in control subjects. However, the angle has a normal range of 70 to 134 degrees, with a mean of about 95 degrees.⁴⁶ When the patient squeezes or lifts the buttocks, the anorectal angle decreases to a mean of 19 degrees in women (range, 6 to 26 degrees) and a mean of 28 degrees in men (range, 12 to 45 degrees).⁴⁴ This angle increases during straining and defecation. The mean anorectal angle during straining in normal young women is 103 degrees, with a range of 75 to 108 degrees. In men, the mean angle is slightly lower, 98 degrees, with a range of 67 to 123 degrees.⁴⁶

ANAL CANAL LENGTH

The anal canal length is easily measured. It is the distance traversed by the parallel borders of the anal canal before they form the diverging walls of the distal rectum. At rest, the mean length

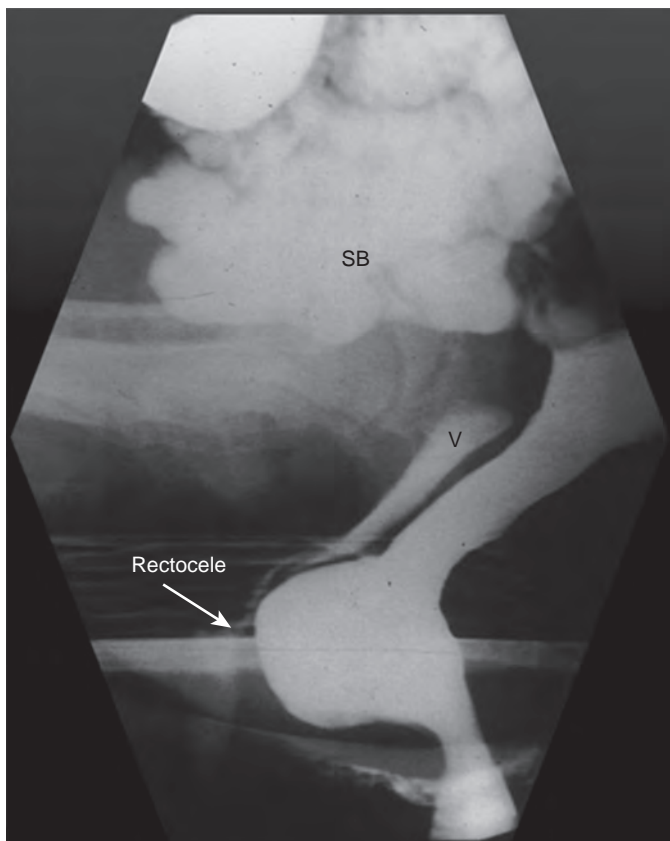


Figure 52-6 Rectocele (R). This is normal, except when it does not empty at the end of defecation. SB, small bowel; V, vagina.

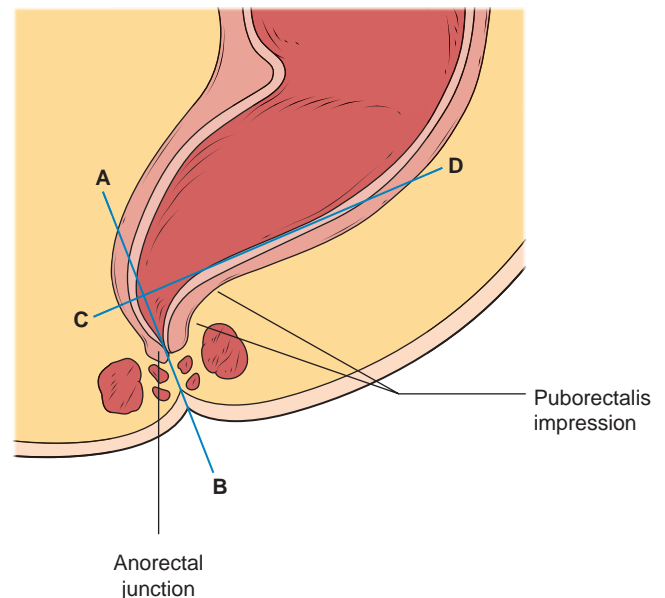


Figure 52-7 Schematic showing the anorectal angle. The lines AB and CD subtend the posterior anorectal angle. The position of AB is easily determined; CD can be much more difficult to draw. The thicker line shows the position of the anorectal junction. Below it are the two parallel lines that form the anal canal. The thinner lines point to the puborectalis impression.

of the anal canal is 16 mm in women (range, 6 to 26 mm) and 22 mm in men (range, 10 to 38 mm). During lifting (squeezing), the anal canal lengthens to a mean of 19 mm in women (range, 9 to 26 mm) and 28 mm in men (range, 12 to 45 mm). During straining, the canal shortens slightly and has a mean length of 14 mm in young women (range, 6 to 20 mm) and 17 mm in young men (range, 9 to 27 mm).⁴⁶

LEVEL OF ANORECTAL JUNCTION

The anorectal junction is the uppermost point of the anal canal. Its position is measured from an easily visualized fixed point, the ischial tuberosity. A positive value indicates a position above the ischial tuberosity, whereas a negative value indicates a position below it. In normal young men at rest, the mean level of the anorectal junction is 16 mm and increases to 28 mm during lifting (squeezing). It drops to -4 mm during defecation. In young women, the mean values for the same maneuvers are 4 mm at rest, 14 mm during lifting (squeezing), and 16 mm during defecation,⁴⁵ measurements significantly different from those of normal young men.

Although these measurements can be made, in routine practice it is not done because of the poor reproducibility, especially the anorectal angle and descent of the anorectal junction.⁴⁸ Occasionally, unusual or unexplained findings are seen on lateral views, and anteroposterior or oblique views are needed for further clarification. Some patients have a history of using a variety of maneuvers to facilitate evacuation. These patients should be encouraged to use these maneuvers during the examination, and the mechanisms aiding evacuation should be identified. When patients have a large anterior rectocele that remains full even after the rectum has completely emptied, they may complain of incomplete emptying. These patients typically empty the rectocele back into the rectum by digital perineal or vaginal pressure. In patients with a history of obstructed defecation, it is sometimes helpful to perform the examination first with liquid barium, which makes expulsion easier. If this approach is successful, the examination should be repeated in the usual way with one of the thick barium pastes.

Pathology

ENTEROCELE AND SIGMOIDOCELE

Enterocoele refers to herniation of the small bowel into the posterior peritoneal cul-de-sac in the rectovaginal space or into the vagina itself. In some patients, both locations become filled with small bowel. Diagnosis depends on opacification of the pelvic small bowel and vagina (Fig. 52-8). The incidence of enterocoele has markedly increased as a result of the widespread performance of hysterectomy and cystourethropepy because both these procedures open up the posterior cul-de-sac. At hysterectomy, the uterosacral ligament complex or adjacent fascia is usually compromised. This leads to enterocoele formation and vaginal vault prolapse because damage occurs at the level of the vaginal apex. In one study,³⁸ defecography showed an enterocoele in 64% of patients who had undergone hysterectomy and 27% of those who had undergone cystopexy. Currently, hysterectomy is not considered a risk factor for future prolapse unless the hysterectomy was performed for prolapse.¹⁹ Patients with prolapse already have an underlying collagen tissue abnormality that predisposes them to further future prolapse. Urethropepy

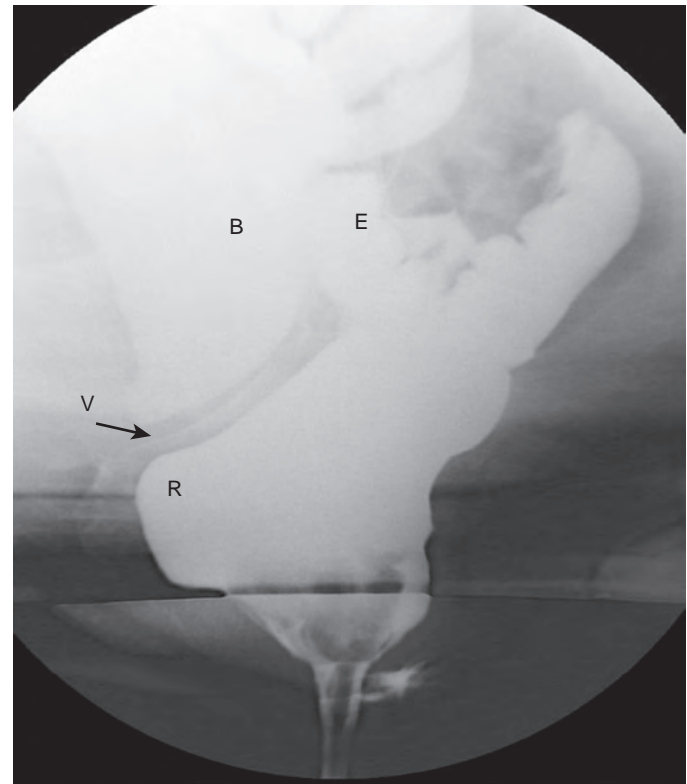


Figure 52-8 Small enterocoele (E). The small bowel has just begun to enter the gap between the vagina (V) and rectum (R). The vagina and bladder (B) have also been opacified.

performed for incontinence predisposes to enterocoele formation by lifting the anterior vaginal wall forward and opening up the cul-de-sac. However, urethropepy has generally been replaced with the urethral sling procedure, which does not increase the frequency of enterocoele formation.¹⁸

Unlike rectoceles, which are generally largest during evacuation, enterocoeles (Fig. 52-9) usually become evident only at the end of evacuation because of the space occupied by the distended rectum. Repeated straining after evacuation may be essential for the recognition of enterocoeles. In one study,⁴⁹ almost half (43%) of the enterocoeles were seen only on post-evacuation radiographs obtained with the patient straining maximally, thus emphasizing the importance of this maneuver. Evacuation should be as complete as possible because the unemptied rectum or rectocele may prevent descent of an enterocoele. Obtaining a post-toilet radiograph (or postcatheterization radiograph in patients with urinary retention) to carry out further rectal evacuation offers the best opportunity to detect an enterocoele. Intravaginal enterocoeles, unlike those that extend into the rectovaginal space, often compete with a cystocele; if the cystocele is not sufficiently drained, the presence of a coexistent enterocoele may be overlooked or minimized. It should be noted, however, that enterocoeles may be overdiagnosed because of the lack of a clear imaging definition of the abnormality because the cul-de-sac can extend down the posterior vaginal wall by 5 cm.

The symptom typically associated with an enterocoele is a sensation of pelvic pressure or dragging, especially when standing or bearing down. Symptoms of vaginal prolapse, pelvic fullness, and lower abdominal pain have been shown to disappear

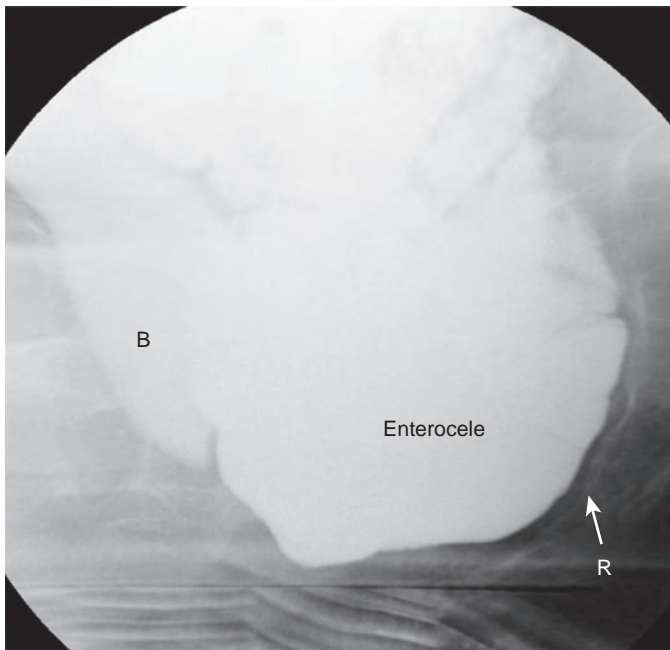


Figure 52-9 Large enterocele. A large enterocele develops if the patient has to strain because of difficulty in evacuation. This can then compress the rectum (R) and prevent further emptying. The bladder (B) has also been opacified. The opacified vagina can barely be seen.

after enterocele repair.⁵⁰ Enteroceles have long been held responsible for causing pressure on the rectum and obstructing rectal evacuation (the so-called defecation block).⁵¹ One study, however, has shown that enteroceles do not impair rectal emptying.⁵² Our observation is that it is the distended rectum, not the obstruction of the rectum by the enterocele, that prevents enterocele descent. Not uncommonly, an enterocele accompanies a rectoanal intussusception or rectal prolapse.

Surgical repair of an enterocele requires obliteration of the herniated, bowel-containing cul-de-sac, resuspension of the unsupported vaginal axis, and repair of other associated defects. Large enteroceles usually require a transabdominal approach so that a concomitant abdominal sacrocolpopexy procedure or similar vaginal suspension procedure can be performed. Defecography is important in this respect because the radiographic detection of a large, previously undiagnosed enterocele may change the surgical approach from a transvaginal to transabdominal route of entry. In many patients referred for defecography, this is the most crucial piece of information needed by the pelvic floor surgeon before surgery.¹⁸

A sigmoidocele is a redundancy of the sigmoid colon that extends caudally into the cul-de-sac.⁵² They are less common than enteroceles and are found on approximately 5% of proctograms.^{49,53,54} This condition will be underdiagnosed at proctography if the sigmoid is not opacified, but a sigmoidocele is suspected on the basis of widening of the rectovaginal septum and air seen within fecal residue. Lax presacral fixation of the rectosigmoid can be seen in some patients. As with other organ prolapses, there is no standard definition for sigmoidocele.⁵⁴ Fenner has defined a sigmoidocele as a sigmoid colon extending more than 4.5 cm below the pubococcygeal line.⁵⁴ According to our definition,²² such a finding would constitute a moderate-sized sigmoid herniation. Sigmoidoceles are usually not detected

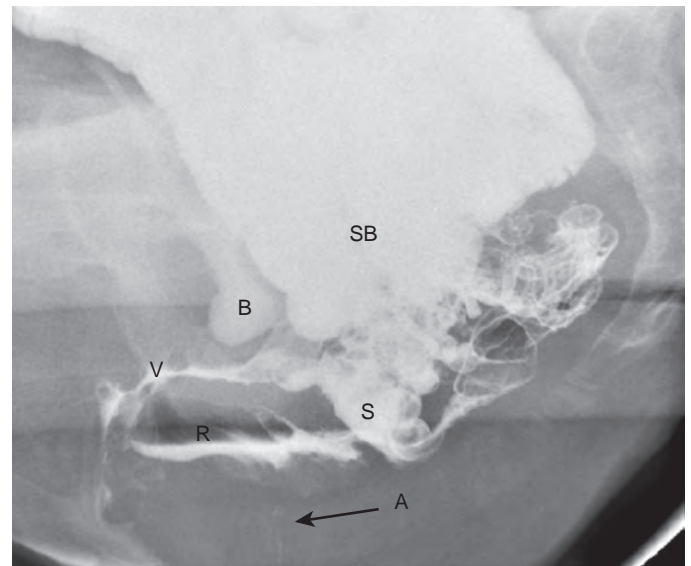


Figure 52-10 Sigmoidocele and rectocele. This image shows a sigmoidocele (S) and rectocele (R). The vagina (V) has been slightly displaced by the rectocele, which has both air and contrast. The bladder (B) and small bowel (SB) have been opacified. The faintly seen anal canal has been marked (A; arrow).

at physical examination, even when large,²² and are often associated with constipation.^{53,54} The redundant sigmoid colon may compress the rectum and obstruct defecation. Stasis of solid debris in the redundant sigmoid may give rise to further discomfort and straining. A large rectocele may be combined with a sigmoidocele, which is known as a rectosigmoidocele (Fig. 52-10).

Sigmoid resection or sigmoidopexy has been shown to provide striking relief of associated constipation. Marked detachment of the sigmoid colon from the sacral hollow is suggestive of the need for concomitant sigmoidopexy. Because bowel surgery is often performed by a colorectal surgeon rather than a pelvic floor reconstructive surgeon, preoperative recognition of a sigmoidocele coexisting with other defects is important so that sigmoid resection or sigmoidopexy, obliteration of the cul-de-sac, and repair of associated pelvic floor defects can be accomplished at one surgical setting.

The term *peritoneocele* has been applied to herniation into the cul-de-sac⁵⁵ defined a peritoneocele as an extension of the rectouterine excavation below the upper third of the vagina. In the series by Bremmer et al., approximately 50% of peritoneoceles were found to contain bowel. In our experience, however, peritoneoceles usually contain small bowel. This probably reflects our routine use of the post-toilet strain sequence following emptying of any filled organ (bladder or rectum). This is readily demonstrated with dynamic MRI.²² A peritoneocele should be suspected at defecography if there is unexplained widening of the rectovaginal space (Fig. 52-11); we have found this on 9% of defecography images.⁴⁹ Recognition of a peritoneocele is important because it predisposes to enterocele formation and suggests the need for surgical closure of the cul-de-sac if reconstructive surgery of the pelvic floor is undertaken.¹⁸

As shown by vaginal markers, the vagina may separate from the anterior wall of the rectum during defecation (see Fig. 52-11), often causing the patient to feel pressure in the perineum.



Figure 52-11 Peritoneocele. A peritoneocele is suspected when there is a widening gap (*double arrow*) between the vagina (V) and rectum. The small bowel (SB) and sigmoid (S) have also been opacified.

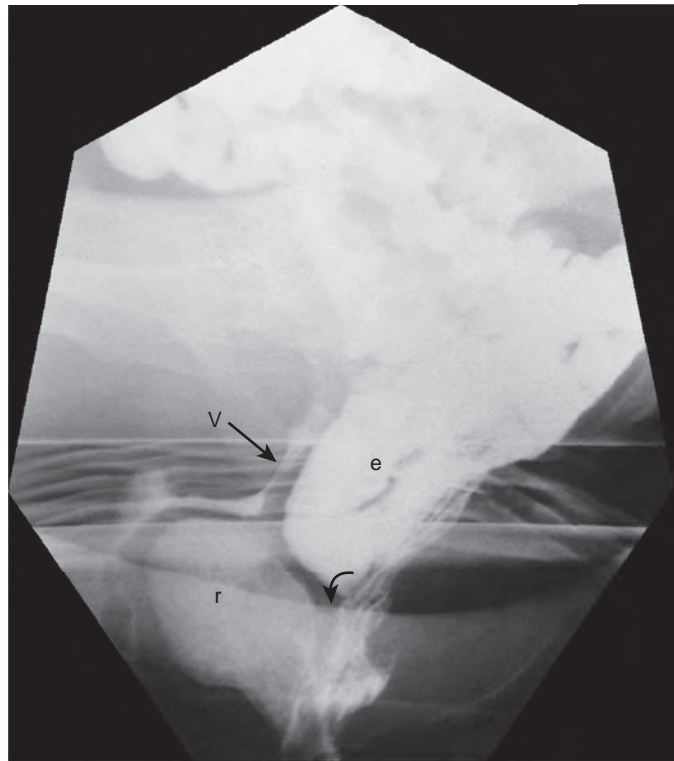


Figure 52-12 Enterocoele. An enterocoele (e) is seen in the gap between the vagina (V) and rectum. There is also a rectocoele (r) present. This has been obstructed from further emptying by an intussusception (*curved arrow*).

When this separation is identified, the examination should be repeated at a later date, after the small bowel or peritoneum has been opacified, as described earlier.^{33,45} If the gap between the vagina and rectum is caused by an enterocoele, the opacified small bowel is seen descending (herniating) into a deep pouch of Douglas (Fig. 52-12). If rectal prolapse is also present, the small bowel may invaginate into the anterior rectal wall and prolapse with the rectum through the anal canal. A sigmoidocele can produce a similar appearance, so the proximal sigmoid colon must be opacified to allow differentiation. Occasionally, an enterocoele and sigmoidocele are present in the same patient (Fig. 52-13).

ANTERIOR MUCOSAL WALL PROLAPSE AND RECTOCELE

In anterior wall prolapse, the anterior rectal wall prolapses toward the external anal orifice during the final stages of evacuation. This prolapse is a frequent finding in women and may be responsible for isolating an anterior rectocoele. As noted, rectoceles are outpouchings of the rectal wall. They are usually anterior, reflecting a relative weakness of the rectovaginal septum. Rectoceles are often accompanied by an intussusception, which may obstruct defecation by occluding the anal canal and neck of the rectocoele.³¹ The anterior wall prolapse may precede an intussusception. Rectoceles are common in women who have had children. It is present in 78% to 99% of women who have given birth.^{56,57}

A rectocoele depth of less than 2 cm is usually considered clinically insignificant.⁴³ A rectocoele may be considered large if

the depth is more than 3.5 cm, as measured from the anterior margin.⁵⁸ Retained contrast material greater than 10% at the end of defecation is indicative of barium trapping. If the patient then believes that she has not emptied her rectum or uses vaginal or perineal pressure to empty the rectocoele, the rectocoele is abnormal. In other words, the size does not matter but symptomatic relief is relied on to make the diagnosis.

RECTAL INTUSSUSCEPTION

Rectal intussusception is a concentric invagination of the entire rectal wall that progresses toward the anal canal.⁵⁹ It is thought to cause rectal prolapse. The intussusception usually begins about 6 to 8 cm above the anal canal as an invagination of one of the valves of Houston.⁶⁰ The infolding of the intussusception is anterior in 62% of patients, annular in 32%, and posterior in only 6%. Minor degrees of infolding of less than 3 mm represent mucosal prolapse and are probably not significant. However, inferior extension of the intussusception into the anal canal is abnormal. When an intussusception plugs the anal canal, the patient may develop symptoms of obstructed defecation⁶¹ and solitary rectal ulcer.¹⁴ The patient sometimes learns to relieve the obstruction by pushing the intussusception plug back with a finger placed in the anal canal. Internal prolapse, as seen with an intussusception plug, is revealed only by evacuation proctography. Occasionally, it is demonstrated during the end of defecation, sometimes only with straining. Spot films depicting postdefecation straining are therefore important (Fig. 52-14A). Complete or external prolapses are clinically obvious (see Fig. 52-14B).

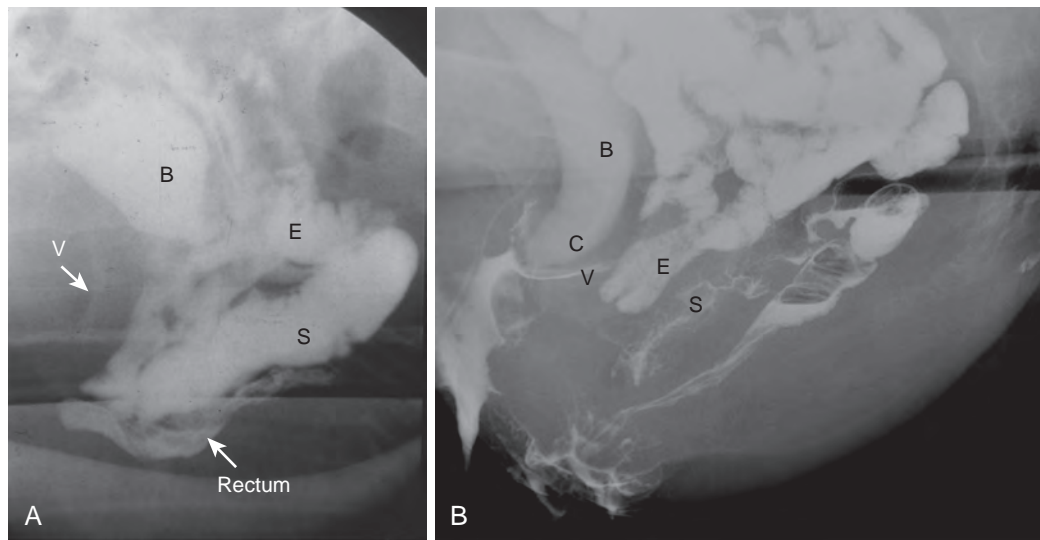


Figure 52-13 Simultaneous sigmoidocele and enterocele. **A.** Simultaneous presence of a sigmoidocele (S) and enterocele (E). The vagina (V) and bladder (B) have been opacified as well. **B.** Another patient with a sigmoidocele, enterocele, and cystocele (C). The bladder and vagina are opacified.

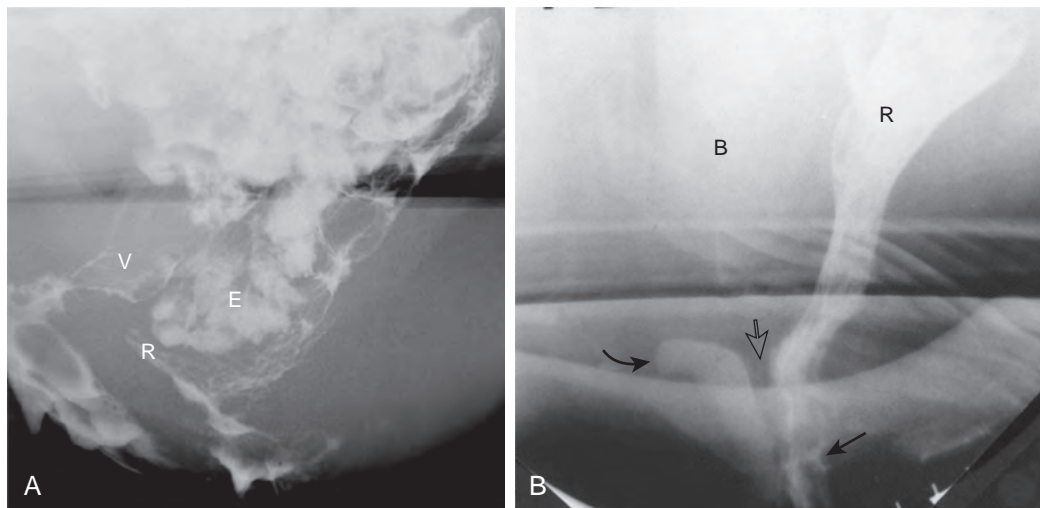


Figure 52-14 Enterocele, rectocele, prolapsed and intussusception. **A.** Postdefecation, there is an enterocele (E), obstructed rectocele (R), and some external prolapse. The vagina (V) has been opacified. **B.** In another patient, there is an intussusception (open arrow), external prolapse (straight solid arrow), and obstructed rectocele (curved arrow). This is the result of continued constant straining. The bladder (B) has been opacified.

Solitary Rectal Ulcer Syndrome

This is almost always associated with rectoanal or extra-anal intussusceptions. There is an increase in sphincter thickness on endosonography.⁶² The clinical findings are chronic straining, with blood and mucus. Endoscopy shows erythema or ulceration at endoscopy. The term *solitary ulcer syndrome* is misleading because erythema, a single erosion, or more than one ulcer may be present.¹⁵ With a double-contrast barium enema, thickening of the valves of Houston (rectal folds) is seen in most patients.¹⁶ However, the best indicators for surgical correction is a clinical or proctographic finding of rectal prolapse and the presence of a solitary rectal ulcer in association with rectal intussusception.⁶³

POSTERIOR-LATERAL RECTAL POUCHES

Posterior-lateral rectal pouches are herniations of rectal mucosa through the pelvic floor. They are often suspected on lateral

views but are confirmed on anteroposterior views during straining. These pouches are usually found in patients who have difficulty with rectal evacuation, which requires excessive straining. Patients who demonstrate excessive straining may have paradoxical contraction of the puborectalis sling or a nonrelaxing anal sphincter.

PELVIC FLOOR DYSSYNERGY (ANISMUS)

Pelvic floor dyssynergy, or anismus, is not a clear-cut diagnosis. Historically, pelvic floor dyssynergy has been diagnosed in those with a history of prolonged straining during defecation if there is inappropriate puborectal contraction and the patient is unable to expel a balloon filled with 50 mL of water. It was initially assumed that this would be shown during defecography as a persistent indentation posteriorly, just above the anorectal junction, but this finding has been poorly predictive of the diagnosis.⁶⁴ In the study by Halligan and associates,⁶⁴ prolonged and/or incomplete evacuation of contrast material was shown

to be a much more sensitive and specific finding; it was present in 83% of patients and none of the control subjects. The combination of prolonged and incomplete evacuation had a positive predictive value of 90% compared with a physiologic diagnosis of anismus. The cause of this syndrome (also known as paradoxical puborectalis contraction, incompletely relaxing puborectalis, and spastic pelvic floor syndrome) is unknown, although a convincing association with sexual abuse is suggestive of a psychological origin. Controversy surrounds its diagnosis. It cannot be demonstrated in many constipated patients and may be found in asymptomatic subjects; it has also been described as a laboratory artifact.⁶⁴ However, there seems to be a generally strong association with symptoms. Most convincingly, the success of biofeedback treatments in these patients supports the value of making this diagnosis¹⁷ and thus the importance of categorizing posterior compartment defects into functional and anatomic abnormalities. Slow colon transit may be improved as a secondary effect to the treatment of poor rectal emptying or by affecting cerebral gut innervation.⁶⁵

In patients with paradoxical contraction of the puborectalis, defecography shows an increased or unchanged anorectal angle during straining and defecation (Fig. 52-15). The puborectalis impression is usually prominent because of persistent contraction and increases when the anorectal angle is decreased. This syndrome is relatively common in patients with normal colonic transit and chronic constipation. Bartolo and co-workers found this syndrome in 11 of 49 patients who were examined by proctography.⁶⁶ As noted, it has also been called anismus and spastic floor syndrome.⁶⁷

In some patients, the puborectalis relaxes during defecation, but the internal or external anal sphincter muscle, or both, fails to open. Sphincters that fail to relax normally may be associated with anal fissures, spinal cord tumors, and painful hemorrhoids.

DESCENDING PERINEUM SYNDROME

Patients with the descending perineum syndrome also have difficulty defecating. This syndrome occurs when there is ballooning of the perineum below the plane of the ischial tuberosities during straining. Perineal descent is usually less than that of the pelvic floor and can be measured with a perineometer.⁶⁸ However, proctography is a more reliable method of assessing pelvic floor descent.⁶⁹ This syndrome may be seen in other

disorders involving obstructed defecation and may subsequently lead to injury of the pudendal nerve.

In younger patients, the pelvic floor is higher at rest and descends more at evacuation, whereas in older patients there is more descent at rest and less change at evacuation.⁷⁰ A low pelvic floor at rest is usually suggestive of muscle weakness and stretching of the elastic tissue in the fascial support.⁵⁶ In perineal descent syndrome, the anorectal junction is more than 3 cm below its normal resting position, as measured at the level of the ischial tuberosities. These measurements only apply if the study is done with defecation being observed in the normal physiologic position (i.e., sitting on a commode). When done with the patient in the left lateral decubitus position, the position of the pelvic floor is significantly higher.⁷¹ Therefore, this affects comparisons with other imaging techniques of the pelvic floor, such as MRI.

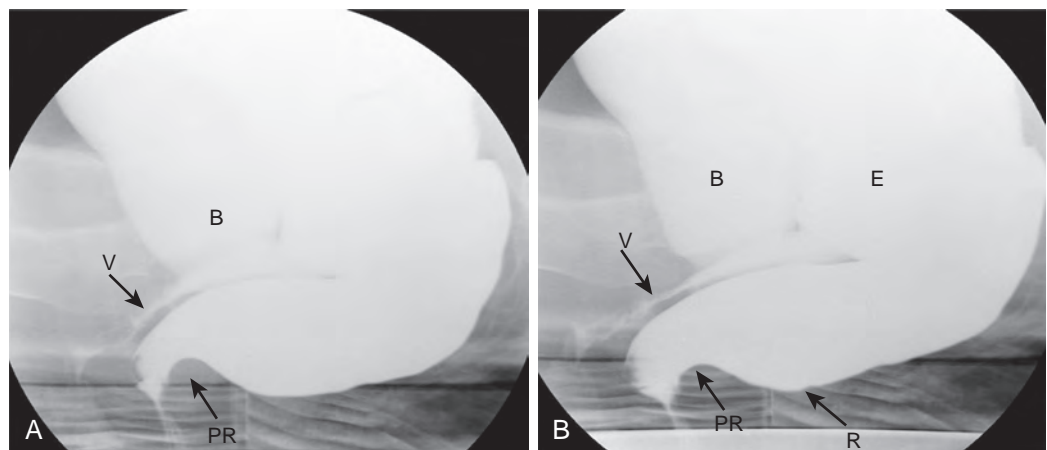
ANTERIOR MUCOSAL PROLAPSE

These patients present with bleeding, pain, and tenesmus. Progression to complications such as prolapse is uncommon.⁷² The characteristics of anterior mucosal prolapse at defecography is variable. A common finding is inversion of the anterior rectal wall over the anal canal with rectoceles.⁷³ Extension of the anterior wall into upper rectum without widening of the canal is suggestive of anterior mucosal prolapse (Fig. 52-16). One study has shown that anterior rectocele and perineal descent are present in 70% of women with anterior mucosal prolapse.⁷⁴ These findings are representative of total pelvic floor descent.

UTERINE AND VAGINAL VAULT PROLAPSE

In uterine prolapse, the uterus and cervix descend in the vagina and sometimes beyond the introitus. The cervix is the most distal point of the prolapse. Prolapse of the vaginal vault involves prolapse of the apex of the vagina through or beyond the introitus after a previous total hysterectomy.⁷⁵ Vaginal vault prolapse is almost always associated with prolapse of other pelvic organs; the most common is an enterocele. These associations usually reflect a loss of support because of damage to the uterosacral-cardinal complex. If the vagina is adequately opacified, the location of the cervix and/or vaginal apex can be determined on the strain images after evacuation by defecography.

Figure 52-15 Pelvic floor dyssynergy. **A.** This patient has pelvic floor dyssynergy or a nonrelaxing puborectalis (PR). The muscle can be seen to be prominent at rest. The vagina (V) and bladder (B) have been opacified. **B.** In pelvic floor dyssynergy, the puborectalis (PR) fails to relax sufficiently, as seen in this patient. With continued straining, a posterior rectocele (R) may appear. E, possible early enterocele.



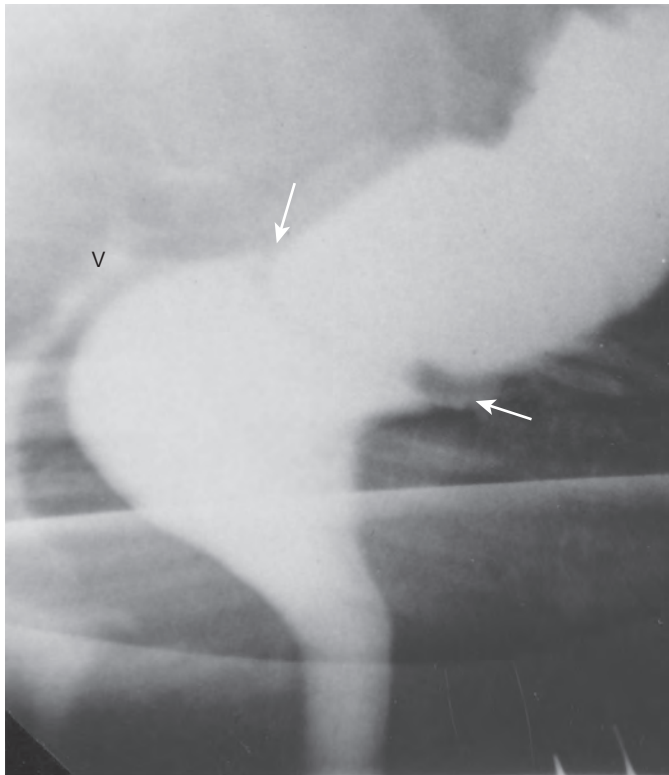


Figure 52-16 Mucosal prolapse (arrows). V, vagina.

CYSTOCELE

A cystocele is diagnosed when the bladder base descends below the pubococcygeal line. It is the result of defects in the pubocervical fascia, which attaches laterally to the arcus tendineus and posteriorly to the cervix. The symptoms from a cystocele are minimal until it reaches the introitus. The most common symptoms are feelings of heaviness or “something bulging.” Voiding dysfunction may occur with large cystoceles.

Cystoceles are larger after rectal emptying and therefore optimally assessed by measuring the depth of the anterior vaginal wall at the end of defecation. If the vagina is well opacified, cystoceles can still be seen, without bladder opacification, by the downward displacement of the vagina. However, if the urinary bladder is too full, it may prevent the detection of a coexistent enterocele. Hypermobility of the bladder neck is diagnosed when the urethrovesical junction descends more than 1 cm from rest to strain, as measured on the postdefecation images (Fig. 52-17).

CONSTIPATION AND INCONTINENCE

Continuous straining stretches the pudendal nerve by causing ballooning of the pelvic floor. This stretching has been shown to increase motor latency of the pudendal nerve.⁷⁶ Continued straining can ultimately lead to permanent pudendal nerve damage and incontinence.

Normal control subjects have an anorectal junction level above the ischial tuberosity and an excursion of about 3 cm during straining and defecation. Constipated patients have a low anorectal junction level and good lift, but little or no movement during straining and defecation. Patients with fecal

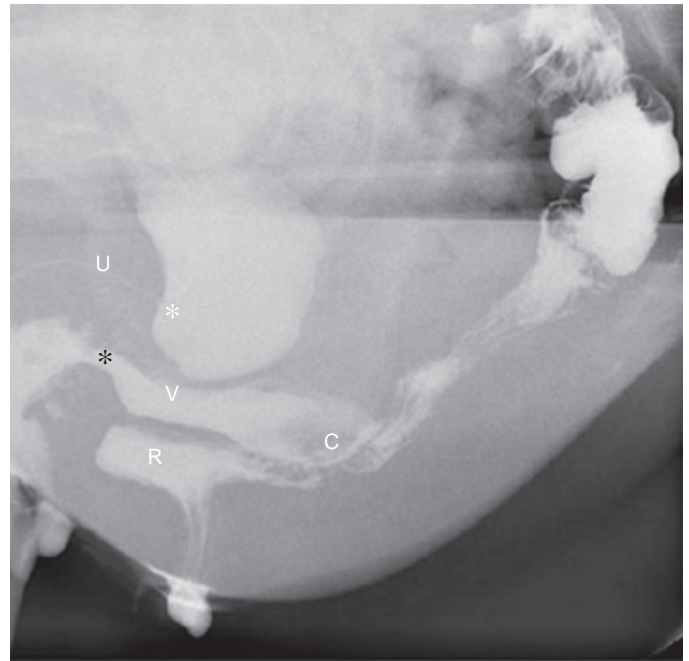


Figure 52-17 Hypermobility of the bladder neck. C, cervix; R, rectocele; U, urethra; V, vagina.

incontinence have a low anorectal junction level (not unlike constipated patients), small lift, and large excursion during straining and defecation. Given that the constipated and incontinent patients both have low anorectal junction levels, it seems reasonable to speculate that these low levels are caused by constant straining and that constipated patients will eventually become incontinent as a result of a pudendal neuropathy. Because lift in the constipated group is still satisfactory, it may be possible to prevent incontinence in this group with a perineal support device, such as the Lesaffer seat (Defecom, Aalst, Belgium). The Lesaffer perineal support device⁷⁷ is designed to prevent excessive descent of the perineum, permit normal relaxation and expulsion, and prevent or minimize nerve damage.

Evacuation proctography for incontinence is of value only in patients with rectal prolapse, anal sphincter trauma, or neurogenic (idiopathic) incontinence. In rectal prolapse, patients are partially incontinent because the intussusception dilates the internal sphincter. When detected by proctography, rectopexy or a postanal repair can be performed.⁷⁸ In neurogenic or idiopathic incontinence, if the anorectal angle is widened, a postanal repair can correct this angle and restore continence.⁷⁹ In sphincteric trauma, proctography is useful for assessing the extent of damage to the pelvic musculature and monitoring healing.

Comparison with Other Methods of Examining the Pelvic Floor

Although incompetence of the internal and external sphincters or atrophy of the external anal sphincter can be predicted with rest, and strain images obtained at defecography,⁸⁰ this study cannot demonstrate the structural sphincter defects that are shown with anal endosonography⁸¹ and does not have the multiplanar imaging capabilities or soft tissue resolution

available with endoanal MRI.^{82,83} Several studies have compared defecography and dynamic MRI.²¹⁻²³ The conclusion by the investigators appears to be conflicting, and there is no consensus about which technique is superior for the evaluation of pelvic floor disorders. Dynamic MRI has considerable advantages.^{26,84} MRI provides a cine loop of pelvic organ and pelvic floor descent. The multiplanar representation has the potential to yield much more anatomic information about the pelvic floor musculature and support structures. It has the advantage of no ionizing radiation. The mean effective dose for defecography has been estimated to be 3.2 ± 2.7 mSv.⁸⁵ The risk with this dose is unknown, but the Health Physics Society⁸⁶ has stated that the risk for developing radiation-induced cancer with doses in this range are too small to measure or are nonexistent. Also, in the age group referred for defecography, radiation should not be a consideration.

Dynamic MRI also has major disadvantages. In most MRI units, the patients are imaged in the supine rather than upright position (this does not apply when imaged in a vertical open magnet).²⁵ In the horizontal magnet, the patient is therefore asked to defecate while lying supine, an unnatural position. A position in which patients are usually asymptomatic, and in an artificial environment, makes an embarrassing examination less acceptable. Evacuation of the rectum is pivotal in this study; if an open vertical magnet is not available, fluoroscopic defecography is preferable.

Additional factors that have to be considered are economics, practicality in everyday practice, and the advantages of one modality over another. In most institutions, the additional cost of MRI versus conventional defecography and the relative lack of time on the MR unit as a result of other clinical demands are major disadvantages.

Normal Variations

The abnormal findings in evacuation proctography, as noted, are much easier to characterize than normal findings. This difficulty in defining normal characteristics is because there are limited data on normal subjects in different age groups⁸⁷ and

only one study of normal volunteers.⁴⁴ The latter study by Shorvon and associates showed that the range of normal characteristics is much greater than originally reported. Several investigators agree that the normal mean anorectal angle is between 90 and 100 degrees.^{31,33,56,88} In the earlier study, the anorectal angle in normal young volunteers had a range of more than 60 degrees around this mean. The same study showed a mean pelvic descent of 2 cm; however, pelvic descent was greater than 5 cm in some women and 4 cm in some men. Many investigators believe that a pelvic descent of 3 to 3.5 cm between rest and defecation is abnormal; this position has been confirmed by clinical estimates.⁸⁹ This discrepancy may be related to the fact that clinical estimates are obtained with the patient lying on a couch in a horizontal lateral position. In this position, the patient may be inhibited from maximal straining for fear of incontinence. In addition, the added weight of the rectal contents that contributes to the downward pull of the pelvic floor is absent. Furthermore, the proximal radiographic anal canal probably becomes incorporated into the distal rectum during evacuation as it forms a cone configuration. These factors increase apparent pelvic descent during evacuation proctography. In the study by Shorvon and co-workers, it was also surprising to find that rectal intussusception occurred in normal subjects.⁴⁵ However, none of these patients had external prolapse.

Summary

In conclusion, evacuation proctography can often provide a unique functional perspective of disorders of defecation, particularly those relating to constipation and obstructed defecation. Some of the problems depicted by this examination are amenable to surgery, and others can use nonsurgical options such as biofeedback and pelvic floor exercises (Kegel exercises). However, because there is considerable overlap between normal and abnormal appearances, it is important to recognize the value of anal manometry, electromyography, colon transit studies, and the patient's clinical findings before making any management decisions.

REFERENCES

- Handa VL, Cundiff G, Chang HH, et al: Female sexual function and pelvic floor disorders. *Obstet Gynaecol* 111:1045-1052, 2008.
- Nygaard I, Barber MD, Burgio KL, et al: Pelvic floor disorders network. Prevalence of symptomatic pelvic floor disorders in US women. *JAMA* 300:1311-1316, 2008.
- MacLennan AH, Taylor AW, Wilson DH, et al: The prevalence of pelvic floor disorders and their relationship to gender, age, parity and mode of delivery. *BJOG* 107:1460-1470, 2000.
- Walters MD: Pelvic floor disorders in women: An overview. *Rev Med Univ Navarra* 48:9-12, 15-17, 2004.
- Borello-France D, Burgio KL, Richter HE, et al: Pelvic floor disorders. Fecal and urinary incontinence in primiparous women. *Obstet Gynecol* 108:863-872, 2006.
- Lukacz ES, Lawrence JM, Contreras R, et al: Parity, mode of delivery and pelvic floor disorders. *Obstet Gynecol* 107:1253-1260, 2006.
- NIH state-of-the-science conference statement on the prevention of fecal and urinary incontinence in adults. *NIH Consens State Sci Statements* 24:1-37, 2007.
- Jorge JM, Habr-Gama A, Raivio R, et al: The role of biofeedback therapy in functional proctologic disorders. *Scand J Surg* 93:184-190, 2004.
- Nichols CM, Ramakrishnan V, Gill EJ, et al: Anal incontinence in women with symptoms of urinary incontinence and genital prolapse. *Obstet Gynecol* 100:1266-1271, 2002.
- Whitehead WE, Wald A, Diamant NE, et al: Functional disorders of the anus and rectum. *Gut* 45(Suppl 2):II55-II59, 1999.
- Whitehead WE: Functional anorectal disorders. *Semin Gastrointest Dis* 7:230-236, 1966.
- Barucha AE, Wald A, Enck P, et al: Functional anorectal disorders. *Gastroenterology* 130:1510-1518, 2006.
- Takao Y, Okano H, Gilliland R, Wexner SD: Cine-defecographic evidence of difficult evacuation in constipated patients with complex symptoms. *Int J Colorectal Dis* 14:291-296, 1999.
- Womack NR, Williams NS, Holmfeld JH, Morrison JF: Pressure and prolapse—the cause of solitary rectal ulceration. *Gut* 28:1228-1233, 1987.
- Goei R, Baeten C, Arends JW: Solitary rectal ulcer syndrome: Findings at barium enema study and defecography. *Radiology* 168:303-306, 1988.
- Mahieu P: Barium enema and defaecography in the diagnosis and evaluation of the solitary ulcer rectal ulcer syndrome. *Int J Colorect Dis* 1:85-90, 1986.
- Stoker J, Bartram CI, Halligan S: Imaging of the posterior pelvic floor. *Eur Radiol* 12:779-788, 2002.
- Hale D: Clinical and surgical pelvic organ prolapse. In Bartram CI, DeLancey JOL, editors: *Medical Radiology Diagnostic and Radiation Oncology: Pelvic Floor Disorders*, ed 2, Heidelberg, Germany, 2008, Springer-Verlag, pp 165-186.
- Maglinte DT, Bartram CI, Hale DA, et al: Functional imaging of the pelvic floor. *Radiology* 258:23-39, 2011.
- Maglinte DD, Bartram C: Dynamic imaging of posterior compartment pelvic floor dysfunction

- by evacuation proctography: Techniques, indications, results and limitations. *Eur J Radiol* 61:454–461, 2007.
21. Lienemann A, Anthuber C, Baron A, et al: Dynamic MR colpocystorectography assessing pelvic-floor descent. *Eur Radiol* 7:1309–1317, 1997.
22. Kelvin FM, Maglinte DD, Hale DS, Benson JT: Female pelvic organ prolapse: A comparison of triphasic dynamic MR imaging and triphasic fluoroscopic cystocolpoproctography. *AJR* 174: 81–88, 2000.
23. Williams AB, Bartram CI, Modhwadia D, et al: Endocoil magnetic resonance imaging quantification of external anal sphincter atrophy. *Br J Surg* 88:853–859, 2001.
24. Silva Ana Caterina A, Maglinte Dean DT: Pelvic floor disorders: What's the best test? *Abdom Imaging* 38:1391–1408, 2013.
25. Roos JE, Weishaupt D, Wildermuth S, et al: Experience of 4 years with open MR defecography: Pictorial review of anorectal anatomy and disease. *Radiographics* 22:817–832, 2002.
26. Law YM, Fielding JR: MRI of pelvic floor dysfunction: Review. *AJR* 191(Suppl):S45–S53, 2008.
27. Maglinte DD, Hale DS, Sandrasegaran K: Comparison between dynamic cystocolpoproctography and dynamic pelvic floor MRI: Pros and cons: Which is the "functional" examination for anorectal and pelvic floor dysfunction? *Abdom Imaging* 38:952–973, 2013.
28. Healy JC, Halligan S, Reznick RH, et al: Patterns of prolapse in women with symptoms of pelvic floor weakness: Assessment with MR imaging. *Radiology* 203:77–81, 1997.
29. Halligan S, Spence-Jones C, Kamm MA, Bartram CI: Dynamic cystoproctography and physiological testing in women with urinary stress incontinence and urogenital prolapse. *Clin Radiol* 51:785–790, 1996.
30. Mahieu PH, Pringot J, Bodart P: Defecography. I. Description of a new procedure and results in normal patients. *Gastrointest Radiol* 9:247–251, 1984.
31. Walden L: Roentgen examination of the deep rectogenital pouch. *Acta Radiol* 39:105–116, 1953.
32. Mahieu PH, Pringot J, Bodart P: Defecography. II. Contribution to the diagnosis of defecation disorders. *Gastrointest Radiol* 9: 253–261, 1984.
33. Ekberg O, Nylander G, Fork F-T: Defecography. *Radiology* 155:45–48, 1985.
34. Shorvon PJ, Stevenson GW: Defaecography: Setting up a service. *Br J Hosp Med* 41:460–466, 1989.
35. Bartram CI, Turnbull GK, Lennard-Jones JE: Evacuation proctography: an investigation of rectal expulsion in 20 subjects without defecatory disturbance. *Gastrointest Radiol* 13:72–80, 1988.
36. Goei R, van Engelshoven J, Schouten H, et al: Anorectal function: Defecographic measurement in asymptomatic subjects. *Radiology* 173:137–141, 1989.
37. Halligan S, Bartram CI: The radiological investigation of constipation. *Clin Radiol* 50:429–435, 1995.
38. Hock D, Lombard R, Jehaes C, et al: Colpocystodefecography. *Dis Colon Rectum* 36:1015–1021, 1993.
39. Sentovich SM, Rivela LJ, Thorson AG, et al: Simultaneous dynamic proctography and peritoneography for pelvic floor disorders. *Dis Colon Rectum* 38:912–915, 1995.
40. Bremmer S, Ahlback SO, Uden R, Mellgren A: Simultaneous defecography and peritoneography in defecation disorders. *Dis Colon Rectum* 38:969–973, 1995.
41. Bartram CI, Mahieu PHG: Evacuation proctography and anal endosonography. In Henry MM, Swash M, editors: *Coloproctology and the Pelvic Floor*, London, 1991, Butterworth, pp 146–172.
42. Archer BD, Somers S, Stevenson GW: Contrast medium gel for marking vaginal position during defecography. *Radiology* 182:278–279, 1992.
43. Bernier P, Stevenson GW, Shorvon P: Defecography commode. *Radiology* 166:891–892, 1988.
44. Hare C, Halligan S, Bartram CI, et al: Dose reduction in evacuation proctography. *Eur Radiol* 11:432–434, 2001.
45. Shorvon PJ, McHugh S, Diamant NE, et al: Defecography in normal volunteers: Results and implications. *Gut* 30:1737–1749, 1989.
46. Bharucha AE, Fletcher JG, Harper CM, et al: Relationship between symptoms and disordered continence mechanisms in women with idiopathic faecal incontinence. *Gut* 54:546–555, 2005.
47. Penninckx F, Debruyne C, Lestar B, Kerremans R: Observer variation in the radiological measurement of the anorectal angle. *Int J Colorectal Dis* 5:94–97, 1990.
48. Goei R: Anorectal function in patients with defecation disorders and asymptomatic subjects: Evaluation with defecography. *Radiology* 174:121–123, 1990.
49. Kelvin FM, Hale DS, Maglinte DD, et al: Female pelvic organ prolapse: Diagnostic contribution of dynamic cystoproctography and comparison with physical examination. *AJR* 173:31–37, 1999.
50. Driebeek-van Dam JH, Schouten WR, Gosselink MJ, et al: Anorectal symptoms in rectoenterocele [abstract]. *Int Urogynecol J Pelvic Floor Dysfunct* 8(Suppl):55, 1997.
51. Walden L: Defecation blocks in cases of deep recto-genital pouch. *Acta Chir Scand* 165(Suppl):1–121, 1952.
52. Halligan S, Bartram CI, Hall C, Wingate J: Enterocoele revealed by simultaneous evacuation proctography and peritoneography: Does "defecation block" exist? *AJR* 167:461–466, 1996.
53. Jorge JM, Yang YK, Wexner SD: Incidence and clinical significance of sigmoidoceles as determined by a new classification system. *Dis Colon Rectum* 37:1112–1117, 1994.
54. Fenner DE: Diagnosis and assessment of sigmoidoceles. *Am J Obstet Gynecol* 175:1438–1441, 1996.
55. Bremmer S, Mellgren A, Holmström B, et al: Peritoneocele: Visualization with defecography and peritoneography performed simultaneously. *Radiology* 202:373–377, 1997.
56. Kelvin FM, Maglinte DD, Hornback JA, Benson JT: Pelvic prolapse: assessment with evacuation proctography (defecography). *Radiology* 184: 547–551, 1992.
57. Kenton K, Shott S, Brubaker L: The anatomic and functional variability of rectoceles in women. *Int Urogynecol J Pelvic Floor Dysfunct* 10:96–99, 1999.
58. Siproudhis L, Robert A, Lucas J, et al: Defecatory disorders, anorectal and pelvic floor dysfunction: A polygamy? Radiologic and manometric studies in 41 patients. *Int J Colorectal Dis* 7:102–107, 1992.
59. Hoffman MJ, Kodner IJ, Fry RD: Internal intussusception of the rectum. Diagnosis and surgical management. *Dis Colon Rectum* 27:435–441, 1984.
60. Broden B, Snellman B: Procidentia of the rectum studied with cineradiography: A contribution to the discussion of causative mechanism. *Dis Colon Rectum* 11:330–347, 1968.
61. Bartolo DC, Roe AM, Virjee J, Mortensen NJ: Evacuation proctography in obstructed defaecation and rectal intussusception. *Br J Surg* 72(Suppl):S111–S116, 1985.
62. Halligan S, Sultan A, Rottenberg G, Bartram CI: Endosonography of the anal sphincters in solitary rectal ulcer syndrome. *Int J Colorectal Dis* 10:79–82, 1995.
63. Gooi R, Baeten C: Rectal intussusception and rectal prolapse: Detection and postoperative evaluation with defecography. *Radiology* 174: 124–126, 1990.
64. Halligan S, Bartram CI, Park HJ, Kamm MA: Proctographic features of anismus. *Radiology* 197:679–682, 1995.
65. Emmanuel AV, Kamm MA: Response to a behavioural treatment, biofeedback, in constipated patients is associated with improved gut transit and autonomic innervation. *Gut* 49:214–219, 2001.
66. Bartolo DC, Roe AM, Virjee J, et al: An analysis of rectal morphology in obstructed defaecation. *Int J Colorectal Dis* 3:17–22, 1988.
67. Kuijpers HC, Bleijenberg G: The spastic pelvic floor syndrome: A cause of constipation. *Dis Colon Rectum* 28:669–672, 1985.
68. Henry MM, Parks AG, Swash M: The pelvic floor musculature in the descending perineum syndrome. *Br J Surg* 69:470–472, 1982.
69. Oettle GJ, Roe AM, Bartolo DC, Mortensen NJ: What is the best way of measuring perineal descent? A comparison of radiographic and clinical methods. *Br J Surg* 72:999–1001, 1985.
70. Pinho M, Yoshioka K, Ortiz J, et al: The effect of age on pelvic floor dynamics. *Int J Colorectal Dis* 5:207–208, 1990.
71. Jorge JM, Ger GC, Gonzalez L, Wexner SD: Patient position during cinedefecography: Influence on perineal descent and other measurements. *Dis Colon Rectum* 37:927–931, 1994.
72. Allen-Mersh TG, Henry MM, Nicholls RJ: Natural history of anterior mucosal prolapse. *Br J Surg* 74:679–682, 1987.
73. Bartram CI, Turnbull GK, Lennard-Jones JE: Evacuation proctography: An investigation of rectal expulsion in 20 subjects without defecatory disturbance. *Gastrointest Radiol* 13:72–80, 1988.
74. Tsiaoussis J, Chrysos E, Glynos M, et al: Pathophysiology and treatment of anterior rectal mucosal prolapse syndrome. *Br J Surg* 85:1699–1702, 1998.
75. Timmons MC, Addison WA: Vaginal vault prolapse. In Brubaker LT, Saclarides TJ, editors: *The female pelvic floor: Disorders of function and support*, Philadelphia, 1996, FA Davis, pp 262–268.
76. Vernava AM, Longo WE, Daniel GL: Pudendal neuropathy and the importance of EMG evaluation of fecal incontinence. *Dis Colon Rectum* 36:23–27, 1993.
77. Lesaffer LPA: Perineal support device. In Smith LE, editor: *Practical Guide to Anorectal Testing*, New York, 1990, Igaku-Shoin, pp 205–208.
78. Penninckx FM: Faecal incontinence: Symposium. *Int J Colorectal Dis* 2:173–186, 1987.
79. Henry MM: Pathogenesis and management of fecal incontinence in the adult. *Gastroenterol Clin North Am* 16:35–45, 1987.
80. Herbst F, Kamm MA, Morris GP, et al: Gastrointestinal transit and prolonged ambulatory

- colonic motility in health and fecal incontinence. *Gut* 41:381–389, 1997.
81. Frudinger A, Bartram CI, Halligan S, Kamm M: Examination techniques for endosonography of the anal canal. *Abdom Imaging* 23:301–303, 1998.
 82. Rociu E, Stoker J, Eijkemans MJ, et al: Fecal incontinence: Endoanal US versus endoanal MR imaging. *Radiology* 212:453–458, 1999.
 83. Malouf AJ, Williams AB, Halligan S, et al: Prospective assessment of accuracy of endoanal MR imaging and endosonography in patients with fecal incontinence. *AJR* 175:741–745, 2000.
 84. Fletcher JG, Busse RF, Riederer SJ, et al: Magnetic resonance imaging of anatomic and dynamic defects of the pelvic floor in defecatory disorders. *Am J Gastroenterol* 98:399–411, 2003.
 85. Goei R, Kemerink G: Radiation dose in defecography. *Radiology* 176:137–139, 1990.
 86. Burk RJ, Jr: Radiation risk in perspective: Position statement of the Health Physics Society. http://www.hps.org/documents/risk_ps0101.pdf. Accessed November 20, 2009.
 87. McHugh SM, Diamant NE: Anal canal pressure profile: A reappraisal as determined by rapid pull-through technique. *Gut* 28:1234–1242, 1987.
 88. Skomorowska E, Hegedus V: Sex differences in anorectal angle and perineal descent. *Gastrointest Radiol* 12:353–355, 1987.
 89. Parks AG, Porter NH, Hardcastle J: The syndrome of the descending perineum. *Proc R Soc Med* 59:477–482, 1966.

Computed Tomography Colonography

DAVID H. KIM | PERRY J. PICKHARDT

CHAPTER OUTLINE

Technical Components

Bowel Preparation
Colonic Distention
Image Acquisition
Alternative Protocols

Interpretation

Detection
Characterization
Polyp Differential
Reporting

CTC Trial Results

Indications and Use

Screening for Colorectal Cancer
Diagnostic Indications
Staging and Surveillance

Pertinent Issues

Complications
Radiation
Extracolonic Findings

Summary

Computed tomography colonography (CTC) is a low-dose, cross-sectional imaging examination optimized for the detection of colorectal polyps and masses. As a result of advanced computer 3D postprocessing, a popular misperception is one of an imaging analogue to optical colonoscopy in which a 3D model is used to view the mucosal surface of the interior of the colon. However, CTC is fundamentally a different examination, using 2D images and 3D datasets in the interpretation of mucosa, deeper structures, and even processes beyond the colon. Since its introduction in 1994, CTC has matured into a clinically effective modality. Central to this transition are technologic advances in computer hardware and software that have allowed the easy acquisition and manipulation of large volumetric CT data sets. Performance in low polyp prevalent screening populations has now been validated in a number of prospective clinical trials,¹⁻⁵ with a general consensus that CTC performs substantially better than double-contrast barium enema⁶ and is equivalent to optical colonoscopy for clinically relevant polyps and masses.

This chapter will provide a comprehensive overview of this modality. The technical components that comprise the examination, including bowel preparation, colonic distention, and image acquisition, as well as alternative CTC approaches such as noncathartic or laxative-free (previously mislabeled as

“prepless”) protocols, will be discussed. Interpretation will be covered in detail, including common strategies currently in use. The mechanics of interpretation will be highlighted, with coverage of the more common and important pitfalls that can affect the accuracy of this process. The indications and uses for CTC will be examined, outlining the optimal screening target and the polyp-carcinoma sequence that forms the underlying rationale of the selective polypectomy strategies for CTC-based screening. In addition to screening, diagnostic applications for CTC and the evaluation of colorectal cancer (CRC) staging will be covered. Finally, pertinent issues central to CTC will be examined, including radiation dose, complications, and extracolonic (incidental) findings.

Technical Components

CT colonography is a multicomponent examination that is undertaken over several days. The major technical components include bowel preparation, colonic distention, and image acquisition. A programmatic or team approach is favored because it allows each portion of the procedure to be optimized for reproducible, high-quality examinations. Thus, a nurse program coordinator can answer patient questions on bowel preparation in the days prior to the scan to minimize preparation failure, and the technologist can optimize the bowel distention while the patient is on the scanner table. The radiologist can interpret the examination and forward the results for further coordination of care to be undertaken by the program nurse. Such division of labor allows the radiologist to concentrate totally on interpretation. Without a team approach, the technical components are often addressed in a less complete fashion. A breakdown in any study component ultimately limits the potential impact of the overall examination.

The traditional approach to CT colonography involves a fully cleansed and tagged colon. Alternate methods have been investigated, including laxative-free techniques, but large multicenter validation studies remain to be done. Once the colon has been prepared, it is distended with gas (carbon dioxide or room air) and finally imaged with a low-dose, thin collimated technique in a minimum of two patient positions. The following sections outline the principles and major strategies in use for the technical components of the examination. In addition, common problems that may arise will be addressed. The protocol at the University of Wisconsin (UW) is highlighted as one specific solution.

BOWEL PREPARATION

The objective of this first portion of the examination is to prepare the colorectum for optimal imaging. Traditionally, this involves oral administration of a cathartic agent to purge the

colon of fecal matter that could mimic or obscure a colonic polyp. Tagging agents are also administered orally to admix with any remaining stool and colonic fluid. Contrast agents increase the attenuation of stool and fluid to allow easy differentiation of soft tissue polyps from stool and detection of polyps submerged in fluid (Fig. 53-1). Bowel preparation is typically undertaken 1 to 2 days prior to the scheduled examination. The specific agents and protocol used in bowel preparation often vary among different institutions.

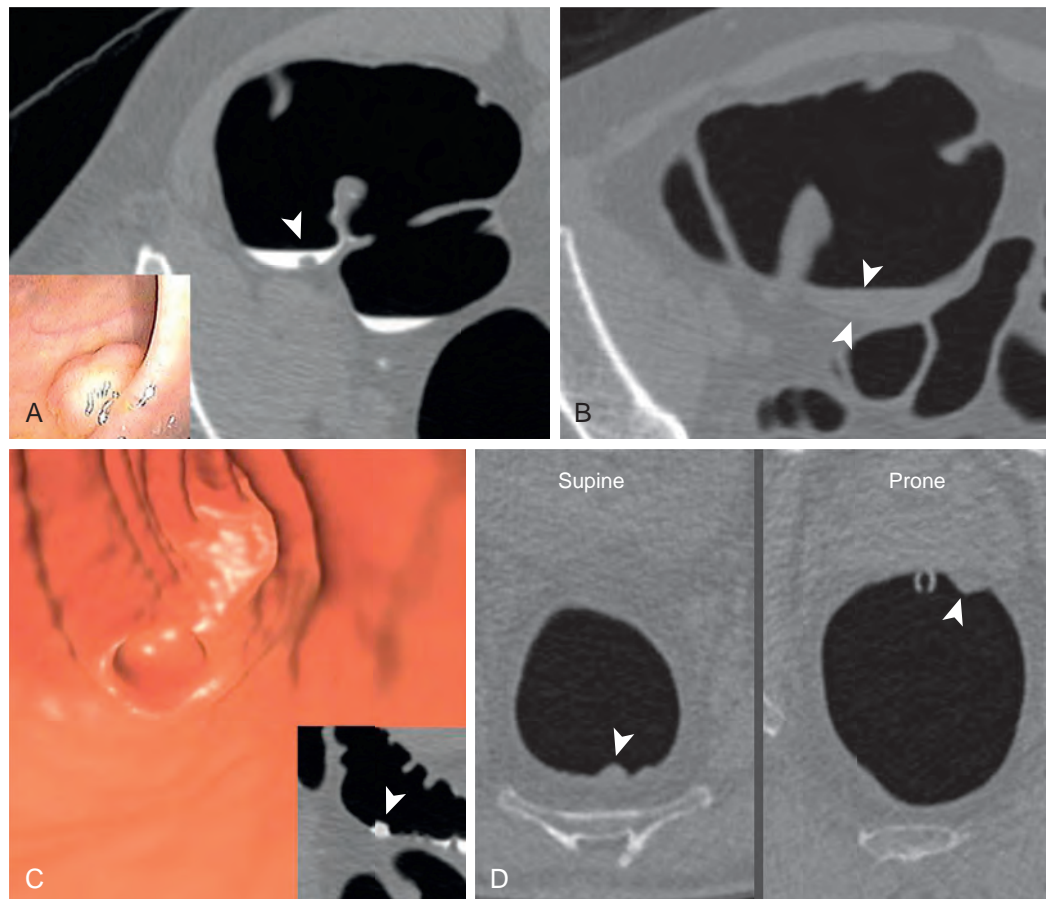
Cathartic agents have traditionally been classified as dry or wet preparations. Both types are in use with CTC. Dry preparations result in only minimal residual colonic fluid and include low-volume osmotic cathartics, such as magnesium citrate; wet preparations often result in larger amounts of residual fluid, occupying up to 50% of the lumen in various segments. Wet preparations include polyethylene glycol (PEG) and formulations based on PEG. Early on, there was an emphasis placed on using dry cathartic preparations with CTC to minimize obscuring polyps by residual fluid.⁷ At this time, tagging agents were not typically used, and any unopacified fluid would obscure a submerged polyp. Although the polyp should theoretically be seen when the patient was imaged in a complementary position (i.e., supine vs. prone), it could be missed when detected only on one view, and the examination became considerably more tedious and difficult to interpret because of the difficulty in determining which portion of the colon mucosa had been interrogated and what remained to be seen. With the addition of colonic tagging, such considerations regarding the amount of residual fluid have become less important because the polyp can

be seen as a soft tissue structure in the high-density colonic fluid (see Fig. 53-1). On the other hand, some reports have suggested that dry formulations remain advantageous over wet preparations because they may promote the phenomenon of polyp contrast coating.⁸ There is increasing recognition that polyp coating is an important aid in polyp detection, particularly those of a flat morphology (see later, "Interpretation").

The major cathartic agents currently in use include magnesium citrate and PEG. Magnesium citrate is an osmotic cathartic agent. It is one of the dry cathartics in which relatively small amounts are ingested and work by means of an osmotic effect. Because of its hypertonicity, fluid is pulled across the colonic mucosa into the colonic lumen. The fluid then serves as an effluent that lavages out the colon. Because of this mechanism of action, it mandates that the patient be well hydrated before catharsis; otherwise, the cleansing action is less than optimal. Furthermore, it is important to maintain hydration throughout the preparation period to maintain effective cathartic action and decrease the possibility of dehydration. Holte and associates have shown that osmotic cathartics can cause significant volume loss over the preparation period, during which a median weight loss of 1 kg was seen, despite fluid intake of 4 L in a series of healthy volunteers.⁹ Typically, a multidose magnesium citrate regimen is undertaken with CTC (e.g., two doses separated by a predetermined time interval) to allow optimal cleansing.¹⁰ Single-dose regimens have shown less effectiveness and more poor preparation outcomes.¹¹ Magnesium citrate has long been used for barium enema examinations,^{12,13} and there is considerable experience with its use in this regard. It is well

Figure 53-1 Advantages of fluid and stool tagging.

A. Supine 2D CTC image with fluid tagging allows easy visualization of a submerged polyp (arrowhead), which was a tubular adenoma at colonoscopy (inset). **B.** Without fluid tagging in another patient, the grey appearance of the fluid (arrowheads) in the cecum would obscure submerged polyps. **C.** Supine 3D CTC image shows a possible sessile polyp, which is easily confirmed as stool (2D inset) because of tagging, which increases the internal attenuation values to create a white appearance (arrowhead). **D.** Without stool tagging, stool (arrowhead) mimics a polyp with a grey appearance, requiring demonstration of movement. Note the dependent location between the supine and prone series.



tolerated, with a favorable safety profile.¹²⁻¹⁴ It can be used in almost all patients aside from those with severe renal dysfunction and those with tenuous fluid balance control.

PEG is a wet-based preparation. In addition to standard PEG, several related formulations are in use with CTC, including Miralax and HalfLytely. PEG is a balanced solution with various electrolytes and a high molecular weight, nonabsorbable polymer that prevents secretion or absorption. Large volumes (4 L) are ingested to create the effluent. PEG is considered the safest of cathartics and can be used even in debilitated, fluid-tenuous patients because negligible fluid and electrolyte shifts occur across the colonic mucosa. When completed, this preparation leads to excellent catharsis in most patients. The major drawback has been compliance with the preparation because of decreased palatability. One study showed that up to 38% of patients failed to complete the entire preparation.¹⁵ As noted, because of its wet preparation nature, there is often a fair amount of residual colonic fluid.

Sodium phosphate is an osmotic cathartic agent that was used widely in the past but is no longer favored. It is mentioned for historical reasons and to highlight its potential dangers. Until 2008, it was one of the major cathartic agents in use for CTC and optical colonoscopy because of its excellent cleansing abilities and high compliance rate. Patients were more likely to complete the regimen, which required ingestion of a small-volume solution or ingestion of multiple pills. However, sodium phosphate had a narrow therapeutic range, with a higher incidence of complications. In 2004, a rare but generally irreversible form of renal failure was identified with sodium phosphate use mediated by a precipitation of calcium phosphate in the renal tubules (so-called phosphate nephropathy).¹⁶ After recognition of this potential complication, a black box warning was issued by the U.S. Food and Drug Administration in 2008, and this agent now requires a prescription. For CTC, sodium phosphate and formulations that contain sodium phosphate are typically no longer used.

Tagging agents include barium formulations and iodine-based solutions. For barium, there are two common densities used, a dilute 2% w/v preparation (CT barium) or a much denser 40% w/v preparation. The primary action of barium is to tag particulate stool internally. It admixes with the stool to increase the attenuation substantially from 40 to 60 HU to well over 200 HU, allowing for easy identification from soft tissue (see Fig. 53-1). Barium can also tag fluid but tends to do so inhomogeneously, with a gradient effect related to gravity, in which the more dependent portions of the fluid are more densely tagged. Iodine-based agents are ionic (e.g., diatrizoate) or nonionic (e.g., iohexol, iopamidol). The primary action is to tag residual colonic fluid (see Fig. 53-1). It can also tag stool but often does less well than barium-based agents in this regard. There is considerable variation in tagging approaches. Some CTC protocols use a single tagging agent (barium or iodine alone), and others use a two-agent approach (both barium and iodine) to take advantage of the benefits of each.

The UW protocol is one of several that have demonstrated excellent results for bowel preparation on a consistent basis, with nondiagnostic rates related to bowel preparation with CTC much less than 1%.¹⁷ The specific protocol is outlined in Table 53-1. It is predicated on the principles of complete colonic catharsis and tagging of residual stool and fluid. The cathartic choice has been magnesium citrate because of its palatability in comparison to PEG. A double-dose regimen is required to

TABLE 53-1 University of Wisconsin Bowel Preparation

Time*	Agent	Amount	Comment
8 AM	Clear liquid diet	Maintain hydrated state. [†]	Beginning with breakfast
11 AM	Bisacodyl (Dulcolax)	2 tablets orally [‡]	Stool softener
3-5 PM	Magnesium citrate	300 mL (one bottle)	Cathartic [§]
After 3 hours, administer	Magnesium citrate	300 mL (one bottle)	Cathartic
	2% w/v Barium sulfate	250 mL (one bottle)	Tagging
After 3 hours, administer	Diatrizoate	60 mL	Tagging
9-11 PM	Preparation is complete for the examination the following morning.		

*Prior to 8 AM, the patient is NPO after midnight.

[†]It is important to maintain hydration to optimize the cathartic action. Recommend hydration prior to cathartics and at least 4-6 cups of liquid with each of the osmotic cathartic

[‡]Does not require the patient to be near a bathroom. Catharsis begins with administration of magnesium citrate.

[§]If polyethylene glycol is substituted, the first dose should be given around noon (16 8-oz cups, one every 10 minutes, for a total of 4 L).

cleanse the colon adequately.¹⁰ As opposed to some protocols, the cathartic is given prior to tagging (as opposed to the reverse situation) to purge the bulk of the stool and increase the effectiveness and efficiency of tagging; a wider window for optimal tagging exists for a given amount of tagging agent. With the reverse situation, larger amounts of tagging agents are needed to tag the bulk colonic contents.

A dual tagging approach is preferred (as opposed to a single agent) to take advantage of the benefits of each agent—barium for stool and iodine for fluid. The dilute formulation of barium (2% w/v) is used in the UW protocol. The 2% version tags the residual stool particles well and is not too dense with CTC. As opposed to the denser 40% preparation, this formulation has not obscured visualization of colonic mucosa or clogged colonoscopic ports; this is important because most patients with CTC-detected polyps undergo same-day colonoscopy to take advantage of the prepped status. Regarding the second tagging agent, the ionic nature of diatrizoate is preferred over a non-ionic solution, despite its less palatable taste. In addition to tagging residual fluid, the increased osmolarity of the solution works like a mild second cathartic, resulting in a final cleansing of the colon. This action is particularly important when a dry cathartic agent is used in the protocol. From the barium enema era, it was noted that use of magnesium citrate promotes excessive barium coating.¹⁸ In the case of CTC, without the final cleansing action of diatrizoate, this can lead a right-sided studding or even a thick film of tagged stool (Fig. 53-2). This pitfall often precludes the use of 3D CTC for polyp detection in this situation (see later), which can lead to decreased sensitivity for lesion detection. It is thought that the substitution of nonionic iodine solutions could lead to a similar situation, in which the final hypertonic cleansing does not occur.

Finally, and perhaps most importantly, the combination of the three agents in this protocol (magnesium citrate, 2% barium, and diatrizoate) appears to promote a polyp-coating phenomenon (Fig. 53-3). The tag appears to adhere to the mucosa

overlying the polyp (CTC equivalent of a polyp etched in white at barium enema) while it is washed away from the normal colonic mucosa.⁸ It is postulated that there is an interaction between a negatively charged mucin film elaborated by polyps and the positively charged barium tag. The diatrizoate washes the tag away from normal mucosa but not from the polyp surface. This phenomenon has been very helpful in detecting polyps, particularly those of a flat nature, which are only

minimally raised from the colonic surface. Whether this phenomenon is reliably seen with wet-based or iodine-only preparations is unknown.

COLONIC DISTENTION

The objective of this portion of the examination is to distend the colorectum optimally to allow the easy detection of

Figure 53-2 Importance of diatrizoate. **A.** Supine 2D CTC image shows right-sided studding of tagged stool in a patient who did not take all the diatrizoate. Note the impact on 3D (*inset*), where it would be difficult to assess for polyps. **B.** Without diatrizoate (in a second patient), this can even lead to a diffusely tagged coating of the mucosa.

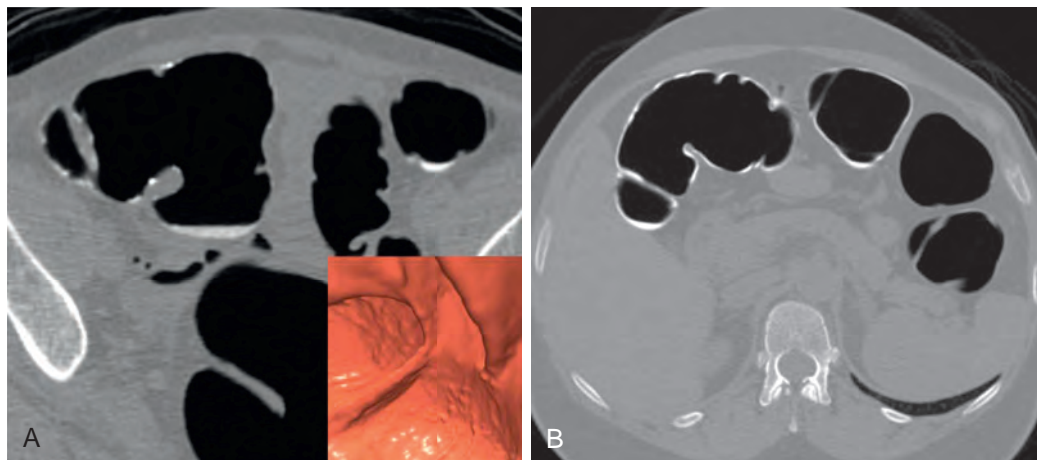
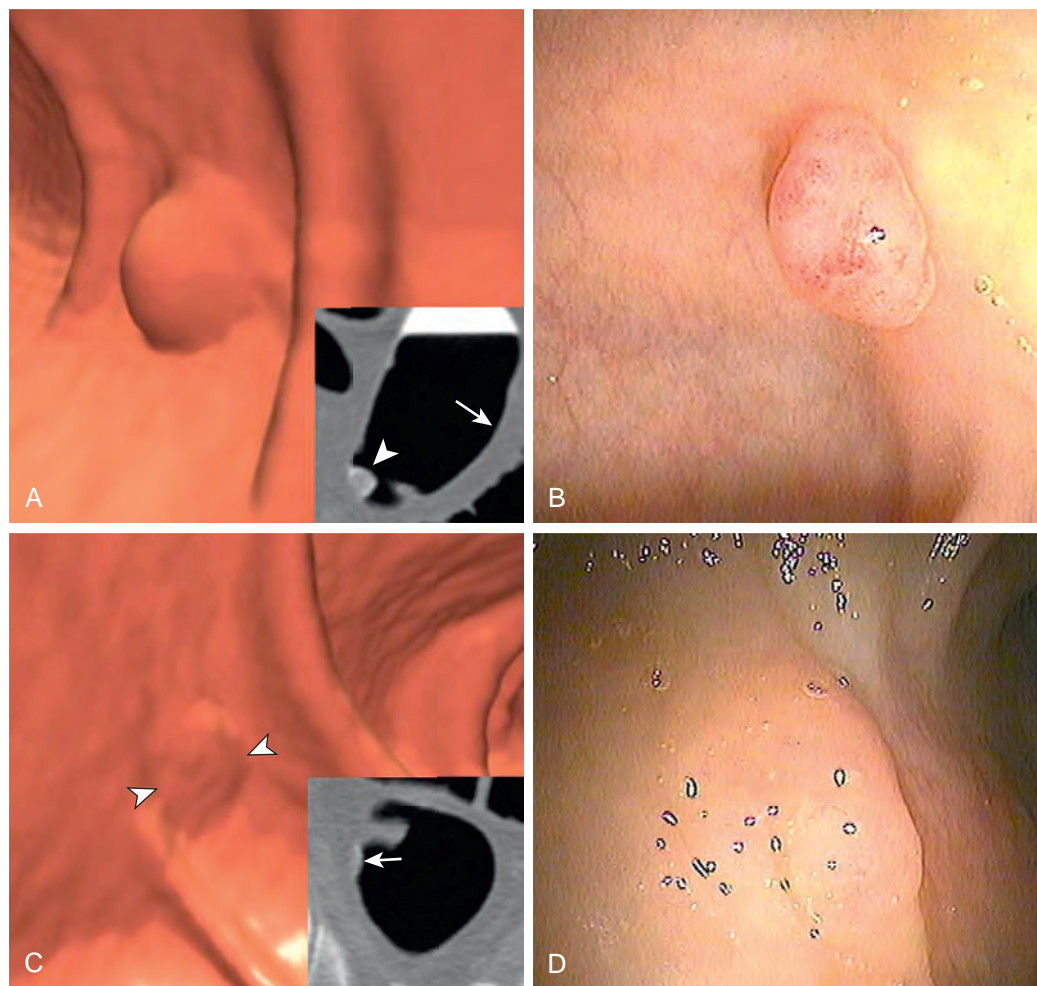


Figure 53-3 Polyp-coating phenomenon. **A.** 3D CTC image shows a sessile polyp. Note the thin barium coat (*arrowhead*) overlying the polyp (*inset*) whereas it has washed away from the colonic wall (*arrow*). **B.** A 10-mm tubular adenoma confirmed at colonoscopy. **C.** 3D CTC image shows a flat polyp (*arrowheads*), which is etched in white (*arrow*) on the 2D inset, increasing conspicuity. **D.** Flat hyperplastic polyp seen at colonoscopy.



intraluminal projections and true wall thickening, but also to balance the degree of distention with acceptable patient discomfort. With optimal distention, the colonic walls are well separated; the walls are thin and almost imperceptible. Thus, polyps are well delineated as they project into the colonic lumen. The high contrast between the gas-filled lumen and soft tissue nature of the polyp allows for even many small diminutive polyps to be seen. It is important to realize that the colon does not have to be completely distended on a given series to be diagnostic in nature. It can be partially underdistended on a single series. However, the corresponding series often shows excellent distention in the same area because of the complementary shifting of gas to nondependent regions, allowing for an interpretable examination (Fig. 53-4). When needed, a decubitus series can be helpful.

There are two gaseous agents available for colonic distention. Of these, carbon dioxide is favored over room air because it is actively absorbed across the colonic mucosa and eventually expelled by the respiratory system. Reduced instillation pressures essentially preclude perforation and promote patient comfort.¹⁹⁻²¹ Because the colon rapidly decompresses, the patient feels relief very quickly after the instillation ceases. In

contrast, room air is composed chiefly of nitrogen, an inert gas in which there is no active reabsorption. Because of this, manual instillation pressures can be very high, with the possibility for perforation. In addition, patients can feel uncomfortable and bloated for several hours after colonic distention with room air until it is passed through the gastrointestinal (GI) tract.

The major strategies for colonic distention include manual room air insufflation and automated carbon dioxide insufflation. Room air insufflation was initially the primary method for distention with CTC. There was considerable prior experience with barium enema, and the equipment was inexpensive and readily accessible. This was undertaken with manual bulb insufflation after the insertion of an enema tip. The air was introduced by staff or by patient self-insufflation. However, there are several major problems with this CTC strategy that led to less than optimal examinations. Most importantly, unlike with barium enema, there was no real time assessment of the degree of colonic distention. With barium enema, distention adequacy could be determined at fluoroscopy. With CTC, no real-time visualization is possible; adequacy was surmised by a set number of puffs relative to patient body habitus or by patient feedback to distention discomfort. Therefore, colonic distention was

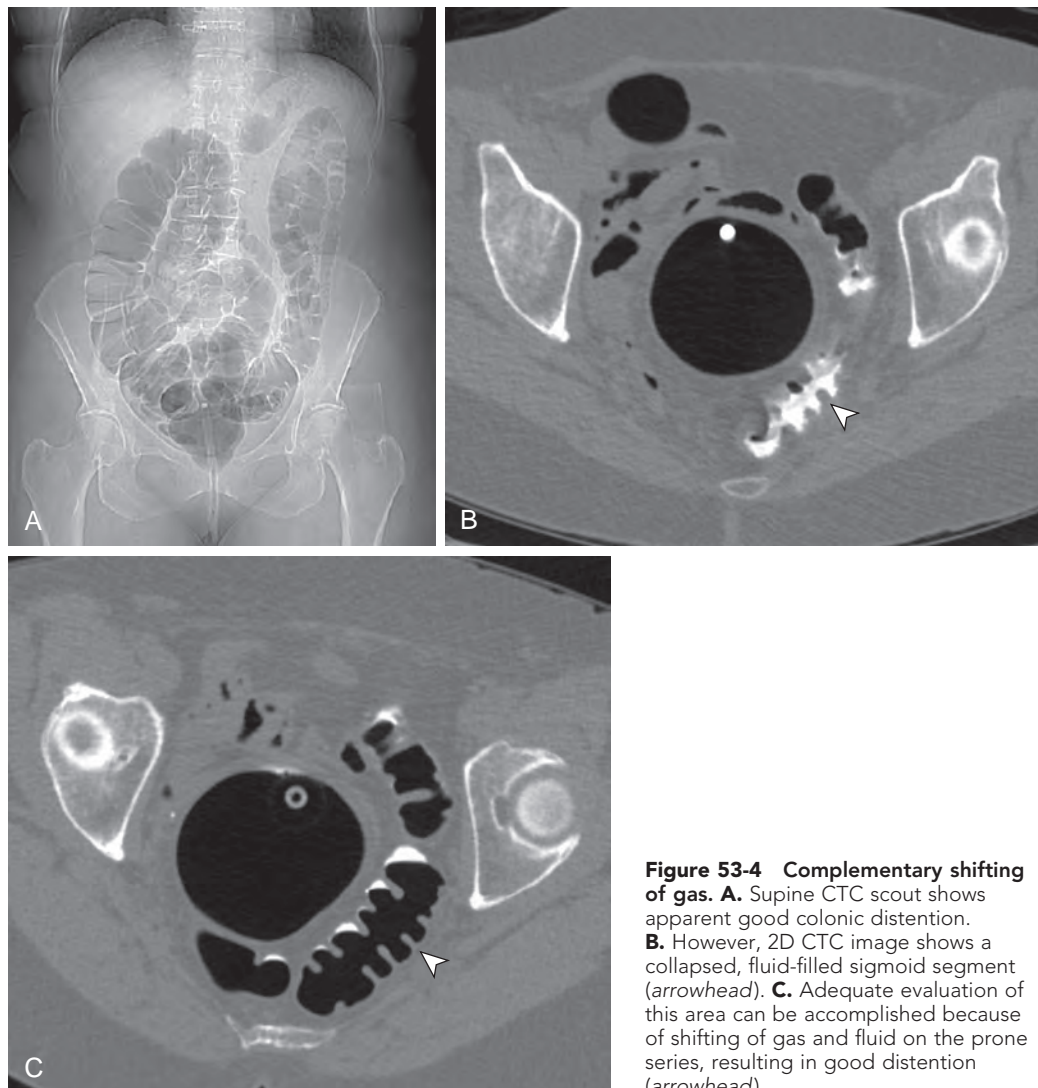


Figure 53-4 Complementary shifting of gas. **A.** Supine CTC scout shows apparent good colonic distention. **B.** However, 2D CTC image shows a collapsed, fluid-filled sigmoid segment (arrowhead). **C.** Adequate evaluation of this area can be accomplished because of shifting of gas and fluid on the prone series, resulting in good distention (arrowhead).

variable, dependent on the administering staff and the patient's individual perception of or tolerance to distention. Also, this was a very labor-intensive method that required individual coaching for each case. In addition to the difficulties of distending the colon, there was the possibility of perforation because fairly high wall pressures could be generated with this "blind" administration. Most institutions have since moved to automated carbon dioxide (CO₂) insufflation because of difficulties with room air insufflation and several recognized advantages with the use of CO₂. However, because of the inert nature of room air, in which there is no active resorption, room air can be used to distend segments that are resistant to CO₂.

CO₂-based distention involves the use of an automated insufflator. Because CO₂ is actively resorbed, it requires continuous low-pressure instillation, which can only be undertaken with automated delivery. After insertion of a small-caliber, flexible-tip catheter, CO₂ is instilled at low pressures, regulated by the machine. During the filling phase, intracolonic pressures (as measured by the insufflator) generally range from 11 to 19 mm Hg. The pressures may transiently increase to 35 to 40 mm Hg with positional change or if colonic spasm occurs, but will quickly decrease as the spasm resolves. At some point, the pressures settle in a range of 20 to 28 mm Hg (with volume measurements typically at 3.5 to 4.0 L) and an equilibrium state is achieved—the CO₂ inflow balances the ongoing losses (resorption by colonic mucosa, as well as potential loss around the catheter and/or reflux into small bowel). At this point, the colon is typically optimally distended. The benefits of this equilibrium state are that it can be maintained as long as the CO₂ remains infusing, and it is easily identified by viewing pressure and volume measurements on the machine console. Thus, distention is much more reproducible and less labor-intensive with this approach. In addition, because of the low-pressure delivery, in which maximum pressures rarely exceed 50 mm Hg for a few moments, complications are almost nonexistent (see later).

The use of spasmolytics is controversial. Glucagon, a polypeptide pancreatic hormone with smooth muscle relaxant effects, has shown mixed results, without definite improvement in distention or improved patient comfort.^{22,23} In addition, it has been reported to increase the incidence of small bowel reflux. It is typically not used with CTC in the vast majority of U.S. institutions. However, in Europe and Canada, Buscopan (hyoscine butylbromide) is widely used. This anticholinergic agent acts on the postganglionic parasympathetic smooth muscle receptors to cause colonic relaxation. Several studies have shown increased distention and patient comfort, however, without a significant increase in polyp detection.^{23,24} Contraindications include a history of glaucoma. It is not available in the United States.

The UW distention protocol is outlined in Table 53-2. Patient discomfort is minimized by setting the instillation pressure at 17 to 18 mm Hg for the average-sized individual, which is adjusted upward as needed. The key for optimal distention is to attain and maintain an equilibrium state prior to imaging. As noted, this is determined by assessing pressure and volume measurements recorded by the insufflator (21 to 29 mm Hg and 4 L, respectively). One key point to optimizing distention is related to volume. Although equilibrium pressures can be seen with volume measurements at 2 L, it has been preferable to wait until 3.5 to 4 L has been reached (Fig. 53-5). In our experience, persons are often imaged too quickly before full distention because of high-volume concerns and the possibility of perforation. It is important to understand that the volume recorded by

TABLE 53-2

University of Wisconsin Distention Protocol

Volume (L)	Pressure (mm Hg)	Patient Positioning and Comments
0.0	0.0	Insert rectal catheter with patient in LLD and inflate balloon.
0.0-2.0	10-19	Fill with patient in LLD.
2.1-4.0	10-19*	Roll RLD and continue filling.
4.0+	20-30	At equilibrium, turn supine to scout and scan.
4.0+†	20-30	Roll prone and do quality check of supine series.
4.0+†	20-30	Wait until equilibrium is reestablished; then scout and scan prone series.
4.0+†	20-30	Quality check of prone series and determine need for decubitus series
6.0-8.0‡	20-30	Typical volume and pressure at end of examination

*May rise to 20 to 30 mm Hg suggesting equilibrium but continue to fill until volume reaches 3.5 to 4 L. If pressures rise to 30 to 40 mm Hg, transient spasm is likely.

†Continuous infusion throughout required to maintain equilibrium. Volume should continue to rise.

‡May see volumes exceeding 10 L if patient has loss around catheter or incompetent ileocecal valve.

LLD, left lateral decubitus; RLD, right lateral decubitus.

the machine does not represent the amount in the person's colon because there is continuing ongoing loss (see earlier). Equilibrium is reached when the infusion is matched by the loss; thus, the low-pressure instillation could be extended indefinitely. As such, it is important to wait until the volume measurements reach about 4 L, even if equilibrium pressures (20 to 25 mm Hg) are attained earlier to allow full distention. Typical recorded volume measurements at the conclusion of the examination range from 5 to 6 L although it is not uncommon to have numbers in the range of 10 to 12 L. The CTC technologist is an important person in this part of the examination; real-time quality assurance checks are carried out by this trained individual to determine whether additional imaging is required (e.g., a decubitus series).

Some common distention difficulties include machine- and patient-related factors. Active problem solving, however, can often salvage an otherwise suboptimal examination. One common situation is frozen or unchanging pressure and volume measurements, in which it does not appear that carbon dioxide is infusing. The cause is an obstruction at some level, usually in the tubing. In addition to factors such as lying on the tubing, a common cause is a column of fluid in the tubing, which can block the CO₂ infusion because of the low-pressure nature of instillation. The patient will often report that the bowel preparation was started late. Once the tubing is cleared of fluid, the infusion will restart. Other situations, in which CO₂ infuses but does not optimally distend the colon, may be related to almost empty tanks or to the patient's underlying colon and decreased distensibility from conditions such as diverticular myochosis or frank stricture.

IMAGE ACQUISITION

Once the colon is optimally distended, the patient is scanned. At a minimum, two series are obtained, with the patient in supine and prone positions. Each series is undertaken in end-expiration to minimize the extrinsic compression of the lungs

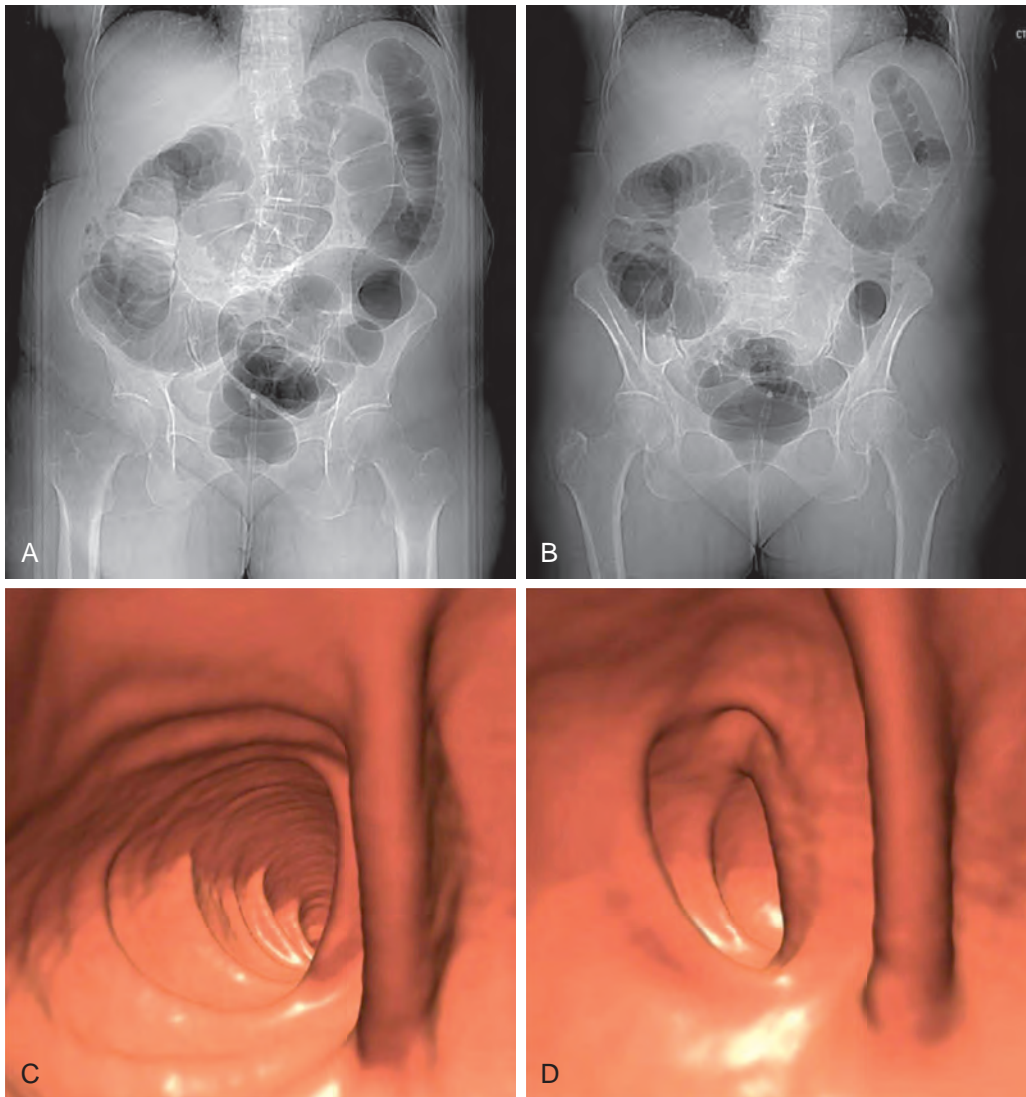


Figure 53-5 Distention at 4 L versus 2 L. **A.** Scout CTC at 4 L shows excellent colonic distention. **B.** Scout CTC at 2 L in the same patient at repeat routine screen 5 years later shows less distention. Although both examinations at 4 L (**C**) and 2 L (**D**) are diagnostic, note how the decreased distention (**D**) leads to prominence of the haustral folds and deeper troughs between them, which may contribute to decreased polyp detection.

on the transverse colon. The datasets should be immediately evaluated to ensure that there is adequate distention and that no colonic segment is collapsed on both views. If this occurs, an additional series (typically with the patient in a right lateral decubitus position) can be undertaken.

CTC represents a low-dose, thinly collimated, and typically noncontrast examination. The optimal parameters represent a balance between maintaining polyp visualization while minimizing dose. Thus, although submillimeter collimation is possible, overlapping 1.0- to 1.25-mm slice thicknesses are adequate, given that the examination positivity size threshold is set at 6 mm for CTC. Overall, the required parameters for the examination are not stringent, and high-quality CTC results can be obtained with basic multidetector CT (MDCT) scanners. As opposed to examinations such as cardiac CT, in which high temporal and spatial resolution are needed (to image small-caliber cardiac vessels on a beating heart), the high-contrast nature of soft tissue polyps projecting into a gas-filled lumen and the static nature of the colon allow the use of standard 16-slice MDCT scanners. The scanning parameters of the UW protocol are given in Table 53-3. Dose exposures are approximately 3 to 5 mSv for the examination.

TABLE 53-3 University of Wisconsin Computed Tomography Colonography Scan Parameters

Parameter*	GE LS VCT 64
Detector configuration	64 × 0.625
Rotation time (sec)	0.5
Pitch	0.984
Speed (mm/rot)	39.36
Slice thickness (mm)	1.25
Interval (mm)	0.75
kV	120
Smart mA/auto mA range	30-120
Noise index	50

*Specific parameters represent a snapshot in time.

ALTERNATIVE PROTOCOLS

In addition to the standard cathartic-tagging regimen, considerable interest has centered on alternative protocols that minimize or eliminate the cathartic portion of the bowel preparation. The cathartic requirement for CRC screening modalities has long been recognized as a major barrier in colorectal cancer

screening compliance.²⁵⁻²⁷ Noncathartic or laxative-free CTC holds the possibility of substantially increasing screening rates by appealing to those who currently refuse screening because of purging requirements. Whether polyp sensitivity can be maintained in this situation is an area of ongoing research.

The typical approach of this modified CTC protocol is to use a low-fiber diet followed by the ingestion of tagging agents. Often, the protocols are multiday regimens, so the popular monikers of “prepless” or “minimal prep” CTC are a misnomer. There is a bowel preparation regimen but the cathartic aspect has been removed. The colon is distended in a fashion similar to that for standard CTC. Often, postprocessing in the form of electronic cleansing or digital subtraction of the tagged feces is used. Single-center feasibility studies have shown excellent results in high-polyp prevalence cohorts.^{28,29} Recently, a multicenter prospective trial in a low-prevalence screening cohort reported per patient sensitivities of 91% for adenomas at the 10-mm threshold, with decreased sensitivities of 59% at the 6-mm threshold.³⁰ This study highlights the current tradeoff with noncathartic protocols. Although perhaps more appealing to patients, there is a real decrease in sensitivity for polyp detection by laxative-free CTC versus the standard cathartic and tagging protocol, particularly for smaller subcentimeter polyps. In addition, these studies are more difficult to read, requiring expertise in distinguishing a postprocessing digital subtraction artifact from subtle polyps at 3D or relying on primary 2D approaches alone.

Interpretation

Once the technical aspects of the CTC examination are complete, the datasets can be networked to a workstation to allow 2D and 3D review. The main objective of interpretation is to identify soft tissue polyps and exclude pseudopolyps, typically related to retained feces or thickened folds. There is general consensus that an unavoidable learning curve exists for CTC.^{31,32} CTC interpretation requires the traditional cross-sectional skills from CT as well as additional CTC-specific skills for accurate interpretation. Two major strategies were initially proposed, defined in terms of detection: (1) a primary 2D approach with 3D problem solving; and (2) a primary 3D approach with 2D confirmation. Most recently, a combined approach has been favored. All detection strategies ultimately use a common characterization pathway, and the process of interpretation (regardless of specific detection approach) can be broken down into two major tasks, as described here.

There are two general tasks of interpretation with CTC. The first is one of detection, in which focal intracolonic structures that potentially represent a polyp are identified (with 2D or 3D review). Once a list of possible polyps is established, the second task is characterizing each of these possible polyps—the soft tissue polyps are confirmed and the pseudopolyps are excluded. It is this step in interpretation in which the true skill in interpretation resides (i.e., achieving high specificity is more challenging than high sensitivity). If this cannot be done well, too many patients are sent on to colonoscopy for false-positive CTC examination results from pseudopolyps. Young and colleagues have shown that nonradiologists can detect potential polyps with similar sensitivities to radiologists at the 8-mm threshold but at the expense of specificity (78% vs. 92.2%, respectively). This suggests that nonradiologists do not have critical cross-sectional characterization skills.

The property of polyp coating from tagging agents is an important phenomenon that has now been recognized.⁸ It positively affects detection and characterization, perhaps most importantly for flat polyps. As noted earlier (see “Bowel Preparation”), tagging agents adhere to true polyps while are washed away from the normal mucosa. This serves to draw attention to possible polyps, particularly on the 2D view, and helps increase confidence that a polyp is real (by demonstrating this property). One pitfall is not to mistake poorly tagged stool or adherent plaques of tagged stool as coated polyps (see later, “Characterization”).

DETECTION

Regarding detection, there had been a heated debate in the literature about the optimal method, a primary 2D approach or primary 3D approach.³³ A primary 2D approach consists of interrogating a stack 2D dataset, typically in the transverse plane (Video 53-1). The mechanics are similar to viewing a standard CT, in which the reader scrolls interactively through a stack of images in polyp window settings (2000 W, 0 L). The colon is traced from rectum to cecum with the intent of detecting focal soft tissue projections into the colonic lumen. The difficulty of this approach is distinguishing between a focal polyp and colonic haustral fold. On a single image, a colonic fold can present as a focal polyp; it requires scrolling through to ascertain its elongated nature (Fig. 53-6). Once experienced, the reader can be very effective at quickly detecting polyps by this approach. However, it requires sustained concentration, which can be somewhat tedious. The 2D search pattern is analogous to detecting pulmonary nodules on a chest CT and distinguishing them from pulmonary vessels.

Additional videos for this topic are available online.



A primary 3D approach uses postprocessing of the 2D dataset into a 3D perspective. The reading mechanics are completely different and involves traveling through a tubular 3D environment, typically on a preprogrammed course (see Video 53-1). When needed, the reader can then break off this fly-through to interact freely in this 3D environment and visualize an area of concern from any angle. The 3D approach holds the advantage that differentiating potential focal polyps from colonic folds is easily done from this perspective (see Fig. 53-6). The mental translation into a 3D structure that is needed for a primary 2D approach has been undertaken by a computer. Whereas from a 2D perspective, a haustral fold can appear polyp-like until assessed in detail, such is not the case at 3D where they are instantly recognizable as different entities. A disadvantage of this approach is that 3D relies on surface morphologic cues only as compared to the 2D approach, which uses morphologic and attenuation cues simultaneously. Thus, any retained stool, despite its tagged status, would appear as a polyp at 3D and require evaluation of the 2D source data for confirmation. Also, areas of colonic collapse or segments with residual fluid are not well evaluated with a 3D approach, and the reader may not be aware of their existence on that series. Typically, however, 3D evaluation is possible on the complementary series as fluid moves away and gas distends these areas on the second series.

The standard 3D viewing option is an endoluminal perspective. Traditionally, a fly-through consists of passage from the

rectum to the cecum and then from the cecum to the rectum to allow both sides of the colonic folds to be visualized. Often, the field of view is widened at 120 degrees. In addition to the standard endoluminal view, there are alternate advanced 3D displays in use, including the filet view, unfolded cube, and band view (Fig. 53-7). These increase visualization (behind folds) and

thus speed of interpretation, but at the cost of increased spatial distortion.

Despite the prior controversy regarding detection approaches, there is now general consensus that a combination of 2D and 3D is required for optimal polyp detection. In practice, it has become obvious that the approaches are

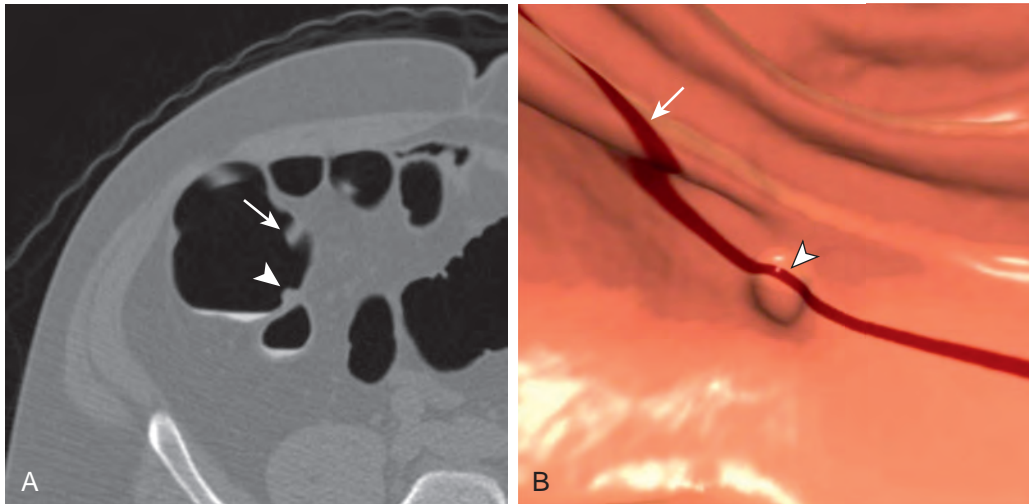


Figure 53-6 Polyp versus haustral fold at 2D. **A.** 2D CTC image shows the difficulty of distinguishing a polyp (arrowhead) from a haustral fold (arrow) on a single image, where they are similar in appearance. **B.** This is not a perceptive concern at 3D, where the haustral morphology (arrow) is clearly different from a polyp (arrowhead). The red line corresponds to the level and orientation of the 2D image.

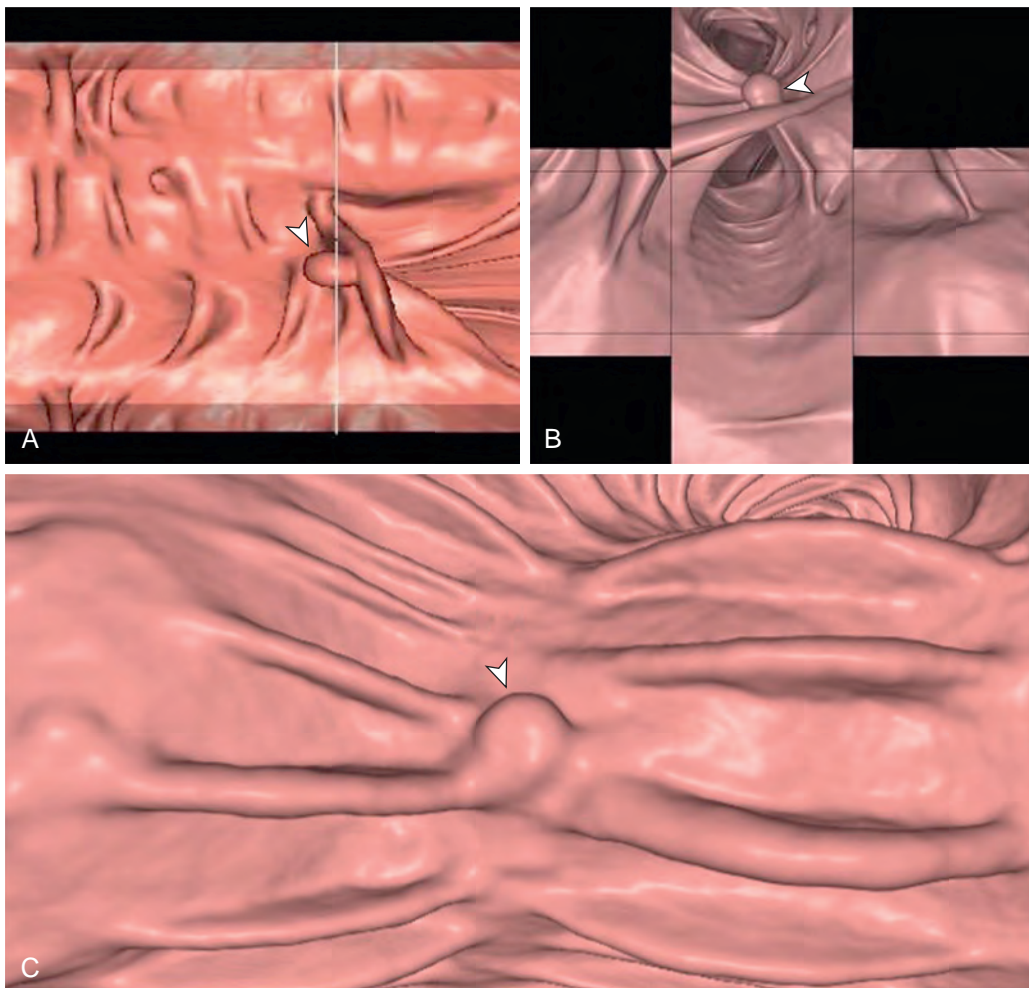


Figure 53-7 Advanced 3D displays. The filet (**A**), unfolded cube (**B**), and band view (**C**) allow examination of both sides of the colonic folds simultaneously to detect a polyp (arrowhead), but at the cost of spatial distortion. (**A** and **B** from Pickhardt PJ, Kim DH: *CT Colonography: Principles and Practice of Virtual Colonoscopy*. Philadelphia, Elsevier, 2010; **C** courtesy Seong Ho Park, MD.)

complementary; polyps or masses that are difficult to visualize by one perspective are easily seen by the other. For the 2D approach, there are some polyps that project off the colonic mucosa or off the end of the fold at an angle relative to the axial plane that are difficult to detect because the reader perceives the polyp as a fold or an extension of the fold (Video 53-2). In addition, polyp shape at 2D can cause difficulties in detection (Video 53-3). Both situations are not problem areas at 3D. For 3D, polyps submerged in the polyp pool can be missed (Video 53-4). In addition, underdistended areas can make the determination of lesions difficult because the walls become irregular as a result of their partially collapsed state. Focal areas of collapse related to an annular cancer with the 3D approach can be misinterpreted and missed if not evaluated with a 2D approach (Fig. 53-8). By combining 2D and 3D detection, the complementary nature of the approaches allows a polyp to be seen when not evident by one perspective. In addition, the added redundancy of interacting with the imaging dataset multiple times during a combined approach further decreases the possibility of missing polyps.

 *Additional videos for this topic are available online.*

Figure 53-8 Collapse at 3D.

A. 3D CTC map shows two innocuous areas of collapse. The 3D endoluminal view (inset) of the inferior collapsed area is unremarkable. One segment (arrow) is simple collapse but the second (arrowhead) is not. **B.** The 2D CTC image depicts the annular cancer (arrowhead), which would be easily ascertained during 2D detection review.

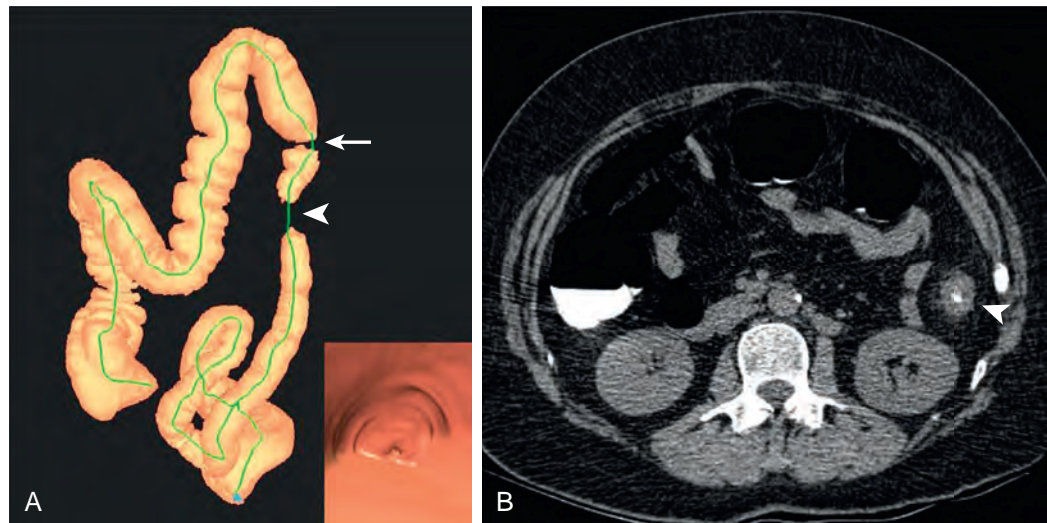
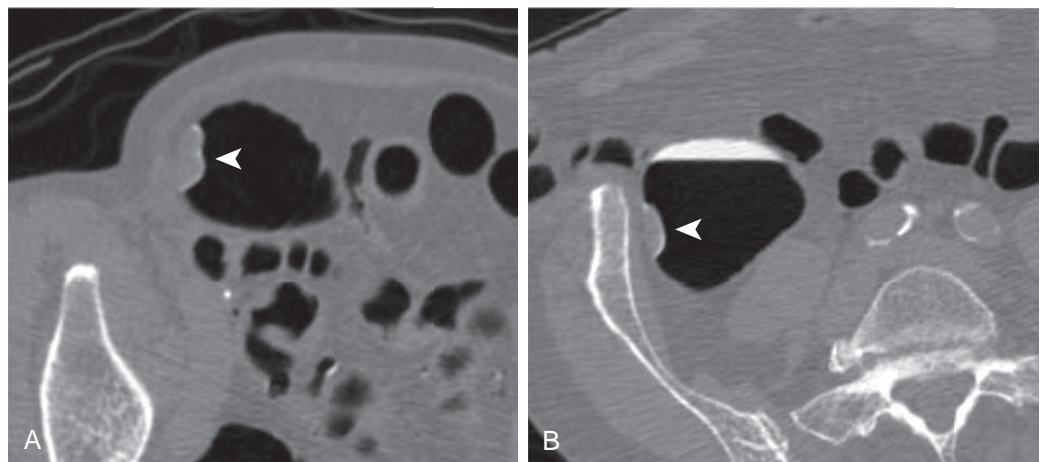


Figure 53-9 Polyp confirmation.

A, B. Supine and prone 2D CTC images show that this cecal polyp candidate (arrowhead) meets the criteria for a true soft tissue polyp. Note the homogenous grey appearance on both views and the fixed location, where it does not fall to a dependent location on either position. There is a thin etching of contrast overlying the polyp (the polyp coating), which is common with the UW bowel preparation.



CHARACTERIZATION

Characterization of suspected polyps is the second and perhaps most important step in interpretation. Each detected polyp candidate must be evaluated to determine if it actually represents a polyp and exclude pseudopolyps related to retained stool or thickened folds. A true soft tissue polyp must fulfill two criteria (Fig. 53-9; see Video 53-1). First, it must be homogenous soft tissue in attenuation when viewed in polyp window settings (2000 W, 0 L). There should be a uniform grey appearance similar in density to the adjacent musculature on all series as opposed to untagged stool, in which internal heterogeneity exists. At times, feces can demonstrate internal homogeneity, particularly small, subcentimeter-sized pieces. However, these pseudopolyps can often be ascertained as they are often mobile in the colorectum (see later, second criterion). Tagged stool is easily determined by its markedly increased attenuation (see Fig. 53-1).

The second criterion relates to a fixed location between the various series. The polyp candidate must be attached to the colonic mucosa at a single point and cannot move. In contrast, stool will fall to a dependent location between the series. Thus, a true soft tissue polyp must be homogenous in attenuation and

fixed in location on all series. When these criteria are used, the concordance at optical colonoscopy is well over 90%.^{34,35} These determinations are made by evaluating the 2D source images and only minimally by the 3D postprocessed dataset (3D tools such as translucency rendering can help in attenuation determination). The ability to confirm suspected polyps accurately requires a strong cross-sectional skill set and grounding in CT principles. There are several pitfalls that can cause misinterpretation, including beam hardening, apparent movement of polyp, and underlying colonic movement. In addition, incompletely tagged stool can at times mimic a coated polyp.

Beam hardening is an important phenomenon that can affect characterization (Fig. 53-10). Because of the low doses used with CTC, beam hardening can cause apparent heterogeneity of soft tissue polyps or even a fatty appearance if adjacent to high-density structures such as tagged fluid pools or bone. Flat polyps are particularly affected by this phenomenon given their lack of soft tissue bulk, in which they have such an appearance because of streak from the overlying contrast coat. It is important to recognize this phenomenon to prevent mischaracterization of a polyp for stool related to its altered internal appearance.

Differentiating apparent movement of a true polyp from a moving pseudopolyp related to untagged stool is key. One

well-recognized pitfall is related to pedunculated polyps with an elongated polyp stalk (Fig. 53-11). If this is not recognized, the polyp head can be mistaken for a sessile polyp candidate. Because it moves with changes in patient position, this true polyp can be mistaken for moving stool. At times, the 3D approach can be helpful to identify the stalk.

Additionally, the colon can shift, move, and twist in position, particularly those segments on a mesentery (cecal apex, transverse, sigmoid). It requires solid localization skills with a 2D approach to confirm that the polyp candidates seen on both views represents the same colonic location because of the shifting underlying colon (Fig. 53-12). The reader must use the few internal landmarks, such as a stray diverticulum, characteristic bend, or haustral fold, to trace the colon in this area to confirm that the candidate is at the same location between the various series. When possible, the ileocecal valve is an excellent landmark to use for polyp candidates in the right colon. One important underrecognized pitfall is the ability of the cecum and ascending colon to rotate on its long axis.^{36,37} There is often a counterclockwise rotation between the supine and prone position, despite the retroperitoneal location of the ascending colon and portions of the cecum. This can cause apparent movement of the polyp candidate (Video 53-5).

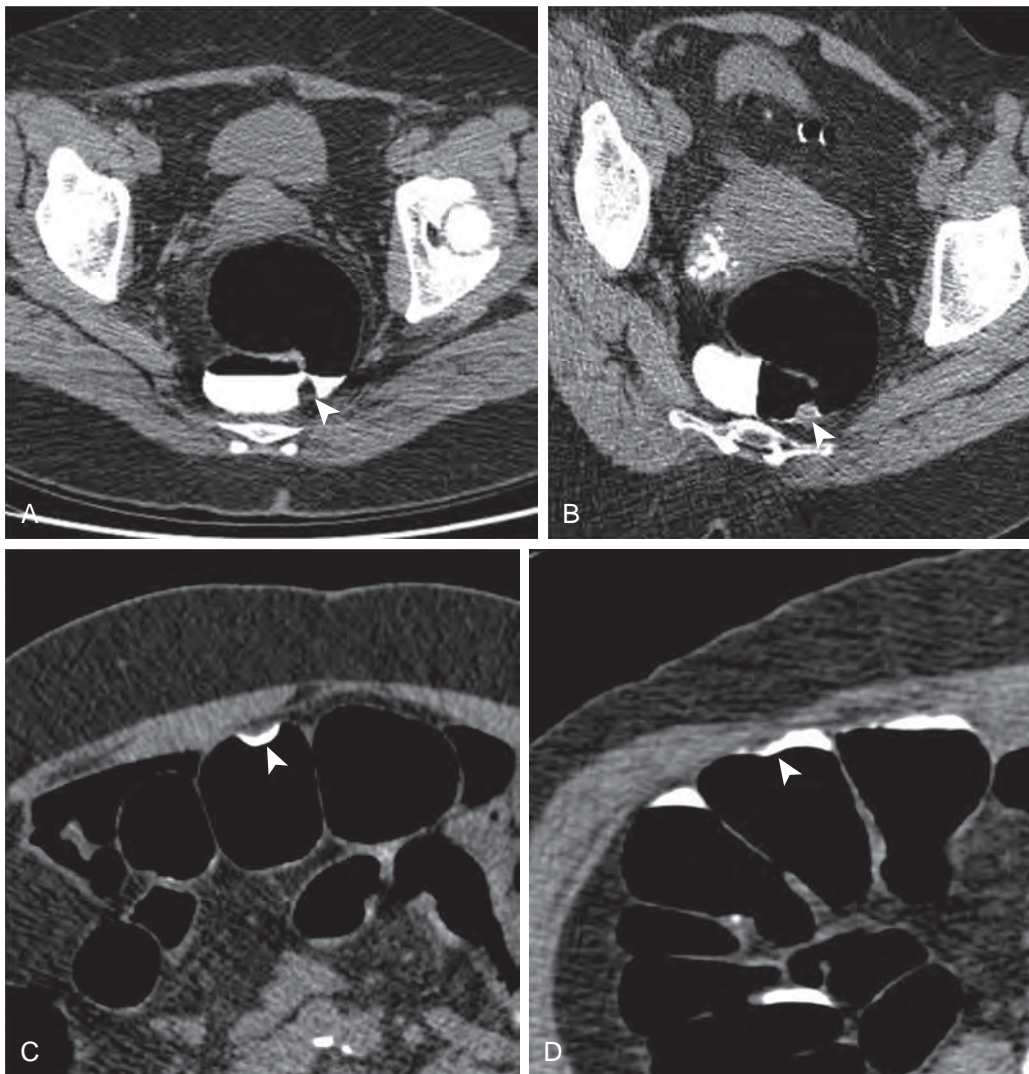


Figure 53-10 Beam hardening.

A. 2D CTC in soft tissue windows suggests that a submerged pedunculated lesion (arrowhead) may be a lipoma. This is an artifactual appearance related to beam hardening from the contrast fluid pool. **B.** The true soft tissue nature of the polyp (arrowhead) is seen on the decubitus view, where the contrasted fluid moves away. **C.** Supine 2D CTC image in another patient with a flat polyp (arrowhead), where beam hardening from the contrast coat and fluid pool on the prone image (**D**, arrowhead), which creates an artifactual fatty appearance of this proven soft tissue polyp.

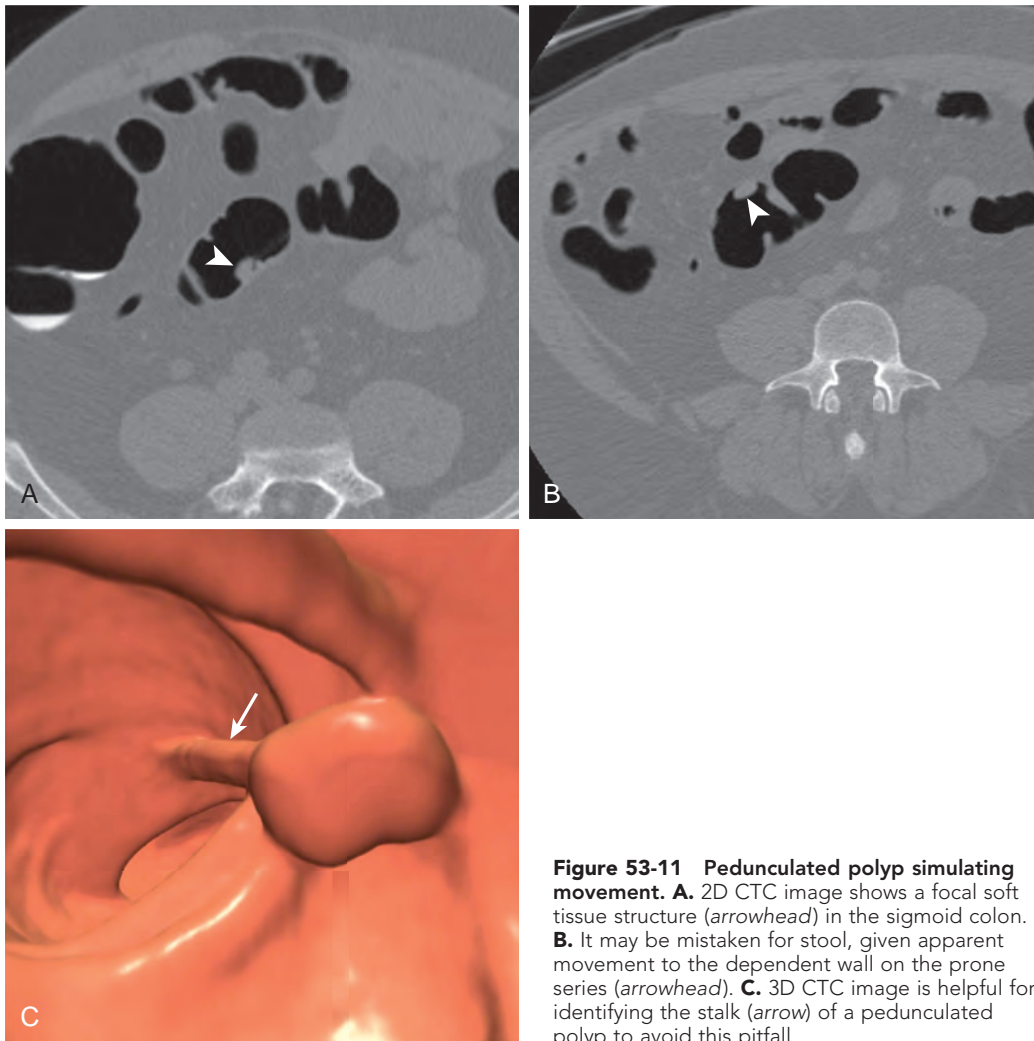


Figure 53-11 Pedunculated polyp simulating movement. **A.** 2D CTC image shows a focal soft tissue structure (arrowhead) in the sigmoid colon. **B.** It may be mistaken for stool, given apparent movement to the dependent wall on the prone series (arrowhead). **C.** 3D CTC image is helpful for identifying the stalk (arrow) of a pedunculated polyp to avoid this pitfall.

 Additional videos for this topic are available online.

Finally, although the coating phenomenon is very important in improving polyp detection and characterization, it is important to recognize that incompletely tagged stool can mimic a coated polyp (Fig. 53-13). With close inspection, there are slight differences where the interface between the polyp and barium coat is sharper and better defined than for stool. The easiest way to distinguish stool is mobility—the tagged stool will move between the supine and prone positions. In these cases, when there is a question between a coated polyp and incompletely tagged stool, the fecal debris tends to be large and not adherent.

POLYP DIFFERENTIAL

At interpretation, the practical differential is between a true soft tissue polyp and pseudopolyp (related to stool or a thickened fold).³⁸ It is not necessary to determine the histology of the polyp (which cannot be determined with CTC or optical colonoscopy) because management is driven by polyp size.³⁹ However, it is important to be aware of the possibilities and future cancer risk for each histologic subtype once it is known

at pathologic evaluation. Polyps typically arise from the mucosal surface. The major histologic subtypes include adenomatous polyps, hyperplastic polyps, and mucosal polyps (in order of decreasing frequency). Adenomatous polyps account for approximately 50% of all polyps, hyperplastic a third, and mucosal 10%.⁴⁰ Although benign, a tiny fraction of adenomatous (and recent evidence also indicates hyperplastic polyps) can progress to cancer over many years.

Deeper lesions from the submucosa, intramural layer, or extrinsic to the colon can present as polyps indistinguishable from mucosal originating lesions. These include lipomas, carcinoid, lymphangiomas, and GI stromal tumors. However, as with principles at barium enema, the lesions can be suggested when they demonstrate obtuse sloping margins, suggesting a deeper origin.

As noted, histologic diagnosis cannot typically be undertaken by imaging. Mucosa-based polyps (adenomas, hyperplastic polyps, mucosal polyps) and deeper colonic lesions present as nondescript focal lesions of soft tissue attenuation. However, image-specific diagnoses can be made in a few rare circumstances without pathologic evaluation, such as a lipoma. Lipomas arise from the submucosal layer but often appear as

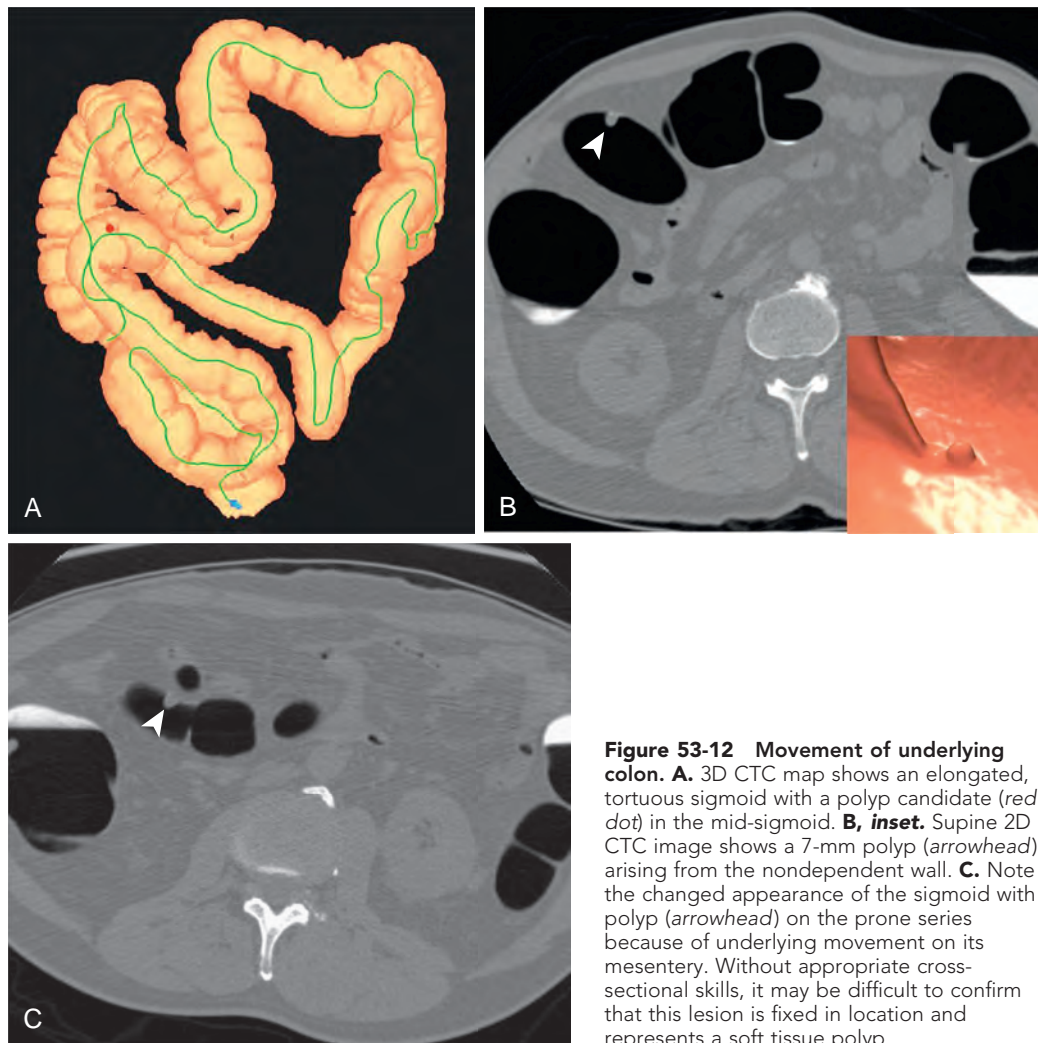


Figure 53-12 Movement of underlying colon. **A.** 3D CTC map shows an elongated, tortuous sigmoid with a polyp candidate (red dot) in the mid-sigmoid. **B, inset.** Supine 2D CTC image shows a 7-mm polyp (arrowhead) arising from the nondependent wall. **C.** Note the changed appearance of the sigmoid with polyp (arrowhead) on the prone series because of underlying movement on its mesentery. Without appropriate cross-sectional skills, it may be difficult to confirm that this lesion is fixed in location and represents a soft tissue polyp.

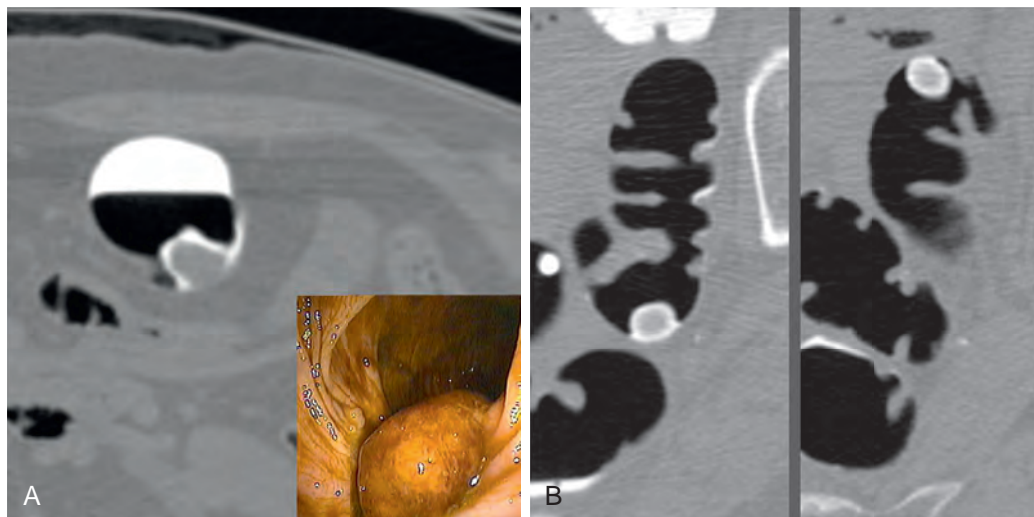


Figure 53-13 Coated polyp versus tagged stool pitfall. **A.** 2D CTC prone image shows a nondependent structure consistent with a polyp with a thick overlying barium coat. Colonoscopy (inset) confirmed a large villous adenoma containing a well-differentiated adenocarcinoma. **B.** Note the similar appearance of incompletely tagged stool. Movement (supine on left side of image, prone on right side) confirms that this is stool.

sessile or even pedunculated lesions of presumed mucosal origin. An image-specific diagnosis can be made when a fatty internal density is seen (Fig. 53-14). In other circumstances, a diagnosis can be highly suspected in entities such as endometriosis, dependent on clinical and imaging factors (Fig. 53-15). This diagnosis can be suggested when a nonspecific soft tissue, broad-based lesion with smooth obtuse margins is seen in a younger female. The overlying folds are often not disrupted. These lesions represent serosal implants that have extended into intramural and submucosal layers. Colonoscopy is often helpful to exclude a mucosal lesion that appears submucosal on CT.

REPORTING

Reporting is a central element in interpretation. C-RADS (CT colonography reporting and data system) is a structured reporting construct in use since 2005. Colonic and extracolonic findings are classified separately by C and E categories (Table 53-4). This allows for standardization of approach and management,⁴¹ which then allows for comparison between institutions clinically and in research.

On the colonic side, C-RADS standardizes polyp sizing, location, and reporting of morphology. For measurement, the longest axis of the polyp is used. For pedunculated lesions, the

longest axis of the polyp head is measured (with exclusion of the stalk). Standardization of sizing is particularly important because polyp management is dependent largely on size. Location is divided into the six colonic segments of cecum—ascending, transverse, descending, sigmoid, and rectum. Polyp morphology includes sessile (dome-shaped, with a broad base of attachment), pedunculated (polyp head with a stalk of variable length attaching to the colonic mucosa), and flat (plaque-like appearance with a height ≤ 3 mm from the colonic surface). Masses are 3 cm or larger.

On the extracolonic side, each finding is classified by clinical significance and the need for further evaluation. By definition, E1 and E2 examinations will not require additional work-up, whereas E3 and E4 can lead to further imaging. The final E category is determined by the most advanced lesion if there are multiple findings. The extracolonic issue is covered in additional detail later in this chapter.

Computer-Aided Detection/Diagnosis

CAD (computer-aided detection or diagnosis) software devices use mathematic algorithms to identify specific patterns in radiologic images. Because the primary objective with CTC involves a repetitive defined task operating within a large dataset, there is considerable interest in using CAD to improve

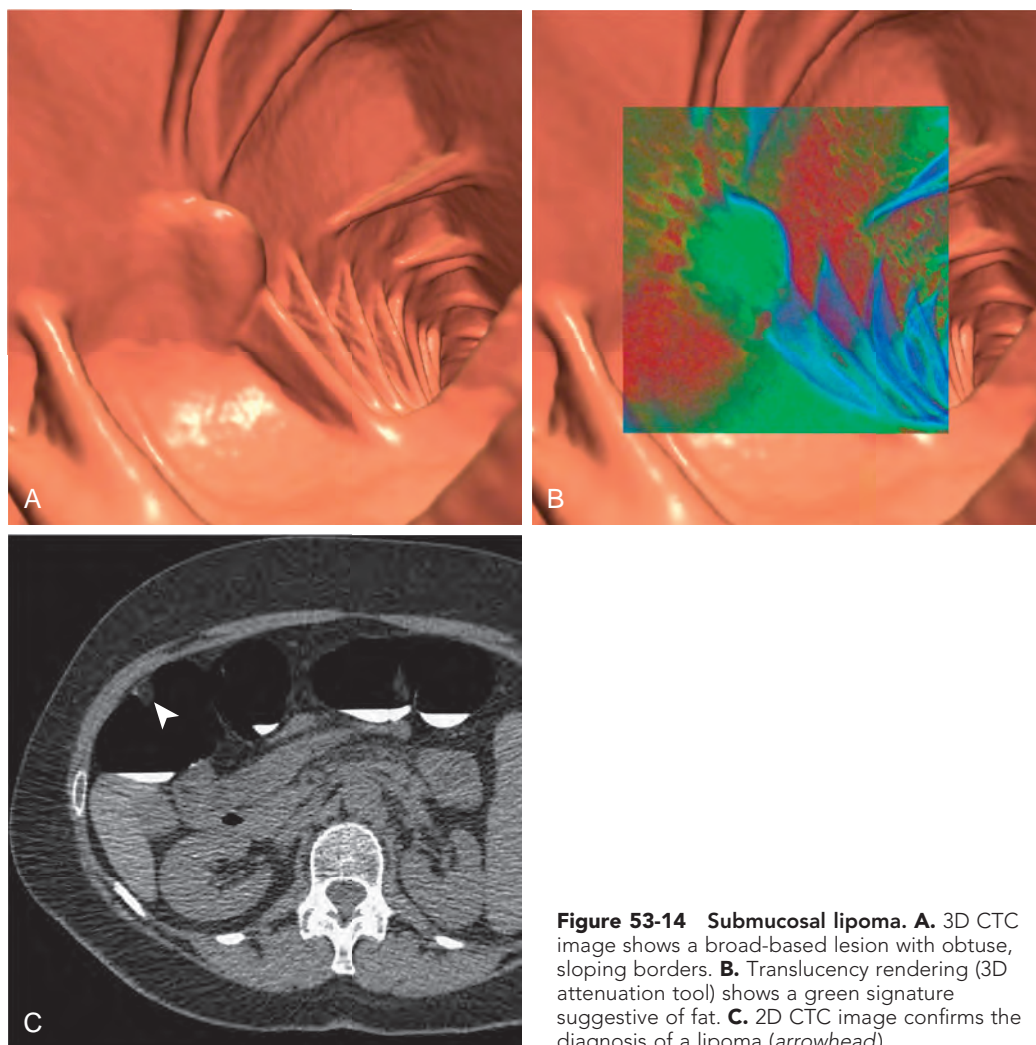


Figure 53-14 Submucosal lipoma. **A.** 3D CTC image shows a broad-based lesion with obtuse, sloping borders. **B.** Translucency rendering (3D attenuation tool) shows a green signature suggestive of fat. **C.** 2D CTC image confirms the diagnosis of a lipoma (arrowhead).

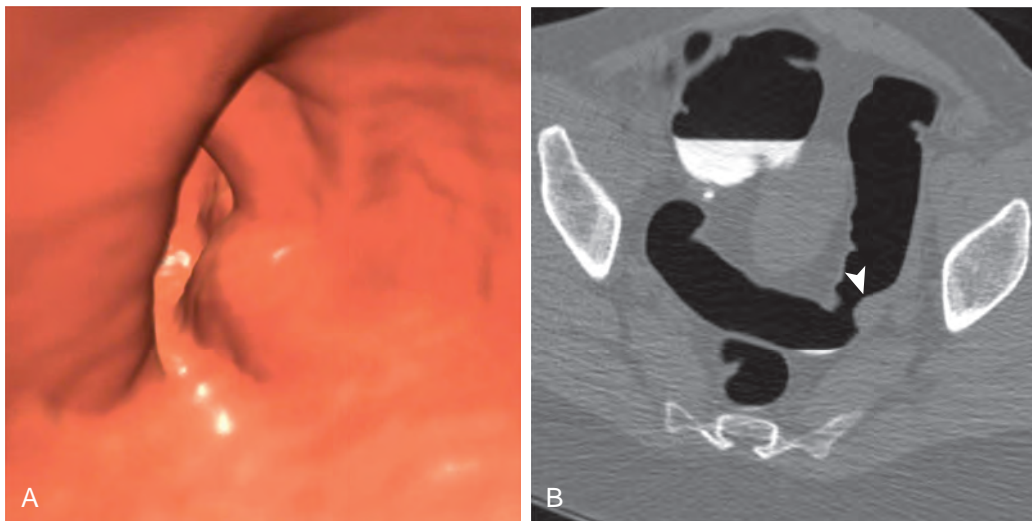


Figure 53-15 Endometrioma. **A.** 3D CTC image shows an apparent submucosal or deeper lesion with obtuse borders. **B.** 2D CTC image shows a nonspecific soft tissue lesion (arrowhead) but in the appropriate clinical situation and history, a diagnosis of endometrioma can be made.

TABLE 53-4

C-RADS

Parameter	Description	Recommendation
Colonic		
C0	Inadequate study or awaiting comparisons	—
C1	Normal colon (no polyp ≥ 6 mm)	Routine screen (5 yr)
C2	Isolated small polyp (one or two 6- to 9-mm polyps)	Imaging surveillance up to 3 yr versus immediate colonoscopic removal
C3	Polyp, possibly advanced adenoma (≥ 10 mm or \geq three 6-9 mm polyps)	Colonoscopic removal
C4	Colonic mass, likely malignant	Surgical consult
Extracolonic		
E1	Normal examination or anatomic variant	—
E2	Clinically unimportant finding (e.g., hepatic or renal cyst)	No work-up indicated
E3	Likely unimportant; incompletely characterized	Work-up may be indicated
E4	Potentially important finding (e.g., solid mass or aneurysm)	Work-up indicated; communication to referring physician

C-RADS, CT colonography reporting and data system.

interpretation. CAD is potentially helpful by reducing perceptual errors (errors in which polyps are not perceived initially but can be identified in retrospect) related to fatigue and inattentiveness on the part of the radiologist. Ultimately, however, the radiologist must have a strong interpretative skill set to determine which CAD prompts represent true polyps; otherwise, the use of CAD simply increases sensitivity at the expense of specificity, without a true improvement in accuracy.

Although the specific algorithms are unique to each CAD system, all systems have some common steps. First, the dataset is postprocessed to facilitate CAD application and may include elements such as edge enhancement and sharpening of interfaces. The area of interest (i.e., the colorectum) is segmented out and a set of specific features are calculated for each voxel. Examples of possible features include shape, size, and curvature. The number and specific features used are different with different CAD systems. These features are then entered into a classifier, which may be a neural network, kernel machine, or decision tree to calculate a numeric value representing the likelihood that the prompt represents a polyp. If the CAD system is intended to be a detection device (CADE), there is a binary reporting of positive or negative according to whether a certain threshold is met; CAD systems intended for diagnosis (CADx) presents likelihood information.

The impact of the use of CAD software is difficult to assess. Stand-alone device performance can be excellent, with sensitivities of 90% for large (≥ 10 mm) polyp and variable lower sensitivities, ranging from 61% to 92% at the 6-mm level, with false-positive marks of 2 to 14 per patient.⁴²⁻⁴⁵ However, ultimately, it is the interaction between the CAD device and radiologist that determines overall performance. There is conflicting evidence whether CAD improves interpretation. Petrick and associates have shown that although sensitivities increased by 15% at the 6-mm threshold versus unassisted reads, it was at the expense of specificity, which decreased by 14%.⁴⁶ Thus, there was no actual improvement but simply a shift in the set point of what was called positive. In contrast, Dachman and co-workers reported true improvement with a small but statistically significant increase in the segment level area under the receiver operating curve (AUC; $p = 0.015$).⁴⁷

CTC Trial Results

CTC performance has been well established by a number of trials in high-polyp prevalence groups and low-prevalence screening cohorts. The high-polyp prevalence population studies represented initial proof of concept studies. Typically performed as single-institution series, these studies showed that CTC could detect polyps with high sensitivities, albeit in the least difficult situation, in which a large percentage of

examinations were positive.⁴⁸⁻⁵² One notable study from this group was a prospective trial from Boston University published in the *New England Journal of Medicine* in 1999. Fenlon and colleagues⁵⁰ enrolled 100 high-risk individuals to undergo both CTC and colonoscopy evaluation. Despite using now older technology and protocols (including no fecal tagging, room air distention, and 5-mm image collimation reconstructed at 2-mm intervals), CTC demonstrated a 91% sensitivity (20 of 22 polyps) at the 10-mm threshold, which decreased to 82% (33 of 40) for 6- to 9-mm polyps. All cancers in the series (3 of 3) were seen with CTC.

The positive results seen in these small, single-institution series then paved the way for large multicenter trials in low polyp prevalence or screening cohorts. These studies assessed whether CTC performance could be maintained in the more challenging and pertinent clinical situation in which most of the examinations would be negative. Here there were discrepant results, leading to controversy regarding the true capabilities of this modality. First, Pickhardt and associates reported the results from the multicenter Department of Defense (DoD) CTC trial in 2003.² In a large cohort ($N = 1233$ screening individuals, three institutions), the per-patient sensitivity for adenomatous polyps was 94% at the 10-mm threshold, decreasing to 89% at the 6-mm threshold. In comparison, optical colonoscopy sensitivity was 88% at the 10-mm level and 92% at the 6-mm level. The lower than traditionally reported sensitivity levels for colonoscopy were likely related to trial design, in which an enhanced polyp validation system of segmental unblinding was used. In contrast to using colonoscopy in isolation as the gold standard, in which colonoscopy misses would be unaccounted, segmental unblinding created an enhanced reference standard in which the CTC results were revealed segmentally at colonoscopy. Thus, if no polyp was initially seen at colonoscopy but noted with CTC, the colonoscopist reexamined the segment for the missed polyp. Such a standard led to more accurate sensitivity and specificity measures for both modalities, correcting the situation in which a false-negative colonoscopy result would be inaccurately counted as a CTC false-positive.

Following the DoD results, however, two smaller multicenter trials demonstrated much poorer results.^{53,54} Rockey and co-workers ($N = 614$)⁵⁴ and Cotton and colleagues ($N = 615$)⁵³ reported poor sensitivities, ranging from 55% to 59% for large polyps (≥ 10 mm) and decreasing to even lower levels for sub-centimeter polyps. At the time, this led to great debate about the adequacy of CTC performance. However, with the results of the subsequent larger validation trials published several years later, it is now evident that the Rockey and Cotton trials were flawed, accounting for the poorer trial results. In addition to using older CTC technology, one major criticism concerned the lack of reader training. For example, the Cotton trial required no prior reader experience or training for the CTC readers. It is now evident that there is a learning curve for CTC interpretation that requires acquisition of CTC-specific skills in addition to existing CT cross-sectional skills. Liedenbaum and associates demonstrated such a learning curve in which substantial improvement among novice readers was seen through a study set of 200 CTC cases.³¹ Sensitivity increased from an initial value of 76% at the 6-mm threshold for the first set of 50 CTC cases to 91% sensitivity for the fourth set of 50 cases. Furthermore, studies suggested that training and experience may not be enough, and that competency testing may ultimately be required.⁵⁵

During this evaluation period of CTC performance, it is important to be aware that CTC was a dynamic technology with continuing changes in the underlying CTC software, hardware, and examination protocol. Technical components were refined, leading to more optimally prepared and tagged bowel, improved and consistent colonic distention, and increased spatial resolution with decreased artifact.^{7,10,56-65} The CTC protocol evolved, such as standardizing the use of both supine and prone imaging for the typical examination, with additional decubitus series for problem solving.^{59,66,67} Underlying improvements in computer hardware allowed easy manipulation of even larger volumetric datasets. The current CTC examination, as noted earlier, now reflects the tremendous advancements over the years.

In 2008, the results of the ACRIN 6664 protocol or National CT colonography trial were published, answering the controversy about the discrepant initial screening results. This landmark trial validated the prior excellent results seen by Pickhardt and co-workers.² It was a large multicenter trial ($N = 2531$ participants, 15 institutions) performed in a low-prevalence or screening cohort. It used state of the art techniques and required a high level of experience and competence testing by the readers. In this trial, a per-patient sensitivity of 90% and specificity of 86% was seen for large polyps (≥ 10 mm). The performance decreased to a sensitivity of 78% at the 6-mm threshold. In addition to the ACRIN trial, other series in Europe corroborated a high level of CTC performance. The Italian IMPACT trial ($N = 937$, 12 institutions)³ showed a 90.8% sensitivity (84.5% specificity) at the 10-mm threshold, and the Munich Colorectal cancer screening trial⁴ also showed similar results (92% sensitivity, 98% specificity). The United Kingdom SIGGAR trial demonstrated equivalent detection rates for cancers and large polyps between CTC and colonoscopy screening programs.⁵

Outside of trial data, actual results from large-scale clinical practices suggested that CTC-based screening could be effective.⁶⁸⁻⁷¹ A large Wisconsin series by Kim and colleagues reported results from parallel operating CTC ($N = 3120$) and colonoscopy ($N = 3163$) colorectal cancer screening programs, in which each drew from the same regional population.⁷⁰ The CTC program reported advanced neoplastic yields equivalent to the colonoscopy program ($n = 123$ CTC; $n = 121$ colonoscopy) but with a fourfold decrease in the number of polypectomies (561 vs. 2434) and subsequent marked decrease in the number of complications (0 vs. 7 perforations). In addition, outcomes data from the negative CTC screening cohort ($N = 1050$) from this program have also been reported. Patients with a negative screen who were followed over a 5-year interval showed a very low interval cancer rate of 0.2 cancers/1000 years of patient follow-up, suggesting that setting examination positivity at a 6-mm threshold and routine screen interval at 5 years is a safe practice.⁷²

Indications and Use

There are three broad categories of use for CTC: (1) screening for colorectal cancer; (2) focused evaluation for various diagnostic reasons, including incomplete colonoscopy; and (3) simultaneous colonic evaluation and distant staging of initially diagnosed CRC or surveillance of known CRC. Many of the indications previously undertaken by barium enema have been now supplanted by CTC at many institutions.

SCREENING FOR COLORECTAL CANCER

Screening for CRC is perhaps the most important indication for CTC, for which its use could have a major public health impact. CRC currently is the second leading cause of cancer in the United States; there are approximately 143,000 new cases/year, leading to almost 52,000 deaths annually.⁷³ It is estimated that of the 80 million U.S. adults eligible for screening, only slightly over 50% participate with any of the traditional options, including optical colonoscopy, fecal occult blood test (FOBT)—fecal immunochemical test (FIT), flexible sigmoidoscopy, and double-contrast barium enema (DCBE).^{74,75} In addition, there are concerns regarding population screening capacity for options such as optical colonoscopy.⁷⁶ This is further accentuated by the growing awareness that specialized GI capacity is uneven and is dependent on geographic region, which is particularly limited in rural areas.⁷⁴ Thus, CTC has the potential to increase screening adherence substantially by appealing to currently noncompliant persons^{77,78} and by increasing the screening capacity, particularly in rural underserved areas (where examinations can be conducted at the local hospital and networked to central areas of expertise for interpretation).⁷⁹

Screening is particularly effective in decreasing CRC mortality because of several favorable factors in its biology: (1) CRC has a stepwise progression, from a benign precursor lesion to cancer; (2) the benign precursor can be identified and removed; and (3) the benign precursor has an extended latent period (10–15 years) prior to transformation to cancer, leading to a wide window for intervention. As opposed to other cancers, such as breast cancer, in which the intent is to detect early cancer to affect future mortality, CRC screening represents true primary prevention, in which the removal of a benign lesion precludes the future development of a cancer.

The benign precursor lesion for CRC arises from a subset of colonic polyps from adenomatous and hyperplastic lineages. Transformation from benign adenomas represent the major pathway, accounting for an estimated 85% of sporadic cancers, and hyperplastic or serrated polyps may account for the remaining 15% of cancers.^{80–82} It has only recently become apparent that hyperplastic polyps hold the possibility of malignant transformation; previously, they were considered to be completely innocuous lesions. Adenomatous polyps typically undergo genetic changes in several key genes, including *APC*, *k-ras*, and *p53*, whereas serrated or hyperplastic polyps undergo a newly discovered pathway mediated by a mutation in the *B-raf* oncogene, followed by epigenetic changes to this cell signaling pathway and microsatellite instability. It is important to realize that only a tiny minority of adenomatous and hyperplastic polyps ultimately go through the entire pathway to cancer; the vast majority regress or remain benign adenomas or hyperplastic polyps. Thus, although up to 40% of adults older than 50 years may harbor adenomas,^{83–85} and approximately 10% to 30% harbor hyperplastic polyps,^{86,87} only a relatively small fraction ends up with cancer. Risk factors suggesting that an adenoma or hyperplastic polyp may progress include larger size (>1 cm) or high-grade dysplasia.^{82,88–90} For adenomas, a villous architecture also increases risk for progression.⁸⁹

Because of these findings, the screening strategy with CTC is based on a selective polypectomy approach; this differs substantially from the universal polypectomy approach with optical colonoscopy, in which all soft tissue polyps regardless of size are removed. In contrast, CTC follows a strategy in

which the higher risk polyps, identified by large size, are initially removed and the polyps at low risk for transformation are followed. Of the low-risk group, those that increase in size at follow-up are then removed, whereas the stable and regressing polyps are not. This allows CTC to maximize the yield of advanced lesions, most likely to transform to a future cancer but avoid numerous polypectomies, which hold no benefit but increase the risk of complications, such as perforation. As noted, results from large screening programs suggest that such a strategy is effective and safe.^{70,72}

Screening by CTC is appropriate for average-risk individuals (≥50 years old), which represents the largest screening cohort. CTC-based screening is also appropriate for individuals of this age group who have a somewhat elevated risk because of a positive family history. Family history can be defined as a history of cancer in one first-degree relative or two second-degree relatives.⁹¹ Although somewhat controversial, CTC can also be used in the FOBT-positive population. Lesion detection and negative predictive value are high, but questions have been raised about cost-effectiveness because of higher underlying polyp and cancer prevalence in this group.^{3,92,93} Finally, CTC can be substituted when screening colonoscopy is contraindicated in a patient because of comorbidities and sedation issues or if the patient is anticoagulated. Particularly in the setting of warfarin use, CTC is an excellent alternative for screening because the anticoagulation therapy does not have to be interrupted for the procedure. For the small percentage of positive patients who require removal of a large polyp, the anticoagulation can be reversed at a future date for the therapeutic polypectomy. In contrast, screening by CTC is not indicated for individuals at high risk for colorectal carcinoma and polyps for whom the pretest probability for a positive examination is substantially high. These include those with a polyposis syndrome (e.g., familial adenomatous polyposis, hereditary nonpolyposis colorectal cancer syndrome) and inflammatory bowel disease. Patients with these underlying diagnoses are better evaluated by colonoscopy.

DIAGNOSTIC INDICATIONS

CTC can also be used for the evaluation of various diagnostic situations. It represents a less invasive alternative to colonoscopy for the work-up of clinical scenarios such as altered bowel habits, iron deficiency anemia, and nonspecific weight loss, in which one of the concerns is cancer. In terms of cancer detection, a large meta-analysis (49 studies; compiled cohort $N = 11,151$) demonstrated that CTC had a high sensitivity of 96.1%.⁹⁴ Unlike colonoscopy, there is less concern that detection ability with CTC decreases for right-sided cancers. Several population-based studies have indicated decreased detection or protective effects of colonoscopy for proximal colorectal cancers.^{95–97}

In addition to symptomatology, CTC is often used to complete colonic evaluation in the situation of an incomplete colonoscopy.^{93,98} Whereas same-day barium enema following incomplete colonoscopy may have been difficult because of incomplete colonic coating caused by air block, this is not a concern with CTC. Typically, same-day CTC examinations of good diagnostic quality can be performed. The bowel preparation is often supplemented by tagging agents prior to scanning. A typical protocol involves administering 30 mL of diatrizoate after the patient recovers from sedation to minimize aspiration

risk. Scanning occurs 2 hours after contrast administration, allowing for complete colonic fluid tagging in most patients.⁹⁹

STAGING AND SURVEILLANCE

CTC offers a unique opportunity for the initial staging of colorectal cancer and for surveillance following surgical resection. Because of its cross-sectional nature, CTC can assess the colon and extracolonic structures. In both situations, the standard protocol is typically altered; the prone series is undertaken first at low dose, without intravenous (IV) contrast. This is followed by the supine series, in which a standard CT dose and IV contrast are used to allow optimal extracolonic evaluation for involved regional lymph nodes and distant metastases.

In staging, CTC excels in the localization of the primary cancer, particularly in tortuous elongated colons, in which such localization is difficult for colonoscopy, and for the detection of synchronous polyps and cancers.¹⁰⁰⁻¹⁰² Although several studies have reported decent discriminatory ability in tumor wall staging,^{100,102,103} there is general consensus that this evaluation is better undertaken by magnetic resonance imaging or transrectal ultrasound (in the specific case of rectal cancer), in which both modalities can resolve the layers of the bowel wall. In addition to colonic evaluation, CTC can evaluate regional lymph node and distant metastases. With minor image parameter changes, CTC is essentially a contrast CT examination, which currently is the modality of choice for this portion of the staging evaluation.¹⁰⁴

Surveillance after colorectal cancer treatment is an emerging application for CTC.^{105,106} Similar to colonoscopy, CTC allows for intraluminal evaluation for anastomotic recurrences as well as for metachronous polyps and cancers, similar to colonoscopy. Unlike colonoscopy, however, CTC is not limited to the colorectum, where its cross-sectional nature allows for extraluminal evaluation, including local pericolonic recurrences, regional adenopathy, and distant metastases. Kim and associates reported a large Asian, single-institution experience in this area.¹⁰⁶ CTC detected 6 metachronous cancers, including 1 anastomotic recurrence in 548 patients undergoing routine surveillance without clinical suspicion or increasing carcinoembryonic antigen (CEA) levels following prior colorectal cancer resection and treatment. The per-patient sensitivity was 81.8% for advanced adenomas (18 of 22) and 100% for cancer. CTC was also able to detect an extracolonic recurrence in an additional 11 patients, which could not be seen at colonoscopy.

Pertinent Issues

COMPLICATIONS

CTC has a wide safety profile; complications are extremely rare. The lack of complications is a major advantage of CTC over colonoscopy. CTC is a minimally invasive technique that requires the insertion of a soft-tipped, small-caliber catheter a few centimeters into the rectum to insufflate the colon. In contrast, colonoscopy requires the manipulation of a fiberoptic scope across the entire length of the colon. Because of the torque and traction to accomplish placement, sedation and pain control are both needed at colonoscopy. In contrast, no sedation or pain control is needed with CTC, and thus the possible adverse effects from these medications are avoided. The avoidance of sedation can preclude a substantial number

of complications. Such incidents have been reported as occurring in 0.5% of cases at colonoscopy.¹⁰⁷

Most complications with CTC occur with the bowel preparation. Dehydration and fluid shifts are possible, which are decreased with the use of PEG. However, even these complications are not common and are typically minor in severity. A large survey of several U.S. and international institutions has reported that significant complications from bowel preparation are extremely rare, at 0.0009% (2 of 21,923).¹⁰⁸

There was initial concern that the use of CO₂ could cause interference with the body's acid-base balance or create difficulties for patients with chronic obstructive pulmonary disease because of the respiratory excretion pathway. However, this has not been found to be a problem in clinical practice.¹⁰⁸ Additionally, as part of a Scandinavian CRC screening trial (NORCCAP), CO₂ insufflation at screening optical colonoscopy was investigated in a small subset of the screening cohort.¹⁰⁹ The end-tidal CO₂ was not elevated despite the respiratory excretion and no adverse events reported.

Unlike colonoscopy, perforation is not a significant concern. The perforation rate is almost nonexistent with CTC, particularly with the low-pressure nature of automated CO₂ instillation. Perforation rates with CTC are typically more than an order of magnitude less than colonoscopy, 0.009% versus 0.1% for colonoscopy.^{108,110} Two series have reported higher perforation rates of 0.03% to 0.06% with CTC.^{111,112} However, these rates are likely not representative in screening average-risk persons using automated CO₂ insufflation. These series represented high-risk patients with a potentially distal obstructing process (e.g., distal cancers, diverticular disease, inguinal hernia with trapped sigmoid colon) and were conducted with manual, staff-controlled room air insufflation, which can generate very high intraluminal pressures.

It is important to be aware of an imaging finding that can mimic or raise the specter of perforation. Incidental colonic pneumatosis can be infrequently seen following CO₂ administration. The calculated incidence has been reported to be 0.1% of screening patients.¹¹³ As opposed to a true perforation, the patient is typically asymptomatic, without complaint. Although a subset of these patients may undergo some additional monitoring postprocedure, no supportive measures or intervention are required. On 2D review, scattered lucent foci can be seen paralleling the colonic wall (Fig. 53-16). The cause of this phenomenon is not completely certain but may be related to the increased mucosal permeability of CO₂ and appears to occur with increased frequency with the use of CO₂ as opposed to room air. It is postulated that this phenomenon occurs with colonoscopy but would not be seen, because asymptomatic postprocedure patients are typically not imaged with CT.

RADIATION

Radiation exposure with CTC is low, typically less than 50% of that received with standard CT. Previously, the dose was equivalent to a barium enema examination (5-8 mSv) but has decreased over time.¹¹⁴ The average dose is slightly less than 1 year of background radiation or less than 3 mSv.¹¹⁵ Such reductions are possible because of the high contrast between the gas-filled lumen and soft tissue mucosa of the bowel wall. With the newer iterative reconstruction techniques and other methods of dose reduction, doses are rapidly decreasing from this low level. Despite this low-dose nature, radiation exposure

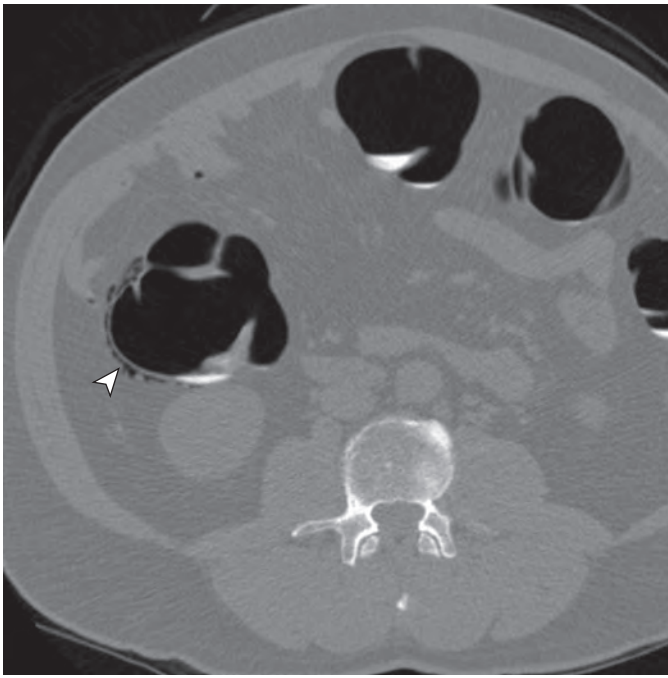


Figure 53-16 Incidental pneumatosis. 2D CTC image shows colonic pneumatosis (arrowhead) in this screening patient. The patient was asymptomatic and remained without complaint with monitoring. No intervention or supportive care needed.

has been raised as an item of concern for CTC, particularly because of its potential application to large portions of the population.^{116,117} This has been fueled by risk prediction models for general CT based on the linear no-threshold theory, which claims a tiny yet finite risk for future cancer induction.¹¹⁸ There is a strong consensus by health radiation physicists that such estimates of quantitative risk should not be done for dose exposures less than 50 mSv because of the range of possible health outcomes, including no or even potentially beneficial health effects at these dose levels.¹¹⁹

It is important to realize that the concerns are theoretical in nature, proposed by one risk model. When looked at directly, in populations with similar dose exposures, there has been no empiric evidence for increased numbers of cancers in these groups. Large studies (up to 174,000 persons) over many years (5 decades in one study) have been conducted in nuclear industry workers, airline pilots, and atomic bomb survivors.¹²⁰⁻¹²² Cancer-related deaths are decreased in nuclear industry personnel compared with the general population. In the atomic bomb survivor data, in which 43% of the entire cohort ($N = 86,572$) received a dose less than 5 mSv, there was no increased incidence of cancer.¹²³ Ironically, it is this dataset from which the linear no-threshold model was developed from the backward extrapolation of the high-dose exposure cohort.

There are additional factors that mitigate risk, even if they are only theoretically true. For example, only the lung bases are included in the imaged field (most theoretically induced cancers are thoracic in origin), and the patient's typical age of 50 years or older further decreases the risk of a future cancer. Furthermore, several studies have modeled the benefit-risk ratio of CTC-based screening versus induced cancers (using the controversial linear risk model). In this worst case theoretical scenario, the benefit highly outweighs the risk. Berrington de González

and co-workers predicted that 24 to 35 colorectal cancers would be prevented for every theoretically induced cancer.¹²⁴

EXTRACOLONIC FINDINGS

The cross-sectional nature of CTC allows for diagnoses outside the colon, despite the lack of IV contrast and low-dose nature of this examination. Because of the potential widespread use of CTC with colorectal screening, this issue has been one of major interest for optimizing the approach to incidental lesions to minimize the cost and complications.^{125,126} There has been increasing recognition that the incidental risks and costs of any imaging examination should be factored into consideration in addition to the primary reason for the examination.¹¹⁷

As with incidental findings in general, there are positive and negative aspects for extracolonic findings. On the one hand, there are many findings that are incompletely evaluated and turn out to be benign after work-up. These incur cost and the potential for complications related to the additional evaluation. On the other hand, a few important unsuspected diagnoses will be made that have substantial impact for the patient. Structured reporting vehicles such as C-RADS and quality metrics help maximize the benefits of extracolonic findings and minimize the disadvantages of this issue.

Although an extensive literature exists specific to extracolonic findings (ECFs) with CTC, there remains debate on the overall benefit-cost balance, which in part is because of heterogeneous results among studies. It is important that population demographics be carefully considered when applying observed ECF rates. The studies reporting very high rates of additional needed work-up typically reflect a study population very disparate from the average-risk screening U.S. population.¹²⁷⁻¹³⁰ When considering low polyp prevalence or screening cohorts that would mirror the U.S. screening population, ECF rates fall into a consistent range. The overall ECF rates are typically 60% to 70% of the population.¹³¹⁻¹³³ However, it is important to recognize that most of these findings do not require additional work-up. For example, when detected, the diagnosis of a renal calculus is made with CTC, and no additional diagnostic work-up is necessary. When ECF rates for findings with potential for additional evaluation are examined, such as the E3-E4 rates in C-RADS, the rates typically range from 7% to 14%.¹³¹⁻¹³⁵ Also, when actual work-up rates are measured, the rates consistently decrease to less than 10%, from 5.5% to 8%.^{30,131-135} In these studies, this has translated into an additional cost of \$24 to \$34 per examination.^{131-133,135} Reasons why recommended work-ups are not undertaken may be that the extracolonic finding is a known finding that has already been evaluated, or because of comorbidities, work-up is not thought to be indicated for the patient.

These costs in regard to the ECF issue are balanced by the detection of clinically significant conditions. Approximately 2% to 3% of the screening cohort will have a clinically important diagnosis made. Two of the more important conditions include extracolonic cancers and abdominal aortic aneurysms (AAAs; Fig. 53-17). One large series of over 10,000 screening patients demonstrated an extracolonic cancer prevalence of 0.35%¹³⁶; AAA prevalence was reported as 0.5%.¹³⁵ Hassan and colleagues proposed that when extracolonic cancers and AAAs are considered, CTC screening strategies are more clinically effective and cost effective colonoscopic screening because of its coincident ability to detect these ECFs.¹³⁷

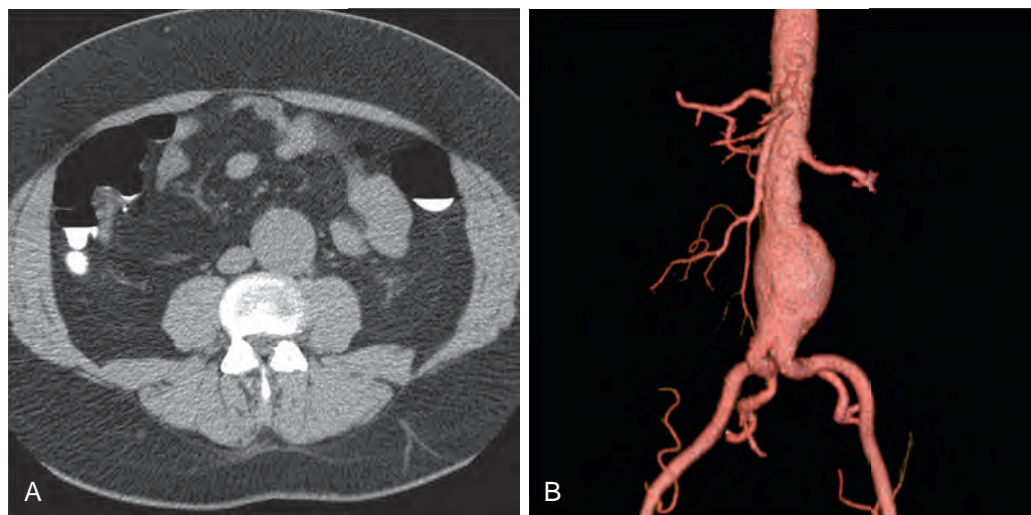


Figure 53-17 Unsuspected extracolonic finding. **A.** 2D CTC image shows an incidental aortic aneurysm during colorectal cancer screening. The patient was asymptomatic and unaware. **B.** The aneurysm was followed and repaired 5 years later as it began to grow.

Summary

CTC has matured into a clinically effective modality for the evaluation of colorectal polyps and masses. It has been validated by several prospective multicenter trials. CTC is a multicomponent examination requiring optimization of bowel preparation, colonic distention, and imaging acquisition parameters to

provide quality images. There is a learning curve for optimal interpretation. With attention to detail, this examination can detect relevant polyps with great sensitivity and specificity, equivalent to colonoscopy but with less invasiveness and risk for complications. Its main use and greatest impact will likely be in screening for colorectal cancer, but additional indications include diagnostic purposes and cancer staging and surveillance.

REFERENCES

- Johnson CD, Chen MH, Toledano AY, et al: Accuracy of CT colonography for detection of large adenomas and cancers. *N Engl J Med* 359:1207–1217, 2008.
- Pickhardt PJ, Choi JR, Hwang I, et al: Computed tomographic virtual colonoscopy to screen for colorectal neoplasia in asymptomatic adults. *N Engl J Med* 349:2191–2200, 2003.
- Regge D, Laudi C, Galatola G, et al: Diagnostic accuracy of computed tomographic colonography for the detection of advanced neoplasia in individuals at increased risk of colorectal cancer. *JAMA* 301:2453–2461, 2009.
- Graser A, Stieber P, Nagel D, et al: Comparison of CT colonography, colonoscopy, sigmoidoscopy, and fecal occult blood tests for the detection of advanced adenoma in an average risk population. *Gut* 58:241–248, 2009.
- Atkin W, Dadswell E, Wooldrage K, et al: Computed tomographic colonography versus colonoscopy for investigation of patients with symptoms suggestive of colorectal cancer (SIGGAR): A multicentre randomised trial. *Lancet* 381:1194–1202, 2013.
- Halligan S, Wooldrage K, Dadswell E, et al: Computed tomographic colonography versus barium enema for diagnosis of colorectal cancer or large polyps in symptomatic patients (SIGGAR): A multicentre randomised trial. *Lancet* 381:1185–1193, 2013.
- Young PE, Ray QP, Hwang I, et al: Gastroenterologists' interpretation of CTC: A pilot study demonstrating feasibility and similar accuracy compared with radiologists' interpretation. *Am J Gastroenterol* 104:2926–2931, 2009.
- O'Connor SD, Summers RM, Choi JR, Pickhardt PJ: Oral contrast adherence to polyps on CT colonography. *J Comput Assist Tomogr* 30:51–57, 2006.
- Holte K, Nielsen KG, Madsen JL, Kehlet H: Physiologic effects of bowel preparation. *Dis Colon Rectum* 47:1397–1402, 2004.
- Borden ZS, Pickhardt PJ, Kim DH, et al: Bowel preparation for CT colonography: Blinded comparison of magnesium citrate and sodium phosphate for catharsis. *Radiology* 254:138–144, 2010.
- Keedy AW, Yee J, Aslam R, et al: Reduced cathartic bowel preparation for CT colonography: Prospective comparison of 2-L polyethylene glycol and magnesium citrate. *Radiology* 261:156–164, 2011.
- Dodds WJ, Scanlon GT, Shaw DK, et al: An evaluation of colon cleansing regimens. *AJR* 128:57–59, 1977.
- Strates BS, Hofmann LM: A randomized study of two preparations for large bowel radiology. *Pharmatherapeutica* 5:57–61, 1987.
- Woodard JA, Shannon M, Lacouture PG, Woolf A: Serum magnesium concentrations after repetitive magnesium cathartic administration. *Am J Emerg Med* 8:297–300, 1990.
- Hookey LC, Depew WT, Vanner SJ: Combined low-volume polyethylene glycol solution plus stimulant laxatives versus standard-volume polyethylene glycol solution: A prospective, randomized study of colon cleansing before colonoscopy. *Can J Gastroenterol* 20:101–105, 2006.
- Markowitz GS, Nasr SH, Klein P, et al: Renal failure due to acute nephrocalcinosis following oral sodium phosphate bowel cleansing. *Hum Pathol* 35:675–684, 2004.
- Kim DH, Pickhardt PJ, Lubner MG, et al: Standardized reporting utilizing CT colonography reporting and data systems (C-RADS) in over 5,000 colorectal cancer screening individuals. Presented at the American Roentgen Ray Society Annual Meeting, San Diego, May 2–7 2010.
- Conry BG, Jones S, Bartram CI: The effect of oral magnesium containing bowel preparation agents on mucosal coating by barium sulphate suspensions. *Br J Radiol* 60:1215–1219, 1987.
- Robson NK, Lloyd M, Regan F: The use of carbon-dioxide as an insufflation agent in barium enema—does it have a role? *Br J Radiol* 66:197–198, 1993.
- Sumanac K, Zealley I, Fox BM, et al: Minimizing postcolonoscopy abdominal pain by using CO₂ insufflation: A prospective, randomized, double blind, controlled trial evaluating a new commercially available CO₂ delivery system. *Gastrointest Endosc* 56:190–194, 2002.
- Church J, Delaney C: Randomized, controlled trial of carbon dioxide insufflation during colonoscopy. *Dis Colon Rectum* 46:322–326, 2003.
- Yee J, Hung RK, Akerkar GA, Wall SD: The usefulness of glucagon hydrochloride for colonic distention in CT colonography. *AJR* 173:169–172, 1999.
- Rogalla P, Lembcke A, Ruckert JC, et al: Spasmodysis at CT colonography: Butyl scopolamine versus glucagon. *Radiology* 236:184–188, 2005.
- Taylor SA, Halligan S, Goh V, et al: Optimizing colonic distention for multidetector row CT colonography: Effect of hyoscine butylbromide and rectal balloon catheter. *Radiology* 229:99–108, 2003.
- Beebe TJ, Johnson CD, Stoner SM, et al: Assessing attitudes toward laxative preparation in colorectal cancer screening and effects on future testing: Potential receptivity to computed tomographic colonography. *Mayo Clin Proc* 82:666–671, 2007.

26. Ho W, Broughton DE, Donelan K, et al: Analysis of barriers to and patients' preferences for CT colonography for colorectal cancer screening in a nonadherent urban population. *AJR* 195:393–397, 2010.
27. McLachlan SA, Clements A, Austoker J: Patients' experiences and reported barriers to colonoscopy in the screening context—a systematic review of the literature. *Pat Educ Counsel* 86:137–146, 2012.
28. Iannaccone R, Laghi A, Catalano C, et al: Computed tomographic colonography without cathartic preparation for the detection of colorectal polyps. *Gastroenterology* 127:1300–1311, 2004.
29. Callstrom MR, Johnson CD, Fletcher JG, et al: CT colonography without cathartic preparation: Feasibility study. *Radiology* 219:693–698, 2001.
30. Zalis ME, Blake MA, Cai WL, et al: Diagnostic accuracy of laxative-free computed tomographic colonography for detection of adenomatous polyps in asymptomatic adults: A prospective evaluation. *Ann Intern Med* 156:692–702, 2012.
31. Liedenbaum MH, Bipat S, Bossuyt PMM, et al: Evaluation of a standardized CT colonography training program for novice readers. *Radiology* 258:477–487, 2011.
32. Soto JA, Barish MA, Yee J: Reader training in CT colonography: How much is enough? *Radiology* 237:26–27, 2005.
33. Pickhardt PJ, Lee AD, Taylor AJ, et al: Primary 2D versus primary 3D polyp detection at screening CT colonography. *AJR* 189:1451–1456, 2007.
34. Pickhardt PJ, Taylor AJ, Kim DH, et al: Screening for colorectal neoplasia with CT colonography: Initial experience from the 1st year of coverage by third-party payers. *Radiology* 241:417–425, 2006.
35. Pickhardt PJ, Wise SM, Kim DH: Positive predictive value for polyps detected at screening CT colonography. *Eur Radiol* 20:1651–1656, 2010.
36. Kim JY, Park SH, Lee SS, et al: Ascending colon rotation following patient positional change during CT colonography: A potential pitfall in interpretation. *Eur Radiol* 21:353–359, 2011.
37. Chen JC, Dachman AH: Cecal mobility: A potential pitfall of CT colonography. *AJR* 186:1086–1089, 2006.
38. Pickhardt PJ: Differential diagnosis of polypoid lesions seen at CT colonography (virtual colonoscopy). *Radiographics* 24:1535–1556, 2004.
39. Pickhardt PJ, Hain KS, Kim DH, Hassan C: Low rates of cancer or high-grade dysplasia in colorectal polyps collected from computed tomography colonography screening. *Clin Gastroenterol Hepatol* 8:610–615, 2010.
40. Vatn MH, Stalsberg H: The prevalence of polyps of the large intestine in Oslo—an autopsy study. *Cancer* 49:819–825, 1982.
41. Zalis ME, Barish MA, Choi JR, et al: CT colonography reporting and data system: A consensus proposal. *Radiology* 236:3–9, 2005.
42. Yoshida H, Nappi J, MacEneaney P, et al: Computer-aided diagnosis scheme for detection of polyps at CT colonography. *Radiographics* 22:963–979, 2002.
43. Taylor SA, Halligan S, Burling D, et al: Computer-assisted reader software versus expert reviewers for polyp detection on CT colonography. *AJR* 186:696–702, 2006.
44. Summers RM, Yao JH, Pickhardt PJ, et al: Computed tomographic virtual colonoscopy computer-aided polyp detection in a screening population. *Gastroenterology* 129:1832–1844, 2005.
45. Kim SH, Lee JM, Lee JG, et al: Computer-aided detection of colonic polyps at CT colonography using a Hessian matrix-based algorithm: Preliminary study. *AJR* 189:41–51, 2007.
46. Petrick N, Haider M, Summers RM, et al: CT colonography with computer-aided detection as a second reader: Observer performance study. *Radiology* 246:148–156, 2008.
47. Dachman AH, Obuchowski NA, Hoffmeister JW, et al: Effect of computer-aided detection for CT colonography in a multireader, multicase trial. *Radiology* 256:827–835, 2010.
48. Hara AK, Johnson CD, Reed JE, et al: Detection of colorectal polyps with CT colonography: Initial assessment of sensitivity and specificity. *Radiology* 205:59–65, 1997.
49. Dachman AH, Kuniyoshi JK, Boyle CM, et al: CT colonography with three-dimensional problem solving for detection of colonic polyps. *AJR* 171:989–995, 1998.
50. Fenlon HM, Nunes DP, Schroy PC, et al: A comparison of virtual and conventional colonoscopy for the detection of colorectal polyps. *N Engl J Med* 341:1496–1503, 1999.
51. Yee J, Akerkar GA, Hung RK, et al: Colorectal neoplasia: Performance characteristics of CT colonography for detection in 300 patients. *Radiology* 219:685–692, 2001.
52. Royster AP, Fenlon HM, Clarke PD, et al: CT colonoscopy of colorectal neoplasms: Two-dimensional and three-dimensional virtual-reality techniques with colonoscopic correlation. *AJR* 169:1237–1242, 1997.
53. Cotton PB, Durkalski VL, Benoit PC, et al: Computed tomographic colonography (virtual colonoscopy): A multicenter comparison with standard colonoscopy for detection of colorectal neoplasia. *JAMA* 291:1713–1719, 2004.
54. Rockey DC, Paulson E, Niedzwiecki D, et al: Analysis of air contrast barium enema, computed tomographic colonography, and colonoscopy: Prospective comparison. *Lancet* 365:305–311, 2005.
55. Fletcher JG, Chen MH, Herman BA, et al: Can radiologist training and testing ensure high performance in CT colonography? Lessons From the National CT Colonography Trial. *AJR* 195:117–125, 2010.
56. Hara AK, Johnson CD, MacCarty RL, et al: CT colonography: Single-versus multidetector row imaging. *Radiology* 219:461–465, 2001.
57. Pineau BC, Paskett ED, Chen GJ, et al: Virtual colonoscopy using oral contrast compared with colonoscopy for the detection of patients with colorectal polyps. *Gastroenterology* 125:304–310, 2003.
58. Macari M, Bini EJ, Xue XN, et al: Colorectal neoplasms: Prospective comparison of thin-section low-dose multidetector row CT colonography and conventional colonoscopy for detection. *Radiology* 224:383–392, 2002.
59. Yee J, Kumar NN, Hung RK, et al: Comparison of supine and prone scanning separately and in combination at CT colonography. *Radiology* 226:653–661, 2003.
60. Thomeer M, Carbone I, Bosmans H, et al: Stool tagging applied in thin-slice multidetector computed tomography colonography. *J Comput Assist Tomogr* 27:132–139, 2003.
61. Taylor SA, Halligan S, Bartram CI, et al: Multidetector row CT colonography: Effect of collimation, pitch, and orientation on polyp detection in a human colectomy specimen. *Radiology* 229:109–118, 2003.
62. Shinnors TJ, Pickhardt PJ, Taylor AJ, et al: Patient-controlled room air insufflation versus automated carbon dioxide delivery for CT colonography. *AJR* 186:1491–1496, 2006.
63. Pickhardt PJ, Choi JHR: Electronic cleansing and stool tagging in CT colonography: Advantages and pitfalls with primary three-dimensional evaluation. *AJR* 181:799–805, 2003.
64. Johnson CD, Fletcher JG, MacCarty RL, et al: Effect of slice thickness and primary 2D versus 3D virtual dissection on colorectal lesion detection at CT colonography in 452 asymptomatic adults. *AJR* 189:672–680, 2007.
65. Burling D, Taylor SA, Halligan S, et al: Automated insufflation of carbon dioxide for MDCT colonography: Distension and patient experience compared with manual insufflation. *AJR* 186:96–103, 2006.
66. Fletcher JG, Johnson CD, Welch TJ, et al: Optimization of CT colonography technique: Prospective trial in 180 patients. *Radiology* 216:704–711, 2000.
67. Buchach CM, Kim DH, Pickhardt PJ: Performing an additional decubitus series at CT colonography. *Abdom Imaging* 36:538–544, 2011.
68. Cash BD, Riddle MS, Bhattacharya I, et al: CT colonography of a Medicare-aged population: Outcomes observed in an analysis of more than 1400 patients. *AJR* 199:W27–W34, 2012.
69. Behrens C, Stevenson G, Eddy R, et al: The benefits of computed tomographic colonography in reducing a long colonoscopy waiting list. *Can Assoc Radiol J* 61:33–40, 2010.
70. Kim DH, Pickhardt PJ, Taylor AJ, et al: CT colonography versus colonoscopy for the detection of advanced neoplasia. *N Engl J Med* 357:1403–1412, 2007.
71. Long JR, Frew MI, Brazaitis MP: Virtual colonoscopy in the US Army: Current utilization at the Walter Reed Army Medical Center. *Abdom Imaging* 36:149–512, 2011.
72. Kim DH, Pooler BD, Weiss JM, Pickhardt PJ: Five year colorectal cancer outcomes in a large negative CT colonography screening cohort. *Eur Radiol* 22:1488–1494, 2012.
73. Siegel R, Naishadham D, Jemal A: Cancer statistics, 2012. *CA Cancer J Clin* 62:10–29, 2012.
74. Steinwachs D, Allen JD, Barlow WE, et al: National Institutes of Health State-of-the-Science Conference Statement: Enhancing use and quality of colorectal cancer screening. *Ann Intern Med* 152:663–667, 2010.
75. Shapiro JA, Klabunde CN, Thompson TD, et al: Patterns of colorectal cancer test use, including CT colonography, in the 2010 National Health Interview Survey. *Cancer Epidemiol Biomarkers Prev* 21:895–904, 2012.
76. Seeff LC, Manninen DL, Dong FB, et al: Is there endoscopic capacity to provide colorectal cancer screening to the unscreened population in the United States? *Gastroenterology* 127:1661–1669, 2004.
77. Moawad FJ, Maydonovitch CL, Cullen PA, et al: CT colonography may improve colorectal cancer screening compliance. *AJR* 195:1118–1123, 2010.
78. Pooler BD, Baumeil MJ, Cash BD, et al: Screening CT colonography: Multicenter survey of patient experience, preference, and potential impact on adherence. *AJR* 198:1361–1366, 2012.

79. Friedman AC, Downing D, Chino J, et al: Feasibility of remote CT colonography at two rural Native American medical centers. *AJR* 195:1110–1117, 2010.
80. Robbins DH, Itzkowitz SH: The molecular and genetic basis of colon cancer. *Med Clin North Am* 86:1467–1495, 2002.
81. Jass JR: Classification of colorectal cancer based on correlation of clinical, morphological and molecular features. *Histopathology* 50: 113–130, 2007.
82. O'Brien MJ: Hyperplastic and serrated polyps of the colorectum. *Gastroenterol Clin N Am* 36:947–968, 2007.
83. Johnson DA, Gurney MS, Volpe RJ, et al: A prospective study of the prevalence of colonic neoplasms in asymptomatic patients with an age-related risk. *Am J Gastroenterol* 85:969–974, 1990.
84. Lieberman DA, Smith FW: Screening for colon malignancy with colonoscopy. *Am J Gastroenterol* 86:946–951, 1991.
85. Lieberman DA, Weiss DG, Bond JH, et al: Use of colonoscopy to screen asymptomatic adults for colorectal cancer. *N Engl J Med* 343:162–168, 2000.
86. Disario JA, Foutch PG, Mai HD, et al: Prevalence and malignant potential of colorectal polyps in asymptomatic, average-risk men. *Am J Gastroenterol* 86:941–945, 1991.
87. Rex DK, Lehman GA, Hawes RH, et al: Screening colonoscopy in asymptomatic average-risk persons with negative fecal occult blood tests. *Gastroenterology* 100:64–67, 1991.
88. O'Brien MJ, Winawer SJ, Zauber AG, et al: The National Polyp Study—patient and polyp characteristics associated with high-grade dysplasia in colorectal adenomas. *Gastroenterology* 98:371–379, 1990.
89. Winawer SJ, Zauber AG: The advanced adenoma as the primary target of screening. *Gastrointest Endosc Clin N Am* 12:1–9, 2002.
90. Cunningham KS, Riddell RH: Serrated mucosal lesions of the colorectum. *Curr Opin Gastroenterol* 22:48–53, 2006.
91. Levin B, Lieberman DA, McFarland B, et al: Screening and surveillance for the early detection of colorectal cancer and adenomatous polyps, 2008: A joint guideline from the American Cancer Society, the US MultiSociety Task Force on Colorectal Cancer, and the American College of Radiology. *CA Cancer J Clin* 58:130–160, 2008.
92. Liedenbaum MH, van Rijn AF, de Vries AH, et al: Using CT colonography as a triage technique after a positive faecal occult blood test in colorectal cancer screening. *Gut* 58:1242–1249, 2009.
93. Sali L, Falchini M, Bonanomi AG, et al: CT colonography after incomplete colonoscopy in subjects with positive faecal occult blood test. *World J Gastroenterol* 14:4499–4504, 2008.
94. Pickhardt PJ, Hassan C, Halligan S, Marmo R: Colorectal cancer: CT colonography and colonoscopy for detection—systematic review and meta-analysis. *Radiology* 259:393–405, 2011.
95. Baxter NN, Goldwasser MA, Paszat LF, et al: Association of colonoscopy and death from colorectal cancer. *Ann Intern Med* 150:1–8, 2009.
96. Singh H, Nugent Z, Demers AA, Bernstein CN: Rate and predictors of early/missed colorectal cancers after colonoscopy in Manitoba: A population-based study. *Am J Gastroenterol* 105:2588–2596, 2010.
97. Bressler B, Paszat LF, Chen Z, et al: Rates of new or missed colorectal cancers after colonoscopy and their risk factors: A population-based analysis. *Gastroenterology* 132:96–102, 2007.
98. Pullens HJ, van Leeuwen MS, Laheij RJ, et al: CT colonography after incomplete colonoscopy: What is the diagnostic yield? *Dis Colon Rectum* 56:593–599, 2013.
99. Chang KJ, Rekh SS, Anderson SW, Soto JA: Fluid tagging for CT colonography: Effectiveness of a 2-hour iodinated oral preparation after incomplete optical colonoscopy. *J Comput Assist Tomogr* 35:91–95, 2011.
100. da Fonte AC, Chojniak R, Ferreira FD, et al: Inclusion of computed tomographic colonography on pre-operative CT for patients with colorectal cancer. *Eur J Radiol* 81:E298–E303, 2012.
101. Neri E, Turini F, Cerri F, et al: Comparison of CT colonography vs. conventional colonoscopy in mapping the segmental location of colon cancer before surgery. *Abdom Imaging* 35:589–595, 2010.
102. Kim JH, Kim WH, Kim TI, et al: Incomplete colonoscopy in patients with occlusive colorectal cancer: Usefulness of CT colonography according to tumor location. *Yonsei Med J* 48:934–941, 2007.
103. Chung DJ, Huh KC, Choi WJ, Kim JK: CT colonography using 16-MDCT in the evaluation of colorectal cancer. *AJR* 184:98–103, 2005.
104. Engstrom PF, Arnoletti JP, Benson AB, et al: Colon cancer. *J Natl Compr Cancer Network* 7:778–831, 2009.
105. Neri E, Vaghi P, Turini F, et al: Post-surgical follow-up of colorectal cancer: Role of contrast-enhanced CT colonography. *Abdom Imaging* 35:669–675, 2010.
106. Kim HJ, Park SH, Pickhardt PJ, et al: CT colonography for combined colonic and extracolonic surveillance after curative resection of colorectal cancer. *Radiology* 257:697–704, 2010.
107. Keefe E, O'Connor K: 1989 A/S/G/E survey of endoscopic sedation and monitoring practices. *Gastrointest Endosc* 36:S13–S18, 1990.
108. Pickhardt PJ: Incidence of colonic perforation at CT colonography: Review of existing data and implications for screening of asymptomatic adults. *Radiology* 239:313–316, 2006.
109. Bretthauer M, Thiis-Evensen E, Huppertz-Hauss G, et al: NORCCAP (Norwegian colorectal cancer prevention): A randomised trial to assess the safety and efficacy of carbon dioxide versus air insufflation in colonoscopy. *Gut* 50:604–607, 2002.
110. Levin TR, Zhao W, Conell C, et al: Complications of colonoscopy in an integrated health care delivery system. *Ann Intern Med* 145:880–886, 2006.
111. Burling D, Halligan S, Slater A, et al: Potentially serious adverse events at CT colonography in symptomatic patients: National survey of the United Kingdom. *Radiology* 239:464–471, 2006.
112. Sosna J, Blachar A, Amitai M, et al: Colonic perforation at CT colonography: Assessment of risk in a multicenter large cohort. *Radiology* 239:457–463, 2006.
113. Pickhardt PJ, Kim DH, Taylor AJ: Asymptomatic pneumatisis at CT colonography: A benign self-limited imaging finding distinct from perforation. *AJR* 190:W112–W117, 2008.
114. Liedenbaum MH, Venema HW, Stoker J: Radiation dose in CT colonography—trends in time and differences between daily practice and screening protocols. *Eur Radiol* 18:2222–2230, 2008.
115. Neri E, Faggioni L, Cerri F, et al: CT colonography versus double-contrast barium enema for screening of colorectal cancer: Comparison of radiation burden. *Abdom Imaging* 35:596–601, 2010.
116. Whitlock EP, Lin JS, Liles E, et al: Screening for colorectal cancer: A targeted, updated systematic review for the U.S. Preventive Services Task Force. *Ann Intern Med* 149:638–658, 2008.
117. Calonge N, Petitti DB, DeWitt TG, et al: Screening for colorectal cancer: U.S. Preventive Services Task Force recommendation statement. *Ann Intern Med* 149:627–637, 2008.
118. Brenner DJ, Hall EJ: Current concepts. Computed tomography—an increasing source of radiation exposure. *N Engl J Med* 357:2277–2284, 2007.
119. Health Physics Society: Radiation risk in perspective. Position statement of the Health Physics Society, 2010. <http://hps.org/documents/risk_ps010-2.pdf>. Accessed March 10, 2014.
120. Muirhead CR, O'Hagan JA, Haylock RGE, et al: Mortality and cancer incidence following occupational radiation exposure: Third analysis of the National Registry for Radiation Workers. *Br J Cancer* 100:206–212, 2009.
121. Pukkala E, Aspholm R, Auvinen A, et al: Incidence of cancer among Nordic airline pilots over five decades: Occupational cohort study. *Br Med J* 325:567–569, 2002.
122. Hammar N, Linnarsjo A, Alfredsson L, et al: Cancer incidence in airline and military pilots in Sweden—1961–1996. *Aviat Space Environ Med* 73:2–7, 2002.
123. Preston DL, Shimizu Y, Pierce DA, et al: Studies of mortality of atomic bomb survivors. Report 13: Solid cancer and noncancer disease mortality: 1950–1997. *Radiat Res* 178:AV146–AV172, 2012.
124. Berrington de González A, Kim KP, Knudsen AB, et al: Radiation-related cancer risks from CT colonography screening: A risk-benefit analysis. *AJR* 196:816–823, 2011.
125. Berland LL, Silverman SG, Gore RM, et al: Managing incidental findings on abdominal CT: White paper of the ACR Incidental Findings Committee. *J Am Coll Radiol* 7:754–773, 2010.
126. Berland LL: Incidental extracolonic findings at CT colonography: The impending deluge and its implications. *J Am Coll Radiol* 6:14–20, 2009.
127. Hellstrom M, Svensson MH, Lasso A: Extracolonic and incidental findings on CT colonography (virtual colonoscopy). *AJR* 182: 631–638, 2004.
128. Xiong T, McEvoy K, Morton DG, et al: Resources and costs associated with incidental extracolonic findings from CT colonography: A study in a symptomatic population. *Br J Radiol* 79:948–961, 2006.
129. Khan KY, Xiong T, McCafferty I, et al: Frequency and impact of extracolonic findings detected at computed tomographic colonography in a symptomatic population. *Br J Surg* 94:355–361, 2007.
130. Spreng A, Netzer P, Mattich J, et al: Importance of extracolonic findings at IV contrast medium-enhanced CT colonography versus those at non-enhanced CT colonography. *Eur Radiol* 15:2088–2095, 2005.

131. Hara AK, Johnson CD, MacCarty RL, Welch TJ: Incidental extracolonic findings at CT colonography. *Radiology* 215:353–357, 2000.
132. Gluecker TM, Johnson CD, Wilson LA, et al: Extracolonic findings at CT colonography: Evaluation of prevalence and cost in a screening population. *Gastroenterology* 124:911–916, 2003.
133. Yee J, Kumar NN, Godara S, et al: Extracolonic abnormalities discovered incidentally at CT colonography in a male population. *Radiology* 236:519–526, 2005.
134. Rajapaksa RC, Macari M, Bini EJ: Prevalence and impact of extracolonic findings in patients undergoing CT colonography. *J Clin Gastroenterol* 38:767–771, 2004.
135. Pickhardt PJ, Hanson ME, Vanness DJ, et al: Unsuspected extracolonic findings at screening CT colonography: Clinical and economic impact. *Radiology* 249:151–159, 2008.
136. Pickhardt PJ, Kim DH, Meiners RJ, et al: Colorectal and extracolonic cancers detected at screening CT colonography in 10,286 asymptomatic adults. *Radiology* 255:83–88, 2010.
137. Hassan C, Pickhardt PJ, Laghi A, et al: Computed tomographic colonography to screen for colorectal cancer, extracolonic cancer, and aortic aneurysm: Model simulation with cost-effectiveness analysis. *Arch Intern Med* 168:696–705, 2008.

Magnetic Resonance Colonography

SOFIA GOURTSOYIANNI | NICKOLAS PAPANIKOLAOU |
NICHOLAS C. GOURTSOYIANNIS

CHAPTER OUTLINE

Prerequisites and Examination Guidelines

Data Analysis

Indications

Accuracy and Clinical Experience

Patient Acceptance

Colonoscopy remains the first and, in most cases, the sole investigation for detection and prevention of colorectal cancer. However, in up to 26% of examinations, the ileocecal valve cannot be reached by the endoscopist because of stenotic lesions or elongated colonic segments.¹⁻³ Although computed tomography colonography (CTC; see Chapter 53) has received great appreciation in the last decade as an alternative colonic cancer screening examination, with a high accuracy for detection of polypoid lesions 1 cm or larger, radiation exposure remains a concern, especially for young patients with colonic pathology who require regular follow-up. In this context, the introduction of magnetic resonance colonography (MRC) holds great promise. The technique is based on the acquisition of MR datasets of the abdomen, with a distinct focus on the large bowel. Because of the noninvasive character and lack of procedural pain and discomfort, patient acceptance is improved compared with colonoscopy. The datasets can be displayed in a multiplanar reformation (MPR) mode on a postprocessing workstation, which enables the analysis of the colonic wall from any desired angle. In addition, virtual endoscopic views can be generated, so lesions may be more accurately defined.⁴ Concurrently with the colonic wall evaluation on MRC images, all abdominal organs within the displayed field of view can be also assessed.⁵

Prerequisites and Examination Guidelines

General contraindications to MR imaging (MRI), including the presence of a pacemaker or metallic, non-MRI-compatible implants, have to be considered prior to MRC referral. In addition, patients with hip prostheses are not considered ideal candidates for MRC because significant artifacts predominantly obscure the anorectal region, downgrading image quality significantly.

A clean colon is required, especially when the clinical question to be answered is in regard to polyp detection. The cleansing method is usually the same, implemented locally for conventional colonoscopy or CTC.

Because most bowel loops are collapsed in their physiologic state, sufficient distention of the bowel is needed to optimize the examination. This allows for reliable differentiation between

the bowel lumen and bowel wall. Most centers use water or barium solutions administered per rectum.⁶⁻⁸ The use of gaseous media has also been proposed, including room air or CO₂.⁹ Prior to rectal filling, spasmolytic agents (e.g., 20 to 40 mg of scopolamine or 1 mg of glucagon) should be administered intravenously. The effect of these agents is threefold:

1. A better degree of bowel distention can be achieved.
2. Bowel spasm is minimized and thereby patient's acceptance is enhanced.
3. Absence of artifacts because bowel motion is reduced.

Patients are positioned in a prone or supine position on the scanner table. If liquid contrast agents are used for luminal distention, 2000 to 2500 mL is administered via a rectal tube, using hydrostatic pressure. The filling procedure should be stopped whenever patients express considerable discomfort. Alternatively, dedicated sequences can be acquired to monitor the filling process, such as nonslice select sequences providing an update image every 2 to 3 seconds.¹⁰ A combination of two large flex surface coils should be used for signal reception to ensure coverage of the entire large bowel. However, use of the body coil may be sufficient, especially for obese patients.

For data acquisition, the use of a 1.5-T scanner equipped with strong gradient systems is preferable. Data collection is mainly performed under breath-hold conditions. Thus, acquisition times of the single sequence should not exceed 20 to 25 seconds. Cardinal sequences used in MRC are the same as the ones used in MRI of the small bowel (MR enterography or enteroclysis; see Chapter 40).¹¹ The acquisition of 2D and/or 3D fast imaging with steady-state precession (FISP) sequences has proven to be quite useful.^{12,13} Image properties are characterized by a mixture of T1-weighted and T2-weighted contrast, leading to a homogenous bright signal of the colonic lumen filled with water and providing good contrast with the colonic wall, which has low signal intensity. Furthermore, 3D T1-weighted MRI scans should be acquired before and at 70 to 80 seconds after intravenous (IV) administration of gadolinium. Data collection is done in coronal and axial planes for all sequences described. Proposed MRC protocol sequence parameters are listed in Table 54-1.

Data Analysis

Whenever a colorectal lesion is found, the analysis has to be repeated using the corresponding, native, T1-weighted dataset. The signal intensities of the lesions should be recorded to calculate the percentage of contrast enhancement. This procedure helps distinguish between residual stool and true colorectal polyps or cancers reliably. Although true colorectal lesions always enhance (Figs. 54-1 and 54-2), residual stool shows the same signal properties on native and contrast-enhanced T1-weighted images. However, scar tissue, (e.g., after appendectomy) may also show a significant percentage of contrast enhancement, thereby mimicking a polyp (Fig. 54-3). In a

TABLE 54-1 Proposed Magnetic Resonance Colonography Sequence Characteristics

Parameter	T1w VIBE	T1w FLASH	True FISP
2D or 3D	3D	2D	3D
Acquisition plane	Coronal	Axial	Coronal
Acquisition time (s)	21	5 × 19*	22
TR (ms)	3.1	158	3.8
TE (ms)	1.1	1.8	1.9
FLIP angle (degrees)	12	70	80
Slice thickness (mm)	1.8	5.0	2.0
No of slices	120	70	96

*Five acquisition blocks of 19 seconds each.
TE, echo time; TR, repetition time.

second step, the FISP sequences should be analyzed. These sequences have been found to be very accurate for the detection of inflammatory bowel lesions.¹²

In contrast to colonoscopy, virtual colonoscopy studies are not limited to endoscopic viewing. In addition, all abdominal organs within the field of view are displayed. This is especially useful in cases of a colorectal carcinoma because the liver and adrenal glands can be evaluated at the same time. Hepatic lesions can be easily detected and characterized because of the availability of dynamic, contrast-enhanced T1-weighted images. Furthermore, relevant lesions in other organs, including the presence of enlarged lymph nodes, may be identified, which helps in accurate colorectal cancer staging.

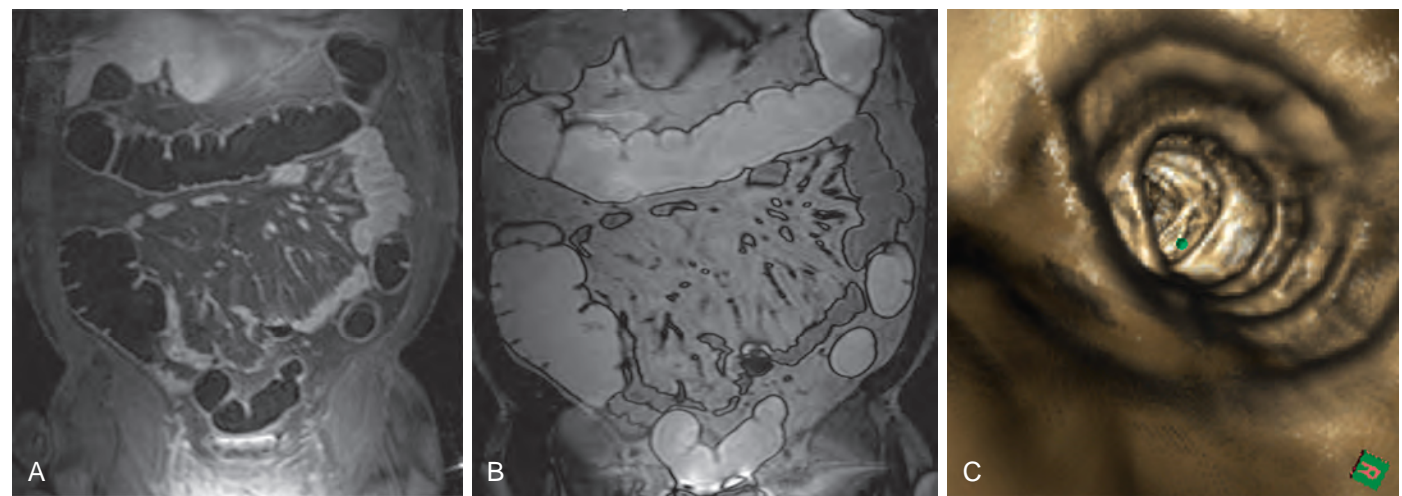


Figure 54-1 MRC sequences. Comprehensive examination protocol of MR colonography should include T1-weighted images (A), true FISP images (B), and virtual endoscopic reconstructions (C).

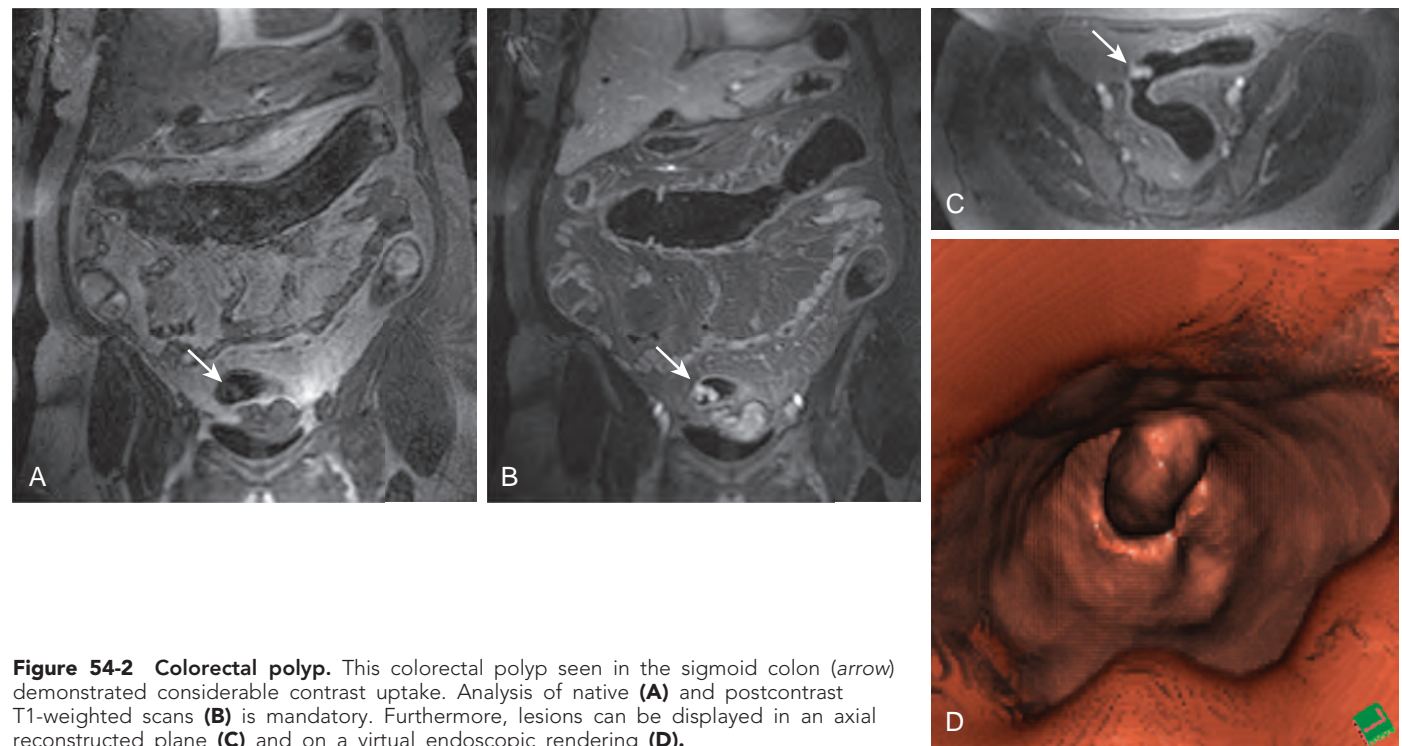


Figure 54-2 Colorectal polyp. This colorectal polyp seen in the sigmoid colon (arrow) demonstrated considerable contrast uptake. Analysis of native (A) and postcontrast T1-weighted scans (B) is mandatory. Furthermore, lesions can be displayed in an axial reconstructed plane (C) and on a virtual endoscopic rendering (D).

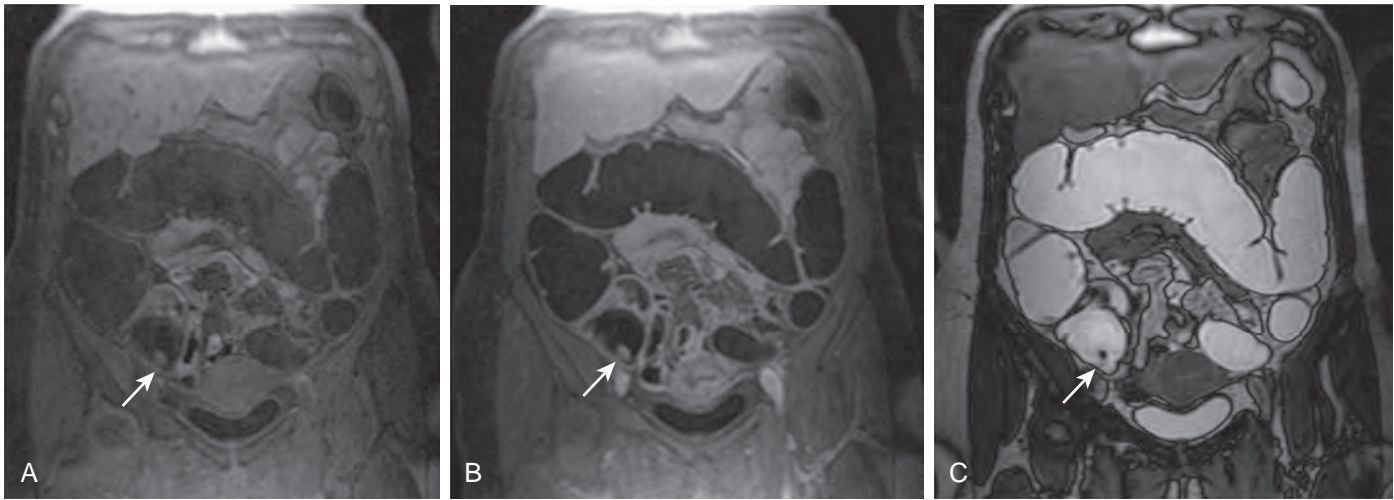


Figure 54-3 Appendectomy scar artifact. Scar tissue following appendectomy (arrow) may mimic a colonic polyp (C) because of strong contrast uptake comparing the pre- (A) and postcontrast (B) T1-weighted scans.

Indications

MRC has proven to be a suitable tool in patients with incomplete colonoscopy. There are several underlying reasons for incomplete colonoscopy, such as strictures, elongated bowel segments, and insufficient patient acceptance. MRC provides significantly higher completion rates—bowel elongation has no influence on the visualization of colonic segments, and only high-grade stenosis might prohibit the passage of water, which is necessary for the distention of prestenotic segments (Fig. 54-4). In a study investigating 37 patients with MRC after incomplete conventional colonoscopy (CC), only 4% of the bowel segments were not assessable by means of MRC, whereas CC had failed to reach almost 50% of the potentially visible colonic segments.¹⁴ In addition, MRC revealed lesions in the prestenotic segments, which had not been depicted by CC, including two carcinomas and five polyps.

Furthermore, MRC has shown to be suitable for the diagnosis and assessment of colonic inflammatory bowel disease (IBD) (Fig. 54-5).¹⁵⁻¹⁷ In a study of 23 patients with suspected IBD of the large bowel with MRC,¹⁵ bowel wall inflammation was quantified according to four imaging characteristics—bowel wall contrast enhancement, bowel wall thickness, presence of regional lymph nodes, and loss of haustral folds. Consequently, an inflammation score was calculated, which was compared with endoscopic results and clinical data. Over 90% of the colonic segments with IBD changes were correctly identified. For severe inflammation, sensitivity approached 100%. Therefore, MRC may be used for monitoring IBD activity. Furthermore, extramural changes, including abscesses, phlegmon, or fistula formation can be easily depicted, which may not indicated by colonoscopy.¹⁸ MRC has an especially high reported accuracy for the diagnosis of disease activity and severity in the proximal colon.¹⁹

Despite promising results in the assessment of prestenotic bowel segments and IBD, there are no reliable data yet on MR colonography supporting colorectal cancer screening applications. Most colorectal cancers develop over a period of several years from adenomatous polyps. This makes colorectal cancer to a large extent preventable because detection and subsequent



Figure 54-4 Adenocarcinoma of the colon. Severe stenosis caused by colonic adenocarcinoma (arrow) does not permit evaluation of prestenotic bowel segments when using colonoscopy. Such a display is much less difficult with MRC.

removal of polyps eliminate the risk of malignant degeneration. MRC actually provides all important properties of a screening tool. It is not associated with ionizing radiation exposure, and no other side effects are known. However, all experimental studies and data analysis of MRC have been performed so far in preselected patient cohorts. Further studies with larger screening cohorts are needed.

Contrast-enhanced MRC has been reported to have a very high accuracy (84%-100%) in detecting colorectal involvement in women presenting with deep pelvic endometriosis, playing an important role in preoperative mapping.²⁰

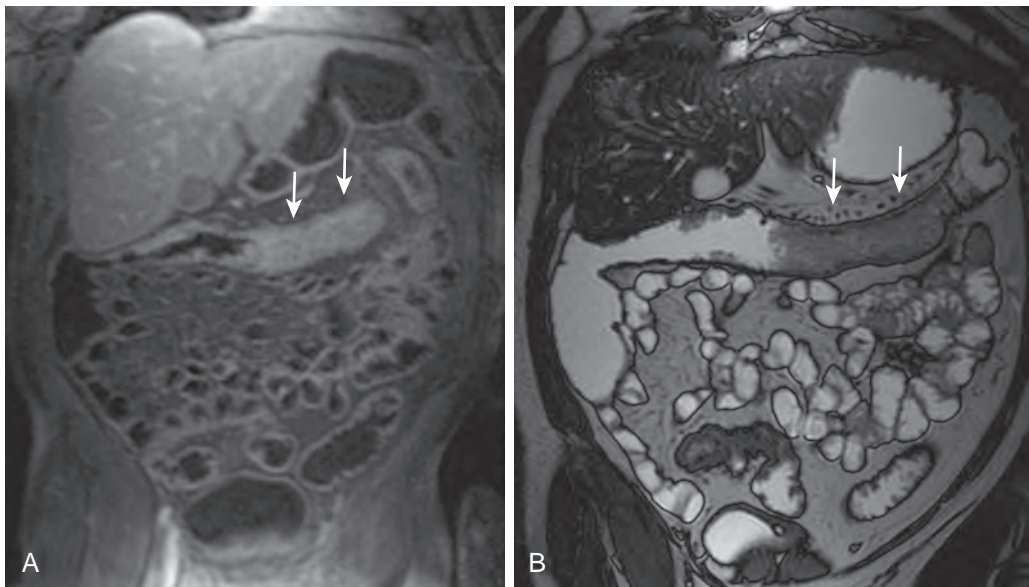


Figure 54-5 Crohn's disease with MRC. This patient with Crohn's disease showed increased contrast enhancement of the transverse colon (arrows) on the T1-weighted image (A) and bowel wall thickening on the true FISP image (B).

Accuracy and Clinical Experience

The accuracy of MRC for the detection of colorectal masses and IBD has been assessed in a number of studies. The largest study to date included 100 patients evaluated with MRC¹⁰; conventional colonoscopy was performed following the MRC examination on the same day and served as the standard of reference. MR data acquisition included pre- and postgadolinium T1-weighted images, which were compared with endoscopic and histologic results. Colonoscopy revealed a total of 107 colorectal masses. MRC was able to identify all masses larger than 10 mm and 84.2% of polyps between 6 and 9 mm in diameter. Overall specificity of MRC amounted to 96.0%, and only a very small number of false-positive results were found. MRC showed a high accuracy for the detection of adenomas and carcinomas larger than 6 mm. These results were confirmed by a study that included patients at high risk.⁵ Over 100 subjects with suspected colorectal disease underwent MRI, with colonoscopy serving as the standard of reference. None of the lesions smaller than 5 mm was identified by MRC, probably because of lower spatial resolution. However, the sensitivity for the detection of lesions between 5 and 10 mm amounted to 89%. Also, all colorectal masses larger than 10 mm, including nine carcinomas, were correctly diagnosed with MRC.

Diagnostic accuracy and image quality appear to be related to the type of MR sequences used. Thus, the application of fast imaging with true FISP or contrast-enhanced, T1-weighted images have been found to result in different image quality and accuracy.¹² Lauenstein et al,¹² in a study comparing MRC and colonoscopy, used true FISP and postcontrast T1-weighted fast low-angle shot (FLASH) images. T1-weighted imaging provided all-over sensitivity values of almost 80% for the detection of colorectal pathologies. Furthermore, there were no false-positive results because residual stool could be easily distinguished from colorectal masses because of the lack of contrast enhancement. True FISP sequences, however, had a lower sensitivity, approximately 70%. False-positive results were identified in 14% of the examinations, most probably related to the

difficulty of distinguishing between residual stool and colorectal masses. Interestingly, image quality of FISP turned out to be significantly better than that of T1-weighted imaging; because of lower motion sensitivity, fewer artifacts caused by respiratory or patient motion were noticed (Fig. 54-6). These results indicate that the main diagnostic evaluation, at present, should be based on the T1-weighted data, although true FISP sequences may provide useful information, especially in uncooperative patients.

One major criticism still relates to the very limited accuracy of MRC to detect colorectal polyps smaller than 5 mm. The clinical significance of these lesions remains controversial, because most of them are not prone to malignant degeneration.²¹ Small polyps will probably become detectable by MRC in the future. Technical improvements, such as parallel acquisition techniques (PATs), have certainly helped increase spatial resolution.²² However, flat adenomas are likely to remain elusive.

A qualitative assessment of diffusion weighted imaging (DWI)—obtained images (highest b value of 1000 s/mm²) was carried out for the detection of clinically significant colorectal polyps (≥ 6 mm) in 26 patients who underwent colonoscopy. On a per-lesion basis, a sensitivity of 80% and a positive predictive value (PPV) of 73% have been reported. As such, DWI cannot be recommended in a clinical setting when CC is to be performed in patients with positive findings on DWI.²³ DWI-MRC, however, has been reported to be a reliable tool for detecting colonic inflammation in ulcerative colitis, even without bowel preparation.²⁴

Patient Acceptance

Bowel cleansing has been a mandatory prerequisite for MRC because fecal material may mimic the appearance of colonic masses. However, bowel preparation is considered unpleasant by most patients and may lead to symptoms ranging from feeling unwell to an inability to sleep.^{25,26} Patient's acceptance for MRC could be significantly increased if bowel preparation

Figure 54-6 Motion artifacts on MRC. True FISP images (**A**) are less prone to motion artifacts than T1-weighted gradient echo images (**B**) and may therefore provide helpful information, especially for patients who are not able to hold their breath.

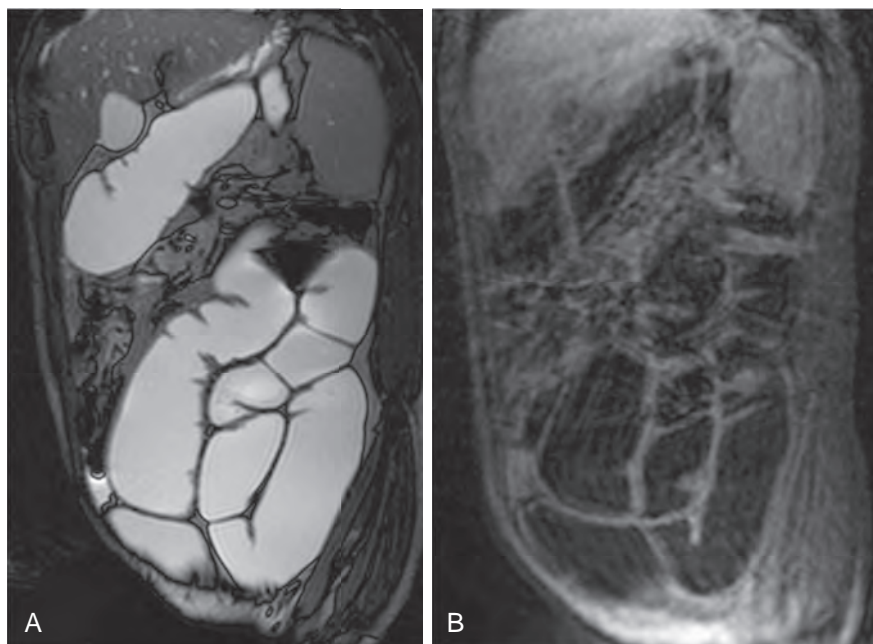
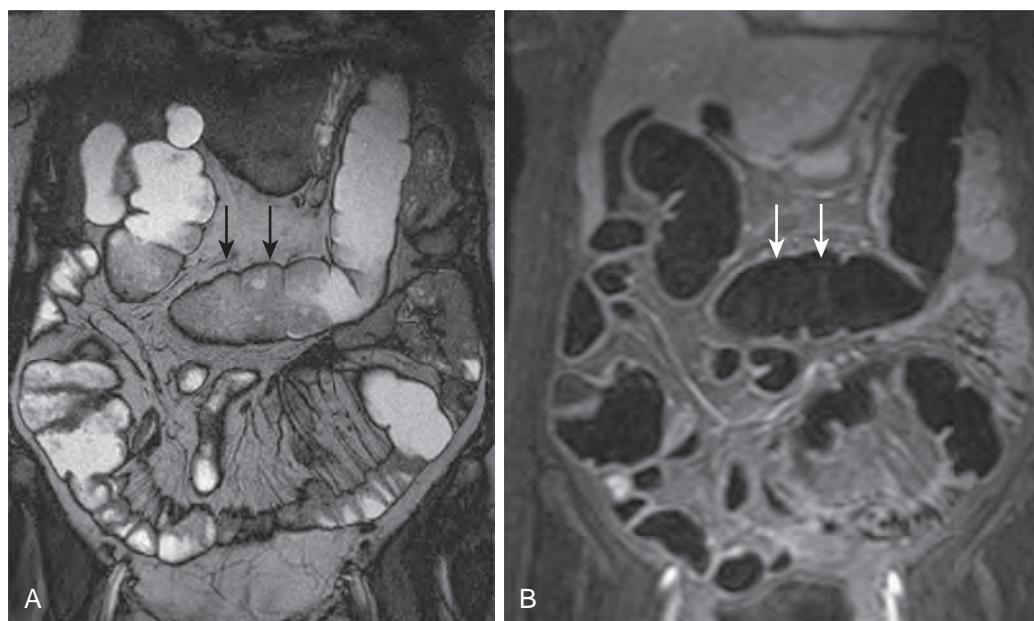


Figure 54-7 Fecal material visibility with tagging. **A.** Note that on the true FISP image the fecal material presents with moderate signal intensity (arrows). **B.** Fecal material (arrows) may be rendered almost invisible on T1-weighted images by means of fecal tagging.



could be eliminated. Different strategies have been proposed and tested to accomplish this. One successful approach is fecal tagging, which leads to a modification of signal characteristics of fecal material. For this, specific oral contrast compounds have to be ingested over 48 hours prior to the MR examination. The signal properties of stool are thereby adapted to the signal characteristics of the rectal enema. Thus, fecal material becomes almost invisible (Fig. 54-7).

Barium sulfate solutions have been used for fecal tagging. Administered orally, with 200 mL given with each of four main meals prior to the MR examination, barium decreases the signal intensity of fecal material on T1-weighted gradient recalled

echo (GRE) images.^{8,26,27} Thus, feces are rendered almost indistinguishable from the water enema administered (Fig. 54-8). Fecal tagging with barium has been successfully tested in volunteer and patient studies.^{8,28} However, ingestion of barium was considered as unpleasant as bowel cleansing.

Patient experiences of MRC and conventional colonoscopy have been compared in small cohorts of those having undergone both examinations, and it has been found that the experience is rather complex and strongly influenced by the clinical indications. IBD patients have reported more physical discomfort during conventional colonoscopy but were more satisfied with received feedback.²⁹

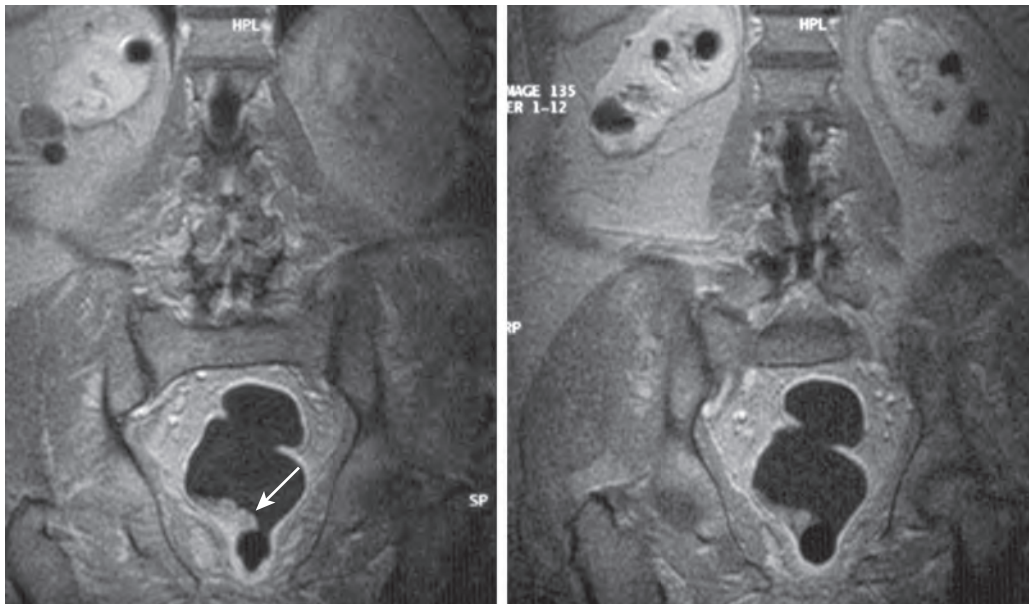


Figure 54-8 Large polyp on MRC. This large polyp (arrow) is depicted in two consecutive turbo FLASH coronal views. Homogeneous suppression of the intraluminal signal can be achieved through optimization of the inversion time, whereas the absence of motion-related artifacts can be explained in the sequential data acquisition of the turbo FLASH sequence.

REFERENCES

- Dafnis G, Granath F, Pahlman L, et al: Patient factors influencing the completion rate in colonoscopy. *Dig Liver Dis* 37:113–118, 2005.
- Cirotto WC, Rusin LC: Factors that predict incomplete colonoscopy. *Dis Colon Rectum* 38:964–968, 1995.
- Marshall JB, Barthel JS: The frequency of total colonoscopy and terminal ileal intubation in the 1990s. *Gastrointest Endosc* 39:518–520, 1993.
- McFarland EG, Brink JA, Pilgram TK, et al: Spiral CT colonography: Reader agreement and diagnostic performance with two- and three-dimensional image-display techniques. *Radiology* 218:375–383, 2001.
- Ajay W, Pelster G, Treichel U, et al: Dark lumen magnetic resonance colonography: Comparison with conventional colonoscopy for the detection of colorectal pathology. *Gut* 52:1738–1743, 2003.
- Pappalardo G, Poletti E, Frattaroli FM, et al: Magnetic resonance colonography versus conventional colonoscopy for the detection of colonic endoluminal lesions. *Gastroenterology* 119:300–304, 2000.
- Lauenstein TC, Herborn CU, Vogt FM, et al: Dark lumen MR-colonography: Initial experience. *Rofo* 173:785–789, 2001.
- Lauenstein T, Holtmann G, Schoenfelder D, et al: MR colonography without colonic cleansing: A new strategy to improve patient acceptance. *AJR* 177:823–827, 2001.
- Ajay W, Lauenstein TC, Pelster G, et al: MR colonography: How does air compare to water for colonic distention? *J Magn Reson Imaging* 19: 216–221, 2004.
- Hartmann D, Bassler B, Schilling D, et al: Colorectal polyps: Detection with dark-lumen MR colonography versus conventional colonoscopy. *Radiology* 238:143–149, 2006.
- Gourtsoyiannis NC, Grammatikakis J, Papamastorakis G, et al: Imaging of small intestinal Crohn's disease: Comparison between MR enteroclysis and conventional enteroclysis. *Eur Radiol* 16:1915–1925, 2006.
- Lauenstein TC, Ajay W, Kuehle CA, et al: Magnetic resonance colonography: Comparison of contrast-enhanced three-dimensional turbo with two-dimensional FISP sequences: Preliminary experience. *Invest Radiol* 40:89–96, 2005.
- Martin DR, Yang M, Thomasson D, Acheson C: MR colonography: Development of optimized method with ex vivo and in vivo systems. *Radiology* 225:597–602, 2002.
- Ajay W, Lauenstein TC, Pelster G, et al: MR colonography in patients with incomplete conventional colonoscopy. *Radiology* 234:452–459, 2005.
- Ajay W, Lauenstein TC, Pelster G, et al: MR colonography for the detection of inflammatory diseases of the large bowel: Quantifying the inflammatory activity. *Gut* 54:257–263, 2005.
- Schreyer AG, Golder S, Scheibl K, et al: Dark lumen magnetic resonance enteroclysis in combination with MRI colonography for whole bowel assessment in patients with Crohn's disease: First clinical experience. *Inflamm Bowel Dis* 11(4):388–394, 2005.
- Schreyer AG, Rath HC, Kikinis R, et al: Comparison of magnetic resonance imaging colonography with conventional colonoscopy for the assessment of intestinal inflammation in patients with inflammatory bowel disease: A feasibility study. *Gut* 54:250–256, 2005.
- Rimola J, Ordás I, Rodríguez S, Panés J: Colonic Crohn's disease: Value of magnetic resonance colonography for detection and quantification of disease activity. *Abdom Imaging* 35:422–427, 2010.
- Ordás I, Rimola J, García-Bosch O, et al: Diagnostic accuracy of magnetic resonance colonography for the evaluation of disease activity and severity in ulcerative colitis: A prospective study. *Gut* 62:1566–1572, 2013.
- Scardapane A, Lorusso F, Bettocchi S, et al: Deep pelvic endometriosis: Accuracy of pelvic MRI completed by MR colonography. *Radiol Med* 118:323–338, 2013.
- Villavicencio RT, Rex DK: Colonic adenomas: Prevalence and incidence rates, growth rates, and miss rates at colonoscopy. *Semin Gastrointest Dis* 11:185–193, 2000.
- Steidle G, Schafer J, Schlemmer HP, et al: Two-dimensional parallel acquisition technique in 3D MR colonography. *Rofo* 176:1100–1105, 2004.
- Leufkens AM, Kwee TC, van den Bosch MA, et al: Diffusion-weighted MRI for the detection of colorectal polyps: Feasibility study. *Magn Reson Imaging* 31:28–35, 2013.
- Oussalah A, Laurent V, Bruot O, et al: Diffusion-weighted magnetic resonance without bowel preparation for detecting colonic inflammation in inflammatory bowel disease. *Gut* 59:1056–1065, 2010.
- Elwood MJ, Ali G, Schlup MT, et al: Flexible sigmoidoscopy or colonoscopy for colorectal screening: A randomized trial of performance and acceptability. *Cancer Detect Prev* 19:337–347, 1995.
- Thomeer M, Bielen D, Vanbekevoort D, et al: Patient acceptance for CT colonography: What is the real issue? *Eur Radiol* 12:1410–1415, 2002.
- Papanikolaou N, Grammatikakis J, Maris T, et al: MR colonography with fecal tagging: Comparison between 2D turbo FLASH and 3D FLASH sequences. *Eur Radiol* 13:448–452, 2003.
- Lauenstein TC, Goehde SC, Ruehm SG, et al: MR colonography with barium-based fecal tagging: Initial clinical experience. *Radiology* 223:248–254, 2002.
- Hafeez R, Wagner CV, Smith S, et al: Patient experiences of MR colonography and colonoscopy: A qualitative study. *Br J Radiol* 85:765–769, 2012.

Diverticular Disease of the Colon

KIRAN H. THAKRAR | RICHARD M. GORE | VAHID YAGHMAI |
EMIL J. BALTHAZAR

CHAPTER OUTLINE

Diverticulosis

Epidemiology
Causative Factors
Pathophysiology
Clinical Findings
Radiologic Findings

Diverticulitis

Epidemiology
Pathophysiology
Clinical Findings
Radiologic Findings
Surgical and Computed Tomography Staging
Differentiation of Diverticulitis from Carcinoma
Chronic Diverticulitis
Differential Diagnosis
Complications

Diverticular Hemorrhage

Pathophysiology
Clinical Findings

Giant Sigmoid Diverticulum

Causative Factors
Pathophysiology and Clinical Findings
Radiologic Findings
Therapy

Colonic diverticula are acquired herniations of the mucosa and of portions¹ of the submucosa through the muscularis propria. Diverticular disease of the colon represents a continuum from an initial, prediverticular phase of marked muscular thickening of the colon wall (myochosis) to frank outpouchings (diverticulosis) and finally to diverticular perforation (diverticulitis). Disease progression from the initial phase to the advanced phases does not necessarily occur.¹ In this chapter, we discuss the natural history of this disease and focus on radiologic diagnosis and intervention.

Diverticulosis

EPIDEMIOLOGY

Diverticular disease is the most common colonic disease in the Western world. Interestingly, this disease was a pathologic curiosity before the 20th century. Its modern development is attributable to the introduction of the roller milling process in 1880, which removes most of the fiber from flour. This process results in a low-residue diet producing low-volume,

tenacious stools that require a high degree of propulsive effort for expulsion.^{2,3}

In Western countries, colonic diverticula occur in 5% of the population by 40 years of age, in 33% to 50% of the population after 50 years of age, and in more than 50% of the population after 80 years of age.^{2,3} Among patients of routine risk, diverticulosis is found in 71% of patients on colonoscopy age 80 years or older.⁴ These findings contrast sharply to the prevalence rate of less than 0.2% in underdeveloped areas of Asia and Africa.⁵ In individuals from low-prevalence areas who migrate to Western communities, the frequency of diverticula increases within 10 years.^{1,6}

The sigmoid colon is involved in up to 95% of patients.⁷ Japan is an interesting exception to other developed countries in that patients with right-sided diverticulosis predominate at younger ages, subsequently becoming more bilateral over time.⁸ Of all patients who harbor diverticula, and 20% of those whose diverticula are clinically recognized, 4% to 5% will develop some complication, 1% to 2% will require hospitalization, and 0.5% will need surgical intervention, radiologic intervention, or both.^{4,5} In 2011, diverticulosis and diverticulitis were listed as the principal discharge diagnosis in 329,165 cases, accumulating over \$11 billion in hospital charges in the United States. In-hospital deaths were listed as 1,858 cases (0.56%).^{9,10}

CAUSATIVE FACTORS

The two fundamental factors contributing to the development of sigmoid diverticula are a pressure gradient between the lumen and serosa and areas of relative weakness in the bowel wall. The first factor can best be appreciated by considering the tendency of the colon to function not as a tube but as small compartments created by the haustra (segmentation). The sigmoid is the narrowest portion of the colon and generates the highest intrasegmental pressures, an example of the law of Laplace. In addition, stool is most dehydrated in the sigmoid colon, further increasing segmentation and motor activity.^{6,10}

The colon wall is weakest where the intramural vasa recta penetrate to the submucosal layers. These points are on either side of the taenia mesocolica and on the mesenteric side of the taenia libera and taenia omentalis (Fig. 55-1).^{2,3} Diverticula do not usually occur on the haustral row between the taenia omentalis and taenia libera.^{2,3}

PATHOPHYSIOLOGY

Most colonic diverticula are false diverticula, or pseudodiverticula, because they contain mucosa and submucosa but not the muscularis propria (Fig. 55-2). They are usually 0.5 to 1.0 cm in size and penetrate the clefts between bundles of circular muscle fibers at points where nutrient arteries pass through the

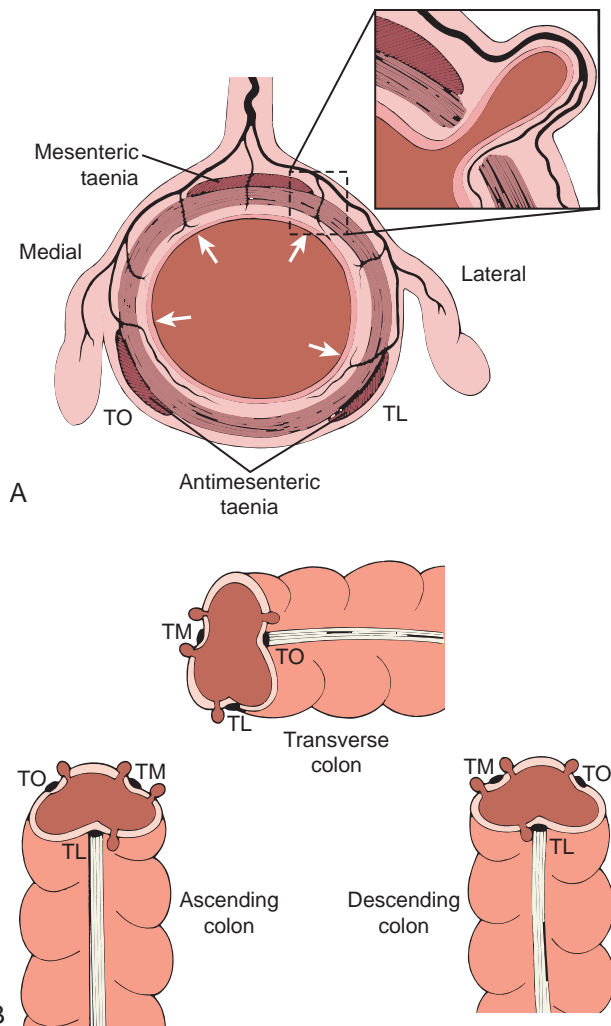


Figure 55-1 Site of origin of colonic diverticula. **A.** Diverticula develop on either side of the mesenteric taenia and on the mesenteric side of the antimesenteric taenia, taenia omentalis (TO), and taenia libera (TL). These are the sites (arrows) at which the vasa recta perforate the muscularis propria and penetrate the submucosa (inset). **B.** The antimesenteric TO-TL haustral row does not give rise to diverticula. TM, mesenteric taenia. (**A** from Dietzen CD, Pemberton JH: Diverticulitis. In Yamada T [ed]: *Textbook of Gastroenterology*. Philadelphia, JB Lippincott, 1991, pp 1734–1748; **B** from Meyers MA, Volberg F, Katzen B, et al: *Haustral anatomy and pathology: A new look: II. Roentgen interpretation of pathologic alterations*. *Radiology* 108:505–512, 1973.)

submucosa. The proximity of the diverticula to the arteries is considered key in the development of hemorrhage.^{2,3,11}

In the uninfamed state, diverticula are elastic and compressible but have a tendency to empty poorly and, as a result, to fill with inspissated stool. This tendency may account for the increased number of lymphoid follicles found in the lining mucosa.^{2,3} Most patients with sigmoid diverticula have myochosis, a disorder in which there is thickening of the circular muscle layer, shortening of the taeniae, and narrowing of the lumen. The circular muscle is often corrugated, and its appearance has been likened to that of a concertina.^{2,3}

Diverticula of the rectum are rare, likely because the taeniae become fused anteriorly and posteriorly at this level, forming a completely encircling, supporting coat. Rectal diverticula are true diverticula and are usually lateral.^{12–14}

CLINICAL FINDINGS

In most patients, diverticulosis is an incidental finding. Patients may complain of symptoms of irritable bowel syndrome, such as chronic or intermittent postprandial lower abdominal pain, which is relieved by defecation.

RADIOLOGIC FINDINGS

Radiographic Studies

More than 50% of patients with significant diverticular disease demonstrate a distinctive bubbly appearance of the sigmoid colon on routine abdominal radiographs. When pelvic phleboliths are present, there is a statistical correlation between their number and size and the degree of diverticular disease. It is postulated that both these common disorders are caused by the long-term effects of a low-fiber diet and straining while defecating.^{15,16}

Barium Studies

Diverticulosis is detected more often by double-contrast studies than by single-contrast studies because of the greater colonic distention and improved visualization of intramural diverticula (Fig. 55-3). When viewed en face, these immature diverticula may simulate aphthae. Their true nature is established when they are viewed in profile, when they are conical or triangular and 1 to 2 mm high.^{17–20}

The mature diverticulum has several characteristic appearances (Fig. 55-4) that depend on the angle with which it is viewed and degree of barium filling. In profile, the diverticulum appears as a flasklike protrusion measuring several millimeters to several centimeters in length, joined to the wall by a fairly long, large neck. En face, it may appear as a ring shadow or a well-margined barium collection or may resemble a bowler hat (Fig. 55-5). The size and form of diverticula vary from one moment to the next, depending on the degree of colonic distention. The alignment of diverticula along the taeniae is usually apparent.^{20–25}

Diagnostic difficulties may arise if the diverticulum inverts into the lumen, and a number of diverticular polypectomies have been described in the endoscopic literature. Also, if feces obstruct the diverticulum, the diverticular orifice may bulge into the lumen, resulting in a ring shadow or filling defect. In profile, only the neck of the diverticulum may be visible. If the obstruction is incomplete, a fine linear strand of barium may penetrate the diverticulum, simulating a spur. Because this strand of barium appears outside the lumen, its presence usually allows the correct diagnosis to be made. For this reason, careful attention to the appearance of polyps and diverticula from film to film is necessary.^{20–26}

A diverticulum with a large neck may resemble a sessile polyp, one with a narrow neck may resemble a pedunculated polyp, and an obstructed diverticulum may resemble a polyp or adherent fecal material. In addition, both polyps and diverticula can produce the so-called bowler hat sign. If the bowler hat points toward the center of the long axis of the colon, it represents a polyp. If it points away from the center of the long axis of the bowel, it represents a diverticulum. If the bowler hat is located in the midline of the bowel, or is directly parallel to the long axis of the bowel, it cannot be confidently classified as representing a polyp or diverticulum.^{20–25}



Figure 55-2 Diverticula: pathologic findings. **A.** Diverticula (black arrow) arise adjacent to the taenia coli, where there is weakness in the bowel wall from penetration of the vasa rectae. The appendices epiploicae (blue arrows) lie adjacent to these diverticula. It is not surprising that epiploic appendagitis and diverticulitis can have similar clinical features. **B.** Histologic image shows that diverticula consist of herniated mucosal and submucosal layers and lack the muscularis propria. **C.** Colonoscopic view of multiple diverticula in the sigmoid colon. The orifice of the diverticula is evident (arrows). **D.** Gross specimen of colon. Diverticula readily fill with stool but empty it poorly.

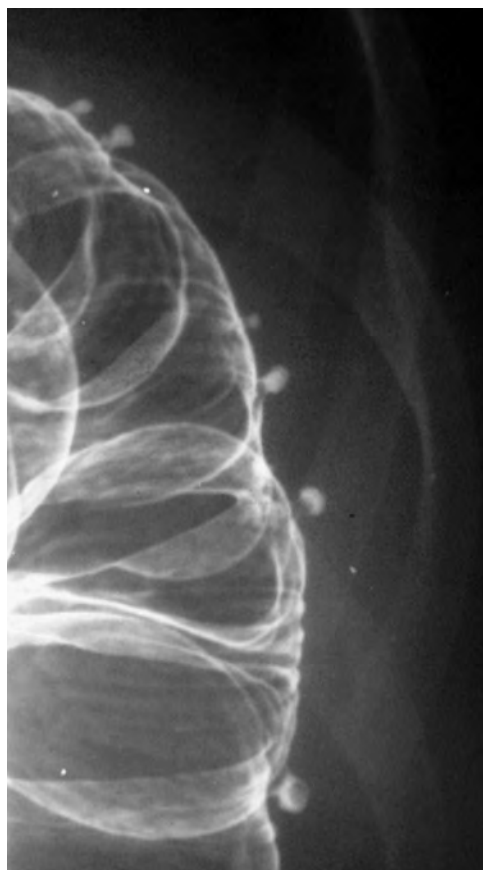


Figure 55-3 Colonic diverticulosis: double-contrast barium enema features. Multiple barium-filled outpouchings are identified along the lateral aspect of the proximal descending colon.

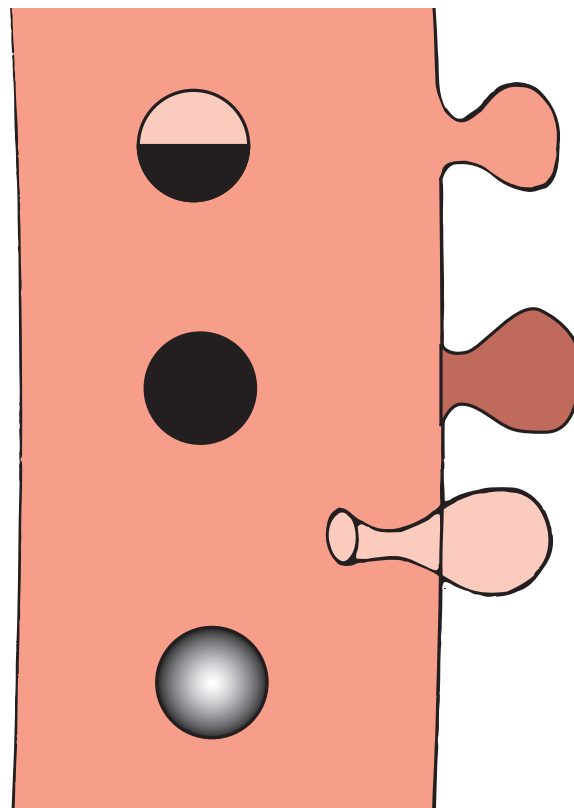


Figure 55-4 Variable appearance of diverticula on double-contrast barium enema. The appearance of diverticula depends on the angle from which they are viewed and how much barium or air they contain. (From Bartram CI, Kumar P: *Clinical Radiology in Gastroenterology*. Oxford, England, Blackwell Scientific, 1981, p 130.)

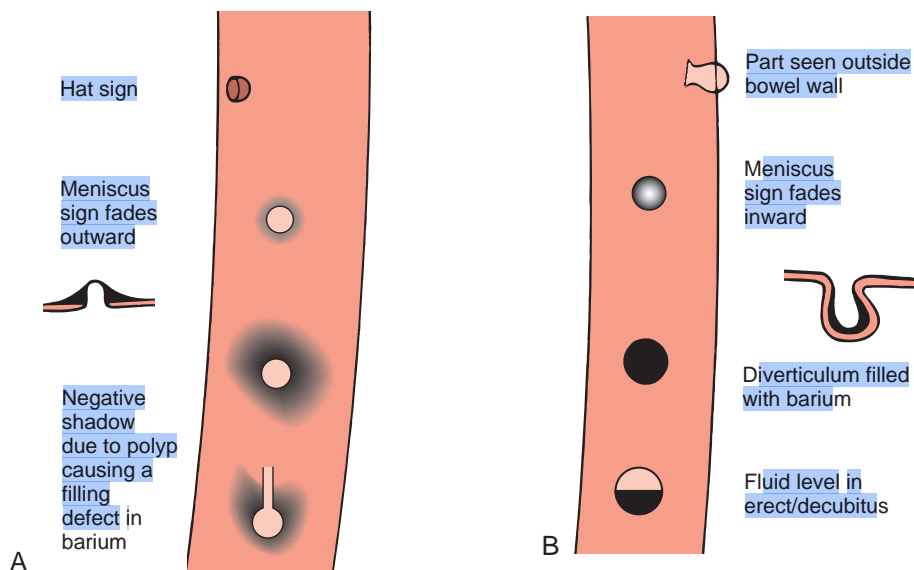


Figure 55-5 Distinguishing features of polyps and diverticula. **A.** Polyps. **B.** Diverticula. (From Bartrum CI, Kumar P: *Clinical Radiology in Gastroenterology*. Oxford, England, Blackwell Scientific, 1981, p 131.)

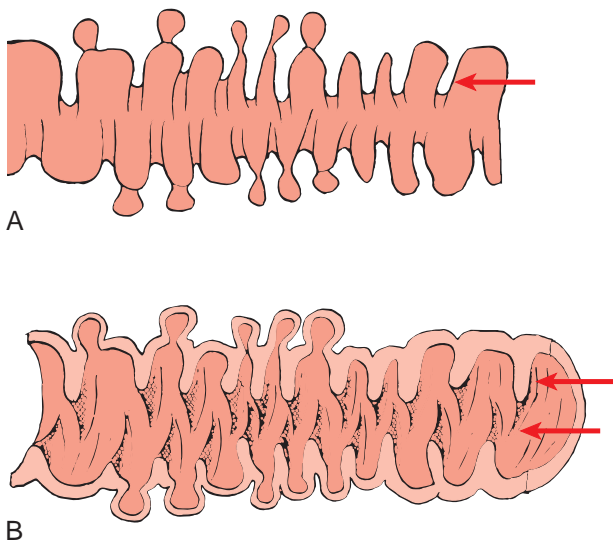


Figure 55-6 Colonic myochosis. **A.** The thickened circular muscle (arrow) and shortened taeniae lead to the appearance of a concertina. **B.** Longitudinal section of the same sigmoid colon segment shows narrowing of the lumen and prominent haustra (arrows), which are staggered. (From Weissman A, Clot M, Brellet J: *Double Contrast Examination of the Colon*. Berlin, Springer-Verlag, 1985, p 150.)

Caliber and haustral abnormalities (Fig. 55-6) usually accompany and often antedate the appearance of diverticula, particularly in the sigmoid colon. Haustral clefts are usually symmetric and face one another in the sigmoid; however, in diverticular or prediverticular disease, they indent alternately from one border to another, creating a staggered effect. The circular muscle is hypertonic and thickened, and the taeniae contract. Diverticula originate at the top of the haustra. With progressive disease, the circular muscle continues to undergo hypertrophy and a concertina or zigzag appearance develops. This appearance is caused by the alternated, highly compact, deep, and uniform haustra that separate and segment the haustral cul-de-sacs.¹⁷⁻²⁵

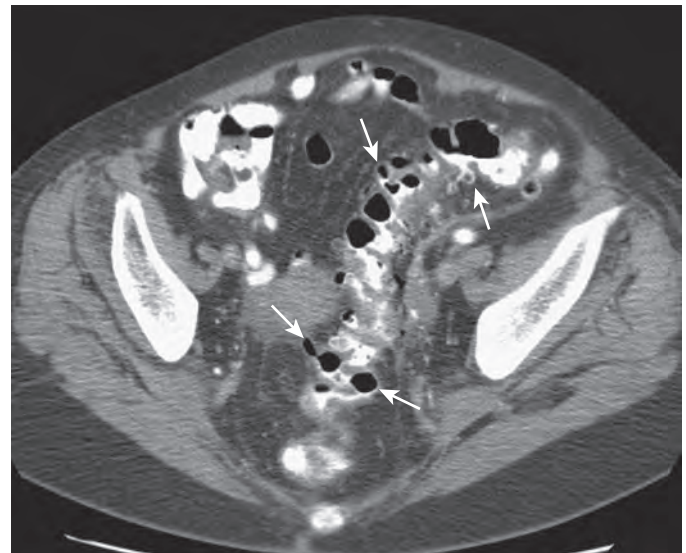


Figure 55-7 Diverticulosis: CT findings. CT scan at the level of the sigmoid colon shows multiple air- and contrast-filled diverticula (arrows).

Computed Tomography

Computed tomography (CT; Fig. 55-7) reveals mural thickening of the colon (>4 mm) in myochosis and in most cases of diverticulosis. The diverticula appear as outpouchings that contain air, stool, and/or contrast agent.

Diverticulitis

EPIDEMIOLOGY

Diverticulitis is the most common complication of diverticulosis. Traditionally, this has been estimated to occur in 10% to 25% of patients with diverticulosis.^{27,28} The true incidence is likely less, with one study of Veterans Administration patients establishing an incidence closer to 4%.²⁹

Simple, or uncomplicated diverticulitis, will occur in 75% of initial presentations. Complicated diverticulitis, defined as the presence of an abscess, fistula, obstruction, or perforation, is seen in the remaining 25%.³⁰

PATHOPHYSIOLOGY

The stagnation of nonsterile, inspissated fecal material within the diverticulum can cause inflammatory erosion of the mucosal lining in early, subclinical stages of diverticulitis. Subsequently, the wall of the diverticulum is eroded. This perforation is the essential feature of diverticulitis (Fig. 55-8A).^{2,3}

This sequence of events can involve an intramural diverticulum, leading to the formation of an intramural abscess. Usually, it occurs extramurally within the pericolic fat, leading to fibrinous exudate, abscess formation, local adhesions, or peritonitis. During surgery and pathologic examination, many juxtacolic abscesses are small and difficult to find in the mass of indurated fat and fibrous tissue. It is important to emphasize that the inflammation begins at the apex of the diverticulum and may spread rapidly into the soft pericolic and mesocolic fat. The inflammatory changes in diverticulitis are therefore mainly pericolic, adjacent but outside the bowel wall.^{2,3}

The colonic mucosa is not affected in diverticulitis, except in the region of the erosion. Most inflammatory complications of clinical significance are secondary to the rupture of a diverticulum, and they occur in a pericolic location in almost all cases. Consequently, these pathologic changes may be better described as peridiverticulitis or pericolitis. True diverticulitis, with inflammation limited to the diverticular lining, was present in 10% of pathologic specimens, and muscular hypertrophy, with distortion alone and without inflammation, accounted for the remaining 25% of cases.^{2,3}

The consequences of diverticular rupture depend on the host response and virulence of the bacterial contamination.^{2,3} Most patients develop sealed-off abscesses or contained sinus tracts and fistulas. Free perforations are uncommon but can lead to

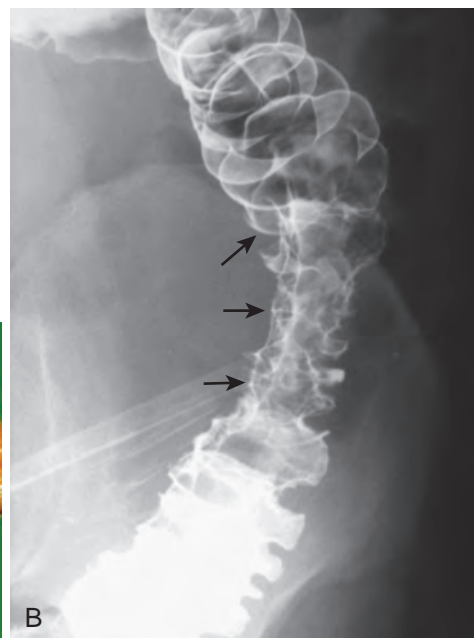
localized pelvic or generalized peritonitis. Fistulas involve adjacent structures, such as the small bowel, urinary bladder, vagina, and anterior abdominal wall. Occasionally, several adjacent diverticula communicate with each other along the outer aspect of the deep muscular layers, forming an intramural fistulous tract. In other cases, fistulas extend deeply into the fatty tissue at the site of the attachment of the sigmoid mesocolon.^{2,3}

CLINICAL FINDINGS

The classic clinical features of sigmoid diverticulitis are left lower quadrant pain, tenderness, fever, and leukocytosis. Because of this clinical constellation, sigmoid diverticulitis has been termed *left-sided appendicitis*. Diverticulitis occurring in other colonic locations is more difficult to diagnose clinically. In one review, the following clinical features were noted: pain in the left iliac fossa in 85% of patients; palpable mass, tenderness, and muscle guarding in 48%; fever in 30%; vomiting in less than 50%; and partial obstruction in 20%. Mild bleeding occurred in 25% of patients, and about 33% of patients had a history of recurrent episodes of similar attacks. Surgical evaluation of this group of 258 patients showed a 20% incidence of pericolic abscess, 8% incidence of fistulas, and 18% incidence of peritonitis. The initial clinical diagnosis was sigmoid carcinoma in 32% of patients, but carcinoma was found in only 2% of patients. The occurrence of malignancy was entirely coincidental, but it highlights the clinical difficulties of diagnosing and evaluating patients with suspected acute diverticulitis. These difficulties are further documented by large surgical series of patients with a clinical diagnosis of acute diverticulitis, in whom 25% to 33% of the resected surgical specimens showed no active inflammation, abscess, or fistulas.^{1-3,26-28,31}

Severe diverticulitis can occur in certain groups of patients and produce only minimal or unremarkable clinical symptoms, such as debilitated older patients, patients who have renal failure, are undergoing dialysis, or have had renal transplantation, and patients receiving corticosteroids. Disease in these

Figure 55-8 Diverticulitis. A. Pathologic specimen showing perforation of a diverticulum into the pericolic fat, a finding diagnostic of diverticulitis. **B.** Double-contrast barium enema shows mass effect on the medial aspect of the junction of the descending colon and sigmoid (arrows). There is distortion of the lumen, but the extent of extracolonic disease cannot be assessed.



patients may progress to free perforation, and the diagnosis is often made only when free intra-abdominal air is detected on abdominal films.^{2,3,30}

Patients younger than 40 years have historically been reported to have more severe forms of diverticulitis, ultimately requiring surgery.³² Some reports have suggested that younger patients follow the same course as older patients, and the decision for surgery should be made similarly.^{33,34}

The clinical management of patients with acute diverticulitis depends on the severity, type, and extent of the pericolic inflammatory changes. Mild forms of disease are managed medically with antibiotic therapy. A large recent Swedish study, however, concluded that mild acute uncomplicated diverticulitis may be successfully treated with anti-inflammatory agents, with no additional benefit from antibiotics.³⁵ In more severe forms, surgical resection may be indicated, either at the time of the diagnosis or after a cooling-off interval of antibiotic therapy and percutaneous abscess drainage. One study demonstrated emergent surgical intervention in 12% of patients admitted for diverticulitis.³⁶ This has decreased over time, partly because of increased use of image-guided percutaneous drainages.^{37,38} Emergent surgery is reserved for Hinchey 3 or 4 acute diverticulitis.

Close clinical and radiologic evaluation are crucial for the triage of patients to conservative, radiologic, or surgical management. The radiologic investigation of these patients has two objectives—to confirm the clinical suspicion of diverticulitis (and rule out other colonic or pelvic disease) and evaluate and stage the severity of the inflammatory disease. Sigmoidoscopy is usually contraindicated and serves no useful purpose except in patients who have more chronic forms of disease and present with bleeding, or in patients in whom polyps or sigmoid carcinoma is suspected.

RADIOLOGIC FINDINGS

Radiographic Studies

Abdominal radiographs taken with the patient supine and upright are usually diagnostic only in the most severe forms of diverticulitis, in which the patient presents with free intraperitoneal air or sealed-off perforations and pelvic extraluminal air. The detection of an ill-defined, left-sided pelvic mass, localized ileus, and fluid in the pelvis suggests the diagnosis in the appropriate clinical setting. In most patients with acute diverticulitis, however, abdominal plain films are unremarkable and do not contribute to the diagnosis.

Contrast Enema Examination

Contrast enema (CE) examination had traditionally been the primary method of examining patients with suspected diverticulitis, but now has been replaced by CT as the initial diagnostic test. It superbly depicts diverticula, colonic mucosa and lumen, spasm, muscle hypertrophy, and sacculations. These findings, however, are indicative of diverticular disease but not diagnostic of acute diverticulitis. Because this procedure primarily evaluates the colonic lumen and mucosal surface, the pericolic inflammatory process present in most patients with diverticulitis can only be inferred (Fig. 55-8B).¹⁷⁻¹⁹

A specific diagnosis of perforated diverticulitis can be made only when there is extravasation of contrast material from a diverticulum into a walled-off abscess, sinus tract, or fistula or free extravasation of contrast material into the peritoneal cavity.

These extraluminal collections of contrast medium vary in size, are usually located adjacent to the colon, compress and displace the colonic wall, and are detected in less than 50% of cases of diverticular perforation. Narrowing of the sigmoid lumen, extrinsic compression, and spasm are present in more than 80% of patients, but these findings are less specific. Similarly, an altered mucosal pattern is present in 68% of patients but is not a reliable indicator of acute inflammation. Lack of mobility with fixation of the sigmoid colon and narrowing, pointing, and distortion of individual diverticula are indirect signs consistent with acute or chronic diverticulitis.¹⁷⁻¹⁹

A contour defect that is smooth, well defined, and associated with adjacent sigmoid diverticula represents an intramural inflammatory mass. The contents of the intramural mass, whether pus, organized abscess, or merely mural fibrosis, are more difficult to characterize. Tracts filled with contrast material passing from ruptured diverticula into the pericolic tissues are common (Fig. 55-9). They may be single or multiple, end blindly (sinuses), or connect with an adjacent hollow viscus or abdominal wall (fistulas). The most common fistulas are colovesical and coloenteric. Colocutaneous fistulas are less frequent and are clinically associated with subcutaneous abscess, emphysema, or fasciitis. Fistulas to the vagina, ureter, appendix, hip, perineum, and soft tissues of the thigh have also been reported. With CE, the fistulous tract between the colon and urinary bladder is visualized in only 20% of patients who have colovesical fistulas.¹⁷⁻¹⁹

Longitudinal intramural fistulous tracts represent ruptured diverticula that communicate with each other. Although this sign has also been reported in carcinoma of the colon and Crohn's disease, longitudinal intramural fistulous tracts most often are caused by diverticulitis unless there is a previous history or radiographic evidence of Crohn's disease in the remainder of the colon or terminal ileum.

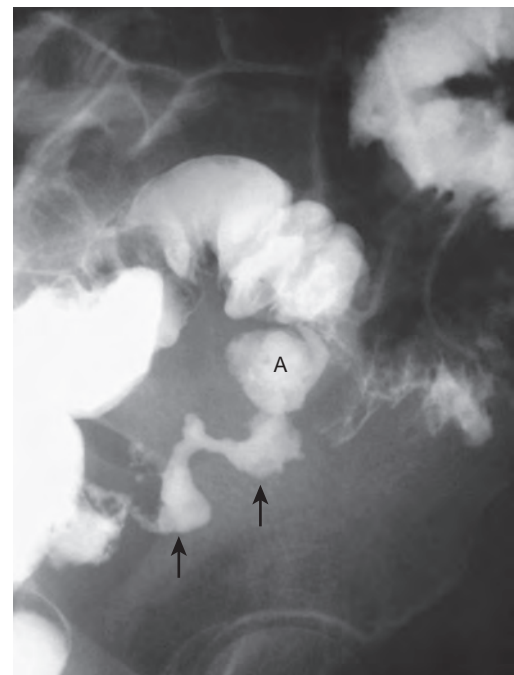


Figure 55-9 Diverticulitis with pericolic abscess: barium enema features. Spot image from a barium enema shows filling of an abscess (A) and a sinus tract (arrows) along the inferior aspect of the sigmoid colon.

Ultrasonography

Although multidetector CT (MDCT) is the primary cross-sectional imaging study for patients with suspected diverticulitis, ultrasonography (US) may be the first study ordered for nondescript abdominal pain and for pregnant patients suspected of having diverticulitis. The advantages of ultrasound are the lack of ionizing radiation and relative lower cost. Ultrasound is practically and technically more difficult in obese and severely ill patients, and is operator-dependent. US should be performed with a graded compression technique. One meta-analysis has demonstrated no significant difference in the accuracy of graded compression US and CT in diagnosing diverticulitis, with CT more likely to find alternative causes of abdominal pain.³⁹ Additionally, CT has been found to be more sensitive in the evaluation of complicated diverticular disease, better demonstrating abscess and free air.⁴⁰

The segmental concentric thickening of the gut wall commonly found in patients with diverticular disease manifests as a hypoechoic segment that reflects the predominant thickening of the muscular layer (Fig. 55-10). Sonographic findings of

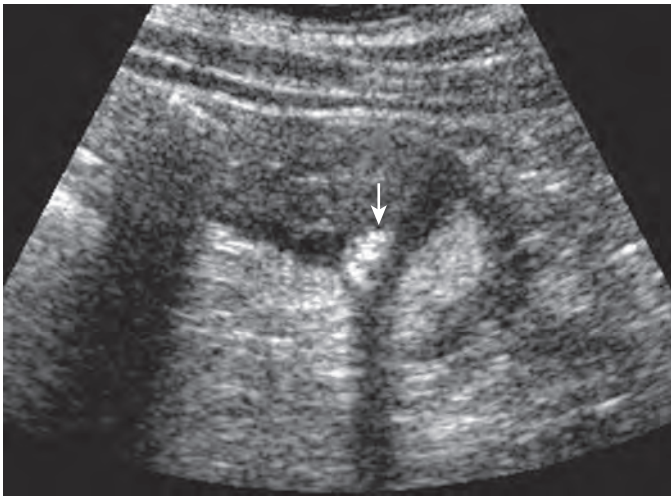
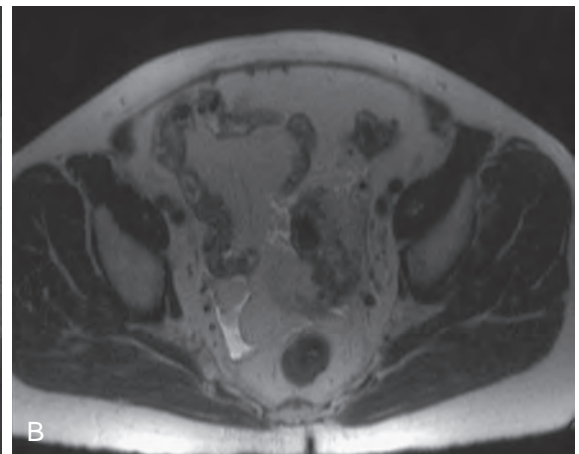
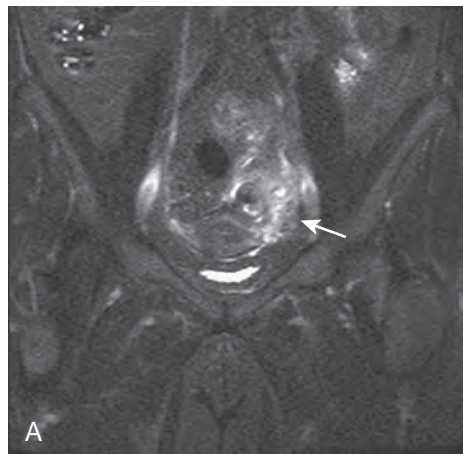


Figure 55-10 Diverticulitis: sonographic features. There is mural thickening of the sigmoid colon associated with a gas-containing intramural abscess (arrow) that casts an acoustic shadow.

Figure 55-11 Diverticulitis: MRI features. **A.** Coronal T2-weighted MRI scan of the descending colon demonstrates mural thickening, increased signal from the colonic mucosa, and abnormal signal in the pericolic fat (arrow). **B.** Axial T2-weighted image without fat suppression demonstrates abnormal T2 signal within the pericolic fat and mural thickening. A small amount of free fluid is also present.



diverticulitis include segmental wall thickening more than 4 mm, echogenic adjacent pericolic fat that is noncompressible, and inflamed diverticula. Local pain on compression is also a typical finding. Inflamed diverticula are brightly echogenic reflectors with acoustic shadowing or a ring-down artifact in or beyond the thickened gut wall. There may be adjacent fluid. Intramural sinus tracts appear as high-amplitude linear echoes that often have a ring-down artifact within the colon wall. A fecalith will be echogenic, with posterior acoustic shadowing. Abscesses appear as loculated, thick-walled fluid collections that may contain gas.⁴¹⁻⁴⁴

Magnetic Resonance Imaging

Mural thickening of the colon (Fig. 55-11) and diverticular abscesses are well visualized on magnetic resonance imaging (MRI), particularly on gadolinium-enhanced, fat-suppressed, T1-weighted spoiled gradient-echo images and T2-weighted, single-shot echo-train spin-echo images. Inflammatory change within the adjacent fat can be seen on non-fat-suppressed and fat-suppressed images. Sinus tracts, fistulas, and the walls of abscesses enhance and are well depicted in a background of suppressed fat on gadolinium-enhanced, fat-suppressed, spoiled gradient-echo images.⁴⁵

The major advantage of MRI is the lack of ionizing radiation. The disadvantages of MRI are longer scan times, greater susceptibility to motion artifact from the adjacent bowel, and relative higher cost. Given the efficiency and effectiveness of CT in the assessment of diverticulitis and its complications, MRI has little role in the primary evaluation of routine patients with known or suspected diverticulitis. MRI could be considered in special situations, such as pregnant patients, because of the lack of ionizing radiation.

Computed Tomography

MDCT has dramatically improved the diagnosis and management of patients with diverticulitis. MDCT is ideally suited for evaluating the intramural component of the inflammatory process and its intraperitoneal or retroperitoneal extension. CT is particularly useful in the evaluation of patients with sepsis who present with left lower quadrant pain, fever, leukocytosis, and a tender, palpable pelvic mass. CT has a reported accuracy, specificity, and sensitivity of up to 99%.^{32,46} Current guidelines recommend a CT with intravenous (IV) contrast as the initial test for patients with suspected diverticulitis.⁴⁷ Oral contrast is

not practically necessary, but may help in the evaluation of fistulas and with bowel distention.

CT findings in acute diverticulitis are listed in Table 55-1. On non-contrast-enhanced scans, the offending diverticulum can often be identified. It is hyperdense and is the nidus of the surrounding inflammation (Fig. 55-12). Diverticula are identified on CT at the site of the perforation or at a site adjacent to it in more than 80% of cases of acute diverticulitis. They appear as small outpouchings filled with air, barium, and/or fecal material projecting through the colonic wall. Symmetric thickening of the colonic wall in excess of 4 mm is seen in about 70% of cases. The thickened wall has a homogeneous density, and its diameter usually measures less than 1 cm in the distended colon. When there is significant muscular hypertrophy, the wall of the colon can be up to 2 or 3 cm thick. In diverticulitis, significant hypertrophy of muscle primarily occurs in the sigmoid

segment, which can mimic carcinoma of the colon. Accurate assessment of colon wall thickness is possible only with proper lumen distention.^{26,48}

The hallmark of acute diverticulitis on CT is the presence of inflammatory changes in the pericolic fat. This sign is seen in 98% of patients. The degree of inflammatory reaction varies, depending on the size of perforation, bacterial contamination, and host response. In mild cases, there is only a slight increase in the attenuation of fat adjacent to the involved colon, with engorgement of the vasa recta (Fig. 55-13). Fine linear strands, small fluid collections, and several bubbles of extraluminal air may be present (Fig. 55-14). In more severe cases, pericolic heterogeneous soft tissue densities representing phlegmons (Fig. 55-15) and/or intramural or extraintestinal loculated fluid collections representing abscess can occur. In sigmoid diverticulitis, fluid in the combined interfascial plane in the pelvis is a common finding.^{26,48}

On CT, abscesses appear filled with fluid and may contain bubbles of air or air-fluid levels (Fig. 55-16). These collections can form at a distance from the involved segment of colon. They may form at the flank, groin, thigh, psoas muscle, subphrenic space, or liver. Most abscesses are contained within the sigmoid mesocolon or are sealed off by the sigmoid colon and adjacent small bowel loops.^{26,48}

A sealed-off perforation with the resulting juxtacolic inflammatory reaction causes thickening of the sigmoid mesocolon or the adjacent parietal peritoneum. Although this is not a specific finding, it is often seen in diverticulitis and helps in identifying the site and focal nature of the inflammatory process. Small, 1- to 2-cm intramural fluid collections representing intramural abscesses can be detected. Intramural or pericolic fistulas can be recognized as linear, fluid-filled tracts within or parallel to the thickened colonic wall. Blind sinus tracts and fistulas manifest as linear or tubular branching structures in the pericolic tissues. They can communicate with adjacent organs or terminate in an abscess cavity.

TABLE 55-1 Multidetector Computed Tomography Findings in Diverticulitis

Finding	No. of Cases (%)
Mural thickening of the colon	96
Fat stranding	95
Adjacent diverticula	91
Fascial thickening	50
Visualization of inflamed diverticulum	43
Pericolic gas bubbles	30
Arrowhead sign	16
Abscess	4
Phlegmon	4
Intramural gas	2
Sinus tracts	2

Modified from Kircher MF, Rhea JT, Kihiczak D, et al: Frequency, sensitivity and specificity of individual signs of diverticulitis on thin-section helical CT with colonic contrast material: Experience with 312 cases. *AJR* 178:1313–1318, 2002.

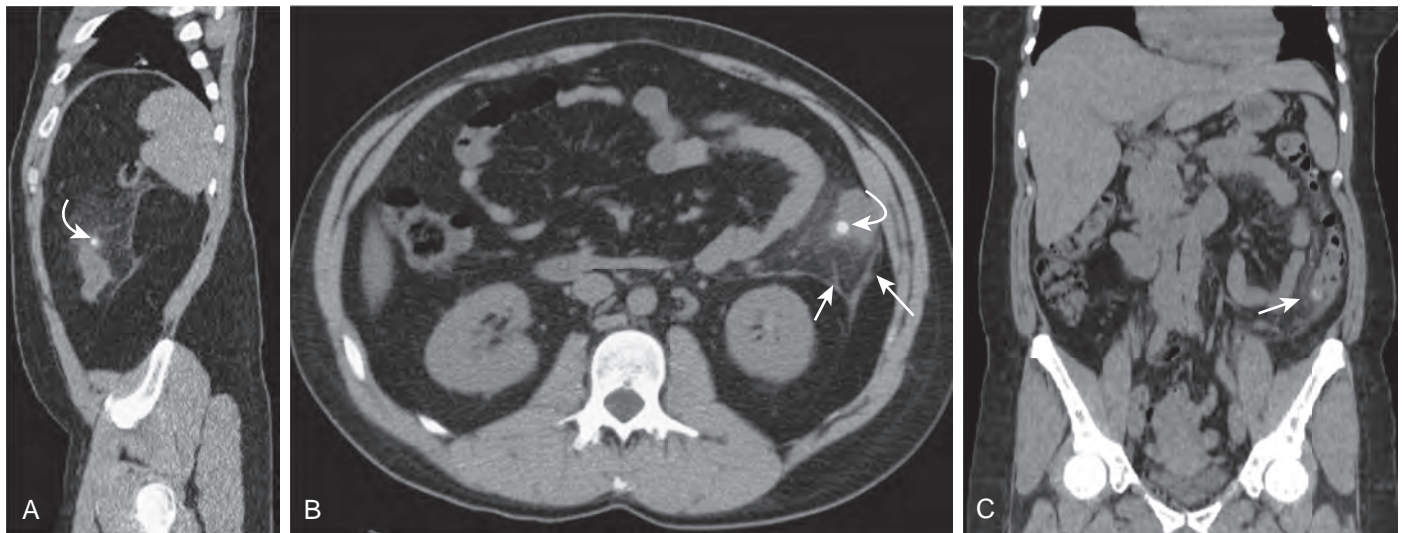


Figure 55-12 Diverticulitis: MDCT findings on non-contrast-enhanced scans. Sagittal (A) and axial (B) images show the hyperdense offending diverticulum (curved arrow) at the center of the pericolic inflammation. Note the thickening of the anterior (small straight arrow) and lateroconal (large straight arrow) interfascial planes. C. Coronal reformatted image in a different patient demonstrates a hyperdense diverticulum with surrounding inflammatory change (arrow).

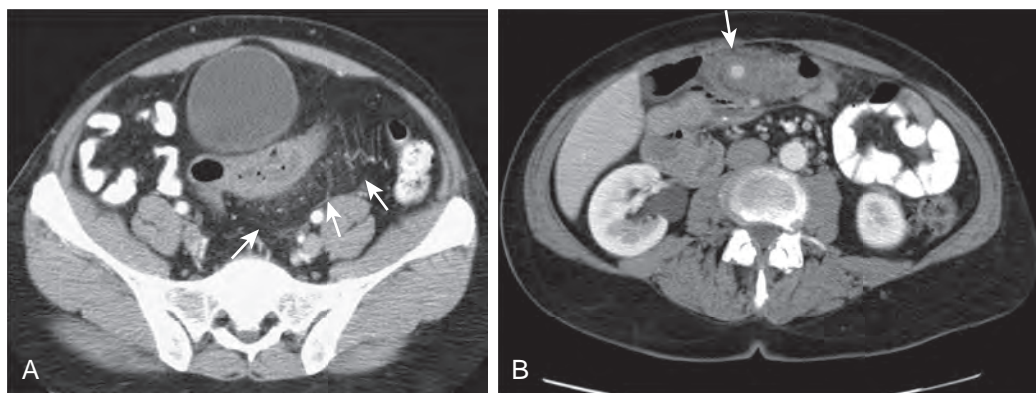


Figure 55-13 MDCT of diverticulitis: early changes. **A.** Axial CT scan of the sigmoid colon demonstrates mural thickening with haziness of the sigmoid mesocolon (arrows) associated with engorged vasa recta. **B.** Axial postcontrast CT scan shows mural thickening and pericolic inflammatory change in the transverse colon, with hyperdense diverticulum (arrow).

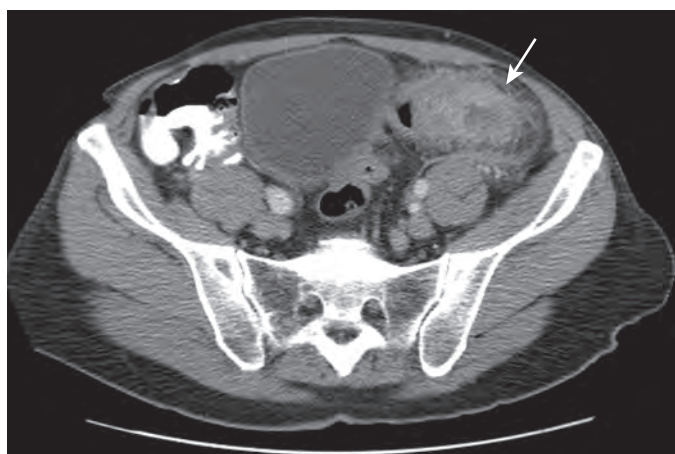


Figure 55-14 MDCT of diverticulitis: intramural abscess. Axial CT of the sigmoid colon shows mural thickening, pericolic inflammatory changes, and fascial thickening with the presence of an intramural abscess (arrow).

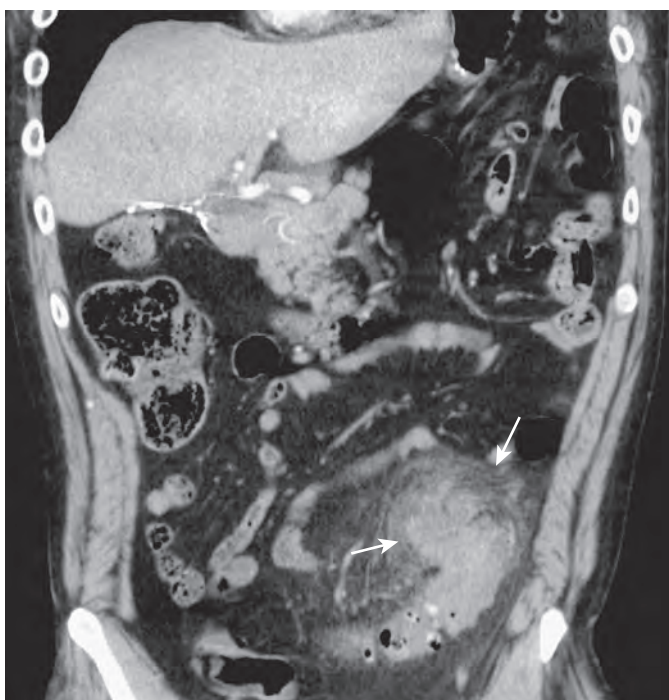
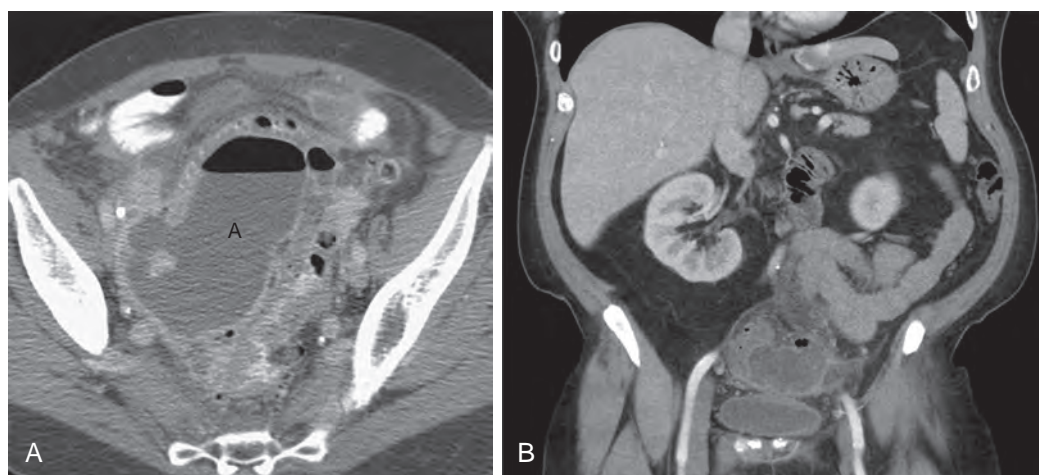


Figure 55-15 MDCT of diverticulitis: pericolic phlegmon. Coronal reformatted image shows intense inflammatory change in the sigmoid mesocolon (arrows), without drainable fluid.

Figure 55-16 MDCT of diverticulitis: abscess. **A.** Axial image in one patient demonstrates a large abscess with an air-fluid level (A) identified in the pelvis. **B.** Coronal image in a different patient demonstrates similar findings.



SURGICAL AND COMPUTED TOMOGRAPHY STAGING

Diverticulitis can be staged surgically (Fig. 55-17) and by CT. Familiarity with the following staging system (modified Hinchey classification) helps in directing therapy and assessing prognosis (Table 55-2):

- **Stage 0 diverticulitis** is the most common form, in which the inflammation is contained within the serosa. This mural inflammation usually responds well to antibiotics. On CT, it appears primarily as mural thickening, with little inflammatory change in the surrounding fat.⁴⁹
- **Stage Ia diverticulitis** denotes confined pericolic inflammation or phlegmon. CT findings demonstrate phlegmonous changes only. These patients do well with antibiotic therapy and seldom progress to stage II or III disease.^{49,50}
- **Stage Ib diverticulitis** denotes diverticulitis with a confined pericolic abscess.⁴⁹ Abscesses smaller than 3 cm can be treated with antibiotics alone. Percutaneous CT guided drainage is usually performed in patients with amenable abscesses larger than 4 cm.^{50,51}
- **Stage II diverticulitis** signifies that the pericolic abscess has broken through the sigmoid mesocolon and has become walled off by the small bowel, greater omentum, fallopian tubes, or other pelvic structures. This stage is associated with abscesses 4 to 15 cm in diameter that are well suited to percutaneous drainage (Fig. 55-18).⁵¹⁻⁵³ Percutaneous drainage is used as a bridge from the acute setting to subsequent elective colon resection. In select patients with comorbidities, however, the need for surgery can be established after successful percutaneous drainage.^{28,49,54,55}
- **Stage III diverticulitis** signifies pelvic abscess that has spread beyond the confines of the pelvis to involve other portions of the peritoneal cavity. CT findings demonstrate changes of diverticulitis with free air and/or free

fluid.⁵⁰ This represents a generalized purulent peritonitis. Fortunately, this form of diverticulitis is relatively infrequent because the body's defenses usually contain the perforation.⁴⁹ Traditionally, this is treated with emergent sigmoid resection in a one- or two-stage procedure. In select patients, the use of laparoscopic peritoneal lavage for patients with stable Hinchey stage 3 can be used as a definitive treatment or as a bridge to subsequent colonic resection.⁵⁶

- **Stage IV diverticulitis** is defined as fecal spread into the peritoneal cavity. A wide-mouthed perforation is usually present. The CT appearance may be similar to that of stage III with free air and/or free fluid, but these patients have acute peritonitis with life-threatening sepsis, so they usually undergo immediate exploratory laparotomy.⁴⁹

Together with the clinical evaluation, CT is used not only to confirm the clinical suspicion but also as a reliable guide to patient management. Patients with mild diverticulitis (pericolic inflammation, small abscess [<3 cm]) are treated conservatively with antibiotic therapy and bowel rest. Patients with larger abscesses (>4 cm) are percutaneously drained. Emergency surgery is reserved for cases of free perforation with peritonitis.²⁸ Elective colonic resection after an episode of complicated diverticulitis or multiple episodes of diverticulitis should be decided on an individual basis.²⁸

DIFFERENTIATION OF DIVERTICULITIS FROM CARCINOMA

Diverticulitis can mimic colon cancer clinically on barium enema examination, US, MRI, and MDCT. On CE studies, the detection of partial colonic obstruction with sigmoid

TABLE 55-2 Staging and Classification of Diverticulitis		
Stage	Modified Hinchey Classification*	CT Staging†
0	Mild clinical diverticulitis	Diverticula, with or without wall thickening
Ia	or	Colonic wall thickening with pericolic soft tissue changes
Ib	Pericolic-mesocolic abscess	Ia changes with pericolic-mesocolic abscess
II	Pelvic, distant intra-abdominal, retroperitoneal abscess	Ia changes with distant abscess
III	Generalized purulent peritonitis	Free air with localized or generalized ascites
IV	Generalized feculent peritonitis	Same findings as III

*Adapted from Wasvary H, Turfah F, Kadro O, Beauregard W: Same hospitalization resection for acute diverticulitis. *Am Surg* 65:632-635, 1999.

†Adapted from Kaiser AM, Jiang JK, Lake JP, et al: The management of complicated diverticulitis and the role of computed tomography. *Am J Gastroenterol* 100:910-917, 2005.

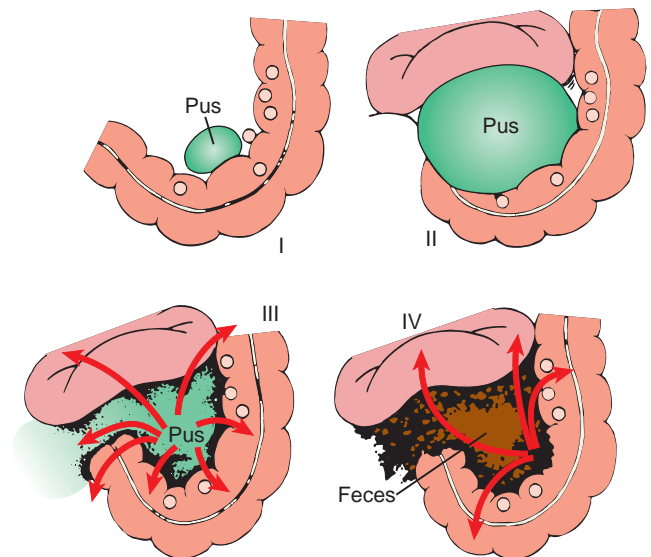
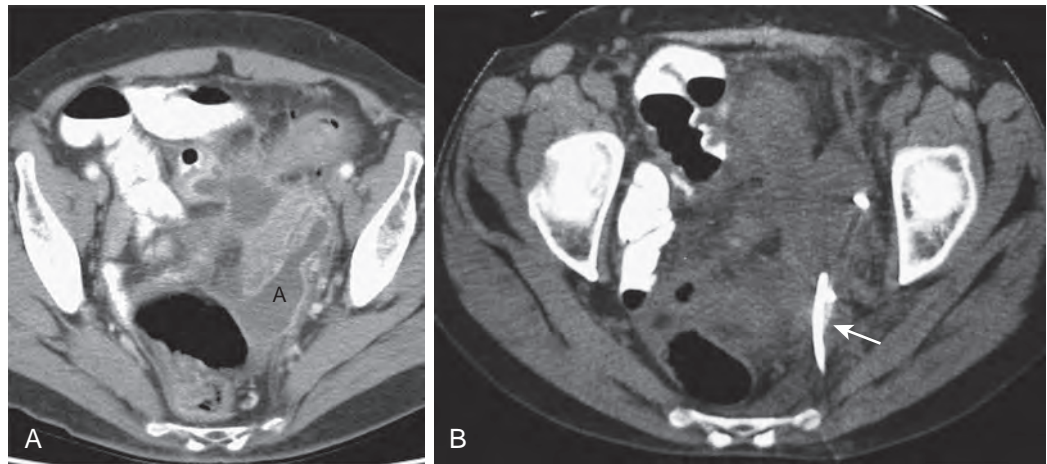


Figure 55-17 Surgical staging of diverticular abscesses. Stage I, A small (<3 cm) pericolic abscess is contained within the sigmoid mesocolon. Stage II, A pelvic abscess has broken out of the sigmoid mesocolon but is contained by the pelvic organs. Stage III, The large pelvic abscess has spread into the rest of the peritoneal cavity. Stage IV, Large diverticular perforation occurs with fecal contamination of the peritoneal cavity. (From Hinchley EJ, Schaaf PGH, Richards GK: Treatment of perforated diverticular disease of the colon. *Adv Surg* 12:85-109, 1978.)

Figure 55-18 MDCT of diverticulitis: abscess drainage.

A. There is a multilocular abscess (A) identified in the left side of the pelvis. **B.** The dominant loculation has been drained with a percutaneous catheter (arrow) introduced via a transgluteal approach.



narrowing, a gradual zone of transition, preservation of the mucosal folds, and associated diverticula indicate diverticulitis (Fig. 55-19). Abrupt transition at the site of obstruction, a rigid, narrowed lumen, destruction of mucosa, and a so-called apple core configuration suggest carcinoma of the colon. CE is valuable in differentiating diverticulitis from carcinoma of the sigmoid colon in most cases. The presence of sigmoid diverticula, however, is not helpful in the differential diagnosis because 28% of sigmoid cancers involve coincidental diverticula.⁵⁷ When the retrograde flow of contrast medium is impeded and the obstructed sigmoid lumen cannot be well visualized, the differentiation of an inflammatory lesion from a malignant lesion cannot be made.

CT features that suggest diverticulitis include identification of the offending hyperdense diverticulum, inflammation of the adjacent fat with engorgement of the vasa recta, fluid at the root of the mesentery (in the combined interfascial plane), fluid and inflammatory changes out of proportion to the mural thickening, abscess formation, extraluminal fluid, and gas. CT features favoring carcinoma include prominent adjacent lymph nodes; symmetric or asymmetric mural thickening with shouldered, nontapered margins; and presence of a luminal mass. There is considerable overlap of CT findings. If there is a long segment of colonic thickening with pericolic inflammatory change and no pericolic lymph nodes, diverticulitis is the most likely diagnosis. When pericolic lymph nodes are seen adjacent to a segment of colonic thickening, colon cancer is the most likely diagnosis.⁵⁸⁻⁶⁰

In approximately 10% of patients, diverticulitis cannot be differentiated from colon carcinoma on the basis of CT scans. Most patients with diverticulitis exhibit only mild circumferential wall thickening, in the range of 4 to 5 mm. Excessive thickening of the colonic wall, concentrically or focally, suggests colonic neoplasm. Although most colon cancers are more than 2 cm thick, neoplastic lesions less than 1 cm in diameter may be seen. These facts account for a significant overlap in colonic wall thickness in diverticulitis and carcinoma, particularly with lesions that are between 1 and 3 cm in thickness. An abrupt zone of transition with overhanging edges and a narrow, rigid lumen indicates carcinoma; a tethered or saw-toothed luminal configuration suggests diverticular disease. Associated inflammatory mesenteric changes favor diverticulitis, whereas regional lymphadenopathy favors carcinoma of the colon.^{58,60,61}

CT perfusion may help in the differentiation between colon cancer and diverticulitis. One small study showed that blood volume, blood flow, and mean transit time and sensitivities of 80%, 80%, and 85%, respectively, could help discriminate between the two. Permeability showed a specificity of 90%.⁶⁰ The incorporation of CT perfusion into routine clinical practice, however, remains a challenge.

The differential diagnosis of cancer versus diverticulitis is extremely difficult in patients presenting with perforated colon carcinoma associated with pericolic inflammation or abscess. An abruptly altered lumen caliber with an asymmetric and lobulated soft tissue mass is diagnostic of perforated sigmoid carcinoma.

After a CT diagnosis of sigmoid diverticulitis, current guidelines recommend follow-up CE or endoscopic visualization.²⁸ This may not be necessary in all cases, particularly acute uncomplicated diverticulitis.⁶²⁻⁶⁴ Lymph nodes, abscess, obstruction, wall thickness more than 6 mm, or other complicating factors of diverticulitis may represent more refined CT criteria requiring near-term (usually 6 weeks) follow-up with CE or colonoscopy.⁶³

CHRONIC DIVERTICULITIS

Chronic diverticulitis, a variant of acute diverticulitis with longer duration of symptoms, is characterized by more obstructive symptoms. CE enema findings demonstrate long segment narrowing with spiculated contour and tapered margins, occasionally with an associated obstruction. CT demonstrates findings similar to those of acute diverticulitis (Fig. 55-20).⁶⁵ One study of CT colonographies demonstrated that the most important discriminator was the presence of diverticula, with the affected segment favoring chronic diverticulitis. This study also reinforced the findings favoring diverticulitis versus carcinoma and vice versa (see earlier).⁶⁶

DIFFERENTIAL DIAGNOSIS

Other conditions such as nonspecific or infectious colitis, ischemic colitis, and Crohn's disease are part of the differential diagnosis of diverticulitis. A long segment of colonic involvement, lack of diverticula, absence of a focal inflammatory pericolic process, or pericolic air collection helps in the CT differential diagnosis. Foreign bodies that escape CT detection

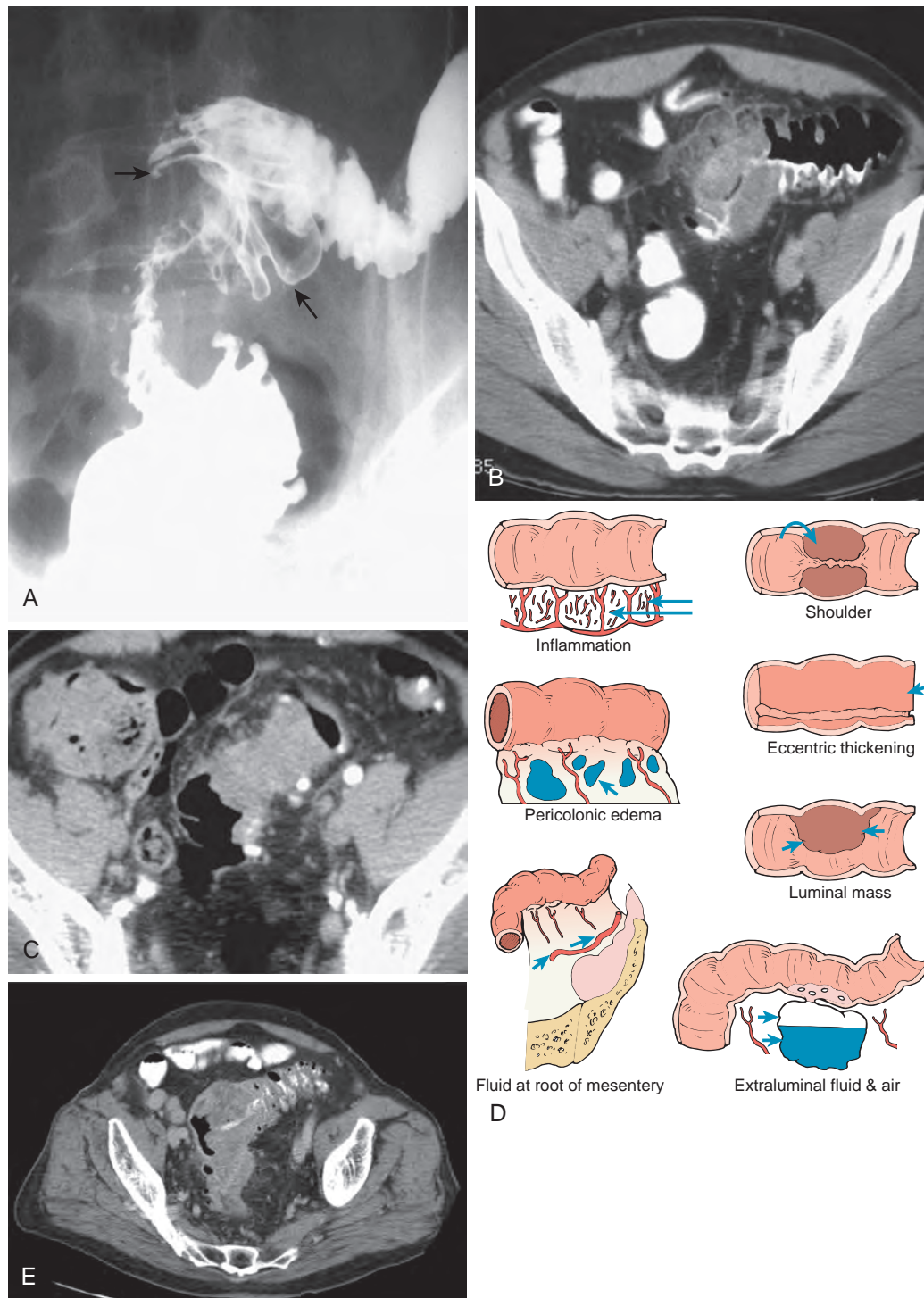


Figure 55-19 Colon cancer versus diverticulitis: imaging considerations. **A.** Barium enema examination demonstrates an indeterminate stricture in the sigmoid colon. Multiple diverticula are present but there is an abrupt, overhanging edge (arrows) along the proximal margin of this lesion. This patient had diverticulitis and carcinoma of the sigmoid colon. **B.** Focal, symmetric mural thickening of the sigmoid colon is present. There are inflammatory changes in the fat of the sigmoid mesocolon. Several diverticula are evident just distal to the region of thickening. This patient had diverticulitis. **C.** There is a mass identified within the lumen of the sigmoid colon, with only minimal haziness of the adjacent fat. This patient had carcinoma of the sigmoid colon. **D.** Line drawings showing features that suggest diverticulitis (inflammation, pericolic edema, fluid in the root of the mesentery—combined interfascial plane, extraluminal fluid and air) versus carcinoma (eccentric thickening, luminal mass). **E.** Axial CT demonstrates an intraluminal mass with diverticula seen along the margins of the mass, but not in the segment with the mass. There are equivocal surrounding inflammatory changes. This patient had carcinoma of the sigmoid colon. (**D** from Chintapalli KN, Chopra S, Ghiatas AA, et al: Diverticulitis versus colon cancer: Differentiation with helical CT findings. *Radiology* 210:429–435, 1999.)

and perforate the colon can mimic the CT findings of acute diverticulitis.

Epiploic Appendagitis

Primary epiploic appendagitis, a relatively common condition resulting from an acute inflammation of appendices epiploicae often associated with torsion and infarction, can be confused as diverticulitis. This is frequently seen in patients younger than those with diverticulitis. CT will show the characteristic appearance of a small, round, or oval fat-containing mass with associated inflammatory reaction adjacent to the colon (Fig. 55-21). Frequently, a central dot representing a thrombosed vessel is seen.⁶⁷ The lack of adjacent colonic wall thickening can differentiate this from acute diverticulitis.⁶⁸ Complications of diverticulitis including abscess, extraluminal gas, and inflamed diverticula are not seen with primary epiploic appendagitis. The

process is self-containing, with clinical resolution within a few days. Follow-up CT examination may show total resolution or shrinkage, with eventual calcification of the inflamed and infarcted epiploic appendage.

Cecal Diverticulitis

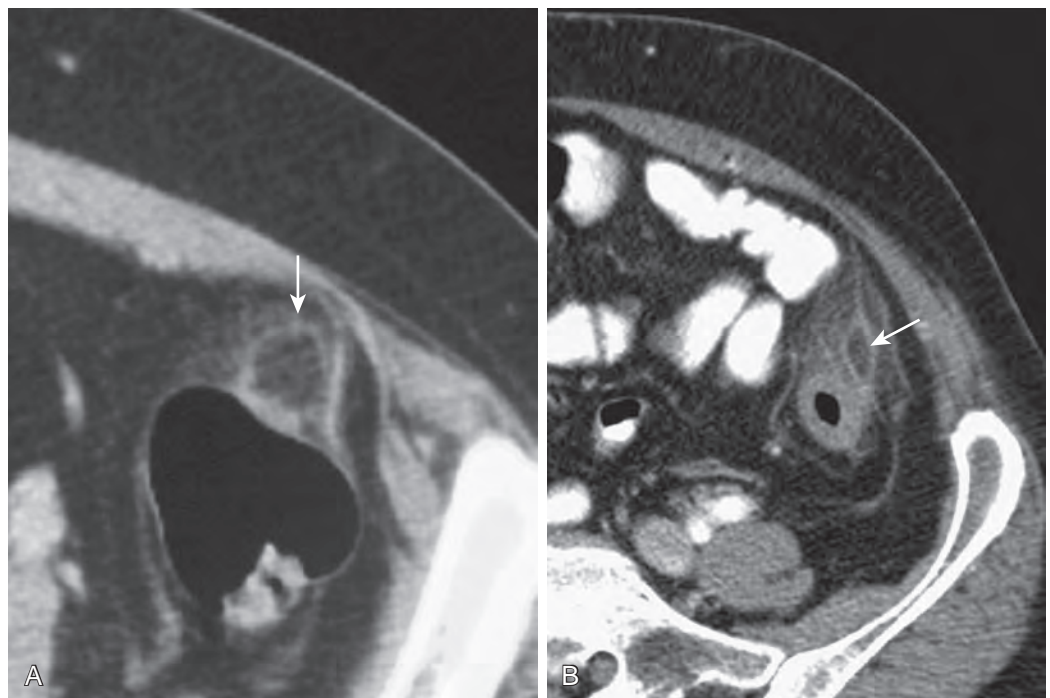
Cecal diverticulitis or right-sided colonic diverticulitis is a relatively rare pathologic entity in which patients present with protean clinical manifestations that are often clinically misdiagnosed as appendicitis. Cecal diverticula are classified as true (congenital) or false (acquired). The congenital variety is usually larger and solitary and is characterized by the presence of a well-developed muscle coat. Most cecal diverticula are acquired and are similar to diverticula present in the remainder of the colon. They are usually multiple, involve the cecum and ascending colon, are formed by herniated mucosa and serosa, and lack a muscular coat. Traditionally, barium examination represented the primary means of preoperative diagnosis, but CT is now the mainstay in the evaluation of cecal diverticulitis and its differential diagnosis, including appendicitis and carcinoma. The characteristic findings of the barium enema examination include a filling defect with an irregular contour, cecal spasm, fixation and spiculation of the cecal wall, visualization of diverticula, and a normal appearance of the appendix.⁶⁹

The CT findings consist of focal pericolic inflammatory changes, slight thickening of the wall of the colon, demonstration of diverticula and, occasionally, an intramural or pericolic fluid collection representing an abscess (Fig. 55-22). When a normal appendix is seen and the focal pericecal inflammatory process is above the cecal caput, a reliable CT diagnosis can be made. If the appendix is not seen, findings similar to those of appendicitis or perforated cecal carcinoma make the CT diagnosis uncertain. Recent experience indicates that the diagnosis of right-sided colonic diverticulitis can be suggested or established by MDCT.⁷⁰



Figure 55-20 Chronic diverticulitis. Axial CT image shows pericolic inflammatory changes, with extensive long segment wall thickening.

Figure 55-21 Epiploic appendagitis: MDCT features. **A, B.** These two different patients have a fat-density mass (arrow) surrounded by increased attenuation adjacent to the sigmoid colon. This fatty mass is the epiploic appendage that has undergone torsion, ischemia, and/or inflammation.



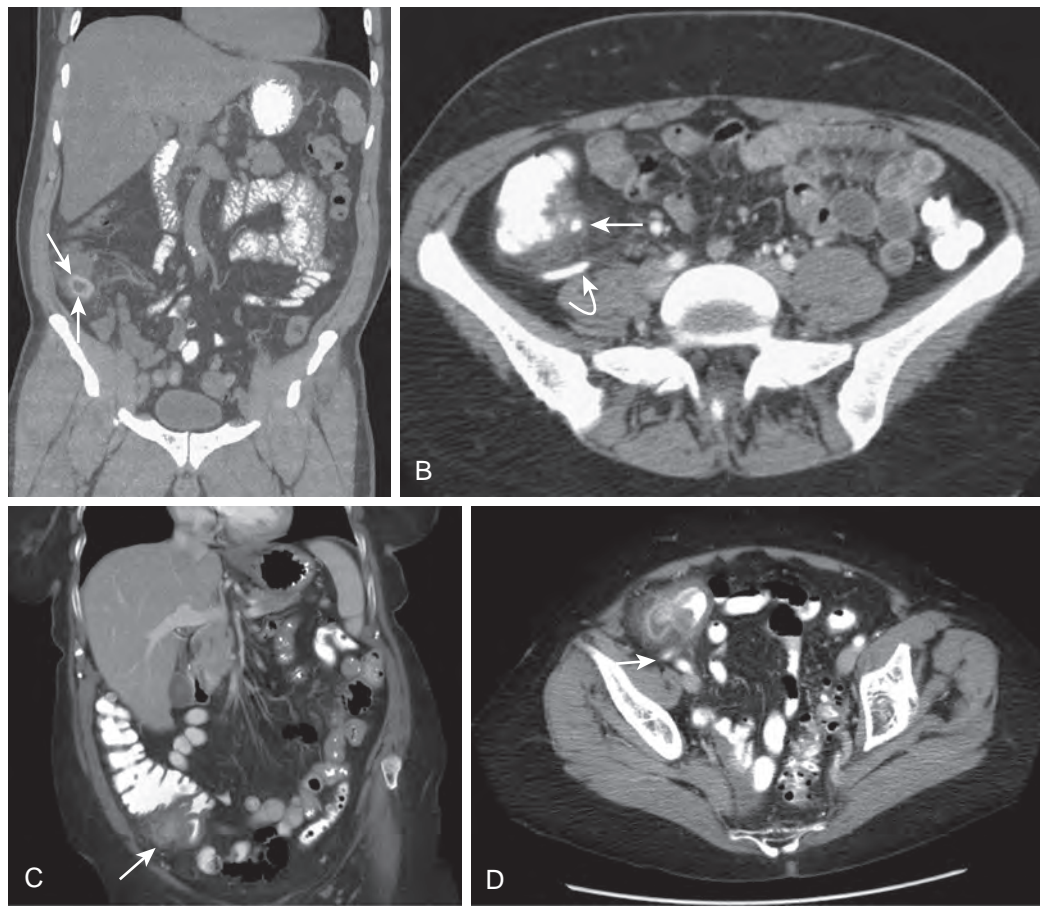


Figure 55-22 Right-sided diverticulitis: imaging considerations. **A.** Coronal reformatted image shows the hyperdense offending diverticulum (arrows) associated with considerable inflammatory change in the adjacent fat. **B.** Axial scan of different patient shows contrast filling a normal appendix (curved arrow) and the offending diverticulum (straight arrow). **C.** Postcontrast coronal reformatted CT image demonstrates focal pericolic inflammatory changes, with wall thickening and suggestion of the inflamed diverticulum (arrow). **D.** Note the contrast-filled posterior to the cecum on the axial image (arrow).

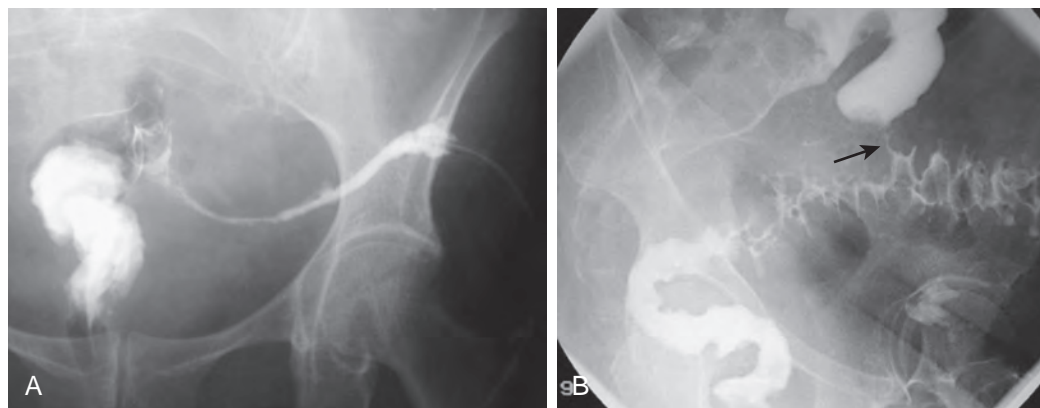


Figure 55-23 Fistulas from diverticulitis. **A.** Fistulogram showing injection of a skin wound and direct communication to the sigmoid colon. **B.** A fistula (arrow) from the sigmoid colon to the ileum is identified on this barium enema examination.

COMPLICATIONS

Perforation of one or several diverticula produces a localized inflammatory reaction and may lead to the development of a sinus tract, intramural tract, or variable-sized intramural or pericolic abscess. Other more unusual complications can sometimes occur.

Fistulas and Sinus Tracts

Fistulas (Fig. 55-23), which are communications between two epithelium-lined surfaces—bowel to another hollow organ, or bowel to skin—can develop and be difficult to detect. Fistulas have been reported in up to 20% of surgical cases of diverticulitis.⁷¹ Diverticulum-related fistulas are usually to the bladder,

but fistulization to the vagina (usually in patients who are status posthysterectomy), uterus, adnexae, small and large bowel, and others is also encountered.⁷²

CT is extremely useful in the evaluation of patients with suspected colovesical fistulas. CT has a high sensitivity and provides useful information about the surrounding anatomic structures.⁷³ It should be used as the first imaging modality in patients suspected of having a colovesical fistula.

In patients presenting with pneumaturia, the pericolic inflammatory mass involving the bladder wall and the presence of intraluminal vesical air confirms the diagnosis. Sigmoid-vesical fistulas rarely occur in the acute setting during the initial attack of diverticulitis and the development of the pelvic abscess. Colovesical fistulas are mostly seen as late sequelae after one or several episodes of diverticulitis, when the acute inflammatory reaction has already subsided. Thickening of the bladder wall, thickening of the bowel wall adjacent to the bladder, gas in the bladder, insinuating mass, and direct adherence of the colon to the bladder are all findings that may indicate a fistula. A discretely opacified fistula and oral contrast medium within the bladder are more direct signs (Fig. 55-24).^{73,74}

Free Intraperitoneal Perforation

As noted, severe forms of diverticulitis, and particularly free perforations, occur rarely and are seen mainly in debilitated

older individuals and patients on corticosteroid therapy. Free diverticular perforation results in extravasation of air and fluid into the pelvis and peritoneal cavity with the development of peritonitis. On CT (Fig. 55-25), bubbles of air are seen floating in the pelvic fluid close to the sigmoid colon, as well as free in the greater peritoneal cavity. Occasionally, a sigmoid diverticulum can perforate into the leaves of the mesosigmoid, and air can dissect into the retroperitoneum of the left pelvis and left upper abdomen. This presentation, when associated with bubbles of air adjacent to the sigmoid colon, is diagnostic of perforated diverticulitis.

Bowel Obstruction

Diverticulitis is the third most common cause of a large bowel obstruction, seen in approximately 10% of cases, behind colorectal cancer and volvulus.⁷⁵ This can be seen in the acute and chronic setting. The colon can become obstructed because of luminal narrowing caused by inflammation or compression by an abscess (Fig. 55-26). Multiple attacks can lead to progressive fibrosis and stricture of the colonic wall. Obstruction generally is self-limited and responds to conservative therapy. If persistent, obstruction of the colon can be treated by a variety of endoscopic and surgical techniques.

Diverticulitis is a rare cause of small bowel obstruction. The small bowel loops become trapped in the perisigmoid

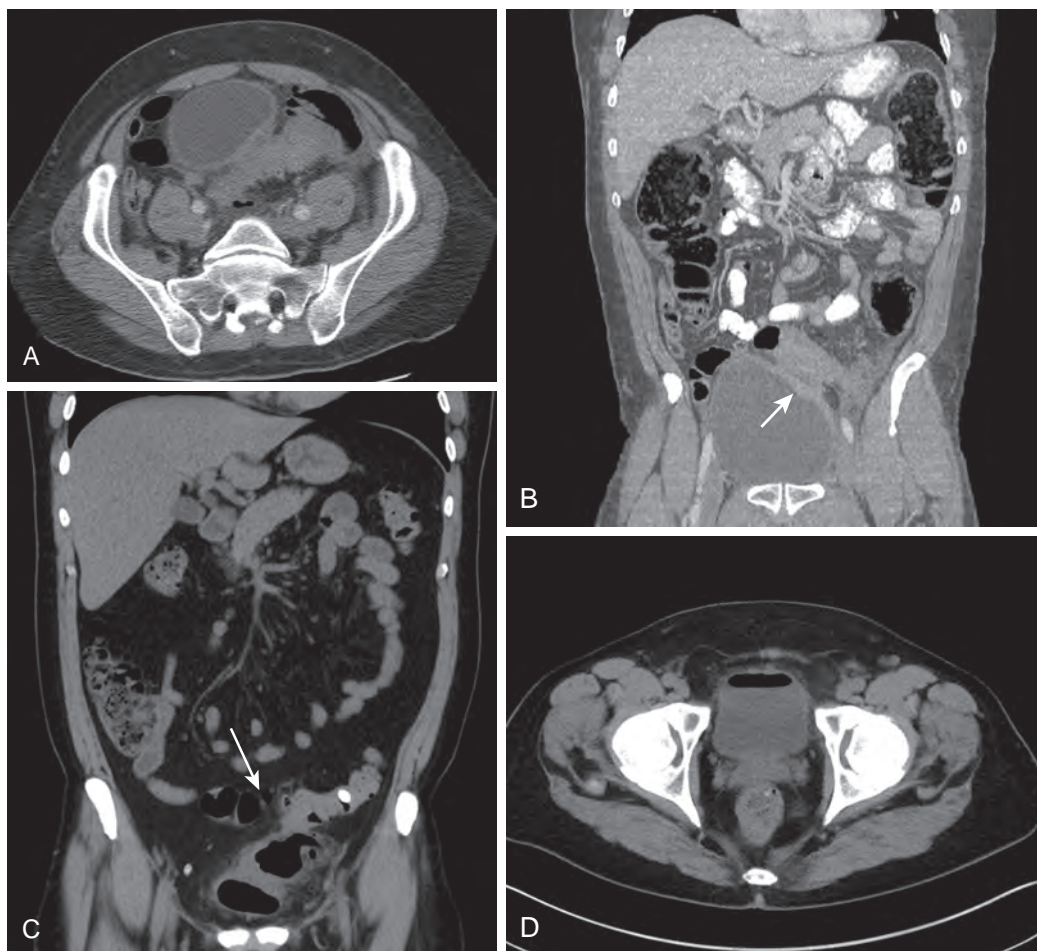


Figure 55-24 Colovesical fistula caused by diverticulitis. **A, B.** Indirect evidence of a fistula with inflammatory changes of the sigmoid colon and adjacent eccentric bladder wall thickening (arrow).⁷³ **C, D.** Direct evidence of a colovesical fistula with an air-filled tract between the sigmoid colon and bladder (arrow), with gas seen in the bladder.

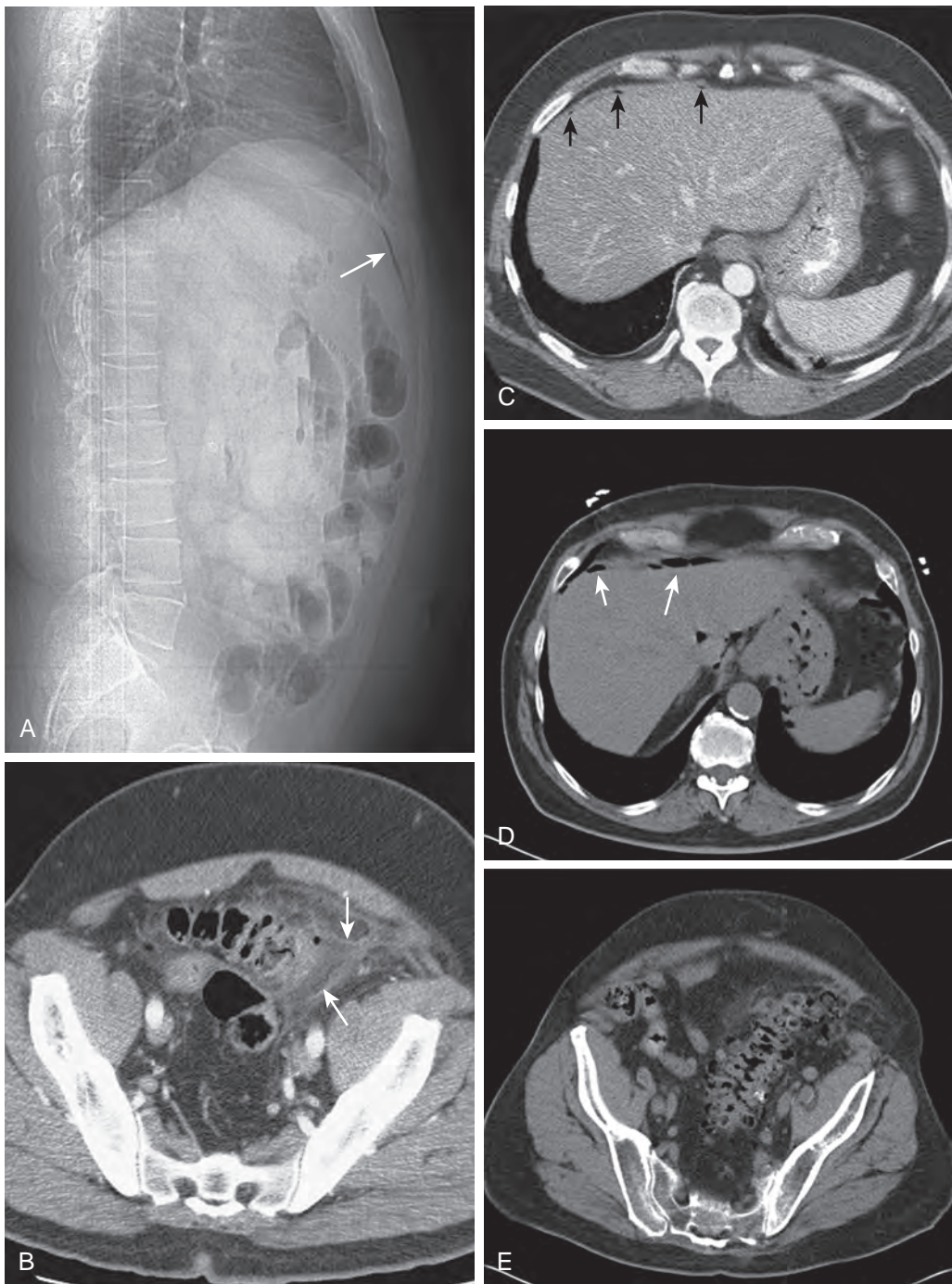


Figure 55-25 Free intraperitoneal perforation.

A. Lateral scout image demonstrates free intraperitoneal gas (arrow). **B.** Axial image of the pelvis demonstrates the gas-containing region of perforation (arrows). **C.** Several bubbles of gas are evident anterior to the liver (arrows). **D.** Noncontrast CT in a different patient demonstrates free air adjacent to the liver (arrows). **E.** Diverticulitis is noted, with extensive diverticulosis in the sigmoid colon.

inflammatory process, and the associated mesenteric changes can be detected by MDCT (Fig. 55-27).⁷⁶

Pylephlebitis and Liver Abscess

The acute infection, originating from a left- or right-sided diverticulitis, can spread into the liver via mesenteric venous drainage and portal vein. The septic thrombosis that develops, called pylephlebitis or septic thrombosis of the portal vein, represents a serious complication seen in severely ill patients with septic manifestations and no localizing signs. CT can reveal air or thrombus in the draining mesenteric veins and

thrombus in the mesenteric and portal veins (Fig. 55-28). Sometimes, during the initial presentation or on follow-up examination, a pyogenic liver abscess may develop (Fig. 55-29). The primary colonic inflammatory process can be detected by CT as an intramural inflammatory mass or pericolic abscess. This complication carries an overall mortality of 32%. Patients should be diagnosed early and be closely monitored and adequately treated with a combination of antibiotic therapy, percutaneous abscess drainage, and surgical intervention, when necessary. Anticoagulant therapy may also be used.^{77,78}



Figure 55-26 Large bowel obstruction caused by diverticulitis. **A.** Scout image demonstrates large and small bowel distention. **B, C.** CT scan demonstrates transition point (arrows) with pericolic inflammatory change, fascial thickening, and luminal narrowing.

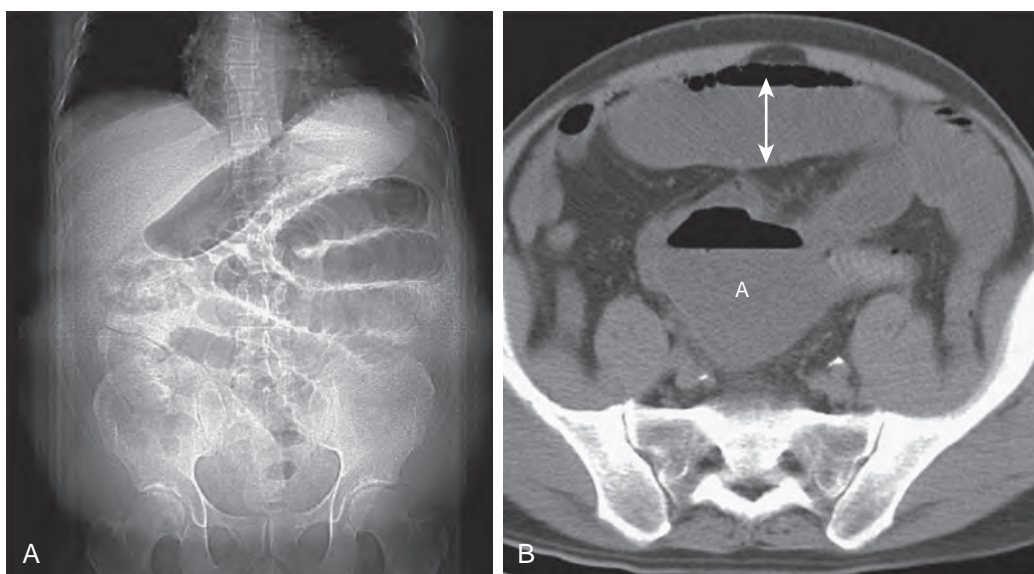


Figure 55-27 Small bowel obstruction caused by diverticulitis abscess. **A.** Scout image demonstrates small bowel obstruction. **B.** An air-fluid level is identified within the abscess (A). Note the dilated, fluid-filled, small bowel loops (double arrow).

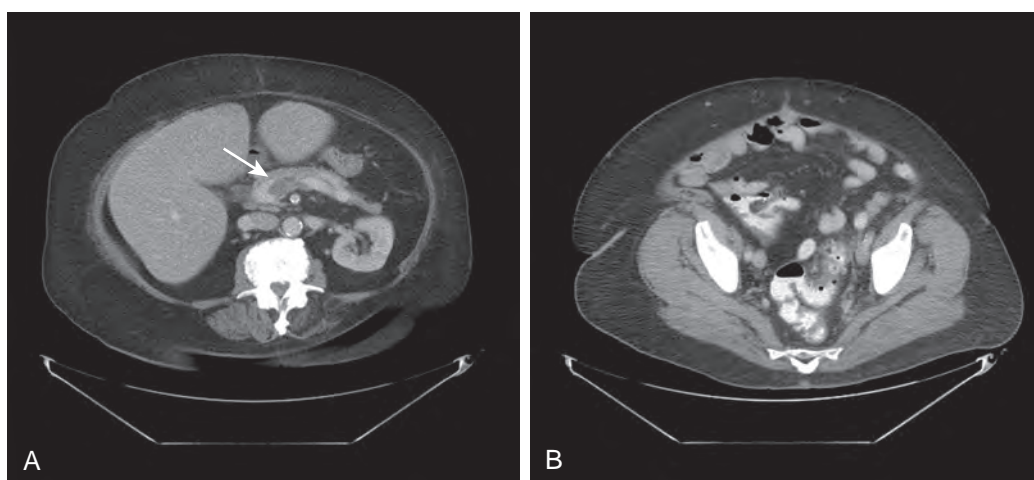


Figure 55-28 Sigmoid diverticulitis with pylephlebitis. **A.** Axial postcontrast portal venous phase image demonstrates a filling defect in the portal vein (arrow). **B.** Mild sigmoid diverticulitis with pericolic inflammatory change.

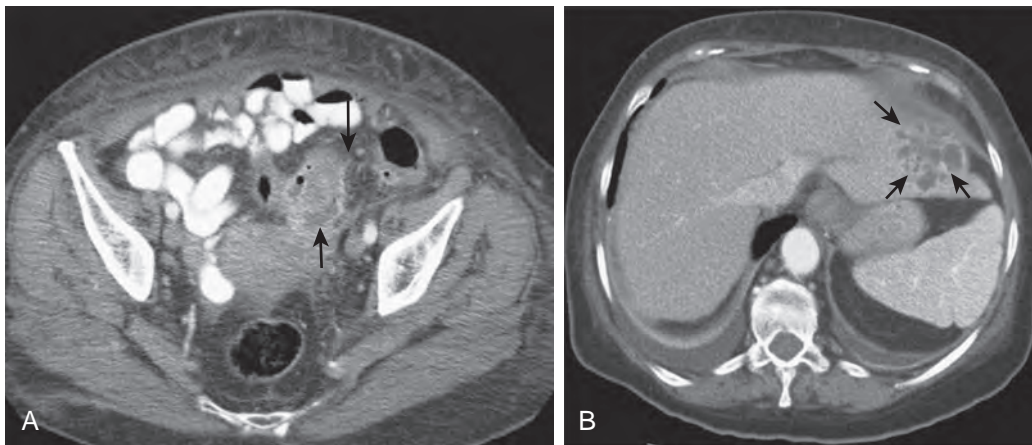


Figure 55-29 Sigmoid diverticulitis leading to the formation of a liver abscess.
A. There is a gas-containing abscess (arrows) in the sigmoid mesocolon. **B.** A multiloculated abscess is identified in the left lobe of the liver (arrows).

Diverticular Hemorrhage

Diverticular disease is the most common cause of lower gastrointestinal bleeding in the United States, accounting for 17% to 40% of cases.⁷⁹ In one study, diverticular disease accounted for 42% of patients hospitalized for lower GI bleeding.⁸⁰ It usually is difficult to confirm the exact cause of bleeding, however. Although diverticula predominate in the sigmoid and descending colon, angiographic confirmation of diverticular bleeding has been documented throughout the colon, with one study noting a 60% incidence in the right colon.⁸¹ One study of 180 patients in Asia demonstrated that right-sided disease was more likely to present with massive hemorrhage and require surgery, whereas left-sided disease was more likely to present with diverticulitis.⁸² The use of nonsteroidal anti-inflammatory drugs (NSAIDs) or aspirin, hypertension, and/or anticoagulation are risk factors.⁸³

PATHOPHYSIOLOGY

The source is typically a single diverticulum, which in 80% of cases is not inflamed. There is minute rupture of one of the vasa recta asymmetrically placed in the wall adjacent to the lumen of the diverticulum (Figs. 55-30 and 55-31). Eccentric intimal thickening, duplication of the internal elastic lamina, and thinning of the media are changes that are all found with the involved artery. An eccentric focus of media thickening, intramural thickening and duplication, and fragmentation of the internal elastic lamina in the wall of the involved artery at the point of its disruption are seen. Some traumatic factor within the lumen of the diverticulum induces this eccentric intimal thickening, which eventually weakens and ruptures the vasa recta. The wider domed necks of right-sided colonic diverticula may expose these vessels to injury over a greater length, explaining the strikingly high incidence of right-sided hemorrhage.⁸⁴

CLINICAL FINDINGS

Most patients with massive diverticular hemorrhage are older adults, with severe coexistent cardiovascular and pulmonary disease, and they present with a sudden onset of mild abdominal cramps and the urge to defecate. Soon after, a large volume of bright red blood, clots, or both, or dark red, maroon or, least commonly, black stool is passed rectally. Bleeding ceases

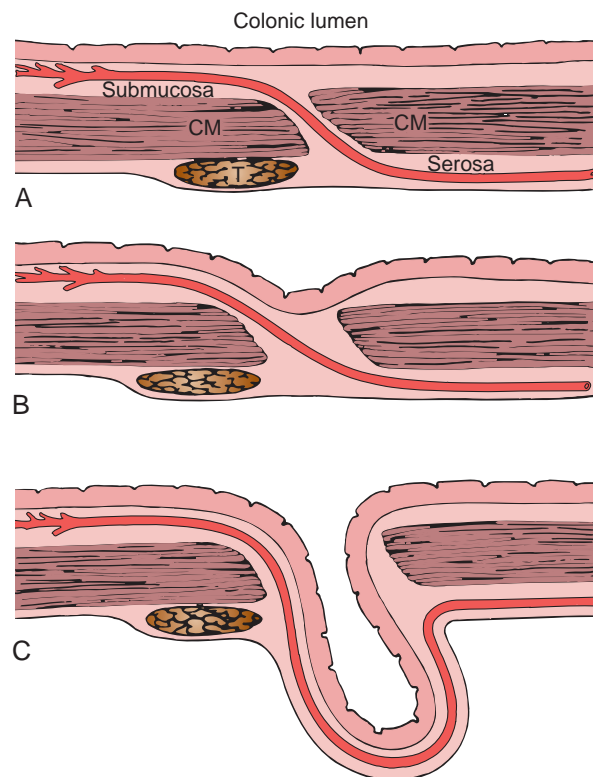


Figure 55-30 Diverticulum formation and vascular relationships.
A. The vas rectum penetrates the colon wall from the serosa to the submucosa through an obliquely oriented connective tissue septum in the circular muscle (CM). This penetration occurs near the mesenteric side of the taenia (T). **B.** The diverticulum develops through and widens this connective tissue cleft. The mucosal protrusion begins to elevate the artery. **C.** As the diverticulum extends transmurally, the vas rectum is placed over its dome, penetrating to the submucosa on the antimesenteric border of its neck and orifice. (From Meyers MA, Volberg F, Katzen B, et al: *Angioarchitecture of colonic diverticula: Significance in bleeding diverticulosis*. Radiology 108:249–261, 1973.)

spontaneously in approximately 75% of patients, but the bleeding may be continuous or intermittent.⁸⁵ The rebleeding rate in patients without definitive therapy was 9% at 1, 10% at 2, 19% at 3, and 25% at 4 years.⁸⁰ The differential diagnosis, radiology, and treatment of diverticular hemorrhage are discussed elsewhere in this text (see Chapter 125).

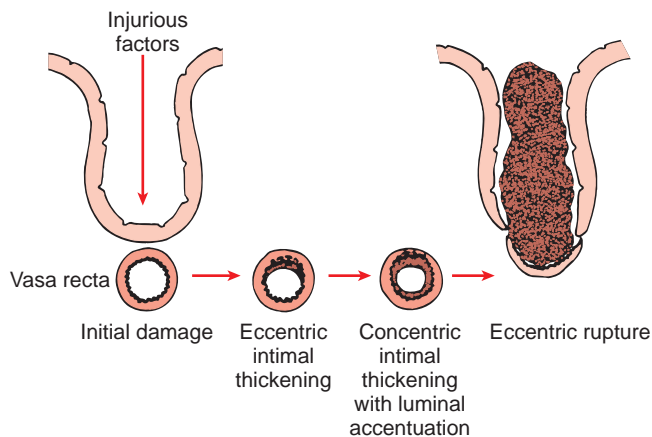


Figure 55-31 Pathogenesis of colonic diverticular hemorrhage. Progressive eccentric changes weaken the wall of the vas rectum, which eventually ruptures into the lumen of the diverticulum. (From Meyers MA, Alonso DR, Gray GF, et al: *Pathogenesis of bleeding colonic diverticulosis*. *Gastroenterology* 71:577–583, 1976.)

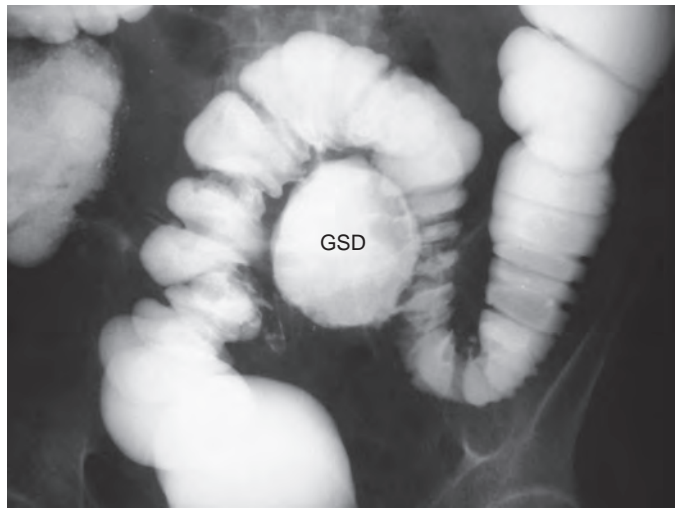


Figure 55-32 Giant sigmoid colon diverticulum. A giant sigmoid colon diverticulum (GSD) is demonstrated in two different patients on a barium enema study.

Giant Sigmoid Diverticulum

CAUSATIVE FACTORS

A giant sigmoid diverticulum is a rare complication of diverticulitis. It is believed to result from subserosal perforation and inflammation of a diverticulum, with subsequent air trapping and eventual formation of a large cyst, which is caused by elevated intraluminal pressure of the colon working in tandem with a ball valve mechanism. In time, inflammatory and granulation tissue replaces the mucosal lining of the cyst wall. The trapped air in the cyst increases during defecation and is vented irregularly.⁸⁶⁻⁸⁸

PATHOPHYSIOLOGY AND CLINICAL FINDINGS

Most patients are elderly and have a history of chronic vague abdominal discomfort or acute symptoms suggesting diverticulitis. A palpable mass is detected in 71% of cases, and anatomic communication between the cyst and the lumen is present in 82%. The cysts range in size between 6 and 27 cm, with a mean diameter of 13 cm. The cyst may be hyperresonant on percussion.⁸⁶⁻⁸⁹

RADIOLOGIC FINDINGS

The barium enema (Fig. 55-31) and plain radiograph findings in giant sigmoid diverticulum are striking. Plain radiographs demonstrate a large gas-filled structure in the lower to middle pelvis that can have an air-fluid level. The gas collections may change in size on interval studies.⁸⁶⁻⁸⁹

Barium enters these collections on contrast agent studies in two thirds of patients, and diverticula are seen elsewhere in the colon in 82% of patients. The differential diagnosis of these large collections includes volvulus, giant Meckel's or other small bowel diverticulum, tubo-ovarian abscess, cystitis, emphysematous cholecystitis, infected pancreatic pseudocyst, and vesicoenteric fistula.⁸⁶⁻⁸⁹ On CT, a giant sigmoid diverticulum appears as a gas- or contrast-filled structure communicating with the colon (Fig 55-32).

THERAPY

Giant colonic diverticula have been reported to perforate, cause volvulus and infarction and small bowel obstruction, and may contain carcinoma. The accepted therapy for giant colonic diverticula is surgical excision.⁸⁶⁻⁸⁹

REFERENCES

- Andeweg CS, Mulder IM, Felt-Bersma RJ, et al: Guidelines of diagnostics and treatment of acute left-sided colonic diverticulitis. *Dig Surg* 30:278–292, 2013.
- Wilkins T, Embry K, George R, et al: Diagnosis and management of acute diverticulitis. *Am Fam Physician* 87:612–620, 2013.
- Fox JA, Stollman NH: Diverticular disease of the colon. In Feldman M, Friedman LS, Brandt LJ, editors: *Sleisenger and Fordtran's Gastrointestinal and Liver Disease: Pathophysiology, Diagnosis, Management*, ed 9, Philadelphia, 2010, Elsevier, pp 2073–2089.
- Bailey MB, Davenport DL, Procter L, et al: Morbid obesity and diverticulitis: Results from the ACS NSQIP dataset. *J Am Coll Surg* 217: 874–880, 2013.
- Painter NS, Burkitt DP: Diverticular disease of the colon: A deficiency disease of Western civilization. *Br Med J* 2:450–454, 1971.
- Hjern F, Johansson C, Mellgren A, et al: Diverticular disease and migration—the influence of acculturation to a Western lifestyle on diverticular disease. *Aliment Pharmacol Ther* 23:797–805, 2006.
- Strate LL, Modi R, Cohen E, Spiegel BM: Diverticular disease as a chronic illness: Evolving epidemiologic and clinical insights. *Am J Gastroenterol* 107:1486–1493, 2012.
- von Rahden BH, Germer CT: Pathogenesis of colonic diverticular disease. *Langenbecks Arch Surg* 397:1025–1033, 2012.
- Fagenholz PJ, de Moya MA: Acute inflammatory surgical disease. *Surg Clin North Am* 94:1–30, 2014.
- West B: The pathology of diverticulosis: Classical concepts and mucosal changes in diverticula. *J Clin Gastroenterol* 40(Suppl 3):S126–S131, 2006.
- Strate LL: Lower GI bleeding: Epidemiology and diagnosis. *Gastroenterol Clin North Am* 34:643–664, 2005.
- Abrisqueta J, Frutos MD, Luján J, et al: Solitary rectal diverticulum. A case presentation. *Cir Esp* 91:128–129, 2013.
- Giffin HZ: VII. Diverticulitis of the rectum: A report of two cases operated upon, one of them with carcinomatous degeneration. *Ann Surg* 53:533–537, 1911.
- Piercy KT, Timaran C, Akin H: Rectal diverticula: Report of a case and review of the literature. *Dis Colon Rectum* 45:1116–1117, 2002.

15. Russin LD: Plain film recognition of air within colonic diverticula. *AJR* 134:176–177, 1980.
16. Hunter TB, Merkley R, Pitt MJ: Relation between pelvic phleboliths and diverticular disease of the colon. *AJR* 143:105–107, 1984.
17. Laufer I, Lavine MS, Laufer I: *Double Contrast Gastrointestinal Radiology*, ed 2, Philadelphia, 1992, WB Saunders.
18. Weissman A, Clot M, Grellet J: *Double Contrast Examination of the Colon: Principles and Practice*, New York, 1985, Springer-Verlag.
19. Gelfand DW: *Gastrointestinal Radiology: Performing and Interpreting Fluoroscopic Examinations*. New York, Churchill Livingstone, 1984.
20. Freeny PC, Walker JH: Inverted diverticula of the gastrointestinal tract. *Gastrointest Radiol* 4:57–59, 1979.
21. Htoo AM, Bartram CI: The radiological diagnosis of polyps in the presence of diverticular disease. *Br J Radiol* 52:263–267, 1979.
22. Glick SN: Inverted colonic diverticulum: Air contrast barium enema findings in six cases. *AJR* 156:961–964, 1991.
23. Keller CE, Halpert RD, Feczko PJ, Simms SM: Radiologic recognition of colonic diverticula simulating polyps. *AJR* 143:93–97, 1984.
24. Baker SR, Alterman DD: False-negative barium enema in patients with sigmoid cancer and coexistent diverticula. *Gastrointest Radiol* 10: 171–173, 1985.
25. Miller WT, Jr, Levine MS, Rubesin SE, Laufer I: Bowler-hat sign: A simple principle for differentiating polyps from diverticula. *Radiology* 173: 615–617, 1989.
26. Gore RM, Miller FH, Pereles FS, et al: Helical CT in the evaluation of the acute abdomen. *AJR* 174:901–913, 2000.
27. Parks TG: Natural history of diverticular disease of the colon. *Clin Gastroenterol* 4:53–69, 1975.
28. Rafferty J, Shellito P, Hyman NH, et al: Practice parameters for sigmoid diverticulitis. *Dis Colon Rectum* 49:939–944, 2006.
29. Shahedi K, Fuller G, Bolus R, et al: Long-term risk of acute diverticulitis among patients with incidental diverticulosis found during colonoscopy. *Clin Gastroenterol Hepatol* 11:1609–1613, 2013.
30. Young-Fadok TM, Sarr MG: Diverticular disease of the colon. In Yamada T, Alpers DH, Kalloo AN, et al, editors: *Textbook of Gastroenterology*, ed 5, Oxford, 2009, Blackwell, pp 1574–1597.
31. Brown DB, Toomey WF: Diverticular disease of the colon. A review of 258 cases. *Br J Surg* 47: 485–493, 1960.
32. Ünlü Ç, van de Wall BJ, Gerhards MF, et al: Influence of age on clinical outcome of acute diverticulitis. *J Gastrointest Surg* 17:1651–1656, 2013.
33. Kotzampassakis N, Pittet O, Schmidt S, et al: Presentation and treatment outcome of diverticulitis in younger adults: A different disease than in older patients? *Dis Colon Rectum* 53:333–338, 2010.
34. Nelson RS, Velasco A, Mukesh BN: Management of diverticulitis in younger patients. *Dis Colon Rectum* 49:1341–1345, 2006.
35. Chabok A, Pählman L, Hjert F, et al: Randomized clinical trial of antibiotics in acute uncomplicated diverticulitis. *Br J Surg* 99:532–539, 2012.
36. Masoomi H, Buchberg BS, Magno C, et al: Trends in diverticulitis management in the United States from 2002 to 2007. *Arch Surg* 146:400–406, 2011.
37. Etzioni DA, Mack TM, Beart RW, Jr, Kaiser AM: Diverticulitis in the United States: 1998–2005: Changing patterns of disease and treatment. *Ann Surg* 249:210–217, 2009.
38. Salem L, Anaya DA, Flum DR: Temporal changes in the management of diverticulitis. *J Surg Res* 124:318–323, 2005.
39. Laméris W, van Randen A, Bipat S, et al: Graded compression ultrasonography and computed tomography in acute colonic diverticulitis: Meta-analysis of test accuracy. *Eur Radiol* 18: 2498–2511, 2008.
40. Pradel JA, Adell JE, Taourel P, et al: Acute colonic diverticulitis: Prospective comparative evaluation with US and CT. *Radiology* 205:503–512, 1997.
41. Ripolles T, Agramunt M, Martínez MJ, et al: The role of ultrasound in the diagnosis, management and evolutive prognosis of acute left-sided colonic diverticulitis: A review of 208 patients. *Eur Radiol* 13:2587–2595, 2003.
42. Baker JB, Mandavia D, Swadron SP: Diagnosis of diverticulitis by bedside ultrasound in the Emergency Department. *J Emerg Med* 30:327–329, 2006.
43. Vijayaraghavan SB: High-resolution sonographic spectrum of diverticulosis, diverticulitis, and their complications. *J Ultrasound Med* 25:75–85, 2006.
44. Hollerweger A, Rettenbacher T, Macheiner P, et al: Sigmoid diverticulitis: Value of transrectal sonography in addition to transabdominal sonography. *AJR* 175:1155–1160, 2000.
45. Buckley O, Geoghegan T, McAuley G, et al: Pictorial review: Magnetic resonance imaging of colonic diverticulitis. *Eur Radiol* 17:221–227, 2007.
46. Rotert H, Nöldge G, Encke J, et al: The value of CT for the diagnosis of acute diverticulitis. *Radiologe* 43:51–58, 2003.
47. ACR Expert Panel on Gastrointestinal Imaging: ACR Appropriateness Criteria: Left Lower Quadrant Pain—Suspected Diverticulitis, 2011. <http://www.acr.org/~media/ACR/Documents/AppCriteria/Diagnostic/LeftLowerQuadrantPainSuspectedDiverticulitis.pdf>. Accessed March 13, 2014.
48. Kaewlai R, Nazinitsky KJ: Acute colonic diverticulitis in a community-based hospital: CT evaluation in 138 patients. *Emerg Radiol* 13: 171–179, 2007.
49. Wasvary H, Turfah F, Kadro O, Beauregard W: Same hospitalization resection for acute diverticulitis. *Am Surg* 65:632–635, 1999.
50. Kaiser AM, Jiang JK, Lake JP, et al: The management of complicated diverticulitis and the role of computed tomography. *Am J Gastroenterol* 100:910–917, 2005.
51. Siewert B, Tye G, Kruskal J, et al: Impact of CT-guided drainage in the treatment of diverticular abscesses: Size matters. *AJR* 186:680–686, 2006.
52. Hall J: Should elective colectomy be routine following percutaneous drainage of a diverticular abscess? *Dis Colon Rectum* 56:533–534, 2013.
53. Gaertner WB, Willis DJ, Madoff RD, et al: Percutaneous drainage of colonic diverticular abscess: Is colon resection necessary? *Dis Colon Rectum* 56:622–626, 2013.
54. Singh B, May K, Coltart I, et al: The long-term results of percutaneous drainage of diverticular abscess. *Ann R Coll Surg Engl* 90:297–301, 2008.
55. Gaertner WB, Willis DJ, Madoff RD, et al: Percutaneous drainage of colonic diverticular abscess: Is colon resection necessary? *Dis Colon Rectum* 56:622–626, 2013.
56. Alamili M, Gogenur I, Rosenberg J: Acute complicated diverticulitis managed by laparoscopic lavage. *Dis Colon Rectum* 52:1345–1349, 2009.
57. Ponka JL, Fox JD, Brush BE: Coexisting carcinoma and diverticula of the colon: A review of three hundred fifty-five cases of carcinoma of the colon. *Arch Surg* 79:373–382, 1959.
58. Chintapalli KN, Chopra S, Ghatas AA, et al: Diverticulitis versus colon cancer: Differentiation with helical CT findings. *Radiology* 210:429–435, 1999.
59. Chintapalli KN, Esola CC, Chopra S, et al: Pericolic mesenteric lymph nodes: An aid in distinguishing diverticulitis from cancer of the colon. *AJR* 169:1253–1255, 1997.
60. Goh V, Halligan S, Taylor SA, et al: Differentiation between diverticulitis and colorectal cancer: Quantitative CT perfusion measurements versus morphologic criteria—initial experience. *Radiology* 242:456–462, 2007.
61. Balthazar EJ, Megibow A, Schinella RA, Gordon R: Limitations in the CT diagnosis of acute diverticulitis: Comparison of CT, contrast enema, and pathologic findings in 16 patients. *AJR* 154:281–285, 1990.
62. Sai VF, Velayos F, Neuhaus J, Westphalen AC: Colonoscopy after CT diagnosis of diverticulitis to exclude colon cancer: A systematic literature review. *Radiology* 263:383–390, 2012.
63. Elmi A, Hedgire SS, Pargaonkar V, et al: Is early colonoscopy beneficial in patients with CT-diagnosed diverticulitis? *AJR* 200:1269–1274, 2013.
64. Brar MS, Roxin G, Yaffe PB, et al: Colonoscopy following nonoperative management of uncomplicated diverticulitis may not be warranted. *Dis Colon Rectum* 56:1259–1264, 2013.
65. Sheiman L, Levine MS, Levin AA, et al: Chronic diverticulitis: Clinical, radiographic, and pathologic findings. *AJR* 191:522–528, 2008.
66. Gryspeerdt S, Lefere P: Chronic diverticulitis vs. colorectal cancer: Findings on CT colonography. *Abdom Imaging* 37:1101–1109, 2012.
67. Almeida AT, Melao L, Viamonte B, et al: Epiploic appendagitis: An entity frequently unknown to clinicians—diagnostic imaging, pitfalls, and look-alikes. *AJR* 193:1243–1251, 2009.
68. Jalaguier A, Zins M, Rodallec M, et al: Accuracy of multidetector computed tomography in differentiating primary epiploic appendagitis from left acute colonic diverticulitis associated with secondary epiploic appendagitis. *Emerg Radiol* 17:51–56, 2010.
69. Katz DS, Lane MJ, Ross BA, et al: Diverticulitis of the right colon revisited. *AJR* 171:151–156, 1998.
70. Jang HJ, Lim HK, Lee SJ, et al: Acute diverticulitis of the cecum and ascending colon: The value of thin-section helical CT findings in excluding colonic carcinoma. *AJR* 174:1397–1402, 2000.
71. Colcock BP, Stahmann FD: Fistulae complicating diverticular disease of the sigmoid colon. *Ann Surg* 175:838–846, 1972.
72. Woods RJ, Lavery IC, Fazio VW, et al: Internal fistulae in diverticular disease. *Dis Colon Rectum* 31:591–596, 1988.
73. Jarrett TW, Vaughan ED, Jr: Accuracy of computerized tomography in the diagnosis of colovesical fistula secondary to diverticular disease. *J Urol* 153:44–46, 1995.
74. Goldman SM, Fishman EK, Gatewood OM, et al: CT in the diagnosis of enterovesical fistulas. *AJR* 144:1229–1233, 1985.

75. Taourel P, Kessler N, Lesnik A, et al: Helical CT of large bowel obstruction. *Abdom Imaging* 28:267–275, 2003.
76. Kim AY, Bennett GL, Bashist B, et al: Small-bowel obstruction associated with sigmoid diverticulitis: CT evaluation in 16 patients. *AJR* 170:1311–1313, 1998.
77. Van De Wauwer C, Irvin TT: Pylephlebitis due to perforated diverticulitis. *Acta Chir Belg* 105:229–230, 2005.
78. Lee BK, Ryu HH: A case of pylephlebitis secondary to cecal diverticulitis. *J Emerg Med* 42:e81–e85, 2012.
79. Zuccaro G, Jr: Management of the adult patient with acute lower gastrointestinal bleeding. American College of Gastroenterology. Practice Parameters Committee. *Am J Gastroenterol* 93:1202–1208, 1998.
80. Longstreth GF: Epidemiology and outcome of patients hospitalized with acute lower gastrointestinal hemorrhage: A population-based study. *Am J Gastroenterol* 92:419–424, 1997.
81. Koval G, Benner KG, Rösch J, Kozak BE: Aggressive angiographic diagnosis in acute lower gastrointestinal hemorrhage. *Dig Dis Sci* 32:248–253, 1987.
82. Wong SK, Ho YH, Leong AP, Seow-Choen F: Clinical behavior of complicated right-sided and left-sided diverticulosis. *Dis Colon Rectum* 40:344–348, 1997.
83. Nishikawa H, Maruo T, Tsumura T, et al: Risk factors associated with recurrent hemorrhage after the initial improvement of colonic diverticular bleeding. *Acta Gastroenterol Belg* 76:20–24, 2013.
84. Meyers MA, Alonso DR, Baer JW: Pathogenesis of massively bleeding colonic diverticulosis: New observations. *AJR* 127:901–908, 1976.
85. McGuire HH, Jr, Haynes BW, Jr: Massive hemorrhage for diverticulosis of the colon: Guidelines for therapy based on bleeding patterns observed in fifty cases. *Ann Surg* 175:847–855, 1972.
86. Abou-Nukta F, Bakhos C, Ikekpeazu N, Ciardello K: Ruptured giant colonic diverticulum. *Am Surg* 71:1073–1074, 2005.
87. Chaiyasate K, Yavuzer R, Mittal V: Giant sigmoid diverticulum. *Surgery* 139:276–277, 2006.
88. Thomas S, Peel RL, Evans LE, Haarer KA: Best cases from the AFIP: Giant colonic diverticulum. *Radiographics* 26:1869–1872, 2006.
89. Zeina AR, Nachtigal A, Matter I, et al: Giant colon diverticulum: Clinical and imaging findings in 17 patients with emphasis on CT criteria. *Clin Imaging* 37:704–710, 2013.

Diseases of the Appendix

DANIEL R. WENZKE | JILL E. JACOBS | EMIL J. BALTHAZAR |
NATASHA WEHRLI

CHAPTER OUTLINE

Embryology

Acute Appendicitis

Epidemiology

Causes

Pathophysiology

Clinical and Radiologic Assessment

Findings

Differential Diagnosis

Crohn's Disease

Ulcerative Colitis

Endometriosis

Appendiceal Diverticulitis

Appendiceal Intussusception

Appendiceal Neoplasms

Mucocele

Mucinous Cystadenoma and Cystadenocarcinoma

Nonmucinous Adenocarcinoma

Carcinoid

Lymphoma

Metastases

The vermiform appendix is the smallest and functionally most irrelevant segment of the gastrointestinal (GI) tract, yet diseases of the appendix are among the most common surgical emergencies in the western world.¹⁻⁵ The appendix arises from the posteromedial aspect of the cecum at the junction of the three taeniae coli. Although the appendix has the same mural layers as those of the remainder of the gut, it is distinguished by extremely rich lymphoid tissue in the mucosa and submucosa. This forms an entire layer of germinal follicles and lymphoid pulp in the young.⁶ With age, this lymphoid tissue underlying the mucosal epithelium and glands undergoes progressive atrophy. The distal portion of the appendix sometimes undergoes fibrous obliteration in older adults.⁶

Embryology

The vermiform appendix and cecum are intestinal derivations of the midgut. During the sixth week of gestational life, the cecum begins to develop as a small bulge in the midgut at the level of the ileocolic junction. This diverticular structure continues to enlarge and assumes a conical shape, with its apex corresponding to the primitive appendix.⁷⁻⁹ The initial cecal and appendiceal structures have been referred to as the "bud of the cecum."¹⁰ The midgut undergoes physiologic umbilical

herniation at approximately gestational week 6 and subsequently begins to relocate into the embryonal body cavity at approximately gestational week 10. This process is accompanied by counterclockwise rotation of the midgut, which results in positioning of the cecal complex in the right lower quadrant (Fig. 56-1). As the colon grows, it moves caudad toward the right iliac fossa, a process known as descensus.¹⁰ Because of differential growth rates during this time, the development of the primitive appendix is slower than that of the rest of the cecum. This differential growth was theorized by Broman to be caused by a mucosal fold in the distal cecum that prevents accumulation of meconium.¹¹ Broman hypothesized that colonic growth is stimulated by intraluminal meconium accumulation. Because this mucosal fold prevents complete filling of the distal cecum and appendix with meconium, growth is retarded in these segments. The appendix subsequently lengthens rapidly but fails to grow in thickness, soon assuming the configuration of a vermiform process.

By birth, the appendix has lengthened and shows a more abrupt transition zone at the junction with the cecum. At this time, the appendix is still attached to the cecal apex. The fully developed adult appendix is uniformly narrow and arises from the left posterior wall of the cecum, rather than the cecal apex, 2.5 to 3.5 cm below the ileocecal valve. The process of migration of the root of the appendix from the cecal tip toward the left, on the same side as the ileocecal valve, is probably related to the upright posture of the child. The right and ventral walls of the cecum grow and distend at the expense of the left and posterior walls. The fixation at the ileocecal junction and weight of the column of feces in the ascending colon explain this additional asymmetric development.

In adults, the root of the appendix can be located anywhere along the medial-posterior wall of the cecum, between the ileocecal valve and the cecal tip. In addition, there is great variation in the position of the appendix in relation to the cecum and ascending colon.^{12,13} More than 60% of appendices are retrocecal or retrocolic, with the remainder in a more inferior pelvic location. A fully developed appendix varies in size and thickness, with an average length of 8 to 10 cm (range, 4-25 cm; Fig. 56-2). The location of the appendix in the peritoneal cavity depends on its length and relationship to the cecum and the extreme variations in the mobility and location of the ascending colon and cecum (Fig. 56-3).¹⁴

Examples of arrest in later phases of development of the appendix are common and can be recognized during barium enema examinations. An arrest in the fetal phase of development is unusual (Fig. 56-4). A conic configuration of the lower cecal segment signifies total absence or hypoplasia of the appendix. Agenesis of the appendix is rare; the reported incidence is about 1 in 100,000 individuals.¹⁵

The ileocolic artery, a branch of the superior mesenteric artery, supplies the appendix, cecum, and ileum via five branches: (1) several ileal rami; (2) anterior cecal artery;

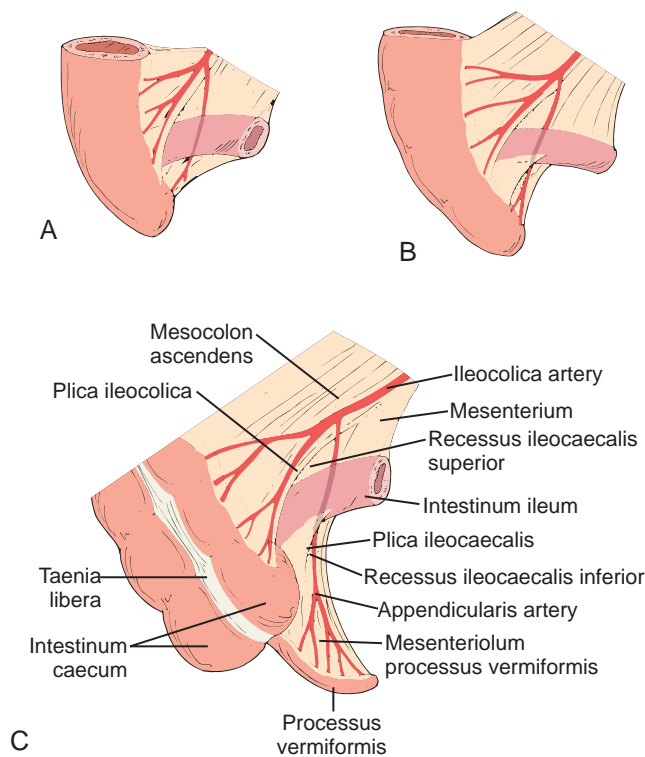


Figure 56-1 Embryology of the appendix. **A.** Growth of the inferior tip of the cecum lags during early intrauterine development. **B.** This produces the infantile appendix. **C.** Continued differential growth of the lateral cecal wall leads to the posteromedial position of the appendix in older children and adults. (From McVay CB: *Anson & McVay Surgical Anatomy*, 6th ed. Philadelphia, WB Saunders, 1984.)

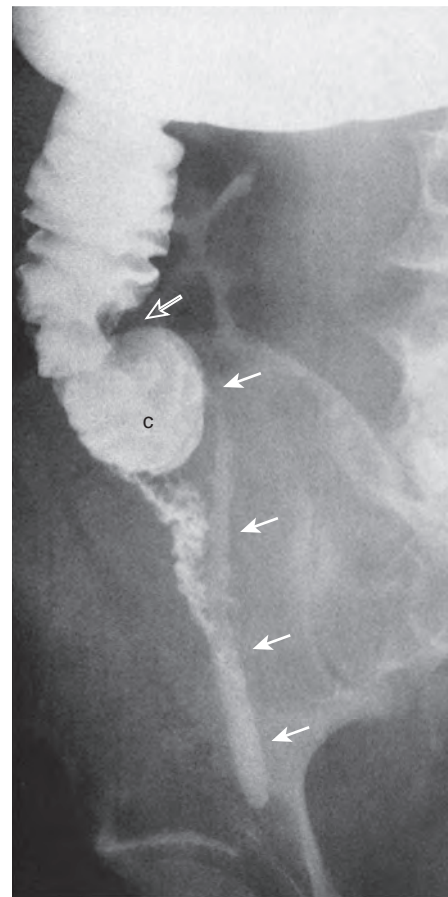


Figure 56-2 Normal appendix: barium enema findings. A long pelvic appendix is present, arising from the medial wall of the cecum (c) below the ileocecal valve (open arrow). The appendix is uniformly narrow and completely filled with barium to the distal tip (solid arrows). This finding rules out appendicitis.

(3) posterior cecal artery; (4) colic ramus; and (5) appendicular artery, which runs through the mesenteriolum to supply the vermiform appendix. Because there are no arterial arcades in the mesenteriolum, the appendicular artery is a terminal artery, predisposing the appendix to ischemia when there is vascular insult.¹⁰ The appendicular artery origin is variable, with the following frequencies: iliac ramus (35%), ileocolic artery (28%), anterior cecal artery (20%), posterior cecal artery (12%), ileocecal artery (3%), and ascending colon ramus (2%).¹⁶ The veins accompany the arteries.

Lymphatic tissue begins to develop in the appendix during the 14th and 15th weeks of gestation.¹⁷ Initial accumulations of lymphatic cells occur directly below the epithelium, but some lymphocytes eventually penetrate the epithelial layer of the appendix. Lymphatic drainage of the appendix is via ileocolic lymph nodes located along the superior mesenteric artery and via celiac nodes into the cisterna chyli.

Unlike the cecal wall, which is composed of a diagonal rhomboid mesh of collagen fibers and allows it to accommodate luminal expansion, the appendiceal wall is composed of horizontal collagen fibers that tolerate only minimal increases in luminal diameter. Although the appendix secretes 2 to 3 mL of mucus daily, its average luminal capacity is only approximately 1 mL.¹⁰ This, in conjunction with the appendix's solitary blood supply, explains its propensity to become ischemic rapidly and perforate after luminal obstruction.

Acute Appendicitis

EPIDEMIOLOGY

Appendicitis was first described and reported by Reginald H. Fitz at the 1886 meeting of the Association of American Physicians.¹⁸ Appendicitis is the most frequent cause of acute abdominal pain requiring surgical intervention in the western world and is the most common abdominal operation performed annually in the United States on an emergency basis.^{19,20}

Appendicitis is rare in infants but becomes increasingly common in childhood. The highest incidence of appendicitis is in individuals aged 10 to 19 years (15.3/10,000 population/year).²¹ Across all age groups, the annual rate is approximately 9.4/10,000.²¹ The lifetime cumulative incidence is approximately 9%.²² There is a slight male predominance, with a ratio of 1.3:1. Mortality and morbidity rates for removal of a normal appendix are 0.14% and 4.6%, respectively, but increase to 0.24% and 6.1% for acute appendicitis and to 1.7% and 19% for perforated appendicitis, respectively.²³ These mortality rates are far better than the 50% mortality seen in the preantibiotic era.¹⁻⁵

Appendiceal perforation occurs in 16% to 39% of patients with a median reported incidence of 20%.²⁴⁻³¹ Risk factors for perforation include very young or old age, Asian or Hispanic

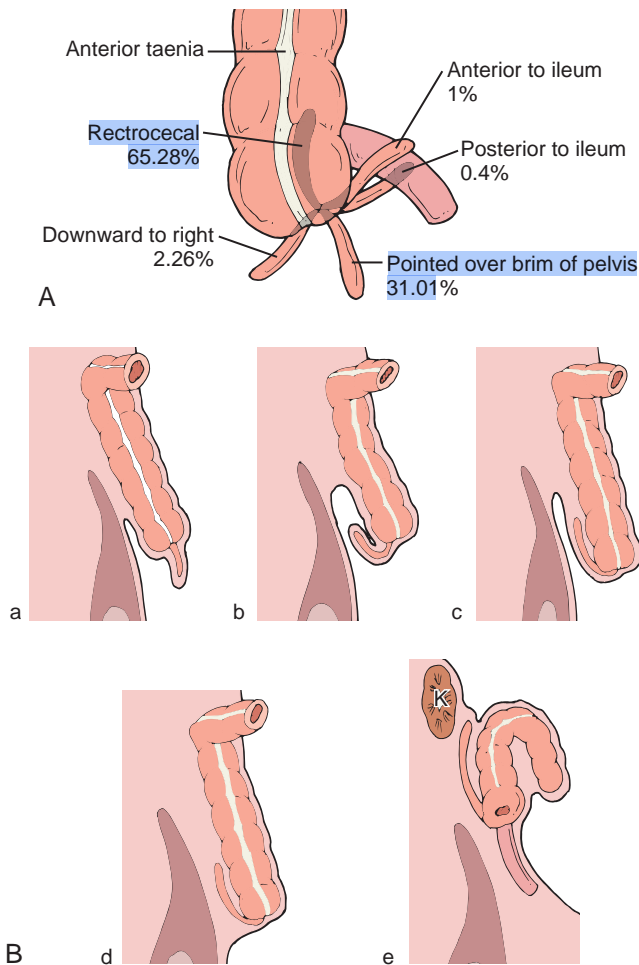


Figure 56-3 Variations in position of the appendix. **A.** Incidence of various positions of the appendix. **B.** Normal variations in the position and peritoneal fixation of the appendix: (a) intraperitoneal, pointing over the brim of the pelvis; (b) intraperitoneal, ascending retrocecal; (c) extraperitoneal, ascending retrocecal, with a paracecal fossa present; (d) extraperitoneal, ascending retrocecal; (e) extraperitoneal, ascending retrocecal, lying anterior to the right kidney (K) deep to the liver, associated with an undescended subhepatic cecum. (The terminal ileum is also extraperitoneal and enters the cecum from behind.) (**A** from Meyers MA: *Dynamic Radiology of the Abdomen*. New York, Springer-Verlag, 1988, p 403; **B** from Meyers MA, Oliphant M: *Ascending retrocecal appendicitis*. *Radiology* 110:295–299, 1974.)

ethnicity, and lower socioeconomic status.^{22,32,33} Although some early studies found a linear correlation between perforation rates and diagnostic accuracy, more recent studies have cast doubt on any relationship.^{28,30} A study of 1486 appendectomy cases found an overall perforation rate of 19%, with higher rates in the very young and older adults.²⁸ Vorhes noted that patients older than 55 years underwent laparotomy on average 2 days later than those younger than 55 years.³⁴ A large retrospective study of children (≤ 18 years) showed that the rate of appendiceal perforation was markedly higher for children younger than 5 years old (71.9% vs. 21.7% for children > 5 years) and that the risk for perforation was inversely proportional to the patient's age.³³

Acute appendicitis is the most common nonobstetric surgical emergency in pregnant patients, occurring in approximately

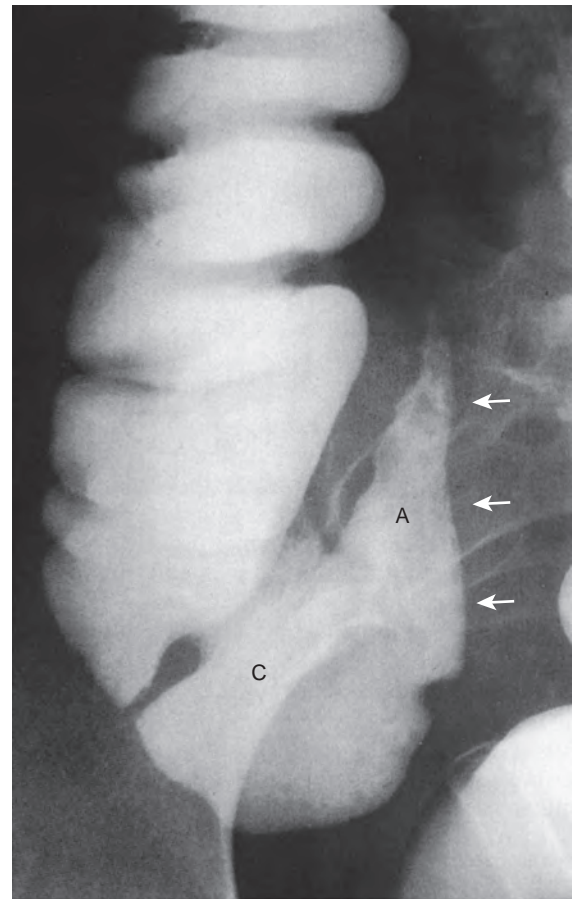


Figure 56-4 Fetal appendix. Barium enema examination in a 21-year-old woman shows arrest in the development of the appendix (A). The cecum (C) has a triangular, funnel-shaped inferior segment (arrows), with gradual transition into an incompletely developed appendix.

1 in 766 pregnancies.³⁵ Complications include premature labor and fetal and maternal death, especially when perforation occurs.³⁶ The fetal loss rate for nonruptured appendicitis is approximately 2%, compared with more than 30% in patients with ruptured appendicitis.³⁷

CAUSES

Acute appendicitis occurs after luminal obstruction. Causes of obstruction include fecalith, lymphoid hyperplasia, primary tumor (e.g., carcinoid, adenocarcinoma, lymphoma, Kaposi's sarcoma) or metastasis, parasitic infection, foreign body, stricture, Crohn's disease, and adhesion (Fig. 56-5). Prolonged retention of barium is no longer considered a risk factor for acute appendicitis.^{38–41}

Of the possible causes of luminal obstruction, fecaliths are the most common, occurring in 11% to 52% of patients with acute appendicitis.^{42,43} Fecalith formation results from inspissation of fecal material and inorganic salts within the appendiceal lumen. As they enlarge, these concretions can obstruct the appendix. Low-fiber diets contribute to low-residue stool, which has a propensity to become impacted in the appendiceal lumen. True appendiceal calculi (hard, noncrushable calcified stones) are less common than fecaliths but, when present, they

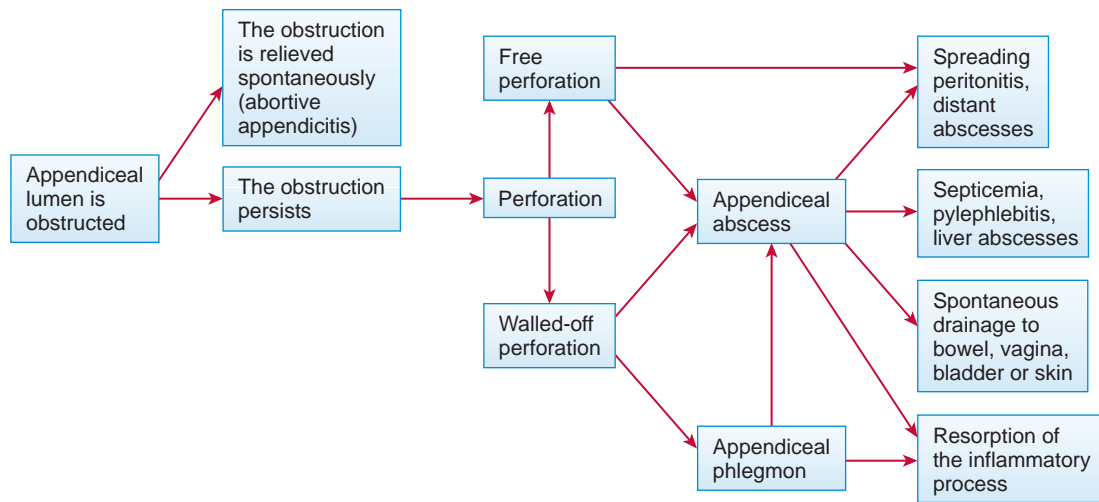


Figure 56-5 Pathophysiologic pathways in untreated appendicitis. (From Puylaert JBCM: *Ultrasound of Appendicitis*. Berlin, Springer-Verlag, 1990, p 5.)

have a higher association with appendiceal perforation and periappendiceal abscess formation.⁴³

Hygiene improvements of the modern world have greatly reduced the exposure of infants and children to enteric organisms. Consequently, when infections do occur, they can elicit an exaggerated lymphoid hyperplasia that may block the appendix or devitalize the appendiceal mucosa, allowing bacterial invasion.³⁸⁻⁴¹

PATHOPHYSIOLOGY

Continued secretion of mucus into the appendix after luminal obstruction results in distention and concurrent elevation of luminal pressures. When the luminal pressure exceeds the capillary perfusion pressure, lymphatic and venous drainage are impaired and arterial compromise and tissue ischemia result. Breakdown of the epithelial mucosal barrier occurs, and luminal bacteria multiply and invade the appendiceal wall, causing transmural inflammation and gangrenous appendicitis (Fig. 56-6). Continued tissue ischemia can result in appendiceal infarction and perforation. Perforation can cause a localized or generalized peritonitis as inflammation extends through the serosa to the parietal peritoneum and adjacent organs (cecum, terminal ileum, pelvic viscera). Although periappendiceal abscess or phlegmon is usually walled off by the adjacent greater omentum or small bowel, some cases will spread through the peritoneum to the paracolic gutters and subphrenic spaces, sigmoid colon, bladder, ovaries, or vagina. Infected thrombus may form in the portal vein, causing pylephlebitis, although this is unusual with modern antibiotics.^{1-5,44}

CLINICAL AND RADIOLOGIC ASSESSMENT

Clinical assessment remains an essential and critical part of the initial evaluation of patients with suspected acute appendicitis. The physician's goal is to confirm or exclude the diagnosis of acute appendicitis expeditiously while minimizing diagnostic delays, negative appendectomy (i.e., surgery for suspected appendicitis yields a normal appendix) and appendiceal perforation rates, and hospital costs. More recently, reducing or

eliminating ionizing radiation dose to the patient has become a major consideration driving the diagnostic approach, particularly in children and pregnant women.⁴⁵⁻⁴⁷ However, despite continued advances in clinical medicine, the diagnosis of acute appendicitis can sometimes remain elusive.⁴⁸⁻⁵¹

Although diagnostic accuracy rates for appendicitis in the United States had improved from 86% to 92% in male patients and from 74% to 83% in female patients between 1970 and 1984,^{14,20} one study suggested that imaging has helped improve accuracy. Perforation and false-negative appendectomy rates have stabilized in recent decades.²⁷ Cases of "missed appendicitis" typically reflect the frequent diagnostic difficulty of differentiating appendicitis from other causes of abdominal pain.^{52,53}

Historically, negative appendectomy rates of as high as 15% to 23% had been acceptable, with rates as high as 45% in patients with an atypical presentation or in women of childbearing age.⁵⁴ Negative laparotomy rates of 10% to 15% have now been considered acceptable, although that number continues to trend downward as imaging improves. Negative laparotomy rates remain higher in women of childbearing age.^{22,55} Diagnostic accuracy can be improved with inpatient observation, subsequently leading to a decreased negative appendectomy rate without a concurrent increase in appendiceal perforation rates.⁵⁶

A large retrospective study found that risk factors for negative appendectomy included very young or advanced age, female gender, and presence of comorbid illness. In that study, the highest rate of negative appendectomy was in women older than 70 years.⁵⁷ Negative appendectomy (compared with positive appendectomy) was associated with a significantly longer length of stay (5.8 vs. 3.6 days), case-fatality rate (1.5% vs. 0.2%), and infectious complication rate (2.6% vs. 1.8%).⁵⁸

Radiologic imaging has become an important adjunct to clinical evaluation. Accurate identification of an inflamed or normal appendix can greatly facilitate appropriate treatment. Imaging can also identify alternate diagnoses in patients with clinically suspected acute appendicitis.^{45,54,55,59-61}

Despite advances in radiologic imaging, controversy still exists in the literature about whether the increased availability

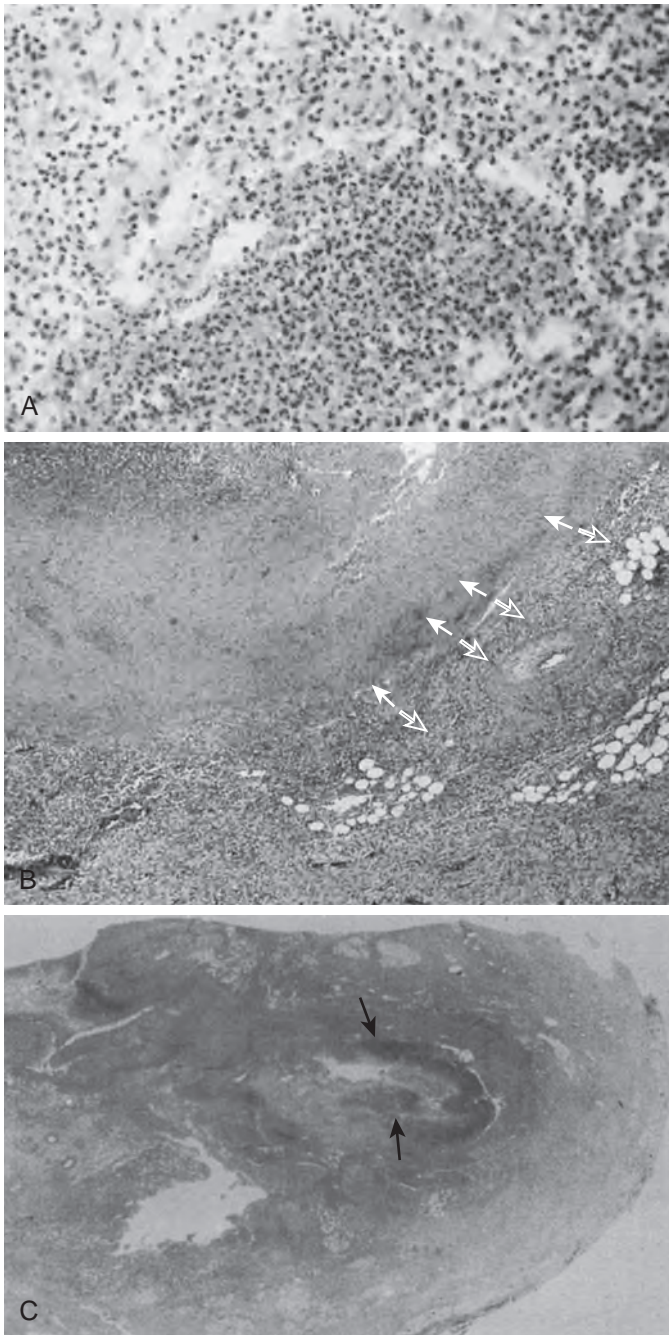


Figure 56-6 Pathology of appendicitis. **A.** The lumen fills with purulent exudate (hematoxylin-eosin, $\times 150$). **B.** Necrosis of the muscularis propria (solid arrows) and inflammation of the periappendiceal fat (open arrows) are seen (hematoxylin-eosin, $\times 80$). **C.** Transmural and periappendiceal inflammation and fibrosis are present with focal destruction (arrows) of the appendiceal wall (hematoxylin-eosin, $\times 6$).

of imaging and laparoscopy has decreased misdiagnoses and negative laparotomy rates. For example, Flum and associates performed a retrospective study of 63,707 appendectomy patients from 1987 to 1998.⁵⁷ They found that, contrary to expectation, the use of computed tomography (CT), ultrasonography (US), and laparoscopy did not change the negative appendectomy or appendiceal perforation rates.

In contrast, many subsequent reports have described reductions in the negative appendectomy rate associated with increased use of imaging. Jones and co-workers found a decrease in the negative appendectomy rate (from 17%-2%) coinciding with increased CT use from 2000 to 2002.⁶² The rate of appendiceal perforation also decreased (from 25%-9%) during the same interval. Rao and colleagues found reductions in the negative appendectomy rate (from 20%-7%) and perforation rate (from 22%-14%) with increased use of CT.⁶³ At Duke University, a 10-year retrospective study published in 2010 found that an increase in preoperative CT use from 18.5% to 93.2% resulted in a reduction of the negative appendectomy rate among 18- to 45-year-old women from 42.9% to 7.1%.⁶⁴ A study by Bendeck and associates showed a lower negative appendectomy rate for women who underwent preoperative CT or US imaging compared with women without preoperative imaging (7% vs. 28%, respectively).⁶²

In a large study of almost 20,000 patients, Drake and co-workers found a negative appendectomy rate of 4.5% in patients who underwent imaging versus 15.4% in patients with only clinical assessment.⁶⁵ Despite imaging, the negative appendectomy remained higher for women compared with men (6.9% vs. 3%).⁶⁶

FINDINGS

Clinical Findings

Most patients with acute appendicitis present with abdominal pain, although the classic presentation sequence of poorly localized periumbilical pain followed by nausea and vomiting and later migration of the pain to the right lower quadrant occurs in only half to two thirds of all patients.⁶⁷ The location of abdominal pain varies and depends on both the position of the inflamed appendix and stage of appendiceal inflammation. With initial distention and increased intraluminal pressure in the obstructed appendix, patients typically perceive visceral epigastric or periumbilical pain. During this time, the disease is usually confined to the appendix. When the inflamed serosa of the progressively inflamed appendix comes into contact with the parietal peritoneum, somatic pain is perceived, with the classic description of pain that shifts to the right lower quadrant.⁶⁸ In patients with a retrocecal appendix, the pain may be referred to the right flank, costovertebral angle or, in males, the right testis. Patients with a pelvic or retroileal appendix may experience pain in the pelvis, rectum, adnexa or, less commonly, left lower quadrant.⁶⁷ Nausea, vomiting, and anorexia are variably present, occurring in more than 50% of all cases.^{31,69}

Signs and symptoms vary with the inflammatory stage of the appendicitis. Abdominal tenderness is the most common physical finding, occurring in more than 95% of patients.⁶⁷ Although the classic teaching is that patients with appendicitis present with localized tenderness at or near McBurney's point (positioned 1.5 cm superior and medial to the anterior superior iliac spine and parallel to a plane drawn from the anterior superior iliac spine to the umbilicus), the point of tenderness will vary, depending on the position of the inflamed appendix. In one series of 275 double-contrast barium enemas, the appendiceal location was within 5 cm of McBurney's point in only 35% of patients and was farther than 10 cm in 15% of cases.⁷⁰ Usually, the appendix is located inferior and medial to McBurney's point.^{70,71} Patients may also present with Rovsing's sign (pain referred to the area of maximal tenderness during palpation or

percussion of the left lower quadrant), positive psoas sign (right lower quadrant pain with extension of the right hip), or obturator sign (right lower quadrant pain with flexion and internal rotation of the right hip). Voluntary muscle guarding in the right lower quadrant is common and typically precedes localized rebound tenderness. Bowel sounds vary but are usually diminished or absent with advanced appendiceal inflammation or perforation.⁶⁷

Most patients with acute appendicitis (70%-90%) present with a white blood cell (WBC) count greater than 10,000/mL and neutrophilia more than 75%.⁷²⁻⁷⁴ Serial WBC counts may be helpful in the diagnosis because it has been shown that patients tend to have an increased WBC count 4 to 8 hours after admission unless the appendix is perforated, in which case the WBC count typically decreases.⁷⁵ Because a minority of patients with acute appendicitis have a normal WBC count, a normal value is not sufficient to exclude the diagnosis.⁷⁶

Urinalysis is positive in 19% to 40% of patients with appendicitis; abnormalities include bacteriuria, mild pyuria, and hematuria.^{77,78} Abnormal urinalysis results are more commonly observed in women with appendicitis than in men.

Elevation of the C-reactive protein (CRP) level more than 0.8 mg/dL has sensitivities of 46% to 75% and specificities of 56% to 82% in acute appendicitis, and elevation is more common when symptoms are present for more than 12 hours.^{75,78-81} The diagnostic sensitivity for acute appendicitis is improved to 97% to 100% when an elevated CRP level, elevated WBC count, and neutrophilia more than 75% are all present.⁸¹

Imaging Findings

Plain Radiographs. The most specific plain film sign is the presence of an appendicolith (Fig. 56-7). However, appendicoliths are only found by radiographs in 10% of patients with acute appendicitis. When present on radiographs, the reported incidence of perforation is almost 50%. Appendicoliths are usually 0.5 to 2 cm in diameter and have a round or oval configuration and laminated rim. The calcified rim assists in differentiating them from bone islands, ureteral stones, and phleboliths. They may be obscured by the bone structures of the pelvis or may be ectopically located in the right upper abdomen in cases of retrocolic appendicitis. Appendicoliths are usually solitary, but two or three adjacent small calcifications are not unusual. Appendicoliths may be detected in asymptomatic individuals and, without associated clinical findings, are not indicative of appendicitis.⁸²⁻⁸⁵

Air in the appendix, particularly in the retrocecal location, is a normal finding. Extraluminal bubbles of air associated with an ill-defined soft tissue mass indicate an abscess (Fig. 56-8). Sometimes, the inflammatory process in the right lower quadrant induces a severe localized ileus, with dilation and air-fluid levels in the ileal loops and cecum. When severe, this process can mimic the appearance of a mechanical distal small bowel obstruction (Fig. 56-9). Dilation of the transverse colon in association with a gasless cecum and ascending colon may result from ileus of the transverse colon and spasm of the ascending colon. Free air in the peritoneal cavity is rare because the base of the appendix is usually occluded when perforation occurs.⁸⁶⁻⁸⁹

Other findings such as partial loss of the right psoas shadow and a lumbar scoliosis concave to the right are common, albeit nonspecific.⁸²⁻⁸⁵ Appendicitis may also cause a distal small bowel obstruction, particularly when perforated.

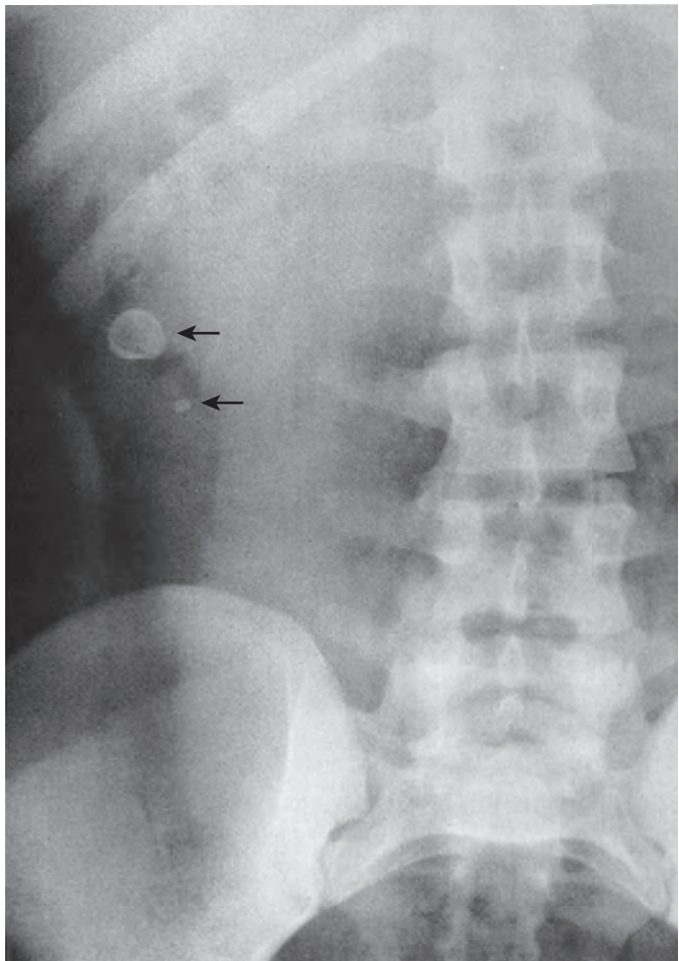


Figure 56-7 Appendicoliths. Two appendicoliths (arrows) are present in the right upper quadrant. The patient had a long retrocolic subhepatic appendix with acute appendicitis.

Plain film radiography is typically inadequate for the diagnosis of appendicitis. Ahn and colleagues retrospectively reviewed the records of 871 adult patients with nontraumatic acute abdominal pain and found that plain radiographs were normal in 23%, nonspecific in 68%, and abnormal in only 10%. The diagnostic sensitivity for appendicitis, pyelonephritis, pancreatitis, and diverticulitis was 0% in the study.⁹⁰

Barium Enema. Before the 1980s, the barium enema was the primary radiologic test used in the diagnosis of appendicitis. This examination can be performed quickly and safely with the single-column technique. Because appendicitis results from luminal obstruction, complete filling of a normal appendix effectively excludes the diagnosis (Fig. 56-10A). Nonfilling or incomplete filling of the appendix in the presence of mass effect (on the caput cecum and adjacent distal ileum indicates inflammation Fig. 56-11; Fig. 56-10B). Studies have reported diagnostic accuracy as high as 91.5%.^{82,83,88,91-97}

A barium enema study may also detect other pathologies of the small and large bowel that can mimic the clinical presentation of acute appendicitis. These include neoplasm, Crohn's disease, ileal diverticulitis, and cecal diverticulitis.^{82,83,88,91-97}

Barium enema is not without major drawbacks. Nonfilling of the appendix can be seen in 15% to 20% of normal patients,



Figure 56-8 Appendiceal abscess: plain radiographic findings.

This abscess manifests as a bubbly collection of extraluminal gas in the right lower quadrant.

and it may be difficult to differentiate a partially filled from a completely filled appendix. Also, a barium enema study provides only inferential information about extracolonic disease and cannot evaluate the nature of appendiceal phlegmons and abscesses. The appendix can also intussuscept (Fig. 56-12) into the cecum, producing a cecal defect unrelated to appendicitis.^{96,98-100}

Computed Tomography. Helical CT imaging has proven to be a highly effective and accurate means of diagnosing acute appendicitis, with reported sensitivities of 90% to 100%, specificities of 91% to 99%, accuracies of 94% to 98%, positive predictive values of 92% to 98%, and negative predictive values of 95% to 100%.¹⁰¹⁻¹⁰⁶ In addition to visualization of the appendix, CT can detect complications of appendiceal perforation, such as abscess or phlegmon (Fig. 56-13). Critically, CT can help diagnose many alternate conditions that might mimic the clinical presentation of acute appendicitis.¹⁰⁷

The goal of CT investigation in patients with right lower quadrant pain is to identify the normal or abnormal appendix. Thin-section (slice thickness ≤ 5 mm) imaging is now standard, providing superior sensitivity compared with older techniques.^{108,109} With the advent of multidetector scanners such as

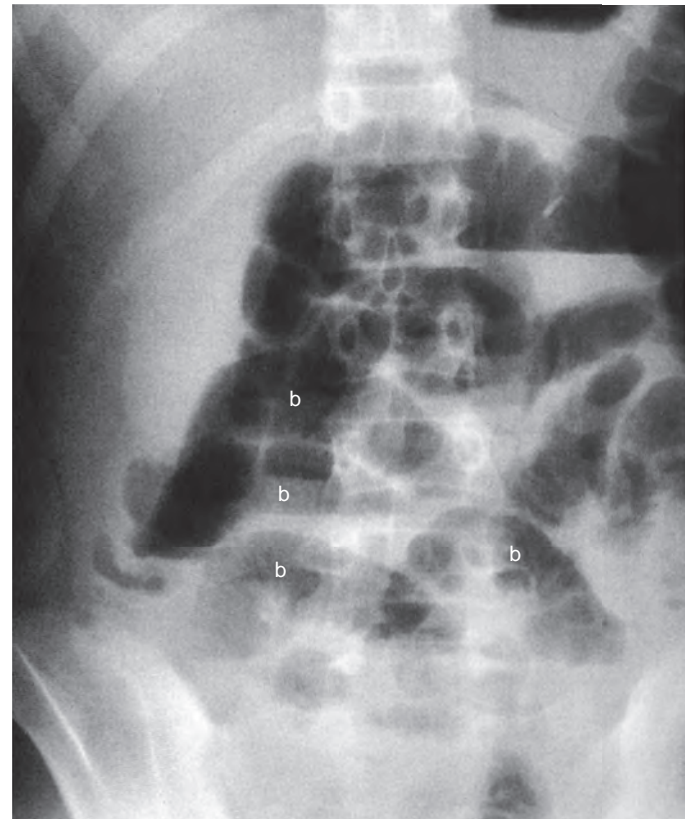


Figure 56-9 Acute appendicitis causing partial small bowel obstruction. Upright radiograph shows dilation and air-fluid levels in multiple lower abdominal small bowel loops (b). The patient presented with fever and leukocytosis, and gangrenous appendicitis was found at surgery.

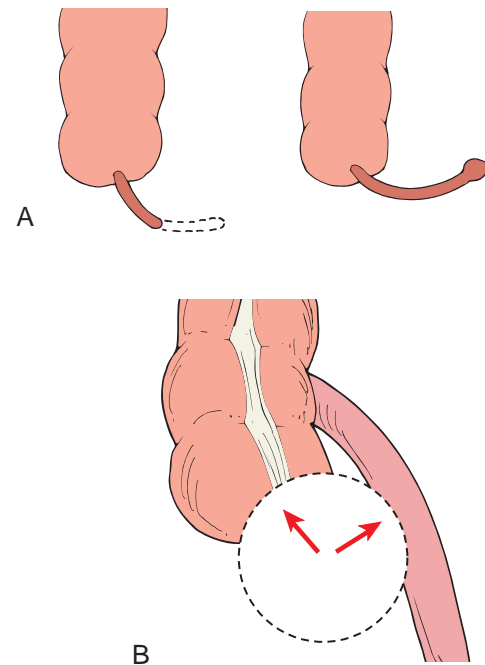


Figure 56-10 Principles of barium enema diagnosis of acute appendicitis. A. Only complete filling of the appendix to its bulbous tip excludes appendicitis. B. Ileocecal deformity (arrows) caused by appendiceal abscess or phlegmon. (From Bartram CI, Kumar P: *Clinical Radiology in Gastroenterology*. Oxford, Blackwell Scientific, 1981, p 219.)

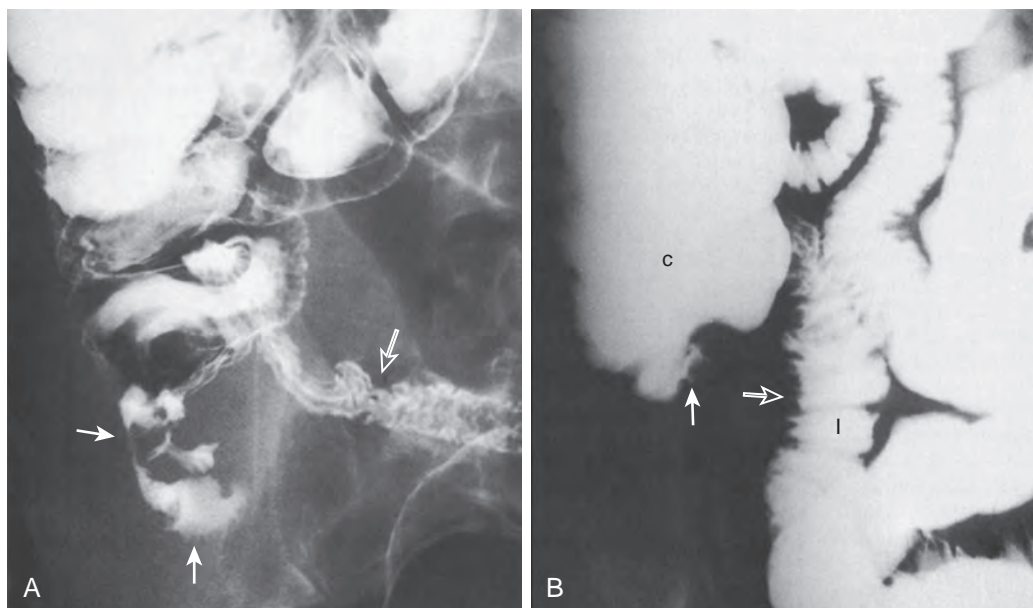


Figure 56-11 Acute appendicitis: barium enema findings. **A.** Extravasation of barium in a patient with sealed-off, perforative appendicitis (solid arrows). The cecum and terminal ileum (open arrow) are unremarkable. **B.** Appendiceal abscess shows compression of the cecal caput, obstruction of the base of the appendix (solid arrow), and a spiculated lateral contour (open arrow) of the terminal ileum. C, cecum; I, ileum.

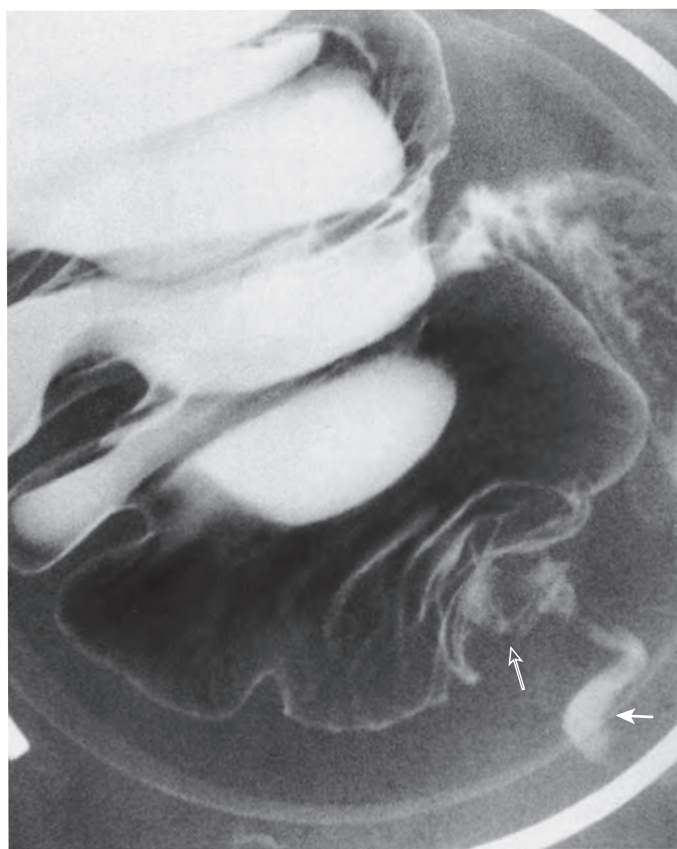


Figure 56-12 Partial appendiceal intussusception. The appendix is incompletely filled (solid arrow) and partially intussuscepting into the cecal caput (open arrow).

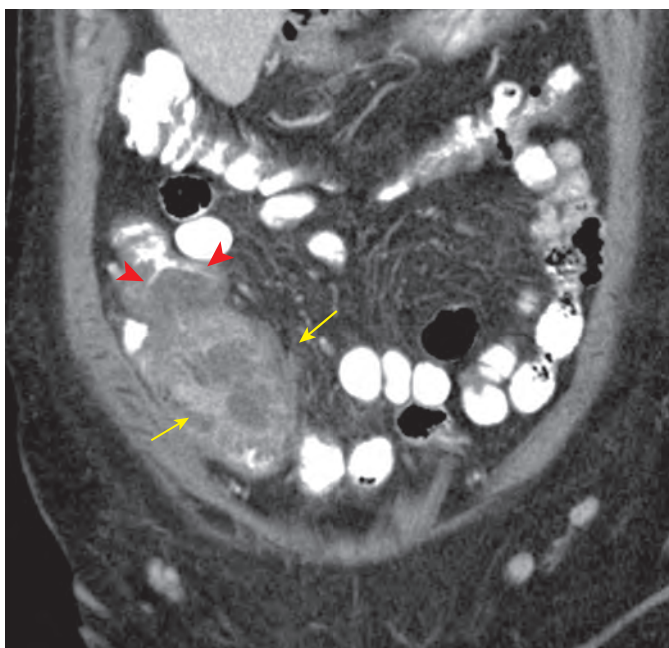


Figure 56-13 Perforated acute appendicitis with abscess. This coronal image from an enhanced CT scan shows extensive right lower quadrant inflammation and a fluid-filled abscess (arrows). Note the thickened, inflamed cecum (arrowheads).

16- and 64-slice multidetector CT (MDCT), high-quality multiplanar reformatted (MPR) images are now possible. Adding coronal reconstructions, for example, can improve appendix visualization and diagnostic confidence.^{110,111}

Radiologists are able to identify a normal appendix in most patients with abdominal pain who undergo abdominal CT (67%-100%), with a trend toward better visualization with thinner section imaging.^{109,112-114} Appendix identification is more difficult in patients with a paucity of retroperitoneal fat, in patients with ascites, and in women compared with men.¹¹²⁻¹¹⁴ With CT, the diameter of a normal appendix ranges from 3 to 10 mm.¹¹²⁻¹¹⁴ In one study, the normal appendix had a diameter more than 6 mm in 42% of cases.¹¹³ Therefore, an appendiceal diameter more than 6 mm is not alone sufficient for the diagnosis of acute appendicitis.

CT findings of appendicitis may include appendiceal distention, wall thickening, appendicolith, periappendiceal fat stranding, periappendiceal fluid, and abscess (Figs. 56-14 to 56-16).^{20,109,115,116} In early or mild cases, the appendix commonly appears as a fluid-filled, minimally distended tubular structure measuring 5 to 6 mm in diameter.²⁰ At this stage, the periappendiceal fat may have a normal appearance (Fig. 56-17).

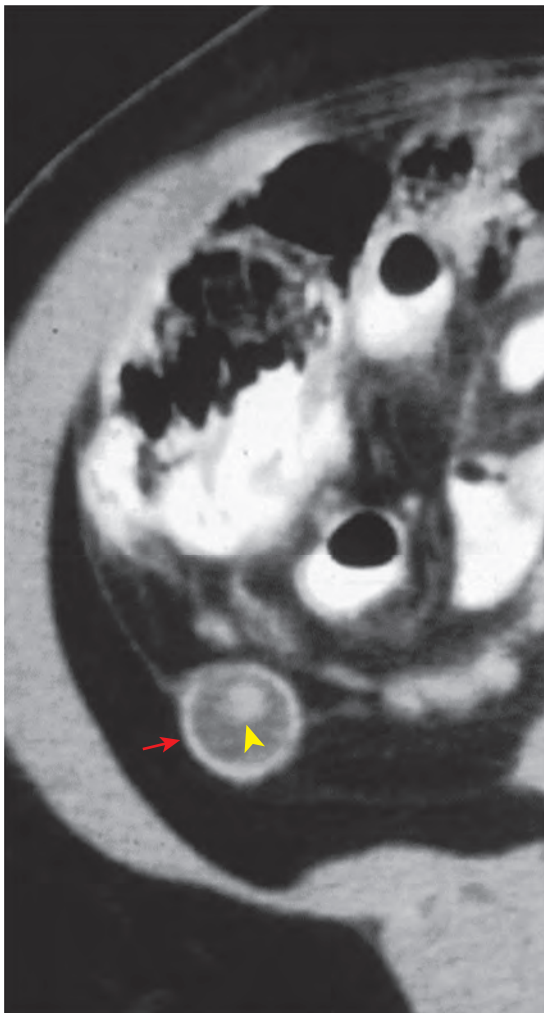


Figure 56-14 Acute appendicitis on enhanced CT. The distended appendix (arrow) is seen in cross section and demonstrates abnormal mural thickening and enhancement. In addition, an intraluminal appendicolith (arrowhead) is present.

Over time, the appendix continues to distend, often measuring 7 to 15 mm in diameter. The appendiceal wall thickens circumferentially and enhances after intravenous (IV) contrast administration. The mural enhancement may be homogeneous or may exhibit a so-called target sign (Fig. 56-18). Periappendiceal inflammation, seen as stranding in the adjacent fat, is present in most patients.²⁰ Lack of IV contrast material limits visualization of mural thickening and mural enhancement in mild cases of appendicitis. As a result, noncontrast CT may result in a higher rate of false-negative interpretations.^{104,116-118} Many investigators consider periappendiceal inflammation a necessary imaging finding when diagnosing acute appendicitis with unenhanced CT imaging.^{101,102,104,105,117}

Inflammation of the appendix may also cause secondary reactive thickening of adjacent structures, including the wall of the terminal ileum or cecal caput. The cecal arrowhead sign refers to a triangular or arrowhead configuration of oral contrast material funneling into a focally thickened cecum, pointing toward the appendiceal orifice (Fig. 56-19). The cecal bar sign refers to linear inflammatory soft tissue at the base of the appendix that separates the contrast-filled cecum from the appendix.^{119,120} With perforated appendicitis, extraluminal air,

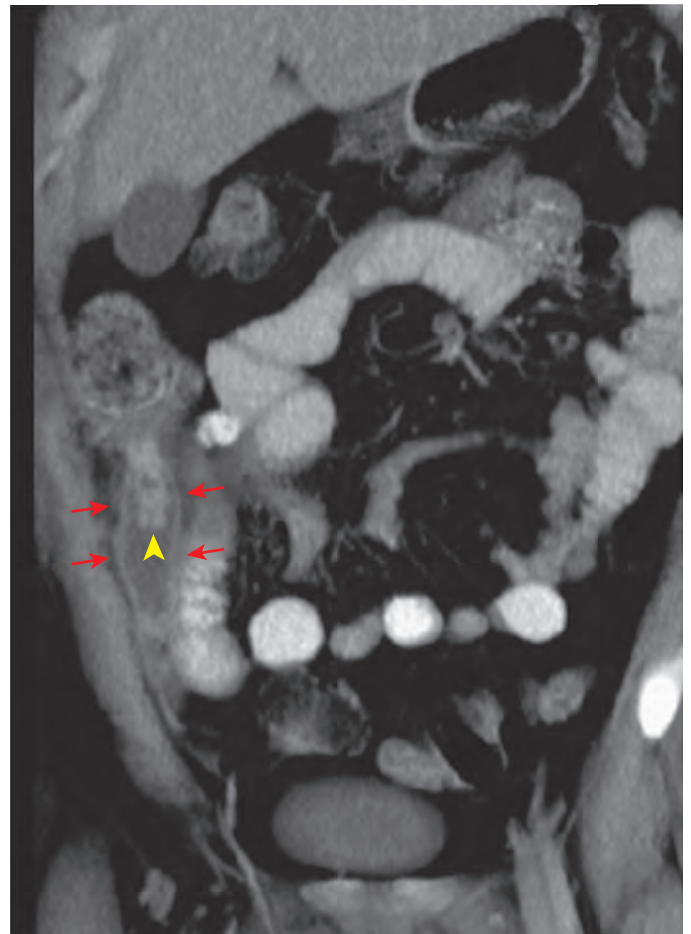


Figure 56-15 Acute appendicitis on enhanced CT. This coronal multiplanar reconstruction image shows the distended appendix (arrows) with multiple obstructing appendicoliths (arrowhead) at the appendiceal orifice. Note the mural wall thickening and enhancement, as well as the periappendiceal soft tissue stranding and fluid. On pathologic examination the appendix was shown to be perforated.

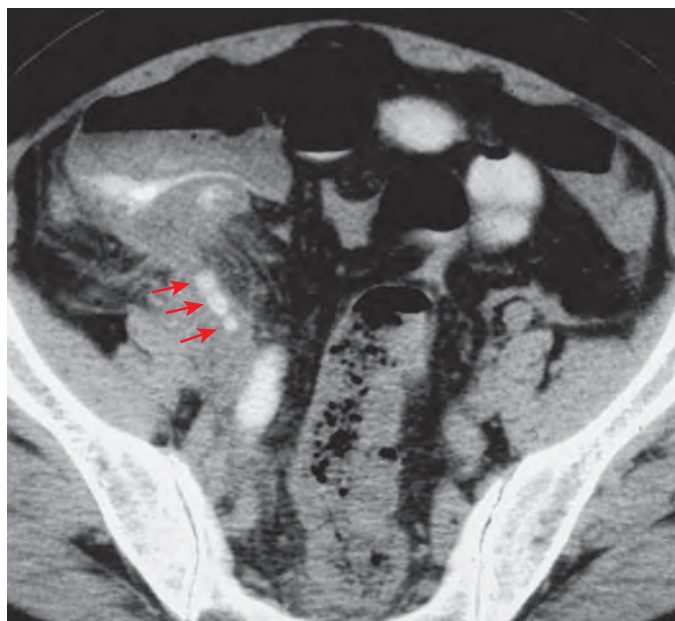


Figure 56-16 Acute appendicitis on CT. Although the appendix itself is not distinctly identified, there are three appendicoliths (arrows) present in association with right lower quadrant inflammation and pericecal thickening. This constellation of findings is diagnostic of acute appendicitis.



Figure 56-17 Acute appendicitis. The abnormal appendix (arrows) is seen in cross section on this enhanced CT scan. Although there is minimal distention of the appendiceal lumen, there is evidence for abnormal mural thickening and enhancement. Note the absence of periappendiceal inflammatory change.

marked ileocecal wall thickening, localized lymphadenopathy, pericecal phlegmon or abscess, peritonitis, and/or small bowel obstruction may be present (Fig. 56-20).¹²¹⁻¹²⁴

Appendicitis may also be confined to the distal appendix, a condition referred to as distal or tip appendicitis (Fig. 56-21). Distal appendicitis (in which at least 3 cm of the proximal appendix is normal) may affect as many as 8% of patients with appendicitis who undergo CT.¹²⁵

Computed Tomography Protocols. Conventional CT protocols for evaluating patients with suspected appendicitis

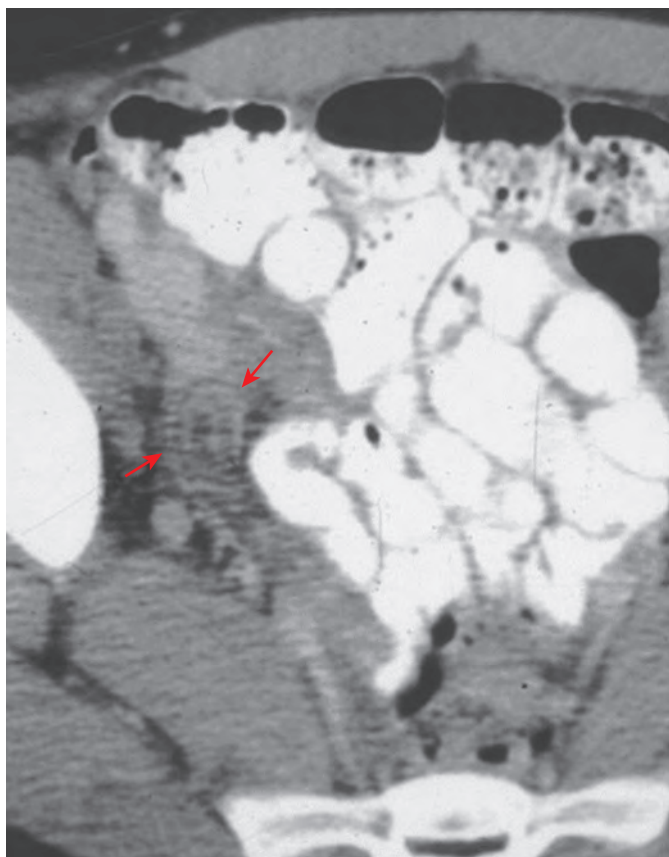


Figure 56-18 Acute appendicitis. The abnormal appendix (arrows) is seen in cross section on this enhanced CT study, which demonstrates a mural stratification pattern of enhancement with alternating high- and low-density rings caused by serosal and mucosal enhancement and submucosal edema.

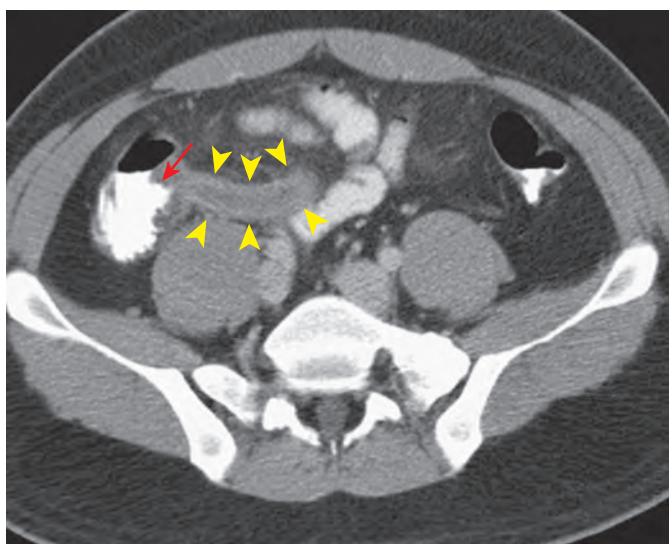


Figure 56-19 Acute appendicitis on enhanced CT. The appendix (arrowheads) is distended, with enhancement of the thickened appendiceal wall and periappendiceal soft tissue stranding. Note the funneling of enteric contrast in the thickened cecum toward the appendiceal orifice, the so-called arrowhead sign (arrow).

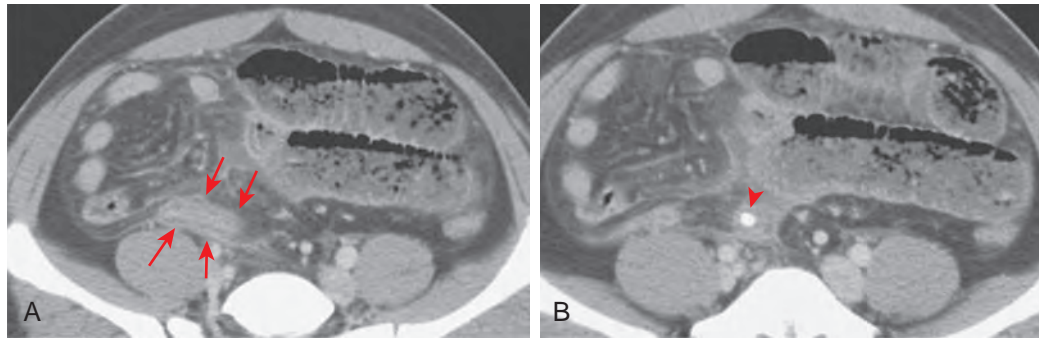


Figure 56-20 Small bowel obstruction from acute appendicitis. **A.** There are multiple dilated small bowel loops in the pelvis to the level of the abnormally distended, thick-walled, and enhancing appendix (arrows). **B.** A more superior CT scan shows a calcified appendicolith (arrowhead) near the appendiceal orifice.

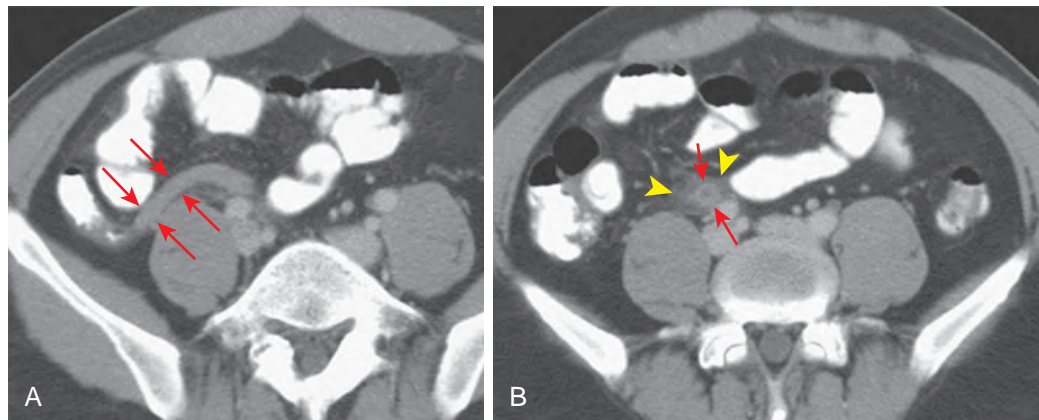


Figure 56-21 Distal or tip appendicitis. **A.** The proximal appendix (arrows) is normal in appearance on this enhanced CT scan. **B.** The distal aspect of the appendix demonstrates abnormal mural thickening and enhancement (arrows); periappendiceal soft tissue stranding is also present (arrowheads).

incorporate abdominal and pelvic imaging after administration of oral and IV contrast material. Many studies have focused on alternate CT protocols in an attempt to reduce radiation dose to the patient, eliminate the patient risks associated with contrast administration, and enable earlier scanning rather than waiting for bowel transit of oral contrast material. Investigated strategies include scanning without IV or oral contrast, using rectal contrast, targeted imaging of the right lower quadrant, and reduced radiation dose scanning techniques.^{4,105,118,126-132}

CT protocols may not include oral or IV contrast. A major advantage of this approach is the ability to scan symptomatic patients immediately without having to wait for oral contrast material ingestion and transit to the cecum. Eliminating IV contrast means avoiding risks of adverse reaction and nephrotoxicity. Noncontrast scans also have lower costs.

Without oral contrast, disadvantages include potential misinterpretation of another structure (e.g., a loop of bowel) as the appendix, or misinterpretation of an abnormal appendix or abscess as a bowel loop.^{117,133} Relative to a contrast-filled appendix, finding the normal appendix without oral contrast is more difficult. Finally, identification of bowel thickening and luminal narrowing, two hallmarks of GI disease on CT, is often very limited without contrast material filling the bowel lumen.¹³⁴

Without IV contrast, disadvantages include limited assessment of wall thickening, inability to assess enhancement, limited differentiation of the appendix from blood vessels, reduced sensitivity for perforation or complication,^{20,118,133,135} and a lesser ability to make an alternate diagnosis. Identification of wall thickening and enhancement is often critical in patients in whom fat stranding is not detected, either because there is a paucity of retroperitoneal fat or because appendicitis is early or mild.^{104,118} One study found that 15% to 22% of patients with proven appendicitis had no detectable periappendiceal inflammation on CT.¹¹⁸

Administration of rectal contrast material permits rapid filling of the cecum, with appendix identification in a large majority of cases. In a study by Rao and associates, use of a focused right lower quadrant technique with rectal contrast material enabled detection of the normal appendix in 94% of patients without appendicitis and visualization of part or all of the abnormal appendix in 96% of patients with acute appendicitis. In their study, 73% of the normal appendices filled with air or rectal contrast.¹⁰⁴ Disadvantages of the rectal contrast technique include the potential for increased patient discomfort,¹³¹ inability to instill rectal contrast material in patients with contraindications to its use, and risk of causing a hydraulic pressure effect and rupturing the appendix.¹³⁶ This technique may also fail if there is leakage of contrast material onto the CT

table or if there is inadequate opacification of the cecum. Wise and co-workers reported that colonic contrast material was not successfully advanced into the cecum in 18% of 100 patients who underwent focused appendiceal CT, usually because of abundant stool in the right colon.¹³¹ One study reported that rectal contrast use resulted in a reduced length of patient stay in the emergency room without significant impact on patient satisfaction or comfort.¹³⁷

The goal of focused scanning is to reduce the portion of the abdomen and pelvis that is scanned, thereby reducing overall radiation dose to the patient. Although early studies showed that focused techniques may have comparable diagnostic accuracy,¹⁰⁵ later investigations found an overall reduction in diagnostic performance. By using a focused technique, the appendix may not be visualized or may only be partially visualized. In addition, evidence of an alternate diagnosis may be excluded from the field of view.¹¹⁸ Brassart and colleagues compared scanning of the whole abdomen and pelvis with focused scanning below the iliac crests in the same set of 152 adult patients by generating two sets of images from the raw data.¹³⁸ They found that the focused technique resulted in exclusion of the appendix from view in 5% of patients and a reduced likelihood of giving a correct diagnosis (from 78%-68%). Common alternative diagnoses include acute gynecologic disorders, inflammatory bowel disease, small bowel obstruction, infectious disorders of the GI tract, and urinary tract conditions.^{45,107}

As of 2013, the consensus position of the American College of Radiology (ACR) expert panel is that IV contrast is preferred but not mandatory when using CT to evaluate for suspected appendicitis in adult patients. The use of oral or rectal contrast is left to institutional preference. For atypical presentations in patients older than 14 years, the use of IV contrast is relatively more valuable. In this group, ultrasound evaluation may be of similar value to noncontrast CT. In pregnant patients and children younger than 14 years, ultrasound is considered first-line imaging. When CT is used, IV contrast is preferred, whereas oral and rectal agents are again left to institutional preference. Magnetic resonance imaging (MRI) evaluation is gaining popularity as the technology evolves, particularly in pregnant patients or those in whom US is inconclusive.⁴⁵

Ultrasonography. Puylaert's introduction of the graded compression ultrasound technique in the 1980s has substantially improved sonographic identification of the appendix.¹³⁹ US is widely available, noninvasive, relatively inexpensive, and poses no ionizing radiation risk to the patient. This latter feature is a major consideration in the most radiation-sensitive individuals, children and pregnant women.¹²⁸

Important limitations of US are reduced sensitivity in obese patients, inability to image beyond bowel gas, technical difficulties in patients with severe pain, and dependence on operator skill. Poor penetration in the obese population limits widespread use of this technique in North America and parts of Europe. Although some authors have reported that the normal appendix is visible in 64% to 72% of patients, others have noted a visualization rate of only 0% to 4% in adult patients, regardless of technique.^{140,141}

The reported diagnostic accuracy of ultrasound varies, depending on the patient population studied. A meta-analysis comparing CT and US in a broad age range found an overall ultrasound sensitivity of 78% and specificity of 83%.¹⁴² A large

study of children aged 3 to 18 years found sensitivity and specificity of 73% and 97%, respectively.¹⁴³

Adherence to optimal scanning techniques is critical. Sagittal, transverse, and oblique imaging should be performed in the abdomen and pelvis, with the addition of a transvaginal examination in women in whom the diagnosis is not clear following the transabdominal approach. A high-frequency linear or curvilinear transducer may be used, depending on the patient's body habitus. A high-frequency transducer typically offers the best image resolution, but a curvilinear probe may be better suited for imaging patients with a poorly compressible right lower quadrant bowel, large patients with their cecum and appendix located deep within the pelvis, patients with poorly defined right lower quadrant anatomy, and patients with a retrocecal or perforated appendix.

The technique of graded compression should be used to displace or compress gas-filled bowel loops in the field of view. This maneuver aids identification of the maximal point of tenderness while helping differentiate abnormal, noncompressible bowel loops or the inflamed appendix from those normally compressible structures. Also, the maintenance of slow and gentle pressure facilitates completion of the examination in uncomfortable and apprehensive patients.²⁰

Color Doppler evaluation may add valuable information by demonstrating hyperemia in the inflamed appendix or bowel wall.¹⁴⁰ This can aid diagnosis in patients with equivocal gray-scale results.

Sonographically, the abnormal appendix appears as a blind-ending, noncompressible, tubular structure larger than 6 mm in diameter with a laminated wall (Figs. 56-22 to 56-24). Progressive ischemia and infarction of the appendiceal wall lead to focal or diffuse loss of definition of the wall layers.¹⁴⁴ Hyperemia may be demonstrated on color Doppler evaluation, but decreased or absent flow may be seen in cases of gangrenous

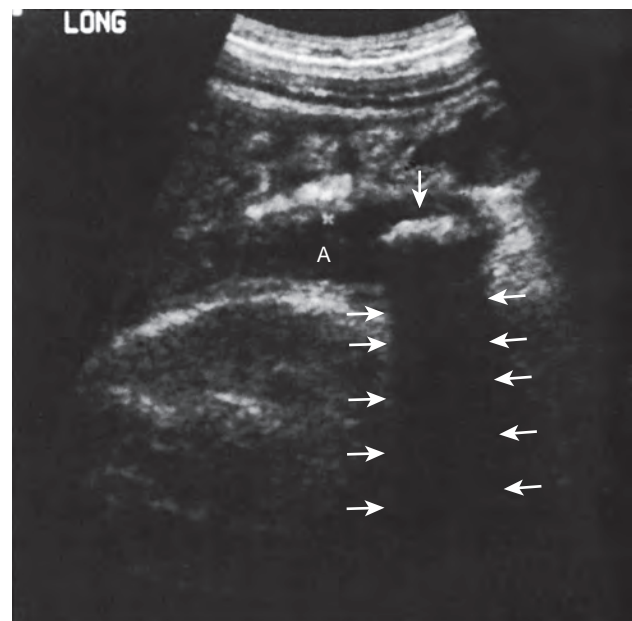


Figure 56-22 Sonogram of an inflamed appendix containing an appendicolith. Longitudinal image shows a thick-walled, fluid-filled appendix (A). The layers of the appendiceal wall are not well defined. An appendicolith (large arrow) is identified as an echogenic focus with acoustic shadowing (small arrows).

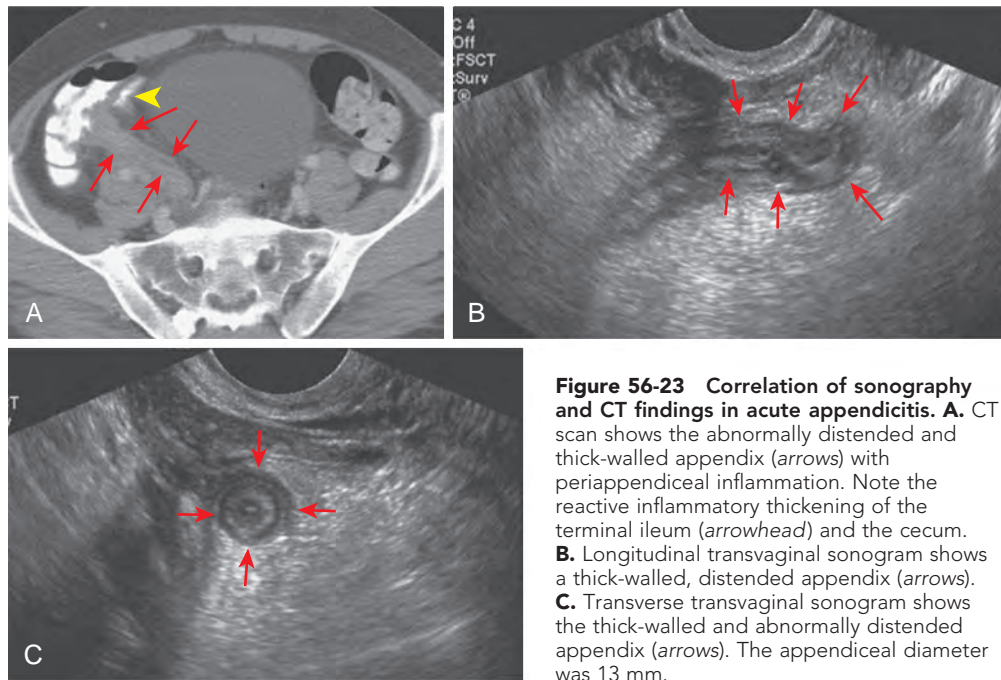


Figure 56-23 Correlation of sonography and CT findings in acute appendicitis. **A.** CT scan shows the abnormally distended and thick-walled appendix (arrows) with periappendiceal inflammation. Note the reactive inflammatory thickening of the terminal ileum (arrowhead) and the cecum. **B.** Longitudinal transvaginal sonogram shows a thick-walled, distended appendix (arrows). **C.** Transverse transvaginal sonogram shows the thick-walled and abnormally distended appendix (arrows). The appendiceal diameter was 13 mm.

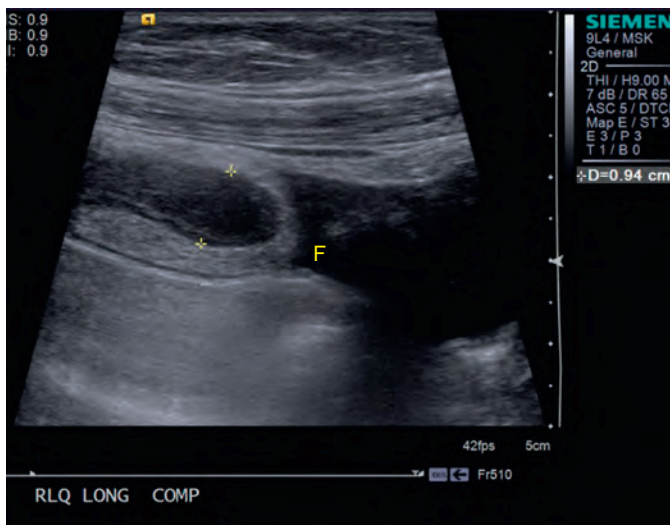


Figure 56-24 Ultrasound of appendicitis with periappendiceal fluid. **A.** Longitudinal imaging with graded compression in a 7-year-old girl demonstrates a dilated appendix with a diameter of 9 mm (cursors). Wall stratification is maintained, and periappendiceal fluid (F) is visualized.

appendicitis.²⁰ With perforation, localized disruption of the appendiceal wall may be seen, and extraluminal pockets of gas may be present. Appendicoliths appear as rounded echogenic foci with clean distal acoustic shadowing, and their presence is highly associated with appendicitis.

In addition to the appendiceal findings present in acute appendicitis, recognition of characteristic periappendiceal findings can aid in its diagnosis and differentiation from other conditions. Inflammation of the periappendiceal fat appears as an echogenic region that may cause mass effect and separate the

inflamed bowel segment(s) from surrounding structures.²⁰ Periappendiceal phlegmon appears as hypoechoic, poorly marginated regions within the fat adjacent to the appendix, and abscesses can be recognized as focal collections of fluid that may or may not contain gas. Reactive inflammatory thickening of the cecal or terminal ileal wall may also be present in patients with appendicitis.

Despite performance of optimized US examinations, US sensitivity for diagnosing perforated appendicitis is lower than that for nonperforated appendicitis. Overall, the noncompressible appendix is visible in only 38% to 55% of patients with perforated appendicitis.^{145,146}

As of 2013, ACR Appropriateness Criteria guidelines recommend ultrasound as the first-choice imaging technique in pregnant women and children younger than 14 years with suspected appendicitis.⁴⁵

Magnetic Resonance Imaging. Recent advances in MRI technology have led to an increased role in the setting of suspected appendicitis. Superior soft tissue contrast resolution, multiplanar imaging capability, and ability to scan without contrast administration make MRI an attractive choice. Unlike CT, MRI does not involve the use of ionizing radiation.¹⁴⁷ Drawbacks to the use of MRI include relatively long imaging times, higher cost, higher dependence on technique for good results, and reduced availability relative to CT.⁵⁷

Successful MRI protocols limit motion artifact and emphasize soft tissue contrast in the region of the appendix. Published protocols typically include single-shot fast spin-echo (SSFSE) sequences with T2 weighting in axial, coronal, and sagittal planes, at least one plane with SSFSE T2 with fat suppression, and one or more planes of T1-weighted imaging.¹⁴⁸ Multiple studies have reported the highest appendix visualization rate with T2-weighted images.^{47,149,150} Others have shown improved sensitivity for acute appendicitis by including a diffusion-weighted sequence.^{151,152}

With MRI, the normal appendiceal walls are isointense to muscle on T1- and T2-weighted images. Luminal contents such as air are typically T1 and T2 hypointense.^{149,153} In pregnant patients, the appendix tends to migrate superiorly in the abdomen over time, often extending superior to the iliac crest by the third trimester.^{154,155}

MRI findings of acute appendicitis include a dilated appendix (>7 mm) filled with T2 hyperintense fluid, wall thickness more than 2 mm, and T2 hyperintense inflammation or fluid in the periappendiceal fat (Fig. 56-25).^{46,151,156,157} The thickened appendiceal wall may also be hyperintense on T2-weighted imaging. MRI is indeterminate if the appendix measures 6 to 7 mm in diameter and contains T2 hyperintense fluid without evidence of wall thickening or a periappendiceal fluid signal.^{46,153}

Although reduction or elimination of ionizing radiation is always desirable, the use of MRI for suspected appendicitis has grown most rapidly in patients for whom radiation concerns are most pronounced, notably pregnant women and pediatric patients.⁴⁵ US remains the initial imaging test of choice in these patients,⁴⁵ but the use of MRI has been growing in popularity, particularly when ultrasound examinations are inconclusive.¹⁵⁸ At one institution, integrating MRI into the workup for suspected appendicitis in pregnant women resulted in a 47% reduction in the negative laparotomy rate (from 55%-29%).¹⁵⁹ Some early studies comparing the two modalities have found better overall diagnostic performance with MRI, suggesting that MRI use may continue trending upward.¹⁶⁰⁻¹⁶²

The clinical diagnosis of acute appendicitis can be more challenging in pregnant patients because of anatomic considerations, presence of leukocytosis in otherwise normal patients, and wide range of alternate pathologies.^{45,59,163} Early studies¹⁶⁴ reported right upper quadrant pain to be the typical presentation of acute appendicitis during pregnancy, with the appendix migrating superiorly as the uterus enlarges.¹⁶⁵ However, more recent investigations have found that right lower quadrant pain remains the most common presenting symptom, even in this patient population.¹⁶⁶

Despite early reports, most recent studies have found poor sensitivity for ultrasound in the diagnosis of acute appendicitis during pregnancy.¹⁶⁷ In a large study by Pedrosa and colleagues,

the normal appendix was only visualized in 2 of 126 pregnant patients without appendicitis ($<2\%$). In patients with appendicitis, sensitivity was only 36% (5 of 14).¹⁵⁷ In another smaller study, US could not identify the appendix in 92% of pregnant patients.³⁶

Theoretical risks to the fetus of MRI during pregnancy include heat deposition, acoustic damage, and gadolinium toxicity. When MRI heat deposition was studied in a pig model, results showed no significant change in amniotic fluid temperature.¹⁶⁸ During an MRI examination, rapid current switching within the gradient coils creates substantial acoustic noise. In clinical use, maximum noise tends to be generated during echoplanar imaging (e.g., diffusion sequences) because of the high-gradient amplitudes and rapid switching required.¹⁶⁹ Despite the theoretical concerns, studies following children exposed to echoplanar MRI in utero did not demonstrate a significant increase in postnatal disease or disability.^{170,171} MRI vendors have begun introducing scanners with reduced acoustic noise.¹⁷² This may help alleviate safety concerns while improving patient comfort and, as a result, motion degradation.¹⁷³⁻¹⁷⁵ Despite the theoretical risks of MRI to the fetus, no studies have shown deleterious long-term effects. MRI has long been used in the obstetric population to evaluate fetal anomalies, without known adverse effects.¹⁷⁶⁻¹⁷⁸

Gadolinium toxicity has garnered attention as our understanding of nephrogenic systemic fibrosis continues to evolve. In the pregnant female, IV gadolinium-based contrast crosses the placenta and is filtered by the fetal kidneys. Subsequently, the gadolinium agent is excreted into the amniotic fluid, where some of it remains in contact with the fetus for a prolonged period. Because there is more time inside the body, there is more time for the chelated agent to break down and release the free gadolinium, which has been implicated in toxicity events.¹⁷⁹⁻¹⁸²

Based on this physiology, the U.S. Food and Drug Administration has classified gadolinium-based contrast agents as category C agents. The 2013 ACR guidance document on safe MR practices stated that "The risk to the fetus of gadolinium-based MR contrast agent administration remains unknown and may be harmful."¹⁸³

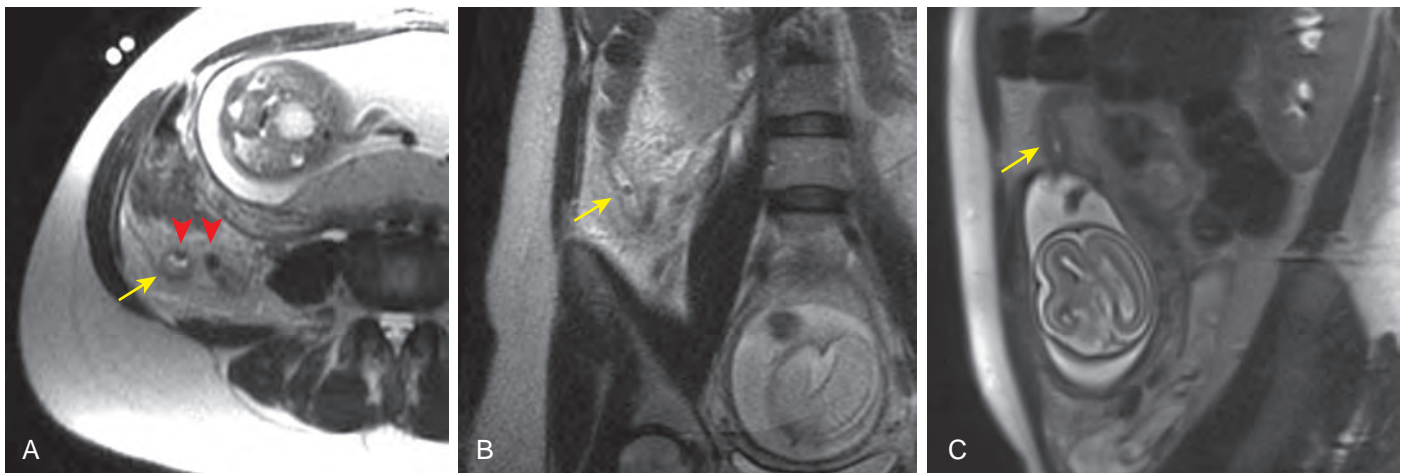


Figure 56-25 MRI scans of acute appendicitis during pregnancy. **A.** Axial T2-weighted HASTE imaging shows a dilated, fluid-filled appendix (arrow) surrounded by low signal fat stranding. There are multiple low signal fecaliths within the appendiceal lumen (arrowheads). **B.** A coronal HASTE image shows the dilated appendix and fecalith (arrow). **C.** In a second patient, sagittal T2-weighted HASTE imaging shows the appendix, with marked, low-signal wall thickening (arrow).

IV gadolinium is not routinely used when using MRI to evaluate for suspected appendicitis.¹⁴⁸ Fortunately, recent studies have demonstrated a similar level of diagnostic accuracy using contrast-enhanced CT and noncontrast MRI to detect acute appendicitis in the pregnant population.^{147,184} A meta-analysis by Blumenfeld and associates noted sensitivity, specificity, and positive and negative predictive values of MRI for diagnosing appendicitis during pregnancy as 95.0%, 99.9%, 90.4%, and 99.5%, respectively, when scans of diagnostic quality were reviewed.¹⁸⁵

DIFFERENTIAL DIAGNOSIS

The presence of inflammatory change adjacent to the cecum is typical of acute appendicitis but is not specific for the diagnosis. The differential diagnosis includes cecal or ileal diverticulitis, Crohn's disease, mesenteric adenitis, epiploic appendagitis, inflamed Meckel's diverticulum, infectious or ischemic ileitis, typhlitis, perforated cecal carcinoma, and pelvic inflammatory disease.

Identification of the normal appendix can facilitate an appropriate alternate diagnosis. The distinction can be critical because, unlike appendicitis, many of the other conditions are treated conservatively.

Mesenteric Adenitis

Mesenteric adenitis is the second most common cause of right lower quadrant pain after acute appendicitis, accounting for 2% to 14% of discharge diagnoses in patients suspected of having appendicitis.¹⁸⁶⁻¹⁸⁹

Primary mesenteric adenitis is diagnosed by CT or US when there are more than three right-sided mesenteric lymph nodes 5 mm or larger without an identifiable acute inflammatory process or with mild (<5-mm) terminal ileal wall thickening. Mesenteric nodes should not be considered responsible for the patient's symptoms unless a primary intestinal inflammatory lesion is excluded. Underlying infectious terminal ileitis is thought to be responsible for most cases of primary mesenteric adenitis.^{186,187,189}

In secondary mesenteric adenitis, the enlarged mesenteric lymph nodes are related to an identifiable underlying condition. Possible causes include acute appendicitis, infectious enteritis or enterocolitis, diverticulitis, Crohn's disease (Fig. 56-26), celiac disease, and neoplasia.¹⁸⁹

Infectious Enterocolitis

Infectious enterocolitis, especially bacterial ileoceitis caused by *Yersinia* spp., *Campylobacter*, or *Salmonella*, can present with symptoms similar to those of acute appendicitis. Imaging studies reveal terminal ileal and cecal wall thickening in association with moderate right lower quadrant mesenteric adenopathy.¹⁹⁰

Crohn's Disease

Crohn's disease is characterized by transmural granulomatous infiltration of the bowel that results in wall thickening secondary to edema, fibrosis, inflammation, and lymphangiectasis. CT is useful in the identification of inflamed segments of bowel in this disease; the terminal ileum and right colon are most commonly affected (Fig. 56-27). The most frequent CT finding in Crohn's disease is homogeneously enhancing thickened bowel, although a mural stratification pattern may be

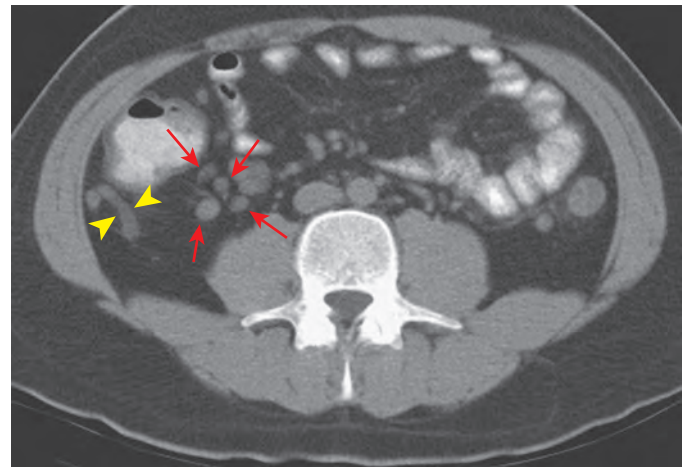


Figure 56-26 Mesenteric adenitis in a patient with Crohn's disease. Enhanced CT scan shows multiple, enlarged, right lower quadrant nodes (arrows) in this patient with Crohn's disease. The appendix was identified (arrowheads) and was normal.

present. The average degree of mural thickening has been noted to range from 11 to 30 mm.¹⁹¹⁻¹⁹⁵ The distribution of bowel involvement is commonly segmental, with interposed loops of normal bowel.

CT is also useful for identifying the many potential complications of this disorder. These include the formation of bowel strictures, mesenteric pathology (e.g., fibrofatty proliferation, inflammation, abscesses, and adenopathy), fistula and sinus tract formation (Fig. 56-28), superimposed neoplasm, renal and gallbladder calculi, hepatic and biliary disease (including hepatitis and pericholangitis), and sacroiliitis.

Epiploic Appendagitis

Primary epiploic appendagitis is the result of ischemia, torsion, or infarction of an epiploic appendage. This self-limiting condition results in focal abdominal pain that can simulate appendicitis when it occurs in the right lower quadrant. It is estimated to be the cause in approximately 1% of patients suspected of having appendicitis.¹⁹⁶ On CT, the inflamed appendage is identified as a round or ovoid fat density structure surrounded by a thickened, high-attenuation rim of thickened visceral peritoneum (Fig. 56-29). A central high-attenuation focus representing a thrombosed vessel or hemorrhage may also be present. Thickening of the adjacent colonic wall is commonly present, along with inflammatory changes in the adjacent fat.

Omental Infarction

An omental infarction is a benign, self-limiting condition caused by torsion or infarction of the greater omentum. Males are affected twice as often as females, and the infarction is usually right-sided.¹⁹⁷ On CT, an omental infarction appears as an inflammatory mass containing variable amounts of fat and fluid (Fig. 56-30). Inflammatory change and small amounts of peritoneal fluid are commonly seen surrounding the omental infarction. The size of the infarct is typically larger than that of an inflamed epiploic appendage; it is more heterogeneous in appearance and lacks a surrounding hyperattenuating rim. Sonographically, an omental infarction appears as a hyperechoic, noncompressible, ovoid mass adherent to the peritoneum.

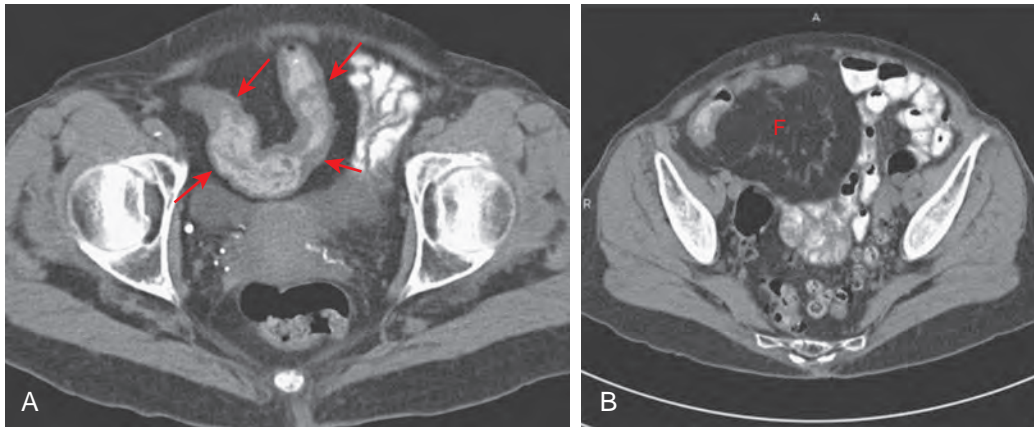


Figure 56-27 Crohn's disease. **A.** This enhanced CT scan shows circumferential mural thickening of the terminal ileum (arrows). **B.** A more cephalad image shows associated fibrofatty proliferation (F) of the mesentery.

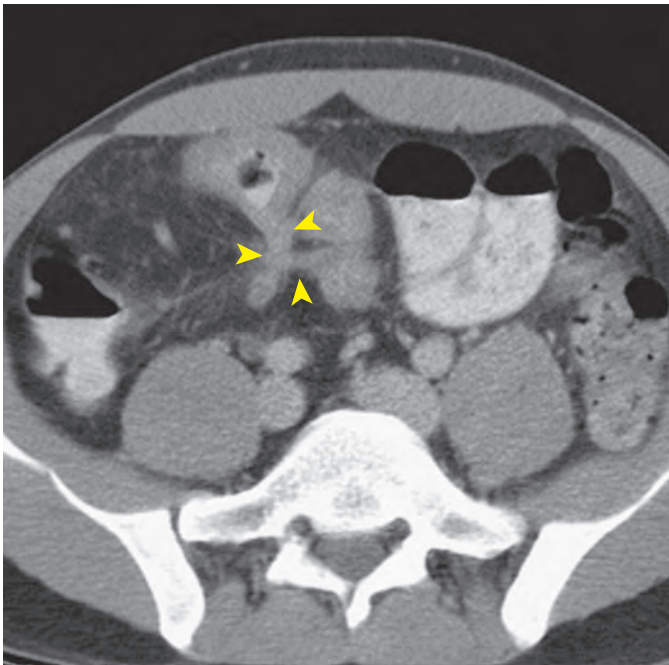


Figure 56-28 Crohn's disease with enteroenteric fistulas. This enhanced CT scan shows circumferential thickening of ileal loops with multiple linear soft tissue tracts extending between the loops representing interloop (enteroenteric) fistulas (arrowheads). Fibrofatty proliferation is also present in the mesentery.

Right-Sided and Ileal Diverticulitis

Right-sided diverticulitis is caused by inflammation of a colonic diverticulum in the cecum or ascending colon. Unlike sigmoid diverticula, right-sided diverticula are usually true diverticula that contain all layers of the colonic wall. Identification of an intramural abscess or cecal diverticulum in association with an inflammatory process located cephalad to a normal-appearing cecal caput and periappendiceal region should suggest the diagnosis. The characteristic findings on US and CT examination are identification of the inflamed diverticulum in association with focal, asymmetric, colonic wall thickening and inflammation of the pericolonic fat (Fig. 56-31).

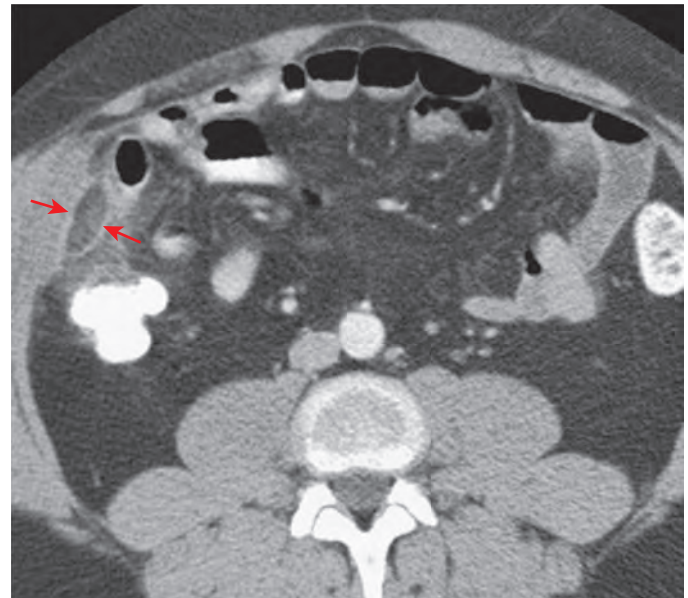


Figure 56-29 Right-sided epiploic appendagitis. On enhanced CT, the inflamed epiploic appendage (arrows) is identified as a homogeneous oval structure surrounded by a thickened, high-attenuation rim of visceral peritoneum contiguous with the ascending colon.

Ileal diverticulitis presents as a focal inflammatory mass or thickening of the terminal ileum with a variable mesenteric inflammatory reaction surrounding an inflamed ileal diverticulum. Acquired ileal diverticula have been reported in 1% to 2% of small bowel series using spot compression radiography.¹⁹⁸

Meckel's Diverticulum

Meckel's diverticulum is a true diverticulum arising from the distal ileum. It is the most common congenital anomaly of the small bowel, affecting approximately 2% of the population.⁶¹

On imaging, an inflamed Meckel's diverticulum appears as a variable-sized, blind-ending structure contiguous with the distal ileum (Fig. 56-32). Generally, the diverticulum itself cannot be identified but the diagnosis can be considered when inflammatory changes are seen adjacent to the distal ileum.

Neutropenic Colitis (Typhlitis)

This type of colitis occurs in profoundly neutropenic patients (especially patients with acute leukemia who are receiving chemotherapy) and results in necrotizing injury to the involved bowel. The inflammatory process may involve the cecum, ascending colon, ileum, or appendix. CT findings are nonspecific and include concentric homogeneous or heterogeneous thickening of the bowel wall, with associated intramural edema and necrosis, pericolic fluid, thickening of the pericolic fascia, and pneumatosis intestinalis (Fig. 56-33).¹⁹⁹ Prompt diagnosis

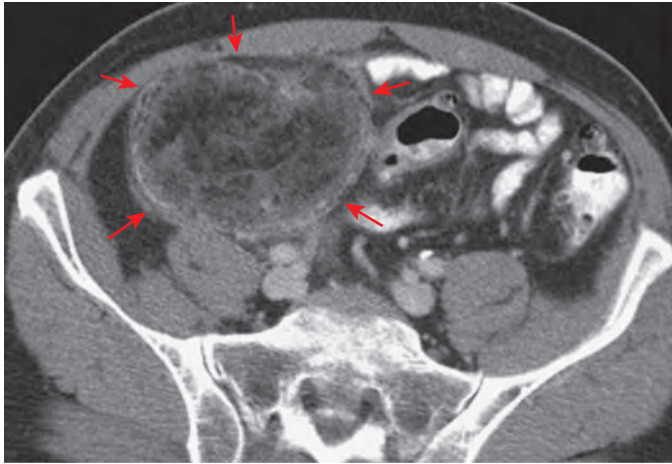


Figure 56-30 Right-sided omental infarct. A heterogeneous inflammatory mass (arrows) composed of fat and soft tissue elements is identified in the right lower quadrant; this represents an omental infarct. The omental infarct is causing displacement of pelvic small bowel loops toward the left abdomen.

is essential to prevent transmural necrosis and subsequent perforation.

Ischemia

Ischemia of the distal small bowel or the right colon may cause localized right lower quadrant pain. Most cases will be caused by a superior mesenteric artery thrombus or embolus or by low perfusion pressure.⁶¹

On enhanced CT examination, the affected bowel will initially demonstrate circumferential bowel wall thickening (Fig. 56-34). A mural stratification pattern is often seen after IV contrast administration. With bowel infarction, pneumatosis intestinalis may develop, and the bowel wall may demonstrate lack of enhancement with IV contrast administration.

Cecal Carcinoma

Cecal carcinoma usually presents as asymmetric nodular mural thickening (typically >1 cm) or a soft tissue attenuation mass (Fig. 56-35). Obstruction of the appendiceal orifice by the mass may lead to the development of appendicitis and appendiceal perforation.^{200,201}

Crohn's Disease

Crohn's disease may involve any part of the GI tract. Involvement of the appendix results in a granulomatous appendicitis that is usually managed conservatively. Pathologic studies have shown appendiceal involvement in 20% to 36% of patients with Crohn's disease (Fig. 56-36).²⁰² Histopathologically, the inflammatory appendiceal changes in Crohn's disease are similar to changes in other intestinal segments involved by this entity—transmural inflammation with wall thickening, epithelioid granulomas, lymphoid aggregates, and mucosal ulcerations.²⁰³

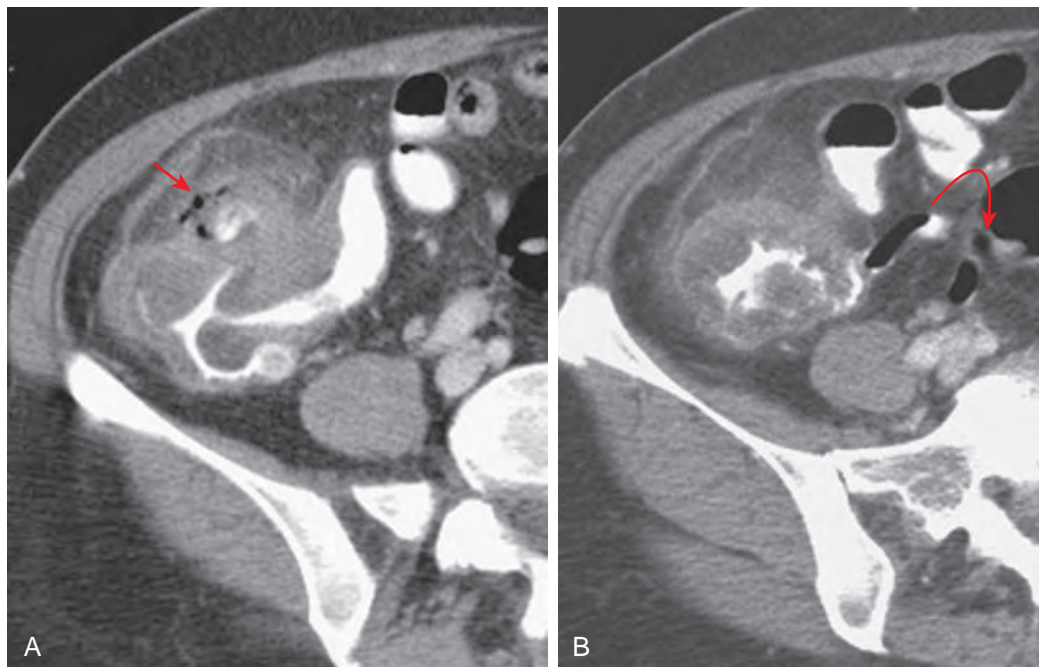


Figure 56-31 Right-sided diverticulitis. A. This enhanced CT scan shows the inflamed diverticulum (arrow) in the proximal ascending colon with surrounding inflammatory changes and associated reactive lateral colonic wall thickening. **B.** This slightly more caudal image shows the normal appendix (curved arrow) medial to the inflamed right colon.

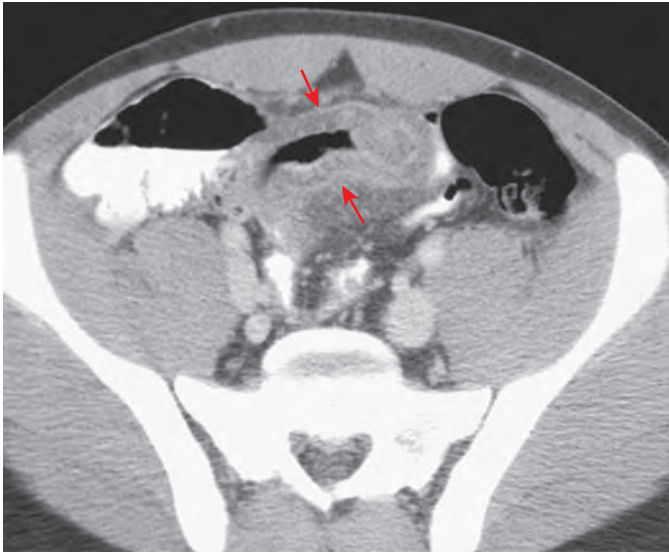


Figure 56-32 Inflamed Meckel's diverticulum. There is a thick-walled, blind-ending tubular structure adjacent to the terminal ileum (arrows) that represents the inflamed Meckel's diverticulum. Inflammatory changes are also identified in the surrounding mesenteric fat.

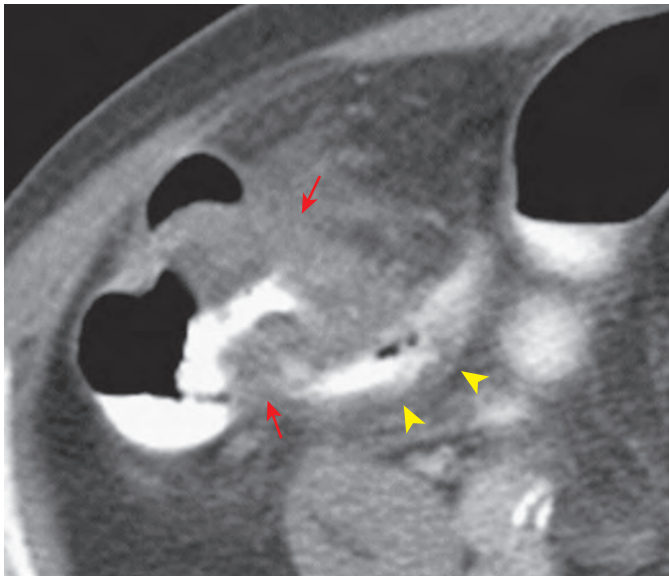


Figure 56-33 Neutropenic colitis (typhlitis) in a patient with acute myelogenous leukemia. There is circumferential mural thickening of the cecum (arrows) and terminal ileum (arrowheads) along with mild perienteric inflammatory change.

Although Crohn's disease frequently causes chronic abdominal symptoms, up to one third of patients with ileocecal Crohn's disease present with right lower quadrant symptoms mimicking those of appendicitis.²⁰⁴

Ripolles and co-workers evaluated 190 patients with Crohn's disease with gray-scale and color Doppler US and found that 20% had appendicular involvement.²⁰² They also found that appendiceal involvement of Crohn's disease was always associated with segmental ileal and/or cecal thickening. There were no cases of isolated appendiceal involvement in their series.

They found that in patients with isolated ileocecal region involvement, terminal ileal wall thickening more than 5 mm and color Doppler flow in the ileum were the most valuable US features for differentiating Crohn's disease from acute appendicitis (positive and negative predictive values as high as 96% and 74%, respectively). Also, they found that irregular thickening of the submucosal layer of the terminal ileum and fibrofatty proliferation of the mesentery around the inflamed terminal ileum were specific findings of Crohn's disease that were absent in acute appendicitis.²⁰²

Isolated appendiceal involvement, also known as idiopathic granulomatous appendicitis, is now believed by many to be a distinct entity from Crohn's disease with appendiceal involvement. Patients with this condition commonly present with symptoms mimicking those of acute appendicitis. Idiopathic granulomatous appendicitis is characterized pathologically by the presence of numerous granulomas and concentric mural fibrosis.²⁰⁵ The histopathologic feature of numerous granulomas differentiates this entity from Crohn's disease, which characteristically has sparse granulomas. Also, unlike patients who have involvement of the appendix from Crohn's disease, patients with idiopathic granulomatous appendicitis rarely have recurrence, fistulization, or extra-appendiceal GI tract involvement after appendectomy.²⁰⁵

Ulcerative Colitis

Ulcerative colitis is characterized by colonic mucosal inflammation and ulceration that typically proceeds in a continuous fashion from the rectum proximally. CT shows bowel wall thickening caused by a combination of infiltration of the lamina propria by round cells, hypertrophy of the muscularis mucosa with resultant separation of the mucosa from the submucosa, and deposition of submucosal fat.¹⁹⁴ The mean bowel wall thickness in ulcerative colitis is approximately 8 mm.^{192,195} In contradistinction to Crohn's disease, which typically shows homogeneous enhancement of the colonic wall after IV contrast administration, approximately 70% of patients with ulcerative colitis demonstrate inhomogeneous mural enhancement after IV contrast administration (Fig. 56-37).^{194,195}

Appendiceal involvement is seen in 61% to 87% of patients with pancolitis caused by ulcerative colitis.²⁰³ The appendiceal involvement may be contiguous with cecal ulcerative colitis or may occur as a skip lesion adjacent to a normal cecum. This latter type has been referred to as ulcerative appendicitis. Appendiceal involvement was found to occur as a skip lesion without associated cecal involvement in 34% to 86% of colons removed for chronic ulcerative colitis.²⁰⁶

On CT examination, the typical features of ulcerative appendicitis are edema and thickening of the appendiceal wall. Appendectomy is thought to be a protective factor in ulcerative appendicitis.²⁰⁶

Endometriosis

GI tract involvement is seen in 5% to 37% of patients with endometriosis. The most commonly involved segments, in order of decreasing frequency, are the rectum and sigmoid colon, small bowel, cecum, and appendix.

Most patients with endometriosis of the appendix will remain asymptomatic. Symptomatic patients usually experience chronic pain; however, some patients may experience acute

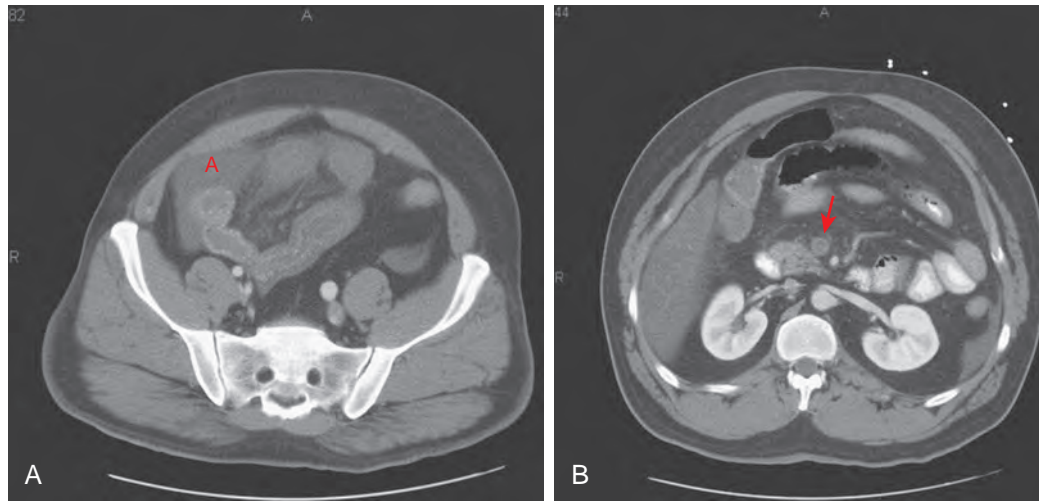


Figure 56-34 Small bowel ischemia due to thrombosis of the superior mesenteric vein. **A.** This enhanced CT scan shows circumferential thickening of ileal small bowel loops within the pelvis. Pelvic ascites (A) is also present. **B.** There is absent enhancement of the superior mesenteric vein (arrow) caused by intraluminal thrombus.

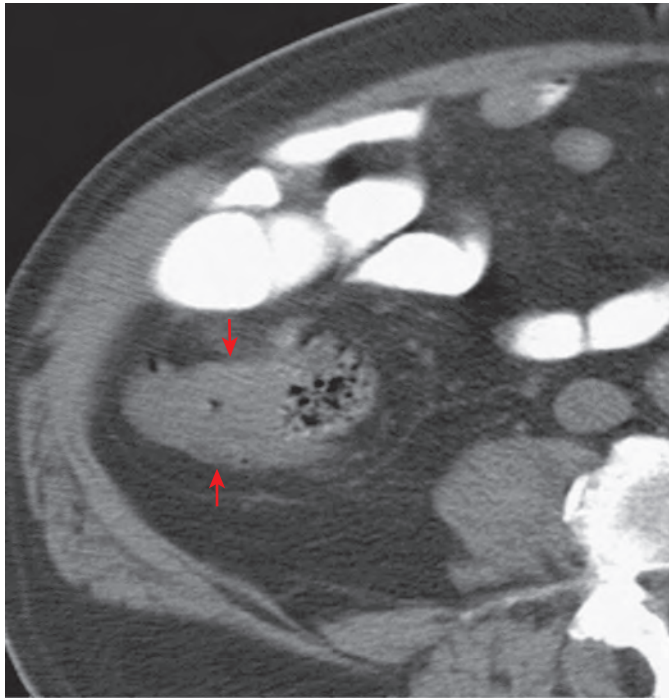


Figure 56-35 Cecal carcinoma. This lobulated, nodular cecal mass causing eccentric wall thickening of more than 1 cm (arrows) was pathologically proven to be a primary cecal adenocarcinoma.

right lower quadrant pain that is clinically indistinguishable from that of acute appendicitis. On CT, a noninflamed, nondistended, and nonopacified appendix is frequently seen.²⁰³

Appendiceal Diverticulitis

Appendiceal diverticula are found in 0.004% to 2.8% of surgical and pathologic specimens.²⁰³ Most are acquired because of intrinsic mural weakness or abnormally raised intraluminal pressure secondary to increased muscular activity or closed

loop obstruction.²⁰⁷⁻²⁰⁹ The diverticula may be solitary or multiple and are found anywhere along the appendix. They are usually 0.2 to 0.5 mm.²⁰³

The presence of appendiceal diverticula may predispose to hemorrhage and diverticulitis. On CT, inflammation of the diverticulum and/or appendix is seen. Clinically, patients can present with symptoms similar to those of acute appendicitis. The pain is often intermittent and insidious and typically occurs 1 to 14 days before presentation. Because the risk of appendiceal perforation in appendiceal diverticulitis is fourfold greater than that for simple appendicitis, prompt surgical resection is advised.²⁰³ Accordingly, some surgeons recommend prophylactic appendectomy when diverticula are discovered during laparotomy for other disorders.^{207,208,210}

Appendiceal Intussusception

Intussusception of the appendix can present clinically in five different ways²¹¹⁻²¹⁴: (1) acute appendicitis; (2) intussusception; (3) recurrent intermittent right lower quadrant pain; (4) intermittent painless rectal bleeding; and (5) asymptotically, with incidental findings at laparotomy, barium enema, or colonoscopy. In the past, appendiceal intussusception was considered rare, being found in only 0.01% of surgical cases. However, the fifth presentation is probably the most common.

Most cases of significant appendiceal intussusception occur in children and are attributed to abnormal peristalsis caused by intraluminal or intramural irritants of the appendix. These include fecaliths, foreign bodies, endometriosis, lymphoid hyperplasia, carcinoid, adenocarcinoma, and mucocoeles.²¹¹⁻²¹⁴

On double-contrast barium enema examination, intussusception causes a characteristic coiled spring appearance of the cecum with nonfilling of the appendix. These findings are best seen en face. In incidental cases, the intussusception usually disappears on delayed overhead or postevacuation films. The coiled spring appearance can also be seen in appendicitis, but it is fixed in these cases, and the patient is symptomatic in the right lower quadrant. There may be only partial intussusception of the appendix, which produces an intraluminal filling defect

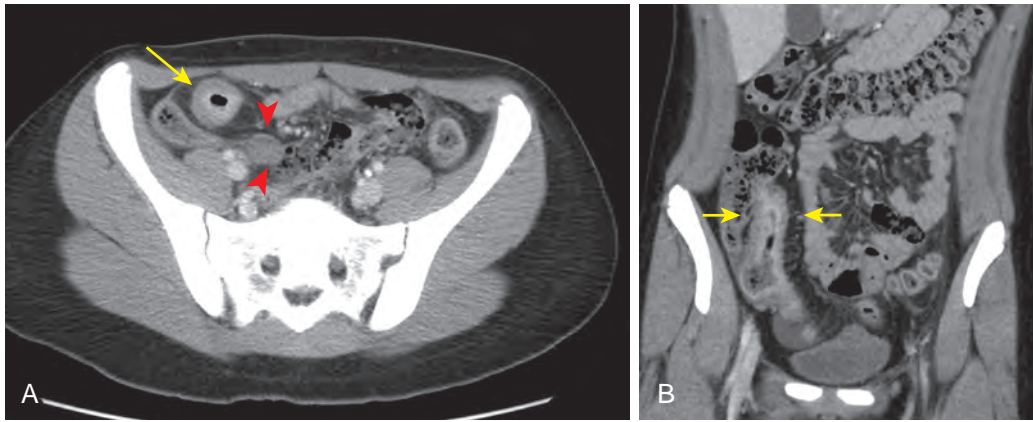


Figure 56-36 Crohn's disease with involvement of the appendix. **A.** There is circumferential wall thickening of the terminal ileum with mucosal hyperenhancement (arrow). The appendix is distended (arrowheads). **B.** On coronal reformatted imaging, the terminal ileum is thickened with mucosal hyperenhancement (arrows).



Figure 56-37 Ulcerative colitis. Enhanced CT scan shows a pancolitis with heterogeneous circumferential wall thickening of the cecum, transverse colon, and descending colon (arrows).

on the medial wall of the cecum and nonfilling of the appendix. The defect may be mistaken for a polyp (Fig. 56-38).²¹¹⁻²¹⁴ On US, the intussusception appears as multiple hypoechoic and hyperechoic rings, similar to intussusceptions elsewhere in the gut.^{211,213}

Hydrostatic reduction of appendiceal intussusceptions has been successful in children and adults. Asymptomatic transient intussusceptions probably do not require therapy or an extensive work-up, however.²¹¹⁻²¹⁴

Appendiceal Neoplasms

Primary neoplasms of the appendix are identified in 0.5% to 1% of appendectomy specimens at pathologic evaluation.²¹⁵⁻²¹⁷ The vast majority of these occur in adults older than 30 years. Of patients with appendiceal tumors, 30% to 50% will present with symptoms of appendicitis, and most of these will have obstruction of the appendiceal lumen by the tumor.^{216,218} Similarly, cecal carcinomas can obstruct the appendiceal lumen, resulting in secondary appendicitis. A study by Peck showed that 11% of right-sided colon cancers clinically presented as

appendicitis, most of which were caused by appendiceal inflammation from obstruction.²¹⁹

Preoperative identification of an appendiceal or cecal neoplasm may change the surgical approach (laparoscopic vs. an open procedure) and procedure performed (appendectomy vs. right hemicolectomy). CT has proven very useful in this regard. In a retrospective review of 22 CT scans in patients with pathologically proven primary appendiceal neoplasms, Pickhardt and colleagues found that the sensitivity of CT for tumor detection was 95% when morphologic appendiceal changes or a threshold appendiceal diameter of 15 mm was used as a diagnostic criterion. In 95% of these patients, soft tissue stranding of the peri-appendiceal fat was also present.²¹⁸

MUCOCELE

Epidemiology, Cause, and Pathology

Mucocele of the appendix is a descriptive term used to indicate dilation of the appendiceal lumen by mucinous secretions. The accumulation of mucin is slow and, if infection does not intervene, the appendix becomes a large, thin-walled, mucin-filled cystic structure.²²⁰⁻²²⁸ Mucoceles are uncommon; they are found in 0.3% of appendectomy specimens, with a 4:1 preponderance in females and a mean age of 55 years at presentation.²²⁸

Histologically, mucoceles are classified into three groups—focal or diffuse hyperplasia, mucinous cystadenoma, and mucinous cystadenocarcinoma. A number of obstructing lesions can lead to mucocele formation, such as postappendicitis scarring (most common), fecalith, appendiceal carcinoma, appendiceal endometrioma, appendiceal carcinoid, carcinoma of the cecum or ascending colon, appendiceal polyp, and appendiceal volvulus. It is unclear whether the cystadenoma or cystadenocarcinoma causes obstruction of the lumen as well or whether the mucosa of the obstructed appendix undergoes neoplastic change. Benign causes of obstruction outnumber malignant causes by a ratio of 4:1 to 10:1.^{222,225,226,229-231}

Most mucoceles are between 3 and 6 cm in diameter. Calcifications may occur in the wall or lumen of the mucocele.^{220,221,223,225,226} Myxoglobulosis is a rare variant in which numerous small globules form in the appendix. They may calcify and produce numerous 1- to 10-mm round or oval mobile

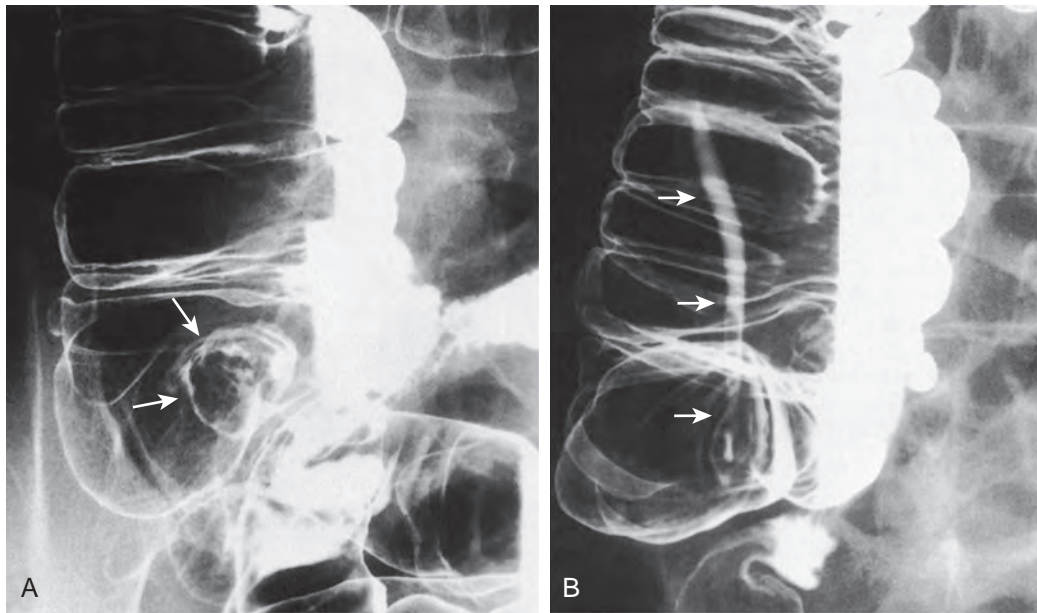


Figure 56-38 Appendiceal intussusception. **A.** Initial barium enema examination reveals a filling defect in the lower cecum that was interpreted as a polypoid mass (arrows). Colonoscopy performed several days later revealed no abnormalities. **B.** Subsequent barium enema examination shows a normal retrocecal appendix (arrows).

calcifications in the right lower quadrant. In myxoglobulosis, the appendiceal lumen has the consistency of tapioca or fish eggs.^{232,233}

Clinical Findings

The dominant complaint is chronic right lower quadrant pain in up to 64% of patients with mucocèles. Almost 23% of patients are asymptomatic. Abdominal swelling, anemia, or a mucous fistula may also be present. Physical examination reveals right lower quadrant tenderness in 38% and a palpable mass in 18% to 50% of patients.^{222,223,225,226,228-231}

The major clinical significance of a mucocèle lies in its complications; these include rupture or leakage leading to pseudomyxoma peritonei, torsion with gangrene and hemorrhage, and intussusception into the cecum, causing various degrees of bowel obstruction. If pseudomyxoma peritonei results from rupture of a benign mucocèle, the prognosis is good with simple removal of the fluid. When it results from a malignant process, it behaves like an invasive neoplasm with adhesions, bowel obstruction, and a 5-year survival rate of only 25%. Because cystadenoma and cystadenocarcinoma are usually indistinguishable radiologically, clinically, and on gross inspection, the surgeon must be warned preoperatively of the presence of a mucocèle.^{234,235}

Radiologic Findings

Plain Radiographs. The plain abdominal radiograph may be normal or may show a well-defined right lower quadrant mass. Rimlike calcifications help establish the diagnosis but are uncommon. In myxoglobulosis, mobile calcifications may be present that must be differentiated from phleboliths, calcified mesenteric lymph nodes, and calcified metastases to the medial wall of the cecum.^{82-84,225,226,230}

Barium Enema. The appendix fails to fill on barium enema examination, and the cecum is indented on its medial aspect by a smooth-walled mass. The cecum is distensible but inseparable

from the mass (Fig. 56-39). The terminal ileum is often displaced as well.^{82-84,225,226,230}

Cross-Sectional Imaging. On US, mucocèles manifest as fluid-filled masses that may be completely anechoic or may have septations and gravity-dependent echoes. These latter findings probably result from inspissated mucoid material that develops as the mucocèle ages and matures. Increased through-transmission is characteristic.^{229,231}

On CT, mucocèles appear as water density or, less often, soft tissue density masses (Fig. 56-40). Calcification may be seen within the wall or lumen (Fig. 56-41).

On MRI, when mucocèles contain predominantly fluid, they have long T1 and T2 relaxation times and low signal intensity on T1-weighted images and high signal intensity on T2-weighted images (Fig. 56-42). If their mucin content is high, mucocèles have short T1 and long T2 times, so they appear intense on both T1- and T2-weighted images.

When pseudomyxoma peritonei develops, malignant-appearing ascites with loculated fluid collections, septations, small calcifications, and a scalloped contour of the liver and spleen are visualized (Fig. 56-43).²³⁶⁻²³⁹ Mucin-producing adenoma, cystadenoma, or mucinous cystadenoma presents as an encapsulated, low-attenuation cyst and cannot be differentiated from a retention mucocèle.²²⁴

Differential Diagnosis

The differential diagnosis for these imaging findings includes ovarian cysts and neoplasms, duplication cyst, mesenteric and omental cysts, mesenteric hematoma or tumor, and abdominal abscess.

MUCINOUS CYSTADENOMA AND CYSTADENOCARCINOMA

The detection of a heterogeneously attenuated mass with nodular areas of soft tissue density or of a cystic mass with

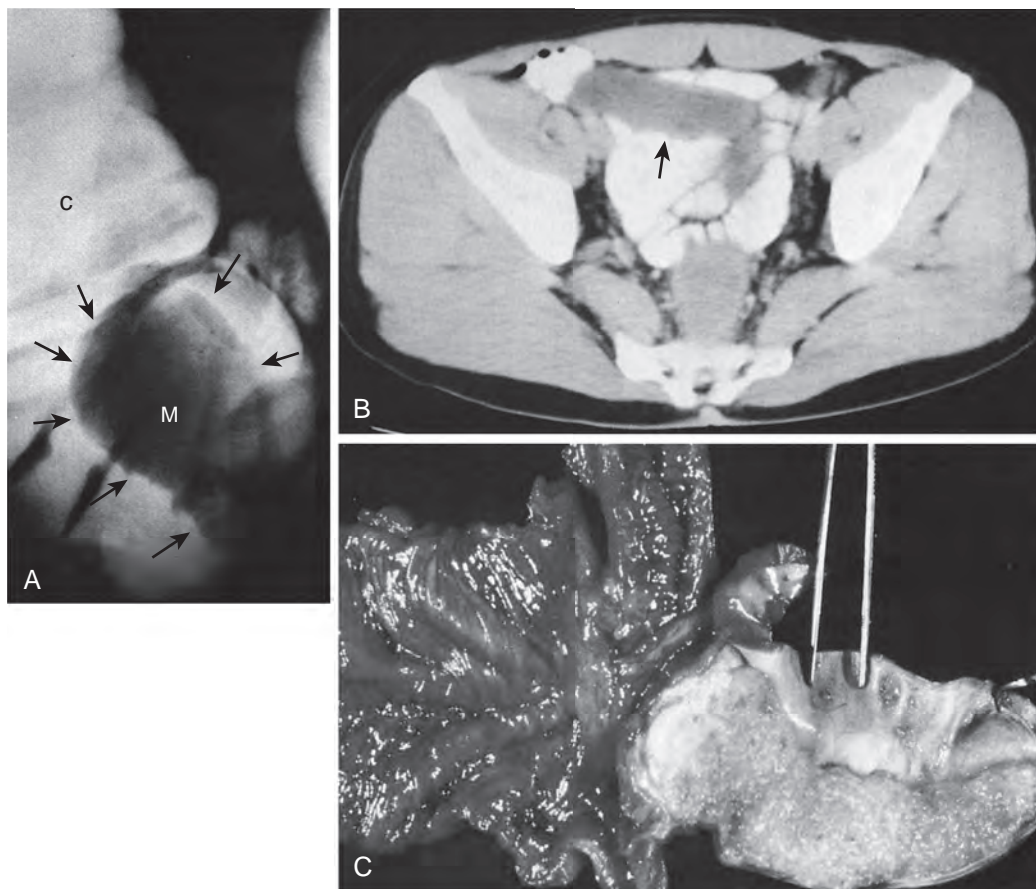


Figure 56-39 Mucocoele of the appendix. **A.** Barium enema study shows a sharply contoured large intraluminal cecal defect (M). Note that the intussuscepting mucocoele arises from the tip of the cecum (c) and the appendix is not filled (arrows). **B.** CT scan shows the pericecal extension of the mucus-filled, distended appendix (arrow). Note that there is no periappendiceal inflammation. **C.** Gross specimen reveals a markedly distended, mucus-filled appendix compressing the base of the cecum. Pathologic study showed benign mucocoele.

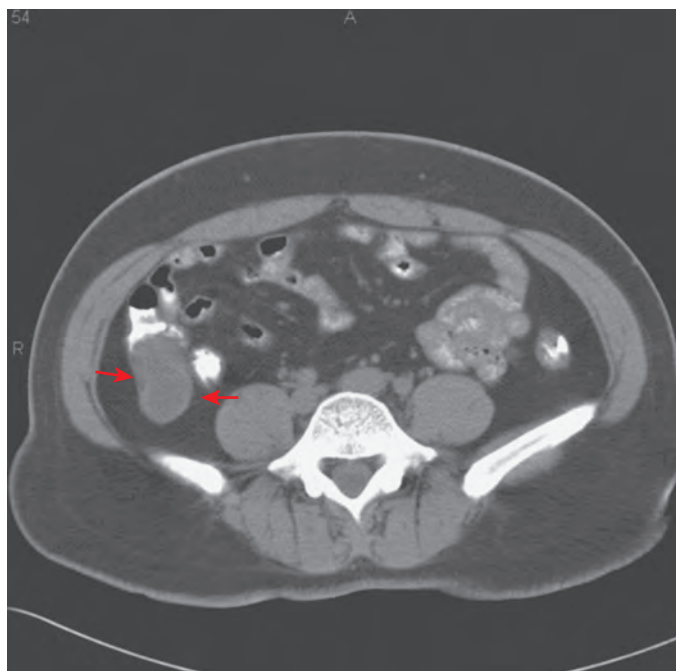


Figure 56-40 Mucocoele of the appendix. This ovoid-shaped fluid-filled mass (arrows) represents an appendiceal mucocoele that is causing a mass effect on the adjacent cecum.

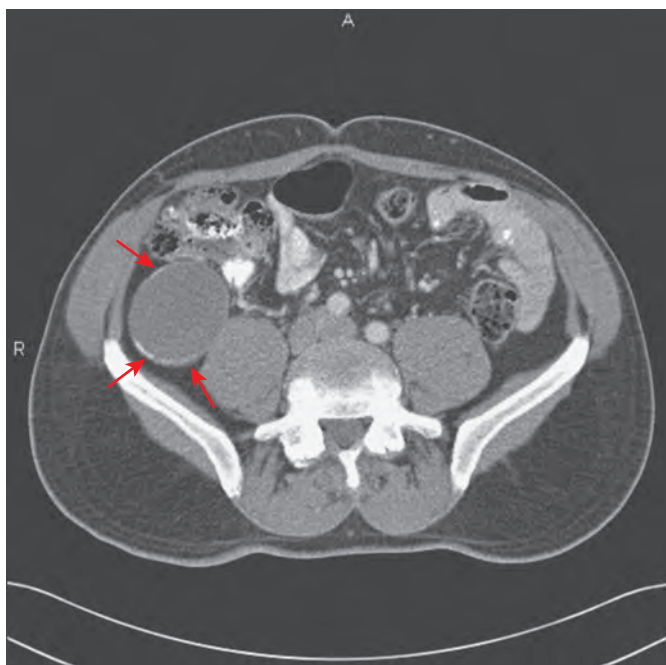


Figure 56-41 Mucocoele of the appendix. This ovoid-shaped, fluid-filled appendiceal mucocoele contains mural calcifications (arrows).

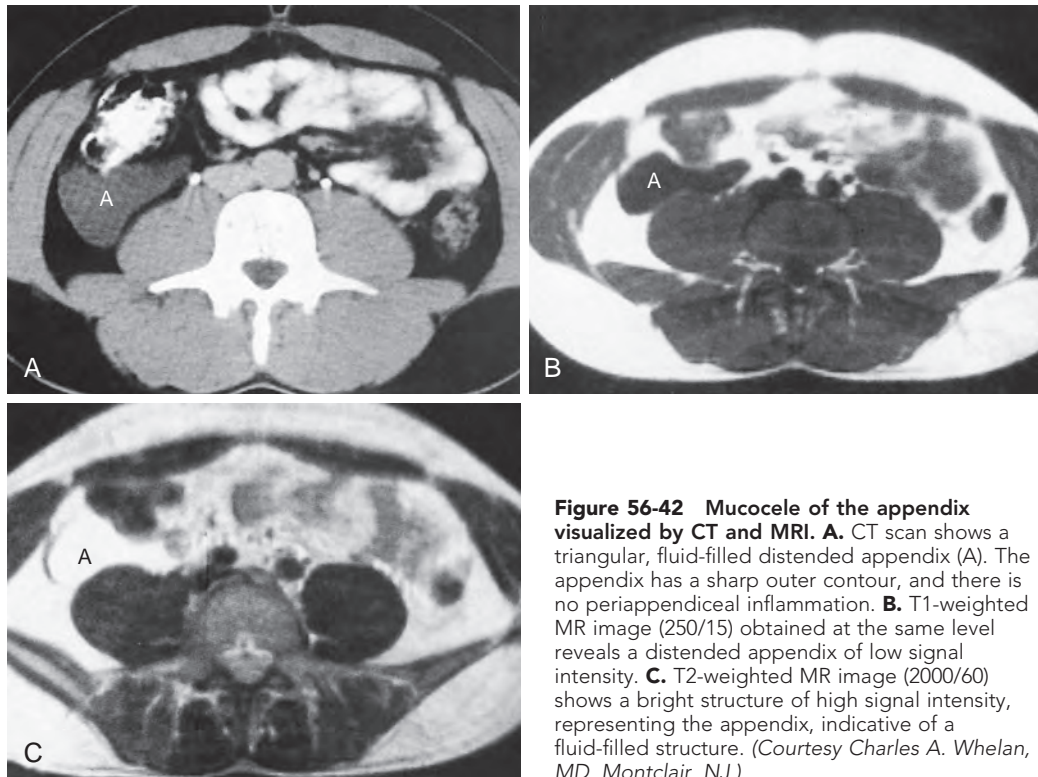


Figure 56-42 Mucocoele of the appendix visualized by CT and MRI. **A.** CT scan shows a triangular, fluid-filled distended appendix (A). The appendix has a sharp outer contour, and there is no periappendiceal inflammation. **B.** T1-weighted MR image (250/15) obtained at the same level reveals a distended appendix of low signal intensity. **C.** T2-weighted MR image (2000/60) shows a bright structure of high signal intensity, representing the appendix, indicative of a fluid-filled structure. (Courtesy Charles A. Whelan, MD, Montclair, NJ.)

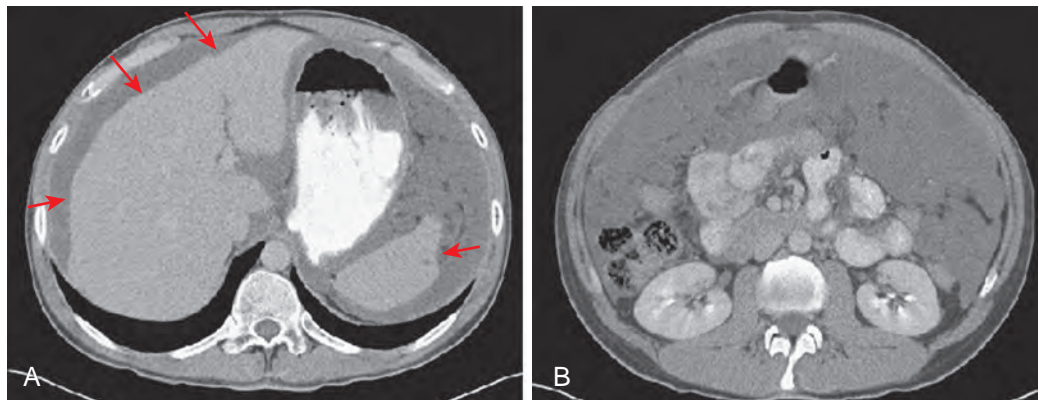


Figure 56-43 Pseudomyxoma peritonei. **A.** Upper abdomen reveals ascites with a scalloped contour to the liver and spleen (arrows). **B.** Midabdomen reveals massive ascites with heterogeneous attenuated fluid and septations causing mass effect on adjacent bowel loops.

associated soft tissue components (Fig. 56-44) is strongly suggestive of a mucinous cystadenocarcinoma of the appendix.^{238,240} Perforation is present in approximately 46% of patients with mucinous cystadenocarcinoma at the time of appendectomy.²⁴¹ Patients with mucinous cystadenocarcinomas associated with pseudomyxoma peritonei have a poor 5-year survival rate of 50%.²⁰³

NONMUCINOUS ADENOCARCINOMA

Primary appendiceal adenocarcinoma is an uncommon tumor, with an incidence of approximately 0.08%.²⁴² Adenocarcinoma of the appendix presents as a soft tissue mass similar to the more

common colonic carcinoma, and it metastasizes hematogenously and lymphatically.

On CT examination, these tumors usually appear as a focal or diffuse soft tissue mass with appendiceal distention (diameter typically >15 mm), wall thickening, and associated soft tissue stranding of the periappendiceal fat (Figs. 56-45 and 56-46). When small, carcinoma of the appendix cannot be differentiated from complicated appendicitis.

Surgical treatment depends on the size and stage of the tumor. Small lesions without lymph node involvement can usually be treated with appendectomy, but more advanced appendiceal carcinoma typically necessitates right hemicolectomy.

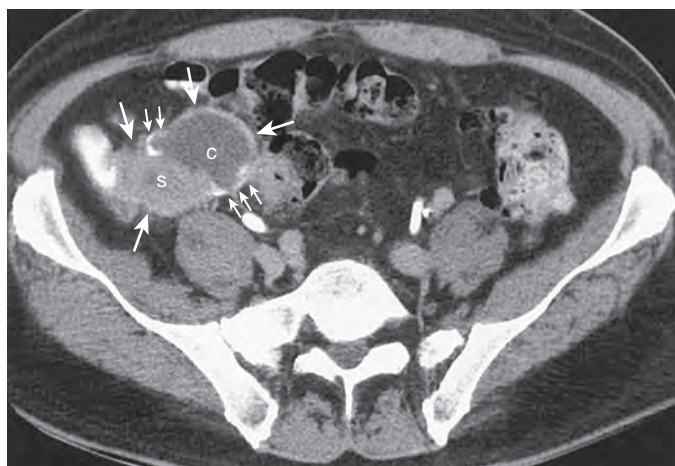


Figure 56-44 Mucinous cystadenocarcinoma of the appendix. CT detects a mass having solid (s) and cystic (c) components in the right pelvis inferior and medial to the cecum (large arrows). Peripheral calcifications are seen in the cystic component (small arrows).

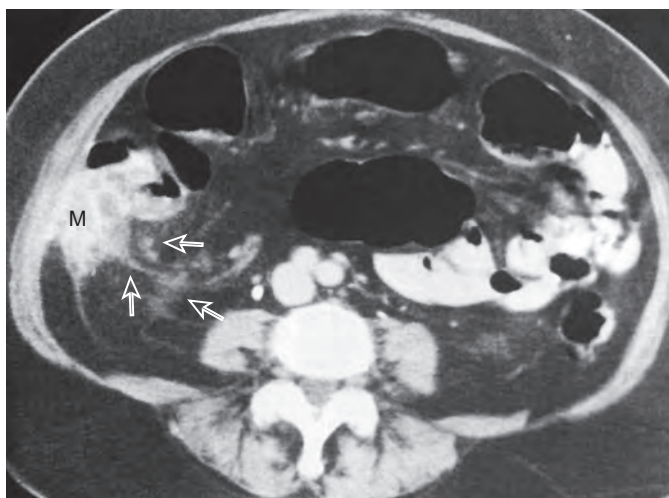


Figure 56-45 CT scan of perforated carcinoma of the appendix. A lobulated, heterogeneous complex mass (M) is seen posterior and caudal to the cecum. The mass has an irregular contour, and periappendiceal inflammatory changes are present (arrows).

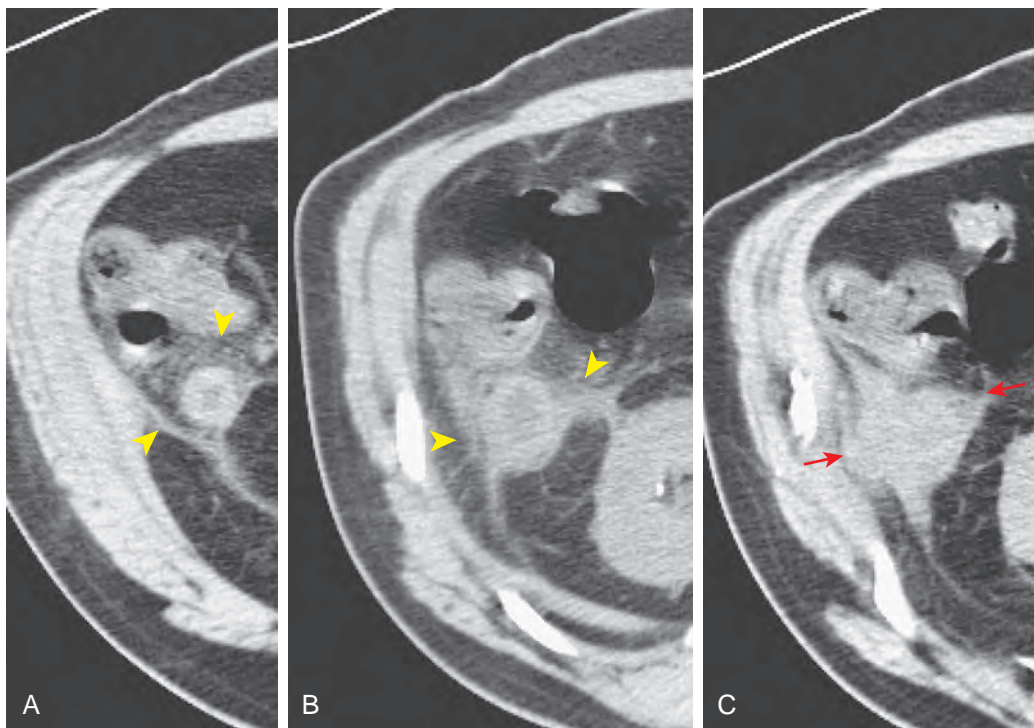


Figure 56-46 CT scans of carcinoma of the distal appendix. A-C. Series axial CT scans of the right, mid, and lower abdomen show that a lobulated soft tissue mass (arrows) is present in the distal aspect of the appendix, with mural thickening identified in the more proximal appendix. Periappendiceal inflammatory changes are also identified (arrowheads).

CARCINOID

Carcinoid tumor is the most common neoplasm of the appendix, with an incidence of 0.32% in appendectomy specimens and 0.054% in an autopsy series.^{203,243} Appendiceal carcinoid tumors comprise 18.9% of all GI carcinoid tumors, but are less biologically aggressive than other GI carcinoid tumors.²⁴⁴ Most are smaller than 2 cm at presentation, and most patients

are asymptomatic. Typically, these lesions are incidentally found at surgery (Fig. 56-47). Appendiceal carcinoids have a lower average age at presentation (average, 42.2 years) than other GI carcinoid tumors (average, 62.9 years) or noncarcinoid appendiceal tumors (average, 61.9 years), have a tendency to present with coexistent tumors, have little metastatic potential, and have a female predominance (male-to-female ratio of 0.47).^{245,246} The 5-year survival for appendiceal

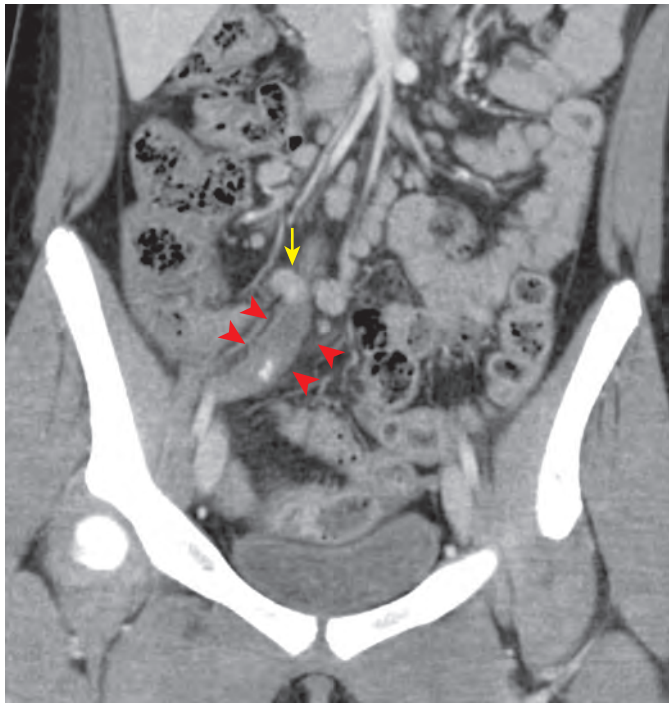


Figure 56-47 Carcinoid tumor of the appendix. An enhancing soft tissue mass (arrow) occludes the lumen of the appendix, which is dilated and fluid-filled (arrowheads). The patient presented with acute appendicitis.

carcinoids (85.9%) is higher than for other GI carcinoid tumors (54%).²⁴⁶

Most appendiceal carcinoid tumors ($\approx 70\%$) are located in the appendiceal tip, followed by the body (approximately 22%) and the base (approximately 7%).²⁰³ The typical CT appearance

is a homogeneous soft tissue mass that may infiltrate into the cecum and mesentery.²⁴⁷

Treatment of appendiceal carcinoid depends on its size. Tumors smaller than 2 cm are usually treated with appendectomy. Tumors larger than 2 cm or with evidence for invasion into the mesoappendix necessitate right hemicolectomy and, unfortunately, have a poorer prognosis.²⁰³

LYMPHOMA

Primary appendiceal lymphoma is a very rare lesion, with an incidence of 1% to 3%.^{248,249} Patients typically present with clinical signs mimicking those of acute appendicitis and with no prior history of lymphoma. At the time of diagnosis, most tumors are larger than 3 cm. All reported cases have been non-Hodgkin's type.²⁵⁰

On CT, there is usually marked mural thickening of the appendix, which maintains its vermiform shape. Aneurysmal luminal dilation may be present, and periappendiceal stranding may also be identified because of secondary appendicitis from luminal obstruction or direct serosal extension of lymphomatous cells.^{250,251}

Metastases

Primary neoplasms that can metastasize to the appendix include those of the breast, lung, bronchus, stomach, colon, pancreas, kidney, ovaries, or prostate. Direct extension of cecal or ileal tumors can also involve the appendix.²⁰³

Metastatic tumors of the appendix usually involve the serosal or submucosal layers and, on CT, they usually appear as a solitary soft tissue mass contiguous with the appendix. These lesions can obstruct the appendiceal lumen, leading to secondary appendicitis and its complications, including perforation.²⁰³

REFERENCES

- Karul M, Berliner C, Keller S, et al: Imaging of appendicitis in adults. *Rofo* 186:551–558, 2014.
- Di Cesare A, Parolini F, Morandi A, et al: Do we need imaging to diagnose appendicitis in children? *Afr J Paediatr Surg*. 10:68–73, 2013.
- Golblatt MI: Appendix. In Shackelford RT, Zuidema GD, editors: *Shackelford's Surgery of the Alimentary Tract*, ed 7, Philadelphia, 2012, Saunders, pp 2019–2029.
- Litz C, Danielson PD, Gould J, et al: Financial impact of surgical technique in the treatment of acute appendicitis in children. *Am Surg* 79:857–860, 2013.
- Stoker ME, Becker JM: Appendicitis. In Brandt LJ, editor: *Clinical Practice of Gastroenterology*, Philadelphia, 1999, Current Medicine, pp 773–778.
- Anson BJ, McVay CB, Callander CL: *Surgical Anatomy*, ed 5, Philadelphia, 1971, Saunders.
- Arey LB: *Developmental Anatomy: A Textbook and Laboratory Manual of Embryology*, ed 7, Philadelphia, 1965, Saunders.
- Voight A: Embryology and anatomy of the appendix. *Southwest Med J* 34:285–287, 1953.
- Balthazar EJ, Gade M: The normal and abnormal development of the appendix. A radiographic assessment. *Radiology* 121(Pt 1): 599–604, 1976.
- Schumpelick V, Dreuw B, Ophoff K, et al: Appendix and cecum. Embryology, anatomy, and surgical applications. *Surg Clin North Am* 80:295–318, 2000.
- Broman I: [Die entwicklung des menschen von der geburt; ein leitfaden zum selbststudium der menschlichen embryologie.] Munich, 1927, JF Bergmann.
- Wakeley CP: The position of the vermiform appendix as ascertained by an analysis of 10,000 Cases. *J Anat* 67(Pt 2):277–283, 1933.
- Maisel H: A note on the vermiform appendix. *S Afr Med J* 32:673–674, 1958.
- Meyers MA: *Dynamic Radiology of the Abdomen: Normal and Pathologic Anatomy*, ed 6, New York, 2010, Springer-Verlag.
- Collins DC: Agenesis of the vermiform appendix. *Am J Surg* 82:689–696, 1951.
- Lippert H, Pabst R: *Arterial Variations in Man: Classification and Frequency*, Munich, 1985, JF Bergmann Verlag.
- Kyriazis AA, Esterly JR: Development of lymphoid tissues in the human embryo and early fetus. *Arch Pathol* 90:348–353, 1970.
- Fitz RH: Perforating inflammation of the vermiform appendix: With special reference to its early diagnosis and treatment. *Am J Med Sci* 92:321–346, 1886.
- Owings MF, Kozak LJ: Ambulatory and inpatient procedures in the United States, 1996. *Vital Health Stat* 13(139):1–119, 1998.
- Birnbaum BA, Wilson SR: Appendicitis at the millennium. *Radiology* 215:337–348, 2000.
- Buckius MT, McGrath B, Monk J, et al: Changing epidemiology of acute appendicitis in the United States: Study period 1993–2008. *J Surg Res* 175:185–190, 2012.
- Anderson JE, Bickler SW, Chang DC, et al: Examining a common disease with unknown etiology: Trends in epidemiology and surgical management of appendicitis in California, 1995–2009. *World J Surg* 36:2787–2794, 2012.
- Velanovich V, Satava R: Balancing the normal appendectomy rate with the perforated appendicitis rate: Implications for quality assurance. *Am Surg* 58:264–269, 1992.
- Berry J, Jr, Malt RA: Appendicitis near its centenary. *Ann Surg* 200:567–575, 1984.
- Shelton T, McKinlay R, Schwartz RW: Acute appendicitis: Current diagnosis and treatment. *Curr Surg* 60:502–505, 2003.

26. Fares A: Summer appendicitis. *Ann Med Health Sci Res* 4:18–21, 2014.
27. Hale DA, Molloy M, Pearl RH, et al: Appendectomy: A contemporary appraisal. *Ann Surg* 225:252–261, 1997.
28. Korner H, Sondenaa K, Soreide JA, et al: Incidence of acute nonperforated and perforated appendicitis: Age-specific and sex-specific analysis. *World J Surg* 21:313–317, 1997.
29. Temple CL, Huchcroft SA, Temple WJ: The natural history of appendicitis in adults. A prospective study. *Ann Surg* 221:278–281, 1995.
30. Andersson RE, Hugander A, Thulin AJ: Diagnostic accuracy and perforation rate in appendicitis: Association with age and sex of the patient and with appendectomy rate. *Eur J Surg* 158:37–41, 1992.
31. Pieper R, Kager L, Nasman P: Acute appendicitis: A clinical study of 1018 cases of emergency appendectomy. *Acta Chir Scand* 148:51–62, 1982.
32. Bratu I, Martens PJ, Leslie WD, et al: Pediatric appendicitis rupture rate: Disparities despite universal health care. *J Pediatr Surg* 43:1964–1969, 2008.
33. Rodriguez DP, Vargas S, Callahan MJ, et al: Appendicitis in young children: Imaging experience and clinical outcomes. *AJR* 186:1158–1164, 2006.
34. Vorhes CE: Appendicitis in the elderly: The case for better diagnosis. *Geriatrics* 42:89–92, 1987.
35. Andersen B, Nielsen TF: Appendicitis in pregnancy: Diagnosis, management and complications. *Acta Obstet Gynecol Scand* 78:758–762, 1999.
36. Cobben LP, Groot I, Haans L, et al: MRI for clinically suspected appendicitis during pregnancy. *AJR* 183:671–675, 2004.
37. Mazze RI, Kallen B: Appendectomy during pregnancy: A Swedish registry study of 778 cases. *Obstet Gynecol* 77:835–840, 1991.
38. Walker AR, Segal I: What causes appendicitis? *J Clin Gastroenterol* 12:127–129, 1990.
39. Larner AJ: The aetiology of appendicitis. *Br J Hosp Med* 39:540–542, 1988.
40. Wangenstein OH, Buirge RE, Dennis C, et al: Studies in the etiology of acute appendicitis: The significance of the structure and function of the vermiform appendix in the genesis of appendicitis: A preliminary report. *Ann Surg* 106:910–942, 1937.
41. Burkitt DP, Moolgaokar AS, Tovey FI: Aetiology of appendicitis. *Br Med J* 1:620, 1979.
42. Jones BA, Demetriades D, Segal I, et al: The prevalence of appendiceal fecaliths in patients with and without appendicitis. A comparative study from Canada and South Africa. *Ann Surg* 202:80–82, 1985.
43. Nitecki S, Karmeli R, Sarr MG: Appendiceal calculi and fecaliths as indications for appendectomy. *Surg Gynecol Obstet* 171:185–188, 1990.
44. Cotran RS, Kumar V, Robbins SL, et al: Robbins Pathologic Basis of Disease, ed 4, Philadelphia, 1989, WB Saunders.
45. Rosen MP, Ding A, Blake MA, et al: ACR Appropriateness Criteria® right lower quadrant pain—suspected appendicitis. *J Am Coll Radiol* 8:749–755, 2011.
46. Pedrosa I, Levine D, Eyvazzadeh AD, et al: MR imaging evaluation of acute appendicitis in pregnancy. *Radiology* 238:891–899, 2006.
47. Johnson AK, Filippi CG, Andrews T, et al: Ultrafast 3-T MRI in the evaluation of children with acute lower abdominal pain for the detection of appendicitis. *AJR* 198:1424–1430, 2012.
48. Trautlein JJ, Lambert RL, Miller J: Malpractice in the emergency department—review of 200 cases. *Ann Emerg Med* 13(Pt 1):709–711, 1984.
49. Trautlein JJ, Lambert R, Miller J: Malpractice in the emergency room: A critical review of undiagnosed appendicitis cases and legal actions. *Qual Assur Util Rev* 2:54–56, 1987.
50. Phillips RL, Jr, Bartholomew LA, Dovey SM, et al: Learning from malpractice claims about negligent, adverse events in primary care in the United States. *Qual Saf Health Care* 13:121–126, 2004.
51. Selbst SM, Friedman MJ, Singh SB: Epidemiology and etiology of malpractice lawsuits involving children in U.S. emergency departments and urgent care centers. *Pediatr Emerg Care* 21:165–169, 2005.
52. Andersson RE: Meta-analysis of the clinical and laboratory diagnosis of appendicitis. *Br J Surg* 91:28–37, 2004.
53. Andersson RE, Hugander AP, Ghazi SH, et al: Why does the clinical diagnosis fail in suspected appendicitis? *Eur J Surg* 166:796–802, 2000.
54. Kharbanda AB, Taylor GA, Fishman SJ, et al: A clinical rule to identify children at low risk for appendicitis. *Pediatrics* 116:709–716, 2005.
55. Kalliakmanis V, Pikoulis E, Karavokyros IG, et al: Acute appendicitis: The reliability of diagnosis by clinical assessment alone. *Scand J Surg* 94:201–206, 2005.
56. White JJ, Santillana M, Haller JA, Jr: Intensive in-hospital observation: A safe way to decrease unnecessary appendectomy. *Am Surg* 41:793–798, 1975.
57. Flum DR, Morris A, Koepsell T, et al: Has misdiagnosis of appendicitis decreased over time? A population-based analysis. *JAMA* 286:1748–1753, 2001.
58. Flum DR, Koepsell T: The clinical and economic correlates of misdiagnosed appendicitis: Nationwide analysis. *Arch Surg* 137:799–804, 2002.
59. Long SS, Long C, Lai H, et al: Imaging strategies for right lower quadrant pain in pregnancy. *AJR* 196:4–12, 2011.
60. Sivit CJ: Imaging the child with right lower quadrant pain and suspected appendicitis: Current concepts. *Pediatr Radiol* 34:447–453, 2004.
61. Macari M, Balthazar EJ: The acute right lower quadrant: CT evaluation. *Radiol Clin North Am* 41:1117–1136, 2003.
62. Bendeck SEJ, Nino-Murcia M, Berry GJ, Jeffrey RB, Jr: Imaging for suspected appendicitis: Negative appendectomy and perforation rates. *Radiology* 225:131–136, 2002.
63. Rao PM, Rhea JT, Rattner DW, et al: Introduction of appendiceal CT: Impact on negative appendectomy and appendiceal perforation rates. *Ann Surg* 229:344–349, 1999.
64. Coursey CA, Nelson RC, Patel MB, et al: Making the diagnosis of acute appendicitis: Do more preoperative CT scans mean fewer negative appendectomies? A 10-year study. *Radiology* 254:460–468, 2010.
65. Drake FT, Florence MG, Johnson MG, et al: Progress in the diagnosis of appendicitis: A report from Washington State's Surgical Care and Outcomes Assessment Program. *Ann Surg* 256:586–594, 2012.
66. Nelson DW, Causey MW, Porta CR, et al: Examining the relevance of the physician's clinical assessment and the reliance on computed tomography in diagnosing acute appendicitis. *Am J Surg* 205:452–456, 2013.
67. Graffeo CS, Counselman FL: Appendicitis. *Emerg Med Clin North Am* 14:653–671, 1996.
68. Kumar V, Abbas AK, Fausto N, et al: Robbins and Cotran Pathologic Basis of Disease, ed 7, Philadelphia, 2005, Elsevier Saunders.
69. Brewer BJ, Golden GT, Hitch DC, et al: Abdominal pain. An analysis of 1,000 consecutive cases in a University Hospital emergency room. *Am J Surg* 131:219–223, 1976.
70. Ramsden WH, Mannion RA, Simpkins KC, et al: Is the appendix where you think it is—and if not does it matter? *Clin Radiol* 47:100–103, 1993.
71. Karim OM, Boothroyd AE, Wyllie JH: McBurney's point—fact or fiction? *Ann R Coll Surg Engl* 72:304–308, 1990.
72. Marchand A, Van Lente F, Galen RS: The assessment of laboratory tests in the diagnosis of acute appendicitis. *Am J Clin Pathol* 80:369–374, 1983.
73. Hoffmann J, Rasmussen OO: Aids in the diagnosis of acute appendicitis. *Br J Surg* 76:774–779, 1989.
74. Raftery AT: The value of the leucocyte count in the diagnosis of acute appendicitis. *Br J Surg* 63:143–144, 1976.
75. Thompson MM, Underwood MJ, Dookeran KA, et al: Role of sequential leucocyte counts and C-reactive protein measurements in acute appendicitis. *Br J Surg* 79:822–824, 1992.
76. Sasso RD, Hanna EA, Moore DL: Leukocytic and neutrophilic counts in acute appendicitis. *Am J Surg* 120:563–566, 1970.
77. Kretschmar LH, McDonald DF: The urine sediment in acute appendicitis. *Arch Surg* 87:209–211, 1963.
78. Thimsen DA, Tong GK, Gruenberg JC: Prospective evaluation of C-reactive protein in patients suspected to have acute appendicitis. *Am Surg* 55:466–468, 1989.
79. Vaughan-Shaw P, Richardson C, Lewis M: White cell count and C-reactive protein measurement in patients with possible appendicitis. *Ann R Coll Surg Engl* 93:183, 2011.
80. Eriksson S, Granstrom L, Bark S: Laboratory tests in patients with suspected acute appendicitis. *Acta Chir Scand* 155:117–120, 1989.
81. Nordback I, Harju E: Inflammation parameters in the diagnosis of acute appendicitis. *Acta Chir Scand* 154:43–48, 1988.
82. Kelvin FM, Gardiner R: Clinical Imaging of the Colon and Rectum, New York, 1987, Raven Press.
83. Marshak RH, Lindner AE, Maklansky D: Radiology of the Colon, Philadelphia, 1980, WB Saunders.
84. Long JA: The appendix. In Dreyfuss JR, Janower ML, editors: Golden's Diagnostic Radiology, Baltimore, 1980, Williams & Wilkins, pp 497–521.
85. Harding JA, Glick SN, Teplick SK, et al: Appendiceal filling by double-contrast barium enema. *Gastrointest Radiol* 11:105–107, 1986.
86. Johnson JF, Coughlin WF: Plain film diagnosis of appendiceal perforation in children. *Semin Ultrasound CT MR* 10:306–313, 1989.
87. Olutola PS: Plain film radiographic diagnosis of acute appendicitis: An evaluation of the signs. *Can Assoc Radiol J* 39:254–256, 1988.

88. Swischuk LE, Hayden CK, Jr: Appendicitis with perforation: The dilated transverse colon sign. *AJR* 135:687–689, 1980.
89. Vaudagna JS, McCort JJ: Plain film diagnosis of retrocecal appendicitis. *Radiology* 117 (Pt 1):533–536, 1975.
90. Ahn SH, Mayo-Smith WW, Murphy BL, et al: Acute nontraumatic abdominal pain in adult patients: Abdominal radiography compared with CT evaluation. *Radiology* 225:159–164, 2002.
91. Shimkin PM: Radiology of acute appendicitis. *AJR* 130:1001–1004, 1978.
92. Sakover RP, Del Fava RL: Frequency of visualization of the normal appendix with the barium enema examination. *Am J Roentgenol Radium Ther Nucl Med* 121:312–317, 1974.
93. Cohen N, Modai D, Rosen A, et al: Barium appendicitis: Fact or fancy? Report of a case and review of the literature. *J Clin Gastroenterol* 9:447–451, 1987.
94. Smith DE, Kirchmer NA, Stewart DR: Use of the barium enema in the diagnosis of acute appendicitis and its complications. *Am J Surg* 138:829–834, 1979.
95. Rajagopalan AE, Mason JH, Kennedy M, et al: The value of the barium enema in the diagnosis of acute appendicitis. *Arch Surg* 112:531–533, 1977.
96. Rice RP, Thompson WM, Fedyschin PJ, et al: The barium enema in appendicitis: Spectrum of appearances and pitfalls. *Radiographics* 4:393–409, 1984.
97. Fedyschin P, Kelvin FM, Rice RP: Nonspecificity of barium enema findings in acute appendicitis. *AJR* 143:99–102, 1984.
98. Gorske K: Intussusception of the proximal appendix into the colon. *Radiology* 91:791, 1968.
99. Demos TC, Flisak ME: Coiled-spring sign of the cecum in acute appendicitis. *AJR* 146:45–48, 1986.
100. Halls JM, Meyers HI: Acute appendicitis with abscess stimulating carcinoma of the sigmoid. *AJR* 129:1057–1059, 1977.
101. Lane MJ, Liu DM, Huynh MD, et al: Suspected acute appendicitis: Nonenhanced helical CT in 300 consecutive patients. *Radiology* 213:341–346, 1999.
102. Lane MJ, Katz DS, Ross BA, et al: Unenhanced helical CT for suspected acute appendicitis. *AJR* 168:405–409, 1997.
103. Schuler JG, Shortsleeve MJ, Goldenson RS, et al: Is there a role for abdominal computed tomographic scans in appendicitis? *Arch Surg* 133:373–376, 1998.
104. Rao PM, Rhea JT, Novelline RA, et al: Helical CT combined with contrast material administered only through the colon for imaging of suspected appendicitis. *AJR* 169:1275–1280, 1997.
105. Rao PM, Rhea JT, Novelline RA, et al: Helical CT technique for the diagnosis of appendicitis: Prospective evaluation of a focused appendix CT examination. *Radiology* 202:139–144, 1997.
106. Rao PM, Rhea JT, Novelline RA: Helical CT of appendicitis and diverticulitis. *Radiol Clin North Am* 37:895–910, 1999.
107. Stoker J, van Randen A, Laméris W, et al: Imaging patients with acute abdominal pain. *Radiology* 253:31–46, 2009.
108. Weltman DI, Yu J, Krumenacker J, Jr, et al: Diagnosis of acute appendicitis: Comparison of 5- and 10-mm CT sections in the same patient. *Radiology* 216:172–177, 2000.
109. Johnson PT, Horton KM, Kawamoto S, et al: MDCT for suspected appendicitis: Effect of reconstruction section thickness on diagnostic accuracy, rate of appendiceal visualization, and reader confidence using axial images. *AJR* 192:893–901, 2009.
110. Lee KH, Kim YH, Hahn S, et al: Added value of coronal reformations for duty radiologists and for referring physicians or surgeons in the CT diagnosis of acute appendicitis. *Korean J Radiol* 7:87–96, 2006.
111. Paulson EK, Harris JP, Jaffe TA, et al: Acute appendicitis: Added diagnostic value of coronal reformations from isotropic voxels at multi-detector row CT. *Radiology* 235:879–885, 2005.
112. Jan YT, Yang FS, Huang JK: Visualization rate and pattern of normal appendix on multidetector computed tomography by using multiplanar reformation display. *J Comput Assist Tomogr* 29:446–451, 2005.
113. Tamburrini S, Brunetti A, Brown M, et al: CT appearance of the normal appendix in adults. *Eur Radiol* 15:2096–2103, 2005.
114. Benjaminov O, Atri M, Hamilton P, et al: Frequency of visualization and thickness of normal appendix at nonenhanced helical CT. *Radiology* 225:400–406, 2002.
115. Balthazar EJ, Megibow AJ, Siegel SE, et al: Appendicitis: Prospective evaluation with high-resolution CT. *Radiology* 180:21–24, 1991.
116. Balthazar EJ, Birnbaum BA, Yee J, et al: Acute appendicitis: CT and US correlation in 100 patients. *Radiology* 190:31–35, 1994.
117. Malone AJ, Jr, Wolf CR, Malmel AS, et al: Diagnosis of acute appendicitis: Value of unenhanced CT. *AJR* 160:763–766, 1993.
118. Jacobs JE, Birnbaum BA, Macari M, et al: Acute appendicitis: Comparison of helical CT diagnosis focused technique with oral contrast material versus nonfocused technique with oral and intravenous contrast material. *Radiology* 220:683–690, 2001.
119. Rao PM: Cecal apical changes with appendicitis: Diagnosing appendicitis when the appendix is borderline abnormal or not seen. *J Comput Assist Tomogr* 23:55–59, 1999.
120. Rao PM, Wittenberg J, McDowell RK, et al: Appendicitis: Use of arrowhead sign for diagnosis at CT. *Radiology* 202:363–366, 1997.
121. Tsuboi M, Takase K, Kaneda I, et al: Perforated and nonperforated appendicitis: Defect in enhancing appendiceal wall—depiction with multi-detector row CT. *Radiology* 246:142–147, 2008.
122. Huynh V, Lalezaradeh F, Lawandy S, et al: Abdominal computed tomography in the evaluation of acute and perforated appendicitis in the community setting. *Am Surg* 73:1002–1005, 2007.
123. Bixby SD, Lucey BC, Soto JA, et al: Perforated versus nonperforated acute appendicitis: Accuracy of multidetector CT detection. *Radiology* 241:780–786, 2006.
124. Sivit CJ, Applegate KE: Imaging of acute appendicitis in children. *Semin Ultrasound CT MR* 24:74–82, 2003.
125. Rao PM, Rhea JT, Novelline RA: Distal appendicitis: CT appearance and diagnosis. *Radiology* 204:709–712, 1997.
126. Kim SY, Lee KH, Kim K, et al: Acute appendicitis in young adults: Low- versus standard-radiation-dose contrast-enhanced abdominal CT for diagnosis. *Radiology* 260:437–445, 2011.
127. Johnson PT, Horton KM, Mahesh M, et al: Multidetector computed tomography for suspected appendicitis: Multi-institutional survey of 16-MDCT data acquisition protocols and review of pertinent literature. *J Comput Assist Tomogr* 30:758–764, 2006.
128. Pinto Leite N, Pereira JM, Cunha R, et al: CT evaluation of appendicitis and its complications: Imaging techniques and key diagnostic findings. *AJR* 185:406–417, 2005.
129. Anderson BA, Salem L, Flum DR: A systematic review of whether oral contrast is necessary for the computed tomography diagnosis of appendicitis in adults. *Am J Surg* 190:474–478, 2005.
130. O'Malley ME, Halpern E, Mueller PR, et al: Helical CT protocols for the abdomen and pelvis: A survey. *AJR* 175:109–113, 2000.
131. Wise SW, Labuski MR, Kasales CJ, et al: Comparative assessment of CT and sonographic techniques for appendiceal imaging. *AJR* 176:933–941, 2001.
132. Rhea JT, Rao PM, Novelline RA, et al: A focused appendiceal CT technique to reduce the cost of caring for patients with clinically suspected appendicitis. *AJR* 169:113–118, 1997.
133. Raman SS, Lu DS, Kadell BM, et al: Accuracy of nonfocused helical CT for the diagnosis of acute appendicitis: A 5-year review. *AJR* 178:1319–1325, 2002.
134. Federle MP: Focused appendix CT technique: A commentary. *Radiology* 202:20–21, 1997.
135. Raman SP, Fishman EK: Imaging: Multidetector CT in the diagnosis of suspected appendicitis. *Nat Rev Gastroenterol Hepatol* 8:607–609, 2011.
136. Wijetunga R, Tan BS, Rouse JC, et al: Diagnostic accuracy of focused appendiceal CT in clinically equivocal cases of acute appendicitis. *Radiology* 221:747–753, 2001.
137. Berg ER, Mehta SD, Mitchell P, et al: Length of stay by route of contrast administration for diagnosis of appendicitis by computed-tomography scan. *Acad Emerg Med* 13:1040–1045, 2006.
138. Brassart N, Winant C, Tack D, et al: Optimised z-axis coverage at multidetector-row CT in adults suspected of acute appendicitis. *Br J Radiol* 86:20130115, 2013.
139. Puylaert JB: Acute appendicitis: US evaluation using graded compression. *Radiology* 158:355–360, 1986.
140. Kessler N, Cyteval C, Gallix B, et al: Appendicitis: Evaluation of sensitivity, specificity, and predictive values of US, Doppler US, and laboratory findings. *Radiology* 230:472–478, 2004.
141. Rettenbacher T, Hollerweger A, Macheiner P, et al: Outer diameter of the vermiform appendix as a sign of acute appendicitis: Evaluation at US. *Radiology* 218:757–762, 2001.
142. van Randen A, Bipat S, Zwinderman AH, et al: Acute appendicitis: Meta-analysis of diagnostic performance of CT and graded compression US related to prevalence of disease. *Radiology* 249:97–106, 2008.
143. Mittal MK, Dayan PS, Macias CG, et al: Performance of ultrasound in the diagnosis of appendicitis in children in a multicenter cohort. *Acad Emerg Med* 20:697–702, 2013.
144. Borushok KF, Jeffrey RB, Jr, Laing FC, et al: Sonographic diagnosis of perforation in patients with acute appendicitis. *AJR* 154:275–278, 1990.
145. Ooms HW, Koumans RK, Ho Kang You PJ, et al: Ultrasonography in the diagnosis of acute appendicitis. *Br J Surg* 78:315–318, 1991.

146. Quillin SP, Siegel MJ, Coffin CM: Acute appendicitis in children: Value of sonography in detecting perforation. *AJR* 159:1265–1268, 1992.
147. Leeuwenburgh MMN, Wiarda BM, Wiezer MJ, et al: Comparison of imaging strategies with conditional contrast-enhanced CT and unenhanced MR imaging in patients suspected of having appendicitis: A multicenter diagnostic performance study. *Radiology* 268:135–143, 2013.
148. Cobben L, Groot I, Kingma L, et al: A simple MRI protocol in patients with clinically suspected appendicitis: Results in 138 patients and effect on outcome of appendectomy. *Eur Radiol* 19:1175–1183, 2009.
149. Baldisserotto M, Valduga SG, da Cunha CF: MR imaging evaluation of the normal appendix in children and adolescents. *Radiology* 249:278–284, 2008.
150. Horowitz JM, Nikolaidis P, Hammond NA, et al: Taking advantage of chemical shift imaging: Using opposed-phase images to locate the normal appendix on MR. *Clin Imaging* 35:424–430, 2011.
151. Leeuwenburgh MMN, Wiarda BM, Bipat S, et al: Acute appendicitis on abdominal MR images: Training readers to improve diagnostic accuracy. *Radiology* 264:455–463, 2012.
152. Inci E, Kilickesmez O, Hocaoglu E, et al: Utility of diffusion-weighted imaging in the diagnosis of acute appendicitis. *Eur Radiol* 21:768–775, 2011.
153. Spalluto LB, Woodfield CA, DeBenedictis CM, et al: MR imaging evaluation of abdominal pain during pregnancy: Appendicitis and other nonobstetric causes. *Radiographics* 32:317–334, 2012.
154. Lee KS, Rofsky NM, Pedrosa I: Localization of the appendix at MR imaging during pregnancy: Utility of the cecal tilt angle. *Radiology* 249:134–141, 2008.
155. Oto A, Srinivasan PN, Ernst RD, et al: Revisiting MRI for appendix location during pregnancy. *AJR* 186:883–887, 2006.
156. Dewhurst C, Beddy P, Pedrosa I: MRI evaluation of acute appendicitis in pregnancy. *J Magn Reson Imaging* 37:566–575, 2013.
157. Pedrosa I, Lafornera M, Pandharipande PV, et al: Pregnant patients suspected of having acute appendicitis: Effect of MR imaging on negative laparotomy rate and appendiceal perforation rate. *Radiology* 250:749–757, 2009.
158. Herliczek TW, Swenson DW, Mayo-Smith WW: Utility of MRI after inconclusive ultrasound in pediatric patients with suspected appendicitis: Retrospective review of 60 consecutive patients. *AJR* 200:969–973, 2013.
159. Rapp EJ, Naim F, Kadivar K, et al: Integrating MR imaging into the clinical workup of pregnant patients suspected of having appendicitis is associated with a lower negative laparotomy rate: Single-institution study. *Radiology* 267:137–144, 2013.
160. Israel GM, Malguria N, McCarthy S, et al: MRI vs. ultrasound for suspected appendicitis during pregnancy. *J Magn Reson Imaging* 28:428–433, 2008.
161. Birchard KR, Brown MA, Hyslop WB, et al: MRI of acute abdominal and pelvic pain in pregnant patients. *AJR* 184:452–458, 2005.
162. Nitta N, Takhashi M, Furukawa A, et al: MR imaging of the normal appendix and acute appendicitis. *J Magn Reson Imaging* 21:156–165, 2005.
163. Oto A, Ernst RD, Shah R, et al: Right-lower-quadrant pain and suspected appendicitis in pregnant women: Evaluation with MR imaging—initial experience. *Radiology* 234:445–451, 2005.
164. Baer JL, Reis RA, Arens RA: Appendicitis in pregnancy: With changes in position and axis of the normal appendix in pregnancy. *JAMA* 98:1359–1364, 1932.
165. Sharp HT: The acute abdomen during pregnancy. *Clin Obstet Gynecol* 45:405–413, 2002.
166. Mourad J, Elliott JP, Erickson L, et al: Appendicitis in pregnancy: New information that contradicts long-held clinical beliefs. *Am J Obstet Gynecol* 182:1027–1029, 2000.
167. Katz DS, Klein MA, Ganson G, et al: Imaging of abdominal pain in pregnancy. *Radiol Clin North Am* 50:149–171, 2012.
168. Levine D, Zuo C, Faro CB, et al: Potential heating effect in the gravid uterus during MR HASTE imaging. *J Magn Reson Imaging* 13:856–861, 2001.
169. Shellock FG, Ziarati M, Atkinson D, et al: Determination of gradient magnetic field-induced acoustic noise associated with the use of echo planar and three-dimensional, fast spin-echo techniques. *J Magn Reson Imaging* 8:1154–1157, 1998.
170. Reeves MJ, Brandreth M, Whitby EH, et al: Neonatal cochlear function: Measurement after exposure to acoustic noise during in utero MR imaging. *Radiology* 257:802–809, 2010.
171. Baker PN, Johnson IR, Harvey PR, et al: A three-year follow-up of children imaged in utero with echo-planar magnetic resonance. *Am J Obstet Gynecol* 170(1 Pt 1):32–33, 1994.
172. Aspelund G, Fingeret A, Gross E, et al: Ultrasonography/MRI versus CT for diagnosing appendicitis. *Pediatrics* 133:586–593, 2014.
173. Idiyatullin D, Corum C, Park JY, et al: Fast and quiet MRI using a swept radiofrequency. *J Magn Reson* 181:342–349, 2006.
174. Edelstein WA, Kidane TK, Taracila V, et al: Active-passive gradient shielding for MRI acoustic noise reduction. *Magn Reson Med* 53:1013–1017, 2005.
175. Katsunuma A, Takamori H, Sakakura Y, et al: Quiet MRI with novel acoustic noise reduction. *MAGMA* 13:139–144, 2002.
176. Oto A, Ernst RD, Ghulmiyyah LM, et al: MR imaging in the triage of pregnant patients with acute abdominal and pelvic pain. *Abdom Imaging* 34:243–250, 2009.
177. Kanal E, Shellock FG: Policies, guidelines, and recommendations for MR imaging safety and patient management. SMRI Safety Committee. *J Magn Reson Imaging* 2:247–248, 1992.
178. ACOG Committee on Obstetric Practice: ACOG Committee Opinion. Number 299, September 2004 (replaces No. 158, September 1995). Guidelines for diagnostic imaging during pregnancy. *Obstet Gynecol* 104:647–651, 2004.
179. Webb JA, Thomsen HS: Gadolinium contrast media during pregnancy and lactation. *Acta Radiol* 54:599–600, 2013.
180. De Santis M, Straface G, Cavaliere AF, et al: Gadolinium periconceptional exposure: Pregnancy and neonatal outcome. *Acta Obstet Gynecol Scand* 86:99–101, 2007.
181. Garcia-Bournissen F, Shrim A, Koren G: Safety of gadolinium during pregnancy. *Can Fam Physician* 52:309–310, 2006.
182. Webb JA, Thomsen HS, Morcos SK, et al: The use of iodinated and gadolinium contrast media during pregnancy and lactation. *Eur Radiol* 15:1234–1240, 2005.
183. Expert Panel on MRS, Kanal E, Barkovich AJ, et al: ACR guidance document on MR safe practices: 2013. *J Magn Reson Imaging* 37:501–530, 2013.
184. Heverhagen JT, Pfestroff K, Heverhagen AE, et al: Diagnostic accuracy of magnetic resonance imaging: A prospective evaluation of patients with suspected appendicitis (diamond). *J Magn Reson Imaging* 35:617–623, 2012.
185. Blumenfeld YJ, Wong AE, Jafari A, et al: MR imaging in cases of antenatal suspected appendicitis—a meta-analysis. *J Matern Fetal Neonatal Med* 24:485–488, 2011.
186. Rao PM, Rhea JT, Novelline RA: CT diagnosis of mesenteric adenitis. *Radiology* 202:145–149, 1997.
187. Puylaert JB, van der Zant FM: Mesenteric lymphadenitis or appendicitis? *AJR* 165:490, 1995.
188. Puylaert JB: Mesenteric adenitis and acute terminal ileitis: US evaluation using graded compression. *Radiology* 161:691–695, 1986.
189. Macari M, Hines J, Balthazar E, et al: Mesenteric adenitis: CT diagnosis of primary versus secondary causes, incidence, and clinical significance in pediatric and adult patients. *AJR* 178:853–858, 2002.
190. van Breda Vriesman AC, Puylaert JB: Mimics of appendicitis: Alternative nonsurgical diagnoses with sonography and CT. *AJR* 186:1103–1112, 2006.
191. Gore RM: CT of inflammatory bowel disease. *Radiol Clin North Am* 27:717–729, 1989.
192. Gore RM: Cross-sectional imaging of inflammatory bowel disease. *Radiol Clin North Am* 25:115–131, 1987.
193. Gore RM, Balthazar EJ, Ghahremani GG, et al: CT features of ulcerative colitis and Crohn's disease. *AJR* 167:3–15, 1996.
194. Gore RM, Marn CS, Kirby DE, et al: CT findings in ulcerative, granulomatous, and indeterminate colitis. *AJR* 143:279–284, 1984.
195. Philpotts LE, Heiken JP, Westcott MA, et al: Colitis: Use of CT findings in differential diagnosis. *Radiology* 190:445–449, 1994.
196. van Breda Vriesman AC, de Mol van Otterloo AJ, Puylaert JB: Epiploic appendagitis and omental infarction. *Eur J Surg* 167:723–727, 2001.
197. Puylaert JB: Right-sided segmental infarction of the omentum: Clinical, US, and CT findings. *Radiology* 185:169–172, 1992.
198. Macari M, Balthazar EJ, Krinsky G, et al: CT diagnosis of ileal diverticulitis. *Clin Imaging* 22:243–245, 1998.
199. Frick MP, Maile CW, Crass JR, et al: Computed tomography of neutropenic colitis. *AJR* 143:763–765, 1984.
200. Peltokallio P: Acute appendicitis associated with carcinoma of the colon. *Dis Colon Rectum* 9:453–456, 1966.
201. Watchorn RE, Ponder L, Wang ZJ, et al: Computed tomography findings mimicking appendicitis as a manifestation of colorectal cancer. *Clin Imaging* 33:430–432, 2009.
202. Ripolles T, Martinez MJ, Morote V, et al: Appendiceal involvement in Crohn's disease: Gray-scale sonography and color Doppler flow features. *AJR* 186:1071–1078, 2006.
203. Chiou YY, Pitman MB, Hahn PF, et al: Rare benign and malignant appendiceal lesions: Spectrum of computed tomography findings

- with pathologic correlation. *J Comput Assist Tomogr* 27:297–306, 2003.
204. Sturm EJ, Cobben LP, Meijssen MA, et al: Detection of ileocecal Crohn's disease using ultrasound as the primary imaging modality. *Eur Radiol* 14:778–782, 2004.
 205. Dudley TH, Jr, Dean PJ: Idiopathic granulomatous appendicitis, or Crohn's disease of the appendix revisited. *Hum Pathol* 24:595–601, 1993.
 206. Scott IS, Sheaff M, Coumbe A, et al: Appendiceal inflammation in ulcerative colitis. *Histopathology* 33:168–173, 1998.
 207. Buffo GC, Clair MR, Bonheim P: Diverticulosis of the vermiform appendix. *Gastrointest Radiol* 11:108–109, 1986.
 208. Sharp JE, Nicholson ML, Fossard DP: Diverticulosis of the appendix. *Scott Med J* 35:50–51, 1990.
 209. Riddell R: Appendix. In Riddell R, Jain D, editors: *Lewin, Weinstein and Riddell's Gastrointestinal Pathology and Its Clinical Implications*, ed 2, Philadelphia, 2014, Wolters, pp 793–874.
 210. Phillips BJ, Perry CW: Appendiceal diverticulitis. *Mayo Clin Proc* 74:890–892, 1999.
 211. Langsam LB, Raj PK, Galang CF: Intussusception of the appendix. *Dis Colon Rectum* 27:387–392, 1984.
 212. Levine MS, Trenkner SW, Herlinger H, et al: Coiled-spring sign of appendiceal intussusception. *Radiology* 155:41–44, 1985.
 213. Maglinte DD, Fleischer AC, Chua GT, et al: Sonography of appendiceal intussusception. *Gastrointest Radiol* 12:163–165, 1987.
 214. Kleinman PK: Intussusception of the appendix: Hydrostatic reduction. *AJR* 134:1268–1270, 1980.
 215. Deans GT, Spence RA: Neoplastic lesions of the appendix. *Br J Surg* 82:299–306, 1995.
 216. Connor SJ, Hanna GB, Frizelle FA: Appendiceal tumors: Retrospective clinicopathologic analysis of appendiceal tumors from 7,970 appendectomies. *Dis Colon Rectum* 41:75–80, 1998.
 217. van den Heuvel MG, Lemmens VE, Verhoeven RH, et al: The incidence of mucinous appendiceal malignancies: A population-based study. *Int J Colorectal Dis* 28:1307–1310, 2013.
 218. Pickhardt PJ, Levy AD, Rohrmann CA, Jr, et al: Primary neoplasms of the appendix manifesting as acute appendicitis: CT findings with pathologic comparison. *Radiology* 224:775–781, 2002.
 219. Peck JJ: Management of carcinoma discovered unexpectedly at operation for acute appendicitis. *Am J Surg* 155:683–685, 1988.
 220. Horgan JG, Chow PP, Richter JO, et al: CT and sonography in the recognition of mucocoele of the appendix. *AJR* 143:959–962, 1984.
 221. Kim SH, Lim HK, Lee WJ, et al: Mucocoele of the appendix: Ultrasonographic and CT findings. *Abdom imaging* 23:292–296, 1998.
 222. Li YP, Morin ME, Tan A: Ultrasound findings in mucocoele of the appendix. *J Clin Ultrasound* 9:406–408, 1981.
 223. Madwed D, Mindelzun R, Jeffrey RB, Jr: Mucocoele of the appendix: Imaging findings. *AJR* 159:69–72, 1992.
 224. McGinnis HD, Chew FS: Mucin-producing adenoma of the appendix. *AJR* 160:1046, 1993.
 225. Ruiz-Tovar J, Teruel DG, Castineiras VM, et al: Mucocoele of the appendix. *World J Surg* 31:542–548, 2007.
 226. Skaane P: Radiological features of mucocoele of the appendix. *Rofo* 149:624–628, 1988.
 227. Soweid AM, Clarkston WK, Andrus CH, et al: Diagnosis and management of appendiceal mucocoeles. *Dig Dis* 16:183–186, 1998.
 228. Wackym PA, Gray GF, Jr: Tumors of the appendix: I. Neoplastic and non-neoplastic mucocoeles. *South Med J* 77:283–287, 1984.
 229. Karakuc RJ: Unusual roentgenographic manifestations of mucocoele of the appendix. *Radiology* 89:886–887, 1967.
 230. Kimura H, Konishi K, Yabushita K, et al: Intussusception of a mucocoele of the appendix secondary to an obstruction by endometriosis: Report of a case. *Surg Today* 29:629–632, 1999.
 231. Sandler MA, Pearlberg JL, Madrazo BL: Ultrasonic and computed tomographic features of mucocoele of the appendix. *J Ultrasound Med* 3:97–100, 1984.
 232. Chan JK: Images in pathology: Myxoglobulosis of the appendix. *Int J Surg Pathol* 9:303, 2001.
 233. Aroukatos P, Verras D, VANDOROS GP, et al: Myxoglobulosis of the appendix: A case associated with ruptured diverticulum. *Case Rep Med* pii: 745021, 2010.
 234. Mayes GB, Chuang VP, Fisher RG: CT of pseudomyxoma peritonei. *AJR* 136:807–808U, 1981.
 235. Novetsky GJ, Berlin L, Epstein AJ, et al: Case report. Pseudomyxoma peritonei. *J Comput Assist Tomogr* 6:398–399, 1982.
 236. Balthazar EJ, Javors BR: The radiology corner. Pseudomyxoma peritonei, clinical and radiographic features. *Am J Gastroenterol* 68:501–509, 1977.
 237. Dachman AH, Lichtenstein JE, Friedman AC: Mucocoele of the appendix and pseudomyxoma peritonei. *AJR* 144:923–929, 1985.
 238. Gustafson KD, Karnaze GC, Hattery RR, et al: Pseudomyxoma peritonei associated with mucinous adenocarcinoma of the pancreas: CT findings and CT-guided biopsy. *J Comput Assist Tomogr* 8:335–338, 1984.
 239. Matsuoka Y, Ohtomo K, Itai Y, et al: Pseudomyxoma peritonei with progressive calcifications: CT findings. *Gastrointest Radiol* 17:16–18, 1992.
 240. Skaane P, Isachsen MM, Hoiseth A: Computed tomography of mucin-producing adenocarcinoma of the appendix presenting as a bladder tumor. *J Comput Assist Tomogr* 9:566–567, 1985.
 241. Nitecki SS, Wolff BG, Schlinkert R, et al: The natural history of surgically treated primary adenocarcinoma of the appendix. *Ann Surg* 219:51–57, 1994.
 242. Collins DC: 71,000 human appendix specimens. A final report, summarizing forty years' study. *Am J Proctol* 14:265–281, 1963.
 243. Moertel CG, Dockerty MB, Judd ES: Carcinoid tumors of the vermiform appendix. *Cancer* 21:270–278, 1968.
 244. Mitra B, Pal M, Paul B, et al: Goblet cell carcinoid of appendix: A rare case with literature review. *Int J Surg Case Rep* 4:334–337, 2013.
 245. Hemminki K, Li X: Incidence trends and risk factors of carcinoid tumors: A nationwide epidemiologic study from Sweden. *Cancer* 92:2204–2210, 2001.
 246. Käser SA, Willi N, Maurer CA: Prevalence and clinical implications of diverticulosis of the vermiform appendix. *J Int Med Res* 41:1350–1368, 2013.
 247. Pelage JP, Soyer P, Boudiaf M, et al: Carcinoid tumors of the abdomen: CT features. *Abdom Imaging* 24:240–245, 1999.
 248. Kitamura Y, Ohta T, Terada T: Primary T-cell non-Hodgkin's malignant lymphoma of the appendix. *Pathol Int* 50:313–317, 2000.
 249. Yilmaz M, Akbulut S, Kutluturk K, et al: Unusual histopathological findings in appendectomy specimens from patients with suspected acute appendicitis. *World J Gastroenterol* 19:4015–4022, 2013.
 250. Pickhardt PJ, Levy AD, Rohrmann CA, Jr, et al: Non-Hodgkin's lymphoma of the appendix: Clinical and CT findings with pathologic correlation. *AJR* 178:1123–1127, 2002.
 251. O'Malley DP, Goldstein NS, Banks PM: The recognition and classification of lymphoproliferative disorders of the gut. *Human Pathol* 45:899–916, 2014.

Ulcerative and Granulomatous Colitis: Idiopathic Inflammatory Bowel Disease

RICHARD M. GORE | JONATHAN W. BERLIN | ALEKSANDAR M. IVANOVIC

CHAPTER OUTLINE

Ulcerative Colitis

Historical Perspective
Epidemiology
Pathogenesis and Causative Factors
Findings
Therapy
Prognosis

Crohn's Disease

Historical Perspective
Pathogenesis and Causative Factors
Epidemiology
Findings
Therapy
Prognosis

Intestinal Complications of Inflammatory Bowel Disease

Carcinoma
Toxic Megacolon

Extraintestinal Complications of Inflammatory Bowel Disease

Hepatobiliary Complications
Pancreatic Complications
Urinary Tract Complications
Musculoskeletal Complications
Pulmonary Complications

Differential Diagnosis of Colitis

Summary

The term *inflammatory bowel disease* encompasses two forms of chronic, idiopathic intestinal inflammation, ulcerative colitis and Crohn's disease. Although many other inflammatory diseases affect the gut, most are distinguished by a specific identifiable causative agent or process or by the nature of the inflammatory activity. The cause of ulcerative colitis and Crohn's disease is unknown, so these disorders are empirically defined by their typical pathologic, radiologic, clinical, endoscopic, and laboratory features.¹⁻⁷ This chapter summarizes the features that usually permit an operational distinction to be made between ulcerative colitis and Crohn's disease. The fundamental validity of this classification is uncertain and will remain so until the cause and pathogenesis of these disorders are better understood.

Ulcerative Colitis

Ulcerative colitis is a diffuse inflammatory disease of unknown origin that primarily involves the colorectal mucosa but later extends to other layers of the bowel wall. The disease characteristically begins in the rectum and extends proximally to involve part or all of the colon. The diagnosis is usually made on the basis of clinical symptoms and the presence of inflamed mucosa on sigmoidoscopy and confirmed by the findings on barium enema and mucosal biopsy.^{5,6}

HISTORICAL PERSPECTIVE

Although Hippocrates was aware that diarrhea was not a single disease, it required more than 2 millennia before ulcerative colitis was distinguished from the very common infectious enteritides. In 1859, Wilks described the case of Mrs. Isabella Banks, who had "inflammation of the large intestine" and was "affected by discharge of mucus and blood, where, after death, the whole internal surface of the colon presented a highly vascular soft, red surface covered with tenacious mucus, adherent lymph."⁸ By 1900, ulcerative colitis was fully characterized in terms of its clinical and pathologic criteria.¹

EPIDEMIOLOGY

Epidemiologic data have yielded some important clues concerning the cause of ulcerative colitis. The salient epidemiologic features of ulcerative colitis are listed in [Box 57-1](#) and will be discussed in more detail.

Ulcerative colitis is more common than Crohn's disease, with an annual incidence of 2 to 10 cases/100,000 population. The worldwide prevalence ranges from 35 to 100 cases/100,000 population. This wide range is probably the result of true differences in disease distribution as well as differences in reporting, diagnostic criteria, and availability of medical care.⁷ The incidence of ulcerative colitis has remained steady. This is in sharp contrast to Crohn's disease, which has shown a sixfold increase in incidence over the past 3 decades.

Ulcerative colitis is most prevalent in the developed countries of northern Europe, Scandinavia, British Isles, United States, and Israel. The incidence of ulcerative colitis in high-prevalence areas has leveled off, whereas the incidence of Crohn's disease has been increasing. In low-prevalence geographic areas, the incidence of ulcerative colitis has been increasing.⁷ Ulcerative colitis is four times more common in whites than in nonwhites, and there is a slight female preponderance.⁷

BOX 57-1 EPIDEMIOLOGY OF ULCERATIVE COLITIS

Worldwide prevalence: 35-100 cases/100,000 population
 Annual incidence: 2-10 cases/100,000 population
 Bimodal age distribution—peak, 15-25 yr; smaller peak, 50-80 yr
 Risk factors
 White (2-5× risk)
 Jewish (2-4× risk)
 Live in developed country
 Urban dweller
 Family history (30-100× risk)
 Sibling with disease (8.8% incidence)
 Single
 Nonsmoker

Adapted from Osterman MT, Lichtenstein GR: Ulcerative colitis. In Feldman M, Friedman LS, Branch LJ (eds): Gastrointestinal and Liver Disease, 8th ed. Philadelphia, Saunders, 2010, pp 1975-2090.

There is a twofold to fourfold increase of ulcerative colitis among Jews. The incidence of ulcerative colitis is much lower among Israeli than among American and European Jews. Furthermore, the incidence of disease is lower in Sephardic than in Ashkenazi Jews in Israel. These disparate rates suggest that a hereditary predisposition may be altered by environmental factors.⁷

The peak age at onset of ulcerative colitis is between 15 and 25 years of age, with a smaller peak at ages 55 to 65 years. Ulcerative colitis is more common than Crohn's disease in children younger than 10 years. Ulcerative colitis is more common in urban than in rural populations.⁷

The incidence of ulcerative colitis among first-degree relatives is 30 to 100 times greater than that of the general population.⁷ Of patients with ulcerative colitis, 10% to 20% have a similarly affected first-degree relative. The lifetime risk of developing ulcerative colitis among first-degree relatives is 8.9% for offspring, 8.8% for siblings, and 3.5% for parents. The child develops the disease at a much younger age than the affected parent—a phenomenon known as genetic anticipation. Familial ulcerative colitis seems to follow a polygenic inheritance pattern.⁷

The risk of developing ulcerative colitis for current smokers compared with lifetime nonsmokers is 59% less, but the risk is elevated by 64% for former smokers. However, smoking is not therapeutic, and there is no strong evidence of a beneficial effect of smoking on the clinical course of ulcerative colitis. Patients who quit smoking before the onset of disease have more frequent hospitalizations and colectomies. This fact raises the possibility that smoking cessation may lead to more severe illness.^{8,9}

The mortality rate of ulcerative colitis has significantly improved, which can be attributed to improvements in diagnosis and management. In the past, ulcerative colitis was responsible for 90% of deaths attributable to inflammatory bowel disease (IBD). More recently, the proportion of ulcerative colitis and Crohn's disease deaths is about equal—1/100,000 for those 20 to 29 years and 3 to 4/100,000 for those 50 to 59 years of age.⁷ Approximately 78% of ulcerative colitis patients die of causes unrelated to bowel disease. Colorectal cancer caused 14% of deaths in ulcerative colitis patients in one study.⁷

PATHOGENESIS AND CAUSATIVE FACTORS

Despite exhaustive work by many investigators, the cause of ulcerative colitis is still unknown. Although the participation of genetic, environmental, neural, hormonal, infectious, immunologic, and psychological factors in the pathogenesis of this disease is well established, none of the mechanisms has proved to be the primary causative agent. In addition, it now appears that distal ulcerative proctitis may have a cause different from that of pancolitis.¹⁻⁴

As noted, familial aggregation of ulcerative colitis is well recognized. The postulated mode of inheritance of susceptibility to ulcerative colitis is through polygenes. The disease occurs with greatest frequency in monozygotic twins. Human leukocyte antigen (HLA) phenotypes B5, Bw52, and DR2 also have a significant association with ulcerative colitis. Ulcerative colitis is often associated with the autoimmune disorders, sacroiliitis, ankylosing spondylitis, enteropathic oligoarthritis, and anterior uveitis, which are associated with HLA-B27 antigen.⁴⁻⁶ Possibly, genes related to ulcerative colitis may encode products that contribute to functional or structural abnormalities in the colon, which render it more susceptible to attack by infection, toxins, and autoimmune actions.⁸

Patients with ulcerative colitis have abnormal mucin production, which may permit various intraluminal bacterial products and toxins to attack the mucosa. It is uncertain whether this defect is a cause or effect of the disease.⁴⁻⁶ An infectious cause for IBD with a direct cause and effect relationship between a single microorganism and inflammation still remains plausible. *Chlamydia*, mycobacteria, gut anaerobes, cytomegalovirus, *Yersinia*, and bacterial cell wall components have all been implicated as a cause of ulcerative colitis. It is also possible that bacteria that normally constitute normal flora may be pathogenic in a susceptible host.⁴⁻⁶

In ulcerative colitis, the enteric nervous system and nerves containing substance P and vasoactive intestinal polypeptide (VIP) become straight, thick, and highly immunoreactive. Substance P and VIP are powerful mediators in neurogenically induced inflammation and cause vasodilation, plasma extravasation, and watery diarrhea. All these factors may have a role in the pathophysiology of IBD.⁴⁻⁶

The immune system provides an important contribution to the pathogenesis of ulcerative colitis because of failure to clear a microbial or toxic agent or because of an inappropriate response to it. The immune system probably mediates the tissue injury as well, regardless of the trigger, and this is the basis of therapy with corticosteroids and other immunosuppressive agents. The colonic inflammation of ulcerative colitis may merely be an exaggerated physiologic response that is always present within the lamina propria of the colon. There is an alteration of the relative representation of macrophages and T-cell and B-cell populations and an increase in the numbers of immunoglobulin G-bearing cells. The disease is also characterized by a fundamental alteration in antigen-presenting activity associated with a reduction of intestinal suppressor T cells and elevated levels of cytotoxic Leu-7-positive cells. Increased levels of specific antibodies to antigens in the gut lumen are also found.¹⁻⁶ These immunologic disturbances offer great potential for therapy with new immunosuppressive and biologic agents (see later).

Ulcerative colitis is a complex disease. It consists of interactions among initiating organisms or antigens, the host's immune

response, and immunologic, environmental, and hereditary influences.

FINDINGS

Clinical Findings

Ulcerative colitis is highly variable in clinical course, severity, and prognosis. Disease activity waxes and wanes and is characterized by acute exacerbations of bloody diarrhea that resolve spontaneously or after therapy. The most common clinical findings are diarrhea, abdominal pain, rectal bleeding, weight loss, and tenesmus; vomiting, fever, constipation, and arthralgias occur less commonly.¹⁰⁻¹²

Ulcerative colitis usually behaves as a chronic low-grade illness in most patients. In 15% of patients, this disease has an acute and fulminating course, with explosive diarrhea, hematochezia, and hypotension. Most patients (60%-75%) have intermittent attacks with complete symptomatic remission between attacks, 4% to 10% have one attack and no subsequent symptoms, and 5% to 15% are troubled by continuous symptoms without remission.^{10,11}

Patients with ulcerative proctitis have disease of mild severity, and the disease usually remains distal. There is extension to the proximal colon in 15% of patients over a 10-year period and extension to the hepatic flexure in 7%. At presentation, 30% of patients have disease limited to the rectum, 40% have disease extending above the rectum but not beyond the hepatic flexure, and the remaining 30% have pancolitis. Extraintestinal manifestations, such as arthralgias, mild arthritis, eye inflammation, and rash, are present in fewer than 10% of patients at initial presentation.^{1-5,10,11}

Physical examination discloses fever, prostration, dehydration, and postural hypotension in the most severe cases. The abdomen may be protuberant because of colonic atony and distention. Abdominal tenderness over the colon and absent bowel sounds are ominous signs suggesting toxic megacolon or early perforation. Patients with milder involvement present with pallor, low-grade fever, weight loss, and mild abdominal tenderness.^{10,11}

Endoscopic Findings

Sigmoidoscopy is helpful in establishing the diagnosis of ulcerative colitis because the distal colon and rectum are involved in 90% to 95% of cases. Early on, the mucosa is edematous and friable, with loss of the normal vascular pattern and bleeding when touched by the endoscope or rubbed with a cotton swab. With disease progression, granular, spontaneously hemorrhagic mucosa is found, associated with a mucopurulent exudate. The haustra are thick and blunted, the lumen seems narrowed and straightened, and the normal thin (<2 mm) mucosal folds are lost. In severe disease, the mucosa is diffusely hemorrhagic, and frank ulceration with loss of mucosal irregularity is seen.^{3,13,14}

Radiologic Findings

Plain Abdominal Radiographs. Considerable information can be gained by carefully scrutinizing the abdominal radiographs of patients with ulcerative colitis. Although attention should be focused on the colon, other abnormalities, such as renal calculi, sacroiliitis, ankylosing spondylitis, and avascular necrosis of the femoral heads, must also be excluded.¹⁵⁻²⁰

Although the extent of ulcerative colitis is generally determined by barium enema and colonoscopy, these procedures carry a higher risk in severely ill patients. The following radiographic features can be used to assess the severity and extent of the colitis: (1) the extent of formed fecal residue; (2) the appearance of the mucosal edge; (3) alterations of the haustra; (4) colonic width; and (5) mural thickness.¹⁵

Colonic Fecal Residue. The distal extent of formed fecal residue provides a good indication, although not absolute, of the proximal extent of the colitis (Fig. 57-1). This approach sometimes overestimates but does not underestimate the extent of disease. The following conclusions can be drawn from the extent of residue¹⁵⁻²³:

1. If no residue is visible, the patient probably has active pancolitis.
2. If the residue extends down into the sigmoid colon, proctitis is present (this may be indistinguishable from normal).

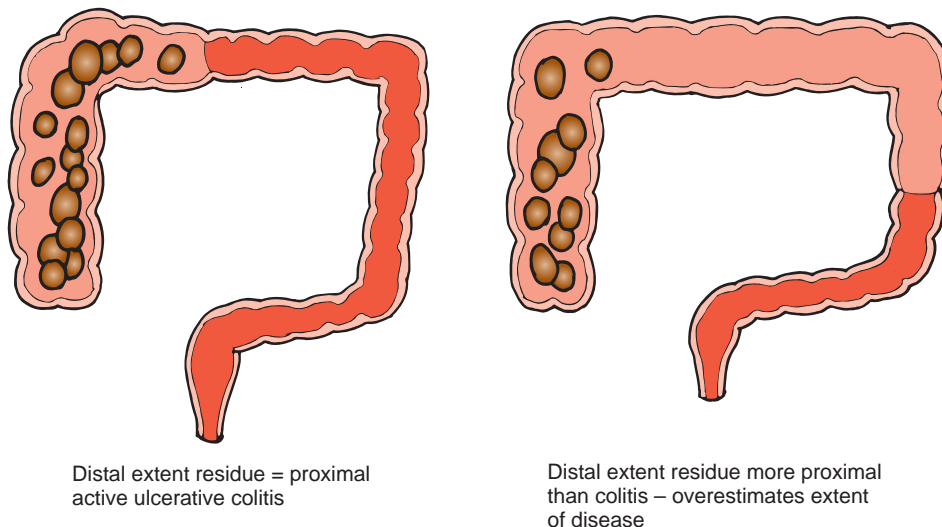


Figure 57-1 Ulcerative colitis: plain film estimation of active disease. The distal extent of fecal residue may overestimate but seldom underestimates the proximal extent of active disease. (From Bartram C, Kumar P: *Clinical Radiology in Gastroenterology*. Oxford, England, Blackwell Scientific, 1981, p 135.)

3. If residue is present only in the proximal colon, the colitis most likely extends to this level but could be more distal.

Mucosa. The colonic mucosal edge is normally smooth. In active colitis, the line is granular, indistinct, and somewhat fuzzy. With frank ulceration, the mucosal line is disrupted, which causes an irregular edge. With extensive ulceration, only edematous mucosal islands remain. Intramural, mottled-appearing gas shadows may be present in fulminating colitis with necrosis of the bowel wall. Linear pneumatosis suggests extremely deep ulceration or extraperitoneal perforation with gas trapped adjacent to the bowel wall.¹⁵⁻²³

Haustration. Normal haustral clefts run in parallel, about 2 to 4 mm apart, across one third of the diameter of the colon. Widening of the haustral clefts with loss of the parallel lines is an early manifestation of ulcerative colitis and is more obvious on radiographs than the mucosal granularity that it accompanies. The haustra may be completely absent as well. Blunting can be confused with underdistention, so it should not be diagnosed if only a small amount of gas is present within the colon.¹⁵⁻²³

Colon Diameter. The upper limit of normal for the diameter of the transverse colon is 5.5 cm. In chronic, “burned out” ulcerative colitis, the colon becomes tubular and narrowed and is considerably less than 5 cm in diameter. In these patients, if the colon is more than 5 cm in diameter, the inflammation has become transmural, which indicates a fulminant colitis at risk for perforation or toxic megacolon.¹⁵⁻²³

Mural Thickness. In the normal colon, the distance between the line of pericolic fat and gas-filled lumen is less than 3 mm. In chronic ulcerative colitis, it increases to more than 3 mm in thickness. In a study assessing these findings, a combination of four features was pathognomonic for disease proximal to the hepatic flexure: irregularity of the mucosal edge, loss of haustral clefts, increased thickness of the colon wall, and an empty right colon.¹⁹

Barium Enema

The barium enema has the following roles in patients with ulcerative colitis: (1) to confirm the clinical diagnosis; (2) to assess the extent and severity of disease; (3) to differentiate ulcerative colitis from Crohn’s disease and other colitides; (4) to follow the course of disease; and (5) to detect complications. The role of barium enema has largely been supplanted by colonoscopy, multidetector computed tomography (MDCT),

and magnetic resonance imaging (MRI) in patients with ulcerative colitis. The major radiographic findings on the barium enema examination in ulcerative colitis are presented in [Box 57-2](#); their anatomic and pathologic origin ([Fig. 57-2](#)) and significance are discussed subsequently.

Granular Pattern. The earliest pathologic changes of ulcerative colitis are hyperemia and the accumulation of inflammatory cells in the mucosa.^{24,25} These changes are manifested by a loss of normal mucosal translucency and obscuration of the submucosal pattern on endoscopy.^{26,27} Subtle thickening of the mucosa or haustral edema may be present radiographically, but these findings are often appreciated only in retrospect.²⁶ With progressive edema and hyperemia, the mucosa develops a granular pattern ([Fig. 57-3A](#)).²⁷⁻²⁹ The smooth, sharp, and distinct appearance of the colonic margin seen on normal double-contrast studies is replaced by an amorphous, thickened, and indistinct mucosal line. There is a gradual transition between the normal and abnormal mucosa that extends for several centimeters. This granularity should be distinguished from the granular appearance of chronic ulcerative colitis (see [Fig. 57-3B](#)). In chronic ulcerative colitis, the mucosal surface pattern is coarser, and there are significant changes in colonic contour.

The granular pattern develops as a result of abnormalities in the quality and quantity of mucus produced by the involved

BOX 57-2 ULCERATIVE COLITIS: BARIUM ENEMA FINDINGS

ACUTE CHANGES

- Mucosal granularity
- Mucosal stippling
- Collar button ulcers
- Haustral thickening or loss
- Inflammatory polyps
- Confluent, contiguous, circumferential disease

CHRONIC CHANGES

- Haustral loss
- Luminal narrowing
- Loss of rectal valves
- Widened presacral space
- Backwash ileitis
- Postinflammatory pseudopolyps

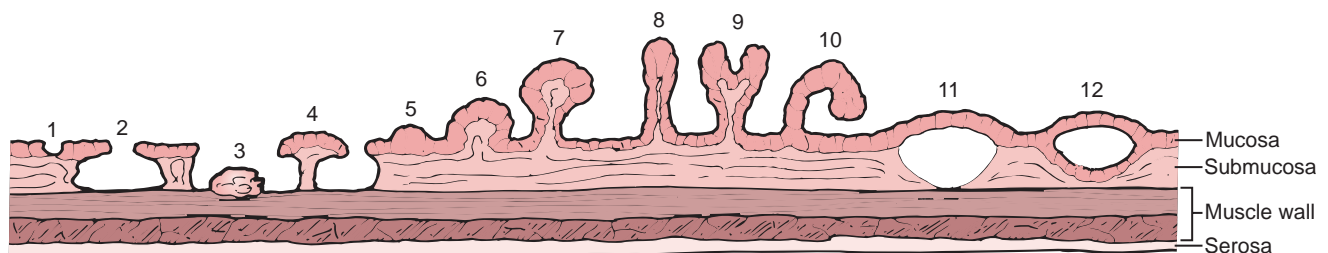


Figure 57-2 Spectrum of mucosal abnormalities in ulcerative colitis. 1, Punctate mucosal ulcer-crypt abscess; 2, collar button ulcer; 3, polypoid accumulation of granulation tissue; 4, mucosal remnant forming inflammatory pseudopolyp; 5 and 6, sessile mucosal polyps (similar morphologic features are seen in hyperplasia, adenoma, and carcinoma); 7, pedunculated polyp (typically hyperplastic or low-grade adenomas); 8, 9, and 10, postinflammatory pseudopolyps of various configurations; 11, mucosal remnant bridging area of active undermining ulceration; 12, mucosal bridge in quiescent state with previously denuded surfaces covered with new epithelium. (From Lichtenstein JE: Radiologic-pathologic correlation of inflammatory bowel disease. *Radiol Clin North Am* 25:324, 1987.)

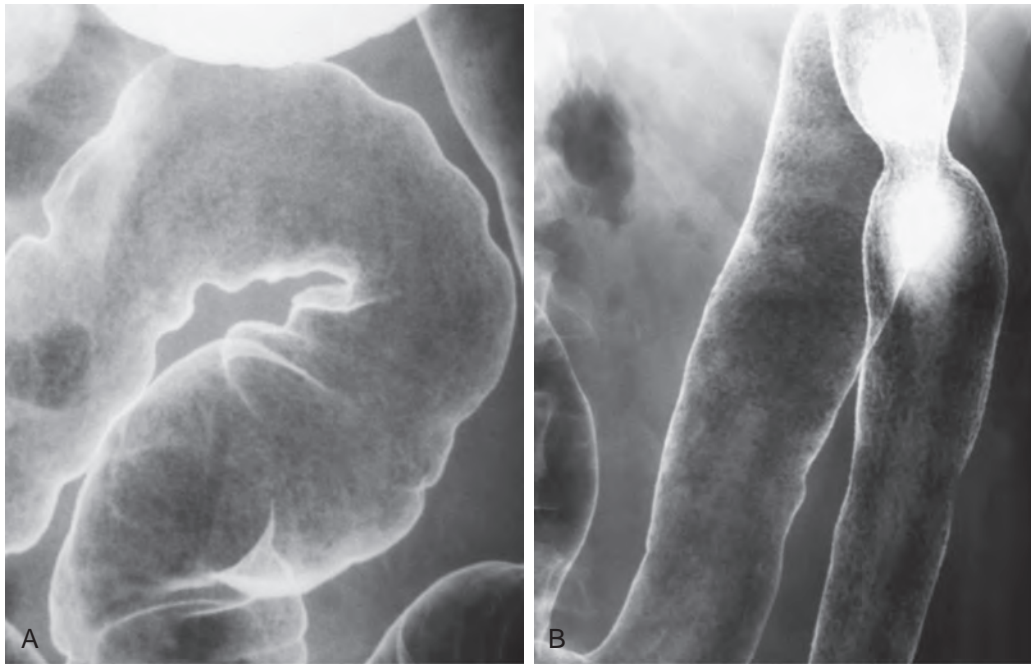


Figure 57-3 Ulcerative colitis: granular mucosal pattern. **A.** Early ulcerative colitis. The blunted haustral clefts are evident on this spot image of the sigmoid colon. The mucosal granularity, attributable to abnormal quantity and quality of mucin, is contiguous, circumferential, and symmetric. **B.** Chronic ulcerative colitis. This spot image of a short, tubular, ahaustral splenic flexure of the colon shows a coarser surface pattern than that seen in acute disease.

mucosa.²⁵ On histologic examination, there is a reduction in the number of goblet cells, which contain less than the normal complement of mucin.^{6,25,30,31} Normal mucus is essential to normal barium coating of the gut. Any process, whether benign or malignant, infectious or inflammatory, that alters mucin production affects mucosal coating and visualization.²⁵

Mucosal Stippling. During the granular phase of ulcerative colitis, inflammatory cells accumulate at the base of the mucosal crypts.^{25,31} Cellular debris tends to block the crypts of Lieberkühn, which leads to the formation of microabscesses, better known as crypt abscesses (Fig. 57-4A). These crypt abscesses eventually erode into the lumen.^{30,31} The ulcers deepen, and barium flecks become adherent to them, producing mucosal stippling (see Fig. 57-4B).²⁵ This stippling resembles white paint applied by dabbing a surface with the end of a fairly dry paintbrush.²⁷

“Collar Button” Ulcers. With disease progression, the ulcers of the crypt abscess breach the lamina propria and muscularis mucosae and cause undermining of the less resistant areolar tissue of the submucosa.³⁰ The involved submucosa becomes necrotic, and the ulcers extend laterally, causing further undermining. This undermining is contained by the muscularis propria on the serosal side and by the muscularis mucosae on the luminal side of the colon.^{32,33} The ulcers are frequently related to the taeniae. The mucosal defect is small relative to the degree of undermining and produces a flasklike, so-called collar button ulcer (Fig. 57-5).²⁵ As these ulcers enlarge and interconnect, the collar button ulcer configuration is lost; a network of residual islands of mucosa and inflammatory pseudopolyps is produced.

Polyps. A variety of different mucosal protrusions may be seen on barium studies in patients with IBD.²⁵ Their appearance and significance depend on the stage of disease and pathologic origin.

Inflammatory Pseudopolyps. In patients with severe ulcerative colitis, there is extensive mucosal and submucosal ulceration in which only small islands of mucosa and submucosa may survive. The inflamed edematous mucosa protrudes above the surrounding areas of ulceration, which gives a polypoid appearance (Fig. 57-6).³¹ Because these represent merely the remnants of preexisting mucosa and submucosa rather than new growths, they are termed *pseudopolyps*.³¹ Inflammatory pseudopolyps are the natural progression of collar button ulcers: the ulcers extend and interconnect so that the pseudopolyp rather than the ulcers becomes the major radiographic finding.³⁴⁻³⁸ Inflammatory pseudopolyps usually occur in ulcerative colitis but may also be seen in Crohn’s disease. The cobblestoning pattern seen in Crohn’s disease is another type of pseudopolyp, in which larger islands of preserved mucosa are surrounded by linear and transverse ulcerations.²⁵

Postinflammatory Pseudopolyps. When IBD goes into remission, the denuded mucosa heals and is covered by granulation tissue that has a granular appearance similar to that observed in the early stages of ulcerative colitis.^{6,31,36-38} In some patients, the regenerated mucosa has a tendency to overgrow (Fig. 57-7). This overgrowth often results in polypoid lesions that may be small and rounded, long and filiform, or proliferate into a bushlike structure simulating a villous adenoma. Because the regenerating mucosa is cytologically normal, it is not a true neoplasm but a pseudopolyp. Because this occurs during mucosal healing, it is termed a *postinflammatory pseudopolyp*.³⁴⁻³⁸ These polyps represent the aftermath of a severe attack of colitis

Figure 57-4 Ulcerative colitis: crypt abscess causing mucosal stippling. **A.** A crypt abscess (arrow) is seen at the base of a crypt of Lieberkühn. **B.** When these abscesses erode into the lumen, they accumulate punctate collections of barium, which produces mucosal stippling.

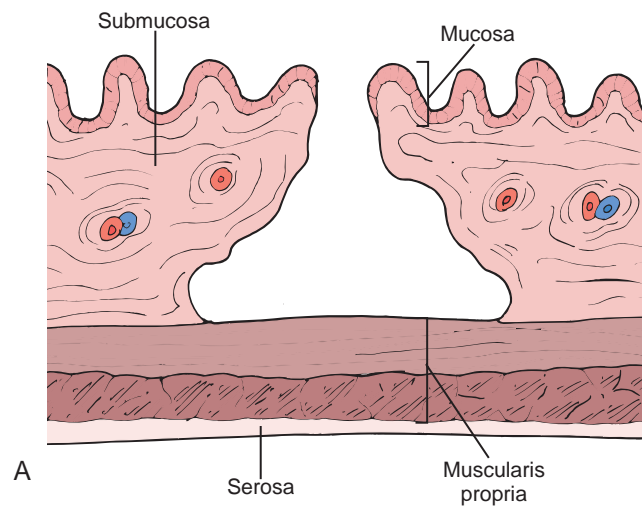
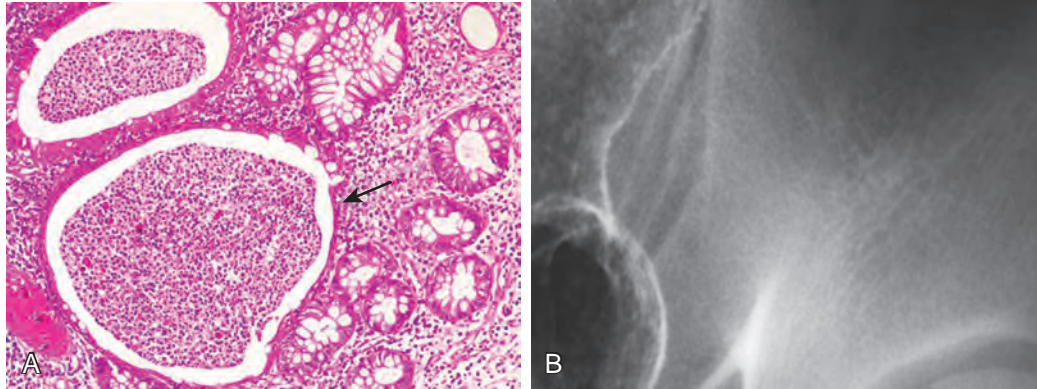
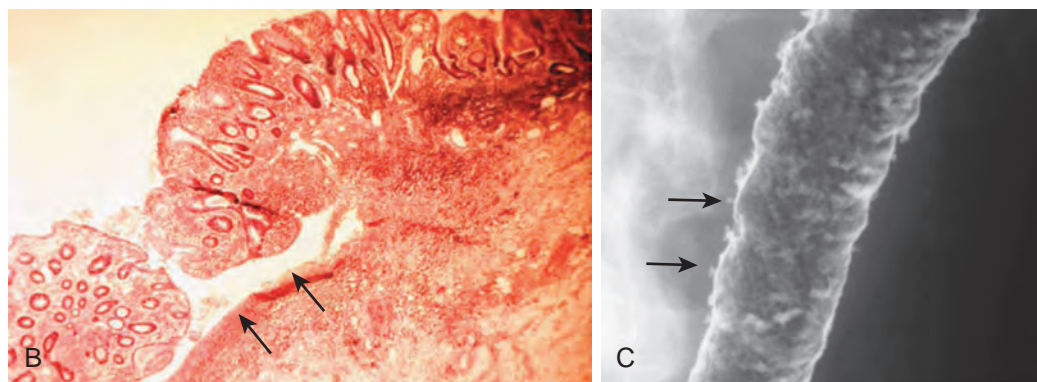


Figure 57-5 Ulcerative colitis: collar button ulcers. **A.** Narrow neck of the crypt abscess erodes through the muscularis mucosae into the submucosa. The ulcer spreads laterally through the submucosa and is contained with a flat base by the resistant inner circular layer of the muscularis propria. **B.** Low-power photomicrograph shows characteristic undermining with a flat base (arrows). **C.** Spot film of the splenic flexure shows multiple flasklike ulcers (arrows) with a flat base. The ulceration is limited to the layers superficial to the muscularis propria. (A from Lichtenstein JE: Radiologic-pathologic correlation of inflammatory bowel disease. *Radiol Clin North Am* 25:324, 1987.)



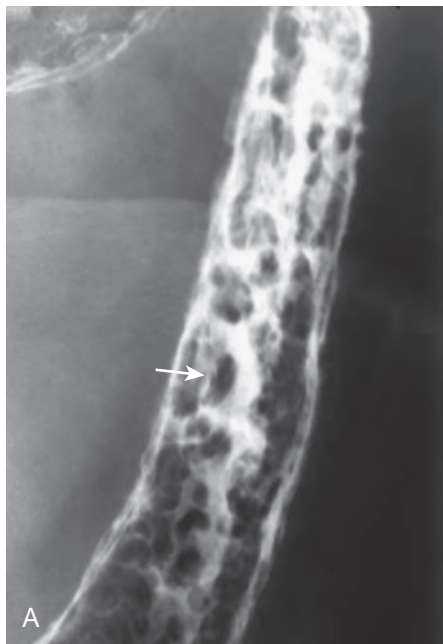
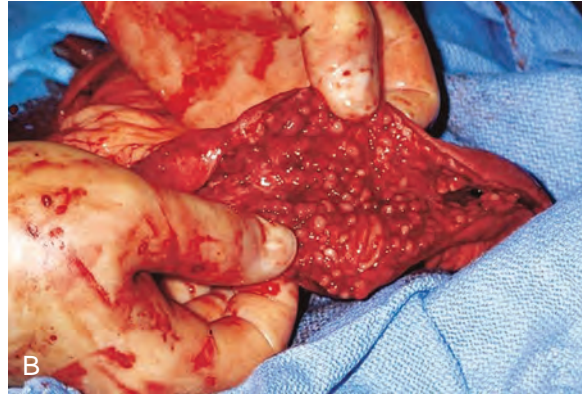


Figure 57-6 Ulcerative colitis: inflammatory pseudopolyps. **A.** Inflammatory pseudopolyps (arrow) are identified on a double-contrast barium enema study. These pseudopolyps are seen when extensive mucosal and submucosal ulcerations leave only small residual islands of surviving mucosa and submucosa. Thus, they represent remnants of preexisting mucosa and submucosa rather than new growths. **B.** Intraoperative image of a diseased colon showing multiple residual islands of whitish mucosa surrounded by hemorrhagic ulcerations.



and may be the only sign of previous disease. Mucosal bridges are also postinflammatory pseudopolyps, in which a bridge of mucosa survives between islands of mucosa surrounded by ulceration. With remission, the underside of the mucosal bridge and underlying ulcer re-epithelialize.^{39,40}

Postinflammatory pseudopolyps can also be seen after ischemia, after severe infection, and in Crohn's disease. Filiform polyps have also been described in the esophagus, stomach, and small bowel in patients with Crohn's disease.²⁵

Backwash Ileitis. In 10% to 40% of patients with chronic ulcerative pancolitis, the distal 5 to 25 cm of ileum is inflamed (Fig. 57-8). This ileitis occurs only in the presence of pancolitis and usually resolves 1 to 2 weeks after colectomy.^{15,26} Although small ulcerations may be present, this is not a primary inflammation of the ileum. The distal ileum can be used to form an ileostomy or pouch. The pathogenesis of this disorder is uncertain but may relate to the reflux of colonic contents into the small bowel, hence the term *reflux* or *backwash ileitis*.¹⁵

Barium studies reveal a chronic pancolitis associated with a patulous and fixed ileocecal valve that easily refluxes and persistent dilation of the terminal ileum. The normal fold pattern is absent, and the mucosa is granular.

Blunting and Lost Haustra. In the course of ulcerative colitis, the haustral folds undergo two major changes (Fig. 57-9; see also Fig. 57-8): (1) early in the disease, they are edematous and thickened; (2) with chronic disease, they become blunted or may be completely lost.¹⁵ This evolution of haustral changes can be understood by a brief review of haustral formation.

At birth, colonic haustra are usually absent, which explains why it is difficult to differentiate colonic from small bowel gas in neonates. As the colon grows, the circular muscle of the muscularis propria outgrows the longitudinal muscle, the taenia coli. This differential growth rate causes the taeniae to shorten the colon in an accordion-like fashion, with production of saccular haustra that usually are first seen by the age of 3 years.⁴¹

Haustra are fixed anatomic landmarks in the proximal colon because the circular muscle is fused to the taeniae. In the distal colon, haustra are created by active contraction of the taeniae. Consequently, the colon can normally be devoid of haustra distal to the midtransverse colon; loss of haustra in the proximal colon is always abnormal.^{41,42}

In early ulcerative colitis, the haustra are deformed and thickened because of edema and may produce a corrugate outline to the colon, which has been called the indenture sign.⁴³ In chronic ulcerative colitis, the haustra are often lost for two reasons, alterations in the muscle tone of the taeniae^{41,42} and the fact that the colon is shortened. In this disease, the taeniae coli become relaxed for some unknown reason. This relaxation is associated with abolition of the haustral pattern. With healing, the haustra may reappear as they gain tone. A second major factor is also at work in chronic ulcerative colitis—massive hypertrophy and fixed contraction of the muscularis mucosae (Fig. 57-10), which causes foreshortening of the colon. Thus, the normal accordion-like array of colon on the relatively shorter taeniae is lost.⁴²⁻⁴⁵

Widened Presacral Space. When the rectum is distended, the retrorectal space as projected on true lateral films obtained during barium enema is usually 7.5 mm or less.⁴⁶ A distance of 1 to 1.5 cm is considered a moderate increase of this space, and a distance greater than 1.5 cm is abnormal. These values are obtained by measuring the shortest distance between the posterior edge of the barium column and the anterior edge of the second sacral segment. The presacral space is frequently widened in chronic ulcerative colitis and Crohn's disease but may also be seen in obese patients and patients with pelvic lipomatosis, pelvic carcinomatosis, radiation fibrosis, inferior vena cava thrombosis, sacral and rectal tumors, chlamydial infection, and other infectious proctitides.⁴⁷⁻⁴⁹

In patients with ulcerative colitis, two processes account for the abnormal presacral space (see Fig. 57-10): (1) narrowing of the rectal lumen and its associated mural thickening; and (2) proliferation, inflammation, and infiltration of perirectal

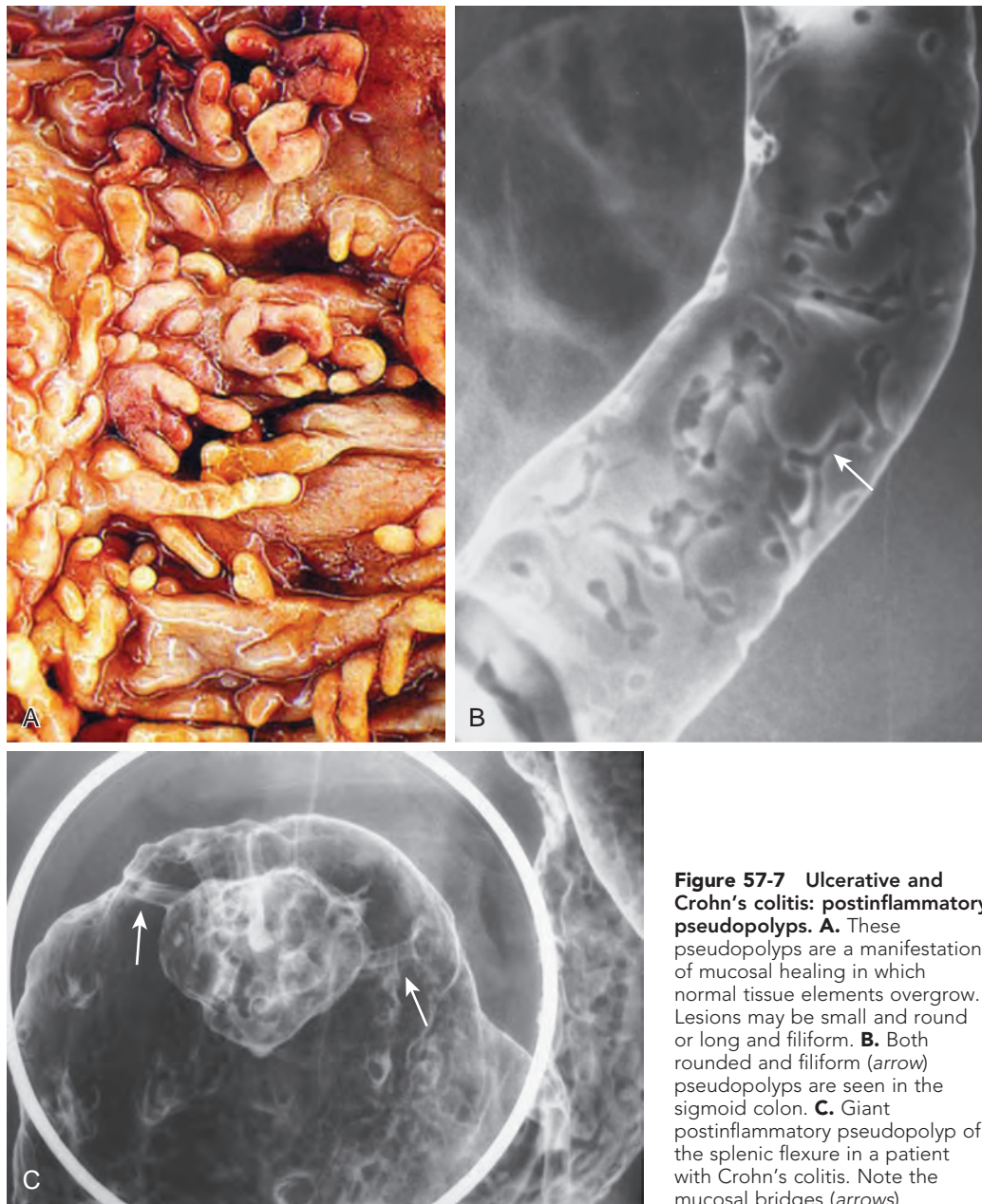


Figure 57-7 Ulcerative and Crohn's colitis: postinflammatory pseudopolyps. **A.** These pseudopolyps are a manifestation of mucosal healing in which normal tissue elements overgrow. Lesions may be small and round or long and filiform. **B.** Both rounded and filiform pseudopolyps are seen in the sigmoid colon. **C.** Giant postinflammatory pseudopolyp of the splenic flexure in a patient with Crohn's colitis. Note the mucosal bridges (arrows).

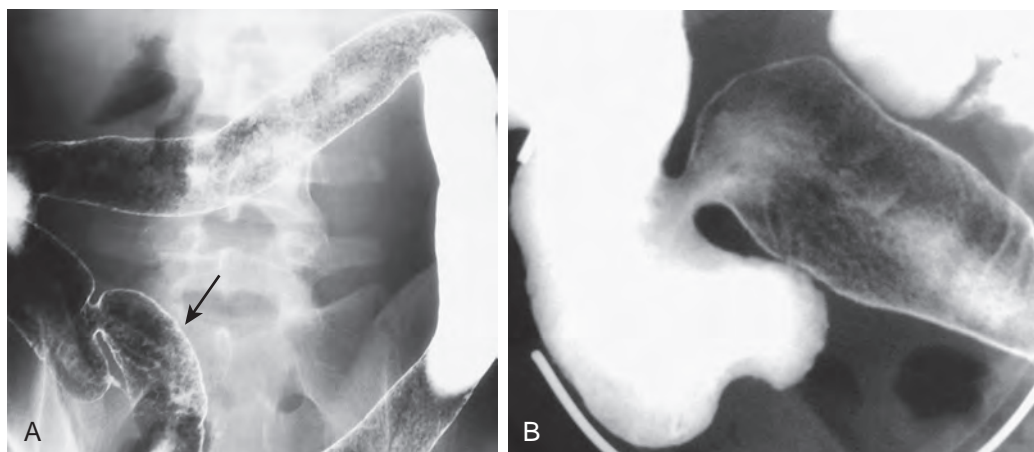


Figure 57-8 Ulcerative colitis: backwash ileitis. **A.** Backwash ileitis (arrow) is demonstrated in this patient with chronic ulcerative pancolitis. **B.** In a different patient, note the patulous ileocecal valve, the dilated, granular-appearing terminal ileum, and the tubular, anastomotic colon.



Figure 57-9 Acute ulcerative colitis: loss of haustra. Haustra distal to the hepatic flexure are absent, and the taeniae coli are relaxed. The mucosa is granular in appearance. The colon is not shortened at this point because thickening and contraction of the muscularis mucosae have not yet developed at this early stage of disease.

fat. These changes are well demonstrated by CT and correlate with the edematous adipose tissue and enlarged perirectal lymph nodes that are commonly observed at the time of abdominoperineal resection in patients with ulcerative colitis. In patients with Crohn's disease, perirectal abscesses may also contribute to this widening.⁵⁰

Rectal Valve Abnormalities. At least one rectal valve should be visible on lateral rectal views of double-contrast enemas. The fold is usually seen at the level of S3 and S4 and should be less than 5 mm thick. The rectal valves are an important indicator of proctitis and should be interpreted with the size of the presacral space. Two situations are indicative of proctitis:

1. The presacral space is more than 1.5 cm, with the valve thicker than 6.5 mm or absent.
2. The presacral space is normal, but the valve thickness is more than 6.5 mm.

Absence of the rectal valves in the presence of a normal presacral space can be a normal variant.¹⁵

Strictures. Benign strictures are local sequelae of ulcerative colitis that occur in approximately 10% of patients.¹⁵ They are usually localized and smoothly tapering and are only rarely sufficiently narrow to cause obstruction. They are sometimes reversible and are usually found in the distal colon. Strictures that are not reversible and are located more proximally in the colon should be viewed with suspicion for a neoplasm. The strictures have been attributed to the changes of the muscularis

mucosae described earlier and are almost invariably associated with mural thickening on cross-sectional imaging.⁵¹⁻⁵⁵

Distribution. Ulcerative colitis originates in the rectum and extends proximally in a continuous fashion. There is often a fairly sharply defined margin between diseased and normal bowel. The affected mucosa is diffusely, contiguously, confluent, circumferentially, and symmetrically involved, without normal intervening mucosa. The rectum is almost invariably involved but may be spared in patients treated with corticosteroid enemas.

Computed Tomography

The subtle mucosal abnormalities that characterize the early stages of ulcerative colitis are beneath the spatial resolution of CT. With progressive disease, severe mucosal ulceration can denude certain portions of the colonic wall, leading to inflammatory pseudopolyps (Fig. 57-11).⁵⁶ When sufficiently large, these pseudopolyps can be visualized on CT. Mural thinning, unsuspected perforations, and pneumatosis can be detected on CT in patients with toxic megacolon.⁵⁷ In this regard, CT can be quite helpful in determining the urgency of surgery in patients with stable abdominal radiographs but a deteriorating clinical course. Postinflammatory pseudopolyps can also be seen on CT.

Mural thickening and luminal narrowing are common CT features of subacute and chronic ulcerative colitis (Fig. 57-12; Box 57-3). The mucosa becomes thickened because of hypertrophy of the muscularis mucosae in chronic ulcerative colitis. Also, the lamina propria is thickened because of round cell infiltration in acute and chronic ulcerative colitis. The submucosa becomes thickened because of the deposition of fat or, in acute and subacute cases, edema. Submucosal thickening further contributes to luminal narrowing.⁵⁸⁻⁶²

On CT, these mural changes produce a target or halo appearance when axially imaged. The lumen is surrounded by a ring of soft tissue density (mucosa, lamina propria, hypertrophied muscularis mucosae), surrounded by a low-density ring (edema or fatty infiltration of the submucosa), which in turn is surrounded by a ring of soft tissue density (muscularis propria).⁵⁸⁻⁶⁴ This mural stratification is not specific and can also be seen in patients with Crohn's disease, infectious enterocolitis, pseudomembranous colitis, ischemic and radiation enterocolitis, mesenteric venous thrombosis, bowel edema, and graft-versus-host disease.⁵⁸⁻⁶⁴

Rectal narrowing and widening of the presacral space are radiologic hallmarks of chronic ulcerative colitis.⁶⁵⁻⁶⁸ MDCT depicts the anatomic alterations that underlie these rather dramatic morphologic changes (see Fig. 57-10). The rectal lumen is narrowed because of the mural thickening that attends chronic ulcerative colitis (see earlier). As a result, the rectum has a target appearance on axial scans, which should not be mistaken for the external anal sphincter, mucosal prolapse, or levator ani muscles. The increase in the presacral space is caused by proliferation of the perirectal fat.

Ultrasonography

IBD alters the thickness and echogenicity of the gut wall or individual layers, integrity of mural stratification, appearance of surrounding tissues, and bowel motility and compressibility (Box 57-4).⁶⁹⁻⁷⁴ Edema is a prominent feature of acute intestinal inflammation. Edema results in thickening of the colon wall and preservation of wall stratification (Fig. 57-13). On

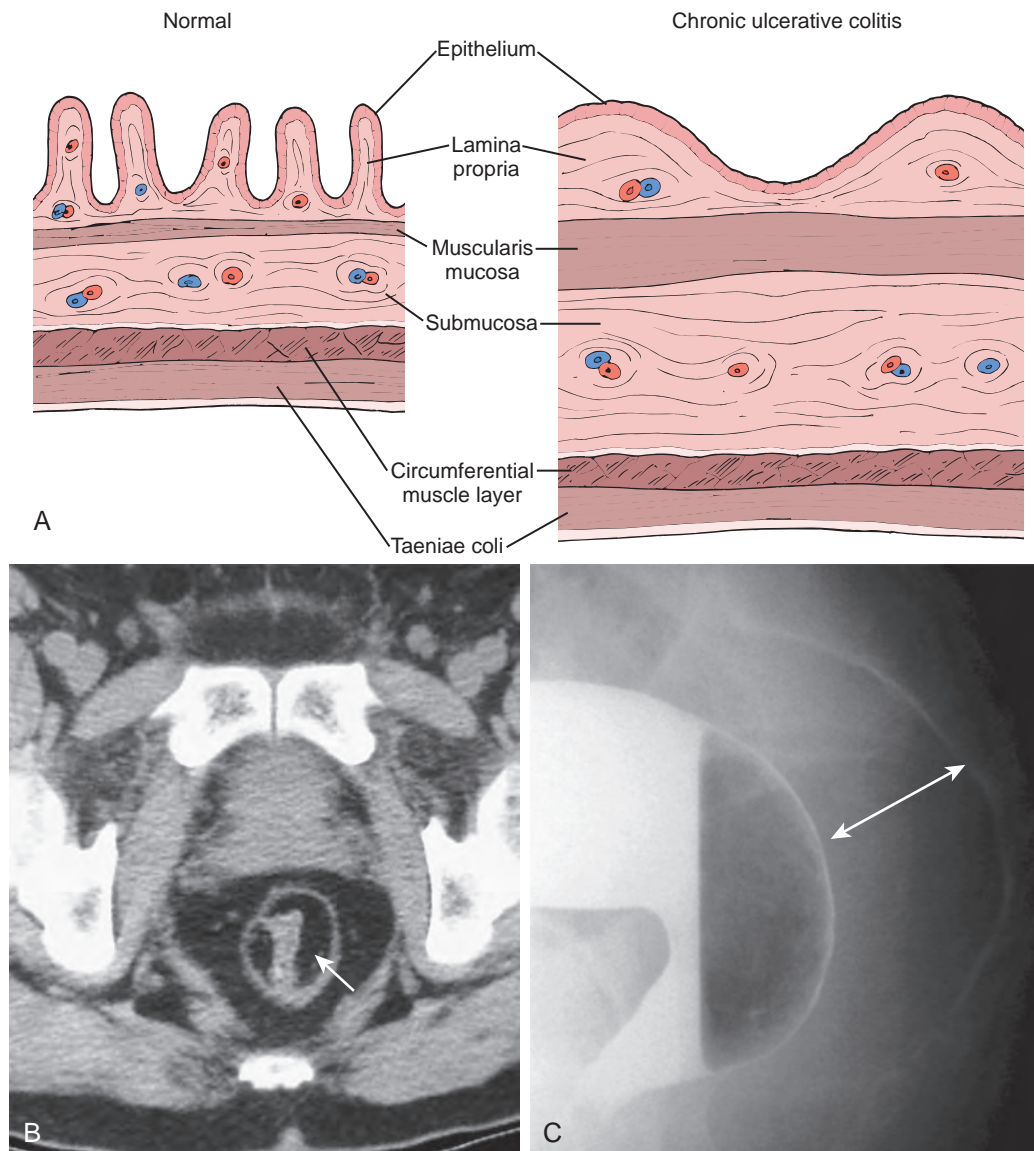


Figure 57-10 Cause of rectal contour changes in chronic ulcerative colitis. **A.** Marked hypertrophy of the muscularis mucosae. This muscle, oriented along the long axis of the colon, is chronically contracted, even after the IV administration of glucagon and in formalin-impregnated specimens. This contraction shortens and narrows the involved colon. The submucosa also widens and shows various degrees of fatty infiltration, further narrowing the lumen. The taeniae coli are relaxed, which abolishes the haustral folds. **B.** Pelvic CT scan shows a characteristic target or ring sign with a thickened, low-density submucosa (arrow) caused by fatty infiltration. The soft tissue density ring on the lumen side of the submucosa represents thickened lamina propria and muscularis mucosae; the ring on the serosal side is muscularis propria. **C.** Corresponding lateral view from an air-contrast barium enema. The mucosa has a granular appearance, the lumen is narrowed, the valves of Houston are absent, and there is significant widening of the presacral space (double arrow). (A from Gore RM: Colonic contour changes in chronic ulcerative colitis: Reappraisal of some old concepts. *AJR* 158:59–61, 1992.)

transverse section, alternate hyperechoic and hypoechoic layers give rise to a target appearance. In ulcerative colitis, the mucosa becomes thickened and hypoechoic as a result of edema.^{73,74} The submucosa also thickens, but colonic motility is maintained. With progressive disease, haustral septations are lost. In patients with well-established disease, bowel wall thickness is approximately 0.6 ± 0.2 cm.⁶²⁻⁶⁷ In one series, these changes were seen in all patients with pancolitis, in 94% of those with left-sided colitis, but in only 50% of patients with rectosigmoiditis. If there is extensive pseudopolypoidosis, the thickness of the wall may increase to 1.5 cm, which is often accompanied by loss of wall stratification.⁶⁸⁻⁷⁴

Magnetic Resonance Imaging

Magnetic resonance imaging is capable of identifying the mural stratification present in ulcerative colitis (Figs. 57-14 and 57-15). MRI demonstrates thickening and abnormal hypointensity of the mucosal and submucosal layers on T1- and T2-weighted images. The T1 shortening probably relates to the severe hemorrhagic phenomena that frequently appear in these layers. The degree of mural enhancement correlates well with the severity of disease activity on fat-suppressed gradient-echo images after the intravenous (IV) administration of gadolinium.⁷⁵⁻⁷⁹

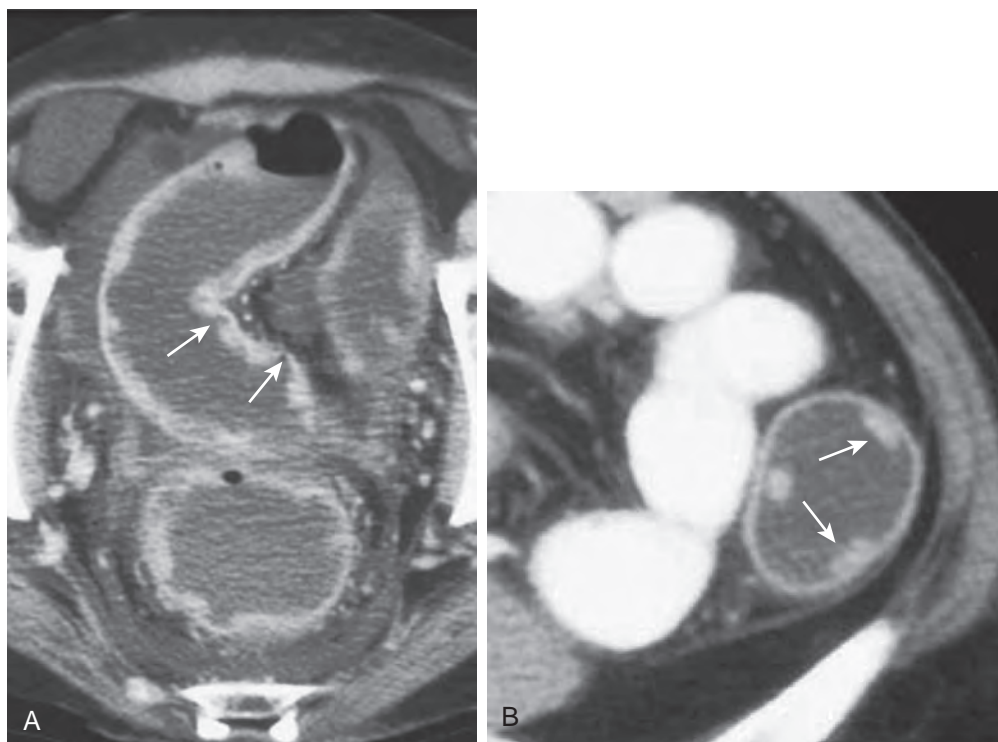


Figure 57-11 Mucosal disease in acute ulcerative colitis: CT features. **A.** Pelvic CT reveals diffuse mucosal thickening of fluid-filled rectum and sigmoid. Deep ulcerations (arrows) are visualized. Note normal lumen caliber and ascites. **B.** Magnified CT image of distal descending colon shows residual islands of inflamed mucosa protruding above the denuded colonic surface, so-called inflammatory pseudopolyps (arrows). (From Gore RM, Balthazar E, Ghahremani GG, et al: CT features of ulcerative colitis and Crohn's disease. *AJR* 167:3–15, 1996.)



Figure 57-12 Subacute ulcerative colitis: CT features. Coronal reformatted image through the rectosigmoid reveals diffusely inflamed and thickened mucosa (arrow). The edematous submucosal layer of low attenuation is paralleled by the external layer of muscularis propria and the internal layer of submucosa, both of which have a higher attenuation.

BOX 57-3 ULCERATIVE COLITIS VERSUS CROHN'S DISEASE: COMPUTED TOMOGRAPHY FINDINGS

ULCERATIVE COLITIS

- Mural thickening <1.5 cm
- Target appearance of wall—submucosal edema (acute)
- Target appearance of wall—submucosal fat (chronic)
- Increased perirectal and presacral fat

CROHN'S DISEASE

- Mural thickening >2 cm
- Target appearance of wall—submucosal edema (acute)
- Target appearance of wall—submucosal fat (chronic)
- Homogeneous CT density of wall
- Mural thickening of small bowel
- Abscesses, fistulas, sinus tracts
- Mesenteric changes (abscess, phlegmon, fibrofatty proliferation)
- Perianal disease

COMMON FINDINGS

- Mural thickening
- Narrowed lumen
- Increased lymph node size and number

BOX 57-4 ULCERATIVE COLITIS VERSUS CROHN'S COLITIS: SONOGRAPHIC FINDINGS**ULCERATIVE COLITIS**

Moderately thick, hypoechoic wall
 Typical wall stratification maintained
 Loss of haustration
 Absent peristaltic motion

CROHN'S COLITIS

Clearly thickened, hypoechoic wall
 Loss of typical wall stratification
 Loss of haustration
 Diminished compressibility
 Absent peristaltic motion
 Increased blood flow of superior mesenteric artery with decreased resistive index

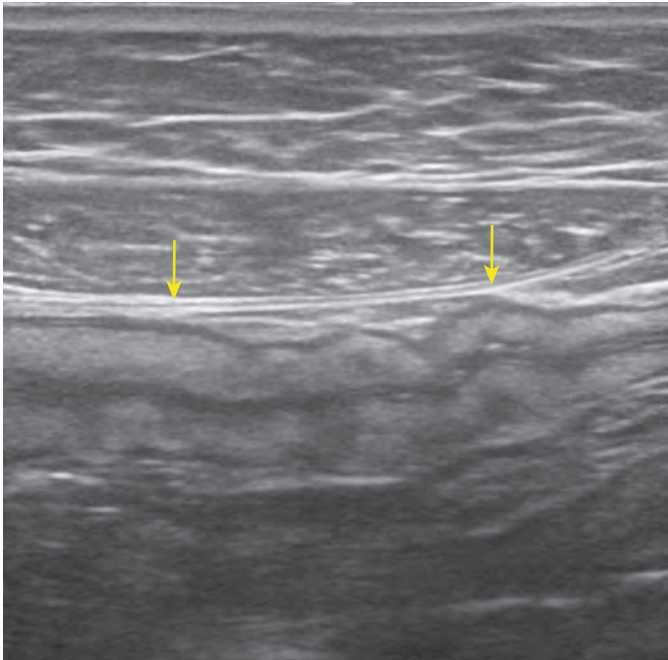


Figure 57-13 Chronic ulcerative colitis: sonographic findings. The descending colon, imaged longitudinally, shows circumferential mural thickening (arrows).

Scintigraphy

Although the diagnosis and assessment of disease activity of ulcerative colitis are made primarily by radiographic and endoscopic techniques, both gallium 67 (^{67}Ga) citrate and indium 111 (^{111}In)-labeled leukocyte scans have proved helpful for patients with IBD. Scintigraphic techniques are useful when there is danger of bowel perforation and the extent and degree of disease activity must be assessed. Positron emission tomography (PET) using ^{18}F -fluorodeoxyglucose (FDG) can also be used to assess disease activity. FDG uptake (Fig. 57-16)

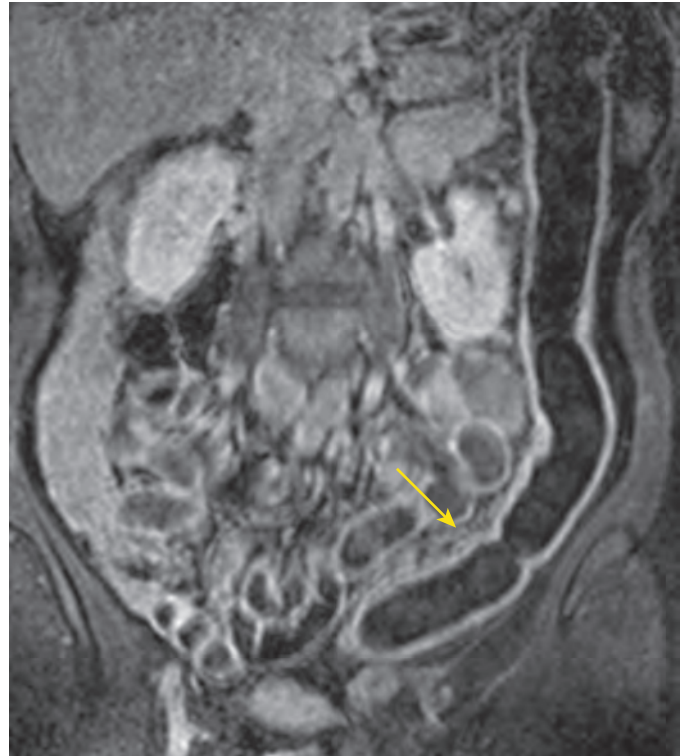


Figure 57-15 Ulcerative colitis: MR features. T1-weighted MR coronal image shows loss of haustration and hyperenhancement of mucosa of the left colon (arrow) in this patient with active ulcerative colitis. (Courtesy Shahid M. Hussain, MD.)

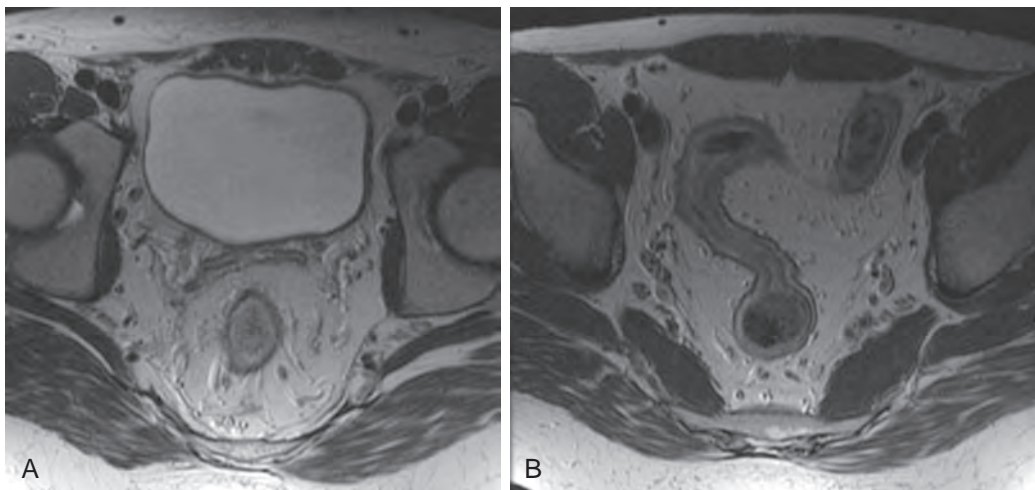


Figure 57-14 Ulcerative colitis: MR findings. T1-weighted axial MR images of the rectum (A) and rectosigmoid junction (B) show mural thickening of the colon, submucosal fat deposition, increased presacral fat, and prominent vessels in the mesorectal fat.

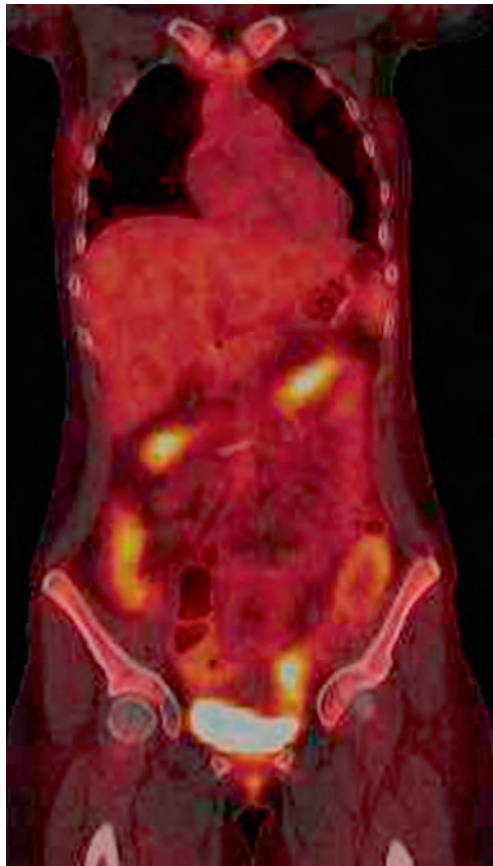


Figure 57-16 Ulcerative colitis: positron emission tomography scanning features. Diffuse increased FDG uptake in the colon is present in this patient with acute, active disease.

is increased in areas of active inflammation resulting from hyperemia and increased metabolic activity.⁸⁰⁻⁸⁴

THERAPY

Medical Management

The treatment of ulcerative colitis depends on the severity, extent, and distribution of disease. Sulfasalazine, a congener of 5-aminosalicylic acid and sulfapyridine, is effective in the treatment of acute ulcerative colitis and in reducing the frequency and severity of recurrent attacks.⁸⁵ Sulfasalazine attenuates the bowel inflammation by a number of actions: (1) reduces production of prostaglandins; (2) diminishes leukotriene production, which activates neutrophils and other constituents of the inflammatory response; (3) blocks the chemotactic activity of formulated bacterial peptides that help recruit neutrophils to the bowel; and (4) acts as a scavenger of oxygen free radicals.⁸⁵ Many patients develop hypersensitivity or less specific forms of intolerance; efforts are now being made to deliver the active component, 5-aminosalicylic acid, without the sulfapyridine moiety, which apparently causes the hypersensitivity.⁸⁵

Corticosteroids are effective in patients with moderate to severe ulcerative colitis. They do not affect the rate or timing of disease recurrence in patients in remission. Topical hydrocortisone in the form of a foam enema is the mainstay of therapy for distal proctocolitis.⁸⁵

Azathioprine, 6-mercaptopurine, chloroquine, hydroxychloroquine sulfate (Plaquenil), methotrexate, and cyclosporine are alternative therapies in patients with refractory disease. Bowel

rest and nutritional therapy also have beneficial effects on this disease.⁸⁵

Increased concentrations of leukotrienes in the inflamed mucosa in ulcerative colitis have suggested the use of inhibitors of leukotriene B₄ (LTB₄) for therapy because this is a highly potent mediator of inflammation. LTB₄ receptor antagonists are under investigation as are inhibitors of platelet-activating factor and mast cell stabilizers.⁸⁵⁻⁸⁷

Anti-tumor necrosis factor (TNF) agents such as Remicade and Humira suppress part of the inflammatory response of IBD. Although used more commonly in patients with Crohn's disease, these agents have been found useful for patients with ulcerative colitis.

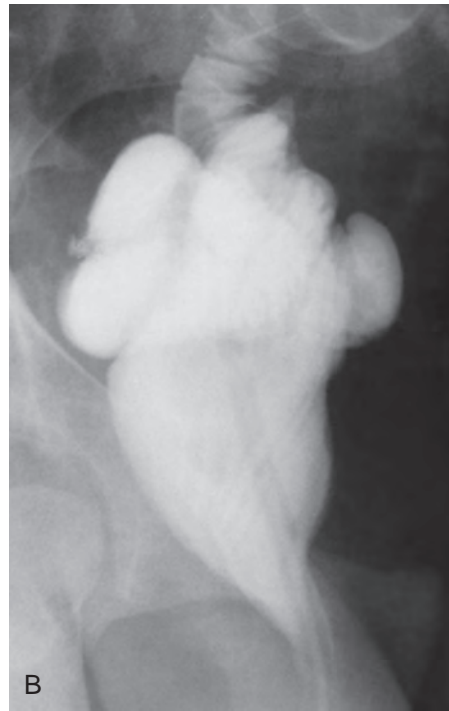
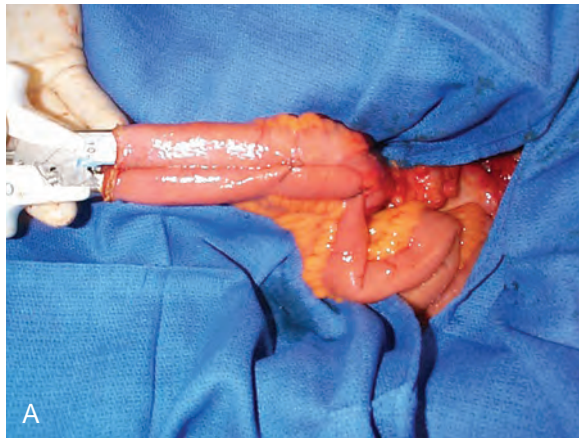
Surgery

Although proctocolectomy is always curative for ulcerative colitis, this procedure carries an operative risk, and not all patients are willing to accept an ileostomy. Consequently, colectomy is not indicated for patients who are easily managed medically. There are several major indications for surgery in ulcerative colitis: (1) massive, unremitting colonic hemorrhage; (2) toxic megacolon with impending or frank perforation; (3) fulminant colitis that is unresponsive to antibiotic, supportive immunosuppressive therapy; (4) obstruction from a stricture; and (5) suspicion or demonstration of colon cancer. Less immediate and definite indications for colectomy are (1) intractable chronic disease that becomes a physical and social burden to the patient and is unresponsive to appropriate therapy, (2) failure of children to mature at an acceptable rate, and (3) high-grade dysplasia in a patient with pancolitis.⁸⁸ Fulminant acute disease accounts for 13% to 25% of colectomies in patients with ulcerative colitis. Many of the extraintestinal complications of ulcerative colitis, such as uveitis and pyoderma gangrenosum, are also eliminated by colectomy. However, the course of hepatobiliary disease and ankylosing spondylitis is usually not altered by surgery.⁸⁸⁻⁹⁰ Since the 1980s, tremendous advances have been made in the surgical approach to ulcerative colitis that offer the patient and surgeon a variety of options.

Proctocolectomy with a Brooke Ileostomy. After a proctocolectomy is performed, the end of the ileum is passed through an opening in the middle aspect of the right rectus muscle at a point beneath the umbilicus that allows convenient placement of the forepiece of an ileostomy bag. This procedure is curative and requires one operation, but the patient must constantly wear an external ileostomy appliance that needs to be emptied four to eight times per day. Perineal wound problems, stoma revision, and small bowel obstruction occur in 10% to 25% of patients. This is the fastest and safest operation, but it dramatically alters body image in many patients, particularly younger ones.⁸⁸⁻⁹⁰

Proctocolectomy with Continent Ileostomy (Kock Pouch). A continent ileostomy is made by creating a pouch out of terminal ileum to hold the intestinal contents, an ileal conduit that leads from the pouch to the stoma, and an intervening intestinal valve. Patients empty the pouch by passing a tube through the valve via the stoma. The ileostomy is continent, so an external appliance is not needed. The nipple valve is created by intussuscepting the terminal ileum in a retrograde manner into the pouch for 3 to 4 cm. Anatomic complications requiring reoperation develop in 40% to 50% of these patients.⁹¹⁻⁹⁵

Figure 57-17 Surgical management of ulcerative colitis ileal pouch-anal anastomosis. **A.** The two-loop ileal J pouch shown in the intraoperative image is simple to construct, provides adequate storage capacity, and is evacuated spontaneously and fully. **B.** Barium enema evaluation of such a pouch.



Total Colectomy with Ileorectal Anastomosis. Total colectomy with ileorectal anastomosis is no longer popular because of a fairly high complication rate and unpredictable functional result.⁹¹⁻⁹⁵

Total Proctocolectomy, Rectal Mucosal Stripping, and Ileal Pouch Formation with Anastomosis to the Sphincter. This is the preferred operation in most patients. An abdominal colectomy and mucosal proctectomy are performed. A J pouch or W-shaped pouch is fashioned out of ileum. This reservoir is then anastomosed to the anus (Fig. 57-17). The endorectal ileal pouch and anal anastomosis are given 8 weeks to heal by diverting the gut through a conventional ileostomy.⁹⁰⁻⁹⁵ The advantages of this procedure are that no stoma is required and that fecal continence is usually maintained, albeit with bowel movements four to eight times per day.

This procedure is technically demanding and requires two operations. Complications include postoperative abscess, pouch fistulas, stenosis, small bowel obstruction, and pouchitis. Approximately 15% of patients require reoperation, and some ultimately require a conventional ileostomy. Pouchitis is an inflammatory process that can cause tenesmus, bloody diarrhea, and constitutional symptoms similar to those of ulcerative colitis.⁹⁵⁻¹⁰⁰

PROGNOSIS

The prognosis in ulcerative colitis has improved dramatically. Most patients have mild to moderate disease, and only 15% to 25% require a colectomy. Mortality associated with ulcerative colitis occurs in the first 2 years of disease, primarily in patients older than 40 years—one third attributable to the colonic disease itself, one third caused by complications of the disease (colorectal cancer, sclerosing cholangitis, thromboembolic disease, medical and surgical therapy), and the remaining third attributable to unrelated causes. Excess mortality of 2.1% for men and 1.5% for women has been reported, but only for the

first 2 years of disease.¹⁰ Most patients with ulcerative colitis can cope with their disease and achieve what is subjectively interpreted as a relatively acceptable lifestyle.¹⁰

Crohn's Disease

Crohn's disease is a chronic, cicatrizing disorder of the alimentary tract characterized by granulomatous inflammation of the mucosa, bowel wall, and surrounding mesentery. Any portion of the alimentary tract may be involved, but the terminal ileum and proximal colon are most frequently diseased.^{2,4,6}

HISTORICAL PERSPECTIVE

It is difficult to decide who described the first case of "regional ileitis" or "ileocolitis."¹ In 1806, Combe and Saunders described "a singular case of stricture and thickening of the ileum." Although similar cases were reported in the 19th century and early years of the 20th century, the first series of satisfactorily documented cases of regional enteritis was described by Crohn, Ginzburg, and Oppenheimer in 1932 at Mount Sinai Hospital in New York.^{2,4,6} Crohn's disease was originally called *terminal ileitis* because these cases were located mainly in the distal ileum in young persons. The outstanding complaints of the patients were diarrhea and weight loss, with progressive anemia and fever. Pathologic examination showed a thickened intestinal wall with subacute or chronic necrotizing inflammation and a greatly enlarged mesentery. Small linear ulcerations with distorted and broken mucosal folds and a cobblestone appearance were noted. The ulceration of the mucosa was accompanied by a disproportionate connective tissue reaction in the bowel wall, leading to stenosis and multiple fistulas. The lumen was "irregularly encroached" with dilation of proximal areas of the bowel.^{2,4,6,101,102} Many years later, it was realized that Crohn's disease might be confined to the colon without affecting the ileum; it is now recognized that Crohn's disease can involve every portion of the gut, from the mouth to the anus.^{2,4,6}

PATHOGENESIS AND CAUSATIVE FACTORS

The cause of Crohn's disease remains unknown. Although the participation of genetic, environmental, infectious, immunologic, and psychologic factors in the pathogenesis is well established, none of these mechanisms has proved to be the primary causative agent.¹⁰² Genetic vulnerability is likely to facilitate the occurrence of the disease, whereas the other factors may play a supportive and superimposed role. A further complicating factor in establishing a cause is the fact that in practice, Crohn's disease does not behave as a single disorder.^{6,11}

More recently, interest has centered on immunologic mechanisms, in particular the role of platelet-activating factor. Platelet-activating factor is a form of phosphatidylcholine that causes inflammation that is detectable in colonic mucosa in IBD but is not present in normal colonic mucosa. Production of platelet-activating factor is stimulated by a number of inflammatory mediators, such as prostaglandin and leukotrienes. In vitro studies have demonstrated that levels of several forms of prostaglandin are significantly elevated in the mucosa in Crohn's colitis and ulcerative colitis. Local release of LTB₄ by the rectal mucosa is considerably increased in ulcerative colitis but is elevated in Crohn's colitis only when frank ulceration is present.^{2,4,6,11} Consequently, safe inhibitors of platelet-activating factor are now being sought, which could prove to be a powerful new form of therapy.

Other immunologic evidence suggests that there is a failure of suppressor cell generation coupled with a hyperactive state of helper T cells in patients with IBD. The activated T cells may then lead to an overactive immune response that is not turned off. This response results in increased macrophage activation, enhanced cytokine production, and augmented antibody secretion. Although immunologic factors are important, no specific antibody-producing antigen has been identified in the intestinal mucosa of patients with IBD. Also, there is still no convincing demonstration of any fundamental underlying immune defect. Further evidence against immunodeficiency as the cause of Crohn's disease comes from the report of a patient who had a prolonged remission coincidental with acquiring human immunodeficiency virus (HIV) infection. Similarly, exhaustive efforts to relate mycobacterial infection to Crohn's disease have been unsuccessful. A defect in mucosal permeability that permits absorption of macromolecules and complex sugars may be another important factor in the pathophysiology of Crohn's disease. Apparently healthy relatives of patients with Crohn's disease show the same intestinal permeability defect. This finding suggests that this defect may antedate intestinal inflammation and may also play a causative role.^{2,4,6,11}

EPIDEMIOLOGY

Although understanding of the epidemiology of Crohn's disease is unclear, investigators hope that more precise information will yield important clues about cause.¹¹ Salient epidemiologic features are listed in [Box 57-5](#).

Crohn's disease is an uncommon but not rare disease, with a reported incidence between 0.6 and 6.3 cases/100,000 population. Worldwide prevalence ranges from 10 to 70 cases/100,000 population; this wide variation is probably because of actual differences in disease distribution, as well as differences in

BOX 57-5 EPIDEMIOLOGY OF CROHN'S DISEASE

Worldwide prevalence: 10-70 cases/100,000 population
 Annual incidence: 0.6-6.3 cases/100,000 population*
 Bimodal age distribution: Peak at 15-25 yr; smaller peak at 50-80 yr
 Risk factors
 White race
 Jewish (eightfold increase)
 Residence in urban area
 Family history of disease
 Sibling with disease (30-fold increase)
 Single
 Oral contraceptive use
 Smoking (fourfold increase)

*Incidence has increased 1.4 to 4 times in past 40 years.

reporting, diagnostic criteria, and availability of medical care.^{2,4,7}

Crohn's disease is most common in the developed countries of Europe and Scandinavia, United States, and Israel. The incidence is lower in Southern and Eastern Europe and the former Soviet Union. The disease is uncommon in Central and South America and Cuba and is rare in Asia and Africa. Crohn's disease has been increasing in incidence over the past 40 years by a factor of 1.4- to 4-fold.^{2,4,7} Crohn's disease is more common in white than in African Americans or Asian, and the gender distribution is equal.^{2,4,7} There is a sevenfold to eightfold increase of Crohn's disease among Jews. The rates are highest for American Jews and much lower in Israeli-born and non-Ashkenazi Jews. These disparate rates found in different countries suggest the likelihood of hereditary predisposition, which may be altered by environmental factors.^{2,4,7} Crohn's disease has a bimodal age distribution. The peak incidence is between the ages of 15 and 25 years, with a lower peak between 50 and 80 years. It occasionally occurs in children as young as 2 years old.^{2,4,7}

Crohn's disease is generally acknowledged to be more common in urban than in rural populations, but the literature is conflicting on this matter.^{2,4,7} Epidemiologic data have shown that 4.5% to 16.6% of patients with Crohn's disease have a positive family history. The disease is 30 times more frequent in siblings than in the general population. Familial IBD seems to follow a polygenic inheritance pattern.^{2,4,7}

Crohn's disease runs a clinical course, with seasonal exacerbations. The highest relapse rate is found in the autumn and winter; the lowest is seen in the summer. This pattern suggests that seasonal or exogenous factors may be involved in relapse.^{2,4,7} Although nonsmoking is a feature of ulcerative colitis, patients with Crohn's disease are four times more likely to be smokers than matched controls.^{2,4,7}

The mortality rate of Crohn's disease has significantly declined, which can be attributed to improvements in diagnosis and management. The mortality rates for all IBDs for white American men were 5.88/1 million in 1970 to 1971 and 2.68/1 million in 1982; the rates for white American women were 7.24 and 3.48/1 million population, respectively.¹²

FINDINGS

Clinical Findings

The clinical manifestations of Crohn's disease are protean.^{2,4,11} The most frequently encountered initial features are rectal

bleeding, diarrhea, and abdominal pain. Two major types of pain occur in patients with Crohn's disease. The first is often mild, colicky, situated in the lower abdomen, and relieved by defecation. It tends to occur in association with diffuse Crohn's disease involving the colon and simulates the pain of ulcerative colitis. The second type is more severe; it is often situated in the right lower quadrant, simulating appendicitis. In a World Gastroenterology Organisation (WGO) survey, 75% of patients with Crohn's disease had abdominal pain at presentation.^{2,4,11}

Some degree of diarrhea usually accompanies active Crohn's disease, but it is less severe than the often explosive diarrhea of ulcerative colitis. Almost 50% of all patients with Crohn's colitis experience at least minor rectal bleeding during the active phase of disease. Profuse bleeding is much more common in ulcerative colitis. The presence of mucus in the stool is also more frequent in ulcerative colitis than in Crohn's disease. Many of the most severe symptoms reflect complications such as abscess, fistula, and perianal lesions rather than Crohn's disease itself.

The physical examination of patients with IBD is often normal in quiescent disease. In severe cases, pallor, dehydration, anemia, weight loss, finger clubbing, abdominal distention, tachycardia, and fever may be found. Abdominal tenderness and distention, pronounced wasting, and emaciation are more frequently found in Crohn's disease than in ulcerative colitis. An intra-abdominal mass is common in Crohn's disease but is rarely present in ulcerative colitis. The masses and tenderness usually occur on the right side in patients with Crohn's disease.

No examination of the patient with possible IBD is complete without a detailed rectal examination, including sigmoidoscopy. Circumferential, confluent, and contiguous inflammatory changes were found in 96% of patients with ulcerative colitis in the WGO series.^{2,4,11} Patchy, inflammatory changes with areas of normal intervening mucosa were highly suggestive of Crohn's disease, occurring in two thirds of patients with Crohn's proctosigmoiditis. Simple inspection may reveal severe perianal disease, which strongly suggests the diagnosis of Crohn's disease.^{2,4,11}

Endoscopic Findings

Aphthoid lesions, cobblestoning, and ulcers in an area of otherwise apparently normal mucosa are diagnostic of Crohn's disease versus ulcerative colitis but can be seen in other colitides. Mucosal granularity and friability are common in early ulcerative colitis but may be a late finding in Crohn's colitis. The rectum is often grossly normal in patients with Crohn's disease, and involvement is typically asymmetric and discontinuous.^{2,4,14}

Radiologic Findings

Radiography. When confined to the colon, Crohn's disease (Fig. 57-18) has features similar to those of ulcerative colitis on radiographs. An extended gas-filled stricture of the colon is suggestive of granulomatous colitis but can also be seen in ulcerative colitis, carcinoma, and healing ischemic colitis.^{16,21}

Small bowel obstruction can be seen on radiographs in patients with Crohn's disease of the small bowel. It is uncommon to identify stenotic small bowel segments on radiographs because gas is not found in the small bowel as often as is found in the colon. Occasionally, a markedly dilated segment of small bowel, reminiscent of a dilated loop of small bowel volvulus or Meckel's diverticulum, can be seen between two stenotic areas.^{16,21} Evidence of nephrolithiasis, gallstones, ankylosing

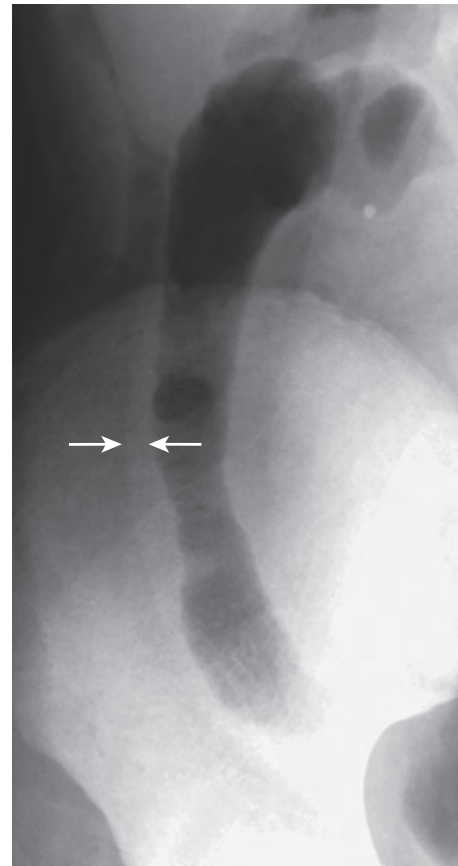


Figure 57-18 Crohn's disease: plain radiograph. The ascending colon is tubular and ahaustral. Note the mural thickening (arrows).

TABLE 57-1

Crohn's Colitis: Findings of Barium Enema

Early Changes	Late Changes
Nodular lymphoid hyperplasia	Fissures
Aphthoid ulcerations	Fistulas
Deep ulcerations	Haustral loss
Confluent ulcerations	Sacculations
"Cobblestone" appearance	Postinflammatory
Asymmetry involvement	Pseudopolyps
Inflammatory pseudopolyps	Intramural abscess strictures
Segmental distribution	
Skip lesions	

spondylitis, sacroiliitis, avascular necrosis of the femoral heads, and disorders associated with Crohn's disease and its therapy should also be sought on abdominal radiographs.

Barium Enema

The barium enema features of Crohn's colitis are listed in Table 57-1 and summarized in Figure 57-19, and will be discussed here in more detail.

Lymphoid Hyperplasia. Lymphoid follicles are a normal component of gut-associated lymphatic tissue. They are aggregates of lymphocytes surrounding germinal centers that straddle the muscularis mucosae. Lymphoid follicles have an average macroscopic density of 3.8/cm of adult human colon.^{25,103} They are

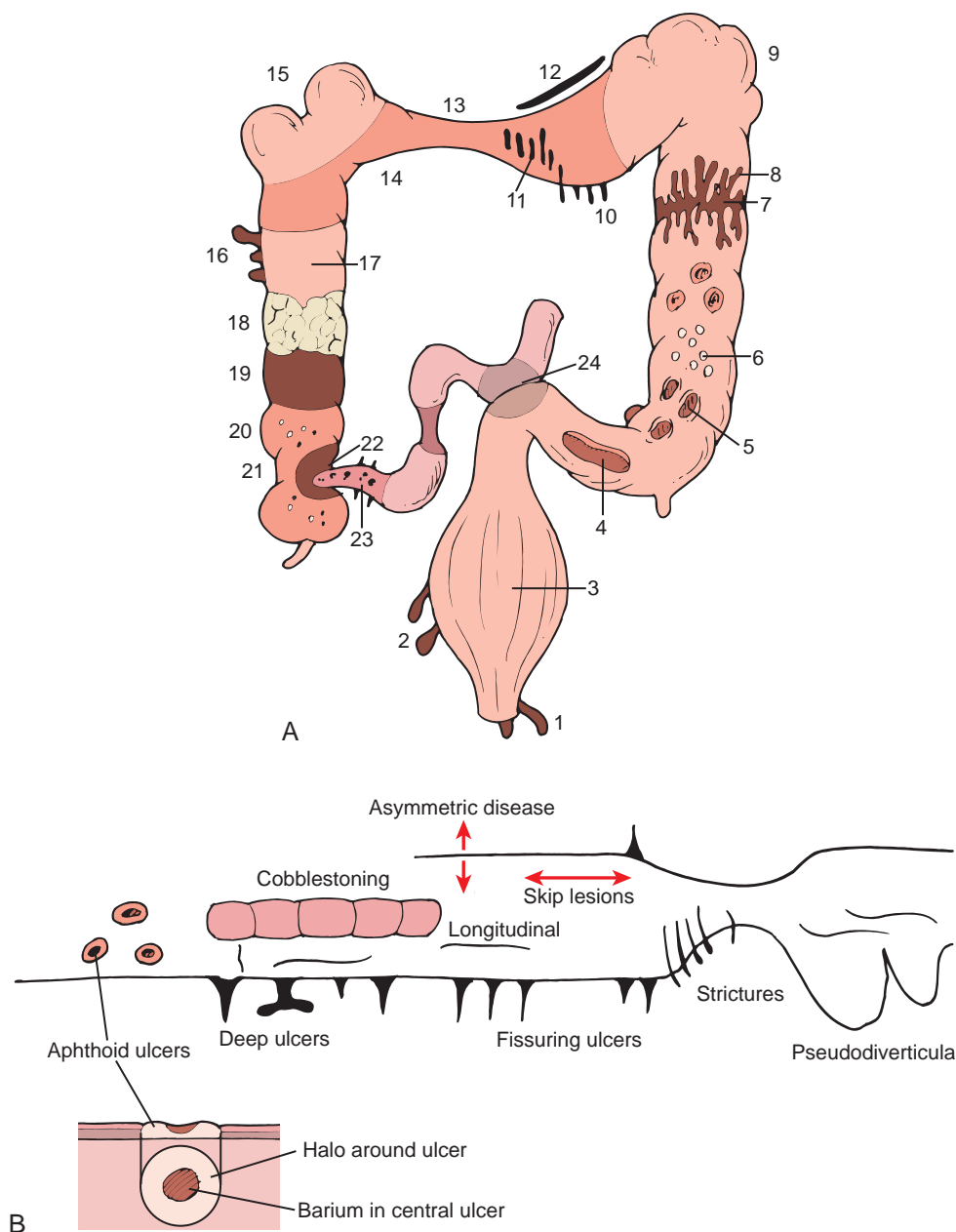


Figure 57-19 Spectrum of radiologic changes in Crohn's colitis on double-contrast barium enema examinations. A. 1, Perianal disease: ulcers, abscess, fissures, anocutaneous fistula; 2, deep rectal ulcers; 3, normal rectum in 50% of cases; 4, island ulcer; 5, circular discrete ulcers; 6, aphthoid ulcers; 7, serpiginous ulceration formed by coalition in a longitudinal form of circular and island ulcers; 8, thickening of the bowel wall; 9, normal skip areas; 10, rose thorn-shaped fissures; 11, transverse stripes of Welin (en face fissures or crevices between adjacent swollen mucosal folds); 12, linear confluent intramural ulceration, "double tracking"; 13, stricture (25% of cases); 14, eccentric disease, not involving the entire circumference; 15, pseudosacculations, produced by fibrosis of the opposite wall; 16, deep pleomorphic ulcers—composite, horned, sacular; 17, a normal patch surrounded by disease (and patches of disease surrounded by normal mucosa also occur); 18, inflammatory and postinflammatory pseudopolyps; 19, cobblestone mucosa— islands of residual swollen mucosa bounded by intersecting linear ulcers; 20, right-sided disease with normal rectum and distal colon; 21, contracted, cone-shaped cecum; 22, enlarged ileocecal valve usually associated with involvement of the terminal ileum; 23, small bowel disease in 60% of cases; 24, ileocolic fistula. **B.** Further depiction of mucosal abnormalities in Crohn's colitis. (**A** from Simpkins KC: *Inflammatory bowel disease: Ulcerative and Crohn's colitis*. In Simpkins KC [ed]: *A Textbook of Radiological Diagnosis*, vol 4, *The Alimentary Tract: The Hollow Organs and Salivary Glands*. London, HK Lewis, 1988, pp 473–498; **B** from Bartram CI, Kumar P: *Clinical Radiology in Gastroenterology*. Oxford, England, Blackwell Scientific, 1981, p 138.)

seen in 50% of barium studies performed on children and 13% of air-contrast barium enemas in adults. Lymphoid follicles appear as 1- to 3-mm elevations in the mucosa, without a ring shadow.^{103,104}

Lymphoid follicles may enlarge in a wide variety of infectious, neoplastic, immunologic, and inflammatory diseases of

the gut, including Crohn's disease.¹⁰⁵ Prominent lymphoid follicles have also been observed in older patients with colonic adenomas and carcinomas.¹⁰⁶

Aphthoid Ulcerations. As the lymphoid follicles enlarge, the overlying mucosa may ulcerate with production of the

aphthous lesion. These small superficial ulcers have erythematous margins and are seen on a background of normal or near-normal mucosa.²⁵ This is in direct contrast to ulcerative colitis, in which ulceration invariably occurs against a background of heavy inflammation. Aphthae are recognized radiographically as punctate central collections of barium surrounded by a radiolucent halo about 1 mm in diameter that produces a target or bull's-eye appearance (Fig. 57-20).¹⁰⁷⁻¹¹³ Aphthae may be isolated, found in clusters, or involve the entire colon.¹⁰⁸

Aphthoid lesions are found in 44% to 72% of patients with Crohn's disease and may be the only abnormality found in an otherwise normal colon.^{2,4,109} These ulcers are nonspecific and occur in amebiasis, salmonellosis, shigellosis, herpes, cytomegalovirus infection, Behçet's disease, ischemic colitis, and *Yersinia* enterocolitis.^{2,4}

Cobblestoning. The aphthous lesions may regress, remain stable or, more commonly, enlarge and deepen.^{111,113} As the aphthae expand, they become irregular in outline and lose their surrounding lucent halo. Adjacent ulcers may coalesce, forming a network of longitudinal linear ulceration and transverse fissuring, with edematous intervening mucosa producing a raised, cobbled appearance (Fig. 57-21).¹⁵ As noted, this condition is actually one of many forms of inflammatory pseudopolyposis.

Deep Ulcerations. Fissuring ulcers (Fig. 57-22) are a distinctive feature of Crohn's disease. They typically penetrate beyond the submucosa, with resultant knife-shaped or rose thorn fistulas.²⁵ These fissures and fistulas do not cause pneumoperitoneum because the surrounding serosa is inflamed, and involved bowel

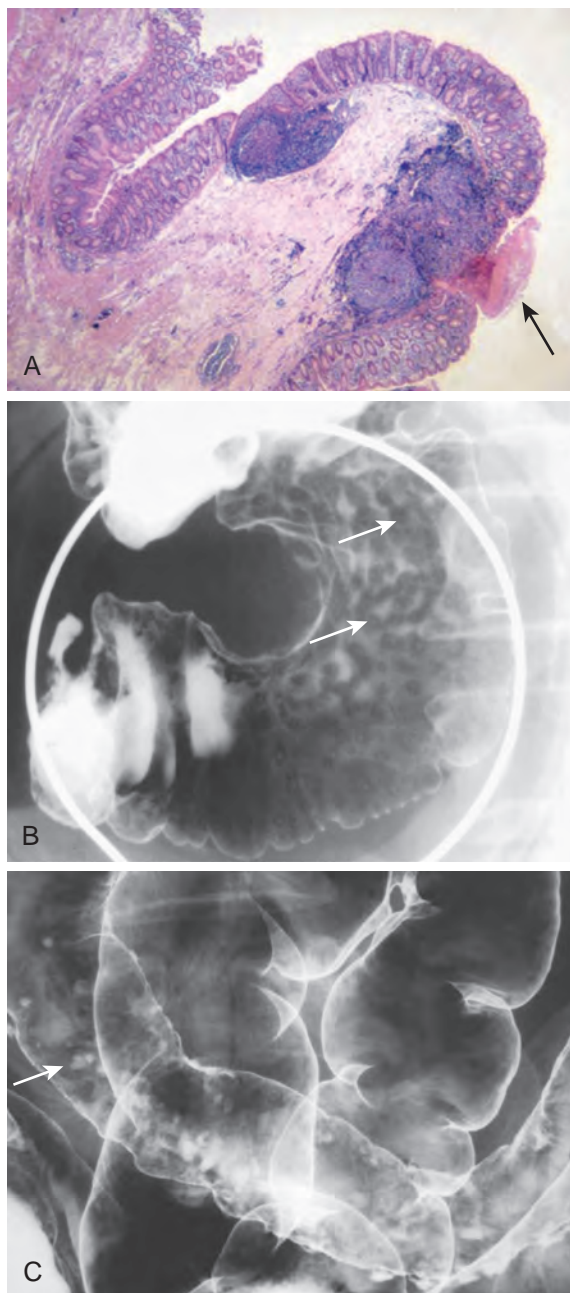


Figure 57-20 Crohn's disease: aphthoid ulcerations. **A.** Photomicrograph demonstrates an enlarged lymphoid follicle with overlying ulceration (arrow). **B to D.** Double-contrast barium enema in different patients demonstrates aphthoid lesions (arrows) of varying sizes in the cecum (**B**), transverse colon (**C**), and sigmoid colon (**D**).

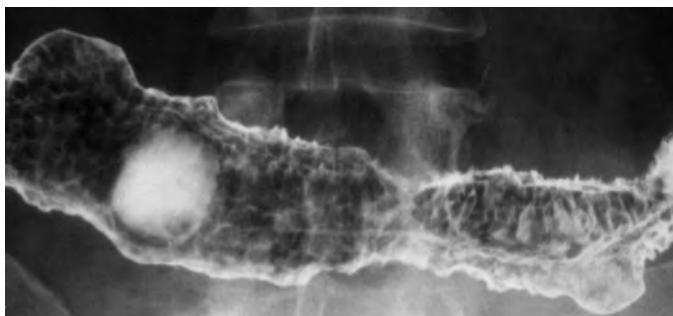


Figure 57-21 Crohn's disease: cobblestone mucosa. Longitudinal and transverse ulcers of the transverse colon produce a cobblestone appearance.



Figure 57-22 Crohn's disease: deep ulcerations. Double-contrast image of the splenic flexure demonstrates deep ulcers (arrow), a large ileocecal valve, and sparing of the sigmoid colon. The appendix is subhepatic in location.

loops become adherent to one another and adjacent peritoneal surfaces.^{25,39,40}

Sinus Tracts, Fissures, and Fistulas. Sinuses, fissures, and fistulas (Fig. 57-23) are a hallmark of Crohn's disease.^{2,4,11} Sinuses and fissures represent blind-ended inflammatory tracts that penetrate through the full thickness of the muscle coat later in the disease course. Fistulas communicate with other structures. Anatomic evidence suggests that mechanical factors, such as elevated intraluminal pressure, rather than any intrinsic pathologic change of Crohn's disease, are responsible for these fissures and fistulas.² This suggestion is based on the fact that there is a significant coincidence of sinuses and strictures and that sinuses arise proximal to the point of maximal stricture. In addition, fissures, sinuses, and fistulas are not constantly associated with myocytolysis, a seemingly necessary process if only the Crohn's inflammation is required for the fissuring.^{2,4}

Long interconnecting fistulas are common in Crohn's colitis and occur in the muscularis mucosae or subserosa paralleling the bowel lumen. When not associated with neoplasia or diverticula, pericolic sinus tracts are suggestive of Crohn's disease.²⁵⁻²⁷

Mural Thickening. The mural thickening that occurs in Crohn's disease is more impressive than that found in ulcerative colitis. It is caused by transmural inflammation and fibrosis. The submucosa may also accumulate fat in Crohn's disease but less commonly than in ulcerative colitis. CT well demonstrates mural thickening of the esophagus, stomach, duodenum, small bowel, and colon when these areas are involved by Crohn's disease.

Luminal Narrowing and Strictures. Crohn's disease is a transmural inflammatory process that produces gut wall thickening and fibrosis, leading to narrowing of the lumen and shortening of the gut as well.^{2,4,6} In ulcerative colitis, narrowing results from thickening and contractions of the muscularis mucosae rather than from fibrosis. Strictures are asymmetric in Crohn's disease and tend to be less smooth and circumferential than those seen in ulcerative colitis. Strictures occur in 21% of patients with small bowel disease and in 8% of patients with Crohn's colitis.²⁸

Sacculations. The transmural fibrosis of Crohn's disease is often asymmetric. It occurs predominantly on the mesenteric side of the gut, where it is often accompanied by creeping fat of the mesentery. The relatively unaffected side (usually antimesenteric) remains pliable and tends to bulge when luminal pressure increases because of peristalsis. Outpouchings may eventually develop. The outpouchings are similar to the so-called pseudosacculations (Fig. 57-24) or pseudodiverticula seen in scleroderma.^{25,27}

Anorectal Disease. Anorectal complications are common in patients with Crohn's disease (Fig. 57-25) and include anal fissures, ulcers, abscess, internal hemorrhoids, and stenosis with induration, skin lesions such as erosion, skin tags, ulceration, maceration, external hemorrhoids, and abscess, and fistulas—anal canal to skin, rectum to skin, and rectovaginal. Anal disease develops in 36% of all patients with Crohn's disease, 25% of those with only small bowel involvement, 67% of those with colonic disease, and nearly all patients with rectal disease.³¹ In approximately 25% of patients, the anal disease may antedate overt intestinal disease, often by 4 years. Accordingly, development of these anorectal disorders warrants radiologic investigation of the entire gastrointestinal tract.^{2,4,31}

Distribution. Any portion of the gut, from the mouth to the anus, may be involved by Crohn's disease. Twenty percent of cases are isolated to the colon, 20% are restricted to the small bowel, and 60% involve the colon and small bowel simultaneously. In 5% to 10% of these patients, upper gastrointestinal tract involvement is seen. It is unusual to see isolated esophageal or gastroduodenal Crohn's disease. Regardless of location, radiographic and pathologic findings are similar; there is discontinuous, patchy, and asymmetric disease involvement.^{2,4,6}

Computed Tomography

Crohn's disease is manifested on CT (see Box 57-3) by bowel wall thickening of 1 to 2 cm.¹¹⁴ This thickening, which occurs

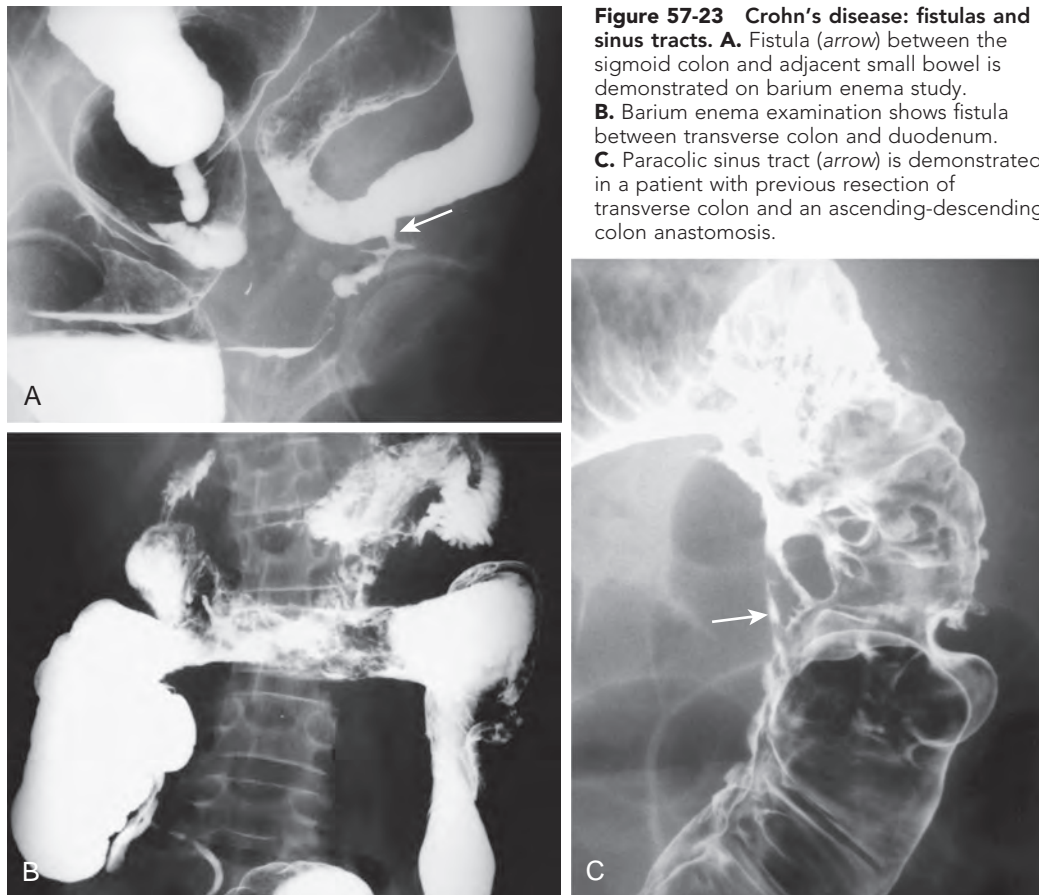


Figure 57-23 Crohn's disease: fistulas and sinus tracts. **A.** Fistula (arrow) between the sigmoid colon and adjacent small bowel is demonstrated on barium enema study. **B.** Barium enema examination shows fistula between transverse colon and duodenum. **C.** Paracolic sinus tract (arrow) is demonstrated in a patient with previous resection of transverse colon and an ascending-descending colon anastomosis.

in 83% of patients, is usually observed in the terminal ileum, but other portions of the small bowel, colon, duodenum, stomach, and esophagus may be similarly affected.^{62,65}

During the acute, noncicatrizing phase of Crohn's disease, the small bowel and colon maintain mural stratification (Fig. 57-26) and often have a target or double halo appearance.^{56,115} As in ulcerative colitis, there is a soft tissue density ring (corresponding to mucosa), which is surrounded by a low-density ring with an attenuation near water or fat (corresponding to submucosal edema or fat infiltration), which in turn is surrounded by a higher density ring (muscularis propria).¹¹⁶ Inflamed mucosa and serosa may show significant contrast enhancement after IV bolus contrast administration; the intensity of enhancement correlates with the clinical activity of disease.¹¹⁷

The CT demonstration of mural stratification (i.e., the ability to visualize distinct mucosal, submucosal, and muscularis propria layers) indicates that transmural fibrosis has not occurred and that medical therapy may be successful in ameliorating lumen compromise.⁵⁶ The edema and inflammation of the bowel wall that cause mural thickening and lumen obstruction are reversible to some extent. A modest decrease in wall thickness often produces dramatic increase in the luminal cross-sectional area and resolution of the patient's obstructive symptoms. In patients with long-standing Crohn's disease and transmural fibrosis, mural stratification is lost, so the affected bowel wall typically has homogeneous attenuation on CT.⁶⁷ Homogeneous attenuation of the thickened bowel wall in the

presence of good intravascular contrast medium levels and thin section scanning suggests irreversible fibrosis, so anti-inflammatory and immunosuppressive agents may not provide significant reduction in bowel wall thickness.⁹⁹ If these segments become sufficiently narrow, surgical resection or strictureplasty may be necessary to relieve the patient's obstruction. Not uncommonly, acute and chronic changes of Crohn's disease can coexist (Fig. 57-27).

Mesenteric Involvement. The palpation of an abdominal mass or separation of bowel loops on a small bowel series in a patient with Crohn's disease evokes a large differential diagnosis—abscess, phlegmon, “creeping fat” or fibrofatty proliferation of the mesentery, bowel wall thickening, and enlarged mesenteric lymph nodes. Each of these disorders has significantly different prognostic and therapeutic implications.^{99,118,119} This diagnostic dilemma is further complicated by the fact that many patients are receiving immunosuppressive therapy that can mask signs and symptoms. CT can readily differentiate the extraluminal manifestations of Crohn's disease.

Fibrofatty Proliferation of the Mesentery. Fibrofatty proliferation, also known as creeping fat of the mesentery, is the most common cause of separation of bowel loops seen on small bowel series in patients with Crohn's disease.^{120,121} On CT, the sharp interface between bowel and mesentery is lost, and the attenuation value of the fat is elevated by 20 to 60 HU as a result of the influx of inflammatory cells and fluid.⁶¹ Mesenteric

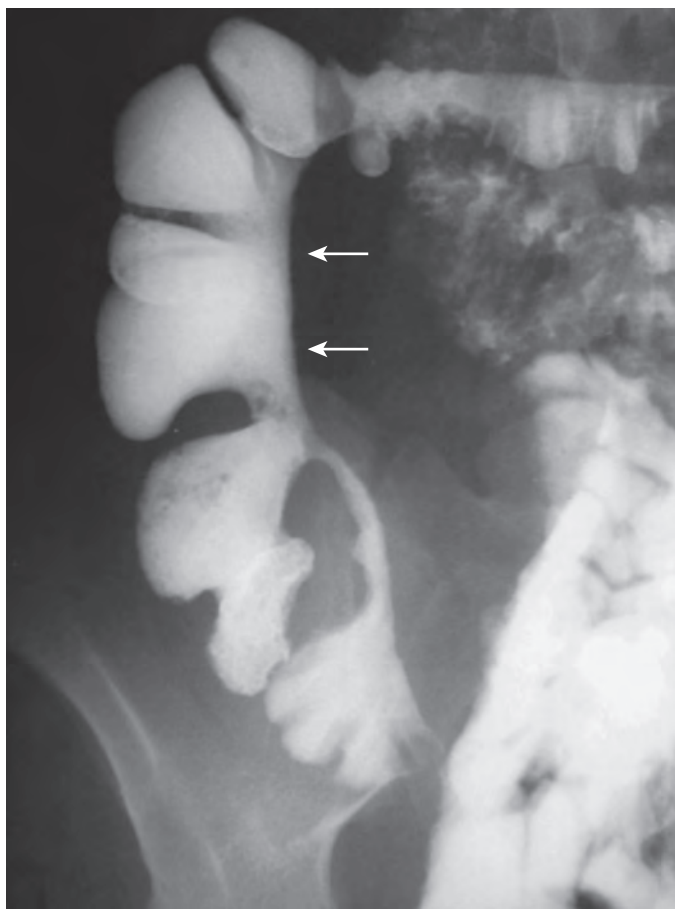


Figure 57-24 Crohn's disease: sacculations. Crohn's disease involves primarily the mesenteric side (arrows) of the gut, leading to fibrosis and ballooning of the antimesenteric border. Crohn's disease is typically discontinuous, patchy, and asymmetric.

adenopathy with lymph nodes ranging in size from 3 to 8 mm may also be present. If these lymph nodes are larger than 1 cm, lymphoma or carcinoma, both of which occur with greater frequency in Crohn's disease, must be excluded.

There is subserosal accumulation of an increased amount of hypertrophied fat as a result of perivascular inflammation with fibrosis and contraction of the muscular properties. The perivascular fibrosis results in the contraction of dilated feeding vessels and hypertrophied mesenteric fat, tethering the mesentery closer to the gut wall. This tethering contributes to the gross appearance of fat wrapping around the gut.¹²²

Contrast-enhanced CT scans often show hypervascularity of the involved mesentery manifesting as vascular dilation, tortuosity, prominence, and wide spacing of the vasa recta. These distinctive vascular changes have been termed *vascular jejunization of the ileum* or the *comb sign*.¹²¹ Identification of this hypervascularity should suggest active disease and may be useful in differentiating Crohn's disease from lymphoma and metastases, which tend to be hypovascular lesions.

Phlegmon. A phlegmon is an ill-defined, inflammatory mass in the mesentery or omentum that may resolve completely with antibiotics or progress to form an abscess.¹⁰⁹ Phlegmons are another common cause of mesenteric mass effect in patients with Crohn's disease. On CT, a phlegmon produces loss of

definition of surrounding organs and a smudgy or streaky appearance of the adjacent mesenteric or omental fat.⁶⁶

Abscess. Of patients with Crohn's disease, 15% to 20% eventually develop an intra-abdominal abscess.¹²² Abscesses are most frequently associated with small bowel disease or ileocolitis.¹²³ Once developed, an abscess can burrow through the adjacent tissue or break open and drain spontaneously into another part of the bowel, adjacent organs, or both. Abscesses usually result from sinus tracts, fistulas, perforations, or surgery for Crohn's disease.

An intra-abdominal abscess may be difficult to diagnose on clinical grounds in patients with Crohn's disease because symptoms may be inconspicuous, masked by corticosteroids, or mistaken for an exacerbation of disease. Barium studies and endoscopy can only suggest the presence of an abscess indirectly by mass effect, spiculation of the mucosa, or identification of a fistula. Also, these studies do not evaluate the ischiorectal fossa, psoas muscle, and solid abdominal organs, which are common locations of abscess formation.^{123,124} Cross-sectional imaging is required to confirm the diagnosis and reveal the full extent and location of the abscess cavity. CT is the primary imaging tool used for percutaneous drainage of Crohn's disease-related abscesses.¹²⁵⁻¹²⁷

Transrectal Ultrasonography

Transrectal ultrasonography can show the following abnormalities in patients with Crohn's disease: (1) mural thickening; (2) perianal and perirectal abscesses and fistulas; and (3) heterogeneity of the anal sphincter.⁷³ Rectal wall thickening (>4 mm) is often accompanied by loss of mural stratification in Crohn's disease.⁷³

The anal sphincter derives from the rectal muscular layer as a sharply delineated ellipsoid that is uniformly hypoechoic. When involved by Crohn's disease, the sphincter becomes heterogeneous, with echogenic zones interspersed between the normal hypoechoic regions. Also in patients with active proctologic disease, the shortening and narrowing of the anal canal during squeezing and elongation with dilation during straining are less pronounced. Fistulas and sinus tracts appear as a dotted column of echo-rich gas bubbles, with reverberation on transrectal ultrasonography. Abscesses are characterized sonographically as predominantly hypoechoic areas that contain echogenic elements corresponding to debris and gas bubbles. The wall of the abscess is usually thick and irregular, and some posterior acoustic enhancement may be seen. Some authors advocate routine screening with transrectal ultrasonography because this technique is capable of defining pararectal and para-anal abscesses and fistulas that develop extramurally without mucosal lesions.^{2,4,11}

Transabdominal Ultrasonography

The thickness of the colonic and small bowel wall can be appreciated sonographically, and the validity of using mural thickening in establishing the diagnosis of IBD has a reported sensitivity of 67% to 86% and specificity of 87% to 100%.⁶⁸⁻⁷² Some authors suggest using ultrasonography as a screen for IBD.⁶⁸⁻⁷² When suspicion of disease is low, normal ultrasonography may be sufficient to avoid barium examination. When abnormal gut is seen or clinical suspicion is high, despite a normal ultrasound study, barium examination should be performed.⁶⁸⁻⁷²

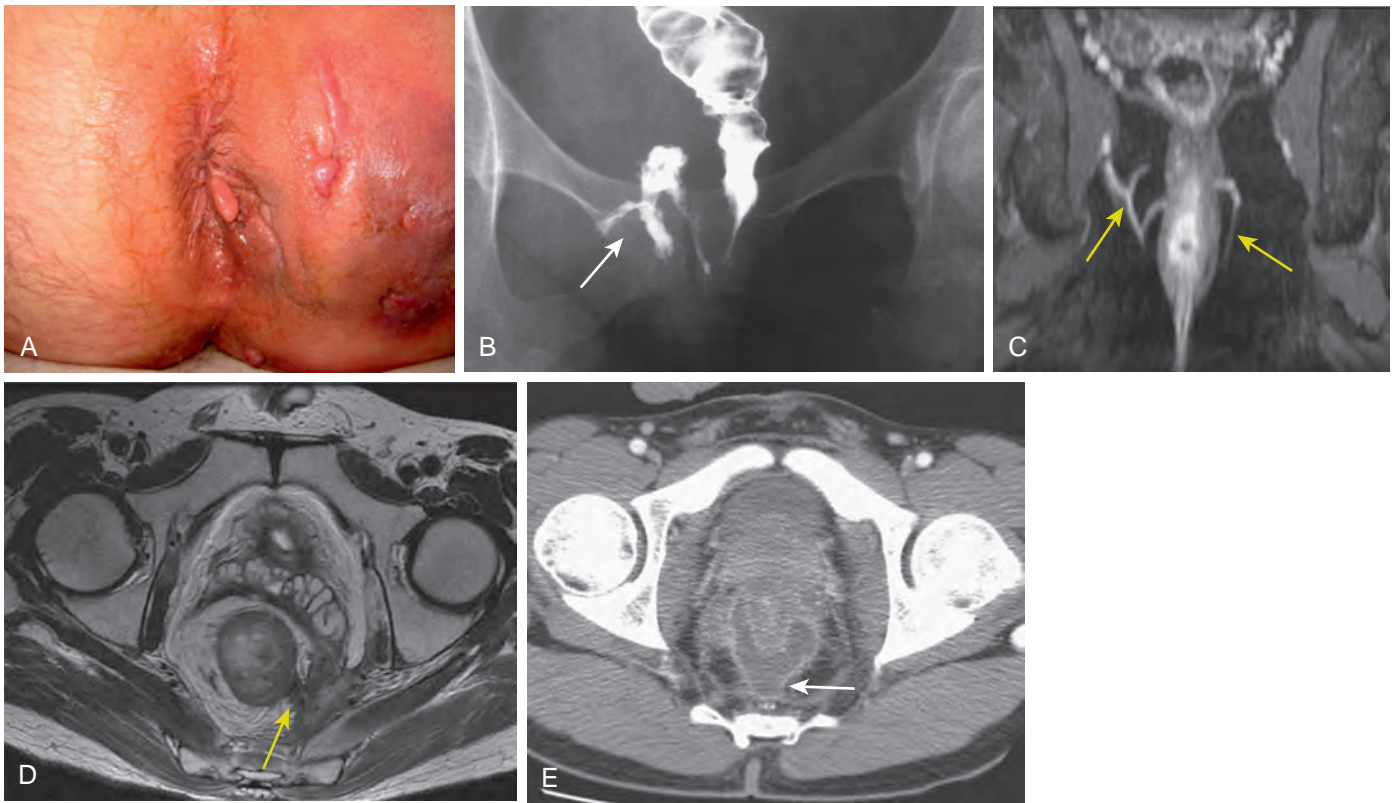


Figure 57-25 Crohn's disease: anorectal pathology. **A.** Multiple cutaneous fistulas are seen in the perianal region. **B.** Barium enema study shows a sinus tract (arrow) into the right perianal soft tissues. **C.** Coronal, fat-suppressed T2-weighted MRI scan of the anorectum shows multiple high signal intensity fistulas (arrows) into the perianal and mesorectal fat. **D.** Axial MRI scan shows mural thickening of the rectum, with a fistula (arrow) extending into the left piriformis muscle. **E.** CT scan shows a U-shaped abscess along the posterior aspect of the anorectal junction (arrow).

In patients with active Crohn's disease, the colon wall can be 1.5 cm thick. Mural stratification is typically lost as well. Using criteria listed in [Box 57-4](#), the sensitivity of ultrasound in detecting active Crohn's disease was 91%, with a specificity of 100%; sensitivity was 89%, with a specificity of 97% for detecting active ulcerative colitis. Several sonographic caveats should be noted. In patients with only aphthoid ulcerations, typical wall stratification is maintained in patients with Crohn's disease, suggesting that the disease is not yet transmural. In patients with ulcerative colitis who have large and extensive pseudopolyps, the thickness of the colon wall may approach 1.5 cm, and mural stratification may be lost.⁶⁸⁻⁷²

Several authors have questioned the usefulness of ultrasound for differentiating ulcerative colitis and Crohn's colitis on the basis of bowel wall changes alone.⁶⁸⁻⁷² Documentation of continuous or discontinuous involvement, combined with evidence of mesenteric disease, abscess, or fistula, can assist differentiation.

In a study using hydrocolonic ultrasonography, 93% of patients with Crohn's disease showed loss of mural stratification, and the wall appeared hypoechoic and clearly thickened. In contrast, mural stratification was maintained in ulcerative colitis.⁶⁸⁻⁷² Hydrocolonic ultrasonography could differentiate Crohn's disease from ulcerative colitis in 93% of cases. Colonic Crohn's disease was detectable by this technique with a sensitivity of 96% and specificity of 91%.⁶⁸⁻⁷²

The thickened bowel wall in Crohn's disease ([Fig. 57-28](#)) produces a target, bull's-eye, or cockade appearance that must be differentiated from chronic ulcerative colitis, diverticulitis, lymphoma, ischemic colitis, and pseudomembranous colitis.⁶⁸⁻⁷² Ultrasonography has also successfully diagnosed recurrent disease in patients who have had surgical resections.⁶⁸⁻⁷² Sonographically, creeping fat of the mesentery is hypoechoic compared with normal fat resulting from edema.⁶⁸⁻⁷²

Doppler sonographic evaluation of the superior mesenteric artery is a promising noninvasive method of detecting ileocolic inflammation in patients with Crohn's disease and assessing disease activity. In patients with active disease, there is an increase in blood flow and decrease of resistive index of the superior mesenteric artery. Scans are performed preprandially, and postprandial scans can provide additional information. In normal subjects, there is a significant difference in the resistive index before and after meals because of the vasodilation and increased diastolic flow that occur after a meal. In patients with Crohn's disease, there is massive and persistent vasodilation, related to the extent and severity of disease, which increases blood flow and decreases the resistive index. Accordingly, a meal in patients with active disease does not produce expected Doppler changes because the vasodilation is already established.¹²⁸⁻¹³⁰

In patients with active ileocecal Crohn's disease, alterations of intestinal vascular impedance may reflect the Doppler waveform of the superior mesenteric artery. This change in vascular

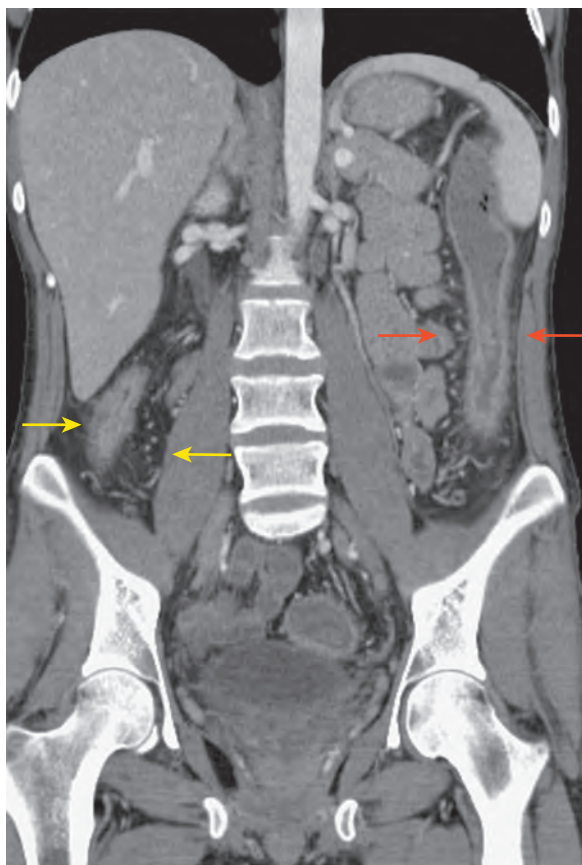


Figure 57-26 Crohn's disease: acute disease on CT. Coronal reformatted image shows mural thickening of the ascending (yellow arrows) and descending (red arrows) colon, with engorgement of the vasa rectae indicating active, acute disease.

impedance is manifest by increased flow velocities (peak systolic and diastolic) in the superior mesenteric artery flow volume to the superior mesenteric artery territory. Increased flow velocities are caused by the hyperemia and increased flow, as well as decreased downstream resistance.¹²⁸⁻¹³⁰

Magnetic Resonance Imaging

MRI provides a similar perspective to CT in that images demonstrate the overall topography of the abdomen. This imaging technique has several inherent advantages—lack of ionizing radiation, multiplanar imaging capability, and superb soft tissue contrast.⁷⁵⁻⁷⁹ Disadvantages that have generally precluded the routine use of MRI in the evaluation of IBD include respiratory and bowel motion artifact, lack of a satisfactory oral contrast agent, high signal intensity of intra-abdominal fat, and long imaging times used in conventional spin-echo sequences.

Many of the limitations of MRI have been overcome by using breath-holding imaging (fast low-angle shot [FLASH]), fat suppression, and an IV contrast agent, gadopentetate dimeglumine (Gd-DTPA).^{131,132} With these new techniques, MRI can show the extent and severity of inflammatory changes of the gut (see Fig. 57-25) that correlate with endoscopic and histologic findings from surgical specimens.⁷⁵⁻⁷⁹ Mural thickening of the gut can also be appreciated with MRI. When fast imaging sequences are combined with IV contrast material (Gd-DTPA) administration and fat-suppressed imaging, a good correlation among

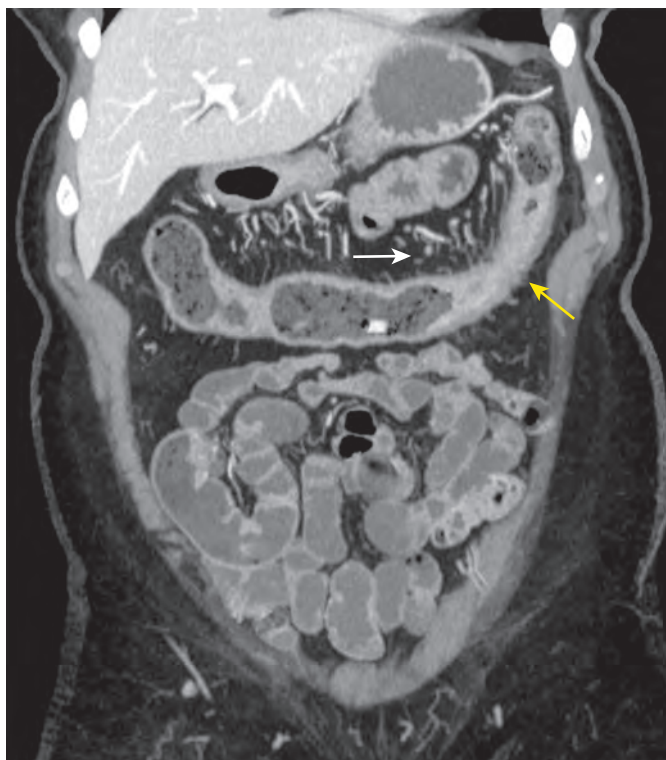


Figure 57-27 Coexisting acute and chronic Crohn's disease: CT findings. There is stenosis of the distal transverse colon (yellow arrow), indicating chronic disease. There is also some hyperenhancement of the mucosa of the more proximal transverse colon with engorgement of the vasa rectae (white arrow), indicating coexisting active disease.

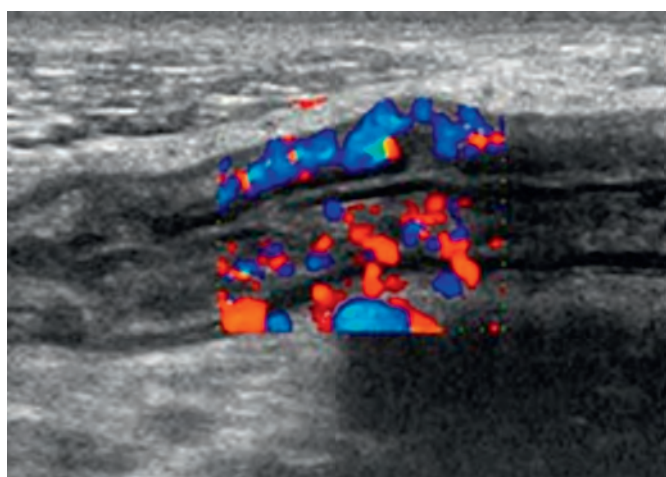


Figure 57-28 Crohn's disease: sonographic findings. Longitudinal sonogram of the ascending colon shows hypervascularity and mural thickening.

bowel wall thickness, length of diseased bowel, and severity of inflammation has been reported.⁷⁵⁻⁷⁹ The percentage contrast enhancement compares well with severity of inflammation based on endoscopic and surgical findings. The actively inflamed wall enhances because of increased delivery of the agent and increased capillary permeability. On T1-weighted MR sequences, the fat may have low signal intensity streaks and strands. These

areas may enhance after Gd-DTPA administration on gradient-echo images. MRI is sensitive for the detection of perianal and perirectal fistulas, sinus tracts, and abscesses that frequently accompany perianal Crohn's disease.^{133,134}

THERAPY

Medical Management

Crohn's disease does not behave clinically as a single disorder, so each patient must receive an individual clinical evaluation and integrated medical and surgical management.^{2,4,11}

Drug Therapy. Corticosteroids are the most effective therapy for producing symptomatic relief in Crohn's disease patients. Although they are effective in preventing relapses, they do not alter the long-term outcome and are associated with complications related to Cushing's disease. Immunosuppressive agents have also been tested, with encouraging results. Several studies have shown that cyclosporine is effective when conventional corticosteroids have failed and that it works more quickly than other immunosuppressive agents. Its efficacy is related to its ability to interfere with T-cell activation. Side effects include malabsorption and renal toxicity, and there is the long-term risk of cyclosporine-induced neoplasm.^{2,4,11}

The role of azathioprine in Crohn's disease remains controversial because it produces a variety of significant side effects. Physicians are often compelled to use azathioprine as a third-line drug, particularly in patients with extensive small bowel disease, recurrence after surgery, and fistulas. In some patients, the use of azathioprine or its active metabolite, 6-mercaptopurine, has permitted reduction in the dose of corticosteroid and even discontinuation of the drug.

Mesalamine decreases recurrence rates in Crohn's colitis, but its value for small bowel disease is uncertain. The use of sulfasalazine is hindered by side effects, which has led to the development of less toxic derivatives of 5-aminosalicylic acid.

The efficacy of metronidazole in Crohn's disease remains unproved, and its use is limited by neurologic toxicity. However, this therapy may lead to complete remission of perianal disease and the closure of fistulas.^{2,4,11}

Total parenteral nutrition (TPN) is useful for maintaining nutritional status when the gut cannot be used during exacerbations of inflammatory or fibrostenotic Crohn's disease. Nevertheless, remission rates while maintained on TPN and bowel are equivalent to those of enteral nutrition. TPN for 5 to 10 days preoperatively can decrease surgical complications in patients who require bowel resection.

Advances in understanding of the role of immune cells, natural killer cells, and macrophages and their soluble mediators, such as cytokines and tumor necrosis factor, have led to the development of specific immunotherapies with improved efficacy and reduced toxicity. As noted, anti-TNFs (chimeric, monoclonal antibody [infliximab]) have proved helpful in patients with advanced Crohn's disease refractory to corticosteroids and immunosuppressive therapy. This recombinant antibody is given as a single IV dose and can rapidly close fistulas, with improvement lasting for 3 months.^{2,4,11}

Surgical Management

There is a high rate of recurrence (30% to 53%) of Crohn's disease after resection of diseased bowel.^{2,4,88,91} It is possible

that Crohn's disease affects, at least at a microscopic level, the entire gut from the outset, so the disease cannot be cured by surgery. Therefore, surgery should be reserved for certain complications of the disease or for unequivocal failure to respond to optimal medical therapy. These guidelines are particularly applicable to two groups of patients, those who have previously undergone small bowel resection and present with recurrent disease of an obstructive nature and those who have diffuse disease and multiple small bowel strictures. Removal of all the diseased areas in these patients may lead to short bowel syndrome.

The major indications for surgery in Crohn's disease are obstruction, perforation, hemorrhage, and carcinoma.^{2,4,88,91} Abscesses and fistulas should first be treated by the interventional radiologist because this may save the patient from having surgery.^{2,4,88,91}

There is considerable interest concerning strictureplasty, and early reports have suggested that this technique is effective in treating short, stenosing Crohn's lesions of the small bowel.^{2,4,88,91} One series reported 24 patients who had 86 strictureplasties.⁸⁸ This procedure was safe and effective for select patients undergoing surgery for obstructive Crohn's disease. Short fibrous strictures in patients who did not have acute inflammatory segments of disease were most amenable to strictureplasty. Another report compared recurrence after strictureplasty with that after primary resection for small intestinal Crohn's disease.⁸⁸ No difference in the rate of recurrence after strictureplasty or resection was found, offering more support to the choice of strictureplasty for select patients with obstructive symptoms.

Reports of radiologically guided balloon dilation of strictures are also of interest, but this method is unlikely to be suitable for many Crohn's strictures, which are located in the small bowel.^{2,4,88,91} Current surgical opinion holds that external fistulas unassociated with residual Crohn's disease should be managed along conventional lines but that fistulas arising from diseased small intestine may require surgery. This surgery should be performed after an associated abscess has been drained, metabolic deficits have been corrected, and the anatomy of the fistula has been defined.⁹¹

Primary fistulotomy has been shown to be a safe procedure in selected patients, provided that aggressive medical treatment is used to control bowel disease preoperatively.^{2,4,88,91} Rectovaginal fistulas are especially difficult to treat, but with prolonged conservative treatment, the rectum can be preserved in many cases.

PROGNOSIS

The manifestations and complications of Crohn's disease are so diverse and unpredictable that for some patients the outlook is bleak. Disease remission can be interrupted by exacerbations at any time. Approximately 50% of patients develop complications that require surgery, and 10% to 20% lead symptom-free lives after one or two attacks. In view of the serious nature of Crohn's disease and its complications, the mortality is low. With proper medical supervision, most patients adjust remarkably well to their chronic illness and lead productive lives.^{2,4,11,133-137} The use of biologic agents such as Remicade and Humira have the potential to improve the natural history of this disease significantly.

Intestinal Complications of Inflammatory Bowel Disease

Table 57-2 summarizes gastrointestinal complications in ulcerative colitis and Crohn’s disease.

CARCINOMA

The risk of developing colorectal cancer is significantly higher in patients with ulcerative colitis and Crohn’s colitis than in the general population, although the precise magnitude of this risk

is uncertain.^{1-6,138} Studies have suggested an annual incidence of 10% after the first decade of ulcerative colitis. The risk of colorectal cancer also increases with increasing extent of disease; 75% to 80% of patients who develop cancer have pancolitis.¹³⁸ Carcinomas associated with ulcerative colitis are multiple in almost 25% of cases; they are more often flat and scirrhous than in patients without colitis and thus harder to detect.

Cancer screening has become a popular and controversial issue in patients with IBD. Since the 1960s, mucosal dysplasia has been considered a precursor of colon cancer or at least a marker of colons at risk for developing cancer. Mucosal dysplasia is often detected near or remote from the neoplasm in ulcerative colitis patients with carcinoma. However, dysplasia is patchy, inconsistent, and unpredictably distributed in the colon. Accordingly, colonoscopy with multiple, random biopsy specimens and biopsy specimens from masses or raised areas is recommended. Flow cytometry searching for aneuploidy has been advocated as a means of increasing the specificity and prognostic significance of the histologic results.

Molecular markers, such as Ki-67, DPC-4, and DYS nuclear matrix proteins, are a means of further refining the diagnosis of dysplasia and may eventually provide an alternate method of predicting colorectal cancer. Clinical studies provide support for the increasingly prevalent recommendation that any dysplasia warrants colectomy.^{2,4,11}

Several studies have shown that certain dysplastic lesions are radiologically visible (Fig. 57-29). When the dysplasia is elevated and plaquelike or multinodular, it manifests en face as irregular nodular areas with sharply angulated borders, having a mosaic tile appearance. Tangentially, these lesions project only 1 to 2 mm above the adjacent normal mucosa. When the dysplasia assumes a more polypoid form, it is indistinguishable from an adenomatous polyp. Most dysplasias occur in flat mucosa and therefore are not detectable on double-contrast barium studies. The management of high-risk patients with

TABLE 57-2 Relative Frequency of Gastrointestinal Complications in Inflammatory Bowel Disease		
Complication	Ulcerative Colitis (%)	Crohn’s Disease (%)
Anorectal lesions	<20	20-80
Fissure in ano	<15	25-30
Perianal abscess	<10	20-25
First symptom	Very infrequent	20-25
Fistula in ano	<6	20-25
Multiple and complex	Never	Common
Multiple anorectal complications	Very infrequent	20
Massive hemorrhage	3	<3
Colon	Never	<2
Small bowel		
Intra-abdominal abscess	Very rare	20-40
Internal fistulas	Very rare	Very uncommon
Free perforation	Uncommon	<8
Toxic megacolon	2-10	Less common
Pseudopolyposis	15-30	Very common
Strictures	11-15	15-25

Adapted from Osterman MT, Lichtenstein GR: Ulcerative colitis. In Feldman M, Friedman LS, Branch LJ (eds): *Gastrointestinal and Liver Disease*, 8th ed. Philadelphia, Saunders, 2010, pp 1975–2090.

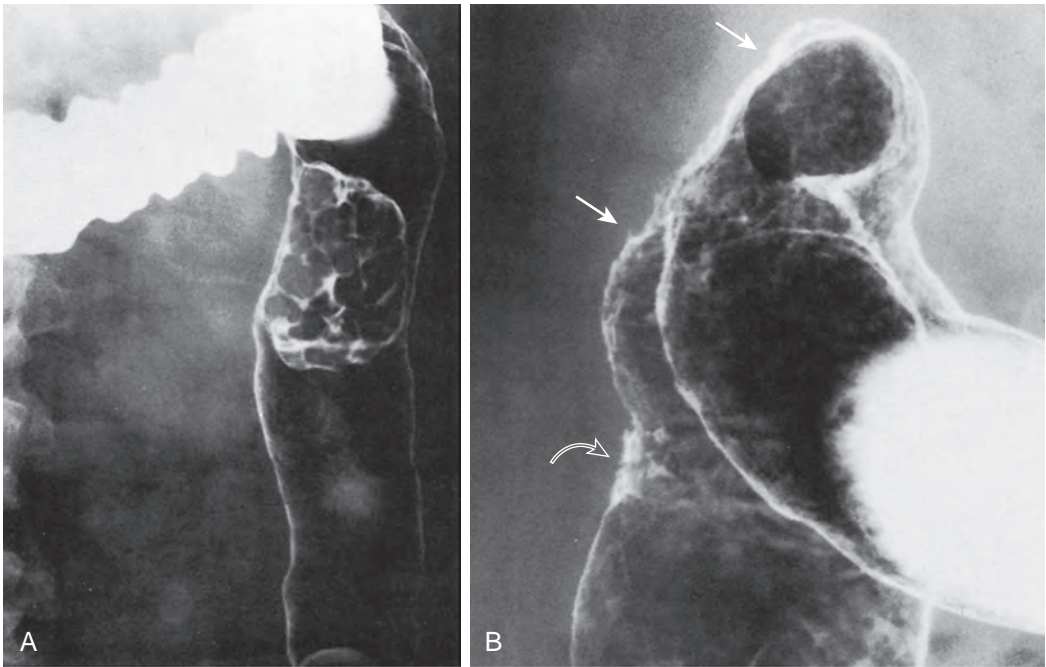


Figure 57-29 Ulcerative colitis: carcinoma. Colitic carcinomas often have an atypical appearance. **A.** Unusual polypoid carcinoma in the proximal descending colon. **B.** There is an infiltrative plaquelike carcinoma of the hepatic flexure (solid arrows). A small macrodysplastic lesion (curved open arrow) is present proximal to the carcinoma.

ulcerative pancolitis requires regular radiologic and endoscopic surveillance for detecting dysplasia.¹³⁸⁻¹⁴⁴

TOXIC MEGACOLON

Toxic megacolon is the most severe, life-threatening complication of IBD. It occurs in 1.6% to 13% of patients with ulcerative colitis and is less common in Crohn's colitis. Toxic megacolon usually occurs in patients in their 30s and may be the initial manifestation of ulcerative colitis. It is the most common cause of death directly related to ulcerative colitis and is an indication for emergency surgery.¹⁴⁵⁻¹⁴⁸

Pathologic Findings

On pathologic examination, there is transmural inflammation with deep fissuring ulcers into the muscularis propria, often with extension to the serosa. These inflammatory changes may be so extensive that large areas of denuded mucosa are seen. The colon undergoes disintegration of normal tissue cohesion, an appearance that surgeons have likened to having the consistency of wet tissue paper on handling. The inflammatory exudate seeps through the serosa and may lead to signs of peritonitis, even without frank perforation. The external surface of the colon shows intense serositis, and the greater omentum and gastrocolic ligament are edematous and inflamed. These changes are accompanied by vasculitis of the small arterioles and inflammation and by destruction of the ganglion cells of the myenteric and submucosal plexuses; there is myocytolysis in the muscularis propria.^{2,4,6} Although the bowel wall appears thickened and nodular on abdominal radiographs, the specimen often shows a mural thickness of only 2 to 3 mm in areas of denuded mucosa.

A number of factors that further contribute to high intraluminal pressures and decreased muscle tone that can lead to colonic distention in toxic megacolon include antidiarrheal drugs (e.g., codeine, morphine, tincture of opium), aerophagia, and hypokalemia. Barium enema has also been implicated as a precipitating factor in toxic megacolon, but this is controversial. Certain evidence suggests that the relationship may be temporal more than a cause and effect phenomenon. Nevertheless, the interdiction concerning barium enema studies in patients who are severely ill with ulcerative colitis is valid.^{2,4,6} Toxic megacolon can also complicate other forms of colitis, such as ischemic colitis, Crohn's disease, pseudomembranous colitis, and amebiasis.

Radiologic Findings

Toxic megacolon (Fig. 57-30) is one of the few life-threatening conditions in which an abdominal radiograph is all that is required to establish a firm diagnosis.¹⁴⁸ Dilation is the hallmark of toxic megacolon; mean diameters of the most dilated segments are between 8.2 and 9.2 cm. Dilation more than 5 cm indicates ulceration to the muscle layer and should be considered the threshold for dilation in fulminating colitis. In the past, the transverse colon was considered the focus of disease, but this only reflects the fact that the transverse colon is the least dependent portion of the large intestine on supine view radiographs. Initially, only a short segment of colon may be involved.^{2,4}

Mucosal islands are a common finding in toxic megacolon and indicate severe disruption of the mucosa. This appearance can be simulated in patients with inflammatory polyps during an acute attack. As noted, although the colon wall is thin

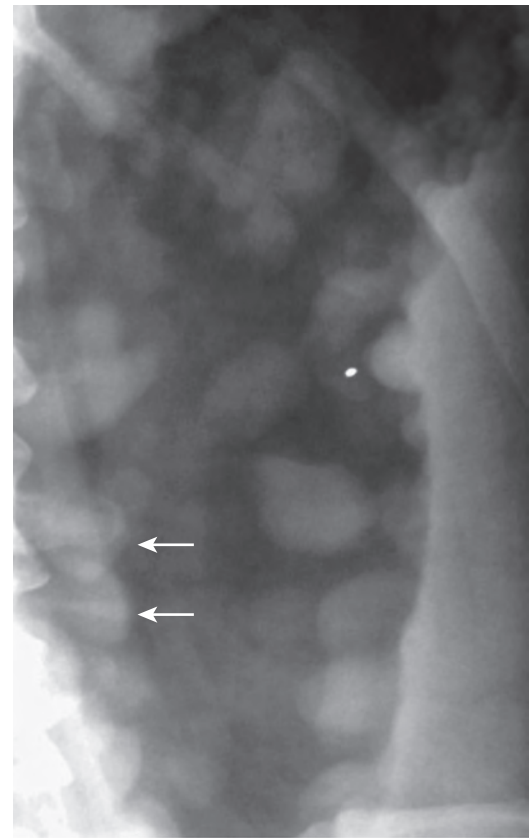


Figure 57-30 Intestinal complications of ulcerative colitis: toxic megacolon. Mucosal islands (arrows), deep ulcerations, and dilation establish the diagnosis.

pathologically, it appears thickened radiologically, presumably as a result of subserosal or omental edema. A radiolucent stripe may be noted running parallel to the colon, which probably represents the pericolic fat line.

The profound inflammation and extensive ulceration of toxic megacolon always abolish the haustral pattern, so that the presence of normal haustra excludes the diagnosis. Long fluid levels can be seen in the colon as well as small bowel distention, in keeping with an ileus.¹⁴⁸

Extraintestinal Complications of Inflammatory Bowel Disease

Extraintestinal manifestations develop in one fourth to one third of patients with IBD (Box 57-6).¹⁻⁷ They can be divided into three categories: (1) those intimately related to disease activity or extent of disease and are responsive to therapy directed at the bowel disease (e.g., arthritis, iritis); (2) those whose course is independent of underlying bowel disease (e.g., sclerosing cholangitis, ankylosing spondylitis); and (3) those caused by inadequate or disordered intestinal function (e.g., cholelithiasis, nephrolithiasis).¹⁻⁷

HEPATOBIILIARY COMPLICATIONS

The most frequent serious manifestations of extraintestinal IBD occur in the liver and biliary tract.¹⁻⁷ As a rule, these

BOX 57-6 EXTRACOLONIC MANIFESTATIONS OF ULCERATIVE COLITIS**HEPATOBIILIARY AND RENAL**

Nonspecific reactive hepatitis
 Sclerosing cholangitis
 Pericholangitis
 Chronic active hepatitis
 Cholangiocarcinoma
 Fatty infiltration
 Musculoskeletal
 Arthritis
 Ankylosing spondylitis
 Sacroiliitis
 Hypertrophic osteoarthropathy
 Avascular necrosis
 Ocular
 Uveitis and iritis
 Episcleritis
 Conjunctivitis
 Mucocutaneous
 Pyoderma gangrenosum
 Erythema nodosum
 Cutaneous vasculitis
 Stomatitis
 Urolithiasis and nephrolithiasis
 Amyloidosis
 Drug-related disease
 Bronchopulmonary
 Pulmonary vasculitis
 Pleuropericarditis

HEMATOLOGIC AND VASCULAR

Anemia from blood loss
 Autoimmune hemolytic anemia
 Thrombocytosis
 Thromboembolic disease
 Increased factors V and VIII
 Accelerated thromboplastin III levels
 Arteritis of aorta and subclavian artery
 Pancreas
 Drug-related pancreatitis

Adapted from Osterman MT, Lichtenstein GR: *Ulcerative colitis*. In Feldman M, Friedman LS, Branch LJ (eds): *Gastrointestinal and Liver Disease*, 8th ed. Philadelphia, Saunders, 2010, pp 1975–2090.

complications generally do not correlate with disease activity, duration, or severity, with the exception of fatty infiltration, which occurs in patients who tend to be more seriously ill, debilitated, and malnourished.¹⁻⁷

Hepatic Steatosis

Fatty liver is found on liver biopsy specimens in 20% to 25% of patients with IBD; it may be caused by fat malabsorption, hyperalimentation, sepsis, protein-losing enteropathy, malnutrition, and corticosteroids.¹⁻⁷ The imaging features of fatty liver are variable and depend on the amount of fat deposited, its distribution within the liver, and presence of associated hepatic disease. CT is the best noninvasive technique for the detection of hepatic steatosis because there is an excellent correlation between hepatic parenchymal CT attenuation and the level of hepatic fat found in liver biopsy specimens. Fatty deposition is usually diffuse; however, involvement can be focal, lobar,

segmental, or scattered in a bizarre pattern that rapidly appears and disappears.¹⁻⁷

Cholelithiasis

Of patients with Crohn's disease, 30% to 50% develop gallstones, especially those with extensive terminal ileal disease or after ileal resection. As a consequence of this ileal disease, these patients form lithogenic bile because of bile salt malabsorption or loss of the enterohepatic circulation. Ultrasonography is the primary modality for diagnosing gallstones.¹⁻⁷

Primary Sclerosing Cholangitis

Primary sclerosing cholangitis occurs in fewer than 2% to 5% of patients with IBD; it is usually associated with ulcerative colitis.¹⁻⁷ Ultrasonography, CT, and MRI (Fig. 57-31) can directly visualize the fibrous mural thickening of the larger bile ducts that characterize this disease.^{1-7,149} The thickening may be concentric or asymmetric and usually measures 2 to 5 mm. Other suggestive diagnostic signs include focal duct dilation, discrepancy between the size of the intrahepatic and extrahepatic bile ducts, focal clustering of intrahepatic ducts, and discontinuous areas of minimal intrahepatic biliary dilation without associated hepatic, porta hepatis, or pancreatic masses. The cholangiographic signs of beading, pruning, and nodular mural thickening can also be seen on cross-sectional imaging, but usually with less detail and precision.¹⁴⁹

CT, ultrasonography, and MRI offer three major advantages in evaluating patients with known or suspected sclerosing cholangitis.¹⁴⁹ First, they are noninvasive techniques that are quite safe in these patients, who often need multiple serial examinations. Second, they can visualize the entire biliary tract in patients in whom strictures obstruct the flow of contrast medium during cholangiography, occasionally leaving large portions of the intrahepatic ducts unexamined. Finally, CT and ultrasonography can depict complications of sclerosing cholangitis, such as cirrhosis and portal hypertension, and soft tissue masses associated with cholangiocarcinoma.¹⁴⁹ Magnetic resonance cholangiopancreatography (MRCP) is the best noninvasive means of establishing the diagnosis.¹⁴⁹ Patients with ulcerative colitis and sclerosing cholangitis are at greater risk for developing cholangiocarcinoma and secondary biliary cirrhosis.

Liver Abscess

Hepatic abscess is an uncommon complication of Crohn's disease. In one institution, they accounted for 8% of all liver abscesses.^{2,4,150} They usually develop in patients with longstanding disease but may occur as the initial manifestation of Crohn's disease.^{2,4,150} Corticosteroids and other immunosuppressive agents, perforation, intra-abdominal abscess, and anastomotic leaks are all predisposing factors to the development of a hepatic abscess in patients with Crohn's disease.^{2,4,150}

PANCREATIC COMPLICATIONS

Of patients with Crohn's disease, 1% to 2% develop pancreatitis from a variety of causes: (1) drugs such as corticosteroids, azathioprine, and metronidazole; (2) choledocholithiasis; (3) fistula from the adjacent gut; (4) sclerosing cholangitis; (5) dysfunction of the sphincter of Oddi or stenosis of the descending duodenum, leading to obstruction of the duct or

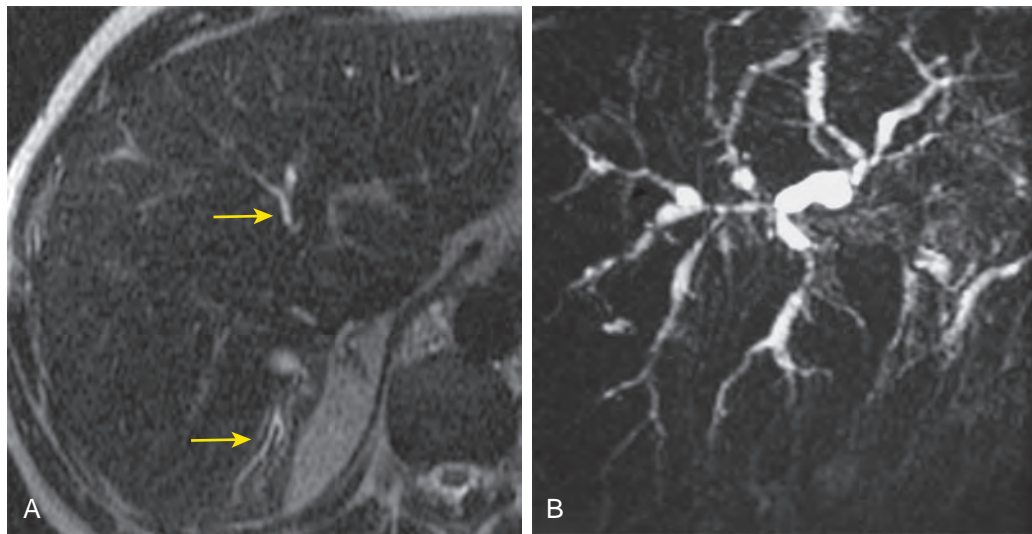


Figure 57-31 Sclerosing cholangitis. Axial T2-weighted MR images shows focal dilation of intrahepatic bile ducts in two areas (arrows). **B.** MRCP image shows multifocal strictures and irregularity of the intrahepatic bile ducts.

reflux of duodenal contents into the duct; and (6) autoantibodies against pancreatic acinar cells. Regardless of the cause, cross-sectional imaging is needed to help confirm the diagnosis of pancreatitis and, more importantly, its complications.¹⁵¹

URINARY TRACT COMPLICATIONS

Nephrolithiasis

Of patients with Crohn's disease, 2% to 10% develop nephrolithiasis as a result of water and electrolyte losses from diarrhea, malabsorption, and large ileostomy output. Oxalate stones are most common and, because they are not calcified, they may not be visible using conventional radiologic techniques.^{152,153} Non-contrast CT scans and, to a lesser degree, ultrasonography detect these stones more readily.

Hydronephrosis

Hydronephrosis may develop in patients with Crohn's disease for a variety of reasons, including calculous disease or obstruction resulting from the inflammatory effect of an abscess or phlegmon or the mass effect of creeping fat of the mesentery.^{152,153} CT is useful in detecting the hydronephrosis and obstructing mass.

Fistulas

Fistulas may develop between diseased gut and the kidney in patients with Crohn's disease, leading to a renal or perinephric abscess.^{2,4,6} Usually, enterovesical fistulas develop. Although these fistulas should first be evaluated with conventional barium studies, excretory urography, and cystography, the origin of the fistula may be edematous and prevent contrast opacification, and tiny fistulous tracts may not be seen. Conventional studies detect fewer than 50% of enterovesical fistulas; CT has an almost 90% success rate.¹⁵⁰ CT scans are initially obtained with only oral and rectal contrast administration. The presence of gas and small amounts of contrast material entering through the fistula may be obscured if the bladder is opacified after the IV injection of iodinated contrast medium.

MUSCULOSKELETAL COMPLICATIONS

Arthropathy

Arthritis is one of the most common extraintestinal manifestations of IBD; it is manifested as a peripheral arthritis or sacroiliitis-spondylitis.¹⁵⁴⁻¹⁵⁹ The radiologic findings of peripheral enteropathic arthritis are usually minimal and best seen, if at all, with conventional radiographs. The changes in the axial skeleton, affecting 3% to 16% of patients with IBD, are similar to those of ankylosing spondylitis.¹⁵⁴⁻¹⁵⁸ CT and MRI can often detect the subtle changes of early sacroiliitis before they become apparent on radiographs—bilateral, usually symmetric joint narrowing with osseous erosions followed by sclerosis are more pronounced on the iliac side of the articulation.¹⁵⁴⁻¹⁵⁸ Eventually, bony ankylosis occurs. T1-weighted fat-suppression images are superior at demonstrating the cortical erosion and subchondral sclerosis of sacroiliitis.

Avascular Necrosis

Osteonecrosis is a rare complication of IBD and usually occurs in the following clinical settings: during or after corticosteroid therapy; during TPN, especially with lipid emulsions; and most recently as a direct complication of the disease, without other precipitating factors.¹⁵⁴⁻¹⁵⁸

MRI is the best technique for establishing this diagnosis, with a reported sensitivity of 97% and specificity of 98%.¹⁵⁴⁻¹⁵⁸ On T1-weighted images, areas of low signal intensity may be seen beneath the articular surface. Alternatively, bands of low signal intensity are seen surrounding a central area of higher signal intensity. On T2-weighted images, areas of low signal intensity can become bright, and regions of high signal intensity remain high.

Asymptomatic and radiologically normal hips may have early signs of avascular necrosis on CT studies. These include subtle alterations in trabecular pattern, joint space integrity, and femoral head and acetabular contour, which may be undetected or ill-defined on radiographs.

Osteomyelitis and Septic Arthritis

Septic arthritis of the hip can complicate a psoas or retroperitoneal abscess tracking through the greater sciatic notch. MRI and CT show these changes before their recognition on radiographs.

The iliac bone and sacrum are the most frequent sites of osteomyelitis in patients with Crohn's disease. They are almost invariably the result of an adjacent pelvic abscess or enteric fistula. Accordingly, osteomyelitis is usually diagnosed on cross-sectional imaging when the abscess is identified. CT findings in osteomyelitis include cortical bone destruction, intraosseous gas, increased attenuation of the bone marrow, narrowing of the medullary cavity, serpentine drainage tracts, and the presence of an involucrum or sequestrum. With MRI, the marrow space of the involved bone demonstrates decreased signal on T1-weighted images and increased signal on T2-weighted images. Cortical destruction or thickening and edema or abscess formation in the soft tissues can also be demonstrated on MRI.

Spinal epidural abscess has been reported from fistulization of a presacral or psoas abscess in patients with Crohn's disease. Prevertebral, intraforaminal, and epidural gas may be seen on CT and MRI studies.

Osteoporosis

Osteoporosis is a common complication of IBD. Osteoporosis and osteomalacia occur secondary to malabsorption with resultant calcium and vitamin D deficiency and can also be related to corticosteroid therapy.

Psoas Abscess

Crohn's disease complications now account for 73% of all psoas abscesses.^{36,160} On the right, a psoas abscess may develop secondary to terminal ileal disease and, on the left, it can result from sigmoid or jejunal involvement. Most patients with psoas abscess have well-established Crohn's disease, but the clinical manifestations may be nonspecific. Occasionally, psoas abscess may be seen at the initial presentation of disease. CT has emerged as the single best examination for its diagnosis. CT can also direct percutaneous abscess drainage in these patients.¹⁶¹ Primary rectus sheath abscesses have also been reported as a complication of Crohn's disease and may be visualized with CT, MRI, or ultrasonography.

PULMONARY COMPLICATIONS

Although clinically significant, pulmonary manifestations are uncommon in patients with IBD. Prospective studies have identified pulmonary abnormalities in 30% to 50% of cases. There are four major clinicopathologic categories of disease: (1) airway disease (chronic bronchitis, bronchiectasis, bronchiolitis); (2) interstitial lung disease (bronchiolitis obliterans, interstitial lung disease); (3) necrobiotic nodules; and (4) serositis. Respiratory or pleuropericardial disease is much more common in ulcerative colitis than in Crohn's disease.¹⁻⁶

Differential Diagnosis of Colitis

Ulcerative colitis and Crohn's disease are responsible for most cases of enterocolitis in North America and Europe. However, infectious enteritis and colitis have been occurring more

frequently because of increased global travel and immigration, the indiscriminate use of antibiotics, and more widespread immunosuppression resulting from the large numbers of those infected by HIV, chemotherapy, and bone marrow, stem cell, and organ transplantation.¹⁻¹² Because the small bowel and colon have only a limited variety of response to a wide variety of insults, it is not surprising that the infectious enterocolitides often simulate the radiologic (Table 57-3) and clinical (Table 57-4) features of IBD. The definitive diagnosis of infectious or idiopathic IBD ultimately rests on histologic and bacteriologic documentation.

The differentiation of Crohn's colitis and ulcerative colitis is important because each disease has different therapeutic and prognostic implications. Patients with ulcerative colitis have a higher risk of developing cancer. They can also have a curative colectomy and are candidates for sphincter-preserving surgery. Patients with Crohn's disease are not candidates for ileal reservoirs because disease may recur in the ileum. The following double-contrast barium enema features enable the correct diagnosis to be made in most patients:

- 1. Ulcerative colitis is a contiguous, confluent, circumferential, and symmetric disease that begins in the rectum and extends proximally.

TABLE 57-3 Inflammatory Bowel Disease: Radiologic Differential Diagnosis		
Feature	Commonly Found In	May Occur In
Granular mucosa	Ulcerative colitis	Early Crohn's colitis (rare)
Ulceration	Crohn's colitis	Amebiasis
Discrete	<i>Yersinia</i> infection	Ischemia
	Behçet's disease	Tuberculosis
	Ulcerative colitis	Crohn's disease
Confluent (shallow)		Amebiasis
Confluent (deep)	Crohn's disease	Ischemia
		Amebiasis
		Tuberculosis
		<i>Strongyloides</i> infection
		Tuberculosis
Stricture	Ulcerative colitis	
Symmetric	Lymphogranuloma venereum	
Asymmetric	Crohn's disease	
	Ischemia	
	Tuberculosis	
Fistula	Crohn's disease	Tuberculosis
	Lymphogranuloma venereum	Actinomycosis
Inflammatory polyps	Ulcerative colitis	Ischemia (rare)
	Crohn's disease	
	Schistosomiasis	
	Colitis cystica profunda	
Small bowel disease	Crohn's disease	Ulcerative colitis (backwash ileitis)
	<i>Yersinia</i> infection	Behçet's disease
	Tuberculosis	Ischemia
	Pseudomembranous enterocolitis	
Skip lesions	Crohn's disease	Lymphogranuloma venereum
	Tuberculosis	
	Amebiasis	
Toxic megacolon	Ulcerative colitis	Crohn's disease
		Ischemia
		Amebiasis

From Bartram CI, Laufer I: Inflammatory bowel disease. In Laufer I, Levine MS (eds): Double Contrast Gastrointestinal Radiology, 2nd ed. Philadelphia, WB Saunders, 1992, pp 579-645.

TABLE 57-4 Inflammatory Bowel Disease: Clinical Differential Diagnosis

Ulcerative Colitis	Crohn's Disease
Pancolitis	Ileal and jejunal
<i>Campylobacter</i> infection	<i>Yersinia enterocolitis</i>
Shigellosis	Salmonellosis
Salmonellosis	Tuberculosis
Cytomegalovirus infection	<i>Strongyloides</i> infection
<i>Escherichia coli</i> infection	Lymphoma
<i>Clostridium difficile</i> infection	Radiation enteritis
Amebiasis	Carcinoid
Behçet's disease	Eosinophilic enteritis
Graft-versus-host disease	Carcinoma (rare)
Radiation colitis	Ileocecal
Diverticular disease	Tuberculosis
Ischemic colitis	Typhlitis
Proctosigmoiditis	Amebiasis
Herpes simplex infection	Graft-versus-host disease
Gonorrhea	Appendicitis
<i>Chlamydia</i> infection	Carcinoma
	Colonic
	Diverticulitis
	Carcinoma
	Amebiasis
	Tuberculosis
	Ischemic colitis
	Radiation colitis
	<i>Chlamydia</i> infection

Adapted from Osterman MT, Lichtenstein GR: Ulcerative colitis. In Feldman M, Friedman LS, Branch LJ (eds): *Gastrointestinal and Liver Disease*, 8th ed. Philadelphia, Saunders, 2010, pp 1975–2090.

- Crohn's disease is a patchy, discontinuous disease with asymmetric involvement that can lead to pseudodiverticula.
- The following types of ulcerations are characteristic of Crohn's disease: aphthoid, discrete, deep (>3 mm), fissuring, and rose thorn.

- Granular mucosa is typical in ulcerative colitis but not in Crohn's colitis.
- Severe anal and perianal disease is characteristic of Crohn's disease but is exceptionally rare in ulcerative colitis.
- Spontaneous fistula and sinus tracts are a hallmark of Crohn's disease.

Certain CT findings can help differentiate granulomatous and ulcerative colitis. Mural stratification is seen in 61% of patients with chronic ulcerative colitis but in only 8% of patients with chronic granulomatous colitis. Also, mean colon wall thickness in chronic ulcerative colitis is 7.8 mm, significantly smaller than that observed in Crohn's colitis (11 mm). Finally, the outer contour of the thickened colonic wall is smooth and regular in 95% of ulcerative colitis cases, whereas serosal and outer mural irregularities are present in 80% of granulomatous colitis patients.

Differentiation between these two diseases can be made on radiologic grounds in 90% to 95% of patients. The distinction is easier to make in the early stages of disease because the early manifestations are particularly distinctive. When the disease is chronic or when there have been numerous exacerbations and remissions, the distinction may be more difficult. For example, ulcerative colitis in remission may become discontinuous, whereas granulomatous colitis may involve the entire colon.^{1-6,162}

Summary

The radiologic diagnosis of ulcerative colitis and Crohn's disease is challenging. It embraces a variety of examination techniques that must be performed and interpreted with care if the radiologist is to make a significant contribution to patient management. An understanding of the anatomic and pathophysiologic basis of the radiologic features of IBD is important to appreciate the natural history and differentiating features of these perplexing diseases fully.¹⁶³⁻¹⁶⁵

REFERENCES

- Adams SM, Bornemann PH: Ulcerative colitis. *Am Fam Physician* 87:699–705, 2013.
- Sands BE, Siegel CA: Crohn's disease. In Feldman MS, Friedman LS, Sleisenger MH, editors: *Gastrointestinal and Liver Disease*, ed 8, Philadelphia, 2010, Saunders, pp 1941–1974.
- Shanahan F: Ulcerative colitis. In Weinstein WM, Hawkey CJ, Bosch J, editors: *Clinical Gastroenterology and Hepatology*, New York, 2005, Elsevier Mosby, pp 341–342.
- Vermeire S, Rutgeerts P: Crohn's disease. In Weinstein WM, Hawkey CJ, Bosch J, editors: *Clinical Gastroenterology and Hepatology*, New York, 2005, Elsevier Mosby, pp 359–376.
- Greeson JK, Odze RD: Inflammatory diseases of the large intestine. In Odze RD, Goldblum JR, Crawford JM, editors: *Surgical Pathology of the GI Tract, Liver, Biliary Tract, and Pancreas*, ed 2, Philadelphia, 2009, Saunders, pp 269–320.
- Robert ME: Inflammatory diseases of the small intestine. In Odze RD, Goldblum JR, Crawford JM, editors: *Surgical Pathology of the GI Tract, Liver, Biliary Tract, and Pancreas*, ed 2, Philadelphia, 2010, Saunders, pp 321–354.
- Ekbom BT: The changing epidemiology of inflammatory bowel diseases. In Cohen RD, editor: *Inflammatory Bowel Disease: Diagnosis and Therapy*, ed 2, New York, 2011, Springer, pp 17–26.
- Mayer L, Agarwal S: Genetic testing for inflammatory bowel disease: Current knowledge and future trends. In Bernstein CN, editor: *The Inflammatory Bowel Disease Yearbook*, London, 2013, Remedica, pp 43–57.
- Mahid SS, Minor KS, Soto RE, et al: Smoking and inflammatory bowel disease: A meta-analysis. *Mayo Clin Proc* 81:1462–1471, 2006.
- Cantor M, Bernstein CN: Clinical course and natural history of ulcerative colitis. In Sartor RB, Sandborn WJ, editors: *Kirsner's Inflammatory Bowel Disease*, ed 6, Edinburgh, 2004, Saunders, pp 245–263.
- Munkholm P, Binder V: Clinical features and natural history of Crohn's disease. In Sartor RB, Sandborn WJ, editors: *Kirsner's Inflammatory Bowel Disease*, ed 6, Edinburgh, 2004, Saunders, pp 289–300.
- Raine T: Insights from immunology: New targets for new drugs? *Best Pract Res Clin Gastroenterol* 28:411–420, 2014.
- Forcione DG, Sands BE: Differential diagnosis of inflammatory bowel disease. In Sartor RB, Sandborn WJ, editors: *Kirsner's Inflammatory Bowel Disease*, ed 6, Edinburgh, 2004, Saunders, pp 370–379.
- Farrell RJ, Peppercorn MA: Endoscopy inflammatory bowel disease. In Sartor RB, Sandborn WJ, editors: *Kirsner's Inflammatory Bowel Disease*, ed 6, Edinburgh, 2004, Saunders, pp 380–398.
- Bartram CI: Ulcerative colitis. In Bartram CI, editor: *Radiology in Inflammatory Bowel Disease*, New York, 1983, Marcel Dekker, pp 31–62.
- Bartram CI: Plain abdominal x-ray in acute colitis. *Proc Soc Med* 69:617–618, 1976.
- Bartram CI: Radiology in the current assessment of ulcerative colitis. *Gastrointest Radiol* 1:383–392, 1977.
- Gabrielsson N, Grandvist S, Sundelin P, et al: Extent of inflammatory lesions in ulcerative colitis assessed by radiology, colonoscopy, and endoscopic biopsies. *Gastrointest Radiol* 4: 395–400, 1979.
- Prantera C, Lorenzetti R, Cerro P, et al: The plain abdominal film accurately estimates

- extent of active ulcerative colitis. *J Clin Gastroenterol* 13:231–234, 1991.
20. Rice RP: Plain abdominal film roentgenographic diagnosis of ulcerative disease of the colon. *Radiology* 104:544–550, 1968.
 21. Simpson SA, Lewis JR: Plain roentgenography in diagnosis of chronic ulcerative colitis and terminal ileitis. *Radiology* 84:306–315, 1960.
 22. McConnell F, Hanelin J, Robbins LL: Plain film diagnosis of fulminating ulcerative colitis. *Radiology* 71:674–682, 1958.
 23. Caprilli R, Vernia P, Latella G, et al: Early recognition of toxic megacolon. *J Clin Gastroenterol* 9:160–164, 1987.
 24. Bartram CI, Herlinger H: Bowel wall thickness as a differentiating feature between ulcerative colitis and Crohn's disease of the colon. *Clin Radiol* 30:15–19, 1979.
 25. Lichtenstein JE: Radiologic-pathologic correlation of inflammatory bowel disease. *Radiol Clin North Am* 25:324, 1987.
 26. Laufer I, Mullens JE, Hamilton J: Correlation of endoscopy and double-contrast radiography in the early stages of ulcerative and granulomatous colitis. *Radiology* 118:15, 1988.
 27. Simpkins KC: Inflammatory bowel disease: Ulcerative and Crohn's colitis. In Simpkins KC, editor: *A Textbook of Radiological Diagnosis, vol 4: The Alimentary Tract: The Hollow Organs and Salivary Glands*, London, 1988, HK Lewis, pp 473–498.
 28. Bartram CI, Laufer I: Inflammatory bowel disease. In Laufer I, Levine MS, editors: *Double Contrast Gastrointestinal Radiology*, ed 2, Philadelphia, 1992, WB Saunders, pp 580–645.
 29. Kelvin FM, Gardiner RH: *Clinical Imaging of the Colon and Rectum*, New York, 1987, Raven, pp 64–119.
 30. Laufer I: The radiologic demonstration of early changes in ulcerative colitis by double contrast techniques. *J Can Assoc Radiol* 26: 116–121, 1975.
 31. Riddell RH: Pathology of idiopathic inflammatory bowel disease. In Sartor RB, Sandborn WJ, editors: *Kirsner's Inflammatory Bowel Disease*, ed 6, Edinburgh, 2004, Saunders, pp 399–424.
 32. Lichtenstein JE, Madewell JE, Feigen DS: The collar button ulcer. *Gastrointest Radiol* 4:79–84, 1979.
 33. Suekane H, Iida M, Matsui T, et al: Radiographic demonstration of longitudinal ulcers in patients with ulcerative colitis. *Gastrointest Radiol* 4:103–112, 1980.
 34. Zegel H, Laufer I: Filiform polypoidosis. *Radiology* 127:615–619, 1978.
 35. Bray JF: Filiform polypoidosis of the small bowel in Crohn's disease. *Gastrointest Radiol* 8:155–156, 1983.
 36. Gardiner GA: "Backwash ileitis" with pseudopolypoidosis. *AJR* 129:506–507, 1977.
 37. Kirks DR, Currarino G, Berk RN: Localized giant pseudopolypoidosis of the colon. *Am J Gastroenterol* 69:609–614, 1978.
 38. Hammerman AM, Shatz BA, Susman N: Radiographic characteristics of colonic "mucosal bridges": Sequelae of inflammatory bowel disease. *Radiology* 127:611–614, 1978.
 39. Bartram CI: Complications of ulcerative colitis. In Bartram CI, editor: *Radiology in Inflammatory Bowel Disease*, New York, 1983, Marcel Dekker, pp 63–118.
 40. Bartram CI: Complications of Crohn's disease. In Bartram CI, editor: *Radiology in Inflammatory Bowel Disease*, New York, 1983, Marcel Dekker, pp 169–202.
 41. Gore RM: Colonic contour changes in chronic ulcerative colitis: Reappraisal of some old concepts. *AJR* 158:59–61, 1992.
 42. Gore RM: Characteristic morphologic changes in chronic ulcerative colitis. *Abdom Imaging* 20:275–278, 1995.
 43. Poppel MH, Beranbaum SL: The indenture sign in acute exudative colitis. *Am J Dig Dis* 1:382–388, 1957.
 44. Campbell WL: Cathartic colon: Reversibility of roentgen changes. *Dis Colon Rectum* 23:445–449, 1983.
 45. Kim SK, Gerle RD, Rozanski R: Cathartic colitis. *AJR* 131:1079–1081, 1978.
 46. Kattan KR, King AY: Presacral space revisited. *AJR* 132:437–439, 1979.
 47. Krestin GP, Beyer D, Steinbrich W: Computed tomography in the differential diagnosis of the enlarged retrorectal space. *Gastrointest Radiol* 11:364–369, 1986.
 48. Edling NPG, Eklof O: The retrorectal soft tissue space in ulcerative colitis. *Radiology* 80:949–953, 1963.
 49. Eklof O, Gierup J: The retrorectal soft tissue space in children: Normal variations and appearance in granulomatous colitis. *AJR* 108:624–627, 1970.
 50. Lew RJ, Ginsberg GG: The role of endoscopic ultrasound in inflammatory bowel disease. *Gastrointest Endosc Clin North Am* 12:561–571, 2002.
 51. Marshak RH, Boch C, Wolf BS: The roentgen findings in strictures of the colon associated with ulcerative and granulomatous colitis. *AJR* 90:709–716, 1963.
 52. Goldberg HI, Gore RM, Margulis AR, et al: Computed tomography in the evaluation of Crohn's disease. *AJR* 140:277–282, 1983.
 53. Dombal FT, Watts JM, Watkinson G, et al: Local complications of ulcerative colitis: Stricture, pseudopolypoidosis, and carcinoma of the colon and rectum. *BMJ* 1:1442–1447, 1966.
 54. Goulston SJM, McGovern VJ: The nature of benign strictures in ulcerative colitis. *N Engl J Med* 281:290–295, 1969.
 55. Antes G: Inflammatory diseases of the large intestine, colon, contrast enema and CT. *Radiology* 38:41–45, 1998.
 56. Gore RM, Balthazar EJ, Ghahremani GG, et al: CT features of ulcerative colitis and Crohn's disease. *AJR* 167:3–15, 1996.
 57. Hoeffel C, Crema MD, Belkacem A, et al: Multi-detector row CT: Spectrum of diseases involving the ileocecal area. *Radiographics* 26:1373–1390, 2006.
 58. Horton KM, Corl FM, Fishman EK: CT evaluation of the colon: Inflammatory disease. *Radiographics* 20:399–418, 2000.
 59. Gore RM, Marn CS, Kirby DE, et al: CT findings in ulcerative, granulomatous, and indeterminate colitis. *AJR* 143:279–284, 1984.
 60. Gore RM, Lichtenstein JE: The gastrointestinal tract: Anatomic-pathologic basis of radiologic findings. In Taveras JM, Ferrucci JT, editors: *Radiology: Diagnosis-Imaging-Intervention*, Philadelphia, 1994, JB Lippincott, pp 1–42.
 61. Gore RM, Goldberg HI: Computed tomographic evaluation of the gastro-intestinal tract in diseases other than primary adenocarcinoma. *Radiol Clin North Am* 20:781–796, 1982.
 62. Gore RM, Ghahremani GG: Radiological investigation of acute inflammatory and infectious bowel disease. *Gastroenterol Clin North Am* 24:353–384, 1995.
 63. Balthazar EJ: CT of the gastrointestinal tract: Principles and interpretation. *AJR* 156:23–32, 1991.
 64. Thoeni RF, Cello JP: CT imaging of colitis. *Radiology* 240:623–638, 2006.
 65. Philpotts LE, Heiken JP, Westcott MA, et al: Colitis: Use of CT findings in differential diagnosis. *Radiology* 190:445–449, 1994.
 66. Gore RM: Cross-sectional imaging of inflammatory bowel disease. *Radiol Clin North Am* 25:115–127, 1987.
 67. Gore RM: CT of inflammatory bowel disease. *Radiol Clin North Am* 27:717–730, 1989.
 68. De Pascale A, Garofalo G, Perna M, et al: Contrast-enhanced ultrasonography in Crohn's disease. *Radiol Med (Torino)* 111:539–550, 2006.
 69. Grand DJ, Harris A, Loftus EV, Jr: Imaging for luminal disease and complications: CT enterography, MR enterography, small-bowel follow-through, and ultrasound. *Gastroenterol Clin North Am* 41:497–512, 2012.
 70. Calabrese E, Zorzi F, Pallone F: Ultrasound in Crohn's disease. *Curr Drug Targets* 13:1224–1233, 2012.
 71. Maconi G, Radice E, Greco S, et al: Bowel ultrasound in Crohn's disease. *Best Pract Res Clin Gastroenterol* 20:93–112, 2006.
 72. Al-Hawary M, Zimmermann EM: A new look at Crohn's disease: Novel imaging techniques. *Curr Opin Gastroenterol* 28:334–340, 2012.
 73. Parente F, Greco S, Molteni M, et al: Imaging inflammatory bowel disease using bowel ultrasound. *Eur J Gastroenterol Hepatol* 17:283–291, 2005.
 74. Ajaj WM, Lauenstein TC, Pelster G, et al: Magnetic resonance colonography for the detection of inflammatory diseases of the large bowel: Quantifying the inflammatory activity. *Gut* 54:257–263, 2005.
 75. Maccioni F, Bruni A, Viscido A, et al: MR imaging in patients with Crohn disease: Value of T2- versus T1-weighted gadolinium-enhanced MR sequences with use of an oral superparamagnetic contrast agent. *Radiology* 238:517–530, 2006.
 76. Low RN, Francis IR: MR imaging of the gastrointestinal tract with IV gadolinium and diluted oral contrast media compared with unenhanced MR imaging and CT. *AJR* 169: 1051–1054, 1997.
 77. Schreyer AG, Rath HC, Kikinis R, et al: Comparison of magnetic resonance imaging colonography with conventional colonoscopy for the assessment of intestinal inflammation in patients with inflammatory bowel disease: A feasibility study. *Gut* 54:250–256, 2005.
 78. Schreyer AG, Golder S, Scheibl K, et al: Dark lumen magnetic resonance enteroclysis in combination with MRI colonography for whole bowel assessment in patients with Crohn's disease: First clinical experience. *Inflamm Bowel Dis* 11:388–394, 2005.
 79. Rottgen R, Herzog H, Lopez-Hanin E, et al: Bowel wall enhancement in magnetic resonance colonography for assessing activity in Crohn's disease. *Clin Imaging* 30:27–31, 2006.
 80. Aburano T, Saito Y, Shuke N, et al: Tc-99m leukocyte imaging for evaluating disease severity and monitoring treatment response in ulcerative colitis: Comparison with colonoscopy. *Clin Nucl Med* 23:509–513, 1998.
 81. Loffler M, Weckesser M, Franzius C, et al: High diagnostic value of ¹⁸F-FDG-PET in pediatric patients with chronic inflammatory bowel disease. *Ann N Y Acad Sci* 1072:379–385, 2006.

82. Annovazzi A, Bagni B, Burrioni L, et al: Nuclear medicine imaging of Inflammatory/infective disorders of the abdomen. *Nucl Med Commun* 26:657–664, 2005.
83. Kerry JE, Marshall C, Griffiths PA, et al: Comparison between Tc-HMPAO labelled white cells and Tc LeukoScan in the investigation of inflammatory bowel disease. *Nucl Med Commun* 26:245–251, 2005.
84. Almer S, Bodemar G, Lindstrom E, et al: Air enema radiology compared with leukocyte scintigraphy for imaging in inflammation in active colitis. *Eur J Gastroenterol Hepatol* 7:59–64, 1995.
85. Shen B, Hao W: Optimizing antitumor necrosis therapy for inflammatory bowel disease. In Bernstein CN, editor: *The Inflammatory Bowel Disease Yearbook*, London, 2013, Remedica, pp 58–59.
86. Sandborn WJ: Medical therapy for Crohn's disease. In Sartor RB, Sandborn WJ, editors: *Kirsner's Inflammatory Bowel Disease*, ed 6, Edinburgh, 2004, Saunders, pp 503–530.
87. Caprilli R, Viscido A, Latella G: Current management of severe ulcerative colitis. *Nat Clin Pract Gastroenterol Hepatol* 4:92–101, 2007.
88. Marion JF, Present DH: Indications for surgery in inflammatory bowel disease from the gastroenterologist's point of view. In Sartor RB, Sandborn WJ, editors: *Kirsner's Inflammatory Bowel Disease*, ed 6, Edinburgh, 2004, Saunders, pp 585–595.
89. Steinhart AJ: Laparoscopic surgery for inflammatory bowel disease. In Bernstein CN, editor: *The Inflammatory Bowel Disease Yearbook*, London, 2013, Remedica, pp 128–161.
90. Cima RR, Pemberton JH: Surgical management of ulcerative colitis. In Sartor RB, Sandborn WJ, editors: *Kirsner's Inflammatory Bowel Disease*, ed 6, Edinburgh, 2004, Saunders, pp 602–614.
91. Bemelman WA, Allez M: The surgical intervention: Earlier or never? *Best Pract Res Clin Gastroenterol* 28:497–503, 2014.
92. Crema MD, Richarme D, Azizi L, et al: Pouchography, CT, and MRI features of ileal J pouch-anal anastomosis. *AJR* 187:594–603, 2006.
93. Nadgir RN, Soto JA, Dendrinos K, et al: MRI of complicated pouchitis. *AJR* 187:386–391, 2006.
94. Gosselink MP, West RL, Kuipers EJ, et al: Integrity of the anal sphincters after pouch-anal anastomosis: Evaluation with three-dimensional endoanal ultrasonography. *Dis Colon Rectum* 48:1728–1735, 2005.
95. Brown JJ, Balfe DM, Heiken JP, et al: Ileal J pouch: Radiologic evaluation in patients with and without postoperative complications. *Radiology* 174:115–120, 1990.
96. Kremers PW, Scholz FJ, Schoetz DJ, et al: Radiology of the ileoanal reservoir. *AJR* 145:559–567, 1985.
97. Lycke KG, Gothlin JH, Jensen JK, et al: Radiology of the continent ileostomy reservoir: I. Method of examination and normal findings. *Abdom Imaging* 19:116–123, 1994.
98. Alfsher MM, Scholz FJ, Robert PL, et al: Radiology of ileal pouch-anal anastomosis: Normal findings, examination pitfalls, and complications. *Radiographics* 17:81–98, 1997.
99. Thoeni RF, Fell C, Engelstad B, et al: Ileoanal pouches: Comparison of CT, scintigraphy and contrast enemas for diagnosing post-surgical complications. *AJR* 154:73–78, 1990.
100. Lycke KG, Gothlin JH, Jensen JK, et al: Radiology of the continent ileostomy reservoir: II. Findings in patients with late complications. *Abdom Imaging* 19:124–131, 1994.
101. Lockhart-Mummery HE, Morson BC: Crohn's disease (regional enteritis) of the large intestine and its distinction from ulcerative colitis. *Gut* 1:87–105, 1960.
102. Crohn BB, Ginzburg L, Oppenheimer GD: Regional ileitis: A pathologic and clinical entity. *JAMA* 99:1323–1329, 1932.
103. Kelvin FM, May RJ, Norton GA: Lymphoid follicular pattern of the colon in adults. *AJR* 133:831–835, 1979.
104. Laufer I, Desa D: Lymphoid follicular pattern: A normal feature of the pediatric colon. *AJR* 130:51–55, 1978.
105. Kenney PJ, Koehler RE, Shackelford GD: The clinical significance of large lymphoid follicles of the colon. *Radiology* 142:41–46, 1982.
106. Bronen RA, Glick SN, Teplick SH: Diffuse lymphoid follicles of the colon. *Radiology* 142:41–46, 1982.
107. Laufer I, Costopoulos L: Early lesions of Crohn's disease. *AJR* 130:307–311, 1978.
108. Simpkins KC: Aphthoid ulcers in Crohn's colitis. *Clin Radiol* 28:601–604, 1977.
109. Ekberg O, Lindstrom C: Superficial lesions in Crohn's disease of the small bowel. *Gastrointest Radiol* 4:389–392, 1979.
110. Degrysa HRM, DeSchepper AMAP: Aphthoid esophageal ulcers in Crohn's disease of ileum and colon. *Gastrointest Radiol* 9:197–201, 1984.
111. Ni XY, Goldberg HI: Aphthoid ulcers in Crohn's disease: Radiographic course and relationship to bowel appearance. *Radiology* 158:589–592, 1986.
112. Hizawa K, Aoyagi K, Fujishima M: The significance of colonic mucosal lymphoid hyperplasia and aphthoid ulcers in Crohn's disease. *Clin Radiol* 51:706–708, 1996.
113. Hizawa K, Iida M, Kohroggi N, et al: Crohn disease: Early recognition and progress of aphthous lesions. *Radiology* 190:451–454, 1994.
114. Goldberg HI, Gore RM, Margulis AR, et al: Computed tomography in the evaluation of Crohn disease. *AJR* 140:277–282, 1983.
115. Raptopoulos V, Schwartz RK, McNicholas MMJ, et al: Multiplanar helical CT enterography in patients with Crohn's disease. *AJR* 169:1545–1550, 1997.
116. Gore RM, Ghahremani GG, Miller FH: Cross-sectional imaging in the evaluation of Crohn's disease. In Prantera C, Korelitz BI, editors: *Crohn's Disease*, New York, 1996, Marcel Dekker, pp 145–185.
117. Jacobs JE, Birnbaum BA: CT of the inflammatory disease of the colon. *Semin Ultrasound CT MRI* 16:91–101, 1995.
118. Fishman EK, Wolf EJ, Jones B, et al: CT evaluation of Crohn's disease: Effect on patient management. *AJR* 148:537–541, 1987.
119. Gossios KJ, Tsianos EV: Crohn disease: CT findings after treatment. *Abdom Imaging* 22:160–163, 1997.
120. Scott EM, Freeman AH: Prominent omental and mesenteric vasculature in inflammatory bowel disease shown by computed tomography. *Eur J Radiol* 22:104–106, 1996.
121. Meyers MA, McGuire PV: Spiral CT demonstration of hypervascularity in Crohn disease: "Vascular jejunalization of the ileum" or the "comb sign." *Abdom Imaging* 20:327–332, 1995.
122. Herlinger H, Furth EE, Rubesin SE: Fibrofatty proliferation of the mesentery in Crohn's disease. *Abdom Imaging* 23:446–448, 1998.
123. Ribeiro MB, Greenstein AJ, Yamazaki Y, et al: Intra-abdominal abscess in regional enteritis. *Ann Surg* 213:32–36, 1991.
124. Lambiase RE, Cronan JJ, Dorfman GS: Percutaneous drainage of abscesses in patients with Crohn disease. *AJR* 150:1043–1045, 1988.
125. Casola G, vanSonnenberg E, Neff CC, et al: Abscess in Crohn's disease: Percutaneous drainage. *Radiology* 163:19–22, 1987.
126. Safrit HD, Mauro MA, Jaques PF: Percutaneous abscess drainage in Crohn's disease. *AJR* 148:859–862, 1987.
127. Doemeny JM, Burke DR, Meranze SG: Percutaneous drainage of abscesses in patients with Crohn's disease. *Gastrointest Radiol* 13:327–341, 1988.
128. Erden A, Cumhur T, Olger T: Superior mesenteric artery Doppler waveform changes in response to inflammation of the ileocecal region. *Abdom Imaging* 22:483–486, 1997.
129. van Oostayen JA, Wasser MNJM, van Hoge-zand RA, et al: Activity of Crohn disease assessed by measurements of superior mesenteric artery flow with Doppler US. *Radiology* 193:551–554, 1994.
130. Nemcek AA: Superior mesenteric artery Doppler waveform changes in response to inflammation of the ileocecal region. *Abdom Imaging* 22:487–488, 1997.
131. Funt SA, Krinsky G, Horowitz L: MR demonstration of submucosal fat in a patient with Crohn's disease. *J Comput Assist Tomogr* 20:940–941, 1996.
132. Ernst O, Asselah T, Cablan X, et al: Breath-hold fast spin-echo MR imaging of Crohn's disease. *AJR* 170:1273–1278, 1998.
133. Spencer JA, Chapple K, Wilson D, et al: Outcome after surgery for perianal fistula value of MR imaging. *AJR* 171:403–408, 1998.
134. Maconi G, Tonolini M, Monteleone M, et al: Transperineal perineal ultrasound versus magnetic resonance imaging in the assessment of perianal Crohn's disease. *Inflamm Bowel Dis* 19:2737–2743, 2013.
135. Vanbeckevoort D, Bielen D, Vanslebrouck R, et al: Magnetic resonance imaging of perianal fistulae. *Magn Reson Imaging Clin N Am* 22:113–123, 2014 Feb.
136. Assadsangabi A, Lobo AJ: Diagnosing and managing inflammatory bowel disease. *Practitioner* 257:13–18, 2013.
137. von Ritter C: Inflammatory bowel disease: Pathophysiology and medical treatment. *Radiologie* 38:3–7, 1998.
138. Milsom JW: Surgery of colorectal cancer and inflammatory bowel disease. *Curr Opin Gastroenterol* 9:42–48, 1993.
139. Doemeny JM, Burke DR, Maranze SG: Percutaneous abscess drainage in Crohn's disease. *AJR* 148:859–862, 1987.
140. Fearnhead NS, Chowdhury R, Box B: Long-term follow-up of stricturoplasty for Crohn's disease. *Br J Surg* 93:475–482, 2006.
141. Sanduleanu S, Rutter MD: Interval colorectal cancers in inflammatory bowel disease: The grim statistics and true stories. *Gastrointest Endosc Clin N Am* 24:337–348, 2014.
142. Stucchi AF, Aarons CB, Becker JM: Surgical approaches to cancer in patients who have inflammatory bowel disease. *Gastroenterol Clin North Am* 35:641–673, 2006.
143. Bernstein CN: Neoplasia in inflammatory bowel disease: Surveillance and management

- strategies. *Curr Gastroenterol Rep* 8:513–518, 2006.
144. Moum B, Ekblom A: Ulcerative colitis, colorectal cancer and colonoscopic surveillance. *Scand J Gastroenterol* 40:881–885, 2005.
145. Autenrieth DM, Baumgart DC: Toxic megacolon. *Inflamm Bowel Dis* 18:5845–5891, 2012.
146. Ausch C, Madoff RD, Gnant M, et al: Aetiology and surgical management of toxic megacolon. *Colorectal Dis* 8:195–201, 2006.
147. Goldberg HI: The barium enema and toxic megacolon: Cause-effect relationship? *Gastroenterology* 68:617–618, 1975.
148. Halpert RD: Toxic dilatation of the colon. *Radiol Clin North Am* 25:147–155, 1987.
149. Tsaitis C, Semertzidou A, Sinakos E: Update of inflammatory bowel disease in patients with primary sclerosing cholangitis. *World J Hepatol* 64:178–187, 2014.
150. Patel TR, Patel KN, Boyarsky AH, et al: Staphylococcal liver abscess and acute cholecystitis in a patient with Crohn's disease receiving infliximab. *J Gastrointest Surg* 10:105–110, 2006.
151. Moonsintong P, Loftus EV, Jr, Chari ST, et al: Acute pancreatitis in patients with Crohn's disease: Clinical features and outcomes. *Inflamm Bowel Dis* 11:1080–1084, 2005.
152. Banner MP: Genitourinary complications of inflammatory bowel disease. *Radiol Clin North Am* 25:199–204, 1987.
153. Mazziotti S, Blandino A, Scribano E, et al: MR enterography findings in abdominopelvic extraintestinal complications of Crohn's disease. *J Magn Reson Imaging* 37:1055–1063, 2013.
154. Al-Jarallah K, Shehab D, Al-Azmi W, et al: Rheumatic complications of inflammatory bowel disease among Arabs: A hospital-based study in Kuwait. *Int J Rheum Dis* 16:134–138, 2013.
155. Björkengren AG, Resnick D, Sartoris DJ: Enteropathic arthropathies. *Radiol Clin North Am* 25:189–198, 1987.
156. McEniff N, Eustace S, McCarthy C: Asymptomatic sacroiliitis in inflammatory bowel disease: Assessment by computed tomography. *Clin Imaging* 19:258–262, 1995.
157. Geijer M, Sihlbom H, Gothlin JH, et al: The role of CT in the diagnosis of sacroiliitis. *Acta Radiol* 39:265–268, 1998.
158. Ghahremani GG: Osteomyelitis of the ilium in patients with Crohn's disease. *AJR* 118:364–370, 1973.
159. Bernstein CN: Osteoporosis and other complications of inflammatory bowel disease. *Curr Opin Gastroenterol* 18:428–434, 2002.
160. Millward SE, Ramsewak W, Fitzsimons P: Percutaneous drainage of iliopsoas abscess in Crohn's disease. *Gastrointest Radiol* 11:289–290, 1986.
161. Boland GW, Mueller PR: Update on abscess drainage. *Semin Intervent Radiol* 13:27–40, 1996.
162. Tremaine WJ: Is indeterminate colitis determinable? *Curr Gastroenterol Rep* 14:162–165, 2012.
163. Kucharzik T, Maaser C, Luger A, et al: Recent understanding of IBD pathogenesis: Implications for future therapies. *Inflamm Bowel Dis* 12:1068–1083, 2006.
164. Lissner D, Siegmund B: Ulcerative colitis: Current and future treatment strategies. *Dig Dis* 31:91–94, 2013.
165. Marchioni Beery R, Kane S: Current approaches to the management of new-onset ulcerative colitis. *Clin Exp Gastroenterol* 7:111–132, 2014.

Other Inflammatory Conditions of the Colon

RICHARD M. GORE | SETH N. GLICK | ALEKSANDAR M. IVANOVIC

CHAPTER OUTLINE

Bacterial Infections

Salmonellosis
Shigellosis
Campylobacteriosis
Yersinia Enterocolitis
Colitis Caused by *Escherichia coli* O157:H7
Tuberculosis
Actinomycosis

Viral Infections

Parasitic Infections

Anisakiasis
Amebiasis
Schistosomiasis
Strongyloidiasis
Trichuriasis

Fungal Infections

Histoplasmosis
Mucormycosis

Noninfectious Colitis

Nonspecific Ulcer
Microscopic (Collagenous) Colitis
Eosinophilic Colitis
Graft-Versus-Host Disease
Retractile Mesenteritis
Reactive Inflammation

Neutrophil and Macrophage Dysfunction

Chronic Granulomatous Disease of Childhood
Glycogen Storage Disease
Malacoplakia

Exogenous Causes of Colitis

Caustic Colitis
Typhlitis (Neutropenic Colitis)
Clostridium difficile Colitis

Infectious and inflammatory disorder of the colon are common and do not require imaging in most cases. In some disorders, imaging has a role in establishing the diagnosis, assessing the severity of the process, monitoring the course of the disease, and determining the presence of complications.

Bacterial Infections

Infectious colitis may be caused by bacterial, viral, fungal, and parasitic organisms.¹⁻⁴ In Western countries, bacterial colitis

represents the most common form of colonic infection, whereas in underdeveloped countries, parasitic infestation occurs most frequently. Imaging studies are not usually performed for patients with bacterial colitis because the diagnosis is readily established with routine stool cultures.

The diagnosis of bacterial colitis should be suggested by the typical presentation of acute onset of dysenteric symptoms, consisting of fever, crampy abdominal pain and tenderness (with or without vomiting), tenesmus, and small-volume diarrhea (frequently bloody). In most cases, the disease is self-limited. Routine cultures may occasionally yield false-negative results, so specialized cultures are required to isolate specific organisms.

SALMONELLOSIS

Salmonella is a gram-negative rod that is ingested with contaminated food or water.¹⁻⁴ Colonic involvement may occur during the course of typhoid fever or as an acute dysentery. Typhoid fever is caused by *Salmonella typhi* or *Salmonella paratyphi*. Presenting symptoms include marked pyrexia, arthralgias, malaise, headaches, and right lower quadrant pain. The organism initially involves the reticuloendothelial system, particularly the spleen, mesenteric lymph nodes, and Peyer patches of the terminal ileum. Splenomegaly may occur after 1 week. Gastrointestinal involvement occurs in the second or third week in approximately 50% of cases, but is obscured by other symptoms. Right lower quadrant pain and tenderness are the most common findings. When colonic involvement is present, the barium enema may reveal narrowing and loss of haustration in the cecum caused by edema and spasm, as well as ileal fold thickening and ulceration. Aphthoid ulcers in the ascending colon have also been reported.⁵ The ileum is invariably involved. Hemorrhage and perforation occur in 1% to 3% of cases. Symptoms begin to resolve in the fourth week, but relapses are common. Blood cultures are positive during the first week in 90% of patients, and the organism may be isolated from stool cultures during the second and third weeks. Chloramphenicol is the treatment of choice.

In most reported cases, barium enemas have revealed a pancolitis with loss of haustration, often associated with superficial or even deep, so-called collar button ulcers.^{6,7} Thumbprinting has also been reported. Other patients may have extensive small bowel thickening and effacement associated with a pancolitis. Double-contrast studies may reveal punctate mucosal stippling, discrete superficial ulcers, or mucosal granularity. The descending and sigmoid colon are usually involved, with variable proximal extension. Although the rectum generally appears spared radiographically, there may be mild inflammation at endoscopy.⁸ A segmental ulcerating colitis in the left colon is rare.⁹

Fulminant disease and even toxic megacolon may occur, particularly in older or debilitated persons. Bacteremia is common, and the infection may spread to the gallbladder, bones, lungs, and kidneys.

SHIGELLOSIS

Infection with *Shigella*, a gram-negative rod, may be caused by three species—*Shigella flexneri*, *Shigella dysenteriae*, and *Shigella sonnei*.¹⁻⁴ In the United States, *S. sonnei* is the offending organism in 70% of cases, whereas in Mexico and Asia, *S. dysenteriae* is most common. As with salmonellosis, infection may occur in outbreaks, particularly in warm weather. The incubation period is 1 to 3 days, and the presentation is usually similar to that of *Salmonella* infection. However, shigellosis produces a toxin that causes increased small bowel secretion and watery diarrhea, which lasts several days and then progresses to dysenteric symptoms. Systemic absorption of the toxin may also cause arthritis, pneumonitis, seizures, peripheral neuropathy, microangiopathy, and hemolytic-uremic syndrome. Bacteremia is rare but may cause vascular collapse. Stool cultures are positive within 1 day of onset and may remain positive for months. Toxic megacolon has also been reported. The disease is usually self-limited, lasting 7 to 10 days, but occasionally as long as 1 month. The mortality rate is 10% to 20% in immunocompromised patients or in patients with bacteremia.

Sigmoidoscopy almost always reveals an inflammatory process simulating ulcerative colitis; it varies from mild granularity and erythema to ulceration.^{10,11} Ulceration is more commonly seen than in salmonellosis. Ulcers are usually superficial and of varying size and shape. They are predominantly stellate but may be linear, serpiginous, or aphthoid and are superimposed on a diffusely friable mucosa. In patients with *S. dysenteriae* infection, the ulcerative phase is most marked in the second and third weeks of the disease, with erythema and edema more prominent in the first week.¹¹ In many cases, the ulceration is most severe distal to the splenic flexure. Healing ensues with gradually decreasing erythema. The process is initially continuous and pancolonic. During recovery, involvement may become patchy. Although healing is usually complete, some patients may have residual strictures, inflammatory polyps, or even persistent colitis.¹²

Barium enema reveals a predominantly left-sided colitis with deep ulcers, which may have a collar button appearance.⁷ Aphthoid ulcers may also be seen.

CAMPYLOBACTERIOSIS

Campylobacter is the most common cause of bacterial colitis. This organism has been isolated in 7% to 10% of stool cultures obtained from patients with diarrhea.¹⁻⁴ The offending agent is *Campylobacter fetus* subspecies *jejuni*. The disease is usually self-limited, lasting less than 7 days, but symptoms may persist as long as 1 month. In some cases, barium enemas reveal a pancolitis with diffuse granularity and loss of haustration simulating ulcerative colitis, whereas in others, barium enemas have revealed aphthoid ulcers, resembling those of Crohn's disease.¹³⁻¹⁶ The left side of the colon is almost always involved. Hemorrhage, perforation, and toxic megacolon have also been reported as complications. The diagnosis requires culture on selective media; serologic studies may also be helpful for confirmation.

YERSINIA ENTEROCOLITIS

Infection by *Yersinia enterocolitica*, a gram-negative rod, tends to be more common in certain regions, such as Japan, Canada, and Scandinavia.^{1-4,17-20} Specific strains may be endemic to each of these locations, and these strains have different clinical and pathologic manifestations. Patients younger than 5 years usually present with acute right lower quadrant pain and fever, simulating appendicitis. In contrast, adults may present with acute or protracted fever, pain, and diarrhea evolving over a 4- to 6-week period. Other patients may have associated arthralgias, arthritis, or rashes, such as erythema nodosum or erythema multiforme.

The terminal ileum is invariably involved on barium enemas; the radiographic findings depend on the stage of the disease.¹⁷ The most common findings include small nodules caused by enlarged lymphoid follicles or discrete punctate, aphthoid, or larger oval ulcers. Folds may also be thickened but, unlike in Crohn's disease, stenosis is not a feature. Colonic changes are manifested by aphthoid ulcers that are predominantly located in the right side of the colon, but left-sided colonic involvement is occasionally noted.²⁰⁻²² The evolution and resolution of these clinical and radiologic abnormalities may require several months. Perforation is rare, but hepatic abscess and septicemia are well-documented complications. Diagnosis requires special culture media or serologic studies. Although no treatment has been proved to be effective, the diagnosis of *Yersinia enterocolitica* is important primarily for the purpose of excluding other entities.

COLITIS CAUSED BY *ESCHERICHIA COLI* O157:H7

Escherichia coli strains are the most common cause of traveler's diarrhea and are usually self-limited. However, the subtype *E. coli* O157:H7 has drawn increased attention because it is associated with a high morbidity and mortality. Outbreaks of this infection have been noted in Canada; residents of nursing homes have been particularly susceptible. Patients typically present with watery diarrhea (without fever) that progresses over several days to a hemorrhagic colitis. The most serious complication, the hemolytic-uremic syndrome, results from a toxin associated with this infection. The overall mortality may be as high as 33%. The findings on barium enemas are similar to those of ischemic colitis, with thumbprinting, narrowing, and spasm of the involved bowel. Computed tomography (CT) may reveal low-density thickening of the wall caused by edema (Fig. 58-1). Most reported cases have involved the transverse colon, often associated with extension to the right, left, or both sides of the colon.²³⁻²⁵ The morphologic changes are caused predominantly by ischemia, and histologic specimens may resemble pseudomembranous colitis. Treatment is supportive, but this diagnosis is important so that isolation procedures can be instituted.

TUBERCULOSIS

Although once considered rare in Western countries, tuberculosis has been increasing in incidence. As a result, reports of gastrointestinal tract involvement have become more common. Patients with AIDS have been noted to be at greater risk than the general population.²⁶ Although most cases are secondary to

a pulmonary source, most patients have no evidence of active or previous pulmonary tuberculosis on chest radiographs. In endemic areas of Asia, most cases of gastrointestinal tuberculosis are caused by ingestion of the bovine bacillus. Colonic involvement is often associated with ileal disease.

Barium studies may reveal abnormalities in the ascending and proximal transverse colon that are indistinguishable from those of Crohn's disease.²⁶ It has been suggested that certain abnormalities are characteristic, such as oval or circumferential transverse ulcers, loss of anatomic demarcation between the ileum and the right colon (Stierlin sign), and a right-angle intersection between the ileum and cecum, with marked hypertrophy of the ileocecal valve (Fleischner's sign). These findings result from the exuberant mural thickening, which tends to be greater than that in Crohn's disease. Other suggestive features include extremely short segments of involvement of the ileum or cecum, markedly enlarged lymph nodes, particularly with low density on CT, and ascites. However, the most frequent findings include some combination of narrowing, deep ulceration, and mucosal granulation with nodularity and inflammatory polyps. Less common findings include aphthous ulcers, diffuse colitis, segmental colitis distal to the hepatic flexure, and short strictures, simulating carcinoma.²⁷⁻³³ Fistulas and sinus tracts are also rare.

The diagnosis can be made on endoscopic biopsy specimens that reveal caseating granulomas or positive cultures for the acid-fast bacilli.³⁴ However, the yield from endoscopy has been variable. As a result, surgical specimens are sometimes required for a definitive diagnosis. Tuberculous colitis is an important diagnosis because of the potentially catastrophic consequences of administering corticosteroids to these patients because of a mistaken diagnosis of inflammatory bowel disease.

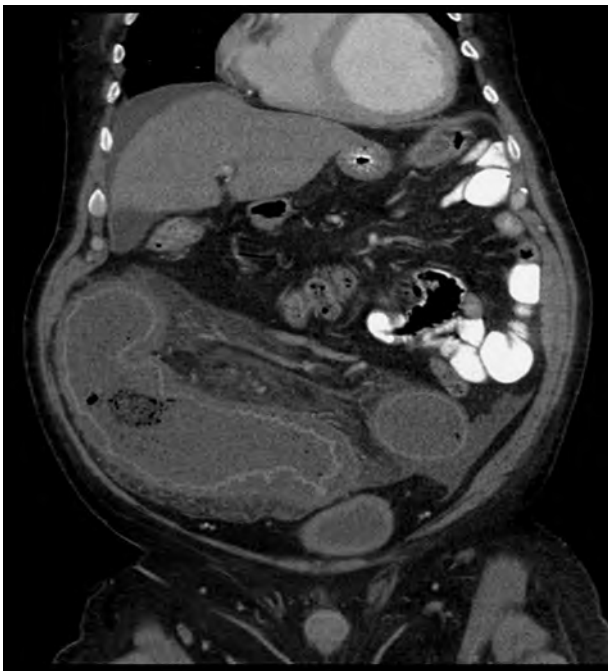


Figure 58-1 Colitis caused by *Escherichia coli* O157:H7. Coronal reformatted CT scan shows marked mural thickening of a redundant sigmoid colon associated with submucosal edema, inflammatory change in the adjacent mesentery, and ascites.

ACTINOMYCOSIS

Actinomyces israelii is an anaerobic bacterium that occurs as part of the normal flora of the bowel but, when there is contact with tissues not normally exposed to this organism, a pathologic process ensues. Gastrointestinal involvement occurs after infection of mesenteric and peritoneal tissues from penetrating trauma, abdominal surgery, or long-standing intrauterine devices. These patients may develop inflammatory masses and fistulas that involve the colon. Presenting symptoms include a palpable mass, vague abdominal pain, and diarrhea.

Barium enemas may reveal extrinsic masses involving the colon with reactive changes, distortion, and strictures, with or without fistula formation.^{35,36} Fistulas can extend to the skin, where characteristic colonies of sulfur granules may be identified. The ileocecal region is the most common site of gastrointestinal involvement. Many of these patients have a history of prior appendectomy. In contrast, the rectosigmoid colon is the usual site of involvement in patients with intrauterine devices. Ultrasonography and CT may also reveal large inflammatory masses. Surgery is often necessary for a definitive diagnosis and for differentiating these inflammatory masses from neoplasms.

Viral Infections

Cytomegalovirus (CMV) infection is a frequent complication of AIDS; the gastrointestinal tract may be focally or diffusely involved. Gastrointestinal abnormalities are thought to result from CMV-induced ischemic vasculitis. When colonic involvement by CMV is suspected, the diagnosis can be confirmed by the presence of characteristic intranuclear inclusions (viral inclusion bodies) on endoscopic brushings or biopsy specimens.

CMV colitis usually involves the cecum and proximal colon, sometimes extending into the distal ileum. Early disease is manifested by diffuse nodular lymphoid hyperplasia. Positive cultures from the colon are diagnostic. With moderate disease, barium enemas may reveal multifocal ulcerations, appearing as shallow, well-defined ulcers scattered on an otherwise normal background mucosa.³⁷ More advanced disease (Fig. 58-2) may

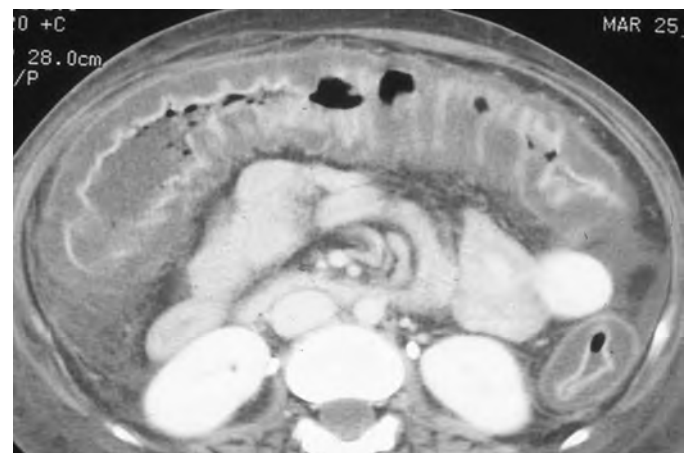


Figure 58-2 Cytomegalovirus (CMV) colitis. CT scan demonstrates severe mural thickening of the transverse colon in this patient with AIDS. Note the edematous low-density submucosa, with enhancement of the mucosa and serosa.

be manifested by deeper ulcers and marked thickening of the colonic wall on barium studies and with CT.³⁷ Some patients have a pancolitis with diffuse, contiguous involvement of bowel. With bolus injection of contrast material, CT may reveal enhancement of the mucosa and serosa with hypodense thickening of the intervening bowel wall caused by edema. With severe disease, however, the bowel wall may have increased attenuation, reflecting a hemorrhagic component of this process. Hemorrhagic CMV colitis can be fatal in patients with AIDS.

Parasitic Infections

ANISAKIASIS

Within 12 to 24 hours after the ingestion of raw fish, infestation by larvae of the nematode *Anisakis* can produce severe abdominal pain, sometimes accompanied by fever, nausea and vomiting, and/or diarrhea.³⁸⁻⁴⁰ Anisakiasis has a predilection for the stomach and small intestine, but the colon may occasionally be involved by this infection. Eosinophilia is not often present in the serum but is invariably identified on biopsy specimens. The ascending colon and, less commonly, the transverse colon are involved; barium enemas may reveal segmental thumbprinting of the affected bowel. The diagnosis of anisakiasis can be suggested when double-contrast barium enemas show the actual larvae as thin, linear filling defects 12 to 20 mm long and 0.7 mm wide at the proximal portion of the diseased segment of bowel.⁴⁰ Serologic studies may be performed to confirm the diagnosis. The worm is present in the stool in less than 25% of cases. The process is self-limited, usually lasting 7 to 10 days.

AMEBIASIS

Colonic amebiasis is rare in the United States. The cysts are ingested and subsequently develop into the invasive trophozoite. This organism is harbored by 20% of the world population. Infestation by this protozoan may vary from the carrier state to fulminant colitis, and symptoms may be indolent or acute. Spread to the liver and then the lungs may result in abscesses in either of these organs.

Colonic amebiasis is usually an acute ulcerative colitis (95%) manifested by skip lesions, although the intervening bowel may be involved to a much lesser extent.⁴¹⁻⁴³ At times, the affected bowel is characterized by short regions of involvement with marked granulation (ameboma).⁴⁴ Such amebomas are seen in approximately 10% of cases and are usually located in the right side of the colon. Although diffuse colitis is not unusual, the right side of the colon tends to be more severely involved. Barium enemas usually reveal deep ulcers or bowel wall edema, but some patients may have aphthous ulcers, discrete ulcers appearing as marginal defects, or granularity with barium flecks.⁴⁵ The terminal ileum is invariably spared. The coned cecum is a suggestive but nonspecific finding. Residual deformity and stricture formation may occur, even after appropriate therapy.⁴⁶ Less than 1% of patients present with toxic megacolon, and approximately 3% present with typhloappendicitis.

The diagnosis of amebiasis is usually established by the presence of trophozoites in the stool or on rectal smear. Serologic studies are also sensitive. When amebiasis is suspected, trial therapy may be warranted, even if the diagnosis is not

confirmed; the disease may progress rapidly if these patients are inappropriately treated with corticosteroids for presumed inflammatory bowel disease.

SCHISTOSOMIASIS

Schistosomiasis belongs to the trematode or fluke group of worms; different strains are endemic to specific geographic areas. *Schistosoma mansoni* is found in the United States, Puerto Rico, and the tropics.³ *Schistosoma haematobium* is the primary form in Africa and southern Asia, and *Schistosoma japonicum* usually occurs in eastern Asia. Mixed infection with *S. mansoni* and *S. haematobium* is not uncommon, particularly in Egypt. The larva penetrates the skin, where it enters the systemic circulation. It eventually reaches the liver and matures into the adult form. Upstream migration occurs through the portal venous system to the colon, where the worms invade the bowel wall and lay eggs. Portal hypertension with secondary hepatosplenomegaly is frequently associated. Although some patients may develop a pancolitis, *S. mansoni* has a predilection for the inferior mesenteric vein and left side of the colon, *S. japonicum* infects the superior mesenteric vein and right side of the colon and terminal ileum, and *S. haematobium* infects the hemorrhoidal veins and rectum and urinary tract. Most patients present with bloody diarrhea, but some may have chronic abdominal pain, intermittent diarrhea, and a palpable abdominal mass.

Barium enema examinations may reveal nonspecific colitis involving a variable extent of colon, with narrowing, loss of haustration, and ulceration.⁴⁶ However, a hallmark of this disease is the presence of inflammatory polyps as a result of granulation reaction to the deposition of eggs in the bowel wall.^{47,48} Another suggestive finding is calcification of the bowel wall or liver, which is usually associated with *S. haematobium* but also with *S. japonicum*.^{48,49} CT is particularly sensitive to these changes. The diagnosis can be established by demonstrating the eggs in biopsy specimens or in the stool. Eosinophilia is frequently present.

STRONGYLOIDIASIS

The nematode *Strongyloides stercoralis* also gains entrance through the skin. It spreads to the lungs, ruptures into the tracheobronchial tree, and is subsequently ingested. The primary sites of involvement are the stomach, duodenum, and proximal small bowel; and a chronic host-parasite relationship ensues. In most cases, eggs are passed into the stool. However, in patients with decreased immunity, the eggs progress to the filariform larval stage and invade the portal system, producing a repeated cycle or autoinfection. The excess parasite load results in a distal accumulation of filariform larvae with subsequent colonic involvement. Because of the setting of severe debilitation, this process is often fatal. Barium enemas typically reveal findings of a diffuse ulcerative colitis.⁵⁰⁻⁵² Aphthoid ulcers may be identified in the colon.⁵³ Fistulas and sinus tracts may also be present. Eosinophilia is the rule, but the diagnosis requires identification of cysts, larvae, or both, in the stool.

TRICHURIASIS

The whipworm *Trichuris trichiura* predominantly involves children in tropical areas. The worm is minimally invasive

but invades the mucosa, with resultant bleeding, anemia, diarrhea, malaise, and cramps. Intussusception and rectal prolapse are common; the adherent worms serve as the lead point for this intussusception. Eosinophilia is usually present. The barium enema shows clumping and granularity of the barium because of excessive production of mucus.^{54,55} The worms are identified as wavy, linear lucencies 3 to 5 cm in length, sometimes terminating in a ring shape, with a central barium collection.

Fungal Infections

HISTOPLASMOSIS

Histoplasma capsulatum is a fungus endemic to river basin areas. The lung and skin are the usual sites of involvement, but the gastrointestinal tract may also be involved.⁵⁶ Gastrointestinal disease usually occurs in the setting of a chronic debilitating illness in which the intestinal symptoms are overlooked. Anemia and leukopenia may be present. Perforation, obstruction, or hemorrhage may direct attention to the alimentary tract. The ileocecal region is the most common site of disease. Other associated findings include mesenteric adenopathy, hepatosplenomegaly (often with calcifications), and abnormal chest radiographs. Barium studies may reveal right-sided colonic filling defects, one or more segments of nonspecific inflammation (e.g., narrowing, mucosal granulation, sinus tracts, ulcers, strictures), diffuse colitis, periceal masses simulating appendicitis, and rectal polyps.⁵⁶⁻⁵⁸ Mucosal biopsy specimens may demonstrate the fungus, which stains with methenamine silver.

MUCORMYCOSIS

Colonic involvement by mucormycosis invariably occurs in a setting of immunosuppression. The diagnosis is rarely made preoperatively, and almost all cases have been fatal. The sinuses, lungs, and central nervous system are the usual sites of involvement. Colonic involvement may be isolated or may be associated with abnormalities elsewhere in the gastrointestinal tract.^{59,60} The right side of the colon is most often affected; findings include a polypoid mass or segmental inflammation, with or without sinus tracts. Rarely, these patients may have a pancolitis.

Noninfectious Colitis

NONSPECIFIC ULCER

Nonspecific colonic ulcer is of unknown cause. More than 50% of these ulcers are located in the right side of the colon near the ileocecal valve, and approximately 20% are multiple.⁶¹ The clinical presentation can mimic that of appendicitis or even carcinoma. The ulceration may be superficial or deep and occurs on the antimesenteric border. The most common finding on barium enema is a focal mass with or without ulceration and, less commonly, a short stricture or segmental colitis.⁶¹⁻⁶⁵ CT scans may show a colonic mass with mesenteric stranding. This condition is rarely diagnosed preoperatively, but a nonspecific ulcer may be suspected when an ulcer is seen at colonoscopy and biopsy results are negative for other causes.

MICROSCOPIC (COLLAGENOUS) COLITIS

Microscopic (collagenous) colitis is a clinicopathologic entity characterized by a history of variable (but usually long) duration, intermittent or chronic watery diarrhea. This condition occurs predominantly in middle-aged and older women. Results of laboratory studies and diagnostic procedures, including endoscopy, are usually normal. The diagnosis is established by endoscopic biopsy specimens, which reveal increased lymphocytes in the surface epithelium and, in the variant, collagenous colitis, an increase in the width of the subepithelial collagen band.^{66,67}

The barium enema had generally been considered to be incapable of detecting changes of microscopic colitis, but double-contrast studies may occasionally reveal nonspecific inflammatory surface abnormalities, predominantly in the rectosigmoid region.^{68,69} In the appropriate clinical setting, microscopic colitis should therefore be considered in the differential diagnosis of these findings, and endoscopic biopsy specimens should be obtained. Sulfasalazine or corticosteroids may be of benefit for the control of symptoms.

EOSINOPHILIC COLITIS

Eosinophilic gastroenteritis is a disease of unknown cause that invariably involves the stomach or small bowel. Ascites is also common, and peripheral eosinophilia is usually present. Occasionally, the colon (particularly the right side of the colon) may be involved. Thumbprinting, spasm, and narrowing are the primary findings on barium study.⁷⁰ These findings may be reversible after treatment with corticosteroids.

GRAFT-VERSUS-HOST DISEASE

One of the complications of bone marrow transplantation is that the donor immune cells may recognize the host tissue as foreign. The small intestine is invariably involved. Barium studies may reveal mural thickening and fold thickening or complete loss of mucosal features (ribbon bowel). Some of these patients also have abnormalities involving the entire colon or, less commonly, selective right-sided colonic disease.⁷¹ The findings on barium enema are those of a nonspecific colitis (e.g., loss of haustration, spasm, ulceration) and, in some cases, a granular surface pattern. CT shows (Fig. 58-3) edema in the mesentery, small and large bowel wall thickening, and mucosal and serosal enhancement. Graft-versus-host disease and viral infection (or both conditions combined) are indistinguishable.

RETRACTILE MESENTERITIS

Retractile mesenteritis is a disease of unknown cause in which a spectrum of inflammatory and fibrotic pathologic changes occurs in the mesenteric fat but can extend to the intestinal wall. Autoimmune factors have been postulated. The patient's age may range from the second to the eighth decades of life, and there is a slight male predominance. Presenting symptoms include abdominal pain, diarrhea, and weight loss. The small bowel is the usual site of involvement, but colonic abnormalities are not uncommon. The sigmoid and transverse colon are most likely to be involved because these segments of bowel are intimately related to a mesentery.

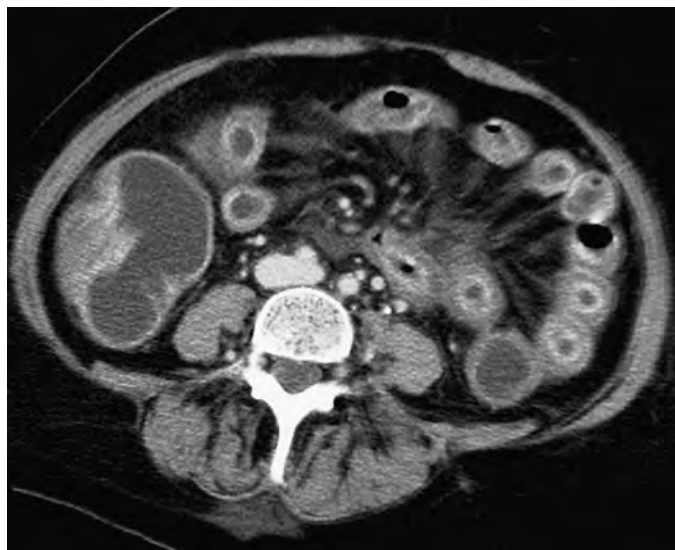


Figure 58-3 Graft-versus-host disease. Axial contrast-enhanced CT scan shows edema in the mesentery, small and large bowel wall thickening, and mucosal and serosal enhancement.

The findings on barium enema may be secondary to ischemia as a result of occlusion of the mesenteric vessels or direct extension of the fibroinflammatory process.⁷²⁻⁷⁵ Barium studies may reveal long segments of mild to moderate narrowing with thumbprinting, strictures of variable length, and/or extrinsic masses with reactive changes on the contiguous margin of the bowel. CT is a complementary imaging study because it may demonstrate markedly increased density in the mesentery, with or without discrete, fibrotic soft tissue masses. Ultrasonography may also reveal solid masses with hypoechoic areas that resemble sarcomas, hematomas, or abscesses.⁷³ Surgery is often performed to relieve obstructive symptoms, but corticosteroid therapy may also be beneficial.

REACTIVE INFLAMMATION

Reactive inflammation may occur in the colon because of extension of primary inflammatory processes from other organs or from adjacent abscesses. The site of colonic disease closely correlates with its anatomic contiguity and mesenteric relationships with these structures. The appearance may vary from an area of extrinsic mass effect with reactive spiculation to long segments of concentric narrowing and spiculation, with or without an adjacent soft tissue mass that fixes and distorts the bowel. For example, appendicitis may involve the ascending colon or sigmoid colon (depending on the location of the appendix), whereas pancreatitis tends to involve a variable length of the transverse colon up to the junction with the descending colon (phrenocolic ligament). Pancreatitis may also cause obstruction (colon cutoff), fistula formation, necrosis and perforation, and strictures. Both these entities may simulate primary colitis with pain and diarrhea.⁷⁶ However, careful interpretation of the barium enema may allow the radiologist to suggest these possibilities, and a CT scan combined with appropriate laboratory studies may allow an accurate diagnosis. Less commonly, inflammatory disease in the kidneys produces reactive changes in the proximal descending or ascending colon, and acute cholecystitis may have a similar

effect on the proximal transverse colon, particularly on its superior border.

Neutrophil and Macrophage Dysfunction

CHRONIC GRANULOMATOUS DISEASE OF CHILDHOOD

In patients with conditions associated with neutrophil dysfunction, a colitis that may be segmental or pancolonic and indistinguishable from Crohn's disease has been reported.⁷⁷ Fistulas and sinuses may be features of this form of colitis. It occurs predominantly in the pediatric population. Chronic granulomatous disease of childhood is an inherited defect of leukocyte function characterized by the inability of phagocytes to kill catalase-positive microorganisms, resulting in multifocal abscesses and granulomas. The presence of lipid-bearing histiocytes in the mucosa is highly suggestive of this entity. Some degree of colonic involvement is common in these patients, but clinically significant colonic disease is rare. Some patients with colonic disease may have associated involvement of the stomach with narrowing of the gastric antrum.

GLYCOGEN STORAGE DISEASE

Glycogen storage disease type Ib is also associated with neutropenia and a metabolic defect in neutrophil activity. Recurrent pyogenic infections are a significant clinical problem in these patients. In the limited number of reported cases, gastrointestinal involvement has been manifested by long or short strictures involving the right side of the colon and even the terminal ileum.⁷⁸

MALACOPLAKIA

Malacoplakia is a granulomatous process that usually involves the genitourinary tract. However, the colon is the most frequent extraurinary site of involvement.⁷⁹ Distinctive macrophages that contain pathognomonic intracytoplasmic calcifications (Michaelis-Gutmann bodies) are present on biopsy specimens. The cause is unknown, but a macrophage defect is most likely. Unlike the urinary tract abnormalities, which tend to occur in older women, colonic disease shows a wide age distribution. Abnormalities may include small polyps or bulky masses occurring in a segmental or diffuse distribution. Barium studies may even reveal a diffuse nonspecific colitis resembling Crohn's disease. Rectal bleeding, diarrhea, and abdominal pain are the most frequent symptoms in these patients.

Exogenous Causes of Colitis

CAUSTIC COLITIS

Direct contact between the colorectal mucosa and caustic substances introduced into the rectum by various types of enemas may produce a colitis that is transient or results in complete mucosal sloughing, with subsequent strictures. The most common causes of caustic colitis are detergent or soapsuds enemas used as laxatives or herbal (ritual) enemas practiced in Third World countries as a form of medical therapy.⁸⁰⁻⁸³ In some cases, the injury has been thermal as a result of the high

temperature of the liquid.⁸⁴ The changes occur predominantly in the distal colon because of the route of entry. However, skip lesions or transverse and right-sided colonic alterations can occur as a result of spasm and prolonged contact. Bloody diarrhea is the usual presenting symptom. Barium studies may demonstrate thumbprinting or severe mucosal necrosis and ulceration that progresses to deformity or strictures. Some patients may require colectomy and colostomy.

A number of cases of colitis secondary to glutaraldehyde exposure have also been reported. This form of colitis occurs when disinfectant is inadequately removed from endoscopes. Radiographic findings include thumbprinting in the rectosigmoid colon on barium enema and a thickened colonic wall on CT.⁸⁵

TYPHLITIS (NEUTROPENIC COLITIS)

Typhlitis (neutropenic colitis) is a potentially fatal infection of the cecum and ascending colon caused by enteric pathogens in patients with severe immunosuppression. It is usually seen in patients with acute leukemia receiving chemotherapy but

also occurs in the setting of AIDS, aplastic anemia, multiple myeloma, or bone marrow transplantation. Bacteria, viruses, and fungi penetrate the damaged cecal mucosa and proliferate because of the profound neutropenia. There is edema and inflammation of the cecum, ascending colon, and occasionally ileum. Fever, abdominal pain, nausea, and diarrhea are presenting symptoms. Prompt diagnosis and supportive therapy with intensive antibiotics and fluids are required to prevent transmural necrosis and perforation. Surgical resection is indicated for patients with transmural necrosis, intramural perforation, abscess, or uncontrolled sepsis and gastrointestinal hemorrhage.

Because of the inherent risks of bowel perforation in performing barium enemas and colonoscopies in these critically ill patients, CT is the study of choice for typhlitis. CT demonstrates circumferential mural thickening (1 to 3 cm) of the cecum (Fig. 58-4), low-density areas within the colonic wall secondary to edema, pericolic inflammation and fluid and, in severe cases, pneumatosis. Clinically, CT is used to monitor decreases in mural thickness with therapy and detect subtle pneumoperitoneum in cases of silent perforation or necrosis.⁷⁷⁻⁸⁰

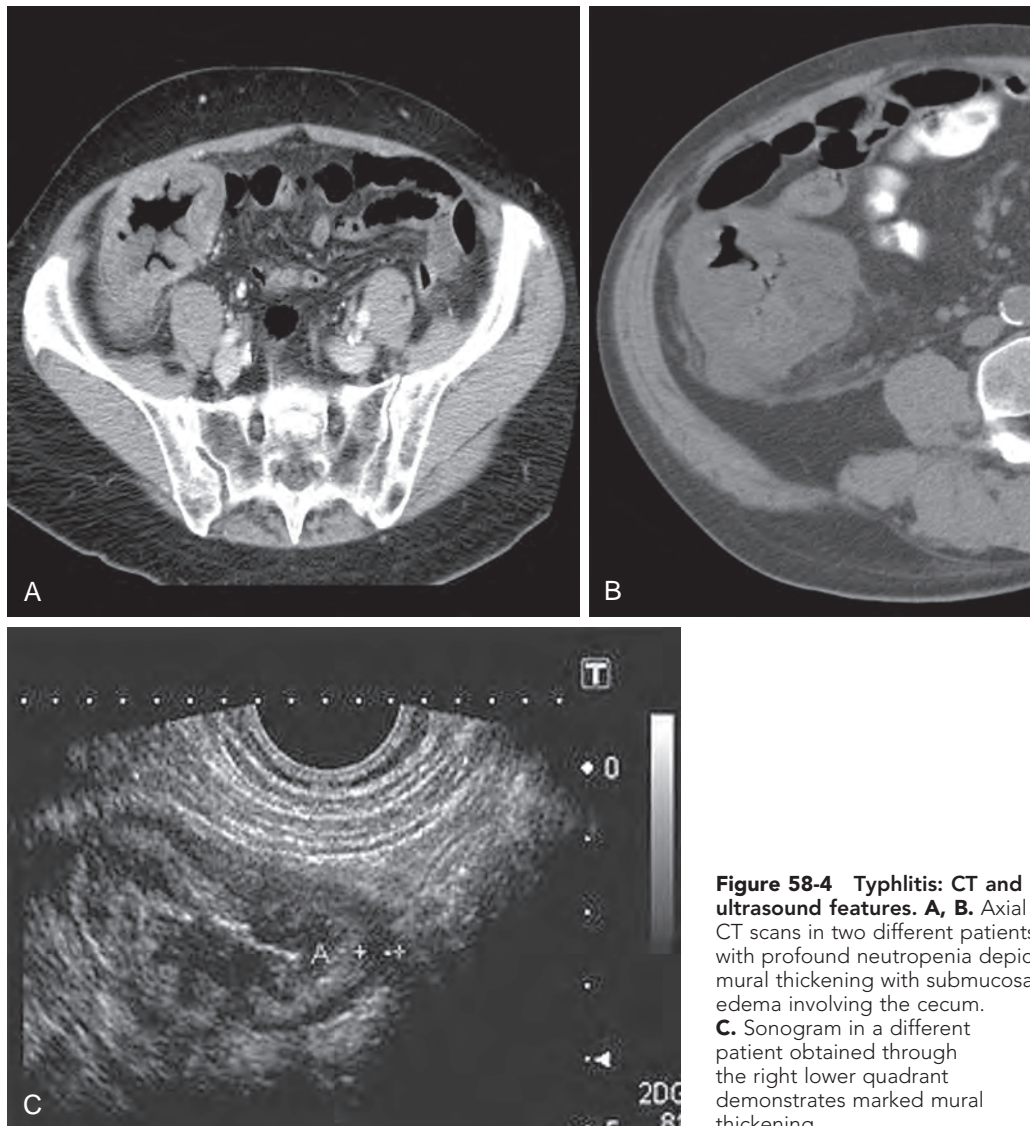


Figure 58-4 Typhlitis: CT and ultrasound features. **A, B.** Axial CT scans in two different patients with profound neutropenia depict mural thickening with submucosal edema involving the cecum. **C.** Sonogram in a different patient obtained through the right lower quadrant demonstrates marked mural thickening.

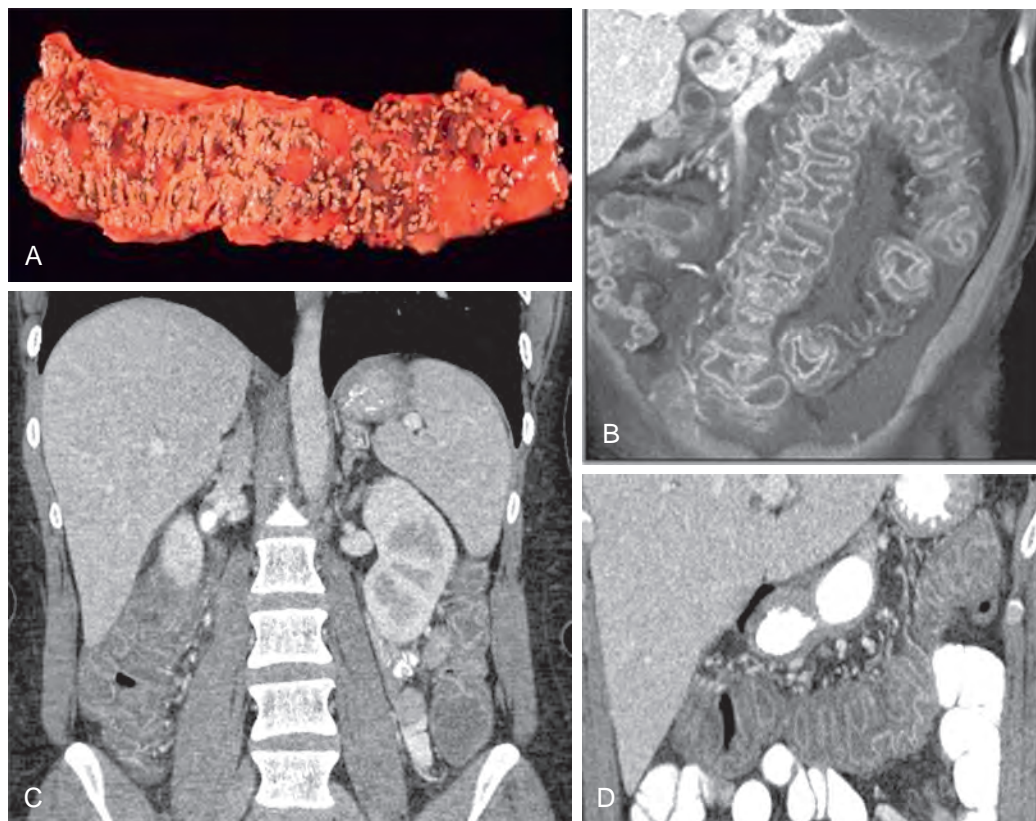


Figure 58-5 Pseudomembranous colitis: pathologic and CT findings. **A.** Surgical specimen shows whitish plaques on a background of hemorrhagic mucosa of the cecum and ascending colon. **B.** Coronal reformatted image shows marked mural thickening of a redundant sigmoid colon with enhancing mucosa and submucosal edema, the so-called accordion appearance. Ascites is also present. In a different patient, coronal reformatted images show mural thickening and submucosal edema of the ascending and descending colon (**C**) and the transverse colon (**D**).

Neutropenic colitis, also known as typhlitis when confined to the cecum, develops in profoundly immunocompromised patients, especially those with leukemia, AIDS, profound neutropenia caused by chemotherapy, or transplantation. A variety of organisms (particularly clostridia) have been isolated from surgical specimens. Presenting symptoms include fever, right lower quadrant pain, and diarrhea.

Plain radiographic findings of typhlitis include ileocecal dilation with air-fluid levels and small bowel obstruction secondary to inflammation. In severe cases, pneumatosis may develop.⁸⁶⁻⁹⁰

The most important consideration in the differential diagnosis is colitis caused by *Clostridium difficile* infection. A diagnosis of typhlitis can be made on the basis of the clinical and imaging findings only after other pathologic entities have been excluded. Surgery may be necessary in severe cases.

CLOSTRIDIUM DIFFICILE COLITIS

Pseudomembranous colitis has been encountered with increasing frequency as a nosocomial infection complicating antibiotic therapy. This potentially life-threatening disorder is caused by overgrowth of *C. difficile* and the subsequent release of a cytotoxic enterotoxin. This enterotoxin causes ulceration of the colonic mucosa and the formation of 2- to 3-mm pseudomembranes, which consist of fibrin, mucus, sloughed epithelial cells, and leukocytes. Mild cases may demonstrate only mucosal irregularity and nodularity with small plaque formation that cannot be detected radiologically. In advanced cases, there is

thickening of haustral folds, a shaggy wall contour, and mucosal plaques.⁹¹⁻⁹⁵

The diagnosis of *C. difficile* colitis should be suggested in patients on antibiotics who develop a sudden onset of watery diarrhea, often associated with fever, abdominal tenderness, and leukocytosis. Many of these patients are hospitalized, and many have had recent surgery. The onset of disease usually occurs within 2 days to 2 weeks after the introduction of antibiotic therapy, but some patients may develop symptoms as late as 8 weeks after these agents are discontinued. In these cases, the temporal relationship to antibiotics may be obscure, and a careful clinical history must be elicited.⁹¹

CT shows a colitis with mural thickening, which may be irregular or polypoid and have a shaggy endoluminal contour. The mural thickening, which is usually 1.6 to 1.8 cm, is a result of submucosal edema. Mucosal and serosal enhancement are seen following intravenous contrast administration. The haustra are also thickened and edematous, producing the accordion pattern, which is highly suggestive of pseudomembranous colitis (Fig. 58-5). This pattern consists of contrast trapped between thickened haustral folds that are aligned in a parallel fashion. This appearance can sometimes simulate that of deep ulcerations or fissures. Pericolonic stranding, ascites, pleural effusions, and subcutaneous edema are other ancillary CT findings.

Complications of untreated pseudomembranous colitis include toxic megacolon and intestinal perforation, with subsequent peritonitis. CT is also useful in monitoring the response to medical therapy with oral vancomycin and metronidazole.⁹¹⁻⁹⁵

REFERENCES

- Fukata M, Arditi M: The role of pattern recognition receptors in intestinal inflammation. *Mucosal Immunol* 6:451–463, 2013.
- Gore RM, Miller FH, Yaghmai V, et al: Inflammatory conditions of the colon. *Semin Roentgenol* 36:126–137, 2001.
- Thoeni RF, Cello JP: CT imaging of colitis. *Radiology* 240:623–638, 2006.
- Tedesco FJ, Hardin RD, Harper RN, et al: Infectious colitis endoscopically simulating inflammatory bowel disease: A prospective evaluation. *Gastrointest Endosc* 29:195–197, 1983.
- Grundy A, Gilks CF: Typhoid: An unusual cause of gastrointestinal bleeding. *Br J Radiol* 57:344–346, 1984.
- Saffouri B, Bartolomeo RS, Fuchs B: Colonic involvement in salmonellosis. *Dig Dis Sci* 24: 203–208, 1979.
- Farman J, Rabinowitz JG, Meyers MA: Roentgenology of infectious colitis. *AJR* 119:375–381, 1973.
- Nakamura S, Iida M, Tominaga M, et al: *Salmonella* colitis: Assessment with double-contrast barium enema examination in seven patients. *Radiology* 184:537–540, 1992.
- Vender RJ, Marignani P: *Salmonella* colitis presenting as a segmental colitis resembling Crohn's disease. *Dig Dis Sci* 28:848–851, 1983.
- Speelman P, Kabir I, Islam M: Distribution and spread of colonic lesions in shigellosis: A colonoscopic study. *J Infect* 150:899–903, 1984.
- Khuroo MS, Mahajan R, Zargar SA, et al: The colon in shigellosis: Serial colonoscopic appearances in *Shigella dysenteriae* I. *Endoscopy* 22:35–38, 1990.
- Zalev AH, Warren RE: *Shigella* colitis with radiological and endoscopic correlation: Case report. *J Can Assoc Radiol* 40:328–330, 1989.
- Lambert JR, Tischler ME, Karmali MA, et al: *Campylobacter* ileocolitis: An inflammatory bowel disease. *Can Med Assoc J* 121:1377–1379, 1979.
- Brodey PA, Fertig S, Aron JM: *Campylobacter* enterocolitis: Radiographic features. *AJR* 139: 1199–1201, 1982.
- Tielbeek AV, Rosenbusch G, Muytjens HL, et al: Roentgenologic changes of the colon in *Campylobacter* infection. *Gastrointest Radiol* 10:358–361, 1985.
- Kollitz JPM, Davis GB, Berk RN: *Campylobacter* colitis: A common infectious form of acute colitis. *Gastrointest Radiol* 6:227–229, 1981.
- Vantrappen G, Agg HO, Ponette E, et al: *Yersinia* enteritis and enterocolitis: Gastroenterological aspects. *Gastroenterology* 72:220–227, 1977.
- Matsumoto T, Iida M, Matsui T, et al: Endoscopic findings in *Yersinia enterocolitica* enterocolitis. *Gastrointest Endosc* 36:583–587, 1990.
- Simmonds SD, Noble MA, Freeman HJ: Gastrointestinal features of culture-positive *Yersinia enterocolitica* infection. *Gastroenterology* 92: 112–117, 1987.
- Shrago G: *Yersinia enterocolitica* ileocolitis findings observed on barium examination. *Br J Radiol* 49:181–183, 1976.
- Atkinson GO, Gay BB, Ball TI, et al: *Yersinia enterocolitica* colitis in infants: Radiographic changes. *Radiology* 148:113–116, 1983.
- Lachman R, Soong J, Wishon G, et al: *Yersinia* colitis. *Gastrointest Radiol* 2:133–135, 1977.
- Kawanami T, Bowen A, Girdany BR: Enterocolitis: Prodrome of the hemolytic-uremic syndrome. *Radiology* 151:91–92, 1984.
- Peterson RB, Meseroll WP, Shrago GG, et al: Radiographic features of colitis associated with the hemolytic-uremic syndrome. *Radiology* 118:667–671, 1976.
- Shortsleeve MJ, Wilson ME, Finklestein M, et al: Radiologic findings in hemorrhagic colitis due to *Escherichia coli* O157:H7. *Gastrointest Radiol* 14:341–344, 1989.
- Balthazar EJ, Gordon R, Hulnick D: Ileocecal tuberculosis: CT and radiologic evaluation. *AJR* 154:499–503, 1990.
- Vaidya MG, Sodhi JS: Gastrointestinal tract tuberculosis: A study of 102 cases including 55 hemicolectomies. *Clin Radiol* 29:189–195, 1978.
- Ehsannullah M, Isaacs A, Filipe MI, et al: Tuberculosis presenting as inflammatory bowel disease: Report of two cases. *Dis Colon Rectum* 27:134–136, 1984.
- Tishler JM: Tuberculosis of the transverse colon. *AJR* 133:229–232, 1979.
- Peh WC: Filiform polyposis in tuberculosis of the colon. *Clin Radiol* 39:534–536, 1988.
- Downey DB, Nakiely RA: Aphthoid ulcers in colonic tuberculosis. *Br J Radiol* 58:561–562, 1985.
- Carr-Locke DL, Finlay DBL: Radiological demonstration of colonic aphthoid ulcers in a patient with intestinal tuberculosis. *Gut* 24:453–455, 1983.
- McDonald JB, Middleton PJ: Tuberculosis of the colon simulating carcinoma. *Radiology* 118: 293–294, 1976.
- Bhargava DK, Tandon HD, Chawla TC, et al: Diagnosis of ileocecal and colonic tuberculosis by colonoscopy. *Gastrointest Endosc* 31:68–70, 1985.
- Maloney JJ, Cho SR: Pelvic actinomycosis. *Radiology* 148:388, 1983.
- Fowler RC, Simpkins KC: Abdominal actinomycosis: A report of three cases. *Clin Radiol* 34:301–307, 1983.
- Balthazar EJ, Megibow AJ, Fazzini E: Cytomegalovirus colitis in AIDS: Radiographic findings in 11 patients. *Radiology* 155:585–589, 1985.
- Higashi M, Tanaka K, Kitada T, et al: Anisakiasis confirmed by radiography of the large intestine. *Gastrointest Radiol* 13:85–86, 1988.
- Matsui T, Iida M, Murakami M, et al: Intestinal anisakiasis: Clinical and radiologic features. *Radiology* 157:299–302, 1985.
- Matsumoto T, Iida M, Kimura Y, et al: Anisakiasis of the colon: Radiologic and endoscopic features in six patients. *Radiology* 183:97–99, 1992.
- Cardoso JM, Kimura K, Stoope M, et al: Radiology of invasive amebiasis of the colon. *AJR* 128:935–941, 1977.
- Balikian JP, Uthman SM, Khouri NF: Intestinal amebiasis: A roentgen analysis of 19 cases including 2 case reports. *AJR* 122:245–256, 1974.
- Kolawole TM, Lewis EA: Radiologic observations on intestinal amebiasis. *AJR* 122:257–265, 1974.
- Cevallos AM, Farthing MJG: Parasitic infections of the gastrointestinal tract. *Curr Opin Gastroenterol* 9:96–102, 1993.
- Matsui T, Iida M, Tata S, et al: The value of double-contrast barium enema in amebic colitis. *Gastrointest Radiol* 14:73–78, 1989.
- Martinez CR, Gilman RH, Rabbani GH, et al: Amebic colitis: Correlation of proctoscopy before treatment and barium enema after treatment. *AJR* 138:1089–1093, 1982.
- Medina JT, Seaman WB, Guzman-Acosta C, et al: The roentgen appearance of *Schistosomiasis mansoni* involving the colon. *Radiology* 85:682–688, 1965.
- Lehman JS, Farid Z, Bassily S, et al: Colonic calcification and polyposis. *Radiology* 98:379–380, 1971.
- Lee RC, Chiang JH, Chou YH, et al: Intestinal schistosomiasis japonica: CT-pathologic correlation. *Radiology* 193:539–542, 1994.
- Yoshida T, Nozaki F, Tanaka K, et al: *Strongyloides stercoralis* hyperinfection: Sequential changes of gastrointestinal radiology after treatment with thiabendazole. *Gastrointest Radiol* 6:223–225, 1981.
- Dallemand S, Waxman M, Farman J: Radiological manifestations of *Strongyloides stercoralis*. *Gastrointest Radiol* 8:45–51, 1983.
- Drasin GF, Moss JB, Cheng SH: *Strongyloides stercoralis* colitis: Findings in four cases. *Radiology* 126:619–621, 1978.
- Stoopack PM, Raufman JP: Aphthoid ulceration of the colon in strongyloidiasis. *Am J Gastroenterol* 86:639–642, 1991.
- Reeder MM, Astacio JE, Theros EG: Case of the month from the AFIP. *Radiology* 90:382–387, 1968.
- Fisher RM, Cremin BJ: Rectal bleeding due to *Trichuris trichiura*. *Br J Radiol* 43:214–215, 1970.
- Cappell MS, Mandell W, Grimes MM, et al: Gastrointestinal histoplasmosis. *Dig Dis Sci* 33: 353–360, 1988.
- Haws CC, Long RF, Caplan GE: *Histoplasma capsulatum* as a cause of ileocolitis. *AJR* 128: 692–694, 1977.
- Dietz MW: Ileocecal histoplasmosis. *Radiology* 91:285–289, 1968.
- De Feo E: Mucormycosis of the colon. *AJR* 86:86–90, 1961.
- Agha FP, Lee HH, Boland CR, et al: Mucormycosis of the colon: Early diagnosis and successful management. *AJR* 145:739–741, 1985.
- Shallman RW, Kuehner M, Williams GH, et al: Benign cecal ulcers. *Dis Colon Rectum* 28:732–737, 1985.
- Huded FV, Posner GL, Tick R: Nonspecific ulcer of the colon in a chronic hemodialysis patient. *Am J Gastroenterol* 77:913–916, 1982.
- Brodey PA, Hill RP, Baron S: Benign ulceration of the cecum. *Radiology* 122:323–327, 1977.
- Gardiner GA, Bird CR: Nonspecific ulcers of the colon resembling annular carcinoma. *Radiology* 137:331–334, 1980.
- Marn CS, Yu BFB, Nostrant TT, et al: Idiopathic cecal ulcer: CT findings. *AJR* 153:761–763, 1989.
- Frick MP, Maile CW, Crass JR, et al: Computed tomography of neutropenic colitis. *AJR* 143: 763–765, 1984.
- Hoeffel C, Crema MD, Belkacem A, et al: Multidetector row CT: Spectrum of diseases involving the ileocecal area. *Radiographics* 26: 1373–1390, 2006.
- Glick SN, Teplick SK, Amenta PS: Microscopic (collagenous) colitis. *AJR* 153:995–996, 1989.
- Feczko PJ, Mezwa DG: Nonspecific radiographic abnormalities in collagenous colitis. *Gastrointest Radiol* 16:128–132, 1991.
- MacCarty RL, Talley NJ: Barium studies in diffuse eosinophilic gastroenteritis. *Gastrointest Radiol* 15:183–187, 1990.
- Kalantari BN, Mortele KJ, Cantisani V, et al: CT features with pathologic correlation of acute gastrointestinal graft-versus-host disease after

- bone marrow transplantation in adults. *AJR* 181:1621–1625, 2003.
72. Han SY, Koehler RE, Keller FS, et al: Retractable mesenteritis involving the colon: Pathologic and radiologic correlation. *AJR* 147:268–270, 1986.
 73. Periz-Fontan FJ, Soler R, Sanchez J, et al: Retractable mesenteritis involving the colon: Barium enema, sonographic, and CT findings. *AJR* 147:937–940, 1986.
 74. Williams RG, Nelson JA: Retractable mesenteritis: Initial presentation as colonic obstruction. *Radiology* 126:35–37, 1978.
 75. Thompson GT, Fitzgerald EF, Somers SS: Retractable mesenteritis of the sigmoid colon. *Br J Radiol* 58:266–267, 1985.
 76. Picus D, Shackelford GD: Perforated appendix presenting with severe diarrhea. *Radiology* 149:141–143, 1983.
 77. Werlin SL, Chusid MJ, Caya J, et al: Colitis in chronic granulomatous disease. *Gastroenterology* 82:328–331, 1982.
 78. Couper R, Kapelushnik J, Griffiths AM: Neutrophil dysfunction in glycogen storage disease Ib: Association with Crohn's-like colitis. *Gastroenterology* 100:549–554, 1991.
 79. Radin DR, Chandrasoma P, Halls JM: Colon malacoplakia. *Gastrointest Radiol* 9:359–361, 1984.
 80. Kim SK, Cho C, Levinsohn EM: Caustic colitis due to detergent enema. *AJR* 134:397–398, 1980.
 81. Pike BF, Phillippi PJ, Lawson EH: Soap colitis. *N Engl J Med* 285:217–218, 1971.
 82. Segal I, Solomon A, Mirwis J: Radiological manifestations of ritual-enema-induced colitis. *Clin Radiol* 32:657–662, 1981.
 83. Young WS: Herbal-enema colitis and stricture. *Br J Radiol* 53:248–249, 1980.
 84. Lee JH, Lim GY, Im SA, et al: Gastrointestinal complications following hematopoietic stem cell transplantation in children. *Korean J Radiol* 9:449–457, 2008.
 85. Altunel E, Yerali N, Isik P, et al: Typhlitis in acute childhood leukemia. *Med Princ Pract* 21:36–39, 2012.
 86. O'Malley ME, Wilson SR: US of gastrointestinal tract abnormalities with CT correlation. *Radiographics* 23:59–72, 2003.
 87. Abramson SJ, Berdon WE, Baker DH: Childhood typhlitis: Its increasing association with acute myelogenous leukemia. *Radiology* 146:61–64, 1983.
 88. Turner DR, Markose G, Arends MJ, et al: Unusual causes of colonic wall thickening on computed tomography. *Clin Radiol* 58:191–200, 2003.
 89. Horton KM, Corl FM, Fishman EK: CT evaluation of the colon: Inflammatory disease. *Radiographics* 20:399–418, 2000.
 90. Shafey A, Ethier MC, Traubici J, et al: Incidence, risk factors, and outcomes of enteritis, typhlitis, and colitis in children with acute leukemia. *J Pediatr Hematol Oncol* 35:514–517, 2013.
 91. Pacheco SM, Johnson S: Important clinical advances in the understanding of *Clostridium difficile* infection. *Curr Opin Gastroenterol* 29:42–48, 2013.
 92. Kirkpatrick ID, Greenberg HM: Gastrointestinal complications in the neutropenic patient: Characterization and differentiation with abdominal CT. *Radiology* 226:668–674, 2003.
 93. Fishman EK, Kavuru M, Jones B, et al: Pseudomembranous colitis: CT evaluation of 26 cases. *Radiology* 180:57–60, 1991.
 94. Ash L, Baker ME, O'Malley CM, Jr, et al: Colonic abnormalities on CT in adult hospitalized patients with *Clostridium difficile* colitis: Prevalence and significance of findings. *AJR* 186:1393–1400, 2006.
 95. Winslow BT, Onysko M, Thompson KA, et al: Common questions about *Clostridium difficile* infection. *Am Fam Physician* 89:437–442, 2014.

Polyps and Colon Cancer

RUEDI F. THOENI

CHAPTER OUTLINE

Epidemiology

Factors Involved

Dietary Factors

Hereditary Factors

Risk Factors

Pathogenesis

Clinical Aspects

Radiology and Diagnostic Methods

Contrast Enema

Colonoscopy

Cross-Sectional Imaging

Benign Epithelial Polyps

Incidence

Pathology

Polyp Detection

Adenocarcinoma

Barium Enema

Computed Tomography

Magnetic Resonance Imaging

Transrectal Ultrasound

Immunoscintigraphy with Monoclonal Antibodies

Positron Emission Tomography

Cross-Sectional Imaging in Primary Colorectal Neoplasm Detection

Postoperative Follow-Up

Contrast Enema

Cross-Sectional Imaging

Cross-Sectional Imaging in Recurrent Colorectal Carcinoma

Epidemiology

Colon cancer is a major public health problem in the United States, one of the most common significant cancers in the U.S. population, and the third most common cause of cancer mortality. It ranks third to lung and prostate cancer in men and third to lung and breast cancer in women.¹ The American Cancer Society estimates that in the year 2014 about 136,830 will be diagnosed with colorectal cancer and that about 50,340 will die of the disease.¹ The distribution of this disease varies widely throughout the world. It is common in North America, Europe, and New Zealand, but the incidence is low in South America, Africa, and Asia. The United States has one of the highest incidences of colorectal cancer in the world. However, even within the United States, the rates of occurrence vary

considerably, being higher in the North, among the urban white population, and among blacks.¹ Viewed in a personal way, U.S. adults have approximately a 1 in 20 chance of developing colorectal cancer during their lifetime and a 1 in 40 chance of dying of this disease.

Colorectal neoplasms account for about 9% of new cancer diagnoses in the United States. The incidence rates (per 100,000) have declined from a high of 71 in 1975 to 55.7 in 2004 to 2008 for men and from 54 in 1975 to 41.4 in 2004 to 2008 for women.¹ This decline was seen mostly in whites, whereas incidence rates for blacks have slightly increased. In the United States, the incidence rates among blacks are about 23% higher than in whites, whereas mortality rates in blacks are about 48% higher than in whites.¹ The decline in whites is probably because of increased screening for colon cancer and subsequent polyp removal. The lack of improvement over time in blacks may reflect historic underdiagnosis of colon cancer in blacks, racial differences in the trends in prevalence of risk factors for colon cancer, and lower access and use of recommended screening tests by blacks. Blacks are more likely to be diagnosed when the disease has spread beyond the colon but, once diagnosed, are less likely than whites to receive recommended surgical treatment and adjuvant therapy.^{2,3}

The distribution of cancer in the large bowel is of considerable importance because it affects the diagnostic approach. Approximately 50% of these cancers occur in the rectum and sigmoid colon, within reach of the short flexible sigmoidoscope (Fig. 59-1).⁴ The remainder are scattered throughout the proximal colon. Some authors suggest that there has been a shift to the right, rendering fewer cancers diagnosable by digital and short sigmoidoscopic examinations.⁵ Although the overall incidence of colorectal tumors increases with age, this increase is greatest for proximal neoplasms beyond the reach of the sigmoidoscope.⁶ Also, race and gender can independently predict the location of the cancer.⁷ Generally, more distal cancers are found in Asians than in blacks or whites. Whites have more distal cancers than blacks, and men have more distal cancers than women.

Factors Involved

DIETARY FACTORS

The wide variation and distribution of colorectal cancer throughout the world is probably related to dietary differences. In general, diets low in fiber and high in fat and animal protein (especially high and prolonged consumption of red or processed meat) are associated with a higher prevalence of colorectal cancer, which is inversely related to the incidence of gastric cancer.⁸ However, these conclusions are based on population studies, and a direct link between diet and colon cancer has not been demonstrated.¹

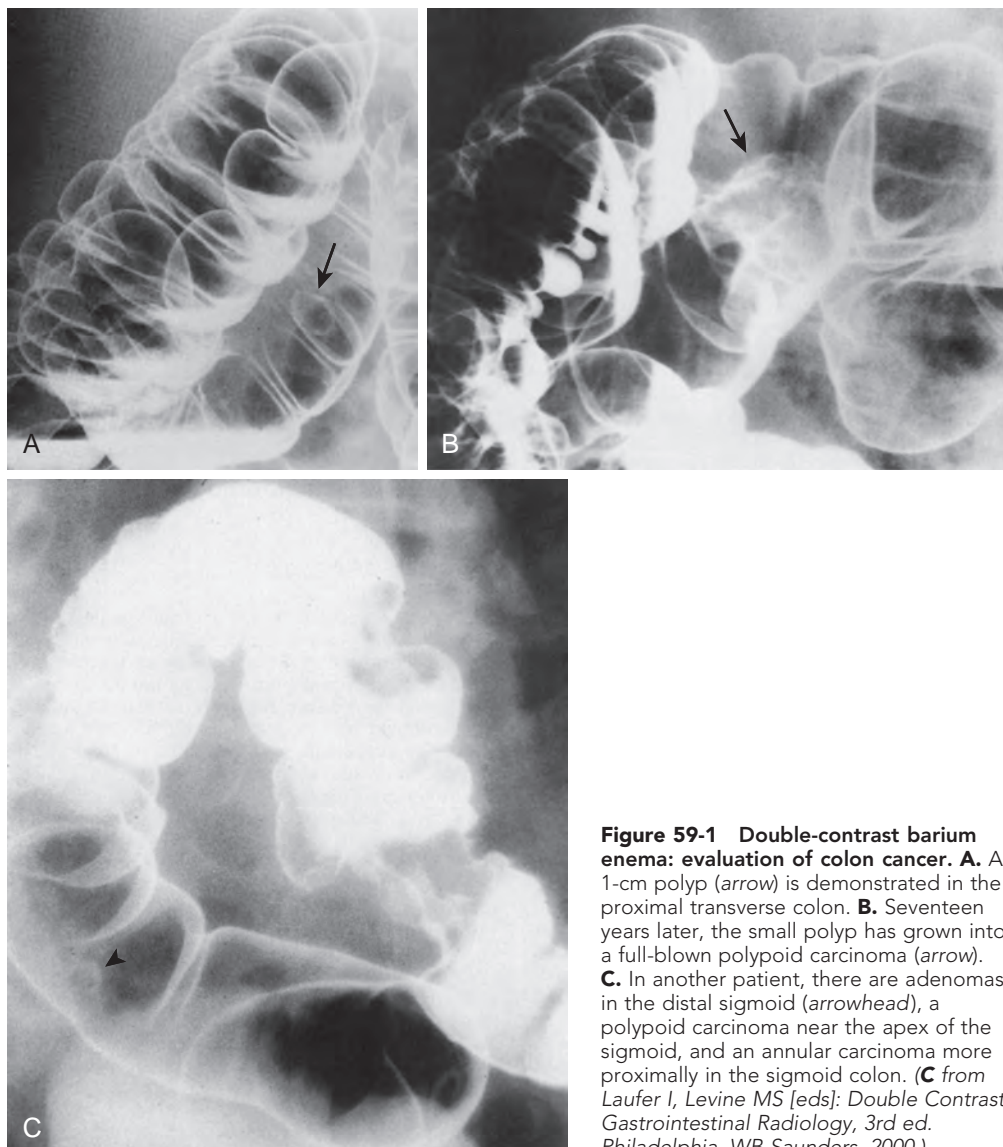


Figure 59-1 Double-contrast barium enema: evaluation of colon cancer. **A.** A 1-cm polyp (arrow) is demonstrated in the proximal transverse colon. **B.** Seventeen years later, the small polyp has grown into a full-blown polypoid carcinoma (arrow). **C.** In another patient, there are adenomas in the distal sigmoid (arrowhead), a polypoid carcinoma near the apex of the sigmoid, and an annular carcinoma more proximally in the sigmoid colon. (C from Laufer I, Levine MS [eds]: *Double Contrast Gastrointestinal Radiology*, 3rd ed. Philadelphia, WB Saunders, 2000.)

HEREDITARY FACTORS

The role of heredity in colorectal cancer has been a subject of considerable interest. Heredity probably plays a role in 5% to 6% of all cases of colorectal cancer. Adenomatous polyposis coli (see Chapter 61) is transmitted by the classic mendelian dominant inheritance pattern, and almost all patients with this condition eventually develop colorectal carcinoma. They account for approximately 1% of colorectal cancers. Another 5% occur in patients with hereditary nonpolyposis colorectal cancer (HNPCC). HNPCCs are subdivided into those in which colorectal cancer is clustered in families (type I) and those in which there is a familial clustering of colorectal cancer with other malignancies, such as carcinomas of the endometrium, ovary, and breast (type II). In all these syndromes, carcinomas tend to occur in the proximal part of the colon and are found at a relatively young age.⁹

It has been suggested that an abnormality in the genetic material may be associated with the development of colorectal cancer.¹⁰ The discovery of four human mismatch repair genes

(*hMSH2*, *hMLH1*, *hPMS1*, and *hPMS2*) has provided novel insight into the genetic basis of this disease and raised the possibility of genetic diagnosis for the management of HNPCC patients and their family members.¹¹ Therefore, it may be important to perform DNA testing in families suspected of having HNPCC.¹²

RISK FACTORS

Although colorectal cancer is common in the U.S. population, several factors place individuals at higher than normal risk. These include older age, a personal or family history of colorectal polyps or cancer, certain hereditary conditions, diets high in saturated fat but low in fiber, excessive alcohol consumption, sedentary lifestyle, obesity, and inflammatory bowel disease (IBD). The onset of colorectal cancer is clearly related to age. The incidence increases markedly in those older than 50 and peaks in those about 70 years old. First-degree relatives of patients with colon cancer have a twofold to threefold increase

in cancer risk, as do patients who have previously been treated for colon cancer.

Patients with chronic ulcerative colitis have a higher incidence of colorectal cancer. The incidence starts to increase after the disease has been present for about 10 years, and approximately 10% develop cancer for every decade after 10 years of disease activity.¹³ These cancers tend to be more uniformly distributed throughout the colon, with a trend toward a more proximal location, and they often have a scirrhous appearance.¹⁴ Patients with pancolitis are predominantly affected. Sclerosing cholangitis is associated with a strong risk of developing colon cancer in patients with IBD; consumption of nonsteroidal anti-inflammatory drugs (NSAIDs) exerts a protective influence.¹⁴ The incidence, characteristics, and prognosis of colorectal carcinoma complicating Crohn's disease are similar to the features of cancer in ulcerative colitis, including young age, multiple neoplasms, long duration of disease, and more than a 50% 5-year survival rate.¹⁵

Pathogenesis

In the past, there was considerable controversy regarding the adenoma-carcinoma sequence. However, it is now believed that at least 70% of colorectal carcinomas start as benign adenomas that undergo malignant transformation (see Fig. 59-1).¹⁶ Up to 30% of cancers arise from a *de novo* sequence—that is, carcinoma developing in normal mucosa without an antecedent adenoma.¹⁵ Larger adenomas (>1 cm) pose a greater cancer risk.¹⁷ Thus, it is vital to detect and remove polypoid lesions larger than 1 cm. Their removal prevents the subsequent development of cancer. If the polyp has become a colon cancer, the earlier it is removed, the less likely it is to have spread.

Cancers that develop in patients with IBD generally arise from areas of high-grade mucosal dysplasia rather than from adenomatous polyps.¹⁸ Therefore, in the surveillance of these patients, blind biopsy specimens are often taken throughout the colon in an attempt to detect severe and persistent dysplasia.

Clinical Aspects

Colorectal cancer is a slow-growing malignancy, requiring a period of 7 to 10 years for a benign adenoma to undergo malignant transformation. Ideally, the disease should be detected before it becomes symptomatic. Colorectal cancer is sufficiently common in the Western world that routine screening is recommended. The American Cancer Society recommends that starting at age 50, men and women at average risk for developing colorectal cancer should follow one of the screening options listed below^{19,20}:

- Fecal occult blood test (FOBT) or fecal immunochemical test (FIT) every year
- Stool DNA test, interval uncertain
- Flexible sigmoidoscopy every 5 years
- FOBT or FIT every year, plus flexible sigmoidoscopy every 5 years
- Double-contrast barium enema every 5 years *or*
- Colonoscopy every 10 years
- Computed tomography colonography (CTC) every 5 years

The American College of Radiology recommends periodic (\approx every 5 years) double-contrast barium enema study,

especially for patients at higher than normal risk of developing colorectal cancer.²¹ A cost-effectiveness study of double-contrast barium enema in the screening for colorectal carcinoma has shown that the double-contrast barium enema is a cost-effective screening procedure in average-risk patients.²² The results were based on the assumption that a missed benign 10-mm adenomatous polyp could become malignant within 5 years. Recent advances with CT colonography should aid in clarifying its exact role and further expands its role in screening and diagnosing patients with colorectal polyps or cancer (see Chapters 53 and 54).²³⁻²⁵

If patients are at an increased risk for colon cancer, they should be tested at an earlier age than 50 years. In this group are patients with IBD, a personal or family history of colorectal polyps or colorectal cancer, and genetic syndromes, such as familial adenomatous polyposis (FAP) or hereditary nonpolyposis colorectal cancer.

Symptomatic colorectal cancer most often presents as bleeding. The severity of bleeding may range from the presence of occult blood in the stool to the passage of bright red blood per rectum to the development of iron deficiency anemia. The patient's symptoms are usually related to the location of the tumor. Approximately one third of carcinomas are in the rectum and can be reached by the examining finger or a rigid proctoscope. About 50% of large bowel cancers are in the left half of the colon and can be reached with the flexible sigmoidoscope. Left-sided tumors often present with bright red rectal bleeding or constipation caused by obstruction. The remaining tumors are scattered throughout the colon. Cecal carcinomas constitute about 10% of the entire group and are most likely to present as iron deficiency anemia caused by chronic blood loss. Other frequent symptoms of colorectal cancer include abdominal pain, which may be related to the development of obstruction or to tumor invasion of adjacent tissues. Patients may also present with a change in bowel habit or nonspecific symptoms, such as weight loss or fever.

Radiology and Diagnostic Methods

Radiology plays a critical role in the diagnosis and management of patients with colorectal cancer. The double-contrast barium enema may be used for screening, especially for patients who are at higher than normal risk.²² It also can be used as a primary method for diagnosing symptomatic colorectal cancer. Single-column studies should be considered for detecting complications, such as obstruction or perforation. Radiology using multidetector computed tomography (MDCT), CTC, magnetic resonance imaging (MRI), and/or transrectal ultrasound (TRUS) also plays an important role in tumor detection and staging.²³⁻²⁸ Treatment decisions are often based on results from positron emission tomography and CT (PET/CT).²⁹ Radiology has a significant role after treatment for colorectal cancer in the detection of recurrent disease, local and distant metastases, and metachronous colon tumors.

CONTRAST ENEMA

Radiologic examination of the colon can be performed with a single- or double-contrast technique. In most cases, double-contrast enema is superior for the examination of the rectum³⁰ and the detection of small lesions.³¹ In most series of double-contrast studies, polyps are demonstrated in 10% to 13% of all

patients,³² whereas in single-contrast studies, polyps are found in 7% of patients.

COLONOSCOPY

Many studies have claimed to show that colonoscopy is superior to contrast enema for the detection of polypoid lesions. However, most of these studies do not compare state of the art barium techniques with operators of similar interest and experience. There is an error rate inherent in colonoscopy. Part of this error rate derives from failure to reach the cecum in 15% of cases.³³ In addition, there are blind spots within the colon. Generally, these are behind folds or around flexures, and polyps or even large cancers in these regions can be missed (Fig. 59-2).³⁴ If there are significant radiologic-endoscopic discrepancies, they should be resolved by consensus or by further examination, and it should not be assumed that the endoscopy result was correct.^{35,36}

Colonoscopy and double-contrast enema examinations have comparable overall accuracy, with detection of approximately 90% of all polypoid lesions if the radiographic examination is performed by an experienced radiologist with special interest in gastrointestinal (GI) radiology.^{37,38} However, the cost and complications of colonoscopy are considerably higher than those for double-contrast barium enema. Colonoscopy or flexible sigmoidoscopy should always be used to evaluate suggestive findings in contrast enema studies, particularly in patients with marked diverticular disease. It should also be used for biopsy of lesions and removal of polypoid lesions.

CROSS-SECTIONAL IMAGING

CT has been used to detect and stage many tumors, including primary and recurrent colorectal neoplasms,³⁹⁻⁴¹ and has been joined by MRI,^{27,42,43} TRUS,^{28,42} scintigraphy with monoclonal antibody (MoAb) imaging,^{44,45} and PET.^{29,46,47} 3D virtual reality

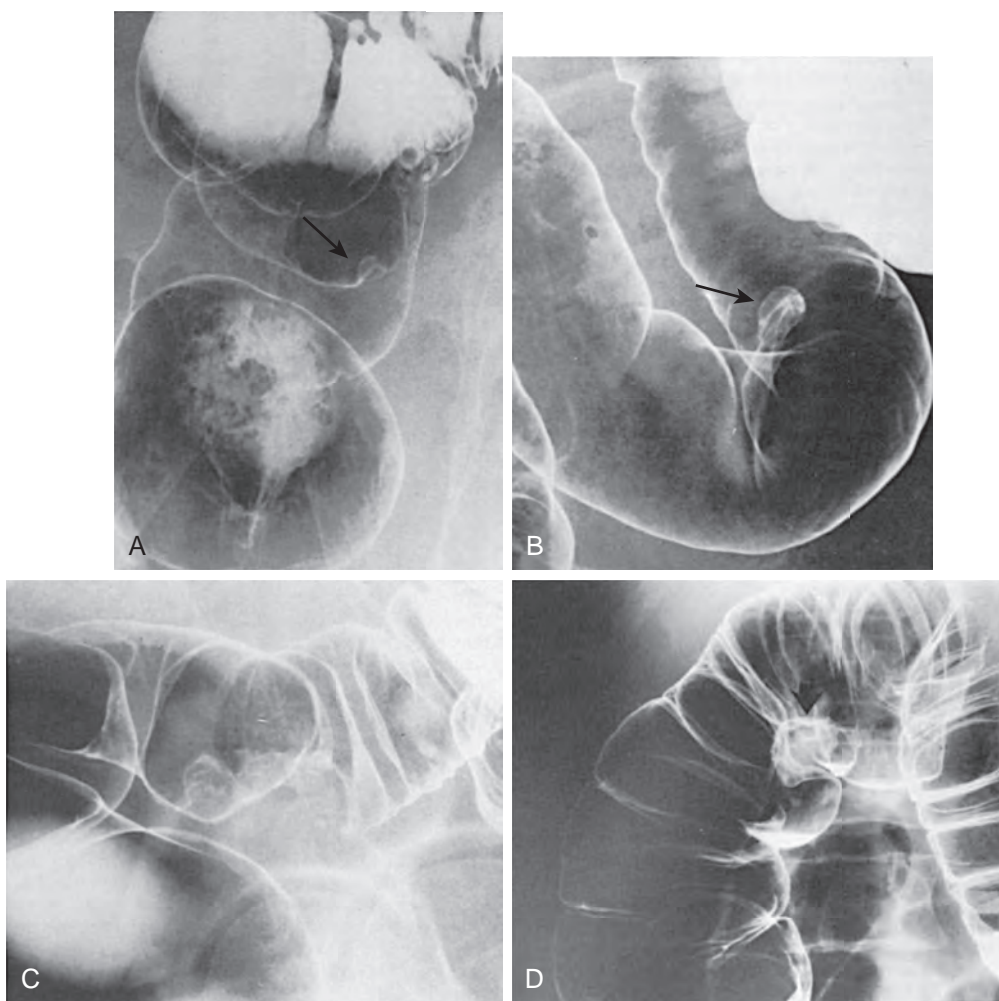


Figure 59-2 Lesions missed at endoscopy identified on barium enema. **A.** There is a small sessile polyp (arrow) behind a fold at the rectosigmoid junction. This lesion was missed twice on sigmoidoscopy and was finally detected at the third sigmoidoscopic examination. **B.** A small polyp (arrow) is situated behind a fold at an area of angulation at the junction of the sigmoid and the descending colon. This polyp was missed on two colonoscopic examinations and was found on the third. **C.** Polypoid carcinoma is just proximal to the rectosigmoid junction. This lesion was missed on several sigmoidoscopic and colonoscopic examinations and was confirmed only at surgery. **D.** Polypoid carcinoma at the hepatic flexure was missed on initial colonoscopy. (**A**, **C**, and **D** from Laufer I, Levine MS [eds]: *Double Contrast Gastrointestinal Radiology*, 3rd ed. Philadelphia, WB Saunders, 2000; **B** from Laufer I, Smith NC, Mullens JE: *The radiological demonstration of colorectal polyps undetected by endoscopy*. *Gastroenterology* 70:167-170, 1976.)

techniques, such as CTC, have been used with increasing frequency, and results are excellent.²³⁻²⁵

Few studies present an in-depth assessment of the value of the various techniques. A review of the large body of literature on this topic reveals many conflicting reports about the effectiveness of the various methods and opposing recommendations for their use. In many cases, this disagreement is because of early, overly enthusiastic conclusions about high success rates with each new imaging technique and underestimation of their pitfalls. Also, some literature reports contain incomplete proof of pathology or neglect to include all factors necessary for complete staging of colon neoplasms.

Benign Epithelial Polyps

INCIDENCE

Benign tumors of the colon are extremely common and usually do not cause symptoms. These polyps are found in 10% to 12.5% of patients studied with double-contrast techniques, and the incidence rises dramatically with increasing age (Fig. 59-3A). Polyps occur most frequently in the left colon and are scattered throughout the remainder of the transverse and right colon (see Fig. 59-3B). As people age, there is a shift in the incidence of polyps to the right side of the colon, coinciding with a shift in the distribution of colon carcinoma to the right.^{48,49}

PATHOLOGY

The term *polyp* refers only to a focal, protruded lesion within the bowel. In general terms, a polyp may be neoplastic or non-neoplastic. Most non-neoplastic polyps are inflammatory or hyperplastic. They are generally small and usually occur in the distal colon. Neoplastic polyps may represent true neoplasms of any component of the bowel wall. Epithelial neoplasms—adenomas—are the most important because they serve as precursors to colorectal carcinoma. The demonstration of a polypoid lesion on a barium enema does not necessarily provide information regarding its pathologic nature. Whenever possible, polyps larger than 1 cm in diameter must be removed, preferably by colonoscopic polypectomy (Fig. 59-4), because of the increased risk of harboring a malignancy.

Most colonic adenomas are tubular adenomas. However, tubular adenomas have various degrees of villous change and, as a polyp becomes larger, the degree of villous change increases. At the other end of the spectrum, some polyps are villous adenomas because the surface consists of frondlike structures arising from the base of the mucosa. Thus, there may be a transition from tubular adenoma to tubulovillous adenoma to villous adenoma. It has been suggested that any adenoma with more than 75% villous change should be referred to as a villous adenoma.⁵⁰ In general, the risk of carcinoma is related to the proportion of villous change in an adenoma.

In small adenomas, it may be impossible to distinguish villous change radiologically. However, as the adenoma becomes larger and the proportion of villous change increases, a reticular or granular mucosal surface may be seen (Fig. 59-5A).⁵¹ Large villous adenomas have an atypical radiologic appearance.⁵² They are large, bulky polypoid masses with barium caught between the frondlike protrusions, producing a lacy surface pattern (see Fig. 59-5B). Large villous tumors should be removed

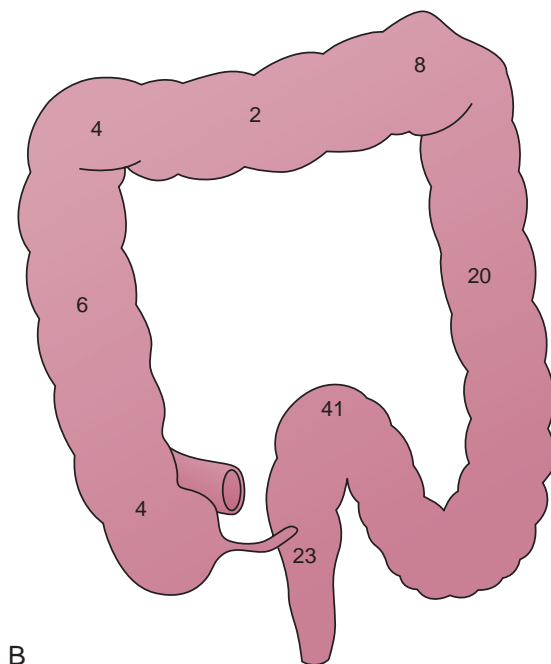
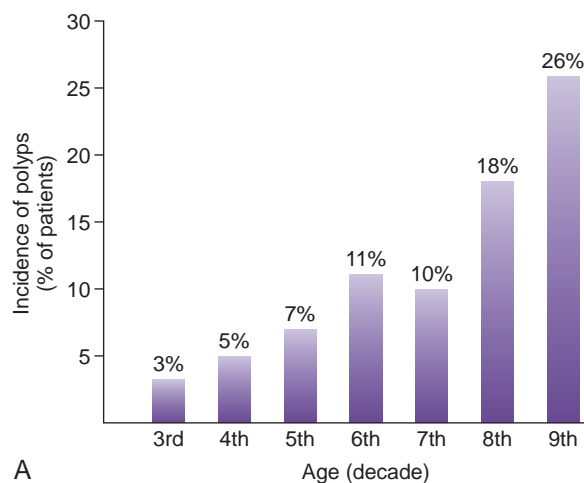


Figure 59-3 Incidence and distribution of colorectal polyps.

A. Incidence of colonic polyps related to age (based on 800 consecutive double-contrast enemas). There is an increasing incidence of colonic polyps, ranging from 3% in those in their 20s to 26% in those in their 80s. **B.** Distribution of colorectal polyps (based on 108 consecutive polyps). Approximately 60% of the polyps are in the rectum and sigmoid colon. (**A** from Laufer I: *The double contrast enema: Myths and misconceptions*. *Gastrointest Radiol* 1:19–31, 1976, with kind permission from Springer Science and Business Media; **B** from Laufer I, Levine MS [eds]: *Double Contrast Gastrointestinal Radiology*, 3rd ed. Philadelphia, WB Saunders, 2000.)

completely because malignant degeneration may occur in only a portion of the tumor, and random biopsy sampling is unreliable for the detection of malignant change.

Other non-neoplastic polyps may also be found in the colon. These include juvenile polyps, which may be single or multiple and may be found in adults and in children. Hamartomatous polyps are found in patients with Peutz-Jeghers syndrome and inflammatory polyps in patients with Cronkhite-Canada syndrome (see Chapter 61).

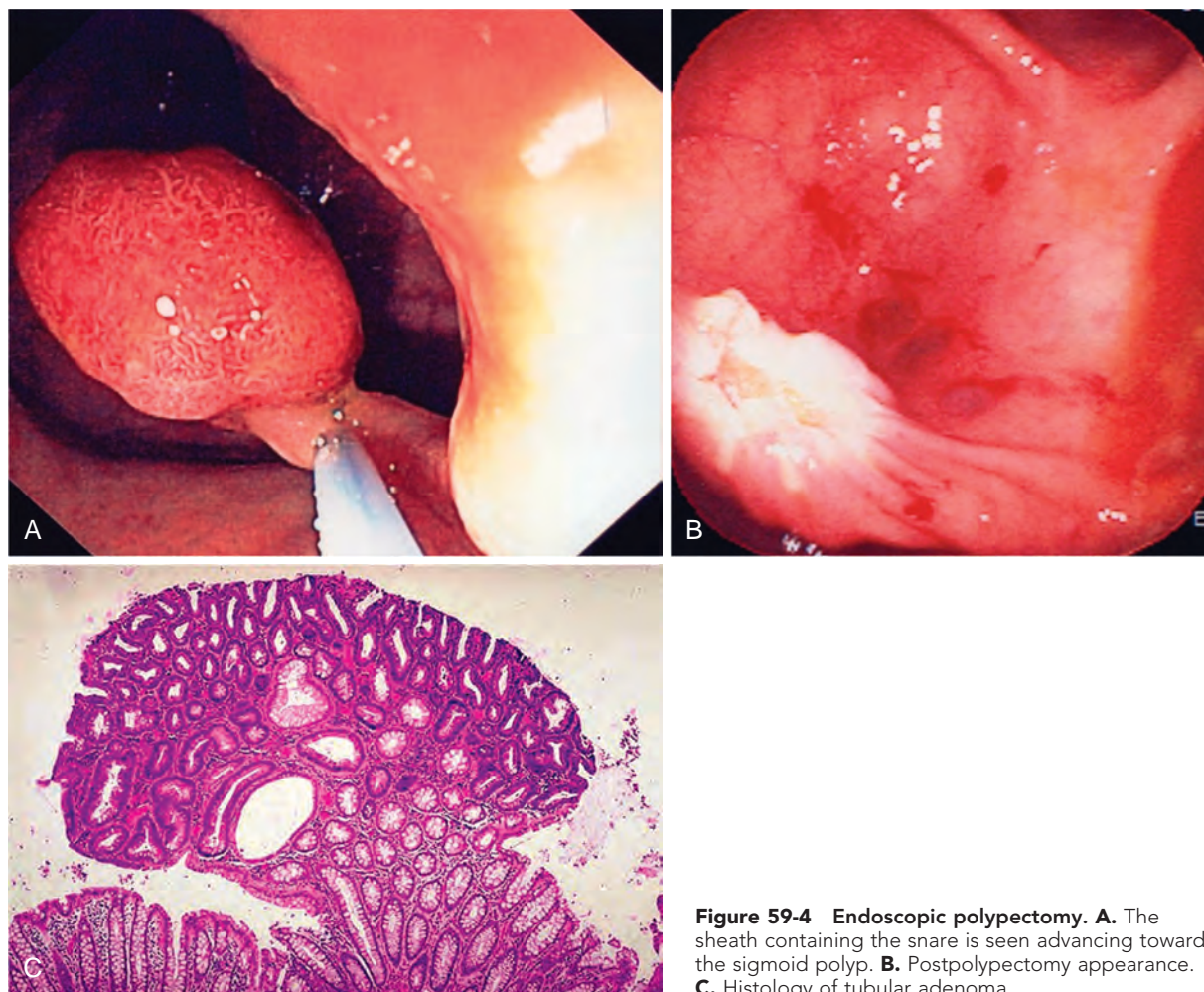


Figure 59-4 Endoscopic polypectomy. **A.** The sheath containing the snare is seen advancing toward the sigmoid polyp. **B.** Postpolypectomy appearance. **C.** Histology of tubular adenoma.

POLYP DETECTION

Barium Enema

A polyp may be demonstrated as a radiolucent filling defect, contour defect, or ring shadow because it is simply a protrusion of the mucosa into the bowel lumen (see Chapter 2). The greatest and most frequent difficulty arises in distinguishing polyps from fecal residue. In general, fecal residue is mobile and is usually found on the dependent surface in the barium pool. In addition, several features may suggest that the filling defect represents a true polyp. These include the bowler hat sign (Fig. 59-6A) and Mexican hat sign (see Fig. 59-6B). Although the bowler hat sign can also be produced by a diverticulum, the direction of the dome of the bowler hat distinguishes a polyp from a diverticulum.⁵³ When the dome of the hat points away from the axis of the bowel, the lesion is a diverticulum; when the dome points toward the lumen of the bowel, it is a polyp. Villous adenomas may have a reticular or granular surface because of barium trapped between the fronds of the tumor.⁵¹ These signs are illustrated and discussed in detail in Chapters 2 and 3. Some hyperplastic polyps may not appear as smooth sessile lesions measuring 5 mm or less, but as larger lobulated lesions that cannot be distinguished morphologically from adenomatous polyps.⁵⁴

Rubenstein and coworkers have used the term *carpet lesion* to describe a flat lobulated lesion that is manifest primarily as an alteration in the surface texture of the bowel (Fig. 59-7A).⁵⁵ These lesions may be large and are mostly tubular adenomas with varying degrees of villous change. In some cases of colorectal carcinoma, the background of a benign carpet lesion can be recognized (see Fig. 59-7B).

Cross-Sectional Imaging

Benign lesions of the colon, such as hyperplastic polyps or adenomatous polyps, are usually not examined by CT or MRI. They are demonstrated by barium examinations or by an endoscopic technique and are seen during CT or MRI examinations only incidentally. These techniques are used only if these benign tumors become large enough to have a high likelihood of harboring a malignancy. Benign polyps appear as sessile soft tissue masses that protrude into the lumen of the bowel on axial images (Fig. 59-8). They are usually detected only if the patient has undergone colonic cleansing or if the polyp is large. If the polyp is pedunculated, CT scans may demonstrate a large polypoid mass that represents the combined polyp and stalk (see Chapter 53).

Kim and colleagues⁵⁶ have suggested that villous adenomas have a characteristic CT appearance based on their high mucus

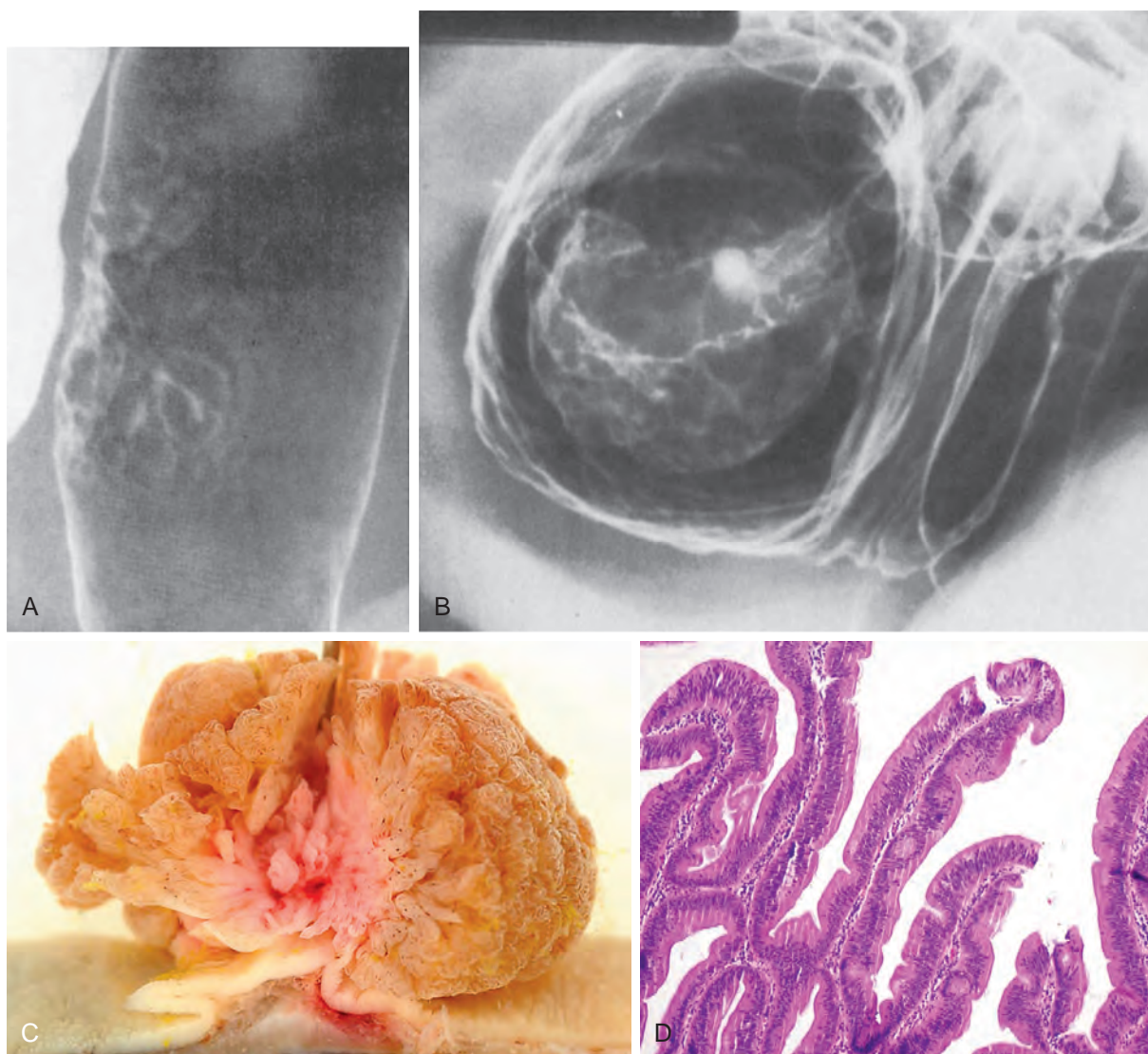


Figure 59-5 Villous adenomas. **A.** A flat tumor in the descending colon with an irregular surface suggestive of a villous adenoma. This was a villoglandular polyp. **B.** Typical villous tumor in the sigmoid colon. This tumor exhibits the typical, irregular, frondlike surface of a villous tumor. It was a malignant villous adenoma. **C.** Gross pathology specimen shows cauliflower-like colon polyp. **D.** Histology reveals frondlike nature of polyp. (**A** and **B** from Laufer I, Levine MS [eds]: *Double Contrast Gastrointestinal Radiology*, 3rd ed. Philadelphia, WB Saunders, 2000.)

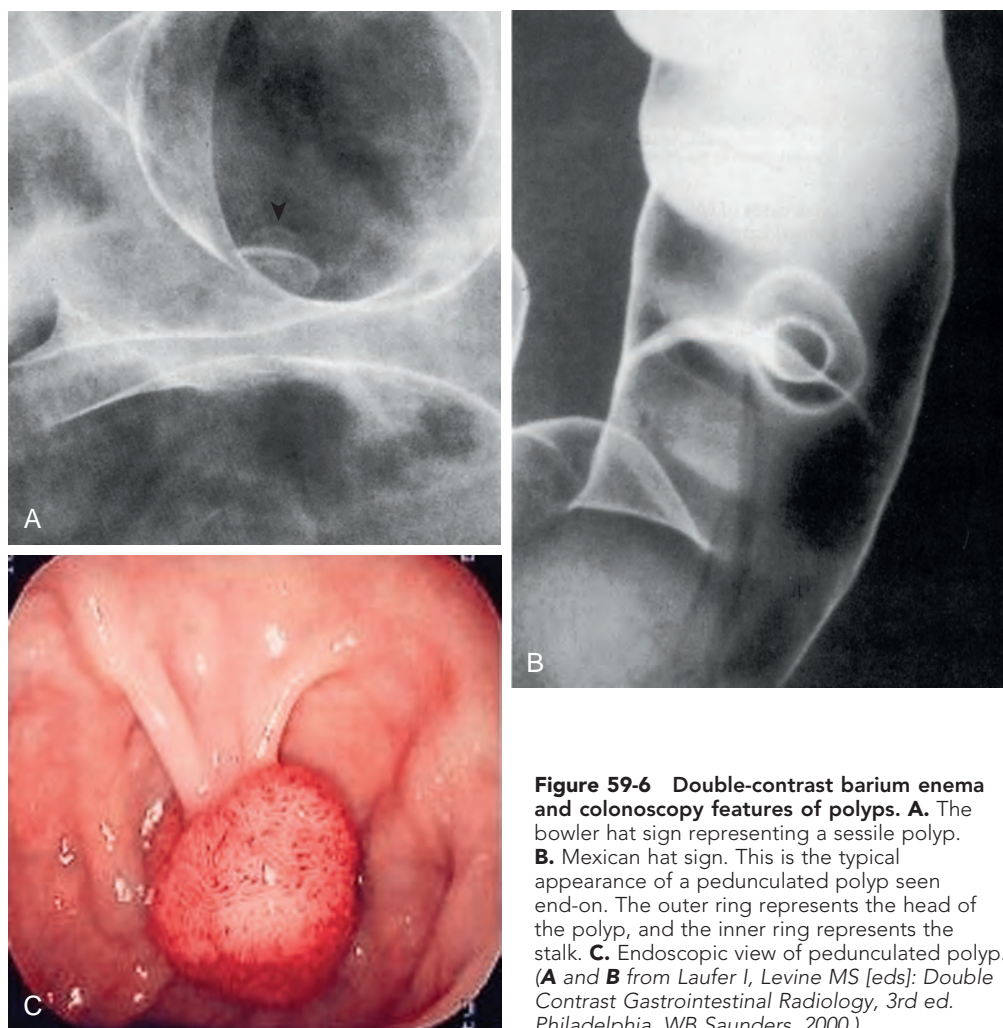
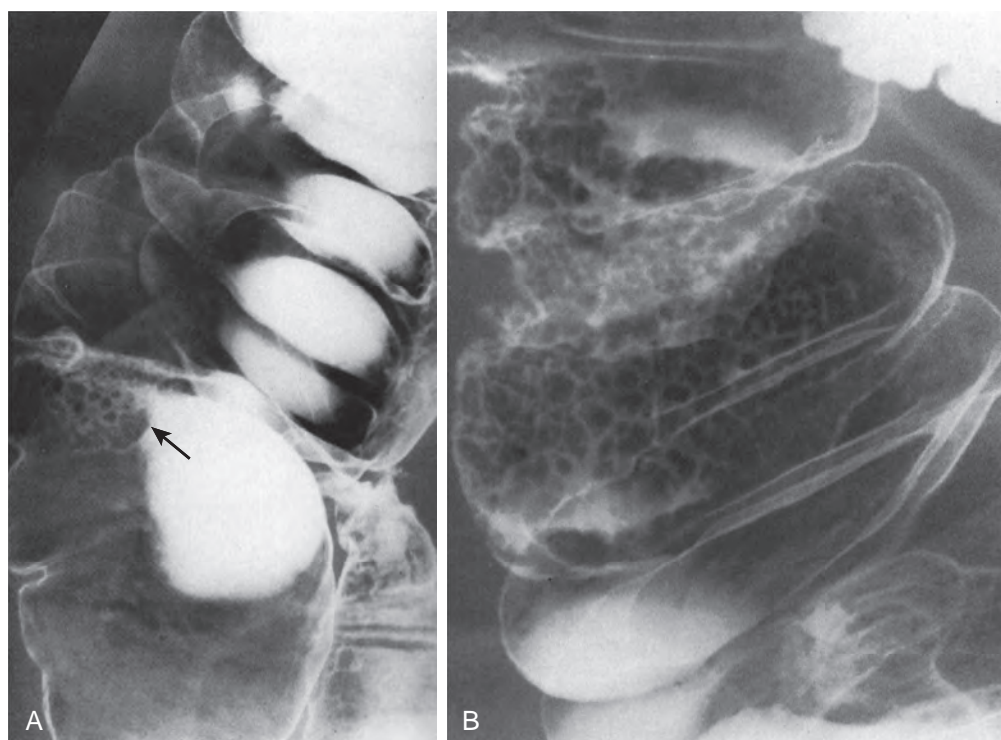


Figure 59-6 Double-contrast barium enema and colonoscopy features of polyps. **A.** The bowler hat sign representing a sessile polyp. **B.** Mexican hat sign. This is the typical appearance of a pedunculated polyp seen end-on. The outer ring represents the head of the polyp, and the inner ring represents the stalk. **C.** Endoscopic view of pedunculated polyp. (A and B from Laufer I, Levine MS [eds]: *Double Contrast Gastrointestinal Radiology*, 3rd ed. Philadelphia, WB Saunders, 2000.)

Figure 59-7 Carpet lesions.

A. Typical carpet lesion (arrow) in the cecum. **B.** Malignant transformation in a carpet lesion. An obvious polypoid carcinoma is seen in the ascending colon. Surrounding the polypoid lesion is the mucosal change representing the underlying adenoma. (From Laufer I, Levine MS [eds]: *Double Contrast Gastrointestinal Radiology*, 3rd ed. Philadelphia, WB Saunders, 2000.)



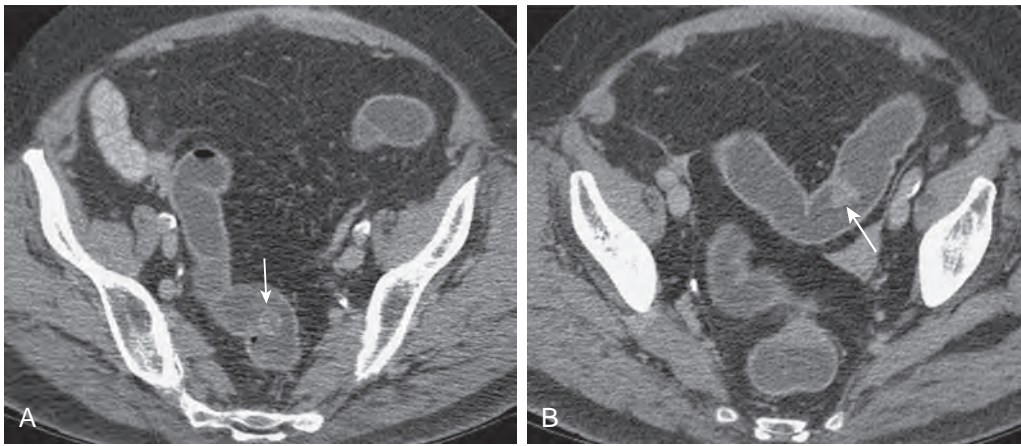


Figure 59-8 CT of benign polyps. **A.** Axial thin-section MDCT scan identifies a sessile polyp (arrow) on the left wall of the proximal sigmoid colon, which was confirmed by colonoscopy in a patient with carcinoma of the cecum and familial polyposis syndrome. **B.** Axial thin-section MDCT below level shown in **A** demonstrates a second polyp (arrow) in the small bowel.

content. The CT features of villous adenomas include homogeneous water density (<10 HU) occupying more than 50% of the lesion and an eccentric location on the luminal side of the mass. No air-fluid level is seen, and the lesion should not have a round cystic configuration. Opaque oral or rectal contrast material should not be used to diagnose a suspected villous adenoma because it obscures the lesion. In these cases, insufflation of air, water, or oily substance administered per rectum may be helpful. Because of their malignant potential, larger villous adenomas should always be staged by CT or TRUS if located in the rectum.⁵⁷

On MRI scans, benign polyps appear as low-intensity structures on T1-weighted spin-echo sequences. If there are many mucin-producing cells, the signal intensity of the polypoid mass increases on T1-weighted sequences. TRUS is used for assessment of sessile polyps large enough to have an increased risk for malignancy. In these cases, TRUS can be used to determine the depth of invasion by a sessile mass that protrudes into the lumen. The depth of invasion is best assessed by TRUS because it is the only method that can demonstrate the various layers of the colonic wall. If the intraluminal component is large, false tumor measurements and erroneous depiction of the surface of the mass can occur because of compression of the tumor by the transrectal probe.

Adenocarcinoma

BARIUM ENEMA

Early Cancer

The radiologic detection of early colorectal cancer is basically an exercise in the detection of polyps. The typical early colon cancer is a flat, sessile lesion that may produce a contour defect (Fig. 59-9). Although most polyps detected radiologically should be removed if they are larger than 5 mm in diameter, a number of radiologic criteria have been used for the detection of malignancy in colorectal polyps.⁵⁸ The size of the polyp is the most important criterion. Carcinoma is very rare in polyps smaller than 5 mm. The incidence of cancer is approximately 1% in polyps in the 5- to 10-mm range (Fig. 59-10), 10% in polyps measuring between 1 and 2 cm, and more than 25% in polyps larger than 2 cm.⁵⁹

Malignant polyps tend to grow more quickly than benign polyps, although there is considerable overlap between the two

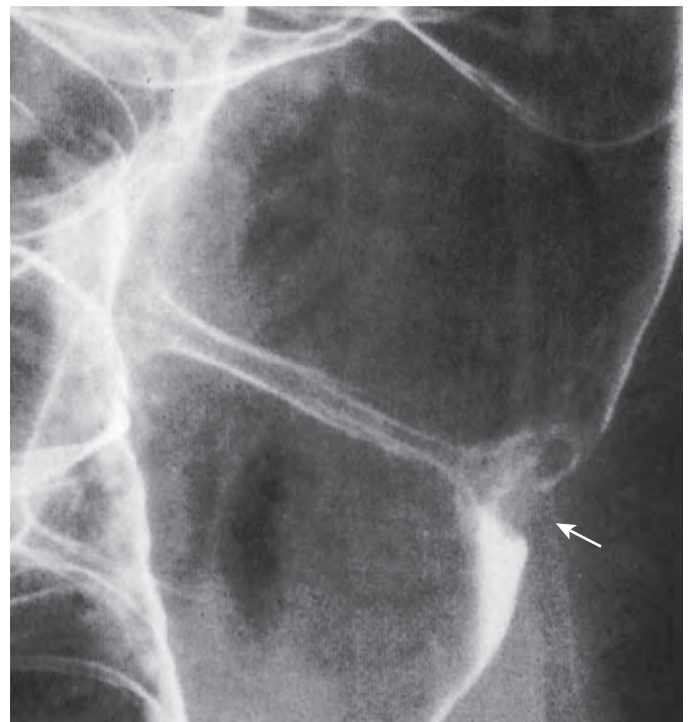


Figure 59-9 Typical early colon cancer. A 1-cm polypoid mass with a contour defect (arrow) is seen along the lateral wall. (From Laufer I, Levine MS [eds]: *Double Contrast Gastrointestinal Radiology*, 3rd ed. Philadelphia, WB Saunders, 2000.)

groups.⁶⁰ If there is definite evidence of polyp growth on serial examinations, malignancy should be suspected. The presence of a long thin stalk is generally a sign of a benign polyp. Rarely, these polyps harbor malignancy.⁶¹ As a rule, the stalk associated with carcinoma is short and thick (Fig. 59-11). If the head of the polyp is irregular or lobulated, the probability of malignancy is greater, although some benign polyps may have an irregular or lobulated surface.

Advanced Cancer

Most patients with symptomatic colorectal carcinoma have advanced lesions. These lesions are generally annular or polypoid tumors seen as filling defects in the barium column or as

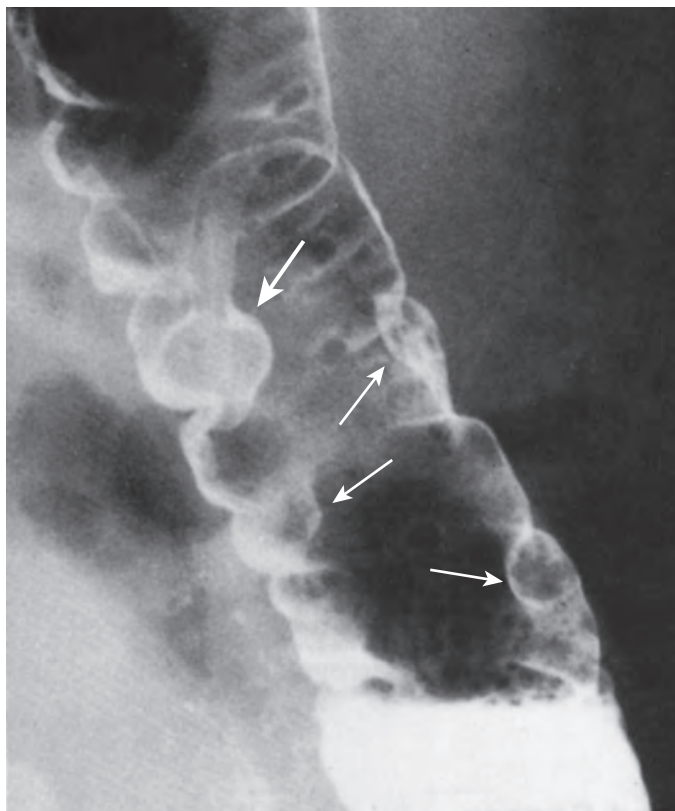


Figure 59-10 Early colon cancers: polypoid carcinoma with a pedicle in 29-year-old man with rectal bleeding. A pedunculated polyp in the descending colon (large arrow) has a typically benign appearance. This was removed at colonoscopy and was found to be a carcinoma with invasion of the stalk. The smaller lesions (small arrows) were hyperplastic polyps. (From Laufer I: *The double contrast enema: Myths and misconceptions*. *Gastrointestinal Radiol* 1:19–31, 1976.)

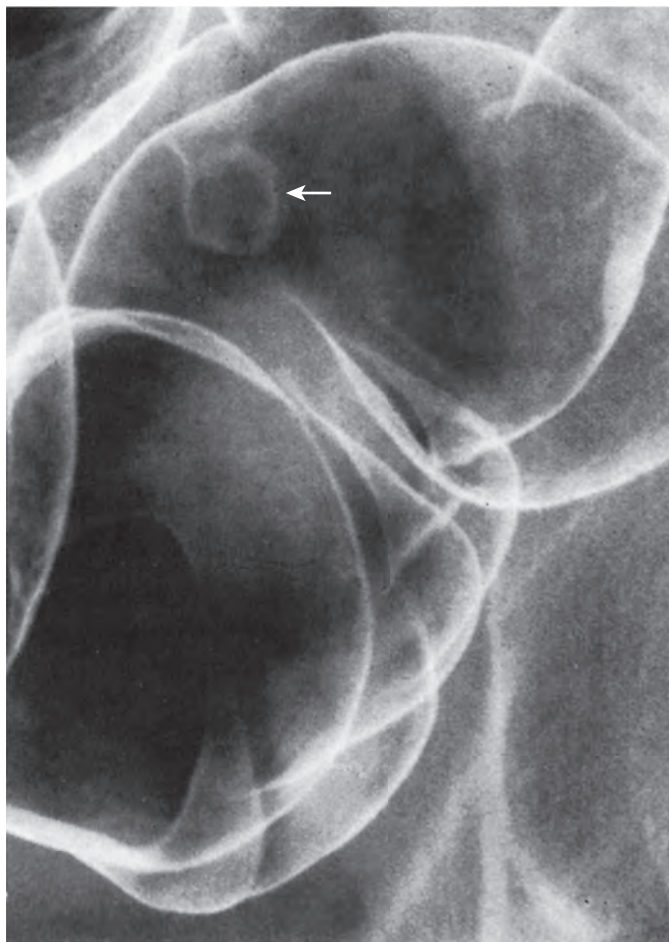


Figure 59-11 Pedunculated early cancer. Early carcinoma (arrow) with a short, thick stalk. (From Laufer I, Levine MS [eds]: *Double Contrast Gastrointestinal Radiology*, 3rd ed. Philadelphia, WB Saunders, 2000.)

contour defects. In addition, plaquelike lesions can produce abnormal lines on double-contrast barium studies (Figs. 59-12 and 59-13).⁶² Annular or semiannular carcinomas as seen with barium enema have a higher rate of serosal invasion and lymph node metastases than polypoid carcinomas.⁶³

Advanced cancers are often associated with sentinel polyps or additional polyps elsewhere in the colon. Approximately 5% of patients who have a colon carcinoma have additional, synchronous carcinomas in the colon (see Fig. 59-13).^{59,64} Therefore, whenever possible, the entire colon should be examined, even when a carcinoma is encountered in the distal bowel. The barium enema may be used to search for neoplastic lesions larger than 1 cm in patients with incomplete colonoscopy.⁶⁵

Carcinomas are particularly difficult to detect in patients with extensive diverticular disease of the sigmoid colon (Fig. 59-14). If the radiologic examination leaves any doubt regarding the presence of a carcinoma, flexible sigmoidoscopy should be recommended to confirm or exclude lesions in the sigmoid colon.⁶⁶

Advanced carcinoma may have an atypical appearance. The linitis plastica type of carcinoma has predominant submucosal infiltration and fibrous reaction.⁶⁷ The radiologic appearance may be suggestive of an inflammatory stricture. This type of carcinoma is particularly likely to develop in patients with ulcerative colitis (see Chapter 57).

Complications

The most important complications of colorectal cancer include bleeding, bowel obstruction, and perforation. Massive rectal bleeding caused by colon carcinoma is rare; the bleeding is more often manifest as occult blood in the stool or as chronic anemia. Colorectal cancer is one of the major causes of large bowel obstruction. Obstruction may be caused by encroachment of the tumor mass on the lumen of the bowel (Fig. 59-15A). Antegrade and retrograde obstruction tend to be poorly correlated. Frequently, there is a high-grade obstruction to the retrograde flow of barium when the patient has few or no symptoms of clinical obstruction. In the case of polypoid tumors, obstruction may also be caused by colocolic intussusception (see Fig. 59-15B). In patients with long-standing obstruction and colon distention, mucosal ischemia may result in an ulcerative form of colitis affecting the colon proximal to the obstruction.

Advanced cancer may result in perforation of the colon and a pericolic abscess (Fig. 59-16A). The signs, symptoms, and radiologic features of a perforated carcinoma may be difficult to distinguish from those of a pericolic abscess associated with diverticulitis (see Fig. 59-16B). However, evidence of GI blood loss makes a malignant origin much more likely.⁶⁸ Perforation of the colon may lead to a fistula to adjacent organs, such as the

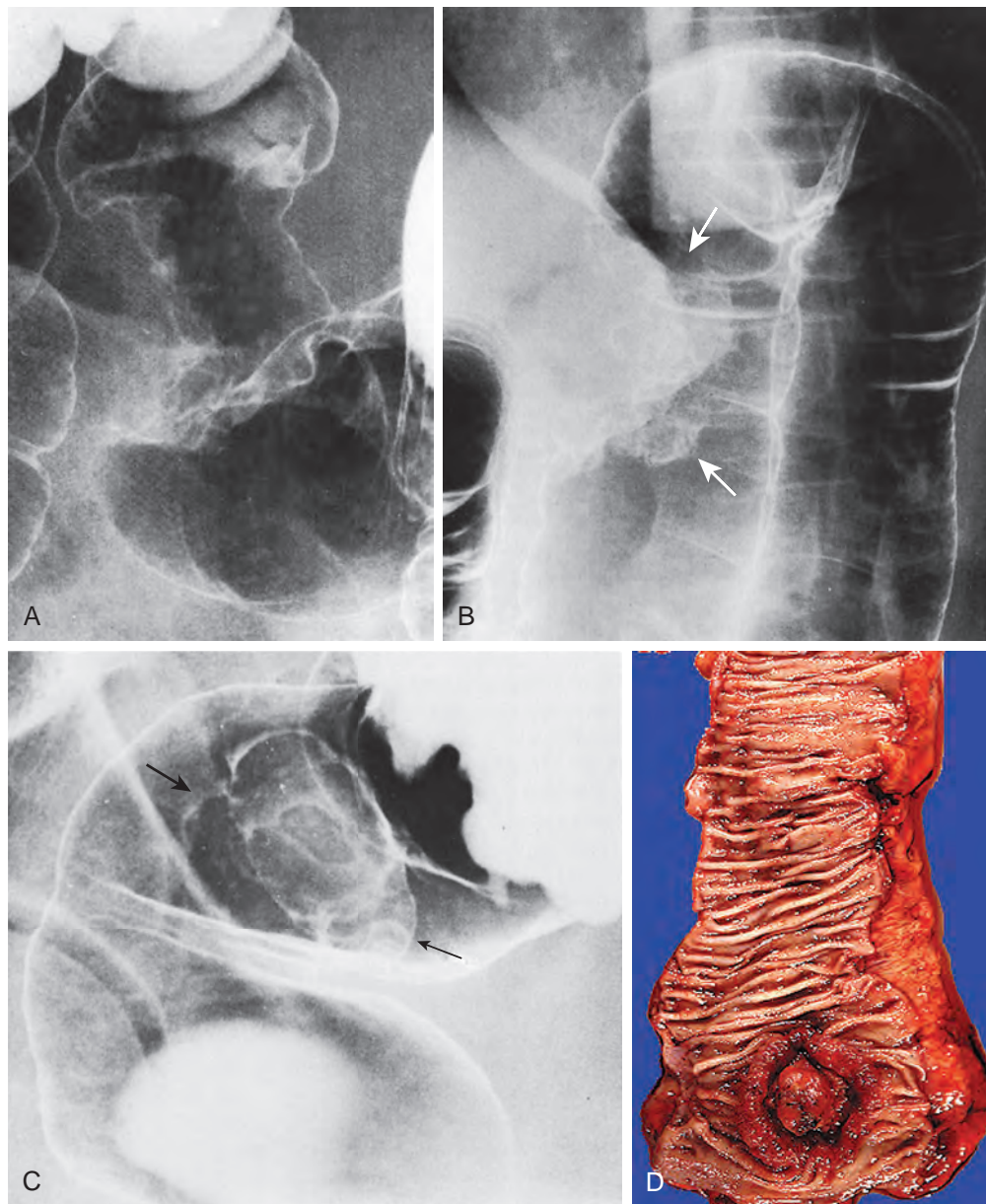


Figure 59-12 Advanced colon cancer. **A.** Annular "apple core" lesion. **B.** Large polypoid carcinoma (arrows) at the splenic flexure. **C.** Lateral view shows an ulcerated plaque-like carcinoma etched in white (arrows) at the rectosigmoid junction. **D.** Specimen shows ulcerating polypoid carcinoma. (**A** and **B** from Laufer I, Levine MS [eds]: *Double Contrast Gastrointestinal Radiology*, 3rd ed. Philadelphia, WB Saunders, 2000.)

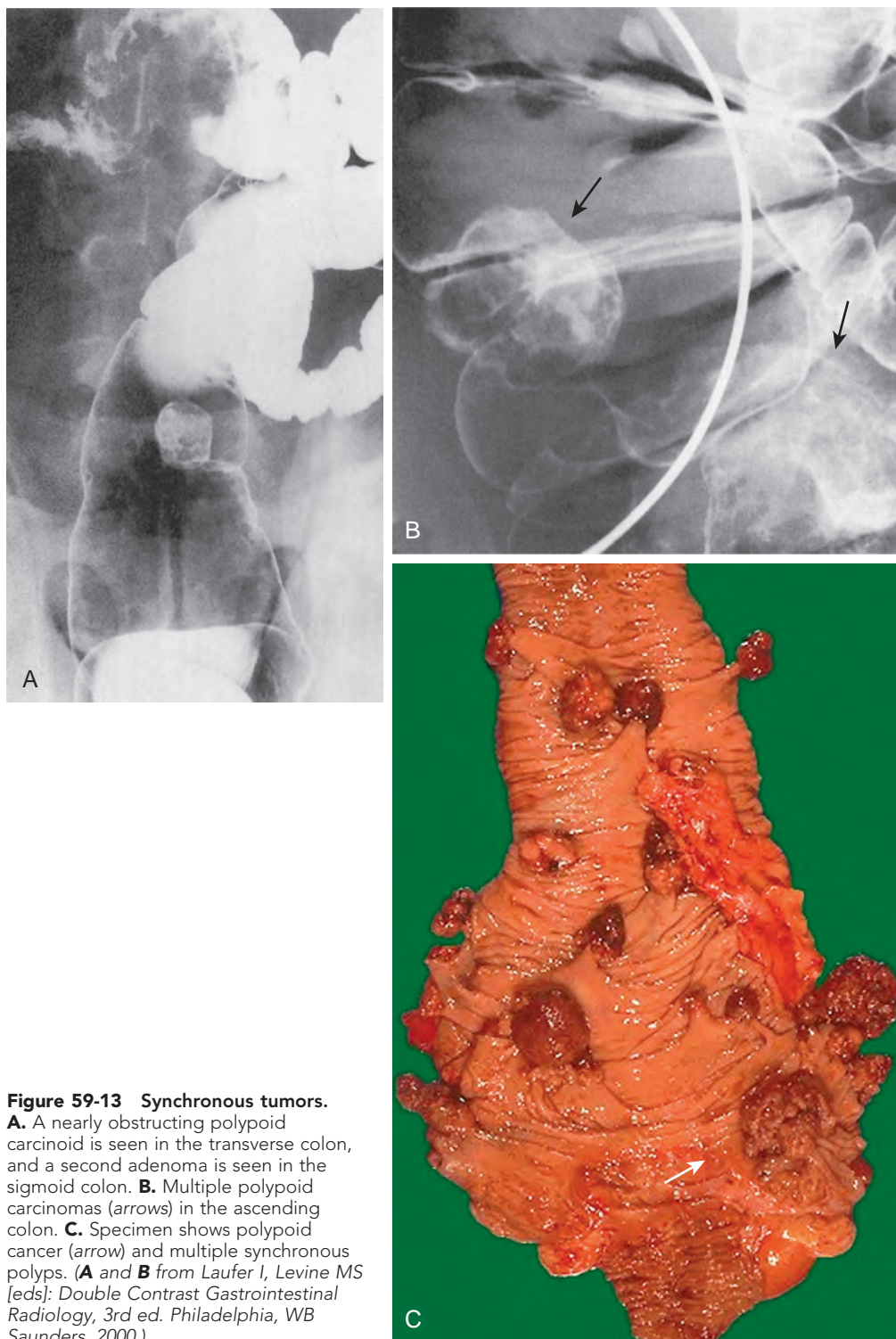


Figure 59-13 Synchronous tumors.

A. A nearly obstructing polypoid carcinoid is seen in the transverse colon, and a second adenoma is seen in the sigmoid colon. **B.** Multiple polypoid carcinomas (arrows) in the ascending colon. **C.** Specimen shows polypoid cancer (arrow) and multiple synchronous polyps. (**A** and **B** from Laufer I, Levine MS [eds]: *Double Contrast Gastrointestinal Radiology*, 3rd ed. Philadelphia, WB Saunders, 2000.)



Figure 59-14 Carcinoma in a patient with diverticulosis. The polypoid carcinoma (arrow) is more difficult to recognize in the presence of extensive diverticulosis. (From Laufer I, Levine MS [eds]: *Double Contrast Gastrointestinal Radiology*, 3rd ed. Philadelphia, WB Saunders, 2000.)

stomach (Fig. 59-17A), duodenum (see Fig. 59-17B), bladder, or vagina. The fistulous communication can be demonstrated by barium study or by the extracolonic presence of gas or contrast medium on CT scans.

COMPUTED TOMOGRAPHY

Primary Colorectal Carcinoma

CT and endoluminal ultrasound are better suited for the evaluation of tumor stage than manual examination, barium enema, or fiberoptic techniques. In the presence of a colorectal cancer, CT and ultrasound may visualize a discrete mass (Fig. 59-18) or focal wall thickening (Fig. 59-19), but this finding is nonspecific and requires further investigation. The wall thickening may be circumferential, with or without extension beyond the bowel wall (Figs. 59-20 and 59-21A). Water introduced per rectum and multiplanar reconstructions often help delineate a tumor better (see Fig. 59-21B). Asymmetric mural thickening, with or without an irregular surface contour, is suggestive of a neoplastic process (see Fig. 59-20), particularly if benign causes can be excluded by history or physical examination. In the anorectal region, internal hemorrhoids must be distinguished from a polypoid malignancy.

With a properly distended lumen, a colonic wall thickness less than 3 mm is normal, 3 to 6 mm is indeterminate, and more than 6 mm is definitely abnormal. If the tumor is contained within the wall of the colon or rectum, the outer margins of the large bowel appear smooth. CT cannot reliably assess the depth of mural penetration. The various layers of bowel wall and depth of mural invasion can be depicted by endoluminal

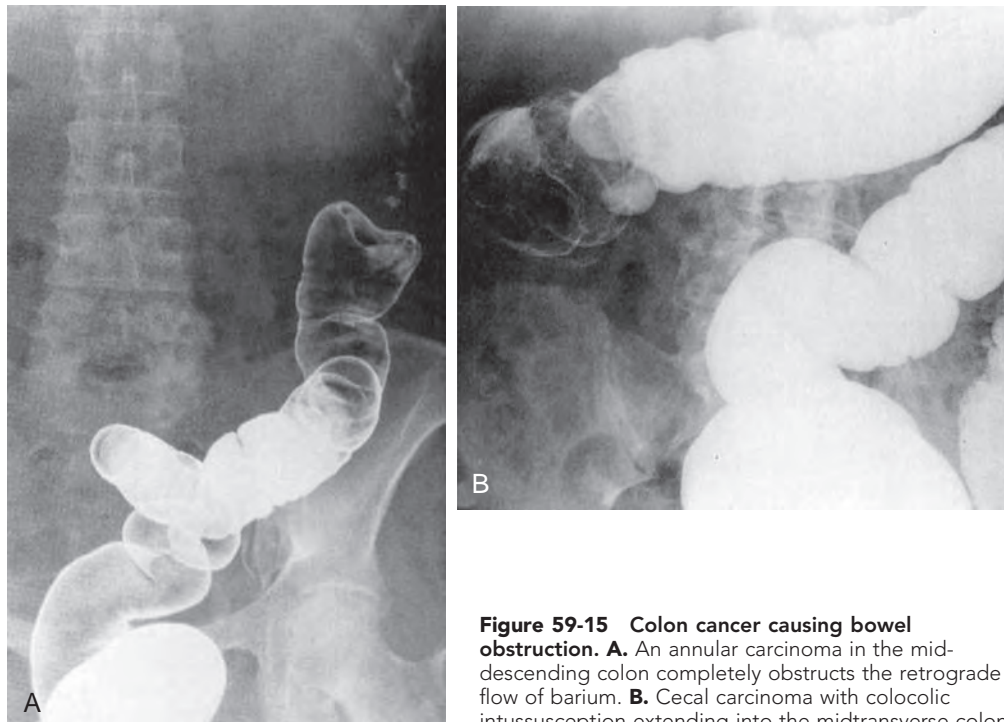


Figure 59-15 Colon cancer causing bowel obstruction. **A.** An annular carcinoma in the mid-descending colon completely obstructs the retrograde flow of barium. **B.** Cecal carcinoma with colocolic intussusception extending into the midtransverse colon.

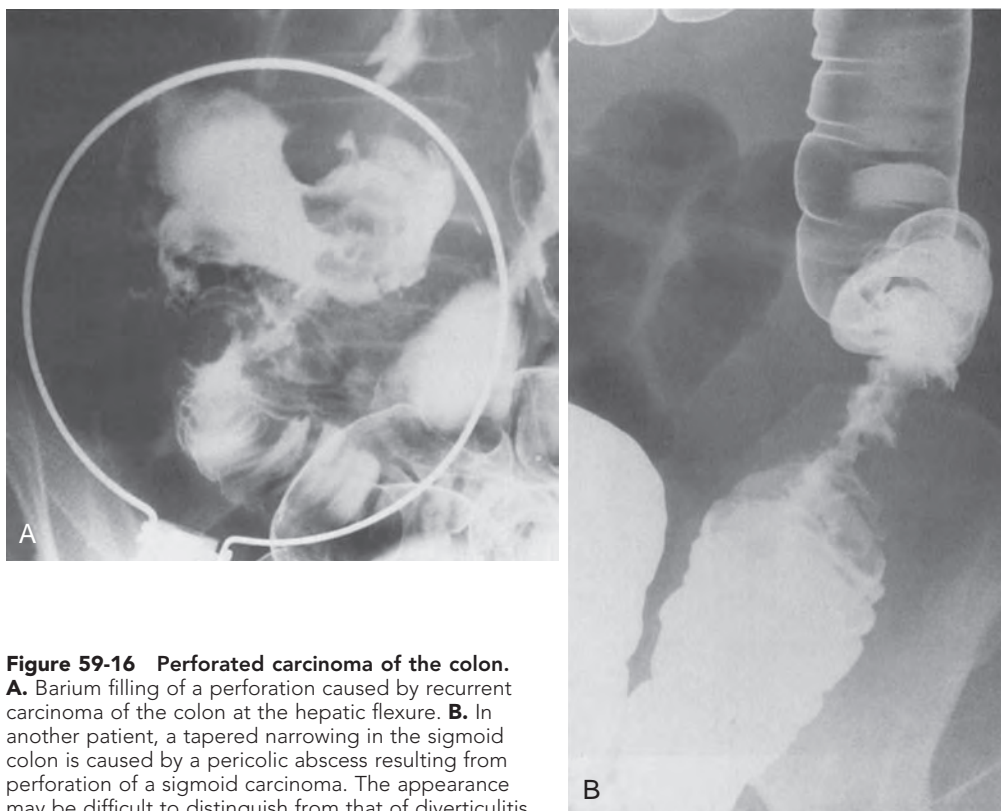


Figure 59-16 Perforated carcinoma of the colon. **A.** Barium filling of a perforation caused by recurrent carcinoma of the colon at the hepatic flexure. **B.** In another patient, a tapered narrowing in the sigmoid colon is caused by a pericolic abscess resulting from perforation of a sigmoid carcinoma. The appearance may be difficult to distinguish from that of diverticulitis.

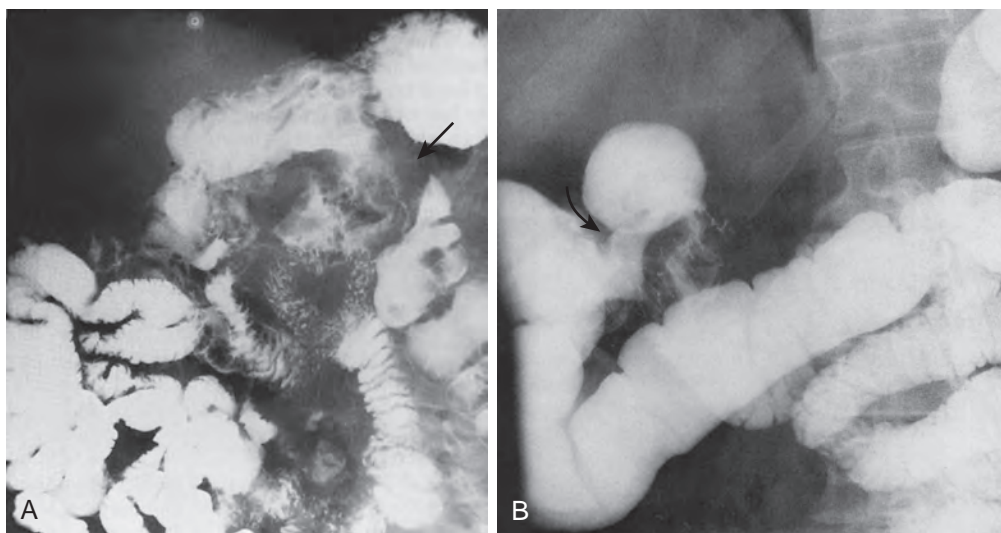


Figure 59-17 Fistulas complicating carcinoma of the colon. **A.** Gastrocolic fistula arising from a carcinoma at the splenic flexure (arrow). **B.** A carcinoma of the transverse colon giving rise to a fistula to the duodenum (arrow).

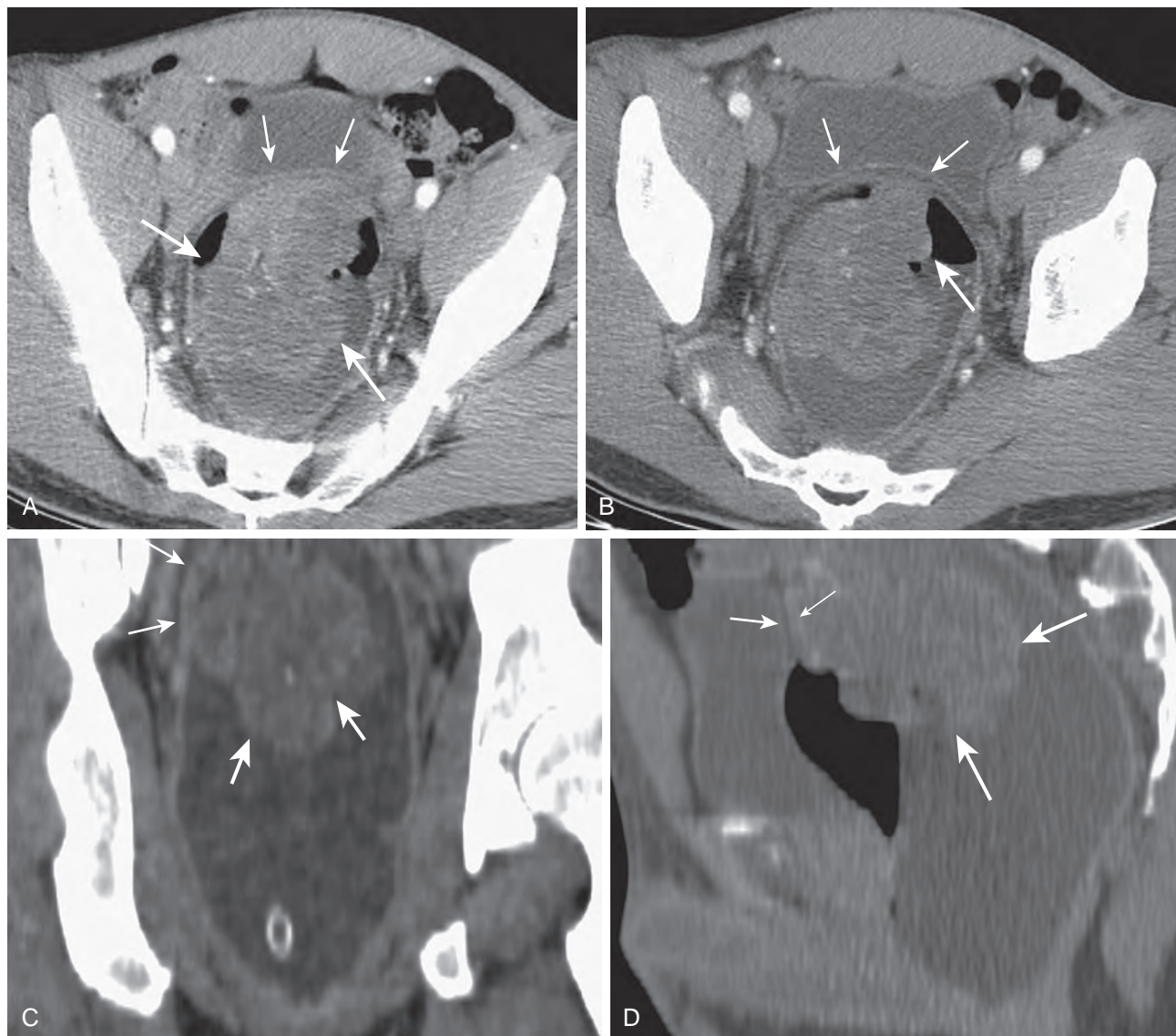


Figure 59-18 Large intraluminal mass in a distended rectum without extension beyond bowel wall (T2N0M0). **A.** A thin-section MDCT scan in the arterial phase demonstrates a very large intraluminal mass (*large arrows*) that appears to arise from the anterior wall of the rectum. Bladder wall (*thin arrows*) is clearly separated from the rectal wall by a thin layer of fat. **B.** Several centimeters below the level of **A**, the fat plane between bladder wall (*thin arrows*) and the mass (*large arrow*) in the anterior rectal wall remains intact. **C.** Coronal MPR demonstrates the large intraluminal component of the mass (*large arrows*) and the wall thickening (*small arrows*), with a smooth outer border. **D.** The sagittal multiplanar reformatted image demonstrates a clear fat plane between the bladder wall (*small arrow*) and thickened rectal wall (*thin arrow*). Both MPRs confirm absence of perirectal infiltration. The large intraluminal mass (*large arrows*) is also appreciated.

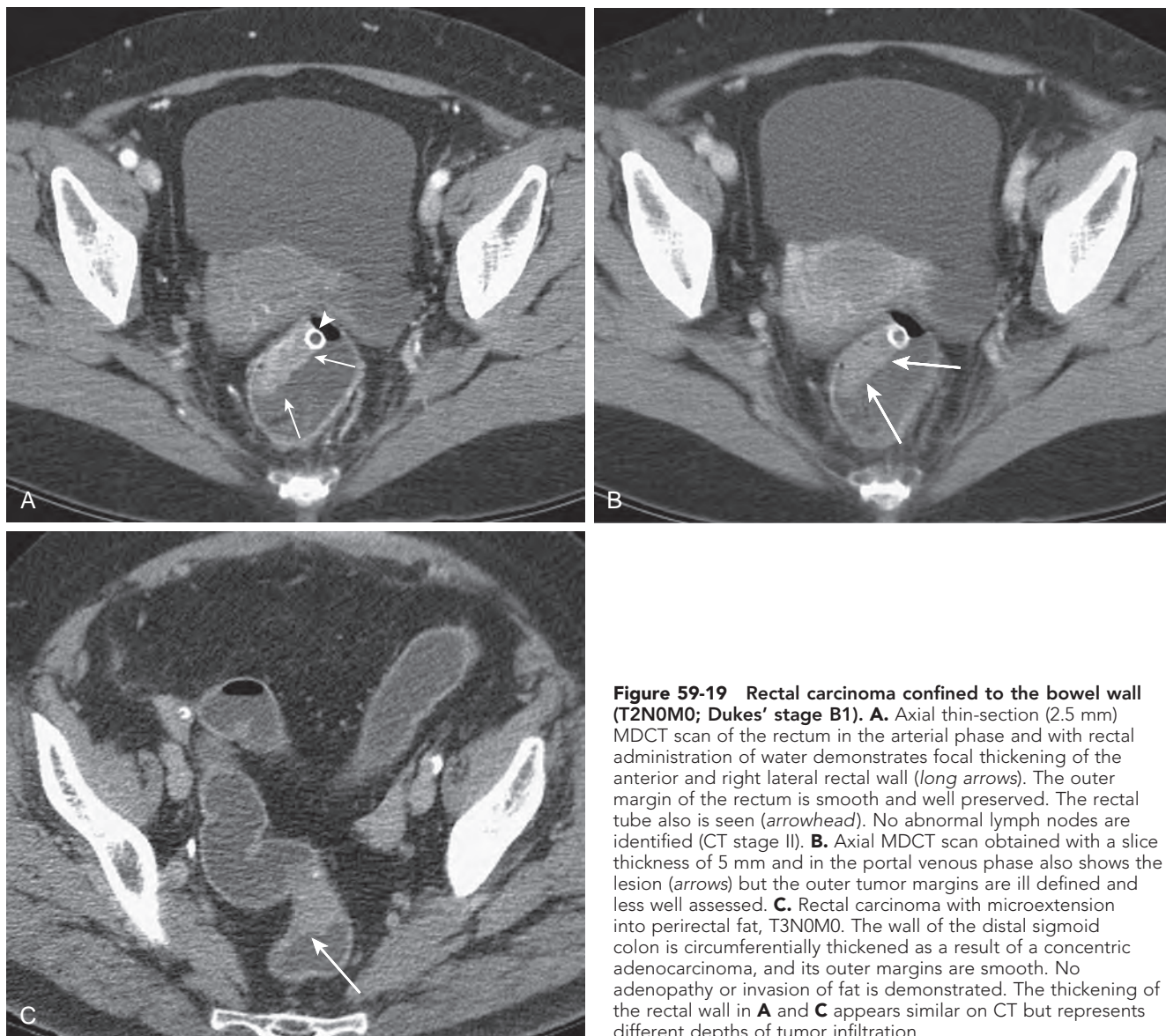


Figure 59-19 Rectal carcinoma confined to the bowel wall (T2N0M0; Dukes' stage B1). **A.** Axial thin-section (2.5 mm) MDCT scan of the rectum in the arterial phase and with rectal administration of water demonstrates focal thickening of the anterior and right lateral rectal wall (long arrows). The outer margin of the rectum is smooth and well preserved. The rectal tube also is seen (arrowhead). No abnormal lymph nodes are identified (CT stage II). **B.** Axial MDCT scan obtained with a slice thickness of 5 mm and in the portal venous phase also shows the lesion (arrows) but the outer tumor margins are ill defined and less well assessed. **C.** Rectal carcinoma with microextension into perirectal fat, T3N0M0. The wall of the distal sigmoid colon is circumferentially thickened as a result of a concentric adenocarcinoma, and its outer margins are smooth. No adenopathy or invasion of fat is demonstrated. The thickening of the rectal wall in **A** and **C** appears similar on CT but represents different depths of tumor infiltration.

ultrasound or MRI with endorectal coils. These techniques can also determine the layer from which the tumor arises, which is important for differentiating an adenocarcinoma from a lymphoma or GI stromal tumor.

Tumor invasion beyond the bowel wall is suggested by a mass with nodular or spiculated borders, associated with strands of soft tissue extending from the muscularis propria into the perirectal fat or from the serosal surface into the pericolic fat (Fig. 59-22). Broad-based soft tissue extensions from the tumor into the perirectal fat are more indicative of tumor extension than spiculation, which often represents a desmoplastic reaction. Desmoplastic reaction frequently leads to overstaging by MRI because it can be difficult to distinguish between fibrosis alone and fibrosis that contains tumor cells (Fig. 59-23).⁴² Extracolonic tumor spread is also suggested by loss of tissue fat planes between the large bowel and surrounding muscles, such as the obturator internus, piriformis (Fig. 59-24), levator ani, puborectalis, coccygeal, and gluteus

maximus. Invasion is definite only when a tumor mass extends directly into an adjacent muscle, obliterating the fat plane and enlarging the individual muscle. Cross-sectional methods such as CT cannot detect microscopic invasion of the fat surrounding the colon or rectum (see Fig. 59-19) and tend to understage these patients. Spread to contiguous organs in the pelvis can be simulated by absence of tissue planes between the viscera and tumor mass, without actual invasion. Vascular or lymphatic congestion, inflammation, or actual absence of fat because of severe cachexia can cause obliteration of fat planes. Therefore, invasion should be diagnosed cautiously and considered definite only if an obvious mass clearly involves an adjacent organ. Distinction between tumor infiltration of adjacent muscle and simple absence of fat separating normal structures is particularly difficult in the area of the lower rectum and anal verge.

In our experience, CT results can be improved through the use of a large, rapidly delivered bolus of intravenous (IV)

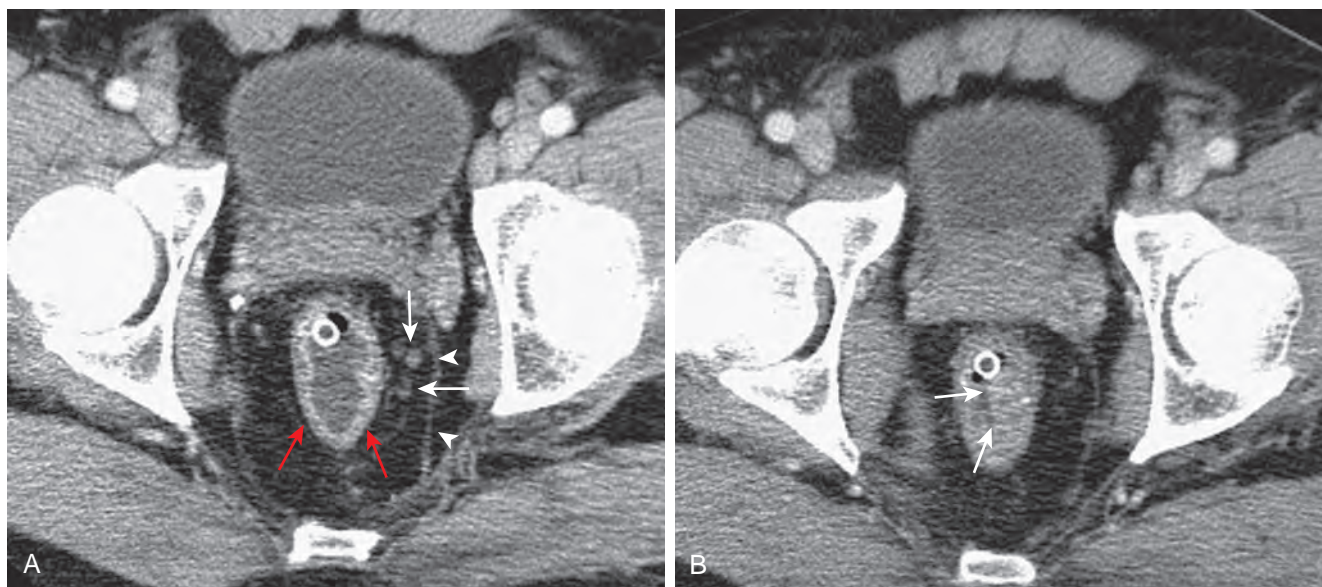


Figure 59-20 Adenocarcinoma of the rectum confined to the rectal wall with perirectal lymph nodes (T2N1M0; Duke's stage C1).
A. MDCT scan demonstrates minimal but diffuse wall thickening (red arrows). Mesorectal fascia is well shown (arrowheads). Perirectal lymph nodes (white arrows) are seen in the perirectal fat adjacent to left lateral wall of rectum. MDCT was performed after one course of radiation, which probably caused the diffuse wall thickening. **B.** MDCT scan slightly below the level in **A** reveals asymmetric nodular thickening of left lateral wall of the rectum (arrows) without extension of tumor into perirectal fat.

contrast agent and MDCT with thin sections and water as rectal and colonic contrast material (see Fig. 59-23). With this approach, the pelvis is scanned at peak enhancement, and the enhanced wall of the rectum can be better distinguished from adjacent levator ani and sphincter muscles. CT generally is used for staging and not for detection of colonic lesions. Nevertheless, ultrathin sections (0.625- to 1.25-mm slices) obtained with MDCT can facilitate the demonstration of even small lesions and increase the accuracy of tumor staging. Staging results can be further improved if multiplanar reformats are used, and interpretation is based on a combination of axial slices and multiplanar reformats (see Fig. 59-18).⁶⁹ Coronal reformats often are helpful to define the relationship of the rectal mass to the levator ani, puborectalis, and sphincter muscles, which is helpful in planning the appropriate surgery. Nevertheless, CT cannot achieve the exquisite soft tissue resolution afforded by MRI with gadolinium contrast enhancement.⁷⁰ Such superior distinction is particularly useful in the lower pelvis for assessing tumor relationship to the mesorectal fascia and invasion into muscle, nerves, bladder, and male or female organs (see later, “Magnetic Resonance Imaging”).⁷¹

Primary and recurrent colon cancer can invade the seminal vesicles, prostate, bladder, uterus (Fig. 59-25), ovaries, small bowel, and sciatic nerves and can obstruct the ureters. Occasionally, tumors of the prostate, uterus, or ovaries that invade or are contiguous with the rectum or sigmoid colon can be indistinguishable from an invasive colon neoplasm. Areas of low attenuation within the mass suggest tumor necrosis; tumor calcifications indicate a mucinous adenocarcinoma. A vesicorectal fistula manifests as air in the tract and bladder. After administration of an IV contrast agent, the wall of the tract may enhance. Alternatively, a jet of positive rectal contrast material can be identified in the bladder. Fistulous tracts can also extend

into the uterus or vagina, and sinus tracts may be seen in the fat of the ischiorectal fossa.

Colon tumors can destroy adjacent bone, usually the sacrum and coccyx. Large tumors can involve the ilium. Advanced bone invasion causes frank bone destruction often associated with a soft tissue mass. Subtle cortical destruction visible only on bone window settings may be the only manifestation of bone invasion.

Liver metastases usually appear hypodense on non-contrast-enhanced scans. Foci of calcification can be seen within primary or metastatic mucinous adenocarcinomas (Fig. 59-26). After a bolus injection of contrast material, the CT density of hepatic colonic metastasis can change rapidly. Compared with the uninvolved liver parenchyma, metastases often show early rim enhancement or become partially hyperdense (Fig. 59-27), go through an isodense phase, and then become low-density lesions again. Optimal bolus and scanning techniques are necessary to minimize false-negative results that can occur when metastases become isodense with normal liver parenchyma when scanning is extended into the equilibrium phase. This isointensity often occurs with small (<2 cm) lesions. If only one to four hepatic metastases are detected (more if they are peripheral and can be easily wedged out), and no extrahepatic disease is present, an aggressive treatment plan appears warranted, because there is improved 5-year survival after removal of isolated metastatic foci by resection or ablation.⁷²⁻⁷⁴

CT with arterial portography (CTAP) was formerly considered the single most accurate means of detecting additional metastatic lesions in the normal-appearing lobe.⁷⁵ However, the general use of CTAP has been abandoned in favor of helical CT. Helical CT can achieve similar sensitivities, has a lower false-positive rate than CTAP, and is noninvasive.^{76,77} In one helical CT study with surgical correlation in all patients, the sensitivity for detecting colonic metastases to the liver was 85% and the

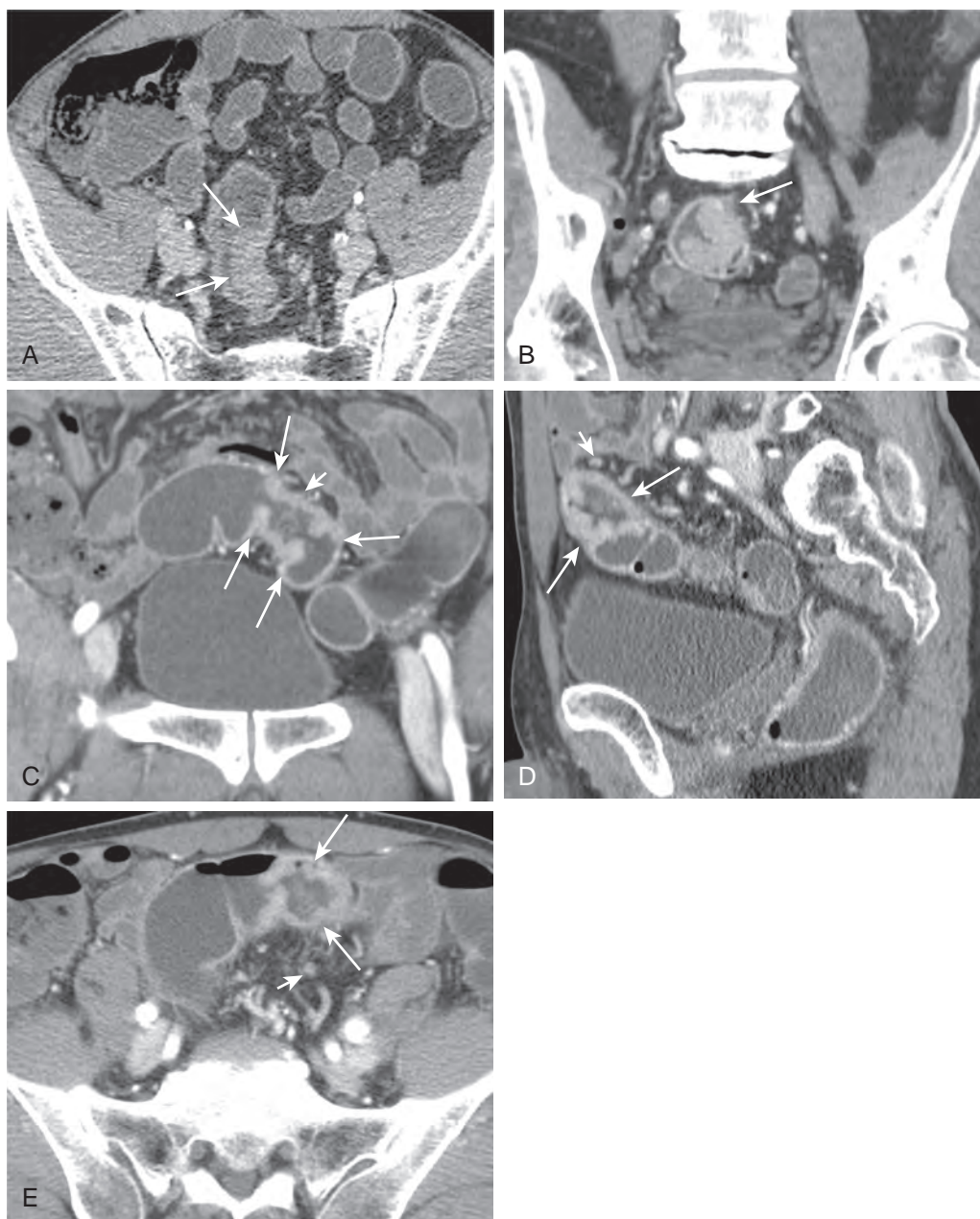


Figure 59-21 Adenocarcinoma of the sigmoid colon, A, B. T3N0 M0 (Dukes' stage B2). **A.** The axial MDCT scan demonstrates a nodular mass along the left lateral wall of the sigmoid colon (arrows) without definite extension beyond the bowel wall. **B.** In the coronal reconstruction a broad based extension of tumor (arrow) into the pericolic fat is seen. **C-E.** T3N1M0 (Dukes' stage C1). **C.** The full extent of the circumferential tumor in the sigmoid colon (arrows) is best demonstrated in the coronal reconstruction. Subtle broad-based stranding (short arrow) suggests extension beyond the bowel wall. **D.** The sagittal reconstruction demonstrates a small lymph node (short arrow) next to the sigmoid neoplasm (long arrows). **E.** The true extent of the tumor (arrows) is more difficult to assess in the axial views but the metastatic lymph node (short arrow) is well shown, demonstrating the complementary nature of the various planes.

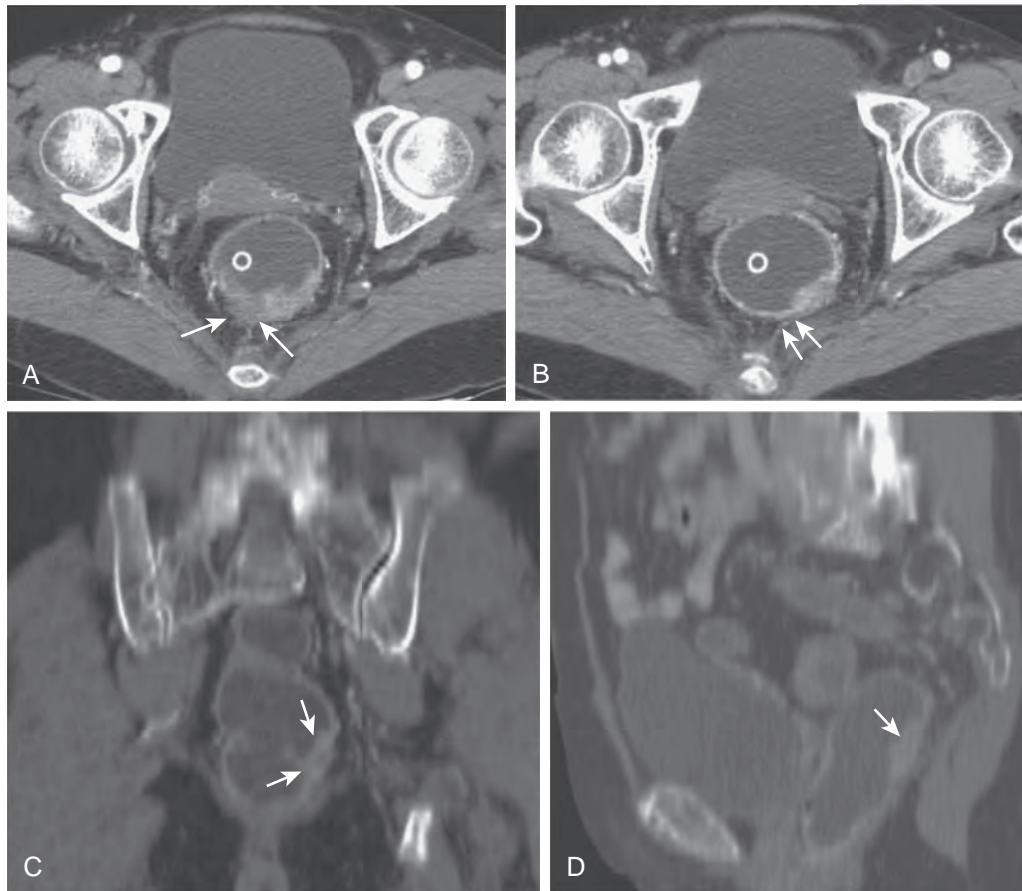


Figure 59-22 CT scan of rectal tumor with extension beyond the wall (T3N0M0; **Dukes' stage B2**). **A.** The thin-section MDCT scan in the arterial phase reveals nodular broad-based extensions of soft tissue density (arrows) into the perirectal fat indicative of tumor invasion. **B.** MDCT scan slightly below the level in **A** shows a focal mass with some spiculation (arrows). This feature is more suggestive of desmoplastic reaction without tumor cells rather than infiltration of tumor into perirectal fat. This distinction is not always possible on MDCT. **C.** The coronal MPR reveals the nodular outer surface of the tumor (arrows). **D.** The sagittal MPR does not demonstrate this feature effectively. The mass is located in posterior wall (arrow) of upper rectum.

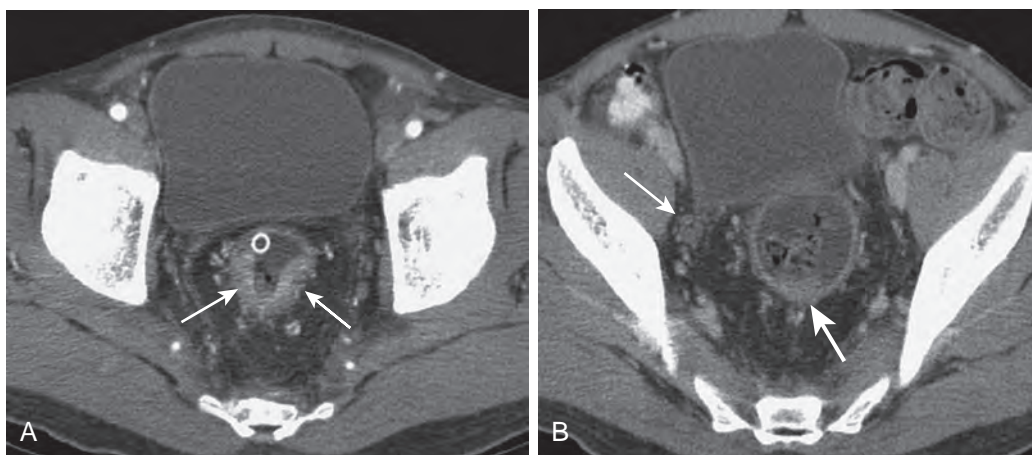


Figure 59-23 Rectal carcinoma in posterior and lateral walls (arrows) of rectum (T3N1M0; **Dukes' stage C1**). **A.** Outer borders (arrows) are slightly irregular, but no definite nodularity can be seen. This makes it difficult to distinguish a desmoplastic reaction from actual tumor extension in this case. The patient was diagnosed by MDCT as probably a T3. **B.** At a level higher than in **A**, tumor is present only in posterior wall (thick arrow). Water facilitates visualization of intraluminal component of tumor in spite of the presence of feces. Also note hypogastric lymph nodes (thin arrow) that are lateral to mesorectal fascia.

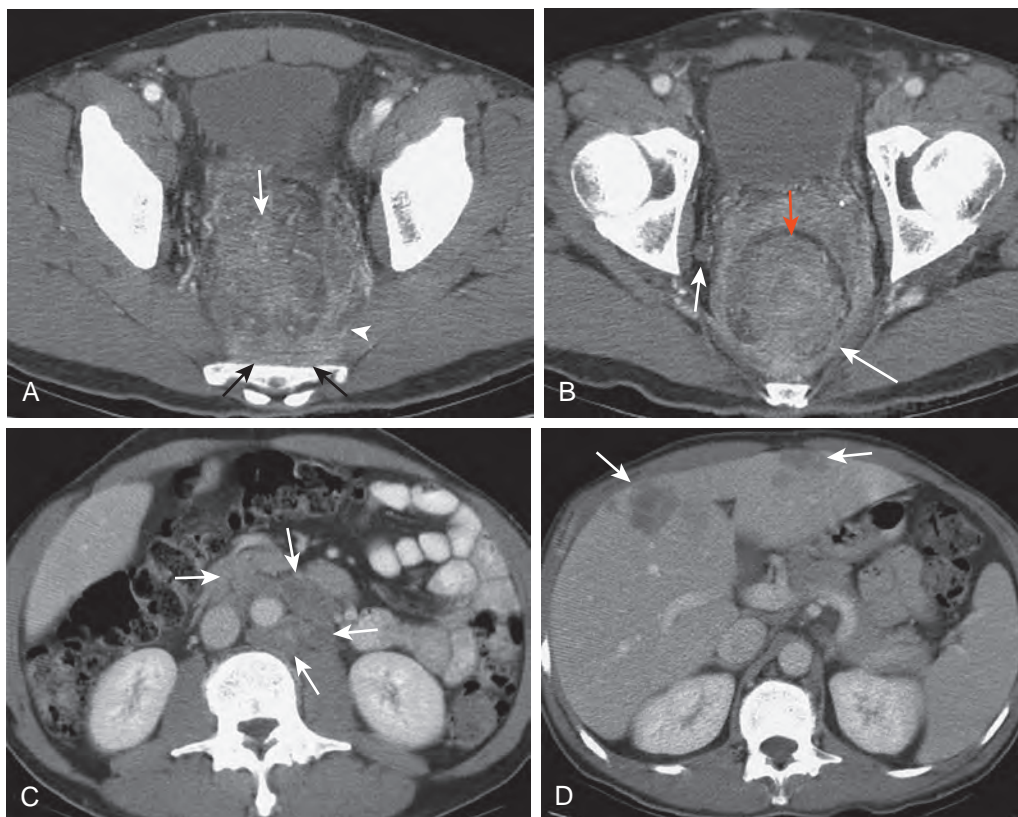


Figure 59-24 CT scan of primary invasive rectal adenocarcinoma (T4bN2M1; Dukes' stage D). **A.** Large enhancing rectal mass (white arrow) with extension to pelvic sidewalls. Enhanced mass is inseparable from the sacrum (black arrows) and piriformis muscle (arrowhead) on left. **B.** Rectal mass (red arrow) directly extends into mesorectal fascia (long arrow). Abnormal internal iliac lymph node (small arrow) also is identified. **C.** At a level just below the midpole of kidneys, extensive retroperitoneal adenopathy (arrows) is demonstrated. **D.** Several hepatic metastases (arrows) are seen.

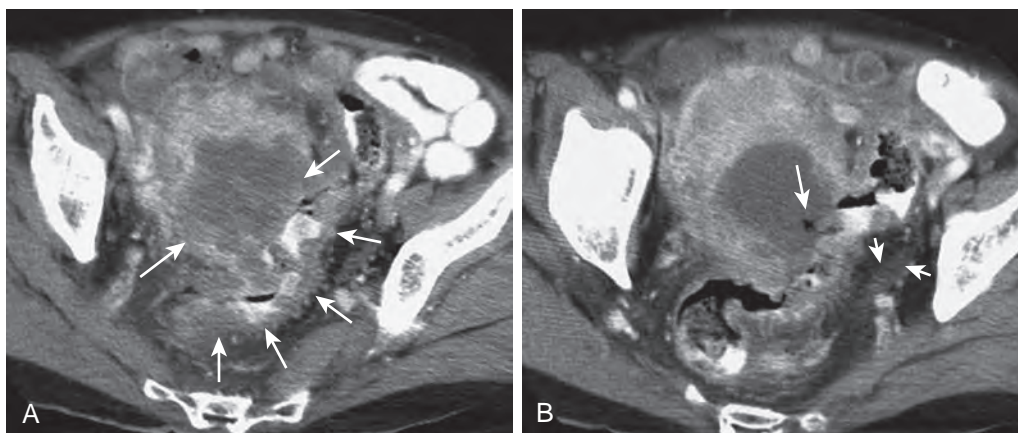


Figure 59-25 Sigmoid carcinoma with invasion of uterus (T4bN1M0; Dukes' stage C2). **A.** Long segmental thickening (small arrows) of sigmoid wall. Note the absence of wall stratification, which can be seen in diverticulitis. The sigmoid tumor is inseparable from the low-density mass in the uterus (large arrows). **B.** At a level 5 mm below **A**, gas (long arrow) is seen, indicating direct invasion of the tumor into uterus with perforation and necrosis. Note ascites (short arrows) along the pelvic sidewall.

positive predictive value was 96%.⁴¹ MRI with ferumoxides or gadolinium enhancement also provides excellent results in distinguishing hepatic metastases from colon carcinoma, but this technique is more expensive and not as widely available as CT.^{78,79} In one series, the MRI sensitivity for colorectal liver metastases was 96.8% but only slightly over one third of patients

underwent curative resection for histologic confirmation.⁷⁸ More recently, MRI enhanced with gadoxetate disodium (Primovist in Europe and Eovist in the United States, Bayer Pharmaceuticals) has shown excellent results for assessing hepatic metastases from colonic carcinoma and were superior to MDCT.⁸⁰ Large series are still needed to establish the true

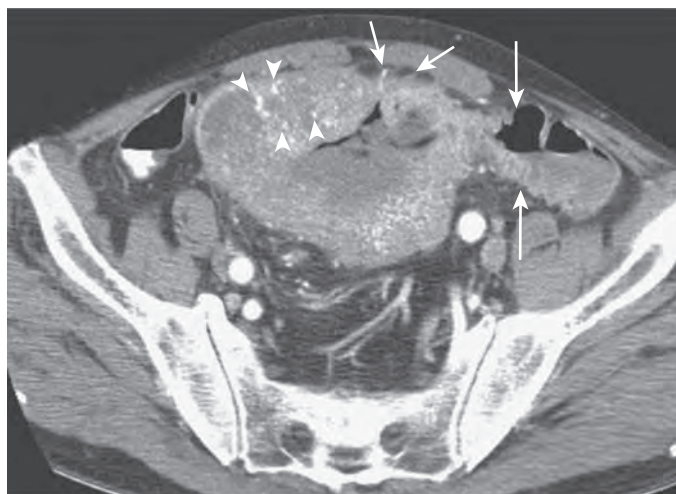


Figure 59-26 Large mucinous sigmoid cancer (T3N1M0; Dukes' stage C2). Large sigmoid mass with pericolic fat infiltration (short arrows) and intramural calcifications (arrowheads) is identified. The transition to normal proximal sigmoid colon (long arrows) can be clearly seen.

cost-effectiveness of the various techniques. Intraoperative ultrasound is often used as the gold standard, but not all published studies had histopathologic correlation.⁴¹ In patients for whom resection is not an option, thermal tumor ablation or selective catheterization and intra-arterial chemotherapy of the liver are often used, but only if there is no evidence of tumor spread to extrahepatic sites. Local or distant adenopathy, adrenal metastases, peritoneal carcinomatosis, metastases to other areas of the GI tract, and lung metastases are some findings that preclude resection or chemoembolization of liver lesions.

Generally, rectal carcinoma metastasizes to lymph nodes along the superior rectal vessels to the mesenteric vessels for upper rectal tumors and along the middle rectal vessels to the internal iliac vessels for lower rectal tumors. Advanced low rectal or anal tumors drain along the inferior rectal vessels into the inguinal nodes. Metastases may be found in nodes in the retroperitoneum (see Fig. 59-24) and porta hepatis. In other areas of the colon, lymph node metastases follow the normal pattern of lymph drainage from the involved area. Local lymph nodes may or may not be demonstrated, depending on separability from the main mass and size of the lymph nodes (Fig. 59-28). In the abdomen and pelvis, lymph nodes more than 1.0 cm in diameter are considered abnormal. The pathologic nature of node enlargement cannot be determined absolutely by CT, although asymmetry, irregularity of the nodal margins and, less reliably, size criteria can be used to establish lymph node abnormality.⁸¹

Benign and malignant disease can produce lymphadenopathy, and often only PET or guided biopsy can provide a definitive diagnosis. Many metastatic foci are found in normal-sized lymph nodes (<1 cm) that cannot be considered abnormal by CT if size is used as the only diagnostic criterion. Pericolic lymph nodes next to a segment of thickened colonic wall are seen much more frequently in patients with colon cancer than in those with diverticulitis. Therefore, the presence of such nodes should lead to further evaluation in patients with suspected diverticulitis.⁸² Additional signs that favor a diagnosis of colon carcinoma over diverticulitis are loss of a

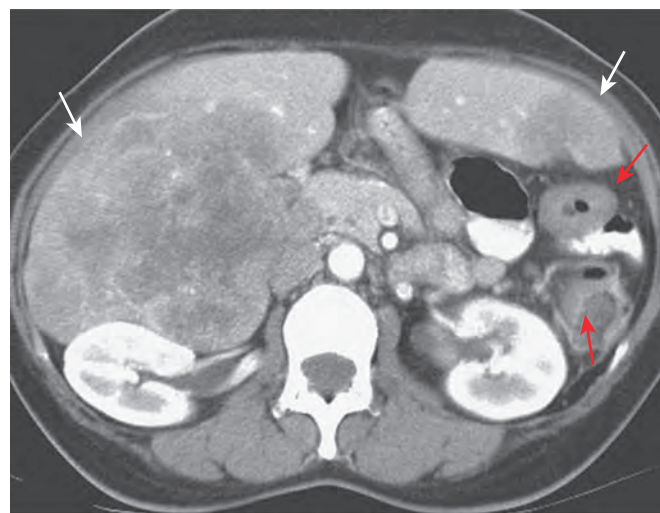


Figure 59-27 Nonobstructing adenocarcinoma in the splenic flexure with liver metastases (T2N0M1; Dukes' stage D). Two hepatic metastases (white arrows) are identified. The primary tumor has smooth outer margins (red arrows) and is located in the splenic flexure. The tumor was first diagnosed by MDCT and surgically confirmed to be stage T2.

normal enhancement pattern in the thickened bowel wall and absence of inflamed diverticula.⁸³ Because hyperplastic or inflammatory nodes are rare in the perirectal area, demonstration of nonenhanced, small (<1 cm), round or oval soft tissue densities suggests the presence of malignant adenopathy (Fig. 59-29).

There are certain pitfalls in the interpretation of CT scans of patients with colon tumors.⁸⁶ CT scans obtained soon after surgery or radiation therapy can demonstrate edema or hemorrhage of the pelvic structures that simulates recurrent neoplasm. Chronic radiation changes in the pelvis may be difficult or impossible to distinguish from colon tumor without CT-guided biopsies.⁸⁵⁻⁸⁸ It is therefore essential to determine the tumor stage by CT or MRI before the patient undergoes radiation. Follow-up CT scans after irradiation are needed only to determine whether the mass seen on the staging scan has sufficiently diminished in size to become resectable. Benign bone defects can simulate metastatic foci, and nonopacified bowel loops can be mistaken for a tumor mass. Perforation of a colon cancer can result in an inflammatory mass or abscess, which makes diagnosis of the underlying cancer difficult (see Fig. 59-29).⁸⁹ Cachexia can lead to loss of fat planes, which mimics direct invasion of tumor into surrounding structures.

Preoperative Staging by Computed Tomography

The staging of colon tumors has usually been based on Dukes' classification⁹⁰ or a modification (Table 59-1).^{91,92} CT staging is based on an analysis of the thickness of the colon wall, extension beyond bowel wall margins, and presence or absence of tumor spread to lymph nodes and adjacent and distant organs.⁹³ The size of a primary or recurrent colon tumor can be measured and the tumor assigned to one of four stages, depending on the CT findings (Table 59-2).

Many surgeons use the tumor, node, metastases (TNM) classification (see Table 59-1) for staging colon neoplasms.⁹⁴ It has the advantage of more precise definition of the depth of infiltration in the bowel wall. Because of the inability of CT to

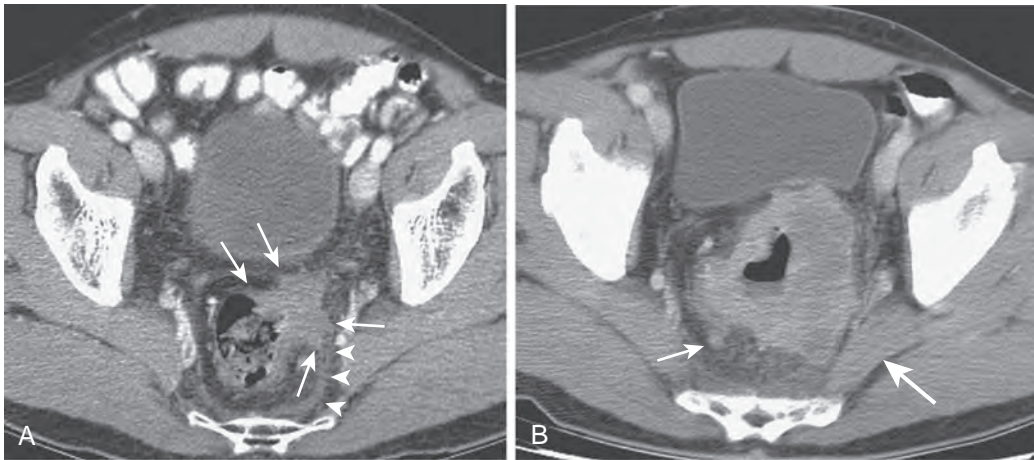


Figure 59-28 Rectal tumor with direct extension to the mesorectal fascia and locoregional lymphadenopathy (T3N1M0 or Dukes' stage C2). **A.** Large rectal mass with broad-based extension of soft tissue (arrows) into perirectal fat and direct invasion of mesorectal fascia (arrowheads). **B.** Several centimeters above the level of **A**, rectal wall is markedly thickened but tumor does not extend into piriform muscle (thick arrow) or bladder. Note enlarged perirectal lymph node (thin arrow).

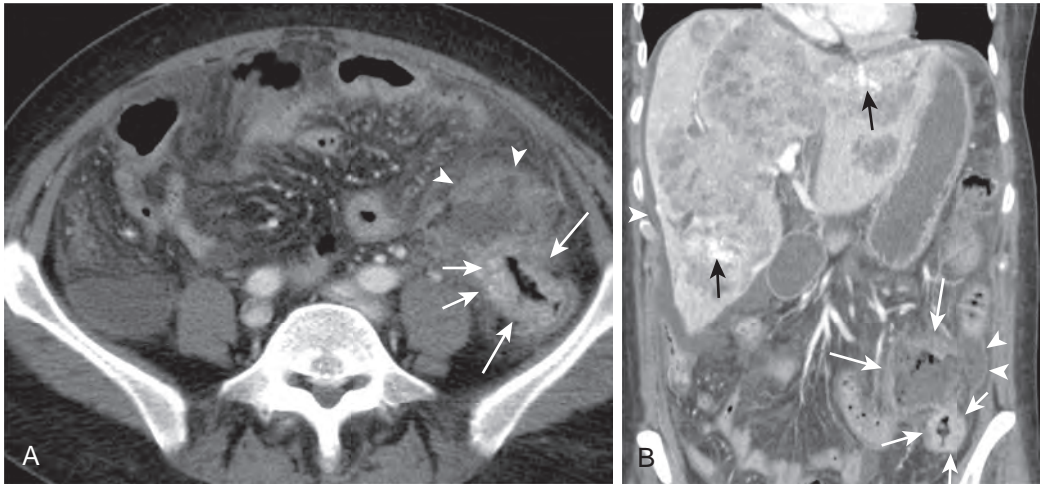


Figure 59-29 Perforation of mucinous adenocarcinoma of the descending colon (T4N0M1). **A.** Nodular thickening of the descending colon (long arrows) is seen with stippled calcifications in the medial wall (short arrows) and a fluid collection with ill-defined rim representing the abscess (arrowheads). **B.** On this coronal reconstruction, the circumferential wall thickening (short arrows) with the perforation and large adjacent abscess (long arrows) is clearly demonstrated. Note also the ascites with enhancing peritoneum (arrowheads) representing peritonitis and the calcifications (black short arrows) within the metastases in the liver.

TABLE 59-1 Surgical-Pathologic Staging of Colorectal Neoplasm (Dukes' and TNM Classification)			
Astler-Coller Classification (Modified from Dukes')	TNM Staging	Description	Approximate 5-Year Survival (%)
A or I	T1N0M0	Nodes (–), limited to mucosa ± submucosa	80
B1 or I	T2N0M0	Nodes (–), limited to muscularis ± serosa	70
B2 or II	T3N0M0	Nodes (–), transmural into subserosa or into nonperitonealized perirectal or pericolic tissue	60-65
C1 or III	T2N1M0	Nodes (+), limited to muscularis ± serosa	35-45
C2 or III	T3N1M0	Nodes (+), transmural into subserosa or into nonperitonealized perirectal or pericolic tissue	25
	T4aN1M0	Nodes (+), perforation of tumor mass	
	T4bN1M0	Nodes (+), extension into adjacent organs or structures (e.g., muscle, nerve, bone)	
D or IV	Any T and N, M1	Any of the above, plus distant metastases	<25

determine depth of invasion to or through the various layers of the colon, CT findings cannot be correlated easily with the TNM classification. For example, tumor limited to mucosa or submucosa (T1N0M0) cannot be distinguished from tumor invading the muscularis or infiltrating to but not through the serosa, if present (T2N0M0). Generally, lesions extending beyond bowel wall (T3 and T4) are correctly identified by CT unless microinvasion by tumor is present. Assessment of regional lymph node (N) involvement and distant metastases (M) must be added to the evaluation of the depth of tumor invasion.

Early reports suggested that CT findings related to local extent and regional spread of tumor correlated well with surgical and histopathologic findings, and accuracy rates of 77% to 100% were reported.^{84,93,95-97} The high accuracy rates of these reports were largely because of the more advanced cases in these series. For primary colon cancer, CT is more accurate in showing extensive invasion of surrounding tissue and distant metastases than in demonstrating local adenopathy or minimal tumor extension.

CT frequently understages patients with microinvasion of pericolic or perirectal fat or small tumor foci in normal-sized nodes. Lymph node metastases were not analyzed separately in some of the earlier studies. In a meta-analysis that analyzed local staging and lymph node involvement in patients with

rectal cancers, summary estimates of sensitivity and specificity for CT in assessing perirectal tissue invasion and invasion of adjacent organs were 79% and 78% and 72% and 96%, respectively.⁴² In the same study, the summary estimates of sensitivity and specificity for CT in detecting lymph node involvement were much lower and reached only 55% and 74%, respectively.⁴² One study found that staging accuracy increased from 17% for Dukes' B lesions to 81% for Dukes' D lesions.⁹⁸ In another meta-analysis, the mean weighted sensitivity of helical CT for detecting hepatic metastases, mostly from colon carcinoma, was 72% at a specificity of higher than 85%.⁹⁹ Some individual studies have reached higher sensitivities for hepatic metastases from colorectal carcinoma.⁴¹

The accuracy of CT assessment of local tumor extent can be improved by prior colonic cleansing, prone positioning of the patient, air distention of the rectum, or administration of water enemas to serve as a low-density intraluminal contrast agent.^{100,101} Also, lowering the size threshold for diagnosing lymph node metastases improves the sensitivity for detecting such deposits, but this approach decreases specificity.

Little information is available about the CT detection and staging of tumors in the cecum or ascending, transverse, and descending colon. Most tumors in these areas are easily demonstrated (Figs. 59-30 and 59-31), but no investigation has analyzed these lesions in detail.

TABLE 59-2 Computed Tomography Staging of Primary or Recurrent Colorectal Tumor with TNM Correlation

CT Stage	TNM Staging	Description
I	T1	Intraluminal mass without thickening of wall
II*	T2	Thickened large bowel wall (>0.6 cm) or pelvic mass, no extension beyond bowel wall
IIIa*	T3	Thickened large bowel wall or pelvic mass with invasion of adjacent pericolic or perirectal tissue but not to mesorectal fascia
IIIb*	T3	Thickened large bowel wall or pelvic mass with invasion of adjacent pericolic or perirectal tissue with extension to mesorectal fascia
IIIc*	T4a and b	Thickened large bowel wall or pelvic mass with perforation or invasion of adjacent organs or structures, with or without extension to pelvic or abdominal walls but without distant metastases
IV*	Any T, M1	Distant metastases with or without local abnormality

*With or without lymphadenopathy (N0 or N1).

Modified from Thoeni RF, Moss AA, Schnyder P, et al: Detection and staging of primary rectal and rectosigmoid cancer by computed tomography. *Radiology* 141:135-138, 1981.

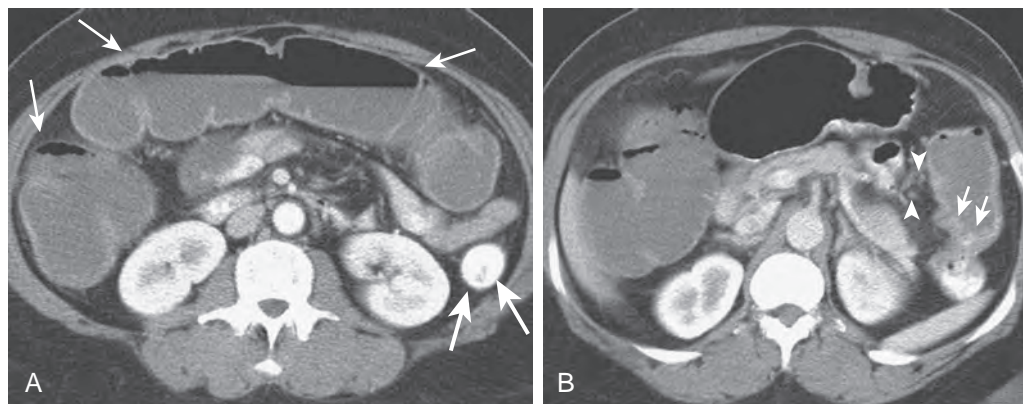


Figure 59-30 Near-complete colonic obstruction caused by tumor near splenic flexure (T3N1M0 or Dukes' stage C1). **A.** Axial MDCT scan demonstrates positive rectal contrast (thick arrows) in descending colon near the splenic flexure but no rectal contrast entering the fluid-filled and distended transverse and ascending colon (thin arrows). **B.** Two centimeters above level of **A**, obstructing tumor is demonstrated and its proximal border well outlined by retained colonic fluid (arrows). Tumor was underestimated by MDCT to be stage T2. Note subcentimeter lymph nodes (arrowheads) near the tumor in mesentery. They were confirmed to be positive for tumor at surgery but not prospectively diagnosed because of their small size.

Further studies are needed to establish whether new-generation CT scanners, especially MDCT with 16- or 64-slice capability, can compete with MRI in staging colorectal tumors. One study has already demonstrated that reformats could significantly increase the accuracy of T staging of rectal tumors

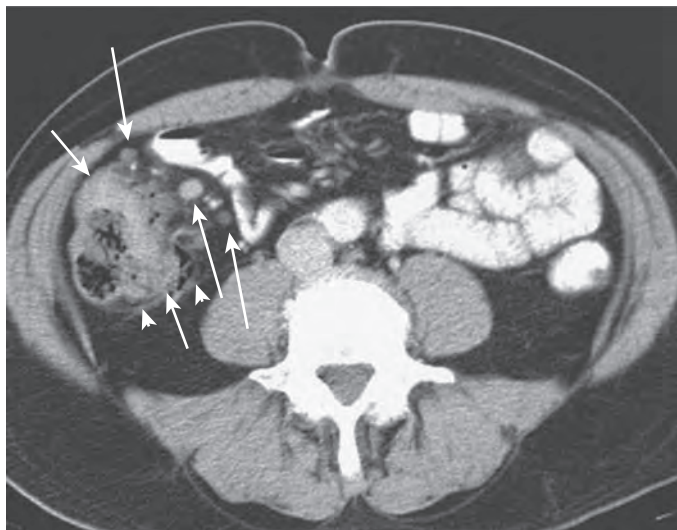
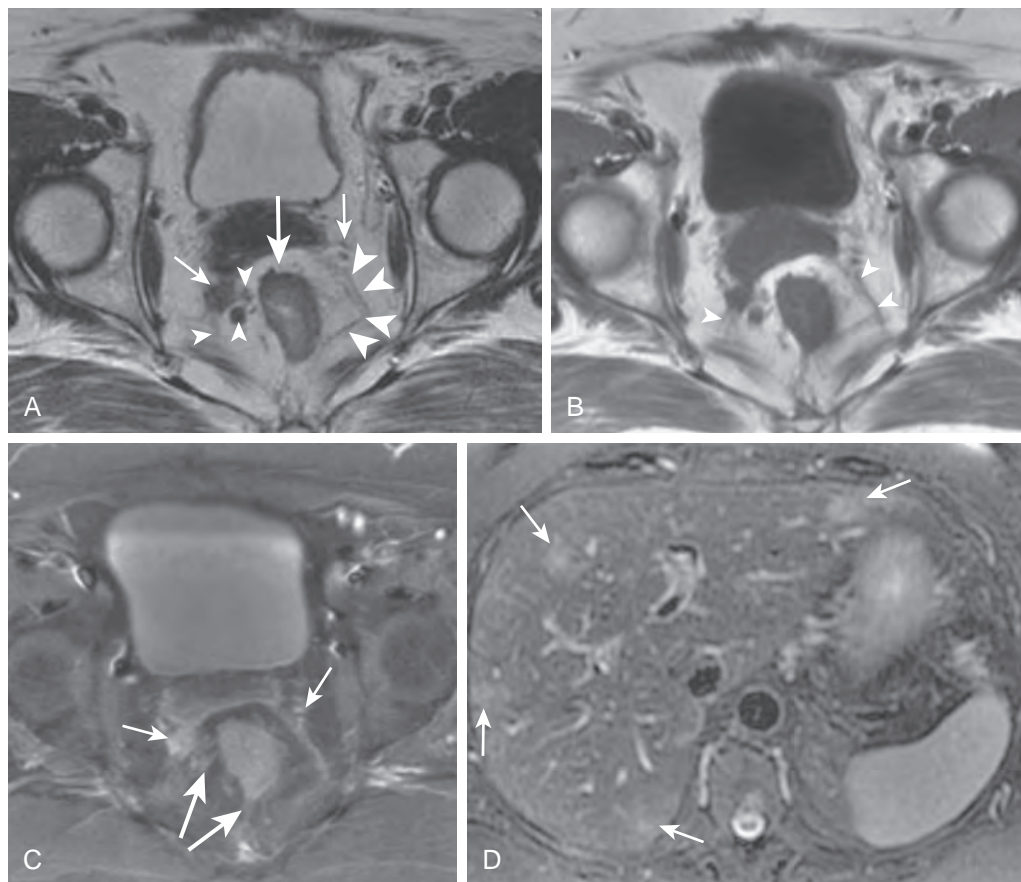


Figure 59-31 Cecal adenocarcinoma (T3N1M0). The cecum demonstrates eccentric wall thickening (*short arrows*) near the ileocecal valve, with nodular outer margins and soft tissue strands (*arrowheads*) extending into pericolic fat, suggestive of infiltration beyond the bowel wall. Abnormal local lymph nodes (*long thin arrows*) are present and were confirmed as pathologic at surgery.

Figure 59-32 MRI scans of adenocarcinoma of the rectum (T3N1M1; Duke's stage D).

A. Axial T2-weighted fast spin-echo image scanned perpendicular to long axis of tumor demonstrates eccentric thickening of anterior rectal wall (*thick arrow*), with extension of tumor to rectal sidewalls. Perirectal lymph nodes (*arrowheads*) are identified. The middle rectal vessels (*thin arrows*) in the lateral ligament are seen lateral to mesorectal fascia (*large arrowheads*). **B.** On this axial T1-weighted spin-echo MR image, the mesorectal fascia (*arrowheads*) is not as clearly delineated as on the T2-weighted image. **C.** Axial T1-weighted fat-suppressed image after administration of gadolinium shows enhancement of mesorectal vessels (*thin arrows*) bilaterally. Extension of tumor into the perirectal fat (*large arrows*) is best seen on this fat-suppressed sequence; however, a desmoplastic reaction alone cannot be definitively distinguished in this case from desmoplastic reaction containing tumor cells. **D.** Axial T2-weighted image with fat suppression identifies multiple liver metastases (*arrows*).



(see Figs. 59-18 and 59-22).⁶⁹ In this study, the staging accuracy based on axial slices ranged from 77% to 81%, whereas it increased to 90% to 98% when axial slices were combined with multiplanar reformats.⁶⁹ These results compare favorably with CT studies from the last decade that did not use MDCT, with accuracy rates ranging from 41% to 82%.^{26,102,103} MDCT offers the advantages of combining local, regional, and distant staging in one study, ultrathin slice capability, very fast imaging times, reconstruction in any desired plane, and lower cost compared with MRI.

MAGNETIC RESONANCE IMAGING

Magnetic resonance imaging can be used to detect and stage rectosigmoid tumors more accurately than tumors in other areas of the colon. As with CT, this increased accuracy is because of the fixed position of the rectosigmoid colon in relation to the pelvis. Therefore, most reports have focused on the depiction and staging of rectal tumors. For accurate depiction of the intraluminal component of rectal tumors, particularly smaller ones, it may be necessary to prepare the colon to avoid confusion with feces. Rectal air insufflation, with prone positioning of the patient and an antispasmodic agent, may be helpful in depicting the tumor better. Other investigators have recommended axial T2-weighted imaging perpendicular to the long axis of the tumor, as seen on sagittal views, for more accurate staging (Fig. 59-32).¹⁰⁴ On T1-weighted spin-echo images, rectosigmoid tumors produce wall thickening with signal intensity similar to or slightly higher than that of skeletal muscle (long T1; see Fig. 59-32A). Because perirectal fat has

high signal intensity (short T1), air has no signal intensity, and tumor has moderate signal intensity (long T1), tumors are shown with high contrast. For the same reason, extension of tumor beyond the colon wall may be seen on T1-weighted images (Fig. 59-33). On T2-weighted spin-echo images, the signal intensity of tumor increases relative to that of muscle (see Fig. 59-33A) and the neoplasm in the rectal wall may be well visualized on high-resolution MRI.

Whereas early studies indicated that T2-weighted images are not as useful as T1-weighted images for determining extracolonic tumor extension (see Fig. 59-32),¹⁰⁵ it is now generally accepted that T2-weighted sequences are superior to T1-weighted scans in evaluating the extent of tumor in relation to the rectal wall layers and mesorectal fascia.^{106,107} Several studies have shown that T2-weighted sequences can demonstrate the mesorectal fascia, which has gained importance since the introduction of total mesorectal excision (TME).¹⁰⁶⁻¹¹⁰

In TME, the entire mesorectal compartment is removed, which consists of the rectum, surrounding mesorectal fat with the perirectal lymph nodes, and a thin fascia that envelops the two former structures; it is known as the mesorectal fascia. The TME procedure reduces the chance that tumor is left behind.

Even without preoperative or postoperative radiation therapy, the recurrence rate after TME is reported to be less than 10%.¹¹¹ If uterine or pelvic sidewall invasion is suspected, T2-weighted sequences also are useful because of the differences in signal intensity among muscle, fat, tumor, and muscle invaded by tumor.

Today, MRI using thin sections and phased-array coils can distinguish between tumors localized to mucosa and submucosa (stage I or T1) and those that infiltrate the entire colonic wall (stage II or T2), with a moderate to good staging accuracy (65%-86%; Table 59-3).¹¹⁰ The detection of the tumor in the bowel wall based on T2-weighted imaging relies on signal intensity differences between the intermediate signal intensity of the tumor, low signal intensity of normal mucosa and muscularis propria, and high signal intensity of the submucosa and perirectal or pericolic fat. Endoluminal MRI coils also make visualization of the layers of the rectal wall feasible and have demonstrated improved accuracy for T staging when compared with phased-array external coils (accuracy ranging from 71%-91%).¹¹² Endoluminal MRI is not widely available and, because of its small field of view, it cannot visualize the mesorectal fascia and surrounding pelvic structures.

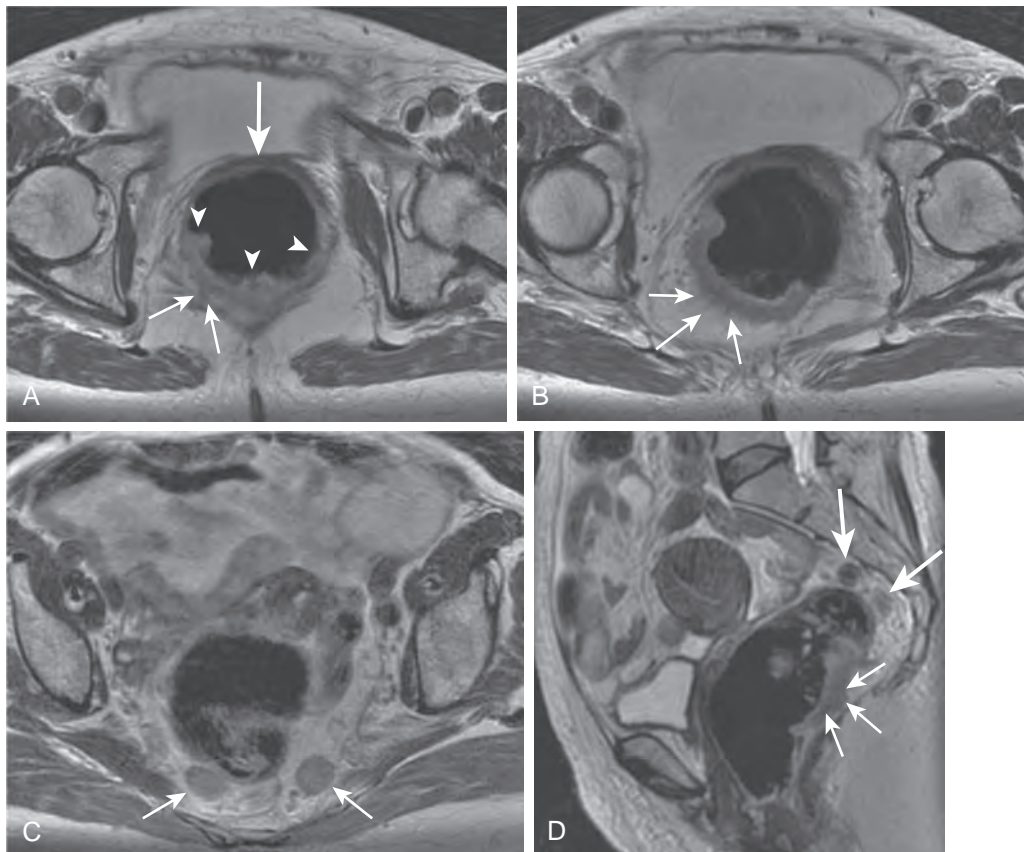


Figure 59-33 MRI scans of rectal adenocarcinoma with extension beyond the bowel wall (T3N1M0; Dukes' stage C2). **A.** Axial T2-weighted fast spin-echo image demonstrates a nodular outer margin of the posterolateral rectal wall with broad-based extension of soft tissue (small arrows) into perirectal fat. The luminal margin of the tumor is irregular (arrowheads), and signal intensity of the tumor is higher than that of the muscularis propria (large arrow). **B.** Axial T2-weighted fast spin-echo image shows spiculated outer margin (arrows) of mass involving posterior and right lateral aspects of the rectum. These features suggest a desmoplastic reaction related to tumor rather than neoplastic infiltration of perirectal fat. **C.** Axial T2-weighted fast spin-echo scan at higher level than **A** and **B** depicts prominent presacral lymph nodes (arrows) indicative of malignant lymphadenopathy slightly remote from primary tumor (N2). **D.** Sagittal T2-weighted fast spin-echo image confirms enlarged lymph nodes (large arrows) in the presacral space. The nodular outer margin of the rectal mass (thin arrows) is well demonstrated on sagittal view, suggesting invasive tumor (T3).

TABLE 59-3 Criteria for Magnetic Resonance Imaging Staging of Rectal Cancer

Tumor (T) Stage	MRI Criteria
T1	Tumor signal intensity confined to mucosal and submucosal layer; signal intensity low compared with high signal intensity of the adjacent submucosa
T2	Tumor signal intensity extends into muscle layer, with loss of interface between submucosa and circular muscle layer
T3	Tumor signal intensity extends through muscle layer into perirectal fat, with obliteration of interface between muscle and perirectal fat
T4	Tumor signal intensity extends into adjacent structure(s) or viscus

Modified from Brown G, Richards CJ, Newcombe RG, et al: Rectal carcinoma: Thin-section MR imaging for staging in 28 patients. *Radiology* 211:215–222, 1999.

Microinvasion into surrounding fat cannot be detected by MRI, which leads to understaging, whereas peritumoral tissue inflammation and fibrosis can lead to overstaging.¹¹³ However, if the feature of a nodular or pushing configuration of an advancing tumor margin is used, tumor extension beyond the bowel wall can be distinguished in most cases from the spiculated and low signal intensity of peritumoral fibrosis.¹⁰⁴ Because the mesorectal fascia can be readily recognized on MRI and the depth of transmural tumor invasion (T3) can usually be diagnosed accurately, MRI is more sensitive and reliable for predicting the circumferential resection margin (CRM) than overall T stage of tumor (Fig. 59-34).¹¹⁴ For the surgeon, it is important to obtain information on the distance between the rectal tumor and mesorectal fascia. A pathologically involved margin in rectal cancer is defined as tumor within 1 mm of the surgical CRM.¹¹⁵

Tumor foci in normal-sized nodes may go unrecognized.¹¹⁶ If the MRI diagnosis of lymph node abnormality is based on mixed signal intensity and irregular outer margins, rather than size of the nodes, the MRI prediction of nodal involvement can be improved.¹¹⁷ In one older series, in five of six cases in which

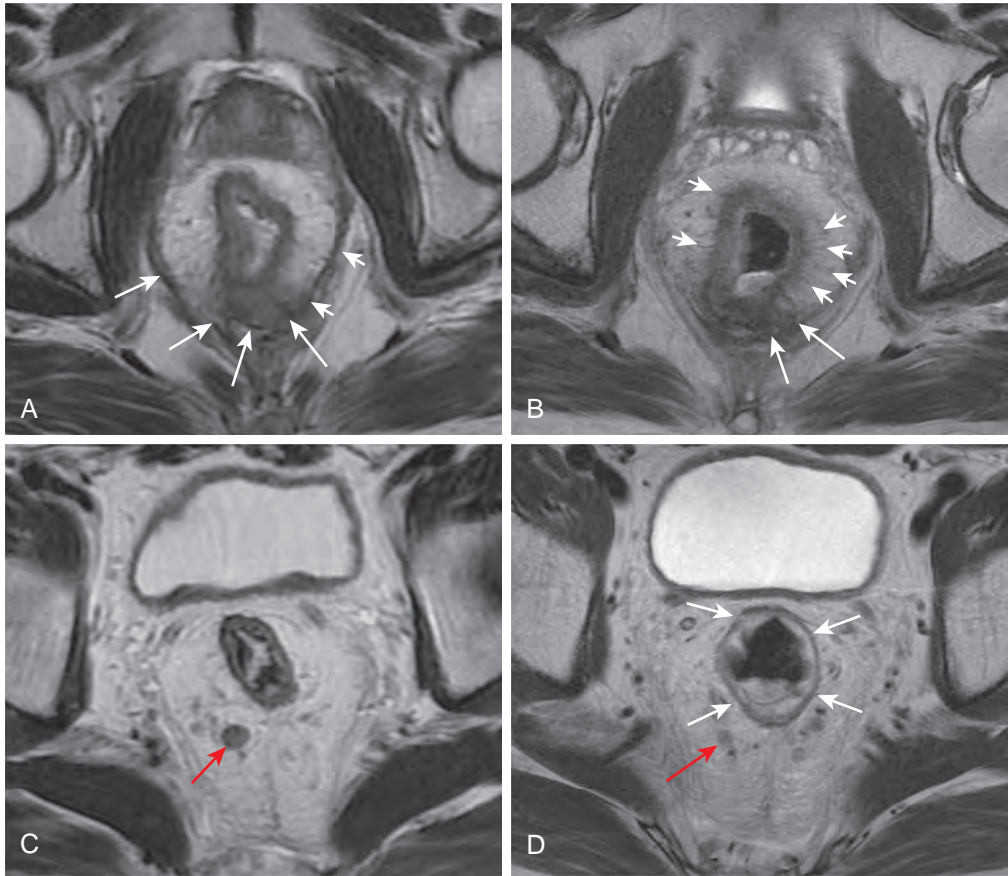


Figure 59-34 MRI scans of rectal adenocarcinoma with extension to mesorectal fascia (T3N2M0) before and after neoadjuvant chemotherapy and radiation). **A.** This T2-weighted MRI scan demonstrates rectal wall thickening with the tumor extending posteriorly beyond the rectal wall (long arrows) and reaching the mesorectal fascia (short arrows), which is well shown in this view. **B.** Following treatment, the rectal wall is less defined on this high-resolution MRI scan and shows multiple thin spicules (short arrows) extending from the rectal wall into the perirectal fat. This represents acute radiation change and not tumor extension. Posteriorly, the tumor extension to the mesorectal fascia (long arrows) is still present but slightly reduced compared to image **A**. **C.** Axial T2-weighted MRI scan demonstrates an enlarged round perirectal node (red arrow). **D.** Following neoadjuvant chemotherapy and radiation, an axial T2-weighted MRI scan close to the same level as **C** shows the same node (red arrow), which now is considerably smaller. Note the edema in the rectal wall (long arrows) above the tumor following radiation.

lymph nodes were seen, the nodes were normal in size but contained tumor and, in the one case with enlarged nodes (>15 mm in diameter), reactive hyperplasia was present.¹⁰⁷ In a more recent series with nodes considered suspicious based on irregular borders and mixed signal intensity, 51 of 60 were correctly identified as malignant (sensitivity, 85%) and 216 of 221 were considered nonmalignant (specificity, 97%).¹¹⁷

For demonstration of liver and adrenal metastases, MRI and CT are comparable if an optimal CT bolus technique is used.⁹⁹ MRI with a liver-specific contrast agent such as mangafodipir (Teslascan, Nycomed, Princeton, NJ) or iron oxide particles (Feridex, Berlex, Wayne, NJ) may render MRI superior to CT, particularly for the detection of small lesions.^{118,119} However, these liver-specific agents have not found wide acceptance, and Teslascan is no longer available. Generally, most MRI for colorectal tumor staging and suspected liver metastases still is performed after administration of gadolinium, and excellent results have been achieved with a newer liver-specific contrast agent, gadoxetate disodium (see earlier).¹²⁰

Invasion of adjacent organs is best demonstrated with transverse or coronal high-resolution MRI. MRI is superior to CT in demonstrating invasion of the levator ani (Fig. 59-35), puborectalis, or internal and external sphincter muscles. Lateral extension of tumor is difficult to detect on sagittal MRI scans but can be assessed accurately with axial images.¹¹⁴ Extension into the prostate, seminal vesicles, vagina, and cervix can be shown well by MRI, but extension into the bladder may be missed if the bladder is not well distended.

Preoperative Staging by Magnetic Resonance Imaging

The introduction of neoadjuvant preoperative radiation and/or chemotherapy and TME has made accurate preoperative staging even more critical in patient management and identifying those at risk for local recurrence. The risk of local recurrence ranges from 3% to 32%, and patients with positive resection margins are much more likely to suffer from local tumor recurrence.¹¹⁴ Based on the different risk categories, the treatment is tailored to the individual patient. In the United States, patients with

fixed T3 tumors and/or positive local nodes routinely undergo postoperative radiation and chemotherapy, but preoperative radiation is reserved for those with tumor extension to the pelvic sidewalls. In Europe, large trials have shown that the recurrence rate is markedly reduced if patients receive preoperative radiation, and therefore it is routinely performed in all patients with rectal cancer.¹²¹ Imaging should provide the following staging information: depth of tumor growth in the rectal wall, circumferential resection margin at the time of TME, degree of tumor invasion into surrounding pelvic structures, and nodal status. Edema, granulation tissue, and fibrosis can lead to overstaging in patients who undergo MRI after neoadjuvant chemotherapy and irradiation (Fig. 59-36).

Endoluminal MR and endoluminal ultrasound (see later) are the two most accurate methods for staging early or superficial rectal cancer that can be treated with surgery alone. Accuracies ranging between 71% to 91% for MRI and 70% to 94% for TRUS have been reported.^{114,122-125} These two methods are considered superior to CT in staging early tumors. However, both techniques have a limited field of view, and neither method can adequately assess the mesorectal fascia and CRM.

At present, for advanced mobile or fixed rectal cancers, MRI with phased-array coils and high spatial resolution (thin sections) generally appears to be better suited for demonstrating the mesorectal fascia and CRM than CT (see Fig. 59-32).¹¹⁴ In a meta-analysis, the sensitivity of MRI for invasion of the muscularis propria was 94%, similar to that of TRUS, but the specificity was significantly lower for MRI (69%) compared with TRUS (86%).⁴² In the same meta-analysis, at comparable specificities, the sensitivity of MRI for perirectal invasion was 82% compared with 79% for CT and 90% for endoluminal ultrasound, whereas the sensitivity of MRI for adjacent organ invasion was 74%, similar to the 72% for CT and 70% for endoluminal ultrasound.⁴² Overall, it appears that MRI may currently be slightly superior to CT in assessing extension of tumor into surrounding pelvic structures, especially for demonstrating direct invasion of tumor into pelvic sidewalls, sciatic nerves, or subtle invasion of bone marrow.¹²⁶ In one study of patients with known peritoneal carcinomatosis, it was shown that MRI had a higher sensitivity (84%) than CT (54%) for detecting peritoneal carcinomatosis if fat-suppressed

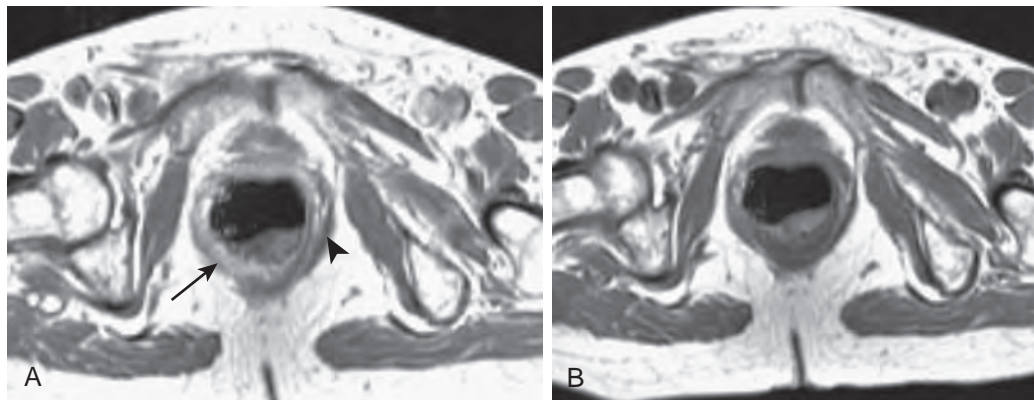


Figure 59-35 MRI scans of rectal adenocarcinoma with extension into the levator ani muscles (T3N0M0; Dukes' stage B2). **A.** Axial T1-weighted spin-echo image after gadolinium demonstrates thickening and enhancement in posterior and right lateral rectal wall administration, with direct invasion of tumor into levator ani. This suggested extension by increased signal intensity of muscle in invaded area (arrow). Compare this appearance to the normal left levator ani, which has low signal intensity (arrowhead). **B.** Tumor invasion into the levator ani is difficult to diagnose on T1-weighted sequence without gadolinium.

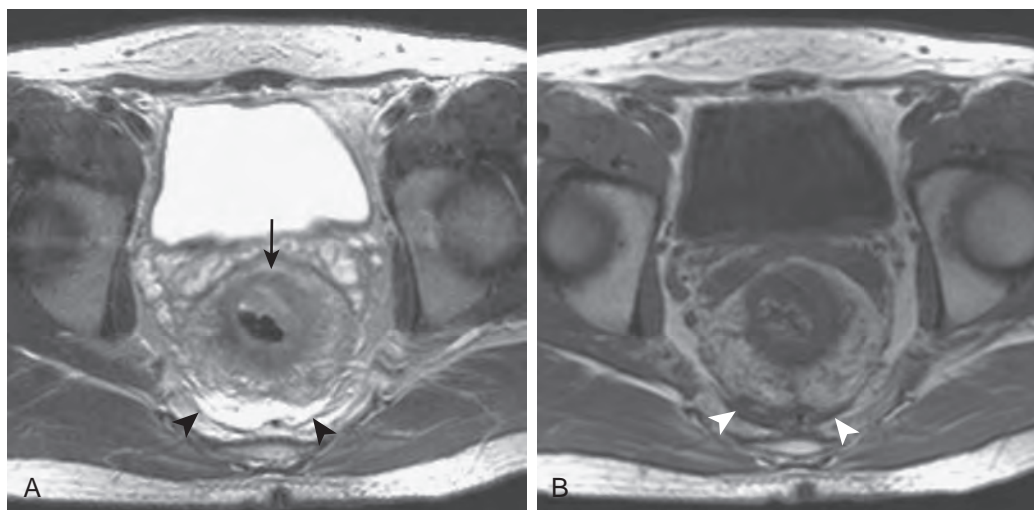


Figure 59-36 MRI scans of rectal adenocarcinoma with extension into the perirectal fat (T3N0M0; Duke's stage B2) in a patient who underwent neoadjuvant chemotherapy and radiation therapy. **A.** Axial T2-weighted spin-echo image shows a lobular wall thickening in anterior rectal wall (arrow) and mild thickening of remainder of rectal wall. Outer rectal wall margins are ill defined because of radiation therapy. Mixed signal intensity of perirectal fat with blurring of outer rectal wall and high signal intensity in presacral space are most likely secondary to post-treatment granulation tissue and retroperitoneal fluid. This makes accurate staging of this tumor more difficult. **B.** T1-weighted image does not suffer from as many postradiation artifacts, as does a T2-weighted sequence. Arrowheads, presacral fluid collection.

T2-weighted and gadolinium-enhanced T1-weighted sequences with breath holding were used.¹²⁷ However, a more recent study concluded that the use of gadolinium enhancement did not improve the diagnostic accuracy of MR for assessing tumor penetration through rectal wall and tumor extension into mesorectal fascia.¹²⁸ Diffusion-weighted imaging can be useful for identifying lymph nodes and, at times, the primary rectal cancer when the tumor is difficult to visualize with other sequences.¹¹⁶

Because the radiologic detection of nodal tumor involvement relies on morphologic criteria such as size, contour margins and signal intensity, it is difficult to distinguish between reactive and metastatic nodes. Also, micrometastases can easily be missed. Rectal tumors tend to produce micrometastases¹²⁹ but, in the perirectal fat, any node can be considered malignant because reactive lymph nodes are rare in this area. Because cross-sectional imaging uses morphology to diagnose metastases to lymph nodes, reliable detection of lymphadenopathy is not possible at present. The accuracy rates for unenhanced MRI for detection of nodal involvement range from 39% to 95%.^{105,114,123} Large variations in the accuracy for detecting nodal metastases also have been published for CT (22%-73%) and TRUS (62%-83%).^{114,130} Some promising results have been reported on the use of ultrasmall superparamagnetic iron oxide particles that are phagocytosed by the reticuloendothelial system and cause shortening of the T2* relaxation time and subsequent decrease of the signal intensity of normal lymph nodes, but not in nodes with metastatic deposits.¹³¹ Uniform and central low signal intensity patterns are suggestive of nonmalignant nodes, whereas eccentric or uniform high signal intensity patterns suggest malignant nodes.¹³² Its use for colorectal cancer needs further investigation.

Overall, for the definitive analysis of these staging results, a comparison between state of the art MDCT and MRI in large clinical trials is needed. At present, most comparative studies

have used state of the art MRI but not the latest imaging technology with CT. The advantages of MDCT with ultrathin sections and very short imaging times, particularly with 64-slice scanners, optimized bolus techniques, and multiplanar reformats have not been fully explored. Although one study indicated that improved staging accuracy could be achieved with the inclusion of multiplanar reformats,⁶⁹ no direct comparison to MRI or TRUS is currently available in larger prospective series.

TRANSRECTAL ULTRASOUND

Primary Tumor

The major advantage of endoluminal ultrasound or TRUS is that it can depict the various layers of the colon wall, which enables determination of the depth of mural tumor penetration. Colorectal tumors present as a hypoechoic mass whose margins can be outlined and related to the layers in the colon or rectal wall. The depth of infiltration can be assessed from evidence of disruption of the different segments of the rectal or colon wall. On images produced with a radial rotating transducer placed in the rectum, the elements of the rectal wall appear as rings of different echogenicities. The transducer is covered with a balloon filled with water. The innermost ring is hyperechoic and represents the interface of the balloon and mucosa. The second ring from the center is hypoechoic and is produced by the muscularis mucosae. The third ring is hyperechoic and consists of the submucosa. The fourth ring is hypoechoic and is formed by the muscularis propria. The fifth ring is hyperechoic and is caused by the perirectal fat or, if it is in an area with peritoneal reflection, by the serosa and fat.

If the examination is performed carefully, even the intraluminal component of the tumor can be clearly demonstrated as a polypoid or exophytic mass. Filling of the balloon attached to the transducer and colorectal lumen with water allows optimal

visualization of mural and nodal abnormalities. In one study, the accuracy of TRUS for local tumor staging was 85% with intrarectal administration of water and only 57% without water administration.¹³³ Pericolonic or perirectal abnormalities can also be seen, but depth of penetration beyond the colon or rectal wall is limited. Whenever possible, the transducer is passed beyond the tumor into the colon proximal to the lesion for more complete assessment of mural and nodal pathology. Peritumoral inflammation and irradiation may simulate more advanced tumor changes because these abnormalities often have a hypoechoic pattern that may be indistinguishable from the echo pattern of tumor. This leads to overestimation of the size of the neoplasm. Tumors that severely narrow the lumen may not be completely assessed by endoluminal ultrasound because it may not be possible to pass the probe through the area of stenosis. Also, high location of the tumor may prevent its evaluation by TRUS.

The ultrasonographic staging system is based on the TNM classification.¹³⁴ Three stages are distinguished by ultrasonography. A T1 tumor is confined to the mucosa and submucosa, with the echogenic layer of the submucosa thinned and irregular. It does not interrupt the middle echogenic interface to the muscularis propria. A T2 lesion is confined to the rectal wall and involves the hypoechoic muscularis propria. The outermost echogenic interface is intact. T3 tumor penetrates into the perirectal fat and is visualized as a disruption of the outermost hyperechoic ring (Fig. 59-37). Stage T4 may be assessed by endoluminal ultrasound but it is often beyond the limited field of view because T4 represents extension into adjacent organs or pelvic sidewall structures.

On TRUS, normal lymph nodes are hyperechoic and bean-shaped and have indistinct margins. Consequently, they are not routinely seen within the echogenic perirectal fat. Tumors containing lymph nodes are spherical hypoechoic structures with distinct margins. According to the TNM classification, stage N1 is present when TRUS visualizes one to three hypoechoic nodes and stage N2 is present if TRUS sees four or more of these hypoechoic lymph nodes.

Smaller probes that can be introduced through the biopsy channel of an endoscope and pass through a severe luminal stenosis allow more accurate staging because the complete tumor extent can be visualized. The echo-endoscope has become the instrument of choice for visualizing proximal colon

neoplasms because the transducer can be maneuvered into the proximal segments of the colon. In one diagnostic and staging procedure, the combination of endoscope and TRUS can serve the following functions: demonstrate the surface of the mucosa, obtain a biopsy specimen, visualize the depth of a lesion within the bowel wall, and determine the presence or absence of adjacent lymphadenopathy.^{135,136} However, CT or MRI is needed for complete staging, especially for detecting distant metastases.

Preoperative Staging by Endoluminal Ultrasound

Although transabdominal sonography may be used to assess the presence or absence of liver metastases, TRUS is increasingly used to detect the depth of tumor infiltration and local adenopathy in patients with rectal carcinomas. As noted, its ability to distinguish the normal layers of the bowel wall and visualize disruption of one or more of these layers by tumor leads to accurate staging of local tumor extent. With this method, sensitivities of 67% to 96% have been reported for assessing perirectal spread but the presence of regional lymph node metastases is less well detected (sensitivity, 50% to 70%).^{42,134,137-140} One study has shown that results were less accurate with T2 carcinomas, which were often accompanied by peritumoral inflammation or abscess.¹⁴¹ Abscesses manifest as fluid-filled structures, usually in the perianal space, that may contain internal echoes but exhibit good posterior acoustic enhancement. In their study of transcolorectal endosonography, the authors achieved an accuracy of 81% for rectal and 93% for colon carcinomas, with overstaging in 13% and understaging in 2% of patients. When lymph node involvement was analyzed separately, the sensitivity was 94% and specificity 55% for an overall accuracy of 70%. When transcolorectal ultrasound was compared with Dukes' classification, the overall accuracy was 67%.

The broad range of sensitivities of TRUS for the detection of tumor extent in and through the bowel wall emphasizes the operator dependence of this method. This fact was well demonstrated in a multicenter trial in which experienced ultrasonographers with a large caseload of patients with rectal cancers achieved the highest accuracy with TRUS.¹⁴² TRUS has expanded the application of ultrasonographic methods to the entire colon, and even ultrasound-guided biopsies of submucosal and extrinsic masses of the colon and rectum have become possible with this technique.^{135,143,144} Spontaneous or iatrogenic inflammation is a major limiting factor affecting diagnostic

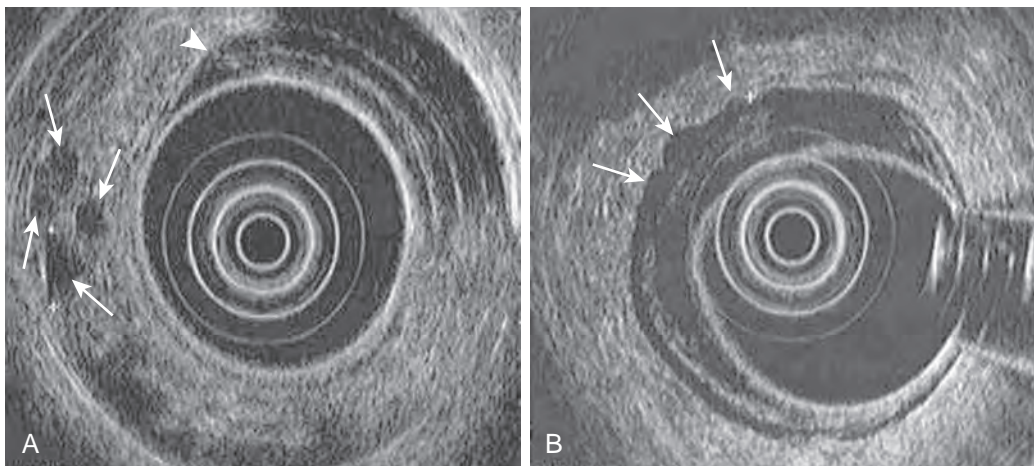


Figure 59-37 Transrectal ultrasound of rectal tumor (T3N1). **A.** TRUS image shows several lymph nodes in perirectal fat (arrows) and marked thickening (arrowhead) of rectal wall. **B.** TRUS image demonstrates thickened anterolateral wall of rectum as a low echogenicity structure with nodular outer margin (arrows) against the surrounding high signal intensity fat. This indicates transmurum tumor extension (T3).

accuracy.¹⁴⁵ Transrectal volume scans obtained using a 3D multiplane transducer (7.5 to 10.0 MHz) permits examination of rectal cancer using previously unattainable planes and 3D views¹⁴⁶ and may help improve tumor staging and treatment planning.¹⁴⁷ Because of the limited penetration of the ultrasound probe, only locoregional staging is possible with TRUS, and CT or MR need to be added for complete tumor staging.

IMMUNOSCINTIGRAPHY WITH MONOCLONAL ANTIBODIES

Detection of Primary Colorectal Neoplasm

Since the mid-1970s, MoAbs have been used in vivo as tumor-localizing agents and in vitro as diagnostic markers with gamma camera imaging to differentiate tumor cell types.^{44,148} Agents used include anticarcinoembryonic antigen (anti-CEA) MoAbs tagged with ¹²³I and ¹²⁵I, anti-CEA MoAbs conjugated with diethylenetriaminepentaacetic acid (DTPA) and labeled with ¹¹¹In, MoAbs B72.3-GYK-DTPA, designated as CYT-103 (¹¹¹In-labeled satumomab pendetide; MoAb B72.3-glycyl-tyrosyl-[N-e-DTPA] lysine), sodium iodide ¹²⁵I-labeled anti-TAG monoclonal antibody CC49, and MoAb ior c5.¹⁴⁹⁻¹⁵¹ The level of serum CEA did not influence tumor detection. MoAb B72.3 targets the high-molecular-weight tumor-associated glycoprotein 72, which is expressed in 80% of colon cancers and reacts with various mucin-producing adenocarcinomas, but has almost no reaction to normal tissues. Some patients require cathartic agents before imaging because of prominent radioactivity in the large bowel. In general, lesion detection is performed with planar imaging 3 to 4 days after MoAb infusion. Single photon emission CT (SPECT) is usually performed 5 to 7 days after MoAb infusion, and its better anatomic definition and determination of approximate size result in improved tumor detection.¹⁵² Most studies attempt to determine the maximum tolerated dose and uptake and retention of isotope in the tumor.¹⁵³

Primary adenocarcinomas of the colon and metastatic foci in liver or lymph nodes are seen as areas of increased radioactivity (hot spots). Depending on the size and degree of necrosis of the liver metastases, neoplastic deposits in the liver may be visualized as areas of intense accumulation of radioactivity, areas with no accumulation of radioactivity surrounded by normal liver uptake, and intermediate lesions, with uptake identical to that of normal liver. In one study using ¹¹¹In-labeled CYT-103, cold defects in the liver shown by immunoscintigraphy were found to represent areas with moderate to severe necrosis, whereas lesions with normal MoAb uptake had only minor degrees of necrosis.¹⁵² The same study revealed a low incidence of human antimouse antibody formation (16%) and an even lower incidence of adverse reactions (3.5%).¹⁵² Radioimmunoguided surgery (RIGS) with the monoclonal antibody CC49 labeled with ¹²⁵I has been used in the treatment of colorectal cancer and appears promising.^{150,154,155}

Preoperative Staging of Primary Colorectal Neoplasm

A number of studies have evaluated the value of isotope-labeled MoAb immunoscintigraphy for the detection of primary colorectal carcinoma and its metastases.¹⁴⁸⁻¹⁶² Sensitivity ranged from 65% to 95% and specificity ranged from 77% to 100% for the detection of primary tumor, local recurrences, and distant

metastases. The major role of immunoscintigraphy is detecting occult tumor lesions and establishing absence of distant disease in patients with isolated, resectable metastases. In one study¹⁶² using ¹¹¹In-labeled CYT-103, extrahepatic lesions undetected by CT and other tests were confirmed by surgery in more than 10% of patients. In another study, RIGS had a sensitivity of 92% and specificity of 88% for the detection of lymph node metastases.¹⁶² Also, immunoscintigraphy contributed beneficially to the management of 27% of patients.¹⁶⁰ It therefore appears reasonable to use immunoscintigraphy in patients with suspected focal or metastatic colorectal neoplasms. However, the validity of this test and low incidence of adverse reactions must be confirmed in larger series before a final conclusion can be drawn.

POSITRON EMISSION TOMOGRAPHY

Primary Colorectal Neoplasm

PET was initially used for the detection of functional abnormalities of the brain and heart, but its use has been expanded to the detection of primary and recurrent tumors as well as metastases. For these tumor studies, ¹⁸F-fluorodeoxyglucose (FDG) has been used, and a remarkable correlation has been found between tumor grade and the degree of glucose uptake.¹⁶³ The new generation of PET scanners has good resolution and can provide high-quality images of any area of the human body; it is possible to use this method to detect distant, residual, or recurrent disease in patients with colorectal carcinomas. With the introduction of the PET/CT system, lesion classification has been significantly improved.¹⁶⁴ Large series in patients with colorectal cancer are still needed to define the role of PET/CT more clearly in staging and treating these patients.

For the purpose of identifying tumor tissue, PET images are evaluated quantitatively in regions of interest and time-activity curves are calculated. Tracer uptake is expressed as a differential absorption ratio calculated as the tissue concentration (in mCi/g) divided by injected dose (mCi) per body weight (g). After IV injection of FDG, PET images show significant uptake by malignant tumors (Fig. 59-38). Quantitative analyses demonstrate rapid uptake of FDG by the tumor, followed by a slight decrease in the differential absorption ratio for up to 40 minutes after FDG administration. In comparison, the FDG concentration is low in nonmalignant lesions and in soft tissue. In general, 1 hour after tracer injection, FDG accumulation in tumors is more than twice as high as in normal tissue or nonmalignant lesions. Tumor imaging is best performed at that time. Colon cleansing and drainage of the bladder with a Foley catheter after administration of the isotope can minimize artifactual accumulation of FDG.¹⁶⁵

Staging of Primary Colorectal Neoplasm

The Centers for Medicare and Medicaid Services (CMS) first approved PET for coverage in 1998 and its guidelines specifically approve the use of FDG-PET for the diagnosis, staging, and restaging of colorectal cancer, but in clinical practice it is rarely used for the diagnosis of primary colorectal cancer unless the diagnosis has not been made pathologically.¹⁶⁶ Most investigations of the applications of FDG-PET for colorectal tumors have focused on the detection of local recurrent or residual disease. PET has also been used to identify distant metastatic foci and occasionally unexpected primary malignant tumors in patients with other colorectal neoplasms.^{47,163,167-173} Most studies

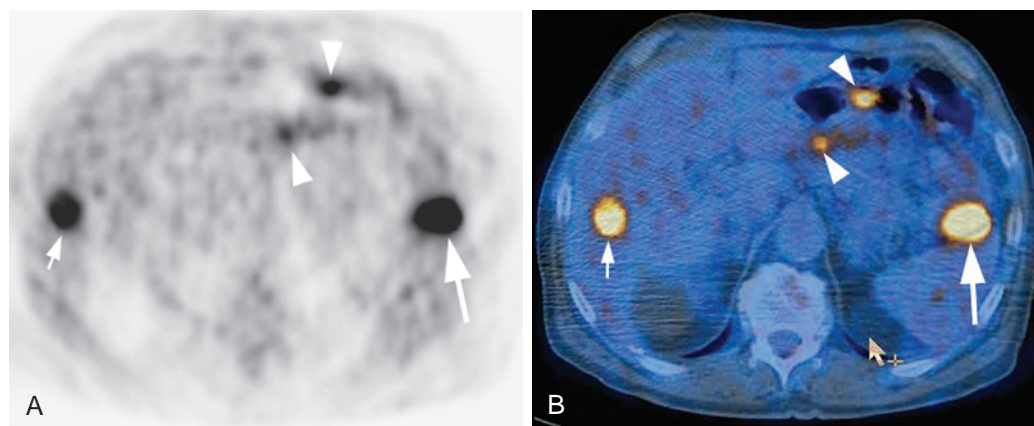


Figure 59-38 PET for staging in patient with history of splenic flexure carcinoma. **A.** Axial FDG-PET image demonstrates increased FDG uptake in anticipated location of splenic flexure (*large arrow*) and in liver (*small arrow*). Two additional areas of increased FDG uptake (*arrowheads*) are seen in expected location of hepatic flexure. **B.** The fused PET/CT scan shows that left flank activity is located in the splenic flexure primary tumor (*large arrow*), and a large area of increased activity on the right corresponds to hepatic lesion (*small arrow*) seen on CT. Two small areas of increased activity (*arrowheads*) were not seen on CT and represent small implants on surface of hepatic flexure. Although CT detected both primary tumor in splenic flexure and hepatic metastasis, serosal colonic implants were missed.

that addressed the sensitivity for identifying primary tumor by PET were retrospective and hampered by physiologic bowel wall accumulation of the isotope. This prevents the use of FDG-PET as an initial diagnostic modality.

Only small series are available, so the accuracy of PET with FDG for staging colorectal tumors remains to be determined. Even smaller numbers are reported for the PET/CT scanner. Nevertheless, the results with PET/CT are promising because of the superior localization of lesions. In one study of asymptomatic patients with colonoscopic correlation, PET/CT detected 13 villous adenomas and 3 adenocarcinomas and had 5 false-positive results.¹⁷² In this study, the authors were able to distinguish adenoma from carcinoma by an increased rate of glycolysis in carcinoma. Metastases have been shown in lymph nodes remote from the primary tumor site and in liver. The results for lymph nodes are not as promising as those for liver metastases. One study showed a sensitivity for regional lymph nodes of only 29% but a specificity of 96%.¹⁶⁸ These disappointing results are probably because many metastatic deposits from colon carcinoma to nodes are in close proximity to the primary tumor, are small, and are often not cell-rich, especially if the tumor is mucinous.

PET is excellent for the depiction of distant nodal or extra-nodal metastases. In one study, the positive predictive value of PET for malignant liver lesions was 93% and was superior to the 78% of CT or MRI.¹⁷⁴ PET is more accurate than CT for depicting hepatic metastases from colon carcinoma larger than 1 cm in diameter but frequently misses lesions smaller than 1 cm.¹⁷⁵ Because PET does not provide accurate information about the location of hepatic metastases according to hepatic anatomy, its best role lies in the detection of extrahepatic disease that precludes resection for cure (see Fig. 59-37). It appears that the addition of PET to the presurgical evaluation of patient with colorectal carcinoma may improve survival by eliminating patients with inoperable disease from consideration for surgical resection of liver lesions.¹⁷⁵ However, in a more recent study, PET/CT changed the treatment of patients with colorectal carcinoma in only 3.2% and the authors recommended against the routine use of PET/CT for primary staging of these tumors.¹⁷⁶

Cross-Sectional Imaging in Primary Colorectal Neoplasm Detection

CTC has been introduced as a method for screening patients at risk for colon cancer and polyps. The introduction of 2D and 3D CTC as complementary techniques has several advantages, including good patient tolerance, excellent visualization of abnormalities within the colon, and accurate detection of pathology proximal to an obstructing lesion (Fig. 59-38).^{177,178} Furthermore, 3D reconstruction with fly-through capability offers the advantage of complete antegrade and retrograde inspection of the entire colon, whereas retroflexion with the endoscope during colonoscopy cannot be achieved for all areas of the large bowel. Various technical approaches are still being explored to facilitate the process of evaluating the colon with CTC and further improve its sensitivity. CTC is discussed in detail in Chapter 53.

Patient prognosis in colorectal cancer is closely related to tumor stage at the time of diagnosis. The overall 5-year survival rate is about 61% (stage A, 81%-85%; stage B, 64%-78%; stage C, 27%-33%; stage D, up to 20%).^{175,179-181} There is consensus that the most important prognostic factor is the presence or absence of lymph node invasion, but malignant fixation of colorectal tumor through direct invasion also appears to be an important sign.¹⁸²

Most patients with colorectal cancer have disease that at the time of diagnosis is limited to the bowel wall and regional pericolic or mesenteric lymph nodes. These patients undergo curative surgery. In patients with advanced disease, surgery is performed to prevent hemorrhage, obstruction, and perforation. Both types of patients need accurate, noninvasive, preoperative assessment of tumor stage based on one or a combination of radiographic techniques to individualize the treatment plan. The rest of this section will analyze the effectiveness of various imaging techniques for detecting and staging primary colorectal neoplasms.

Endoluminal or endoscopic ultrasound is useful for determining local tumor extent within and beyond the bowel wall but may miss regional lymph node metastases, which develop in 14% of patients with primary tumors confined to the rectal

BOX 59-1 DIFFERENTIAL DIAGNOSIS OF COLONIC WALL THICKENING

Neoplasm (primary, including lymphoma and secondary)
 Neoplasm from adjacent tissue or organs invading colon and/or rectum
 Neoplasm metastatic to the colon or rectum
 Muscular hypertrophy (particularly sigmoid colon)
 Crohn's disease
 Ulcerative colitis
 Infectious colitides (including pseudomembranous colitis)
 Diverticulitis
 Intramural abscess or hematoma (trauma, coagulopathy)
 Perforation with inflammation
 Ischemia
 Vasculitis (with focal involvement)
 Endometriosis
 Amyloidosis
 Focal chronic inflammation from pancreatitis
 Plication defects after surgery

wall. At present, endoluminal sonography is superior to CT and equal to MRI in demonstrating the T stage of tumors confined to the bowel wall (T1 and T2) and has a higher specificity.⁴² Endoluminal ultrasound appears to be more sensitive in assessing early perirectal invasion, but its sensitivity does not reach 100%.

Based on the available results, routine CT or MRI staging is not recommended for early primary colorectal tumors. Wall thickening alone is a nonspecific finding that occurs in many different diseases (Box 59-1). Endoluminal MRI can achieve results for T1 and T2 staging similar to endoluminal ultrasound, but this method is rather invasive and not widely used. Both endoluminal techniques are limited when a large obstructing colorectal mass is present. MRI with phased-array coils is capable of demonstrating the layers of the rectal wall.

Overall, CT and MRI should be reserved for patients with suspected locally invasive (T3 or T4) or metastatic disease. If CT or MRI shows extensive local tumor, these patients can be treated with neoadjuvant radiation therapy and chemotherapy with subsequent tumor resection. In the United States, chemotherapy and radiation therapy are reserved for patients with T3 disease, but in Europe all patients with rectal carcinoma receive preoperative irradiation, with or without chemotherapy. Neoadjuvant therapy has proven to reduce rectal tumor recurrence dramatically.¹²¹

If a colon resection is planned, the decision to use local tumor excision by surgery or colonoscopy cannot be based on CT alone. CT has poor sensitivity in depicting depth of mural tumor penetration and is less sensitive than other techniques for assessing invasion of the mesorectal fascia and regional lymph nodes. CT can be used to guide fine-needle aspiration of suspected metastases and assess complications, such as abscess formation. When the primary neoplasm arises in the abdomen, pelvic metastases are uncommon, and isolated pelvic metastases are rare, which focuses the metastatic work-up on the abdomen.^{183,184} Subtle extension of tumor beyond the bowel wall may be better recognized by MRI than by CT, whereas advanced T3 usually is diagnosed equally well by both techniques. In these cases, the choice of method is largely determined by the operator's skills and experience. At present, MRI is considered superior to CT in demonstrating the mesorectal fascia and determining the exact distance of the tumor from it.

Invasion of the muscles, nerves, and bones may be better delineated on MRI than on CT.¹²⁶ Because in-depth studies are not available that compare MDCT with 16 or 64 detector rows to state of the art MRI, a definitive assessment of the respective advantages of the two techniques cannot be made.

Large variations in sensitivity and specificity for detecting metastases in lymph nodes have been published for all three techniques. Endoluminal ultrasound has limited depth penetration and therefore can only be used for the detection of locoregional nodes. All techniques suffer from the fact that small metastatic deposits in lymph nodes may go undetected. MR lymphangiography may improve staging of colorectal tumors, but MR lymphangiography with target-specific contrast material is not yet commercially available.

The role of MoAb immunoscintigraphy and PET in the evaluation of patients with primary colorectal tumors is still uncertain. Results with immunoscintigraphy are encouraging, with sensitivities for detecting primary colorectal tumor ranging from 65% to 95% and specificity from 77% to 100%. Furthermore, RIGS was shown to guide resection of malignant lymph nodes successfully.¹⁶² Specifically, this test may lead to more accurate assessment of distant disease for resection. Similarly, PET has become an accurate method for staging colorectal neoplasms because the resolution of PET scanners has improved, and combined PET/CT provides more accurate lesion localization. Although the sensitivity of PET for detecting hepatic metastases larger than 1 cm in diameter is superior to that of CT or MRI, CT or MRI should be used initially for detecting liver metastases and localize them precisely to the various liver segments. MRI with a liver-specific contrast agent has the advantage of detecting liver metastases with a high sensitivity and can readily detect lesions smaller than 1 cm. The most important role of PET in the presurgical evaluation of patients with colorectal cancer is in the detection of extrahepatic disease that precludes resection for cure.

In conclusion, a combination of endoluminal ultrasound (or endoluminal MRI) for local and CT for overall staging is optimal for early colorectal cancer. Whether the addition of PET is beneficial and cost-effective in these patients remains to be seen. In suspected advanced disease, MRI appears to be superior to CT for local staging and assessing the presence or absence of liver metastases, and it should be combined with PET/CT for complete staging and preoperative treatment planning. Intraoperative ultrasound can be used to confirm the presence or absence of hepatic metastases.

Postoperative Follow-Up

CONTRAST ENEMA

Patients who have had surgery for colorectal carcinoma should undergo frequent postoperative examinations because of their relatively high risk for developing a recurrent and metachronous carcinoma.¹⁸⁵ Ileocolic (Fig. 59-39) and colocolic anastomoses are well depicted on double-contrast enema examination, particularly after the use of IV glucagon. Plication defects are frequently identified. In some patients, a filling defect resulting from a stitch granuloma may be seen in the early postoperative period (Fig. 59-40). This defect regresses and becomes less prominent on follow-up studies.¹⁸⁶ It is important to obtain a postoperative study within approximately 3 months of surgery to establish the baseline appearance of the

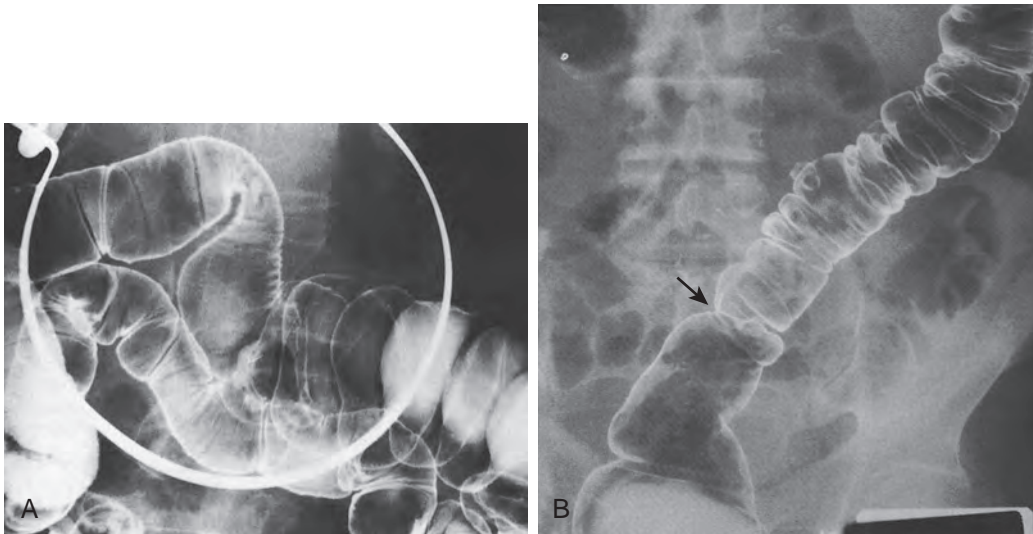


Figure 59-39 Normal postoperative appearances.
A. Normal ileocolic anastomosis in the transverse colon.
B. Example of a normal colocolic anastomosis (arrow). (From Laufer I, Levine MS [eds]: *Double Contrast Gastrointestinal Radiology*, 3rd ed. Philadelphia, WB Saunders, 2000.)

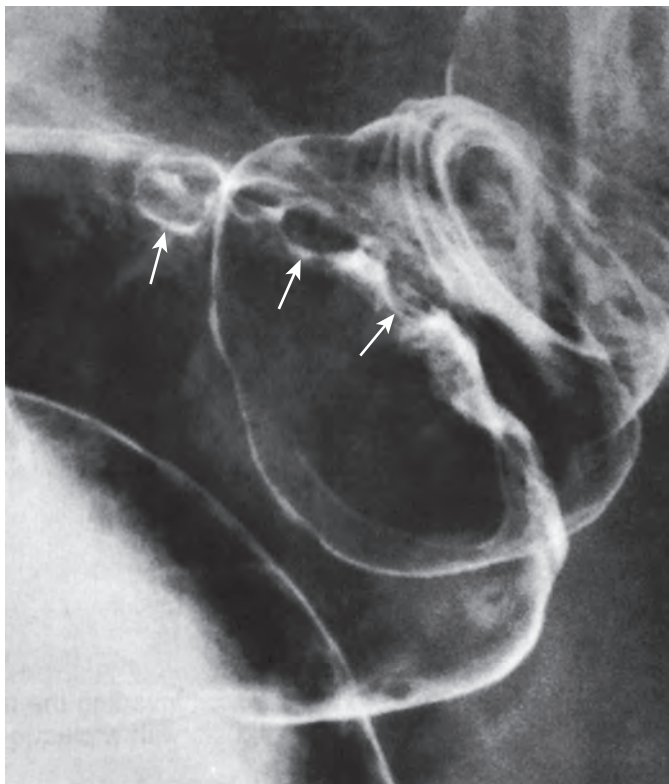


Figure 59-40 Stitch granuloma. Colocolic anastomosis with identifiable plication defects caused by sutures (arrows). (From Laufer I, Levine MS [eds]: *Double Contrast Gastrointestinal Radiology*, 3rd ed. Philadelphia, WB Saunders, 2000.)

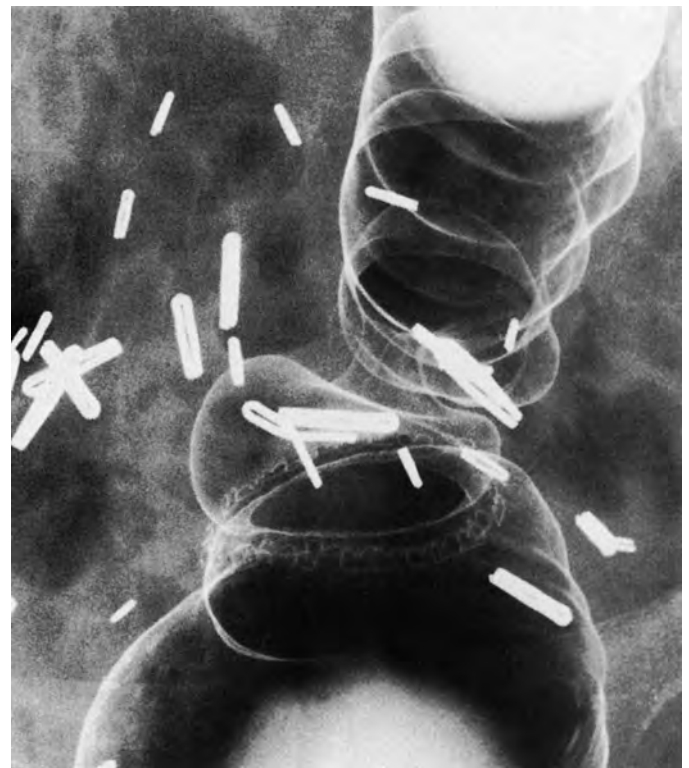


Figure 59-41 Low anterior resection. Double-contrast barium enema shows normal appearance of low anterior resection using staple gun. (From Laufer I, Levine MS [eds]: *Double Contrast Gastrointestinal Radiology*, 3rd ed. Philadelphia, WB Saunders, 2000.)

anastomosis for comparison with subsequent studies. The surgical anastomoses of low anterior resections performed with a surgical stapler are beautifully demonstrated by double-contrast technique (Fig. 59-41).¹⁸⁷ CT is the examination of choice for the detection of recurrence remote from the anastomotic line and detection of distant metastases (see later).^{188,189}

The double-contrast enema is the primary diagnostic procedure for the detection of local and anastomotic recurrences (Fig. 59-42), as well as metachronous lesions (Fig. 59-43). It is

particularly important to examine the anastomotic site because metastatic deposits tend to be implanted there.^{190,191} Welch and Donaldson have shown that 20% of recurrences after colon resection and anastomosis are found at the anastomotic site.¹⁹² When the anastomotic site appears eccentric or irregular or has nodular filling defects, recurrent tumor should be suspected. Colonoscopy may be helpful, although in some cases it may be misleading because recurrent tumor may be submucosal and biopsy findings may be negative for malignancy. CT and

Figure 59-42 Local recurrence of colon carcinoma. **A.** Soft tissue mass represents recurrent colon carcinoma invading rectosigmoid. **B.** Anastomotic recurrence of colon cancer. A narrowing of the anastomosis with a plaquelike extension of recurrent tumor is seen proximally (arrow).

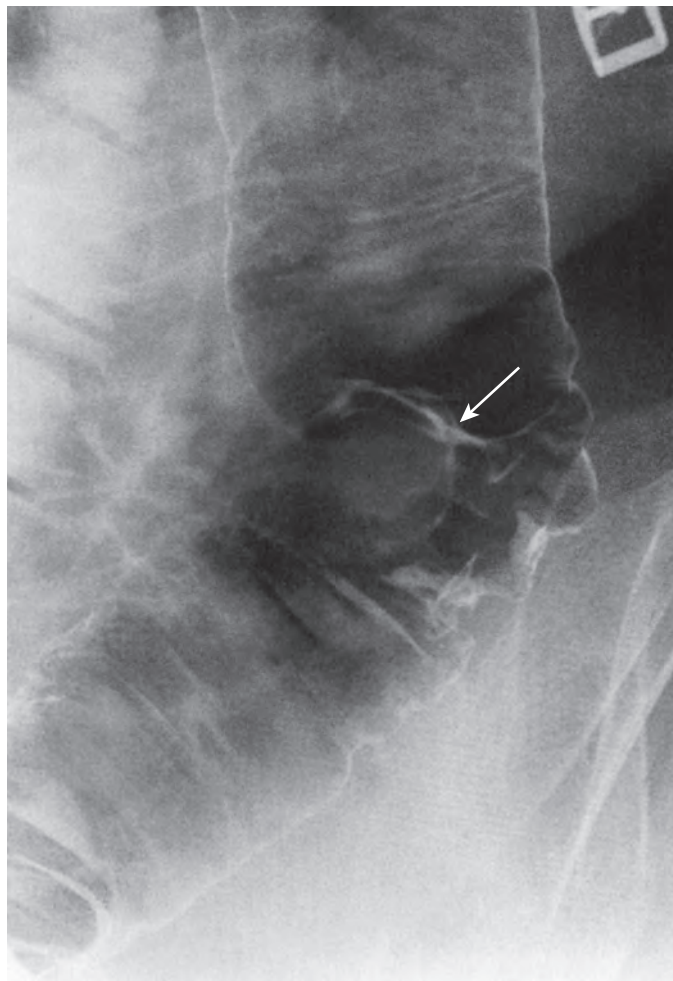
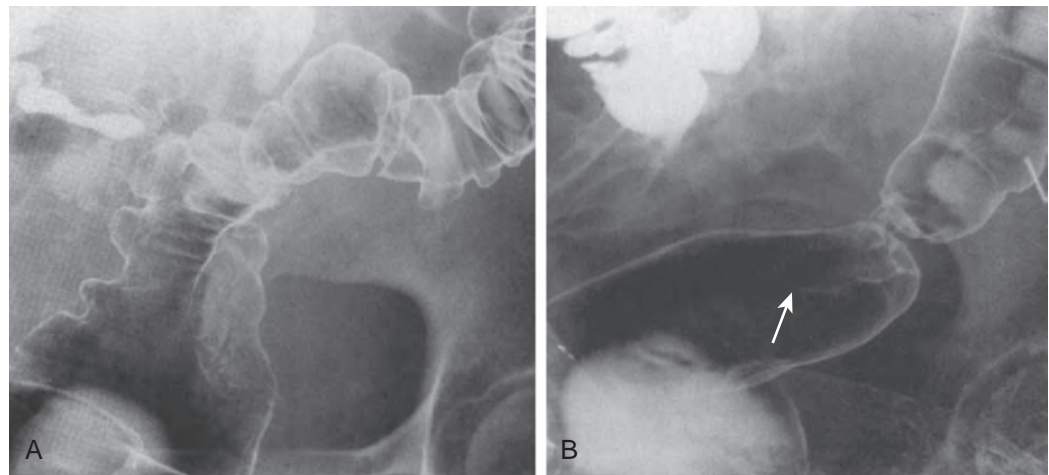


Figure 59-43 Metachronous carcinoma. A colostomy enema study performed after total proctectomy for carcinoma shows new primary carcinoma (arrow) in the descending colon.

CT-guided biopsy may be needed to determine the presence and nature of an extracolonic mass, which cannot be appreciated to its full extent, if at all, by the barium enema.

Patients who have undergone abdominoperineal resection with colostomy must also be examined regularly because of the

possibility of developing a second tumor. Double-contrast examination of the residual colon can usually be performed through the colostomy (see Fig. 59-43 and Chapter 55). CT and MRI are of particular value for the detection of pelvic recurrence of tumor in patients who have undergone abdominoperineal resection.

CROSS-SECTIONAL IMAGING

CT and MRI have been used extensively to identify recurrent colorectal cancer, and both methods can detect recurrent tumor when CEA titers are normal and symptoms are absent.^{193,194} They are particularly useful in patients who have had total abdominoperineal resection. Follow-up studies of patients with potentially curative resection of recurrent tumor demonstrated an average symptom-free period of 38 months, compared with an average survival of 8 months for patients without resection of recurrent tumor.¹⁹⁵⁻¹⁹⁷ CT and MRI are accepted methods for detecting recurrent tumor that develops extraluminally. There is an ongoing debate on the appropriate timing and cost-effectiveness of these imaging tests. Rectal tumors have significantly more locoregional and pulmonary recurrences, whereas colon carcinomas have more hepatic and intra-abdominal recurrences.¹⁹⁷ Testing for asymptomatic recurrence during the first follow-up year is usually less fruitful than in the second through fourth follow-up years.^{185,198} Patients with local recurrence in the first year are less likely to have a successful second “curative resection.” Patients with low tumor grade at initial diagnosis are more likely to have a successful second surgical resection and a better prognosis.¹⁹⁹ Young patients with colon cancer have an increased prevalence of isolated local recurrences and a lower rate of liver metastases than older patients.²⁰⁰

The stage, histology, and site of primary tumor at the time of diagnosis have been found to be most predictive of eventual relapse.^{185,198,201} Anastomotic recurrence usually occurs after low anterior resection of a rectal tumor and is usually related to residual tumor outside the colorectal wall that grows into the suture site. Since the introduction of total mesorectal excision, the incidence of local relapse has been markedly reduced.²⁰² Pelvic tumor recurrence limited to the axial location or axial and anterior locations is more likely to be resectable than those involving the sidewalls.²⁰³ Because tumor recurrence develops in 30% to 50% of patients who have undergone apparently

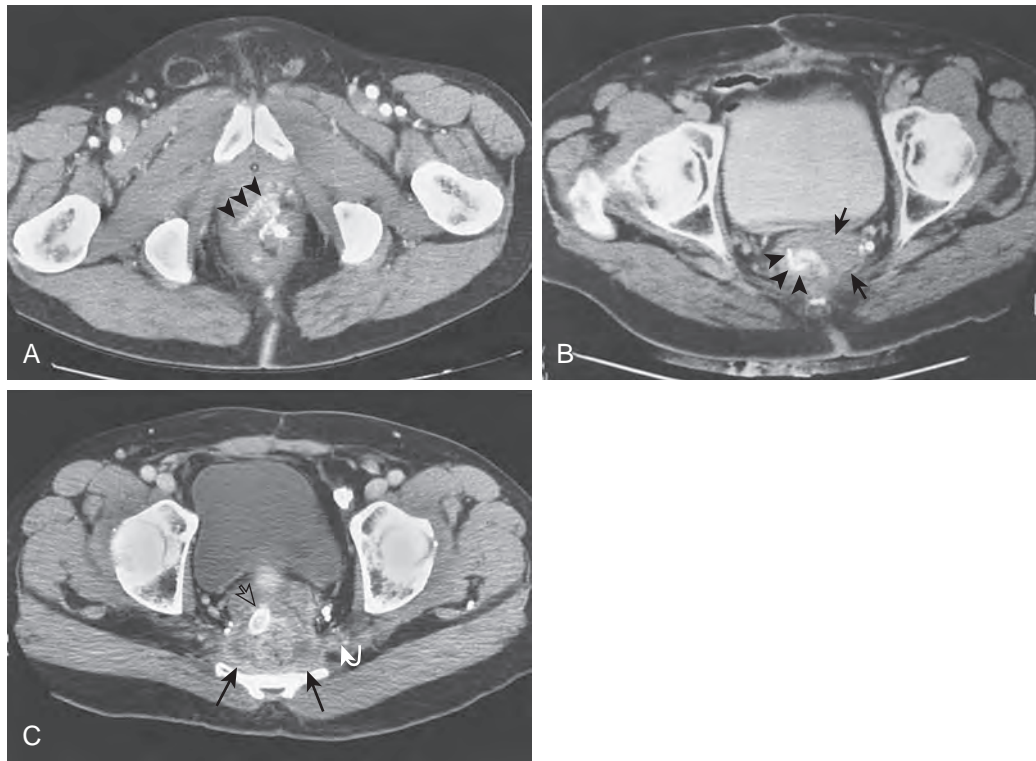


Figure 59-44 Postoperative appearance of pelvis after rectal carcinoma resection and reanastomosis. **A.** Status postresection without recurrence. The staple line (arrowheads) is clearly identified. **B.** Recurrent rectal carcinoma with extension into perirectal fat (T3N0M0). Thickening of the rectal wall is seen on the left side (arrows). There is also extension into perirectal fat. Staples (arrowheads) outline the area of anastomosis. Note the largely extrinsic component of the recurrence. **C.** Advanced recurrent rectal carcinoma (T4bN1M0). The rectal wall is markedly thickened, and a tumor mass is noted to extend to the sacrum (straight arrows) and piriformis muscle on the left (curved arrow). Adenopathy is inseparable from the mass. A rectal tube (open arrow) is also seen on this section.

curative resection, and 80% of these recurrences develop within the first 2 years,²⁰⁴ early and frequent follow-up studies are recommended. Many cancer centers observe a frequent follow-up program that includes serum CEA level determination, chest radiography, colonoscopy, and imaging.^{185,205} The most commonly recommended sequence of imaging follow-up studies consists of baseline CT or MRI at 3 to 4 months, with subsequent imaging examinations at 6-month intervals for 3 years and then at yearly intervals for 5 years. PET/CT has proven that it can distinguish between surgical scar and tumor recurrence with a high degree of accuracy.⁴⁷

Computed Tomography

Early studies established the usefulness of CT in detecting local recurrence and metastases to lymph nodes, liver, peritoneal cavity, retroperitoneum, and lung.^{206,207} Sensitivities as high as 93% to 95% were initially reported for the detection of locally recurrent tumor.^{208,209} Later investigations indicated accuracy rates ranging from 53% to 88%.^{205,210-212} Most diagnostic errors are a result of the inability to detect microscopic invasion of perirectal or pericolic fat in patients with reanastomoses, assess presence or absence of metastatic foci in normal-sized lymph nodes, and visualize minimal local tumor recurrence at the anastomotic site, particularly if the postoperative scar has not changed in size.

The CT features of recurrent anastomotic tumor are similar to those of the primary tumors, but the recurrence may be largely extrinsic. MDCT often can demonstrate the staple line at the anastomosis (Fig. 59-44). In these patients, wall



Figure 59-45 Postsurgical scar in patient with total abdominoperineal resection. A small area of soft tissue density (arrows) is seen in the presacral region.

thickening caused by plication defects must be differentiated from recurrent tumor. The presence of streaky densities or a clean operative bed suggests fibrosis, whereas the presence of a mostly globular mass favors the diagnosis of tumor recurrence.⁸⁷ However, other studies have indicated that a globular soft tissue mass may represent granulation tissue, hemorrhage, edema, or fibrosis in the early postoperative period (Fig. 59-45 and Box 59-2).⁹³ Postradiation fibrosis can also cause streaky densities or a presacral mass.^{208,213,214} Pelvic radiation causes an inflammatory reaction in the soft tissue of the pelvis, which

BOX 59-2 DIFFERENTIAL DIAGNOSIS OF COLORECTAL MASS WITH SOFT TISSUE STRANDING

Neoplasm (primary and secondary)
 Focal colitis (e.g., ameboma, Crohn's disease, neutropenic colitis)
 Abscess
 Diverticulitis
 Pelvic inflammatory disease with contiguous colorectal inflammation
 Rectal perforation and inflammation
 Prostatitis, with contiguous inflammation and/or abscess
 Status postradiation
 Endometriosis
 Pancreatitis in transverse colon or splenic flexure
 Transplants of pancreas and kidney with rejection or pancreatitis and contiguous involvement of colon or rectum
 Peritonitis with infected fluid in pouch of Douglas

leads to increased fat attenuation and thickening of the perirectal fascia. These changes persist for many years and may be indistinguishable from tumor recurrence. In a study that compared CT with PET, presacral soft tissue masses were seen by CT in 48% of patients with suspected tumor recurrence, and these findings were caused by actual tumor recurrence in only 23%.⁴⁷

Benign postoperative masses may persist on CT more than 24 months after abdominoperineal resection.²¹⁴ A baseline CT study 3 to 4 months after surgery frequently demonstrates the presence of a mass, which by 4 to 9 months decreases in size and develops sharper margins. In the absence of symptoms and elevated CEA titers, this change in the appearance of the mass should not cause concern about local tumor recurrence. However, any increase in mass size, even in the absence of local invasion, lymphadenopathy, or perineal soft tissue density, should suggest recurrence, prompting percutaneous biopsy (Fig. 59-46).^{213,214} Biopsy results may be negative if the recurrent tumor incites a substantial fibrous reaction.

With TME, the primary tumor is removed together with the perirectal lymph nodes but the internal iliac nodes are left in place. Positive lymph nodes left behind at TME substantially increase the risk for local recurrence in patients with lower rectal cancer. In one study, it was shown that 28% of patients with distal rectal cancers and positive lymph nodes had involvement of the internal iliac nodes, and in 6% these lateral chains were the only nodes involved.²¹⁵ These patients are staged as lymph node–negative at TME. In a large TME trial, it was shown that nodal disease is a prognostic indicator for local recurrence and distant metastases.²¹⁶ Detection of these nodes is essential if preoperative radiation and chemotherapy are considered for patients at high risk for recurrence. If postoperative radiation and chemotherapy is chosen for patients with advanced node-positive disease, preoperative detection of positive lymph nodes is not as crucial.

For 2 decades, CT was considered the best modality for detecting and staging recurrent rectal or rectosigmoid carcinomas. In patients who have had sphincter-saving resection of rectal and rectosigmoid carcinomas, almost all recurrent tumors develop extraluminally and subsequently infiltrate the suture lines. These extraluminal recurrences are missed on endoscopy and barium enema. In these patients, the rectum must be

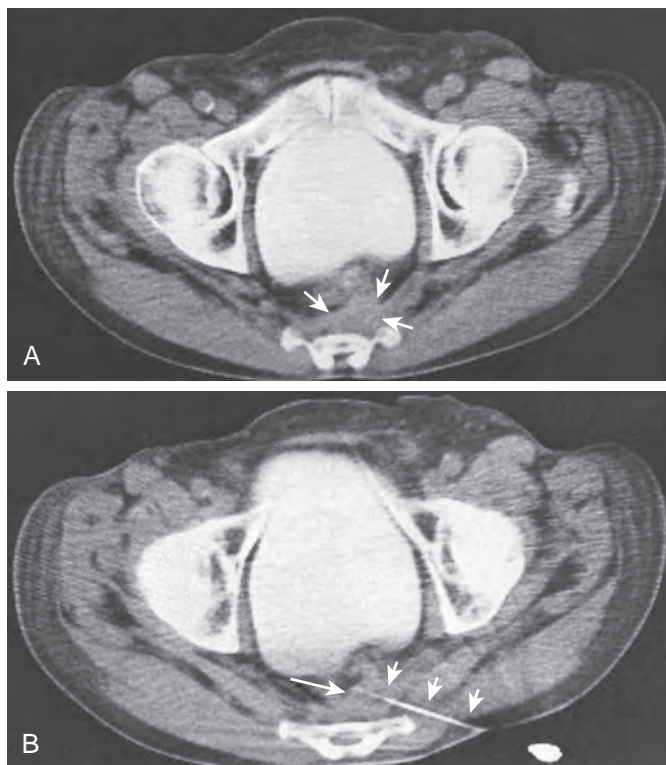


Figure 59-46 CT scan of recurrent rectal mass in patient after total abdominoperineal resection. **A.** Irregular soft tissue mass (arrows) is identified in the rectal bed. Size of mass has increased slightly compared with baseline CT study obtained 1 year before present examination. **B.** Percutaneous biopsy confirms presence of recurrent tumor. Short arrows outline the needle, with its tip in the mass of recurrent tumor (arrow).

distended with negative contrast material to detect subtle lesions.²¹¹ Glucagon helps the patient retain the rectal contrast medium but its administration is optional. More recently, comparison of contrast-enhanced CT with PET revealed CT sensitivities for local tumor recurrence that were lower than those for MRI and PET.^{205,217,218} However, results obtained with MDCT and thin sections in large series are not currently available for local tumor recurrence.

Colonoscopy and barium enemas provide exquisite mucosal detail but cannot assess extraluminal disease and remote metastases. Therefore, barium enema and CT are complementary radiologic methods for evaluating patients with suspected recurrent colon tumor. In patients with abdominoperineal resections, CT and MRI are the primary imaging tests for evaluating recurrent tumor (Fig. 59-47). Definition of the full extent of disease, particularly to distant sites, is necessary if another resection is contemplated.

Magnetic Resonance Imaging

MRI has slightly superior results to CT in detecting recurrent tumor in patients who have undergone a low anterior resection or transanal local excision.^{217,218} In some cases, large surgical clips slightly impair the quality of MRI scans, but CT scans may also be difficult to analyze when large clips are present at an anastomotic site or in an area of lymphadenectomy. After total resection of the rectum, presacral masses are readily detected and staged with MRI. Initial reports have suggested

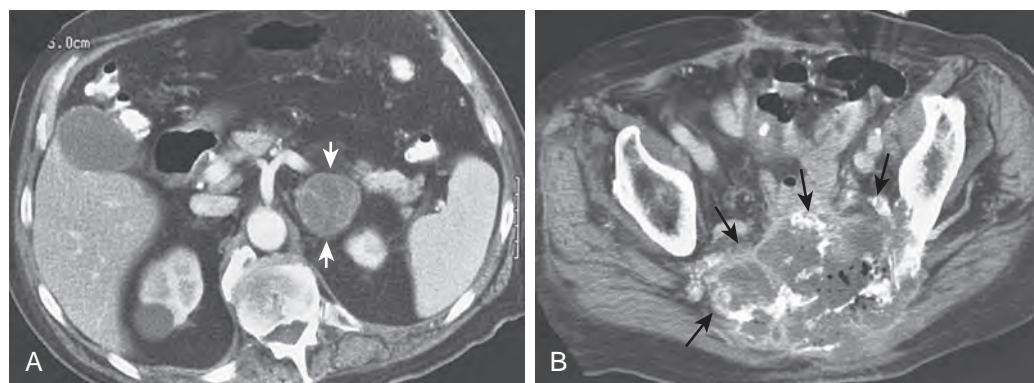


Figure 59-47 CT scan of recurrent rectal carcinoma with adrenal metastasis (T4bN1M1). **A.** Low-density mass (arrows) is seen in left adrenal gland. A cyst also is present in the right kidney. **B.** Large, irregular mass present in presacral space (arrows) with destruction of sacrum. Air bubbles within the mass indicate necrosis in the absence of clinical evidence of infection.

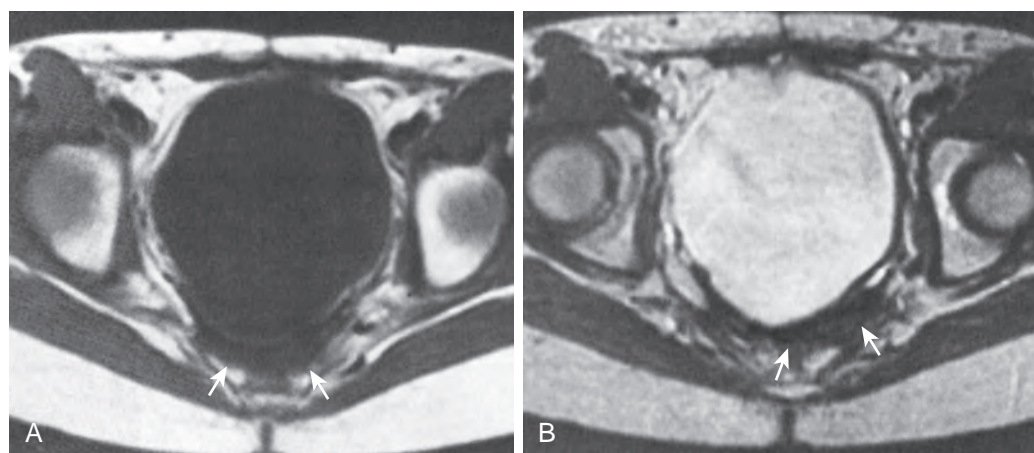


Figure 59-48 MRI of a postsurgical scar in patient with total colectomy. **A.** T1-weighted spin-echo image (600/11). Area posterior to the bladder has low signal intensity (arrows). **B.** T2-weighted spin-echo image (2500/80). Low signal intensity area on T1-weighted image remains dark (arrows) on T2-weighted scan, suggesting fibrosis in the surgical bed.

that postoperative and postradiation fibrosis have a low signal intensity on T1- and T2-weighted sequences (Fig. 59-48), whereas tumor recurrence has a high signal intensity on T2-weighted images.²¹⁹⁻²²³ However, it now appears doubtful that MRI cannot reliably distinguish among recurrent tumor, fibrosis, and inflammation (Figs. 59-48 and 59-49).^{224,225}

One study using T2-weighted sequences with long repetition and long echo times examined the value of MRI in distinguishing early fibrosis (1 to 6 months after first treatment), tumor or late fibrosis (>12 months), and recurrent tumor.²²⁶ The authors found higher signal intensity values for early fibrosis compared with late fibrosis, probably because of increased vascularity, edema, and the presence of immature mesenchymal cells in granulation tissue. Radiation-induced necrosis and postsurgical inflammatory reaction can also contribute to an increase in signal intensity on T2-weighted images. The increase in tissue fluids seen in granulation tissue and necrosis caused by radiation makes distinguishing early fibrosis from tumor recurrence difficult or even impossible (Fig. 59-50). However, late fibrosis and tumor recurrence could be clearly distinguished from one another (see Fig. 59-48).²²⁴ Other studies found similar results, but one showed that the accuracy of MRI in differentiating between radiation damage and residual or recurrent tumor varied with the primary site.^{100,222,225}

It was excellent for cervical carcinoma but suboptimal for rectal carcinoma.²²⁶

De Lange and colleagues²²⁷ compared MRI results with histologic sections from tissue obtained during radical pelvic exenteration or extensive partial resection of a mass in patients with suspected recurrent rectosigmoid carcinoma. They found that the signal intensities on T2-weighted images do not permit prediction of the histologic diagnosis of a lesion. High signal intensity was found in areas of viable tumor (Figs. 59-51 and 59-51C), tumor necrosis, benign inflammation, and edematous tissue (Fig. 59-52). Because a desmoplastic reaction is a common response to many benign and malignant processes, including tumors of the colon and rectum, areas of low signal intensity on T2-weighted images were also nonspecific, and the differential diagnosis included tumor-induced fibrosis and non-neoplastic, benign fibrotic tissue. However, MRI can reveal a presacral mass accurately and depict its complete extent. If such a mass consists mainly of desmoplastic tissue, with only small strands of interspersed tumor tissue, even a percutaneous biopsy specimen may show fibrous tissue alone and no malignant cells. In these cases, a definitive diagnosis may be made by PET, possibly with surgical removal of the mass or biopsy at laparotomy. It has been shown that if the mass enhances with gadolinium (>40%), it most likely represents tumor recurrence

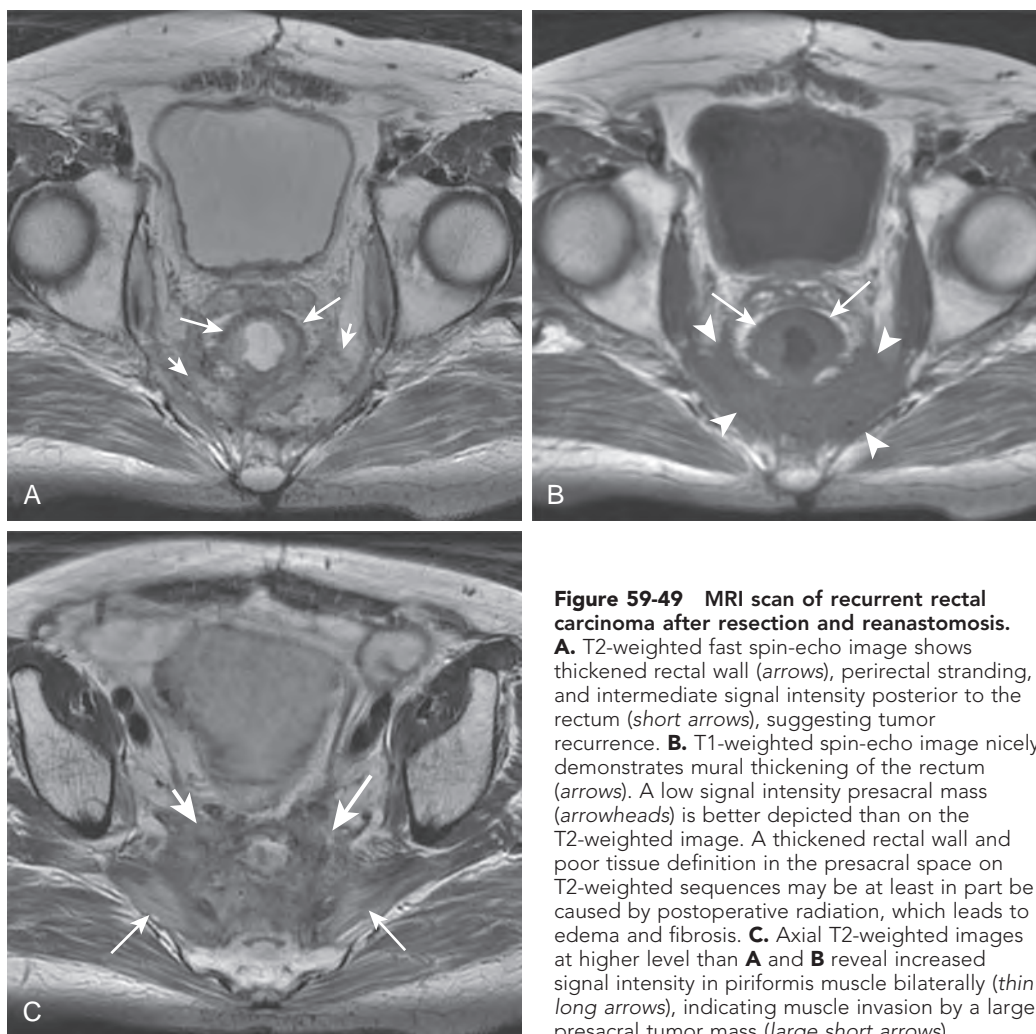


Figure 59-49 MRI scan of recurrent rectal carcinoma after resection and reanastomosis. **A.** T2-weighted fast spin-echo image shows thickened rectal wall (*arrows*), perirectal stranding, and intermediate signal intensity posterior to the rectum (*short arrows*), suggesting tumor recurrence. **B.** T1-weighted spin-echo image nicely demonstrates mural thickening of the rectum (*arrows*). A low signal intensity presacral mass (*arrowheads*) is better depicted than on the T2-weighted image. A thickened rectal wall and poor tissue definition in the presacral space on T2-weighted sequences may be at least in part be caused by postoperative radiation, which leads to edema and fibrosis. **C.** Axial T2-weighted images at higher level than **A** and **B** reveal increased signal intensity in piriformis muscle bilaterally (*thin long arrows*), indicating muscle invasion by a large presacral tumor mass (*large short arrows*).

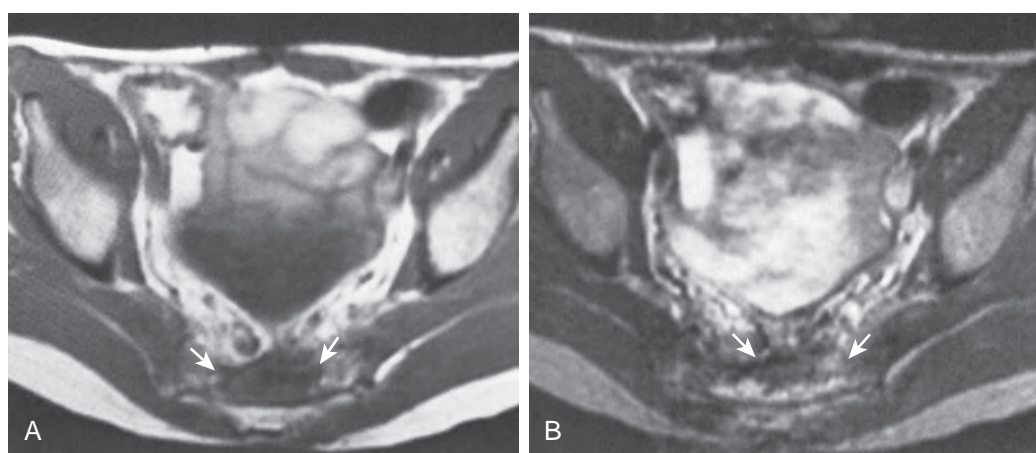


Figure 59-50 Indeterminate MRI scans of recurrent carcinoma after total colectomy. **A.** T1-weighted spin-echo image (700/20). An area of low signal intensity mixed with some intermediate signal intensity (*arrows*) is seen in the presacral space. **B.** T2-weighted spin-echo image (2500/70). The presacral soft tissue mass has intermediate signal intensity on T2-weighted scans (*arrows*). This is an indeterminate result and could represent recurrent viable tumor with a moderate amount of fibrous stroma, mild tumor necrosis, inflammation, or granulation tissue after surgery, irradiation, or both.

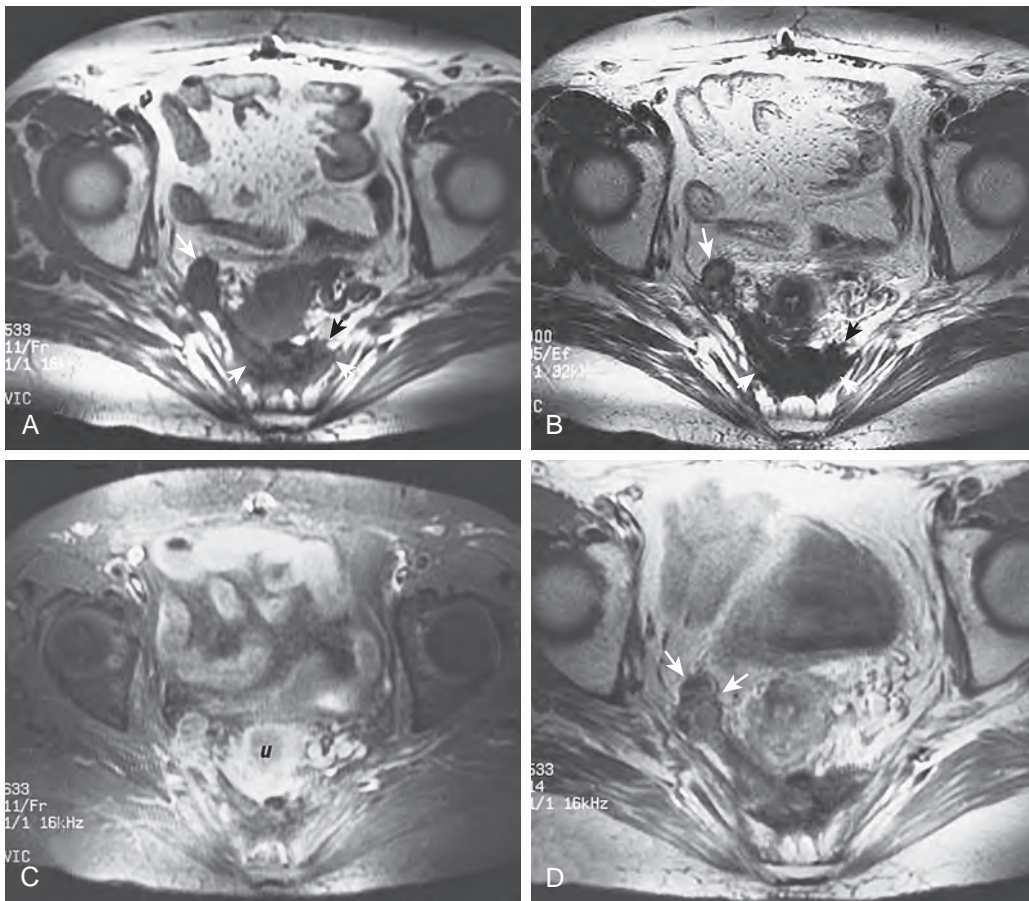


Figure 59-51 MRI scans of recurrent rectal carcinoma.
A. T1-weighted spin-echo image (533/11). An area of low signal intensity (black arrow) representing scar tissue is seen in presacral space. In addition, a slightly irregular, oval mass (white arrows) is seen immediately anterior to piriformis muscle, owing to recurrent tumor.
B. T2-weighted fast spin-echo image (4000/105). Scar tissue (black arrow) is clearly identified as an area of low signal intensity, and the recurrent tumor mass (white arrow) has intermediate signal intensity.
C. T1-weighted spin-echo image with fat suppression. Scar tissue remains largely dark, but the recurrent tumor and the uterus (u) demonstrate increased signal intensity.
D. T1-weighted spin-echo image after gadolinium (533/11). Enhancing recurrent mass is slightly larger 3 months later (arrows).

if the patient is at least 1 year postsurgery or irradiation.²²⁸ Nevertheless, published result with gadolinium enhancement are conflicting.^{217,229}

One MRI study demonstrated good distinction between scar tissue and recurrence based on measurements of the time-intensity curve and the ratio of signal intensity of the lesion to the signal intensity of the iliac artery at 60 seconds, but not for the maximum change in signal intensity as other studies have demonstrated.²²⁹ Whether an MR perfusion study can be used to distinguish between tumor recurrence and scar tissue remains to be seen. One study using MDCT with kinetic scanning and maximum density measurements did not show a significant difference between patients with and without tumor recurrence.²³⁰ However, CT perfusion studies in primary rectal tumors to assess response to chemotherapy and irradiation have shown promising results.^{231,232} In one prospective study, diffusion-weighted MRI with measurement of apparent diffusion coefficient (ADC) values was valuable in distinguishing between local recurrence of colorectal neoplasms and post-therapeutic soft tissue changes, except in mucinous adenocarcinomas, in which the high ADC values could be confused with benign lesions.²³³

MRI is a sensitive method for detecting masses after colorectal surgery, and its specificity is slightly higher than that of CT.²¹⁷ In these patients, benign and malignant processes cannot be distinguished solely on the basis of morphologic appearance and signal intensity on MRI scans. MDCT may be more helpful in evaluating anastomoses in patients with suture material or

multiple clips from lymphadenectomies because susceptibility artifacts may be problematic at a high magnetic field strength. MDCT may be more valuable than MRI for the detection of nonlocal recurrence, but more studies are needed to determine the efficacy of these procedures and their possibly complementary natures. Further technical advances may improve MRI results.

Transrectal Ultrasound

The findings and results of TRUS for recurrent colorectal malignancy are similar to those for primary carcinoma, but the examination can be done only for patients who have had a transanal local excision, low anterior resection or, in women, an abdominoperineal resection. In patients with total abdominoperineal resection and colostomy, the recurrent tumor should be assessed by CT, MR, PET, or scintigraphy with MoAb.

TRUS provides a highly accurate assessment of local recurrence. In one study, TRUS revealed all 15 recurrences of rectal neoplasm.²³⁴ In four cases, CEA titers were not elevated, and rectal or vaginal digital examination, rigid rectoscopy examination, and pelvic CT scans were negative. In these four patients, TRUS was the only method that detected recurrence. Therefore, endoluminal sonography should be used for evaluating patients when early or limited recurrence is suspected or the patients had a tumor grade or stage with a high prognostic factor for recurrence, even if the results of initial tests in routine follow-up examinations are negative.

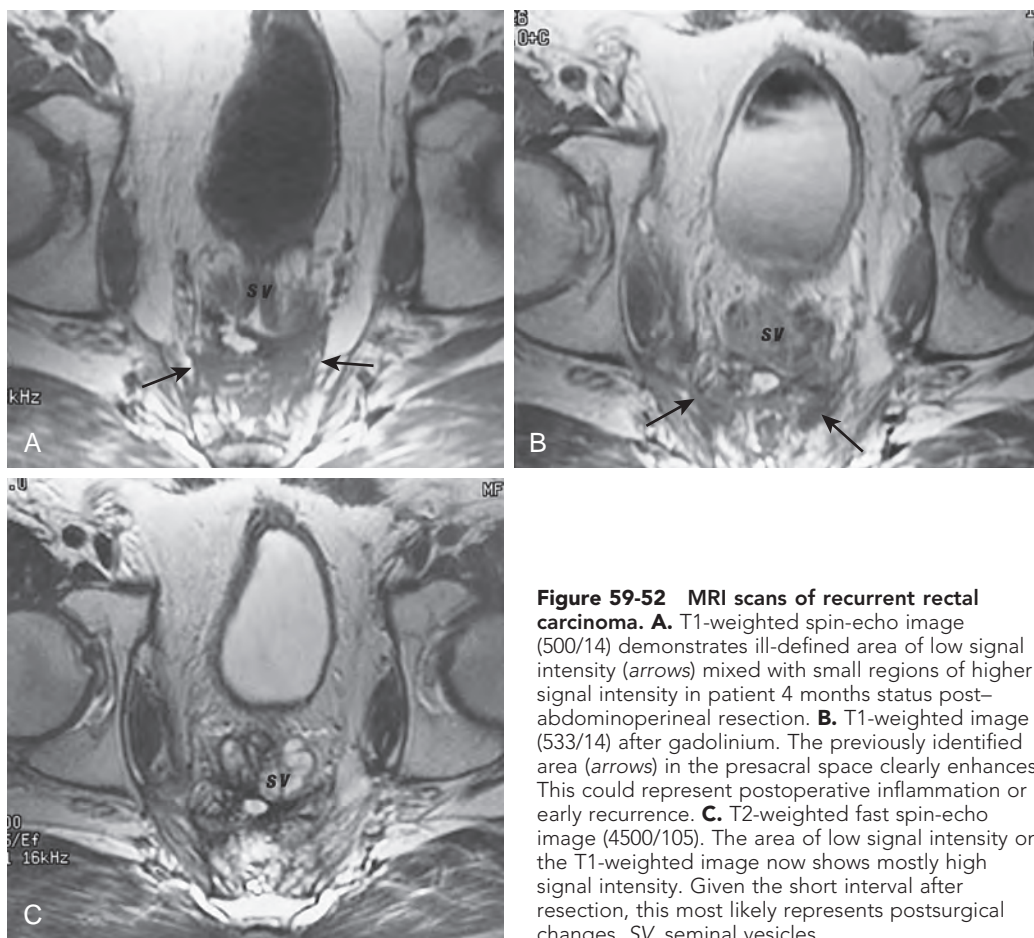


Figure 59-52 MRI scans of recurrent rectal carcinoma. **A.** T1-weighted spin-echo image (500/14) demonstrates ill-defined area of low signal intensity (arrows) mixed with small regions of higher signal intensity in patient 4 months status post-abdominoperineal resection. **B.** T1-weighted image (533/14) after gadolinium. The previously identified area (arrows) in the presacral space clearly enhances. This could represent postoperative inflammation or early recurrence. **C.** T2-weighted fast spin-echo image (4500/105). The area of low signal intensity on the T1-weighted image now shows mostly high signal intensity. Given the short interval after resection, this most likely represents postsurgical changes. SV, seminal vesicles.

Immunoscintigraphy

Most results of MoAb immunoscintigraphy have been for patients with primary colorectal tumors, and only studies of small numbers of patients with recurrent or residual tumor have been published.^{148-150,159} In one study using ¹¹¹In-labeled MoAb ZCE-025,¹⁵⁰ recurrences were found in 79.4% of 16 patients, and immunoscintigraphy was beneficial for their management (Fig. 59-53). Other immunoscintigraphic studies that focused on recurrent colorectal tumor showed similar sensitivities, with a high negative predictive value.^{150,159,235} One study compared the sensitivity and specificity of imaging with a ^{99m}Tc-labeled Fab fragment of anti-CEA IMMU-4 with that achieved with CT for detecting pelvic recurrence of colorectal tumor.²³⁶ The sensitivity and specificity for antibody scanning alone was 79% and 84% and improved to 83% and 81% when combined with CT, but did not reach statistical significance.

Positron Emission Tomography

PET has been used extensively for assessing patients with suspected recurrence or residual tumor from colorectal neoplasms. In several studies, the distinction between neoplasm and scar tissue was made with a high degree of accuracy, with lesion-to-soft tissue ratios of 1.19 to 4.94.¹⁶⁶ However,

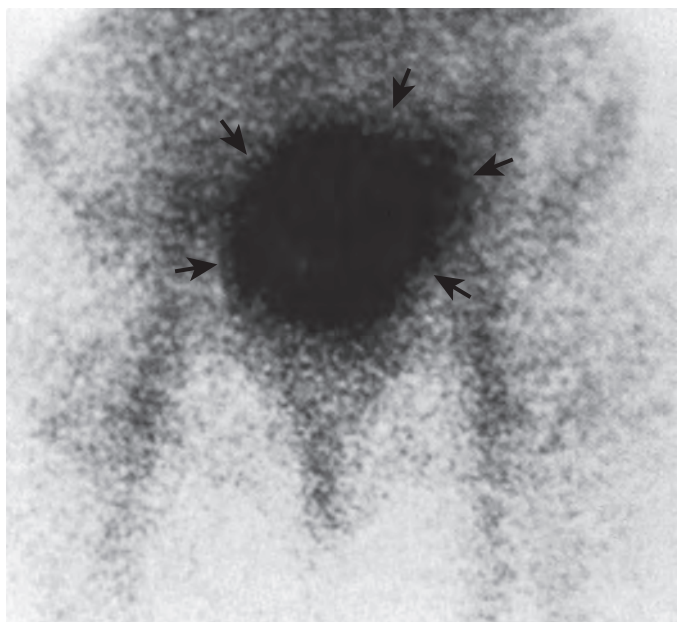


Figure 59-53 Immunoscintigraphy of recurrent rectal carcinoma. A large mass of high uptake (arrows) is seen in the pelvis of a patient with recurrent rectal tumor.

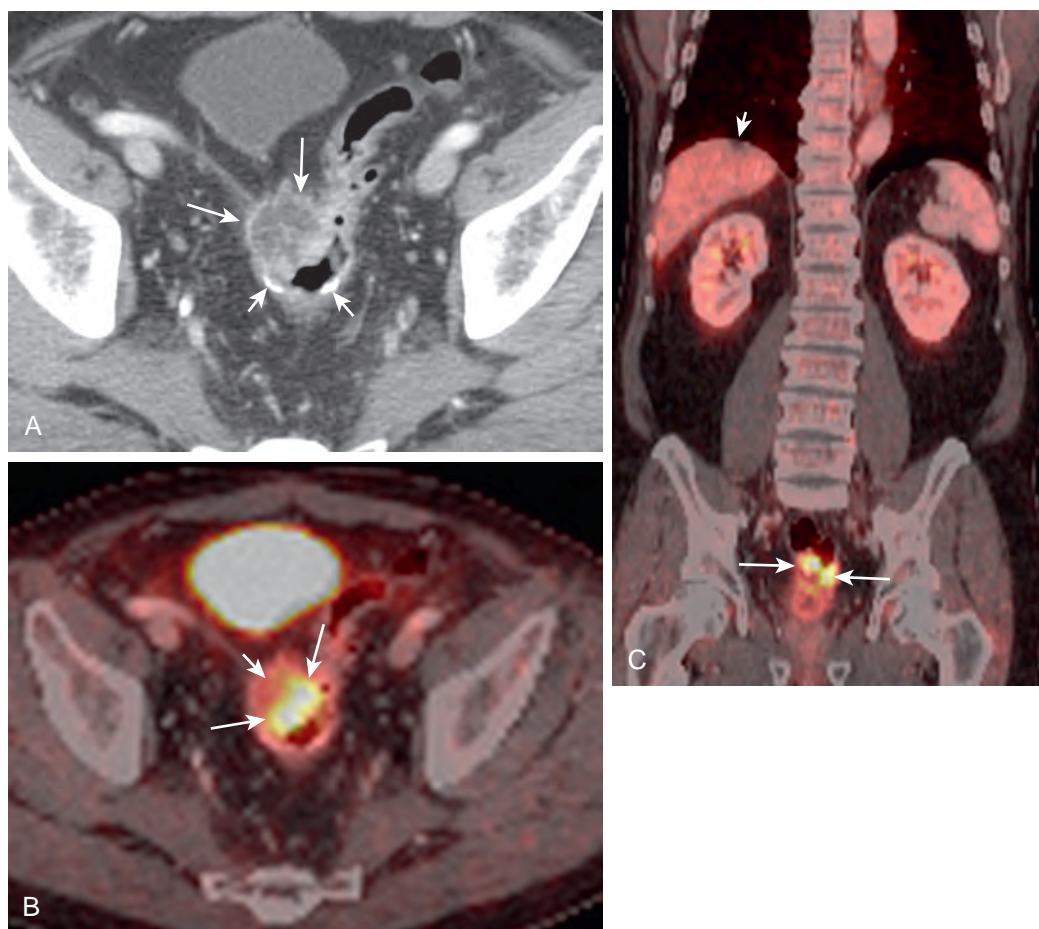


Figure 59-54 PET/CT scan of recurrence of tumor at the anastomosis in the rectosigmoid colon. This patient had undergone resection for sigmoid carcinoma and presents now with rising CEA levels. **A.** MDCT scan in the pelvis obtained in the axial plane demonstrates the partially necrotic recurrent tumor with a large extrinsic component (*large arrows*). The staple lines (*short arrows*) are also seen. **B.** The corresponding fusion image demonstrates markedly increased FDG uptake of the recurrent tumor at the anastomosis (*arrows*) but not in the necrotic component (*short arrow*). **C.** The coronal fusion image again demonstrates local recurrence (*long arrows*). A low-attenuation lesion seen on CT in the dome of the liver (*short arrow*) was not positive for a liver metastasis.

based on the FDG differential absorption ratio values, one patient was misclassified because of low FDG uptake. All scars in the pelvis after abdominoperineal resection were correctly identified. In another study, in five patients whose CT and PET results were similar, three recurrences and two scars were correctly identified.¹⁶⁷ In four patients with negative or equivocal CT scans, PET correctly identified all tumors and, in three patients whose CT scans raised suspicion of recurrence, PET correctly excluded recurrence. Other studies have confirmed these early results.²¹² PET appears to have an advantage over CT in the detection of recurrent hepatic metastases after partial hepatectomy, extrahepatic metastases, and local recurrence (see Fig. 59-54).²¹² In one study comparing PET alone to PET/CT, the sensitivity, specificity, and overall accuracy of PET in diagnosing intra-abdominal extrahepatic recurrence of colorectal cancer were 82%, 88%, and 86%, respectively, which was lower than 88%, 94%, and 92%, respectively, reported for PET/CT.²³⁷ It appears that PET/CT is an accurate method for detecting recurrent colorectal neoplasms (Fig. 59-55) and may offer an alternative to biopsy because it successfully excludes recurrence in patients with suspicious masses in the surgical bed. Nevertheless, larger series are needed to confirm these results.

Cross-Sectional Imaging in Recurrent Colorectal Carcinoma

Based on current literature, it is difficult to compare CT and MRI, used alone or in combination, for the detection of recurrent disease. This difficulty is mainly because of the great variations in both techniques and types of scanners used, scanning protocols, and methods of administering the contrast agent. Even the diagnostic criteria, study population, and analysis of the data vary greatly. Although MRI demonstrates excellent results for local tumor recurrence detection, especially if diffusion-weighted sequences were included, results of MRI combined with FDG-PET are not yet available. CT has the major advantage that the entire abdomen and pelvis can be scanned within a few seconds, much shorter than the acquisition time for an abdominal and pelvic MR study.

Based on currently available data, it appears that a combination of CT and PET would be most beneficial for imaging of possible recurrent colorectal tumor. CT should be performed with contrast enhancement. Any suspicious area on CT can thus be clarified by PET. If PET/CT is not available, CT or MRI combined with immunoscintigraphy could be helpful. All these imaging protocols should be accompanied with frequent

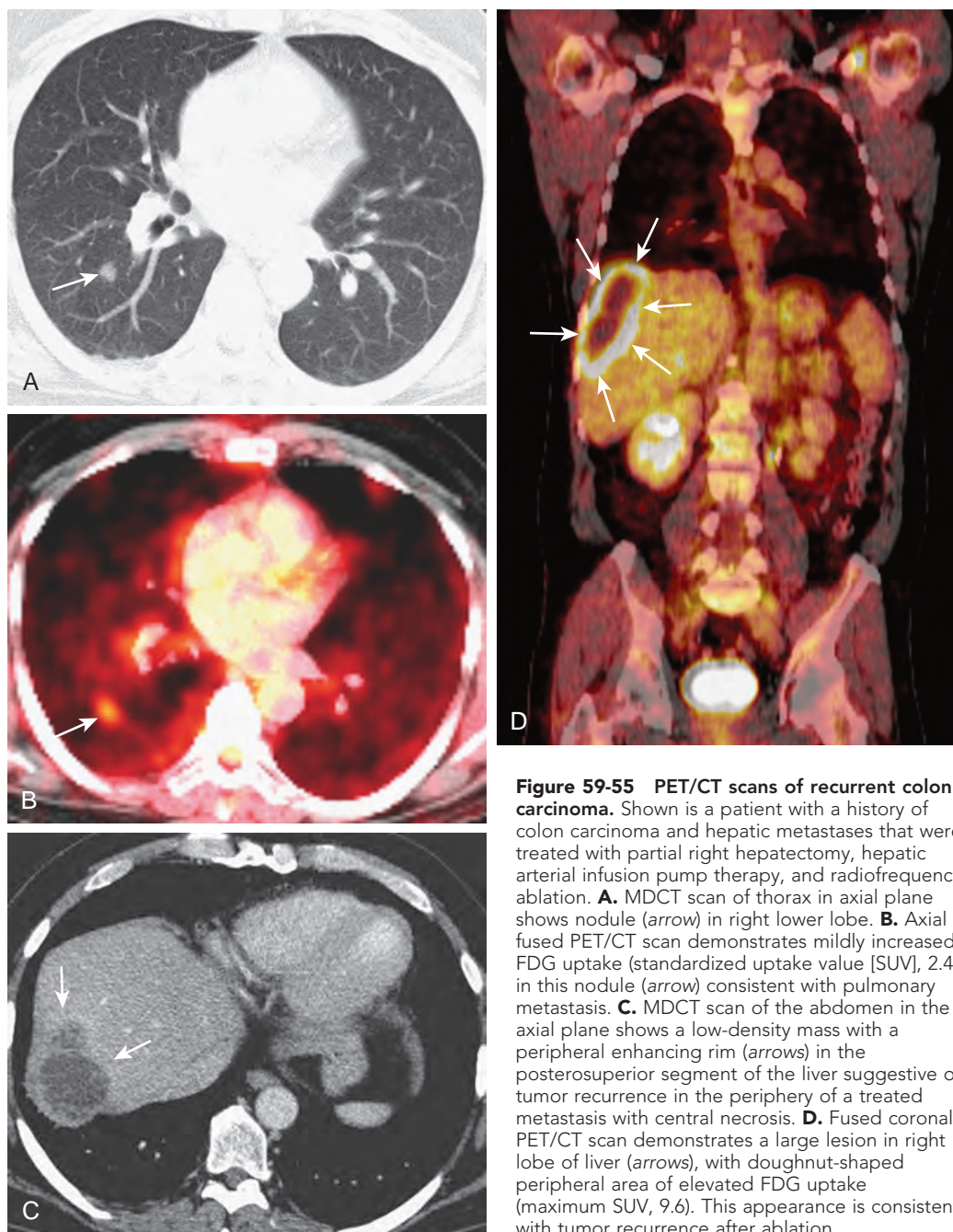


Figure 59-55 PET/CT scans of recurrent colon carcinoma. Shown is a patient with a history of colon carcinoma and hepatic metastases that were treated with partial right hepatectomy, hepatic arterial infusion pump therapy, and radiofrequency ablation. **A.** MDCT scan of thorax in axial plane shows nodule (arrow) in right lower lobe. **B.** Axial fused PET/CT scan demonstrates mildly increased FDG uptake (standardized uptake value [SUV], 2.4) in this nodule (arrow) consistent with pulmonary metastasis. **C.** MDCT scan of the abdomen in the axial plane shows a low-density mass with a peripheral enhancing rim (arrows) in the posterosuperior segment of the liver suggestive of tumor recurrence in the periphery of a treated metastasis with central necrosis. **D.** Fused coronal PET/CT scan demonstrates a large lesion in right lobe of liver (arrows), with doughnut-shaped peripheral area of elevated FDG uptake (maximum SUV, 9.6). This appearance is consistent with tumor recurrence after ablation.

clinical visits, laboratory tests (serum CEA levels), and colonoscopy, where feasible. In general, MRI is used in selected cases and is not recommended for routine follow-after curative resection for colorectal cancer.^{127,238,239}

Because of the high frequency of tumor recurrence in the first 24 to 36 months after surgery, a series of follow-up CT examinations at 6-month intervals should be obtained to detect early tumor recurrence.¹⁷³ In addition, a CT scan is indicated whenever a patient has a rising CEA titer or symptoms. Because local recurrence of cancer occurs in 50% of patients within the first year and in 80% within the second year,¹⁹² patients with suspected recurrence should have a baseline study 3 to 4 months after initial surgery. This time frame is chosen because

postsurgical acute changes, such as edema and hemorrhage, have substantially resolved. Follow-up examinations should be compared with those of the baseline study to avoid unnecessary biopsies. A study is considered positive if masses or nodes are detected that were not seen on the baseline study or have become larger since the original study. Biopsy specimens should be obtained of any new or enlarging mass or lymph nodes or confirmed with PET. Any clinical signs, elevated CEA levels, or suspicious CT or MRI findings should lead to a FDG-PET examination for further evaluation to ensure early detection of recurrence, with possible curative resection. If CT or MRI diagnoses resectable recurrence of colorectal tumor that is confirmed by PET, a biopsy should be avoided for fear of tumor seeding.

REFERENCES

1. Siegel R, Desantis CE, Jemal A: Colorectal cancer statistics, 2014. *CA Cancer J Clin* 64: 104–117, 2014.
2. Du XL, Meyer TE, Franzini L: Meta-analysis of racial disparities in survival in association with socioeconomic status among men and women with colon cancer. *Cancer* 109:2161–2170, 2007.
3. Ananthkrishnan AN, Schellhase KG, Sparapani RA, et al: Disparities in colon cancer screening in the Medicare population. *Arch Intern Med* 167:258–264, 2007.
4. Bond JH: Colonic tumors. *Endoscopy* 30:150–157, 1998.
5. Bond JH: Adenomatous polyps and adenocarcinoma of the colon. In DiMarino AJ, Benjamin SB, editors: *Gastrointestinal Disease: An Endoscopic Approach*, Oxford, England, 1998, Blackwell Scientific, pp 610–624.
6. Fisher JA, Fikry C, Troxel AB: Cutting cost and increasing access to colorectal cancer screening: Another approach to following the guidelines. *Cancer Epidemiol Biomarkers Prev* 15:108–113, 2006.
7. Nelson RL, Dollear T, Freels S, et al: The relation of age, race, and gender to the subsite location of colorectal carcinoma. *Gut* 80:193–197, 1997.
8. Calle EE, Rodriguez C, Walker-Thurmond K, Thun MJ: Overweight, obesity, and mortality from cancer in a prospectively studied cohort of US adults. *N Engl J Med* 348:1625–1638, 2003.
9. Lagerstedt Robinson K, Liu T, Vandrovicova J, et al: Lynch syndrome (hereditary nonpolyposis colorectal cancer) diagnostics. *J Natl Cancer Inst* 21:291–299, 2007.
10. Vogelstein B: A model of colorectal tumorigenesis. *Adv Oncol* 7:2–6, 1991.
11. Joyce T, Pintzas A: Microarray analysis to reveal genes involved in colon carcinogenesis. *Expert Opin Pharmacother* 8:895–900, 2007.
12. Yuan Y, Han HJ, Zheng S, et al: Germline mutations of hMLH1 and hMSH2 genes in patients with suspected hereditary nonpolyposis colorectal cancer and sporadic early-onset colorectal cancer. *Dis Colon Rectum* 41:434–440, 1998.
13. Solomon MJ, Schnitzler M: Cancer and inflammatory bowel disease: Bias, epidemiology, surveillance, and treatment. *World J Surg* 22: 352–358, 1998.
14. Bansal P, Sonnenberg A: Risk factors of colorectal cancer in inflammatory bowel disease. *Am J Gastroenterol* 91:44–48, 1996.
15. Svrcek M, Cosnes J, Beaugerie L, et al: Colorectal neoplasia in Crohn's colitis: A retrospective comparative study with ulcerative colitis. *Histopathology* 50:574–583, 2007.
16. Chen CD, Yen MF, Wang WM, et al: A case-cohort study for the disease natural history of adenoma-carcinoma and de novo carcinoma and surveillance of colon and rectum after polypectomy: Implication for efficacy of colonoscopy. *Br J Cancer* 88:1866–1873, 2003.
17. Winawer SJ, Zaubler AG, O'Brien MJ, et al: The national polyp study: Design, methods, and characteristics of patients with newly diagnosed polyps. *Cancer* 70:1236–1245, 1992.
18. Thomas T, Abrams KA, Robinson RJ, et al: Meta-analysis: Cancer risk of low-grade dysplasia in chronic ulcerative colitis. *Aliment Pharmacol Ther* 15:657–668, 2007.
19. Smith RA, Cokkinides V, Durado B, et al: Cancer screening in the United States, 2010: A review of current American Cancer Society guidelines and issues in cancer screening. *CA Cancer J Clin* 60:99–119, 2010.
20. Levin B, Lieberman DA, McFarland B, et al; American Cancer Society Colorectal Cancer Advisory Group; U.S. Multi-Society Task Force; American College of Radiology Colon Cancer Committee: Screening and surveillance for the early detection of colorectal cancer and adenomatous polyps, 2008: A joint guideline from the American Cancer Society, the U.S. Multi-Society Task Force on Colorectal Cancer, and the American College of Radiology. *Gastroenterology* 134:1570–1595, 2008.
21. Eddy DM, Nugent FW, Eddy JF, et al: Screening for colorectal cancer in a high-risk population. *Gastroenterology* 92:682–692, 1987.
22. Glick S, Wagner JL, Johnson CD: Cost-effectiveness of double-contrast barium enema in screening for colorectal cancer. *AJR* 170: 629–636, 1998.
23. Knudsen AB, Lansdorp-Vogelaar I, Rutter CM, et al: Cost-effectiveness of computed tomographic colonography screening for colorectal cancer in the Medicare population. *J Natl Cancer Inst* 102:1238–1252, 2010.
24. Pickhardt PJ: Computed tomography colonography: Emerging evidence to further support clinical effectiveness. *Curr Opin Gastroenterol* 29:55–59, 2013.
25. Yee J, Keysor KJ, Kim DH: The time has arrived for national reimbursement of screening CT colonography. *AJR Am J Roentgenol* 201:73–79, 2013.
26. Thoeni RF: Colorectal cancer: Radiological staging. *Radiol Clin North Am* 35:457–458, 1997.
27. Low RN, McCue M, Barone R, et al: MR staging of primary colorectal carcinoma: Comparison with surgical and histopathologic findings. *Abdom Imaging* 28:784–793, 2003.
28. Fuchsjager MH, Maier AG, Schima W, et al: Comparison of transrectal sonography and double-contrast MR imaging when staging rectal cancer. *AJR* 181:421–427, 2003.
29. Chen YK, Kao CH, Liao AC, et al: Colorectal cancer screening in asymptomatic adults: The role of FDG PET scan. *Anticancer Res* 23:4357–4361, 2003.
30. Levine MS, Laufer I: Rectum. In Laufer I, Levine MS, editors: *Double Contrast Gastrointestinal Radiology*, ed 2, Philadelphia, 1992, WB Saunders, pp 647–686.
31. Ott DJ, Chen YM, Gelfand DW, et al: Single-contrast vs. double-contrast barium enema in the detection of colonic polyps. *AJR* 146:993–996, 1986.
32. Fork FT, Lindstrom C, Ekelund GR: Reliability of routine double-contrast examination (DCE) of the large bowel in polyp detection: A prospective clinical study. *Gastrointest Radiol* 8:163–172, 1983.
33. Anderson ML, Heigh RI, McCoy GA, et al: Accuracy of assessment of the extent of examination by experienced colonoscopists. *Gastrointest Endosc* 38:560–563, 1992.
34. Robertson DJ, Lieberman DA, Winawer SJ, et al: Colorectal cancers soon after colonoscopy: A pooled multicohort analysis. *Gut* 63:949–956, 2014.
35. Rockey DC, Koch J, Yee J, et al: Prospective comparison of air-contrast barium enema and colonoscopy in patients with fecal occult blood: A pilot study. *Gastrointest Endosc* 60: 953–958, 2004.
36. Le Clercq CM, Bouwens MW, Rondagh EJ, et al: Postcolonoscopy colorectal cancers are preventable: A population-based study. *Gut* 63:957–963, 2014.
37. Law RL, Longstaff AJ, Slack N: A retrospective 5-year study on the accuracy of the barium enema examination performed by radiographers. *Clin Radiol* 54:80–83, 1999.
38. Rex DK, Rahmani EY, Haseman JH, et al: Relative sensitivity of colonoscopy and barium enema for detection of colorectal cancer in clinical practice. *Gastroenterology* 11:17–23, 1997.
39. Burling D, Halligan S, Atchley J, et al: CT colonography: Interpretative performance in a non-academic environment. *Clin Radiol* 62: 424–429, 2007.
40. Ng CS, Doyle TC, Courtney HM, et al: Extracolonic findings in patients undergoing abdominopelvic CT for suspected colorectal carcinoma in the frail and disabled patient. *Clin Radiol* 59:421–430, 2004.
41. Dighe S, Purkayastha S, Swift I, et al: Diagnostic precision of CT in local staging of colon cancers: A meta-analysis. *Clin Radiol* 65:708–719, 2010.
42. Bipat S, Glas AS, Slors FJ, et al: Rectal cancer: Local staging and assessment of lymph node involvement with endoluminal US, CT, and MR imaging—a meta-analysis. *Radiology* 232:773–783, 2004.
43. Halefoglu AM, Atasoy ST, Sakiz D, et al: Accuracy of thin-section magnetic resonance imaging with a pelvic phased-array coil in the local staging of rectal cancer. *J Comput Assist Tomogr* 37:58–64, 2013.
44. Murcia Duréndez MJ, Frutos Esteban L, Luján J, et al: The value of 18F-FDG PET/CT for assessing the response to neoadjuvant therapy in locally advanced rectal cancer. *Eur J Nucl Med Mol Imaging* 40:91–97, 2013.
45. Agnese DM, Abdessalam SF, Burak WE, Jr, et al: Pilot study using a humanized CC49 monoclonal antibody (HuCC49DeltaCH2) to localize recurrent colorectal carcinoma. *Ann Surg Oncol* 11:197–202, 2004.
46. Huh JW, Min JJ, Lee JH, et al: The predictive role of sequential FDG-PET/CT in response of locally advanced rectal cancer to neoadjuvant chemoradiation. *Am J Clin Oncol* 35:340–344, 2012.
47. Even-Sapir E, Parag Y, Lerman H, et al: Detection of recurrence in patients with rectal cancer: PET/CT after abdominoperineal or anterior resection. *Radiology* 232:815–822, 2004.
48. Gupta S, Balasubramanian BA, Fu T, et al: Polyps with advanced neoplasia are smaller in the right than in the left colon: Implications for colorectal cancer screening. *Clin Gastroenterol Hepatol* 10:1395–1401, 2012.
49. Qumseya BJ, Coe S, Wallace MB: The effect of polyp location and patient gender on the presence of dysplasia in colonic polyps. *Clin Transl Gastroenterol* 3:e20, 2012.
50. Rubesin SE, Levine MS, Laufer I, et al: Villous adenomas: The scientific and the practical. *Radiology* 167:869–870, 1988.
51. Iida M, Iwashita A, Yao T, et al: Villous tumor of the colon: Correlation of histologic, macroscopic, and radiographic features. *Radiology* 167:673–677, 1988.

52. Delamarre J, Descombes P, Marti R, et al: Villous tumor of the colon: Double-contrast study of 47 cases. *Gastrointest Radiol* 5:69–73, 1980.
53. Miller WT, Jr, Levine MS, Rubesin SE, et al: Bowler hat sign: A simple principle for differentiating polyps from diverticula. *Radiology* 173:615–617, 1989.
54. Levine MS, Barnes MJ, Bronner MP, et al: Atypical hyperplastic polyps at double-contrast barium enema examination. *Radiology* 175:691–694, 1990.
55. Rubesin SE, Sul SH, Laufer I, et al: Carpet lesions of the colon. *Radiographics* 5:537–552, 1985.
56. Kim DH, Pickhardt PJ, Taylor AJ: Characteristics of advanced adenomas detected at CT colonographic screening: Implications for appropriate polyp size thresholds for polypectomy versus surveillance. *AJR* 188:940–944, 2007.
57. Pikarsky A, Wexner S, Lebansart P, et al: The use of rectal ultrasound for the correct diagnosis and treatment of rectal villous tumors. *Am J Surg* 179:261–265, 2000.
58. Kolligs FT, Crispin A, Graser A, et al: Risk factors for advanced neoplasia within subcentimetric polyps: Implications for diagnostic imaging. *Gut* 62:863–870, 2013.
59. Muto T, Bussey HJR, Morson BC: The evolution of cancer of the colon and rectum. *Cancer* 36:2251–2270, 1975.
60. Welin S, Youker J, Spratt JS, Jr: The rates and patterns of growth of 375 tumors of the large intestine and rectum observed serially by double contrast enema study (Malmo technique). *AJR* 90:673–687, 1963.
61. Smith TR: Pedunculated malignant colonic polyps with superficial invasion of the stalk. *Radiology* 115:593–596, 1975.
62. Levine MS, Rubesin SE, Laufer I, et al: Diagnosis of colorectal neoplasms at double-contrast barium enema examination. *Radiology* 216:11–18, 2000.
63. McCarthy PA, Rubesin SE, Levine MS, et al: Colon cancer: Morphology detected by barium enema examination versus histopathologic stage. *Radiology* 197:683–687, 1995.
64. Fischel RE, Dermer R: Multifocal carcinoma of the large intestine. *Clin Radiol* 26:495–498, 1975.
65. Chong A, Shah JN, Levine MS, et al: The diagnostic yield of barium enema examination after incomplete colonoscopy. *Radiology* 223:620–624, 2002.
66. Gazelle GS, McMahon PM, Scholz FJ: Screening for colorectal cancer. *Radiology* 215:327–335, 2000.
67. Raskin MM, Viamonte M, Viamonte M, Jr: Primary linitis plastica carcinoma of the colon. *Radiology* 113:17–22, 1974.
68. Laufer I, Joffe N: Some roentgenologic aspects of chronic perforating carcinoma of the colon. *Dis Colon Rectum* 16:127–135, 1973.
69. Kulinna C, Eibel R, Matzek W, et al: Staging of rectal cancer: Diagnostic potential of multiplanar reconstructions with MDCT. *AJR* 183:421–427, 2004.
70. Yee J, Thoeni RF, Gorcezyka DP, et al: Value of contrast-enhanced MRI for TNM staging of regional disease in primary and recurrent rectal and rectosigmoid tumors. *AJR* 162:66, 1994.
71. Nougaret S, Reinhold C, Mikhael HW, et al: The use of MR imaging in treatment planning for patients with rectal carcinoma: Have you checked the “DISTANCE”? *Radiology* 268:330–344, 2013.
72. Fong Y, Kemeny N, Paty P, et al: Treatment of colorectal cancer: Hepatic metastases. *Semin Surg Oncol* 12:219–252, 1996.
73. Zhang S, Gao F, Luo J, Yang J: Prognostic factors in survival of colorectal cancer patients with synchronous liver metastasis. *Colorectal Dis* 12:754–761, 2010.
74. Low SC, Lo RH, Lau TN, et al: Image-guided radiofrequency ablation of liver malignancies: Experience at Singapore General Hospital. *Ann Acad Med Singapore* 35:851–857, 2006.
75. Thoeni RF, Bangard C, Heller DND, et al: Dynamic CT versus MRI versus CTAP for diagnosing colorectal metastases: A cost comparison analysis. *AJR* 170:9, 1998.
76. Valls C, Lopez E, Guma A, et al: Helical CT versus CT arterial portography in the detection of hepatic metastasis of colorectal carcinoma. *AJR* 170:1341–1347, 1998.
77. Onishi H, Murakami T, Kim T, et al: Hepatic metastases: Detection with multi-detector row CT, SPIO-enhanced MR imaging, and both techniques combined. *Radiology* 239:131–138, 2006.
78. Semelka RC, Cance WG, Marcos HB, et al: Liver metastases: Comparison of current MR techniques and spiral CT during arterial portography for detection in 20 surgically staged cases. *Radiology* 213:86–91, 1999.
79. Kim YK, Ko SW, Hwang SB, et al: Detection and characterization of liver metastases: 16-slice multidetector computed tomography versus super-paramagnetic iron oxide-enhanced magnetic resonance imaging. *Eur Radiol* 16:1337–1345, 2006.
80. Kim YK, Park G, Kim CS, et al: Diagnostic efficacy of gadoteric acid-enhanced MRI for the detection and characterisation of liver metastases: Comparison with multidetector-row CT. *Br J Radiol* 85:539–547, 2012.
81. Farouk R, Nelson H, Radice E, et al: Accuracy of computed tomography in determining resectability for locally and advanced primary or recurrent colorectal cancers. *Am J Surg* 175:283–287, 1998.
82. Chintapalli KN, Esola CC, Chopra S, et al: Pericolic mesenteric lymph nodes: An aid in distinguishing diverticulitis from cancer of the colon. *AJR* 169:1253–1255, 1997.
83. Goh V, Halligan S, Taylor SA, et al: Differentiation between diverticulitis and colorectal cancer: Quantitative CT perfusion measurements versus morphologic criteria—initial experience. *Radiology* 242:456–462, 2007.
84. Scharling ES, Wolfman NT, Bechtold RE: Computed tomography evaluation of colorectal carcinoma. *Semin Roentgenol* 31:125–141, 1996.
85. Sinha R, Verma R, Rajesh A, et al: Diagnostic value of multidetector row CT in rectal cancer staging: Comparison of multiplanar and axial images with histopathology. *Clin Radiol* 61:924–931, 2006.
86. Frommhold W, Hubener KH: The role of computerized tomography in the aftercare of patients suffering from a carcinoma of the rectum. *Comput Tomogr* 5:161–168, 1981.
87. Lee JKT, Stanley RJ, Sagel SS, et al: CT appearance of the pelvis after abdominoperineal resection for rectal carcinoma. *Radiology* 141:737–741, 1981.
88. Doubleday LC, Bernardino ME: CT findings in the perirectal area following radiation therapy. *J Comput Assist Tomogr* 4:634–638, 1980.
89. Colley DP, Farrell JA, Clark RA: Perforated colon carcinoma presenting as a suprarenal mass. *J Comput Assist Tomogr* 5:55–58, 1981.
90. Dukes CE: The classification of cancer of the rectum. *J Pathol* 35:323–332, 1932.
91. Astler VB, Coller FA: The prognostic significance of direct extension of carcinoma of the colon and rectum. *Ann Surg* 139:846–851, 1954.
92. Turnbull RB, Jr: The no-touch isolation technique of resection. *JAMA* 231:1181–1182, 1975.
93. Thoeni RF, Moss AA, Schnyder P, et al: Detection and staging of primary rectal and rectosigmoid cancer by computed tomography. *Radiology* 141:135–138, 1981.
94. Compton CC, Fielding LP, Burgart LJ, et al: Prognostic factors in colorectal cancer. College of American Pathologists Consensus Statement 1999. *Arch Pathol Lab Med* 124:979–994, 2000.
95. Dixon AK, Fry IK, Morson BC, et al: Preoperative computed tomography of carcinoma of the rectum. *Br J Radiol* 54:655–659, 1981.
96. Grabbe E, Lierse W, Winkler R: The perirectal fascia: Morphology and use in staging of rectal carcinoma. *Radiology* 149:241–246, 1983.
97. Van Waes PF, Koehler PR, Feldberg MA: Management of rectal carcinoma: Impact of computed tomography. *AJR* 140:1137–1142, 1983.
98. Balthazar EJ, Megibow AJ, Hynick D, et al: Carcinoma of the colon: Detection and preoperative staging by CT. *AJR* 150:301–306, 1988.
99. Kinkel K, Lu Y, Both M, et al: Detection of hepatic metastases from cancers of the gastrointestinal tract by using noninvasive imaging methods (US, CT, MR imaging, PET): A meta-analysis. *Radiology* 224:748–756, 2002.
100. Megibow AJ, Zerhouni EA, Hynick DH, et al: Air insufflation of the colon as an adjunct to computed tomography of the pelvis. *J Comput Assist Tomogr* 8:797–800, 1984.
101. Gazelle GS, Saini S, Shellito P: Staging of colon carcinoma using water enemas CT. *J Comput Assist Tomogr* 19:87–91, 1995.
102. Hundt W, Braunschweig R, Reiser M: Evaluation of spiral CT in staging of colon and rectum carcinoma. *Eur J Radiol* 9:78–84, 1999.
103. Chiesura-Corona M, Muzzio PC, Giust G, et al: Rectal cancer: CT local staging with histopathologic correlation. *Abdom Imaging* 26:134–138, 2001.
104. Wieder HA, Rosenberg R, Lordick F, et al: Rectal cancer: MR imaging before neoadjuvant chemotherapy and radiation therapy for prediction of tumor-free circumferential resection margins and long-term survival. *Radiology* 243:744–751, 2007.
105. Butch RJ, Stark DD, Wittenberg J, et al: Staging rectal cancer by MR and CT. *AJR* 146:1155–1160, 1986.
106. Beets-Tan RG, Beets GL, Vliegen RF, et al: Accuracy of magnetic resonance imaging in prediction of tumour-free resection margin in rectal cancer surgery. *Lancet* 357:497–504, 2001.
107. Brown G, Kirkham A, Williams GT, et al: High-resolution MRI of the anatomy important in total mesorectal excision of the rectum. *AJR* 182:431–439, 2004.
108. Blomqvist I, Rubio C, Holm T, et al: Rectal adenocarcinoma: Assessment of the lateral resection margin by MRI of resected specimens. *Br J Radiol* 72:18–23, 1999.
109. Bissett IP, Fernando CC, Hough DM, et al: Identification of the fascia propria by magnetic

- resonance imaging and its relevance to preoperative assessment of rectal cancer. *Dis Colon Rectum* 44:259–265, 2001.
110. Brown G, Radcliffe AG, Newcombe RG, et al: Preoperative assessment of prognostic factors in rectal cancer using high-resolution magnetic resonance imaging. *Br J Surg* 90:355–364, 2003.
 111. Heald RJ, Ryall RD: Recurrence and survival after total mesorectal excision for rectal cancer. *Lancet* 1:1479–1482, 1986.
 112. Akasu T, Iinuma G, Fujita T, et al: Thin-section MRI with a phased-array coil for preoperative evaluation of pelvic anatomy and tumor extent in patients with rectal cancer. *AJR* 184:531–538, 2005.
 113. MERCURY Study Group: Extramural depth of tumor invasion at thin-section MR in patients with rectal cancer: Results of the MERCURY study. *Radiology* 243:132–139, 2007.
 114. Beets-Tan RG, Beets GL: Rectal cancer: Review with emphasis on MR imaging. *Radiology* 232:335–346, 2004.
 115. Taylor FG, Quirke P, Heald RJ, et al: MERCURY study group: One millimetre is the safe cut-off for magnetic resonance imaging prediction of surgical margin status in rectal cancer. *Br J Surg* 98:872–879, 2011.
 116. Kaur H, Choi H, You YN, et al: MR imaging for preoperative evaluation of primary rectal cancer: Practical considerations. *Radiographics* 32:389–409, 2012.
 117. Brown G, Richards CJ, Bourne MW, et al: Morphologic predictors of lymph node status in rectal cancer with use of high-spatial resolution MR imaging with histopathologic comparison. *Radiology* 227:371–377, 2003.
 118. Birnbaum BA, Weinreb JC, Fernandez MP, et al: Comparison of contrast enhanced CT and Mn-DPDP enhanced MRI for detection of focal hepatic lesions: Initial findings. *Clin Imaging* 18:21–27, 1994.
 119. Schwartz LH, Seltzer SE, Tempny CM, et al: Superparamagnetic iron oxide hepatic MR imaging: Efficacy and safety using conventional and fast spin-echo pulse sequences. *J Magn Reson Imaging* 5:566–570, 1995.
 120. Nickel MC, Bipat S, Stoker J: Diagnostic imaging of colorectal liver metastases with CT, MR imaging, FDG PET, and/or FDG PET/CT: A meta-analysis of prospective studies including patients who have not previously undergone treatment. *Radiology* 257:674–684, 2010.
 121. Improved survival with preoperative radiotherapy in resectable rectal cancer. Swedish Rectal Cancer Trial. *N Engl J Med* 336:980–987, 1997.
 122. Gualdi GF, Casciani E, Guadalajara A, et al: Local staging of rectal cancer with transrectal ultrasound and endorectal magnetic resonance imaging: Comparison with histologic findings. *Dis Colon Rectum* 43:338–345, 2000.
 123. Zagoria RJ, Schlarb CA, Ott DJ, et al: Assessment of rectal tumor infiltration utilizing endorectal MR imaging and comparison with endoscopic rectal sonography. *J Surg Oncol* 64:312–317, 1997.
 124. Maldjian C, Smith R, Kilger A, et al: Endorectal surface coil MR imaging as a staging technique for rectal carcinoma: A comparison study to rectal endosonography. *Abdom Imaging* 25:75–80, 2000.
 125. Schnall MD, Furth EE, Rosato EF, et al: Rectal tumor stage: Correlation of endorectal MR imaging and pathologic findings. *Radiology* 190:709–714, 1994.
 126. Beets-Tan RG, Beets GL, Borstlap AC, et al: Preoperative assessment of local tumor extent in advanced rectal cancer: CT or high-resolution MRI? *Abdom Imaging* 25:533–541, 2000.
 127. Low RN, Barone RM, Lacey C, et al: Peritoneal tumor: MR imaging with dilute oral barium and intravenous gadolinium-containing contrast agents compared with unenhanced MR imaging and CT. *Radiology* 204:513–520, 1997.
 128. Vliegen RF, Beets GL, von Meyenfeldt MF, et al: Rectal cancer: MR imaging in local staging—is gadolinium-based contrast material helpful? *Radiology* 234:179–188, 2005.
 129. Chang GJ, Rodriguez-Bigas MA, Skibber JM, Moyer VA: Lymph node evaluation and survival after curative resection of colon cancer: Systematic review. *J Natl Cancer Inst* 21:433–441, 2007.
 130. de Lange EE, Gechnier RE, Edge SB, et al: Preoperative staging of rectal carcinoma with MR imaging: Surgical and histopathologic correlation. *Radiology* 176:623–628, 1990.
 131. Harisinghani MG, Saini S, Slater GJ, et al: MR imaging of pelvic lymph nodes in primary pelvic carcinoma with ultrasmall superparamagnetic iron oxide (Combidex): Preliminary observations. *J Magn Reson Imaging* 7:161–163, 1997.
 132. Koh DM, Brown G, Temple L, et al: Rectal cancer: Mesorectal lymph nodes at MR imaging with USPIO versus histopathologic findings—initial observations. *Radiology* 231:91–99, 2004.
 133. Kim S, Lim HK, Lee SJ, et al: Depiction and local staging of rectal tumors: Comparison of transrectal US before and after water installation. *Radiology* 231:117–122, 2004.
 134. Fuchsjäger MH, Maier AG, Schima W, et al: Comparison of transrectal sonography and double-contrast MR imaging when staging rectal cancer. *AJR* 181:421–427, 2003.
 135. Sasaki Y, Niwa Y, Hirooka Y, et al: The use of endoscopic ultrasound-guided fine-needle aspiration for investigation of submucosal and extrinsic masses of the colon and rectum. *Endoscopy* 37:154–160, 2005.
 136. Stergiou N, Haji-Kermani N, Schneider C, et al: Staging of colonic neoplasms by colonoscopic miniprobe ultrasonography. *Int J Colorectal Dis* 18:445–449, 2003.
 137. Dewhurst C, Rosen MP, Blake MA, et al: ACR Appropriateness Criteria pretreatment staging of colorectal cancer. *J Am Coll Radiol* 9:775–781, 2012.
 138. Rafaelsen SR, Vagn-Hansen C, Sørensen T, et al: Transrectal ultrasound and magnetic resonance imaging measurement of extramural tumor spread in rectal cancer. *World J Gastroenterol* 18:5021–5026, 2012.
 139. Thaler W, Watzka S, Martin F, et al: Preoperative staging of rectal cancer by endoluminal ultrasound vs. magnetic resonance imaging: Preliminary results of a prospective, comparative study. *Dis Colon Rectum* 37:1189–1193, 1994.
 140. Kim NK, Kim NJ, Yun SH, et al: Comparative study of transrectal ultrasonography, pelvic computerized tomography, and magnetic resonance imaging in preoperative staging of rectal cancer. *Dis Colon Rectum* 42:770–775, 1999.
 141. Tio TL, Coene PPL, Van Delden OM, et al: Colorectal carcinoma: Preoperative TNM classification with endosonography. *Radiology* 179:165–170, 1991.
 142. Marusch F, Koch A, Schmidt U, et al: Routine use of transrectal ultrasound in rectal carcinoma: Results of a prospective multicenter study. *Endoscopy* 34:385–390, 2002.
 143. Wolfman NT, Ott DJ: Endoscopic ultrasonography. *Semin Roentgenol* 31:154–161, 1996.
 144. Lim JH: Colorectal cancer: Sonographic findings. *AJR* 167:45–47, 1998.
 145. Hulsmans FJ, Tio TL, Fockens P, et al: Assessment of tumor infiltration depth in rectal cancer with transrectal sonography: Caution is necessary. *Radiology* 190:715–720, 1994.
 146. Hünnerbein M, Schlag PM: Three-dimensional endosonography for staging of rectal cancer. *Ann Surg* 225:432–438, 1997.
 147. Ivanov KD, Diavoc CD: Three-dimensional endoluminal ultrasound: New staging technique in patients with rectal cancer. *Dis Colon Rectum* 40:47–50, 1997.
 148. Delaloye B, Bischof-Delaloye A, Buchegger F, et al: Detection of colorectal carcinoma by emission computerized tomography after injection of I-123 labeled Fab or F(ab)2 fragments from monoclonal anti-carcinoembryonic antigen antibodies. *J Clin Invest* 77:301–311, 1986.
 149. Agnese DM, Abdessalam SF, Burak WE, Jr, et al: Pilot study using a humanized CC49 monoclonal antibody (HuCC49DeltaCH2) to localize recurrent colorectal carcinoma. *Ann Surg Oncol* 11:197–202, 2004.
 150. Avital S, Haddad R, Troitsa A, et al: Radioimmunoguided surgery for recurrent colorectal cancer manifested by isolated CEA elevation. *Cancer* 89:1692–1698, 2000.
 151. Ramos-Suarez M, Pintado AP, Mesa NR, et al: Diagnostic efficacy and safety of 99mTc-labeled monoclonal antibody for c5 in patients with colorectal and anal carcinomas: Final report clinical trial phase I/II. *Cancer Biol Ther* 6:22–29, 2007.
 152. Hansen JE, Fischer LK, Chan G, et al: Antibody-mediated p53 protein therapy prevents liver metastasis in vivo. *Cancer Res* 67:1769–1774, 2007.
 153. Baranda J, Williamson S: The new paradigm in the treatment of colorectal cancer: Are we hitting the right target? *Expert Opin Investig Drugs* 16:311–324, 2007.
 154. Manayan RC, Hart MJ, Friend WG: Radioimmunoguided surgery for colorectal cancer. *Am J Surg* 173:386–389, 1997.
 155. Cote RJ, Houchens DP, Hitchcock CL, et al: Intraoperative detection of occult colon cancer micrometastases using 125 I-radiolabeled monoclonal antibody CC49. *Cancer* 77:613–620, 1996.
 156. Mach JP, Buchegger F, Forni M, et al: Use of radiolabeled monoclonal anti-CEA antibodies for the detection of human carcinomas by external photoscanning and tomoscintigraphy. *Immunol Today* 2:239–249, 1981.
 157. Abdel-Nabi HH, Schwartz AN, Higano CS, et al: Colorectal carcinoma detection with indium-111 anticarcinoembryonic antigen monoclonal antibody ZCE 025. *Radiology* 164:617–621, 1987.
 158. Patt YZ, Lamki LM, Haynie TP, et al: Improved tumor localization with increasing dose of indium-111-labeled anti-carcinoembryonic antigen monoclonal antibody ZCE-025 in metastatic colorectal cancer. *J Clin Oncol* 6:1220–1230, 1988.
 159. Lunniss PJ, Skinner S, Britton KE, et al: Effect of radioimmunoscintigraphy on the management of recurrent colorectal cancer. *Br J Surg* 86:244–249, 1999.

160. Collier BD, Abdel-Nabi H, Doerr RJ, et al: Immunoscintigraphy performed with In-111-labeled CYT-103 in the management of colorectal cancer: Comparison with CT. *Radiology* 185:179–186, 1992.
161. Lamki LM, Patt YZ, Rosenblum MG, et al: Metastatic colorectal cancer: Radioimmunosintigraphy with a stabilized In-111-labeled F(ab')₂ fragment of an anti-CEA monoclonal antibody. *Radiology* 174:147–151, 1990.
162. Gu J, Zhao J, Li Z, et al: Clinical application of radioimmunoguided surgery in colorectal cancer using 125I-labeled carcinoembryonic antigen-specific monoclonal antibody submucosally. *Dis Colon Rectum* 46:1659–1666, 2003.
163. Okuno T, Fu KI, Sano Y, et al: Early colon cancers detected by FDG-PET: A report of two cases with immunohistochemical investigation. *Hepatogastroenterology* 51:1323–1325, 2004.
164. Hany TF, Steinert HC, Goerres GW, et al: PET diagnostic accuracy: Improvement with in-line PET-CT system: Initial results. *Radiology* 225:575–581, 2002.
165. Miraldi F, Vesselle H, Faulhaber PF, et al: Elimination of artifactual accumulation of FDG in PET imaging of colorectal cancer. *Clin Nucl Med* 23:3–7, 1998.
166. Rohren EM, Turkington TG, Coleman RE: Clinical applications of PET in oncology. *Radiology* 231:305–332, 2004.
167. Flanagan FL, Dehdashti F, Ogunbiyi OA, et al: Utility of FDG-PET for investigating unexplained plasma CEA elevation in patients with colorectal cancer. *Ann Surg* 227:319–323, 1998.
168. Schaefer O, Langer M: Detection of recurrent rectal cancer with CT, MRI and PET/CT. *Eur Radiol* 17:2044–2054, 2007.
169. Moore HG, Akhurst T, Larson SM, et al: A case-controlled study of 18-fluorodeoxyglucose positron emission tomography in the detection of pelvic recurrence in previously irradiated rectal cancer patients. *J Am Coll Surg* 197:22–28, 2003.
170. Belkacemi Y, Lartigau E, Kerrou K, et al: The contribution of PET to radiation treatment planning. *Bull Cancer* 94:99–108, 2007.
171. Ishimori T, Patel PV, Wahl RL: Detection of unexpected additional primary malignancies with PET/CT. *J Nucl Med* 46:752–757, 2005.
172. Chen YK, Kao CH, Liao AC, et al: Colorectal cancer screening in asymptomatic adults: The role of FDG PET scan. *Anticancer Res* 23:4357–4361, 2003.
173. Gutman F, Alberini JL, Wartski M, et al: Incidental colonic focal lesions detected by FDG PET/CT. *AJR* 185:495–500, 2005.
174. Rydzewski B, Dehdashti F, Gordon BA, et al: Usefulness of intraoperative sonography for revealing hepatic metastases from colorectal cancer in patients selected for surgery after undergoing FDG PET. *AJR* 178:353–358, 2002.
175. Blodgett TM, Meltzer CC, Townsend DW: PET/CT: Form and function. *Radiology* 242:360–385, 2007.
176. Cipe G, Ergul N, Hasbahceci M, et al: Routine use of positron-emission tomography/computed tomography for staging of primary colorectal cancer: Does it affect clinical management? *World J Surg Oncol* 11:49, 2013.
177. Mang T, Maier A, Plank C, et al: Pitfalls in multi-detector row CT colonography: A systematic approach. *Radiographics* 27:431–454, 2007.
178. Macari M, Bini EJ, Jacobs SL, et al: Significance of missed polyps at CT colonography. *AJR* 183:127–134, 2004.
179. Kelvin FM, Maglinte DT: Colorectal carcinoma: A radiologic and clinical review. *Radiology* 164:1–8, 1987.
180. Zinkin LD: A critical review of the classifications and staging of colorectal cancer. *Dis Colon Rectum* 26:37–43, 1983.
181. Nauta R, Stablein D, Holyoke D: Survival of patients with stage B2 colon carcinoma: The gastrointestinal tumor study group experience. *Arch Surg* 124:180–182, 1989.
182. Durdey P, Williams NS: The effect of malignant and inflammatory fixation of rectal carcinoma on prognosis after rectal excision. *Br J Surg* 71:787–790, 1984.
183. Giess CS, Schwartz LH, Bach AM, et al: Patterns of neoplastic spread in colorectal cancer: Implications for surveillance CT studies. *AJR* 170:987–991, 1998.
184. Hamlin DF, Burgener FA, Sischy B: New techniques to stage early rectal carcinoma by computed tomography. *Radiology* 141:539–540, 1981.
185. Figueredo A, Rumble RB, Maroun J, et al: Follow-up of patients with curatively resected colorectal cancer: A practice guideline. *BMC Cancer* 3:26–31, 2003.
186. Shauver IA, Sequeira J: Suture granuloma simulating recurrent carcinoma. *AJR* 128:856–857, 1977.
187. Daly BD, Crowley BM: Radiological appearances of colonic ring staple anastomoses. *Br J Radiol* 62:256–259, 1989.
188. Chen YM, Ott DJ, Wolfman NT, et al: Recurrent colorectal carcinoma: Evaluation with barium enema examination and CT. *Radiology* 163:307–310, 1987.
189. McCarthy SM, Barnes D, Deveney K, et al: Detection of recurrent rectosigmoid carcinoma: Prospective evaluation of CT and clinical factors. *AJR* 144:577–579, 1985.
190. Sharpe M, Golden R: End-to-end anastomosis of the colon following resection: A roentgen study of 42 cases. *AJR* 64:769–777, 1950.
191. Fleischner FG, Berenberg AL: Recurrent carcinoma of the colon at the site of anastomosis. *Radiology* 66:540–547, 1956.
192. Welch JP, Donaldson GA: Detection and treatment of recurrent cancer of the colon and rectum. *Am J Surg* 135:505–511, 1978.
193. Thoeni RF, Moss AA: The gastrointestinal tract. In Moss AA, Gamsu G, Genant H, editors: *Computed Tomography of the Body*, Philadelphia, 1992, WB Saunders, pp 643–734.
194. Kelvin FM, Korobkin M, Breiman RS, et al: Recurrent rectal carcinoma in an asymptomatic patient. *J Comput Assist Tomogr* 6:186–188, 1982.
195. Shoemaker D, Black R, Giles L, et al: Yearly colonoscopy, liver CT, and chest radiography do not influence 5-year survival of colorectal cancer patients. *Gastroenterology* 114:7–14, 1998.
196. Kjeldsen BJ, Kronborg O, Fenger C, et al: Careful follow-up for patients undergoing curative resections in colorectal carcinoma: How careful is "careful"? *Br J Surg* 84:666–669, 1997.
197. Stulc JP, Petrelli NJ, Herrera L, et al: Anastomotic recurrence of adenocarcinoma of the colon. *Arch Surg* 121:1077–1080, 1986.
198. Flamen P, Stroobants S, Van Cutsem E, et al: Additional value of whole body positron emission tomography with fluorine-18-2-fluoro-2-deoxy-D-glucose in recurrent colorectal cancer. *J Clin Oncol* 17:894–901, 1999.
199. Peethambaram P, Weiss M, Loprinzi CL, et al: An evaluation of postoperative follow-up tests in colon cancer patients treated for cure. *Oncology* 54:287–292, 1997.
200. Earls JP, Colon-Negron E, Dachman AH: Colorectal carcinoma in young patients: CT detection of an atypical pattern of recurrence. *Abdom Imaging* 19:441–445, 1994.
201. Olson RM, Perencevich P, Malcolm AW, et al: Patterns of recurrence following curative resection of adenocarcinoma of the colon and rectum. *Cancer* 45:2969–2974, 1980.
202. Christoforidis E, Kanellos I, Tsachalis T, et al: Locally recurrent rectal cancer after curative resection. *Tech Coloproctol* 8(Suppl 1):S132–S134, 2004.
203. Moore HG, Shoup M, Riedel E, et al: Colorectal cancer pelvic recurrences: Determinants of resectability. *Dis Colon Rectum* 47:1599–1606, 2004.
204. Cass AW, Million RR, Pfaff W: Patterns of recurrence following surgery alone for adenocarcinoma of the colon and rectum. *Cancer* 37:1861–1865, 1976.
205. Ntinas A, Zambas N, Al Mogrambi S, et al: Postoperative follow-up of patients with colorectal cancer: A combined evaluation of CT scan, colonoscopy and tumour markers. *Tech Coloproctol* 8(Suppl 1):S190–S192, 2004.
206. Husband JE, Hodson NJ, Parsons CA: The use of computed tomography in recurrent rectal tumors. *Radiology* 134:677–682, 1980.
207. Ellert J, Kreel L: The value of CT in malignant colonic tumors. *J Comput Assist Tomogr* 4:225–240, 1980.
208. Moss AA, Thoeni RF, Schnyder P, et al: Value of computed tomography in the detection and staging of recurrent rectal carcinomas. *J Comput Assist Tomogr* 5:870–874, 1981.
209. Adalsteinsson B, Glimelius B, Graffan S, et al: Computed tomography of recurrent renal carcinoma. *Acta Radiol Diagn* 22:669–672, 1981.
210. Bachmann G, Pfeifer T, Bauer T: [MRT and dynamic CT in the diagnosis of a recurrence of rectal carcinoma.] *Rofo* 161:214–219, 1994.
211. Chen YM, Ott DJ, Wolfman N: Recurrent colorectal carcinoma evaluation with barium enema examination and CT. *Radiology* 163:307–310, 1987.
212. Selzner M, Hany TF, Wildbrett P, et al: Does the novel PET/CT imaging modality impact on the treatment of patients with metastatic colorectal cancer of the liver? *Ann Surg* 240:1027–1034, 2004.
213. Reznick RH, White FE, Young JW, et al: The appearances on computed tomography after abdomino-perineal resection for carcinoma of the rectum: A comparison between the normal appearances and those of recurrence. *Br J Radiol* 56:237–240, 1983.
214. Kelvin FM, Korobkin M, Heaston DK, et al: The pelvis after surgery for rectal carcinoma: Serial CT observations with emphasis on non-neoplastic features. *AJR* 141:959–964, 1983.
215. Moriya Y, Sugihara K, Akasu T, et al: Importance of extended lymphadenectomy with lateral node dissection for advanced lower rectal cancer. *World J Surg* 21:728–732, 1997.
216. Kapiteijn E, Maaijnen CA, Nagtegaal ID, et al: Preoperative radiotherapy combined with total mesorectal excision for resectable rectal cancer. *N Engl J Med* 345:638–646, 2001.

217. Torricelli P, Pecchi A, Luppi G, et al: Gadolinium-enhanced MRI with dynamic evaluation in diagnosing the local recurrence of rectal cancer. *Abdom Imaging* 28:19–27, 2003.
218. Robinson P, Carrington BM, Swindell R, et al: Recurrent or residual pelvic bowel cancer: Accuracy of MRI local extent before salvage surgery. *Clin Radiol* 57:514–522, 2002.
219. Ebner F, Kressel HY, Mintz MC, et al: Tumor recurrence versus fibrosis in the female pelvis: Differentiation with MR imaging at 1.5 T. *Radiology* 166:333–340, 1988.
220. Gomberg JS, Friedman AC, Radecki PD: MRI differentiation of recurrent colorectal carcinoma from postoperative fibrosis. *Gastrointest Radiol* 11:361–363, 1986.
221. Glazer HS, Lee JKT, Levitt RG, et al: Radiation fibrosis: Differentiation from recurrent tumor by MR imaging. *Radiology* 156:721–726, 1985.
222. Yamashita S, Masui T, Katayama M, et al: T2-weighted MRI of rectosigmoid carcinoma: Comparison of respiratory-triggered fast spin-echo, breath-hold fast-recovery fast spin-echo, and breath-hold single-shot fast spin-echo sequences. *J Magn Reson Imaging* 25:511–516, 2007.
223. Heiken JP, Lee JKT: MR imaging of the pelvis. *Radiology* 166:11–16, 1988.
224. Ebner F, Kressel HY, Mintz MC, et al: Tumor recurrence versus fibrosis in the female pelvis: Differentiation with MR imaging at 1.5T. *Radiology* 166:333–340, 1988.
225. Rafto SE, Amendola MA, Gefter WB: MR imaging of recurrent colorectal carcinoma versus fibrosis. *J Comput Assist Tomogr* 12: 521–523, 1988.
226. Sugimura K, Carrington BM, Quivey JM, et al: Postirradiation changes in the pelvis: Assessment with MR imaging. *Radiology* 175:805–813, 1990.
227. De Lange EE, Fechner RE, Wanebo HJ: Suspected recurrent rectosigmoid carcinoma after abdominoperineal resection: MR imaging and histopathologic findings. *Radiology* 170:323–328, 1989.
228. Markus J, Morrissey B, deGara C, et al: MRI of recurrent rectosigmoid carcinoma. *Abdom Imaging* 22:338–342, 1997.
229. Dicle O, Obuz F, Cakmakci H: Differentiation of recurrent rectal cancer and scarring with dynamic MR imaging. *Br J Radiol* 72:1155–1159, 1999.
230. Stueckle CA, Koenig M, Haegeler KF, et al: Contrast media kinetic in multi-slice helical CT cannot detect rectal cancer recurrence with certainty. *Rofo* 177:893–899, 2005.
231. Sahani DV, Kalva SP, Hamberg LM, et al: Assessing tumor perfusion and treatment response in rectal cancer with multisection CT: Initial observations. *Radiology* 234:785–792, 2005.
232. Goh V, Halligan S, Daley F, et al: Colorectal tumor vascularity: Quantitative assessment with multidetector CT—do tumor perfusion measurements reflect angiogenesis? *Radiology* 249:510–517, 2008.
233. Nural MS, Danaci M, Soyucok A, et al: Efficiency of apparent diffusion coefficients in differentiation of colorectal tumor recurrences and posttherapeutic soft-tissue changes. *Eur J Radiol* 82:1702–1709, 2013.
234. Assenat E, Thezenas S, Samalin E, et al: The value of endoscopic rectal ultrasound in predicting the lateral clearance and outcome in patients with lower-third rectal adenocarcinoma. *Endoscopy* 39:309–313, 2007.
235. Baulieu F, Bourlier P, Scotto B, et al: The value of immunoscintigraphy in the detection of recurrent colorectal cancer. *Nucl Med Commun* 22:1295–1304, 2001.
236. Yao YF, Yang Z, Li ZF, et al: Immunoscintigraphy of local recurrent rectal cancer with 99m Tc-labeled anti-CEA monoclonal antibody CL58. *World J Gastroenterol* 12:1841–1846, 2007.
237. Votruba J, Belohlavek O, Jaruskova M, et al: The role of FDG-PET/CT in the detection of recurrent colorectal cancer. *Eur J Nucl Med Mol Imaging* 33:779–784, 2006.
238. Titu LV, Nicholson AA, Hartley JE, et al: Routine follow-up by magnetic resonance imaging does not improve detection of resectable local recurrences from colorectal cancer. *Ann Surg* 243:348–352, 2006.
239. Colosio A, Fornès P, Soyer P, et al: Local colorectal cancer recurrence: Pelvic MRI evaluation. *Abdom Imaging* 38:72–81, 2013.

Other Tumors of the Colon

STEPHEN E. RUBESIN

CHAPTER OUTLINE

Lymphoma

Pathologic Findings

Clinical Findings

Radiographic Findings and Differential Diagnosis

Vascular Lesions

Hemangioma

Lymphangioma

Angiodysplasia

Kaposi's Sarcoma

Endocrine (Carcinoid) Tumors

Pathologic Findings

Endocrine Cell Tumors of the Rectum

Endocrine Tumors (Exclusive of the Rectum)

Fatty Lesions

Lipoma

Fatty Infiltration of the Ileocecal Valve

Stromal Tumors

Pathologic Findings

Small Stromal Tumors

Large Stromal Tumors

Squamous Cell Carcinoma

Cloacogenic Carcinoma

Metastases

Direct Invasion from Contiguous Primary Tumors

Direct Invasion from Noncontiguous Primary Tumors

Intraperitoneal Seeding

Embolic Metastases

This chapter discusses a variety of benign and malignant tumors of the colon as separate entities. Although these tumors are associated with a wide range of clinical and radiologic manifestations, they may have typical features on imaging studies that suggest the correct diagnosis.

Lymphoma

PATHOLOGIC FINDINGS

Malignant lymphomas involve the gastrointestinal (GI) tract as primary neoplasms or as part of a disseminated disease. The colon is the third most common primary site of lymphoma involving the GI tract (after the stomach and small bowel); colonic involvement occurs in 6% to 12% of cases.¹⁻³ Primary lymphoma of the colon is rare, comprising less than 1% of all primary malignant tumors of the colon.^{4,5} Colonic involvement by systemic lymphoma is relatively common, with microscopic

evidence of tumor in up to 44% of cases at autopsy.³ Non-Hodgkin's lymphoma accounts for almost all colonic lymphomas; Hodgkin's lymphoma involving the colon is extremely rare.^{1,6,7} Primary colonic lymphoma is usually a B-cell lymphoma; diffuse large B-cell lymphoma is the most common primary colonic subtype.²

CLINICAL FINDINGS

Primary non-Hodgkin's lymphoma involving the colon is usually seen in middle-aged or older persons.² Men are more frequently affected than women by a ratio of 2:1.^{6,8} Abdominal pain, weight loss, and altered bowel habits occur in 60% to 90% of patients, and rectal bleeding or diarrhea occur in 25%.^{6,9} A palpable abdominal mass is the most frequent physical finding.⁶ Long-standing ulcerative colitis appears to be a predisposing condition, but the development of lymphoma in these patients may be related more to treatment with immunosuppressive agents than to the disease itself.^{6,8,10,11} Extranodal presentation of post-transplantation lymphoproliferative disorders is typical, and B-cell lymphomas may arise in the colon after solid organ transplantation.¹² Anorectal lymphoma is seen in HIV-infected patients, but this has been decreasing in frequency.¹³

RADIOGRAPHIC FINDINGS AND DIFFERENTIAL DIAGNOSIS

The primary form of colonic lymphoma usually involves the ileocecal valve, cecum, or rectum.¹²⁻¹⁵ In contrast, systemic lymphoma usually involves the entire colon or long segments of bowel.^{7,16-18} The primary localized form of colonic lymphoma may be manifested by a variety of radiographic findings, including a polypoid or cavitory mass or circumferential mural lesion. Bulky polypoid masses represent the most common form of primary colonic lymphoma.^{5,9,18-20} These tumors usually appear as smooth-surfaced, broad-based sessile lesions, with or without central depressions or ulcerations.¹⁴ These lesions vary from 4 to 20 cm in size and are usually located near the ileocecal valve (Fig. 60-1).¹⁵ Extension of cecal lymphoma into the terminal ileum is not uncommon (see Fig. 60-1).

The annular infiltrating form of colonic lymphoma usually involves a long segment of colon, appearing as a concentric area of narrowing or as a cavitory mass (Fig. 60-2).^{5,20} Although the colonic lumen may be narrowed, obstruction is uncommon. The infiltrating form is usually characterized by a discrete lesion, with thickened, irregular haustral folds and a nodular surface pattern. Although the contour is irregular, the mucosal surface is smooth, suggesting submucosal infiltration rather than mucosal ulceration. Thus, the major considerations in the differential diagnosis of the annular infiltrating form of lymphoma include submucosal hemorrhage and edema (caused by ischemia or a bleeding diathesis) and an unusual colonic carcinoma.⁵

Large infiltrating tumors may extend into the mesentery or exhibit central cavitation, resulting in a bulky, cavitary mass lesion. The major considerations in the differential diagnosis of the cavitary form of lymphoma include a perforated colonic carcinoma and a mesenchymal tumor, such as a GI stromal tumor.

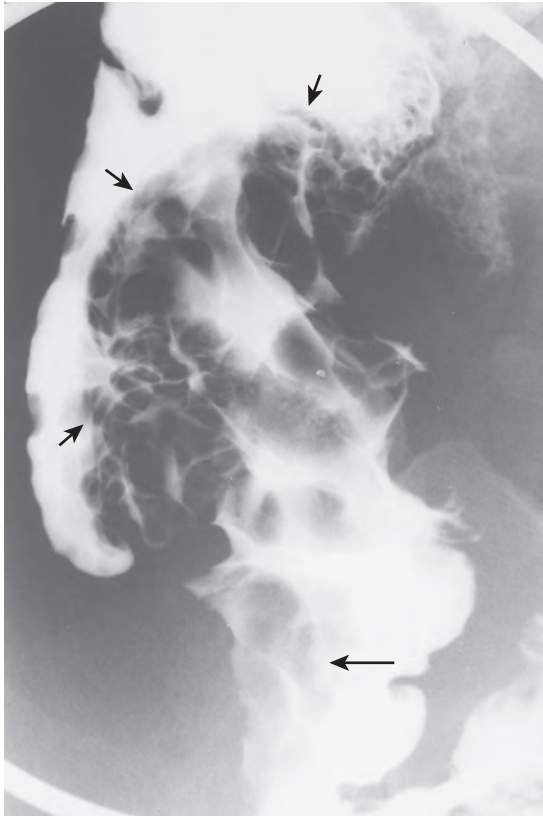


Figure 60-1 Lymphoma of the terminal ileum and ileocecal valve. Spot image from a small bowel follow-through shows a smooth-polypoid fold (arrow) in the terminal ileum and a coarsely lobulated mass (small arrows) replacing the ileocecal valve.

The diffuse multinodular form of colonic lymphoma (lymphomatous polyposis) is associated with disseminated disease from a nodal primary lymphoma or occurs as a true primary GI lymphoma. Histologically, this form of lymphoma is usually a mantle cell lymphoma derived from a subpopulation of mantle zone cells.^{21,22} These multinodular lymphomas involve long segments of the colon or the entire colon. The small intestine may be simultaneously involved. The tumors disseminate rapidly to the liver, spleen, peripheral lymph nodes, and bone marrow.²² More than 100 nonuniform, smooth, sessile nodules varying from 2 to 25 mm in size carpet the colonic surface.^{15,19} The nodules are occasionally elongated, pedunculated, umbilicated, or filiform.¹⁹ A conglomerate cecal mass is seen in almost 50% of cases.¹⁹ Associated mesenteric lymph nodes are usually enlarged.²² The multinodular form of colonic lymphoma may be confused radiographically with familial polyposis, lymphoid hyperplasia, inflammatory bowel disease, or infectious diseases, such as pseudomembranous colitis or schistosomiasis. The nodules of colonic lymphoma are nonuniform and relatively large in comparison to the uniform, 1- to 2-mm nodules of lymphoid hyperplasia. Unlike the pseudopolyposis in inflammatory bowel disease, the haustral pattern is also preserved in colonic lymphoma, and ulceration is uncommon.^{7,15} Conglomerate cecal masses are more frequent in disseminated lymphoma than in the polyposis syndromes.^{7,19} Rarely, diffuse colonic lymphoma may be associated with acute toxic dilation or pneumatosis coli.¹⁵

Vascular Lesions

HEMANGIOMA

Clinical and Pathologic Findings

Hemangiomas of the colon are rare vascular lesions, but the radiologic diagnosis is important because these lesions may be misdiagnosed at endoscopy and have a high mortality rate related to severe GI bleeding.²³ Patients with colonic hemangiomas usually present at a young age with acute, recurrent, or chronic rectal bleeding.^{24,25} Some patients may have severe,

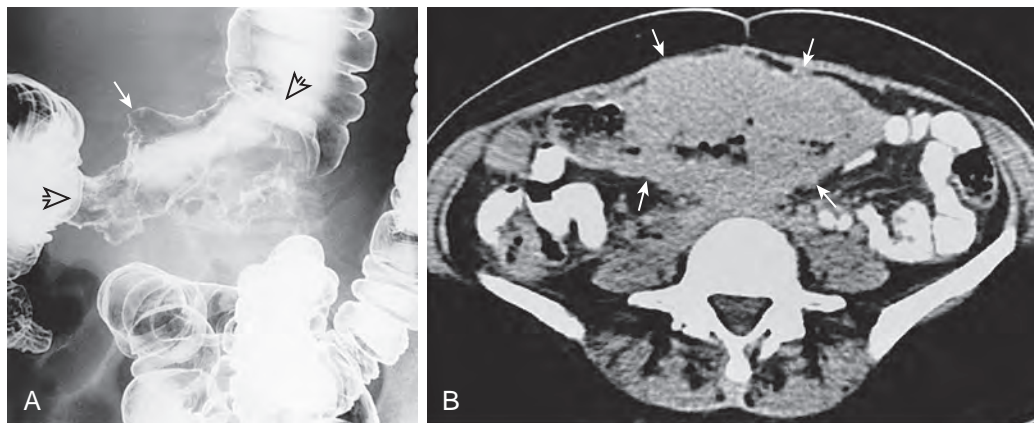


Figure 60-2 Lymphoma of the transverse colon. **A.** Spot image from a double-contrast barium enema shows a long (limits denoted by open arrows) concentric lesion in the transverse colon, with an irregular contour. Note protrusion of the contour superiorly outside the expected lumen of the bowel (arrow); this finding indicates cavitation of the mass. **B.** CT scan shows a large soft tissue mass (arrows) with lobular thickening of the walls of the transverse colon.

life-threatening rectal bleeding²⁵; mortality rates for this tumor approach 50%.²⁶ Obstructive symptoms and diarrhea are uncommon, occurring in 15% to 20% of cases.^{24,27} Occasionally, patients with anorectal lesions may complain of tenesmus or constipation.

Cavernous hemangiomas are the most common form; capillary hemangiomas are second in frequency.^{27,28} Cavernous hemangiomas are unencapsulated lesions, usually arising in the submucosa. They are composed of large, multiloculated, thin-walled vessels²⁶ separated by loose connective tissue. They usually occur in the rectum or sigmoid colon,²⁹ appearing as discrete submucosal masses²⁷ or, more frequently, as diffuse, infiltrative lesions.²⁵ Polypoid tumors may intussuscept, causing obstruction, whereas infiltrative lesions often ulcerate and bleed.²⁵

Capillary hemangiomas usually occur as solitary, sharply circumscribed submucosal masses in asymptomatic patients. The tumors are composed of small vessels lined by well-differentiated endothelial cells.²⁶ The vessels are packed together, with scant surrounding connective tissue. These tumors are occasionally associated with cutaneous or visceral hemangiomas.^{25,30} Colonic hemangiomas may occur in the Klippel-Trenaunay syndrome, manifested by the triad of cutaneous hemangiomas, soft tissue hypertrophy of the involved lower extremity, and congenital varicose veins.^{29,31} Cavernous hemangiomas of the colon are also seen in the blue rubber bleb nevus syndrome and in some patients with Peutz-Jeghers syndrome.³² Hemangiomas have also been reported in 5% to 8% of patients with Turner's syndrome.³³ Colonic hemangiomas have no propensity for malignant transformation and should therefore be distinguished from their true neoplastic counterpart, angiosarcomas.

Radiographic Findings and Differential Diagnosis

Rectal hemangiomas are frequently misdiagnosed on endoscopy as hemorrhoids or proctitis.^{26,34} As a result, the radiologist may be the first physician to suggest the correct diagnosis. Plain abdominal radiographs may show multiple phleboliths along the course of the bowel in 50% of cases.^{25,26,30} Hemangiomas should therefore be suspected if abdominal radiographs demonstrate phleboliths in young patients with GI bleeding or clusters of phleboliths in atypical locations or along the expected course of the rectosigmoid colon.

Barium enema examinations usually reveal a circumferential lesion, with scalloped contours and a nodular mucosal surface pattern.²⁵ The colonic lumen is narrowed in 50% of cases. If the tumor is in its usual rectosigmoid location, a wide presacral space may be seen. If phleboliths are visible, they are seen in the expected location of the colonic tumor (Fig. 60-3).²⁹ The polypoid form of hemangioma is usually manifested by smooth, sessile, broad-based submucosal masses.

Although hemangiomas are usually vascular at angiography, they may occasionally be hypovascular or avascular because of vessel thrombosis and sclerosis.²³ Computed tomography (CT) better delineates the true dimensions of the mass (see Fig. 60-3) and involvement of adjacent structures, such as the urinary bladder.³⁰ Hemangioma is included in the differential diagnosis of polypoid submucosal masses, but the most common submucosal mass in the colon is a lipoma. Hemangioma is also included in the differential diagnosis of infiltrative submucosal rectosigmoid lesions, such as those found in solitary rectal ulcer syndrome or lymphoma. However, the clinical history and presence of phleboliths should suggest the correct diagnosis.

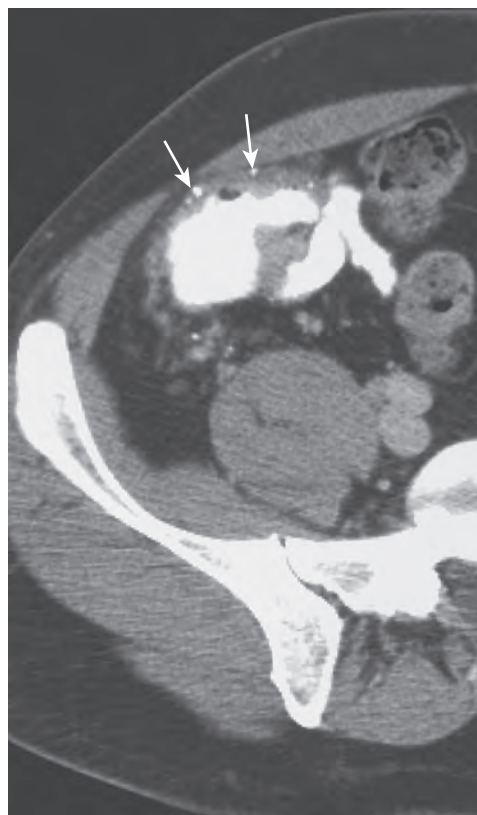


Figure 60-3 Hemangioma of the colon. CT scan shows lobulated thickening of the circumference of the wall of the cecum with numerous calcified phleboliths (arrows) in the subserosa.

LYMPHANGIOMA

Lymphangiomas of the colon are extremely rare benign lesions of neoplastic or hamartomatous origin.³⁵ The lesions are composed of a cluster of lymphatic spaces lined by endothelial cells and separated by connective tissue septa.³² These dilated lymphatics are usually found in the muscularis mucosae or submucosa. Some lymphangiomas arise in the colonic mesentery.³⁶ Patients with colonic lymphangiomas usually present in the fourth to sixth decade of life with abdominal pain, rectal bleeding, watery diarrhea, and/or altered bowel habits.^{36,37} Lymphangiomas may appear radiographically as solitary, 2- to 4-cm, often pedunculated polypoid lesions³⁷ or as smooth submucosal masses.^{35,38} These soft tumors are pliable, changing in size or shape with compression or varying luminal distention, and they may be compressible during endoscopic ultrasound.³⁹ A cystic or multicystic mass is often found on endoscopic ultrasonography or CT. The smooth unilocular or multilocular submucosal mass is of water attenuation (0-20 HU) on CT.^{39,40}

ANGIODYSPLASIA

Clinical and Pathologic Findings

Angiodysplasia is a common cause of chronic low-grade or acute massive lower GI bleeding in older patients.^{41,42} These lesions are acquired vascular ectasias, possibly caused by chronic, low-grade colonic obstruction.⁴¹ Angiodysplasias are composed of clusters of dilated, tortuous, thin-walled veins,

venules, and capillaries localized in the colonic mucosa and submucosa. The mucosal layer overlying the vascular tuft may be thin or ulcerated. These lesions are single or multiple and small (usually <5 mm), usually found in the cecum or ascending colon.⁴¹

Angiodysplasias may coexist with other causes of GI bleeding. These lesions have been found at autopsy in 2% of asymptomatic older patients and, in one series, angiodysplasias were present in the resected specimens in 12 of 15 patients who had undergone surgery for colonic carcinoma.⁴¹ Angiodysplasias are not associated with angiomatous lesions of the skin or other viscera.⁴¹

Radiographic Findings

Angiodysplasias may be detected during the work-up of patients with severe or recurrent lower GI bleeding after a normal barium enema or colonoscopy.⁴² During the arterial phase of angiography, a focus of angiodysplasia usually appears as a tangle of small vessels at the end of a cecal or right colonic artery. Early filling of draining veins with contrast medium is usually seen, but extravasation of contrast medium rarely occurs.⁴³ The radiologist is critical to the diagnosis of angiodysplasia because the surgeon is unable to see or palpate these lesions during surgery. The pathognomonic histologic findings are not usually present on endoscopic biopsy specimens. As a result, the decision for surgery is made on the basis of the radiographic findings and the clinical history of severe or recurrent lower GI bleeding.

KAPOSI'S SARCOMA

Kaposi's sarcoma involving the colon usually occurs in patients with AIDS. Kaposi's sarcoma has also been reported in HIV-negative patients with Crohn's disease or ulcerative colitis and in patients who have undergone solid organ transplantation.^{44,45} Colonic Kaposi's sarcoma is associated with human herpesvirus 8 infection. Kaposi's sarcoma in the colon is manifested radiographically by a flat or plaque-like lesion, small polypoid nodule, or polypoid submucosa-appearing mass, with or without central umbilication.³² The tumor is usually confined to the mucosa and submucosa.

Endocrine (Carcinoid) Tumors

PATHOLOGIC FINDINGS

Endocrine cells are scattered throughout the GI tract. These cells synthesize and secrete a variety of peptide hormones and biogenic amines. The endocrine cells give rise to GI tumors traditionally termed *carcinoid tumors* but now preferably termed *endocrine cell tumors*. The most common sites of endocrine cell tumors include the appendix (35%), ileum (16%), lung (14%), and rectum (13%).⁴⁶ Endocrine cell tumors arising in the remainder of the colon constitute only 2% to 3% of all carcinoid tumors.⁴⁶⁻⁵⁰

The most common sites of endocrine cell tumors in the colon are the rectum and cecum. Endocrine tumors involving the cecum and ascending or transverse colon are of midgut origin. These midgut lesions may synthesize, store, and secrete serotonin. Although serotonin may be produced, carcinoid syndrome is rare.⁵¹ If carcinoid syndrome is present, it is usually associated with liver metastases.

Hindgut endocrine cell tumors involve the descending colon, sigmoid colon, and rectum. They primarily synthesize and store a variety of polypeptide hormonal substances, including gastrin, somatostatin, glucagon, and vasoactive intestinal polypeptide.^{47,52} These tumors do not usually produce serotonin or cause carcinoid syndrome.

ENDOCRINE CELL TUMORS OF THE RECTUM

Endocrine cell tumors arising in the rectum are usually small, smooth, submucosal polypoid lesions less than 2 cm in diameter and are located in the lower two thirds of the rectum. Most cases are discovered incidentally during a screening barium enema examination or endoscopy or during work-up for rectal pain or bleeding.^{53,54} Small rectal carcinoids have low malignant potential and are cured by simple and complete excision. As with any carcinoid tumor, the larger the tumor, the greater the chance of metastases at the time of diagnosis. Although rare, large rectal endocrine cell tumors are associated with a much greater frequency of metastases at the time of diagnosis.⁵⁴ Large rectal carcinoids may appear as irregular ulcerated masses.⁵⁴ If all rectal endocrine cell tumors are considered, patients with rectal carcinoids have an overall 5-year survival rate of about 85%.^{46,54}

ENDOCRINE TUMORS (EXCLUSIVE OF THE RECTUM)

Endocrine cell tumors of the remainder of the colon have a very different clinical history, morphology, and prognosis than small low-grade endocrine tumors of the rectum. Endocrine cell tumors in the colon (exclusive of the rectum) are usually large aggressive lesions associated with a poor prognosis. Patients usually present in the sixth decade of life with symptoms similar to those of colonic adenocarcinoma, including abdominal pain, distention, and a palpable abdominal mass. Rectal bleeding and diarrhea are seen in approximately one third of patients.⁵⁵

Endocrine cell tumors of the colon are usually located in the cecum or ascending colon.^{51,55} These tumors appear on barium enemas as large (>5 cm), fungating intraluminal masses or as irregular annular lesions (Fig. 60-4)^{48,51,56} that are indistinguishable from those of colonic carcinoma. In other patients, these endocrine cell tumors may appear as smooth, polypoid submucosal masses. At the time of diagnosis, 50% to 60% of patients with large endocrine tumors have metastases to the liver, lymph nodes, mesentery, or peritoneum.^{46,51,55} Overall, 5-year survival rates of approximately 50% have been reported.⁴⁶

Fatty Lesions

LIPOMA

Clinical Findings

Colonic lipomas are benign uncommon lesions, occurring at autopsy in less than 1% of patients.⁵⁷⁻⁵⁹ Colonic liposarcomas are exceedingly rare. However, the colon is the most frequent site of GI involvement by lipomas.^{60,61} Most patients are asymptomatic, and the tumors are detected during studies performed for symptoms ultimately attributed to other causes.^{57,59} When these patients are symptomatic, they usually present with



Figure 60-4 Endocrine carcinoma of the colon. Spot image from a double-contrast barium enema shows a short annular lesion (arrow) with shelflike margins in the hepatic flexure of the colon. These radiographic findings are similar to those of an annular carcinoma of the colon, but the mucosa is smoother than that usually found with an annular carcinoma. (Courtesy Seth N. Glick, MD, Philadelphia.)

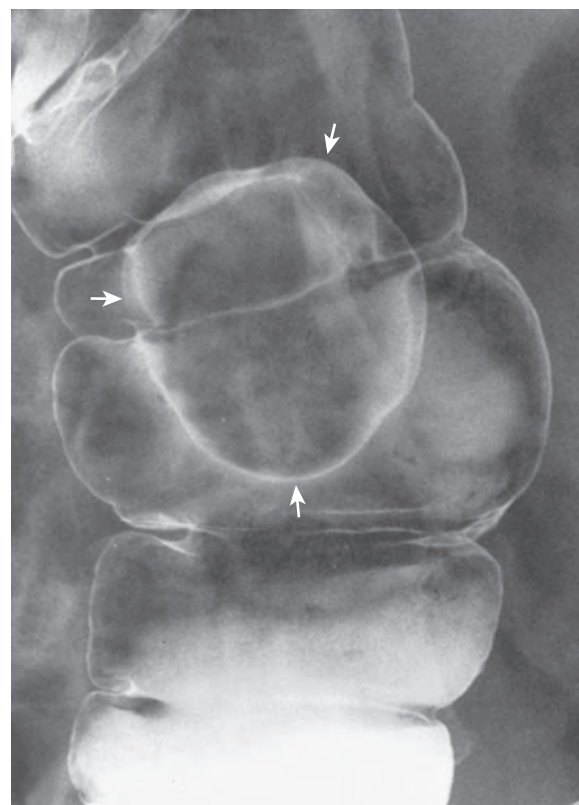


Figure 60-5 Lipoma of the descending colon. Spot image from a double-contrast barium enema shows a 3-cm, smooth-surfaced, submucosal mass (arrows) with a slightly lobulated contour.

abdominal pain and discomfort.⁵⁹ Rectal bleeding and pain related to intussusception are less common.

Pathologic Findings

Most colonic lipomas are found in the right colon, and 90% originate in the submucosa.^{14,57,59} The remaining 10% arise in the appendices epiploicae. Multiple tumors are found in up to 25% of patients.⁵⁹ Colonic lipomas are usually smaller than 3 cm in diameter, but those that cause symptoms tend to be larger lesions.

Colonic lipomas are encapsulated masses of mature adipose tissue usually confined to the submucosa. Approximately two thirds of these tumors are pedunculated, with a broad-based pedicle covered by normal colonic mucosa. Because of this pedunculation, local trauma and mechanical irritation may lead to focal ulceration and fat necrosis. Continuing inflammation may cause fibrosis and calcification.

Radiographic Findings

Colonic lipomas usually appear on barium enemas as smooth, sessile submucosal masses or as smooth polypoid lesions on a broad-based pedicle (Fig. 60-5).¹⁴ Lipomas may be round, ovoid, or pear-shaped. They are sharply demarcated masses that form obtuse angles with the adjacent colonic wall.⁶² Although these lesions may have a lobulated contour, the mucosal surface is smooth (see Fig. 60-5). Because of the pliable nature of fat, lipomas change shape with palpation, position of the patient,

or varying degrees of colonic distention.^{58,62} These tumors may also elongate during colonic spasm or after colonic evacuation. Some lipomas may serve as the lead point for colocolic intussusceptions.⁶³⁻⁶⁵

Before the advent of CT, the barium enema was considered to be a relatively accurate test for the diagnosis of colonic lipoma.^{62,66} However, a definitive diagnosis of a colonic lipoma can be made on CT when it shows a mass of uniform fat density (60-120 HU) without septa or other large areas of nonfatty tissue (Fig. 60-6).^{39,65,67-69}

When colonic lipomas intussuscept, they can ulcerate and undergo fat necrosis, resulting in CT attenuation numbers higher than those of fat. As a result, an intussuscepting lipoma appearing as a soft tissue mass or having only a small focus of fat attenuation may be confused with an intussuscepting carcinoma.⁶⁵ The radiologist can also confuse any intussuscepting tumor with a lipoma if the eccentrically invaginating mesenteric fat associated with the intussuscepting tumor mass is mistaken for the fat of a lipoma.⁶⁵ Lipomas can also be diagnosed via endoscopic ultrasound as smooth hemispheric polyps with a broad base containing hyperechoic tissue or tissue of intermediate echogenicity.³⁹

FATTY INFILTRATION OF THE ILEOCECAL VALVE

Pathologic, Clinical, and Radiographic Findings

Fatty infiltration (also known as lipohyperplasia or lipomatous infiltration) of the ileocecal valve results from a localized



Figure 60-6 Lipoma of the cecum. CT scan shows a 1.5-cm, smooth-surfaced, ovoid mass (arrow) in the cecum with the same attenuation value as nearby mesenteric fat.

massive accumulation of submucosal fat in this region. The lack of a capsule differentiates this fatty proliferation pathologically from a true lipoma.^{28,70} Fatty infiltration of the ileocecal valve is associated with obesity.²¹ The diagnosis is suggested on barium enema when there is a large ileocecal valve with smooth or lobulated contours and a smooth mucosal surface without a discrete polypoid mass. Although rigid measurements are not reliable in distinguishing a normal-sized ileocecal valve from an enlarged valve, some investigators have suggested that a normal ileocecal valve should be 4 cm or less.⁷¹ Others have found that one lip of a normal valve should be 1.5 cm or less.⁷² A normal ileocecal valve may also have stellate folds radiating toward its center.⁷²

Differential Diagnosis

The radiologist must first decide whether the polypoid projection in the cecum arises on or near the ileocecal valve or actually represents the valve. The normal ileocecal valve is usually located at the level of the first complete haustral fold on the medial or posterior colonic wall at the junction of the cecum and ascending colon.⁷² Filling of the terminal ileum with barium confirms the location of the ileocecal valve. If an ileocecal valve is mildly enlarged (>4 cm) and has a smooth or slightly lobulated contour and smooth mucosal surface, the most likely diagnosis is fatty infiltration of the valve (Fig. 60-7). In contrast, a focal polypoid projection from the ileocecal valve may represent a tumor, such as an adenoma or lipoma (Fig. 60-8).⁷² Any

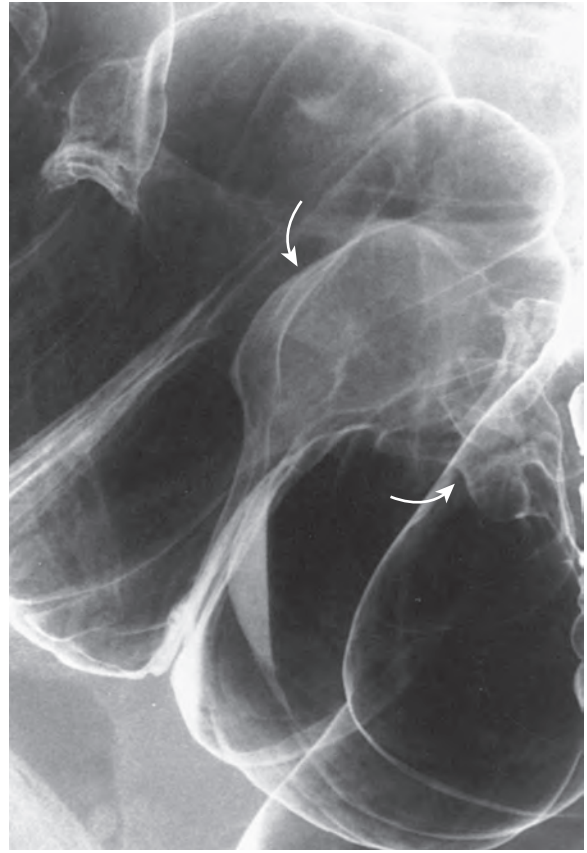


Figure 60-7 Fatty infiltration of the ileocecal valve. Close-up view from a right side-down decubitus overhead radiograph of the colon shows smooth, slightly lobulated enlargement of the ileocecal valve (arrows). Fatty infiltration was confirmed at colonoscopy performed for other reasons.

mucosal surface irregularity of the ileocecal valve should also suggest the possibility of tumor involving the valve, including an adenocarcinoma. The ileocecal valve may also be involved by Crohn's disease or lymphoma. In Crohn's disease, there is fatty hypertrophy of the valve, usually associated with other radiographic findings of Crohn's disease in the terminal ileum and ileocecal fistulas. In lymphoma, the ileocecal valve is moderately enlarged and has a lobulated contour, usually because of the spread of lymphoma from the terminal ileum.

Stromal Tumors

PATHOLOGIC FINDINGS

Historically, most spindle and epithelioid cell tumors of the GI tract have erroneously been termed *smooth muscle tumors* (leiomyoma or leiomyosarcoma). Only a small percentage of all spindle cell tumors, however, are recognized as arising from smooth muscle cells or neural cells by ultrastructural or immunohistochemical means.⁷³⁻⁷⁶ Most spindle cell tumors are undifferentiated stromal neoplasms, termed *gastrointestinal stromal tumors* (GISTs).⁷³⁻⁷⁶ GISTs originate from the interstitial cells of Cajal or a progenitor of these cells. The interstitial cells of Cajal are within the interstices of the muscularis propria. These cells act as a pacemaker, coordinating peristalsis. GIST development depends on a proto-oncogenic receptor, tyrosine kinase (*KIT*). GISTs usually express CD34 and many have been found to

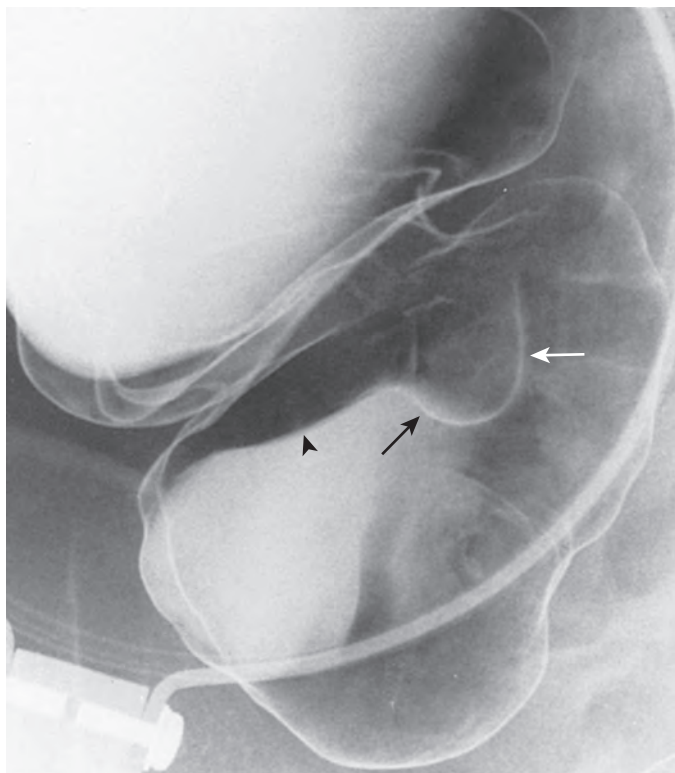


Figure 60-8 Lipoma of the ileocecal valve. A small, smooth-surfaced, submucosal lesion (arrows) is seen arising from the inferior lip of the ileocecal valve (arrowhead).

contain mutations in *KIT*.⁷⁷ The likelihood of recurrent tumor or metastases with GISTs is based on their mitotic index, size, and location.⁷⁸

SMALL STROMAL TUMORS

Only 1% of all GI tumors are of stromal origin, and these tumors are least commonly found in the colon.⁷⁹ Colonic stromal tumors are usually located in the rectum.⁸⁰ In general, there are two macroscopic types of colonic stromal tumors, small polypoid lesions and large bulky masses. Small polypoid lesions may be sessile or pedunculated and usually arise in the rectum. They probably arise from the muscularis mucosae, are histologically benign, and do not recur after excision.⁸¹ These small polypoid lesions are often true leiomyomas of the colon because they demonstrate smooth muscle differentiation by their desmin positivity and ultrastructural characteristics. These tumors are distinct from GISTs and have essentially no malignant potential. These small rectal lesions appear on barium enema as sessile or pedunculated polyps, with a smooth or slightly irregular surface. Small polypoid leiomyomas have also been reported in patients with AIDS.⁸² Multiple small polypoid neurofibromas may be seen in patients with neurofibromatosis (Fig. 60-9).

LARGE STROMAL TUMORS

Large (>2 cm) stromal tumors probably arise from the muscularis propria. They have a high rate of local recurrence (60%), regardless of histologic differentiation, and are associated with



Figure 60-9 Neurofibromatosis of the colon. Spot image from a double-contrast barium enema shows numerous small, smooth-surfaced filling defects (arrows) and hemispheric lines in the descending colon. Neurofibromatosis is a rare cause of colonic polyposis.

a poor prognosis.⁸¹ These bulky lesions are usually found in the rectum, with the remainder evenly distributed throughout the colon. Large stromal tumors may appear on barium enema or CT as annular lesions, cavitating masses with a prominent extraluminal component, or submucosal masses with or without central ulceration (Fig. 60-10). Cavitation may lead to superimposed infection or perforation with abscess formation.⁷⁹ These lesions may be confused radiographically with colonic lymphomas or perforated colonic carcinomas. Stromal lesions typically metastasize to peritoneal surfaces and to the lungs and liver.⁷⁵

Squamous Cell Carcinoma

Squamous cell carcinomas of the colon are extremely rare tumors. Most squamous cell carcinomas arise in the rectum and cause symptoms identical to those of rectal adenocarcinomas.⁸³ Squamous cell carcinomas of the colon should be distinguished from squamous cell carcinomas invading the colon from the anal canal or from squamous mucosa-lined fistulas. These lesions must also be distinguished from squamous cell carcinomas that have metastasized to the colon and from poorly differentiated adenocarcinomas that show focal squamous differentiation. Squamous cell carcinomas have been detected in patients with a history of ulcerative colitis, pelvic irradiation, and schistosomiasis.⁸⁴ Squamous cell carcinoma arising in the anal canal is often seen in patients with HIV infection, hematologic malignancy, and a solid organ

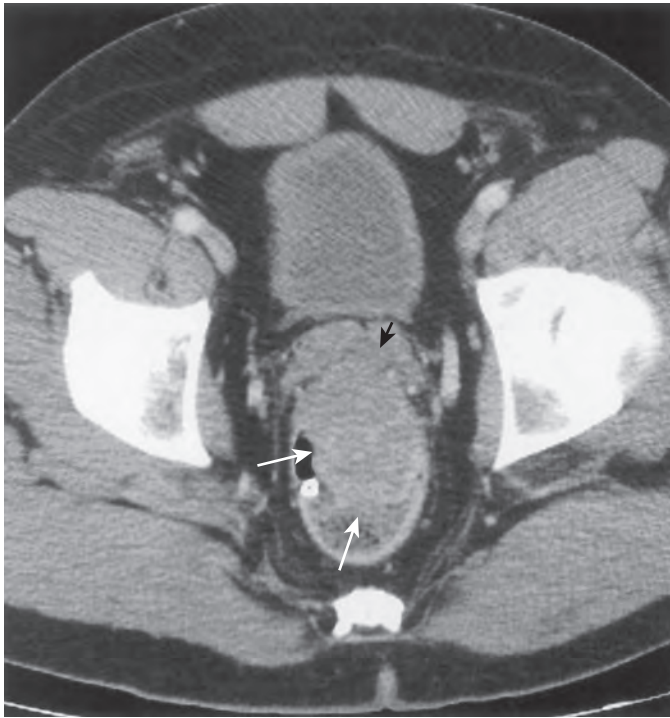


Figure 60-10 Malignant gastrointestinal stromal tumor of the rectum. CT scan shows a large soft tissue mass (white arrows) arising from the left anterolateral wall of the rectum. The mass enhances to the same degree as adjacent muscle. Infiltration of the fat plane between the rectum and seminal vesicles (black arrow) is present. (From Forbes A, Rubesin SE, et al: *Colon II*. In Forbes A, Misiewicz J, Compton C, et al [eds]: *Atlas of Clinical Gastroenterology*, 3rd ed. Edinburgh, Elsevier Mosby, 2005, p 183.)

transplant.⁸⁵ Squamous cell carcinomas may appear on barium enemas as large, bulky, ulcerated masses grossly identical to rectal adenocarcinomas (Fig. 60-11).⁸³ Hematogenous, lymphatic, and local metastases are frequently present.

Cloacogenic Carcinoma

The epithelium at the junction of the anal canal and rectum is composed of squamous and stratified columnar epithelium, as well as scattered goblet cells. This transitional zone has features of both urothelium and squamous epithelium compatible with a cloacogenic origin.⁸⁶ As a result, many tumors in this region were previously termed *cloacogenic carcinomas*. Primary tumors at the anorectal junction are currently classified according to architectural and cellular differentiation indicative of their cellular origin, including terms such as *squamous cell carcinoma*, *basaloid carcinoma*, *transitional cell carcinoma*, *mucoepidermoid carcinoma*, and *adenoid cystic carcinoma*. Most tumors have a mixture of histologic growth patterns. Tumors with squamous differentiation are termed *squamous cell carcinoma*, as noted earlier. Tumors that arise from submucosal glands in this region are salivary gland-type tumors, such as adenoid cystic carcinoma and mucoepidermoid carcinoma. The most common malignant tumor of the anal canal, however, is not of cloacogenic origin but is an adenocarcinoma arising from the rectal mucosa that subsequently invades the anal canal.

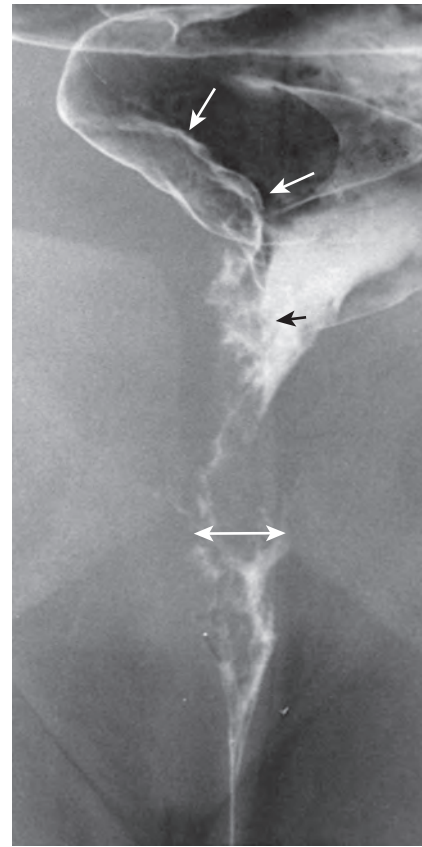


Figure 60-11 Verrucous squamous cell carcinoma arising in a condyloma acuminatum. This young woman had been treated for 5 years for perianal, vaginal, cervical, and vulvar condylomata. A spot image of the distal rectum and anal canal from a double-contrast barium enema shows a polypoid mass (white arrows) in the distal rectum and nodular mucosa extending to the anorectal junction (black arrow), with abnormal mucosa distending the anal canal (double arrow).

The transitional zone is an area in which metaplasia and reserve cell hyperplasia occur in a manner similar to that in the transitional zone of the uterine cervix and gastroesophageal junction.⁸⁶ It has therefore been postulated that some tumors arise in this region in areas of chronic inflammation, squamous metaplasia, and reserve cell hyperplasia, resulting in dysplasia and subsequent carcinoma. For example, homosexual men have a high incidence of squamous cell carcinoma of the anus. These tumors are associated with venereally transmitted human papillomavirus.⁸⁷⁻⁸⁹ Other oncogenic viruses, carcinogens in lubricants and cleansers, and mechanical irritation may also play a role.⁸⁷⁻⁹²

Cloacogenic carcinomas have no distinctive gross pathologic or radiologic features. Patients usually present with rectal bleeding or pain or altered bowel habits. These tumors may be flat, infiltrative, annular, or ulcerative lesions with rolled borders. The tumors may appear on barium enema as submucosal masses with a smooth or ulcerated surface, as broad-based, sessile polypoid masses, or as infiltrative lesions (Fig. 60-12).^{93,94}

Metastases to sacral, internal iliac, and common iliac lymph nodes are found in approximately 50% of patients.

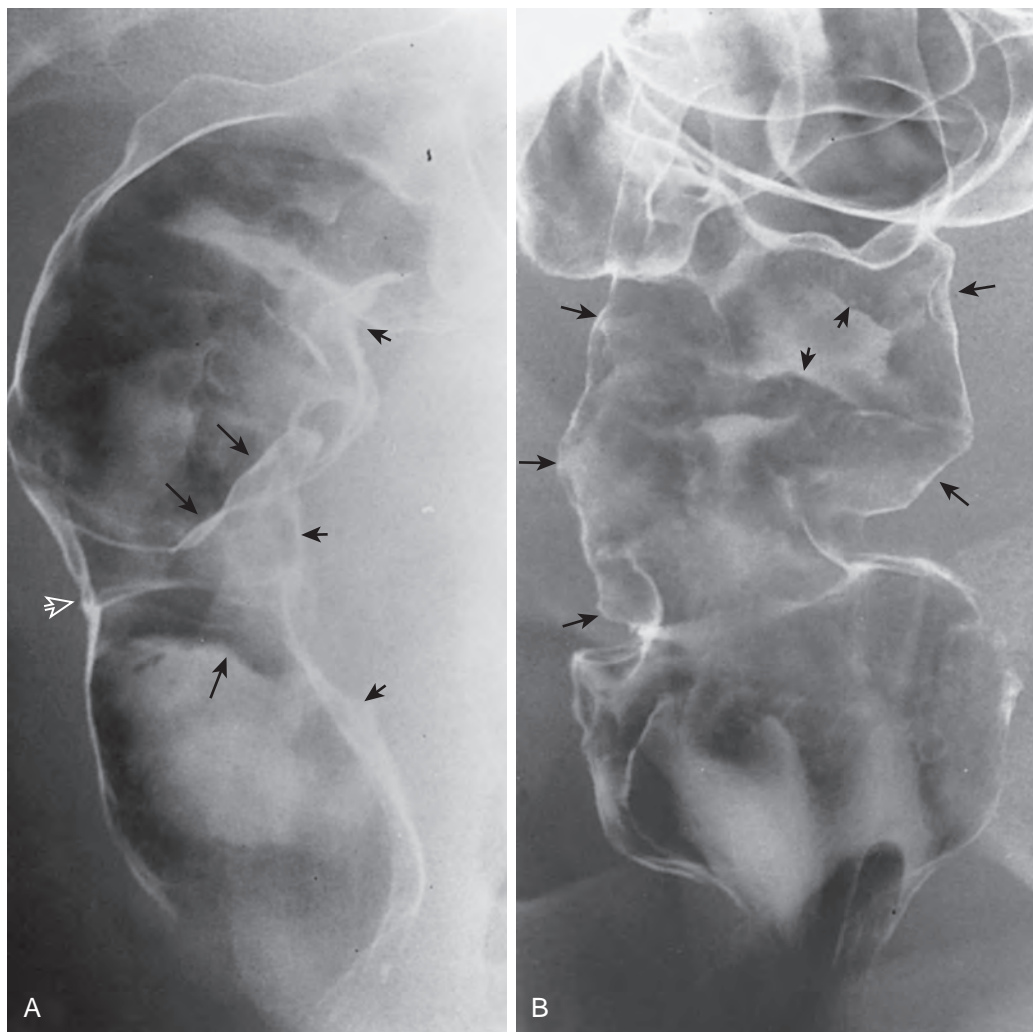


Figure 60-12 Basaloid carcinoma. **A.** Lateral view of the rectum shows the infiltrative pattern of cloacogenic carcinoma. The anterior wall of the rectum is moderately flattened and lobulated (*short arrows*), with thickened nodular folds traversing the rectum (*long arrows*). The rectal mucosa is relatively smooth. Focal circumferential extension of tumor around the rectum is seen as flattening of the posterior rectal wall (*open arrow*). **B.** Prone view of the rectum shows mild inbowing and irregularity of the contour of the lateral walls of the rectum (*long arrows*) and thickened nodular folds en face (*short arrows*).

Hematogenous metastases may also result from spread of tumor via the portal venous system and inferior vena cava. Patients with basaloid carcinoma have a 5-year survival rate of approximately 50%.³²

Metastases

Metastases to the colon are not uncommon.⁹⁵ It also is not uncommon for symptoms produced by GI metastases to occur as the initial manifestation of a primary malignancy. Colonic metastases are classified by their mode of dissemination as follows⁹⁶: (1) direct invasion from a contiguous primary tumor or noncontiguous primary tumor; (2) intraperitoneal seeding; and (3) embolic metastases.

Imaging studies may not only identify the lesion as a metastasis to the colon, but also indicate the mode of dissemination and most likely origin of malignancy.⁹⁷ Detection of these

metastases is also important because localized embolic metastases may be resected for cure or for control of complications, such as GI bleeding or obstruction. Recognition of colonic invasion by tumor also enables the surgeon to perform a wider excision or, if necessary, a diverting colostomy.⁹⁸

DIRECT INVASION FROM CONTIGUOUS PRIMARY TUMORS

The most common tumors that directly invade the colon include carcinoma of the ovary, kidney, uterus, cervix, prostate, and gallbladder, as discussed here.

Prostatic carcinoma may spread via Denonvillier's fascia to invade the rectum anteriorly or circumferentially.⁹⁹ Rectal involvement by prostatic carcinoma occurs in 0.5% to 11.5% of patients.¹⁰⁰⁻¹⁰² Affected individuals may present with obstructive symptoms, constipation, or rectal bleeding.¹⁰²

Although the normal prostate abuts the distal rectum, most patients with prostatic carcinoma invading the colon have involvement of the rectosigmoid junction, with distal rectal sparing.^{99,104} Prostatic carcinoma usually spreads cranially to involve the seminal vesicles before invading the rectum posteriorly. Thus, on barium enema examination, early cases may manifest an extrinsic mass effect, predominantly on the anterior border of the rectosigmoid junction. With colonic invasion, mucosal pleating and tethering are seen en face and a spiculated contour is seen in profile. In advanced cases, the rectum is circumferentially narrowed, with a widened presacral space and spiculated contour.^{99-101,103} In some cases, prostatic carcinoma invades posteriorly to involve the lower rectum (Fig. 60-13). The major consideration in the differential diagnosis is direct invasion of the rectum by a contiguous pelvic tumor such as carcinoma of the urinary bladder.

When left-sided ovarian carcinoma directly invades the colon, it first involves the inferior border of the sigmoid colon.¹⁰⁴ Colonic wall invasion is indicated by angulation of the affected sigmoid loops, spiculation of the colonic contour, and tethering and angulation of mucosal folds en face (Fig. 60-14). Rarely, a fistula to the sigmoid colon may be seen.¹⁰⁵

Renal cell carcinoma or recurrent renal cell carcinoma in the retroperitoneum may directly invade the colon.^{96,104,106} Left-sided renal cell carcinomas usually invade the splenic flexure or the distal transverse or proximal descending colon,⁹⁶ whereas right-sided renal cell carcinomas invade the descending duodenum. Colonic invasion by renal cell carcinoma is usually

manifested on barium enema by bulky intraluminal masses, without signs of obstruction.⁹⁶

DIRECT INVASION FROM NONCONTIGUOUS PRIMARY TUMORS

Malignancies may spread in the subperitoneal space or by lymphatic permeation.⁹⁶ Examples of this mode of dissemination include colonic carcinoma invading the stomach via the gastocolic ligament,¹⁰⁷ pancreatic carcinoma invading the transverse colon via the transverse mesocolon, gastric carcinoma invading the transverse colon via the gastocolic ligament,⁹⁶ and colonic carcinoma invading contiguous loops of small bowel or colon.¹⁰⁸ The gastocolic ligament (the proximal part of the greater omentum) is the anatomic bridge between the greater curvature of the stomach and superior border of the transverse colon (Fig. 60-15).¹⁰⁴ When gastric carcinoma spreads to the transverse colon via the gastocolic ligament, mass effect, fixation, and fold spiculation are initially seen along the superior border of the transverse colon, with sacculation of the uninvolved inferior border. Rarely, the involved colon may have a cobblestone-like appearance indistinguishable from that of Crohn's disease. The major considerations in the differential diagnosis include gastric carcinoma invading the transverse colon and an omental cake from peritoneal metastasis secondarily invading the transverse colon.¹⁰⁹

The transverse mesocolon courses from the retroperitoneum overlying the pancreas to the inferior border of the transverse colon.⁹⁷ Therefore, when pancreatic carcinoma invades

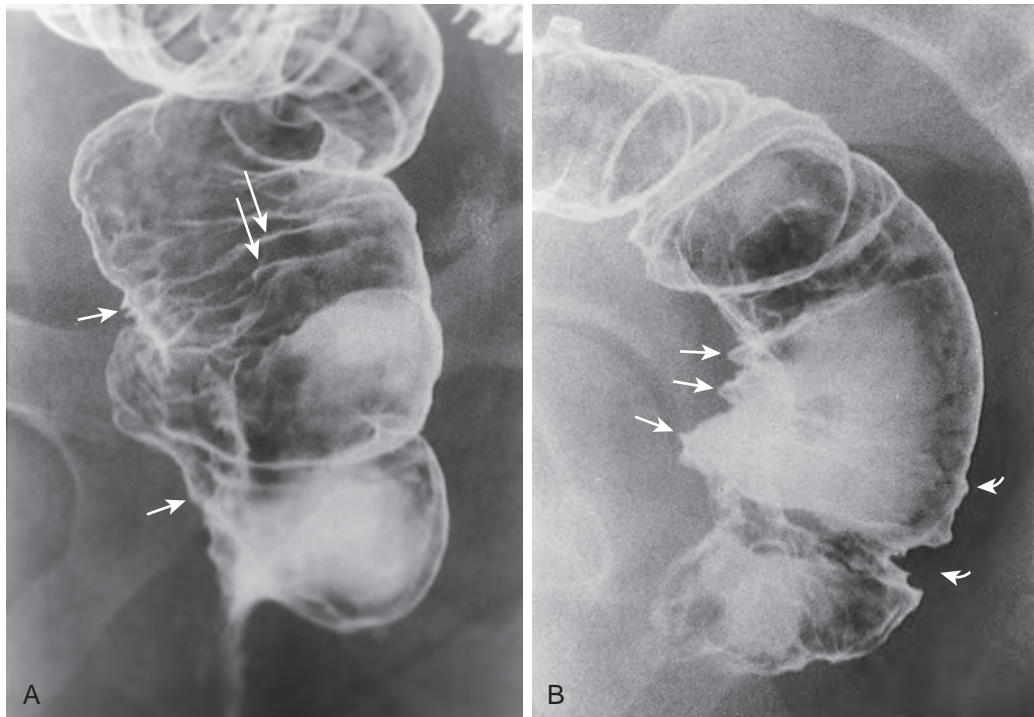


Figure 60-13 Rectal invasion by prostatic carcinoma. **A.** Frontal view of the rectum shows mass effect and spiculation predominantly along the right lateral wall of the rectum (short arrows) and pleating of the mucosa en face (long arrows). Invasion of the mucosa and submucosa was confirmed on biopsy specimens of the right lateral rectal wall. **B.** Lateral view of the rectum shows mass effect along the anterior rectal wall and spiculation of the mucosal contour (straight arrows). Mild circumferential extension is seen distally (curved arrows). (From Rubesin SE, Levine MS, Bezzi M, et al: Rectal involvement by prostatic carcinoma: Radiographic findings. *AJR* 152:53-57, 1989.)



Figure 60-14 Direct colonic invasion by left ovarian carcinoma. Close-up view of an overhead radiograph from a double-contrast barium enema shows spiculation and mass effect along the inferior border of the sigmoid colon (open arrows) and pleating of the mucosa of the rectosigmoid junction en face (solid arrow).

the transverse colon via the transverse mesocolon, the initial radiographic changes occur on the inferior border of the transverse colon.⁹⁶ Despite these anatomic attachments, pancreatic carcinoma may occasionally spread to the superior border of the transverse colon (Fig. 60-16). Carcinoma of the pancreatic tail may extend along the phrenicocolic ligament to invade the medial border of the splenic flexure.⁹⁷

INTRAPERITONEAL SEEDING

The most common primary tumors that seed the peritoneal cavity are ovarian carcinoma in women and gastric, pancreatic, and colonic carcinomas in men. When appendiceal mucinous adenocarcinomas spread intraperitoneally, they result in a condition termed *pseudomyxoma peritonei*. Occasionally, lymph node metastases to the retroperitoneum or mesentery from breast carcinoma or other malignant tumors may secondarily seed the peritoneal cavity. Other tumors that spread intraperitoneally include carcinoma of the bladder, uterus, and cervix and hepatocellular carcinoma.

The peritoneal cavity is separated into various compartments by peritoneal reflections and mesenteries (Fig. 60-17).¹¹³ The transverse mesocolon divides the abdomen into the supramesocolic and inframesocolic spaces.^{110,111} The small bowel mesentery divides the inframesocolic space into small right

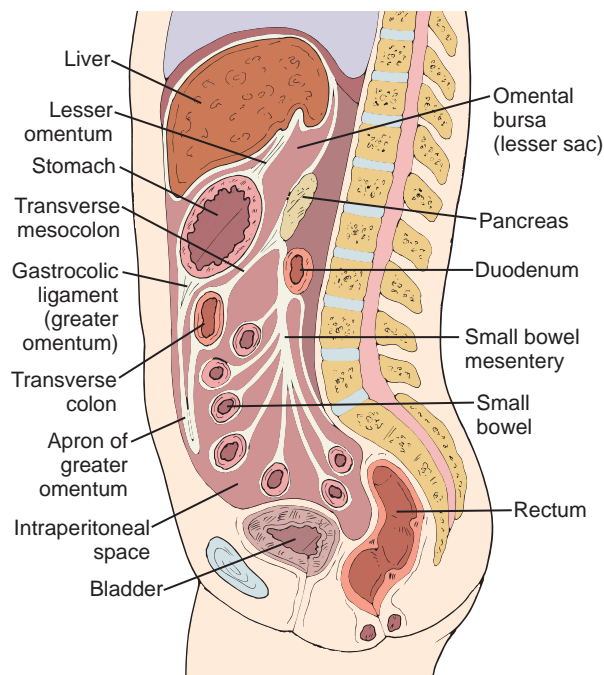


Figure 60-15 Sagittal line drawing of the abdomen. The proximal part of the greater omentum (gastrocolic ligament) bridges the greater curvature of the stomach with the anterosuperior border of the transverse colon. Thus, when gastric or omental processes directly invade the colon, the superior border of the transverse colon is involved first. The transverse mesocolon suspends the transverse colon from the retroperitoneum overlying the pancreas. (Adapted from Rubesin SE, Fishman EK: *Peritoneal metastasis*. In Fishman EK, Jones B [eds]: *Computed Tomography of the Gastrointestinal Tract*. New York, Churchill Livingstone, 1986.)



Figure 60-16 Pancreatic carcinoma invading the transverse colon. Overhead radiograph from a double-contrast barium enema shows extrinsic mass effect and spiculation along the superior border of the transverse colon (arrow). Contrast medium is present in the renal collecting systems from a prior intravenous urogram.

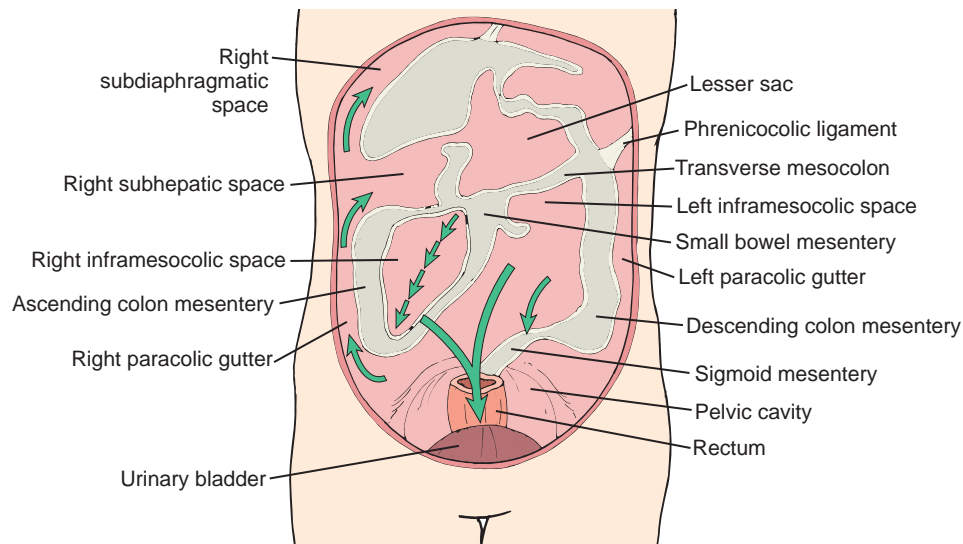


Figure 60-17 Directed flow of intraperitoneal fluid. The peritoneal reflections direct the flow of intraperitoneal fluid within the peritoneal cavity. Flow from the left inframesocolic space pools in the sigmoid mesentery along the superior border of the sigmoid colon and then courses into the pelvic cavity (pouch of Douglas in women, rectovesical space in men, and pararectal spaces). Flow in the right inframesocolic space courses down the ruffles of the small bowel mesentery into the right lower quadrant along distal small bowel loops and medial border of the cecum and then into the pelvic cavity from this region. Fluid from the pelvic cavity then courses up the right paracolic gutter to the right subhepatic space and right subdiaphragmatic space. Thus, the sites of pooling of ascitic fluid (superior border of the sigmoid colon, pouch of Douglas or rectovesical space, medial border of the cecum, mesenteric border of the distal small bowel, and right paracolic gutter) are the predominant sites for intraperitoneal seeding by tumor.

and large left regions.¹¹¹ The phrenicocolic ligament partially separates the left subphrenic space from the left paracolic gutter, extending from the splenic flexure of the colon to the peritoneum overlying the 11th rib.¹¹⁰ These peritoneal reflections direct the flow of intraperitoneal fluid, affecting the distribution and deposition of intraperitoneal-seeded infections and metastases. Directed flow results in characteristic sites of tumor deposition. As the most dependent portion of the peritoneal cavity in the supine and upright positions, the pouch of Douglas or rectovesical space is the most common site for intraperitoneal metastases (occurring in 56% of cases) (Fig. 60-18).¹¹⁰ Other sites include the right lower quadrant small bowel loops and medial border of the cecum (41%), superior border of the sigmoid colon (21%), lateral border of the ascending colon (the right paracolic gutter) (18%), and transverse colon.¹¹⁰

Radiographic Findings

Independent of the site of intraperitoneal-seeded metastases, the radiographic findings are similar. Initially, there is extrinsic mass effect along the side of the bowel wall bathed in peritoneal fluid. Direct invasion of the serosa or muscular layers of the bowel wall by tumor incites a desmoplastic reaction. On barium enema, this desmoplastic reaction is manifested in profile by spiculation of the luminal contour and en face by tethering and pleating of mucosal folds in a fixed, parallel, or angulated pattern.^{109,112} Angulation of bowel loops occurs predominantly in the sigmoid colon and small bowel. The major considerations in the differential diagnosis of serosal desmoplastic disease in the pouch of Douglas (or rectovesical space in men) include endometriosis, prostatic or cervical carcinoma invading the rectum, and an inflammatory process in the pouch of Douglas or rectovesical space such as a tubo-ovarian abscess or abscess caused by diverticulitis, appendicitis,

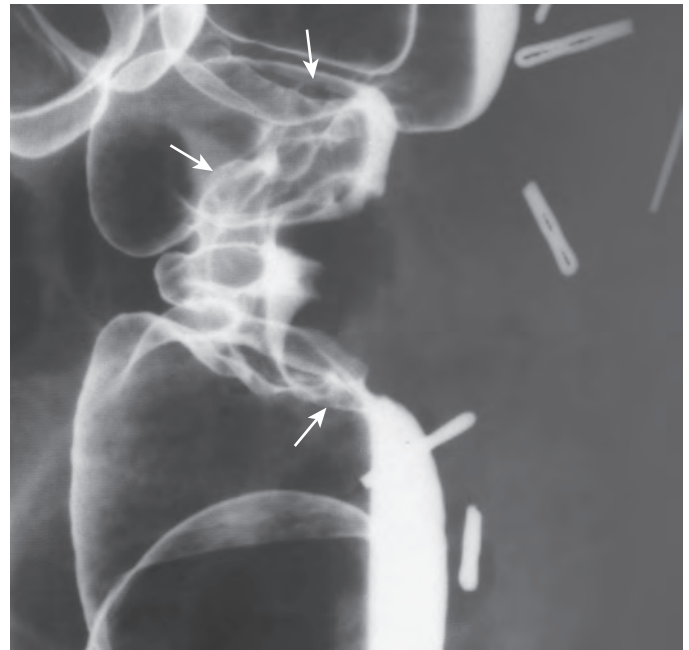


Figure 60-18 Intraperitoneal metastases from ovarian cancer invading the rectosigmoid junction. Left side-down decubitus radiograph from double-contrast barium enema shows mass effect (arrows) on the left anterolateral wall of the rectosigmoid junction. The contour is spiculated. The mucosa, although thrown into thick folds, is smooth.

or Crohn's disease. The clinical history, physical findings, and age of the patient usually allow differentiation of the various causes.

Cecal metastases are invariably accompanied by small bowel changes, including scalloping of the mesenteric border of right

lower quadrant ileal loops, fixation and angulation of loops, and spiculation of the luminal contour.¹⁰⁴

When peritoneal metastases involve the greater omentum, they may secondarily abut and invade the serosa of the transverse colon.¹¹³ These omental cakes initially involve the superior border of the transverse colon at the site of attachment of the greater omentum.¹⁰⁹ Mass effect may be seen along the superior border of the transverse colon on barium enema, with spiculation of the luminal contour and pleating and tethering of mucosal folds (Fig. 60-19). The major consideration in the differential diagnosis is gastric carcinoma invading the transverse colon via the gastocolic ligament. The clinical history and presence of metastases involving other portions of the colon should suggest the correct diagnosis.^{109,113} Inflammatory processes involving the gastocolic ligament, such as cholecystitis, pancreatitis, or diverticulitis, may produce identical radiographic findings.

EMBOLIC METASTASES

The most common primary tumors resulting in embolic metastases to the colon include malignant melanoma and breast and lung carcinoma. Carcinoma of the breast is the most common primary malignant tumor that spreads to the colon, but breast metastases to the colon are usually small lesions that cause no symptoms. More than 5% of those who die of metastatic breast carcinoma are found to have metastases to the colon at autopsy.¹¹⁴ These metastases may appear on barium enema as mural nodules, eccentric strictures, or irregular areas of circumferential narrowing, producing a linitis plastica appearance.⁹⁷ Hematogenous metastases may occasionally simulate Crohn's disease of the colon.

Metastases to the colon from carcinoma of the lung are usually small serosal deposits that cause no symptoms.⁹⁷ Occasionally, however, lung metastases cause GI bleeding or obstruction.¹¹⁵ These metastases may appear radiographically as ulcerated submucosal masses (target lesions), short eccentric segments of narrowing, or large mesenteric masses with secondary desmoplastic serosal changes.⁹⁷

Malignant melanoma involves the small intestine more frequently than it involves the colon. Metastatic melanoma is usually manifested on barium enemas by umbilicated or ulcerated submucosal masses or by bulky, polypoid intraluminal masses.

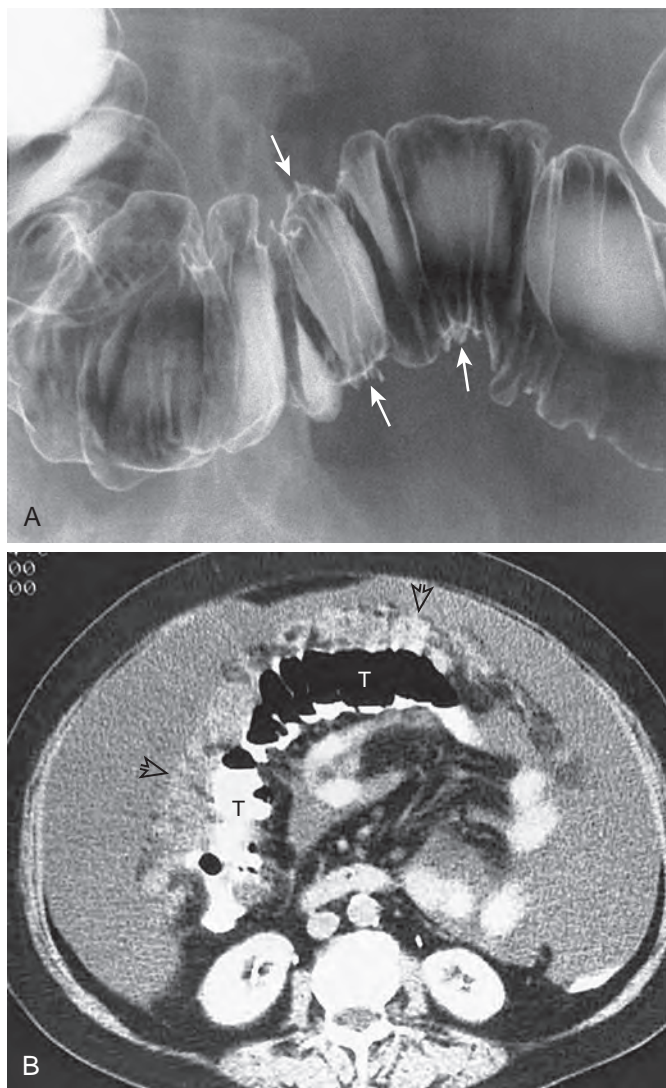


Figure 60-19 Omental cake from ovarian carcinomatosis invading the transverse colon. **A.** Spot image from a double-contrast barium enema shows spiculation of the colonic contour (arrows) and thin transverse stripes traversing the colon as a result of pleating of the mucosa. **B.** CT scan shows enlargement and increased attenuation of greater omentum caused by an omental cake (open arrows) along the anterior border of the transverse colon (T). A large amount of malignant ascites deviates the colon and small bowel loops medially. At surgery, intraperitoneal and greater omental metastases from ovarian carcinoma were found.

REFERENCES

- Weinsrad D, DeCosse JJ, Sherlock P, et al: Primary gastrointestinal lymphoma. *Cancer* 49:1258–1265, 1982.
- Lewin KJ, Ranchod M, Dorfman RF: Lymphomas of the gastrointestinal tract: A study of 117 cases presenting with gastrointestinal disease. *Cancer* 42:693–707, 1978.
- Herrman R, Panahon AM, Barcos MP, et al: Gastrointestinal involvement in non-Hodgkin's lymphoma. *Cancer* 46:215–222, 1980.
- Dragosics B, Bauer P, Radaszkiewicz T: Primary gastrointestinal non-Hodgkin's lymphomas: A retrospective clinicopathologic study of 150 cases. *Cancer* 55:1060–1073, 1985.
- Messinger NH, Bobroff LM, Beneventano TC: Lymphosarcoma of the colon. *AJR* 117:281–286, 1973.
- Wychulis AR, Beahrs OH, Woolner LB: Malignant lymphoma of the colon. *Arch Surg* 93:215–225, 1966.
- Wolf BS, Marshak RH: Roentgen features of diffuse lymphosarcoma of the colon. *Radiology* 75:733–740, 1960.
- Cornes JS, Wallace MH, Morson BC: Benign lymphomas of the rectum and anal canal. *J Pathol Bacteriol* 82:371–382, 1961.
- Marshak RH, Lindner AE, Maklansky D: Lymphoreticular disorders of the gastrointestinal tract: Roentgenographic features. *Gastrointest Radiol* 4:103–120, 1979.
- Shepherd NA, Hall PA, Williams GT, et al: Primary malignant lymphoma of the large intestine complicating chronic inflammatory bowel disease. *Histopathology* 15:325–327, 1989.
- Hill DH, Mill M, Maxwell RJ: Metachronous colonic lymphomas complicating ulcerative colitis. *Abdom Imaging* 18:369–370, 1993.
- Horton KM, Fishman EK: Multifocal primary colonic lymphoma in a patient with posttransplantation lymphoproliferative disease: CT findings. *AJR* 170:1998, 1672.

13. Heise W: GI-lymphomas in immunosuppressed patients (organ transplantation, HIV). *Best Pract Res Clin Gastroenterol* 24:57–59, 2010.
14. Kawamoto K, Motooka M, Hirata N, et al: Colonic submucosal tumors: New classification based on radiologic characteristics. *AJR* 160:315–320, 1993.
15. O'Connell DJ, Thompson AJ: Lymphoma of the colon: The spectrum of radiologic changes. *Gastrointest Radiol* 2:377–385, 1978.
16. Zornoza J, Dodd GD: Lymphoma of the gastrointestinal tract. *Semin Roentgenol* 15:272–287, 1980.
17. Bragg DG, Colby TV, Ward JH: New concepts in the non-Hodgkin lymphomas: Radiologic implications. *Radiology* 159:289–304, 1986.
18. Pochaczewsky R, Sherman RS: Diffuse lymphomatous disease of the colon: Its roentgen appearance. *AJR* 87:670–684, 1962.
19. Williams SM, Berk RN, Harned RK: Radiologic features of multinodular lymphoma of the colon. *AJR* 143:87–91, 1984.
20. Wyatt SH, Fishman EK, Jones B: Primary lymphoma of the colon and rectum: CT and barium correlation. *Abdom Imaging* 18:376–380, 1993.
21. Fléjou J-F: Non-epithelial tumors of the large intestine. In Shepherd NA, Warren BF, Williams GT, et al, editors: *Morson and Dawson's Gastrointestinal Pathology*, ed 5, Chichester, England, 2013, Wiley-Blackwell, pp 733–747.
22. Issacson PG, Wright DH: Gut-associated lymphoid tumors. In Whitehead R, editor: *Gastrointestinal and Oesophageal Pathology*, Edinburgh, 1995, Churchill Livingstone, pp 755–775.
23. Harned RK, Doby CA, Farley GE: Cavernous hemangioma of the rectum and appendix. *Dis Colon Rectum* 17:759–762, 1974.
24. Camilleri M, Chadwick VS, Hodgson HJ: Vascular anomalies of the gastrointestinal tract. *Hepatogastroenterology* 31:149–153, 1984.
25. Dachman AH, Ros PR, Shekitka KM, et al: Colorectal hemangioma: Radiologic findings. *Radiology* 167:31–34, 1988.
26. Lyon DT, Mantea AG: Large-bowel hemangiomas. *Dis Colon Rectum* 27:404–414, 1984.
27. Allred HW, Jr, Spencer JC: Hemangiomas of the colon, rectum, and anus. *Mayo Clin Proc* 49:739–741, 1974.
28. Mills CS, Lloyd TV, Van Aman ME, Lucas J: Diffuse hemangiomatosis of the colon. *J Clin Gastroenterol* 7:416–421, 1985.
29. Ghahremani GG, Kangaroo H, Volberg F, et al: Diffuse cavernous hemangioma of the colon in the Klippel-Trenaunay syndrome. *Radiology* 118:673–678, 1976.
30. Perez C, Andreu J, Llauger J, et al: Hemangioma of the rectum: CT appearance. *Gastrointest Radiol* 12:347–349, 1987.
31. Gandolfi L, Rossi A, Stasi G, Tonti R: The Klippel-Trenaunay syndrome. *Gastrointest Endosc* 33:442–445, 1987.
32. Goboes K: Rare and secondary (metastatic) tumors. In Whitehead R, editor: *Gastrointestinal and Oesophageal Pathology*, Edinburgh, 1995, Churchill Livingstone, pp 910–924.
33. Reinhart WH, Staubli M, Mordasini C, et al: Abnormalities of the gut vessels in Turner's syndrome. *Postgrad Med J* 59:122–124, 1983.
34. Margulis AR: Case: Hemangioma of the rectum. *Gastrointest Radiol* 6:363–364, 1981.
35. Lawson JP, Myerson PJ, Myerson DA: Colonic lymphangioma. *Gastrointest Radiol* 1:85–89, 1976.
36. Camilleri M, Satti MB, Wood CB: Cystic lymphangioma of the colon. *Dis Colon Rectum* 25:813–816, 1982.
37. Arnet NL, Friedman PS: Lymphangioma of the colon: Roentgen aspects, a case report. *Radiology* 67:882–885, 1956.
38. Agha FP, Francis IR, Simms SM: Cystic lymphangioma of the colon. *AJR* 141:709–710, 1983.
39. Kawamoto K, Ueyama T, Iwashita I, et al: Colonic submucosal tumors: Comparison of endoscopic US and target air-enema CT with barium enema study and colonoscopy. *Radiology* 192:697–702, 1994.
40. Young T-H, Ho A-S, Tang HS, et al: Cystic lymphangioma of the transverse colon: Report of a case and review of the literature. *Abdom Imaging* 21:415–417, 1996.
41. Price AB: Angiodysplasia of the colon. *Int J Colorectal Dis* 1:121–128, 1986.
42. Baum S, Athanasoulis C, Waltman A, et al: Angiodysplasia of the right colon: A cause of gastrointestinal bleeding. *AJR* 129:789–794, 1977.
43. Galloway SJ, Casarella WJ, Shimkin PM: Vascular malformations of the right colon as a cause of bleeding in patients with aortic stenosis. *Radiology* 113:11–15, 1974.
44. Thompson GB, Pemberton JH, Morris S, et al: Kaposi's sarcoma of the colon in a young HIV-negative man with chronic ulcerative colitis. *Dis Colon Rectum* 32:73–76, 1989.
45. Mesri EA, Cesarman E, Boshoff C: Kaposi's sarcoma and its associated herpesvirus. *Nat Rev Cancer* 10:707–719, 2010.
46. Godwin DJ: Carcinoid tumors: An analysis of 2837 cases. *Cancer* 36:560–569, 1975.
47. Martensson H, Nobin A, Sundler F: Carcinoid tumours in the gastrointestinal tract—an analysis of 156 cases. *Acta Chir Scand* 149:607–616, 1983.
48. Shulman H, Giustra P: Invasive carcinoids of the colon. *Radiology* 98:139–143, 1971.
49. Williams GT: Endocrine tumors of the gastrointestinal tract—selected topics. *Histopathology* 50:30–41, 2007.
50. Modlin IM, Sandor A: An analysis of 8305 cases of carcinoid tumors. *Cancer* 79:813–829, 1997.
51. Balthazar EJ: Carcinoid tumors of the alimentary tract. *Gastrointest Radiol* 3:47–56, 1978.
52. Fioca R, Capella C, Bufta R, et al: Glucagon-like, glycerin-like and pancreatic polypeptide-like immunoreactivities in rectal carcinoids and related colorectal cells. *Am J Pathol* 100: 81–92, 1980.
53. Jetmore AB, Ray JE, Gathright JB, et al: Rectal carcinoids: The most frequent rectal tumor. *Dis Colon Rectum* 35:717–725, 1992.
54. Sato T, Sakai Y, Sonoyama A, et al: Radiologic spectrum of rectal carcinoid tumors. *Gastrointest Radiol* 9:23–26, 1984.
55. Berardi RS: Carcinoid tumors of the colon (exclusive of the rectum): Review of the literature. *Dis Colon Rectum* 15:383–391, 1972.
56. Crittenden JJ, Byllesby J, Dodds W: Carcinoid tumor presenting as an annular lesion in the ascending colon. *Radiology* 97:85–86, 1970.
57. Haller JD, Roberts TW: Lipomas of the colon: A clinicopathologic study of 40 cases. *Surgery* 55:773–781, 1964.
58. Hurwitz MH, Redleaf PD, Williams HJ, et al: Lipomas of the gastrointestinal tract. *AJR* 99:84–89, 1967.
59. Castro DB, Stearns MW: Lipomas of the large intestine. *Dis Colon Rectum* 15:441–444, 1972.
60. Michowitz M, Lazebnik N, Noy S, Lazebnik R: Lipoma of the colon. A report of 22 cases. *Ann Surg* 51:449–454, 1985.
61. Ryan J, Martin JE, Pollock DJ: Fatty tumors of the large intestine: A clinicopathological review of 13 cases. *Br J Surg* 76:793–796, 1989.
62. Margulis AR, Jovanovich A: The roentgen diagnosis of submucous lipomas of the colon. *AJR* 84:1114–1120, 1960.
63. Kabaalioglu A, Gelen T, Aktan S, et al: Acute colonic obstruction caused by intussusception and extrusion of a sigmoid lipoma through the anus after barium enema. *Abdom Imaging* 22:389–391, 1997.
64. Wulff C, Jespersen N: Colocolic intussusception caused by lipoma: Case report. *Acta Radiol* 36:478–480, 1995.
65. Buetow PC, Buck JL, Carr NJ, et al: Intussuscepted colonic lipomas: Loss of fat attenuation on CT with pathologic correlation in 10 cases. *Abdom Imaging* 21:153–156, 1996.
66. Deeths TM, Dodds WJ: Lipoma of the colon. *Am J Gastroenterol* 58:326–331, 1972.
67. Heiken JP, Forde KA, Gold RP: Computed tomography as a definitive method for diagnosing gastrointestinal lipomas. *Radiology* 142:409–414, 1982.
68. Megibow AJ, Redmond PE, Bosniak MA, et al: Diagnosis of gastrointestinal lipomas by CT. *AJR* 133:743–745, 1979.
69. Liessi G, Pavanello M, Cesari S, et al: Large lipomas of the colon: CT and MR findings in three symptomatic cases. *Abdom Imaging* 21:150–152, 1996.
70. Geboes K: Rare and secondary (metastatic) tumors. In Whitehead R, editor: *Gastrointestinal and Oesophageal Pathology*, Edinburgh, 1989, Churchill Livingstone, pp 779–786.
71. Hinkel CL: Roentgenological examination and evaluation of the ileocecal valve. *AJR* 68:171–182, 1952.
72. El-Amin LC, Levine MS, Rubesin SE, et al: Ileocecal valve: Spectrum of normal findings at double-contrast barium enema examination. *Radiology* 227:52–58, 2003.
73. Rubin BP: Gastrointestinal stromal tumors: an update. *Histopathology* 48:83–96, 2006.
74. Miettinen M, Lasota J: Gastrointestinal stromal tumors: Review on morphology, molecular pathology, prognosis, and differential diagnosis. *Arch Pathol Lab Med* 130:1466–1478, 2006.
75. Downs-Kelly E, Rubin BP, Goldblum JR: Stromal tumors of the stomach. In Shepherd NA, Warren BF, Williams GT, et al, editors: *Morson and Dawson's Gastrointestinal Pathology*, ed 5, Chichester, England, 2013, Wiley-Blackwell, pp 223–240.
76. Sugimura H, Tamura S, Yamada H, et al: Benign nerve sheath tumor of the sigmoid colon. *Clin Imaging* 17:64–66, 1993.
77. Hirtola S, Isozaki K, Moriyama Y, et al: Gain-of-function mutations of *c-kit* in human gastrointestinal stromal tumors. *Science* 279: 577–580, 1998.
78. Ma CK, De Peralta MN, Amin MB, et al: Small intestinal stromal tumors: A clinicopathologic study of 20 cases with immunohistochemical assessment of cell differentiation and the prognostic role of proliferation antigens. *Am J Clin Pathol* 108:641–651, 1997.
79. Rao BK, Kapur MM, Roy S: Leiomyosarcoma of the colon: A case report and review of literature. *Dis Colon Rectum* 23:184–190, 1980.

80. Miettinen M, Sarlomo-Rikala M, Sobin LH, Lasota J: Gastrointestinal stromal tumors and leiomyosarcomas in the colon. A clinicopathologic, immunohistochemical, and molecular genetic study of 44 cases. *Am J Surg Pathol* 24:1339–1352, 2000.
81. Miettinen M, Sarlomo-Rikala M, Sobin LH: Mesenchymal tumors of muscularis mucosae of colon and rectum are benign leiomyomas that should be separated from gastrointestinal stromal tumors—a clinicopathologic and immunohistochemical study of eighty-eight cases. *Mod Pathol* 14:950–956, 2001.
82. Radin DR, Kiyabu M: Multiple smooth-muscle tumors of the colon and adrenal gland in an adult with AIDS. *AJR* 159:545–546, 1992.
83. Williams GT, Blackshaw AJ, Morson BC: Squamous carcinoma of the colorectum and its genesis. *J Pathol* 129:139–147, 1979.
84. Guenther T: Tumours and tumour-like conditions of the anorectal junction. In Shepherd NA, Warren BF, Williams GT, et al, editors: *Morson and Dawson's Gastrointestinal Pathology*, ed 5, Chichester, England, 2013, Wiley-Blackwell, pp 771–792.
85. Sunesen K, Norgaard M, Thorlacius-Ussing O, Laurberg S: Immunosuppressive disorders and risk of anal squamous cell carcinoma. A nationwide cohort study in Denmark, 1979–2005. *Int J Cancer* 127:675–684, 2009.
86. Fenger C: The anal canal epithelium: A review. *Scand J Gastroenterol* 14(Suppl):114–117, 1979.
87. Vernon SD, Unger ER, Reeves WC: Human papillomaviruses and anogenital cancer. *N Engl J Med* 338:921–922, 1998.
88. Shah KV: Human papillomaviruses and anogenital cancers. *N Engl J Med* 337:1386–1388, 1997.
89. Frisch M, Glimelius B, van den Brule AJ, et al: Sexually transmitted infection as a cause of anal cancer. *N Engl J Med* 337:1350–1359, 1997.
90. Austin DR: Etiological clues from descriptive epidemiology: Squamous carcinoma of the rectum or anus. *Natl Cancer Inst Monogr* 62:89–90, 1982.
91. Peters RK, Mack TM: Patterns of anal carcinoma by gender and marital status in Los Angeles County. *Br J Cancer* 48:629–636, 1983.
92. Daling JR, Weiss NS, Klopfenstein LL, et al: Correlates of homosexual behavior and the incidence of anal cancer. *JAMA* 247:1988–1990, 1982.
93. Kyaw MM, Gallagher T, Haines JO: Cloacogenic carcinoma. *AJR* 115:384–391, 1972.
94. Glickman MG, Margulis AR: Cloacogenic carcinoma. *AJR* 107:175–180, 1969.
95. Wigh R, Tapley ND: Metastatic lesions to the large intestine. *Radiology* 70:222–229, 1958.
96. Meyers MA, McSweeney J: Secondary neoplasms of the bowel. *Radiology* 105:1–11, 1972.
97. Meyers MA: *Dynamic Radiology of the Abdomen: Normal and Pathologic Anatomy*, ed 3, New York, 1988, Springer.
98. Gedgaudas RK, Kelvin FM, Thompson WM, et al: The value of pre-operative barium enema in the assessment of pelvic masses. *Radiology* 146:609–613, 1983.
99. Becker JA: Prostatic carcinoma involving the rectum and sigmoid colon. *AJR* 94:421–428, 1965.
100. Gengler L, Baer J, Finby N: Rectal and sigmoid involvement secondary to carcinoma of the prostate. *AJR* 125:910–917, 1975.
101. Winter CC: The problem of rectal involvement by prostatic cancer. *Surg Gynecol Obstet* 105:136–140, 1957.
102. Fry DE, Amin M, Harbrecht PJ: Rectal obstruction secondary to carcinoma of the prostate. *Ann Surg* 189:488–492, 1979.
103. Rubesin SE, Levine MS, Bezzi M, et al: Rectal involvement by prostatic carcinoma: Radiographic findings. *AJR* 152:53–57, 1989.
104. Meyers MA: Intraperitoneal spread of malignancies and its effect on the bowel. *Clin Radiol* 32:129–146, 1981.
105. Honda H, Lu CH, Barloon TT, et al: Sigmoid colon fistula complicating ovarian cystadenocarcinoma—a rare finding. *Gastrointest Radiol* 15:78–81, 1990.
106. Khilnani MT, Wolf BS: Late involvement of the alimentary tract by carcinoma of the kidney. *Am J Dig Dis* 5:529–540, 1960.
107. Bachman AL: Roentgen appearance of gastric invasion from carcinoma of the colon. *Radiology* 63:814–822, 1954.
108. Goodman P, Balachandran S: Direct invasion of the transverse colon by a cecal tumor. *Abdom Imaging* 18:20–22, 1993.
109. Rubesin SE, Levine MS: Omental cakes: Colonic involvement by omental metastases. *Radiology* 154:593–596, 1985.
110. Meyers MA: Distribution of intraabdominal malignant seeding: Dependency on dynamics of flow of ascitic fluid. *AJR* 119:198–206, 1973.
111. Meyers MA: The spread and localization of acute intraperitoneal effusions. *Radiology* 95:547–554, 1970.
112. Ginaldi S, Lindell MM, Zornoza J: The striped colon: A new radiographic observation in metastatic serosal implants. *AJR* 134:453–455, 1980.
113. Krestin GP, Beyer D, Lorenz R: Secondary involvement of the transverse colon by tumors of the pelvis: Spread of malignancies along the greater omentum. *Gastrointest Radiol* 10:283–288, 1985.
114. Asch MJ, Wiedel PD, Habif DV: Gastrointestinal metastases from carcinoma of the breast: Autopsy study and 18 cases requiring operative intervention. *Arch Surg* 96:840–843, 1968.
115. Smith HJ, Vlask MG: Metastasis to the colon from bronchogenic carcinoma. *Gastrointest Radiol* 2:393–396, 1978.

Polyposis Syndromes

ANGELA D. LEVY | CARINA L. BUTLER | JAMES L. BUCK

CHAPTER OUTLINE

Familial Adenomatous Polyposis Syndrome

Colonic Manifestations

Extracolonic Gastrointestinal Manifestations

Extraintestinal Manifestations

Hamartomatous Polyposis Syndromes

Peutz-Jeghers Syndrome

Multiple Hamartoma Syndrome (Cowden Disease)

Juvenile Polyposis

Cronkhite-Canada Syndrome

Bannayan-Riley-Ruvalcaba Syndrome

The polyposis syndromes are rare but fascinating conditions. A thorough knowledge of the clinical and radiographic manifestations of these syndromes and their complications is required to provide optimal care for affected individuals and their families.

Familial Adenomatous Polyposis Syndrome

Familial polyposis coli, attenuated familial adenomatous polyposis, and Gardner syndrome are varying expressions of the same disease. Most cases are caused by the presence of an abnormal tumor suppressor gene (the *APC* gene) located on the long arm of chromosome 5.¹ As a result, the term *familial adenomatous polyposis syndrome* (FAPS) is used to refer to the entire spectrum of this disease.

FAPS is a relatively rare condition, but it is the most common of the polyposis syndromes.² Males and females are equally affected. FAPS has an autosomal dominant pattern of inheritance when associated with the *APC* gene mutation. However, up to 30% of patients have no family history of polyposis, suggesting the presence of spontaneous mutations or an association with a different mutation.^{3,4} A family history of polyposis or colorectal cancer therefore is not required for the diagnosis of FAPS. Penetrance is generally thought to be in the range of 80% to 100%, although in one series it was calculated to be less than 60%.⁵ In most families, comparative DNA testing alone can determine whether a family member is carrying the abnormal *APC* gene.⁶

In 5% to 30% of patients with FAPS, however, no *APC* mutation can be identified by current genetic testing.⁴ A different gene (the *MUTYH* gene) has also been linked to *APC*-negative patients with FAPS.⁴ Interestingly, FAPS associated with the *MUTYH* gene is thought to be inherited in an autosomal recessive fashion. The acronym MAP is used for *MUTYH*-associated polyposis. Synonyms include colorectal

adenomatous polyposis, autosomal recessive, multiple colorectal adenomas, autosomal recessive, and *MHY*-associated polyposis. Patients with the *MUTYH* mutation appear to have a milder form of the disease than those with the *APC* mutation.^{7,8} Patients with MAP have fewer polyps (10 to a few hundred, and occasionally few or none) compared to patients with FAP and an older mean age of 50 years at presentation.⁹ Extracolonic manifestations similar to those of FAP may occur, but with decreased incidence.

COLONIC MANIFESTATIONS

As the name implies, FAPS is predominantly associated with the development of adenomas. In the colon, where the polyposis is most severe, the polyps are usually tubular or tubulovillous adenomas. Occasionally, villous adenomas are also seen. The polyps usually appear at or near puberty and, eventually, an average of about 1000 colonic adenomas will develop.¹⁰ The adenomas of FAPS are usually small (80% are <5 mm in diameter) and sessile. The polyps involve all portions of the colon but may first appear distally. Rectal sparing occasionally may be seen.

A milder phenotype of FAPS, known as attenuated familial adenomatous polyposis syndrome (AFAPS), has recently been described. These patients generally present with 100 or fewer colonic adenomas.^{11,12} The adenomas tend to be located more proximally than those in classic FAPS, so sigmoidoscopy alone is inadequate for evaluating these patients.^{13,14} Colonic carcinoma also develops at an older age, with an average age of 55 years in patients with AFAPS versus an average age of 40 years in patients with classic FAPS. There is no current consensus on the diagnostic criteria for AFAPS, but it should be considered in a patient with a personal history of colorectal cancer before 60 years of age and a family history of multiple adenomatous polyps and in those with more than 10 but less than 100 polyps.¹⁵

The most common clinical symptoms encountered in FAPS are rectal bleeding and diarrhea, which occur in more than 75% of patients. Abdominal pain, anemia, and mucous discharge are less frequently noted.^{16,17} However, many patients with FAPS are asymptomatic. Regardless of symptoms, colonic carcinomas develop in almost every untreated patient and at a much younger age than in the general population.³ The average age of colon cancer in untreated patients is 39 years.^{17,18} Thus, DNA testing or serial colonic examinations after 10 years of age are recommended for other family members at risk for the disease.¹³

Total colectomy with mucosal proctectomy and ileoanal anastomosis is the procedure of choice for treatment because it eliminates all colonic and rectal mucosa.¹⁹ Surgical intervention should be performed by the late teenage years.¹⁷ After surgery, continued surveillance is necessary because any surgical procedure that restores intestinal continuity bears a continued risk of malignancy in the surgical remnant. For patients who have

undergone ileorectal anastomoses prior to current surgical recommendations for total colectomy with mucosal proctectomy and ileoanal anastomosis, completion surgery should be considered because recurring adenomas in the remaining rectal mucosa cannot be adequately controlled endoscopically.

The radiographic appearance of the colon in FAPS varies. Typically, innumerable small or moderate-sized sessile filling defects carpet the entire colon (Fig. 61-1A). Larger pedunculated polyps are less common. In some younger patients, however, the polyps may be more widely scattered (Fig. 61-1B). Correlation with colectomy specimens has shown that barium enemas markedly underestimate the number of polyps, especially in young patients, whose polyps are often smaller than 3 mm in diameter.¹⁸ Unfortunately, carcinomas still develop because of inadequate screening of family members at risk for

the disease. Carcinoma may be manifested by a dominant polyp (Fig. 61-2), saddle lesion, or advanced annular lesion (Fig. 61-3). As in the general population, carcinomas are usually found in the left side of the colon.

EXTRACOLONIC GASTROINTESTINAL MANIFESTATIONS

Extracolonic gastrointestinal (GI) manifestations of FAPS are well recognized.²⁰⁻²⁸ Fundic gland polyps are the most common gastric manifestation of FAPS in Western countries, occurring in up to 84% of patients.^{29,30} In FAPS, both genders are equally involved, whereas in the absence of FAPS, fundic gland polyps are more common in females.^{31,32} The polyps are frequently discovered in asymptomatic patients at an average age of 25 to

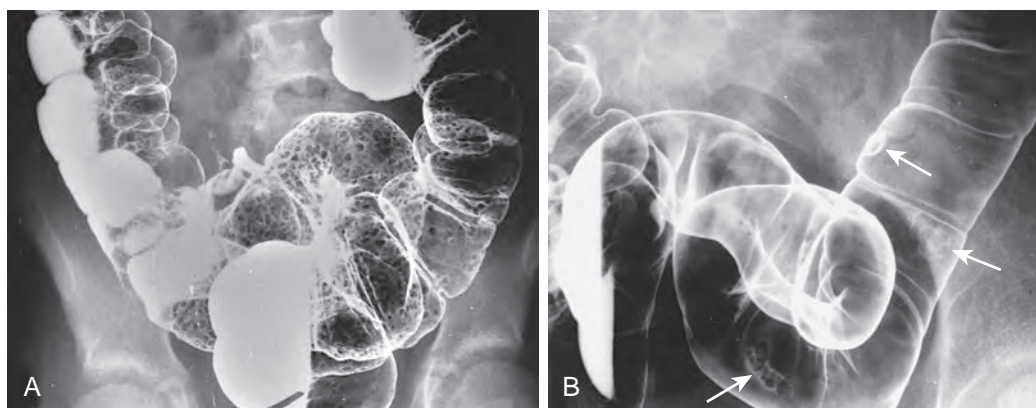


Figure 61-1 Various appearances of colonic involvement by familial adenomatous polyposis syndrome. **A.** In a 10-year-old boy, a double-contrast barium enema demonstrates innumerable small polyps in the colon, particularly carpeting the rectosigmoid region. **B.** In a 17-year-old girl, a double-contrast barium enema shows scattered, small to moderate-sized polyps (arrows) in the sigmoid colon.

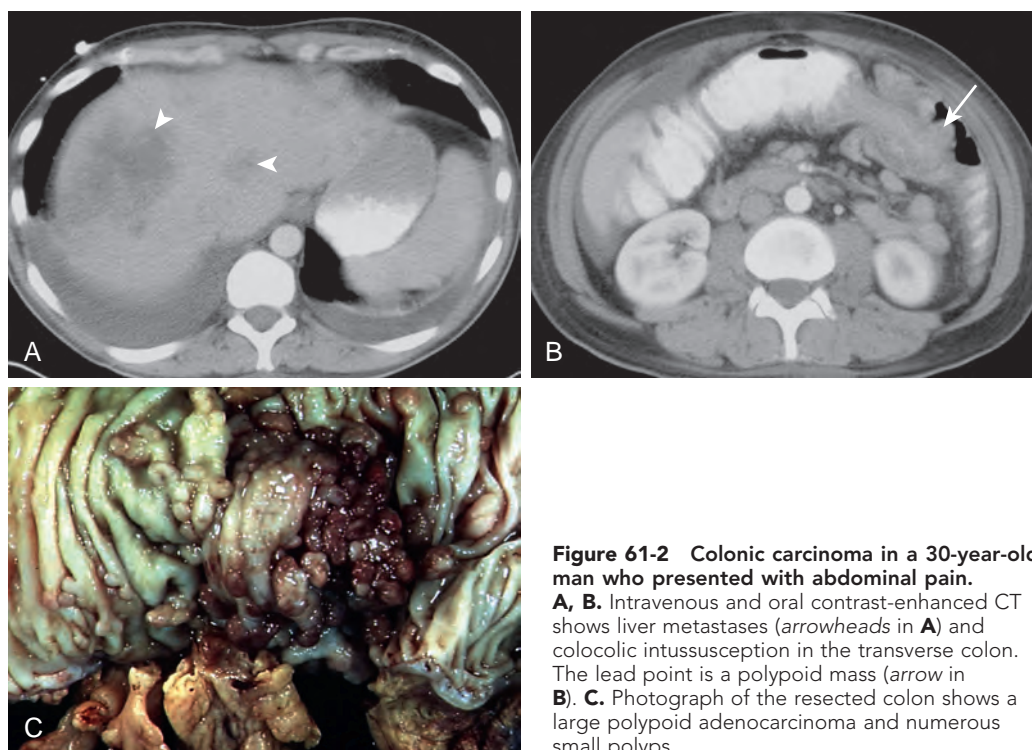


Figure 61-2 Colonic carcinoma in a 30-year-old man who presented with abdominal pain. **A, B.** Intravenous and oral contrast-enhanced CT shows liver metastases (arrowheads in **A**) and colocolic intussusception in the transverse colon. The lead point is a polypoid mass (arrow in **B**). **C.** Photograph of the resected colon shows a large polypoid adenocarcinoma and numerous small polyps.



Figure 61-3 Colonic carcinoma in familial adenomatous polyposis syndrome. An annular lesion is present in the sigmoid colon (arrow). Scattered small polyps are also present.

30 years and are almost invariably multiple, appearing as small sessile lesions ranging from 1 to 5 mm in diameter.³³ They are almost always confined to the fundus and body of the stomach. They are characteristically small (5–10 mm), smooth, sessile nodules protruding into the gastric lumen. There may be few or hundreds, which carpet the gastric fundus. On subsequent examinations, the polyps may progress, remain stable, or even resolve.^{34,35} These polyps have little tendency for malignant transformation, although gastric cancer has occasionally been reported in patients with preexisting fundic gland polyps.³²

Tubular and villous adenomas are also found in the stomach in patients with FAPS. In Japan, the incidence of gastric adenomas in FAPS ranges from 40% to 50%, whereas in Europe and North America, a lower incidence is reported.^{24,29} The higher incidence of adenomas associated with FAPS in Japan may be related to the higher frequency of adenomas and adenocarcinomas in the general population of that country.³⁷ Gastric adenomas are typically sessile polyps, ranging from 5 to 10 mm in diameter, and are multiple in over 50% of reported cases.³⁵ The adenomas are usually located in the distal stomach.³⁵ Unlike fundic gland polyps, gastric adenomas are premalignant lesions, so that periodic surveillance of the stomach is required.

The duodenum is the second most common site of GI disease in FAPS. Endoscopic examinations of asymptomatic patients in Japan have revealed tubular adenomas in more than 90% of cases.^{36–38} Other screening studies from Western countries have revealed adenomas in 47% to 72% of cases.^{39–41} The adenomas range from microscopic to 2 cm in diameter, with most being 5 mm or less. The polyps are usually found in the second portion of the duodenum, clustered around the papilla.³⁹

This differs from the typically bulbar distribution of adenomas in patients without FAPS.⁴⁰ Villous adenomas are also commonly found and, as in patients without FAPS, they tend to be located in the periampullary region of the duodenum. Villous adenomas are typically large and are even more likely to undergo malignant degeneration. It has been estimated that the lifetime incidence of periampullary carcinoma is as high as 12%, and that it is now the leading cause of cancer deaths in patients who have had a colectomy. It is therefore advocated that surveillance of the upper GI tract be performed in asymptomatic patients with FAPS beginning at 25 years of age.¹³

Adenomas in the jejunum and ileum have been identified in most patients in Japan who have undergone intraoperative small bowel endoscopy.³⁹ Small bowel endoscopy performed through a cutaneous ileostomy or ileoproctostomy has also revealed adenomas in approximately 20% of FAPS patients in Western countries.³⁶ As in the duodenum, these premalignant lesions are typically small and numerous. Although several cases of adenocarcinoma of the jejunum or ileum have been reported—coexisting adenomas have been found in all of these cases—the need for routine screening of the small bowel beyond the duodenum has not been established.⁴¹ Ileal lymphoid hyperplasia occurs more frequently in patients with FAPS than in the general population. The gross appearance of these lesions is similar to that of adenomas.⁴¹ However, lymphoid hyperplasia has no apparent clinical significance in these patients.

Biliary polyps are often found in patients with FAPS studied by endoscopic retrograde cholangiopancreatography.²⁶ Not surprisingly, cholangiocarcinoma and gallbladder carcinoma have also been reported in FAPS.^{42–47} Several cases of pancreatic carcinoma have been reported, and there is an increased incidence of pancreatitis in these patients.⁴⁹

EXTRAINTESTINAL MANIFESTATIONS

It was not until the 1950s that the extraintestinal manifestations of FAPS were well established. Gardner and Richards initially described a family of patients with adenomatous polyps of the colon, sebaceous cysts, and osteomas.^{48–50} Later, fibrous tumors and dental abnormalities were added to the list of lesions included in what was subsequently called *Gardner syndrome*.⁵¹ Numerous reports have subsequently confirmed the occurrence of these and other extraintestinal manifestations that have a tendency to appear in certain kindred affected by FAPS. The location of the defect in the *APC* gene and other intracellular factors appear to determine whether these manifestations are likely to appear.^{52,53} It is unusual to see all manifestations in the same patient.⁵⁴

Epidermoid (sebaceous) cysts are the skin lesions usually encountered in patients with FAPS. The cysts tend to be located on the face and scalp rather than on the back, as in the general population.⁴⁸ They are uncommon before puberty, but the presence of these cysts often precedes the recognition of colonic polyps. Otherwise, they have no clinical significance. Lipomas and small fibrous tumors of the skin are also found in FAPS.⁴⁸

Osteomas are another well-known manifestation of FAPS. Like epidermoid cysts, osteomas are usually unimportant unless they cause symptoms because of mass effect. In FAPS patients, these dense cortical lesions are usually found in the angle of the mandible, sinuses, and outer table of the skull (Fig. 61-4).^{55–60} Other flat bones and long bones may be involved. Bone islands are also quite common in the maxilla and mandible and may

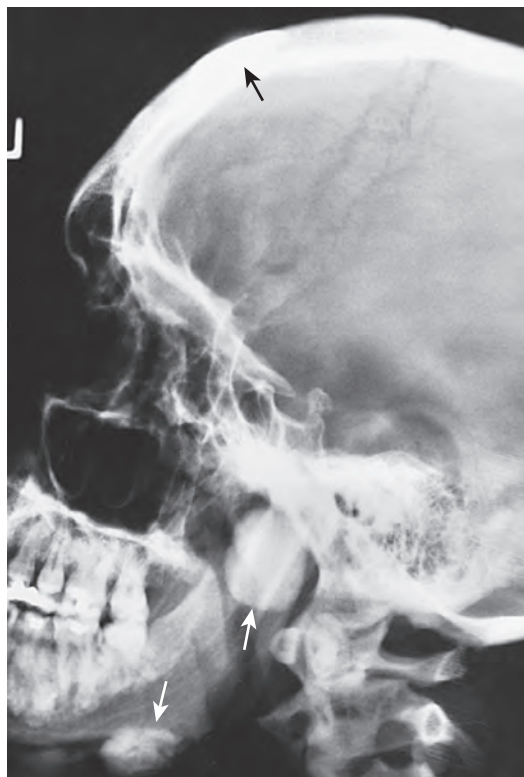


Figure 61-4 Multiple osteomas in a 23-year-old man with familial adenomatous polyposis syndrome. Lateral radiograph of the face and skull demonstrates two dense bony lesions (white arrows) arising from the mandible. A subtle lesion (black arrow) is also seen in the frontal bone.

be seen in other flat bones as well.⁵⁸⁻⁶⁰ In one series, localized or diffuse cortical thickening of the long bones was the most commonly identified bone abnormality in FAPS.⁵⁵ Dental abnormalities, particularly unerupted teeth, supernumerary teeth, dentigerous cysts, and odontomas, are also common.⁵⁹

Fibrous proliferation is a less common but more important feature of FAPS. An increased incidence of postoperative peritoneal adhesions occurs in FAPS, and retroperitoneal fibrosis has also been reported.⁶¹⁻⁶³ Usually, these patients develop fibrous tumors (particularly desmoid tumors of the abdominal wall) and mesenteric fibromatosis (Fig. 61-5). Histologically, desmoids are benign lesions but are nonencapsulated. In FAPS, these tumors often develop postoperatively, occurring within abdominal incisions, the peritoneal cavity, or the retroperitoneum.⁶² They usually develop in women of childbearing age and may grow rapidly or may first appear during pregnancy or after exposure to oral contraceptives.⁶² These tumors may recur locally after resection, and invasion of bowel is common. Death may result from intestinal or vascular obstruction, particularly when the lesions are located within the peritoneal cavity. With improvements in computed tomography (CT), more subtle, diffuse soft tissue infiltration of the mesentery can be identified, but this appearance is less likely to be associated with symptoms than is an actual mesenteric mass.⁶²

Congenital pigmented lesions of the retina are common in patients with FAPS; the prevalence of these lesions may be higher than 90%.⁶⁴⁻⁶⁸ Although similar lesions are occasionally found in the general population, the presence of large,

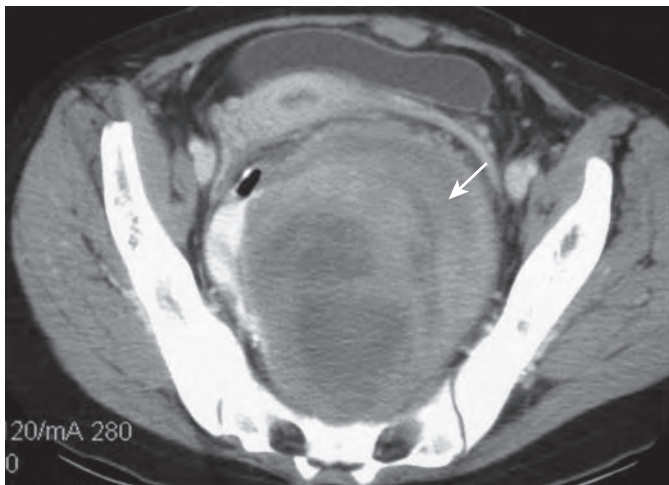


Figure 61-5 Mesenteric fibromatosis in a 25-year-old woman with familial adenomatous polyposis syndrome. She is status post total colectomy with ileoanal anastomosis. Intravenous and oral contrast-enhanced CT shows a large heterogeneous mass (arrow) arising in the small bowel mesentery adjacent to the ileoanal anastomosis.

multifocal, or bilateral pigmented lesions on fundoscopic examination is a strong indicator of FAPS. These lesions may occur before the development of colonic polyposis, serving as a marker for FAPS, but the absence of these lesions does not exclude FAPS.⁶⁸

Much has been learned about the association between colonic carcinoma and central nervous system malignancies, a condition traditionally known as Turcot syndrome.⁶⁹⁻⁷² Evidence suggests that many, if not most, of these cases (including those in the family first described by Turcot) are actually related to the hereditary nonpolyposis colon cancer syndrome (HNPCCS) and do not have abnormalities of the *APC* gene.⁷⁰ Nevertheless, central nervous system tumors are important extraintestinal manifestations of FAPS. There is clearly an increased incidence of medulloblastomas. There have also been case reports of benign intracranial tumors associated with FAPS, including intracranial epidermoid cysts and meningiomas.⁷¹ Glial tumors such as ependymomas and astrocytomas also occur in FAPS.⁷¹ However, many cases of glioblastoma multiforme associated with colonic adenomas or carcinomas that were reported in the past were probably related to HNPCCS.

The prevalence of thyroid carcinoma in FAPS has been calculated to be 160 times greater than that in the general population. Almost all reported cases are papillary, and they are frequently multifocal.⁷³⁻⁷⁵ In most series, affected individuals are girls or young women, and the thyroid carcinoma is usually detected before colonic polyposis becomes apparent. FAPS therefore should be suspected in young women with papillary carcinoma of the thyroid.⁷⁵ In one series, however, there was no female predominance in patients with thyroid carcinoma and FAPS.⁷⁴ Other endocrine tumors, including multiple endocrine neoplasia type 2, carcinoid tumors, and adrenocortical adenomas and carcinomas, have also been reported in patients with FAPS.⁷⁶⁻⁸⁰

Several tumors of the pancreas and liver have been reported in FAPS, including pancreatic carcinoma.⁸¹ Solid and papillary epithelial neoplasm, neuroendocrine tumors, and intraductal

papillary mucinous tumors of the pancreas have also been reported. Because of the rarity of these tumors, screening of FAPS patients for pancreatic lesions does not appear to be warranted. Hepatoblastomas have also been reported with increased frequency in the children of patients with FAPS.⁸²

Hamartomatous Polyposis Syndromes

The other polyposis syndromes, which occur less frequently than FAPS, include Peutz-Jeghers syndrome (PJS), multiple hamartoma syndrome (MHS), juvenile polyposis (JP), Cronkhite-Canada syndrome (CCS), and Bannayan-Riley-Ruvalcaba syndrome (BRRS). These conditions are collectively known as the hamartomatous polyposis syndromes.⁸²⁻⁸⁵ The term *hamartoma* implies a non-neoplastic tumor composed of normal tissue elements. Hamartomatous polyps may coexist with adenomatous polyps, explaining the association of alimentary tract adenocarcinoma with most of these syndromes, although they account for less than 1% of all colorectal carcinomas in North America.⁸⁶

PEUTZ-JEGHERS SYNDROME

PJS is an inherited condition characterized by a unique type of GI hamartoma, mucocutaneous pigmentation, neoplasms outside the alimentary tract, and an increased risk for GI carcinoma. PJS has an autosomal dominant pattern of inheritance and affects both genders equally. The only gene associated with PJS is a tumor suppressor gene, *STK11*, previously known as *LKB1* gene, located on chromosome 19.⁸⁵⁻⁸⁸ There are, however, a substantial number of PJS patients in whom there is no linkage to chromosome 19, suggesting that other genes also play a role in the development of this syndrome.

The characteristic feature of the PJS hamartoma is a smooth muscle core arising from the muscularis mucosae and extending into the polyp, much like the trunk and branches of a tree. The mucosa covering the polyp is similar to that normally found in the portion of the gut in which the polyp arises. Some PJS polyps may cause displacement of the epithelial elements within the submucosa, muscularis propria, and subserosa; this finding should not be mistaken for an invasive mucinous adenocarcinoma.⁸⁴

Mucocutaneous pigmentation is one of the most characteristic features of PJS. Brown or bluish-black macules usually occur on the lips and buccal mucosa (Fig. 61-6) and, less commonly, on the eyelids and dorsal surfaces of the fingers and soles of the feet. The pigmentation is rarely present at birth, usually appearing after the first or second year of life. The skin and lip pigmentation fades gradually in adulthood, whereas the macules on the buccal mucosa remain unchanged.^{83,86}

Most patients have recurrent episodes of abdominal pain related to small bowel intussusceptions caused by the hamartomatous polyps. These intussusceptions usually resolve spontaneously. However, persistent intussusceptions may cause small bowel obstruction, necessitating surgical intervention. Less frequently, patients may have rectal bleeding or melena. Life-threatening GI hemorrhage is extremely uncommon.⁸⁶

Patients with PJS are at increased risk for developing adenocarcinoma of the GI tract. Most of these carcinomas are located in the colon, followed in decreasing order of frequency, by the stomach, duodenum, and esophagus.⁸⁶ Although the exact prevalence of GI carcinoma is unclear, studies suggest that at least



Figure 61-6 Classic mucocutaneous pigmentation of Peutz-Jeghers syndrome. Bluish black macules are seen on the lips and buccal mucosa.

10% of patients with PJS develop GI cancer^{88,89} and that females with PJS are more likely to develop these tumors.^{86,90} It is uncertain whether carcinoma in PJS develops from malignant transformation of a hamartomatous polyp, from a coexisting adenomatous polyp, or de novo. However, cases of dysplasia and carcinoma occurring within a PJS hamartoma are well documented.⁹¹⁻⁹⁸

Patients with PJS are also at increased risk for developing extraintestinal malignancies, which have a reported prevalence of 10% to 30%. The most commonly implicated tumors include carcinoma of the pancreas, breast, and ovary.⁹⁹⁻¹⁰³ Pancreatic cancers in PJS have a tendency to develop at an unusually early age, with the risk estimated to be 200 times greater than that in the general population.^{99,101-105} Breast cancer tends to occur in young women, is usually ductal, and is commonly bilateral.¹⁰⁶ The risk for breast cancer in patients with PJS is similar in magnitude to that in patients with hereditary breast cancer (*BRCA1* and *BRCA2*).¹⁰⁷

Rare neoplasms of the reproductive tract may also occur in patients with PJS. Adenoma malignum is a uterine cervix cancer with a relatively benign histologic appearance but an aggressive biologic behavior.¹⁰⁸⁻¹¹¹ A benign ovarian tumor, designated as sex cord tumor with annular tubules (SCTAT), also commonly occurs in women with PJS.¹¹¹⁻¹¹³ These tumors are often bilateral, small or microscopic, and calcified, whereas in patients with SCTAT without PJS, the tumors are usually larger and unilateral.¹¹⁰ These benign ovarian tumors are capable of producing both estrogen and progesterone. In fact, hyperestrogenism may contribute to the increased incidence of breast carcinoma in patients with PJS. More common benign and malignant ovarian neoplasms also occur. Sertoli cell tumors of the testes have occasionally been reported in males with PJS. Like SCTAT, these tumors are benign, microscopic, and often bilateral. They may also produce estrogen, leading to gynecomastia.¹¹⁵ Other neoplasms reported less frequently in patients with PJS include benign and malignant tumors of the thyroid gland, gallbladder, ureter, urinary bladder, bronchus, and nasal cavity.^{99,101,114-118}

PJS hamartomas are found predominantly in the jejunum and ileum, followed by the duodenum, colon, and stomach (Figs. 61-7 and 61-8).¹¹⁹ Individual polyps vary in size and may be pedunculated or sessile. Pedunculated polyps are usually

Figure 61-7 Fluoroscopic features of Peutz-Jeghers syndrome. **A.** Spot radiograph from a double-contrast upper gastrointestinal series in a patient with Peutz-Jeghers syndrome shows a multilobulated polyp (arrow) on a stalk (arrowhead) in the stomach. **B.** Radiograph from a small bowel series in a different patient shows a lobular filling defect (arrowhead) in the jejunum from a hamartomatous polyp and intussusception (arrows).

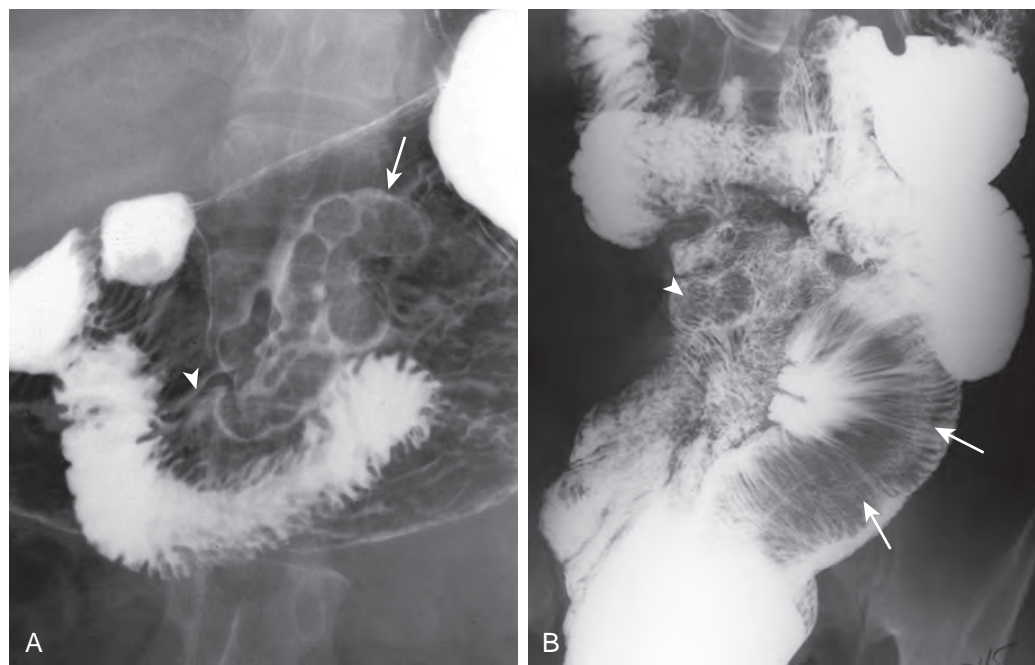
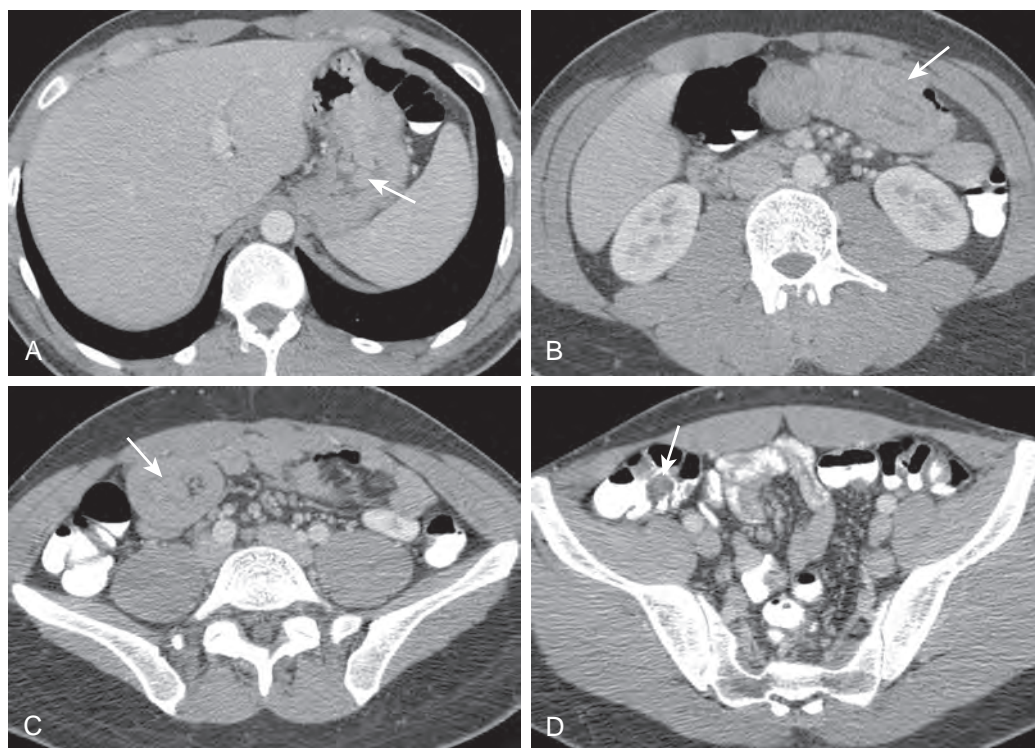


Figure 61-8 Peutz-Jeghers syndrome in a 22-year-old man who presented with acute abdominal pain, nausea, and vomiting. **A-D.** Intravenous and oral contrast-enhanced CT shows multiple hamartomas polyps throughout the gastrointestinal tract. Polyps are present in the stomach and colon (arrows in **A** and **D**). Two small bowel intussusceptions are present (arrows in **B** and **C**).



located in the small bowel or colon, whereas sessile polyps are more common in the stomach.¹²⁰ Larger hamartomas often have a lobulated surface (see Fig. 61-7A). It is more common for PJS polyps to occur in clusters than for the lesions to carpet the bowel.⁸⁸ A solitary hamartoma involving one segment of the GI tract may occur but is uncommon. Intussusception caused by small bowel hamartomas is an important radiologic feature of PJS. Transient intussusceptions may occasionally be observed on barium studies, ultrasonograms, and CT scans.¹¹⁸

A combination of radiologic and endoscopic studies should be used to diagnose these polyps. Upper endoscopy and screening of the small bowel with capsule endoscopy, magnetic resonance (MR) enterography, or CT enterography is recommended for surveillance beginning at 8 years of age or when symptoms occur.¹²² Colonoscopy should also begin at age 8 and repeated every 3 years.¹²² Ultrasonography is particularly useful for detecting ovarian and testicular tumors. The role of screening mammography for young women (25-35 years of age) with

PJS remains controversial. Screening with breast MR imaging (MRI) in addition to self-examination has been recommended.¹¹⁹ Cross-sectional imaging studies may be helpful for the diagnosis of extraintestinal abnormalities.

When a preoperative diagnosis of PJS is made, these patients can benefit from intraoperative endoscopic removal of small bowel polyps, a procedure that reduces the risk of adenocarcinoma and further intussusceptions. This form of treatment is preferable to small bowel resection because some patients with PJS develop short bowel syndrome from multiple enterectomies.¹²²

MULTIPLE HAMARTOMA SYNDROME (COWDEN DISEASE)

MHS is a genodermatosis characterized by hamartomas and neoplasms of ectodermal, mesodermal, and endodermal origin, affecting multiple organs and organ systems.¹²³⁻¹²⁷ The prevalence of MHS is 1 per 200,000. Patients usually present in their late teens or early 20s, with almost all patients presenting by their late 30s.¹²⁸ The most consistent clinical features are mucocutaneous lesions associated with thyroid gland abnormalities, breast carcinoma, hamartomatous polyposis of the GI tract, and abnormalities of the central nervous system. This syndrome has an autosomal dominant pattern of inheritance. As many as 80% of patients with MHS have a mutation in the tumor suppressor gene *PTEN* located on the long arm of chromosome 10.¹²⁹ As a result, patients with MHS and *PTEN* mutation are classified as part of the *PTEN* hamartoma syndrome, which also includes patients with *PTEN* mutations and BRRS, *PTEN*-related Proteus syndrome, and Proteus-like syndrome.¹²⁹

Mucocutaneous lesions are present in almost all patients with MHS and are considered the hallmark of the disease. Facial trichilemmomas are pathognomonic of MHS and can develop before the internal manifestations of this condition. Keratotic papules around the mouth and nose, labial and oral mucosal papillomatoses, acral keratoses, and multiple sclerotic fibromas are the most characteristic lesions, serving as external markers for the syndrome.¹³⁰⁻¹³⁸ These benign mucocutaneous lesions almost always develop early in the disease (usually in the third decade of life) before the neoplastic manifestations have developed.¹³⁹ Recognition of these features is therefore essential for the early diagnosis of MHS and initiation of screening programs for associated neoplasia.

Thyroid disease is the most frequent extracutaneous abnormality, occurring in about 65% of patients with MHS. Goiters and adenomas are the most common lesions, and men and women are affected equally.^{123,131} Thyroid carcinoma has been reported in about 10% of patients, with the most common subtypes being follicular and papillary carcinoma. Almost all cases of thyroid carcinoma have been reported in women.^{126,134}

About 70% of women with MHS have breast lesions. Fibrocystic disease is the most common finding, occurring in at least 50% of patients.^{126,137,140,141} Carcinoma of the breast (often bilateral ductal cancer) is the most common malignant tumor in MHS, occurring in 25% to 50% of patients.¹³⁷ The age at onset is 38 to 46 years, which is earlier than expected for the general population. Breast screening with self-examination, MRI, and possibly mammography, as in patients with PJS, should be encouraged in young women with MHS.

Multiple central nervous system abnormalities have also been described in patients with MHS. Lhermitte-Duclos disease (dysplastic gangliocytomas of the cerebellar cortex) is readily diagnosed by MRI of the brain and is now considered one of the major criteria for the diagnosis of MHS.¹⁴⁰⁻¹⁴³ After MHS or Lhermitte-Duclos disease has been diagnosed, careful evaluation of the patient for the other entity is therefore crucial.¹⁴⁸ Meningiomas and vascular malformations, including venous angiomas and cavernous angiomas, have also been found to occur in patients with MHS.^{144,145}

Many patients with MHS have facial or skeletal abnormalities. Macrocephaly, with a high broad forehead, is one of the most characteristic features.¹⁴⁵ Progressive macrocephaly may be accompanied by a delay in psychomotor development.¹⁴⁵

Genitourinary lesions are frequent and include uterine leiomyomas, endometrial and cervical carcinomas, and transitional cell carcinomas of the renal pelvis and urinary bladder.¹³⁹ Renal cell carcinomas have also been reported.

Polyps of the GI tract occur in 70% to 85% of patients with MHS.¹⁴⁶⁻¹⁵² They occur in all segments of the GI tract with variable reported histology, including hamartomas, hyperplastic polyps, and adenomatous polyps, followed less frequently by lipomas, ganglioneuromas, and inflammatory fibroid polyps. When present, hyperplastic polyps are usually located in the stomach, and adenomatous polyps are usually located in the stomach or colon.^{150,151} The hamartomas in MHS differ histologically from the hamartomas in PJS. They are usually sessile and smaller, with less exophytic and arborizing proliferation of the muscularis mucosae. Hamartomatous polyps are the most commonly described polyps in MHS and are the predominant lesions in the rectosigmoid colon.^{151,156} Although hamartomas occur in the esophagus, glycogenic acanthosis appears to be a more consistent finding in the esophagus and is considered by some to be another characteristic feature of MHS (Fig. 61-9).¹⁵²

The GI polyps of MHS usually appear radiographically as multiple small, sessile lesions with a segmental or diffuse distribution. They are usually located in the rectosigmoid colon followed, in decreasing order of frequency, by the stomach, duodenum, small bowel, and esophagus.^{151,152}

In most patients, GI polyps cause no symptoms and are usually found incidentally or during screening for MHS. Rare cases of colon and gastric carcinoma have been described in MHS, but an increased risk of developing these malignancies in patients with MHS has not been established.^{150,151,153}

JUVENILE POLYPOSIS

Although an isolated juvenile polyp is the most common tumor of the colon in children, JP is a rare disease. The age at onset is variable, but most patients present during the second decade of life.^{154-159,161} The criteria for establishing a diagnosis of JP include the following: (1) more than five juvenile polyps in the colon or rectum; (2) juvenile polyps throughout the GI tract; and/or (3) any number of juvenile polyps in a patient with a family history of juvenile polyps.¹⁵⁸ Affected individuals may present with bleeding, obstruction, and intussusception, but many patients are asymptomatic.

The genetics are not precisely defined, but JP appears to have an autosomal dominant pattern of inheritance.¹⁵⁸ About 25% of newly diagnosed cases of JP are sporadic; the remaining 75% of patients have a family history of JP. Two genes have been

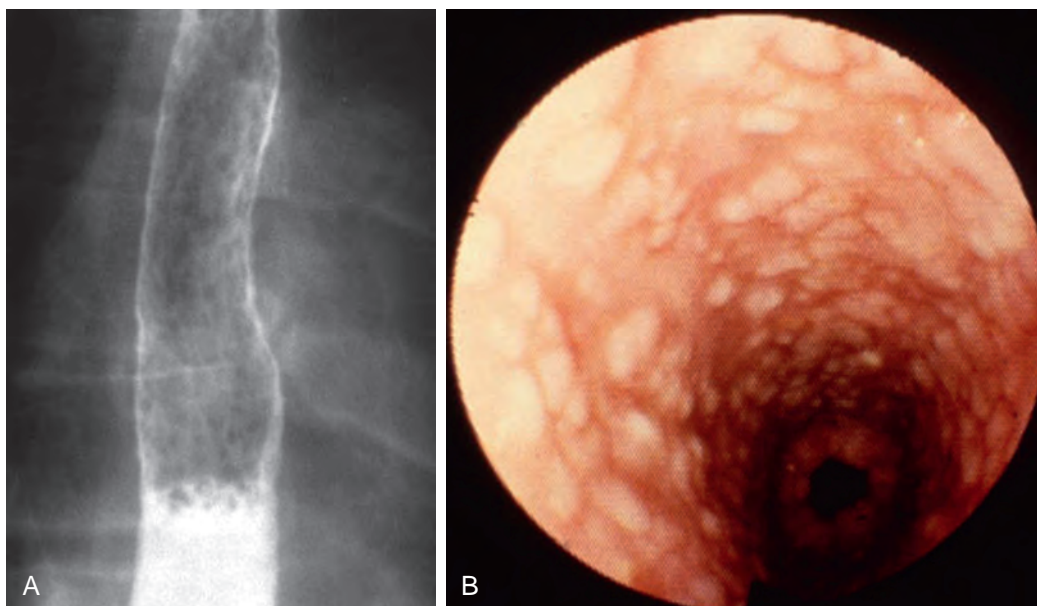


Figure 61-9 Glycogen acanthosis in multiple hamartoma syndrome. **A.** Multiple lucent plaque-like filling defects are present in the esophagus on a double-contrast esophagram. **B.** Endoscopic photograph shows characteristic white plaques with normal surrounding mucosa.

implicated in the development of JP. One gene is located on chromosome 18 (*SMAD4*) and the other on chromosome 10 (*BMPRIA*).¹⁵⁸ Approximately 20% of patients with JP have mutations in *BMPRIA* and 20% have mutations in *SMAD4*.¹⁵⁸ Various congenital anomalies, including hydrocephalus and pulmonary venous malformations, occur in 25% of nonfamilial cases of JPS but are rare in patients with the familial form of the disease.^{159,160}

Patients with JP are at increased risk for developing malignant tumors of the colon, stomach, small intestine, and pancreas.¹⁶¹⁻¹⁶⁸ Evidence indicates that the risk of colon cancer is 17% to 22% by 35 years of age and as high as 68% by 60 years of age. In patients with gastric polyps, the incidence of gastric carcinoma is more than 20%.^{158,162} Precancerous dysplasia in juvenile polyps has been well documented and suggests that carcinoma may arise in such lesions. Current screening recommendations for patients with JP include colonoscopy every 1 to 2 years beginning at 15 years of age and upper endoscopy beginning at 25 years of age.¹⁵⁸ Investigators have found that family members of patients with JP may also be at risk for developing malignant tumors of the GI tract, so the families of these patients should also be evaluated carefully.¹⁶⁵

In the colon, the polyps vary in size but, as in patients with isolated juvenile polyps, they tend to be large lesions with a diameter of 1 cm or more. These polyps can be sessile or pedunculated. When the polyps are distributed throughout the GI, they are still more likely to be clustered than to carpet the mucosa. In decreasing order of frequency, the polyps in JP occur in the colon, stomach, small bowel, and duodenum. Gastric polyps in JP are predominantly located in the gastric antrum (Fig. 61-10).¹⁶⁹⁻¹⁷⁵

JP of infancy is a severe disease.¹⁷⁶⁻¹⁸⁰ Most patients present in the first 2 years of life with a devastating mucoid or bloody diarrhea. There is usually no family history of JP. Anemia, hypoproteinemia, and repeated episodes of bronchopulmonary infection and small bowel intussusception result in early death

for most patients. Ectodermal changes resembling those of adult Cronkhite-Canada syndrome and congenital anomalies, including clubbing of the fingers, macrocephaly, and arachnoid cysts, have been reported in a small number of patients.¹⁸⁰ Juvenile polyps vary in size and are distributed throughout the GI tract, except for the esophagus. The small bowel and colon are most severely affected.¹⁸¹

CRONKHITE-CANADA SYNDROME

Unlike most of the other polyposis syndromes, CCS is not familial and occurs in older adults.¹⁸²⁻¹⁸⁸ The average age at onset is 60 years, with an age distribution of 31 to 76 years. (A condition known as Cronkhite-Canada syndrome of infancy is probably the same disease as infantile juvenile polyposis.) Mental and physical stress has been suggested as an important factor in the development of this disorder.¹⁸⁵

The histologic appearance of the GI polyps was not characterized in the first reported cases, but it is generally thought that the lesions of CCS are inflammatory polyps.¹⁸⁸ Adenomatous, hyperplastic, and hamartomatous polyps have also been reported in smaller numbers in patients.¹⁸⁸⁻¹⁹⁰ Colon cancer has been reported in about 12% of the 387 documented cases of CCS to date.¹⁹⁰

Patients with CCS typically present with abdominal pain, anorexia, a severe protein-losing diarrhea, malabsorption, and weight loss. This severe diarrhea causes electrolyte disturbances, anemia, and hypoproteinemia. Ectodermal abnormalities of the skin, hair, and nails generally follow the onset of GI symptoms. Hair loss involving the scalp or body occurs abruptly. Brown macules develop on the palmar and plantar skin surfaces. Dys-trophic changes in the nails may lead to complete nail loss (Fig. 61-11). Rarely, the ectodermal manifestations precede the onset of GI disease.^{189,191} The ectodermal changes and even the GI polyps may regress when clinical remission occurs.^{187,190,191} The prognosis is usually poor, with a mortality rate of more than

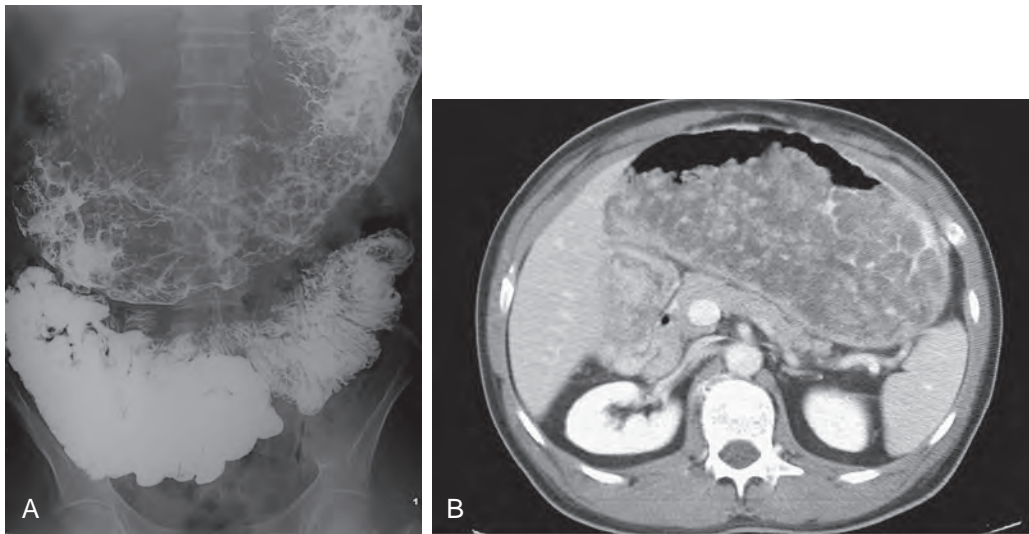


Figure 61-10 Juvenile polyposis in a 52-year-old man presenting with hematemesis. He had a family history of juvenile polyposis and a history of colonic juvenile polyp resection.
A. Radiograph from an upper gastrointestinal series shows innumerable filling defects in a distended stomach.
B. Intravenous contrast-enhanced CT shows innumerable low-attenuation polyps nearly filling the stomach.

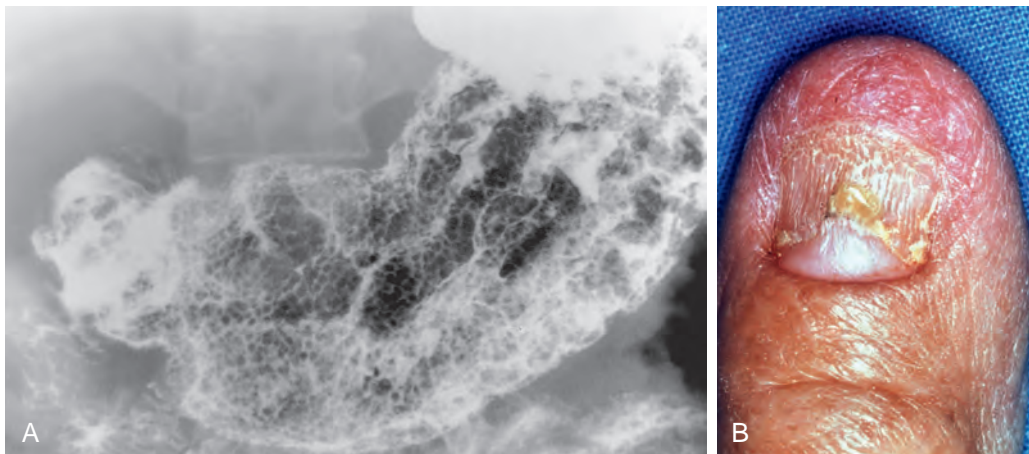


Figure 61-11 Radiographic and clinical features of Cronkhite-Canada syndrome.
A. In a 34-year-old woman, a double-contrast study of the stomach shows carpeting of the mucosa with hamartomatous polyps superimposed on enlarged rugal folds.
B. Dystrophic nail changes are seen in a different patient with Cronkhite-Canada syndrome.

50%. However, evidence has suggested a more favorable prognosis after intense therapy with corticosteroids and nutritional support.^{191,192}

Polyyps in CCS usually appear on barium studies as small, sessile or, less commonly, pedunculated lesions. They are almost always distributed throughout the stomach, small bowel, and colon.¹⁹³ Definite esophageal involvement has not been reported. In the stomach, small to moderate-sized polyps carpet the mucosal surface, usually superimposed on thickened rugal folds (see Fig. 61-11). The small bowel may contain multiple small polyps from the duodenum to the terminal ileum. The colon and rectum may also be diffusely involved, but carpeting of the mucosa is not as extensive as that in the stomach.¹⁹³

BANNAYAN-RILEY-RUVALCABA SYNDROME

Because of overlapping clinical features, three syndromes—Riley-Smith syndrome, Bannayan-Zonana syndrome, and Ruvalcaba-Myhre-Smith syndrome—have been combined into

a single entity, the Bannayan-Riley-Ruvalcaba syndrome (BRRS).^{194,195} This syndrome has an autosomal dominant pattern of inheritance.^{194,195} A *PTEN* gene mutation is present in 50% to 60% of patients with BRRS, the same gene associated with MHS.¹³⁸ Some authors now believe that BRRS and MHS may be the same syndrome, because there is overlap in the genetic and clinical manifestations of these diseases.⁸³ Also, families have been reported in which some members had MHS and others had BRRS.¹⁴²

The most common clinical features of BRRS include macrocephaly and multiple subcutaneous and visceral lipomas and hemangiomas. About 50% of patients have delayed psychomotor development, hypotonia, and mild to severe mental deficiency. Male patients may have pigmented spotting of the penis.

Hamartomatous intestinal polyps are present in about 45% of patients with BRRS.¹⁹⁴ They are usually located in the distal ileum and colon but can be found throughout the GI tract.^{83,195-198} An increased risk of GI malignancy has not been described in these patients.

REFERENCES

- Bertorelle R, Rampazzo E, Pucciarelli S, et al: Telomeres, telomerase and colorectal cancer. *World J Gastroenterol* 20:1940–1950, 2014.
- Barrow P, Khan M, Lalloo F, et al: Systematic review of the impact of registration and screening on colorectal cancer incidence and mortality in familial adenomatous polyposis and Lynch syndrome. *Br J Surg* 100:1719–1731, 2013.
- Bussey JHR, Veale AMO, Morson BC: Genetics of gastrointestinal polyposis. *Gastroenterology* 74:1325–1330, 1978.
- Varesco L: Familial adenomatous polyposis: Genetics and epidemiology. *Tech Coloproctol* 8:S305–S308, 2004.
- Pierce ER: Some genetic aspects of familial multiple polyposis of the colon in a kindred of 1,422. *Dis Colon Rectum* 11:321–327, 1968.
- Petersen GM: Genetic testing and counseling in familial adenomatous polyposis. *Oncology* 10:89–94, 1996.
- Siebert OM, Lipton L, Crabtree M, et al: Multiple colorectal adenomas, classic adenomatous polyposis, and germ-line mutations in *MYH*. *N Engl J Med* 348:791–799, 2003.
- Brand R, Nielsen M, Lynch H, et al: *MUTYH-associated polyposis* (review), 2012. <http://www.ncbi.nlm.nih.gov/books/NBK107219>. Accessed December 26, 2013.
- Bussey HJR: *Familial Polyposis Coli*, Baltimore, 1975, John Hopkins University Press.
- Giardiello FM, Brensinger JD, Luce MC, et al: Phenotypic expression of disease in families that have mutations in the 5 region of the adenomatous polyposis coli gene. *Ann Intern Med* 126:514–519, 1997.
- Ibrahim A, Barnes DR, Dunlop J, et al: Attenuated familial adenomatous polyposis manifests as autosomal dominant late-onset colorectal cancer. *Eur J Hum Genet* 2014. doi: 10.1038/ejhg.2014.20. [Epub ahead of print.]
- Hernegger GS, Moore HG, Guillem JG, et al: Attenuated familial adenomatous polyposis: An evolving and poorly understood entity. *Dis Colon Rectum* 45:127–134, 2002.
- Jasperson KW, Burt RW: *APC-associated polyposis conditions* (review), 2011. <http://www.ncbi.nlm.nih.gov/books/NBK1345>. Accessed December 10, 2013.
- Watne AL: The syndromes of intestinal polyposis. *Curr Probl Surg* 24:269–340, 1987.
- Nandakumar G, Morgan J, Silverberg D, et al: Familial polyposis coli: Clinical manifestations, evaluation, management and treatment. *Mt Sinai J Med* 71:384–391, 2004.
- Sarre RG, McGannon E, Jagelman DG, et al: Colectomy with ileorectal anastomosis for familial adenomatous polyposis. *Surgery* 101:20–26, 1987.
- Welling DR, Beart RW: Surgical alternatives in the treatment of polyposis coli. *Semin Surg Oncol* 3:99–104, 1987.
- Bartram CI, Thornton A: Colonic polyp patterns in familial polyposis. *AJR* 142:305–308, 1984.
- Hoffman DC, Goligher JC: Polyposis of the stomach and small intestine in association with familial polyposis coli. *Br J Surg* 58:126–128, 1971.
- Bulow S, Lauritsen KB, Johnsen A, et al: Gastrointestinal polyps in familial polyposis coli. *Dis Colon Rectum* 28:90–93, 1985.
- Ushio K, Sasagawa M, Doi H, et al: Lesions associated with familial polyposis coli: Studies of lesions of the stomach, duodenum, bones, and teeth. *Gastrointest Radiol* 1:67–80, 1976.
- Utsunomiya J, Maki T, Iwama T, et al: Gastric lesion of familial polyposis. *Cancer* 34:745–754, 1974.
- Burt RW, Berenson MM, Lee RG, et al: Upper gastrointestinal polyps in Gardner's syndrome. *Gastroenterology* 86:295–301, 1984.
- Shemesh E, Bat L: A prospective evaluation of the upper gastrointestinal tract and perianal region in patients with Gardner syndrome. *Am J Gastroenterol* 80:825–827, 1985.
- Arnason T, Liang WY, Alfaro E, et al: Morphology and natural history of familial adenomatous polyposis associated dysplastic fundic gland polyps. *Histopathology* 2014. doi: 10.1111/his.12393. [Epub ahead of print.]
- Tonelli F, Nardi E, Becchi P, et al: Extracolonic polyps in familial polyposis coli and Gardner's syndrome. *Dis Colon Rectum* 28:664–668, 1985.
- Watanabe H, Enjoji M, Yao T, et al: Gastric lesions in familial adenomatous coli. *Hum Pathol* 9:269–283, 1978.
- Burt RW: Gastric fundic gland polyps. *Gastroenterology* 125:1462–1469, 2003.
- Iida M, Yao T, Watanabe H, et al: Fundic gland polyposis in patients without familial adenomatous coli. *Gastroenterology* 86:1437–1442, 1984.
- Tatsuta M, Okuda S, Tamura H: Gastric hamartomatous polyps in the absence of familial polyposis coli. *Cancer* 45:818–823, 1980.
- Nishiur M, Hirota T, Itabashi M, et al: A clinical and histopathological study of gastric polyps in familial polyposis coli. *Am J Gastroenterol* 79:98–103, 1984.
- Iida M, Yao T, Itoh H, et al: Natural history of fundic gland polyposis in patients with familial adenomatous coli/Gardner's syndrome. *Gastroenterology* 89:1021–1025, 1985.
- Itai Y, Kogure T, Okuyama Y, et al: Radiographic features of the gastric polyps in familial adenomatous coli. *AJR* 128:73–76, 1977.
- Iida M, Yao T, Watanabe H, et al: Spontaneous disappearance of the fundic gland polyposis: Report of three cases. *Gastroenterology* 79:725–728, 1980.
- Denzler TB, Harned RK, Pergam CJ: Gastric polyps in familial polyposis coli. *Radiology* 130:63–66, 1979.
- Alderlieste YA, Rauws EA, Mathus-Vliegen EM, et al: Prospective enteroscopic evaluation of jejunal polyposis in patients with familial adenomatous polyposis and advanced duodenal polyposis. *Fam Cancer* 12:51–56, 2013.
- Wallace MH, Phillips RKS: Upper gastrointestinal disease in patients with familial adenomatous polyposis. *Br J Surg* 85:742–750, 1998.
- Qizilbash AH: Epithelial neoplasms of the duodenum and perianal region. In Appelman HD, editor: *Pathology of the Esophagus, Stomach and Duodenum*, New York, 1984, Churchill Livingstone, p 145.
- Iida M, Yao T, Ohsata K, et al: Diagnostic value of intraoperative fiberoscopy for small-intestinal polyps in familial adenomatous coli. *Endoscopy* 12:161–165, 1980.
- Ross JE, Mara JE: Small bowel polyps and carcinoma in multiple intestinal polyposis. *Arch Surg* 108:736–738, 1974.
- Phillips LG: Polyposis and carcinoma of the small bowel and familial colonic polyposis. *Dis Colon Rectum* 24:478–481, 1981.
- Scully RE, Galdabini JJ, McNeely BU: Case records of the Massachusetts General Hospital. Weekly clinicopathological exercises. Case 47-1978. *N Engl J Med* 299:1237–1244, 1978.
- Jarvinen HJ, Nyberg M, Peltokallio P: Biliary involvement in familial adenomatous coli. *Dis Colon Rectum* 26:525–528, 1983.
- Less CD, Hermann RE: Familial polyposis coli associated with bile duct cancer. *Am J Surg* 141:378–380, 1981.
- Burney B, Assor D: Polyposis coli with adenocarcinoma associated with carcinoma in situ of the gallbladder. *Am J Surg* 132:100–102, 1976.
- Willson SA, Princethal RA, Law B, et al: Gallbladder carcinoma in association with polyposis coli. *Br J Radiol* 60:771–773, 1987.
- Futami H, Furuta T, Hanai H, et al: Adenoma of the common human bile duct in Gardner's syndrome may cause relapsing acute pancreatitis. *J Gastroenterol* 32:558–561, 1997.
- Gardner EJ, Richards RC: Multiple cutaneous and subcutaneous lesions occurring simultaneously with hereditary polyposis and osteomatosis. *Am J Hum Genet* 5:139–148, 1953.
- Gardner EJ: Follow-up study of a family group exhibiting dominant inheritance for a syndrome including intestinal polyps, osteomas, fibromas and epidermal cysts. *Am J Hum Genet* 14:376–390, 1962.
- Scott RJ, Taeschner W, Heinemann K, et al: Association of extracolonic manifestations of familial adenomatous polyposis with acetylation phenotype in a large FAP kindred. *Eur J Hum Genet* 5:43–49, 1997.
- Davies DR, Armstrong JG, Thakker N, et al: Severe Gardner syndrome in families with mutations restricted to a specific region of the APC gene. *Am J Hum Genet* 57:1151–1158, 1995.
- Jagelman DG: Extracolonic manifestations of familial polyposis coli. *Cancer Genet Cytogenet* 27:319–325, 1987.
- Lal G, Gallinger S: Familial adenomatous polyposis. *Semin Surg Oncol* 18:314–323, 2000.
- Gorlin RJ, Chaudhry AP: Multiple osteomatosis, fibromas, lipomas and fibrosarcomas of the skin and mesentery, epidermoid inclusion cysts of the skin, leiomyomas and multiple intestinal polyposis. *N Engl J Med* 263:1151–1158, 1960.
- Chang CH, Piatt ED, Thomas KE, et al: Bone abnormalities in Gardner's syndrome. *AJR* 103:645–652, 1968.
- Utsunomiya J, Nakamura T: The occult osteomatous changes in the mandible in patients with familial polyposis. *Br J Surg* 62:45–51, 1975.
- Cankaya AB, Erdem MA, Isler SC, et al: Oral and maxillofacial considerations in Gardner's syndrome. *Int J Med Sci* 9(2):137–141, 2012.
- Woods RJ, Sarre RG, Ctercteko GC, et al: Occult radiologic changes in the skull and jaw in familial adenomatous polyposis coli. *Dis Colon Rectum* 32:304–306, 1989.
- Fader M, Kline SN, Spatz SS, et al: Gardner's syndrome (intestinal polyposis, osteomas, sebaceous cysts) and a new dental discovery. *Oral Surg Oral Med Oral Pathol* 15:153–172, 1962.
- Sondergaard JO, Bulow S, Wolf J, et al: Dental anomalies in familial adenomatous polyposis coli. *Acta Odontol Scand* 45:61–63, 1987.

61. Huges LE: Abdominal fibrodysplasia and polyposis coli. *Dis Colon Rectum* 13:121–123, 1970.
62. Jones IT, Fazio VW, Weakley FL, et al: Desmoid tumors in familial polyposis coli. *Ann Surg* 204:94–97, 1986.
63. Johnson-Smith TGP, Katz DE, Clark SK, et al: Spiral CT scanning in detection of desmoid tumors in familial adenomatous polyposis. Presented at the American Roentgen Ray Society Annual Meeting, San Francisco, April 26–May 1, 1998.
64. Iwamma T, Mishima Y, Okamoto N, et al: Association of congenital hypertrophy of the retinal pigment epithelium with familial adenomatous polyposis. *Br J Surg* 77:273–276, 1990.
65. Traboulsi EI, Maumenee IH, Krush AJ, et al: Congenital hypertrophy of the retinal pigment epithelium predicts colorectal polyposis in Gardner's syndrome. *Arch Ophthalmol* 108:525–526, 1990.
66. Baker RH, Heinemann MH, Miller HH, et al: Hyperpigmented lesions of the retinal pigment epithelium in familial adenomatous polyposis. *Am J Med Genet* 31:427–435, 1988.
67. Romania A, Zakov ZN, McGannon E, et al: Congenital hypertrophy of the retinal pigment epithelium in familial adenomatous polyposis. *Ophthalmology* 96:879–884, 1989.
68. Baba S, Tsuchiya M, Watanabe I, et al: Importance of retinal pigmentation as a subclinical marker in familial adenomatous polyposis. *Dis Colon Rectum* 33:660–664, 1990.
69. Turcot J, Depres JP, Pierre F: Malignant tumors of the central nervous system associated with familial polyposis of the colon. *Dis Colon Rectum* 2:465–468, 1959.
70. Fritch Lilla SA, Yi JS, Hall BA, et al: A novel APC gene mutation associated with a severe phenotype in a patient with Turcot syndrome. *J Pediatr Hematol Oncol* 36:e177–e179, 2014.
71. Leblanc R: Familial adenomatous polyposis and benign intracranial tumors: A new variant of Gardner's syndrome. *Can J Neurol Sci* 27:341–346, 2000.
72. Torres CF, Korones DN, Pilcher W: Multiple ependymomas in a patient with Turcot's syndrome. *Med Pediatr Oncol* 28:59–61, 1997.
73. Plail RO, Bussey JH, Glazer G, et al: Adenomatous polyposis: An association with carcinoma of the thyroid. *Br J Surg* 74:377–380, 1987.
74. Delamarre J, Capron J, Armand A, et al: Thyroid carcinoma in two sisters with familial polyposis of the colon: Case reports and review of the literature. *J Clin Gastroenterol* 10:659–662, 1988.
75. Hizawa K, Iida M, Aoyagi K, et al: Thyroid neoplasia and familial adenomatous polyposis/Gardner's syndrome. *J Gastroenterol* 32:196–199, 1997.
76. Schneider NR, Cubilla AL, Chaganti RS: Association of endocrine neoplasia with multiple polyposis of the colon. *Cancer* 51:1171–1175, 1983.
77. Perkins JT, Backstone MO, Riddell RH: Adenomatous polyposis coli and multiple endocrine neoplasia type 2b: A pathogenic relationship. *Cancer* 55:375–381, 1985.
78. Painter TA, Jagelman DG: Adrenal adenomas and adrenal carcinomas in association with hereditary adenomatosis of the colon and rectum. *Cancer* 55:2001–2004, 1985.
79. Bulow S: Familial adenomatous polyposis. *Ann Med* 21:299–307, 1989.
80. Schneider NR, Cubilla AL, Chaganti RS: Association of endocrine neoplasia with multiple polyposis of the colon. *Cancer* 51:1171–1175, 1983.
81. Maire F, Hammel P, Terris B, et al: Intraductal papillary and mucinous pancreatic tumour: A new extracolonic tumour in familial adenomatous polyposis. *Gut* 51:446–449, 2002.
82. LeSher AR, Castronuovo JJ, Jr, Filippone AL, Jr: Hepatoblastoma in a patient with familial polyposis coli. *Surgery* 105:668–670, 1989.
83. Schreiber IR, Baker M, Amos C, McGarrity TJ: The hamartomatous polyposis syndromes: A clinical and molecular review. *Am J Gastroenterol* 100:476–490, 2005.
84. Boardman LA, Thibodeau SN, Schaid DJ, et al: Increased risk for cancer in patients with the Peutz-Jeghers syndrome. *Ann Intern Med* 128:896–899, 1998.
85. Dai L, Fu L, Liu D, et al: Novel and recurrent mutations of STK11 gene in six Chinese cases with Peutz-Jeghers syndrome. *Dig Dis Sci* 2014. [Epub ahead of print.]
86. Buck JL, Harned RK, Lichtenstein JE, et al: Peutz-Jeghers syndrome. *Radiographics* 12:365–378, 1992.
87. Hizawa K, Matsumoto T, Iida M, et al: Neoplastic transformation arising in Peutz-Jeghers polyposis. *Dis Colon Rectum* 36:953–957, 1993.
88. Schumacher V, Vogel T, Leube B, et al: STK11 genotyping and cancer risk in Peutz-Jeghers syndrome. *J Med Genet* 42:428–435, 2005.
89. Niimi K, Tomoda H, Furusawa M, et al: Peutz-Jeghers syndrome associated with adenocarcinoma of the cecum and focal carcinomas in hamartomatous polyps of the colon: A case report. *Jpn J Surg* 21:220–223, 1991.
90. Visvanathan R, Thambidorai CR, Myint H: Do dysplastic and adenomatous changes in large bowel hamartomas predispose to malignancy? A report of two cases. *Ann Acad Med Singapore* 21:830–832, 1992.
91. Laughlin EH: Benign and malignant neoplasms in a family with Peutz-Jeghers syndrome: Study of three generations. *South Med J* 84:1205–1209, 1991.
92. Spiegelman AD, Ares P, Phillips RKS: Polyposis: The Peutz-Jeghers syndrome. *Br J Surg* 82:1311–1314, 1995.
93. Luk GD: Diagnosis and therapy of hereditary polyposis syndromes. *Gastroenterologist* 3:153–167, 1995.
94. Perzin KH, Bridge MF: Adenomatous and carcinomatous changes in hamartomatous polyps of the small intestine (Peutz-Jeghers) syndrome: Report of a case and review of the literature. *Cancer* 49:971–983, 1982.
95. Miller LJ, Bartholomew LG, Dozois RR, et al: Adenocarcinoma of the rectum arising in a hamartomatous poly in a patient with Peutz-Jeghers syndrome. *Dig Dis Sci* 28:1047–1051, 1983.
96. Flageole H, Stavros R, Trude JL, et al: Progression toward malignancy of hamartomas in a patient with Peutz-Jeghers syndrome: Case report and literature review. *Can J Surg* 37:231–236, 1994.
97. Utsunomiya J, Gocho H, Miyanaga T, et al: Peutz-Jeghers syndrome: Its natural course and management. *John Hopkins Med J* 136:71–82, 1975.
98. Linos DA, Dozois RR, Dahlin DC, et al: Does Peutz-Jeghers syndrome predispose to gastrointestinal malignancy? A later look. *Arch Surg* 116:1182–1184, 1981.
99. Spiegelman AD, Murday V, Phillips RK: Cancer and the Peutz-Jeghers syndrome. *Gut* 30:1588–1590, 1989.
100. Giardiello FM, Welsh SB, Hamilton SR, et al: Increased risk of cancer in the Peutz-Jeghers syndrome. *N Engl J Med* 316:1511–1514, 1987.
101. Hizwa K, Matsumoto T, Iida M, et al: Cancer in Peutz-Jeghers syndrome. *Cancer* 72:2777–2781, 1993.
102. Thatcher BS, May ES, Taxier MS, et al: Pancreatic adenocarcinoma in a patient with Peutz-Jeghers syndrome: A case report and literature review. *Am J Gastroenterol* 81:594–597, 1986.
103. Bowlby LS: Pancreatic adenocarcinoma in an adolescent male with Peutz-Jeghers syndrome. *Hum Pathol* 17:97–99, 1986.
104. Martin-Odegard B, Svane S: Peutz-Jeghers syndrome associated with bilateral synchronous breast carcinoma in a 30-year-old woman. *Eur J Surg* 160:511–512, 1994.
105. Giardiello FM, Brensinger JD, Tersmette AC, et al: Very high risk of cancer in familial Peutz-Jeghers syndrome. *Gastroenterology* 119:1447–1453, 2000.
106. Chen KTK: Female genital tract tumors in Peutz-Jeghers syndrome. *Hum Pathol* 17:858–861, 1986.
107. Choi CG, Kim SH, Kim JS, et al: Adenoma malignum of uterine cervix in Peutz-Jeghers syndrome: CT and US features. *J Comput Assist Tomogr* 17:819–821, 1993.
108. Tsuruchi N, Tsukamoto N, Kaku T, et al: Adenoma malignum of the uterine cervix detected by imaging methods in a patient with Peutz-Jeghers syndrome. *Gynecol Oncol* 54:232–236, 1994.
109. Sirvatsa PJ, Keeney GL, Podratz KC: Disseminated cervical adenoma malignum and bilateral ovarian sex cord tumors with annular tubules associated with Peutz-Jeghers syndrome. *Gynecol Oncol* 53:256–264, 1994.
110. Young RH, Welch WR, Dickersin GR, et al: Ovarian sex cord tumor with annular tubules: Review of 74 cases including 27 with Peutz-Jeghers syndrome and four with adenoma malignum of the cervix. *Cancer* 50:1384–1402, 1982.
111. Podczaski E, Kaminski PF, Pees RC, et al: Peutz-Jeghers syndrome with ovarian sex cord tumor with annular tubules and cervical adenoma malignum. *Gynecol Oncol* 42:74–78, 1991.
112. Young RH, Welch WR, Dickersin GR, et al: Ovarian sex cord tumor with annular tubules: Review of 74 cases including 27 with Peutz-Jeghers syndrome and four with adenoma malignum of the cervix. *Cancer* 50:1384–1402, 1982.
113. Cooper ML, Kaefer M, Fan R, et al: Testicular microlithiasis in children and associated testicular cancer. *Radiology* 270:857–863, 2014.
114. Wada K, Tanaka M, Yamaguchi K, et al: Carcinoma and polyps of the gallbladder associated with Peutz-Jeghers syndrome. *Dig Dis Sci* 32:943–946, 1987.
115. Yamamoto M, Hoschino H, Onizuka T, et al: Thyroid papillary adenocarcinoma in a woman with Peutz-Jeghers syndrome. *Intern Med* 31:1117–1119, 1992.
116. De Faq L, De Sutter J, De Man M, et al: A case of Peutz-Jeghers syndrome with nasal polyposis, extreme iron deficiency anemia, and hamartoma-adenoma transformation: Management by combined surgical and endoscopic approach. *Am J Gastroenterol* 90:1330–1332, 1995.

117. McGarrity TJ, Kulin HE, Zaino RJ: Peutz-Jeghers syndrome. *Am J Gastroenterol* 95:596–604, 2000.
118. Sener RN, Kumcuoglu Z, Elmasn N, et al: Peutz-Jeghers syndrome: CT and US demonstration of small bowel polyps. *Gastrointest Radiol* 16:21–23, 1991.
119. McGarrity TJ, Amos CI, Frazier ML, et al: *Peutz-Jeghers syndrome* (review), 2013. <http://www.ncbi.nlm.nih.gov/books/NBK1266>. Accessed December 10, 2013.
120. Corredor J, Wambach J, Barnard J, et al: Gastrointestinal polyps in children: Advances in molecular genetics, diagnosis, and management. *J Pediatr* 138:621–628, 2001.
121. Parker MC, Michell MJ: Polyposis: The Peutz-Jeghers syndrome. *Br J Surg* 83:865–875, 1996.
122. Panos RG, Opelka FG, Nogueras JJ: Peutz-Jeghers syndrome: A call for intraoperative enteroscopy. *Am Surg* 56:331–333, 1990.
123. Starink TM, van Der Veen JW, DeWaal LP, et al: The Cowden syndrome: A clinical and genetic study in 21 patients. *Clin Genet* 29:222–233, 1986.
124. Mallory SB: Cowden syndrome (multiple hamartoma syndrome). *Dermatol Clin* 13:27–31, 1995.
125. Eng C: Cowden syndrome. *J Gen Counsel* 6:181–192, 1997.
126. Nelen MR, Padberg GW, Peeters EAJ, et al: Localization of the gene for Cowden disease to chromosome 10q22–23. *Nat Genet* 13:114–116, 1996.
127. Liaw D, March DJ, Li J, et al: Germline mutations of the *PTEN* gene in Cowden disease, an inherited breast and thyroid cancer syndrome. *Nat Genet* 16:64–67, 1997.
128. Nelen MR, van Staveren WCG, Peeters EAJ, et al: Germline mutations in the *PTEN/MMAC1* gene in patients with Cowden disease. *Hum Mol Genet* 6:1383–1387, 1997.
129. Eng C: *PTEN* hamartoma tumor syndrome (PHTS) (review), 2012. <http://www.ncbi.nlm.nih.gov/books/NBK1488>. Accessed December 18, 2013.
130. Salem OS, Steck WD: Cowden's disease (multiple hamartoma and neoplasia syndrome): A case report and review of the English literature. *J Am Acad Dermatol* 8:686–696, 1983.
131. Starink TM: Cowden's disease: Analysis of fourteen new cases. *J Am Acad Dermatol* 11:1127–1141, 1984.
132. Hauck RM, Manders EK: Familial syndromes with skin markers. *Ann Plast Surg* 33:102–111, 1994.
133. Flores IL, Romo SA, Tejeda Nava FJ, et al: Oral presentation of 10 patients with Cowden syndrome. *Oral Surg Oral Med Oral Pathol Oral Radiol* 117:e301–e310, 2014.
134. Brownstein MH, Mehregan AH, Bikowski JB: The dermatopathology of Cowden's disease: Analysis of fourteen new cases. *Br J Dermatol* 111:1127–1134, 1984.
135. Schreibman IR, Baker M, Amos C, et al: The hamartomatous polyposis syndromes: A clinical and molecular review. *Am J Gastroenterol* 100:476–490, 2005.
136. Shapiro SD, Lambert WC, Schwartz RA: Cowden's disease: A marker for malignancy. *Int J Dermatol* 27:232–237, 1988.
137. Brownstein MH, Wolfe M, Bokowski JB: Cowden's disease: A cutaneous marker of breast cancer. *Cancer* 41:2393–2398, 1978.
138. Pilarski R, Eng C: Will the real Cowden syndrome please stand up (again)? Expanding mutational and clinical spectra of the *PTEN* hamartoma tumour syndrome. *J Med Genet* 41:323–326, 2004.
139. Coriat R, Mozer M, Caux F, et al: Endoscopic findings in Cowden syndrome. *Endoscopy* 43:723–726, 2011.
140. Thomas DW, Lewis MAO: Lhermitte-Duclos disease associated with Cowden's disease. *Int J Oral Maxillofac Surg* 24:369–371, 1995.
141. Lyons CJ, Wilson CB, Horton JC: Association between meningioma and Cowden's disease. *Neurology* 43:1436–1437, 1993.
142. Wells GB, Lasner TM, Yousem DM, et al: Association of Lhermitte-Duclos and Cowden's disease in an adolescent patient. *J Neurosurg* 81:133–136, 1994.
143. Vinchon M, Blond S, Lejeune JP, et al: Association of Lhermitte-Duclos and Cowden disease: Report of a new case and review of the literature. *J Neurol Neurosurg Psychiatry* 57:699–704, 1994.
144. Koeller KK, Henry JM: From the archives of the AFIP: Superficial gliomas: Radiologic-pathologic correlation. *Radiographics* 21:1533–1566, 2001.
145. Lok C, Viseux V, Avril MF, et al: Brain magnetic resonance imaging in patients with Cowden syndrome. *Medicine* 84:129–136, 2005.
146. Hizawa K, Iida M, Matsumoto T, et al: Gastrointestinal manifestations of Cowden's disease, report of four cases. *J Clin Gastroenterol* 18:13–18, 1994.
147. Marra G, Armelao F, Vecchio FM, et al: Cowden's disease with extensive gastrointestinal polyposis. *J Clin Gastroenterol* 18:42–47, 1994.
148. Carlson GJ, Nivatongs S, Snover DC: Colorectal polyps in Cowden's disease multiple hamartoma syndrome. *Am J Pathol* 8:703–707, 1984.
149. Lashner BA, Riddell RH, Winans CS: Ganglioneuromatosis of the colon and extensive glycogenic acanthosis in Cowden's disease. *Dig Dis Sci* 31:212–216, 1986.
150. Kay PS, Soetikno RM, Mindelzum R, et al: Diffuse esophageal glycogenic acanthosis: An endoscopic marker of Cowden's disease. *Am J Gastroenterol* 92:1038–1040, 1997.
151. Taylor AJ, Dodds WJ, Stewart ET: Alimentary tract lesions in Cowden's disease. *Br J Radiol* 62:890–892, 1989.
152. Hauser H, Ody B, Plojoux O, Wettstein P: Radiological findings in multiple hamartoma syndrome (Cowden disease): A report of 3 cases. *Radiology* 137:317–323, 1980.
153. Hambry LS, Lee EY, Schwartz RW: Parathyroid adenoma and gastric carcinoma as manifestations of Cowden's disease. *Surgery* 118:115–117, 1997.
154. Jass JR, Williams CB, Bussey HR, et al: Juvenile polyposis: A precancerous condition. *Histopathology* 13:619–630, 1988.
155. Wu TT, Rezai B, Rashed A, et al: Genetic alterations and epithelial dysplasia in juvenile polyposis syndrome and sporadic juvenile polyps. *Am J Pathol* 150:939–947, 1997.
156. Bussey HR, Veale AO, Morson BC: Genetics of gastrointestinal polyposis. *Gastroenterology* 74:1325–1330, 1978.
157. Hess KF, Schaffner D, Ricketts RR, et al: Malignant risk in juvenile polyposis coli: Increasing documentation in the pediatric age group. *J Pediatr Surg* 28:1188–1193, 1993.
158. Larsen Haidle J, Howe JR: Juvenile polyposis syndrome (review), 2011. <http://www.ncbi.nlm.nih.gov/books/NBK1469>. Accessed December 18, 2013.
159. Desai DC, Neale KF, Talbot IC, et al: Juvenile polyposis. *Br J Surg* 82:14–17, 1995.
160. Radin DR: Hereditary generalized juvenile polyposis: Association with arteriovenous malformation and risk of malignancy. *Abdom Imaging* 19:140–142, 1994.
161. O'Riordain DS, O'Dwyer PJ, Cullen AF, et al: Familial juvenile polyposis coli and colorectal cancer. *Cancer* 68:889–892, 1991.
162. Coburn MC, Pricolo VE, Deluca FG, et al: Malignant potential in intestinal juvenile polyposis syndromes. *Ann Surg Oncol* 2:386–391, 1995.
163. Stemper TJ, Kent THE, Summers RW: Juvenile polyposis and gastro-intestinal carcinoma: A study of a kindred. *Ann Intern Med* 83:639–646, 1975.
164. Grigioni WF, Alampi G, Martinelli G, et al: Atypical juvenile polyposis. *Histopathology* 5:361–376, 1981.
165. Rozen P, Baratz M: Familial juvenile polyposis coli: Increased risk of cancer. *Cancer* 49:1500–1503, 1984.
166. Brosens LA, Langeveld D, van Hattem WA, et al: Juvenile polyposis syndrome. *World J Gastroenterol* 17:4839–4844, 2011.
167. Subramony C, Scoot-Conner CEH, Skelton D, et al: Familial juvenile polyposis, study of a kindred: Evolution of polyps and relationship to gastrointestinal carcinoma. *Am J Clin Pathol* 102:91–97, 1994.
168. Vaiphei K, Thapa BR: Juvenile polyposis (coli)—high incidence of dysplastic epithelium. *J Pediatr Surg* 32:1287–1290, 1997.
169. Yoshida T, Haraguchi A, Tanaka A, et al: A case of generalized juvenile gastrointestinal polyposis associated with gastric carcinoma. *Endoscopy* 20:33–35, 1988.
170. Walpole IR, Cullity G: Juvenile polyposis: A case with early presentation and death attributable to adenocarcinoma of the pancreas. *Am J Med Genet* 32:1–8, 1989.
171. Sassatelli R, Bertoni G, Serra L, et al: Generalized juvenile polyposis with mixed pattern and gastric cancer. *Gastroenterology* 110:910–915, 1993.
172. Haggitt RC, Reid BJ: Hereditary gastrointestinal polyposis syndromes. *Am J Surg Pathol* 101:871–887, 1986.
173. Covarrubias D, Huprich J: Best cases from the AFIP: Juvenile polyposis of the stomach. *Radiographics* 22:415–420, 2002.
174. Berk RN, Rush JL, Elson EC, et al: Multiple inflammatory polyps of the small intestine with cachexia and protein-losing enteropathy. *Radiology* 95:611–612, 1970.
175. Ray JE, Heald RJ: Growing up with juvenile gastrointestinal polyposis: Report of a case. *Dis Colon Rectum* 14:375–380, 1971.
176. Soper RT, Kent THE: Fatal juvenile polyposis of infancy. *Surgery* 169:692–698, 1971.
177. Schwart AM, McCauley RK: Juvenile gastrointestinal polyposis. *Radiology* 121:441–444, 1976.
178. Le Luyer B, Le Bihan M, Metayer P, et al: Generalized juvenile polyposis in an infant: Report of a case and successful management by endoscopy. *J Pediatr Gastroenterol Nutr* 4:128–134, 1985.
179. Ruymann FB: Juvenile polyp with cachexia: Report of an infant and comparison with Cronkhite-Canada syndrome in adults. *Gastroenterology* 57:431–438, 1969.
180. Scharf GM, Becker JHR, Lage NJ: Juvenile gastrointestinal polyposis of the infant:

- Cronkhite-Canada syndrome. *J Pediatr Surg* 21:953–954, 1986.
181. Sachatello CR, Hahn IS, Carrington CB: Juvenile gastrointestinal polyposis in a female patient: Report of a case and review of the literature of a recently recognized syndrome. *Surgery* 175:107–114, 1974.
 182. Goto A: Cronkhite-Canada syndrome: Epidemiological study of cases reported in Japan. *Arch Jpn Chir* 64:3–14, 1995.
 183. Bettington M, Brown IS, Kumarasinghe MP, et al: The challenging diagnosis of Cronkhite-Canada syndrome in the upper gastrointestinal tract: A series of 7 cases with clinical follow-up. *Am J Surg Pathol* 38:215–223, 2014.
 184. Diner WC: The Cronkhite-Canada syndrome. *Radiology* 105:715–716, 1972.
 185. Daniel ES, Ludwig SL, Lewin KL, et al: The Cronkhite-Canada syndrome: An analysis of clinical and pathological features and therapy in 55 patients. *Medicine (Baltimore)* 61:293–309, 1982.
 186. Kilcheski T, Kressel HY, Laufer I, et al: The radiographic appearance of the stomach in the Cronkhite-Canada syndrome. *Radiology* 141: 57–60, 1981.
 187. Murai N, Fukuzaki T, Nakamura T, et al: Cronkhite-Canada syndrome associated with colon cancer: Report of a case. *Jpn J Surg* 23:825–829, 1993.
 188. Burke AP, Sobin LH: The pathology of Cronkhite-Canada syndrome polyps. *Am J Surg Pathol* 13:940–946, 1989.
 189. Kopáčová M, Urban O, Cyrany J, et al: Cronkhite-Canada syndrome: Review of the literature. *Gastroenterol Res Pract* 2013:856–873, 2013.
 190. Yashiro M, Kobayashi H, Kubo N, et al: Cronkhite-Canada syndrome containing colon cancer and serrated adenoma lesions. *Digestion* 69:57–62, 2004.
 191. Russell D, Bhatthal PS, St. John JB: Complete remission in Cronkhite-Canada syndrome. *Gastroenterology* 85:180–185, 1983.
 192. Peart AG, Jr, Sivak MV, Rankin GB, et al: Spontaneous improvement of Cronkhite-Canada syndrome in a postpartum female. *Dig Dis Sci* 29:470–474, 1984.
 193. Dachman AH, Buck JL, Burke AP, et al: Cronkhite-Canada syndrome: Radiologic features. *Gastrointest Radiol* 14:3–14, 1995.
 194. Gorlin RJ, Cohen MM, Condon LM, et al: Bannayan-Riley-Ruvalcaba syndrome. *Am J Med Genet* 44:307–314, 1992.
 195. Fargnoli MC, Orlow SJ, Semel-Concepcion J, Bologna JL: Clinicopathologic findings in the Bannayan-Riley-Ruvalcaba syndrome. *Arch Dermatol* 132:1214–1218, 1996.
 196. Arch EM, Goodman BK, Van Sesep RA, et al: Depletion of PTEN in a patient with Bannayan-Riley-Ruvalcaba syndrome suggests allelism with Cowden disease. *Am J Med Genet* 71:489–493, 1997.
 197. Shah KR, Boland CR, Patel M, et al: Cutaneous manifestations of gastrointestinal disease: Part I. *J Am Acad Dermatol* 68(2):189.e1–189.e21, 2013.
 198. Foster MA, Kilcoyne RF: Ruvalcaba-Myhre-Smith syndrome: A new consideration in the differential diagnosis of intestinal polyposis. *Gastrointest Radiol* 11:349–350, 1986.

Miscellaneous Abnormalities of the Colon

RICHARD M. GORE | RICHARD A. SZUCS | ELLEN L. WOLF |
FRANCIS J. SCHOLZ | RONALD L. EISENBERG | STEPHEN E. RUBESIN

CHAPTER OUTLINE

Colonic Obstruction

Pathophysiology
Clinical Findings
Radiologic Approach to Suspected Large Bowel Obstruction
Major Types of Colonic Obstruction

Extracolonic Diseases Involving the Colon

Endometriosis
Malignant Gynecologic Tumors
Ovarian Carcinoma
Other Gynecologic Malignancies
Benign Gynecologic Tumors
Pelvic Inflammatory Disease and Tubo-Ovarian Abscess
Sexually Transmitted Diseases
Pancreatitis
Metastases

Colonic Ischemia

Clinical Findings
Pathologic Findings
Radiologic Findings

Radiation Colitis

Pathogenesis
Findings
Treatment

Vascular Lesions of the Anorectum

Internal Hemorrhoids
Rectal Varices
Cloacogenic (Basaloid) Carcinoma
Rectal Mucosal Prolapse Syndromes

Functional Disorders of the Colon

Irritable Bowel Syndrome
Chronic Constipation
Nonobstructive Megacolon
Collagen Vascular Disorders
Diabetes

Pneumatosis Intestinalis

Primary Intestinalis
Secondary Intestinalis

Other Colon Abnormalities

Diversion Colitis
Behçet's Syndrome
Amyloidosis
Cathartic Colon
Urticaria
Colitis Cystica Profunda
Diarrhea

Colonic Obstruction

Mechanical large bowel obstruction is four to five times less common than small bowel obstruction and differs significantly in terms of cause (Table 62-1), pathophysiology, therapy, and prognosis.¹⁻⁴ Colon obstruction is most often the result of a neoplasm (Table 62-2), whereas most small bowel obstructions are caused by adhesions.^{5,6} A number of extracolonic disease processes, including gynecologic diseases, can secondarily involve the large bowel, leading to obstruction or formation of strictures and fistulas.⁷

PATHOPHYSIOLOGY

When colonic obstruction is caused by diverticulitis or cancer, symptoms are usually subacute or chronic. Swallowed air proximal to the obstruction causes dilation, but third spacing of fluid in the gut lumen characteristic of small bowel obstruction is not seen. Strangulation rarely occurs, except in occasional

cases of volvulus.⁸ Colonic response to the mechanical obstruction depends on the competency of the ileocecal valve (Fig. 62-1). The small bowel serves to decompress the colon when the valve is incompetent. A closed loop obstruction develops when the valve is competent because the colon cannot decompress.

The cecum has the largest diameter of the colon, and therefore its wall develops the highest tension, according to Laplace's law (wall tension = intraluminal pressure \times radius). The increased pressure may cause separation of the muscle fibers, leading to cecal diastatic perforation. Dissection of air into the wall results in pneumatosis, which may precede frank perforation.^{9,10} The risk of perforation increases when the cecum reaches a diameter of 9 to 12 cm.¹¹ The duration and rapidity of onset of the distention are also important.^{12,13} The intraluminal pressure needed to produce perforation is between 20 and 55 mm Hg.¹⁴ Ischemia and bacterial overgrowth also play a role in cecal perforation, and the systemic effects seen with strangulating obstruction.^{15,16}

TABLE 62-1 Causes of Mechanical Large Bowel Obstruction

Intrinsic Defects	Extrinsic Defects
Neoplasms	Volvulus
Benign	Secondary
Malignant	Primary
Inflammatory	Hernias
Diverticulitis	Internal
Ulcerative colitis	External
Crohn's disease	Adhesions
Amebiasis	Mass compression
Tuberculosis	Carcinomatosis
Intussusception	Abscess
Obturation	Pregnancy
Gallstones	Cysts
Foreign bodies	Pancreatitis
Meconium	Endometriosis
Medications	
Enteroliths	
Bezoars	
Worms	
Congenital	
Atresia	
Stenosis	
Imperforate anus	
Cysts and duplications	
Miscellaneous	
Post-traumatic events	
Pneumatosis intestinalis	

TABLE 62-2 Incidence of Colonic Obstruction by Cause

Cause	Incidence (%)
Carcinoma	55
Volvulus	11
Diverticulitis	9
Extrinsic cancer	8
Adhesions	4
Impaction	3
Hernia	2
Intrinsic	4

CLINICAL FINDINGS

Because most colonic obstructions are caused by cancer, patients are usually older adults and have symptoms related to tumor location. Signs and symptoms are often insidious with right colon lesions because the lumen is large and the contents are semiliquid. These patients often present with pain, a palpable mass, and anemia.¹⁷ Left-sided lesions cause progressive constipation and, ultimately, obstipation, with abdominal distention and pain. If the ileocecal valve is incompetent, retrograde decompression produces the gradual onset of distention and, eventually, feculent vomiting.^{18,19} Lesions occurring at the ileocecal valve or ileocolic intussusception cause more acute symptoms of small bowel obstruction—abdominal pain, distention, vomiting, and obstipation.^{18,19} Patients with volvulus may develop pain and distention rapidly if a closed loop obstruction and bowel ischemia are present.²⁰ On physical examination, an abdominal mass may be present (e.g., advanced right-sided colon cancer) and distention may be most marked in one region (e.g., the left upper quadrant in cecal volvulus). Bowel sounds are often hyperactive, particularly with superimposed small

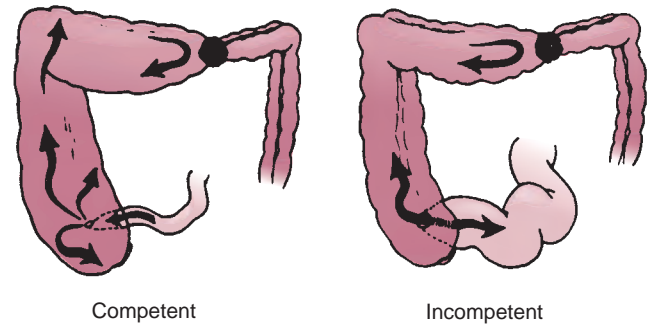


Figure 62-1 Importance of the ileocecal valve to the radiologic findings in large bowel obstruction. If the ileocecal valve is competent (left), pronounced cecal dilation can occur. An incompetent valve (right) allows retrograde decompression into the small bowel. (From Welch JP [ed]: *Bowel Obstruction*. Philadelphia, WB Saunders, 1990.)

bowel obstruction. Marked tenderness or rebound suggests perforation or strangulation.^{18,19}

RADIOLOGIC APPROACH TO SUSPECTED LARGE BOWEL OBSTRUCTION

Radiography

Abdominal radiographs obtained in the supine and erect or left lateral decubitus positions are often the initial means of imaging patients with suspected obstruction.²¹ These radiographs may confirm the diagnosis, locate the site of obstruction and, in some cases, identify the nature of the obstructing lesion.²²⁻²⁵ The colon is usually dilated proximal to the obstruction; however, if the ileocecal valve is incompetent, the appearance may mimic that of small bowel obstruction.²⁶⁻²⁸ The radiographic findings on plain radiographs in bowel obstruction are discussed in detail in Chapter 10.

Contrast Enemas

If the plain abdominal radiographs show convincing evidence of large bowel obstruction caused by volvulus or ileocolic intussusception, a contrast enema, preferably with a water-soluble medium, is the next step in patients with suspected large bowel obstruction. Although barium is inherently a better contrast agent, it may interfere with future studies, such as computed tomography (CT) or colonoscopy. If the patient proves to have a pseudo-obstruction rather than true obstruction, the barium may remain within the colon for days.²⁹ A water-soluble enema can also be therapeutic in patients with fecal impactions.²⁹ Because oral barium can inspissate proximal to a partial or complete large bowel obstruction, it is important to exclude an obstructing colonic lesion before the small bowel is examined with barium.^{30,31}

Computed Tomography

CT is now the imaging modality of choice for patients with known or suspected obstruction. It is the best noninvasive means of answering the following key questions:

- Is the bowel obstructed?
- What is the level of the obstruction?
- What is the cause of the obstruction?
- Is the obstruction simple or closed loop?

- Are ischemic changes present?
- Does the patient need immediate surgery, or should a trial of conservative therapy be attempted first?

CT is most valuable when there are systemic signs suggesting infection, bowel infarction, or an associated palpable mass.³² CT identifies bowel obstruction as distended bowel loops seen proximal to collapsed loops and can reveal the cause of obstruction, such as tumor, volvulus, diverticulitis, or appendicitis.³³ The transitional zone should be carefully evaluated for masses.³²

Ultrasonography and Magnetic Resonance Imaging

Although CT is the best examination for evaluating patients with suspected colon obstruction, ultrasonography and magnetic resonance imaging (MRI) can also determine the level and cause of obstruction, particularly in children and pregnant women.^{34,35}

MAJOR TYPES OF COLONIC OBSTRUCTION

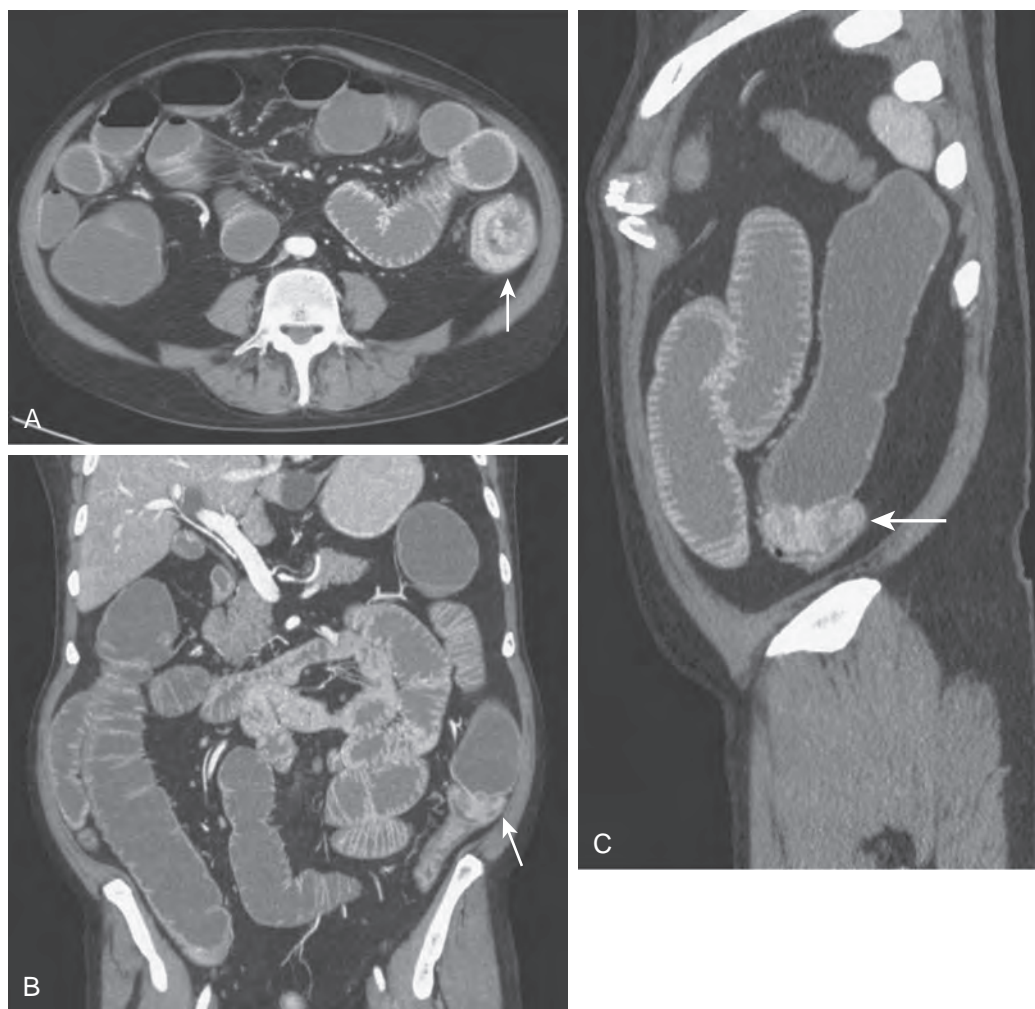
Carcinoma of the Colon

Large bowel obstruction is caused by intrinsic colon carcinoma in approximately 55% of cases.^{36,37} Almost 20% of colon cancers are complicated by some degree of obstruction; 5% to 10% are complicated by complete obstruction, which requires emergent

surgical intervention.³⁸ The mortality rate is high (10%-30%) in patients requiring emergency surgery, regardless of the site of tumor.^{38,39} This is a reflection of advanced tumor stage, advanced patient age, and associated cardiorespiratory disease, malnutrition, sepsis, and surgical stress.^{40,41} Mortality is even higher if there is concurrent perforation. Patients who present with obstructing colon carcinoma have low curability and survival rates because of advanced disease at the time of diagnosis.⁴²

The sigmoid colon is the most common site of obstructive colon cancer because of its relatively narrow diameter and solid fecal contents. The location of obstruction in one series was as follows: cecum, 11%; right colon, 5%; hepatic flexure, 3%; transverse colon, 11%; splenic flexure, 12%; descending colon, 10%; sigmoid colon, 35%; and rectum, 13%.³⁷ The ratio of obstructing carcinomas to total tumors is similar in the right (Fig. 62-2) and left colon but lower for rectal lesions.¹⁷ Tumors of the transverse colon and splenic flexure are at particular risk for obstruction before clinical detection.⁴³ The risk of developing obstruction in tumors at a particular site has been estimated as 50% for splenic flexure lesions, 25% for right- and left-sided ones, and 6% for rectal tumors.^{17,44} Perforation occurs in 3% to 8% of patients with malignant obstruction.³⁸ The most common site of perforation is the cecum rather than adjacent to the tumor.^{45,46}

Figure 62-2 CT in the evaluation of large bowel obstruction. **A.** Axial image shows an enhancing, obstructing mass (arrow) at the junction of the descending colon and sigmoid colon. **B.** Coronal reformatted image demonstrates the obstructing cancer (arrow) and dilated, fluid-filled colon, and small bowel. **C.** Sagittal depiction of the cancer (arrow) and dilated, fluid-filled colon, and small bowel.



The clinical presentation of obstructive colon cancer depends on the location, duration, and completeness of obstruction, as well as on the competency of the ileocecal valve. Tumors located near the ileocecal valve can produce symptoms suggesting a distal small bowel obstruction. Some right colon tumors act as lead points for colocolic intussusception; others may perforate, causing abscess formation and obstruction. Left-sided colon tumors tend to obstruct in an annular fashion or by a polypoid lesion that reaches a size sufficient to obstruct the lumen. The rectum is not a common site of obstruction because of its greater diameter and distensibility and because rectal cancers often cause rectal bleeding, prompting earlier medical attention. The usual treatment of obstructive colon cancer is surgical resection or diverting colostomy; however, expandable metallic stents can be used for palliation or to allow bowel cleansing before surgical resection.^{47,48}

Diverticulitis

Large bowel obstruction is the result of diverticular disease in about 12% of cases. Diverticulitis can cause small and large bowel obstruction. Partial colonic obstruction can complicate acute diverticulitis as a consequence of edema and pericolic inflammation or abscess formation. High-grade obstruction is uncommon; it is far more frequently caused by carcinoma of the colon. Usually, obstruction follows recurrent attacks of diverticulitis, with marked fibrosis of the colon wall leading to narrowing and eventually stricture formation. The site of obstruction is usually in the sigmoid colon, near the site of inflammation. Obstruction of the transverse or right colon attributable to diverticulitis is rare.^{49,50}

Clinically, patients with sigmoid diverticulitis complain of left lower quadrant pain, fever, and abnormal bowel habits. It is important for these symptoms to be differentiated from those of carcinoma of the colon, an often difficult task clinically and radiologically (Fig. 62-3 and Table 62-3). Symptoms of sigmoid colon cancer are usually more insidious, with rectal bleeding, constipation, and weight loss.⁵¹⁻⁵⁶ A more complete discussion of diverticular disease can be found in Chapter 55.

Volvulus

Volvulus refers to torsion or twist of an organ on a pedicle to a degree sufficient to cause symptoms. Large bowel volvulus (Fig. 62-4) accounts for about 10% of colon obstructions and can affect the sigmoid colon (Fig. 62-5), cecum (Figs. 62-6 and 62-7), transverse colon and, rarely, the splenic flexure. Symptoms are caused by narrowing and obstruction of the gut, strangulation of the blood vessels, or both.⁵⁷⁻⁵⁹

The major predisposing factors necessary for colonic volvulus are a segment of redundant mobile colon on a mesentery or mesocolon and a fixed point around which rotation can occur. The sigmoid colon (Fig. 62-8) is therefore the most frequent site of colonic volvulus, especially in patients older than 60 years.^{60,61} Sigmoid volvulus is not caused by a congenital defect but by dietary and behavioral factors, including increased fiber in the diet, which increases the bulk of stool and elongates the colon. Cecal or ascending colon volvulus occurs in patients with a congenital defect in attachment of the right colon or postpartum ligamentous laxity and a mobile cecum.⁶² Anything that causes colon distention, including pseudo-obstruction, distal tumor, endoscopy, enemas, and postoperative ileus, may precipitate cecal volvulus in susceptible individuals. Transverse colon volvulus occurs in patients with a redundant transverse

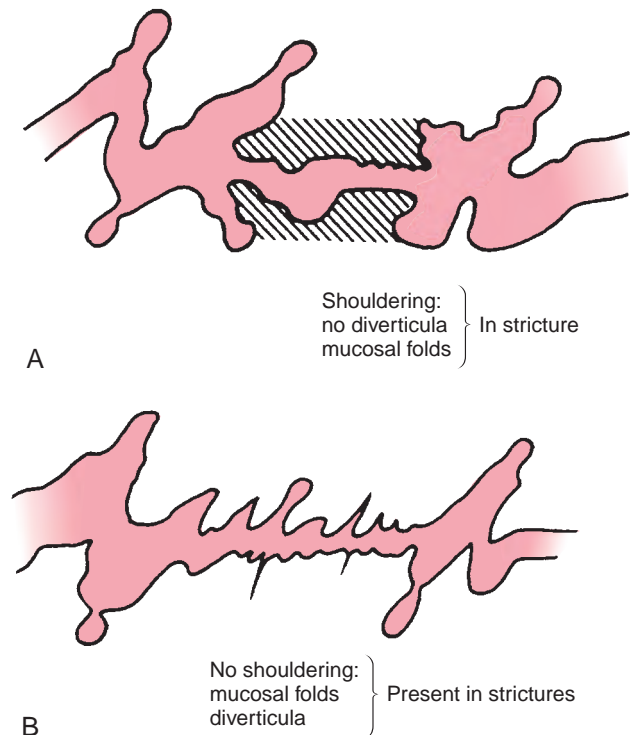


Figure 62-3 Sigmoid diverticulitis versus carcinoma: barium enema findings. A. Carcinoma in diverticular disease. **B.** Stricturing attributable to diverticular disease. (From Bartram CT, Kumar P: *Clinical Radiology in Gastroenterology*. Oxford, England, Blackwell Scientific, 1981, p 132.)

TABLE 62-3 Radiologic Differentiation of Sigmoid Diverticulitis from Carcinoma

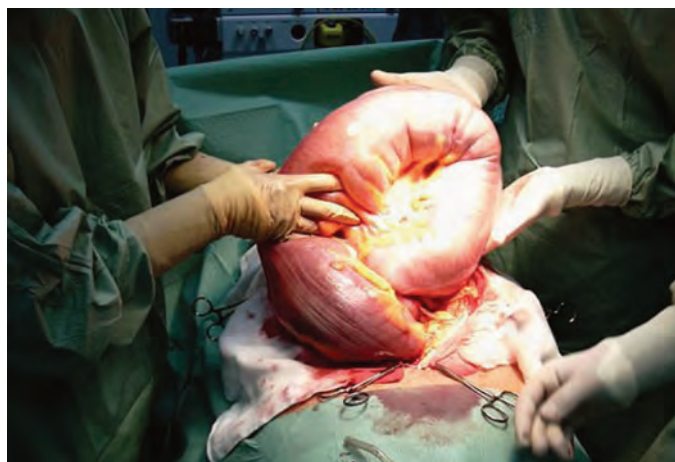
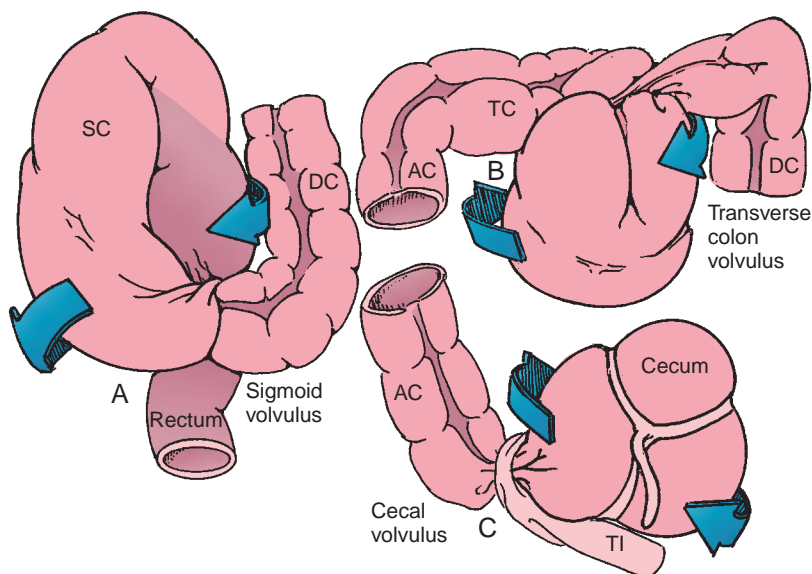
Diverticulitis	Carcinoma
Spastic bowel	Normal adjacent bowel
Cone-shaped edges	Sharp margins, shelflike
Long segments	Short segments
Mucosa preserved	Mucosa destroyed
Variable constriction between examinations	Progressive obstruction
Diverticula present	Occasional diverticula
Obstruction without tumor	Obstruction with tumor

colon on a long mesentery,⁶³ and splenic flexure volvulus occurs in patients with deficiency of the normal attachments of the splenic flexure to the posterior peritoneal wall, usually as a result of prior surgery.^{64,65} The frequency of colon volvulus is as follows: sigmoid colon, 50% to 75%; cecum, 25% to 40%; and transverse colon, 0% to 10%. A rare cause of combined colon and small bowel obstruction is the ileosigmoid knot.⁶⁶⁻⁶⁸ A detailed discussion of colonic volvulus and its conventional radiographic features can be found in Chapter 10.

On CT, a whirl sign has been described in volvulus. The whirl is constituted by the afferent and efferent limbs leading into the volvulus. Tightly twisted mesentery and bowel compose the central portion of the whirl. The progressive tapering of the two limbs leading to the twist on CT corresponds to the so-called beak seen on barium enema. The distended and redundant sigmoid colon may overlie the liver and extend cephalad to the transverse colon (the so-called northern exposure sign).⁶⁹⁻⁷¹

Figure 62-4 The three major sites of colonic volvulus.

A. Sigmoid volvulus. Adjacent middle walls of the dilated sigmoid colon (SC) form a double line on radiographs that converges on the point of twist in the sigmoid mesocolon. **B.** Transverse colonic volvulus. The caudal border of this ptotic colon is rounded, and the central double bowel wall does not extend to the sigmoid mesentery. **C.** Cecal volvulus. The dilated cecum twists clockwise, obstructing the ascending colon, and the terminal ileum (TI) swings around the dilated bowel. AC, Ascending colon; DC, descending colon; TC, transverse colon.

**Figure 62-5 Sigmoid volvulus: intraoperative image.** A massively dilated sigmoid colon is identified twisted on itself.

Adult Intussusception

Intussusception is defined as the invagination of one segment of the gastrointestinal (GI) tract into an adjacent one (Fig. 62-9). It accounts for 80% to 90% of bowel obstruction in infants and children and ranks second only to appendicitis as the most common cause of an acute abdominal emergency in children. In children, intussusception usually begins in the distal ileum, and in 90% of cases the cause is idiopathic.^{1-4,20} A complete discussion of childhood intussusception can be found in Chapter 121.

In contrast, intussusception in adults accounts for only 1% to 3% of mechanical intestinal obstruction, and a demonstrable cause is found in 80% of adult cases. Colonic intussusception is usually caused by a primary colon cancer, whereas small bowel intussusception is generally related to a benign tumor and less often to a malignancy, usually a metastatic lesion.⁷²⁻⁸⁴ Postoperative intussusceptions usually occur in the small bowel and are related to a number of factors, such as suture lines, ostomy closure, adhesions, long intestinal tubes,

bypassed intestinal segments, submucosal edema, abnormal bowel motility, electrolyte imbalance, and chronic dilation of the bowel.^{84,85}

Benign lesions that can serve as lead points in colonic intussusception include adenomatous polyps, lipomas, gastrointestinal stromal tumors (Fig. 62-10), appendiceal stump granulomas, and villous adenomas of the appendix.⁸⁴ The normal appendix may transiently intussuscept, although clinically significant appendiceal intussusception usually occurs in the setting of appendiceal inflammation, infestation, neoplasm, or endometriosis deposition.⁸⁶ A more complete discussion of diseases of the appendix can be found in Chapter 56. Colonic intussusception has also been reported as a complication of eosinophilic colitis, epiploic appendagitis, and pseudomembranous colitis.⁸⁷⁻⁸⁹

In children, the diagnosis is suggested by the presence of an abdominal mass and passage of blood per rectum. Because adult intussusception is often chronic and relapsing, the diagnosis is suggested by recurrent episodes of subacute obstruction and variable abdominal signs. During the height of an attack, a palpable mass may be present but may disappear completely when the patient is reexamined several hours later, by which time the symptoms have resolved.^{3,20} In infants and young children, hydrostatic or pneumatic intussusception reduction should be attempted and may be definitive therapy because the cause is usually idiopathic. In adults, the high incidence of organic lesions, often malignant, precludes this approach.

If the intussusception is of the ileocolic or colocolic variety, the pathognomonic crescent sign may be seen. This sign is produced when the intussusciens invaginates into the intussusceptum and stretches the outer wall. Intraluminal gas trapped between the two intestinal surfaces can appear as a semilunar lucency lacking haustral septa or valvulae conniventes. This lucent crescent is wider than normal bowel in diameter and is often superimposed on a round soft tissue density representing the mass created by the intussusception. A more central and less distinct lucency may be seen, representing gas trapped in the lumen of the intussusciens. On supine views, the transverse colon gas shadow is often absent because this segment of colon is usually displaced distally.^{21,90,91}

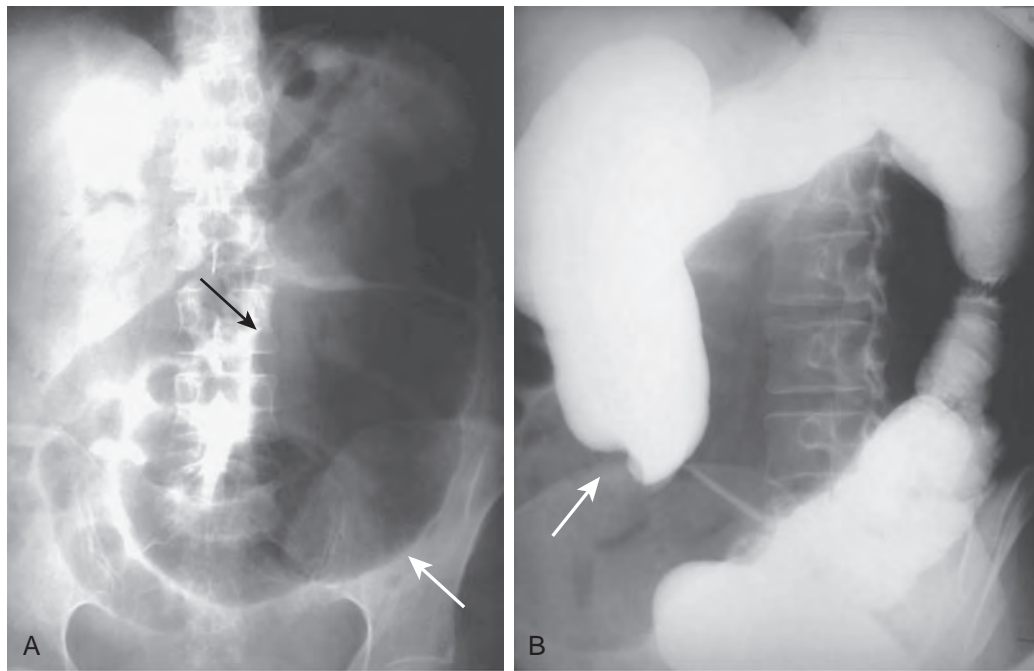


Figure 62-6 Cecal volvulus: plain radiograph and barium enema features. **A.** A distended cecum (arrows) is present in the left lower quadrant. Dilated small bowel is evident proximally. There is a relative paucity of colonic gas distal to the volvulus. **B.** Barium enema shows the contrast column ending abruptly (arrow) at the level of the twist.

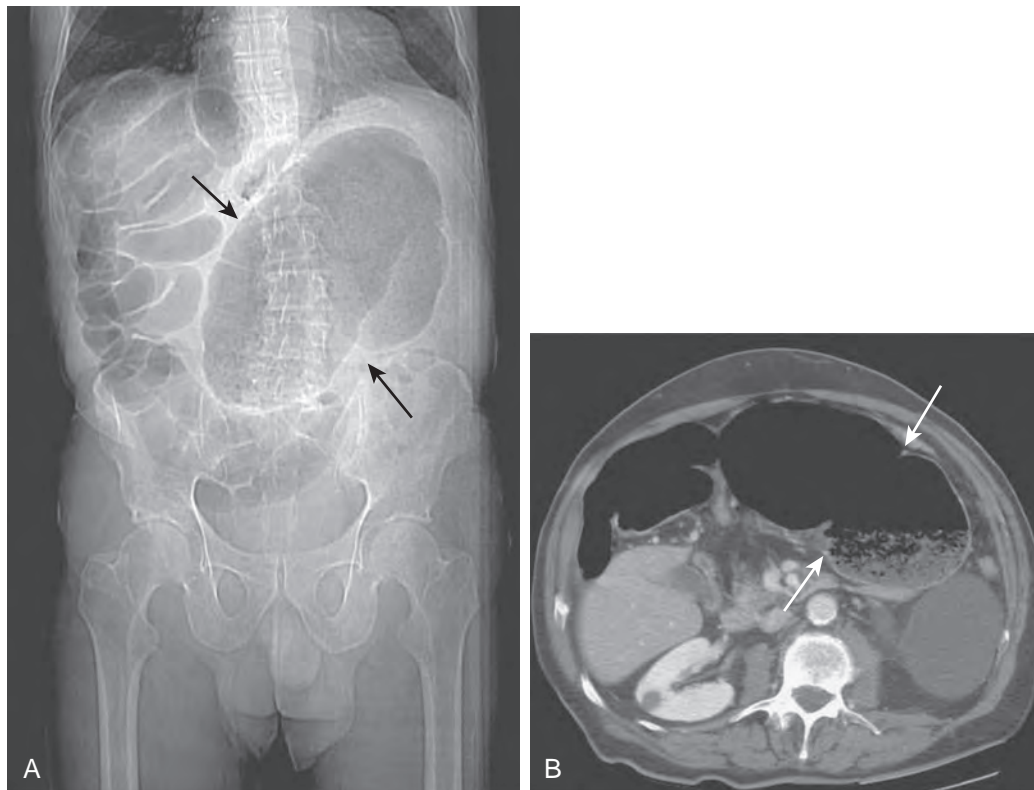


Figure 62-7 Cecal volvulus: CT features. **A.** Scout image shows that a distended cecum (arrows) is present in the left upper quadrant, with multiple dilated small bowel loops in the right upper quadrant. **B.** CT scan demonstrates the malpositioned cecum (arrows) and swirling of the mesentery.

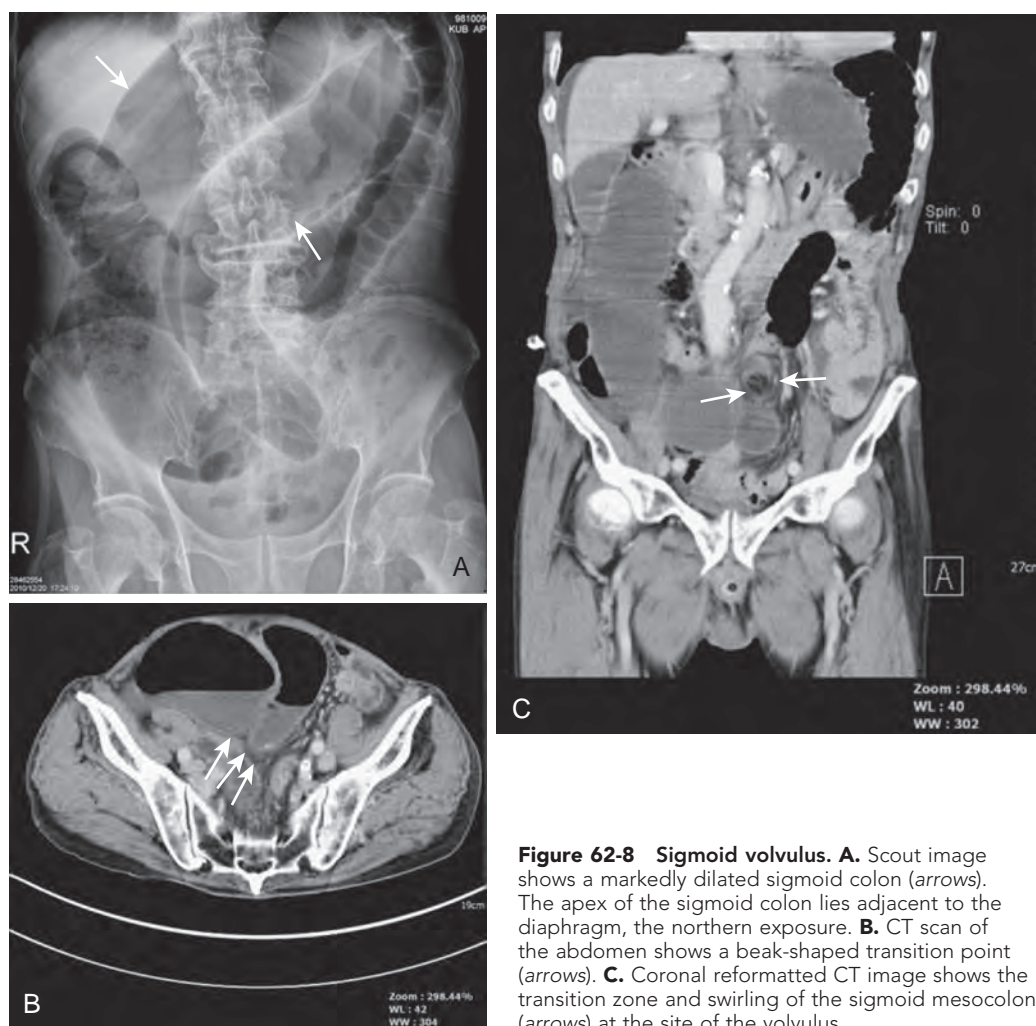


Figure 62-8 Sigmoid volvulus. **A.** Scout image shows a markedly dilated sigmoid colon (arrows). The apex of the sigmoid colon lies adjacent to the diaphragm, the northern exposure. **B.** CT scan of the abdomen shows a beak-shaped transition point (arrows). **C.** Coronal reformatted CT image shows the transition zone and swirling of the sigmoid mesocolon (arrows) at the site of the volvulus.

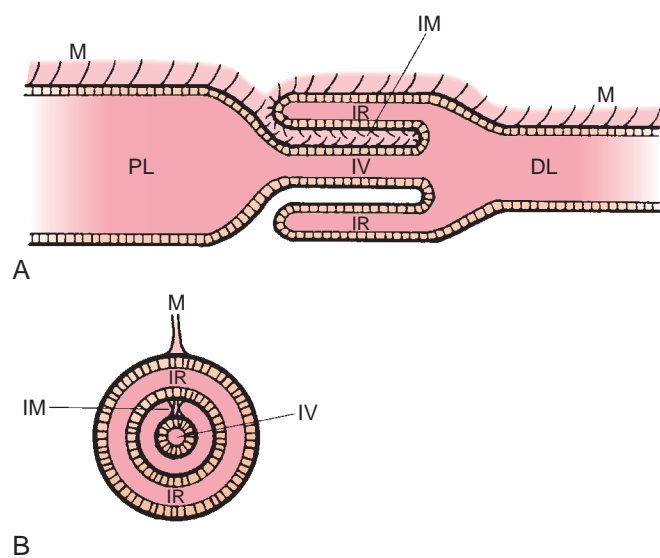


Figure 62-9 Intussusception. Longitudinal (**A**) and cross-sectional (**B**) diagrams of antegrade intussusception. DL, distal intestinal loops; IM, intussuscepted mesentery; IR, intussusciens; IV, intussusceptum; M, mesentery; PL, proximal intestinal loops. (From Iko BO, Teal JS, Siram SM, et al: Computed tomography of adult colonic intussusception: Clinical and experimental studies. *AJR* 143:769-772, 1984.)



Figure 62-10 Ileocolic intussusception. The ileum is intussuscepting (arrow) into the colon. The lead point was a small gastrointestinal stromal tumor of the distal ileum.

The classic appearance of intussusception on barium studies is the coil spring appearance as contrast is trapped between the intussusceptum and intussusciens (Fig. 62-11).

Ultrasound shows a target-like lesion (Fig. 62-12), in which the hypoechoic halo is produced by the mesentery and edematous wall of the intussusciens, and the hyperechoic center is produced by multiple interfaces of compressed mucosal, submucosal, and serosal surfaces of the intussusceptum. Multiple concentric rings, best seen on transverse scans, are also characteristic. The corresponding appearance on longitudinal scans is that of multiple, thin, parallel, hypoechoic, and echogenic stripes.⁹²⁻⁹⁶

On CT, intussusceptions appear as three different patterns, which reflect their severity and duration: (1) the target sign; (2) a sausage-shaped mass, with alternating layers of low and high attenuation; and (3) a reniform mass. Pathophysiologically, the target is the earliest stage of intussusception. As it progresses, a layering pattern develops, with alternating low-attenuation (mesenteric fat) and high-attenuation areas (bowel wall), (Fig. 62-13). If intussusception is untreated, edema and mural thickening develop. An intussusception with a reniform appearance is caused by severe edema and vascular compromise, which constitutes a surgical emergency.⁹⁷ Intussusception is almost invariably associated with acute intestinal obstruction or partial and recurrent obstruction, air-fluid levels, and proximal bowel distention. The mesenteric arcade associated with the intussusciens may show traction. If infarction occurs, this

mass may be surrounded by intraperitoneal fluid, edema, hemorrhage in the mesentery, and even perforation.⁹⁸⁻¹⁰⁴ CT can diagnose lipoma as the lead point; however, with varying degrees of infarction and fat necrosis, lipomas may have an atypical appearance.^{105,106}

Adhesions

Adhesions are the result of inflammation that heals with fibrosis. They are usually the result of surgical trauma but may be congenital. Adhesional large bowel obstruction is unusual because the colon is characteristically fixed and of large caliber and has thick walls. The small bowel, in contrast, has an inherently small caliber and high degree of mobility and is therefore very prone to obstruction by adhesions. A more complete discussion of small bowel obstruction can be found in Chapter 46. The mobile redundant portions of the colon are most likely to be involved.¹⁰⁷ Adhesive obstructions of the right colon, transverse colon, and sigmoid colon have been reported.^{108,109}

Folding of the cecum on itself, the cecal bascule, often occurs at the site of an adhesive band.¹¹⁰ The ascending colon can be obstructed by congenital bands or adhesions caused by inflammatory changes after colonoscopy and polypectomy.^{111,112} Inflammation of the appendices epiploicae can rarely cause obstruction in the rectosigmoid, and ischemia and inflammation of the greater omentum can cause obstruction in the transverse colon.^{113,114} On barium enema, adhesions can appear as an area of circumferential narrowing, usually short, with intact

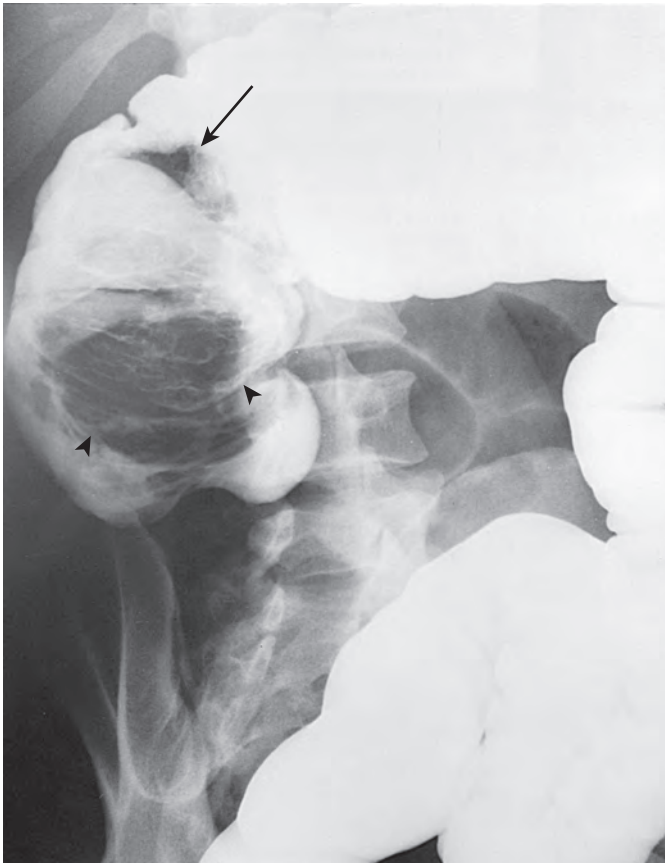


Figure 62-11 Colonic intussusception: barium enema findings. A cecal neoplasm is intussuscepting into the ascending colon (arrow). Note the coiled spring appearance (arrowheads).

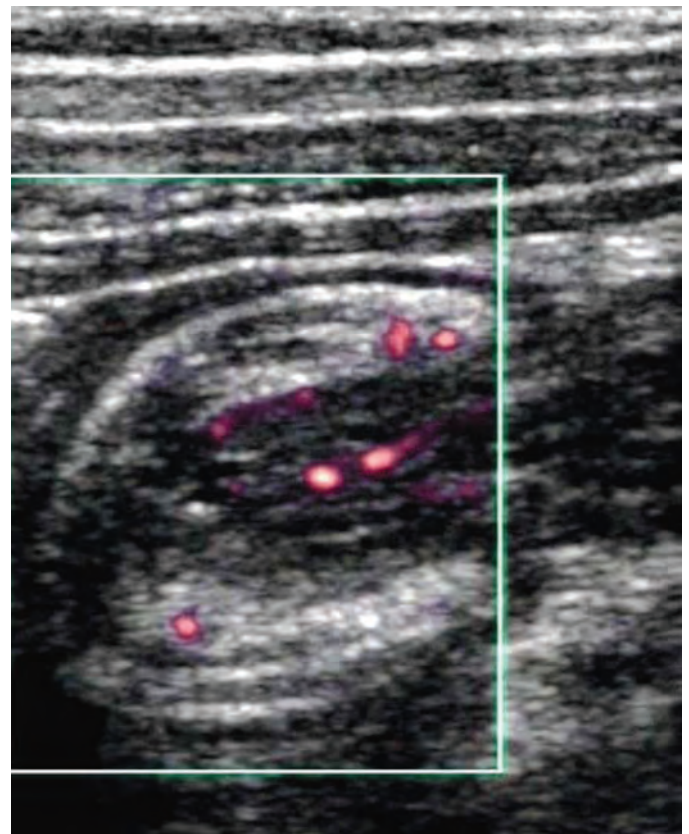
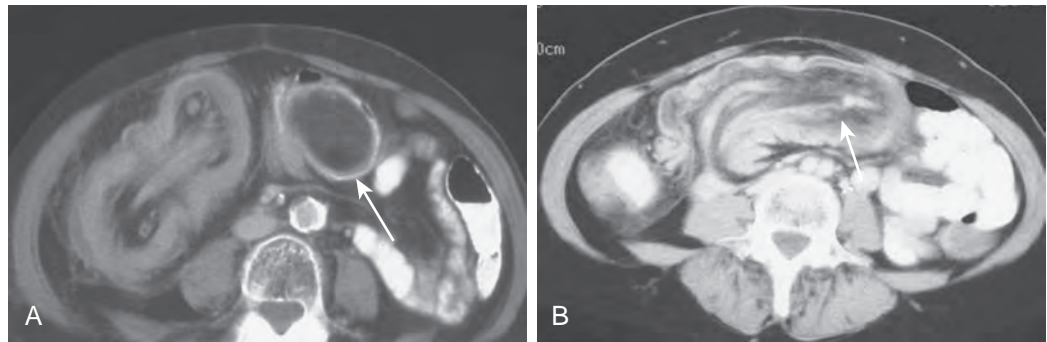


Figure 62-12 Intussusception: sonographic findings. This color Doppler scan, longitudinally imaging the intussusception, shows a central hypoechoic area that is the intussusceptum telescoping into the intussusciens.

Figure 62-13 Colonic intussusception: CT findings.

A. The lead point of this colonic intussusception is a lipoma (arrow). The outer layer represents the intussusciens and the inner layer represents the intussusceptum. **B.** In a different patient, the cigar-shaped intussusceptum (arrow) is seen within the intussusciens.



mucosa, or as a smooth, broad-based filling defect. They may produce partial or complete colonic obstruction.¹¹⁵

Hernias

Hernias cause large bowel obstruction less often than small bowel obstruction because of the relatively fixed nature of the colon and its larger caliber. Inguinal, femoral, umbilical, spigelian, incisional, lumbar, and diaphragmatic hernias (congenital or post-traumatic) can all contain colon and cause bowel obstruction.¹¹⁶⁻¹²⁵ Internal hernias, such as through the foramen of Winslow, can contain colon and cause obstruction as well.¹²⁶⁻¹²⁹ The diagnosis may be made by radiography, barium enema, or CT. A complete discussion of hernias can be found in Chapter 112.

Obturation Obstruction

The terminal ileum is the narrowest portion of the gut and, as a result, is the most common site of obturation obstruction. The sigmoid colon, measuring 2.5 cm in diameter, only slightly larger than the distal ileum, is the narrowest portion of the colon, followed by the hepatic and splenic flexures. These are the most likely points of colonic impaction of an intraluminal object.¹³⁰

Of patients with gallstone ileus, 3% to 5% have colonic obstruction.¹³¹ In these patients, the gallstone most often bypasses the ileocecal valve through a cholecystocolic fistula and usually impacts in the sigmoid colon, which may be narrowed by prior diverticulitis.¹³²

Bezoars, foods, and enteroliths usually do not obstruct the colon unless there is a stricture.^{133,134} Patients with cystic fibrosis (see Chapter 118) tend to form large cecal masses of inspissated feces that can cause the meconium ileus equivalent syndrome.¹³⁵

Sufficient amounts of various medications or diagnostic agents can cause colonic obturation obstruction. Antacid impactions containing nonabsorbable aluminum hydroxide antacid gels, given to prevent hyperphosphatemia, can develop in the right colon of patients with renal failure. These impactions can be treated with orally or rectally administered hyperosmolar diatrizoate meglumine (Gastrografin).¹³⁶

Barium retained in the colon for several days is desiccated and can form impactions in any part of the colon, usually the proximal portion. These impactions can also be treated by hyperosmolar Gastrografin, which stimulates peristalsis and draws fluid into the bowel.^{137,138} Foreign bodies entering via an oral or transanal route can cause obstruction or perforation.¹³⁹

Older, inactive, debilitated, and mentally challenged patients, drug addicts in methadone maintenance programs, transplantation and hemodialysis patients, and those with adult Hirschsprung's disease are at risk for developing fecal

BOX 62-1 COLONIC ISCHEMIA: RISK FACTORS

- Inferior mesenteric artery ligation, thrombosis, or embolus
- Superior mesenteric artery ligation, thrombosis, or embolus
- Cardiac arrhythmia
- Congestive heart failure
- Shock
- Digitalis toxicity
- Collagen vascular disease
- Strangulated hernia
- Oral contraceptives
- Polycythemia vera
- Trauma
- Diabetes
- Amyloidosis
- Radiation

impaction. The most common sites are the rectum (70%) and sigmoid colon (20%). A fecaloma or stercoroma is a mass of fecal material that develops the characteristics of an intraluminal tumor. These are composed primarily of an accumulation of undigested food forming a nucleus around which fecal material accumulates. Obstruction, volvulus, stercoral ulceration, perforation, rectal prolapse, and rectal fissure are potential complications of fecalomas.^{140,141}

Strictures

Colonic strictures can result from a variety of disorders (Boxes 62-1 to 62-3). These strictures often cause chronic obstructive symptoms and may cause acute obstruction from the presence of impacted feces or as a result of obturation in the stricture by a foreign object.

Other Causes

Pelvic lipomatosis, in which there is benign fatty tissue infiltration into the perirectal and perivesical spaces, usually causes straightening, narrowing, and rigidity of the rectum but occasionally can cause obstruction.¹⁴² Pregnancy, mesenteric cysts, wandering spleen, retroperitoneal tumors, retractile mesenteritis, and retroperitoneal fibrosis are rarer causes of large bowel obstruction.¹⁴³⁻¹⁴⁵

Extracolonic Diseases Involving the Colon

Benign and malignant extrinsic disease processes can involve the colon. Endometriosis, ovarian carcinoma, other benign and malignant gynecologic diseases, pancreatic disease, prostate

BOX 62-2 GENERAL, SYSTEMIC, AND PSYCHOLOGIC CAUSES OF CONSTIPATION

LIFESTYLE

- Inadequate fiber
- Little food
- Repressing or ignoring urge to defecate
- Immobility

EXTERNAL FACTORS

- Drugs (including opiates, anticholinergics, antidepressants, anti-convulsants)

ENDOCRINE AND METABOLIC FACTORS

- Hypothyroidism
- Hypercalcemia
- Porphyria
- Neurologic
- Parkinson's disease
- Multiple sclerosis
- Spinal lesions
- Damage to sacral parasympathetic nerves
- Autonomic neuropathy
- Autonomic failure

PSYCHOLOGIC FACTORS

- Depression
- Eating disorders (e.g., anorexia nervosa)
- Obsession about "inner cleanliness"
- Denied bowel actions

From Lembo AJ, Ullman SP: Constipation. In Feldman M, Friedman LS, (eds): *Gastrointestinal and Liver Disease*, 9th ed. Philadelphia, Saunders, 2010, pp 259–284.

BOX 62-3 GASTROINTESTINAL CAUSES OF CONSTIPATION AND RELATED SYMPTOMS

GASTROINTESTINAL TRACT

- Obstruction
- Aganglionosis (Hirschsprung's disease, Chagas' disease)
- Myopathy
- Neuropathy
- Systemic sclerosis

MEGARECTUM AND COLON

- Anal atresia or malformation
- Hereditary internal anal sphincter myopathy
- Anal stenosis
- Weak pelvic floor
- Large rectocele
- Internal intussusception
- Anterior mucosal prolapse
- Prolapse
- Solitary rectal ulcer

From Lembo AJ, Ullman SP: Constipation. In Feldman M, Friedman LS, (eds): *Gastrointestinal and Liver Disease*, 9th ed. Philadelphia, Saunders, 2010, pp 259–284.

carcinoma, and other abdominal malignancies can present as colon involvement. This involvement may cause obstruction and can mimic primary colon pathology. Obstruction usually occurs in the pelvis, where the colon is fixed and confined by the bony pelvis. The transverse colon is another common site

of involvement because of its omental and mesenteric attachments (see Chapter 108). Barium enema, CT, and endoscopic ultrasonography may be helpful in the assessment of colonic wall invasion by adjacent disease processes.¹⁴⁶

ENDOMETRIOSIS

Endometriosis is a disease that affects 8% to 18% of women during their active menstrual years, usually between the ages of 30 and 45 years.^{147,148} GI tract involvement has been reported in 5% to 37% of patients.¹⁴⁹ In one large retrospective review of over 7000 patients with endometriosis, 12% of the patients had gut involvement. The rectosigmoid colon was the most frequently involved site (72% of cases), followed by the rectovaginal septum (14%), small intestine (7%), cecum (4%), and appendix (3%).¹⁵⁰ Rare cases of involvement of the stomach, pancreas, proximal small bowel, and transverse colon have been reported.

The anterior wall of the rectosigmoid colon adjacent to the pouch of Douglas is the most frequent site of GI tract involvement. Endometrial implants on the bowel are usually extrinsic or serosal but may be intramural or, rarely, intraluminal.¹⁵¹ Implants typically appear as an extrinsic serosal mass effect with mucosal preservation on double-contrast barium enema studies (Fig. 62-14). This appearance, although characteristic of endometriosis, is not specific because other extrinsic processes in the cul-de-sac, such as drop metastases or an abscess, can produce an identical appearance. Serosal spiculation and fine crenulations of the mucosa can usually be identified when there is involvement of the bowel wall.¹⁵² Less frequently, manifestations of endometriosis on barium enema are a polypoid mass extending into the lumen of the colon, stricture, or short annular lesion. These cases may be difficult to distinguish clinically and radiographically from carcinoma.¹⁵³ Rarely, endometriosis presents as acute obstruction, GI bleeding, or perforation, necessitating resection.^{7,154-157} Endometriomas usually appear as solid or complex cystic masses on ultrasound or CT, but the appearance is not specific and may be indistinguishable from a neoplasm or abscess.¹⁵⁸⁻¹⁶⁰ MRI (see Fig. 62-14) is more sensitive and specific for detection of hemorrhage within these masses.¹⁶⁰

MALIGNANT GYNECOLOGIC TUMORS

Malignant gynecologic neoplasms spread within the peritoneal cavity by direct invasion, intraperitoneal seeding, hematogenous metastasis, and lymphatic extension. Intraperitoneal seeding of malignant cells is dependent on the natural pathways of flow of ascitic fluid as demonstrated by Meyers.¹⁶¹ The characteristic patterns of spread vary depending on the origin of the primary tumor. See Chapter 109 for a more complete discussion of pathways of abdominal and pelvic spread of disease.

OVARIAN CARCINOMA

Ovarian carcinoma is the fifth leading cause of cancer deaths in women; the prevalence increases with age and peaks around age 60 years.¹⁶²⁻¹⁶⁴ Most patients with ovarian carcinoma have relatively few symptoms, and in over 50% the disease is in an advanced stage at the time of initial presentation. Patients usually have vague abdominal symptoms and present with

increasing abdominal girth and a large palpable mass, although some tumors are detected earlier on routine pelvic examination. Occasionally, intestinal symptoms or colonic obstruction may be the first manifestation of ovarian cancer.¹⁶⁵

Ovarian carcinoma is the most common primary malignancy to invade the colon directly. The subperitoneal space forms a pathway for the spread of disease processes from the pelvis to the abdomen.^{166,167} Direct invasion from the left ovary through the sigmoid mesocolon usually involves the inferior border of the sigmoid colon. Direct invasion from the right ovary usually involves the cecum and distal ileum by means of extension through the small bowel mesentery of the ileum. Direct invasion of the colon by ovarian cancer can be readily

demonstrated on barium enema, with appearances ranging from serosal spiculation with tethering and fixation to gross invasion and annular constriction to complete obstruction.¹⁶⁸ Mural involvement may produce narrowing with mucosal crenulations or, in more severe cases, marked narrowing with spiculation. Annular constriction may simulate carcinoma or diverticulitis, and complete obstruction may mimic an obstructing colon carcinoma.

Ovarian carcinoma frequently spreads by intraperitoneal seeding. The colon is the portion of the GI tract most frequently involved by intraperitoneal seeding of ovarian carcinoma. Peritoneal implants, which may be multiple, are seen as extrinsic masses, often with serosal spiculation and tethering (Fig. 62-15)

Figure 62-14 Pelvic endometriosis. **A.** Barium enema examination shows an extrinsic mass on the serosal aspect of the rectum (arrow). **B.** Pelvic ultrasound depicts a well-margined pelvic mass (arrow) with multiple fine, homogenous, low-level echoes. **C.** Sagittal MRI scan demonstrates invasive endometriosis along the anterior aspect of the rectum (arrow).

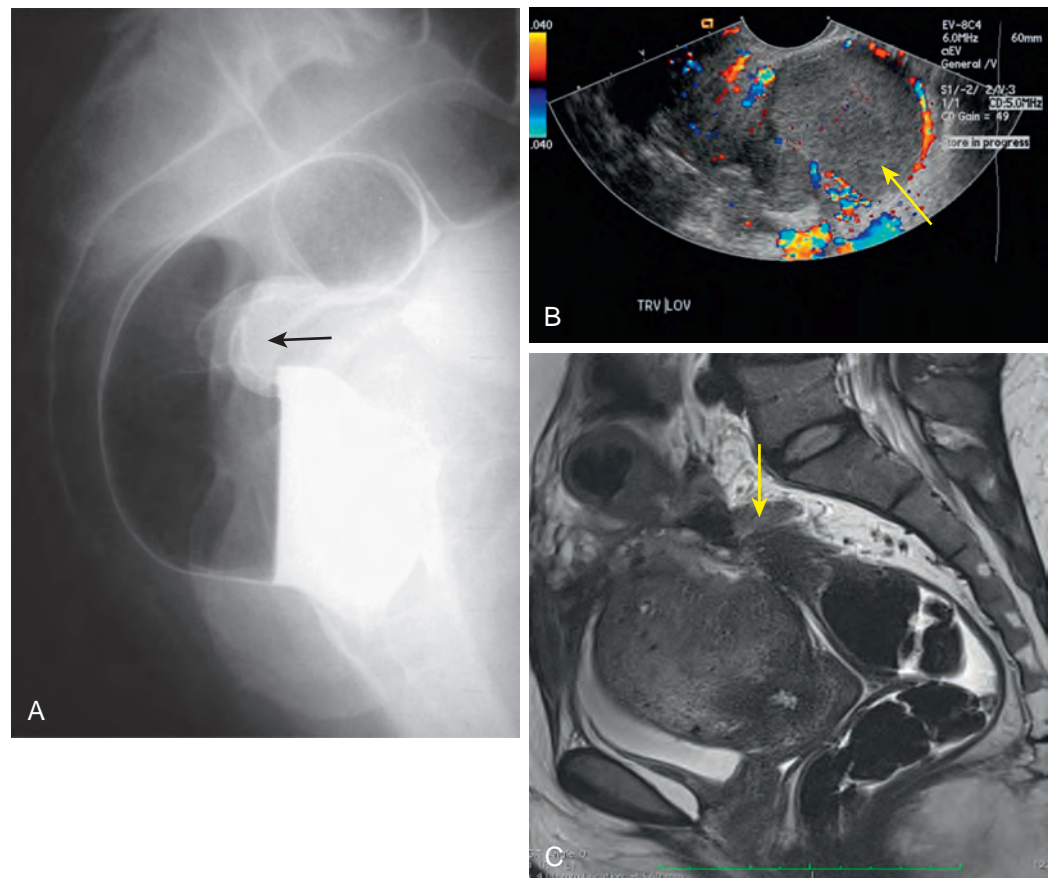
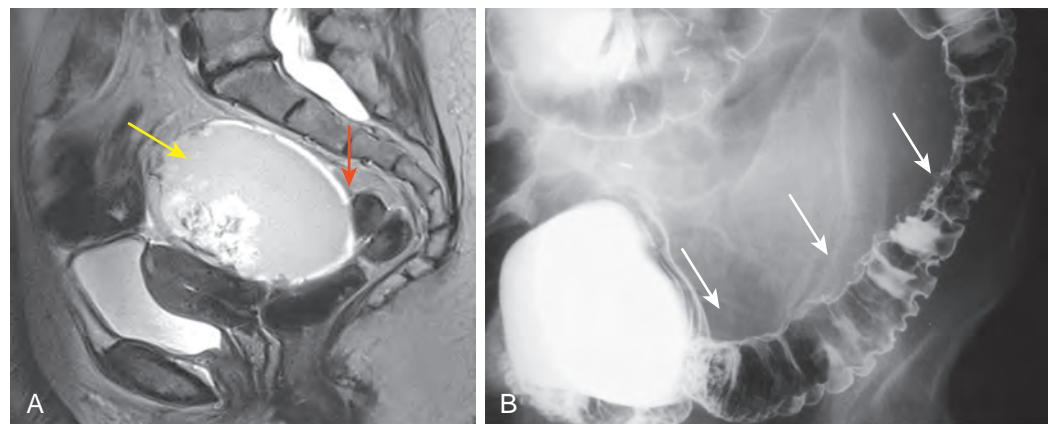


Figure 62-15 Ovarian carcinoma. **A.** Sagittal T2-weighted MRI scan shows a complex cystic mass (yellow arrow) compressing the anterior wall of the rectum (red arrow). **B.** In a different patient with ovarian carcinomatosis, multiple serosal implants (arrows) are identified along the medial aspect of the sigmoid colon.



on barium enema studies. An implant in the cul-de-sac may be indistinguishable from an abscess or endometrioma. In addition, ovarian carcinoma frequently seeds the greater omentum, producing a so-called omental cake, which can secondarily involve the transverse colon or stomach. The appearance in these cases can simulate gastric cancer with extension to the transverse colon through the gastrocolic ligament or colon cancer with extension to the stomach.¹⁶⁹⁻¹⁷¹

OTHER GYNECOLOGIC MALIGNANCIES

Cervical carcinoma spreads by direct extension to the pelvic sidewall and adjacent structures, including the rectum. Demonstration of rectal involvement is an important finding because hysterectomy is reserved for patients with tumor localized to the cervix or extension confined to the parametrium or upper two thirds of the vagina (stage IIB or less). All others are treated with radiation therapy.¹⁷²

Carcinoma of the endometrium, vagina, and fallopian tubes can also invade the rectosigmoid colon directly. Barium enema examination provides important information for staging and planning surgical resection of these pelvic malignancies. These tumors can also spread by peritoneal seeding or lymphatic extension. Leiomyosarcoma of the uterus, like other sarcomas, may spread by hematogenous metastasis to the gut, producing submucosal masses that can ulcerate and bleed.

BENIGN GYNECOLOGIC TUMORS

Benign ovarian tumors, including serous and mucinous cystadenomas and teratomas, may produce an extrinsic impression on the rectosigmoid colon that is recognizable on CT and barium enema. These masses, which are purely extrinsic to the bowel, have a smooth interface with the colonic wall and are usually asymptomatic but, if very large, may produce symptoms of partial obstruction. Teratomas usually contain fat or calcification that can be detected on plain films or CT. Uterine fibroids are present in 25% to 50% of women and are the most common pelvic tumor, with a peak incidence in the fifth decade of life. Most are small and asymptomatic. Fibroids may present as vaginal bleeding if they are submucosal or may become symptomatic if they grow to a large size. Barium enema in these cases demonstrates a smooth extrinsic mass effect on the sigmoid colon, with marked displacement and stretching of the colon if the tumor is large. Rupture of an ovarian cystadenoma into the peritoneal cavity may result in pseudomyxoma peritonei.

PELVIC INFLAMMATORY DISEASE AND TUBO-OVARIAN ABSCESS

Pelvic inflammatory disease has a variety of causative organisms, including *Chlamydia trachomatis*, *Neisseria gonorrhoeae*, and a number of other aerobic and anaerobic bacteria. The tubo-ovarian abscesses that result may secondarily involve the bowel and may be indistinguishable on barium enema from endometrial or metastatic implants on the serosal surface. The cul-de-sac is a frequent site of involvement. Ultrasonography, CT, or MRI shows a thick-walled fluid collection that may be difficult or impossible to differentiate from cystic neoplasm or endometrioma.^{173,174}

SEXUALLY TRANSMITTED DISEASES

Lymphogranuloma venereum is a sexually transmitted disease caused by infection of lymphatic tissue by *C. trachomatis*. The site of primary infection is usually around the genitals, but the rectum may be the primary site of involvement. Primary infection of the rectum is usually acquired by anal intercourse, but proctitis may also result from the spread of an infected vaginal discharge to the anal canal or by lymphatic extension from inguinal lymph nodes. Patients present with inguinal adenopathy and deep rectal ulceration. The disease may progress to form a fistula, perirectal abscess, or stricture (Fig. 62-16).¹⁷⁵ Other sexually transmitted diseases, including *N. gonorrhoeae* or herpes simplex infection and syphilis, can infect the rectum and cause proctitis.¹⁷⁶ Barium enema demonstrates mucosal ulceration or a granular mucosal pattern. CT typically shows non-specific mural thickening of the rectum and anus.

PANCREATITIS

Approximately 1% of patients with acute pancreatitis have significant colonic problems. These complications usually occur 10 to 21 days after disease onset and may relate to compression caused by a pancreatic phlegmon or abscess and widespread fat necrosis, or by mural thickening caused by edema and necrosis secondary to pancreatic enzymes dissecting down the transverse mesocolon or phrenicocolic ligament.¹⁷⁷ Occasionally, a high-grade obstruction or perforation may occur that requires surgical intervention.¹⁷⁸⁻¹⁸² For a more complete discussion of pancreatitis, see Chapter 97.

METASTASES

High-grade colonic obstruction is attributable much less often to metastatic than to primary tumors.¹⁸³ Renal and prostate neoplasms can directly invade the colon.¹⁸⁴ Carcinoma of the prostate involves the rectum in 0.5% to 11% of cases and may simulate rectal carcinoma clinically. Rectal obstruction occurs when there is direct extension through the thick, double-layered



Figure 62-16 Chlamydial infection (lymphogranuloma venereum). Barium enema examination demonstrates a stricture of the rectum, with fistulas and sinus tracts.

Denonvillier's fascia or by rectal compression caused by a massively enlarged prostate gland.^{185,186} Gastric and pancreatic neoplasms can invade the colon directly or narrow it by serosal metastases.¹⁸⁷⁻¹⁸⁹

Colonic Ischemia

CLINICAL FINDINGS

Colonic ischemia is the most common vascular disorder of the GI tract and the most common cause of colitis in older adults.^{189,190} Although many conditions have been implicated in the pathogenesis of colonic ischemia (see Box 62-1), the cause is unclear in most patients, and no precipitating event or condition can be identified. Most patients have no major vascular occlusion, so the condition is attributed to low flow states, small vessel disease, or both. In about 20% of cases, an obstructive or potentially obstructive colonic lesion is present.

Colonic ischemia produces a wide spectrum of disease, ranging from gangrene of the colon to transient ischemic colitis. Colonic ischemia is classified as follows: (1) reversible ischemic colopathy; (2) reversible or transient ischemic colitis; (3) chronic ulcerative ischemic colitis; (4) ischemic colonic stricture; (5) colonic gangrene; or (6) fulminant universal ischemic colitis.¹⁹¹

The underlying pathophysiology of colonic ischemia is insufficient blood supply to the bowel to meet the needs of the mucosa. The mucosa receives most of the intestinal blood flow and is most susceptible to damage. Injury may be confined to the mucosa and submucosa or may extend transmurally. The degree of damage depends on the rate of onset of the ischemic event and extent of the vascular deprivation. The outcome may be complete healing, reversible or chronic colitis, stricture formation, or gangrene. About 50% of patients fall into the first category, with mild disease that resolves in 1 to 2 weeks. The clinical course is highly variable. In one series, the outcomes were as follows: reversible hemorrhage and edema, 33%; transient or reversible colitis, 16%; reversible or persistent strictures, 12%; persistent colitis, 21%; and gangrene or perforation, 18%.¹⁹⁰

Most patients with colonic ischemia are older than 50 years and present with mild lower abdominal pain and rectal bleeding or bloody diarrhea. Those with transmural disease have more impressive findings, with peritoneal signs. The frequency of distribution of ischemic colitis is as follows: left colon (32.6%), distal colon (24.6%), right colon (25.2%), transverse colon

(10.2%), and pancolitis (7.3%). The diagnosis is usually based on colonoscopy and CT results.

PATHOLOGIC FINDINGS

Acute ischemic lesions of the colon show necrosis (Fig. 62-17) of the superficial portion of the mucosa, which often spares the deeper portions of the colonic crypts. The remaining crypts typically have an atrophic or withered appearance that reveals striking cytoplasmic atypia, which may be mistaken for dysplasia. Pseudomembranes, hemorrhage into the lamina propria, and hyalinization of the lamina propria may also be seen. These lesions may regress on their own, or frank gangrene with perforation or stricture formation may occur.

The chronic phase of ischemic colitis may be more difficult to diagnose, because the only histologic findings may be areas of submucosal fibrosis and stricture, which are nonspecific.

RADIOLOGIC FINDINGS

Radiography

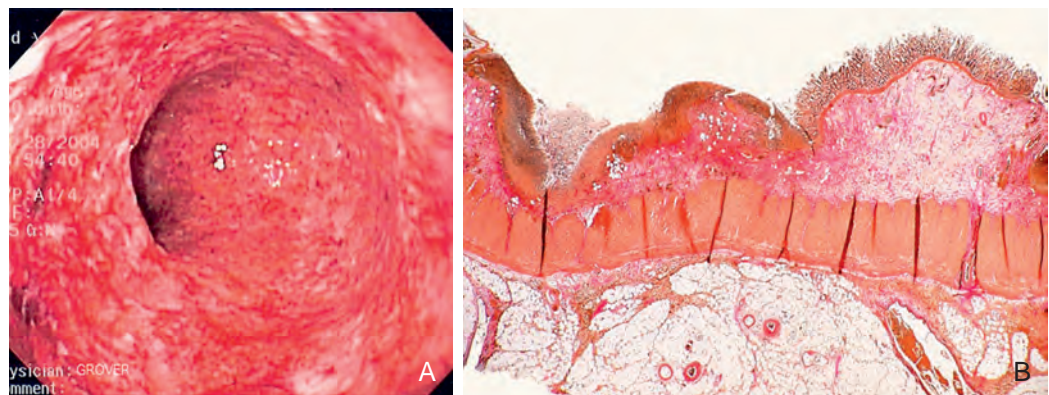
Abdominal radiographs are usually nondiagnostic and are normal or show a nonspecific ileus. In a series of 41 patients with colonic ischemia, only 21% had radiographic findings suggesting ischemia. Radiographic findings in colonic ischemia include normal, nonspecific ileus, thumbprinting, transverse ridging, and fixed loops with tubulation and lack of haustra. The most characteristic finding on radiographic and barium enema examination is thumbprinting, which consists of multiple round, smooth, scalloped defects projecting into the air-filled colonic lumen (Fig. 62-18). Thumbprinting is caused by submucosal bleeding, edema, or both, and usually occurs within the first 24 hours after the insult to the bowel.¹⁹² Experimental work has shown that thumbprinting results from extravasation of blood around small blood vessels that are reperfused after losing their integrity during the ischemic period.¹⁹⁰ Thickening of the bowel wall secondary to edema and hemorrhage may be observed; this is reflected by luminal narrowing or transverse ridging. As the edema progresses or mucosal sloughing occurs, fixed rigid, tubular, ahaustral loops may develop.¹⁹³ Rarely, pneumatosis or portal venous gas can be identified. These findings generally indicate necrotic bowel.

Barium Enema

Colonoscopy and CT are the primary means of establishing the diagnosis of ischemic colitis. The barium enema findings

Figure 62-17 Ischemic colitis.

A. Colonoscopy shows a diffusely ulcerative, hyperemic mucosa.
B. The mucosal surface of the colon shows necrosis and hyperemia extending from the mucosa to the serosa of the colon. Frank ulceration is present.



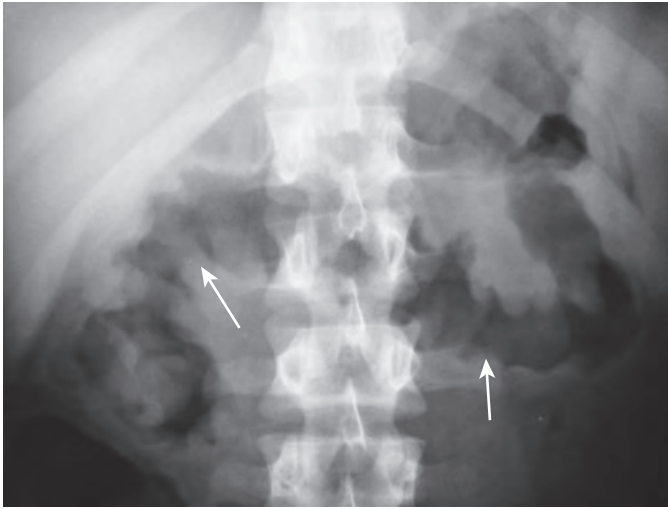


Figure 62-18 Colonic ischemia: narrowing and thumbprinting on plain abdominal radiograph. Supine radiograph of the abdomen shows marked narrowing and thumbprinting of the transverse colon (arrows) caused by colonic ischemia.

depend on the extent of the ischemic process, degree of damage, and stage at which the examination is performed. The hallmark of colonic ischemia is serial changes on examinations performed over days, weeks, or months.¹⁹⁴⁻¹⁹⁶

The classic barium enema findings in colonic ischemia are thumbprinting, transverse ridging, spasm, ulceration, intramural barium, and strictures. The most consistent and characteristic finding on the barium enema examination early in the course of the disease is thumbprinting, which is seen in 75% of patients.¹⁹⁶ Thumbprinting on a barium enema study corresponds to the radiographic findings of smooth, round, polypoid, and scalloped filling defects projecting into the opacified colonic lumen as a result of submucosal edema or hemorrhage (Fig. 62-19). Edema and hemorrhage may be soft and compressible, and taking films with maximal distention may affect the findings. Because spasm often accompanies ischemia, maximal distention may be hard to maintain, making thumbprinting easier to see. Careful fluoroscopy with imaging during the filling stage of the examination and postevacuation radiographs should be obtained to document the presence of thumbprinting. Intraluminal pressures during single- and double-contrast examinations are fairly equivalent, so there is no advantage to performing a single-contrast study in this regard. Thumbprinting characteristically resorbs in less than 1 week but may persist for weeks in some patients.¹⁹⁵ Thumbprinting, although characteristic of ischemia, may also be observed in other conditions, including inflammatory bowel disease and the infectious colitides.

Transverse ridging is a less common finding, observed in 13% of patients with colonic ischemia.¹⁹⁵ Transverse ridging is caused by edema or spasm and is characterized by parallel, symmetric thickened folds running perpendicular to the bowel lumen. Like thumbprinting, it is generally an early finding and usually resolves rapidly.¹⁹⁶

Ulceration is present in 46% to 60% of patients with colonic ischemia, and is caused by sloughing of the mucosa.¹⁹⁶ Ulceration generally develops 1 to 3 weeks after the onset of disease and may heal completely, continue into a chronic



Figure 62-19 Colonic ischemia: thumbprinting. Single-contrast barium enema study shows extensive thumbprinting caused by hemorrhage or edema in colonic ischemia.

ulcerative ischemic phase, or heal with stricture formation. The ulcerations are characteristically longitudinal but may also be discrete, superficial, deep, small, or large. Differential diagnosis from other forms of colitis, particularly Crohn's disease and ulcerative colitis, can be made on the basis of sequential changes on barium enema examination, age of the patient, distribution of disease, clinical history, and endoscopic and biopsy findings.¹⁹⁶

Intramural barium is an unusual manifestation of ischemia and is caused by sloughing of a necrotic portion of the wall, with subsequent tracking of barium intramurally. Intramural barium can also be seen in other conditions, such as Crohn's disease and diverticulitis.

About 12% of patients with severe colonic ischemia heal with stricture formation.¹⁹⁰ Strictures can develop rapidly in the course of disease and may be identified as early as 3 weeks after initial presentation. Strictures may be reversible or irreversible and characteristically lead to few obstructive symptoms. In some patients, postischemic strictures may be encountered without a clear antecedent episode. The strictures may be smooth and tapering or eccentric, with sacculations.

About 20% of cases of colonic ischemia occur proximal to an obstructive or potentially obstructive colonic lesion. In about 50% of patients, the lesion is a colon carcinoma; diverticulitis and volvulus are the other major causes. In this setting, the typical findings of thumbprinting and ulceration can

develop or an urticarial pattern can be seen. This consists of bleblike mounds on the mucosal surface caused by early ischemia.¹⁹⁷ It is thought that increased intraluminal pressure proximal to the obstruction decreases mucosal perfusion.

Colonoscopy is useful in the diagnosis of colonic ischemia; the findings vary, depending on the stage at which the examination is performed. Initially, purplish blebs resulting from hemorrhage may be seen, corresponding to the radiographic findings of thumbprinting. As the hemorrhage is resorbed, varying degrees of ulceration, mucosal sloughing, and inflammation develop. The colonoscopic findings at this stage may resemble those in other forms of colitis. As with the barium enema, sequential studies demonstrate a changing pattern.¹⁹⁸

Computed Tomography, Ultrasonography, and Magnetic Resonance Imaging

Because CT is often the initial radiologic procedure in patients presenting with abdominal pain, colonic ischemia may first be suspected on the basis of this study. Symmetric bowel thickening is the major CT finding of colonic ischemia (Fig. 62-20A). In some cases, a target or double halo pattern and polypoid defects associated with thumbprinting may be seen.¹⁹⁹ Mural thickening (>3 mm) of the colon is a nonspecific finding that can also be seen in carcinoma, lymphoma, metastatic disease, diverticulitis, Crohn's disease, and appendicitis. When the ischemia is severe, pneumatosis intestinalis may be seen (Fig. 62-20B; also see later).

Abnormal colonic wall thickening can also be identified by ultrasound.²⁰⁰ Again, this is a nonspecific finding but should lead to further studies of the colon when identified. Doppler ultrasound may show diminished perfusion to the involved segment.²⁰¹⁻²⁰³

Radiation Colitis

The colon is often affected by radiation for pelvic genitourinary tract tumors. Patients with carcinoma of the rectum may also receive radiotherapy before or after surgery. Acute symptoms of

proctitis and diarrhea are common during therapy and usually resolve within weeks after completion of the therapy.

PATHOGENESIS

Radiation can injure and kill cells by two methods. The first is a direct cytotoxic effect, in which the ionizing radiation absorbed by these cells generates a series of biochemical events that progress to cell disruption and death. Free radicals derived from intracellular water interact with DNA to prevent replication, transcription, and protein synthesis. These cytotoxic effects predominate in cells that replicate rapidly. Accordingly, the intestine has the following radiation tolerance (in decreasing order): duodenum, jejunum, ileum, transverse colon, sigmoid colon, esophagus, and rectum. Pathologically, abnormal epithelial cell proliferation and maturation are associated with decrease in crypt cell mitosis. Edema, hyperemia, and extensive inflammatory cell infiltration are often present as well.

The second major mechanism of radiation injury is more insidious and involves damage to the fine vasculature and connective tissue of the intestine. A low-grade ischemia is caused by medial wall thickening and subendothelial proliferation producing endarteritis obliterans of the smallest arterial branches. This chronic ischemia often leads to a fibrotic reaction that can result in contraction, stricture formation, perforation, fistula, or hemorrhage.

The usual dose for treating abdominal and pelvic malignancies is between 3000 and 7000 cGy (1 cGy = 1 rad) and is delivered in fractions over an interval of 4 to 8 weeks. Lower total dosage, lower rates, and smaller treatment volumes minimize damage. Inherent differences in tissue susceptibility also determine which organ is affected most severely by a given dose. Rubin and Casarett have defined the concept of the tolerance dose.²⁰³ A minimal tolerance dose is usually expressed as TD_{5/5}, which represents the total dose that produces radiation damage in 5% of patients within 5 years. This dose has been determined to be 4500 cGy for the small bowel and colon and 5000 cGy for the rectum.²⁰⁵

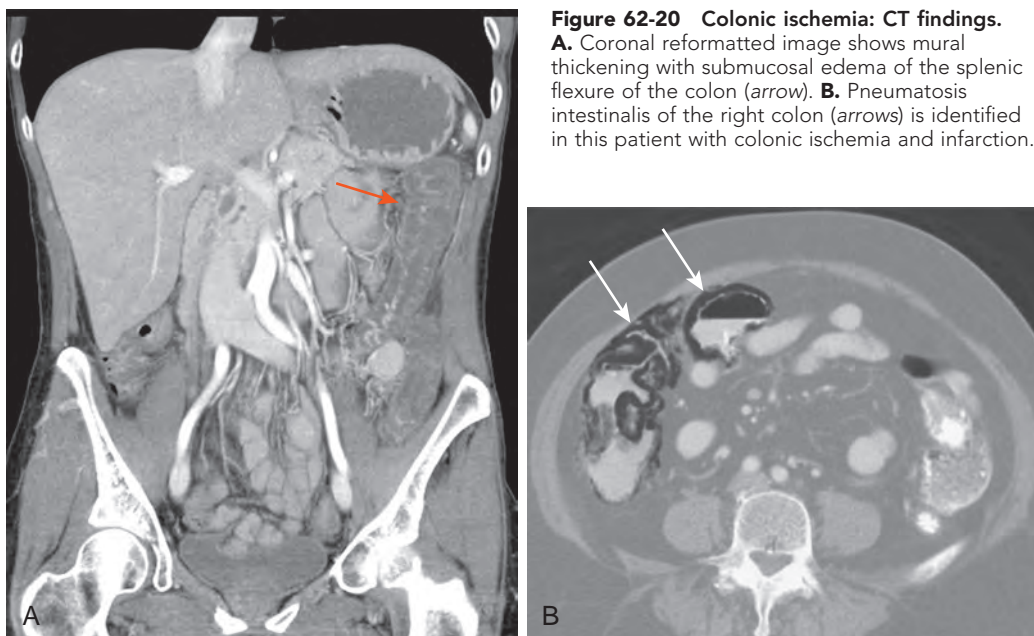


Figure 62-20 Colonic ischemia: CT findings.

A. Coronal reformat image shows mural thickening with submucosal edema of the splenic flexure of the colon (arrow). **B.** Pneumatosis intestinalis of the right colon (arrows) is identified in this patient with colonic ischemia and infarction.

FINDINGS

Clinical Findings

Radiation colitis typically develops after a 2-year latency period. Patients present with rectal bleeding, pain, and diarrhea, evoking a differential diagnosis that includes recurrent tumor, postoperative stricture in a colonic anastomosis, or regional inflammatory change resulting from pelvic abscess. Proctitis is usually seen sigmoidoscopically.²⁰⁴

Radiologic Findings

In acute radiation colitis, mural thickening of the involved segment of colon may be seen, associated with submucosal edema and hyperenhancement of the mucosa (Fig. 62-21A). In patients with chronic radiation proctosigmoiditis, barium enema examination can show diffuse or focal narrowing of the rectum and sigmoid colon, usually with tapered margins (Fig. 62-21B). The mucosal pattern is usually preserved but may be distorted or disrupted because of edema or intramural hemorrhage resulting from radiation-induced ischemic changes. Rectal stricture or rectovaginal fistula may be seen, and the presacral space is widened on the lateral view of the rectum and on CT.¹⁹⁹⁻²⁰² A recurrent tumor usually produces an eccentric mass effect and mucosal destruction and involves a relatively short segment of the colon. The radiologic differential diagnosis includes ulcerative colitis, Crohn's disease, and scarring by chlamydial proctitis.

TREATMENT

When symptoms such as obstruction or fistula become intolerable, surgical resection may be needed. Initially, a diversion colostomy is formed. After healing has occurred, an abdominal pull-through procedure with coloanal anastomosis between the nonirradiated colon and anus usually provides permanent relief. Attempts to resect strictures or fistulas are less likely to

succeed because of poor healing of the irradiated rectosigmoid tissue. Development of colon carcinoma has been suggested as a possible late sequela of pelvic irradiation.^{201,203}

Vascular Lesions of the Anorectum

INTERNAL HEMORRHOIDS

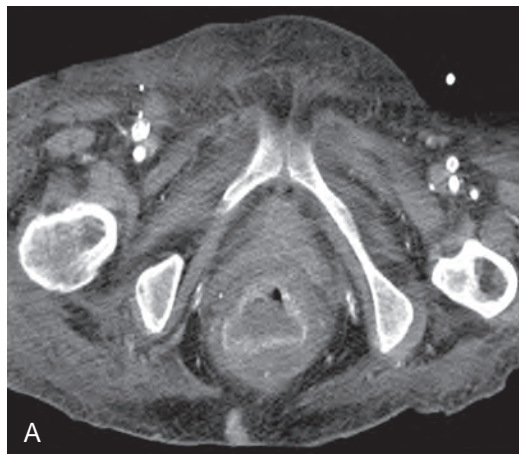
Internal hemorrhoids are dilated vascular spaces of the internal hemorrhoidal plexus in the submucosal layer of the upper anal canal and lower rectum. Normally, the submucosa of the upper anal canal has three distinct vascular cushions—along the left lateral, right anterior, and right posterior wall.²⁰⁴ It is postulated that these anal cushions aid in anal continence. The pathogenesis of hemorrhoids is multifactorial. With age, the connective tissue tethering the mucosa to the submucosa and muscular layer of the anal canal becomes lax. With excessive straining during defecation, prolapse of anal canal mucosa occurs, leading to congestion of vascular cushions and internal hemorrhoids. Pathologically, internal hemorrhoids appear as thick-walled submucosal veins, with accompanying arteries and dilated capillaries. Abundant arteriovenous anastomoses are present.

Hemorrhoids (piles) are extremely common and can cause brisk rectal bleeding, blood staining on toilet tissue, or painful swelling. With strangulation of hemorrhoids, mucosal infarction, necrosis, and superinfection may occur. Internal hemorrhoids may also be a complication of distal rectal carcinoma. Internal hemorrhoids are not varicose veins, and their incidence is not increased in patients with portal hypertension. Hemorrhoids are frequently diagnosed by digital examination, anoscopy, and flexible sigmoidoscopy.

Internal hemorrhoids have a varying radiographic appearance.^{205,206} When mild lobulation of anorectal folds (the columns of Morgagni) extends less than 3 cm from the radiographic anorectal junction, radiographic diagnosis of internal

Figure 62-21 Radiation-induced proctitis.

A. There is mural thickening with submucosal edema and hyperenhancement of the rectum in this patient with acute radiation proctitis undergoing therapy for rectal cancer. **B.** In a different patient with chronic radiation proctitis, there is a long segment of narrowing in the rectosigmoid demonstrated on this barium enema examination. The presacral space is also widened.



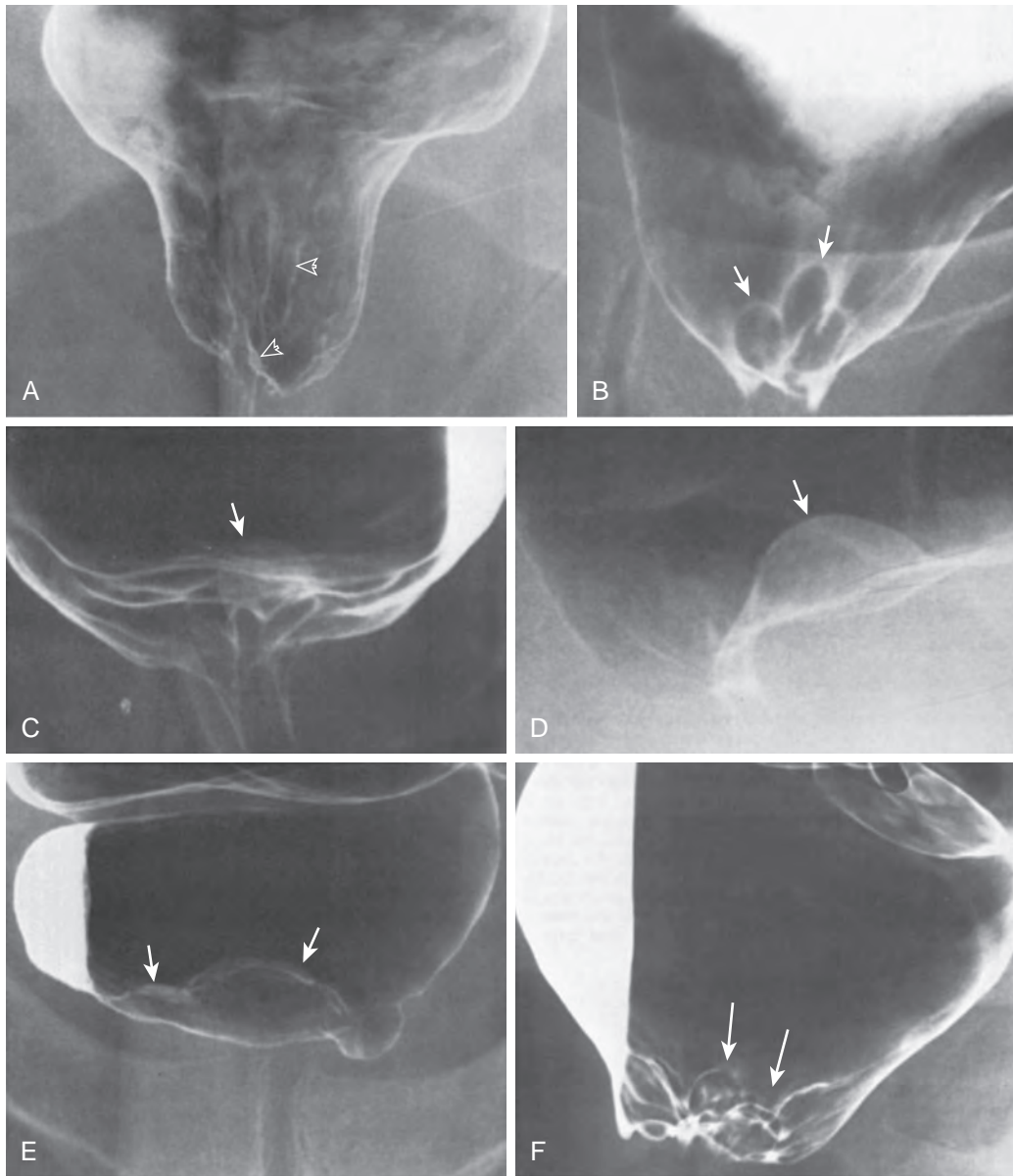


Figure 62-22 Radiographic appearance of internal hemorrhoids. **A.** Lobulated folds. Mild lobulation of anorectal folds (arrowheads) that extends less than 3 cm above the anorectal junction is a typical radiographic finding for internal hemorrhoids. **B.** "Bunch of grapes." Three smooth-surfaced polyps (arrows) are clustered above the anorectal junction. This radiographic appearance is typical of internal hemorrhoids. **C.** Solitary polyp. A smooth-surfaced polyp (arrow) projects from mildly lobulated columns of Morgagni. This is a nonspecific radiographic appearance that requires endoscopy. **D.** Submucosal mass. A smooth-surfaced mass (arrow) with relatively abrupt angulation to the colonic contour is typical of a submucosal mass. Although this is a typical radiographic appearance of internal hemorrhoids, other submucosal rectal masses include lymphoid polyps and solitary rectal ulcers. **E.** Masslike internal hemorrhoid. A large mass (arrows) in the distal rectum has a focally irregular surface pattern. This huge internal hemorrhoid cannot be distinguished from other rectal masses, such as carcinoma or cloacogenic carcinoma. Endoscopy and biopsy are necessary. **F.** Multiple polypoid folds. Large polypoid folds (arrows) with a nodular surface pattern in the distal rectum. Although these radiographic findings are typically seen with internal hemorrhoids, they may also be caused by solitary rectal ulcer syndrome, various forms of proctitis, or an unusual infiltrating tumor.

hemorrhoids is confident (Fig. 62-22A). Another diagnostic appearance of internal hemorrhoids is a cluster of smooth-surfaced polyps smaller than 1 cm abutting the anorectal junction (Fig. 62-22B). Internal hemorrhoids may have nonspecific appearances as well, including a solitary polyp (Fig. 62-22C); solitary submucosal mass (Fig. 62-22D); mass (Fig. 62-22E); or large, infiltrative lobulated folds extending more than 3 cm from the anorectal junction (Fig. 62-22F). Internal hemorrhoids seen as solitary polyps cannot be distinguished from inflammatory, benign, or neoplastic rectal polyps. Internal

hemorrhoids appearing as large, lobulated infiltrative folds extending more than 3 cm above the anorectal junction are indistinguishable from proctitis or infiltrating neoplasm.²⁰⁶

RECTAL VARICES

Rectal varices are a rare cause of lower GI bleeding and are usually seen in patients with portal hypertension. Rectal varices have been associated with adhesions.^{207,208} Radiologically, smooth serpiginous folds course along the rectal mucosa

(Fig. 62-23). When seen in profile, rectal varices may appear as small, smooth-surfaced submucosal nodules. Like esophageal varices, rectal varices may change in size and shape with luminal distention.²⁰⁹

CLOACOGENIC (BASALOID) CARCINOMA

The transitional epithelium of the anal canal contains squamous, transitional, and stratified columnar epithelium, as well as scattered goblet cells. Various neoplasms of controversial origin arise in this transitional epithelium. The transitional zone has features of urothelium and squamous epithelium consistent with a cloacogenic origin.²¹⁰ Hence, many tumors in this region were previously termed *cloacogenic carcinomas*. However, the transitional zone also has features suggesting that it is an area in which metaplasia and reserve cell hyperplasia occur, similar to the transitional zone in the uterine cervix or transitional zone at the esophagogastric junction.²¹¹ Thus, it has also been postulated that tumors in this region are caused by dysplasia and, hence, carcinoma arising in squamous metaplasia and reserve cell hyperplasia. For example, homosexual men have a high incidence of anal transitional cell carcinoma and squamous cell carcinoma in this region. These tumors may be related to venereally transmissible agents, such as oncogenic viruses, carcinogens in lubricants and cleansers, or mechanical irritation.²¹² Tumors at the anorectal junction have been described by a wide variety of names, including squamous cell carcinoma, basaloid carcinoma, transitional cell carcinoma, mucoepidermoid carcinoma, adenoid cystic carcinoma, and verrucous carcinoma. Basaloid carcinoma and cloacogenic carcinoma are probably equivalent terms. Most tumors, however, have a mixture of growth patterns, including basaloid areas, transitional cell carcinomas with squamous differentiation, adenoid cystic carcinoma, and mucoepidermoid carcinoma. The most common tumor of the anal canal is adenocarcinoma of the rectal mucosa invading the anal canal.

Cloacogenic (basaloid) carcinoma has no distinctive clinical, gross pathologic, or radiologic features. Patients usually

complain of rectal bleeding, rectal pain, or a change in bowel habits. These tumors may be flat, infiltrative, annular, or ulcerative lesions, with rolled borders. Radiographically, the tumor may appear as a submucosal mass with a smooth or ulcerated surface (Fig. 62-24), broad-based sessile polyps, or infiltrative lesions (Fig. 62-25).^{211,212}

Metastases occur in approximately 50% of patients to the sacral lymph nodes, internal and common iliac lymph nodes, and superficial inguinal lymph nodes. Venous drainage and hematogenous metastasis are to both the inferior vena cava and the portal system. Five-year survival in patients with basaloid carcinoma is approximately 50%.²¹²

RECTAL MUCOSAL PROLAPSE SYNDROMES

Chronic prolapse of rectal mucosa may result in chronic inflammation, ulceration, and hyperplastic reparative response. During defecation, rectal mucosa passing inferiorly through a contracted puborectalis sling may experience trauma, especially along the anterior and anterolateral wall. Chronic intussusception may also result in mucosal damage. The mucosal response to chronic defecatory problems results in a spectrum of syndromes, including solitary rectal ulcer syndrome, colitis cystica profunda, hypertrophied anal papilla, and inflammatory cloacogenic polyp.²¹³ A similar histologic response may be seen with prolapsing internal hemorrhoids and prolapsing colostomies.²¹³

Solitary rectal ulcer syndrome is an uncommon, chronic benign condition. The term *solitary ulcer syndrome* is a misnomer because multiple small ulcers may be present, or the colon may not be grossly ulcerated at all. Although the syndrome is typically seen in young adults, it may occur at any age. Patients commonly complain of rectal bleeding, rectal pain, and passage of mucus. At sigmoidoscopy, single or multiple well-demarcated, shallow ulcers may be found on the anterolateral or anterior wall of the distal half of the rectum.²¹⁴ An ulcer may not be visible; rather, the mucosa may appear diffusely erythematous, friable, or even polypoid.²¹⁴

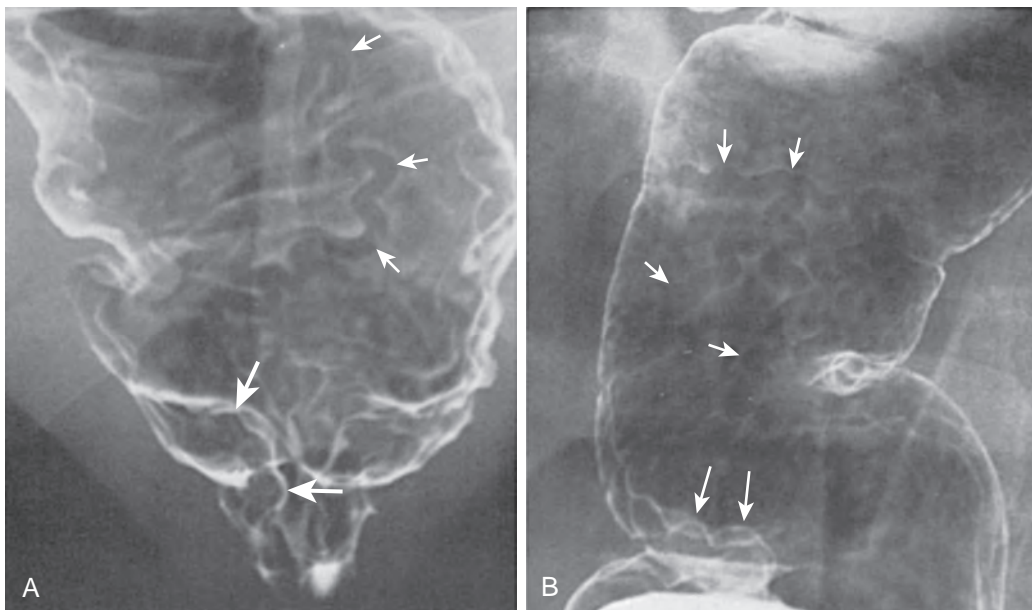
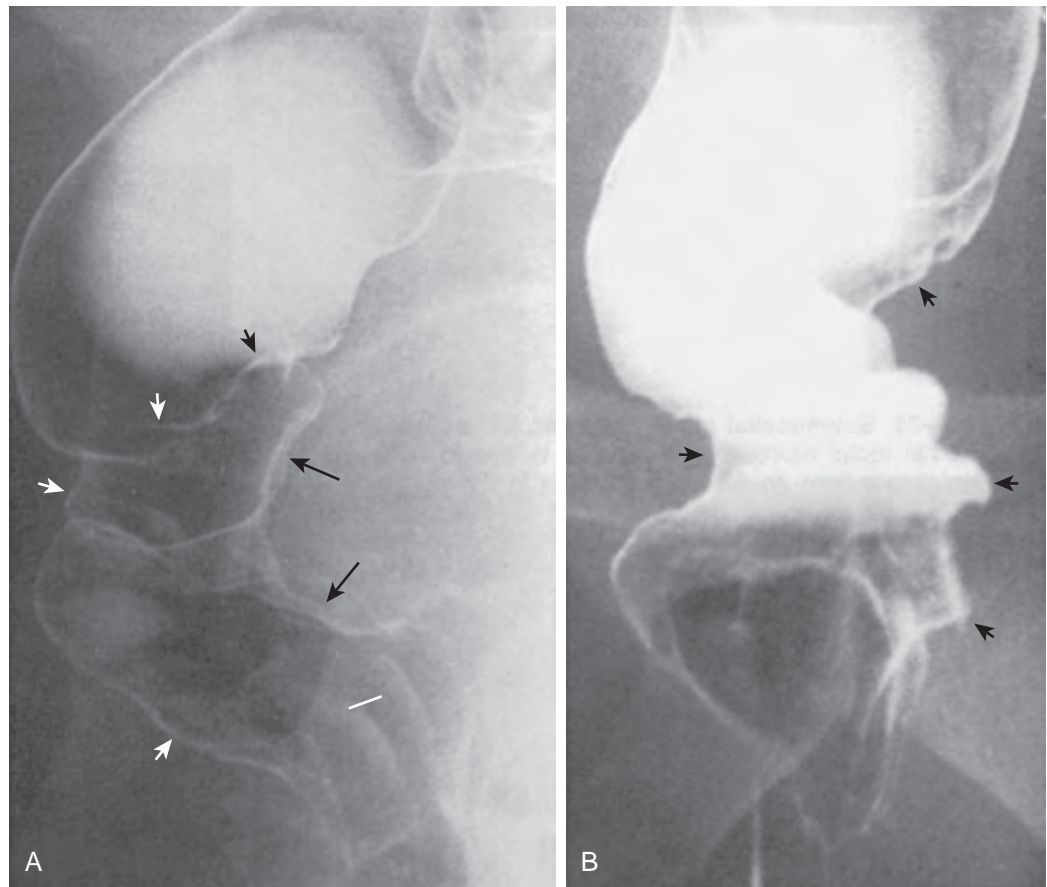


Figure 62-23 Rectal varices.
A. Spot radiograph of the distal rectum shows the en face appearance of rectal varices as serpentine folds etched in white (small arrows). In profile, smooth lobulated folds disrupt the contour of the bowel, extending from the anorectal junction proximally (large arrows). **B.** In another patient, spot radiograph of the proximal rectum shows serpentine folds etched in white (short arrows). In profile, a valve of Houston is expanded by a smooth, lobulated submucosal process compatible with a rectal varix (long arrows). (From Rubesin SE, Saul SH, Laufer I, et al: *Carpet lesions of the colon*. *RadioGraphics* 5:537-552, 1985.)

Figure 62-24 Cloacogenic carcinoma. **A.** Lateral spot view of the rectum shows a dominant, large submucosal mass (*large arrows*) indenting the anterior wall of the midrectum. Diffuse infiltration of the remainder of the distal rectum is manifested by smooth narrowing of the distal rectum (*small arrows*). **B.** Supine view of the distal rectum shows diffuse narrowing of the rectal ampulla and a diffusely irregular contour (*arrows*).



Pathologically, the mucosa is mildly inflamed. The glandular epithelium may be hyperplastic, occasionally showing villous formation, which may even be mistaken for villous adenoma.¹¹⁹ The muscularis mucosae is disorganized, and there may be extension of the smooth muscle of the muscularis mucosae into the lamina propria. When mucin-filled glands become cystically dilated, a diagnosis of localized colitis cystica profunda may be made.²¹³ Solitary rectal ulcer syndrome and colitis cystica profunda have been confused with villous adenoma or infiltrating adenocarcinoma. However, the glandular epithelium is not dysplastic in solitary rectal ulcer syndrome and colitis cystica profunda.

The radiographic findings are variable.²¹⁵ The rectal mucosa may appear normal in up to 50% of cases.²¹⁶ Diffuse, finely nodular mucosa in the distal rectum may be seen, correlating with the friable erythematous mucosa seen at proctoscopy (Fig. 62-26). A focal small ulcer may be found on the anterior or anterolateral wall. Redundant prolapsing mucosa may appear as a polypoid mass. Localized colitis cystica profunda may have the appearance of a submucosal mass (Fig. 62-27). The valves of Houston may be markedly enlarged with a nodular contour. Rarely, a stricture may be seen.

Functional Disorders of the Colon

IRRITABLE BOWEL SYNDROME

Epidemiology

Irritable bowel syndrome (IBS) is one of the most common yet least understood conditions encountered in clinical practice. It

is characterized by altered bowel habits and abdominal pain in the absence of detectable structural abnormalities. It occurs with surprising frequency in the general population, as high as 14% in one series, and accounts for one third to one half of outpatient referrals to gastroenterologists.²¹⁷ IBS ranks close to the common cold as a leading cause of absenteeism from work because of illness.²¹⁸ The symptoms of IBS begin before the age of 35 years in 50% of patients, and 40% of patients are 35 to 50 years of age. Female patients outnumber male patients 2:1, and the disease is more common in white and Jewish populations than in persons of color.²¹⁹

Clinical Findings

The clinical findings in irritable syndrome include the following:

1. Abdominal pain relieved by defecation or associated with a change in frequency or consistency of stool
2. Disturbed defecation associated with two more of the following: altered stool frequency, altered stool form (loose and watery or hard), and altered stool passage (straining or urgency, feeling of incomplete evacuation, passage of mucus)
3. Bloating or feeling of abdominal distention

Between 25% and 50% of IBS patients complain of dyspepsia, nausea and vomiting, and heartburn, suggesting that a portion of the gut other than the colon may be involved.²¹⁹

Pathophysiology

Although extensive clinical and laboratory investigations have failed to discover any microbiologic, histologic, or biochemical

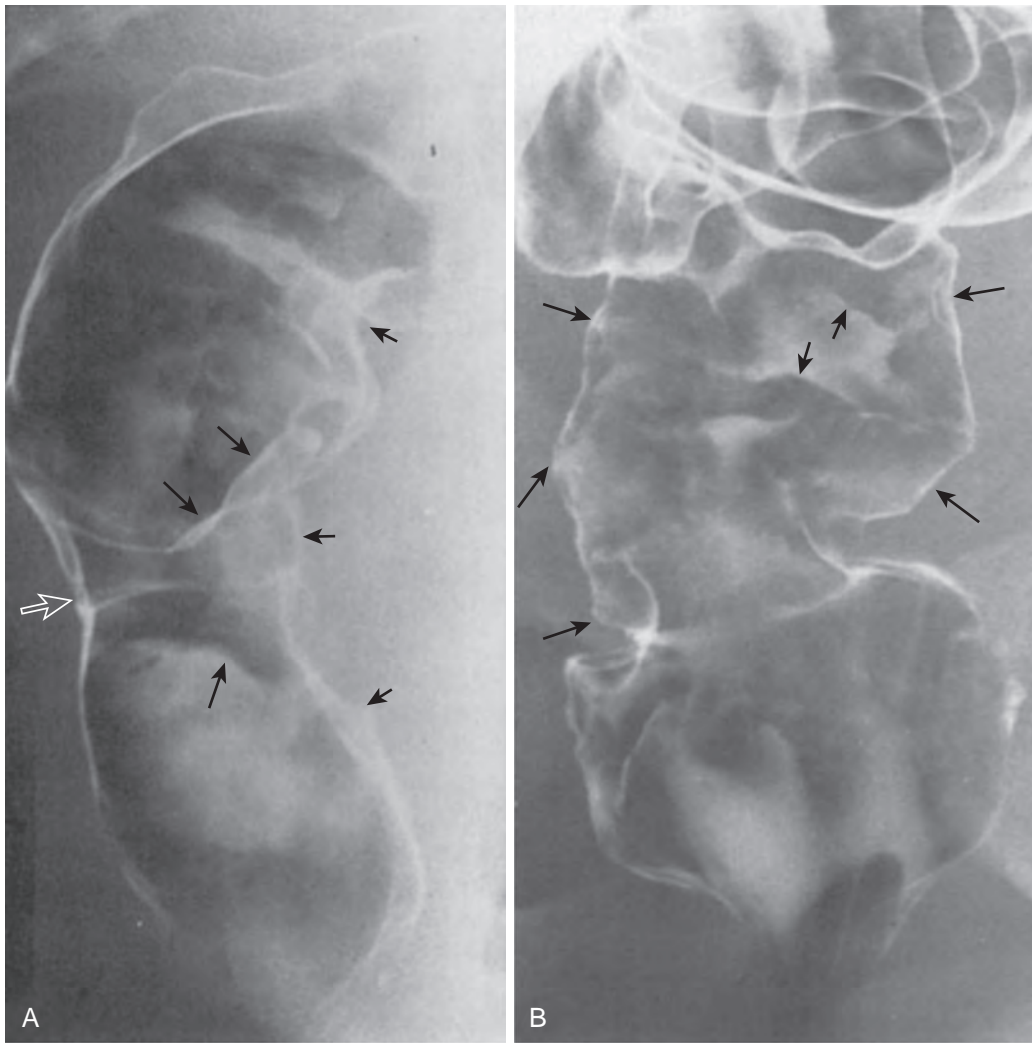


Figure 62-25 Cloacogenic carcinoma. **A.** Lateral view of the rectum demonstrates the infiltrative pattern of cloacogenic carcinoma. The anterior wall of the rectum is moderately flattened and lobulated (*short arrows*), and thick nodular folds cross the rectum (*long arrows*). The rectal mucosa is relatively smooth. Focal circumferential extension of tumor around the rectum is seen as flattening of the posterior rectal wall (*open arrow*). **B.** Prone view of the rectum shows mild inbowing and irregularity of the contour of the lateral walls of the rectum (*long arrows*) and thick nodular folds en face (*short arrows*).

abnormalities in patients with IBS, evidence suggests that this disorder is caused by abnormal myoelectric and motor activities in the gut. The myoelectric rhythm of the colon in normal patients has a frequency of 6 cycles/min; most patients with IBS have a predominant frequency of 3 cycles/min. Patients with IBS also have an abnormal gastrocolic reflex, such that the postprandial increase in colonic spike activity and intraluminal pressure is delayed by 30 to 60 minutes. Patients with IBS have a lower threshold for pain and for induction of spastic colonic contraction during rectal distention. It is postulated that this abnormal response is mediated through the autonomic nervous system, as in patients with diffuse esophageal spasm. This exaggerated motor response to colonic distention may explain why patients with spastic colons have symptoms when even small amounts of gas or stool are present.²¹⁷

Recordings of small bowel motility in ambulatory patients with IBS show a high incidence of abnormal activity during waking hours. There are frequent episodes of clustered contractions that occur at 0- to 9-minute intervals, and these are often associated with abdominal pain and discomfort.²¹⁸ Superimposed on these myoelectric abnormalities are environmental factors such as stress and diet, which can also alter motility.

Diagnostic Procedures

IBS is a diagnosis of exclusion, and there is always a nagging fear about missing an organic lesion. In the young patient, inflammatory bowel disease is the primary concern. In patients older than 40 years, the risk of occult colon cancer is such that complete evaluation of the colon by CT colonography, double-contrast barium enema, or colonoscopy is indicated.

There are no typical features of IBS on barium enema studies, which are usually normal in these patients. Some authors have reported a correlation between exaggerated haustral markings and scybalous (pellet-like) stool. Regions of hypertonicity and spasm, sigmoid myochosis, and diverticula have also been associated with IBS, but these findings can be present in patients without IBS and absent in patients with classic IBS. Clearly, the role of radiology in IBS is to exclude structural abnormalities such as inflammatory bowel disease, strictures, and cancer.²¹⁹

Therapy

The first step in therapy of IBS is to reassure the patient and explain the functional nature of this disorder. Foods that can cause symptoms (e.g., caffeine) are eliminated from the diet. Artificial sweeteners, legumes, carbonated beverages, and foods

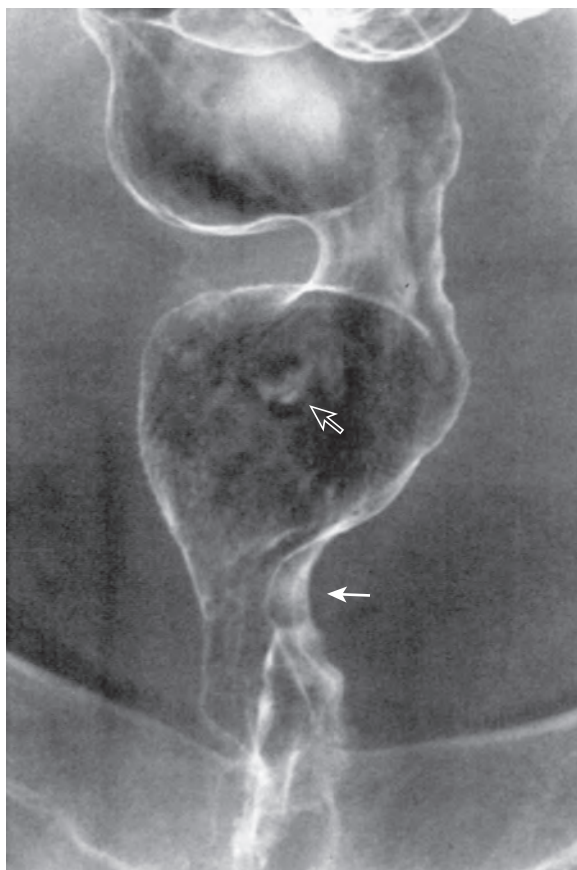


Figure 62-26 Solitary rectal ulcer syndrome: solitary ulcer. An irregular barium collection (open arrow) 1 cm in diameter is surrounded by a radiolucent halo of edema. Also note mild granularity of the distal rectal mucosa and focal submucosal mass effect (solid arrow).

of the cabbage family are proscribed. Dietary fiber and bulking agents are given because they have been shown to lower pressure in the sigmoid colon. Antispasmodic agents such as tincture of belladonna and dicyclomine (Bentyl) are also helpful. When diarrhea is the presenting symptom, antidiarrheal agents such as loperamide (Imodium) can be used during periods of stress.

CHRONIC CONSTIPATION

Most patients with chronic constipation respond to simple dietary and, if necessary, medical therapy consisting of natural bulk-forming laxatives and stool softeners.^{220,221} Anatomic disorders must be ruled out by colonoscopy, CT colonography, or double-contrast barium enema; metabolic, endocrine, drug-induced, and neurologic causes must be excluded by careful history, physical, and laboratory examinations. Functional evaluation of the colon and anorectum is generally reserved for patients who do not respond to initial therapy and express continued dissatisfaction with their bowel movements.²²¹ The causes of constipation are listed in Boxes 62-2 and 62-3.

Colorectal Transit Studies

The transit of stool through the colon is evaluated by following the progression of swallowed radiopaque markers on radiographs over several days. Patients ingest 20 small radiopaque

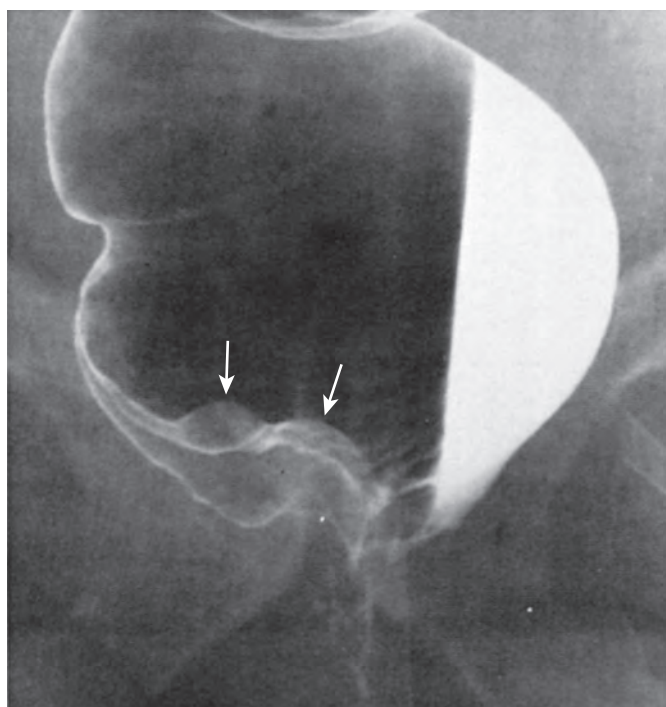


Figure 62-27 Solitary rectal ulcer syndrome: colitis cystica profunda. Two smooth-surfaced, polypoid, submucosal-appearing masses (arrows) are seen in the distal rectum. These masses were caused by mucus-filled, epithelium-lined cysts in the submucosa (colitis cystica profunda). (From Levine MS, Piccoletto M, Sollenberger LC, et al: Solitary rectal ulcer syndrome: A radiologic diagnosis? *Gastrointest Radiol* 11:187-193, 1986.)

markers with breakfast food. These markers (Sitzmarks) are commercially available. Abdominal radiographs are taken at 24-hour intervals until all the markers are evacuated or until 7 days pass. If markers are still present, films are obtained at days 10 and 15 to reduce the radiation received by the patient.²²¹

The large bowel is divided into three segments (the right colon, left colon, and rectosigmoid) by the spinous process, and imaginary lines are drawn from L5 to the left iliac crest and pelvic outlet (Fig. 62-28). Sample transit time studies are illustrated in Figure 62-29.

With this test, colonic inertia can be distinguished from normal transit with outlet obstruction. In the latter case, anorectal manometry and defecography are then required. Surprisingly, many studies are normal, and many of these patients have major psychologic factors influencing their symptoms.

Anorectal Manometry

Anorectal manometry is performed to characterize sensory and motor function of the gut, such as rectal sensation and viscoelasticity. Rectal distention produced by a rectal balloon normally initiates a reflex that contracts the external anal sphincter and relaxes the internal anal sphincter. Loss of this reflex suggests Hirschsprung's disease, which must be confirmed by biopsy. Severe idiopathic constipation is usually accompanied by impaired rectal sensation to balloon distention. Paradoxical contraction of the external sphincter and pool relaxation of the internal sphincter during defecation are often associated with constipation. An overall compliant rectum in combination with sensory loss may interfere with the normal urge to defecate.²²⁰

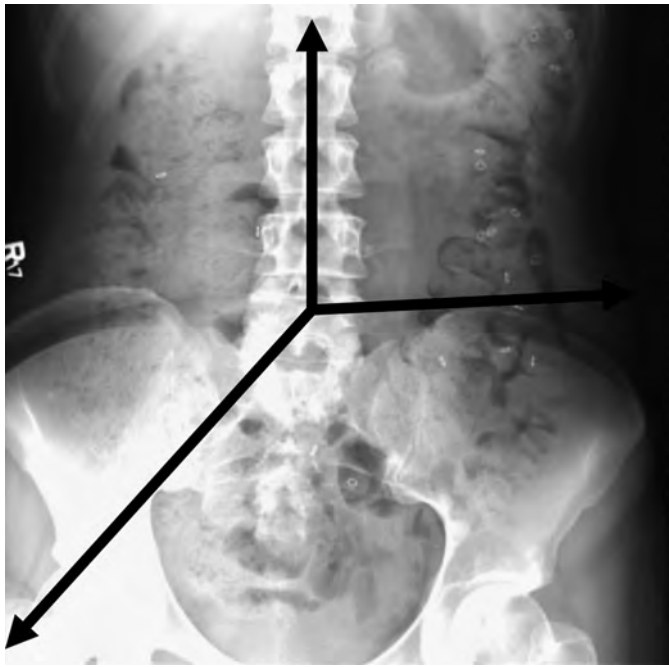


Figure 62-28 Colon transit study. Plain film demonstrates radiopaque markers. For the purpose of counting, the colon is divided into three segments—left colon, right colon, and rectosigmoid.

Evacuation Proctography

Evacuation proctography (defecography) permits dynamic evaluation of the defecation process. It assesses the anorectal angle and status of the puborectalis sling and can diagnose rectal prolapse, rectal intussusception, rectoceles, obstructive enteroceles, and abnormal perineal descent. This test is especially important if there is manometric or electromyographic evidence of hyperactive rectosigmoid junction, abnormal anorectal motility, or anismus and clinical evidence of descending perineum syndrome, prolapse, and the solitary rectal ulcer syndrome. Chapter 52 is devoted to a discussion of this procedure.²²²

The combination of transit studies, anorectal manometry, and evacuation proctography can often identify the type and cause of constipation, which greatly assists further therapy.

NONOBSTRUCTIVE MEGACOLON

Chronic constipation may be caused by a mechanical obstruction (e.g., carcinoma, stricture) or may be of functional origin, as in bedridden older patients or those with improper bowel habits. In Chagas' disease, destruction of the colonic myenteric plexuses by the protozoan *Trypanosoma cruzi* causes striking elongation and dilation, especially of the rectosigmoid and descending colon. Acquired nonobstructive megacolon in adults can also be found in patients with severe neurologic or psychologic disorders and in patients with abnormal colonic motility (e.g., myxedema, infiltrative disease, such as amyloidosis and scleroderma, narcotic drugs). Regardless of the underlying cause, plain abdominal radiographs and CT scans demonstrate a tremendously dilated tortuous colon and rectum filled with a large fecal residue.²²³

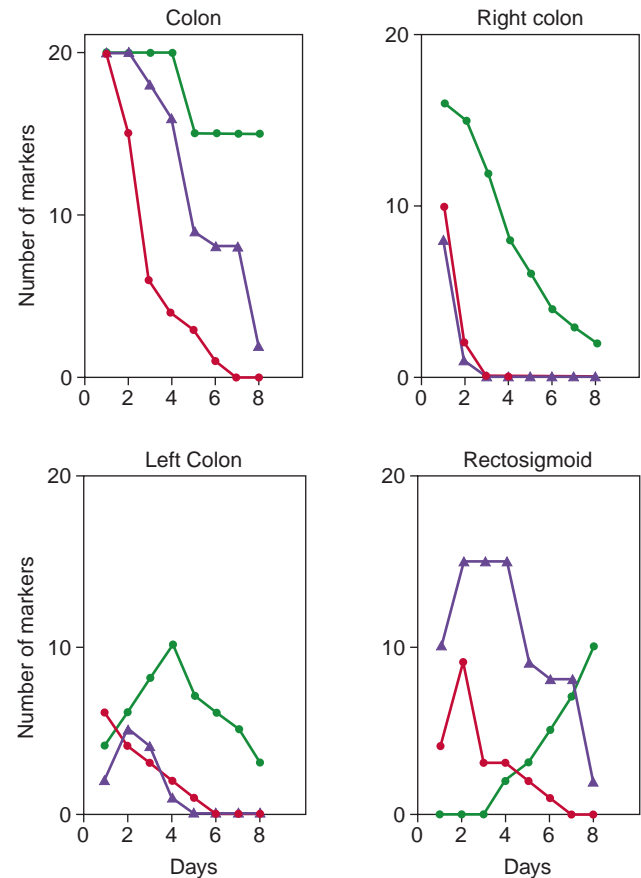


Figure 62-29 Abnormal colon transit studies. Diagram depicts characteristic transit patterns of 20 radiopaque markers through the colon during an 8-day period in three groups of constipated patients. With normal transit (red circles), the markers disappear rapidly from the colon. With colon inertia (green circles), there is prolonged transit through the right and left colon segments with delayed appearance in the rectosigmoid. With outlet obstruction (triangles), transit is normal in the right and left colon but there is stagnation of the rectosigmoid. (From Wald A: Colonic transit and anorectal manometry in chronic idiopathic constipation. *Arch Intern Med* 146:1713-1716, 1986.)

Incomplete evacuation of feces over a prolonged period can result in the formation of a fecal impaction—a large, firm, immovable mass of stool in the rectum that may cause large bowel obstruction. Fecal impactions most commonly develop in older, debilitated, or sedentary persons. They can occur in patients who have been inactive for long periods (e.g., because of myocardial infarction, traction), narcotic addicts, patients on large doses of tranquilizers, and children with megacolon or psychologic problems.²²⁴

The symptoms of fecal impaction usually consist of vague rectal fullness and nonspecific abdominal discomfort. A common complaint is overflow diarrhea, the uncontrolled passage of small amounts of watery and semiformal stool around a large obstructing impaction. In bedridden older patients, it is essential that this overflow phenomenon be recognized as secondary to fecal impaction rather than perceived as true diarrhea.

Intestinal myopathy patients have aperistalsis of the esophagus with low pressure of the lower esophageal sphincter, a variable degree of dilation and dysmotility of the stomach, duodenum, small bowel, and colon, and ureteral and bladder enlargement.²²⁵⁻²²⁷

COLLAGEN VASCULAR DISORDERS

Colonic involvement in scleroderma occurs less frequently than is observed in the esophagus and small bowel. Patchy smooth muscle atrophy and fibrotic replacement cause wide-mouthed diverticula at the weakened sites. These are true diverticula that contain all three layers of bowel wall. The smooth muscle is replaced by connective tissue, however. These smooth and wide diverticula retain barium on the postevacuation films.²²⁶

The normal postprandial gastrocolic reflex is decreased in scleroderma patients. This colonic dysmotility may be clinically latent early in disease and manifest only with further smooth muscle atrophy. Similarly, manometric studies have shown decreased pressure of the smooth muscle internal anal sphincter and abnormal relaxation after rectal distention. The external anal sphincter, which is skeletal muscle, responds appropriately. Manometric studies have shown a correlation between the relaxation of the lower esophageal sphincter and dysfunction of the internal anal sphincter in patients with scleroderma. Symptoms from colonic involvement are nonspecific, but decreased motility causes constipation and may result in impaction of fecal contents.²²⁸

Benign pneumoperitoneum can be seen in patients with scleroderma and may be asymptomatic for years. The cause is probably slow passage of bowel gas through minute or microperforations in colonic or small bowel sacculations. Clinically symptomatic and significant bowel perforations may occur in scleroderma from stercoral ulcerations, bowel impactions, and focal vasculitis. These usually require surgical intervention. It may not be possible to differentiate clinically benign pneumoperitoneum from that caused by perforation.²²⁸

Systemic lupus erythematosus can cause a variety of abdominal problems—peritoneal serositis, pancreatitis, ascites, and enteritis. There is a small vessel arteritis of the small bowel and colon that causes ischemia, which leads to edema, hemorrhage, mucosal ulceration, and, ultimately, necrosis and perforation. The radiologic findings are those expected with hemorrhage and ischemia—ileus, thumbprinting, pneumatosis intestinalis, and pseudo-obstruction. The radiologic findings may be indistinguishable from those of ischemia, hemorrhage, or inflammatory bowel disease. Aspirin and corticosteroids are used in the therapy of lupus, and these drugs often aggravate the underlying GI disease.²²⁶

DIABETES

Constipation is the most common GI symptom of the diabetic patient, and it appears to be directly related to autonomic neuropathy. Only 29% of patients without neuropathy symptoms are constipated. This figure increases to 88% in patients with five symptoms of neuropathy. Constipation typically is intermittent and alternates with diarrhea in almost one third of patients. Fecal impaction may be sufficiently severe to produce mechanical obstruction. This autonomic neuropathy leads to the loss of the postprandial gastrocolic response, similar to that observed in patients with intestinal pseudo-obstruction. This is explained pathophysiologically by the inflammatory changes demonstrated in the autonomic ganglia; the cholinergic postganglionic neurons are intact, with a normally responsive smooth muscle.^{204,226}

Pneumatosis Intestinalis

Gas in the bowel wall (pneumatosis intestinalis) can exist as an isolated entity or in conjunction with a broad spectrum of disease of the GI tract or respiratory system. In primary pneumatosis (about 15% of cases), no respiratory or other gastrointestinal abnormality is present. Primary pneumatosis usually occurs in adults and involves mainly the colon. Secondary pneumatosis intestinalis (about 85% of cases) more commonly affects the small bowel and is associated with a wide variety of preexisting disorders. In the primary form, gas collections usually appear cystic; in the secondary type, a linear distribution of gas is generally seen.²²⁹

PRIMARY INTESTINALIS

Primary pneumatosis intestinalis is a relatively rare benign condition characterized pathologically by multiple thin-walled, noncommunicating, gas-filled cysts in the subserosal or submucosal layer of the bowel. The overlying mucosa is entirely normal, as is the muscularis. The appearance of radiolucent clusters of cysts along the contours of the bowel is diagnostic of primary pneumatosis intestinalis. On barium examinations, the filling defects are seen to lie between the lumen (outlined by contrast material) and the water density of the outer wall of the bowel.

The radiographic pattern of pneumatosis can simulate that of more severe GI conditions. Small cysts may be confused with tiny polyps. Larger cysts can produce scalloped defects simulating inflammatory pseudopolyps or the thumbprinting seen with intramural hemorrhage. At times, the cysts of pneumatosis intestinalis concentrically compress the lumen, producing gas shadows that extend on either side of the bowel contour, surrounding a thin, irregular stream of barium and simulating the appearance of an annular carcinoma. To differentiate pneumatosis intestinalis from these other conditions, it is important to note the striking lucency of the gas-filled cysts in contrast to the soft tissue density of an intraluminal or intramural lesion. Other distinguishing factors are the compressibility of the cysts on palpation and the not infrequent occurrence of asymptomatic pneumoperitoneum. Primary pneumatosis intestinalis (Fig. 62-30) usually requires no treatment and resolves spontaneously.²²⁹

SECONDARY INTESTINALIS

Secondary pneumatosis intestinalis usually reflects GI disease with bowel necrosis. In infants, pneumatosis intestinalis suggests an underlying necrotizing enterocolitis, which occurs primarily in premature or debilitated infants, usually affects the ileum and right colon, and has a very low survival rate. This condition is characterized by a frothy or bubbly appearance of gas in the wall of the diseased bowel loops. The appearance often resembles fecal material in the right colon. However, it must be remembered that although this feces-like appearance is normal in adults, it is always abnormal in premature infants. The gas in the wall of the colon in necrotizing enterocolitis is probably related to mucosal necrosis and subsequent passage of intraluminal gas into the bowel wall. This may be complicated by intraluminal gas-forming organisms that also penetrate the diseased mucosa to reach the inner layers of the intestinal wall. Dissection of air into the

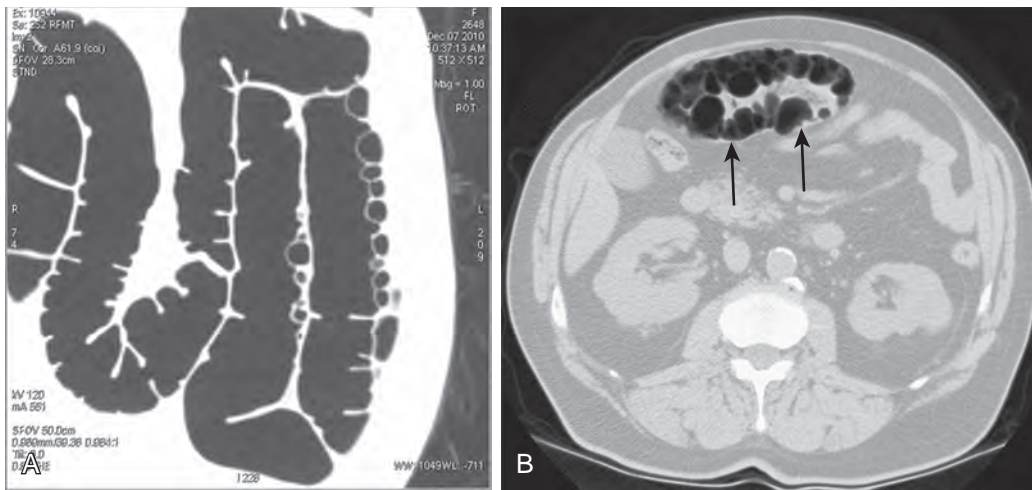


Figure 62-30 Primary pneumatosis cystoides intestinalis. **A.** Coronal reformatted image from a CT colonography study in an asymptomatic outpatient shows multiple intramural cystic lucencies. **B.** Axial imaging in another asymptomatic patient demonstrates multiple large gas-filled cysts (arrows), which produced scalloped defects in the transverse colon.

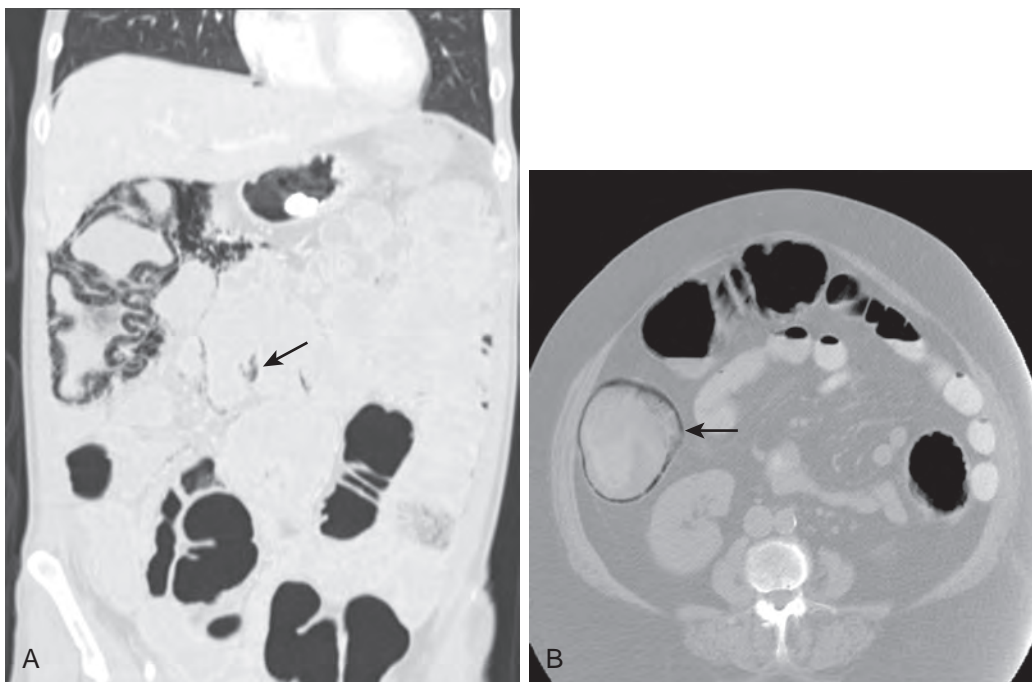


Figure 62-31 Secondary pneumatosis intestinalis. **A.** Coronal reformatted image in a patient with bowel ischemia shows linear intramural lucencies in the right colon. Gas is seen within the mesenteric vessels (arrow) as well. **B.** Linear pneumatosis (arrow) is seen in the ascending colon in this relatively asymptomatic patient undergoing targeted therapy with imatinib for a gastric gastrointestinal stromal tumor.

intrahepatic branches of the portal vein is an ominous prognostic finding.²³⁰

In adults, secondary pneumatosis intestinalis (Fig. 62-31) suggests bowel necrosis caused by mesenteric arterial or venous thrombosis. Secondary pneumatosis intestinalis may be related to mucosal ischemia, as in strangulating obstructions, or to mucosal destruction by infectious organisms or powerful corrosive agents.

Secondary pneumatosis intestinalis may also develop in the absence of necrosis of the bowel wall. Any lesion of the GI tract that results in mucosal ulceration or intestinal obstruction (obstructive bowel disease) can cause secondary pneumatosis intestinalis. Gas in the bowel wall is an uncommon complication of GI endoscopy. Severe obstructive pulmonary disease can also be associated with the development of pneumatosis intestinalis. Partial bronchial obstruction and coughing presumably cause alveolar rupture, with gas dissecting along peribronchial and perivascular tissue planes into the mediastinum. Gas then enters the retroperitoneal area via the

hiatus of the esophagus and aorta, from which it dissects between the leaves of the mesentery to eventually reach subserosal and submucosal locations in the bowel wall.^{231,232}

Patients undergoing molecular targeted therapy with agents such as imatinib, sunitinib, bevacizumab, sorafenib, cetuximab, and erlotinib may develop pneumatosis, perforation, and fistula formation. These patients may be relatively asymptomatic, with these complications found during routine cancer follow-up imaging. Most patients with these therapy-associated intestinal complications can be treated conservatively after discontinuation of molecular targeted therapy.^{231,232}

Other Colon Abnormalities

DIVERSION COLITIS

Diversion colitis is a nonspecific inflammation in a segment of colon that has been surgically isolated from the fecal stream by placement of a proximal colostomy or ileostomy. It is unknown

whether lack of contact of the distal colonic segment to feces somehow deprives the colonic mucosa of necessary exposure to enteric bacteria, bacterial by-products, or nutrients. Conversely, it is conceivable that diversion colitis results from stasis within the inactive segment, causing excessive mucosal exposure to unrecognized intraluminal toxins. Radiographically, diversion colitis resembles ulcerative or Crohn's colitis with punctate or aphthoid ulcerations, which may produce a diffuse, granular mucosal appearance in severe or long-standing cases. Isolated inflammatory polyps or diffuse mucosal nodularity may occur.²³³⁻²³⁶

BEHÇET'S SYNDROME

Behçet's syndrome is a systemic inflammatory disease involving a triad of uveitis, oral ulcers, and genital ulcers, as well as involvement of the central nervous system, joints, kidneys, skin, and GI tract. It is unclear whether the cause of this disorder is viral, allergic, environmental, or autoimmune.²³⁷

Abdominal pain occurs in up to 75% of patients, and the clinical course can be complicated by diarrhea, malabsorption, bleeding, perforation, fistulas, and toxic megacolon. Ulcerations tend to involve the terminal ileum, cecum, and ascending colon, simulating Crohn's disease and some infectious colitides. Diffuse colonic involvement can mimic ulcerative colitis.²³⁸

The barium enema appearance of Behçet's disease varies from mild proctitis to pancolitis with multiple discrete ulcers and inflammatory polyposis. Aphthoid ulcerations and skip lesions are typical. The ulcers in Behçet's syndrome tend to be larger and deeper than those in Crohn's colitis, leading to a higher incidence of perforation and hemorrhage.^{239,240}

AMYLOIDOSIS

As in other parts of the bowel, amyloidosis involving the colon can produce a broad spectrum of radiographic abnormalities. Narrowing and rigidity of the colon, especially in the rectum and sigmoid colon, can result from direct deposition of amyloid within the mucosal and muscular layers of the bowel or can be secondary to extensive amyloid deposition in blood vessel walls and subsequent ischemic colitis. The resulting thickening of the bowel with effacement of haustral markings can closely simulate the radiographic appearance of chronic ulcerative colitis. Less commonly, amyloidosis can produce an acute ulcerating process, single or multiple discrete colonic filling defects, or an appearance simulating the thumbprinting seen with ischemic colitis.²⁴¹⁻²⁴⁴

CATHARTIC COLON

Cathartic colon is caused by the prolonged use of stimulant or irritant cathartics (e.g., castor oil, phenolphthalein, cascara, senna, podophyllum). The radiographic appearance of cathartic colon is similar to that of burned-out chronic ulcerative colitis. In contrast to ulcerative colitis, however, the absent or diminished haustral markings, bizarre contractions, and inconstant areas of narrowing primarily involve the right colon (Fig. 62-32). In severe cases, the left side of the colon can also be affected, although the sigmoid colon and rectum usually appear normal. The mucosal pattern is linear or smooth; ulcerations are not seen. The ileocecal valve is frequently flattened and gaping, simulating the backwash ileitis seen in ulcerative colitis.



Figure 62-32 Cathartic colon. Contractions with irregular areas of narrowing are seen in the right colon, and there is a paucity of haustra in the transverse colon.

Shortening of the ascending colon can be severe but, unlike the rigidity of the tubular bowel in chronic ulcerative colitis, the shortened segment in a cathartic colon remains remarkably distensible. Inconstant areas of narrowing of the bowel lumen can be seen at fluoroscopy and on radiographs of patients with cathartic colon. These pseudostrictures primarily involve the hepatic flexure, vary in length, have a concentric lumen with tapering margins, and often disappear during a single examination.²⁴⁵⁻²⁴⁷

URTICARIA

A characteristic mucosal pattern of large, round or polygonal, raised plaques in a grossly dilated bowel was first described as an allergic reaction of the colonic mucosa to medication. This so-called colonic urticaria predominantly involves the right colon, can be seen without concomitant cutaneous lesions, and regresses once the offending medication is withdrawn.²⁴⁸

A pattern similar to colonic urticaria has been reported in several other conditions for which the common denominator seems to be submucosal edema. In herpes zoster, an exanthematous neurocutaneous disorder secondary to reactivation or reinfection by a large poxvirus, colonic mucosal blebs infrequently appear as multiple small, discrete, polygonal filling defects, with sharp angular margins (Fig. 62-33). These blebs correspond morphologically and temporarily to the vesicular phase of the cutaneous lesion and are segmentally arrayed in a corresponding or noncorresponding dermatome. In *Yersinia* colitis, submucosal edema is caused by an alteration in vascular permeability. A similar radiographic pattern has also been observed in patients with submucosal colonic edema secondary

to obstructing carcinoma, cecal volvulus, ischemia, colonic ileus, and benign colonic obstruction.²⁴⁹

COLITIS CYSTICA PROFUNDA

Colitis cystica profunda is a rare benign disease in which large, mucous epithelium-lined cysts up to 2 cm in diameter form in the submucosal layer of the colon. These cysts are usually seen in the rectum and pelvic colon, and usually only a short segment of colon is involved. Colitis cystica profunda is associated with solitary rectal ulcer syndrome and rectal prolapse, as well as other proctitides. This suggests that these cysts are formed when surface mucosa is implanted into the colonic submucosa during the healing phase of an ulcerative inflammatory process. Because these cells cannot be shed into the lumen and mucus cannot be discharged, a cystic mass develops.^{250,251}

Patients with colitis cystica profunda present with hematochezia, passage of mucus or pus per rectum, diarrhea, constipation, tenesmus, and rectal, sacral, or abdominal pain. On barium studies, multiple, irregular, rectal filling defects suggesting adenomatous polyps are seen. Barium filling clefts between these polyps can simulate mucosal ulcerations. Ischemic colitis can be mimicked when sufficient scalloping of the colon occurs.^{252,253}

As with solitary rectal ulcer syndrome, conservative treatment is the initial approach. Surgery to correct rectal prolapse may lead to resolution of cysts in certain patients



Figure 62-33 Colonic urticaria. Raised polygonal plaques are present in the ascending colon in this patient with *Yersinia* colitis.

with refractory symptoms and rectal prolapse evident on defecography.²⁵⁴⁻²⁵⁶

DIARRHEA

In Western countries, most cases of diarrhea are self-limited (Box 62-4) and seldom come to radiologic attention. When the diarrhea persists (Box 62-5), radiology plays an important part in diagnosis. Radiologic findings, however, must be interpreted in view of clinical and laboratory findings. There are three fundamental types of diarrhea—osmotic, secretory, and inflammatory.

Osmotic Diarrhea

Osmotic diarrhea usually occurs as a result of malabsorption or ingestion of certain chemicals in which a high osmotic load is presented to the gut. Small bowel series and enteroclysis are superb means of demonstrating causes of malabsorption, such as sprue, amyloidosis, mastocytosis, intestinal lymphangiectasia, intestinal anastomoses, small bowel diverticula, and abnormal motility, which predispose to bacterial overgrowth. Chronic

BOX 62-4 MAJOR CAUSES OF ACUTE DIARRHEA*

INFECTIONS (INCLUDING TRAVELERS' DIARRHEA)

Bacterial

Campylobacter species
Clostridium difficile
Escherichia coli (ET, EI, EH, O157:H7)
Salmonella enterocolitidis
Shigella species

Parasitic and Protozoal

Entamoeba histolytica
Giardia lamblia
Cryptosporidium
Cyclospora

Viral

Adenovirus
 Norwalk virus
 Rotavirus

Fungal

FOOD POISONING

Bacillus cereus
Clostridium perfringens
Salmonella species
Staphylococcus aureus
Vibrio species
Shigella species
Campylobacter jejuni
Escherichia coli
Yersinia enterocolitidis
Listeria monocytogenes

OTHER CAUSES

Medications
 Recent ingestion of large amounts of poorly absorbable sugars
 Intestinal ischemia
 Fecal impaction
 Pelvic inflammation

From Schiller LR, Sellin JH: Constipation. In Feldman M, Friedman LS, (eds): *Gastrointestinal and Liver Disease*, 9th ed. Philadelphia, Saunders, 2010, pp 211–232.

*(<2-3 wk duration).

BOX 62-5 MAJOR CAUSES OF CHRONIC DIARRHEA***NO PREVIOUS WORK-UP**

Irritable bowel syndrome
 Inflammatory bowel disease
 Ischemic bowel disease
 Chronic bacterial or mycobacterial infection
 Parasitic and fungal infection
 Radiation enteritis
 Malabsorption syndromes
 Medications
 Alcohol
 Intestinal lymphoma
 Colon cancer
 Villous adenoma
 Diverticulitis
 Previous surgery (e.g., gastrectomy, vagotomy, intestinal resection, cholecystectomy)
 Endocrine causes
 Hyperthyroidism
 Hypothyroidism
 Addison's disease

Diabetes mellitus
 Pheochromocytoma
 Ganglioneuroma
 Fecal impaction
 Heavy metal poisoning
 Epidemic idiopathic chronic diarrhea

PREVIOUS WORK-UP FAILED TO REVEAL DIAGNOSIS

Surreptitious laxative abuse
 Defective anal continence masquerading as severe diarrhea
 Microscopic colitis (with or without subepithelial collagen)
 Previously unrecognized malabsorption
 Pseudopancreatic cholera syndrome
 Idiopathic chronic diarrhea
 Neuroendocrine tumor
 Systemic mastocytosis
 Amyloidosis
 Idiopathic bile acid malabsorption
 Food allergy

From Schiller LR, Sellin JH: Constipation. In Feldman M, Friedman LS, (eds): *Gastrointestinal and Liver Disease*, 9th ed. Philadelphia, Saunders, 2010, pp 211–232.

*(>4-wk duration).

pancreatitis, cystic fibrosis, the Shwachman-Diamond syndrome, and other causes of pancreatic insufficiency have characteristic appearances on imaging studies that can specifically establish the cause of the diarrhea.²⁵⁷

Secretory Diarrhea

Secretory diarrhea stimulates intestinal secretion or inhibits absorption. Enterotoxins produced by certain infections, certain irritant laxatives, metals, and toxins, and tumors that elaborate secretagogues, such as vasoactive intestinal polypeptide (pancreatic cholera), are major causative factors in

secretory diarrheas. Radiology has only a small role in the assessment of these patients unless the diarrhea is caused by a pancreatic tumor.²⁵⁸

Inflammatory Diarrhea

Radiology is most useful for evaluating inflammatory diarrhea, in which inflammatory damage and death of the brush border and epithelium occur. This diarrhea occurs in patients with inflammatory bowel disease, certain infections, and radiation enteritis and as a complication of chemotherapy and graft-versus-host disease.^{259,260}

REFERENCES

- Shah S: An update on common gastrointestinal emergencies. *Emerg Med Clin North Am* 31:775–793, 2013.
- Hucl T: Acute GI obstruction. *Best Pract Res Clin Gastroenterol* 27:639–647, 2013.
- Ellis H: *Intestinal Obstruction*, New York, 1982, Appleton-Century-Crofts.
- Cohn I, Chappuis CW: Bowel obstruction. In Taylor MB, editor: *Gastrointestinal Emergencies*, ed 2, Baltimore, 1997, Williams & Wilkins, pp 515–536.
- Richards WO, Williams LF, Jr: Obstruction of the large and small intestine. *Surg Clin North Am* 68:355–376, 1988.
- Smith GA, Perry JF, Jr, Yonehiro EG: Mechanical intestinal obstructions: A study of 1252 cases. *Surg Gynecol Obstet* 100:651–660, 1955.
- Szucs RA, Turner MA: Gastrointestinal tract involvement by gynecological diseases. *Radiographics* 6:1251–1270, 1996.
- Russell JC, Welch JP: Pathophysiology of bowel obstruction. In Welch JP, editor: *Bowel Obstruction*, Philadelphia, 1990, WB Saunders, pp 28–58.
- Kottler RE, Lee GK: The threatened cecum in acute large-bowel obstruction. *Br J Radiol* 57:989–990, 1984.
- Schmidt AG: Intramural gas proximal to obstructing carcinoma. *Radiology* 91:784–785, 1968.
- Mak SY, Roach SC, Sukumar SA: Small bowel obstruction: Computed tomography features and pitfalls. *Curr Probl Diagn Radiol* 35:65–74, 2006.
- Meyers MA: Colonic ileus. *Gastrointest Radiol* 2:37–40, 1997.
- Lowman RM, Davis L: An evaluation of cecal size in impending perforation of the cecum. *Surg Gynecol Obstet* 103:711–718, 1956.
- Novy S, Rogers LF, Kirkpatrick W: Diastatic rupture of the cecum in obstructing carcinoma of the left colon: Radiographic diagnosis and surgical implications. *AJR* 123:281–286, 1975.
- Chappuis CW, Cohn J, Jr: Pathophysiological effects on intraluminal contents. In Fielding LP, Welch JP, editors: *Intestinal Obstruction*, Edinburgh, 1987, Churchill Livingstone, pp 32–40.
- Sugerman HJ: Systemic effects of intestinal obstruction. In Fielding LP, Welch JP, editors: *Intestinal Obstruction*, Edinburgh, 1987, Churchill Livingstone, pp 32–40.
- Vanek VW, Whitt CL, Abdu RA, et al: Comparison of right colon, left colon and rectal carcinoma. *Am Surg* 52:504–509, 1986.
- Welch JP: General considerations and mortality. In Welch JP, editor: *Bowel Obstruction*, Philadelphia, 1990, WB Saunders, pp 59–95.
- Nadrowski L: Clinical presentation and preoperative management of bowel obstruction. In Fielding LP, Welch JP, editors: *Intestinal Obstruction*, Edinburgh, 1987, Churchill Livingstone, pp 67–77.
- Ellis H: Special forms of intestinal obstruction. In Schwartz SI, Ellis H, editors: *Maingot's Abdominal Operations*, East Norwalk, CT, 1989, Appleton & Lange, pp 905–932.
- Baker SR, Cho KC: The Abdominal Plain Film with Correlative Imaging, East Norwalk, CT, 1998, Appleton & Lange.
- Siter FMH, Jr: Radiologic diagnosis: Small bowel. In Welch JP, editor: *Bowel Obstruction*, Philadelphia, 1990, WB Saunders, pp 96–107.
- Markowitz KS: Radiologic diagnosis: Colon. In Welch JP, editor: *Bowel Obstruction*, Philadelphia, 1990, WB Saunders, pp 108–122.
- Love L: Large bowel obstruction. *Semin Roentgenol* 8:299–321, 1973.
- Levin B: Mechanical small bowel obstruction. *Semin Roentgenol* 8:281–297, 1983.
- Love L: The role of the ileocecal valve in large bowel obstruction: A preliminary report. *Radiology* 75:391–397, 1960.

27. Kent KH, Raskowski HJ: Colon lesions masquerading as small bowel obstruction on the plain roentgenogram of the abdomen. *AJR* 88:671–676, 1962.
28. Fataar S, Schulman A: Small bowel obstruction masking synchronous large bowel obstruction: A need for emergency barium enema. *AJR* 140:1159–1162, 1983.
29. Ott DJ, Gelfand DW: Gastrointestinal contrast agents: Indications, uses and risks. *JAMA* 249:2380–2384, 1983.
30. Grossman RI, Miller WT, Dann RW: Oral barium sulfate in partial large bowel obstruction. *Radiology* 136:327–331, 1980.
31. Frimann-Dahl JC: The administration of barium orally in acute obstructions: Advantages and risks. *Acta Radiol* 42:285–288, 1954.
32. Filippone A, Iezzi R, Di Fabio F, et al: Multidetector-row computed tomography of focal liver lesions treated by radiofrequency ablation: Spectrum of findings at long-term follow-up. *J Comput Assist Tomog* 31:42–52, 2007.
33. Yaghamai V, Nikolaidis P, Hammond NA, et al: Multidetector-row computed tomography diagnosis of small bowel obstruction: Can coronal reformations replace axial images? *Emerg Radiol* 13:69–72, 2006.
34. Lim JH, Ko YT, Lee DH, et al: Determining the site and causes of colonic obstruction with sonography. *AJR* 163:1113–1117, 1994.
35. Thompson WM: Gasless abdomen in the adult: What does it mean? *AJR* 191:1093–1099, 2008.
36. Hucl T: Acute GI obstruction. *Best Pract Res Clin Gastroenterol* 27:691–707, 2013.
37. Welch JP, Donaldson GA: Management of severe obstruction of the large bowel due to malignant disease. *Am J Surg* 127:492–499, 1974.
38. Welch JP: Carcinoma of the colon. In Welch JP, editor: *Bowel Obstruction*, Philadelphia, 1990, WB Saunders, pp 546–574.
39. Irvin GL, III, Horsely JS, III, Caruana JA, Jr: The morbidity and mortality of emergent operations for colorectal disease. *Ann Surg* 199:598–603, 1984.
40. Cortet M, Grimault A, Cheyrel N, et al: Patterns of recurrence of obstructing colon cancers after surgery for cure: A population-based study. *Colorectal Dis* 15:1100–1106, 2013.
41. Gandrup P, Lund L, Balslev I: Surgical treatment of acute malignant large bowel obstruction. *Eur J Surg* 158:427–430, 1992.
42. Ohman U: Prognosis in patients with obstructing colorectal carcinoma. *Am J Surg* 143:742–747, 1982.
43. Umpleby HC, Williamson RCN, Chir M: Survival in acute obstructing colorectal carcinoma. *Dis Colon Rectum* 27:299–304, 1984.
44. Turunen JM: Colorectal cancer obstruction: A challenge to improve diagnosis. *Ann Chir Gynaecol* 72:317–323, 1983.
45. Desai MG, Rodko EA: Perforation of the colon in malignant tumors. *J Can Assoc Radiol* 24:344–349, 1973.
46. Paine JR: Cancer of the colon: Treatment of large bowel obstruction. *Postgrad Med* 39:596–600, 1966.
47. Canon CL, Baron TH, Morgan DE, et al: Treatment of colonic obstruction with expandable metal stents: Radiologic features. *AJR* 168:199–205, 1997.
48. Mainar A, Tejero E, Maynar M, et al: Colorectal obstruction: Treatment with metallic stents. *Radiology* 198:761–764, 1996.
49. Hughes LE: Complications of diverticular disease: Inflammation, obstruction, and bleeding. *Clin Gastroenterol* 4:147–170, 1975.
50. Welch JP: Diverticular disease. In Welch JP, editor: *Bowel Obstruction*, Philadelphia, 1990, WB Saunders, pp 589–599.
51. Morton DL, Goldman L: Differential diagnosis of diverticulitis and carcinoma of the sigmoid colon. *Am J Surg* 103:55–61, 1962.
52. Schnyder P, Moss AA, Thoeni RF, et al: A double-blind study of radiologic accuracy in diverticulitis, diverticulosis, and carcinoma of the sigmoid colon. *J Clin Gastroenterol* 1:55–66, 1979.
53. Schatzki R: The roentgenologic differential diagnosis between cancer and diverticulitis of the colon. *Radiology* 34:651–662, 1940.
54. Balthazar EJ, Megibow A, Schinella RA, et al: Limitations in the CT diagnosis of acute diverticulitis: Comparison of CT, contrast enema and pathologic findings in 16 patients. *AJR* 154:281–285, 1990.
55. Cho KC, Morehouse HT, Alterman DD, et al: Sigmoid diverticulitis: Diagnostic role of CT: Comparison with barium enema studies. *Radiology* 176:111–115, 1990.
56. Welch JP: Volvulus. In Welch JP, editor: *Bowel Obstruction*, Philadelphia, 1990, WB Saunders, pp 575–588.
57. Kerry RL, Ransom HK: Volvulus of the colon: Etiology, diagnosis and treatment. *Arch Surg* 99:215–222, 1969.
58. Ballantyne GH, Brandner ML, Beart RW, et al: Volvulus of the colon: Incidence and mortality. *Ann Surg* 202:83–92, 1985.
59. Khoury GA, Pickard R, Knight M: Volvulus of the sigmoid colon. *Br J Surg* 64:587–589, 1977.
60. Hirao K, Kikawada M, Hanyu H, et al: Sigmoid volvulus showing “a whirl sign” on CT. *Intern Med* 45:331–332, 2006.
61. Hoeffel C, Crema MD, Belkacem A, et al: Multi-detector row CT: Spectrum of diseases involving the ileocecal area. *Radiographics* 26:1373–1390, 2006.
62. Gumbs MA, Kashan F, Shumofsky E, et al: Volvulus of the transverse colon: Reports of cases and review of the literature. *Dis Colon Rectum* 26:825–828, 1983.
63. Hsueh CC, Jaw TS, Lin JY, et al: Splenic flexure colonic volvulus: A pediatric case report. *Kaohsiung J Med Sci* 23:207–210, 2007.
64. Ballantyne G: Volvulus of the splenic flexure: Report of a case and review of the literature. *Dis Colon Rectum* 24:630–632, 1981.
65. Frimann-Dahl J: Roentgen findings in intestinal knots. *Acta Radiol* 23:22–33, 1942.
66. Selguk Atamanalp S: Treatment for ileosigmoid knotting: A single-center experience of 74 patients. *Tech Coloproctol* 18:233–237, 2014.
67. Baheti AD, Patel D, Hira P, et al: Ileosigmoid knot: A case report. *Indian J Radiol Imaging* 21:147–149, 2011.
68. Delabrousse E, Saguet O, Destrumelle N, et al: Sigmoid volvulus: Value of CT. *J Radiol* 82: 930–932, 2001.
69. Lin MP, Chen YL, Tzeng WS: Diagnosis of sigmoid volvulus using the coffee bean, northern exposure sign, whirl sign and transition point. *BMJ Case Rep* 2011:24, 2011.
70. Matsumoto S, Mori H, Okino Y, et al: Computed tomographic imaging of abdominal volvulus: Pictorial essay. *Can Assoc Radiol J* 55:297–303, 2004.
71. Javors BR, Baker SR, Miller JA: The northern exposure sign: A newly described finding in sigmoid volvulus. *AJR* 173:571–574, 1999.
72. Erkan N, Hacıyanlı M, Yildirim M, et al: Intussusception in adults: An unusual and challenging condition for surgeons. *Int J Colorectal Dis* 20:452–456, 2005.
73. Dick A, Green CJ: Large bowel intussusception in adults. *Br J Radiol* 34:769–777, 1961.
74. Yamada H, Morita T, Fujita M, et al: Adult intussusception due to enteric neoplasms. *Dig Dis Sci* 52:764–766, 2007.
75. Briggs DF, Carpathios J, Zollinger RW: Intussusception in adults. *Am J Surg* 101:109–113, 1961.
76. McKay R: Ileocecal intussusception in an adult: The laparoscopic approach. *JLS* 10:250–253, 2006.
77. Lou CJ: Intussusception in adults: An analysis of 92 cases. *Clin Med J* 95:297–300, 1982.
78. Bocker J, Vasile J, Zager J, et al: Intussusception: An uncommon cause of postoperative small bowel obstruction after gastric bypass. *Obes Surg* 14:116–119, 2004.
79. Stubenbord WT, Thorbjarnarson B: Intussusception in adults. *Ann Surg* 172:306–310, 1970.
80. Burmeister RW: Intussusception in the adult: An elusive case of recurrent abdominal pain. *Am J Dig Dis* 7:360–374, 1962.
81. Cotlar AM, Cohn I: Intussusception in adults. *Am J Surg* 101:114–120, 1961.
82. Dean D, Ellis FH, Sauer WG: Intussusception in adults. *Arch Surg* 73:6–11, 1956.
83. Orlando R, III: Intussusception in adults. In Welch JP, editor: *Bowel Obstruction*, Philadelphia, 1990, WB Saunders, pp 229–240.
84. Sarr MG, Nagorney DM, McIlrath DC: Postoperative intussusception in the adult: A previously unrecognized entity? *Arch Surg* 116: 144–148, 1981.
85. Levine MS, Trenkner SW, Herlinger H, et al: Coiled-spring sign of appendiceal intussusception. *Radiology* 155:41–44, 1985.
86. Wilson A, Elias G, Dupiton R: Adult colocolic intussusception and literature review. *Case Rep Gastroenterol* 7:381–387, 2013.
87. Harte MS: Chronic partial intestinal obstruction due to intussusception of an appendix epiploica. *Surgery* 55:55–60, 1942.
88. Ikukara M, Tsang TK, Tosiou A, et al: Intussusception in an adult with pseudomembranous colitis. *J Clin Gastroenterol* 21:336–338, 1995.
89. Jackson H: A sign of intussusception. *Br J Radiol* 26:323–325, 1953.
90. Schatzki R: The roentgenologic appearance of intussuscepted tumors of the colon with and without barium examination. *AJR* 41:549–563, 1939.
91. Verbanck JJ, Rutgeerts LJ, Douterlungne PH, et al: Sonographic and pathologic correlation intussusception of the bowel. *J Clin Ultrasound* 14:393–397, 1986.
92. Parienty RA, LePreux JF, Gruson B: Sonography and CT features of ileocolic intussusception. *AJR* 136:608–610, 1981.
93. Alessi V, Salerno G: The “hay-fork” sign in the ultrasonographic diagnosis of intussusception. *Gastrointest Radiol* 10:177–179, 1985.
94. Rao BK, Fleischer AC: Sonography of the gastrointestinal tract. *Curr Opin Radiol* 2:207–212, 1990.
95. Del-Pozo G, Albillos JC, Tejedor MD: Intussusception: US findings with pathologic correlation—the crescent-in-doughnut-sign. *Radiology* 199:688–692, 1996.
96. Iko BO, Teal JS, Siram SM, et al: Computed tomography of adult colonic intussusception:

- Clinical and experimental studies. *AJR* 143:769–772, 1984.
97. Park SB, Ha HK, Kim AY, et al: The diagnostic role of abdominal CT imaging findings in adult intussusception: Focused on the vascular compromise. *Eur J Radiol* 62:406–415, 2007.
 98. Bar-Ziv J, Solomon A: Computed tomography in adult intussusception. *Gastrointest Radiol* 10:355–357, 1985.
 99. Pottmeyer A, McDowell J, Lang EK: CT findings of a rectal intussusception. *AJR* 156:870, 1991.
 100. Skaane P, Schindler G: Computed tomography of adult ileocolic intussusception. *Gastrointest Radiol* 10:355–357, 1985.
 101. Yoshimitsu F, Fukuya T, Onitsuka H, et al: Computed tomography of ileoileocolic intussusception caused by a lipoma. *J Comput Assist Tomogr* 13:704–706, 1989.
 102. Styles RA, Larsen CR: CT appearance of adult intussusception. *J Comput Assist Tomogr* 7:331–333, 1983.
 103. Balthazar EJ: CT of the gastrointestinal tract: Principles and interpretation. *AJR* 156:23–32, 1991.
 104. Hodgman CG, Lantz EJ, Maus TP, et al: Computed tomography of intussusception due to colon lipoma. *J Comput Assist Tomogr* 11:740–741, 1987.
 105. Buetow PC, Buck JL, Carr NJ, et al: Intussuscepted colonic lipomas: Loss of fat attenuation on CT with pathologic correlation in 10 cases. *Abdom Imaging* 21:153–156, 1996.
 106. Welch JP: Extrinsic causes. In Welch JP, editor: *Bowel Obstruction*, Philadelphia, 1990, WB Saunders, pp 640–653.
 107. Holt RW, Wagner RC: Adhesional obstruction of the colon. *Dis Colon Rectum* 27:314–315, 1984.
 108. Agrawal NW, Akdamar K, Litwin MS: Postoperative adhesions causing colon obstruction. *Am Surg* 50:479–481, 1984.
 109. Bobroff LM, Messinger NH, Subbarao K, et al: The cecal bascule. *AJR* 115:249–252, 1972.
 110. Twersky J, Himmelfarb E: Right colonic adhesions. *Radiology* 120:37–40, 1976.
 111. Bonello JC, Kasten MJ, Slezak FA: Large bowel obstruction following colonoscopic polypectomy. *Contemp Surg* 29:39–41, 1986.
 112. Hwang JA, Kim SM, Song HJ, et al: Differential diagnosis of left-sided abdominal pain: Primary epiploic appendagitis vs colonic diverticulitis. *World J Gastroenterol* 19:6842–6848, 2013.
 113. McCann JC: Omental adhesions syndrome: Postoperative dysfunction of the transverse colon. *Surg Gynecol Obstet* 72:707–721, 1941.
 114. Brodey PA, Scholdt DR, Magnuson A, et al: Complete colonic obstruction secondary to adhesions. *AJR* 133:917–918, 1979.
 115. Farrell B, Gerard PS, Bryk D: Paraesophageal hernia causing colonic obstruction. *J Clin Gastroenterol* 13:188–190, 1991.
 116. Javors BR, Bryk D: Colonic obstruction with inguinal hernia. *J Can Assoc Radiol* 32:162–163, 1981.
 117. Ben Dov D, Rosenblatt M, Rothfeld H: Large-bowel dilatation due to non-incarcerated hernias. *Mt Sinai J Med* 53:99–102, 1986.
 118. Bryk D: Spigelian hernia containing sigmoid colon. *AJR* 99:71–73, 1962.
 119. Hunter TB, Freundlich IM, Zukoski CF: Preoperative radiographic diagnosis of a Spigelian hernia containing large and small bowel. *Gastrointest Radiol* 1:379–381, 1977.
 120. Ghiassi S, Nguyen SQ, Divino CM: Internal hernias: Clinical findings, management, and outcomes in 49 nonbariatric cases. *J Gastrointest Surg* 11:291–295, 2007.
 121. Cruz CJ, Minagi H: Large-bowel obstruction resulting from traumatic diaphragmatic hernia: Imaging findings in four cases. *AJR* 162:843–845, 1994.
 122. Schulman A, van Gelderen F: Bowel herniation through the torn diaphragm: II. Intestinal herniation. *Abdom Imaging* 21:400–403, 1996.
 123. Blatt ES, Schneider H, Wiot JF, et al: Roentgen findings in obstructed diaphragmatic hernia. *Radiology* 79:649–657, 1962.
 124. Gravier L, Freemark RJ: Traumatic diaphragmatic hernia. *Arch Surg* 86:363–373, 1963.
 125. Evrard V, Vielle G, Buyck A, et al: Herniation through the foramen of Winslow: Report of two cases. *Dis Colon Rectum* 39:1055–1057, 1996.
 126. Schuster MR, Tu RK, Scanlan KA: Cecal herniation through the foramen of Winslow: Diagnosis by computed tomography. *Br J Radiol* 65:1047–1048, 1992.
 127. Zink LD, Moore D: Herniation of the cecum through the foramen of Winslow. *Dis Colon Rectum* 23:276–279, 1980.
 128. Pritchard GA, Price-Thomas JM: Internal hernia of the transverse colon. *Dis Colon Rectum* 29:658–659, 1986.
 129. Welch JP: Intrinsic causes. In Welch JP, editor: *Bowel Obstruction*, Philadelphia, 1990, WB Saunders, pp 654–671.
 130. Chou JW, Hsu CH, Liao KF, et al: Gallstone ileus: Report of two cases and review of the literature. *World J Gastroenterol* 13:1295–1298, 2007.
 131. Young WV: Gallstone ileus of the colon: Report of an unusual type of colon obstruction. *Arch Surg* 82:333–336, 1961.
 132. Price JE, Michel SL, Morgenstern L: Fruit pit obstruction: "The propitious pit." *Arch Surg* 111:773–775, 1976.
 133. Cotner M: Fecal impaction due to bubblegum bezoar. *South Med J* 75:775–776, 1982.
 134. Matseshe JW, Go VLW, DiMaggio EP: Meconium ileus equivalent complicating cystic fibrosis in post neonatal children and young adults. *Gastroenterology* 72:732–736, 1977.
 135. Welch JP, Schweitzer RT, Bartus SA: Management of antacid impactions in hemodialysis and renal transplant patients. *Am J Surg* 139: 561–568, 1980.
 136. Culp WC: Relief of severe rectal impactions with water-soluble contrast enemas. *Radiology* 115:9–12, 1975.
 137. Kurer MA, Chintapata S: Images in clinical medicine. Intestinal obstruction due to inspissated barium. *N Engl J Med* 356:1656–1657, 2007.
 138. Eftaiha M, Hambrick E, Abcarian H: Principles of management of colorectal foreign bodies. *Arch Surg* 112:691–695, 1977.
 139. Segall H: Obstruction of large bowel due to fecaloma: Successful medical treatment in two cases. *Calif Med* 108:54–56, 1968.
 140. Welch JP: Constipation. In Welch JP, editor: *Bowel Obstruction*, Philadelphia, 1990, WB Saunders, pp 616–626.
 141. Jones DJ, Dharmeratnam R, Langstaff RJ: Large bowel obstruction due to pelvic lipomatosis. *Ann Surg* 71:309–311, 1985.
 142. Leffall LD, White JE, Mann M: Retroperitoneal fibrosis: Two unusual cases. *Arch Surg* 89: 1070–1076, 1964.
 143. Williams RG, Nelson JA: Retractable mesenteritis: Initial presentation as colonic obstruction. *Radiology* 126:35–37, 1978.
 144. Sirinek KR, Livingston CD, Bova JG, et al: Bowel obstruction due to infarcted splenosis. *South Med J* 77:764–767, 1984.
 145. Hirata N, Kawamoto K, Ueyama T, et al: Endoscopic ultrasonography in the assessment of colonic wall invasion by adjacent diseases. *Abdom Imaging* 19:21–26, 1994.
 146. Wu MH, Shoji Y, Chuang PC, et al: Endometriosis: Disease pathophysiology and the role of prostaglandins. *Expert Rev Mol Med* 9:1–20, 2007.
 147. Mirkin D, Murphy-Barron C, Iwasaki K: Actuarial analysis of private payer administrative claims data for women with endometriosis. *J Manag Care Pharm* 13:262–272, 2007.
 148. Farquhar C: Endometriosis. *BMJ* 334:249–253, 2007.
 149. McCaffee CHG, Greer HLH: Intestinal endometriosis: A report of 29 cases and a survey of the literature. *J Obstet Gynecol* 67:539–555, 1960.
 150. Fagan CJ: Endometriosis: Clinical and roentgenographic manifestations. *Radiol Clin North Am* 12:109–125, 1974.
 151. Gordon RL, Evers K, Kressel HY, et al: Double-contrast enema in pelvic endometriosis. *AJR* 138:549–552, 1982.
 152. Sievert W, Sellin JH, Stringer CA: Pelvic endometriosis simulating colonic malignant neoplasm. *Arch Intern Med* 149:935–938, 1989.
 153. Tate GT: Acute obstruction of the large bowel due to endometriosis. *Br J Surg* 50:771–773, 1963.
 154. Goodman P, Raval B, Zimmerman G: Perforation of the colon due to endometriosis. *Gastrointest Radiol* 15:346–348, 1990.
 155. Coronado C, Franklin RR, Lotze EC, et al: Surgical treatment of symptomatic colorectal endometriosis. *Fertil Steril* 53:411–416, 1990.
 156. Nezhad F, Nezhad C, Pennington E, et al: Laparoscopic segmental resection for infiltrating endometriosis of the rectosigmoid colon: A preliminary report. *Surg Laparosc Endosc* 2:212–216, 1992.
 157. Athey PA, Diment DD: The spectrum of sonographic findings in endometriomas. *J Ultrasound Med* 8:487–491, 1989.
 158. Brown DL, Frates MC, Laing FC, et al: Ovarian masses: Can benign and malignant lesions be differentiated with color and pulsed Doppler US? *Radiology* 190:333–336, 1994.
 159. Fishman EK, Scatarige JC, Saksouk FA, et al: Computed tomography of endometriosis. *J Comput Assist Tomogr* 7:257–264, 1983.
 160. Togashi K, Nishimura K, Kimura I, et al: Endometrial cysts: Diagnosis with MR imaging. *Radiology* 180:73–78, 1991.
 161. Meyers MA: Intraperitoneal spread of malignancies and its effect on the bowel. *Clin Radiol* 32:129–146, 1981.
 162. Levitt RG, Koehler RE, Sagel SS, et al: Metastatic disease of the mesentery and omentum. *Radiol Clin North Am* 20:501–510, 1982.
 163. Landis SH, Murray T, Bolden S, et al: Cancer statistics, 2006. *CA* 48:6–29, 2006.
 164. Feller E, Schiffman FJ: Colonic obstruction as the first manifestation of ovarian carcinoma. *Am J Gastroenterol* 82:25–28, 1987.
 165. Oliphant M, Berne AS, Meyers MA: Imaging the direct bidirectional spread of disease between the abdomen and the female pelvis via the subperitoneal space. *Gastrointest Radiol* 13:285–298, 1988.

166. Oliphant M, Berne AS, Meyers MA: Bidirectional spread of disease via the subperitoneal space: The lower abdomen and left pelvis. *Abdom Imaging* 18:117-125, 1993.
167. Gedgaudas K, Kelvin FM, Thompson WM, et al: The value of the pre-operative barium-enema examination in the assessment of pelvic masses. *Radiology* 146:609-613, 1983.
168. Rubesin SE, Levine MS: Omental cakes: Colonic involvement by omental metastases. *Radiology* 154:593-596, 1985.
169. Rubesin SE, Levine MS, Glick SN: Gastric involvement by omental cakes: Radiographic findings. *Gastrointest Radiol* 11:223-228, 1986.
170. Krestin GP, Beyer D, Lorenz R: Secondary involvement of the transverse colon by tumors of the pelvis: Spread of malignancies along the greater omentum. *Gastrointest Radiol* 10:283-288, 1985.
171. Hawnaur JM: Staging of cervical and endometrial carcinoma. *Clin Radiol* 47:7-13, 1993.
172. Ellis JH, Francis IR, Rhodes M, et al: CT findings in tuboovarian abscess. *J Comput Assist Tomogr* 15:589-592, 1991.
173. Adelson MA, Adelson KL: Miscellaneous benign disorders of the upper genital tract. In Copeland LJ, editor: *Textbook of Gynecology*, Philadelphia, 1993, WB Saunders, pp 857-870.
174. Quinn TC, Goodell SE, Mkrtichian E, et al: *Chlamydia trachomatis* proctitis. *N Engl J Med* 305:195-200, 1981.
175. Wexner SD: Sexually transmitted diseases of the colon, rectum, and anus. *Dis Colon Rectum* 33:1048-1062, 1990.
176. Hunt DR, Mildenhall P: Etiology of strictures of the colon associated with pancreatitis. *Dig Dis Sci* 20:941-946, 1975.
177. Aronson AR, Davis DA: Obstruction near hepatic flexure in pancreatitis: A rarely reported sign. *JAMA* 176:451-454, 1961.
178. Brearly S, Campbell DJ: Stenosis of the colon following acute pancreatitis. *Postgrad Med J* 58:293-296, 1982.
179. Thompson WM, Kelvin FM, Rice RP: Inflammation and necrosis of the transverse colon secondary to pancreatitis. *AJR* 128:943-948, 1977.
180. Mann NS: Colonic involvement in pancreatitis. *Am J Gastroenterol* 73:357-362, 1980.
181. Adams DB, Davis BR, Anderson MC: Colonic complications of pancreatitis. *Am Surg* 60:44-49, 1994.
182. Meyers MA, McSweeney J: Neoplasms of the bowel. *Radiology* 105:1-11, 1972.
183. Khilnani MT, Wolf BS: Late involvement of the alimentary tract by carcinoma of the kidney. *Am J Dig Dis* 5:529-540, 1960.
184. Fry DE, Amin M, Harbrecht PJ: Rectal obstruction secondary to carcinoma of the prostate. *Ann Surg* 189:488-492, 1979.
185. Ruggiero RP, Chang H: Rectal involvement by carcinoma of the prostate. *Am J Gastroenterol* 81:372-374, 1986.
186. Lasser A: Adenocarcinoma of the prostate involving the rectum. *Dis Colon Rectum* 21:23-25, 1978.
187. Welch JP: Acute large intestinal obstruction as the initial sign of pancreatic carcinoma. *Dis Colon Rectum* 22:425-427, 1979.
188. Brandt JL: Intestinal ischemia. In Feldman M, Friedman LS, Sleisenger MH, editors: *Sleisenger and Fordtran's Gastrointestinal and Liver Disease*, ed 8, Philadelphia, 2006, Saunders, pp 2563-2586.
189. Greenwald DA, Brandt LJ: Colonic ischemia. *J Clin Gastroenterol* 27:122-128, 1998.
190. Barbagelatta M: Pathologic diagnosis of ischemic colitis. *J Chir* 134:97-102, 1997.
191. Levine JS, Jacobson ED: Intestinal ischemic disorders. *Dig Dis* 13:3-24, 1995.
192. Parfitt JR, Driman DK: Pathological effects of drugs on the gastrointestinal tract: A review. *Hum Pathol* 38:527-536, 2007.
193. Wittenberg J, Athanasoulis CA, Williams LE, et al: Ischemic colitis: Radiology and pathophysiology. *AJR* 123:287-300, 1975.
194. Gore RM, Calenoff L, Rogers LF: Roentgenographic manifestations of ischemic colitis. *JAMA* 241:1171-1173, 1979.
195. Iida M, Matsui T, Fuchigami T, et al: Ischemic colitis: Serial changes in double contrast barium enema examinations. *Radiology* 159:337-341, 1986.
196. Greenberg HM, Goldberg HI, Axel L: Colonic "urticaria" pattern due to early ischemia. *Gastrointest Radiol* 6:145-149, 1981.
197. Noyer CM, Brandt LJ: Systemic, iatrogenic, and unusual disorders of the colon. In DiMarino AJ, Benjamin SB, editors: *Gastrointestinal Disease: An Endoscopic Approach*, Oxford, England, 1997, Blackwell Scientific, pp 684-706.
198. Koehler RE, Memel DS, Stanley RJ: Gastrointestinal tract. In Lee JKT, Sagel SS, Stanley JR, et al, editors: *Computed Body Tomography with MRI Correlation*, ed 3, Philadelphia, 1998, Lippincott-Raven, pp 637-700.
199. Jeffrey RB, McGahan JP: Gastrointestinal tract and peritoneal cavity. In McGahan JP, Goldberg BB, editors: *Diagnostic Ultrasound: A Logical Approach*, Philadelphia, 1998, Lippincott-Raven, pp 511-560.
200. Wilson SR: The gastrointestinal tract. In Rumack CM, Wilson SR, Charboneau JW, editors: *Diagnostic Ultrasound*, ed 2, St. Louis, 1998, Mosby-Year Book, pp 279-328.
201. Donner CS: Pathophysiology and therapy of chronic radiation-induced injury to the colon. *Dig Dis* 16:253-258, 1998.
202. Capps GW, Fulcher AS, Szucs RA, et al: Imaging features of radiation-induced changes in the abdomen. *Radiographics* 17:1455-1473, 1997.
203. Carr ND, Pullen BR, Hasleton PS, et al: Microvascular studies in human radiation bowel disease. *Gut* 25:448-454, 1984.
204. Hull TL: Diseases of the anorectum. In Feldman M, Friedman LS, Sleisenger MH, editors: *Gastrointestinal and Liver Disease*, ed 8, Philadelphia, 2006, Saunders, pp 2833-2856.
205. Thoeni RF, Venbrux AC: The anal canal: Distinction of internal hemorrhoids from small cancers by double-contrast barium enema examination. *Radiology* 145:17-19, 1982.
206. Levine MS, Kam LW, Rubesin SE, et al: Internal hemorrhoids: Diagnosis with double-contrast barium enema examinations. *Radiology* 177:141-144, 1990.
207. Manzi D, Samanta AK: Adhesion-related colonic varices. *J Clin Gastroenterol* 7:71-75, 1985.
208. McCormack TT, Bailey HR, Simms JM, et al: Rectal varices are not piles. *Br J Surg* 71:163-168, 1984.
209. Kelvin FM, Gardiner R: *Clinical Imaging of the Colon and Rectum*, New York, 1987, Raven Press, pp 422-460.
210. Kyaw MM, Gallagher T, Haines JO: Cloacogenic carcinoma of the anorectal junction: Roentgenologic diagnosis. *AJR* 115:384-391, 1972.
211. Glickman MG, Margulis AR: Cloacogenic carcinoma. *AJR* 107:175-180, 1969.
212. Gillespie JJ, Mackay B: Histogenesis of cloacogenic carcinoma: Fine structure of anal transitional epithelium and cloacogenic carcinoma. *Hum Pathol* 9:579-587, 1978.
213. Vaizey CJ, van den Bogaerde JB, Emmanuel AV, et al: Solitary rectal ulcer syndrome. *Br J Surg* 85:1617-1623, 1998.
214. Feczko PJ, O'Connell DJ, Riddell RH, et al: Solitary rectal ulcer syndrome: Radiologic manifestations. *AJR* 135:499-506, 1980.
215. Millward SF, Bayjoo P, Dixon MF, et al: The barium enema appearances in solitary rectal ulcer syndrome. *Clin Radiol* 36:185-189, 1985.
216. Levine MS, Piccolo ML, Sollenberger LC, et al: Solitary rectal ulcer syndrome: A radiologic diagnosis? *Gastrointest Radiol* 11:187-193, 1986.
217. Chang FY, Lu CL: Irritable bowel syndrome in the 21st century: Perspectives from Asia or Southeast Asia. *J Gastroenterol Hepatol* 22:4-12, 2007.
218. Podovei M, Kuo B: Irritable bowel syndrome: A practical review. *South Med J* 99:1235-1242, 2006.
219. Henningsen P, Zipfel S, Herzog W: Management of functional somatic syndromes. *Lancet* 369:946-955, 2007.
220. Lennard-Jones JE: Constipation. In Feldman M, Scharschmidt BF, Sleisenger MH, editors: *Gastrointestinal and Liver Disease*, ed 6, Philadelphia, 1998, WB Saunders, pp 174-197.
221. Greenfield SM: The management of constipation in hospital inpatients. *Br J Hosp Med (Lond)* 68:145-147, 2007.
222. Karasick S, Ehrlich SM: Is constipation a disorder of defecation or impaired motility? Distinction based on defecography and colonic transit studies. *AJR* 166:63-67, 1996.
223. Schuffler MD: Chronic intestinal pseudo-obstruction. In Feldman M, Scharschmidt BF, Sleisenger MH, editors: *Gastrointestinal and Liver Disease*, ed 6, Philadelphia, 1998, WB Saunders, pp 1820-1830.
224. Phillips SF: Motility disorders of the colon. In Yamada T, editor: *Textbook of Gastroenterology*, ed 2, Philadelphia, 1995, JB Lippincott, pp 1856-1875.
225. Phillips SF, Pemberton JH: Megacolon: Congenital and acquired. In Feldman M, Scharschmidt BF, Sleisenger MH, editors: *Gastrointestinal and Liver Disease*, ed 6, Philadelphia, 1998, WB Saunders, pp 1810-1819.
226. Sartor RB, Murphy ME, Rydzak E: Miscellaneous inflammatory and structural disorders of the colon. In Yamada T, editor: *Textbook of Gastroenterology*, ed 2, Philadelphia, 1995, JB Lippincott, pp 1806-1831.
227. Chiao GZ, Rey D: Motor disorders of the colon. In DiMarino AJ, Benjamin SB, editors: *Gastrointestinal Disease: An Endoscopic Approach*, Malden, MA, 1997, Blackwell Scientific, pp 659-683.
228. Rose S, Young MA, Reynolds JC: Gastrointestinal manifestations of scleroderma. *Gastroenterol Clin North Am* 27:563-594, 1998.
229. Brandt LS, Simon DM: Pneumatosis cystoides intestinalis. In Haubrich WS, Schaffner F, Berk JE, editors: *Gastroenterology*, ed 5, Philadelphia, 1995, WB Saunders, pp 1685-1693.
230. Eisenberg RL: *Gastrointestinal Radiology: A Pattern Approach*, Philadelphia, 1996, Lippincott-Raven, pp 925-937.

231. Feczko PJ, Mezwa DG, Farah MC, et al: Clinical significance of pneumatosis of the bowel wall. *Radiographics* 12:1069–1084, 1992.
232. Shinagare AB, Howard SA, Krajewski KM, et al: Pneumatosis intestinalis and bowel perforation associated with molecular targeted therapy: An emerging problem and the role of radiologists in its management. *AJR* 199:1259–1265, 2012.
233. Komorowski RA: Histologic spectrum of diversion colitis. *Am J Surg Pathol* 14:548–554, 1990.
234. Lechner GL, Frank W, Jantsch H, et al: Lymphoid follicular hyperplasia in excluded colonic segments: A radiologic sign of diversion colitis. *Radiology* 176:135–136, 1990.
235. Whelan RL, Abramson D, Kim DS, et al: Diversion colitis: A prospective study. *Surg Endosc* 8:19–24, 1994.
236. Scott RL, Pinstein ML: Diversion colitis demonstrated by double-contrast barium enema. *AJR* 143:767–771, 1984.
237. Stanley RJ, Teseco FJ, Melson GL, et al: The colitis of Behçet's disease: A clinical-radiographic correlation. *Radiology* 114:603–608, 1975.
238. Molean AM, Simms DM, Homer MJ: Ileal ring ulcers in Behçet's syndrome. *AJR* 140:947–951, 1983.
239. Mendoza-Pinto C, García-Carrasco M, Jiménez-Hernández M, et al: Etiopathogenesis of Behçet's disease. *Autoimmun Rev* 9:241–245, 2010.
240. Kim JH, Choi BJ, Han JK, et al: Colitis in Behçet's disease: Characteristics on double-contrast barium enema examinations in 20 patients. *Abdom Imaging* 19:132–136, 1994.
241. Kim SH, Kim JH, Gu MJ: Secondary intestinal amyloidosis presenting with intractable hematochezia. *Int J Exp Pathol* 15:1805–1808, 2014.
242. Tada S, Iida M, Yao T, et al: Gastrointestinal amyloidosis: Radiologic features by chemical types. *Radiology* 190:37–42, 1994.
243. Moller JM, Santoni-Rugiu E, Chabanova E, et al: Magnetic resonance imaging with liver-specific contrast agent in primary amyloidosis and intrahepatic cholestasis. *Acta Radiol* 48:145–149, 2007.
244. Ogasawara N, Kitagawa W, Obayashi K, et al: Solitary amyloidosis of the sigmoid colon featuring submucosal tumor caused hematochezia. *Intern Med* 52:2523–2527, 2013.
245. Urso FP, Urso JM, Lee CH: The cathartic colon: Pathological findings and radiological pathological correlation. *Radiology* 116:557–561, 1975.
246. Puy-Montbrun T, Delechenault P, Ganansia R, et al: Rectal stenosis due to Vegainin suppositories. *Gastrointest Radiol* 15:169–173, 1990.
247. Kim SK, Gerle RD, Rozanski R: Cathartic colitis. *AJR* 130:825–831, 1978.
248. Seaman WB, Clements JL: Urticaria of the colon: A nonspecific pattern of submucosal edema. *AJR* 138:545–551, 1982.
249. Miller VE, Han SY, Witten DM: Reticular mosaic (urticarial) pattern of the colon mucosa in *Yersinia* colitis. *Radiology* 146:307–309, 1983.
250. Schuster MM, Raytch RE: Anorectal disease. In Haubrich WS, Schaffner F, Berk JE, editors: *Gastroenterology*, ed 5, Philadelphia, 1995, WB Saunders, pp 1773–1789.
251. Walker P, Wiener I, Rave EB: Colitis cystica profunda: Diagnosis and management. *South Med J* 79:1167–1170, 1986.
252. Laurent V, Corby S, Meyer-Bisch L, et al: MRI aspect of rare rectal pseudotumor associated with dyschezia: Colitis cystica profunda. *J Radiol* 88:585–588, 2007.
253. Sarzo G, Finco C, Parise P, et al: Colitis cystica profunda of the rectum: Report of a case and review of the literature. *Chir Ital* 57:789–798, 2005.
254. Dewandel P, Schraepen T, Vanbeckevoort D, et al: Colitis cystica profunda. *JBR-BTR* 84:111–113, 2001.
255. Noyer CM, Brandt LJ: Systemic, iatrogenic, and unusual disorders of the colon. In DiMarino AJ, Benjamin SB, editors: *Gastrointestinal Disease: An Endoscopic Approach*, Malden, MA, 1997, Blackwell Scientific, pp 684–706.
256. Wald A: Other diseases of the colon and rectum. In Feldman M, Friedman LS, Sleisenger MH, editors: *Gastrointestinal and Liver Disease*, ed 8, Philadelphia, 2006, Saunders, pp 2811–2832.
257. Martin SP, Gianella RA: Infectious disease of the colon. In DiMarino AJ, Benjamin SB, editors: *Gastrointestinal Disease: An Endoscopic Approach*, Malden, MA, 1997, Blackwell Scientific, pp 593–609.
258. Banks MR, Farthing MJG: Diarrhea. In Weinstein WM, Hawkey CJ, Bosch J, editors: *Clinical Gastroenterology and Hepatology*, St. Louis, 2005, Elsevier Mosby, pp 37–44.
259. Schiller LR, Sellin JH: Diarrhea. In Feldman M, Friedman LS, editors: *Sleisenger and Fordtran's Gastrointestinal and Liver Disease*, ed 9, Philadelphia, 2010, Saunders Elsevier, pp 211–232.
260. Saha L: Irritable bowel syndrome: Pathogenesis, diagnosis, treatment, and evidence-based medicine. *World J Gastroenterol* 20:6759–6773, 2014.

Postoperative Colon

CHRISTOPHER D. SCHEIREY | JALIL AFNAN | FRANCIS J. SCHOLZ

CHAPTER OUTLINE

Segmental Resection

Side-to-Side Enterocolic Anastomosis

Colostomy

End-Colostomy

Loop Colostomy

Double-Barreled Colostomy

Divided Colostomy and Mucous Fistula

Cecostomy

Low Anterior Resection

Proctectomy and Coloanal Anastomoses

Abdominoperineal Resection

Hartmann Procedure

Mucous Fistula

Appendectomy

Ileal Pouch–Anal Anastomosis

Colonic Stents

Radiologists are often asked to evaluate the postoperative colon to exclude complications such as fistula, dehiscence, stricture, and abscess formation. Radiologists are also called on to assess the colon in the asymptomatic patient for anastomotic healing or resolution of inflammatory disease before a colostomy is closed. The radiologist must be familiar with the details of the surgical procedure, terminology, and individual surgeon's modifications to render an intelligent consultation. The major surgical procedures performed on the colon are discussed in this chapter. Although there is increasing use of the laparoscopic approach to colonic surgeries, the structural end results are similar to those of their open counterparts. The minute intraoperative technical details have been well described in classic surgical textbooks.¹⁻⁴

Segmental Resection

Segmental resection entails surgical removal of a diseased segment of the colon. Colonic continuity is usually restored with an end-to-end colocolic or ileocolic anastomosis (Figs. 63-1 and 63-2). The latter is created for patients who undergo resection of the cecum or right colon. In some patients, the anastomotic line may be seen as a short-segment, ringlike indentation during contrast examination of the colon (Fig. 63-3), but in many patients the site of the anastomosis may not be discernible unless defined by surgical staples. Currently, most

surgeons use stapling devices rather than traditional hand-sewn anastomoses to reestablish bowel continuity. The stapling units usually create a uniform ring of staples. Disruption of the ring on a plain film of the abdomen may indicate disruption of the anastomosis. A segmental resection may be performed in conjunction with an upstream diverting ileostomy or colostomy (see later).

Prior to colostomy takedown, the surgeon may request a preoperative examination of the anastomosis to ensure integrity. In terms of technique, the examination is performed after placement of a rectal tube or Foley catheter into the rectum, with instillation of water-soluble contrast material under fluoroscopy. The examination should focus on the region of the anastomosis, with imaging performed in multiple projections and with the patient in a variety of positions. In particular, the examination should be performed with a mild degree of stress to the anastomosis. For example, rather than performing an examination of a sigmoid anastomosis entirely in the recumbent position, a high-pressure view of the sigmoid in a right posterior oblique and/or reverse Trendelenburg position should be performed. This will create a column of contrast at the level of the anastomosis, potentially revealing a leak that could be missed if the contrast flowed past the anastomosis in a low-pressure position (left posterior oblique and Trendelenburg position).

Side-to-Side Enterocolic Anastomosis

A side-to-side enterocolic anastomosis (Fig. 63-4) may be created when a diseased segment of distal small bowel (as in Crohn's disease or radiation enteritis) is bypassed or when the length of the functional small bowel is shortened for treatment of morbid obesity. Currently, this procedure is rarely performed in isolation. Surgeons prefer to resect rather than bypass small bowel involved by Crohn's disease. Gastric restrictive surgeries, including gastric stapling and Roux-en-Y gastric bypass, are much preferred over a small bowel bypass procedure as therapy for morbid obesity (see Chapter 35).

Colostomy

A colostomy is a colcutaneous opening, or stoma, created to decompress a colonic obstruction or divert the fecal stream away from the distal colon. Diverting colostomies may be performed to protect a distal anastomosis that has recently been created and requires time to heal or to direct the fecal stream away from a segment of distal colon that is too inflamed to be resected at the time of the initial operation. If the surgeon elects to resect the diseased segment, he or she may choose to perform an end-to-end anastomosis and divert the fecal stream with a temporary colostomy. The colon proximal to the stoma is often evaluated radiographically to rule out

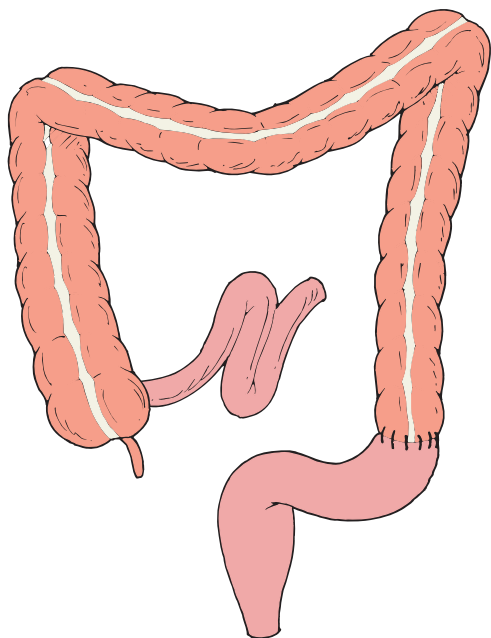


Figure 63-1 Segmental sigmoid resection and end-to-end colocolic anastomosis. Foreshortening of the sigmoid colon may or may not be apparent radiographically, depending on the length of colon resected.



Figure 63-2 Ileal-transverse colonic anastomosis. The small bowel proximal to the anastomosis (*long arrow*) has an abnormal appearance with pseudohaustra (*short arrows*) and dilation, an appearance known as *colonization*.

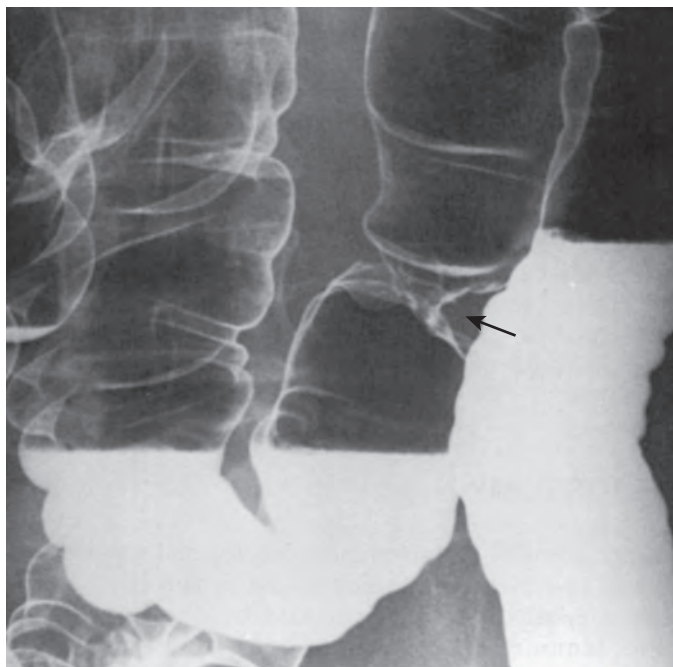


Figure 63-3 Postoperative deformity after closure of prior diverting colostomy. A prominent short-segment annular constriction (*arrow*) is present in the transverse colon with intact mucosa. Serosal metastatic disease can have the same appearance.

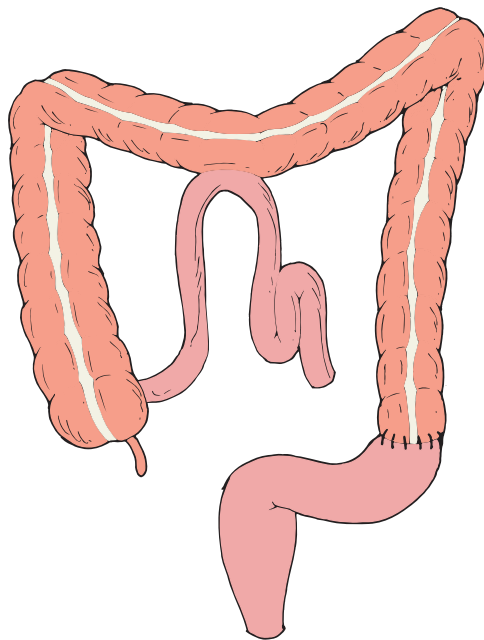


Figure 63-4 Side-to-side enterocolic anastomosis. Evaluation of the colon proximal to the anastomosis may be technically difficult because of preferential filling of the distal small bowel.

additional colonic lesions, whereas the distal colon is evaluated to assess the status of a distal anastomosis or a previously inflamed segment.

Stomal creation is associated with a number of complications. Necrosis may occur if the blood supply is compromised by tension or compression during formation of the stoma. The stoma may become detached from the abdominal wall and migrate into the abdominal cavity. With stomal recession, it may remain attached to the abdominal wall but retract into the abdomen, causing inflammation of the surrounding skin. The bowel may also prolapse or intussuscept through the stoma. When they occur, parastomal hernias may contain small or, rarely, large bowel that passes through an enlarged fascial defect adjacent to the stoma. The hernia may remain in the subcutaneous tissues (Fig. 63-5) or may protrude externally beside the stoma. In obese patients, these hernias can be difficult to detect clinically but are readily apparent on abdominal computed tomography (CT) scans. Parastomal hernias can result in bowel obstructions and can be difficult for the surgeon to repair. Parastomal hernias causing stomal obstruction or dysfunction may be intermittent. When examining a stoma at fluoroscopy, tangential views should be obtained with and without a Valsalva maneuver to elicit bowel herniation into a parastomal hernia. Stomal ulceration may occur because of mechanical irritation from the stomal appliance. The choice of colostomy depends on whether it is to be permanent or temporary, the patient's body habitus, previous operations, and the surgeon's preference.

END-COLOSTOMY

An end-colostomy may be performed as a definitive procedure in patients with distal rectal carcinoma or as part of a two-stage procedure for diverticulitis. The stoma is usually in the left lower quadrant, and the descending colon or residual sigmoid colon is the portion that forms the stomal opening. This procedure is often performed in association with the Hartmann

procedure to close off the rectal stump, so only one stoma is present.

LOOP COLOSTOMY

A loop colostomy is usually performed for the following indications: (1) as a temporary procedure to relieve an acute obstruction of the distal colon or to protect a new distal colonic anastomosis; and (2) as a permanent procedure for unresectable advanced lesions. A loop of transverse or sigmoid colon is brought to the surface of the abdominal wall, sutured in place on the outside, and then opened up, creating afferent and efferent stomas. The mucosa connecting the two stomal openings is the posterior wall of the colon. Patients are usually aware of which stoma produces feces and are able to direct the radiologist to examine the correct portion of the colon.

DOUBLE-BARRELED COLOSTOMY

A double-barreled colostomy is created when the colon is divided completely and the two cut ends are sewn side by side to each other, but this type of colostomy is rarely performed. This type of stoma also has two openings, and the patient can usually tell which one is the productive orifice. This procedure is chosen because the stoma can be closed without reentering the abdomen. The apposed common walls are cut, and the stoma closes spontaneously, or the margins of the two stomal openings can be pursed together with minimal suturing under local anesthesia.

DIVIDED COLOSTOMY AND MUCOUS FISTULA

A divided colostomy and mucous fistula operation creates two separate colostomies—one for the proximal colon, creating an efferent or productive stoma, and one for the distal colon, creating an afferent stoma (Fig. 63-6). From the afferent stoma, the



Figure 63-5 Parastomal hernia. Large parastomal hernia (arrows) containing unobstructed small bowel in this patient status total proctocolectomy and end-ileostomy for Crohn's disease.

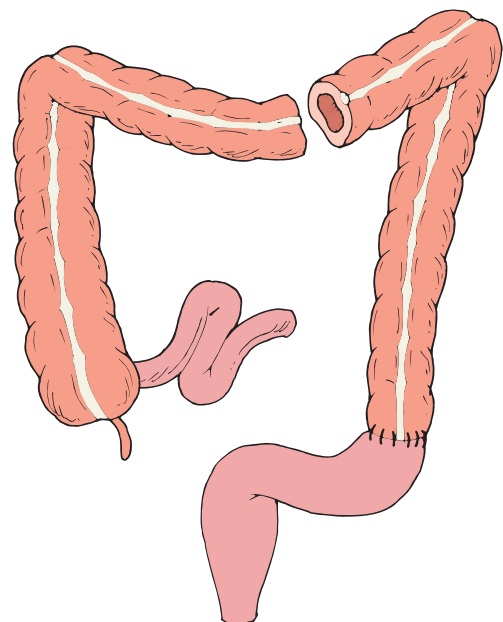


Figure 63-6 Typical diverting transverse colostomy. This demonstrates a fecal stoma, mucous fistula stoma, and end-to-end sigmoid anastomosis.

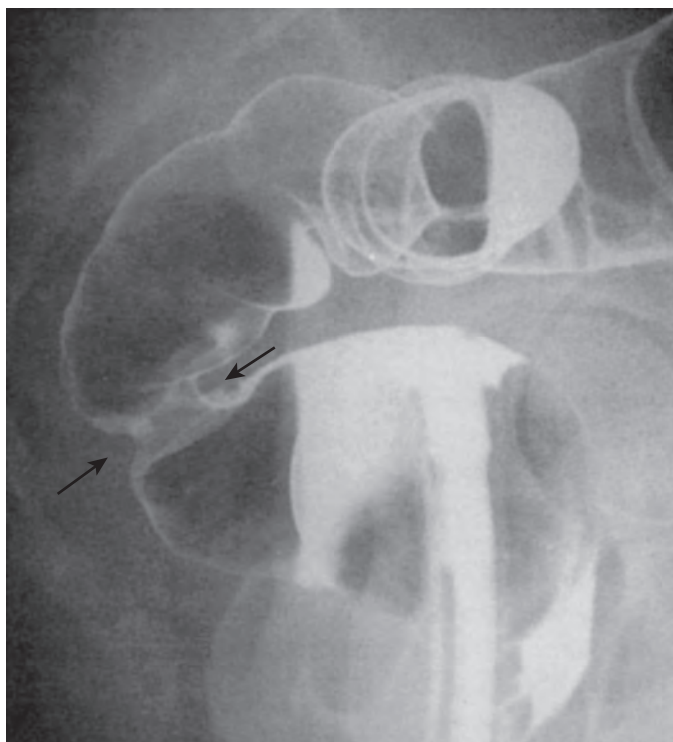


Figure 63-7 Rectal deformity caused by prior abscess and drainage. Examination performed because of a family history of colonic carcinoma demonstrates a short, annular constriction (arrows) in the midrectum that was not present on an examination performed 6 years earlier. Endoscopy showed normal mucosa in the contracted segment. Additional history was obtained before ordering further studies. An intervening appendectomy at another institution 4 years earlier required postoperative transrectal drainage of a perirectal abscess. This case represents residual deformity from that abscess and its treatment.

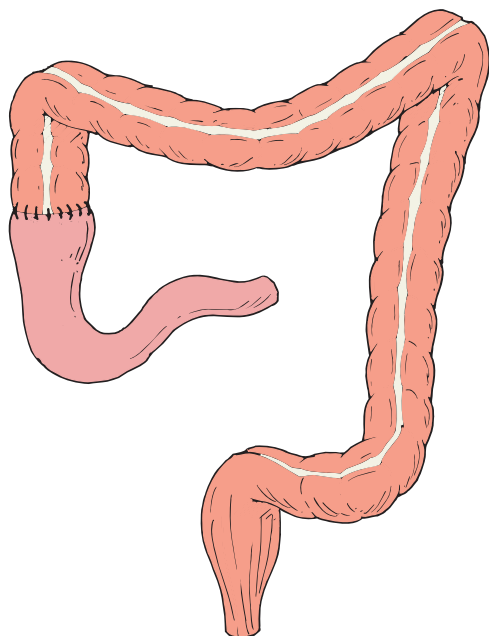


Figure 63-8 Ileal-ascending colonic anastomosis. This procedure is performed after resection of a right colonic tumor or ileocecal Crohn's disease.

colon carries only mucus to the rectum; this stoma has been called a *mucous stoma* or *mucous fistula*. This procedure is not commonly performed but may be chosen to ensure that no fecal debris enters the distal colon.

At 6 to 8 weeks, the colon is usually reexamined before closing the diverting colostomy to ensure that there is no leakage and that regional inflammatory changes have subsided. When the colon is evaluated to exclude a fistula, a single-contrast rather than a double-contrast barium enema study should be performed. Barium is safe to use in the asymptomatic patient because extravasation, when it occurs, has a well-formed sinus tract, and barium does not enter the peritoneal cavity. Also, barium has contrast characteristics superior to those of water-soluble contrast agents, which may not be sufficiently dense and can become diluted in such a tract, making it difficult to visualize tiny tracts during fluoroscopy of organs low in the bony pelvis.

After diversion of the fecal stream with a colostomy, the distal colon may have an abnormal appearance when examined before closure. The unused segment of the colon may appear nondistensible and may have an abnormal mucosal pattern, with nodularity and lymphoid follicular hyperplasia.⁵ This condition is known as *diversion colitis*. The apparent absence of distensibility is probably the result of chronic lack of distention, and the mucosal irregularity is likely secondary to adherent mucus in a contracted and unprepared colon. Patients may be asymptomatic; this entity likely represents a radiographic phenomenon rather than a true colitis. With restoration of the fecal stream after closure of the colostomy, the morphologic features of the colon return to normal unless underlying colonic inflammatory disease is present. A deformity may be created at the site of the previous colostomy and may cause radiographic confusion when the history is not correlated with the radiographic examination. The appearance is variable and may resemble that of a polypoid filling defect, smooth or nodular annular lesion, or submucosal or serosal process (see Fig. 63-3). Any colonic operative or endoscopic procedure may also produce a persistent deformity that can mimic disease (Fig. 63-7). Careful review of the patient's history should prevent a misdiagnosis.

Cecostomy

Cecostomy is a surgical procedure in which an opening is created in the cecum to relieve cecal distention produced by intestinal pseudo-obstruction, profound paralytic ileus, or, rarely, distal obstruction (e.g., tumor, cecal volvulus). It is a temporizing or palliative measure in acutely ill patients and in those who would not tolerate a definitive but more prolonged right hemicolectomy and ileal ascending colonic anastomosis (Fig. 63-8) or resection of a distal colonic obstructive process. A tube is placed in the cecum and brought to the abdominal surface to relieve colonic distention. A cecostomy may be performed by the surgeon, interventional radiologist, or gastroenterologist. A definitive surgical procedure can later be performed when the patient's condition permits.

Low Anterior Resection

Low anterior resection, performed for carcinoma of the proximal rectum and midrectum, entails resection of the rectosigmoid and anastomosis of a cuff of the proximal colon to the distal rectum below the peritoneal reflection. It involves an

anastomosis deep within the pelvis and may be difficult to perform. The surgeon must determine how low a resection to perform; this decision depends on the patient's body habitus, nature of the lesion to be resected, and skill of the surgeon. Depending on the amount of residual rectum, a straight colorectal anastomosis or pouch to rectal anastomosis may be performed (see later, "Proctectomy and Coloanal Anastomoses"). Stapling devices greatly facilitate the technical performance of low anterior resection. A temporary, protective diverting ileostomy or colostomy may be created in conjunction with this procedure.

Preoperatively, the surgeon may wish to obtain a proctoscopic measurement or radiographic estimation of the distance from the anal canal to the lesion. Postoperatively, the status of the anastomosis may require evaluation with a water-soluble contrast enema before closure of the ostomy. The examination is performed with a gently placed 12F Foley or small-caliber red rubber catheter that is taped onto the adjacent gluteal skin; inflation of the balloon could disrupt the anastomosis. Leakage from a low anastomosis within the pelvis may produce a pelvic abscess, perirectal abscess, or colovaginal fistula (Fig. 63-9).

Proctectomy and Coloanal Anastomoses

A proctectomy with coloanal anastomosis is a means of removing the rectum while preserving colonic continuity and anal sphincter function. This is performed primarily in patients with rectal carcinoma involving the mid and lower thirds of the rectum. Total mesorectal excision is preformed to reduce the risk of local recurrence. The tumor is excised with a relatively

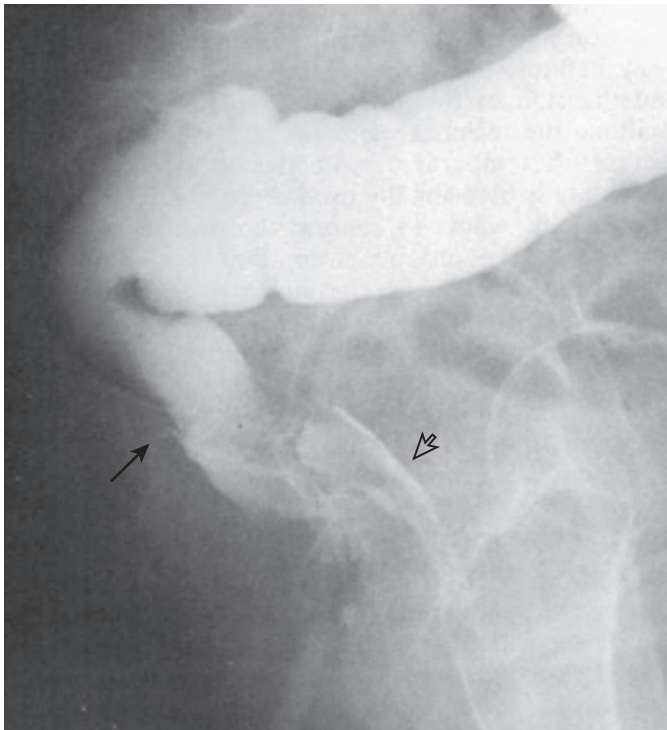


Figure 63-9 Rectovaginal fistula. Contrast material is identified in the vagina (open arrow). Surgical clips (solid arrow) seen posteriorly define the level of the anastomosis and level of the fistula.

short distal margin while preserving the anal sphincter. Previously, the colon was reattached to the anus via a straight coloanal anastomosis, but the current procedure of choice is the colonic J-pouch anastomosis (Fig. 63-10). This has improved functional outcome over a straight anastomosis, particularly in the first postoperative year.^{6,7} The technique involves folding the distal aspect of the residual colon upon itself and dividing the septum to create a reservoir for fecal material. The pouch is hand-sewn or stapled directly to the anus. A diverting colostomy or ileostomy may also be performed. Similar to other colonic anastomoses, the surgeon may request a water-soluble contrast examination prior to ileostomy takedown (Fig. 63-11).

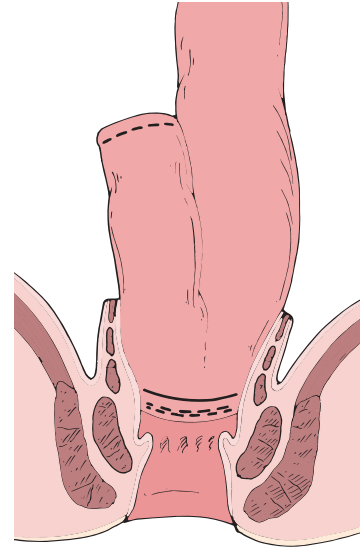


Figure 63-10 Colon J pouch. A segment of distal colonic is folded upon itself, divided, and anastomosed to the anus, creating a reservoir for fecal material after low anterior resection.



Figure 63-11 Colon J pouch. This is the normal appearance of a colon J pouch on a retrograde water-soluble contrast study performed prior to takedown of a diverting ileostomy.



Figure 63-12 Colon J pouch leak and inflammation. CT scan of the pelvis in a patient status postproctectomy and colon J pouch for a low rectal cancer shows a leak and presacral inflammation at the blind-ending stump of the J pouch (arrowhead) that was not detected prior to ileostomy takedown.

Another surgical technique in patients with difficult anatomy is the coloplasty pouch. This involves a longitudinal incision in the descending colon, which is then closed transversely. This creates a pouch that may be technically easier to anastomose to the anus in patients with a narrow pelvis. Early studies indicated a higher rate of anastomotic leaks, particularly at the distal end of the incision, but improved functional results compared with a straight coloanal anastomosis.^{8,9}

All types of coloanal anastomoses can be complicated by anastomotic leaks and associated abscesses (Fig. 63-12).

Abdominoperineal Resection

Lesions involving the anal sphincter complex usually require an abdominoperineal resection. In this procedure, the rectum and anal sphincter complex are removed via an abdominal and perineal approach, with creation of a permanent colostomy. Major radiologic complications are related to abdominal or pelvic abscesses.¹⁰ Colostomy complications can also arise, similar to those discussed earlier.

Hartmann Procedure

During the Hartmann procedure, a tumor or segment of sigmoid diverticulitis is resected, an end colostomy is created, and the distal rectal stump is closed by stapled sutures or sewn by hand (Fig. 63-13). The resulting Hartmann pouch becomes a blind segment of colon from the anus to the sealed stump. The procedure is used when a primary reanastomosis is thought

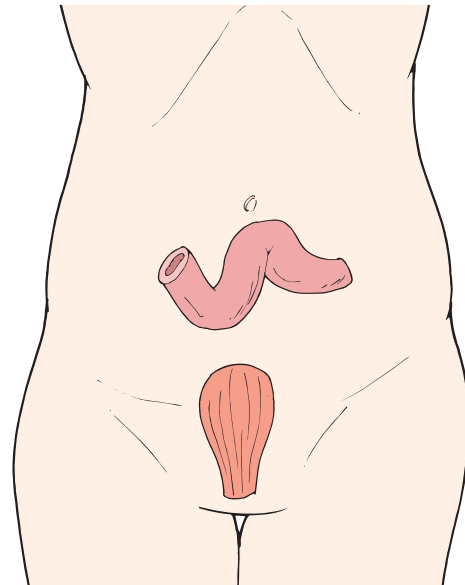


Figure 63-13 Closed rectal pouch. This line drawing shows a Hartmann pouch with a terminal ileostomy.

to be unsafe and is usually performed with complicated diverticulitis, but may also be performed for other indications, including colon and rectal cancers, inflammatory bowel disease, and trauma. Bowel continuity can subsequently be reestablished by a colorectal anastomosis. In some patients, however, the surgeon may elect not to reestablish continuity for medical or technical reasons. The blind pouch normally may contain fecal debris, inspissated mucus, or enteroliths. Polyps or carcinoma can also develop in this segment.¹¹ Patients may be asymptomatic until the tumor has become far advanced. Although the classic Hartmann pouch involves only a portion of the rectum, in practice the pouch may be much longer and include part or all of the sigmoid colon. A Hartmann pouch may also be created after total colectomy and creation of an ileostomy for Crohn's disease or ulcerative colitis.

Mucous Fistula

Rather than closing off the rectal stump, a rectosigmoid stoma or mucous fistula may be created by bringing out the proximal cut end of the distal sigmoid colon or rectum, which results in a stoma that produces only mucus. The distal colon extends from the stoma of the mucous fistula distally to the anus.

Appendectomy

Appendectomy is a procedure in which the appendix is tied at its junction with the cecum and is resected. The stump is ligated and inverted. Occasionally, this operation may produce a sizable, smooth polypoid defect at the base of the cecum (Fig. 63-14). A history of appendectomy and the typical location of the defect at the apex of the cecum should help prevent a mistaken diagnosis of cecal polyp. Nodularity, mucosal disruption, or a location away from the cecal apex should arouse suspicion that it is a true polyp requiring colonoscopic evaluation.

Ileal Pouch–Anal Anastomosis

Ileal pouch–anal anastomosis is performed in patients who have ulcerative colitis (see Chapter 57) or familial polyposis (see Chapter 61).^{12,13} It is an alternative to proctocolectomy that offers the potential for nearly normal defecation through an intact anus. Careful radiographic and clinical evaluation of the patient to exclude Crohn's disease is essential. Patients with Crohn's disease may not tolerate extensive pelvic surgery, and perineal fistulas and sinus tracts, inflammation of the pouch, and anastomotic strictures may develop. The procedure consists of colectomy, mucosal proctectomy, and creation of a small bowel reservoir. The colon and most of the rectum are removed, leaving the distal portion of the rectum in place. The mucosa is dissected from this rectal remnant, leaving a cuff of denuded rectum with intact muscularis propria, based on the concept that the intact sensory innervation of this segment enables the patient to sense bowel distention and have the urge to

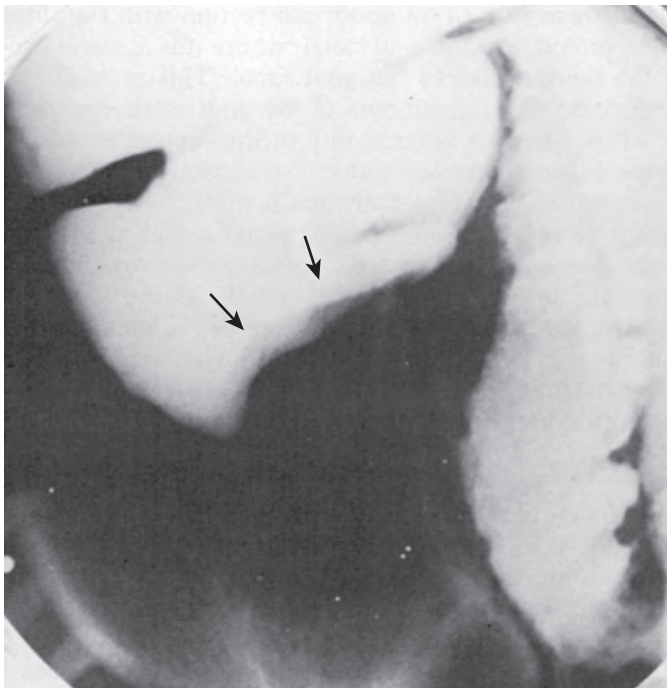


Figure 63-14 Appendiceal stump deformity. A broad-based defect (arrows) at the apex of the cecum is caused by a previous appendectomy. Most appendectomies produce minimal or no deformity of the cecum.

defecate. Although bowel movements may be increased in frequency, patients may need to defecate no more often than they normally urinate. Some patients have nocturnal soiling, but the quality of life of patients who had ulcerative colitis is greatly enhanced, and the risk of developing colonic carcinoma is eliminated.

The most common pouch is a J pouch, although an S or side-to-side (Fonkalsrud) pouch may be created (Fig. 63-15). The J pouch is formed when the distal ileum is closed and the ileum is doubled on itself, forming a J configuration. The apposed walls of the two limbs are stapled to each other, and the two segments are opened, creating a pouch that has the volume of two limbs (Fig. 63-16). The staples delineate the length of the pouch. The pouch is placed into the rectal cuff, a hole is created at the apex of the pouch, and the pouch is stapled to the anal mucosa.

The S pouch is created by apposing and suturing three limbs of the distal ileum to each other. The common walls are opened, creating a pouch with the diameter of three segments of small bowel. This pouch and the Fonkalsrud pouch have an efferent limb that is brought into the rectal cuff, and its mucosa is sutured to the dentate line of the anal canal.

The Fonkalsrud pouch is created by resecting a segment of the distal ileum. This segment is placed next to another loop of ileum, and a side-to-side anastomosis is created.

The ileal pouch–anal anastomosis procedure is usually performed in two stages. The first stage consists of a total colectomy, creation of the pouch and pouch–anal anastomosis, and creation of a protective diverting ileostomy. The second stage is ileostomy closure, which is performed after a period of 6 to 8 weeks, allowing suture lines to mature. Before closure, the surgeon examines the anorectum. If the anorectum is normal, a barium enema is performed to rule out small leaks from the pouch staple lines or pouch–anal anastomosis. If the clinical examination is abnormal, the barium enema is delayed or CT is performed. Abscesses tend to occur later and are best seen on CT examination.

A three-stage procedure may be required when the patient is weakened by fulminant colitis and is receiving high-dose corticosteroid therapy. The first stage consists of creation of a simple ileostomy, colectomy, and Hartmann closure of the rectum. The second stage is performed several months later, when healing and recovery of electrolyte and endocrine integrity have occurred (usually after corticosteroid withdrawal). The remainder of the rectum is resected, mucosal proctectomy is performed, and a pouch with pouch–anal anastomosis is created. The third stage is closure of the ileostomy 6 to 8 weeks later.

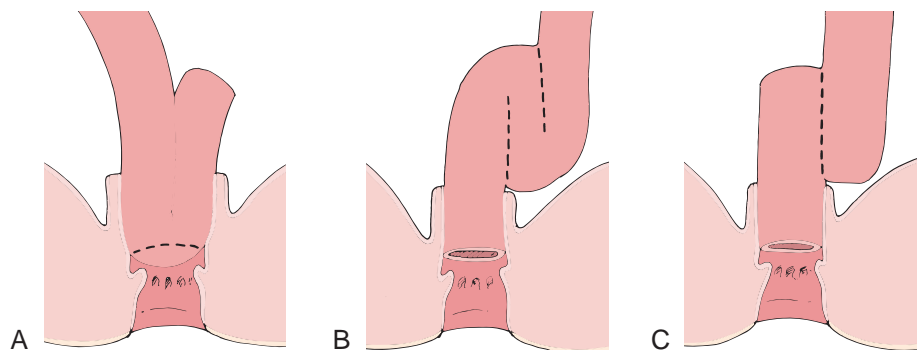


Figure 63-15 Three major types of ileal pouch–anal anastomosis. A. J pouch. B. S pouch. C. Side-to-side (Fonkalsrud) pouch.

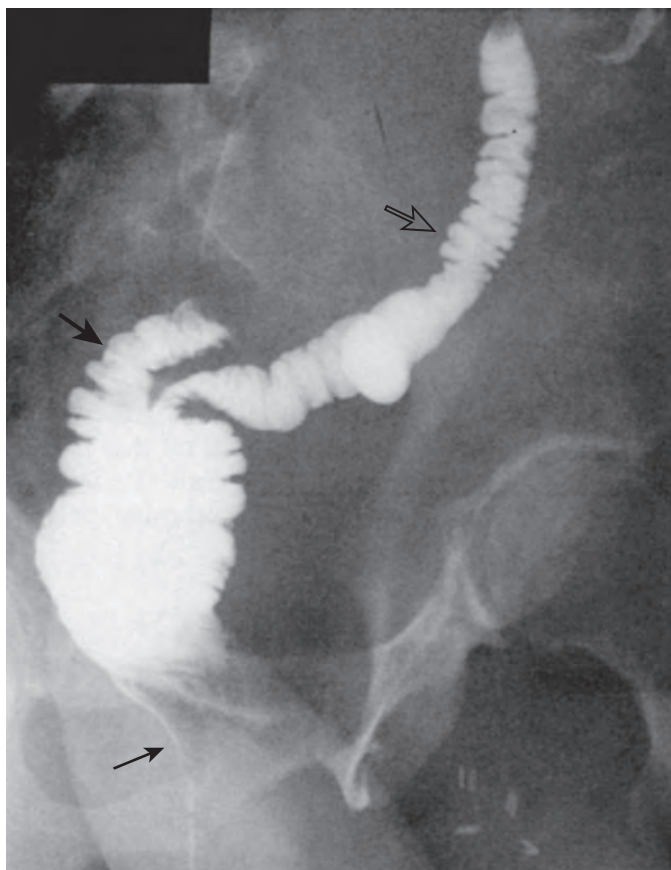


Figure 63-16 Normal J-pouch reservoir before closure of the diverting ileostomy. Note the long J-pouch appendage (top solid arrow) and the efferent limb (open arrow) leading from the ileostomy to the pouch. In this supine oblique view, air is present (bottom solid arrow) in the anterior portion of the pouch at the pouch–anal anastomotic region. Contrast material should be positioned at the pouch–anal anastomosis by placing the patient in a 45-degree erect position or turning the patient toward the prone position until air is displaced by contrast material.

Any of the complications that attend all major abdominal operations may develop after ileal pouch–anal anastomosis, including abscesses, ileus, or small bowel obstruction.^{14,15} The small bowel mesentery limits mobility of the ileum, and the small bowel may have to be manipulated extensively to create the ileal pouch–anal anastomosis. This manipulation may contribute to the prolonged ileus seen in some patients. Small bowel obstruction may develop in the immediate postoperative period, in the period between creation of the pouch and closure of the ileostomy, or at any time during the remainder of the patient's life. A mesenteric hematoma may occur if small mesenteric vessels rupture because of manipulation of or prolonged tension on the mesentery. The superior mesenteric artery syndrome can develop if tension placed on the mesentery in an attempt to position the pouch in the lowest portion of the pelvis retracts the superior mesenteric artery against the aorta.^{15,16} Prophylactic release of the small bowel mesentery at the ligament of Treitz, mesenteric lengthening incisions, and judicious suturing and resection of stretched branch mesenteric vessels facilitate mobilization of the terminal ileal pouch into the pelvis.¹⁷

Although leakage may occur from the suture lines of the pouch (Fig. 63-17), this complication usually occurs at the ileal

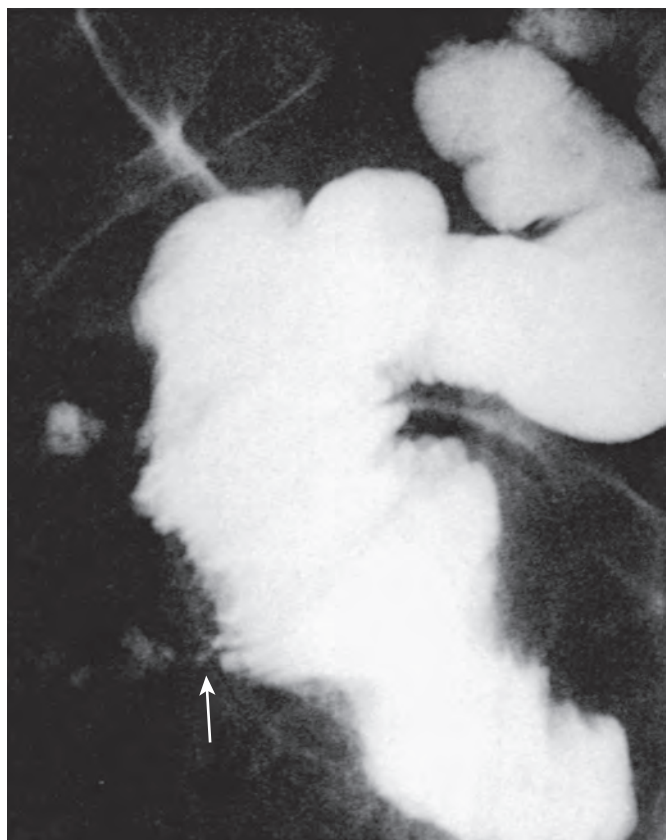


Figure 63-17 Pouch leak. Leakage (arrow) from a J-pouch reservoir with a presacral fistula and collection.

pouch–anal anastomosis (Figs. 63-18 and 63-19). Anteroposterior, oblique, and lateral views of the distended, gas-free pouch in a 30- to 45-degree upright position must be obtained low enough to include the ileal pouch–anal canal junction. CT scans may also depict pouch leaks (Fig. 63-20). Leakage from the pouch or from the ileal pouch–anal anastomosis requires that closure of the diverting ileostomy be postponed until healing of the leak has been confirmed. Small leaks and collections may be treated by endoscopic drainage, suturing, or antibiotic therapy if they do not resolve spontaneously.¹⁸ A small length of closed reflected ileum often is not incorporated into the J pouch, termed the *J-pouch appendage* (Fig. 63-21; see also Fig. 63-16). This appendage may leak, may be long enough to twist and necrose, or may simulate leakage (see Fig. 63-21).¹⁹ The S pouch and Fonkalsrud pouch have efferent limbs that pass from the pouch to the anus. These pouches, when distended with fecal contents, may compress the efferent limb and interfere with pouch emptying. Some patients with this condition succeed in emptying their pouch by self-catheterization.

Patients who tolerate the complete procedure may return with so-called pouchitis, complaining of tenesmus and diarrhea and, rarely, with bleeding, fever, arthralgias, and other systemic symptoms.^{20,21} Endoscopic examination of the pouch may reveal redness and ulceration.²² Pouchitis is not associated with consistent radiographic findings, and its cause is unknown.

With time, accommodation of the small bowel to the pouch leads to an increased capacity and small bowel dilation, which can simulate small bowel obstruction on abdominal radiographs. When clinical and radiographic findings are confusing,

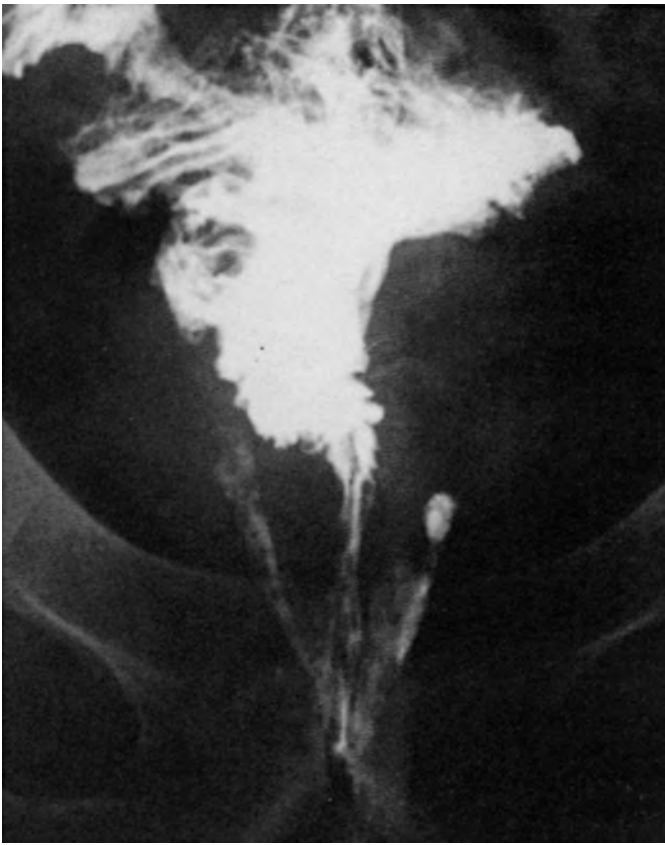


Figure 63-18 Pouch leak. Leakage from the J-pouch–anal anastomosis of a J-pouch reservoir is seen. Leakage from any anal anastomosis has a typical chevron appearance resulting from tracking of the extravasated contrast material between the rectal cuff and the pouch or efferent limb inserted into the cuff. (From Kremers PW, Scholz FJ, Schoetz DJ Jr, et al: *Radiology of the ileoanal reservoir*. AJR 145:559–567, 1985.)



Figure 63-20 CT scan of pouch leak. CT scan with oral and IV contrast depicts a leak (arrows) at the pouch–anal anastomosis on this coronal reformatted image.

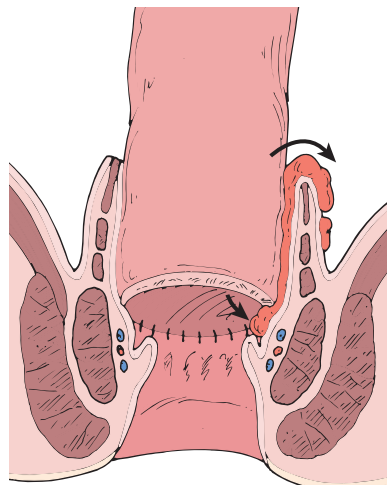
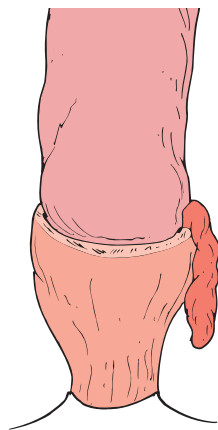


Figure 63-19 Chevron configuration of ileoanal anastomotic leak. Diagrammatic illustration of the mechanism of extravasation from a pouch–anal anastomosis. *Right*, Mucus (or contrast material) passes from the point of disruption (short curved arrow) and courses between the cuff and the cuff of rectum, producing the chevron configuration seen in [Figure 63-18](#). Purulent material eventually dissects beyond the cuff and spills (long curved arrow) into the perirectal soft tissues. (From Kremers PW, Scholz FJ, Schoetz DJ Jr, et al: *Radiology of the ileoanal reservoir*. AJR 145:559–567, 1985.)

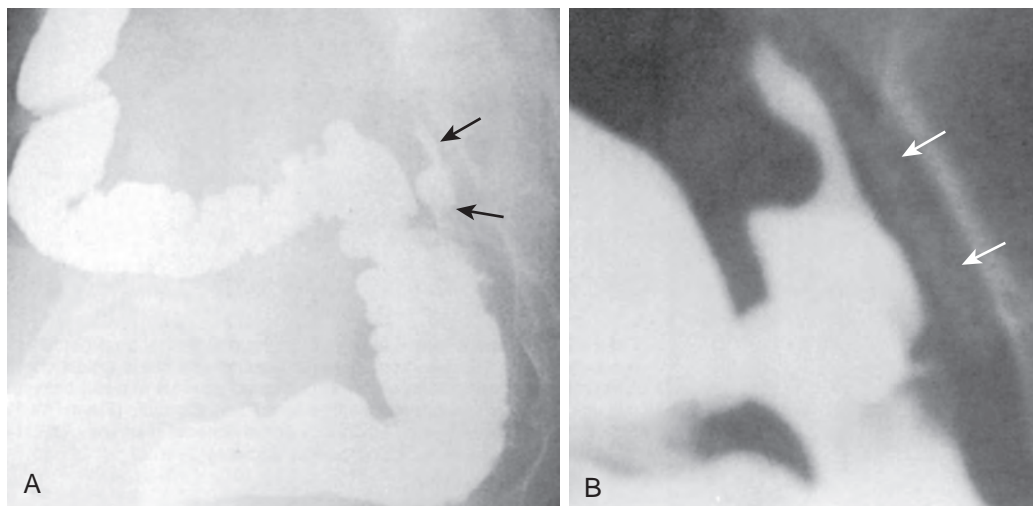


Figure 63-21 Pseudoleakage. This appearance is commonly seen with a J-pouch reservoir in which there is incomplete filling of the J-pouch appendage and represents a potential radiographic pitfall. **A.** Traces of contrast material (arrows) appear to extravasate from the proximal posterior part of the J-pouch reservoir. **B.** Additional spot image with further distention shows contrast material surrounded by a faintly visible suture line (arrows) just anterior to the sacrum. The lateral view also demonstrates the anterior position of the lower portion of the pouch, which traps air in the supine position, impairing visualization of the J pouch–anal anastomosis. (From Kremers PW, Scholz FJ, Schoetz DJ Jr, et al: *Radiology of the ileoanal reservoir*. AJR 145:559–567, 1985.)

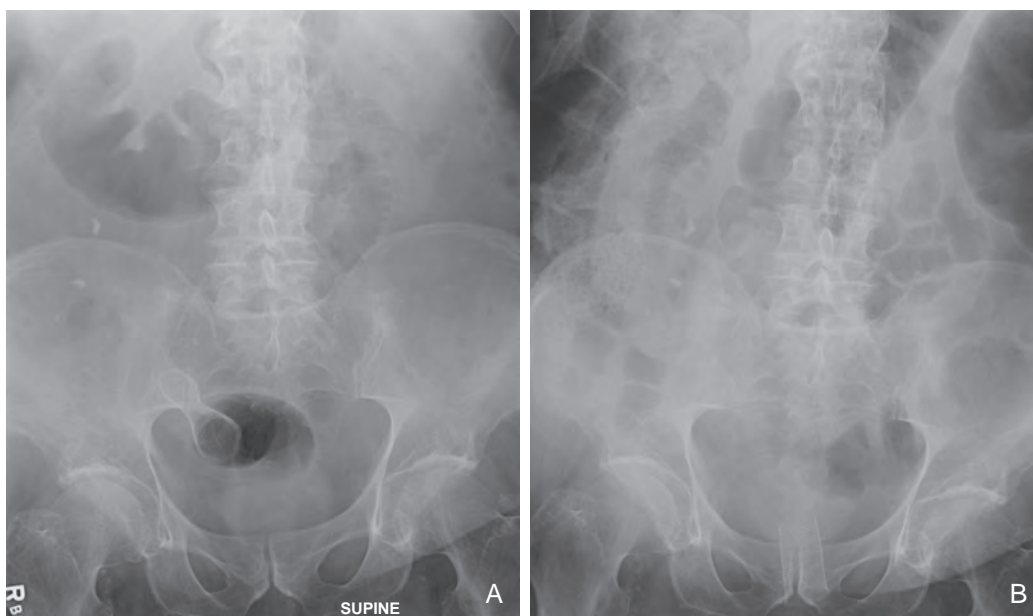


Figure 63-22 Colonic stent. **A.** Normal appearance of stent with central waistlike narrowing. **B.** Recurrent large bowel obstruction with migrated colonic stent currently located in distal rectum. Note the absence of waistlike narrowing.

enteroclysis or retrograde small bowel enema examination may be required to rule out mechanical obstruction.

Occasionally, patients post–pouch procedure for ulcerative colitis return years later with symptoms and are found by radiography to have small bowel Crohn's disease. Further review of the original pathology may show sparse granulomas in the colon.

Colonic Stents

Colonic stents are sometimes placed for treatment of large bowel obstruction.^{23,24} These procedures are usually palliative and are

performed in patients with colon cancer or obstructing colonic metastases whose condition is deemed unresectable or who are unable to tolerate definitive resection. On occasion, stents are a temporal bridge to definitive colonic resection, avoiding emergency surgery. Obstructing lesions are traversed with a guide wire, and metallic stents are deployed to relieve the obstruction. Postprocedural radiographs demonstrate waistlike midstent narrowing that indicates satisfactory placement across the stricture (Fig. 63-22A). The most common complications of colon stent placement seen on radiographic studies include perforation, stent migration (Fig. 63-22B), and recurrent obstruction.²⁵

REFERENCES

1. Wolff BG, Fleshman JW, Beck DE: The ASCRS Textbook of Colon and Rectal Surgery, New York, 2007, Springer.
2. Benyon J, Carr ND: Progress in Colorectal Surgery, New York, 2006, Springer.
3. Killingback M: Colorectal Surgery: Living Pathology in the Operating Room, New York, 2006, Springer.
4. Phillips RKS: Colorectal Surgery: A Companion to Specialist Surgical Practice, New York, 2005, Elsevier.
5. Lechner GL, Frank W, Jantsch H, et al: Lymphoid follicular hyperplasia in excluded colonic segments: A radiologic sign of diversion colitis. *Radiology* 176:135–136, 1990.
6. Parc R, Tiret E, Frileux P, et al: Resection and coloanal anastomosis with colonic reservoir for rectal carcinoma. *Br J Surg* 73:139–141, 1986.
7. Lazorthes F, Fages P, Chiotasso P, et al: Resection of the rectum with construction of a colonic reservoir and coloanal anastomosis for carcinoma of the rectum. *Br J Surg* 73:136–138, 1986.
8. Ho YH, Brown S, Heah SM, et al: Comparison of J-pouch and coloplasty pouch for low rectal cancers: A randomized, controlled trial investigating functional results and comparative anastomotic leak rates. *Ann Surg* 236:49–55, 2002.
9. Remzi FH, Fazio VW, Gorgun E, et al: Quality of life, functional outcome, and complications of coloplasty pouch after low anterior resection. *Dis Colon Rectum* 48:735–743, 2005.
10. Murrell ZA, Dixon MR, Vargas H, et al: Contemporary indications for and early outcomes of abdominoperineal resection. *Am Surg* 71:837–840, 2005.
11. Haas PA, Fox TA, Jr: The fate of the forgotten rectal pouch after Hartmann's procedure without reconstruction. *Am J Surg* 159:106–110, discussion 110–111, 1990.
12. Schoetz DJ, Jr, Collier JA, Veidenheimer MC: Proctocolectomy with ileoanal reservoir: An alternative to permanent ileostomy. *Postgrad Med* 75:123–127, 130–132, 137–138, 1984.
13. Schoetz DJ, Jr, Collier JA, Veidenheimer MC: Ileoanal reservoir for ulcerative colitis and familial polyposis. *Arch Surg* 121:404–409, 1986.
14. Hillard AE, Mann FA, Becker JM, Nelson JA: The ileoanal J pouch: Radiographic evaluation. *Radiology* 155:591–594, 1985.
15. Kremers PW, Scholz FJ, Schoetz DJ, Jr, et al: Radiology of the ileoanal reservoir. *AJR* 145:559–567, 1985.
16. Ballantyne GH, Graham SM, Hammers L, Modlin IM: Superior mesenteric artery syndrome following ileal J-pouch anal anastomosis: An iatrogenic cause of early postoperative obstruction. *Dis Colon Rectum* 30:472–474, 1987.
17. Burnstein MJ, Schoetz DJ, Jr, Collier JA, Veidenheimer MC: Technique of mesenteric lengthening in ileal reservoir-anal anastomosis. *Dis Colon Rectum* 30:863–866, 1987.
18. Schoetz DJ, Jr, Collier JA, Veidenheimer MC: Can the pouch be saved? *Dis Colon Rectum* 31:671–675, 1988.
19. Pezim ME, Taylor BA, Davis CJ, Beart RW, Jr: Perforation of terminal ileal appendage of J-pelvic ileal reservoir. *Dis Colon Rectum* 30:161–163, 1987.
20. Franceschi D, Chen PF, Yuh JN: Solitary J-pouch ulcer causing pouchitis-like syndrome. *Dis Colon Rectum* 29:515–517, 1986.
21. Iwata T, Yamamoto T, Umegae S, et al: Pouchitis and pre-pouch ileitis developed after restorative proctocolectomy for ulcerative colitis: A case report. *World J Gastroenterol* 13:643–646, 2007.
22. Stucchi AF, Aarons CB, Becker JM: Surgical approaches to cancer in patients who have inflammatory bowel disease. *Gastroenterol Clin North Am* 35:641–673, 2006.
23. Soto S, Lopez-Roses L, Gonzalez-Ramirez A, et al: Endoscopic treatment of acute colorectal obstruction with self-expandable metallic stents: Experience in a community hospital. *Surg Endosc* 20:1072–1076, 2006.
24. Dafnis G: Repeated coaxial colonic stenting in the palliative management of benign colonic obstruction. *Eur J Gastroenterol Hepatol* 19:83–86, 2007.
25. Watt AM, Faragher IG, Griffin TT, et al: Self-expanding metallic stents for relieving malignant colorectal obstruction: A systematic review. *Ann Surg* 246:24–30, 2007.

Colon: Differential Diagnosis

RICHARD M. GORE

CHAPTER OUTLINE

- | | |
|---|---|
| Table 64-1. Multiple Colonic Filling Defects | Table 64-19. Rectovaginal Fistula |
| Table 64-2. Solitary Colonic Filling Defects | Table 64-20. Double Tracking in the Sigmoid Colon |
| Table 64-3. Mosaic-Submucosal Edema Pattern | Table 64-21. Colonic Thumbprinting |
| Table 64-4. Segmental Colonic Narrowing | Table 64-22. Large Lymphoid Follicles |
| Table 64-5. Annular "Apple-Core" Colonic Lesion | Table 64-23. Aphthoid Ulcerations |
| Table 64-6. Causes of Large Bowel Obstruction in an Adult | Table 64-24. Ulcerative Colonic Lesions |
| Table 64-7. Intestinal Pseudo-Obstruction: Ogilvie's Syndrome | Table 64-25. Smooth Colon |
| Table 64-8. Colon Distention Without Obstruction | Table 64-26. Pericolonic Abscess |
| Table 64-9. Large Bowel Obstruction in a Newborn | Table 64-27. Widened Presacral Space |
| Table 64-10. Intestinal Obstruction in a Postneonatal Child | Table 64-28. Anterior Indentation on the Rectosigmoid Junction |
| Table 64-11. Toxic Megacolon | Table 64-29. Congenital Syndromes Associated with Colonic Malrotation |
| Table 64-12. Enlarged Ileocecal Valve | Table 64-30. Mural Thickening of the Colon on Computed Tomography, Ultrasound, and Magnetic Resonance Imaging |
| Table 64-13. Appendiceal Lesions | Table 64-31. "Bull's-Eye" Lesions |
| Table 64-14. Coned Cecum | Table 64-32. Microcolon |
| Table 64-15. Cecal Filling Defects | Table 64-33. Colon Cutoff Sign |
| Table 64-16. Gas in the Colon Wall | Table 64-34. Classification Scheme for Mural Thickening of the Gastrointestinal Tract |
| Table 64-17. Pneumatosis Cystoides Coli (Non-Necrotizing) | |
| Table 64-18. Fistula Involving the Colon | |

TABLE 64-1 Multiple Colonic Filling Defects

Artifacts
Feces
Mucus strands
Oil droplets
Ingested foreign bodies
Air bubbles
Neoplasms and Tumors
Multiple adenomatous polyps
Hemangiomas
Familial adenomatous polyposis
Cronkhite-Canada syndrome
Disseminated gastrointestinal polyposis
Juvenile polyposis coli
Turcot's syndrome
Neurocrest and colonic tumors
Ruvalcaba-Myhre-Smith syndrome
Lymphoma
Metastases
Multiple adenocarcinomas
Cowden's syndrome
Leukemic infiltration
Blue nevus syndrome
Neurofibromas, neurofibromatosis
INFLAMMATORY DISORDERS
Ulcerative colitis
Crohn's disease
Diversion colitis
<i>Colitis cystica profunda</i>
<i>Malacoplakia</i>
Behçet's syndrome
INFECTIOUS DISORDERS
Pseudomembranous colitis
Amebiasis
Schistosomiasis
Trichuriasis
<i>Strongyloides</i> infection
Cytomegalovirus infection
Ascariasis
Herpes zoster
MISCELLANEOUS DISORDERS
Lymphoid follicular pattern
Nodular lymphoid hyperplasia
Hemorrhoids
Diverticula
Pneumatosis intestinalis
Cystic fibrosis
Endometriosis
Colonic varices
Amyloidosis
Hemangiomas
Urticaria

TABLE 64-2 Solitary Colonic Filling Defects

BENIGN TUMORS
Hyperplastic polyp
Adenomatous polyp
Villous adenoma
Villoglandular polyp
Hamartoma
Peutz-Jeghers polyp
Spindle cell tumor (lipoma, gastrointestinal stromal tumor, fibroma, neurofibroma, cystic lymphangioma)
Traumatic neuroma
Carcinoid tumor
MALIGNANT TUMORS
Carcinoma
Lymphoma
Metastases
Kaposi's sarcoma
INFECTIOUS DISORDERS
Ameboma
Tuberculosis
Mucormycosis
Periappendiceal abscess
Diverticular abscess
Schistosomiasis (polypoid granuloma)
<i>Ascaris lumbricoides</i> (bolus of worms) infection
Intramural hematoma
INFLAMMATORY DISORDERS
Colitis cystica profunda
Solitary rectal ulcer syndrome
Foreign body perforation and abscess
Crohn's disease
MISCELLANEOUS DISORDERS
Endometrioma
Intussusception
Bezoar
Suture granuloma
Inverted appendiceal stump
Hypertrophied anal papilla
Stool, vegetable material
Amyloidosis
Varix, hemorrhoid

TABLE 64-3 Mosaic-Submucosal Edema Pattern

Obstructive colon cancer
Colonic urticaria
Herpes zoster
Ischemia
Cecal volvulus
Colonic ileus
<i>Yersinia</i> infection

TABLE
64-4**Segmental Colonic Narrowing****MALIGNANT DISORDERS**

Primary adenocarcinoma
Metastases
Kaposi's sarcoma
Lymphoma
Carcinoma
Carcinoid
Direct spread from renal, duodenal, pancreatic, ovarian tumor

INFLAMMATORY DISORDERS

Crohn's disease
Ulcerative colitis
Cathartic colon
Caustic colon
Retractile mesenteritis
Typhlitis
Solitary rectal ulcer syndrome

INFECTIOUS DISORDERS

Amebiasis
Schistosomiasis
Strongyloides infection
Tuberculosis
Gonorrheal proctitis
Chlamydia infection (lymphogranuloma venereum)
Herpes zoster
Cytomegalovirus infection
Bacillary dysentery
Actinomycosis
Giant anorectal condyloma acuminatum
Pericolic abscess

VASCULAR DISORDERS

Ischemic colitis
Radiation colitis
Intramural hematoma

MISCELLANEOUS DISORDERS

Pancreatitis
Pelvic lipomatosis
Endometriosis
Amyloidosis
Adhesive band
Postoperative deformity
Myochosis

TABLE
64-6**Causes of Large Bowel Obstruction in an Adult****INFLAMMATORY DISORDERS**

Diverticulitis
Inflammatory bowel disease
Retractile mesenteritis

INFECTIOUS DISORDERS

Ascaris bolus
Chagas' disease
Amebiasis
Schistosomiasis
Actinomycosis
Tuberculosis

EXTRINSIC BOWEL LESIONS

Adhesions
Hernias
Volvulus
Endometriosis
Neoplasms
Appendiceal abscess
Tubo-ovarian abscess
Distended bladder

NEOPLASTIC LESIONS

Adenocarcinoma of the colon
Lymphoma
Spindle cell tumor
Gastrointestinal stromal tumor
Carcinoid
Metastases

VASCULAR DISORDERS

Intramural hematoma
Vascular occlusion, infarction

OBTURATION OF LUMEN

Bezoar
Gallstone
Enterolith
Fecal impaction
Foreign body
Intussusception

MISCELLANEOUS DISORDERS

Amyloidosis
Colonic pseudo-obstruction

TABLE
64-5**Annular "Apple-Core" Colonic Lesion**

Carcinoma
Diverticulitis
Chronic Crohn's disease
Chronic ulcerative colitis
Ischemic colitis
Chlamydia infection (lymphogranuloma venereum)
Lymphoma
Tuberculosis
Villous adenoma
Helminthoma
Ameboma

**TABLE
64-7****Intestinal Pseudo-Obstruction: Ogilvie's Syndrome**

DRUG REACTION Phenothiazine Antidepressants Morphine Antiparkinsonian	NEUROMUSCULAR DISORDERS Parkinson's disease Chagas' disease Myotonic dystrophy
PARALYTIC ILEUS Hypokalemia Pancreatitis Pneumonia Myocardial infarction Trauma	MISCELLANEOUS DISORDERS Amyloidosis Sprue Scleroderma Retractile mesenteritis Vitamin D deficiency
ENDOCRINE DISEASE Myxedema Diabetes Hypoparathyroidism Pheochromocytoma	

**TABLE
64-8****Colon Distention Without Obstruction**

PARALYTIC ILEUS After operation Peritonitis Appendicitis Pancreatitis	TRAUMA Spinal cord injury Intramural hematoma Lower rib injury Retroperitoneal hemorrhage
ELECTROLYTE IMBALANCE Hypokalemia Hypochloremia Calcium abnormality	URINARY TRACT DISORDERS Ureteral colic Renal failure, uremia Urine retention
ENDOCRINE DISORDERS Diabetes Adrenal insufficiency Myxedema Hypoparathyroidism	COLLAGEN-VASCULAR DISEASE Scleroderma Dermatomyositis Polyarteritis nodosa Kawasaki's syndrome
NEUROMUSCULAR DISORDERS Hirschsprung's disease Parkinson's disease Multiple sclerosis Riley-Day syndrome Amyotonia congenita Chagas' disease	ACUTE THORACIC DISEASE Myocardial infarction Congestive heart failure
DRUG THERAPY Morphine, L-dopa, chlorpromazine, benztropine, atropine, propantheline bromide Hexamethonium	MISCELLANEOUS DISORDERS Chronic constipation Chronic laxative, cathartic abuse Aerophagia Mesenteric infarction Shock Septicemia Toxic megacolon Cystic fibrosis Amyloidosis

**TABLE
64-9****Large Bowel Obstruction in a Newborn**

Hernia, incarcerated, internal or external Congenital stenosis or atresia Hernia, incarcerated, internal or external Hirschsprung's disease Imperforate anus Rectal atresia Intussusception Midgut volvulus with malrotation Small left colon syndrome Megacystis-microcolon syndrome Intraluminal web, diaphragm, or band Duplication

**TABLE
64-10****Intestinal Obstruction in a Postneonatal Child**

Hirschsprung's disease Imperforate anus with fistula Hernia Appendicitis Duplication Intussusception Midgut volvulus Tuberculosis Cystic fibrosis Crohn's disease Fecal impaction Foreign body, bezoar Ascaris bolus Neoplasm
--

TABLE 64-11 Toxic Megacolon

Bacillary dysentery
 Pseudomembranous colitis
 Ulcerative colitis
 Crohn's disease
 Ischemic colitis
 Amebic colitis
 Bacillary dysentery
 Typhoid fever
 Cholera
 Strongyloidiasis
Campylobacter colitis
 Pseudomembranous colitis
 Behçet's disease

TABLE 64-12 Enlarged Ileocecal Valve

Normal variant
 Crohn's disease
 Amebiasis
 Fatty infiltration, lipoma
 Intussusception
 Villous adenoma
 Adenocarcinoma
 Lymphoma
Yersinia enterocolitis
 Actinomycosis
 Cathartic abuse
 Tuberculosis
 Typhoid fever
 Intramural hematoma
 Anisakiasis
 Ileocolic prolapse
 Carcinoid
 Lymphoid hyperplasia

TABLE 64-13 Appendiceal Lesions

After operation (inverted stump, adhesions)
 Abscess
 Acute appendicitis
 Calculus, fecalith
 Crohn's disease
 Metastasis
 Intussusception, invagination
 Endometrial implantation
 Mucocele
 Myxoglobulosis
 Adenocarcinoma
 Spindle cell tumor
 Carcinoid tumor
 Diverticulosis
 Amebiasis
 Ascariasis
 Ulcerative colitis
 Tuberculosis
 Lymphoma
 Trichuriasis
 Typhoid fever

TABLE 64-14 Coned Cecum

Crohn's disease
 Amebiasis
 Appendicitis
 Carcinoma of the cecum
 Ulcerative colitis
 Diverticulitis
 Cathartic abuse
 Actinomycosis
 Tuberculosis
 Metastasis
 Anisakiasis
 Typhoid fever
Yersinia enterocolitis
 Cytomegalovirus infection
 Typhlitis
 Radiation therapy
 South American blastomycosis

TABLE 64-15 Cecal Filling Defects

Appendiceal lesions
 Metastases (pancreas, ovary, colon, stomach)
 General causes of colonic filling defects
 Intussusception of appendix, Meckel's diverticulum, lymphoma, distal ileum
 Diverticulitis
 Endometriosis
 Solitary benign ulcer
 Adherent fecalith (cystic fibrosis)
 Burkitt's lymphoma
 Ameboma
 Lipomatous ileocecal valve

TABLE 64-16 Gas in the Colon Wall

Ischemic colitis
 Necrotizing enterocolitis
 Pseudomembranous colitis
 Toxic megacolon
 Large bowel obstruction
 Inflammatory bowel disease
 Molecular targeted therapy

TABLE 64-17 Pneumatosis Cystoides Coli (Non-Necrotizing)

Colonoscopy
 Colonic irrigation or enema
 Pneumomediastinum with abdominal extension
 Emphysema, asthma
 Molecular targeted therapy
 Scleroderma
 Dermatomyositis
 Juvenile rheumatoid arthritis
 Pyloric obstruction
 Imperforate anus
 Hirschsprung's disease
 After operation (intestinal bypass)
 Blunt abdominal trauma
 Cystic fibrosis
 Peptic ulcer with intramural perforation
 Hydrogen peroxide enema
 Inflammatory bowel disease

TABLE 64-18 **Fistula Involving the Colon****INFLAMMATORY DISORDERS**

Crohn's disease
Diverticulitis
Biliary fistula
Peptic ulcer, marginal ulcer
Aspirin, nonsteroidal anti-inflammatory drugs
Pancreatitis

INFECTIOUS DISORDERS

Actinomycosis
Pelvic inflammatory disease
Tuberculosis
Amebiasis
Chlamydia infection (lymphogranuloma venereum)
Appendiceal abscess
Renal abscess

MALIGNANT DISORDERS

Adenocarcinoma of the colon
Lymphoma
Metastasis

MISCELLANEOUS DISORDERS

After operation
Ischemic colitis
Infarction
Foreign body (pin, bone, toothpick)
Abdominal trauma
Iatrogenic trauma

TABLE 64-19 **Rectovaginal Fistula****INFLAMMATORY DISORDERS**

Crohn's disease
Diverticulitis

NEOPLASTIC DISORDERS

Carcinoma of the rectum
Carcinoma of the cervix
Carcinoma of the vagina

INFECTIOUS DISORDERS

Chlamydia infection (lymphogranuloma venereum)
Appendiceal abscess
Tubo-ovarian abscess
Actinomycosis
Schistosomiasis
Tuberculosis

TRAUMA

External
Sexual
Puerperal
Iatrogenic

MISCELLANEOUS DISORDERS

Endometriosis
Radiation therapy
Foreign body
Imperforate anus or other cloacal anomaly

TABLE 64-20 **Double Tracking in the Sigmoid Colon**

Carcinoma of the colon
Crohn's disease
Diverticulitis

TABLE 64-21 **Colonic Thumbprinting****VASCULAR DISORDERS**

Occlusive vascular disease
Intramural hemorrhage (anticoagulants, bleeding diathesis)
Traumatic intramural hematoma
Hemolytic uremic syndrome
Hereditary angioneurotic edema

INFLAMMATORY DISORDERS

Ulcerative colitis
Crohn's disease
Retractile mesenteritis

INFECTIOUS DISORDERS

Amebiasis
Schistosomiasis
Cytomegalovirus infection
Strongyloidiasis
Pseudomembranous colitis
Typhlitis
Staphylococcus colitis
Anisakiasis

NEOPLASTIC DISORDERS

Lymphoma
Hematogenous metastases

MISCELLANEOUS DISORDERS

Amyloidosis
Endometriosis
Diverticulosis or diverticulitis
Mesenteric or peritoneal lesions
Pneumatosis cystoides coli

TABLE 64-22 **Large Lymphoid Follicles****INFLAMMATORY DISORDERS**

Crohn's disease
Behçet's syndrome
Nodular lymphoid hyperplasia

INFECTIOUS DISORDERS

Campylobacter colitis
Yersinia colitis
Amebic colitis
Herpes colitis
Salmonella colitis
Shigella colitis
Tuberculosis

NEOPLASTIC DISORDERS

Lymphoma
Adenocarcinoma
Adenoma
Leukemia

IMMUNOLOGIC DISORDERS

AIDS
Immunoglobulin E deficiency

TABLE 64-23 **Aphthoid Ulcerations**

Crohn's disease
Yersinia enterocolitis
Amebic colitis
Behçet's disease
Ischemic colitis

Lymphoma
Salmonella colitis
Shigella colitis
Herpes colitis
Cytomegalovirus colitis

TABLE 64-24 Ulcerative Colonic Lesions**INFLAMMATORY DISORDERS**

Ulcerative disorders
 Crohn's disease
 Caustic colitis
 Behçet's syndrome
 Diversion colitis
 Solitary rectal ulcer syndrome
 Diverticulitis
 Pancreatitis
 Stercoral colitis

INFECTIOUS DISORDERS

Pseudomembranous colitis
 Amebiasis
Campylobacter colitis
 Schistosomiasis
 Shigellosis
 Tuberculosis
 Gonorrhea
 Staphylococcal colitis
Yersinia colitis
Chlamydia infection (lymphogranuloma venereum)
 Herpes zoster
 Herpes simplex
 Rotavirus infection
 Cytomegalovirus infection
 Strongyloidiasis
 Histoplasmosis
 Candidiasis
 Actinomycosis
 Mucormycosis

VASCULAR DISORDERS

Ischemic colitis
 Uremic colitis
 Hemolytic uremic syndrome

MALIGNANT DISORDERS

Carcinoma
 Lymphoma
 Leukemic infiltration
 Gastrointestinal stromal tumor

MISCELLANEOUS DISORDERS

Drug-induced colitis (corticosteroids, antibiotics, chemotherapy)
 Inorganic mercury poisoning
 Chemical (paraldehyde) proctitis
 Amyloidosis

TABLE 64-25 Smooth Colon

Ulcerative colitis	Amyloidosis
Crohn's disease	Radiation colitis (late)
Cathartic or enema abuse	Schistosomiasis
Ischemic colitis (late)	

TABLE 64-26 Pericolic Abscess

Diverticulitis
 Appendicitis
 Crohn's disease
 Perforated primary or metastatic neoplasm
 Tubo-ovarian abscess
 Pancreatitis
 Trauma
 Foreign body perforation
 Ischemic colitis
 Amebiasis
 Schistosomiasis
 Helminthoma
Chlamydia infection (lymphogranuloma venereum)
 Actinomycosis
 Tuberculosis
 Renal infection

TABLE 64-27 Widened Presacral Space

Normal variant

INFLAMMATORY DISORDERS

Ulcerative colitis
 Crohn's disease
 Retroperitoneal fibrosis
 Pelvic lipomatosis
 Colitis cystica profunda
 Chemical (paraldehyde) proctitis

INFECTIOUS DISORDERS

Presacral abscess
 Diverticulitis
 Appendicitis
 Tuberculosis
 Amebiasis
Chlamydia infection (lymphogranuloma venereum)
 Presacral abscess (diverticular, appendiceal)
 Gonorrheal proctitis

TUMORS

Primary rectal tumors (adenocarcinoma, lymphoma, sarcoma, cloacogenic carcinoma)
 Invasion by adjacent tumors (bladder, prostate, ovary, cervix, myeloma)
 Sacral or coccygeal neoplasm (osteogenic sarcoma, chondrosarcoma, giant cell tumor) or teratoma
 Neurogenic tumors (chordoma, neurofibroma, schwannoma)
 Lipoma
 Multiple myeloma
 Sacral metastases
 Ovarian cyst or neoplasm

VASCULAR DISORDERS

Hematoma
 Radiation fibrosis
 Inferior vena cava obstruction (pelvic edema)
 Hemorrhoidal injection

MISCELLANEOUS DISORDERS

Urinoma
 Lymphocele
 Inguinal hernia with rectal traction
 Cushing's disease
 Sacral fracture
 Duplication (tailgut) cyst
 Amyloidosis

TABLE 64-28 Anterior Indentation on the Rectosigmoid Junction

Peritoneal metastases (stomach, colon, pancreas, ovary, Blumer shelf)
 Extrinsic invasion from prostate, uterus, bladder, vagina, neoplasms
 Abscess
 Hematoma
 Ascites
 Iliac artery aneurysm
 Pelvic lipomatosis, retroperitoneal fibrosis
 Lymphadenopathy
 Surgical sling repair
 Lymphocele
 Hematocolpos

TABLE 64-29 Congenital Syndromes Associated with Colonic Malrotation

Marfan's syndrome
 Mobile cecum
 Prune-belly syndrome
 Asplenia or polysplenia
 Trisomy 21
 Thoracoabdominal wall defect
 Eagle-Barrett syndrome
 Cornelia de Lange's syndrome
 Abdominal heterotaxy

TABLE 64-30 Mural Thickening of the Colon on Computed Tomography, Ultrasound, and Magnetic Resonance Imaging**NEOPLASMS**

Carcinoma
 Lymphoma
 Polyposis syndromes
 Metastases
 Gastrointestinal stromal tumor

INFLAMMATORY DISORDERS

Ulcerative colitis
 Crohn's disease
 Behçet's disease
 Diverticulosis, diverticulitis
 Typhlitis

INFECTIOUS DISORDERS

Pseudomembranous colitis
 Amebic colitis
 Any infectious colitis

MISCELLANEOUS DISORDERS

Intussusception
 Hematoma
 Low-protein states

TABLE 64-31 "Bull's-Eye" Lesions

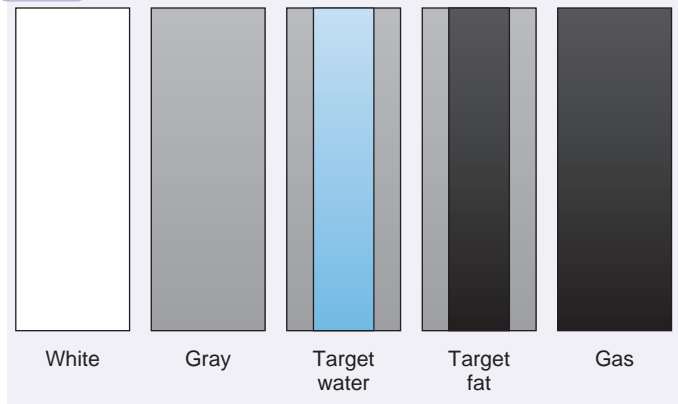
Metastases (especially melanoma)
 Kaposi's sarcoma
 Lymphoma
 Carcinoma
 Carcinoid
 Ulcerating submucosal tumor (e.g., leiomyosarcoma)

TABLE 64-32 Microcolon

Meconium ileus
 Ileal atresia
 Megacystis-microcolon-hypoperistalsis syndrome
 Colonic atresia
 Hirschsprung's disease

TABLE 64-33 Colon Cutoff Sign

Acute pancreatitis
 Ischemic colitis
 Colon obstruction
 Mesenteric thrombosis

TABLE 64-34 Classification Scheme for Mural Thickening of the Gastrointestinal Tract**SUGGESTED READINGS**

1. Eisenberg RL: Gastrointestinal Radiology: A Pattern Approach, ed 4, Philadelphia, 2003, Lippincott Williams & Wilkins.
2. Reeder MM: Reeder and Felson's Gamuts in Radiology, ed 4, New York, 2003, Springer-Verlag.
3. Dähnert W: Radiology Review Manual, ed 6, Philadelphia, 2007, Wolters Kluwer/Lippincott Williams & Wilkins.
4. Wittenberg J, Harisinghani MG, Jhaveri K, et al: Algorithmic approach to CT diagnosis of the abnormal bowel wall. Radiographics 22:1093–1107, 2002.
5. Horton KM, Corl FM, Fishman EK: CT evaluation of the colon: Inflammatory disease. Radiographics 20:399–419, 2000.
6. Lee KS, Hwang S, Rúa SM, et al: Distinguishing benign and life-threatening pneumatosis intestinalis in patients with cancer by CT imaging features. AJR Am J Roentgenol 200:1042–1047, 2013.

SECTION
VIII

**General Radiologic
Principles for
Imaging and Intervention
of the Solid Viscera**

Computed Tomography of the Solid Abdominal Organs

CECIL G. WOOD III | SENTA BERGGRUEN

CHAPTER OUTLINE

Historical Perspective

Creating the Computed Tomography Image

Data Acquisition

Image Reconstruction

Image Display

Helical Computed Tomography

Multidetector Computed Tomography

Dual-Energy Computed Tomography

Dosimetry and Dose Reduction

Intravenous Contrast Principles

Interpretation Principles

Image Postprocessing

Scanning Protocols

Abdominopelvic Survey

Computed Tomography of the Liver

Computed Tomography of the Pancreas

Future Directions

Historical Perspective

The practice of medicine has been transformed by computed tomography (CT). In recognition of the importance of this technique, Cormack and Hounsfield were awarded the Nobel Prize in 1979 for their role in its development.¹ The first clinical CT unit was placed at Atkinson Morley Hospital in England on October 1, 1971.¹ Each image took 4 minutes to be acquired, and 2 days were needed to reconstruct the series. The clinical importance of CT was immediately appreciated; by 1976, 22 companies were manufacturing CT scanners, and in 1979, more than 1000 scanners were in use throughout the world. Since then, there has been continuous and dramatic improvement in both spatial and temporal resolution as a result of advances in both hardware and software design, particularly the development of helical and multidetector helical CT and dual-energy CT.

Creating the Computed Tomography Image

The fundamental concept of CT is to use multiple projections of an object to reconstruct the internal structure of that object.^{2,3} The creation of a CT image can be divided into three steps. Data

acquisition involves the actual exposure to radiation (scanning of the patient) with the creation of raw data; image reconstruction involves processing of the raw data into a numerical matrix revealing the internal structure; and image display involves converting the numerical data matrix to a gray-scale image. Each of these is discussed with conventional CT, and then the changes created by the advent of helical and multidetector helical CT are described.

DATA ACQUISITION

An x-ray tube and an opposing array of detectors as well as the associated electronics are mounted on a track or frame called a gantry. The x-ray tube produces a fan-shaped beam of x-rays that interact with the patient by absorption or scattering; some of the x-rays pass through the patient to interact with the detector array. During data acquisition, the tube and detectors rotate around the patient, and the detectors repeatedly measure the amount of x-ray energy transmitted through the patient. The amount of x-ray energy received by the detector and the gantry angle at the time of the measurement are recorded (Fig. 65-1). Typically, the detector array contains 500 to 1000 detectors, each of which is sampled approximately 1000 times per revolution.³ Each line of this information reflects the summation of the attenuation coefficients of all structures in that x-ray path. The entire data set forms the “raw data” from which an image is reconstructed. Conventional or incremental scanning is obtained by performing a series of individual scans during suspended respiration. After each scan, the patient breathes; the table is advanced; and in most machines, the tube and detector apparatus rewinds to begin another scan.⁴

IMAGE RECONSTRUCTION

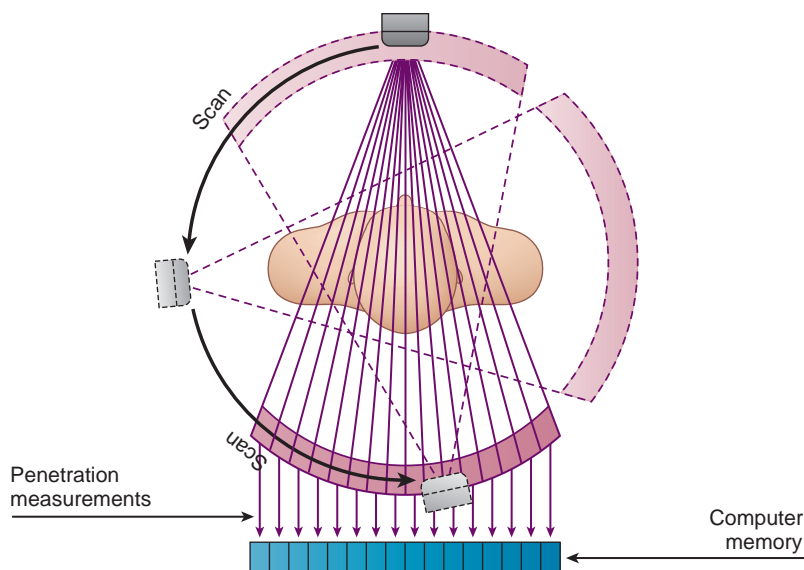
From the raw data, a digital image is created. A variety of techniques can be used to accomplish this; these rely on the principles of back projection, iterative formulas, or analytic formulas, either with or without Fourier transformation.⁵ The result is a matrix of numbers; in general, a 512×512 matrix is used in abdominopelvic CT. Each number in this matrix is called a pixel, or picture element. Each pixel corresponds to a volume of tissue or voxel within the patient; the average density of the tissue within the voxel is represented by the pixel value. The difference in attenuation of the contents of a voxel relative to water is defined as the CT attenuation number and expressed in Hounsfield units (HU).⁶

IMAGE DISPLAY

This digital image or number matrix is converted to a visual format for interpretation. A gray scale is used with the densest

Figure 65-1 Three sample positions of data measurement in obtaining a single image.

Data are collected from approximately 1000 positions during each revolution. At each position, measurements are obtained from each detector in the array; although the example shows 16 detectors, in actuality 500 to 1000 are used. The entire group of measurements forms the raw data used to reconstruct the internal structure of the scanned object. (Modified from Sprawls P: *Physical Principles of Medical Imaging*. Gaithersburg, Md, Aspen, 1987.)



materials, such as bone (highest HU), being assigned lighter shades, whereas the least dense, such as air (most negative HU), are assigned darker shades. A problem arises in that display devices are limited to demonstrating approximately 60 shades of gray, and the human eye may distinguish as few as 30 shades; the 4096 CT numbers cannot be simply mapped without conversion. The wide range of numbers is converted for display by window width and level controls. The window level specifies the centering of the gray scale, and the choice of width specifies the numbers over which the gray scale is to extend. For example, if the window level is set to 0 and the width is set to 500, every pixel number below 250 will be black and every pixel greater than 250 will be white; if there are 50 shades of gray, each would be assigned a range of 10 numbers with the middle gray used for the numbers adjacent to 0.

Helical Computed Tomography

Helical or spiral CT involves a continuous rotation of the gantry as the patient is advanced at a steady rate through it, dispensing with the discrete steps of data acquisition in conventional CT.^{4,7} This continuous rotation creates a volume set of raw data that must then be segmented to create planar images. Introduced in 1989, the technology was rapidly accepted and distributed. The major advantages of helical scanning include rapid acquisition, unlimited ability to obtain overlapping images without increased radiation exposure, high-quality multiplanar reconstruction, and absence of respiratory misregistration.⁸

Helical CT introduced several unique new concepts that the physician must understand. The first reflects the relationship between the speed of the table and the speed of the gantry. This is described as the pitch and is defined as the table feed per 360-degree tube revolution divided by the width of the collimated beam (Fig. 65-2). When the patient's movement is equal to the beam collimation, the pitch is 1. Increasing the pitch allows increased coverage in the z direction but with some increase in image noise. Use of pitches greater than 1 also decreases the radiation dose to the patient.⁷

A second important new concept introduced by helical CT is that of reconstruction increment and overlapping

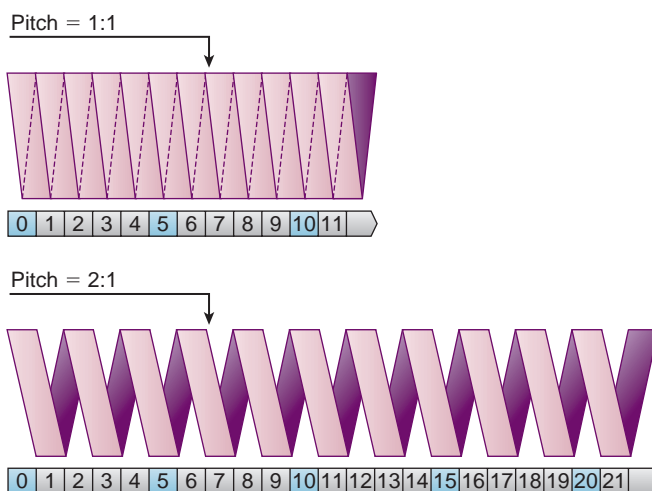


Figure 65-2 Concept of pitch (table increment per revolution of the gantry over collimation). Pitch of 1:1 (top). The table increment is a constant 1 cm/s with a collimation of 1 cm. Pitch of 2:1 (bottom). The table increment is 2 cm/s with the 1-cm collimation. Advantages of pitches greater than 1 include increased coverage (20 cm versus 10 cm in this example with a 10-second acquisition) and decreased radiation exposure. However, there is increased noise and slice profile broadening with increased pitches. In clinical scanning of the abdomen, pitches of 1.3 to 2.0 are frequently used with single-detector helical CT. (Modified from Zeman RK, Fox SH, Silverman PM, et al: *Helical [spiral] CT of the abdomen*. *AJR Am J Roentgenol* 160:719-725, 1993.)

reconstructions. As with conventional CT, once the scan has been obtained, the image thickness cannot be changed. However, because the data acquisition is continuous, the location of the image center along the z-axis may be altered. This has two practical applications: it allows overlapping reconstructions for use in postprocessing without any increase in radiation dose to the patients, and it reduces volume averaging effect, which may lead to improved detection of small lesions⁹ (Fig. 65-3).

The demand to scan faster continued despite the dramatic improvement resulting from helical CT. This demand was met by increasing the rotational speed of the gantry and increasing

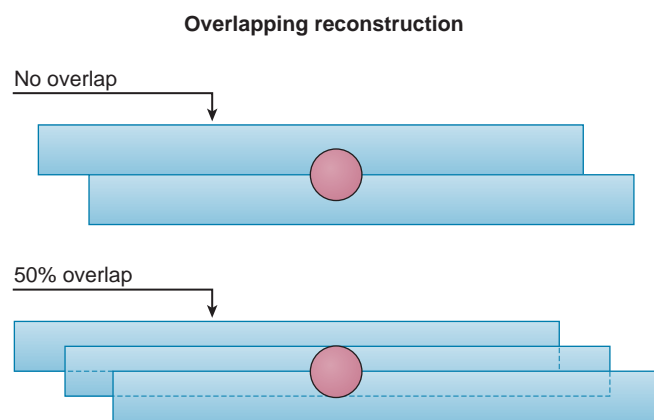


Figure 65-3 Use of overlapping images with helical CT. A small lesion may be difficult to visualize because of volume averaging effects if it is centered between two adjacent images (*upper example*), where the “nodule” is centered between the top and bottom images. With the use of a 50% overlap, the nodule would be well visualized on the middle of the three images (*lower example*). There is no additional scanning time or radiation exposure to the patient.

the number of slices obtained with each revolution.¹⁰ Rotation speed has been reduced to a fraction of a second, with most high-end scanners having speeds of less than 0.5 s/rotation. Increasing the number of slices obtained per revolution was the next evolution of CT technology: multidetector helical CT (MDCT), also called multidetector-row CT and multislice CT.¹¹

Multidetector Computed Tomography

MDCT machines segment the detector array along the z-axis of the patient, allowing multiple rows of data in this plane to be obtained simultaneously. Elscint (Haifa, Israel) introduced the first MDCT machine, a dual-slice unit, in 1992. However, it was not until several manufacturers introduced four-channel machines in 1998 that the technology exploded. The technology behind MDCT is fascinating but largely beyond the scope of this chapter. Several reviews and books have been published to which the interested reader is referred.¹²⁻¹⁵ As with other improvements in CT technology, the major advantage of multiple detector rows is an increase in performance that can be used to shorten scan duration, to increase scan range, and to improve resolution. In imaging of the solid abdominal organs, radiologists have exploited both the improved resolution and speed afforded by this new technology.¹⁶ A significant portion of the performance gain has been used to obtain images of the organs multiple times during a single bolus of contrast material.¹⁷

In discussing MDCT, it is important to distinguish between the number of channels and the number of detector rows. For example, manufacturers and radiologists often refer to 4-row or 16-row MDCT; however, this is a misnomer, and referring to 4-channel or 16-channel MDCT is more accurate. The number of data channels determines the number of data streams that can be acquired simultaneously from the detector. The number of detector rows is the number of segmented detectors in the z-axis; this number is often greater than the number of channels¹⁸ (Fig. 65-4). However, as the number of channels increases, this discrepancy decreases.

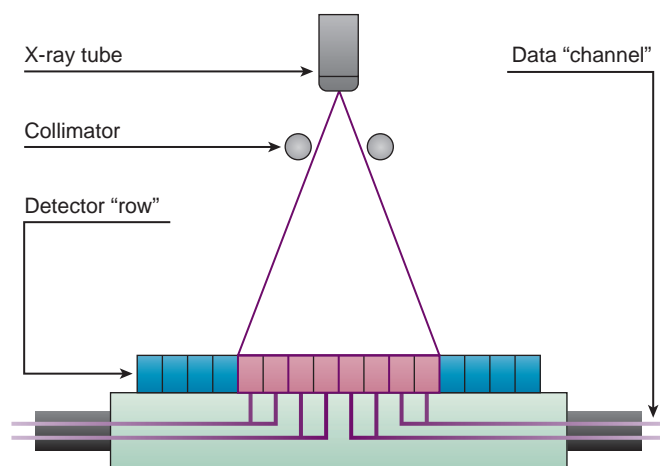


Figure 65-4 Differentiation of channel from row. Four-channel, 16-row MDCT. In this example, the blue and light purple boxes represent the 16 detector rows. The x-ray beam is collimated to expose the central eight rows. The radiation information obtained from each pair of central detector rows is combined electronically behind the detector to create four data streams, one for each of the four channels. Common usage is to refer to this as four-row MDCT, meaning four-channel MDCT.

Another important new concept must be considered with MDCT: acquisition thickness versus image thickness. Before MDCT, image thickness was an acquisition parameter. Once this was chosen and the patient was scanned, it could not be altered. However, with multidetector machines, image thickness is a reconstruction parameter; that is, one can change the image thickness after the patient has been scanned. Various reconstructed section widths are available; the number of choices varies by the manufacturer. An image cannot be created with an image width thinner than the acquisition collimation. As long as the raw data are available, additional images can be created at a different thickness.

MDCT has been used in imaging of the solid abdominal organs in several ways. There has been a reduction in slice width and scan acquisition time for routine abdomen and pelvis imaging. Scanning of a single organ, such as the liver or the pancreas, at multiple times during the rapid administration of intravenous contrast material (multiphase studies) is much easier to accomplish than on single-detector helical CT and has become part of the routine armamentarium of the radiologist. Finally, the use of very thin images during the arterial phase of injection has become helpful in CT angiography, often combined with routine images of the organ of interest.

Dual-Energy Computed Tomography

Dual-energy CT (DECT) is an emerging technology that promises to add a new dimension to CT imaging. Its utility is based on the principle that the attenuation of each element varies by the energy of the x-ray used to image it. The relationship between x-ray attenuation and x-ray energy is not linear. Rather, because of the photoelectric effect, attenuation spikes when the energy of the x-ray is at or just above the k-shell binding energy of the element. This energy level is known as the k-edge. The k-edge varies from element to element but increases with the atomic number of the element.¹⁹ DECT takes advantage of this phenomenon by imaging the patient at two different tube

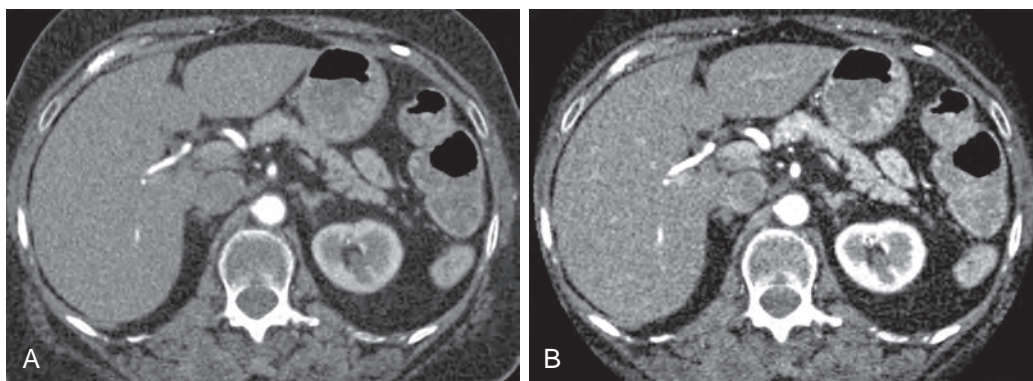


Figure 65-5 Increased attenuation of iodine at 80 kVp compared with 140 kVp. Two axial contrast-enhanced images of the abdomen obtained at the same time at 140 kVp (A) and 80 kVp (B). Note the increased attenuation of the aorta and solid organs on the 80-kVp image resulting from the increased attenuation of iodine at 80 kVp. When measured, the attenuation of the aorta increased from 420 to 835 HU. The attenuation of the pancreas increased from 119 to 184 HU.

voltages. This is accomplished either by rapidly switching the tube voltage of a single x-ray tube as it rotates around the patient (rapid switching DECT) or by imaging the patient with a pair of x-ray tubes and detectors oriented at 90 degrees to each other (dual-source DECT). The lower tube voltage is most commonly 80 kVp, and the higher voltage is 140 kVp. Whereas the energy of the x-rays emitted by the x-ray tube is a spectrum of varying energies, the lower the tube voltage, the lower the average energy of the spectrum.²⁰

By determining the attenuation of a voxel at two different tube voltages, DECT has several potential benefits. The first is increased sensitivity to iodinated contrast media. When imaging at 80 kVp, a larger portion of the x-ray spectrum is near the k-edge of iodine (33.2 keV). Therefore, the attenuation of iodine is greater than at higher tube voltages. This increases the sensitivity of the detection of iodinated contrast media (Fig. 65-5).¹⁹ Unfortunately, imaging at 80 kVp generates inherently noisier images than those obtained at a higher tube voltage. This disadvantage is mitigated by blending the noisy 80-kVp image with the “cleaner” 140-kVp image to create an acceptable image quality.²¹ This increased sensitivity to contrast media has been shown to increase the conspicuity of hypervascular lesions in the liver and hypovascular lesions in the pancreas.²⁰

DECT also has the ability to detect certain substances on the basis of their differing attenuation at different x-ray energies. With respect to gastrointestinal imaging, there have been investigations into use of DECT to detect and to quantify hepatic iron and fat stores.²²⁻²⁴ In addition, DECT has been used to detect iodine and to create iodine-only images that aid in lesion detection. Conversely, DECT has also been used to create virtual unenhanced images by removing the iodine from a single-pass contrast-enhanced DECT. These two techniques allow detection of lesion enhancement without the need for a noncontrast CT scan.²¹

Dosimetry and Dose Reduction

There has been a significant increase in both the public and professional awareness of radiation dose in medical imaging.²⁵ As CT is a procedure of relatively high dose and is used for a widening array of applications, it has received a large share of the attention.²⁶ CT scanning is now the highest single

contributor to human-made radiation exposure to the population.²⁶ The National Radiological Protection Board in Great Britain estimated that in 1999, although only 4% of diagnostic procedures were CT scans, they contributed to 40% of overall medical radiation exposure.²⁷ Unfortunately, calculating the radiation dose in CT is complex, leading to difficulty in providing simple answers to questions of dose.²⁸ Important principles include the following: the dose is administered only to a certain volume of the body, not to the entire patient; the dose can vary considerably from scanner to scanner and from image to image, depending on the technical parameters set; and the percentage of the dose delivered centrally compared with the skin dose is much greater with CT than with conventional radiography.^{2,3}

Absorbed dose is the energy absorbed per unit mass; it is measured in the SI unit gray (Gy). Fundamental CT absorbed dose descriptors include volume CT dose index (mGy), which reflects the average radiation dose within a scan volume, and dose-length product (mGy-cm), which reflects the radiation dose over the entire scan length. One or both of these values is displayed on the operator console of newer CT machines.

The other descriptor of importance is the effective dose (mSv), which estimates biologic risk. Effective dose may be calculated by multiplying the dose-length product by a conversion factor that is based on the body part being scanned and the size of the patient. For an adult, the conversion factor for abdominal CT is 0.15.²⁹ The effective dose is almost always the number a clinician or patient wants to know when they ask what the radiation dose of a CT examination is. Typical effective dose values for abdominopelvic CT scans range from 8 to 16 mSv.^{26,30} It is often helpful to remember that the range of background radiation in the United States is 1 to 10 mSv, with an average of about 3.6 mSv. Several excellent reviews are available for those interested in further information.³¹⁻³³

Several strategies exist to reduce radiation exposure due to CT both at the population level and during a given CT examination. Emphasis by the radiologist on performing a CT examination only to provide clinically useful information that will affect the course of treatment is the first step in reducing CT use as a population. Optimizing the study to answer the clinical question the first time avoids radiation from repeated CT studies. Limiting scan length to the area of interest also avoids excess radiation. Finally, consideration of alternative imaging

modalities, such as ultrasound and magnetic resonance (MR), which do not use ionizing radiation, is also important.

In performing a given study, there are several parameters that may be adjusted to reduce the dose to the patient. The key tradeoff involved is between radiation dose and image quality. In general, parameters that reduce radiation exposure to the patient also reduce the number of photons that reach the detector. This reduced sample size increases statistical noise, which is manifested as reduced image quality. Therefore, it is important for the radiologist to understand that although the highest possible image quality is desirable, it often comes at the expense of increased radiation exposure.

Three key parameters that influence both radiation dose and image quality are the tube current-time product, tube voltage, and pitch. The tube current-time product measured in milliamperere-seconds (mAs) is the product of the tube current and the time of rotation. Peak tube voltage (kVp) measured in kilovolts (kV) is the voltage applied to the x-ray tube. Decreases in current-time product result in a linearly proportional decrease in radiation dose. However, this results in an increase in image noise proportional to the inverse of the square root of the decrease in current-time product (e.g., a reduction in half of the current-time product would result in a $1/\sqrt{.5}=1.41$ or a 41% increase in image noise).³⁴ Similarly, a decrease in tube voltage results in reduced radiation dose at the expense of increased noise and other artifacts.³⁴ Finally, pitch is inversely proportional to radiation dose and directly proportional to image noise.³⁴

Although there is no agreed-on value of these parameters that will produce the optimal image, they may be adjusted to yield the lowest radiation dose possible while still achieving diagnostic image quality in a given clinical scenario. One of the most important factors to take into account is the patient's size. Smaller pediatric patients will require a lower tube current-time product, depending on their size.³⁵ Conversely, the obese adult patient will often require an increased tube current-time product and tube voltage for a diagnostic image to be obtained.³⁶

Reconstructed slice thickness is another factor that may influence radiation dose. As discussed before, with MDCT, a given CT data set may be reconstructed at varying slice thicknesses. However, for a given data set, a thinner reconstruction will have more noise than a thicker one. Conversely, given a desired level of image noise, a thinner reconstruction will require a higher dose than a thicker one.³⁷

CT scanner manufacturers have recently implemented a feature known as automated exposure control, which attempts to simplify the process of optimizing dose reduction. With automated exposure control, the operator sets an image quality parameter, the tube voltage, and the desired slice thickness. Then, as the gantry rotates around the patient, the scanner modulates the tube current such that the lowest necessary current is used to obtain the desired image quality. Determining what represents acceptable image quality may be difficult as image quality parameters vary between manufacturers, and individual radiologists interpret image quality differently.³⁴ However, as this technology becomes more commonplace, automated exposure control should become increasingly useful to limit radiation dose in CT.

One additional dose reduction technique on the horizon is iterative reconstruction. Iterative reconstruction is an alternative reconstruction algorithm that requires less radiation exposure than filtered back projection to generate images of similar

quality. The details of this algorithm are beyond the scope of this text. However, the main limitation of iterative reconstruction is that it is a computationally intensive technique that results in long reconstruction times. Although this is an old technique that was used to reconstruct the first CT images, this limitation caused it to fall out of favor. Recent increased interest in reduction of radiation exposure combined with increasing computational processing power has renewed interest in this method. Methods that combine traditional filtered back projection with iterative reconstruction have been found to reduce radiation dose by as much as 25% to 40% while maintaining image quality and acceptable reconstruction times.³⁸ Recent research reports 57% to 88% dose reduction with use of a pure form of iterative reconstruction (model-based iterative reconstruction), albeit with long reconstruction times and some loss of image quality.³⁸ However, with increasing computation power and improving algorithms, iterative reconstruction holds great promise for dose reduction in CT.

Intravenous Contrast Principles

Iodine-based intravenous contrast material is routinely used in CT of the solid abdominal organs. When it is properly used, such contrast material improves lesion detection and characterization. However, when it is used improperly, contrast material can actually decrease lesion detection.³⁹ In the early days of conventional CT, abdominal enhancement was described as consisting of three phases: bolus, nonequilibrium, and equilibrium.^{40,41} Whereas these phases are no longer as critical in protocol planning as they were with conventional CT, scanning of the liver should be completed before the equilibrium phase, which generally begins about 90 to 120 seconds after injection.⁴² This could be relevant when either patient or technical problems cause an unplanned increase in the scan delay.

With helical CT and MDCT, enhancement characteristics of abdominal structures have been more completely studied⁴³ (Fig. 65-6). The *early arterial phase* is a common name given to the period when a significant amount of contrast material is in the

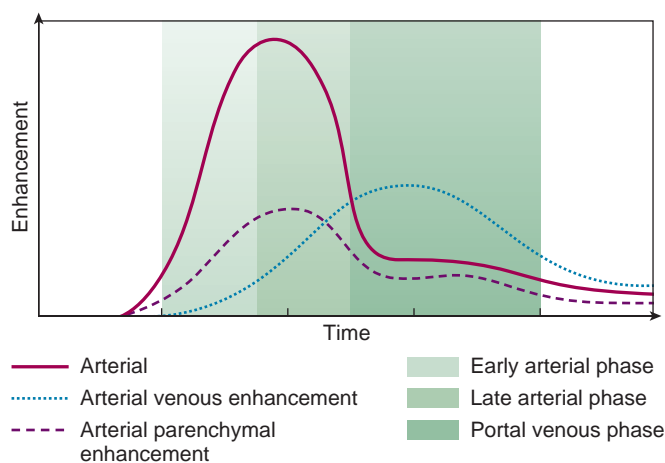


Figure 65-6 Phases of enhancement. The curves display the density of arteries, arterial parenchymal enhancement (such as in hypervascular tumors or the pancreas), and portal venous enhancement of the liver. The boxes demonstrate the timing of acquisition of each phase for a hypothetical scanner. Each of the three phases is acquired while contrast enhancement difference is greatest between the desired structure and other structures.

arterial system but little or no contrast material is in the venous system or organs. In the abdomen, this generally occurs 15 to 25 seconds after the initiation of injection in most patients. The *late arterial phase* describes the time when contrast material is entering hypervascular tumors and vascular organs in significant amounts; this is generally 30 to 45 seconds after the beginning of the injection. Some have termed this the *portal inflow phase*, as contrast material is generally seen in the portal vein also but not in the hepatic veins; however, the enhancement of the liver parenchyma in this phase is primarily due to hepatic arterial flow. Finally, the period from 50 to 80 seconds after the injection is referred to as the *portal venous phase* and is the time during which the liver is maximally enhanced; this delay reflects the predominant portal venous supply of the liver. Contrast material reaches the liver through the portal vein only after it traverses the mesentery and bowel. This phase has also been called the *hepatic parenchymal phase* and the *hepatic venous phase*.⁴³

Iodinated contrast material is available in varying concentrations. Sixty percent iodine concentrations (300 mg/mL) are most commonly used for abdominal applications. However, varying concentrations have been studied, with a recent trend in use of higher concentrations.⁴⁴ One rationale for use of higher concentrations (350 to 370 mg/mL available in the United States, 400 mg/mL elsewhere) is the ability to get a greater number of iodine atoms into the organ of interest with the same injection rate.⁴⁵ Lower injection rates may be safer and easier to use.⁴⁶ Use of higher concentrations has been shown to improve detection of hypervascular hepatocellular carcinoma compared with preparations of 300 mg/mL.⁴⁷

Injection of contrast material should always be performed with a power injector. This ensures that the desired injection rates and timing are achieved. Both the rate at which the contrast material should be administered and the length of the scan delay (time from initiation of the injection of the contrast agent to time of initiation of scanning) have been studied extensively.⁴⁸ As the rapidity of acquisition increased with helical CT and MDCT, a complete reevaluation of contrast agent administration strategies has been required.⁴² Before helical CT, the greatest concern was administration of the contrast agent to maximize the time to equilibrium phase to allow scan completion before equilibrium began. This is now easily accomplished, and the focus has been on determining the strategies to maximize visualization of various normal and pathologic structures at certain points of enhancement.

There are two additional questions to be answered with regard to intravenous administration of contrast material: the amount and method of administration. All currently used iodine-based contrast agents distribute rapidly into the extracellular space. Thus, the enhancement of vessels and organs depends not only on the dose but also on the rate of injection and the length of time from the beginning of the injection to imaging (scan delay) (Fig. 65-7).

The dose of contrast material administered depends on scanner type and the specific organ of interest. Because of the various concentrations available, dose is best considered in grams of iodine. The increased speed of helical CT and MDCT has allowed dose reductions when the primary purpose of contrast is vascular opacification. However, adequate opacification of the hepatic parenchyma to optimize detection of focal lesions probably is not as dependent on speed; it has been recommended that a minimum dose of 38 g (125 mL of a

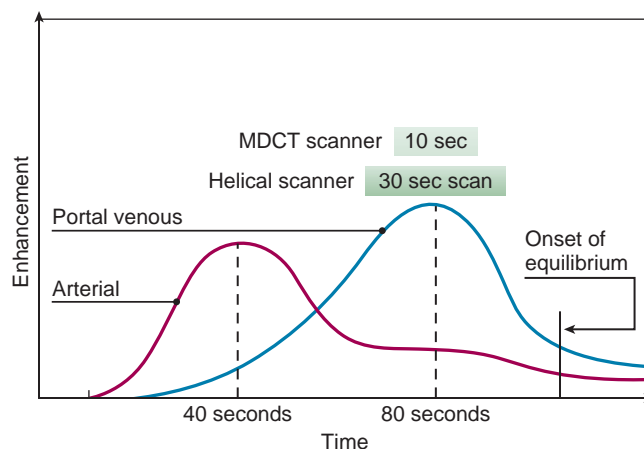


Figure 65-7 Phases of enhancement with demonstration of timing differences based on machine type. If a series of images through the liver is desired at peak parenchymal enhancement, the scan delay will vary with the length of time the scanner takes to image the entire organ. Shown are two examples: a four-channel MDCT scanner that requires 10 seconds to scan the liver and a single-channel helical scanner that requires 30 seconds to complete the images.

300 mg/mL formulation) should be used with helical scanning.⁴⁹ For general parenchymal organ imaging, a dose of 120 to 150 mL of 300 to 370 mg/mL contrast material is generally used.⁵⁰

The volume of contrast material administered to adults undergoing CT has routinely been held constant regardless of the patient's size. By adjustment of the dose according to the patient's weight, a lower overall amount of contrast material may be used, creating a cost savings while maintaining image quality. A weight-based dose of 1.5 mL/kg was found acceptable in most patients for routine survey examinations.⁵¹

In general, contrast material is injected at relatively high rates to obtain rapid opacification of vessels and organs and to avoid imaging during the equilibrium phase. The degree of enhancement and the time of maximum enhancement are both directly related to the injection rate.⁵² Rates for routine abdominal studies generally are 2 to 3 mL/s; this is adequate to image the abdomen during the portal venous phase of enhancement. With multiphasic imaging, a more rapid bolus helps separate the different phases; for example, with a higher rate, a greater volume of contrast material is administered to obtain a high degree of hepatic arterial enhancement in the liver before portal venous contamination begins.⁵³ Rates for hepatic examinations generally range from 3 to 6 mL/s.

The scan delay is defined as the time between the initiation of injection and the initiation of image acquisition. The delay chosen depends primarily on the phase of enhancement one wishes to image. Routine abdominal studies are ideally performed during the portal venous phase; CT angiographic images are obtained during the early arterial phase and hepatic parenchymal arterial studies during the late arterial phase. The scan delay also depends on how fast the scanner is—one must consider the contrast enhancement at the end of the scan as well as at the beginning. Ideally, the scan is centered at the peak of the desired phase. Thus, with the slowest scanners, one might have to begin before the ideal opacification is reached to ensure that at the end of the scan, the

enhancement phase is still appropriate; conversely, with the fastest scanners, the delay is greater to center the acquisition at the desired enhancement peak (Fig. 65-7). The optimal scan delay depends on the injection rate and volume administered; when the rate is changed, the delay may require adjustment as well.⁵⁴⁻⁵⁷

The terminology used to describe the administration of contrast material in CT varies in the literature, by local custom, and with the organ of interest. Multiphase studies are usually referred to by the number of series obtained after the injection of contrast material; for example, "biphasic" CT of the liver usually includes two contrast-enhanced scans; it may or may not include a precontrast scan. If a precontrast scan were included, some would term this a triphasic examination, whereas others would not.

As the science of contrast agent administration has progressed, patient-dependent factors have become more obvious. Most institutions use nearly the same technique for most adult patients. However, differences in cardiac output, weight, time from last meal, and fluid status affect the actual enhancement obtained on the images.^{58,59} In an effort to tailor the examination to the specific patient, bolus tracking systems are available that initiate scanning when the optimal enhancement has been reached.^{60,61} In general, these systems use a series of low-dose scans obtained at a single location within the abdomen. A region of interest cursor is placed on the aorta or liver, and a threshold density level is set. After the beginning of the contrast agent administration, scans are obtained every second or so until the density measured within the region of interest reaches a threshold value. At that time, the diagnostic scan is begun.

Another technique becoming more popular, particularly with the use of 64-channel CT machines and in CT angiography, is the use of a "saline chaser." This was originally described with a technique of placing both the contrast agent and saline in one injector chamber, but now dual-bore (one piston for the contrast agent and one for the saline) injectors are available as well.⁶² The saline serves two functions: it increases the efficiency of the contrast agent used as no contrast material will remain in the tubing or in the peripheral circulation of the arm at the end of the injection, and it maintains high concentrations of contrast material in the circulation longer by preserving the bolus shape. This in turn has been used to decrease the total dose of contrast material administered.⁶³

Other intravenous contrast agents are being explored, primarily to image the liver with the goal of improving lesion detection and characterization. These contrast agents target either the reticuloendothelial system (Kupffer cells) or hepatocytes. However, iodine is the only intravenous agent currently used routinely in abdominopelvic CT.

Interpretation Principles

The conventional approach to CT interpretation is based on "hard-copy" film. A number of forces have changed interpretation from a film-based environment to a "soft-copy" or monitor-based environment. The number of images obtained in abdominal studies is climbing as multidetector techniques allow the creation of more (usually thinner) images. Multiple phase acquisitions and use of multiplanar reformations have led to the creation of even more images. Filming this number of images is not practical. Picture archiving and communications

system (PACS) methods have helped manage these images as well as allowed enterprise-wide simultaneous visualization of images with central secure data storage.

Certain principles are the same with both film and monitor interpretation. Images should be displayed with window width and level settings appropriate for differentiation of solid-containing, fluid-containing, and air-containing structures (body window: level = 40-70, width = 380-550). Many radiologists find narrower width (liver window: level = 60-80, width = 125-150) images of the upper abdomen helpful, and viewing of these windows is suggested to aid in identification of lesions with minimal density difference from normal liver.^{64,65} Varieties of measurements are made to clarify findings and to include objective data in the radiology report. Regions of interest are created to obtain the average density of the contents inscribed to help lesion characterization. Size measurements on helical data sets are accurate in the axial, longitudinal, or z-axis.⁶⁶ Bidimensional measurements are made by determining the longest single diameter, then the longest dimension that is perpendicular to the first.⁶⁷

Image Postprocessing

One of the most important advantages of helical acquisition is that a true volume data set is obtained. This allows several postprocessing options. The most basic option is planar reformations in the sagittal and coronal planes. These may be helpful in a variety of circumstances. For example, in attempting to delineate the origin of a mass, coronal or sagittal reformations may better demonstrate a fat plane separating the mass from an adjacent organ. In addition, certain structures, such as small vessels or the common bile duct, are often more readily assessed in the sagittal or coronal plane.

Curved planar reformations are another postprocessing option in which a single image is created representing the anatomy along a curved line. This is useful in depicting biliary and pancreatic ductal anatomy and the relationship of tumor to these structures. Curved planar reformation is also useful in depicting stenosis, thrombosis, and aneurysms in vascular structures.⁶⁸ In addition, the ability to depict complex anatomy on a single image is appreciated by referring clinicians.⁶⁸

Maximum intensity projection renderings generate images in which each pixel represents the highest attenuation voxel in a slab of tissue of a set thickness. This slab can be oriented in any plane. Maximum intensity projection reformations are often used with CT angiography to aid in evaluating small vascular structures that are accentuated by this technique. They are also used in surgical planning to help resolve questions of vascular anatomy and the relationship of tumor with adjacent vasculature.⁶⁹

Minimum intensity projection renderings conversely generate images in which each pixel represents the lowest attenuation voxel in a slab of tissue of a set thickness. Minimum intensity projection images are useful in evaluating low-attenuation structures, such as the pancreatic ducts and the biliary tree.⁷⁰

Volume rendering encompasses a wide array of techniques in which a three-dimensional model of the structures of interest is created. With respect to the imaging of the solid organs, it is mainly used with CT angiography to depict vessels. Volume rendering is used in conjunction with maximum intensity projection in addressing questions of vascular anatomy and the relationship of vessels to adjacent tumor.⁶⁹ It is therefore useful

for surgical planning before liver transplantation, liver donation, partial hepatectomy, and partial pancreatectomy.

Volumetry is another postprocessing technique used to calculate the volume of a structure. The structure may be outlined manually or automatically at a workstation over contiguous slices throughout its entire volume. The workstation software then calculates the estimated volume of the structure. Estimation of tumor volume may be useful in assessing response to treatment.⁷¹ Volumetry has also proved useful in presurgical planning before living related liver donation to estimate the volume of the donated liver and the remaining liver after donation.⁷² It is also useful in planning before partial hepatectomy to estimate liver volume after resection.⁷³

These are just some of the more common available postprocessing options. Some, such as multiplanar reformations, may be performed routinely, whereas others are performed only for certain indications. They are often of great utility to the referring clinician as they may depict anatomy and pathology in a manner more easily interpreted by the nonradiologist.

Scanning Protocols

Exact scanning protocols depend on many variables, including the clinical indication, patient-related factors such as weight and venous access, and scanner type and manufacturer. Scanning protocols should be tailored for the specific clinical indication.⁷⁴ Some basic principles are provided here from which exact CT protocols may be derived.

ABDOMINOPELVIC SURVEY

Survey examinations of the abdomen are often obtained for conditions such as abdominal pain, possible abscess, or malignant disease. For general survey examinations, the study is best performed with both oral and intravenous contrast material unless it is contraindicated.⁷⁵ The use of 5-mm-thick images obtained every 5 mm through the abdomen is standard. An injection of 125 mL of intravenous contrast material is used with an injection rate of 3 mL/s. A scan delay of 70 seconds is used for most patients. Approximately 900 mL of oral contrast material is used for most patients, if they can tolerate the enteric intake. However, acquisition section thickness may range from 0.5 to 2.5 mm. The images created for interpretation are usually thicker, from 3 to 5 mm.⁷⁶

As long as the raw data are still in the scanner memory, additional thinner images can be created later if needed. One should be cognizant of the length of time of the injection versus scanning speed. This is usually an issue only in patients with poor intravenous access requiring lower injection rates. For example, if the injection rate is reduced to 1.5 mL/s, the injection will last about 90 seconds. Depending on the acquisition collimation and gantry rotation speed, a scan initiated at 70 seconds could be complete before all the intravenous contrast material has entered the abdominal circulation. To avoid this, one may increase the delay, slow the scanner, or reduce the volume of contrast material. Sample abdominopelvic survey protocols may be found in Table 65-1.

COMPUTED TOMOGRAPHY OF THE LIVER

Specific CT techniques to better evaluate the liver have become routine with helical CT and especially MDCT (Table 65-2).

TABLE 65-1 Abdominal CT Survey Protocols			
	4-Slice	16-Slice	64-Slice
Intravenous contrast agent (300 mg/mL)*	125 mL	125 mL	125 or 100 mL + 50 mL saline chaser
Injection rate	2-3 mL/s	2-3 mL/s	2-4 mL/s
Scan delay	60-70 s	60-70 s	60-70 s
Detector collimation	2.5-5 mm	1-1.5 mm	0.5-0.625 mm
Image thickness	5 mm	5 mm	5 mm

Oral and intravenous contrast agents should be used unless contraindicated.

*Other concentrations of the contrast agent may be used; the volume can be adjusted to keep grams of iodine constant.

Conventional CT cannot be used for specific hepatic imaging protocols. Whereas certain principles of hepatic CT imaging exist, the specific techniques used will vary slightly by the exact indication. Specific protocols may focus on lesion characterization, screening for hepatocellular carcinoma in high-risk individuals, evaluation of cholangiocarcinoma, or preoperative staging and planning. In addition, there are also special techniques involving catheter angiography with CT.

The general principle from which most specific protocols are derived is based on the dual blood supply of the liver.⁷⁷ The normal liver receives approximately 25% of its blood supply from the hepatic artery and 75% from the portal vein. The hepatic arteries will receive contrast material after a peripheral venous injection first, generally beginning at 15 to 25 seconds, depending on injection rate and the patient's circulation time.⁷⁸ Contrast material reaches the portal venous system later as it must first traverse the mesenteric vessels and bowel capillaries. The portal vein begins to enhance about 35 to 40 seconds after the injection of contrast material begins. Finally, at about 60 to 70 seconds, contrast material is identified in the hepatic veins.

In contrast to the hepatic parenchyma, most hepatic tumors are supplied by the hepatic artery exclusively. The appearance of a focal hepatic mass depends on its vascularity and the delay after administration of contrast material.⁷⁹ Hepatic tumors that are hypervascular are generally best seen on late arterial phase images, which are obtained near the end of the phase of exclusive enhancement of the liver by the hepatic arteries, that is to say, when the contrast material just reaches the portal vein, at about 35 to 40 seconds (Fig. 65-8). Images obtained at this time have been referred to in the literature as arterial, late arterial, or portal venous inflow images.⁷⁹ Hepatic tumors that are hypovascular are generally best seen when there is good opacification of the liver by both the hepatic artery and portal vein, but before the onset of equilibrium. This is at 60 to 70 seconds and is identified by contrast material in the hepatic veins. Images obtained at this time may be varyingly referred to as portal venous, parenchymal, or hepatic venous phase images. However, these tumors may not be visualized during earlier phases (Fig. 65-9). This is because the hypovascular tumor receiving a large amount of contrast material may become isodense to the hypervascular liver, which is receiving contrast material from only a portion of its blood supply. The exact timing of each phase in a particular patient may be determined by a test bolus technique.⁷⁷

TABLE 65-2 Hepatic CT Protocols		4-Slice	16-Slice	64-Slice
Precontrast images	Detector collimation	5 mm	1.5 mm	0.5-0.625 mm
	Image thickness	5 mm	5 mm	5 mm
Injection	Contrast volume (300 mg/mL)	125 mL	125 mL	125 mL
	Injection rate	3-4 mL/s	3-4 mL/s	3-4 mL/s
Early arterial phase* (CT angiography)	Scan delay	15 s	15 s	15 s
	Detector collimation	1-1.25 mm	0.75 mm	0.5-0.625 mm
	Image thickness	2 mm	1 mm	1 mm
Late arterial phase (arterial, portal venous inflow)	Scan delay	30 s	30 s	30 s
	Detector collimation	1-2.5 mm	0.75 mm	0.5-0.625 mm
	Image thickness	2-4 mm [†]	2 mm [†]	2 mm [†]
Portal venous phase (hepatic venous, parenchymal)	Scan delay	60-70 s	70 s	70 s
	Detector collimation	5 mm	1.5 mm	0.5-0.625 mm
	Image thickness	5-7 mm	2-5 mm	2-5 mm
Delayed phase [‡]	Scan delay	10-20 min	10-20 min	10-20 min
	Detector collimation	5 mm	0.75 mm	0.5-0.625 mm
	Image thickness	5-7 mm	2-5 mm	2-5 mm

For most indications, three phases are chosen, generally precontrast, late arterial, and portal venous phases. Early arterial images may be performed if desired for surgical planning, and delayed phase images are generally added in evaluation of cholangiocarcinoma.

*With single channel, cannot be combined with arterial phase. Positive enteric contrast material should not be used; neutral or negative enteric contrast material may be administered. A 50% image overlap should be used (reconstruction interval equal to half of image thickness).

[†]Thinner slice images with a softer kernel are created for use in maximum intensity projection and volume rendering angiographic images.

[‡]For use in identification or evaluation of cholangiocarcinoma.

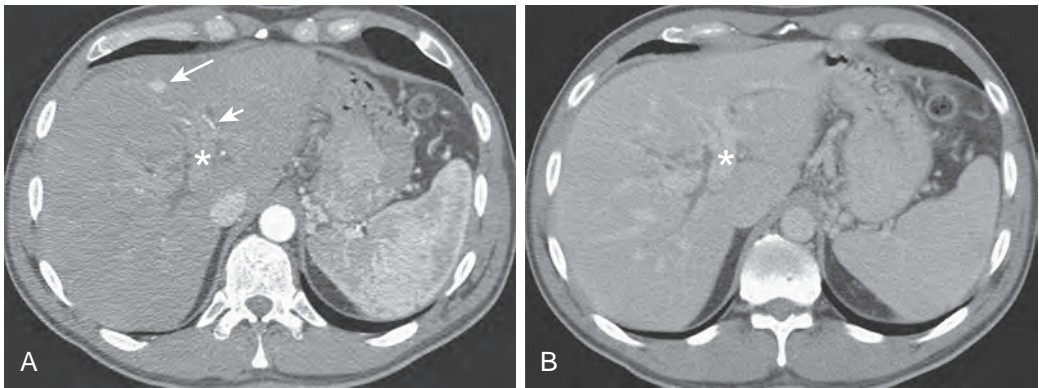


Figure 65-8 Biphasic liver examination of a hypervascular metastasis. **A.** On this late arterial phase image, a 1-cm hypervascular metastasis is identified in the medial segment of the left lobe (*long arrow*). Note that portions of the hepatic artery (*short arrow*) are well seen and contrast material is just entering the portal vein (*asterisk*). **B.** On this portal venous phase image obtained at the same location as in **A**, the lesion cannot be easily identified (*asterisk*).

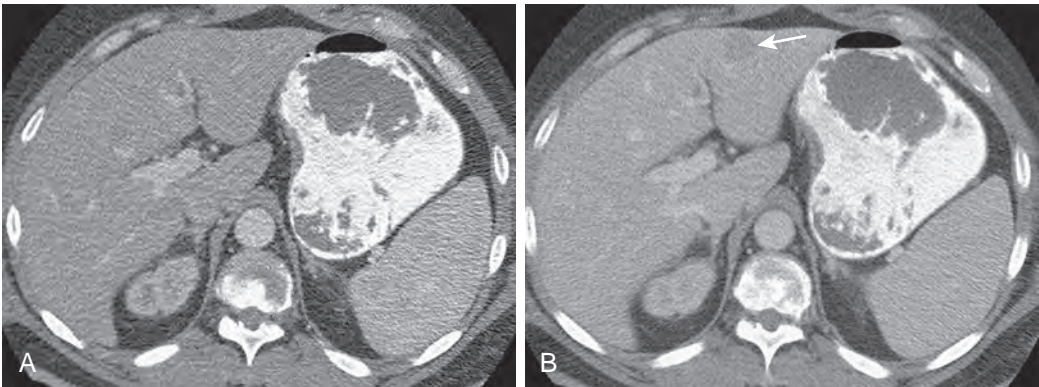


Figure 65-9 Biphasic liver examination of a hypovascular metastasis. **A.** On this late arterial phase image in a patient with metastatic colon cancer, no hepatic lesion can be identified. **B.** On the portal venous phase image obtained at the same location, the hypovascular metastasis on the lateral segment of the left lobe is easily seen (*arrow*).

The specific acquisition collimation, pitch, gantry rotation, and table speed will vary by scanner type and manufacturer. In general, these parameters are adjusted such that each phase can be accomplished within a 10- to 15-second breath hold. Increasing pitch decreases the radiation dose but increases image noise; in general, pitch should vary from 0.75 to 1.5 for most protocol phases. The reconstruction interval is generally equal to the image thickness, resulting in contiguous images, with the exception of early arterial images to be used for CT angiographic reconstruction, in which the reconstruction interval is generally 50% of the image thickness.

The usefulness of precontrast images has been the subject of some debate. Proponents note the increased sensitivity for certain malignant lesions.⁸⁰ Precontrast images can also be helpful in the identification of focal calcifications. Detractors focus on the relatively small incremental advantages compared with the additional cost and radiation exposure.⁸¹ Acquisition collimation is also generally kept relatively large and image thickness is usually kept at 3 to 5 mm (see Table 65-2).

Early arterial phase images can be separately obtained for three-dimensional reconstructions of the upper abdominal and hepatic arterial trees for use in surgical planning. When these are desired, a high rate of injection (4-6 mL/s) is important. As thin an acquisition collimation and as rapid a gantry speed as possible are used. If three-dimensional reconstructions are anticipated, positive oral contrast material should not be given as it interferes with reconstructions.

Late arterial phase images are used for identification of hypervascular lesions as well as for lesion characterization.⁴³ This requires high injection rates of 4 to 6 mL/s to get adequate amounts of iodine into the liver before portal venous contamination. With higher concentrations of contrast material, slightly slower injection rates introduce the same amount of iodine per unit time. Acquisition thickness ranges from 2.5 mm on 4-channel units to 0.5 mm on 64-channel units. The general principle used is to obtain as thin of a collimation as possible that will allow completion of the scan before a large amount of contrast material has entered the liver through the portal vein. This allows excellent spatial resolution that can be exploited to evaluate the arterial tree during this phase, negating the need for early arterial images. Image thickness of 2.5 to 5 mm may be used. Thinner images may help with identification of small vessels; however, one study demonstrated no improvement in the detection of hypervascular hepatocellular carcinoma with images thinner than 5 mm.⁸²

Portal venous phase images are obtained with parameters similar to those used for routine survey examination of the abdomen. MDCT is begun at 60 to 70 seconds with an acquisition collimation of 0.5 to 5 mm, depending on the number of channels. With MDCT, the image thickness is generally larger than the collimator thickness, usually 3 to 5 mm. Results from several studies comparing different image thickness have had varying results. A study of small lesions (defined as ≤ 10 mm) found that 2.5-mm image thickness was more sensitive than 5-, 7.5-, or 10-mm image thickness.⁸³ However, a later study comparing images of 5-, 3.75-, and 2.5-mm thickness showed no improvement in detection of small metastases with the thinner image thickness, possibly because of increased noise on the thinner images.⁸⁴ Finally, one must consider that 80% of small (10 mm) liver lesions in patients with known malignant neoplasms are benign, and differentiation of small benign lesions from small malignant lesions can be difficult or impossible.⁸⁵ It

is possible that in evaluating for small and very small metastases, an approach different from the routine anatomic one, such as perfusion imaging, will be required.⁸⁶

Delayed scanning can be performed at 10 to 20 minutes after the injection, particularly for the detection or evaluation of cholangiocarcinoma.^{87,88} At this time, contrast material persists in fibrous, dense structures but is decreasing in concentration in most tissues because of renal excretion. Such a delayed acquisition generally would have the same parameters as the portal venous phase sequence.

If bolus tracking or a test bolus is used to optimize timing of the study, the region of interest may be placed over the upper abdominal aorta and a trigger of 100 HU may be used. For the late arterial phase, a delay of 16 seconds from the trigger is recommended. For the portal venous phase, a delay of 50 seconds from the trigger is recommended.⁸⁹ If delayed scanning to assess for cholangiocarcinoma is to be performed, timing of the delayed phase based on the test bolus or bolus tracking is not necessary.

A significant challenge in liver imaging is imaging of sick patients with decreased liver perfusion. This includes patients with cirrhosis, cardiac dysfunction, and portal vein thrombosis. These comorbidities are common in patients undergoing liver imaging. These patients may have decreased enhancement of the liver parenchyma in the portal venous phase that may obscure hypovascular liver lesions. This effect may be partially mitigated by the use of contrast media with higher concentration of iodine or higher volumes of contrast material.⁹⁰

Additional specialized hepatic CT imaging techniques exist but are not routinely used at most institutions. Delayed images at 6 hours after injection demonstrate focal lesions as slightly hypodense as the liver is slightly increased in density because of active excretion of the contrast material by the hepatocytes into the bile.⁹¹ CT angiography and CT portography employ the use of an arterial catheter placed in the hepatic, splenic, or superior mesenteric artery. Images are obtained either during the direct arterial opacification of the liver (CT hepatic angiography) or during the first pass of contrast material through the portal venous system of the liver (CT arterial portography).^{92,93} These techniques have been shown to be most sensitive for focal lesion detection; however, most comparisons predate MDCT.⁹⁴

COMPUTED TOMOGRAPHY OF THE PANCREAS

MDCT scanners have improved pancreatic imaging because of reduced acquisition time, ability to image during multiple phases of enhancement, and excellent multiplanar image reconstructions. MDCT imaging of the pancreas is based on the enhancement pattern of the pancreas in its normal and diseased states. Noncontrast images can be helpful in identifying pancreatic calcifications and calcified common bile duct stones. However, full MDCT evaluation of the pancreas requires the use of intravenous contrast material. Water or negative oral contrast media may be used to distend the stomach and duodenum to make it easier to evaluate for gastric and duodenal wall lesions. Compared with positive oral contrast agents, negative oral contrast agents do not mask possible radiopaque stones in the common bile duct or pancreatic calcifications.⁹⁵ Sample pancreatic CT protocols may be found in Table 65-3.

Contrast-enhanced CT pancreatic imaging is based on multiple parameters, such as iodine concentration, contrast

material volume, and injection rate. The maximum iodine dosage should not exceed 35 to 45 g.⁹⁶ Achieving high-contrast pancreatic enhancement is possible by increasing the injection rate or the concentration of iodine in the intravenous contrast material while keeping the total iodine dose constant. If the injection rate of the contrast material and the total iodine dose are constant, the use of higher concentration contrast media significantly improves pancreatic enhancement compared with lower concentration contrast media.⁹⁷ As a result, high-concentration intravenous contrast media improve pancreatic lesion detection. A weight-based approach to administration of intravenous contrast media may also be used to optimize the iodine dose. An iodine dose of 550 mg/kg can be used for both pancreatic and vascular enhancement, which translates into 1.8 to 2.0 mL/kg, depending on the iodine concentration in the contrast media.⁹⁸

Precontrast CT of the upper abdomen is first performed with 5- to 10-mm slice thickness to cover the pancreas. Subsequent contrast-enhanced imaging of the pancreas has three possible phases: the early arterial phase, the pancreatic phase

(also known as the delayed arterial phase), and the portal venous phase.⁹⁹

The early arterial phase is obtained approximately 20 seconds after the bolus administration of 125 to 150 mL of contrast medium, injected at a rate of 4 to 5 mL/s. This is almost a purely arterial phase with little if any pancreatic enhancement. This phase, although it is not always obtained, allows assessment of the arterial tree in relation to pancreatic disease and may be useful in surgical planning.¹⁰⁰ However, there may not be enough contrast material present within the pancreas for identification of hypervascular or hypovascular lesions.^{100,101}

The pancreatic (delayed arterial) phase is acquired nearly 35 to 40 seconds after administration of the contrast medium. The scan extends from the level of the diaphragm to the inferior aspect of the duodenum with 2-mm slice thickness. During this phase, there is peak enhancement of the pancreas and good opacification of the arterial vascular system.¹⁰² Images obtained in the pancreatic phase can be particularly helpful in identifying both hypervascular and hypovascular pancreatic lesions or vascular involvement by tumor or inflammation¹⁰³ (Fig. 65-10).

TABLE 65-3 Pancreatic CT Protocols

		4-Slice	16-Slice	64-Slice
Precontrast ^{*,†}	Detector collimation	5 mm	1.5 mm	0.5-0.625 mm
	Image thickness	5 mm	5 mm	5 mm
Injection	Contrast volume (300 mg/mL)	125 mL	125 mL	125 mL
	Injection rate	4-6 mL/s	4-6 mL/s	4-6 mL/s
Arterial phase (CT angiography)	Scan delay	15 s	15 s	15 s
	Detector collimation	1-1.25 mm	0.75 mm	0.5-0.625 mm
Parenchymal phase ^{‡,§}	Image thickness	1.25 mm	1 mm	1 mm
	Scan delay	35-45 s	35-45 s	35-45 s
Portal venous phase	Detector collimation	2.5 mm	0.75 mm	0.5-0.625 mm
	Image thickness	2-3 mm	2 mm	2 mm
	Scan delay	60-70 s	70 s	70 s
	Detector collimation	5 mm	0.75 mm	0.5-0.625 mm
	Image thickness	5-7 mm	2-3 mm	2-3 mm

Up to four phases may be obtained through the pancreas; however, most institutions perform only three (choosing either the arterial phase or parenchymal phase) to limit radiation dose. Enteric contrast agents should be neutral or negative.

^{*}Most useful in evaluating patients with chronic pancreatitis or biliary obstruction; not generally used for routine mass evaluation.

[†]This may be restricted in the z-axis to cover only the pancreas.

[‡]In many circumstances, this can also be used for vascular assessment and reconstructions (CT angiography) with minimal venous contamination.

The raw data can be reconstructed into an additional data set with image thickness equal to detector collimation and with 50% overlap.

[§]In cases of known or suspected hypervascular pancreatic tumor (i.e., neuroendocrine), this phase can be expanded to include the liver for assessment for metastasis.

^{||}Generally includes the entire abdomen.

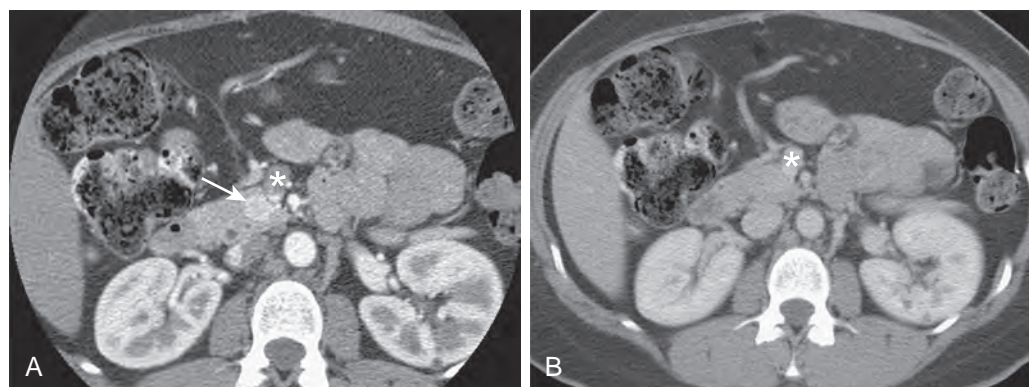


Figure 65-10 Patient with symptoms and laboratory abnormalities consistent with an insulinoma. **A.** Image obtained during the pancreatic phase clearly demonstrates the hypervascular tumor (arrow) in the pancreatic head adjacent to the superior mesenteric vein. **B.** The tumor is almost impossible to identify on the portal venous phase image obtained at the same level. *, superior mesenteric vein.

The portal venous phase is acquired at 70 to 80 seconds after the administration of the contrast medium. For the portal venous phase, an acquisition is performed covering the entire upper abdomen with 2.5- to 5-mm slice collimation. Portal venous phase images improve visualization of the hepatic parenchyma, hypovascular hepatic metastases, and involvement of venous structures by tumor.⁹⁹

If a bolus tracking or test bolus technique is used, the region of interest is placed over the aorta just above the pancreas and a threshold of 50 to 100 HU is used to trigger the study. With this technique, scanning for the arterial phase begins 8 seconds after the trigger, the pancreatic phase starts 25 seconds after the trigger, and the portal venous phase begins 50 seconds after the trigger.⁸⁹

Future Directions

The history of CT has been one of continuous improvement, usually measured in resolution and speed. Several significant leaps forward have occurred, most notably the introduction of helical and multidetector technologies. Although one major goal, the isotropic voxel, has been achieved with 64-channel machines, the demand for continued improvement persists.

Whereas machines with even greater numbers of channels have been developed, the pursuit of speed and anatomic detail is only one avenue of future development and one that has led to its own set of questions. How can the new larger data sets generated by these machines be interpreted efficiently? With the potential for thousands of images to be generated for a single examination, what are the optimal reformations of the CT data set that will maximize efficiency of interpretation without sacrificing the diagnostic accuracy of the examination? Finally, what are we to make of those small findings of questionable clinical significance that are now being revealed with the improved anatomic detail offered by modern CT (e.g., the small pancreatic cystic lesion)?

Another area of future development is in the techniques that provide the radiologist with information beyond anatomy and attenuation. DECT is in its early stages, and although a few applications of abdominal imaging have been conceived, this is an area of active investigation that has the potential to provide the radiologist with increased contrast sensitivity as well as potentially clinically relevant information about the chemical composition of the tissue being imaged. Another area of active interest is the development of perfusion CT in the abdomen and pelvis, particularly of the liver.¹⁰⁴⁻¹⁰⁶ Following the pathway of many CT innovations, this technique is becoming increasingly important in neuroradiology, and applications in the body (where cardiac and respiratory motion as well as greater z-axis coverage presents additional challenges) may not be far behind. Perfusion is an area of great research interest that may have practical clinical benefits as well. Comparison with MR perfusion techniques will have to be made, particularly in light of the potentially high radiation dose of perfusion CT.

Finally, the central issue facing CT is that of radiation. As the number of CT examinations performed annually continues to increase and the radiation dose from these examinations increases as well, CT faces increasing scrutiny from public health officials, the media, and the general public. In the near future, CT will surely remain the predominant cross-sectional imaging modality, but in the long run, concerns about the effects of radiation as well as the increasing availability of MR and improvements in ultrasound have the potential to decrease the dominance of CT in the imaging armamentarium. As might be expected, manufacturers have stepped up to the plate, offering techniques such as automated exposure control and iterative reconstruction as described earlier. Improvements in these techniques as well as the development of new hardware- and software-based techniques to decrease radiation dose will be crucial to maintaining the long-term relevance of CT.

REFERENCES

- Friedland GW, Thurber BD: The birth of CT. *AJR Am J Roentgenol* 167:1365-1370, 1996.
- Miraldi F: Imaging principles in computed tomography. In Haaga JR, Lanzieri CF, editors: *CT and MR Imaging of the Whole Body*, ed 4, Philadelphia, 2002, Lippincott, pp 3-36.
- Bae KT, Whiting BR: Basic principles of computed tomography physics and technical considerations. In Lee JKT, Sagel SS, Stanley RJ, et al, editors: *Computed Tomography with MRI Correlation*, Philadelphia, 2006, Lippincott Williams & Wilkins, pp 1-29.
- Heiken JP, Brink JA, Vannier MW: Spiral (helical) CT. *Radiology* 189:647-656, 1993.
- Seeram E: *Computed Tomography: Physical Principles, Clinical Applications and Quality Control*, Philadelphia, 1994, WB Saunders, pp 125-138.
- Barnes JE: Characteristics and control of contrast in CT. *Radiographics* 12:825-837, 1992.
- Kalender WA, Seissler W, Klotz E, Vock P: Spiral volumetric CT with single-breath-hold technique, continuous transport, and continuous scanner rotation. *Radiology* 176:181-183, 1990.
- Herts BR, Einstein DM, Paushter DM: Spiral CT of the abdomen: Artifacts and potential pitfalls. *AJR Am J Roentgenol* 161:1185-1190, 1993.
- Urban BA, Fishman EK, Kuhlman JE, et al: Detection of focal hepatic lesions with spiral CT: Comparison of 4- and 8-mm interscan spacing. *AJR Am J Roentgenol* 160:783-785, 1993.
- Foley WD: Technology/contrast: Current state of the art. In Fishman EK, Federle MP, editors: *Body CT Categorical Course Syllabus*, Reston, Va, 1994, American Roentgen Ray Society, pp 1-4.
- Silverman PM, Kalender WA, Hazle JD: Common terminology for single and multislice helical CT. *AJR Am J Roentgenol* 176:1135-1136, 2001.
- Flohr TG, Schaller S, Stierstorfer K, et al: Multi-detector row CT systems and image-reconstruction techniques. *Radiology* 235:756-773, 2005.
- Prokop M: Principles of CT, spiral CT and multislice CT. In Prokop M, Galanski M, editors: *Spiral and Multislice Computed Tomography of the Body*, Stuttgart, 2003, Thieme, pp 1-43.
- Fishman EK, Jeffrey RB, editors: *Multidetector CT: Principles, Techniques, and Clinical Applications*, Philadelphia, 2004, Lippincott Williams & Wilkins.
- Prokop M: General principles of MDCT. *Eur J Radiol* 45:S4-S10, 2003.
- Ros PR, Hoon J: Multisession (multidetector) CT: Applications in the abdomen. *Radiographics* 22:697-700, 2002.
- Saini S: Multi-detector row CT: Principles and practice for abdominal applications. *Radiology* 233:323-327, 2004.
- Napel S: Basic principles of MDCT. In Fishman EK, Jeffrey RB, editors: *Multidetector CT: Principles, Techniques, and Clinical Applications*, Philadelphia, 2004, Lippincott Williams & Wilkins, pp 3-13.
- Coursey CA, Nelson RC, Boll DT, et al: Dual-energy multidetector CT: How does it work, what can it tell us, and when can we use it in abdominopelvic imaging? *Radiographics* 30:1037-1055, 2010.
- Morgan DE: Dual-energy CT of the abdomen. *Abdom Imaging* 39:108-134, 2014.
- Johnson TR: Dual-energy CT: General principles. *AJR Am J Roentgenol* 199:S3-S8, 2012.

22. Fischer MA, Reiner CS, Raptis D, et al: Quantification of liver iron content with CT—added value of dual-energy. *Eur Radiol* 21:1727–1732, 2011.
23. Xiangpeng Z, Ren Y, Phillips WT, et al: Assessment of hepatic fatty infiltration using spectral computed tomography imaging: A pilot study. *J Comput Assist Tomogr* 37:134–141, 2013.
24. Joe E, Kim SH, Lee KB, et al: Feasibility and accuracy of dual-source dual-energy CT for noninvasive determination of hepatic iron accumulation. *Radiology* 262:126–135, 2012.
25. Amis ES, Butler PF: ACR white paper on radiation dose in medicine: Three years later. *J Am Coll Radiol* 7:865–870, 2010.
26. Maccougall RD, Strauss KJ, Lee EY: Managing radiation dose from thoracic multidetector computed tomography in pediatric patients: Background, current issues, and recommendations. *Radiol Clin North Am* 51:743–760, 2013.
27. Crawley MT, Booth A, Wainwright A: A practical approach to the first iteration in the optimization of radiation dose and image quality in CT: Estimates of the collective dose savings achieved. *Br J Radiol* 74:607–614, 2001.
28. Minhas AS, Frush DP: Compendium of resources for radiation safety in medical imaging using ionizing radiation. *J Am Coll Radiol* 10:354–360, 2013.
29. The Measurement, Reporting, and Management of Radiation Dose in CT. Report No. 96. College Park, Md, 2008, American Association of Physicists in Medicine.
30. Huda W: Radiation dosimetry in diagnostic radiology. *AJR Am J Roentgenol* 169:1487–1488, 1997.
31. Kalra MK, Maher MM, Toth TL, et al: Techniques and applications of automatic tube current modulation for CT. *Radiology* 233:649–657, 2004.
32. Nagel HD, editor: Radiation Exposure in Computed Tomography: Fundamentals, Influencing Parameters, Dose Assessment, Optimization, Scanner Data, Terminology, ed 2, Frankfurt, 2000, COCIR.
33. McNitt-Gray MF: Radiation dose in CT. *Radiographics* 22:1541–1553, 2002.
34. Tamm EP, Rong XJ, Cody DD, et al: Quality initiatives: CT radiation dose reduction: How to implement change without sacrificing diagnostic quality. *Radiographics* 31:1823–1832, 2011.
35. Siegel MJ, Schmidt B, Bradley D, et al: Radiation dose and image quality in pediatric CT: Effect of technical factors and phantom size and shape. *Radiology* 233:515–522, 2004.
36. Schindera ST, Nelson RC, Lee ER, et al: Abdominal multislice CT for obese patients: Effect on image quality and radiation dose in phantom study. *Acad Radiol* 14:486–494, 2007.
37. Kanal KM, Stewart BK, Kolokythas O, Shuman WP: Impact of operator-selected image noise index and reconstruction slice thickness on patient radiation dose in 64-MDCT. *AJR Am J Roentgenol* 189:219–225, 2007.
38. Pickhardt PJ, Lubner MG, Kim DH, et al: Abdominal CT with model-based iterative reconstruction (MBIR): Initial results of a prospective trial comparing ultralow-dose with standard-dose imaging. *AJR Am J Roentgenol* 199:1266–1274, 2012.
39. Burgener FA, Hamlin DJ: Contrast enhancement in abdominal CT: Bolus versus infusion. *AJR Am J Roentgenol* 137:351–358, 1981.
40. Foley WD, Berland LL, Lawson TL, et al: Contrast enhancement technique for dynamic hepatic computed tomographic scanning. *Radiology* 147:797–803, 1983.
41. Wang L: Morphological and functional MDCT: Problem-solving tool and surrogate biomarker for hepatic disease clinical care and drug discovery in the era of personalized medicine. *Hepat Med* 2:111–124, 2010.
42. Silverman PM: Pharmacokinetics of contrast enhancement in body CT: Implications for spiral (helical) scanning. In Fishman EK, Jeffrey RB, editors: *Spiral CT: Principles, Techniques and Clinical Applications*, New York, 1995, Raven, pp 11–23.
43. Foley WD, Mallisee TA, Hohenwarter MD: Multiphase hepatic CT with a multirow detector CT scanner. *AJR Am J Roentgenol* 175:679–685, 2000.
44. Hanninen EL, Vogl TF, Felfe R: Detection of focal liver lesions at biphasic spiral CT: Randomized double-blind study of the effect of iodine concentration in contrast material. *Radiology* 216:403–409, 2000.
45. Fleischman D: Use of high concentration contrast media: Principles and rationale. *Eur J Radiol* 45:S88–S93, 2003.
46. Harris JP, Nelson RC: Abdominal imaging with multidetector computed tomography. *J Comput Assist Tomogr* 28:S1–S19, 2004.
47. Yagyu Y, Awai K, Inoue M, et al: MDCT of hypervascular hepatocellular carcinomas: A prospective study using contrast materials with different iodine concentrations. *AJR Am J Roentgenol* 184:1535–1540, 2005.
48. Laghi A: Multidetector CT (64 slices) of the liver: Examination techniques. *Eur Radiol* 17:675–683, 2007.
49. Small WC, Nelson RC, Bernardino ME: Contrast-enhanced spiral CT of the liver: Effect of different amounts and injection rates of contrast material on early contrast enhancement. *AJR Am J Roentgenol* 163:87–92, 1994.
50. Jeffrey RB: Multidetector CT of hepatic tumors. In Fishman EK, Jeffrey RB, editors: *Multidetector CT: Principles, Techniques, and Clinical Applications*, Philadelphia, 2004, Lippincott Williams & Wilkins, pp 185–198.
51. Megibow AJ, Jacob G, Heiken JP, et al: Quantitative and qualitative evaluation of volume of low osmolality contrast medium needed for routine helical abdominal CT. *AJR Am J Roentgenol* 176:583–589, 2001.
52. Tublin ME, Tessler FN, Cheng SL, et al: Effect of injection rate of contrast medium on pancreatic and hepatic helical CT. *Radiology* 210:97–101, 1999.
53. Morden P, Sokhandon F, Miller L, et al: The role of saline flush injection rate in displacement of CT-injectable peripherally inserted central catheter tip during power injection of contrast material. *AJR Am J Roentgenol* 202:W13–W18, 2014.
54. Oliver JH, Baron RL: Helical biphasic contrast-enhanced CT of the liver: Technique, indications, and pitfalls. *Radiology* 201:1–14, 1996.
55. Garcia PA, Bonaldi VM, Bret PM, et al: Effect of rate of contrast medium injection on hepatic enhancement at CT. *Radiology* 199:185–189, 1996.
56. Chambers TP, Baron RL, Lush RM: Hepatic CT enhancement: Part I. Alterations in the volume of contrast material within the same patients. *Radiology* 193:513–517, 1994.
57. Chambers TP, Baron RL, Lush RM: Hepatic CT enhancement: Part II. Alterations in the contrast material volume and rate of injection within the same patients. *Radiology* 193:518–522, 1994.
58. Sheafor DH, Keogan MT, DeLong DM, et al: Dynamic helical CT of the abdomen: Prospective comparison of pre- and postprandial contrast enhancement. *Radiology* 206:359–363, 1998.
59. Bae KT, Heiken JP, Brink JA: Aortic and hepatic contrast medium enhancement at CT: Part II. Effect of a reduced cardiac output in a porcine model. *Radiology* 207:657–662, 1998.
60. Silverman PM, Roberts SC, Ducic I, et al: Assessment of a technology that permits individualized scan delays on helical hepatic CT: A technique to improve efficiency of contrast material. *AJR Am J Roentgenol* 167:79–84, 1996.
61. Silverman PM, Brown B, Wray H, et al: Optimal contrast enhancement of the liver using helical (spiral) CT of the liver: Value of SmartPrep. *AJR Am J Roentgenol* 164:1169–1171, 1995.
62. Dorio PJ, Lee FT, Henseler KP, et al: Using a saline chaser to decrease contrast media in abdominal CT. *AJR Am J Roentgenol* 180:929–934, 2003.
63. Haage P, Schmitz-Rode T, Hubner D, et al: Reduction of contrast material dose and artifacts by a saline flush using a double power injector in helical CT of the thorax. *AJR Am J Roentgenol* 174:1049–1053, 2000.
64. Federle MP: Liver windows in body CT. *AJR Am J Roentgenol* 163:1525, 1994.
65. White T: A plea for narrow windows. *AJR Am J Roentgenol* 165:1307–1308, 1995.
66. Van Hoe L, Van Cutsem E, Vergote I, et al: Size quantification of liver metastasis in patients undergoing cancer treatment: Reproducibility of one-, two- and three-dimensional measurements determined with spiral CT. *Radiology* 202:671–675, 1997.
67. Fornage BD: Measuring masses on cross-sectional images [letter]. *Radiology* 189:289, 1993.
68. Dresser TS, Sommer GF, Jeffrey RB: Value of curved planar reformations in MDCT of abdominal pathology. *AJR Am J Roentgenol* 182:1477–1484, 2004.
69. Fishman EK, Ney DR, Heath DG, et al: Volume rendering versus maximum intensity projection in CT angiography: What works best, when and why. *Radiographics* 26:905–922, 2006.
70. Takeshita K, Furui S, Takada K: Multidetector row helical CT of the pancreas: Value of three-dimensional images, two-dimensional reformations, and contrast-enhanced multiphase imaging. *J Hepatobiliary Pancreat Surg* 9:576–582, 2002.
71. Yaghamai V, Miller FH, Rezai P, et al: Response to treatment series: Part 2, tumor response assessment—using new and conventional criteria. *AJR Am J Roentgenol* 197:18–27, 2011.
72. Kamel IR, Kruskal JB, Warmbrand G, et al: Accuracy of volumetric measurements after virtual right hepatectomy in potential donors undergoing living adult liver transplantation. *AJR Am J Roentgenol* 176:483–487, 2001.
73. Van der Vorst JR, van Dam RM, van Stiphout RS, et al: Virtual liver resection and volumetric analysis of the future liver remnant using open source image processing software. *World J Surg* 34:2426–2433, 2010.
74. Zeman RK, Baron RL, Jeffery RB, et al: Helical body CT: Evolution of scanning protocols. *AJR Am J Roentgenol* 170:1427–1437, 1998.

75. Ros PR, Hoon J: Multisection (multidetector) CT: Applications in the abdomen. *Radiographics* 22:697–700, 2002.
76. Saini S: Multi-detector row CT: Principles and practice for abdominal applications. *Radiology* 233:323–327, 2004.
77. Foley WD: Multidetector CT: Abdominal visceral imaging. *Radiographics* 22:701–709, 2002.
78. Bader TR, Prokesch RW, Grabenwoger F: Timing of the hepatic arterial phase during contrast enhanced computed tomography of the liver: Assessment of normal values in 25 volunteers. *Invest Radiol* 35:486–492, 2000.
79. Kopp AF, Heuschmid M, Claussen CD: Multi-detector helical CT of the liver for tumor detection and characterization. *Eur Radiol* 12:745–752, 2002.
80. Schiavon G, Ruggiero A, Bekers DJ, et al: The effect of baseline morphology and its change during treatment on the accuracy of Response Evaluation Criteria in Solid Tumours in assessment of liver metastases. *Eur J Cancer* 50:972–980, 2014.
81. Miller FH, Butler RS, Hoff FL, et al: Using triphasic helical CT to detect focal hepatic lesions in patients with neoplasms. *AJR Am J Roentgenol* 171:643–649, 1998.
82. Kawata S, Murakami T, Kim T, et al: Multidetector CT: Diagnostic impact of slice thickness on detection of hypervascular hepatocellular carcinoma. *AJR Am J Roentgenol* 179:61–66, 2002.
83. Weg N, Scheer MR, Gabor MP: Liver lesions: Improved detection with dual-detector-array CT and routine 2.5-mm thin collimation. *Radiology* 209:417–426, 1998.
84. Haider MA, Amitai MM, Rappaport DC, et al: Multi-detector row helical CT in preoperative assessment of small (≤ 1.5 cm) liver metastasis: Is thinner collimation better? *Radiology* 225: 137–142, 2002.
85. Schwartz LH, Gandras EJ, Colangelo SM, et al: Prevalence and importance of small hepatic lesions found at CT in patients with cancer. *Radiology* 210:71–74, 1999.
86. Robinson PJA: Imaging liver metastasis: Current limitations and future prospects. *Br J Radiol* 73:234–241, 2000.
87. Keogan MT, Seabourn JT, Paulson EK, et al: Contrast-enhanced CT of intrahepatic and hilar cholangiocarcinoma: Delay time for optimal imaging. *AJR Am J Roentgenol* 169: 1493–1499, 1997.
88. Valls C, Ruiz S, Martinez L, et al: Radiological diagnosis and staging of hilar cholangiocarcinoma. *World J Gastrointest Oncol* 5:115–126, 2013.
89. Fleischmann D, Kamaya A: Optimal vascular and parenchymal contrast enhancement: The current state of the art. *Radiol Clin North Am* 47:13–26, 2009.
90. Awai K, Takada K, Onishi H, Hori S: Aortic and hepatic enhancement and tumor to liver contrast: Analysis of the effect of different concentrations of contrast media at multidetector row helical CT. *Radiology* 224:757–763, 2002.
91. Miller DL, Simmons JT, Chang R, et al: Hepatic metastasis detection: Comparison of three CT contrast enhancement methods. *Radiology* 165:785–790, 1987.
92. Bluemke DA, Soyer PA, Chan BW, et al: Spiral CT during arterial portography: Techniques and applications. *Radiographics* 15:623–637, 1995.
93. Lupetin AR, Cammisa BA, Beckman I, et al: Spiral CT during arterial portography. *Radiographics* 16:723–724, 1996.
94. Hori M, Murakami T, Oi H, et al: Sensitivity in detection of hypervascular hepatocellular carcinoma by helical CT with intra-arterial injection of contrast medium, and by helical CT and MR imaging with intravenous injection of contrast medium. *Acta Radiol* 39:144–151, 1998.
95. Tunaci M: Multidetector row CT of the pancreas. *Eur J Radiol* 52:18–30, 2004.
96. Fenchel S, Boll DT, Fleiter TR: Multislice helical CT of the pancreas and spleen. *Eur J Radiol* 45:S59–S72, 2003.
97. Fenchel S, Fleiter TR, Aschoff AL, et al: Effect of iodine concentration of contrast media on contrast enhancement in multislice CT of the pancreas. *Br J Radiol* 77:821–830, 2004.
98. Sahani D, Shah ZK: Soft-organ MDCT imaging: Pancreas and spleen. In Sahani S, Rubin GD, Kalra MK, editors: *MDCT: A Practical Approach*, Berlin, 2006, Springer.
99. McNulty NJ, Francis IR, Platt JF, et al: Multidetector row helical CT of the pancreas: Effect of contrast enhanced multiphasic imaging on enhancement of the pancreas, peripancreatic vasculature, and pancreatic adenocarcinoma. *Radiology* 220:97–102, 2001.
100. Schima W, Ba-Ssalamah A, Kolblinger C, et al: Pancreatic adenocarcinoma. *Eur Radiol* 17: 638–649, 2007.
101. Satoi S, Yamamoto H, Takai S, et al: Clinical impact of multidetector row computed tomography on patients with pancreatic cancer. *Pancreas* 34:175–179, 2007.
102. Fishman EK, Jeffrey RB, Jr: *Multidetector CT: Principles, Techniques and Clinical Applications*, Philadelphia, 2004, Lippincott Williams & Wilkins.
103. Vargas R, Nino-Murcia M, Trueblood W, et al: MDCT in pancreatic adenocarcinoma: Prediction of vascular invasion and resectability using a multiphasic technique with curved planar reformations. *AJR Am J Roentgenol* 182:419–425, 2004.
104. Fujishiro T, Shuto K, Hayano K, et al: Preoperative hepatic CT perfusion as an early predictor for the recurrence of esophageal squamous cell carcinoma: Initial clinical results. *Oncol Rep* 31:1083–1088, 2014.
105. Pandharipande PV, Krinsky GA, Rusinek H, et al: Perfusion imaging of the liver: Current challenges and future goals. *Radiology* 234: 661–673, 2005.
106. Hatwell C, Zappa M, Wagner M, et al: Detection of liver micrometastases from colorectal origin by perfusion CT in a rat model. *Hepatobiliary Pancreat Dis Int* 13:303–308, 2014.

Ultrasound Examination of the Solid Abdominal Viscera

STUART A. BARNARD | PATRICK M. VOS | PETER L. COOPERBERG

CHAPTER OUTLINE

Basic Physics

Recent Developments

Doppler Ultrasound

Ultrasound Contrast Media

Ultrasound Artifacts

Liver

Gallbladder and Biliary Tract

Pancreas

Spleen

Ultrasound is an ideal modality for examination of the solid abdominal viscera. It is relatively inexpensive and portable and does not require the use of potentially harmful ionizing radiation or contrast agents. It enables real-time examination and can be used in the emergency department and by the bedside in the wards. Continual improvements in ultrasound technology and computing during the six decades since medical ultrasound was first developed have ensured that it remains the first-choice modality for many applications within the abdomen. Ultrasound has several advantages over computed tomography (CT) and magnetic resonance imaging (MRI), including cost (and hence ease of access), real-time imaging, portability, lack of ionizing radiation, and absence of contraindications, although the cross-sectional modalities are often complementary. Further advances in ultrasound technology will ensure that it retains a central role in abdominal imaging for the foreseeable future.

The first use of medical ultrasound was documented in Austria in 1942 by Karl Dussik, who imaged the ventricles of the brain and brain tumors. Another pioneer of medical ultrasound, Ian Donald in Glasgow, built on innovations in the fields of sonar, radar, and ultrasonic flaw detection in metals to image uterine fibroids and ovarian cysts. He also published a paper entitled "The Investigation of Abdominal Masses by Pulsed Ultrasound" in 1958.¹ Several technologic innovations were necessary to drive ultrasound forward as the commonplace medical imaging technique we know today. The first static arm commercial medical scanners were marketed in the 1960s, but the technique was slow and the machines were cumbersome. Real-time scanners soon replaced static arm scanners. These early scanners used the A-mode technique, in which the amplitude of returning echoes along a single line was displayed on an oscilloscope screen. Later B-mode compound scan images were composed of only black and white. Gray-scale imaging improved

interpretation and is now the standard for abdominal imaging. The development of the transistor and later the integrated circuit improved signal generation and amplification. All modern machines now employ digital signal processing techniques, and improvements in the design and manufacture of probes have allowed the development of compact, robust, and versatile probes for a variety of applications.

The real-time nature of imaging with ultrasound lends itself particularly well to problem solving. Movement with respiration can be examined, tubular structures can be followed, and structures can be examined in different planes. Ultrasound can aid interventional procedures, such as fine-needle aspiration, core biopsy, and drain placement, and it is the modality of choice for guiding interventional procedures within the abdominal solid organs,² although on occasion it may be necessary to supplement it with fluoroscopy, CT, or MRI. However, the real-time nature of ultrasound requires competence on the part of the ultrasonographer or sonologist performing the examination. Although the examination is performed in real time with up to 60 frames per second, only a fraction of these are saved as representative images for future review. Thus the experience of the operators is important because they will decide on the images to store. Picture archiving and storage (PACS) systems have enabled more still images to be stored without incurring the cost of printing film and may also allow the storage of cine loops to show dynamic processes.

Ultrasound enables blood flow to be easily demonstrated without the need for nephrotoxic contrast agents, and neither the patient nor the operator is exposed to harmful ionizing radiation. The ability of ultrasound to differentiate between solid and cystic structures is a particular strength.

Basic Physics

Medical ultrasound uses short pulses of sound waves that are transmitted and received by the transducer (Fig. 66-1). A coupling gel is used to facilitate the transmission of sound waves to and from the probe. This matches the acoustic impedance of the probe to that of tissue and eliminates air gaps between the probe and the skin. The basic element of most current transducers is a piezoelectric crystal that emits a sound wave when a voltage is applied to it (transmission) and generates a voltage when the reflected sound wave returns to it (reception). The voltages produced by each crystal on receiving reflected sound waves are converted into digital signals by an analog to digital signal converter and processed by the ultrasound machine to form the image. Future transducer designs may use alternative methods of transducer construction,³ but the principles of sound wave generation and reception will remain the same. The probe contains multiple crystals arranged in a strip or a grid. There are typically 128 individual crystals within a transducer

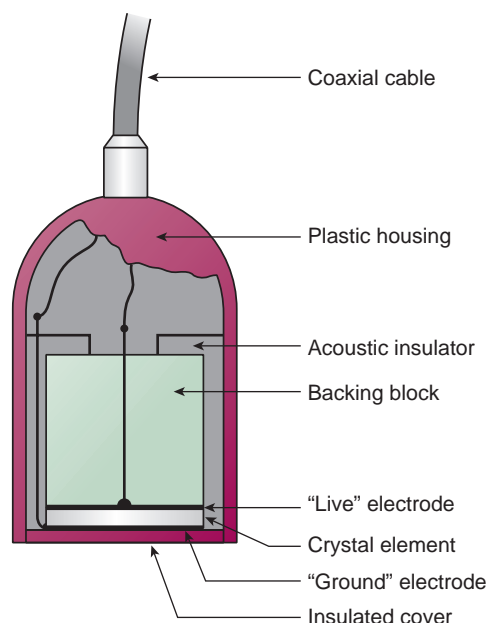


Figure 66-1 Components of an ultrasound transducer. The crystal element has piezoelectric properties. (From Curry TS, Dowdey JE, Murry RC: *Christensen's Physics of Diagnostic Radiology*, 2nd ed. Philadelphia, Lea & Febiger, 1990, p 328.)

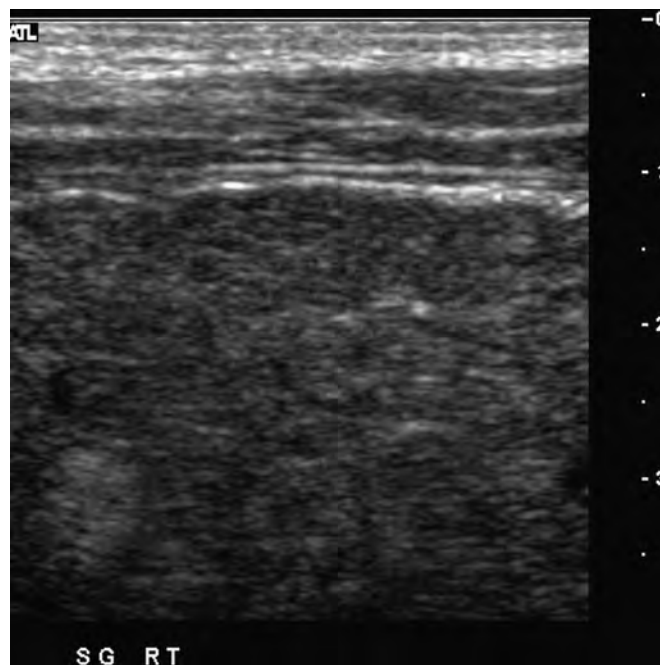


Figure 66-2 Hepatic cirrhosis. Superficial aspect of the liver scanned with a 7-MHz linear transducer showing nodular surface due to cirrhosis.

array, and they can be independently activated; this allows the ultrasound beam to be electronically steered and focused. Earlier designs used mechanical devices to steer and focus the beam, but these have largely been superseded by electronic controls. The best resolution of an image is within the focal zone, and focusing allows the focal zone to be varied according to the area of interest being examined. The beams of array transducers can be focused on both transmit and receive. Some transducers allow multiple focal zones to be selected to increase the effective focal zone, but this will reduce the frame rate or temporal resolution of the scan.

Several factors have to be taken into account in considering the most appropriate choice of transducer for a given application. Modern transducers suitable for abdominal imaging include linear arrays, curved linear arrays, and sector scanners. Linear arrays (typically 7–12 MHz) provide excellent resolution at the expense of penetration and field of view. They are ideal for superficial lesions or for examining the surface of abdominal viscera, such as the liver (Fig. 66-2). The field of view can be extended by the use of trapezoidal imaging (Fig. 66-3) or compound (or extended field of view) imaging, in which the probe is moved across a structure and the ultrasound machine “stitches together” the images to produce a panoramic image. This is useful for large superficial lesions, such as soft tissue tumors (Fig. 66-4). Curved linear (or curvilinear) arrays are less effective for the examination of superficial structures but provide better penetration (because of their lower frequencies) and a wider field of view. Sector scanners have a limited role in routine abdominal ultrasound but do provide a wide field of view with a small footprint, which can be useful when access is limited, for example, in examining the pediatric abdomen. A compromise must be reached between penetration and resolution, which are inversely proportional. Raising the frequency of the transmitted ultrasound pulse will improve resolution because



Figure 66-3 Trapezoid scan. A trapezoid scan area can be selected with some linear transducers to extend the field of view but maintain the resolution of a high-frequency linear transducer.

of shortening of the wavelength, but it will also decrease the penetration as high frequencies are attenuated more than low frequencies are (attenuation of the sound wave is proportional to frequency). Many modern transducers allow the operator to vary the transmitted frequency within a certain range without having to change probes, for example, from 1 to 5 MHz for a typical curvilinear probe. Most modern ultrasound machines will select the transmitted frequency on the basis of the user's selection of presets, optimizing the image for detail or resolution (high frequency) or penetration (low frequency).



Figure 66-4 Extended field of view demonstration of abdominal wall desmoid tumor.

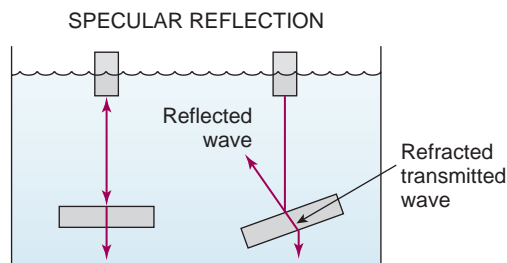


Figure 66-5 Specular versus nonspecular echoes. Specular reflectors are large interfaces that must be close to the perpendicular of the beam path for the reflected wave in many directions. Some of the wave returns to the transducer. (From Sarti DA: *Diagnostic Ultrasound: Text and Cases*, 2nd ed. Chicago, Year Book Medical, 1987, p 10.)

Sound waves interact with the tissues of the body in three main ways: reflection, absorption, and scatter. The terminology used to describe ultrasound findings is a description of the brightness of the structure; the more sound energy reflected back to the transducer, the brighter the object on the image. Objects are described as hypoechoic (darker than adjacent structures), isoechoic (the same brightness as adjacent structures), or hyperechoic (brighter than adjacent structures). Anechoic structures appear black and indicate fluid. Internal echoes may be caused by debris, septations, or artifacts. Often the liver is chosen as a reference in the abdomen, but care must be taken to ensure that the reference organ is of normal reflectivity and not abnormal due to fatty infiltration, for example. The amount of energy reflected back to the transducer depends on several factors. The simplest form of reflection occurs when sound waves encounter a flat interface perpendicular to the beam with a large disparity in the velocity of sound between the adjacent tissues; this is termed a specular reflector and will appear as a well-defined bright line (Fig. 66-5). Smaller interfaces (0.1-1 mm in diameter) may cause scattering in all directions. Only a small fraction of the transmitted energy is returned to the probe, but when multiple such structures are present, the interference pattern between echoes produces a visible texture.

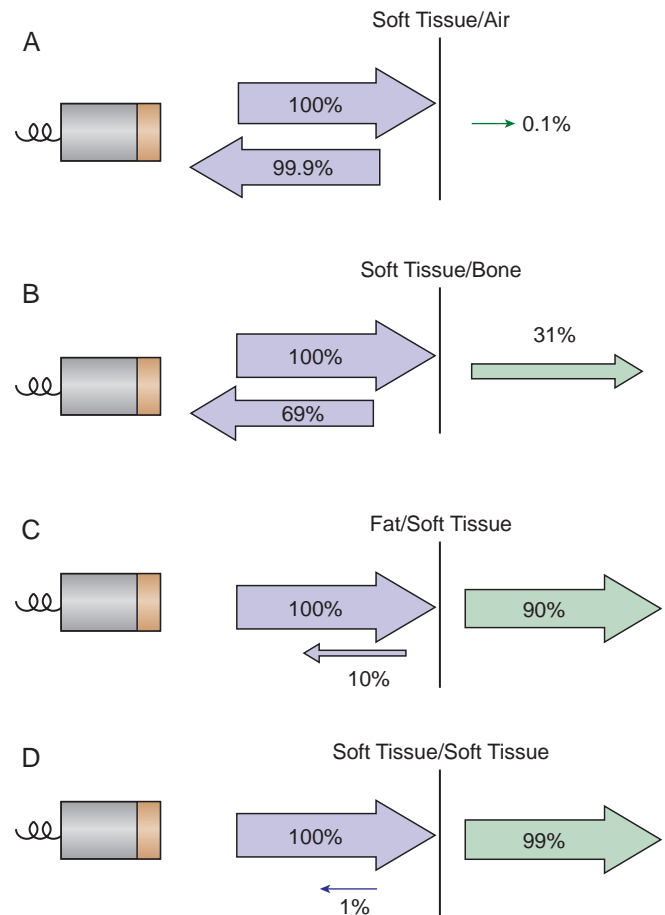


Figure 66-6 Sound wave transmission and reflection. The percentages of sound transmission and reflection at different interfaces (A-D) are illustrated. This is for the amplitude of a wave. (From Sarti DA: *Diagnostic Ultrasound: Text and Cases*, 2nd ed. Chicago, Year Book Medical, 1987, p 8.)

This process is responsible for the ultrasound appearance of liver, spleen, and kidney parenchyma.

Sound waves propagate through tissues at different velocities, and when there is an interface between different tissues, the sound may be reflected or refracted (just as light may be reflected or refracted by a prism of glass). The greater the difference in velocity between the adjacent tissues, the greater proportion is reflected (if the incident angle of the beam is large) or the more the beam is refracted (if the incident angle of the beam is smaller) (Fig. 66-6).

Recent Developments

Ultrasound machines continue to rapidly evolve with the introduction of new technology. Although the principles of physics remain the same, manufacturers have developed new methods of probe construction, ultrasound generation, and postprocessing algorithms. Often these are assigned brand-specific trademarked titles that may be rather opaque to the user.

Many ultrasound machines now allow the user to select a real-time compound imaging mode, whereby the area to be examined is insonated from several different directions by electronic beam steering for transmission and reception. The

displayed image is an average of the images derived from different insonation angles. This has been shown to improve overall image quality, to increase lesion conspicuity, and to reduce artifact.⁴ However, it does reduce the frame rate and can lead to image blurring if the transducer or the subject is moving.

A recent development that is now standard on most machines is tissue harmonic imaging. “Conventional” imaging without harmonics is known as fundamental imaging because only the fundamental transmitted frequency is used for transmission and reception. Tissue harmonic imaging was originally proposed for use with an ultrasound contrast agent, but it has been shown to improve visualization of abdominal structures without the use of contrast agents.^{5,6} The shape of the transmitted waveform changes as a sound wave is propagated through tissue, particularly in the focal zone, where the intensity is high. Tissues resist compression more than expansion. This is termed nonlinear behavior. The waveform of the reflected pulse is altered and contains higher frequencies than the transmitted pulse. The higher frequencies are multiples of the transmitted fundamental frequency, called harmonic frequencies. At present, it is usually the second harmonic (twice the fundamental frequency) that is used for imaging, but higher multiples may also be used. The fundamental frequencies are electronically filtered out after reception, leaving only the harmonic frequencies. The harmonic frequencies travel through the tissues only once on the return to the probe and therefore are attenuated half as much as an identical frequency transmitted and received by the probe. There is less scatter, particularly in obese patients, in whom subcutaneous fat and superficial muscle layers cause scatter and attenuation of the fundamental frequencies, which may cause a haze of echoes, degrading the image on fundamental imaging. Artifacts such as side and grating lobe artifacts that degrade fundamental images are also reduced because the weak side and grating lobes are not powerful enough to produce harmonic frequencies. The images are clearer, and tissue harmonic imaging may improve diagnostic ability in challenging patients.⁷ Phase inversion imaging also exploits the nonlinear behavior of tissues but employs a different technique from frequency-based tissue harmonic imaging.^{8,9} Two pulses are sent with 180-degree phase difference. If the pulse is reflected in a linear fashion, the reflected waves will cancel each other out. If the waves are reflected in a nonlinear fashion, the waves will not cancel out and are used to form the image. Phase inversion harmonic imaging reduces the frame rate because of the need to transmit twice as many pulses, but the spatial resolution is better than that of frequency-based tissue harmonic imaging.

Three-dimensional and four-dimensional ultrasound applications are established in obstetric ultrasound,¹⁰ but their value is yet to be proved in abdominal imaging.¹¹ Improvements in processing and probe technology have made real-time three-dimensional volume rendered and multiplanar reconstruction imaging possible. An acquisition of a volume of data in a fashion akin to helical CT allows retrospective reconstruction of multiplanar reconstruction views and surface rendered images.

Doppler Ultrasound

The examination of blood flow with Doppler techniques is a valuable addition to real-time gray-scale abdominal ultrasound. The wavelengths of a transmitted sound pulse and the received pulse differ when sound waves are reflected from a moving surface. The wavelength shortens when the reflector is moving

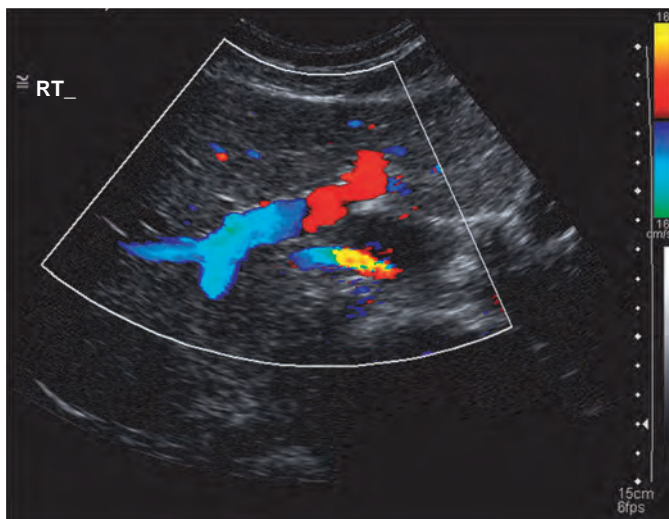


Figure 66-7 Color Doppler ultrasound scan showing normal flow in the left and right branches of the portal vein. Red represents flow toward the transducer, and blue, flow away from the transducer.

toward the transducer and lengthens when it is moving away. The change in wavelength is accompanied by a change in frequency and phase and is termed the Doppler effect. The Doppler frequency (or phase) shift is measured, and the velocity and direction of blood flow can be calculated. One method of displaying the information is as color flow, in which a color map of flow is superimposed on a gray-scale real-time image. Convention dictates that blood flow toward the transducer is red and blood flow away from the transducer is blue, although the operator may invert this. Color flow Doppler is used in the abdomen to examine the arterial tree, the portal venous system, and the systemic veins (Fig. 66-7). It may also be used to examine vascularity within the solid organs, for example, within or surrounding a mass lesion. The box displaying the color information can be resized and moved to include different parts of the image. A compromise between the color box size and the refresh rate of the image must be reached as an increased color box size will slow down the refresh rate of the image.

Power Doppler is a similar technique, but the total power of the reflected Doppler signal is displayed. There are no velocity data and therefore no indication of the direction of flow, but there are some advantages of power Doppler over color flow Doppler in certain situations.¹² Power Doppler is more sensitive to slow flow and, unlike color Doppler, can display flow that is almost perpendicular to the beam. Background noise appears as brightly colored speckles in color Doppler that can be distracting, whereas in power Doppler the background noise is dark, allowing higher gains to be used. It is thus a useful technique when the demonstration of low flow is needed but the direction of flow is not important.

The waveform and the direction of flow in vessels may change in disease states, such as portal hypertension. Pulsed-wave Doppler displays the flow velocity as a waveform, and this is often combined with gray-scale imaging as duplex imaging (Fig. 66-8). The flow is measured in a small sample volume that can be placed on the region of interest. The operator can adjust the position and the size of the sample volume. If quantitative measurement of flow is required, a correction has to be made as the Doppler beam is at an angle to the blood flow. The angle

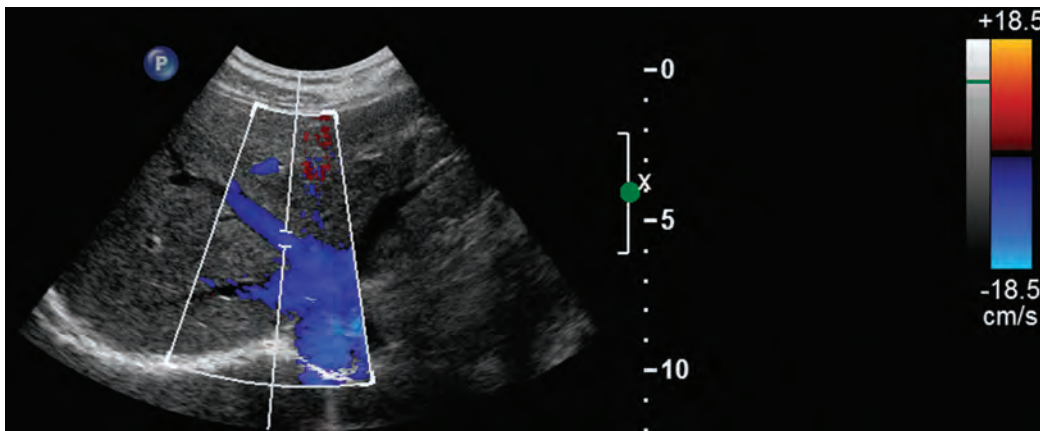


Figure 66-8 Color and pulsed-wave Doppler examination of the liver illustrating normal flow in the middle hepatic vein.

between the blood flow and the interrogating Doppler beam should be kept as small as possible; it is not possible to obtain a reliable Doppler velocity measurement if this angle exceeds 60 degrees.¹³ This quantitative data can be used to assess vascular resistance, for example, within a transplanted liver.

Ultrasound Contrast Media

Conventional ultrasound does have some limitations in the detection and characterization of liver lesions. Alternative cross-sectional imaging techniques, such as CT and MRI, have often been used to complement ultrasound to overcome these limitations. Ultrasound contrast agents have been developed to increase the sensitivity of ultrasound to small liver lesions and to improve the characterization when lesions are detected on the basis of their perfusion properties. The first-generation ultrasound contrast agents were based on air-filled bubbles and required high acoustic pressures (high mechanical index) to break the bubbles. Contrast enhancement was short-lived. Second-generation contrast agents are now available. These form small bubbles filled with gases other than air, such as sulfur hexafluoride,¹⁴ and allow real-time scanning at a low mechanical index depicting the different phases of blood flow, which is particularly useful in the liver. The appearances of a lesion in arterial, portal venous, and sinusoidal phases (15-35, 35-90, and 90-240 seconds, respectively) can be observed.¹⁵

Most modern ultrasound machines include technology that will allow imaging with contrast agents, but an estimated 60% of ultrasound machines currently in use worldwide do not have the capability.¹⁶ The contrast agent is administered through an intravenous cannula as a rapid bolus followed by a saline flush. The area is then scanned continuously to depict the different vascular phases, and the images are often recorded as a cine clip to allow later playback. Repeated injections of contrast agent are possible, if necessary, as the agents are of low toxicity.¹⁷

The detection of subcentimeter liver metastases is improved when contrast media are used.¹⁸ Contrast media can also be useful in differentiating benign from malignant tumors and characterizing the lesions.^{19,20} It has been suggested that a contrast agent should also be used in the assessment of abdominal trauma,²¹ in which it may be added to the FAST (focused assessment with sonography in trauma) protocol.²²

The use of ultrasound contrast agents remains highly variable, despite some encouraging clinical results. This is due to

many factors, including workflow issues, availability of suitable ultrasound machines, and remuneration. It seems unlikely that they will become a method of choice for characterization of liver lesions, as some proponents suggest.²³

Ultrasound Artifacts

The sonologist should be familiar with common artifacts to minimize their effect on image quality and to avoid confusion with significant pathologic changes,²⁴ although some of the processes described as artifacts can be helpful in interpreting images.

Several assumptions are made in forming an ultrasound image. It is assumed that the ultrasound beam travels in a straight line from the probe and in the body. The velocity of the sound wave is assumed to be constant on the path, and the received echoes are assumed to have traveled in a straight line back to the probe. If any of these assumptions are incorrect, an artifact will be produced.

If the ultrasound wave is propagated through a substance with reduced attenuation compared with the surrounding tissues, the region beyond it will appear brighter or more echogenic. This is due to the fact that a time gain compensation function is applied to the image, whereby the received echoes are amplified proportional to the time interval between pulse transmission and echo reception. The sound wave is attenuated as it passes through a structure, and the reflected echoes are also attenuated on their return to the transducer. If time gain compensation were not applied, deeper structures would appear unacceptably dark. If a structure, for example, a fluid-filled cyst, transmits sound waves effectively with little attenuation, the tissue beyond the cyst will appear brighter than equivalent adjacent tissue (Fig. 66-9). This phenomenon is called acoustic enhancement, and it is an important feature of fluid-filled lesions. Conversely, if a structure attenuates more than the surrounding tissue, tissues beyond it will appear darker and lie within the acoustic shadow. This is typical of solid lesions (Fig. 66-10). A very reflective surface, such as bone or air, will reflect the ultrasound beam and appear as a bright line with a very dark shadow beyond (Fig. 66-11). The ability to differentiate between solid and cystic lesions is an important strength of ultrasound. Gas collections and gas within the bowel tend to produce "dirty" shadows, which are less clear than the shadows produced by a solid lesion such as a calculus.²⁵

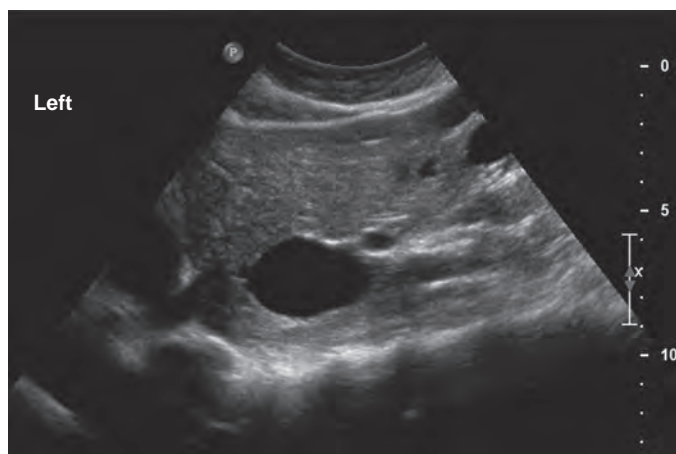


Figure 66-9 Simple hepatic cyst. Note the lack of perceptible wall, the anechoic contents, and the posterior acoustic enhancement.



Figure 66-10 Multiple solid hepatic lesions from metastatic neuroendocrine tumor. Note the hypoechoic rims, echoes within the lesions, and lack of posterior enhancement, differentiating them from cystic structures.

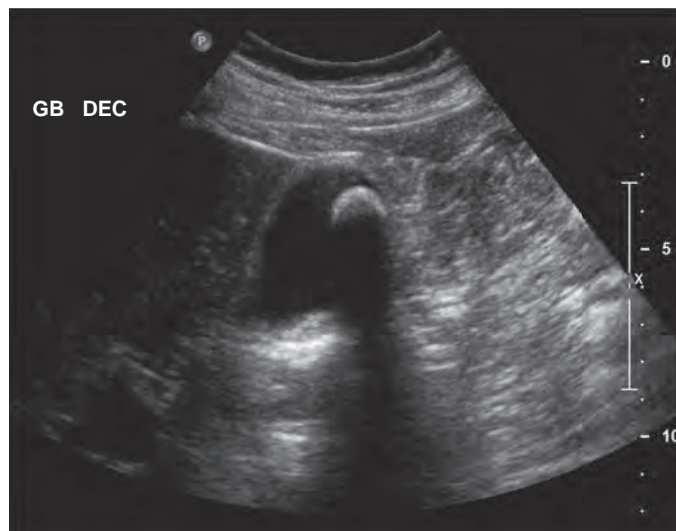


Figure 66-11 Single large gallstone. Note the bright anterior surface due to strong reflection and the posterior acoustic shadow.

Reverberation artifacts are a common source of image degradation that may mask disease. They occur when sound waves bounce back and forth between a strong interface and the transducer. As the reflections increase the length of the path, the artifact is seen deep to the interface. Such artifacts are commonly seen in the superficial aspect of the urinary bladder or in the near field of the liver.

Large specular reflectors, such as the air-pleura interface at the diaphragm, can produce artifactual structures to appear beyond them. As an example, the sound wave passes through the structure, such as a lesion in the liver, on the transmission path. Part of the sound wave is reflected back to the transducer and produces the appearance of the lesion in the correct location, but some passes through the lesion and is then reflected back toward the transducer by the right pleural-aerated lung interface acting as reflector. These sound waves will arrive at the transducer later than the “true” echoes from the liver lesion, and thus the artifactual structure will be placed deeper in the body on the display, beyond the reflecting surface. Common examples include liver lesions reflected posterior to the right hemidiaphragm (Fig. 66-12) and apparent pelvic masses reflected posterior to gas-containing loops of bowel in the pelvis.

If there are two or more reflectors close to each other, the sound waves may bounce back and forth between them and produce a comet-tail or ring-down artifact. Ring-down is an ultrasound artifact that appears as a solid streak or a series of parallel bands radiating away from the causative structure, which appears as bands of bright lines posterior to the reflector, the lines becoming shorter and less intense the deeper they are. Examples of causative structures include Rokitsky-Aschoff sinuses within the gallbladder wall (Fig. 66-13), gas in the biliary tree (Fig. 66-14), and surgical clips. Color Doppler will show a twinkle artifact analogous to a comet tail.

Refraction occurs when there is an oblique interface between tissues with different acoustic velocities. This is most commonly seen when the beam passes through the rectus muscles and can

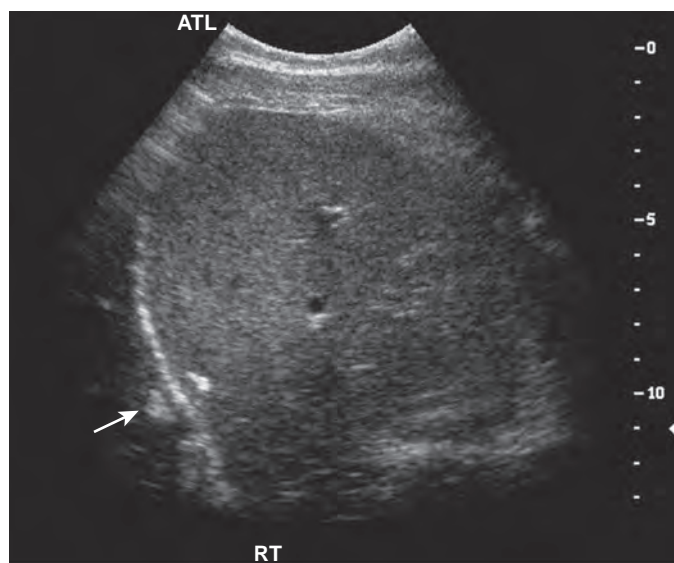


Figure 66-12 Mirror image artifact. Hemangioma (arrow) within the right lobe of the liver reflected in the right pleura-lung interface (the bright line curving superior to the liver) to produce an apparent, artifactual lesion in the right lung base.

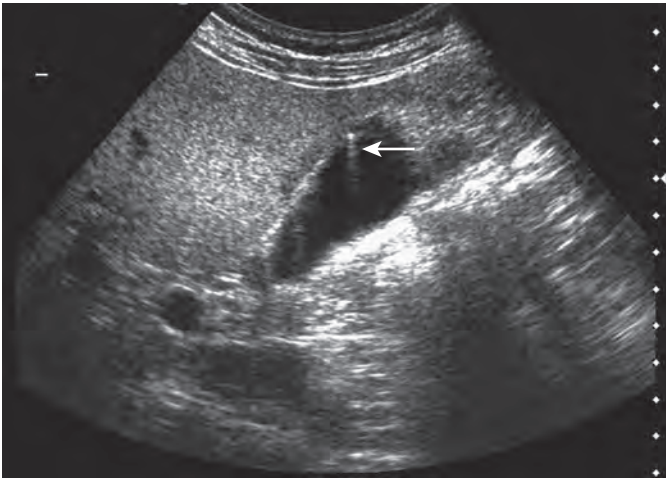


Figure 66-13 Comet-tail or ring-down artifact. Comet-tail artifact (arrow) arising from strongly reflective small cholesterol crystals in Rokitansky-Aschoff sinuses in the anterior gallbladder wall.

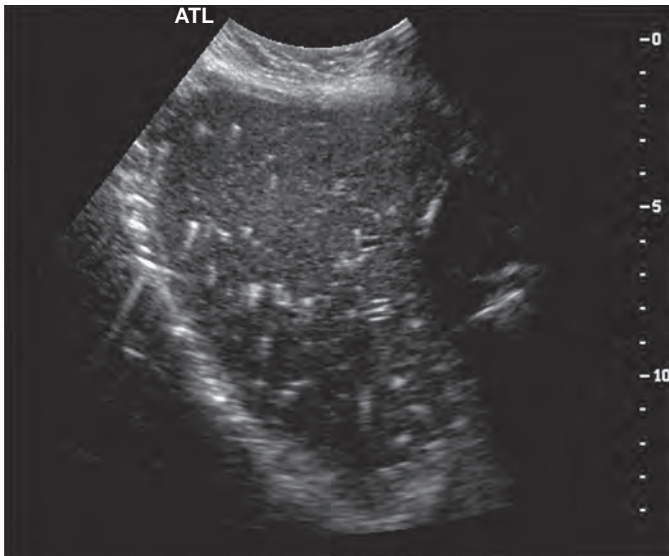


Figure 66-14 Intrabiliary gas. Gas in the biliary tract after endoscopic sphincterotomy, producing bright linear shadows with posterior ring-down artifact.

produce duplication of deeper structures. Movement of the probe eliminates the artifact.

Liver

Ultrasound of the liver is one of the most common examinations in a general ultrasound practice. Information can be gained about the liver echotexture in diffuse liver disease, and focal liver lesions can be characterized as cystic or solid. It may be used as an alternative or an adjunct to CT, and ultrasound is frequently used to guide needle biopsy and drainage procedures.

It is important to ensure that all segments of the liver are examined. Representative images are captured and recorded on film or a PACS system, but these serve only to demonstrate key anatomic structures or selected views of pathologic findings.

The operator makes use of the dynamic nature of real-time ultrasound to differentiate between normal and abnormal. The person reporting static images must therefore be satisfied that the operator has covered the entire liver and has sufficient experience to recognize pathologic changes. A cross section of a fluid-filled structure, such as a hepatic vein, may have similar appearance to a cystic lesion on a static image; but in real time, it can be followed by sweeping the transducer from side to side or turning the transducer through 90 degrees, and the tubular nature is appreciated in longitudinal section. A sweeping motion may also make subtle areas of altered echogenicity more apparent.

Appreciation of the anatomy of the liver is important for ensuring adequate coverage of the liver and for localizing lesions. The porta hepatis is the point at which the portal vein and hepatic artery enter the liver and the common hepatic duct leaves the liver. The plane of the porta hepatis lies approximately transversely. The portal vein divides into left and right branches before entering the liver itself; the anatomy of the hepatic artery is subject to much variation but always lies anterior to the portal vein. The artery lies medial to the common hepatic duct; in 90% it passes posterior to the duct, but in 10% it passes anteriorly. The right portal vein passes laterally in the liver before dividing into anterior and posterior branches; the left passes anteriorly and superiorly in a C shape.

The vascular structures of the liver are important in dividing the liver into the hepatic segments as defined by Couinaud,^{26,27} which enables accurate localization and assessment of the resectability of lesions, although the system is based on the fetal rather than on the adult pattern of circulation. Segment I is the caudate lobe, which receives blood from both the right and left portal veins; it also drains into the inferior vena cava (IVC) through its own short veins (often not visible on ultrasound). It is often spared in early diffuse liver disease, such as cirrhosis, or in hepatic vein occlusion (Budd-Chiari syndrome). Segments II and III are supplied by the left portal vein and divided by the plane of the left hepatic vein. Segment IV corresponds to the quadrate lobe and is separated from segments II and III by the umbilical fissure. A plane between the IVC posteriorly and the gallbladder fossa anteriorly divides the left and right lobes of the liver and corresponds to the line of the middle hepatic vein. The plane of the right branch of the portal vein may be used to divide segment IV into IVa superiorly and IVb inferiorly. The right lobe of the liver consists of segments V to VIII. The plane of the anterior and posterior branches of the right portal vein divides the right lobe into superior (VIII anterior and VII posterior) and inferior (V anterior and VI posterior) segments. The right hepatic vein divides the anterior from the posterior segment. The use of segments to describe liver anatomy has become more important with increasing correlation between different cross-sectional modalities and the use of interventions such as segmental resection and radiofrequency ablation of focal hepatic lesions (Fig. 66-15).

As the liver is a large organ, a systematic approach to its assessment with ultrasound is required to show representative images of the liver segments. The patient is initially positioned supine, although it may be necessary to rotate the patient onto the left side or into the left posterior oblique position during the examination. The patient is asked to take a deep breath in and to hold it as inspiration will move the liver and spleen caudally, making them more amenable to examination from the subcostal position. If it is not possible to image the entire liver

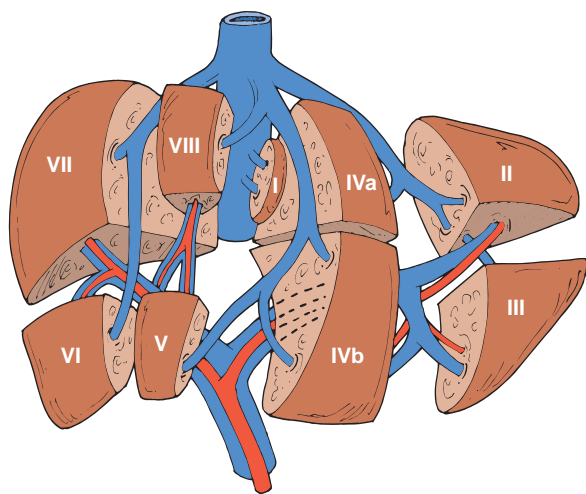


Figure 66-15 Segments of the liver as described by Couinaud. (From Meire H, Cosgrove D, Dewbury K, Farrant P: *Clinical Ultrasound: A Comprehensive Text—Abdominal and General Ultrasound*, vol 1, 2nd ed. London, Churchill Livingstone, 2001, p 167.)

from a subcostal transducer position, an intercostal approach may be necessary. This is best achieved with the patient in a left posterior oblique or left lateral decubitus (left side down) position. The liver should be thoroughly assessed in both transverse and longitudinal planes with a curvilinear transducer (5-1 MHz). Before any images are taken, the liver is quickly surveyed in both the longitudinal and transverse planes with a maximum sector width. This gives the operator an opportunity to view the liver parenchymal characteristics and to adjust the system settings accordingly to optimize the image, to check for any masses or cysts and abnormal liver contour and abnormal areas of echogenicity to determine whether the scan will be intercostal or subcostal, and to determine if there is hepatomegaly or a Riedel lobe and therefore take additional images to document this.

The transducer is obliquely positioned and angled subcostally toward the patient's right shoulder. With a continuous sweeping motion, the transducer is moved from the most lateral portion of the right lobe of liver through to the porta hepatis. When the most lateral portion of the left lobe of liver has been visualized, the transducer is rotated 90 degrees clockwise into a transverse position. The transducer is then angled in a cranial direction from a subcostal position to visualize beyond the superior portion of the left liver lobe. From this position, the transducer is moved caudally through the superior portion to the inferior aspect of the left liver lobe. This transverse scan is repeated on suspended inspiration throughout the whole liver, finishing at the inferior aspect of the right liver lobe. As soon as this general liver survey is over, the transducer is returned to the initial oblique position and angled subcostally toward the patient's right shoulder.

With the transducer in a sagittal orientation, the patient inhales and the depth of the image is adjusted so that the most lateral aspect of the right liver lobe dome and the diaphragm are shown. Adjusting the gain and time gain compensation to optimize the image will ensure an even distribution of echoes from the near field to the far field, thus giving the liver its normal homogeneous echotexture. If the liver is of a heterogeneous echotexture, this must be shown with careful adjustment of the gain and time gain compensation. The liver echogenicity

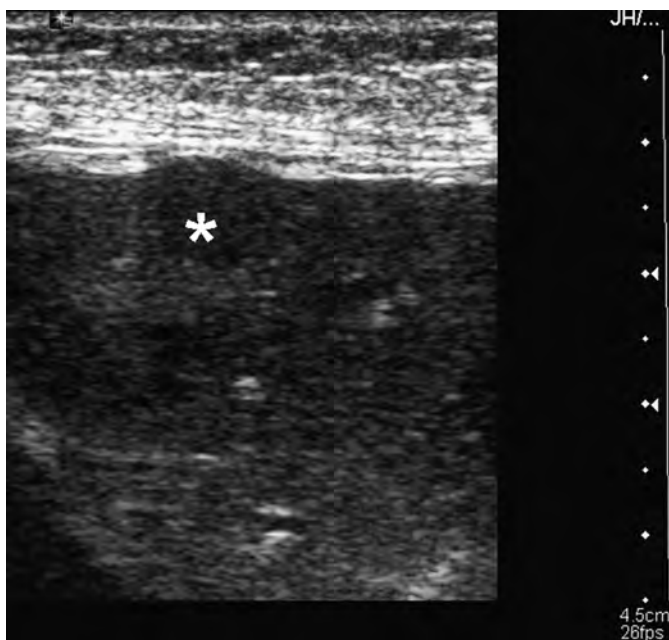


Figure 66-16 A linear transducer (7-12 MHz) probe was used to examine this cholangiocarcinoma metastasis (*) close to the surface of the liver. Linear transducers have better near-field resolution but are limited in their penetration. They are therefore suited to superficial lesions.

should be compared with that of the right kidney and an image recorded including both in one view. The liver parenchyma is normally less echogenic than the kidney. If the liver is more echogenic than the kidney, it may be due to fatty infiltration of the liver parenchyma. The transducer is moved more medially until the IVC is visualized with the caudate lobe anterior and posterior to it. The portal triad (portal vein, hepatic artery, and common bile duct) is demonstrated at the porta hepatis. Medial to this is the gallbladder fossa, the ligamentum venosum, and a complete view of the caudate lobe. The left lobe including the left hepatic vein is then imaged.

From the longitudinal position, the transducer is rotated 90 degrees clockwise into a transverse position. The left lobe of the liver is imaged to show the left hepatic vein and the left portal vein. The next image is of the left, main, and right hepatic veins draining into the IVC. These are imaged in gray scale and with color Doppler to show nonobstructed venous flow. The next image should document the ligamentum venosum and caudate lobe. Overall gain and time gain compensation adjustment may be required to adequately visualize the caudate lobe as it may appear hypoechoic compared with the rest of the liver because of attenuation of the ultrasound beam by the left portal vein or the liver fissures. The hockey stick-shaped bifurcation of the main portal vein (MPV) into the left and right branches should then be imaged. The right lobe, including the right branch of the portal vein and the right hepatic vein, is examined.

A higher frequency linear probe (8-4 MHz) may be used to examine the surface of the liver for nodularity or superficial lesions (Fig. 66-16). Fine surface nodularity in cirrhosis appears as a broken line on the surface of the liver.²⁸

Any masses, cystic lesions, or abnormal liver areas that are discovered during the scan are imaged separately in both the

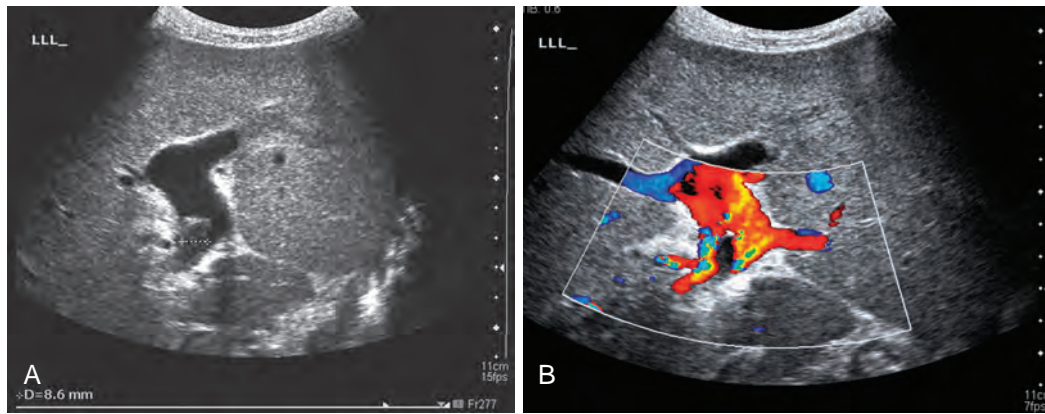


Figure 66-17 Nonocclusive thrombus in the right portal vein. Nonocclusive thrombus in the right portal vein (calipers in **A**) seen on gray-scale (**A**) and color Doppler (**B**) images.

longitudinal and transverse planes and characterized. They should be labeled according to the liver segment. Measurements should be taken and the lesions interrogated with color Doppler or power Doppler to check for unusual vascularity or mass effects on adjacent liver parenchyma. Image optimization of liver cysts can be achieved by reduction of the sector width, adjustment of the focal zone to the level of the cyst, write-zoom magnification, and removal of spatial compounding imaging to show the enhanced through-transmission of the ultrasound beam.

The hepatic vasculature should also be interrogated with color and pulsed Doppler. Color flow will give an indication of the direction of flow (which should be toward the liver), and thrombus may be apparent as filling defects (Fig. 66-17). The MPV should be assessed coronally and sagittally with the patient in the left lateral decubitus position. The coronal approach allows visualization of the longitudinal axis of the MPV. Normal portal venous flow is of low velocity toward the liver with a gentle respiratory variation (Fig. 66-18). In portal hypertension, the flow may become “to and fro,” then reversed (Fig. 66-19). The pulsatility of the MPV flow is assessed with spectral Doppler; the mean velocity in the fasted state is between 15 and 18 cm/s, which increases by 50% to 100% after eating.²⁹ The pulsed-wave sample volume is placed within the lumen of the MPV (before it bifurcates into the right and left branches) on a longitudinal view of the MPV without including the vessel wall and ensuring that the Doppler angle between the axis of the MPV and the Doppler beam is always less than 60 degrees. The velocity scale should be adjusted to improve sensitivity. The waveform of normal hepatopetal flow is monophasic flow toward the liver. As portal hypertension develops, the flow may become biphasic (forward flow in systole and reverse flow in diastole), then eventually reverse (hepatofugal).

Hepatofugal MPV flow is indicative of severe portal hypertension, and the common cause of this is liver cirrhosis. If hepatofugal portal vein flow is identified, recanalization of the umbilical vein and other portosystemic shunts may occur, and evidence of this should be sought (Fig. 66-20). The remainder of the abdomen should be examined, looking for splenomegaly and ascites. Hepatofugal flow may alternatively be due to occlusion of the MPV by thrombus or a mass. Multiple small tortuous vessels may be seen around the thrombosed MPV in cavernous transformation of the portal vein.

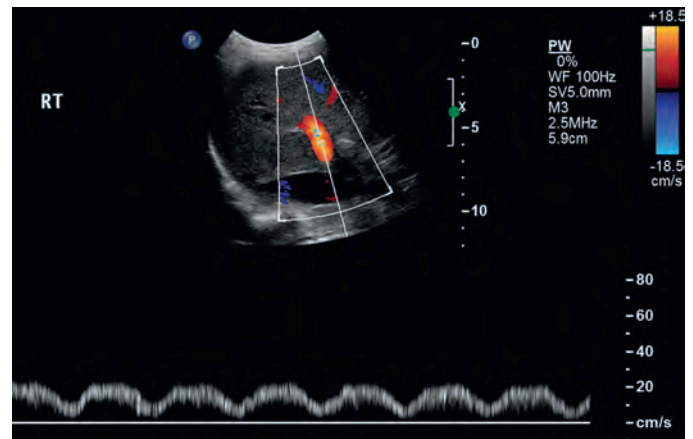


Figure 66-18 Color and pulsed-wave Doppler examination of the right portal vein showing normal flow.

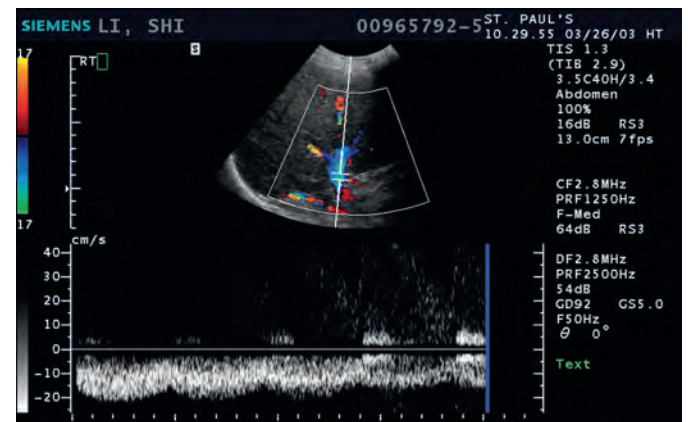


Figure 66-19 Color and pulsed-wave Doppler examination of the right portal vein showing reversed flow in a patient with cirrhosis and portal hypertension.

The sagittal approach allows the measurement of the diameter of the MPV at the porta hepatis where the MPV enters the liver. This is achieved by positioning the transducer just inferior to the xiphisternum and scanning subcostally. The diameter of the portal vein is measured at the point where it crosses the IVC

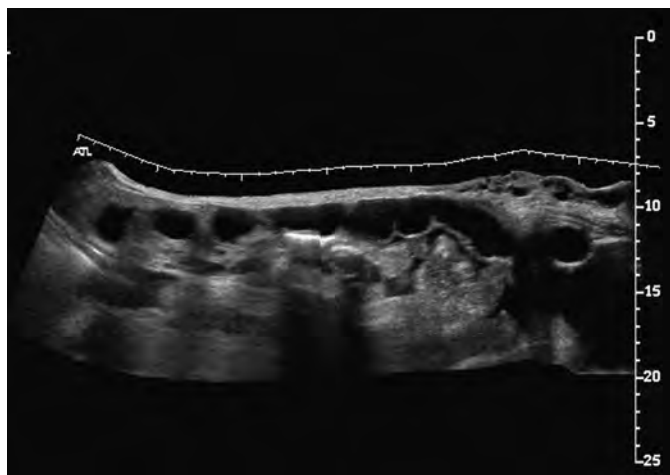


Figure 66-20 Dilated recanalized umbilical vein seen on an extended field of view image heading from the liver toward the umbilicus.



Figure 66-21 Fold in the neck of the gallbladder. This may cast a shadow and simulate calculi in the transverse plane.

(i.e., between the intrahepatic portion and the portal confluence). The measurement of the MPV is performed on the B-mode image; the calipers are positioned perpendicular to the vessel to exclude the echogenic portal vein walls and to measure only the portal vein lumen. This is performed while the patient is maintaining gentle respiration. A measurement greater than 13 mm is considered abnormal.³⁰

The hepatic artery should normally not exceed 6 mm in diameter, but it may enlarge in cases of alcoholic hepatitis or cirrhosis.³¹ The hepatic venous flow is normally triphasic, but the waveform may be altered by right-sided heart failure (which may also cause dilation of the veins), or thrombosis may occur. The thrombus may be isoechoic with liver parenchyma and missed unless the hepatic veins are deliberately sought, and color flow may help visualize hypoechoic or isoechoic thrombus. Occlusion of the veins may lead to Budd-Chiari syndrome with the development of congestive hepatopathy.

Gallbladder and Biliary Tract

Ultrasound has long been accepted as an excellent method of examining the gallbladder and the biliary tract.³² It is often performed with examination of the liver and pancreas, but a focused study of the gallbladder and biliary tree is occasionally performed, for example, immediately before elective cholecystectomy to determine the need for bile duct exploration.

The patient should fast before the examination to ensure adequate distention of the gallbladder. A 5-1 MHz curved linear array probe is sufficient for most examinations, but a higher frequency transducer (9-4 MHz) can be used to assess the fundus in some slimmer patients or children. Tissue harmonic imaging may be useful to demonstrate the gallbladder and biliary tree,³³ although care is needed with use of tissue harmonics as it will remove reverberation artifacts from the gallbladder lumen in the near field and may also obscure fine calculi or "sludge." The patient is placed supine initially, although the patient should be rolled into a right anterior oblique or left lateral decubitus position during the course of the examination. This maneuver will help unfold the gallbladder, allowing it to shift from being embedded on the visceral surface of the right

liver lobe to a more accessible midline position. It also allows further assessment of the neck. The movement from supine to left lateral decubitus position will cause any mobile stones or sludge to move into the new gravity-dependent position. Erect positioning should be performed to look for mobile gallstones; it may also be necessary to visualize the distal common bile duct through a water-filled stomach and duodenum. It should also be noted if the patient has any tenderness over the gallbladder during the scan (positive sonographic Murphy's sign).

The transducer is placed in the right midclavicular line in a parasagittal orientation and the long axis of the gallbladder is sought. Long-axis views are supplemented with short-axis views, and the entire gallbladder should be inspected. Suspended inspiration will help move the gallbladder caudally, and intercostal views may be useful. The size, shape, and position of the gallbladder are highly variable, but a diameter of more than 5 cm is considered abnormal and indicates a distended gallbladder. It is commonly pear shaped, with the neck found near the porta hepatis and the fundus in a fossa on the undersurface of the right lobe of the liver; but it may be found in an intrahepatic position or on a mesentery, and the fundus may reach the right iliac fossa, especially in the elderly. The fundus of the gallbladder may be folded (the phrygian cap); maneuvers to unfold the fundus include further fasting to distend the gallbladder and placement of the patient in the left lateral position. The wall is usually thin and uniform, and bile should appear hypoechoic. Particular attention should be paid to the neck of the gallbladder because stones may collect there in the supine position. Failure to demonstrate the gallbladder may be due to prior cholecystectomy, nonfasting state, calculous disease, shadowing or reverberation from the near wall of the gallbladder, or congenital absence of the gallbladder.³⁴

Gallstones will appear as echogenic structures with distal acoustic shadowing. They are highly variable in size and shape and will usually move if the patient is rolled unless they are impacted in the neck of the gallbladder. A higher frequency transducer may be used to look for small stones in a superficial gallbladder. False positives include folds in the wall of the gallbladder, which can be differentiated from stones by turning the transducer through 90 degrees (Fig. 66-21) or by repositioning

the patient, and loops of echogenic bowel indenting the posterior wall of the gallbladder, which on peristalsis may cast a dirty shadow, unlike the clean shadow of a gallstone. A wall-echo-shadow pattern may be seen when a contracted gallbladder is full of calculi³⁵ (Fig. 66-22). Polyps are echogenic but less echogenic than stones; they do not cast distal acoustic shadows and are not mobile. They may be single or multiple, and most are benign. The probability of malignancy increases with the size of the polyp (most malignant polyps are more than 10 mm in diameter), age, and the presence of gallstones and if there are fewer than three polyps.³⁶⁻³⁸

The wall of the gallbladder may be generally thickened (>2 mm) in acute cholecystitis, but this is not a specific sign.³⁹ It may also occur in the postprandial state and in other conditions including ascites, hypoalbuminemia, and hepatitis. Other signs of acute cholecystitis are gallbladder wall edema (Fig. 66-23), positive sonographic Murphy's sign, and pericholecystic

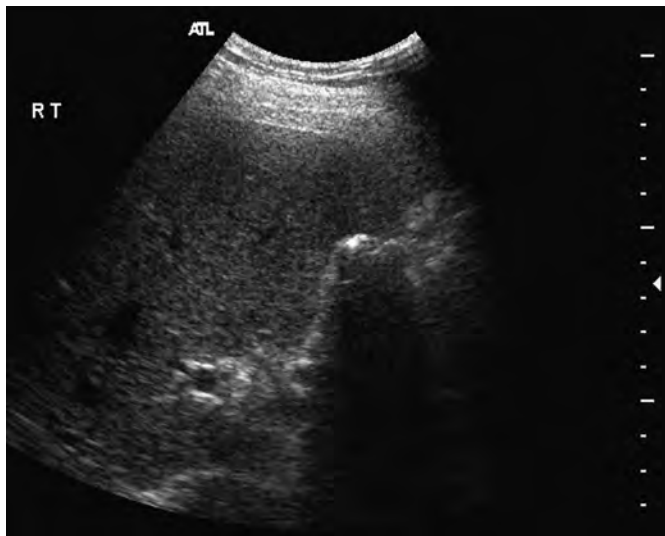


Figure 66-22 The wall-echo-shadow complex seen when a gallbladder full of calculi contracts. This may be confused for an echogenic gas-filled segment of bowel.



Figure 66-23 Transverse view of the gallbladder fundus showing a thickened edematous gallbladder wall.

fluid. Focal gallbladder wall thickening may be seen in adenomyomatosis, gallbladder carcinoma, and metastatic deposits. The gallbladder fills and drains by the cystic duct, which joins the common hepatic duct to form the common bile duct after a variable distance. The exact level at which this occurs is often not visible, and the extrahepatic bile duct may be referred to as the common duct when it is not clear where the cystic duct joins the common hepatic duct to form the common bile duct.

The biliary tree should be examined both within the liver and in the extrahepatic course. Normal intrahepatic bile ducts more peripheral than the left and right hepatic ducts are usually not visualized even with modern equipment. When the intrahepatic bile ducts are dilated, they can be recognized adjacent to the portal venous branches (which are visible even when of normal caliber and can be recognized by their echogenic borders due to the presence of adjacent fat); this appearance has been likened to a double-barreled shotgun.⁴⁰ The dilation may be generalized if the obstruction is central at the porta or distally within the common duct, or it may be localized to a segment or lobe if there is a more proximal obstruction. A more patchy distribution of dilation may be seen where a diffuse process affects the bile ducts, such as diffuse cholangiocarcinoma. An attempt should be made to follow the extrahepatic common duct to the ampulla of Vater if possible. Shadowing from bowel gas may obscure the mid and distal duct, but changing of the patient's position, use of the gallbladder as an acoustic window, or ingestion of water can improve visualization. This is particularly important when proximal dilation of the biliary tract is encountered and the level and cause of the obstruction are sought. Calculi within the distal duct and pancreatic head masses are common causes of distal common bile duct obstruction. The common duct is measured close to the porta just distal to the point at which the right hepatic artery crosses between the portal vein and the duct (Fig. 66-24). The duct then continues in the free edge of the lesser omentum to the head of the pancreas and the sphincter of Oddi, and the diameter of the duct increases in the extrahepatic section before tapering in the head of the pancreas. The normal caliber varies with age but should be less than 5 mm in adults.⁴¹ The duct does dilate with



Figure 66-24 Normal hepatoduodenal ligament anatomy. Normal common duct showing the right hepatic artery crossing between the common hepatic duct (anterior) and the portal vein (posterior).

age, and the upper limit of normal should be increased to 8 mm in the elderly. If the patient has a dilated duct before cholecystectomy, the duct may not return to normal diameter postoperatively, and a diameter of up to 10 mm may be considered normal after cholecystectomy.^{42,43}

Pancreas

Ultrasound examination of the pancreas can be a useful technique,⁴⁴ but views of the pancreas can be limited by overlying bowel gas. Improved views may be obtained by displacing gas-filled loops of bowel by pressure, sitting the patient up, or administering gasless fluid and scanning the pancreas through the fluid-filled stomach. The pancreas has an oblique transverse lie and is divided into the head (including the uncinate process), the neck, the body, and the tail. The head is situated to the right of the midline in the C of the duodenum. The uncinate process passes posteriorly and medially behind the superior mesenteric vein (Fig. 66-25). The neck of the pancreas connects the body to the tail anterior to the superior mesenteric artery and vein. The body then passes transversely and slightly cranially, and the tail ends in the splenic hilum. For the whole organ to be adequately assessed, the curvilinear 5-1 MHz transducer is positioned obliquely from the left upper quadrant to the right iliac fossa, inferior to the xiphisternum (Fig. 66-26). Sweeping the transducer cranially, then caudally will allow a full assessment of the head and uncinate process to check for masses, focal changes in echotexture, prominent lymph nodes, and any peripancreatic fluid. The tortuous splenic artery passes along the superior margin of the pancreas, whereas the splenic vein follows a straight course posterior to the gland and is a useful landmark. The splenic vein joins the superior mesenteric vein to form the portal vein posterior to the neck; the uncinate process may pass posterior to this junction. The normal outline of the pancreas is slightly lobular, and if the echogenicity of the gland is compared with the liver parenchyma, it is normally slightly more echogenic than the liver; but obviously care must be taken if the echogenicity of the liver is abnormal, for example, in fatty infiltration. The pancreas may also become more echogenic with fatty infiltration. The uncinate process

and the posterior part of the head may be relatively hypoechoic (Fig. 66-27), and this should not be confused with a tumor.⁴⁵ The main pancreatic duct may be visualized in normal individuals, but the diameter in the head should not exceed 3 mm. Dilation of the duct should prompt a search for an obstructing lesion.

Acute pancreatitis is a common condition often associated with gallstones or a history of alcohol use. There may be no abnormalities on ultrasound or CT for 24 to 48 hours. Areas of the gland then become swollen and edematous, manifested by hypoechoic areas on ultrasound. The duct can be obstructed by the swelling, leading to ductal dilation. Fluid collections may be seen in the peripancreatic retroperitoneal space or in the lesser sac. A search should always be made for gallstones as a treatable cause of pancreatitis, and elective cholecystectomy after the pancreatitis has resolved may prevent further episodes. Complications of pancreatitis include pseudocyst and pseudoaneurysm formation. Chronic pancreatitis may produce an enlarged



Figure 66-26 Transverse view of normal pancreas. The probe has been angled obliquely to include the tail of the pancreas, which passes laterally and cranially.



Figure 66-25 Normal pancreas. Transverse view of the pancreas illustrating the normal uncinate process (U) passing posterior to the superior mesenteric vein.



Figure 66-27 Hypoechoic uncinate process of the pancreas. This is a normal variant seen in up to 25% of patients.



Figure 66-28 Left basal pleural effusion seen above the diaphragm. There is also some ascites adjacent to the spleen.



Figure 66-29 Splenomegaly in a patient with cirrhosis and portal hypertension. Note also the dilated splenic vein branches at the splenic hilum.

gland in the early stages; in the later stages, shrinkage, calcifications, and increased echogenicity are more common. Duct strictures and dilations are seen, often with calculi, and are characteristic of the disease but are better demonstrated with pancreatography.

Pancreatic adenocarcinoma most commonly arises in the head and may cause dilation of the common bile duct and the pancreatic duct. The tumors are typically hypoechoic but attenuating and can be detected when they are as small as 1 cm in diameter. Endoscopic or intraoperative ultrasound may be used to improve lesion detection and characterization. The reduced need for penetration enables the use of higher frequencies and hence better resolution. Other tumors found in the pancreas include intraductal papillary mucinous tumors and endocrine tumors (of which insulinoma is the most common).

Spleen

The spleen is well protected by the lower left ribs, and this can pose a challenge to the ultrasonographer. The patient is placed in the right posterior oblique or right lateral decubitus position, and the spleen is scanned from the subcostal or intercostal approach. The spleen moves caudally on inspiration, and often this movement can be used to achieve a thorough examination of the entire spleen through a single intercostal space by a combination of breathing instructions to the patient and a sweeping movement of the transducer. The subphrenic space above the spleen should be examined for collections, and a left pleural effusion can often be seen above the diaphragm (Fig. 66-28). The spleen moves anterior to the left kidney on inspiration, a fact that should be borne in mind when attempting to establish the origin of a mass in the left upper quadrant.

The echotexture of the spleen is homogeneous; it is normally slightly hyperechoic compared with the kidney and isoechoic with the liver. The outer surface is smooth and convex, whereas the visceral surface is concave and may show indentations for the adjacent organs. The splenic artery and vein enter and leave

the spleen at the hilum, which is found on the visceral surface. Accessory spleens are common (10% of subjects in autopsy series) and are often seen in the region of the hilum or within the lienorenal ligament or the gastrosplenic ligament. They are rounded or oval, measuring 1 to 2 cm in diameter, and isoechoic with spleen.⁴⁶ Vessels can often be traced from the splenic artery and vein to the accessory spleen.⁴⁷ It is important to differentiate accessory spleens from lymph nodes or masses; in patients undergoing splenectomy for hematologic disease, the presence of accessory spleens should be carefully documented before surgery. On occasion, the spleen may have a long vascular pedicle and is described as wandering.⁴⁸ It may then be found in locations other than the left upper quadrant and is prone to torsion.

Assessment of splenic size by physical examination is inaccurate and requests for evaluation with imaging are common. A single ultrasonic measurement of splenic length has been shown to be an accurate predictor of splenic volume,⁴⁹ and ultrasound is cheaper and more accessible than CT scanning without the risks of ionizing radiation. The longitudinal diameter of the spleen should measure less than 11 cm.⁵⁰ There are many causes of diffuse splenic enlargement, including infection, liver disease, portal hypertension, lymphoma and other metastatic and primary neoplasms, hematopoietic disease, and splenic vein thrombosis (Fig. 66-29).

Ultrasound may be used to detect free fluid in an unstable trauma patient, and although large splenic lacerations may be visible, the sensitivity of ultrasound to splenic injuries (even with the use of contrast agents) is unacceptably low.⁵¹ CT is the investigation of choice in the acute setting. In the nontraumatic setting, focal splenic lesions are divided into cystic and solid lesions. Cystic lesions may be congenital, infectious (echinococcal), or secondary to trauma. Solid lesions may be benign or malignant. Splenic hemangiomas and hamartomas can be differentiated by the presence of vascular flow on Doppler imaging. Infarcts are typically peripheral, wedge shaped, and hypoechoic in the acute stage but later may become hyperechoic. Common malignant solid lesions include primary lymphoma and metastases. These are typically hypoechoic.^{52,53}

REFERENCES

- Donald I, Macvicar J, Brown TG: The investigation of abdominal masses by pulsed ultrasound. *Lancet* 271:188–195, 1958.
- Sammon J, Twomey J, Crush L, et al: Image-guided percutaneous splenic biopsy and drainage. *Semin Intervent Radiol* 301–310, 2012.
- Lewin PA: Quo vadis medical ultrasound? *Ultrasonics* 42:1–7, 2004.
- Oktar SO, Yucel C, Ozdemir H, et al: Comparison of conventional sonography, real-time compound sonography, tissue harmonic sonography, and tissue harmonic compound sonography of abdominal and pelvic lesions. *AJR Am J Roentgenol* 181:1341–1347, 2003.
- Song P, Zhao H, Urban M, et al: Improved shear wave motion detection using pulse-inversion harmonic imaging with a phased array transducer. *IEEE Trans Med Imaging* 2013. [Epub ahead of print.]
- Choudhry S, Gorman B, Charboneau JW, et al: Comparison of tissue harmonic imaging with conventional US in abdominal disease. *Radiographics* 20:1127–1135, 2000.
- Sodhi KS, Sidhu R, Gulati M, et al: Role of tissue harmonic imaging in focal hepatic lesions: Comparison with conventional sonography. *J Gastroenterol Hepatol* 20:1488–1493, 2005.
- Rosenthal SJ, Jones PH, Wetzel LH: Phase inversion tissue harmonic sonographic imaging: A clinical utility study. *AJR Am J Roentgenol* 176:1393–1398, 2001.
- Hong HS, Han JK, Kim TK, et al: Ultrasonographic evaluation of the gallbladder: Comparison of fundamental, tissue harmonic, and pulse inversion harmonic imaging. *J Ultrasound Med* 20:35–41, 2001.
- Ness A, Blumenfeld YJ, Platt LD: Maternal-fetal medicine fellowship 3- and 4-dimensional ultrasound experience: Room for improvement. *J Ultrasound Med* 32:949–953, 2013.
- Downey DB, Fenster A, Williams JC: Clinical utility of three-dimensional US. *Radiographics* 20:559–571, 2000.
- Murphy KJ, Rubin JM: Power Doppler: It's a good thing. *Semin Ultrasound CT MR* 18:13–21, 1997.
- Lunt MJ: The optimum frequency and angle of insonation for a Doppler ultrasonic flow velocity meter. *Phys Med Biol* 25:839–848, 1980.
- Schneider M, Arditi M, Barrau MB, et al: BR1: A new ultrasonographic contrast agent based on sulfur hexafluoride-filled microbubbles. *Invest Radiol* 30:451–457, 1995.
- Solbiati L, Tonolini M, Cova L, et al: The role of contrast-enhanced ultrasound in the detection of focal liver lesions. *Eur Radiol* 11(Suppl 3):E15–E26, 2001.
- Leen E, Moug SJ, Horgan P: Potential impact and utilization of ultrasound contrast media. *Eur Radiol* 14(Suppl 8):P16–P24, 2004.
- Bokor D, Chambers JB, Rees PJ, et al: Clinical safety of SonoVue, a new contrast agent for ultrasound imaging, in healthy volunteers and in patients with chronic obstructive pulmonary disease. *Invest Radiol* 36:104–109, 2001.
- Albrecht T, Hoffmann CW, Schmitz SA, et al: Phase-inversion sonography during the liver-specific late phase of contrast enhancement: Improved detection of liver metastases. *AJR Am J Roentgenol* 176:1191–1198, 2001.
- Bryant TH, Blomley MJ, Albrecht T, et al: Improved characterization of liver lesions with liver-phase uptake of liver-specific microbubbles: Prospective multicenter study. *Radiology* 232:799–809, 2004.
- Migaleddu V, Virgilio G, Turilli D, et al: Characterization of focal liver lesions in real time using harmonic imaging with high mechanical index and contrast agent Levovist. *AJR Am J Roentgenol* 182:1505–1512, 2004.
- Catalano O, Lobianco R, Raso MM, Siani A: Blunt hepatic trauma: Evaluation with contrast-enhanced sonography: Sonographic findings and clinical application. *J Ultrasound Med* 24:299–310, 2005.
- Blaivas M, Lyon M, Brannam L, et al: Feasibility of FAST examination performance with ultrasound contrast. *J Emerg Med* 29:307–311, 2005.
- Catalano O, Nunziata A, Lobianco R, Siani A: Real-time harmonic contrast material-specific US of focal liver lesions. *Radiographics* 25:333–349, 2005.
- Keogh CF, Cooperberg PL: Is it real or is it an artifact. *Ultrasound Q* 17:201–210, 2001.
- Sommer FG, Taylor KJ: Differentiation of acoustic shadowing due to calculi and gas collections. *Radiology* 135:399–403, 1980.
- Couinaud C: *Le foie: Etudes anatomiques et chirurgicales*, Paris, 1957, Masson.
- Lafortune M, Madore F, Patriquin H, Breton G: Segmental anatomy of the liver: A sonographic approach to the Couinaud nomenclature. *Radiology* 181:443–448, 1991.
- Colli A, Fraquelli M, Andreoletti M, et al: Severe liver fibrosis or cirrhosis: Accuracy of US for detection—analysis of 300 cases. *Radiology* 227:89–94, 2003.
- Patriquin H, Lafortune M, Burns PN, et al: Duplex Doppler examination in portal hypertension: Technique and anatomy. *AJR Am J Roentgenol* 149:71–76, 1987.
- Haag K, Rössle M, Ochs A, et al: Correlation of duplex sonography findings and portal pressure in 375 patients with portal hypertension. *AJR Am J Roentgenol* 172:631–635, 1999.
- Wing VW, Laing FC, Jeffrey RB, et al: Sonographic differentiation of enlarged hepatic arteries from dilated intrahepatic bile ducts. *AJR Am J Roentgenol* 145:57–61, 1985.
- Cooperberg PL, Burhenne HJ: Real-time ultrasonography. Diagnostic technique of choice in calculous gallbladder disease. *N Engl J Med* 302:1277–1279, 1980.
- Ortega D, Burns PN, Hope Simpson D, et al: Tissue harmonic imaging: Is it a benefit for bile duct sonography? *AJR Am J Roentgenol* 176:653–659, 2001.
- Hammond DI: Unusual causes of sonographic nonvisualization or nonrecognition of the gallbladder: A review. *J Clin Ultrasound* 16:77–85, 1988.
- MacDonald FR, Cooperberg PL, Cohen MM: The WES triad—a specific sonographic sign of gallstones in the contracted gallbladder. *Gastrointest Radiol* 6:39–41, 1981.
- Lee KF, Wong J, Li JC, et al: Polypoid lesions of the gallbladder. *Am J Surg* 188:186–190, 2004.
- Persley KM: Gallbladder polyps. *Curr Treat Options Gastroenterol* 8:105–108, 2005.
- Shinkai H, Kimura W, Muto T: Surgical indications for small polypoid lesions of the gallbladder. *Am J Surg* 175:114–117, 1998.
- Sanders RC: The significance of sonographic gallbladder wall thickening. *J Clin Ultrasound* 8:143–146, 1980.
- Weill F, Eisencher A, Zeltner F: Ultrasonic study of the normal and dilated biliary tree. The “shotgun” sign. *Radiology* 127:221–224, 1978.
- Cooperberg PL, Li D, Wong P, et al: Accuracy of common hepatic duct size in the evaluation of extrahepatic biliary obstruction. *Radiology* 135:141–144, 1980.
- Graham MF, Cooperberg PL, Cohen MM, et al: The size of the normal common hepatic duct following cholecystectomy: An ultrasonographic study. *Radiology* 135:137–139, 1980.
- Wedmann B, Borsch G, Coenen C, et al: Effect of cholecystectomy on common bile duct diameters: A longitudinal prospective ultrasonographic study. *J Clin Ultrasound* 16:619–624, 1988.
- Walls WJ, Gonzalez G, Martin NL, et al: B-scan ultrasound evaluation of the pancreas. Advantages and accuracy compared to other diagnostic techniques. *Radiology* 114:127–134, 1975.
- Donald JJ, Shorvon PJ, Lees WR: A hypoechoic area within the head of the pancreas—a normal variant. *Clin Radiol* 41:337–338, 1990.
- Subramanyam BR, Balthazar EJ, Horii SC: Sonography of the accessory spleen. *AJR Am J Roentgenol* 143:47–49, 1984.
- Bertolotto M, Gioulis E, Ricci C, et al: Ultrasound and Doppler features of accessory spleens and splenic grafts. *Br J Radiol* 71:595–600, 1998.
- Phillips GW, Hemingway AP: Wandering spleen. *Br J Radiol* 60:188–190, 1987.
- Loftus WK, Chow LT, Metreweli C: Sonographic measurement of splenic length: Correlation with measurement at autopsy. *J Clin Ultrasound* 27:71–74, 1999.
- Frank K, Linhart P, Kortsik C, et al: Sonographic determination of spleen size: Normal dimensions in adults with a healthy spleen. *Ultraschall Med* 7:134–137, 1986.
- Poletti PA, Platon A, Becker CD, et al: Blunt abdominal trauma: Does the use of a second-generation sonographic contrast agent help to detect solid organ injuries? *AJR Am J Roentgenol* 183:1293–1301, 2004.
- Goerg C, Schwerk WB, Goerg K: Sonography of focal lesions of the spleen. *AJR Am J Roentgenol* 156:949–953, 1991.
- Caremani M, Occhini U, Caremani A, et al: Focal splenic lesions: US findings. *J Ultrasound* 16:65–74, 2013.

Magnetic Resonance Imaging of the Solid Parenchymal Organs

JENNIFER W. UYEDA | SANDEEP S. HEDGIRE |
MUKESH G. HARISINGHANI | RAJ R. CHINNAPPAN | PRITESH PATEL

CHAPTER OUTLINE

Magnetic Resonance Imaging Technique

Field Strength

Surface Coils

Magnetic Resonance Sequences

Magnetic Resonance Contrast Agents

Imaging of Abdominal Organs

Liver

Bile Ducts and Gallbladder

Pancreas

Adrenal Glands

Kidneys

Summary

Magnetic resonance imaging (MRI) is frequently used as a problem-solving tool for the evaluation of disease processes throughout the body and is a powerful imaging modality to characterize disease in the solid abdominal organs. With widespread availability, technologic advances, and increasing familiarity of ordering physicians and radiologists alike, MRI is becoming the modality of choice for parenchymal lesion detection, anatomic localization, and lesion characterization. MRI has high spatial and temporal resolution without exposure to ionizing radiation, allowing accurate imaging on a wide spectrum of patients, including pregnant women and children.

Various technologic advances in MRI have been made in recent years, including increased magnetic strength, improved coil technology, and advanced imaging sequences. The purpose of this chapter is to discuss commonly used imaging sequences and protocols as well as recent developments in advanced sequences in MRI of the abdomen. An all-encompassing summary of each pathologic diagnosis in the abdomen is beyond the scope of this chapter; the chapter reviews solid abdominal organ lesions and pathologic processes in which MRI is crucial for accurate diagnosis and characterization.

Magnetic Resonance Imaging Technique

FIELD STRENGTH

Of the recent advances in MRI, the most significant is the increasing magnetic field strength. The most common field strengths in clinical use in MRI are 1.5T and 3.0T. Higher magnetic field strengths allow increased longitudinal magnetization and signal intensity, resulting in increased signal-to-noise ratio

(SNR). The resulting increased SNR can be used to increase spatial resolution or to decrease imaging acquisition time, allowing improved imaging.

There are disadvantages to higher magnetic field strengths. Higher purchasing prices in addition to higher maintenance prices are among the disadvantages. Reduced T1 contrast secondary to lengthening of T1 is a limitation of higher magnetic field strengths. Increased susceptibility from magnetic field inhomogeneity, patient motion, and chemical shift are also a disadvantage of higher magnetic field strengths.

SURFACE COILS

For imaging of the abdomen, the goal is to maximize SNR for a large area of interest, and a multichannel phased-array body coil is typically used. Flexible coils are used to maintain the contour of the torso, which allows high-resolution imaging of the abdomen and pelvis. Phased-array coils allow parallel imaging, in which each channel has its own receiver, and the multichannel system increases the number of receiver coils. Advances in phased-array coil technology have resulted in increased SNR and improved image quality, faster scan time, and larger scan area.

Other body parts, such as the rectum or the female pelvis, can be imaged with a phased-array body coil that covers a smaller field of view with high-resolution images. Intraluminal coils are also used to image pelvic organs such as the prostate gland, yielding images with high SNR and high resolution. Anatomy, extracapsular extension, perivascular invasion, and lymphadenopathy can be readily assessed by MRI of the prostate.

MAGNETIC RESONANCE SEQUENCES

The basic MR sequences employed in imaging of solid abdominal organs are fairly standard. These include axial and coronal T2-weighted images with and without fat suppression, diffusion-weighted images with apparent diffusion coefficient (ADC) maps, in- and out-of-phase gradient-echo images, and dynamic contrast-enhanced three-dimensional T1 gradient-echo images with fat saturation. Two- and three-dimensional free-breathing navigator-triggered magnetic resonance cholangiopancreatography (MRCP) sequences may also be obtained if clinically indicated. Additional sequences, such as balanced fast field echo or fast imaging employing steady-state acquisition sequences, can be obtained for evaluation of vascular anatomy, delineation of bowel and mesentery, and quantification of fat by T2*.

Single-shot T2-weighted images are rapidly acquired, heavily T2-weighted images that are useful for evaluating fluid and structures with short T2 values. The benefit of this sequence is

the speed with which images are acquired; however, the contrast-to-noise ratio is not as high as in other T2-weighted fast spin-echo sequences. Axial T2 fast spin-echo sequences with fat suppression have the benefit of increased liver-to-spleen contrast and are useful for detection of lesions. Lymph nodes are also easily detected on this sequence. PROPELLER (periodically rotated overlapping parallel lines with enhanced reconstruction) is a fast imaging technique whereby a fraction of k space is acquired in each frame. Each imaging acquisition in a PROPELLER sequence acquires a rectangular portion of k space, with each acquisition acquiring images through the k space center, and can reduce artifact from respiratory motion (Fig. 67-1). Other T2-weighted sequences, such as the three-dimensional turbo spin-echo sequence known as SPACE (sampling perfection with application-optimized contrast with different flip-angle evolutions), have been developed to decrease image acquisition times. With this sequence, the acquired images serve as a data set that can be used to create postprocessed reformatted images in axial, coronal, and sagittal planes. The SPACE sequence decreases the number of T2-weighted image acquisitions and can potentially replace two-dimensional T2-weighted images.

Diffusion-weighted imaging with varying diffusion gradient strengths has become important for evaluating malignant neoplasms and inflammatory conditions.¹ The principle of diffusion-weighted imaging is based on random motion of microscopic water molecules and diffusion of water in body tissues. Diffusion of water molecules is based on cell membrane integrity and tissue cellularity. Diffusion-weighted imaging provides functional information about tissue cellularity along with the ADC values, which are calculated from diffusion-weighted imaging data. An increase in the number of cells in conditions such as primary malignant neoplasms, metastases, and infection or abscesses leads to crowding of extracellular spaces and further restriction of water molecules.

T1-weighted in-phase and opposed-phase gradient-echo images are useful for detection of focal and diffuse hepatic steatosis, but the T2* effects and susceptibility artifact are also useful components of this sequence. There is signal loss on the opposed-phase images at water-fat interfaces, resulting in the India ink artifact or fat-water cancellation artifact, whereby a sharply defined black rim is seen at water-fat interfaces. Water and fat protons precess at different frequencies, and in spin-echo sequences, a 180-degree refocusing pulse causes the protons to be in phase when the echo is acquired; however, gradient-echo images lack the 180-degree refocusing pulse. Focal and diffuse hepatic steatosis is manifested as loss of signal

on the opposed-phase images (Fig. 67-2). The dual gradient-echo images also provide information by T2* effects, whereby hepatic parenchymal storage diseases, such as hemochromatosis and hemosiderosis, decrease in signal intensity with the longer time to echo secondary to continued transverse magnetization decay (Fig. 67-2). Susceptibility artifacts result from field inhomogeneities occurring at interfaces of materials with varying magnetic susceptibility, such as metallic objects, gas-filled bowel, and pneumobilia (Fig. 67-3). The difference in precession rates of fat and water protons is proportional to the magnetic field strength and is 3.5 ppm or 225 Hz at 1.5T. At 3T, the difference in precession rates is 450 Hz, and the protons are out of phase at 1.1 ms, 3.4 ms, 5.6 ms, and so forth, whereas the protons are in phase at 2.2 ms, 4.5 ms, 6.7 ms, and so forth. Acquiring the out-of-phase image at a short time interval of 1.1 ms followed by the in-phase image at 2.2 ms can be challenging, and the second- or third-order echo may need to be obtained. The DIXON method uses the T1 in-phase and out-of-phase images to mathematically calculate “fat-only” and “water-only” images, which is particularly useful in areas with high magnetic susceptibility (Fig. 67-4).

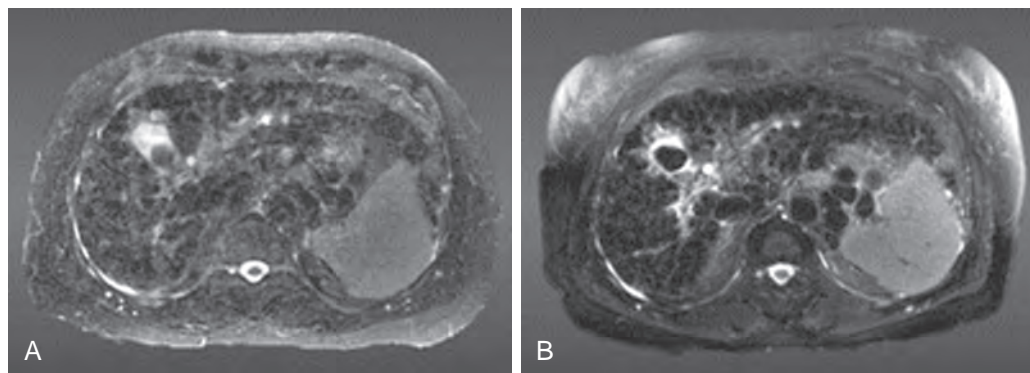
Dynamic contrast-enhanced three-dimensional T1-weighted gradient-echo images with fat saturation sequences are helpful in assessing for the presence of enhancement as well as characteristic enhancement patterns of certain lesions. Dynamic imaging with arterial, portal venous, equilibrium, and delayed phases is useful for evaluation of all upper abdominal organs, including the liver, spleen, pancreas, adrenal glands, and kidneys. Images are performed with a breath hold of approximately 15 to 20 seconds. Subtraction images are obtained by subtracting the images made before the administration of gadolinium from the dynamic contrast-enhanced images and are helpful in assessing for the presence and degree of enhancement.

Two- and three-dimensional free-breathing navigator-triggered MRCP sequences have excellent spatial and temporal resolution. Accurate assessment of the hepatobiliary and pancreatic ducts with MRCP has replaced endoscopic retrograde cholangiopancreatography (ERCP) and percutaneous transhepatic cholangiography as the initial study of choice in the evaluation of hepatobiliary and pancreatic ducts.

MAGNETIC RESONANCE CONTRAST AGENTS

Multiple MR contrast agents are currently in use. They can be categorized into five classes: extracellular, hepatobiliary, reticuloendothelial, blood pool, and combined agents.²⁻⁶ A complete list and thorough review of the mechanism of action and side

Figure 67-1 Respiratory motion artifact. **A.** Axial T2 image with fat saturation is degraded secondary to respiratory motion. **B.** Rapid acquisition PROPELLER technique reduces artifact from respiratory motion.



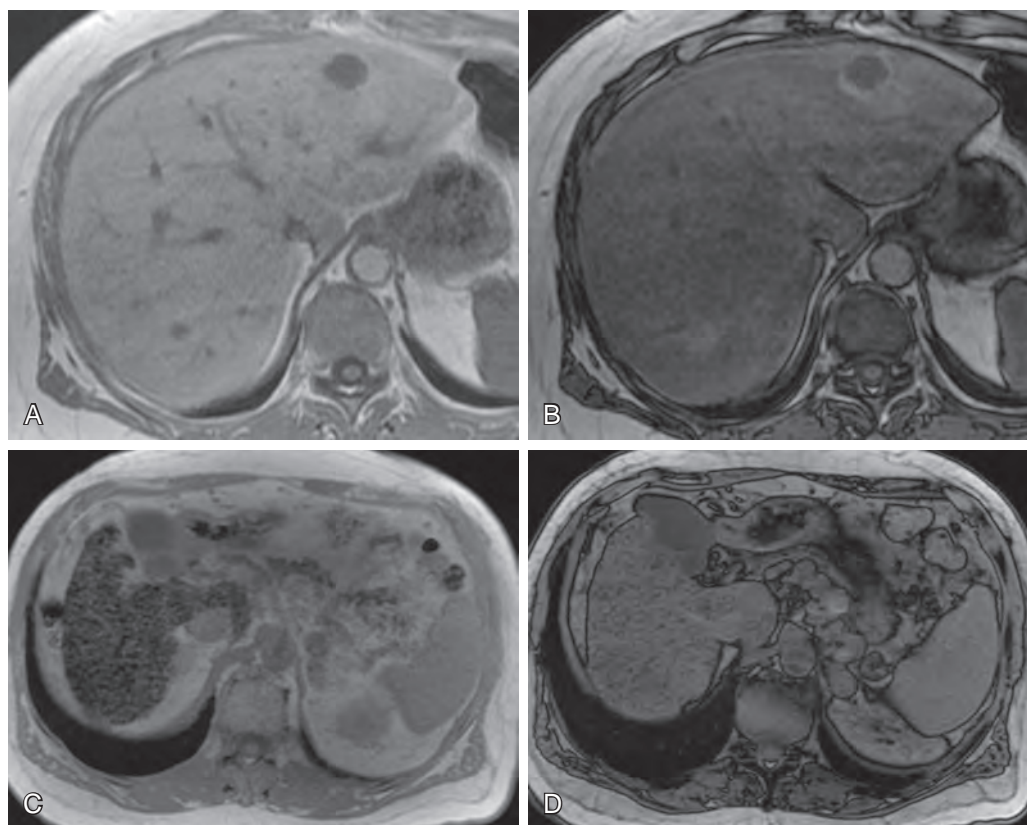


Figure 67-2 Hepatic steatosis and hemochromatosis. Axial gradient-echo in-phase (A) and opposed-phase (B) images show loss of signal intensity on the opposed-phase image, consistent with hepatic steatosis. The liver lesion in the left lobe is a hemangioma with surrounding focal fatty sparing. In a different patient, axial in-phase (C) and opposed-phase (D) images demonstrate decreased signal on the in-phase images, with the longer echo time reflecting the T2* shortening in a patient with hemochromatosis.

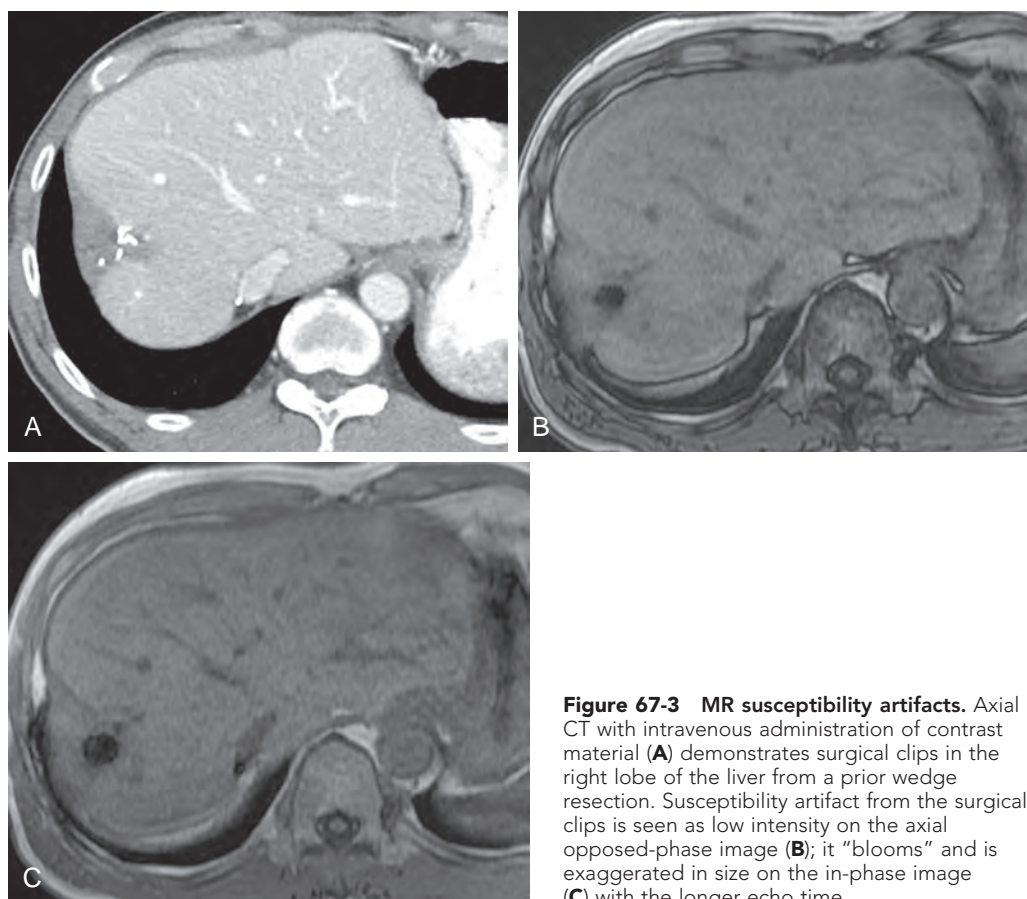


Figure 67-3 MR susceptibility artifacts. Axial CT with intravenous administration of contrast material (A) demonstrates surgical clips in the right lobe of the liver from a prior wedge resection. Susceptibility artifact from the surgical clips is seen as low intensity on the axial opposed-phase image (B); it "blooms" and is exaggerated in size on the in-phase image (C) with the longer echo time.

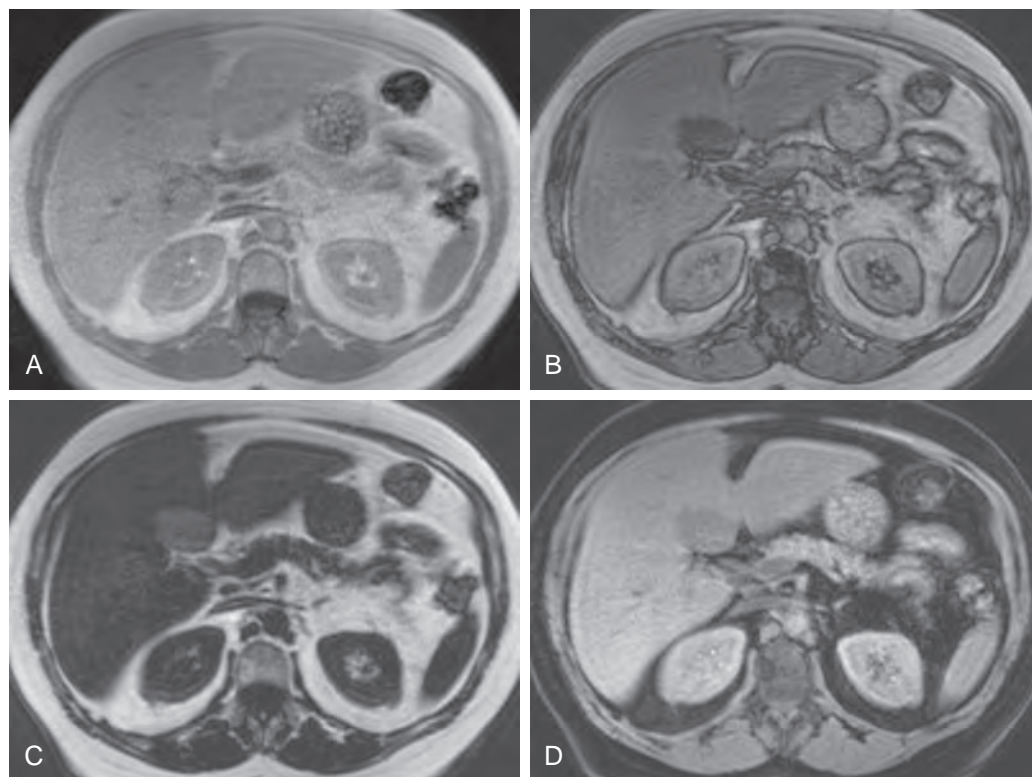


Figure 67-4 DIXON sequence. Axial T1 in-phase image (A) demonstrates an oval area in segments IV and V that decreases in signal on the opposed-phase image (B), consistent with focal fat. On the axial fat-only image (C), the focal fat is hyperintense relative to liver parenchyma compared with low signal on the water-only image (D).

effects are beyond the scope of this chapter; however, the indications for and MR techniques used to enhance these agents are briefly reviewed.

Extracellular agents such as gadopentetate dimeglumine (Magnevist) have been in use for the longest time clinically. These agents are distributed in the extracellular space; 20 mL is administered and nearly entirely excreted by the kidneys.⁶

Hepatobiliary agents such as gadoxetic acid (Eovist) are taken up by hepatocytes and excreted through the biliary system, which causes the liver, biliary ducts, and hepatocyte-containing lesions to be T1 hyperintense.³⁻⁶ The average dose is 0.025 mmol/kg for approximately 10 mL, and there is around 50% hepatic and 50% renal excretion. The delayed hepatobiliary phase ranges from 10 minutes to hours, which is significantly shorter compared with the combined agent gadobenate dimeglumine (MultiHance).⁶

Blood pool agents stay intravascular for a longer time compared with the extravascular agents and are used for angiography.^{2,3} Although use of blood pool agents is limited in imaging of solid abdominal organs, it is listed here for completeness.

Combined agents have extracellular, blood pool, and hepatobiliary characteristics. Gadobenate dimeglumine (MultiHance) is taken up by hepatocytes, and 5% of the administered dose is excreted in bile; the remaining 95% is excreted renally. A limitation of this agent is that the hepatobiliary phase occurs approximately 1 to 2 hours after ingestion of the contrast agent, which is significantly longer compared with hepatobiliary agents.^{2,6}

Imaging of Abdominal Organs

A complete summary of each pathologic diagnosis in the abdomen is beyond the scope of this chapter, and as such, this

chapter reviews solid abdominal organ lesions for which classic MRI characteristics are diagnostic. MRI features are crucial for narrowing the differential diagnosis and making accurate diagnoses.

LIVER

The three most common benign hepatic lesions encountered are cavernous hemangiomas, focal nodular hyperplasia (FNH), and hepatic adenomas. FNH and adenomas share imaging characteristics but can be accurately differentiated by various MR sequences and contrast agents. FNH can also be differentiated from fibrolamellar hepatocellular carcinoma (HCC) on the basis of MR characteristics.

Cavernous Hemangiomas

Cavernous hemangiomas, the most common primary liver tumor, occur in 20% of the general population.⁷⁻⁹ On histologic examination, hemangiomas are composed of large blood-filled vascular channels of varying sizes and shapes.⁷ Typically, they are solitary and small; however, multiplicity can occur, and giant cavernous hemangiomas can be larger than 20 cm. On imaging, hemangiomas have characteristic appearances. On ultrasound (US), hemangiomas are focal, homogeneous, and echogenic and can have varying appearances, depending on the degree of background hepatic steatosis, which can be easily assessed on MRI. MRI shows typical features of hemangiomas, which include T1 hypointensity and marked T2 hyperintensity; on the dynamic contrast-enhanced images, hemangiomas have peripheral nodular enhancement with progression in a centripetal distribution (Fig. 67-5).⁷⁻⁹ Flash-filling hemangiomas can be seen, in which the entire lesion homogeneously enhances in the arterial phase. In addition, the very bright T2 hyperintense

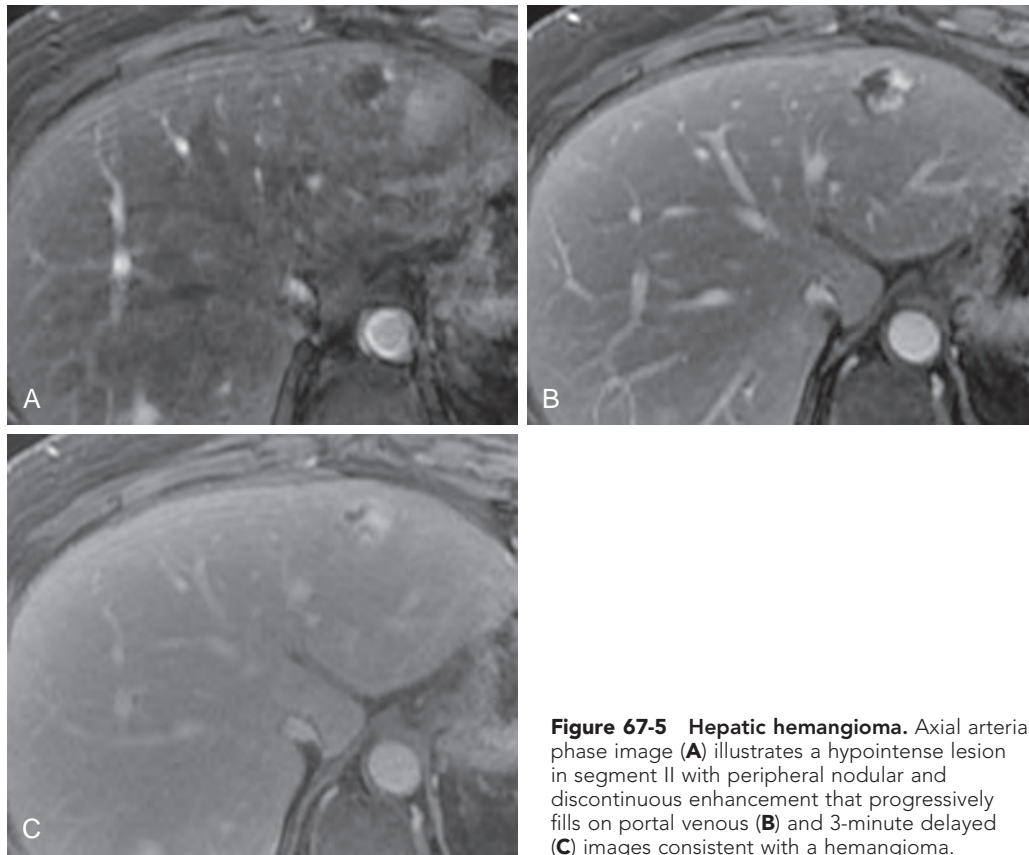


Figure 67-5 Hepatic hemangioma. Axial arterial phase image (A) illustrates a hypointense lesion in segment II with peripheral nodular and discontinuous enhancement that progressively fills on portal venous (B) and 3-minute delayed (C) images consistent with a hemangioma.

signal has a high sensitivity (100%) and specificity (92%) for differentiation of hemangiomas from hepatic metastases.

Focal Nodular Hyperplasia

FNH is the second most common benign hepatic tumor after hemangiomas. It is an aggregate of hepatocytes that form in response to a “central scar,” which represents an underlying vascular malformation or clusters of blood vessels and bile ducts.⁷⁻¹⁰ FNH is hypointense to isointense on T1-weighted images and isointense to mildly hyperintense on T2-weighted images with a T2 hyperintense scar.⁷⁻⁹ After the administration of gadolinium, there is brisk, homogeneous, and intense arterial enhancement of the lesion with the exception of the central scar, which has gradual delayed enhancement (Fig. 67-6).

Approximately 20% of FNH cases are atypical and do not have characteristic imaging features.⁷ The three subtypes include telangiectatic FNH, FNH with cytologic atypia, and mixed hyperplastic and adenomatous FNH, all of which do not possess the central vascular malformation and are often challenging to diagnose on imaging.^{7,9} These three nonclassic FNH types have bile ducts and some degree of normal hepatocytes, allowing uptake and excretion of hepatobiliary contrast agents.

The delayed enhancement of the central scar helps differentiate FNH from fibrolamellar HCC, which is an uncommon type of HCC. Fibrolamellar HCC usually is manifested as a large heterogeneous T1 hypointense and T2 hyperintense mass, and a majority (80%) of fibrolamellar HCCs contain a true central scar (Fig. 67-7).⁹ In contradistinction to FNH, the central scar is a true scar that is T2 hypointense and demonstrates minimal or no enhancement after gadolinium administration.⁹

Hepatic Adenoma

Hepatic adenomas are rare benign tumors containing well-differentiated hepatocytes with few or no biliary ducts. Most adenomas are single, and 90% of adenomas occur in women. On the basis of recent pathologic and genetic evaluation of hepatic adenomas, four subtypes of adenomas have been developed: inflammatory hepatocellular adenoma, hepatocyte nuclear factor 1 α (HNF-1 α)–mutated hepatocellular adenoma, β -catenin–mutated hepatocellular adenoma, and unclassified.^{8,11-14} Each type should be considered a different entity because imaging appearances as well as management options vary according to the subtype.

Inflammatory adenomas were previously known as telangiectatic adenomas or telangiectatic FNH. This subtype commonly occurs in young women taking oral contraceptive medications and obese patients. On MRI, inflammatory adenomas are T1 isointense to mildly hyperintense and T2 diffusely intense to hyperintense. T1-weighted in-phase and opposed-phase gradient-echo images show little or no loss of signal. After the administration of gadolinium, inflammatory adenomas enhance on the arterial phase and persist on the portal venous and delayed phases (Fig. 67-8).⁸ Two complications of hepatic adenomas are intratumoral bleeding and development of HCC. Bleeding occurs in 25% to 50% of adenomas, and tumors larger than 5 cm are at increased risk for bleeding and rupture. Inflammatory adenomas have the highest risk of bleeding of all subtypes.

HNF-1 α –mutated hepatocellular adenoma accounts for 30% to 35% of all adenomas and is the second most common subtype. This subtype occurs almost exclusively in women, with

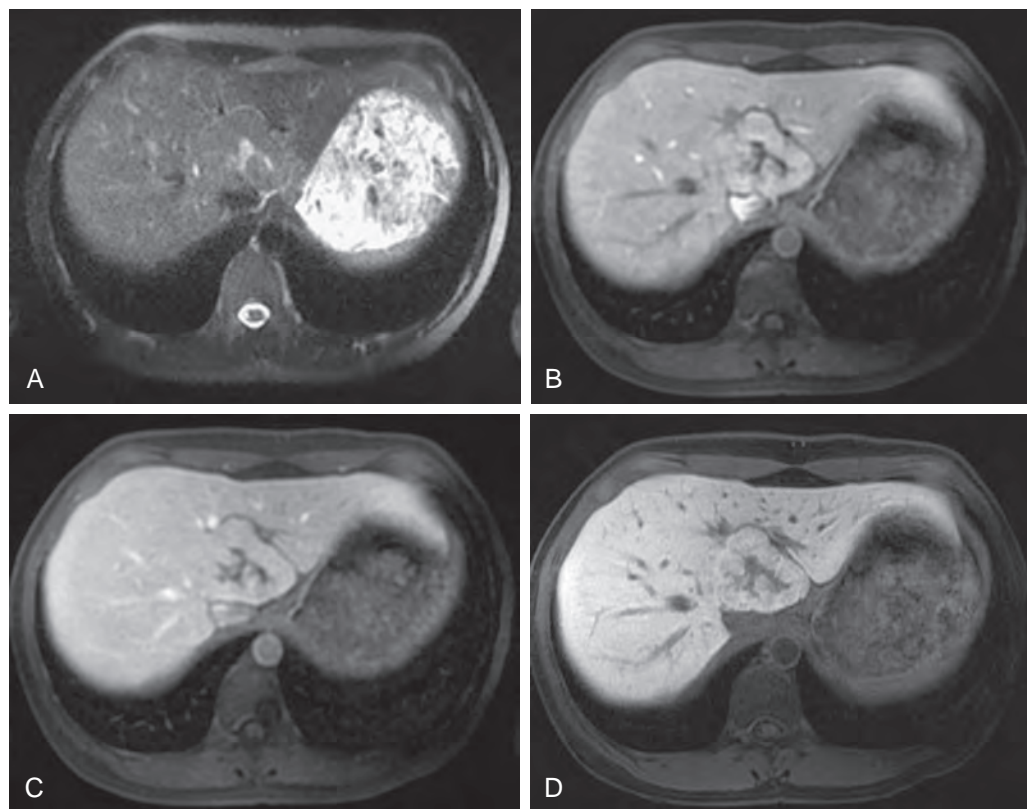


Figure 67-6 Focal nodular hyperplasia. Axial T2 fat-saturated image (**A**) demonstrates a T2 isointense lesion with a central T2 hyperintense "scar." After the administration of gadolinium, axial fat-saturated images in 25-second (**B**), 70-second (**C**), and hepatobiliary (**D**) delayed phases show brisk, homogeneous, and intense arterial enhancement of the lesion with the liver parenchyma.

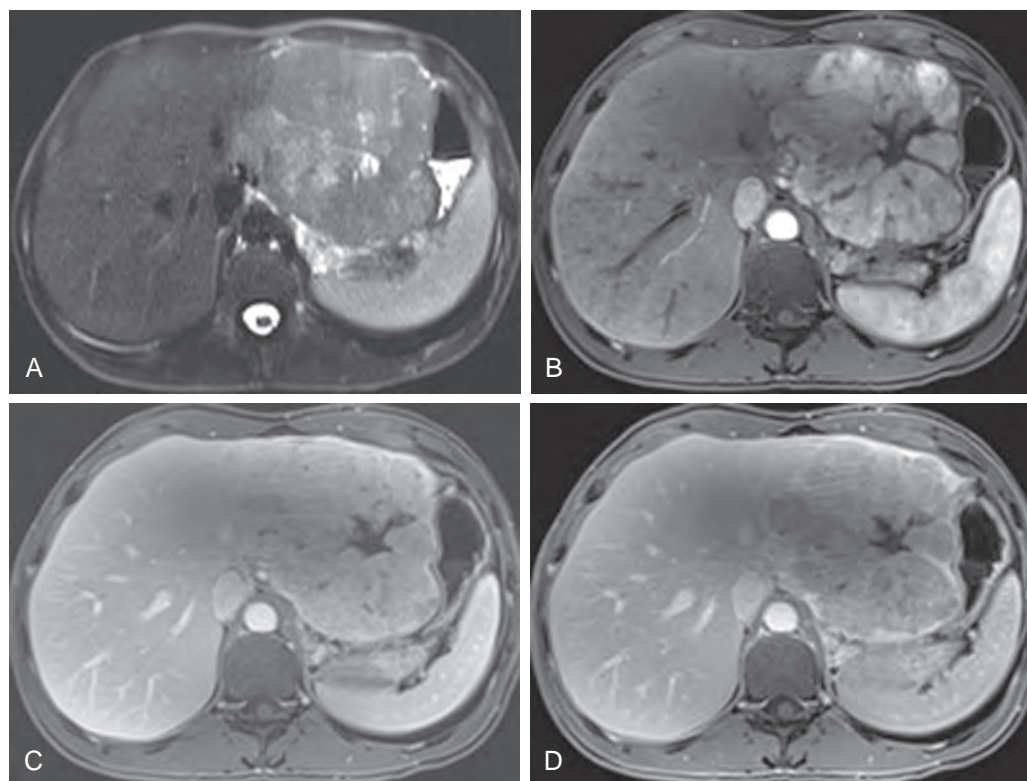


Figure 67-7 Fibrolamellar hepatocellular carcinoma. Axial T2 fat-saturated image (**A**) shows a mildly T2 hyperintense lesion that is large and with a true central scar. Axial dynamic images after the administration of gadolinium (**B-D**) show early heterogeneous arterial enhancement with minimal or no enhancement of the true central scar.

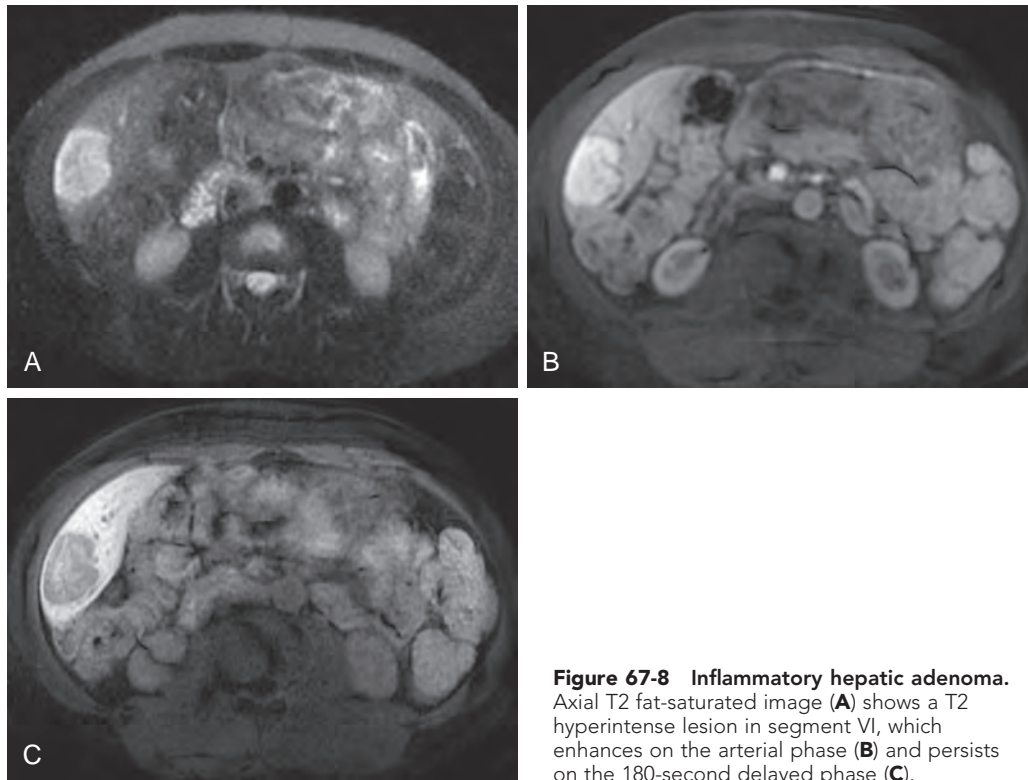


Figure 67-8 Inflammatory hepatic adenoma. Axial T2 fat-saturated image (A) shows a T2 hyperintense lesion in segment VI, which enhances on the arterial phase (B) and persists on the 180-second delayed phase (C).

the majority of patients taking oral contraceptive medications. Estrogens in these medications have been postulated to cause somatic mutations in HNF-1 α adenomas, and inactivation of *HNF1A* gene results in nonfunctioning HNF-1 α protein, which subsequently promotes proliferation of hepatocytes and lipogenesis with impaired fatty acid regulation in hepatocytes, resulting in fat deposition within the hepatocytes. On MRI, HNF-1 α -mutated hepatocellular adenomas are T1 hyperintense to isointense and T2 isointense to slightly hyperintense; after the administration of contrast material, there is moderate arterial enhancement with no persistent portal venous or delayed phase enhancement.⁸ Diffuse signal loss on out-of-phase gradient recalled echo images is seen because of intracellular steatosis, with sensitivity and specificity as high as 85% and 100%, respectively. HNF-1 α -mutated hepatocellular adenomas, even lesions larger than 5 cm, have minimal risk of bleeding, and there is minimal or no risk for development of HCC.

β -Catenin-mutated hepatocellular adenoma accounts for 10% to 15% of all adenomas. This subtype occurs more commonly in men and is associated with exogenous testosterone use, familial adenomatous polyposis, and glycogen storage disease. There is overexpression of the glutamate-ammonia lipase gene, resulting in elevated levels of glutamine synthetase, which has been used recently in immunohistochemical analysis for definitive diagnosis. This subtype has homogeneous or heterogeneous T1 and T2 hyperintense signal, depending on the presence of blood and necrosis. These lesions enhance intensely on the arterial phase, with variable persistence on the portal venous and delayed phases. The imaging appearance can be confused with that of HCC. This subtype has the highest risk of malignant transformation, with an overall risk of 5% to 10%

as the β -catenin pathway is involved in the pathogenesis of HCC. Other risk factors for malignant transformation are male sex, glycogen storage disease, tumors larger than 5 cm, and exogenous anabolic steroid use.

Focal and Diffuse Steatosis

Various manifestations of fatty infiltration include focal, patchy, and diffuse.^{15,16} Focal fat deposition and focal fat sparing can be mistaken for a focal hepatic lesion.¹⁵ MRI is helpful in differentiating a true hepatic lesion from focal fat deposition and focal fat sparing, particularly the T1-weighted in-phase and opposed-phase gradient-echo images. Focal fat deposition is lower in intensity on the opposed-phase images compared with the in-phase images and has high signal on the DIXON fat-only images (see Fig. 67-4). In contradistinction, focal fat sparing does not decrease in intensity on the opposed-phase images but instead appears hyperintense relative to the surrounding hepatic steatosis.

Another helpful differentiating imaging feature is the location, which typically is in the gallbladder fossa, in the medial aspect of the left hepatic lobe, along the falciform ligament, and in the central aspect of segment IV.¹⁵ Also, no mass effect is seen on adjacent structures or hepatic parenchyma, and blood vessels course through areas of focal hepatic steatosis and focal fat sparing. The presence of normal enhancing liver is helpful in accurate diagnosis of focal fat and focal fat sparing.

Diffuse hepatic steatosis involves a majority of the hepatic parenchyma, and on MRI, the liver intensity decreases on the opposed-phase images relative to the in-phase images (see Fig. 67-2A, B).^{15,16} Rather than appearing as focal hepatic signal abnormality, the entire hepatic parenchyma is diffusely involved.

Cholangiocellular Origin Lesions

MRI is extremely helpful in diagnosing and characterizing lesions of cholangiocellular origin, including simple hepatic cysts, biliary hamartomas, peribiliary cysts, biliary cystadenoma, and biliary cystadenocarcinoma.⁷ MRCP sequences are useful to assess the relationship of these lesions to the biliary tree.

Simple hepatic cysts are lined by biliary epithelium and originate from precursor microhamartomas.⁷ Cysts are usually round, well defined, and larger than 1 cm, and they can be single or multiple. Multiple simple hepatic cysts may be seen in adult polycystic kidney disease. On MRI, simple hepatic cysts have classic imaging characteristics with T1 hypointensity, T2 hyperintensity, and no associated enhancement.

Biliary hamartomas are also known as von Meyenburg complexes. They represent rare benign malformations of the biliary system secondary to failed involution of embryonic biliary ducts.⁷ Hamartomas are usually numerous, subcentimeter, well-defined T1 hypointense, T2 hyperintense, nonenhancing lesions with no connection to the biliary tree (Fig. 67-9A).

Peribiliary cysts are benign cystic dilations of obstructed glands around the biliary duct walls.⁷ Inflammation and disturbed periportal circulation lead to gland obstruction and result in peribiliary cyst formation. These lesions are typically associated with cirrhosis with portal hypertension and portal vein thrombosis. Peribiliary cysts are usually multiple T1 hypointense, T2 hyperintense tubular structures coursing along the bile ducts (Fig. 67-9B). They typically have smooth walls with no internal components, and they do not communicate with the biliary system.

Biliary cystadenoma, a rare benign cystic neoplasm, is a precursor to the malignant form of biliary cystadenocarcinoma.^{7,17} A majority of these lesions originate from the intrahepatic bile

ducts and are complex, multiloculated, cystic masses with enhancing internal septations (Fig. 67-9C). The MRI findings are variable, depending on the internal composition of the lesion, specifically if the lesion is composed of mucinous or serous fluid. The presence of enhancing nodular septations in the lesion is suggestive of the malignant biliary cystadenocarcinoma. These tumors tend to recur after complete surgical excision, and biliary cystadenomas can undergo malignant degeneration even after years of stability.

Cirrhosis and Hepatocellular Carcinoma

Cirrhosis is associated in up to 90% of patients with HCC and is characterized by irreversible disruption of the normal hepatic architecture with fibrosis and hepatic nodules.^{6,18-23} The most common causes of cirrhosis worldwide, in order of decreasing frequency, are hepatitis C virus, hepatitis B virus, alcohol, and nonalcoholic steatohepatitis; in the United States and Europe, the most common cause of cirrhosis is alcohol. Hepatitis B and C increase the risk of HCC 20 times, and the rate of HCC development once a diagnosis of cirrhosis is made is 1% to 4% per year.

The development of HCC is a multistep continuous carcinogenic process whereby multiple alterations lead to malignant transformation of the hepatocyte.^{6,18-23} The hepatocarcinogenesis has been arbitrarily divided for diagnostic and practical purposes. There are two types of hepatocellular nodules, regenerative and dysplastic nodules. Regenerative nodules result from proliferation of hepatocytes and supporting stroma, leading to nodular transformation of hepatic parenchyma with no fibrous septations between the nodules. These nodules can be mononodular or multinodular and can also be micronodular (<3 mm) or macronodular (>3 mm). Dysplastic nodules result from hepatocyte proliferation with abnormal growth or dysplasia,

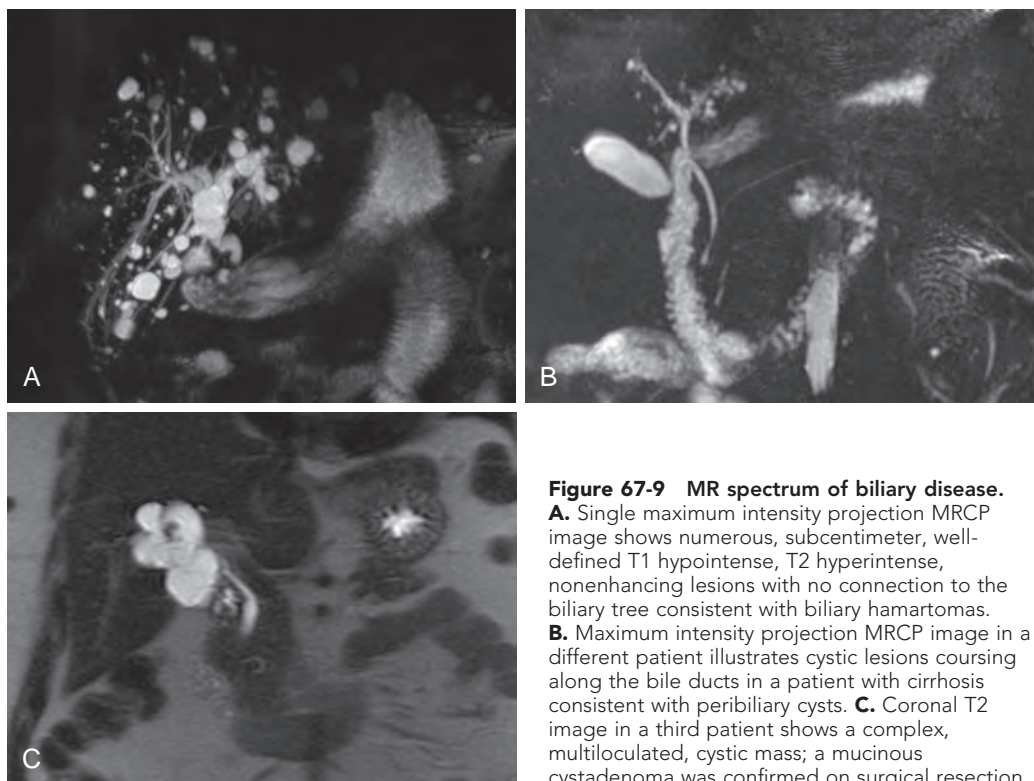


Figure 67-9 MR spectrum of biliary disease.

A. Single maximum intensity projection MRCP image shows numerous, subcentimeter, well-defined T1 hypointense, T2 hyperintense, nonenhancing lesions with no connection to the biliary tree consistent with biliary hamartomas. **B.** Maximum intensity projection MRCP image in a different patient illustrates cystic lesions coursing along the bile ducts in a patient with cirrhosis consistent with peribiliary cysts. **C.** Coronal T2 image in a third patient shows a complex, multiloculated, cystic mass; a mucinous cystadenoma was confirmed on surgical resection.

with derangement of normal architecture and cellular atypia. HCC is a malignant neoplasm with hepatocellular differentiation and development of neoangiogenesis with progressive loss of portal venous blood flow and increased arterial vascularity.

Cirrhosis on imaging is characterized by atrophy and hypertrophy of certain segments, liver contours, presence of hepatic nodules, fibrotic and fatty changes, and signs of portal hypertension. The right lobe of the liver and the medial segment of the left hepatic lobe (segment IV) atrophy, whereas the caudate and lateral segments of the left hepatic lobe (segments II and III) hypertrophy. The liver contour tends to be nodular, although this may not be apparent in all cirrhotics, and there is widening of the fissures between lobes and segments. Regenerative nodules are seen, and diffuse lacelike bands of fibrosis may be present; diffuse or geographic areas of fatty change have also been seen in cirrhosis. Signs of portal hypertension, including splenomegaly, enlargement of the portal vein, presence of varices (gastric, splenic, esophageal, caput medusae), and peribiliary cysts, are present in varying degrees in cirrhotic patients.

MRI has revolutionized the diagnostic and treatment implications involved in the care of cirrhotic patients.¹⁸⁻²² MRI can accurately characterize cirrhosis-associated liver nodules, with the critical role being early detection of HCC. The MRI examination is easily and accurately reproducible, allowing staging of HCC, planning of treatment options, and assessment of response to treatment. HCC is T2 hyperintense with avid arterial enhancement that shows washout or becomes hypointense relative to the surrounding liver on the delayed phase (Fig. 67-10).

Regenerative nodules are T1 variable, T2 hypointense, and after the administration of gadolinium, these nodules are usually isointense to surrounding parenchyma as they maintain

hepatocellular function. Dysplastic nodules have variable imaging appearances that overlap with both regenerative nodules and HCC. Low-grade dysplastic nodules are usually T2 hypointense, in contradistinction to high-grade dysplastic nodules, which have high signal on T2. Low- and high-grade dysplastic nodules have variable T1 signal intensity but usually have T1 high signal. Also, low-grade dysplastic nodules share enhancement patterns with regenerative nodules, and high-grade dysplastic nodules share enhancement patterns with HCC, but low- and high-grade dysplastic nodules typically enhance as much as hepatic parenchyma. Siderotic nodules are characterized by high iron content and can be either regenerative or dysplastic nodules. On MRI, siderotic nodules are low T1 and T2 because of magnetic susceptibility from local field inhomogeneities. It is difficult to differentiate regenerative siderotic nodules from dysplastic siderotic nodules on imaging.

A dysplastic nodule may contain a focus of HCC and have a nodule-in-nodule appearance. The dysplastic nodule has low T2 signal, and after the administration of gadolinium, a focus of arterial enhancement is visualized, resulting in the so-called nodule-in-nodule appearance. HCC appearance on MRI depends on the size and grade of the malignant neoplasm. Small HCCs are less than 2 cm and are classified into early and progressed categories. Early HCCs are T1 hyperintense and T2 hypointense to isointense with relative hypoenhancement on the arterial phase but are hypointense on the portal venous phase. The arterial hypovascularity is thought to be secondary to decreased portal venous vascularity but insufficient arterial supply. The use of hepatobiliary contrast agents increases the detection of these early HCCs, in which normal hepatocytes will have enhancement, whereas the HCC will not enhance and will be hypointense. However, well-differentiated early HCCs may have residual hepatocyte function and have uptake of contrast

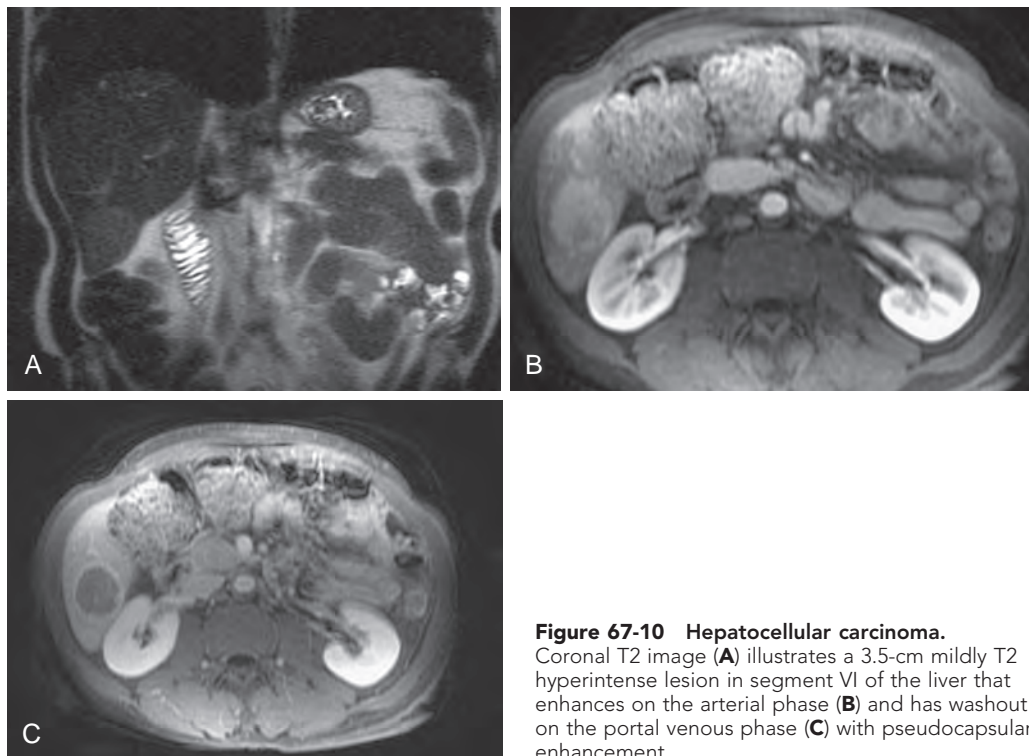


Figure 67-10 Hepatocellular carcinoma.

Coronal T2 image (A) illustrates a 3.5-cm mildly T2 hyperintense lesion in segment VI of the liver that enhances on the arterial phase (B) and has washout on the portal venous phase (C) with pseudocapsular enhancement.

material, with false-negative results. Progressed HCCs are less of a diagnostic dilemma in that they are well-defined, small T1 isointense and T2 moderately hyperintense nodular lesions with avid arterial enhancement and washout on the portal venous and delayed phases. On the basis of the new Organ Procurement and Transplantation Network policy for liver transplantation, small HCCs can be diagnosed on imaging alone if the lesion is at least 1 cm and less than 2 cm with arterial enhancement and washout on portal venous or delayed phase and has peripheral rim enhancement. Large lesions between 2 and 5 cm must have arterial enhancement and either washout on portal venous or delayed phase or peripheral rim enhancement or growth by 50% or more on serial imaging less than 6 months apart.

Iron Depositional Disease

Hemochromatosis can be primary, originating from a genetic disorder causing increased intestinal absorption of iron, or secondary, which is related to transfusions or chronic disease. Iron is normally stored in hepatocytes and in the reticuloendothelial cells, but excess iron can act as a catalyst of hydrogen peroxide into free radicals, resulting in cellular damage. MRI can noninvasively quantify the amount of iron in the liver and assess for response to treatment with high sensitivity and specificity.²⁴⁻²⁷ Primary hemochromatosis follows a hepatic parenchymal deposition pattern whereby iron is deposited in hepatocytes, then spread to the remainder of the liver, pancreas, thyroid, and cardiac tissue. Secondary hemochromatosis follows a reticuloendothelial deposition pattern whereby cells of the reticuloendothelial system of the liver, bone marrow, and spleen accumulate iron. Because the iron is not deposited in the hepatocytes, there is no associated tissue damage with secondary hemochromatosis. In advanced cases of secondary hemochromatosis, the iron deposition may exceed the storage capacity of the reticuloendothelial cells and may result in parenchymal deposition.

Hemochromatosis can be accurately and quickly diagnosed with MRI because of the shortening of T1 and T2 as well as the T2* shortening due to field inhomogeneities caused by superparamagnetic effects of iron.²⁴⁻²⁷ On T1-weighted in-phase and opposed-phase gradient-echo images, there is diffuse decreased intensity on images with the longer echo time, which is usually the in-phase images on 1.5T MRI (see Fig. 67-2C, D). This effect is due to the increased sensitivity to field inhomogeneities on the longer echo time sequence from increased T2* effect. Iron quantification can readily be performed with MRI with a high degree of accuracy on routine T1-weighted in-phase and opposed-phase gradient-echo images and T2* imaging.^{24,25}

BILE DUCTS AND GALLBLADDER

US is the initial imaging study of choice in the evaluation of gallbladder disease because of the high sensitivity and specificity. However, there are limitations of US, including operator dependence and degradation of image quality in obese patients. An increasing role of MRI has evolved with improved technology and faster acquisition times whereby MRI is a valuable imaging complement to US and computed tomography (CT).²⁸⁻³¹ MRI provides a comprehensive and detailed assessment of the biliary tree, including anatomic evaluation as well as disease processes, and is an established alternative to ERCP.²⁸⁻³¹

Cholelithiasis and Choledocholithiasis

Cholelithiasis is the concretion of bile in the biliary system, of which there are two types: cholesterol stones (75%-80%) and pigmented stones (20%-25%). Gallstones can form from cholesterol supersaturation; risk factors include obesity, pregnancy, rapid weight loss, high-fat diet, female gender, and advanced age. Gallstones can also form secondary to decreased gallbladder motility, which leads to crystallization of bile and predisposes to stone formation; risk factors include rapid weight loss, use of total parenteral nutrition, pregnancy, and oral contraceptive use. Pigmented stones can be of the black stone variety, which is caused by increased unconjugated bilirubin from chronic hemolytic states, or brown stones, which are associated with recurrent cholangitis or parasitic infections.

Stones within the intrahepatic and extrahepatic biliary tree can be primary, which form within the biliary ducts, or secondary, whereby stones from the gallbladder migrate into the common bile duct. Predisposing factors of primary choledocholithiasis include parasitic infections or recurrent cholangitis, congenital abnormalities, and prior surgery.

MRI accurately and consistently detects gallstones, which are best appreciated on T2-weighted images, where they appear as multiple filling defects in a gallbladder filled with T2 hyperintense bile.^{28,30} MRI can also differentiate the types of gallstones because both cholesterol and pigmented stones are T2 hypointense; however, pigmented stones are higher in T1 signal compared with cholesterol stones, and they also have a larger range of signal intensities.³⁰ MRI and MRCP heavily T2-weighted sequences also detect choledocholithiasis with a high sensitivity and specificity (>95%); the stones are seen as filling defects within the bile ducts (Fig. 67-11).²⁸⁻³³

Acute Cholecystitis

Acute cholecystitis is one of the most common causes of hospital admission from the emergency department and is the most common complication of cholelithiasis; up to 95% of cases are associated with gallstones. US is the traditional imaging modality of choice for gallbladder disease in patients thought to have acute cholecystitis. MRI is increasingly used in the emergency setting, given the faster acquisition sequences and improved technology. Imaging of suspected cases of acute cholecystitis assists in planning of immediate or delayed cholecystectomy and of the surgical approach (laparoscopic or open). MRI is particularly useful in clinically and sonographically equivocal cases of acute cholecystitis, with sensitivities up to 95% and specificities up to 89%,²⁹ and in the assessment of the bile ducts for possible choledocholithiasis. MRI and MRCP performed within 24 hours of arrival to the emergency department provide additional information in the evaluation of acute biliary disease, particularly with equivocal or inconclusive sonographic findings.²⁹ MRI has a sensitivity of 95% and specificity of 90% for diagnosis of acute cholecystitis.

MRI findings of uncomplicated acute cholecystitis include the presence of a gallstone usually impacted in the gallbladder neck or cystic duct, gallbladder distention (transverse diameter >4 cm), wall thickening (>3 mm), abnormal T2 hyperintense mural thickening and edematous stratification, wall hyperemia, and pericholecystic fluid.²⁸⁻³¹ MRI has excellent tissue contrast that increases the detection of gallbladder wall edema and pericholecystic fluid, which is manifested as T2 hyperintensity around the gallbladder (Fig. 67-12). A highly specific sign

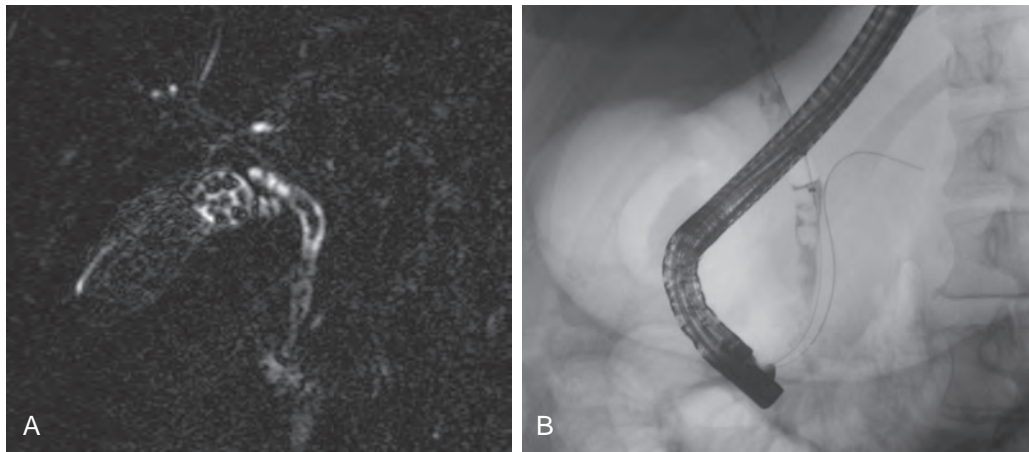


Figure 67-11 Cholelithiasis and choledocholithiasis. Coronal MRCP image (A) shows multiple filling defects within the gallbladder and bile ducts, which were confirmed at ERCP (B).

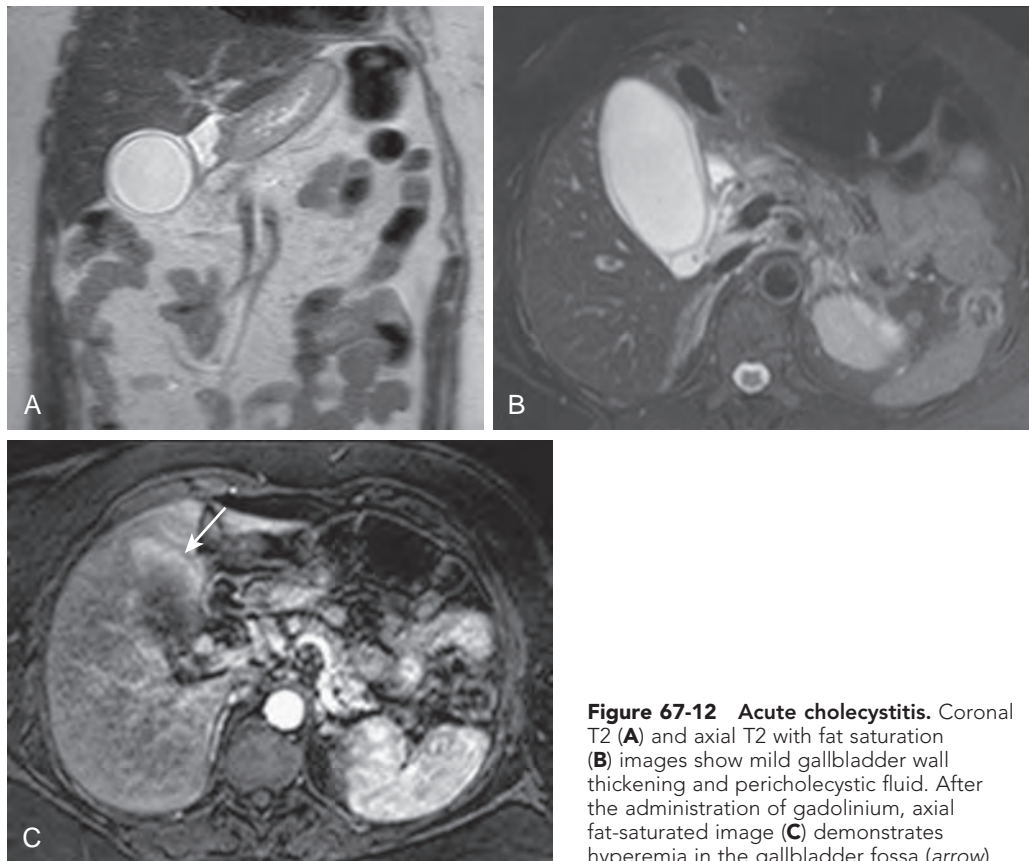


Figure 67-12 Acute cholecystitis. Coronal T2 (A) and axial T2 with fat saturation (B) images show mild gallbladder wall thickening and pericholecystic fluid. After the administration of gadolinium, axial fat-saturated image (C) demonstrates hyperemia in the gallbladder fossa (arrow).

(specificity of 70%) for acute cholecystitis is transient enhancement of the pericholecystic liver parenchyma seen immediately after the administration of gadolinium; this is thought to be secondary to reactive hyperemia of the hepatic parenchyma surrounding the acutely inflamed gallbladder.

Complications of acute cholecystitis are seen in up to 40% of cases and include gallbladder perforation with pericholecystic abscess formation, gangrenous cholecystitis, emphysematous cholecystitis, hemorrhagic cholecystitis, and perforation with bilioenteric fistula formation.^{30,31} Most complications can

be readily identified by MRI with the exception of emphysematous cholecystitis, for which CT is the best imaging modality to detect air within the gallbladder lumen and wall.

Gallbladder Carcinoma

Gallbladder malignant disease is the most common biliary tree carcinoma and the fifth most common gastrointestinal neoplasm.^{30,34} The prognosis is poor, with an estimated patient survival time of 3 months after diagnosis and a 5% 5-year survival rate.³⁴ At the time of initial presentation, there is usually

advanced disease with infiltration into the adjacent liver parenchyma and lymph node metastases. The thin gallbladder wall and the continuity of the connective tissue around the gallbladder with that of the liver allow invasion of the hepatic parenchyma and lymphatics. A majority of the cases (approximately 90%) are associated with gallstones, probably secondary to chronic inflammation; other risk factors include porcelain gallbladder and long common pancreatic-biliary channel.

Focal or diffuse gallbladder wall thickening of more than 1 cm is seen in early gallbladder malignant disease; however, the typical imaging appearance is an infiltrating mass in the gallbladder fossa. The mass is T1 isointense to hypointense and T2 heterogeneously hyperintense compared with adjacent liver, which enhances after the administration of gadolinium. Intrahepatic biliary dilation, best seen on MRCP images, may be seen secondary to hepatic duct compression directly by the tumor, direct invasion by the tumor, or lymphadenopathy, and MRCP images are helpful in localizing the site of obstruction. In cases in which the gallbladder is indistinct and replaced diffusely with neoplasm, the presence of gallstones within the mass can be helpful in making the diagnosis (Fig. 67-13).

In 25% of cases, an intraluminal polypoid mass is confined to the muscle layer. These cases are associated with a better prognosis compared with the diffusely infiltrating pattern of malignant disease. The polypoid masses are T1 isointense, T2 hyperintense compared with liver, and the mass projects into the gallbladder lumen. After the administration of gadolinium, the polypoid masses enhance early with prolonged enhancement.

Cholangiocarcinoma

Cholangiocarcinoma, a primary malignant neoplasm arising from the biliary epithelium, is the second most common primary hepatic tumor after HCC.^{35,36} The peak age prevalence is in the sixth to seventh decades; risk factors include choledochal cysts, primary sclerosing cholangitis, familial polyposis, chronic infection, and congenital hepatic fibrosis. Most cases (95% of cases) are histologically adenocarcinoma. Cholangiocarcinoma can be anatomically classified as intrahepatic, including central and peripheral, or extrahepatic.^{35,36} Central intrahepatic cholangiocarcinoma arises from the hepatic duct bifurcation and proximal common hepatic duct, whereas peripheral intrahepatic tumors involve the second-order bile ducts. Tumor growth has been described as polypoid

(intraductal), infiltrative (periductal), or exophytic (mass forming); infiltrating central intrahepatic tumors (Klatskin tumors) have been subclassified according to the Bismuth-Corlette classification.

On MRI, mass-forming cholangiocarcinomas are T1 hypointense to isointense and have variable T2 signal, depending on the amount of tumoral fibrosis, hemorrhage, and necrosis. After gadolinium administration, the masses have little arterial enhancement with increased progressive enhancement on the delayed phases owing to the presence of fibrosis and central tumoral necrosis and desmoplastic response (Fig. 67-14). Smaller tumors may demonstrate homogeneous and avid arterial enhancement that persists on subsequent phases because of the absence of fibrosis. Intraductal tumors are T1 hypointense to isointense with mild T2 hyperintensity with heterogeneous enhancement. On MRCP sequences, the area of biliary ductal narrowing with upstream ductal dilation can be readily detected to localize and to characterize the tumor.

PANCREAS

MRI is a valuable imaging tool to assess a wide spectrum of pancreatic disease.^{37,38} Specific morphologic features and signal intensity characteristics allow diagnosis of pathologic processes such as acute and chronic pancreatitis, adenocarcinoma, neuroendocrine tumors, microcystic and macrocystic cystadenoma, serous cystadenoma, intraductal papillary mucinous neoplasms, and solid pseudopapillary neoplasms (or solid and papillary epithelial neoplasms). Ductal anatomy and pathologic processes can be readily assessed on MRCP with sensitivity similar to that of ERCP. The pancreas has inherent high signal on T1-weighted images and enhances maximally during the pancreatic arterial phase around 15 to 20 seconds, subsequently becoming isointense on later dynamic contrast-enhanced images.

Acute Pancreatitis

Acute pancreatitis is an acute inflammatory process involving the pancreatic parenchyma and surrounding organs. The diagnosis is made by clinical and laboratory findings; however, imaging is used to confirm the diagnosis and to detect complications. CT is the most common imaging modality used, but MRI has an increasing role, particularly because patients with acute pancreatitis tend to be younger and require multiple

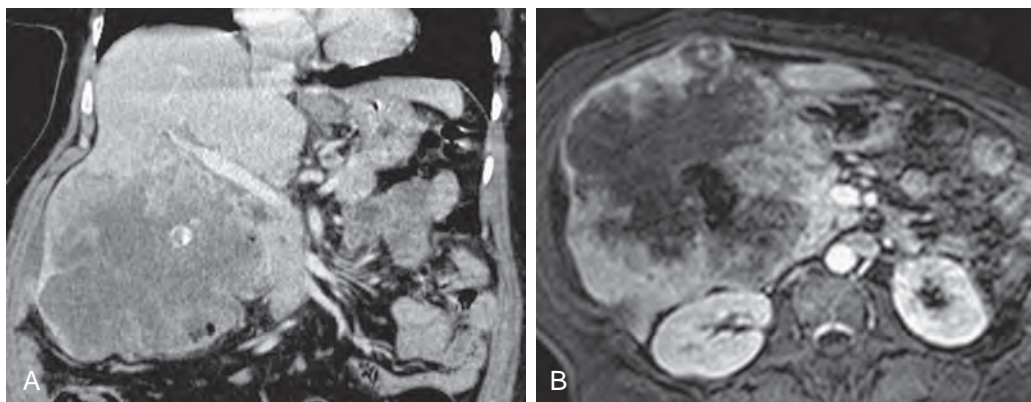


Figure 67-13 Gallbladder adenocarcinoma. Coronal CT (A) and axial post-gadolinium fat-saturated (B) images demonstrate a large heterogeneous mass originating in the gallbladder fossa. Calcified gallstones within the center of the mass are seen on the CT image.

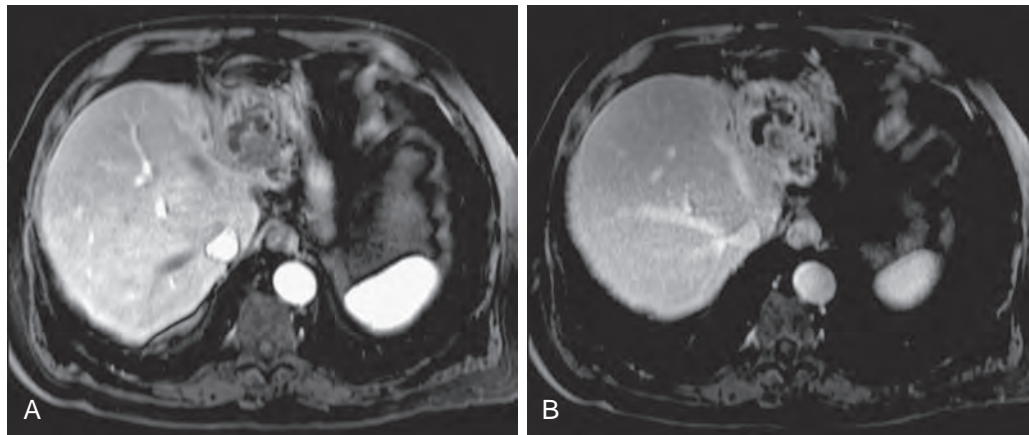


Figure 67-14 Cholangiocarcinoma. Axial arterial (A) and portal venous (B) phase images after the administration of gadolinium show a mass in the atrophied right lobe of the liver with associated biliary dilation and capsular retraction. The mass enhances minimally on the arterial phase, with progressively increasing enhancement on the portal venous phase.

examinations.³⁸⁻⁴² Moreover, advances in MRI technology allow excellent pancreatic imaging and detection of associated complications, such as necrosis, fluid collections, and vascular complications including thrombi and pseudoaneurysms.³⁹⁻⁴¹ Causes of acute pancreatitis include alcohol, gallstones, metabolic abnormalities, infection, trauma, and medications.

Anatomic variations of the pancreatic duct, including pancreas divisum and a long common pancreatic-biliary channel, have been associated with acute pancreatitis⁴² and can readily be assessed with MRCP. Pancreas divisum is the most common congenital anomaly; the ventral and dorsal pancreatic buds do not fuse, and the ventral duct (duct of Wirsung) drains the ventral anlage and the dorsal duct (duct of Santorini) drains a majority of the pancreas, which empties into the minor papilla. Pancreas divisum is detected on MRCP with high sensitivity and specificity. The presence of a long common channel (>15 mm) allows reflux of bile into the pancreatic duct, resulting in acute pancreatitis.

Typical MRI findings of acute pancreatitis are focal or diffuse enlargement of the pancreas with heterogeneous areas of low T1 signal and high T2 signal and normal homogeneous or slightly heterogeneous enhancement.³⁷⁻⁴⁰ Peripancreatic stranding in mild acute pancreatitis is best seen on T1 as peripancreatic hypointensity; in more severe pancreatitis, T2-weighted images show peripancreatic T2 hyperintensity.³⁷⁻⁴⁰

Necrotizing pancreatitis occurs in 20% to 30% of cases and increases the mortality associated with acute pancreatitis. There are three types according to the revised Atlanta classification system: pancreatic parenchymal necrosis, peripancreatic necrosis, and combined pancreatic parenchymal necrosis with peripancreatic necrosis; these types can be sterile or infected. Assessment of the extent of necrosis is important as there is a correlation with overall prognosis. Areas of necrosis on T2 sequences are low intensity, but when liquefied, necrosis is T2 hyperintense. Necrosis is best depicted on post-gadolinium images as areas of decreased enhancement.

Pancreatic and peripancreatic collections can be seen in acute pancreatitis.^{39,40} Acute collections are classified as acute pancreatic fluid collection (APFC) if there is no necrosis or acute necrotizing collection (ANC) if necrosis is present. With time, after 4 weeks, acute pancreatitis without necrosis and APFC are associated with pseudocysts, whereas pancreatic

necrosis and ANC are associated with walled-off necrosis. On MRI, APFC has liquefied components and conforms to anatomic boundaries around the pancreas with no discernible wall, which are T1 hypointense and T2 hyperintense. With time, APFC may develop into pseudocysts, which are unilocular encapsulated fluid collections with T1 hypointensity and T2 hyperintensity. ANC is a persistent collection of fluid and necrotic material that replaces pancreatic parenchyma after necrotizing pancreatitis. ANC over time develops into walled-off necrosis, which is heterogeneous on MRI due to the presence of nonliquefied necrotic pancreatic parenchyma and necrotic fat.

Vascular complications of acute pancreatitis include venous thrombus formation and pseudoaneurysms. Venous thrombi are the most common vascular complication of acute pancreatitis and affect the splenic, superior mesenteric, and portal veins; on MRI, thrombi are best seen on post-gadolinium images. Pseudoaneurysms are caused by blood vessel wall weakening from the proteolytic enzymes and most frequently involve the splenic, pancreaticoduodenal, and gastroduodenal arteries. Pseudoaneurysms are readily detected on post-gadolinium images and opacify during the early arterial phase. Pseudoaneurysms can rupture, with resulting peripancreatic hemorrhagic fluid collections that are high signal on T1 due to methemoglobin with a T2 hypointense hemosiderin rim. MRI has the benefit of persistent signal abnormalities compared with CT.

Pancreatic Cystic Lesions

Accurate characterization of pancreatic cystic lesions is crucial to create a differential diagnosis and to guide subsequent treatment, and MRI has been shown to be the optimal imaging modality for complete assessment.⁴³ Pancreatic cystic lesions can be primary, such as pseudocysts, serous cystadenomas, and mucinous lesions, including mucinous cystadenoma, cystadenocarcinoma, and intraductal papillary mucinous neoplasms; or they can be cystic changes in a solid neoplasm, including adenocarcinoma, neuroendocrine tumors, and solid pseudopapillary neoplasms (or solid and papillary epithelial neoplasms).⁴³⁻⁴⁶

Serous cystadenomas are benign cystic neoplasms composed of numerous small cysts, typically less than 1 cm, that are

separated by fibrous septa radiating from a central scar.⁴⁵ These neoplasms occur in older women, typically older than 65 years, and are typically incidentally found. On MRI, these lesions appear as a cluster of small T2 hyperintense cysts with thin enhancing fibrous septa separating the cysts; a central calcified scar with signal void may be seen. There is no connection to the main pancreatic duct (Fig. 67-15).^{43,45}

Mucinous cystadenomas are thick-walled, uniloculated or multiloculated cystic masses in the pancreatic body or tail that are lined by mucin-producing columnar epithelium with no communication to the pancreatic ducts. Most are incidentally found in women. Mucinous cystadenomas have malignant potential and are surgically resected.⁴³ On MRI, these lesions are uniloculated or multiloculated, with signal intensity that follows simple fluid despite the presence of mucin, and are T1 hypointense and T2 hyperintense, although intrinsic T1 hyperintense signal has been described (Fig. 67-16).⁴³ The thick wall has enhancement in the delayed phases because of the presence of fibrosis, and the internal septa enhance. Intracystic nodular soft tissue components suggest the presence of invasive carcinomatous components. Mucinous cystadenocarcinomas have intracystic nodular soft tissue components in a mucinous cyst with surrounding ovarian-type stroma.

Intraductal papillary mucinous neoplasms (IPMNs) are mucin-producing tumors arising from the epithelial lining of the main or side branch pancreatic ducts.⁴³ The pancreatic ductal epithelial cells are transformed into neoplastic mucin, producing cells that form papillary projections, and the excess mucin results in cystic dilation of the ducts (Fig. 67-17). At ERCP, spillage of mucin into the ampulla of Vater is classically

seen.⁴³ An association between IPMN and concomitant pancreatic ductal adenocarcinoma and pancreatic ductal adenocarcinoma arising from IPMN has been described, both of which are thought to have favorable biologic behavior or to be diagnosed at an earlier stage.^{43,47,48} IPMNs are classified as involved with the main pancreatic duct or isolated to the side branch ducts, which has important implications because 60% to 70% of main duct IPMNs have invasive carcinoma, as opposed to 20% of side branch IPMNs containing invasive carcinoma.^{43,49} MRI is the imaging modality of choice in the evaluation of IPMNs to determine the location and type of the lesion. Main duct IPMNs have focal or diffuse enlargement of the main pancreatic duct, and although chronic pancreatitis can be manifested with diffuse enlargement of the pancreatic duct, helpful differentiating imaging features are associated parenchymal changes in chronic pancreatitis with T1 hypointensity and delayed contrast uptake secondary to fibrosis. Multiple dilated side branch T2 hyperintensities are seen in side branch IPMNs. Enhancing and nodular soft tissue components in IPMNs are suggestive of concomitant adenocarcinoma, which can arise from the IPMN or at a different site along the pancreatic duct.

Pancreatic Solid Lesions

Solid pancreatic lesions include pancreatic adenocarcinoma, neuroendocrine tumors, solid pseudopapillary neoplasms (or solid and papillary epithelial neoplasms), and metastases, all of which have different appearances on MRI. As described previously, these masses may have cystic components from tumor degeneration.

Figure 67-15 Pancreatic serous cystadenoma. Axial T2 fat-saturated MR image (A) demonstrates a cluster of small T2 hyperintense cysts with thin septations. No communication or dilation of the main pancreatic duct is visualized on the maximum intensity projection MRCP image (B).

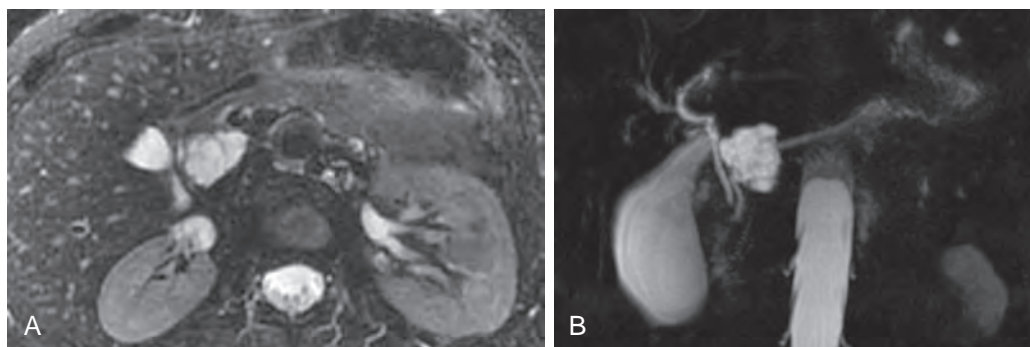
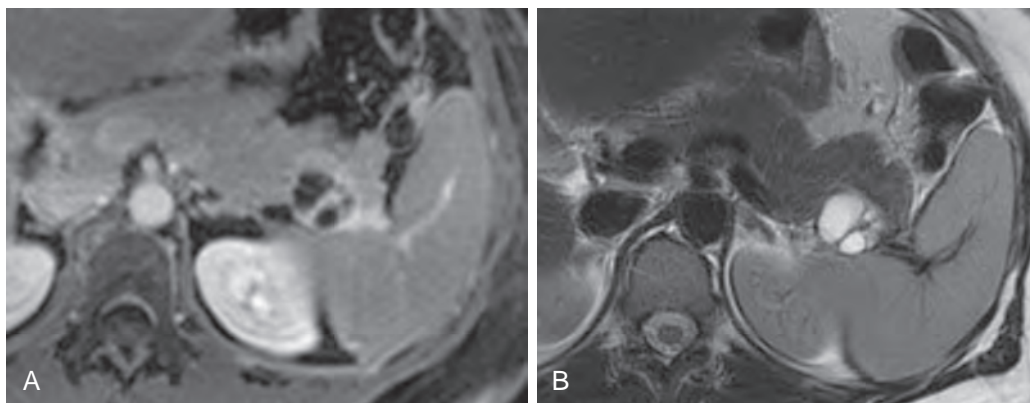


Figure 67-16 Pancreatic mucinous cystadenoma. Axial post-gadolinium fat-saturated (A) and axial T2 (B) images show a lobulated T1 hypointense and T2 hyperintense lesion in the pancreatic tail. There are thick-walled septations, which enhance.



Pancreatic Adenocarcinoma

Pancreatic adenocarcinoma is the most common malignant neoplasm of the pancreas and arises from the ductal epithelium. Pancreatic adenocarcinoma carries a very poor prognosis with a 5-year survival rate of approximately 6%.^{50,51} It is often locally progressed at the time of diagnosis.

The normal pancreatic parenchyma is T1 hyperintense; however, adenocarcinoma will appear as an irregular T1 hypointense mass relative to normal pancreas on T1-weighted fat-suppressed images because of an intense fibrotic, desmoplastic reaction. After the administration of contrast material, adenocarcinomas usually have less enhancement on the arterial phase and occasionally demonstrate delayed enhancement. Diffusion-weighted imaging and ADC reconstruction maps are particularly helpful in detecting small adenocarcinomas as pancreatic adenocarcinomas exhibit restricted diffusion, probably attributable to the associated fibrosis, with high signal on diffusion-weighted imaging with associated low ADC values.⁵² Pancreatic ductal abrupt obstruction with upstream dilation is commonly seen, which can be readily assessed on MRCP images, and the common bile duct is usually dilated with an abrupt termination, resulting in the so-called double duct sign.

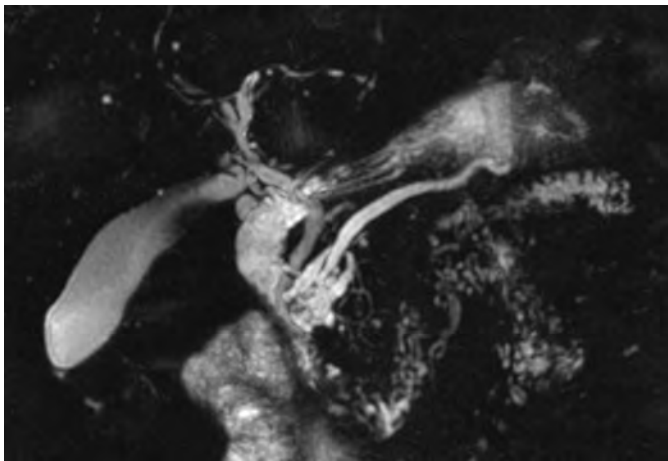


Figure 67-17 Mixed main and side branch IPMN. Maximum intensity projection MRCP image demonstrates a multilobulated cystic mass in the uncinate process that has a direct connection to the main pancreatic duct, which is dilated.

Neuroendocrine Neoplasms

Pancreatic neuroendocrine neoplasms are rare; neuroendocrine carcinoma accounts for 1% to 2% of all pancreatic tumors, but the incidence has increased as a result of increased detection.⁵³ Pancreatic neuroendocrine neoplasms are tumors that arise from neuroendocrine cells and include a range of tumors. They can be functioning or nonfunctioning; the two most common types are insulinomas and gastrinomas. Functioning tumors tend to be small at presentation, in contradistinction to nonfunctioning tumors, which are larger with possible venous invasion and metastatic lesions. Like adenocarcinoma, these lesions have low signal intensity on T1-weighted fat-suppressed images. Lesions are hyperintense on T2 with hyperenhancement on the arterial phase, which is one of the typical MRI features. Preoperative MRI assists in accurate diagnosis and may be helpful in determining tumor stage and grade.⁵³

Solid Pseudopapillary Neoplasms

Solid pseudopapillary neoplasms are rare, accounting for 1% of all pancreatic neoplasms, and have a low malignant potential.⁴³ They typically occur in young women (average age of 30 years). On imaging, these lesions are well-defined, heterogeneous, large masses with central cystic areas of T2 hyperintensity from tumor degeneration. These masses can be completely solid with mild T2 high signal, whereas masses that are mostly cystic are T2 hyperintense. Thick enhancing capsule of enhancing soft tissue is usually seen on post-gadolinium images.

ADRENAL GLANDS

The most valuable MRI sequence in imaging of the adrenal glands is chemical shift T1-weighted in-phase and opposed-phase gradient-echo imaging. This sequence is particularly useful in determining the presence of fat within adrenal lesions. Fat-containing adrenal masses can be classified into two groups: lesions with intravoxel fat, such as adenomas; and lesions with macroscopic fat, such as myelolipomas.⁵⁴ Pheochromocytomas have typical MRI characteristics, but not all lesions have diagnostic features.

Adrenal Adenoma

Adrenal adenomas are the most common lesions found in the adrenal glands.⁵⁴ The presence of intracellular fat is diagnostic of adrenal adenomas, and this can be accurately detected on the opposed-phase gradient-echo image (Fig. 67-18).^{54,55} A 20%

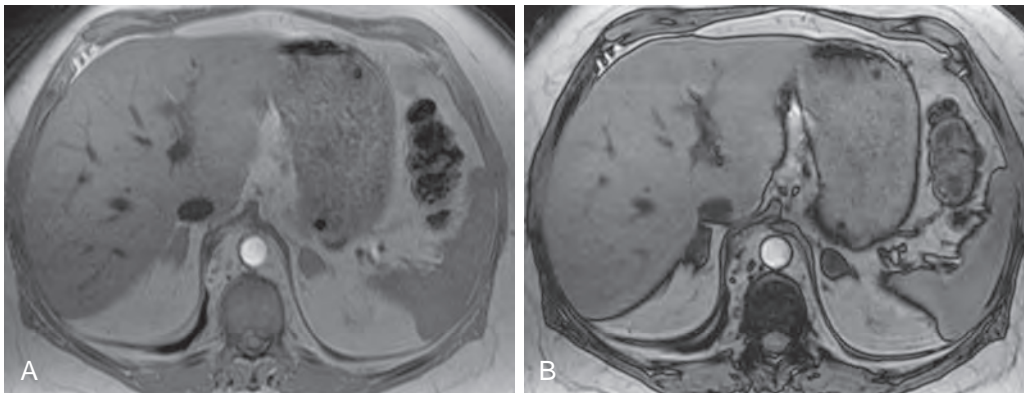


Figure 67-18 Bilateral adrenal adenomas. Axial T1 in-phase image (A) shows bilateral adrenal nodules that decrease in signal on the opposed-phase sequence (B), consistent with fat-containing adenomas.

decrease in signal intensity on the opposed-phase image compared with the in-phase image is diagnostic of an adrenal adenoma. Adenomas typically have homogeneous enhancement in the early arterial phase with more than 50% washout on the delayed phase images.

Myelolipoma

Myelolipomas are rare benign tumors of the adrenal gland and account for 7% to 15% of incidentally found adrenal masses.⁵⁴ Myelolipomas are composed of adipocytes and hematopoietic tissue (myeloid and erythroid cells) and are non-functioning.^{54,56} A tumor with a major fat component is found on diagnostic MRI, and on the basis of the MR appearances, myelolipomas can be categorized into three main categories.⁵⁶ Myelolipomas can be homogeneous and T1 hyperintense with intermediate T2 signal, suggestive of a large fat component; heterogeneous mass with T1 hyperintense foci, corresponding to foci of fat, and T2 hyperintense foci, which have mixed fat and myeloid components; and nodules that are T1 hypointense and T2 hyperintense compared with liver, corresponding to lesions composed of predominantly myeloid components. Adrenal myelolipomas rarely spontaneously rupture, resulting in hemorrhage.

Pheochromocytoma

Pheochromocytomas are tumors arising from chromaffin cells of the adrenal medulla. Most pheochromocytomas, approximately 90%, arise from the adrenal gland; the remaining 10% of lesions are extra-adrenal and arise along the sympathetic chain. On MRI, pheochromocytomas are intensely T2 hyperintense, the so-called light bulb sign, and enhance intensely. Approximately 33% of pheochromocytomas do not have the light bulb sign and instead are heterogeneous on T2-weighted images. Pheochromocytomas are the tumors with the “rule of 10s” or the “10% tumor”; 10% are extra-adrenal, 10% are familial, 10% are malignant, 10% are bilateral, and 10% occur in children.

KIDNEYS

MRI is helpful in diagnosis, in assessing enhancement of renal lesions, and in determining the presence of intralesional fat.⁵⁷ Different lesions in the kidneys, including cysts, angiomyolipoma, oncocytoma, renal cell carcinoma (RCC), and transitional cell carcinoma (TCC), have characteristic MRI findings.^{57,58}

Renal Cysts

Renal cysts are common and are present in 20% to 30% of the middle-aged adult population. Simple renal cysts are round, homogeneously hypointense on T1 and T2 hyperintense, with imperceptible walls that do not enhance. Complicated cysts can be hemorrhagic, infected, or proteinaceous, which would alter the signal characteristics accordingly.

Angiomyolipoma

Angiomyolipomas are benign renal tumors composed of blood vessels, smooth muscle, and fatty components and are the most common benign renal tumor; 90% of angiomyolipomas are unilateral and single, whereas the remaining 10% are multiple and bilateral and associated with tuberous sclerosis complex. A renal mass containing fat on imaging is diagnostic of an angiomyolipoma; however, 5% do not have detectable fat. On MRI, these lesions follow fat signal on all sequences, and the most reliable method of detecting bulk fat is to compare images before and after application of a fat-suppressed pulse sequence (Fig. 67-19).

Oncocytoma

Oncocytoma is a benign renal tumor composed of eosinophilic epithelial cells arising from collecting ducts; it is the second most common benign renal tumor next to angiomyolipoma. A central stellate fibrosis with compressed blood vessels is known as the central scar and is seen in approximately half of the cases. These lesions are T1 isointense to hypointense and slightly T2 hyperintense compared with renal cortex. The central scar is manifested as a stellate area of low T1 intensity and high T2 signal.

Renal Cell Carcinoma

RCC is a malignant tumor of the renal tubular epithelium. It projects from the cortical surface and deforms the renal cortex (Fig. 67-20). The subtypes of RCC include clear cell (70%), papillary (10%-15%), granular cell (7%), chromophobe cell (5%), sarcomatoid (2%), and collecting duct (<1%). MRI appearances vary by the subtype, but the most common, clear cell, has T1 isointense signal relative to renal parenchyma with increased T2 signal. Clear cell RCC has areas of low signal on opposed-phase images indicating the presence of fat, which is seen in 60% of tumors. Marked enhancement in viable areas of tumor is seen. Papillary RCC is the second most common subtype and has

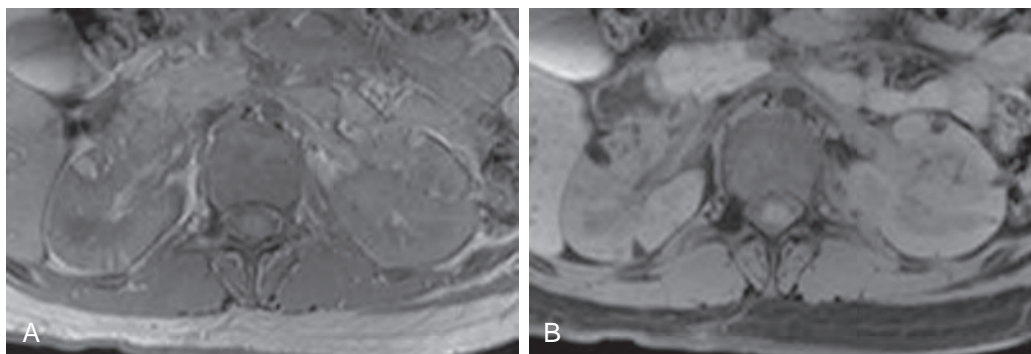


Figure 67-19 Bilateral renal angiomyolipoma. Axial T1 images without (A) and with fat saturation (B) show bilateral small T1 hyperintense lesions that drop in signal on the fat-saturated sequences, confirming the presence of intralésional fat.

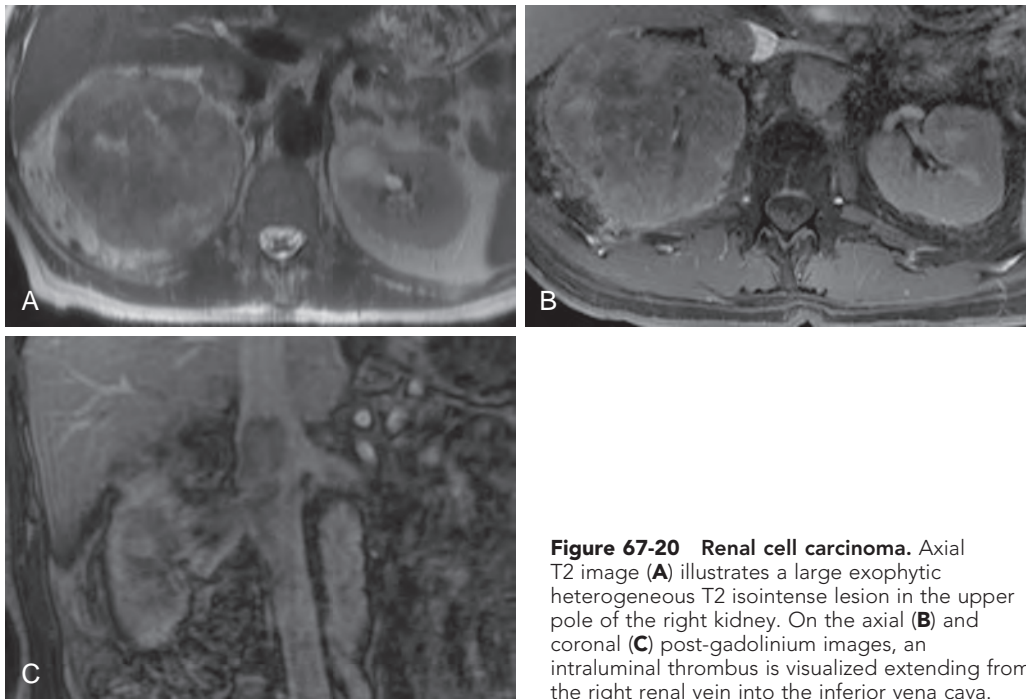


Figure 67-20 Renal cell carcinoma. Axial T2 image (A) illustrates a large exophytic heterogeneous T2 isointense lesion in the upper pole of the right kidney. On the axial (B) and coronal (C) post-gadolinium images, an intraluminal thrombus is visualized extending from the right renal vein into the inferior vena cava.

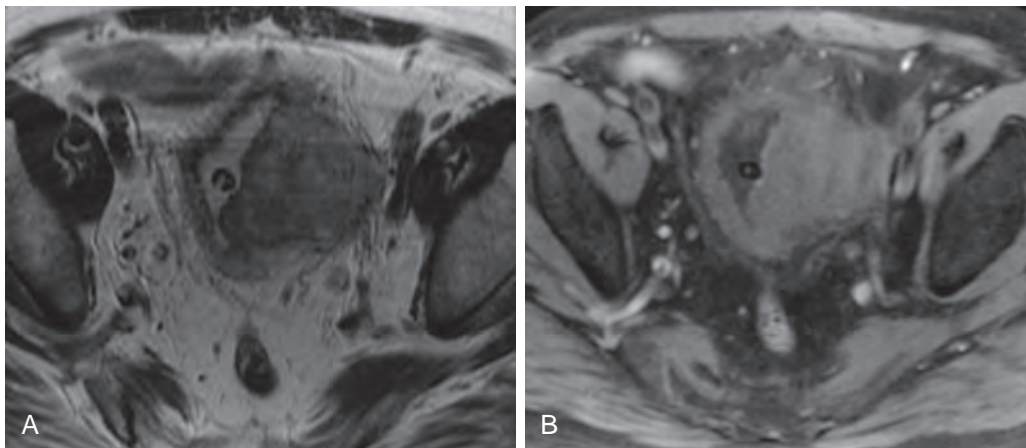


Figure 67-21 Bladder transitional cell carcinoma. Axial T2 (A) and axial T1 post-gadolinium (B) images show a large, homogeneously enhancing T2 heterogeneous mass arising from the left side of the bladder, extending toward the left pelvic side wall, and closely approximating the left external iliac artery and vein.

low T2 signal with low levels of enhancement after gadolinium administration.

Transitional Cell Carcinoma

TCC most commonly occurs in the bladder but accounts for 90% of all tumors arising from the urothelium lining the renal pelvis. Of the two subtypes, papillary and nonpapillary, papillary TCC is more common. TCC tends to be multifocal and can involve the entire collecting system. TCC is T1 isointense to the renal medulla and can infiltrate the renal sinus; it is seen as a filling defect on T2-weighted images because of the high signal T2 intensity of urine (Fig. 67-21). TCCs are hypoenhancing

masses, but avid enhancement may occur, and a focal filling defect that has enhancement is highly suggestive of a TCC. MRI is also helpful in assessing renal vein or inferior vena cava tumor extension.

Summary

MRI is a commonly used imaging modality, particularly in the evaluation of solid abdominal organs. With the increasing use of MRI, familiarity with imaging sequences and technique is imperative. In addition, knowledge of and familiarity with typical MRI features of various solid organ pathologic processes are crucial.

REFERENCES

- Sinha R, Rajiah P, Ramachandran I, et al: Diffusion-weighted MR imaging of the gastrointestinal tract: Technique, indications, and imaging findings. *Radiographics* 33:655–676, 2013.
- Gandhi SN, Brown MA, Wong JG, et al: MR contrast agents for liver imaging: What, when, how. *Radiographics* 26:1621–1636, 2006.
- Seale MK, Catalano OA, Saini S, et al: Hepatobiliary-specific MR contrast agents: Role in imaging the liver and biliary tree. *Radiographics* 29:1725–1748, 2009.
- Motosugi U, Ichikawa T, Araki T: Rules, roles, and room for discussion in gadoteric acid-enhanced magnetic resonance liver imaging: Current knowledge and future challenges. *Magn Reson Med* 12:161–175, 2013.
- Reimer P, Vosschenrich R: Detection and characterization of liver lesions using gadoteric acid as a tissue-specific contrast agent. *Biologics* 4:199–212, 2010.
- LeBedis C, Luna A, Soto JA: Use of magnetic resonance imaging contrast agents in the liver and biliary tract. *Magn Reson Imaging Clin N Am* 20:715–737, 2012.
- Anderson SW, Kruskal JB, Kane RA: Benign hepatic tumors and iatrogenic pseudotumors. *Radiographics* 29:211–229, 2009.
- Fowler KJ, Brown JJ, Narra VR: Magnetic resonance imaging of focal liver lesions: Approach to imaging diagnosis. *Hepatology* 54:2227–2237, 2011.
- Elsayes KM, Narra VR, Yin Y, et al: Focal hepatic lesions: Diagnostic value of enhancement pattern approach with contrast-enhanced 3D gradient-echo MR imaging. *Radiographics* 25:1299–1320, 2005.
- Nguyen BN, Flejou JF, Terris B, et al: Focal nodular hyperplasia of the liver: A comprehensive pathologic study of 305 lesions and recognition of new histologic forms. *Am J Surg Pathol* 23:1441–1454, 1999.
- Katabathina VS, Menias CO, Shanbhogue AKP, et al: Genetics and imaging of hepatocellular adenomas: 2011 update. *Radiographics* 31:1529–1543, 2011.
- Ronot M, Bahrani S, Calderaro J, et al: Hepatocellular adenomas: Accuracy of magnetic resonance imaging and liver biopsy in subtype classification. *Hepatology* 53:1182–1191, 2011.
- Zucman-Rossi J, Jeannot E, Nhieu JT, et al: Genotype-phenotype correlation in hepatocellular adenoma: New classification and relationship with HCC. *Hepatology* 43:515–524, 2006.
- Lewin M, Handra-Luca A, Arrivé L, et al: Liver adenomatosis: Classification of MR imaging features and comparison with pathologic findings. *Radiology* 241:433–440, 2006.
- Chundru S, Kalb B, Arif-Tiwari H, et al: MRI of diffuse liver disease: The common and uncommon etiologies. *Diagn Interv Radiol* 19:479–487, 2013.
- Reeder SB, Sirlin CB: Quantification of liver fat with magnetic resonance imaging. *Magn Reson Imaging Clin N Am* 18:337–357, 2010.
- Buetow PC, Buck JL, Pantongrag-Brown L, et al: Biliary cystadenoma and cystadenocarcinoma: Clinical-imaging-pathologic correlations with emphasis on the importance of ovarian stroma. *Radiology* 196:805–810, 1995.
- Parente B, Perez RM, Eiras-Araujo A, et al: MR imaging of hypervascular lesions in the cirrhotic liver: A diagnostic dilemma. *Radiographics* 32:767–787, 2012.
- Hussain SM, Reinhold C, Mitchell DG: Cirrhosis and lesion characterization at MR imaging. *Radiographics* 29:1637–1652, 2009.
- Hanna RF, Aguirre DA, Kased N, et al: Cirrhosis-associated hepatocellular nodules: Correlation of histopathologic and MR imaging features. *Radiographics* 28:747–769, 2008.
- Lutz AM, Willmann JK, Goepfert K, et al: Hepatocellular carcinoma in cirrhosis: Enhancement patterns at dynamic gadolinium- and superparamagnetic iron oxide-enhanced T1-weighted MR imaging. *Radiology* 237:520–528, 2005.
- Lee JM, Yoon JH, Kim KW: Diagnosis of hepatocellular carcinoma: Newer radiological tools. *Semin Oncol* 39:399–409, 2012.
- Ward C, Russo MW, Heimbach JK, et al: New OPTN/UNOS policy for liver transplant allocation: Standardization of liver imaging, diagnosis, classification, and reporting of hepatocellular carcinoma. *Radiology* 266:376–382, 2013.
- Lim RP, Tuvia K, Hadju CH, et al: Quantification of hepatic iron deposition in patients with liver disease: Comparison of chemical shift imaging with single-echo T2*-weighted imaging. *AJR Am J Roentgenol* 194:1288–1295, 2010.
- Queiroz-Andrade M, Blasbalg R, Ortega CD, et al: MR imaging findings of iron overload. *Radiographics* 29:1575–1589, 2009.
- Alústiza JM, Artetxe J, Castiella A, et al: MR quantification of hepatic iron concentration. *Radiology* 230:479–484, 2004.
- Sirlin CB, Reeder SB: Magnetic resonance imaging quantification of liver iron. *Magn Reson Imaging Clin N Am* 18:359–381, 2010.
- Kondo S, Isayama H, Akahane M, et al: Detection of common bile duct stones: Comparison between endoscopic ultrasonography, magnetic resonance cholangiography, and helical-computed-tomographic cholangiography. *Eur J Radiol* 54:271–275, 2005.
- Tonolini M, Ravelli A, Villa C, et al: Urgent MRI with MR cholangiopancreatography (MRCP) of acute cholecystitis and related complications: Diagnostic role and spectrum of imaging findings. *Emerg Radiol* 19:341–348, 2012.
- Catalano OA, Sahani DV, Kalva SP, et al: MR imaging of the gallbladder: A pictorial essay. *Radiographics* 28:135–155, 2008.
- Watanabe Y, Nagayama M, Okumura A, et al: MR imaging of acute biliary disorders. *Radiographics* 27:477–495, 2007.
- Yeh BM, Liu PS, Soto JA, et al: MR imaging and CT of the biliary tract. *Radiographics* 29:1669–1688, 2009.
- Soto JA, Barish MA, Alvarez O, et al: Detection of choledocholithiasis with MR cholangiography: Comparison of three-dimensional fast spin-echo and single- and multisection half-Fourier rapid acquisition with relaxation enhancement sequences. *Radiology* 215(30):737–745, 2000.
- Bartlett DL: Gallbladder cancer. *Semin Surg Oncol* 19:145–155, 2000.
- Sainani NI, Catalano OA, Holalkere N, et al: Cholangiocarcinoma: Current and novel imaging techniques. *Radiographics* 28:1263–1287, 2008.
- Nakeeb A, Pitt HA, Sohn TA, et al: Cholangiocarcinoma: A spectrum of intrahepatic, perihilar, and distal tumors. *Ann Surg* 224:463–475, 1996.
- Ly JN, Miller FH: MR imaging of the pancreas: A practical approach. *Radiol Clin North Am* 40:1289–1306, 2002.
- Pamuklar E, Semelka RC: MR imaging of the pancreas. *Magn Reson Imaging Clin N Am* 13:313–330, 2005.
- Miller FH, Keppke AL, Dalal K, et al: MRI of pancreatitis and its complications: Part 1, acute pancreatitis. *AJR Am J Roentgenol* 183:1637–1644, 2004.
- Thoeni RF: The revised Atlanta classification of acute pancreatitis: Its importance for the radiologist and its effect on treatment. *Radiology* 262:751–764, 2012.
- Czakó L: Diagnosis of early-stage chronic pancreatitis by secretin-enhanced magnetic resonance cholangiopancreatography. *J Gastroenterol* 42(Suppl 17):113–117, 2007.
- Soto JA, Lucey BC, Stuhlfaut JW: Pancreas divisum: Depiction with multi-detector row CT. *Radiology* 235:503–508, 2005.
- Kalb B, Sarmiento JM, Kooby DA, et al: MR imaging of cystic lesions of the pancreas. *Radiographics* 29:1749–1765, 2009.
- Kim JH, Eun HW, Kim YJ, et al: Staging accuracy of MR for pancreatic neuroendocrine tumor and imaging findings according to the tumor grade. *Abdom Imaging* 38:1106–1114, 2013.
- Choi JY, Kim MJ, Lee JY, et al: Typical and atypical manifestations of serous cystadenoma of the pancreas: Imaging findings with pathologic correlation. *AJR Am J Roentgenol* 193:136–142, 2009.
- Balci NC, Semelka RC: Radiologic features of cystic, endocrine and other pancreatic neoplasms. *Eur J Radiol* 38:113–119, 2001.
- Salvia R, Fernandez-del Castillo C, Bassi C, et al: Main-duct intraductal papillary mucinous neoplasms of the pancreas: Clinical predictors of malignancy and long-term survival following resection. *Ann Surg* 239:678–685, discussion 685–687, 2004.
- Yamaguchi K, Kanemitsu S, Hatori T, et al: Pancreatic ductal adenocarcinoma derived from IPMN and pancreatic ductal adenocarcinoma concomitant with IPMN. *Pancreas* 40:571–580, 2011.
- Terris B, Ponsot P, Paye F, et al: Intraductal papillary mucinous tumors of the pancreas confined to secondary ducts show less aggressive pathologic features as compared with those involving the main pancreatic duct. *Am J Surg Pathol* 24:1372–1377, 2000.
- National Cancer Institute: SEER stat fact sheets: Pancreas cancer, <http://seer.cancer.gov/statfacts/html/pancreas.html>.
- Park HS, Lee JM, Choi HK, et al: Preoperative evaluation of pancreatic cancer: Comparison of gadolinium-enhanced dynamic MRI with MR cholangiopancreatography versus MDCT. *J Magn Reson Imaging* 30:586–595, 2009.
- Lee SS, Byun JH, Park BJ, et al: Quantitative analysis of diffusion-weighted magnetic resonance imaging of the pancreas: Usefulness in characterizing solid pancreatic masses. *J Magn Reson Imaging* 28:928–936, 2008.

53. Kim JH, Eun HW, Kim YJ, et al: Staging accuracy of MR for pancreatic neuroendocrine tumor and imaging findings according to the tumor grade. *Abdom Imaging* 38:1106–1114, 2013.
54. Elsayes KM, Mukundan G, Narra VR, et al: Adrenal masses: MR imaging features with pathologic correlation. *Radiographics* 24:S73–S86, 2004.
55. Mitchell DG, Crovello M, Matteucci T, et al: Benign adrenocortical masses: Diagnosis with chemical shift MR imaging. *Radiology* 185:345–351, 1992.
56. Boraschi P, Braccini G, Gigoni R, et al: Adrenal myelolipomas: Their magnetic resonance assessment. *Clin Ter* 147:549–557, 1996.
57. Pedrosa I, Sun MR, Spencer M, et al: MR imaging of renal masses: Correlation with findings at surgery and pathologic analysis. *Radiographics* 28:985–1003, 2008.
58. Dyer R, DiSantis DJ, McClennan BL: Simplified imaging approach for evaluation of solid renal masses in adults. *Radiology* 247:331–333, 2008.

Positron Emission Tomography/ Computed Tomography of the Solid Parenchymal Organs

SHAUNAGH McDERMOTT | SELIM R. BUTROS | MICHAEL A. BLAKE

CHAPTER OUTLINE

Gallbladder and Biliary Tract

Cholangiocarcinoma
Gallbladder Carcinoma
Pitfalls

Liver

Hepatocellular Carcinoma
Metastases
Lymphoma
Pitfalls

Spleen

Lymphoma
Metastases
Pitfalls

Pancreas

Pancreatic Adenocarcinoma
Cystic Neoplasms
Pitfalls

Adrenal Glands

Metastases
Adrenocortical Carcinoma
Pheochromocytoma
Lymphoma
Pitfalls

In this chapter, we discuss fluorine-18-deoxyglucose positron emission tomography (FDG PET) and positron emission tomography/computed tomography (PET/CT) of the solid parenchymal organs of the abdomen and highlight in particular the advantages and pitfalls of hepatopancreatobiliary, splenic, and adrenal PET imaging.

Gallbladder and Biliary Tract

The gallbladder and biliary tract are essentially indistinguishable from the liver because of minimal physiologic FDG activity in these structures.

CHOLANGIOCARCINOMA

Several studies have shown that FDG PET has a 90% or greater sensitivity for primary cholangiocarcinoma.¹⁻⁴ However, the accuracy of FDG PET for detection of cholangiocarcinoma

appears to be dependent on the anatomic location, growth pattern, and pathologic characteristics. Studies have shown that the sensitivity of FDG PET for detection of intrahepatic cholangiocarcinoma is relatively higher than that for perihilar and extrahepatic tumors (Fig. 68-1). For example, Corvera and associates⁵ found that the sensitivity of PET for detecting intrahepatic cholangiocarcinoma was 95% compared with only 69% for extrahepatic cholangiocarcinoma. Petrowsky and colleagues⁶ and Lee and coworkers⁷ also found that the sensitivity for detecting intrahepatic cholangiocarcinoma was higher than that for extrahepatic cholangiocarcinoma (93% vs 55% and 100% vs 78%, respectively). Furthermore, Moon and colleagues⁴ found that the site of the primary tumor affected sensitivity of FDG PET; the sensitivity of FDG PET was lower for perihilar tumors compared with intrahepatic and common bile duct cancers (83% vs 91%, 91%). Moreover, in cases of perihilar tumors, the sensitivity of PET was lower than that of CT (83% vs 92%). Yamada and coworkers⁸ also concluded that the sensitivity for the detection of hilar cholangiocarcinomas was less than that for the detection of intrahepatic and extrahepatic cholangiocarcinoma (78% vs 100% and 84%, respectively). However, Reinhardt and associates⁹ were able to differentiate 12 patients with extrahepatic cholangiocarcinoma from 8 patients without cholangiocarcinoma by PET/CT with a delayed timing of FDG uptake and a maximum standardized uptake value (SUV_{max}) cutoff of 3.6.

The diagnostic accuracy of FDG PET in cholangiocarcinoma is also related to the growth pattern of the tumor. Anderson and coworkers¹⁰ reported a sensitivity of 85% for nodular morphology but only 18% for infiltrating morphology. Kato and associates¹¹ similarly found that 11 of 13 tumors (85%) found to be a tumoral mass in the bile duct on CT were identified on PET, whereas only 4 of 11 infiltrating-type tumors (36%) were detected by PET. The diagnostic accuracy of FDG PET may also differ on the basis of the histopathologic findings. Fritscher-Ravens and coworkers¹² found that whereas all true-positive PET results were seen in the tubular type of cholangiocarcinoma with a high amount of tumor cells and only low production of mucus, false-negative PET results were observed in three patients with mucinous adenocarcinoma.

Cholangiocarcinoma is a well-documented malignant complication of primary sclerosing cholangitis (PSC). The average prevalence of cholangiocarcinoma in PSC is approximately 10%.¹³ The detection of cholangiocarcinoma in patients with PSC remains challenging, despite improvements in morphologic imaging. Alkhawaldeh and colleagues¹⁴ found that by using the SUV_{max} cutoff of more than 3.9 in patients with PSC

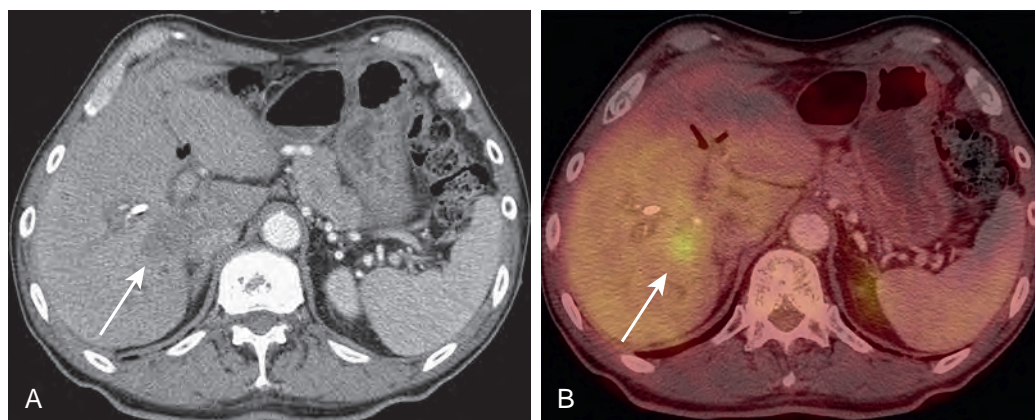


Figure 68-1 Cholangiocarcinoma. **A.** Contrast-enhanced CT demonstrates an ill-defined area of low attenuation in the right lobe of the liver (arrow). Note is also made of a biliary stent. **B.** This area demonstrates increased FDG avidity on PET/CT (arrow). Cholangiocarcinoma was confirmed on biopsy.

and suspected cholangiocarcinoma, FDG PET/CT had a sensitivity, specificity, and accuracy of 94%, 83%, and 91%, respectively. However, an earlier study by Fevery and coworkers¹⁵ found that PET is not reliable in the diagnosis of cholangiocarcinoma in patients with PSC as there were two false-positive and one false-negative results in the 10 patients in their study.

The resectability of cholangiocarcinoma depends on its regional and distant spread. Advances in surgery have increased the likelihood of achieving local disease control. Accurate staging is critical for surgical planning and also to prevent unnecessary surgical intervention in those with advanced disease. Compared with CT, PET has been found to have a higher specificity but lower sensitivity in the diagnosis of regional lymph node metastases.^{6,11,16,17} Another study found that FDG PET could detect lymph node metastases undetected by CT and changed the treatment plan in a significant number of cases.⁴ With regard to distant metastases, several studies have demonstrated the high accuracy of FDG PET in the detection of unsuspected distant metastasis.^{4,10,17,18} This revealing of otherwise undetected distant metastases has also been shown to play a significant role in clinical decision-making.

For the detection of recurrent cholangiocarcinoma, PET/CT may be beneficial in detecting disease recurrence for which anatomic imaging can be limited because of distortion and fibrotic changes after surgery. Jadvar and colleagues¹⁹ assessed the role of PET/CT in detecting recurrence after surgery and found a sensitivity and specificity of 94% and 100% for PET/CT compared with 82% and 43% for CT alone.

PET/CT may have a role in predicting survival in patients with cholangiocarcinoma undergoing treatment. Zhu and associates²⁰ found that a decrease in SUV_{max} after treatment of advanced biliary tract cancers with combined gemcitabine, oxaliplatin, and bevacizumab was associated with disease control and an increase in progression-free and overall survival. Furthermore, Haug and coworkers²¹ found that changes in SUV_{max} , SUV_{mean} , and metabolically active tumor volume at 3 months after yttrium 90 (⁹⁰Y) radioembolization for intrahepatic cholangiocarcinoma were able to predict patient outcome.

GALLBLADDER CARCINOMA

FDG PET has been found useful in the characterization of gallbladder lesions (Fig. 68-2). Koh and associates,²² in a study

of 16 patients, found that FDG PET had a sensitivity of 68% and a specificity of 88%. In another case series of 16 patients by Rodriguez-Fernandez and coworkers,²³ in which SUV in the gallbladder of more than 2.5 was considered positive for neoplasm, FDG PET was found to have a sensitivity of 80% and a specificity of 82%. In a study by Oe and colleagues,²⁴ PET had a sensitivity of 75% and a specificity of 100% in distinguishing between malignant and benign gallbladder wall thickening.

Nishiyama and coworkers²⁵ found that delayed FDG PET was more helpful than early FDG PET for evaluating malignant lesions because of increased lesion uptake and increased lesion-to-background contrast. When a threshold of SUV_{early} of 4.5, $SUV_{delayed}$ of 2.9, and retention index of -8 were chosen as arbitrary cutoffs for differentiating between malignant and benign conditions, sensitivity increased from 83% to 96% and 100% for delayed imaging and combined early and delayed imaging, respectively. However, few centers perform delayed FDG PET scanning, in large part because of workflow logistics.

Lee and coworkers⁷ found that in 16 patients with gallbladder cancer, PET/CT detected 14 cases (88%), whereas multidetector CT identified 15 cases (94%). In a study by Corvera and associates,⁵ FDG PET/CT identified 100% of the 15 primary gallbladder carcinomas left in situ. In a study by Petrowsky and colleagues,⁶ PET/CT detected each primary or recurrent gallbladder cancer (100%), whereas contrast-enhanced CT identified tumor in only 10 of 14 patients (71%).

In patients diagnosed with incidental gallbladder cancer after cholecystectomy for presumed benign disease, PET/CT may be a useful tool for the selection of patients for potentially curative treatment and may help reduce the number of patients undergoing nontherapeutic reexploration.^{26,27}

The presence of distant metastases in biliary tract cancers is associated with poor survival, regardless of treatment. It is therefore important to detect distant metastases so that surgery is offered only to those who may benefit from it. A study by Albazaz and colleagues¹⁸ on the clinical impact of FDG PET/CT in management decisions found that PET/CT had a major impact on management in 39% of cases in patients with gallbladder cancer, including upstaging of 27% of the scans performed for initial staging. Corvera and associates⁵ also found that among patients with gallbladder cancer,

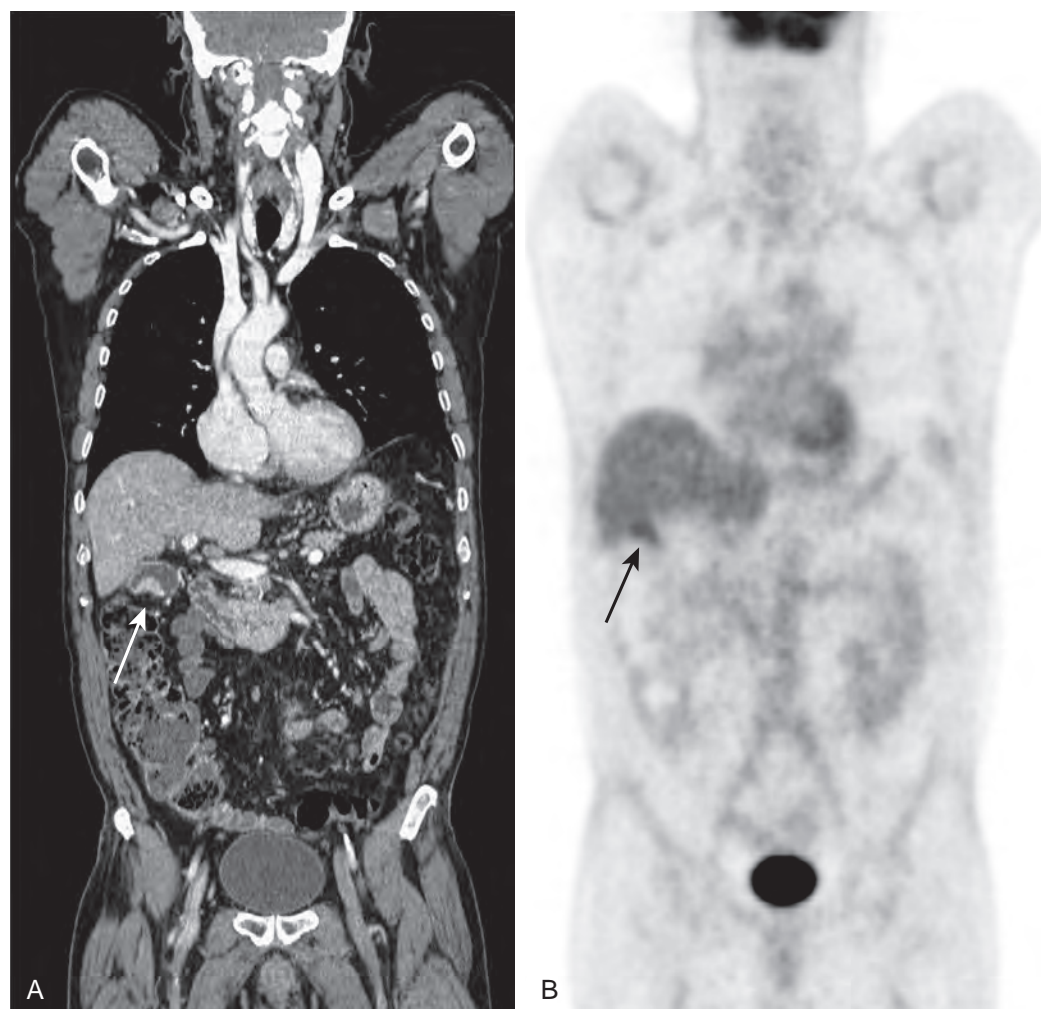


Figure 68-2 Gallbladder carcinoma. **A.** Contrast-enhanced CT demonstrates focal thickening of the inferior wall of the gallbladder (arrow). **B.** This region demonstrated increased FDG avidity on PET (arrow), without evidence of distant metastases. This was confirmed as gallbladder carcinoma on surgical resection.

PET changed management in 23% by showing metastatic disease not seen on other imaging, preventing futile and unnecessary explorations.

FDG PET/CT has a role to play in the detection of recurrent gallbladder carcinoma. Kumar and colleagues²⁸ found that FDG PET/CT had a sensitivity of 98% and a specificity of 90% in detecting tumor recurrence. They also concluded that when comparable conventional imaging (contrast-enhanced CT, MRI) was available, PET/CT had a better sensitivity for the detection of recurrence.

Interestingly, FDG PET/CT may also have a role in risk stratification of patients with gallbladder polyps. A study by Lee and colleagues²⁹ found that visual grading, polyp SUV_{max} cutoff of 2.14, and polyp-to-liver ratio cutoff of 1.14 yielded accuracy of 80%, 78%, and 84%, respectively, in diagnosis of malignant gallbladder polyps in the 1- to 2-cm size range.

PITFALLS

FDG PET must be interpreted carefully in patients with PSC and patients with other biliary strictures as biliary stents, known granulomatous disease, or other benign inflammatory conditions may accumulate FDG. In the cases of gallbladder cancer, false-positive FDG PET results have been reported with

xanthogranulomatous cholecystitis,²² tuberculoid granulomatosis of the gallbladder,²³ and adenomyomatosis.^{23,30}

Liver

At the standard image acquisition of approximately 1 hour after FDG administration, hepatic activity is usually mildly intense with a relatively uniformly mottled appearance.

HEPATOCELLULAR CARCINOMA

Well-differentiated hepatocellular carcinoma (HCC) has a high level of glucose-6-phosphatase, which results in dephosphorylation of FDG-6-phosphate and thus low FDG accumulation compared with poorly differentiated HCC, which has a low level of glucose-6-phosphatase and tends to be FDG avid.³¹ Because of the variable glucose metabolism of HCC, FDG PET has shown mixed utility in the detection of HCC. Initial studies on PET-only scanners reported a detection rate of primary untreated HCC of 50% to 70%.³¹⁻³³ A more recent study on PET/CT for the detection of primary HCC reported a sensitivity of 61%.³⁴ The investigators also found that advanced tumor stage, portal vein thrombosis, large tumors, and multiple tumors were significantly associated with positive FDG PET/CT results. With

respect to the size of the lesion, the sensitivity was 27%, 48%, and 93% for index lesions measuring 1 to 2 cm, 2 to 5 cm, and more than 5 cm, respectively.

Even though the sensitivity of FDG PET has been found to be lower than that of other imaging modalities, it still plays an important role in management and prognosis. The detection of extrahepatic metastases, although rare, can significantly affect management. Kawaoka and associates³⁵ compared the efficacy of PET/CT with CT for the detection of extrahepatic metastases (lung, lymph node, and bone) and found that CT was more sensitive than PET/CT for the detection of lung metastases and performed equally well for nodal metastases; however, bone metastases were more accurately detected by PET/CT. The three PET false-negative lung metastases in the study were less than 8 mm. Sugiyama and coworkers³⁶ found a similar pattern, in which the detection rate of FDG PET was 83% for extrahepatic metastases larger than 1 cm but only 13% for lesions of 1 cm or less.

Shiomi and coworkers³⁷ found that the SUV ratio (SUV ratio of tumor to nontumor in the liver) correlated with tumor volume doubling time and that the cumulative survival rate could be predicted on the basis of the SUV ratio. Kawamura and associates³⁸ also found that the SUV ratio was associated with survival, with people with SUV ratio of more than 1.6 having a lower survival rate. Another study found that patients with tumor SUV of more than 7 had a significantly lower median survival time (4 vs 15 months).³⁹ Hatano and colleagues⁴⁰ evaluated the role of preoperative PET in predicting the prognosis of patients after resection. In patients with SUV ratio of more than 2, the overall survival was significantly shorter than in those with a lower SUV ratio (182 vs 2310 days). Seo and coworkers⁴¹ had similar results, concluding that the overall survival and disease-free survival were significantly lower in the high SUV ratio group (>2) compared with the low SUV ratio group.

HCC is one of the major indications for liver transplantation; however, appropriate patient selection can be difficult. A study of 43 patients with HCC who underwent PET before liver transplantation found that patients with advanced PET-negative tumors and patients with HCC meeting the Milan criteria had a comparable 3-year survival rate (80% vs 94%).⁴² The HCC recurrence rate in this study was 50% in the PET-positive group compared with 3.8% in the PET-negative group. Another study by Lee and colleagues⁴³ attempted to evaluate FDG PET as a prognostic factor in predicting HCC recurrence after liver transplantation. They found that the ratio of tumor SUV_{max} to normal liver SUV_{max} was the most significant parameter for the

prediction of tumor recurrence, with a cutoff value of 1.15. Among the tumor recurrence patients, 93% had a value of 1.15 or more, whereas just 18% of the nonrecurrence patients had a value of 1.15 or more. The 1- and 2-year recurrence-free survival rates were significantly different between the two groups.

Patients with HCCs that are nonresectable or those awaiting transplantation can be treated with ablation or embolization. PET has been shown to play a role in monitoring response to such treatments. Torizuka and coworkers⁴⁴ found that after transarterial chemoembolization, increased or similar FDG uptake relative to normal liver was suggestive of residual viable tumor, whereas decreased or absent FDG uptake indicated more than 90% necrosis. Paudyal and coworkers⁴⁵ found that after radiofrequency ablation, PET detected recurrence earlier than CT and had a higher overall detection rate (92% for PET vs 75% for CT). Han and colleagues⁴⁶ found that PET/CT was valuable in patients who had unexplained serum α -fetoprotein elevation after either transarterial chemoembolization or radiofrequency ablation and a normal multiphasic CT scan.

For patients with advanced-stage HCC or with disease progression after locoregional therapy, treatment options are limited. However, studies have recently demonstrated survival benefit with sorafenib for patients with advanced HCC. PET/CT may have a role in monitoring of patients treated with sorafenib and for predicting response to treatment. A report of two patients with positive FDG PET at baseline found that a PET scan early after the start of treatment seemed to be a promising technique for monitoring early response.⁴⁷ A more recent study by Lee and colleagues⁴⁸ concluded that the degree of FDG uptake on baseline PET scan significantly correlated with overall survival and progression-free survival for such patients receiving sorafenib treatment.

METASTASES

Metastatic disease accounts for the majority of malignant hepatic lesions. The presence of liver metastases often guides the management of patients and is one of the main determinants of survival. FDG PET has been shown to be highly sensitive in detecting liver metastases (Fig. 68-3). Delbeke and coworkers³³ found that FDG PET detected all liver metastases larger than 1 cm from a number of different primary tumors. A meta-analysis by Kinkel and associates⁴⁹ found that at equivalent specificity, FDG PET was the most sensitive noninvasive imaging modality for the diagnosis of hepatic metastases from cancers of the gastrointestinal tract. Another meta-analysis by Bipat and colleagues⁵⁰ concluded that FDG PET had

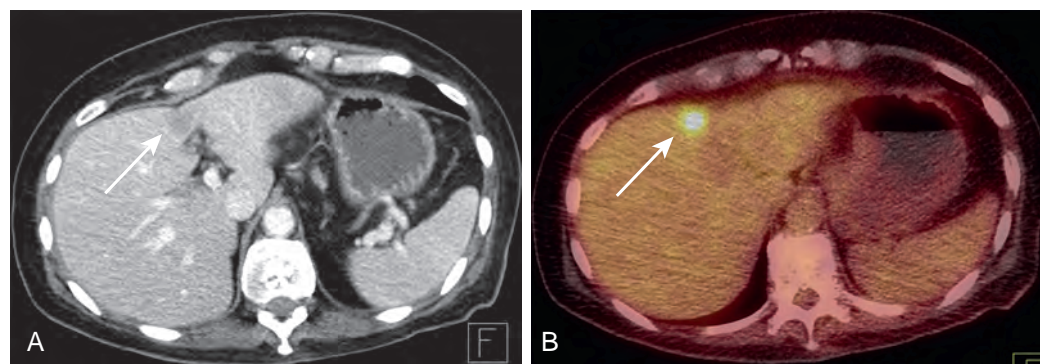


Figure 68-3 Liver metastasis.

A. Contrast-enhanced CT demonstrates an ill-defined area of low attenuation adjacent to the falciform ligament (arrow), which was previously attributed to focal fat. **B.** However, PET/CT demonstrates increased FDG avidity (arrow), consistent with a metastasis in this patient with a history of colon cancer.

significantly higher sensitivity on a per-patient basis compared with CT and MRI, but not on a per-lesion basis, in patients with colorectal liver metastases.

Hepatic resection is the most effective therapy for a subset of patients with liver metastases; however, strict selection criteria are paramount as there is no survival benefit if residual disease remains after hepatectomy. Arulampalam and colleagues⁵¹ found that preoperative FDG PET in patients with colorectal liver metastases altered management in 39% of patients, with avoidance of unnecessary surgery being the most common change. A study by Fernandez and colleagues⁵² found that use of FDG PET to assess patients with colorectal liver metastases being considered for partial hepatectomy was associated with excellent postresection 5-year survival.

Complete surgical resection is the best chance of cure in patients with liver metastases. However, in some patients, this is not feasible because of location of the tumor, multifocality, or insufficient functional liver reserve. In these cases, local ablative techniques may have a role to play. PET may have a role in follow-up of patients who underwent ablation (Fig. 68-4). Donckier and coworkers⁵³ compared PET and CT in 28 metastatic tumors 1 week, 1 month, and 3 months after radiofrequency ablation. The PET scan performed at 1 week found residual disease in 4 cases that was not identified on any of the CT scans at 1 week, 1 month, and 3 months.

Radioembolization with ⁹⁰Y microspheres has emerged as a palliative treatment for hepatic metastases of various tumors.

Szyszkowski and colleagues⁵⁴ performed a study evaluating the role of PET compared with Response Evaluation Criteria in Solid Tumors (RECIST) in early response assessment after ⁹⁰Y radioembolization in 21 patients. They found that 86% of patients demonstrated decreased PET activity at 6 weeks, whereas only 13% showed a partial response in the size of tumor on CT scan. A study by Haug and coworkers⁵⁵ in 58 patients with breast cancer metastases treated with ⁹⁰Y radioembolization found that PET/CT performed 3 months after treatment was the strongest predictor of survival (67 weeks in responders vs 43 weeks in nonresponders). Furthermore, they found that a pretreatment SUV_{max} of more than 20 was associated with a significantly shorter median survival than was SUV_{max} of 20 or less (21 vs 52 weeks). Another study comparing FDG PET/CT with RECIST and tumor density criteria found that PET/CT significantly predicted progression-free survival (the median progression-free survival in patients with a partial response was 12 months compared with 5 months in those with stable disease), whereas RECIST and tumor density criteria did not.⁵⁶

During the last few years, the addition of biologic agents (anti-epidermal growth factor receptor antibodies and anti-vascular endothelial growth factor antibodies) to conventional chemotherapy has increased overall survival in patients with metastatic colorectal cancer; it also has improved response rates and can render unresectable liver metastases resectable. A report by Bertolini and coworkers⁵⁷ found that patients with nonoptimally resectable colorectal metastases treated with FOLFOX

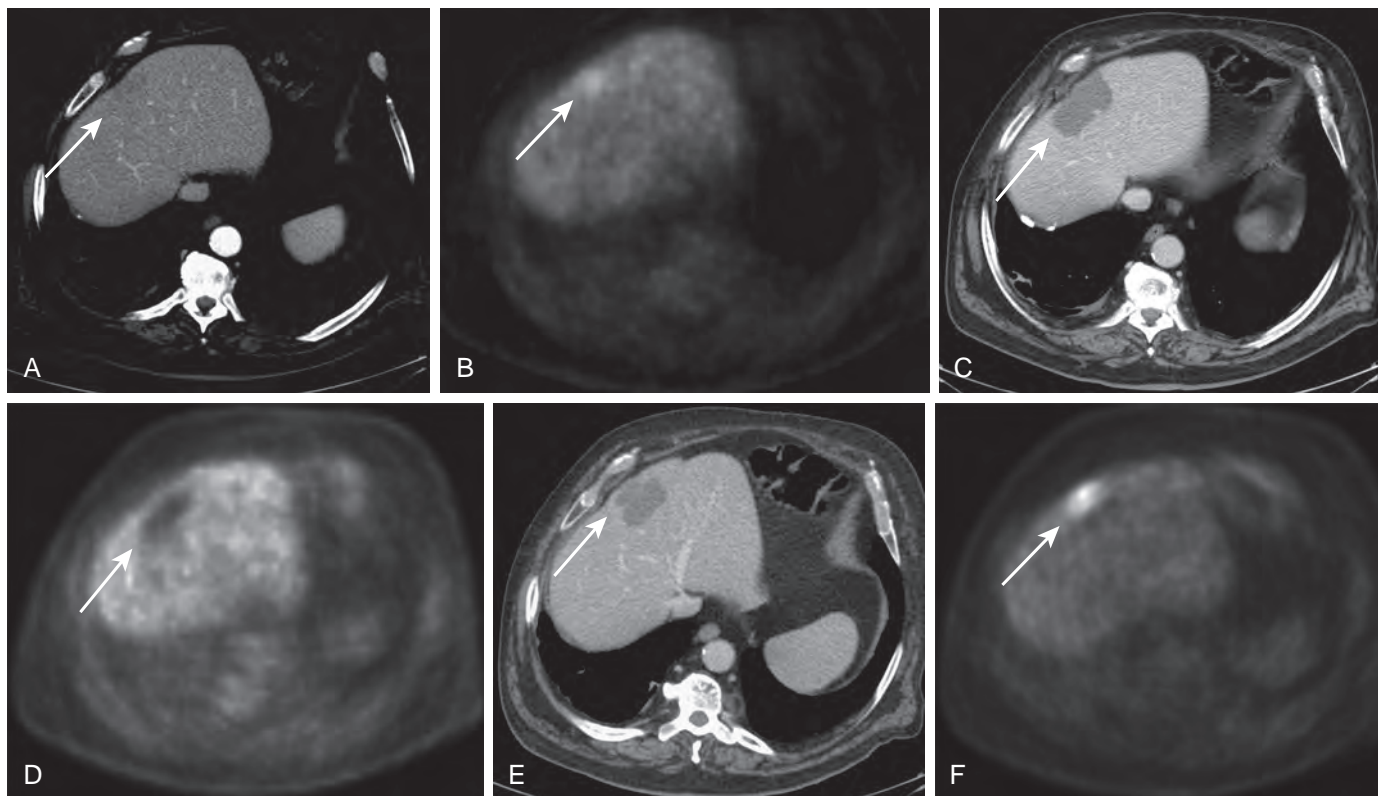


Figure 68-4 Recurrent hepatic tumor. Contrast-enhanced CT demonstrates an ill-defined low-attenuation lesion in the periphery of the liver (**A**, arrow), which demonstrated increased FDG avidity on PET (**B**, arrow). Biopsy confirmed a metastasis from colon cancer, which was treated with radiofrequency ablation. Contrast-enhanced CT 1 month after ablation demonstrated a nonenhancing low-attenuation ablation zone (**C**, arrow), which is photopenic on PET (**D**, arrow), consistent with treatment response. Contrast-enhanced CT 9 months after ablation demonstrates a low-attenuation area adjacent to the ablation zone (**E**, arrow), which demonstrated increased FDG avidity (**F**, arrow). Findings are consistent with local recurrence.

(folinic acid, fluorouracil, oxaliplatin) and bevacizumab who achieved at least 1 unit reduction in SUV_{max} had longer progression-free survival (median progression-free survival of 22 vs 14 months). Another study found that low follow-up SUV_{max} and complete metabolic response were favorable prognostic factors in patients with metastatic colorectal cancer who underwent liver surgery with curative intent after neoadjuvant chemotherapy with bevacizumab.⁵⁸

LYMPHOMA

Primary hepatic lymphoma is defined as a lesion or lesions confined to the liver only without the involvement of any other organ or lymph nodes; it is extremely rare, representing less than 1% of all extranodal lymphomas. It usually is manifested as a solitary mass (Fig. 68-5) or as multiple discrete masses.⁵⁹ Rarely, the disease is manifested as diffuse involvement of the liver.⁶⁰ Case reports have found the lesions to be hypermetabolic on PET/CT.^{61,62}

PITFALLS

Causes of false-negative FDG PET findings include small size of lesion, underestimation of uptake, misregistration of foci, and recent completion of chemotherapy. Underestimation of FDG uptake and misregistration of foci are caused by the physiologic motion of the liver during emission scans. False-positive findings for malignant changes on PET have also been reported. Causes include intrahepatic abscess and benign inflammatory lesions, such as regenerative nodules in a cirrhotic liver.

Spleen

There is usually slightly less FDG uptake in the normal spleen than in the liver.

LYMPHOMA

Splenic involvement in lymphoma can be primary or secondary; secondary splenic lymphoma is much more common. The spleen is involved in one third of all Hodgkin's lymphoma and 30% to 40% of non-Hodgkin's lymphoma at presentation. Primary splenic lymphoma is defined as lymphomatous involvement of the spleen with or without splenic hilar lymphadenopathy and is rare, accounting for 1% to 2% of all lymphomas at presentation.⁶³ The two patterns of splenic lymphomatous infiltration on FDG PET/CT are a diffusely FDG-avid spleen,

with more FDG activity than in liver and normal bone marrow and often with a normal CT appearance (Fig. 68-6), and solitary or multiple FDG-avid splenic lesions.⁶⁴ A study has found the sensitivity and specificity of CT, PET, and PET/CT for identification of splenic involvement at initial staging in lymphoma to be 91% and 96%, 75% and 99%, and 100% and 95%, respectively.⁶⁵

Primary nonhematopoietic tumors of the spleen are extremely rare. They may arise from the sinus epithelium (angiosarcoma and hemangioendotheliomas) or from connective tissue (spindle cell sarcoma and fibrosarcoma).

METASTASES

Splenic metastases are encountered in 2.3% to 12.9% of post-mortem examinations in cancer patients; melanoma and lung, breast, and ovarian cancer are the most common malignant neoplasms to metastasize to the spleen (Fig. 68-7). Metser and associates⁶⁶ found that the sensitivity, specificity, positive predictive value, and negative predictive value of FDG PET/CT in differentiating benign from malignant solid splenic lesions in patients with and without malignant disease were 100%, 100%, 100%, and 100% versus 100%, 83%, 80%, and 100%, respectively. They also concluded that in patients with known malignant disease, an SUV threshold of 2.3 correctly differentiated benign from malignant lesions with sensitivity, specificity, positive predictive value, and negative predictive value of 100%, 100%, 100%, and 100%, respectively. They also found that in patients without known malignant disease, false-positive results were due to granulomatous disease.

PITFALLS

Increased splenic activity can be seen in the post-therapy period, especially after hematopoietic stimulants, and can limit the evaluation of splenic involvement by lymphoma or can result in a false-positive finding. However, associated diffuse symmetric FDG uptake in bone marrow of the axial skeleton can suggest hematopoietic stimulation instead of true splenic lymphomatous involvement.⁶³

Most benign solid splenic lesions, such as hamartomas and hemangiomas of the spleen, are not expected to demonstrate abnormal FDG uptake. However, some benign lesions exhibit abnormal uptake of FDG, most commonly splenic abscess and active granulomatous disease involving the spleen. Conversely, non-FDG-avid tumors, such as some renal and thyroid cancers, may metastasize to the spleen. Therefore,

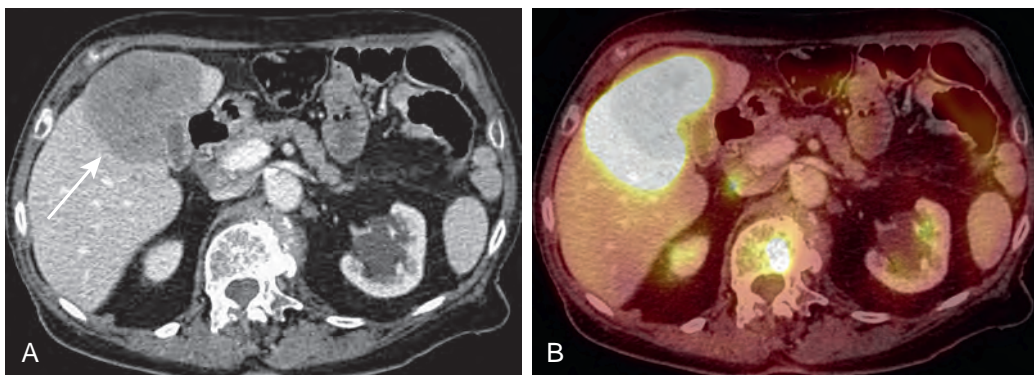


Figure 68-5 Hepatic lymphoma. **A.** Contrast-enhanced CT demonstrates a solitary, large, low-attenuation lesion in the liver (arrow) adjacent to the gallbladder. **B.** PET/CT demonstrates the increased FDG avidity of the lesion. Percutaneous biopsy confirmed lymphoma.

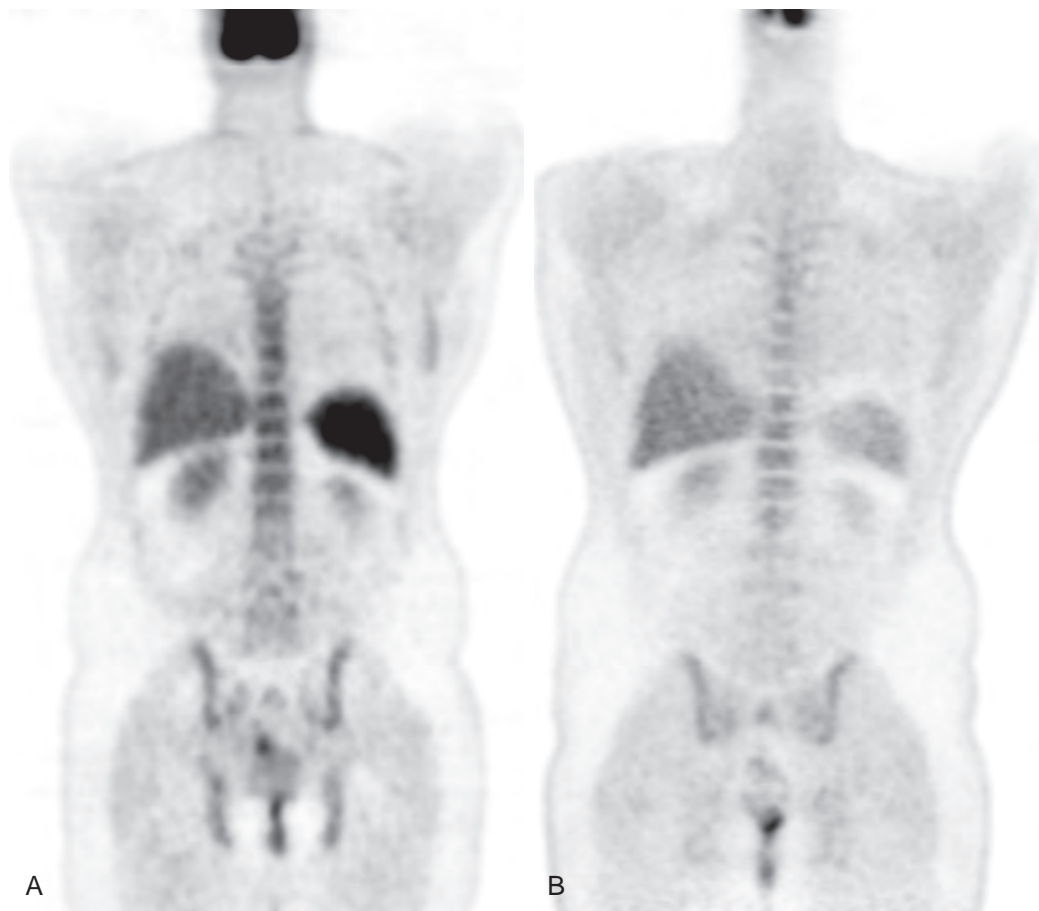


Figure 68-6 Splenic lymphoma. **A.** PET scan demonstrated abnormal increased FDG avidity in the spleen compared with the liver, consistent with lymphoma. **B.** PET scan 1 month after chemotherapy demonstrates resolution of increased FDG avidity consistent with treatment response.

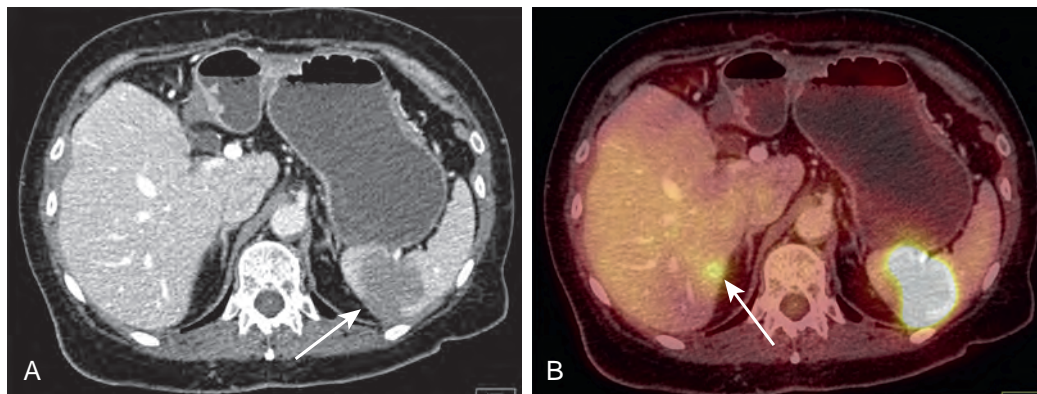


Figure 68-7 Splenic metastasis. **A.** Contrast-enhanced CT demonstrates a low-attenuation mass in the spleen (arrow). **B.** This splenic mass demonstrates increased FDG avidity on PET/CT. Findings are consistent with a splenic metastasis in a patient with known colon carcinoma. The apparent focal area of FDG uptake in the periphery of the liver (arrow) without a CT correlate is due to misregistration from excreted FDG in the right renal collecting system.

when a non-FDG-avid splenic lesion is encountered, the CT portion of the PET/CT study should be assessed for potential non-FDG-avid malignant lesions.⁶⁷

Pancreas

Minimal physiologic uptake is identified in the pancreas on PET/CT. The average SUV_{max} for normal pancreas is calculated as 2.7 ± 1.3 (range, 1.8-5.1).⁶⁸

PANCREATIC ADENOCARCINOMA

The role of imaging in patients with suspected pancreatic cancer is to depict lesions and to determine whether tumors are resectable. Pancreatic adenocarcinoma usually is manifested as an area of increased uptake (Fig. 68-8); however, it may demonstrate a low level of FDG uptake or no uptake based on the degree of desmoplastic response and tumor biology.⁶⁹ Irrespective of size, the SUV_{max} is typically higher in malignant lesions,

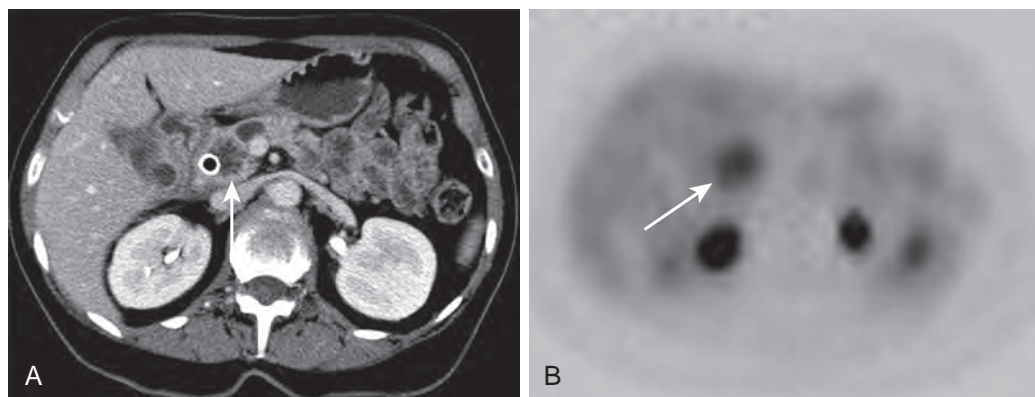


Figure 68-8 Pancreatic adenocarcinoma. **A.** Contrast-enhanced CT demonstrates a 2-cm mass in the head of the pancreas (arrow) with a stent in the adjacent common bile duct. **B.** PET demonstrates increased FDG avidity in the mass (arrow). Endoscopic biopsy confirmed pancreatic adenocarcinoma.

and therefore FDG PET may be useful in depicting small pancreatic lesions (<2 cm) and those that are isoattenuating to adjacent normal pancreatic parenchyma, which are difficult to detect at CT. Okano and associates⁷⁰ reported sensitivities of 100% for FDG PET and 40% for contrast-enhanced CT for depicting lesions smaller than 2 cm. Delbeke and coworkers⁷¹ demonstrated that FDG PET had a higher sensitivity, specificity, and accuracy than CT in diagnosis of pancreatic carcinoma (92%, 85%, and 91% for FDG/PET vs 65%, 61%, and 65% for CT, respectively). In another study, Lemke and colleagues⁷² compared the diagnostic value of CT, PET, and PET/CT fusion in 104 patients with pancreatic cancer and reported that the image fusion improved the sensitivity of detection of malignant disease from 77% (CT) and 84% (PET) to 89% (image fusion). Kauhanen and associates⁷³ found that diagnostic accuracy of FDG PET/CT for pancreatic malignant disease was 89% compared with 76% and 79% for multidetector CT and magnetic resonance imaging, respectively. Buchs and colleagues⁷⁴ concluded that enhanced PET/CT seemed to be superior to unenhanced PET/CT in the detection of pancreatic cancer, with the sensitivity of enhanced PET/CT being 96% compared with 72% for unenhanced PET/CT and the specificity being 67% versus 33%.

To determine the resectability of the tumor, it is crucial that the presence or absence of metastasis be determined and that the degree of venous (superior mesenteric vein and portal vein) involvement and relationship to adjacent arteries (superior mesenteric artery, celiac axis, hepatic artery, gastroduodenal artery) be evaluated.⁷⁵ Strobel and coworkers⁷⁶ concluded that contrast-enhanced PET/CT was significantly superior to PET alone for the preoperative assessment of cancer resectability, and there was a trend for enhanced PET/CT to be superior to unenhanced PET/CT. PET and unenhanced PET/CT both had sensitivities of 100%, but PET alone had specificity of 44%, whereas unenhanced PET/CT had 56% specificity. Contrast-enhanced PET/CT was superior to unenhanced PET/CT with a sensitivity of 96% and a specificity of 82%. Regarding the presence of nodal metastases (N stage), FDG PET/CT has been found to have a sensitivity of 30% to 42%, whereas sensitivity for distant metastases (M stage) has been found to be 88% to 94%.^{73,77}

FDG PET/CT may also have a role in planning the radiation field in patients with pancreatic cancer. A study by Topkan and

coworkers⁷⁸ in 14 patients undergoing radiation planning for unresectable pancreatic cancer found that the addition of PET resulted in an average 30% increase in gross tumor volume in 5 patients. Another role for FDG PET/CT is in predicting pathologic response to preoperative chemoradiation therapy (CRT). Kittaka and associates⁷⁹ found that a better pathologic response can be expected in pancreatic cancer patients who have a high pre-CRT SUV (≥ 4.7) and a high regression index (≥ 0.46), determined by $1 - \text{post-CRT SUV/pre-CRT SUV}$.

FDG PET/CT has also been shown to have a role in the diagnosis of recurrent pancreatic cancer. Sperti and coworkers⁸⁰ found that tumor relapse after pancreatic cancer resection was detected by CT in 35 patients and by PET in 61 of 63 patients with recurrence and that PET results influenced treatment strategies in 44% of patients. Casneuf and associates⁸¹ concluded that in assessing for recurrence, the sensitivity (90%) and accuracy rate (92%) were highest for PET and PET/CT, whereas CT yielded a lower sensitivity (80%). A study by Ruf and colleagues⁸² demonstrated that 96% of local recurrences were detected by PET compared with 39% by CT or MRI. Asagi and colleagues⁷⁷ found that enhanced PET/CT correctly detected local recurrence in all of the 11 cases of recurrence, whereas enhanced CT detected only 7 of 11 cases.

CYSTIC NEOPLASMS

Cystic neoplasms of the pancreas encompass a wide range of pathologic conditions from benign lesions to malignant, potentially malignant, and borderline tumors. Sperti and coworkers⁸³ found that FDG-avid intraductal papillary mucinous neoplasms are frankly malignant or invasive, and conversely, FDG-negative lesions may be benign, borderline malignant, or noninvasive malignant. Other studies have found that by use of a cutoff SUV of 2.5, it was feasible to differentiate between benign and malignant intraductal papillary mucinous neoplasms.⁸⁴⁻⁸⁶

PITFALLS

Serum glucose levels can affect FDG PET findings. One study found that FDG PET has better sensitivity (86%) for pancreatic tumor depiction in patients who are euglycemic than in those with elevated glucose levels (42%).⁸⁷ False-positive results can

be due to inflammation or infection (Fig. 68-9), inflammatory pseudotumor, pancreatic tuberculosis, chronic pancreatitis, and focal high-grade dysplasia.⁸⁸

Adrenal Glands

Adrenal incidentalomas are found in approximately 4% to 10% of all CT examinations in the general population⁸⁹; 80% of incidentally found adrenal masses in healthy individuals and 40% to 57% of adrenal incidentalomas in those with a known primary malignant neoplasm are benign.⁹⁰ The normal adrenal gland is usually barely visible on FDG PET, and normal mild FDG uptake in the location of the glands can be visible on the coregistered CT scan of a combined PET/CT scan. The maximum SUVs of normal adrenal glands range from 0.95 to 2.46.⁹¹

METASTASES

An adrenal lesion is usually considered malignant if its intensity is higher than that of liver; however, because the average mean SUV of the liver is 1.5 to 2.0, physiologic adrenal uptake may be in the range of malignant lesions in some cases. Jana and colleagues⁹² reported 93% sensitivity and 96% specificity with

use of lesion activity higher than liver uptake as a criterion for malignancy (Fig. 68-10). Metser and coworkers⁹³ found that when 3.1 was used as a cutoff for SUV_{max} PET/CT had a sensitivity and specificity of 98.5% and 92% in the differentiation of malignant from benign lesions. Watanabe and coworkers⁹⁴ concluded that the adrenal-to-liver SUV ratio is the best parameter for differentiation of adrenal metastases from adenomas; use of an adrenal-to-liver SUV ratio cutoff value of 1.37 yielded a sensitivity of 96% and specificity of 100%. A meta-analysis by Boland and colleagues⁹⁵ found that FDG PET had 97% sensitivity and 91% specificity in the differentiation between malignant and benign adrenal disease.

ADRENOCORTICAL CARCINOMA

Adrenocortical carcinoma is the most common primary malignant neoplasm of the adrenal cortex but still accounts for less than 5% of all adrenal incidentalomas. Groussin and coworkers⁹⁶ found that with use of a cutoff value above 1.45 for adrenal-to-liver SUV_{max} ratio, the sensitivity and specificity to distinguish adrenal adenoma from adrenocortical carcinoma were, respectively, 100% and 88%. Becherer and colleagues⁹⁷ evaluated FDG PET in patients with known adrenocortical carcinoma and reported that FDG PET had a sensitivity and specificity of 100%

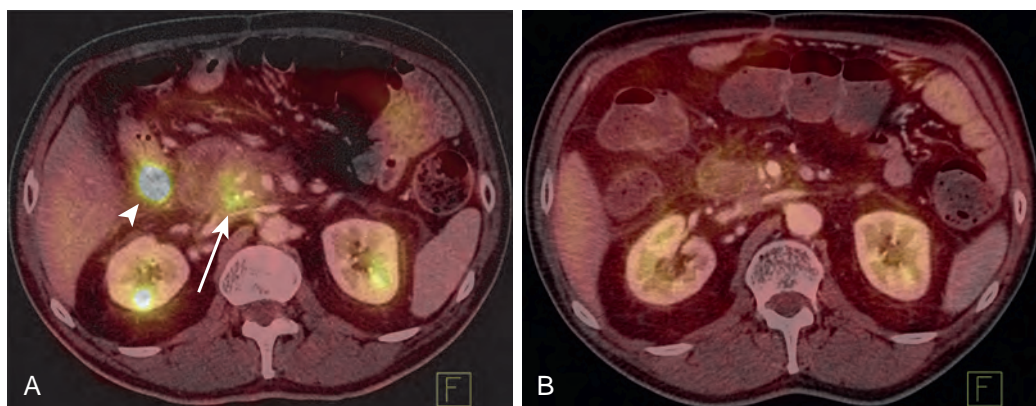


Figure 68-9 Infection simulating recurrent pancreatic adenocarcinoma. **A.** PET/CT in a patient 9 months after a Whipple procedure for ampullary carcinoma demonstrates soft tissue with increased FDG avidity surrounding the superior mesenteric vessels (arrow). Focal uptake in the renal parenchyma bilaterally is secondary to misregistration of excreted isotope in the renal collecting system bilaterally. Note is also made of increased FDG uptake in the duodenum (arrowhead). Percutaneous biopsy found actinomycosis. Infection is one of the causes of pancreatic FDG PET/CT false-positive findings. **B.** PET/CT after treatment with intravenous penicillin demonstrates resolution of FDG avidity.

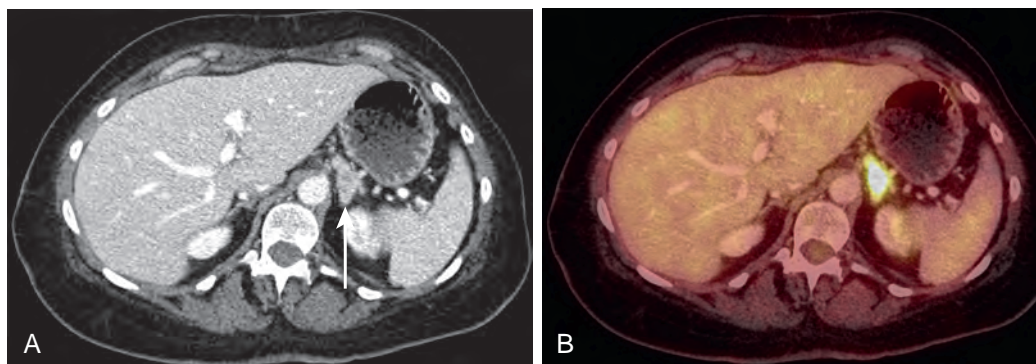


Figure 68-10 Adrenal metastasis from lung cancer. **A.** Contrast-enhanced CT demonstrates a 2.9-cm left adrenal nodule (arrow) that is incompletely characterized. **B.** PET/CT demonstrates increased FDG avidity in the nodule. Percutaneous biopsy was positive for adenocarcinoma from a lung primary.

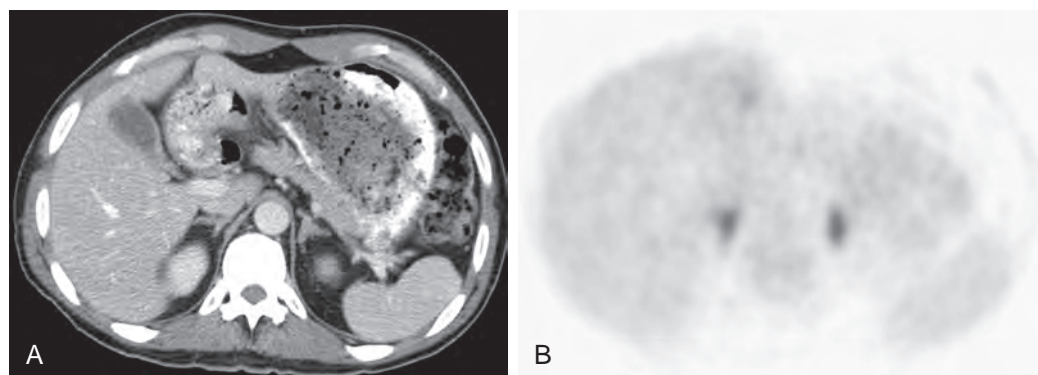


Figure 68-11 Adrenal lymphoma. **A.** Contrast-enhanced CT demonstrates essentially normal-appearing bilateral adrenal glands. **B.** PET scan demonstrates increased FDG avidity in the glands bilaterally (arrow indicating right uptake). Percutaneous biopsy of the left adrenal gland confirmed lymphoma.

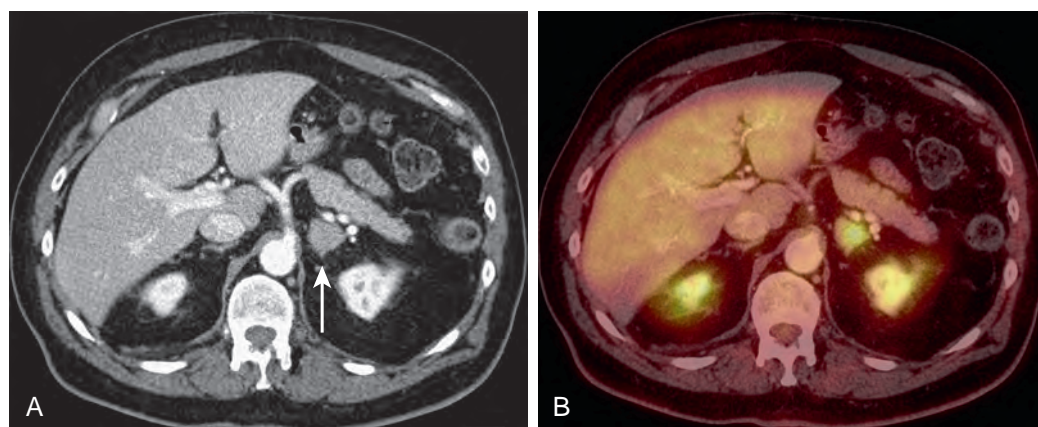


Figure 68-12 Adrenal adenoma. **A.** Contrast-enhanced CT demonstrating a 2.2-cm left adrenal nodule (arrow) that is incompletely characterized. **B.** Left adrenal nodule demonstrates increased FDG avidity, greater than that of the liver, on PET/CT. On resection, this was shown to be an adenoma; 5% of adrenal adenomas may show increased FDG uptake falsely positive for malignancy as was evident in this case.

and 95%, respectively. The addition of PET detected additional lesions compared with anatomic imaging in 30% of patients and modified treatment in 20%. Patients with initial complete surgery have a high risk of relapse within the first 2 years of follow-up. One study found that 38% of patients with local relapses were detected with PET/CT and not with CT, which led to change in treatment in three of these five patients.⁹⁸ They also found that the intensity of FDG uptake (SUV_{max}) and the FDG uptake volume were significantly associated with survival.⁹⁸

PHEOCHROMOCYTOMA

Pheochromocytomas are relatively rare catecholamine-secreting neuroendocrine tumors that arise from the chromaffin cells of the adrenal medulla. Shulkin and coworkers⁹⁹ compared FDG PET with metaiodobenzylguanidine (MIBG) scintigraphy for the detection of pheochromocytomas. They found that for benign pheochromocytomas, MIBG scintigraphy had a sensitivity of 83%, whereas FDG PET had a sensitivity of 58%. However, for malignant pheochromocytomas, MIBG scintigraphy had a sensitivity of 88% and FDG PET had a sensitivity of 82%. Although MIBG scintigraphy had a better sensitivity than FDG PET, all of the MIBG-negative lesions showed avid FDG uptake. A more recent, large prospective study in patients with pheochromocytomas and paragangliomas found that primary tumors are equally well identified by FDG PET/CT and ¹²³I-MIBG single photon emission computed tomography (SPECT), currently the standard imaging modality. The investigators also found that metastases are better detected by FDG

PET than by ¹²³I-MIBG SPECT, with sensitivities of 80% and 49%, respectively.¹⁰⁰

LYMPHOMA

Primary adrenal lymphomas are rare and typically bilateral, homogeneous, and infiltrating, with the enlarged adrenal glands tending to maintain their overall shape (Fig. 68-11). Secondary adrenal involvement has been reported in 1% to 4% of affected patients. PET/CT has been found to be valuable in distinguishing nonfunctioning adrenal neoplasms or hyperplasia from lymphomatous involvement.⁹⁰

PITFALLS

Both false-positive and false-negative adrenal FDG PET findings have been reported. Causes of false-positive results include significant FDG uptake in some adrenal adenomas (Fig. 68-12), adrenal endothelial cysts, and inflammatory and infectious lesions. Increased FDG uptake in the suprarenal or retrocrural region due to brown fat may mimic an adrenal lesion and is another pitfall of PET; however, such patients should be readily recognized as they have the characteristic brown fat pattern of FDG uptake in the neck and mediastinum. Adrenal metastatic lesions with hemorrhage or necrosis, small metastatic lesions, and metastases from non-FDG-avid primary tumors, such as pulmonary bronchoalveolar carcinoma and carcinoid tumors, may be causes of false-negative PET adrenal findings.¹⁰¹

REFERENCES

- Kluge R, Schmidt F, Caca K, et al: Positron emission tomography with [^{18}F]fluoro-2-deoxy-D-glucose for diagnosis and staging of bile duct cancer. *Hepatology* 33:1029–1035, 2001.
- Keiding S, Hansen SB, Rasmussen HH, et al: Detection of cholangiocarcinoma in primary sclerosing cholangitis by positron emission tomography. *Hepatology* 28:700–706, 1998.
- Widjaja A, Mix H, Wagner S, et al: Positron emission tomography and cholangiocarcinoma in primary sclerosing cholangitis. *Z Gastroenterol* 37:731–733, 1999.
- Moon CM, Bang S, Chung JB, et al: Usefulness of ^{18}F -fluorodeoxyglucose positron emission tomography in differential diagnosis and staging of cholangiocarcinomas. *J Gastroenterol Hepatol* 23:759–765, 2008.
- Corvera CU, Blumgart LH, Akhurst T, et al: ^{18}F -Fluorodeoxyglucose positron emission tomography influences management decisions in patients with biliary cancer. *J Am Coll Surg* 206:57–65, 2008.
- Petrowsky H, Wildbrett P, Husarik DB, et al: Impact of integrated positron emission tomography and computed tomography on staging and management of gallbladder cancer and cholangiocarcinoma. *J Hepatol* 45:43–50, 2006.
- Lee SW, Kim HJ, Park JH, et al: Clinical usefulness of ^{18}F -FDG PET-CT for patients with gallbladder cancer and cholangiocarcinoma. *J Gastroenterol* 45:560–566, 2010.
- Yamada I, Ajiki T, Ueno K, et al: Feasibility of ^{18}F -fluorodeoxyglucose positron-emission tomography for preoperative evaluation of biliary tract cancer. *Anticancer Res* 32:5105–5110, 2012.
- Reinhardt MJ, Strunk H, Gerhardt T, et al: Detection of Klatskin's tumor in extrahepatic bile duct strictures using delayed ^{18}F -FDG PET/CT: Preliminary results for 22 patient studies. *J Nucl Med* 46:1158–1163, 2005.
- Anderson CD, Rice MH, Pinson CW, et al: Fluorodeoxyglucose PET imaging in the evaluation of gallbladder carcinoma and cholangiocarcinoma. *J Gastrointest Surg* 8:90–97, 2004.
- Kato T, Tsukamoto E, Kuge Y, et al: Clinical role of ^{18}F -FDG PET for initial staging of patients with extrahepatic bile duct cancer. *Eur J Nucl Med Mol Imaging* 29:1047–1054, 2002.
- Fritscher-Ravens A, Bohuslavizki KH, Broering DC, et al: FDG PET in the diagnosis of hilar cholangiocarcinoma. *Nucl Med Commun* 22:1277–1285, 2001.
- Siqueira E, Schoen RE, Silverman W, et al: Detecting cholangiocarcinoma in patients with primary sclerosing cholangitis. *Gastrointest Endosc* 56:40–47, 2002.
- Alkhalwaleh K, Faltten S, Biersack HJ, Ezziddin S: The value of F-18 FDG PET in patients with primary sclerosing cholangitis and cholangiocarcinoma using visual and semiquantitative analysis. *Clin Nucl Med* 36:879–883, 2011.
- Fevry J, Buchel O, Nevens F, et al: Positron emission tomography is not a reliable method for the early diagnosis of cholangiocarcinoma in patients with primary sclerosing cholangitis. *J Hepatol* 43:358–360, 2005.
- Seo S, Hatano E, Higashi T, et al: Fluorine-18 fluorodeoxyglucose positron emission tomography predicts lymph node metastasis, P-glycoprotein expression, and recurrence after resection in mass-forming intrahepatic cholangiocarcinoma. *Surgery* 143:769–777, 2008.
- Kim JY, Kim MH, Lee TY, et al: Clinical role of ^{18}F -FDG PET-CT in suspected and potentially operable cholangiocarcinoma: A prospective study compared with conventional imaging. *Am J Gastroenterol* 103:1145–1151, 2008.
- Albazaz R, Patel CN, Chowdhury FU, et al: Clinical impact of FDG PET-CT on management decisions for patients with primary biliary tumours. *Insights Imaging* 4:691–700, 2013.
- Jadvar H, Henderson RW, Conti PS: [^{18}F] fluorodeoxyglucose positron emission tomography and positron emission tomography: Computed tomography in recurrent and metastatic cholangiocarcinoma. *J Comput Assist Tomogr* 31:223–228, 2007.
- Zhu AX, Meyerhardt JA, Blaszkowsky LS, et al: Efficacy and safety of gemcitabine, oxaliplatin, and bevacizumab in advanced biliary-tract cancers and correlation of changes in 18-fluorodeoxyglucose PET with clinical outcome: A phase 2 study. *Lancet Oncol* 11:48–54, 2010.
- Haug AR, Heinemann V, Bruns CJ, et al: ^{18}F -FDG PET independently predicts survival in patients with cholangiocellular carcinoma treated with ^{90}Y microspheres. *Eur J Nucl Med Mol Imaging* 38:1037–1045, 2011.
- Koh T, Taniguchi H, Yamaguchi A, et al: Differential diagnosis of gallbladder cancer using positron emission tomography with fluorine-18-labeled fluoro-deoxyglucose (FDG-PET). *J Surg Oncol* 84:74–81, 2003.
- Rodriguez-Fernandez A, Gomez-Rio M, Llamas-Elvira JM, et al: Positron-emission tomography with fluorine-18-fluoro-2-deoxy-D-glucose for gallbladder cancer diagnosis. *Am J Surg* 188:171–175, 2004.
- Oe A, Kawabe J, Torii K, et al: Distinguishing benign from malignant gallbladder wall thickening using FDG-PET. *Ann Nucl Med* 20:699–703, 2006.
- Nishiyama Y, Yamamoto Y, Fukunaga K, et al: Dual-time-point ^{18}F -FDG PET for the evaluation of gallbladder carcinoma. *J Nucl Med* 47:633–638, 2006.
- Shukla PJ, Barreto SG, Arya S, et al: Does PET-CT scan have a role prior to radical re-resection for incidental gallbladder cancer? *HPB (Oxford)* 10:439–445, 2008.
- Butte JM, Redondo F, Waugh E, et al: The role of PET-CT in patients with incidental gallbladder cancer. *HPB (Oxford)* 11:585–591, 2009.
- Kumar R, Sharma P, Kumari A, et al: Role of ^{18}F -FDG PET/CT in detecting recurrent gallbladder carcinoma. *Clin Nucl Med* 37:431–435, 2012.
- Lee J, Yun M, Kim KS, et al: Risk stratification of gallbladder polyps (1–2 cm) for surgical intervention with ^{18}F -FDG PET/CT. *J Nucl Med* 53:353–358, 2012.
- Maldjian PD, Ghesani N, Ahmed S, Liu Y: Adenomyomatosis of the gallbladder: Another cause for a “hot” gallbladder on ^{18}F -FDG PET. *AJR Am J Roentgenol* 189:W36–W38, 2007.
- Khan MA, Combs CS, Brunt EM, et al: Positron emission tomography scanning in the evaluation of hepatocellular carcinoma. *J Hepatol* 32:792–797, 2000.
- Trojan J, Schroeder O, Raedle J, et al: Fluorine-18 FDG positron emission tomography for imaging of hepatocellular carcinoma. *Am J Gastroenterol* 94:3314–3319, 1999.
- Delbeke D, Martin WH, Sandler MP, et al: Evaluation of benign vs malignant hepatic lesions with positron emission tomography. *Arch Surg* 133:510–515, discussion 515–516, 1998.
- Park JW, Kim JH, Kim SK, et al: A prospective evaluation of ^{18}F -FDG and ^{11}C -acetate PET/CT for detection of primary and metastatic hepatocellular carcinoma. *J Nucl Med* 49:1912–1921, 2008.
- Kawaoka T, Aikata H, Takaki S, et al: FDG positron emission tomography/computed tomography for the detection of extrahepatic metastases from hepatocellular carcinoma. *Hepatol Res* 39:134–142, 2009.
- Sugiyama M, Sakahara H, Torizuka T, et al: ^{18}F -FDG PET in the detection of extrahepatic metastases from hepatocellular carcinoma. *J Gastroenterol* 39:961–968, 2004.
- Shiomi S, Nishiguchi S, Ishizu H, et al: Usefulness of positron emission tomography with fluorine-18-fluorodeoxyglucose for predicting outcome in patients with hepatocellular carcinoma. *Am J Gastroenterol* 96:1877–1880, 2001.
- Kawamura E, Habu D, Ohfuji S, et al: Clinical role of FDG-PET for HCC: Relationship of glucose metabolic indicator to Japan Integrated Staging (JIS) score. *Hepatogastroenterology* 55:582–586, 2008.
- Kong YH, Han CJ, Lee SD, et al: [Positron emission tomography with fluorine-18-fluorodeoxyglucose is useful for predicting the prognosis of patients with hepatocellular carcinoma.] *Korean J Hepatol* 10:279–287, 2004.
- Hatano E, Ikai I, Higashi T, et al: Preoperative positron emission tomography with fluorine-18-fluorodeoxyglucose is predictive of prognosis in patients with hepatocellular carcinoma after resection. *World J Surg* 30:1736–1741, 2006.
- Seo S, Hatano E, Higashi T, et al: Fluorine-18 fluorodeoxyglucose positron emission tomography predicts tumor differentiation, P-glycoprotein expression, and outcome after resection in hepatocellular carcinoma. *Clin Cancer Res* 13(Pt 1):427–433, 2007.
- Kornberg A, Freesmeyer M, Barthel E, et al: ^{18}F -FDG-uptake of hepatocellular carcinoma on PET predicts microvascular tumor invasion in liver transplant patients. *Am J Transplant* 9:592–600, 2009.
- Lee JW, Paeng JC, Kang KW, et al: Prediction of tumor recurrence by ^{18}F -FDG PET in liver transplantation for hepatocellular carcinoma. *J Nucl Med* 50:682–687, 2009.
- Torizuka T, Tamaki N, Inokuma T, et al: Value of fluorine-18-FDG-PET to monitor hepatocellular carcinoma after interventional therapy. *J Nucl Med* 35:1965–1969, 1994.
- Paudyal B, Oriuchi N, Paudyal P, et al: Early diagnosis of recurrent hepatocellular carcinoma with ^{18}F -FDG PET after radiofrequency ablation therapy. *Oncol Rep* 18:1469–1473, 2007.
- Han AR, Gwak GY, Choi MS, et al: The clinical value of ^{18}F -FDG PET/CT for investigating unexplained serum AFP elevation following interventional therapy for hepatocellular carcinoma. *Hepatogastroenterology* 56:1111–1116, 2009.

47. Siemerink EJ, Mulder NH, Brouwers AH, Hospers GA: ^{18}F -Fluorodeoxyglucose positron emission tomography for monitoring response to sorafenib treatment in patients with hepatocellular carcinoma. *Oncologist* 13:734–735, author reply 736–737, 2008.
48. Lee JH, Park JY, Kim do Y, et al: Prognostic value of ^{18}F -FDG PET for hepatocellular carcinoma patients treated with sorafenib. *Liver Int* 31:1144–1149, 2011.
49. Kinkel K, Lu Y, Both M, et al: Detection of hepatic metastases from cancers of the gastrointestinal tract by using noninvasive imaging methods (US, CT, MR imaging, PET): A meta-analysis. *Radiology* 224:748–756, 2002.
50. Bipat S, van Leeuwen MS, Comans EF, et al: Colorectal liver metastases: CT, MR imaging, and PET for diagnosis—meta-analysis. *Radiology* 237:123–131, 2005.
51. Arulampalam TH, Francis DL, Visvikis D, et al: FDG-PET for the pre-operative evaluation of colorectal liver metastases. *Eur J Surg Oncol* 30:286–291, 2004.
52. Fernandez FG, Drebin JA, Linehan DC, et al: Five-year survival after resection of hepatic metastases from colorectal cancer in patients screened by positron emission tomography with F-18 fluorodeoxyglucose (FDG-PET). *Ann Surg* 240:438–447, discussion 447–450, 2004.
53. Donckier V, Van Laethem JL, Goldman S, et al: [F-18]fluorodeoxyglucose positron emission tomography as a tool for early recognition of incomplete tumor destruction after radiofrequency ablation for liver metastases. *J Surg Oncol* 84:215–223, 2003.
54. Szyszko T, Al-Nahhas A, Canelo R, et al: Assessment of response to treatment of unresectable liver tumours with ^{90}Y microspheres: Value of FDG PET versus computed tomography. *Nucl Med Commun* 28:15–20, 2007.
55. Haug AR, Tiega Donfack BP, Trumm C, et al: ^{18}F -FDG PET/CT predicts survival after radioembolization of hepatic metastases from breast cancer. *J Nucl Med* 53:371–377, 2012.
56. Zerizer I, Al-Nahhas A, Towey D, et al: The role of early ^{18}F -FDG PET/CT in prediction of progression-free survival after ^{90}Y radioembolization: Comparison with RECIST and tumour density criteria. *Eur J Nucl Med Mol Imaging* 39:1391–1399, 2012.
57. Bertolini F, Malavasi N, Scarabelli L, et al: FOLFOX6 and bevacizumab in non-optimally resectable liver metastases from colorectal cancer. *Br J Cancer* 104:1079–1084, 2011.
58. De Bruyne S, Van Damme N, Smeets P, et al: Value of DCE-MRI and FDG-PET/CT in the prediction of response to preoperative chemotherapy with bevacizumab for colorectal liver metastases. *Br J Cancer* 106:1926–1933, 2012.
59. Elsayes KM, Menias CO, Willatt JM, et al: Primary hepatic lymphoma: Imaging findings. *J Med Imaging Radiat Oncol* 53:373–379, 2009.
60. Gazelle GS, Lee MJ, Hahn PF, et al: US, CT, and MRI of primary and secondary liver lymphoma. *J Comput Assist Tomogr* 18:412–415, 1994.
61. Pan B, Wang CS, Han JK, et al: ^{18}F -fluorodeoxyglucose PET/CT findings of a solitary primary hepatic lymphoma: A case report. *World J Gastroenterol* 18:7409–7412, 2012.
62. Bangerter M, Moog F, Griesshammer M, et al: Usefulness of FDG-PET in diagnosing primary lymphoma of the liver. *Int J Hematol* 66:517–520, 1997.
63. Saboo SS, Krajewski KM, O'Regan KN, et al: Spleen in haematological malignancies: Spectrum of imaging findings. *Br J Radiol* 85:81–92, 2012.
64. Paes FM, Kalkanis DG, Sideras PA, Serafini AN: FDG PET/CT of extranodal involvement in non-Hodgkin lymphoma and Hodgkin disease. *Radiographics* 30:269–291, 2010.
65. de Jong PA, van Ufford HM, Baarslag HJ, et al: CT and ^{18}F -FDG PET for noninvasive detection of splenic involvement in patients with malignant lymphoma. *AJR Am J Roentgenol* 192:745–753, 2009.
66. Metser U, Miller E, Kessler A, et al: Solid splenic masses: Evaluation with ^{18}F -FDG PET/CT. *J Nucl Med* 46:52–59, 2005.
67. Metser U, Even-Sapir E: The role of ^{18}F -FDG PET/CT in the evaluation of solid splenic masses. *Semin Ultrasound CT MR* 27:420–425, 2006.
68. Komar G, Kauhanen S, Liukko K, et al: Decreased blood flow with increased metabolic activity: A novel sign of pancreatic tumor aggressiveness. *Clin Cancer Res* 15:5511–5517, 2009.
69. Sahani DV, Bonaffini PA, Catalano OA, et al: State-of-the-art PET/CT of the pancreas: Current role and emerging indications. *Radiographics* 32:1133–1158, discussion 1158–1160, 2012.
70. Okano K, Kakinoki K, Akamoto S, et al: ^{18}F -fluorodeoxyglucose positron emission tomography in the diagnosis of small pancreatic cancer. *World J Gastroenterol* 17:231–235, 2011.
71. Delbeke D, Rose DM, Chapman WC, et al: Optimal interpretation of FDG PET in the diagnosis, staging and management of pancreatic carcinoma. *J Nucl Med* 40:1784–1791, 1999.
72. Lemke AJ, Niehues SM, Hosten N, et al: Retrospective digital image fusion of multidetector CT and ^{18}F -FDG PET: Clinical value in pancreatic lesions—a prospective study with 104 patients. *J Nucl Med* 45:1279–1286, 2004.
73. Kauhanen SP, Komar G, Seppanen MP, et al: A prospective diagnostic accuracy study of ^{18}F -fluorodeoxyglucose positron emission tomography/computed tomography, multidetector row computed tomography, and magnetic resonance imaging in primary diagnosis and staging of pancreatic cancer. *Ann Surg* 250:957–963, 2009.
74. Buchs NC, Buhler L, Bucher P, et al: Value of contrast-enhanced ^{18}F -fluorodeoxyglucose positron emission tomography/computed tomography in detection and presurgical assessment of pancreatic cancer: A prospective study. *J Gastroenterol Hepatol* 26:657–662, 2011.
75. Callery MP, Chang KJ, Fishman EK, et al: Pre-treatment assessment of resectable and borderline resectable pancreatic cancer: Expert consensus statement. *Ann Surg Oncol* 16:1727–1733, 2009.
76. Strobel K, Heinrich S, Bhure U, et al: Contrast-enhanced ^{18}F -FDG PET/CT: 1-stop-shop imaging for assessing the resectability of pancreatic cancer. *J Nucl Med* 49:1408–1413, 2008.
77. Asagi A, Ohta K, Nasu J, et al: Utility of contrast-enhanced FDG-PET/CT in the clinical management of pancreatic cancer: Impact on diagnosis, staging, evaluation of treatment response, and detection of recurrence. *Pancreas* 42:11–19, 2013.
78. Topkan E, Yavuz AA, Aydin M, et al: Comparison of CT and PET-CT based planning of radiation therapy in locally advanced pancreatic carcinoma. *J Exp Clin Cancer Res* 27:41, 2008.
79. Kittaka H, Takahashi H, Ohigashi H, et al: Role of ^{18}F -fluorodeoxyglucose positron emission tomography/computed tomography in predicting the pathologic response to preoperative chemoradiation therapy in patients with resectable T3 pancreatic cancer. *World J Surg* 37:169–178, 2013.
80. Sperti C, Pasquali C, Bissoli S, et al: Tumor relapse after pancreatic cancer resection is detected earlier by ^{18}F -FDG PET than by CT. *J Gastrointest Surg* 14:131–140, 2010.
81. Casneuf V, Delrue L, Kelles A, et al: Is combined ^{18}F -fluorodeoxyglucose-positron emission tomography/computed tomography superior to positron emission tomography or computed tomography alone for diagnosis, staging and restaging of pancreatic lesions? *Acta Gastroenterol Belg* 70:331–338, 2007.
82. Ruf J, Lopez Hanninen E, Oettle H, et al: Detection of recurrent pancreatic cancer: Comparison of FDG-PET with CT/MRI. *Pancreatology* 5:266–272, 2005.
83. Sperti C, Bissoli S, Pasquali C, et al: ^{18}F -Fluorodeoxyglucose positron emission tomography enhances computed tomography diagnosis of malignant intraductal papillary mucinous neoplasms of the pancreas. *Ann Surg* 246:932–937, discussion 937–939, 2007.
84. Hong HS, Yun M, Cho A, et al: The utility of F-18 FDG PET/CT in the evaluation of pancreatic intraductal papillary mucinous neoplasm. *Clin Nucl Med* 35:776–779, 2010.
85. Takanami K, Hiraide T, Tsuda M, et al: Additional value of FDG PET/CT to contrast-enhanced CT in the differentiation between benign and malignant intraductal papillary mucinous neoplasms of the pancreas with mural nodules. *Ann Nucl Med* 25:501–510, 2011.
86. Tomimaru Y, Takeda Y, Tatsumi M, et al: Utility of 2-[^{18}F] fluoro-2-deoxy-D-glucose positron emission tomography in differential diagnosis of benign and malignant intraductal papillary-mucinous neoplasm of the pancreas. *Oncol Rep* 24:613–620, 2010.
87. Diederichs CG, Staib L, Glatting G, et al: FDG PET: Elevated plasma glucose reduces both uptake and detection rate of pancreatic malignancies. *J Nucl Med* 39:1030–1033, 1998.
88. Heinrich S, Goerres GW, Schafer M, et al: Positron emission tomography/computed tomography influences on the management of resectable pancreatic cancer and its cost-effectiveness. *Ann Surg* 242:235–243, 2005.
89. Young WF, Jr: Clinical practice. The incidentally discovered adrenal mass. *N Engl J Med* 356:601–610, 2007.
90. Blake MA, Prakash P, Cronin CG: PET/CT for adrenal assessment. *AJR Am J Roentgenol* 195:W91–W95, 2010.
91. Bagheri B, Maurer AH, Cone L, et al: Characterization of the normal adrenal gland with ^{18}F -FDG PET/CT. *J Nucl Med* 45:1340–1343, 2004.
92. Jana S, Zhang T, Milstein DM, et al: FDG-PET and CT characterization of adrenal lesions in cancer patients. *Eur J Nucl Med Mol Imaging* 33:29–35, 2006.
93. Metser U, Miller E, Lerman H, et al: ^{18}F -FDG PET/CT in the evaluation of adrenal masses. *J Nucl Med* 47:32–37, 2006.

94. Watanabe H, Kanematsu M, Goshima S, et al: Adrenal-to-liver SUV ratio is the best parameter for differentiation of adrenal metastases from adenomas using F-FDG PET/CT. *Ann Nucl Med* 27:648–653, 2013.
95. Boland GW, Dwamena BA, Jagtiani Sangwaiya M, et al: Characterization of adrenal masses by using FDG PET: A systematic review and meta-analysis of diagnostic test performance. *Radiology* 259:117–126, 2011.
96. Groussin L, Bonardel G, Silvera S, et al: ¹⁸F-Fluorodeoxyglucose positron emission tomography for the diagnosis of adrenocortical tumors: A prospective study in 77 operated patients. *J Clin Endocrinol Metab* 94:1713–1722, 2009.
97. Becherer A, Vierhapper H, Potzi C, et al: FDG-PET in adrenocortical carcinoma. *Cancer Biother Radiopharm* 16:289–295, 2001.
98. Leboulleux S, Dromain C, Bonniaud G, et al: Diagnostic and prognostic value of 18-fluorodeoxyglucose positron emission tomography in adrenocortical carcinoma: A prospective comparison with computed tomography. *J Clin Endocrinol Metab* 91:920–925, 2006.
99. Shulkin BL, Thompson NW, Shapiro B, et al: Pheochromocytomas: imaging with 2-[fluorine-18]fluoro-2-deoxy-D-glucose PET. *Radiology* 212:35–41, 1999.
100. Timmers HJ, Chen CC, Carrasquillo JA, et al: Staging and functional characterization of pheochromocytoma and paraganglioma by ¹⁸F-fluorodeoxyglucose (¹⁸F-FDG) positron emission tomography. *J Natl Cancer Inst* 104:700–708, 2012.
101. Chong S, Lee KS, Kim HY, et al: Integrated PET-CT for the characterization of adrenal gland lesions in cancer patients: Diagnostic efficacy and interpretation pitfalls. *RadioGraphics* 26:1811–1824, discussion 1824–1826, 2006.

Diffusion-Weighted Imaging of the Abdomen

YEE LIANG THIAN | DOW-MU KOH

CHAPTER OUTLINE

Principles of Diffusion-Weighted Imaging

Observing and Measuring Water Diffusion with Magnetic Resonance Imaging
Intravoxel Incoherent Motion Model

Technical Considerations

Image Acquisition and Sequence Optimization
Compensation for Physiologic Motion
Choice of b Values

Image Interpretation

Qualitative Assessment
Quantitative Assessment
Imaging Artifacts
Diagnostic Pitfalls

Clinical Application in the Abdomen

Liver
Pancreas
Gallbladder
Spleen
Lymph Nodes
Peritoneum
Gastrointestinal Tract

Future Directions

Summary

Diffusion-weighted magnetic resonance imaging (MRI) was introduced into clinical practice in the mid-1990s, primarily in brain imaging because of its exquisite sensitivity to detect ischemic infarcts. In the past decade, technical advancements have allowed the technique to be translated to body imaging, and abdominal diffusion-weighted imaging (DWI) is now well established. The clinical applications of abdominal DWI are both oncologic and nononcologic; the oncologic applications have been especially helpful.

DWI provides a contrast mechanism for the qualitative and quantitative assessment of tissues. The technique is complementary to and in some situations a viable alternative to gadolinium-enhanced MRI. Abdominal DWI does not require contrast media to be administered, yet it frequently highlights pathologic processes visible on contrast-enhanced techniques with increased conspicuity. The technique allows disease detection and assessment beyond that achievable by morphologic imaging alone.

This chapter discusses the principles of DWI, technical implementation, image interpretation, clinical applications,

and potential pitfalls of the technique as applied to imaging of the abdomen.

Principles of Diffusion-Weighted Imaging

At its most fundamental level, DWI uses an imaging sequence that probes the microscopic mobility of water. The true diffusion coefficient of water is a measure of the effective displacement of water molecules per unit time, which is a random process (brownian motion) and is temperature dependent. Conceptually, it may be useful to consider the diffusion coefficient as a reflection of the freedom of movement of water molecules in a particular volume.

Several biophysical mechanisms can alter the random brownian motion of water molecules in tissues. These include cellular density, cell membrane integrity, cellular structural organization, and the presence of macromolecules that bind to water.¹ The term *apparent diffusion coefficient* (ADC) represents the observed diffusion constant as the water molecules in tissues are modified by these biophysical interactions.

The image contrast on diffusion-weighted images is based on the differences in the diffusivity of water molecules. For example, tumor tissues exhibit low water diffusivity (or “impeded diffusion”) because of the relatively high density of cellular membranes. This increases the frequency of water proton–cell membrane interactions, which thus impedes water mobility. By contrast, a simple cyst containing water only would show high diffusivity as there are no barriers to water diffusion (Fig. 69-1).

OBSERVING AND MEASURING WATER DIFFUSION WITH MAGNETIC RESONANCE IMAGING

The quantification of diffusion with MRI on current clinical systems is based on experiments by Stejskal and Tanner in the 1960s.² The introduction of a pair of symmetric gradients before and after the 180-degree refocusing pulse of a conventional T2-weighted spin-echo sequence “sensitizes” the sequence to water motion (Fig. 69-2). Static water spins dephased by the first gradient lobe would experience a complete rephasing by the second gradient lobe, thereby maintaining their signal. However, moving water spins will be in a different position at the time of the second lobe and thus not be rephased by the same degree, resulting in signal attenuation. Thus the presence of water diffusion is observed as signal loss on DWI. The greater the displacement of water molecules (i.e., the higher their diffusivity), the greater will be the degree of signal attenuation.

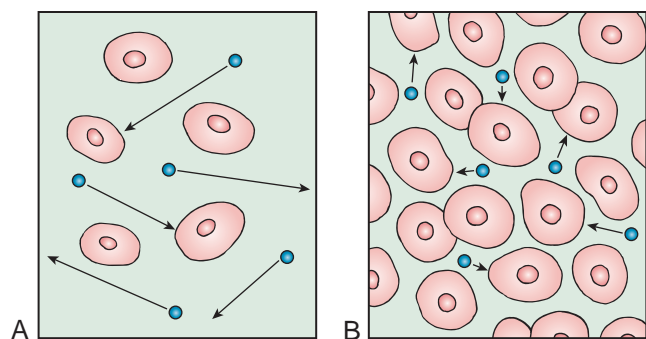


Figure 69-1 Diffusion of water molecules within schematized voxels of interest. **A.** Free diffusion. Water molecules (small blue circles) have relatively unimpeded motion in a hypocellular environment, with the majority of the molecules diffusing freely within the extracellular space. The voxel would return a high apparent diffusion coefficient. **B.** Restricted diffusion. In a hypercellular environment, such as within viable tumor, water molecules encounter frequent collisions with cell membranes. This impedes the free movement of water molecules, which is quantified as a low apparent diffusion coefficient within the voxel.

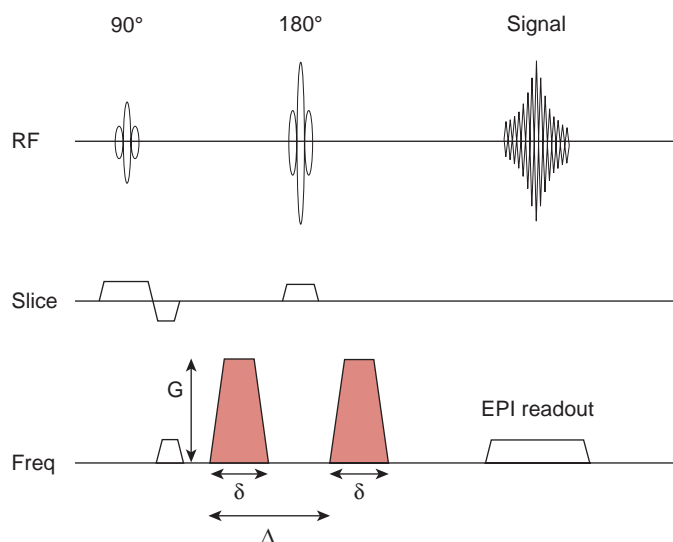


Figure 69-2 Stejskal-Tanner diffusion-weighted spin-echo MR pulse sequence diagram. The time line for the phase-encoding gradient is omitted to simplify the diagram. Two symmetric diffusion-sensitizing gradients (red) are inserted before and after the 180-degree radiofrequency (RF) refocusing pulse. The diffusion sensitivity or b value of the sequence is determined by G, amplitude; δ , duration of the sensitizing gradient; and Δ , time between the two sensitizing gradient lobes. EPI, Echo planar imaging.

As with any MR sequence, the image contrast on DWI results from a combination of different tissue magnetic properties. In DWI, as this is significantly affected by water diffusion, the term *diffusion weighted* is used. However, the image contrast is influenced by both the underlying sequence (usually a T2-weighted sequence with a relatively long repetition time) and the strength of the diffusion weighting, which is given by the b value (diffusion weighting factor). The b value on a clinical scanner is usually altered by changing the amplitude of the diffusion sensitizing gradient, although it may be possible to vary the gradient duration and time interval between the paired gradients.

A b factor of zero ($b = 0 \text{ s/mm}^2$) indicates no diffusion weighting, and the image is analogous to a T2-weighted image. In the abdomen, lower b values applied often range from 50 to 150 s/mm^2 ; higher b values typically range between 500 and 1000 s/mm^2 . DWI in the abdomen is usually performed with use of at least two b values, a lower and a higher b value. To calculate the quantitative ADC value, the relative signals of each voxel at different b value are mathematically fitted by an exponential function according to the following equation:

$$\text{ADC} = \ln(S_1/S_0)/(b_1 - b_0)$$

where S_0 is the signal intensity with the b value of 0 and S_1 is the signal intensity with b value = b (this equation assumes the repetition time and echo time are held constant). A graphic representation of this formula is shown in Figure 69-3A.

INTRAVOXEL INCOHERENT MOTION MODEL

In certain organs such as the liver, the measured signal declines sharply with increasing diffusion weighting over the lower range of b values (typically $0\text{--}100 \text{ s/mm}^2$); the signal then attenuates more gradually with further increase in the b values. This biexponential behavior of signal attenuation is attributed to intravoxel incoherent motion (IVIM),³ in which intravascular microcapillary perfusion generates a pseudodiffusion effect at low b values. Thus, in calculating ADC values, the inclusion of these low b values can result in overestimation of tissue diffusivity. At higher b values, the pseudodiffusion effect is largely negated, and estimation of tissue diffusivity in tissues with significant tissue perfusion may be more reliable if the lower b values are excluded. However, the more sophisticated approach is to apply the biexponential IVIM model to the data fitting, from which the pseudodiffusion coefficient (D^*), perfusion fraction (f), and tissue diffusion coefficient (D) are derived (Fig. 69-4). Both D^* and f reflect tissue perfusion and can vary independently.

The contribution of microcapillary perfusion may be considered in quantitative DWI analysis and is more significant in certain organs and pathologic processes. However, the utility of IVIM-based quantitative metrics is still largely confined to research,⁴ as accurate estimation of the perfusion-sensitive parameters can be challenging, particularly in lesions with inherently low vascular perfusion. Furthermore, there is currently a lack of commercial software for data analysis. Nonetheless, emerging observations suggest that in well-conducted studies with sufficient image signal-to-noise ratio (SNR) and in diseases or organs with significant perfusion effects, IVIM analysis may provide additional information to aid disease characterization.

Technical Considerations

IMAGE ACQUISITION AND SEQUENCE OPTIMIZATION

DWI sequences for clinical imaging of the abdomen are available on most current 1.5T and 3.0T MRI scanners. As in any MR sequence, tradeoffs between image spatial resolution, image SNR, and scan duration are often made, depending on the clinical indication. The technique that is most widely applied is single-shot fat-suppressed spin-echo echo planar imaging

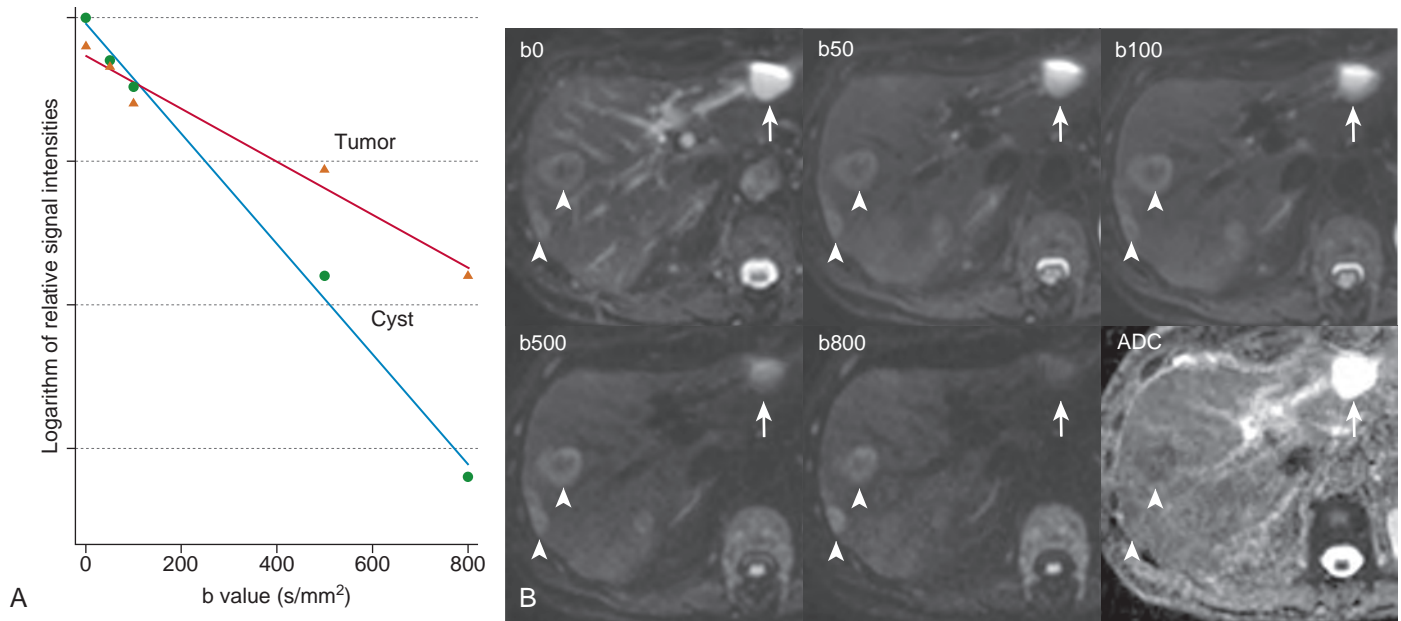


Figure 69-3 **A.** Graph schematic of measured signal intensities (in logarithmic scale) over the range of b values illustrating the concept of apparent diffusion coefficient (ADC). The ADC value represents the slope of the line that describes this relationship within each voxel. A voxel within a cyst would show greater signal attenuation with each incremental increase in the b value, resulting in a high measured ADC (steeper slope). The signal attenuates less sharply as the b value increases within voxels containing a tumor microenvironment, which corresponds to a lower ADC (more gentle slope). **B.** Series of diffusion-weighted images of the liver showing the marked signal attenuation of a cyst (arrow) as the b value increases. The tumor deposits (arrowheads) show more gradual signal attenuation and are conspicuous on the b800 image because of a relatively higher lesion-to-background contrast. Derived ADC map shows the higher ADC of the cyst represented by high signal intensity, compared with the lower ADC of the tumor represented by low signal intensity.

(SS-EPI). The primary merit of this technique is the speed of acquisition (with subsecond acquisitions of the entire k -space), but the sequence is prone to low SNR as well as ghosting, image distortion, blurring, and susceptibility artifacts.⁵ Other k -space acquisition techniques, such as multishot EPI DWI, turbo spin-echo DWI, and radial schemes of k -space acquisition (PROPELLAR DWI), may have potential to reduce some of the artifacts associated with the SS-EPI technique but are not widely implemented.

The underlying principles that guide imaging parameter selection in SS-EPI should be optimized for good SNR and reduction of artifacts. It is beyond the scope of this chapter to discuss the broader MR principles that affect image SNR and artifacts, but a few points that are particularly relevant to EPI DWI are mentioned here. First, fat suppression is routinely used to reduce the large chemical shifts in EPI and to increase the dynamic range of DWI images. This can be achieved either by inversion recovery (e.g., short tau inversion recovery) technique, which gives more uniform fat suppression but less SNR, or with chemical fat-selective saturation (e.g., spectral selected attenuation with inversion recovery or chemical shift selective imaging), which yields better SNR but is more susceptible to magnetic field inhomogeneities. Second, the echo time should be minimized as this increases the SNR; the repetition time should be sufficiently long to avoid T1 saturation effects (at least three to five times that of the T1 relaxation time of the imaged tissue). Use of a simultaneous gradient scheme (e.g., tetrahedral encoding or three-scan trace) allows the echo time to be reduced. Third, the number of signal averages can be increased to achieve better SNR, although at a cost of increased scan time. Some scanners allow the

number of averages performed to vary with the b value, with more averages performed for SNR-poor high- b value DWI images. Last, parallel imaging should always be applied for body DWI as it shortens the echo train lengths, thereby reducing susceptibility and field inhomogeneity-related artifacts as well as reducing the acquisition time (Tables 69-1 and 69-2). The reader is referred to the review article by Koh and associates⁶ for a more detailed discussion of the technical parameters that influence the imaging quality of EPI DWI images.

COMPENSATION FOR PHYSIOLOGIC MOTION

Unlike in the brain, which is a reasonably static organ, several physiologic processes create motion-related phase artifacts in the abdomen that degrade image quality. This includes coherent movement, such as respiratory motion and bowel peristalsis, and noncoherent motion, such as cardiac pulsation.

Strategies to overcome artifacts arising from respiratory motion include breath-hold DWI, respiratory or navigator triggered/controlled DWI, and free-breathing DWI with multiple signal averages. Of these three techniques, breath-hold SS-EPI DWI of the abdomen is the fastest to perform, with coverage of the entire liver or abdomen over two breath-holds, each lasting approximately 20 seconds. The images retain good anatomic detail and are not degraded by respiratory averaging. However the major drawback is the lower SNR of the source data, which imposes limits on the acceptable spatial resolution (typically wider section thicknesses of 8 to 10 mm) and the maximum b value used (as higher b factors decrease the SNR). Fewer b values are obtained with this technique because of the limited number of b -value acquisitions that can be

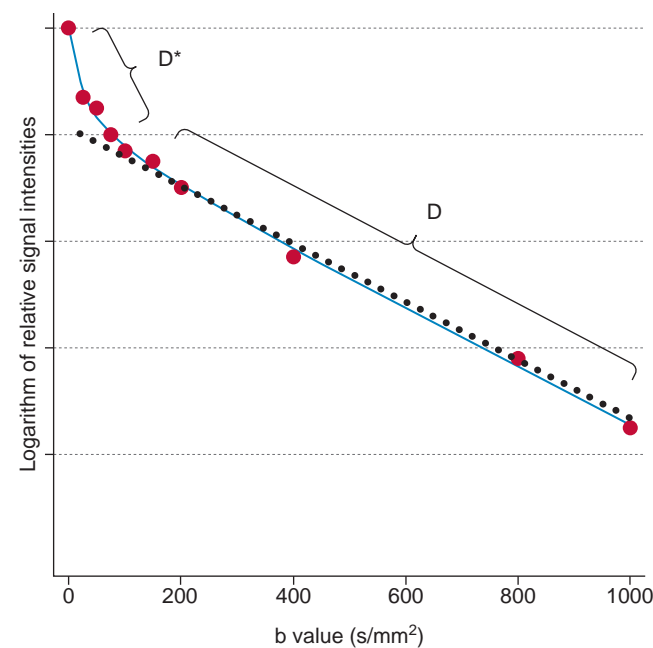


Figure 69-4 Graph schematic shows calculation of diffusion parameters by intravoxel incoherent motion (IVIM) analysis. Plot shows the logarithm of the signal intensity for each image voxel acquired at the same anatomic position across the range of b values applied. A biexponential behavior of signal attenuation is observed because of the different predominant processes at low and high b values causing signal attenuation. D* represents the slope at the range of low b values (typically 0-100 s/mm²). The more rapid loss of signal (steeper slope) at lower b values is attributed to the dominant effect of microcirculatory perfusion, producing a pseudodiffusion effect. D represents the slope at the range of high b values (more than 100 s/mm²). The more gradual decline in signal at this portion of the curve reflects true diffusivity effects. Note that a higher concentration of data points is acquired in the lower range of b values to improve the accuracy of the calculation of D*. (Modified from Koh DM, Collins DJ, Orton MR: Intravoxel incoherent motion in body diffusion-weighted MRI: Reality and challenges. *AJR Am J Roentgenol* 196:1351-1361, 2011.)

accommodated within a breath-hold. Breath-holding techniques may also be more sensitive to susceptibility and pulsation artifacts.¹

Respiratory or navigator triggered/controlled techniques synchronize data acquisition with respiratory movement, and data are acquired only within a certain period of the respiratory cycle (usually the expiratory phase). The advantages of this method include better subjective image quality, higher SNR, higher lesion-to-liver contrast ratio, and more precise ADC quantification compared with breath-hold DWI.^{7,8} However acquisition times are increased substantially (up to 5 to 6 minutes), and ADC measurements may be less reproducible compared with breath-hold and free-breathing DWI.⁹ In addition, the technique may result in pseudo-anisotropy artifacts related to the gated image acquisition.¹⁰

In free-breathing EPI DWI, signal averaging from multiple acquisitions of the same imaging volume produces images with high SNR. Thin slice partitions (4-5 mm) are possible, and this allows multiplanar reconstructions of reasonable quality. A larger number of b values can be accommodated, which enables evaluation of ADC as well as IVIM parameters of lesions. However, image acquisition time is longer compared with

TABLE 69-1 List of Recommended Optimizations of Echo Planar Diffusion-Weighted Imaging	
Problem	Solution
Poor signal-to-noise ratio	Use shortest echo time available Echo time can be reduced with the following techniques : Parallel imaging (maximum 2x) Simultaneous gradient application scheme (e.g., three-scan trace) Increase of receiver bandwidth Use of monopolar gradient scheme Use multiple averages (maximum 6) Choose larger voxel size (increase field of view, smaller matrix, increase section thickness) Choose lower b values Image at higher field (3T) Optimize receiver bandwidth
Poor fat suppression and chemical shift artifact	Use nonchemical selective fat suppression scheme (e.g., short tau inversion recovery) Increase receiver bandwidth Use combination fat suppression schemes at 3T
Eddy current artifacts (geometric distortion, image shearing)	Optimize/increase receiver bandwidth Use of bipolar gradient scheme Use of parallel imaging Simultaneous gradient application scheme
Nyquist (N/2) ghosting	Decrease receiver bandwidth

TABLE 69-2 Typical Scan Parameters Used to Perform Abdominal Diffusion-Weighted Magnetic Resonance Imaging	
Parameter	Value
Pulse sequence	Single-shot spin-echo echo planar imaging
Imaging plane	Axial
Field of view, mm	380 × 380
Matrix size	150 × 256
Repetition time (TR), ms	14,000
Echo time (TE), ms	72
Echo planar imaging factor	150
Parallel imaging factor	2
Number of signals averaged	4
Section thickness, mm	5
Direction of motion-probing gradients	3-scan trace
Receiver bandwidth	1800 Hz/pixel
Fat suppression	Short tau inversion recovery (inversion time, 180 ms)
b value, s/mm ²	0, 100, 900
Breathing technique	Free breathing
Acquisition time	4 minutes 30 seconds

breath-hold imaging (in the region of 3 to 6 minutes to cover the liver), and signal/volume averaging may result in suboptimal characterization of lesion heterogeneity, especially for smaller lesions. Even allowing for the presence of motion, ADC measurements in free-breathing DWI have been shown to be robust and comparable or even superior to breath-hold DWI.⁹

Cardiac pulsation results in spin dephasing, which is most prominent in the structures immediately inferior to the heart, such as the left lobe of the liver, resulting in severe signal loss

and overestimation of ADC.¹¹ Cardiac gating seems intuitive to reduce cardiac motion effects in the liver, but some authors have found it difficult to find a phase of the cardiac cycle that yields diffusion-weighted images free of signal dropout artifact.¹² Moreover, the combination of respiratory and cardiac gating will significantly prolong scan time to clinically unfeasible levels. Low-*b* value images are less prone to cardiac motion-induced signal loss and are therefore invaluable for lesion detection in susceptible areas.¹³

Bulk motion from bowel peristalsis can be reduced by administration of antiperistaltic drugs (e.g., hyoscine butylbromide and glucagon). However, these are not routinely administered for the evaluation of the upper abdominal viscera.

CHOICE OF *b* VALUES

There is no clear consensus on the precise number and magnitude of *b* values that should be used for abdominal DWI. Considerations include the target organ being evaluated, the image SNR, and whether DWI is primarily used for qualitative or quantitative analysis. For ADC quantification, three or more *b* values are generally recommended, with one being a lower *b* factor (≤ 100 s/mm²) and one being a higher *b* factor (> 500 s/mm²). Additional *b* values can be considered to increase the accuracy of ADC estimation or if IVIM parameters need to be extracted with biexponential modeling.¹⁴ Increasing the number of *b* values results in increase in the imaging time. Some researchers now favor omitting *b* = 0 s/mm² in their ADC calculations to obtain perfusion-insensitive values for comparison between serial measurements.

Image Interpretation

QUALITATIVE ASSESSMENT

The source *b*-value diffusion-weighted images and the ADC maps are both useful for visual assessment. The degree of signal attenuation from water molecules at high *b* values is less in areas of impeded diffusion (in other words, these water molecules produce higher signal on native high-*b* value images). Most pathologic processes, such as tumors, inflammation, and infection, show greater impeded water diffusion compared with normal tissues and thus return higher signal on diffusion-weighted images.

In the abdomen, native *b*-value diffusion-weighted images are used for detection of lesions and pathologic changes because of their excellent suppression of the normal background signal, which increases the conspicuity of tumors and inflammatory processes. Even with minimal diffusion weighting, the signal from vasculature structures is suppressed ("black blood"), and intrinsic fat suppression of diffusion-weighted sequences widens the dynamic range considerably. On low-*b* value images, there is high lesion-to-background contrast, good anatomic information, and fewer eddy current-induced distortions.¹³ However, a "T2 shine-through" effect is present because of the preservation of signal in areas with prolonged T2 relaxation times (e.g., contents of the gallbladder, cystic or mucinous lesions). The use of a high-*b* value image (e.g., *b* = 1000 s/mm²) decreases the relative contribution of T2 signal intensity to diffusion-weighted images, and the T2 shine-through effect may be mitigated if not removed completely. Several investigators have relied on a very high-*b* value approach for detection

of lesions (e.g., *b* value > 1000 s/mm²) in other parts of the body,^{15,16} although this approach has not been shown to confer additional advantages in abdominal diseases.

Inspection of the corresponding ADC map will usually distinguish areas of true impeded diffusion from areas of T2 shine-through. Areas of true impeded diffusion have lower absolute ADC values and by convention appear "dark" on the ADC maps, whereas areas of T2 shine-through have high ADC values and appear "bright." Even when the ADC maps are not available, the reviewer may infer the degree of impeded diffusion on the basis of relative signal attenuation at different *b* values. This concept is illustrated in Figure 69-3B.

However, the diffusion-weighted images should always be interpreted in conjunction with their morphologic counterparts. The background anatomy is better demonstrated on conventional MR sequences, allowing localization of any diffusion abnormality and exclusion of normal and physiologic causes of impeded diffusion. Many of the pitfalls of DWI interpretation detailed later in this section can be avoided by correlation with the morphologic images. Some have proposed a "fusion" approach to image assessment, whereby the functional diffusion information is fused with morphologic data, similar to the creation of positron emission tomography/computed tomography images.

QUANTITATIVE ASSESSMENT

ADC maps are postprocessed representations of the ADC values calculated for each voxel from the source *b*-value images. The mean or median ADC values in areas of interest are derived by drawing regions of interest on these parametric maps. These values can aid lesion characterization as well as provide clues to tissue microstructure, for example, in liver cirrhosis. Lower ADC values imply greater impeded water mobility. However, as ADC values can be dependent on a multitude of scan parameters, there has been difficulty in prescribing a cutoff value between benign and malignant or pathologic and nonpathologic. Reported ranges of ADC in abdominal organs are presented in Table 69-3 for reference.¹⁷

One of the most promising developments in DWI is the use of ADC as a quantifiable biomarker for response assessment. In

TABLE 69-3
Reported Normal Ranges of Apparent Diffusion Coefficient Values for Abdominal Viscera

Organ	Values in Organs without Disease ($\times 10^{-3}$ mm ² /s)	Values in Diseased Organs ($\times 10^{-3}$ mm ² /s)
Liver	1.55 \pm 0.30 to 1.63 \pm 0.31	Cirrhosis 1.45 \pm 0.13 to 1.60 \pm 0.19
Kidney	2.60 \pm 0.32 to 2.67 \pm 0.29	Chronic renal failure 2.11 \pm 0.25 to 2.15 \pm 0.30
Pancreas		Chronic pancreatitis
Head	1.82 \pm 0.40	1.71 \pm 0.20
Body	1.81 \pm 0.41	1.67 \pm 0.17
Tail	1.65 \pm 0.37	1.58 \pm 0.39
Spleen	1.26 \pm 0.23	
Gallbladder	3.50 \pm 0.51	

Modified from Yoshikawa T, Kawamitsu H, Mitchell DG, et al: ADC measurement of abdominal organs and lesions using parallel imaging technique. *AJR Am J Roentgenol* 187:1521–1530, 2006.

general, therapy response is associated with significant increases in tumor ADC, which can be seen as early as within the first week after therapy. The ADC increase is postulated to be due to cellular damage leading to necrosis¹⁸ and has been demonstrated in a variety of tumors, including breast, cervical, prostate, and liver cancers.¹⁹⁻²³ One of the advantages of obtaining longitudinal measurements of ADC is that changes are detected earlier than morphologic changes, potentially allowing earlier assessment of treatment response and potential alterations to management. Baseline ADC measurements are also being investigated as pretreatment predictors of the effectiveness of tumor therapy because diffusivity reflects tissue cellularity, microcirculation, and necrosis, which affect response to chemotherapy. More sophisticated methods of quantitative ADC analysis currently under research include ADC histogram analysis, IVIM analysis, and even textural analysis, but these are beyond the scope of this chapter.

IMAGING ARTIFACTS

Artifacts Related to Echo Planar Imaging

Most DWI for abdominal clinical applications is performed by single-shot echo planar imaging–based sequences. This ultrafast method of k-space acquisition requires large gradient reversals and results in accumulation of phase shift errors because of the prolonged readout. This results in eddy current–induced geometric distortions, image shearing, and Nyquist or N/2 ghosting (Fig. 69-5).⁵ These effects are even more pronounced at higher field strengths because of greater nonuniformities in the magnetic field (B₀), greater diamagnetic susceptibility effects, and shorter T2* relaxation time. On modern scanners, improvements in hardware and sequence optimization have reduced these artifacts. Multishot imaging techniques are being explored, which may further reduce artifacts in the future.

Susceptibility-Related Signal Loss

Diffusion-weighted sequences are prone to susceptibility effects because of the echo planar readout. Hypointensity on DWI may be due to T2 or T2* shortening from abnormal iron deposition, hemorrhage, and inflammation²⁴ (so-called T2 dark-through or T2 blackout). ADC measurements in such areas may be

spuriously low.²⁵ In the abdomen, gas-filled viscera such as bowel and structures close to the lungs can also produce spuriously low or high signals, resulting in missed lesions or false positives. Pathologic iron depositions in the abdominal viscera (most commonly in the liver) and metal implants are other potential sources of susceptibility that could obscure lesion detection.

Physiologic Motion

Ultrafast methods of MRI such as EPI are resistant to but not invulnerable to physiologic motion. Motion degrades image quality in two ways, depending on when it occurs during the scan. Motion during data acquisition introduces additional phase terms, whereas motion between acquisition intervals causes inconsistencies in the data before and after the movement. In both cases, the decreased coherence of the acquired signals produces ghosting, blurring, and lower image SNR. Motion-related data inconsistencies also make ADC assessment of small target lesions inaccurate.

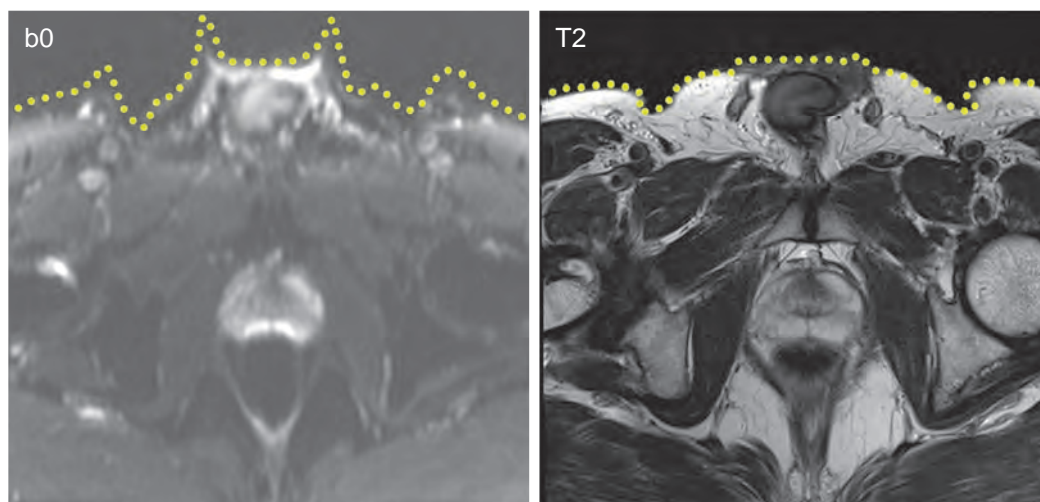
In the abdomen, the main causes of bulk motion are respiratory motion, cardiac motion, and peristalsis. Strategies to minimize the effects of these in the abdomen have been discussed earlier. It is particularly difficult to compensate for the spin dephasing from cardiac pulsation that results in signal loss in the left liver lobe. This decreases the detectability of lesions and impairs the reliability of ADC measurements in the left lobe immediately inferior to the heart.

DIAGNOSTIC PITFALLS

T2 Shine-Through

Tissues with long intrinsic T2 relaxation times (such as free water) may appear hyperintense on diffusion-weighted images even at high b values. This may be falsely ascribed to impeded water diffusion. Comparison with ADC maps or the exponential images (formed by taking the ratio of a diffusion-weighted image divided by an unweighted image from the same image series and slice position) helps avoid this pitfall. In cases of true impeded diffusion, the region of increased DWI signal will demonstrate low ADC values compared with T2 shine-through, which would return a relatively high ADC value.

Figure 69-5 Diffusion-weighted image (b0) through the pelvis obtained with single-shot echo planar imaging technique. Note the geometric distortion, which is especially pronounced at the air-skin interface (dotted line). An artifactual exaggerated concavity is also seen at the posterior border of the prostate. The T2 morphologic image is shown for reference.



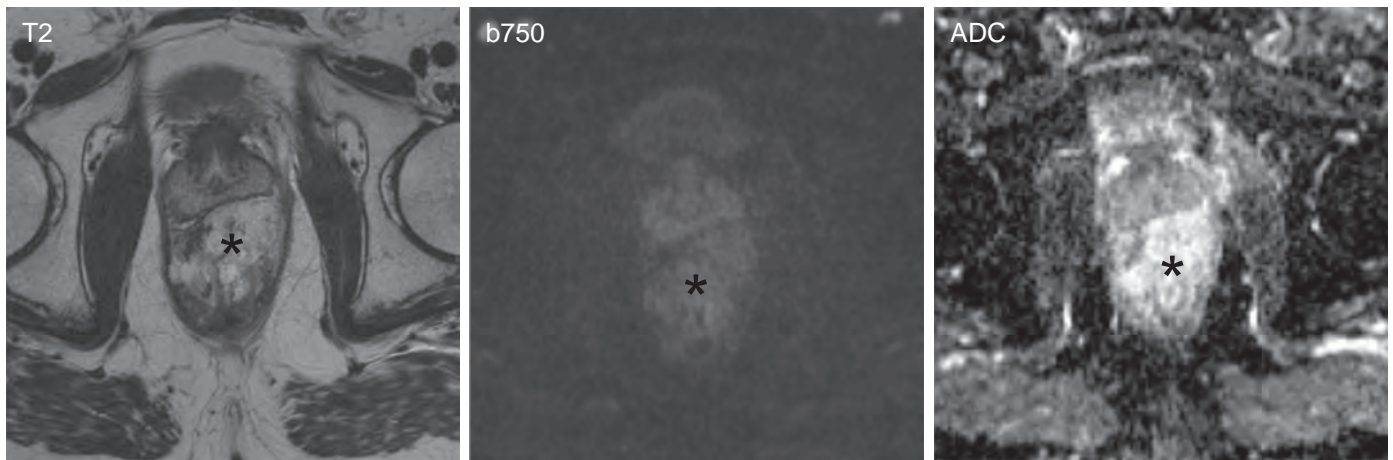


Figure 69-6 Diagnostic pitfall of diffusion-weighted imaging. Axial images of the distal rectum in a 64-year-old woman with mucinous rectal carcinoma. The tumor (*) is markedly hyperintense on the T2-weighted images, characteristic of mucinous histology. The high-*b* value diffusion-weighted image (b750) shows very little tumor signal, and the apparent diffusion coefficient (ADC) is high because of the large proportion of freely diffusing water molecules within extracellular mucin deposits.

Normal and Benign Structures Showing Impeded Diffusion

Certain physiologic tissues appear hyperintense on DWI even at high *b* values because of their intrinsic hypercellularity. These include the spleen, lymph nodes, ganglia, spinal cord, bowel mucosa, endometrium, testes, and ovaries. On occasion, tiny foci (1–2 mm) of impeded diffusion are detected on *b*-value images that are difficult to correlate with structures on corresponding morphologic sequences. These may be due to small nerves or venules, which are benign. Apart from malignant or inflammatory processes, benign tumoral lesions with high cellularity, such as liver adenomas, focal nodular hyperplasia, and sclerosed hemangiomas, may show varying degrees of impeded diffusion as well.

Tumors Showing Unimpeded Diffusion

Lesions with mucinous or cystic contents are a potential pitfall on DWI as there is relatively unimpeded diffusion of their internal contents, whereas the cellular portion of tumor may not be evident or is confined only to the lesion wall (Fig. 69-6). Hypocellular tumors, such as low-grade tumors, may not be depicted on DWI. Tumors or abscesses that have been treated may also not show impeded diffusion, but this allows DWI to be used as a marker for treatment response. Knowledge of the relevant clinical history is important, particularly the histologic subtype and treatment history at image interpretation.

Pitfalls of Quantitative Assessment

An important challenge to overcome is the implementation of quantitative ADC measurements in a multicenter setting across different imaging platforms. However, it is encouraging that in well-controlled imaging studies, ADC quantification shows good measurement reproducibility, with coefficient of repeatability as low as 8% to 10% being achievable. Furthermore, interscanner measurement variability of ADC was shown to be 12% across scanners using analogous imaging parameters.²⁶

Radiology departments should verify their MR scanner ADC measurement reproducibility and standardize their own protocols to enable pretreatment and post-treatment ADC measurements to be obtained with confidence in the assessment of

therapeutic response.²⁷ Pooled analysis of data acquired from different centers using analogous technique may be performed by adapting the measurement reproducibility of the worst-performing platform to determine the threshold of significant ADC change. Clearly, such an approach needs to be verified in future clinical trials.

Another potential confounding factor in quantitative ADC assessment is the variability in defining the size and position of the region of interest. This can particularly be a problem for very small residual tumors after therapy. The variations in regions of interest have been shown to have a significant effect on tumor ADC values and interobserver variability.²⁸ The analysis of heterogeneous lesions with DWI can also be challenging as summary values, such as mean or median ADC, may not be representative of the underlying changes. For this reason, more sophisticated methods of data analysis are now being evaluated to better describe lesion heterogeneity and the heterogeneity of tumor response.

In summary, diagnostic characterization with DWI requires integration of morphologic sequences and clinical information and awareness of the artifacts and pitfalls associated with the technique.

Clinical Application in the Abdomen

DWI is useful in a broad spectrum of diseases in the abdomen as the most common pathologic processes, such as neoplasia, inflammation, and infection, alter their microenvironments in such a way as to impede water diffusion. Currently, the most common applications of DWI of the abdomen are for disease detection and disease characterization. However, there is increasing evidence that the quantitative parameters obtained from DWI are also helpful in assessment of response to treatment and as a potential predictive biomarker.

LIVER

Lesion Detection

The background signal suppression in diffusion-weighted images results in excellent conspicuity of focal liver lesions and high lesion-to-background contrast. This coupled with the fact

that the SS-EPI technique used for DWI is inherently less vulnerable to respiratory motion-related blurring provides for a robust sequence for lesion detection. This has been shown in many publications that have demonstrated DWI to be more sensitive in detecting metastases than conventional T2-weighted imaging and at least comparable to extracellular gadolinium contrast-enhanced sequences.²⁹⁻³⁴ A combination of DWI with hepatocellular contrast agents appears to provide the best performance for detection of metastases,³⁵ and the sequence is particularly helpful for detection of lesions less than 10 mm (Fig. 69-7).

DWI may also improve the detection of hepatocellular carcinomas (HCCs). A meta-analysis showed DWI sensitivity to be 81% with 89% specificity, comparable to that of imaging with conventional gadolinium-based contrast agents.³⁶ However, some authors have found DWI to be less sensitive than conventional contrast-enhanced T1-weighted imaging.³⁷ Missed lesions arise in a fibrotic or cirrhotic liver, which creates a background of limited water diffusivity, or are well differentiated, thus diminishing the contrast between lesion and background. The sensitivity of DWI for HCC decreases with increasing cirrhosis³⁸ and lower histopathologic tumor grades.³⁹

Although DWI has not been officially incorporated into the American Association for the Study of Liver Diseases or European Association for the Study of the Liver guidelines on HCC diagnosis, it has been shown to be useful for the diagnosis of hypovascular HCCs when it is interpreted in conjunction with the hepatocellular contrast agents.⁴⁰ Hyperintensity on diffusion-weighted images and hypointensity in the hepatocellular phase imaging (using Gd-EOB-DTPA) favors the diagnosis of HCC over dysplastic or regenerative nodules. Whereas DWI is certainly a useful adjunct, there are insufficient grounds to recommend DWI as a replacement for contrast-enhanced imaging for HCC diagnosis.

Lesion Characterization

DWI is able to distinguish reliably between cystic and solid lesions as cysts show signal suppression at higher b values and return very high ADC values. However, the technique has been less successful at differentiating between benign and malignant solid lesions as all solid lesions appear relatively high signal on DWI, and there is substantial overlap of the ADC values between benign cellular lesions (such as focal nodular hyperplasia and adenomas) and malignant lesions.^{41,42} Moreover, any prescriptive ADC cutoff is itself vulnerable to erroneous lesion

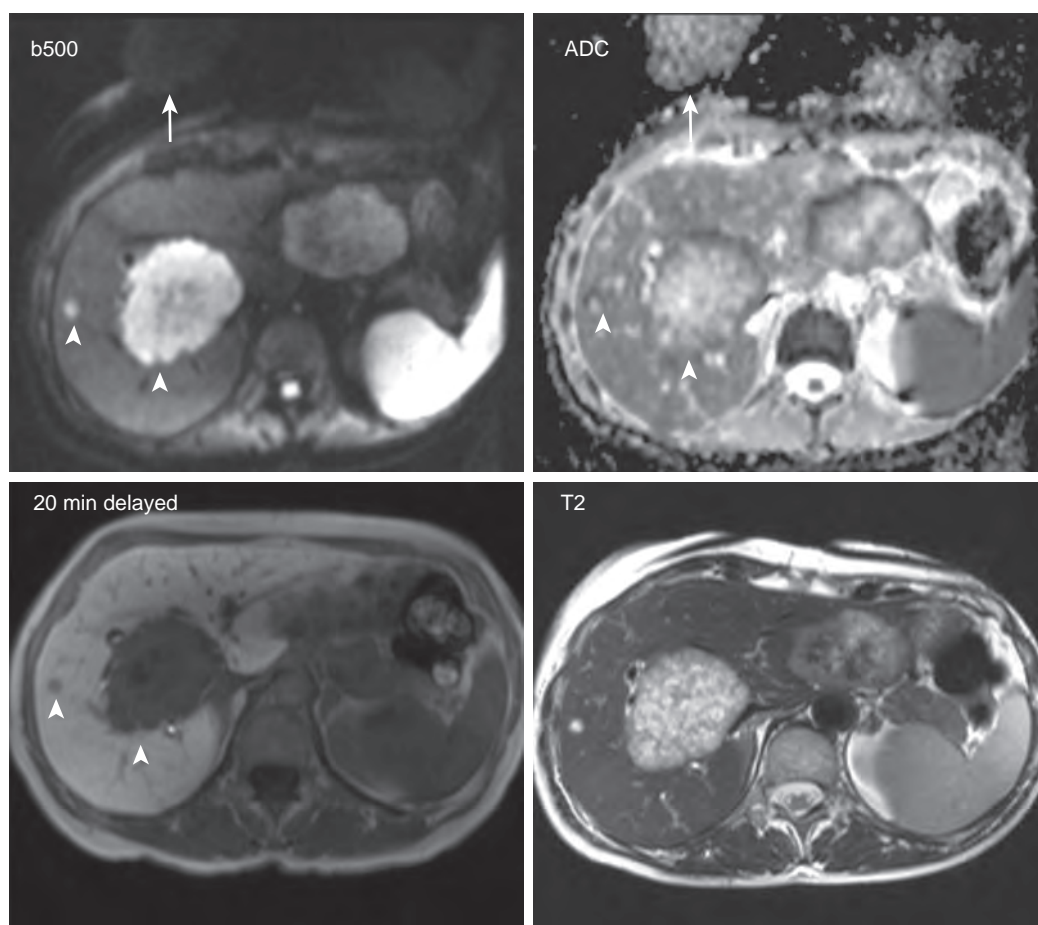


Figure 69-7 Hepatic metastases from colorectal carcinoma. Top panel, Diffusion-weighted image (b500) demonstrates high contrast of lesion (arrowheads) to background liver. The apparent diffusion coefficient (ADC) map shows hypointensity of the wall of each lesion, indicating that viable hypercellular tumor is at the periphery of the lesion, whereas necrotic tumor tissue is in the core. Note the presence of Nyquist ghost artifact (arrow) shifted from the true image by half of the field of view. Bottom panel, left, Hepatocellular phase image obtained 20 minutes after injection of a hepatocellular-specific agent showing relative hypointensity of the metastases (arrowheads); right, T2-weighted image for correlation.

classification because of the variability of ADC quantification. For this reason, one should combine DWI with conventional morphologic MR images for optimal assessment.

Interestingly, liver abscesses return markedly low ADC values because of cellular and viscous debris as well as exudates within the abscess cavity. This can be helpful in distinguishing them from necrotic or cystic tumors, which have necrotic central portions with high ADC.⁴³ Furthermore, the wall of an abscess is often isointense to liver parenchyma, whereas the wall of a cystic or necrotic tumor is hyperintense at DWI owing to its cellularity. However, early abscess formation may be associated with elevated ADC values, thus leading to misinterpretation.⁴⁴

Assessment of Tumor Response to Treatment

It is intuitive that ADC should increase with response to therapy because of cell death and reduced tumor cellularity. Indeed, tumor ADC increase among responders has been observed in several studies with liver metastases and HCC.^{22,45,46} The ADC change is observed earlier than morphologic alterations and as early as 3 days after therapy.⁴⁷ An increase in ADC has been observed in responders of both systemic treatment (chemotherapy) and local-regional therapies (radiofrequency ablation and chemoembolization). However, the exact evolution of ADC after treatment is complex because of concurrent processes, such as acute cell swelling, fibrosis, and perfusional changes, that may affect the diffusion coefficients.

It has been reported that colorectal metastases with high pretreatment ADC values respond poorly to chemotherapy.^{45,48} This may be attributed to more necrotic tumors, which infer a more aggressive phenotype or confer treatment resistance due to diminished drug penetration to the center of the tumors. However, studies correlating pretreatment ADC and long-term clinical outcomes are lacking.

Diagnosis of Liver Fibrosis and Cirrhosis

The noninvasive diagnosis of liver fibrosis and cirrhosis is challenging with conventional MRI as changes are apparent only when fibrosis is relatively advanced. The ADC values obtained by DWI in cirrhotic livers are significantly lower than those in nonfibrotic livers,⁴⁹⁻⁵¹ but distinguishing between the different grades of fibrosis with DWI has been difficult because of the substantial overlap of ADC values between fibrosis grades and the relatively narrow dynamic range of the ADC values in this disease setting. The impeded diffusion observed in cirrhosis has been suggested by IVIM analysis to be in part due to reduction in capillary perfusion.^{52,53}

PANCREAS

Diffusion-weighted MRI has been used to detect pancreatic lesions and to distinguish between solid and cystic pancreatic lesions. Pathologic entities such as pancreatic adenocarcinoma, pancreatic neuroendocrine tumors, solid pseudopapillary tumors of the pancreas, acute pancreatitis, and autoimmune pancreatitis all show impeded diffusion.⁵⁴⁻⁵⁷ Consequently, differentiation between these entities by DWI has been less successful because of substantial overlap in their ADC values. Despite initial enthusiasm, ADC quantification has not been successful in differentiating between pancreatic adenocarcinoma and mass-forming pancreatitis. More recently, the use of IVIM analysis has shown that the perfusion fraction of

pancreatic cancer is lower compared with normal pancreas or mass-forming pancreatitis. However, it is not yet practical to implement this technique in the routine clinical setting.^{58,59}

The conspicuity of pancreatic adenocarcinoma on DWI is also variable. In one series of 80 patients with pancreatic adenocarcinoma,⁵⁵ only about half of pancreatic adenocarcinomas were hyperintense and clearly demarcated from the surrounding pancreatic parenchyma, although overall about 80% of the pancreatic cancers were hyperintense. This was thought to be related to tumor-associated pancreatitis affecting the regions of the pancreas distal to the tumor, which resulted in reduced contrast differentiation between tumoral tissue and inflamed pancreatic parenchyma because both processes impeded diffusion (Fig. 69-8).

With regard to cystic lesions of the pancreas, such as mucinous cystic neoplasm, serous cystadenomas, and intraductal papillary mucinous neoplasms, these demonstrate elevated ADC values. Studies that aimed to differentiate malignant from benign cystic pancreatic lesions have met with limited success,⁶⁰ although it is conceivable that DWI may be able to demonstrate solid components within a cystic pancreatic lesion, such as when there is malignant transformation within an intraductal papillary mucinous neoplasm.

GALLBLADDER

Ultrasound remains the initial investigation of choice for diagnosis of gallbladder disease. However, with the ubiquity of DWI in abdominal MR protocols, a few studies have retrospectively examined the performance of DWI in this area. As can be expected, gallbladder carcinomas show low ADC values, signifying impeded diffusion.⁶¹⁻⁶³ However, it may not always be possible to distinguish gallbladder carcinoma from other polypoidal lesions, adenomyomatosis, and hyperplastic polyps or adenomas.^{63,64} There have been no large-scale studies to date of the findings of acute cholecystitis on DWI, but this remains a potential cause of a false-positive diagnosis of malignant disease. In some patients in whom gas-filled large bowel abuts the gallbladder, EPI-related artifacts might cause spurious signal changes, which confound evaluation of the gallbladder.

SPLEEN

There are very few published studies on the clinical utility of DWI in the spleen. This is because the spleen is hypercellular and therefore shows substantial impeded diffusion and inherently high signal intensity on high-*b* value sequences, rendering any cellular lesions within it less conspicuous. The spleen has been used as an internal reference organ for normalization of ADC values,⁶⁵ an approach favored by some authors but that has inherent limitations. ADC normalization is more susceptible to image noise, and the ADC value of the spleen may not be invariate with antitumor therapies. Interestingly, some studies suggest that ADC values in the spleen may correlate with the severity of liver fibrosis and cirrhosis.^{66,67}

LYMPH NODES

DWI is exquisitely sensitive for the detection of lymph nodes, both normal and pathologic. As even normal and reactive lymph nodes are densely packed with lymphoid elements, they return high signal intensity on diffusion-weighted images. DWI

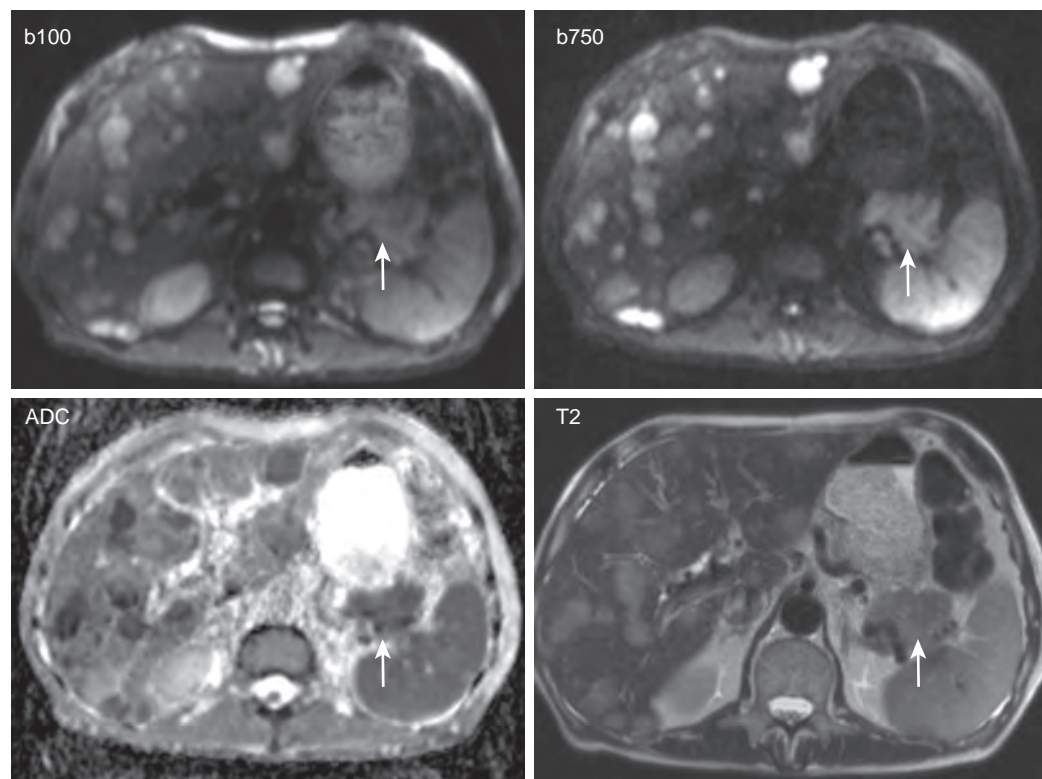


Figure 69-8 A 70-year-old man with pancreatic tail glucagonoma. Axial diffusion-weighted images (b100 and b750) show the conspicuity of the tumor (arrow) and the multiple hepatic metastases, which show restricted diffusion. Note that the normal spleen also returns a low apparent diffusion coefficient (ADC) value similar to that of tumor because of its inherent hypercellularity.

often reveals normal lymph nodes that are not apparent on other morphologic sequences.⁶⁸

Most studies have shown that malignant nodes return lower ADC values compared with benign lymph nodes,⁶⁸⁻⁷⁰ which may improve size and morphologic criteria for nodal classification. Although there is a distinct trend toward lower ADC values in malignant nodes,⁷¹ there remains a wide range of ADC values in both categories.^{72,73} This makes it difficult to confidently classify any single node prospectively as benign or malignant. The limited spatial resolution of DWI also hinders the accuracy of ADC measurements of small nodes because of partial volume effects. At present, DWI is best used in detection of abdominal nodes, and characterization should be made in conjunction with morphologic sequences. However, the combination of DWI with ultrasmall iron oxide particle-enhanced imaging⁷⁴ shows substantial promise in the detection of lymph node metastases.

PERITONEUM

Small-volume metastatic deposits in the peritoneum or even large peritoneal masses can be missed with computed tomography or conventional MR sequences because they are frequently isodense or isointense with adjacent bowel loops and vessels, affording little contrast to enable their detection. The images on DWI provide effective background suppression in the abdomen by a combination of fat suppression and nulling the signal from bowel viscera and mesenteric vasculature. Any ascites that may be present will be of low signal intensity on high-*b* value images. Therefore, even small-volume peritoneal disease stands out as hyperintense foci in the abdomen.

Several studies have corroborated the sensitivity of DWI for depiction of peritoneal tumors,⁷⁵⁻⁷⁷ with sensitivity ranging from 84% to 90% when it is used in conjunction with conventional MR sequences. The technique has also been used with gadolinium-enhanced imaging to accurately predict the peritoneal cancer index before surgery in patients undergoing evaluation for cytoreductive surgery.⁷⁸ This may potentially differentiate patients who are good surgical candidates from those who may be candidates for neoadjuvant chemotherapy to reduce tumor burden (Fig. 69-9).

GASTROINTESTINAL TRACT

Detection and Characterization of Disease

DWI has been successfully applied in the gastrointestinal tract for detection of malignant lesions as well as bowel inflammation. The speed of *k*-space acquisition with the SS-EPI technique makes bowel peristalsis less of an issue compared with other MR sequences, in which shot-to-shot differences produce blurring of moving structures such as bowel.

DWI has been shown to be able to depict tumors in the esophagus, stomach, small bowel, and large bowel.^{15,72,79-84} High-*b* value diffusion-weighted images are the most effective in this regard as hypercellular tumors appear hyperintense, with corresponding low ADC values. It is particularly useful in regions where pseudothickening of bowel wall due to muscle contraction or benign inflammatory processes may mimic malignant neoplasms. For example, in the stomach, low ADC values have helped differentiate gastric wall thickening due to malignant disease from benign causes, such as gastritis and portal gastropathy.⁸⁰ In the ampullary region, DWI improves the diagnosis of ampullary carcinomas over

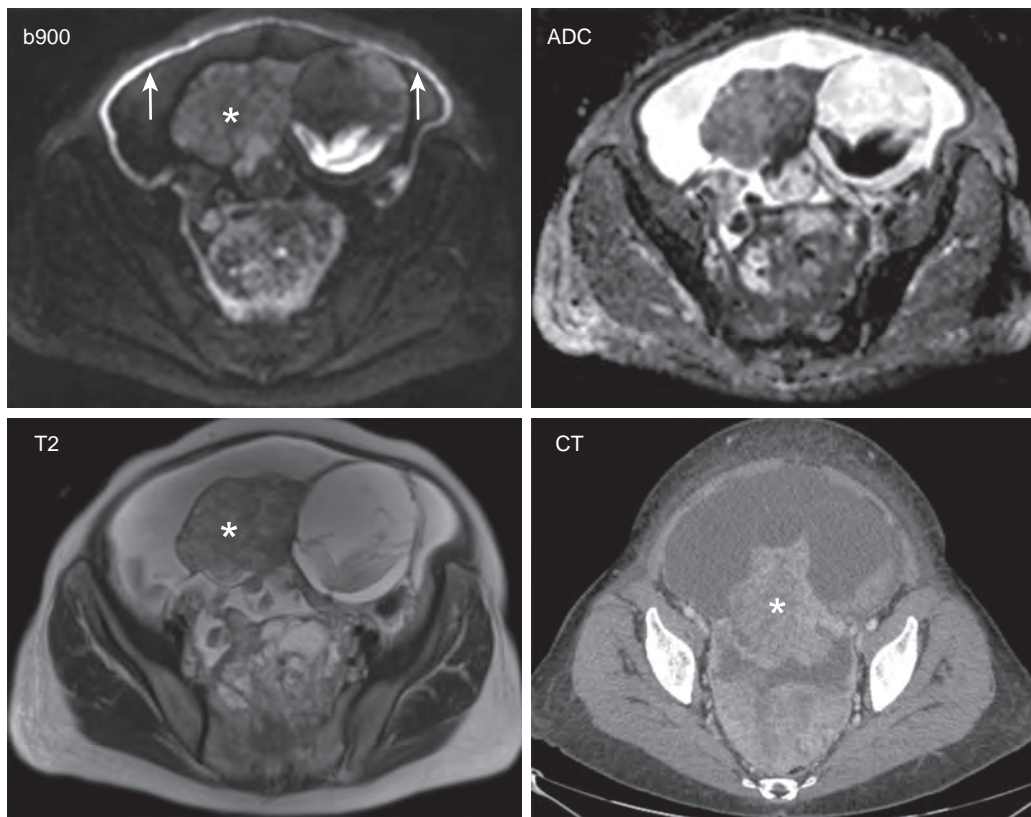


Figure 69-9 A 52-year-old woman with ovarian carcinoma and peritoneal carcinomatosis. The high- b value diffusion-weighted image (b900) shows excellent contrast between the hyperintense tumor coating the peritoneal lining (arrows) and ascites in the pelvis, which is almost completely attenuated in signal. The large primary ovarian mass (*) is also seen on the b900 image. In comparison, the true extent of peritoneal disease is easily underestimated on morphologic T2-weighted and computed tomography (CT) images. ADC, Apparent diffusion coefficient.

conventional MR sequences as it is able to differentiate malignant from benign papillary lesions, such as papillary stenosis and papillitis.⁸¹

A few caveats regarding the use of DWI in the gastrointestinal tract are worth noting. Early tumors (T1 and T2) are generally difficult to detect. In the esophagus, there is particularly poor sensitivity of DWI for detection of primary tumors (49% in one series⁷²). This has been attributed to signal loss from adjacent “incoherent” cardiac motion. Another problem is the hyperintensity of viscous bowel content, which may mask underlying mucosal lesions. Gaseous contents within bowel can also cause susceptibility artifacts that can obscure pathologic changes or produce spurious signals. Last, the ability of DWI to detect premalignant lesions, such as small polyps, has thus far been disappointing.⁸³ This may be related to current technical limitations with DWI resolution as well as the tissue architecture of adenomas, which may be less cellular than their malignant counterparts.

Assessment of Treatment Response and Disease Recurrence

In rectal cancer, MRI performed after neoadjuvant chemoradiotherapy can be challenging to interpret with morphologic sequences (T2-weighted imaging) because it is frequently difficult to differentiate between post-treatment fibrosis and residual tumor. The addition of DWI to T2-weighted imaging has been shown to be invaluable in post-treatment imaging as residual tumor will be expected to show impeded diffusion, whereas fibrosis is relatively hypointense on high- b value images. DWI has been shown to improve diagnostic performance in the prediction of tumor clearance in the mesorectal fascia,⁸⁵ assessment

of complete pathologic response,⁸⁶ and detection of areas of viable tumor⁸⁷ (Fig. 69-10).

ADC as a Prognostic Biomarker

To date, the value of ADC as a prognostic quantitative biomarker in patients with rectal cancer is unclear. In one series, lower tumor ADC values were found to correlate with involvement of the mesorectal fascia, higher nodal stage, and poorer histologic differentiation of the neoplasm.⁸⁸ Studies investigating the role of pretreatment tumor ADC as a prognostic factor in terms of prediction of response to chemoradiation have generally shown that tumors with lower ADC values respond more favorably.^{18,89} A possible hypothesis for this is that nonresponding tumors have higher ADC values due to internal necrosis and are therefore hypoxic and poorly perfused, resulting in a poor response to chemotherapy.

Utility in Nononcologic Bowel Disease

DWI has also been successfully applied to the imaging of inflammatory bowel disease. DWI hyperintensity is associated with active inflammation in ulcerative colitis and Crohn's disease.^{90,91} The sequence facilitates detection of complications, such as abscesses, fistulas, and stenotic segments,⁹² and provides sensitivity comparable to that of contrast-enhanced MRI. Impeded diffusion in inflamed bowel may result from reduced extracellular space secondary to cell swelling or increased cell density caused by migration of lymphocytes into the bowel wall. The absence of need for ionizing radiation, intravenous contrast administration, and bowel preparation are major advantages of DWI in regular imaging follow-up for this patient population.

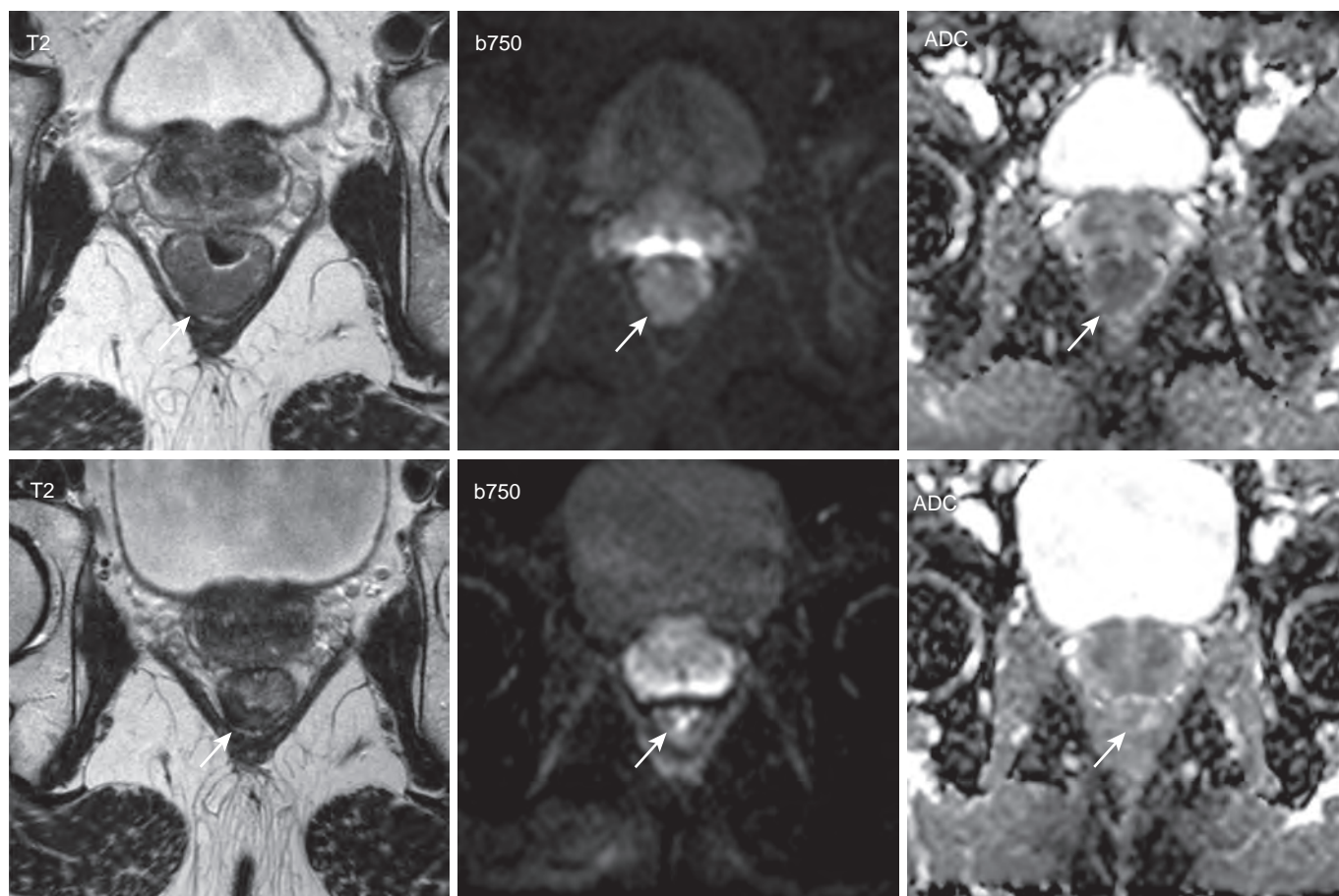


Figure 69-10 Changes in diffusion-weighted imaging in response to treatment. *Top panel,* Pretreatment appearance of the distal rectal adenocarcinoma (arrow). The primary tumor is hyperintense on diffusion-weighted imaging (b750) and hypointense on the apparent diffusion coefficient (ADC) map, indicating restricted diffusion. *Bottom panel,* Appearance 3 months after chemoradiotherapy. The tumor shows marked hypointensity on the T2-weighted image, indicating fibrosis. The mass is isointense to the surrounding rectal wall on diffusion-weighted images, as would be expected for response due to loss of cellularity.

Low- b value imaging may be used to study alterations in bowel peristalsis, such as in the diagnosis of bowel strangulation.⁹³ In normal bowel showing motility, the turbulent flow of the intraluminal contents results in suppression of their signal at low- b value DWI. In contrast, strangulated bowel segments have severely impaired or absent peristalsis, resulting in relative preservation of signal of their contents.

Future Directions

In the past decade, DWI has been rapidly adopted for the evaluation of abdominal disease. It is a powerful qualitative tool, but the use of quantitative ADC values for disease characterization and tumor response assessment is not fully realized.²⁷

The pathway to technical optimization and standardization has seen developments broadly along two ideologies. One school of thought suggests that all technical details should be strictly prescribed, including all the b values, and implemented rigorously across all scanners. Another school of thought reasons that it may be sufficient to recommend a range and number of b values to be used for the DWI measurements, taking into account the tumor ADC values that are likely to be encountered. The former approach may find difficulties in implementing exactly the same imaging protocol across

different MR systems; these MR systems have different gradient performance, which would affect the choice of scan settings and hence the ADC results. The latter approach may be more practical but may introduce more ADC variability across centers. At the moment, it is probably reasonable that both approaches be pursued to allow us to have a sense of the “best case” versus “worst case” ADC variability that may be encountered in a multicenter setting with these approaches so that an informed decision can be made as to how prescriptive the choice of scan parameters should be to ensure practical comparison across a range of imaging departments.

For ADC data analysis, it is recognized that the summary values of mean or median ADC values may not adequately reflect lesion heterogeneity. New approaches, such as volumetric or histogram ADC analysis, are also being tested that may allow robust comparison of data.^{94,95} However, such complex methods of diffusion-weighted MRI data analysis are not currently available on commercial MRI platforms.

Last but not least, whereas diffusion-weighted MRI has high diagnostic accuracy and utility on its own, it may be combined with other functional MRI techniques, such as dynamic contrast-enhanced MR imaging, MR elastography, or MR spectroscopy. This multi-parametric imaging paradigm has been adopted for prostate imaging and shown to improve diagnostic

performance,⁹⁶ and it would be exciting to see more applications and research developed in the abdomen to further enhance disease assessment.

Summary

Diffusion-weighted MRI provides a unique and effective contrast mechanism for detection and characterization of

abdominal disease that is easily incorporated into standard abdominal imaging protocols.⁹⁷ Optimization of acquisition technique and understanding of its limitations and pitfalls are critical in successful implementation of DWI in clinical practice. Diffusion-weighted images should always be interpreted in the appropriate clinical context and in combination with conventional MR images. It has great potential as a quantitative biomarker, and future developments should consolidate that role.

REFERENCES

- Koh DM, Collins DJ: Diffusion-weighted MRI in the body: Applications and challenges in oncology. *AJR Am J Roentgenol* 188:1622–1635, 2007.
- Stejskal EO, Tanner JE: Spin diffusion measurements: Spin echoes in the presence of a time-dependent field gradient. *J Chem Phys* 42:288–292, 1965.
- Le Bihan D, Breton E, Lallemand D, et al: Separation of diffusion and perfusion in intravoxel incoherent motion MR imaging. *Radiology* 168:497–505, 1988.
- Koh DM, Collins DJ, Orton MR: Intravoxel incoherent motion in body diffusion-weighted MRI: Reality and challenges. *AJR Am J Roentgenol* 196:1351–1361, 2011.
- Tsao J: Ultrafast imaging: Principles, pitfalls, solutions, and applications. *J Magn Reson Imaging* 32:252–266, 2010.
- Koh DM, Takahara T, Imai Y, Collins DJ: Practical aspects of assessing tumors using clinical diffusion-weighted imaging in the body. *Magn Reson Med* 62:11–224, 2007.
- Taouli B, Sandberg A, Stemmer A, et al: Diffusion-weighted imaging of the liver: Comparison of navigator triggered and breathhold acquisitions. *J Magn Reson Imaging* 30:561–568, 2009.
- Dyvorne HA, Galea N, Nevers T, et al: Diffusion-weighted imaging of the liver with multiple b values: Effect of diffusion gradient polarity and breathing acquisition on image quality and intravoxel incoherent motion parameters—a pilot study. *Radiology* 266:920–929, 2013.
- Kwee TC, Takahara T, Koh DM, et al: Comparison and reproducibility of ADC measurements in breathhold, respiratory triggered, and free-breathing diffusion-weighted MR imaging of the liver. *J Magn Reson Imaging* 28:1141–1148, 2008.
- Nasu K, Kuroki Y, Fujii H, Minami M: Hepatic pseudo-anisotropy: A specific artifact in hepatic diffusion-weighted images obtained with respiratory triggering. *MAGMA* 20:205–211, 2007.
- Kwee TC, Takahara T, Niwa T, et al: Influence of cardiac motion on diffusion-weighted magnetic resonance imaging of the liver. *MAGMA* 22:319–325, 2009.
- Liau J, Lee J, Schroeder ME, et al: Cardiac motion in diffusion-weighted MRI of the liver: Artifact and a method of correction. *J Magn Reson Imaging* 35:318–327, 2012.
- Takahara T, Kwee TC: Low b-value diffusion-weighted imaging: Emerging applications in the body. *J Magn Reson Imaging* 35:1266–1273, 2012.
- Penner A-H, Sprinkart AM, Kukuk GM, et al: Intravoxel incoherent motion model-based liver lesion characterisation from three b-value diffusion-weighted MRI. *Eur Radiol* 23:2773–2783, 2013.
- Hosonuma T, Tozaki M, Ichiba N, et al: Clinical usefulness of diffusion-weighted imaging using low and high b-values to detect rectal cancer. *Magn Reson Med* 5:173–177, 2006.
- Koh DM, Blackledge M, Padhani AR, et al: Whole-body diffusion-weighted MRI: Tips, tricks, and pitfalls. *AJR Am J Roentgenol* 199:252–262, 2012.
- Yoshikawa T, Kawamitsu H, Mitchell DG, et al: ADC measurement of abdominal organs and lesions using parallel imaging technique. *AJR Am J Roentgenol* 187:1521–1530, 2006.
- Sun Y-S, Zhang X-P, Tang L, et al: Locally advanced rectal carcinoma treated with preoperative chemotherapy and radiation therapy: Preliminary analysis of diffusion-weighted MR imaging for early detection of tumor histopathologic downstaging. *Radiology* 254:170–178, 2010.
- Pickles MD, Gibbs P, Lowry M, Turnbull LW: Diffusion changes precede size reduction in neoadjuvant treatment of breast cancer. *Magn Reson Imaging* 24:843–847, 2006.
- Kim HS, Kim CK, Park BK, et al: Evaluation of therapeutic response to concurrent chemoradiotherapy in patients with cervical cancer using diffusion-weighted MR imaging. *J Magn Reson Imaging* 37:187–193, 2013.
- Nilsen L, Fangberget A, Geier O, et al: Diffusion-weighted magnetic resonance imaging for pre-treatment prediction and monitoring of treatment response of patients with locally advanced breast cancer undergoing neoadjuvant chemotherapy. *Acta Oncol* 49:354–360, 2010.
- Kamel IR, Reyes DK, Liapi E, et al: Functional MR imaging assessment of tumor response after ⁹⁰Y microsphere treatment in patients with unresectable hepatocellular carcinoma. *J Vasc Interv Radiol* 18(Pt 1):49–56, 2007.
- Song I, Kim CK, Park BK, Park W: Assessment of response to radiotherapy for prostate cancer: Value of diffusion-weighted MRI at 3 T. *AJR Am J Roentgenol* 194:W477–W482, 2010.
- Hiwatashi A, Kinoshita T, Moritani T, et al: Hypointensity on diffusion-weighted MRI of the brain related to T2 shortening and susceptibility effects. *AJR Am J Roentgenol* 181:1705–1709, 2003.
- Chandarana H, Do RKG, Mussi TC, et al: The effect of liver iron deposition on hepatic apparent diffusion coefficient values in cirrhosis. *AJR Am J Roentgenol* 199:803–808, 2012.
- Corona-Villalobos CP, Pan L, Halappa VG, et al: Agreement and reproducibility of apparent diffusion coefficient measurements of dual-b-value and multi-b-value diffusion-weighted magnetic resonance imaging at 1.5 Tesla in phantom and in soft tissues of the abdomen. *J Comput Assist Tomogr* 37:46–51, 2013.
- Padhani AR, Liu G, Koh DM, et al: Diffusion-weighted magnetic resonance imaging as a cancer biomarker: Consensus and recommendations. *Neoplasia* 11:102–125, 2009.
- Lambrechts DMJ, Beets GL, Maas M, et al: Tumour ADC measurements in rectal cancer: Effect of ROI methods on ADC values and interobserver variability. *Eur Radiol* 21:2567–2574, 2011.
- d'Assignies G, Fina P, Bruno O, et al: High sensitivity of diffusion-weighted MR imaging for the detection of liver metastases from neuroendocrine tumors: Comparison with T2-weighted and dynamic gadolinium-enhanced MR imaging. *Radiology* 268:390–399, 2013.
- Parikh T, Drew SJ, Lee VS, et al: Focal liver lesion detection and characterization with diffusion-weighted MR imaging: Comparison with standard breath-hold T2-weighted imaging. *Radiology* 246:812–822, 2008.
- Bruegel M, Gaa J, Waldt S, et al: Diagnosis of hepatic metastasis: Comparison of respiration-triggered diffusion-weighted echo-planar MRI and five T2-weighted turbo spin-echo sequences. *AJR Am J Roentgenol* 191:1421–1429, 2008.
- Hardie AD, Naik M, Hecht EM, et al: Diagnosis of liver metastases: Value of diffusion-weighted MRI compared with gadolinium-enhanced MRI. *Eur Radiol* 20:1431–1441, 2010.
- Koh DM, Brown G, Riddell AM, et al: Detection of colorectal hepatic metastases using MnDPDP MR imaging and diffusion-weighted imaging (DWI) alone and in combination. *Eur Radiol* 18:903–910, 2008.
- Low RN, Gurney J: Diffusion-weighted MRI (DWI) in the oncology patient: Value of breath-hold DWI compared to unenhanced and gadolinium-enhanced MRI. *J Magn Reson Imaging* 25:848–858, 2007.
- Koh DM, Collins DJ, Wallace T, et al: Combining diffusion-weighted MRI with Gd-EOB-DTPA-enhanced MRI improves the detection of colorectal liver metastases. *Br J Radiol* 85:980–989, 2012.
- Wu L-M, Xu J-R, Lu Q, et al: A pooled analysis of diffusion-weighted imaging in the diagnosis of hepatocellular carcinoma in chronic liver diseases. *J Gastroenterol Hepatol* 28:227–234, 2013.
- Park M-S, Kim S, Patel J, et al: Hepatocellular carcinoma: Detection with diffusion-weighted versus contrast-enhanced magnetic resonance imaging in pretransplant patients. *Hepatology* 56:140–148, 2012.
- Kim AY, Kim YK, Lee MW, et al: Detection of hepatocellular carcinoma in gadoteric acid-enhanced MRI and diffusion-weighted MRI with respect to the severity of liver cirrhosis. *Acta Radiol* 53:830–838, 2012.
- Nasu K, Kuroki Y, Tsukamoto T, et al: Diffusion-weighted imaging of surgically resected hepatocellular carcinoma: Imaging characteristics and relationship among signal intensity, apparent

- diffusion coefficient, and histopathologic grade. *AJR Am J Roentgenol* 193:438–444, 2009.
40. Park MJ, Kim YK, Lee MH, Lee JHWJ: Validation of diagnostic criteria using gadoxetic acid-enhanced and diffusion-weighted MRI imaging for small hepatocellular carcinoma (≤ 2.0 cm) in patients with hepatitis-induced liver cirrhosis. *Acta Radiol* 54:127–136, 2013.
 41. Miller FH, Hammond N, Siddiqi AJ, et al: Utility of diffusion-weighted MRI in distinguishing benign and malignant hepatic lesions. *J Magn Reson Imaging* 32:138–147, 2010.
 42. Cieszanowski A, Anysz-Grodzicka A, Szeszkowski W, et al: Characterization of focal liver lesions using quantitative techniques: Comparison of apparent diffusion coefficient values and T2 relaxation times. *Eur Radiol* 22:2514–2524, 2012.
 43. Chan JH, Tsui EY, Luk SH, et al: Diffusion-weighted MR imaging of the liver: Distinguishing hepatic abscess from cystic or necrotic tumor. *Abdom Imaging* 26:161–165, 2001.
 44. Holzapfel K, Rummeny E, Gaa J: Diffusion-weighted MR imaging of hepatic abscesses: Possibility of different apparent diffusion coefficient (ADC)—values in early and mature abscess formation. *Abdom Imaging* 32:538–539, 2007.
 45. Cui Y, Zhang X-P, Sun Y-S, et al: Apparent diffusion coefficient: Potential imaging biomarker for prediction and early detection of response to chemotherapy in hepatic metastases. *Radiology* 248:894–900, 2008.
 46. Chen C-Y, Li C-W, Kuo Y-T, et al: Early response of hepatocellular carcinoma to transcatheter arterial chemoembolization: Choline levels and MR diffusion constants—initial experience. *Radiology* 239:448–456, 2006.
 47. Kamel IR, Bluemke DA, Ramsey D, et al: Role of diffusion-weighted imaging in estimating tumor necrosis after chemoembolization of hepatocellular carcinoma. *AJR Am J Roentgenol* 181:708–710, 2003.
 48. Koh DM, Scurr E, Collins D, et al: Predicting response of colorectal hepatic metastasis: Value of pretreatment apparent diffusion coefficients. *AJR Am J Roentgenol* 188:1001–1008, 2007.
 49. Bakan AA, Inci E, Bakan S, et al: Utility of diffusion-weighted imaging in the evaluation of liver fibrosis. *Eur Radiol* 22:682–687, 2012.
 50. Sandrasegaran K, Akisik FM, Lin C, et al: Value of diffusion-weighted MRI for assessing liver fibrosis and cirrhosis. *AJR Am J Roentgenol* 193:1556–1560, 2009.
 51. Soyulu A, Kilickesmez O, Poturoğlu S, et al: Utility of diffusion-weighted MRI for assessing liver fibrosis in patients with chronic active hepatitis. *Diagn Interv Radiol* 16:204–208, 2010.
 52. Luciani A, Vignaud A, Cavet M, et al: Liver cirrhosis: Intravoxel incoherent motion MR imaging—pilot study. *Radiology* 249:891–899, 2008.
 53. Chow AM, Gao DS, Fan SJ, et al: Liver fibrosis: An intravoxel incoherent motion (IVIM) study. *J Magn Reson Imaging* 36:159–167, 2012.
 54. Wiggermann P, Grützmann R, Weissenböck A, et al: Apparent diffusion coefficient measurements of the pancreas, pancreas carcinoma, and mass-forming focal pancreatitis. *Acta Radiol* 53:135–139, 2012.
 55. Fukukura Y, Takumi K, Kamimura K, et al: Pancreatic adenocarcinoma: Variability of diffusion-weighted MR imaging findings. *Radiology* 263:732–740, 2012.
 56. Hur BY, Lee JM, Lee JE, et al: Magnetic resonance imaging findings of the mass-forming type of autoimmune pancreatitis: Comparison with pancreatic adenocarcinoma. *J Magn Reson Imaging* 36:188–197, 2012.
 57. Thomas S, Kayhan A, Lakadamyali H, Oto A: Diffusion MRI of acute pancreatitis and comparison with normal individuals using ADC values. *Emerg Radiol* 19:5–9, 2012.
 58. Lemke A, Laun FB, Klauss M, et al: Differentiation of pancreas carcinoma from healthy pancreatic tissue using multiple b-values: Comparison of apparent diffusion coefficient and intravoxel incoherent motion derived parameters. *Invest Radiol* 44:769–775, 2009.
 59. Graf M, Simon D, Lemke A, et al: Toward a non-invasive screening tool for differentiation of pancreatic lesions based on intra-voxel incoherent motion derived parameters. *Z Med Phys* 23:46–55, 2013.
 60. Sandrasegaran K, Akisik FM, Patel AA, et al: Diffusion-weighted imaging in characterization of cystic pancreatic lesions. *Clin Radiol* 66:808–814, 2011.
 61. Kim SJ, Lee JM, Kim H, et al: Role of diffusion-weighted magnetic resonance imaging in the diagnosis of gallbladder cancer. *J Magn Reson Imaging* 38:127–137, 2013.
 62. Ogawa T, Horaguchi J, Fujita N, et al: High b-value diffusion-weighted magnetic resonance imaging for gallbladder lesions: Differentiation between benignity and malignancy. *J Gastroenterol* 47:1352–1360, 2012.
 63. Irie H, Kamochi N, Nojiri J, et al: High b-value diffusion-weighted MRI in differentiation between benign and malignant polypoid gallbladder lesions. *Acta Radiol* 52:236–240, 2011.
 64. Kang TW, Kim SH, Park HJ, et al: Differentiating xanthogranulomatous cholecystitis from wall-thickening type of gallbladder cancer: Added value of diffusion-weighted MRI. *Clin Radiol* 68:992–1001, 2013.
 65. Do RKG, Chandarana H, Chandarana H, et al: Diagnosis of liver fibrosis and cirrhosis with diffusion-weighted imaging: Value of normalized apparent diffusion coefficient using the spleen as reference organ. *AJR Am J Roentgenol* 195:671–676, 2010.
 66. Klasen J, Lanzman RS, Wittsack H-J, et al: Diffusion-weighted imaging (DWI) of the spleen in patients with liver cirrhosis and portal hypertension. *Magn Reson Imaging* 31:1092–1096, 2013.
 67. Cece H, Ercan A, Yildiz S, et al: The use of DWI to assess spleen and liver quantitative ADC changes in the detection of liver fibrosis stages in chronic viral hepatitis. *Eur J Radiol* 82:e307–e312, 2013.
 68. Cheng J, Wang Y, Deng J, et al: Discrimination of metastatic lymph nodes in patients with gastric carcinoma using diffusion-weighted imaging. *J Magn Reson Imaging* 37:1436–1444, 2013.
 69. Beer AJ, Eiber M, Souvatzoglou M, et al: Restricted water diffusibility as measured by diffusion-weighted MR imaging and choline uptake in ^{11}C -choline PET/CT are correlated in pelvic lymph nodes in patients with prostate cancer. *Mol Imaging Biol* 13:352–361, 2011.
 70. Yasui O, Sato M, Kamada A: Diffusion-weighted imaging in the detection of lymph node metastasis in colorectal cancer. *Tohoku J Exp Med* 218:177–183, 2009.
 71. Akduman EI, Momtahan AJ, Balci NC, et al: Comparison between malignant and benign abdominal lymph nodes on diffusion-weighted imaging. *Acad Radiol* 15:641–646, 2008.
 72. Sakurada A, Takahara T, Kwee TC, et al: Diagnostic performance of diffusion-weighted magnetic resonance imaging in esophageal cancer. *Eur Radiol* 19:1461–1469, 2009.
 73. Lambregts DMJ, Maas M, Riedl RG, et al: Value of ADC measurements for nodal staging after chemoradiation in locally advanced rectal cancer—a per lesion validation study. *Eur Radiol* 21:265–273, 2011.
 74. Thoeny HC, Triantafyllou M, Birkhaeuser FD, et al: Combined ultrasmall superparamagnetic particles of iron oxide-enhanced and diffusion-weighted magnetic resonance imaging reliably detect pelvic lymph node metastases in normal-sized nodes of bladder and prostate cancer patients. *Eur Urol* 55:761–769, 2009.
 75. Bozkurt M, Doganay S, Kantarci M, et al: Comparison of peritoneal tumor imaging using conventional MR imaging and diffusion-weighted MR imaging with different b values. *Eur J Radiol* 80:224–228, 2011.
 76. Low RN, Sebrechts CP, Barone RM, Muller W: Diffusion-weighted MRI of peritoneal tumors: Comparison with conventional MRI and surgical and histopathologic findings—a feasibility study. *AJR Am J Roentgenol* 193:461–470, 2009.
 77. Satoh Y, Ichikawa T, Motosugi U, et al: Diagnosis of peritoneal dissemination: Comparison of ^{18}F -FDG PET/CT, diffusion-weighted MRI, and contrast-enhanced MDCT. *AJR Am J Roentgenol* 196:447–453, 2011.
 78. Low RN, Barone RM: Combined diffusion-weighted and gadolinium-enhanced MRI can accurately predict the peritoneal cancer index preoperatively in patients being considered for cytoreductive surgical procedures. *Ann Surg Oncol* 19:1394–1401, 2012.
 79. Avcu S, Arslan H, Unal O, et al: The role of diffusion-weighted MR imaging and ADC values in the diagnosis of gastric tumors. *JBR-BTR* 95:1–5, 2012.
 80. Onur MR, Ozturk F, Aygun C, et al: Role of the apparent diffusion coefficient in the differential diagnosis of gastric wall thickening. *J Magn Reson Imaging* 36:672–677, 2012.
 81. Jang KM, Kim SH, Lee SJ, et al: Added value of diffusion-weighted MR imaging in the diagnosis of ampullary carcinoma. *Radiology* 266:491–501, 2013.
 82. Kilickesmez O, Atilla S, Soyulu A, et al: Diffusion-weighted imaging of the rectosigmoid colon: Preliminary findings. *J Comput Assist Tomogr* 33:863–866, 2009.
 83. Leufkens AM, Kwee TC, van den Bosch MAAJ, et al: Diffusion-weighted MRI for the detection of colorectal polyps: Feasibility study. *Magn Reson Imaging* 31:28–35, 2013.
 84. Ichikawa T: High-b-value diffusion-weighted MRI in colorectal cancer. *AJR Am J Roentgenol* 187:181–184, 2006.
 85. Curvo-Semedo L, Lambregts DMJ, Maas M, et al: Rectal cancer: Assessment of complete response to preoperative combined radiation therapy with chemotherapy—conventional MR volumetry versus diffusion-weighted MR imaging. *Radiology* 260:734–743, 2011.
 86. Lambregts DMJ, Vandecaveye V, Barbaro B, et al: Diffusion-weighted MRI for selection of complete responders after chemoradiation for locally advanced rectal cancer: A multicenter study. *Ann Surg Oncol* 18:2224–2231, 2011.
 87. Song I, Kim SH, Lee SJ, et al: Value of diffusion-weighted imaging in the detection of viable tumour after neoadjuvant chemoradiation therapy in patients with locally advanced rectal cancer: Comparison with T2 weighted and PET/CT imaging. *Br J Radiol* 85:577–586, 2012.

88. Curvo-Semedo L, Lambregts DMJ, Maas M, et al: Diffusion-weighted MRI in rectal cancer: Apparent diffusion coefficient as a potential noninvasive marker of tumor aggressiveness. *J Magn Reson Imaging* 35:1365–1371, 2012.
89. Dzik-Jurasz A, Domenig C, George M, et al: Diffusion MRI for prediction of response of rectal cancer to chemoradiation. *Lancet* 360:307–308, 2002.
90. Oussalah A, Laurent V, Bruot O, et al: Diffusion-weighted magnetic resonance without bowel preparation for detecting colonic inflammation in inflammatory bowel disease. *Gut* 59:1056–1065, 2010.
91. Kiryu S, Dodanuki K, Takao H, et al: Free-breathing diffusion-weighted imaging for the assessment of inflammatory activity in Crohn's disease. *J Magn Reson Imaging* 29:880–886, 2009.
92. Neubauer H, Pabst T, Dick A, et al: Small-bowel MRI in children and young adults with Crohn disease: Retrospective head-to-head comparison of contrast-enhanced and diffusion-weighted MRI. *Pediatr Radiol* 43:103–114, 2013.
93. Takahara T, Kwee TC, Sadahiro S, et al: Low b-value diffusion-weighted imaging for diagnosing strangulated small bowel obstruction: A feasibility study. *J Magn Reson Imaging* 34:1117–1124, 2011.
94. Downey K, Riches SF, Morgan VA, et al: Relationship between imaging biomarkers of stage I cervical cancer and poor-prognosis histologic features: Quantitative histogram analysis of diffusion-weighted MR images. *AJR Am J Roentgenol* 200:314–320, 2013.
95. Gowdra Halappa V, Corona-Villalobos CP, Bonekamp S, et al: Neuroendocrine liver metastasis treated by using intraarterial therapy: Volumetric functional imaging biomarkers of early tumor response and survival. *Radiology* 266:502–513, 2013.
96. Hoeks CMA, Barentsz JO, Hambrock T, et al: Prostate cancer: Multiparametric MR imaging for detection, localization, and staging. *Radiology* 261:46–66, 2011.
97. Tsien C, Cao Y, Chenevert T: Clinical applications for diffusion magnetic resonance imaging in radiotherapy. *Semin Radiat Oncol* 24:218–226, 2014.

Perfusion Computed Tomography and Magnetic Resonance Imaging in the Abdomen and Pelvis

SURABHI BAJPAI | DUSHYANT V. SAHANI | AVINASH KAMBADAKONE

CHAPTER OUTLINE

Basic Principles

Perfusion Computed Tomography

Technical Principles

Protocol

Postprocessing

Clinical Applications

Perfusion Magnetic Resonance Imaging

Technical Principles

Protocol

Data Analysis

Clinical Applications

Summary

Perfusion imaging is an exciting new radiologic investigation that allows functional evaluation of tissue vascularity by measuring the changes in the tissue characteristics after administration of intravenous contrast medium (IVCM). Rapid technologic advancements in both computed tomography (CT) and magnetic resonance imaging (MRI) coupled with innovations in postprocessing capabilities have widened the scope of perfusion imaging in a wide range of research and clinical applications.¹⁻¹⁰

Early in its development, perfusion imaging demonstrated significant applications in the evaluation of stroke patients because of its ability to accurately depict the structural and functional status of cerebral vasculature.¹¹⁻¹³ With improved understanding of the tissue vascular physiology, perfusion imaging has been used extensively in various other body applications. In an oncologic setting, perfusion imaging plays a key role not only in the diagnosis and staging of malignant neoplasms but also in prognostic evaluation and monitoring of treatment response in various cancers.^{3,6,9,10,14-27} In addition, the ability of perfusion imaging to evaluate tumor biology and function has a promising role in providing early surrogate biomarkers for treatment response, thereby facilitating customized patient therapeutic options. In this chapter, we review the basic principles of perfusion CT and MRI and discuss their clinical applications in the management of diseases of the abdomen and pelvis.

Basic Principles

Perfusion imaging, either CT or MRI, essentially involves sequential acquisition of images through a particular tissue in

question after the administration of IVCM.^{7,8,22,28,29} After intravenous administration, the contrast medium travels through the vascular system, leaks from the tissue vasculature, accumulates in the tissue, and then diffuses back into the vascular system before being ultimately eliminated through the urinary system.^{7,8,22,28,29} By measurement of the changes in tissue density or signal intensity during the movement of contrast material with sequential images, perfusion CT or MRI is able to estimate various semiquantitative measurements of perfusion, which allows evaluation of the tissue vascularity.^{7,8,22,28,29} Objective measurement of tissue enhancement by placement of region of interest (ROI) over the tissue allows generation of graphs of tissue density or signal intensity versus time, which enables measurement of semiquantitative values.

Perfusion Computed Tomography

Perfusion CT provides estimation of tissue vascularity by measurement of the progressive changes in tissue density after injection of iodinated IVCM. This functional CT technique is usually performed for evaluation of tissue perfusion in day-to-day clinical practice because of its widespread availability and presence of better experience. The speed of image acquisition and round-the-clock accessibility are particularly valuable in a neurologic setting for the evaluation of stroke patients, in whom it allows institution of immediate therapeutic interventions.²¹ The simple linear relationship between iodine concentration and tissue density changes and the easy availability of commercial software for postprocessing render quantification of vascularity easier with CT.^{7,21,22,30} In addition, the routine use of multidetector CT (MDCT) for tumor diagnosis and response assessment makes perfusion CT a preferred choice in an oncologic setting because it allows easier integration into treatment protocols.²¹

TECHNICAL PRINCIPLES

The basic principle of CT perfusion is the depiction of temporal changes in tissue attenuation after intravenous administration of iodine-based contrast medium (Fig. 70-1).²⁹ Tissue enhancement, which refers to increase in tissue attenuation after administration of IVCM, is proportional to the iodine concentration of tissues. Dynamic CT acquisition after IVCM administration thereby allows assessment of tissue enhancement, which represents an indirect measure of tissue vascularity and vascular physiology.²⁹ Tissue enhancement after IVCM administration can be divided into two phases based on distribution characteristics of the contrast medium in the intravascular and extravascular compartments.^{8,29} The initial phase of enhancement or the first pass (usually lasting 30-60 seconds after influx of the

contrast medium) is mainly due to distribution of contrast medium within the intravascular space.^{8,29} In the second phase, tissue enhancement is secondary to distribution of contrast medium between both intravascular and extravascular compartments due to movement of contrast medium from the intravascular to the extravascular compartment across the capillaries.^{8,29} Accordingly, tissue enhancement in the first phase is determined primarily by tissue blood flow and blood volume, whereas capillary permeability to the IVC contributes to enhancement in the later phase.^{8,29} Semiquantitative assessment of tissue perfusion based on dynamic CT acquisition can be accomplished by analytical methods, and the two most commonly used analytical methods are deconvolution and compartmental analysis.^{8,21,22,31}

Both the deconvolution and compartmental modeling methods are broadly equivalent, with few differences in their theoretical assumptions and susceptibility to noise and motion.^{8,21,22,31} Compartmental analysis (single- and

double-compartment methods) is based on the assumption that the bolus of contrast material is retained within the organ of interest at the time of measurement, and this can at times result in underestimation of perfusion values in organs with rapid vascular transit.^{8,21,22,31} Compartmental analysis uses three sets of images for perfusion estimation, including the baseline image and images before and after the maximal rate of contrast enhancement, and is therefore not usually degraded by patient motion.^{8,21,22,31} However, the presence of higher image noise adversely affects perfusion value calculation for the compartmental model, and therefore a higher tube current with lower image frequency is preferred for the dynamic CT technique.^{8,21,22,31}

Deconvolution analysis is based on the use of arterial and tissue time-concentration curves to calculate tissue perfusion and relative blood volumes.^{8,22,32} Although this modeling technique works well for most organs, it might not be suitable for assessing perfusion in organs such as the spleen and kidney, which have complex microcirculations, for which compartmental analysis is preferred.^{8,22,32} Deconvolution methods are suitable for measuring lower perfusion values (<20 mL/min/100 mL); this method tolerates greater image noise because the complete time series of images is included for calculation.^{8,22,32} As a result, deconvolution analysis is particularly beneficial for monitoring treatment response because of its ability to accurately measure lower perfusion values typically seen after successful treatment. The inclusion of the complete series of images, however, renders this method susceptible to image misregistration from patient motion and therefore erroneous calculation.^{8,22,32} As the deconvolution method is less sensitive to noise, it allows use of a lower tube current and permits scanning with higher temporal resolution for dynamic cine CT acquisition.^{8,22,32} The various analytical methods, the acquisition protocols, and the software packages differ between scanner technologies and the commercial vendors (Table 70-1). Nevertheless, irrespective of the technology used, perfusion CT allows estimation of various qualitative and quantitative measures of tissue perfusion.^{8,22,32}

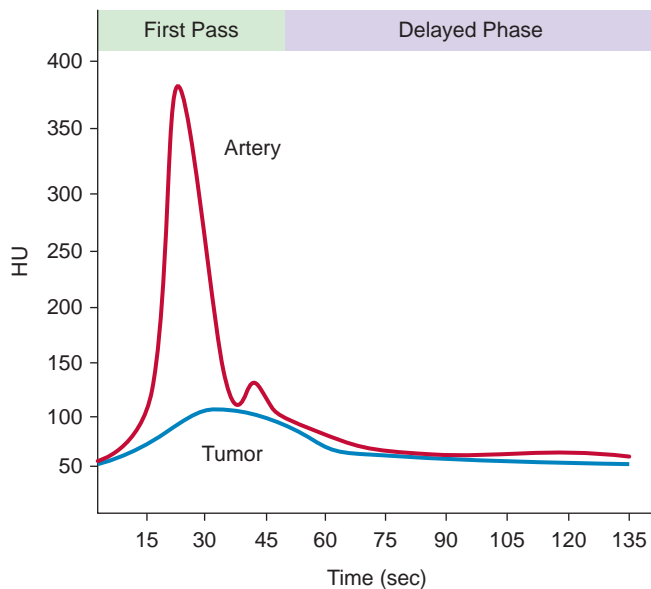


Figure 70-1 Time-attenuation curves showing enhancement characteristics of the artery and the tumor during the first pass and the delayed phase of the perfusion CT acquisition.

PROTOCOL

The perfusion CT protocol needs to be tailored to the clinical objective in question, body part being scanned, mathematical

TABLE 70-1 Comparison of Various CT Perfusion Analytical Models

Mathematical Model	Deconvolution Method	Two-Compartment Model	Slope Method
Vendors	GE Healthcare	Siemens	Philips, Toshiba, Siemens
Basic principle	Uses arterial and tissue time-concentration curves to estimate tissue perfusion	Based on Patlak analysis and assumes one-way transfer of contrast medium from IVS and EVS proportional to blood clearance constant	Perfusion is estimated as a maximum slope of tissue concentration curve normalized to maximum arterial enhancement
Parameters measured	BF, BV, MTT, PS	BV and permeability	BF, MTT, time to peak enhancement
Advantages	The perfusion parameters can be calculated by a single CT study	Simple analysis Efficient in calculation of rate constant value	Short scan duration Assumption of no venous outflow and no recirculation; less sensitive to movement
Limitations	Partial volume averaging correction required	Based on assumption that back-flux of contrast medium from EVS to IVS is negligible in the initial 1-2 minutes	Sensitive to image noise

Data from references 4, 5, 8, 17, 21, 29, 30, 70, and 71. Adapted from reference 21.

BF, Blood flow; BV, blood volume; EVS, extravascular space; IVS, intravascular space; MTT, mean transit time; PS, permeability–surface area product.

modeling technique employed, CT scan configuration, and radiation dose considerations.^{8,21,22,32,33} A typical dynamic CT protocol consists of a preliminary noncontrast scan followed by a dynamic acquisition performed after administration of IVCN. The noncontrast CT scan serves as a localizer for selecting the appropriate tissue area to be included in the dynamic CT acquisition. A 2- to 4-cm area of tumor tissue is routinely selected for dynamic scanning on the basis of the scanner configuration (16-slice or 64-slice CT scanner).²¹ With the introduction of 128-slice to 320-slice MDCT scanners, larger areas of tumor tissue (8-16 cm) can be interrogated for assessment of tissue perfusion.^{21,34} Several techniques have been introduced to allow perfusion imaging of a volume of tissue or entire organ, including axial shuttle mode (repeated axial scans at two adjacent table positions in a to-and-fro manner to double detector coverage) and helical shuttle mode (continuous bidirectional table movement with variable pitch).³⁴⁻³⁸

The dynamic CT acquisition consists of a first-pass phase, a delayed phase, or both, depending on the pertinent physiologic parameters that need to be analyzed and the tissue in question.²¹ The first-pass phase or the initial cine phase consists of CT images acquired for a total of 40 to 60 seconds after the injection of IVCN.^{8,29-31} For obtaining permeability measurements, a second delayed phase ranging from 2 to 10 minutes follows the first phase.^{8,29-31} In the first-pass phase, the MDCT images are acquired every 1 to 3 seconds; in the second phase, the images are acquired every 5 to 15 seconds.^{8,29-31} A key consideration for optimal evaluation of tissue perfusion is the IVCN bolus used for dynamic CT acquisition (Table 70-2). An additional consideration in dynamic CT evaluation of the upper abdomen

is the need for appropriate breath-holding instructions to patients to limit the potential deleterious effects of motion on estimated perfusion values.^{8,21,29-31} Some authors recommend use of motility-inhibiting agents, such as glucagon, to limit peristaltic movements of bowel during image acquisition.^{1,19-21,39}

POSTPROCESSING

The dynamic CT data obtained after a perfusion CT study are processed on dedicated workstations using specific vendor-based perfusion software.²¹ The postprocessing of the CT perfusion data generates colored parametric perfusion maps. Quantitative tissue perfusion measurements are then obtained from these perfusion maps by ROI placement over the tissue in question. The various quantitative perfusion parameters estimated depict various aspects of tissue or tumor vascular physiology²¹ (Table 70-3). With the increasing use of CT perfusion in various body applications, several non-vendor-based software models are available that allow estimation of tissue perfusion irrespective of the method of scanning.

CLINICAL APPLICATIONS

Perfusion CT has been established as a valuable technique for estimation of tissue vascularity. The validity and reproducibility of this functional CT technique have been proved in several animal and human studies and tested against other techniques, such as xenon washout methods.^{12,21,40-42} Early studies have demonstrated the value of this technique in quantifying tissue perfusion in solid visceral organs such as liver, pancreas, spleen, and kidney.* Ever since, perfusion CT has found a wide range of applications in oncology, such as determining tumor biology including lesion characterization, risk stratification and staging, monitoring response to various treatment regimens (chemoradiation and antiangiogenic drugs), and predicting treatment outcome.^{21,22,33,44} In addition to the overwhelming amount of research performed in oncology, this technique has also been explored in the assessment of tissue perfusion in various non-oncologic applications, such as in patients with cirrhosis and renal artery stenosis.

Tumor Biology

One of the key elements of tumor physiology that influences the aggressiveness of tumors and their response to treatment is

*References 9, 10, 15, 19-21, 24, 27, 43.

TABLE 70-2	Technical Parameters of a Typical CT Perfusion Protocol
Kilovoltage*	100-120
Milliamperes-seconds* (mAs)	50-150
Iodine concentration† (mg I/mL)	370-400
Contrast bolus (mL)	40-70
Injection rate‡ (mL/s)	4-10
Scan delay (s)	5-10

Data from references 8, 21, 29-31.
*Lower kilovoltage peak and milliamperes-seconds are recommended to reduce the radiation exposure.
†A higher iodine concentration of 370 mg I/mL is preferred because of the linear relationship between iodine concentration and tissue enhancement.
‡Higher injection rates are preferable to maximize tissue enhancement and to improve signal-to-noise ratio.

TABLE 70-3	Various CT Perfusion Parameter Terminologies for Description of Tissue Vascular Physiology		
Perfusion Parameter	Definition	Marker (in Oncology)	Units
Blood flow or perfusion (BF)	Flow rate through tissue vasculature in the region of interest	Tumor vascularity	mL per 100 g/min
Blood volume (BV)	Volume of blood flowing within the tissue vasculature in the region of interest	Tumor grade	mL per 100 g
Mean transit time (MTT)	Average time taken to travel from artery to vein	Tumor vascularity	Seconds
Permeability-surface area product (PS)	Total flux from plasma to interstitial space	Perfusion pressure	mL per 100 g/min
Time to peak (TTP)	Time from arrival of the contrast medium in major arterial vessels to the peak enhancement	Immature leaky vessels	Seconds
Peak enhancement intensity (PEI)	Maximum increase in tissue density after injection of contrast medium	Perfusion pressure	
		Tissue blood volume	HU

Data from references 4, 5, 8, 17, 21, 29, 30, 70, 71. Adapted from reference 21.

the status of tumor microvasculature (neoangiogenesis).^{*} Tumor angiogenesis refers to the development of new blood vessels in the tumor, resulting in vascularization.^{*} Histopathologic markers, such as tumor microvessel density count, are established markers of tumor angiogenesis. Despite the “gold standard” attributes of microvessel density, it is invasive to obtain tissue, often in regions that are difficult to approach, and fraught with sampling error. Moreover, it lacks the functional information about angiogenesis and is often impractical for monitoring of response at several time points. Because the perfusion profile of a lesion on dynamic contrast-enhanced CT (CECT) is a reflection of its underlying vascular signature, CT perfusion can be exploited to predict the status of tissue vascularity and therefore predict tumor biology.^{*} Several studies have demonstrated the role of perfusion CT in evaluating tumor biology, including lesion characterization and assessment of tumor grade.[†]

Several studies have shown significant differences in tissue perfusion values between normal tissue and benign and malignant tumors in the liver, pancreas, and colon.[‡] In general, malignant tumors demonstrate higher perfusion values (increased tumor perfusion and capillary permeability). In bowel, colorectal cancers demonstrate higher tumor perfusion compared with normal colonic wall.^{5,10,39} Higher tumor perfusion can also be used to differentiate between colonic wall thickening in diverticulitis and colorectal cancer.^{5,10,39} In the liver, perfusion CT allows an earlier detection of hepatic metastases because hepatic arterial perfusion in these patients is increased.⁴⁶⁻⁵⁰ The lesions are seen as an area with increased blood flow in comparison to the rest of the liver parenchyma. The baseline tumor perfusion in hepatic metastases can also be used to predict treatment outcome as metastatic lesions with higher perfusion have improved prognosis compared with those with lower perfusion.⁴⁶⁻⁵⁰ In patients with hepatocellular carcinoma (HCC), differentiation from background liver is possible because of the higher perfusion seen in HCC (higher blood flow, blood volume, and permeability–surface area product).^{9,24}

Perfusion CT also aids in evaluating tumor aggressiveness and helps differentiate between well-differentiated and moderately to poorly differentiated tumors.^{9,24} In the pancreas, dynamic CECT allows characterization of hypervascular pancreatic tumors, such as insulinoma, that show higher perfusion.^{15,51} The perfusion measurements of pancreatic neuroendocrine tumors also correlate with histoprosthetic factors.^{15,51} In the prostate, malignant foci have shown considerably increased perfusion values, and this potentially would allow identification of tumor foci, thus enabling targeted radiotherapy with minimal radiation to the surrounding tissues.⁵²

Risk Stratification and Staging

Tumor vascularity is a marker of tumor aggressiveness, and higher tumor vascularity is often indicative of aggressive biology and often associated with a poor outcome compared with less vascular tumors.^{21,33} By depicting the vascular signature of tumors, CT perfusion has been shown to be valuable in risk

stratification and tumor staging.^{21,33} Patients with metastatic renal cell carcinoma with higher baseline tumor perfusion have been shown to have a poor prognosis.⁵³ In patients with rectal cancer, dynamic CECT has been shown to be more accurate and specific than conventional CT in characterizing local invasion.⁵⁴ In HCC, baseline perfusion parameters have been shown to correlate with clinical outcome.^{9,27}

Even in nononcologic settings, perfusion CT has been shown to be helpful in risk stratification. In patients with cirrhosis, perfusion changes depicted on CT correlate well with the severity of chronic liver disease.^{55,56} In patients with acute pancreatitis, perfusion CT has been found to be sensitive for detection of pancreatic ischemia, which demonstrates reduced perfusion values compared with normal pancreas.²⁴ The identification of ischemic areas can help predict the later development of pancreatic necrosis, which has therapeutic implications because its early detection and identification will allow induction of intensive care for these patients at the earliest to prevent infective complications and to improve the prognosis.²⁴ In patients with mesenteric ischemia, dynamic CECT has the potential role of identifying bowel at risk of ischemic injury.

Monitoring Treatment Response

Novel antiangiogenic drugs target tumor neoangiogenesis, which is mediated by circulating factors, such as vascular endothelial growth factor, fibroblast growth factor, and platelet-derived endothelial cell growth factor.^{*} After successful response to therapy, there is a reduction in tumor perfusion, vascularity, and vascular permeability that precedes changes in tumor size.[†] Conventionally, therapeutic response to various treatment regimens has been monitored by serial assessment of tumor burden on CT or MRI according to criteria such as the Response Evaluation Criteria in Solid Tumors (RECIST) or World Health Organization criteria.^{2,44,58} However, these traditional methods of response assessment are not effective in demonstrating early changes after treatment with targeted therapies because the functional and perfusional changes precede morphologic changes.^{2,44,58} An ideal imaging marker for these therapies needs to be noninvasive, reproducible, readily available, and repeatable and should dynamically reflect the microcirculatory function in a living individual.^{2,44,58} Perfusion CT has particularly seen rising utility in monitoring treatment response in various cancers to a number of therapeutic regimens, including chemoradiation and novel antiangiogenic drugs. In addition to monitoring treatment response, dynamic CECT could be used to predict response and prognosis.

After a combined chemotherapy regimen of oxaliplatin and bevacizumab in HCC, CT perfusion demonstrated reduction in tumor vascularity that correlated with clinical response (Fig. 70-2).²⁷ In rectal cancer, after combined chemoradiation including antiangiogenic therapy, a consistent decrease in tumor perfusion (fall in blood flow and increase in mean transit time) was shown on CT (Fig. 70-3).^{10,25,45} There is also evidence that CT perfusion has shown reduction in tumor perfusion after antiangiogenic therapy in renal cell carcinoma and neuroendocrine tumors.^{59,60}

^{*}References 7, 21, 22, 30, 31, 33, 44.

[†]References 5, 9, 10, 15, 18, 24, 27, 33, 45.

[‡]References 5, 9, 10, 15, 18, 24, 27, 33, 45.

^{*}References 14, 21, 25, 33, 45, 57.

[†]References 2, 14, 21, 25, 33, 44, 45, 57.

Figure 70-2 CT perfusion images obtained before and after treatment with antiangiogenic agent in a 56-year-old man with hepatocellular carcinoma. Axial contrast-enhanced CT image in the dynamic phase (**A**) shows the avidly enhancing rounded hepatocellular carcinoma in the left lobe; corresponding colored perfusion map (**B**) demonstrates increased blood flow (102 mL/100 g/min). After antiangiogenic therapy, axial contrast-enhanced CT image (**C**) shows reduced enhancement; corresponding colored perfusion map (**D**) demonstrates reduction in the blood flow (15 mL/100 g/min).

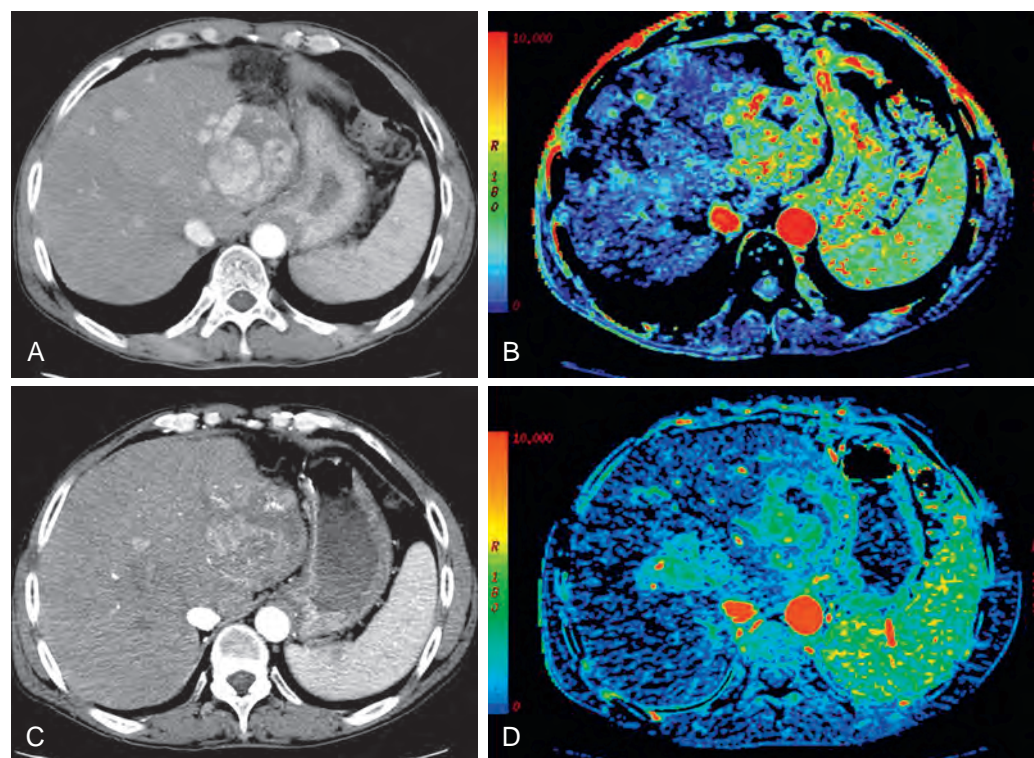
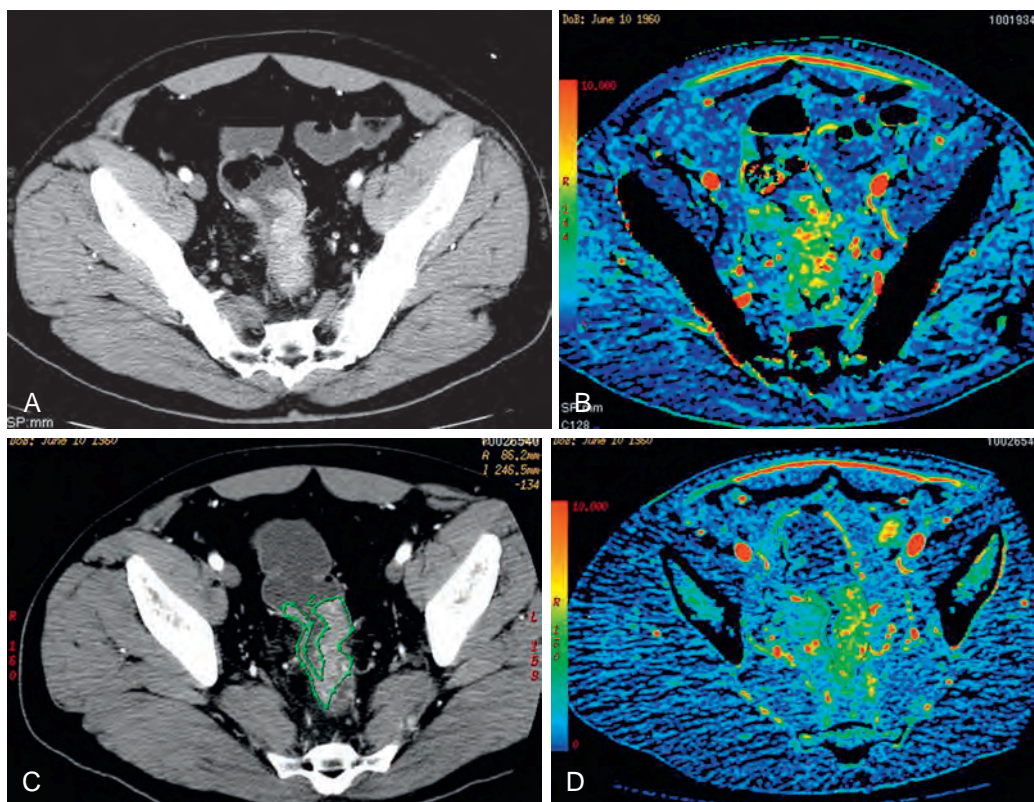


Figure 70-3 CT perfusion images obtained before and after treatment with antiangiogenic agent in a 72-year-old man with rectal cancer. Axial contrast-enhanced CT image in the dynamic phase (**A**) shows the avidly enhancing tumor in the rectum; corresponding colored perfusion map (**B**) demonstrates increased blood flow (78 mL/100 g/min). After treatment with bevacizumab, axial contrast-enhanced CT image (**C**) shows reduced enhancement; corresponding colored perfusion map (**D**) demonstrates reduction in the blood flow (20 mL/100 g/min).



Perfusion Magnetic Resonance Imaging

Perfusion MRI is a dynamic imaging technique that allows noninvasive characterization of tissue vasculature after the intravenous administration of a paramagnetic tracer.^{28,61-65} By quantifying the signal changes induced by the tracer in the tissue as a function of time, perfusion MRI allows evaluation of tumor perfusion and capillary permeability.^{28,61-65} Gadolinium-based contrast agents, such as gadopentetate dimeglumine, are frequently used because they have a sufficiently small molecular weight to allow visualization of lesion vasculature.^{28,61-65} Perfusion MRI has several advantages over perfusion CT, including lack of ionizing radiation, superior soft tissue contrast resolution, and improved coverage of anatomy. The additional advantage includes the capability of performing functional imaging techniques, such as diffusion-weighted imaging and magnetic resonance spectroscopy, which provide complementary information in evaluation of tumor physiology and in monitoring treatment response.

TECHNICAL PRINCIPLES

Perfusion MRI involves sequential acquisition of images during the passage of gadolinium-based contrast agents through the particular tissue of interest and measures variations in vessel and tissue enhancement over time.^{28,61-65} It depicts the signal changes induced by gadolinium as it moves through the tissue as a function of time.^{28,61-65} Perfusion MRI or dynamic contrast-enhanced MRI (DCE-MRI) is typically performed with T1-weighted imaging.^{28,61,65} In general, T2-weighted images are not useful because of loss of T2 weighting after extravasation of tracer into the interstitial space despite the strong T2 effects of intravascular tracers.⁶⁵ On the other hand, T1 weighting is not affected by tracer extravasation and therefore allows derivation of permeability measurements by analyzing the slow component of the signal.⁶⁵ For the same reason, the use of protein-bound gadolinium tracers must be avoided to allow permeability measurements.^{28,61,65}

PROTOCOL

The selection of the appropriate DCE-MRI technique should be tailored to the organ under investigation and involves selection of the appropriate MRI sequences, contrast agent, injection protocol, and robust postprocessing software.⁶⁵ Because of improved contrast-to-noise ratio, 3T scanners are generally preferred to 1.5T scanners for perfusion MRI.⁶⁵ A typical MRI perfusion sequence includes a precontrast T1-weighted image followed by a series of T1-weighted images after gadolinium administration.⁶⁵ Data acquisition is started 10 to 20 seconds before the bolus is injected to allow acquisition of a sufficient amount of precontrast data. A typical injection protocol includes injection of 0.1 mmol per kilogram of body weight of gadolinium-diethylenetriaminepentaacetic acid (Gd-DTPA).⁶⁵ The gadolinium agent is generally injected at a rate of 2 mL/s.^{65,66} The bolus of contrast material is flushed with 20 to 30 mL of saline at the same injection rate.^{65,66} The acquisition time is similar to that of CT perfusion; an acquisition time of 1 minute is usually adequate for perfusion measurements, with a longer time for permeability measurements, usually up to 5 minutes.⁶⁵ In tissues with slower enhancement,

longer acquisitions may be required.⁶⁵ A sampling interval of less than 2 seconds is usually recommended for measurement of perfusion because the tracer transit time in the capillary bed is usually in the range of 3 to 5 seconds.⁶⁵ An optimum balance of the sampling interval is necessary as slower sampling permits improved spatial resolution and signal-to-noise ratio.⁶⁵ Lower temporal resolution with longer sampling interval may be used for permeability measurements because the transit times in the extravascular space are longer on the order of minutes.⁶⁵

The DCE-MRI sequences are most commonly either two-dimensional or three-dimensional gradient-echo sequences.⁶⁵ The earliest perfusion MRI sequences had limited number of slices in the two-dimensional sequence because of the need to achieve higher temporal resolution.⁶⁵ However, with the introduction of parallel imaging and faster MRI sequences, three-dimensional gradient-echo sequences are increasingly used.⁶⁵ Multiecho sequences are typically preferred because they eliminate any T2 effects.⁶⁵ Technologic advancements in DCE-MRI leading to shorter echo times and higher field strengths have improved the image quality.⁶⁵ One of the major impediments to perfusion MRI in the abdomen is the adverse effect of breathing motion.⁶⁵ This can be minimized by data acquisition in the breath-hold or triggering mechanism to ensure that the data are always acquired at the same point in the breathing cycle.⁶⁵ Multiple breath-holds are usually necessary, which runs the risk of misregistration between different breath-holds and might affect quantification.⁶⁵ Triggering mechanism can reduce temporal resolution to below the requirements for accurate perfusion measurement.⁶⁵

DATA ANALYSIS

The analysis of the perfusion MRI data sets is usually performed on sophisticated workstations with dedicated perfusion software. The perfusion data set can be interrogated to obtain descriptive parameters, such as time to peak enhancement, area under the curve, or maximum enhancement, by use of the shape and structure of curves, plotting the signal intensity changes as a function of time.⁶¹⁻⁶⁵ More robust evaluation of the tissue vascularity can be obtained by performing quantitative analysis to measure physiologic parameters, such as tissue blood flow, blood volume, and interstitial volume or permeability surface area.⁶¹⁻⁶⁵ Determination of quantitative or descriptive parameters can be done by ROI analysis or voxel-based analysis.⁶¹⁻⁶⁵ ROI analysis involves manually or semiautomatically performing a ROI in the tissue of interest or lesion on one of the parametric maps, and this takes into account the average signal-time curves of all voxels in the ROI and gives the average over the ROI.⁶¹⁻⁶⁵ Voxel-based analysis involves application of the postprocessing algorithm to each individual voxel, which allows depiction of the heterogeneity of perfusion or permeability within the organ or tumor.⁶¹⁻⁶⁵ Motion correction can also be applied at the postprocessing level to account for the misregistration artifacts.⁶⁵ This is performed by coregistration techniques with use of a reference image to apply corrections.⁶⁵ This avoids the tedious process of redrawing the ROI for every individual dynamic image.⁶⁵ The various quantitative perfusion parameters include the blood flow, blood volume, permeability-surface area product, volume transfer constant (K^{trans}), and rate transfer constant (K_{ep}).⁶⁵

CLINICAL APPLICATIONS

The perfusion characteristics of tumors depicted on MRI have been shown to correlate with prognostic factors, such as histologic grade and overall survival.^{61-64,66} Several studies have shown the value of DCE-MRI in monitoring tumor response to therapy and its role as an early indicator of treatment response.^{61-64,66} The studies have been predominantly performed in cancers of the breast, cervix, bowel, liver, lung, and head and neck.^{61-64,66}

Perfusion MRI not only estimates the tissue perfusion but also visualizes the heterogeneity in the angiogenic properties within an individual tumor.^{61-64,66} The determination of heterogeneity within the tumor tissue is crucial in assessing early therapy response and individualizing treatment regimens because it allows identification of a small subpopulation of tumor cells that are resistant to treatment.^{61-64,66} However, generalization of these results is difficult because of the differences in technique and population studied.^{61-64,66}

In a study of perfusion MRI in patients with rectal cancer, George and associates⁶⁷ showed that patients with higher baseline permeability measurements responded better to chemoradiation than those with lower permeability. Mayr and coworkers⁶⁸ showed that perfusion MRI could predict tumor

recurrence on the basis of the enhancement rate within 2 weeks of radiotherapy in cervical cancer patients, with poor enhancement having a high recurrence rate of 78%. Lancaster and colleagues⁶⁹ showed in a study of patients with cervical cancer that small tumors with enhancement showed a better survival (92%) versus larger poorly enhancing tumors (55%). Perfusion MRI has been found to be helpful in detecting residual disease and in predicting early recurrence and identifying patients who are likely to benefit from salvage treatment.⁶¹⁻⁶³ Persistent enhancement at the end of the treatment regimen is more likely to be associated with increased risk of recurrence and poor survival.⁶¹⁻⁶³ In patients with cervical cancer, Boss and coworkers showed that early onset of enhancement after completion of a 6-week course of radiation treatment predicted recurrence and poor survival.^{61,63} Perfusion MRI has been studied as a potential biomarker for antiangiogenic therapy.⁶⁴ Liu and associates, in a study of patients with cancers of the liver and lung, showed that K^{trans} and initial area under the curve had inverse correlation with axitinib plasma exposure.⁶⁴ In HCC, Sahani and colleagues⁶⁶ showed that perfusion MRI is a more sensitive biomarker in predicting early response and progression-free survival after sunitinib therapy compared with RECIST criteria (Fig. 70-4).

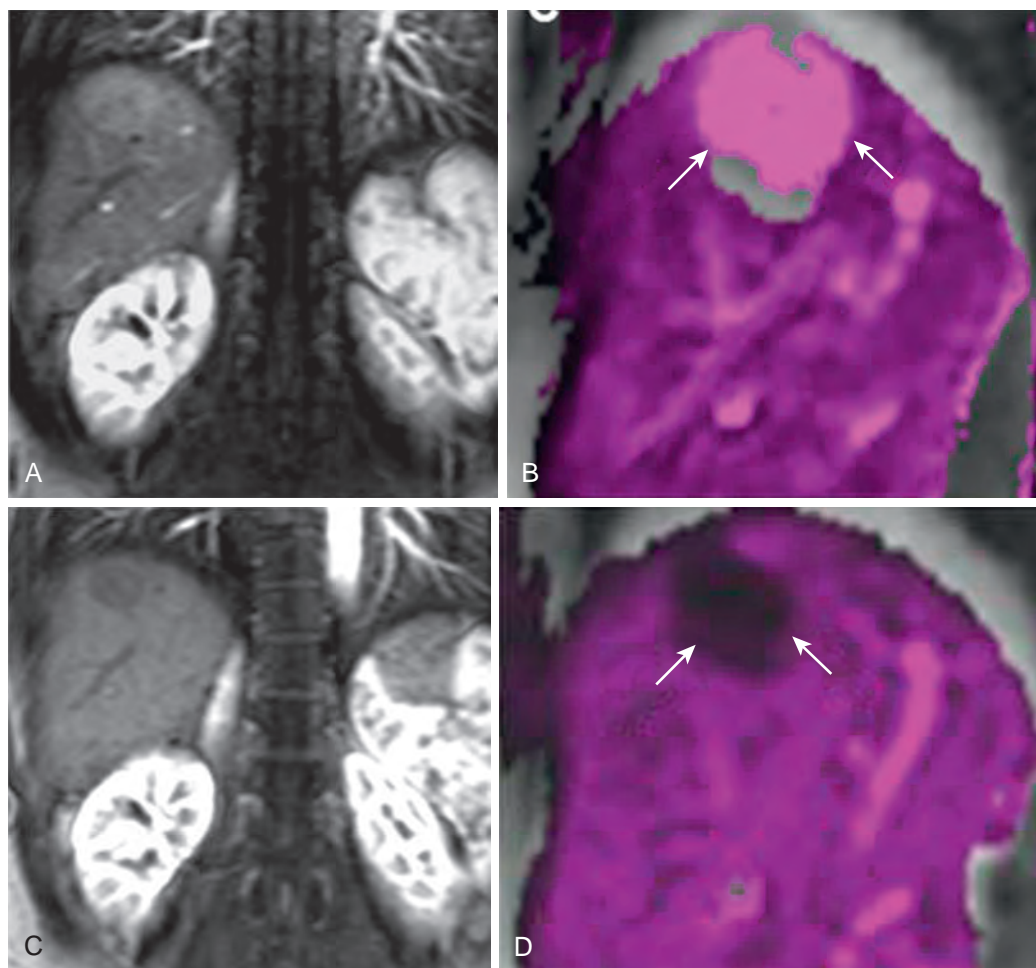


Figure 70-4 MR perfusion images before and after sunitinib therapy in a 47-year-old man with hepatocellular carcinoma. Pretreatment gadolinium-enhanced coronal T1-weighted image (A) shows the enhancing mass in the dome of the liver; the corresponding functional transfer constant (K^{trans}) map (B) was obtained after postprocessing. Two weeks after sunitinib therapy, the tumor demonstrated a reduction in enhancement (C) and a 96% drop in K^{trans} (D).

Summary

Perfusion imaging is finding increasing applications as a functional imaging tool in the field of oncology. Despite their shortcomings, perfusion CT and MRI have the potential to play a crucial role in the management of patients with cancer,

particularly as a biomarker for monitoring response to newer targeted therapies, such as antiangiogenic drugs. However, more collaborative research and robust validation are imperative before this innovative technique can find its utility in routine clinical practice.

REFERENCES

- Goh V, Halligan S, Hugill JA, et al: Quantitative assessment of colorectal cancer perfusion using MDCT: Inter- and intraobserver agreement. *AJR Am J Roentgenol* 185:225–231, 2005.
- Jiang T, Kambadakone A, Kulkarni NM, et al: Monitoring response to antiangiogenic treatment and predicting outcomes in advanced hepatocellular carcinoma using image biomarkers, CT perfusion, tumor density, and tumor size (RECIST). *Invest Radiol* 47:11–17, 2012.
- Li Y, Yang ZG, Chen TW, et al: Peripheral lung carcinoma: Correlation of angiogenesis and first-pass perfusion parameters of 64-detector row CT. *Lung Cancer* 61:44–53, 2008.
- Li Y, Yang ZG, Chen TW, et al: Whole tumour perfusion of peripheral lung carcinoma: Evaluation with first-pass CT perfusion imaging at 64-detector row CT. *Clin Radiol* 63:629–635, 2008.
- Li ZP, Meng QF, Sun CH, et al: Tumor angiogenesis and dynamic CT in colorectal carcinoma: Radiologic-pathologic correlation. *World J Gastroenterol* 11:1287–1291, 2005.
- Meijerink MR, van Crujisen H, Hoekman K, et al: The use of perfusion CT for the evaluation of therapy combining AZD1775 with gefitinib in cancer patients. *Eur Radiol* 17:1700–1713, 2007.
- Kim SH, Kamaya A, Willmann JK: CT perfusion of the liver: Principles and applications in oncology. *Radiology* 272:322–344, 2014.
- Miles KA: Perfusion CT for the assessment of tumour vascularity: Which protocol? *Br J Radiol* 76(Spec No 1):S36–S42, 2003.
- Sahani DV, Holalkere NS, Mueller PR, Zhu AX: Advanced hepatocellular carcinoma: CT perfusion of liver and tumor tissue—initial experience. *Radiology* 243:736–743, 2007.
- Sahani DV, Kalva SP, Hamberg LM, et al: Assessing tumor perfusion and treatment response in rectal cancer with multisection CT: Initial observations. *Radiology* 234:785–792, 2005.
- Wintermark M, Chioloro R, Van Melle G, et al: Cerebral vascular autoregulation assessed by perfusion-CT in severe head trauma patients. *J Neuroradiol* 33:27–37, 2006.
- Wintermark M, Thiran JB, Maeder P, et al: Simultaneous measurement of regional cerebral blood flow by perfusion CT and stable xenon CT: A validation study. *AJNR Am J Neuroradiol* 22:905–914, 2001.
- Wintermark M, van Melle G, Schnyder P, et al: Admission perfusion CT: Prognostic value in patients with severe head trauma. *Radiology* 232:211–220, 2004.
- Cuenod CA, Fournier L, Balvay D, Guinebreliere JM: Tumor angiogenesis: Pathophysiology and implications for contrast-enhanced MRI and CT assessment. *Abdom Imaging* 31:188–193, 2006.
- d'Assignies G, Couvelard A, Bahrami S, et al: Pancreatic endocrine tumors: Tumor blood flow assessed with perfusion CT reflects angiogenesis and correlates with prognostic factors. *Radiology* 250:407–416, 2009.
- Dugdale PE, Miles KA, Bunce I, et al: CT measurement of perfusion and permeability within lymphoma masses and its ability to assess grade, activity, and chemotherapeutic response. *J Comput Assist Tomogr* 23:540–547, 1999.
- Ellika SK, Jain R, Patel SC, et al: Role of perfusion CT in glioma grading and comparison with conventional MR imaging features. *AJNR Am J Neuroradiol* 28:1981–1987, 2007.
- Goh V, Halligan S, Bartram CI: Quantitative tumor perfusion assessment with multidetector CT: Are measurements from two commercial software packages interchangeable? *Radiology* 242:777–782, 2007.
- Goh V, Halligan S, Gartner L, et al: Quantitative colorectal cancer perfusion measurement by multidetector-row CT: Does greater tumour coverage improve measurement reproducibility? *Br J Radiol* 79:578–583, 2006.
- Goh V, Halligan S, Gharpuray A, et al: Quantitative assessment of colorectal cancer tumor vascular parameters by using perfusion CT: Influence of tumor region of interest. *Radiology* 247:726–732, 2008.
- Kambadakone AR, Sahani DV: Body perfusion CT: Technique, clinical applications, and advances. *Radiol Clin North Am* 47:161–178, 2009.
- Miles KA: Functional CT imaging in oncology. *Eur Radiol* 13(Suppl 5):M134–M138, 2003.
- Ng CS, Charnsangavej C, Wei W, Yao JC: Perfusion CT findings in patients with metastatic carcinoid tumors undergoing bevacizumab and interferon therapy. *AJR Am J Roentgenol* 196:569–576, 2011.
- Sahani DV, Holalkere NS, Kambadakone A, et al: Role of computed tomography perfusion in the evaluation of pancreatic necrosis and pancreatitis after endoscopic ultrasound-guided ablation of the pancreas in a porcine model. *Pancreas* 38:775–781, 2009.
- Willett CG, Duda DG, di Tomaso E, et al: Efficacy, safety, and biomarkers of neoadjuvant bevacizumab, radiation therapy, and fluorouracil in rectal cancer: A multidisciplinary phase II study. *J Clin Oncol* 27:3020–3026, 2009.
- Wintermark M, Smith WS, Ko NU, et al: Dynamic perfusion CT: Optimizing the temporal resolution and contrast volume for calculation of perfusion CT parameters in stroke patients. *AJNR Am J Neuroradiol* 25:720–729, 2004.
- Zhu AX, Holalkere NS, Muzikansky A, et al: Early antiangiogenic activity of bevacizumab evaluated by computed tomography perfusion scan in patients with advanced hepatocellular carcinoma. *Oncologist* 13:120–125, 2008.
- Cha S: Perfusion MR imaging: Basic principles and clinical applications. *Magn Reson Imaging Clin N Am* 11:403–413, 2003.
- Miles KA: Tumour angiogenesis and its relation to contrast enhancement on computed tomography: A review. *Eur J Radiol* 30:198–205, 1999.
- Miles KA, Griffiths MR: Perfusion CT: A worthwhile enhancement? *Br J Radiol* 76:220–231, 2003.
- Miles KA, Charnsangavej C, Lee FT, et al: Application of CT in the investigation of angiogenesis in oncology. *Acad Radiol* 7:840–850, 2000.
- Kambadakone AR, Sharma A, Catalano OA, et al: Protocol modifications for CT perfusion (CTp) examinations of abdomen-pelvic tumors: Impact on radiation dose and data processing time. *Eur Radiol* 21:1293–1300, 2011.
- Garcia-Figueiras R, Goh VJ, Padhani AR, et al: CT perfusion in oncologic imaging: A useful tool? *AJR Am J Roentgenol* 200:8–19, 2013.
- Rogalla P, Kloeters C, Hein PA: CT technology overview: 64-slice and beyond. *Radiol Clin North Am* 47:1–11, 2009.
- Goetti R, Leschka S, Desbiolles L, et al: Quantitative computed tomography liver perfusion imaging using dynamic spiral scanning with variable pitch: Feasibility and initial results in patients with cancer metastases. *Invest Radiol* 45:419–426, 2010.
- Haberland U, Klotz E, Abolmaali N: Performance assessment of dynamic spiral scan modes with variable pitch for quantitative perfusion computed tomography. *Invest Radiol* 45:378–386, 2010.
- Morhard D, Wirth CD, Fesl G, et al: Advantages of extended brain perfusion computed tomography: 9.6 cm coverage with time resolved computed tomography—angiography in comparison to standard stroke-computed tomography. *Invest Radiol* 45:363–369, 2010.
- Youn SW, Kim JH, Weon YC, et al: Perfusion CT of the brain using 40-mm-wide detector and toggling table technique for initial imaging of acute stroke. *AJR Am J Roentgenol* 191:W120–W126, 2008.
- Goh V, Halligan S, Taylor SA, et al: Differentiation between diverticulitis and colorectal cancer: Quantitative CT perfusion measurements versus morphologic criteria—initial experience. *Radiology* 242:456–462, 2007.
- Gobbel GT, Cann CE, Fike JR: Comparison of xenon-enhanced CT with ultrafast CT for measurement of regional cerebral blood flow. *AJNR Am J Neuroradiol* 14:543–550, 1993.
- Gobbel GT, Cann CE, Iwamoto HS, Fike JR: Measurement of regional cerebral blood flow in the dog using ultrafast computed tomography. Experimental validation. *Stroke* 22:772–779, 1991.
- Purdie TG, Henderson E, Lee TY: Functional CT imaging of angiogenesis in rabbit VX2 soft-tissue tumour. *Phys Med Biol* 46:3161–3175, 2001.
- Blomley MJ, Coulters R, Bufkin C, et al: Contrast bolus dynamic computed tomography for the measurement of solid organ perfusion. *Invest Radiol* 28(Suppl 5):S72–S77, discussion S8, 1993.
- Jiang T, Zhu AX, Sahani DV: Established and novel imaging biomarkers for assessing

- response to therapy in hepatocellular carcinoma. *J Hepatol* 58:169–177, 2013.
45. Willett CG, Boucher Y, di Tomaso E, et al: Direct evidence that the VEGF-specific antibody bevacizumab has antivascular effects in human rectal cancer. *Nat Med* 10:145–147, 2004.
 46. Leggett DA, Kelley BB, Bunce IH, Miles KA: Colorectal cancer: Diagnostic potential of CT measurements of hepatic perfusion and implications for contrast enhancement protocols. *Radiology* 205:716–720, 1997.
 47. Meijerink MR, van Waesberghe JH, van der Weide L, et al: Total-liver-volume perfusion CT using 3-D image fusion to improve detection and characterization of liver metastases. *Eur Radiol* 18:2345–2354, 2008.
 48. Miles KA, Hayball MP, Dixon AK: Functional images of hepatic perfusion obtained with dynamic CT. *Radiology* 188:405–411, 1993.
 49. Pandharipande PV, Krinsky GA, Rusinek H, Lee VS: Perfusion imaging of the liver: Current challenges and future goals. *Radiology* 234:661–673, 2005.
 50. Perkins AC, Whalley DR, Ballantyne KC, Hardcastle JD: Reliability of the hepatic perfusion index for the detection of liver metastases. *Nucl Med Commun* 8:982–989, 1987.
 51. Miles KA, Hayball MP, Dixon AK: Measurement of human pancreatic perfusion using dynamic computed tomography with perfusion imaging. *Br J Radiol* 68:471–475, 1995.
 52. Henderson E, Milosevic MF, Haider MA, Yeung IW: Functional CT imaging of prostate cancer. *Phys Med Biol* 48:3085–3100, 2003.
 53. Fournier LS, Oudard S, Thiam R, et al: Metastatic renal carcinoma: Evaluation of antiangiogenic therapy with dynamic contrast-enhanced CT. *Radiology* 256:511–518, 2010.
 54. Sun CH, Feng ST, Xiao P, et al: Quantitative assessment of perirectal tumor infiltration with dynamic contrast-enhanced multi-detector row CT in rectal cancer. *Eur J Radiol* 80:279–283, 2011.
 55. Tsushima Y, Blomley JK, Kusano S, Endo K: The portal component of hepatic perfusion measured by dynamic CT: An indicator of hepatic parenchymal damage. *Dig Dis Sci* 44:1632–1638, 1999.
 56. Van Beers BE, Leconte I, Materne R, et al: Hepatic perfusion parameters in chronic liver disease: Dynamic CT measurements correlated with disease severity. *AJR Am J Roentgenol* 176:667–673, 2001.
 57. Phongkitkarun S, Kobayashi S, Kan Z, et al: Quantification of angiogenesis by functional computed tomography in a Matrigel model in rats. *Acad Radiol* 11:573–582, 2004.
 58. Suzuki C, Jacobsson H, Hatschek T, et al: Radiologic measurements of tumor response to treatment: Practical approaches and limitations. *Radiographics* 28:329–344, 2008.
 59. Han KS, Jung DC, Choi HJ, et al: Pretreatment assessment of tumor enhancement on contrast-enhanced computed tomography as a potential predictor of treatment outcome in metastatic renal cell carcinoma patients receiving antiangiogenic therapy. *Cancer* 116:2332–2342, 2010.
 60. van der Veldt AA, Haanen JB, van den Eertwegh AJ, Boven E: Targeted therapy for renal cell cancer: Current perspectives. *Discov Med* 10:394–405, 2010.
 61. Harry VN: Novel imaging techniques as response biomarkers in cervical cancer. *Gynecol Oncol* 116:253–261, 2010.
 62. Harry VN, Deans H, Ramage E, et al: Magnetic resonance imaging in gynecological oncology. *Int J Gynecol Cancer* 19:186–193, 2009.
 63. Boss EA, Massuger LF, Pop LA, et al: Post-radiotherapy contrast enhancement changes in fast dynamic MRI of cervical carcinoma. *J Magn Reson Imaging* 13:600–606, 2001.
 64. Liu Y, Ramirez J, Ratain MJ: Inhibition of paracetamol glucuronidation by tyrosine kinase inhibitors. *Br J Clin Pharmacol* 71:917–920, 2011.
 65. Sourbron S: Technical aspects of MR perfusion. *Eur J Radiol* 76:304–313, 2010.
 66. Sahani DV, Jiang T, Hayano K, et al: Magnetic resonance imaging biomarkers in hepatocellular carcinoma: Association with response and circulating biomarkers after sunitinib therapy. *J Hematol Oncol* 6:51, 2013.
 67. George ML, Dzik-Jurasz AS, Padhani AR, et al: Non-invasive methods of assessing angiogenesis and their value in predicting response to treatment in colorectal cancer. *Br J Surg* 88:1628–1636, 2001.
 68. Mayr NA, Yuh WT, Arnholt JC, et al: Pixel analysis of MR perfusion imaging in predicting radiation therapy outcome in cervical cancer. *J Magn Reson Imaging* 12:1027–1033, 2000.
 69. Lancaster JA, Carrington BM, Sykes JR, et al: Prediction of radiotherapy outcome using dynamic contrast enhanced MRI of carcinoma of the cervix. *Int J Radiat Oncol Biol Phys* 54:759–767, 2002.
 70. Gandhi D, Hoeffner EG, Carlos RC, et al: Computed tomography perfusion of squamous cell carcinoma of the upper aerodigestive tract. Initial results. *J Comput Assist Tomogr* 27:687–693, 2003.
 71. Ma SH, Xu K, Xiao ZW, et al: Peripheral lung cancer: Relationship between multi-slice spiral CT perfusion imaging and tumor angiogenesis and cyclin D1 expression. *Clin Imaging* 31:165–177, 2007.

Techniques of Percutaneous Tissue Acquisition

STEVEN Y. HUANG | ERIK K. PAULSON

CHAPTER OUTLINE

Preprocedure Evaluation

Choice of Modality for Image Guidance

Fluoroscopy
 Ultrasonography
 Computed Tomography
 Magnetic Field–Based Electronic Guidance System
 Magnetic Resonance Imaging

Choice of Needles

Biopsy Planning

Acceptable Routes
 Routes to Avoid

Specific Organ-Related Techniques

Liver
 Adrenal Glands
 Pancreas
 Bowel
 Lymph Nodes
 Spleen

Complications

The acquisition of tissue from lesions that are neither visually apparent nor palpable has evolved from being performed in the operating room by surgeons to being performed percutaneously by radiologists with image guidance. Image-guided percutaneous biopsies have also evolved from being reserved for large and superficial lesions to include small, deep, and precariously positioned lesions. With these changes has come a trend toward more outpatient procedures, fewer complications, and lower cost. Because radiologists are willing to perform biopsy of more challenging lesions, there has also been a trend toward imaging techniques with real-time guidance, such as ultrasonography (US) or computed tomography (CT) fluoroscopy. In the past, the success of image-guided biopsies has depended not only on the expertise of the radiologist but also on that of the cytopathologist. Whereas a proficient cytopathologist is extremely advantageous, often enabling a sample consisting of only a minimal amount of tissue to be diagnostic, the increased use of core or cutting biopsy needles has diminished the overall impact of that contribution.¹

The role of image-guided percutaneous biopsy is mainly to diagnose or to exclude the presence of malignant disease, to stage patients with a known malignant neoplasm, to monitor the response to tumor therapy, to confirm or to exclude recurrent tumor, and to differentiate whether nodal enlargement is due to tumor or infection. Furthermore, biopsy techniques can

be used to diagnose nonmalignant medical diseases in the liver and kidneys. For these “medical”-type biopsies, larger bore needles are generally required to obtain specimens for histology.

The challenge facing radiologists is to provide a biopsy service whereby adequate tissue can be readily obtained from almost any lesion in the abdomen and pelvis, on almost any patient, with near real-time needle-tip visualization during both placement and sampling. This has numerous implications related to the coagulation status and condition of the patient, the choice of imaging modality, the choice of type and gauge of needles, and the transgression of normal structures. This chapter discusses the details of these techniques in a systematic fashion including the preprocedural evaluation, choice of modality for image guidance, choice of needles, biopsy planning, specific organ-related details, and complications.

Preprocedure Evaluation

A complete preprocedure evaluation is an important component of an efficient and effective biopsy service. This evaluation should consist of reviewing prior diagnostic imaging studies, obtaining a bleeding history and appropriate laboratory studies, and obtaining written informed consent. We have found that incorporating physician extenders into the procedural approval process helps ensure that biopsies are performed as efficiently and safely as possible. Integration of physician assistants, nurse practitioners, and nurse coordinators allows the radiologist to focus on the procedure, improving throughput. Furthermore, many of these patient encounters, whether they are performed on an inpatient or elective outpatient basis, can be coded and billed as a specialty consultation, allowing the radiology group to be reimbursed appropriately.

Review of prior diagnostic imaging studies will confirm the presence of a lesion suitable for biopsy and help in planning of a specific approach, choice of the appropriate guidance modality, and characterization of the lesion to provide the pathologist with an appropriate differential diagnosis. The importance of reviewing prior imaging studies cannot be overstated. For example, a radiologist may be asked to biopsy a lesion that, on review, proves to be a benign hemangioma or cyst.

The appropriate laboratory investigation of the patient before a biopsy remains the subject of debate. No single published guideline is widely accepted or used. This lack of consensus stems from the fact that no prospective evaluation of a large number of patients has been performed in which various factors, including patient history, specific type of procedure, and laboratory tests, have been compared with outcome.^{2,3}

Silverman and colleagues² proposed a strategy for screening laboratory tests for abdominal interventional procedures based primarily on the bleeding risk of the procedure and screening

of patients for bleeding tendencies. Since the work by Silverman and coworkers, consensus guidelines have been published by the Society of Interventional Radiology^{4,5} (Table 71-1). The recommendations are based on available literature and consensus expert opinion but, admittedly, lack high-level evidence. As a result, the recommendations can conflict with other publications. For example, in a review by O'Connor and associates,⁶ the international normalized ratio (INR) and platelet transfusion threshold for percutaneous liver biopsy were 2.0 or lower and 25,000/mL or higher, respectively, whereas, the Society of Interventional Radiology guidelines^{4,5} recommend an INR and platelet transfusion threshold of 1.5 or lower and 50,000/mL or higher, respectively. The lack of high-level data contributes to the nonuniform pattern regarding management of hemostatic defects. It is likely that individual practitioners will tailor their guidelines to local expertise and patient comorbidities.

A patient's bleeding risk is also influenced by medication use, with emphasis on anticoagulant and antiplatelet agents. Anticoagulant medications have traditionally included warfarin and unfractionated heparin. Newer anticoagulants include low-molecular-weight heparin (e.g., enoxaparin), indirect factor Xa inhibitors (e.g., fondaparinux, idraparinux, idrabiotaparinux), direct Xa inhibitors (e.g., rivaroxaban and apixaban), and direct thrombin inhibitors (e.g., lepirudin, argatroban, bivalirudin, dabigatran). The lack of objective data evaluating the periprocedural management of patients receiving anticoagulant or antiplatelet agents⁷⁻⁹ makes the proposal of general recommendations for the interventionalist difficult. The American College of Chest Physicians has proposed stratifying patients on the basis of risk for perioperative thromboembolism.¹⁰ Patients are classified as being at low, moderate, or high risk for thromboembolic events (Table 71-2). By use of this classification scheme,

TABLE 71-1 Hematologic and Coagulation Parameters for Interventions

Category	1	2	3
Procedure	Low bleeding risk, easily detected and controllable (e.g., paracentesis, superficial aspiration, and biopsy)	Moderate bleeding risk (e.g., intra-abdominal or retroperitoneal biopsy)	Significant bleeding risk, difficult to detect or to control (e.g., renal biopsy)
Tests	INR: recommended only for patients receiving warfarin or with known or suspected liver disease aPTT: recommended only for patients receiving unfractionated heparin	INR: recommended aPTT: recommended only for patients receiving unfractionated heparin	INR: recommended aPTT: recommended
	Platelet count: not routinely recommended	Platelet count: not routinely recommended	Platelet count: recommended
	Hematocrit: not routinely recommended	Hematocrit: not routinely recommended	Hematocrit: recommended
Management	INR: correct to ≤ 2.0 Platelets: recommend transfusion $\leq 50,000/\mu\text{L}$ aPTT: no consensus Hematocrit: no consensus	INR: correct to ≤ 1.5 Platelets: recommend transfusion $\leq 50,000/\mu\text{L}$ aPTT: no consensus Hematocrit: no consensus	INR: correct to ≤ 1.5 Platelets: recommend transfusion $\leq 50,000/\mu\text{L}$ aPTT: correct so that value is ≤ 1.5 times control Hematocrit: no consensus

aPTT, Activated partial thromboplastin time; INR, international normalized ratio.

Modified from Society of Interventional Radiology consensus guidelines for periprocedural management of coagulation status and hemostasis risk in percutaneous image-guided interventions.^{4,5}

TABLE 71-2 Risk Stratification for Perioperative Thromboembolism

Risk Stratum	INDICATION FOR ANTICOAGULATION		
	Mechanical Heart Valve	Atrial Fibrillation	VTE
High (>10% annual risk of thromboembolism)	Any mitral valve prosthesis Any caged-ball or tilting-disk aortic valve prosthesis Recent (within 6 months) stroke or TIA	CHADS ₂ score of 5-6 Recent (within 3 months) stroke or TIA Rheumatic valvular heart disease	Recent (within 3 months) VTE Severe thrombophilia (e.g., deficiency of protein C or S or antithrombin, antiphospholipid antibodies)
Moderate (5%-10% annual risk of thromboembolism)	Bileaflet aortic valve prosthesis and one or more of the following risk factors: atrial fibrillation, prior stroke or TIA, hypertension, diabetes, congestive heart failure, age >75 years	CHADS ₂ score of 3-4	VTE within 3-12 months No severe thrombophilia (e.g., heterozygous factor V Leiden or prothrombin gene mutation) Recurrent VTE Active cancer (treated within 6 months or palliative)
Low (<5% annual risk of thromboembolism)	Bileaflet aortic valve prosthesis without atrial fibrillation and no other risk factors for stroke	CHADS ₂ score of 0-2 (assuming no history of stroke or TIA)	VTE > 12 months previous and no other risk factors

CHADS₂: 1 point is allotted for congestive heart failure, hypertension, age older than 75 years, and diabetes; 2 points are allotted for stroke or transient ischemic attack.

TIA, Transient ischemic attack; VTE, venous thromboembolism.

Modified from the 2012 American Association of Chest Physicians guidelines for perioperative management of antithrombotic therapy.¹⁰

TABLE
71-3

Management of Commonly Used Anticoagulant and Antiplatelet Agents

Medications	Category 1 Procedure (Low Bleeding Risk)	Category 2 Procedure (Moderate Bleeding Risk)	Category 3 Procedure (Significant Bleeding Risk)
Warfarin	Withhold 3-5 days (INR \leq 2.0)	Withhold 5 days (INR \leq 1.5)	Withhold 5 days (INR \leq 1.5)
Heparin (unfractionated)	No consensus	No consensus	Withhold 2-4 hours before procedure
Low-molecular-weight heparin (therapeutic dose)	Withhold 1 dose or 12 hours before procedure	Withhold 1 dose or 12 hours before procedure	Withhold 2 doses or 24 hours before procedure
Aspirin*	Do not withhold	Do not withhold	Withhold 5 days before procedure
Clopidogrel*	Withhold 0-5 days before procedure	Withhold days before procedure	Withhold for 5 days before procedure

INR, International normalized ratio.

*Patients unable to safely discontinue medications for any number of medical reasons, including but not limited to recent coronary or cerebrovascular stents, should be afforded a degree of variance from these guidelines.

Modified from Society of Interventional Radiology consensus guidelines for periprocedural management of coagulation status and hemostasis risk in percutaneous image-guided interventions.^{4,5}

patients with the highest thromboembolic risk and scheduled to undergo a procedure with a high hemorrhagic risk (e.g., renal biopsy) stand to benefit the most from interruption of anticoagulation and bridging with an anticoagulant with a short half-life (e.g., enoxaparin). In observational studies, this regimen was associated with a 1% to 2% incidence of thromboembolic events in the high-risk group.^{11,12} There is a paucity of evidence to guide the use of bridging anticoagulation for moderate- and low-risk categories.

If anticoagulation can be withheld, it is frequently helpful to allow a time lapse of five half-lives, which corresponds to a residual drug activity of 3% from the initial dose. Whereas making decisions based on the half-life of a drug is reasonable, clearance can be affected by drug-drug interactions, differences in metabolism, and genetic influences.⁵ If a procedure requires more urgency, an elevated INR may be reversed immediately by administering fresh frozen plasma. Alternatively, vitamin K can be used to reverse the effects of warfarin.¹³ An elevation of partial thromboplastin time induced by heparin may be reversed with protamine, a heparin antagonist. Low-molecular-weight heparin (i.e., enoxaparin) has a half-life of 4.5 to 7 hours, based on anti-Xa activity. In general, most percutaneous interventions in the abdomen and pelvis can be performed after withholding of the therapeutic dose on the morning of the procedure.

Similar to anticoagulants, antiplatelet agents can also increase a patient's hemorrhagic risk during surgery.^{14,15} Platelet inhibitors include aspirin, thienopyridines (clopidogrel, prasugrel, ticlopidine), and glycoprotein IIb/IIIa inhibitors (e.g., abciximab, eptifibatide, tirofiban). Appropriate management of antiplatelet agents is determined by the indication. Most common indications include secondary prevention of ischemic cardiac events, post-coronary stenting, and secondary prevention of cerebrovascular events.¹⁶ Stopping of these agents should be considered carefully. At our institution, it is common to consult the treating cardiologist before cessation to better understand the risks associated with stopping of the medication against the hemorrhagic risk of the procedure. If a cardiac event occurred within 1 year and the patient is taking aspirin or clopidogrel, we generally perform the biopsy without stopping the medication but inform the patient of the increased hemorrhagic risk. Aspirin, clopidogrel, prasugrel, and ticlopidine irreversibly inhibit platelet function, making the half-life of the drug irrelevant.¹⁷ For each day that one of these agents is withheld,

approximately 10% to 14% of the normal platelet function is restored, taking 7 to 10 days for the entire platelet pool to be replenished.^{18,19} On the other hand, dipyridamole, cilostazol, and nonsteroidal anti-inflammatory drugs reversibly inhibit platelet function, and their effects are dependent on the elimination half-life.¹⁰ The Society of Interventional Radiology has published consensus guidelines on appropriate management of anticoagulant and antiplatelet medications (Table 71-3).

Written informed consent should be obtained from each patient. The biopsy procedure should be described to the patient thoughtfully in layman's terms. Patients should be informed of the risk of bleeding and infection and that biopsy of upper abdominal lesions may result in a pneumothorax and possibly chest tube placement. Patients should be informed that multiple needle passes may be required, the specimen may not be diagnostic, and additional work-up may be necessary. Patients with lesions near bowel are at risk of bowel injury and abscess, although this complication, surprisingly, has only rarely been reported. The preprocedure visit is also an excellent opportunity to assess various factors, such as the patient's airway, ability to lie in the desired position, and level of anxiety. All these variables play a role in deciding the level of sedation (i.e., moderate sedation, often administered by the radiologist, or a higher level of sedation requiring an anesthesiologist). A detailed home care instruction form is reviewed with each patient before the biopsy that explains which symptoms are to be expected after the biopsy and which symptoms raise the question of a complication. This form provides a list of contact telephone numbers in case a complication occurs.

Choice of Modality for Image Guidance

Numerous modalities are available for performing image-guided percutaneous biopsies: fluoroscopy, US, CT (with or without fluoroscopic capability), and magnetic resonance imaging (MRI). Each of these techniques has strengths and weaknesses as well as specific indications, and they are discussed next.

FLUOROSCOPY

Fluoroscopy is used sparingly within the abdomen and pelvis and is reserved for lesions that are large, superficial, or calcified.

Fluoroscopy can also be used on occasion to perform a biopsy of obstructing lesions, such as a cholangiocarcinoma located adjacent to or surrounding a surgically or endoscopically placed stent. US, however, can also accomplish this task. Preliminary cross-sectional imaging with CT, US, or MRI is important to determine which intervening structures the needle may transgress en route to the lesion.

ULTRASONOGRAPHY

The use of US for image-guided biopsies is generally preferred for its accuracy, safety, decreased costs, decreased procedure time, widespread availability, multiplanar capabilities, and flexible patient positioning. US has the major advantage of direct real-time visualization of the needle tip during both placement and sampling.²⁰ This advantage not only aids in avoiding blood vessels but also helps ensure that sampling is restricted to the lesion. Furthermore, compression with the US transducer is a major advantage in that it not only reduces the distance between the skin surface and the lesion but also displaces bowel and other structures. Color Doppler US should be used to assess lesion vascularity and to avoid transgression of nearby vascular structures.

Careful sampling of the lesion alone is particularly important in certain scenarios, such as in differentiating a hepatocellular adenoma from focal nodular hyperplasia. The conspicuous absence of bile duct epithelium in adenomas is the key to differentiating these two hepatocyte-containing lesions. Therefore, if one is performing a biopsy of an adenoma and the needle tip ventures beyond the margins of the lesion into normal hepatic parenchyma, the bile duct constituents that are aspirated may cause the cytopathologist to inadvertently diagnose the lesion as a focal nodular hyperplasia. This could lead to an error in diagnosis, which is important to avoid; many adenomas are surgically resected because they are considered to be premalignant and can undergo spontaneous hemorrhage.

The disadvantages of US include the obscuration of some lesions by intervening lung, bone, or bowel. An angled approach or transducer compression can be used to improve visualization. Needle-tip visualization can be difficult with modern transducers that are narrowly collimated. This difficulty can be reduced by using an attached needle guide. Visualization can also be poor in larger patients, in whom sonographic tissue penetration is poor. Finally, ultrasound of solid abdominal viscera is limited in the setting of tissue heterogeneity (e.g., liver cirrhosis). Contrast-enhanced CT and MRI are excellent tools to detect lesions within solid organs.^{21,22} Image fusion of contrast-enhanced CT or MRI examinations with US allows ultrasound-guided biopsies to be performed with high success²³; however, the technique requires additional hardware for needle tracking and software for coregistration.

The two main techniques of US-guided biopsies are the freehand technique and the attached needle guide technique.^{8,9} The freehand technique has the advantages of allowing many more degrees of freedom and the ability to separate the needle and the transducer, an approach that often results in better needle visualization. The main disadvantage is the steep learning curve because needle-tip visualization can be difficult and time-consuming. The attached needle guide has the advantages of a shallow learning curve with easier and quicker needle-tip visualization. Disadvantages include a significant reduction in the degrees of freedom and the modest cost of the apparatus.

COMPUTED TOMOGRAPHY

CT is widely used for image guidance in the United States primarily because of equipment availability and user preference. CT has the advantages of very high spatial resolution and lack of imaging “blind spots.” Furthermore, the depiction of intervening structures is superb. Disadvantages include the exposure to ionizing radiation, the lack of direct real-time needle-tip visualization, the difficulty encountered in the biopsy of moving lesions, and the high cost. Although CT is limited to the axial plane, the ability to angle the gantry up to 30 degrees allows some limited flexibility in needle placement, particularly in the cephalocaudal direction. An alternative to angling the gantry is to use the triangulation method, in which three points composed of the lesion (A), the skin overlying the lesion (B), and a point either cranial or caudal to the lesion (C) are selected in the same parasagittal plane. The position of C should be selected such that a line formed between A and C does not transgress any critical structures (see later, routes to avoid). These three points form a right triangle, and by trigonometry, the length and angle of insertion can be calculated (Fig. 71-1).²⁴

CT fluoroscopy is capable of providing six to eight lower resolution and low-milliamperage images and near real-time needle-tip visualization.¹⁰ This technique reduces the time advantages of US considerably and improves the targeting of moving lesions. It is particularly useful for procedures involving deep structures, such as retroperitoneal masses, or for procedures involving organs prone to respiratory motion, such as the liver. CT fluoroscopy may use a quick check technique, which is analogous to conventional CT. This technique uses single-section CT fluoroscopic images to check needle location and to confirm appropriate alignment. Continuous CT fluoroscopic images may be obtained in the region of the needle when the needle tip is difficult to localize, such as when it is in an oblique or a transverse plane. This technique is analogous to conventional CT, except reconstruction times are faster and

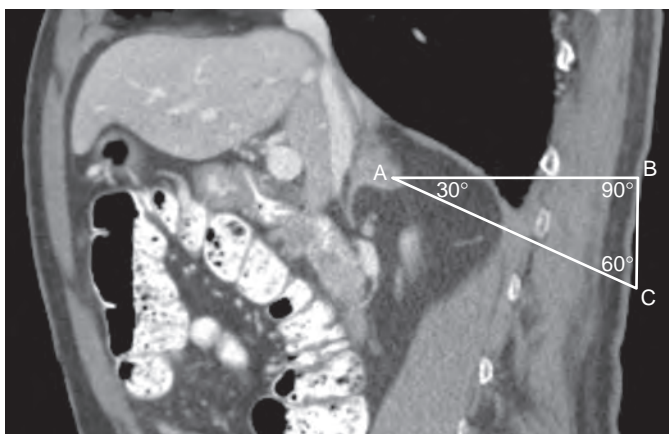


Figure 71-1 An 87-year-old man with melanoma. Parasagittal reformation of an intravenous and oral contrast-enhanced CT of the upper abdomen reveals a right adrenal mass. Because biopsy of the lesion through an axial approach would have transgressed lung, the triangulation method was used. Three points are selected: A, the lesion; B, the skin overlying the lesion; and C, a point either cranial or caudal to the lesion. The position of C was selected such that a line formed between A and C did not transgress any critical structures. These three points form a right triangle, and by trigonometry, the needle length distance and angle of insertion were appropriately calculated. Fine-needle aspiration revealed metastatic melanoma.

the radiologist may manually position the table. Continuous fluoroscopy denotes the use of continuous fluoroscopic exposure during needle advancement or manipulation. It is wise to use forceps as a needle holder to prevent primary beam irradiation of the radiologist's hands.

Radiation doses to the patient and radiologist are higher in CT fluoroscopy than in conventional CT; however, observed doses have fallen with the trend toward the quick check technique and modulation of two scanner parameters, which are usually readily displayed: CT dose index and dose-length product. These parameters can be lowered by modifying the longitudinal scan length, number of scans, and tube current-exposure time product (milliamperage \times second [mAs]).²⁵

Solid masses, which are isodense to surrounding organ parenchyma, are difficult to biopsy. Intravenous contrast material may be administered to increase lesion conspicuity. We recommend administering intravenous contrast material after placement of the guide needle or biopsy needle near the lesion, based on anatomic landmarks.

MAGNETIC FIELD-BASED ELECTRONIC GUIDANCE SYSTEM

Electromagnetic navigation systems have been developed to aid in near real-time needle tracking. The technology uses real-time positioning information obtained when a probe containing embedded sensors is moved within a magnetic field during CT- or US-guided procedures.^{26,27} The postprocessed images allow the operator to quickly assess the needle trajectory before entering the patient's skin. As the needle is advanced down to the lesion, the screen displays the real-time needle position by overlaying it on a preprocedural CT or US set of images. This technology helps facilitate out-of-plane biopsy approaches.

MAGNETIC RESONANCE IMAGING

MRI has been used sparingly for guiding percutaneous biopsies, although the roadblocks to use of this modality are diminishing. The advantages of MRI include high spatial resolution, very high inherent tissue contrast, lack of ionizing radiation, real-time capability, and virtually unlimited multiplanar imaging planes, which facilitates needle placement for lesions not readily accessible with a traditional axial approach (Fig. 71-2).

Disadvantages include the requirement for MR-compatible supplies and monitoring equipment, the considerable time commitment, and the high cost. Many of these disadvantages, however, are significantly reduced or eliminated with the open or dedicated interventional units, which allow placement of the needle while the patient is in the bore of the magnet and use fast imaging sequences that provide near real-time guidance.²⁸ The use of lower field strength in an open system decreases the signal-to-noise ratio and results in longer acquisition times but may still be sufficient for lesion visualization.²⁹ The high inherent tissue contrast attainable on noncontrast MRI can be a major advantage; in most practices, this modality is used selectively in patients with lesions that are not well seen on US and CT. This imaging scenario, however, is infrequent in the abdomen.

Choice of Needles

In choosing a needle for image-guided biopsy, the first issue to address is what technique will be used to acquire the sample. A single-needle technique uses a new needle for each pass. This is limited by the necessity of imaging guidance for each pass, resulting in long procedure times, need to traverse structures with each pass, increase in the risk of complications, and increased radiation exposure when CT guidance is used.³⁰ In the tandem technique, a small-caliber needle is first used to localize the lesion with image guidance. A larger caliber biopsy needle is then advanced parallel to the localizing needle without imaging guidance. This technique is limited by multiple organ punctures and imprecise needle-tip localization.³⁰ At our institution, most operators use a coaxial technique, during which a guide needle is advanced down to the lesion under imaging guidance. Biopsy needles are then advanced coaxially through the guide needle. The drawbacks include having to use a larger caliber guide needle to accommodate the biopsy needle and that subsequent passes may follow the same path and yield little diagnostic tissue.^{30,31}

Guide needles are available in a wide range of size, length, and tip configuration. In general, the needles used for biopsies in the abdomen and pelvis range in size from 16- to 19-gauge and 5 to 20 cm in length. The tips of the guide needles may have an angled bevel or a stylet with a sharp point. A drawback of the beveled needles is that they may deflect away from the

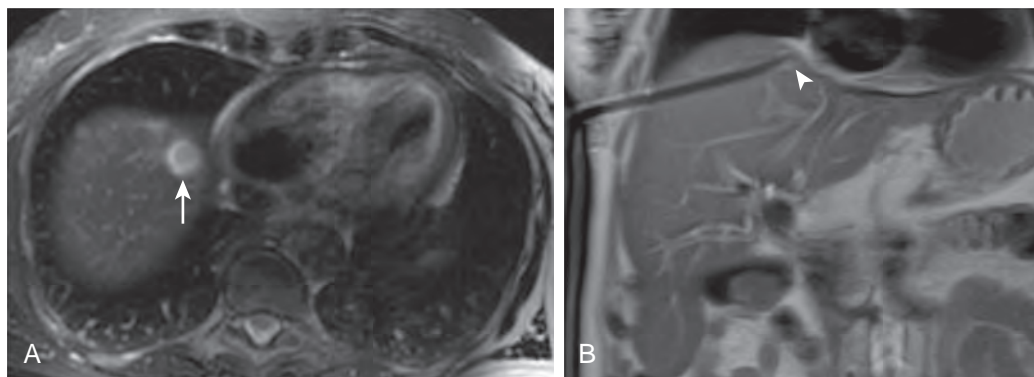


Figure 71-2 MRI of a 76-year-old woman with ampullary carcinoma. **A.** Axial T2-weighted MRI demonstrates a 1.2-cm T2 hyperintense lesion in the hepatic dome (arrow). **B.** Coronal MRI demonstrates the biopsy needle within the hepatic dome lesion (arrowhead). Given its multiplanar capabilities, MRI facilitates biopsy of lesions that would be difficult to target by conventional axial approaches. Fine-needle aspiration revealed hepatocytes with focal chronic inflammatory cells.

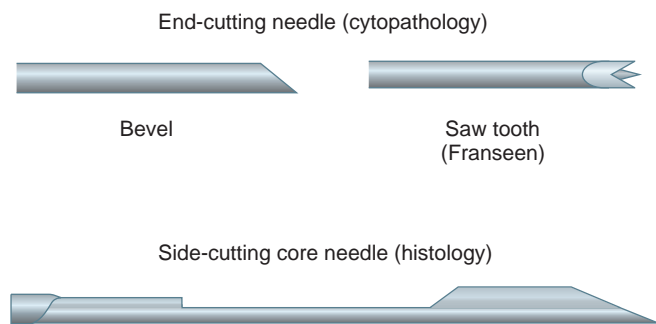


Figure 71-3 Biopsy needles.

intended target as they pass through tissue interfaces, which renders accurate needle placement somewhat more difficult. Needles with a pointed stylet tend to track along a straight line. The Hawkins-Akins needle (Cook Medical, Inc., Bloomington, Ind) also contains an interchangeable blunt stylet, which reduces the risk of injury to bowel, nerves, and blood vessels.³²⁻³⁴

Many biopsy needles are available. These can be broadly grouped into aspirating and cutting needles (Fig. 71-3). The aspirating needles are usually 20- to 25-gauge and are designed to yield individual cells or small clumps of cells that can be spread into a single cell layer for cytopathologic analysis. The “skinny” 22- or 25-gauge needle, although in widespread use, is very flexible and particularly susceptible to bending and deflection. At times, however, the purposeful bending of such a thin-gauge needle can aid in targeting lesions that would be difficult to access otherwise. A curved needle placed coaxially through a straight needle is advantageous because it can compensate for inaccurate guide needle placement and can also sample different regions of a lesion without having to manipulate the outer needle.³⁵ If a curved needle is used without a guide needle, care should be taken in inserting the needle as rotation of the needle may result in a lacerating effect.³⁶

Many radiologists attach a syringe and tube to the needle to apply suction during the actual biopsy. We have abandoned the use of this suction method in favor of simply removing the stylet and relying on natural capillary forces and mechanical agitation to draw tissue into the needle.³⁷ The main advantage of the nonsuction technique is that the specimens are usually free of blood. Fibrin clots form quickly within bloody aspirates, rendering them difficult to smear onto a glass slide. Also, the presence of abundant erythrocytes obscures cellular detail.

The cutting needles, usually 14- to 20-gauge, are designed to obtain a core of tissue suitable for histologic analysis. Most radiologists have adopted the use of automated cutting needles.^{38,39} These automated needles have an inner slotted stylet for the specimen and an outer cutting stylet. They consistently provide an excellent core of tissue. Manufacturers have designed single-use automated or semiautomated cutting needles that are so lightweight they will maintain their position during the movement of patients in and out of the CT gantry. Cutting needles with a short, long, or adjustable excursion are available. Many of these needles lend themselves to a coaxial technique, permitting several biopsy samples to be obtained from a single skin and organ puncture. In a blinded evaluation of 20 automated cutting biopsy devices, the best overall performance was obtained with 18-gauge needles with at least a 2-cm excursion.³⁸

It has been suggested that radiologists should use the smallest gauge needle possible in performing biopsy procedures. Researchers have explored the effect of needle gauge on organ bleeding in the pig model.^{40,41} This work shows that in general, larger needles produce greater bleeding. The research also shows that large needles yield greater amounts of tissue. To the extent that each needle pass carries risk, the maximum tissue yield can be obtained at minimum risk by performing fewer passes with a larger needle. There are two caveats to consider. First, cytopathologists prefer to analyze a thin layer of single cells or clumps of cells. Samples obtained from thin needles (i.e., 20- to 25-gauge) may be easier to smear into a single cell layer than samples from larger needles (14- or 18-gauge). Second, use of cutting needles is riskier than use of aspirating needles. If the knifelike blade of the cutting needle encounters an artery or a vein, the vessel will be lacerated and bleed. In contrast, aspirating needles tend to displace rather than to cut tissue.

MRI is used to guide tissue biopsies particularly in the central nervous system and breast.^{29,42} Dedicated MR-specific needles are now available,⁴³ although the selection of biopsy needles and sizes is considerably more limited than with the ferromagnetic needles traditionally used in US and CT cases. These nonferromagnetic needles are readily visualized as a signal void and are safe to use in the magnetic field. Use of a ferromagnetic needle, on the other hand, can cause considerable image distortion that may obscure the lesion of interest and hinder precise needle localization. In addition, they may be torqued or deflected in the magnetic field, raising questions about their safety.

It is vital to coordinate needle selection with the pathologist who will interpret the case. If the pathologist is skilled in cytopathology, small-bore (20- to 25-gauge) aspirating needles are recommended. If the pathologist prefers samples for histologic analysis, larger bore cutting needles are appropriate. Some groups perform a cytopathologic touch preparation for samples obtained with core needles. This technique allows a rapid preliminary diagnosis and preserves the core material for permanent fixation and sectioning.⁴⁴

Biopsy Planning

In planning the approach to a lesion, one must decide not only on the needle type but also on the needle route, the guidance modality, and the most efficient and comfortable patient position. The choice of needle route to a lesion will be based on the presence of intervening structures. Because needle passage through an organ creates both an entrance and an exit wound, this is indeed an important consideration. Whereas some organs tolerate this type of transgression, others do not, and henceforth these are referred to as acceptable and unacceptable transgressions.

ACCEPTABLE ROUTES

Organs through which needle transgression is acceptable include the liver, lungs, and gastrointestinal tract. The liver, because of its size and solid nature, provides not only a window for sonographic imaging of the upper abdomen but also an access route for the biopsy of deep masses. This includes masses involving the gallbladder, pancreatic head and body, porta hepatitis, adrenal gland (Fig. 71-4), and, on occasion, right kidney. Needles ranging up to 14-gauge in caliber and of all

types are usually well tolerated as long as blood vessels are avoided.

The lungs can usually be avoided when US is used for guidance because an off-axis approach allows one to angle the transducer cranially to avoid the pleural space. Even when the pleural space is violated, the lung parenchyma itself is often spared, reducing the risk of pneumothorax considerably. When CT is used to biopsy subdiaphragmatic lesions, lung transgression is sometimes unavoidable, although this is usually well tolerated when needles of 20-gauge or smaller are used, and, typically, chest tube placement is unnecessary.

The gastrointestinal tract can also tolerate needle transgression. The stomach, being thick walled, can tolerate puncture with needles up to 18-gauge or even larger. Transgression of the

stomach, however, can be challenging because the wall is resilient and the needle may induce a peristaltic contraction.

Some interventionalists hesitate to transgress the small bowel because of its thin wall and fear of perforation and abscess formation. However, in our experience using 20-gauge needles, such transgressions are well tolerated. Newer 20-gauge automated cutting needles are particularly useful for the biopsy of deep lesions or lymph nodes because transenteric excursion is virtually unavoidable. Transducer compression effectively reduces lesion depth by displacing or flattening bowel and adipose tissue (Fig. 71-5).^{45,46}

Transcolonic needle excursion is somewhat more controversial because of the fear of bacterial contamination within the peritoneal cavity. However, as with the small bowel, the colon is undoubtedly violated at times during US-guided biopsies using transducer compression. Passing a needle through stool-filled bowel, which may be unavoidable with CT, may be another issue, at least empirically (Fig. 71-6). In this scenario, it may be prudent to administer antibiotics (e.g. gentamicin 80 mg intramuscularly within 60 minutes prior to the procedure plus 250 mg ciprofloxacin twice daily orally for 5 days following the procedure). As with the small bowel, whenever colon transgression is anticipated, a needle on the order of 20-gauge or smaller is recommended.

Hydrodissection is a technique in which structures can be safely displaced away from the targeted mass.³⁴ Fluids, such as physiologic sterile saline, can be safely infused to create an artificial space and allow safe passage of a biopsy needle (Fig. 71-7). Hydrodissection generally works well in the retroperitoneum (e.g., to widen the paravertebral space before adrenal biopsy or to displace the ascending colon, descending colon, or second portion of the duodenum).³⁶ In the peritoneum, however, this technique is limited as fluid diffusion within the peritoneal cavity and mesenteric folds becomes difficult to control.⁴⁷

Transgression of vascular structures should be avoided whenever possible. Nevertheless, there is anecdotal evidence to suggest that the aorta is tolerant of needle transgression (Fig. 71-8). Certainly, early interventional experience with translumbar aortography using 16- and 18-gauge needles corroborates this contention.⁴⁸ Additional reports describe transaortic endoscopic US (EUS)-guided fine-needle aspiration of thoracic para-aortic lesions using 22- and 25-gauge needles as safe.^{49,50} Transgression of the inferior vena cava is also feasible, safe, and

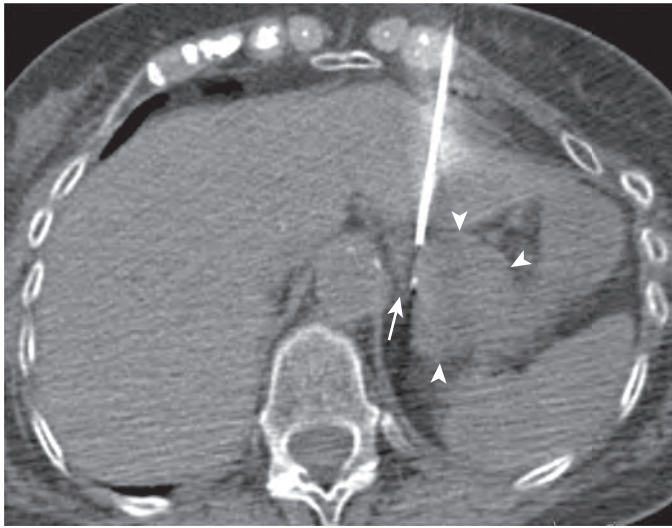


Figure 71-4 CT scan of a 66-year-old man with lung carcinoma. Axial noncontrast CT of the upper abdomen reveals an enlarged left adrenal gland (arrow) adjacent to the gastric fundus/proximal gastric body (arrowheads). The left adrenal gland was biopsied with a transhepatic approach. The liver tolerates needle transgression well as long as blood vessels are avoided. Fine-needle aspiration revealed metastatic carcinoma. Of note, the patient was initially scanned in the prone and left lateral decubitus positions in the hope of accessing the lesion posteriorly, but the intervening left kidney prevented this approach.

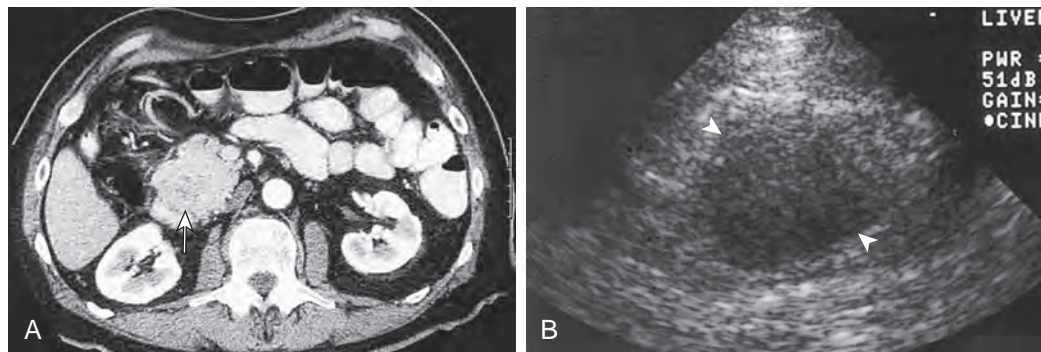


Figure 71-5 Images of a 57-year-old man with abdominal pain and weight loss. **A.** Axial CT of the upper abdomen with contrast material reveals a rounded fullness in the pancreatic head with subtle hypoattenuation changes (arrow). Note numerous blood vessels anterolateral to the pancreatic head as well as colon and jejunum anteromedially. **B.** Gray-scale ultrasound in the transverse plane reveals a hypoechoic, rounded mass in the region of the pancreatic head (arrowheads). Note that with transducer compression, there has been considerable decrease in the distance from the skin to the mass as well as displacement of intervening bowel. Fine-needle aspiration revealed adenocarcinoma.



Figure 71-6 CT of a 70-year-old woman with abdominal pain and jaundice. The patient underwent preliminary endoscopic retrograde cholangiography (not shown) suggesting a mass involving the distal common bile duct. A plastic biliary stent was inserted. Follow-up noncontrast axial CT scan of the upper abdomen reveals some rounded fullness of the pancreatic head but no obvious mass. Percutaneous biopsy was performed by an anterior transcolonic approach. Because no obvious mass was identified, biopsy samples were taken adjacent to the stent (arrow). Fine-needle aspiration revealed adenocarcinoma. There were no hemorrhagic or infectious complications.

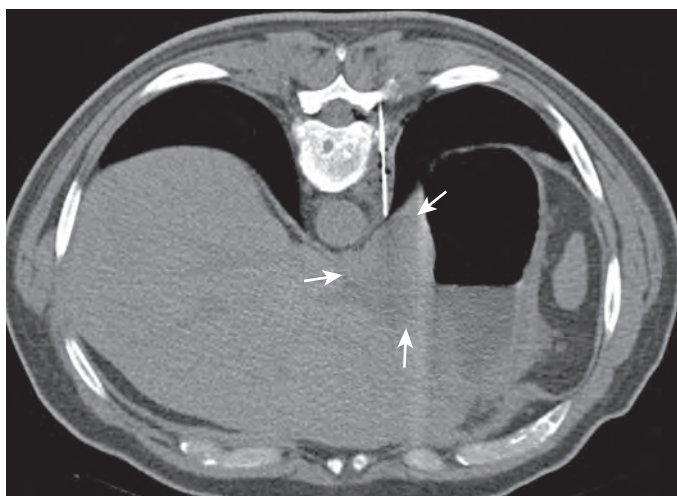


Figure 71-7 CT of a 55-year-old man with confluent adenopathy along the lesser curvature of the stomach (arrows). An 18-gauge Hawkins-Akins needle was advanced into the left paravertebral space, and approximately 30 mL of sterile 0.9% saline was injected to create an artificial space to avoid pulmonary transgression. Fine-needle aspiration biopsy revealed diffuse large B-cell lymphoma. A chest radiograph after the procedure demonstrated no pneumothorax.

well tolerated, as illustrated by studies using CT-guided fine-needle aspiration biopsy of pancreatic and peripancreatic lesions by a posterior transcaval approach.^{51,52} The 18-, 20-, and 22-gauge needles have been used with diagnostic accuracy rates of 86%.⁵¹ At our institution, we advance an 18-gauge Chiba guide needle to the posterior wall of the cava and traverse the cava wall with a 22-gauge aspirating needle and have expanded the use of this technique to other retroperitoneal lesions along the inferior vena cava (Fig. 71-9).



Figure 71-8 CT of a 59-year-old man with back pain and weight loss. Preliminary CT revealed a mass in the pancreatic head and neck encasing the celiac axis and superior mesenteric artery. The mass subsequently underwent biopsy percutaneously in the prone position by a retroperitoneal approach. Initial needle placement revealed aortic violation. The needle was subsequently repositioned into the pancreatic mass, and fine-needle aspiration revealed adenocarcinoma. There were no hemorrhagic complications as a result of aortic transgression.



Figure 71-9 CT of a 76-year-old woman with non-small cell lung carcinoma. Axial CT of the abdomen with contrast material reveals a small lymph node anterior to the inferior vena cava (arrow). An 18-gauge Chiba needle was advanced to the posterior wall of the inferior vena cava, and multiple passes were obtained with a 22-gauge Chiba needle through the inferior vena cava into the lymph node. Cytology revealed metastatic carcinoma. Follow-up CT imaging obtained 15 minutes after biopsy demonstrated no hemorrhage.

ROUTES TO AVOID

A needle path through the pancreas should be absolutely avoided. In a review of percutaneous abdominal sampling by Smith,⁵³ pancreatic biopsy accounted for the second-most number of deaths. Whereas liver biopsy is associated with a higher number of deaths, it is important to consider that the liver is the most commonly sampled abdominal organ. In Smith's review, there were six deaths from pancreatic biopsy, and five were due to pancreatitis. In each of these five cases, no

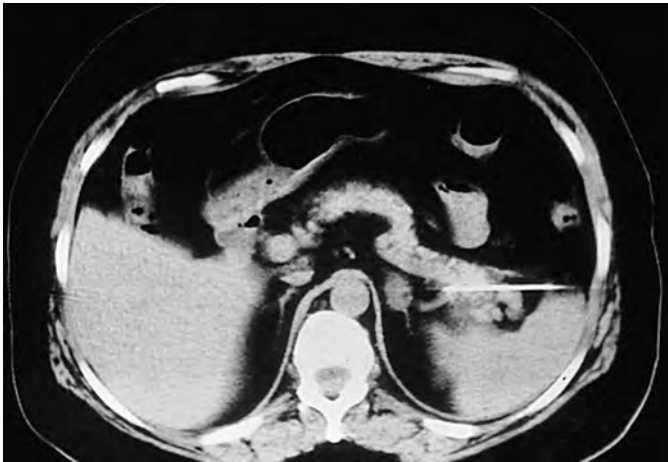


Figure 71-10 CT of a 48-year-old woman with breast carcinoma. Axial CT of the upper abdomen with contrast material reveals a small nodule in the left adrenal gland. The right adrenal gland was normal. The left adrenal mass underwent biopsy percutaneously through an intercostal and transpancreatic approach. Because normal pancreatic parenchyma is prone to development of pancreatitis when it is transgressed, this technique is not recommended. Fine-needle aspiration revealed no evidence of malignant transformation.

tumor was found. One plausible explanation is that when small lesions are biopsied, the needle probably transgresses normal pancreatic parenchyma, causing enzyme release. Thus, at our institution, it is our policy to avoid needle paths through normal pancreas. This is true for both dedicated pancreatic biopsies and transpancreatic biopsies of deeper lesions (Fig. 71-10).

The following needle paths should be avoided, if possible: through the spleen, adrenals, and kidneys. The spleen is a solid but soft organ that, like the liver, can provide a window to the left upper quadrant, particularly when it is enlarged. However, because of its well-known susceptibility to blunt trauma, there is concern that a splenic biopsy might result in capsular rupture. Transsplenic needle excursion is even more of a concern than splenic biopsies because the capsule is punctured twice. Although complications related to needles and the spleen may be overestimated, we recommend avoiding this organ when needles are placed in the left upper quadrant. The adrenals and kidneys are both associated with hemorrhagic complications of biopsy. Although retroperitoneal hemorrhage after these types of biopsies is often asymptomatic, even when it is substantial, transadrenal or transrenal needle excursion is not recommended.

Specific Organ-Related Techniques

LIVER

The liver is a vascular but relatively resilient organ that tolerates needle placement well, whether for biopsy of a focal liver abnormality, for biopsy of hepatic parenchyma, or to be traversed en route to a deeper lesion. Needles up to 14-gauge are commonly used without difficulty. The liver capsule is richly innervated; therefore, copious infiltration of the capsule with a local anesthetic, such as lidocaine, is necessary to achieve adequate pain control during needle placement. The liver can usually be accessed through a subcostal, subxiphoid, or intercostal approach. The last approach is typically the most difficult, and

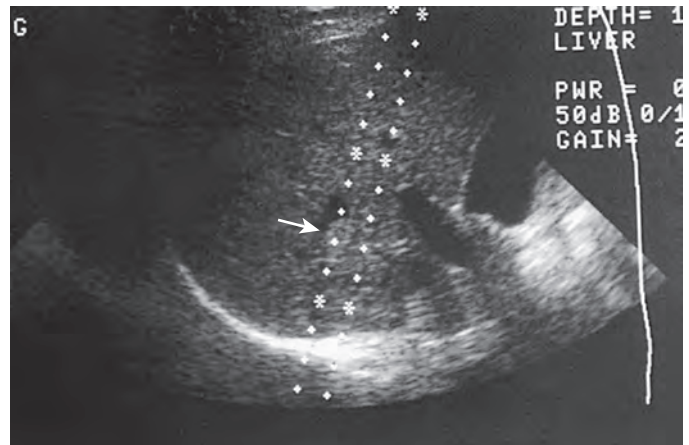


Figure 71-11 Ultrasonogram of a 63-year-old man with small cell lung cancer. Gray-scale ultrasound reveals a large hypoechoic mass located deep in the left hepatic lobe (arrow). The mass underwent biopsy percutaneously by a subcostal approach. Fine-needle aspiration revealed metastasis.

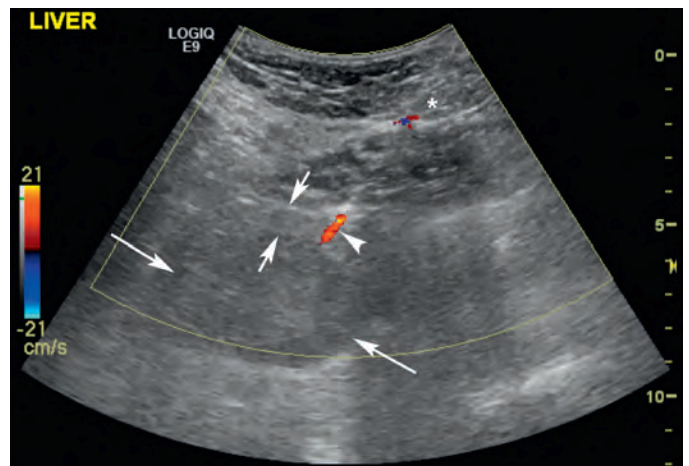


Figure 71-12 Ultrasonogram of a 51-year-old man with melanoma. Color ultrasound of the liver following percutaneous needle biopsy of a hypoechoic hepatic mass (long arrows). The needle transgressed approximately 1 cm of normal hepatic parenchyma (short arrows). As the needle (asterisk) was removed from the liver, a tract of blood was evident along the needle path (arrowhead) toward the liver capsule. There was, however, no evidence of subcapsular accumulation of blood, and the track resolved within 30 to 60 seconds.

care should be taken to avoid the intercostal neurovascular bundle, which courses along the inferior margin of each rib. Real-time guidance during needle placement is also helpful for avoidance of major portal and hepatic veins. It is advantageous to interpose a cuff of normal parenchyma (at least 1 cm) between the liver capsule and the margin of a lesion, and this task is more easily accomplished with US by an off-axis approach (Fig. 71-11).

Fine-needle aspiration of focal abnormalities for cytology is typically performed with a 20- to 22-gauge aspirating needle, either a Chiba or Franseen. Medical biopsy of hepatic parenchyma for histology is typically performed with a 20-gauge cutting needle, many of which have a spring-loaded rapid-fire mechanism. Routine assessment of the liver with color Doppler US after withdrawal of one of these larger gauge cutting needles can demonstrate a linear track of blood flowing toward the capsule (Fig. 71-12). These tracks, however, typically resolve

within 2 to 3 minutes without evidence of subcapsular accumulation of blood. Plugging of biopsy tracks with gelatin particles,⁵⁴⁻⁵⁷ gelatin particles and thrombin,⁵⁴ or coils⁵⁸ has been described. Whereas these studies were limited by small numbers of patients, use of these agents appears to be safe and well tolerated.⁵⁴⁻⁵⁸

There has been considerable controversy about the biopsy of hepatic hemangiomas, whether inadvertent or intentional. Because these benign tumors consist of a tangle of thin-walled endothelium-lined blood vessels, there is presumed to be an increased risk for hemorrhagic complications. Several studies have shown, however, that hemangiomas can be biopsied safely with an acceptable complication rate (Fig. 71-13).⁵⁹⁻⁶² This includes the use of 18-gauge aspirating needles and 18-gauge cutting needles. These studies have also emphasized the importance of interposing a cuff of normal hepatic parenchyma between the capsule and the margin of the lesion. Although these results are encouraging, the number of patients included in each of these studies is relatively small, and it is presumed that a large-scale comparative trial of the biopsy of hemangiomas and metastases would reveal a slightly higher complication rate for the biopsy of hemangiomas. Whereas the noninvasive work-up of these common and, in most cases, inconsequential lesions cannot be overemphasized, it is comforting to know that if a hemangioma is biopsied, whether inadvertently or because of nonclassic imaging features, the complication rate is low.⁵⁹

Another issue is the safety of performing a liver biopsy in the presence of ascites. It is presumed that direct contact with the diaphragm or abdominal wall functions to tamponade the capsular injury, thereby preventing significant subcapsular or intraperitoneal hemorrhage. Therefore, when the capsule is in contact with a layer of fluid, the risk of hemorrhagic complications is increased, particularly if patients have a tenuous coagulation status (Fig. 71-14). Two studies in particular have addressed the issue of ascites in patients with cirrhosis.^{63,64} In both reports, the complication rate was low, and when

complication rates were compared between those with ascites and those without ascites, there was no statistically significant difference.

Hepatocellular carcinoma is a locally invasive tumor that often infiltrates and obstructs portal veins, hepatic veins, and even bile ducts. The presence of underlying cirrhosis often excludes a patient from hepatic tumor resection, either because of inadequate residual function or because hepatomas in these patients are typically more aggressive. However, patients with little or no parenchymal dysfunction may be candidates for resection. In these patients, it is imperative to determine if portal or hepatic venous thrombosis is bland or malignant. There are noninvasive means of making this determination, such as enhancement during the hepatic arterial dominant phase of a dynamic bolus CT with iodinated contrast material or MRI with a gadolinium chelate. However, these signs of unresectability are not often present. Biopsy of the intraluminal mass may be requested both to diagnose and to stage this malignant neoplasm. It is useful to use a guidance technique with real-time capability, in biopsy of an intraluminal mass, to ensure that the needle tip does not venture beyond the wall of the vein into an adjacent parenchymal tumor deposit.⁶⁵ US-guided biopsy of portal vein thrombus is safe, accurate, and well tolerated.⁶⁵⁻⁶⁷

In addition to biopsy of focal hepatic masses, US is used to guide random liver biopsies in medical liver disease, such as hepatitis or hemochromatosis. For diffuse liver disease, most hepatopathologists are satisfied with a specimen containing at least six to eight portal triads.⁶⁸ Biopsy is considered the “gold standard” for assessment and grading of liver fibrosis. However, the accuracy of histologic assessment has been challenged because of the nonuniform pattern of liver fibrosis.⁶⁹ For this reason, techniques using US and magnetic resonance elastography have been developed.



Figure 71-13 CT of a 61-year-old woman with vague right upper quadrant pain. Axial noncontrast CT of the upper abdomen reveals a large hypoattenuating mass occupying most of the right hepatic lobe. A central hypoattenuating scar is noted within the mass. Although the mass is large and easily approached through an intercostal space, it underwent biopsy anteriorly, for a cuff of normal hepatic parenchyma to be interposed between the capsule and the mass. Fine-needle aspiration revealed a hemangioma.

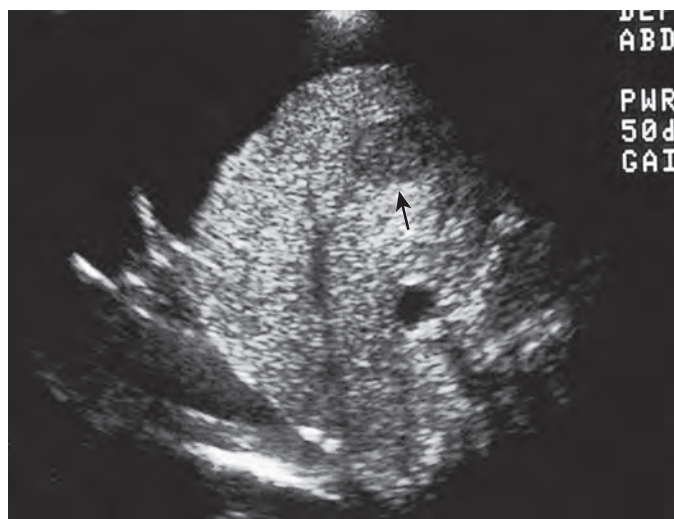


Figure 71-14 Ultrasonography of a 42-year-old man with cirrhosis and portal hypertension. Gray-scale ultrasound of the liver in the longitudinal plane revealed a small, shrunken liver with heterogeneous echotexture consistent with cirrhosis. There is also a considerable amount of perihepatic ascites and a 2-cm hypoechoic nodule in the right hepatic lobe anteriorly (arrow). The mass underwent biopsy with ultrasound guidance by an intercostal space through the ascites. Fine-needle aspiration revealed hepatocellular carcinoma. There were no hemorrhagic complications.

ADRENAL GLANDS

The possibility of malignant disease is the primary concern when adrenal masses are discovered. In a study by Young,⁷⁰ incidental adrenal masses were detected in 2005 patients; adrenal cortical carcinoma was diagnosed in 4.7% and metastatic disease in 2.5%. For patients with a history of malignant disease, however, metastatic disease accounts for nearly half of the causes.⁷¹ The role of fine-needle aspiration biopsy is to delineate adrenal and nonadrenal tissue.⁷² Many routes have been used with success. Whereas an anterior approach through the liver (for right adrenal biopsy), stomach, and pancreas has also been described,⁷³ this is rarely used. Patients are most often placed in the prone or lateral position, and a guide needle is generally advanced from a posterior approach. Out-of-plane access is used because of interposed, aerated lung. Methods to circumvent puncture of the lung include the triangulation method,²⁴ angling of the CT gantry,⁷⁴ injection of medical-grade carbon dioxide into the pleural space,⁷⁵ and placement of the patient in the ipsilateral decubitus position.⁷⁶ At our institution, we generally place the patient in the ipsilateral decubitus position to immobilize the diaphragm and to minimize lung aeration. In our experience, this results in a direct, non-transpulmonary route for biopsy, reduces the need for out-of-plane approaches, and is as reliable and safe as the prone position.⁷⁶

Technical success of adrenal biopsy ranges from 80% to 95%.^{77,78} Risks include adrenal hematoma, abdominal pain, hematuria, pancreatitis, pneumothorax, adrenal abscess, and needle track seeding.^{70,74,78} The possibility of pheochromocytoma should be excluded with biochemical testing before biopsy as fine-needle aspiration biopsy can result in adrenal hemorrhage and hypertensive crisis.^{79,80}

PANCREAS

The pancreas is a relatively soft, unencapsulated organ located deep in the upper retroperitoneum that is prone to development of inflammation. Acute pancreatitis can occur not only after a needle biopsy but also after blunt trauma or the direct injection of contrast media into the pancreatic duct during endoscopic retrograde cholangiopancreatography.⁸¹ Pancreatic tumors, including both adenocarcinomas and islet

cell tumors, are often difficult to visualize because there may not be a contour abnormality or there is little tissue contrast compared with adjacent nontumorous parenchyma. Furthermore, pancreatic adenocarcinomas are associated with a considerable amount of tissue desmoplasia, which can increase sampling error.¹

Both EUS-guided FNA and percutaneous image-guided FNA are similarly accurate for the diagnosis for exocrine pancreatic cancer when the lesion is more than 3 cm in size. One advantage of EUS-guided sampling is that it can often find small pancreatic or ampullary lesions that are not clearly visible with CT, MRI, or transabdominal US, thus providing a better guide for biopsy.^{82,83} Also, EUS-guided pancreatic biopsy through the duodenum provides a theoretical decreased risk of malignant seeding intraperitoneally or along the needle path. Despite the advantages of EUS-guided pancreatic sampling, there are still occasions when percutaneous pancreatic biopsy is indicated. In general, small-caliber needles, on the order of 20- to 22-gauge, are used to biopsy the pancreas. Although there is concern about development of a fistula to the pancreatic duct with larger caliber needles, 14-, 16-, and 18-gauge cutting needles can be used to safely biopsy large pancreatic masses.⁸⁴ In general, however, 20-gauge cutting needles are preferred in this scenario. Many of the needles used for fine-needle aspiration are designed to be self-aspirating, although it may be advantageous to use suction in performing a biopsy of pancreatic tumors that are desmoplastic.

Biopsy of pancreatic masses is usually performed by an anterior approach, through either the left lobe of the liver or the gastrointestinal tract, typically the stomach or small bowel. Fine-needle aspiration biopsy of lesions in or around the pancreatic head by a transcaecal approach has also been shown to be safe and effective in obtaining diagnostic tissue.^{51,52} Approaching a mass in the head of the pancreas through the right hepatic lobe, duodenum, or gallbladder is generally not recommended. Furthermore, approaching a mass in the tail of the pancreas through the spleen is not recommended.

In our practice, we prefer US for guidance as it is generally easier than with CT to navigate a needle into the lesion without traversing the numerous peripancreatic blood vessels. Furthermore, perivascular tumor encasement can be biopsied directly and can serve both to diagnose and to stage the tumor (Fig. 71-15). With an anterior approach, compression with the US

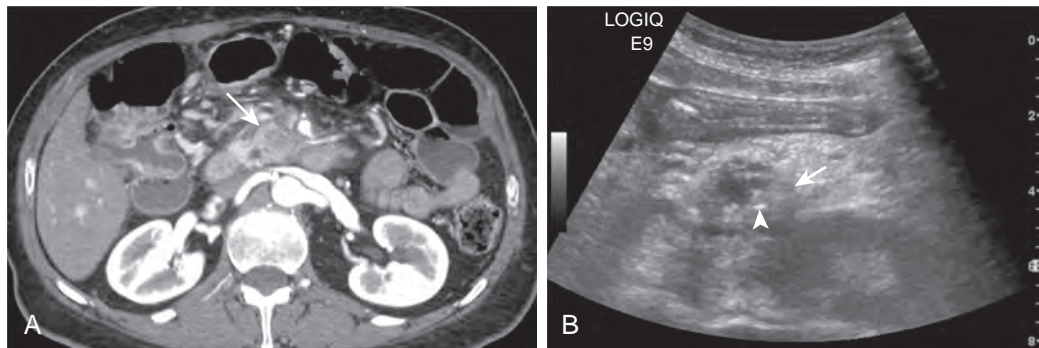


Figure 71-15 Images of a 64-year-old woman with vague upper abdominal pain and weight loss. **A.** Preliminary axial CT scan with contrast material revealed a pancreatic head mass (arrow). **B.** This mass (arrow) was subsequently biopsied percutaneously under ultrasound guidance by an anterior approach. The needle tip (arrowhead) is placed directly in this soft tissue. Fine-needle aspiration revealed adenocarcinoma. There were no hemorrhagic complications, and real-time guidance prevented transgression of the artery.

transducer not only reduces the depth of needle placement but also displaces many intervening structures, particularly the transverse colon and jejunum. In some cases, a discrete mass may not be appreciated, yet diagnostic tissue can still be obtained by looking for indirect signs, such as abrupt termination of a dilated duct, or taking a biopsy sample adjacent to a biliary stent. The biopsy of peripancreatic lymph nodes or liver nodules in the setting of pancreatic carcinoma is often productive as well, especially for staging.

A concern about pancreatic biopsies is the potential for peritoneal tumor seeding.⁸⁵ This theory, however, is difficult to substantiate because most patients are inoperable and do not have surgical confirmation, and most do not survive long enough for the implants to reach a size detectable with cross-sectional imaging. It is doubtful that the biopsy of pancreatic adenocarcinoma negatively affects outcome.

BOWEL

Biopsies of the digestive tract are almost always performed endoscopically and, when that is not possible, usually open or laparoscopically. However, endoscopic biopsy may be impossible when the lesion or involved bowel segment lies between the ligament of Treitz and the ileocecal valve. In many of these cases, there may be metastases elsewhere that are better suited to endoscopic biopsy. However, when an isolated bowel wall mass is not amenable to endoscopic biopsy, percutaneous sampling is appropriate.⁸⁶⁻⁸⁸ For example, submucosal lesions such as gastrointestinal stromal tumors may not be easily identified endoscopically.

Percutaneous bowel wall biopsy may be performed with either US or CT guidance, depending on the lesion's characteristics and the patient's body habitus. Our group prefers US guidance as compression with the US transducer may displace overlying bowel loops and anchor the targeted bowel segment, which may otherwise be displaced by the biopsy needle. Color Doppler US may also be used to identify and to avoid adjacent mesenteric vessels. In addition, percutaneous bowel wall biopsy can be performed with either fine-needle aspiration or core needles.^{86,89}

Potential complications particular to biopsies of the digestive tract include bowel hematoma, bowel perforation, and peritonitis. Choosing a biopsy route that does not traverse the bowel lumen may minimize the risk of bowel perforation. Even when the bowel lumen is traversed, the risk of perforation remains low. The study of Marco-Doménech and associates⁸⁷ included eight patients whose histologic samples contained mucosa, indicating that the mucosa and lumen were perforated; however, none had an adverse outcome.

LYMPH NODES

Lymph nodes represent the most common site of metastatic disease. With improvements in image guidance and needle design, radiologists are increasingly requested to biopsy lymph nodes to diagnose and to stage a suspected malignant neoplasm or to obtain samples for culture. This increase in the number of requests for lymph node biopsy may be attributed to discovery of normal-sized but hypermetabolic nodes on positron emission tomography.

We have found US guidance to be accurate and safe for biopsy of abdominal and retroperitoneal nodes with a success

rate of 86%, similar to results from other institutions.^{45,46} Real-time needle-tip visualization helps ensure that sampling will be limited to the lesion; samples are far less likely to be contaminated with extraneous tissue or blood and thus may be easier to interpret by the cytopathologist. With real-time visualization, it is also possible to ensure that the needle excursions are short of adjacent critical structures, such as blood vessels and the common bile duct. We have found that lymph node visualization is improved markedly by applying firm pressure with the transducer to compress and to displace overlying fatty tissue and bowel loops, decreasing the necessary depth for sound penetration and length of needle excursion by approximately 50%. For biopsy of lymph nodes, it is vital to review CT scans before the procedure to choose the optimal site and route.

A special consideration is lymphoma, which can be broadly classified into mature B-cell and T-cell neoplasms. At our institution, the majority of both superficial and deep lymphomatous masses are approached with image-guided biopsy. The combination of cytology fine-needle aspiration and flow cytometry to differentiate reactive lymphoid hyperplasia from a mature B-cell lymphoma has a high sensitivity and specificity (ranging from 94% to 100%) to appropriately classify the disease.⁹⁰⁻⁹³ We attempt to collect at least 1 million lymphocytes, which can be quickly quantified with an automated cell counter. Obtaining sufficient material allows the cytopathologists to perform immunophenotyping and additional ancillary studies, such as immunocytochemistry, fluorescence in situ hybridization, and polymerase chain reaction. Hodgkin's lymphoma patients typically present with supradiaphragmatic lymphadenopathy, with inguinal adenopathy seen in a minority of cases. For Hodgkin's lymphoma, we generally perform a concurrent core needle biopsy. Other groups, however, argue that the initial diagnosis of Hodgkin's lymphoma should be made with a surgical specimen as fine-needle aspiration and core needle samples fail to appropriately depict the architecture of the lymph node, which is important for an accurate diagnosis.⁹⁴ Ultimately, consultation with local experts is necessary to ensure that appropriate specimens are obtained at your institution.

SPLEEN

Requests for percutaneous splenic biopsies are uncommon. This relates to the relative infrequency of isolated splenic disease and the perceived risk of hemorrhagic complications in this soft, encapsulated organ. However, in a meta-analysis to determine the diagnostic accuracy and complication rate of percutaneous image biopsy of the spleen, pooled sensitivity and specificity measured 87.0% and 96.4%, respectively.⁹⁵ The pooled complication rate was 1.3% when needles were 18-gauge or smaller, and the most common complication was hemorrhage followed by pain. The advantages of interposing a cuff of normal splenic parenchyma between the capsule and the lesion are controversial (Fig. 71-16). Unless it is large, the spleen is approached through the intercostal space, and at times, pleural transgression is necessary. This is less of a problem with US than with CT because an off-axis or angled approach can be used.

Complications

In general, abdominal biopsies are safe. Minor complications include pain, vasovagal reactions, small hematomas, pneumothorax, bacteremia, and pancreatitis.^{41,96} The most common

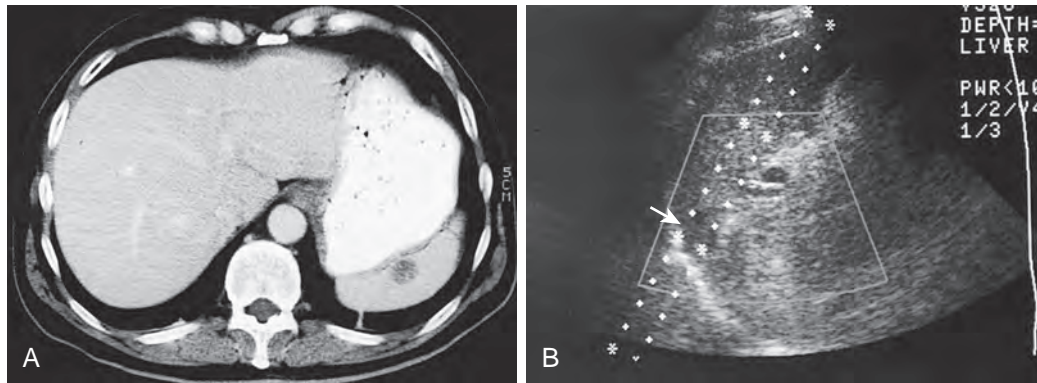


Figure 71-16 Images of a 52-year-old man with melanoma. **A.** Axial CT of the upper abdomen with contrast material reveals a 1.5-cm hypoattenuating mass in the spleen. **B.** Gray-scale ultrasound of the spleen in the longitudinal plane reveals a hypoechoic mass located deep in the splenic parenchyma (arrow). By an intercostal approach, the mass underwent biopsy percutaneously with the attached needle guide. Note that the mass is aligned within the parallel dotted lines, which represent the proposed path of the needle when it is advanced through the attached guide. Fine-needle aspiration revealed metastatic melanoma.

minor complication is pain or vasovagal reaction, which occurs in approximately 1% to 5% of patients. Fortunately, less than 1% of patients will have a hematoma large enough to require a transfusion. An additional minor complication of biopsies in the upper abdomen is pneumothorax.⁹⁶ Whereas there is a theoretical risk of pneumothorax when the potential space of the pleura is transgressed, pneumothorax is extremely rare unless the aerated pulmonary parenchyma is transgressed as well. It is our impression that the risk of pneumothorax is decreased with the use of US compared with CT guidance. Pancreatitis after biopsy is a well-described complication. Paradoxically, pancreatitis tends to occur only when the normal pancreatic parenchyma is transgressed; biopsies of the diseased pancreas (chronic pancreatitis or cancer) are usually well tolerated and rarely result in pancreatitis. Although pancreatitis is often considered a minor complication, some patients with biopsy-related pancreatitis may be critically ill, requiring prolonged hospitalization.

When the bowel is transgressed, there is a risk of microperforation and subsequent abscess formation. Theoretically, the risk of peritonitis is increased when the colon is transgressed compared with when the small bowel or stomach is transgressed because of the relatively sterile contents of the last two structures. With the use of US guidance and abdominal wall compression, it is often not possible to differentiate collapsed loops of small bowel from mesenteric fatty tissues. There is no doubt that needle transgression of bowel occurs more frequently with

US guidance than with CT guidance. Despite the increased use of US for guidance at our institution, we have not detected an increase in abscess formation or peritonitis. In support of this observation, Petit and associates⁹⁷ found that in pigs, transgression of the large and small bowel with 8F catheters was not associated with peritonitis or abscess formation. Care should be exercised, however, when there is transgression of colon for biopsy of a fluid-containing structure as the sample and lesion can become contaminated.³⁶

Fortunately, serious complications are rare.^{53,97-99} The mortality rate from an image-guided percutaneous abdominal biopsy is widely considered to be 0.1%. However, a retrospective review of complications by Smith⁵³ suggested that the mortality rate from abdominal fine-needle aspirations may in fact be as low as 0.006% to 0.031%. The majority of reported deaths from biopsies are from hemorrhage after a liver biopsy. Interestingly, most of the reported deaths from liver biopsies occurred with use of skinny needles of only 20- to 22-gauge. The second most frequent cause of death after an abdominal guided biopsy is pancreatitis due to transgression of normal pancreatic parenchyma.

Needle track seeding is also a rare but major complication with a frequency ranging from 0.003% to 0.009%.¹⁰⁰ Most of the reported needle track seedings are the result of biopsies of pancreatic cancer, although virtually any tumor may spread along a needle track.

REFERENCES

- Hébert-Magee S: Basic technique for solid lesions: Cytology, core, or both? *Endosc Ultrasound* 3:28-34, 2014.
- Silverman SG, Mueller PR, Pfister RC: Hemostatic evaluation before abdominal interventions: An overview and proposal. *AJR Am J Roentgenol* 154:233-238, 1990.
- Rapaport SI: Assessing hemostatic function before abdominal interventions. *AJR Am J Roentgenol* 154:239-240, 1990.
- Patel IJ, Davidson JC, Nikolic B, et al: Consensus guidelines for periprocedural management of coagulation status and hemostasis risk in percutaneous image-guided interventions. *J Vasc Interv Radiol* 23:727-736, 2012.
- Patel IJ, Davidson JC, Nikolic B, et al: Addendum of newer anticoagulants to the SIR consensus guideline. *J Vasc Interv Radiol* 24:641-645, 2013.
- O'Connor SD, Taylor AJ, Williams EC, et al: Coagulation concepts update. *AJR Am J Roentgenol* 193:1656-1664, 2009.
- Ansell JE: The perioperative management of warfarin therapy. *Arch Intern Med* 163:881-883, 2003.
- Douketis JD, Spyropoulos AC: Vitamin K to reverse the anticoagulant effect of vitamin K antagonists: Can you teach an old dog new tricks? *J Thromb Haemost* 8:496-498, 2010.
- Douketis JD, Berger PB, Dunn AS, et al: The perioperative management of antithrombotic therapy: American College of Chest Physicians Evidence-Based Clinical Practice Guidelines (8th Edition). *Chest* 133(Suppl):299S-339S, 2008.
- Douketis JD, Spyropoulos AC, Spencer FA, et al: Perioperative management of antithrombotic therapy: Antithrombotic Therapy and Prevention of Thrombosis, 9th ed: American College of Chest Physicians Evidence-Based Clinical Practice Guidelines. *Chest* 141(Suppl):e326S-e350S, 2012.
- Douketis JD, Johnson JA, Turpie AG: Low-molecular-weight heparin as bridging

- anticoagulation during interruption of warfarin: Assessment of a standardized periprocedural anticoagulation regimen. *Arch Intern Med* 164:1319–1326, 2004.
12. Spyropoulos AC, Turpie AG, Dunn AS, et al: Clinical outcomes with unfractionated heparin or low-molecular-weight heparin as bridging therapy in patients on long-term oral anticoagulants: the REGIMEN registry. *J Thromb Haemost* 4:1246–1252, 2006.
13. Dezee KJ, Shimeall WT, Douglas KM, et al: Treatment of excessive anticoagulation with phytonadione (vitamin K): A meta-analysis. *Arch Intern Med* 166:391–397, 2006.
14. Ferraris VA, Ferraris SP, Lough FC, et al: Preoperative aspirin ingestion increases operative blood loss after coronary artery bypass grafting. *Ann Thorac Surg* 45:71–74, 1988.
15. Yusuf S, Zhao F, Mehta SR, et al: Effects of clopidogrel in addition to aspirin in patients with acute coronary syndromes without ST-segment elevation. *N Engl J Med* 345:494–502, 2001.
16. McKenzie JL, Douglas G, Bazargan A: Perioperative management of anticoagulation in elective surgery. *ANZ J Surg* 83:814–820, 2013.
17. Harder S, Klinkhardt U, Alvarez JM: Avoidance of bleeding during surgery in patients receiving anticoagulant and/or antiplatelet therapy: Pharmacokinetic and pharmacodynamic considerations. *Clin Pharmacokinet* 43:963–981, 2004.
18. Roth GJ, Majerus PW: The mechanism of the effect of aspirin on human platelets. I. Acetylation of a particulate fraction protein. *J Clin Invest* 56:624–632, 1975.
19. Roth GJ, Stanford N, Majerus PW: Acetylation of prostaglandin synthase by aspirin. *Proc Natl Acad Sci U S A* 72:3073–3076, 1975.
20. Sheafor DH, Paulson EK, Simmons CM, et al: Abdominal percutaneous interventional procedures: Comparison of CT and US guidance. *Radiology* 207:705–710, 1998.
21. Kehagias D, Metafa A, Hatzioannou A, et al: Comparison of CT, MRI and CT during arterial portography in the detection of malignant hepatic lesions. *Hepatogastroenterology* 47:1399–1403, 2000.
22. Ichikawa T, Saito K, Yoshioka N, et al: Detection and characterization of focal liver lesions: A Japanese phase III, multicenter comparison between gadoxetic acid disodium-enhanced magnetic resonance imaging and contrast-enhanced computed tomography predominantly in patients with hepatocellular carcinoma and chronic liver disease. *Invest Radiol* 45:133–141, 2010.
23. Jung EM, Friedrich C, Hoffstetter P, et al: Volume navigation with contrast enhanced ultrasound and image fusion for percutaneous interventions: First results. *PLoS ONE* 7:e33956, 2012.
24. van Sonnenberg E, Wittenberg J, Ferrucci JT, Jr, et al: Triangulation method for percutaneous needle guidance: The angled approach to upper abdominal masses. *AJR Am J Roentgenol* 137:757–761, 1981.
25. Chintapalli KN, Montgomery RS, Hatab M, et al: Radiation dose management: Part 1, minimizing radiation dose in CT-guided procedures. *AJR Am J Roentgenol* 198:W347–W351, 2012.
26. Howard MH, Nelson RC, Paulson EK, et al: An electronic device for needle placement during sonographically guided percutaneous intervention. *Radiology* 218:905–911, 2001.
27. Paltiel Y, Degani S, Zrayek A, et al: A new guidance system for freehand, obstetric ultrasound-guided procedures. *Ultrasound Obstet Gynecol* 19:269–273, 2002.
28. Silverman SG, Collick BD, Figueira MR, et al: Interactive MR-guided biopsy in an open-configuration MR imaging system. *Radiology* 197:175–181, 1995.
29. Kariniemi J, Blanco Sequeiros R, Ojala R, et al: MRI-guided abdominal biopsy in a 0.23-T open-configuration MRI system. *Eur Radiol* 15:1256–1262, 2005.
30. Gupta S, Madoff DC: Image-guided percutaneous needle biopsy in cancer diagnosis and staging. *Tech Vasc Interv Radiol* 10:88–101, 2007.
31. Sheiman RG, Fey C, McNicholas M, et al: Possible causes of inconclusive results on CT-guided thoracic and abdominal core biopsies. *AJR Am J Roentgenol* 170:1603–1607, 1998.
32. Akins EW, Hawkins IF, Jr, Mladinich C, et al: The blunt needle: A new percutaneous access device. *AJR Am J Roentgenol* 152:181–182, 1989.
33. Heavner JE, Racz GB, Jenigiri B, et al: Sharp versus blunt needle: A comparative study of penetration of internal structures and bleeding in dogs. *Pain Pract* 3:226–231, 2003.
34. Gupta S, Nguyen HL, Morello FA, Jr, et al: Various approaches for CT-guided percutaneous biopsy of deep pelvic lesions: Anatomic and technical considerations. *Radiographics* 24:175–189, 2004.
35. Gupta S, Ahrar K, Morello FA, Jr, et al: Using a coaxial technique with a curved inner needle for CT-guided fine-needle aspiration biopsy. *AJR Am J Roentgenol* 179:109–112, 2002.
36. Sainani NI, Arellano RS, Shyn PB, et al: The challenging image-guided abdominal mass biopsy: Established and emerging techniques 'if you can see it, you can biopsy it'. *Abdom Imaging* 38:672–696, 2013.
37. Hopper KD, Grenko RT, Fisher AI, et al: Capillary versus aspiration biopsy: Effect of needle size and length on the cytopathological specimen quality. *Cardiovasc Intervent Radiol* 19:341–344, 1996.
38. Hopper KD, Abendroth CS, Sturtz KW, et al: Automated biopsy devices: A blinded evaluation. *Radiology* 187:653–660, 1993.
39. Parker SH, Hopper KD, Yakes WF, et al: Image-directed percutaneous biopsies with a biopsy gun. *Radiology* 171:663–669, 1989.
40. Plecha DM, Goodwin DW, Rowland DY, et al: Liver biopsy: Effects of biopsy needle caliber on bleeding and tissue recovery. *Radiology* 204:101–104, 1997.
41. Gazelle GS, Haaga JR, Rowland DY: Effect of needle gauge, level of anticoagulation, and target organ on bleeding associated with aspiration biopsy. *Work in progress. Radiology* 183:509–513, 1992.
42. Daniel BL, Birdwell RL, Ikeda DM, et al: Breast lesion localization: A freehand, interactive MR imaging-guided technique. *Radiology* 207:455–463, 1998.
43. Moscatel MA, Shellock FG, Morisoli SM: Biopsy needles and devices: Assessment of ferromagnetism and artifacts during exposure to a 1.5-T MR system. *J Magn Reson Imaging* 5:369–372, 1995.
44. Diederich S, Padge B, Vossas U, et al: Application of a single needle type for all image-guided biopsies: Results of 100 consecutive core biopsies in various organs using a novel tri-axial, end-cut needle. *Cancer Imaging* 6:43–50, 2006.
45. Memel DS, Dodd GD, 3rd, Esola CC: Efficacy of sonography as a guidance technique for biopsy of abdominal, pelvic, and retroperitoneal lymph nodes. *AJR Am J Roentgenol* 167:957–962, 1996.
46. Fisher AJ, Paulson EK, Sheafor DH, et al: Small lymph nodes of the abdomen, pelvis, and retroperitoneum: Usefulness of sonographically guided biopsy. *Radiology* 205:185–190, 1997.
47. Arellano RS, Gervais DA, Mueller PR: CT-guided drainage of abdominal abscesses: Hydrodissection to create access routes for percutaneous drainage. *AJR Am J Roentgenol* 196:189–191, 2011.
48. Bakal CW, Friedland RJ, Sprayregen S, et al: Translumbar arch aortography—a retrospective controlled-study of usefulness, technique, and safety. *Radiology* 178:225–228, 1991.
49. von Bartheld MB, Rabe KF, Annema JT: Transaortic EUS-guided FNA in the diagnosis of lung tumors and lymph nodes. *Gastrointest Endosc* 69:345–349, 2009.
50. Wallace MB, Woodward TA, Raimondo M, et al: Transaortic fine-needle aspiration of centrally located lung cancer under endoscopic ultrasound guidance: The final frontier. *Ann Thorac Surg* 84:1019–1021, 2007.
51. Sofocleous CT, Schubert J, Brown KT, et al: CT-guided transvenous or transcaval needle biopsy of pancreatic and peripancreatic lesions. *J Vasc Interv Radiol* 15:1099–1104, 2004.
52. Gupta S, Ahrar K, Morello FA, Jr, et al: Masses in or around the pancreatic head: CT-guided coaxial fine-needle aspiration biopsy with a posterior transcaval approach. *Radiology* 222:63–69, 2002.
53. Smith EH: Complications of percutaneous abdominal fine-needle biopsy. *Review. Radiology* 178:253–258, 1991.
54. Zins M, Vilgrain V, Gayno S, et al: US-guided percutaneous liver biopsy with plugging of the needle track: A prospective study in 72 high-risk patients. *Radiology* 184:841–843, 1992.
55. Riley SA, Ellis WR, Irving HC, et al: Percutaneous liver biopsy with plugging of needle track: A safe method for use in patients with impaired coagulation. *Lancet* 2:436, 1984.
56. Chuang VP, Alspaugh JP: Sheath needle for liver biopsy in high-risk patients. *Radiology* 166(Pt 1):261–262, 1988.
57. Tobin MV, Gilmore IT: Plugged liver biopsy in patients with impaired coagulation. *Dig Dis Sci* 34:13–15, 1989.
58. Allison DJ, Adam A: Percutaneous liver biopsy and track embolization with steel coils. *Radiology* 169:261–263, 1988.
59. Nelson RC, Chezmar JL: Diagnostic approach to hepatic hemangiomas. *Radiology* 176:11–13, 1990.
60. Cronan JJ, Esparza AR, Dorfman GS, et al: Cavernous hemangioma of the liver: Role of percutaneous biopsy. *Radiology* 166(Pt 1):135–138, 1988.
61. Solbiati L, Livraghi T, De Pra L, et al: Fine-needle biopsy of hepatic hemangioma with sonographic guidance. *AJR Am J Roentgenol* 144:471–474, 1985.
62. Heilo A, Stenwig AE: Liver hemangioma: US-guided 18-gauge core-needle biopsy. *Radiology* 204:719–722, 1997.
63. Little AF, Ferris JV, Dodd GD, 3rd, et al: Image-guided percutaneous hepatic biopsy: Effect of ascites on the complication rate. *Radiology* 199:79–83, 1996.

64. Murphy FB, Barefield KP, Steinberg HV, et al: CT- or sonography-guided biopsy of the liver in the presence of ascites: Frequency of complications. *AJR Am J Roentgenol* 151:485–486, 1988.
65. Dodd GD, 3rd, Carr BI: Percutaneous biopsy of portal vein thrombus: A new staging technique for hepatocellular carcinoma. *AJR Am J Roentgenol* 161:229–233, 1993.
66. Dusenbery D, Dodd GD, 3rd, Carr BI: Percutaneous fine-needle aspiration of portal vein thrombi as a staging technique for hepatocellular carcinoma. Cytologic findings of 46 patients. *Cancer* 75:2057–2062, 1995.
67. De Sio I, Castellano L, Calandra M, et al: Ultrasound-guided fine needle aspiration biopsy of portal vein thrombosis in liver cirrhosis: Results in 15 patients. *J Gastroenterol Hepatol* 10:662–665, 1995.
68. Bravo AA, Sheth SG, Chopra S: Liver biopsy. *N Engl J Med* 344:495–500, 2001.
69. Bedossa P, Dargere D, Paradis V: Sampling variability of liver fibrosis in chronic hepatitis C. *Hepatology* 38:1449–1457, 2003.
70. Young WF, Jr: Management approaches to adrenal incidentalomas. A view from Rochester, Minnesota. *Endocrinol Metab Clin North Am* 29:159–185, x, 2000.
71. Lener JT, Barnett CC, Jr, Kudelka AP, et al: Evaluation and surgical resection of adrenal masses in patients with a history of extra-adrenal malignancy. *Surgery* 130:1060–1067, 2001.
72. Kloos RT, Gross MD, Francis IR, et al: Incidentally discovered adrenal masses. *Endocr Rev* 16:460–484, 1995.
73. Mody MK, Kazerooni EA, Korobkin M: Percutaneous CT-guided biopsy of adrenal masses: Immediate and delayed complications. *J Comput Assist Tomogr* 19:434–439, 1995.
74. Arellano RS, Harisinghani MG, Gervais DA, et al: Image-guided percutaneous biopsy of the adrenal gland: Review of indications, technique, and complications. *Curr Probl Diagn Radiol* 32:3–10, 2003.
75. Favelier S, Guiu S, Cherblanc V, et al: Transthoracic adrenal biopsy procedure using artificial carbon dioxide pneumothorax as outpatient procedure. *Cardiovasc Intervent Radiol* 36:1184–1187, 2013.
76. Odisio BC, Tam AL, Avritscher R, et al: CT-guided adrenal biopsy: Comparison of ipsilateral decubitus versus prone patient positioning for biopsy approach. *Eur Radiol* 22:1233–1239, 2012.
77. Boland GW, Blake MA, Holalkere NS, et al: PET/CT for the characterization of adrenal masses in patients with cancer: Qualitative versus quantitative accuracy in 150 consecutive patients. *AJR Am J Roentgenol* 192:956–962, 2009.
78. Welch TJ, Sheedy PF, 2nd, Stephens DH, et al: Percutaneous adrenal biopsy: Review of a 10-year experience. *Radiology* 193:341–344, 1994.
79. Casola G, Nicolet V, van Sonnenberg E, et al: Unsuspected pheochromocytoma: Risk of blood-pressure alterations during percutaneous adrenal biopsy. *Radiology* 159:733–735, 1986.
80. McCorkell SJ, Niles NL: Fine-needle aspiration of catecholamine-producing adrenal masses: A possibly fatal mistake. *AJR Am J Roentgenol* 145:113–114, 1985.
81. Cohen SA, Siegel JH, Kasmin FE: Complications of diagnostic and therapeutic ERCP. *Abdom Imaging* 21:385–394, 1996.
82. Cannon ME, Carpenter SL, Elta GH, et al: EUS compared with CT, magnetic resonance imaging, and angiography and the influence of biliary stenting on staging accuracy of ampullary neoplasms. *Gastrointest Endosc* 50:27–33, 1999.
83. Agarwal B, Abu-Hamda E, Molke KL, et al: Endoscopic ultrasound-guided fine needle aspiration and multidetector spiral CT in the diagnosis of pancreatic cancer. *Am J Gastroenterol* 99:844–850, 2004.
84. Zech CJ, Helmberger T, Wichmann MW, et al: Large core biopsy of the pancreas under CT fluoroscopy control: Results and complications. *J Comput Assist Tomogr* 26:743–749, 2002.
85. Smith FP, Macdonald JS, Schein PS, et al: Cutaneous seeding of pancreatic cancer by skin-needle aspiration biopsy. *Arch Intern Med* 140:855, 1980.
86. Farmer KD, Harries SR, Fox BM, et al: Core biopsy of the bowel wall: Efficacy and safety in the clinical setting. *AJR Am J Roentgenol* 175:1627–1630, 2000.
87. Marco-Doménech SF, Gil-Sanchez S, Fernandez-Garcia P, et al: Sonographically guided percutaneous biopsy of gastrointestinal tract lesions. *AJR Am J Roentgenol* 176:147–151, 2001.
88. Tudor GR, Rodgers PM, West KP: Bowel lesions: Percutaneous US-guided 18-gauge needle biopsy—preliminary experience. *Radiology* 212:594–597, 1999.
89. Carson BW, Brown JA, Cooperberg PL: Ultrasound-guided percutaneous biopsy of gastric, small bowel, and colonic abnormalities: Efficacy and safety. *J Ultrasound Med* 17:739–742, 1998.
90. Schmid S, Tinguely M, Cione P, et al: Flow cytometry as an accurate tool to complement fine needle aspiration cytology in the diagnosis of low grade malignant lymphomas. *Cytopathology* 22:397–406, 2011.
91. Bangerter M, Brudler O, Heinrich B, et al: Fine needle aspiration cytology and flow cytometry in the diagnosis and subclassification of non-Hodgkin's lymphoma based on the World Health Organization classification. *Acta Cytol* 51:390–398, 2007.
92. Demurtas A, Accinelli G, Pacchioni D, et al: Utility of flow cytometry immunophenotyping in fine-needle aspirate cytologic diagnosis of non-Hodgkin lymphoma: A series of 252 cases and review of the literature. *Appl Immunohistochem Mol Morphol* 18:311–322, 2010.
93. Liu K, Stern RC, Rogers RT, et al: Diagnosis of hematopoietic processes by fine-needle aspiration in conjunction with flow cytometry: A review of 127 cases. *Diagn Cytopathol* 24:1–10, 2001.
94. Ansell SM: Hodgkin lymphoma: 2012 update on diagnosis, risk-stratification, and management. *Am J Hematol* 87:1096–1103, 2012.
95. McInnes MD, Kielar AZ, Macdonald DB: Percutaneous image-guided biopsy of the spleen: Systematic review and meta-analysis of the complication rate and diagnostic accuracy. *Radiology* 260:699–708, 2011.
96. Nyman RS, Cappelen-Smith J, Brismar J, et al: Yield and complications in ultrasound-guided biopsy of abdominal lesions. Comparison of fine-needle aspiration biopsy and 1.2-mm needle core biopsy using an automated biopsy gun. *Acta Radiol* 36:485–490, 1995.
97. Petit P, Bret PM, Lough JO, et al: Risks associated with intestinal perforation during experimental percutaneous drainage. *Invest Radiol* 27:1012–1019, 1992.
98. Nolsoe C, Nielsen L, Torp-Pedersen S, et al: Major complications and deaths due to interventional ultrasonography: A review of 8000 cases. *J Clin Ultrasound* 18:179–184, 1990.
99. Drinkovic I, Brkljacic B: Two cases of lethal complications following ultrasound-guided percutaneous fine-needle biopsy of the liver. *Cardiovasc Intervent Radiol* 19:360–363, 1996.
100. Maxwell AW, Klein JS, Dantey K, et al: CT-guided transthoracic needle aspiration biopsy of subsolid lung lesions. *J Vasc Interv Radiol* 25:340–346, 2014.

Abdominal Abscess

AVINASH KAMBADAKONE | PETER R. MUELLER

CHAPTER OUTLINE

Pathogenesis

Imaging Techniques

Plain Radiography or Fluoroscopy

Ultrasound

Computed Tomography

Magnetic Resonance Imaging

Scintigraphy

Imaging-Guided Intervention

Diagnostic Aspiration

Percutaneous Abscess Drainage: Clinical Considerations

Percutaneous Abscess Drainage: Technique

Additional Techniques for Abscess Drainage

Catheter Management after Drainage

Factors Affecting Outcome of Abscess Drainage

Tips and Tricks to Improve Outcome

Abscesses at Specific Locations

Conclusion

Intra-abdominal abscesses occur from a wide variety of causes and are characterized by accumulation of an infected fluid collection within the structures of the abdomen and pelvis. Depending on the etiology, the abscesses can develop either within the solid or hollow visceral organs or within the intraperitoneal and retroperitoneal spaces. Without timely and adequate drainage, intra-abdominal abscesses cause increased morbidity and mortality in spite of appropriate antibiotic coverage.¹⁻⁵ Image-guided percutaneous drainage provides a safe substitute to surgical débridement in the management of these abscesses.^{2-4,6-8} Advances in percutaneous techniques have resulted in abscess cure rates of more than 90%, and image-guided drainage is currently considered the preferred treatment option in the management of intra-abdominal abscesses.²⁻⁸ Higher cure rates in treatment of intra-abdominal abscesses have also resulted from improved diagnostic imaging techniques, such as computed tomography (CT) and magnetic resonance imaging (MRI), which allow early diagnosis and thereby timely intervention. Percutaneous catheter drainage of abscesses has several advantages over surgical lavage for treatment of intra-abdominal abscess. These include absence of a laparotomy scar, shorter hospital stay, avoidance of general anesthesia, lower risk of complications, and lower morbidity and mortality.^{3,7-10}

Rising use of CT and MRI in patients thought to have intra-abdominal sepsis has permitted early and accurate detection of abscesses. This is particularly true in patients with predisposing factors for development of abdominal abscesses, such as individuals with Crohn's disease, diverticulitis, and appendicitis,

and in postoperative patients after abdominal surgery.^{7-9,11,12} Imaging not only provides precise diagnosis but also guides interventional radiologists in safely draining the infected fluid collections. Despite the high success rates reported for percutaneous abscess drainage, it can at times be technically challenging because of the presence of fistulas, inaccessible locations, and comorbidities of the patient. In this chapter, our endeavor is to provide the reader with a synopsis of a radiologist's role in the diagnosis and management of intra-abdominal abscesses, particularly focusing on percutaneous abscess drainage.

Pathogenesis

The development of abscesses in the abdomen and pelvis is pathophysiologically similar to that elsewhere in the body, although the cause is often multifactorial.^{3,8,13} Intra-abdominal abscesses can arise from a wide variety of conditions but are commonly encountered in postoperative patients or in patients with infective or inflammatory diseases, such as inflammatory bowel disease, acute diverticulitis, or acute appendicitis.^{3,8,11-13} They can result from superinfection of a previously sterile fluid collection (e.g., postoperative biloma, hematoma) or arise de novo from an infectious nidus in a solid or hollow visceral organ (e.g., pyogenic liver abscess). In gross appearance, abscesses can have varied size and shape. Abscesses developing within solid visceral organs, such as liver and spleen, are often spherical or ovoid in configuration because of uniform pressure from surrounding tissue.^{3,14} Intraperitoneal and retroperitoneal abscesses have varied morphologic features and shape, depending on their location, spread along various fascial spaces, and pressure of surrounding structures.³ Mature abscesses often have a well-defined capsule composed of connective tissue (fibrin, collagen), blood vessels, and leukocytes.³ The contents of the abscess cavity gradually undergo liquefaction due to the enzymatic action of leukocytes.³ Bacterial isolates from abscess confirm the predominance of polymicrobial microorganisms in intra-abdominal infection.^{3,15}

Imaging Techniques

Technologic advancements in imaging techniques, particularly CT and MRI, have greatly enhanced their ability to accurately diagnose intra-abdominal abscesses. In addition to detection, imaging permits accurate depiction of extension of abscess across various fascial spaces in the abdomen.^{5,9,14,16} Imaging also aids the interventional radiologist in planning of interventional procedures for safe and effective drainage of the abscesses (Table 72-1).

PLAIN RADIOGRAPHY OR FLUOROSCOPY

Plain film radiography has a limited role in the diagnosis and management of intra-abdominal abscess. The radiographic

TABLE
72-1**Advantages and Disadvantages of Various Imaging Modalities in the Diagnosis and Management of Abscesses**

	Advantages	Disadvantages
Ultrasound	No radiation exposure Real-time nature helps avoid vessels, bowel, or pleural cavity Helps identify loculations and septations within abscesses Preferred for draining of superficial and unilocular abscesses	Limited role in drainage of collections deep in the abdomen Does not allow identification of complex abdominal fluid collections Limited role in the presence of ileus or extensive surgical wounds
Computed tomography	Modality of choice to drain complex abscesses in the retroperitoneum and mesentery Ideal for drainage of abscesses in postoperative patients with ileus and surgical wounds	Ionizing radiation exposure Considerable overlap in CT appearance of sterile and infected collections Abscesses of solid visceral organs can simulate soft tissue masses, often necessitating needle aspiration for differentiation
Magnetic resonance	Superior soft tissue resolution allows accurate diagnosis	Expensive Requires MR-compatible equipment
Fluoroscopy	When combined with ultrasound, fluoroscopy can be useful for performing drainage with Seldinger technique Helps demonstrate fistulous communication of abscesses with bowel and surrounding structures Helps in manipulation and repositioning of catheters with Seldinger technique	Lacks superior soft tissue resolution of cross-sectional imaging Accurate localization of catheter position often not possible

signs that are helpful in the diagnosis of intra-abdominal abscesses include an abnormal gas pattern, extraluminal air-fluid level, free intraperitoneal air, soft tissue mass, and loss of normal fat planes and interfaces.³ Nonetheless, plain radiography is an insensitive technique that is not reliable in day-to-day practice.³ Real-time fluoroscopy, on the other hand, is useful in guiding percutaneous drainage of abscesses in specific locations; for example, it can be used in conjunction with ultrasound to facilitate drainage of subphrenic abscesses while avoiding pleural transgression. Fluoroscopic guidance is also useful for aiding catheter manipulations, such as catheter repositioning and exchanges after initial placement of the percutaneous catheter.

ULTRASOUND

Ultrasound is often used as a screening modality for initial diagnosis of intra-abdominal fluid collections. Ultrasound has

several advantages over other imaging modalities; it is relatively inexpensive, easily available, and portable and does not use ionizing radiation.³ Ultrasound is particularly beneficial in rapid bedside diagnosis of abscesses in seriously ill patients in hospital intensive care units who are unable to travel to the radiology department for a CT scan.^{3,17} The ability to perform bedside ultrasound scans is especially valuable for guiding placement of percutaneous drainage catheters into abdominal abscesses in intensive care unit patients.^{3,17}

Ultrasound is also the preferred imaging modality for diagnosis and for guiding percutaneous drainage of superficially located abscesses and multiloculated collections.^{3,17,18} Because of its real-time nature, it also confers a low risk for traversing vascular structures, bowel, or the pleural cavity during ultrasound-guided abscess drainage.^{3,5,9,17,18} In patients with deep-seated pelvic abscesses, ultrasound also provides the opportunity for drainage through the transrectal or transvaginal route.^{9,17,18} In experienced hands, ultrasound allows rapid and accurate drainage of intra-abdominal abscesses compared with CT.^{3,17}

The sonographic appearance of abdominal and pelvic abscesses depends on their location and internal contents. In general, the abscesses are seen as anechoic to hypoechoic cystic collections with internal echoes and debris.^{3,5,18} More complex abscesses can have variegated hypoechoic and solid cystic appearance with irregular margins, internal septation, and debris (Fig. 72-1).^{3,5,18} Presence of gas within a fluid collection often demonstrates “dirty” shadowing and is highly suggestive of infection.^{3,5,18} The demonstration of multiloculations within a fluid collection is a valuable feature of ultrasound, which has important treatment implications because such abscesses often require insertion of multiple catheters or instillation of thrombolytic agents to facilitate optimal drainage.^{3,5,18-21} On occasion, the diagnosis of intraperitoneal abscesses can be challenging on ultrasound because of the need to differentiate these collections from surrounding fluid-filled bowel loops.^{3,18} The real-time nature of ultrasound aids in this differentiation by demonstrating peristalsis within bowel loops.^{3,18} The characteristic sonographic signature of the bowel wall is an additional differentiating feature. Doppler interrogation of intra-abdominal fluid collections is essential to rule out the possibility of pseudoaneurysms. This is particularly relevant in fluid collections adjacent to major vessels or in conditions with a high incidence of pseudoaneurysm formation, such as acute pancreatitis.

Ultrasound, however, has several limitations. Despite its value in abscess detection, ultrasound has a limited ability to define the spread of abscesses and inflammation across fascial planes within the abdomen. Ultrasound is highly operator dependent, and detection of fluid collections is rendered challenging in patients with ileus or those with extensive surgical wounds.^{3,18} For the same reason, ultrasound fares poorly in the detection of deep-seated abscesses in the retroperitoneum because of overlying bowel gas. Wound dressings and postsurgical drains also limit adequate visualization of intra-abdominal abscess.^{3,18}

COMPUTED TOMOGRAPHY

CT is the imaging modality of choice for initial diagnosis and management of patients with suspected intra-abdominal abscess.* CT allows precise anatomic localization of the abscess,

*References 3, 4, 9, 13, 18, 22-26.

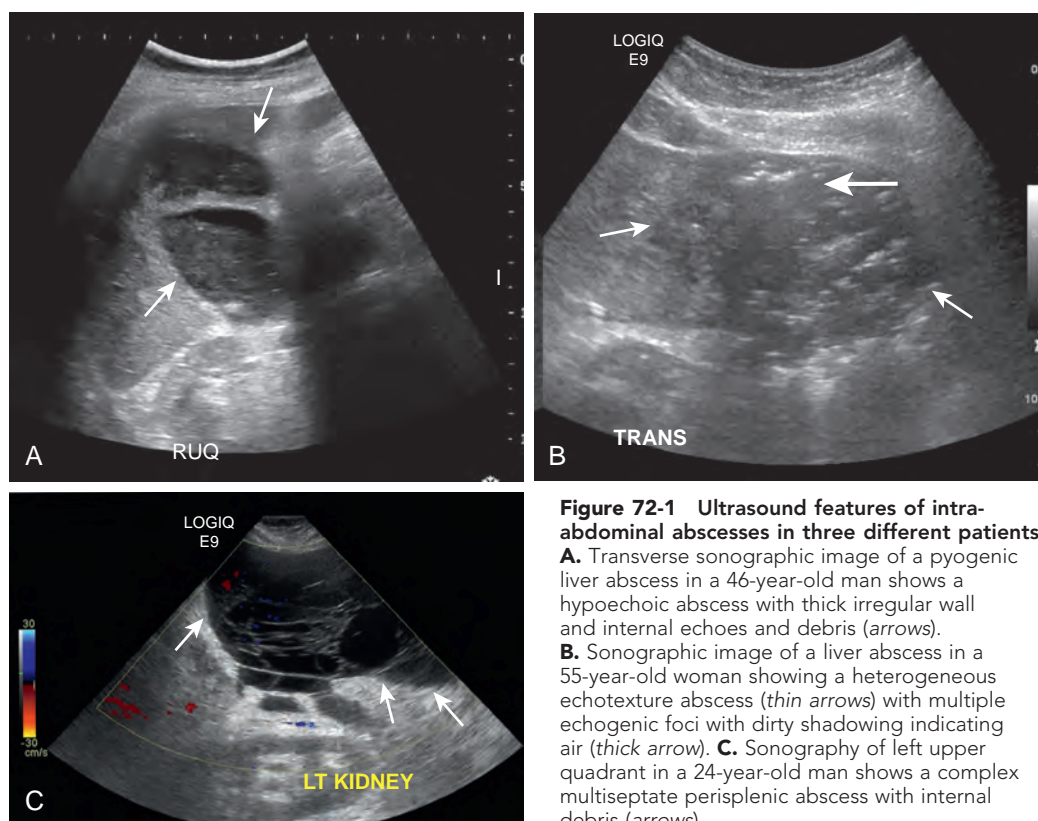


Figure 72-1 Ultrasound features of intra-abdominal abscesses in three different patients.

A. Transverse sonographic image of a pyogenic liver abscess in a 46-year-old man shows a hypoechoic abscess with thick irregular wall and internal echoes and debris (arrows).

B. Sonographic image of a liver abscess in a 55-year-old woman showing a heterogeneous echotexture abscess (thin arrows) with multiple echogenic foci with dirty shadowing indicating air (thick arrow). **C.** Sonography of left upper quadrant in a 24-year-old man shows a complex multiseptate perisplenic abscess with internal debris (arrows).

defines its extent, and delineates its relationship to other intra-abdominal structures, such as bowel loops and vascular structures.* Multiplanar reformations (coronal and sagittal) are extremely valuable in defining abscess extent and in assessment of collections in the subphrenic location around the dome of the liver and the spleen. In patients with intra-abdominal sepsis and in postoperative patients, CT affects management by allowing detection of multifocal abscesses at distant locations within the abdomen and pelvis. CT is valuable not only for diagnosis of intra-abdominal abscess but also in the planning of percutaneous interventions.* CT is less successful in the depiction of internal septations within an abscess, a feature better visualized on ultrasound.

In patients thought to have an infected intra-abdominal process, CT should ideally be performed after the administration of intravenous and oral contrast media.^{3,4,26} Intravenous injection of contrast media not only improves abscess detection but also is essential for enhanced characterization of the abscess features, such as the abscess wall.^{3,5,18} The wall of a mature abscess demonstrates enhancement after injection of contrast media, and it remains a key feature in the diagnosis of intra-abdominal abscess.^{3,5,18} Ingestion of positive oral contrast media is preferred before the CT scan as it allows differentiation of abscesses from adjacent bowel loops because unopacified bowel loops can mimic an abscess^{2,3,5,18} (Fig. 72-2). Some authors advocate the use of delayed scans in different positions for differentiation of questionable areas of abscess from bowel loops as bowel loops generally change in position and configuration with change in the patient's position.³ Positive oral contrast media are often helpful in detecting the presence of

bowel perforation, particularly in patients presenting with intra-abdominal sepsis after bowel surgeries. Bowel perforation is diagnosed by extraluminal leak of the orally administered contrast material. Colonic perforations are less reliably depicted with orally administered contrast material and might require administration of rectal contrast. Instillation of rectal contrast material is optional but can be helpful in the differentiation of deep pelvic and perirectal abscesses.

Administration of an oral contrast agent, is however, not recommended for patients presenting for follow-up CT examination after initial catheter drainage of abdominal abscess. Because these patients might require catheter manipulations for optimal positioning of the drainage catheter, oral contrast media ingestion is not recommended if the patient is to shortly receive conscious sedation.

On CT, abscesses often have fluid attenuation with internal attenuation measurements ranging between 0 and 25 HU.^{3-5,18} The density of an abscess largely depends on the abscess contents, degree of liquefaction, and presence of gas (Fig. 72-3).^{3-5,18} The abscess wall often appears as a high-density irregular peripheral rim that enhances after contrast medium injection.^{3-5,18} Abscess wall enhancement is considered to be a sign of abscess wall maturation and therefore predicts favorable response to percutaneous drainage.^{3-5,18} The abscess contents often do not enhance because of the ongoing process of liquefaction and lack of internal vascularity; internal enhancement in a suspected abscess should therefore raise concern for underlying tumor.³ Gas within a fluid collection is highly diagnostic of an abscess and is seen in up to 50% of infected intra-abdominal fluid collections (Fig. 72-3).^{3-5,18} Gas can be seen as either small locules and air pockets or air-fluid levels. Presence of gas within a collection could be due to infection with anaerobic organisms, fistulous communication with bowel, or prior

*References 3, 4, 9, 13, 18, 22-26.

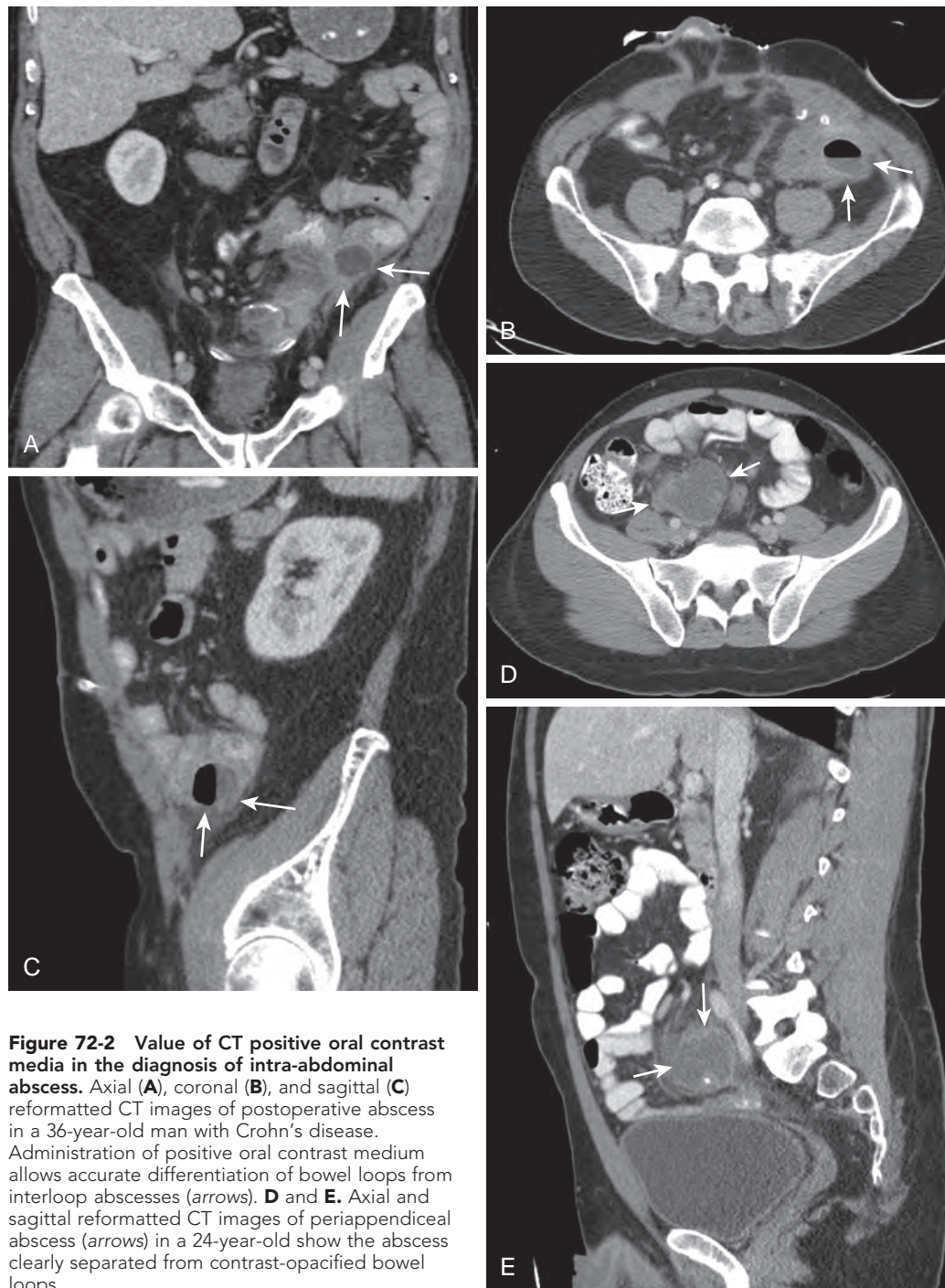


Figure 72-2 Value of CT positive oral contrast media in the diagnosis of intra-abdominal abscess. Axial (A), coronal (B), and sagittal (C) reformatted CT images of postoperative abscess in a 36-year-old man with Crohn's disease. Administration of positive oral contrast medium allows accurate differentiation of bowel loops from interloop abscesses (arrows). D and E. Axial and sagittal reformatted CT images of periappendiceal abscess (arrows) in a 24-year-old show the abscess clearly separated from contrast-opacified bowel loops.

interventions. Demonstration of large amounts of air in intra-peritoneal or retroperitoneal collections should raise concern for possible fistulous communication with bowel loops.^{3-5,18,27,28} Bowel communication could be due to either bowel perforation or the primary cause of the abscess itself, such as Crohn's disease or diverticulitis.^{3,27-29}

Typically, an abscess within a solid visceral organ is ovoid or spherical in shape, whereas intraperitoneal or retroperitoneal abscesses have varied morphology because they conform to the shape of the compartment in which they are located and often displace surrounding structures. The adjacent fascial planes may be obliterated or thickened by spread of inflammation, and surrounding mesenteric fat can show increased

attenuation.^{3,18,24,26} The CT appearance of sterile and infected fluid collections can show a substantial degree of overlap. On CT, abscesses of solid visceral organs can simulate soft tissue masses.^{2,7,18} Not infrequently, needle aspiration is required to differentiate between an abscess and solid mass.^{2,7,18}

MAGNETIC RESONANCE IMAGING

In the past few years, there has been an increasing trend in the use of MRI for diagnosis of intra-abdominal abscesses. MRI offers several advantages over CT, the chief ones being the absence of ionizing radiation and the superior soft tissue resolution. MRI is particularly preferred in pediatric patients and

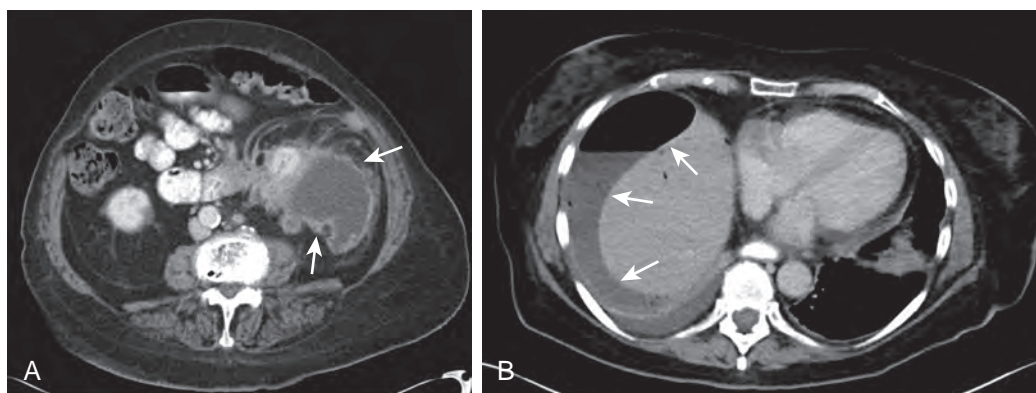


Figure 72-3 CT features of intra-abdominal abscesses in two different patients. **A.** Axial CT image in a 62-year-old man with perinephric abscess shows a low-attenuation collection in the left perinephric space with enhancing wall (arrows) at the periphery and mild surrounding fat stranding. **B.** Axial CT image in a 65-year-old woman with a postoperative abscess after laparoscopic cholecystectomy shows a perihepatic abscess with air-fluid level (arrows).

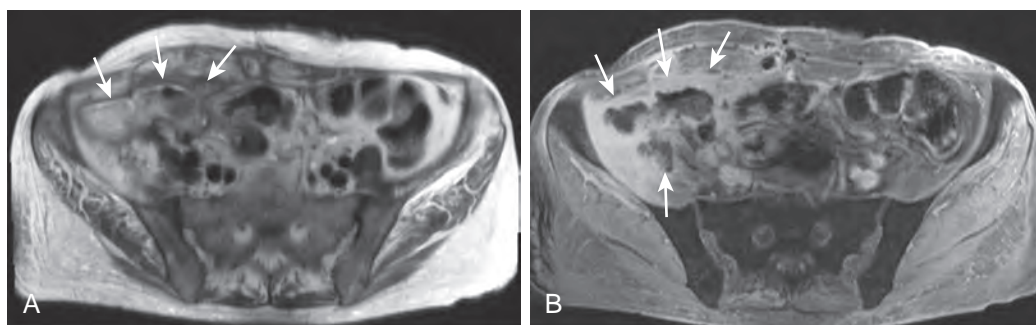


Figure 72-4 MRI in diagnosis of intraperitoneal abscess. **A.** Axial T2-weighted image demonstrates a right lower quadrant abscess (arrows) in a 24-year-old man with Crohn's disease. The abscess demonstrates heterogeneous T2 hyperintensity. **B.** Post-gadolinium-enhanced fat-suppressed T1-weighted image shows intense peripheral enhancement of the abscess wall and the surrounding structures, indicating inflammatory involvement (arrows).

young adults because of the concerns about the harmful effects of ionizing radiation. This is particularly true in patients with Crohn's disease, who often undergo multiple cross-sectional imaging studies in their lifetime, and intra-abdominal abscesses frequently complicate their clinical course. MRI has a problem-solving role in the characterization of complex adnexal lesions in women of reproductive age and aids in the diagnosis of tubo-ovarian abscesses.

The routine use of MRI for detection of abscess is however limited by the lack of MRI expertise, high cost, and long scanning times in abdominal MRI examinations. It is also difficult to perform good-quality examinations on critically ill patients.

On MRI, intra-abdominal abscesses typically demonstrate inhomogeneous areas of hypointensity on T1-weighted images and intermediate intensity to hyperintensity on T2-weighted images (Fig. 72-4).^{3,4} After intravenous administration of gadolinium, the abscess demonstrates intense wall enhancement as on CT.^{3,4}

SCINTIGRAPHY

Nuclear scintigraphy has a limited role in the diagnosis of intra-abdominal abscesses and is often not the first-line imaging investigation to be performed. Scintigraphic studies are often obtained in patients with suspected intra-abdominal sepsis or abscess when other diagnostic modalities, such as ultrasound, CT, or MRI, have yielded negative results.^{3,18,30} The most

commonly used isotopes for detection of abscess are gallium (Ga 67) and indium (In 111) to label white blood cells.^{3,18,30,31} Newer scintigraphic agents, such as technetium Tc 99m HMPAO-labeled white blood cells, ¹¹¹In-labeled polyclonal immunoglobulin G, and ^{99m}Tc-labeled monoclonal antibodies, have also been reported to improve diagnosis of intra-abdominal abscess.³ ⁶⁷Ga scans, although sensitive, have limited specificity for abscess diagnosis because of false-positive results in conditions such as granulomatous disease, lymphoma, and normal gut.³ One of the main limitations of nuclear scintigraphic studies in the characterization of abdominal abscesses is the poor anatomic detail of these scans, which limits their value in planning of percutaneous interventional procedures.^{3,18}

Imaging-Guided Intervention

Percutaneous catheter drainage is a safe and effective means for treatment of the entire gamut of intra-abdominal abscesses irrespective of their cause and anatomic location.* Percutaneous catheter drainage is widely considered the first-line treatment option for management of intra-abdominal abscesses, superseding surgical drainage.* Percutaneous catheter drainage of abscesses is less invasive compared with surgery and is associated with fewer postprocedural complications, such as

*References 1, 2, 5, 7-10, 18, 24, 32, 33.

atelectasis, pneumonia, pain, and venous thrombosis.^{3,9,10,18} A combination of high success rate and low complication rate has made percutaneous drainage a mainstay in the treatment of abdominal abscess.

DIAGNOSTIC ASPIRATION

In patients with clinical and imaging confirmation of an intra-abdominal abscess, the definitive treatment is percutaneous drainage through a catheter. However, in certain circumstances in which the imaging features are not conclusive for the presence of pus, simple diagnostic aspiration of the fluid collection is indicated.^{2,9,18} Fine-needle aspiration of small amounts of fluid permits laboratory evaluation of fluid chemistry and microbiology.^{2,18} Diagnostic needle aspiration of fluid collections is also valuable as a temporizing measure before surgical intervention in anatomically difficult locations like the pelvis to render the surgical field clean.^{2,9,18}

Diagnostic needle aspiration of fluid collections is usually accomplished with a 20- or 22-gauge Chiba needle.^{2,9,18} The placement of the needle into the collection can be guided with either ultrasound or CT (Fig. 72-5). The type of fluid aspirated from the needle often dictates the next strategy. If pure pus is extracted, the drainage catheter is immediately placed. If no pus is obtained, a Gram stain can be performed to assess the origin and cause of the contents. If Gram stain of the contents reveals leukocytes without bacteria, it is likely to be a sterile abscess, which is typically seen in hospitalized patients who have already been administered antibiotics.⁹ If Gram staining reveals leukocytes and bacteria, it is likely to be an abscess and requires catheter drainage.⁹ If there are bacteria without leukocytes, the possibilities include abscess in an immunocompromised patient and a likelihood of fistulous communication with bowel. Aspiration is not indicated if the collection has potential

communications with bowel, the biliary system, or the urinary tract.^{2,9,18} Aspiration is ineffective in these situations as immediate reaccumulation of the collection occurs after initial successful percutaneous aspiration and needle removal.² In addition to Gram stain, the extracted fluid should also be sent for fluid chemistry analysis to study fluid characteristics because the radiologic signs of abscesses, hematomas, urinomas, bilomas, postoperative seromas, and even loculated ascites can often overlap.^{2,9,18} Accordingly, analysis of fluid chemistry leads to recognition of the source of the fluid collection (e.g., urinomas demonstrate elevated creatinine concentration, bilomas are characterized by elevated bilirubin levels, and pseudocysts show amylase).^{2,9,18}

PERCUTANEOUS ABSCESS DRAINAGE: CLINICAL CONSIDERATIONS

Indications

Appropriate patient selection is important before percutaneous drainage as improper patient selection with incomplete drainage often leads to an increase in morbidity. The typical indication for image-guided percutaneous drainage is the presence of an intra-abdominal fluid collection with features of abscess in the background of abdominal pain, fever, and leukocytosis.^{2,3,9,18} The goal of drainage in these circumstances is palliation and treatment of sepsis associated with the infected fluid collection. Another common indication for percutaneous drainage is for alleviation of symptoms caused by the size of the fluid collection (e.g., in pancreatic pseudocysts).^{34,35}

Contraindications

Percutaneous abscess drainage is contraindicated in patients with severe uncorrectable coagulopathy and thrombocytopenia as they predispose to increased risk of bleeding.³⁶ Other relative

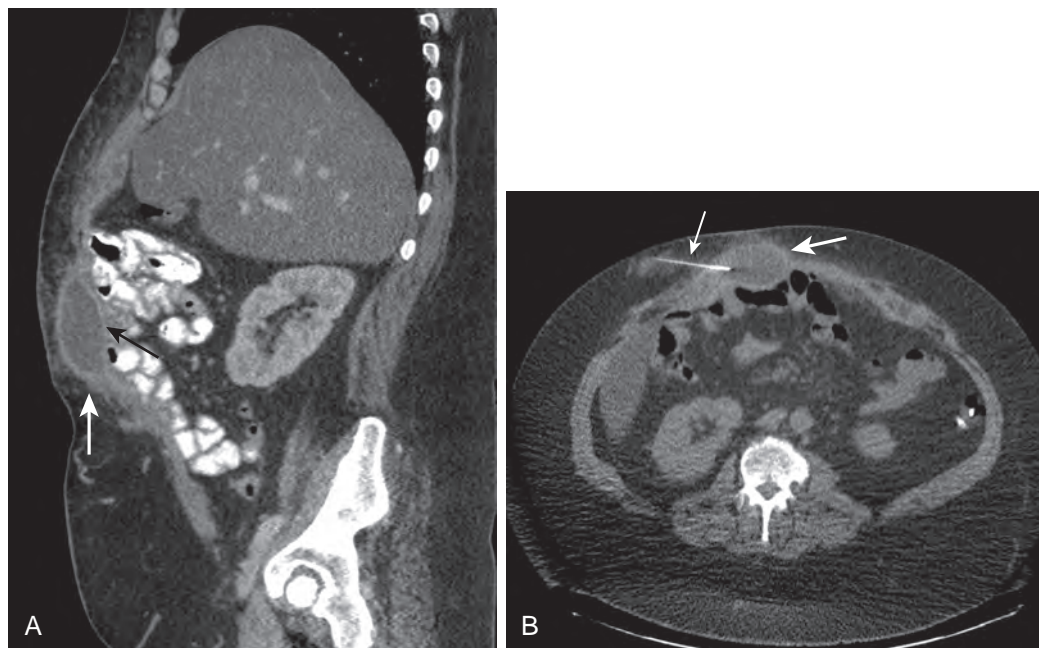


Figure 72-5 Diagnostic aspiration of postoperative fluid collection after mesh repair. **A.** Sagittal reformatted CT image shows an anterior abdominal wall fluid collection (white arrow) in a 75-year-old man after ventral hernia mesh repair (black arrow). **B.** Diagnostic aspiration was performed under CT guidance with a 20-gauge needle (thin arrow) to confirm presence of infection in the collection (thick arrow). Gram stain showed gram-negative rods and a percutaneous drainage catheter was subsequently placed.

contraindications for abscess drainage are severely compromised cardiopulmonary function and hemodynamic instability.³⁶ In these situations, efforts should be made to improve clinical status to a level at which the drainage procedure can be safely performed. Lack of a safe trajectory to the abscess for optimal drainage because of overlying vital structures is another relative contraindication.^{2,3,36} However, in many of these situations, changes in the patient's position or other maneuvers can often create a safe pathway for successful drainage.

There are several situations in which image-guided abscess drainage, although not contraindicated, should be avoided.² When free hollow organ perforation occurs as evidenced by a large amount of intraperitoneal free air, an open surgical procedure should be primarily considered.² Similarly, acute peritonitis is best managed by immediate surgical intervention, although in dire settings when a patient is considered unfit for surgical treatment, percutaneous catheter drainage could be performed.² Symptomatic noninfected fluid collections in the vicinity of surgical implants of any type, including vascular grafts, hernia repair mesh, and joint prosthesis, should not be drained unless they are superinfected.² Percutaneous catheter drainage of these noninfected fluid collections could potentially risk infection of the implants.² In these situations, infection can be confirmed with diagnostic fine-needle aspiration (Fig. 72-5).² In addition, drainage of noninfected pelvic collections through a transvaginal route is not appropriate.^{2,5,18} Collections related to pancreatic abscess or pancreatitis are usually refractory to percutaneous drainage compared with intra-abdominal abscesses from other sources.^{2,5,18} A multidisciplinary approach is needed in these patients, that is, collaboration with endoscopic methods to facilitate resolution of the collections by placement of cystogastrostomy stents.^{2,5,18}

Role of Antibiotics

Effective management of intra-abdominal abscess needs administration of intravenous antibiotics in addition to prompt percutaneous drainage. Prophylactic antibiotic coverage is also essential before image-guided abscess drainage to prevent septic complications due to transient bacteremia resulting from the drainage of intra-abdominal abscess.^{2,3,18} Adjunctive antimicrobial therapy must be directed at enteric gram-negative rods, gram-positive cocci, and anaerobes.^{2,3,18}

Preprocedure Work-up

A comprehensive patient work-up including informed consent is indispensable before the procedure.³⁷ Before abscess drainage, details including the technique and the complications and effectiveness of the procedure should be explained to the patient and the family, and written informed consent should be obtained. During the consent process, it is essential to explain to the patient and the family about the need for regular care of the drainage catheter after the procedure. It is equally important to communicate to the patient and the family that often the drainage catheters need to be retained in place at least for a few weeks before they are removed.

The necessary preliminary work-up includes laboratory evaluation of complete blood count, coagulation profile (international normalized ratio should be <1.5, activated partial thromboplastin time normal 25-35 sec, platelet count >50,000).^{3,7,9,38} The recent imaging studies including CT and MRI should be carefully reviewed to determine the abscess number, size, and location and the extent of involvement.^{3,7,9} In

general, the yield of drainage in abdominal abscesses smaller than 2 cm is low because the diameter of the pigtail catheter is more than 2 cm.* Preprocedure imaging should be carefully reviewed to plan the drainage procedure by giving special consideration to the proposed path of the drainage catheter. Careful interrogation is also essential to avoid inadvertent catheter drainage of infected pseudoaneurysms, which can lead to catastrophic bleeding. Color Doppler ultrasound and contrast-enhanced CT or MRI are key to making this diagnosis. It is also important to carefully review the preprocedural diagnostic imaging studies to avoid bowel transgression and vascular injury. To avoid inadvertent injury to superficial vessels in the abdominal wall, such as epigastric arteries, it is crucial to review the diagnostic contrast-enhanced CT or MRI study to map the location of these vessels. In addition, one can perform color Doppler ultrasound before the percutaneous drainage to map the location of these vessels.

Catheter Selection

Wide ranges of drainage catheters are available with diameters varying from 6F to 18F.[†] The selection of catheter is performed on the basis of several factors, including the size of the collection and the nature and the viscosity of the fluid obtained during initial needle placement immediately before catheter placement.[†] In general, smaller 8F to 12F catheters can be used successfully for initial percutaneous drainage. The newer catheters have hydrophilic coating (capability of absorbing and retaining water when wet), which reduces their friction coefficient and substantially improves the ease of insertion. Catheters with an internal locking pigtail configuration are preferred for retention. Larger catheters are generally preferred in abscesses with thick and viscous abscess contents.^{18,19} Percutaneous drainage of complex abscesses is sometimes limited despite appropriate positioning of catheters.¹⁹ Catheter selection in such situations is of crucial importance as increasing catheter size and number of catheter side holes often allows effective drainage of difficult abscesses.¹⁹

Patient Positioning

Planning of the patient's position is vital to successful abscess drainage; not only does this determine a safe percutaneous path to the abscess, but optimal positioning ensures the patient's comfort and minimizes motion during the procedure. An ideal position is one that allows the shortest and least complicated access to the abscess by avoiding vital structures such as bowel and vessels. The positioning during the procedure is often dependent on the location of the abscess and the planned percutaneous path for the drainage catheter. In most cases, successful drainage of the abscess can be performed with the patient in the supine position. The other common positions are prone, lateral decubitus, and lateral oblique positions.

Patient Preparation

Percutaneous drainage of intra-abdominal abscess is often performed in hospitalized patients but can also be done on an outpatient basis. When it is performed on an outpatient basis, it might be necessary to admit the patient for overnight observation on the basis of the patient's clinical condition. Before the

*References 5, 6, 9, 18, 32, 39.

†References 2, 5-9, 18, 19, 32, 39.

procedure, the patient should be fasting for at least 8 hours, and anticoagulant medications should be discontinued before the procedure. The patient should, however, continue other medications in the preoperative period. The procedure is mostly performed under intravenous conscious sedation, but general anesthesia should be considered in critically ill patients. Cardio-respiratory monitoring including electrocardiography, blood pressure, and pulse oximetry are crucial for monitoring of the patient during the procedure.

PERCUTANEOUS ABSCESS DRAINAGE: TECHNIQUE

After the details of the procedure and the associated risks are explained, the patient is placed on the procedure table in a position most optimal for a safe drainage as determined by the preprocedural imaging. During ultrasound-guided abscess drainage, a preliminary real-time scan is performed to identify the percutaneous needle path to the abscess. After the path is identified, color Doppler ultrasound should be used to determine if any intervening vessel lies in the proposed path. It is also crucial to interrogate the abscess with color Doppler to avoid placing a drainage catheter in a pseudoaneurysm, which could lead to catastrophic bleeding. Once a safe path is identified, the skin over the needle entry site is marked with a skin marker. Similarly, during CT-guided procedures, a preliminary CT scan is obtained to localize the abscess and to determine the path of the needle. Just as in ultrasound, review of the preprocedural imaging is critical to identify any vessels in the needle path. The skin entry site for the needle and the catheter are then cleansed with antiseptic solution, and the site is draped with sterile drapes to create a sterile field.

There are two basic techniques for percutaneous drainage of intra-abdominal abscesses, namely, the trocar technique and the Seldinger technique. Both these techniques are equally effective and have their distinct advantages and disadvantages (Table

72-2). The choice of technique to drain a particular abscess is mostly dependent on the preference of the interventionalist and the size, shape, and location of the abscess.

Trocar Technique

In this technique, a catheter is mounted on a metal cannula–sharp trocar system and introduced into the abscess directly or in tandem with a guiding needle.^{2,25} Direct trocar technique is often performed when the abscess drainage is performed under ultrasound guidance (Fig. 72-6). In this technique, after the

TABLE 72-2

Advantages and Disadvantages of Image-Guided Percutaneous Drainage Catheter Techniques

	Advantages	Disadvantages
Trocar technique	Allows rapid deployment of catheters Best suited for uncomplicated well-defined collections, particularly in solid organs	Difficulty of repositioning a catheter that has been initially deployed suboptimally Not preferred for complicated ill-defined collections in open spaces (retroperitoneum or mesentery)
Seldinger technique	Allows the ability to direct the wire to the precise location desired for catheter deployment Allows accurate placement in large complex abscesses, such as those in subphrenic locations and where access is tightly restricted	Difficulty in working in confined spaces Multiple steps involved in dilation Under CT guidance, any buckling or kinking of the wire and dilators can be a problem

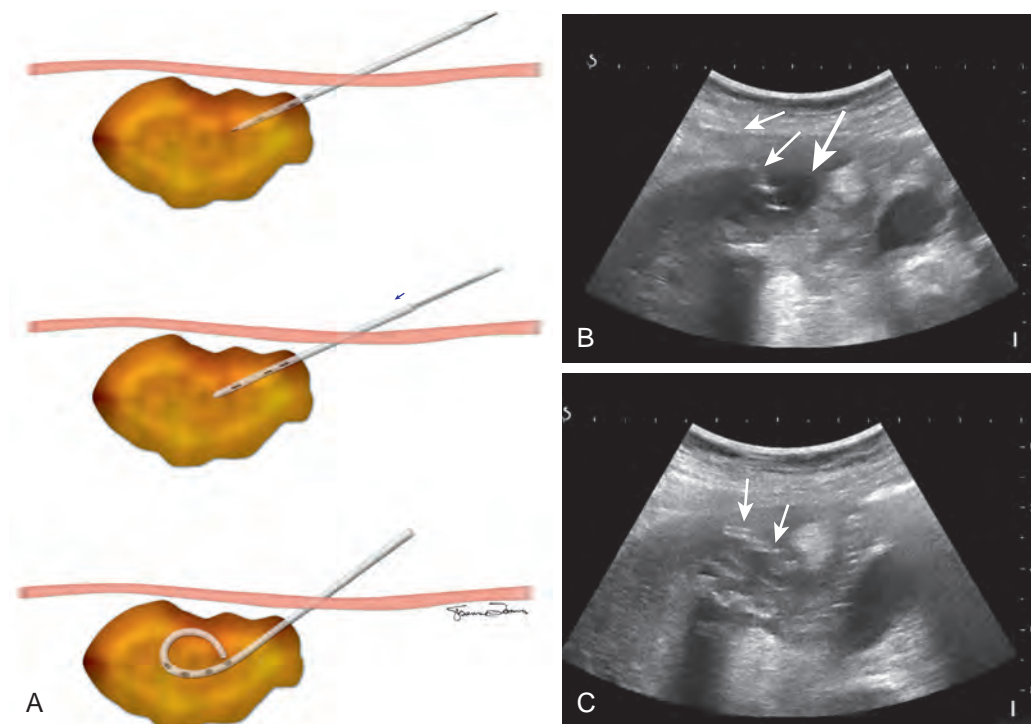


Figure 72-6 Trocar technique for placement of percutaneous drainage catheter. **A.** Illustration shows the placement of the catheter-cannula-trocar system into the abscess. This is followed by the catheter being fed off over the cannula-trocar. The final image shows the catheter positioned within the abscess cavity. **B and C.** Ultrasound-guided placement of drainage catheter (thin arrow) into a liver abscess (thick arrow).

direct path to the abscess is identified, local anesthetic is administered and a skin incision is made at the planned skin entry site wide enough to accommodate the catheter. Blunt dissection is then performed at the incision site to facilitate easy passage of the catheter.²⁵ The preselected drainage catheter is then mounted onto a metal stiffening cannula and inner trocar.^{2,25} Subsequently, the catheter loaded on the trocar and the cannula are then advanced into the abscess under direct visualization by real-time ultrasound.²⁵ Once the tip of the catheter-trocar system is within the abscess, the catheter is fed off of the cannula and trocar into the abscess cavity.²⁵ Pulling on the string then forms the pigtail of the catheter, and the catheter is connected to a bag for gravity drainage.²⁵

The tandem trocar technique is most often employed when the drainage catheter placement is performed under CT guidance, during which the catheter-trocar system is inserted into the abscess parallel to a guiding needle.^{25,36} The initial step in this technique involves placement of a guiding needle at the planned skin entry site after subcutaneous infiltration with 1%

lidocaine.²⁵ The guiding needle, which is usually a 20-gauge needle (Chiba biopsy needle), is slowly advanced under imaging guidance into the abscess. Accurate placement of the guiding needle is crucial to ensure safety of this technique and also permits precise deployment of the catheter in an appropriate position.^{25,36} Because the portion of the needle outside the body serves as a guide for subsequent catheter placement, the length of the needle should be appropriately selected such that a substantial portion of the needle extends outside the skin as the needle is firmly positioned inside the abscess (Fig. 72-7).^{25,36} It is key to have several centimeters of the guiding needle outside the skin because the outer portion of the localizer needle directs the appropriate trajectory and angle of entry of the catheter into the abscess even if the shape of the abscess is affected by respiratory or other motion.^{25,36} After accurate positioning of the needle within the abscess is confirmed, the catheter is placed adjacent to the needle in tandem to it.³⁶ A small incision is made in the skin adjacent to the needle, and blunt dissection is done to allow placement of the catheter.^{25,36} For accurate positioning

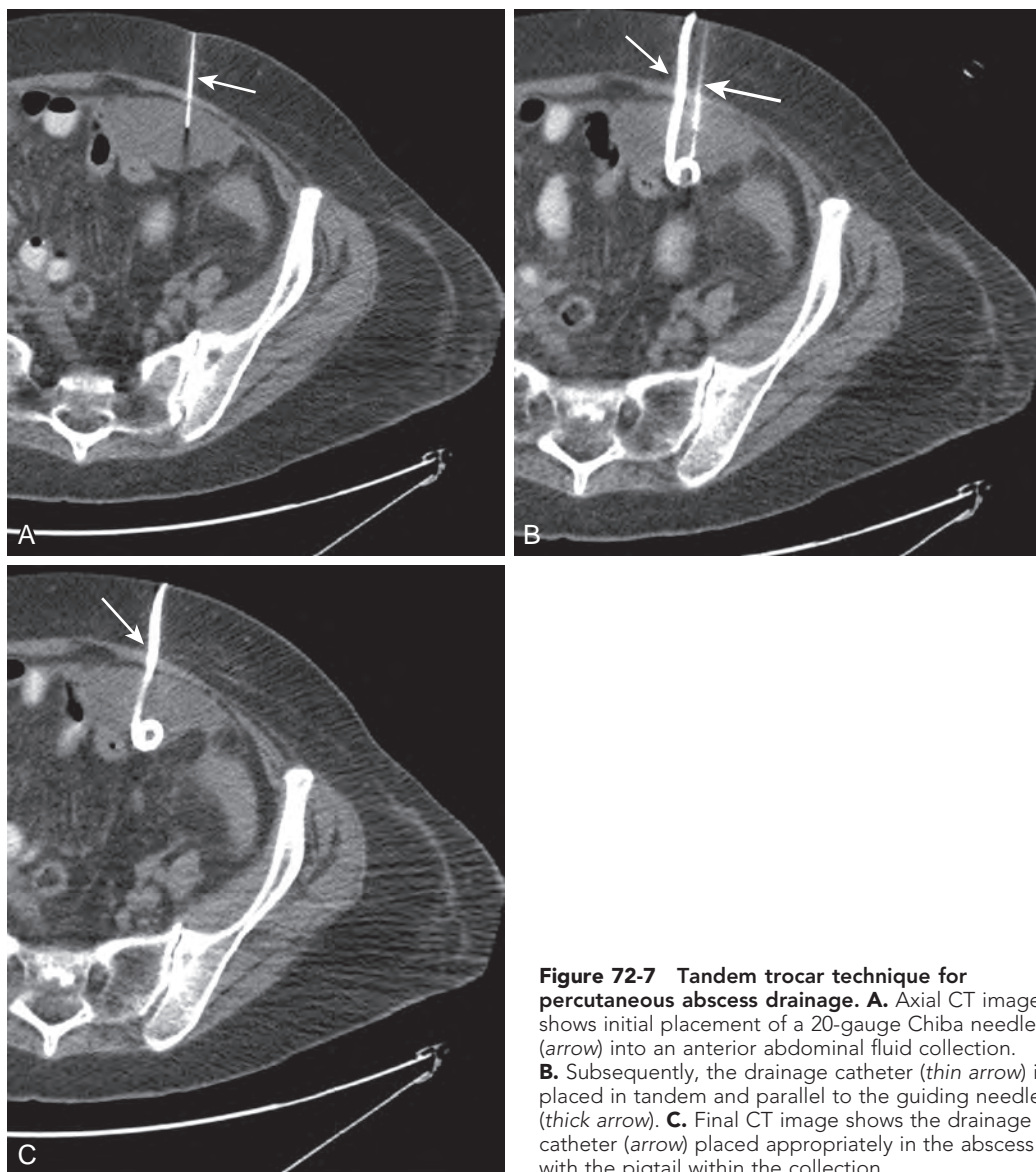


Figure 72-7 Tandem trocar technique for percutaneous abscess drainage. **A.** Axial CT image shows initial placement of a 20-gauge Chiba needle (arrow) into an anterior abdominal fluid collection. **B.** Subsequently, the drainage catheter (thin arrow) is placed in tandem and parallel to the guiding needle (thick arrow). **C.** Final CT image shows the drainage catheter (arrow) placed appropriately in the abscess with the pigtail within the collection.

of the catheter, the depth of the abscess cavity from the skin entry site is measured and appropriate marking is made on the catheter. The catheter-trocar system is then advanced alongside the needle, holding it perfectly parallel to the guiding needle to the predetermined depth.^{25,36} When the catheter has been advanced to the premeasured depth, feeding the catheter over the trocar-cannula system deploys the catheter. The catheter tip position within the abscess cavity is then ascertained by obtaining postprocedure CT images. If the position of the catheter is deemed satisfactory, it is secured externally and connected to a bag drainage system.

Seldinger Technique

The Seldinger technique encompasses the placement of a drainage catheter into an abscess over a guidewire, which is positioned into the abscess through a needle (Fig. 72-8).^{25,36,40} The first step in this procedure involves introduction of a needle into the abscess cavity through a safe percutaneous path as described before.^{25,36,40} The needle should be an 18-gauge or 19-gauge sheathed needle to accommodate a 0.035- or 0.038-inch guidewire for placement of 8F to 14F catheters (Fig. 72-9).^{25,36,40} Once the position of the needle in the abscess cavity is confirmed, the inner stylet of the needle is removed, and the guidewire is threaded into the needle and positioned within the abscess cavity.^{25,36,40} The catheter is then deployed into the abscess cavity over the guidewire after serial dilation with fascial dilators to the required catheter size.^{25,36,40}

Despite the technique used (i.e., trocar or Seldinger), it is essential to ensure that the catheter is appropriately positioned within the abscess.³ In general, for effective drainage, the

catheter tip should be ideally positioned within the most dependent portion of the abscess.³ In abscesses with complex shape, the catheter tip should be positioned within a location distal to the catheter entry site, and preferably the side holes should be spread out within the abscess to help effective drainage.³

Catheter Fixation

After placement of the abscess drainage catheter, the catheters are retained in place within the abscess cavity by internal and external retention mechanisms. Internal retention is achieved by the nature of the locking pigtail catheters, which prevents inadvertent catheter withdrawal.³⁶ The pigtail is formed with the help of a string, which courses through the catheter and is secured near the catheter hub.³⁶ The string has a protective mechanism as well to prevent catheter rupture within the patient as the string usually breaks when excessive tension or pressure is applied.³⁶ For external fixation, the catheter is fixed outside the body by taping or sewing it to different types of fixation devices that are left adherent to the skin.³⁶ External fixation devices preclude the need for suturing of the catheter to the patient's skin, which not only can be an irritant but also can be a focus of infection.³⁶

ADDITIONAL TECHNIQUES FOR ABSCESS DRAINAGE

Organ Traversal

On occasion, percutaneous access into abdominal abscesses is not possible without crossing an intervening organ.² In several

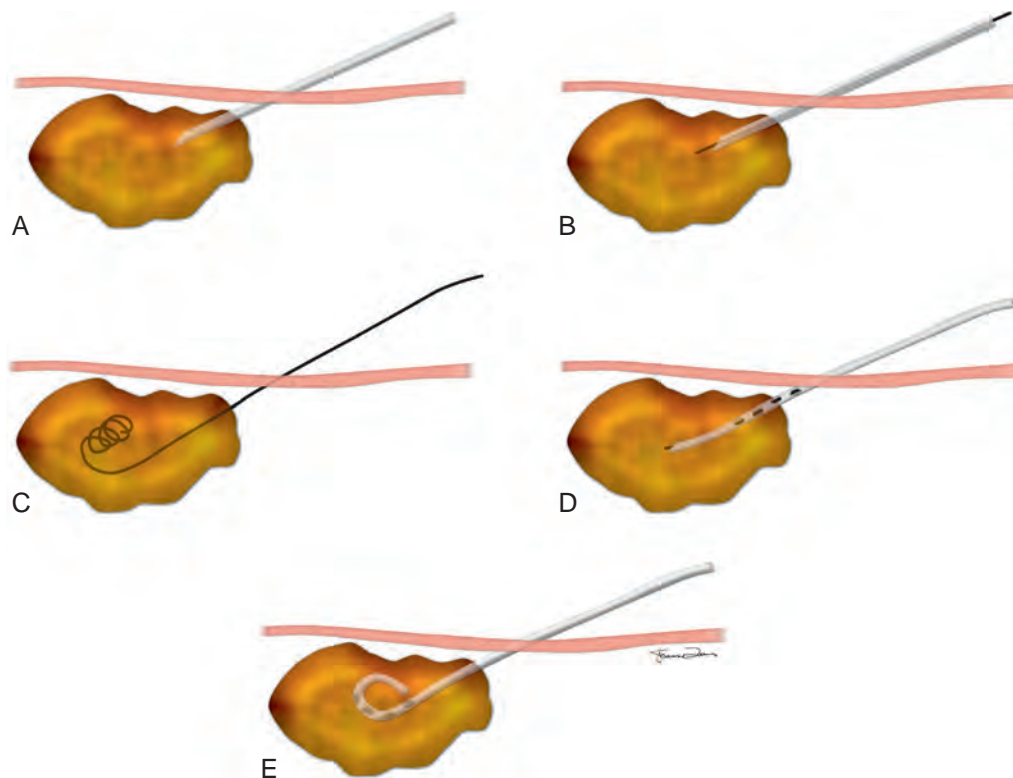


Figure 72-8 Seldinger technique for percutaneous abscess drainage. **A.** Illustration shows initial placement of a 19-gauge needle into the abscess. **B.** In the next step, a guidewire is introduced through the needle into the abscess cavity. **C.** After a sufficient length of guidewire is coiled in the abscess cavity, the track is serially dilated over the guidewire using fascial dilators to enable placement of a drainage catheter. **D.** The percutaneous drainage catheter is then placed into the abscess after passing over the guidewire. **E.** The final image shows appropriate positioning of the percutaneous catheter within the abscess.

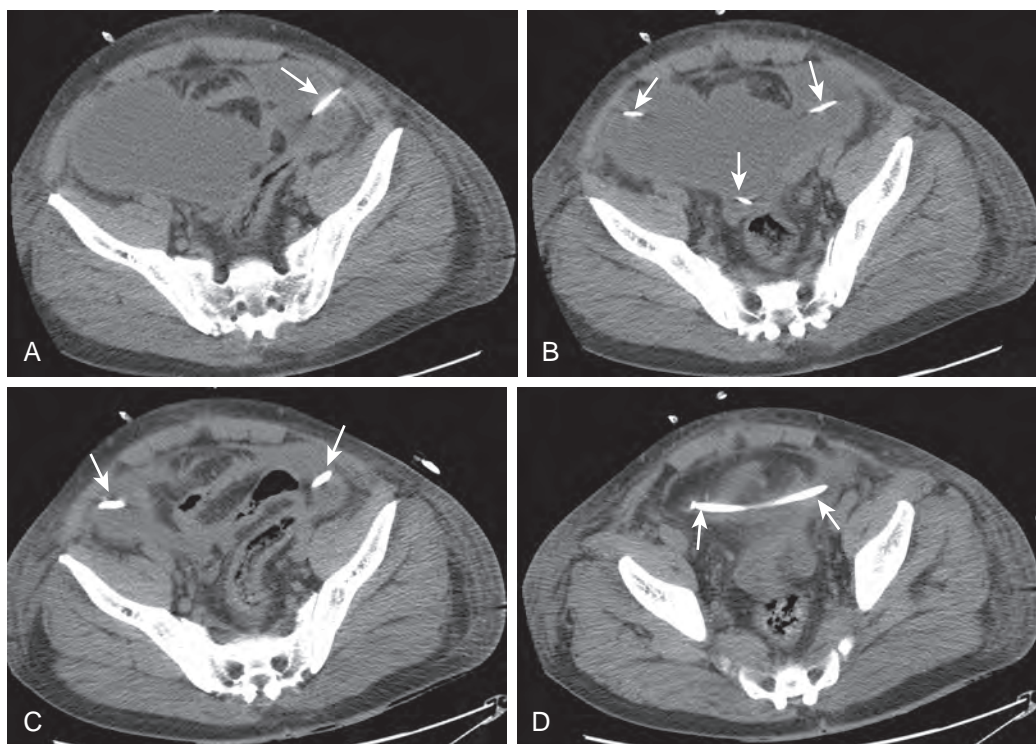


Figure 72-9 Seldinger technique for drainage of a large intraperitoneal abscess. **A.** Preliminary axial CT image shows the placement of an 18-gauge needle (arrow) into the intraperitoneal abscess. **B.** Subsequently, a guidewire (arrows) was introduced into the collection through the needle. **C** and **D.** After serial dilation over the guidewire, a 12F multi-side hole drainage catheter (arrows) was placed into the collection, resulting in adequate drainage.

circumstances, the drainage catheter can traverse intervening organs without undue complications.²

The organs that can be safely traversed in most circumstances are the stomach and the liver (Fig. 72-10).² It is also safe to traverse the rectum and the vagina with use of the transcavitary approach for abscess drainage.²

Several organs, however, should not be traversed and should be carefully avoided during percutaneous abscess drainage, namely, the pancreas, spleen, gallbladder, small and large bowel, urinary bladder, uterus and ovaries, prostate, and blood vessels.² Although percutaneous drainage of abscesses within these organs is safe, these organs should not be transgressed in an attempt to reach a deep-seated abscess.²

It is important to take several important precautions to ensure safe traversal of intervening organs.² In traversing structures such as the liver, it is important to make sure that the coagulation parameters are normal.² Also ensure that the catheter has the shortest possible course through the liver, at a safe distance from major blood vessels, dilated biliary ducts, and gallbladder.² In addition, care should be taken that the catheter side holes are totally confined within the abscess cavity to avoid contamination of the adjacent liver or biliary tract.²

The stomach is frequently traversed for percutaneous drainage of pancreatic abscess or pseudocysts.² In these situations, a multi-side hole catheter is used, and it is positioned such that the side holes are situated within both the pancreatic or peripancreatic collection and the stomach.² To promote formation of a cystogastrostomy track, the catheter should be left in place for 6 weeks. This allows drainage of the pancreatic duct secretions into the stomach because of the presence of a communication between the pancreatic duct and the pseudocyst.²

CT Gantry Angulation

Angulation of the CT gantry is a useful technique to create a safe pathway for drainage of deep-seated abscesses when all the planned access routes in the axial planes have bowel, bone, and blood vessels in their paths.^{2,41,42} Angling of the gantry in a cranial or caudal direction generally helps create a safe path to the abscess that avoids vital organs.^{2,41,42} For example, if an abscess is located high in the pelvis, angulation of the CT gantry in the cephalic direction can facilitate transgluteal drainage (Fig. 72-11).^{2,41,42} When this approach is used, careful attention to technique is required because the needle and the catheter should be aligned parallel to the angled gantry for optimal positioning.^{2,41,42}

Surgical Drains as Access Route for Abscess Drainage

Preexisting surgical drains provide a safe and effective alternative access route for percutaneous drainage of less accessible deep-seated postoperative abdominal abscesses (Fig. 72-12).⁴³ This is particularly true for deep-seated intra-abdominal fluid collections that cannot be accessed safely from a percutaneous approach.⁴³

Combined Modality Approach

Abscesses in difficult locations that cannot be accessed with guidance from a single imaging modality can be effectively drained by a combination of imaging modalities, like ultrasound and fluoroscopy.^{2,3,9,18,36} In these situations, after initial placement of the needle into the abscess with ultrasound, fluoroscopy allows real-time navigation of the catheter and

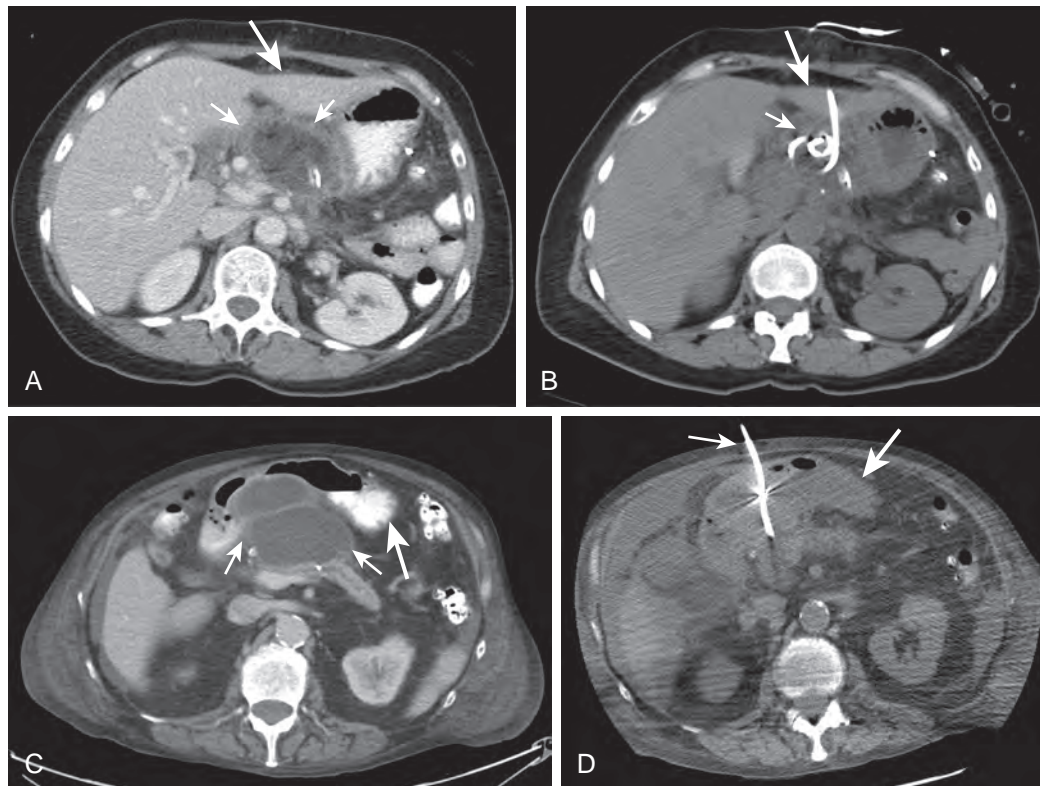


Figure 72-10 Organ traversal technique for percutaneous abscess drainage. **A.** Contrast-enhanced axial CT image shows an abscess (*thin arrows*) posterior to the left lobe of the liver (*thick arrow*). **B.** Percutaneous abscess drainage was performed with successful placement of the drainage catheter into the abscess (*thin arrow*) after traversing the lateral portion of the left lobe of the liver (*thick arrow*). **C.** Contrast-enhanced axial CT image shows a bilobed infected pancreatic pseudocyst (*thin arrows*). The drainage catheter is indicated by the thin arrow. **D.** Percutaneous drainage of this abscess necessitated traversal of the stomach (*thick arrow*). The stomach is indicated by the thick arrow.

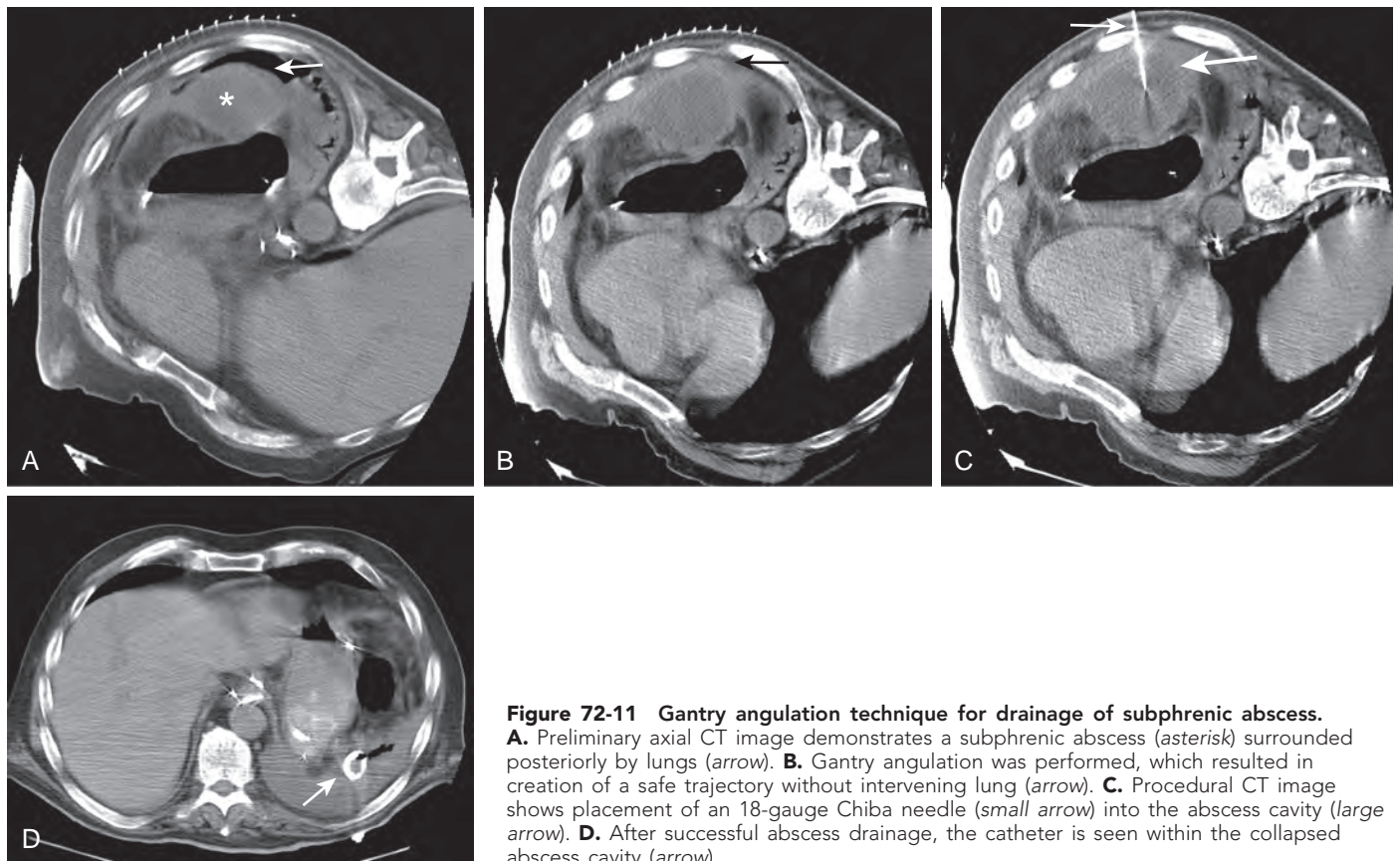


Figure 72-11 Gantry angulation technique for drainage of subphrenic abscess. **A.** Preliminary axial CT image demonstrates a subphrenic abscess (*asterisk*) surrounded posteriorly by lungs (*arrow*). **B.** Gantry angulation was performed, which resulted in creation of a safe trajectory without intervening lung (*arrow*). **C.** Procedural CT image shows placement of an 18-gauge Chiba needle (*small arrow*) into the abscess cavity (*large arrow*). **D.** After successful abscess drainage, the catheter is seen within the collapsed abscess cavity (*arrow*).

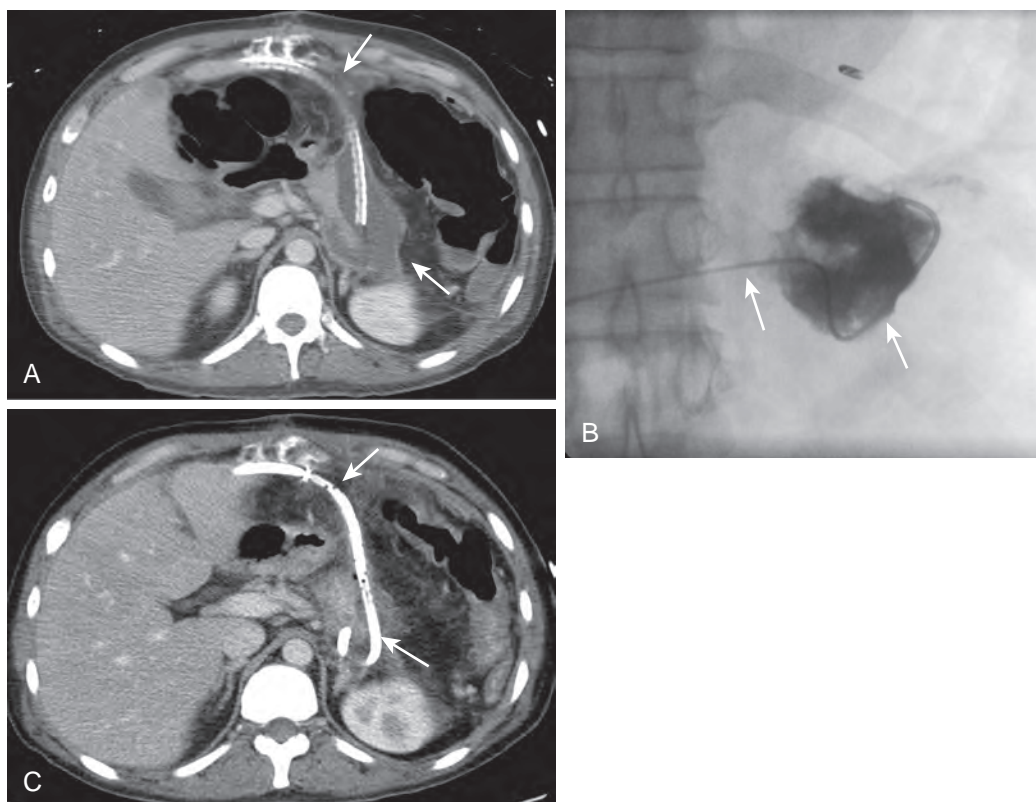


Figure 72-12 Use of surgical drain as an access for percutaneous drainage. **A.** Contrast-enhanced CT image shows a postoperative abscess (arrows) in the pancreatic bed not effectively drained by a surgical drain. **B.** Under fluoroscopic guidance, a guidewire was passed through the surgical drain to gain access into the abscess cavity. A Kumpke catheter was then passed over the wire into the abscess. Injection of contrast material in the image shows the peripancreatic abscess (arrows). **C.** Subsequently, the Kumpke catheter was exchanged for a wire, and a 12F multi-side hole drainage catheter was placed into the deep peripancreatic abscess with decompression of the abscess cavity (arrows).

guidewire into the desired location within the abscess.^{2,3,9,18,36} For example, fluoroscopy and ultrasound or CT can be used in combination to successfully drain abscesses in the subphrenic location while at the same time avoiding pleural transgression (Fig. 72-13).^{2,3,9,18,36}

Hydrodissection

Hydrodissection is an organ displacement method for creating a safe percutaneous trajectory for abscess drainage when adjunctive measures such as gantry angulation and patient positioning are not successful.⁴⁴ It involves instillation of 0.9% saline solution with a 20-gauge Chiba needle into the planned path for placement of the drainage catheter (Fig. 72-14).⁴⁴ The instilled saline then displaces the intervening structures away from the path to the abscess, allowing safe placement of the drainage catheter.⁴⁴ Hydrodissection is most effective for displacement of retroperitoneal structures, such as colon and duodenum, away from the path to deeper intraperitoneal abscesses.⁴⁴

CATHETER MANAGEMENT AFTER DRAINAGE

Immediately after Drainage

After initial catheter drainage, it is essential to completely evacuate the abscess contents and to irrigate the abscess cavity with saline several times until the aspirate becomes clear.^{8,18} The irrigation of the abscess must be performed with saline flushes

with a volume smaller than the abscess volume to avoid an ensuing increase in intracavitary pressure, which could potentially lead to bacteremia and sepsis.^{5,8,9,18,36} The catheter tip is positioned in a gravity-dependent location of the abscess to facilitate effective drainage.^{8,18} After successful placement of the drainage catheter and evacuation of the abscess cavity, it is essential to obtain postprocedure imaging to identify any additional collections or undrained loculations before completion of the procedure.^{8,18} Postprocedure imaging also allows detection of any complications related to the procedure, such as bleeding or pneumothorax.

Regular Catheter Care

After percutaneous abscess drainage, daily ward rounds are imperative to assess the patient's clinical response and to monitor catheter functioning.^{18,45} Daily rounds are also critical in fostering a good patient-physician relationship because a majority of patients are unaware of the existence of the interventional radiology service.^{18,45} The patients also appreciate the opportunity to interact with the radiologists, and the interaction in turn helps the radiologist to educate the patients about regular catheter care. The daily rounds should be used to assess the patient's clinical status, including the development of any postprocedure complications.^{18,45} The catheter function should be monitored to document drain output and any change in appearance of drain fluid.^{18,45} The catheter should be irrigated at least a few times daily with saline flushes (5-10 mL) to avoid

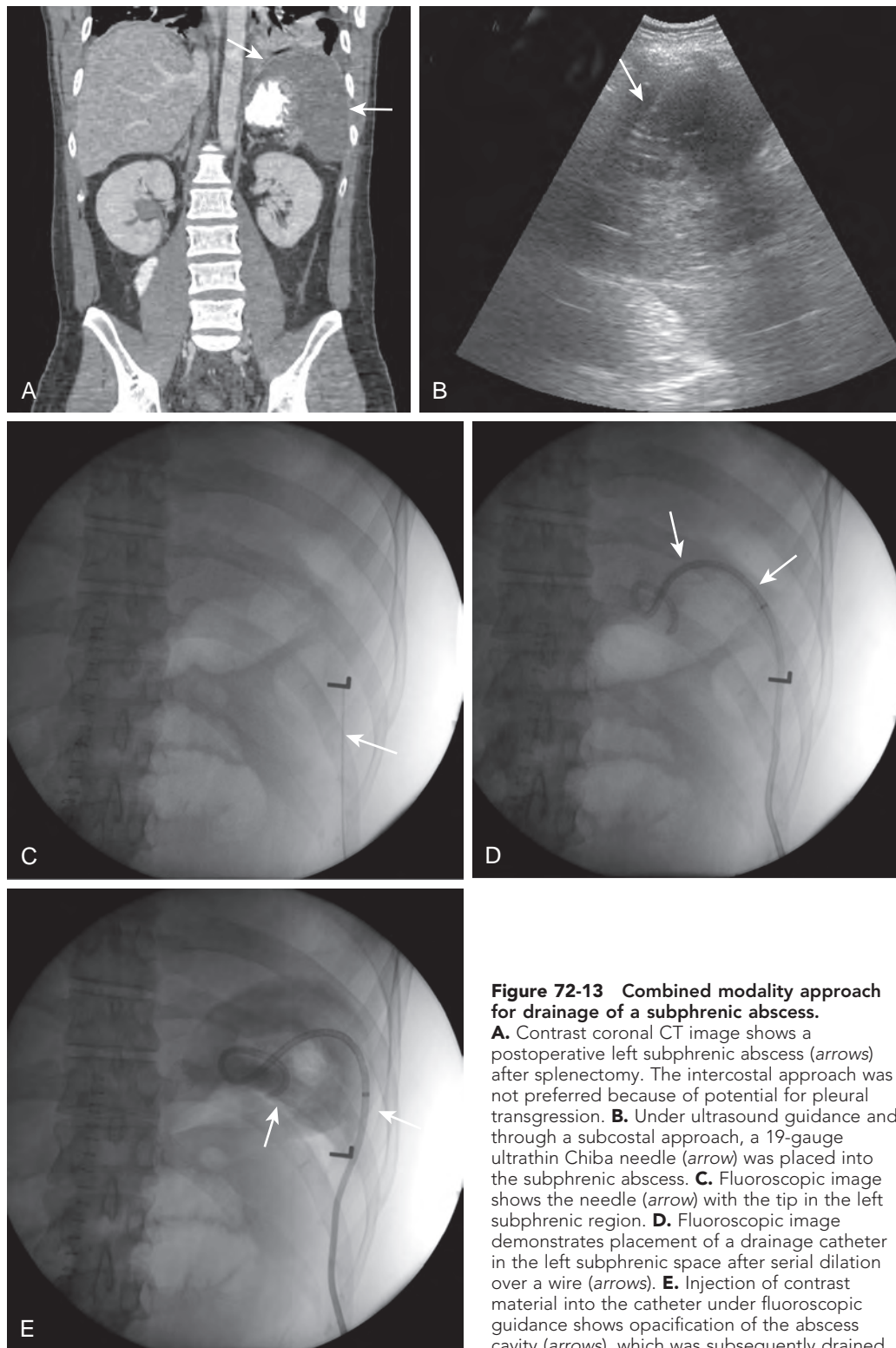


Figure 72-13 Combined modality approach for drainage of a subphrenic abscess.

A. Contrast coronal CT image shows a postoperative left subphrenic abscess (arrows) after splenectomy. The intercostal approach was not preferred because of potential for pleural transgression. **B.** Under ultrasound guidance and through a subcostal approach, a 19-gauge ultrathin Chiba needle (arrow) was placed into the subphrenic abscess. **C.** Fluoroscopic image shows the needle (arrow) with the tip in the left subphrenic region. **D.** Fluoroscopic image demonstrates placement of a drainage catheter in the left subphrenic space after serial dilation over a wire (arrows). **E.** Injection of contrast material into the catheter under fluoroscopic guidance shows opacification of the abscess cavity (arrows), which was subsequently drained.

clogging of the catheter and connecting tubing.^{18,45} The catheter position, exit site, and dressing should be carefully examined to ensure that the catheter is not retracting from the abscess.^{2,3,8,18} The daily rounds are also helpful to review the need for follow-up imaging and to decide the timing of catheter removal.^{18,45}

Post-Catheter Drainage Imaging and Catheter Removal

The timing for imaging assessment of the abscess after catheter drainage depends on several factors, including the patient's clinical status, laboratory findings, and daily drain output. In

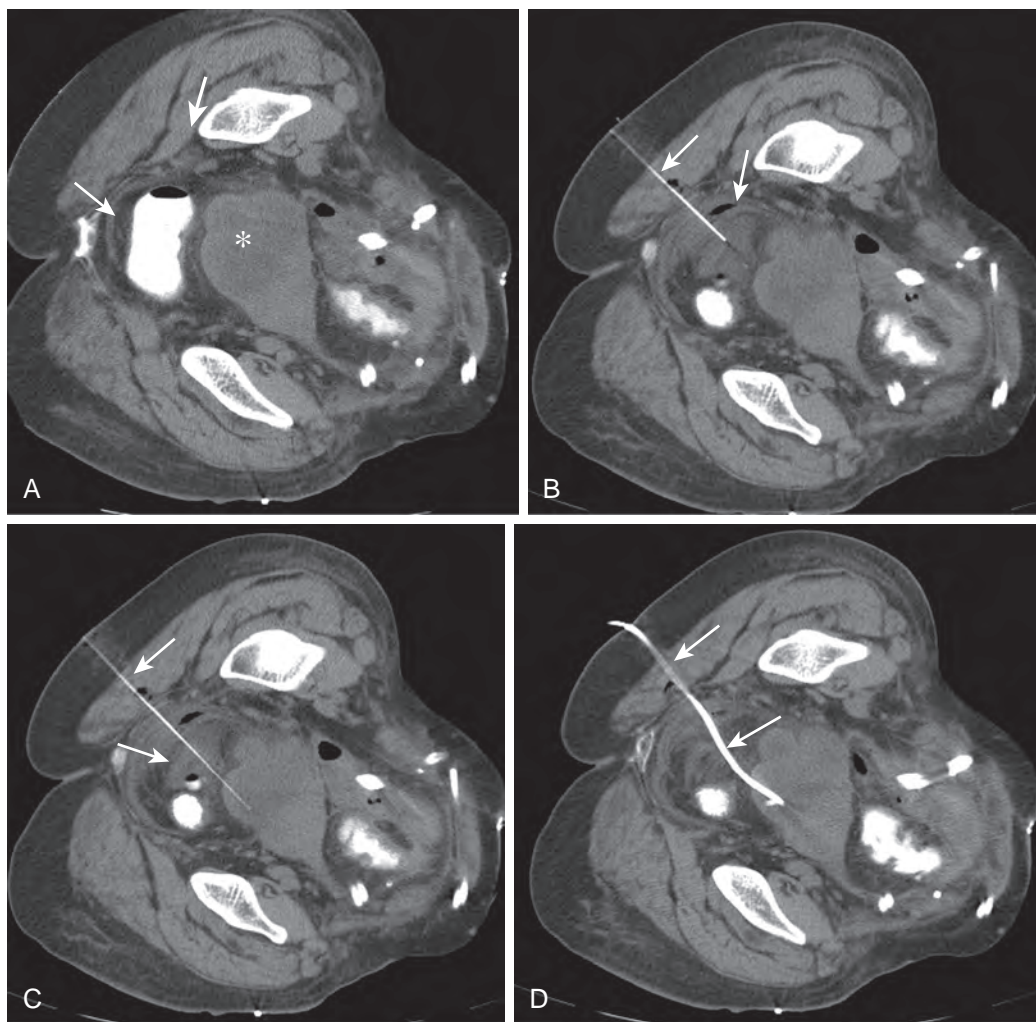


Figure 72-14 Hydrodissection technique for drainage of deep pelvic abscess. **A.** Preliminary CT image shows a deep pelvic abscess (asterisk). A safe pathway to the abscess is blocked by the rectum posteriorly (thin arrow). A lateral percutaneous access to the abscess (thick arrow) is hindered by presence of blood vessels. **B.** A 20-gauge Chiba needle was introduced lateral to the rectum, and saline (arrows) was instilled through the needle to displace the rectum medially. **C.** Subsequent CT image shows the needle placed into the abscess through the percutaneous path created by saline instillation (arrows). **D.** Procedural axial CT image shows a safe pathway created by hydrodissection, which allowed placement of the drainage catheter (arrows) into the abscess through the transgluteal approach.

general, repeat imaging is often performed 1 to 2 weeks after initial abscess drainage. Cross-sectional imaging techniques such as CT are most commonly used to monitor the adequacy of drainage by determining the residual abscess volume as well as the development of new abscesses.^{9,18} However, MRI could be used for postprocedure imaging, particularly in pediatric patients. If CT shows that the abscess is totally resolved, catheter removal could be contemplated on the basis of the nature and quantity of drainage fluid (Fig. 72-15). If CT shows residual abscess in spite of optimum position of the catheter, the patency of the catheter should be confirmed by a 5- to 10-mL saline flush.^{9,18-20,29} If the catheter is patent and well positioned within the abscess but imaging shows persistence of the abscess, the catheter should be exchanged for a larger catheter or a catheter with more side holes to improve drainage.^{9,18-20,29} Fluoroscopic injection of iodinated contrast medium through the catheter should also be performed on the same day as the CT scan to look for any residual abscess and to document presence of a fistulous communication.^{9,18-20,29}

The percutaneous drainage catheter can generally be safely removed when the following criteria are met: resolution of clinical findings, including fever, pain, and leukocytosis; minimal drainage output (<10 mL in 24 hours); imaging findings demonstrating resolution of the abscess with absence of any residual collection; and fluoroscopically guided injection of contrast material demonstrating absence of fistulous communication of the abscess cavity with bowel or other structures close to the abscess cavity. Although diminishing drain output is an important indicator of effective abscess drainage, it is important to ensure that the reduction in drain output from the catheter is not due to other reasons, such as catheter malpositioning or blockage. In fact, whenever there is a sudden decrease in drain output, the possibility of catheter obstruction or kinking should be considered. Sudden increases in drainage could indicate fistulous communication with bowel or ascites drainage. These facts underscore the value of obtaining repeated imaging after catheter drainage to confirm abscess resolution and appropriate catheter position before contemplating catheter removal.

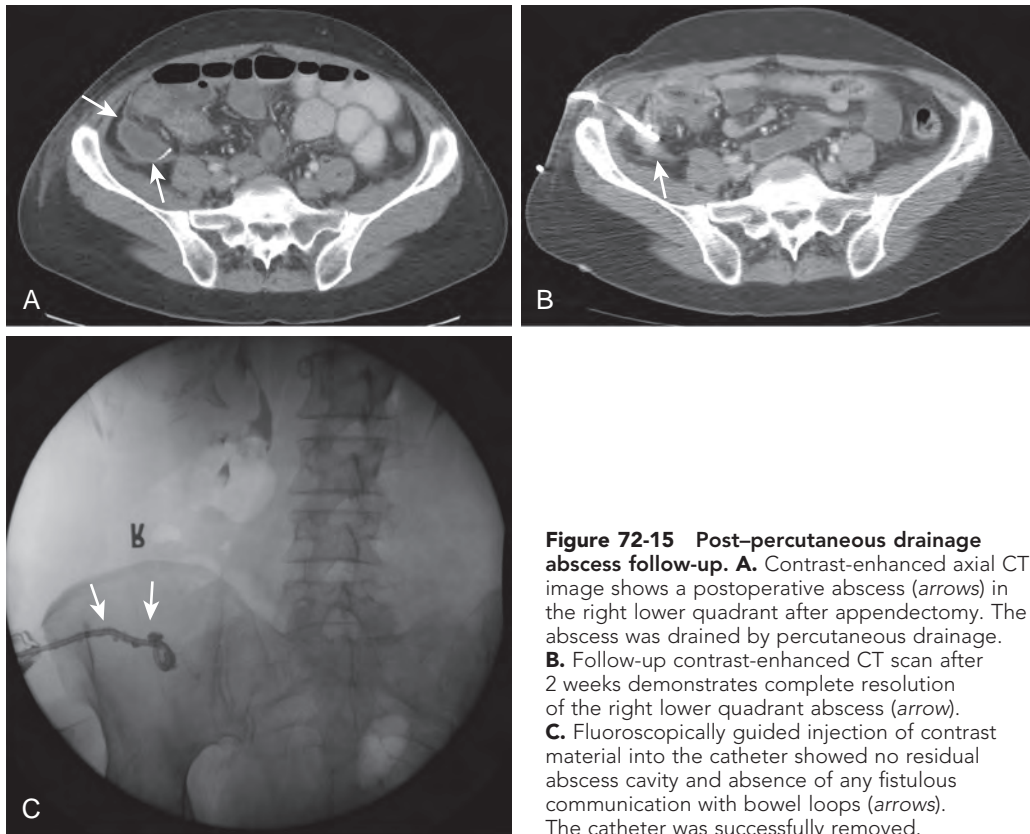


Figure 72-15 Post-percutaneous drainage abscess follow-up. **A.** Contrast-enhanced axial CT image shows a postoperative abscess (arrows) in the right lower quadrant after appendectomy. The abscess was drained by percutaneous drainage. **B.** Follow-up contrast-enhanced CT scan after 2 weeks demonstrates complete resolution of the right lower quadrant abscess (arrow). **C.** Fluoroscopically guided injection of contrast material into the catheter showed no residual abscess cavity and absence of any fistulous communication with bowel loops (arrows). The catheter was successfully removed.

FACTORS AFFECTING OUTCOME OF ABSCESS DRAINAGE

Successful drainage of intra-abdominal abscesses by percutaneous catheters relies on several important factors.^{6,19,20} A key factor facilitating adequate drainage is the appropriate placement of the catheter within the abscess cavity.^{6,19,20} The abscess size or volume as estimated by imaging is also important for selecting the catheters of appropriate size and length to enable unimpeded drainage.^{18,20,46} The density of abscess contents on CT has been reported to influence the success of abscess drainage.² An abscess with an attenuation of more than 20 HU has a higher failure rate compared with an abscess with a fluid attenuation of less than 20 HU.^{6,19} Abscesses with higher fluid attenuation might have increased levels of protein, blood products, and bacteria, which can impede catheter drainage.^{2,3,6,18,19} Complexity of abscess fluid, such as multiloculation and increased viscosity of internal contents, is associated with a lower rate of success.^{2,3,6,18,19} The relative efficacy of the initial drainage catheter is an important predictor of response to abscess drainage.^{2,3,6,18,19} This means that the abscesses that have a lower residual abscess volume as a percentage of initial volume have better treatment success than those with larger volume^{2,3,6,18,19} (Table 72-3).

After successful drainage of intra-abdominal abscesses, they can often recur at the same location.^{18,20,46} In such circumstances, repeated abscess drainage should be performed. However, if more than two drainage attempts have been made, consideration needs to be given to open operative drainage.^{2,18,20,46} Multiple abscess recurrence after successful evacuation of the abscess contents should prompt consideration of an

TABLE 72-3 Causes of Unsuccessful Drainage

	Cause
Causes due to catheter	Catheter blocked Catheter in improper position Small catheter for the collection Too few side holes in the catheter
Causes due to abscess	Multiloculated collection Presence of fistula, particularly enteric fistula Infection with fungal organisms Pancreatic origin

unsuspected diagnosis.^{18,20,46} The presence of fistula between the abscess cavity and another body cavity (bowel, biliary tree, or bladder) has a higher failure rate.^{18,20,46}

TIPS AND TRICKS TO IMPROVE OUTCOME

Catheter Blockage and Improper Position

A clogged or occluded catheter is often diagnosed when there is difficulty in flushing a catheter.³⁶ An occluded or clogged catheter needs to be exchanged for a new catheter for effective drainage.³⁶ However, before catheter exchange, a diagnostic imaging study, preferably CT, is necessary to confirm the position of the drainage catheter tip. Sometimes, the reason for ineffective drainage is abnormal position of the drainage catheter (Fig. 72-16).^{19,36} If the catheter is abnormally positioned or pulled out, repositioning and catheter rescue might be required.^{19,36} A new percutaneous drainage might be

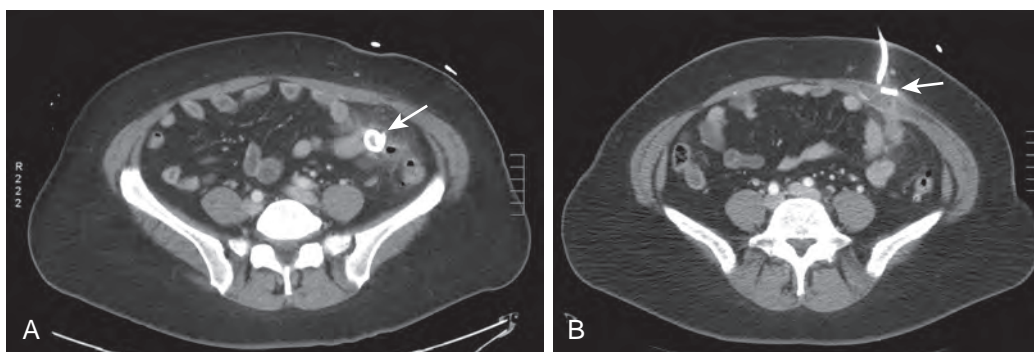


Figure 72-16 Catheter dislodgment after percutaneous drainage. **A.** Axial CT image shows a left lower quadrant percutaneous drainage catheter placed in a 65-year-old man with diverticular abscess. The catheter tip is in the appropriate position within the abscess (arrow). The patient presented 2 weeks later with decreasing drainage from the catheter. **B.** Follow-up CT showed that the catheter had retracted from an intra-abdominal location into the subcutaneous tissues (arrow). The catheter was successfully repositioned into the abscess under fluoroscopic guidance.

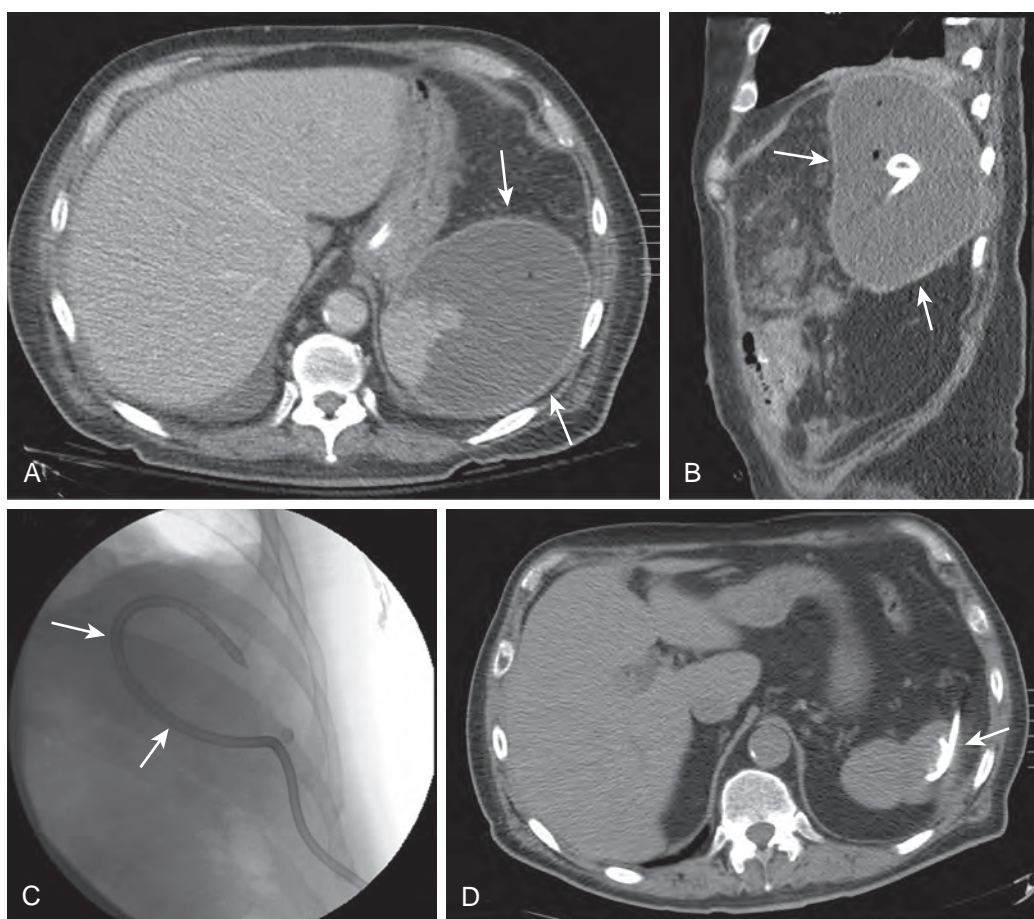


Figure 72-17 Improved drainage of a perisplenic abscess after catheter exchange for a larger catheter with more side holes. **A.** Axial contrast-enhanced CT image in a 54-year-old man shows a large perisplenic abscess (arrows). **B.** Sagittal CT image shows persistent abscess despite adequate positioning of the catheter (arrows). **C.** Fluoroscopic image shows placement of a larger bore catheter with more side holes into the abscess over a guidewire (arrows). **D.** CT obtained 2 weeks later showed complete resolution of the abscess (arrow).

necessitated in situations in which catheter rescue is not possible and a substantial abscess cavity remains.^{19,36}

Increasing Catheter Drainage Surface Area

Percutaneous catheter exchange over a guidewire is the favored intervention for suboptimally drained abscesses despite adequate catheter placement.^{19,36} When postprocedure imaging

demonstrates reduction in abscess volume without significant resolution and appropriate positioning of the catheter within the collection, increasing the number of catheter side holes and increasing the catheter diameter improve drainage and have a higher rate of success^{19,36} (Fig. 72-17). Use of a longer drainage catheter with multiple side holes increases the drainage surface area, and therefore drainage of the abscess is more

effective.^{19,36} For example, a multi-side hole drainage catheter (e.g., 32-side hole biliary drainage catheter) provides better drainage than a five-side hole drainage catheter because of an increase in the number of side holes for drainage along the length of the catheter and decreased risk of catheter occlusion.¹⁹

Thrombolytic Agents

Certain abscesses are refractory to simple percutaneous drainage and benefit from instillation of thrombolytic agents, which improves percutaneous drainage, thereby avoiding surgical débridement.^{3,21,36,47} Thrombolytic therapy is particularly helpful in multiloculated abscesses or abscesses with extremely viscous contents that result in limited or no drainage from the catheter despite the presence of a large residual collection and proper catheter positioning. The difficulty in drainage is due to fibrin matrix deposition in the abscess, which causes loculations interfering with simple catheter drainage.^{3,21,36,47} The basic principle of the use of thrombolytic agents is their ability to cause fibrinolysis, which involves degradation of fibrin through activation of plasmin from plasminogen (Fig. 72-18). The fibrinolysis results in lysis of the septations and loculations, mobilizing abscess fluid.^{3,21,36,47} Thrombolytic agents such as tissue plasminogen activator (tPA) and urokinase also act to reduce the viscosity of abscess contents, thereby facilitating catheter drainage.^{3,21,36,47} It is a proven safe therapy for management of abscesses and is associated with only minimal risk of bleeding, even in patients who are receiving prophylactic anticoagulation.^{3,21,36,47}

At our institution, tPA is the preferred agent for thrombolytic therapy. The preferred dosage in our institution is 4 to 6 mg of tPA reconstituted in 50 mL of 0.9% saline per administration.^{21,47} The volume of instilled tPA is adjusted on the basis of the size of the cavity and usually should be 30% to 50% of the initial cavity volume.^{21,47} The reconstituted tPA is instilled into the abscess cavity, and the catheter is clamped for approximately 30 minutes to 1 hour.^{21,47} At the end of this period, the tube is opened to gravity drainage. We routinely administer six doses of tPA during a period of 3 days (two doses per day). After completion of the administration of tPA, diagnostic imaging with CT is performed to assess the efficacy of the thrombolytic therapy. Instillation of the thrombolytic agents early in the course of drainage therapy improves the likelihood of success compared with later instillation.^{3,21,36,47} The dosing of urokinase is 250,000 units reconstituted in 250 mL of sterile saline to achieve a concentration of 1000 U/mL and divided into three equal aliquots administered during a period of 24 hours.⁴⁸ After administration of each aliquot, the catheter is clamped for 30 minutes to 2 hours before the catheter is opened for gravity drainage.⁴⁸

Fungal Abscesses

Fungal abscesses are increasingly encountered in hospitalized patients, mostly in immunocompromised patients and elderly and intensive care unit patients.^{49,50} Although technically highly successful, percutaneous drainage of fungal abscesses has limited success because of the higher clinical failure rate.^{49,50} The most common fungal organism isolated from these abscesses is

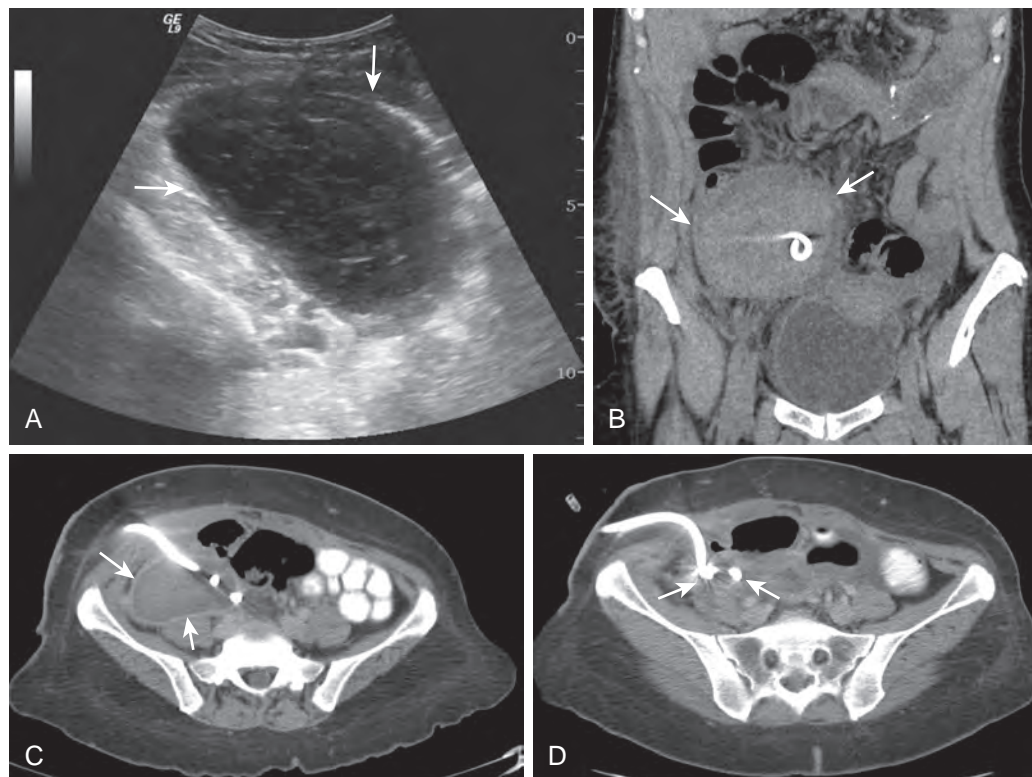


Figure 72-18 Thrombolytic therapy for effective abscess drainage. **A.** Transverse ultrasound image of a 67-year-old man with an intraperitoneal abscess shows multiple internal septations (arrows). Percutaneous abscess drainage was performed. **B.** CT obtained 2 weeks later shows persistent abscess despite adequate catheter positioning (arrows). High density of the internal contents of the abscess suggests viscous contents. tPA instillation was performed into the abscess. **C.** CT obtained after six doses of tPA showed improved liquefaction of the abscess contents (arrows). **D.** Follow-up CT obtained 1 week later showed complete collapse of the abscess cavity (arrows).

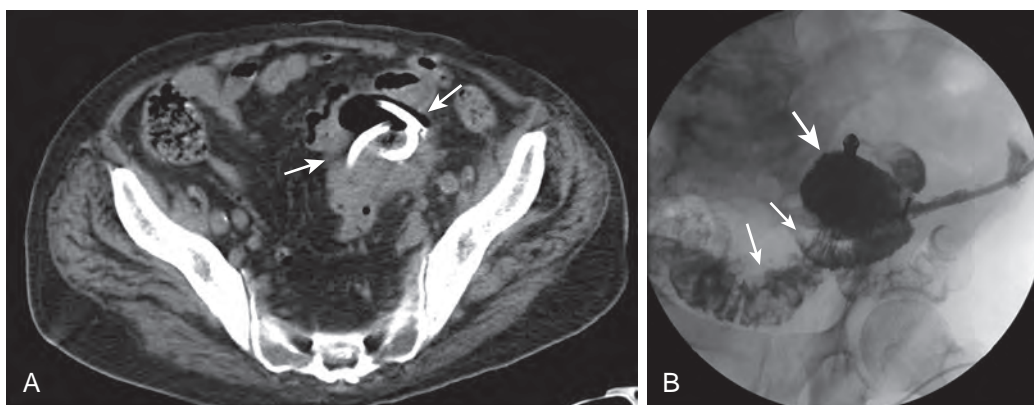


Figure 72-19 Diverticular abscess with fistulous communication to sigmoid colon. **A.** Axial CT image shows a percutaneous drainage catheter within a diverticular abscess associated with sigmoid diverticulitis (arrows). The patient continued to have persistent drainage from the catheter for 4 weeks. **B.** Fluoroscopically guided injection of contrast material into the abscess cavity (thick arrow) showed fistulous communication of the abscess cavity with the sigmoid colon (thin arrows).

Candida albicans (79%), followed by *Candida glabrata*.^{49,50} Varghese and colleagues reported a technical success rate of 79% and a clinical success rate of 57% for percutaneous drainage of fungal abscesses. The predictors of poor clinical outcome in fungal abscess include presence of loculations at imaging, history of malignant disease, and admission to the intensive care unit.^{49,50} Drainage can be optimized in such situations by placement of larger bore catheters with larger diameter or catheters with an increased number of side holes.^{49,50}

Abscesses with Fistulous Communication

Intra-abdominal abscesses are often complicated by fistulous communication with surrounding structures within the abdomen, which can often impede effective drainage.* The risk factors for fistulous communication include abscesses developing in patients with Crohn's disease, diverticulitis, pancreatic duct injuries, and postoperative abscesses after bowel surgery.* The presence of a fistulous communication should be suspected in these patients during the management of their intra-abdominal abscesses. The diagnosis of fistulous communication is normally made during fluoroscopically guided injection of contrast material into the drainage catheter (Fig. 72-19).^{3,36} CT with positive oral contrast agents can also be performed to confirm the diagnosis in suspected fistulization to the bowel. The presence of a fistula is also indicated by the change in the nature and appearance of the drainage fluid. For example, the initial purulent drainage from an abscess transforms into fluid resembling origin from other body cavities, such as bile, bowel contents, urine, or pancreatic fluid.^{3,36} An additional sign that is highly suggestive of fistulous communication is a persistently high drain output from the catheter.^{3,36}

The management of an abscess with fistulous communication to other abdominal structures, particularly bowel, is complex and challenging. The presence of a fistulous communication usually necessitates prolonged catheter drainage because premature catheter removal results in abscess recurrence due to reaccumulation of fluid. Surgery remains the definitive treatment option in these patients. In patients who are poor surgical candidates, the management strategy often

involves prolonged catheter drainage for several weeks to months to allow healing and the fistula to close. In many situations in which the patient is unfit for surgical intervention, adjunctive procedures may facilitate fistula healing.^{18,20,29,36} For example, sphincterotomy with endoscopic biliary stent placement for biliary diversion is effective in patients with infected bilomas from biliary injury as this allows internal biliary drainage and curtails bile leakage into the abscess cavity, promoting healing.^{18,20,29,36} Similarly, in patients with infected urinomas caused by post-traumatic urine leaks, urinary diversion away from the urinoma can be achieved with a ureteral stent or a percutaneous nephrostomy catheter to aid closure of the fistula.^{18,20,29,36} In patients with high-output enteric fistula, prolonged parenteral nutrition and exclusion of oral nutrition may be necessary.^{18,20,29,36}

ABSCESSSES AT SPECIFIC LOCATIONS

Liver Abscess

Liver abscesses are often either pyogenic or amebic in origin.^{3,51-54} Other causes, such as fungal and protozoan, are uncommon. Pyogenic liver abscess most commonly occurs in the United States, whereas amebic liver abscesses account for most cases of hepatic abscess throughout the world.^{3,51-54} Hepatic abscesses cause significant morbidity and mortality despite advances in antibiotic therapy.^{3,51-54}

Pyogenic liver abscesses usually result from prior abdominal surgery, trauma, neoplastic disease, biliary tract disease, or bacteremia in immunocompromised patients.^{3,18,51-54} Intra-abdominal infections such as diverticulitis and appendicitis often result in hepatic abscess by bacteremia from the portal vein; however, their incidence has fallen because of improved management of these conditions with antibiotic therapy.^{3,18,51-54} Hepatic abscesses can also result from complications of prior hepatobiliary surgeries involving biliary-enteric anastomoses, liver transplantation, and locoregional therapies such as transarterial chemoembolization and percutaneous tumor ablation.^{3,18,51-54} In addition to features of abdominal sepsis, such as abdominal pain, fever, and chills, the patients with hepatic abscess present with leukocytosis and elevated bilirubin and alkaline phosphatase.^{3,18,51-54} Pyogenic abscesses can be single or multiple (46%-71%).¹⁸ *Klebsiella pneumoniae* is the most

*References 2, 9, 19, 20, 29, 36.

common microbe in solitary abscesses, whereas *Escherichia coli* is most often involved in multiple abscess groups.^{3,18,51-54} Single pyogenic abscesses are usually located in the right lobe of the liver, whereas multiple abscesses usually occur in both lobes.^{3,51-54} Untreated pyogenic abscesses are almost uniformly fatal.¹⁸ On ultrasound, pyogenic abscesses have a cystic or hypoechoic appearance with internal debris and often demonstrate posterior acoustic enhancement.¹⁸ Amebic abscesses are manifested as rounded or oval lesions with a homogeneous hypoechoic appearance without irregular walls as seen with pyogenic abscess.¹⁸ On CT, they are manifested as low-attenuation masses with a rim of peripheral enhancement surrounded by a hypodense halo due to surrounding edema.^{3,18}

The cardinal rule in the management of pyogenic liver abscess is early intervention with either surgical or percutaneous drainage and parenteral antibiotics.^{7,9,18,54-57} A single abscess can be drained by ultrasound, whereas multiple abscesses are drained with CT guidance (Fig. 72-20).⁷⁻⁹ Percutaneous drainage is effective in treatment of 70% to 94% of patients.^{7-9,18,53,58-60} Higher rates of morbidity and mortality are seen in patients with multiple or multiseptate abscesses and with underlying comorbidities, systemic sepsis, delayed diagnosis, or fungal superinfection.^{7-9,18,53,58-60}

Amebic liver abscesses are common worldwide and caused by *Entamoeba histolytica*.^{9,18,61} They are common in individuals living in or with history of recent travel to endemic areas and in immunocompromised individuals.^{9,18,61} Amebic liver abscesses are often single and seen in the right lobe of the liver in a subcapsular location.^{9,18,61} The cornerstone of therapy in patients with amebic liver abscess is medical management with metronidazole.^{9,57} The option of drainage is restricted to patients in whom medical therapy fails, to those with abscesses larger than 6 to 8 cm, and to those in whom there is increased risk of rupture.^{9,57,61,62} Amebic abscesses have a better response rate than pyogenic abscesses do.^{9,57,61,62}

Splenic Abscess

Splenic abscess is a rare condition with an incidence of less than 1%; however, an increasing number of cases are being reported in immunocompromised patients.^{3,18,63-66} Splenic abscesses most often result from metastatic hematogenous infections secondary to endocarditis, contiguous sites of infection, and

trauma.^{18,63-66} Splenic abscess can be associated with a high degree of morbidity and mortality because of the risk of sepsis and splenic rupture.^{3,18,63-66} Early diagnosis and intervention are imperative to improve outcome. Patients usually present with left upper quadrant pain, fever, and leukocytosis.^{3,18,63-66} Imaging has a high sensitivity in the diagnosis of splenic abscess ranging from 75% to 96%, with CT performing better than ultrasound.^{18,63-66} Percutaneous drainage of splenic abscess has success rates between 75% and 100% and is an effective treatment strategy for single lesions along with antibiotic therapy because it precludes splenectomy and preserves splenic function.^{3,18,63-66} In patients with multiple splenic abscesses, splenectomy might be the preferred option, except in patients with high risk for surgery.^{3,18,63-66} For percutaneous drainage, the subcostal approach is preferred to avoid traversing the pleural space, but the intercostal approach might be required because of the subphrenic location of the spleen.³ Multiloculations, septations, viscous contents, and abscess rupture with bleeding are considered to be relative contraindications to catheter drainage, and the surgical option is preferred.^{18,63-66}

Peripancreatic Abscess

Peripancreatic fluid collections, pancreatic pseudocysts, pancreatic abscess, and pancreatic necrosis are common findings in patients with acute pancreatitis.^{18,35,67-71} Percutaneous drainage of peripancreatic fluid collections and pseudocysts should be considered a treatment option when these collections become superinfected.^{18,35,67-71} Noninfected pancreatic pseudocysts or peripancreatic fluid collections can be observed conservatively, and percutaneous drainage may be indicated only in the presence of symptoms such as recurrent abdominal pain, mass effect causing biliary or bowel obstruction, intracystic hemorrhage, or increasing size of the collections.^{9,67,68,71,72} Superinfection is often suspected clinically, and contrast-enhanced CT scans can help in diagnosis.¹⁸ However, percutaneous aspiration with Gram stain and culture could be performed for confirmation before percutaneous drainage.^{3,34,35} Percutaneous drainage has reported cure rates of 65% to 90%, and surgical intervention is reserved for unresponsive collections.^{18,35,67-71} CT is preferred for percutaneous drainage of peripancreatic collections because they are often deep seated and have a complex anatomy (Fig. 72-21).^{18,35,67-71} Fluid collections or abscesses related to

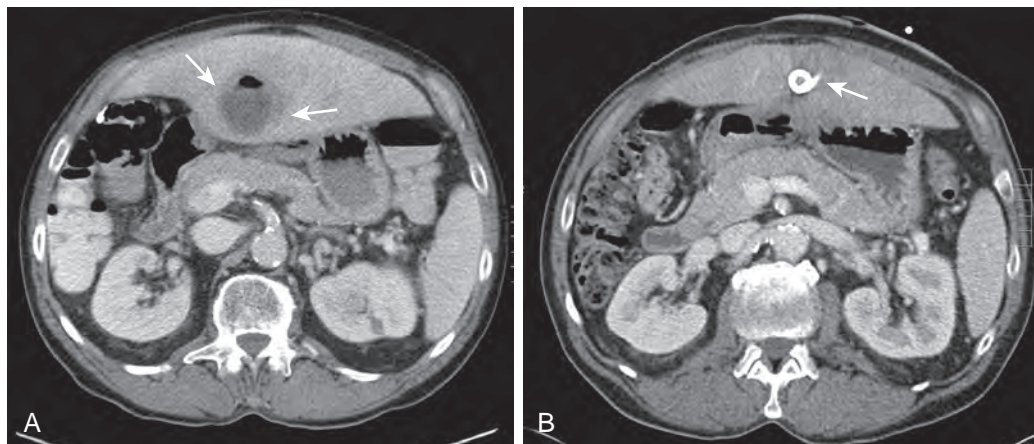


Figure 72-20 Pyogenic hepatic abscess drained by percutaneous drainage. **A.** Contrast-enhanced axial CT image shows a peripherally enhancing air-containing abscess in the left hepatic lobe (arrows). **B.** Contrast-enhanced axial CT image 2 weeks after abscess drainage shows resolution of the left hepatic lobe abscess (arrow).

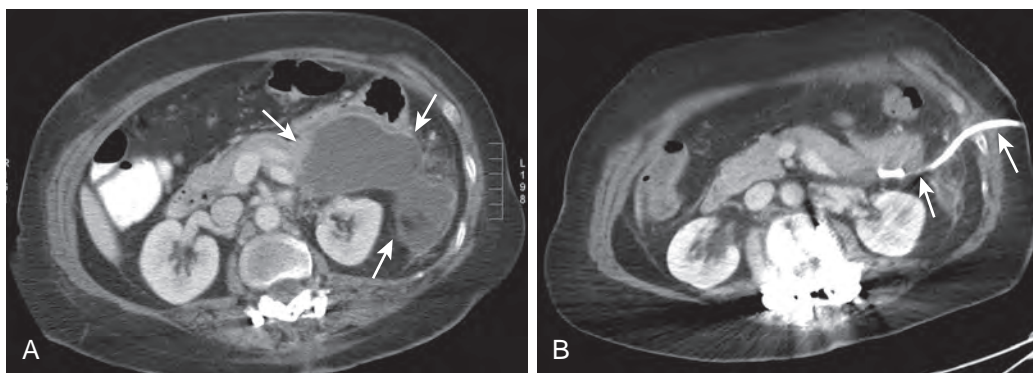


Figure 72-21 Percutaneous drainage of infected peripancreatic fluid collection. **A.** Contrast-enhanced axial CT image in a 45-year-old man with acute pancreatitis shows a large fluid collection adjacent to the pancreatic tail (arrows). **B.** Axial CT image after percutaneous drainage shows resolution of the peripancreatic abscess (arrows).

pancreatitis often result in catheter drainage for longer periods (weeks to months), particularly in collections with fistulous communications to bowel or pancreatic duct.^{3,19,67} Successful repeated percutaneous drainage is possible in some patients with fistulas.¹⁸

Pancreatic and peripancreatic necrosis may result in accumulations of material with fluid attenuation at CT. This necrotic material is viscous and often does not drain completely through the catheter.^{3,9,67,68,71,72} In suspected cases of infected pancreatic necrosis, needle aspiration can be performed for confirmation of infection.^{3,9,67,68,70-72} If the area of necrosis is not infected, the recommended treatment is supportive care.^{3,9,67,68,70-72} If the area becomes infected, surgery is indicated. Percutaneous drainage can be offered as a temporizing measure before surgical intervention in critically ill patients unfit for surgery.^{3,9,67,68,70-72} Large-bore catheters, such as 20F to 30F catheters, are often required for drainage of infected pseudocysts or infected pancreatic necrosis if significant debris is present or if the abscess contents are thick and viscous.^{18,35,67-71} Aggressive catheter management with irrigation is often helpful.³

Retroperitoneal Abscess

Abscesses in the retroperitoneum most often arise from the pancreas or are renal in origin. Renal abscesses are common in patients with preexisting renal diseases, such as nephrolithiasis, hydronephrosis, septicemia, and diabetes mellitus.¹⁸ Renal abscesses can be localized within the renal parenchyma or can rupture externally to be manifested as a perinephric abscess.¹⁸ If renal or perirenal abscess is associated with a urinary obstruction, a percutaneous nephrostomy is needed to relieve the obstruction and could also be used as an access for stone removal.¹⁸ Infected urinomas can also manifest as retroperitoneal abscesses. For infected urinomas resulting from post-traumatic urine leaks, urinary diversion through either a ureteral stent or percutaneous nephrostomy might be required to facilitate healing.^{18,20,29,36,73}

Abscesses in the iliopsoas compartment constitute an important entity and may develop secondary to previous surgery, penetrating trauma, hematogenous spread, contiguous spread from spinal osteomyelitis or tuberculosis, renal abscess, or inflammatory bowel disease.^{18,74} Abscesses in the iliopsoas compartment should preferably be drained under CT guidance because of their ability to demonstrate the location and extent of the abscess and its relationship to nearby structures.¹⁸

Pelvic Abscess

The pelvis is a frequent site of abscess formation, particularly in postoperative patients, because of its dependent location.¹⁸ The other common causes of pelvic abscesses include diverticulitis, appendicitis, Crohn's disease, postirradiation enteric fistulas, and pelvic inflammatory disease.^{3,18} Several safe approaches can be used for effective drainage of pelvic abscess, including the transgluteal, transvaginal, and transrectal route, as the presence of overlying bowel loops and bladder precludes a direct anterior or anterolateral approach.^{2,3,9,18,36} Sonographic guidance is used for drainage by the transvaginal or transrectal route, whereas CT guidance is used for transgluteal drainage.

In the transgluteal approach, the needle is directed caudal to the sacrospinous ligament, and it passes through the sciatic foramen (Fig. 72-22).^{2,25,40,75} To avoid transgression of sciatic nerves and superior and inferior gluteal vessels, the catheter must pass as close to the sacrum as possible while sparing the rectum.^{2,25,40,75} A common disadvantage of the transgluteal route is the significant discomfort and buttock pain.^{2,25,40}

The transvaginal approach provides the most direct access for drainage of abscesses situated close to the apex of the vaginal vault.^{2,76-78} The transvaginal approach is performed with an endoluminal ultrasound probe with a guide, which facilitates needle access for trocar-catheter insertion.^{2,76-78} However, this approach cannot be used for inaccessible collections in the presacral space or ischiorectal fossa.^{2,76-78} The transvaginal route is also not preferred for abscesses located high in the pelvis because of the risk of injury to urinary bladder, bowel, or vascular structures.² Technically, because the vagina is a muscular structure, puncture, dilation, and catheter placement may be difficult.^{2,76-78}

Enteric Abdominal Abscesses

Diverticular Abscess. Acute diverticulitis complicated by abscess formation is seen in nearly 25% of cases. Diverticular abscesses initially start as a microperforation at the site of inflammation with formation of a microabscess, which gradually grows in size to form a larger abscess.^{3,9,12,79} Without definitive treatment, these abscesses can potentially rupture, resulting in gross fecal peritonitis.^{3,9,12,79} Whereas acute diverticulitis is treated medically with antibiotics, development of abscess necessitates drainage either percutaneously or surgically.^{12,28,40} The role of percutaneous drainage in diverticular abscesses is

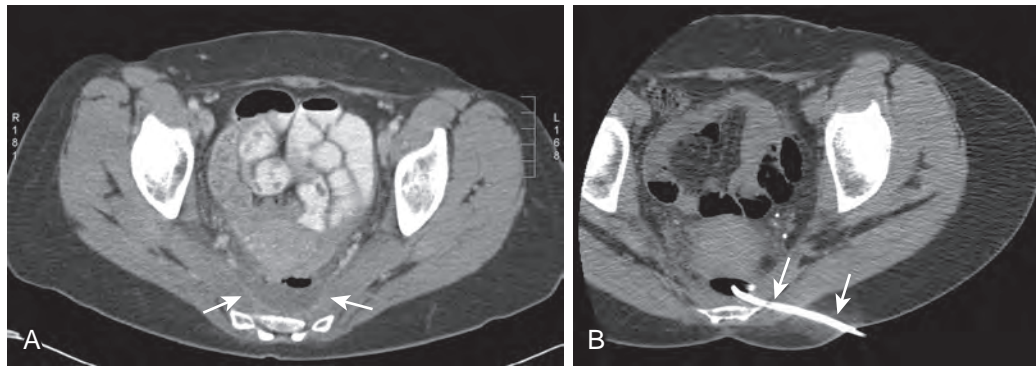


Figure 72-22 Transgluteal drainage of presacral abscess. **A.** Contrast-enhanced axial CT image shows a presacral abscess with an air-fluid level (arrows) in a 67-year-old patient with rectal cancer after rectal cancer surgery. **B.** CT-guided transgluteal drainage of the abscess was performed with placement of the catheter into the presacral abscess (arrows).

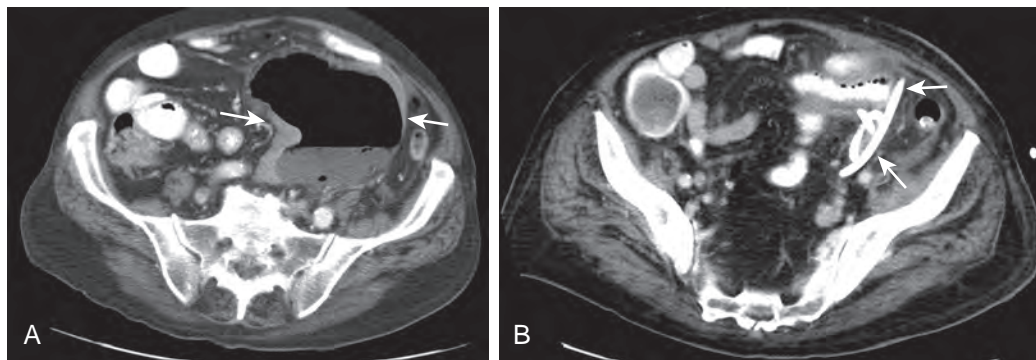


Figure 72-23 Percutaneous drainage of diverticular abscess. **A.** Contrast-enhanced CT image shows a large diverticular abscess (arrows) in a 51-year-old woman. **B.** Axial CT image obtained 2 weeks after percutaneous drainage shows complete collapse of the diverticular abscess cavity (arrows).

usually temporizing to relieve fever and other symptoms before definitive surgery, which involves resection of the affected segment of colon.^{3,12,28,40} Percutaneous drainage is primarily beneficial in cases with limited perforation without gross fecal spillage.^{3,12,28,40} Percutaneous drainage is effective in treatment of diverticular abscess with success rates of up to 90% and can decompress the abscess cavities well (Fig. 72-23).^{*} Percutaneous drainage combined with antibiotic therapy limits morbidity resulting from multistaged colonic surgeries for acute complicated diverticulitis.^{3,12,28,40}

Appendicular Abscess. Periappendiceal abscess may arise as a complication of acute appendicitis (preoperatively) or appendectomy (postoperatively) and is seen in up to 2% to 3% of cases (see Fig. 72-15).^{9,18,79,82,83} In patients with appendiceal rupture from acute perforated appendicitis, surgical drainage of periappendiceal abscesses has a high rate of morbidity.⁸⁴ Percutaneous drainage of the periappendiceal abscess as a temporizing measure allows the acute inflammation to subside, thereby limiting the degree of postoperative morbidity.^{9,18} In poor surgical candidates, percutaneous catheter drainage may be an alternative to surgery.³

Crohn's Disease. In patients with Crohn's disease, abscesses may occur either spontaneously or postoperatively.¹⁸ Abscess

formation in Crohn's disease patients can be multifactorial; causative factors include direct disease extension from an involved loop of bowel, hematogenous seeding, peritoneal contamination, and anastomotic breakdown after surgery.^{9,11,18,29,85} Abscesses most frequently occur between the leaves of the mesentery, between adjacent bowel loops, in the anterior peritoneum, in the right iliac fossa, in the retroperitoneum, or in the pelvis.¹⁸ Because of concurrent bowel involvement, intra-abdominal abscesses in Crohn's patients are often associated with fistula formation to the bowel, which is a predictor of the need for surgery.^{18,29} Percutaneous drainage of intra-abdominal abscesses in Crohn's patients often has a temporizing role before definite surgical intervention, given the relapsing chronic nature of the disease itself.^{11,18,29,85} Catheter drainage for several weeks is required in this group to allow fistulous communication with the bowel to heal.^{11,29,85} Fistulas tend to close on their own with bowel rest, parenteral nutrition, and long-term catheter drainage for healing.^{11,29,85} Success rates for percutaneous drainage are higher for postoperative abscess compared with spontaneous abscess.^{9,11,18,29,85}

Intraperitoneal Abscess

Infected intra-abdominal collections in the postoperative period are a common occurrence and often prolong hospital stay and increase morbidity and mortality. Early intervention and treatment are necessary in these patients because of the high mortality of up to 30% associated with postoperative intra-abdominal sepsis.^{5,18,86,87} Percutaneous catheter drainage is

*References 3, 12, 27, 28, 40, 80, 81.

the preferred treatment for management of postoperative abscesses because of the high morbidity associated with repeated surgeries.^{5,18} However, accurate diagnosis of a postoperative abscess is important to avoid drainage of noninfected inflammatory fluid collections. The diagnosis is rendered difficult in the immediate postoperative period because of fluid collections resulting from intraoperative irrigation, edema, old blood, and inflammatory changes.¹⁸ CT imaging is generally recommended on the eighth postoperative day for accurate characterization of intra-abdominal abscess.¹⁸ After recognition of intra-abdominal abscesses, percutaneous drainage is performed either as a definitive treatment or as a temporizing procedure before the surgical revision.¹⁸ The limiting factors for successful drainage of postoperative fluid collections include anastomotic dehiscence, multiple loculations, and increased viscosity of fluid contents.¹⁸ Abscesses at sites of enteric anastomoses often have fistulous communication to the bowel, which necessitates prolonged catheter drainage or corrective surgical intervention.¹⁸ At times, however, the anastomotic leak may heal and seal by percutaneous drainage alone.¹⁸

Intraperitoneal abscesses can also result from superinfection of preexisting fluid collections, such as hematomas, bilomas, urinomas, and even ascitic fluid, and these can be successfully treated by percutaneous drainage.³ Bilomas resulting from iatrogenic bile duct injury during hepatobiliary surgeries commonly have a persistent biliary fistula in more than 45% of cases.⁸⁸ To facilitate adequate healing, drainage of infected bilomas should be complemented by additional endoscopic or percutaneous procedures, such as biliary stent or percutaneous transhepatic biliary drain for biliary diversion away from the site of injury.^{3,88} Infected hematomas often do not drain well despite adequate liquefaction and might require the administration of thrombolytic agents such as tPA to improve drainage.^{3,21} Effective percutaneous drainage of infected large intraperitoneal fluid collections often necessitates placement of multiple catheters.^{3,8,39} The access route for drainage of a large intraperitoneal abscess is often straightforward and can be accomplished without difficulty by ultrasound or CT guidance.³ However, it is important to carefully select the percutaneous path for drainage to avoid vascular injury or bowel transgression.

Epigastric abscesses often result from hepatic, gastric, or colonic pathologic processes and have complex anatomic features because of their extent of involvement and proximity to several important structures.^{2,36} This necessitates use of CT guidance for safe percutaneous drainage of these complex abscesses, particularly for drainage of abscesses in the posterior epigastric region as they are surrounded by stomach anteriorly, liver and spleen laterally, and kidneys and bones posteriorly.³⁶ A transhepatic and transgastric route may be used that transgresses the periphery of the liver.³⁶

Subphrenic abscesses are manifested by their own unique challenges for percutaneous drainage because of their location and the necessity to transgress the pleura in most of the cases.^{2,36} Transgression of pleura can result in complications

such as pneumothorax, hemothorax, and conversion of a pleural effusion into an empyema.^{2,36} Left subphrenic abscesses usually develop after splenectomy, whereas a right subphrenic abscess may be related to liver trauma or liver surgery.^{2,36} Abscesses in the subphrenic location should ideally be drained through a subcostal approach to avoid the pleura, although an intercostal access may be necessary in the absence of a suitable subcostal window.^{2,36} In such circumstances, it is safer to be as caudal and anterior as possible with the drainage path to avoid the pleura because the anterior pleural reflection is cephalad compared with the posterior one.^{2,36} Combined ultrasound and fluoroscopic guidance is most suitable for drainage of a subphrenic abscess through the subcostal approach (see Fig. 72-13).^{2,36} In this procedure, a needle is initially placed through a subcostal route under ultrasound guidance into the most caudal aspect of the fluid collection. The needle is then used to manipulate a guidewire to a position beneath the diaphragm under fluoroscopic guidance. The guidewire access is then used to place a catheter into the subphrenic location by the Seldinger technique.^{2,36} Percutaneous drainage can also be performed under CT guidance, during which gantry angulation is used to place the catheter in the subphrenic location.^{2,36} Patients may complain of referred pain in the shoulder or scapular region during drainage of subphrenic abscesses, which usually resolves after drainage of the abscess.^{2,36}

Tumor Abscess

Tumor abscess is a rare occurrence and involves superinfection of a necrotic tumor.² In the majority of the cases, the diagnosis is straightforward as superadded infection develops in patients with a known malignant tumor.² A high degree of suspicion is warranted in other circumstances because abscess can develop in the postoperative bed after tumor resection.² Contrast-enhanced CT and MRI provide helpful clues to the diagnosis as they show irregularly enhancing solid areas within the abscess. The diagnosis of tumor abscess is crucial because percutaneous drainage in these cases should be avoided. Percutaneous drainage is not curative for tumor abscesses, and most often the catheters need to be in place indefinitely.² It can be performed in patients with sepsis or in those critically ill before definitive surgery. A frank discussion with the patient, the family, and the referring physicians is often necessary before percutaneous drainage of tumor abscesses to ensure appropriate education of the patient.²

Conclusion

Intra-abdominal abscesses have a high rate of morbidity and mortality if they are left untreated. Image-guided percutaneous drainage is a minimally invasive technique valuable in management of infected fluid collections. The intent of this chapter is to provide the radiologist with a bird's-eye view of percutaneous management of intra-abdominal abscesses to deal with both routine and challenging cases.

REFERENCES

1. Elagili F, Stocchi L, Ozuner G, et al: Outcomes of percutaneous drainage without surgery for patients with diverticular abscess. *Dis Colon Rectum* 57:331–336, 2014.
2. Maher MM, Gervais DA, Kalra MK, et al: The inaccessible or undrainable abscess: How to drain it. *Radiographics* 24:717–735, 2004.
3. Chen R, Sato KT, Chrisman HB: Abdominal abscess. In Gore RM, Levine MS, editors: *Textbook of Gastrointestinal Radiology*, Philadelphia, 2007, WB Saunders, pp 1315–1330.

4. Burke C, Maura M, Molina PL: Interventional computed tomography. In Lee J, Sagel SS, Stanley RJ, editors: *Computed Body Tomography*, Philadelphia, 2006, Lippincott Williams & Wilkins, pp 95–144.
5. Montgomery RS, Wilson SE: Intraabdominal abscesses: Image-guided diagnosis and therapy. *Clin Infect Dis* 23:28–36, 1996.
6. Kumar RR, Kim JT, Haukoos JS, et al: Factors affecting the successful management of intra-abdominal abscesses with antibiotics and the need for percutaneous drainage. *Dis Colon Rectum* 49:183–189, 2006.
7. Mueller PR, vanSonnenberg E, Ferrucci JT, Jr: Percutaneous drainage of 250 abdominal abscesses and fluid collections. Part II: Current procedural concepts. *Radiology* 151:343–347, 1984.
8. vanSonnenberg E, Mueller PR, Ferrucci JT, Jr: Percutaneous drainage of 250 abdominal abscesses and fluid collections. Part I: Results, failures, and complications. *Radiology* 151:337–341, 1984.
9. vanSonnenberg E, Wittich GR, Goodacre BW, et al: Percutaneous abscess drainage: Update. *World J Surg* 25:362–369, discussion 370–372, 2001.
10. Lee H, Kim YH, Kim JH, et al: Nonsurgical treatment of abdominal or pelvic abscess in consecutive patients with Crohn's disease. *Dig Liver Dis* 38:659–664, 2006.
11. Rypens F, Dubois J, Garel L, et al: Percutaneous drainage of abdominal abscesses in pediatric Crohn's disease. *AJR Am J Roentgenol* 188:579–585, 2007.
12. Siewert B, Tye G, Kruskal J, et al: Impact of CT-guided drainage in the treatment of diverticular abscesses: Size matters. *AJR Am J Roentgenol* 186:680–686, 2006.
13. Gazelle GS, Haaga JR, Stellato TA, et al: Pelvic abscesses: CT-guided transrectal drainage. *Radiology* 181:49–51, 1991.
14. Gerzof SG, Robbins AH, Birkett DH: Computed tomography in the diagnosis and management of abdominal abscesses. *Gastrointest Radiol* 3: 287–294, 1978.
15. Konig C, Simmen HP, Blaser J: Bacterial concentrations in pus and infected peritoneal fluid—implications for bactericidal activity of antibiotics. *J Antimicrob Chemother* 42:227–232, 1998.
16. Koehler PR, Moss AA: Diagnosis of intra-abdominal and pelvic abscesses by computerized tomography. *JAMA* 244:49–52, 1980.
17. Sheafor DH, Paulson EK, Simmons CM, et al: Abdominal percutaneous interventional procedures: Comparison of CT and US guidance. *Radiology* 207:705–710, 1998.
18. Men S, Akhan O, Koroglu M: Percutaneous drainage of abdominal abscess. *Eur J Radiol* 43:204–218, 2002.
19. Gee MS, Kim JY, Gervais DA, et al: Management of abdominal and pelvic abscesses that persist despite satisfactory percutaneous drainage catheter placement. *AJR Am J Roentgenol* 194:815–820, 2010.
20. Gervais DA, Ho CH, O'Neill MJ, et al: Recurrent abdominal and pelvic abscesses: Incidence, results of repeated percutaneous drainage, and underlying causes in 956 drainages. *AJR Am J Roentgenol* 182:463–466, 2004.
21. Shenoy-Bhangle AS, Gervais DA: Use of fibrinolytics in abdominal and pleural collections. *Semin Interv Radiol* 29:264–269, 2012.
22. Buckley O, Geoghegan T, Ridgeway P, et al: The usefulness of CT guided drainage of abscesses caused by retained appendicoliths. *Eur J Radiol* 60:80–83, 2006.
23. Gervais DA, Hahn PF, O'Neill MJ, Mueller PR: CT-guided transluteal drainage of deep pelvic abscesses in children: Selective use as an alternative to transrectal drainage. *AJR Am J Roentgenol* 175:1393–1396, 2000.
24. Haaga JR, Weinstein AJ: CT-guided percutaneous aspiration and drainage of abscesses. *AJR Am J Roentgenol* 135:1187–1194, 1980.
25. Harisinghani MG, Gervais DA, Hahn PF, et al: CT-guided transluteal drainage of deep pelvic abscesses: Indications, technique, procedure-related complications, and clinical outcome. *Radiographics* 22:1353–1367, 2002.
26. Koehler PR, Knochel JQ: Computed tomography in the evaluation of abdominal abscesses. *Am J Surg* 140:675–678, 1980.
27. Bruscianno L, Maffettone V, Napolitano V, et al: Management of colorectal emergencies: Percutaneous abscess drainage. *Ann Ital Chir* 75:593–597, 2004.
28. Durmishi Y, Gervaz P, Brandt D, et al: Results from percutaneous drainage of Hinchey stage II diverticulitis guided by computed tomography scan. *Surg Endosc* 20:1129–1133, 2006.
29. Gervais DA, Hahn PF, O'Neill MJ, Mueller PR: Percutaneous abscess drainage in Crohn disease: Technical success and short- and long-term outcomes during 14 years. *Radiology* 222:645–651, 2002.
30. Levitt RG, Biello DR, Sagel SS, et al: Computed tomography and ⁶⁷Ga citrate radionuclide imaging for evaluating suspected abdominal abscess. *AJR Am J Roentgenol* 132:529–534, 1979.
31. Knochel JQ, Koehler PR, Lee TG, Welch DM: Diagnosis of abdominal abscesses with computed tomography, ultrasound, and ¹¹¹In leukocyte scans. *Radiology* 137:425–432, 1980.
32. Lambiase RE: Percutaneous abscess and fluid drainage: A critical review. *Cardiovasc Intervent Radiol* 14:143–157, 1991.
33. Lambiase RE, Deyoe L, Cronan JJ, Dorfman GS: Percutaneous drainage of 335 consecutive abscesses: Results of primary drainage with 1-year follow-up. *Radiology* 184:167–179, 1992.
34. Torres WE, Evert MB, Baumgartner BR, Bernardino ME: Percutaneous aspiration and drainage of pancreatic pseudocysts. *AJR Am J Roentgenol* 147:1007–1009, 1986.
35. vanSonnenberg E, Wittich GR, Casola G, et al: Percutaneous drainage of infected and noninfected pancreatic pseudocysts: Experience in 101 cases. *Radiology* 170:757–761, 1989.
36. Gervais DA, Brown SD, Connolly SA, et al: Percutaneous imaging-guided abdominal and pelvic abscess drainage in children. *Radiographics* 24:737–754, 2004.
37. O'Dwyer HM, Lyon SM, Fotheringham T, Lee MJ: Informed consent for interventional radiology procedures: A survey detailing current European practice. *Cardiovasc Intervent Radiol* 26:428–433, 2003.
38. Payne CS: A primer on patient management problems in interventional radiology. *AJR Am J Roentgenol* 170:1169–1176, 1998.
39. vanSonnenberg E, Ferrucci JT, Jr, Mueller PR, et al: Percutaneous drainage of abscesses and fluid collections: Technique, results, and applications. *Radiology* 142:1–10, 1982.
40. Harisinghani MG, Gervais DA, Maher MM, et al: Transluteal approach for percutaneous drainage of deep pelvic abscesses: 154 cases. *Radiology* 228:701–705, 2003.
41. Arellano RS, Maher M, Gervais DA, et al: The difficult biopsy: Let's make it easier. *Curr Probl Diagn Radiol* 32:218–226, 2003.
42. Sainani NI, Arellano RS, Shyn PB, et al: The challenging image-guided abdominal mass biopsy: Established and emerging techniques 'if you can see it, you can biopsy it'. *Abdom Imaging* 38:672–696, 2013.
43. Kim YJ, Han JK, Lee JM, et al: Percutaneous drainage of postoperative abdominal abscess with limited accessibility: Preexisting surgical drains as alternative access route. *Radiology* 239:591–598, 2006.
44. Arellano RS, Gervais DA, Mueller PR: CT-guided drainage of abdominal abscesses: Hydrodissection to create access routes for percutaneous drainage. *AJR Am J Roentgenol* 196:189–191, 2011.
45. Goldberg MA, Mueller PR, Saini S, et al: Importance of daily rounds by the radiologist after interventional procedures of the abdomen and chest. *Radiology* 180:767–770, 1991.
46. Gobien RP, Stanley JH, Schabel SI, et al: The effect of drainage tube size on adequacy of percutaneous abscess drainage. *Cardiovasc Intervent Radiol* 8:100–102, 1985.
47. Beland MD, Gervais DA, Levis DA, et al: Complex abdominal and pelvic abscesses: Efficacy of adjunctive tissue-type plasminogen activator for drainage. *Radiology* 247:567–573, 2008.
48. Moulton JS, Moore PT, Mencini RA: Treatment of loculated pleural effusions with transcatheter intracavitary urokinase. *AJR Am J Roentgenol* 153:941–945, 1989.
49. Varghese JC, Hahn PF, Harisinghani MG, et al: Fungus-infected fluid collections in thorax or abdomen: Effectiveness of percutaneous catheter drainage. *Radiology* 236:730–738, 2005.
50. Cinat ME, Wilson SE, Din AM: Determinants for successful percutaneous image-guided drainage of intra-abdominal abscess. *Arch Surg* 137:845–849, 2002.
51. Kaplan GG, Gregson DB, Laupland KB: Population-based study of the epidemiology of and the risk factors for pyogenic liver abscess. *Clin Gastroenterol Hepatol* 2:1032–1038, 2004.
52. Kim SB, Je BK, Lee KY, et al: Computed tomographic differences of pyogenic liver abscesses caused by *Klebsiella pneumoniae* and non-*Klebsiella pneumoniae*. *J Comput Assist Tomogr* 31:59–65, 2007.
53. Wong WM, Wong BC, Hui CK, et al: Pyogenic liver abscess: Retrospective analysis of 80 cases over a 10-year period. *J Gastroenterol Hepatol* 17:1001–1007, 2002.
54. Yu SC, Ho SS, Lau WY, et al: Treatment of pyogenic liver abscess: Prospective randomized comparison of catheter drainage and needle aspiration. *Hepatology* 39:932–938, 2004.
55. Giorgio A, de Stefano G, Di Sarno A, et al: Percutaneous needle aspiration of multiple pyogenic abscesses of the liver: 13-year single-center experience. *AJR Am J Roentgenol* 187:1585–1590, 2006.
56. Giorgio A, Tarantino L, Mariniello N, et al: Pyogenic liver abscesses: 13 years of experience in percutaneous needle aspiration with US guidance. *Radiology* 195:122–124, 1995.
57. Sharma MP, Ahuja V: Management of amebic and pyogenic liver abscess. *Indian J Gastroenterol* 20(Suppl 1):C33–C36, 2001.
58. Liao WI, Tsai SH, Yu CY, et al: Pyogenic liver abscess treated by percutaneous catheter drainage: MDCT measurement for treatment outcome. *Eur J Radiol* 81:609–615, 2012.

59. Liu CH, Gervais DA, Hahn PF, et al: Percutaneous hepatic abscess drainage: Do multiple abscesses or multiloculated abscesses preclude drainage or affect outcome? *J Vasc Interv Radiol* 20:1059–1065, 2009.
60. Ramos A, Gazapo T, Murillas J, et al: [Pyogenic liver abscess. A descriptive study of 35 cases.] *Gastroenterol Hepatol* 19:292–296, 1996.
61. vanSonnenberg E, Mueller PR, Schiffman HR, et al: Intrahepatic amebic abscesses: Indications for and results of percutaneous catheter drainage. *Radiology* 156:631–635, 1985.
62. Goessling W, Chung RT: Amebic liver abscess. *Curr Treat Options Gastroenterol* 5:443–449, 2002.
63. Farres H, Felsher J, Banbury M, Brody F: Management of splenic abscess in a critically ill patient. *Surg Laparosc Endosc Percutan Tech* 14:49–52, 2004.
64. Lieberman S, Libson E, Sella T, et al: Percutaneous image-guided splenic procedures: Update on indications, technique, complications, and outcomes. *Semin Ultrasound CT MR* 28:57–63, 2007.
65. Tasar M, Ugurel MS, Kocaoglu M, et al: Computed tomography-guided percutaneous drainage of splenic abscesses. *Clin Imaging* 28:44–48, 2004.
66. Thanos L, Dailiana T, Papaioannou G, et al: Percutaneous CT-guided drainage of splenic abscess. *AJR Am J Roentgenol* 179:629–632, 2002.
67. Freeny PC: Percutaneous management of pancreatic fluid collections. *Baillieres Clin Gastroenterol* 6:259–272, 1992.
68. Freeny PC, Lewis GP, Traverso LW, Ryan JA: Infected pancreatic fluid collections: Percutaneous catheter drainage. *Radiology* 167:435–441, 1988.
69. Guittet V, Menager C, Missotte I, et al: [Hepatic abscesses in childhood: Retrospective study about 33 cases observed in New-Caledonia between 1985 and 2003.] *Arch Pediatr* 11:1046–1053, 2004.
70. Mithofer K, Mueller PR, Warshaw AL: Interventional and surgical treatment of pancreatic abscess. *World J Surg* 21:162–168, 1997.
71. vanSonnenberg E, Wittich GR, Chon KS, et al: Percutaneous radiologic drainage of pancreatic abscesses. *AJR Am J Roentgenol* 168:979–984, 1997.
72. Neff R: Pancreatic pseudocysts and fluid collections: Percutaneous approaches. *Surg Clin North Am* 81:399–403, xii, 2001.
73. Tittton RL, Gervais DA, Hahn PF, et al: Urine leaks and urinomas: Diagnosis and imaging-guided intervention. *Radiographics* 23:1133–1147, 2003.
74. Pombo F, Martin-Egana R, Cela A, et al: Percutaneous catheter drainage of tuberculous psoas abscesses. *Acta Radiol* 34:366–368, 1993.
75. Cantwell CP, Pena CS, Gervais DA, et al: Thirty years' experience with balloon dilation of benign postoperative biliary strictures: Long-term outcomes. *Radiology* 249:1050–1057, 2008.
76. Goharkhay N, Verma U, Maggiorotto F: Comparison of CT- or ultrasound-guided drainage with concomitant intravenous antibiotics vs. intravenous antibiotics alone in the management of tubo-ovarian abscesses. *Ultrasound Obstet Gynecol* 29:65–69, 2007.
77. Sudakoff GS, Lundeen SJ, Otterson MF: Transrectal and transvaginal sonographic intervention of infected pelvic fluid collections: A complete approach. *Ultrasound Q* 21:175–185, 2005.
78. vanSonnenberg E, D'Agostino HB, Casola G, et al: US-guided transvaginal drainage of pelvic abscesses and fluid collections. *Radiology* 181:53–56, 1991.
79. Rao PM, Rhea JT, Novelline RA: Helical CT of appendicitis and diverticulitis. *Radiol Clin North Am* 37:895–910, 1999.
80. Brandt D, Gervaz P, Durmishi Y, et al: Percutaneous CT scan-guided drainage vs. antibiotic therapy alone for Hinchey II diverticulitis: A case-control study. *Dis Colon Rectum* 49:1533–1538, 2006.
81. Mueller PR, Saini S, Wittenburg J, et al: Sigmoid diverticular abscesses: Percutaneous drainage as an adjunct to surgical resection in 24 cases. *Radiology* 164:321–325, 1987.
82. Balthazar EJ, Megibow AJ, Siegel SE, Birnbaum BA: Appendicitis: Prospective evaluation with high-resolution CT. *Radiology* 180:21–24, 1991.
83. Nunez D, Jr, Huber JS, Yrizarry JM, et al: Non-surgical drainage of appendiceal abscesses. *AJR Am J Roentgenol* 146:587–589, 1986.
84. Deakin DE, Ahmed I: Interval appendectomy after resolution of adult inflammatory appendix mass—is it necessary? *Surgeon* 5:45–50, 2007.
85. Rypens F, Dubois J, Garel L: The place of interventional radiology in Crohn disease in children. *Pediatr Radiol* 37:1093–1095, 2007.
86. Butler JA, Huang J, Wilson SE: Repeated laparotomy for postoperative intra-abdominal sepsis. An analysis of outcome predictors. *Arch Surg* 122:702–706, 1987.
87. vanSonnenberg E, Wing VW, Casola G, et al: Temporizing effect of percutaneous drainage of complicated abscesses in critically ill patients. *AJR Am J Roentgenol* 142:821–826, 1984.
88. Mueller PR, Ferrucci JT, Jr, Simeone JF, et al: Detection and drainage of bilomas: Special considerations. *AJR Am J Roentgenol* 140:715–720, 1983.

SECTION

IX

Gall Bladder and Biliary Tract

Gallbladder and Biliary Tract: Normal Anatomy and Examination Techniques

MARY ANN TURNER | ANN S. FULCHER

CHAPTER OUTLINE

Normal Anatomy

Gallbladder
Cystic Duct
Bile Ducts

Examination Techniques: Gallbladder

Plain Radiography
Ultrasound
Computed Tomography
Cholescintigraphy
Magnetic Resonance Imaging

Examination Techniques: Biliary Tract

Plain Radiography
Ultrasound
Computed Tomography
Computed Tomography Cholangiography
Magnetic Resonance Cholangiopancreatography
Direct Cholangiography
Biliary Scintigraphy

Rapid advances in technology and refinements in both noninvasive and invasive techniques have improved the ability of imaging methods to make more precise diagnoses in disorders of the biliary tract. Ultrasound and computed tomography (CT), because of wide availability and ease of performance as well as high diagnostic accuracy, are the first-line imaging techniques. Magnetic resonance cholangiopancreatography (MRCP) has assumed a larger role as a rapid, accurate, and noninvasive method of evaluating the bile ducts and has replaced diagnostic endoscopic retrograde cholangiopancreatography (ERCP) in most instances. Modern magnetic resonance (MR) and CT techniques including use of biliary-excreted contrast agents and postprocessing reformation methods, such as multiplanar reformation (MPR), maximum intensity projection (MIP), and volume rendering, allow detailed evaluation of the biliary tract with excellent accuracy and patient tolerance as well as three-dimensional data sets that can be cholangiographically displayed. Percutaneous transhepatic cholangiography (PTC) and ERCP are methods of direct cholangiography used for evaluation of biliary ductal disease. These techniques are invasive, but they are also safe and widely available. Improvements in the technical aspects of PTC and ERCP have led to the development of various interventional biliary procedures performed from both percutaneous and endoscopic routes. Plain radiography plays a minor role in imaging of the gallbladder and bile ducts. The traditional indications for operative and postoperative cholangiography remain unchanged; both techniques allow

direct opacification of the biliary tree but require surgical access and have limited diagnostic use. Biliary scintigraphy also has a limited role in biliary imaging, mainly for confirming acute cholecystitis and identifying bile leaks.¹⁻¹⁷

Normal Anatomy

GALLBLADDER

The gallbladder is an elliptical organ located in a fossa on the undersurface of the liver between the right and left lobes. Although size and shape vary, the relaxed gallbladder is approximately 10 cm long and 3 to 5 cm in diameter. Size may increase after vagotomy, in diabetes, or after cystic duct or common duct obstruction. Normal capacity is approximately 50 mL. The normal gallbladder wall is 2 to 3 mm thick, and the mucosa is composed of simple columnar epithelium. The gallbladder is usually apposed to the liver surface by parietal peritoneum. Rarely, the peritoneal reflection may be loose, forming a mesentery that allows the gallbladder enough mobility to extend into the pelvis or left abdomen, herniate into the lesser sac, or undergo torsion. The gallbladder is positioned partially or completely in an intrahepatic location in 10% of cases.

The gallbladder is divided into four parts—fundus, body, infundibulum, and neck (Fig. 73-1). The fundus is the rounded distal tip, which may project below the anterior inferior liver edge (Fig. 73-2). A characteristic deformity associated with septation and partial folding over of the gallbladder, the phrygian cap, may be found in the fundus. The body is the mid-portion of the gallbladder, which may be in contact with the duodenum and hepatic flexure. The infundibulum (Hartmann's pouch) is the focally enlarged segment between the body and the neck. The neck of the gallbladder lies between the body and the cystic duct and points toward the porta hepatis. A mucosal fold, the junctional fold, is frequently seen near the gallbladder neck. The gallbladder neck bears a constant relationship to the major interlobar fissure and undivided right portal vein or main portal vein, an important anatomic relationship for imaging.¹⁸⁻²⁵

CYSTIC DUCT

The gallbladder is attached to the common bile duct (CBD) by the cystic duct, which is usually 2 to 4 cm long and contains tortuous folds, the spiral valves of Heister (see Fig. 73-1). The cystic duct usually joins the common hepatic duct (CHD) from the right lateral aspect approximately halfway between the porta hepatis and the ampulla of Vater to form the CBD. The point at which the cystic duct joins the CHD is variable, from high in the upper extrahepatic bile duct or one of the intrahepatic ducts (more often the right) to low at the ampulla. The cystic duct

usually runs parallel to the CHD at least for a short distance and may insert either anteriorly or posteriorly or spiral around to insert on the medial aspect. The two ducts may have a long parallel course and can be encircled in a common connective tissue sheath²⁰⁻²³ (Fig. 73-3).

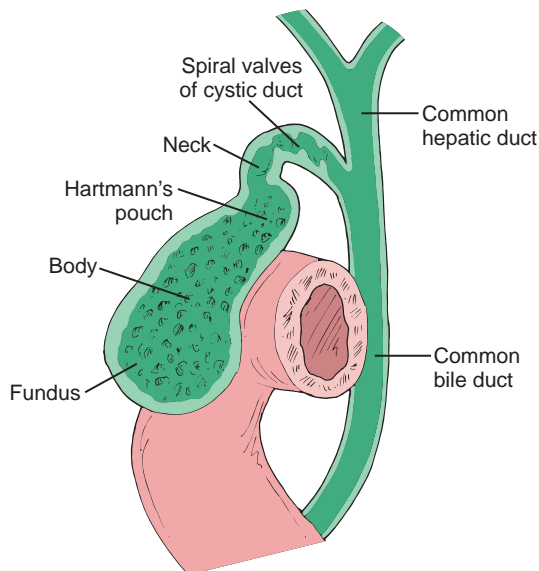


Figure 73-1 Normal anatomy of the gallbladder and cystic duct. (From Linder HH: *Clinical Anatomy*. East Norwalk, Ct: Appleton & Lange, 1989, p 421.)

BILE DUCTS

Intrahepatic Ducts

The liver is divided into right and left lobes on the basis of portal vein anatomy and biliary drainage. The right lobe is divided into anterior and posterior segments, and the left lobe is divided into medial and lateral segments by the fissure of the ligamentum teres. The bile ducts generally follow the internal hepatic segmental anatomy; however, marked variation in the branching pattern is common. Small branching interlobar bile ducts merge into larger ducts until the major left and right hepatic ducts are formed. A left medial segment duct and a left lateral segment duct normally join to form the main left hepatic duct. The right hepatic duct branches near its takeoff from the CHD. In approximately 60% of patients, the right hepatic duct has a dorsocaudal branch, with a characteristic hooklike configuration proximally, draining the posterior segment of the right lobe, and a ventrocranial branch, draining the anterior segment of the right lobe. Variations in the anatomic arrangement of the bifurcation branches are common, however, and it may be impossible to differentiate the anterior and posterior segmental branches on frontal cholangiograms. Common bifurcation variations include drainage of either anterior or posterior right lobe segmental ducts into the left hepatic duct, or a trifurcation configuration may occur. The left hepatic duct is more anterior and is usually longer and wider than the right hepatic duct. The left hepatic duct has a longer extrahepatic course and tends to dilate more with obstruction than the right

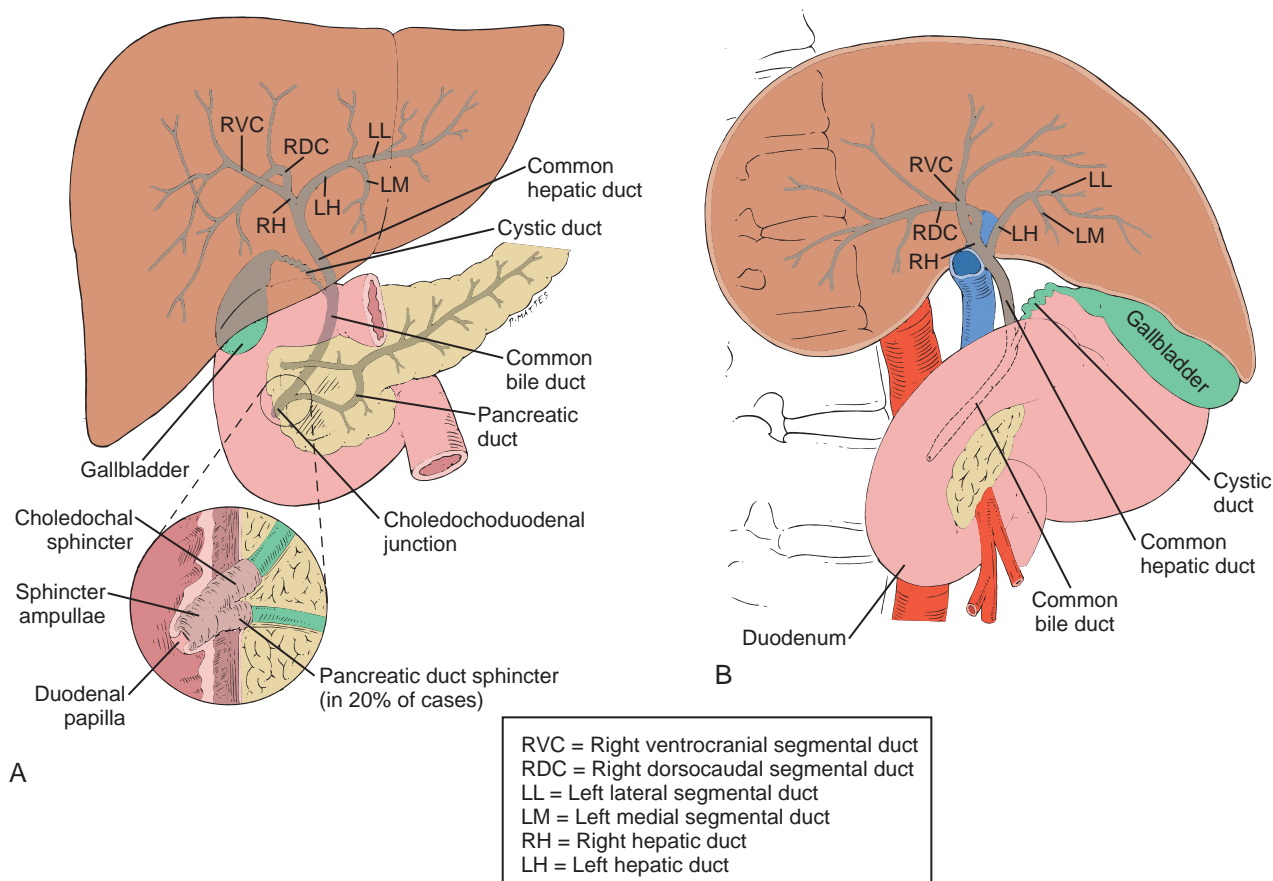


Figure 73-2 Normal anatomy of biliary tract. **A.** Frontal view. **B.** Parasagittal view.

hepatic duct does, presumably because there is less surrounding liver. Ductal drainage of the caudate lobe is variable and may be related to the left or right ductal system.¹⁸⁻²⁹

Extrahepatic Ducts

The right and left hepatic ducts emerge from the liver and unite to form the 3- to 4-cm-long CHD, which then joins the cystic duct to form the CBD. The union of the right and left main hepatic ducts is usually just outside the liver but may be lower, resulting in a shorter CHD or CBD. The CHD courses ventrally and inferiorly from the porta hepatis in the hepatoduodenal ligament accompanied by the portal vein, which lies posteriorly, and the hepatic artery, which lies medially. As the CHD passes inferiorly, it angles anteriorly and then posteriorly, crossing over the right portal vein and joining the cystic duct to form the CBD as it courses behind the postbulbar duodenum (see Fig. 73-1). The CBD averages 6 to 7 cm in length and is usually divided into suprapancreatic, intrapancreatic, and ampullary segments. In approximately 70% of patients, the distal CBD courses through the pancreatic head; in a smaller percentage, the CBD is located in a groove on the posterior surface of the pancreas. The CBD enters the posterior medial aspect of the

second portion of the duodenum through an oblique, 1- to 2-cm-long intramural tunnel terminating at the papilla of Vater.¹⁸⁻²⁴

The exact union of the CBD and the pancreatic duct at the ampulla varies. Most commonly, the two ducts join in the duodenal wall and have a short common channel (<5 mm). On occasion, separate orifices are present at the ampulla, or the ducts unite, forming a long common channel before entering the duodenal wall (Fig. 73-4). The sphincter of Oddi surrounds the common channel, and the choledochal sphincter (sphincter of Boyden) surrounds the CBD from its entrance into the duodenal wall to its junction with the pancreatic duct.³⁰⁻³² The extrahepatic ducts are sparse in muscle fibers (except in the cystic duct and the sphincter areas) and are composed primarily of elastic fibers. This allows relatively rapid change in size in response to fluctuations in intraductal pressure. With age, loss of elasticity may occur, resulting in enlargement of the duct, so-called ductomegaly of aging.³³⁻³⁶

Anatomic Variations

Anatomic variations and anomalies of bile duct anatomy are common (see Chapter 76). Although most are of no pathologic significance, an understanding of these variations is important to avoid misdiagnosis. Anatomic variations have been reported in 23% to 46% of cholangiograms, with the most common sites of involvement at the hepatic bifurcation and in the insertion of the cystic duct.³⁷ An aberrant right hepatic duct (4.6%) entering at a variety of locations (including low along the CHD or into the cystic duct), an accessory right hepatic duct (1.9%), and a high or low insertion of the cystic duct are congenital anomalies of significance because of the potential for injury at biliary surgery.^{20,22,24,25,37} (see Chapter 81).

Examination Techniques: Gallbladder

Modern gallbladder imaging involves primarily ultrasound and CT. Although the gallbladder is readily imaged by MR, this technique is less often used in gallbladder diagnosis because CT and ultrasound are accurate, quicker, less expensive, and easier to obtain. MR and MRCP, however, may be used as the initial imaging study in patients with suspected gallbladder carcinoma because of the greater ability to assess extent of disease and vascular involvement. Real-time sonography is the dominant screening method for the detection of gallbladder disease. Multidetector CT (MDCT) is commonly used to initially evaluate gallbladder disease, particularly neoplastic conditions and complicated cholecystitis, because of its ability to rapidly produce isotropic images of the upper abdomen.^{1-6,10,16,17}

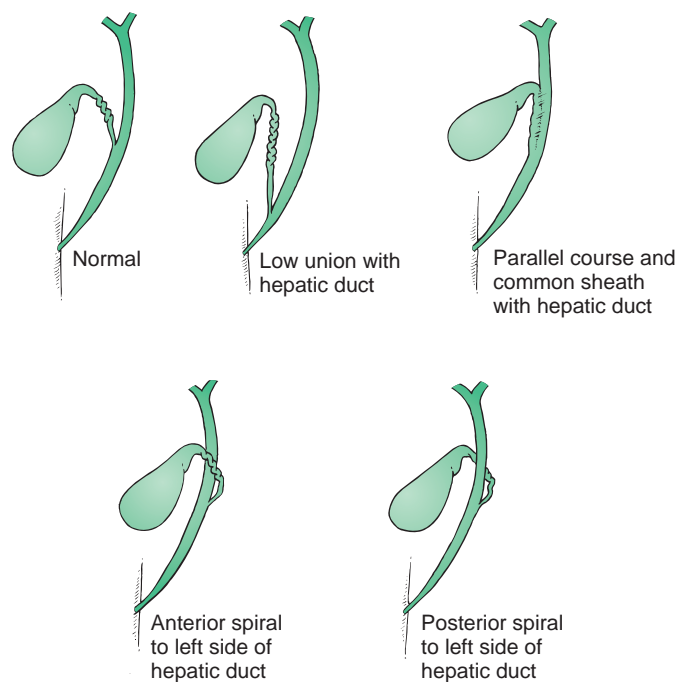


Figure 73-3 Variations in cystic duct insertion.

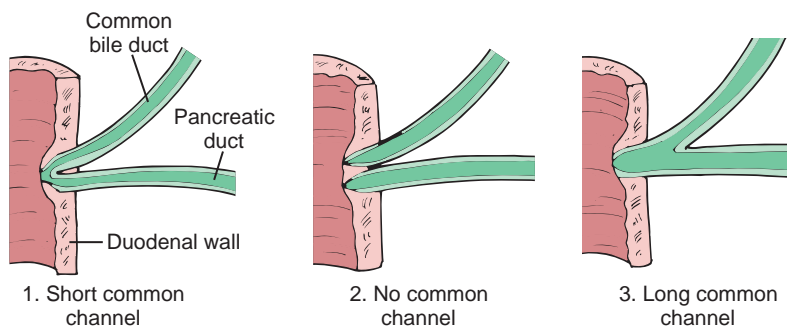


Figure 73-4 Types of union of common bile duct and pancreatic duct.

PLAIN RADIOGRAPHY

Plain abdominal radiography is the simplest and least expensive imaging method that may identify gallbladder disease, but the yield is low, and this study is not used as a primary technique for assessment of suspected biliary or gallbladder disease. However, it is frequently the first study obtained in patients with upper abdominal pain, and gallbladder disease is occasionally apparent on the study. The normal gallbladder is not visible on plain radiographs. Only 10% to 15% of gallstones are sufficiently calcified to be visualized on the plain abdominal radiograph. “Porcelain” gallbladder, emphysematous cholecystitis, and milk of calcium bile (see Chapter 77) are other pathologic gallbladder conditions with characteristic findings that can be diagnosed on plain radiographs. A soft tissue mass in the right upper quadrant may be seen with hydrops of the gallbladder and gallbladder carcinoma.³⁸ Rarely, noncalcified cholesterol gallstones are visible on the abdominal radiograph as a result of nitrogen-containing clefts that produce a lucent, triradiate appearance, the “Mercedes-Benz” sign.³⁹

ULTRASOUND

Real-time sonography is the most widely used diagnostic study for the gallbladder and is the primary screening examination for gallbladder disease. The gallbladder is visible on sonograms in virtually all fasting patients despite body habitus or clinical condition. Gallbladder sonography is noninvasive, quick, and easy to perform. The examination can be performed portably and, because no ionizing radiation is used, is safe in pregnant and pediatric patients. Adjacent upper abdominal organs can be imaged simultaneously. The success rate of obtaining a diagnostic study is more than 95%.^{4,5,40-43}

By far the most common indication for gallbladder sonography is the detection of gallstones. Overall, the sensitivity, specificity, and accuracy of ultrasound for detection of gallstones is 95% to 99% in most series.^{4-6,10,40-43} The frequency of indeterminate studies with ultrasound is low.^{40,41} False-positive ultrasound findings are uncommon and are due primarily to polyps, folds, or cholesterosis of the gallbladder.⁴⁴ Although ultrasound is excellent for the demonstration of calculi, it does not provide direct information about gallbladder function or cystic duct patency. Sonography does have limitations in assessing the size and number of stones in cases of multiple stones. Sonography is useful to confirm the diagnosis of acute cholecystitis. Ultrasound has been shown to have a positive predictive value of 92% and a negative value of 95% for diagnosis of acute cholecystitis in patients with gallstones and a positive sonographic Murphy’s sign.⁴⁵ Complications of cholecystitis, including gallbladder perforation, gangrenous cholecystitis, and emphysematous cholecystitis, are usually readily seen by ultrasound. Gallbladder carcinoma, polyps, metastatic nodules, and adenomyomatosis are uncommon conditions of the gallbladder with characteristic findings on sonography^{4-6,42,43} (see Chapters 77 and 79).

Technique

The gallbladder is examined after the patient has fasted for at least 6 hours. This allows maximal distention of the gallbladder and enhances the detectability of stones. For most patients, real-time scanning is performed with a 3.5- or 4-MHz transducer. In thin patients or those with an anteriorly positioned

gallbladder, a 5-MHz transducer provides superior resolution. A transducer of the highest possible frequency should be used because spatial resolution is improved when the transducer focal zone is the same depth as the gallbladder.^{4,10,46} The examination is begun with the patient in the supine position. Scanning is performed in the right subcostal region or in one of the lower intercostal spaces, in approximately the anterior axillary line. The gallbladder is located in the longitudinal axis by identifying the major interlobar fissure of the liver (Fig. 73-5A). Views are obtained in the longitudinal and transverse planes to allow visualization of the entire gallbladder. Different degrees of inspiration may be necessary to move the gallbladder away from the overlying costal cartilage (Fig. 73-5B, C). Various scanning positions are used; decubitus positioning is often helpful in displaying the gallbladder, displacing bowel gas, unfolding kinks, and allowing small stones hidden in the neck to roll into the fundus to become detectable. The dependent portion of the gallbladder, particularly the neck, should be scrutinized for hidden stones (Fig. 73-5D). Suspended deep inspiration often serves to move the gallbladder into a more accessible position below the ribs. Magnified views, high-frequency transducers, and upright or Trendelenburg positioning are helpful adjuncts. Color Doppler sonography may be used in assessing cystic artery and wall flow in patients with acute cholecystitis or gangrenous cholecystitis and in evaluation of gallbladder carcinoma and metastatic disease to the gallbladder.⁴⁷⁻⁴⁹ If the gallbladder is not readily identified in its usual subhepatic position, other locations must be evaluated to exclude a positional anomaly. Examination of the gallbladder is always accompanied by evaluation of the bile ducts.

Normal Anatomy

The normal gallbladder in the fasting patient appears as an oval sonolucent structure with a thin (2-3 mm), uniformly smooth wall (see Fig. 73-5B, C). It is located by identifying the major interlobar fissure of the liver, which is apparent as a highly reflective line (because of periportal fat extending into the fissure)⁵⁰ (see Fig. 73-5A). The interlobar fissure is an important sonographic landmark because of its constant relationship to the gallbladder neck. Although gallbladder shape and size vary, the sonographic upper limits of normal size are approximately 8 to 10 cm in length and 4 to 5 cm in anterior-posterior diameter. Folds are commonly seen as echogenic foci adjacent to the wall. The junctional fold is a fold between the body and the infundibulum of the gallbladder, a common anatomic variant seen on sonography. If the gallbladder is not visualized by ultrasound, the most likely cause is prior resection or a scarred contracted gallbladder containing calculi. Agenesis of the gallbladder, calcification of the gallbladder wall, and intramural or intraluminal gas are other causes of nonvisualization⁵¹ (see Chapter 82).

COMPUTED TOMOGRAPHY

The gallbladder in fasting patients is nearly always identified on CT scans of the upper abdomen. Although gallstones are frequently visible, CT is not used as a primary examination for detection of gallstones because of its lower sensitivity (80%-85%) and higher cost compared with ultrasound.^{12,41,42,52-55} Calcified gallstones are manifested as high-density foci within the gallbladder lumen, and noncalcified stones are seen as low-attenuation filling defects within the surrounding bile. Although

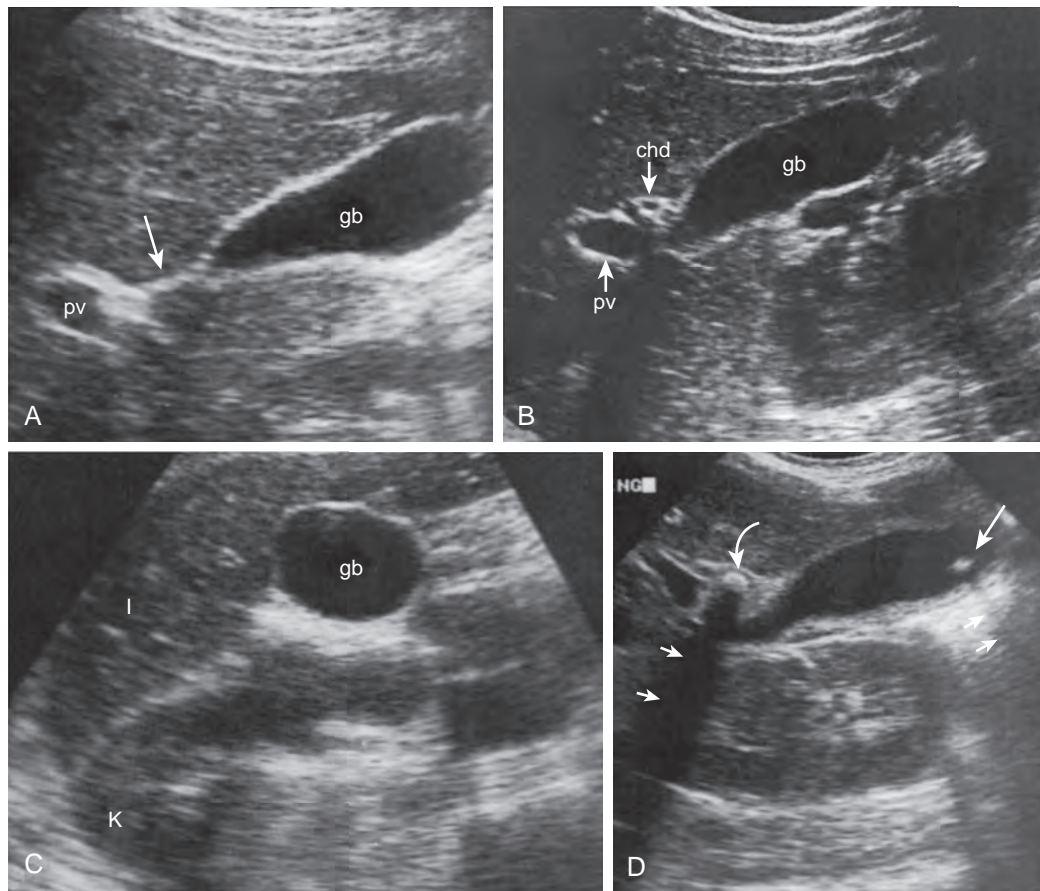


Figure 73-5 Normal gallbladder anatomy: sonography. **A.** The linear echogenic line (arrow) of the interlobar fissure bears a constant relationship to the gallbladder neck and aids in sonographic localization of the gallbladder (gb). pv, Portal vein. **B.** Longitudinal sonogram of the normal gallbladder (gb). Note the relationship of the gallbladder neck to the portal vein (pv, arrow) and common hepatic duct (chd, arrow). **C.** Transverse sonogram of the normal gallbladder (gb). Note the relationship to the liver (l) and the kidney (K). **D.** Sonogram shows a stone in a dependent position in the gallbladder (long arrow). A second stone behind the fold and impacted in the neck of the gallbladder (curved arrow) was seen only after careful evaluation of the neck in the erect position. Both stones cast characteristic acoustic shadows (short arrows).

acute cholecystitis is accurately evaluated with sonography or scintigraphy, CT is often used if the upper abdominal pain is nonspecific or if complicated cholecystitis is suspected. CT easily depicts mural thickening, gallbladder dilation, wall edema, septation, and increased bile density, which allows diagnosis. The main indication for CT in gallbladder disease is for the diagnosis and staging of gallbladder carcinoma (see Chapter 79) and evaluation of the complications of cholecystitis, such as perforation and pericholecystic abscess. Less common entities, such as porcelain gallbladder, milk of calcium bile, and emphysematous cholecystitis, are readily identified and have characteristic CT findings^{12,40-42,53,56,57} (see Chapter 77).

Technique

The gallbladder is usually scanned as part of a routine upper abdominal examination. Multislice CT scanning of the upper abdomen is performed during a single breath-hold after rapid bolus intravenous infusion of contrast material. This permits visualization of the gallbladder and optimal delineation of the gallbladder wall, intrahepatic biliary ducts, and extrahepatic bile duct by enhancing the contiguous liver and pancreatic parenchyma as well as blood vessels. Volumetric imaging with the latest generation scanners allows reconstruction in multiple

planes and different slice thicknesses. Images of 2- to 5-mm slice thickness are used routinely for review. Postprocessing with reconstruction of axial images at 1.5 to 3 mm can be performed and may be helpful in clarifying suspicious areas and in maximizing stone detection. Oral contrast material is routinely used in scanning the upper abdomen. However, in searching for smaller noncalcified stones, scans obtained without contrast material using thin sections filmed at narrow window settings optimize stone detection.^{55,57}

Normal Anatomy

The normal gallbladder on CT scans is a low-density, fluid-filled, elliptical structure in the interlobar fissure of the liver (Fig. 73-6A). A thin (2-3 mm) wall is often seen in normal patients and may show contrast enhancement. The gallbladder neck is superior and medial to the fundus. The gallbladder neck is often folded, and a portion may be cut in cross section. More caudally, the fundus of the gallbladder projects anteriorly and laterally and may touch the anterior abdominal wall or the colon. The duodenal sweep, hepatic flexure, and gastric antrum are contiguous structures (Fig. 73-6B-D). Significant variations in gallbladder size, shape, and position may be seen; however, the gallbladder neck maintains a constant position relative to

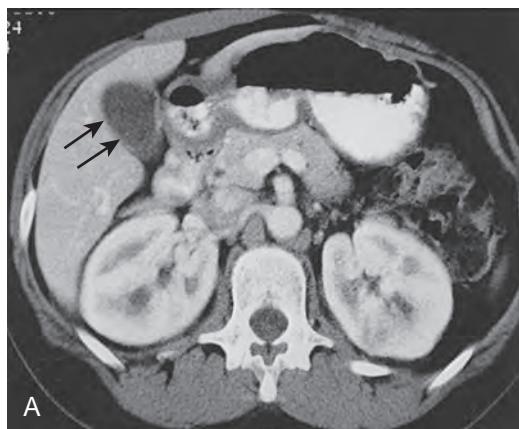
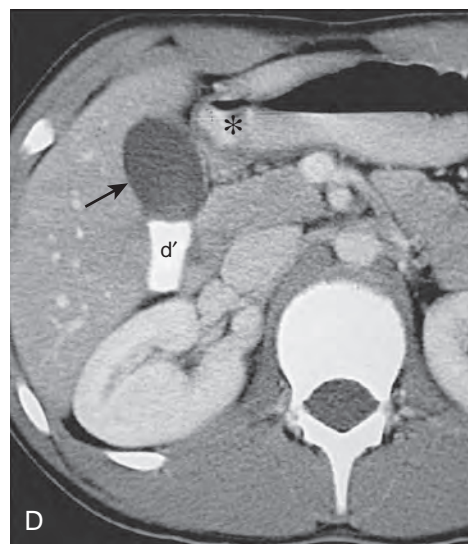
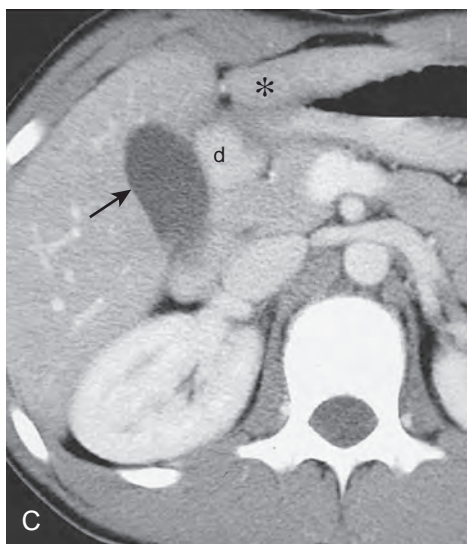
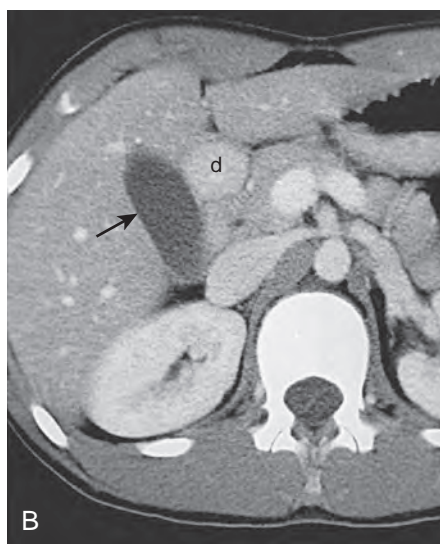


Figure 73-6 Normal gallbladder anatomy: CT. **A.** The gallbladder appears as a fluid-filled ovoid structure (arrows) in the interlobar fossa of the liver. **B-D.** Sequential CT scans show the normal position of the gallbladder (arrows) between the right and left lobes of the liver and the relationship of the gallbladder to the antrum (asterisk in **C** and **D**), duodenal bulb (d in **B** and **C**), and C-sweep of the duodenum (d').



the major interlobar fissure. The collapsed gallbladder may be more difficult to identify on CT scans.^{12,57}

CHOLESCINTIGRAPHY

Cholescintigraphy is used primarily for the diagnosis of acute cholecystitis; 3 to 5 mCi of technetium Tc 99m iminodiacetic acid (^{99m}Tc-IDA) compounds is injected intravenously, and the tracer is taken up by the liver and rapidly excreted into bile without undergoing conjugation, allowing visualization of the gallbladder and bile ducts (Fig. 73-7). Frequent anterior images are obtained up to 1 hour. Delayed imaging up to 4 hours and possibly 24 hours may be necessary in some instances. Nonfilling of the gallbladder on cholescintigraphy indicates functional obstruction of the cystic duct and is considered diagnostic of acute cholecystitis in the appropriate clinical setting. If the gallbladder fills, the cystic duct is deemed to be patent and acute cholecystitis is not present. This technique is highly sensitive and specific for the diagnosis of acute cholecystitis (95%-98%), and it is the procedure of choice to confirm the diagnosis.⁵⁸⁻⁶¹ Intravenous morphine sulfate and sincalide can assist gallbladder filling. Sincalide is a cholecystikinin analogue that produces gallbladder contraction and empties the gallbladder before the study, allowing the gallbladder to more readily fill with the tracer.

MAGNETIC RESONANCE IMAGING

The technology of MRI of the gallbladder and biliary ductal system has continued to evolve since the early 1990s. The gallbladder is routinely imaged on conventional MR studies of the liver and upper abdomen with T1- and T2-weighted sequences. Techniques for imaging of the gallbladder or bile ducts may be tailored to delineate either the wall of the gallbladder and bile ducts and the surrounding soft tissue or the biliary fluid within the lumen (see Chapter 75).

Imaging of the lumen requires optimal contrast between the biliary fluid and the surrounding tissues. Bright signal fluid techniques are generally used with heavily T2-weighted sequences to produce an MR cholangiopancreatogram. The development of MRCP has expanded the role of MRI as a non-invasive method to examine the biliary system. MRCP is performed with heavily T2-weighted sequences that depict fluid in the biliary ducts, pancreatic duct, and gallbladder as high signal intensity, whereas adjacent solid organs and flowing blood have little or no signal. The images produced resemble those of ERCP (Fig. 73-8). Although the primary goal of MRCP is to delineate the biliary and pancreatic ducts, incidental and intentional imaging of the gallbladder is possible even in the nonfasting patient. In many cases, the cystic duct and its site of insertion into the bile duct are also visualized. Although MRCP results in



Figure 73-7 Normal cholescintigram. Frontal view taken 30 minutes after injection of radioisotope shows normal visualization of the gallbladder (long arrow), bile ducts (short arrows), and bowel (curved arrow).



Figure 73-8 MRCP: normal gallbladder and bile duct. Heavily T2-weighted coronal image shows the gallbladder, hepatic confluence, and extrahepatic bile duct.

high-resolution images of the gallbladder, its role relative to ultrasound and CT for evaluation of gallbladder disease is limited primarily to problem solving, not to primary diagnosis, with the exception of gallbladder carcinoma. MR provides comprehensive imaging of the gallbladder and bile ducts as well as

of the surrounding structures, a feature most helpful in staging of tumors arising from or involving the gallbladder.^{12,16,62-66}

Technique

Conventional MRI of the gallbladder and bile ducts frequently combines the use of T1- and T2-weighted sequences. T1-weighted fat suppression sequences with and without intravenous gadolinium chelates may be helpful in demonstrating the lumen as well as the wall of the gallbladder and the bile ducts. T2-weighted sequences may be used in evaluating the surrounding soft tissues. Heavily T2-weighted MR sequences are used to perform MRCP. A number of sequences have been used since its introduction, including two-dimensional fast spin-echo and three-dimensional fast spin-echo. Technical refinements provided by the half-Fourier rapid acquisition with relaxation enhancement (RARE) sequence allow rapid imaging, such that the entire biliary tract can be imaged during an 18-second breath-hold.⁶⁴⁻⁶⁷ A typical MRCP examination comprises multiple acquisitions obtained at variable angles that optimally delineate the biliary tract and gallbladder. The half-Fourier RARE sequence minimizes magnetic susceptibility artifacts, such as those associated with surgical clips and bowel gas. A thin-slab, multislice technique is often used in both axial and coronal planes. From these source images, three-dimensional reconstructions may be generated with an MIP algorithm. No intravenous or oral contrast material is administered.

Normal Anatomy

On MRI, the gallbladder lumen can have a high or low signal intensity, depending on the chemical composition of bile and the pulse sequence used (Fig. 73-9). Concentrated bile is high signal intensity on T1- and T2-weighted images, whereas dilute bile is low in signal intensity on T1-weighted images because of its higher water content. Because concentrated bile has a greater specific gravity than dilute bile, concentrated bile settles in the dependent portion of the gallbladder. On MRCP, gallbladder calculi, regardless of composition, appear as low signal intensity filling defects within the high signal intensity bile (Fig. 73-10). Calculi as small as 2 mm can be identified. In addition to calculi, MRCP can depict neoplastic disease of the gallbladder and its extent. Adenomyosis of the gallbladder may be incidentally identified when the fluid-filled Rokitsky-Aschoff sinuses are seen within the gallbladder wall.^{16,62,64,66,68-71}

Examination Techniques: Biliary Tract

A number of examination techniques are available for evaluation of the biliary ducts. In selection of an imaging technique, several factors must be considered, including clinical presentation, diagnostic information desired, body habitus, and anatomic alterations from previous surgery. If direct cholangiography with PTC or ERCP is used, the potential for conversion to a therapeutic intervention must be considered.

Ultrasound and CT are frequently used as the primary non-invasive methods for screening of patients with suspected ductal disease, although MRCP is being used more often and is now considered the primary evaluation method of choice for biliary ductal disease. MRCP is noninvasive and can be performed rapidly, depicting the intrahepatic and extrahepatic bile ducts as well as the pancreatic duct and surrounding structures. Although CT cholangiography has been widely used in Europe and on a limited basis in the United States for ductal evaluation,

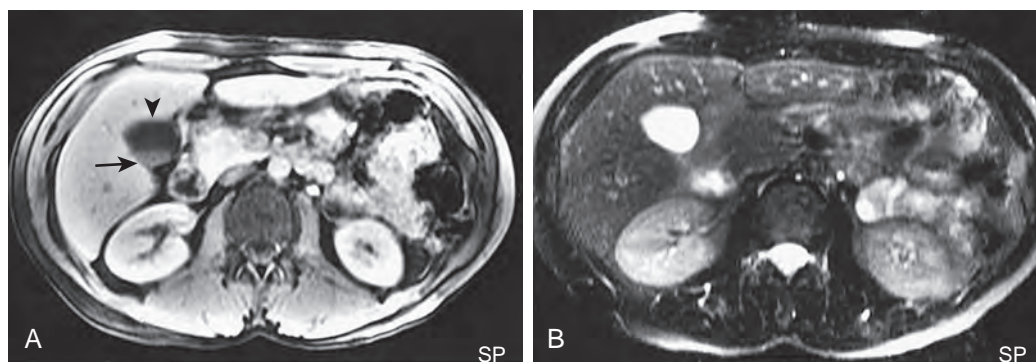


Figure 73-9 Normal gallbladder: MRI. **A.** T1-weighted fat suppression image shows high signal intensity, concentrated bile in the dependent portion of the gallbladder (arrow) and low signal intensity, less concentrated bile in the nondependent portion of the gallbladder (arrowhead). **B.** T2-weighted fat suppression image depicts bile in the gallbladder as high signal intensity.



Figure 73-10 Gallbladder calculi. MR cholangiogram shows multiple gallbladder calculi as multiple filling defects in high signal intensity bile. The extrahepatic bile duct (arrowhead) is noted.

this technique is rarely used in current practice. CT cholangiography provides information similar to that of MRCP but requires intravenous administration of a cholecystographic agent before the CT study. This technique has several limitations, including use of contrast agents with the associated risk of reaction, lack of ready availability of the contrast agents used, inconsistent opacification of the ducts from the contrast agents, and limited opacification of the ducts in patients with biliary obstruction.

Direct opacification of the bile ducts by PTC or ERCP can provide detailed information about ductal anatomy or pathologic changes; however, these are invasive procedures. PTC or ERCP may also serve as a preliminary step to

nonsurgical therapeutic interventions, such as biliary drainage, stent placement, stone removal, or stricture dilation. Biliary scintigraphy is occasionally useful in detection of bile leaks, evaluation of biliary enteric anastomoses, or diagnosis of early or segmental biliary obstruction. Operative cholangiography and postoperative cholangiography are standard methods to evaluate the bile ducts after surgical access to the ductal system. Plain radiography has a limited role and is rarely useful in defining bile duct disease.

PLAIN RADIOGRAPHY

The biliary ductal system is visible on plain radiographs only when it is outlined with air or calcification. Air in the biliary tree most commonly results from a surgically created biliary-enteric anastomosis. Erosion of a gallstone into the gastrointestinal tract and erosion of a peptic ulcer or tumor into the biliary tree are other causes of biliary-enteric fistula that may result in biliary air. Rarely, calcified stones in the bile ducts are visible on plain film.³⁸

ULTRASOUND

Evaluation of the bile ducts in search of stones, mass, or obstruction is one of the main applications for ultrasound. Real-time ultrasound readily depicts dilated biliary ducts, which in most instances is indicative of biliary obstruction. The extrahepatic bile duct can be seen in most patients regardless of body habitus or clinical condition. Because the bile duct is oval in cross section in the majority of patients, measurement of the transverse diameter on axial images correlates more closely with ductal diameters measured on ERCP.⁷² The CHD is the most easily visualized portion of the extrahepatic biliary system and can be rapidly visualized and measured in virtually all patients.^{1,4-9,73} Intrahepatic ducts are rarely seen unless they are dilated. The distal CBD may be obscured by gas in the duodenum. The primary goal of biliary sonography is the detection of dilated ducts because the size of the extrahepatic duct is a fairly sensitive indicator of the presence of biliary obstruction. Early changes of intrahepatic and extrahepatic ductal dilation are readily seen with ultrasound. Frequently, the lesion causing the biliary obstruction is identified as well.^{4,5,73} Ultrasound is an accurate and reliable technique to assess the intrahepatic and extrahepatic ducts as well as adjacent structures, such as the pancreas.

Technique

The bile ducts are best evaluated with high-resolution real-time equipment and the highest frequency transducer possible: 3.5 MHz in obese patients and 5 MHz in thin patients. Optimal imaging of the CHD and proximal CBD is obtained by parasagittal scanning with the patient in the supine left posterior oblique or left lateral decubitus position.⁷⁴ The CHD is identified as a tubular sonolucency anterior and lateral to the proximal main portal vein or the undivided right portal vein (Fig. 73-11A). The right hepatic artery passes between the posteriorly located portal vein and the anteriorly located CHD. In 10% to 15% of patients, the artery is anterior to the CHD. The standard measurement of the CHD is made at this level. The measurement is made from interior wall to interior wall perpendicular to the scan plane. Doppler sonography of the porta hepatis may be needed to distinguish the bile ducts from adjacent vascular structures.⁷⁵

The distal CBD is more difficult and frequently impossible to image because of overlying gas in the duodenum and hepatic flexure. Visualization can be improved by scanning with the patient in the semierect (60 degrees to the vertical) right posterior oblique position in the transverse rather than in the parasagittal plane⁷⁶ (Fig. 73-11B). This position minimizes antral and duodenal gas, allows fluid to enter the antrum and duodenum, and allows the left lobe of the liver to descend, creating an acoustic window. With this technique, the distal duct can be seen in up to 90% of cases.⁷⁷ The specific point of union of the CHD with the cystic duct is usually not seen.

After examination of the extrahepatic ductal system, the proximal ducts and intrahepatic ducts are examined with the patient in the supine or left posterior oblique position. The normal right and left main hepatic ducts can be visualized coursing anterior to the undivided right portal vein and the initial segment of the left portal vein, respectively.

Normal Anatomy

The normal intrahepatic ducts are less than 1 to 2 mm in diameter and are usually not visible. Although visualization

of intrahepatic ducts generally implies biliary dilation, larger central intrahepatic ducts can occasionally be visualized anterior to the portal veins in the right and left lobes near the porta hepatis in normal thin patients with use of a 5-MHz transducer. Gross intrahepatic duct dilation is easy to detect sonographically as the “parallel-channel” sign, formed by dilated intrahepatic ducts running anterior and parallel to the portal vein tributaries.^{1,2,4-7} Dilated intrahepatic ducts tend to have acoustic enhancement posteriorly, which distinguishes them from veins. The use of color Doppler is helpful to distinguish bile ducts from small hepatic vessels. This is especially so for the left lobe of the liver, where parallel branching hepatic anterior and portal veins may mimic dilated left intrahepatic ducts.⁷⁵

The normal CHD measures 4 to 5 mm or less on sonograms. The CBD measures 4 to 6 mm normally, with a 6- to 7-mm diameter considered equivocal. These measurements reflect the internal dimension of the duct. A diameter of more than 8 mm is indicative of ductal dilation.^{4-6,78-80} Sonographic measurements of duct size are smaller than those obtained by direct cholangiography because there is no radiographic magnification or distention resulting from injected contrast material.^{81,82} Some variation in extrahepatic ductal diameter may be due to elastic properties of the bile ducts, which can expand and contract rapidly during normal physiologic filling and emptying, with Valsalva maneuver, or with deep inspiration. There is controversy about whether extrahepatic ductal diameter increases with aging. In a study by Wu and coworkers³³ of 256 normal patients, the CBD size was shown to increase roughly 1 mm per decade after the age of 50 years, indicating that an apparently enlarged CBD may be seen in normal elderly patients. This study also suggested that the upper limit of normal may be up to 10 mm in the elderly population. Two additional studies, one with a cohort of 350 patients³⁶ and another with a cohort of 45 patients,³⁵ support these data. These findings, however, were refuted in a study by Horrow and colleagues³⁴ of 258 patients that did not confirm an association between age and size of the extrahepatic bile duct in an asymptomatic adult population.

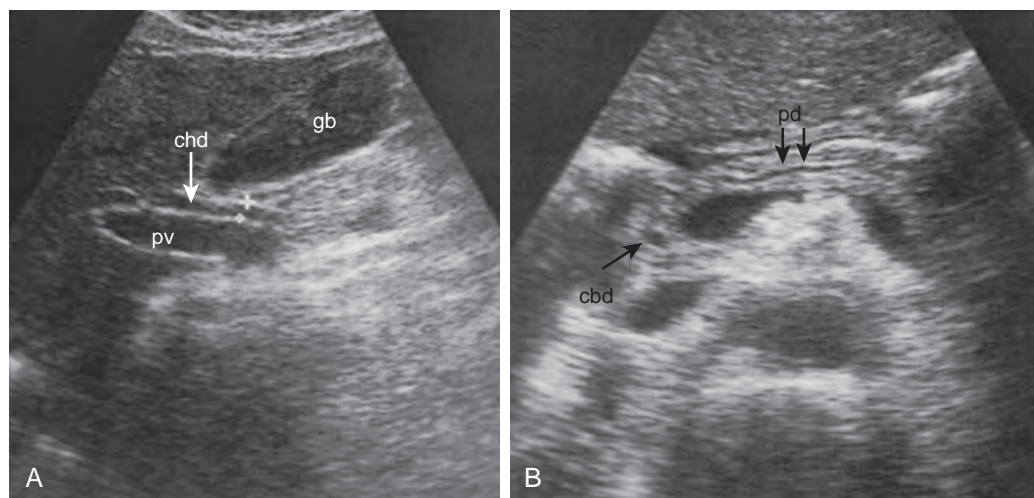


Figure 73-11 Extrahepatic biliary anatomy: ultrasound. **A.** Sonographic demonstration of the common hepatic duct (chd, arrow) located anterior to the portal vein (pv). Note the gallbladder (gb) anteriorly. **B.** Normal distal common bile duct (cbd, arrow) is seen in the head of the pancreas on a semierect transverse sonogram. Pancreatic duct (pd, arrows) is also seen.

Ductal Diameter and Biliary Obstruction: Limitations

Sonography has an overall accuracy of more than 95% in the detection of dilated ducts and diagnosis of biliary obstruction.^{73,78,80,83} However, bile duct caliber does not always correlate with the presence or absence of biliary obstruction. Biliary obstruction without dilation may be seen in patients with low-grade or intermittent obstruction resulting from stricture or small stones and in patients with sclerosing cholangitis.^{84,85} Alternatively, dilated ducts may be seen in the absence of obstruction in patients with prior biliary surgery or patients with resolved obstruction.^{86,87} The decreased elasticity of a dilated duct may result in persistent dilation despite relief of the obstruction. Intestinal hypomotility, recent laparotomy, hyperalimentation, and prolonged fasting can cause ductal dilation presumably secondary to factors that inhibit relaxation of the sphincter of Oddi. An enlarged CBD may be seen in normal, unobstructed elderly patients.³³ Ultrasound is accurate in diagnosing the level of obstruction in 92% to 95% of cases and identifying the cause of obstruction in 70% to 88%.^{5,6,73,77}

Postcholecystectomy Dilation

Whether dilation of the duct occurs after cholecystectomy has been debated in the literature for years. It has been proposed that in the absence of a gallbladder, the CBD dilates to function as a reservoir. Two studies, however, suggest that if the CBD is normal before surgery, it generally remains so after surgery unless disease intervenes.^{78,88,89} A reassessment of the effect of cholecystectomy on duct size found that after cholecystectomy, most patients did not have significant compensatory dilation of the duct.^{79,89} Once a duct dilates, it may lose elastic recoil and never return to normal. Accordingly, some postcholecystectomy patients have biliary “dilation” but nonobstructed ducts. The maximal upper limit of the CBD allowed after cholecystectomy is 10 mm.⁴ The general recommendation is that further studies are warranted if the CHD measures 6 mm or greater in symptomatic patients.

Fatty Meal or Cholecystokinin Sonography

Administration of a fatty meal followed by sonography is an adjunctive maneuver that provides functional information, helps identify patients who require further evaluation with direct cholangiography, and increases the accuracy of ultrasound in detecting obstruction. This technique is helpful in postcholecystectomy patients with suspected obstruction in the absence of ductal dilation, in patients with equivocal duct size, and in asymptomatic patients with abnormal results of liver function studies suggesting occult obstruction. Magnified views of the CHD are obtained, and the internal diameter is measured at a fixed point. A fatty meal or intravenous cholecystokinin is administered, and another measurement of CHD caliber is obtained 30 to 45 minutes later if a fatty meal is used and 5 to 10 minutes later if cholecystokinin is used. A fatty meal and cholecystokinin cause gallbladder contraction, sphincter of Oddi relaxation, and increased bile flow. The normal, nonobstructed duct decreases in size or does not change in caliber. An increase in caliber—or, if the duct is initially dilated, a failure to decrease in caliber—suggests some degree of ductal obstruction and the need for further evaluation. A true change in ductal diameter occurs only if the size changes by 2 mm or more.^{58,90-92} Using these criteria, Simeone and colleagues⁹⁰ reported 84%

sensitivity for fatty meal sonography in predicting the presence or absence of CBD obstruction.

COMPUTED TOMOGRAPHY

Continued evolution of CT technology, including refinements of multidetector scanning technology, has enhanced the utility of CT for evaluation of biliary duct disease. With the use of high-resolution scanners and fine collimation, minimally dilated intrahepatic and extrahepatic ducts are now easily visible. Visualization of the entire CBD is routine on CT scans of the upper abdomen.^{2,93,94} Imaging is not inhibited by overlying gas. CT is more reliable than sonography in determining the caliber of intrahepatic and extrahepatic ducts. In addition, because of more complete delineation of the total length of the CBD, CT is also more useful than sonography for precisely defining the site and cause of biliary obstruction. Whereas ultrasound has been used to screen patients with biliary obstruction in the past, CT and MR are now the first-line diagnostic studies and are no longer used as a follow-up study after ultrasound to refine the data or to confirm anatomy.^{2,11,12,95} CT has an accuracy of 96% to 100% in detecting the presence of biliary obstruction, 90% in determining the level of obstruction, and 70% in identifying the cause of obstruction.^{2,94,96,97} The reported sensitivity of CT for detection of bile duct stones is 72% to 88%.⁹⁵ In addition, CT can often differentiate benign from malignant causes of obstruction and can provide guidance for biopsy and staging of malignant neoplasms.⁹⁸

Technique

Optimal CT scanning of the bile ducts requires rapid intravenous infusion of a bolus of contrast material combined with rapid scanning in the portal venous phase, usually 70 to 80 seconds after bolus injection of contrast material (100-150 mL). With current volumetric MDCT technology, the entire abdomen, with complete depiction of the intrahepatic and extrahepatic biliary tree, can be imaged in less than 5 seconds. MDCT scanners produce a volumetric data set that can be reconstructed in multiple dimensions for interpretation. Standard reconstruction includes 2- to 5-mm-thick axial images. High-quality multiplanar (MPR) coronal, coronal oblique, and curved planar reformatted images as well as three-dimensional reconstructions of the biliary ductal system may be helpful in defining complex anatomy or to map the ducts for planning of therapy. In cases of biliary obstruction, coronal reconstruction or three-dimensional reformations of the dilated bile ducts from data obtained during routine scanning can be produced successfully by taking advantage of the “negative” contrast effect of low-attenuation bile in dilated ducts relative to the adjacent enhanced visceral organs and vessels.*

In searching for CBD stones, scanning may be performed initially without oral or intravenous contrast material. Although dense contrast medium in the bowel has the potential to cause streak artifacts across the CBD, obscuring detail, such artifacts are rarely a problem with MDCT scanners. Duodenal contrast medium may obscure an impacted stone in the ampulla, and contrast medium in a perivaterian duodenal diverticulum can simulate a stone. Contrast enhancement of the vasa vasorum of the CBD wall may also mimic

*References 2, 73, 93, 94, 99, 100.

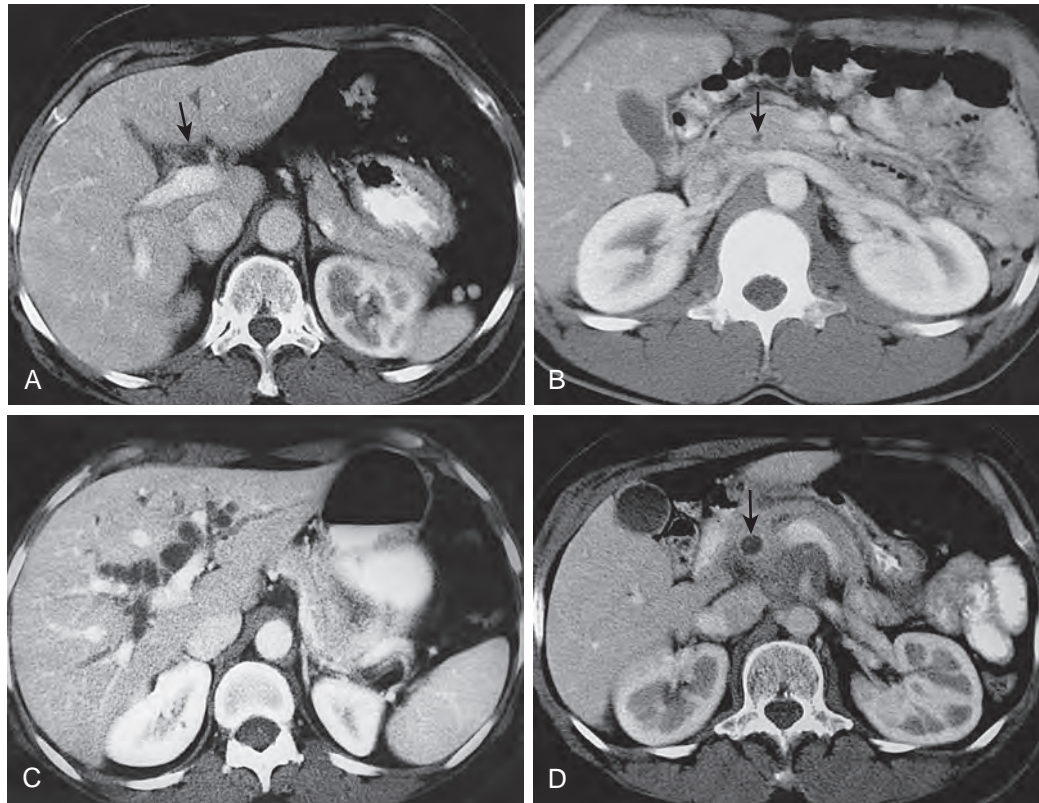


Figure 73-12 Extrahepatic biliary anatomy: CT. **A.** CT scan at the level of the porta hepatis shows the normal common hepatic duct (arrow). **B.** CT scan of the normal common bile duct (arrow) in cross section in the pancreatic head. **C.** Dilated intrahepatic bile ducts are seen as low-density branching structures adjacent to enhanced portal veins. **D.** CT scan of the dilated common bile duct (arrow) seen in the pancreatic head.

choledocholithiasis. Reconstruction in thin slices of 1 to 2 mm or the use of coronal reconstructions may allow better demonstration of calculi.* Proper selection of the correct window width and level is necessary to optimize visualization of the CBD throughout its entire course from the porta hepatis to the intrapancreatic portion.

Multiphase imaging during late arterial and portal venous phase imaging may improve visualization of hypovascular tumors involving the bile ducts. Delayed imaging (10-20 minutes after administration of contrast material) has been shown to be helpful in diagnosis of cholangiocarcinoma. The tumor demonstrates increased retention of contrast material compared with the adjacent liver.^{103,104}

Normal Anatomy

On MDCT scans of the liver and upper abdomen, the CHD and CBD are usually visualized throughout their entire course (Fig. 73-12A-D). Visualization of intrahepatic ducts on CT has been considered evidence of biliary dilation and obstruction. However, with MDCT scanners, bolus contrast enhancement, and 2- to 5-mm-thick scans, visualization of normal intrahepatic ducts may be seen in 40% of normal individuals.¹⁰⁵ The average size of the normal intrahepatic ducts is 2 mm in the central liver and 1.8 mm in the periphery. Demonstration of intrahepatic bile ducts on CT scans does not necessarily indicate biliary obstruction; however, few normal intrahepatic ducts

should be seen. Truly dilated intrahepatic ducts are readily apparent and, when present, indicate biliary tract disease. Bile ducts appear as water-density tubular branching structures converging at the porta hepatis. The left and right hepatic bile ducts course through the porta hepatis and join to form the CHD lying anterior to the portal vein.^{3,73}

The CHD and CBD are usually visible within the hepatoduodenal ligament^{3,73,106,107} (see Fig. 73-12A). The proximal extrahepatic duct forms a fairly straight, thin-walled, low-density tube anterior lateral to the portal vein, angling toward the midline. A more transverse orientation is present in approximately 6% of normal persons and 18% of those with dilated ducts.¹⁰⁷ The distal CBD appears on cross section as a circular, low-density structure in the pancreatic head or in a groove posterior lateral to the pancreatic head (see Fig. 73-12B, D). Visibility of the normal CBD is increased by contrast enhancement of adjacent vascular structures, pancreas, and liver parenchyma. The normal CBD is seen on CT scans at least 50% of the time. However, this figure is higher with contrast-enhanced MDCT, especially when reconstructed thin-slice thickness (2-5 mm) images and coronal reconstructed images are used. In a study using optimal technique, the normal CHD and CBD were visualized in 66% and 82% of cases, respectively.^{73,108} The duct wall may be discerned separately with a mean thickness of 1 mm and a maximal thickness of 1.5 mm. Contrast enhancement of the duct wall may occur in normal patients and should not be confused with peripheral calcification or stone. An isolated finding of duct wall enhancement should not be considered abnormal, although it can occur in

*References 2, 53, 55, 57, 73, 94, 101, 102.

pancreatitis, choledocholithiasis, sclerosing cholangitis, and cholangiocarcinoma.

The normal CHD on CT is 3 to 6 mm in diameter. A CBD diameter of 7 to 8 mm is generally considered upper limit of normal, and 8 to 9 mm is considered dilated.^{95,108} Anterior-posterior measurements are most accurate because the oblique segment of the CHD, when it is measured transversely, may give an artifactually large diameter. Axial CT images of the extrahepatic duct show sequential low-density circles that gradually taper as the duct courses through the head of the pancreas. The level of obstruction corresponds to the transition from dilated to nondilated duct.

COMPUTED TOMOGRAPHY CHOLANGIOGRAPHY

CT cholangiography, obtained after intravenous administration of contrast material that is excreted in the bile, displays biliary ductal anatomy and pathologic changes similar to direct cholangiography. This technique has been used for the noninvasive detection of biliary anatomy and variations before laparoscopic cholecystectomy and in living donor candidates for right hepatic lobe transplantation.¹⁰⁹⁻¹¹² CT cholangiography has also been used for noninvasive detection of bile leaks and bile duct stones and for evaluation of suspected biliary obstruction.¹¹³⁻¹¹⁵ Most reported studies have used intravenous contrast material, meglumine iodipamide, which is the same agent used in the past for intravenous cholangiography. The agent is infused during 20 to 30 minutes, and scanning is performed 15 minutes after the end of the infusion.^{114,115}

After administration of the contrast material, multislice CT images are obtained. Three-dimensional images are reconstructed with MIP and volume rendered techniques (Fig. 73-13). CT cholangiography is not commonly used because of the increased reaction rate associated with intravenous biliary contrast agents, the increased study time necessitated by the administration of the contrast material, the lack of effectiveness

in patients with jaundice or elevated serum bilirubin concentration, and the increased utility of MRCP, which provides similar information more quickly and without the use of contrast agents.¹⁰⁹⁻¹¹⁵

MAGNETIC RESONANCE CHOLANGIOPANCREATOGRAPHY

MRCP uses heavily T2-weighted sequences to generate bright signal from fluid in the bile and pancreatic ducts, allowing delineation of the ducts from surrounding tissues. An image of the ducts similar to that of ERCP is produced. Since its introduction in 1991, MRCP has undergone a number of technical refinements that now allow rapid imaging of the biliary system with consistent visualization of the entire extrahepatic ducts and most of the intrahepatic ducts in 90% to 100% of patients with normal-caliber ducts (see Fig. 73-8). Dilated ducts proximal to an obstruction are well visualized in virtually 100% of cases. The diagnostic accuracy of MRCP is comparable to that of ERCP in the evaluation of choledocholithiasis, malignant obstruction, and anatomic variants of the biliary tract. Simultaneous evaluation of the pancreatic duct is also obtained. The usefulness and accuracy of MRCP have been established in the evaluation of choledocholithiasis, malignant obstruction, congenital anomalies, and postsurgical alterations of the biliary tract¹¹⁶⁻¹²⁶ (Fig. 73-14). The improved spatial resolution afforded by recent refinements in MRCP permits visualization of calculi as small as 2 mm. In addition, MRCP depicts not only the dilated ducts proximal to a stricture but also the stricture itself. MRCP is particularly advantageous in the evaluation of patients who have experienced failed or incomplete ERCP.¹²² MRCP has a reported sensitivity of 89% to 100% and specificity of 83% to 100% for the detection of calculi.¹²⁵ MRCP is now considered to be the diagnostic imaging test of choice in the evaluation of biliary ductal disease. The major disadvantage of MRCP is that it is purely diagnostic and does not provide an access for therapeutic intervention (see Chapter 75).

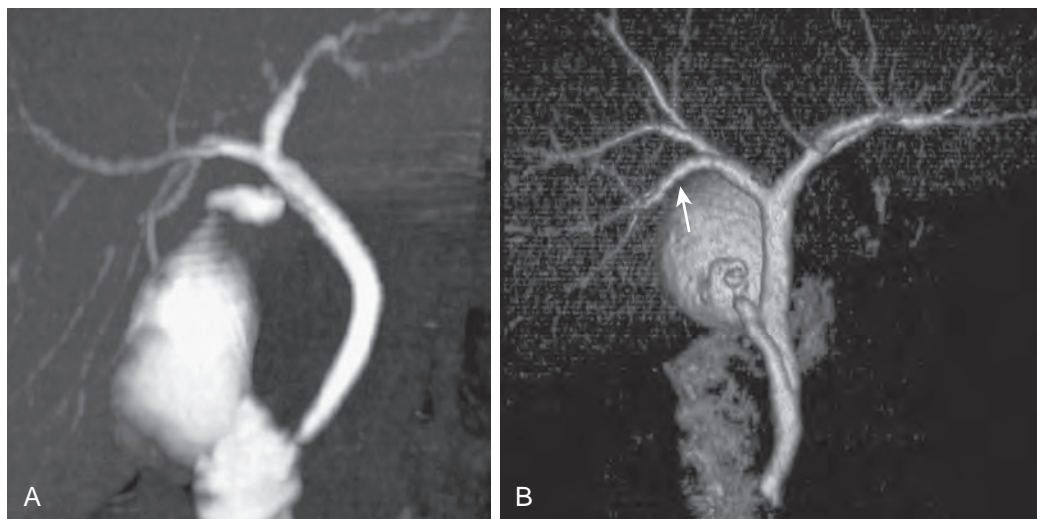


Figure 73-13 CT cholangiography. **A.** Coronal MIP CT cholangiogram acquired with 2.5-mm section thickness after intravenous administration of contrast material. **B.** Reconstructed oblique coronal volume rendered CT cholangiogram in a potential right hepatic lobe donor demonstrates normal branching anatomy of the bile ducts. (**A** from Wang ZJ, Yeh BM, Roberts JP, et al: Living donor candidates for right hepatic lobe transplantation: Evaluation at CT cholangiography—initial experience. *Radiology* 235:899–904, 2005. Reprinted with permission. **B** courtesy Benjamin Yeh, MD, and Z. J. Wang, MD.)

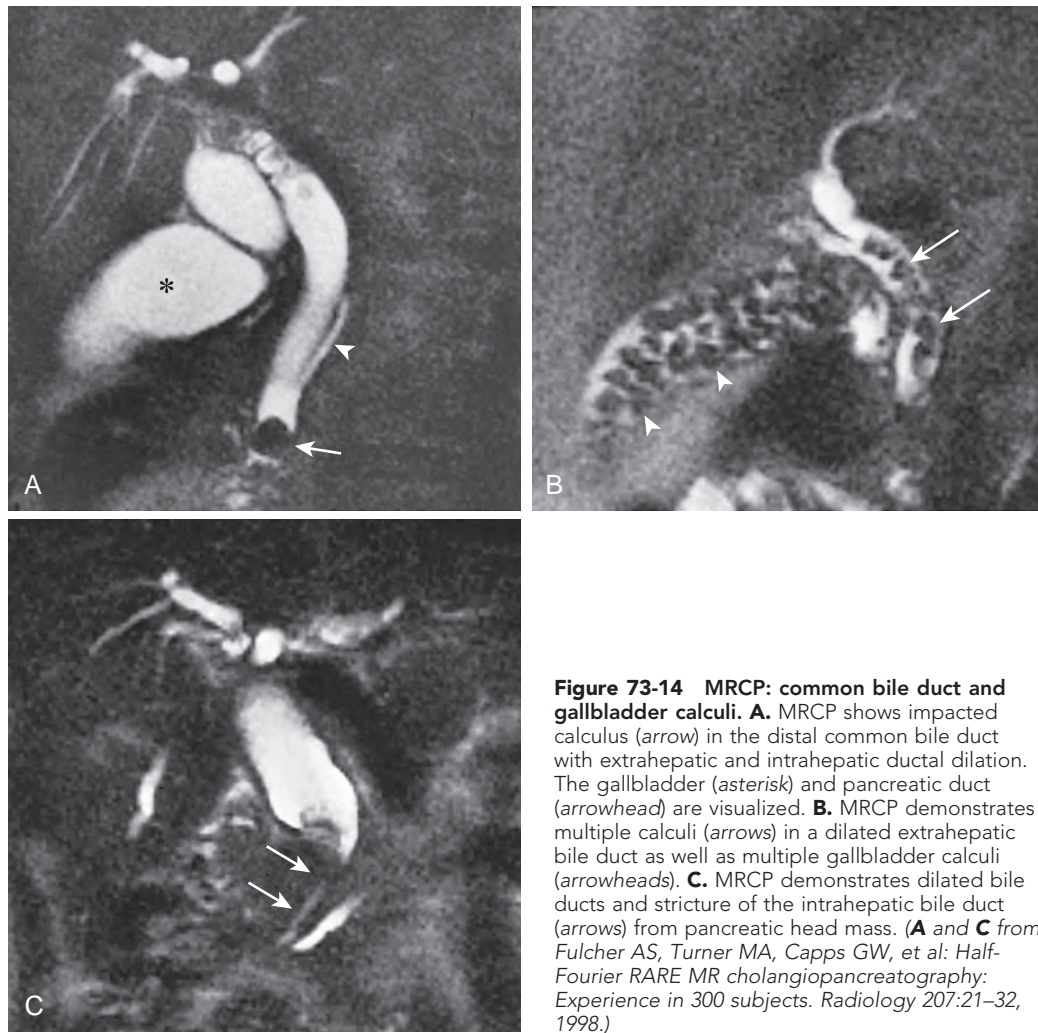


Figure 73-14 MRCP: common bile duct and gallbladder calculi. **A.** MRCP shows impacted calculus (arrow) in the distal common bile duct with extrahepatic and intrahepatic ductal dilation. The gallbladder (asterisk) and pancreatic duct (arrowhead) are visualized. **B.** MRCP demonstrates multiple calculi (arrows) in a dilated extrahepatic bile duct as well as multiple gallbladder calculi (arrowheads). **C.** MRCP demonstrates dilated bile ducts and stricture of the intrahepatic bile duct (arrows) from pancreatic head mass. (A and C from Fulcher AS, Turner MA, Capps GW, et al: Half-Fourier RARE MR cholangiopancreatography: Experience in 300 subjects. *Radiology* 207:21–32, 1998.)

Technique

State-of-the-art MRCP can now be performed with both two-dimensional and three-dimensional heavily T2-weighted sequences, usually RARE (fast spin-echo or turbo spin-echo) techniques.¹²⁴ Variants include single-shot fast spin-echo (also known as half-Fourier acquisition single-shot turbo spin-echo; Siemens Medical Solutions, Malvern, Pa) and fast-recovery fast spin-echo.¹²⁴⁻¹²⁷ The heavily T2-weighted sequences depict the bile ducts as high signal intensity structures against the low signal intensity of the liver (see Fig. 73-8). MRCP offers several advantages over direct cholangiography in general and ERCP in particular in that it avoids the administration of contrast material and exposure to ionizing radiation. The risks of pancreatitis, sepsis, and perforation associated with ERCP are avoided because the examination is performed without instrumentation. Because MRCP is entirely noninvasive, the high cost of sedation and postsedation recovery is eliminated.

MRCP may be performed with a variety of techniques. The multislice technique involves the acquisition of multiple 3- to 5-mm-thick source images of the biliary tract, which may be obtained during breath-hold or shallow respiration.^{16,116,117} With this technique, the biliary tract is first localized by obtaining a thick-slab image in the coronal plane (Fig. 73-15A). The

middle third of the extrahepatic bile duct is localized, and a thick-slab axial image is obtained at this level (Fig. 73-15B). This axial image is used as a guide to prescribe the appropriate angles for optimal delineation of the bile ducts with thin-slab (3- to 5-mm) images in the coronal oblique plane (Fig. 73-15C, D). Although imaging is most often conducted in the coronal plane, axial images may prove useful in confirming suspected CBD stones. From the thin-slab source images, three-dimensional images may be generated with an MIP algorithm or with MPR techniques. An alternative MRCP technique is that of single-shot projection.^{62,125,127} With the projection technique, a single thick (30- to 70-mm) image is generated during a 2-second acquisition.

Technical advances, such as improvements in software and the use of phased array surface coils, have resulted in high-resolution images of the biliary tract that can be acquired during a single breath-hold. When rapid imaging is obtained during a breath-hold, artifacts resulting from respiratory excursion are eliminated. Although the breath-hold technique is recommended, high-quality MRCP images can be obtained in critically ill or ventilator-dependent patients who are not able to cooperate for a breath-hold. Whereas MRCP is a focused examination of the biliary tract, conventional MRI with T1- and T2-weighted sequences may show normal bile ducts as low

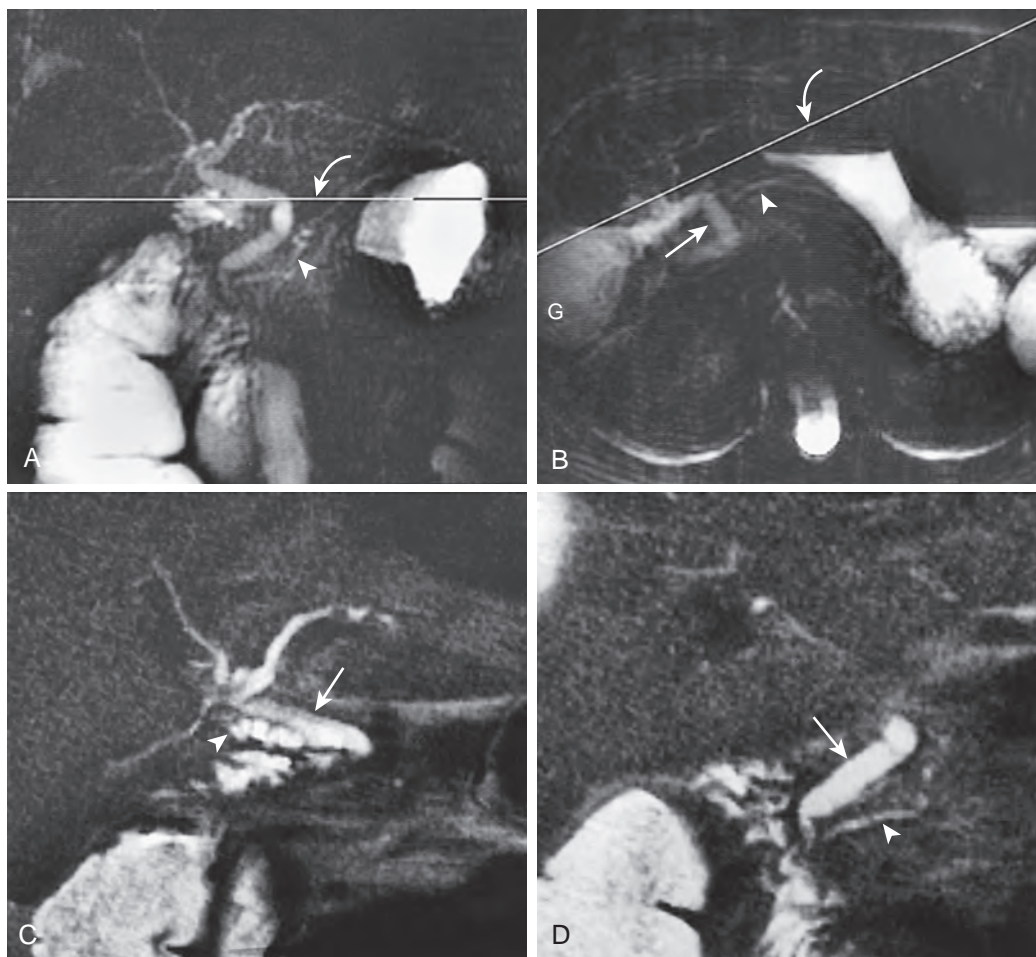


Figure 73-15 MR cholangiogram: technique. **A.** Coronal thick-slab (7-cm) MR cholangiogram with a localizer (*curved arrow*) placed at the level of the middle third of the extrahepatic bile duct demarcates the area through which an axial thick-slab image will be obtained. The pancreatic duct (*arrowhead*) is noted. **B.** Axial thick-slab (7-cm) MR cholangiogram obtained at the level of the middle third of the extrahepatic bile duct is used as a reference from which angles (*curved arrow*) are prescribed to obtain thin-slab images of the duct in the coronal oblique plane. The bile duct (*straight arrow*) and pancreatic duct (*arrowhead*) are shown. **C.** Coronal oblique thin-slab (5-cm) MR cholangiogram demonstrates the proximal extrahepatic bile duct (*arrow*) and the cystic duct remnant (*arrowhead*). **D.** Coronal oblique thin-slab (5-cm) MR cholangiogram image obtained posterior to **C** shows the distal bile duct (*arrow*) and the pancreatic duct (*arrowhead*).

signal intensity tubular structures on T1-weighted images and high signal intensity structures on T2-weighted images. Conventional MRI with T1- and T2-weighted sequences also provides complementary information about the adjacent hepatic and pancreatic parenchyma (Fig. 73-16).

Contrast-Enhanced Magnetic Resonance Cholangiography.

The use of intravenous contrast agents to enhance ductal visualization continues to be investigated. Paramagnetic or T1 relaxation-enhancing agents, which are substantially excreted in the bile, may be used to obtain bright signal delineation of the bile ducts. Gadobenate dimeglumine (Gd-BOPTA, Multi-Hance; Bracco Diagnostics, Princeton, NJ), gadoxetic acid disodium (gadoxetate disodium [Gd-EOB-DTPA], Eovist or Primovist; Bayer Healthcare, Leverkusen, Germany), and mangafodipir trisodium (Teslascan; Nycomed, Zurich, Switzerland; not available in the United States) are three such agents that result in contrast-enhanced high signal bile, permitting good visualization of the biliary tract. These agents shorten the T1 relaxation time of bile, resulting in high signal intensity bile at

T1-weighted imaging. Imaging is performed 15 to 90 minutes after intravenous injection. These agents have been used for anatomic mapping of bile ducts before living donor liver transplantation and for the detection of bile leaks after transplantation. Disadvantages include the need to wait for sufficient biliary excretion of the contrast agent, the need for intravenous access, and the potential risk of the contrast agents.^{12,128} It is uncertain whether these agents have any significant advantage over the inherent contrast and clear ductal delineation provided by the currently used heavily T2-weighted sequences of MRCP.

Normal Anatomy

Normal-caliber proximal intrahepatic bile ducts and the entire extrahepatic bile duct are routinely visualized at MRCP. The intrahepatic bile ducts are depicted as high signal intensity branching tubular structures against the low signal intensity background of the solid parenchymal organs. The intrahepatic bile ducts can be distinguished from the low signal portal veins, which contain rapidly flowing blood. The high signal extrahepatic bile duct is seen throughout its course from the porta

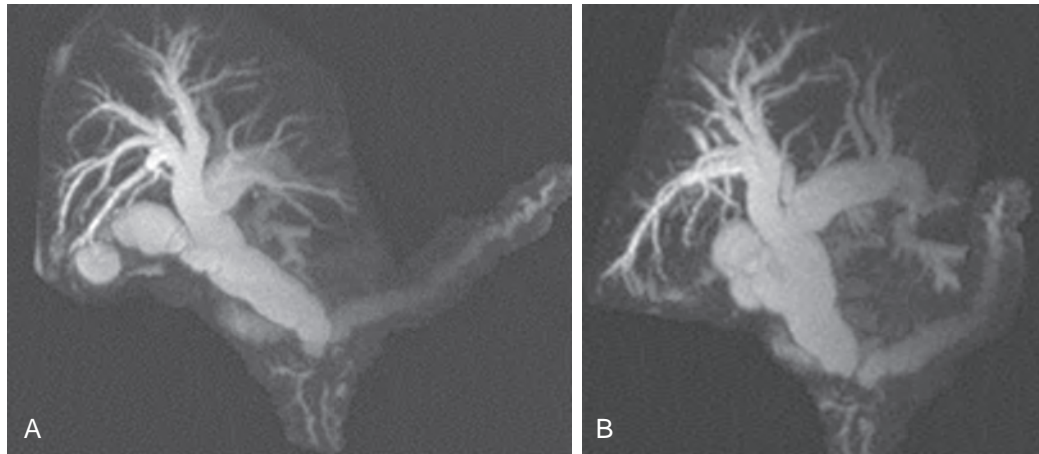


Figure 73-16 MR cholangiogram: enhanced three-dimensional technique. **A.** Three-dimensional MIP image from T2-weighted MRCP in a patient with obstruction and dilated ducts from pancreatic carcinoma better demonstrating detail of the dilated bile ducts. **B.** Slightly rotated view demonstrates distal bile duct and pancreatic duct junction to better advantage.

hepatitis to the duodenum and is distinguished from the lower signal intensity solid organs.^{16,62-64,66} On conventional MRI, the normal extrahepatic duct is seen in approximately 50% of cases. The CBD is more readily depicted on axial projections in its intrapancreatic portion on conventional MRI of the upper abdomen, whereas normal intrahepatic ducts are not usually seen.¹²⁴⁻¹²⁶

DIRECT CHOLANGIOGRAPHY

Despite the high accuracy of ultrasound, CT, and MRCP in biliary disease, direct cholangiography (PTC or ERCP) may be needed when findings on cross-sectional imaging are equivocal or discrepant or when a therapeutic intervention is needed. Direct cholangiography is used to verify the presence or absence of biliary obstruction and to more precisely define the site and cause of an obstructive lesion. Direct cholangiography has a more than 95% success rate in determining the site and a more than 90% success rate in determining the cause of biliary obstruction. Direct cholangiography should always be preceded by ultrasound, CT, or MRCP to reveal unusual anatomy, areas of segmental ductal obstruction, and intrahepatic or extrahepatic mass lesions that would alter the manner in which cholangiography is performed and interpreted. Direct cholangiography clearly delineates biliary anatomy, an essential factor in planning surgical, radiologic, or endoscopic therapy. With the large variety of endoscopic and radiologic therapeutic interventions now available, direct cholangiography often serves as a prelude to nonsurgical biliary interventional procedures^{7,15,128-132} (see Chapters 74 and 78). Direct cholangiography by PTC or ERCP for purely diagnostic purposes is rarely done, having been replaced in current clinical practice by noninvasive imaging, particularly MRCP.

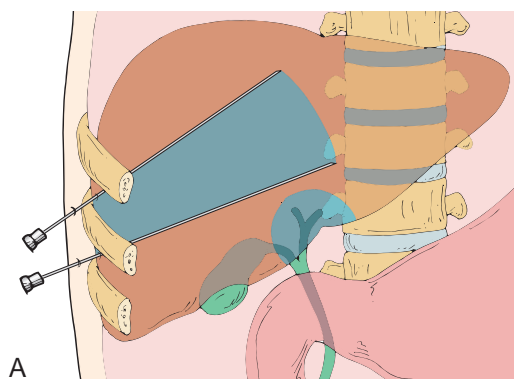
Percutaneous Transhepatic Cholangiography Versus Endoscopic Retrograde Cholangiopancreatography

The choice of procedure for direct cholangiography depends on a number of factors: the clinical situation, the potential for therapeutic intervention, and the availability of a skilled endoscopist or radiologist.

Although there are many similarities in the information provided by antegrade (PTC) and retrograde (ERCP) cholangiography, the advantages and disadvantages of each procedure must be carefully weighed before a decision is made. Both methods provide high-quality images of the ducts and are capable of evaluating intrahepatic and extrahepatic stenoses, ductal dilation, filling defects, and leaks. Both procedures allow transformation of a diagnostic study to a variety of therapeutic maneuvers.

PTC is easier and quicker to perform and is less costly. It has a high success rate; dilated ducts are opacified in virtually 100% and nondilated ducts in 80% to 85% of patients^{129,131} (Fig. 73-17). The complication rate is low (3.4%), and the procedure is performed by the radiologist.^{133,134} Therapeutic transhepatic options after PTC require a higher skill level. These include biliary drainage; stone extraction, crushing, contact dissolution, laser fragmentation, and contact lithotripsy; stent placement; stricture dilation; and biopsy. ERCP is more time-consuming, more expensive, and more dependent on the skill of the endoscopist. The success rate for cannulation of the bile duct varies from 80% to 95%, depending on the experience of the endoscopist.^{14,132,135-139} ERCP offers the advantages of direct pancreatic duct visualization and inspection of the upper gastrointestinal tract and ampulla. The complication rate is comparable to that of PTC (3%-5%).¹⁴⁰⁻¹⁴³ Therapeutic options at ERCP include sphincterotomy for stone extraction or ampullary stenosis, biliary stent placement, and balloon dilation of strictures.^{132,144,145} The procedure is performed by the endoscopist using fluoroscopic monitoring and usually in conjunction with the radiologist.

ERCP is preferred for evaluation of patients with nondilated ducts or more distal lesions. It is the procedure of choice if a primary pancreatic process is suspected and opacification of the pancreatic duct is desired (Fig. 73-18). ERCP is also recommended for patients with bleeding disorders, for whom PTC may be risky. PTC is generally preferred in the evaluation of more proximal lesions involving the hepatic duct bifurcation, which may be difficult or impossible to delineate with a retrograde approach. PTC is recommended when endoscopy is not available or previous biliary enteric surgery has been performed. PTC is also used if ERCP fails, and vice versa.

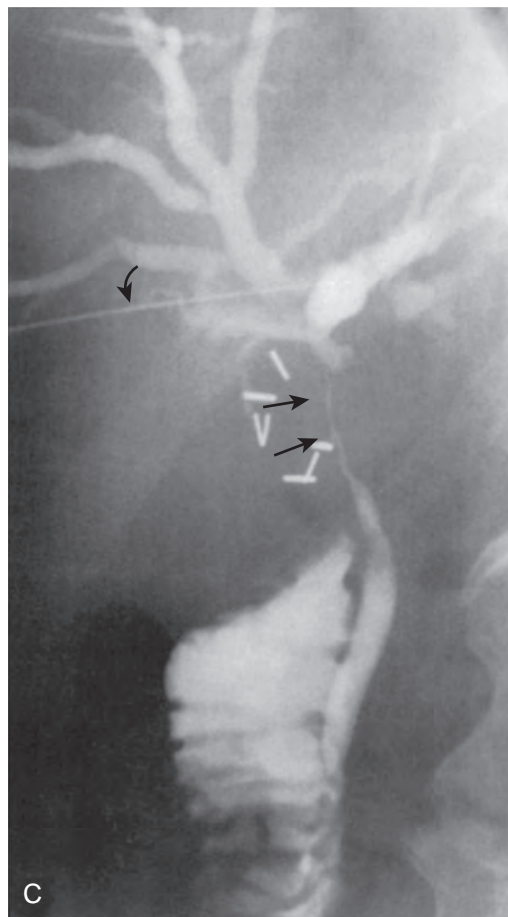


A

Figure 73-17 PTC. **A.** Diagram depicts the PTC technique. Shaded area between the needles is the preferred region for needle insertion. The circular shaded area should be avoided. **B.** PTC outlines the normal biliary ductal system. Note the needle (arrow) with the tip cannulating the small peripheral intrahepatic biliary radicle. **C.** PTC with the needle (curved arrow) in place shows the obstructive lesion (straight arrows) of the common hepatic duct and dilated intrahepatic ducts from metastatic periportal adenopathy. (A from Kadir S: *Diagnostic Angiography*. Philadelphia, WB Saunders, 1986.)



B



C

The choice of diagnostic PTC or ERCP also depends on the therapeutic plan for the patient. If a CBD stone is suspected, ERCP should be used to perform a sphincterotomy and endoscopic stone extraction (see Chapters 74 and 78). If imaging studies indicate a lesion at the hepatic duct bifurcation, PTC is more likely to outline the extent of involvement, to show the presence of segmental occlusions, and to define drainage options.

Percutaneous Transhepatic Cholangiography

PTC is a widely used, successful, and safe method of directly opacifying the biliary ductal system. Its relative ease and safety are related to the use of a fine, 22-gauge, highly flexible Chiba or “skinny” needle, introduced by Okuda and associates in

1974.¹⁴⁶ The small caliber and flexibility of the needle decrease the likelihood of hepatic injury during respiratory motion and decrease procedure-related complications. The success of ductal opacification with PTC is virtually 100% for dilated ducts and 80% to 85% for nondilated ducts.^{15,130,132} The success rate is improved with an increased number of needle passes. Failure of the ducts to opacify during PTC should not be misinterpreted as absence of obstruction or dilated ducts; rather, it may indicate an inconclusive study.

The overall complication rate for PTC is 3.5%.^{15,134,135} The most common serious complications include sepsis (1.4%), bile leak (1.45%), and intraperitoneal hemorrhage (0.35%). Rare complications include pneumothorax, hepatic arteriovenous fistula, reactions to contrast material, and death (0.2%).^{15,132-135}

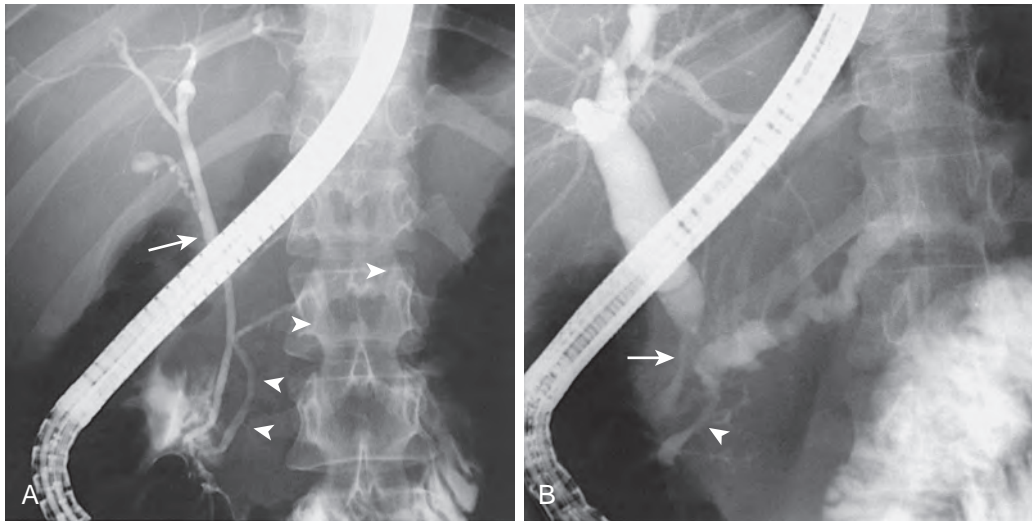


Figure 73-18 ERCP. **A.** Filling of a normal nondilated bile duct (arrow) and normal pancreatic duct (arrowheads). **B.** The bile duct and pancreatic duct are dilated as a result of a distal common bile duct stricture (arrow) and pancreatic duct stricture (arrowhead) in a patient with chronic pancreatitis.

There are no absolute contraindications to PTC except uncorrectable bleeding disorders. Ascites makes the procedure more difficult but is not an absolute contraindication.

Technique. Before the procedure, clotting studies are obtained, and any disorder should be corrected with fresh frozen plasma and platelets. Mild analgesia is provided. The patient should be well hydrated. Broad-spectrum antibiotics are routinely used; the data suggest that 80% of patients with biliary obstruction by CBD stones and 25% to 30% of patients with malignant obstruction may have infected bile, and sepsis is a potential risk.^{15,129,132} Positive organisms are usually *Escherichia coli* and *Klebsiella pneumoniae*. The procedure is performed under fluoroscopic guidance. A percutaneous transhepatic puncture is made with the skinny needle by a right midaxillary approach (see Fig. 73-17A). Alternatively, a left-sided subxiphoid approach can be used if cannulation of the left hepatic duct is desired. The needle is inserted into the liver during suspended respiration, and contrast material is injected as the needle is slowly withdrawn until a duct is opacified. More than one puncture may be necessary, and there is no limit to the number of passes as long as the patient tolerates the procedure.

After cannulation of an intrahepatic biliary radicle, contrast material is injected, outlining the biliary ductal system (see Fig. 73-17B). Images of the opacified biliary tree are obtained in the supine, both oblique, and, if necessary, upright projections. In the presence of obstruction, it may be necessary to tilt the table upright or to turn the patient to the left lateral decubitus position to allow contrast medium to fill the left hepatic ducts or to flow to the site of a distal obstruction. Overdistention of the ductal system can cause sepsis and should be avoided. Contrast material is heavier than bile and may not mix readily with viscid bile in an obstructed system. In the supine patient, the posteriorly positioned right hepatic ducts are dependent and tend to fill preferentially, and the left ductal system may fail to opacify. Turning the patient to the left posterior oblique or left lateral decubitus position facilitates filling of the left duct. Failure of the right hepatic ducts to fill in the supine position is abnormal

and suggests a lesion obstructing the right hepatic duct. Erect or partially upright views may be necessary for adequate filling of the CHD and distal CBD. Coned-down views of the ampulla region may be helpful in clarifying the cause of obstruction in this area. In cases of hepatic bifurcation obstruction or segmental occlusions, multiple passes may be necessary to map the extent of involvement and to determine operability and surgical approach to the lesion.

Transcholecystic Cholangiography

If the percutaneous transhepatic route is unsuccessful, transcholecystic cholangiography can be used to opacify the biliary tree when the gallbladder is present. The technique is simple and involves puncture of the gallbladder aided by ultrasonic guidance to place the needle directly into the gallbladder. Contrast material is then injected into the gallbladder to fill the bile ducts. This technique more easily opacifies the distal bile duct but gives inconsistent intrahepatic ductal opacification^{132,147-149} (see Chapter 78).

Endoscopic Retrograde Cholangiopancreatography

Endoscopic cannulation of the papilla of Vater was first described in the United States by McCune and coworkers in 1968.^{13,133} Advances in technique and improvement in design of the side-viewing endoscope since that time have made ERCP a reliable and safe procedure for evaluation of both the pancreatic and the bile ducts. The primary indications for its use in the biliary tract are extrahepatic biliary obstruction, investigation of unexplained upper abdominal pain in patients with previous cholecystectomy, evaluation of cholangitis, suspected bile duct injury by previous surgery, and choledocholithiasis.^{14,136,138} The performance, interpretation, and complications of this procedure are discussed in Chapter 74.

Normal Cholangiographic Anatomy

The main intrahepatic ducts as well as the cystic duct, CHD, and CBD are routinely opacified. Normal intrahepatic ducts measure 1 to 2 mm in diameter; however, the size is

dependent on technical factors such as injection pressure, runoff into the gallbladder, and geometric magnification during filming. Second- and third-order branches are usually seen. The normal intrahepatic ducts branch regularly and smoothly. The extrahepatic bile duct is a smooth-walled, tubular structure extending from the porta hepatis to the duodenum. Distally, the intramural segment may be slightly narrowed and should not be confused with stricture. When it is partially relaxed, the choledochal sphincter (sphincter of Boyden) can create a wavy or narrowed appearance that may be mistaken for ampullary stenosis or neoplasm.³¹ When it is contracted, its upper rounded border produces a pseudocalculus defect, mimicking an impacted stone.^{150,151} This pseudocalculus defect disappears spontaneously after intravenous injection of glucagon, which relaxes the sphincter (Fig. 73-19). Contrast material should flow freely from the CBD into the duodenum during normal cholangiography. Normally, no splaying or crowding of ducts, caliber irregularity, strictures, or filling defects are seen.

The mean ductal diameter on direct cholangiography is less than 8 mm, with 10 mm considered the upper limit of normal. Magnification and injection pressure account for some of the discrepancy between cholangiographic and ultrasonic measurements. Studies have demonstrated a caliber increase of up to 5 to 6 mm simply as a result of the ERCP procedure.¹⁵² Often, the normal common duct is quite small (<4 mm). The prepancreatic portion of the CBD tends to be the widest segment.

Operative and Postoperative Cholangiography

Operative Cholangiography. Operative cholangiography was first described by Mirizzi in 1932,¹⁵³ and since that time, it has been an important adjunct to biliary tract surgery. The procedure is done at the time of cholecystectomy to detect biliary stones and to determine the need for CBD exploration, a maneuver that substantially increases the time, morbidity, and mortality of gallbladder surgery.

Technique. The bile duct is opacified during operative cholangiography by insertion of a needle or cannula directly into the cystic duct or CBD and injection of contrast material. This technique can be used with open cholecystectomy or with laparoscopic cholecystectomy. However, the rate of successful cannulation and opacification of the ducts is lower with the laparoscopic approach. Common duct exploration is difficult by the laparoscopic approach and is rarely performed laparoscopically. During operative cholangiography, a small volume of contrast material (5-7 mL) is injected initially, followed by the first radiograph. A second radiograph is taken after an additional 5 to 7 mL of contrast material is injected. Because air bubbles can simulate stones, the injection system should be cleared of air. Most operative cholangiography is performed with digital fluoroscopy. A portable radiographic unit with either a fixed or a movable table grid may also be used. The patient should be rotated slightly to the right to project the duct away from the spine. If common duct exploration is necessary, a T tube (usually 12F to 16F) is placed

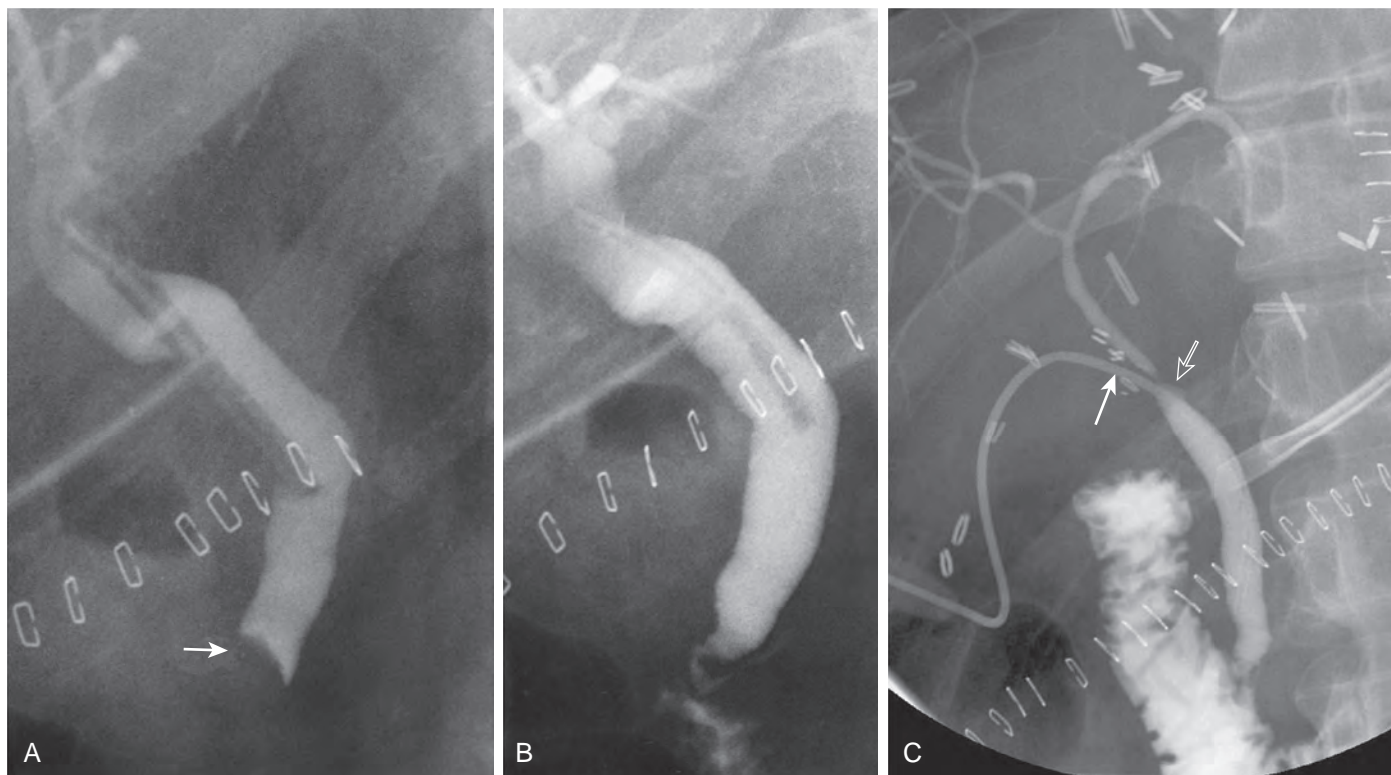


Figure 73-19 Postoperative cholangiogram. A. T-tube cholangiogram demonstrates pseudocalculus defect. Note meniscoid configuration (arrow) of the distal common bile duct from the contracted choledochal sphincter mimicking an impacted stone. **B.** Spot image taken during the same examination after intravenous administration of glucagon shows disappearance of the pseudocalculus defect after relaxation of the choledochal sphincter. **C.** Biliary tube cholangiogram after liver transplantation with duct-to-duct anastomosis demonstrates straight, small-caliber tube entering the cystic duct remnant of the donor duct (arrow). Injected contrast material outlines the ductal system, demonstrating mild narrowing at the duct-to-duct anastomosis (open arrow).

after the procedure and a completion cholangiogram is obtained before closing. The cholangiogram should be free of motion, grid lines, and superimposed tubes or instruments. Adequate exposure factors and proper collimation should be used.^{154,155} The study is considered suboptimal unless complete filling of the intrahepatic and extrahepatic ducts is accomplished (Fig. 73-20). Spasm of the sphincter occurs in as many as 25% of cases after CBD exploration.¹⁵⁶ This may be related to rapid or forceful contrast medium injection or surgical manipulation. Anesthetic agents, such as morphine sulfate and fentanyl citrate, are known to produce spasm.¹⁵⁷ If spasm is present, glucagon should be administered intravenously to relax the sphincter.¹⁵⁸

Postoperative Cholangiography. After common duct exploration for stone disease or after liver transplantation with biliary ductal anastomosis, a surgically placed biliary catheter or T tube is usually left in the extrahepatic bile duct to allow ductal decompression and to provide access for postoperative cholangiography. Postoperative cholangiograms are obtained through the indwelling biliary tube. In the case of stone disease, a T tube is usually left in place and the study is performed 5 to 10 days after surgery to check for retained stones or fragments. If none are identified, the T tube is removed. If stones are present, they may be removed endoscopically or radiologically after maturation of the T-tube track (see Chapter 78). In the case of liver transplantation, a small-caliber biliary tube is left in place for a longer time, usually 2 to 6 months, and cholangiography may be performed at any time to assess the status of the bile ducts and the anastomosis.

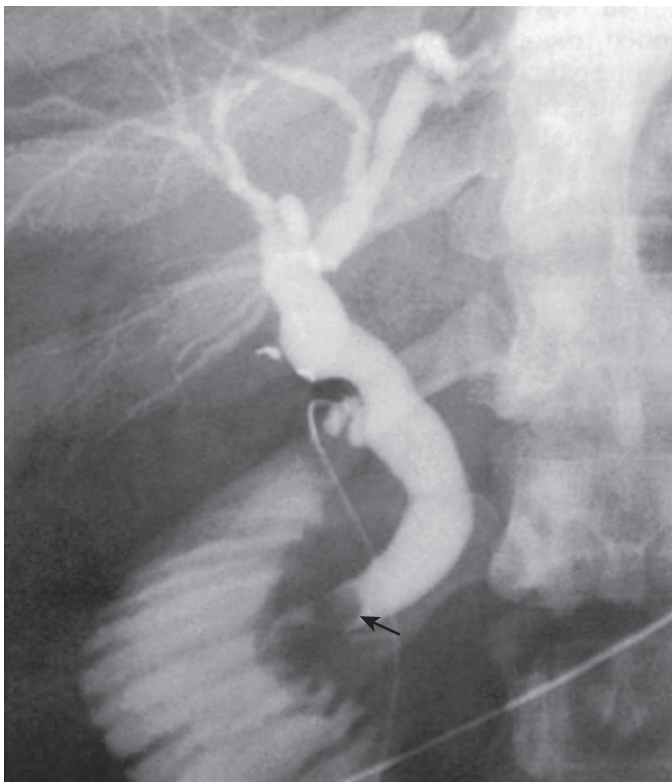


Figure 73-20 Operative cholangiogram. Note the cannula in the cystic duct remnant with filling of the bile duct. There is a retained distal common bile duct stone (arrow).

Contrast medium is administered by hand injection or by gravity drip infusion under fluoroscopic monitoring. Because of the risk of bacteremia, some authors recommend coverage with antibiotics.^{11,154,155} Antibiotics are routinely administered before postoperative cholangiography in patients after liver transplantation. During cholangiography, both the intrahepatic and extrahepatic ducts should be opacified. Use of the upright or tilted position may be necessary to fill the distal CBD. Also, bubbles rise in the upright position, whereas stones gravitate into the distal duct. The Trendelenburg position facilitates intrahepatic ductal filling, and placement of the patient in the left posterior oblique or left lateral decubitus position helps opacify the left ducts. Oblique views minimize superimposition of intrahepatic branches. The optimal study is free of air bubbles, with adequate filling of the intrahepatic and extrahepatic biliary tree. Air bubbles may mimic stones but are usually differentiated by a smooth, round appearance and a tendency to cluster. Sphincter of Oddi spasm is relieved by increased injection pressure or the use of glucagon^{154,155} (see Fig. 73-19).

The accepted radiographic technique for this examination includes low kilovolts peak (70-75 kVp) exposures and dilute contrast material (10%-15% iodine). This technique frequently necessitates a long exposure time (2-4 seconds) to ensure good radiographic quality. The use of high kilovolts peak (100-110 kVp) exposures and full-strength contrast material (30%-38% iodine) has been advocated to improve overall film quality with less motion, to enhance stone detectability, and to decrease radiation to the patient and personnel.¹⁵⁹

BILIARY SCINTIGRAPHY

Although it is used primarily to diagnose acute cholecystitis, biliary scintigraphy has several applications in the evaluation of biliary ductal disease. It is a noninvasive method of evaluating biliary drainage and segmental obstruction and can assess patency or bile leak after cholecystectomy or biliary enteric anastomoses^{8,59,61} (Fig. 73-21). Biliary

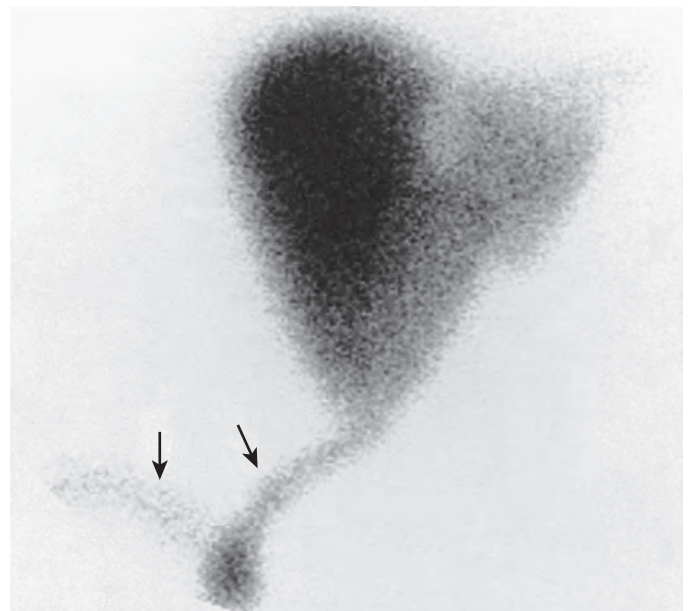


Figure 73-21 Biliary scintigraphy. This study demonstrates bile leak along the right upper quadrant drain (arrows) from a choledochojejunal anastomosis.

scintigraphy may also play a role in evaluating early biliary obstruction when ultrasound results are indeterminate and do not correspond to clinical or laboratory parameters.¹⁶⁰⁻¹⁶² Other uses for scintigraphic evaluation of the biliary tract

include noninvasive evaluation of sphincter of Oddi dysfunction, assessment of bile duct injury and duodenogastric reflux, and evaluation for congenital biliary anomalies.^{59,163,164}

REFERENCES

- Watanabe Y, Nagayama M, Okumura A, et al: MR imaging of acute biliary disorders. *Radiographics* 27:477-495, 2007.
- Shin SM, Kim S, Lee JW, et al: Biliary abnormalities associated with portal biliopathy: Evaluation on MR cholangiography. *AJR Am J Roentgenol* 188:W341-W347, 2007.
- Friedman AC, Dachman AH, editors: *Radiology of the Liver, Biliary Tract, and Pancreas*. St. Louis, 1994, CV Mosby.
- Inoue T, Kitano M, Kudo M, et al: Diagnosis of gallbladder diseases by contrast-enhanced phase-inversion harmonic ultrasonography. *Ultrasound Med Biol* 33:353-361, 2007.
- Laing FC: The gallbladder and bile ducts. In Rumack CM, Wilson SR, Charboneau JW, editors: *Diagnostic Ultrasound*, ed 2, St. Louis, 1998, CV Mosby, pp 175-224.
- Mittelstaedt CA: Ultrasound of the bile ducts. *Semin Roentgenol* 32:161-171, 1997.
- Yu J, Turner MA, Fulcher AS, et al: Congenital anomalies and normal variants of the pancreaticobiliary tract and the pancreas in adults: Part 1: Biliary tract. *AJR Am J Roentgenol* 187:1536-1543, 2006.
- Rubens DJ: Hepatobiliary imaging and its pitfalls. *Radiol Clin North Am* 24:257-278, 2004.
- Burrell MI, Zeman RK, Simeone JE, et al: The biliary tract: Imaging for the 1990s. *AJR Am J Roentgenol* 157:223-233, 1991.
- Cooperberg PL, Gibney RG: Imaging of the gallbladder. *Radiology* 163:605-613, 1987.
- Wyatt SH, Fishman EK: Biliary tract obstruction: The role of spiral CT in detection and definition of disease. *Clin Imaging* 21:27-34, 1997.
- Yeh B, Lui PS, Soto JA, et al: MR imaging and CT of the biliary tract. *Radiographics* 29:1669-1688, 2009.
- Jacobson IM, editor: *ERCP and Its Applications*. Philadelphia, 1997, Lippincott-Raven.
- Silvis SE, Rohrmann CA, Jr, Ansel HJ, editors: *Text and Atlas of Endoscopic Retrograde Cholangiopancreatography*. New York, 1995, Igaku-Shoin.
- Yedlicka JW, Tadararthy SM, Letourneau JG, et al: Interventional techniques in the hepatobiliary system. In Castaneda-Zuniga WR, editor: *Interventional Radiology*, ed 3, Baltimore, 1997, Williams & Wilkins, pp 1439-1573.
- Reinhold C, Bret PM: Current status of MR cholangiopancreatography. *AJR Am J Roentgenol* 166:1285-1295, 1996.
- Barish MA, Soto JA: MR cholangiopancreatography: Techniques and clinical applications. *AJR Am J Roentgenol* 169:1295-1303, 1997.
- Friedman AC, Sachs L: Embryology, anatomy, histology and radiologic anatomy. In Friedman AC, editor: *Radiology of the Liver, Biliary Tract, Pancreas and Spleen*, Baltimore, 1987, Williams & Wilkins, pp 305-332.
- Netter FH: *The Ciba Collection of Medical Illustrations*, Volume III, Digestive System, Part III, Liver, Biliary Tract and Pancreas, Summit, NJ, 1957, Ciba Pharmaceutical Products, pp 22-24.
- Schulte SJ: Anatomy and anomalies of the biliary tract. In *Radiology of the Liver, Biliary Tract, and Pancreas. Categorical Course Syllabus*. American Roentgen Ray Society 96th Annual Meeting, 1996, pp 107-117.
- Balfe DM, Molmenti EP, Bennett HF: Normal abdominal and pelvic anatomy. In Lee JKT, Sagel SS, Stanley RJ, et al, editors: *Computed Body Tomography with MRI Correlation*, ed 3, Philadelphia, 1998, Lippincott-Raven, pp 573-635.
- Schulte SJ: Embryologic and congenital anomalies of the biliary and pancreatic ducts. In Silvis SE, Rohrmann CA, Ansel HJ, editors: *Technique and Interpretation of Endoscopic Retrograde Cholangiopancreatography with Endoscopic Intervention*. New York, 1995, Igaku-Shoin, pp 114-115.
- Turner MA, Fulcher AS: The cystic duct: Normal anatomy and disease processes. *Radiographics* 21:3-22, 2001.
- Linder HH, Green RB: Embryology and surgical anatomy of the extrahepatic biliary tree. *Surg Clin North Am* 44:1273-1285, 1964.
- Hatfield PM, Wise RE: Anatomy variation in the gallbladder and the bile ducts. *Semin Roentgenol* 11:157-164, 1976.
- Healey JE, Jr, Schnoy PC: Anatomy of the biliary ducts within the liver: Analysis of prevailing patterns of branchings and the major variations of the biliary ducts. *Arch Surg* 66:599-616, 1953.
- Schein CJ, Stern WZ, Jacobsen HG: The hepatic ductal system: A correlation of endoscopic and roentgenographic findings. *Surgery* 51:718-723, 1962.
- Silvis SE: The normal bile duct. In Silvis SE, Rohrmann CA, Jr, Ansel HJ, editors: *Text and Atlas of Endoscopic Retrograde Cholangiopancreatography*. New York, 1995, Igaku-Shoin, pp 168-192.
- Bret PM, de Stempel JV, Atri M, et al: Intrahepatic bile duct and portal vein anatomy revisited. *Radiology* 169:405-407, 1988.
- Sterling JA: The common channel for bile and pancreatic ducts. *Surg Gynecol Obstet* 98:420-424, 1954.
- Boyden EA: The anatomy of the choledochoduodenal junction. *Surg Gynecol Obstet* 104:641-652, 1957.
- Hand BH: An anatomical study of the choledochoduodenal junction. *Br J Surg* 50:486-494, 1963.
- Wu CC, Ho VH, Chen CY: Effect of aging on common bile duct diameter: A real-time ultrasonographic study. *J Clin Ultrasound* 12:473-478, 1984.
- Horrow MM, Horrow JC, Niekosari A, et al: Is age associated with size of adult extrahepatic bile duct? Sonographic study. *Radiology* 221:411-414, 2001.
- Kaim A, Steinke K, Frank M, et al: Diameter of the common bile duct in the elderly patient: Measurement by ultrasound. *Eur J Radiol* 8:1413-1415, 1983.
- Kaude JV: The width of the common bile duct in relation to age and stone disease: An ultrasonographic study. *Eur J Radiol* 3:115-117, 1983.
- Puente SG, Bannuraga C: Radiological anatomy of the biliary tract: Variations and congenital abnormalities. *World J Surg* 7:261-266, 1983.
- Berk RN: The plain abdominal radiograph. In Berk RN, Ferrucci JT, Jr, Leopold GR, editors: *Radiology of the Gallbladder and Bile Ducts: Diagnosis and Intervention*. Philadelphia, 1983, WB Saunders, pp 1-29.
- Meyers MA, O'Donahue N: The Mercedes-Benz sign: Insight into the dynamics of formation and disappearance of gallstones. *AJR Am J Roentgenol* 119:63-70, 1973.
- Cooperberg PL: Sonography of the gallbladder and biliary tract. In *Radiology of the Liver, Biliary Tract, and Pancreas. Categorical Course Syllabus*. American Roentgen Ray Society 96th Annual Meeting, 1996, pp 95-105.
- Zeman RK: Cholelithiasis and cholecystitis. In Gore RM, Levine MS, editors: *Textbook of Gastrointestinal Radiology*, ed 2, Philadelphia, 2000, WB Saunders, pp 1321-1345.
- Gore RM, Vaghmai V, Newmark G, et al: Imaging benign and malignant disease of the gallbladder. *Radiol Clin North Am* 40:1307-1328, 2002.
- Bortoff GA, Chen MY, Ott DJ, et al: Gallbladder stones: Imaging and intervention. *Radiographics* 20:751-766, 2000.
- Rosenthal SJ, Cox GG, Wetzel LH, et al: Pitfalls and differential diagnosis in biliary sonography. *Radiographics* 10:285-311, 1990.
- Rall PW, Colletti PM, Lapin SA, et al: Real-time sonography in suspected acute cholecystitis. *Radiology* 155:767-771, 1985.
- Colhoun EN, Fitzgerald EJ, McKnight L: The importance of appropriate frequency selection in sonographic gallstone detection. *Br J Radiol* 60:645-648, 1987.
- Lee FJ, Delone DR, Bean DW: Acute cholecystitis in an animal model: Findings on color Doppler sonography. *AJR Am J Roentgenol* 165:85-90, 1995.
- Jeffrey RB, Nino MM, Ralls PW, et al: Color Doppler sonography of the cystic artery: Comparison of normal controls and patients with acute cholecystitis. *J Ultrasound Med* 14:33-36, 1995.
- Wilbur AC, Sagireddy PB, Aizenstein RI: Carcinoma of the gallbladder: Color Doppler US and CT findings. *Abdom Imaging* 22:187-190, 1997.
- Callen PW, Filly RA: Ultrasonic localization of the gallbladder. *Radiology* 133:687-691, 1979.
- Hammond DI: Unusual causes of sonographic nonvisualization of the gallbladder: A review. *J Clin Ultrasound* 16:77-85, 1988.

52. Barakos JA, Ralls PW, Lapin SA, et al: Cholelithiasis: Evaluation with CT. *Radiology* 162:415–418, 1987.
53. Van Beers BE, Pringot JH: Imaging of cholelithiasis: Helical CT. *Abdom Imaging* 26:15–20, 2001.
54. Baron RL: Diagnosing choledocholithiasis: How far can we push helical CT? *Radiology* 203:601–603, 1997.
55. Neitlich JD, Topazian M, Smith RC, et al: Detection of choledocholithiasis: Comparison of unenhanced helical CT and endoscopic retrograde cholangiopancreatography. *Radiology* 203:753–757, 1997.
56. Gale ME, Robbins AH: CT of the gallbladder: Unusual diseases. *J Comput Assist Tomogr* 9:439–443, 1985.
57. Brink JA, Semin MD: Biliary stone disease. In Gazelle GS, Saini S, Mueller PR, editors: *Hepatobiliary and Pancreatic Radiology: Imaging and Intervention*, New York, 1998, Thieme, pp 590–629.
58. Barr RG, Taka K, Grajo JR: Comparison of sonography and scintigraphy in the evaluation of gallbladder functional studies with cholecystokinins. *J Ultrasound Med* 28:1143–1147, 2009.
59. Thrall JH, Zeisman HA: Hepatobiliary system. In Gay S, editor: *Nuclear Medicine*, St. Louis, 1995, Mosby-Year Book, pp 199–204.
60. Rosenthal L: Nuclear medicine. In Margulis AR, Burhenne HJ, editors: *Alimentary Tract Radiology*, St. Louis, 1989, CV Mosby, pp 1341–1365.
61. Kim EE, Moon TY, Delpassand ES, et al: Nuclear hepatobiliary imaging. *Radiol Clin North Am* 31:923–933, 1993.
62. Reinhold C, Bret PM, Guiband L, et al: MR cholangiopancreatography: Potential clinical application. *Radiographics* 16:309–320, 1996.
63. Reinhold C, Bret C: MR cholangiopancreatography. *Abdom Imaging* 21:105–116, 1996.
64. Catalano OA, Sahani DV, Kalva SP, et al: MR imaging of the gallbladder: A pictorial essay. *Radiographics* 28:135–155, 2008.
65. Barish MA, Yucel EK, Soto JA, et al: MR cholangiopancreatography: Efficacy of three-dimensional turbo spin-echo technique. *AJR Am J Roentgenol* 165:295–300, 1995.
66. Fulcher AS, Turner MA, Capps GW, et al: Half-Fourier RARE MR cholangiopancreatography: Experience in 300 subjects. *Radiology* 207:21–32, 1998.
67. Glockner JF: Hepatobiliary MRI: Current concepts and controversies. *J Magn Reson Imaging* 25:681–695, 2007.
68. Moon KL, Hricak H, Margulis AR, et al: Nuclear magnetic resonance imaging characteristics of gallstones in vitro. *Radiology* 148:753–756, 1983.
69. Sagoh T, Itoh K, Togashi K, et al: Gallbladder carcinoma: Evaluation with MR imaging. *Radiology* 174:131–136, 1990.
70. Rossman MD, Friedman AC, Radecki PD, et al: MR imaging of gallbladder carcinoma. *AJR Am J Roentgenol* 148:143–145, 1987.
71. Fulcher AS, Turner MA: MR cholangiopancreatography. *Radiol Clin North Am* 40:1363–1370, 2002.
72. Wachsberg RH, Kim KH, Sundaram W: Sonographic versus endoscopic retrograde cholangiographic measurements of the bile duct revisited: Importance of the transverse diameter. *AJR Am J Roentgenol* 170:669–674, 1998.
73. Baron RL, Tublin ME, Peterson MS: Imaging the spectrum of biliary tract disease. *Radiol Clin North Am* 40:1325–1354, 2002.
74. Behan M, Kazam E: Sonography of the common bile duct: Value of the right anterior oblique view. *AJR Am J Roentgenol* 130:701–709, 1978.
75. Berland LL, Lawson TL, Foley WP: Porta hepatis: Sonographic discrimination of bile ducts from arteries with pulsed Doppler with new anatomic criteria. *AJR Am J Roentgenol* 138:833–840, 1982.
76. Laing FC, Jeffrey RB, Wing VW: Improved visualization of choledocholithiasis by sonography. *AJR Am J Roentgenol* 143:949–952, 1984.
77. Laing FC, Jeffrey RB, Wing VW, et al: Biliary dilatation: Defining the level and cause by real-time US. *Radiology* 160:39–42, 1986.
78. Niederau C, Muller J, Sonnenberg A, et al: Extrahepatic bile ducts in healthy subjects, in patients with cholelithiasis and post-cholecystectomy patients: A prospective ultrasonic study. *J Clin Ultrasound* 11:23–27, 1983.
79. Majed AW, Ross B, Johnson AG: The preoperatively normal bile duct does not dilate after cholecystectomy: Results of a five year study. *Gut* 45:741–743, 1999.
80. Reinus WR, Shady K, Lind M, et al: Ultrasound evaluation of the common duct in symptomatic and asymptomatic patients. *Am J Gastroenterol* 87:489–492, 1992.
81. Sauerbrei E, Cooperberg P, Gordon P, et al: The discrepancy between radiographic and sonographic bile duct measurements. *Radiology* 137:751, 1980.
82. Davies RP, Downey PR, Moore WR, et al: Contrast cholangiography versus ultrasonographic measurement of the “extrahepatic” bile duct: A two-fold discrepancy revisited. *J Ultrasound Med* 10:653–657, 1991.
83. Cooperberg P, Li D, Wong P, et al: Accuracy of common hepatic duct size in the evaluation of extrahepatic biliary obstruction. *Radiology* 135:141, 1980.
84. Muhletaler CA, Gerlock AJ, Jr, Fleischer AC, et al: Diagnosis of obstructive jaundice with non-dilated bile ducts. *AJR Am J Roentgenol* 134:1149–1152, 1980.
85. Beinart C, Efremidis S, Cohen B, et al: Obstruction without dilatation. *JAMA* 245:353–356, 1981.
86. Weinstein BJ, Weinstein DP: Biliary tract dilatation in the non-jaundiced patient. *AJR Am J Roentgenol* 134:899–901, 1980.
87. Zeman RK, Taylor KJW, Burrell MI, et al: Ultrasound demonstration of anicteric dilatation of the biliary tree. *Radiology* 134:689, 1980.
88. Graham MF, Cooperberg PL, Cohen MM, et al: The size of the normal common hepatic duct following cholecystectomy: An ultrasonographic study. *Radiology* 135:137–139, 1980.
89. Feng B, Song Q: Does the common bile duct dilate after cholecystectomy? Sonographic evaluation in 234 patients. *AJR Am J Roentgenol* 165:859–861, 1995.
90. Simeone JF, Butch RJ, Mueller PR, et al: The bile ducts after a fatty meal: Further sonographic observations. *Radiology* 154:763–768, 1985.
91. Wilson SA, Gosink BB, van Sonnenberg E: Unchanged size of dilated common duct after fatty meal: Results and significance. *Radiology* 160:29–31, 1986.
92. Darweesh RMA, Dodds WJ, Hogan WJ: Fatty meal sonography for evaluating patients with suspected partial common duct obstruction. *AJR Am J Roentgenol* 151:63–68, 1988.
93. Zeman RK, Silverman PM, Ascher SM, et al: Helical (spiral) CT of the pancreas and biliary tract. *Radiol Clin North Am* 33:887–890, 1995.
94. Baron RL: Computed tomography of the bile ducts. *Semin Roentgenol* 32:172–187, 1997.
95. Anderson SW, Lucey BC, Varghese JC, Soto JA: Accuracy of MDCT in the diagnosis of choledocholithiasis. *AJR Am J Roentgenol* 187:174–180, 2006.
96. Pedrosa CS, Casanova R, Rodriguez R, et al: Computed tomography in obstructive jaundice. Part I. The level of obstruction. *Radiology* 139:627–634, 1981.
97. Pedrosa CS, Casanova R, Lezana AH, et al: Computed tomography in obstructive jaundice. Part II. The cause of obstruction. *Radiology* 139:635–645, 1981.
98. Gibson RN, Young E, Thompson JN, et al: Bile duct obstruction: Radiologic evaluation of level, cause and tumor resectability. *Radiology* 160:43–47, 1986.
99. Zeman RK, Berman PM, Silverman PM, et al: Biliary tract: Three-dimensional helical CT without cholangiographic contrast material. *Radiology* 196:865–867, 1995.
100. Fleishmann D, Ringle H, Schoff R, et al: Three-dimensional spiral CT cholangiography in patients with suspected obstructive biliary disease: Comparison with endoscopic retrograde cholangiography. *Radiology* 198:861–868, 1996.
101. Baron RL: Common bile duct stones: Re-assessment of criteria for CT diagnosis. *Radiology* 162:419–424, 1987.
102. Stockberger SM, Sherman S, Kopecky KK: Helical CT cholangiography. *Abdom Imaging* 21:98–104, 1996.
103. Keogan MR, Seabourn JT, Paulson EK, et al: Contrast-enhanced CT of intrahepatic and hilar cholangiocarcinoma: Delay time for optimal imaging. *AJR Am J Roentgenol* 169:1493–1499, 1997.
104. Anderson SW, Rho E, Soto JA: Detection of biliary ductal narrowing and choledocholithiasis: Accuracy of portal venous phase multidetector CT. *Radiology* 247:418–421, 2008.
105. Liddell RM, Baron RL, Ekston JE, et al: Normal intrahepatic bile ducts: CT depiction. *Radiology* 176:633–635, 1990.
106. Weinstein JB, Heiken JP, Lee JKT, et al: High resolution CT of the porta hepatis and hepatoduodenal ligament. *Radiographics* 6:55–74, 1986.
107. Foley WD, Wilson CR, Quiroz FA: Demonstration of the normal extrahepatic biliary tree with computed tomography. *J Comput Assist Tomogr* 4:48–52, 1980.
108. Shulte SJ, Baron RL, Teefey SA, et al: CT of the extrahepatic bile ducts: Wall thickness and contrast enhancement in normal and abnormal ducts. *AJR Am J Roentgenol* 154:79–85, 1990.
109. Kim HJ, Park DI, Park JH, et al: Multidetector computed tomography cholangiography with multiplanar reformation for the assessment of patients with biliary obstruction. *J Gastroenterol Hepatol* 22:400–405, 2007.
110. Van Beers BE, Lacrosse M, Trigaux JP, et al: Noninvasive imaging of the biliary tree before or after laparoscopic cholecystectomy: Use of three-dimensional spiral CT cholangiography. *AJR Am J Roentgenol* 162:1331–1335, 1994.

111. Yeh BM, Breiman RS, Taouli B, et al: Biliary tract depiction in living potential liver donors: Comparison of conventional MR, mangafodipir trisodium-enhanced excretory MR, and multi-detector row CT cholangiography—initial experience. *Radiology* 230:645–651, 2004.
112. Wang ZJ, Yeh BM, Roberts JP, et al: Living donor candidates for right hepatic lobe transplantation: Evaluation at CT cholangiography—initial experience. *Radiology* 235:899–904, 2005.
113. Dinkel HP, Moll R, Gassel HJ, et al: Helical CT cholangiography for the detection and localization of bile duct leakage. *AJR Am J Roentgenol* 173:613–617, 1999.
114. Cabada Giasas T, Sarria O, Martinez-Berganza A: Helical CT cholangiography in the evaluation of the biliary tree: Application to the diagnosis of choledocholithiasis. *Abdom Imaging* 27:61–70, 2002.
115. Caoli EM, Paulson EK, Heyneman L, et al: Helical CT cholangiography with three-dimensional volume rendering using an oral biliary contrast agent: Feasibility of a novel technique. *AJR Am J Roentgenol* 174:487–492, 2000.
116. Soto JA, Barish MA, Yacel EK, et al: Pancreatic duct: MR cholangiopancreatography with a three-dimensional fast spin echo technique. *Radiology* 196:459–464, 1995.
117. Guibaud L, Bret PM, Reinhold C, et al: Bile duct obstruction and choledocholithiasis: Diagnosis with MR cholangiography. *Radiology* 197:109–115, 1995.
118. Miller JC, Harisinghani M, Richter JM, et al: Magnetic resonance cholangiopancreatography. *J Am Coll Radiol* 4:133–136, 2007.
119. Wielopolski PA, Gaa J, Wielopolski DR, et al: Breath-hold MR cholangiopancreatography with three-dimensional, segmented, echo-planar imaging and volume rendering. *Radiology* 210:247–252, 1999.
120. Taourel P, Bret PM, Reinhold C, et al: Anatomic variants of the biliary tree: Diagnosis with MR cholangiopancreatography. *Radiology* 199:521–527, 1996.
121. Fulcher AS, Turner MA, Capps GW: MR cholangiography: Technical advances and clinical applications. *Radiographics* 19:25–41, 1999.
122. Soto JA, Yucel EK, Barish MA, et al: MR cholangiopancreatography after unsuccessful or incomplete ERCP. *Radiology* 199:91–98, 1996.
123. Schmidt S, Chevallier P, Novellas S, et al: Choledocholithiasis: Repetitive thick-slab single-shot projection magnetic resonance cholangiopancreatography versus endoscopic ultrasonography. *Eur Radiol* 17:241–250, 2007.
124. Vitellas KM, Keogan MT, Spritzer CE, Nelson RC: MR cholangiopancreatography of bile and pancreatic duct abnormalities with emphasis on the single shot fast spin-echo technique. *Radiographics* 20:939–957, 2000.
125. Fulcher AS, Turner MA, Capps GW, et al: Half-Fourier RARE MR cholangiopancreatography: Experience in 300 subjects. *Radiology* 207:21–32, 1998.
126. Nandurkar KR, Hussain HK, Weadock WJ: Possible biliary disease: Diagnostic performance of high-spatial resolution isotropic 3D T-2 weighted MRCP. *Radiology* 249:883–890, 2008.
127. Sodickson A, Morteale KJ, Barish MA, et al: Three-dimensional fast-recovery fast spin-echo MRCP: Comparison with two-dimensional single-shot fast spin-echo techniques. *Radiology* 238:549–559, 2006.
128. Seale MK, Catalano OA, Saini S, et al: Hepatobiliary-specific MR contrast agents: Role in imaging the liver and biliary tree. *Radiographics* 29:1725–1748, 2009.
129. Matzen P, Hanberg A, Holst-Christensen J, et al: Accuracy of direct cholangiography by endoscopic or transhepatic route in jaundice: A prospective study. *Gastroenterology* 81:237–241, 1981.
130. Mueller PR, Harbin WP, Ferrucci JT, Jr, et al: Fine needle transhepatic cholangiography: Reflections after 450 cases. *AJR Am J Roentgenol* 136:85–90, 1981.
131. Tobin RS, Vogelzang RL, Gore RM, et al: A comparative study of computed tomography and ERCP in pancreaticobiliary disease. *J Comput Assist Tomogr* 11:1–3, 1987.
132. Wall SD, Yee J: Diagnostic ERCP and PTC. In Gazelle GS, Saini S, Mueller PR, editors: *Hepatobiliary and Pancreatic Radiology: Imaging and Intervention*, New York, 1998, Thieme, pp 154–170.
133. Ahmad NA, Shah JN, Kochman ML: Endoscopic ultrasonography and endoscopic retrograde cholangiopancreatography imaging for pancreaticobiliary pathology: The gastroenterologist's perspective. *Radiol Clin North Am* 40:1377–1395, 2002.
134. McNichols MMJ, Lee MJ, Dawson SL, et al: Complications of percutaneous biliary drainage and stricture dilatation. *Semin Interv Radiol* 11:242–253, 1994.
135. Harbin WP, Mueller PR, Ferrucci JT, Jr: Transhepatic cholangiography: Complications and use patterns of the fine needle technique. A multi-institutional survey. *Radiology* 135:15–22, 1980.
136. Shapiro RH: ERCP in the diagnosis of pancreatic and biliary disease. In Jacobson IM, editor: *ERCP: Diagnostic and Therapeutic Implications*, New York, 1989, Elsevier Science, pp 9–39.
137. Connors PJ, Carr-Locke DL: Biliary endoscopy. *Curr Opin Gastroenterol* 6:697–707, 1990.
138. Stewart ET: Radiographic technique for endoscopic retrograde cholangiopancreatography and endoscopic retrograde sphincterotomy. In Silvis SE, Rohrmann CA, Jr, Ansel HJ, editors: *Text and Atlas of Endoscopic Retrograde Cholangiopancreatography*, New York, 1995, Igaku-Shoin, pp 51–77.
139. Silvis SE, Meier PB: Technique for endoscopic retrograde cholangiopancreatography. In Silvis SE, Rohrmann CA, Jr, Ansel HJ, editors: *Text and Atlas of Endoscopic Retrograde Cholangiopancreatography*, New York, 1995, Igaku-Shoin, pp 22–35.
140. Cohen SA, Siegel JH, Kasmin FE: Complications of diagnostic and therapeutic ERCP. *Abdom Imaging* 21:385–394, 1996.
141. Rochester JS, Jaffe DL: Minimizing complications in endoscopic retrograde cholangiopancreatography and sphincterotomy. *Gastrointest Endosc Clin N Am* 17:105–127, 2007.
142. Vandervoort J, Soetikno RM, Tham TC, et al: Risk factors for complications after performance of ERCP. *Gastrointest Endosc* 56:652–656, 2002.
143. Anacker H, Weiss HD, Kramann B: Indications, contraindications and complications. In Anacker H, Weiss HD, Kramann B, editors: *Endoscopic Retrograde Pancreaticocholangiography*, New York, 1977, Springer-Verlag, pp 25–30.
144. Ott DJ, Gillian JH, Zagoria RJ, et al: Interventional endoscopy of the biliary and pancreatic ducts: Current indications and methods. *AJR Am J Roentgenol* 158:243–250, 1992.
145. Kozarek R: Biliary ERCP. *Endoscopy* 39:11–16, 2007.
146. Okuda K, Tanikawa K, Emura T, et al: Nonsurgical percutaneous transhepatic cholangiography: Diagnostic significance in medical problems of the liver. *Am J Dig Dis* 19:21–36, 1974.
147. Teplick SK, Haskin PH, Sammon JK, et al: Common bile duct obstruction. Assessment by transcholecystic cholangiography. *Radiology* 161:135–138, 1986.
148. Vogelzang RL, Nemcek AA, Jr: Percutaneous cholecystostomy: Diagnostic and therapeutic efficacy. *Radiology* 168:29–34, 1988.
149. van Sonnenberg E, Wittich GR, Casola G, et al: Diagnostic and therapeutic percutaneous gallbladder procedures. *Radiology* 160:23–26, 1986.
150. Beneventano TC, Schein CJ: The pseudocalculus sign in cholangiography. *Arch Surg* 98:731–733, 1969.
151. Mujahed Z, Evans JA: Pseudocalculous defect in cholangiography. *AJR Am J Roentgenol* 116:337–341, 1972.
152. Chang VH, Cunningham JJ, Frankes JJ: Sonographic measurement of the extrahepatic bile duct before and after retrograde cholangiography. *AJR Am J Roentgenol* 144:753–755, 1985.
153. Mirizzi PL: La cholangiografia durante las operaciones de las vias biliares. *Bol Soc Cir Buenos Aires* 16:1133–1136, 1932.
154. Thompson WM: The optimal radiographic technique for operative and T-tube cholangiography. *Crit Rev Diagn Imaging* 26:107–176, 1986.
155. Letourneau JG, Thompson WM: Intraoperative and postoperative cholangiography. *Semin Ultrasound CT MR* 8:126–133, 1987.
156. Chessick KC, Black S, Hoy SJ: Spasm and operative cholangiography. *Arch Surg* 110:53–57, 1975.
157. Chisholm RJ, Davis FM, Billings JD, et al: Narcotics and spasm of the sphincter of Oddi: A retrospective study of operative cholangiograms. *Anesth* 38:689–691, 1986.
158. Jones RM, Coultras JR, Pollard BJ, et al: Reversal of biliary sphincter spasm with low dose glucagon during operative cholangiography. *Anaesth Intensive Care* 11:175–177, 1983.
159. Thompson WM, Halvorsen RA, Gedgaudis RK, et al: High KVP vs low KVP for T-tube and operative cholangiography. *Radiology* 146: 635–642, 1983.
160. Kaplan L, Weismann HS, Rosenblatt R: The early diagnosis of common bile duct obstruction using cholescintigraphy. *JAMA* 254:2431–2434, 1985.
161. Zeman RK, Lee C, Jaffe MH, et al: Hepatobiliary scintigraphy and sonography in early biliary obstruction. *Radiology* 153:793–798, 1984.
162. Noel AW, Velchik MG, Alava A: The “liver scan” appearance in cholescintigraphy, a sign of complete bile duct obstruction. *Clin Nucl Med* 10:264–269, 1985.
163. Negrin JA, Zanzi I, Margouleff D: Hepatobiliary scintigraphy after biliary tract surgery. *Semin Nucl Med* 25:28–35, 1995.
164. Sevilla A, Howman-Giles R, Saleh H, et al: Hepatobiliary scintigraphy with SPECT in infancy. *Clin Nucl Med* 32:16–23, 2007.

Endoscopic Retrograde Cholangiopancreatography

ANDREW J. TAYLOR

CHAPTER OUTLINE

Technique

Anatomy

Biliary Tract

Pancreatic Duct

Biliary Tract Neoplasia

Biliary Tract Infection and Inflammation

Pancreas Neoplasia

Pancreas Inflammation

Complications of Endoscopic Retrograde Cholangiopancreatography

Since the implementation of endoscopic retrograde cholangiopancreatography (ERCP) into clinical practice in the late 1960s, ERCP has allowed exquisite display of the biliary tract and the pancreatic duct systems. The ducts were displayed with great spatial and contrast resolution; however, the ductal findings at times were also used as surrogates for parenchymal or local anatomic abnormalities.

Much of this information is now rightly being obtained non-invasively by the continued development of ultrasound, multi-detector computed tomography (MDCT), and especially magnetic resonance imaging (MRI) and magnetic resonance cholangiopancreatography (MRCP). However, the ERCP examination has continued to change as well, now providing critical advancements in endoscopic therapeutic uses. The continued important presence of ERCP in clinical practice still demands radiology expertise for the interpretation of the findings of this examination.

Technique

Communication between the gastroenterologist and radiologist is critical, for both patient care and medical-legal reasons. With both services usually on busy schedules and frequently being physically separated, the radiologist can obtain information through the dedicated imaging technologist associated with the examination, closed-circuit television, and the gastroenterologist's dictation from the electronic medical record system.

The examination should begin with an image centered over the patient's right upper quadrant even before the patient is endoscoped. This image will allow the gastrointestinal service to appreciate any radiopaque material that might obscure ERCP imaging. This image will also display any calcifications related to the pancreatic and biliary systems that might be covered up

with the injected 150 to 300 mg iodine/mL concentration of contrast medium that is typically used to opacify either system. This image and subsequent images are best obtained at 90 to 100 kVp, depending on the patient's size. However, the fluoroscopic and imaging techniques are frequently adjusted automatically by the fluoroscopic unit.

The duct system is ideally imaged with the cannula placed initially at the level of the sphincter. However, the gastroenterologist will frequently feel more comfortable with the cannula advanced into the duct system for better purchase. Relatively slow injection rate with sequential imaging documentation is most useful for the interpreting radiologist. For example, biliary tract stones tend to congregate distally. A deep cannulation and rapid injection of contrast material can make display of these filling defects difficult.

The patient is typically placed in the prone oblique position for this examination. This results in flowing of the relatively heavier contrast agent away from the cannula, coursing "upstream." With the injection, admixture artifacts may develop both at the cannula tip and at the site of inflow from the cystic duct into the biliary tract.

Also, because of the patient's prone position, the left hepatic duct system will fill before the right. If the right duct system fills first, as is usual for T-tube cholangiography, in which the patient is typically supine, careful examination for left-sided obstruction is needed. A normal cystic duct and gallbladder should be filled during this examination. Images of early filling of the gallbladder may demonstrate the relatively heavy contrast agent's beginning to outline the dependent gallstones in the gallbladder if it is present.

Imaging in multiple projections can be helpful in laying out normal or any abnormal anatomy. An attempt should be made to identify all of the central intrahepatic bile ducts. Lateral positioning of the patient can be helpful in distinguishing right from left ducts. In this position, the more anterior ducts belong to the left system (Fig. 74-1).

Finally, delayed images can be helpful. Allowing some of the contrast agent to flow out of the duct system, greatly facilitated by supine positioning, can bring out findings lost in the dense contrast. Delayed imaging can also help confirm obstruction even if the ducts themselves do not appear to be dilated. A normal pancreatic duct should be drained of contrast material within 10 minutes from injection; the biliary tract, without a gallbladder, should take no more than 45 minutes.¹

Anatomy

BILIARY TRACT

The biliary tract can be divided into the intrahepatic and extrahepatic systems. The intrahepatic biliary tract follows

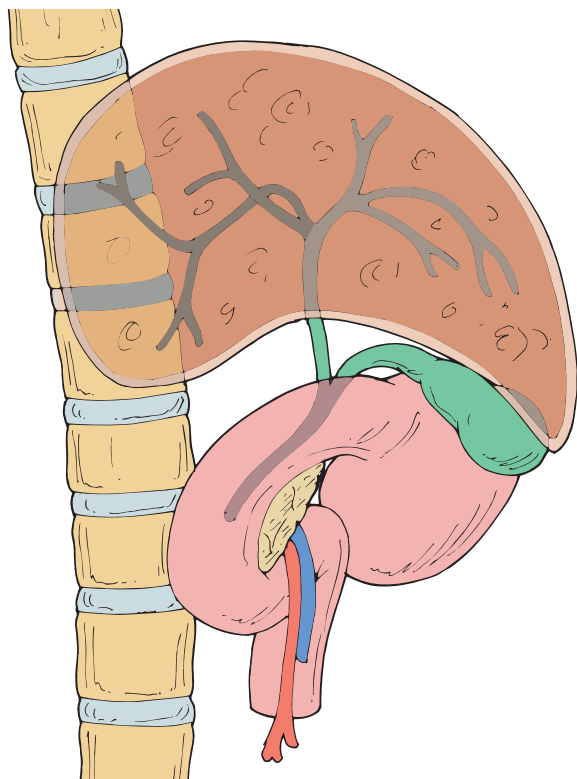


Figure 74-1 Schematic of the biliary tract. A view from the lateral projection, with the patient prone, demonstrates that the left intrahepatic biliary tract (light gray) will fill before the right intrahepatic duct system (dark gray). Also in the prone position, injected contrast medium will flow away from the sphincteric segment because of the gentle downward course of the extrahepatic biliary tract.

the arterial blood supply of the liver draining the eight hepatic segments. There is, however, moderate variability in the intrahepatic duct network; for example, the duct draining the right posterior segment is frequently aberrant (Fig. 74-2). The intrahepatic ducts should appear smooth and gently taper as they course peripherally. The angles formed by these branches should be acute. Changes resulting in pruning of peripheral ducts, stiffening of the duct system, or deviation of the “flowing” appearance of this duct network should raise concern.

The extrahepatic ductal system actually begins with the right and left hepatic ducts, both of which have components outside the liver. The union of these two duct segments forms the common hepatic duct (CHD), which is approximately 2 to 4 cm in length.

The cystic duct joins the CHD at an acute angle, typically on the CHD’s right side. The cystic duct insertion may be anomalous. It may insert abnormally upstream in the CHD or even into the right posterior intrahepatic duct (see Fig. 74-2). It may also join the extrahepatic duct very distally or medially (Fig. 74-3). This variant anatomy can lead to anatomic confusion and possible surgical mishap, or it may predispose to the development of complications, such as the Mirizzi syndrome.

The common bile duct (CBD) is formed with the union of the cystic duct and CHD. This 10-cm duct segment courses caudally and gently anteriorly when the patient is in the usual prone position during the ERCP examination (see Fig. 74-1).



Figure 74-2 Bile duct aberrancy. The duct serving the right posterior hepatic segment is the most common anomalous intrahepatic biliary tree duct segment. A post-liver transplantation T-tube cholangiogram shows the right posterior duct (straight arrow) exiting below the bifurcation (arrowhead), in this case consisting of the right anterior segment and the left hepatic duct. Also note that the transplant’s cystic duct (curved arrow) originates from this aberrant duct.

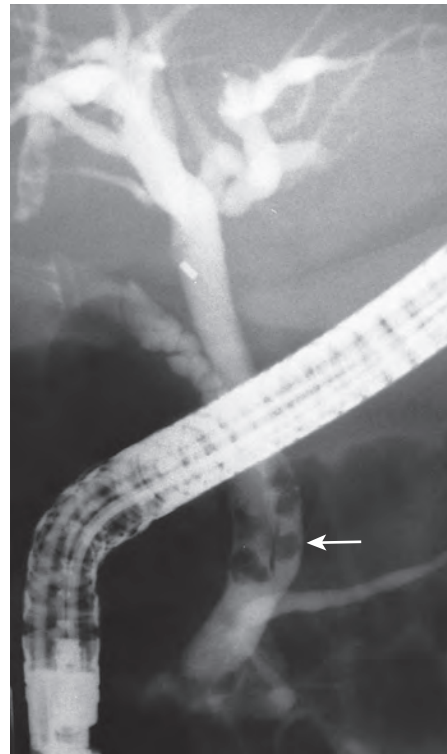


Figure 74-3 Aberrant cystic duct. A magnified view of the distal common duct shows the cystic duct (arrow) originating medially from the intrapancreatic portion of the extrahepatic biliary tree. This anatomy is important to identify, alerting the surgeon before possible laparoscopic cholecystectomy. Numerous faceted gallstones are present in both the cystic and common ducts.

The combined CHD and CBD segments may be referred to as the common duct or extrahepatic biliary tree.

The distal CBD courses into the duodenal wall and into the major duodenal papilla, also named the papilla of Vater. This distal segment is usually smooth, but it may appear finely pleated or may contain a small diverticulum.

The distal CBD is usually met distally by the main pancreatic duct (MPD), the union of which forms a common channel, also known as the ampulla of Vater, of variable length (Fig. 74-4A). In approximately 10% to 20% of cases, each duct system enters the papilla and drains into the duodenum separately. This common channel varies in length from 2 to 15 mm but averages 5 mm.^{2,3}

These two ductal systems are wrapped in smooth muscle called the sphincter of Oddi (Fig. 74-4B), measuring 5 to 15 mm in length.⁴ This muscle segment has a constant, tonic basal pressure on which interval phasic contractions of approximately two or three times per minute are superimposed. These contractions can be appreciated at fluoroscopy during injection of contrast material. This phasic contraction can squeeze the ductal segments together to create the convex-upward

appearance of a stone. This so-called pseudocalculus sign is reversed with the contraction's end (Fig. 74-5).

The diameter of the biliary tract should be measured at the CBD. Most authors suggest a maximal diameter, corrected for magnification with the known 12-mm-diameter of the therapeutic endoscope, to be less than 12 mm.^{1,3} With age, presumably related to degeneration of the duct's elastic fiber network, the CBD may increase in diameter, resulting in a "floppy duct." The normal CBD diameter of ERCP imaging will be greater than that of ultrasound, CT, and MRI, most likely related to the combination of active injection of contrast material and duct relaxation produced by conscious sedation used at ERCP.

PANCREATIC DUCT

The length of the MPD varies from 10 to 25 cm,^{5,6} but it averages 16 to 17 cm.⁷ It typically has an S-shaped configuration (Fig. 74-6). The "toe" of the S courses horizontally from the sphincter, then ascends cranially. This segment drains the pancreatic head. The MPD then again turns into a horizontal

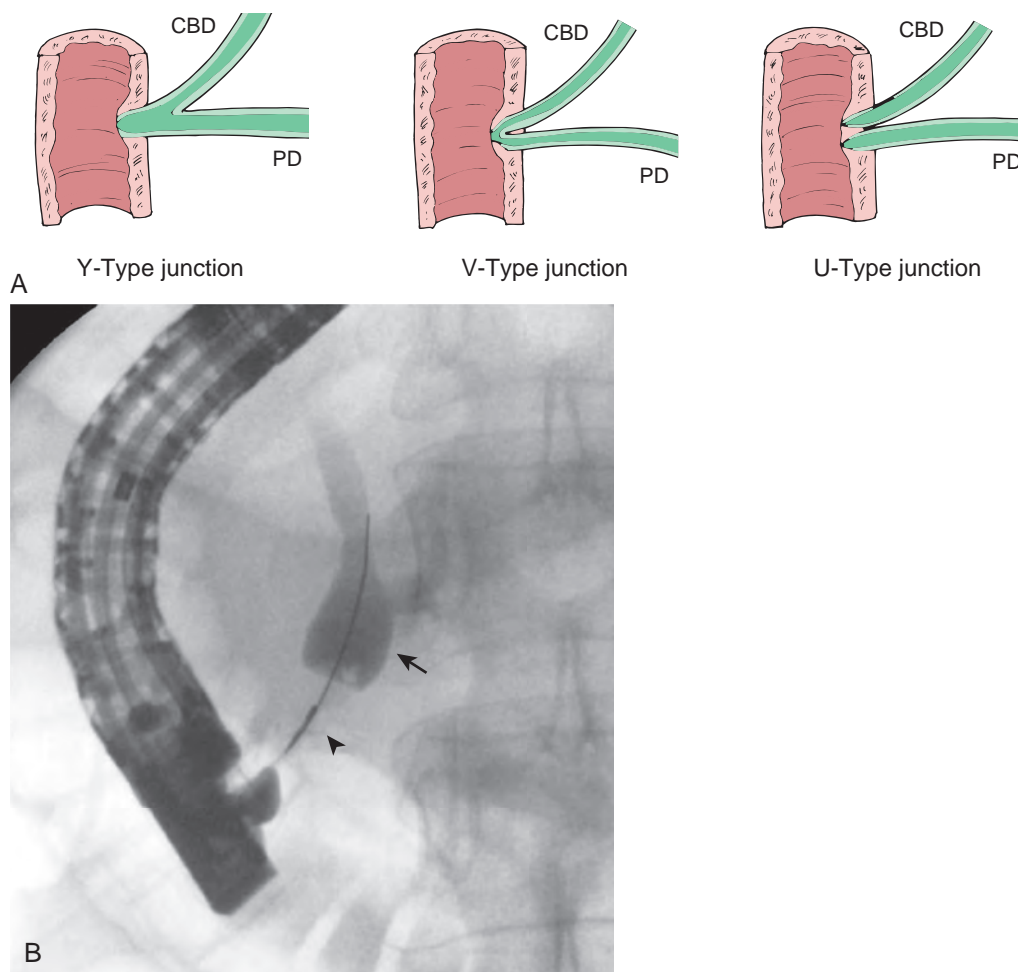


Figure 74-4 Sphincter segment anatomy. **A.** A schematic demonstrates the three types of duct unions: the Y type, with a relatively long common channel; a short common channel, leading to a V appearance; and, in a minority of cases, the two ducts enter the papilla separately in a U appearance. CBD, Common bile duct; PD, pancreatic duct. **B.** An abnormally long and ectatic channel is seen in this ERCP image. The sphincter is contracted (arrowhead), but the common channel (arrow) extends beyond the muscle wrap, allowing direct communication of the two duct systems. This is thought to be the anatomic origin of choledochal cyst development.

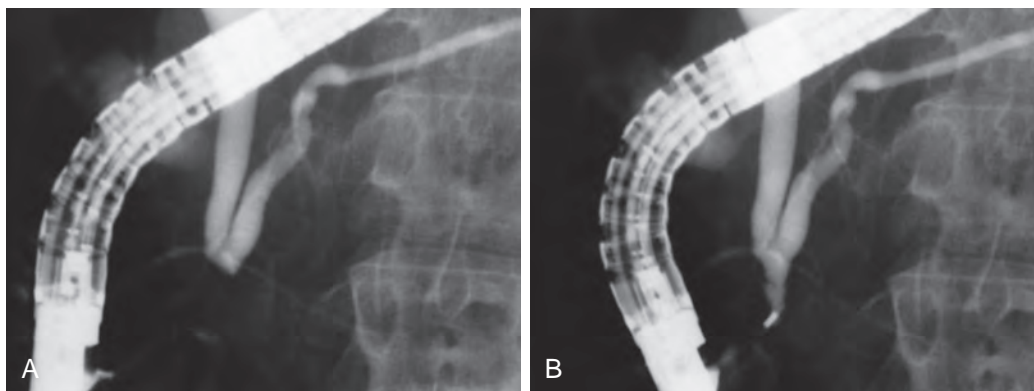


Figure 74-5 The pseudocalculus appearance. **A.** The initial ERCP image is obtained with the sphincter contracted, causing the appearance of an impacted stone. **B.** Seconds later, the sphincter relaxes, showing the normal, patent duct systems.

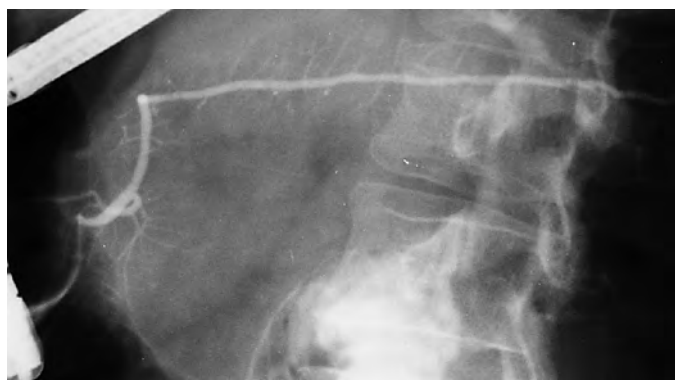


Figure 74-6 Normal ERCP appearance. The main pancreatic duct has an S-shaped appearance, gently tapering as it courses from the head to the tail. In this particular patient, the normal side branches are homogeneously gracile in appearance.

direction corresponding to the “shoulder,” running anterior to the superior mesenteric artery and its vein. The transition from the ascending to the horizontal segment is designated the neck. The remainder of the pancreas is divided between the body and the tail, either with the left side of the spine being the transition point or by simply dividing the duct from the neck to the end of the tail in half.⁸

The neck of the MPD may have a subtle, circumferential narrowing without upstream dilation. This normal variant is thought to represent the union of the embryonic dorsal and ventral ducts. Toward the upstream segment of the MPD, there is often bifurcation of the duct as it nears its termination. Anatomically, the tail is proximal and the head is considered distal, although some use upstream to describe anatomy toward the tail and downstream to refer to the anatomy coursing toward the pancreatic head.

The MPD results from the union of the embryologic ventral duct, Wirsung, and the dorsal duct, Santorini. The MPD has a smooth, gentle narrowing from the head to the tail. The maximum diameter, again magnification corrected, at the head is less than 6 mm.³ The ERCP normal values will again be less than those related to ultrasound, CT, and MRI. With age, the MPD may normally develop a more “stiff” appearance with some subtle ductal irregularity.

There is no “normal” side branch appearance on ERCP. Side branches may have a fine, slender appearance (Fig. 74-6), or

they may be wider in diameter. However, a given patient’s side branches should be uniform in appearance and should have a smooth, gentle tapering configuration as they head into the pancreatic parenchyma. Display of the side branch system, as well as of the MPD, to assess for various abnormalities is infrequent in today’s practice with the other imaging methods now available and because the risk of producing pancreatitis is relatively great with MPD injection.

Biliary Tract Neoplasia

Malignant neoplasms involving the biliary tract, both intrahepatic and extrahepatic, usually are manifested as stricture disease and less commonly as filling defects. The strictured biliary tract segment can be the result of direct mural involvement by the tumor or of compression or infiltration from adjacent diseased lymph nodes or hepatic parenchymal tumor. Unfortunately, benign disease involving the biliary tract also frequently results in a strictured appearance (Box 74-1). The different causes of the biliary stricture must be differentiated for appropriate management.

Morphologic appearance can be of some help in this differentiation. Malignant strictures tend to be long (≥ 1.5 cm), have an irregular, eccentric mural surface, and have a short (< 1 cm) transitional zone with a nodular or shouldered appearance.⁹⁻¹² The addition of contrast-enhanced MDCT or MRI can add criteria for a malignant appearance with increasing mural thickness, irregularity of the external mural border, and mural enhancement.^{12,13}

The cholangiographic appearance in identifying a malignant stricture is only approximately 70% to 85% for sensitivity, specificity, positive predictive value, and accuracy,⁹ so the added benefit of tissue sampling at ERCP can be important. Cells and tissue can be acquired by various methods: aspirated bile for cytology, brush cytology, fine-needle aspiration of the stricture for cytology, endobiliary forceps biopsy, and even analysis of material clinging to a retrieved plastic stent. Multiple types of acquisition methods will increase return. The sensitivity of either brush cytology or biopsy is approximately 56%, but their combined use improves the return to 73%.¹⁴ It has now been reported that the previous practice of sampling after stricture dilation does not increase the return on sampling.¹⁵ These results can be compared with the use of fine-needle aspiration at endoscopic ultrasound (EUS), which has a high return, at

BOX 74-1 BILE DUCT STRICTURES**INFECTIOUS, INFLAMMATORY, MISCELLANEOUS**

Postsurgical
 Pancreatitis
 Primary sclerosing cholangitis
 Immunoglobulin G4-related disease
 AIDS cholangiopathy
 Recurrent pyogenic cholangitis
 Post-liver transplantation
 Sphincter of Oddi dysfunction
 Cirrhosis
 Intra-arterial chemotherapy
 Primary biliary cirrhosis
 Inflammatory pseudotumor (malignant masquerade)
 Cystic fibrosis
 Radiation therapy
 Post-traumatic
 Post-percutaneous ablation of hepatic tumor
 Sarcoidosis
 Tuberculosis
 Eosinophilic cholangiopathy
 Portal biliopathy
 Secondary sclerosing cholangitis
 Duodenal diverticula
 Adjacent abscess or pseudocyst

NEOPLASTIC: MALIGNANT, AGGRESSIVE

Pancreatic cancer
 Cholangiocarcinoma
 Biliary papilloma or papillomatosis
 Gallbladder carcinoma
 Periapillary tumors
 Hepatocellular carcinoma
 Metastatic disease
 Lymphoma
 Biliary cystadenoma or cystadenocarcinoma

NEOPLASTIC: BENIGN, NONAGGRESSIVE

Granular cell tumor

least 80%, for distal malignant strictures from pancreatic cancer or cholangiocarcinoma.¹⁵

Endoscopic techniques are also useful for stent placement in lower duct malignant strictures. The clinical views of what type of stent to use and when to use stents in malignant strictures are continuing to evolve.^{14,16,17}

Pancreatic cancer is the most common cause of malignant biliary tract obstruction. Cholangiocarcinoma and gallbladder cancer are the most common primary bile duct tumors.¹⁰ A group of four different types of tumors, including pancreatic cancer and distal cholangiocarcinoma, can occur at the ampullary site to also cause bile duct obstruction, called periampullary tumors. Metastatic disease also is a common cause of malignant biliary tract obstruction, with gastrointestinal tract tumors, hepatocellular carcinoma, and lymphoma being common causes.

Pancreatic cancer involvement of the biliary tract is usually seen in the distal CBD segment, the intrapancreatic portion of the CBD (Fig. 74-7A, B). The length of bile duct stricture depends on both the tumor size within the pancreatic head and the nearness of the bile duct to the tumor's center. The transition of the strictured segment is usually rapid, with a nodular or shouldered appearance. However, as discussed before, pancreatic carcinoma can involve the proximal extrahepatic biliary tree from adjacent peribiliary lymph node involvement, and it

can also involve the intrahepatic ducts if there is hepatic metastatic disease (Fig. 74-7C, D).

Cholangiocarcinoma can be intrahepatic or extrahepatic in location. It is classified into one of three types: mass forming, periductal infiltrating, and intraductal growth. The mass-forming type of cholangiocarcinoma arises from small intrahepatic ducts. The carcinoma forms a hepatic parenchymal mass; MDCT and MRI are the most appropriate modalities for its detection and assessment for extent of disease. Cholangiography does not play a significant role in imaging.

The tumor associated with the periductal infiltrating cholangiocarcinoma grows within the wall of the biliary tract, causing mural thickening with an irregular (Fig. 74-8A) or smooth (Fig. 74-8B) stricture. It spreads in a submucosal manner and tends to infiltrate the periductal anatomy. This tumor frequently begins in the hilar region, where it is referred to as a Klatskin tumor. The tumor can grow upstream or downstream. Unfortunately, it also tends to extend into the periductal and perineural tissues as well as into the lymphatics, where MDCT or MRI may better define the extramural disease. ERCP does have a place if resection is anticipated (Fig. 74-8C). Cholangiography can be used to better define the biliary tract anatomy involvement by the Bismuth classification (Fig. 74-9). The Bismuth classification is used to evaluate proximal biliary tract resection of strictures or obstructions of various causes. ERCP can provide important information about the local anatomy through its exquisite spatial display of the duct system.¹⁶

At ERCP, the early periductal infiltrating type of cholangiocarcinoma can be manifested as a relatively short, smooth appearance to simulate a benign stricture.¹⁸ However, because cholangiocarcinoma is usually appreciated later in the disease process, this stricture tends to be longer and more irregular in appearance.

The much less common type of cholangiocarcinoma, the intraductal growing type (also referred to as papillary cholangiocarcinoma), is the most likely type of cholangiocarcinoma to be manifested relatively early in its course. It tends to spread superficially and not invade the bile duct wall. It has a better prognosis compared with the other types of cholangiocarcinoma.¹⁹ At ERCP, this tumor may be a well-defined, smooth, intraluminal papillary protrusion (see Fig. 74-8C); but there can be multiple papillary projections, and some of these papillary projections may have an irregular surface. The intraductal growing type of cholangiocarcinoma may cause obstruction of the upstream ductal system without clear definition of the tumor itself. This type of cholangiocarcinoma can also produce mucin to cause biliary dilation. There is a complex relationship between the intraductal growing type of cholangiocarcinoma, biliary papilloma or papillomatosis (Fig. 74-10), and intraductal papillary mucinous neoplasm of the bile duct (Fig. 74-11), all of which can be seen as a papillary projection on cholangiography.^{18,19}

Gallbladder carcinoma is the other primary biliary tract malignant neoplasm. Local disease from this primary may spread to the mid or proximal extrahepatic biliary tree by direct extension along the cystic duct, by lymphatics, or by enlarged peribiliary lymph nodes. The stricture may extend to the hilar bifurcation or into the right or left hepatic duct system. The intrahepatic ducts may also be compromised by the cancer's predilection to invade the adjacent hepatic parenchyma or from metastatic deposits within the liver, which can displace, infiltrate, or obstruct the intrahepatic duct system.

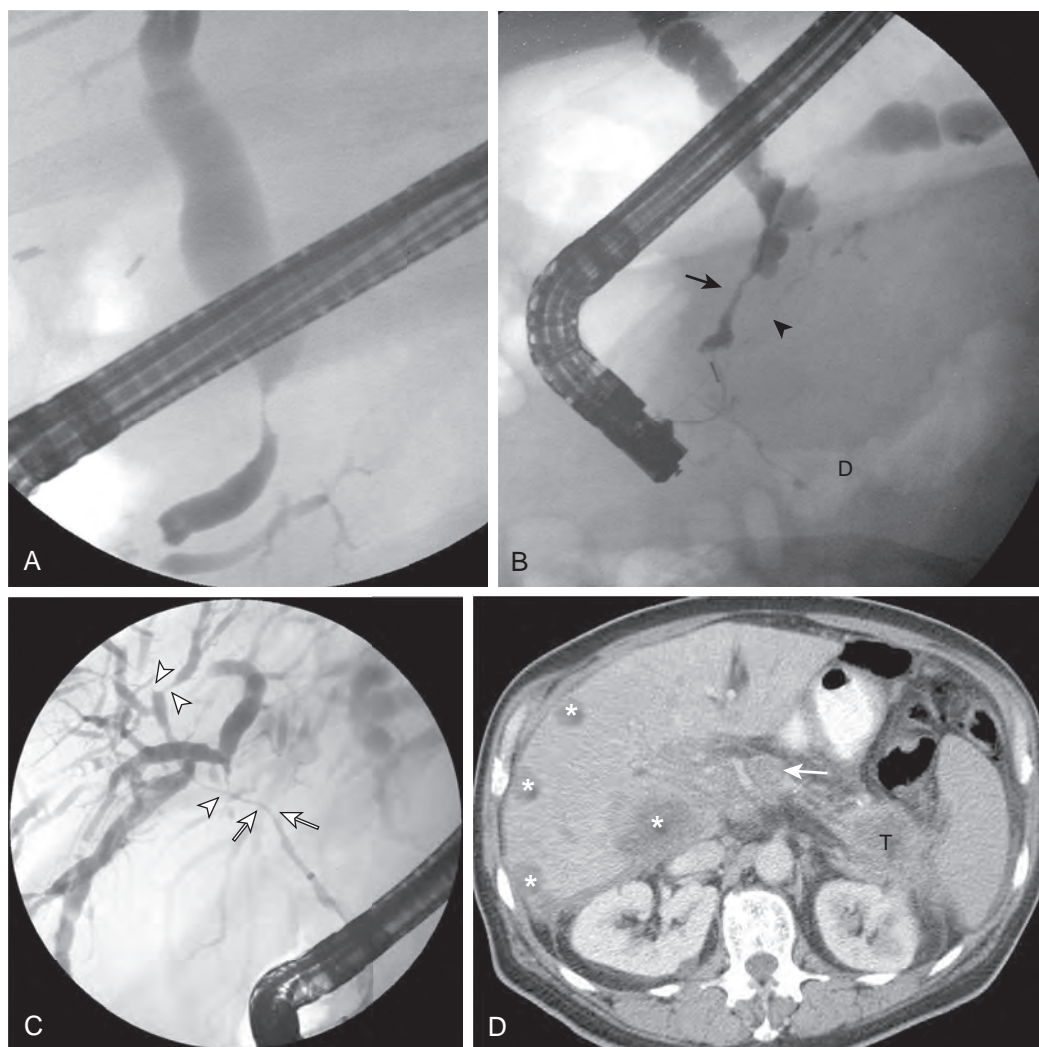


Figure 74-7 Biliary tract strictures from pancreatic carcinoma. **A.** The pancreatic cancer causes a rapid transition to a tight stricture in the intrapancreatic portion of the bile duct with marked upstream dilation. **B.** In this case, the pancreatic cancer has a longer bile duct stricture that is irregular in appearance (arrow). There is also a long diffuse narrowing of the pancreatic cancer in the adjacent main pancreatic duct (arrowhead). There is dilation of the upstream main pancreatic duct. There is also nodular effacement of the gas-filled duodenum from the pancreatic cancer. **C.** In a different patient, the proximal extrahepatic biliary tree (arrows) and intrahepatic bile ducts (arrowheads) are narrowed by metastatic disease to hilar lymph nodes and hepatic metastatic disease, respectively. **D.** The corresponding CT section demonstrates the pancreatic tail primary (T), metastatic hilar lymph nodes (arrow), and hepatic metastases (asterisks).

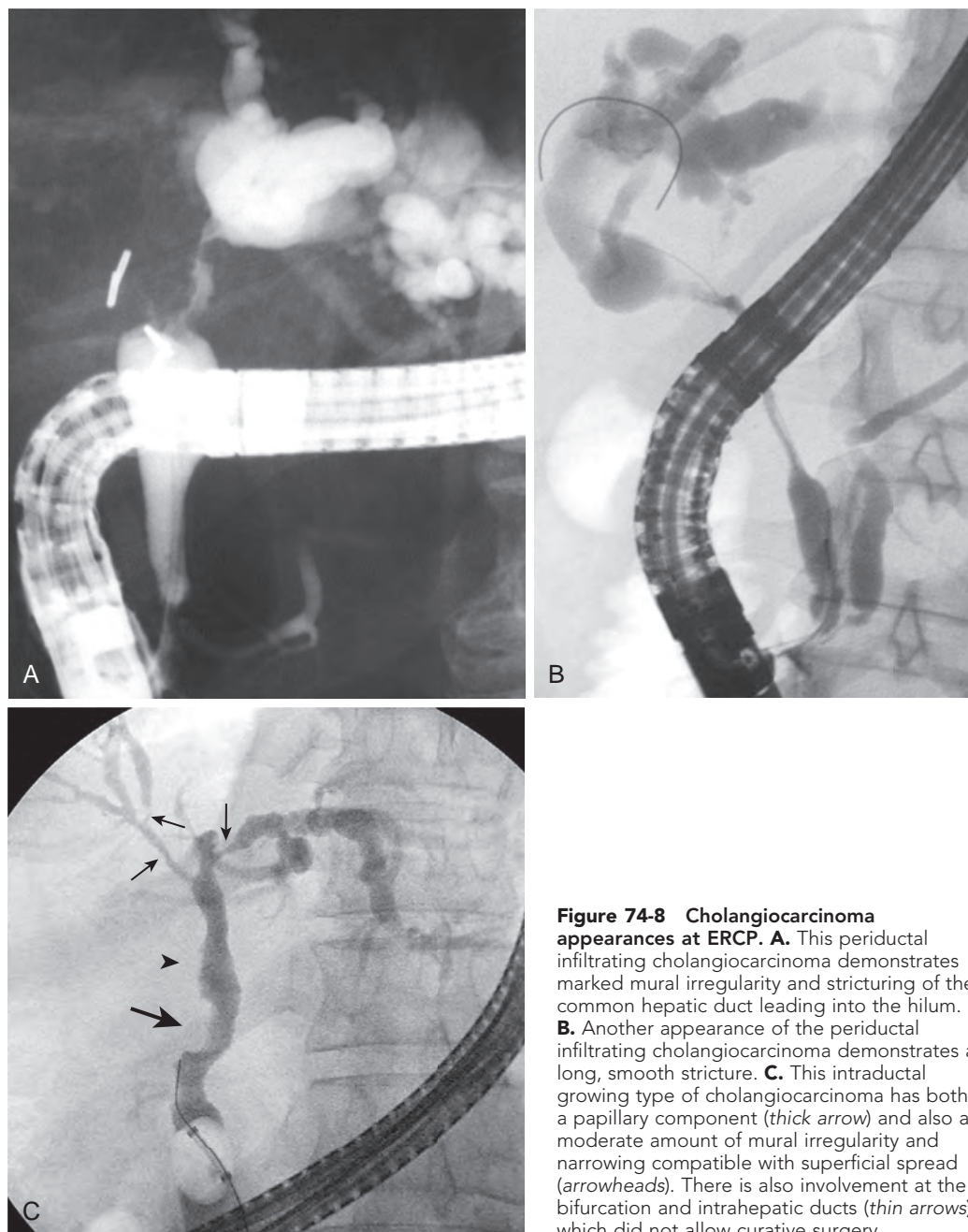


Figure 74-8 Cholangiocarcinoma appearances at ERCP. **A.** This periductal infiltrating cholangiocarcinoma demonstrates marked mural irregularity and stricturing of the common hepatic duct leading into the hilum. **B.** Another appearance of the periductal infiltrating cholangiocarcinoma demonstrates a long, smooth stricture. **C.** This intraductal growing type of cholangiocarcinoma has both a papillary component (*thick arrow*) and also a moderate amount of mural irregularity and narrowing compatible with superficial spread (*arrowheads*). There is also involvement at the bifurcation and intrahepatic ducts (*thin arrows*), which did not allow curative surgery.

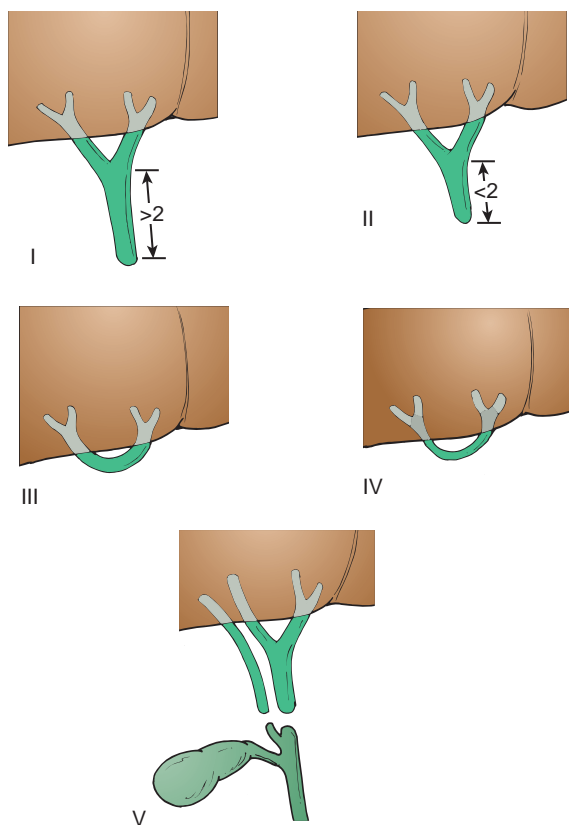


Figure 74-9 Schematic of the Bismuth classification. A type I configuration represents occurrence of the stricture 2 cm or more from the common hepatic duct bifurcation. A type II configuration has less than 2 cm of normal duct before the bifurcation. The type III configuration leaves only the bifurcation intact. Type IV has narrowing of the bifurcation. Type V refers to injury of aberrant branches of the biliary tree. (From Taylor AJ, Bohorfoush AG III: *Interpretation of ERCP*. Philadelphia, Lippincott-Raven, 1997.)

At ERCP, the cystic duct may not fill or only partially fill. The mid to proximal duct can be splayed, be diffusely narrowed, or demonstrate an irregular stricture (Fig. 74-12). Some mass effect, stricture, or obstruction can also be related to enlarged hepatobiliary lymph nodes.

Distal CBD obstruction, and potentially downstream MPD obstruction, can be caused by a variety of tumors that can occur at the papilla of Vater. Because of the difficulty in imaging, endoscopy, surgery, and even histology to separate these tumors, these tumors are combined under the heading of periampullary tumors. These tumors can be either benign or malignant. Benign tumors in this area are less common and include the ampullary adenoma, local geographic benign tumors, and carcinoid.²⁰

Periampullary cancer refers to cancers from one of four structures: the pancreatic head, distal bile duct, duodenum, and ampulla. There are other, rare malignant neoplasms that can occur here as well, such as metastatic disease and lymphoma.²⁰ Even though these cancers share a similar location and clinical presentation, the underlying histologic type can dictate prognosis. The ampullary and duodenal cancers have the best prognosis, whereas the distal bile duct and pancreatic cancers have the worst.



Figure 74-10 Biliary papillomatosis. The multiple papillary projections protruding into the extrahepatic biliary tree are compatible with papillomatosis.

Although some authors suggest that contrast-enhanced MDCT with three-dimensional reconstruction is the preoperative imaging examination of choice for the periampullary tumor, CT can have difficulty in both the visualization and the accurate assessment of local disease.²¹ Biliary or pancreatic duct dilation may be visualized but the underlying tumor not appreciated.

ERCP can be of great help by directly visualizing the periampullary tumor at the time of endoscopy and display the possible intraductal involvement of the tumor during ductal injection of contrast material (Fig. 74-13). Tissue retrieval can also be obtained as well as stenting, if necessary, and even local endoscopic resection in the appropriate case.²⁰ However, EUS and even transpapillary intraductal ultrasound are frequently used by endoscopists for better assessment of local tissue

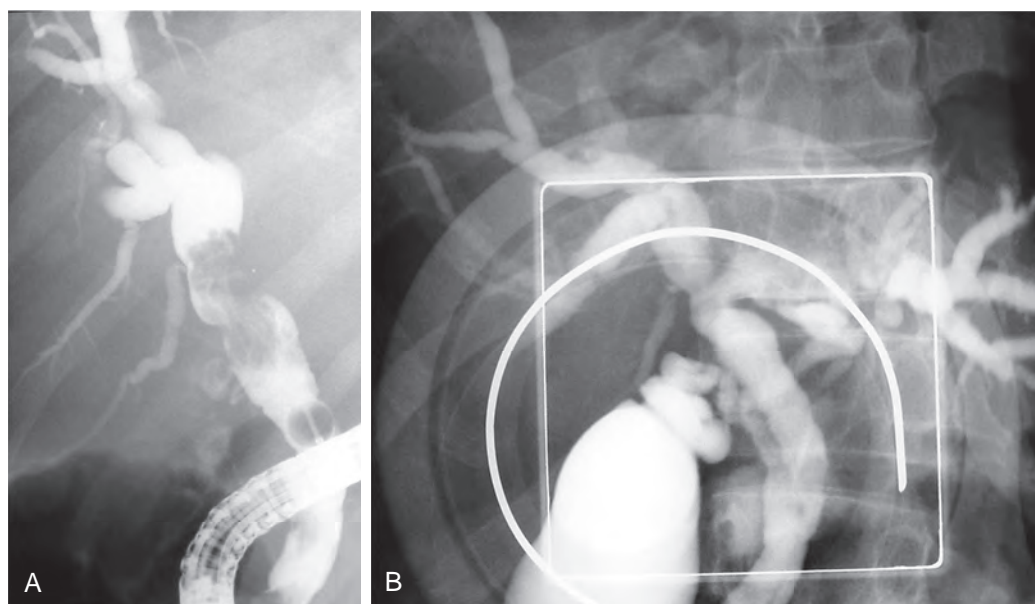


Figure 74-11 Intraductal papillary mucinous neoplasm of the biliary tract. **A.** Initial injection demonstrates an irregular filling defect in the common hepatic duct. This was a jellylike material with strands of contrast medium visualized in its interstices. **B.** After removal of this viscid material with a retrieval balloon, the left hepatic ducts and the common hepatic duct are now widely patent. There was no papillary tumor visualized.

involvement and possible local lymph node spread.²⁰ EUS can also be used for fine-needle aspiration of the tumor for histologic diagnosis. A periampullary tumor may not have an intraluminal component. The cholangiogram or pancreatogram may demonstrate only a narrowing without an intraluminal mass. In these cases, tissue retrieval is critical.

There are also less common malignant neoplasms that can affect the biliary tree. Hepatocellular carcinoma can affect the biliary tract by hepatic parenchyma compression, enlarged hilar lymph nodes, or rarely intraluminal growth. Metastatic disease may cause narrowing by hepatic parenchymal or lymph node extrinsic compression (see Fig. 74-7C, D), but it can also have direct mural involvement and possibly intraluminal growth (Fig. 74-14). Lymphoma can affect the intrahepatic or the extrahepatic bile duct. Lymphoma tends to displace and narrow but not invade the duct system (Fig. 74-15). It also tends to have relatively less obstruction for the degree of narrowing. Biliary cystadenoma or cystadenocarcinoma is an unusual tumor, typically seen in the middle-aged woman, that can splay the biliary tract or rarely have an intraductal component.

A final neoplasm of the biliary tract is the granular cell tumor. This is a submucosal, neurogenic tumor that typically is manifested in a young to middle-aged African American woman. When it is visualized at ERCP, it is a smooth, polypoid, or possibly annular-appearing stricture. It is important to raise the possibility of this tumor in this specific patient demographic because the tumor is benign in nature (Fig. 74-16).

Biliary Tract Infection and Inflammation

There are numerous causes of infectious and inflammatory biliary tract disease (see Box 74-1). The various infectious and inflammatory processes usually are manifested as a stricture. Typically, it is a combination of clinical history (i.e., patient

demographic, significant past medical history, and certain specific laboratory values) and imaging features that suggests the correct diagnosis.

The postoperative biliary tract stricture is by far the most common inflammatory stricture.²² Most of these strictures are related to laparoscopic cholecystectomy. Approximately 0.3% to 0.6% of surgeries result in biliary stricture.^{23,24} Although the duct compromise may be appreciated at the time of surgery or soon thereafter, the stricture may take weeks or years to be manifested. Although MRI and MRCP are now the imaging examinations of choice to assess for these delayed stricture presentations,²⁵ ERCP can help display and treat this injury.

The postoperative stricture is typically short and smooth and is located at the extrahepatic biliary tree at the site of the cystic duct takeoff or above (Fig. 74-17). Treatment of the stricture will depend on the type and complexity of injury, timing of discovery of the injury, and position of the stricture within the biliary tract. However, endoscopic treatment with dilation and plastic stent placement can be effective in establishing and maintaining duct patency.²⁶

Another major area of postoperative bile duct complication is in the post-liver transplantation patient. These complications consist of biliary tract obstruction, stricture formation, filling defects, sphincter of Oddi dysfunction, leaks, and necrosis. A varied rate of 5% to 32% is reported for bile duct complications in this patient population, ranking only second to rejection as the most common problem in this population.^{27,28}

Whereas MRCP has a place in imaging of this patient population,²⁹⁻³¹ ERCP continues to play a critical role in management and diagnosis. The better spatial resolution and the possible interventional therapies provided by ERCP are advantages over the noninvasive MRCP. Also, at times, bile duct obstruction is not reflected in biliary tract dilation (Fig. 74-18).^{17,28} ERCP will be needed to accurately assess for obstruction in these cases. Obversely, bile duct dilation can be present without obstruction, which can also be confusing at MRCP.

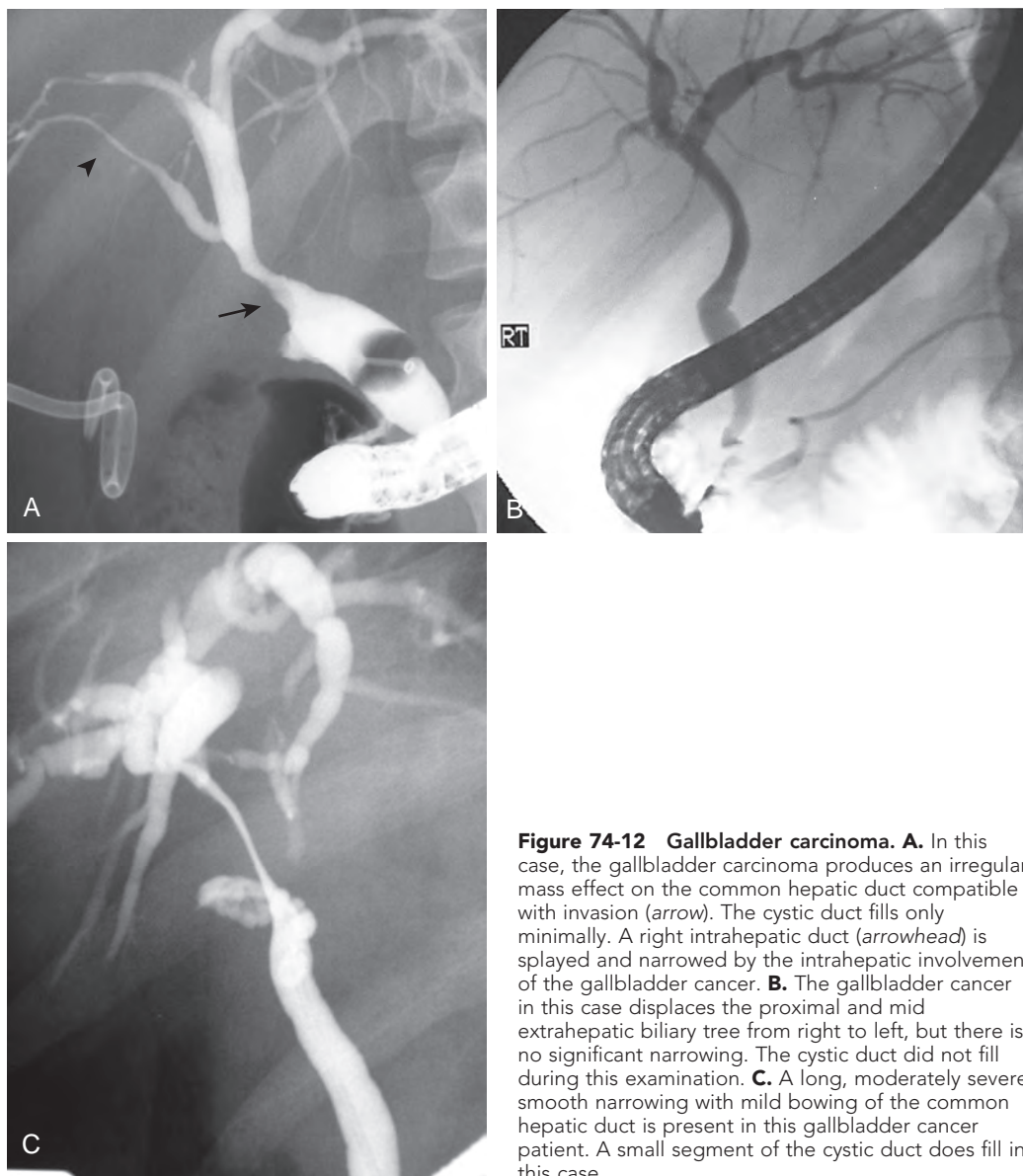


Figure 74-12 Gallbladder carcinoma. **A.** In this case, the gallbladder carcinoma produces an irregular mass effect on the common hepatic duct compatible with invasion (arrow). The cystic duct fills only minimally. A right intrahepatic duct (arrowhead) is splayed and narrowed by the intrahepatic involvement of the gallbladder cancer. **B.** The gallbladder cancer in this case displaces the proximal and mid extrahepatic biliary tree from right to left, but there is no significant narrowing. The cystic duct did not fill during this examination. **C.** A long, moderately severe, smooth narrowing with mild bowing of the common hepatic duct is present in this gallbladder cancer patient. A small segment of the cystic duct does fill in this case.

Biliary strictures account for just less than half of all post-liver transplantation biliary complications.³² These strictures are divided into anastomotic and nonanastomotic. The non-anastomotic strictures are typically longer, multiple, and intrahepatic. They are usually related to a macroangiopathic or microangiopathic etiology or immunogenic (e.g., recurrent disease, such as primary sclerosing cholangitis) in origin.³² Treatment for this type of stricture formation is more difficult and less successful with endoscopic or percutaneous approaches. The presence of these strictures frequently heralds the eventual loss of the transplant liver.

The anastomotic stricture is a short, focal narrowing at the surgical anastomosis (see Fig. 74-18). This stricture has a fibrotic component and is more amenable to endoscopic dilation and

plastic stent placement. The common edematous band at the anastomotic site seen within the first 2 weeks of surgery should not be mistaken for a true stricture. This band will usually spontaneously resolve but may rarely require a temporary plastic stent without balloon dilation for treatment.³²

The filling defects in the post-liver transplantation patient can be related to stones, biliary casts, blood clots, or debris and sludge. These intraluminal filling defects can usually be removed endoscopically. The possible underlying causes of these filling defects, such as stricture, bacterial infection, or ischemia, also need to be ruled out.^{26,32}

Although the etiology is poorly understood, sphincter of Oddi dysfunction accounts for approximately 2% to 3.5% of post-transplantation complications.³³ Bile duct dilation can be

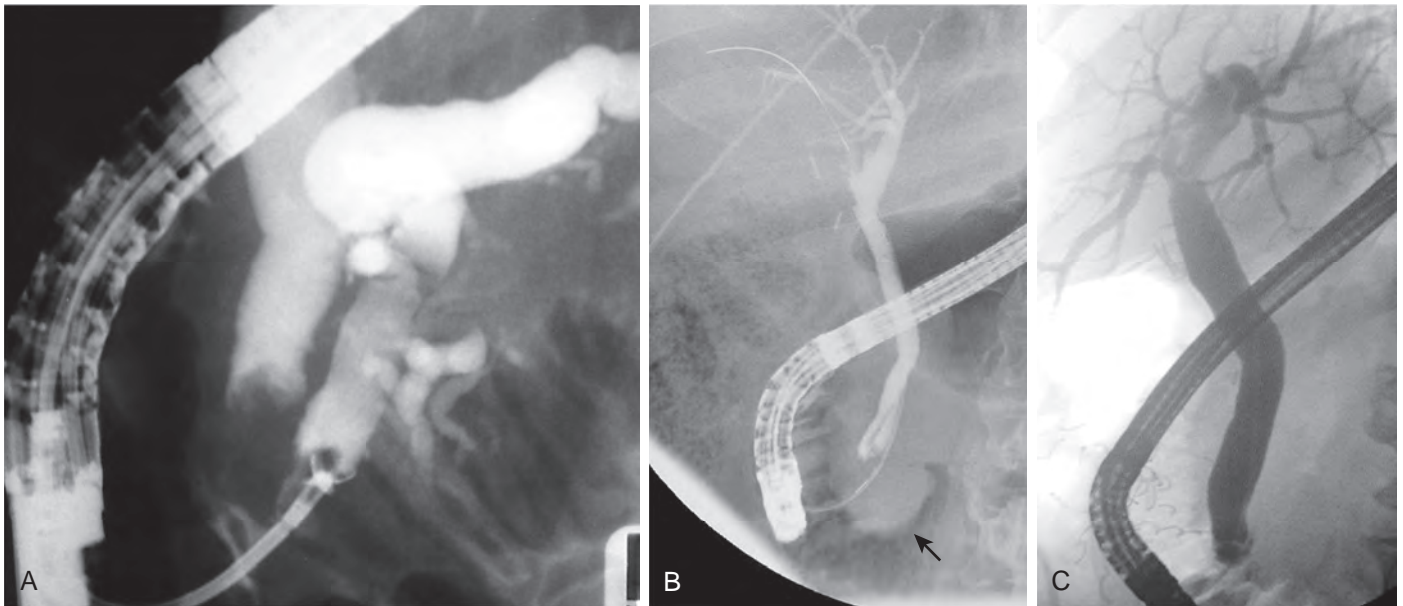


Figure 74-13 Perampullary tumors. **A.** In this case of ampullary carcinoma, nodular filling defects are seen in both the common bile duct and main pancreatic duct. Forceps biopsy confirmed the diagnosis. **B.** In another case, a perampullary duodenal villous adenoma can be visualized from its relief within the duodenal gas (arrow). This patient presented with recurrent bouts of acute pancreatitis without biliary symptoms. **C.** No definite mass is seen at ERCP in this patient with an ampullary tumor. There is only the rounded configuration of a very distal common bile duct obstruction.

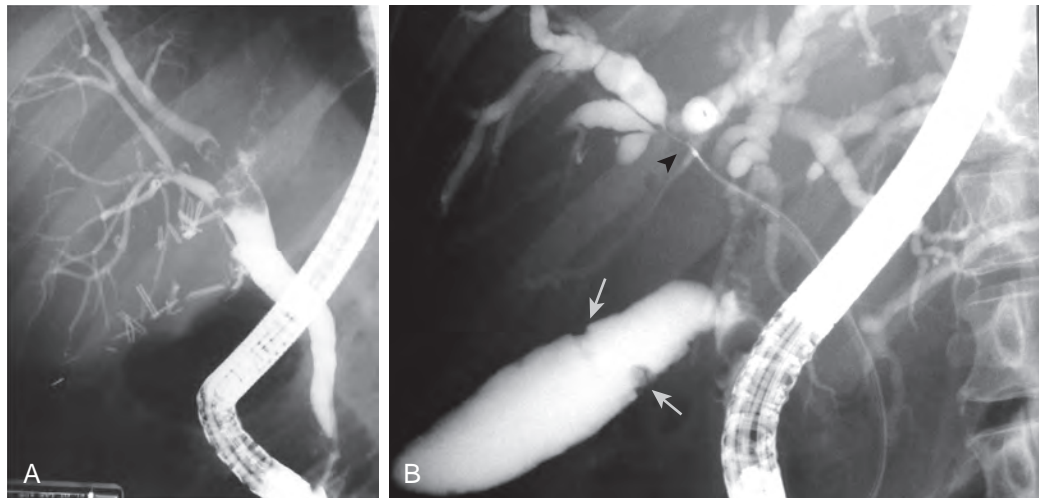


Figure 74-14 Metastatic disease and the biliary tract. **A.** In this patient with partial hepatectomy for metastatic colon cancer, the colon cancer recurrence has grown intraluminally. Colon cancer is a fairly common cause of intraductal growth. **B.** Cervical cancer metastatic disease not only obstructs the hilum by enlarged lymphadenopathy (arrowhead) but also has metastatic deposits directly to the gallbladder wall (arrows).

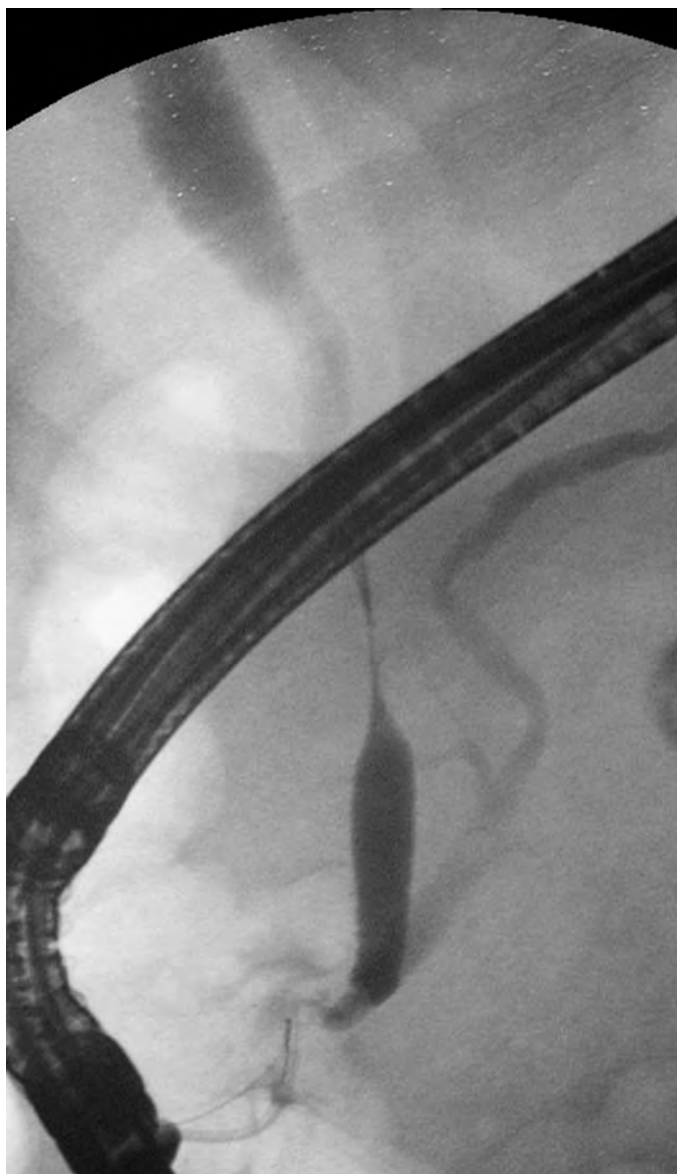


Figure 74-15 Lymphoma of the biliary tract. The long, smooth, common duct narrowing is caused by extrinsic mass effect from adjacent lymphoma.

seen in the donor or recipient duct system. Endoscopic sphincterotomy is appropriate therapy if this is clinically significant.

Post-liver transplantation biliary leaks usually occur at a cystic duct stump, the T-tube insertion site, or the anastomotic site. These leaks are readily treated with sphincterotomy or plastic stent placement. If the leak is related to ischemia, endoscopic treatment will not provide adequate treatment.²⁶

Biliary strictures can be associated with chronic pancreatitis. These strictures are present in the intrapancreatic portion of the CBD, being caused by the surrounding pancreatic fibrosis and occasionally a combination of fibrosis superimposed with edematous change from acute pancreatitis. The biliary tree can also be narrowed by an adjacent pseudocyst in this patient population.

Approximately 25% of chronic pancreatitis patients will develop a stricture in the intrapancreatic segment,³⁴ although the incidence varies from 3% to 46%.³⁵ The recurrent acute

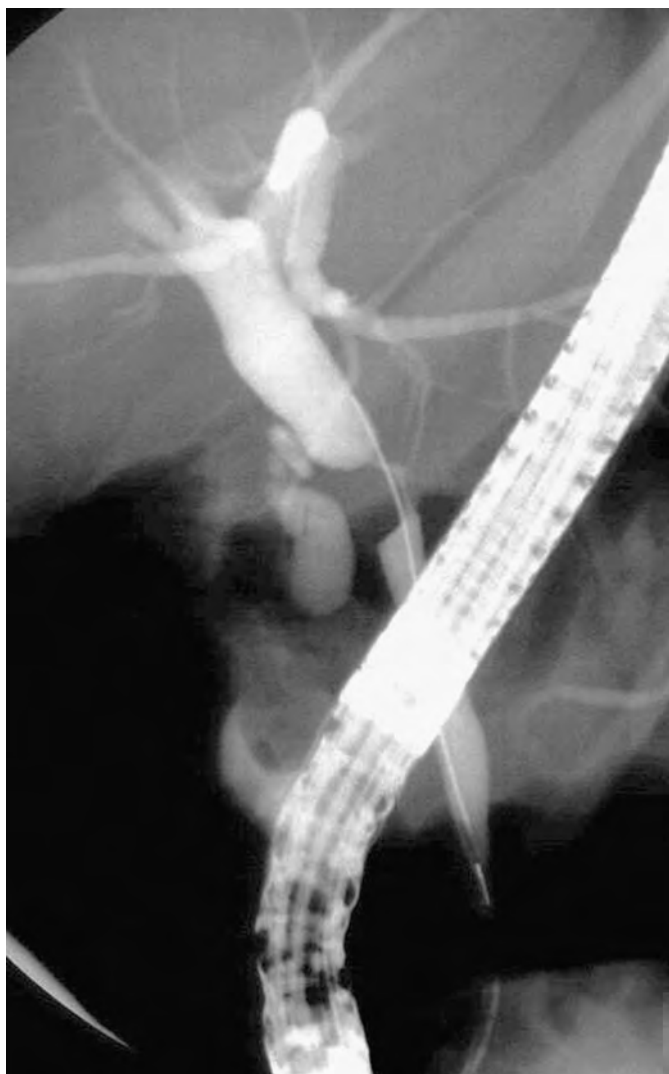


Figure 74-16 ERCP in this young woman with incidental elevated liver function test results demonstrates a smooth, submucosal/extrinsic-appearing common bile duct narrowing. A granular cell tumor was found at surgery.

inflammatory attacks lead to increasing fibrosis in the pancreas that includes the periductal parenchyma. Not all such narrowings need to be treated, but clinical correlation is needed to make sure that the untreated stricture does not result in one of the potential complications of bile duct narrowing: secondary biliary cirrhosis, ascending cholangitis, or choledocholithiasis.^{34,36} For the relatively unusual bile duct stricture that requires treatment, endoscopic dilation with multiple plastic stent placements can be tried. With increasing fibrotic change in the surrounding pancreas, this endoscopic approach can be less effective.^{34,37,38}

The biliary tract stricture in chronic pancreatitis typically has an hourglass appearance of the long, smooth stricture in the distal CBD (Fig. 74-19A). There are various appearances of bile duct stricture in chronic pancreatitis,³⁵ with one series suggesting that up to one third of the bile duct strictures related to chronic pancreatitis had a more aggressive appearance with a short, abruptly narrowing stricture and even shouldering to cause significant upstream dilation³⁹ (Fig. 74-19B).

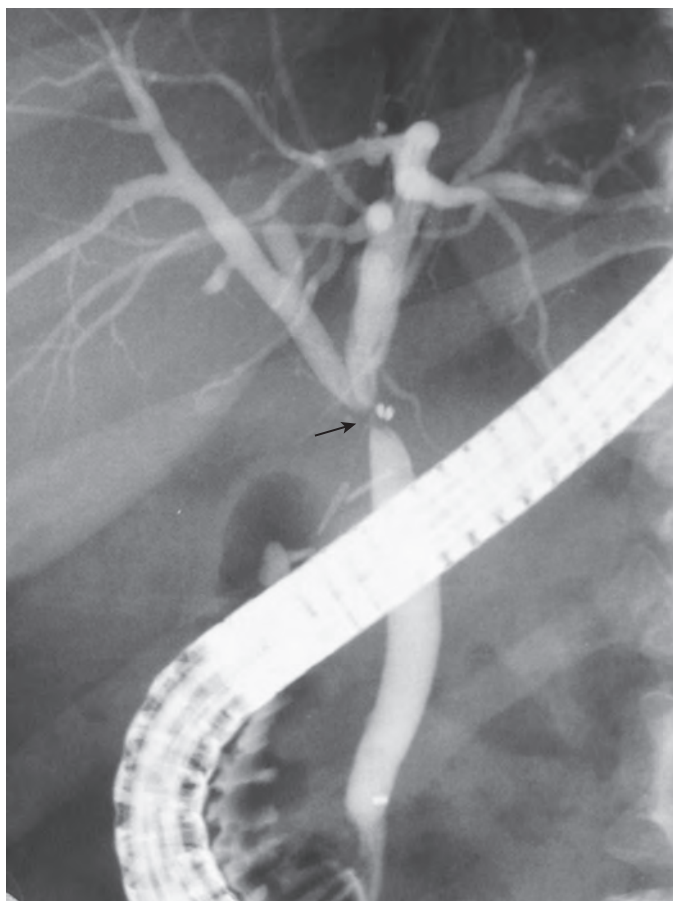


Figure 74-17 This postoperative stricture (arrow) is approximately 1 year after laparoscopic cholecystectomy. This stricture is very short and smooth and located at the common hepatic duct bifurcation.

Choledocholithiasis is another common entity causing obstruction and possible infection. Most of these ductal stones are secondary, that is, they migrate from the gallbladder into the extrahepatic biliary tree. Anywhere from 5% to 18% of cholecystectomy patients will have choledocholithiasis.⁴⁰

“Primary” stones may also develop, causing choledocholithiasis. These stones originate within the lumen of the bile duct itself. These are typically calcium bilirubinate stones seen in patients with increased red blood cell breakdown, alcoholic patients, senescent patients, or cirrhotic patients.⁴¹

Imaging and management of choledocholithiasis can be stratified according to age (increased chance in patients older than 55 years), elevated bilirubin concentration (>1.8 mg/dL), and duct dilation (>6 mm).⁴² However, even if this combination of clinical data suggests a high likelihood of choledocholithiasis, this assessment may be incorrect in more than two thirds of patients.⁴³ Thus, imaging with either MRCP or the more invasive EUS, both being equally the best imaging modalities for choledocholithiasis diagnosis,⁴⁴ is usually obtained before management with ERCP.

With the present use of accurate imaging for choledocholithiasis before ERCP and stone removal, the meticulous ERCP technique, previously needed to identify the stone, is now usually lacking. Ideally, the cannula should be placed with its tip in the most distal portion of the CBD with slow injection of contrast material. The early duct filling is imaged to best



Figure 74-18 Post-liver transplantation patient. There is a very tight anastomotic stricture (arrow) in this liver transplant patient with no upstream dilation. There is also ectasia of the recipient duct without evidence of obstruction. Subsequent balloon dilation and plastic stent placement were used in treatment.

display the offending stone, which has typically migrated to the distal duct. Present practice frequently has a deeper cannula placement and minimal injection of contrast material. These images are used to verify the cannula's position within the CBD so sphincterotomy and stone removal can continue. The decreased amount of intraluminal injection of contrast material is of clinical benefit to decrease the chance of sepsis. Endoscopic management of choledocholithiasis is 90% successful with an approximate 10% complication rate.⁴⁰

In the acute time frame, choledocholithiasis can lead to ascending cholangitis. If ascending cholangitis is suspected, the endoscopist needs to be wary of overinjection of contrast material. Changes of ascending cholangitis can be seen at ERCP: a variable degree of duct dilation with normal-appearing wall; mild irregularity of the wall with “pleating” of diverticula; or marked irregularity of the wall, which may represent necrosis, leading to communicating cavities in the liver from hepatic abscess formation. If the ductal stones go untreated, chronic changes of diffuse stricturing can occur, resulting in secondary sclerosing cholangitis.

Gallstones still residing in the gallbladder can also affect the extrahepatic biliary tree in the Mirizzi syndrome. This is a rare manifestation of gallstone disease, seen in only 0.1% to 0.7% of patients with gallstones.⁴⁵ This syndrome is thought to develop from recurrent bouts of cholecystitis, which contracts the gallbladder around and pushes a stone into Hartmann's pouch or the cystic duct. This pressure, combined with the relatively parallel orientation of the cystic duct with the CHD, can initially

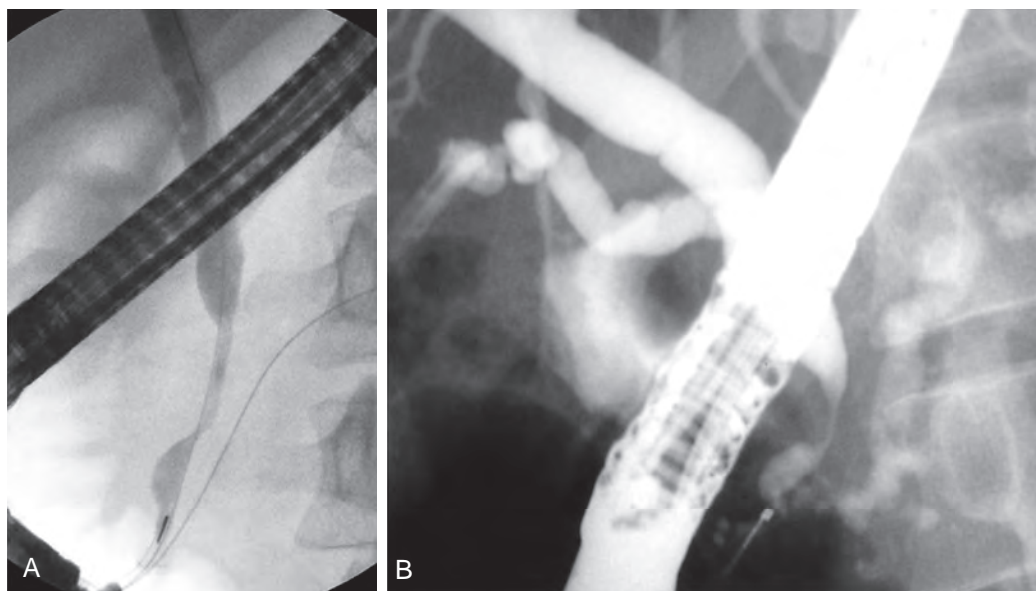


Figure 74-19 Chronic pancreatitis causing distal common duct stricturing. **A.** The hourglass appearance is typical for distal ductal stricture in the chronic pancreatitis patient. **B.** In another patient, there is a rapidly progressive, focal narrowing that could suggest pancreatic carcinoma. However, this aggressive-looking stricture is related to chronic pancreatitis.

cause a lateral to medial indentation on the CHD. With continuing pressure, the stone can be driven progressively into the CHD or CBD lumen. When it is completely intraluminal, this stone can cause obstruction, frequently at the junction of the suprapancreatic and intrapancreatic portion of the common duct. Various classifications have been used to describe this syndrome.⁴⁵ This syndrome has also been associated with an increased chance of cholangiocarcinoma.^{45,46}

MRI and MRCP are the imaging modalities of choice to make the diagnosis of Mirizzi syndrome. ERCP can also be used both for diagnosis and for possible decompression of the bile duct obstruction before surgery (Fig. 74-20).

Autoimmune processes can also lead to biliary stricture disease. Primary sclerosing cholangitis is thought to have at least some component of autoimmune disease. More recently, immunoglobulin G4-related sclerosing disease (formally called autoimmune pancreatitis) has become more widely appreciated as a cause of pancreaticobiliary disease as well as of other disease processes associated with this entity.

In primary sclerosing cholangitis, an inflammatory or fibrotic process diffusely affects the biliary tree, with rare sparing of the extrahepatic duct (Fig. 74-21). Early on, there will be a lack of distensibility of the most peripheral intrahepatic duct system, causing a pruned appearance at ERCP. In the gentle flowing appearance, the intrahepatic ducts lose their normal acute angles and become stiff. As the disease progresses, short focal strictures develop with the defining characteristic of a relative lack of significant upstream dilation. With further progression, there is some interval dilation between the series of focal strictures, leading to a beaded appearance. Diverticula as well as small intraductal stones can develop.

The strictures inexorably progress to cause worsening obstruction. Major central strictures can be targeted for endoscopic dilation to provide some relief. The stricture disease progresses, at a variable rate, leading to end-stage liver disease. Death occurs without liver transplantation. Cholangiocarcinoma is

another potentially lethal complication, being seen in 5% to 20% of patients with primary sclerosing cholangitis.^{47,48}

Although MRCP has replaced ERCP in the initial work-up for suspected primary sclerosing cholangitis, a false-negative MRCP study can be obtained in the early time course of this disease.⁴⁸ The greater spatial resolution at ERCP and the increased pressure from active injection at ERCP will enable the subtle pruning of early primary sclerosing cholangitis to be visualized. Central dominant stricture dilation and brushings of suspicious strictures can also be obtained during ERCP.

Immunoglobulin G4-related sclerosing disease has become much better recognized as a cause of biliary tract strictures. Lymphoplasmacytic cells can infiltrate the biliary tree to create various morphologic appearances of the stricture: a single intrapancreatic CBD stricture simulating pancreatic cancer; multiple strictures in both the intrahepatic and extrahepatic biliary tree that could suggest primary sclerosing cholangitis; multiple intrahepatic strictures only; a hilar stricture to suggest a Klatskin tumor; and a combination of both a hilar and a distal CBD stricture.^{49,50}

The cholangiographic appearance of the biliary tract findings by itself will not allow the diagnosis of immunoglobulin G4-related sclerosing disease to be made. Information obtained from histology, imaging, serology, other organ involvement, and response to steroid therapy (HISORT criteria) in various combinations is required for the diagnosis.^{49,51} ERCP can display the bile duct abnormalities as well as the pancreatic duct findings of this disease (Fig. 74-22). MDCT and MRI are also helpful in displaying not only potential duct abnormalities but also any other abdominal organs that may be involved in this disease complex: pancreatic parenchyma, renal parenchyma, and retroperitoneal fibrosis.

Acquired immunodeficiency syndrome (AIDS) is another immunologic disease that affects the biliary tract, causing AIDS cholangiopathy. Even as the successful treatment of AIDS decreases the incidence of this cholangiopathy, it can still be seen in the severely immunocompromised AIDS patient

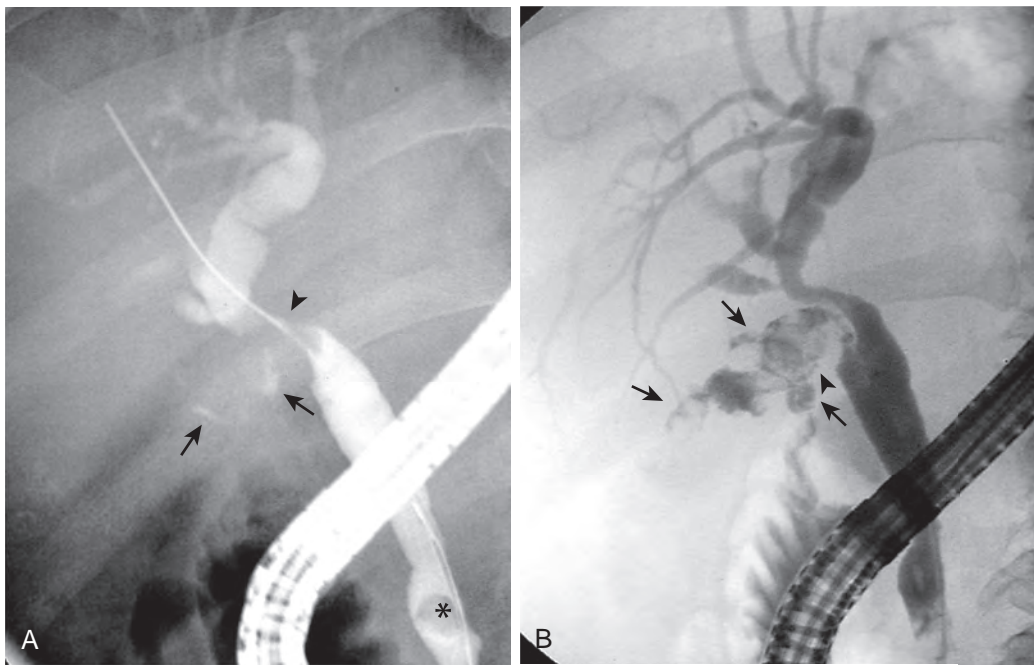


Figure 74-20 Mirizzi syndrome. **A.** A 54-year-old woman with 10 years of intermittent right upper quadrant pain now presents with increasing right upper quadrant pain and elevated liver function test results. The initial ERCP shows proximal common hepatic duct obstruction (arrowhead) with adjacent curvilinear calcifications (arrows). Also note the distal common duct stone (asterisk). **B.** After drainage with a plastic stent for 1 month, ERCP demonstrates a contracted gallbladder (arrows) with a moderate-sized stone at the gallbladder neck (arrowhead). The common hepatic duct is now patent but still narrowed by the adjacent inflammatory process.

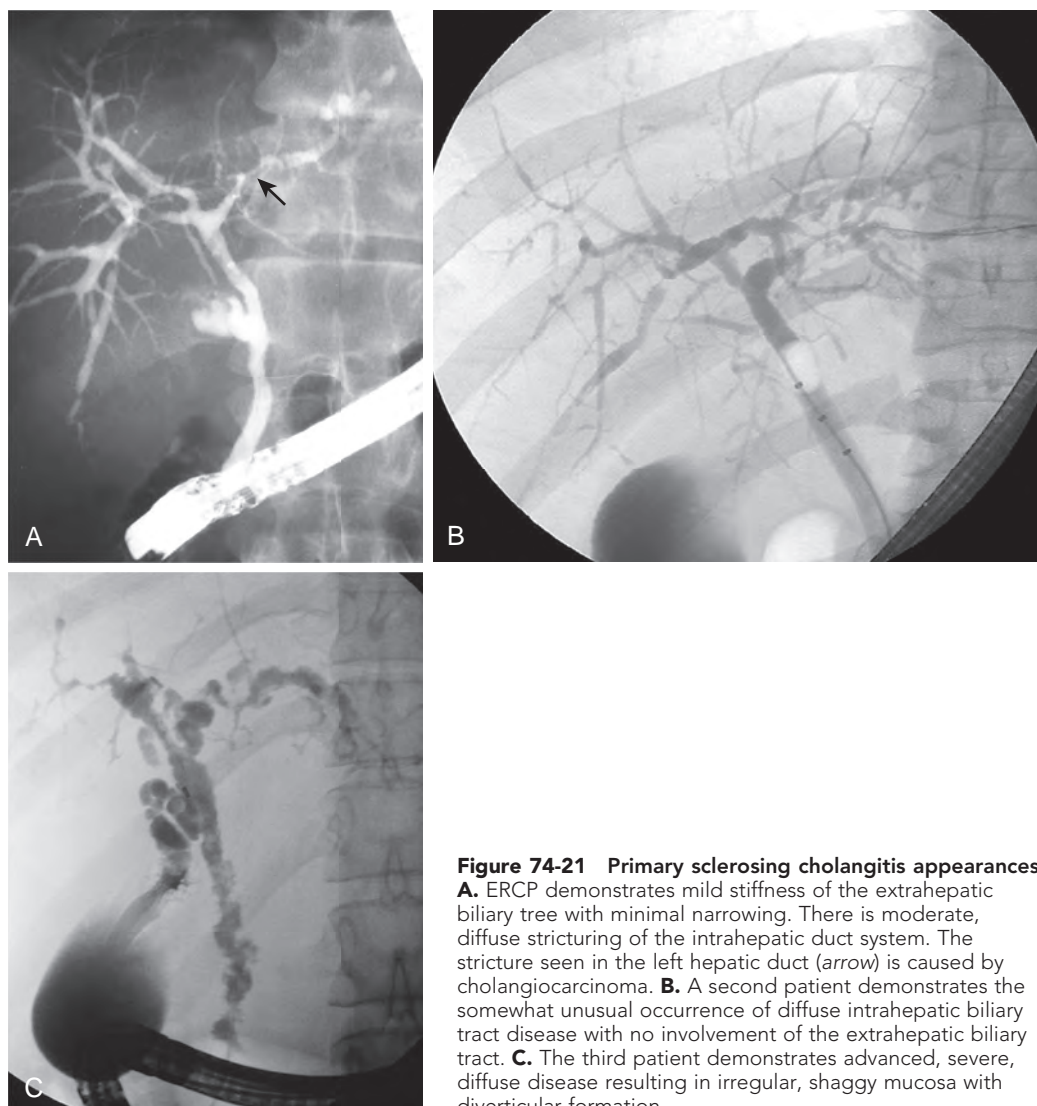


Figure 74-21 Primary sclerosing cholangitis appearances.

A. ERCP demonstrates mild stiffness of the extrahepatic biliary tree with minimal narrowing. There is moderate, diffuse stricturing of the intrahepatic duct system. The stricture seen in the left hepatic duct (arrow) is caused by cholangiocarcinoma. **B.** A second patient demonstrates the somewhat unusual occurrence of diffuse intrahepatic biliary tract disease with no involvement of the extrahepatic biliary tract. **C.** The third patient demonstrates advanced, severe, diffuse disease resulting in irregular, shaggy mucosa with diverticular formation.

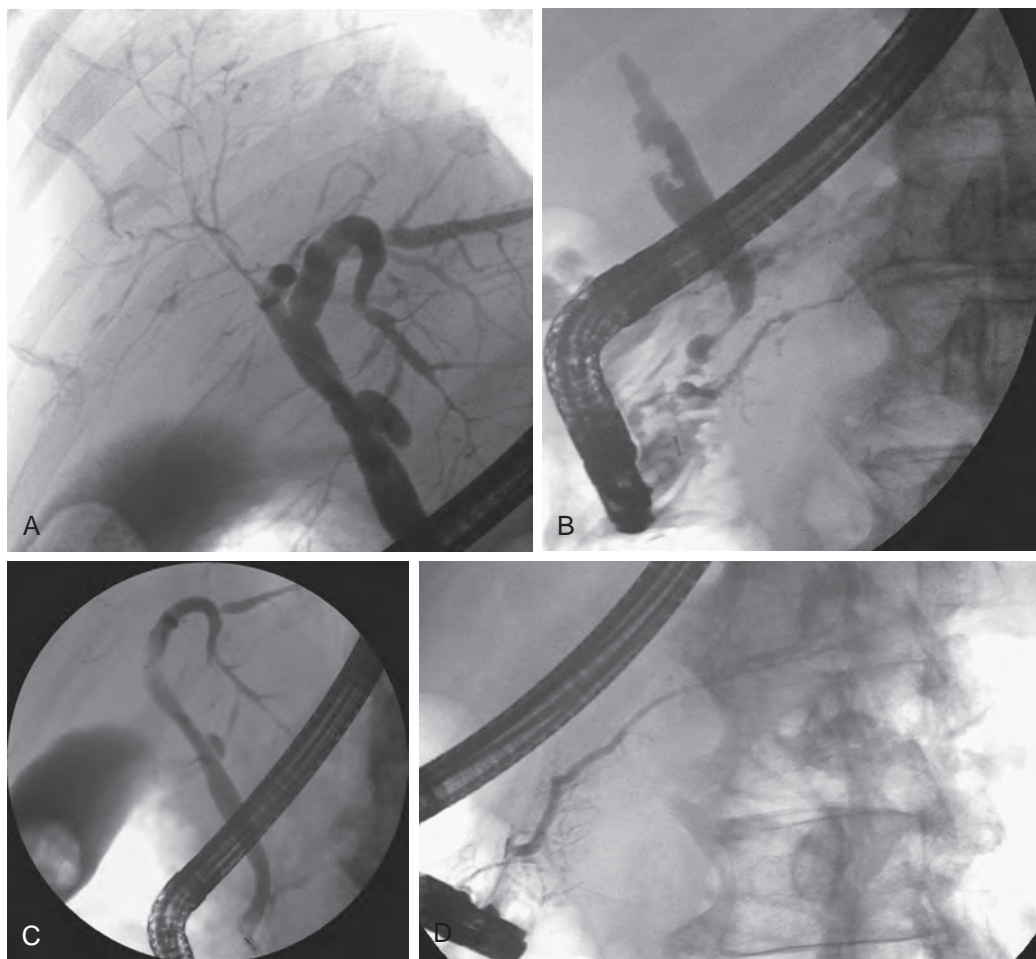


Figure 74-22 Immunoglobulin G4–related sclerosing disease. **A.** There is severe intrahepatic biliary tract stricturing of the right intrahepatic duct system with mild irregularity of the extrahepatic biliary tract that simulates primary sclerosing cholangitis. **B.** The distal extrahepatic biliary tract is strictured along with the diffusely irregular and narrowed pancreatic duct. **C.** After steroid therapy, there has been a marked improvement of the biliary tract. **D.** The pancreatic duct is now nearly normal after steroid treatment.

(CD4 count $<100/\text{mm}^3$) and in the patient population with better preserved immunologic function but not responding to first-line therapies for human immunodeficiency virus infection.⁵² Imaging is still a critical part in the diagnosis of AIDS cholangiopathy; however, clinical information and biochemical data are also important in establishing this diagnosis.

AIDS cholangiopathy can be manifested by a variety of stricture types occurring alone or in combination: a short, papillary stenosis type of narrowing; a longer, 1- to 2-cm extrahepatic biliary tree stricture; or an intrahepatic biliary component that simulates primary sclerosing cholangitis findings (Fig. 74-23).

MRCP is again the imaging examination of choice to display the stricture disease of the biliary tract. ERCP with endoscopic sphincterotomy can relieve the papillary stenosis type of stricture; endoscopic balloon dilation, possibly with stent placement, can be used for the longer extrahepatic biliary tree stricture. Endoscopic brushings can also be obtained to sample areas suspicious for malignant transformation.

The papillitis present in AIDS cholangiopathy can be similar to another distal duct disorder, sphincter of Oddi dysfunction, a nebulous disorder thought to have a mechanical narrowing or an abnormally contracting sphincter of Oddi. Various combinations of “biliary pain,” elevated liver function test results,

increased bile duct diameter, and abnormal sphincter of Oddi manometry are used to place a patient into a type I through type III classification,^{53,54} although this classification has undergone further examination, with some suggesting the need for revision.^{55,56}

Noninvasive tests using nuclear medicine and MRI have been tried to diagnose sphincter of Oddi dysfunction, with mixed results.⁵⁵ ERCP, including sphincter of Oddi manometry when necessary, gives the best results for this diagnosis while also allowing treatment with biliary or, rarely, pancreatic endoscopic sphincterotomy.⁵⁵

ERCP can demonstrate a short, tight stricture at the sphincteric segment (Fig. 74-24) or may be unremarkable. An upstream, dilated CBD may be present. Previously, 12 mm or more was used for abnormal ductal dilation, but now some experts have decreased this diameter to 8 mm or more.⁵⁴ Delayed drainage of either duct system can also be important. The biliary tract, after cholecystectomy, should be completely drained of injected contrast material by 45 minutes. The pancreatic duct should be emptied by 10 minutes after injection. Another important aspect of ERCP is to rule out other diagnoses that may simulate sphincter of Oddi dysfunction. Stones, sludge, and periampullary tumors can all cause sphincter of Oddi dysfunction symptoms and findings.

With increased immigration from Southeast Asia, the inflammatory process of recurrent pyogenic cholangitis, previously referred to as Oriental cholangitis, is more frequently seen in the United States. The presumed combination of infection and obstruction causes the development of intrahepatic and extrahepatic calcium bilirubinate pigment stones.



Figure 74-23 AIDS cholangiopathy. ERCP demonstrates a long stricture of the distal common bile duct (arrow) continuing into the sphincteric segment. The biliary tract above this is mildly dilated with diffuse irregularity of both the intrahepatic and extrahepatic biliary tree. Subsequent endoscopic balloon dilation was used to treat this stricture.

These “stones” tend to be relatively soft, being of mud or paste consistency.

Although CT or MRI may be the first imaging test that can help in the diagnosis and serve as a roadmap for stone location, ERCP can successfully remove the extrahepatic biliary tree stones. The intrahepatic ducts will usually demonstrate angled branching, with stenotic segments making the location of these stones difficult to remove from below. At cholangiography, the left and right posterior duct systems tend to be more heavily involved. Not only does the infection’s fibrotic process cause more central duct strictures, but the peripheral ducts rapidly taper, resulting in the so-called arrowhead sign (Fig. 74-25). The

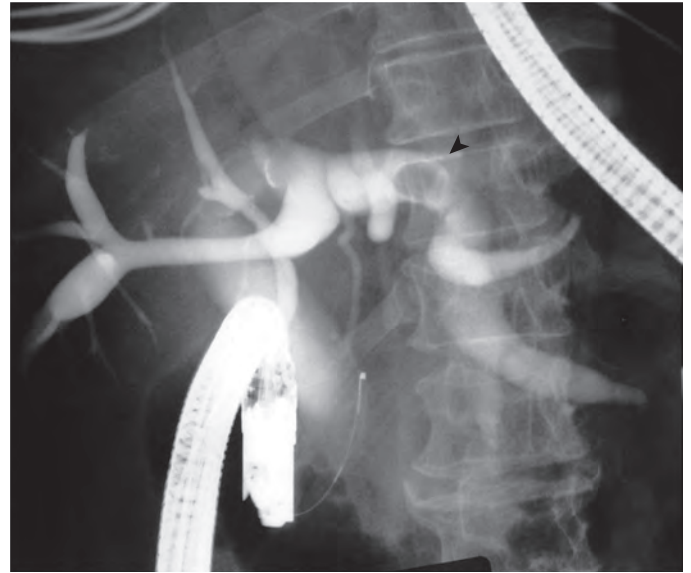


Figure 74-25 Recurrent pyogenic cholangitis. ERCP demonstrates many cholangiographic findings of this disease: diffuse ductal dilation that results from an inflammatory papillitis; a moderate-sized intrahepatic stone (arrowhead); and rapidly tapering peripheral intrahepatic ducts, creating the arrowhead appearance.

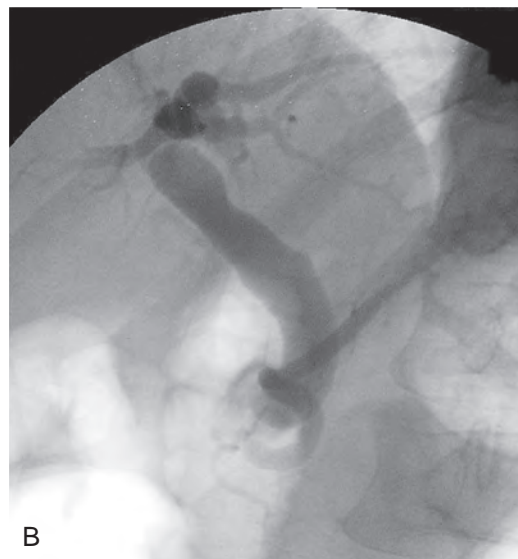
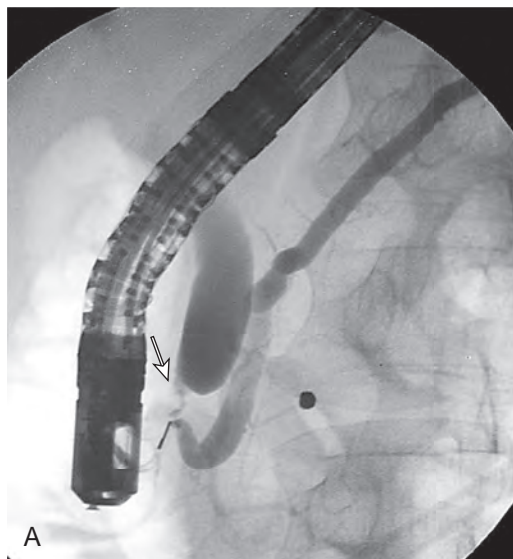


Figure 74-24 Sphincter of Oddi dysfunction. **A.** ERCP shows tight, focal narrowing of the distal common bile duct (arrow). There is upstream dilation. **B.** An image 45 minutes after examination termination reveals contrast material remaining in both the biliary tree and pancreatic duct to confirm obstruction of both systems.

arrowhead appearance is made even more prominent by the tendency of the biliary tract to be diffusely dilated, presumably because of an inflammatory papillitis.

Some other infectious and inflammatory agents can cause biliary narrowing at the hilum from enlarged lymph nodes, such as sarcoid or tuberculosis. Another rare hilar inflammatory process of unknown etiology is the inflammatory pseudotumor or the malignant masquerade. This infiltrating, cicatrizing process tends to occur at the hilum and may extend to the first or second order of the intrahepatic biliary tree. Its appearance is impossible to differentiate from hilar cholangiocarcinoma (Fig. 74-26).



Figure 74-26 Inflammatory pseudotumor. The 78-year-old man presented with jaundice. At cholangiography, there is a tight stricture of the most proximal common hepatic duct (arrow) with upstream dilation. At surgery, a focal inflammatory process was seen in this area, and only inflammatory tissue was found at histology.

Various prior therapeutic treatments can cause biliary strictures. External beam radiation therapy can stricture the bile duct segment within the radiation field (Fig. 74-27A). Strictures can also be seen with the use of intra-arterial chemotherapy (Fig. 74-27B). The bile duct segment near the site of percutaneous ablation can also be narrowed.

There are a number of other inflammatory causes of biliary stricture formation. Cirrhosis can affect the intrahepatic biliary tree with a corkscrew appearance. Cystic fibrosis can have both intrahepatic and extrahepatic biliary tree involvement. Primary biliary cirrhosis will cause diffuse intrahepatic duct strictures as a manifestation of developing cirrhosis. Blunt trauma, with its shearing forces, can produce stricturing at either the hilum or the junction of the suprahepatic and intrahepatic biliary tract. Eosinophilic cholangiopathy is a rare cause of biliary tract stricturing.⁵⁷ Portal biliopathy is a rare condition that occurs with portal hypertension as the recruited bile duct wall vessels enlarge and narrow the extrahepatic duct but do not cause obstruction.⁵⁸ Secondary sclerosing cholangitis can be meant for many of the diseases described so far, but some use this term for the stricturing specifically related to chronic choledocholithiasis. Even periampullary duodenal diverticula may cause extrinsic narrowing of the adjacent biliary tract segment.

Pancreas Neoplasia

Primary pancreatic ductal adenocarcinoma represents more than 90% of pancreatic tumors. Previously, ERCP was an important imaging tool in its diagnosis, having a sensitivity and specificity of 92% and 96%, respectively.⁵⁹ During the past decade, ERCP has steadily been replaced by MDCT, MRI and MRCP, and EUS for diagnosis.^{60,61} MPD injection for diagnostic purposes is no longer used. As discussed earlier, ERCP is now used only in a therapeutic role if treatment for obstructive jaundice is needed, when tissue may also be obtained.

ERCP previously also had a role in the interrogation of the intraductal papillary mucinous neoplasm. ERCP would be used to show ectasia of the MPD or its side branches, to establish the communication of cysts with the MPD, to demonstrate the rare

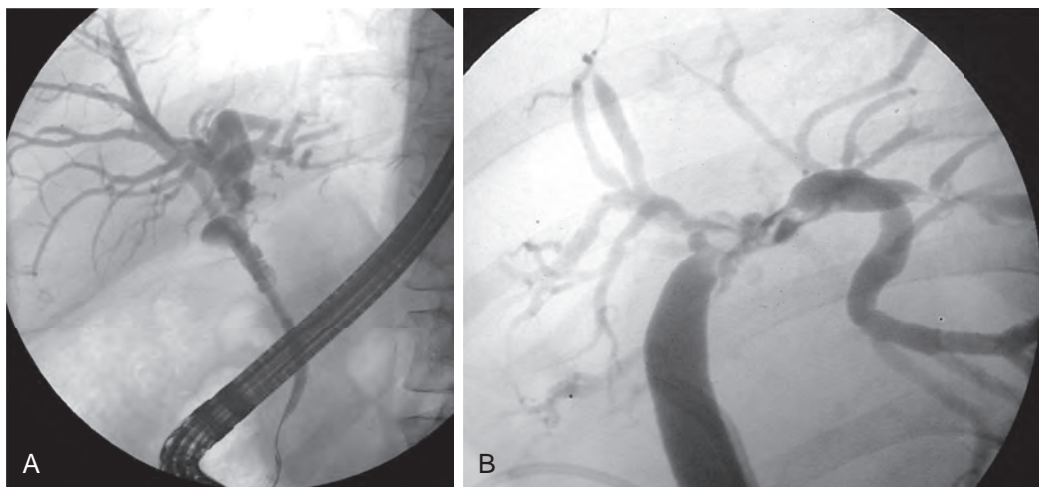


Figure 74-27 Post-therapy biliary tract changes. **A.** ERCP in this patient having undergone radiation therapy for gastric carcinoma demonstrates diffuse extrahepatic biliary tree narrowing, worse distally. **B.** This patient has central duct narrowing after undergoing intra-arterial hepatic chemotherapy for colon cancer.

ductal filling defect, or to obtain brushings or pancreatic fluid samples. However, MDCT, MRI, and MRCP as well as EUS, when it is needed, have replaced ERCP to the extent that it is no longer recommended for imaging of intraductal papillary mucinous neoplasm.⁶²

Numerous other tumors affect the pancreas: serous microcystic adenoma, mucinous cystic neoplasm, neuroendocrine tumor, solid and pseudopapillary endothelial neoplasm, lymphoma, and metastatic disease. ERCP has again been replaced by MDCT, MRI and MRCP, and EUS. In general, all of these tumors tend to displace the MPD. They may cause a variable amount of upstream obstruction from extrinsic pressure, but they do not tend to invade the MPD.

Pancreas Inflammation

Inflammation of the pancreas can be divided into acute and chronic pancreatitis. Idiopathic pancreatitis is used when the etiology of recurrent bouts of acute pancreatitis is not found on the initial work-up. As has been true in many aspects of the pancreaticobiliary tract, the use of ERCP for diagnosis has given way to noninvasive imaging procedures. ERCP is again left mainly for its therapeutic potential.

Although acute pancreatitis has numerous possible causes, alcohol use and gallstones make up the majority of causes. As previously noted, MRCP or EUS now is the first choice in imaging for the diagnosis of choledocholithiasis. In the management of acute pancreatitis, there is still debate as to the necessity of obtaining ERCP with stone removal in biliary pancreatitis. ERCP with endoscopic sphincterotomy and stone removal is not thought to be of help in mild pancreatitis, in which the offending stone presumably is relatively small and passes spontaneously from the biliary tree.^{63,64} However, some would suggest that with a component of biliary tract obstruction or cholangitis, ERCP with stone removal is warranted.⁶³ For any use of ERCP in acute pancreatitis, injection into the MPD is to be avoided.

Previously, ERCP played a prominent role in the diagnosis of chronic pancreatitis (Fig. 74-28) by assessing side branch and main duct changes according to the Cambridge classification.⁶⁵ EUS and MRCP, with the possible addition of secretin with MRCP, are the relatively noninvasive first choices in



Figure 74-28 Mild chronic pancreatitis. The main pancreatic duct is stiff, and there are scattered abnormal side branches (arrow).

imaging of chronic pancreatitis.^{63,66} ERCP, with its endoscopic interventional procedures, can be used to help decompress the MPD and to decrease the pain associated with chronic pancreatitis: endoscopic pancreatic sphincterotomy; balloon dilation of MPD strictures; long-term pancreatic stent placement; and ductal stone or concretion removal (usually made more successful with prior stone extracorporeal shock wave lithotripsy).⁶⁷⁻⁷⁰

Idiopathic pancreatitis is used to describe the 10% to 30% of recurrent acute pancreatitis in which no etiology is found on initial work-up. ERCP can be helpful here as well. Pancreatic sphincter of Oddi manometry can establish the diagnosis of pancreatic sphincter of Oddi dysfunction with subsequent treatment with endoscopic sphincterotomy. ERCP can also be used to aspirate bile to make the diagnosis of microlithiasis, which should lead to cholecystectomy.

Interventional ERCP is also used in the management of pancreatic duct leaks. Most of these leaks are related to severe acute or chronic pancreatitis (Fig. 74-29), but there are other causes as well, such as prior surgery, trauma, or tumor.^{67,71,72} Most success is obtained by extending a pancreatic duct stent across the affected duct segment.⁷³ This pancreatic duct stenting, however, does not provide effective treatment for complete duct disruption, which can lead to the disconnected duct syndrome. In this situation, the leaking pancreatic enzymatic digestive secretions contaminate the pancreatic bed and possibly beyond.⁶⁷ More aggressive measures will be needed with complete disruption.

Endoscopic intervention can also be used in the effective treatment of peripancreatic pseudocysts. Previously, pseudocyst size, reaching 6 cm, was thought to be a major indication for treatment.⁷⁴ Some now suggest that treatment should be reserved for persistent pain, local gastrointestinal tract or biliary tract obstruction, increasing abdominal or pleural fluid, increasing cyst diameter, or signs of pseudocyst complication (such as hemorrhage or infection).⁷⁵

The use of transmural endoscopic treatment requires the pseudocyst to be closely applied with the stomach or duodenum, usually considered to be within 1 cm.⁷⁶ Endoscopy alone or with EUS is used to facilitate the puncture from the gastrointestinal tract segment into the cyst. At least two stents are subsequently placed for adequate drainage. If necrotic debris is present, more stents can be placed or a nasocystic tube can be added.⁷⁵ If needed, subsequent removal of nondrained necrotic material can be obtained by aggressive balloon dilation at the original puncture site with advancement of the endoscope into the cavity for debris removal.⁷⁵

Transpapillary drainage of pseudocysts can also be obtained if the cyst is less than 6 cm and communicates with the MPD.^{75,77,78} A large-bore stent is placed across the segment of duct disruption or into the cyst itself.

Complications of Endoscopic Retrograde Cholangiopancreatography

The major complications occurring with ERCP are pancreatitis, hemorrhage, perforation, and biliary tract infection. Pancreatitis is the most common, ranging from approximately 2% to 16% but most commonly reported in 3.5% of cases.⁷⁹⁻⁸²

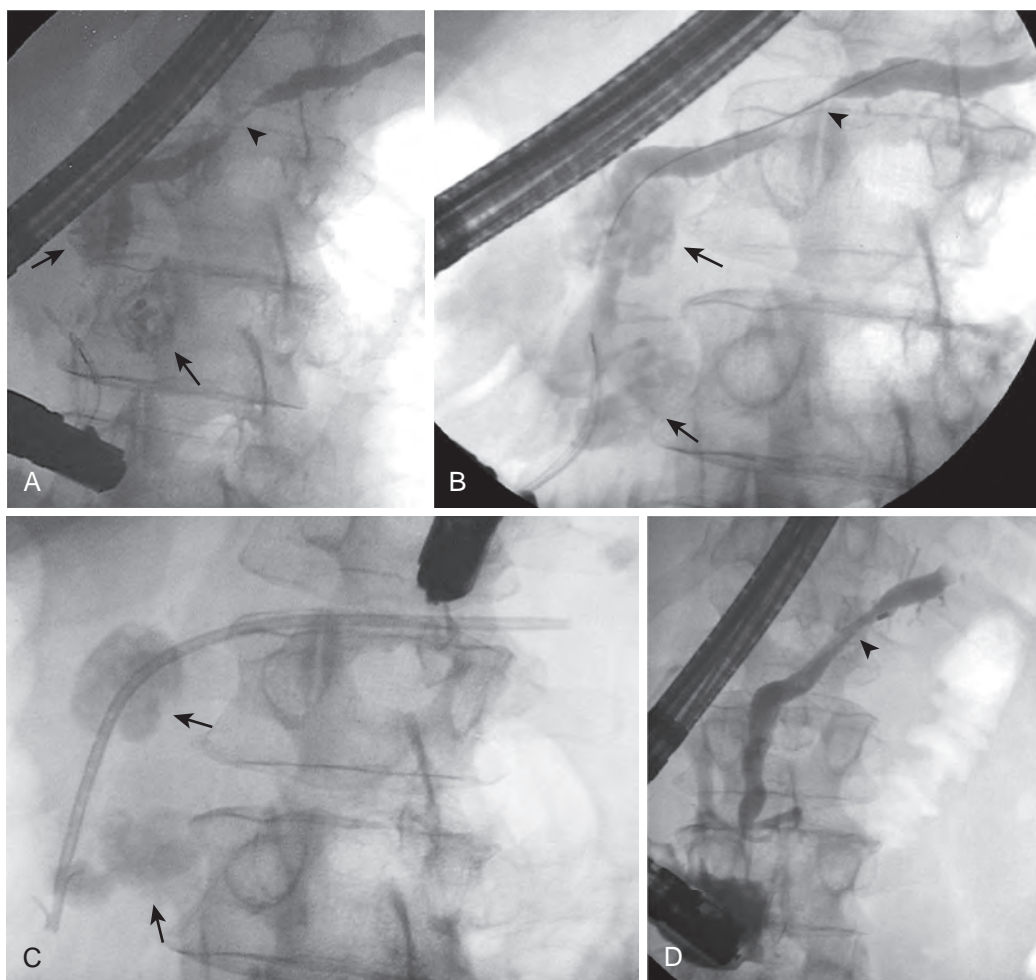


Figure 74-29 Chronic pancreatitis and endoscopic intervention. **A.** On initial ERCP, there is a subtle extravasation into two pseudocysts (arrows) and a stricture in the mid main pancreatic duct (arrowhead). **B.** Subsequently, a wire is placed into the pancreatic duct across the two segments communicating with the pseudocysts (arrows) and stricture (arrowhead). **C.** A final image from this first examination demonstrates the plastic stent crossing the area of the two pseudocysts (arrows) and projecting across the presumed area of main pancreatic duct stricture. **D.** ERCP 5 months after the initial examination demonstrates that there is no filling of either pseudocyst, and the mid main pancreatic duct stricture (arrowhead) has improved.

Hemorrhage after ERCP occurs in about 1.3% of cases, with the majority of bleeding episodes being minor.⁸² This complication is much more likely to be related to sphincterotomy than when only a diagnostic examination is obtained. The bleeding usually exits into the gastrointestinal tract and much less commonly into the ductal system.⁷⁹

Perforation is seen in 0.1% to 0.6% of examinations.⁷⁹ It can be related to guidewire manipulation or perforation at

the ampulla of Vater during endoscopic sphincterotomy or at a site separate from the papilla in the gastrointestinal tract.⁸³

Infection is related to the biliary tract or even the gallbladder. Cholangitis is present in less than 1% of cases and appears to be related to extent of ductal manipulation, patient factors, and operator experience.^{79,84-86} Cholangitis is reported in 0.2% to 0.5% of examinations.^{84,85}

REFERENCES

1. Belsito AA, Marta JB, Cramer GG, et al: Measurements of biliary tract size and drainage time. Composition of endoscopic and intravenous cholangiography. *Radiology* 122:65, 1977.
2. Kim OH, Chung HJ, Choi BG: Imaging of the choledochal cyst. *Radiographics* 15:69-88, 1995.
3. Wiedmeyer DA, Stewart ET, Geenen JE, et al: Choledochal cyst: Findings on cholangiopancreatography with emphasis on ectasia of the common channel. *AJR Am J Roentgenol* 153: 969-972, 1989.
4. Dodds WJ: Biliary tract motility and its relationship to clinical disorders. *AJR Am J Roentgenol* 155:247-258, 1990.
5. Classen M, Hellwig H, Rosch W: Anatomy of the pancreatic duct, a duodenoscopic-radiological study. *Endoscopy* 5:14-17, 1973.
6. Cotton PB: The normal endoscopic pancreatogram. *Endoscopy* 6:65-70, 1974.
7. Kasugai T, Kuno N, Kobayashi S, et al: Endoscopic pancreatocholangiography. *Gastroenterology* 63:217-226, 1972.
8. Mortelé K, Rocha T, Streeter J, et al: Multimodality imaging of pancreatic and biliary congenital anomalies. *Radiographics* 26:715, 2006.
9. Yoon WJ, Brugge WR: Endoscopic evaluation of bile duct strictures. *Gastrointest Endosc Clin N Am* 23:277-293, 2013.
10. Stroszczynski C, Hunerbein M: Malignant biliary obstruction: Value of imaging findings. *Abdom Imaging* 30:314-323, 2005.
11. Park M-S, Kim TK, Kim KW, et al: Differentiation of extrahepatic bile duct cholangiocarcinoma. *Gastrointest Endosc* 79:100-108, 2014.

- noma from benign stricture: Findings at MRCP versus ERCP. *Radiology* 233:234–240, 2004.
12. Choi SH, Han JK, Lee JM, et al: Differentiating malignant from benign common bile duct stricture with multiphasic helical CT. *Radiology* 236:178–183, 2005.
 13. Lalani T, Couto CA, Rosen MP, et al: ACR appropriateness criteria jaundice. *J Am Coll Radiol* 10:402–409, 2013.
 14. Costamagna G, Familiari P, Marchese M, Tringali A: Endoscopic biliopancreatic investigations and therapy. *Best Pract Res Clin Gastroenterol* 22(5):865–881, 2008.
 15. Coté GA, Sherman S: Biliary stricture and negative cytology: What next? *Clin Gastroenterol Hepatol* 9:739–743, 2011.
 16. Akoad M, Jenkins R: Proximal biliary malignancy. *Surg Clin North Am* 88:1409–1428, 2008.
 17. Ray CE, Lorenz JM, Burke CT, et al: ACR Appropriateness Criteria: Radiologic management of benign and malignant biliary obstruction, <<http://www.acr.org/Quality-Safety/Appropriateness-Criteria/AmericanCollegeofRadiology>>. Accessed November 5, 2013.
 18. Joo I, Lee JM: Imaging bile duct tumors: Pathologic concepts, classification, and early tumor detection. *Abdom Imaging* 38:1334–1350, 2013.
 19. Zen Y, Fujii T, Itatsu K, et al: Biliary papillary tumors share pathological features with intra-ductal papillary mucinous neoplasm of the pancreas. *Hepatology* 44:1333–1343, 2006.
 20. Kim HK, Lo SK: Endoscopic approach to the patient with benign or malignant ampullary lesions. *Gastrointest Endosc Clin N Am* 23:347–383, 2013.
 21. Fong ZV, Tan WP, Lavu H, et al: Preoperative imaging for resectable periampullary cancer: Clinicopathologic implications of reported radiographic findings. *J Gastrointest Surg* 17:1098–1106, 2013.
 22. Shanbhoque AKP, Tirumani SH, Prasad SR, et al: Benign biliary strictures: A current comprehensive clinical and imaging review. *AJR Am J Roentgenol* 197:W295–W306, 2011.
 23. Flenn DR, Cheadle A, Prela C, et al: Bile duct injury during cholecystectomy and survival in Medicare beneficiaries. *JAMA* 290:2168–2173, 2003.
 24. Krohenbuhl L, Sclobos C, Wente MN, et al: Incidence, risk factors and prevention of bile duct injuries during laparoscopic cholecystectomy in Switzerland. *World J Surg* 25:1325–1330, 2001.
 25. Jablonska B, Lampe P: Iatrogenic bile duct injuries: Etiology, diagnosis and management. *World J Gastroenterol* 15:4097–4104, 2009.
 26. Baillie J: Endoscopic approach to the patient with bile duct injury. *Gastrointest Endosc Clin N Am* 23:461–472, 2013.
 27. Ayoub WS, Esquivel CO, Martin P: Biliary complications following liver transplantation. *Dig Dis Sci* 55:1540–1546, 2010.
 28. Singh AK, Nachiappan AC, Verma HA, et al: Postoperative imaging in liver transplantation: What radiologists should know. *Radiographics* 30:339–351, 2010.
 29. Jorgensen JE, Waljee AK, Volk ML, et al: Is MRCP equivalent to ERCP for diagnosing biliary obstruction in orthotopic liver transplant recipients? A meta-analysis. *Gastrointest Endosc* 73:955–962, 2011.
 30. Katazono MT, Qayyum A, Yeh BM, et al: Magnetic resonance cholangiography of biliary strictures after liver transplantation: A prospective double-blind study. *J Magn Reson Imaging* 25:1168–1173, 2007.
 31. Novellas S, Caramella T, Fournol M, et al: MR cholangiopancreatography features of the biliary tree after liver transplantation. *AJR Am J Roentgenol* 191:221–227, 2008.
 32. Nasr JY, Slivka A: Endoscopic approach to the post liver transplant patient. *Gastrointest Endosc Clin N Am* 23:473–481, 2013.
 33. Guichelaar MM, Benson JT, Malinchoc M, et al: Risk factors for the clinical course of non-anastomotic biliary strictures after liver transplantation. *Am J Transplant* 3:885–890, 2003.
 34. Baron TH, DeVee T: Endoscopic management of benign bile duct strictures. *Gastrointest Endosc Clin N Am* 23:295–311, 2013.
 35. Abdallah AA, Krige JEJ, Bornman PC: Biliary tract obstruction in chronic pancreatitis. *HPB (Oxford)* 9:421–428, 2007.
 36. Deviere J, Devaere S, Baize M, et al: Endoscopic biliary drainage in chronic pancreatitis. *Gastrointest Endosc* 36:96–100, 1990.
 37. Pozsar J, Sahin P, Laszlo F, et al: Medium-term results of endoscopic treatment of common bile duct strictures in chronic calcifying pancreatitis with increasing numbers of stents. *J Clin Gastroenterol* 38:118–123, 2004.
 38. Kahl S, Zimmermann S, Genz I, et al: Risk factors for failure of endoscopic stenting of biliary strictures in chronic pancreatitis: A prospective follow-up study. *Am J Gastroenterol* 98:2448–2453, 2003.
 39. Petrosz JA, Dutta SK: The variable appearance of distal common bile duct stenosis in chronic pancreatitis. *J Clin Radiol* 7:447, 1985.
 40. Kroh M, Chand B: Choledocholithiasis, endoscopic retrograde cholangiopancreatography, and laparoscopic common bile duct exploration. *Surg Clin North Am* 88:1019–1031, 2008.
 41. Buxbaum J: Modern management of common bile duct stones. *Gastrointest Endosc Clin N Am* 23:251–275, 2013.
 42. Barkun AN, Barkun JS, Fried GM, et al: Useful predictors of bile duct stones in patients undergoing laparoscopic cholecystectomy. *McGill Gallstone Treatment Group. Ann Surg* 220:32–39, 1994.
 43. Tham TC, Lichtenstein DR, Vandervoort J, et al: Role of endoscopic retrograde cholangiopancreatography for suspected choledocholithiasis in patients undergoing laparoscopic cholecystectomy. *Gastrointest Endosc* 47:50–56, 1998.
 44. Ainsworth AP, Rafaelsen SR, Wamberg PA, et al: Is there a difference in diagnostic accuracy and clinical impact between endoscopic ultrasonography and magnetic resonance cholangiopancreatography? *Endoscopy* 35:1029–1032, 2003.
 45. Zalikas J, Monson JL: Complications of gallstones: The Mirizzi syndrome, gallstone ileus, gallstone pancreatitis, complications of “lost” gallstones. *Surg Clin North Am* 88:1345–1368, 2008.
 46. Redaelli CA, Buchler MW, Schilling MK, et al: High coincidence of Mirizzi syndrome and gallbladder cancer. *Surgery* 121:58–63, 1997.
 47. Razumilava N, Gores GJ, Lindor KD: Cancer surveillance in patients with primary sclerosing cholangitis. *Hepatology* 55:1842–1852, 2011.
 48. Weber C, Kuhlencordt R, Grotelueschen R, et al: Magnetic resonance cholangiopancreatography in the diagnosis of primary sclerosing cholangitis. *Endoscopy* 40:739–745, 2008.
 49. Ghazale A, Chari ST, Zhang L, et al: Immunoglobulin G4-associated cholangitis: Clinical profile and response to therapy. *Gastroenterology* 134:706–715, 2008.
 50. Nakazawa T, Ohara H, Sano H, et al: Schematic classification of sclerosing cholangitis with autoimmune pancreatitis by cholangiography. *Pancreas* 32:229, 2006.
 51. Babakhanian Z, Donovan JA: Biliary manifestations of systemic diseases. *Gastrointest Endosc Clin N Am* 23:333–346, 2013.
 52. Tonolini M, Bianco R: HIV-related/AIDS cholangiopathy: Pictorial review with emphasis on MRCP findings and differential diagnosis. *Clin Imaging* 37:219–226, 2013.
 53. Geenen JE, Hogan WJ, Dodds WJ, et al: The efficacy of endoscopic sphincterotomy after cholecystectomy in patients with sphincter-of-Oddi dysfunction. *N Engl J Med* 320:82–87, 1989.
 54. Baillie J: Sphincter of Oddi dysfunction. *Curr Gastroenterol Rep* 12:130–134, 2010.
 55. Leung WD, Sherman S: Endoscopic approach to the patient with motility disorders of the bile duct and sphincter of Oddi. *Gastrointest Endosc Clin N Am* 23:405–434, 2013.
 56. Freeman ML, Gill M, Overby C, et al: Predictors of outcomes after biliary and pancreatic sphincterotomy for sphincter of Oddi dysfunction. *J Clin Gastroenterol* 41:94–102, 2007.
 57. Vauthey JN, Loyer E, Chokshi P, Lohoti S: Case 57: Eosinophilic cholangiopathy. *Radiology* 227:107–112, 2003.
 58. Dhiman RK, Behera A, Chawla YK, et al: Portal hypertensive biliopathy. *Gut* 56:1001–1008, 2007.
 59. Niederau C, Grendell JH: Diagnosis of pancreatic carcinoma. Imaging techniques and tumor markers. *Pancreas* 7:66–86, 1992.
 60. Adamek HE, Albert J, Breer H, et al: Pancreatic cancer detection with magnetic resonance cholangiopancreatography and endoscopic retrograde cholangiopancreatography: A prospective controlled study. *Lancet* 356:190–193, 2000.
 61. Michl P, Pauls S, Gress TM: Evidence-based diagnosis and staging of pancreatic cancer. *Best Pract Res Clin Gastroenterol* 20:227–251, 2006.
 62. Tanaka M, Fernández-del Castillo C, Adsay V, et al: International consensus guidelines 2012 for the management of IPMN and MCN of the pancreas. *Pancreatol* 12:183–197, 2012.
 63. Lee LS, Conwell DL: Update on advanced endoscopic techniques for the pancreas: endoscopic retrograde cholangiopancreatography, drainage and biopsy, and endoscopic ultrasound. *Radiol Clin N Am* 50:547–561, 2012.
 64. Petrov MS, van Santvoort HC, Besselink MG, et al: Early endoscopic retrograde cholangiopancreatography versus conservative management in acute biliary pancreatitis without cholangitis: a meta-analysis of randomized trials. *Ann Surg* 247:250–257, 2008.
 65. Axon ATR: Endoscopic retrograde cholangiopancreatography in chronic pancreatitis. Cambridge classification. *Radiol Clin N Am* 27:39, 1989.
 66. Sanyal R, Stevens T, Novak E, et al: Secretin-enhanced MRCP: review of technique and application with proposal for quantification of exocrine function. *AJR* 198:124–132, 2012.
 67. Buxbaum J: The role of endoscopic retrograde cholangiopancreatography in patients with pancreatic disease. *Gastroenterol Clin N Am* 41:23–45, 2012.
 68. Delhaye M, Arvanitakis M, Verset G, et al: Long-term clinical outcome after endoscopic pancreatic ductal drainage for patients with painful chronic pancreatitis. *Clin Gastroenterol Hepatol* 2:1096–1106, 2004.
 69. Smits ME, Badiga SM, Rauws EA, et al: Long-term results of pancreatic stents in chronic

- pancreatitis. *Gastrointest Endosc* 42:461–467, 1995.
70. Eleftheriadis N, Dinu F, Delhay M, et al: Long-term outcome after pancreatic stenting in severe chronic pancreatitis. *Endoscopy* 37:223–230, 2005.
71. Deviere J, Bueso H, Baize M, et al: Complete disruption of the main pancreatic duct: endoscopic management. *Gastrointest Endosc* 42:445–451, 1995.
72. Varadarajulu S, Noone TC, Tutuian R, et al: Predictors of outcome in pancreatic duct disruption managed by endoscopic transpapillary stent placement. *Gastrointest Endosc* 61:568–575, 2005.
73. Telford JJ, Farrell JJ, Saltzman JR, et al: Pancreatic stent placement for duct disruption. *Gastrointest Endosc* 56:18–24, 2002.
74. Bergman S, Melvin WS: Operative and nonoperative management of pancreatic pseudocysts. *Surg Clin N Am* 87:1447–1460, 2007.
75. Samuelson AL, Shah RJ: Endoscopic management of pancreatic pseudocysts. *Gastroenterol Clin N Am* 41:47–62, 2012.
76. Rosso E, Alexakis N, Ghaneh P, et al: Pancreatic pseudocyst in chronic pancreatitis: endoscopic and surgical treatment. *Dig Surg* 20:397–406, 2003.
77. Catalano MF, Geenen JE, Schmalz MJ, et al: Treatment of pancreatic pseudocysts with ductal communication by transpapillary pancreatic duct endoprosthesis. *Gastrointest Endosc* 42:214–218, 1995.
78. Binmoeller KF, Seifert H, Walter A, et al: Transpapillary and transmural drainage of pancreatic pseudocysts. *Gastrointest Endosc* 42:219–224, 1995.
79. Anderson MA, Fisher L, Jain R, et al: Complications of ERCP. *Gastrointest Endosc* 75:467–473, 2012.
80. Cotton PB, Garrow DA, Gallagher J, et al: Risk factors for complications after ERCP: a multivariate analysis of 11,497 procedures over 12 years. *Gastrointest Endosc* 70:80–88, 2009.
81. Barthet M, Lesavre N, Desjeux A, et al: Complications of endoscopic sphincterotomy: results from a single tertiary referral center. *Endoscopy* 34:991–997, 2002.
82. Andriulli A, Loperfido S, Napolitano G, et al: Incidence rates of post-ERCP complications: a systematic survey of prospective studies. *Am J Gastroenterol* 102:1781–1788, 2007.
83. Howard TJ, Tan T, Lehman GA, et al: Classification and management of perforations complicating endoscopic sphincterotomy. *Surgery* 126:658–663; discussion 64–65, 1999.
84. Freeman ML, Nelson DB, Sherman S, et al: Complications of endoscopic biliary sphincterotomy. *N Engl J Med* 335:909–918, 1996.
85. Masci E, Toti G, Mariani A, et al: Complications of diagnostic and therapeutic ERCP: a prospective multicenter study. *Am J Gastroenterol* 96:417–423, 2001.
86. Loperfido S, Angelini G, Benedetti G, et al: Major early complications from diagnostic and therapeutic ERCP: a prospective multicenter study. *Gastrointest Endosc* 48:1–10, 1998.

Magnetic Resonance Cholangiopancreatography

ANN S. FULCHER | MARY ANN TURNER

CHAPTER OUTLINE

Technique

Clinical Applications

Bile Duct Calculi

Neoplasms

Congenital Anomalies

Postoperative Alterations of the Pancreaticobiliary Tract and Gastrointestinal Tract

Primary Sclerosing Cholangitis

Pancreatitis

Acute Pancreatitis

Chronic Pancreatitis

Gallbladder Diseases

Since the first clinical application of magnetic resonance cholangiopancreatography (MRCP) in the early 1990s, MRCP has evolved from a technique with questionable potential for imaging of the biliary tract and pancreatic duct to one that is now recognized as a pivotal tool for diagnosis of pancreaticobiliary disease. In fact, the evolution of MRCP has been such that at many centers, MRCP has replaced diagnostic endoscopic retrograde cholangiopancreatography (ERCP) in a number of clinical scenarios. A prospective survey revealed that MRCP findings enhance the diagnostic confidence of gastroenterologists and decrease the need for invasive procedures.¹

For many years, ERCP has been considered the standard of reference for imaging of the biliary tract and pancreatic duct because of its ability to render high-quality images of the ducts. However, ERCP is an invasive examination associated with complications that occur in up to 5% of all attempts and that range from subclinical to life-threatening.² Those complications include pancreatitis, hemorrhage, cholangitis, and gastrointestinal tract perforation.

The relatively rapid acceptance of MRCP is related, in large part, to its ability to provide images of the ducts similar to those of ERCP. These images can be obtained without the associated complications of ERCP while offering comparable sensitivity, specificity, and accuracy. In addition, MRCP is readily performed in the outpatient setting and does not expose patients to ionizing radiation. In most instances, performance of MRCP does not require administration of sedation. In contrast to ERCP, MRCP readily depicts ducts proximal to a high-grade obstruction as well as ducts in patients with surgical alterations of the biliary tract and gastrointestinal tract, such as biliary-enteric anastomoses. Although ERCP yields exquisite images of the ductal systems, it provides no direct information about the

solid organs and vessels of the abdomen. However, when MRCP is performed in conjunction with conventional magnetic resonance imaging (MRI) and, when necessary, magnetic resonance angiography (MRA), a comprehensive examination is achieved. This information assists in determining resectability of neoplasms, such as pancreatic carcinoma, and in detecting complications of primary sclerosing cholangitis, such as cirrhosis and cholangiocarcinoma.

Technique

Before acquisition of the MRCP image, many advocate the use of heavily T2-weighted, non-fat-suppressed sequences, such as the half-Fourier acquisition single-shot turbo spin-echo (HASTE) sequence, to provide an overview of the entire abdomen (Fig. 75-1A). These comprehensive images allow visualization of the solid organs as well as of the pancreaticobiliary tract and gallbladder. The MRCP image is then acquired. This can be achieved by use of a two-dimensional (2D), heavily T2-weighted, fat-suppressed, breath-hold sequence. This sequence can provide single thick-slab images with slice thicknesses ranging from 10 to 70 mm and multiple thin-slab images with slice thicknesses ranging from 2 to 5 mm^{3,4} (Fig. 75-1B-D). The images depict the biliary tract, pancreatic duct, and gallbladder as high signal intensity structures. Multiple acquisitions are conducted in the coronal and coronal oblique planes to optimally image the ducts. In addition, the axial plane is useful in distinguishing stones, which layer in the dependent portion of the duct, from pneumobilia, which is nondependent. In general, the thin-slab images allow improved delineation of the finer details of the ductal systems, whereas the thick-slab images provide comprehensive views of the ducts that assist in the depiction of diffuse ductal diseases, such as primary sclerosing cholangitis. Although the thin-slab images may be manipulated with a maximum intensity projection (MIP) algorithm, most diagnostic decisions are made directly from the 2D images. In interpreting MIP images, it should be remembered that at times the high signal intensity that is characteristic of MIPs may obscure subtle intraductal filling defects, such as small stones.

More recently, three-dimensional (3D) sequences used in conjunction with respiratory triggering, thin sections (1-2 mm), and high matrices have been used to generate MRCP images. With this technique, the source images can be viewed as individual images, much like MRCP images acquired with 2D sequences. The advantage of 3D imaging is that it yields isotropic images that can be reformatted in any plane, thereby obviating the need to acquire images in multiple planes.

Some investigators advocate the performance of contrast-enhanced MRCP with 3D T1-weighted sequences and hepatocyte-specific contrast agents that are excreted into the biliary tract. These agents are divided into two major

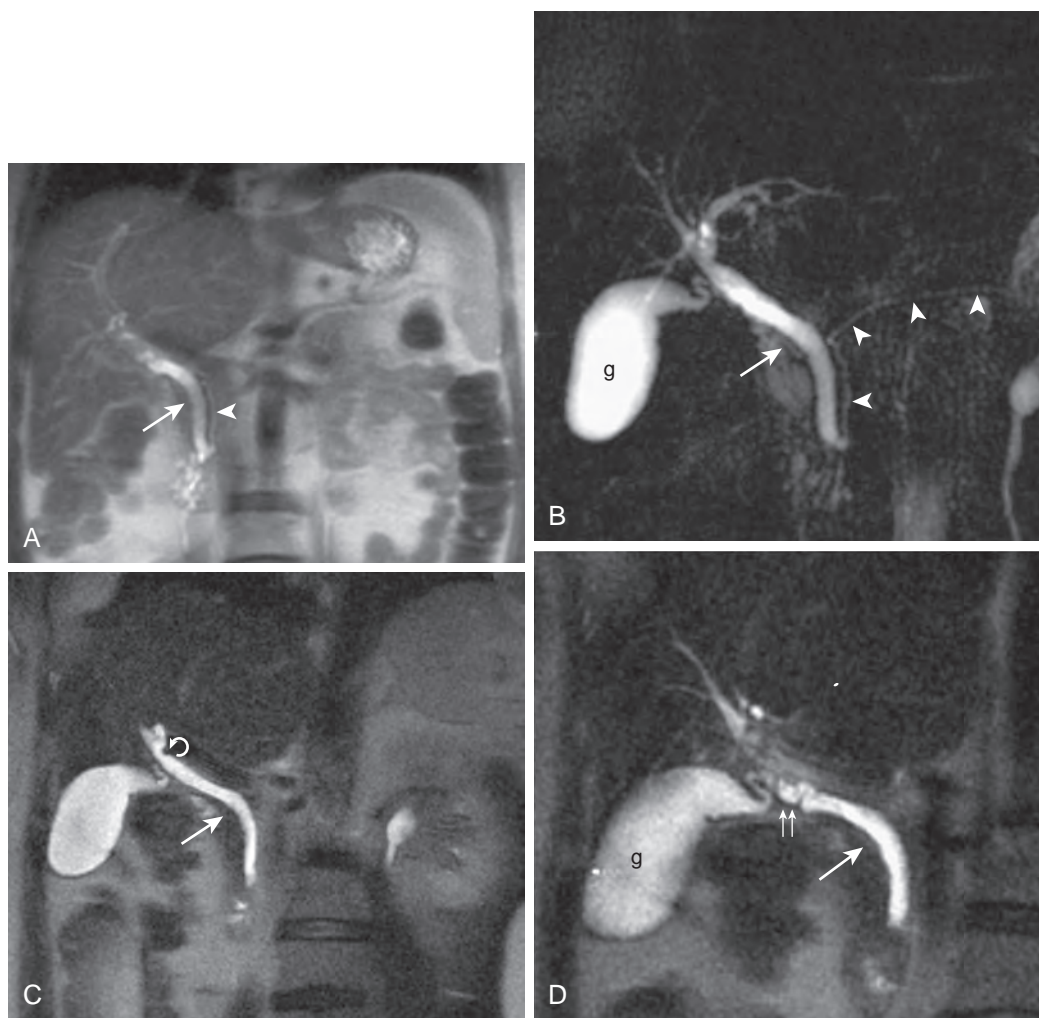


Figure 75-1 MRCP technique: normal anatomy. **A.** Coronal, non-fat-suppressed HASTE image provides an overview of the abdomen by depicting the liver and spleen as well as the distal half of the bile duct (arrow) and pancreatic duct (arrowhead) in the head of the pancreas. **B.** Coronal, fat-suppressed, thick-slab (40 mm) MRCP shows the intrahepatic bile ducts, extrahepatic bile duct (arrow), pancreatic duct (arrowheads), and gallbladder (g) in a single image. **C.** Coronal oblique, fat-suppressed, thin-slab (5 mm) MRCP demonstrates the finer details of the extrahepatic bile duct (arrow) compared with the thick-slab MRCP. Extrinsic compression (curved arrow) of the proximal extrahepatic bile duct by the crossing hepatic artery is noted. **D.** Coronal oblique, fat-suppressed, thin-slab (5 mm) MRCP reveals the gallbladder (g), the cystic duct (double arrow), and a portion of the extrahepatic bile duct (arrow).

categories: manganese-based agents (no longer available in the United States) and gadolinium-based agents, such as gadobenate dimeglumine and gadoxetate.⁵ MRCP performed with T1-weighted sequences and a manganese-based agent has been shown useful in the detection of biliary complications after laparoscopic cholecystectomy and in depicting the intrahepatic bile ducts in living liver transplant donor candidates.^{6,7}

The 2D and 3D techniques allow excellent depiction of the pancreatic duct in most cases. However, in those instances in which the pancreatic duct is not well visualized or determination of pancreatic exocrine function is desired, secretin-enhanced MRCP may prove useful.⁸

Whereas the majority of MRCP studies are performed on 1.5T MRI scanners, a growing number of MRCP studies are being performed on 3.0T MRI scanners, given their increased availability and use. Although 3T scanners may improve image quality and therefore improve ductal delineation, 3T scanners produce increased susceptibility artifacts compared with 1.5T scanners.⁹

Clinical Applications

BILE DUCT CALCULI

Historically, many patients with suspected choledocholithiasis and a normal sonogram or computed tomography (CT) scan underwent diagnostic ERCP to determine the presence or absence of stones. The introduction of MRCP provided a long-awaited, noninvasive alternative to diagnostic ERCP for the detection and exclusion of common bile duct stones. However, for MRCP to gain widespread acceptance, it had to compare favorably with ERCP. In an analysis of 72 patients studied with intraoperative cholangiography and ERCP, Frey and associates¹⁰ found a sensitivity of 90% and a specificity of 98% for ERCP in the setting of suspected choledocholithiasis.

Initial reports of MRCP in the detection of common bile duct stones noted sensitivities as low as 81%.¹¹ However, technical advances in MR hardware and the introduction of sequences that allowed breath-hold imaging and that suppressed artifacts

arising from surgical clips and bowel gas improved MRCP image quality substantially, which in turn enhanced the MRCP diagnosis of common bile duct stones. Subsequent studies performed with state-of-the-art scanners and sequences demonstrated sensitivities of 90% to 100%, specificities of 92% to 100%, and positive predictive value of 96% to 100%, matching and in most cases exceeding those of ERCP.^{3,12-16} Although many physicians focus on the sensitivity offered by a technique, it is equally important to consider the negative predictive value. The negative predictive values of MRCP are high, ranging from 96% to 100%.^{3,14,17} Therefore, if an MRCP study is interpreted as negative for common duct stones, one can be confident that stones are not present in most cases and ERCP can be avoided.^{3,17} In fact, one of the major benefits of MRCP in the setting of suspected biliary calculi is the reduction of unnecessary ERCP studies.¹⁶

In the setting of symptomatic gallstones, MRCP has been shown to be highly accurate in the detection of coexistent choledocholithiasis in patients with high, moderate, and low risks for harboring common bile duct stones based on clinical, laboratory, and sonographic findings.¹² Kim and colleagues¹²

recommended that MRCP be performed before cholecystectomy in patients with a moderate or high risk of common bile duct stones in an effort to reduce morbidity associated with undetected choledocholithiasis and to decrease the performance of purely diagnostic ERCP.

In addition to the detection of common bile duct stones, MRCP performs well in the detection of intrahepatic stones. One study revealed that the sensitivity and specificity of MRCP for detection of intrahepatic stones were 97% and 93%, respectively, whereas those of ERCP were 59% and 97%, respectively.¹⁸

Both extrahepatic and intrahepatic bile duct stones are seen as well-defined, low signal intensity filling defects in the high signal intensity bile (Fig. 75-2). MRCP has been shown to detect stones as small as 2 mm even in normal-caliber ducts.³ Although the coronal and coronal oblique planes demonstrate stones in most instances, at times it is helpful to acquire MRCP images in the axial plane to detect small stones and to differentiate stones that lie in the dependent portion of the duct from pneumobilia that lies in the nondependent portion of the duct (Fig. 75-3).

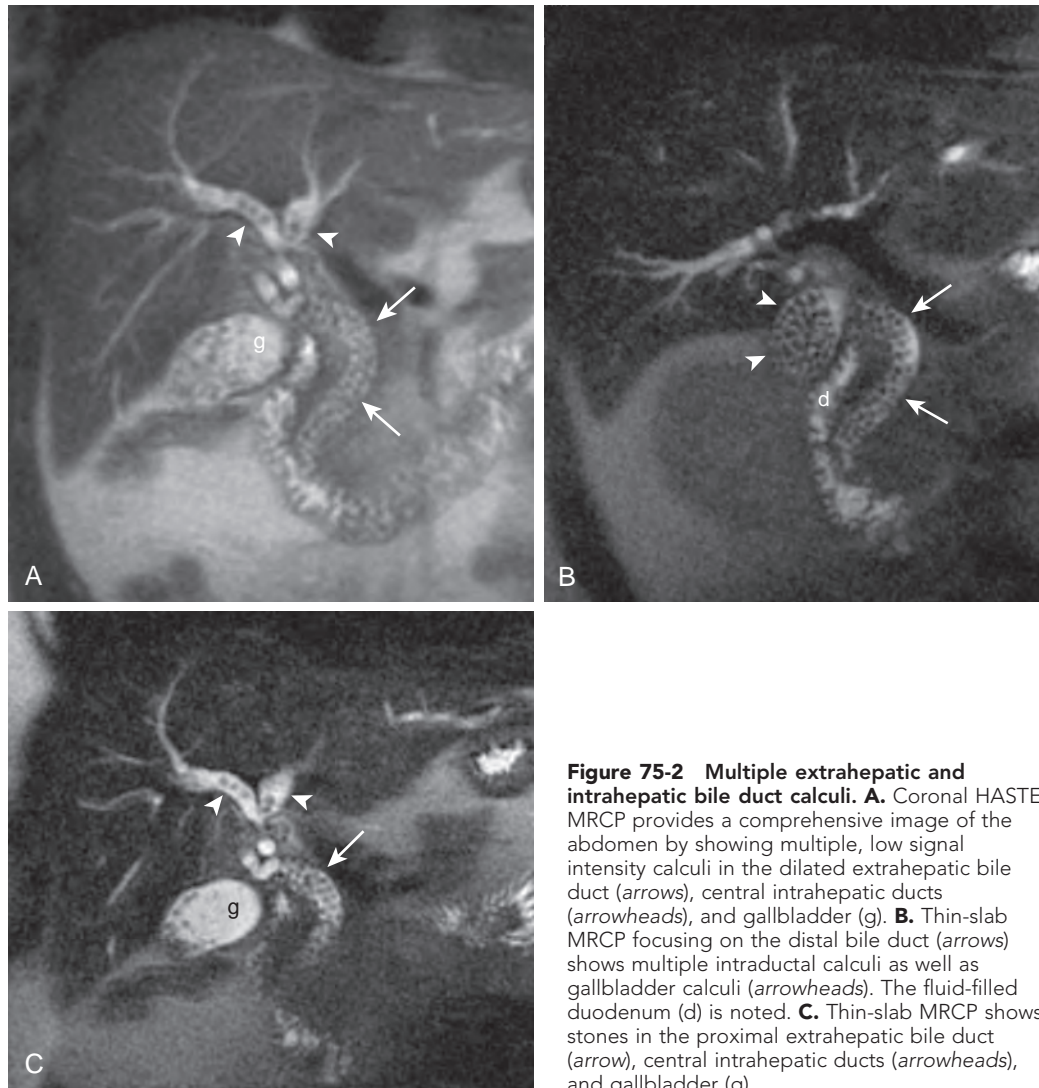


Figure 75-2 Multiple extrahepatic and intrahepatic bile duct calculi. **A.** Coronal HASTE MRCP provides a comprehensive image of the abdomen by showing multiple, low signal intensity calculi in the dilated extrahepatic bile duct (arrows), central intrahepatic ducts (arrowheads), and gallbladder (g). **B.** Thin-slab MRCP focusing on the distal bile duct (arrows) shows multiple intraductal calculi as well as gallbladder calculi (arrowheads). The fluid-filled duodenum (d) is noted. **C.** Thin-slab MRCP shows stones in the proximal extrahepatic bile duct (arrow), central intrahepatic ducts (arrowheads), and gallbladder (g).

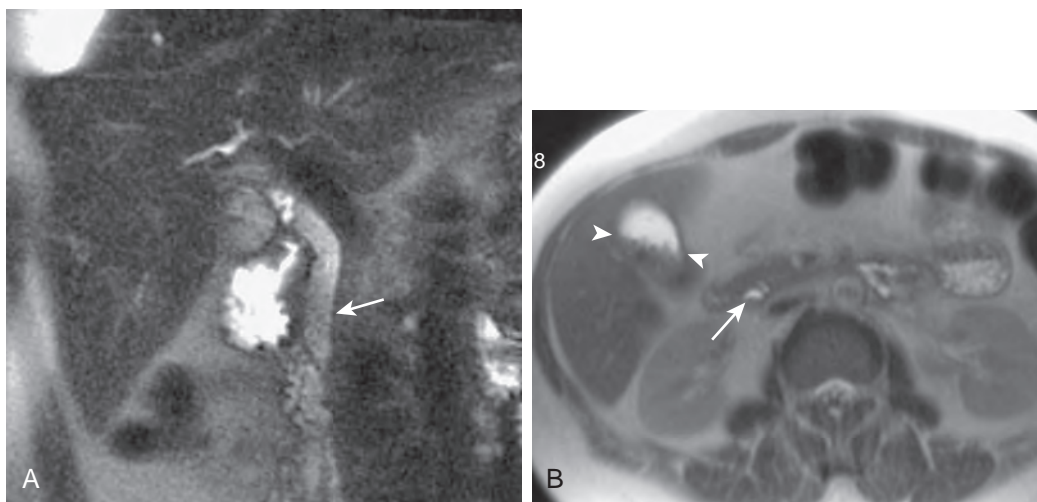


Figure 75-3 Small bile duct calculi: value of axial MRCP. **A.** Thin-slab MRCP reveals small, low signal intensity foci in the distal bile duct (arrow) later removed during therapeutic ERCP. **B.** Axial MRCP shows the small, low signal intensity stones layering in the dependent portion of the intrapancreatic bile duct (arrow), with high signal intensity bile seen anteriorly in the duct. A similar stone-bile level (arrowheads) is noted in the gallbladder.

Although MRCP performs well in the detection of stones, one must be aware of mimickers of stones that may result in false-positive diagnoses. These include pneumobilia, en face visualization of the cystic duct inserting into the bile duct, and compression of the duct by an adjacent vessel.^{19,20}

NEOPLASMS

MRCP is useful in the evaluation of suspected malignant neoplasms of the pancreaticobiliary tract. Multiple studies have demonstrated the ability of MRCP to determine the presence, level, and type of malignant disease with a high degree of accuracy.^{3,21-25} In a study of 62 patients with biliary obstruction, Kim and associates²⁶ demonstrated that the addition of conventional MRI to MRCP significantly improves the accuracy in the diagnosis of pancreaticobiliary disease and aids in the differentiation of benign from malignant causes of biliary dilation. When MRCP is supplemented by conventional MRI and MRA, a comprehensive examination results that allows depiction of the pancreaticobiliary tract, solid organs, and vasculature, which in turn permits determination of resectability of neoplastic disease. This comprehensive examination is most beneficial for patient care. Specifically, if a neoplasm is deemed resectable, the patient should be spared an unnecessary ERCP examination and stent placement as there is no established role for preoperative biliary drainage by ERCP in these patients.²⁷ On the other hand, if a neoplasm is deemed unresectable, the patient may be spared an unnecessary laparotomy. An additional advantage of MRCP offered in the setting of pancreaticobiliary tract malignant neoplasms is that MRCP depicts the entire biliary and pancreatic duct even in the presence of high-grade strictures and allows planning of surgical and percutaneous interventions.

Pancreatic Carcinoma

With the use of newer scanners and sequences that afford high-resolution imaging, MRCP not only readily identifies the ductal dilation that occurs as the result of pancreatic carcinoma but also depicts the malignant ductal strictures themselves and localizes the neoplastic process to the pancreas. MRCP depicts

bile duct involvement by pancreatic carcinoma as an abrupt transition between the dilated suprapancreatic duct and the markedly narrowed intrapancreatic duct, often referred to as a rat-tail configuration (Fig. 75-4A, B). In the case of pancreatic head carcinoma obstructing the bile and pancreatic ducts, MRCP shows dilation of both ducts, known as the double duct sign. Whereas the double duct sign is often seen in association with pancreatic head carcinoma, it is a nonspecific sign that may be due to a benign or malignant process involving the pancreatic head.²⁸ In the setting of carcinoma involving the body or tail of the pancreas, the ductal dilation is limited to the pancreatic duct proximal to the obstruction. Because the entire pancreatic duct is rarely depicted on a single 2D MRCP image, axial MRCP images are often useful in demonstrating the obstructing tumor and the transition between the dilated and nondilated pancreatic duct.

The performance of conventional MRI and MRA in conjunction with MRCP allows determination of resectability (Fig. 75-4C, D). T1-weighted, fat-suppressed, unenhanced sequences are particularly helpful in depicting even small tumors in the pancreas. Pancreatic adenocarcinomas are manifested as areas of low signal intensity against the high signal intensity of the normal pancreatic parenchyma. In addition to detection of the primary tumor, conventional MRI is useful in detecting liver metastases, nodal enlargement, and peritoneal carcinomatosis. MRA plays an important role in detecting neoplastic involvement of the celiac axis, hepatic artery, superior mesenteric artery and vein, and portal vein. In patients with unresectable pancreatic carcinoma, MRCP yields information important in planning of palliative and endoscopic drainage procedures.

In a prospective study of 124 patients with clinical and sonographic findings strongly suggestive of pancreatic neoplasia, Adamek and associates²³ showed that the sensitivity and specificity of MRCP in diagnosis of pancreatic carcinoma (84% and 97%) exceeded those of ERCP (70% and 94%). Unfortunately, the distinction between pancreatic carcinoma and focal chronic pancreatitis will likely remain a problem in some instances despite technical improvements in MRI, MRA, and MRCP.²⁹

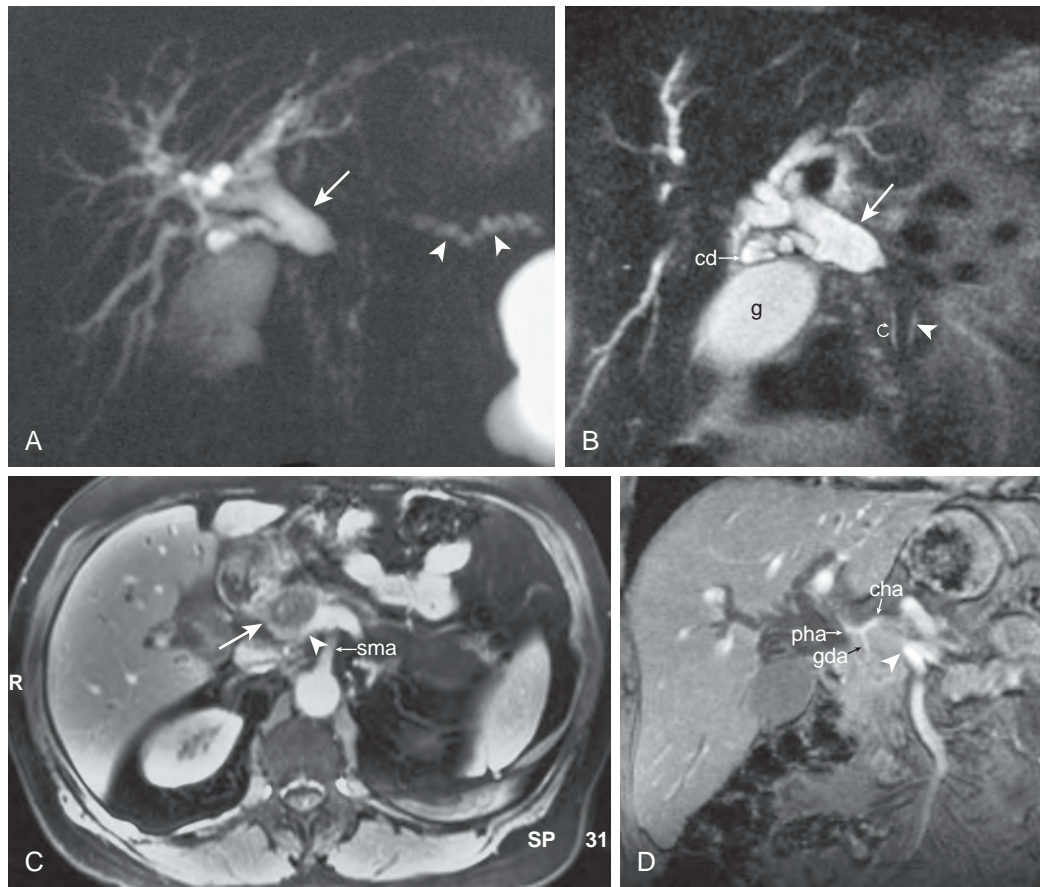


Figure 75-4 Unresectable pancreatic head carcinoma: MRCP, MRI, and MRA. **A.** Thick-slab MRCP provides a comprehensive image of the pancreaticobiliary tract that demonstrates high-grade obstruction of the extrahepatic bile duct (arrow) and minor dilation of the pancreatic duct (arrowheads) in the body and tail of the pancreas. **B.** Thin-slab MRCP reveals the finer details of the ductal systems and shows that the extrahepatic bile duct (arrow) is obstructed at the pancreatic head. The intrapancreatic portion of the bile duct (curved arrow) and the pancreatic duct (arrowhead) in the head of the pancreas are narrowed. The distended gallbladder (g) and cystic duct (cd) are shown. **C.** Transverse, T1-weighted, enhanced abdominal MRI shows that the cause of the obstruction is a low signal intensity pancreatic head carcinoma (arrow) that has occluded the distal superior mesenteric vein (arrowhead). There is no evidence of tumor surrounding the superior mesenteric artery (sma). **D.** Coronal, 2D time-of-flight MRI angiogram shows that the pancreatic head mass has occluded the distal superior mesenteric vein (arrowhead) and is inseparable from the common hepatic artery (cha), proximal proper hepatic artery (pha), and gastroduodenal artery (gda). (From Fulcher AS, Turner MA: MR cholangiopancreatography. *Radiol Clin North Am* 40:1367, 2002.)

Cholangiocarcinoma: Hilar and Distal Duct

Hilar cholangiocarcinoma is the most common manifestation of cholangiocarcinoma and is depicted as a high-grade stricture of the confluence of the right and left hepatic ducts. In the past, much emphasis was placed on palliative procedures, such as percutaneous biliary drainage and endoscopic stent placement, because of the poor prognosis associated with this neoplasm. However, with the advent of improved surgical and radiation therapy techniques, greater attention is directed toward imaging examinations that assist in determining disease extent and resectability.

During the past decade, MRCP has become an important tool in the evaluation of cholangiocarcinoma in general and hilar cholangiocarcinoma in particular. Like direct cholangiography, MRCP demonstrates the marked narrowing of the proximal extrahepatic bile duct, the often-present extension to the central right and left hepatic ducts, and the dilation proximal to the obstruction^{30,31} (Fig. 75-5A, B). Because MRCP readily depicts ducts proximal to high-grade obstructions that are

often not opacified at ERCP, MRCP typically is superior in determining disease extent and resectability.^{30,31} As with other pancreaticobiliary tract neoplasms, MRI performed in association with MRCP offers the added advantage of demonstrating disease that has extended from the ducts into the liver and adjacent structures (Fig. 75-5C). These factors have allowed MRCP to assume an important role in the noninvasive evaluation of hilar cholangiocarcinoma and to facilitate planning of surgical, percutaneous, and radiation therapy procedures. Park and coworkers³² demonstrated that MRCP combined with MRI provides information about cholangiocarcinoma extent and resectability comparable to that of multidetector CT with direct cholangiography.

Cholangiocarcinomas that involve the extrahepatic duct distal to the confluence are often referred to as the distal duct type. Distal duct cholangiocarcinomas are seen as strictures or intraductal polypoid masses resulting in biliary obstruction on both MRCP and ERCP. In a retrospective study of 50 patients with extrahepatic bile duct cholangiocarcinoma and 23 patients with benign strictures, MRCP was shown to have

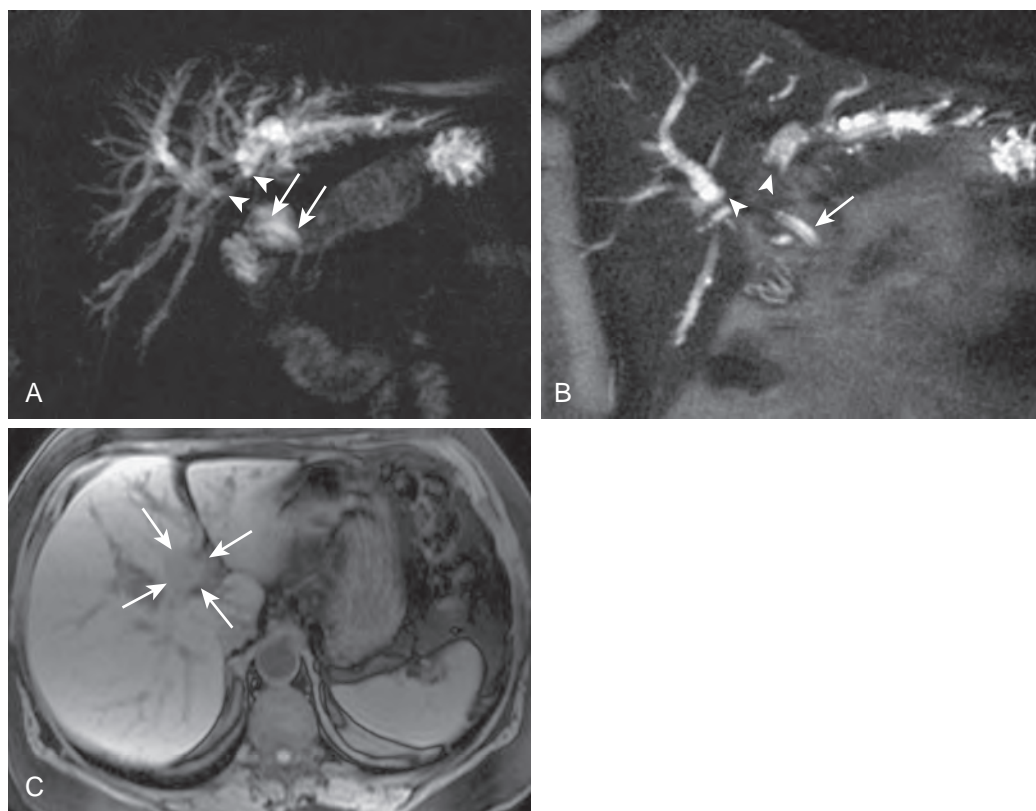


Figure 75-5 Hilar cholangiocarcinoma. **A.** Coronal thick-slab MRCP reveals high-grade isolated obstructions of the central right and left hepatic ducts (arrowheads) due to hilar cholangiocarcinoma. The extrahepatic bile duct distal to the obstruction (arrows) is seen adjacent to the fluid-filled duodenal bulb. **B.** Thin-slab MRCP reveals in greater detail the points of obstruction of the central right and left hepatic ducts (arrowheads) due to cephalad extension of the hilar cholangiocarcinoma. The normal-caliber extrahepatic bile duct (arrow) located just distal to the tumor is noted. **C.** T1-weighted, fat-suppressed, unenhanced abdominal MRI reveals low signal intensity tumor (arrows) that has extended beyond the confines of the biliary tract to invade the hepatic parenchyma.

an accuracy comparable to that of ERCP in making the distinction between cholangiocarcinoma and benign strictures.³² Distal duct cholangiocarcinoma confined to the intrapancreatic bile duct is difficult to distinguish from pancreatic head carcinoma with either MRCP or ERCP (Fig. 75-6). However, the clinical impact of this deficiency is of no consequence as the treatment of both tumors is identical and is predicated on resectability.

Intraductal Papillary Mucinous Neoplasm of the Pancreas

Intraductal papillary mucinous neoplasms (IPMNs) are categorized as main duct type and branch duct type, depending on the duct of origin, and may be benign or malignant. IPMNs are well demonstrated on MRCP because they produce mucin, which appears as high signal intensity within the ducts.³³⁻³⁵ MRCP can reveal the entire spectrum of IPMNs—main duct dilation, cystic dilation of the side branches, nodules, septa, and intraductal filling defects—and is able to show communication between the tumor and the pancreatic duct (Fig. 75-7). A study of 34 IPMNs in 31 patients examined with MRCP and correlated with surgical and pathologic findings revealed that intraductal filling defects are indicative of malignant disease and that diffuse dilation of the main pancreatic duct of more than 15 mm in main duct-type tumors is strongly associated with malignant transformation.³³ In branch duct-type tumors, the absence of main pancreatic duct dilation suggests a benign tumor.

CONGENITAL ANOMALIES

Choledochal or Bile Duct Cysts

MRCP reliably detects choledochal or bile duct cysts in adults and children and provides diagnostic information equivalent to that of ERCP without the risk of complications³⁶⁻³⁹ (Fig. 75-8). MRCP nicely delineates the extent of the cyst and detects anomalous pancreaticobiliary junctions, critical factors in planning of cyst excision and bile duct reconstruction.⁴⁰ Matos³⁶ and Yu⁴¹ and their colleagues noted that the accuracy of MRCP in the detection of anomalous pancreaticobiliary junctions is comparable to that of ERCP. For these reasons, MRCP has been proposed as the imaging modality of choice in evaluation of choledochal cysts.^{37,38}

Anatomic Variants of the Biliary Tract

Anatomic variations of the biliary tract occur in up to 37% of individuals. These include crossover anomalies, such as the dorso-caudal branch of the right hepatic duct entering the central left hepatic duct; trifurcations; accessory or aberrant ducts that enter the extrahepatic duct or cystic duct; and cystic duct variants.⁴² MRCP has been shown to accurately detect these variants.^{43,44} Although ductal variants are usually of no consequence in the general population, they are of great importance in patients undergoing cholecystectomy because some variants predispose to ductal injury.⁴⁵ Ductal variants posed less risk in the era of open cholecystectomy because the biliary tract was

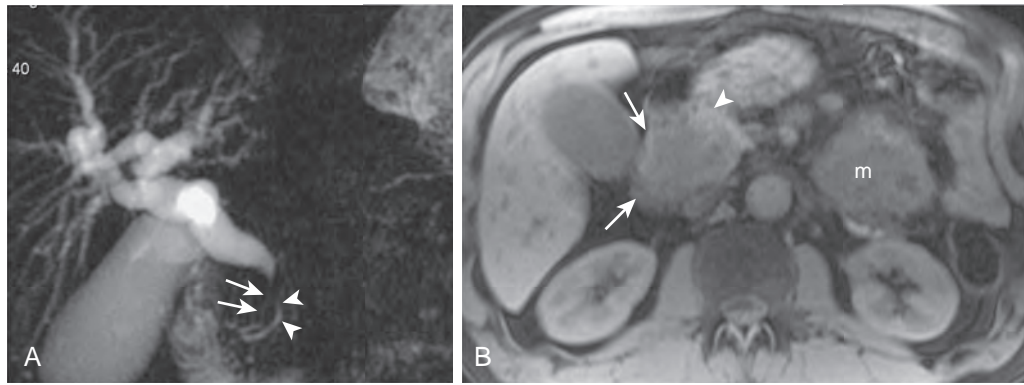


Figure 75-6 Distal duct cholangiocarcinoma. **A.** Coronal thick-slab MRCP shows a high-grade stricture of the intrapancreatic bile duct (arrows) resulting in proximal biliary ductal dilation. The pancreatic duct (arrowheads) is normal in caliber. **B.** T1-weighted, fat-suppressed, unenhanced abdominal MRI shows a mass (arrows) involving the pancreatic head that is low in signal intensity relative to the adjacent normal pancreatic parenchyma (arrowhead). Pathologic analysis revealed cholangiocarcinoma. A large, mesenteric metastasis (m) was present at the time of diagnosis.

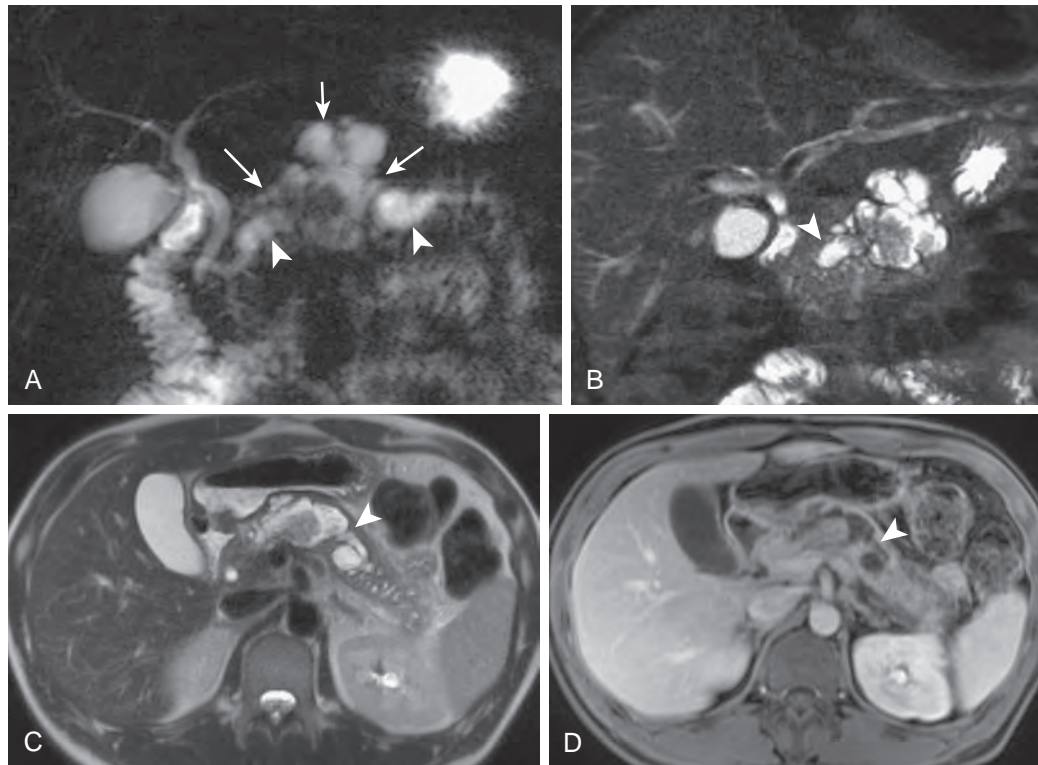


Figure 75-7 Malignant intraductal papillary mucinous neoplasm of the pancreas, main duct type. **A.** Coronal thick-slab MRCP reveals a large cystic lesion (arrows) that contains nodular filling defects and that communicates with the main pancreatic duct in the pancreatic body (arrowheads). Incidental note is made of pancreas divisum as evidenced by the horizontal orientation of the main pancreatic duct in the pancreatic head. **B-D.** Coronal oblique thin-slab MRCP, axial HASTE image, and axial T1-weighted, fat-suppressed, contrast-enhanced abdominal MRI show in detail the lobulated cystic mass and the nodular filling defects as well as the dilated pancreatic duct (arrowhead) from which the mass arises.

directly visualized. Because most cholecystectomies are now performed laparoscopically, which does not provide the same degree of direct visualization of the biliary tract, the preoperative recognition of these anomalies is paramount. The increasing use of right lobe living donor liver transplantations has heightened the awareness of radiologists and surgeons alike to the importance of ductal variants such as crossover anomalies (Fig. 75-9). Whereas these variants do not preclude

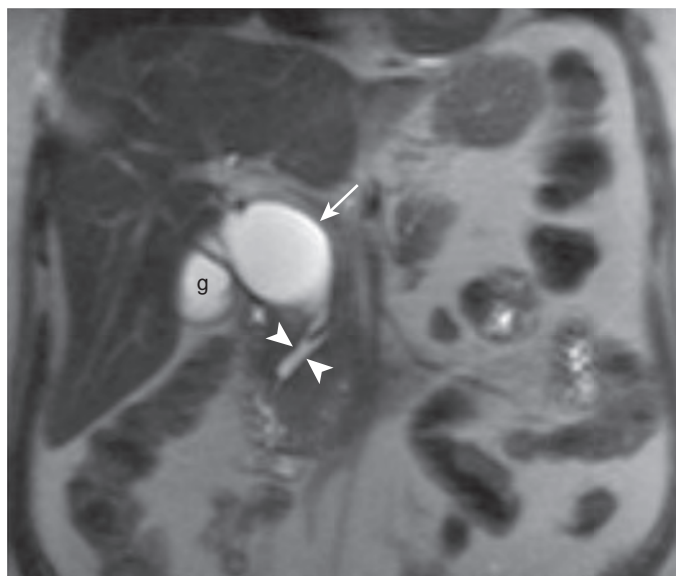


Figure 75-8 Type 1 choledochal or bile duct cyst. Coronal HASTE MRCP shows fusiform dilation of the majority of the extrahepatic bile duct (arrow) indicative of a type 1 choledochal or bile duct cyst. An anomalous pancreaticobiliary junction (arrowheads) is present. The gallbladder (g) is noted.

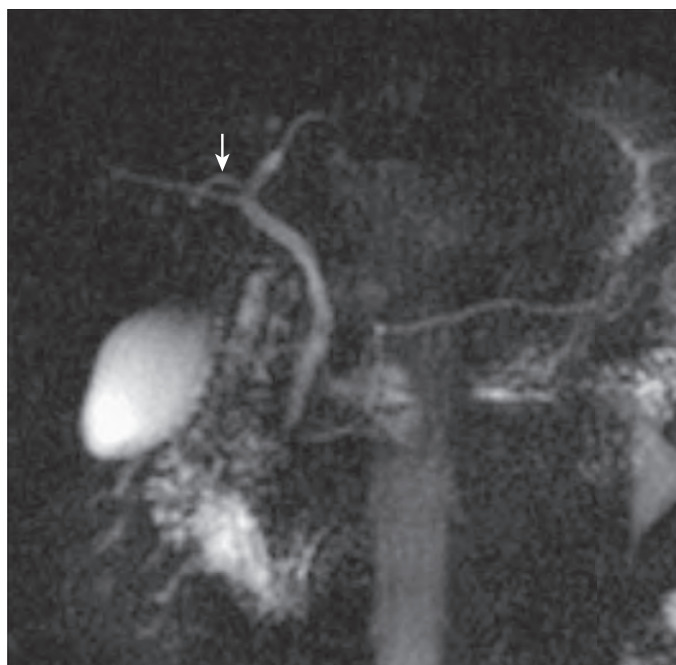


Figure 75-9 Aberrant bile duct: crossover anomaly. Coronal thick-slab MRCP depicts the dorsocaudal branch of the right hepatic duct (arrow) entering the central left hepatic duct.

transplantation in most cases, preoperative identification assists in avoidance of inadvertent surgical ligations. Awareness of ductal variants is also important in the planning of complex percutaneous and endoscopic biliary interventions.

Pancreas Divisum

Pancreas divisum occurs in up to 5.5% to 7.5% of the general population.^{46,47} Although most individuals with pancreas divisum demonstrate no symptoms referable to the pancreas, others present with recurrent bouts of unexplained pancreatitis. In fact, pancreas divisum has been shown to occur with significantly greater frequency in patients with acute idiopathic pancreatitis than in the general population.⁴⁶ MRCP has gained an increasingly prominent role in the evaluation of patients with idiopathic pancreatitis because this technique can detect pancreas divisum and other ductal anomalies with a high degree of accuracy. Unlike diagnostic ERCP, MRCP does not carry the risk of inducing pancreatitis in this group of patients who are predisposed to its development.³⁸ Manfredi and associates⁴⁸ noted that secretin-enhanced MRCP assists in identifying pancreas divisum and sometimes the associated cystic dilation of the distal dorsal duct, often referred to as a santorinicele. MRCP is also useful in delineating the ductal changes of chronic pancreatitis: dilation of the main pancreatic duct, side branch ectasia, strictures, and intraductal stones. In addition, T1-weighted, fat-suppressed, unenhanced sequences performed in conjunction with MRCP assist in detecting associated pancreatic atrophy and fibrosis. With these sequences, fibrosis is seen as decreased signal intensity of the pancreas compared with that of the liver secondary to replacement of aqueous protein in the pancreatic parenchyma.

At MRCP, pancreas divisum is usually depicted as two separate drainage systems of the pancreas (Fig. 75-10). The larger dorsal duct drains the majority of the pancreas and enters the duodenum at the minor papilla cephalad to and separate from the ventral duct. The smaller ventral duct drains the inferior pancreatic head and uncinate process and enters the duodenum at the major ampulla with the distal bile duct. For the diagnosis of pancreas divisum to be established at MRCP, care must be taken to ensure that there is no communication between the dorsal and ventral ducts. This is most readily achieved by reviewing the images at a workstation rather than on film.

Postoperative Alterations of the Pancreaticobiliary Tract and Gastrointestinal Tract

Multiple studies have demonstrated the utility and accuracy of MRCP in depicting normal anatomy and pathologic changes of the ducts in patients with postsurgical alterations of the pancreaticobiliary tract and gastrointestinal tract.⁴⁹⁻⁵⁴ Specifically, MRCP readily depicts anastomotic strictures, intraductal stones, bile plugs, and, in some cases, injuries of the ducts after cholecystectomy with sensitivities up to 100%.^{50,52}

MRCP has been used successfully in imaging of patients after cadaveric and living donor liver transplantations, hepatic resection, pancreatoduodenectomy, and creation of a biliary-enteric anastomosis (Fig. 75-11). MRCP is particularly well suited to the evaluation of patients with biliary-enteric anastomoses. The performance of ERCP is difficult if not impossible in these patients because of the surgical alteration of the gastrointestinal

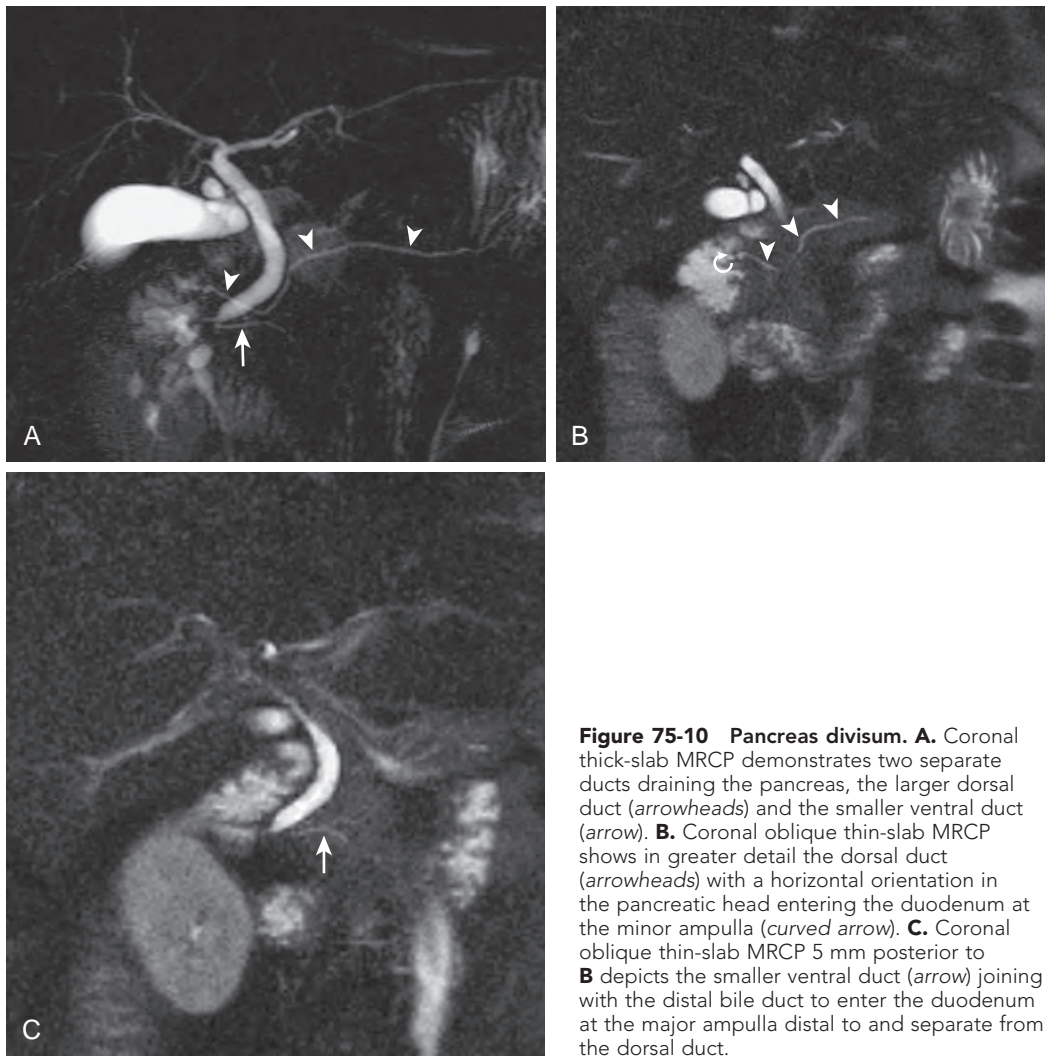


Figure 75-10 Pancreas divisum. **A.** Coronal thick-slab MRCP demonstrates two separate ducts draining the pancreas, the larger dorsal duct (arrowheads) and the smaller ventral duct (arrow). **B.** Coronal oblique thin-slab MRCP shows in greater detail the dorsal duct (arrowheads) with a horizontal orientation in the pancreatic head entering the duodenum at the minor ampulla (curved arrow). **C.** Coronal oblique thin-slab MRCP 5 mm posterior to **B** depicts the smaller ventral duct (arrow) joining with the distal bile duct to enter the duodenum at the major ampulla distal to and separate from the dorsal duct.

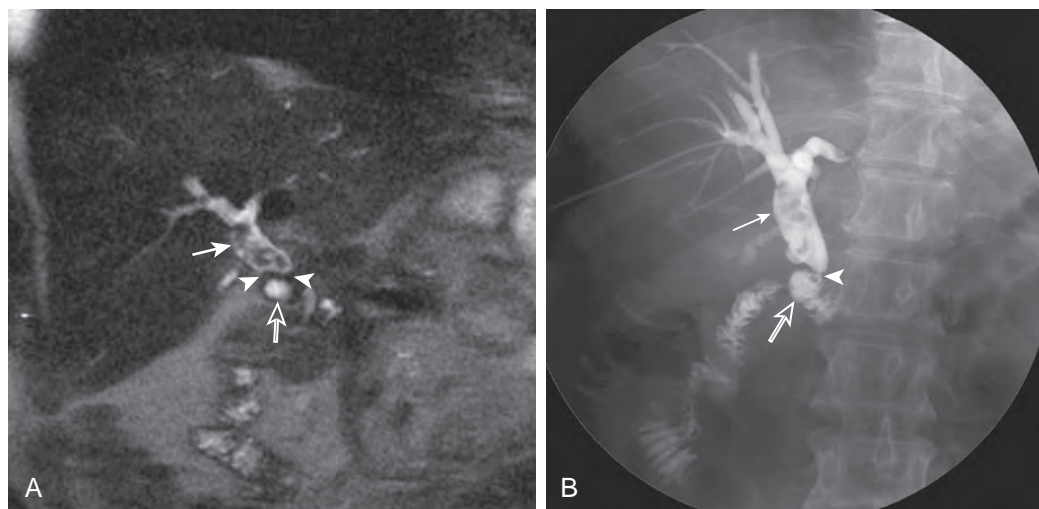


Figure 75-11 Biliary-enteric anastomotic stricture and intraductal stones. **A.** Coronal oblique thin-slab MRCP shows dilation of the residual proximal extrahepatic bile duct (arrow) indicative of a stricture of the biliary enteric anastomosis (arrowheads). Intraductal filling defects represent stones that have formed secondary to stasis. The rounded, fluid-filled structure (open arrow) represents the proximal aspect of the jejunal limb. **B.** Direct cholangiography performed during a percutaneous biliary drainage procedure confirms the biliary enteric anastomotic stricture (arrow), intraductal stones (arrowhead), and proximal jejunal limb (open arrow). Slow passage of contrast material occurred from the duct to the jejunal limb.

tract. Before the advent of MRCP, depiction of the ducts in patients with biliary-enteric anastomoses could be achieved only by performing percutaneous transhepatic cholangiography (PTC), which is an invasive procedure associated with complications such as bleeding and infection.

MRCP is often used to evaluate the biliary tract after liver transplantation for complications such as strictures and stones.⁵⁵ ERCP and PTC may lead to serious complications in this group of seriously ill patients. If complications are detected with MRCP, patients can then be referred for therapeutic ERCP or PTC. If complications are excluded with MRCP, the patient will be spared an unnecessary invasive procedure and its attendant complications.

Although MRCP is highly accurate in imaging of the post-operative pancreaticobiliary tract, it is associated with a number of pitfalls and limitations. In patients with biliary-enteric anastomoses, pneumobilia may mimic intraductal stones as both appear as filling defects in the high signal intensity bile. In most instances, the distinction can be made by observing that pneumobilia is located in the nondependent portion of the duct and stones are located in the dependent portion of the duct on coronal and axial images.^{49,50} A limitation of MRCP in the assessment of biliary strictures was noted by Ward and associates,⁴⁹ who found a tendency of MRCP to overestimate the grade of strictures. Finally, despite studies reporting the utility of MRCP performed in conjunction with agents excreted into the biliary tract for detection of bile duct leaks,⁵⁶ it is likely that diagnostic ERCP may remain the primary means of detecting leaks as ERCP also provides access for stent placement in the same setting as the diagnostic ERCP examination. Nevertheless, MRCP has emerged as an accurate, noninvasive means of evaluating the ductal systems in patients with postsurgical alterations of the pancreaticobiliary tract and gastrointestinal tract.

Primary Sclerosing Cholangitis

For many years, direct cholangiography (ERCP and, to a lesser extent, PTC) has been considered the imaging examination of choice for diagnosis of primary sclerosing cholangitis (PSC)

and observation of its progression. Although both ERCP and PTC yield exquisite images of the ducts and provide access for interventions, these invasive examinations place patients at risk of complications such as cholangitis, pancreatitis, hemorrhage, and infection. MRCP provides a noninvasive diagnostic alternative for the evaluation of patients with known or suspected PSC.

Direct cholangiographic findings of PSC include multifocal, annular strictures of the intrahepatic or extrahepatic bile ducts that alternate with normal or slightly dilated segments, resulting in a beaded appearance of the ducts; diverticulum-like outpouchings; mural irregularities; and pruning of the peripheral intrahepatic bile ducts.⁵⁷ Due to technical advances, MRCP is able to depict the fine details of the ducts and to demonstrate the typical ductal abnormalities of PSC with a high degree of accuracy⁵⁸⁻⁶¹ (Figs. 75-12 and 75-13). Vitellas and associates^{60,61} showed that MRCP is superior to ERCP for depiction of intrahepatic ducts and intrahepatic ductal strictures in part because of the ability of MRCP to demonstrate ducts proximal to a high-grade obstruction. MRCP also is useful in detecting recurrent PSC after liver transplantation as MRCP readily depicts the intrahepatic and extrahepatic bile ducts in these patients with a biliary-enteric anastomosis who would otherwise require PTC for the biliary tract to be visualized.⁵⁸ Despite the utility and accuracy of MRCP in the diagnosis of PSC, the distinction between a benign stricture due to PSC and a malignant stricture related to cholangiocarcinoma will likely remain a problem.

A prospective case-control study in which 102 patients (34 with PSC and 68 age-matched controls with hepatobiliary diseases other than PSC) underwent MRCP revealed that MRCP was accurate in detecting and localizing PSC.⁵⁸ In the detection of PSC, for two independent readers, the sensitivities were 85% and 88%; specificities, 92% and 97%; positive predictive value, 85% and 94%; and negative predictive value, 93% and 94%. Interobserver agreement was excellent. All false-positive diagnoses were related to distortion of the ducts by underlying cirrhosis. Five false-negative diagnoses occurred and were related to marked cirrhosis that obscured the intrahepatic ducts in two patients and early changes of PSC that were limited to the peripheral intrahepatic ducts in the remaining three patients.

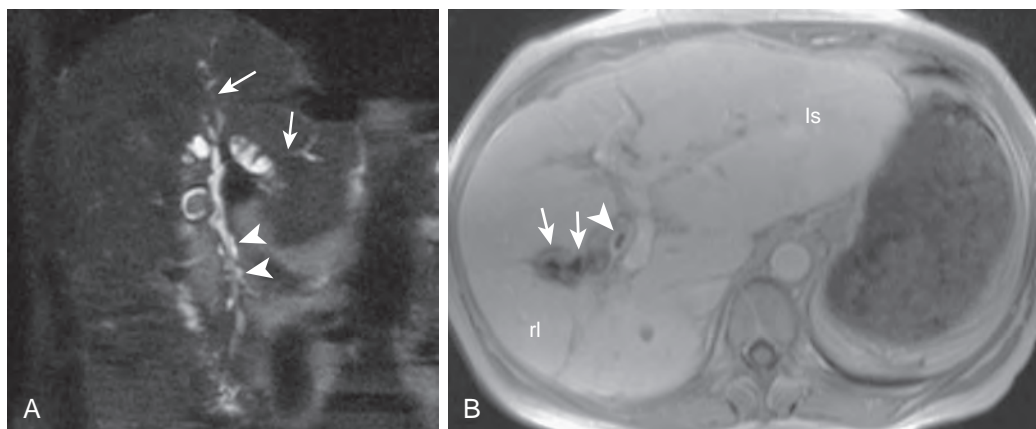


Figure 75-12 Intrahepatic and extrahepatic primary sclerosing cholangitis. **A.** Coronal oblique thin-slab MRCP depicts strictures (arrows) and dilation of the intrahepatic bile ducts and marked mural irregularity and diverticulum-like outpouchings of the extrahepatic bile duct (arrowheads). **B.** Axial, T1-weighted, fat-suppressed, enhanced image of the abdomen reveals cirrhosis complicating PSC as evidenced by lateral segment (ls) hypertrophy and right lobe (rl) atrophy. Thickening and enhancement of the wall of the proximal extrahepatic bile duct (arrowhead) is noted as well as intrahepatic ductal dilation (arrows).

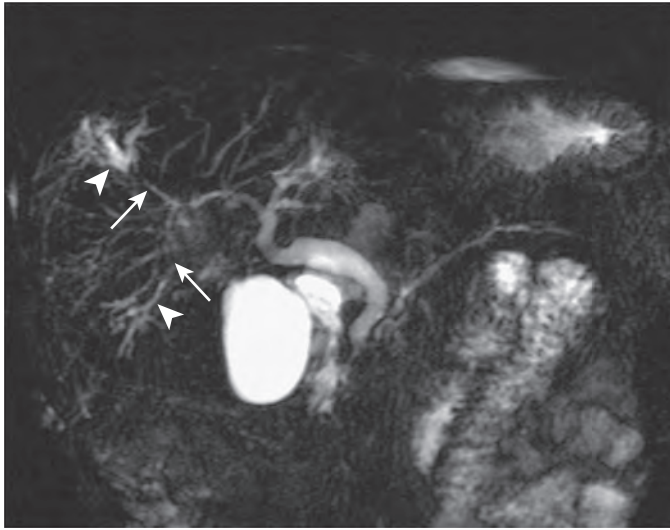


Figure 75-13 Intrahepatic primary sclerosing cholangitis. Coronal thick-slab MRCP shows dilation (arrowheads) and multiple strictures (arrows) of the intrahepatic bile ducts. The slightly dilated extrahepatic bile duct shows no evidence of PSC.

Talwalkar and colleagues⁵⁹ proposed to determine the average cost per correct diagnosis with MRCP or ERCP as the initial means for the diagnosis of PSC. Seventy-three patients with clinically suspected PSC formed the basis of the study; the prevalence of PSC in the study cohort was 32%. The sensitivity and specificity of MRCP for the diagnosis of PSC were 82% and 98%, respectively. Talwalkar and colleagues⁵⁹ found that the accuracy of MRCP was comparable to that of ERCP and that MRCP resulted in cost savings when it was used as the initial test for diagnosis of PSC in their study population. The value of MRCP in the patient with PSC is enhanced when it is performed in association with conventional MRI, which can demonstrate cirrhosis, portal hypertension, cholangiocarcinoma, and hepatic parenchymal changes related to altered perfusion and inflammation of the bile ducts⁶² (see Fig. 75-12B).

MRCP has emerged as a viable alternative to ERCP in the diagnosis of PSC. The utility of MRCP in this setting is related to its accuracy and noninvasive nature and its ability to depict ducts proximal to a high-grade obstruction. As a result, at some centers, ERCP is now used primarily as a means of gaining access for interventions such as stent placements instead of as a diagnostic tool. Nevertheless, ERCP, and at times PTC, may prove useful in detecting PSC in problematic cases, such as in patients with minor changes of PSC limited to the peripheral intrahepatic ducts.

Pancreatitis

ACUTE PANCREATITIS

The primary role of MRCP in the setting of acute pancreatitis is the identification of structural abnormalities that predispose to its development, such as common bile duct stones, pancreas divisum, and tumors obstructing the pancreatic duct. Depending on the severity of acute pancreatitis, edema of the pancreatic parenchyma may result in smooth narrowing of the

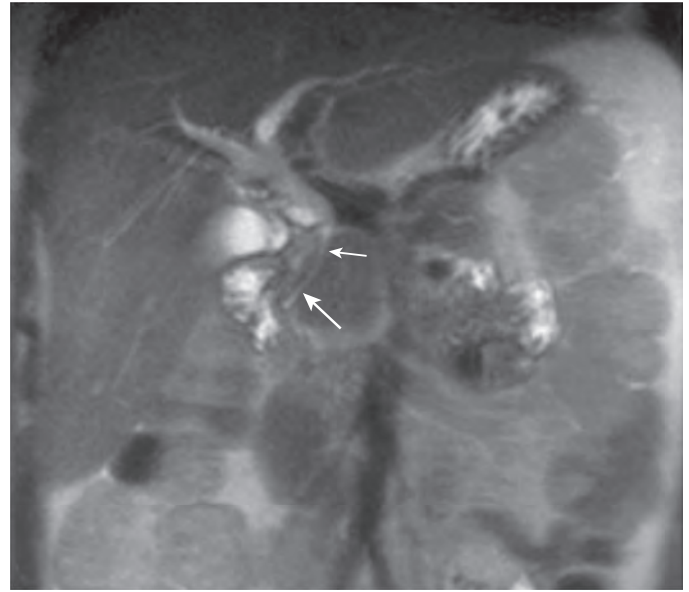


Figure 75-14 Acute pancreatitis. Coronal HASTE reveals dilation of the intrahepatic and suprapancreatic bile ducts and smooth narrowing of the intrapancreatic bile duct (arrows) due to compression by the edematous pancreas. MRCP performed after resolution of acute pancreatitis showed that the duct returned to a normal caliber (not shown).

intrapancreatic bile duct or pancreatic duct (Fig. 75-14). When these findings are confined to the pancreatic head, the ductal narrowing and the pancreatic parenchymal enlargement may mimic pancreatic neoplasia. However, as the edema resolves, the ducts and parenchyma return to normal.

In the setting of acute pancreatitis, the combined MRI and MRCP examinations assist in detecting the cause, extent, and complications of this inflammatory process. Pancreatic enlargement, simple and infected fluid collections, necrosis, thoracopancreatic fistulas, vascular thrombosis, and pseudoaneurysms are well depicted. In fact, MRI has been shown to perform well compared with CT in the evaluation of inflammation and necrosis and in the calculation of the severity index.⁶³ In one study, MRI was superior to CT and ultrasonography for detection of debris in subacute pancreatic fluid collections, an important factor in assessing drainability.⁶⁴

Therefore, an examination including both MRCP and MRI, and at times MRA, yields information about the pancreaticobiliary tract, pancreatic parenchyma, surrounding tissues, and vessels in a single, noninvasive examination that does not expose the patient to radiation or iodinated contrast material. The disadvantages of MRI in the setting of severe acute pancreatitis include the fact that MRI cannot be performed as rapidly as CT and that CT must be used for critically ill patients on ventilators.

CHRONIC PANCREATITIS

MRCP and MRI have emerged as useful tools in demonstrating the ductal and parenchymal manifestations of chronic pancreatitis.^{3,65} The ductal features include dilation of the main pancreatic duct and its side branches, mural irregularity, intraductal stones, and strictures of the pancreatic duct and the intrapancreatic bile duct (Fig. 75-15). A study comparing ERCP with

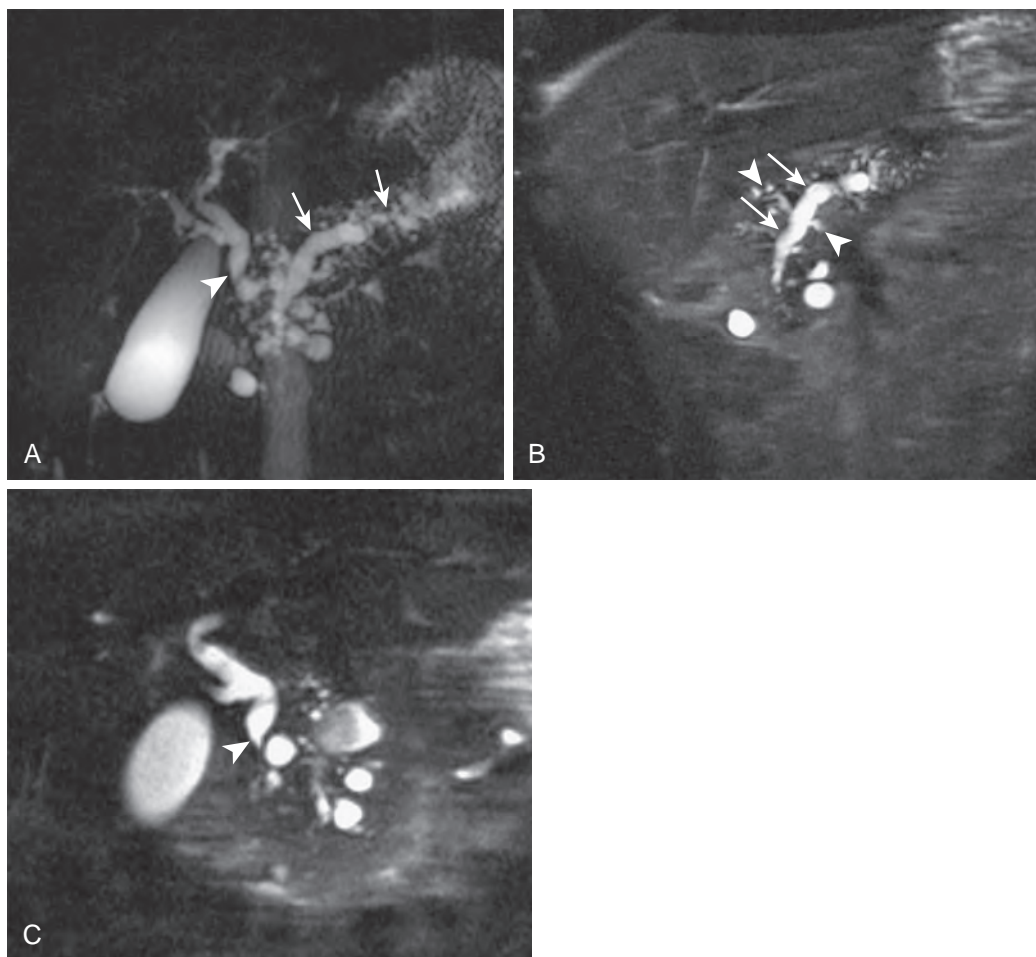


Figure 75-15 Chronic pancreatitis. **A.** Coronal thick-slab MRCP provides a comprehensive image of the pancreaticobiliary tract by demonstrating marked dilation of the main pancreatic duct (arrows) and its side branches and a tapered stricture of the intrapancreatic bile duct (arrowhead). **B.** Coronal oblique thin-slab MRCP focusing on the pancreatic body depicts the dilation of the main pancreatic duct (arrows), its dilated side branches (arrowheads), and rounded intrapancreatic pseudocysts. **C.** Coronal oblique thin-slab MRCP focusing on the pancreatic head demonstrates the smooth, tapered stricture of the intrapancreatic bile duct (arrowhead) that results in dilation of the suprapancreatic bile duct. Again noted are the intrapancreatic pseudocysts and the dilated pancreatic duct and its side branches.

MRCP revealed very good correlation between MRCP and ERCP findings but showed that both modalities failed to depict some abnormalities depicted by the other technique.⁶⁵ In another study including 36 patients with chronic pancreatitis, MRCP identified biliary strictures in 16 and correctly classified all as benign.³ MRCP provides accurate delineation of the ductal manifestations of chronic pancreatitis, which is of utmost importance in determining disease extent and in planning surgical drainage procedures. In some instances, MRCP demonstrates the ductal disease more completely than ERCP does because MRCP readily demonstrates ducts proximal to a high-grade stricture.

MRI is helpful in showing parenchymal manifestations of chronic pancreatitis, such as atrophy and fibrosis, as well as peripancreatic findings, such as pseudocysts. T1-weighted, fat-suppressed, unenhanced sequences are particularly useful in delineating fibrosis and atrophy that result in diminished signal intensity of the pancreas relative to the liver because of the replacement of aqueous protein in the pancreatic parenchyma.^{66,67} Pancreatic enhancement is reduced in patients with chronic calcific pancreatitis compared with

glands without calcifications.⁶⁶ This is presumably due to more severe disease.

Secretin-enhanced MRCP improves visualization of the morphologic features of chronic pancreatitis and can assist in determining function of the exocrine pancreas by assessing fluid output.^{8,68-70}

Gallbladder Diseases

Sonography is the initial modality used to evaluate the gallbladder as it is accurate, relatively inexpensive, readily available, rapidly performed, and portable. MRCP is useful in detecting abnormalities including gallstones, acute cholecystitis (Fig. 75-16), gangrenous cholecystitis, gallbladder perforation, Mirizzi syndrome, carcinoma, and adenomyomatosis (Fig. 75-17).^{3,71-73} In the setting of acute cholecystitis, MRCP coupled with MRI is useful in detecting bile duct stones and in demonstrating extension of infection from the gallbladder to the adjacent hepatic parenchyma. When gallbladder carcinoma is suspected, MRI used in conjunction with MRCP assists in staging.⁷²⁻⁷⁴

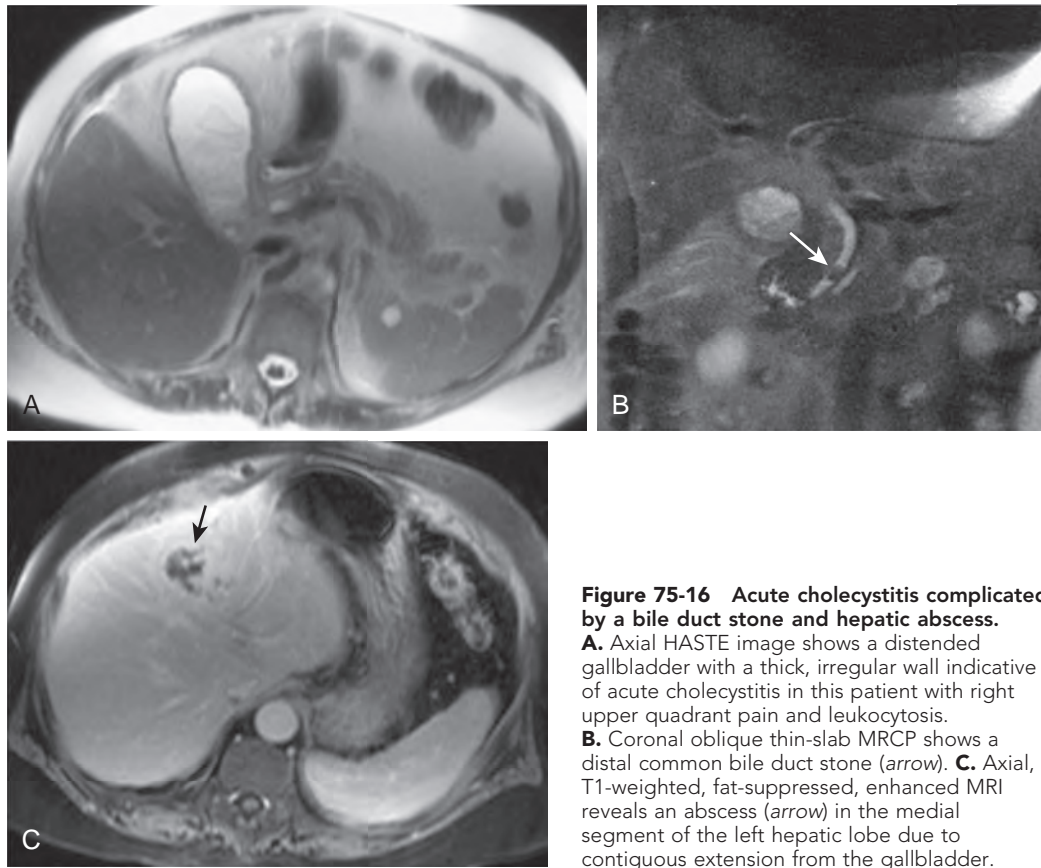


Figure 75-16 Acute cholecystitis complicated by a bile duct stone and hepatic abscess.

A. Axial HASTE image shows a distended gallbladder with a thick, irregular wall indicative of acute cholecystitis in this patient with right upper quadrant pain and leukocytosis.

B. Coronal oblique thin-slab MRCP shows a distal common bile duct stone (*arrow*). **C.** Axial, T1-weighted, fat-suppressed, enhanced MRI reveals an abscess (*arrow*) in the medial segment of the left hepatic lobe due to contiguous extension from the gallbladder.

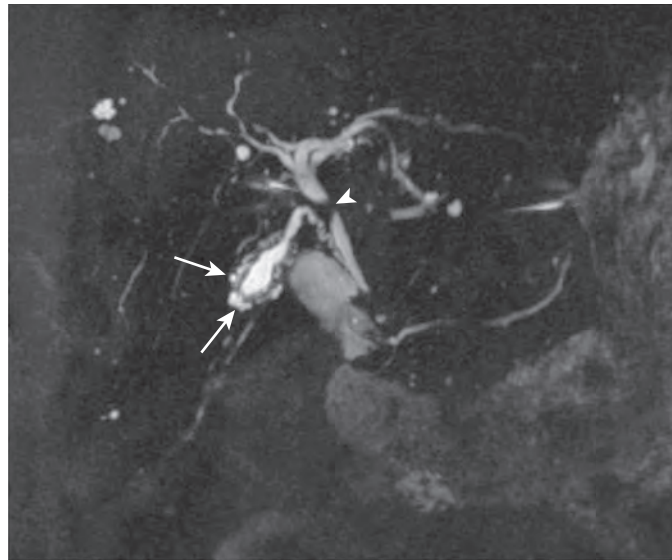


Figure 75-17 Adenomyomatosis. MIP image shows the “pearl necklace” sign of adenomyomatosis that represents dilated Rokitsky-Aschoff sinuses (*arrows*). Artifactual narrowing of the proximal extrahepatic bile duct (*arrowhead*) is noted.

REFERENCES

- Akisik MF, Jennings SG, Aisen AM, et al: MRCP in patient care: A prospective survey of gastroenterologists. *AJR Am J Roentgenol* 201;573–577, 2013.
- Guda NM, Reddy DN, Kumar A: Complications of ERCP. *Indian J Gastroenterol* 33:1–9, 2014.
- Fulcher AS, Turner MA, Capps GW, et al: Half-Fourier RARE MR cholangiopancreatography: Experience in 300 subjects. *Radiology* 207:21–32, 1998.
- Irie H, Honda H, Tajima T, et al: Optimal MR cholangiopancreatographic sequence and its clinical application. *Radiology* 206:379–387, 1998.
- Gupta RT, Brady CM, Lotz J, et al: Dynamic MR imaging of the biliary system using hepatocyte-specific contrast agents. *AJR Am J Roentgenol* 195:405–413, 2010.
- Park MS, Kim KW, Yu JS, et al: Early biliary complications of laparoscopic cholecystectomy: Evaluation on T2-weighted MR cholangiography in conjunction with mangafodipir trisodium-enhanced 3D T1-weighted MR cholangiography. *AJR Am J Roentgenol* 183:1559–1566, 2004.
- Lee VS, Krinsky GA, Nazzaro CA, et al: Defining intrahepatic biliary anatomy in living liver transplant donor candidates at mangafodipir trisodium-enhanced MR cholangiography versus conventional T2-weighted MR cholangiography. *Radiology* 233:659–666, 2004.
- Sanyal R, Stevens T, Novak E, et al: Secretin-enhanced MRCP: Review of technique and application with proposal for quantification of exocrine function. *AJR Am J Roentgenol* 198:124–132, 2012.
- Patel HT, Shah AJ, Khandelwal SR, et al: MR cholangiography at 3.0T. *Radiographics* 29:1689–1706, 2009.
- Frey CF, Burbige EJ, Meinke WB, et al: Endoscopic retrograde cholangiopancreatography. *Am J Surg* 144:109–114, 1982.
- Guibaud L, Bret PM, Reinhold C, et al: Bile duct obstruction and choledocholithiasis: Diagnosis with MR cholangiography. *Radiology* 197:109–115, 1995.
- Kim JH, Kim MJ, Park SI, et al: MR cholangiography in symptomatic gallstones: Diagnostic accuracy according to clinical risk group. *Radiology* 224:410–416, 2002.
- Soto JA, Barish MA, Alvarez O, et al: Detection of choledocholithiasis with MR cholangiography: Comparison of three-dimensional fast spin-echo and single- and multisection half-Fourier rapid acquisition with relaxation enhancement sequences. *Radiology* 215:737–745, 2000.
- Reinhold C, Taourel P, Bret PM, et al: Choledocholithiasis: Evaluation of MR cholangiography for diagnosis. *Radiology* 209:435–442, 1998.
- Becker CD, Grossholz M, Becker M, et al: Choledocholithiasis and bile duct stenosis: Diagnostic accuracy of MR cholangiopancreatography. *Radiology* 205:523–530, 1997.
- Demartines N, Eisner L, Schnabel K, et al: Evaluation of magnetic resonance cholangiography in the management of bile duct stones. *Arch Surg* 135:148–152, 2000.
- Hallal AH, Amortegui JD, Jeroukhimov IM, et al: Magnetic resonance cholangiopancreatography accurately detects common bile duct stones in resolving gallstone pancreatitis. *J Am Coll Surg* 200:869–875, 2005.
- Kim TK, Kim BS, Kim JH, et al: Diagnosis of intrahepatic stones: Superiority of MR cholangiography over endoscopic retrograde cholangiopancreatography. *AJR Am J Roentgenol* 179:429–434, 2002.
- Fulcher AS, Turner MA: Pitfalls of magnetic resonance cholangiopancreatography (MRCP). *J Comput Assist Tomogr* 22:845–850, 1998.
- Watanabe Y, Dohke M, Ishimori T, et al: Pseudo-obstruction of the extrahepatic bile duct due to artifact from arterial pulsatile compression: A diagnostic pitfall of MR cholangiopancreatography. *Radiology* 214:856–860, 2000.
- Soto JA, Alvarez O, Lopera JE, et al: Biliary obstruction: Findings at MR cholangiography and cross-sectional MR imaging. *Radiographics* 20:353–366, 2000.
- Schwartz LH, Coakley FV, Sun Y, et al: Neoplastic pancreaticobiliary duct obstruction: Evaluation with breath-hold MR cholangiopancreatography. *AJR Am J Roentgenol* 170:1491–1495, 1998.
- Adamek HE, Albert J, Breer H, et al: Pancreatic cancer detection with magnetic resonance cholangiopancreatography and endoscopic retrograde cholangiopancreatography: A prospective controlled study. *Lancet* 356:190–193, 2000.
- Magnuson TH, Bender JS, Duncan MD, et al: Utility of magnetic resonance imaging in the evaluation of biliary obstruction. *J Am Coll Surg* 189:63–71, 1999.
- Park HS, Lee JM, Choi JY, et al: Preoperative evaluation of bile duct cancer: MRI combined with MR cholangiopancreatography versus MDCT with direct cholangiography. *AJR Am J Roentgenol* 190:396–405, 2008.
- Kim MJ, Mitchell DG, Ito K, et al: Biliary dilatation: Differentiation of benign from malignant causes—value of adding conventional MR imaging to MR cholangiopancreatography. *Radiology* 214:173–181, 2000.
- Gornals JB, Moreno R, Castellote J, et al: Single-session endosonography and endoscopic retrograde cholangiopancreatography for biliaryopneumatic diseases is feasible, effective and cost beneficial. *Dig Liver Dis* 45:578–583, 2013.
- Plumley TF, Rohrmann CA, Freeny PC, et al: Double duct sign: Reassessed significance in ERCP. *AJR Am J Roentgenol* 138:31–35, 1982.
- Johnson PT, Outwater EK: Pancreatic carcinoma versus chronic pancreatitis: Dynamic MR imaging. *Radiology* 212:213–218, 1999.
- Fulcher AS, Turner MA: HASTE MR cholangiography in the evaluation of hilar cholangiocarcinoma. *AJR Am J Roentgenol* 169:1501–1505, 1997.
- Lopera JE, Soto JA, Múnera F: Malignant hilar and perihilar biliary obstruction: Use of MR cholangiography to define the extent of biliary ductal involvement and plan percutaneous interventions. *Radiology* 220:90–96, 2001.
- Park MS, Kim TK, Kim KW, et al: Differentiation of extrahepatic bile duct cholangiocarcinoma from benign stricture: Findings at MRCP versus ERCP. *Radiology* 233:234–240, 2004.
- Irie H, Honda H, Aibe H, et al: MR cholangiopancreatographic differentiation of benign and malignant intraductal mucin-producing tumors of the pancreas. *AJR Am J Roentgenol* 174:1403–1408, 2000.
- Koito K, Namieno T, Ichimura T, et al: Mucin-producing pancreatic tumors: Comparison of MR cholangiopancreatography with endoscopic retrograde cholangiopancreatography. *Radiology* 208:231–237, 1998.
- Onaya H, Itai Y, Niitsu M, et al: Ductectatic mucinous cystic neoplasms of the pancreas: Evaluation with MR cholangiopancreatography. *AJR Am J Roentgenol* 171:171–177, 1998.
- Matos C, Nicaise N, Devière J, et al: Choledochal cysts: Comparison of findings at MR cholangiopancreatography and endoscopic retrograde cholangiopancreatography in eight patients. *Radiology* 209:443–448, 1998.
- Lam WWM, Lam TPW, Saing H, et al: MR cholangiography and CT cholangiography of pediatric patients with choledochal cysts. *AJR Am J Roentgenol* 173:401–405, 1999.
- Yu J, Turner MA, Fulcher AS, et al: Congenital anomalies and normal variants of the pancreaticobiliary tract and the pancreas in adults. Part 2: Pancreatic duct and pancreas. *AJR Am J Roentgenol* 187:1544–1553, 2006.
- Chavhan GB, Babyn PS, Manson D, et al: Pediatric MR cholangiopancreatography: Principles, technique, and clinical applications. *Radiographics* 28:1951–1962, 2008.
- Okada A, Oguchi Y, Kamata S, et al: Common channel syndrome—diagnosis with endoscopic retrograde cholangiopancreatography and surgical management. *Surgery* 93:634–642, 1983.
- Yu ZL, Zhang LJ, Fu JZ, et al: Anomalous pancreaticobiliary junction: Image analysis and treatment principles. *Hepatobiliary Pancreat Dis Int* 3:136–139, 2004.
- Huang TL, Cheng YF, Chen CL, et al: Variants of the bile ducts: Clinical application in the potential donor of living-related hepatic transplantation. *Transplant Proc* 28:1669–1670, 1996.
- Taourel P, Bret PM, Reinhold C, et al: Anatomic variants of the biliary tree: Diagnosis with MR cholangiopancreatography. *Radiology* 199:521–527, 1996.
- Fulcher AS, Szucs RA, Bassignani MJ, et al: Right lobe living donor liver transplantation: Preoperative evaluation of the donor with MR imaging. *AJR Am J Roentgenol* 176:1483–1491, 2001.
- Suhocki PV, Meyers WC: Injury to aberrant bile ducts during cholecystectomy: A common cause of diagnostic error and treatment delay. *AJR Am J Roentgenol* 172:955–959, 1999.
- Wang DB, Yu J, Fulcher AS, Turner MA: Pancreatitis in patients with pancreas divisum: Imaging features at MRI and MRCP. *World J Gastroenterol* 19:4907–4916, 2013.
- Millbourn E: On the excretory ducts of the pancreas in man, with special reference to their relations to each other, to the common bile duct and to the duodenum. *Acta Anat* 9:1–34, 1950.
- Manfredi R, Costamagna G, Brizi MG, et al: Pancreas divisum and “santorinicele”: Diagnosis with dynamic MR cholangiopancreatography with secretin stimulation. *Radiology* 217:403–408, 2000.
- Ward J, Sheridan MB, Guthrie JA, et al: Bile duct strictures after hepatobiliary surgery: Assessment with MR cholangiography. *Radiology* 231:101–108, 2004.
- Fulcher AS, Turner MA: Orthotopic liver transplantation: Evaluation with MR cholangiography. *Radiology* 211:715–722, 1999.
- Valls C, Alba E, Cruz M, et al: Biliary complications after liver transplantation: Diagnosis with MR cholangiopancreatography. *AJR Am J Roentgenol* 184:812–820, 2005.

52. Tang Y, Yamashita Y, Arakawa A, et al: Pancreaticobiliary ductal system: Value of half-Fourier rapid acquisition with relaxation enhancement MR cholangiopancreatography for postoperative evaluation. *Radiology* 215:81–88, 2000.
53. Ragozzino A, De Ritis R, Mosca A, et al: Value of MR cholangiography in patients with iatrogenic bile duct injury after cholecystectomy. *AJR Am J Roentgenol* 183:1567–1572, 2004.
54. Monill J, Pernas J, Clavero J, et al: Pancreatic duct after pancreatoduodenectomy: Morphologic and functional evaluation with secretin-stimulated MR pancreatography. *AJR Am J Roentgenol* 183:1267–1274, 2004.
55. Novellas S, Caramella T, Fournol M, et al: MR cholangiopancreatography features of the biliary tree after liver transplantation. *AJR Am J Roentgenol* 191:221–227, 2008.
56. Vitellas KM, El-Dieb A, Vaswani KK, et al: Using contrast-enhanced MR cholangiography with IV mangafodipir trisodium (Teslascan) to evaluate bile duct leaks after cholecystectomy: A prospective study of 11 patients. *AJR Am J Roentgenol* 179:409–416, 2002.
57. MacCarty RL, LaRusso NF, Wiesner RH, Ludwig J: Primary sclerosing cholangitis: Findings on cholangiography and pancreatography. *Radiology* 149:39–44, 1983.
58. Fulcher AS, Turner MA, Franklin KJ, et al: Primary sclerosing cholangitis: Evaluation with MR cholangiography—a case-control study. *Radiology* 215:71–80, 2000.
59. Talwalkar JA, Angulo P, Johnson CD, et al: Cost-minimization analysis of MRC versus ERCP for the diagnosis of primary sclerosing cholangitis. *Hepatology* 40:39–45, 2004.
60. Vitellas KM, El-Dieb A, Vaswani KK, et al: MR cholangiopancreatography in patients with primary sclerosing cholangitis: Interobserver variability and comparison with endoscopic retrograde cholangiopancreatography. *AJR Am J Roentgenol* 179:399–407, 2002.
61. Vitellas KM, Enns RA, Keogan MT, et al: Comparison of MR cholangiopancreatographic techniques with contrast-enhanced cholangiography in the evaluation of sclerosing cholangitis. *AJR Am J Roentgenol* 178:327–334, 2002.
62. Elsayes KM, Oliveira EP, Narra VR, et al: MR and MRCP in the evaluation of primary sclerosing cholangitis: Current applications and imaging findings. *J Comput Assist Tomogr* 30:398–404, 2006.
63. Lecesne R, Taourel P, Bret PM, et al: Acute pancreatitis: Interobserver agreement and correlation of CT and MR cholangiopancreatography with outcome. *Radiology* 211:727–735, 1999.
64. Morgan DE, Baron TH, Smith JK, et al: Pancreatic fluid collections prior to intervention: evaluation with MR imaging compared with CT and US. *Radiology* 203:773–778, 1997.
65. Sugiyama M, Haradome H, Atomi Y: Magnetic resonance imaging for diagnosing chronic pancreatitis. *J Gastroenterol* 42(Suppl 17):108–112, 2007.
66. Trout AT, Podberesky DJ, Serai SD, et al: Does secretin add value in pediatric magnetic resonance cholangiopancreatography? *Pediatr Radiol* 43:479–486, 2013.
67. Gallix BP, Bret PM, Atri M, et al: Comparison of qualitative and quantitative measurements on unenhanced T1-weighted fat saturation MR images in predicting pancreatic pathology. *J Magn Reson Imaging* 21:583–589, 2005.
68. Kinney TP, Punjabi G, Freeman M: Technology insight: Applications of MRI for the evaluation of benign disease of the pancreas. *Nat Clin Pract Gastroenterol Hepatol* 4:148–159, 2007.
69. Heverhagen JT, Müller D, Battmann A, et al: MR hydrometry to assess exocrine function of the pancreas: Initial results of noninvasive quantification of secretion. *Radiology* 218:61–67, 2001.
70. Manfredi R, Costamagna G, Brizi MG, et al: Severe chronic pancreatitis versus suspected pancreatic disease: Dynamic MR cholangiopancreatography after secretin stimulation. *Radiology* 214:849–855, 2000.
71. Choi BW, Kim MJ, Chung JJ, et al: Radiologic findings of Mirizzi syndrome with emphasis on MRI. *Yonsei Med J* 41:144–146, 2000.
72. Schwartz LH, Black J, Fong Y, et al: Gallbladder carcinoma: Findings at MR imaging with MR cholangiopancreatography. *J Comput Assist Tomogr* 26:405–410, 2002.
73. Haradome H, Ichikawa T, Sou H, et al: The pearl necklace sign: An imaging sign of adenomyomatosis of the gallbladder at MR cholangiopancreatography. *Radiology* 227:80–88, 2003.
74. Wathle GK, Tjora E, Ersland L, et al: Assessment of exocrine pancreatic function by secretin-stimulated magnetic resonance cholangiopancreatography and diffusion-weighted imaging in healthy controls. *J Magn Reson Imaging* 39:448–454, 2014.

Anomalies and Anatomic Variants of the Gallbladder and Biliary Tract

RICHARD M. GORE | ANDREW J. TAYLOR | GARY G. GHAREMANI

CHAPTER OUTLINE

Embryology

Agenesis of the Gallbladder

Duplication of the Gallbladder

Anomalies of Gallbladder Shape

Phrygian Cap

Multiseptate Gallbladder

Diverticula

Abnormalities of Gallbladder Position

Wandering Gallbladder

Gallbladder Torsion

Ectopic Gallbladder

Abnormalities in Gallbladder Size

Cholecystomegaly

Microgallbladder

Biliary Tract Anomalies

Choledochal Cysts

Choledochoceles

Caroli's Disease

There are many congenital abnormalities of the gallbladder and bile ducts, which, excluding biliary atresia and choledochal cysts, are usually of no clinical or functional significance.¹ These anomalies are usually found in the course of evaluating biliary disease in an adult patient and are of interest primarily to the surgeon, who must deal with the anatomic variation during the course of surgery.²⁻⁶

Embryology

When the human embryo is 2.5 mm in size, a bifid bud forms along the anterior margin of the primitive foregut and proliferates laterally into the septum transversum. The more cephalad of these two diverticula is responsible for the formation of the liver and intrahepatic bile ducts, whereas the caudal diverticulum develops into the gallbladder and extrahepatic biliary tree. At the 5-mm stage of development, the originally hollow primordium of the gallbladder and common bile duct becomes occluded with endodermal cells but is soon revacuolated. If recanalization is incomplete, a compartmentalized multiseptate gallbladder results. A single, transversely oriented septum results in the phrygian cap deformity, whereas longitudinal septa produce a bifid or triple gallbladder. The lumen of the common bile duct is reestablished at the 7.5-mm stage and the

gallbladder and duodenal lumen somewhat later. Bile is secreted by the 12th week.^{4,5}

At the 10- to 15-mm stage (6-7 weeks), the gallbladder has formed and is connected to the duodenum by a canalized choledochocystic duct. This duct originates from the lateral aspect of the primitive foregut and eventually terminates on the medial or posteromedial aspect of the descending portion of the duodenum after the foregut completes its 270-degree rotation.⁴⁻⁶

The formation of the intrahepatic ducts is preceded by the development of the portal and hepatic veins and the formation of the hepatocytes and Kupffer cells. The intrahepatic ducts by the 18-mm stage consist only of a blindly ending solid core of cells that extends from the junction of the cystic and common ducts toward the liver hilum. At the point of contact between this blindly ending ductal anlage and the hepatocytes, the intrahepatic ducts develop along the framework of the previously formed portal vein branches similar to vines on a trellis. Significant variation in the configuration of the intrahepatic ducts can be accounted for by the unpredictable manner in which they wind around pre-existing portal veins.⁴⁻⁶

Agenesis of the Gallbladder

Agenesis of the gallbladder is caused by failure of development of the caudal division of the primitive hepatic diverticulum or failure of vacuolization after the solid phase of embryonic development. Atresia or hypoplasia of the gallbladder also represents aborted development of the organ.⁷⁻⁹ Other congenital anomalies are present in two thirds of these patients, including congenital heart lesions, polysplenia, imperforate anus, absence of one or more bones, and rectovaginal fistula.¹⁰ There appears to be a genetic input as well because several families with multiple individuals having agenesis have been identified.¹⁰ This malformation is reported in 0.013% to 0.155% of autopsy series, but many of these cases are in stillborn and young infants. The surgical incidence of gallbladder agenesis is approximately 0.02%.^{10,11} Nearly two thirds of adult patients with agenesis of the gallbladder have biliary tract symptoms, and extrahepatic biliary calculi are reported in 25% to 50% of these patients.¹²⁻¹⁴

Preoperative diagnosis of gallbladder agenesis is difficult, and the absence of the gallbladder is often an intraoperative finding.^{2,8,14} Ultrasound or computed tomography (CT) may suggest the diagnosis, but this disorder is usually diagnosed at surgery when the gallbladder is not found at cholangiography.¹⁵ Intraoperative ultrasound may be helpful in establishing the diagnosis and excluding a completely intrahepatic gallbladder.¹⁶ Agenesis of the gallbladder is a rare cause of false-positive hepatobiliary scintiscans.¹⁷

Duplication of the Gallbladder

Gallbladder duplication occurs in about 1 in 4000 people and 4.8% of domestic animals.¹⁸⁻²⁰ This anomaly is caused by incomplete revacuolization of the primitive gallbladder, resulting in a persistent longitudinal septum that divides the gallbladder lengthwise. Another possible mechanism is the occurrence of separate cystic buds. To establish the diagnosis, two separate gallbladder cavities, each with its own cystic duct, must be present. These duplicated cystic ducts may enter the common duct separately or form a Y configuration before a common entrance.²¹

Most reported cases of gallbladder duplication have a clinical picture of cholecystitis with cholelithiasis in at least one of the gallbladders. Sometimes one of the gallbladders appears normal on oral cholecystography, whereas the second, diseased, nonvisualized, and unsuspected gallbladder produces symptoms.²²⁻²⁴

A number of entities can mimic the double gallbladder at sonography: folded gallbladder, bilobed gallbladder, choledochal cyst, pericholecystic fluid, gallbladder diverticulum, vascular band across the gallbladder, and focal adenomyomatosis.²⁵⁻²⁸ Complications associated with double gallbladder include torsion and the development of papilloma, carcinoma, common duct obstruction, and secondary biliary cirrhosis.²⁷ Treatment of this disorder consists of removal of both gallbladders.

Triple and quadruple gallbladders have also been reported.²⁸ Diverticular gallbladders without cystic ducts are classified as accessory gallbladders.

Anomalies of Gallbladder Shape

PHRYGIAN CAP

Phrygian cap is the most common abnormality of gallbladder shape, occurring in 1% to 6% of the population.²⁹ It is named after the headgear worn by ancient Greek slaves as a sign of liberation. This deformity is characterized by a fold or septum of the gallbladder between the body and fundus. Two variations of this anomaly have been described. In the retroserosal or concealed type, the gallbladder is smoothly invested by peritoneum, and the mucosal fold that projects into the lumen may not be visible externally. In the serosal or visible type, the peritoneum follows the bend in the fundus, then reflects on itself as the fundus overlies the body. This anomaly is of no clinical significance unless it is mistaken for a layer of stones or hyperplastic cholecystosis.^{3,15,24-29}

MULTISEPTATE GALLBLADDER

The multiseptate gallbladder is a solitary gallbladder characterized by multiple septa of various sizes internally and a faintly bosselated surface externally.²⁸⁻³⁰ The gallbladder is usually normal in size and position, and the chambers communicate with one another by one or more orifices from fundus to cystic duct. These septations lead to stasis of bile and gallstone formation.³¹ On ultrasound studies, multiple communicating septations and locules are seen bridging the gallbladder lumen.³² Oral cholecystography reveals the "honeycomb" multicystic character of the gallbladder. The sonographic

differential diagnoses are desquamated gallbladder mucosa and hyperplastic cholecystoses.

DIVERTICULA

Gallbladder diverticula are rare and usually clinically silent. They can occur anywhere in the gallbladder and are usually single and vary greatly in size. Congenital diverticula are true diverticula and contain all the mural layers, as opposed to the pseudodiverticula of adenomyomatosis, which have little or no smooth muscle in their walls. Acquired traction diverticula from adjacent adhesions or duodenal disease must also be excluded.^{7,8,15}

Abnormalities of Gallbladder Position

WANDERING GALLBLADDER

When the gallbladder has an unusually long mesentery, it can "wander" or "float."³³⁻³⁷ The gallbladder may "disappear" into the pelvis on upright radiographs or wander in front of the spine or to the left of the abdomen. Rarely, the gallbladder can herniate through the foramen of Winslow into the lesser sac. In these cases, cholecystography reveals an unusual angulation of the gallbladder, which lies parallel and adjacent to the duodenal bulb with its fundus pointing to the left upper quadrant. The herniation can be intermittent and may be responsible for abdominal pain. It is best seen by a barium meal in conjunction with oral cholecystography. Cross-sectional imaging may not be specific, showing only a cystic structure in the lesser sac.

GALLBLADDER TORSION

Three unusual anatomic situations give rise to torsion of the gallbladder, and they all produce twisting of an unusually mobile gallbladder on a pedicle: (1) a gallbladder that is completely free of mesenteric or peritoneal investments except for its cystic duct and artery, (2) a long gallbladder mesentery sufficient to allow twisting, and (3) the presence of large stones in the gallbladder fundus that cause lengthening and torsion of the gallbladder mesentery. Kyphosis, vigorous gallbladder peristalsis, and atherosclerosis have also been implicated as other predisposing or contributing factors.³⁸ The mesentery is sufficiently long to permit torsion in 4.5% of the population. Most cases of gallbladder torsion occur in women (female-to-male ratio of 3:1).³⁹ The usual preoperative diagnosis is acute cholecystitis. The presence of fever is variable, leukocytosis is common, and one third of patients have a right upper quadrant mass. Gangrene develops in more than 50% of cases and is extremely common when the pain has been present for more than 48 hours. On cross-sectional imaging, the gallbladder is distended and may have an unusual location and show mural thickening. The diagnosis is seldom made preoperatively, however.^{40,41}

ECTOPIC GALLBLADDER

The gallbladder can be located in a variety of anomalous positions. In patients with an intrahepatic gallbladder, the gallbladder is completely surrounded by hepatic parenchyma. The intrahepatic gallbladder usually presents little difficulty in imaging, but it may complicate the clinical diagnosis of acute

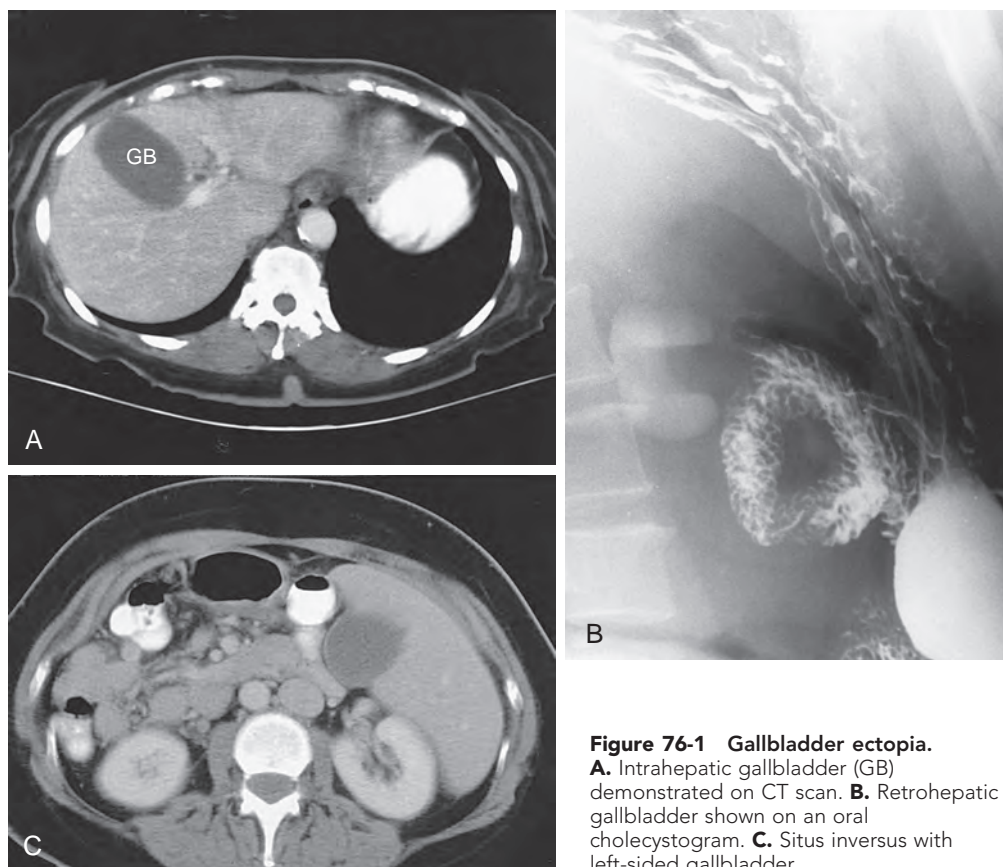


Figure 76-1 Gallbladder ectopia.

A. Intrahepatic gallbladder (GB) demonstrated on CT scan. **B.** Retrohepatic gallbladder shown on an oral cholecystogram. **C.** Situs inversus with left-sided gallbladder.

cholecystitis because of a paucity of peritoneal signs resulting from the long distance between the gallbladder and peritoneum. This anomaly also makes cholecystectomy more difficult. On sulfur colloid scans, the intrahepatic gallbladder presents as a cold hepatic defect.

The gallbladder has also been reported in the following positions: suprahepatic, retrohepatic (Fig. 76-1), supradiaphragmatic, and retroperitoneal. In patients with cirrhosis, small or absent right lobes, or chronic obstructive pulmonary disease, the gallbladder together with the colon is often interposed between the liver and the diaphragm.⁴² Left-sided gallbladders may occur in situs inversus or as an isolated finding. They can also lie in the falciform ligament, transverse mesocolon, and anterior abdominal wall.

Abnormalities in Gallbladder Size

CHOLECYSTOMEGALY

Enlargement of the gallbladder has been reported in a number of disorders including diabetes (because of an autonomic neuropathy) and after truncal and selective vagotomy. The gallbladder also becomes larger than normal during pregnancy, in patients with sickle hemoglobinopathy, and in extremely obese people.⁴³⁻⁴⁶

MICROGALLBLADDER

In patients with cystic fibrosis, the gallbladder is typically small, trabeculated, contracted, and poorly functioning. It often

contains echogenic bile, sludge, and cholesterol gallstones. These changes are presumably due to the thick, tenacious bile that is characteristic of this disease.^{47,48}

Biliary Tract Anomalies

Anomalies of the biliary system are found in 2.4% of autopsies, 28% of surgical dissections, and 5% to 13% of operative cholangiograms.⁶ The most common anomaly is an aberrant intrahepatic duct draining a circumscribed portion of the liver, such as an anterior or posterior segment right lobe duct that drains into the left main rather than the right main hepatic duct. The aberrant main can join the common hepatic duct, common bile duct, or cystic duct or insert into a low right hepatic duct. Rarely, it may run through the gallbladder fossa or into the gallbladder, predisposing it to injury at cholecystectomy.

The hepatic ducts may join either higher or lower than normal. Surgical difficulties may arise when the cystic duct enters into a low inserting right hepatic duct or when the right hepatic duct enters into the cystic duct before joining the left hepatic duct. Duplications of the cystic duct and common bile duct are rare. Anomalies of cystic duct insertion occur as well (Fig. 76-2).

Congenital tracheobiliary fistula is a rare disorder that is manifested with respiratory distress and cough with bilious sputum. The fistula begins near the carina, traverses the diaphragm, and usually communicates with the left hepatic duct. Pneumobilia may be seen on plain radiography, and the diagnosis is confirmed with biliary scintigraphy.

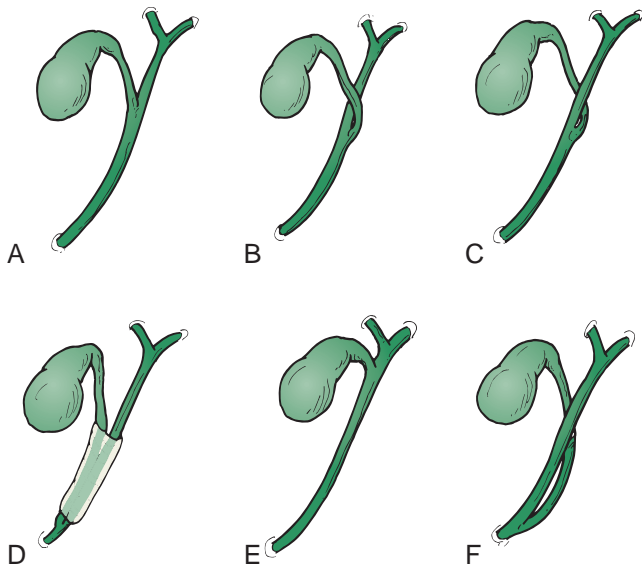


Figure 76-2 Anatomic variants in the cystic duct. Drawings illustrate how the cystic duct may insert into the extrahepatic bile duct with a right lateral insertion (A), anterior spiral insertion (B), posterior spiral insertion (C), low lateral insertion with a common sheath (D), proximal insertion (E), or low medial insertion (F). (From Turner MA, Fulcher AS: *The cystic duct: Normal anatomy and disease processes*. RadioGraphics 21:3–22, 2001.)

Choledochal cysts, choledochoceles, and Caroli's disease are a part of a spectrum of biliary anomalies that produce dilation of the biliary tree. They are discussed individually in the following section, and their relationship is illustrated in Figure 76-3.

CHOLEDOCHAL CYSTS

Choledochal cysts (Figs. 76-4 to 76-6) are congenital cystic dilations of any portion of the extrahepatic bile ducts, most commonly the main portion of the common bile duct.^{49–55} It is postulated that this condition begins with an anomalous junction of the common bile duct and pancreatic duct proximal to the duodenal papilla. Higher pressure in the pancreatic duct combined with an absent ductal sphincter allows free reflux of enzymes into the biliary tree, weakening the wall of the common bile duct. There is a 3:1 female predominance, and 60% of patients present before the age of 10 years, although choledochal cysts can present from birth to old age. This anomaly is associated with an increased incidence of gallbladder anomalies, other biliary anomalies (e.g., biliary stenosis or atresia), and congenital hepatic fibrosis. Complications of choledochal cysts in adults include rupture with bile peritonitis, secondary infection (cholangitis), biliary cirrhosis and portal hypertension, calculus formation, portal vein thrombosis, liver abscess, hemorrhage, and malignant transformation into cholangiocarcinoma.^{55–57}

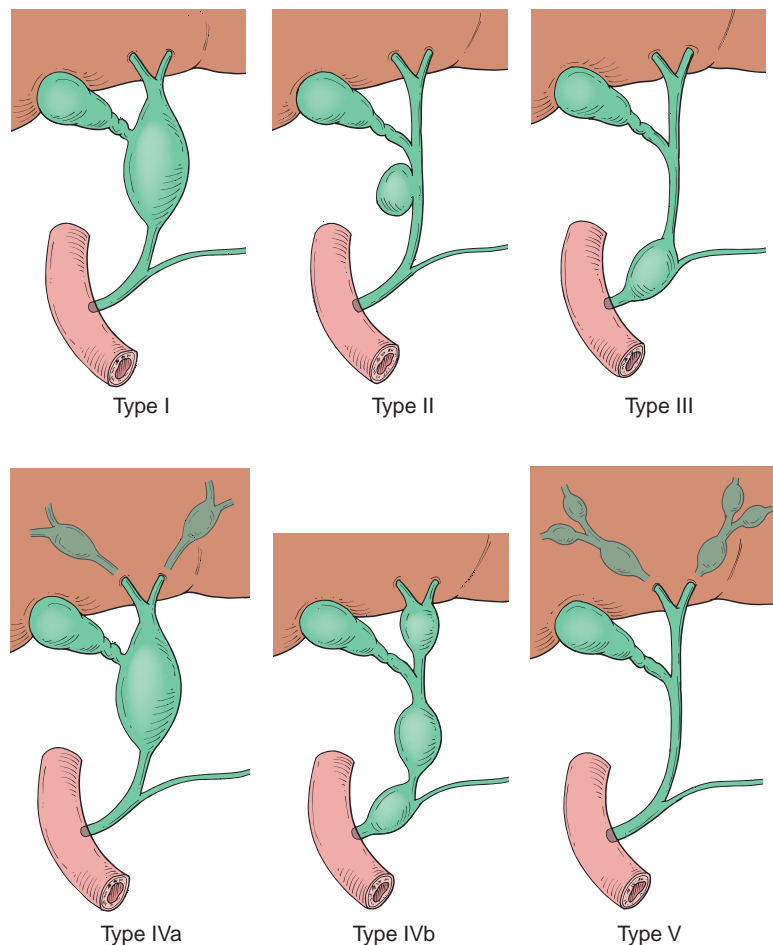


Figure 76-3 Classification of choledochal cysts.

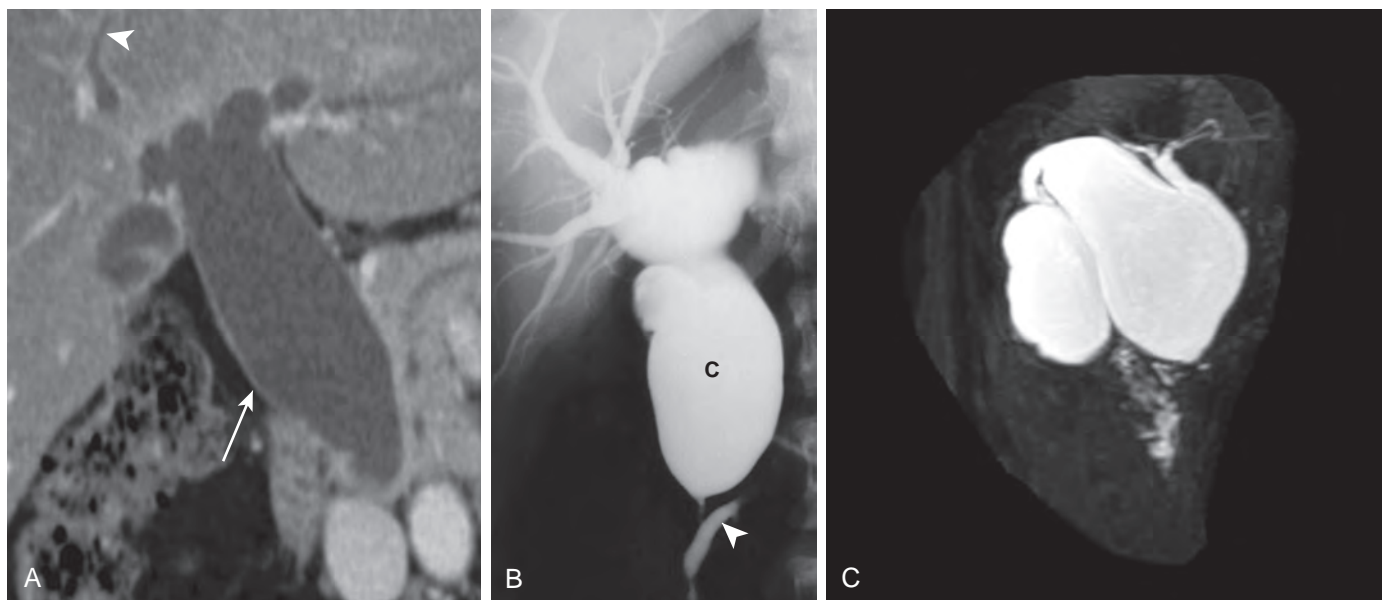


Figure 76-4 Type I choledochal cysts. **A.** Coronal oblique multiplanar reformatted CT image shows fusiform dilation of the common bile duct (arrow). Note also the dilation of the intrahepatic biliary tract (arrowhead). **B.** Percutaneous transhepatic cholangiogram in the same patient shows a large choledochal cyst (c) at the level of the extrahepatic bile duct. Note the aberrant entry of the common bile duct at the side of the pancreatic duct (arrowhead). **C.** MRCP in a different patient shows a dilated main common bile duct.

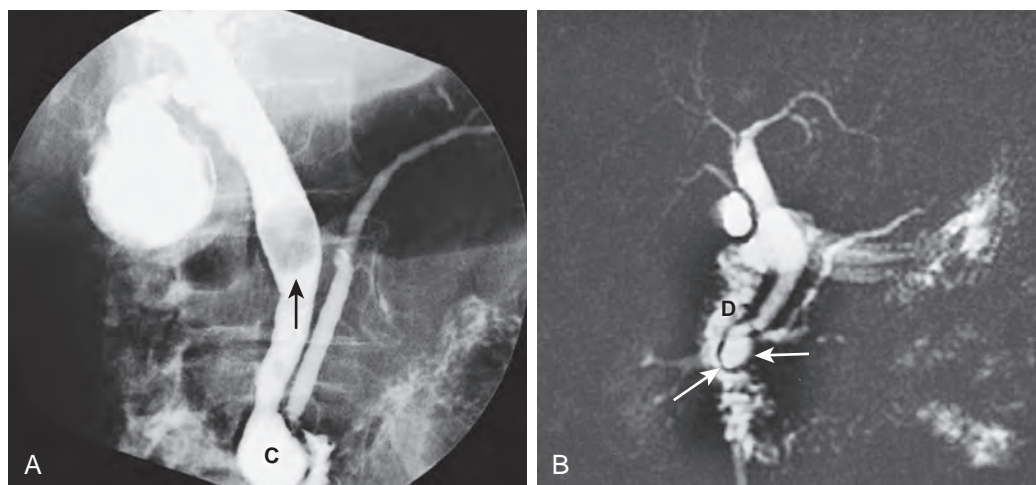


Figure 76-5 Type III choledochal cyst: choledochoceles. **A.** ERCP shows saccular dilation of the distal common bile duct (c) and choledocholithiasis (arrow). **B.** Coronal MRCP image demonstrates bulbous dilation of the intramural segment of the distal common bile duct (arrows), which protrudes into the duodenum (D).

Newborns and infants present with obstructive jaundice.^{54,55} Older children and adults may have the classic triad of right upper quadrant pain, intermittent jaundice, and a palpable right upper quadrant mass. In adult patients, a choledochal cyst is often first diagnosed on cross-sectional imaging. CT (see Fig. 76-4) and ultrasound demonstrate a fluid-filled structure beneath the porta hepatis separate from the gallbladder that communicates with the hepatic ducts. An abrupt change in the caliber of the ducts occurs at the site of the cysts. Intrahepatic ductal dilation may be present as well.

Cholangiography is necessary to confirm the diagnosis. It demonstrates a cystic structure 2 to 15 cm in diameter that communicates with the hepatic ducts. An abrupt change in ductal caliber occurs at the site of the cyst. Mild intrahepatic ductal dilation, stones, or sludge may be present as well. Cholangiography is useful for fully defining ductal anatomy.

Upper gastrointestinal series may show a soft tissue mass in the right upper quadrant that causes anterior displacement of the second portion of the duodenum and antrum or inferior

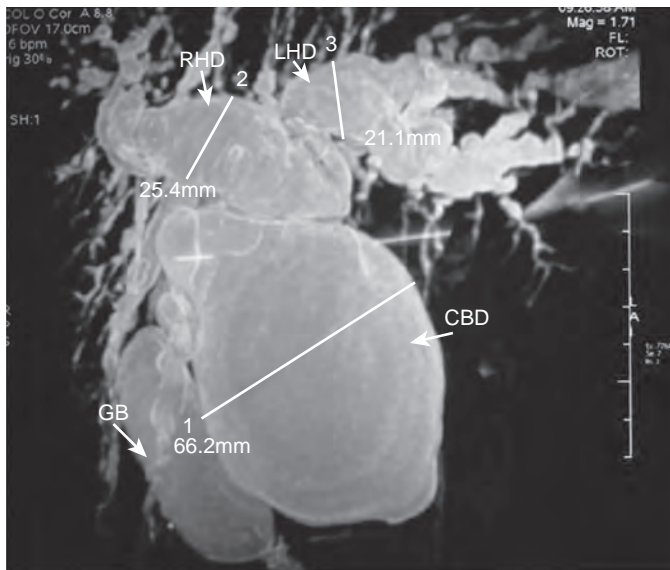


Figure 76-6 Type IV choledochal cyst. MRCP image shows massive dilation of the common bile duct (CBD) as well as the right (RHD) and left (LHD) intrahepatic ducts. GB, Gallbladder.

displacement of the duodenum or widening of the duodenal sweep.⁵⁴⁻⁵⁶

Ultrasound findings reflect the specific type of choledochal cyst, although a cystic extrahepatic mass is typically present. A portion of the proximal bile duct can often be seen extending into the choledochal cyst. Hepatobiliary scans show late filling and stasis of the isotope within the choledochal cyst.⁵³ They are useful in excluding hepatic cyst, pancreatic pseudocyst, and enteric duplication.

Direct coronal magnetic resonance (MR) imaging demonstrates a dilated tubular structure that follows the expected course of the common bile duct. MR cholangiopancreatography (MRCP) can also demonstrate these dilated biliary structures because the luminal contents of the bile appear hyperdense in contrast to the portal vein. MRCP can also diagnose biliary calculi and stricture formation that frequently complicate cystic disease of the bile ducts. Two studies showed that MRCP offered equivalent information to endoscopic retrograde cholangiopancreatography (ERCP), without the potential complications inherent in the latter procedure. In patients with choledochal cysts who are reluctant to undergo surgical resection, periodic follow-up ultrasound and MRCP may help achieve early detection of malignant change.⁵² The management of choledochal cysts is surgical, with excision of all cyst tissue and reconstruction of continuity between the liver and gut by a Roux-en-Y hepaticojejunostomy.⁵⁷

CHOLEDOCHOCES

A choledochocoele is a rare, easily overlooked anomaly of unknown cause. This anomaly has been called variously an intraduodenal choledochal cyst, duodenal duplication cyst, diverticulum of the common bile duct, and enterogenous cyst of the duodenum. It is a protrusion of a dilated intramural segment of common bile duct into the duodenum, analogous

to a ureterocele.⁵⁸⁻⁶⁰ It is often seen on cholangiograms in patients who have had a cholecystectomy, so that the lesion may be partly acquired.

Choledochoceles usually are manifested in adulthood with long-standing nausea, vomiting, and episodic abdominal pain. Stones and sludge are often present, and patients often have episodes of biliary colic, intermittent jaundice, and pancreatitis as well.^{54,55}

Cholangiography shows smooth clublike or saclike dilation of the intramural segment of the common bile duct (see Fig. 76-5A). Barium studies demonstrate a smooth, well-defined intraluminal duodenal filling defect in this region of the papilla that changes in shape with compression and peristalsis. In contrast to intraluminal diverticula, choledochoceles do not fill with barium.⁵⁸⁻⁶⁰ On MRCP images, they have a high signal intensity, “cobra-head” appearance bulging into the duodenum (see Fig. 76-5B).

CAROLI'S DISEASE

Caroli's disease, also known as communicating cavernous ectasia, is characterized by multifocal segmental saccular dilation of the intrahepatic bile ducts, a predisposition to biliary calculi and cholangitis, and an association with various forms of cystic renal disease. Caroli's disease usually is manifested in adulthood; however, it can be seen in newborns and infants. Adult patients present with recurrent attacks of cholangitis and crampy right upper quadrant pain with occasional fever and mild jaundice. Infants and children may present with hematemesis caused by portal hypertension from hepatic fibrosis.^{54,55,61-63} This disease appears to be autosomal recessively inherited in most cases. Complications of Caroli's disease include stone formation (95%) within the dilated intrahepatic ducts, recurrent cholangitis, and liver abscess. There is also a 100-fold increase in the incidence of bile duct carcinoma, occurring in 7% of patients.

Caroli's disease is best demonstrated by cholangiography (Fig. 76-7), which shows saccular dilations of the intrahepatic ducts, stones, strictures, and communicating hepatic abscesses. CT can also demonstrate tiny dots with strong contrast enhancement within dilated intrahepatic bile ducts (the central dot sign). These intraluminal dots correspond to intraluminal portal veins.⁶⁴⁻⁶⁸ CT and ultrasound demonstrate multiple cystic areas within the liver.⁶⁹⁻⁷¹ (Fig. 76-8). Technetium Tc 99m sulfur colloid scans show multiple cold defects, and hepatobiliary scans show an unusual pattern of retained activity throughout the liver.^{54,55}

MRCP with three-dimensional display is an accurate method for demonstrating Caroli's disease because the luminal contents of the bile ducts appear hyperintense in contrast to the portal vein, which usually appears as signal void. Cystic expansions of the intrahepatic biliary tract are depicted as oval structures in continuity with the biliary tract (Fig. 76-9). They are nearly signal void on black bile techniques and have a high signal intensity on bright bile or MRCP sequences.⁷²

Treatment depends on the clinical features and location of the biliary abnormality. When the disease is localized to one hepatic lobe, hepatectomy relieves symptoms and appears to remove the risk of malignancy. In diffuse Caroli's disease, treatment options include conservative or endoscopic therapy, internal biliary bypass procedures, and liver transplantation in carefully selected cases.

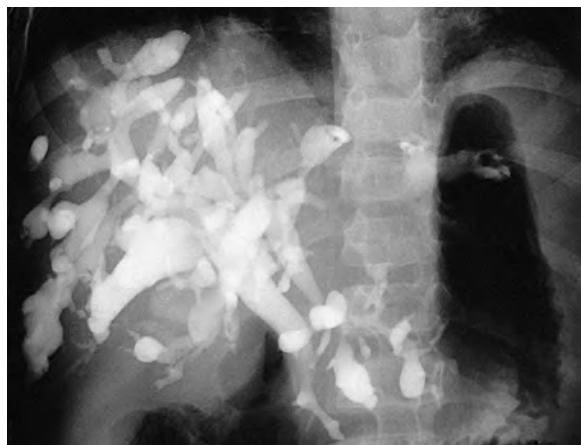


Figure 76-7 Caroli's disease: cholangiographic findings. ERCP demonstrates bulbous dilations of the peripheral intrahepatic biliary radicles characteristic of Caroli's disease. (From Taylor AJ, Bohorfoush AG: *Interpretation of ERCP with Associated Digital Imaging*. Philadelphia, Lippincott-Raven, 1997, p 52, with permission.)

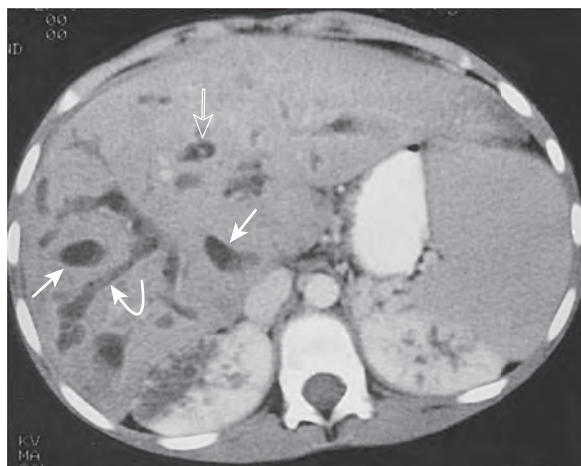


Figure 76-8 Caroli's disease: CT findings. The dilated segments of the intrahepatic biliary tract may be visualized as "cysts" (straight arrows), which are occasionally attached to more proximal ectatic segments of the biliary radicles (curved arrow). The defining CT feature of Caroli's disease is the central dot sign (open arrow). There is ectasia of the distal nephrons in the kidneys. (From Taylor AJ, Bohorfoush AG: *Interpretation of ERCP with Associated Digital Imaging*. Philadelphia, Lippincott-Raven, 1997, p 52, with permission.)

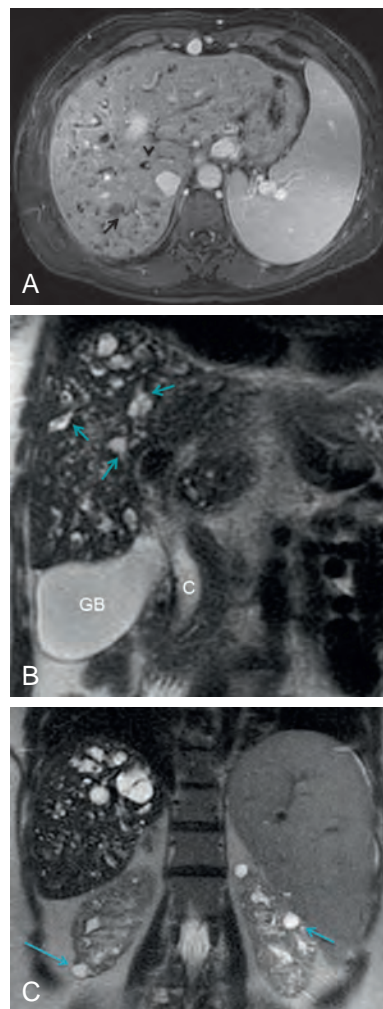


Figure 76-9 Caroli's disease: MR findings. **A.** Portal venous phase contrast enhanced T1 gradient echo axial image shows scattered cystic dilated intrahepatic bile ducts, some leading into mildly dilated ducts (arrow). Also present is the low signal intensity dilated duct surrounding the enhanced portal vein radicle forming the "central dot sign" (arrowhead). **B.** Coronal T2-weighted image shows multiple saccular dilatation of the intrahepatic biliary tree some demonstrating a connection with the more normal diameter ducts (arrows). **C.** Coronal T2-weighted MRI more posteriorly located in this patient with the intrahepatic cystic ductal changes of Caroli's disease shows cystic change in both kidneys (arrows). Also present is an enlarged spleen as a manifestation of portal hypertension, which has developed in this patient.

REFERENCES

1. Keplinger KM, Bloomston M: Anatomy and embryology of the biliary tract. *Surg Clin North Am* 94:203–217, 2014.
2. Savader SJ, Venbrux AC, Faerber AC, et al: Biliary tract anomalies, congenital and neonatal disorders, and hepatobiliary cystic malformations. In Friedman AC, Dachman AH, editors: *Radiology of the Liver, Biliary Tract, and Pancreas*, St. Louis, 1994, CV Mosby, pp 397–444.
3. Kamath BM, Piccoli DA: Heritable disorders of the bile ducts. *Gastroenterol Clin North Am* 32:857–875, 2003.
4. Taylor AJ, Bohorfoush AG: *Interpretation of ERCP with Associated Digital Imaging Correlation*, Philadelphia, 1997, Lippincott-Raven, pp 41–58.
5. Akisik MF, Jennings SG, Aisen AM, et al: MRCP in patient care: A prospective survey of gastroenterologists. *AJR Am J Roentgenol* 201:573–577, 2013.
6. Lack EE: *Pathology of the Pancreas, Gallbladder, Extrahepatic Biliary Tract, and Ampullary Region*, Oxford, 2003, Oxford University Press, pp 395–413.
7. Haller JO, Slovis TL: Pediatric gallbladder and biliary tract: Sonographic evaluation. *Ultrasound Q* 9:271–311, 1992.
8. Kamath BM, Piccoli DA: Heritable disorders of the bile ducts. *Gastroenterol Clin North Am* 32:857–875, 2003.
9. Coughlin JP, Rector FE, Klein MD: Agenesis of the gallbladder in duodenal atresia: Two case reports. *J Pediatr Surg* 27:1304, 1992.
10. Bani-Hani KE: Agenesis of the gallbladder: Difficulties in management. *J Gastroenterol Hepatol* 20:671–675, 2005.

11. Senecail B, Nonent M, Kergastel I, et al: Ultrasonic features of congenital anomalies of the gallbladder. *J Radiol* 81:1591–1594, 2000.
12. Vijay KT, Kocher HH, Koti RS, et al: Agenesis of gallbladder: A diagnostic dilemma. *J Postgrad Med* 42:80–82, 1996.
13. Bartone NF, Grieco RV: Absent gallbladder and cystic duct. *AJR Am J Roentgenol* 110:252–255, 1970.
14. Fisichella PM, Di Stefano A, Di Carlo I: Isolated agenesis of the gallbladder: Report of a case. *Surg Today* 32:78–80, 2002.
15. Berk RN: Oral cholecystography. In Berk RN, Ferrucci JT, Leopold GR, editors: *Radiology of the Gallbladder and Bile Ducts*, Philadelphia, 1983, WB Saunders, pp 83–162.
16. Bayraktar Y, Balaban HY, Arslan S, et al: Agenesis of gallbladder and multiple anomalies of the biliary tree in a patient with portal thrombosis: A case report. *Turk J Gastroenterol* 17:212–215, 2006.
17. Warshaw DM, Sulzer JL: Agenesis of the gallbladder: A rare cause for a false-positive hepatobiliary image. *Clin Nucl Med* 13:468, 1988.
18. Meilstrup JW, Hopper KD, Thieme GA: Imaging of gallbladder variants. *AJR Am J Roentgenol* 157:1205–1208, 1991.
19. Paciorek ML, Lackner D, Daley C, et al: A unique presentation of multiseptate gallbladder. *Dig Dis Sci* 42:2519–2523, 1997.
20. Geremia P, Tomà P, Martinoli C, et al: Multiseptate gallbladder: Clinical and ultrasonographic follow-up for 12 years. *J Pediatr Surg* 48:e25–e28, 2013.
21. Udelsman R, Sugerbaker PH: Congenital duplication of the gallbladder associated with an anomalous right hepatic artery. *Am J Surg* 149:812–815, 1985.
22. Gocmen R, Yesilkaya Y: Imaging findings of gallbladder duplication due to two cases: Case report and review of literature. *Med Ultrason* 14:358–360, 2012.
23. Ozgen A, Akata D, Arat A, et al: Gallbladder duplication: Imaging findings and differential considerations. *Abdom Imaging* 24:285–288, 1999.
24. Chawla Y, Makharia G, Gupta S, et al: Bilobed gallbladder with gallstones and choledocholithiasis. *Trop Gastroenterol* 19:64–66, 1998.
25. Chiba T, Shinozaki M, Kato S, et al: Caroli's disease: Central dot sign re-examined by CT arteriography and CT during arterial portography. *Eur Radiol* 12:701–702, 2002.
26. Takayashiki T, Miyazaki M, Kato A, et al: Double cancer of gallbladder and bile duct associated with anomalous junction of the pancreaticobiliary ductal system. *Hepatogastroenterology* 49:109–112, 2002.
27. Oyar O, Yesildag A, Gulsoy U, et al: Bilobed gallbladder diagnosed by oral cholecysto-CT. *Comput Med Imaging Graph* 27:315–319, 2003.
28. Foster DR: Triple gallbladder. *Br J Radiol* 54:817–818, 1981.
29. Boyden EA: The "phrygian cap" in cholecystography. *Am J Roentgenol* 33:589–596, 1935.
30. Paciorek ML, Lackner D, Daly G, et al: A unique presentation of multiseptate gallbladder. *Dig Dis Sci* 42:2519–2523, 1997.
31. Saddik D: Multiseptate gallbladder: Incidental diagnosis on ultrasound. *Australas Radiol* 42:374–376, 1998.
32. Lev-Toaff AS, Friedman AC, Rindsberg SN, et al: Multiseptate gallbladder: Incidental diagnosis on sonography. *AJR Am J Roentgenol* 14:1119–1120, 1987.
33. Blanton DE, Bream CA, Mandel SR: Gallbladder ectopia: A review of anomalies of position. *Am J Roentgenol Radium Ther Nucl Med* 121:296–300, 1974.
34. Van Gansbeke D, de Toef J, Engelholm L, et al: Suprahepatic gallbladder: A rare congenital anomaly. *Gastrointest Radiol* 9:941–943, 1984.
35. Senecail B, Texier F, Kergastel I, et al: Anatomic variability and congenital anomalies of the gallbladder: Ultrasonographic study of 1823 patients. *Morphologie* 84:35–39, 2000.
36. Naganuma S, Ishida H, Konno K, et al: Sonographic findings of anomalous position of the gallbladder. *Abdom Imaging* 23:67–72, 1998.
37. Strong RW, Fawcett J, Hatzifotis M, et al: Surgical implications of a left-sided gallbladder. *Am J Surg* 206:59–63, 2013.
38. Yeh HC, Weiss MF, Gerson CD: Torsion of the gallbladder: The ultrasonographic features. *J Clin Ultrasound* 17:123–125, 1989.
39. Quinn SF, Fazio F, Jones E: Torsion of the gallbladder: Findings on CT and sonography and role of percutaneous cholecystostomy. *AJR Am J Roentgenol* 148:881–882, 1987.
40. Reilly DJ, Kalogeropoulos G, Thiruchelvam D: Torsion of the gallbladder: A systematic review. *HPB (Oxford)* 14:669–672, 2012.
41. Wellstad M, Kam L, Funstom MR: Radiological pointers to pre-operative diagnosis of torsion of the gallbladder. A case report. *S Afr Med J* 58:980–982, 1980.
42. Gore RM, Ghahremani GG, Joseph AE, et al: Acquired malposition of the colon and gallbladder in patients with cirrhosis: CT findings and clinical implications. *Radiology* 171:739–742, 1989.
43. Bartoli E, Calonaci N, Nenci R: Ultrasonography of the gallbladder in pregnancy. *Gastrointest Radiol* 9:35–38, 1984.
44. Everson GT, Nemeth A, Kourourian S, et al: Gallbladder function is altered in sickle hemoglobinopathy. *Gastroenterology* 96:1307–1316, 1989.
45. Mitsukawa T, Takemura J, Ohgo S: Gallbladder function and plasma cholecystokinin levels in diabetes mellitus. *Am J Gastroenterol* 85:981–984, 1990.
46. Vezina WC, Paradis RL, Grace DM, et al: Increased volume and decreased emptying of the gallbladder in large (morbidly obese, tall normal and muscular normal) people. *Gastroenterology* 98:1000–1007, 1990.
47. McHugo JM, McKeown C, Brown MT, et al: Ultrasound findings in children with cystic fibrosis. *Br J Radiol* 60:137–141, 1987.
48. Willi UV, Reddish JM, Teele RL: Cystic fibrosis: Its characteristic appearance on abdominal sonography. *AJR Am J Roentgenol* 131:1005–1010, 1980.
49. Kim WS, Kim IO, Yeon KM, et al: Choledochal cyst with or without biliary atresia in neonates and young infants: US differentiation. *Radiology* 209:465–469, 1998.
50. Lam WW, Lam TP, Saing H, et al: MR cholangiography and CT cholangiography of pediatric patients with choledochal cysts. *AJR Am J Roentgenol* 173:401–405, 1999.
51. Krause D, Cercueil JP, Dransart M, et al: MRI for evaluating congenital bile duct abnormalities. *J Comput Assist Tomogr* 26:541–552, 2002.
52. Trinidad-Hernandez M, Rivera-Perez VS, Hermosillo-Sandoval JM: Adult choledochal cyst. *Am J Surg* 193:221–222, 2007.
53. Arshanskiy Y, Vyas PK: Type IV choledochal cyst presenting with obstructive jaundice: Role of MR cholangiopancreatography. *AJR Am J Roentgenol* 171:457–459, 1998.
54. Matos C, Nicaise N, Deviere J, et al: Choledochal cysts: comparison of findings at MR cholangiopancreatography and endoscopic retrograde cholangiopancreatography in eight patients. *Radiology* 209:443–448, 1998.
55. Brancatelli G, Federle MP, Vilgrain V, et al: Fibropolycystic liver disease: CT and MR imaging findings. *Radiographics* 25:659–670, 2005.
56. Irie H, Honda H, Jimi M, et al: Value of MR cholangiopancreatography in evaluating choledochal cysts. *AJR Am J Roentgenol* 171:1381–1385, 1998.
57. Wang HP, Wu MS, Lin CC, et al: Pancreaticobiliary diseases associated with anomalous pancreaticobiliary ductal union. *Gastrointest Endosc* 48:184–189, 1998.
58. Jabłońska B: Biliary cysts: Etiology, diagnosis and management. *World J Gastroenterol* 18:4801–4810, 2012.
59. Catalano O: Conventional x-ray and CT findings in a case of intraluminal choledochocoele. *Rofo* 169:210–212, 1998.
60. Woon CY, Tan YM, Oei CL, et al: Adult choledochal cysts: An audit of surgical management. *ANZ J Surg* 76:981–986, 2006.
61. Krepel HP, Siersema PD, Tilanus HW, et al: Choledochocoele presenting with anaemia. *Eur J Gastroenterol Hepatol* 9:641–643, 1997.
62. Bockhorn M, Malago M, Lang H, et al: The role of surgery in Caroli's disease. *J Am Coll Surg* 202:928–932, 2006.
63. Madjov R, Chervenkov P, Madjova V, et al: Caroli's disease. Report of 5 cases and review of literature. *Hepatogastroenterology* 52:606–609, 2005.
64. Levy AD, Rohrmann CA, Jr, Murakata LA, et al: Caroli's disease: Radiologic spectrum with pathologic correlation. *AJR Am J Roentgenol* 179:1053–1057, 2002.
65. Sood GK, Mahapatra JR, Khurana A, et al: Caroli disease: Computed tomographic diagnosis. *Gastrointest Radiol* 16:243–244, 1991.
66. Chiba T, Shinozaki M, Kato S, et al: Caroli's disease: Central dot sign re-examined by CT arteriography and CT during arterial portography. *Eur Radiol* 12:701–702, 2002.
67. Venkatanarasimha N, Thomas R, Armstrong EM, et al: Imaging features of ductal plate malformations in adults. *Clin Radiol* 66:1086–1093, 2011.
68. Ahmadi T, Itai Y, Minami M: Central dot sign in entities other than Caroli's disease. *J Clin Ultrasound* 26:283–287, 1998.
69. Breysam L, Opendakker G, Smet M, et al: Caroli's syndrome. *J Belge Radiol* 81:1–2, 1998.
70. Venkatanarasimha N, Thomas R, Armstrong EM, et al: Imaging features of ductal plate malformations in adults. *Clin Radiol* 66:1086–1093, 2011.
71. Lefere M, Thijs M, De Hertogh G, et al: Caroli disease: Review of eight cases with emphasis on magnetic resonance imaging features. *Eur J Gastroenterol Hepatol* 23:578–585, 2011.
72. Martin RF: Biliary cysts: A review and simplified classification scheme. *Surg Clin North Am* 94:219–232, 2014.

Cholelithiasis, Cholecystitis, Choledocholithiasis, and Hyperplastic Cholecystoses

GENEVIEVE L. BENNETT

CHAPTER OUTLINE

Cholelithiasis

Pathogenesis and Epidemiology
Imaging

Biliary Sludge

Pathogenesis
Imaging

Acute Cholecystitis

Pathogenesis and Epidemiology
Imaging

Acute Acalculous Cholecystitis

Pathogenesis and Epidemiology
Imaging

Complications of Acute Cholecystitis

Gangrenous Cholecystitis
Hemorrhagic Cholecystitis
Emphysematous Cholecystitis
Gallbladder Perforation

Chronic Cholecystitis

Pathogenesis and Epidemiology
Imaging

Chronic Acalculous Cholecystitis

Xanthogranulomatous Cholecystitis

Choledocholithiasis

Pathogenesis and Epidemiology
Imaging

Intrahepatic Biliary Calculi

Recurrent Pyogenic Cholangitis
Imaging

Other Conditions Related to Gallstones

Spilled Gallstones after Laparoscopic Cholecystectomy
Mirizzi Syndrome
Gallstone Ileus

Hyperplastic Cholecystoses

Cholesterosis
Adenomyomatosis

Milk of Calcium Bile

Gallbladder Hydrops

This chapter provides a review of the imaging assessment of gallbladder and biliary calculi. Cholecystitis, both acute and chronic, and associated complications are discussed. Other disorders related to gallstones, including spilled gallstones after laparoscopic surgery, Mirizzi syndrome, and gallstone ileus, are also reviewed. The chapter concludes with a discussion of the spectrum of noninflammatory gallbladder conditions referred to as the hyperplastic cholecystoses.

The imaging evaluation of cholelithiasis and associated complications has evolved significantly in the past decade. Cholescintigraphy and sonography continue to serve as the primary imaging modalities for the initial assessment of most suspected gallbladder disorders. Computed tomography (CT) and magnetic resonance imaging (MRI), however, have proved to be of considerable value in certain circumstances. These may be performed for initial evaluation or serve as an important adjunct to other imaging modalities when further information is required. The role of CT and MRI in the evaluation of cholecystitis, choledocholithiasis, and the hyperplastic cholecystoses is discussed.

Cholelithiasis

PATHOGENESIS AND EPIDEMIOLOGY

The prevalence of gallstones varies with age and gender. Gallstones are present in an estimated 10% to 15% of men and 20% to 40% of women older than 60 years.¹ In general, the risk for stones increases with history of childbearing, estrogen replacement therapy, oral contraceptive use, and obesity. Stones are also associated with hypertriglyceridemia, Crohn's disease, and parenteral hyperalimentation. Gallstones are symptomatic in 20% to 30% of patients; biliary pain or colic is the most common symptom. This is most often related to impaction of a stone in the cystic duct. The most common acute complications of gallstones are acute cholecystitis, acute pancreatitis, and ascending cholangitis. Chronic complications include chronic cholecystitis, Mirizzi syndrome, cholecystenteric fistula, and gallstone ileus.

Gallstones are composed mainly of cholesterol, bilirubin, and calcium salts with smaller amounts of protein and other

materials, including bile acids, fatty acids, and inorganic salts.² Stones form when there is supersaturation of various bile components. Lithogenic bile usually results from increased biliary cholesterol output, but decreased bile acid synthesis or a combination defect may play a role in stone development.¹ Biliary dysmotility and prolonged intestinal transit may also be contributing factors.³

In Western countries, cholesterol is the principal constituent of more than 75% of gallstones. Many stones are more than 80% cholesterol with smaller amounts of calcium bilirubinate. Pure cholesterol stones contain more than 90% cholesterol and are relatively uncommon, accounting for less than 10% of biliary calculi.² Pigment stones contain less than 25% cholesterol and are relatively uncommon, representing 10% to 25% of gallstones in North America.⁴ These stones consist of calcium salts of bilirubin and are categorized as black or brown pigment stones. Black pigment stones consist of polymers of bilirubin with large amounts of mucin glycoproteins. These are more common in patients with cirrhosis or chronic hemolytic anemias in whom biliary excretion is increased. Brown pigment stones are made up of calcium salts of unconjugated bilirubin, with variable amounts of protein and cholesterol, and are more commonly associated with bacterial infection. The deconjugation of bile by bacterial enzymes is also considered an etiologic factor.

IMAGING

Abdominal Radiography

Only about 15% to 20% of gallstones are calcified enough to be visualized on conventional abdominal radiographs⁵ (Fig. 77-1). Therefore, abdominal radiographs have a limited role in the detection of gallstones. Oral cholecystography was introduced in the 1920s and for many years was the primary modality for evaluation of gallbladder disease, including stones. However, this technique has largely been replaced by sonography.

Ultrasound

Sonography is now considered the imaging tool of choice for the detection of gallstones, with a reported accuracy of 96%.⁵⁻⁷ However, recent advances in sonographic technology resulting in improved spatial resolution may allow even higher diagnostic accuracy. Other advantages of sonography include the ability to perform studies at the bedside and lack of ionizing radiation. Sonography can also evaluate other structures in the right upper quadrant when alternative diagnoses are under consideration.

At sonography, a gallstone appears as a highly reflective echo that is generally mobile and associated with posterior acoustic shadowing (Fig. 77-2). Both mobility and acoustic shadowing are important features that help differentiate gallstones from other echogenic foci in the gallbladder lumen, such as sludge or solid masses. An aggregate of sludge or sludge ball (also referred to as tumefactive sludge) may be mobile but will not cast an acoustic shadow (Fig. 77-3). A solid mass will not be mobile and will not shadow and may exhibit vascularity on color Doppler interrogation.

Very small stones may not always cast a shadow. Ex vivo studies have demonstrated that calculi larger than 3 mm produce acoustic shadowing regardless of composition.^{8,9} The demonstration of a posterior acoustic shadow, however, also depends on transducer frequency and beam width. In a study



Figure 77-1 Gallstones: abdominal radiograph. Multiple calcified gallstones are identified.

by Grossman,¹⁰ when a 5-MHz transducer was used, 0.2- to 0.3-cm stones were associated with shadowing, whereas when a 2.25-MHz transducer was used, only stones measuring at least 0.4 cm cast a shadow. Using a tissue phantom, Filly and associates⁹ found that acoustic shadowing was present when the stone was at or near the center of the beam but not at the periphery. These studies demonstrate that to maximize detection, the highest frequency transducer possible should be used with the focal zone placed at the level of the stone. In recent years, tissue harmonic imaging has been shown to improve the detection rate of gallbladder calculi^{11,12} (Fig. 77-4).

Gallstones may not be detected at sonography if they are small or hidden behind a gallbladder fold or in the cystic duct, if intraluminal sludge is present, or if the examination is technically suboptimal related to the patient's body habitus or the operator's inexperience. Chintapalli and colleagues¹³ studied 946 patients with surgically proved gallstones. In 98.7%, preoperative sonography showed single or multiple echogenic foci with or without acoustic shadowing in the gallbladder for a false-negative rate of 1.3%. In the patients with false-negative examinations, sonographic findings were consistent with polyps (five cases), sludge, or both, and the ultrasound was interpreted as normal in one patient. Missed stones were 5 mm or smaller in 10 patients and smaller than 1.0 cm in all 12 patients. Stones located in the gallbladder neck or trapped behind a fold may be overlooked when the patient is evaluated only in the supine position. Also, small stones may become more conspicuous when the patient is evaluated in the decubitus or upright position as they produce a shadow only when they are imaged in

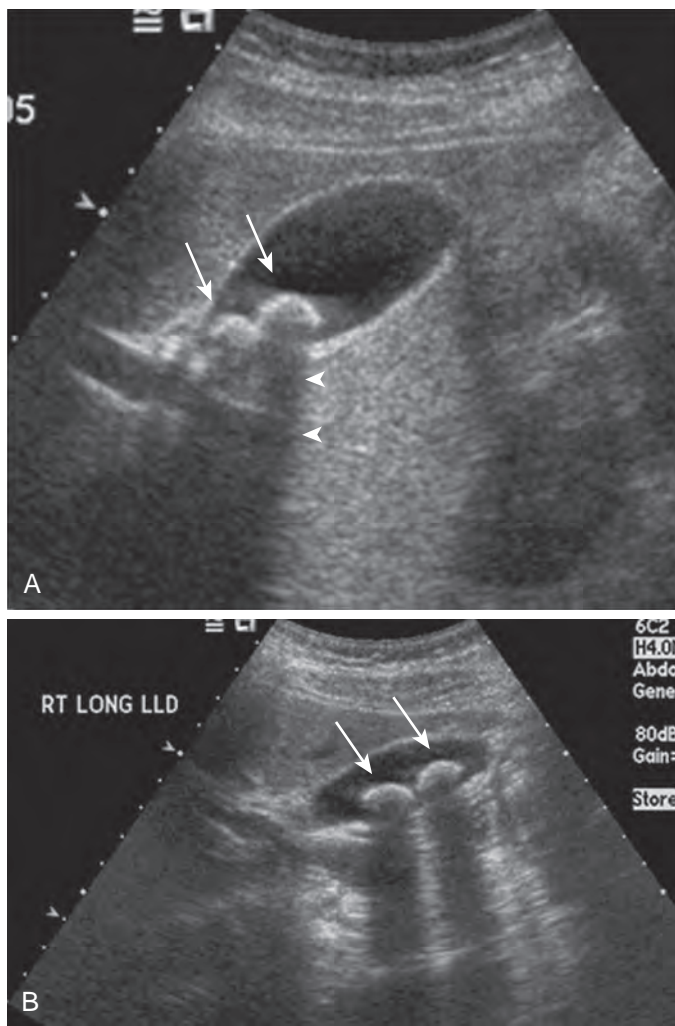


Figure 77-2 Gallstones: sonography. **A.** Two highly reflective echoes (arrows) are located in the dependent portion of the gallbladder lumen with posterior acoustic shadowing (arrowheads). **B.** When the patient is imaged in the left lateral decubitus position (LLD), the gallstones (arrows) change location, indicating mobility.

aggregate (Fig. 77-5). Therefore, it is always important to evaluate the patient in more than one position in assessing for the presence of gallstones. A follow-up study may be suggested if the clinical index of suspicion is high and the initial examination is negative.

If the gallbladder is contracted and the lumen is filled with shadowing stones, a high-amplitude echo results that is usually linear or curvilinear in configuration and associated with posterior acoustic shadowing. Careful observation will demonstrate a perceivable gallbladder wall separate from the intraluminal stones, sometimes facilitated by the use of a high-resolution linear transducer (Fig. 77-6). This appearance has been called the wall-echo-shadow sign.¹⁴ The main differential diagnostic considerations are a porcelain gallbladder, with calcification in the gallbladder wall, and air in the gallbladder, such as in emphysematous cholecystitis. Correlation with abdominal radiography or CT can be helpful as a problem-solving tool (Fig. 77-7).

Computed Tomography

The ability to detect gall stones at CT depends on differing density of the stone with respect to bile.^{15,16} The reported sensitivity of CT for detection of gallstones is approximately 75%.¹⁷ Calcified stones are readily identified as they are denser than bile (Fig. 77-8A). Stones with high concentration of cholesterol may also be readily identified as these stones are less dense than bile (Fig. 77-8B). When stones degenerate, nitrogen gas may collect in central fissures and create the Mercedes-Benz sign. This may be the only visualized evidence of a gallstone and appear as a focal collection of gas in the nondependent gallbladder lumen (Fig. 77-8C). Noncalcified pigment stones are soft tissue attenuation density (Fig. 77-8D). Many stones are composed of a mixture of calcium, bile pigments, and cholesterol and may be similar in density to bile and therefore not visible at CT (Fig. 77-9). The size of the stone is also an important factor determining if a stone is visible at CT. Small stones are frequently missed unless the density differs markedly from bile. In one series, only 78.9% of patients with stones demonstrated at sonography were found to have stones at CT.¹⁸ Most stones missed prospectively were faintly calcified and were retrospectively detected only as subtle defects within the gallbladder. A phantom study demonstrated that the sensitivity of CT for

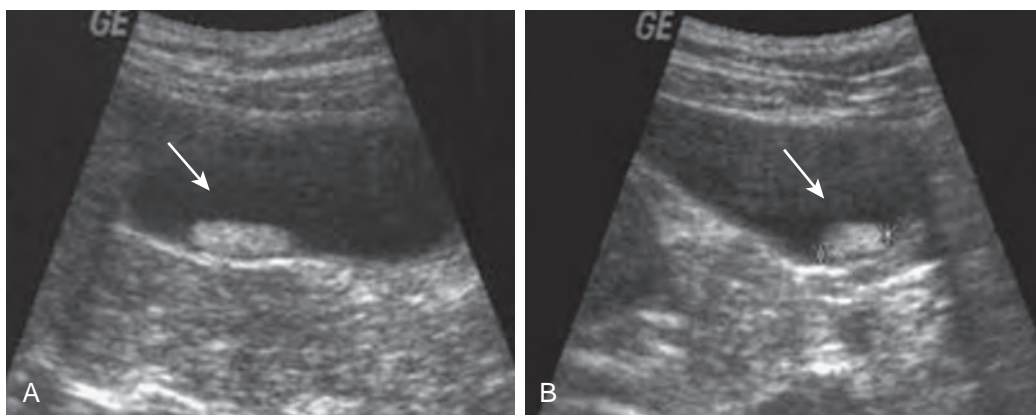


Figure 77-3 Tumefactive sludge: sonography. **A.** In the supine position, there is an echogenic nonshadowing focus (arrow) in the dependent portion of the gallbladder lumen. There is no posterior acoustic shadowing. **B.** In the upright position, the sludge ball moved into the gallbladder fundus (arrow).

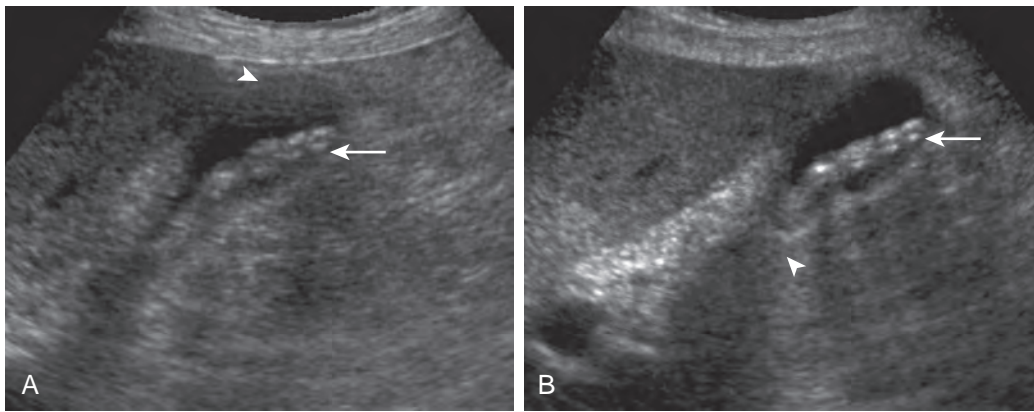


Figure 77-4 Gallstones: improved sonographic visualization with tissue harmonic imaging. **A.** Image obtained with 4-MHz transducer demonstrates gallstones (arrow). Near-field echoes (arrowhead) correspond to reverberation artifact. **B.** Image obtained with tissue harmonic imaging eliminates reverberation artifact. Gallstones are better delineated (arrow), and posterior acoustic shadowing is more evident (arrowhead).

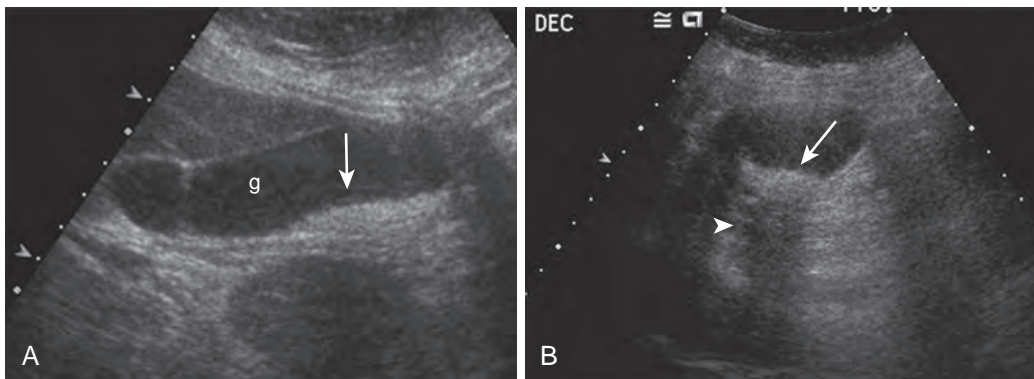


Figure 77-5 Gravel: sonographic appearance. **A.** Supine scan of the gallbladder (g) demonstrates echogenic layering material in the lumen (arrow) with no posterior acoustic shadowing. **B.** In the decubitus position, the material pools in the fundus of the gallbladder (arrow), and a shadow is now demonstrated (arrowhead) consistent with small stones or gravel.

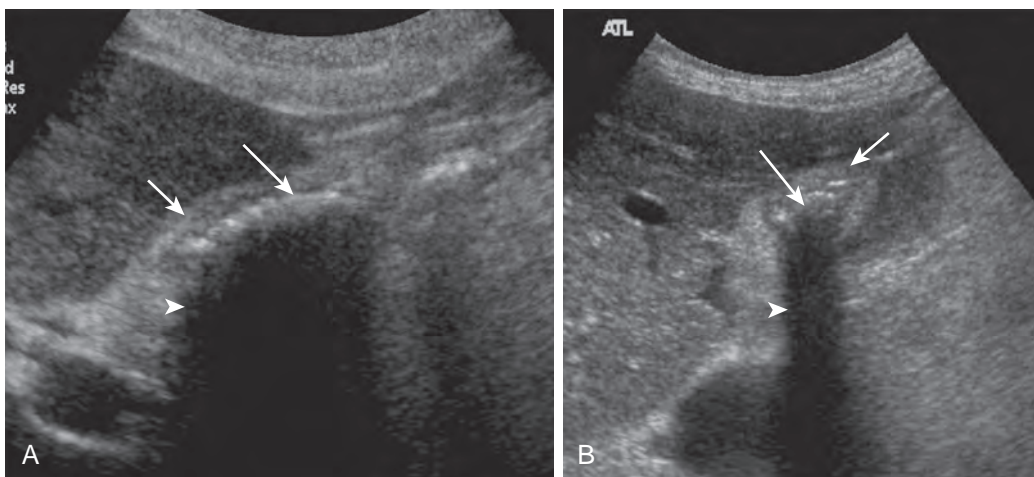


Figure 77-6 Wall-echo-shadow sign on ultrasound. Multiple gallstones are present within a contracted gallbladder. Sagittal (**A**) and transverse (**B**) views. Short arrow points to gallbladder wall that appears as an echogenic arc. Long arrow points to gallstones that appear as bright echoes. The arrowhead points to posterior acoustic shadowing.

detection of gallstones varies with peak voltage and is highest when CT is performed at 140 kVp rather than at lower voltage settings.¹⁹

Magnetic Resonance Imaging

On T2-weighted MRI, gallstones are manifested as signal voids in the high signal intensity bile (Fig. 77-10). Cholesterol stones are generally isointense or hypointense on T1-weighted images, whereas pigment stones have been shown to have high signal intensity on T1-weighted images. This signal hyperintensity is

caused by the presence of metal ions in the pigment stones, shortening the T1 relaxation time.^{20,21} Another study of gallstone appearance at MRI also correlated signal intensity with chemical composition.²² T2-weighted central high signal intensity corresponded to fluid-filled clefts in the stones, whereas central and peripheral high signal areas on T1-weighted images corresponded to fluid clefts as well as regions high in copper content. Other intraluminal filling defects that may mimic gallstones on T2-weighted images include tumor, blood clot, and gas bubbles.

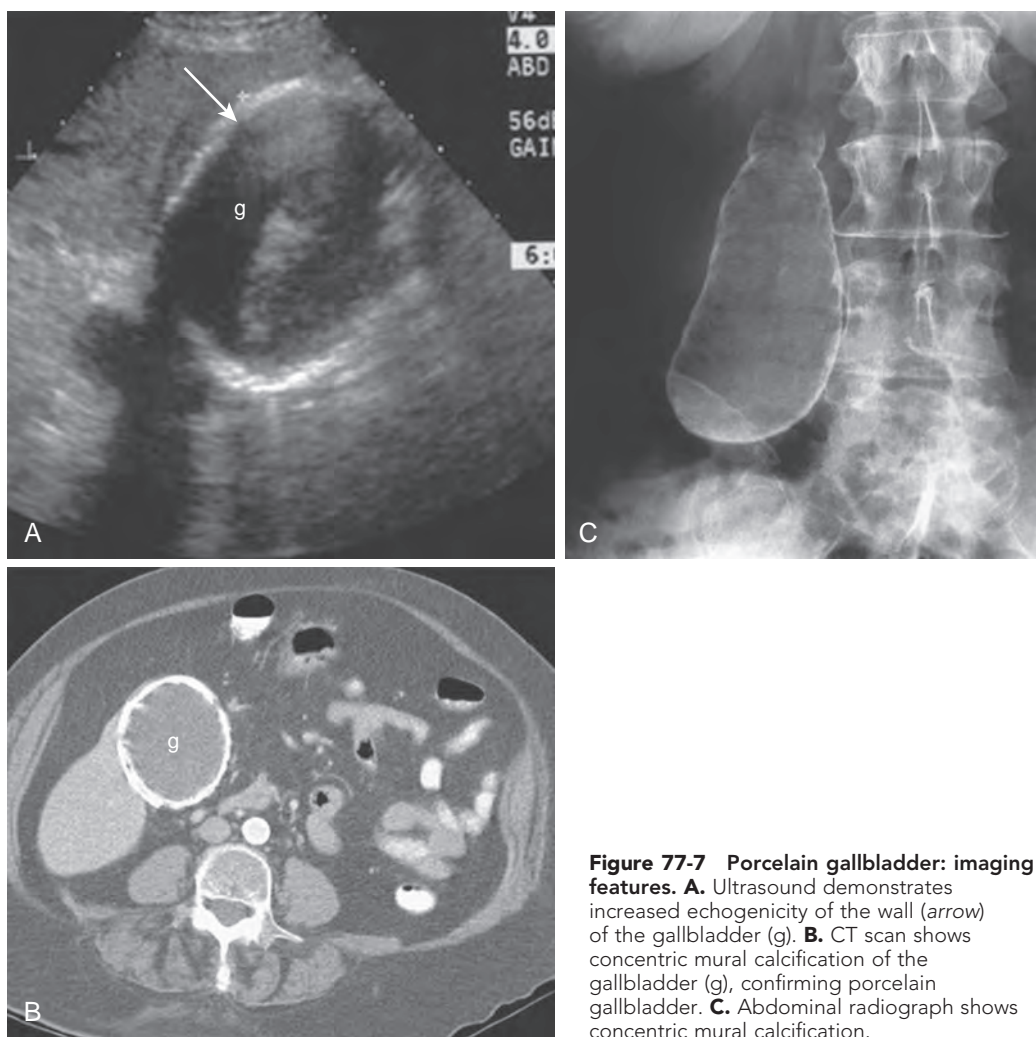


Figure 77-7 Porcelain gallbladder: imaging features. **A.** Ultrasound demonstrates increased echogenicity of the wall (arrow) of the gallbladder (g). **B.** CT scan shows concentric mural calcification of the gallbladder (g), confirming porcelain gallbladder. **C.** Abdominal radiograph shows concentric mural calcification.

Biliary Sludge

PATHOGENESIS

Biliary sludge, also referred to as microlithiasis, biliary sand or sediment, pseudolithiasis, and microcrystalline disease, is a suspension of bile and particulate material in the gallbladder.²³ The chemical composition consists of various proportions of calcium bilirubinate and cholesterol monohydrate crystals and gallbladder mucus. The proposed pathogenesis is similar to that of gallstones. A combination of impaired gallbladder motility and alteration in nucleation factors leads to the formation of sludge, with additional precipitate aggregation resulting in gallstone formation.²⁴ Clinical conditions that increase sludge formation include fasting, pregnancy, total parenteral nutrition, and critical illness. Sludge may resolve, have a cyclic pattern of appearance and disappearance, or progress to stone formation.²⁵ Although patients may generally be asymptomatic, symptoms can include biliary pain, cholecystitis, cholangitis, or pancreatitis. Treatment is symptom directed.

IMAGING

At sonography, sludge typically appears as low-level echoes that layer dependently within the gallbladder lumen (Fig. 77-11).

When the gallbladder lumen is entirely filled with sludge, this yields an appearance referred to as hepatization of the gallbladder. In this situation, the gallbladder assumes the same echotexture as the liver parenchyma (Fig. 77-12A, B). The use of color Doppler imaging is important to exclude other more significant disease, such as intraluminal soft tissue masses. If findings are equivocal and there is suspicion for a possible intraluminal mass, MRI with contrast and subtraction images can be helpful (Fig. 77-12C, D). An aggregate of intraluminal sludge can also mimic a soft tissue density mass (tumefactive sludge). As discussed, gravity dependence should be demonstrated to differentiate sludge from a gallbladder polyp or mass (Fig. 77-13). Doppler demonstration of vascularity within the abnormality confirms the presence of a soft tissue mass. However, absence of demonstrable vascularity is less helpful, and short-interval follow-up examination or assessment with precontrast and postcontrast CT or MRI may be indicated.

Acute Cholecystitis

PATHOGENESIS AND EPIDEMIOLOGY

Acute cholecystitis occurs in approximately one third of patients with gallstones. It results from persistent obstruction of the

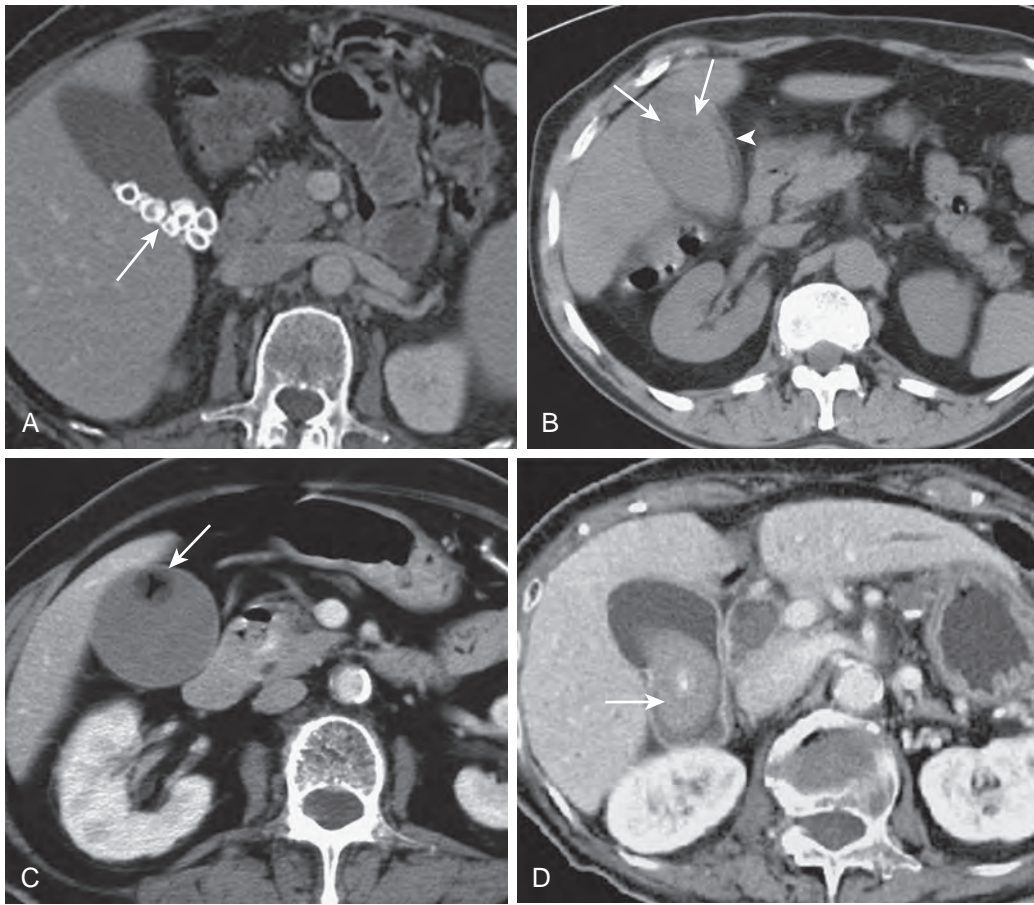


Figure 77-8 CT appearance of gallstones. **A.** Calcified stones depicted as calcified dependent densities in gallbladder lumen (arrow). **B.** Noncalcified stones may be visible if they are less dense than bile (arrows). This patient also had acute cholecystitis. Note thickened gallbladder wall (arrowhead). **C.** Mercedes-Benz sign. Gas-containing stone floating in bile (arrow). **D.** Pigment stone (arrow) is soft tissue density with only small central nidus of calcification.

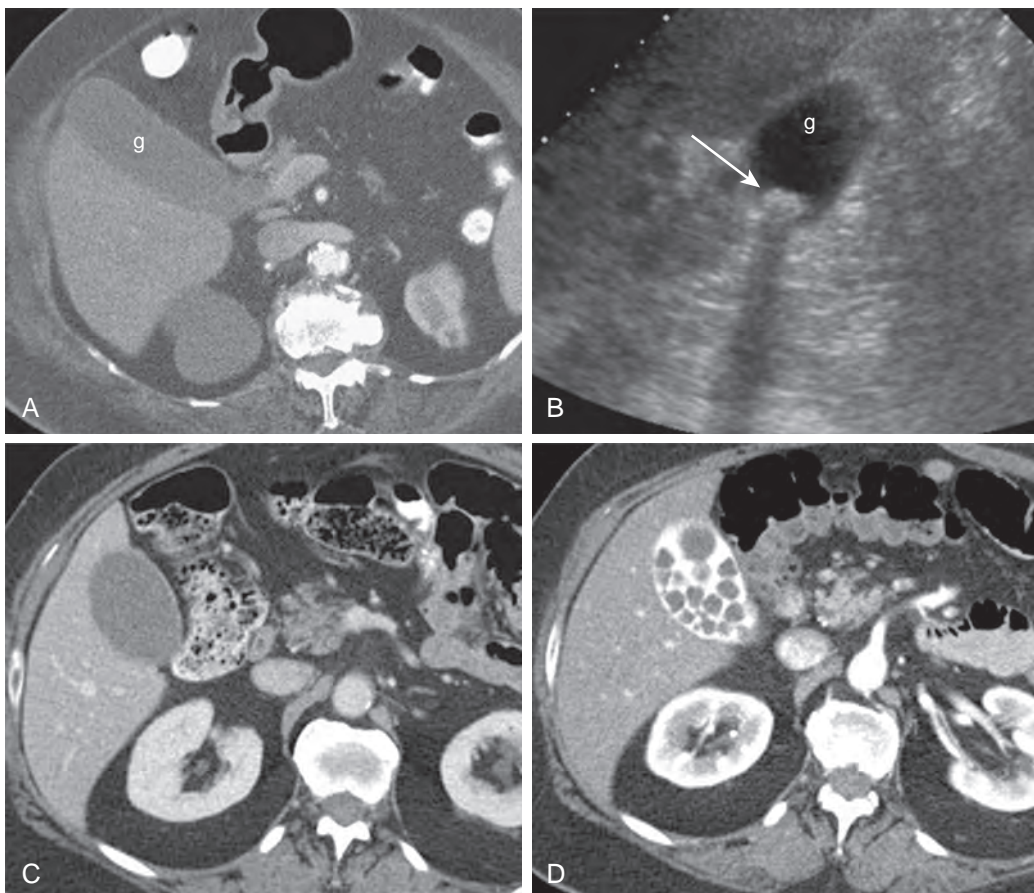


Figure 77-9 Noncalcified gallstones not visualized at CT. **A.** CT scan demonstrates no stones in the gallbladder (g). **B.** Ultrasound performed immediately after CT demonstrates shadowing stone (arrow) in gallbladder (g) lumen. **C.** CT scan in a different patient demonstrates no stones in the gallbladder. **D.** CT performed several days later in the same patient now demonstrates multiple stones in the gallbladder because of vicarious excretion of previously administered intravenous contrast material in the gallbladder.

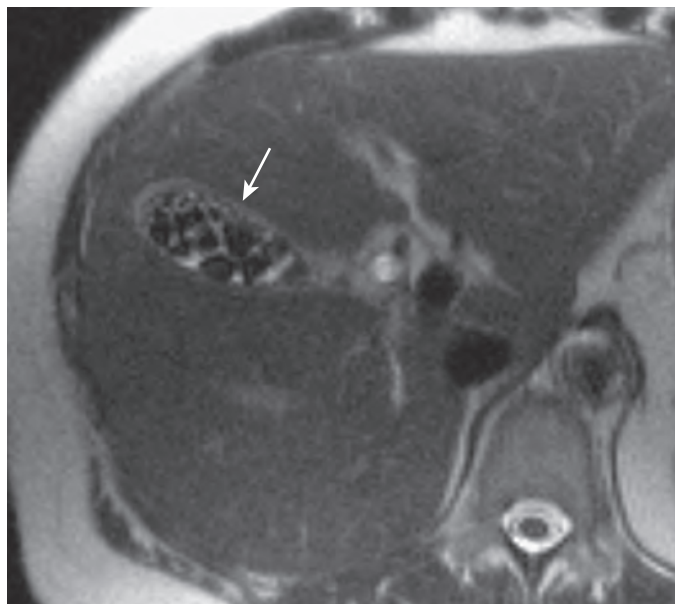


Figure 77-10 MRI appearance of gallstones. Axial T2-weighted HASTE image demonstrates multiple low signal intensity filling defects in gallbladder lumen (arrow).

cystic duct or gallbladder neck, with distention of the gallbladder and increased intraluminal pressure.^{26,27} Inflammation of the gallbladder mucosa may result from chemical injury caused by bile salts or superimposed infection. If left untreated, the inflammation eventually progresses to involve all layers of the gallbladder wall and may lead to necrosis, gangrene, and gallbladder perforation. In most patients, acute cholecystitis is associated with gallstones.

Acute cholecystitis is the most common cause of right upper quadrant pain, and the primary mode of treatment is laparoscopic cholecystectomy. Clinical findings include fever, right upper quadrant pain, and elevated white blood cell count. Approximately one third of patients have a clinically positive Murphy sign, which refers to focal tenderness over the gallbladder on inspiration. However, the clinical manifestations may overlap considerably with other intra-abdominal processes not related to the biliary tract, such as acute hepatitis, primary liver disease including abscess and neoplasm, peptic ulcer disease, and pancreatitis. Also, clinical findings in the elderly or critically ill patient may be more subtle. Approximately one third of patients with the presumptive diagnosis of acute cholecystitis will not have acute cholecystitis on follow-up, and 20% to 25% of patients who have surgery for acute cholecystitis will ultimately have a different diagnosis.²⁸ In a series of 52 patients with right upper quadrant pain thought to have acute cholecystitis, acute cholecystitis was confirmed in 34.6%, chronic cholecystitis was confirmed in 32.7%, and 32.7% had normal gallbladders.²⁹ Therefore, imaging evaluation is critical to provide prompt diagnosis and appropriate intervention.

In 2007, the Tokyo Guidelines that describe the diagnostic and severity assessment criteria for acute cholecystitis were published, and these were recently updated in 2013.^{30,31} According to these guidelines, the diagnostic criteria for acute cholecystitis are one local sign of inflammation (Murphy sign; mass, pain, or tenderness in right upper quadrant), one systemic sign of inflammation (fever, elevated C-reactive protein level,

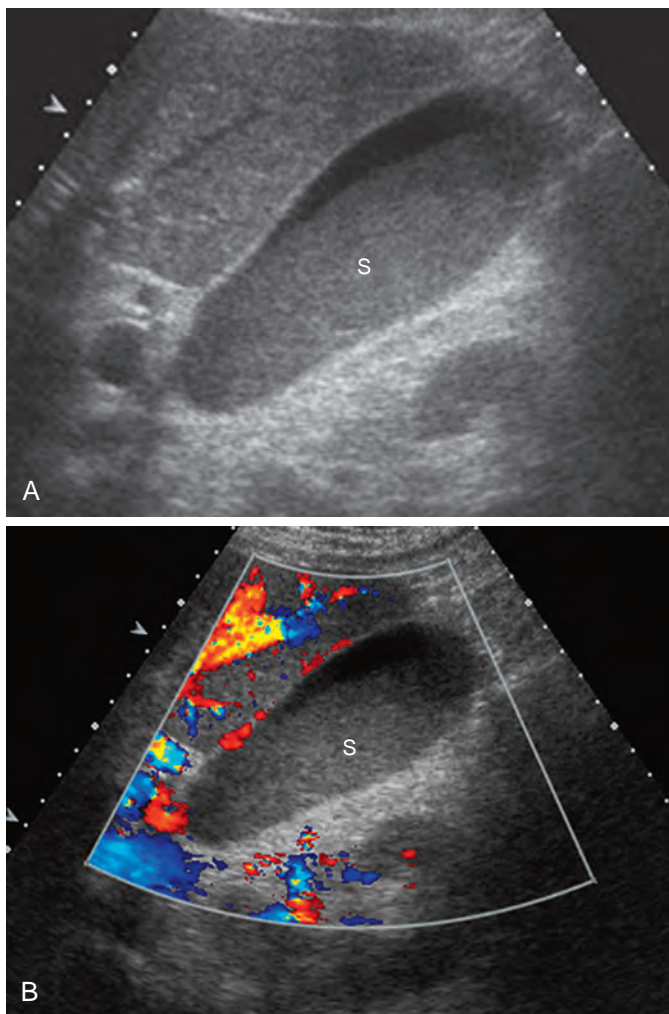


Figure 77-11 Sludge: sonographic findings. **A.** Ultrasound shows low-level, nonshadowing intraluminal echoes (s). **B.** Color Doppler shows no vascularity in sludge (s), helping to exclude a solid, intraluminal mass.

elevated white blood cell count), and confirmatory imaging findings. Cholecystitis severity is classified as mild, moderate, or severe (stages I, II, III, respectively). Mild cholecystitis is defined as cholecystitis with mild inflammatory changes adjacent to the gallbladder without organ dysfunction. Moderate cholecystitis includes elevated white blood cell count, palpable tender mass in the right upper quadrant, duration of symptoms longer than 72 hours, and marked local inflammation. Severe cholecystitis is defined as cholecystitis combined with multiple organ dysfunction. Radiologic findings may have an important impact on how a patient with acute cholecystitis is treated once the diagnosis is established. In a patient with sepsis and organ failure, percutaneous drainage with delayed cholecystectomy may be the best option. Patients without severe inflammation may be best managed with early laparoscopic cholecystectomy. Up to 30% of patients treated laparoscopically may undergo conversion to an open procedure, usually in the setting of severe complicated cholecystitis with dense pericholecystic inflammation and adhesions. Preoperative imaging may also help predict which patients are likely to require conversion to an open procedure.³²

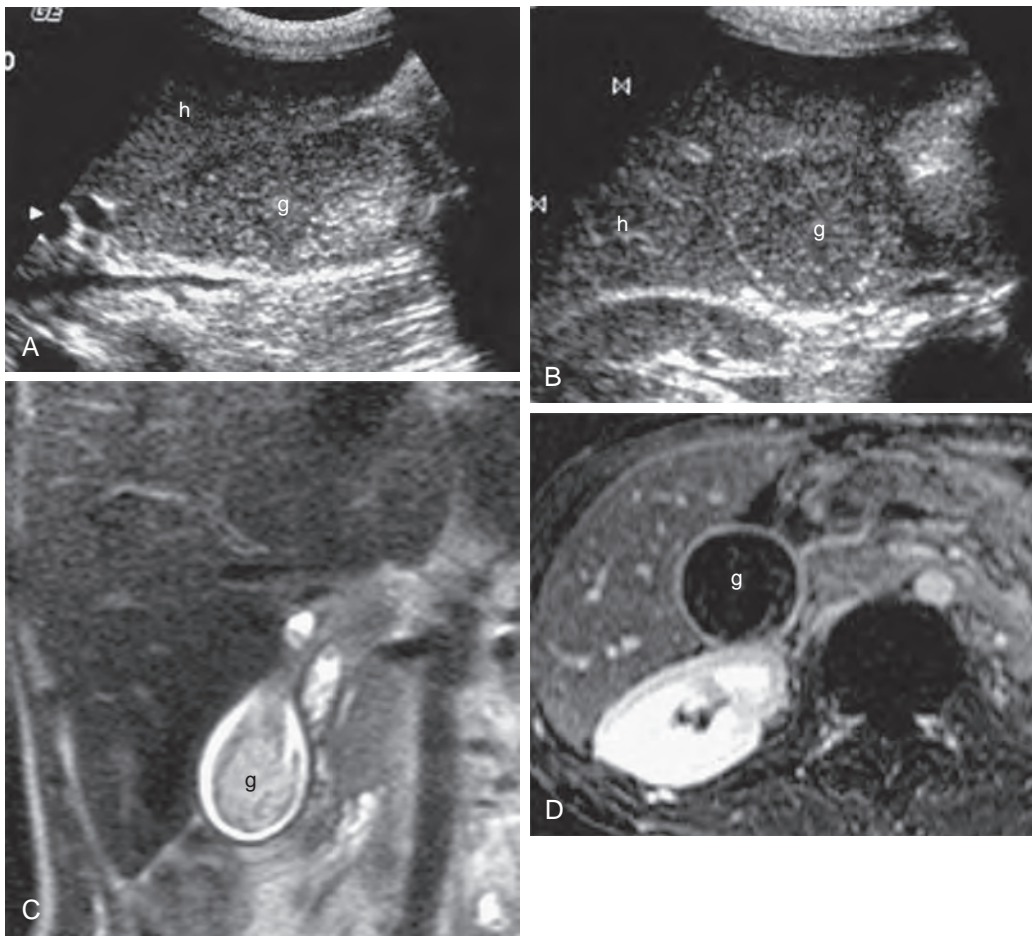


Figure 77-12 Sludge-filled gallbladder: sonography and MR features. Sagittal (A) and transverse (B) sonograms demonstrate gallbladder lumen (g) filled with echogenic material. The echotexture is similar to that of the adjacent liver parenchyma (h). This appearance is referred to as hepatization of the gallbladder. C. Coronal T2-weighted HASTE MR image demonstrates intermediate signal intensity material in the gallbladder lumen (g). D. Axial contrast-enhanced T1-weighted fat-suppressed MR image with subtraction shows no enhancement of gallbladder lumen (g), excluding an intraluminal mass.

IMAGING

The relative role of ultrasonography versus cholescintigraphy with technetium-tagged iminodiacetic acid (IDA) and IDA-like agents for the diagnosis of acute cholecystitis has been extensively addressed in the literature. In an early study published in 1982, the accuracy of scintigraphy with IDA compared with sonography showed similar excellent results in 91 patients with suspected acute cholecystitis, with accuracy of ultrasound of 88% and of scintigraphy of 85%.³³ A study in 1983 of 194 patients showed that sensitivity of both modalities was high, but the specificity of ultrasound was lower at 64%, with a positive predictive value of 40%.³⁴ The sonographic Murphy sign, however, was not evaluated in this study, and there was no correlation with clinical data. More recent studies comparing cholescintigraphy and sonography for diagnosis of acute cholecystitis showed an accuracy of scintigraphy of 91% versus 77% for sonography and sensitivity of scintigraphy of 90.9% versus 62% for ultrasound.^{35,36} Most recently, a systematic review and meta-analysis of diagnostic performance of imaging in acute cholecystitis was performed.³⁷ Fifty-seven studies were included with evaluation of 5859 patients. The sensitivity and specificity were 96% and 90% for cholescintigraphy compared with 81% and 83% for ultrasound.

Although it is possibly somewhat less sensitive and specific for the diagnosis of acute cholecystitis compared with cholescintigraphy, ultrasound does have the advantages of being

readily available and rapidly performed, involving no radiation, and allowing detection of cholecystitis-related complications as well as alternative diagnoses. Ultrasound can confirm the diagnosis of acute cholecystitis and distinguish it from chronic cholecystitis with an accuracy of 95% to 99%.²⁶ The disadvantages of radionuclide scintigraphy include the time to perform the examination (up to 4 hours) and the inability to evaluate for nonbiliary conditions. Furthermore, false-positive results can occur in patients with high bilirubin levels and severe intercurrent illnesses. False-negative results, however, are rare.

Depending on the clinical circumstances, a combination of both cholescintigraphy and sonography may be required to make a definitive diagnosis of acute cholecystitis. The American College of Radiology appropriateness criteria for evaluation of patients with right upper quadrant pain, most recently updated in 2010,²⁸ score ultrasound higher than cholescintigraphy for evaluation of the patient with fever, elevated white blood cell count, and positive Murphy sign and state that cholescintigraphy should generally follow ultrasound on the basis of ultrasound findings. If there is pain but no fever or leukocytosis, ultrasound is given the highest score and may allow detection of stones and bile duct obstruction. If there are only gallstones and pain, cholescintigraphy, CT, and MRI are given equal scores. CT and MRI may allow detection of other causes of pain, improved detection of choledocholithiasis, and further evaluation when it is required, such as when complications are suspected (discussed further later).

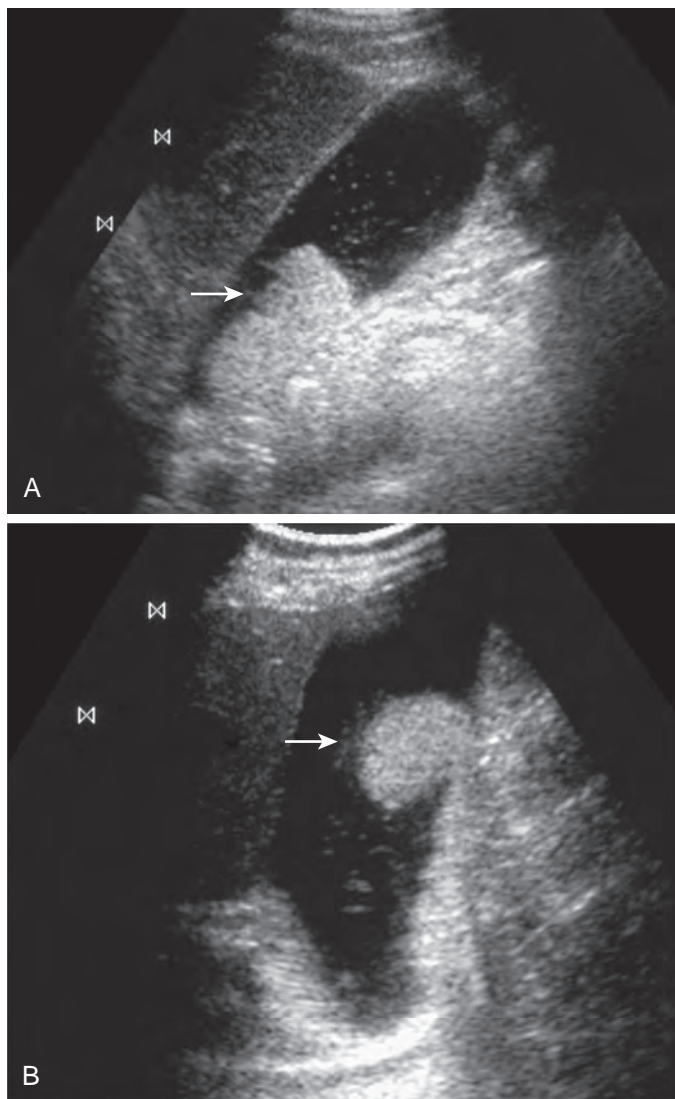


Figure 77-13 Aggregate of sludge on ultrasound. **A.** Sagittal ultrasound image of the gallbladder demonstrates an echogenic nonshadowing abnormality located dependently within the gallbladder lumen (arrow). **B.** When the patient is imaged in the upright position, this abnormality changes location and configuration (arrow), confirming aggregate of sludge rather than soft tissue mass.

Cholescintigraphy

The hepatic parenchyma is normally observed within 1 minute, with peak activity at 10 to 15 minutes.³⁸ The bile ducts are usually visible within 10 minutes, and the gallbladder should appear within 1 hour if the cystic duct is patent (Fig. 77-14A). If the gallbladder has not been defined, imaging should be carried out farther, up to 4 hours. Prompt biliary excretion of tracer without demonstration of the gallbladder is the hallmark of acute cholecystitis (Fig. 77-14B). As noted before, false-positive results may occur in patients with abnormal bile flow because of liver disease or a prolonged fast with distended sludge-filled gallbladder. Also, delayed gallbladder filling can occur in the setting of chronic cholecystitis. If the gallbladder is not visualized after 1 hour and there is visualization of the biliary tree and duodenum, intravenous morphine may be administered, which causes spasm of the sphincter of Oddi,

raising pressure within the bile ducts and increasing the likelihood of bile flow into the gallbladder. If the patient has been fasting for more than 24 hours, an oral fatty meal or intravenous cholecystokinin may be administered, resulting in gallbladder contraction so that the gallbladder can empty and then refill.

Ultrasound

The ultrasound findings in acute uncomplicated cholecystitis are well described and include gallstones, sonographic Murphy sign, gallbladder distention, wall thickening, and pericholecystic fluid^{26,27,39-41} (Figs. 77-15 and 77-16). The sonographic Murphy sign refers to maximum tenderness during compression with the ultrasound transducer placed directly over the gallbladder. Of these findings, the first two are considered the most specific. In a study by Ralls and coworkers,⁴² the sonographic Murphy sign and the presence of gallstones had a positive predictive value of 92% for the diagnosis of acute cholecystitis. It is cautioned that the sonographic Murphy sign may be blunted if the patient has received pain medication before ultrasound evaluation. Furthermore, impaired mental status may preclude evaluation of this sign. Last, the sonographic Murphy sign may be absent in the setting of gangrenous cholecystitis (see later). If it can be demonstrated that a stone is impacted in the gallbladder neck or cystic duct, this is also an important finding that increases the likelihood of acute cholecystitis (Fig. 77-15B). To determine that a stone is impacted in the gallbladder neck or cystic duct requires evaluating the patient in the left lateral decubitus or upright position to assess for mobility of the stone.

Less specific ultrasound findings of acute cholecystitis include gallbladder distention, wall thickening, pericholecystic fluid, and the presence of other intraluminal material such as sludge. In most cases of acute cholecystitis, the gallbladder will be distended. An exception to this occurs when acute cholecystitis complicates chronic cholecystitis, when there may be mural fibrosis impeding distention. Also, if there has been free perforation of the gallbladder, it may appear completely collapsed (discussed further later). Diffuse gallbladder wall thickening, measuring more than 3 mm, is present in 50% to 75% of patients with acute cholecystitis but may also be associated with chronic inflammation.²⁶ Furthermore, gallbladder wall thickening may be associated with many other conditions, including liver disease such as acute hepatitis (Fig. 77-17), ascites, hypoalbuminemia, and alcoholism as well as congestive heart failure, acquired immunodeficiency syndrome (AIDS), and sepsis. In patients with AIDS, cholangiopathy may be related to infection with organisms such as *Cryptosporidium*. Other causes include adenomyomatosis and gallbladder neoplasm. In acute cholecystitis, wall thickening is generally diffuse; if it is more focal, a complication such as gangrenous change or another cause, such as neoplasm, should be considered. Pericholecystic fluid is generally associated with more severe cholecystitis and may be associated with perforation or abscess formation. However, this may also be nonspecific, especially in the setting of generalized ascites. Other entities that clinically can mimic acute cholecystitis, such as peptic ulcer disease and pancreatitis, may also be associated with pericholecystic fluid. Sludge, related to bile stasis, can develop in patients with acute cholecystitis due to gallbladder obstruction.

The role of color and power Doppler evaluation as an adjunct to gray-scale imaging in the diagnosis of acute cholecystitis is somewhat controversial. Although there may be overlap between findings in acute and chronic cholecystitis,⁴³ there may be a

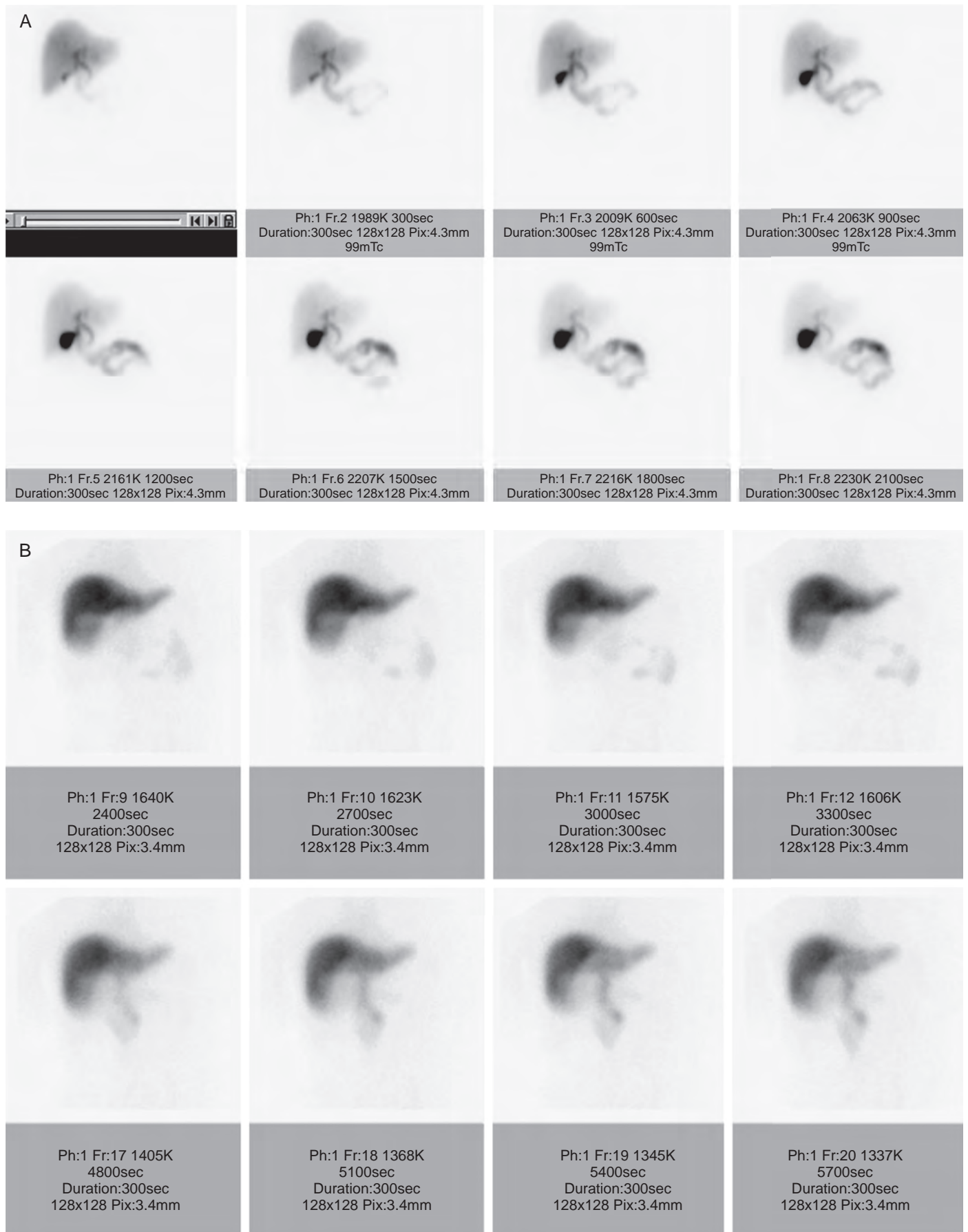


Figure 77-14 Cholescintigraphy. **A.** Negative hydroxy iminodiacetic acid (HIDA) scintiscan shows prompt filling of the gallbladder lumen with tracer, confirming patency of the cystic duct. **B.** Positive HIDA scan. There is no filling of the gallbladder, confirming obstruction of the cystic duct and the presence of acute cholecystitis. (Images courtesy Dr. Elissa Kramer, Department of Nuclear Medicine, New York University Medical Center.)

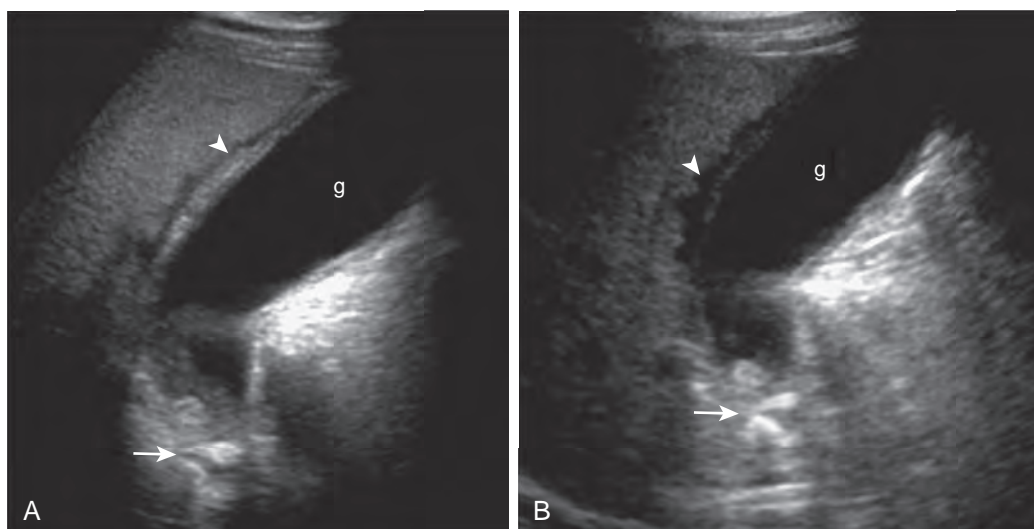


Figure 77-15 Acute cholecystitis: ultrasound. **A.** Gallbladder (g) is distended, with mural thickening (arrowhead) and a stone in the gallbladder neck (arrow). Sonographic Murphy sign was present. **B.** In the upright position, the gallbladder (g) is distended, and pericholecystic fluid is evident (arrowhead). Stone (arrow) does not change location, confirming impaction in gallbladder neck.

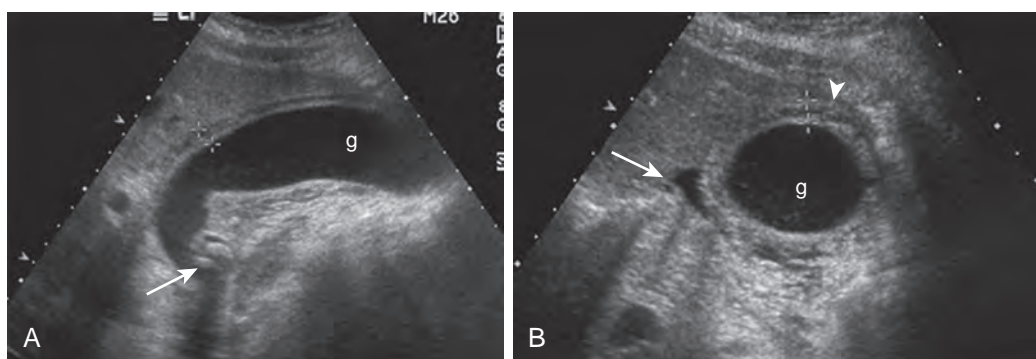


Figure 77-16 Acute cholecystitis: ultrasound. **A.** Sagittal scan demonstrates gallbladder distention (g) and wall thickening (calipers). Arrow, Stones in gallbladder neck. **B.** Transverse scan of gallbladder (g) demonstrates wall thickening (arrowhead) and pericholecystic fluid (arrow). A sonographic Murphy sign was demonstrated.

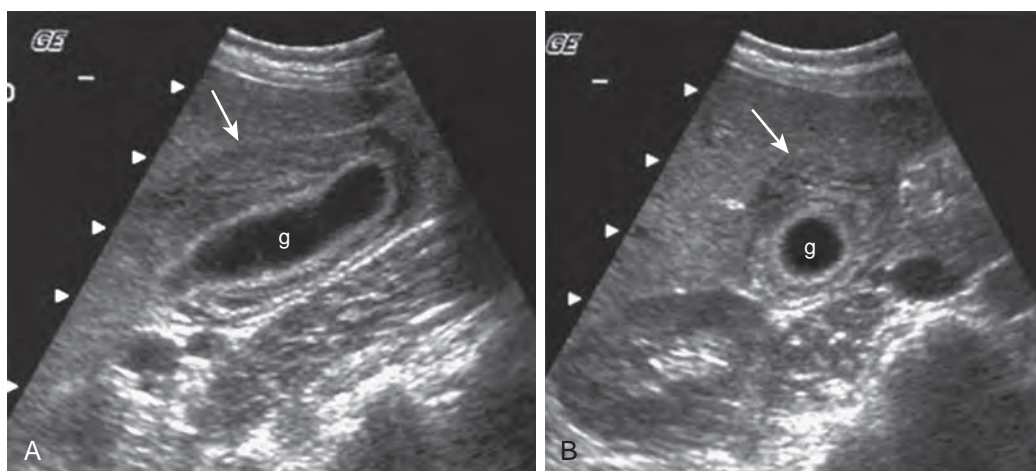


Figure 77-17 Gallbladder manifestations of acute hepatitis: ultrasound findings. Sagittal (**A**) and transverse (**B**) images of the gallbladder demonstrate that the gallbladder lumen (g) is not significantly distended. The wall is markedly thickened (arrows) and has a striated appearance, indicating mural edema.

potential role for Doppler evaluation of the inflamed gallbladder⁴⁴ (Fig. 77-18).

Computed Tomography

Although it is not the first-line imaging modality for the evaluation of suspected acute gallbladder disease, the role of CT in the evaluation of the patient with acute abdominal pain continues to expand. The cause of the patient's symptoms may initially be unclear because of nonspecific clinical findings. In this setting, CT may be the initial study performed as it allows more comprehensive evaluation of the abdomen and pelvis and can identify other acute inflammatory processes that may simulate acute cholecystitis. Therefore, it is important to become familiar with the spectrum of CT findings in acute cholecystitis. CT is also a useful adjunct to ultrasound when ultrasound findings are equivocal or when a complicated form of cholecystitis is suspected⁴⁵ (see later). In a retrospective study at the author's institution,⁴⁶ the overall sensitivity, specificity, and accuracy of CT for the diagnosis of acute cholecystitis were 91.7%, 99.1%, and 94.3%, respectively.

The CT findings of acute cholecystitis include gallstones, gallbladder distention, thickening of the gallbladder wall, pericholecystic inflammation, and fluid^{17,41,47-50} (Fig. 77-19). The CT findings of acute cholecystitis have been divided into major and minor criteria.⁵¹ Major findings include calculi, mural thickening of the gallbladder, pericholecystic fluid, and subserosal edema. Minor findings are gallbladder distention and sludge. CT is limited with respect to detection of gallstones as only up to 75% are visualized.¹⁷ Of these signs, the presence of pericholecystic inflammatory change is believed to be the most

specific.^{17,48} Gallbladder wall thickening on CT is a nonspecific finding and may be secondary to a broad spectrum of both inflammatory and neoplastic disorders.⁵² Gallbladder carcinoma tends to cause greater mural thickening than benign disorders do.⁵³

On occasion, it may be difficult to differentiate gallbladder wall thickening from pericholecystic fluid. Pericholecystic fluid tends to be more focal and irregularly margined, whereas mural thickening is concentric. Punctate foci of contrast enhancement corresponding to enhancing vessels within the gallbladder wall may be observed. A target appearance corresponds to an inner layer of enhancing mucosa and an outer layer of enhancing serosa with hypoattenuating submucosal edema between the two.

An ancillary CT finding of gallbladder inflammation is increased contrast enhancement in the liver parenchyma adjacent to the gallbladder^{50,54,55} (Fig. 77-20). This finding results from hepatic arterial hyperemia secondary to gallbladder inflammation. Increased density of the gallbladder wall has been described as a finding on unenhanced CT, found in approximately 51% of patients.⁵⁶ This is found in patients with mucosal hemorrhage and necrosis and may be a predictor of gangrenous change.

A study evaluating the use of 64-section helical CT for quantitative and qualitative assessment of acute cholecystitis found that pericholecystic fat stranding, mural stratification, pericholecystic hypervascularity, spontaneous hyperattenuation of the gallbladder wall, short (≥ 32 mm) and long (≥ 74 mm) gallbladder axis enlargement, and gallbladder wall thickening (≥ 3.6 mm) were the most discriminating and independent variables for the

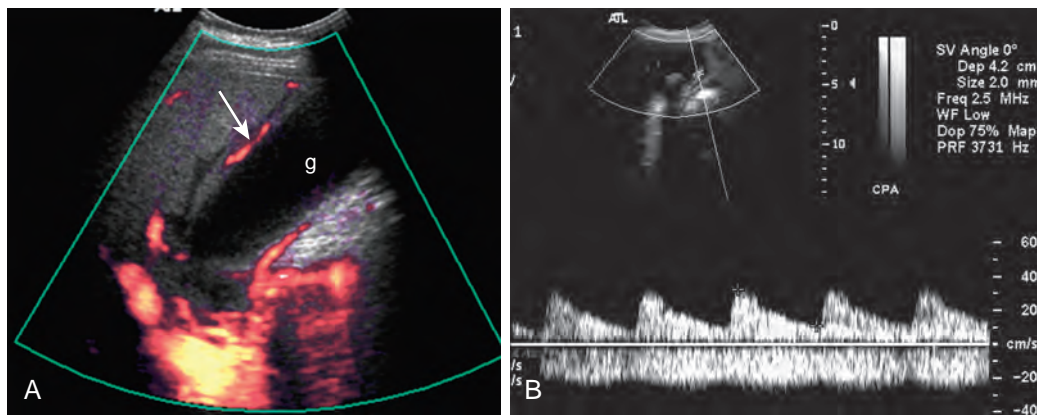


Figure 77-18 Acute cholecystitis: Doppler ultrasound. **A.** Sagittal scan of the gallbladder (g) demonstrates distention and wall thickening. Increased mural vascularity is demonstrated (arrow) with power Doppler. **B.** Spectral Doppler tracing confirms arterial waveform.

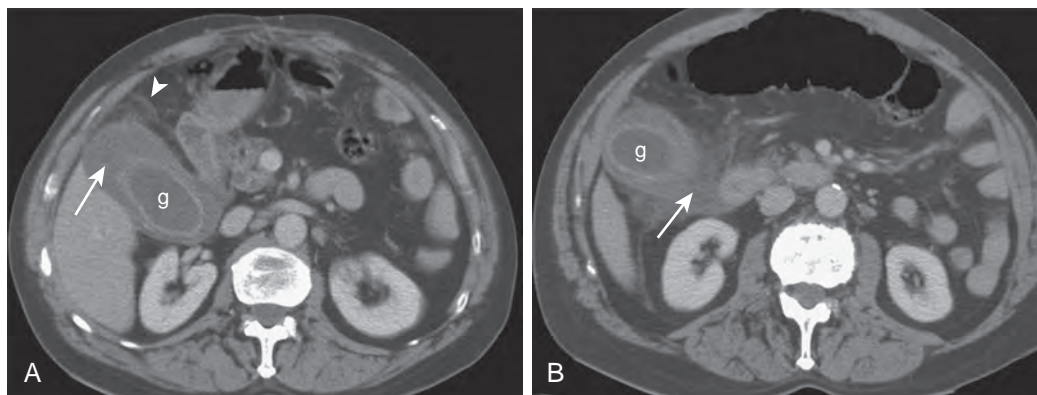


Figure 77-19 Acute cholecystitis: CT features. **A.** The gallbladder lumen (g) is distended with marked mural thickening (arrow) and pericholecystic inflammatory changes (arrowhead). **B.** Slightly more inferior image demonstrates pericholecystic fluid (arrow).



Figure 77-20 Acute cholecystitis: CT demonstration of transient hepatic attenuation difference. Gallbladder (g) is distended with mural thickening. There is focal increase in contrast enhancement of the liver parenchyma adjacent to the gallbladder (arrow), representing hyperemia related to adjacent gallbladder inflammation.

CT diagnosis of acute cholecystitis.⁵⁷ Comparative studies assessing accuracy of CT versus ultrasound for diagnosis of acute cholecystitis are limited. In a study by van Randen and associates⁵⁸ that compared CT and ultrasound in 52 patients with acute cholecystitis, diagnostic accuracy did not differ significantly between the two modalities. However, in their meta-analysis, Kiewiet and colleagues³⁷ cautioned that additional studies evaluating the diagnostic accuracy of CT for acute cholecystitis are needed and that there is currently not enough evidence to support indiscriminate use of this modality in patients suspected of having acute cholecystitis.

Brook and associates⁵⁹ reviewed 14 cases of misdiagnosis of acute cholecystitis at both ultrasound and CT in their practice during a 5-year period. Eight cases of misdiagnosis involved ultrasound and six cases involved CT. Three cases of overcall on ultrasound included cases of gallbladder wall edema that ultimately were diagnosed as hepatitis, sepsis, and chronic cholecystitis. In none of these patients was the gallbladder distended. Therefore, if the gallbladder wall is thickened but there is no distention, an alternative diagnosis should be considered. Two cases of undercall at ultrasound were in patients in the intensive care unit, and two cases were due to lack of wall edema. In an additional patient, diagnosis was delayed because the ultrasound report was not definitive. All of the misdiagnoses at CT were due to undercalls; in one patient, lack of intra-abdominal fat hindered recognition of pericholecystic fat stranding. In another patient, pericholecystic increased arterial enhancement in the liver was mistaken for fatty sparing, and in an additional patient, wall edema and mucosal enhancement were mistaken for a calculus.

Magnetic Resonance Imaging

Like CT, MRI is usually used in the setting of suspected acute cholecystitis when other imaging findings are equivocal or the clinical setting is ambiguous.⁶⁰⁻⁶⁴ Magnetic resonance cholangiopancreatography (MRCP) is sensitive in the diagnosis of

choledocholithiasis, which is particularly important if laparoscopic cholecystectomy is performed. In addition to gallstones, MR readily demonstrates gallbladder wall edema, which is manifested as high signal intensity on T2-weighted images.^{62,65} In one series, pericholecystic high signal intensity on single-shot fast spin-echo (SSFSE) images had an overall accuracy of 89%, specificity of 79%, positive predictive value of 87%, and negative predictive value of 85% for the diagnosis of acute cholecystitis.⁶⁶ Loud and associates⁶¹ found contrast-enhanced T1-weighted images useful for the diagnosis of acute cholecystitis. Patients with surgically proved acute cholecystitis had greater than 80% contrast enhancement of the wall, which helped differentiate acute from chronic cholecystitis. A transient increase in hepatic enhancement may be seen around the gallbladder in 70% of cases during the arterial phase of enhancement and, as with CT, may be an important indicator of acute gallbladder inflammation^{61,62} (Fig. 77-21). Altun and colleagues⁶⁷ found that increased gallbladder wall enhancement and increased transient pericholecystic hepatic enhancement had the highest combination of sensitivity and specificity for the diagnosis and differentiation of acute and chronic cholecystitis. MR has been shown to be superior to ultrasound for detection of obstructing calculi in the gallbladder neck and the cystic duct (Fig. 77-21C, D).⁶⁸ MRI may also be helpful to identify complications of acute cholecystitis. In the meta-analysis by Kiewiet and colleagues,³⁷ diagnostic accuracy of MR for diagnosis of acute cholecystitis was found to be comparable to that of ultrasound, and it is suggested as a helpful imaging modality when ultrasound is technically limited. MRCP is more completely discussed in Chapter 75.

Acute Acalculous Cholecystitis

PATHOGENESIS AND EPIDEMIOLOGY

The reported incidence of acute cholecystitis in the absence of gallstones ranges from approximately 5% to 10%.²⁶ In one large surgical series,⁶⁹ acute acalculous cholecystitis (AAC) represented 14% of cases of acute cholecystitis and was responsible for 2% of all cholecystectomies. Bile stasis, gallbladder ischemia, cystic duct obstruction, and systemic infection are considered to be the most important factors in pathogenesis of AAC.^{70,71} Histologic features include gallbladder wall inflammation, with necrosis of blood vessels in the muscularis and serosa of the gallbladder.⁷² AAC occurs with increased incidence in patients who are critically ill or with prolonged illness, such as in the setting of trauma or after prolonged stay in the intensive care unit. Other risk factors include major cardiovascular disorders, cardiopulmonary bypass, diabetes, autoimmune disease, bacterial and fungal sepsis, hyperalimentation, and AIDS. Although it is much less common, the disease can occur *de novo* in the absence of these other risk factors in otherwise apparently healthy individuals.^{73,74}

AAC is a more fulminant form of acute cholecystitis with higher morbidity and mortality and rapid progression to gangrene and perforation. Mortality is reported to be as high as 65%⁷⁵; therefore, early diagnosis is important. The diagnosis of AAC, however, often presents a challenge, particularly if there are no apparent risk factors. Clinical findings, such as fever and leukocytosis, are nonspecific. The diagnosis should be suspected in critically ill or injured patients who have fever or infection with no other apparent source.

IMAGING

Ultrasound

The reported sensitivity of ultrasound in AAC varies widely from 36% to 92%⁶⁹ (Fig. 77-22). Gallstones are not present, and afflicted patients are often insensitive to pain because of altered mental status or medications, thus making the sonographic

Murphy sign unreliable.⁷⁶ These patients may also have hypoalbuminemia, congestive heart failure, and long-standing parenteral nutrition, all of which are associated with gallbladder wall thickening, distention, and sludge. There is a great degree of overlap in ultrasound findings of intensive care unit patients with AAC and those without. In one study evaluating the ultrasound findings in intensive care unit patients, the majority of

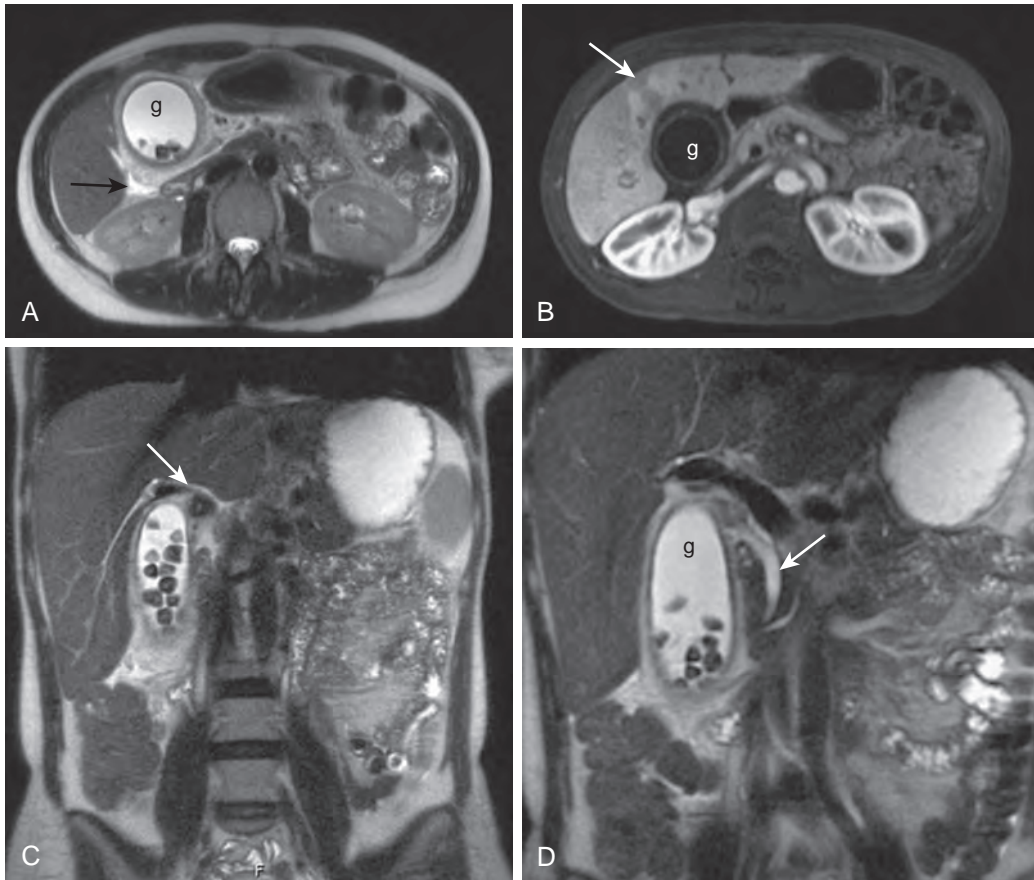


Figure 77-21 Acute cholecystitis: MR findings.
A. T2-weighted HASTE image demonstrates gallbladder distention (g). Dependent low signal gallstones are evident. Gallbladder wall is thickened, and there is pericholecystic fluid (arrow). **B.** Contrast-enhanced T1-weighted gradient-echo fat-suppressed image demonstrates gallbladder distention (g) with wall thickening. Increased enhancement is present in adjacent liver parenchyma (arrow). **C.** Coronal HASTE image demonstrates distended gallbladder with multiple stones. Arrowhead, Stone in gallbladder neck. **D.** Coronal HASTE image demonstrates normal common bile duct (arrow).

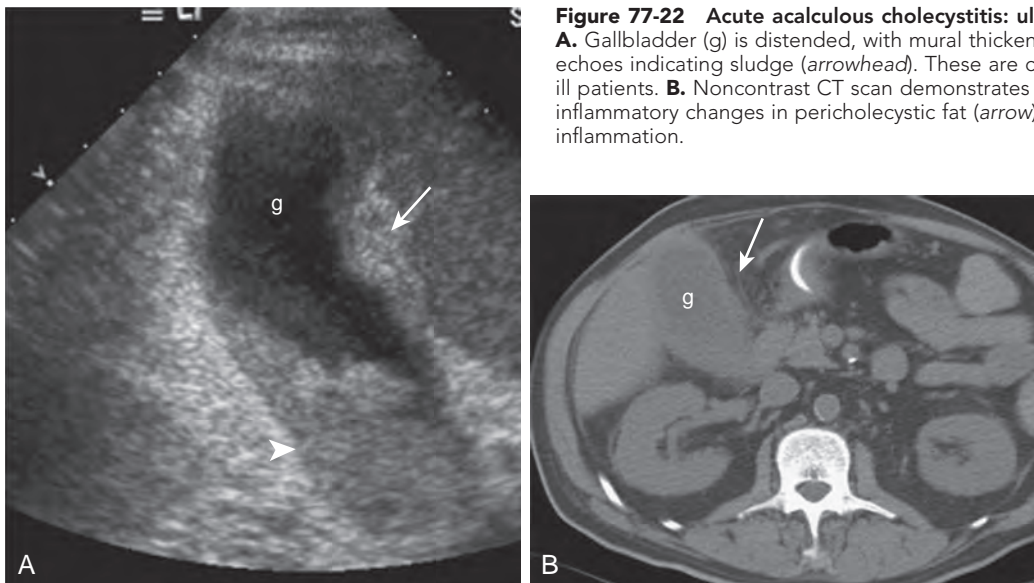


Figure 77-22 Acute acalculous cholecystitis: ultrasound and CT findings.
A. Gallbladder (g) is distended, with mural thickening (arrow), and contains dependent echoes indicating sludge (arrowhead). These are common ultrasound findings in acutely ill patients. **B.** Noncontrast CT scan demonstrates gallbladder distention (g) with inflammatory changes in pericholecystic fat (arrow), confirming presence of gallbladder inflammation.

patients had some abnormality of the gallbladder.⁷⁷ Nevertheless, ultrasound has the advantage of being performed portably at the bedside and remains a reasonable first study for the diagnosis of AAC. Despite limitations, the American College of Radiology appropriateness criteria assign ultrasound the highest ranking for diagnosis of AAC.²⁸

Cholescintigraphy is also of limited value in the diagnosis of AAC, with a significant false-positive rate (nonvisualization of the gallbladder) of up to 40% in patients with hepatocellular dysfunction, prolonged fasting, or severe illness.^{76,78} A negative study is useful for excluding acalculous cholecystitis; however, a positive study must be interpreted with caution. The specificity can be improved to 88% with the use of morphine.⁷⁹ A prospective study comparing ultrasound and morphine scintigraphy in the diagnosis of AAC found the sensitivity of ultrasound and morphine scintigraphy to be 50% and 67%, specificity 94% and 100%, positive predictive value 86% and 100%, negative predictive value 71% and 80%, and accuracy 75% and 86%, respectively.⁸⁰ Combining the two modalities may lead to greater diagnostic accuracy.

Computed Tomography and Magnetic Resonance Imaging

CT or MRI may be helpful in the diagnosis of AAC in the patient who is stable enough to undergo imaging but should generally be performed as an adjunct to ultrasound. With the exception of the absence of gallstones, the CT and MRI findings of AAC are similar to those of calculous cholecystitis. The advantage of these modalities is that they may demonstrate pericholecystic inflammatory change and fluid and abnormalities of the gallbladder wall or adjacent hepatic parenchyma that may not be appreciated at sonography, allowing a more specific diagnosis^{60,62,81-83} (Fig. 77-23). However, as at sonography, less specific findings that may be observed include gallbladder distention, sludge, and wall thickening. A study demonstrated,

however, that a totally normal gallbladder at CT excluded the diagnosis of AAC.⁸⁴

Many times, these patients are too ill for additional cross-sectional imaging evaluation. If no other source of sepsis is discovered, it may be prudent to proceed with percutaneous cholecystostomy, which can be performed at the bedside. This has been shown to be a safe and effective procedure in the patient with acute cholecystitis who is not a surgical candidate.⁸⁵ This can be helpful, for both diagnosis and treatment, in patients with sepsis of unknown cause and equivocal imaging findings of AAC.^{86,87} A study showed that percutaneous cholecystostomy was superior to gallbladder aspiration in terms of clinical effectiveness and was associated with the same complications.⁸⁸

Complications of Acute Cholecystitis

GANGRENOUS CHOLECYSTITIS

Gangrenous cholecystitis is a severe form of acute cholecystitis associated with vascular compromise and intramural hemorrhage, necrosis, and intramural abscess formation. This is usually caused by a stone impacting the cystic duct, with progressive distention of the gallbladder and ultimately ischemic necrosis of the wall.⁸⁹ The incidence ranges from 2% to approximately 30% in various surgical series.⁹⁰⁻⁹² The incidence is increased in men, patients of advanced age, and those with cardiovascular disease. Once it is diagnosed, treatment is generally emergency cholecystectomy to avoid life-threatening complications, such as perforation. There is a higher rate of conversion to open cholecystectomy than in uncomplicated acute cholecystitis.⁹³⁻⁹⁵

At sonography, the features of gangrenous cholecystitis include heterogeneous, striated thickening and irregularity of the gallbladder wall and intraluminal membranes resulting from desquamation of the gallbladder mucosa^{96,97} (Figs. 77-24

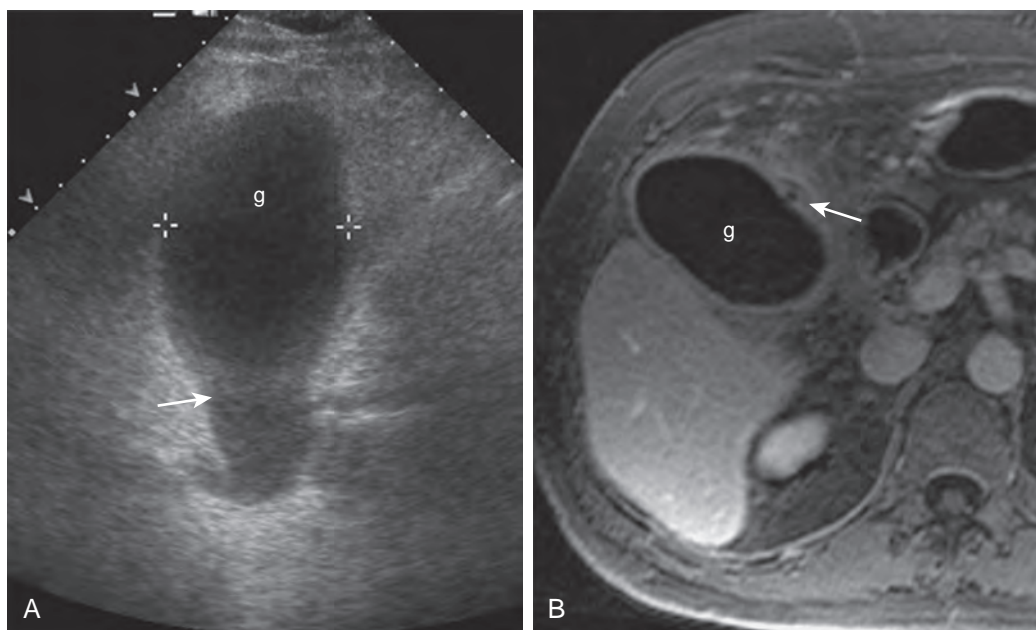


Figure 77-23 Acute acalculous cholecystitis: ultrasound and MR features. **A.** Ultrasound demonstrates markedly distended gallbladder (g) with layering sludge (arrow). **B.** Axial T1-weighted fat-suppressed gradient-echo image with gadolinium enhancement demonstrates distended gallbladder (g), wall thickening, and pericholecystic inflammatory change. Arrow points to small intramural abscess not suspected clinically.

and 77-25). The irregular or asymmetric thickening of the gallbladder wall probably results from ulceration, hemorrhage, necrosis, or microabscess formation. In a series by Jeffrey and colleagues,⁹⁷ these findings were present in 50% of patients. A striated appearance of the gallbladder wall was found in 40% of patients in the series by Teefey and associates.⁹⁶ However, in a more recent analysis by this author, this finding was nonspecific for the presence of gangrenous cholecystitis and found in nongangrenous cholecystitis and other conditions that cause gallbladder wall edema, such as hepatitis.⁹⁸ The presence of

intraluminal membranes is considered a more specific finding (see Fig. 77-25). The sonographic Murphy sign may not be present because of associated denervation of the gallbladder wall. In a series by Simeone and colleagues,⁹⁹ the sonographic Murphy sign was present in only 33% of patients with gangrenous cholecystitis. Additional findings include intramural abscess formation and pericholecystic fluid collection or abscess formation caused by perforation of the gallbladder.

CT findings of gangrenous cholecystitis parallel findings at sonography and include intraluminal membranes, intraluminal

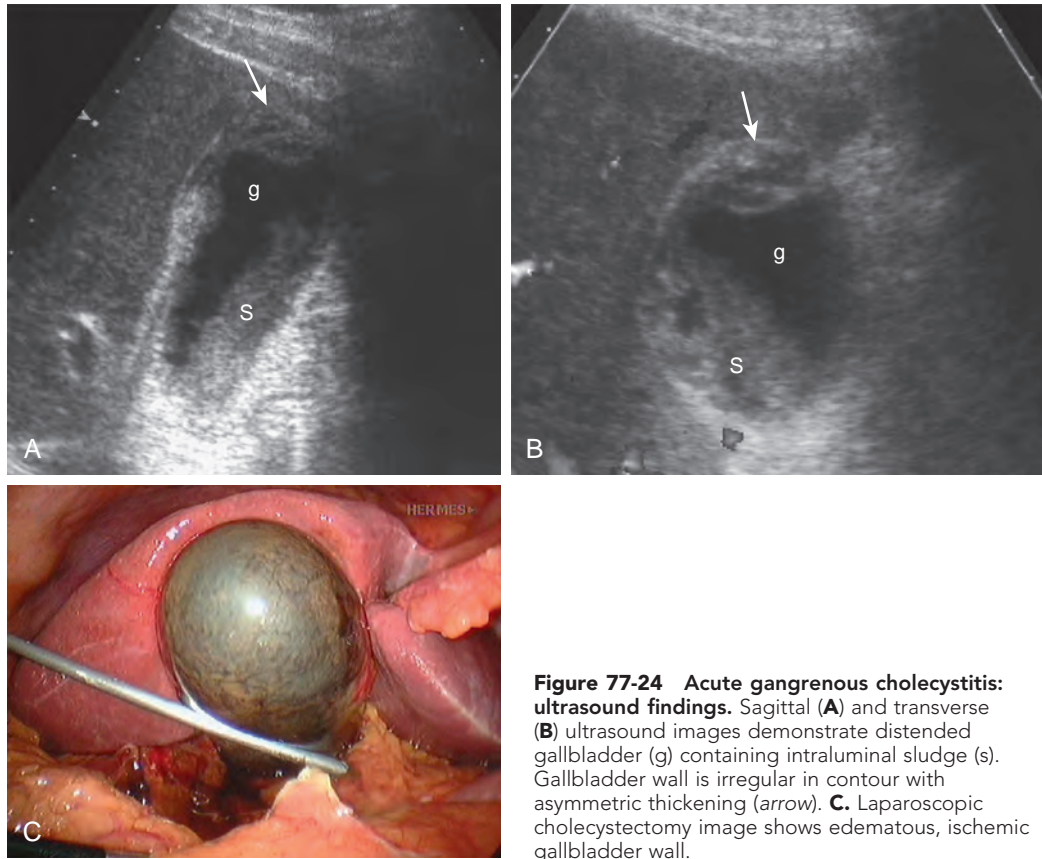


Figure 77-24 Acute gangrenous cholecystitis: ultrasound findings. Sagittal (A) and transverse (B) ultrasound images demonstrate distended gallbladder (g) containing intraluminal sludge (s). Gallbladder wall is irregular in contour with asymmetric thickening (arrow). C. Laparoscopic cholecystectomy image shows edematous, ischemic gallbladder wall.

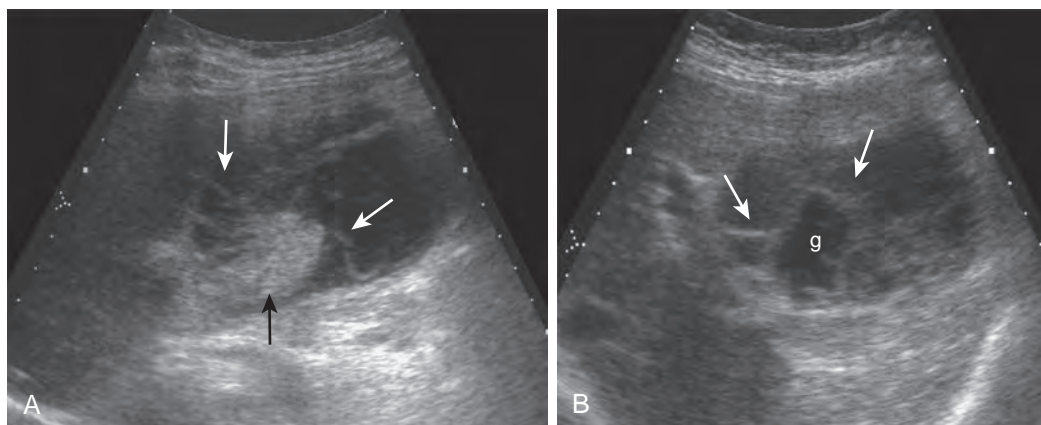


Figure 77-25 Acute gangrenous cholecystitis: ultrasound features. A. Sagittal image demonstrates echogenic, nonshadowing intraluminal material indicating aggregates of sludge (black arrow). Curvilinear intraluminal echogenic regions (white arrows) represent intraluminal membranes secondary to sloughed mucosa. B. Transverse image demonstrates intraluminal membranes (arrows) in gallbladder (g) lumen.

hemorrhage, irregularity or disruption of the gallbladder wall, and pericholecystic abscess^{17,46,48,100-102} (Fig. 77-26). An additional finding detectable at CT is irregular or lack of gallbladder wall enhancement^{46,102} (Fig. 77-27). A study by the author evaluated the sensitivity and specificity of CT for the diagnosis of gangrenous cholecystitis.⁴⁶ CT was highly specific for identifying acute gangrenous cholecystitis (96%) but had low sensitivity (29.3%). The most specific findings at CT for the presence of gangrenous cholecystitis were gas in the gallbladder wall or lumen, intraluminal membranes, irregularity or absence of the gallbladder wall, pericholecystic abscess, and lack of gallbladder wall enhancement. In this study, the presence of pericholecystic fluid, degree of gallbladder distention in the short axis, and degree of mural thickening were also predictive of the severity of gallbladder inflammation. In a more recent study by Wu and associates,¹⁰³ the presence of a perfusional defect of the gallbladder wall (discontinuity or decreased enhancement of the gallbladder wall) was associated with CT diagnosis of gangrenous cholecystitis with accuracy of 80%, sensitivity of 70.6%, specificity of 100%, and positive predictive value of 100%. Therefore, when CT is performed to evaluate for cholecystitis, contrast material should be administered intravenously if possible because this improves delineation of the wall and identification of lack of enhancement, intramural abscess, and focal disruption, which are important features of gangrenous cholecystitis.

Gallbladder carcinoma may be mimicked by the mural changes in acute cholecystitis, particularly gangrenous cholecystitis, and this is an important potential pitfall. If there is concern on the basis of ultrasound findings, CT may be of benefit in demonstrating an enhancing gallbladder mass and

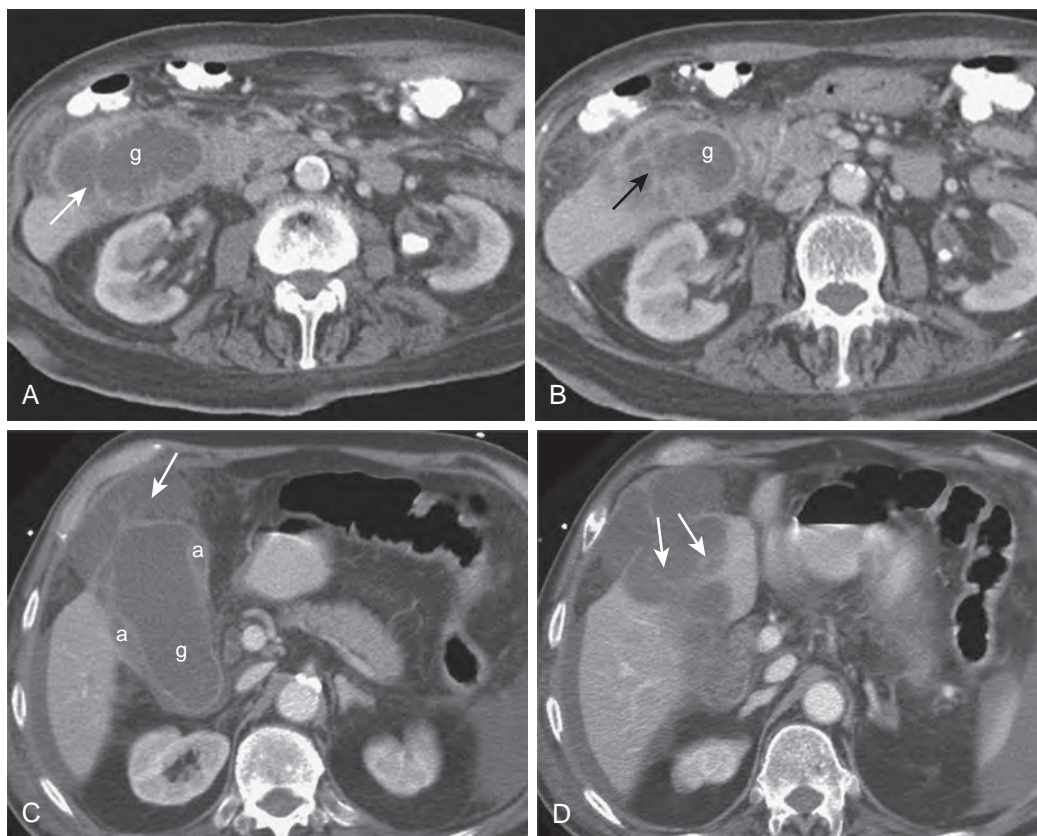
detecting direct invasion of the liver and presence of liver metastases.⁴⁵ Liang and colleagues¹⁰⁴ found that in the differentiation of acute cholecystitis and gallbladder carcinoma, features that favored carcinoma included focal gallbladder wall thickening, intraluminal mass, nondistended gallbladder with diffuse wall thickening, and enlarged regional lymph nodes.

HEMORRHAGIC CHOLECYSTITIS

Hemorrhagic cholecystitis is an uncommon complication of acute cholecystitis and usually occurs in the setting of cholelithiasis and gangrenous cholecystitis. Transmural inflammation causes mural necrosis and ulceration and results in hemorrhage into the gallbladder lumen.¹⁰⁵⁻¹⁰⁷ Atherosclerotic change in the gallbladder wall may be a predisposing factor.¹⁰⁷ Blood clots in the lumen may become impacted in the cystic duct or common bile duct (CBD) or pass into the small bowel. The clinical presentation may be identical to uncomplicated acute cholecystitis with fever and right upper quadrant pain but may also include biliary colic, jaundice, hematemesis, and melena.¹⁰⁸ Massive upper gastrointestinal bleeding and hemoperitoneum rarely occur.¹⁰⁹ Prompt diagnosis is essential because of the associated high mortality rate.

At sonography, blood in the gallbladder lumen can be recognized as hyperechoic material that demonstrates greater echogenicity than sludge (Fig. 77-28). This may form a dependent layer; however, clotted blood may appear as a clump or mass adherent to the gallbladder wall or heterogeneous echogenic material.^{105,108,110} An organized clot may simulate a polypoid, intraluminal mass.¹¹¹ As the hemorrhage evolves, the clot may become more cystic in appearance.¹¹² In addition to

Figure 77-26 Acute gangrenous cholecystitis: CT findings. **A** and **B.** Gallbladder (g) is distended with thickened, irregularly enhancing wall. Arrow, Intraluminal membranes. **C.** Scan obtained in a different patient shows distended gallbladder (g) with thickened wall, which demonstrates heterogeneous contrast enhancement. Low-attenuation areas correspond to intramural abscesses (a). Arrow, Loculated pericholecystic fluid collection secondary to contained gallbladder perforation. **D.** Slightly more inferior image demonstrates intraluminal membranes (arrows).



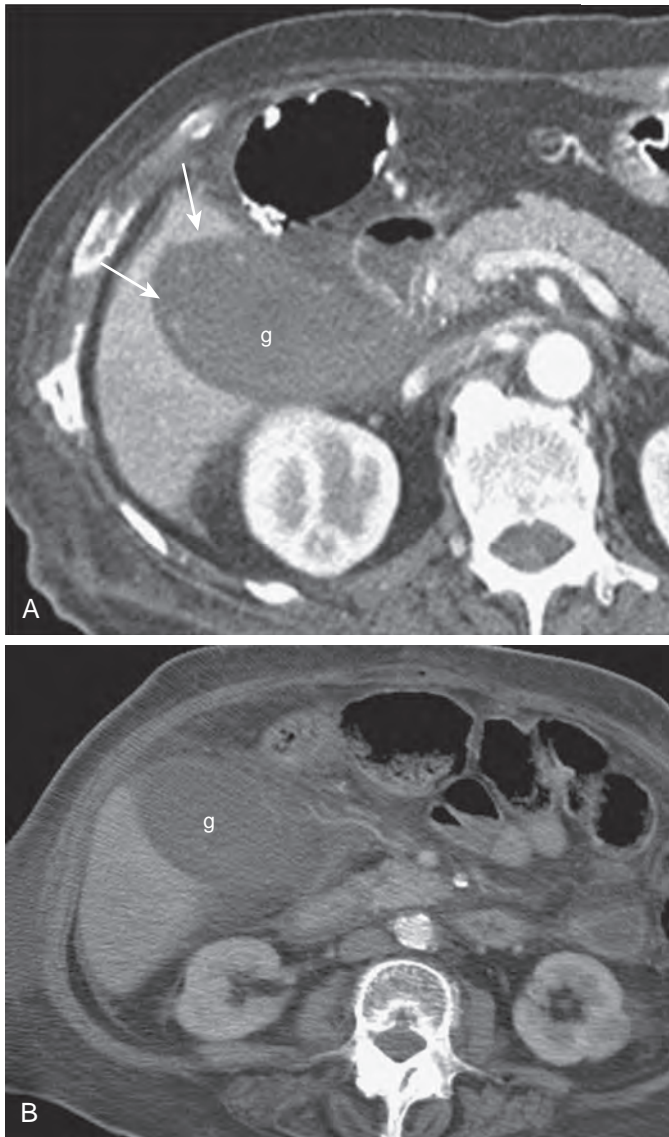


Figure 77-27 CT of gangrenous cholecystitis: lack of mural contrast enhancement. **A.** There is apparent discontinuity of the gallbladder wall (arrows) where no mucosal enhancement is noted. *g*, Distended gallbladder. **B.** Contrast-enhanced CT scan in a second patient demonstrates distended gallbladder (*g*) with extensive pericholecystic inflammatory change. There is no contrast enhancement of gallbladder wall.

other findings of cholecystitis, CT shows increased density of bile¹⁰⁵ (see Fig. 77-28B). A fluid-fluid level may be observed with a high-attenuation dependent component simulating the hematocrit effect observed in acute hemorrhage¹⁰⁸ (Fig. 77-29A). Other causes of high-density bile include biliary excretion of iodinated contrast material and milk of calcium; these do not generally appear as echogenic at sonography, nor is a fluid-fluid level observed. If there is associated perforation of the gallbladder, hemoperitoneum will also be observed (Fig. 77-29B). If there is active bleeding at the time of contrast-enhanced CT, this may appear as active extravasation of intravenous contrast material inside the gallbladder lumen.¹¹³ On MRI, blood products appear as high signal intensity within the gallbladder lumen on T1-weighted images and moderate to high heterogeneous signal intensity on T2-weighted images.⁶²

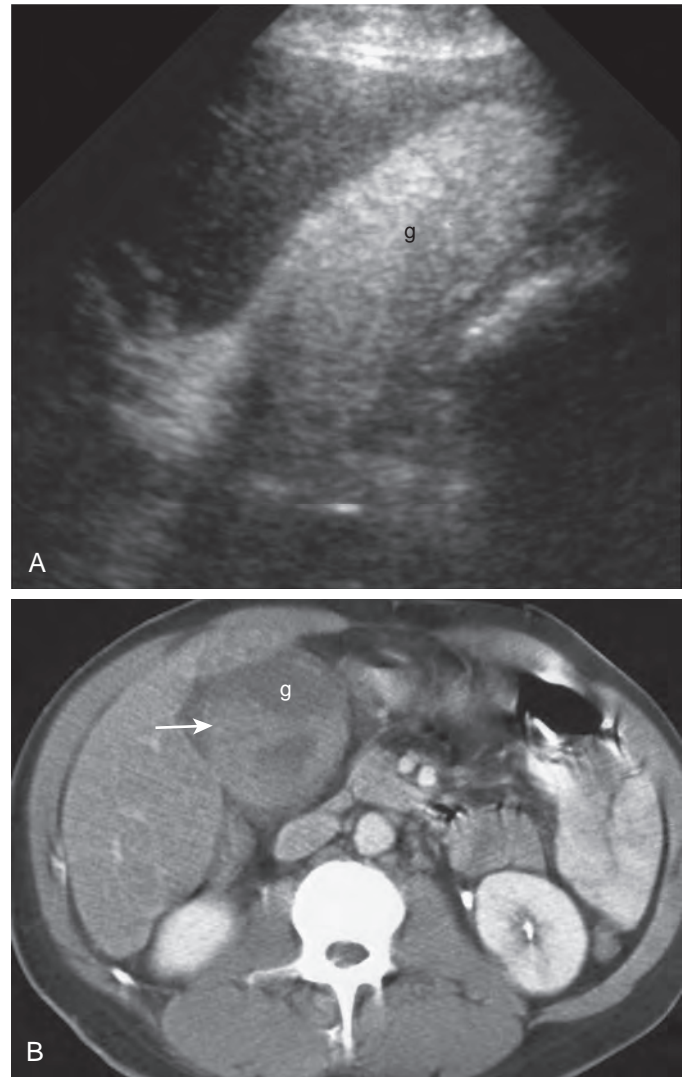


Figure 77-28 Hemorrhagic cholecystitis: ultrasound and CT findings. **A.** Sagittal ultrasound scan demonstrates distended gallbladder (*g*) with lumen completely filled with echogenic material corresponding to hemorrhagic bile. **B.** CT scan demonstrates distended gallbladder (*g*) with fluid-fluid level (arrow) with high-attenuation dependent component. These findings represent intraluminal blood clot.

The multiplanar capability of MRI may help differentiate intraluminal blood from hemorrhage in the wall. MR angiography may supplement conventional imaging if vascular disease is suspected.

EMPHYSEMATOUS CHOLECYSTITIS

Emphysematous cholecystitis is a rare life-threatening and rapidly progressive complication of acute cholecystitis. Cystic artery compromise is thought to promote the proliferation of gas-producing organisms in an anaerobic environment and penetration of gas into the gallbladder wall.^{114,115} The organisms most commonly isolated are *Clostridium welchii* and *Escherichia coli*.¹¹⁵ At pathologic examination, gallbladders with emphysematous cholecystitis have a higher incidence of endarteritis obliterans, supporting vascular insufficiency as a causative factor. This complication occurs with higher frequency in

patients with diabetes (up to 50%) and male patients (up to 71%).¹¹⁶ Gallstones may be absent in up to one third of patients, and there is a high risk of gangrene and a perforation rate five times higher than in acute uncomplicated cholecystitis.^{116,117}

The mortality rate for emphysematous cholecystitis is 15% versus 4% in uncomplicated acute cholecystitis.¹¹⁶ Therefore, prompt diagnosis is critical. The clinical presentation is often indistinguishable from uncomplicated acute cholecystitis. In the diabetic patient, in particular, severe symptoms may be absent, and there needs to be a high clinical index of suspicion. Before cross-sectional imaging, emphysematous cholecystitis

was diagnosed on the abdominal radiograph and classically described in three stages: stage 1, gas in the gallbladder lumen; stage 2, gas in the gallbladder wall; and stage 3, gas in the pericholecystic soft tissues. Ultrasound and CT are now considered more sensitive in the detection of smaller amounts of gas.

Ultrasound findings vary by the amount and location of gas.^{26,27,118,119} A small amount of gas in the wall may appear as an echogenic focus with associated ring-down or comet-tail artifact. Larger amounts of gas and intraluminal gas may appear as a curvilinear arc of increased echogenicity with associated “dirty” posterior acoustic shadowing²⁶ (Fig. 77-30A). In this setting, the

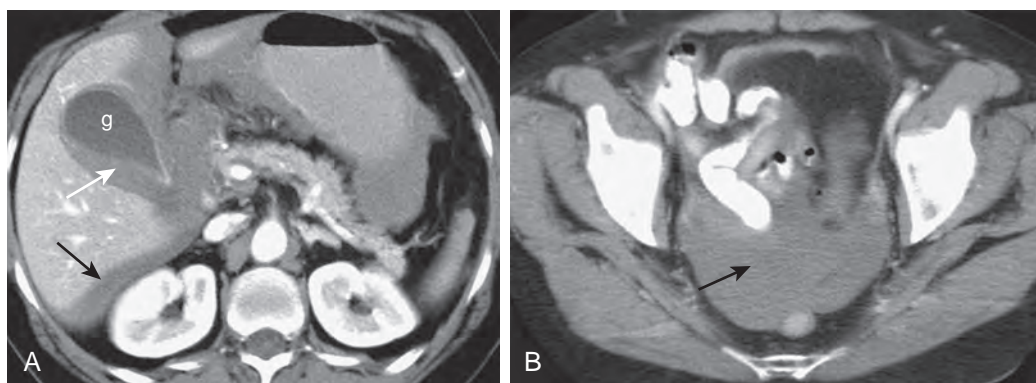


Figure 77-29 Hemorrhagic cholecystitis: CT findings. **A.** CT demonstrates distended gallbladder containing layering material of high attenuation corresponding to intraluminal blood (white arrow). There has been perforation of the gallbladder, resulting in hemoperitoneum (black arrow). **B.** Additional blood is demonstrated in the pelvis (arrow).

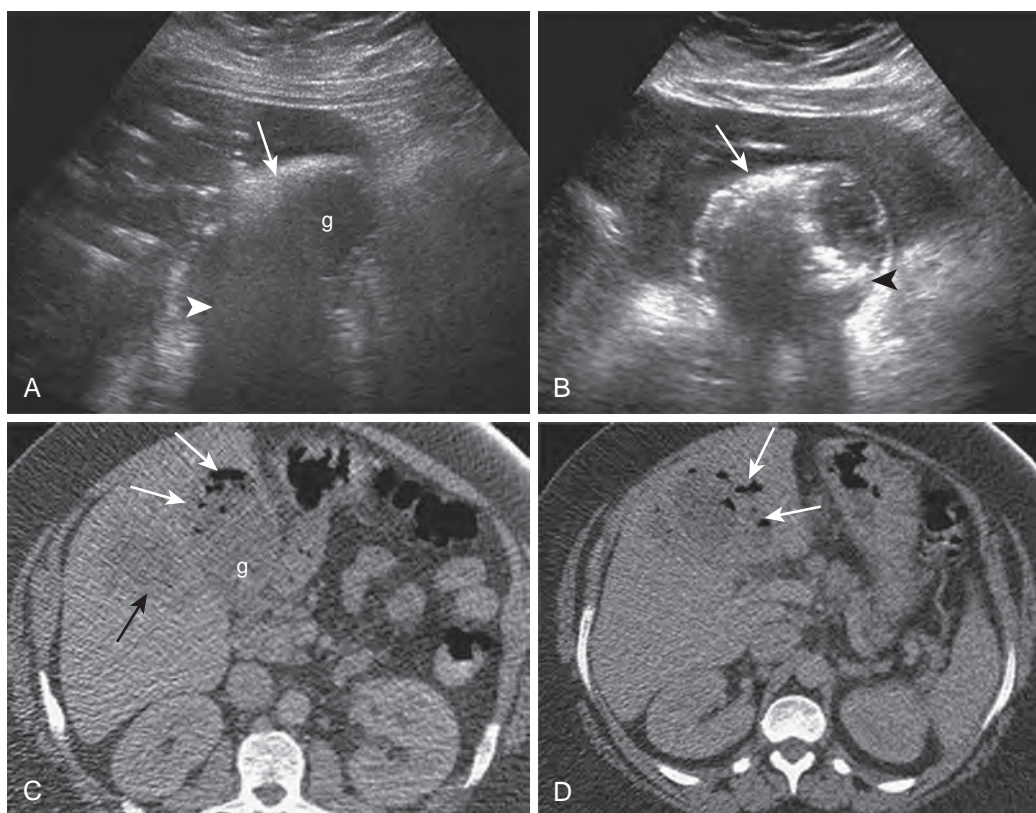


Figure 77-30 Emphysematous cholecystitis: ultrasound and CT features. **A.** Sagittal gallbladder (g) scan demonstrates an arc of increased echogenicity (arrow) in expected location of the gallbladder wall. This is associated with “dirty” posterior acoustic shadowing (arrowhead), suggesting intramural gas. **B.** Transverse image demonstrates intramural gas (arrow) and intraluminal echogenic foci with posterior acoustic shadowing (arrowhead), indicating gallstones. **C.** Noncontrast CT demonstrates gas (white arrows) within lumen and wall of gallbladder (g). Low-attenuation area in the adjacent liver is due to an abscess (black arrow). **D.** Gas (arrows) is present in the pericholecystic soft tissues.

gallbladder may be difficult to visualize owing to associated acoustic shadowing. On sonographic evaluation, it may be difficult to differentiate emphysematous cholecystitis from a contracted gallbladder with stones or a porcelain gallbladder with calcified wall.¹¹⁸

CT has a higher sensitivity than sonography for the identification of emphysematous cholecystitis and plays an important complementary role to ultrasound.¹²⁰ If emphysematous cholecystitis is suspected at sonography or there is a high clinical index of suspicion and ultrasound findings are equivocal, CT should be performed. CT is also indicated when the gallbladder cannot be adequately visualized at sonography. CT findings include gas within the gallbladder wall or nondependent portion of the lumen^{45,121,122} (Fig. 77-31). There may be extension into the pericholecystic soft tissues. CT may also demonstrate other complications, such as abscess formation and perforation (Fig. 77-30C, D and Fig. 77-31B, C). Free intraperitoneal gas indicates associated free gallbladder perforation and constitutes a surgical emergency.

The MRI features of emphysematous cholecystitis have not yet been well described. A report describing MRI features in a case of emphysematous cholecystitis included (1) a signal void in the nondependent portion of the gallbladder and intermediate signal intensity fluid in the dependent portion of the gallbladder, representing a gas-fluid level; (2) a low signal intensity rim surrounding the gallbladder, indicating gas in the gallbladder wall; and (3) regions of very low signal intensity in the pericholecystic soft tissues, indicating extraluminal gas due to

perforation.¹²³ Gas can be recognized as blooming artifact on gradient-echo and echo planar sequences.

GALLBLADDER PERFORATION

Gallbladder perforation can occur in the setting of cholelithiasis, cholecystitis, trauma, neoplasm, steroid use, or vascular compromise. Perforation is most often a complication of severe acute cholecystitis, occurring in approximately 8% to 12% of cases.^{124,125} In one series, associated mortality was 24.1%.¹²⁴ In acute cholecystitis, progressive gallbladder distention and inflammation is followed by vascular compromise, gangrene, necrosis, and ultimately perforation.^{125,126} The fundus is the most frequent site of perforation because of the relatively poor blood supply in this area. Associated complications include bacteremia, septic shock, bile peritonitis, and abscess formation, with mortality rates ranging from 6% to 70%.^{124,127-130}

Gallbladder perforation has been classified into three types¹²⁷: (1) acute free perforation into the peritoneal cavity, (2) subacute perforation with pericholecystic abscess, and (3) chronic perforation with cholecystenteric fistula formation. Subacute perforation with pericholecystic abscess formation is the most common type.¹²⁸ Abscess formation may be confined to the gallbladder fossa or spread into the peritoneal cavity or involve the liver.^{131,132} Type 1 free perforation is associated with the highest mortality rate.¹²⁸ Type 3 perforation is associated with gallstone ileus, discussed later in this chapter.

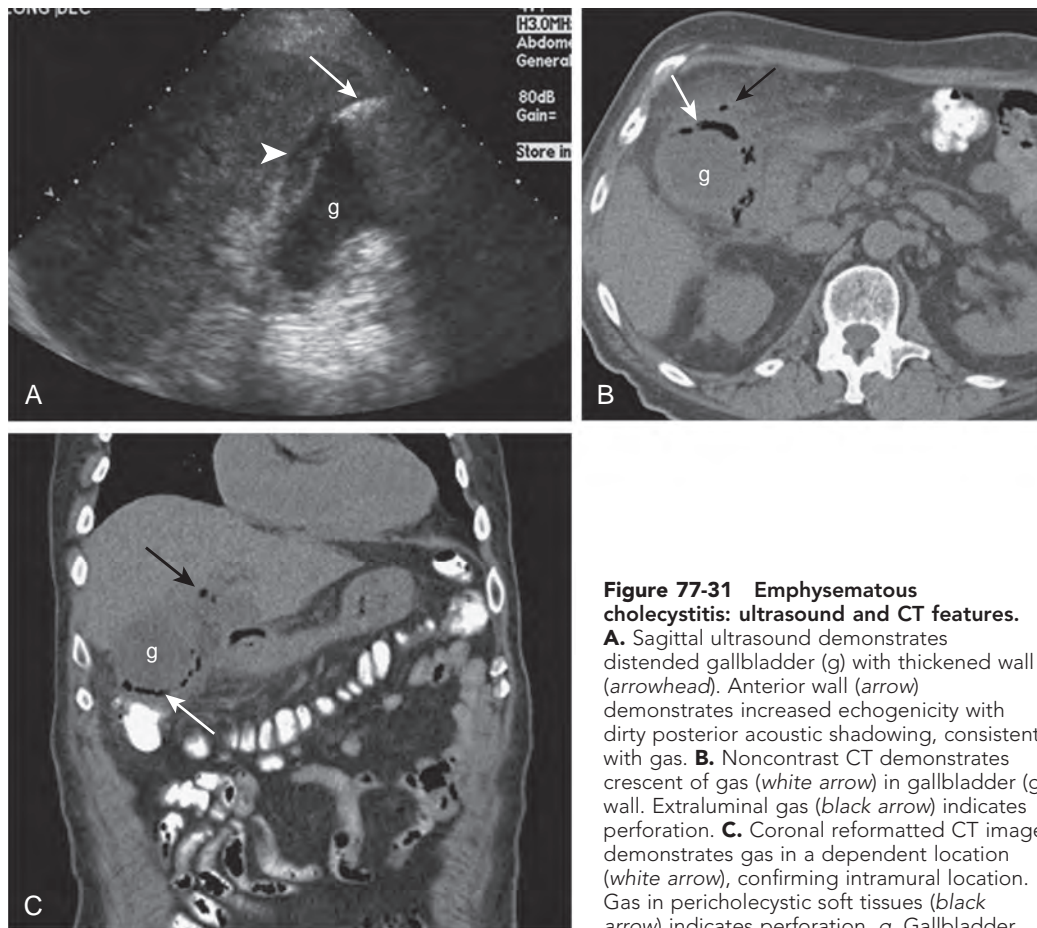


Figure 77-31 Emphysematous cholecystitis: ultrasound and CT features.

A. Sagittal ultrasound demonstrates distended gallbladder (g) with thickened wall (arrowhead). Anterior wall (arrow) demonstrates increased echogenicity with dirty posterior acoustic shadowing, consistent with gas. **B.** Noncontrast CT demonstrates crescent of gas (white arrow) in gallbladder (g) wall. Extraluminal gas (black arrow) indicates perforation. **C.** Coronal reformatted CT image demonstrates gas in a dependent location (white arrow), confirming intramural location. Gas in pericholecystic soft tissues (black arrow) indicates perforation. g, Gallbladder.

Prompt diagnosis of gallbladder perforation is imperative. Emergent cholecystectomy is the treatment of choice. Clinical signs and symptoms may be nonspecific and may be indistinguishable from uncomplicated cholecystitis, particularly in the diabetic patient, so that imaging plays an important diagnostic role.¹³³ At sonography, the gallbladder wall is irregular or ill-defined with focal or global loss of its normal sonorefectivity.⁴⁵ There is a large amount of pericholecystic fluid or a loculated pericholecystic collection¹²⁶ (Fig. 77-32A). A focal defect in the wall of the gallbladder is a more specific finding but may not always be visualized¹³⁴ (Fig. 77-33A, B).

CT plays an important role in the evaluation of suspected gallbladder perforation when ultrasound findings are equivocal.^{131,135,136} Interruption of the gallbladder wall or a focal mural defect may be more readily identified at CT (Fig. 77-33C). Associated findings include pericholecystic or intrahepatic abscess and spilled stones (see Fig. 77-32B). Free gallbladder perforation is identified when there is free intraperitoneal fluid corresponding to bile (Fig. 77-34). In this setting, the gallbladder may be collapsed, which may provide an additional diagnostic challenge as the diagnosis of acute cholecystitis may not be readily apparent. In these instances, presence of localized pericholecystic inflammatory change offers a diagnostic

Figure 77-32 Gallbladder perforation. **A.** Ultrasound demonstrates complex fluid collection in gallbladder fossa (arrow). Gallbladder wall is not delineated, and perforated gallbladder with abscess was suspected. Arrowhead, Gallstones. **B.** Noncontrast CT image demonstrates a large complex fluid collection in gallbladder fossa (arrow). There are spilled gallstones (arrowheads) due to gallbladder perforation.

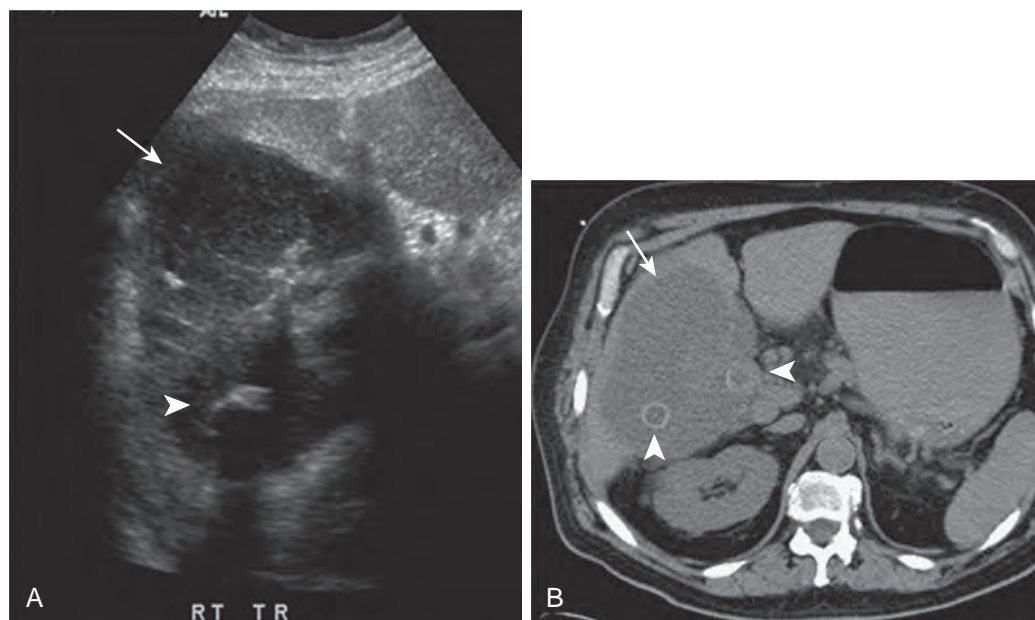
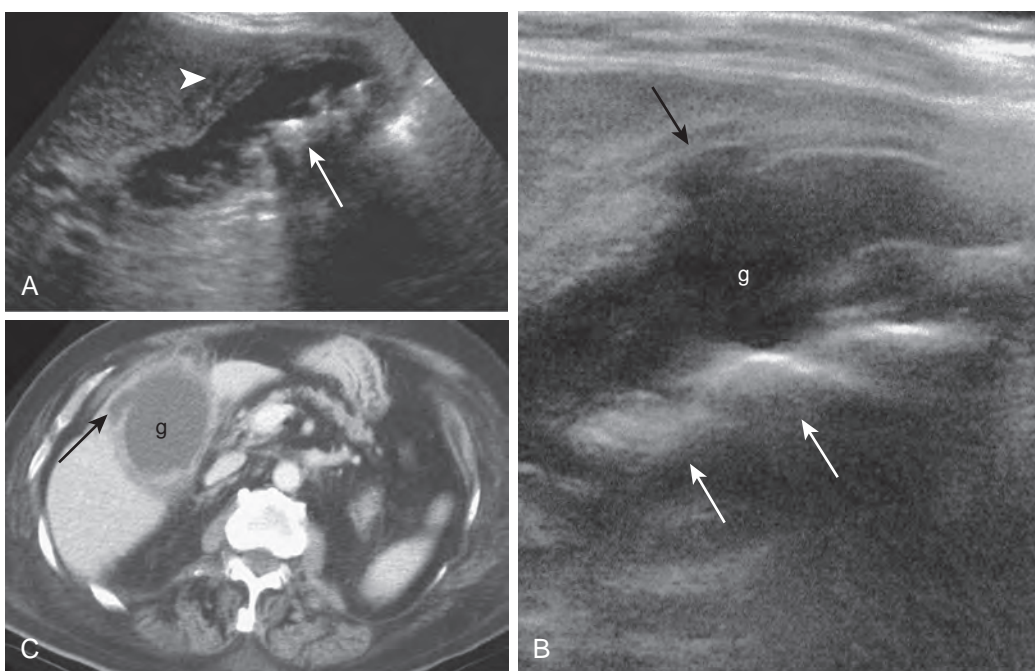


Figure 77-33 Gallbladder perforation. **A.** Sagittal scan shows mural thickening with striations (arrowhead). Arrow, Multiple gallstones. **B.** Sagittal scan obtained with a linear transducer (8 MHz) produces higher resolution image. Focal defect in gallbladder wall (black arrow) is now evident. This indicates a focal intramural abscess or contained perforation. White arrows, Gallstones. **C.** Contrast-enhanced CT confirms focal defect (arrow) in gallbladder (g) wall. Mural thickening and pericholecystic inflammatory changes are present, consistent with acute cholecystitis.



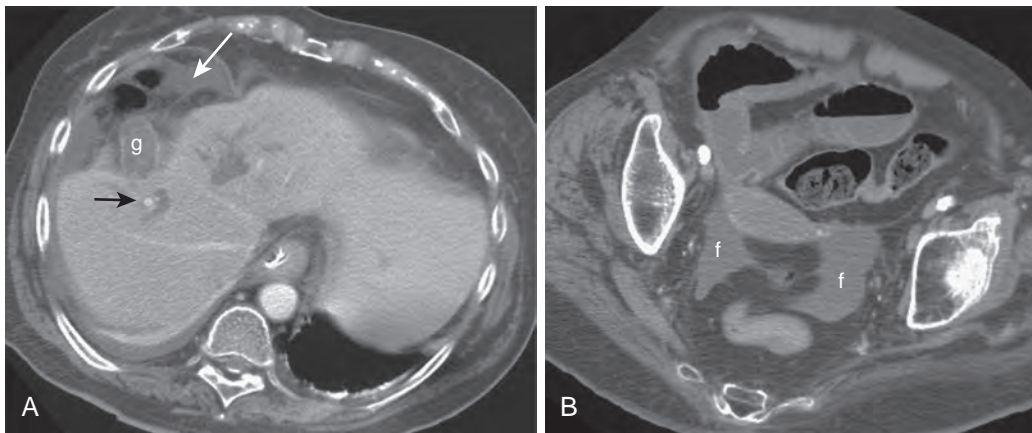


Figure 77-34 Free perforation of the gallbladder with associated bile peritonitis.

Patient presented with several days of right upper quadrant pain and fever. **A.** Contrast-enhanced CT demonstrates that the gallbladder (g) is not distended. Calcified stone (black arrow) appears to be outside of gallbladder lumen. White arrow, Perihepatic free fluid. **B.** Image of the pelvis demonstrates moderate free fluid (f) corresponding to bile.

clue as to the etiology of free fluid and peritoneal inflammatory changes.

In a study comparing ultrasound with CT in 13 patients with surgically proven gallbladder perforation, a mural defect was visualized in 7 patients (53.8%) at CT but in no patient on ultrasound.¹³⁶ Ultrasound and CT were similar in demonstrating pericholecystic fluid collections, gallbladder wall thickening, and cholelithiasis. Bulging or irregular contour of the gallbladder was demonstrated on ultrasound in five cases and on CT in two cases. In all cases, the site of the gallbladder wall defect or bulging on ultrasound or CT corresponded to the site of perforation. These authors concluded that CT was superior to ultrasound for the diagnosis of gallbladder perforation because of improved ability to demonstrate a focal wall defect. A more recent study by Sood and associates,¹³⁷ however, found that there was no statistically significant difference in the ability of ultrasound or CT to detect a focal wall defect in 18 patients evaluated with both modalities. This may be due to recent improvements in ultrasound technology, allowing better resolution and definition of the gallbladder wall. MR, because of its superior soft tissue resolution and multiplanar imaging capability, may also be a useful adjunct if ultrasound and CT findings remain equivocal.

Chronic Cholecystitis

PATHOGENESIS AND EPIDEMIOLOGY

Chronic cholecystitis is associated with cholelithiasis in 95% of cases and may occur after a single bout or multiple recurrent episodes of acute cholecystitis. Etiology is related to intermittent obstruction of the cystic duct or neck as well as gallbladder dysmotility.² Chronic inflammatory changes cause the gallbladder wall to become thickened and fibrotic, and with increasing fibrosis, the gallbladder eventually becomes shrunk and distorted. If there are coexisting acute and chronic inflammatory changes at pathologic examination, the term *chronic active cholecystitis* may be used.¹³⁸

IMAGING

A diagnosis of chronic cholecystitis is difficult to establish with imaging, and clinical correlation is required. Ultrasound findings include gallstones and thickened gallbladder wall with contraction of the gallbladder that persists in the

fasting state (Fig. 77-35). On CT, pericholecystic inflammatory change may be absent.⁵⁰ On MR, gallbladder wall thickening related to chronic inflammation will demonstrate low signal intensity, whereas acute cholecystitis is associated with edema in the wall, which demonstrates increased signal intensity on T2-weighted images.⁶² Also, the increased perihepatic contrast enhancement observed with acute cholecystitis can be helpful in differentiating acute from chronic inflammation.^{61,62,67}

CHRONIC ACALCULOUS CHOLECYSTITIS

Chronic acalculous cholecystitis, a disorder characterized by recurrent biliary colic in a patient without radiographic evidence of gallstones, often creates a diagnostic dilemma for clinicians. In the absence of gallstones, it is often difficult to attribute a patient's symptoms to gallbladder inflammation. However, these patients may benefit from cholecystectomy for relief of symptoms.¹³⁹ A specific diagnosis may require nuclear medicine evaluation, including evaluation of the gallbladder ejection fraction. A decrease in gallbladder ejection fraction is a common feature of both calculous and acalculous chronic cholecystitis.¹⁴⁰ Cholecystokinin cholescintigraphy with calculation of gallbladder ejection fraction has been shown to be a predictor of disease as well as of subsequent symptom relief after cholecystectomy.¹⁴¹

XANTHOGRANULOMATOUS CHOLECYSTITIS

Xanthogranulomatous cholecystitis (XGC) is a rare chronic inflammatory condition of the gallbladder, representing a form of chronic cholecystitis. Goodman and Ishak¹⁴² reported the first series of cases at the Armed Forces Institute of Pathology in 1981. The estimated incidence is 1% to 2% of all cases of cholecystitis,¹⁴³ and most patients present in the sixth or seventh decade.¹⁴⁴ In one surgical review, this disorder was found in 1.46% of all cholecystectomy specimens and was associated with gallstones in 85%, with average age at presentation of 52 years.¹⁴⁵ The proposed etiology of this disorder involves chronic gallbladder infection, usually in the setting of cholelithiasis, with mural microabscesses that involve Rokitsansky-Aschoff sinuses. This may result from obstruction of gallbladder outflow, extravasation of bile into the gallbladder wall, and mucosal ulceration. Histiocytes accumulate in the gallbladder wall as a reaction to the extravasated bile,

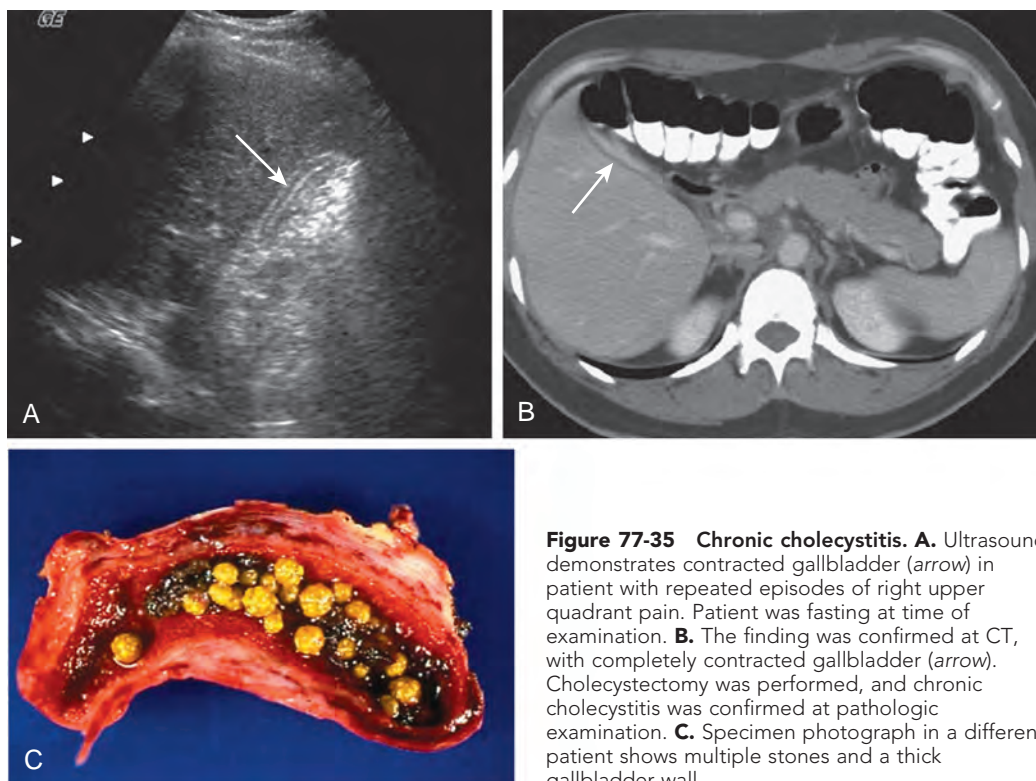


Figure 77-35 Chronic cholecystitis. **A.** Ultrasound demonstrates contracted gallbladder (arrow) in patient with repeated episodes of right upper quadrant pain. Patient was fasting at time of examination. **B.** The finding was confirmed at CT, with completely contracted gallbladder (arrow). Cholecystectomy was performed, and chronic cholecystitis was confirmed at pathologic examination. **C.** Specimen photograph in a different patient shows multiple stones and a thick gallbladder wall.

and ultimately xanthogranulomatous nodules form in addition to extensive fibrous reaction.¹⁴⁶ On gross examination, the wall is thickened and irregular with yellow or brown nodules of varying sizes. On microscopic examination, the xanthogranulomatous nodules are composed of histiocytes, giant cells, and other chronic inflammatory cells such as lymphocytes and plasma cells. Hemosiderin and extravasated bile along with cholesterol clefts are present in the gallbladder wall. There may be associated biliary obstruction secondary to extrinsic compression of the bile duct and associated Mirizzi syndrome. The gallbladder often becomes adherent to adjacent organs and may be associated with fistula formation. There are no specific clinical or laboratory features, and presentation may be similar to acute or chronic cholecystitis from any cause. Clinical symptoms may include right upper quadrant pain, nausea, vomiting, fever, anorexia, and weight loss.¹⁴⁶

Both the ultrasound and CT features of XGC have been described¹⁴⁶⁻¹⁵¹ and overlap with findings of acute and chronic cholecystitis. On both modalities, the gallbladder wall is often markedly thickened and irregular with loss of normal planes with adjacent structures. An infiltrating mass may be apparent. More recent studies have described the presence of intramural nodules visualized on both sonography and CT (Fig. 77-36). In their series, Chun and colleagues¹⁵⁰ found low-density nodules in 11 cases of XGC, compared with only 7 of 17 cases of carcinoma. Intramural nodules are also a prominent finding of XGC described in other series¹⁴⁷⁻¹⁵¹ as well as a hypoechoic band around the gallbladder.^{147,148} By performing ultrasound on pathologic specimens, Parra and associates¹⁴⁷ showed that the intramural hypoechoic nodules correspond to xanthogranulomatous nodules and the hypoechoic band may correspond to more generalized involvement. However, these nodules may also be confused with intramural abscesses in

gangrenous cholecystitis and large Rokitansky-Aschoff sinuses in adenomyomatosis.

It can be very difficult to prospectively distinguish between XGC and gallbladder carcinoma on cross-sectional imaging studies because of many overlapping features, such as marked gallbladder wall thickening, irregularity, nodularity, and infiltration of the pericholecystic soft tissues. There is a 10% incidence of carcinoma in XGC,¹⁴⁴ and fine-needle aspiration biopsy has been successful in establishing the diagnosis.¹⁵² Surgery is often difficult in these patients, with a high conversion rate to open cholecystectomy. A potential role for diffusion-weighted MRI has recently been proposed, with diffusion restriction seen more frequently in patients with carcinoma and higher apparent diffusion coefficient values in patients with XGC in one series¹⁵³; however, further work in this area is needed.

Choledocholithiasis

PATHOGENESIS AND EPIDEMIOLOGY

Biliary stones that form de novo within the biliary tract are referred to as primary stones, whereas those that migrate from the gallbladder through the cystic duct or a cholecystocholedochal fistula are referred to as secondary stones.¹⁵⁴ The majority of stones within the bile ducts are secondary stones, and pathogenesis is similar to that of gallstones. Migration of gallstones among asymptomatic patients is estimated to occur in 3% to 5% of patients per year, with 1% to 2% of patients per year developing symptoms, including biliary colic or acute pancreatitis.^{155,156} Between 7% and 20% of patients undergoing cholecystectomy are found to have one or more stones in the CBD, and these may be clinically silent.¹⁵⁷ Twenty percent to 30% of patients with gallstone pancreatitis have persistent CBD

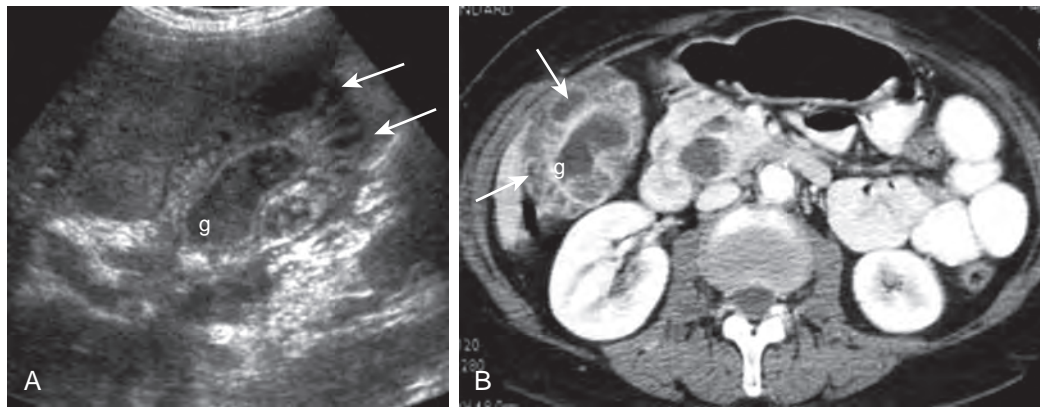


Figure 77-36 Xanthogranulomatous cholecystitis. **A.** Ultrasound demonstrates intraluminal echogenic material due to sludge. Gallbladder (g) wall is markedly thickened and contains hypoechoic nodules (arrows). **B.** Contrast-enhanced CT demonstrates marked gallbladder (g) wall thickening and hypoattenuating mural nodes (arrows).

stones that fail to traverse the ampulla.¹⁵⁸ If a stone remains lodged in the CBD, this can also lead to a potentially life-threatening emergency because of associated cholangitis.

Primary stones are classified according to their location within the biliary tract: intrahepatic, extrahepatic, or ampullary. These develop in the setting of bile stasis and colonization of the bile with enteric organisms. Obstruction of bile may be related to inflammatory or iatrogenic strictures, congenital strictures, or perampullary diverticula.¹⁵⁴ These stones are frequently associated with parasitic infections of the biliary tree, such as *Ascaris lumbricoides*. These worms become the nidus for stone and inflammatory stricture formation.

IMAGING

Endoscopic Retrograde Cholangiopancreatography

Endoscopic retrograde cholangiopancreatography (ERCP) and percutaneous transhepatic cholangiography are highly accurate for the detection of choledocholithiasis and also provide access for therapeutic intervention. However, these are invasive procedures with associated risks, including pancreatitis, sepsis, and hemorrhage. The reported complication rate of ERCP ranges from 3.0% to 5.5%, and mortality rate ranges from 0.2% to 1.0%.^{159,160} Therefore, ERCP is generally reserved for patients who require therapy, such as secondary to an impacted stone, or with a high probability of stones and normal findings on prior examinations. Stones within the biliary tract may be readily detected with MRCP but less accurately with ultrasound and CT.

Ultrasound

Ultrasound is the primary imaging modality for evaluation of right upper quadrant pain and is considered superior to CT in the initial imaging evaluation of biliary disease.^{41,161} The reported sensitivity of ultrasound ranges from 22% to 75% for CBD stones.^{3,162-164} Limited sensitivity results in part from inability to completely visualize the duct, particularly distally, because of interposed bowel gas, and distal stones are most commonly overlooked. In a study by Laing and colleagues,¹⁶⁵ 8 of 9 (89%) proximal and 16 of 23 (70%) distal CBD stones were visualized at sonography. Scanning the patient in the erect right posterior oblique or right lateral decubitus position minimizes gas in the gastric antrum and duodenum and improves visualization of the distal duct. Water may also be administered orally

to provide an acoustic window in the gastric antrum or duodenum.²⁷ Improved contrast enhancement and reduction of side lobe artifacts afforded by tissue harmonic imaging improve the sonographic detection of choledocholithiasis.¹⁶⁶ CBD stones appear as echogenic foci, which may or may not cause posterior acoustic shadowing, depending on size and composition (Figs. 77-37 and 77-38). As with cholelithiasis, nonshadowing stones may be difficult to differentiate from aggregates of sludge or soft tissue masses. Improved accuracy can be accomplished with the use of endoscopic ultrasound,¹⁶⁷ but this is more invasive and operator dependent.

Computed Tomography

Unenhanced conventional CT has a sensitivity of 75% in the detection of choledocholithiasis.¹⁶⁸⁻¹⁷⁰ Indirect signs, such as ductal dilation and abrupt termination of the duct, may be useful but are not conclusive. Multidetector CT (MDCT) has a higher sensitivity, ranging from 65% to 88%.¹⁷¹⁻¹⁷⁴ Multiplanar reconstruction coronal images through the CBD may be useful in depicting stones (Fig. 77-39; see also Fig. 77-37C). In specifically evaluating for choledocholithiasis, water should be used to opacify the bowel because positive oral contrast material may obscure visualization of distal CBD stones and fill perivaterian duodenal diverticula. In a study comparing MDCT and ERCP for the detection of CBD calculi, CT had a sensitivity of 88%, specificity of 97%, and accuracy of 94%.¹⁷¹ Bile window settings (adjustment of the window level setting to the mean attenuation of the CBD and the window width to 150 HU) improve visualization of noncalcified stones by creating better contrast between bile and soft tissues.

The CT appearance of CBD stones is variable. Depending on their composition, stones may be calcified or soft tissue or low density with respect to bile. Calcified stones are the most readily identified (Fig. 77-40A). Unenhanced images are better for detection as most stones are slightly hyperdense. Four CT criteria for detection of CBD stones are (1) a target sign, which refers to a central density, corresponding to the stone, surrounded by hypoattenuating bile or ampullary soft tissue; (2) the rim sign, which corresponds to a faint rim of increased density along the margin of a low-density area (Fig. 77-40B); (3) the crescent sign, which refers to a calculus with increased density surrounded by a crescent of hypoattenuating bile (Fig. 77-40C); and (4) indirect signs, which include abrupt

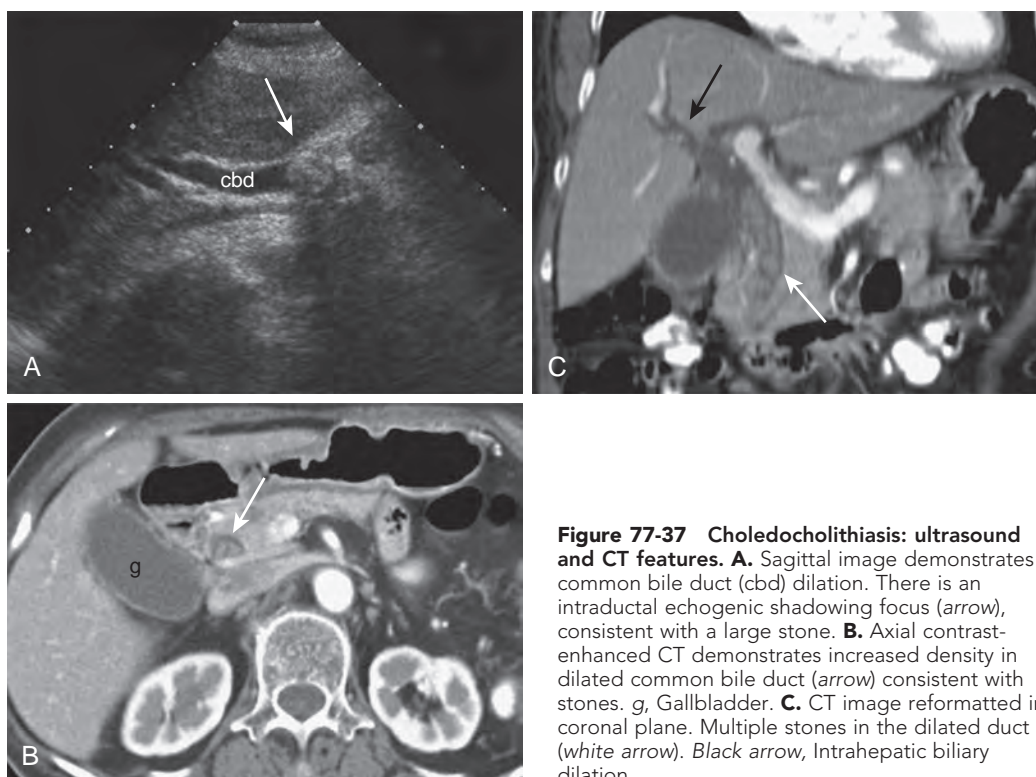


Figure 77-37 Choledocholithiasis: ultrasound and CT features. **A.** Sagittal image demonstrates common bile duct (cbd) dilation. There is an intraductal echogenic shadowing focus (arrow), consistent with a large stone. **B.** Axial contrast-enhanced CT demonstrates increased density in dilated common bile duct (arrow) consistent with stones. g, Gallbladder. **C.** CT image reformatted in coronal plane. Multiple stones in the dilated duct (white arrow). Black arrow, Intrahepatic biliary dilation.

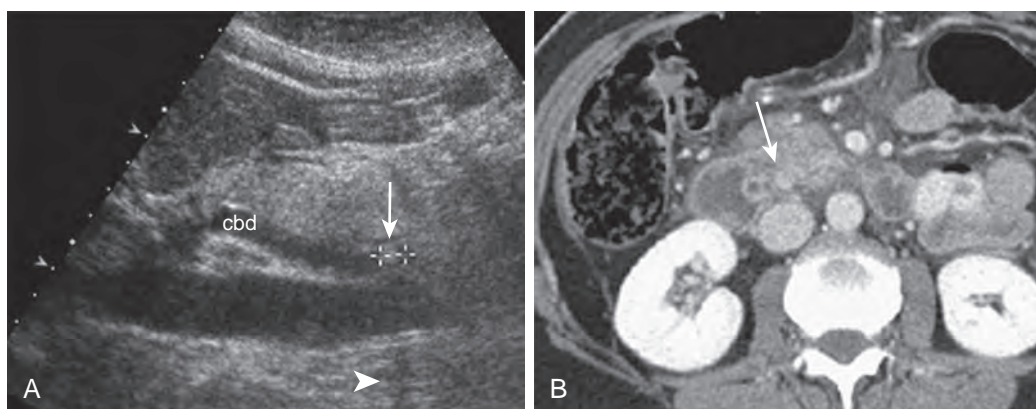


Figure 77-38 Choledocholithiasis: ultrasound and CT findings. **A.** Ultrasound demonstrates dilated common bile duct (cbd) with small stone located distally (arrow). Note posterior acoustic shadowing (arrowhead). **B.** Contrast-enhanced CT demonstrates small distal stone (arrow) that was not identified prospectively.

termination of a dilated distal CBD without visible surrounding mass or biliary dilation.¹⁶⁸ By use of these criteria, 76% of stones were detected in one series.¹⁶⁸ The investigator found that abrupt termination of the CBD without soft tissue mass was most often associated with pancreatic carcinoma; CBD stones manifested either as a densely calcified object or as a target sign.

CT cholangiography is redefining the role of CT as a technique for visualizing the biliary tract and choledocholithiasis. MDCT is performed after indirect opacification of the biliary tract with oral or intravenous iodinated cholangiographic agents.^{175,176} Improved z-axis resolution is achieved with multi-detector array scanners and high-resolution reconstructions of the biliary tract.¹⁷⁷ In one series, CT cholangiography was shown to provide excellent visualization of biliary anatomy and

filling defects, with 95% sensitivity for choledocholithiasis.¹⁷⁸ Other more recent series also show promise of these techniques in evaluation of choledocholithiasis.¹⁷⁹⁻¹⁸² A major drawback of this technique is the associated risk of allergic reactions induced by contrast material.¹⁸³ At the author's institution, this technique is currently used primarily to define donor biliary anatomy before liver transplantation and does not play a role in evaluation of choledocholithiasis.

Magnetic Resonance Imaging

MRCP was introduced in the 1990s as a noninvasive and low-risk technique to evaluate the biliary system and is an excellent modality for the detection of CBD stones.^{184,185} Reported sensitivity, specificity, and accuracy of MRCP for choledocholithiasis



Figure 77-39 Choledocholithiasis: CT appearance. **A.** There are multiple small stones in gallbladder with dilation of CBD (arrow). **B.** More caudal image demonstrates small stone at level of ampulla (arrow). **C.** Coronal reformatted image shows CBD stone (arrow).

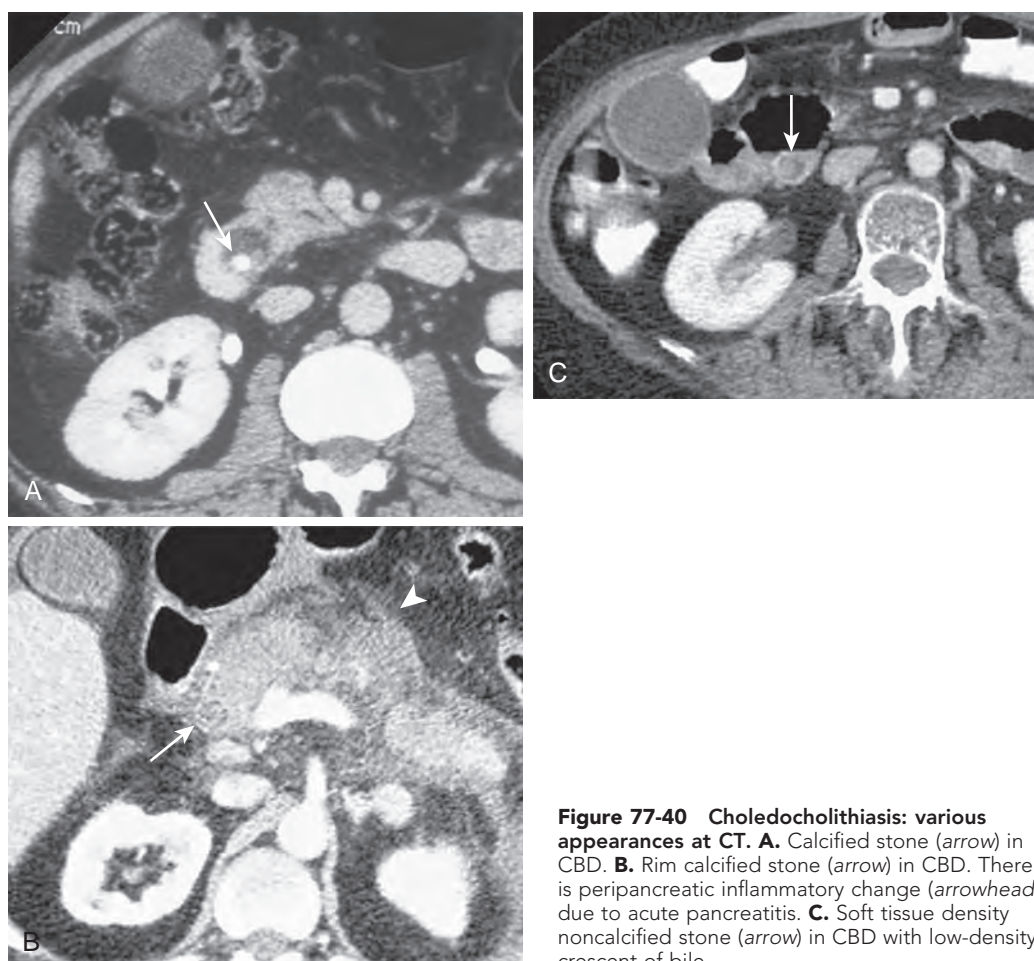


Figure 77-40 Choledocholithiasis: various appearances at CT. **A.** Calcified stone (arrow) in CBD. **B.** Rim calcified stone (arrow) in CBD. There is peripancreatic inflammatory change (arrowhead) due to acute pancreatitis. **C.** Soft tissue density noncalcified stone (arrow) in CBD with low-density crescent of bile.

range from 85% to 100%, 90% to 90%, and 89% to 97%, respectively.^{186,187} MRCP has been shown to be more sensitive than ultrasound and CT²¹ for the detection of CBD stones and is highly accurate for the detection of CBD stones in patients with symptomatic gallstones.¹⁸⁷ The MRCP technique is discussed more fully in Chapter 75.

Thin-slice (3 or 4 mm) half-Fourier acquisition single-shot turbo spin-echo (HASTE) sequences, also referred to as half-Fourier rapid acquisition with relaxation enhancement (RARE), allow rapid acquisition, with imaging of the biliary tract in a single breath hold, decreasing motion artifact.^{186,188-190} Conventional unenhanced T1- and T2-weighted MR images are also usually performed. Gadolinium-enhanced images are helpful if neoplasm or inflammatory disease is suspected.¹⁹⁰ High-resolution fat-suppressed T1-weighted three-dimensional gradient-echo sequences allow high-resolution images of the biliary tree that can be reconstructed in any plane. Additional techniques include the use of contrast agents that are taken up by hepatocytes and excreted through the biliary system, such as manganese dipyrroxy diphosphate, and the use of oral contrast agents, such as ferumoxsil (GastroMark; Mallinckrodt, Maryland Heights, MO), or diluted intravenous contrast material, such as gadopentetate dimeglumine (Magnevist; Berlex Laboratories, Wayne, NJ). Pineapple juice, which has a high manganese content, can also be used to decrease signal from hyperintense bowel fluid.¹⁸⁶ Recently, three-dimensional T2-weighted turbo spin-echo is also promising and offers improved anatomic accuracy, higher signal-to-noise ratio, and thinner sections without gaps.¹⁹¹⁻¹⁹³ When it is combined with new techniques, such as parallel acquisition technique, data acquisition time is shortened while spatial resolution and contrast are retained.¹⁹⁴ Faster gradients and navigator-based respiratory triggering also allow improved image quality.¹⁸⁶

AT MRCP, stones will generally appear as well-circumscribed low signal intensity filling defects in the biliary tract (Fig. 77-41). MRCP can detect stones as small as 2 mm²¹ and may be a helpful adjunct to ultrasound and CT when biliary calculi are suspected but not definitively visualized (Fig. 77-42). MRCP may also be helpful if a noncalcified stone is difficult to differentiate from a soft tissue mass. Diagnostic pitfalls include gas,

blood, and other abnormality within the duct simulating stones as well as signal loss due to surgical clips after cholecystectomy. High signal from adjacent fluid collections, ascites, or edema may also interfere with biliary signal. Pseudo-obstruction of the extrahepatic bile duct may be caused by arterial pulsatile compression, most commonly at the common hepatic duct, by the right hepatic artery,¹⁹⁵ and flow artifacts may mimic filling defects.¹⁹⁶ It is important to review coronal source and transverse T2-weighted images to avoid these pitfalls.

Intrahepatic Biliary Calculi

RECURRENT PYOGENIC CHOLANGITIS

The presence of calculi within the intrahepatic bile ducts is uncommon in patients with gallstones. This can occur in the setting of biliary strictures with long-standing obstruction, such as after biliary surgery or in the setting of Caroli's disease.¹⁹⁷ In the Asian population, the most common entity associated with the formation of primary intrahepatic stones is recurrent pyogenic cholangitis, also referred to as Oriental cholangiohepatitis. This is an endemic disease in Southeast Asia that is more frequently encountered in the United States because of increased immigration from Asia.^{198,199} The hallmark features of this disorder include pigment stone formation within the intrahepatic and extrahepatic bile ducts, stricture development, and biliary dilation. This disorder is characterized clinically by recurrent attacks of fever, chills, jaundice, and abdominal pain. The cause of this disorder is not entirely clear, although it is postulated that infection of the biliary tract with parasitic organisms such as *Clonorchis sinensis* results in biliary stasis and stone formation. Ultimately, there is progression to stricture formation, biliary obstruction, and hepatic cirrhosis with an increased risk of cholangiocarcinoma.

IMAGING

Although imaging of this disorder has traditionally been performed with invasive cholangiographic methods, noninvasive cross-sectional imaging techniques, including CT, ultrasound,

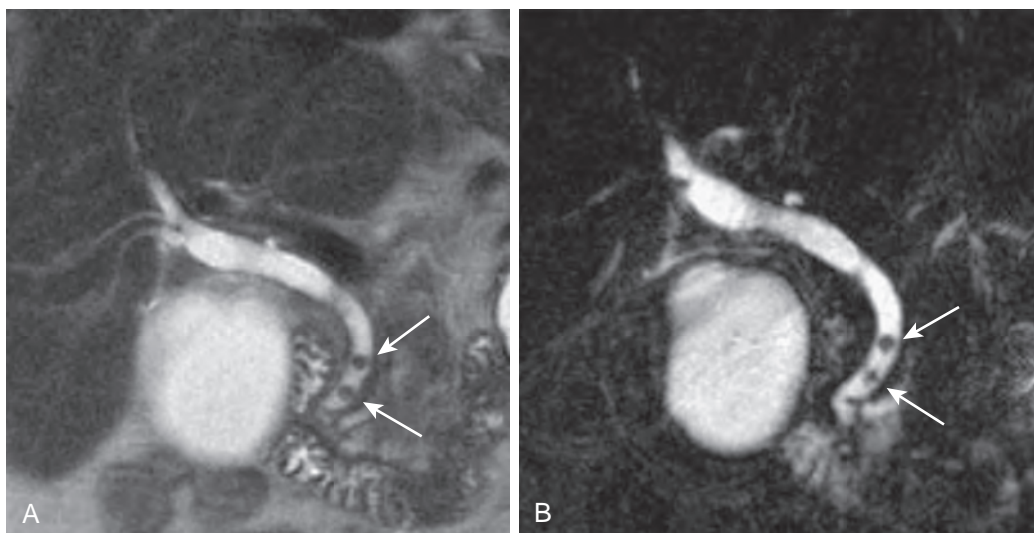


Figure 77-41 Choledocholithiasis: MR findings. A. T2-weighted coronal HASTE image shows low signal intensity CBD stones (arrows). **B.** Two-dimensional thick-slab image demonstrates stones (arrows).



Figure 77-42 Choledocholithiasis: imaging features. An 80-year-old woman with right upper quadrant pain. **A.** CT shows small density suggestive of stone in distal CBD (arrow). **B.** Coronal T2-weighted HASTE MR image confirms the presence of stones in the distal duct (arrow). **C.** Stones (arrow) demonstrated on two-dimensional thick-slab MR image. **D.** ERCP confirms stone (arrow). Sphincterotomy and stone retrieval were performed.

and MRI, now play a more important role.²⁰⁰⁻²⁰⁴ Ultrasonography is usually the initial imaging modality and demonstrates intrahepatic and extrahepatic biliary dilation, with intrahepatic stones that may or may not shadow (Fig. 77-43A). A nonshadowing stone may mimic an echogenic soft tissue mass. CT provides more complete evaluation of the full extent of disease and associated complications, such as liver abscess and pancreatitis (Fig. 77-43B). CT can be particularly helpful if the patient has already undergone biliary enteric bypass surgery, in which case associated pneumobilia may obscure findings at sonography. Noncontrast images may be helpful to identify noncalcified pigment stones that are soft tissue density²⁰⁰ (Fig. 77-44). The use of intravenous contrast agents allows better detection of complications, such as cholangitis, with improved visualization of ductal wall and periductal enhancement indicating active infection or inflammation²⁰² as well as abscess formation (Fig. 77-45). The left hepatic lobe, particularly the lateral segment, most often shows biliary dilation and stone disease. This is an important distinguishing feature of this disorder. Chronic findings include segmental lobe atrophy involving the lateral left lobe, portal vein thrombosis, and ultimately changes of

cirrhosis. Hepatic atrophy has been shown to correlate with portal vein occlusion and is usually most prominent in the lateral segment of the left lobe.²⁰⁵ MR and MRCP methods have also proved useful in the identification of intrahepatic biliary calculi and associated parenchymal abnormalities.²⁰¹

Other Conditions Related to Gallstones

SPILLED GALLSTONES AFTER LAPAROSCOPIC CHOLECYSTECTOMY

Gallbladder perforation during laparoscopic cholecystectomy is reported to occur in 10% to 40% of cases, with spillage of gallstones occurring less frequently, approximately 6% to 8% of the time.²⁰⁶ This complication occurs more frequently during surgery for an acutely inflamed gallbladder and may occur during dissection of the gallbladder from the hepatic bed or removal through the umbilical incision. Late abscess formation due to spilled stones is rare, with an incidence of less than 1%,²⁰⁷⁻²⁰⁹ occurring more frequently when spillage of both bile

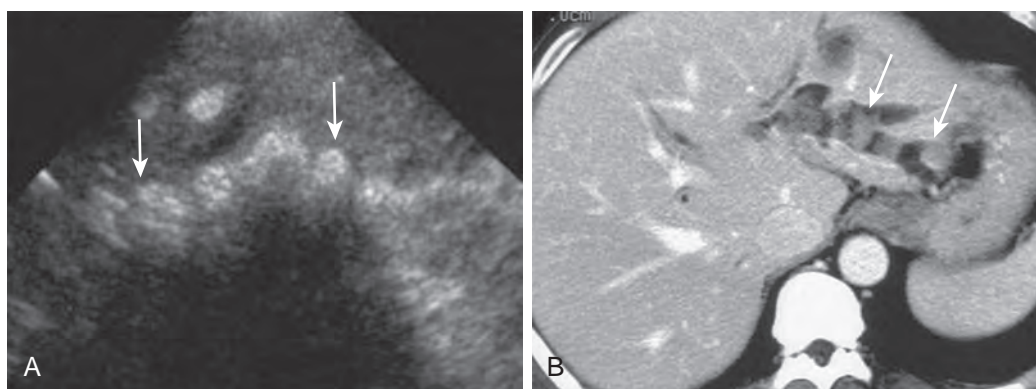


Figure 77-43 Recurrent pyogenic cholangitis. **A.** Hepatic ultrasound demonstrates cast of stones in intrahepatic ducts of left lateral segment (arrows). These appear as echogenic material with posterior acoustic shadowing. **B.** Contrast-enhanced CT demonstrates soft tissue density material in dilated ducts (arrows) corresponding to pigment stones. The lateral segment is primarily involved, a typical feature of recurrent pyogenic cholangitis.

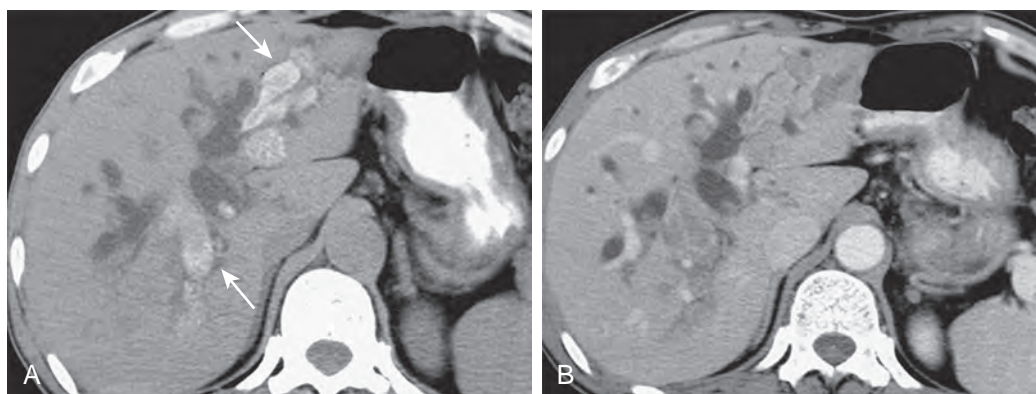


Figure 77-44 Recurrent pyogenic cholangitis: utility of noncontrast CT. **A.** Precontrast CT scan shows cast of stones in dilated intrahepatic ducts (arrows). **B.** After intravenous administration of contrast material, stones are less conspicuous.

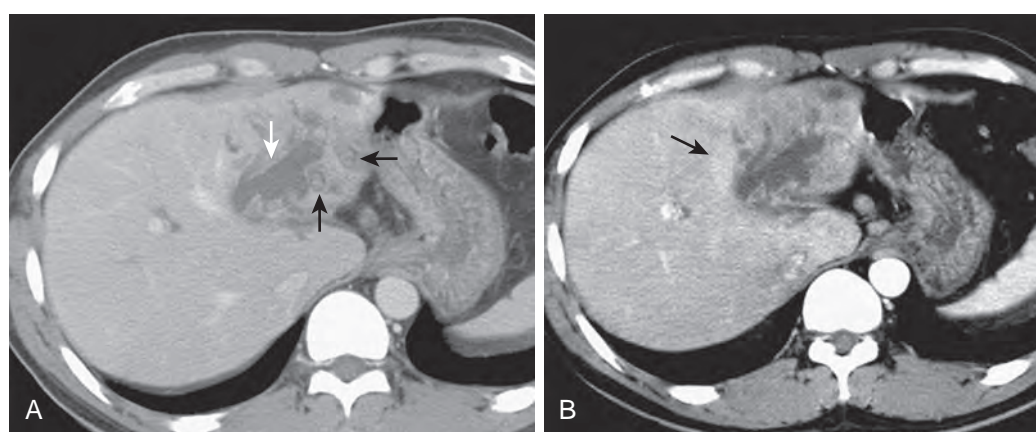


Figure 77-45 Recurrent pyogenic cholangitis with abscess. **A.** CT scan obtained during portal venous phase demonstrates stones in dilated intrahepatic ducts of left lateral segment (black arrows). There is an abscess with fluid attenuation in the liver parenchyma (white arrow). **B.** Scan obtained during the arterial phase demonstrates increased contrast enhancement around the abscess (arrow) related to hyperemia (transient hepatic attenuation difference).

and calculus occurs. Infectious complications are more likely to occur with bilirubinate stones because they contain viable bacteria. The spilled stones may remain in the peritoneal cavity adjacent to the liver and cause a subhepatic abscess or abscess in the retroperitoneum below the subhepatic space. However, because of pneumoperitoneum and peritoneal irrigation at the time of laparoscopy, stones may also migrate to distant sites. More unusual locations for abscess formation include the pleural space, the abdominal wall at the trocar site, and within an incisional hernia. Because of the indolent nature of the infection, the time interval for presentation after surgery is variable, ranging from 1 month to 10 years, with a reported peak incidence around 4 months.²⁰⁶ The patient usually presents with vague constitutional symptoms, such as nausea, anorexia, and low-grade fever.

Ultrasound, CT, and MRI are effective in identifying the abscess and associated dropped gallstones. The abscess appears as a thick-walled fluid collection, most commonly located posterior to the right lobe of the liver (Fig. 77-46). Stones appear as echogenic foci on ultrasound and as calcified densities at CT. At MRI, stones may be identified as low signal intensity foci on T2-weighted images. In a series of five patients by Morrin and associates,²¹⁰ the diagnosis of abscess formation secondary to dropped stones was made in only two of five patients prospectively by a combination of imaging modalities. In retrospect, however, the diagnosis could be made in all patients. Recognizing the history of prior laparoscopic cholecystectomy and careful search for spilled stones, particularly when an abscess is identified in the subhepatic space, are important in making the diagnosis. The abscess may be misdiagnosed as tumor or abscess from another cause if the stones are not radiopaque or not recognized or if they are located in an atypical location (Fig. 77-47). If stones are found in other locations, such as the pelvis, the presence of clips in an otherwise empty gallbladder fossa may help confirm the diagnosis (Fig. 77-48). Surgical or percutaneous removal of the stones is necessary for complete cure as infected stones cannot be sterilized with antibiotic therapy.^{211,212}

MIRIZZI SYNDROME

Mirizzi syndrome refers to common hepatic duct or CBD obstruction due to extrinsic compression from an impacted gallstone in the gallbladder neck or cystic duct or from associ-

ated inflammatory changes. This may be complicated by a cholecystocholedochal fistula.²¹³⁻²¹⁵ Mirizzi syndrome is an uncommon complication of long-standing cholelithiasis; the usual clinical presentation is recurrent episodes of jaundice and cholangitis. This syndrome is reported in up to 2% of patients operated on for symptomatic gallstone disease.²¹⁶ Preoperative diagnosis is important because standard cholecystectomy technique is associated with an increased risk of extrahepatic bile duct injury secondary to dense fibrosis and edema around the hepatoduodenal ligament.²¹⁷

Mirizzi syndrome may be diagnosed with ultrasound, CT, or MRI.^{218,219} The hallmark is intrahepatic biliary dilation and dilation of the common hepatic duct to the level of the porta hepatis with normal caliber of the more distal CBD. A stone may be identified in the gallbladder neck or cystic duct (Fig. 77-49). Multiplanar reconstruction imaging with either CT or MR can be particularly helpful to identify the extrinsic nature of the obstruction. MRI has been proposed as most useful for demonstrating dilation of the intrahepatic ducts, level of obstruction, and location of gallstones.²¹⁹

GALLSTONE ILEUS

Gallstone ileus is mechanical obstruction of the bowel by an impacted gallstone and results from perforation of the gallbladder and fistula formation between the gallbladder and an adjacent viscus. Fistula formation most commonly occurs between the gallbladder and duodenum, followed by the colon and stomach.^{3,220} Obstruction usually occurs in the small intestine when a gallstone larger than 2.5 cm lodges in the lumen. The most common sites of gallstone impaction are the ileum (54%-65%), the jejunum (27%), and the duodenum (1%-3%).²²¹ The term *Bouveret's syndrome* refers to proximal gallstone impaction resulting in duodenal or pyloric obstruction. Gallstone ileus accounts for approximately 1% to 5% of all cases of nonmalignant small bowel obstruction, increasing up to 25% in patients older than 65 years.²²¹

Less than half of patients presenting with gallstone ileus have a known history of preexisting gallbladder disease. Patients usually present with clinical symptoms of bowel obstruction, and abdominal radiography may be the initial imaging study performed. The classic triad of findings, referred to as Rigler's triad,²²² includes presence of bowel obstruction, pneumobilia,

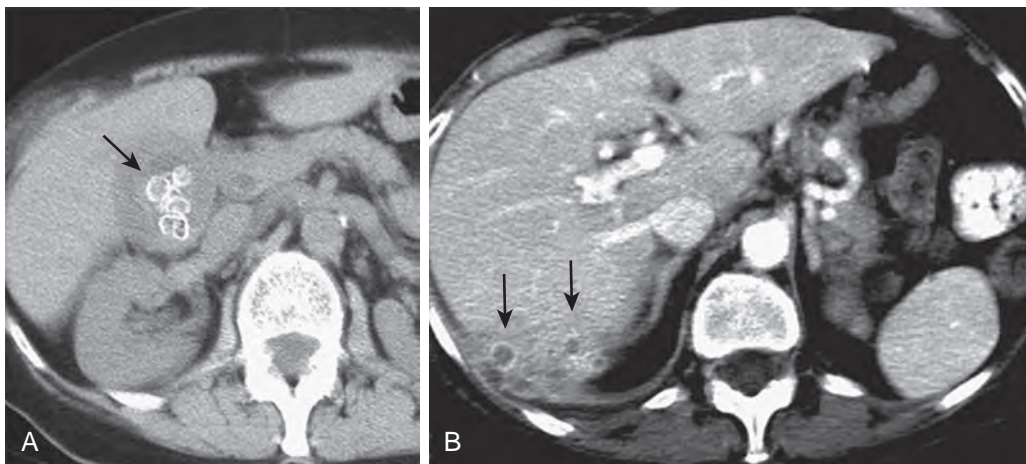


Figure 77-46 Spilled gallstones after laparoscopic cholecystectomy. **A.** Contrast-enhanced CT obtained before surgery demonstrates multiple calcified stones in thick-walled gallbladder (arrow) with pericholecystic fluid, indicating acute cholecystitis. **B.** CT obtained 1 year after cholecystectomy when the patient returned with right upper quadrant pain demonstrates abscess posterior to the right hepatic lobe containing spilled stones (arrows).

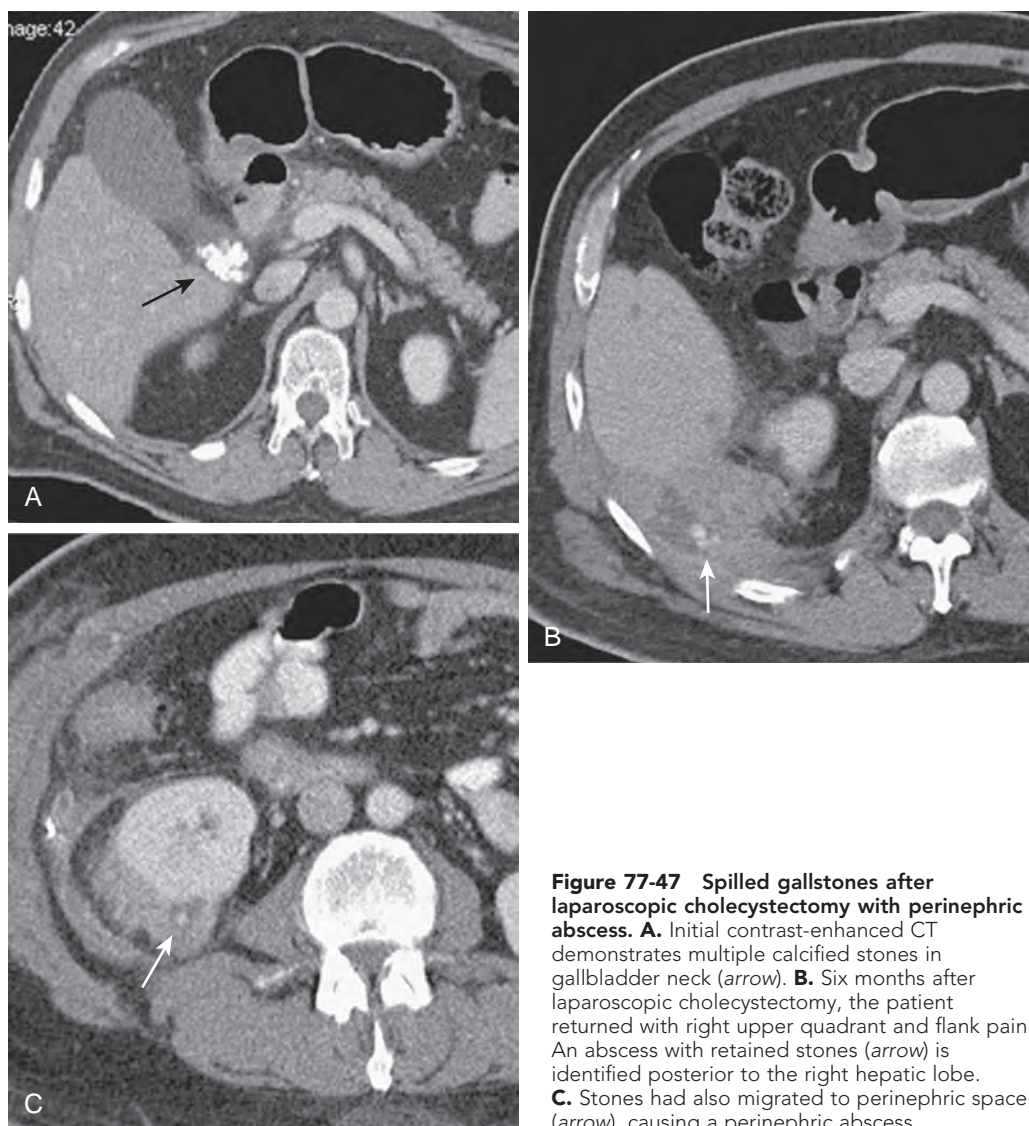


Figure 77-47 Spilled gallstones after laparoscopic cholecystectomy with perinephric abscess. **A.** Initial contrast-enhanced CT demonstrates multiple calcified stones in gallbladder neck (arrow). **B.** Six months after laparoscopic cholecystectomy, the patient returned with right upper quadrant and flank pain. An abscess with retained stones (arrow) is identified posterior to the right hepatic lobe. **C.** Stones had also migrated to perinephric space (arrow), causing a perinephric abscess.

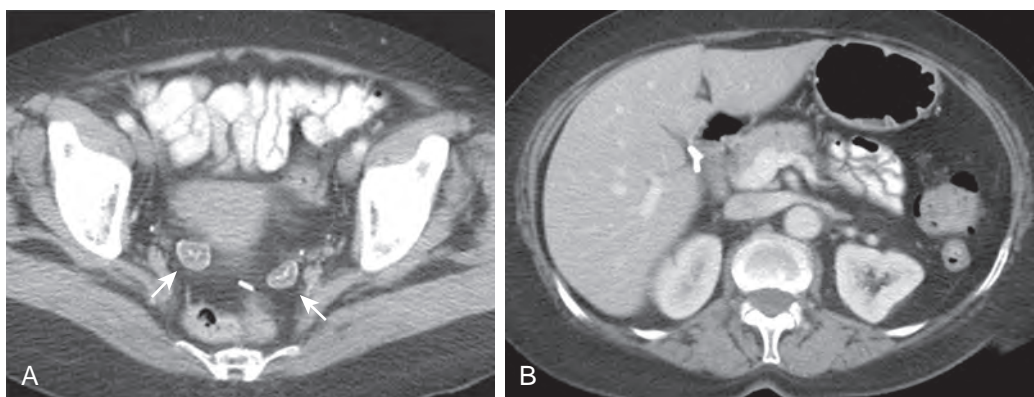


Figure 77-48 Spilled gallstones after laparoscopic cholecystectomy with stones located in the pelvis. **A.** Contrast-enhanced CT demonstrates two partially calcified stones in the pelvis (arrows). A surgical clip is also noted. **B.** Clips are present in the otherwise empty gallbladder fossa, compatible with prior cholecystectomy.

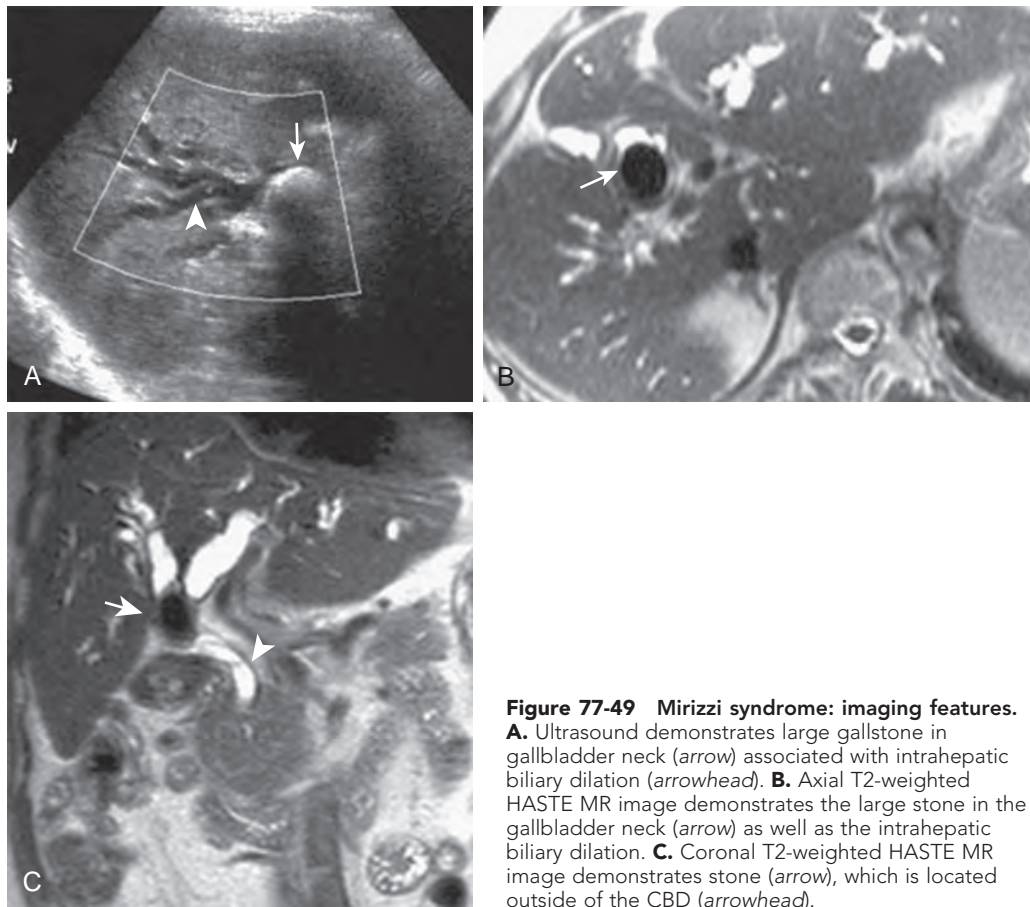


Figure 77-49 Mirizzi syndrome: imaging features.

A. Ultrasound demonstrates large gallstone in gallbladder neck (arrow) associated with intrahepatic biliary dilation (arrowhead). **B.** Axial T2-weighted HASTE MR image demonstrates the large stone in the gallbladder neck (arrow) as well as the intrahepatic biliary dilation. **C.** Coronal T2-weighted HASTE MR image demonstrates stone (arrow), which is located outside of the CBD (arrowhead).

and the obstructing gallstone. However, this is visualized in only 30% to 35% of patients²²³ (Fig. 77-50). CT is frequently used to evaluate patients with bowel obstruction to confirm diagnosis, to determine etiology of obstruction, and to evaluate for complications. CT is superior to plain abdominal radiography for visualization of the obstructing gallstone and detection of small amounts of gas in the gallbladder and biliary tree^{221,224-226} (Fig. 77-51). The cholecystenteric fistula may also be demonstrated. Cholecystenteric fistula may develop in the absence of gallstone ileus, usually resulting from chronic gallbladder inflammation. CT findings include a contracted gallbladder containing air and visualization of a fistulous track (Fig. 77-52).

Hyperplastic Cholecystoses

The term *hyperplastic cholecystoses* was introduced in 1960 by Jutras²²⁷ to designate a spectrum of gallbladder abnormalities separate from inflammatory disease. Hyperplastic refers to a benign proliferation of normal tissue elements, and cholecystoses are pathologic processes distinct from inflammation.²²⁸ The two major conditions within this spectrum of disorders are cholesterosis and adenomyomatosis.

CHOLESTEROSIS

Pathogenesis and Epidemiology

Cholesterosis results from the accumulation of neutral lipid, in particular cholesterol esters and triglyceride, within

macrophages in the lamina propria of the gallbladder.² The cholesterol is probably deposited in the epithelium initially, accumulates in the lamina propria, and subsequently is taken up by the macrophages.²²⁸ The accumulation of lipid creates yellow excrescences on the surface of the mucosa that can be seen by the naked eye. Associated hyperemia of the mucosa gives the appearance of a strawberry, and the term *strawberry gallbladder* has been used to describe the appearance of the gallbladder in this disorder.²²⁹ The pathogenesis of this disorder is not completely understood. Altered hepatic cholesterol synthesis may play an etiologic role leading to increased cholesterol levels in the bile.²³⁰ Impaired cholesterol transport out of the mucosa may also play a role. This disorder is not associated with cholesterol gallstones, hyperlipidemia, or atherosclerosis. There may be an increased incidence of gallstones, present in 50% in one surgical series.²³¹ In an autopsy study involving 1319 cases, there were 165 cases of cholesterosis for an incidence of 12.5%.²³² There are no specific clinical findings, and presentation is usually the result of a complicating disorder, such as cholelithiasis or cholecystitis.

On pathologic examination, cholesterosis is defined by the deposition of lipid within the gallbladder mucosa in one of four patterns: (1) diffuse involvement (80%); (2) cholesterol polyps resulting from focal excrescences of lipid-containing epithelium projecting into the gallbladder lumen, usually measuring 2 to 10 mm; (3) combined diffuse and polypoid form (10%); and (4) focal cholesterosis with only a portion of the gallbladder affected.²³³ Cholesterol polyps account for 60% to 90% of

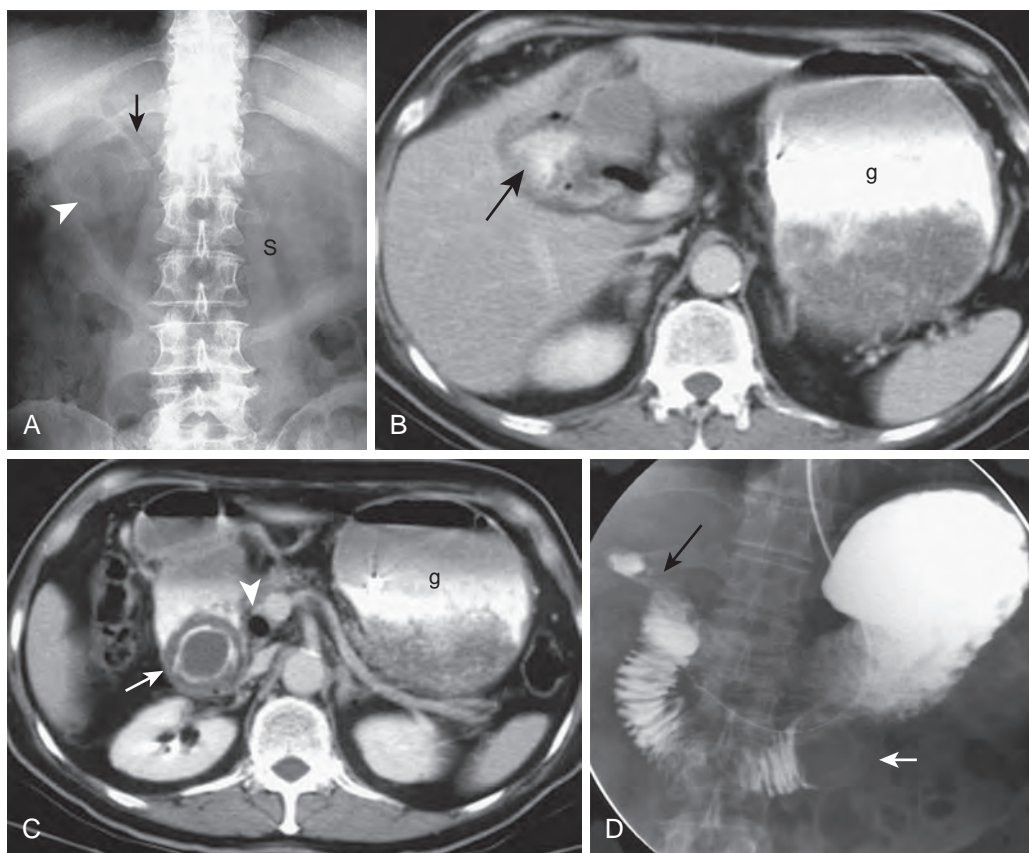


Figure 77-50 Gallstone ileus: Bouveret's syndrome. **A.** Abdominal radiograph demonstrates dilated, gas-filled stomach (S). Rounded calcified density (arrowhead) represents a large stone in the region of the distal gastric antrum. There is pneumobilia (arrow). The presence of bowel obstruction, pneumobilia, and obstructing gallstone constitutes Rigler's triad. **B.** Oral and intravenous contrast-enhanced CT demonstrates distended, contrast-filled stomach (g) consistent with gastric outlet obstruction. There is oral contrast material and bubbles of air in gallbladder fossa (arrow) consistent with cholecystenteric fistula. **C.** Slightly more inferior CT image demonstrates large obstructing gallstone (arrow) within the proximal duodenum. Air is also present in the CBD (arrowhead). **D.** Upper gastrointestinal series demonstrates stone as large filling defect that has migrated to duodenal-jejunal junction (white arrow). Fistula between the gallbladder and proximal duodenum is also demonstrated (black arrow).

gallbladder polyps and are not true neoplasms.² They may be solitary but are most commonly multiple. At histologic evaluation, the polyp has a vascular connective tissue stalk and a branching villous or complex papillary pattern; however, foamy macrophages within the lamina propria are the dominant cellular component.²

Imaging

The diffuse form of cholesterosis cannot be diagnosed at imaging. Traditionally, oral cholecystography was used to diagnose the polypoid variety, which appears as numerous fixed filling defects in the lumen of the gallbladder. As this technique is no longer widely performed, findings are now apparent primarily at sonography. Cholesterol polyps may appear as single or multiple nonshadowing foci adherent to the gallbladder wall and projecting into the gallbladder lumen (Fig. 77-53). Gallbladder polyps may also be visible at CT (Fig. 77-54). It is estimated that polypoid lesions of the gallbladder are seen in approximately 1.4% to 7% of the adult population undergoing abdominal sonography.^{234,235} When polypoid lesions in the gallbladder are identified at either ultrasound or CT, small (<1 cm) and multiple, the diagnosis of benign cholesterol polyps is most likely.²³⁶ The management of gallbladder polyps detected at

imaging remains somewhat controversial. Initial 3- to 6-month ultrasound follow-up can be performed for 1 to 2 years to ensure stability, and this approach has been advocated by many. A study evaluating 346 patients with incidentally detected gallbladder polyps at ultrasound with ultrasound follow-up in 149 patients, 42 patients with cholecystectomy, and 155 patients with clinical follow-up concluded that the incidence of neoplasm in gallbladder polyps 6 mm or smaller is negligible and that these polyps require no further follow-up.²³⁷ Others have proposed that follow-up may not be necessary for polyps of 5 mm or smaller.²³⁸ However, when polyps are single, are larger than 10 mm, are sessile, occur in individuals older than 50 years, or demonstrate interval increase in size during surveillance, differentiation from other polypoid neoplasms such as adenomas or primary or metastatic neoplasm is not possible and surgical evaluation may be required.²³⁸⁻²⁴⁰ In a surgical series of gallbladder polypoid lesions, with use of size larger than 10 mm, a 100% sensitivity and 86.95% specificity in the diagnosis of malignant disease were achieved.²⁴¹ A more recent surgical series recommended that ultrasound size larger than 9 mm, ultrasound suggestion of invasion at the liver interface, and wall thickening of more than 5 mm, especially in the presence of gallstones, should increase suspicion of malignant disease.²³⁵

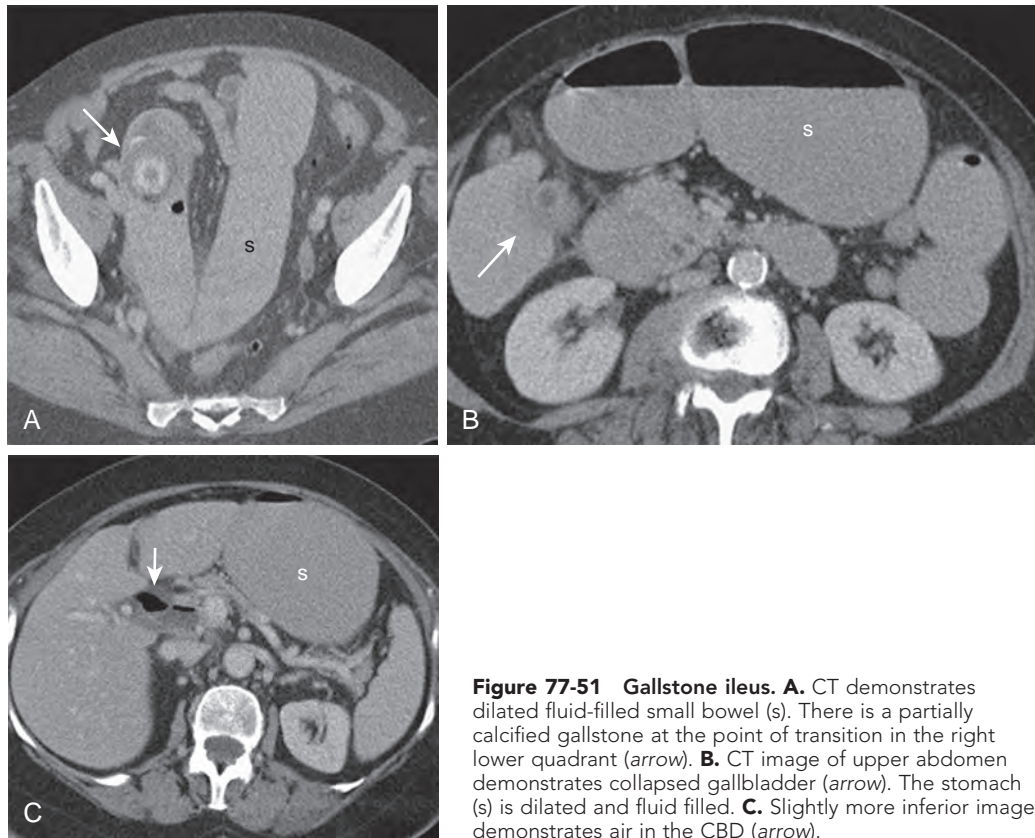


Figure 77-51 Gallstone ileus. **A.** CT demonstrates dilated fluid-filled small bowel (s). There is a partially calcified gallstone at the point of transition in the right lower quadrant (arrow). **B.** CT image of upper abdomen demonstrates collapsed gallbladder (arrow). The stomach (s) is dilated and fluid filled. **C.** Slightly more inferior image demonstrates air in the CBD (arrow).

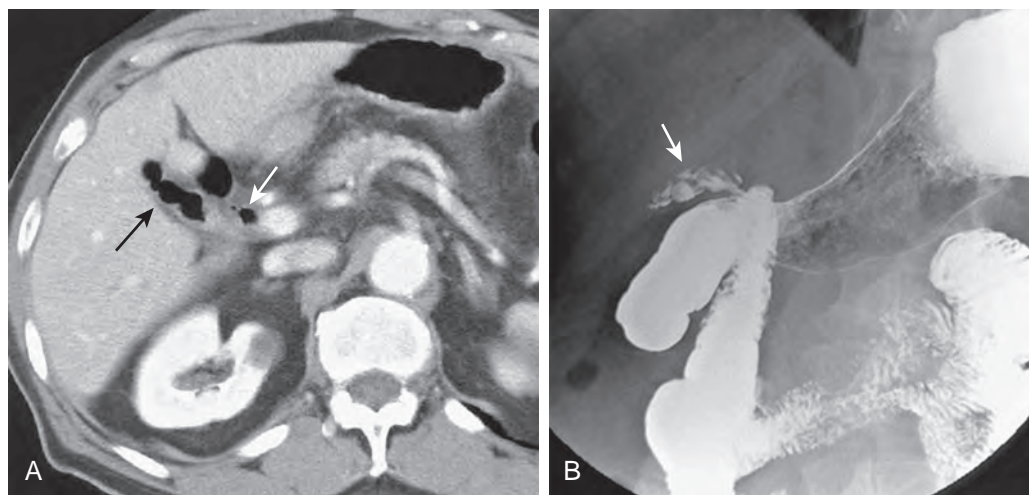


Figure 77-52 Cholecystoduodenal fistula secondary to chronic cholecystitis. **A.** CT demonstrates contracted gallbladder containing air (black arrow). There is also air in the CBD (white arrow). **B.** Upper gastrointestinal series demonstrates fistula between gallbladder and proximal duodenum (arrow).

ADENOMYOMATOSIS

Pathogenesis and Epidemiology

Adenomyomatosis of the gallbladder, also referred to as adenomyomatous hyperplasia and intramural diverticulosis, is an acquired, hyperplastic lesion of the gallbladder characterized by excessive proliferation of surface epithelium with invaginations into the thickened, hypertrophied muscularis

propria.²³³ The intramural diverticula formed by epithelial invaginations into the muscularis are referred to as Rokitansky-Aschoff sinuses (RAS), and dilated RAS are a prominent feature of this disorder. The pathophysiologic mechanism of this disorder is not entirely certain. It is not usually associated with cholesterosis, indicating a separate pathophysiologic process. Pathogenesis has been postulated to result from mechanical obstruction of the gallbladder (from stones,

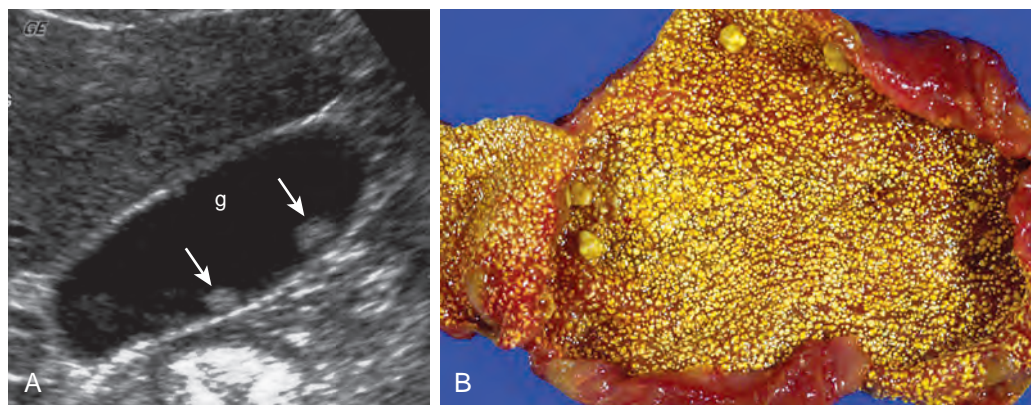


Figure 77-53 Cholesterol polyps: ultrasound and pathology findings. **A.** Sagittal ultrasound image demonstrates two echogenic nonshadowing foci (arrows) adherent to the posterior wall of the gallbladder (g), consistent with cholesterol polyps. **B.** Specimen image in a different patient demonstrates a diffuse granular pattern of cholesterosis with several cholesterol polyps.



Figure 77-54 Cholesterol polyp: CT. CT demonstrates polypoid excrescence arising from the gallbladder wall (arrow).

cystic duct kinking, or congenital septum), chronic inflammation, and anomalous pancreaticobiliary ductal union.²³³ The functional obstruction to bile outflow causes increased pressure within the gallbladder lumen and results in invagination of the mucosa through the muscularis, forming the dilated RAS. The reported incidence of adenomyomatosis in cholecystectomy specimens is up to 8%.²⁴² The association of this disorder with clinical findings is controversial. The disorder may be asymptomatic or associated with symptoms of chronic cholecystitis. More than 90% of cases are associated with gallstones, which may be responsible for biliary symptoms.² Adenocarcinoma of the gallbladder has been found in association with adenomyomatosis; however, a causal link has not been established.²³³ In a surgical series of 3000 resected gallbladders, there was a higher frequency of gallbladder carcinoma (6.4%) in gallbladders with segmental adenomyomatosis than in those without.

Adenomyomatosis may be generalized, segmental, or focal, and the focal form is most common.²⁴³ Diffuse adenomyomatosis causes thickening and irregularity of the mucosa

and muscle layer with associated RAS, which on gross inspection appear as collections of bile in the gallbladder wall. In the segmental or annular form, a focal circumferential stricture divides the gallbladder lumen into separate compartments. The focal form, which causes a focal mass or nodule, usually is fundal in location, frequently referred to as an adenomyoma.

Imaging

In the past, oral cholecystography played an important role in the diagnosis of adenomyomatosis.²²⁸ The hallmark of this disorder is the filling of intramural diverticula with contrast material, which are manifested as radiopaque dots that parallel the gallbladder lumen. In the fundal form, findings may mimic a polyp or other mass. The segmental form may be manifested as circumferential narrowing of the lumen.

Ultrasound. The ultrasound findings in adenomyomatosis have been well described and include diffuse or segmental thickening of the gallbladder wall and anechoic intramural diverticula.²⁴⁴⁻²⁴⁷ Biliary sludge or gallstones within the diverticula may appear as echogenic foci.^{244,247} A V-shaped reverberation or comet-tail artifact may emanate from small cholesterol stones that are lodged in the RAS (Fig. 77-55). This artifact is a result of sound reverberating within or between cholesterol crystals²⁷ and helps differentiate gallbladder wall thickening related to adenomyomatosis from other abnormalities (Fig. 77-56A). The use of high-resolution transducers has been shown to increase detection of intramural cysts or echogenic foci, enabling a more confident diagnosis of adenomyomatosis.²⁴⁸ An additional diagnostic clue is the presence of color Doppler twinkling artifacts in the gallbladder wall that probably result from calcifications or cholesterol depositions with rough interfaces present in the RAS^{249,250} (see Fig. 77-55C, D). This feature may be better demonstrated with a lower frequency transducer.²⁵¹ If these features are not identified, there may be nonspecific thickening of the gallbladder wall. This mural thickening may be indistinguishable from acute or chronic cholecystitis or gallbladder carcinoma on the basis of imaging; therefore, knowledge of the clinical setting is essential. The segmental form of adenomyomatosis results in annular narrowing, usually of the body of the gallbladder, with resulting compartmentalization or segmentation of the gallbladder lumen. In this setting,

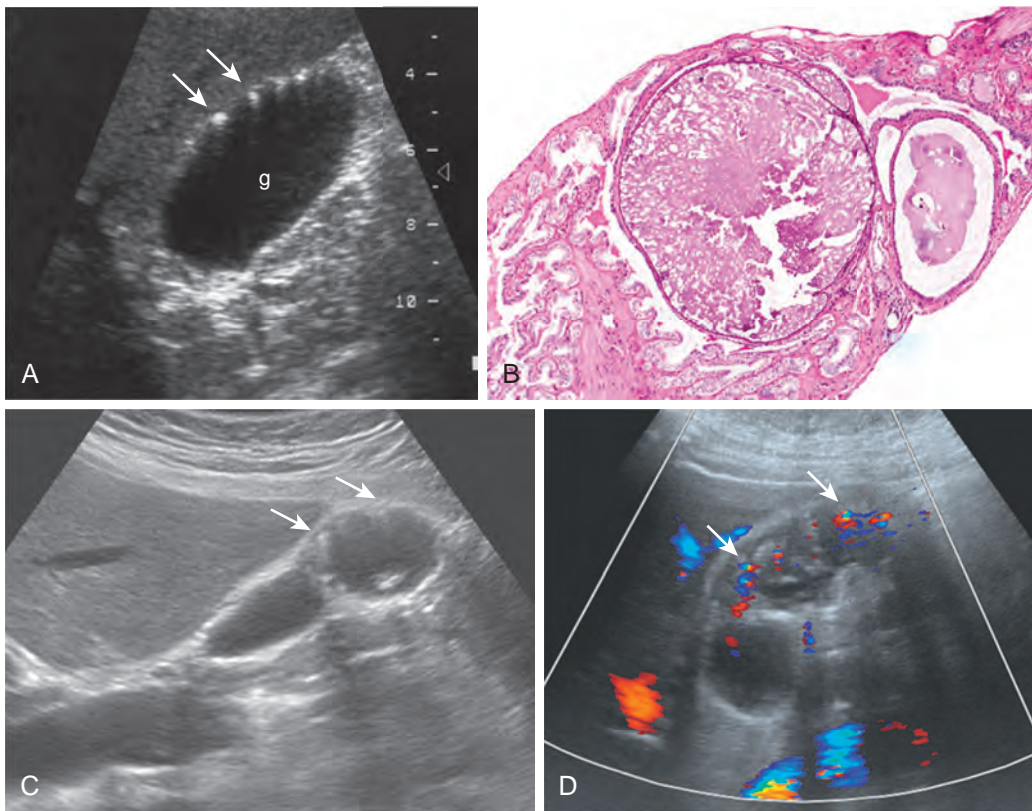


Figure 77-55
Adenomyomatosis: ultrasound and pathologic features.
A. Ultrasound demonstrates multiple comet-tail artifacts (arrows) arising from the wall of the gallbladder (g). **B.** Histologic specimen in a different patient demonstrates debris in a Rokitansky-Aschoff sinus. **C.** Comet-tail artifacts are present only in the superior aspect of the gallbladder in this patient with segmental adenomyomatosis (arrows). **D.** Color Doppler demonstrates twinkling artifact (arrows).

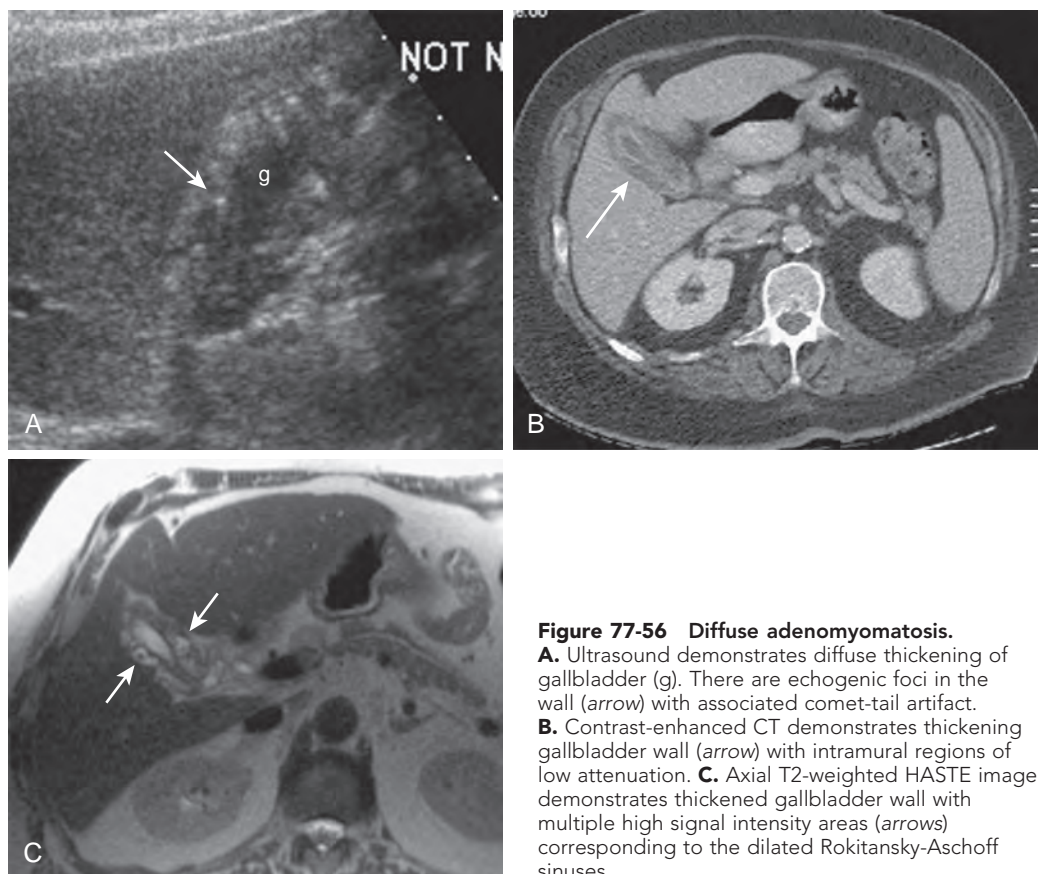


Figure 77-56 **Diffuse adenomyomatosis.**
A. Ultrasound demonstrates diffuse thickening of gallbladder (g). There are echogenic foci in the wall (arrow) with associated comet-tail artifact. **B.** Contrast-enhanced CT demonstrates thickening gallbladder wall (arrow) with intramural regions of low attenuation. **C.** Axial T2-weighted HASTE image demonstrates thickened gallbladder wall with multiple high signal intensity areas (arrows) corresponding to the dilated Rokitansky-Aschoff sinuses.

the fundal compartment may be overlooked. Stones are often trapped within this fundal compartment and are not readily visualized. Again, if the reverberation artifact is not observed, this focal mural thickening may be indistinguishable from gallbladder carcinoma (Fig. 77-57A). The focal form of adenomyomatosis most commonly appears as a sessile, polypoid mass in the region of the fundus, protruding into the gallbladder lumen (Fig. 77-58A). This may mimic other gallbladder masses, including neoplasm. Coexisting gallstones are a frequent finding, with increased incidence in patients with the segmental form.²⁵²

Computed Tomography. On CT, the diffuse form of gallbladder adenomyomatosis is manifested with gallbladder wall thickening and visualization of intramural diverticula^{245,253,254} (see Fig. 77-56B). The segmental and focal forms can be particularly difficult to differentiate from carcinoma because they appear as

focal thickening of the gallbladder wall or a fundal intraluminal mass (Figs. 77-57B and 77-58B). A study addressing the CT differentiation of adenomyomatosis and gallbladder cancer concluded that the diagnosis of adenomyomatosis can be made with reasonable accuracy when diffuse or focal thickening of the gallbladder wall is seen in association with small cystic-appearing spaces.²⁵⁵ In this study, specificity for diagnosis of adenomyomatosis ranged from 79% to 93%. When the findings at CT are not diagnostic, follow-up with ultrasound is necessary. The advantage of ultrasound is that the reverberation artifact related to the RAS may be demonstrated. This finding is not seen with adenocarcinomas. However, small RAS may be overlooked.²⁵³

Magnetic Resonance Imaging. MR has been shown to serve as a helpful problem-solving tool in patients with

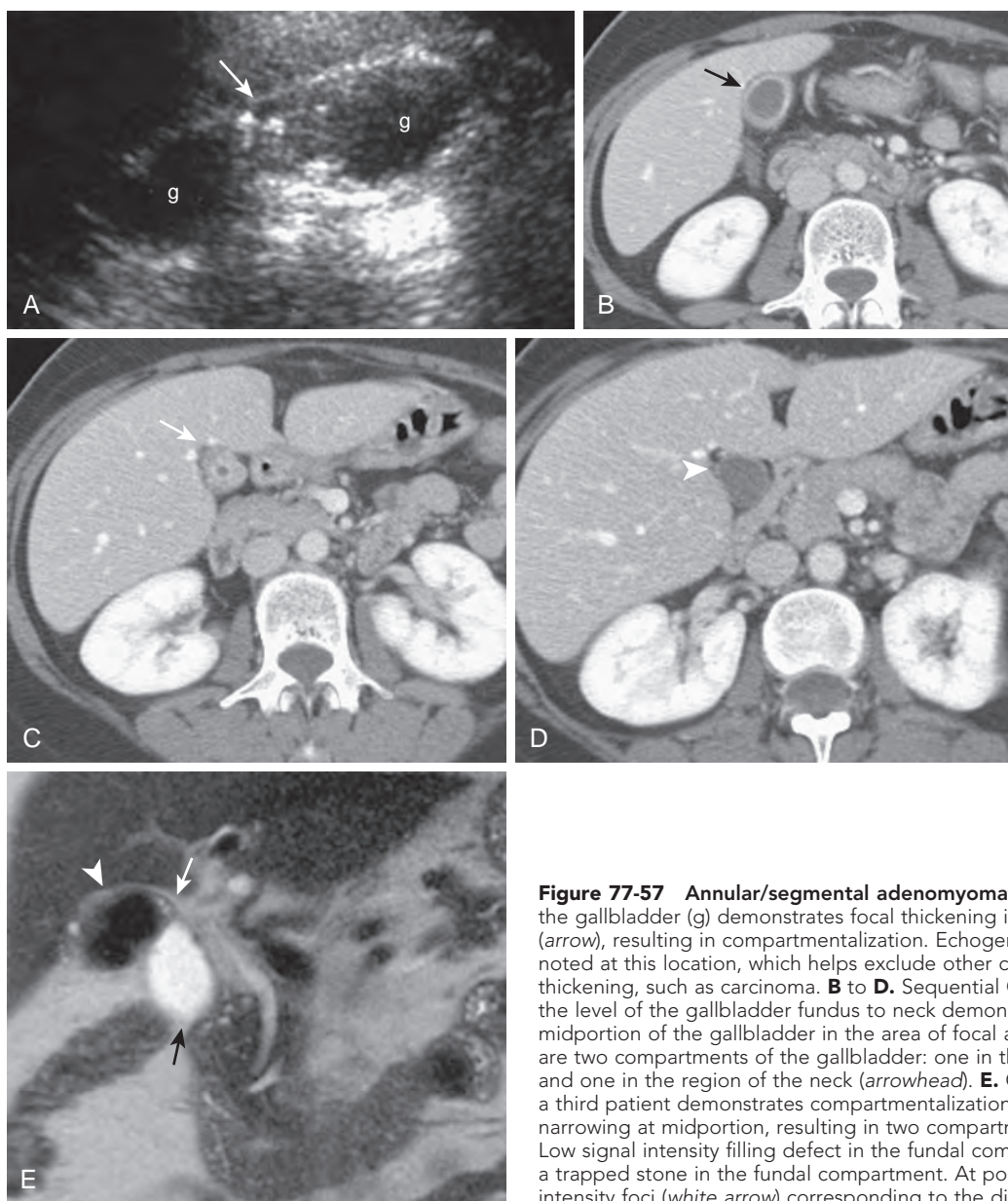


Figure 77-57 Annular/segmental adenomyomatosis. **A.** Sagittal ultrasound image of the gallbladder (g) demonstrates focal thickening in the midportion of the gallbladder (arrow), resulting in compartmentalization. Echogenic foci with ring-down artifact are noted at this location, which helps exclude other causes of focal gallbladder wall thickening, such as carcinoma. **B to D.** Sequential CT images in a second patient from the level of the gallbladder fundus to neck demonstrate focal mural thickening at the midportion of the gallbladder in the area of focal adenomyomatosis (white arrow). There are two compartments of the gallbladder: one in the region of the fundus (black arrow), and one in the region of the neck (arrowhead). **E.** Coronal T2-weighted HASTE image in a third patient demonstrates compartmentalization of the gallbladder with annular narrowing at midportion, resulting in two compartments (arrowhead and black arrow). Low signal intensity filling defect in the fundal compartment (arrowhead) corresponds to a trapped stone in the fundal compartment. At point of narrowing, there are high signal intensity foci (white arrow) corresponding to the dilated Rokitsky-Aschoff sinuses.

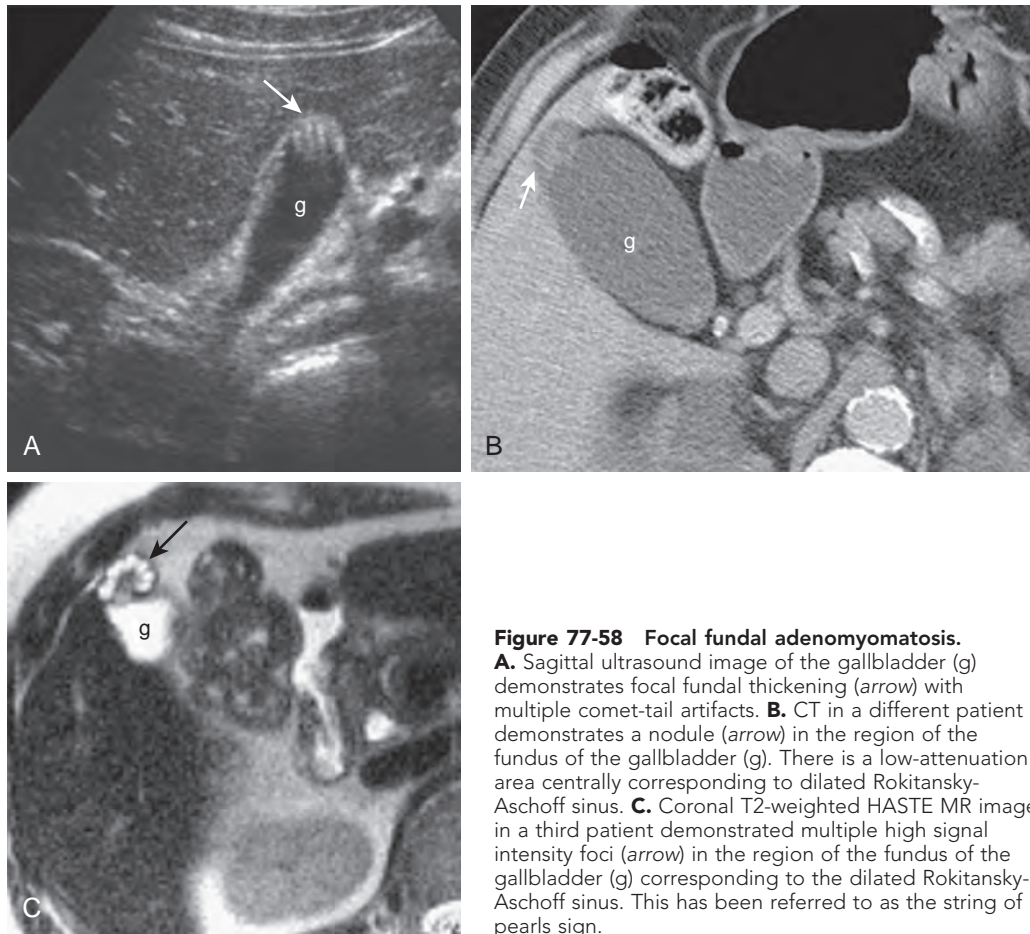


Figure 77-58 Focal fundal adenomyomatosis. **A.** Sagittal ultrasound image of the gallbladder (g) demonstrates focal fundal thickening (arrow) with multiple comet-tail artifacts. **B.** CT in a different patient demonstrates a nodule (arrow) in the region of the fundus of the gallbladder (g). There is a low-attenuation area centrally corresponding to dilated Rokitansky-Aschoff sinus. **C.** Coronal T2-weighted HASTE MR image in a third patient demonstrated multiple high signal intensity foci (arrow) in the region of the fundus of the gallbladder (g) corresponding to the dilated Rokitansky-Aschoff sinus. This has been referred to as the string of pearls sign.

gallbladder adenomyomatosis.⁶⁴ The demonstration of RAS on T2-weighted images is critical in diagnosis of this disorder.²⁵⁶ These appear as high signal intensity foci in the gallbladder wall (Figs. 77-56C, 77-57E, and 77-58C). In a study comparing ultrasound, CT, and MRI,²⁵⁷ MRI using a half-Fourier RARE sequence was superior to helical CT and trans-abdominal ultrasound in establishing the diagnosis of adenomyomatosis. Helical CT showed most lesions as a thickened wall or mass, with limited ability to delineate the RAS. MRI was found to have an accuracy of 93% versus 75% for CT and 66% for ultrasound. MRI offers more complete visualization of the gallbladder and more definitive identification RAS. Yoshimitsu and colleagues²⁵⁶ also found a higher sensitivity of MRI for detection of the RAS in the thickened gallbladder wall and referred to this finding as the “string of pearls” sign (see Fig. 77-58C). The specificity of this sign for adenomyomatosis is 92%, helpful in the differentiation from gallbladder carcinoma, in which this sign is never observed. If findings on ultrasound are equivocal, MR with MRCP is the next best test. There is an increased incidence of gallbladder carcinoma reported in patients with segmental adenomyomatosis²⁴²; therefore, these patients should be closely observed.

Acute cholecystitis may occur in a gallbladder with adenomyomatosis, and there may be overlap in imaging features, such as wall thickening. If ultrasound findings are equivocal, cross-sectional imaging with CT or MR, which

may demonstrate additional features, such as hyperemia in the adjacent liver, may be used as a problem-solving tool (Fig. 77-59).

Milk of Calcium Bile

When the cystic duct is obstructed by a gallstone, the gallbladder may become chronically inflamed, filling with a putty-like material consisting of calcium carbonate. This dense material can be visualized on abdominal plain films (Fig. 77-60) and CT.

Gallbladder Hydrops

Massive enlargement of the gallbladder can develop proximal to an obstructing stone in the gallbladder neck or cystic duct. If there is no supervening infection, the gallbladder lumen becomes progressively distended from the accumulation of sterile mucus secreted by the epithelial cells (Fig. 77-61). The patient usually has few symptoms but may have chronic right upper quadrant discomfort. A right upper quadrant mass may be palpable.

Plain radiographs may show a right upper quadrant mass indenting the lateral border of the duodenum. Sonography shows a distended gallbladder (>5 cm) with a biconvex shape and normal wall thickness. Sludge may be present. CT shows lumen distention and normal mural thickness.

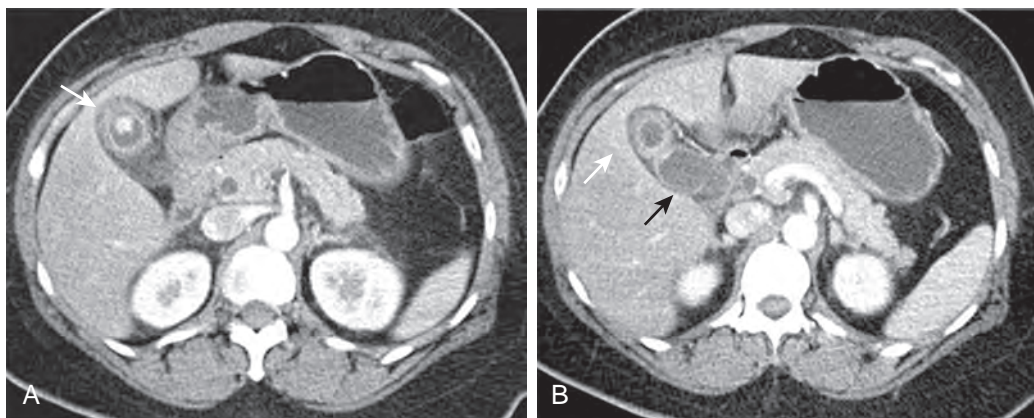


Figure 77-59 Segmental adenomyomatosis with associated acute cholecystitis. A. Contrast-enhanced CT demonstrates focal gallbladder wall thickening and stone in the fundal compartment (*arrow*). **B.** There is hyperemia in the adjacent liver, compatible with active inflammation, helping to confirm diagnosis of acute cholecystitis (*white arrow*). The inferior portion of the gallbladder demonstrates normal wall thickness (*black arrow*).

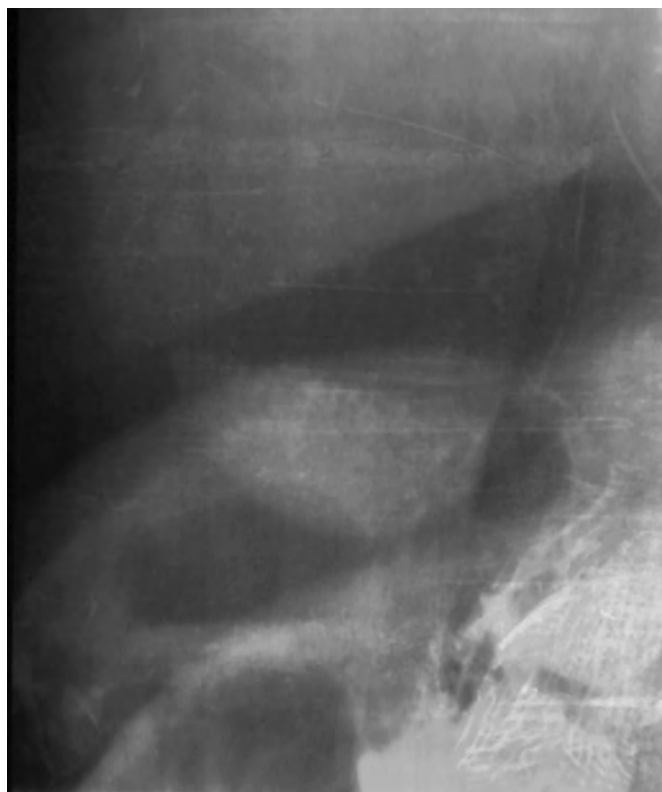


Figure 77-60 Milk of calcium gallbladder. Calcium carbonate layers dependently on this upright radiograph.

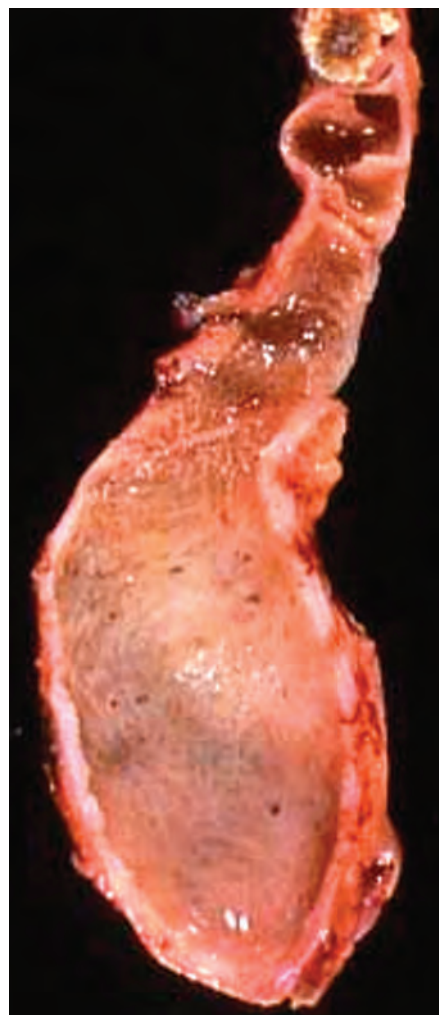


Figure 77-61 Hydrops of gallbladder: gross specimen.

REFERENCES

1. Tazuma S: Gallstone disease: Epidemiology, pathogenesis, and classification of biliary stones (common bile duct and intrahepatic). *Best Pract Res Clin Gastroenterol* 20:1075–1083, 2006.
2. Lack EE: Cholecystitis, cholelithiasis and unusual infections of the gallbladder. In Lack EE, editor: *Pathology of the Pancreas, Gallbladder, Extrahepatic Biliary Tract, and Ampullary Region*, New York, 2003, University Press, pp 414–452.
3. Bortoff GA, Chen MYM, Ott DJ, et al: Gallbladder stones: Imaging and intervention. *Radiographics* 20:751–766, 2000.
4. Trotman BW: Pigment gallstone disease. *Gastroenterol Clin North Am* 20:111–126, 1991.
5. Weltman DI, Zeman RK: Acute diseases of the gallbladder and biliary ducts. *Radiol Clin North Am* 32:933–950, 1994.
6. Cooperberg P: Imaging of the gallbladder. *Radiology* 163:605, 1987.
7. McIntosh DM, Penney HF: Gray-scale ultrasonography as a screening procedure in the detection of gallbladder disease. *Radiology* 136:725–727, 1980.
8. Carroll BA: Gallstones: In vitro comparison of physical, radiographic and ultrasonic characteristics. *AJR Am J Roentgenol* 131:223, 1978.
9. Filly RA, Moss AA, Way LW: In vitro investigation of gallstone shadowing with ultrasound tomography. *J Clin Ultrasound* 7:255–262, 1979.
10. Grossman M: Cholelithiasis and acoustic shadowing. *J Clin Ultrasound* 6:182, 1978.
11. Dessler TS, Jeffrey RB, Jr, Lane MJ, et al: Tissue harmonic imaging: Utility in abdominal and pelvic sonography. *J Clin Ultrasound* 27:135–142, 1999.
12. Oktar SO, Yucel C, Ozdemir H, et al: Comparison of conventional sonography, real-time compound sonography, tissue harmonic sonography, and tissue harmonic compound sonography of abdominal and pelvic lesions. *AJR Am J Roentgenol* 181:1341–1347, 2003.
13. Chintapalli KN, Ghiatas AA, Chopra S, et al: Sonographic findings in cases of missed gallstones. *J Clin Ultrasound* 27:117–121, 1999.
14. MacDonald FR, Cooperberg PL, Cohen MM: The WES triad: A specific sonographic sign of gallstones in the contracted gallbladder. *Gastrointest Radiol* 6:39–41, 1981.
15. Baron RL, Rohrmann CA, Lee SP, et al: CT evaluation of gallstones in vitro: Correlation with chemical analysis. *AJR Am J Roentgenol* 151:1123–1128, 1988.
16. Brakel K, Lameris JS, Nijs HG, et al: Predicting gallstone composition with CT: In vivo and in vitro analysis. *Radiology* 174:337–341, 1990.
17. Paulson EK: Acute cholecystitis: CT findings. *Semin Ultrasound CT MR* 21:56–63, 2000.
18. Barakos JA, Ralls PW, Lapin SA, et al: Cholelithiasis: Evaluation with CT. *Radiology* 162:415–418, 1987.
19. Chan WC, Joe BN, Coakley FV, et al: Gallstone detection at CT in vitro: Effect of peak voltage setting. *Radiology* 241:546–553, 2006.
20. Tsai HM, Lin XZ, Chen CY, et al: MRI of gallstones with different compositions. *AJR Am J Roentgenol* 182:1513–1519, 2004.
21. Hartman EM, Barish MA: MR cholangiography. *Magn Reson Imaging Clin N Am* 4:841–855, 2001.
22. Ukayi M, Ebara M, Tsuchiya Y, et al: Diagnosis of gallstone composition in magnetic resonance imaging: In vitro analysis. *Eur J Radiol* 41:49–56, 2002.
23. Ko CW, Sekijima JH, Lee SP: Biliary sludge. *Ann Intern Med* 130:301–311, 1999.
24. Lee SP: Pathogenesis of biliary sludge. *Hepatology* 12:2005–2035, 1990.
25. Jain R: Biliary sludge: When should it not be ignored? *Curr Treat Options Gastroenterol* 7:105–109, 2004.
26. Laing FC: Ultrasonography of the acute abdomen. *Radiol Clin North Am* 30:389–404, 1992.
27. Laing FC: The gallbladder and bile ducts. In Rumack CM, Wilson SR, Charboneau JW, editors: *Diagnostic Ultrasound*, ed 2, St. Louis, 1998, Mosby, pp 187–193.
28. American College of Radiology: Acute right upper quadrant pain. ACR Appropriateness Criteria, 2010. <<http://www.acr.org>>.
29. Laing FL, Federle MP, Jeffrey RB, et al: Ultrasonic evaluation of patients with acute right upper quadrant pain. *Radiology* 140:449–455, 1981.
30. Hirota M, Takada T, Kawarada Y, et al: Diagnostic criteria and severity assessment of acute cholecystitis: Tokyo guidelines. *J Hepatobiliary Pancreat Surg* 14:78–82, 2007.
31. Kimura Y, Takada T, Strasberg SM, et al: TG13 current terminology, etiology, and epidemiology of acute cholangitis and cholecystitis. *J Hepatobiliary Pancreat Sci* 20:8–23, 2013.
32. Fuks D, Mouly C, Robert B, et al: Acute cholecystitis: Preoperative CT can help the surgeon consider conversion from laparoscopic to open cholecystectomy. *Radiology* 263:128–138, 2012.
33. Ralls PW, Colletti PM, Halls JM, et al: Prospective evaluation of ^{99m}Tc-IDA cholescintigraphy and gray-scale ultrasound in the diagnosis of acute cholecystitis. *Radiology* 144:369–371, 1982.
34. Samuels BI, Freitas JE, Bree RL, et al: Comparison of radionuclide hepatobiliary imaging and real-time ultrasound for the detection of acute cholecystitis. *Radiology* 147:207–210, 1983.
35. Chatziioannou SN, Moire WH, Ford PV, et al: Hepatobiliary scintigraphy is superior to abdominal ultrasonography in suspected acute cholecystitis. *Surgery* 127:609–613, 2000.
36. Alobaidi M, Gupta R, Jafri SZ, et al: Current trends in imaging evaluation of acute cholecystitis. *Emerg Radiol* 10:256–258, 2004.
37. Kiewiet JJS, Leeuwenburgh MMN, Bipat S, et al: A systematic review and meta-analysis of diagnostic performance of imaging in acute cholecystitis. *Radiology* 264:708–720, 2012.
38. Palmer EL, Scott JA, Strauss HW: Abdominal imaging. In Palmer EL, Scott JA, Strauss HW, editors: *Practical Nuclear Medicine*, Philadelphia, 1992, WB Saunders, pp 275–285.
39. Sherman M, Ralls PW, Quinn M, et al: Intravenous cholangiography and sonography in acute cholecystitis: Prospective evaluation. *AJR Am J Roentgenol* 135:311–313, 1980.
40. Laing FC, Federle MP, Jeffrey RB, Jr, et al: Ultrasonic evaluation of patients with acute right upper quadrant pain. *Radiology* 140:449–455, 1981.
41. Hanbidge A, Buckler PM, O'Malley ME, et al: Imaging evaluation for acute pain in the right upper quadrant. *Radiographics* 24:1117–1135, 2004.
42. Ralls PW, Colletti PM, Lapin SA, et al: Real-time sonography in suspected acute cholecystitis. *Radiology* 155:767–771, 1985.
43. Paulson EK, Kliever MA, Hertzberg BS, et al: Diagnosis of acute cholecystitis with color Doppler sonography: Significance of arterial flow in thickened gallbladder wall. *AJR Am J Roentgenol* 162:1105–1108, 1994.
44. Schiller VL, Turner RR, Sarti DA: Color Doppler imaging of the gallbladder wall in acute cholecystitis: Sonographic-pathologic correlation. *Abdom Imaging* 21:233–237, 1996.
45. Charalal RA, Jeffrey RB, Shin LK: Complicated cholecystitis: The complementary roles of sonography and computed tomography. *Ultrasound Q* 27:161–170, 2011.
46. Bennett GL, Rusinek H, Lisi V, et al: CT findings of acute gangrenous cholecystitis. *AJR Am J Roentgenol* 178:275–281, 2002.
47. Kane RA, Costello P, Duszak E: Computed tomography in acute cholecystitis: New observations. *AJR Am J Roentgenol* 141:697–701, 1983.
48. Fidler J, Paulson EK, Layfield L: CT evaluation of acute cholecystitis: Findings and usefulness in diagnosis. *AJR Am J Roentgenol* 166:1085–1088, 1996.
49. Gore RM, Yaghami V, Newmark GM, et al: Imaging benign and malignant disease of the gallbladder. *Radiol Clin North Am* 40:1307–1323, 2002.
50. Grand D, Horton KM, Fishman E: CT of the gallbladder: Spectrum of disease. *AJR Am J Roentgenol* 183:163–170, 2004.
51. Gore RM, Thakrar KH, Newmark GM, et al: Gallbladder imaging. *Gastroenterol Clin North Am* 39:265–287, 2010.
52. Zissin R, Osadchy A, Shapiro-Feinberg M, Gayer G: CT of thickened-wall gall bladder. *Br J Radiol* 76:137–143, 2003.
53. Rooholamini SA, Tehrani NS, Razavi MK, et al: Imaging of gallbladder carcinoma. *Radiographics* 14:291–306, 1994.
54. Yamashita K, Jin MJ, Hirose Y, et al: CT findings of transient focal increased attenuation of the liver adjacent to the gallbladder in acute cholecystitis. *AJR Am J Roentgenol* 164:343–346, 1995.
55. Ito K, Awaya H, Mitchell DG, et al: Gallbladder disease: Appearance of associated transient increased attenuation in the liver at biphasic, contrast-enhanced dynamic CT. *Radiology* 204:723–728, 1997.
56. Cheng SM, Ng SP, Shih SL: Hyperdense gallbladder sign: An overlooked sign of acute cholecystitis on unenhanced CT examination. *Clin Imaging* 28:128–131, 2004.
57. Soyer P, Hoeffel C, Dohan A, et al: Acute cholecystitis: Quantitative and qualitative evaluation with 64-section helical CT. *Acta Radiol* 54:477–486, 2013.
58. van Randen A, Lameris W, van Es HW, et al: A comparison of the accuracy of ultrasound and computed tomography in common diagnoses causing acute abdominal pain. *Eur Radiol* 21:1535–1545, 2011.
59. Brook OR, Kane RA, Tyagi G, et al: Lessons learned from quality assurance: Errors in the diagnosis of acute cholecystitis on ultrasound and CT. *AJR Am J Roentgenol* 196:597–604, 2011.
60. Yam BL, Siegelman ES: MR imaging of the biliary system. *Radiol Clin North Am* 52:725–755, 2014.

61. Tonolini M, Ravelli A, Villa C, et al: Urgent MRI with MR cholangiopancreatography (MRCP) of acute cholecystitis and related disorders. *Emerg Radiol* 19:341–348, 2012.
62. Pedrosa I, Rofsky NM: MR imaging in abdominal emergencies. *Magn Reson Imaging Clin N Am* 12:603–635, 2004.
63. Watanabe Y, Nagayama M, Okumura A, et al: MR imaging of acute biliary disorders. *Radiographics* 27:477–495, 2007.
64. Catalano OA, Sahani DV, Kalva SP, et al: MR imaging of the gallbladder: A pictorial essay. *Radiographics* 28:135–155, 2008.
65. Hakansson K, Leander P, Ekberg O, et al: MR imaging in clinically suspected acute cholecystitis. A comparison with ultrasonography. *Acta Radiol* 41:322–328, 2000.
66. Regan F, Schaefer DC, Smith DP, et al: The diagnostic utility of HASTE MRI in the evaluation of acute cholecystitis. Half-Fourier acquisition single-shot turbo SE. *J Comput Assist Tomogr* 22:638–642, 1998.
67. Altun E, Semelka RC, Elias J, Jr, et al: Acute cholecystitis: MR findings and differentiation from chronic cholecystitis. *Radiology* 244:174–183, 2007.
68. Park MS, Yu JS, Kim YH, et al: Acute cholecystitis: Comparison of MR cholangiography and US. *Radiology* 209:781–785, 1998.
69. Kalliafas S, Ziegler DW, Flancbaum L, et al: Acute acalculous cholecystitis: Incidence, risk factors, diagnosis, and outcome. *Am Surg* 64:471–475, 1998.
70. Barie PS, Eachempati SR: Acute acalculous cholecystitis. *Gastroenterol Clin North Am* 39:343–357, 2010.
71. Kang JY, Williamson RC: Cholecystitis without gallstones. *HPB Surg* 2:83–103, 1990.
72. Glenn F, Becker CG: Acute acalculous cholecystitis. An increasing entity. *Ann Surg* 195:131–136, 1982.
73. Parithivel VS, Gerst PH, Banerjee S, et al: Acute acalculous cholecystitis in young patients without predisposing factors. *Am Surg* 65:366–368, 1999.
74. Savoca PE, Longo WE, Zucker KA, et al: The increasing prevalence of acalculous cholecystitis in outpatients. *Ann Surg* 211:433–437, 1990.
75. Flancbaum L, Choban PS: Use of morphine cholescintigraphy in the diagnosis of acute cholecystitis in critically ill patients. *Intensive Care Med* 21:120–124, 1995.
76. Shuman WP, Rogers JV, Rudd TG, et al: Low sensitivity of sonography and cholescintigraphy in acalculous cholecystitis. *AJR Am J Roentgenol* 142:531–534, 1984.
77. Boland GWL, Slater G, Lu DSK, et al: Prevalence and significance of gallbladder abnormalities seen on sonography in intensive care unit patients. *AJR Am J Roentgenol* 174:973–977, 2000.
78. Kalf V, Froelich JW, Lloyd R, et al: Predictive value of an abnormal hepatobiliary scan in patients with severe intercurrent illness. *Radiology* 146:191–194, 1983.
79. Flancbaum L, Alden SM: Morphine cholescintigraphy. *Surg Gynecol Obstet* 171:227–232, 1990.
80. Mariat G, Mahul P, Prevot N, et al: Contribution of ultrasonography and cholescintigraphy to the diagnosis of acute acalculous cholecystitis in intensive care patients. *Intensive Care Med* 26:1658–1663, 2000.
81. Mirvis SE, Vainright JR, Nelson AW, et al: The diagnosis of acute acalculous cholecystitis: A comparison of sonography, scintigraphy and CT. *AJR Am J Roentgenol* 147:1171–1175, 1986.
82. Mirvis SE, Whitley NO, Miller JW: CT diagnosis of acalculous cholecystitis. *J Comput Assist Tomogr* 11:83–87, 1987.
83. Blankenberg F, Wirth R, Jeffrey RB, et al: Computed tomography as an adjunct to ultrasound in the diagnosis of acute acalculous cholecystitis. *Gastrointest Radiol* 16:149–153, 1991.
84. Havenjarvi L, Koivukangas V, Jartti A, et al: Diagnostic accuracy of computed tomography imaging of surgically treated acute acalculous cholecystitis in critically ill patient. *J Trauma* 70:183–188, 2011.
85. McGahan JP, Lindfors KK: Percutaneous cholecystostomy: An alternative to surgical cholecystectomy for acute cholecystitis? *Radiology* 173:481–485, 1989.
86. Boland GW, Lee MJ, Mueller PR, et al: Gallstones in critically ill patients with acute acalculous cholecystitis treated by percutaneous cholecystostomy: Nonsurgical therapeutic options. *AJR Am J Roentgenol* 162:1101–1103, 1994.
87. Lo LD, Vogelzang RL, Braun MA, et al: Percutaneous cholecystostomy for the diagnosis and treatment of acute calculous and acalculous cholecystitis. *Vasc Interv Radiol* 6:629–634, 1995.
88. Ito K, Fujita N, Noda Y, et al: Percutaneous cholecystostomy versus gallbladder aspiration for acute cholecystitis: A prospective randomized controlled trial. *AJR Am J Roentgenol* 183:193–196, 2004.
89. Cotran RS, Kumar V, Robbins SL: *Pathologic Basis of Disease*, ed 4, Philadelphia, 1989, WB Saunders.
90. Morfin E, Ponka J, Brush B: Gangrenous cholecystitis. *Arch Surg* 96:567–572, 1968.
91. Wilson AK, Kozol RA, Salwen WA, et al: Gangrenous cholecystitis in an urban VA hospital. *J Surg Res* 56:402–404, 1994.
92. Ahmad MM, Macon WL: Gangrene of the gallbladder. *Am Surg* 49:155–158, 1983.
93. Merriam LT, Kanaan SA, Dawes LG, et al: Gangrenous cholecystitis: Analysis of risk factors and experience with laparoscopic cholecystectomy. *Surgery* 126:680–686, 1999.
94. Jacobs M, Verdeja J, Goldstein HS: Laparoscopic cholecystectomy in acute cholecystitis. *J Laparoendosc Surg* 1:175–177, 1991.
95. Singer JA, McKeen RV: Laparoscopic cholecystectomy for acute or gangrenous cholecystitis. *Am Surg* 60:326–328, 1994.
96. Teefey SA, Baron RL, Radke HM, et al: Gangrenous cholecystitis: New observations on sonography. *J Ultrasound Med* 134:191–194, 1991.
97. Jeffrey RB, Laing FC, Wong W, et al: Gangrenous cholecystitis: Diagnosis by ultrasound. *Radiology* 148:219–221, 1983.
98. Teefey SA, Dahiya N, Middleton WD, et al: Acute cholecystitis: Do sonographic findings and WBC count predict gangrenous changes? *AJR Am J Roentgenol* 200:363–369, 2013.
99. Simeone J, Brink J, Mueller P, et al: The sonographic diagnosis of acute gangrenous cholecystitis: Importance of the Murphy sign. *AJR Am J Roentgenol* 152:209–290, 1989.
100. Lamki N, Raval B, St. Ville E: Computed tomography of complicated cholecystitis. *J Comput Assist Tomogr* 10:319–324, 1986.
101. Varma DGK, Faust JM: Computed tomography of gangrenous acute postoperative acalculous cholecystitis. *J Comput Tomogr* 12:29–31, 1988.
102. Bridges MD, Jones BC, Morgan DE, et al: Acute cholecystitis and gallbladder necrosis: Value of contrast enhanced CT [abstract]. *AJR Am J Roentgenol* 172:34–35, 1999.
103. Wu CH, Chen CC, Wang CJ, et al: Discrimination of gangrenous from uncomplicated acute cholecystitis: Accuracy of CT findings. *Abdom Imaging* 36:174–178, 2011.
104. Liang JL, Chen MC, Huang HY, et al: Gallbladder carcinoma manifesting as acute cholecystitis: Clinical and computed tomographic features. *Surgery* 146:861–868, 2009.
105. Jenkins M, Golding RH, Cooperberg PL: Sonography and computed tomography of hemorrhagic cholecystitis. *AJR Am J Roentgenol* 140:1197–1198, 1983.
106. Shah VR, Clegg JF: Haemorrhagic cholecystitis. *Br J Surg* 66:404–405, 1979.
107. Hudson PB, Johnson PP: Hemorrhage from the gallbladder. *N Engl J Med* 234:438–441, 1946.
108. Moskos MM, Eschelmann DJ: Hemorrhagic cholecystitis. *AJR Am J Roentgenol* 156:1304–1305, 1991.
109. Polse S, Stoney RJ, Baldwin JN: Hemorrhage from the gallbladder. *Calif Med* 107:51–53, 1967.
110. Chinn DH, Miller EI, Piper N: Hemorrhagic cholecystitis. Sonographic appearance and clinical presentation. *J Ultrasound Med* 6:313–317, 1987.
111. Gremmels JM, Kruskal JB, Parangi S, et al: Hemorrhagic cholecystitis simulating gallbladder carcinoma. *J Ultrasound Med* 23:993–995, 2004.
112. Yiu-Chiu VS, Chiu LC, Wedel VJ: Current cases and concepts: Acalculous hemorrhagic cholecystitis. *J Comput Tomogr* 4:201–206, 1980.
113. Tavernarakis K, Sykara A, Tavernarakis E, et al: Massive intraperitoneal bleeding due to hemorrhagic cholecystitis and gallbladder rupture: CT findings. *Abdom Imaging* 36:565–568, 2011.
114. Jacob H, Appelman R, Stein HD: Emphysematous cholecystitis. *Am J Gastroenterol* 71:325–330, 1979.
115. May RE, Strong R: Acute emphysematous cholecystitis. *Br J Surg* 58:453–458, 1971.
116. Mentzer RM, Jr, Golden GT, Chandler JG, et al: A comparative appraisal of emphysematous cholecystitis. *Am J Surg* 129:10–15, 1975.
117. Garcia-Sancho Tellez L, Rodriguez-Montes JA, Fernandez de Lis S, et al: Acute emphysematous cholecystitis: Report of twenty cases. *Hepatogastroenterology* 46:2144–2148, 1999.
118. Konno K, Ishida H, Naganuma H, et al: Emphysematous cholecystitis: Sonographic findings. *Abdom Imaging* 27:191–195, 2002.
119. Bloom RA, Libson E, Lebensart PD, et al: The ultrasound spectrum of emphysematous cholecystitis. *J Clin Ultrasound* 17:251–256, 1989.
120. Gill KS, Chapman AH, Weston MJ: The changing face of emphysematous cholecystitis. *Br J Radiol* 70:986–991, 1997.
121. McMillin K: Computed tomography of emphysematous cholecystitis. *J Comput Assist Tomogr* 9:330–332, 1985.
122. Chiu HH, Chen CM, Mo LR: Emphysematous cholecystitis. *Am J Surg* 188:325–326, 2004.
123. Koenig T, Tamm EP, Kawashima A: Magnetic resonance imaging findings in emphysematous cholecystitis. *Clin Radiol* 59:455–458, 2004.
124. Diffenbaugh WG: Gangrenous perforation of the gallbladder. *Arch Surg* 59:743–749, 1949.

125. Seyal AR, Parekh K, Gonzalez-Guindalini FD, et al: Cross-sectional imaging of perforated gallbladder. *Abdom Imaging* 39:855–874, 2014.
126. Madrazo BL, Francis I, Hricak H, et al: Sonographic findings in perforation of the gallbladder. *AJR Am J Roentgenol* 139:491–496, 1982.
127. Niemeier OW: Acute free perforation of the gallbladder. *Am Surg* 99:922–924, 1934.
128. Fletcher AG, Ravdin IS: Perforation of the gallbladder. *Am J Surg* 81:178–185, 1951.
129. Heuer GJ: The factors leading to death in operations upon the gallbladder and bile ducts. *Ann Surg* 99:881–892, 1934.
130. Cowley LL, Harkins HN: Perforation of the gallbladder. *Surg Gynecol Obstet* 77:661–668, 1943.
131. Peer A, Witz E, Manor H, et al: Intrahepatic abscess due to gallbladder perforation. *Abdom Imaging* 20:452–455, 1995.
132. Chen JJ, Lin HH, Chiu CT, et al: Gallbladder perforation with intrahepatic abscess formation. *J Clin Ultrasound* 18:43–45, 1990.
133. Ikard RW: Gallstones, cholelithiasis and diabetes surgery. *Gynecol Obstet* 171:528–532, 1990.
134. Chau WK, Na WT, Feng TT, et al: Ultrasound diagnosis of perforation of the gallbladder: Real time application and the demonstration of a new sonographic sign. *J Clin Ultrasound* 16:358–360, 1988.
135. Fitoz S, Erden A, Karagulle T, et al: Interruption of gallbladder wall with pericholecystic fluid: A CT finding of perforation. *Emerg Radiol* 7:253–255, 2000.
136. Kim PN, Lee KS, Kim IY, et al: Gallbladder perforation: Comparison of US findings with CT. *Abdom Imaging* 19:239–242, 1994.
137. Sood BP, Kalra N, Gupta S, et al: Role of sonography in the diagnosis of gallbladder perforation. *J Clin Ultrasound* 30:270–274, 2002.
138. Saul SH: Gallbladder and extrahepatic biliary tree. In Steinberg SS, editor: *Diagnostic Surgical Pathology*, ed 3, Philadelphia, 1999, Lippincott, pp 1629–1670.
139. Jagannath SB, Singh V, Cruz-Correa M, et al: A long-term cohort study of outcome after cholecystectomy for chronic acalculous cholecystitis. *Am J Surg* 185:91–95, 2003.
140. Krishnamurthy GT, Krishnamurthy S, Brown PH: Constancy and variability of gallbladder ejection fraction: Impact on diagnosis and therapy. *J Nucl Med* 45:1872–1877, 2004.
141. Poynter MT, Saba AK, Evans RA, et al: Chronic acalculous biliary tract disease: Cholecystokinin cholescintigraphy is useful in formulating treatment strategy and predicting success after cholecystectomy. *Am Surg* 68:382–384, 2002.
142. Goodman ZD, Ishak KG: Xanthogranulomatous cholecystitis. *Am J Surg Pathol* 5:653–659, 1981.
143. Ros PR, Goodman ZD: Xanthogranulomatous cholecystitis versus gallbladder carcinoma. *Radiology* 203:10–12, 1997.
144. Reed A, Ryan C, Schwartz SI: Xanthogranulomatous cholecystitis. *J Am Coll Surg* 179:249–252, 1994.
145. Guzman-Valdivia G: Xanthogranulomatous cholecystitis: 15 years' experience. *World J Surg* 28:254–257, 2004.
146. Hsu CH, Hurwitz JL, Schuss A, et al: Radiology-Pathology Conference: Xanthogranulomatous cholecystitis. *J Clin Imaging* 27:421–425, 2003.
147. Parra JA, Acinas O, Bueno J, et al: Xanthogranulomatous cholecystitis: Clinical, sonographic, and CT findings in 26 patients. *AJR Am J Roentgenol* 174:979–983, 2000.
148. Casas D, Perez-Andres R, Jimenez JA, et al: Xanthogranulomatous cholecystitis: A radiological study of 12 cases and a review of the literature. *Abdom Imaging* 21:456–460, 1996.
149. Kim PN, Lee SH, Gong GY, et al: Xanthogranulomatous cholecystitis: Radiologic findings with histologic correlation that focuses on intramural nodules. *AJR Am J Roentgenol* 172:949–953, 1999.
150. Chun KA, Ha HK, Yu ES, et al: Xanthogranulomatous cholecystitis: CT features with emphasis on differentiation from gallbladder carcinoma. *Radiology* 203:93–97, 1997.
151. Lichtman JB, Varma VA: Ultrasound demonstration of xanthogranulomatous cholecystitis. *J Clin Ultrasound* 15:342–345, 1987.
152. Shukla S, Krishnani N, Jain M, et al: Xanthogranulomatous cholecystitis. Fine needle aspiration cytology in 17 cases. *Acta Cytol* 41:413–418, 1997.
153. Kang TW, Kim SH, Park HJ, et al: Differentiating xanthogranulomatous cholecystitis from wall-thickening type of gallbladder cancer: Added value of diffusion-weighted MRI. *Clin Radiol* 68:992–1001, 2013.
154. Liu TH, Moody FG: Pathogenesis and presentation of common bile duct stones. *Semin Laparosc Surg* 7:224–231, 2000.
155. Lamont JT, Afidhal NH: Cholesterol gallstone disease: From pancreatitis to prevention. *Curr Opin Gastroenterol* 10:523–525, 1994.
156. Hermann RE: The spectrum of biliary stone disease. *Am J Surg* 158:171–173, 1989.
157. Raraty MG, Finch M, Neoptolemos JP: Acute cholangitis and pancreatitis secondary to common duct stones: Management update. *World J Surg* 22:1155–1161, 1998.
158. Makary MA, Duncan MD, Harmon JW, et al: The role of magnetic resonance cholangiography in the management of patients with gallstone pancreatitis. *Ann Surg* 241:119–124, 2005.
159. Bilbao MK, Dotter CT, Lee TG, et al: Complications of endoscopic retrograde cholangiopancreatography. A study of 10,000 cases. *Gastroenterology* 70:314–320, 1976.
160. Lo SK, Chen J: The role of ERCP in choledocholithiasis. *Abdom Imaging* 21:120–132, 1996.
161. Harvey RT, Miller WT, Jr: Acute biliary disease: Initial CT and follow-up US versus initial US and follow-up CT. *Radiology* 213:831–836, 1999.
162. Pasanen P, Partanen K, Pikkarainen P, et al: Ultrasonography, CT and ERCP in the diagnosis of choledochal stones. *Acta Radiol* 33:53–56, 1992.
163. Stott MA, Farrands PA, Guyer PB, et al: Ultrasound of the common bile duct in patients undergoing cholecystectomy. *J Clin Ultrasound* 19:73–76, 1991.
164. Dong B, Chen M: Improved sonographic visualization of choledocholithiasis. *J Clin Ultrasound* 15:185–190, 1987.
165. Laing FC, Jeffrey RB, Wing VW: Improved visualization of choledocholithiasis by sonography. *AJR Am J Roentgenol* 143:949–952, 1984.
166. Ortega D, Burns PN, Simpson DH, et al: Tissue harmonic imaging: Is it a benefit for bile duct sonography? *AJR Am J Roentgenol* 176:653–665, 2001.
167. Amouyal P, Amouyal G, Levy P, et al: Diagnosis of choledocholithiasis by endoscopic ultrasonography. *Gastroenterology* 106:1062–1067, 1994.
168. Baron RL: Common bile duct stones: Reassessment of criteria for CT diagnosis. *Radiology* 162:419–424, 1987.
169. Baron RL: Diagnosing choledocholithiasis: How far can we push helical CT? *Radiology* 203:601–603, 1997.
170. Pickuth D: Radiologic diagnosis of common bile duct stones. *Abdom Imaging* 25:618–621, 2000.
171. Neitlich JD, Topazian M, Smith RC, et al: Detection of choledocholithiasis: Comparison of unenhanced helical CT and endoscopic retrograde cholangiopancreatography. *Radiology* 203:753–757, 1997.
172. Soto JA, Alvarez O, Munera F, et al: Diagnosing bile duct stones: Comparison of unenhanced helical CT, oral contrast-enhanced CT cholangiography, and MR cholangiography. *AJR Am J Roentgenol* 175:1127–1134, 2000.
173. Jimenez Cuenca I, del Olmo Martinez L, Perez Horns M: Helical CT without contrast in choledocholithiasis diagnosis. *Eur Radiol* 11:197–201, 2001.
174. Van Beers BE, Pringot JH: Imaging of cholelithiasis: Helical CT. *Abdom Imaging* 26:15–20, 2001.
175. Klein HM, Wein B, Truong S, et al: Computed tomographic cholangiography using spiral scanning and 3D imaging processing. *Br J Radiol* 66:762–767, 1993.
176. Breen DJ, Nicholson AA: The clinical utility of spiral CT cholangiography. *Clin Radiol* 55:733–739, 2000.
177. Xu AM, Cheng HY, Jiang WB, et al: Multislice three-dimensional spiral CT cholangiography: A new technique for diagnosing biliary disease. *Hepatobiliary Pancreat Dis Int* 1:595–603, 2002.
178. Cabada Giasas T, Sarria Octavio de Toledo L, Martinez-Berganza Asensio MT, et al: Helical CT cholangiography in the evaluation of the biliary tract: Application to the diagnosis of choledocholithiasis. *Abdom Imaging* 27:61–70, 2002.
179. Okada M, Fukada JJ, Toya K, et al: The value of drip infusion cholangiography using multidetector-row helical CT in patients with choledocholithiasis. *Eur Radiol* 15:2140–2145, 2005.
180. Zandrino F, Curone P, Benzi L, et al: MR versus multislice CT cholangiography in evaluating patients with obstruction of the biliary tract. *Abdom Imaging* 30:77–85, 2005.
181. Gibson RN, Vincent JM, Speer T, et al: Accuracy of computed tomographic intravenous cholangiography (CT-IVC) with iotroxate in the detection of choledocholithiasis. *Eur Radiol* 15:1634–1642, 2005.
182. Ahmetoglu A, Kosucu P, Kul S, et al: MDCT cholangiography with volume rendering for the assessment of patients with biliary obstruction. *AJR Am J Roentgenol* 183:1327–1332, 2004.
183. Baille J, Paulson EK, Vitellas KM: Biliary imaging: A review. *Gastroenterol Clin North Am* 124:1686–1699, 2003.
184. Fulcher AS, Turner MA: Benign disease of the biliary tract: Evaluation with MR cholangiography. *Semin Ultrasound CT MR* 20:294–303, 1999.
185. Reinhold C, Taourel P, Bret PM, et al: Choledocholithiasis: Evaluation of MR cholangiography for diagnosis. *Radiology* 209:435–442, 1998.

186. Heller SL, Lee VS: MR imaging of the gallbladder and biliary system. *Magn Reson Imaging Clin N Am* 13:295–311, 2005.
187. Kim JH, Kim MJ, Park S, et al: MR cholangiography in symptomatic gallstones: Diagnostic accuracy according to clinical risk group. *Radiology* 224:410–416, 2002.
188. Schmidt S, Chevallier P, Novellas S, et al: Choledocholithiasis: Repetitive thick-slab single-shot projection magnetic resonance cholangiopancreatography versus endoscopic ultrasonography. *Eur Radiol* 17:241–250, 2007.
189. Regan F, Smith D, Khazan R, et al: MR cholangiography in biliary obstruction using half-Fourier acquisition. *J Comput Assist Tomogr* 20:627–632, 1996.
190. Kim M-J, Mitchell DG, Ito K, et al: Biliary dilatation: Differentiation of benign from malignant causes—value of adding conventional MR imaging to MR cholangiography. *Radiology* 214:173–181, 2000.
191. Wielopolski PA, Gaa J, Wielopolski DR, et al: Breath-hold MR cholangiopancreatography with three-dimensional, segmented, echo-planar imaging and volume rendering. *Radiology* 210:247–252, 1999.
192. Soto JA, Barish MA, Yucel E, et al: Pancreatic duct: MR cholangiopancreatography with a three-dimensional fast spin-echo technique. *Radiology* 196:459–464, 1995.
193. Barish M, Yucel E, Soto J, et al: MR cholangiopancreatography: Efficacy of three-dimensional turbo spin-echo technique. *AJR Am J Roentgenol* 196:459–464, 1995.
194. McKenzie CA, Lim D, Ransil BJ, et al: Shortening MR image acquisition time for volumetric interpolated breath-hold examination with a recently developed parallel imaging reconstruction technique: Clinical feasibility. *Radiology* 230:589–594, 2003.
195. Watanabe Y, Dohke M, Ishimori T, et al: Pseudo-obstruction of the extrahepatic bile duct due to artifact from arterial pulsatile compression: A diagnostic pitfall of MR cholangiopancreatography. *Radiology* 214:856–860, 2000.
196. Sugita R, Sugimura E, Itoh M, et al: Pseudolesion of the bile duct caused by flow effect: A diagnostic pitfall of MR cholangiopancreatography. *AJR Am J Roentgenol* 180:467–471, 2003.
197. Menu Y, Lorphelin JM, Scherrer A, et al: Sonographic and computed tomographic evaluation of intrahepatic calculi. *AJR Am J Roentgenol* 145:579–583, 1985.
198. Carmona RH, Crass RA, Lim RC, Jr, et al: Oriental cholangitis. *Am J Surg* 148:117–124, 1984.
199. Sperling RM, Koch J, Sandhu JS, et al: Recurrent pyogenic cholangitis in Asian immigrants to the United States. Natural history and role of therapeutic ERCP. *Dig Dis Sci* 42:865–871, 1997.
200. Yassa NA, Stain S, Ralls PW: Recurrent pyogenic cholangitis. *Ultrasound Q* 14:41–47, 1998.
201. Kim M-J, Cha S-W, Mitchell DG, et al: MR imaging findings in recurrent pyogenic cholangitis. *AJR Am J Roentgenol* 173:1545–1549, 1999.
202. Chan F-L, Man S-W, Leong LLY, et al: Evaluation of recurrent pyogenic cholangitis with CT: Analysis of 50 patients. *Radiology* 170:165–169, 1989.
203. Federle MP, Cello JP, Laing FC, et al: Recurrent pyogenic cholangitis in Asian immigrants. Use of ultrasonography, computed tomography and cholangiography. *Radiology* 143:151–156, 1982.
204. Lim JH, Ko YT, Lee DH, et al: Oriental cholangiohepatitis: Sonographic findings in 48 cases. *AJR Am J Roentgenol* 155:511–514, 1990.
205. Kusano S, Okada Y, Endo T, et al: Oriental cholangiohepatitis: Correlation between portal vein occlusion and hepatic atrophy. *AJR Am J Roentgenol* 158:1011–1014, 1992.
206. Sathesh-Kumar T, Saklani AP, Vinayagam R, et al: Spilled gallstones during laparoscopic cholecystectomy: A review of the literature. *Postgrad Med J* 80:77–79, 2004.
207. Litwin DEM, Girotti MJ, Poulin EC, et al: Laparoscopic cholecystectomy: Trans-Canada experience with 2201 cases. *Can J Surg* 35:291–296, 1992.
208. Larson GM, Vitale GC, Casey J, et al: Multi-practice analysis of laparoscopic cholecystectomy in 1,983 patients. *Am J Surg* 163:221–226, 1992.
209. Cuschieri A, Dubois F, Mouiel J, et al: The European experience with laparoscopic cholecystectomy. *Am J Surg* 161:385–387, 1991.
210. Morrin MM, Kruskal JB, Hochman MG, et al: Radiologic features of complications arising from dropped gallstones in laparoscopic cholecystectomy patients. *AJR Am J Roentgenol* 174:1441–1445, 2000.
211. Trerotola SO, Lillemoe KD, Malloy PC, et al: Percutaneous removal of “dropped” gallstones after laparoscopic cholecystectomy. *Radiology* 188:419–421, 1993.
212. Campbell WB, McGarity WC: An unusual complication of laparoscopic cholecystectomy. *Am Surg* 184:195–200, 1992.
213. Mirizzi PC: Syndrome del conducto hepatico. *J Int Chir* 8:731–777, 1948.
214. McSherry C, Ferstenberg H, Virshup M: The Mirizzi syndrome: Suggested classification and surgical therapy. *Surg Gastroenterol* 1:219–225, 1982.
215. Abou-Saif A, Al-Kawas FH: Complications of gallstone disease: Mirizzi syndrome, cholecystocholedochal fistula and gallstone ileus. *Am J Gastroenterol* 97:249, 2002.
216. Sharma AK, Rangan HK, Choubey RP, et al: Pitfalls in the management of Mirizzi’s syndrome. *Trop Gastroenterol* 19:72–74, 1998.
217. Karademir S, Astarioglu H, Sokmen S, et al: Mirizzi’s syndrome: Diagnostic and surgical considerations in 25 patients. *J Hepatobiliary Pancreat Surg* 7:72–77, 2000.
218. Berland LL, Lawson TL, Stanley RJ: CT appearance of Mirizzi syndrome. *J Comput Assist Tomogr* 8:165–166, 1984.
219. Kim PN, Outwater EK, Mitchell DG: Mirizzi syndrome: Evaluation by MR imaging. *Am J Gastroenterol* 94:2546–2550, 1999.
220. Wakefield EG, Vickers PM, Walters W: Intestinal obstruction caused by gallstones. *Surgery* 5:670–673, 1939.
221. Chen MYM: Gallstone ileus: CT findings. *Appl Radiol* 20:37–38, 1991.
222. Rigler LG, Borman CN, Noble JF: Gallstone obstruction: Pathogenesis and roentgen manifestations. *JAMA* 117:1753–1759, 1941.
223. Balthazar EJ, Schechter LS: Air in gallbladder: A frequent finding in gallstone ileus. *AJR Am J Roentgenol* 131:219–222, 1978.
224. Delabrousse E, Bartholomot B, Sohm O, et al: Gallstone ileus: CT findings. *Eur Radiol* 10:938–940, 2000.
225. Loren I, Lasson A, Nilsson A, et al: Gallstone ileus demonstrated by CT. *J Comput Assist Tomogr* 18:262–265, 1994.
226. Swift SE, Spencer JA: Gallstone ileus: CT findings. *Clin Radiol* 53:451–456, 1998.
227. Jutras JA: Hyperplastic cholecystosis. *AJR Am J Roentgenol* 83:795–827, 1960.
228. Berk RN, van der Vegt JH, Lichtenstein JE: The hyperplastic cholecystoses: Cholesterosis and adenomyomatosis. *AJR Am J Roentgenol* 146:593–601, 1983.
229. Kopp JG: The strawberry gallbladder. *Arch Klin Chir* 151:411–429, 1928.
230. Tilvis RS, Aro J, Strandberg TE, et al: Lipid composition of bile and gallbladder mucosa in patients with acalculous cholesterosis. *Gastroenterology* 82:607–615, 1982.
231. Judd ES, Mentzer SH: Cholesterosis of the gallbladder. I. A clinical study. Collected papers. *Mayo Clin Proc* 19:310–316, 1927.
232. Feldman M, Feldman M, Jr: Cholesterosis of the gallbladder. An autopsy study of 165 cases. *Gastroenterology* 27:641–648, 1954.
233. Owen CC, Bilhartz LE: Gallbladder polyps, cholesterosis, adenomyomatosis and acute acalculous cholecystitis. *Semin Gastrointest Dis* 14:178–188, 2003.
234. Ito H, Hann LE, D’Angelica M, et al: Polypoid lesion of the gallbladder. *J Am Coll Surg* 208:570–575, 2009.
235. Konstantinidis IT, Bajpai S, Kambadakone AR, et al: Gallbladder lesions identified on ultrasound. Lessons from the last 10 years. *J Gastrointest Surg* 16:549–553, 2012.
236. Lee KF, Wong J, Li JCM, et al: Polypoid lesions of the gallbladder. *Am J Surg* 188:186–190, 2004.
237. Corwin MT, Siewart B, Sheiman RG, Kane RA: Incidentally detected gallbladder polyps: Is follow-up necessary? Long-term clinical and US analysis of 346 patients. *Radiology* 258:277–282, 2011.
238. Cairns V, Neal CP, Dennison AR, Garcea G: Risk and cost-effectiveness of surveillance followed by cholecystectomy for gallbladder polyps. *Arch Surg* 147:1078–1083, 2012.
239. Terzi C, Sokmen S, Seckin S, et al: Polypoid lesions of the gallbladder: Report of 100 cases with special reference to operative indications. *Surgery* 127:622–627, 2000.
240. Park JK, Yoon YB, Kim YT, et al: Management strategies for gallbladder polyps: Is it possible to predict malignant gallbladder polyps? *Gut Liver* 2:88–94, 2008.
241. Chattopadhyay D, Lochan R, Balupuri S, et al: Outcome of gallbladder polypoid lesions detected by transabdominal ultrasound scanning: A nine year experience. *World J Gastroenterol* 11:2171–2173, 2005.
242. Ootani T, Shirai Y, Muto T, et al: Relationship between gallbladder carcinoma and the segmental type of adenomyomatosis. *Cancer* 69:2647–2652, 1992.
243. Colquhoun J: Adenomyomatosis of the gallbladder (intramural diverticulosis). *Br J Radiol* 34:101–112, 1961.
244. Raghavendra BN, Subramanyam BR, Balthazar EJ, et al: Sonography of adenomyomatosis of the gallbladder: Radiologic-pathologic correlation. *Radiology* 146:747–752, 1983.
245. Hwang JI, Chou SH, Tsay SH, et al: Radiologic and pathologic correlation of adenomyomatosis of the gallbladder. *Abdom Imaging* 23:73–77, 1998.
246. Halpert RD, Bedi DG, Tirman PJ, et al: Segmental adenomyomatosis of the gallbladder. A

- radiologic, sonographic and pathologic correlation. *Am Surg* 55:570–572, 1989.
247. Yoon JH, Cha SS, Han SS, et al: Gallbladder adenomyomatosis: Imaging findings. *Abdom Imaging* 31:555–563, 2006.
 248. Joo I, Lee Y, Kim JH, et al: Differentiation of adenomyomatosis of the gallbladder from early-stage, wall-thickening-type gallbladder cancer using high resolution ultrasound. *Eur Radiol* 23:730–738, 2013.
 249. Ghersin E, Soudack M, Gaitini D: Twinkling artifact in gallbladder adenomyomatosis. *J Ultrasound Med* 22:229–231, 2003.
 250. Kim HC, Yang DM, Jin W, et al: Color Doppler twinkling artifacts in various conditions during abdominal and pelvic sonography. *J Ultrasound Med* 29:621–632, 2010.
 251. Yu MH, Lee JY, Yoon JH, et al: Color Doppler twinkling artifacts from gallbladder adenomyomatosis with 1.8 MHz and 4.0 MHz color Doppler frequencies. *Ultrasound Med Biol* 7:1188–1194, 2012.
 252. Nishimura A, Shirai Y, Hatakeyama K: Segmental adenomyomatosis of the gallbladder predisposes to cholecystolithiasis. *J Hepatobiliary Pancreat Surg* 11:342–347, 2004.
 253. Gerard PS, Berman D, Zafaranloo S: CT and ultrasound of gallbladder adenomyomatosis mimicking carcinoma. *J Comput Assist Tomogr* 14:490–491, 1990.
 254. Boscak AR, Al-Hawary M, Ramsburgh SR: Best cases from the AFIP: Adenomyomatosis of the gallbladder. *Radiographics* 26:941–946, 2006.
 255. Ching BH, Yeh BM, Westphalen AC, et al: CT differentiation of adenomyomatosis and gallbladder cancer. *AJR Am J Roentgenol* 189:62–66, 2007.
 256. Yoshimitsu K, Honda H, Jimi M, et al: MR diagnosis of adenomyomatosis of the gallbladder and differentiation from gallbladder carcinoma: Importance of showing Rokitansky-Aschoff sinuses. *AJR Am J Roentgenol* 172:1535–1540, 1999.
 257. Bang SH, Lee JY, Woo H, et al: Differentiating between adenomyomatosis and gallbladder cancer: Revisiting a comparative study of high resolution ultrasound, multidetector CT, and MR imaging. *Korean J Radiol* 15:226234, 2014.

Interventional Radiology of the Gallbladder and Biliary Tract

THOMAS A. FARRELL | MIKIN V. PATEL

CHAPTER OUTLINE

Preprocedural Management

Percutaneous Cholecystostomy

Technique

Percutaneous Gallbladder Aspiration

Acalculous Cholecystitis

Percutaneous Transhepatic Cholangiography and Drainage

Technique

Complications

Biliary Strictures

Malignant Stricture

Benign Stricture

Common Duct Stone Removal

Bile Duct Injury

Primary Sclerosing Cholangitis

Biopsy

Interventional radiology continues to play a key role in the management of patients with gallbladder and biliary tract disease. Advances in techniques and technologies have improved patient care with the availability of minimally invasive procedures that include percutaneous drainage, biopsy, and stone removal. Diagnostic procedures include percutaneous transhepatic cholangiography and intraluminal biopsy. Therapeutic procedures include percutaneous drainage-decompression of the biliary tree or gallbladder, dilation of a bile duct stenosis or surgical anastomosis, placement of endobiliary plastic or metallic stents, removal of gallstones, and, finally, percutaneous intraluminal treatment of biliary tumors. This chapter reviews the indications, techniques, outcomes, and recent advances of these interventional procedures in a multidisciplinary setting.

Preprocedural Management

The interventionalist should be familiar with the patient's history, notably previous interventions including surgery. A recent physical examination is useful in evaluating the patient's general condition and is necessary if moderate conscious sedation is being used, in which case the patient should be fasting for at least 6 hours. Review of previous imaging is also helpful for clarification of anatomy and prior procedures.

The clinical practice guidelines of the Society of Interventional Radiology attempt to define practice principles that

generally should assist in producing high-quality medical care. The membership of the Society of Interventional Radiology Standards of Practice Committee represents experts in a broad spectrum of interventional procedures from both the private and academic sectors of medicine, and as such they represent a valid expertise on preprocedural coagulation status and antibiotic prophylaxis.

A platelet count of 50,000/ μ L or lower requires a platelet infusion at the time of the interventional procedure.¹ We generally prefer a prothrombin time of 18 seconds or less and will recommend administration of vitamin K and fresh frozen plasma in the nonacute and acute settings, respectively, to achieve this. Cessation of warfarin and clopidogrel is recommended for 4 to 5 days before the procedure. Unfractionated heparin should be stopped at least 4 hours and low-molecular-weight heparin should be stopped at least 12 hours in advance of the procedure.²

Although the risk is low in nonobstructed ductal systems, infection is a significant contributor to morbidity and mortality, particularly in elderly or immunocompromised patients with gallbladder and hepatobiliary disease. We recommend prophylactic intravenous antibiotics in all patients undergoing procedures with few exceptions.³ Our preferred antibiotics are 1 g of ceftriaxone and 1.5 to 3 g of ampicillin/sulbactam. The hospital pharmacy and the infectious disease service are useful resources for appropriate antibiotic use.

Preprocedural verification and skin marking should be standard as part of the Universal Protocol.⁴ The Universal Protocol was created to address the continuing occurrence of wrong site, wrong procedure, and wrong person surgery in Joint Commission–accredited organizations. The three principal components of the Universal Protocol include a preprocedure verification, site marking as previously mentioned, and a time-out. A time-out for patient safety is called immediately before the procedure, which includes identifying the patient by name and the type and site of procedure to be done.⁵

Percutaneous Cholecystostomy

Acute cholecystitis is the most common cause of acute right upper quadrant pain and occurs in approximately one third of patients with gallstones. In most cases, the condition is due to calculous obstruction of the gallbladder neck or cystic duct, leading to increased intraluminal pressure and distention of the gallbladder.

Although early laparoscopic cholecystectomy is typically the preferred and definitive treatment for acute cholecystitis, the morbidity and mortality increase with the patient's age and complexity, and percutaneous cholecystostomy (PC) has been used as a temporizing and sometimes definitive therapy in high-risk patients. This is a minimally invasive method of

percutaneous placement of a drainage catheter in the gallbladder lumen under ultrasound and fluoroscopic guidance. A positive clinical response, which varies between 56% and 100%, is considered when there is a decrease in white blood cell count, defervescence, and decrease in the need for vasopressors. The risks of PC (bleeding, infection, and visceral perforation) are low. Mortality is associated mainly with the underlying medical conditions. PC can be followed by elective cholecystectomy at a later stage if the patient's condition permits or by expectant or conservative management in those with acalculous cholecystitis.

The earliest reports describing PC for the treatment of acute cholecystitis date back some 30 years.^{6,7} Since then, multiple relatively small and predominantly single-institution series have been published, collectively supporting a role for imaging-guided percutaneous gallbladder decompression in high-risk patients.⁸⁻¹²

In a review of Medicare data between 1994 and 2009, annual PC procedures increased by 567% (from 1085 to 7239). During the same period, laparoscopic cholecystectomy procedures increased by 3% (from 203,836 to 209,650), and open procedures declined by 73%.¹³ Clinical acceptance of PC and the availability and expertise of interventional radiologists have both contributed to an increased use of PC. Expanding the availability of PC may have acted as a "convenience factor" as well, lowering thresholds for use over time and thus contributing to PC's growth. Some growth is also attributable to an aging population with an increasing number of comorbidities.

Traditionally, it was believed that whereas percutaneous drainage represented a valuable intervention, secondary cholecystectomy was mandatory in cases of acute calculous cholecystitis.¹⁴ However, considering limited survival and a low recurrence rate of cholecystitis in elderly high-risk patients with acute cholecystitis, PC is increasingly being accepted as a definitive treatment, and cholecystectomy may not be necessary after resolution of the acute symptoms with gallbladder drain exchanges every 6 to 8 weeks.¹⁵⁻¹⁷

Without evidence from randomized controlled trials comparing PC with surgery in such populations, however, the optimal role and timing of PC remain unclear. Historically, PC has been used in higher risk, often elderly and critically ill patients. As a result, studies comparing the percutaneous technique with cholecystectomy have shared a retrospective study design and selection bias as they have not evaluated comparable groups. Abi-Haidar and colleagues¹⁸ described a 10-year cohort of patients who underwent both techniques. As in other studies, the PC patients were older, had higher American Society of Anesthesiologists classification, and had more comorbidities.¹⁹ Not surprisingly, they experienced more readmissions and complications and had a longer hospital stay. The Cochrane Database Review Group compared two randomized prospective studies, PC followed by early laparoscopic cholecystectomy versus delayed laparoscopic cholecystectomy (70 patients) and PC versus conservative treatment (86 patients), and concluded that the studies had high risk of bias.²⁰⁻²² There was no significant difference in overall morbidity between the two intervention groups. On the basis of available evidence from these randomized clinical trials, the Cochrane Review Group was unable to determine the role of PC in the clinical management of high-risk surgical patients with acute cholecystitis and expressed a need for adequately powered randomized clinical trials of low risk of bias.

Two patient populations deserve consideration for this procedure: those with critical illness and those with a high likelihood of conversion from a laparoscopic to an open procedure. In the case of critical illness, particularly patients who develop acute cholecystitis during an intensive care unit stay, PC has a continued role in light of evidence that emergency cholecystectomy in the critically ill is associated with higher mortality rates than cholecystectomy.²³

An international consensus panel of hepatobiliary surgeons defined the diagnostic criteria and severity assessment of acute cholecystitis as part of the Tokyo Guidelines (TG07) in January 2007. In the TG07, PC should be used in patients with grade II (moderate) cholecystitis only when they do not respond to conservative treatment and for patients with grade III (severe) disease. For patients with severe (grade III) disease, gallbladder drainage is recommended, followed by intensive care.

The updated Tokyo Guidelines 2013 (TG13) describe the surgical treatment for acute cholecystitis according to the grade of severity, the timing, and the procedure used for cholecystitis in a question-and-answer format using the evidence concerning surgical management of acute cholecystitis. Consequently, it was agreed that cholecystectomy is preferable early after admission. However, literature concerning the surgical treatment according to the grade of severity could not be quoted because there have been no publications on this topic, but the consensus was to perform percutaneous drainage when conservative treatment is failing. One prospective study showed that predictors for failure of conservative treatment are age older than 70 years, diabetes, tachycardia, and distended gallbladder at admission. Likewise, white blood cell count ($>15,000$ cells/mL), elevated temperature, and age older than 70 years were found to be predictors for the failure of conservative treatment at 24- and 48-hour follow-up.²⁴

The CHOCOLATE trial is a current randomized controlled, parallel-group, superiority multicenter trial in The Netherlands in which high-risk patients with acute calculous cholecystitis will be randomized to laparoscopic cholecystectomy or PC.²⁵

TECHNIQUE

Work-up includes review of the patient's clinical status and imaging. The authors use a combination of ultrasound and fluoroscopic guidance to place a locking pigtail catheter in the gallbladder by a modified Seldinger technique. Liberal use of subcutaneous lidocaine is recommended in addition to conscious sedation with intravenous midazolam and fentanyl. Typically, an 18-gauge needle is advanced percutaneously into the gallbladder, after which the track is dilated over a short Amplatz stiff guidewire (Cook Medical, Bloomington, IN) with 6F and 8F dilators, followed by placement of an 8F locking pigtail that is connected to gravity drainage (Fig. 78-1). Speed is of the essence during the procedure as bile leakage during dilator exchange and catheter placement may be very painful. Technique modifications include use of a transhepatic instead of a transperitoneal route because of a higher risk of complications due to drain dislocation and also the use of a single-stick or trocar method to access the gallbladder instead of the Seldinger technique. Intuitively, the trocar or single-stick technique should be less painful and is preferred by some to the Seldinger technique for catheter placement. However, we think that the trocar technique may be more difficult in patients whose gallbladders are small or thick walled.

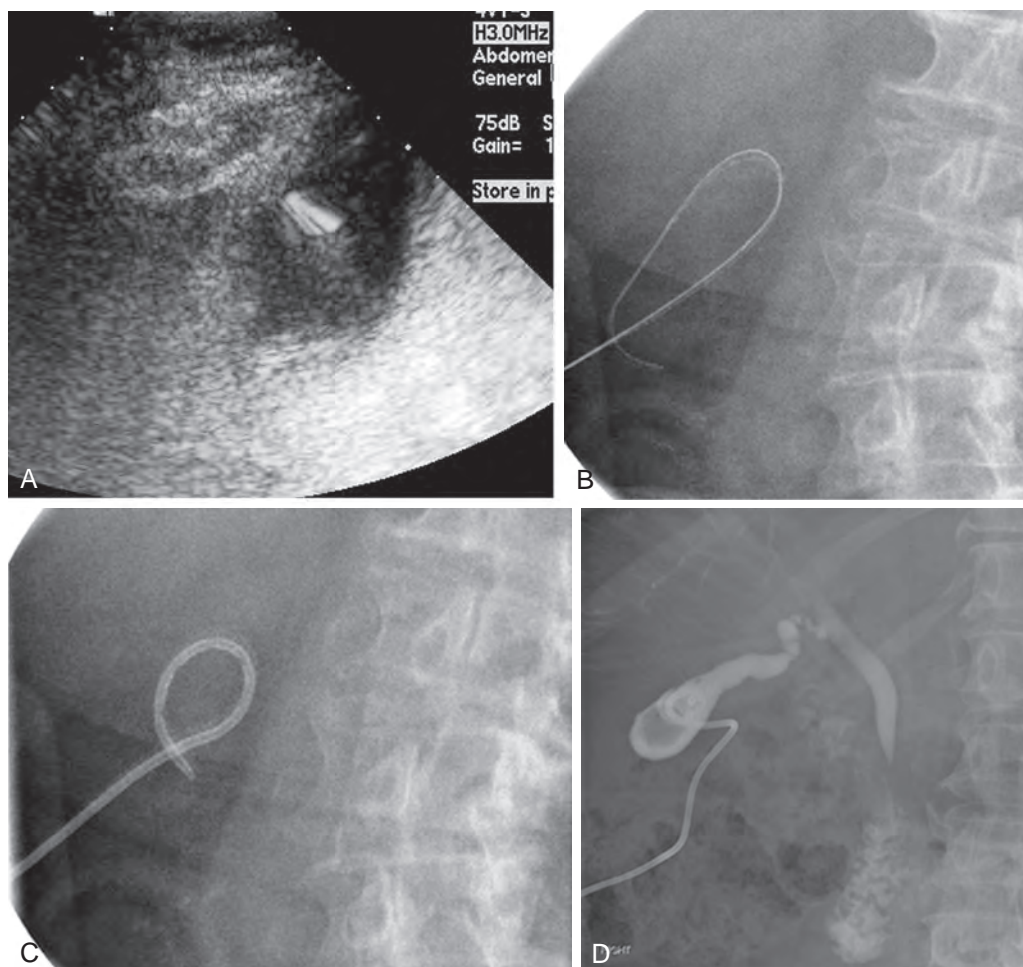


Figure 78-1 Percutaneous cholecystostomy. **A.** Ultrasound confirms position of needle in the gallbladder. **B.** Placement of a guidewire in the gallbladder. **C.** Placement of 8F pigtail drain in the gallbladder. **D.** Tube check several days later confirms a gallstone in the gallbladder and patency of the cystic duct. The tube was capped, and the patient had a cholecystectomy.

We rarely inject more than a few milliliters of contrast material to confirm the location of the tube to avoid bacteremia. A tube check is better done within 5 to 7 days to evaluate for cystic and common duct patency, followed by capping of the tube to promote internal drainage.

Percutaneous Gallbladder Aspiration

Ultrasound-guided aspiration of gallbladder contents offers a less invasive and sometimes just as effective an alternative to percutaneous gallbladder drainage for acute cholecystitis. The procedure can be performed at the bedside under ultrasound guidance with either a 21- or 18-gauge needle and has two main advantages over PC. First, the quoted complication rate is lower because aspiration involves fewer steps than drainage and the needle is narrower than any drainage catheter placed. Second, the patient's comfort and convenience are better with aspiration as the presence of a drainage catheter and bag may be cumbersome. In certain situations, however, PC is preferable to gallbladder aspiration. Aspiration may not be technically feasible in patients with viscous bile. Also, because it does not provide

continuous drainage, gallbladder aspiration is inappropriate in patients in whom the indication for gallbladder drainage is to provide relief from a distal biliary obstruction.

In a meta-analysis of 11 studies comparing aspiration with PC, the clinical response to PC was slightly better compared with aspiration.²⁶ However, the complication rate of PC was also higher than that of aspiration, with 4 of the 11 studies in this review having a complication rate in the range of 10% to 23%, which is well above the threshold set by the Society of Interventional Radiology Standards Committee.²⁷

In one of these comparative studies, the authors recommended that aspiration should be the procedure of choice in high-risk patients, reserving PC as a salvage procedure if aspiration is technically or clinically unsuccessful.²⁸ Interestingly, almost one quarter of patients in this study did not show a clinical response within 72 hours of gallbladder aspiration and had a salvage PC. Using this approach of gallbladder aspiration with salvage PC, the authors avoided PC in 77% of patients while obtaining the overall positive clinical response rate close to that of PC.

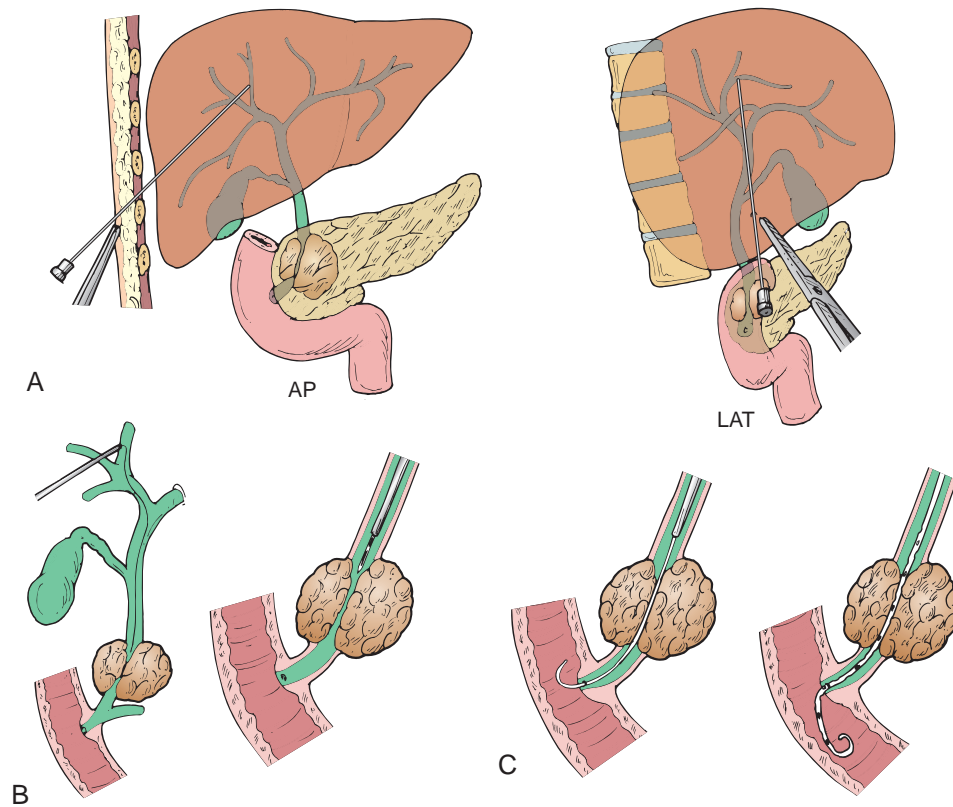


Figure 78-2 One-stick percutaneous transhepatic biliary drainage (PTBD). **A.** The 22-gauge needle tip is advanced into an appropriate duct for conversion. AP, Anteroposterior view; LAT, lateral view. **B.** After removal of the stylet, a 0.018-inch guidewire is inserted and advanced into the common bile duct. The 22-gauge needle is removed, and coaxial dilators are inserted. **C.** The inner dilator is removed, which permits placement of larger guidewires that negotiate the obstruction into the duodenum. Subsequently, a PTBD catheter is inserted. (From Kadir S: Percutaneous transhepatic cholangiography and biliary drainage. In Kadir S [ed]: *Current Practice of Interventional Radiology*. Philadelphia, BC Decker, 1991, pp 497–510.)

Acalculous Cholecystitis

Acute cholecystitis can develop without gallstones in critically ill or injured patients.²⁹ However, the development of acute acalculous cholecystitis is not limited to surgical or injured patients or even to the intensive care unit. Diabetes, malignant disease, abdominal vasculitis, congestive heart failure, cholesterol embolization, and shock or cardiac arrest have been associated with acute acalculous cholecystitis. Children may also be affected, especially after a viral illness. The pathogenesis of acalculous cholecystitis is thought to include ischemia and reperfusion injury, but opioids, positive pressure ventilation, and total parenteral nutrition have been implicated. The clinical presentation is nonspecific, and significant delays in diagnosis result in a high incidence of gangrene, perforation, abscess, and death.^{30,31} To improve outcome, a high index of suspicion with early imaging, often using multiple studies, is necessary. Ultrasound of the gallbladder is the most accurate diagnostic modality in the critically ill patient, with gallbladder wall thickness of 3.5 mm or greater and pericholecystic fluid being the two most reliable findings.³²

Boland and associates⁹ recommend prophylactic PC for all intensive care unit patients with abdominal sepsis who are not improving and for whom no other etiology can be found. In their series, almost 60% of these patients improved

without further treatment. In the rest, the gallbladder was excluded as the source of sepsis, redirecting the search elsewhere.

Interval cholecystectomy is usually not indicated after acalculous cholecystitis in survivors. If the absence of gallstones is confirmed and the precipitating disorder has been controlled, the cholecystostomy tube can be removed once a track has formed after the patient has recovered.³²

Percutaneous Transhepatic Cholangiography and Drainage

Percutaneous transhepatic cholangiography (PTC) is used to visualize the intrahepatic and extrahepatic ductal system, most commonly to identify the nature and location of biliary obstruction due to stones, tumor, or benign stricture and less commonly to detect a bile leak (Fig. 78-2). If either obstruction or leak is diagnosed, percutaneous biliary drainage, with or without adjunctive stenting, is usually attempted at the same time. Although magnetic resonance cholangiopancreatography (MRCP) also visualizes the ductal system, the combination of PTC and drainage (PTCD) allows a one-step diagnosis and treatment procedure. The majority of patients requiring drainage have malignant disease and eventually have a metallic stent

placed. Percutaneous transhepatic access is also useful for balloon dilation of strictures and biopsy.

TECHNIQUE

For a right-sided fluoroscopic approach, an intercostal point in the midaxillary line is marked in the mid liver with attention paid to the locations of the pleura and colon. The patient should have received antibiotics and conscious sedation. After liberal injection of local anesthetic subcutaneously and down to the hepatic capsule, a 15-cm 22-gauge needle is advanced into the liver in a slightly cephalad direction. The needle obturator is removed and the needle is gradually withdrawn while contrast material is injected gently. Opacification of a bile duct is characterized by an accumulation of contrast material, which persists, unlike vascular opacification, which is transient. Another confirmatory feature is that contrast material in the biliary system drains toward the hilum, in contrast to hepatic arterial or portal venous flow, which is away from the hilum. However, if the biliary tract is occluded, flow of contrast material within it may be very slow. Nondilated ducts are more difficult to access. Next, having confirmed that the opacified bile duct has been accessed peripherally, one should advance a 0.018-inch guidewire into the ductal system as far as the obstruction under fluoroscopic guidance. The authors prefer to use a Neff set (Cook), which is a tapered triaxial access system. Once the Neff dilator is in the duct, its inner two components can be removed, and a 5F Kumpe catheter (Cook) and guidewire can be used to traverse the duct obstruction and to access the duodenum. Once the catheter is in the duodenum, the guidewire can be changed for a stiffer version over which an 8F or 10F internal/external biliary drainage catheter is advanced and the pigtail loop formed in the duodenum. This drainage catheter has multiple side holes allowing drainage above and below the biliary tract obstruction. If traversal of the biliary obstruction is not possible initially, placement of a pigtail drain above the obstruction allows external decompression, and traversal of the obstruction is reattempted after several days.

A left-sided PTC is usually under ultrasound guidance with a subcostal approach to access a segment II or III duct. Once the intraductal needle tip location is confirmed on ultrasound, contrast material is injected, outlining the duct. Again, placement of an internal/external or external biliary drainage catheter is as previously described.

COMPLICATIONS

Important complications include bleeding, infection, and visceral perforation.³³ Significant bleeding, which occurs in 2% to 3%, may be classified on the basis of its source: perihepatic bleed sites (hemothorax, hemoperitoneum, subcapsular hepatic hematoma); gastrointestinal bleeding (hemobilia or melena); and bleeding from the percutaneous biliary drain itself, which is the most common clinical presentation.³⁴ Methods to evaluate and to treat this complication include tractography, angiography, track embolization, arterial embolization, and track site changes.³⁵ Bleeding is more common when the ductal system is accessed centrally than peripherally. Left-sided PTCD is associated with a higher bleeding complication rate than a right-sided approach, presumably because of the greater proximity to larger vessels.³⁶

Significant pain can occur after removal of transhepatic catheters from biliary access tracks, after percutaneous biliary drainage or stenting. The track may be embolized to prevent bile leak and bleeding, reducing the patient's pain.³⁷

Biliary Strictures

MALIGNANT STRICTURE

Bile duct obstruction is commonly caused by pancreaticobiliary malignant neoplasms including gallbladder cancer, cholangiocarcinoma, and pancreatic neoplasms that are frequently unresectable at the time of diagnosis. Inoperable malignant bile duct obstruction can be palliated with surgical bypass, placement of percutaneous biliary drainage catheters, and endoscopic or percutaneous biliary stenting. Indications for biliary drainage/stenting include pruritus, cholangitis, and lowering of bilirubin concentration (<2 mg/dL) before chemotherapy.

Percutaneous biliary drainage is achieved by placement of an internal/external or external plastic pigtail drain after PTC as outlined before. In a review of patients with malignant biliary obstruction who had placement of internal/external biliary drains for lowering of bilirubin concentration, pericatheter leakage occurred in nearly one third of cases, requiring three visits per 100 catheter-days, or approximately one per month.³⁸ Only 31% of patients attained a normal serum bilirubin level by 100 days, and median overall survival was 107 days. Careful patient selection is warranted before biliary drainage for this indication. Maximal biliary drainage, a preprocedure total serum bilirubin concentration of less than 9 mg/dL, and a lower international normalized ratio were factors associated with normalization of the serum bilirubin level in this cohort. In another study from the same institution, it was found that the patient's "quality of life" did not improve after catheter drainage regardless of technical success. Whereas palliation of pruritus was probable, the procedure was less successful in lowering the serum bilirubin concentration to a level that permitted the administration of chemotherapy. The authors concluded that biliary drainage without a clear clinical indication was not supported.³⁹

Internalization of drainage may be achieved with either plastic or metal stents. Compared with plastic stents, metal stents are of larger diameter, have better long-term patency, and are more expensive. The use of metal stents is preferred for patients who are expected to survive for more than 6 months, whereas for patients who are likely to survive for less than 6 months, the use of plastic stents is appropriate. Obstruction in a metal stent may be caused by bile sludge, food debris, or tumor ingrowth. To overcome the last problem, covered metal stents were developed, and these stents are now used in patients with malignant distal biliary obstruction. However, despite their superiority over noncovered stents in terms of improved patency, the incidence of acute cholecystitis and stent migration is higher.⁴⁰

Traditionally, endoscopic stent placement was the preferred method to treat bile duct obstruction because it had higher success and lower complication rates and did not require an external drainage catheter.⁴¹ More recent studies reflect a reversal of this experience, with percutaneous stent placement being more successful and associated with fewer complications than endoscopic procedures, with the main procedural complication, cholangitis, occurring almost five times more commonly with

endoscopically placed stents than with percutaneously placed ones.⁴²⁻⁴⁴ Percutaneous transcholecystic placement of metallic stents is a feasible and effective method to manage malignant obstruction at the lower level of the common bile duct when conventional biliary drainage through transhepatic or endoscopic access is technically difficult.⁴⁵

In primary stenting, the stent is placed at the same session as the initial biliary system access, and this has been found to be effective and safer than a staged procedure with secondary stenting. In a review of 61 patients stented transhepatically for malignant biliary duct obstruction, the rate of major complications was 23% in the primarily stented group and 54% in the secondarily stented group.⁴⁶ Primary stenting is also more cost-effective because of a shorter hospital stay. Reduced morbidity and hospital stay with this technique has been corroborated by other investigators.⁴⁷⁻⁴⁹

A reasonable approach to draining patients with bilobar biliary obstruction may be to insert only a single metallic stent into a liver lobe that constitutes 70% or more of the liver volume, is less involved by tumor than the other lobe, and is supplied by a patent lobar portal vein branch.⁵⁰ Patients with liver lobes of similar size and patent lobar portal vein branches might benefit from bilobar drainage. Drainage of more than two biliary segments is best avoided, except in patients presenting with cholangitis, because of a higher complication rate. The main predictive factor for drainage effectiveness in patients with hilar tumors was a drained liver volume of more than 50%, especially in Bismuth III strictures, which may require bilateral stent placement.⁵¹ Draining an atrophic lobe (<30% of volume) is ineffective and increases the risk of cholangitis.

BENIGN STRICTURE

Percutaneous balloon dilation has become a safe and effective long-term alternative to endoscopic or surgical treatment for benign biliary strictures of various causes.^{52,53} According to the location of the involved duct, the strictures can be categorized as duct anastomotic, biliary-enteric anastomotic, and duct non-anastomotic. The anastomotic strictures represent localized narrowing caused by fibrosis, whereas the nonanastomotic strictures are likely to be associated with ductal ischemia from damage to the bile duct arteries from a variety of causes, including hepatic artery thrombosis. A stricture developing after biliary-enteric anastomosis after low division of the bile duct may be explained by damage to the bile duct artery. Recent experience suggests that anastomotic strictures are more amenable than nonanastomotic strictures to balloon dilation⁵⁴ (Fig. 78-3).

The dilation of the benign stricture is usually performed with a noncompliant balloon (8- to 12-mm diameter) and may be repeated at regular intervals until cholangiography demonstrates free drainage of contrast material to the bowel and no residual stenosis. The internal/external biliary drain is removed after a clinical trial of catheter clamping and a normal cholangiogram.

Percutaneous treatment of benign biliary strictures with extended use of a calibrated internal/external (up to 15F) plastic drain has also had good long-term results.⁵⁵ Endoscopically placed retrievable covered self-expandable metal stents are a recent alternative to progressive plastic stenting for the treatment of benign strictures with the prospect of a higher treatment efficacy and the need for fewer tube changes.⁵⁶

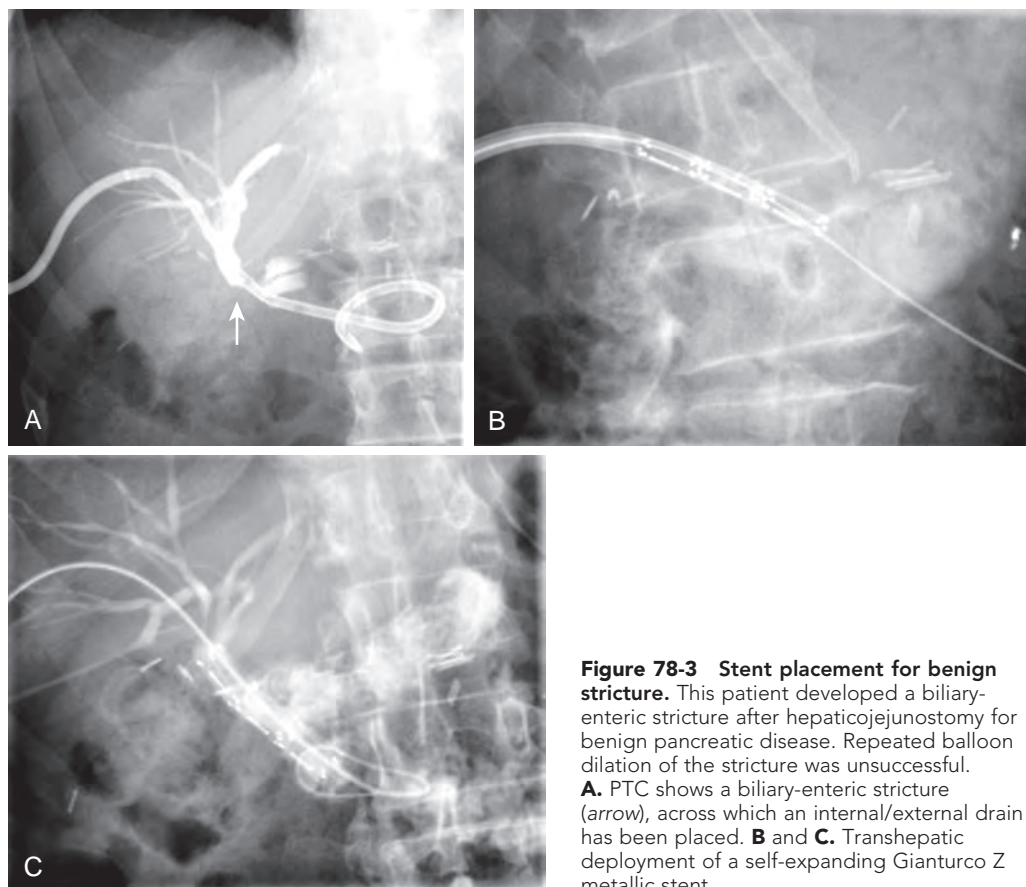


Figure 78-3 Stent placement for benign stricture. This patient developed a biliary-enteric stricture after hepaticojejunostomy for benign pancreatic disease. Repeated balloon dilation of the stricture was unsuccessful. **A.** PTC shows a biliary-enteric stricture (arrow), across which an internal/external drain has been placed. **B** and **C.** Transhepatic deployment of a self-expanding Gianturco Z metallic stent.

Endoscopic intervention is frequently not possible after a Roux-en-Y hepaticojejunostomy or choledochojejunostomy, and percutaneous transhepatic biliary intervention is limited by its inability to access all segments of the biliary tree in a single puncture and carries morbidity as well as discomfort for the patient. A percutaneous transjejunal approach uses an efferent or afferent limb of the Roux-en-Y loop, which is fixed to the peritoneum with the fixation site marked with surgical clips (Hutson loop). Radiologic access is provided to the biliary tree for diagnostic cholangiography, stricture dilation, and intrahepatic stone clearance. Percutaneous catheters need be left in place only for short-term planned repeated interventions (usually in the same admission) for stone disease or for adequate drainage in the case of purulent cholangitis. High success rates and short hospitalizations together with few complications make this option a well-accepted and integral part of managing complex biliary problems.^{57,58}

Common Duct Stone Removal

Up to 18% of people undergoing cholecystectomy for gallstones have common duct stones, which may be treated with exploration (open or laparoscopic) or with endoscopic retrograde cholangiopancreatography (ERCP) before or after cholecystectomy in two stages, usually combined with either sphincterotomy (most common) or sphincteroplasty (papillary dilation) for common bile duct clearance.

The interventionalist may be asked to treat retained bile duct stones through a postoperative drain (T tube or transcystic) placed during cholecystectomy. A less commonly used alternative to these approaches is percutaneous transhepatic removal of bile duct stones when the endoscopic approach fails because of anatomic anomalies or is refused by the patient. Percutaneous transhepatic balloon dilation of the papilla of Vater is performed, followed by pushing of the stones out into the duodenum with a Fogarty balloon catheter. If the stone diameter is larger than 15 mm, basket lithotripsy is recommended before balloon dilation. The overall success rate is greater than 95%, with cholangitis occurring in less than 3% of patients.^{59,60}

Transhepatic cholangioscopy may be necessary for treatment of patients with intrahepatic lithiasis or common bile duct calculi not approachable with retrograde endoscopy, in which direct vision is essential. In patients with very large ductal stones, cholangioscopy combined with percutaneous intracorporeal lithotripsy equipment remains a useful tool.^{61,62}

Percutaneous cholecystolithotomy represents a minimally invasive alternative to cholecystectomy with the disadvantage that gallstones may recur. The procedure consists of three parts: initial PC, track dilation and stone removal, and track evaluation and tube removal. The success rate is as high as 97%, with the main major complication of bile leakage after tube removal reported in less than 10% of patients.^{63,64}

Bile Duct Injury

Bile duct injury (BDI) may occur after gallbladder, pancreas, colonic, and gastric surgery, with laparoscopic cholecystectomy responsible for 80% to 85% of occurrences. Although rare, BDI during laparoscopic cholecystectomy is twice as frequent compared with injury during an open procedure (0.3% open vs. 0.6% laparoscopic), a difference that is not statistically significant. Historically, most BDIs were surgical in nature, with laparoscopic cholecystectomy and liver transplantation

accounting for the majority of cases. Increasingly, ischemic bile duct strictures and bilomas are recognized as a result of hepatic artery chemoembolization and radioembolization treatments for hepatic malignant neoplasms.⁶⁵⁻⁶⁷

Only one third of laparoscopic BDIs are recognized during operation. The majority of patients present initially with non-specific symptoms. Management depends on timing of recognition and the type, extent, and level of the injury. Immediate recognition and repair are associated with improved outcome, and the standard of care after recognition of BDI is referral to a tertiary care hospital that can provide a multidisciplinary approach. Inadequate management may lead to severe complications, with the late clinical course of BDI resulting in chronic liver disease, cirrhosis, and portal hypertension, for which liver transplantation is an option.⁶⁸

BDI may cause bile leakage, abscesses, cholangitis, and secondary biliary cirrhosis due to chronic strictures. The role of interventional radiology in managing patients with BDI is to document the location and nature of the injury, to drain or divert bile, and to promote and provide long-term biliary drainage when appropriate.⁶⁹ Imaging is essential for the evaluation of BDI and subsequent treatment and includes cholescintigraphy, ultrasonography, computed tomography, ERCP, PTCD, and fluoroscopy with a contrast medium injected through a surgically or percutaneously placed biliary drainage catheter.

PTC accurately depicts the location and nature of major BDIs in most patients but may not reliably distinguish injuries at the confluence of the lobar ducts from injuries involving the cephalad 2 cm of the common hepatic duct.⁷⁰ MRCP is replacing PTC as the main diagnostic technique for detecting and localizing bile leaks and has become a reliable and non-invasive way of evaluating the intrahepatic and extrahepatic system.⁷¹⁻⁷³

Depending on the type of injury, management may include endoscopic, percutaneous, and open surgical interventions or a combination of all three options. Percutaneous interventions include drainage of bilomas, abscesses, and obstructed ducts. Additional percutaneous procedures include U-tube placement and balloon dilation and stenting of bile duct strictures. Endoscopic and percutaneous interventional procedures may be performed for definitive treatment in patients with biliary-enteric continuity or as adjuncts to definitive surgical repair. The interventionalist is sometimes challenged to restore biliary-enteric continuity with remarkable ingenuity and innovation.^{74,75}

In a 10-year review of 51 patients with intact biliary-enteric continuity referred for management of BDI, all patients had PTCD followed by balloon dilation and long-term internal/external catheter drainage.⁷⁶ Fifty patients (98%) were drain free at mean follow-up of 76 months, and the success rate of percutaneous management was 58%, without need for subsequent intervention. Percutaneous treatment was more likely to fail in patients who had an internal/external drain for less than 4 months.

Multiple BDI classifications have been developed before and during the laparoscopic era. The Bismuth-Corlette classification was introduced before laparoscopy and is based on the complete section of the common bile duct and the length of the proximal bile duct stump.⁷⁷ Type I is a low injury with a stump length of more than 2 cm. Type II is a middle-level injury with a stump length of less than 2 cm. Type III is a high-level injury without common hepatic duct available but preserved confluence. Type IV involves loss of hepatic confluence with no communication

between right and left ducts. There is no Type V. It is difficult to apply this classification system to laparoscopic BDI as most of the technical factors and mechanisms of injury are different from open surgery.

The Strasberg classification offers a comprehensive classification of laparoscopic BDI.⁷⁸ Injuries are divided into five groups (A to E); the E class is similar to the Bismuth classification, a complex BDI with a complete transection of the duct. Only right and left partial injuries (which account for less than 10% in most series) are not included in this classification. Class A represents a bile leak from the cystic duct or an accessory duct. In both conditions, there is continuity with the common bile duct. Class B is the section of an accessory duct with no continuity with the common bile duct. Class C represents a leak from a bile duct with no continuity with the common bile duct. Class D is a partial section of a bile duct with no complete loss of continuity with the rest of the bile duct system. Class E is a complete transection of the bile duct with subtypes according to the length of the stump (E1-E5) (Strasberg types E1-E4 correspond to Bismuth types I-V).

BDIs are frequently accompanied by vascular injuries, which may worsen the injury and cause liver ischemia.⁷⁹ Right hepatic artery vasculobiliary injury is the most common variant and extends the biliary injury to a higher level than the grossly observed mechanical injury. Vasculobiliary injury results in slow hepatic infarction in about 10% of patients. Repair of the artery is rarely possible and the overall benefit is unclear. Injuries involving the portal vein or common or proper hepatic arteries are much less common but have more serious effects, including rapid infarction of the liver. Routine arteriography is recommended in patients with a biliary injury if early repair is contemplated. Consideration should be given to delaying repair of a biliary injury in patients with occlusion of the right hepatic artery. Patients with injuries to the portal vein or proper or common hepatic artery should be emergently referred to tertiary care centers.

A Strasberg class E5 injury is defined by a complete loss of biliary-enteric continuity and is best treated surgically. Devascularization and loss of bile duct tissue necessitate creation of a Roux-en-Y hepatojejunostomy, a procedure that guarantees well-perfused bile ducts and a low-tension anastomosis (Fig. 78-4). Partial resection of IV and V segments may be necessary to facilitate identification of bile ducts and proper positioning of the jejunal loop. By contrast, the less preferable choledochocolocholedochal or hepatoduodenal anastomoses involve devascularized ducts and the duodenum tends to move caudally, increasing the anastomotic tension.

In a meta-analysis of 31 studies, a total of 99 partial hepatectomies were reported among 1756 (5.6%) patients referred for postcholecystectomy BDI.⁸⁰ Multivariate analysis showed that hepatic arterial and Strasberg E4 and E5 injuries were independent factors associated with partial hepatectomy, and those patients with combined arterial and Strasberg E4 or E5 injury were 43.3 times more likely to undergo partial hepatectomy than were patients without complex injury. Despite the high postoperative morbidity, mortality rates were comparable with those of hepaticojejunostomy.

Primary Sclerosing Cholangitis

Primary sclerosing cholangitis (PSC) is a chronic inflammatory disease characterized by the destruction of medium-sized to large bile ducts and intense concentric fibrosis. Complications



Figure 78-4 Bile duct injury. Right-sided PTC shows a complete occlusion at the duct confluence due to a surgical clip. Traversal of this occlusion and placement of an internal/external drain were not possible, and the patient required a hepaticojejunostomy.

of PSC include bacterial cholangitis, cirrhosis, and cholangiocarcinoma. BDI results from the sustained inflammation and production of inflammatory cytokines. Biliary strictures may cause further damage as a result of bile stasis and recurrent secondary bacterial cholangitis. A retrospective study of 71 patients with PSC showed no additional benefit from stenting after balloon dilation in the treatment of dominant strictures. Stenting was associated with more complications.⁸¹ The only proven curative treatment for PSC is liver transplantation.

Patients with PSC are at risk for development of superimposed cholangiocarcinoma with a 10-year cumulative incidence of approximately 7% to 9%. Cholangiocarcinoma mimics the stricturing process of PSC, and the diagnosis of cholangiocarcinoma in the setting of PSC remains challenging if a mass lesion is not identified by imaging studies. The most definitive evidence of cholangiocarcinoma is a mass lesion with delayed venous phase enhancement on imaging and a positive cytology or biopsy finding.⁸²

Biopsy

Malignant disease of the biliary tract may be a difficult diagnosis to make as radiologic features are nonspecific. Biliary strictures may be directly sampled by brushing, forceps biopsy, fine-needle aspiration, or a combination of these. Cytologic evaluation of brushings obtained endoscopically from the biliary tree is currently the standard of care in most institutions. However, this technique has been plagued by low sensitivity and interpretative difficulties in differentiating reactive from malignant cytologic features. Simply submitting the entire cytology brush for histologic sectioning may increase the sensitivity to 90%.⁸³ The use of fluorescent in situ hybridization technique also increases the sensitivity of cytology.

Alternatively, percutaneous transluminal forceps biopsy is a safe procedure that is easy to perform through a transhepatic biliary drainage tract, in which it is relatively accurate in the diagnosis of malignant biliary obstructions.⁸⁴ In a comparative study, 108 patients underwent forceps biopsy plus cytologic sampling by washing of the forceps device in cytologic solution.⁸⁵ Histologic diagnosis after forceps biopsy was more successful than cytology, with a sensitivity of 78% versus 61% and negative predictive value of 30% versus 19%. Cytology results were never positive when the forceps biopsy finding was negative.

Photodynamic therapy (PDT) is a local, minimally invasive palliative treatment for unresectable cholangiocarcinoma. PDT

uses a photosensitive molecule that accumulates in tumors. Activation of the photosensitizer by a laser introduced endoscopically or percutaneously generates reactive oxygen radicals, leading to selective tumor cell death. Results from two prospective randomized controlled trials comparing PDT after stent insertion with stents alone for patients with unresectable cholangiocarcinoma have shown dramatically prolonged median survival and improved performance status in the PDT group compared with the non-PDT group.^{86,87} The procedures were generally well tolerated and are associated with outcomes as favorable as those of adjuvant and neoadjuvant therapy for cholangiocarcinoma.

REFERENCES

- Patel IJ, Davidson JC, Nikolic B, et al: Consensus guidelines for periprocedural management of coagulation status and hemostasis risk in percutaneous image-guided interventions. *J Vasc Interv Radiol* 23:727–736, 2012.
- Patel IJ, Davidson JC, Nikolic B, et al: Addendum of newer anticoagulants to the SIR consensus guideline. *J Vasc Interv Radiol* 24:641–645, 2013.
- Venkatesan AM, Kundu S, Sacks D, et al: Practice guidelines for adult antibiotic prophylaxis during vascular and interventional radiology procedures. Written by the Standards of Practice Committee for the Society of Interventional Radiology and Endorsed by the Cardiovascular Interventional Radiological Society of Europe and Canadian Interventional Radiology Association [corrected]. *J Vasc Interv Radiol* 21:1611–1630, quiz 1631, 2010.
- The Joint Commission: Universal protocol for preventing wrong site, wrong procedure, wrong person surgery. http://www.jointcommission.org/standards_information/up.aspx.
- Angle JF, Nemcek AA, Jr, Cohen AM, et al: Quality improvement guidelines for preventing wrong site, wrong procedure, and wrong person errors: Application of the Joint Commission “universal protocol for preventing wrong site, wrong procedure, wrong person surgery” to the practice of interventional radiology. *J Vasc Interv Radiol* 20(Suppl):S256–S262, 2009.
- Radder RW: Ultrasonically guided percutaneous catheter drainage for gallbladder empyema. *Diagn Imaging* 49:330–333, 1980.
- Shaver RW, Hawkins IF, Jr, Soong J: Percutaneous cholecystostomy. *AJR Am J Roentgenol* 138:1133–1136, 1982.
- Browning PD, McGahan JP, Gerscovich EO: Percutaneous cholecystostomy for suspected acute cholecystitis in the hospitalized patient. *J Vasc Interv Radiol* 4:531–537, discussion 537–538, 1993.
- Boland GW, Lee MJ, Leung J, Mueller PR: Percutaneous cholecystostomy in critically ill patients: Early response and final outcome in 82 patients. *AJR Am J Roentgenol* 163:339–342, 1994.
- Lo LD, Vogelzang RL, Braun MA, Nemcek AA, Jr: Percutaneous cholecystostomy for the diagnosis and treatment of acute calculous and acalculous cholecystitis. *J Vasc Interv Radiol* 6:629–634, 1995.
- Cherng N, Witkowski ET, Sneider EB, et al: Use of cholecystostomy tubes in the management of patients with primary diagnosis of acute cholecystitis. *J Am Coll Surg* 214:196–201, 2012.
- Joseph T, Unver K, Hwang GL, et al: Percutaneous cholecystostomy for acute cholecystitis: Ten-year experience. *J Vasc Interv Radiol* 23:83–88.e1, 2012.
- Duszak R, Jr, Behrman SW: National trends in percutaneous cholecystostomy between 1994 and 2009: Perspectives from Medicare provider claims. *J Am Coll Radiol* 9:474–479, 2012.
- Melloul E, Denys A, Demartines N, et al: Percutaneous drainage versus emergency cholecystectomy for the treatment of acute cholecystitis in critically ill patients: Does it matter? *World J Surg* 35:826–833, 2011.
- Griniatsos J, Petrou A, Pappas P, et al: Percutaneous cholecystostomy without interval cholecystectomy as definitive treatment of acute cholecystitis in elderly and critically ill patients. *South Med J* 101:586–590, 2008.
- Li M, Li N, Ji W, et al: Percutaneous cholecystostomy is a definitive treatment for acute cholecystitis in elderly high-risk patients. *Am Surg* 79:524–527, 2013.
- de Mestral C, Gomez D, Haas B, et al: Cholecystostomy: A bridge to hospital discharge but not delayed cholecystectomy. *J Trauma Acute Care Surg* 74:175–179, discussion 179–180, 2013.
- Abi-Haidar Y, Sanchez V, Williams SA, Itani KM: Revisiting percutaneous cholecystostomy for acute cholecystitis based on a 10-year experience. *Arch Surg* 147:16–22, 2012.
- Smith TJ, Manske JG, Mathiason MA, et al: Changing trends and outcomes in the use of percutaneous cholecystostomy tubes for acute cholecystitis. *Ann Surg* 257:1112–1115, 2013.
- Gurusamy KS, Rossi M, Davidson BR: Percutaneous cholecystostomy for high-risk surgical patients with acute calculous cholecystitis. *Cochrane Database Syst Rev* (8):CD007088, 2013.
- Akyurek N, Salman B, Yüksel O, et al: Management of acute calculous cholecystitis in high-risk patients: Percutaneous cholecystostomy followed by early laparoscopic cholecystectomy. *Surg Laparosc Endosc Percutan Tech* 15:315–320, 2005.
- Hatzidakis AA, Prassopoulos P, Petinarakis I, et al: Acute cholecystitis in high-risk patients: Percutaneous cholecystostomy vs conservative treatment. *Eur Radiol* 12:1778–1784, 2002.
- Orlando R: Cholecystectomy or percutaneous cholecystostomy for acute cholecystitis: Is it any clearer which to choose? comment on “revisiting percutaneous cholecystostomy for acute cholecystitis based on a 10-year experience.” *Arch Surg* 147:422, 2012.
- Barak O, Elazary R, Appelbaum L, et al: Conservative treatment for acute cholecystitis: Clinical and radiographic predictors of failure. *Isr Med Assoc J* 11:739–743, 2009.
- Kortram K, van Ramshorst B, Bollen TL, et al: Acute cholecystitis in high risk surgical patients: Percutaneous cholecystostomy versus laparoscopic cholecystectomy (CHOCOLATE trial): Study protocol for a randomized controlled trial. *Trials* 13:7, 2012.
- Chung JH, Kim SG, Kim YS, et al: Clinical usefulness of percutaneous transhepatic gallbladder aspiration in patients with acute calculous cholecystitis. *J Clin Gastroenterol* 47:288–290, 2013.
- Saad WE, Wallace MJ, Wojak JC, et al: Quality improvement guidelines for percutaneous transhepatic cholangiography, biliary drainage, and percutaneous cholecystostomy. *J Vasc Interv Radiol* 21:789–795, 2010.
- Chopra S, Dodd GD, 3rd, Mumbower AL, et al: Treatment of acute cholecystitis in non-critically ill patients at high surgical risk: Comparison of clinical outcomes after gallbladder aspiration and after percutaneous cholecystostomy. *AJR Am J Roentgenol* 176:1025–1031, 2001.
- Huffman JL, Schenker S: Acute acalculous cholecystitis: A review. *Clin Gastroenterol Hepatol* 8:15–22, 2010.
- Kalliafas S, Ziegler DW, Flancbaum L, Choban PS: Acute acalculous cholecystitis: Incidence, risk factors, diagnosis, and outcome. *Am Surg* 64:471–475, 1998.
- Ryu JK, Ryu KH, Kim KH: Clinical features of acute acalculous cholecystitis. *J Clin Gastroenterol* 36:166–169, 2003.
- Barie PS, Eachempati SR: Acute acalculous cholecystitis. *Curr Gastroenterol Rep* 5:302–309, 2003.
- Winick AB, Waybill PN, Venbrux AC: Complications of percutaneous transhepatic biliary interventions. *Tech Vasc Interv Radiol* 4:200–206, 2001.
- Saad WEA, Davies MG, Darcy MD: Management of bleeding after percutaneous transhepatic cholangiography or transhepatic biliary drain placement. *Tech Vasc Interv Radiol* 11:60–71, 2008.
- Choi SH, Gwon DI, Ko GY, et al: Hepatic arterial injuries in 3110 patients following percutaneous transhepatic biliary drainage. *Radiology* 261:969–975, 2011.
- Rivera-Sanfeliz GM, Assar OS, LaBerge JM, et al: Incidence of important hemobilia following transhepatic biliary drainage: Left-sided

- versus right-sided approaches. *Cardiovasc Intervent Radiol* 27:137–139, 2004.
37. Lyon SM, Terhaar O, Given MF, et al: Percutaneous embolization of transhepatic tracks for biliary intervention. *Cardiovasc Intervent Radiol* 29:1011–1014, 2006.
 38. Thornton RH, Ulrich R, Hsu M, et al: Outcomes of patients undergoing percutaneous biliary drainage to reduce bilirubin for administration of chemotherapy. *J Vasc Interv Radiol* 23:89–95, 2012.
 39. Robson PC, Heffernan N, Gonen M, et al: Prospective study of outcomes after percutaneous biliary drainage for malignant biliary obstruction. *Ann Surg Oncol* 17:2303–2311, 2010.
 40. Tsuyuguchi T, Takada T, Miyazaki M, et al: Stenting and interventional radiology for obstructive jaundice in patients with unresectable biliary tract carcinomas. *J Hepatobiliary Pancreat Surg* 15:69–73, 2008.
 41. Speer AG, Cotton PB, Russell RC, et al: Randomised trial of endoscopic versus percutaneous stent insertion in malignant obstructive jaundice. *Lancet* 2:57–62, 1987.
 42. Saluja SS, Gulati M, Garg PK, et al: Endoscopic or percutaneous biliary drainage for gallbladder cancer: A randomized trial and quality of life assessment. *Clin Gastroenterol Hepatol* 6:944–950.e3, 2008.
 43. Kloek JJ, van der Gaag NA, Aziz Y, et al: Endoscopic and percutaneous preoperative biliary drainage in patients with suspected hilar cholangiocarcinoma. *J Gastrointest Surg* 14:119–125, 2010.
 44. Walter T, Ho CS, Horgan AM, et al: Endoscopic or percutaneous biliary drainage for Klatskin tumors? *J Vasc Interv Radiol* 24:113–121, 2013.
 45. Yasumoto T, Yokoyama S, Nagaïke K: Percutaneous transcholecystic metallic stent placement for malignant obstruction of the common bile duct: Preliminary clinical evaluation. *J Vasc Interv Radiol* 21:252–258, 2010.
 46. Chatzis N, Pfiffner R, Glenck M, et al: Comparing percutaneous primary and secondary biliary stenting for malignant biliary obstruction: A retrospective clinical analysis. *Indian J Radiol Imaging* 23:38–45, 2013.
 47. Lee MJ, Dawson SL, Mueller PR, et al: Palliation of malignant bile duct obstruction with metallic biliary endoprostheses: Technique, results, and complications. *J Vasc Interv Radiol* 3:665–671, 1992.
 48. Inal M, Aksungur E, Akgül E, et al: Percutaneous placement of metallic stents in malignant biliary obstruction: One-stage or two-stage procedure? Pre-dilate or not? *Cardiovasc Intervent Radiol* 26:40–45, 2003.
 49. Yoshida H, Mamada Y, Taniai N, et al: One-step palliative treatment method for obstructive jaundice caused by unresectable malignancies by percutaneous transhepatic insertion of an expandable metallic stent. *World J Gastroenterol* 12:2423–2426, 2006.
 50. Veal DR, Lee AY, Kerlan RK, Jr, et al: Outcomes of metallic biliary stent insertion in patients with malignant bilobar obstruction. *J Vasc Interv Radiol* 24:1003–1010, 2013.
 51. Vienne A, Hobeika E, Gouya H, et al: Prediction of drainage effectiveness during endoscopic stenting of malignant hilar strictures: The role of liver volume assessment. *Gastrointest Endosc* 72:728–735, 2010.
 52. Cantwell CP, Pena CS, Gervais DA, et al: Thirty years' experience with balloon dilation of benign postoperative biliary strictures: Long-term outcomes. *Radiology* 249:1050–1057, 2008.
 53. House MG, Cameron JL, Schulick RD, et al: Incidence and outcome of biliary strictures after pancreaticoduodenectomy. *Ann Surg* 243:571–576, discussion 576–578, 2006.
 54. Cho KJ: Biliary stricture dilation: Are the unknowns known? *J Vasc Interv Radiol* 23:1355–1357, 2012.
 55. Glas L, Courbière M, Ficarella S, et al: Long-term outcome of percutaneous transhepatic therapy for benign bilioenteric anastomotic strictures. *J Vasc Interv Radiol* 19:1336–1343, 2008.
 56. Poley JW, Cahen DL, Metselaar HJ, et al: A prospective group sequential study evaluating a new type of fully covered self-expandable metal stent for the treatment of benign biliary strictures (with video). *Gastrointest Endosc* 75:783–789, 2012.
 57. Fontein DB, Gibson RN, Collier NA, et al: Two decades of percutaneous transjejunal biliary intervention for benign biliary disease: A review of the intervention nature and complications. *Insights Imaging* 2:557–565, 2011.
 58. Eschelman DJ, Sullivan KL: Retrograde placement of biliary endoprostheses through a Hutson loop. *J Vasc Interv Radiol* 5:633–635, 1994.
 59. Szulman C, Giménez M, Sierre S: Antegrade papillary balloon dilation for extrahepatic bile duct stone clearance: Lessons learned from treating 300 patients. *J Vasc Interv Radiol* 22:346–353, 2011.
 60. Ozcan N, Kahriman G, Mavili E: Percutaneous transhepatic removal of bile duct stones: Results of 261 patients. *Cardiovasc Intervent Radiol* 35:890–897, 2012.
 61. Hatzidakis AA, Alexandrakis G, Kouroumalis H, Gourtsoyannis NC: Percutaneous cholangioscopy in the management of biliary disease: Experience in 25 patients. *Cardiovasc Intervent Radiol* 23:431–440, 2000.
 62. Hatzidakis A, Krokidis M, Gourtsoyannis N: Percutaneous removal of biliary calculi. *Cardiovasc Intervent Radiol* 32:1130–1138, 2009.
 63. Picus D, Hicks ME, Darcy MD, et al: Percutaneous cholecystolithotomy: Analysis of results and complications in 58 consecutive patients. *Radiology* 183:779–784, 1992.
 64. Kim YH, Kim YJ, Shin TB: Fluoroscopy-guided percutaneous gallstone removal using a 12-Fr sheath in high-risk surgical patients with acute cholecystitis. *Korean J Radiol* 12:210–215, 2011.
 65. Miyayama S, Yamashiro M, Okuda M, et al: Main bile duct stricture occurring after transcatheter arterial chemoembolization for hepatocellular carcinoma. *Cardiovasc Intervent Radiol* 33:1168–1179, 2010.
 66. Atassi B, Bangash AK, Lewandowski RJ, et al: Biliary sequelae following radioembolization with yttrium-90 microspheres. *J Vasc Interv Radiol* 19:691–697, 2008.
 67. Ito K, Ito H, Kemeny NE, et al: Biliary sclerosis after hepatic arterial infusion pump chemotherapy for patients with colorectal cancer liver metastasis: Incidence, clinical features, and risk factors. *Ann Surg Oncol* 19:1609–1617, 2012.
 68. Lau WY, Lai EC, Lau SH: Management of bile duct injury after laparoscopic cholecystectomy: A review. *ANZ J Surg* 80:75–81, 2010.
 69. Thompson CM, Saad NE, Quazi RR, et al: Management of iatrogenic bile duct injuries: Role of the interventional radiologist. *Radiographics* 33:117–134, 2013.
 70. Fidelman N, Kerlan RK, Jr, Laberge JM, Gordon RL: Accuracy of percutaneous transhepatic cholangiography in predicting the location and nature of major bile duct injuries. *J Vasc Interv Radiol* 22:884–892, 2011.
 71. Hoeftel C, Azizi L, Lewin M, et al: Normal and pathologic features of the postoperative biliary tract at 3D MR cholangiopancreatography and MR imaging. *Radiographics* 26:1603–1620, 2006.
 72. Alegre Castellanos A, Molina Granados JF, Escribano Fernandez J, et al: Early phase detection of bile leak after hepatobiliary surgery: Value of Gd-EOB-DTPA-enhanced MR cholangiography. *Abdom Imaging* 37:795–802, 2012.
 73. Kantarci M, Pirimoglu B, Karabulut N, et al: Non-invasive detection of biliary leaks using Gd-EOB-DTPA-enhanced MR cholangiography: Comparison with T2-weighted MR cholangiography. *Eur Radiol* 23:2713–2722, 2013.
 74. Lim JB, Andrews RT, Geschwind JF: Balloon tamponade: A novel technique for visualizing and catheterizing the common bile duct after partial transection. *J Vasc Interv Radiol* 12:117–120, 2001.
 75. Arellano RS, Gervais DA, Boland GW, Mueller PR: Percutaneous reconstruction of isolated bile ducts: Combination of percutaneous and endoscopic biliary techniques. *Cardiovasc Intervent Radiol* 25:527–529, 2002.
 76. Misra S, Melton GB, Geschwind JF, et al: Percutaneous management of bile duct strictures and injuries associated with laparoscopic cholecystectomy: A decade of experience. *J Am Coll Surg* 198:218–226, 2004.
 77. Bllumgart LH: Postoperative strictures of the bile ducts. *The Biliary Tract*, New York, 1982, Churchill Livingstone. *Clinical Surgery International*, vol 5.
 78. Strasberg SM, Hertl M, Soper NJ: An analysis of the problem of biliary injury during laparoscopic cholecystectomy. *J Am Coll Surg* 180:101–125, 1995.
 79. Strasberg SM, Helton WS: An analytical review of vasculobiliary injury in laparoscopic and open cholecystectomy. *HPB (Oxford)* 13:1–14, 2011.
 80. Truant S, Boleslawski E, Lebuffe G, et al: Hepatic resection for post-cholecystectomy bile duct injuries: A literature review. *HPB (Oxford)* 12:334–341, 2010.
 81. Kaya M, Petersen BT, Angulo P, et al: Balloon dilation compared to stenting of dominant strictures in primary sclerosing cholangitis. *Am J Gastroenterol* 96:1059–1066, 2001.
 82. Chapman R, Fevery J, Kalloo A, et al: Diagnosis and management of primary sclerosing cholangitis. *Hepatology* 51:660–678, 2010.
 83. Chadwick BE: Beyond cytology: Expanding the diagnostic potential for biliary cytology. *Diagn Cytopathol* 40:536–541, 2012.
 84. Jung GS, Huh JD, Lee SU, et al: Bile duct: Analysis of percutaneous transluminal forceps biopsy in 130 patients suspected of having malignant biliary obstruction. *Radiology* 224:725–730, 2002.
 85. Tapping CR, Byass OR, Cast JE: Cytological sampling versus forceps biopsy during percutaneous transhepatic biliary drainage and analysis of factors predicting success. *Cardiovasc Intervent Radiol* 35:883–889, 2012.
 86. Ortnier ME, Caca K, Berr F, et al: Successful photodynamic therapy for nonresectable cholangiocarcinoma: A randomized prospective study. *Gastroenterology* 125:1355–1363, 2003.
 87. Zoepf T, Jakobs R, Arnold JC, et al: Palliation of nonresectable bile duct cancer: Improved survival after photodynamic therapy. *Am J Gastroenterol* 100:2426–2430, 2005.

Neoplasms of the Gallbladder and Biliary Tract

BYUNG IHN CHOI | JEONG MIN LEE

CHAPTER OUTLINE

Gallbladder Carcinoma

Epidemiology

Etiology

Pathologic Findings

Clinical Findings

Radiographic Findings

Treatment and Prognosis

Other Malignant Gallbladder Neoplasms

Benign Gallbladder Neoplasms

Cholangiocarcinoma

Epidemiology

Pathologic Findings

Clinical Findings

Radiographic Findings

Treatment

Periapillary Carcinoma

Cystic Bile Duct Neoplasms: Cystadenoma and Cystadenocarcinoma

Other Malignant Neoplasms of the Bile Ducts

Benign Bile Duct Neoplasms

Most neoplasms that arise from the gallbladder and bile ducts are malignant. Although infrequent, gallbladder and bile duct carcinomas are not rare. Gallbladder carcinoma is the seventh most common malignant neoplasm of the gastrointestinal tract and the most common biliary malignant neoplasm; bile duct carcinoma occurs less often.¹ Familiarity with the imaging characteristics of gallbladder and bile duct neoplasms is important to expedite diagnosis and appropriate treatment of patients, who often present with nonspecific symptoms of right upper quadrant pain, jaundice, and weight loss.

Gallbladder Carcinoma

EPIDEMIOLOGY

Carcinoma of the gallbladder is responsible for at least 3000 deaths per year in the United States.¹ Gallbladder cancer is the sixth most common cancer of the digestive system but accounts for only 3% to 4% of all gastrointestinal cancers. Carcinoma of the gallbladder is two to three times more common in women than in men, and its incidence steadily increases with age, although it varies greatly in different parts of the world.²⁻⁶ More than 90% of patients are older than 50 years; the peak incidence

is 70 to 75 years. Some geographic areas have a high incidence of gallbladder cancer, including South America and India.⁵ Certain groups, such as Israelis, Native Americans, Spanish Americans in the southwest United States, and Eskimos in Alaska, have a significantly higher incidence of gallbladder carcinoma and cholelithiasis than do populations.^{7,8}

ETIOLOGY

Several factors have been associated with an increased risk for development of gallbladder carcinoma. The presence of gallstones is considered to be an important risk factor for gallbladder carcinoma. Of patients with gallbladder carcinoma, 65% to 90% have gallstones, an incidence considerably higher than that for age- and sex-matched control groups.^{6,9} Many gallbladder cancers are unsuspected and found incidentally during surgery for gallstones or on final histologic analysis of the specimen. Diffuse mural calcification, the “porcelain” gallbladder, is another predisposing factor, ranging from 20% to 50% leading to cancer.^{10,11} Other risk factors include the presence of gallbladder adenomas, an anomalous pancreaticobiliary duct junction, and exposure to carcinogenic chemicals.^{6,12,13}

PATHOLOGIC FINDINGS

Most carcinomas of the gallbladder are adenocarcinomas (85%-90%) and can be papillary, tubular, mucinous, or signet cell type. The remainder are anaplastic, squamous cell, or adenosquamous carcinomas.^{14,15} On macroscopic examination, carcinomas of the gallbladder can appear as poorly defined areas of diffuse gallbladder wall thickening (infiltrating), often with a desmoplastic reaction, or as a cauliflower mass (fungating) that grows into the gallbladder lumen. The infiltrating type invades the gallbladder wall and ultimately replaces the lumen with a tumor mass. The papillary form grows into and eventually fills the lumen.¹⁶ Some tumors may show a combination of the infiltrating and fungating patterns. Approximately 60% of carcinomas originate in the fundus, 30% in the body, and 10% in the neck.¹⁷ In some cases, the tumor may diffusely infiltrate the entire gallbladder, making its organ of origin impossible to identify.

The gallbladder has unique anatomic features; the wall consists of a mucosa, lamina propria, smooth muscle layer, perimuscular connective tissue, and serosa without a submucosa. Furthermore, no serosa exists at the attachment to the liver and along the hepatic surface. The connective tissue is continuous with the interlobular connective tissue of the liver.¹⁷ Gallbladder carcinoma is staged surgically by the depth of invasion, extension of disease into adjacent structures, involvement of lymph nodes, and presence of metastases by the American Joint Committee on Cancer TNM staging system.^{2,18}

BOX 79-1 TNM CLASSIFICATION SYSTEM FOR STAGING GALLBLADDER CARCINOMA**PRIMARY TUMOR (T)**

TX	Primary tumor cannot be assessed
T0	No evidence of primary tumor
Tis	Carcinoma in situ
T1	Tumor invades mucosa or muscle layer
T1a	Tumor invades the mucosa
T1b	Tumor invades the muscle layer
T2	Tumor invades the perimuscular connective tissue; no extension beyond the serosa or into the liver
T3	Tumor perforates the serosa (visceral peritoneum) and/or directly invades the liver and/or one other adjacent organ or structure such as stomach, duodenum, colon, pancreas, omentum, or extrahepatic bile ducts
T4	Tumor invades main portal vein or hepatic artery or invades two or more extrahepatic organs or structures

REGIONAL LYMPH NODES (N)

NX	Regional lymph nodes cannot be assessed
N0	No regional lymph node metastasis
N1	Metastases to nodes along the cystic duct, common bile duct, hepatic artery, and/or portal vein
N2	Metastases to periaortic, pericaval, superior mesenteric artery and/or celiac artery lymph nodes

DISTANT METASTASIS (M)

M0	No distant metastasis
M1	Distant metastasis

STAGE GROUPING

Stage 0	Tis	N0	M0
Stage I	T1	N0	M0
Stage II	T2	N0	M0
Stage IIIA	T3	N0	M0
Stage IIIB	T1-3	N1	M0
Stage IVA	T4	N0-1	M0
Stage IVB	Any T	N2	M0
	Any T	Any N	M1

From Edge SB, Byrd DR, Compton CC, et al (eds): *AJCC Cancer Staging Manual*, 7th ed. Chicago, Springer, 2010, pp 211–217.

(Box 79-1). Invasion of the muscularis mucosa distinguishes T1 from T2 cancers.

CLINICAL FINDINGS

Gallbladder carcinoma most often is manifested with right upper quadrant abdominal pain simulating more common biliary and nonbiliary disorders.¹⁹ Weight loss, jaundice, and an abdominal mass are less common presenting symptoms. Patients may have long-standing symptoms of chronic cholecystitis with a recent change in the quality or frequency of the painful episodes. Other common presentations are similar to either acute cholecystitis or symptoms of biliary malignant disease. Hepatomegaly and ascites suggest liver invasion. Gallbladder carcinoma is occasionally an incidental finding on abdominal imaging studies. Elevated serum levels of α -fetoprotein and carcinoembryonic antigen have been reported in association with gallbladder carcinoma.^{17,20}

RADIOGRAPHIC FINDINGS

Traditional plain oral cholecystography and barium studies of the gastrointestinal tract have a limited role in the imaging of

gallbladder carcinoma. Abdominal radiographs may show calcified gallstones, porcelain gallbladder, or, rarely, punctate calcifications from mucinous carcinomas.²¹ Biliary gas from malignant gallbladder–enteric fistula is another rare finding.²² The gallbladder fails to opacify in at least two thirds of patients with carcinoma of the gallbladder, usually because of cystic duct obstruction.¹⁶ Barium study findings are abnormal in limited cases, showing displacement or direct invasion of the duodenum or anterior limb of the hepatic flexure.

Ultrasound, computed tomography (CT), and magnetic resonance imaging (MRI) are the most valuable imaging modalities for evaluation of patients with gallbladder carcinoma. Patients with right upper quadrant pain should initially be examined with ultrasound. Ultrasound can detect lesions suggestive of gallbladder cancer, such as a wide polyp base and irregular borders. The diagnostic accuracy of ultrasound in gallbladder cancer is more than 80%, but it has limitations in tumor staging.²³ Ultrasound can be useful for differentiating adenomyomatosis from the wall-thickening type of gallbladder cancer by detecting intramural cystic spaces or echogenic foci within the wall.^{24–28} Doppler imaging can be useful for differentiating polyp from tumefactive sludge by demonstrating blood flow to the polypoid tumors (Fig. 79-1). Endoscopic ultrasound is useful in depicting the depth of tumor invasion and for characterizing polypoid lesions.^{26,27} CT is superior to ultrasound in assessing lymphadenopathy and spread of the disease into the liver, porta hepatis, or adjacent structures and is useful in predicting which patients will benefit from surgical therapy (Fig. 79-2).^{28,29} Although MRI can be useful in assessing the cause of focal or diffuse mural thickening and helps differentiate gallbladder cancer from adenomyomatosis and chronic cholecystitis,^{30,31} magnetic resonance cholangiopancreatography (MRCP) provides more detailed information than ultrasound or CT about biliary involvement of the tumor. In addition, adding diffusion-weighted imaging to the standard MRI protocol may improve sensitivity for distinguishing gallbladder cancers from benign gallbladder diseases with wall thickening (Fig. 79-3).^{32–34} Although direct cholangiographic techniques such as endoscopic retrograde cholangiopancreatography (ERCP) and percutaneous transhepatic cholangiography are of little value in detecting the presence of gallbladder carcinoma, they are helpful in planning the surgical procedure because they can show tumor growth into adjacent intrahepatic ducts or into the common bile duct.⁶ The cholangiographic differential diagnosis includes cholangiocarcinoma, metastases, Mirizzi syndrome, and pancreatic carcinoma.

Radiologic Evaluation of the Primary Tumor

Gallbladder carcinomas have three major histologic and imaging presentations: focal or diffuse thickening or irregularity of the gallbladder wall; polypoid mass originating in the gallbladder wall and projecting into the lumen; and most commonly, a mass obscuring or replacing the gallbladder, often invading the adjacent liver.^{25,28,30}

Carcinoma Manifesting as Mural Thickening. Focal or diffuse thickening of the gallbladder wall is the least common presentation of gallbladder carcinoma and is the most difficult to diagnose, particularly in the early stages. Gallbladder carcinoma may cause mild to marked mural thickening in a focal or diffuse pattern. This thickening is best appreciated sonographically; the gallbladder wall is normally 3 mm or less in

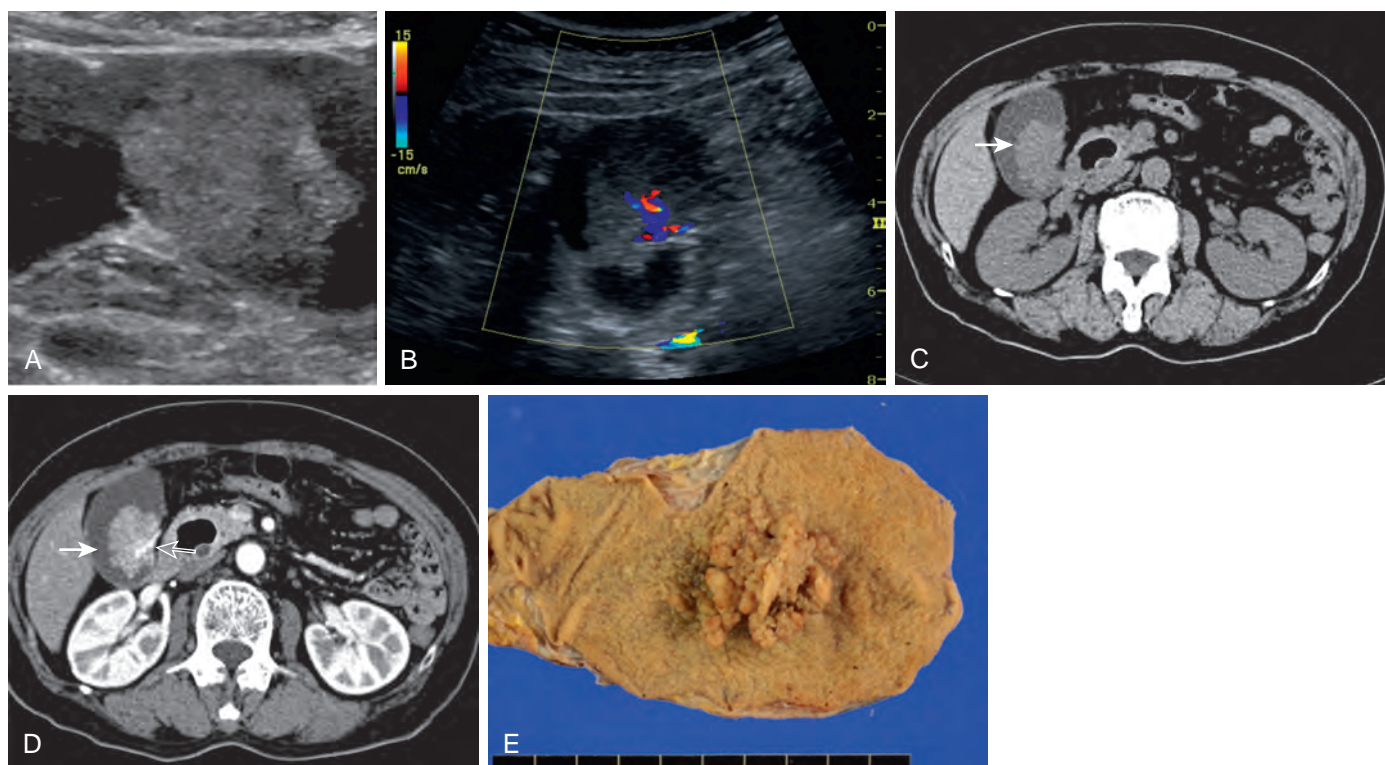


Figure 79-1 Ultrasound and Color Doppler imaging findings of polypoid gallbladder carcinoma. **A.** Subcostal sonogram shows a polypoid mass with a homogeneous tissue texture that is fixed to the gallbladder wall at its base. **B.** Color Doppler imaging shows blood flow signals in the polypoid mass. **C.** Precontrast axial CT scan demonstrates a polypoid mass (arrow) showing hyperattenuation to surrounding bile of the gallbladder. **D.** Axial CT scan demonstrates a homogeneously enhancing polypoid gallbladder carcinoma (arrow) with an enhancing vessel (open arrow). **E.** Photograph of the opened resected specimen shows the cauliflower-like intraluminal growth of a papillary adenocarcinoma.

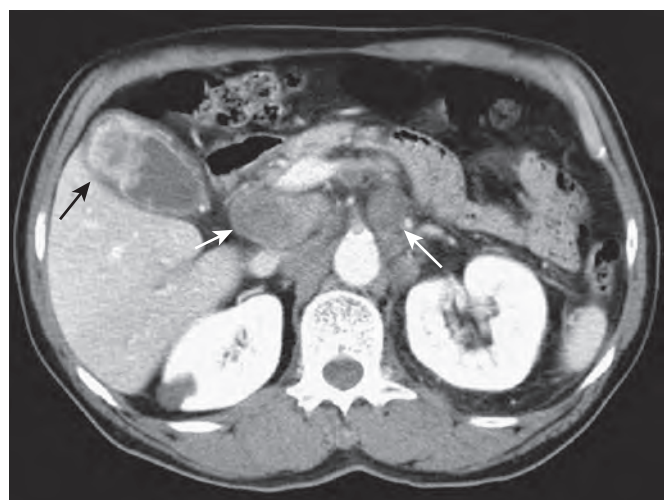


Figure 79-2 Polypoid gallbladder carcinoma with nodal metastasis. CT scan demonstrates a polypoid gallbladder carcinoma (black arrow) and low-density portocaval and para-aortic lymph nodes containing metastases (white arrows).

thickness.³⁵ Carcinomas confined to the gallbladder mucosa may be manifested as flat or slightly raised lesions with mucosal irregularity that are difficult to appreciate sonographically. In one sonographic series, half the patients with these early carcinomas had no protruding lesions, and fewer than one third were identified preoperatively.³⁶ More advanced gallbladder carcinomas can cause marked mural thickening, often with

irregular and mixed echogenicity (Fig. 79-4). The gallbladder may be contracted, normal sized, or distended, and gallstones are usually present. When cancer occurs in the neck portion of the gallbladder, identification of cystic duct involvement by the tumor on imaging merits consideration of focal bile duct resection to achieve a negative resection margin (see Fig. 79-4).

Four factors interfere with the sonographic recognition of carcinoma as the cause of gallbladder wall thickening:

1. Changes of early gallbladder carcinoma may be only subtle mucosal irregularity or mural thickening.
2. Gallbladder wall thickening is a nonspecific finding that can also be caused by acute or chronic cholecystitis, hyperalimentation, portal hypertension, adenomyomatosis, inadequate gallbladder distention, hypoalbuminemia, hepatitis, hepatic failure, cardiac failure, or renal failure. The echo architecture of the wall can sometimes help narrow the differential diagnosis.^{37,38} In acute cholecystitis, the wall often has irregular, discontinuous hypoechoic and echogenic bands. Chronic cholecystitis often results in a uniformly echodense band surrounding the mucosa, and hypoproteinemia may have a hypoechoic central band. Pronounced wall thickening (>1.0 cm) demonstrated by ultrasonography with associated mucosal irregularity or marked asymmetry should raise concerns for malignant disease or complicated cholecystitis.^{24,25}
3. Chronic cholecystitis is often present in patients with gallbladder carcinoma.
4. Shadowing stones or gallbladder wall calcification may obscure the carcinoma.

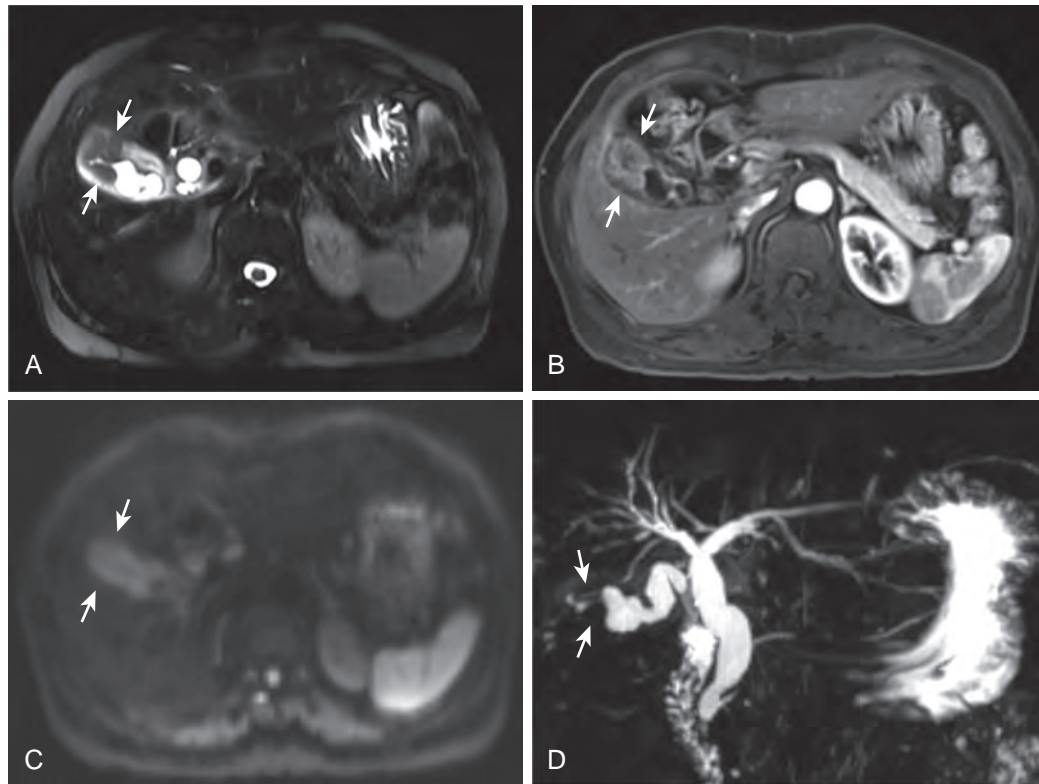


Figure 79-3 Gallbladder cancer showing enhancement on MRI and a high signal intensity on diffusion-weighted imaging. **A.** Fat-suppressed T2-weighted MR image shows an asymmetrically thickened gallbladder wall with hypointensity (arrows) compared with edematous surrounding wall. **B.** Postgadolinium fat-suppressed T1-weighted image reveals slightly heterogeneous enhancement of the thickened gallbladder wall (arrows). **C.** High b value ($b = 1000$) diffusion-weighted imaging demonstrates a high signal intensity of the tumor (arrows) involving the fundus of the gallbladder. **D.** MRCP demonstrates a luminal narrowing of the fundus (arrows) caused by the tumor and a normal appearance of the bile duct.

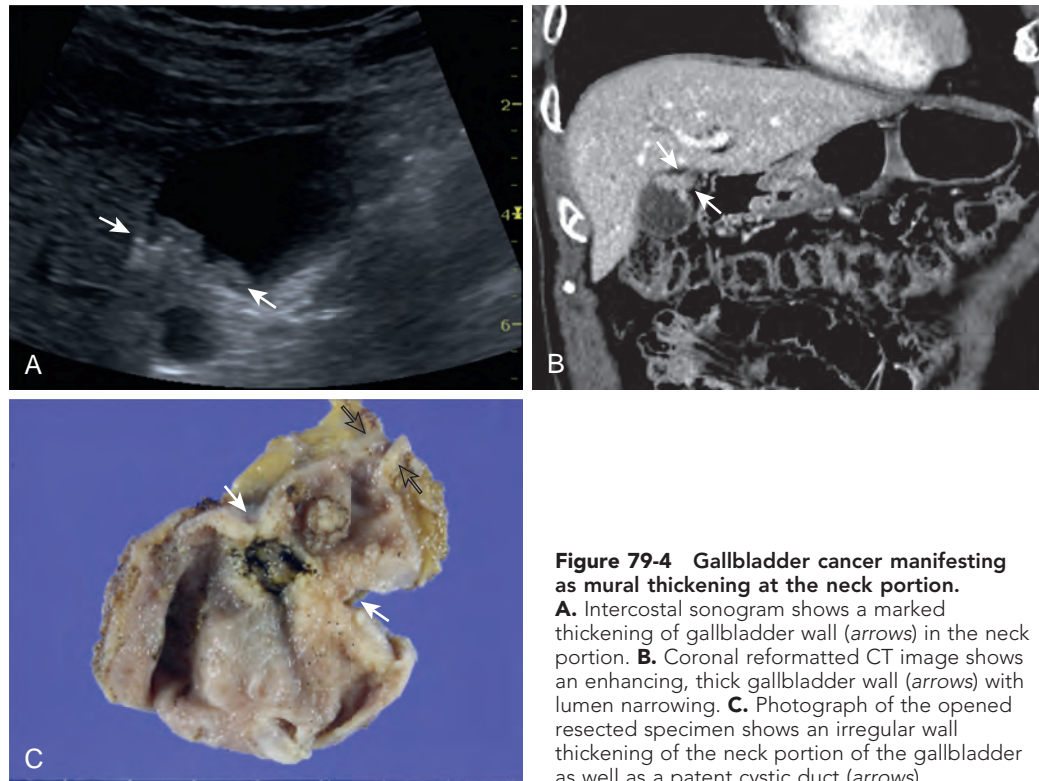


Figure 79-4 Gallbladder cancer manifesting as mural thickening at the neck portion. **A.** Intercostal sonogram shows a marked thickening of gallbladder wall (arrows) in the neck portion. **B.** Coronal reformatted CT image shows an enhancing, thick gallbladder wall (arrows) with lumen narrowing. **C.** Photograph of the opened resected specimen shows an irregular wall thickening of the neck portion of the gallbladder as well as a patent cystic duct (arrows).

Although CT is inferior to ultrasound for evaluating the gallbladder wall for mucosal irregularity, mural thickening, and cholelithiasis, it is superior for evaluating the thickness of portions of the gallbladder wall that are obscured by interposed gallstones or mural calcifications on ultrasound.^{28,37,39} On contrast-enhanced CT, thick (>2.5 mm) and strong enhancement of the inner wall and irregular contour of the affected wall are significant predictors for a malignant cause of gallbladder wall thickening (Fig. 79-5).^{29,40} When focal or irregular thickening of the gallbladder wall is encountered on CT, the images should be carefully inspected for bile duct dilation, local invasion, metastasis, or adenopathy.^{29,40} Multiplanar reformatted images of multidetector CT (MDCT) scans could be valuable for demonstrating extent of gallbladder cancers as well as relationship with adjacent organs, similar to biliary malignant tumors⁴¹⁻⁴⁴ (see Fig. 79-4). Studies have also demonstrated that diffusion-weighted MRI could contribute to the improvement of the diagnostic capability for gallbladder wall thickening or polypoid lesions by demonstrating high signal intensity on high b value diffusion-weighted imaging and a lower apparent diffusion coefficient value of gallbladder cancers than that of benign gallbladder diseases (see Fig. 79-3).^{32,33}

Carcinoma Manifesting as a Polypoid Mass. About one fourth of gallbladder carcinomas are manifested as a polypoid mass projecting into the gallbladder lumen. Identification of these neoplasms is particularly important because they are well differentiated and are more likely to be confined to the gallbladder mucosa or muscularis when discovered.^{36,45}

Polypoid carcinomas on ultrasound usually have a homogeneous tissue texture, are fixed to the gallbladder wall at their base, and do not cast an acoustic shadow^{25,27} (Fig. 79-6; see also Fig. 79-1). Most are broad based with smooth borders, although occasional tumors have a narrow stalk or villous fronds. The

polyp may be hyperechoic, hypoechoic, or isoechoic relative to the liver. Gallstones are usually present, and the gallbladder is either normal sized or expanded by the mass. A small polypoid carcinoma can be indistinguishable from a cholesterol polyp, adenoma, or adherent stone. Most benign polyps are small, measuring less than 1 cm.^{26,27,37} If a gallbladder polyp is larger than 1 cm in diameter and is not clearly benign, cholecystectomy should be considered.³⁶ Tumefactive sludge or blood clot can simulate a polypoid carcinoma.²⁵ Positional maneuvers usually differentiate these entities; clots and sludge move, albeit slowly, whereas cancers do not. Color Doppler imaging is also valuable for differentiating a polypoid tumor from tumefactive sludge by demonstrating vascular flow within tumors²⁸ (see Fig. 79-1). When polypoid carcinomas are sufficiently large, they are manifested as soft tissue masses that are denser than surrounding bile on CT scans or show a hypointensity to surrounding bile on T2-weighted MR imaging (see Fig. 79-6).³⁰ The polypoid cancer usually enhances homogeneously after administration of contrast medium, and the adjacent gallbladder wall may be thickened (see Figs. 79-1 and 79-6). Necrosis or calcification is uncommon.

Carcinoma Manifesting as a Gallbladder Fossa Mass. A large mass obscuring or replacing the gallbladder is the most common (42%-70%) presentation of gallbladder carcinoma.^{28,30} On sonographic examination, the mass is often complex, with regions of necrosis, and small amounts of pericholecystic fluid are often present. Gallstones are commonly seen within the ill-defined mass, which typically invades hepatic parenchyma.

On CT scans, infiltrating carcinomas that replace the gallbladder often show irregular contrast enhancement with scattered regions of internal necrosis (Fig. 79-7).³⁰ Unless the associated gallstones are densely calcified, they may be difficult to identify. Invasion of the liver or hepatoduodenal ligament,

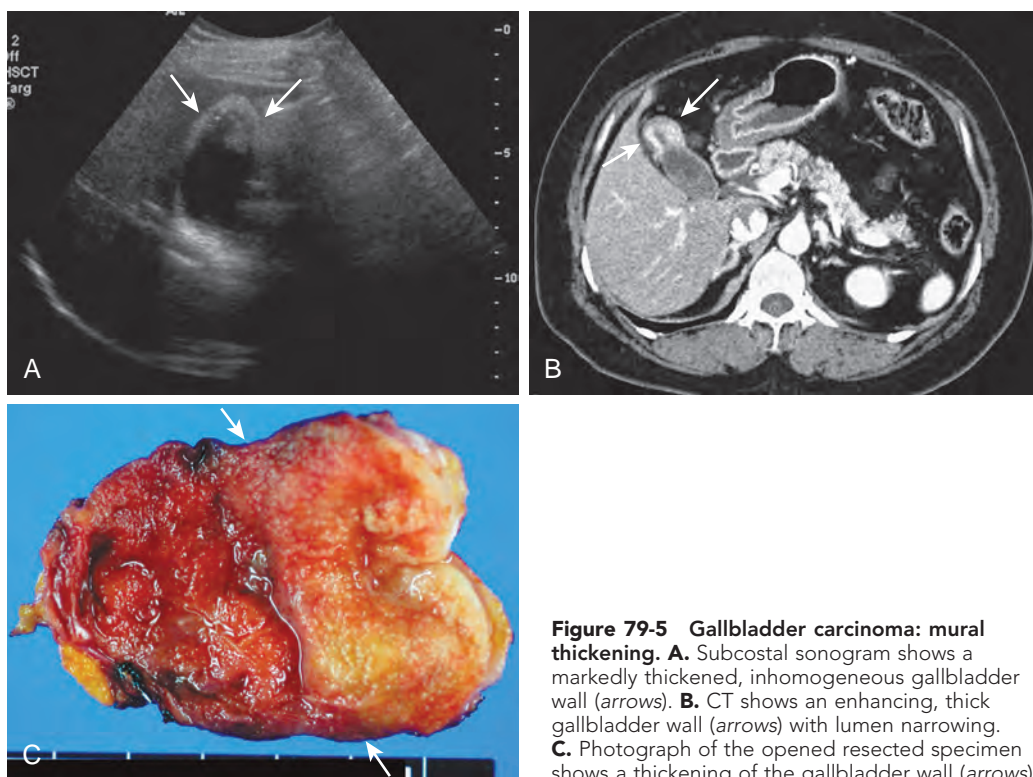


Figure 79-5 Gallbladder carcinoma: mural thickening. **A.** Subcostal sonogram shows a markedly thickened, inhomogeneous gallbladder wall (arrows). **B.** CT shows an enhancing, thick gallbladder wall (arrows) with lumen narrowing. **C.** Photograph of the opened resected specimen shows a thickening of the gallbladder wall (arrows).

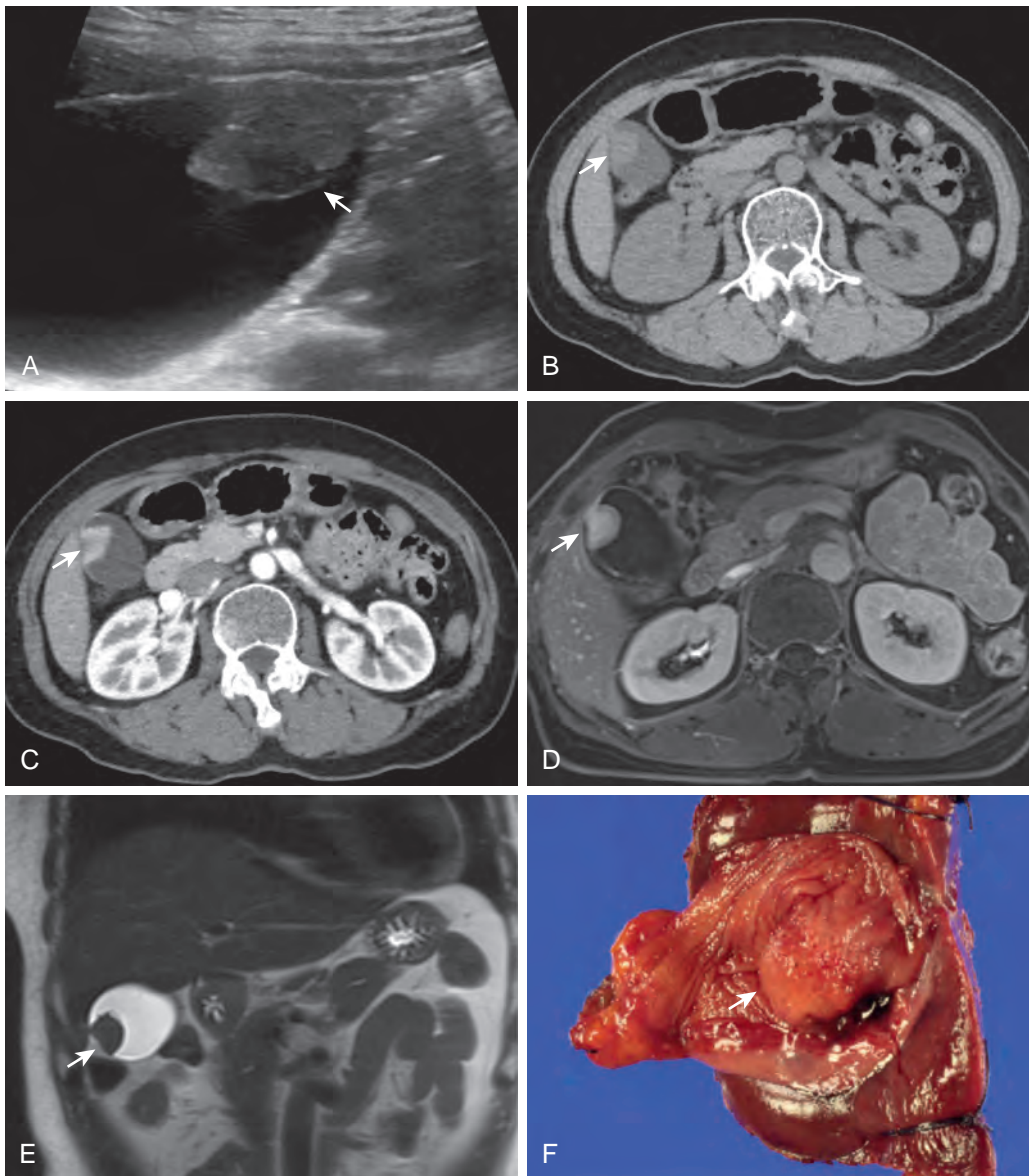


Figure 79-6 Polypoid gallbladder carcinoma having a wide base with a gallbladder wall. **A.** Sonogram shows a large homogeneous, hyperechoic polypoid gallbladder carcinoma (arrow) relative to surrounding bile. The mass was immobile with changes in the patient's position. **B.** Precontrast axial CT scan demonstrates a hyperattenuated soft tissue density polypoid tumor (arrow) in the gallbladder. **C.** Postcontrast axial CT scan demonstrates a homogeneously enhancing polypoid gallbladder carcinoma that is broad based with smooth border (arrow). **D.** Postcontrast T1-weighted MR image also demonstrates a polypoid mass showing hyperenhancement (arrow). **E.** Coronal T2-weighted image demonstrates a hypointense polypoid tumor (arrow) in the gallbladder. **F.** Photograph of the opened resected specimen shows a polypoid gallbladder cancer (arrow).

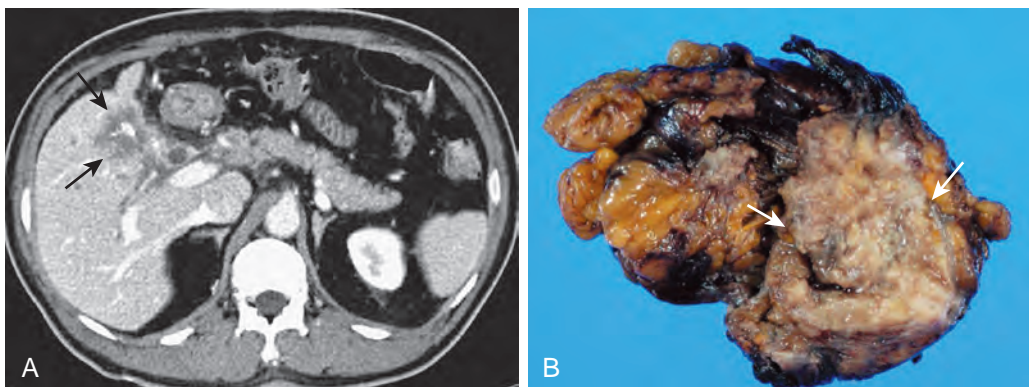


Figure 79-7 Gallbladder carcinoma manifesting as a gallbladder fossa mass. **A.** CT scan demonstrates an irregular hypodense mass replacing the gallbladder extending into the hepatic parenchyma (arrows). Note dilated common duct with wall thickening, suggesting spreading to the extrahepatic bile duct. **B.** Photograph of the resected specimen shows a large mass replacing the gallbladder (arrows).

satellite lesions, hepatic or nodal metastases, and bile duct dilation are also common.

MRI findings in gallbladder carcinoma are similar to those reported with CT. MRI demonstrates prolongation of the T1 and T2 relaxation time in gallbladder carcinoma. These lesions are heterogeneously hyperintense on T2-weighted images and hypointense on T1-weighted images compared with liver parenchyma.⁴⁶ Ill-defined early enhancement is a typical appearance of gallbladder carcinoma on dynamic gadolinium-enhanced MRI²⁹ (Fig. 79-8). MRI with MRCP offers the potential of evaluating parenchymal, vascular, biliary, and nodal involvement with a single noninvasive examination (Fig. 79-9).³⁰ On the basis of MRI alone, it may be difficult to distinguish carcinoma of the gallbladder from inflammatory and metastatic disease.

Differential Diagnosis

The differential diagnosis of infiltrating gallbladder carcinomas includes more common inflammatory and noninflammatory causes of wall thickening. These include heart failure, cirrhosis, hepatitis, renal failure, complicated cholecystitis, xanthogranulomatous cholecystitis, and adenomyomatosis.^{28,38,39} Clinically and radiologically, gallbladder carcinoma can be difficult to differentiate from cholecystitis with pericholecystic fluid and abscess. A increased attenuation intrahepatic halo surrounding the gallbladder wall on contrast-enhanced CT scans or MRI is fairly specific for complicated cholecystitis.^{46,47,48} Gallbladder carcinoma should be suspected when there are features of a focal mass, lymphadenopathy, hepatic metastases, and biliary obstruction at the level of the porta hepatis. Diffuse gallbladder wall thickening and streaky densities in the pericholecystic fat are seen with both inflammation and carcinoma.⁴⁰ Xanthogranulomatous cholecystitis is a pseudotumoral inflammatory

condition of the gallbladder that radiologically simulates gallbladder carcinoma.⁴⁹ In the few cases in which it is impossible to distinguish complicated cholecystitis from neoplasm, ultrasound-directed or CT-directed needle biopsy can provide a tissue diagnosis. Adenomyomatosis, which is characterized by focal or diffuse gallbladder wall thickening with dilated Rokitansky-Aschoff sinuses, may simulate gallbladder carcinoma on CT. MRI can be useful for distinguishing this entity from gallbladder carcinoma.^{30,31}

The differential diagnosis of those tumors that are manifested as an intraluminal polypoid mass includes adenomatous, hyperplastic, and cholesterol polyps; carcinoid tumor; metastatic melanoma; and hematoma.²⁸ The differential diagnosis for a mass replacing the gallbladder fossa includes hepatocellular carcinoma, cholangiocarcinoma, and metastatic disease to the gallbladder fossa.³⁰ Hepatomas occurring near the gallbladder fossa may be confused with gallbladder cancer radiographically, but they usually occur in cirrhotic livers and do not typically invade the gallbladder. Patients with liver metastases to the gallbladder fossa usually have a known primary neoplasm.

Pathways of Tumor Spread

Gallbladder carcinoma spreads beyond the wall by several routes: direct invasion of the liver, hepatoduodenal ligament, duodenum, or colon; lymphatic spread to regional lymph nodes; hematogenous spread to the liver; intraductal tumor extension; and metastasis to the peritoneum.^{50,51} Distant metastases are unusual.

Gallbladder carcinoma spreads most commonly by direct invasion of the liver.⁵⁰⁻⁵² Liver invasion is facilitated by its proximity and the thin gallbladder wall, which lacks a submucosa and has only a single muscle layer. Invasion of the gastrohepatic

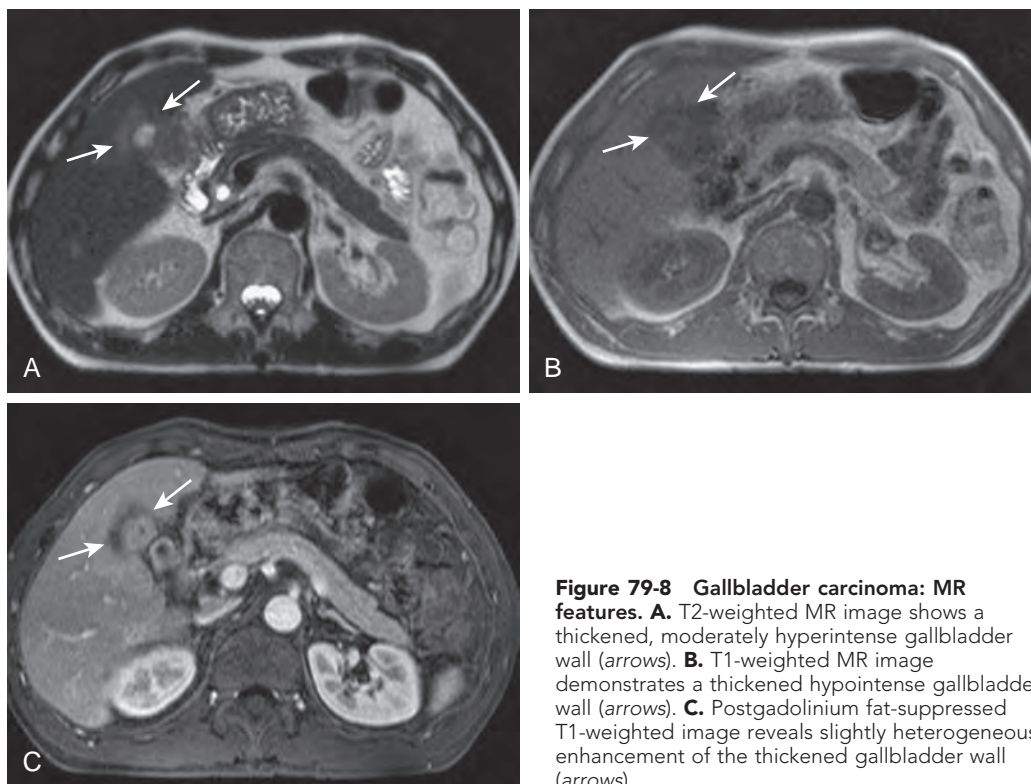


Figure 79-8 Gallbladder carcinoma: MR features. **A.** T2-weighted MR image shows a thickened, moderately hyperintense gallbladder wall (arrows). **B.** T1-weighted MR image demonstrates a thickened hypointense gallbladder wall (arrows). **C.** Postgadolinium fat-suppressed T1-weighted image reveals slightly heterogeneous enhancement of the thickened gallbladder wall (arrows).

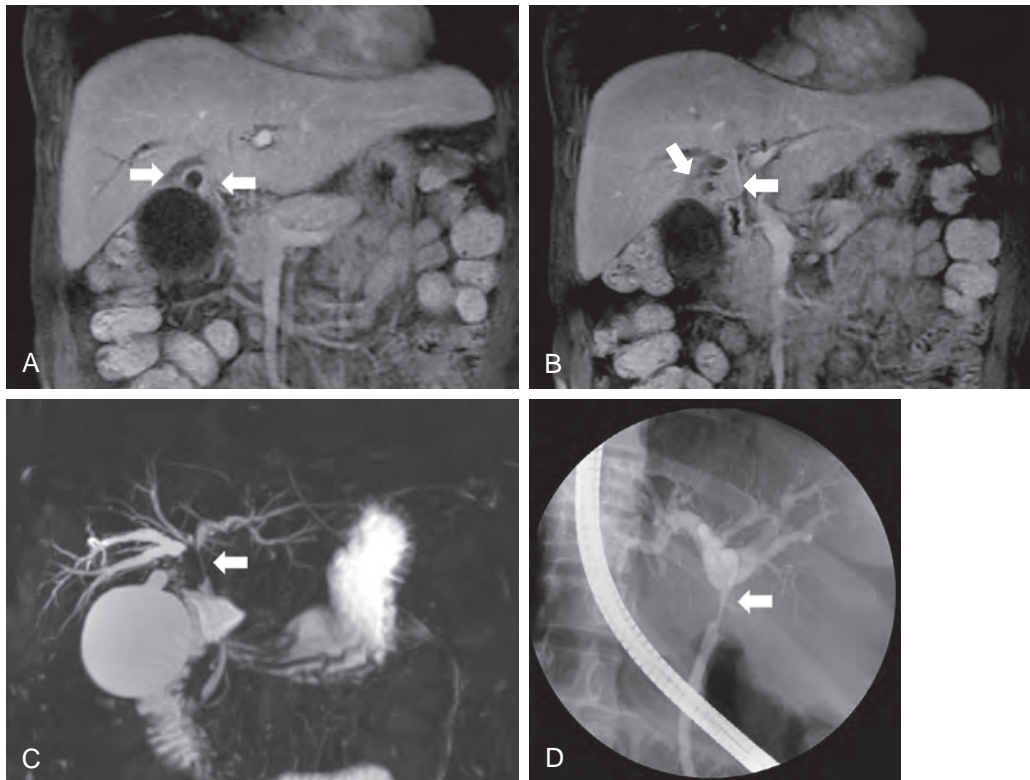


Figure 79-9 Gallbladder carcinoma with direct spread to the bile duct. **A** and **B.** Coronal MR images demonstrate an enhancing gallbladder carcinoma with involvement of adjacent bile duct (arrows). **C.** MRCP maximum intensity projection image demonstrates a malignant stricture involving the common hepatic duct as well as narrowing of the lumen at neck portion of the gallbladder (arrow). **D.** Direct cholangiography also demonstrates the stricture (arrow) involving the confluence of the right and left hepatic ducts (hilum of the bile duct), with dilation of the intrahepatic bile ducts.

ligament is also common and may cause biliary obstruction at the porta hepatis. Invasion into the duodenum or colon is less common. On ultrasound images, the gallbladder wall becomes ill-defined as an inhomogeneous mass extends into the liver parenchyma. On CT scans, portions of the invading tumor show enhancement after administration of contrast medium.⁵³ The gallbladder wall is poorly defined adjacent to the carcinoma invading liver parenchyma. Detection of subtle hepatic invasion is improved by use of narrow collimation to avoid partial volume averaging and by coronal or sagittal reformations.⁵⁴ On MRI, direct hepatic invasion and distant liver metastases are well shown on T2-weighted or gadolinium-enhanced images. The tumor has the same signal intensity as the primary tumor in most cases.³⁰

The prevalence of lymphatic spread is high in gallbladder carcinoma⁵⁵ (see Fig. 79-2). Lymphatic metastases progress from the gallbladder fossa through the hepatoduodenal ligament to nodal stations near the head of the pancreas. The cystic and pericholedochal lymph nodes are the most commonly involved at surgery and are a critical pathway to involvement of the celiac, superior mesenteric, and para-aortic lymph nodes.⁵²⁻⁵⁵ Because the gallbladder drains into these more distal nodes, hepatic hilar nodes are usually not involved. Positive lymph nodes are more likely to be greater than 10 mm in anteroposterior diameter and have heterogeneous contrast material enhancement.^{53,54}

Dilated bile ducts are present in about half the patients at the time of presentation.^{28,53,54} Biliary obstruction may develop

in patients with gallbladder cancer for a variety of reasons: lymphadenopathy, usually surrounding the common bile duct; tumor invasion into the hepatoduodenal ligament, often at the porta hepatis (see Fig. 79-9); intraductal tumor growth; or rarely, choledocholithiasis. Adenopathy and invasion into the hepatoduodenal ligament are the most common causes of obstruction; intraductal spread is infrequent but may be seen as a polypoid mass extending into the common bile duct. Ultrasound, CT, and MRI reveal biliary dilation and can usually show the level of obstruction. Invasion of the hepatoduodenal ligament is often better demonstrated with coronal reformatted CT or MRI than with axial CT.⁵⁶⁻⁵⁸

TREATMENT AND PROGNOSIS

Survival in patients with gallbladder carcinoma is strongly influenced by the pathologic stage at presentation.^{16,59} Patients with cancer limited to the gallbladder mucosa have an excellent prognosis, but most patients with gallbladder carcinoma have advanced, unresectable disease at the time of presentation. As a result, less than 15% of all patients with gallbladder carcinoma are alive after 5 years. Surgical management of gallbladder carcinoma is based on the local extension of the tumor. If there is direct extension of disease to the muscularis propria, a radical cholecystectomy is necessary. When disease extends through the serosa, more radical procedures including extended cholecystectomy, pancreatoduodenectomy, and major hepatic resection can be performed. However, radical tumor resection in this

setting is associated with a high operative mortality and few long-term survivors.

Other Malignant Gallbladder Neoplasms

A number of malignant diseases can metastasize to the gallbladder. Among the most common primary malignant neoplasms are melanoma, breast carcinoma, hepatocellular carcinoma, and lymphoma.^{57,60-62} On cross-sectional images, metastases show focal wall thickening, one or more polypoid masses, or replacement of the gallbladder by neoplasm (Fig. 79-10). Metastatic neoplasms of the gallbladder may be indistinguishable from primary gallbladder carcinoma except that gallstones are less frequently seen in patients with metastases.

Primary carcinoid tumors, lymphomas, and sarcomas of the gallbladder have also been reported.^{16,54} Carcinoids and lymphomas are manifested as polypoid masses that sometimes obstruct the cystic duct.⁶³ Sarcomas are bulky polypoid masses that are indistinguishable from primary gallbladder carcinoma.

Benign Gallbladder Neoplasms

A diverse spectrum of benign tumors arise from the gallbladder. Benign neoplasms are derived from the epithelial and non-epithelial structures that compose the normal gallbladder.⁶⁴ Although these lesions are relatively uncommon, their

importance lies in their ability to mimic malignant lesions of the gallbladder. Most benign neoplasms of the gallbladder are adenomas. At gross examination, gallbladder adenomas appear as polypoid structures and may be sessile or pedunculated. They are generally smaller than 2 cm. Tubular adenomas are typically lobular in contour, whereas papillary adenomas have a cauliflower-like appearance.⁶⁴

On ultrasound, adenomas appear as small, broad-based, nonshadowing, sessile or pedunculated polypoid filling defects that do not move with gravitational maneuvers. The echotexture of adenomas is typically homogeneous and hyperechoic. Adenomas tend to be less echogenic and more heterogeneous as they increase in size⁶⁴ (Fig. 79-11). Focal gallbladder wall thickening adjacent to a polypoid mass should raise concern for malignant disease. These polyps are manifested as enhancing intraluminal soft tissue masses. They are difficult to distinguish from the more common cholesterol polyp. Cholesterol polyps are more often smaller and multiple. Other rare benign neoplasms of the gallbladder include cystadenoma, granular cell tumors, hemangioma, lipoma, and leiomyoma.⁶⁴⁻⁶⁶

Cholangiocarcinoma

EPIDEMIOLOGY

Cholangiocarcinoma is a malignant tumor arising from the epithelium of the bile ducts and is the second most common primary hepatobiliary cancer after hepatocellular carcinoma. Cholangiocarcinoma is an uncommon tumor; between 2500

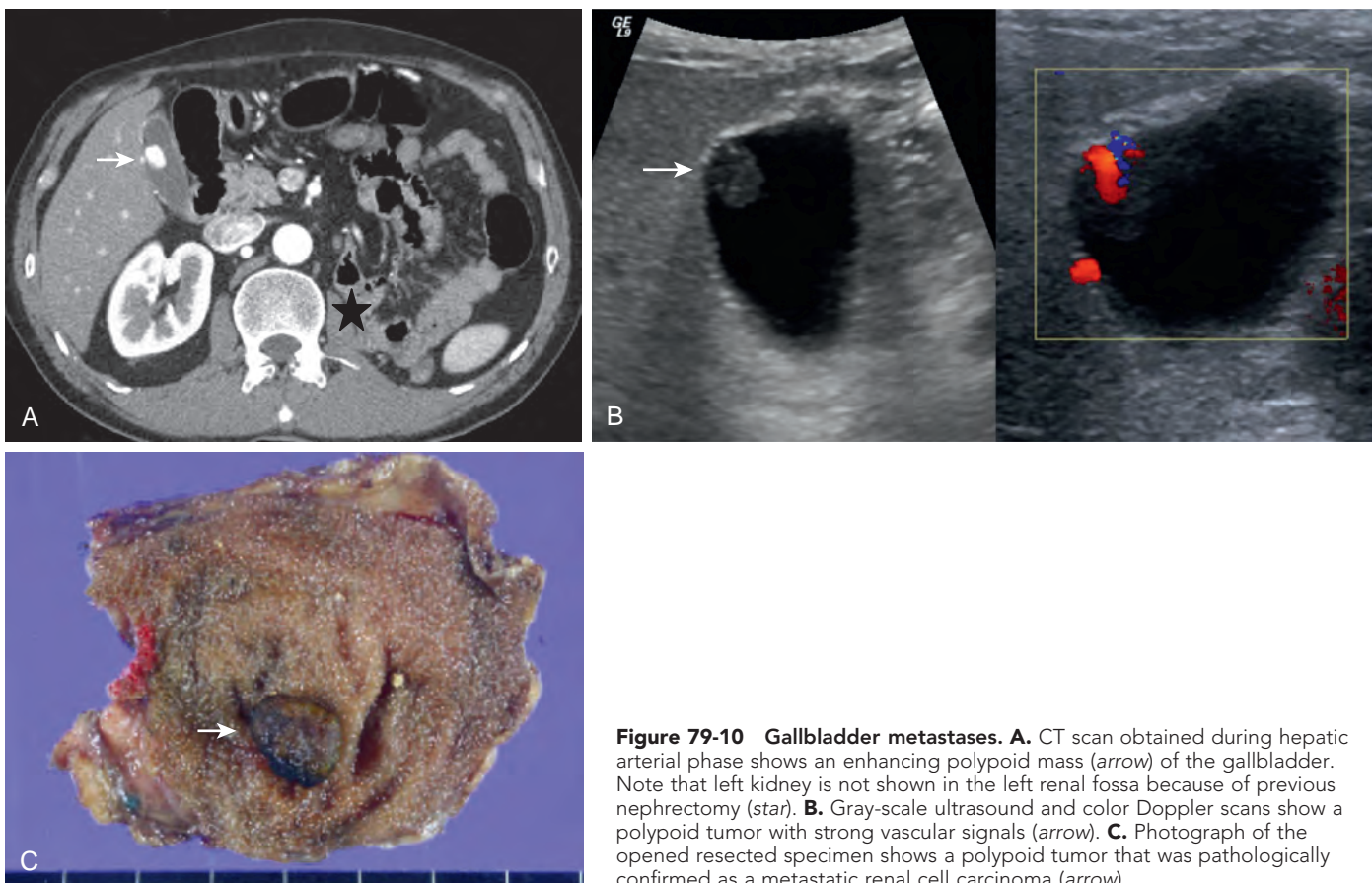


Figure 79-10 Gallbladder metastases. **A.** CT scan obtained during hepatic arterial phase shows an enhancing polypoid mass (arrow) of the gallbladder. Note that left kidney is not shown in the left renal fossa because of previous nephrectomy (star). **B.** Gray-scale ultrasound and color Doppler scans show a polypoid tumor with strong vascular signals (arrow). **C.** Photograph of the opened resected specimen shows a polypoid tumor that was pathologically confirmed as a metastatic renal cell carcinoma (arrow).

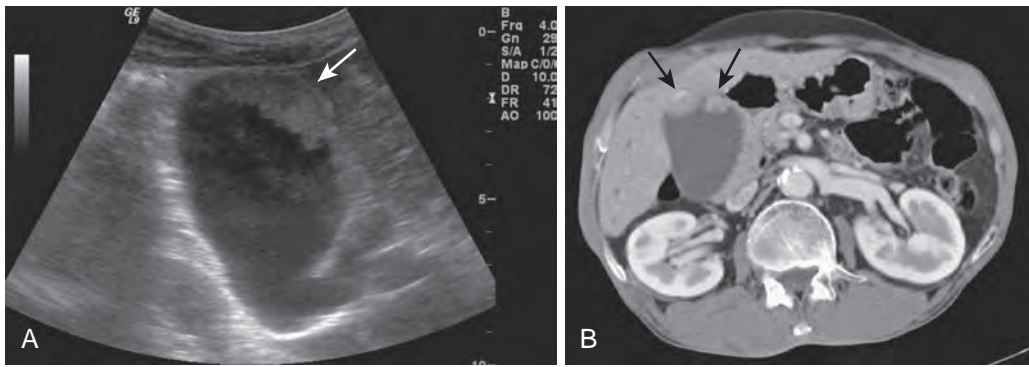


Figure 79-11 Gallbladder adenoma. **A.** Sonogram shows a sessile polypoid mass (arrow). **B.** CT scan demonstrates an enhancing polypoid gallbladder adenoma (arrows).

and 3000 new cases of cholangiocarcinoma are diagnosed annually in the United States.^{4,18,19} This tumor is more prevalent in the Far East and Southeast Asia, where liver fluke infection and choledocholithiasis are common. Cholangiocarcinomas occur slightly more often in men, with a male-to-female ratio of 1.3:1; the average age at diagnosis is between 50 and 70 years.⁶⁷ Risk factors for this neoplasm include primary sclerosing cholangitis, choledochal cyst, familial polyposis, congenital hepatic fibrosis, bile duct stone disease, prior biliary-enteric anastomosis, infection with the Chinese liver fluke *Clonorchis sinensis*, and history of exposure to thorium dioxide (Thorotrast).^{68,69}

PATHOLOGIC FINDINGS

More than 95% of cholangiocarcinomas are adenocarcinomas originating from bile duct epithelium. Most cholangiocarcinomas are well to moderately differentiated adenocarcinomas with a tendency to develop desmoplastic reactions and early perineural invasion.⁶⁹ Cholangiocarcinoma is classified anatomically into three groups: intrahepatic and peripheral to the liver hilum, hilar, or extrahepatic. These three types of cholangiocarcinoma are regarded as distinct disease entities therapeutically. Intrahepatic tumors are treated with hepatectomy, when possible, and hilar tumors are managed with resection of the bile duct, preferably with hepatectomy. Extrahepatic tumors are treated in a fashion similar to other periaampullary malignant neoplasms with pancreaticoduodenectomy. Although their precise definitions are controversial, a tumor that arises peripheral to the secondary bifurcation of the left or right hepatic duct is considered an intrahepatic cholangiocarcinoma. A tumor that arises from one of the hepatic ducts or from the bifurcation of the common hepatic duct is classified as a hilar cholangiocarcinoma.⁷⁰ Peripheral intrahepatic cholangiocarcinoma accounts for 10% of all cholangiocarcinomas, hilar cholangiocarcinoma for 25%, and extrahepatic cholangiocarcinoma for 65%.⁷¹

Cholangiocarcinomas are also divided into three types on the basis of their morphology: mass forming; periductal infiltrating, causing stricture; and intraductal growing.⁷¹⁻⁷⁵ This morphologic classification of cholangiocarcinoma is of great importance as it reflects biologic behavior and mode of spread of the tumor, and different types of cholangiocarcinoma may need different staging systems or different treatment strategies.^{73,74} Mass-forming intrahepatic cholangiocarcinoma is a gray-white mass often accompanied by satellite nodules (Fig. 79-12). Fibrosis and necrosis are frequently seen centrally. The

periductal infiltrating type of cholangiocarcinoma grows along the bile duct wall, resulting in concentric mural thickening and proximal dilation.⁷³ A dense fibroblastic reaction may encase the adjacent hepatic artery or portal vein, complicating surgical resection (Fig. 79-13).⁷⁵⁻⁷⁷ Intraductal growing papillary cholangiocarcinoma is characterized by the presence of intraluminal papillary tumors of the intrahepatic or extrahepatic bile ducts with partial obstruction and dilation of the bile ducts (Fig. 79-14).⁷² The tumors are usually small but often spread superficially along the mucosal surface, resulting in multiple tumors along the adjacent segments of the bile ducts or a tumor cast.⁷⁸ Some papillary tumors of the bile ducts produce a large amount of mucin and may impede the flow of bile.^{74,75,78} Ducts both proximal and distal to the tumor can be dilated because mucin may obstruct the papilla of Vater.

CLINICAL FINDINGS

Patients with hilar or extrahepatic cholangiocarcinomas usually present with painless jaundice. Anorexia, weight loss, vague gastrointestinal symptoms, ill-defined upper abdominal discomfort, and elevated serum alkaline phosphatase and bilirubin levels also can be seen. Cholangitis is unusual as a presenting symptom but most commonly develops after biliary manipulation. Patients with intrahepatic cholangiocarcinoma are usually asymptomatic and are rarely jaundiced until late in the course of disease.

RADIOGRAPHIC FINDINGS

The radiologic evaluation of patients with cholangiocarcinoma should delineate the overall extent of the tumor, including involvement of the bile ducts, liver, and portal vessels and distant metastases.¹⁹ Various imaging tests are available to assess patients with cholangiocarcinoma, and the initial radiographic studies consist of either ultrasound or CT. Ultrasound can quickly establish the level of biliary obstruction. Nowadays, MDCT has become the noninvasive diagnostic test of choice for detailed evaluation and staging of cholangiocarcinoma^{76,77} as it is widely available and able to indicate the location of the tumor and show the relationship between adjacent tissues, such as hepatic artery, portal vein, and liver parenchyma. In addition, it also helps survey the entire abdomen for disease staging. In most centers, ERCP or percutaneous transhepatic cholangiography is used to evaluate the extent of biliary involvement and to provide palliation for jaundice.⁷⁶⁻⁷⁸ MRI with MRCP offers the potential of evaluating parenchymal, vascular, biliary, and

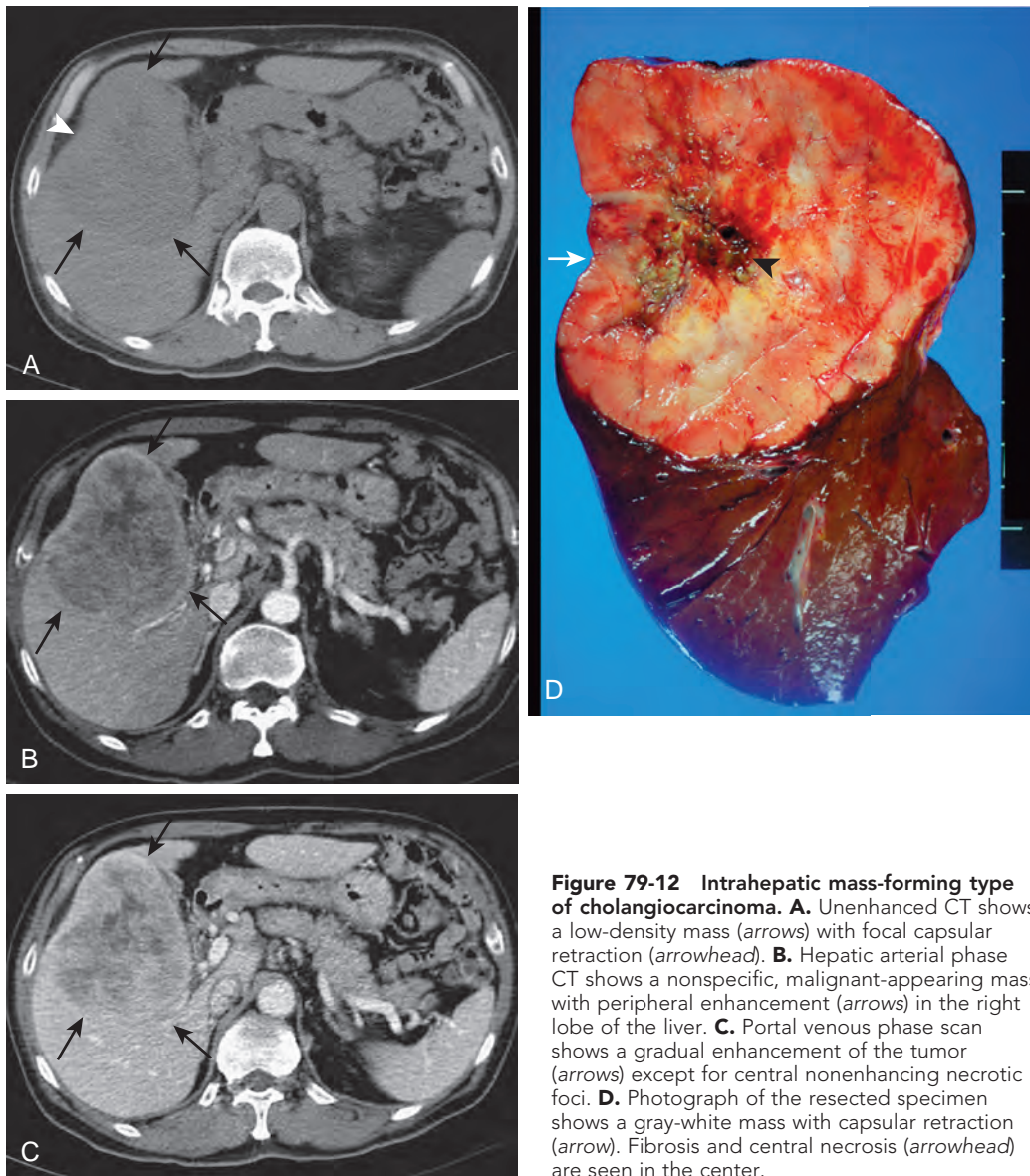


Figure 79-12 Intrahepatic mass-forming type of cholangiocarcinoma. **A.** Unenhanced CT shows a low-density mass (arrows) with focal capsular retraction (arrowhead). **B.** Hepatic arterial phase CT shows a nonspecific, malignant-appearing mass with peripheral enhancement (arrows) in the right lobe of the liver. **C.** Portal venous phase scan shows a gradual enhancement of the tumor (arrows) except for central nonenhancing necrotic foci. **D.** Photograph of the resected specimen shows a gray-white mass with capsular retraction (arrow). Fibrosis and central necrosis (arrowhead) are seen in the center.

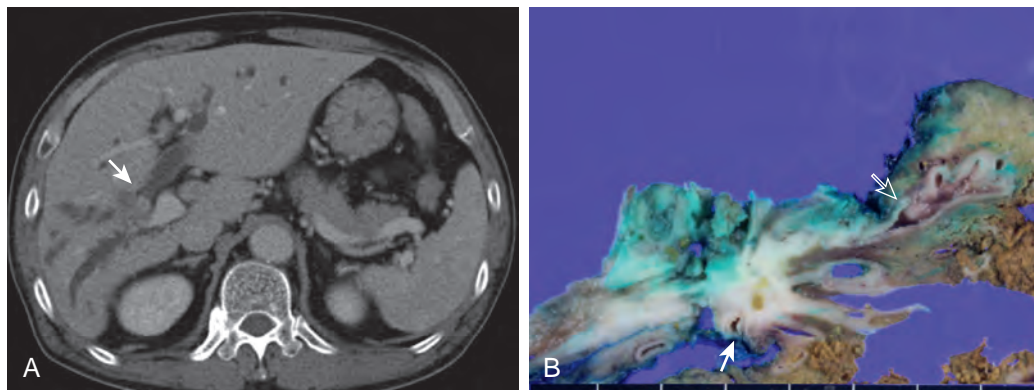


Figure 79-13 Periductal infiltrating type of cholangiocarcinoma. **A.** Portal venous phase scan shows a luminal narrowing of right intrahepatic bile duct with wall thickening (arrow) with invasion into adjacent hepatic parenchyma and upstream ductal dilation. Note dilation of left intrahepatic bile duct, suggestive of liver fluke (*Clonorchis sinensis*) infestation. **B.** Photograph of the resected specimen of a periductal infiltrating cholangiocarcinoma shows irregular thickening of the right main hepatic duct, with parenchymal invasion (arrow) as well as upstream ductal dilation (open arrow).

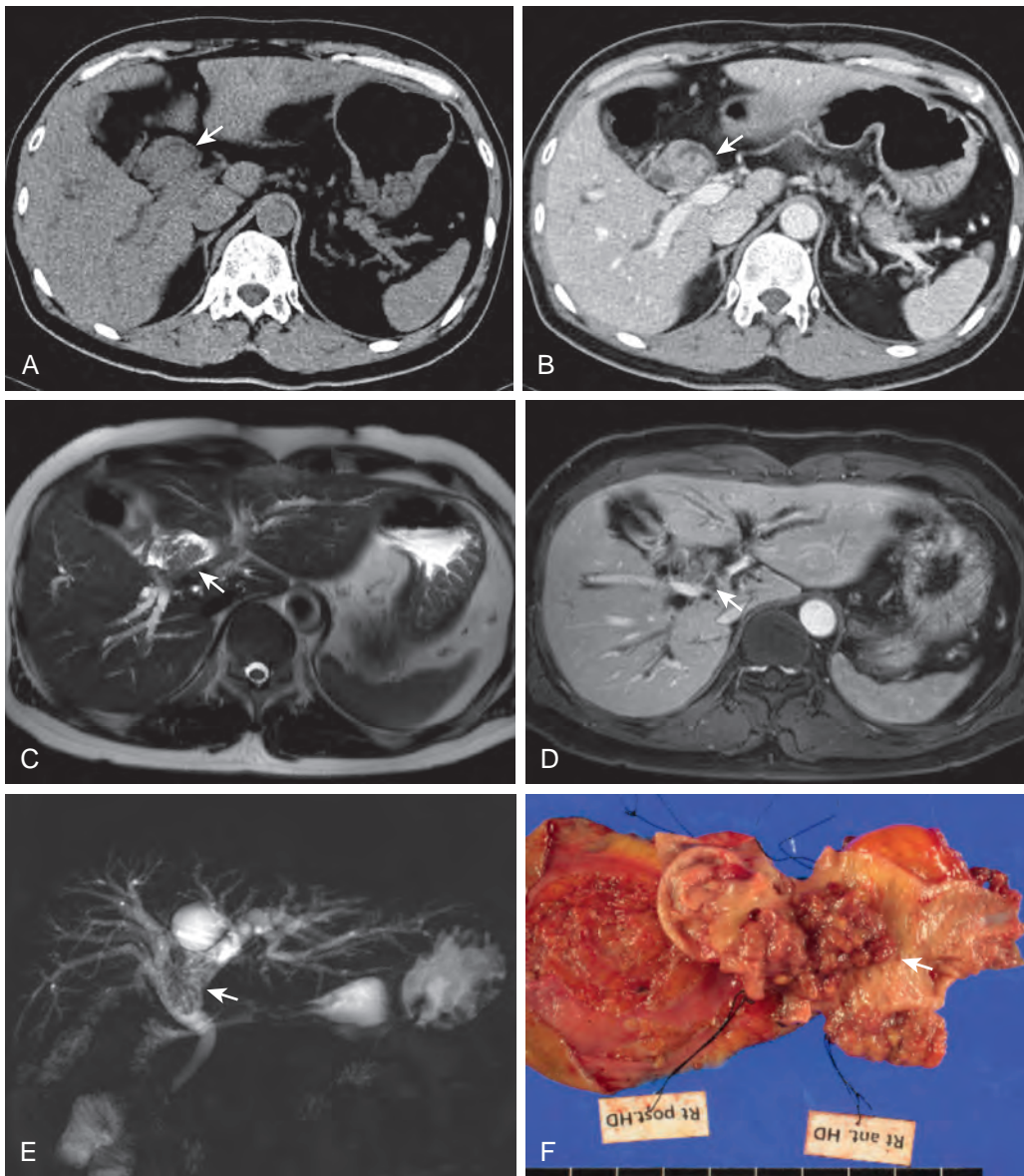


Figure 79-14 Intraductal growing papillary cholangiocarcinoma. **A** and **B**. Precontrast and postcontrast CT scans show an intraluminal tumor with papillary projections with weak enhancement (arrow) in the dilated hilar duct. **C**. Axial T2-weighted image shows a papillary cholangiocarcinoma (arrow) in the hilar duct. **D**. Contrast-enhanced axial T1-weighted image demonstrates a heterogeneously enhancing polypoid tumor (arrow) in the dilated common bile duct. **E**. MR cholangiography shows a papillary intraductal mass (arrow) at the hilar portion of the common bile duct with dilation of bilateral intrahepatic duct. **F**. Photograph of the resected specimen shows a large papillary tumor in left hepatic duct and common bile duct (arrow).

nodal involvement with a single noninvasive examination⁷⁷ (see Chapter 80). Although both MDCT and MRI with MRCP showed excellent diagnostic capability for assessing the longitudinal extent and tumor resectability of bile duct cancer, in general, MDCT or MRI generally underestimates the tumor involvement of vessels and lymph nodes.^{79,80} The imaging features of cholangiocarcinoma depend on tumor location and type.

Intrahepatic Type

The most common appearance of a mass-forming cholangiocarcinoma on sonography, CT, and MRI is a well-defined, predominantly homogeneous mass with irregular borders.^{81,82} On sonographic examination, these masses may have mixed echogenicity or may be predominantly hypoechoic or hyperechoic. Because of the peripheral location of the mass, bile duct obstruction is uncommon. Unenhanced CT scans show a hypoattenuating mass, either solitary or with satellite lesions (see Fig. 79-12). After the administration of contrast medium, there is

irregular peripheral and patchy enhancement in the tumor. The dense fibrotic nature of the tumor often produces capsular retraction. Small necrotic regions and focal intrahepatic bile duct dilation around the mass are common.⁸² A higher incidence of cholangiocarcinoma is associated with clonorchiasis (Fig. 79-15). The CT appearance of clonorchiasis is diffuse, mild dilation of the intrahepatic biliary ducts, especially the peripheral portions, without any evidence of obstruction.⁸³ Capsular retraction, dilation of the peripheral bile ducts, and presence of satellite nodules are frequent findings accompanying mass-forming intrahepatic cholangiocarcinoma.⁸²⁻⁸⁵

The typical appearance of cholangiocarcinoma on MRI is a nonencapsulated mass that is hypointense on T1-weighted images and hyperintense on T2-weighted images⁸⁴ (Fig. 79-16). Central hypointensity corresponding to fibrosis may be seen on T2-weighted images. Capsular retraction is found in 21% of mass-forming cholangiocarcinomas and seems to be related to the dense fibrotic nature of the tumor.^{84,86} In addition, in patients with associated clonorchiasis, dilation of the peripheral

portion of the intrahepatic bile ducts is occasionally seen. Cholangiography demonstrates displacement of bile ducts away from the intrahepatic cholangiocarcinoma, obstruction of an intrahepatic duct, or a polypoid mass in the intrahepatic ducts.

Exophytic, intrahepatic cholangiocarcinomas simulate other hepatic malignant neoplasms, particularly hepatocellular carcinoma, on cross-sectional imaging. Most cholangiocarcinomas,



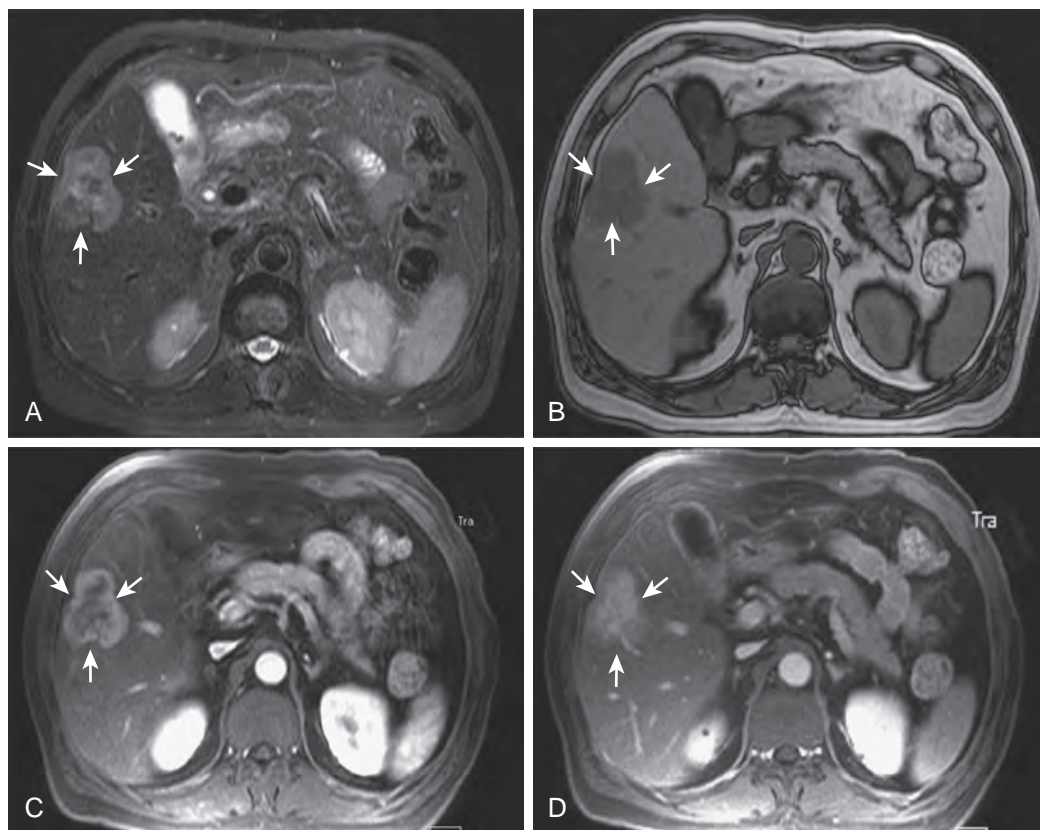
Figure 79-15 Intrahepatic cholangiocarcinoma associated with clonorchiasis. Contrast-enhanced CT scan shows an irregular low-density cholangiocarcinoma (arrows) in the right lobe of the liver and mild, diffuse dilation of intrahepatic bile ducts, suggesting clonorchiasis.

however, occur in noncirrhotic livers. In addition, on dynamic CT or MRI, typical mass-forming cholangiocarcinoma shows thin rimlike or thick bandlike enhancement around the tumor during the hepatic arterial and portal venous phases.^{82,83,87} On delayed (10–15 minutes) scans, there is progressive and concentric filling of the contrast material^{81,86} (see Fig. 79-16). The enhancement pattern of cholangiocarcinoma is explained by slow diffusion of contrast material into the interstitial spaces of the tumor.⁸⁴ This pattern differs from that of hepatocellular carcinoma, which typically shows robust enhancement in the hepatic arterial phase and isoattenuation or low attenuation on the portal venous phase.⁸⁵ A study⁸⁶ reported that hepatobiliary phase imaging of gadoxetic acid-enhanced MRI could improve detection of daughter nodules and intrahepatic metastases compared with dynamic phase images, which might be beneficial for staging and surgical planning of mass-forming cholangiocarcinomas. Hypovascular metastases, especially from adenocarcinoma of the gastrointestinal tract, may show an enhancement pattern similar to that of peripheral cholangiocarcinomas. Absence of a known primary malignant neoplasm, relatively large tumor size, and bile duct dilation favor mass-forming cholangiocarcinomas over metastases.⁸¹

Intrahepatic cholangiocarcinomas may also be polypoid or focally stenotic (Fig. 79-17). If exophytic intrahepatic cholangiocarcinomas are excluded, about three fourths of cholangiocarcinomas are manifested as a focal stricture, and one fourth are polypoid or diffusely stenotic.⁸⁷ Focally stenotic or papillary cholangiocarcinomas often cause segmental bile duct dilation and may induce lobar atrophy if the tumor is central in location. Papillary intrahepatic cholangiocarcinoma occasionally produces abundant mucin, resulting in a well-margined cystic

Figure 79-16 Intrahepatic cholangiocarcinoma.

A. T2-weighted turbo spin-echo image shows a heterogeneously hyperintense cholangiocarcinoma (arrows) in the right lobe of the liver. **B.** Opposed-phase T1-weighted MR image demonstrates a hypointense mass (arrows). **C** and **D.** Dynamic gadolinium-enhanced T1-weighted gradient-echo images at 1 and 5 minutes after injection of contrast material reveal progressive centripetal enhancement of the tumor (arrows).



mass that resembles biliary cystadenocarcinoma (Fig. 79-18). A correct diagnosis of intraductal cholangiocarcinoma can be made by demonstrating direct continuity of the peripheral bile ducts with the tumor and incorporated hepatic parenchyma between cysts.^{88,89} Mucin may result in tumor calcification and can also obstruct the duct lumen distal to the carcinoma (Fig. 79-19).

Hilar Type

Cholangiocarcinomas most often occur at the confluence of the right and left bile ducts and the proximal common hepatic duct.

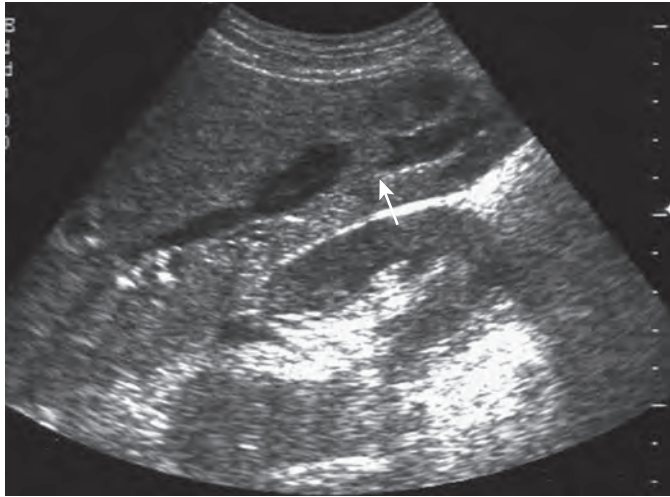


Figure 79-17 Papillary cholangiocarcinoma. Sonogram shows a papillary cholangiocarcinoma filling the dilated right intrahepatic bile duct (arrow).

These so-called Klatskin's tumors are usually periductal infiltrating types.⁹⁰⁻⁹² The sonographic features of Klatskin's tumors include duct dilation, isolation of the right and left bile duct segments, mass or bile duct wall thickening at the hilum, and lobar atrophy with crowded, dilated bile ducts.^{92,93} Klatskin's tumors almost invariably cause biliary dilation. Although the tumor can appear as mural thickening or an encircling mass along the bile duct wall, a definite mass is rarely seen on ultrasound⁹⁰⁻⁹⁴ (Fig. 79-20). Less often, a polypoid mass can cause hilar obstruction.

CT is more sensitive than ultrasound in detecting obstructing ductal masses, which are usually small (Fig. 79-21). MDCT allows more accurate evaluation of these small lesions and better demonstrates the status of the hepatic arterial or portal venous circulation.⁹² The mass is hypodense to liver on most scans before administration of contrast material.⁸¹ On contrast-enhanced CT, infiltrating tumors are seen as a focal thickening of the duct wall, obliterating the lumen. About 80% of these tumors are hyperattenuating relative to the liver on arterial or portal phase or both (see Fig. 79-13).^{91,92,95} Because of their sclerotic nature, most lesions show delayed tumor enhancement up to 8 to 15 minutes after injection of contrast medium (Fig. 79-22).^{95,96}

Cholangiocarcinomas are either isointense or low in signal intensity relative to the liver on T1-weighted images. On T2-weighted images, the tumor signal intensity ranges from markedly increased to mildly increased relative to liver. Tumors with high fibrous content tend to have lower signal intensity on T2-weighted images⁹⁸ (Fig. 79-23). Cholangiocarcinomas enhance to a moderate degree on gadolinium-enhanced T1-weighted MR images. MRI with MR cholangiography can provide comprehensive evaluation of axial and longitudinal tumor extent of hilar cholangiocarcinomas as well as of vascular

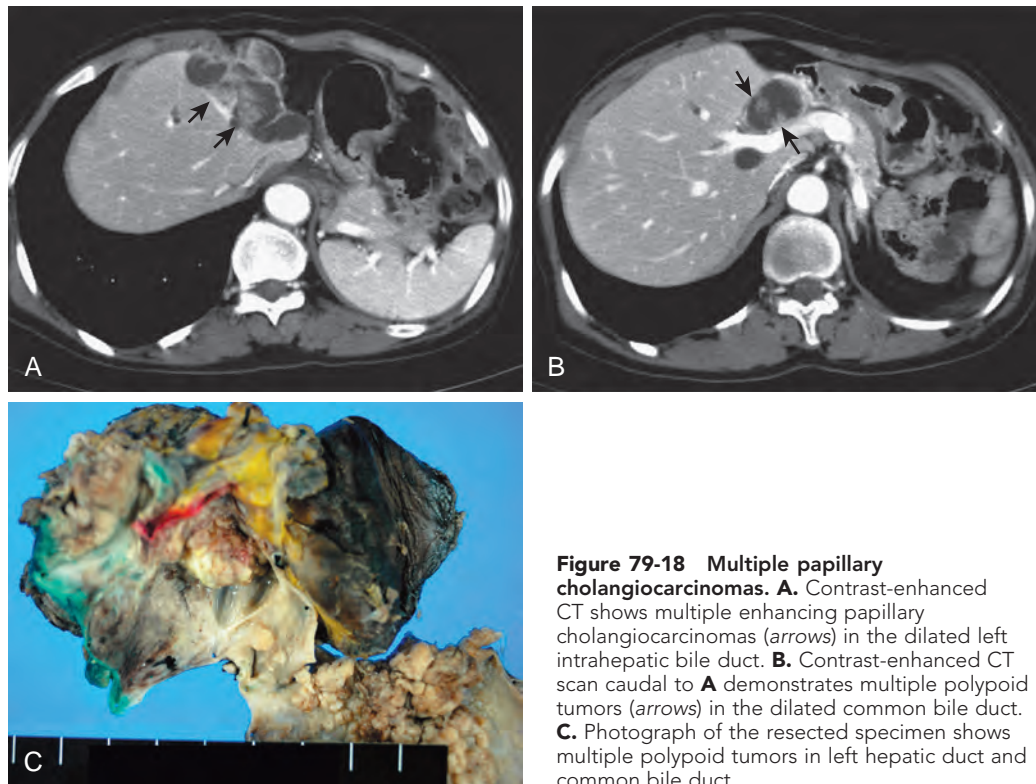


Figure 79-18 Multiple papillary cholangiocarcinomas. **A.** Contrast-enhanced CT shows multiple enhancing papillary cholangiocarcinomas (arrows) in the dilated left intrahepatic bile duct. **B.** Contrast-enhanced CT scan caudal to **A** demonstrates multiple polypoid tumors (arrows) in the dilated common bile duct. **C.** Photograph of the resected specimen shows multiple polypoid tumors in left hepatic duct and common bile duct.

Figure 79-19 Mucin-secreting cholangiocarcinoma. **A.** CT

shows a polypoid mass (arrow) in the left hepatic lobe and dilated left and right intrahepatic bile ducts (curved arrows) and dilated left and common hepatic bile ducts. **B.** ERCP demonstrates mucin expanding the extrahepatic bile ducts (arrows). At endoscopy, mucin was seen coming from the common bile duct.

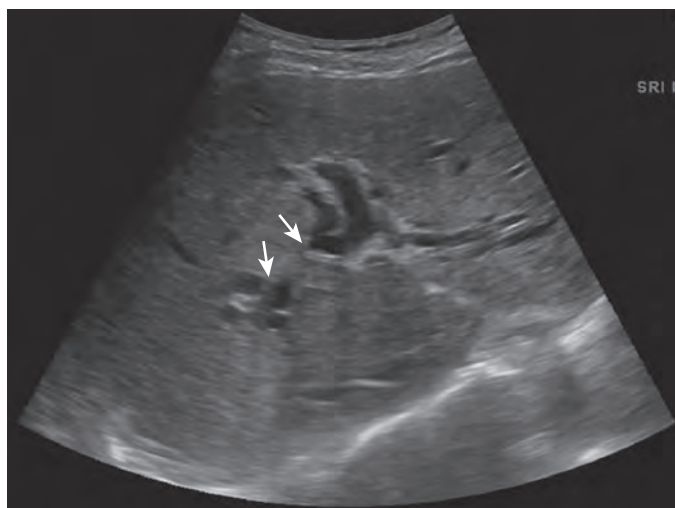
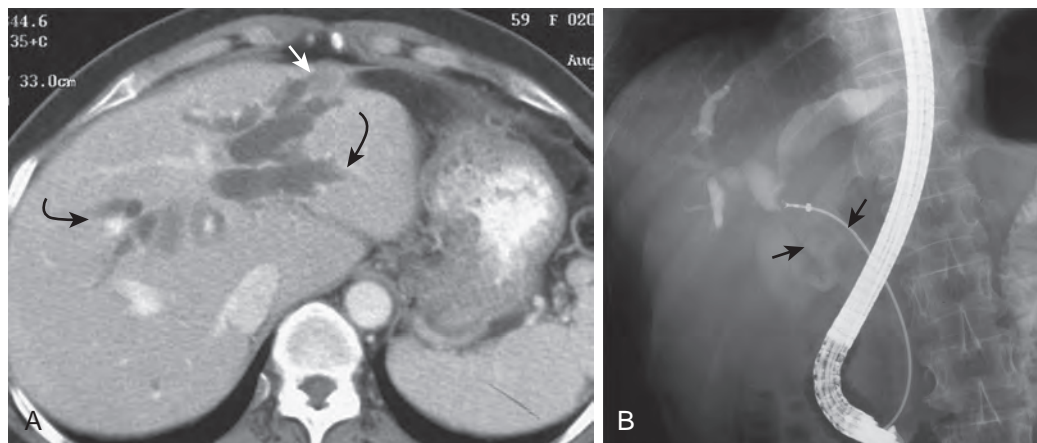


Figure 79-20 Klatskin's tumor. Sonography of Klatskin's tumor shows dilation of intrahepatic bile ducts and nonunion of right and left intrahepatic bile ducts (arrows).

involvement by the tumors^{77,99,100} (Fig. 79-24). As with CT, contrast enhancement is better appreciated on delayed images because of the nature of the tumor (Fig. 79-25).

Lobar hepatic atrophy with marked dilation and crowding of bile ducts is seen on CT and MRI in approximately one fourth of patients with hilar cholangiocarcinomas.⁹⁴ There is dominant involvement of the duct supplying the atrophied segment. Lobar hepatic atrophy with biliary dilation strongly suggests cholangiocarcinoma, although long-standing biliary obstruction from surgical trauma or focal biliary obstruction can cause similar findings (see Fig. 79-24).^{58,92,100} The liver parenchyma and hepatoduodenal ligaments are commonly invaded by Klatskin's tumors.^{70,90,92,101} Lymphatic metastases most commonly involve the portocaval, superior pancreaticoduodenal, and posterior pancreaticoduodenal lymph nodes.⁵⁴ Retroperitoneal lymphadenopathy, peritoneal spread, and proximal intestinal obstruction occur in advanced stages of hilar cholangiocarcinoma.

Although periductal infiltrating cholangiocarcinoma is the most common type of hilar cholangiocarcinoma, less often,

intraductal growing cholangiocarcinoma can occur in the hilar duct. The intraductal tumors may show higher attenuation than bile on precontrast CT images and hypoenhancement with regard to the hepatic parenchyma on contrast-enhanced images, probably because of lack of fibrotic stroma⁹⁷ (see Fig. 79-14). When intraductal tumors are developed as multiple intraluminal lesions, they can be easily mistaken for intrahepatic duct stones or extrahepatic bile duct stones.^{98,99} Contrast enhancement of the intraluminal lesions on contrast-enhanced CT or MRI can differentiate intraductal growing type cholangiocarcinoma from stones (see Fig. 79-14).^{97,98}

In patients with hilar cholangiocarcinoma, accurate evaluation of tumor extent is necessary for proper treatment and assessment of resectability.¹⁹ Nonresectability of hilar cholangiocarcinoma is suggested by cholangiographic evidence of severe bilateral involvement of the secondary confluence (see Fig. 79-24), involvement of the main trunk of the portal vein, involvement of both branches of the portal vein or bilateral involvement of the hepatic artery and portal vein, or vascular involvement on one side of the liver and extensive bile duct involvement on the other side.¹⁰⁰⁻¹⁰² Unilateral involvement of the hepatic artery or portal vein or both vessels is compatible with resection.^{18,19,100} Precise preoperative evaluation of tumor extent often requires several imaging studies.⁷⁷

Direct cholangiography (Fig. 79-26) is used to evaluate the extent of hilar cholangiocarcinomas.^{77,79} There is characteristic stenosis of the central, right, and left common hepatic ducts, with smooth shoulders or irregular tapering of ducts. These neoplastic strictures tend to branch and may extend into second-order biliary radicles. Direct cholangiography is of limited value in assessing submucosal tumor spread and lesions that extend beyond the porta hepatis because of incomplete filling of bile ducts proximal to the tumor. In addition, CT is ineffective in detecting superficially spreading tumors that extend above the level of biliary obstruction because tumor with a superficial spreading pattern shows enhancement of the inner wall of the bile duct with a preserved lumen.⁷⁰ Therefore, combined assessment with CT and state-of-the-art cholangiography or choledochoscopy (through the percutaneous transhepatic biliary drainage tract) and biopsy are needed to evaluate tumor extent.^{70,81} Along these lines, a combination of MRCP and conventional MRI can provide complete tumor staging

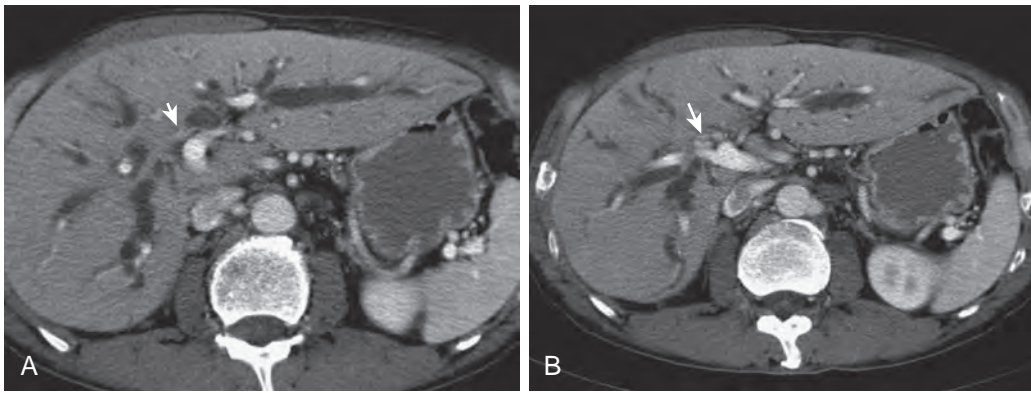


Figure 79-21 Contrast-enhanced CT scans reveal a small enhancing hilar cancers causing biliary strictures (arrow) involving central portion of the left (A) and right (B) bile duct.

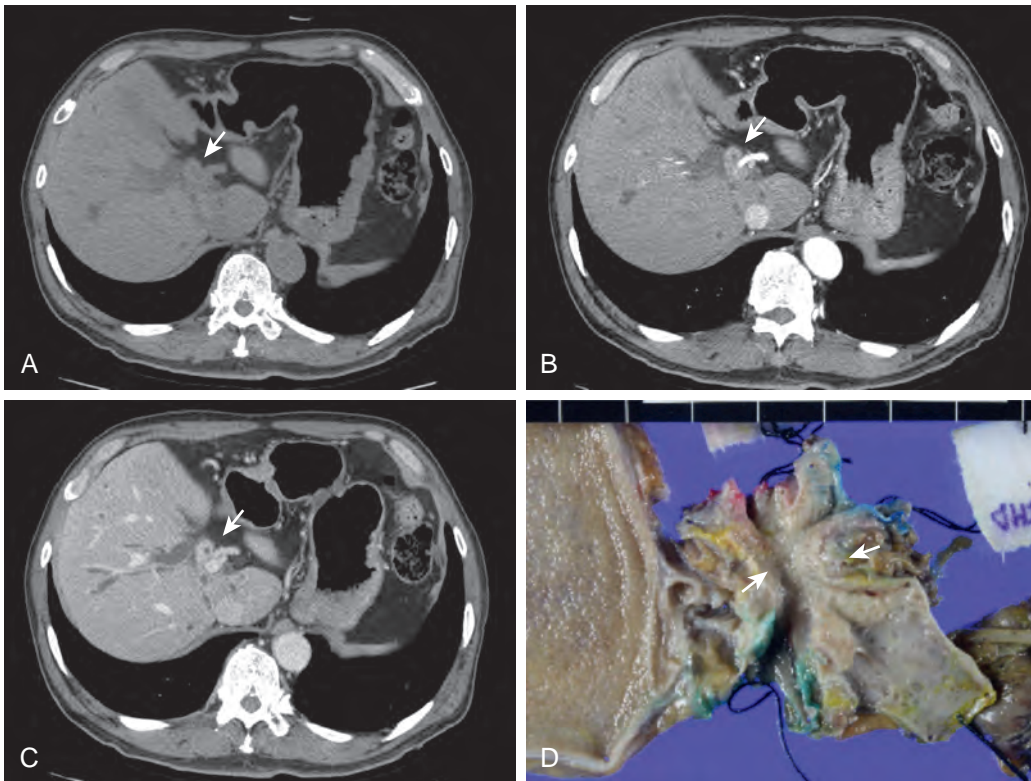


Figure 79-22 Hilar cholangiocarcinoma showing delayed hyperenhancement on CT. Contrast-enhanced CT scans during arterial phase (A and B) and delayed phase (C) reveal a homogeneously hyperenhancing, circumferential wall thickening of the hilar duct (arrow) with dilation of both the right and left bile ducts (not shown). Photograph of the resected specimen (D) shows a luminal narrowing and wall thickening (arrows) caused by an infiltrating cholangiocarcinoma involving the proximal common duct as well as bilateral main hepatic ducts.

that assesses liver, portal node, and portal vein involvement^{79,102} (Fig. 79-27).

Hilar cholangiocarcinomas can usually be differentiated cholangiographically from hilar lymphadenopathy or benign stricture. However, differentiating between benign and malignant biliary strictures is sometimes challenging. Indeed, periductal infiltrating type cholangiocarcinomas, especially in the early stage, may be difficult to differentiate from benign strictures.^{80,103,104} Lymphadenopathy compresses and displaces rather than invades the extrahepatic ducts. Benign strictures complicating cholecystectomy or distal gastric surgery are typically short and cause symmetric narrowing of the common hepatic bile duct.¹⁰³ Rarely, lymphoma or sarcoidosis of the bile ducts may be indistinguishable from cholangiocarcinoma.¹⁰² Longer and thicker involvement, luminal irregularity, asymmetric

narrowing, hyperenhancement during portal venous phase, periductal soft tissue lesion, and lymph node enlargement suggest a malignant stricture rather than a benign stricture¹⁰³⁻¹⁰⁵ (see Figs. 79-25 and 79-26). Recently, great attention has focused on immunoglobulin G4 (IgG4)-related sclerosing cholangitis, which can often mimic periductal infiltrating cholangiocarcinoma. Imaging findings such as involvement of intrapancreatic common duct, smooth outer margin, symmetric narrowing of bile ducts, lower degree of dilation of upstream duct, and lower degree of contrast enhancement are more frequent in IgG4-related sclerosing cholangitis than in cholangiocarcinoma^{106,107} (Fig. 79-28). In addition, coexisting autoimmune pancreatitis, good response to steroid therapy, and increase in IgG and IgG4 are helpful clinical and laboratory findings for the diagnosis of IgG4-related sclerosing cholangitis.^{106,107}

Figure 79-23 Hilar cholangiocarcinoma: MR findings. **A.** T2-weighted MR image shows a slightly hyperintense hilar cholangiocarcinoma (arrow). **B.** Fat-suppressed T1-weighted MR image reveals a hypointense hilar cholangiocarcinoma (arrow). **C.** Gadolinium-enhanced T1-weighted image demonstrates an enhancing mass (arrow) in left main hepatic duct. **D.** Photograph of the resected specimen shows an infiltrating cholangiocarcinoma involving the left main hepatic duct and proximal common duct.

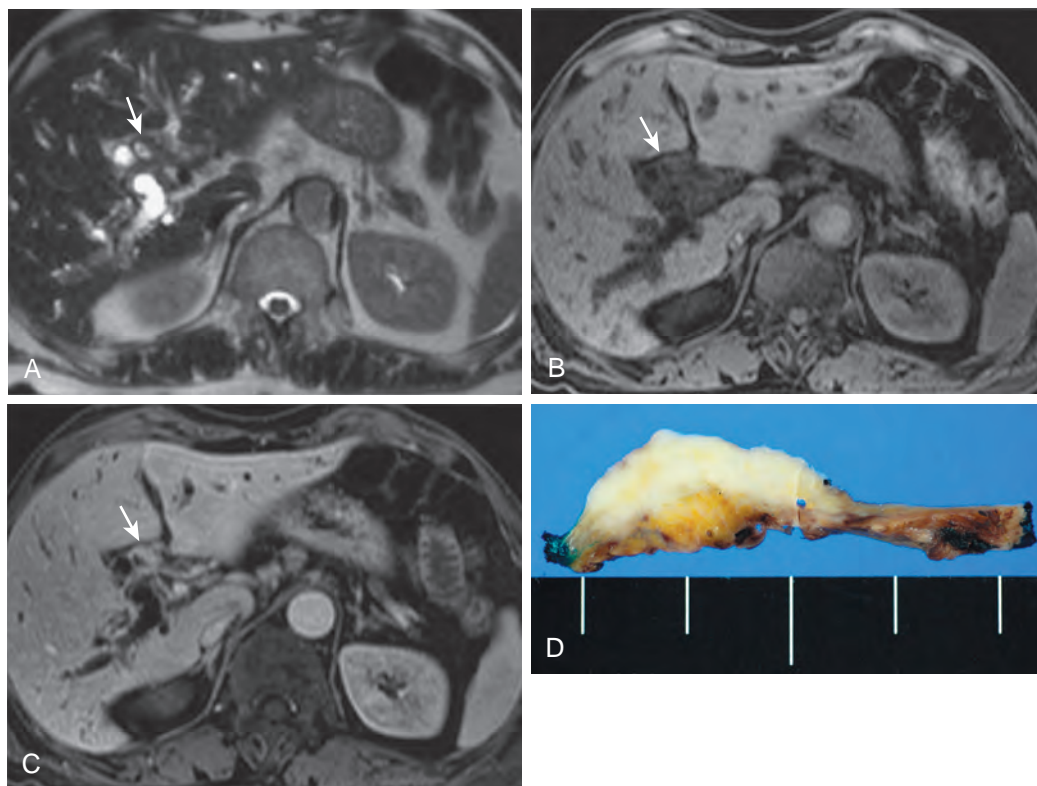
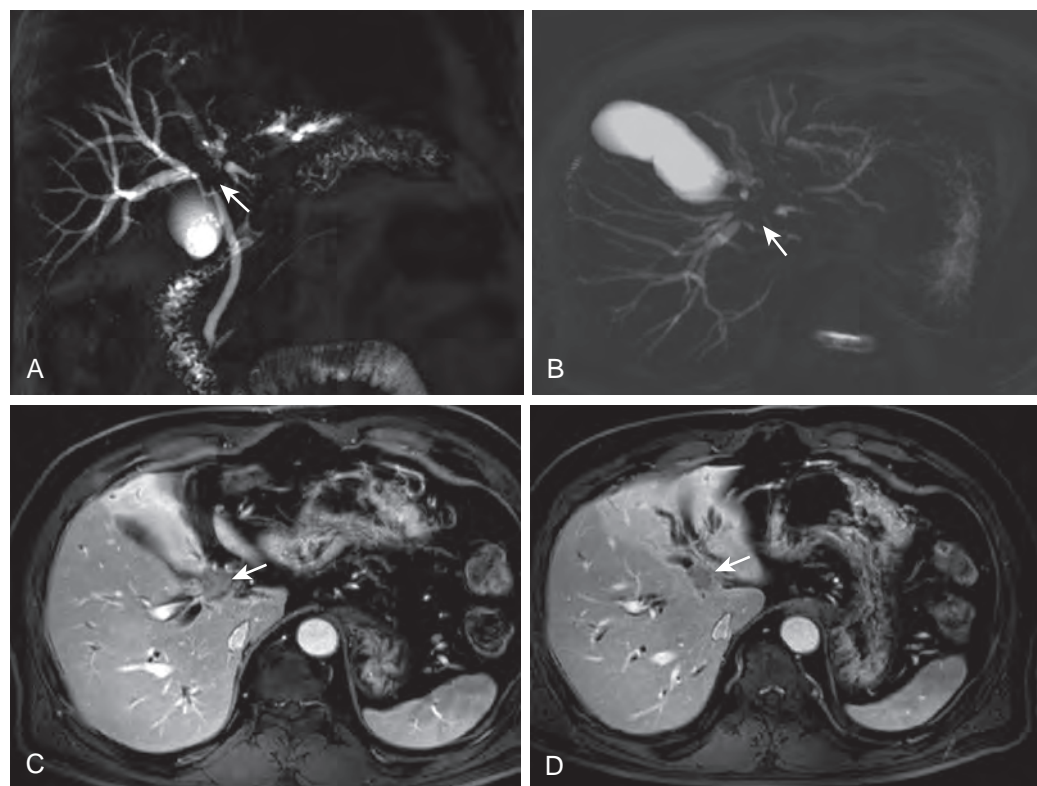


Figure 79-24 Comprehensive evaluation of hilar cholangiocarcinoma by MRI with MR cholangiography for surgical resectability. **A and B.** Coronal and axial thick-slab single-shot MR cholangiograms demonstrate hilar cholangiocarcinoma involving both secondary biliary confluences with upstream ductal dilation. Note that segmental intrahepatic ducts of the left lobe are separated by the tumor (arrow). **C and D.** Postcontrast T1-weighted MR images demonstrate a periductal infiltrating hilar cholangiocarcinoma involving ductal bifurcation area and both main hepatic ducts (arrow). The mass (arrow) shows hypoenhancement compared with adjacent liver parenchyma.



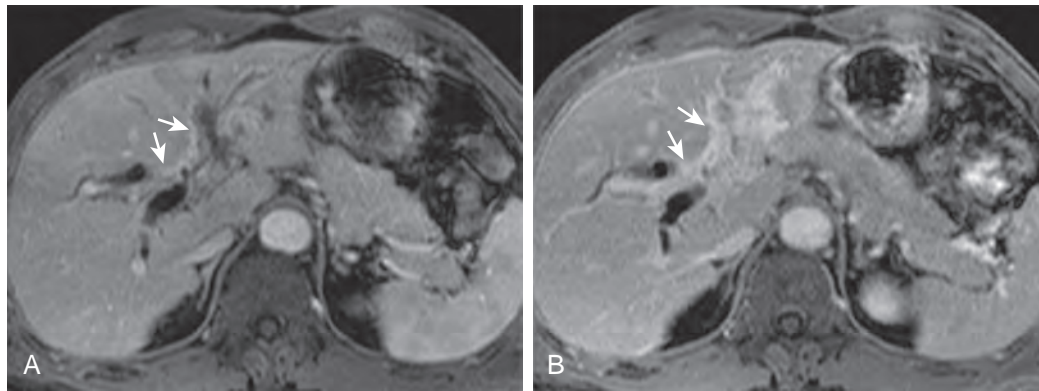


Figure 79-25 Delayed contrast enhancement of cholangiocarcinoma: MRI. **A.** Gadolinium-enhanced T1-weighted image obtained during portal venous phase shows an infiltrating hilar cholangiocarcinoma involving ductal bifurcation area and both main hepatic ducts (arrows). **B.** A 10-minute delayed T1-weighted MR image shows delayed enhancement of the mass (arrows). Tumor involves periportal fat with encased left portal vein.

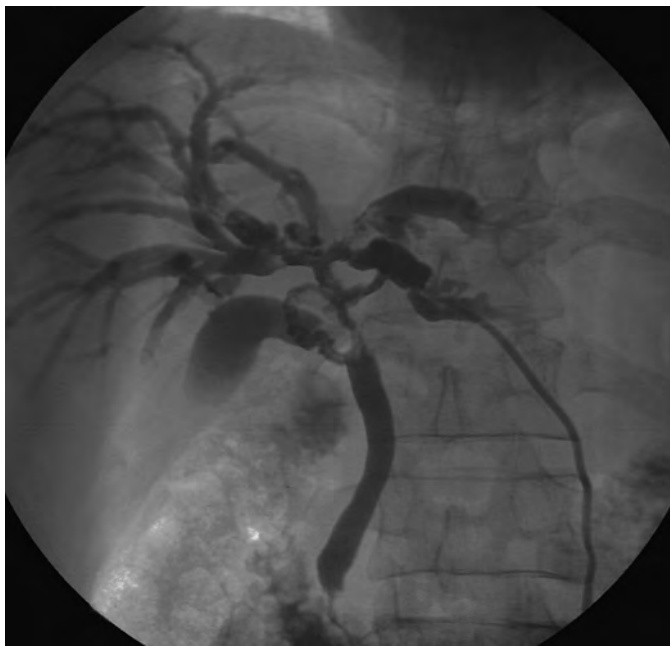


Figure 79-26 Cholangiogram of Klatskin's tumor. Hilar strictures are associated with proximal bile duct dilation.

Extrahepatic Type

Carcinomas of the distal common hepatic or common bile duct are usually small and have a better prognosis than the more central Klatskin's tumor.^{18,19} Fifty percent to 75% of extrahepatic cholangiocarcinomas occur in the upper third, 10% to 30% in the middle third, and 10% to 20% in the lower third of the extrahepatic duct.¹⁰⁸ Cholangiography, either direct cholangiography or MR cholangiography, demonstrates a short stricture or, less often, a polypoid mass, which almost always causes biliary obstruction. CT and MRI can depict an obstructing nodular mass or a concentric or asymmetric thickening of the bile duct wall with enhancement at the transition zone or intraductal polypoid tumors as well as biliary ductal dilation¹⁰⁹ (Fig. 79-29). Adjacent periductal fat may be infiltrated by direct invasion, and lymph node metastasis is relatively frequent. Cholangiocarcinomas that arise in the intrapancreatic portion of the

common bile duct are well depicted as low signal intensity masses against the background of the high signal intensity head of the pancreas on T1-weighted fat-suppressed images and as hyperenhanced thickening of the involved bile duct wall on contrast-enhanced T1-weighted images¹¹⁰ (Fig. 79-30).

For patients with advanced primary sclerosing cholangitis, the risk for development of cholangiocarcinoma is significant. In one study, careful pathologic examination of the native liver removed for transplantation showed that 8% of patients with primary sclerosing cholangitis had coexisting cholangiocarcinoma.¹¹¹ It is often difficult to appreciate malignant degeneration in sclerosing cholangitis. Features that suggest malignancy include progression of strictures on serial cholangiograms, marked biliary dilation above a dominant stricture, and a polypoid ductal mass of 1 cm in diameter or greater¹¹² (Fig. 79-30).

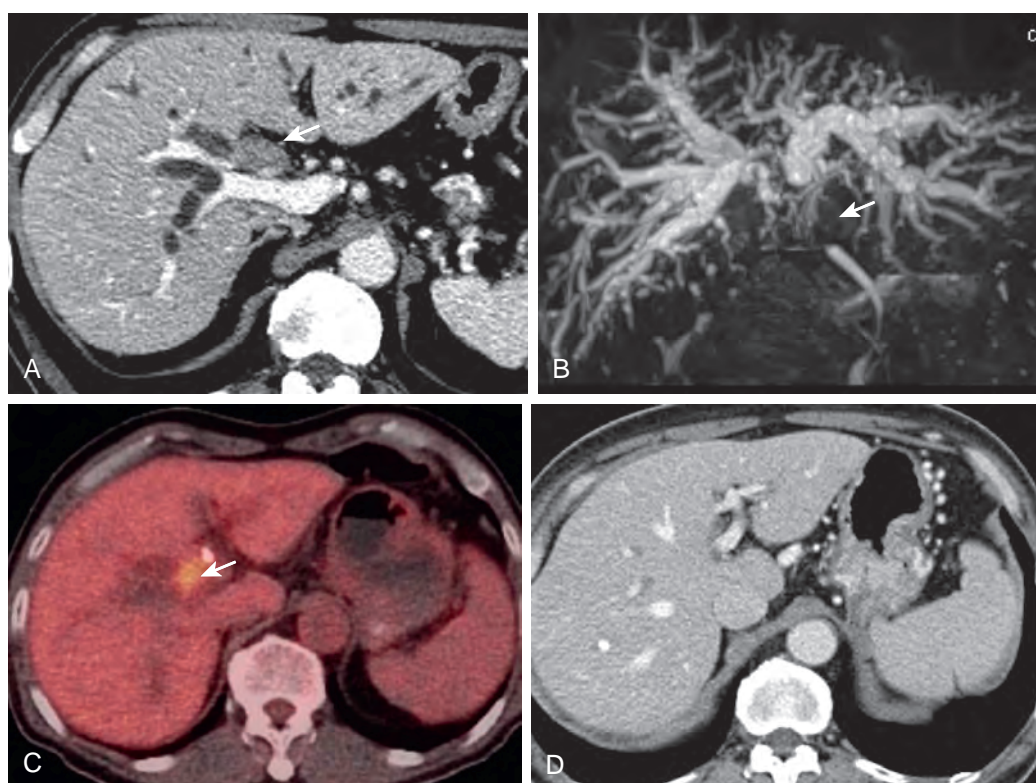
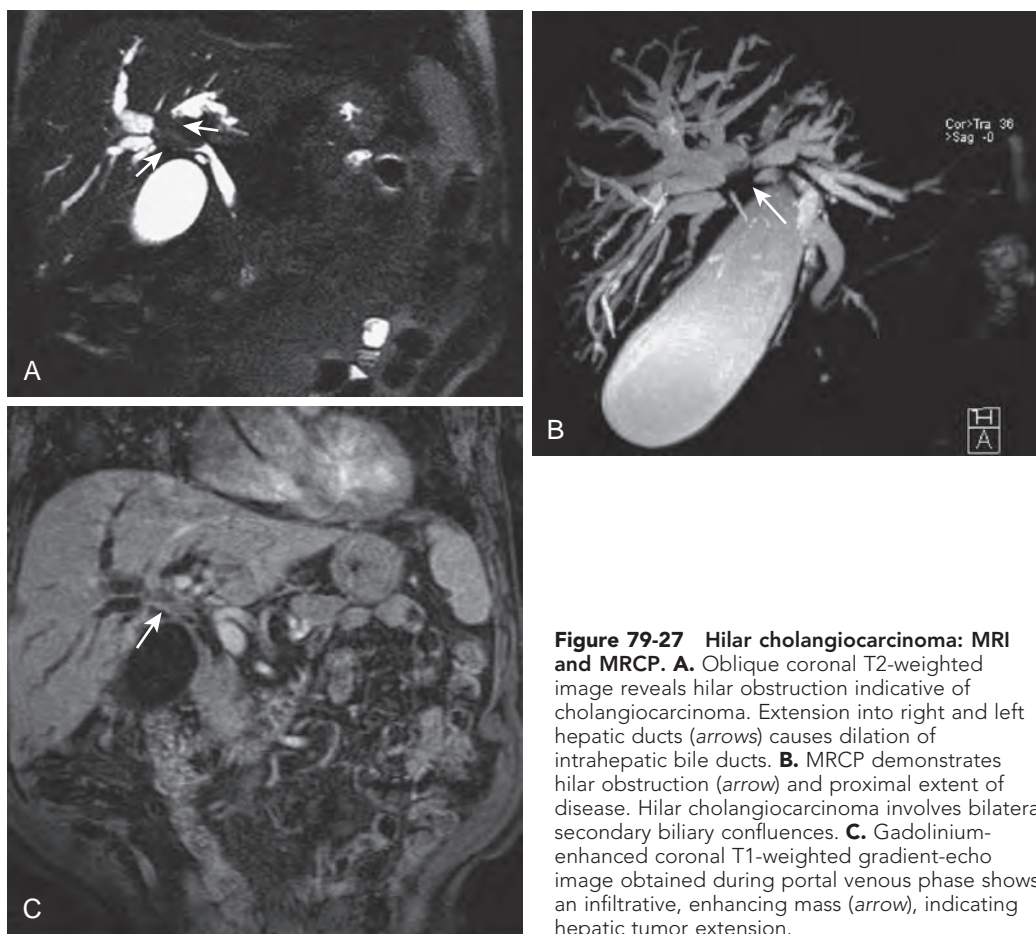
Adults with fusiform extrahepatic choledochal cysts also are at increased risk for development of cholangiocarcinoma (Fig. 79-31). These neoplasms develop within the cyst itself in only about 50% of cases and elsewhere in the biliary system in the remainder. In fact, the cancer can occur after resection of the cyst.¹¹³ Most are manifested as polypoid masses that may be large enough to be visible on cross-sectional imaging.

TREATMENT

Treatment of cholangiocarcinoma includes surgical resection, radiation, laser therapy, biliary stenting, systemic chemotherapy, and liver transplantation.^{18,19,114} There are some long-term survivors after resection, and radiation and bile duct stenting may palliate symptoms for months to years.

Periampullary Carcinoma

Periampullary carcinomas are those tumors arising from or within 1 cm of the papilla of Vater and include ampullary, pancreatic, bile duct, and duodenal cancers.¹¹⁵ It is often impossible by histologic examination to be certain of the origin of the tumor. There is a high incidence of these tumors in patients with familial adenomatous polyposis, and cancer is often preceded by ampullary or duodenal adenomas.¹¹⁵ Periampullary neoplasms tend to be polypoid and lower in grade than more proximal biliary neoplasms.



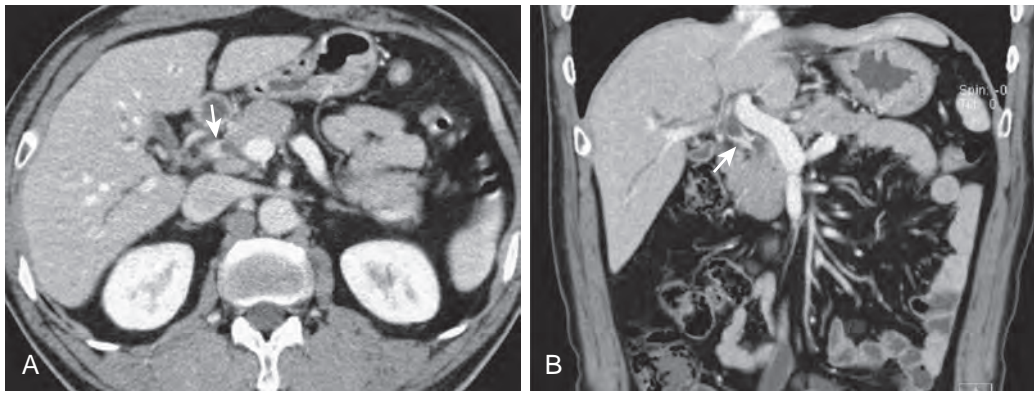


Figure 79-29 Extrahepatic cholangiocarcinoma. **A.** Axial CT during the portal venous phase shows an enhancing mass (arrow) in common bile duct. **B.** Coronal multiplanar reconstructed (MPR) image demonstrates focal mural thickening and enhancement (arrow) of common bile duct.

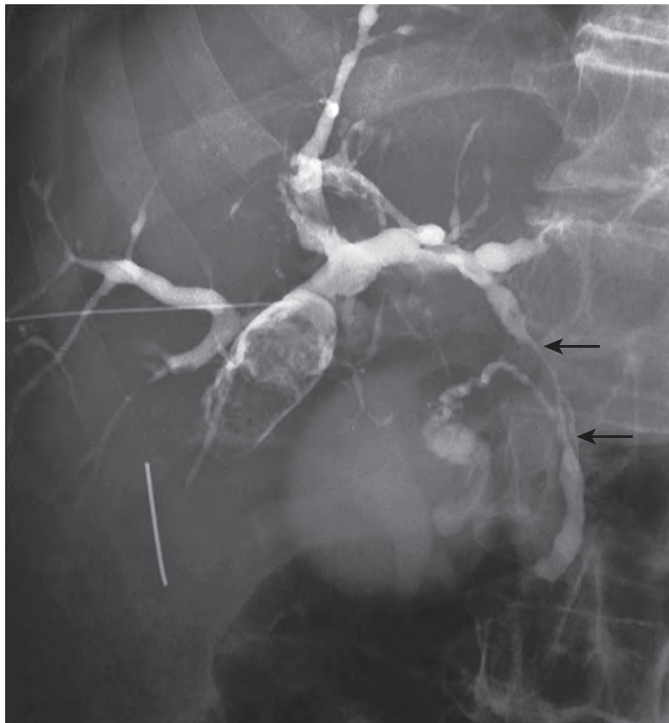


Figure 79-30 Cholangiocarcinoma complicating sclerosing cholangitis. Cholangiocarcinoma is causing a stricture (arrows) in the common hepatic duct in a patient with primary sclerosing cholangitis. Despite the dominant stricture with some biliary dilation proximally, this narrowing could be inflammatory or neoplastic. Calculi are present in the right intrahepatic bile ducts.

Biliary dilation to the level of the ampulla of Vater is seen in 75% of cases, and pancreatic ductal dilation is seen in 67%.¹¹⁵ These masses tend to be small and may not be seen on CT scans, in which case abrupt termination of a dilated bile duct in the head of the pancreas is demonstrated, or abrupt termination of the common bile duct without mass may be seen on cholangiography.¹¹⁶ Ampullary cancer can often be manifested as a polypoid mass at the ampulla with dilation of both main pancreatic duct and common bile duct on three-dimensional contrast-enhanced CT or MRI with MRCP¹¹⁶ (Fig. 79-32). On occasion, a villous polypoid lesion may be seen in the distal common bile duct and duodenum. Liver metastasis or lymphadenopathy is

present at the time of diagnosis in only a small percentage of cases.

On T1-weighted fat-suppressed images, periampullary tumors appear as a low signal intensity mass in the region of the ampulla. On immediate postgadolinium T1-weighted images, these lesions are often visualized as areas of low signal intensity, reflecting their hypovascular character compared with background pancreatic tissue.¹¹⁶ On 2-minute postgadolinium fat-suppressed images, a thin rim of enhancement is commonly observed along the periphery of the tumor⁵⁸ (Fig. 79-33). MRCP and sectional MRI can be useful in determining the origins of periampullary carcinomas.

Cystic Bile Duct Neoplasms: Cystadenoma and Cystadenocarcinoma

Biliary cystadenoma and cystadenocarcinoma are rare cystic neoplasms lined by mucin-secreting columnar epithelium.⁶³ On histologic evaluation, they are similar to cystadenomas and cystadenocarcinomas of the ovary and pancreas. They are usually seen in middle-aged women, who present with abdominal pain, distention, and occasionally jaundice. Most cystadenomas and cystadenocarcinomas are manifested as intrahepatic masses that are hypoechoic on ultrasound and have a low-attenuation, uniloculated or multiloculated, cystic appearance on CT.⁶³ The CT attenuation of the fluid component in a biliary cystadenoma depends on the fluid content. Whereas CT is usually superior in demonstrating the size and extent of these tumors, sonography is superior to CT in depicting internal morphology¹¹⁷ (Fig. 79-34). Irregular, papillary growths and mural nodules along the internal septa and wall are seen in cystadenoma and cystadenocarcinoma, although papillary excrescences and solid portions are more common in cystadenocarcinoma¹¹⁷⁻¹¹⁹ (Fig. 79-35). Cystadenomas occasionally have fine septal calcifications; cystadenocarcinomas may have thick, coarse, mural, and septal calcifications.^{117,118} Communication of these tumors with large intrahepatic ducts is rare. Several case reports have suggested malignant transformation of cystadenomas to cystadenocarcinomas on the basis of several years of follow-up after resection.^{120,121} The differential diagnosis of biliary cystadenoma and cystadenocarcinoma includes hepatic cysts, hydatid cysts, liver abscesses, cystic metastases, hematoma, cystic sarcomas, and choledochal cysts.¹¹⁷

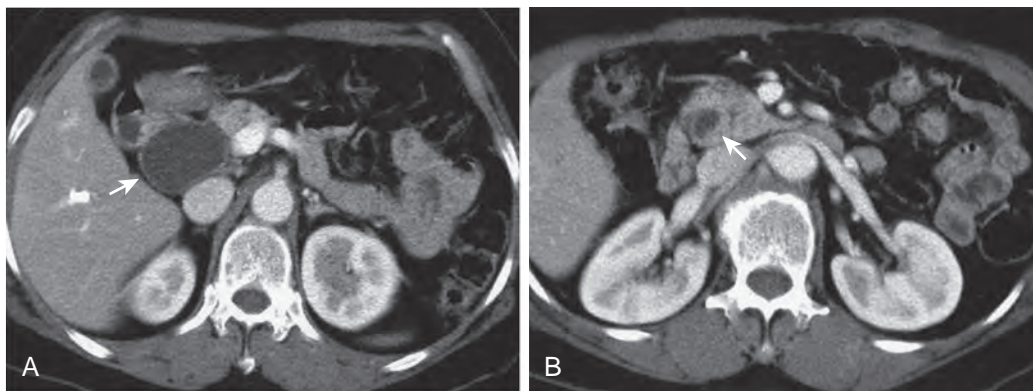


Figure 79-31 Cholangiocarcinoma complicating choledochal cyst. **A.** Contrast-enhanced axial CT scan shows a choledochal cyst (arrow). **B.** CT scan caudal to **A** shows an asymmetric thickening (arrow) of intrapancreatic common bile duct with enhancement.

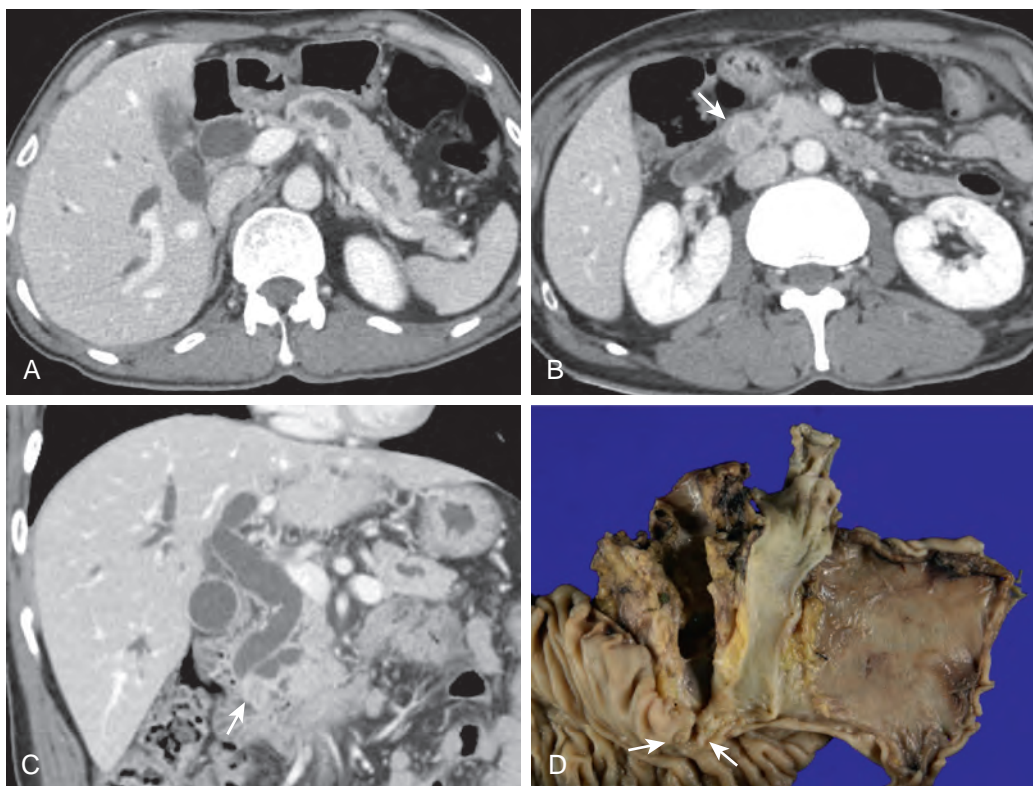


Figure 79-32 Ampulla of Vater cancer. **A.** Axial contrast-enhanced CT scan shows a dilation of the common bile duct and the main pancreatic duct. **B** and **C.** Axial and coronal contrast-enhanced CT scans show a hyperenhancing tumor (arrow) of the ampulla with extension into the main pancreatic duct. **D.** Photograph of the resected specimen shows an irregular mass of the ampulla of Vater (arrows) involving the distal common duct as well as the main pancreatic duct.

Other Malignant Neoplasms of the Bile Ducts

In adults, cholangiocarcinoma and biliary cystadenocarcinoma account for most malignant bile duct neoplasms. Lymphomas, leiomyosarcomas, carcinoid tumors, and metastases rarely occur in the bile ducts (Fig. 79-36). Non-Hodgkin's lymphoma of the bile ducts can rarely mimic cholangiocarcinoma or primary sclerosing cholangitis.^{122,123} In a patient with known lymphoma, cholangiographic findings of smooth, tapered strictures combined with the absence of a portal mass on CT should

suggest the diagnosis. Sarcomas and metastases are manifested as masses projecting into the bile duct lumen, causing biliary obstruction.^{124,125}

After choledochal cyst, embryonal rhabdomyosarcoma is the second most common cause of jaundice in the pediatric population. After infancy, it usually occurs between the ages of 4 and 6 years but has been reported in children aged 1 to 11 years. Sonography and CT will show intrahepatic duct dilation and a soft tissue mass in the region of the common bile duct or porta hepatis. The radiologic appearance of the lesion is similar to that of congenital choledochal cyst if there is no local invasion to adjacent tissues.¹²⁶

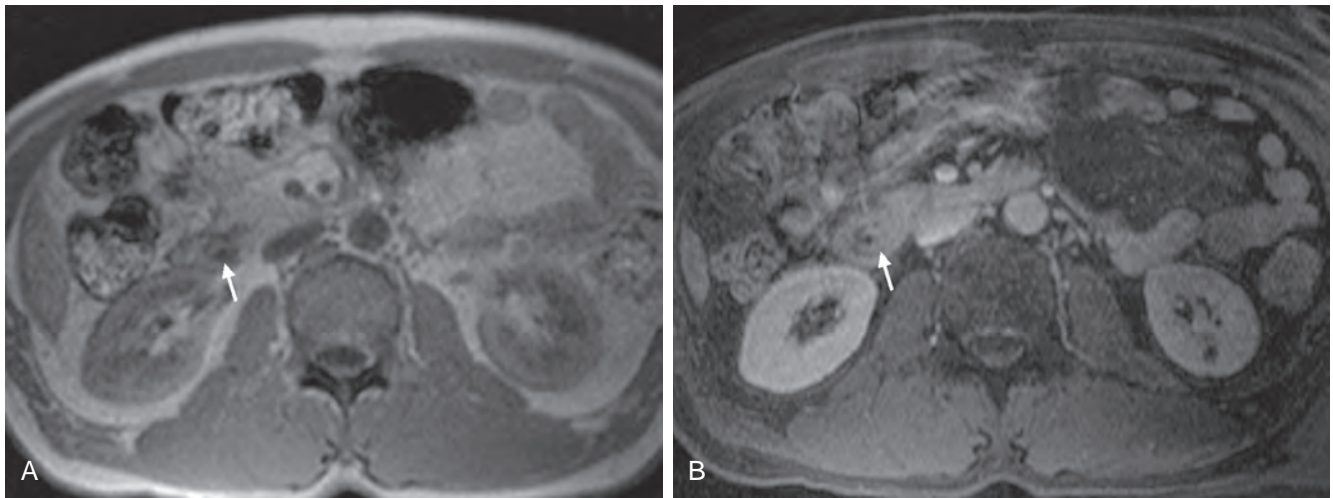


Figure 79-33 Ampullary cancer: MR findings. **A.** T1-weighted image shows a hypointense ampullary tumor (arrow). **B.** Postgadolinium fat-suppressed image demonstrates a thin rim of enhancement (arrow) along the periphery of the tumor.

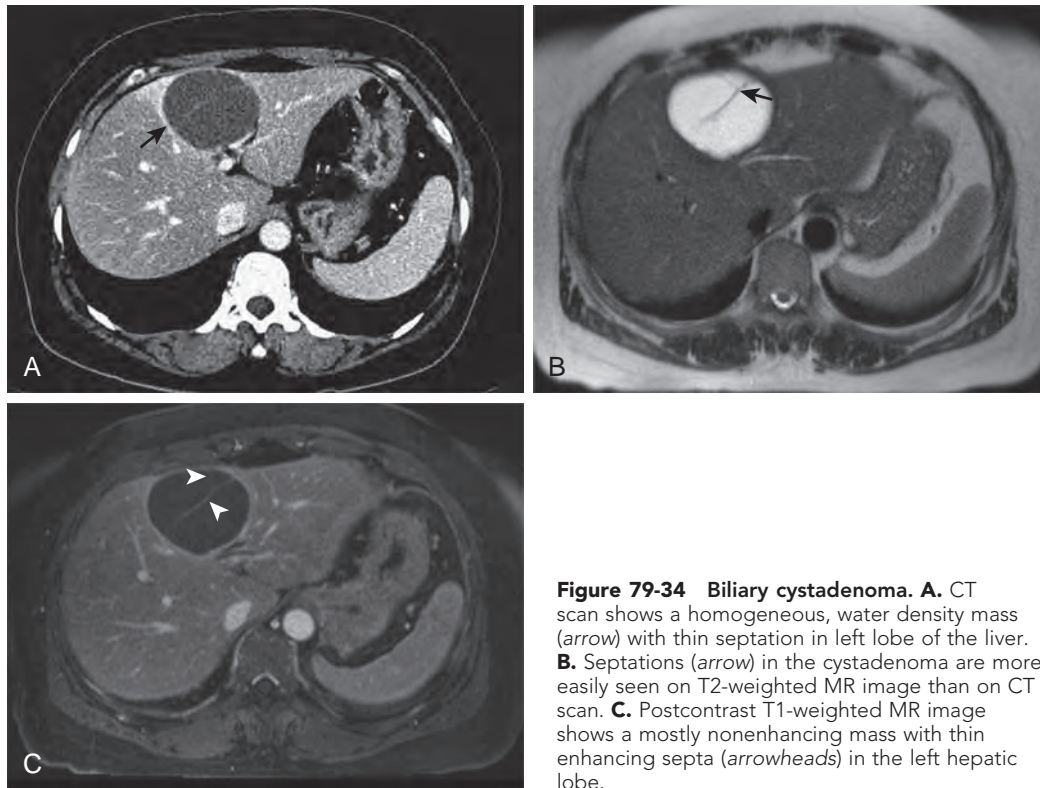


Figure 79-34 Biliary cystadenoma. **A.** CT scan shows a homogeneous, water density mass (arrow) with thin septation in left lobe of the liver. **B.** Septations (arrow) in the cystadenoma are more easily seen on T2-weighted MR image than on CT scan. **C.** Postcontrast T1-weighted MR image shows a mostly nonenhancing mass with thin enhancing septa (arrowheads) in the left hepatic lobe.

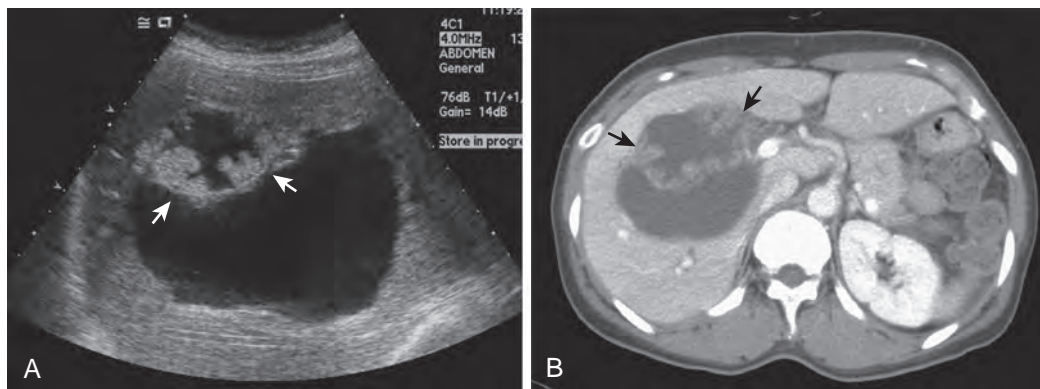


Figure 79-35 Biliary cystadenocarcinoma. **A.** Transverse sonogram shows a large, lobulated cystic mass with thick septation and multiple mural nodules (arrows). **B.** CT scan shows a lobulated cystic mass with thick septation and enhancing mural nodules (arrows).

Figure 79-36 Leiomyosarcoma metastatic to the common hepatic duct. **A.** CT scan shows an enhancing polypoid tumor (black arrow) in dilated common bile duct. White arrow indicates a liver metastasis. **B.** Cholangiography shows an intraluminal mass (arrow) of the common bile duct.

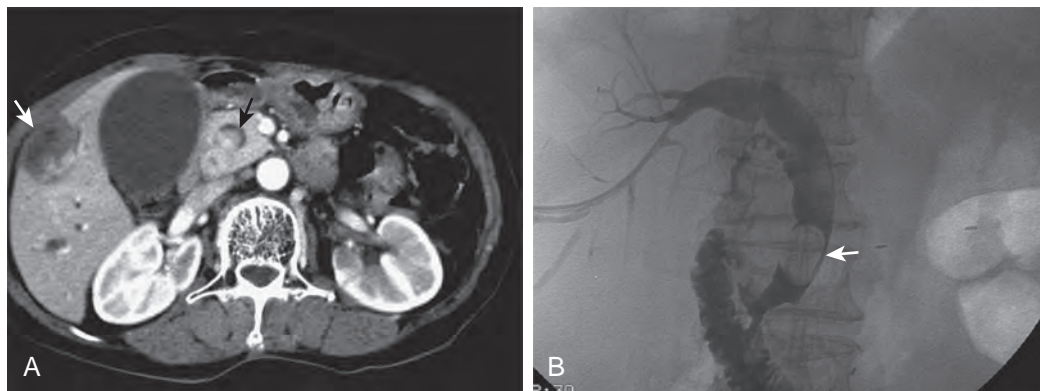
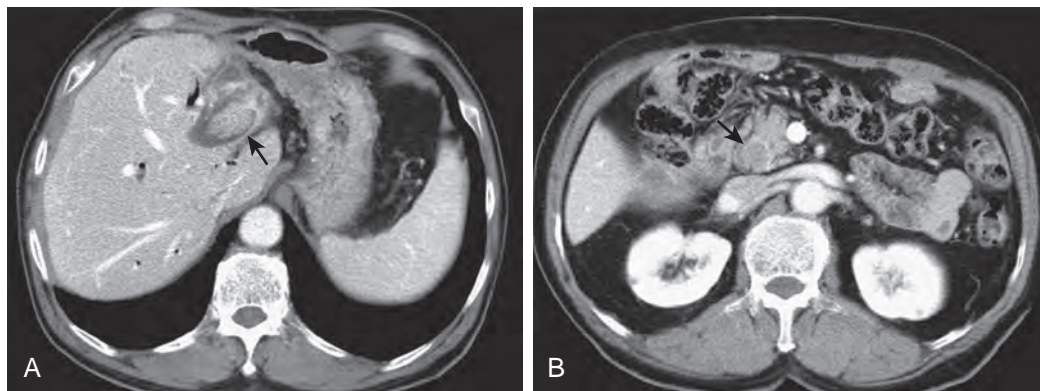


Figure 79-37 Multiple bile duct adenomas. **A.** Contrast-enhanced axial CT scan shows an intraluminal polypoid tumor (arrow) with homogeneous enhancement in dilated left intrahepatic bile duct. **B.** CT scan caudal to A demonstrates similar intraductal mass (arrow) in the common bile duct.



Benign Bile Duct Neoplasms

Benign neoplasms of the bile ducts are rare.⁶⁴ Adenomas are the most common type; others include granular cell tumors, hamartomas, fibromas, neuromas, lipomas, and heterotopic gastric or pancreatic mucosal rests.

Most adenomas are manifested as small asymptomatic polyps in the extrahepatic bile ducts that are found incidentally at surgery (Fig. 79-37). On occasion, they become large and cause biliary obstruction. Multiple papillary adenomas have

been reported in association with obstructive biliary villous adenoma and ampullary carcinoma.^{64,127,128} Granular cell tumors of the bile ducts occur most often in young African American women and cause abdominal pain and jaundice.⁶⁵ Most granular cell tumors are extrahepatic masses and are less than 3 cm in greatest dimension, and as the cell infiltrates the wall of the bile duct, the lumen is obliterated. CT and ultrasound usually show bile duct obstruction without identifying the mass. Cholangiography demonstrates either the extrahepatic bile ducts or a small polypoid mass.⁶⁴ Surgical resection is curative.

REFERENCES

1. Jemal A, Siegel R, Xu J, et al: Cancer statistics, 2010. *CA Cancer J Clin* 60:133–134, 2011.
2. American Joint Committee on Cancer: Gallbladder and extrahepatic bile ducts. In Edge SB, Byrd DR, Compton CC, et al, editors: *AJCC Cancer Staging Manual*, ed 7, Chicago, 2010, Springer, pp 211–217.
3. Meyers MA: Carcinoma of the gallbladder: Imaging, staging, and management. In Meyers MA, editor: *Neoplasms of the Digestive Tract*, Philadelphia, 1998, Lippincott-Raven, pp 479–484.
4. Carriaga MT, Henson DE: Liver, gallbladder, extrahepatic bile ducts, and pancreas. *Cancer* 75:171–190, 1995.
5. Kiran RP, Pokala N, Dudrick SJ: Incidence pattern and survival for gallbladder cancer over three decades—an analysis of 10301 patients. *Ann Surg Oncol* 14:827–832, 2007.
6. Misra S, Chaturvedi A, Misra NC, Sharma ID: Carcinoma of the gallbladder. *Lancet Oncol* 4:167–176, 2003.
7. Foster JM, Hoshi H, Gibbs JF, et al: Gallbladder cancer: Defining the indications for primary radical resection and radical re-resection. *Ann Surg Oncol* 14:833–840, 2007.
8. Roa I, Araya JC, Villaseca M, et al: Gallbladder cancer in a high risk area: Morphologic features and spread patterns. *Hepatogastroenterology* 46:1540–1546, 1999.
9. Maringhini A, Moreau JA, Melton J, et al: Gallstones, gallbladder cancer, and other gastrointestinal malignancies. *Ann Intern Med* 107:30–35, 1987.
10. Berk RN, Armbruster TG, Saltzstein SL: Carcinoma in the porcelain gallbladder. *Radiology* 106:29–31, 1973.
11. Stephen AE, Berger DL: Carcinoma in the porcelain gallbladder: A relationship revisited. *Surgery* 129:699–703, 2001.
12. Aldridge MC, Bismuth H: Gallbladder cancer: The polyp cancer sequence. *Br J Surg* 77:363–364, 1990.
13. Chijiwa K, Kimura H, Tanaka M: Malignant potential of the gallbladder in patients with anomalous pancreaticobiliary ductal junction. *Int Surg* 80:61–64, 1995.
14. Albores-Saavedra J, Henson DE, Sobin LH: The WHO histological classification of tumours of the gallbladder and extrahepatic bile duct. A commentary on the second edition. *Cancer* 70:410–414, 1992.
15. Henson DE, Albores-Saavedra J, Corle D: Carcinoma of the gallbladder. Histologic types, stage of disease, grade and survival rates. *Cancer* 70:1493–1497, 1992.

16. Dachman AH: Benign and malignant tumors of the gallbladder. In Friedman AC, Dachman AH, editors: *Radiology of the Liver, Biliary Tract, and Pancreas*, St Louis, 1994, Mosby-Year Book, pp 155–576.
17. Albores-Saavedra J, Henson DE: Tumors of the Gallbladder and Extra-hepatic Bile Ducts. *Atlas of Tumor Pathology, Fascicle 22, 2nd Series*, Washington, DC, 1986, Armed Forces Institute of Pathology.
18. Rubin P, Hansen JT, editors: *TNM Staging Atlas with Oncoanatomy*, ed 2, Philadelphia, 2011, Lippincott Williams & Wilkins, pp 300–309.
19. Ahrendt SA, Pitt HA: Biliary tract. In Townsend CM, Beauchamp RD, Evers BM, Mattox KL, editors: *Sabiston Textbook of Surgery*, ed 17, Philadelphia, 2004, Elsevier Saunders, pp 1112–1143.
20. Brown JA, Roberts CS: Elevated serum alpha-fetoprotein levels in primary gallbladder carcinoma without hepatic involvement. *Cancer* 70:1838–1840, 1992.
21. Cho KC: Plain films of the liver, bile ducts and spleen. In Baker SR, Choi KC, editors: *The Abdominal Plain Film with Correlative Imaging*, ed 2, Stamford, CT, 1999, Appleton & Lange.
22. Berk RN, Ferrucci JT, Leopold GR: *Radiology of the Gallbladder and Bile Ducts*, Philadelphia, 1983, WB Saunders, p 54.
23. Bach AM, Loring LA, Hann LE, et al: Gallbladder cancer: Can ultrasonography evaluate extent of disease? *J Ultrasound Med* 17:303–309, 1998.
24. Joo I, Lee JY, Kim JH, et al: Differentiation of adenomyomatosis of the gallbladder from early-stage, wall-thickening-type gallbladder cancer using high-resolution ultrasound. *Eur Radiol* 23:730–738, 2013.
25. Soyer P, Gouhiri M, Boudiaf M, et al: Carcinoma of the gallbladder: Imaging features with surgical correlation. *AJR Am J Roentgenol* 169:781–784, 1997.
26. Sadamoto Y, Kubo H, Harada N, et al: Preoperative diagnosis and staging of gallbladder carcinoma by EUS. *Gastrointest Endosc* 58:536–541, 2003.
27. Azuma T, Yoshikawa T, Araidai T, Takasaki K: Differential diagnosis of polypoid lesions of the gallbladder by endoscopic ultrasonography. *Am J Surg* 181:65–70, 2001.
28. Wilbur AC, Sagireddy PB, Aizenstein RI: Carcinoma of the gallbladder: Color Doppler ultrasound and CT findings. *Abdom Imaging* 22:187–190, 1997.
29. Kim SJ, Lee JM, Lee JY, et al: Accuracy of preoperative T-staging of gallbladder carcinoma using MDCT. *AJR Am J Roentgenol* 190:74–78, 2008.
30. Levy AD, Murakata LA, Rohrmann CA, Jr: Gallbladder carcinoma: Radiologic-pathologic correlation. *Radiographics* 21:295–314, 2001.
31. Yoshimitsu K, Honda H, Jimi M, et al: MR diagnosis of adenomyomatosis of the gallbladder and differentiation from gallbladder carcinoma: Importance of showing Rokitsansky-Aschoff sinuses. *AJR Am J Roentgenol* 172:1535–1540, 1999.
32. Kim SJ, Lee JM, Kim H, et al: Role of diffusion-weighted magnetic resonance imaging in the diagnosis of gallbladder cancer. *J Magn Reson Imaging* 38:127–137, 2013.
33. Ogawa T, Horaguchi J, Fujita N, et al: High b-value diffusion-weighted magnetic resonance imaging for gallbladder lesions: Differentiation between benignity and malignancy. *J Gastroenterol* 47:1352–1360, 2012.
34. Sugita R, Yamazaki T, Furuta A, et al: High b-value diffusion-weighted MRI for detecting gallbladder carcinoma: Preliminary study and results. *Eur Radiol* 19:1794–1798, 2009.
35. Demach H, Matsui O, Hoshida K, et al: Dynamic MRI using a surface coil in chronic cholecystitis and gallbladder carcinoma: Radiologic and histopathologic correlation. *J Comput Assist Tomogr* 21:643–651, 1997.
36. Onoyama H: Diagnostic imaging of early gallbladder cancer: Retrospective study of 53 cases. *World J Surg* 23:708–712, 1999.
37. Tsuchiya Y: Early carcinoma of the gallbladder: Macroscopic features and ultrasonography findings. *Radiology* 179:171–175, 1991.
38. Mizuguchi M, Kudo S, Fukahori T, et al: Endoscopic ultrasonography for demonstrating loss of multiple-layer pattern of the thickened gallbladder wall in preoperative diagnosis of gallbladder cancer. *Eur Radiol* 7:1323–1328, 1997.
39. Teehey SA, Baron RL, Bigler SA: Sonography of the gallbladder: Significance of striated (layered) thickening of the gallbladder wall. *AJR Am J Roentgenol* 156:945–947, 1991.
40. Kim SJ, Lee JM, Lee JY, et al: Analysis of enhancement pattern of flat gallbladder wall thickening on MDCT to differentiate gallbladder cancer from cholecystitis. *AJR Am J Roentgenol* 191:765–771, 2008.
41. Lee HY, Kim SH, Lee JM, et al: Preoperative assessment of resectability of hepatic hilar cholangiocarcinoma: Combined CT and cholangiography with revised criteria. *Radiology* 239:113–121, 2006.
42. Ryoo I, Lee JM, Park HS, et al: Preoperative assessment of longitudinal extent of bile duct cancers using MDCT with multiplanar reconstruction and minimum intensity projections: Comparison with MR cholangiography. *Eur J Radiol* 81:2020–2026, 2012.
43. Kakiyama D, Yoshimitsu K, Irie H, et al: Usefulness of the long-axis and short-axis reformatted images of multidetector-row CT in evaluating T-factor of the surgically resected pancreaticobiliary malignancies. *Eur J Radiol* 63:96–104, 2007.
44. Kim HJ, Kim AY, Hong SS, et al: Biliary ductal evaluation of hilar cholangiocarcinoma: Three-dimensional direct multi-detector row CT cholangiographic findings versus surgical and pathologic results—feasibility study. *Radiology* 238:300–308, 2006.
45. Ouchi K, Owada Y, Matsuno S, et al: Prognostic factors in the surgical treatment of gallbladder carcinoma. *Surgery* 101:731–737, 1987.
46. Schwartz LH, Black J, Fong Y, et al: Gallbladder carcinoma: Findings at MR imaging with MR cholangiopancreatography. *J Comput Assist Tomogr* 26:405–410, 2002.
47. Yamashita K, Jin MJ, Hirose Y, et al: CT finding of transient focal increased attenuation of the liver adjacent to the gallbladder in acute cholecystitis. *AJR Am J Roentgenol* 164:343–346, 1995.
48. Choi SH, Lee JM, Lee KH, et al: Relationship between various patterns of transient increased hepatic attenuation on CT and portal vein thrombosis related to acute cholecystitis. *AJR Am J Roentgenol* 183:437–442, 2004.
49. Ros PR, Goodman ZD: Xanthogranulomatous cholecystitis versus gallbladder carcinoma [editorial]. *Radiology* 203:10–12, 1997.
50. Ogura Y, Mizumoto R, Isaji S, et al: Radical operations for carcinoma of the gallbladder: Present status in Japan. *World J Surg* 15:337–343, 1991.
51. Kondo S, Nimura Y, Kamiya J, et al: Mode of tumor spread and surgical strategy in gallbladder carcinoma. *Langenbecks Arch Surg* 387:222–228, 2002.
52. Ohtsuki M, Miyazaki M, Itoh H, et al: Routes of hepatic metastasis of gallbladder carcinoma. *Am J Clin Pathol* 109:62–68, 1998.
53. Ohtani T, Shirai Y, Tsukada K, et al: Spread of the gallbladder carcinoma: CT evaluation with pathologic correlation. *Abdom Imaging* 21:195–199, 1996.
54. Engels JT, Balfe DM, Lee JKT: Biliary carcinoma: CT evaluation of extrahepatic spread. *Radiology* 172:35–40, 1989.
55. Tsukada K, Kurosaki I, Uchida K, et al: Lymph node spread from carcinoma of the gallbladder. *Cancer* 80:661–667, 1997.
56. Thorsen MK, Quiroz F, Lawson TL, et al: Primary biliary carcinoma: CT evaluation. *Radiology* 152:479–483, 1984.
57. Yoshimitsu K, Honda H, Kaneko K, et al: Dynamic MRI of the gallbladder lesions: Differentiation of benign from malignant. *J Magn Reson Imaging* 7:696–703, 1997.
58. Bader TR, Semelka RC, Reinhold C: Gallbladder and biliary system. In Semelka RC, Reinhold C, editors: *Abdominal-Pelvic MRI*, New York, 2002, Wiley-Liss, pp 319–371.
59. Fong Y, Jarnagin W, Blumgart LH: Gallbladder cancer: Comparison of patients presenting initially for definitive operation with those presenting after prior noncurative intervention. *Ann Surg* 232:557–569, 2000.
60. Terasaki S, Nakanuma Y, Terada T, Unoura M: Metastasis of hepatocellular carcinoma to the gallbladder presenting massive intraluminal growth: Report of an autopsy case. *J Clin Gastroenterol* 12:714–715, 1990.
61. Holloway BJ, King DM: Ultrasound diagnosis of metastatic melanoma of the gallbladder. *Br J Radiol* 70:1122–1126, 1997.
62. Inoue T, Kitano M, Kudo M, et al: Diagnosis of gallbladder diseases by contrast-enhanced phase-inversion harmonic ultrasonography. *Ultrasound Med Biol* 33:353–361, 2007.
63. Anjaneyulu V, Shankar-Swarnalatha G, Rao SC: Carcinoid tumor of the gall bladder. *Ann Diagn Pathol* 11:113–116, 2007.
64. Levy AD, Murakata LA, Abbott RM, Rohrmann CA: Benign tumors and tumorlike lesions of the gallbladder and extrahepatic bile ducts: Radiologic-pathologic correlation. *Radiographics* 22:387–413, 2002.
65. Simmons TC, Miller C, Pesigan AM, et al: Cystadenoma of the gallbladder. *Am J Gastroenterol* 84:1427–1430, 1989.
66. Butterly LF, Schapiro RH, LaMuraglia GM, et al: Biliary granular cell tumor: A little-known curable bile duct neoplasm of young people. *Surgery* 103:328–334, 1988.
67. Henson DE, Albores-Saavedra J, Corle D: Carcinoma of the extrahepatic bile ducts: Histologic types, stage of disease, grade, and survival rates. *Cancer* 70:1498–1501, 1992.
68. de Groen PC, Gores GJ, LaRusso NF, et al: Biliary tract cancers. *N Engl J Med* 341:1368–1378, 1999.
69. Khan ZR, Neugut AI, Ahsan H, et al: Risk factors for biliary tract cancers. *Am J Gastroenterol* 94:149–152, 1999.
70. Han JK, Choi BI, Kim AY, et al: Cholangiocarcinoma: Pictorial essay of CT and cholangiographic findings. *Radiographics* 22:173–187, 2002.
71. Nakanuma Y, Minato H, Kida T, Terada T: Pathology of cholangiocarcinoma. In Tobe T, Kameda H, Okudaira M, Ohto M, editors:

- Primary Liver Cancer in Japan, Tokyo, 1994, Springer-Verlag, pp 39–50.
72. Liver Cancer Study Group of Japan: The General Rules for the Clinical and Pathological Study of Primary Liver Cancer, ed 4, Tokyo, 2000, Kanehara.
 73. Lim JH: Cholangiocarcinoma: Morphologic classification according to growth pattern and imaging findings. *AJR Am J Roentgenol* 181: 819–827, 2003.
 74. Lim JH, Park CK: Pathology of cholangiocarcinoma. *Abdom Imaging* 29:540–547, 2004.
 75. Anthony PP: Tumors and tumor-like lesions of the liver and biliary tract: Aetiology, epidemiology and pathology. In MacSween RNM, Burt AD, Portmann BC, et al, editors: *Pathology of the Liver*, ed 4, Edinburgh, 2002, Churchill Livingstone, pp 743–747.
 76. Sainani NI, Catalano OA, Holakere NS, et al: Cholangiocarcinoma: Current and novel imaging techniques. *Radiographics* 28:1263–1287, 2008.
 77. Choi JY, Kim MJ, Lee JM, et al: Hilar cholangiocarcinoma: Role of preoperative imaging with sonography, MDCT, MRI and direct cholangiography. *AJR Am J Roentgenol* 191:1448–1457, 2008.
 78. Lim JH, Yoon KH, Kim SH: Intraductal papillary mucinous tumor of the bile ducts. *Radiographics* 24:53–67, 2004.
 79. Park HS, Lee JM, Choi JY, et al: Preoperative evaluation of bile duct cancer: MRI combined with MR cholangiopancreatography versus MDCT with direct cholangiography. *AJR Am J Roentgenol* 190:396–405, 2008.
 80. Ryoo I, Lee JM, Chung YE, et al: Gadobutrol-enhanced, three-dimensional, dynamic MR imaging with MR cholangiography for the preoperative evaluation of bile duct cancer. *Invest Radiol* 45:217–224, 2010.
 81. Heller SL, Lee VS: MR imaging of the gallbladder and biliary system. *Magn Reson Imaging Clin N Am* 13:295–311, 2005.
 82. Choi BI, Lee JM, Han JK: Imaging of intrahepatic and hilar cholangiocarcinoma. *Abdom Imaging* 29:548–557, 2004.
 83. Kim TK, Choi BI, Han JK, et al: Peripheral cholangiocarcinoma of the liver: Two phase spiral CT findings. *Radiology* 204:539–543, 1997.
 84. Choi BI, Kim TK, Han JK, et al: MRI of clonorchiasis and cholangiocarcinoma. *J Magn Reson Imaging* 8:359–366, 1998.
 85. Honda H, Onitsuka H, Yasumori K, et al: Intrahepatic peripheral cholangiocarcinoma: Two-phased dynamic incremental CT and pathological correlation. *J Comput Assist Tomogr* 17:397–402, 1993.
 86. Kang Y, Lee JM, Kim SH, et al: Intrahepatic mass-forming cholangiocarcinoma: Enhancement patterns on gadoxetic acid-enhanced MR Images. *Radiology* 264:751–760, 2012.
 87. Choi BI, Han JK, Cho JM, et al: Characterization of focal hepatic tumors: Value of two-phase scanning with spiral computed tomography. *Cancer* 76:2434–2442, 1995.
 88. Kokubo T, Itai Y, Ohtomo K, et al: Mucin-hypersecreting intrahepatic biliary neoplasms. *Radiology* 168:609–614, 1988.
 89. Han JK, Lee JM: Intrahepatic intraductal cholangiocarcinoma. *Abdom Imaging* 29:558–564, 2004.
 90. Klatzkin G: Adenocarcinoma of the hepatic duct at its bifurcation with the porta hepatis. *Am J Med* 38:241–256, 1965.
 91. Tillich M, Mischinger H-J, Preisengger K-H, et al: Multiphasic helical CT in diagnosis and staging of hilar cholangiocarcinoma. *AJR Am J Roentgenol* 171:651–656, 1998.
 92. Soyer P, Bluemke DA, Reichle R, et al: Imaging of intrahepatic cholangiocarcinoma. 2. Hilar cholangiocarcinoma. *AJR Am J Roentgenol* 165:1433–1436, 1995.
 93. Garber SJ, Donald JJ, Lees WR: Cholangiocarcinoma: Ultrasound features and correlation with survival. *Abdom Imaging* 18:66–69, 1993.
 94. Hamer OW, Schlottmann K, Sirlin CB, et al: Technology insight: Advances in liver imaging. *Nat Clin Pract Gastroenterol Hepatol* 4:215–228, 2007.
 95. Lacomis JM, Baron RL, Oliver JH, et al: Cholangiocarcinoma: Delayed CT contrast enhancement patterns. *Radiology* 203:98–102, 1997.
 96. Keogan MT, Seabourn JT, Paulson EK, et al: Contrast-enhanced CT of intrahepatic and hilar cholangiocarcinoma: Delay time for optimal imaging. *AJR Am J Roentgenol* 169: 1491–1496, 1997.
 97. Lee JW, Han JK, Kim TK, et al: CT features of intraductal intrahepatic cholangiocarcinoma. *AJR Am J Roentgenol* 175:721–725, 2000.
 98. Kim JE, Lee JM, Kim SH, et al: Differentiation of intraductal growing type cholangiocarcinomas at biliary MR imaging with MR cholangiography. *Radiology* 257:364–372, 2010.
 99. Kim H, Lim JH, Jang KT, et al: Morphology of intraductal papillary neoplasms of the bile ducts: Radiologic-pathologic correlation. *Abdom Imaging* 36:438–446, 2011.
 100. Manfredi R, Masselli G, Maresca G, et al: MR imaging and MRCP of hilar cholangiocarcinoma. *Abdom Imaging* 28:319–325, 2003.
 101. Stain SC, Baer HU, Dennison AR, Blumgart LH: Current management of hilar cholangiocarcinoma. *Surg Gynecol Obstet* 175:579–588, 1992.
 102. Hanninen EL, Jonas PS, Ricke JJ, et al: Magnetic resonance imaging including magnetic resonance cholangiopancreatography for tumor localization and therapy planning in malignant hilar obstructions. *Acta Radiol* 46: 461–470, 2005.
 103. Choi SH, Han JK, Lee JM, et al: Differentiating malignant from benign common bile duct stricture with multiphasic helical CT. *Radiology* 236:178–183, 2005.
 104. Kim JY, Lee JM, Han JK, et al: Contrast-enhanced MRI combined with MR cholangiopancreatography for the evaluation of patients with biliary strictures: Differentiation of malignant from benign bile duct strictures. *J Magn Reson Imaging* 26:304–312, 2007.
 105. Park MS, Kim TK, Kim KW, et al: Differentiation of extrahepatic bile duct cholangiocarcinoma from benign stricture: Findings at MRCP versus ERCP. *Radiology* 233:234–240, 2004.
 106. Tabata T, Kamisawa T, Hara S, et al: Differentiating immunoglobulin G4-related sclerosing cholangitis from hilar cholangiocarcinoma. *Gut Liver* 7:234–238, 2013.
 107. Nakazawa T, Ando T, Hayashi K, et al: Diagnostic procedures for IgG4-related sclerosing cholangitis. *J Hepatobiliary Pancreat Sci* 18: 127–136, 2011.
 108. Chung YE, Kim MJ, Park YN, et al: Staging of extrahepatic cholangiocarcinoma. *Eur Radiol* 18:2182–2195, 2008.
 109. Alexander F, Rossil RL, O'Bryan M, et al: Biliary carcinoma. A review of 109 cases. *Am J Surg* 147:503–509, 1984.
 110. Lim JH, Lee WJ, Takehara Y, Lim HK: Imaging of extrahepatic cholangiocarcinoma. *Abdom Imaging* 29:565–571, 2004.
 111. Goss JA, Shackleton CR, Farmer DG, et al: Orthotopic liver transplantation for primary sclerosing cholangitis. A 12-year single center experience. *Ann Surg* 225:472–481; discussion 481–483, 1997.
 112. Campbell WL, Ferris JV, Holbert BL, et al: Biliary tract carcinoma complicating sclerosing cholangitis: Evaluation with CT, cholangiography, ultrasonography, and MR imaging. *Radiology* 207:41–45, 1998.
 113. Visser BD, Suh I, Way LW, Kang SM: Congenital choledochal cysts in adults. *Arch Surg* 139:855–862, 2004.
 114. Skipworth JR, Keane MG, Pereira SP: Update on the management of cholangiocarcinoma. *Dig Dis* 32:570–578, 2014.
 115. Ditttrick GW, Mallat DB, Lamont JP: Management of ampullary lesions. *Curr Treat Options Gastroenterol* 9:371–376, 2006.
 116. Kim JH, Kim MJ, Chung JJ, et al: Differential diagnosis of periampullary carcinomas at MR imaging. *Radiographics* 22:1335–1352, 2002.
 117. Choid BI, Lim JH, Han MC, et al: Biliary cystadenoma and cystadenocarcinoma: CT and sonographic findings. *Radiology* 171:57–61, 1989.
 118. Meyer X, Henry L, Garcia P, et al: Microcystic variant of biliary mucinous cystadenoma: Ultrasonography, CT, and MR findings. *J Comput Assist Tomogr* 21:1015–1019, 1997.
 119. Korobkin M, Stephens DH, Lee JKT, et al: Biliary cystadenoma and cystadenocarcinoma: CT and sonographic findings. *AJR Am J Roentgenol* 153:507–511, 1989.
 120. Coulter GN, Baxter JN: Cystadenoma of the common bile duct with malignant transformation. *Aust N Z J Surg* 59:291–294, 1989.
 121. O'Shea JS, Shah D, Cooperman AM: Biliary cystadenocarcinoma of extrahepatic duct origin arising in previously benign cystadenoma. *Am J Gastroenterol* 82:1306–1310, 1987.
 122. Lewis RB, Lattin GE, Jr, Makhlof HR, Levy AD: Tumors of the liver and intrahepatic bile ducts: radiologic-pathologic correlation. *Magn Reson Imaging Clin N Am* 18:587–609, 2010.
 123. Cho YH, Byun JH, Kim JH, et al: Primary malt lymphoma of the common bile duct. *Korean J Radiol* 14:764–768, 2013.
 124. Whitcomb FF, Corley GJ, Babigian DN, et al: Leiomyosarcoma of the bile ducts. *Gastroenterology* 52:94–97, 1967.
 125. Katabathina VS, Dasyam AK, Dasyam N, Hosseinzadeh K: Adult bile duct strictures: role of MR imaging and MR cholangiopancreatography in characterization. *Radiographics* 34(3):565–586, 2014. doi: 10.1148/rg.343125211.
 126. Tireli GA, Sander S, Dervisoglu S, et al: Embryonal rhabdomyosarcoma of the common bile duct mimicking choledochal cyst. *J Hepatobiliary Pancreat Surg* 12:263–265, 2005.
 127. Kawakatsu M, Vilgrain V, Zins M, et al: Radiologic features of papillary adenoma and papillomatosis of the biliary tract. *Abdom Imaging* 22:87–93, 1997.
 128. Gulluoglu MG, Ozden I, Poyanli A, et al: Intraductal growth-type mucin-producing peripheral cholangiocarcinoma associated with biliary papillomatosis. *Ann Diagn Pathol* 11: 34–38, 2007.

Inflammatory Disorders of the Biliary Tract

BENJAMIN M. YEH | WEI-CHOU CHANG

CHAPTER OUTLINE

Primary Sclerosing Cholangitis

Epidemiology and Clinical Findings

Pathology

Radiographic Findings

Fluoroscopic Cholangiography

Ultrasound, Computed Tomography, and Magnetic Resonance Imaging

Differential Diagnosis

Primary Biliary Cirrhosis

Epidemiology and Clinical Findings

Radiographic Findings

Obstructive Cholangitis

Recurrent Pyogenic Cholangitis (Oriental Cholangiohepatitis)

Cholangitis Related to Acquired Immunodeficiency Syndrome

Floxuridine Cholangitis

Parasitic Infestation

Ascariasis

Clonorchiasis

Infestation with Other Liver Flukes

Echinococcal Cholangitis

Primary Sclerosing Cholangitis

EPIDEMIOLOGY AND CLINICAL FINDINGS

Primary sclerosing cholangitis (PSC) is a chronic cholestatic liver disease of unknown cause. This disease has a typical onset from 20 to 30 years of age but may begin in childhood; it has a 2:1 male-to-female predilection.¹ PSC is commonly associated with inflammatory bowel disease, particularly ulcerative colitis but also, to a much lesser extent, Crohn's disease. Approximately 70% of patients with PSC have ulcerative colitis. In patients with ulcerative colitis, 3% to 7.5% have or will develop PSC.² The term *primary* is used even when there is associated ulcerative colitis because there is no convincing evidence that PSC is caused by or is secondary to inflammatory bowel disease. In fact, the hepatobiliary disease precedes the clinical onset of the bowel disease in some patients. Other associated conditions include sicca complex, Riedel's struma, retroperitoneal fibrosis, and mediastinal fibrosis, but none of these has been reported consistently.^{3,4} Patients with PSC also have an increased risk for cholangiocarcinoma, with a lifetime risk of 10% to 15%.

Approximately 25% of patients with PSC are asymptomatic at presentation.² Clinical features of PSC include fatigue, pruritus, jaundice, right upper quadrant pain, and hepatosplenomegaly. Elevations of serum bilirubin concentration and serum aspartate transaminase activity are usually not as marked or as consistent as increased serum alkaline phosphatase activity. There is strong evidence that genetic and immunologic factors are important in the pathogenesis of PSC. There is no specific serologic marker for PSC.^{5,6} However, approximately 80% of PSC patients have perinuclear antineutrophil cytoplasmic antibodies, also called antimitochondrial antibodies; antinuclear antibodies and anti-smooth muscle antibody are found in 20% to 50% of PSC patients. These markers are nonspecific.

The natural history of PSC is variable but usually progressively downhill, with a 5-year survival of 88% and a median survival of 11.9 years from the time of diagnosis.³ No known therapy, short of liver transplantation, has been proved effective.

PATHOLOGY

PSC is characterized by fibrosing inflammation of the biliary tree (Fig. 80-1). Inflammatory cells are scanty on microscopic examinations, however, and ductal fibrosis is nonspecific and difficult to quantitate pathologically. The diagnosis therefore cannot be made solely on the basis of an extrahepatic duct biopsy specimen.⁷ In fact, biopsy specimens of the extrahepatic ducts should not be obtained unless cholangiocarcinoma must be ruled out.

Tissue samples from the liver may rarely show specific findings of PSC: cholangiectasis in combination with fibrous obliteration of large intrahepatic bile ducts.^{7,8} These tissue samples are generally available only at autopsy or transplantation and not during routine clinical work-up of the patient. Histologic changes found on conventional needle liver biopsy, although not diagnostic, may strongly support the diagnosis of PSC (nonsuppurative, nongranulomatous destruction of septal or interlobular bile ducts in some portal tracts). Other portal tracts in the same patient may demonstrate ductal proliferation and periportal edema secondary to large duct obstruction.⁹ The histologic stages of PSC are as follows: portal hepatitis or cholangitis (stage 1); periportal hepatitis or fibrosis (stage 2); septal fibrosis or bridging necrosis, or both (stage 3); and cirrhosis (stage 4). The injury to the liver in PSC is the result of both a chronic hepatitis and bile duct obstruction, and the staging system applies to the liver disease, not the bile duct lesions.

The term *pericholangitis* has been used when features of stage 1 and stage 2 disease are seen. These changes are now considered to be part of the spectrum of PSC, and patients are classified as having small duct PSC (visible microscopically) or large duct PSC (visible cholangiographically), or both.

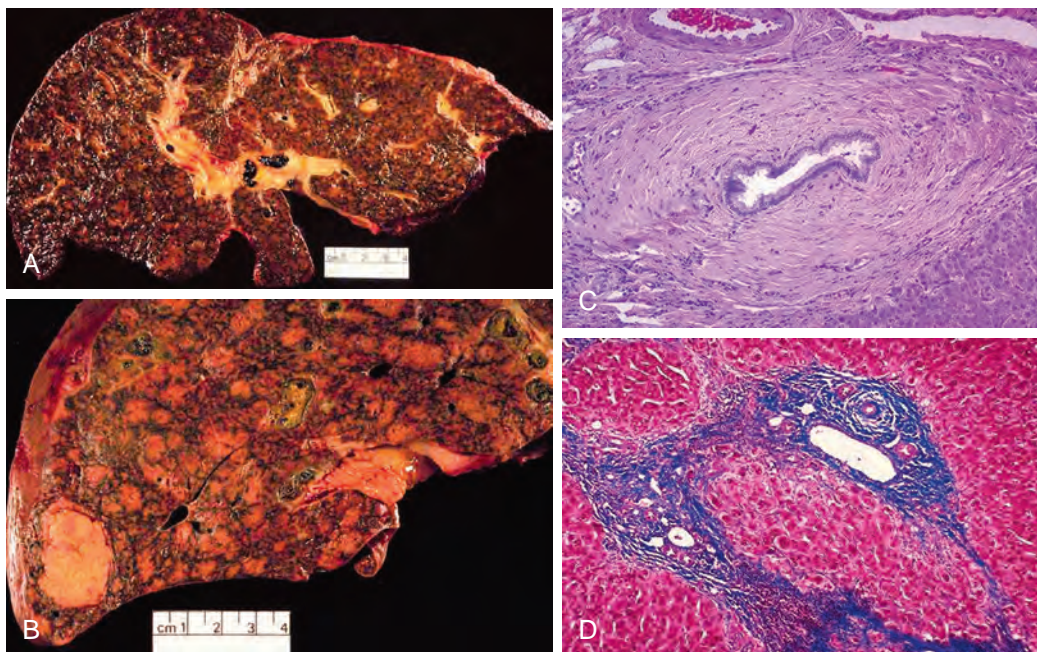


Figure 80-1 PSC: pathologic findings. **A.** Cirrhosis from PSC is illustrated here. The liver in PSC typically is green and becomes progressively darker green with advancing stage. **B.** In this advanced case, a peripheral cholangiocarcinoma is present. **C.** Early phases of ductal fibrous cholangitis show concentric periductal fibrosis and mild epithelial atrophy. **D.** Trichrome stain shows dense fibrosis (blue) in this liver.

Large duct PSC virtually always involves the intrahepatic ducts and almost always the extrahepatic ducts. The common bile duct, the common hepatic duct, and the first 1 cm of the left and right hepatic ducts (which are truly anatomically extrahepatic in most patients) are spared cholangiographically in only 1% to 2% of patients. In 20% of patients, the disease is confined cholangiographically to the intrahepatic and hilar ducts.

In the absence of complicating cholangiocarcinoma, large duct PSC progresses slowly. In one series, 80% of patients with uncomplicated PSC showed no change on serial cholangiograms during a period of 6 months to 6.5 years.¹⁰

Gallbladder abnormalities occur in 40% of patients with PSC; the most common abnormality is gallstones (26%). Direct involvement of the gallbladder wall by PSC occurs in about 15% of patients, and approximately 4% of patients have gallbladder neoplasms, such as adenoma and adenocarcinoma.¹¹

RADIOGRAPHIC FINDINGS

Whereas findings from liver biopsy may be compatible with PSC, they alone are not diagnostic. In general, the diagnostic criteria for PSC should include the following: typical radiographic appearance of cholangiographic abnormalities; appropriate clinical, biochemical, and histologic findings obtained from liver biopsy; and exclusion of secondary causes of sclerosing cholangitis. Of these, typical radiographic cholangiographic abnormalities are crucial for the diagnosis of PSC.

FLUOROSCOPIC CHOLANGIOGRAPHY

Although features of PSC can be demonstrated on a variety of imaging modalities, the most important and most

characteristic radiographic findings are seen at fluoroscopic cholangiography¹² (Fig. 80-2). Fluoroscopic cholangiography is usually accomplished by endoscopic retrograde cholangiopancreatography (ERCP). If certain segments of the biliary tract are unable to be visualized by ERCP, percutaneous transhepatic cholangiography may be performed.

Multiple segmental strictures involving both the intrahepatic and extrahepatic bile ducts are the hallmark of PSC. The fluoroscopic cholangiographic findings in PSC depend on the stage of the disease process. Random segments of the biliary tree may be involved by periductal inflammation and fibrosis. In the early phases of PSC, normal or less-involved duct segments may alternate with segmental strictures, producing the classic beaded appearance. Stricture length can vary from 1 to 2 mm (so-called band strictures) to several centimeters; the most common length is 1 to 1.5 cm. Strictures usually occur at the bifurcation of bile ducts and are out of proportion to upstream ductal dilation. When the periductal fibrosis worsens, the bile ducts take on a “pruned tree” appearance that reflects peripheral duct obliteration. In addition, the angles formed with the central ducts become more obtuse.

Diverticular outpouchings, varying in size from 1 to 2 mm to 1 cm, are seen in about 25% of patients on high-quality cholangiograms and are a characteristic feature of PSC. Some diverticula appear to develop as herniations adjacent to strictures, whereas others arise in the absence of strictures, apparently as mucosal extensions into the thickened duct wall.

Almost half of patients with PSC have some degree of mural irregularity varying from a fine, brush-border appearance to a coarse, shaggy, or frankly nodular appearance. The combined findings of short strictures, beading, pruning, diverticula, and mural irregularities often result in a composite cholangiographic appearance that is nearly pathognomonic for PSC.

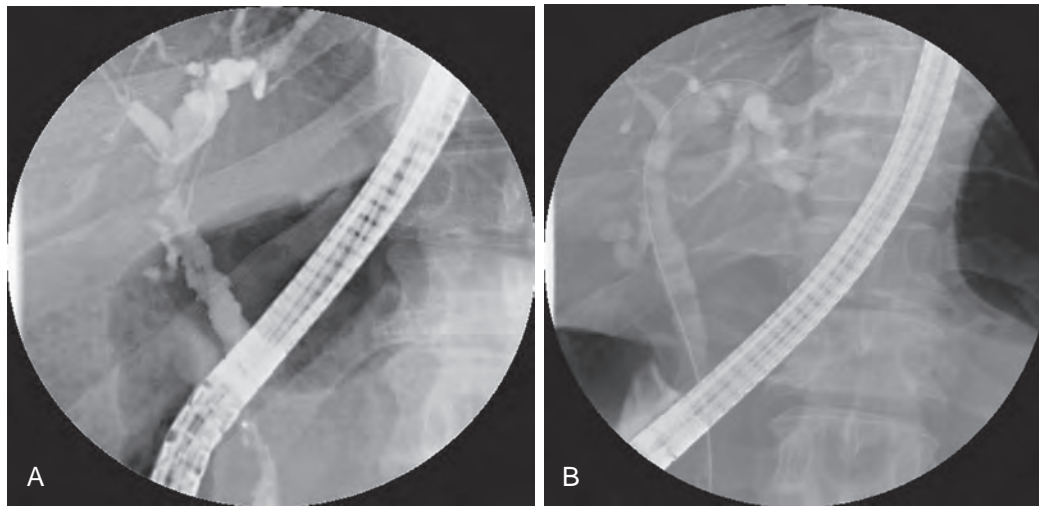


Figure 80-2 PSC: ERCP findings. **A** and **B.** There are multifocal, irregular strictures and dilations involving the intrahepatic and extrahepatic bile ducts. The strictures are usually short and annular, may appear as webs, and alternate with normal or slightly dilated segments, producing a beaded appearance. Coarse nodular mural irregularities as well as small eccentric outpouchings are often seen.

ULTRASOUND, COMPUTED TOMOGRAPHY, AND MAGNETIC RESONANCE IMAGING

Ultrasound, computed tomography (CT), and magnetic resonance imaging (MRI) are common first-line imaging tests for abnormal liver function. These modalities can assess for the presence of biliary tract abnormalities. Cross-sectional imaging allows evaluation of not only the bile duct but also the bile duct wall and the surrounding liver parenchyma. In patients with PSC, cross-sectional imaging allows detection of complications such as cirrhosis and malignant disease.

Because ultrasound (Fig. 80-3) is relatively inexpensive and can effectively evaluate the biliary system, it is commonly the initial imaging modality used in the evaluation of cholestatic liver disease. Findings of PSC by ultrasound evaluation include duct dilation and wall thickening of the common bile duct or the intrahepatic ducts in a smooth or irregular manner. The normal intrahepatic bile ducts have a wall thickness of less than 1 mm and appear sonographically as a thin echogenic line. Thickened bile ducts appear as two parallel echogenic lines with a central hypoechoic stripe.¹³ Bile duct wall thickening in PSC usually measures 2 to 5 mm. Common bile duct wall thickening, when it is present, can be easily seen by ultrasound examination. Detection of intrahepatic bile duct wall thickening, on the other hand, is difficult as this modality is operator dependent and this is a subtle finding not always readily apparent.

With ever-improving technology, CT scanning continues to serve as one of the primary imaging modalities for the evaluation of abdominal disease. Current-generation multidetector CT scanners allow rapid acquisition of data and the creation of high-resolution reformatted images for the evaluation of the biliary system, a technique known as CT cholangiography. CT cholangiography uses axial CT data, which are then reconstructed into two-dimensional and three-dimensional images to evaluate the biliary tree, particularly the extrahepatic bile ducts. Oral or intravenous cholangiographic contrast material is used to opacify the bile ducts before scanning. CT cholangiography allows cross-sectional imaging of the biliary tree in patients who do not qualify for MRI, such as patients who have aneurysm clips or a pacemaker, who are claustrophobic, or who

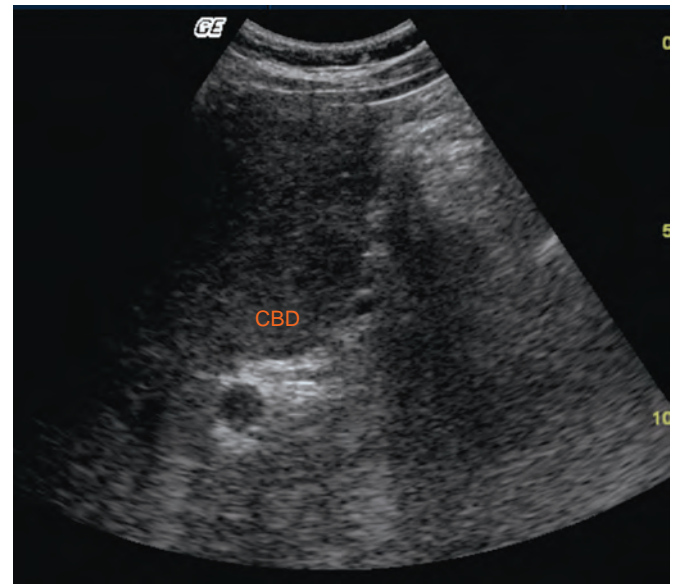


Figure 80-3 PSC: sonographic findings. Mural thickening of the common bile duct (CBD) is identified on this transverse sonogram.

have too many surgical clips within the porta hepatis from prior surgery.¹⁴

CT findings of PSC are similar to ERCP findings and include segmental intrahepatic biliary duct disproportional dilation with focal constrictions (Fig. 80-4). The common hepatic duct and common bile duct can also demonstrate alternating narrowing and dilation. Mural contrast enhancement of the extrahepatic bile ducts can be seen, although this is a nonspecific finding that can be seen with other causes of cholangitis (see Fig. 80-10). Intrahepatic bile duct calculi are present in approximately 8% of patients with PSC. These calculi appear as foci of faint high attenuation or as coarse calcifications and are best seen on non-contrast-enhanced images.¹⁵ Upper abdominal lymphadenopathy is frequently seen in patients with PSC, although this is nonspecific. The presence of lymphadenopathy

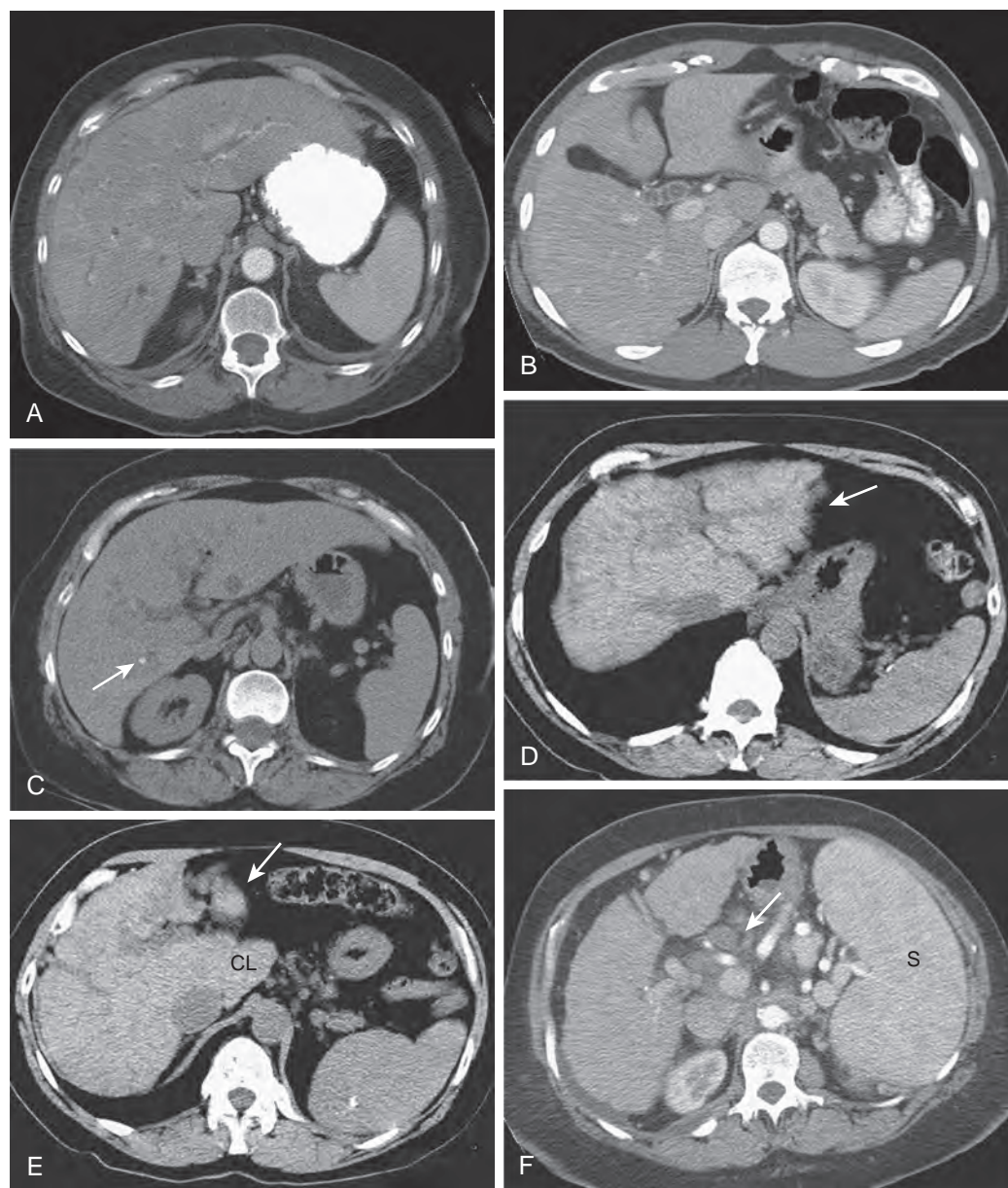


Figure 80-4 PSC: CT findings.

A. Irregular intrahepatic bile duct dilation with periductal hyperenhancement is seen. **B.** Abnormal mural thickening and enhancement are identified in the common bile duct. **C.** Non-contrast-enhanced scan shows an intrahepatic bile duct stone (arrow). **D** and **E.** In a different patient, non-contrast-enhanced CT scan shows a nodular liver with marked atrophy of the lateral segment of the left lobe (arrow) and enlargement of the caudate lobe (CL). **F.** Contrast-enhanced scan in a different patient shows cirrhosis of the liver, splenomegaly (S), and adenopathy in the porta hepatis (arrow), a common finding in patients with PSC.

does not necessarily indicate the development of cholangiocarcinoma and should not be regarded as an exclusion criterion for liver transplantation.¹⁶

There are unique hepatic morphologic changes associated with PSC-induced cirrhosis that can be seen with CT. The liver is markedly deformed with severe contour lobulations, creating an organ that appears rounded. This is due to atrophy of both the posterior segment of the right hepatic lobe and the lateral segment of the left lobe and marked hypertrophy of the caudate lobe. In addition, the atrophied right hepatic lobe may be hypodense (due to fibrosis) relative to the hypertrophied caudate lobe, creating the effect of a pseudotumor. When these morphologic changes are seen in conjunction with scattered, dilated intrahepatic bile ducts and intrahepatic bile duct stones, PSC can be suggested as the cause of the cirrhosis.¹⁷ There is substantial overlap in the appearance of livers affected by cirrhosis due to PSC and those affected by end-stage cirrhosis

caused by the usual factors (alcohol and hepatitis). The typical findings of cirrhosis due to any cause include a nodular liver surface from variably sized regenerative nodules, areas of confluent fibrosis, atrophy of the right hepatic lobe, and hypertrophy of the caudate lobe.

Introduced in 1991, magnetic resonance cholangiopancreatography (MRCP) is a technique that uses heavily T2-weighted pulse sequences to depict the bile and pancreatic ducts. MRCP is noninvasive and does not require the use of iodinated contrast material or ionizing radiation.¹⁸ Studies have shown good correlation between MRCP and ERCP in the diagnosis of PSC.¹⁹⁻²² MRCP findings of PSC are similar to ERCP findings and include multifocal segmental strictures alternating with normal or slightly dilated bile duct segments (Fig. 80-5). The strictures are usually out of proportion to the degree of upstream ductal dilation. Periductal inflammation and fibrosis prevent the ducts from dilating; therefore, high-grade strictures can be

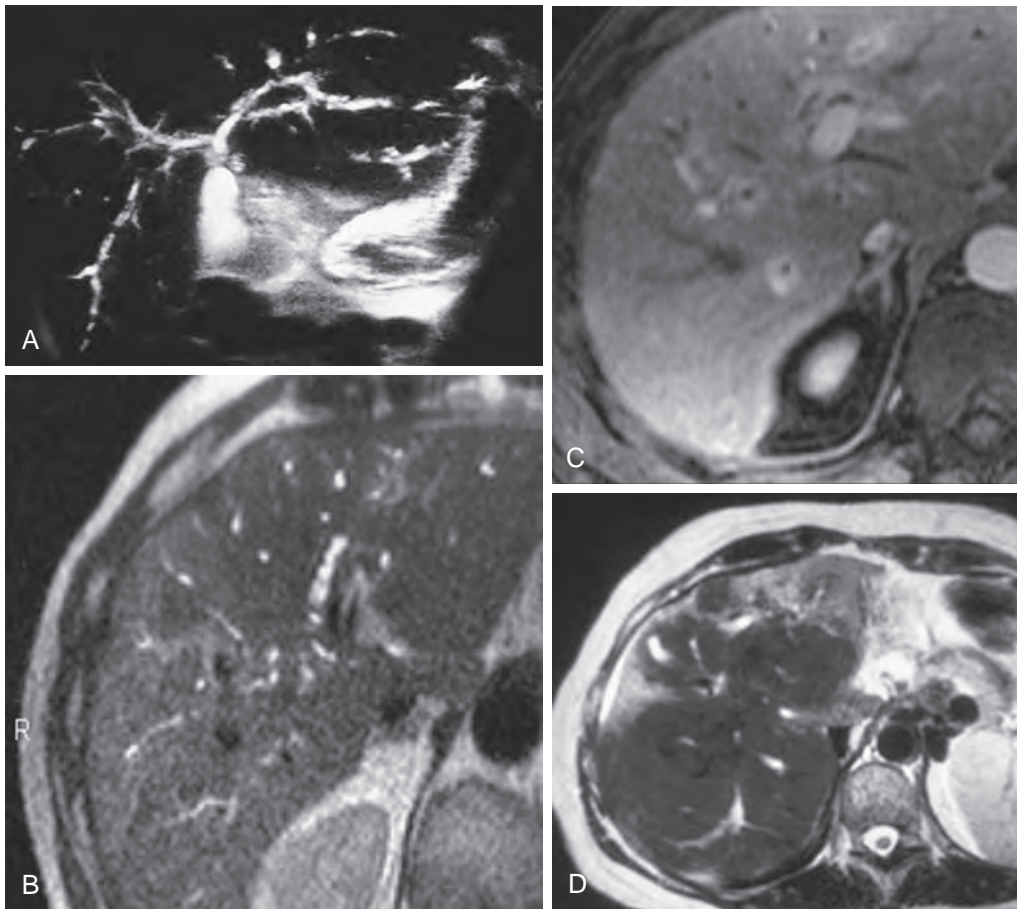


Figure 80-5 PSC: MR findings. **A** and **B.** MR cholangiogram shows characteristic irregular strictures and segmental dilations of the intrahepatic and extrahepatic ducts. **C.** Abnormal periductal enhancement is seen after contrast enhancement. **D.** MR image of patient with secondary biliary cirrhosis due to sclerosing cholangitis.

present with only minimal proximal dilation. With progressive fibrosis, the peripheral bile ducts are obliterated, resulting in a pruned tree appearance at MRCP, similar to findings at fluoroscopic cholangiography. Other findings include mural irregularities, webs, diverticula, and stones.²³

Hepatic parenchymal changes associated with PSC can be observed by MRI. Extension of the ductal inflammation into the hepatic parenchyma, retention of bile salts, and accumulation of copper in hepatocytes are thought to be responsible for the parenchymal changes seen on MRI.²⁴ The extrahepatic bile duct demonstrates wall thickening (1.5 mm or more) and enhancement. On T1-weighted images, randomly distributed areas of high signal intensity can be seen in a minority of patients. This abnormal signal is assumed to be due to cholestasis and lipofuscin deposits in atrophic liver cells.²⁵ T2-weighted images may demonstrate increased signal intensity in a peripheral wedge-shaped or fine reticular pattern. Extension of periductal inflammation to involve the vascular and lymphatic channels is considered to be the reason for the signal abnormality. Inflammatory changes of the hilar bile ducts result in a high T2 signal along the porta hepatis.²⁴ Postcontrast images can demonstrate peripheral areas of enhancement possibly due to alterations in blood flow in response to regional inflammation.²⁵

The morphologic changes of the liver affected by cirrhosis from chronic PSC have been previously discussed with respect to CT. These similar changes and others can be observed by MRI. A macronodular pattern of cirrhosis can be demonstrated

in patients with PSC. These large nodules (usually more than 3 cm) can be found predominantly within the central portion of the liver. The nodules are typically isointense on T1-weighted images and hypointense on T2-weighted images. After the administration of contrast material, the nodules are hypointense immediately after the injection and 2 minutes afterward, eventually becoming isointense.²⁶ The peripheral wedge-shaped areas of parenchymal atrophy seen with PSC-induced cirrhosis are typically hypointense on T1-weighted images and hyperintense on T2-weighted images. Corresponding areas demonstrate hypoenhancement on images obtained immediately after administration of contrast material and hyperenhancement on images obtained 2 minutes afterward.²⁶

DIFFERENTIAL DIAGNOSIS

Cholangiocarcinoma

In 90% of cases, cholangiocarcinoma is manifested cholangiographically either as a focal stricture or, less often, as a polypoid mass, neither of which should be confused with PSC. In about 10% of cases, however, there is metastatic spread or multicentricity, or both, such that the tumor involves the biliary tree diffusely and simulates PSC. When diffuse band strictures and multiple diverticula are identified by cholangiography, PSC may be confidently diagnosed because these findings do not occur in cholangiocarcinoma. Only one fourth of patients with PSC demonstrate these findings, leaving a large percentage of PSC patients in whom cholangiocarcinoma cannot be excluded.

Even more of a problem is the fact that cholangiocarcinoma complicates PSC in about 10% to 15% of patients, and when the two diseases coexist, the duct alterations from the underlying PSC can easily mask the presence of the carcinoma.¹⁰ Because of the segmental nature of PSC, some portions of the biliary tree remain relatively free of fibrosis and retain the ability to dilate in response to obstruction. Cholangiocarcinomas usually obstruct more completely than the fibrous strictures of PSC do. Unfortunately, there is no cholangiographic feature that is specific for cholangiocarcinoma. The clinical manifestations of the two diseases are somewhat different; cholangiocarcinoma is more likely when a patient has rapid clinical deterioration of jaundice, pruritus, and weight loss in combination with a rapid rise in serum bilirubin concentration and liver function test results. With regard to cholangiographic findings, more markedly dilated ducts should be viewed as a worrisome sign of complicating carcinoma.

Because PSC is usually a slowly progressive disease, interval stricture formation and biliary dilation on serial cholangiograms favor the presence of superimposed malignant disease, especially in association with clinical deterioration.^{10,27} Intraluminal filling defects occur in 5% to 10% of PSC patients but are usually small, measuring 2 to 5 mm in diameter.

Filling defects of 1 cm or larger occur in about 50% of patients with PSC complicated by cholangiocarcinoma. When they are present, a presumptive diagnosis of malignant disease should be made if choledocholithiasis can be excluded.

On cholangiographic examination, about 25% of patients with PSC show a *dominant stricture*, in which a segment of the biliary tree, often near the hilum, appears more severely strictured than the remainder of the ducts. Although the concept of the dominant stricture was originally proposed to justify aggressive surgical approaches for management of benign strictures of PSC, some dominant strictures actually represent cholangiocarcinomas.²⁸ If cholangiography or clinical course suggests the possibility of complicating cholangiocarcinoma, ultrasound, CT, or MRI should be performed. Cross-sectional imaging can confirm the presence of neoplasm in 50% to 80% of cases,^{29,30} particularly neoplasms arising from intrahepatic ducts, where cholangiocarcinomas often form bulky, exophytic masses. Mural thickening of the extrahepatic bile ducts of 5 mm or more is presumptive evidence of cholangiocarcinoma.³¹ Periportal soft tissue of 1.5 cm or more in thickness is also suggestive of malignant tumor.³² Contrast-enhanced CT and MRI with thin sections and delayed images are superior to 10-mm-thick, unenhanced images and increase the sensitivity for detection of malignant tumors in patients with PSC.

Benign Ductal Diseases

Primary biliary cirrhosis (PBC), secondary sclerosing cholangitis (from a variety of known causes), and some parasitic infestations all share some pathologic, clinical, and imaging features with PSC. The differential diagnostic considerations for these disorders are discussed under their separate headings.

Thiabendazole (Mintezol), an anthelmintic medication, has been reported to cause a cholestatic disorder characterized histologically by destruction of interlobular bile ducts, possibly with an autoimmune basis.³³ Although the microscopic findings can be confused with small duct PSC, the large ducts are normal on cholangiograms, and the history of thiabendazole treatment is diagnostic.

Hepatic sarcoidosis can lead to a granulomatous cholangitis, which on liver biopsy resembles PSC or PBC in some cases.³⁴ In addition, strictures of the extrahepatic bile ducts have been reported in sarcoidosis. The diagnosis is usually known because clinical evidence of sarcoidosis has preceded the onset of cholestasis in reported cases.

Eosinophilic cholangitis is another rare cause of extrahepatic biliary obstruction. Marked wall thickening of the extrahepatic ducts can be seen on CT and sonography.³⁵

Arteriohepatic dysplasia (Alagille's syndrome) is a rare familial cholestatic syndrome characterized by abnormalities of the heart, skeleton, and eyes; characteristic physiognomy including a broad forehead, flattened malar eminence, and pointed mandible; and loss of interlobular bile ducts as seen on liver biopsy.³⁶ Cholangiograms show segmental strictures of both the intrahepatic and extrahepatic bile ducts, resembling PSC. These ductal changes, however, appear to be due to a defect in duct development, leading to segmental hypoplasia or atresia, rather than to be secondary to fibrosis or ductal destruction as found in PSC. The familial inheritance, onset during infancy, absence of associated ulcerative colitis, and characteristic facies should allow easy distinction from PSC (see Chapter 119).

Allograft rejection after liver transplantation can lead to loss of interlobular bile ducts and strictures of the intrahepatic and extrahepatic bile ducts, closely resembling PSC.³⁷ Similar changes in the large bile ducts can result from ischemia if there is a delay in reestablishment of hepatic arterial circulation or if hepatic artery thrombosis occurs after transplantation.³⁷ Other causes of biliary ischemia may also result in biliary strictures resembling PSC.³⁸ In transplantation for PSC, recurrent disease should be considered in patients in whom strictures occur in the absence of rejection, infection, or ischemia. A complete discussion of biliary complications of liver transplantation can be found in Chapter 92.

A spontaneous stricture of the biliary tree, usually a major duct, occasionally causes diagnostic confusion. In most cases, focal biliary strictures have a malignant cause. Some cholangiocarcinomas induce so much fibrosis that biopsy results are falsely negative, leading to an erroneous diagnosis of benign stricture. Nevertheless, benign, focal biliary strictures do occur rarely in the absence of previous surgery, known infection, or other injury. These are sometimes labeled PSC but probably represent a different disease process or at most a *forme fruste* of PSC.

Primary Biliary Cirrhosis

EPIDEMIOLOGY AND CLINICAL FINDINGS

Although the term *primary biliary cirrhosis* was first used in 1950, the condition was originally described nearly 100 years earlier.^{39,40} Similar to PSC, PBC is a chronic cholestatic syndrome of unknown cause characterized by destruction of small bile ducts, portal inflammation, and progressive scarring, with four histologic stages seen on liver biopsy.⁴¹ Chronic cholestasis leads to hepatic copper overload in both PBC and PSC, but the role of copper in duct injury remains unclear (Fig. 80-6).

PBC is the cause of 1% to 2% of deaths from cirrhosis. The disease typically is manifested in middle-aged women with symptoms of fatigue and pruritus and laboratory test evidence of cholestasis. The clinical presentation of PBC is often

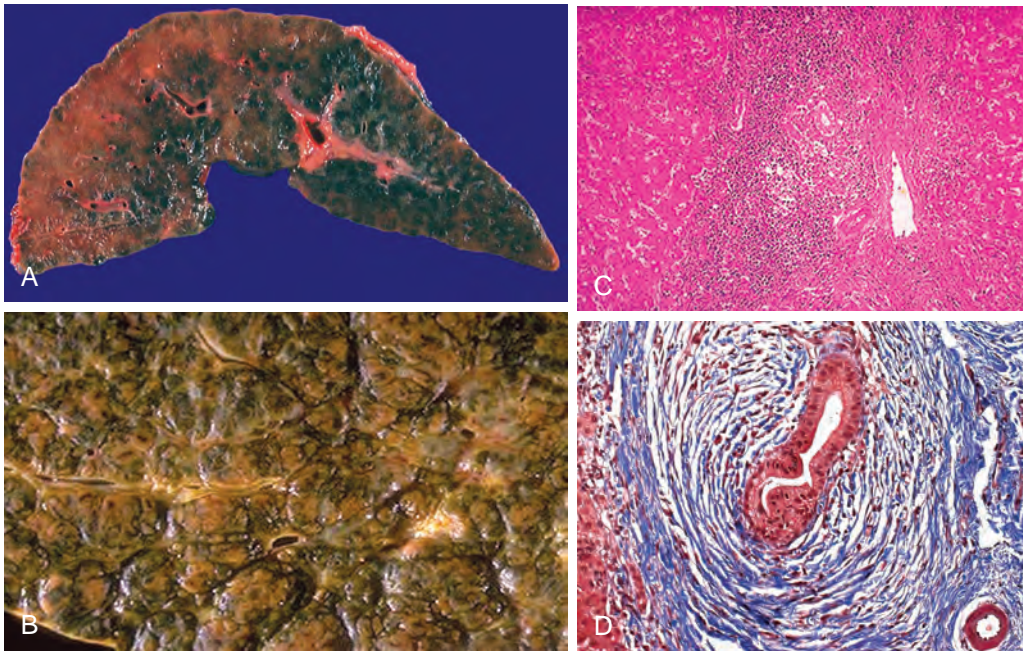


Figure 80-6 PBC: pathologic findings. **A** and **B.** Gross appearance of stage 4 disease; a mixture of tan and green regenerative nodules is typical. **C.** Histologic specimen showing periportal inflammation with lymphocytes and plasma cells. **D.** Periductal lymphocytic infiltration is present.

dominated by the insidious onset of diffuse pruritus owing to cutaneous accumulation of bile salts. Itching generally precedes the onset of cutaneous jaundice by 6 months to 2 years. In later stages of the disease, osteomalacia, liver failure, and portal hypertension are seen.

Alterations of cell-based immunity are an important feature of PBC. Sensitized T lymphocytes and possibly B lymphocytes may mediate the duct injury.⁴² PBC is often associated with other autoimmune diseases, and serum antimitochondrial antibody tests are highly sensitive for PBC. Associated autoimmune and collagen-vascular diseases include rheumatoid arthritis, Sjögren's syndrome, Hashimoto's thyroiditis, dermatomyositis, scleroderma, CRST (calcinosis cutis, Raynaud's phenomenon, sclerodactyly, and telangiectasia) syndrome, and systemic lupus erythematosus.

As in PSC, serum alkaline phosphatase activity is reliably increased, whereas serum bilirubin concentration is more likely to fluctuate and is seldom significantly elevated at presentation. Serum bilirubin is an important prognostic indicator; elevated levels are inversely related to life expectancy.

Despite some similarities to patients with PSC, patients with PBC exhibit important differences clinically and pathologically. About 90% of patients with PBC are female; the ratio of males to females in PSC is more than 2:1. Ulcerative colitis is common in PSC but is not associated with PBC. Serologic markers, especially antimitochondrial antibody, are frequently present in PBC, often in high titers, whereas they are not consistently present in PSC. On pathologic examination, small duct destruction in PBC is accompanied by inflammatory cellular infiltrate, including lymphocytes, plasma cells, histiocytes, and eosinophils, and by granuloma formation. In contrast, the destructive cholangitis in PSC is relatively hypocellular and lacks granuloma formation. The conspicuous fibrous thickening of bile duct walls seen in PSC is absent in PBC. The natural history of PBC is variable but usually inexorably downhill; the mean survival in symptomatic patients is 5.5 to 6 years, with a range of 3 to 11 years.⁴³

RADIOGRAPHIC FINDINGS

Imaging typically plays a minor role in the diagnosis of PBC. The diagnosis is usually based on clinical features and laboratory evaluation. Cross-sectional imaging has traditionally been used to stage liver disease by demonstrating portal hypertension and cirrhosis. Imaging is useful to detect the development of hepatic malignant neoplasms.

In most patients with PBC, cholangiograms are normal, especially during the early stages of the disease. With disease progression, the intrahepatic bile ducts can become tortuous and attenuated in response to the surrounding cirrhosis (Fig. 80-7). In areas of parenchymal atrophy, the ducts become crowded and tortuous; in areas of compensatory hypertrophy or nodular regeneration, the ducts become splayed or displaced. There can be extrinsic compression of the common bile duct due to lymphadenopathy within the porta hepatis.⁴⁴

CT and ultrasound scans performed at the time of diagnosis usually demonstrate hepatomegaly (Fig. 80-8). With progression of PBC, the liver volume decreases with atrophy of the right liver lobe and relative hypertrophy of the caudate and left lobes. Several different patterns of fibrosis can be seen in patients with PBC, but the one that seems characteristic is the lacelike pattern of thin or thick bands of low attenuation that surround regenerating nodules. Regenerating nodules are seen as small, rounded, hyperdense foci on unenhanced scans. Fibrosis is best demonstrated on non-contrast-enhanced examinations. Lymphadenopathy is seen in 80% to 90% of patients with PBC and is typically present within the porta hepatis and portacaval locations.⁴⁵ Ascites, splenomegaly, and varices are findings indicative of portal hypertension. These findings can sometimes be observed before clinical and CT findings of cirrhosis develop.

MRI findings are similar to CT scan findings in patients with PBC, demonstrating morphologic changes associated with cirrhosis and lymphadenopathy. An MRI sign that has been described as the "periportal halo sign" can aid in the diagnosis

of end-stage PBC (Fig. 80-9). The periportal halo sign is considered present when a small (5-mm to 1-cm) rounded lesion of decreased T1 and T2 signal intensity is seen surrounding a portal venous branch. Typically, the lesions are numerous, involve all hepatic segments, and fail to exert mass effect.⁴⁶ The

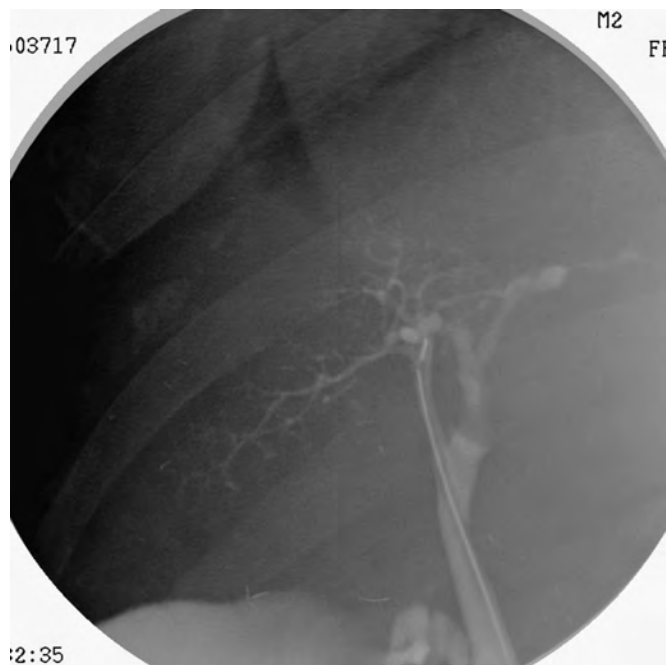


Figure 80-7 PBC: ERCP findings. The intrahepatic bile ducts are small and attenuated, giving the “pruned tree” appearance. The extrahepatic ducts are normal. In PSC, the intrahepatic and extrahepatic ductal systems are usually both involved.

lesions must be differentiated from regenerating nodules, which are usually variable in size and signal intensity and may exhibit mass effect. The sign should also not be confused with periportal edema, which is seen as high signal intensity on T2-weighted images in a periportal distribution. Histologic examination reveals that the periportal halo sign correlates with periportal hepatocellular parenchymal extinction, which is encircled by regenerating nodules.⁴⁶

Cholangiography can be helpful in differentiating PSC from PBC. Strictures are the hallmark of PSC by cholangiography. With PBC, the bile duct deformities are less severe and mainly confined to the intrahepatic bile ducts.¹² The diverticular outpouchings and mural irregularities that are classic in PSC are not seen with PBC.

Obstructive Cholangitis

Biliary obstruction induces bile stasis and predisposes to bacterial infection. Although bacterial cholangitis is nearly always associated with biliary obstruction, benign causes (choledocholithiasis, surgical anastomotic stricture, papillary stenosis) are much more likely to lead to clinical infection than are malignant causes (cholangiocarcinoma, pancreatic carcinoma, malignant hilar lymphadenopathy).⁴⁷

Patients present clinically with right upper quadrant abdominal pain, chills, fever, and jaundice. *Escherichia coli* is the most common infecting organism, but most infections are polymicrobial.⁴⁷ In acute ascending cholangitis, purulent bile may be identified as intraluminal echogenic material within involved ducts by ultrasound or as high-density intraductal material by CT. Cholangiography may demonstrate irregular tubular filling defects in dilated ducts above the obstruction. Hepatic abscesses

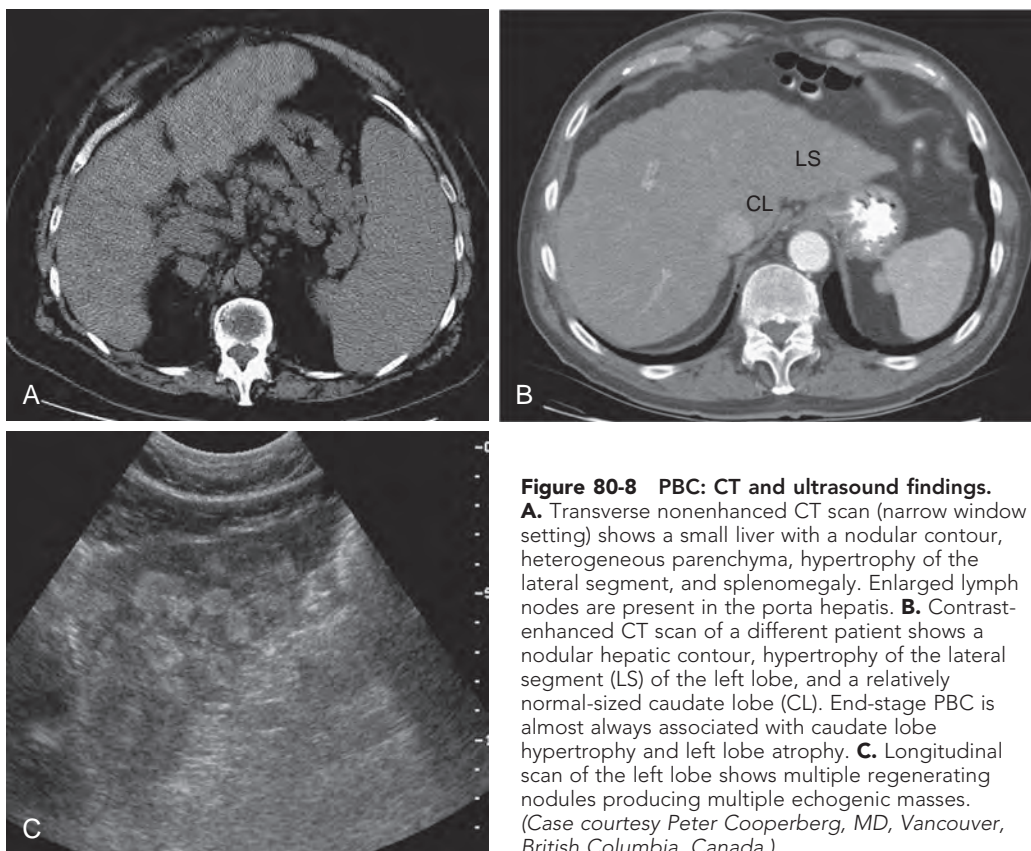


Figure 80-8 PBC: CT and ultrasound findings.

A. Transverse nonenhanced CT scan (narrow window setting) shows a small liver with a nodular contour, heterogeneous parenchyma, hypertrophy of the lateral segment, and splenomegaly. Enlarged lymph nodes are present in the porta hepatis. **B.** Contrast-enhanced CT scan of a different patient shows a nodular hepatic contour, hypertrophy of the lateral segment (LS) of the left lobe, and a relatively normal-sized caudate lobe (CL). End-stage PBC is almost always associated with caudate lobe hypertrophy and left lobe atrophy. **C.** Longitudinal scan of the left lobe shows multiple regenerating nodules producing multiple echogenic masses. (Case courtesy Peter Cooperberg, MD, Vancouver, British Columbia, Canada.)

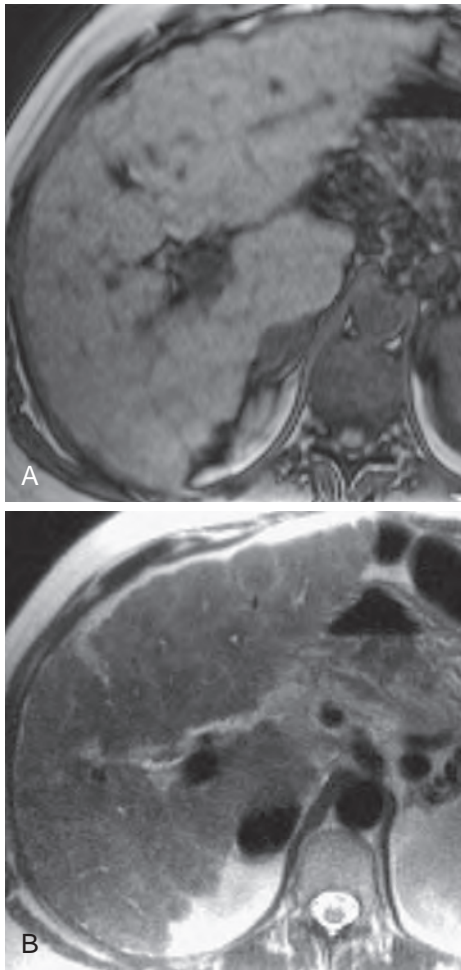
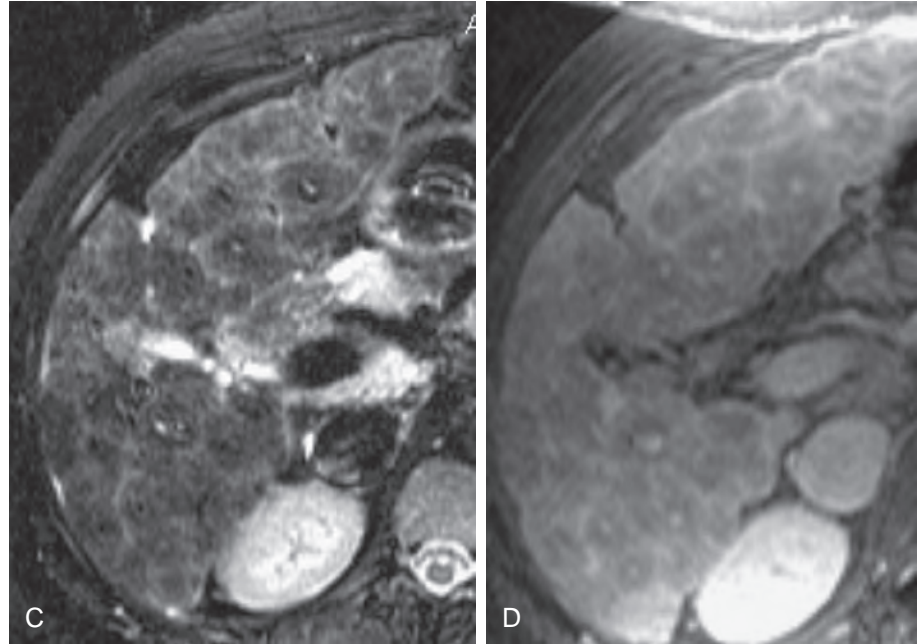


Figure 80-9 PBC: MR features. A to D. Patients with PBC may have a distinctive, conspicuous abnormality of low signal intensity centered around portal venous branches on T1- and T2-weighted MR images, the “periportal halo sign.” This abnormality consists of a rounded lesion centered on a portal venous branch, 5 mm to 1 cm in size. This pattern may involve all hepatic segments and appear as foci of low signal intensity on T1- and T2-weighted images with no mass effect. These criteria allow differentiation of this finding from regenerating nodules, which are usually of various sizes and signal intensity, may exert mass effect, and are not centered on portal venous branches. (Case courtesy Glenn Krinsky, MD, New York, NY.)



not uncommonly complicate the bacterial cholangitis. They are readily demonstrated by ultrasound and CT, and communication with the biliary tree can be documented on fluoroscopic cholangiography (Fig. 80-10).

Although all of the aforementioned are important radiologic signs in obstructive cholangitis, the most important diagnostic objective is to identify the nature and level of the obstruction and to decide the best means of relieving the obstruction. Injection of contrast medium under pressure above an obstruction may exacerbate an existing infection or introduce an infection into a previously sterile biliary tree. If intraductal pressure exceeds portal venous pressure or if communication to the hepatic venous system becomes established, life-threatening septicemia may ensue. Thus, prompt biliary drainage and broad-spectrum antibiotic coverage are mandatory whenever an obstructed infected biliary system is identified on direct cholangiography.⁴⁷

Chronic obstructive cholangitis with repeated episodes of infection may lead to duct strictures, peripheral attenuation of the intrahepatic bile ducts, and biliary cirrhosis. The appearances may resemble PSC, but the cause of obstruction, such as choledocholithiasis or postoperative stricture, is usually clinically or radiologically obvious.

Bacterial infection, usually accompanied by stone formation, may complicate a preexisting biliary tract disease. Congenital cystic disease, including Caroli's disease, is frequently

complicated by choledocholithiasis, infection, and stricture formation, which may potentially mask the underlying disease. Similarly, patients with PSC often form pigment stones within poorly draining portions of the biliary tree, which makes it difficult to establish a primary diagnosis. If clinical and radiologic evidence of an underlying disease is compelling, however, pigmented duct stones and clinical infection should be considered secondary phenomena.^{15,48} Intrahepatic duct stones in PSC patients may be subtle and are often overlooked on contrast-enhanced CT.

Recurrent Pyogenic Cholangitis (Oriental Cholangiohepatitis)

Certain Asian populations have a propensity to form pigmented stones in the intrahepatic and extrahepatic bile ducts that are commonly accompanied by recurrent gram-negative bacterial infections.^{47,49-53} This condition has been variously termed Oriental cholangiohepatitis, Oriental cholangitis, Hong Kong disease, and biliary obstruction of the Chinese. A more inclusive name, recognizing the sporadic occurrence in non-Asians, is recurrent pyogenic cholangitis (RPC). The pattern of stone disease in RPC differs from that in typical Western populations, in which the ductal stones are primarily extrahepatic, are predominantly composed of cholesterol, and most often originate

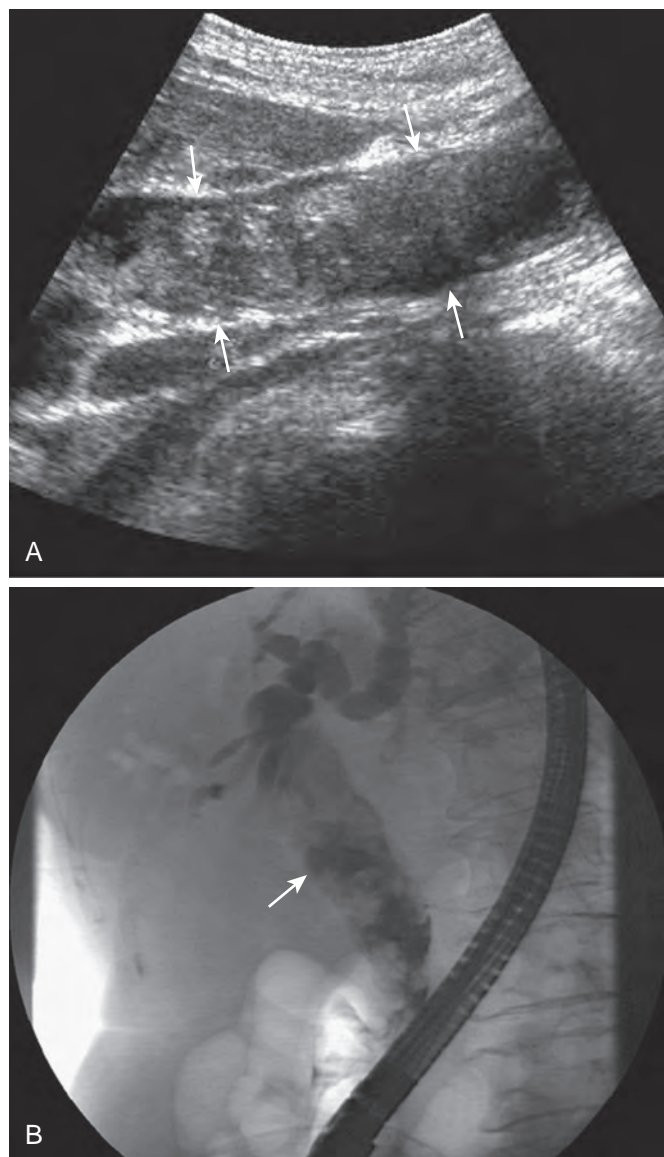


Figure 80-10 Ascending obstructive cholangitis. **A.** Sagittal sonogram shows a markedly dilated common bile duct (arrows) filled with sludge and stones. **B.** ERCP shows a dilated intrahepatic and extrahepatic biliary system with multiple filling defects (arrow). The patient recovered after urgent papillotomy and administration of antibiotics and intravenous fluids. (From Hanbidge AE, Buckler PM, O'Malley ME, et al: Imaging evaluation for acute pain in the upper abdomen. *RadioGraphics* 24:1117–1135, 2004.)

in the gallbladder.⁵³ Parasitic infestation (*Clonorchis sinensis*, *Ascaris lumbricoides*), malnutrition, and portal bacteremia have been etiologically implicated in RPC, but the cause and pathogenesis remain unproved.

Right upper quadrant pain, chills, fever, and jaundice are the common clinical features of RPC; the natural history is characterized by exacerbations and remissions of cholangitis, with duct injury and cholestasis leading to biliary cirrhosis. During the acute phases, sepsis may be life-threatening.

A suggestive diagnostic finding for RPC is intrahepatic and extrahepatic biliary dilation due to multilevel strictures with associated variable density biliary calculi and sludge.

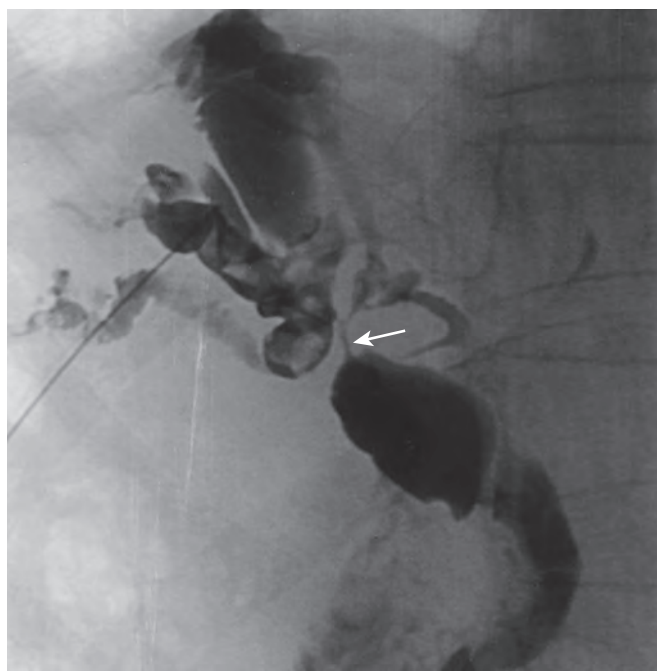


Figure 80-11 Oriental cholangiohepatitis. Percutaneous transhepatic cholangiography shows severe stricture (arrow), with dilated ducts, multiple filling defects, and abrupt tapering in the right anterior segment. (From Mi-Suk Park M-S, Yu J-S, Kim KW, et al: Recurrent pyogenic cholangitis: Comparison between MR cholangiography and direct cholangiography. *Radiology* 220:677–681, 2001.)

Dilated ducts containing stones and sludge are usually identifiable by CT and ultrasound, although large amounts of nonshadowing, isodense material may mask duct dilation on ultrasound evaluation. All segments of the biliary tree may be involved, but the lateral segment of the left lobe is most often and extensively involved. Additional cross-sectional imaging findings of RPC include parenchymal atrophy, fatty metamorphosis, duct wall enhancement, segmental parenchymal enhancement, hepatic abscess, biloma, and pneumobilia.^{50,51} Strictures are suggested by the presence of abruptly tapered ducts. Cholangiography provides the best detail on the status of the ducts (Fig. 80-11) and is a necessary component of the radiologic interventional management of stones and strictures.^{49,54}

Cholangitis Related to Acquired Immunodeficiency Syndrome

A secondary cholangitis resembling PSC is an uncommon but well-recognized component of acquired immunodeficiency syndrome (AIDS). The condition is thought to be secondary to opportunistic infection by *Cryptosporidium*, cytomegalovirus, or both.⁵⁵⁻⁵⁷ In addition to biliary tract signs and symptoms, patients with AIDS-related cholangitis may have abdominal pain and diarrhea from cryptosporidial enteritis.

Cholangiograms typically show irregularities and strictures of the intrahepatic and extrahepatic bile ducts with associated ductal dilation. Papillary stenosis can occur as an isolated phenomenon or in conjunction with more proximal ductal



Figure 80-12 AIDS-related papillitis. ERCP shows marked dilation of the common bile duct and pancreatic duct, a finding indicating low obstruction.

strictures (Fig. 80-12). Polypoid intraluminal filling defects resulting from granulation tissue have been reported in one fourth of patients on ERCP.⁵⁸ CT and ultrasound may demonstrate mural thickening of the gallbladder and bile ducts as well as other extraductal manifestations of AIDS. A hyperechoic nodule at the distal end of the common duct, attributed to inflammation and edema of the papilla of Vater, has been reported in one series of patients.⁵⁹

Floxuridine Cholangitis

Intra-arterial infusion of chemotherapeutic agents for the treatment of liver metastasis has been shown to cause bile duct strictures.^{38,60-63} In one series, 15% of patients receiving intra-arterial therapy showed abnormalities on cholangiograms in the absence of tumor progression.⁶³ Floxuridine (5-fluorodeoxyuridine) has been the offending agent in almost all cases. Ductal damage is believed to be due to chemical toxic effects of the drug on the ducts or drug-induced intravascular thrombosis of hilar vessels.³⁸ Histologic examination of strictured areas shows dense fibrosis of involved bile ducts and surrounding liver parenchyma. Nevertheless, cholangiograms obtained after cessation of chemotherapy have shown reversibility of some strictures.

In patients with chemotherapy-related cholangitis, direct cholangiography shows segmental strictures of variable length, similar to those seen in PSC. Floxuridine-associated strictures have a marked propensity to involve the hilar area and to spare the lower common duct and the peripheral intrahepatic ducts.⁶³ The gallbladder and cystic duct are also usually more severely involved in floxuridine cholangitis than in PSC. The clinical setting leaves no doubt about the diagnosis if tumor progression can be excluded by CT, MRI, ultrasound, or other means.

Parasitic Infestation

ASCARIASIS

Ascaris lumbricoides is the most prevalent human helminth worldwide (Fig. 80-13). Infestation results from ingestion of ova, with adult worms becoming established in the small bowel after larval migration through the liver and lungs. Clinical symptoms depend on the magnitude of infestation and are generally more frequent and severe in children. The most common clinical presentation is intestinal obstruction secondary to obstruction of the small bowel lumen by a mass of entangled worms. Acute appendicitis and pancreatitis also occur. Biliary colic develops when worms occupy and obstruct the common duct. Surgical removal is curative, but if worms become trapped in the biliary tree and are not removed, thousands of eggs may be released as the worms disintegrate, leading to acute and chronic suppurative cholangitis. In mild cases, ascaridic cholangitis resolves with granuloma formation and scarring. In more severe cases, life-threatening complications may ensue. Extension into the portal or hepatic veins may lead to inflammation and thrombosis (pyelephlebitis). Liver abscesses can potentially perforate into the peritoneal cavity and extend into the pleural space.

Worms may be seen as longitudinal filling defects up to several inches in length on direct or intravenous cholangiograms or as thin, long, or coiled echogenic intraluminal structures on ultrasound scans.^{64,65} The diagnosis of biliary ascariasis is usually made by ultrasound. The roundworms can be observed by ultrasound as intrabiliary tubular structures with echogenic walls and an anechoic line inside. An echogenic focus within a duct can have a “bull’s-eye” appearance.⁶⁶ A central anechoic component, probably representing the worm’s digestive tract, has also been described. Worms may occupy any portion of the biliary tree, including the gallbladder. Real-time ultrasound confirms the diagnosis by demonstrating the worm’s motility.^{66,67} Coexisting intrahepatic and extrahepatic biliary stones may be seen. Uncommonly, roundworms may be found in the liver parenchyma, where they cause secondary hepatic abscesses. This unusual condition is more commonly seen in children with malnutrition.

CLONORCHIASIS

The most clinically important liver fluke is *Clonorchis sinensis*, for which humans are the definitive host (Fig. 80-14). The eggs of *C. sinensis* are passed in human feces, and infestation occurs by ingestion of fish after an initial intermediate phase hosted by one of several types of freshwater snails. Clonorchiasis is endemic in Asia but may be seen in Western countries as a result of travel and immigration.

Within the biliary tree, the worms obstruct the flow of bile and incite an inflammatory cell infiltrate. In later stages, periductal fibrosis, ductal epithelial hyperplasia, and cholangiocarcinoma are seen.⁴⁷ Clinical symptoms depend on the number of flukes, the duration of infestation, and the presence of complications. With mild infections, patients may be asymptomatic. Early symptoms associated with moderate disease are nonspecific and include anorexia, dyspepsia, abdominal fullness, and right upper quadrant discomfort. Severe disease induces more significant systemic symptoms, including palpitations, weight loss, and diarrhea. Jaundice results from obstruction of the

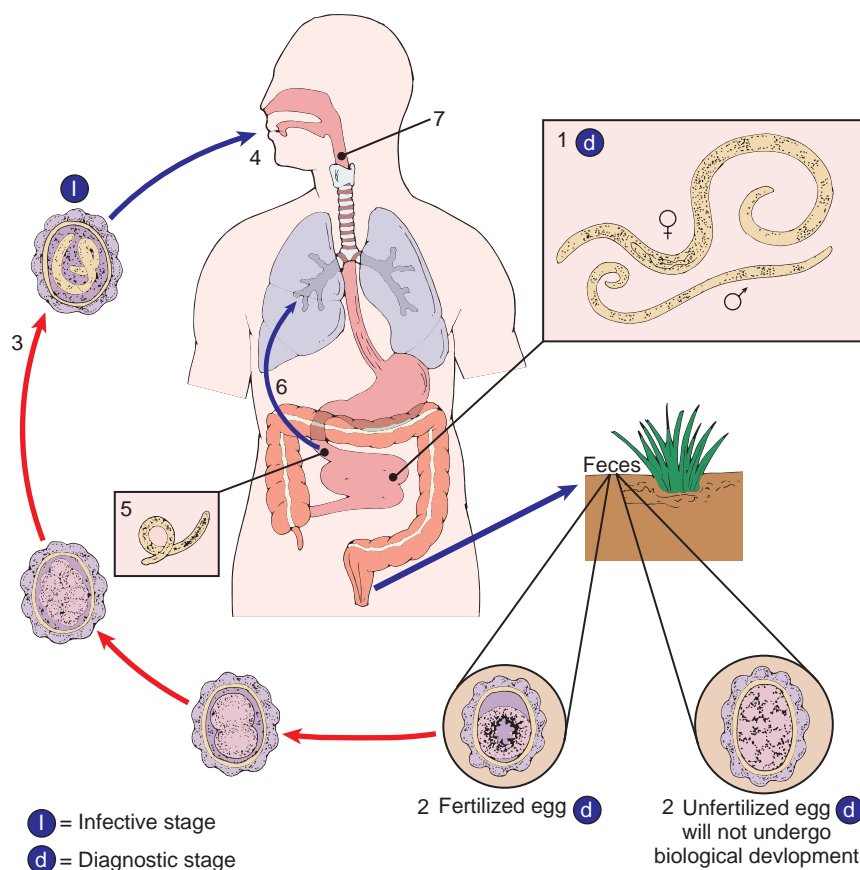
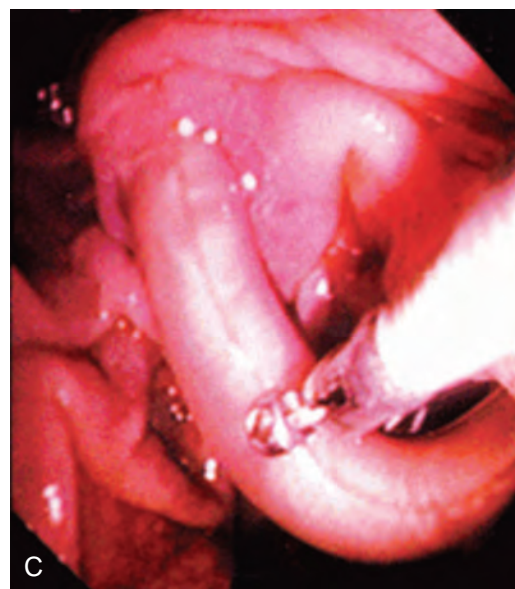
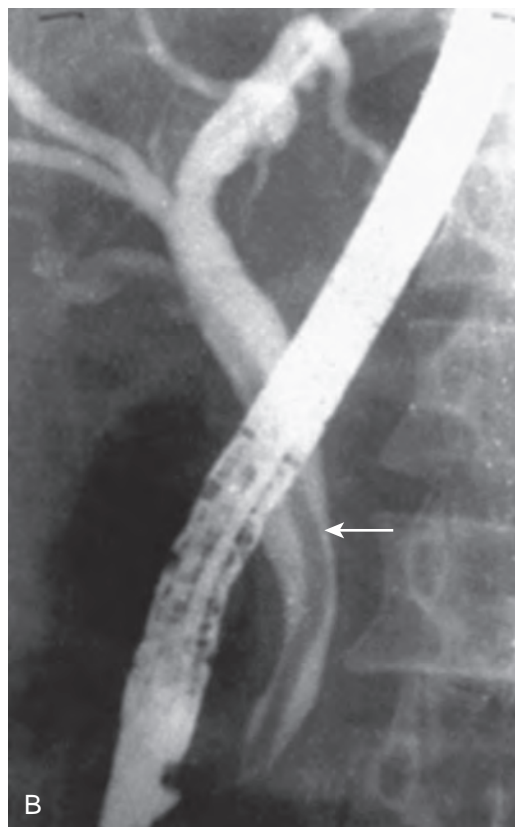
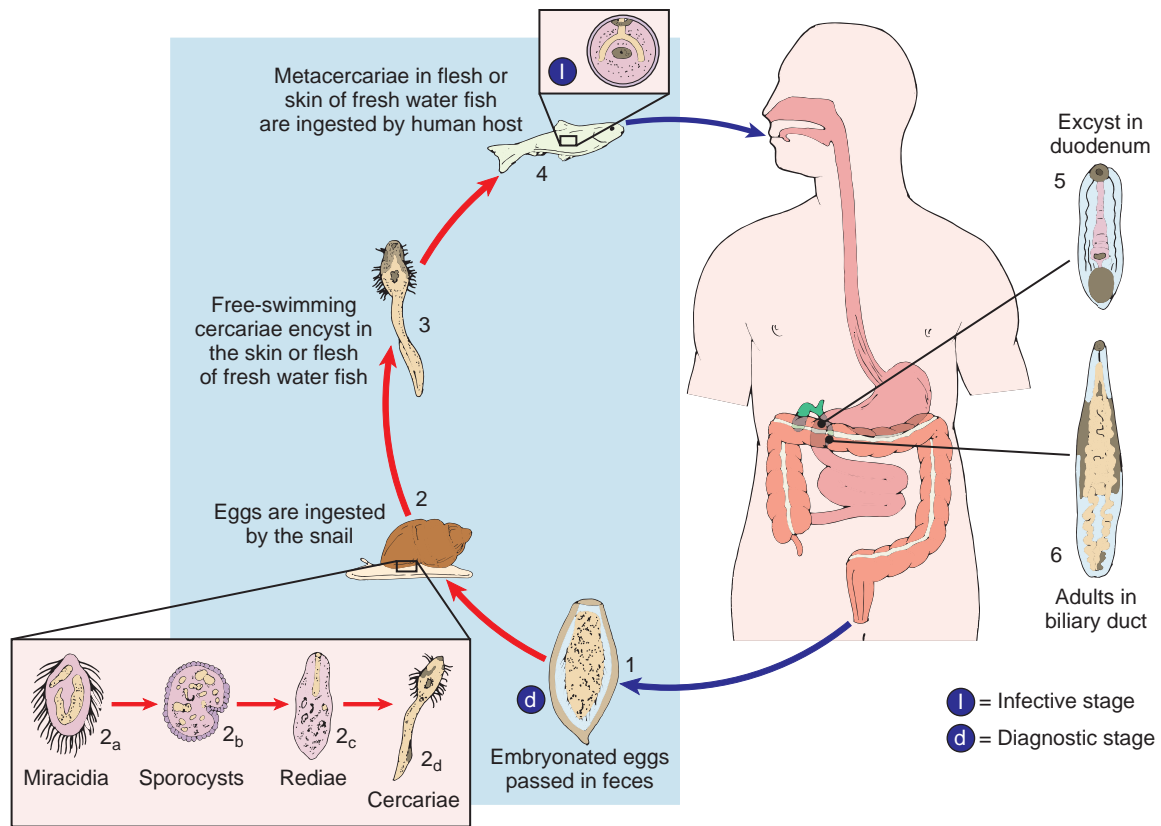


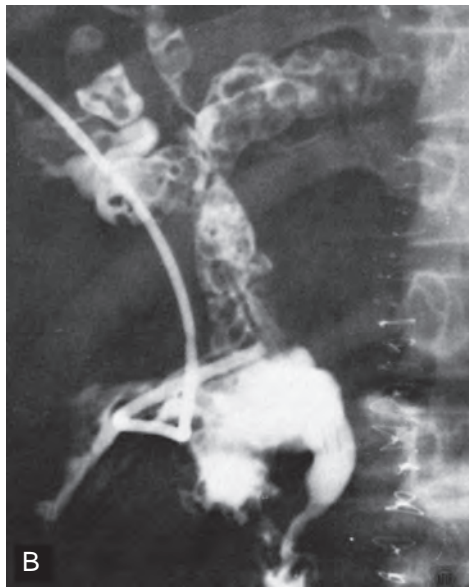
Figure 80-13 Ascariasis. A. Life cycle: Adult worms (1) live in the lumen of the small intestine. A female may produce approximately 200,000 eggs per day, which are passed with the feces (2). Unfertilized eggs may be ingested but are not infective. Fertile eggs embryonate and become infective after 18 days to several weeks (3), depending on the environmental conditions (optimum: moist, warm, shaded soil). After infective eggs are swallowed (4), the larvae hatch (5), invade the intestinal mucosa, and are carried through the portal and then the systemic circulation to the lungs (6). The larvae mature further in the lungs (10 to 14 days), penetrate the alveolar walls, ascend the bronchial tree to the throat, and are swallowed (7). On reaching the small intestine, they develop into adult worms (1). Between 2 and 3 months are required from ingestion of the infective eggs to oviposition by the adult female. Adult worms can live 1 to 2 years. (Source: CDC; available at <http://www.dpd.cdc.gov/>)

B. ERCP shows a linear filling defect in the common bile duct, which is the ascaris worm (arrow).
C. Worm extracted with biopsy forceps from the papilla of Vater during ERCP.

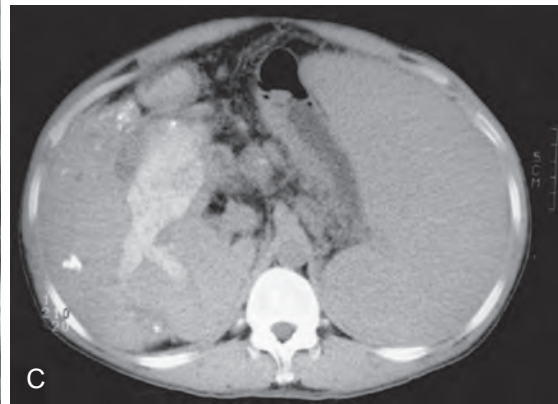




A



B



C

Figure 80-14 Clonorchiasis. **A.** Life cycle. Embryonated eggs are discharged from the biliary ducts and in the stool (1). Eggs are ingested by a suitable snail intermediate host; there are more than 100 species of snails that can serve as intermediate hosts. Each egg releases miracidia (2_a), which go through several developmental stages [sporocysts (2_b), rediae (2_c), and cercariae (2_d)]. The cercariae are released from the snail, and after a short period of free-swimming time in water, they come in contact and penetrate the flesh of freshwater fish, where they encyst as metacercariae (3). Infection of humans occurs by ingestion of undercooked, salted, pickled, or smoked freshwater fish (4). After ingestion, the metacercariae excyst in the duodenum (5) and ascend the biliary tract through the ampulla of Vater (6). Maturation takes approximately 1 month. The adult flukes (measuring 10 to 25 mm long by 3 to 5 mm wide by 1 mm thick) reside in small and medium-sized biliary ducts. In addition to humans, carnivorous animals can serve as reservoir hosts. (Source: CDC; available at <http://www.dpd.cdc.gov>.) **B.** T-tube cholangiogram shows innumerable 1- to 2-cm filling defects within the dilated bile ducts. The flukes can be identified by their typical comma-shaped or crescentic outlines; other filling defects may represent associated stones and biliary sludge. Short strictures and gross dilations of the ducts are present as the result of chronic obstruction and cholangitis. **C.** Nonenhanced CT scan in the same patient shows hyperdense material within grossly distended major intrahepatic bile ducts that on pathologic examination was proved to be a combination of pigmented biliary stones and sludge and *Clonorchis* flukes. Several calcified stones can be seen in peripheral ducts. The spleen is enlarged. (**B** and **C** courtesy Joan A. Kendall, MD, Honolulu, HI.)

biliary tree by the worms, periductal tissue reaction, or cholangiocarcinoma.

The normal habitat of *C. sinensis* is the intrahepatic bile ducts, where on cholangiograms they appear as ellipsoid, leaf-like filling defects measuring 2 to 10 mm in length.⁶⁸ Contrast opacification of the peripheral intrahepatic ducts is impeded by the worms and periductal tissue reaction.

CT and ultrasound show characteristic dilation of the small intrahepatic ducts with accompanying thickening of the duct wall and periductal tissues. The extrahepatic ducts are typically spared.⁶⁹ Flukes and fluke aggregates are more easily identified within the ducts by ultrasound than by CT. Unenhanced CT scans demonstrate branching low-density structures representing a combination of dilated ducts and periductal inflammatory fibrosis. With contrast enhancement, the apparent diameter of these structures diminishes as the periductal tissue component increases in density and blends in with the surrounding parenchyma.

The association of *C. sinensis* and cholangiocarcinoma is well known.^{68,70} Carcinomas in this setting tend to occur peripherally, where the flukes are most concentrated. Therefore, jaundice is often absent, and the tumors may reach considerable size before detection. Stippled or powder-like areas of high attenuation, corresponding to mucin on pathologic examination, have been reported within cholangiocarcinomas associated with clonorchiasis but not in cholangiocarcinomas without clonorchiasis.⁷⁰ Additional complications of clonorchiasis include

intraductal calculus formation, suppurative cholangitis, cholangiohepatitis, and liver abscess, all of which may yield positive findings on cross-sectional imaging and cholangiography.⁷¹

INFESTATION WITH OTHER LIVER FLUKES

Other liver flukes known to infest humans share many features with *C. sinensis*, including similar life cycles and morphologic features, mode of infestation, and pathologic alterations in the liver and biliary tree with the exception of cholangiocarcinoma. *Opisthorchis felinus* and *Opisthorchis viverrini* gain access to the biliary tree through the ampulla of Vater; *Fasciola hepatica* gains access transperitoneally, by penetrating the liver capsule.^{47,72}

ECHINOCOCCAL CHOLANGITIS

Echinococcus granulosus and *Echinococcus multilocularis* are small tapeworms whose larvae may lodge in human livers.⁴⁷ *E. granulosus* produces hydatid cysts in the liver; *E. multilocularis* produces “alveolar” echinococcosis, a more aggressive, invasive form with much tissue destruction. Either form may compress the biliary tract or rupture into it, producing obstruction, inflammation, and secondary bacterial infection.⁷³ Acute cholangitis may occur when a hepatic hydatid cyst ruptures into the bile ducts. A more complete discussion of hepatobiliary echinococcosis can be found in Chapter 88.

REFERENCES

- Yimam KK, Bowlus CL: Diagnosis and classification of primary sclerosing cholangitis. *Autoimmun Rev* 13:445–450, 2014.
- Zein CO, Lindor KD: Primary sclerosing cholangitis. *Semin Gastrointest Dis* 12:103–112, 2001.
- Wiesner RH: Current concepts in primary sclerosing cholangitis. *Mayo Clin Proc* 69:969–982, 1994.
- Lee YM, Kaplan MM: Primary sclerosing cholangitis. *N Engl J Med* 332:924–933, 1995.
- Charatcharoenwitthaya P, Lindor KD: Primary sclerosing cholangitis: Patients with a rising alkaline phosphatase at annual follow-up. *Clin Gastroenterol Hepatol* 5:32–36, 2007.
- Abdalian R, Heathcote EJ: Sclerosing cholangitis: A focus on secondary causes. *Hepatology* 44:1063–1074, 2006.
- LaRusso NF: The Fifth Carlos E. Rubio Memorial Lecture. Sclerosing cholangitis: Pathogenesis, pathology, and practice. *P R Health Sci J* 18:11–17, 1999.
- Ludwig J, MacCarty RL, LaRusso NF, et al: Intrahepatic cholangiectases and large-duct obliteration in primary sclerosing cholangitis. *Hepatology* 6:560–568, 1986.
- Ludwig J, Barham SS, LaRusso NF, et al: Morphologic features of chronic hepatitis associated with primary sclerosing cholangitis and chronic ulcerative colitis. *Hepatology* 1:632–640, 1981.
- MacCarty RL, LaRusso NF, May GR, et al: Cholangiocarcinoma complicating primary sclerosing cholangitis: Cholangiographic appearances. *Radiology* 156:43–46, 1985.
- Brandt DJ, MacCarty RL, Charboneau JW, et al: Gallbladder disease in patients with primary sclerosing cholangitis. *AJR Am J Roentgenol* 150:571–574, 1988.
- MacCarty RL, LaRusso NF, Wiesner RH, et al: Primary sclerosing cholangitis: Findings on cholangiography and pancreatography. *Radiology* 149:39–44, 1983.
- Parulekar SG: Transabdominal sonography of bile ducts. *Ultrasound Q* 18:187–202, 2002.
- Caoili EM, Paulson EK, Heyneman LE, et al: Helical CT cholangiography with three-dimensional volume rendering using an oral biliary contrast agent: Feasibility of a novel technique. *AJR Am J Roentgenol* 174:487–492, 2000.
- Dodd GD, 3rd, Niedzwiecki GA, Campbell WL, et al: Bile duct calculi in patients with primary sclerosing cholangitis. *Radiology* 203:443–447, 1997.
- Johnson KJ, Olliff JF, Olliff SP: The presence and significance of lymphadenopathy detected by CT in primary sclerosing cholangitis. *Br J Radiol* 71:1279–1282, 1998.
- Dodd GD, 3rd, Baron RL, Oliver JH, 3rd, et al: End-stage primary sclerosing cholangitis: CT findings of hepatic morphology in 36 patients. *Radiology* 211:357–362, 1999.
- Silva AC, Friese JL, Hara AK, et al: MR cholangiopancreatography: Improved ductal distention with intravenous morphine administration. *Radiographics* 24:677–687, 2004.
- Ernst O, Asselah T, Sergent G, et al: MR cholangiography in primary sclerosing cholangitis. *AJR Am J Roentgenol* 171:1027–1030, 1998.
- Fulcher AS, Turner MA, Franklin KJ, et al: Primary sclerosing cholangitis: Evaluation with MR cholangiography—a case-control study. *Radiology* 215:71–80, 2000.
- Vitellas KM, Enns RA, Keogan MT, et al: Comparison of MR cholangiopancreatographic techniques with contrast-enhanced cholangiography in the evaluation of sclerosing cholangitis. *AJR Am J Roentgenol* 178:327–334, 2002.
- Vitellas KM, El-Dieb A, Vaswani KK, et al: MR cholangiopancreatography in patients with primary sclerosing cholangitis: Interobserver variability and comparison with endoscopic retrograde cholangiopancreatography. *AJR Am J Roentgenol* 179:399–407, 2002.
- Vitellas KM, Keogan MT, Freed KS, et al: Radiologic manifestations of sclerosing cholangitis with emphasis on MR cholangiopancreatography. *Radiographics* 20:959–975, quiz 1108–1109, 1112, 2000.
- Meagher S, Yusoff I, Kennedy W, et al: The roles of magnetic resonance and endoscopic retrograde cholangiopancreatography (MRCP and ERCP) in the diagnosis of patients with suspected sclerosing cholangitis: A cost-effectiveness analysis. *Endoscopy* 39:222–228, 2007.
- Ito K, Mitchell DG, Outwater EK, et al: Primary sclerosing cholangitis: MR imaging features. *AJR Am J Roentgenol* 172:1527–1533, 1999.
- Bader TR, Beavers KL, Semelka RC: MR imaging features of primary sclerosing cholangitis: Patterns of cirrhosis in relationship to clinical severity of disease. *Radiology* 226:675–685, 2003.
- Hultcrantz R, Olsson R, Danielsson A, et al: A 3-year prospective study on serum tumor markers used for detecting cholangiocarcinoma in patients with primary sclerosing cholangitis. *J Hepatol* 30:669–673, 1999.
- Gossard AA, Talwalkar JA: Cholestatic liver disease. *Med Clin North Am* 98:73–85, 2014.
- Nesbit GM, Johnson CD, James EM, et al: Cholangiocarcinoma: Diagnosis and evaluation of

- resectability by CT and sonography as procedures complementary to cholangiography. *AJR Am J Roentgenol* 151:933–938, 1988.
30. Campbell WL, Ferris JV, Holbert BL, et al: Biliary tract carcinoma complicating primary sclerosing cholangitis: Evaluation with CT, cholangiography, US, and MR imaging. *Radiology* 207:41–50, 1998.
 31. Schulte SJ, Baron RL, Teeffey SA, et al: CT of the extrahepatic bile ducts: Wall thickness and contrast enhancement in normal and abnormal ducts. *AJR Am J Roentgenol* 154:79–85, 1990.
 32. Matsui O, Kadoya M, Takashima T, et al: Intrahepatic periportal abnormal intensity on MR images: An indication of various hepatobiliary diseases. *Radiology* 171:335–338, 1989.
 33. Manivel JC, Bloomer JR, Snover DC: Progressive bile duct injury after thiabendazole administration. *Gastroenterology* 93:245–249, 1987.
 34. Ishak KG: Sarcoidosis of the liver and bile ducts. *Mayo Clin Proc* 73:467–472, 1998.
 35. Song HH, Byun JY, Jung SE, et al: Eosinophilic cholangitis: US, CT, and cholangiography findings. *J Comput Assist Tomogr* 21:251–253, 1997.
 36. Gorelick FS, Dobbins JW, Burrell M, et al: Biliary tract abnormalities in patients with arteriohepatic dysplasia. *Dig Dis Sci* 27:815–820, 1982.
 37. Ward EM, Kiely MJ, Maus TP, et al: Hilar biliary strictures after liver transplantation: Cholangiography and percutaneous treatment. *Radiology* 177:259–263, 1990.
 38. Batts KP: Ischemic cholangitis. *Mayo Clin Proc* 73:380–385, 1998.
 39. Ahrens EH, Jr, Payne MA, Kunkel HG, et al: Primary biliary cirrhosis. *Medicine (Baltimore)* 29:299–364, 1950.
 40. Hiramatsu K, Aoyama H, Zen Y, et al: Proposal of a new staging and grading system of the liver for primary biliary cirrhosis. *Histopathology* 49:466–478, 2006.
 41. Bowlus CL, Gershwin ME: The diagnosis of primary biliary cirrhosis. *Autoimmun Rev* 13:441–444, 2014.
 42. Nakanuma Y: Distribution of B lymphocytes in nonsuppurative cholangitis in primary biliary cirrhosis. *Hepatology* 18:570–575, 1993.
 43. van Dam GM, Gips CH, Reisman Y, et al: Major clinical events, signs and severity assessment scores related to actual survival in patients who died from primary biliary cirrhosis. A long-term historical cohort study. *Hepatogastroenterology* 46:108–115, 1999.
 44. Summerfield JA, Elias E, Hungerford GD, et al: The biliary system in primary biliary cirrhosis. A study by endoscopic retrograde cholangiopancreatography. *Gastroenterology* 70:240–243, 1976.
 45. Blachar A, Federle MP, Brancatelli G: Primary biliary cirrhosis: Clinical, pathologic, and helical CT findings in 53 patients. *Radiology* 220:329–336, 2001.
 46. Wenzel JS, Donohoe A, Ford KL, 3rd, et al: Primary biliary cirrhosis: MR imaging findings and description of MR imaging periportal halo sign. *AJR Am J Roentgenol* 176:885–889, 2001.
 47. Carpenter HA: Bacterial and parasitic cholangitis. *Mayo Clin Proc* 73:473–478, 1998.
 48. Pokorny CS, McCaughan GW, Gallagher ND, et al: Sclerosing cholangitis and biliary tract calculi—primary or secondary? *Gut* 33:1376–1380, 1992.
 49. vanSonnenberg E, Casola G, Cubberley DA, et al: Oriental cholangiohepatitis: Diagnostic imaging and interventional management. *AJR Am J Roentgenol* 146:327–331, 1986.
 50. Chan FL, Man SW, Leong LL, et al: Evaluation of recurrent pyogenic cholangitis with CT: Analysis of 50 patients. *Radiology* 170:165–169, 1989.
 51. Lim JH, Ko YT, Lee DH, et al: Oriental cholangiohepatitis: Sonographic findings in 48 cases. *AJR Am J Roentgenol* 155:511–514, 1990.
 52. Kusano S, Okada Y, Endo T, et al: Oriental cholangiohepatitis: Correlation between portal vein occlusion and hepatic atrophy. *AJR Am J Roentgenol* 158:1011–1014, 1992.
 53. Schulman A: Non-Western patterns of biliary stones and the role of ascariasis. *Radiology* 162:425–430, 1987.
 54. Kerlan RK, Jr, Pogany AC, Goldberg HI, et al: Radiologic intervention in Oriental cholangiohepatitis. *AJR Am J Roentgenol* 145:809–813, 1985.
 55. Dolmatch BL, Laing FC, Federle MP, et al: AIDS-related cholangitis: Radiographic findings in nine patients. *Radiology* 163:313–316, 1987.
 56. Cockerill FR, 3rd, Hurley DV, Malagelada JR, et al: Polymicrobial cholangitis and Kaposi's sarcoma in blood product transfusion-related acquired immune deficiency syndrome. *Am J Med* 80:1237–1241, 1986.
 57. McCarty M, Choudhri AH, Helbert M, et al: Radiological features of AIDS related cholangitis. *Clin Radiol* 40:582–585, 1989.
 58. Collins CD, Forbes A, Harcourt-Webster JN, et al: Radiological and pathological features of AIDS-related polypoid cholangitis. *Clin Radiol* 48:307–310, 1993.
 59. Da Silva F, Boudghene F, Lecomte I, et al: Sonography in AIDS-related cholangitis: Prevalence and cause of an echogenic nodule in the distal end of the common bile duct. *AJR Am J Roentgenol* 160:1205–1207, 1993.
 60. Pien EH, Zeman RK, Benjamin SB, et al: Iatrogenic sclerosing cholangitis following hepatic arterial chemotherapy infusion. *Radiology* 156:329–330, 1985.
 61. Andrews JC, Kuntsen C, Terio P, et al: Hepatobiliary toxicity of 5-fluoro-2'-deoxyuridine. Intra-arterial versus portal venous routes of infusion. *Invest Radiol* 26:461–464, 1991.
 62. Botet JF, Watson RC, Kemeny N, et al: Cholangitis complicating intraarterial chemotherapy in liver metastasis. *Radiology* 156:335–337, 1985.
 63. Shea WJ, Jr, Demas BE, Goldberg HI, et al: Sclerosing cholangitis associated with hepatic arterial FUDR chemotherapy: Radiographic-histologic correlation. *AJR Am J Roentgenol* 146:717–721, 1986.
 64. Schulman A: Ultrasound appearances of intra- and extrahepatic biliary ascariasis. *Abdom Imaging* 23:60–66, 1998.
 65. Das AK: Hepatic and biliary ascariasis. *J Glob Infect Dis* 6:65–72, 2014.
 66. Cremin BJ: Ultrasonic diagnosis of biliary ascariasis: "A bull's eye in the triple O." *Br J Radiol* 55:683–684, 1982.
 67. Cerri GG, Leite GJ, Simoes JB, et al: Ultrasonographic evaluation of ascariasis in the biliary tract. *Radiology* 146:753–754, 1983.
 68. Lim JH: Radiologic findings of clonorchiasis. *AJR Am J Roentgenol* 155:1001–1008, 1990.
 69. Choi BI, Kim HJ, Han MC, et al: CT findings of clonorchiasis. *AJR Am J Roentgenol* 152:281–284, 1989.
 70. Choi BI, Park JH, Kim YI, et al: Peripheral cholangiocarcinoma and clonorchiasis: CT findings. *Radiology* 169:149–153, 1988.
 71. Choi BI, Kim TK, Han JK: MRI of clonorchiasis and cholangiocarcinoma. *J Magn Reson Imaging* 8:359–366, 1998.
 72. Van Beers B, Pringot J, Geubel A, et al: Hepatobiliary fascioliasis: Noninvasive imaging findings. *Radiology* 174:809–810, 1990.
 73. Rinaldi F, Brunetti E, Neumayr A, et al: Cystic echinococcosis of the liver. A primer for hepatologists. *World J Hepatol* 27:293–305, 2014.

Postsurgical and Traumatic Lesions of the Biliary Tract

SIVA P. RAMAN | ELLIOT K. FISHMAN | GABRIELA GAYER

CHAPTER OUTLINE

Laparoscopic Cholecystectomy

Technical Considerations of Laparoscopic Cholecystectomy

Normal Imaging Findings after Uncomplicated Laparoscopic Cholecystectomy

General Postsurgical Complications

Biliary Tract Complications

Biliary-Enteric Anastomosis

Background, Indications, and Technical Considerations
Complications

Post-Traumatic Lesions of the Biliary Tree

Imaging of Post-Traumatic Lesions

The two most common surgical procedures of the biliary tract likely to be encountered in day-to-day practice are laparoscopic cholecystectomy (LC) and biliary-enteric anastomosis. Specifically, given the high prevalence of cholelithiasis or gallstones in the United States, with roughly 20 to 25 million people affected, a large number of patients undergo cholecystectomy each year (~700,000). The revolutionary development and refinement of laparoscopic techniques during the last two decades have allowed LC to largely supplant open surgery.¹⁻³ The creation of a biliary-enteric anastomosis (most often hepaticojejunostomy), on the other hand, can be performed for any number of different indications, the most common of which include liver transplantation, resection of tumors involving the biliary tree, benign or malignant biliary obstruction, biliary stones, and bile duct injuries.^{4,5}

Whereas LC and hepaticojejunostomy are both relatively well tolerated procedures with a low risk of complications, the large number of these procedures performed in the United States each year makes it critical for radiologists to recognize the different complications that may be associated with these surgical procedures and to understand the basic diagnostic and treatment algorithms for each of these complications. This chapter discusses a number of complications associated with LC and hepaticojejunostomy and illustrates their appearances by a number of different radiologic modalities. In addition, this chapter concludes with a discussion of the radiologic diagnosis of post-traumatic lesions of the biliary tree. These traumatic injuries to the bile ducts and gallbladder are relatively rare but can carry a high morbidity and mortality in cases of missed or delayed diagnosis.⁶⁻⁸

Laparoscopic Cholecystectomy

TECHNICAL CONSIDERATIONS OF LAPAROSCOPIC CHOLECYSTECTOMY

The most common indication for LC is symptomatic cholelithiasis, although the procedure is also commonly performed for acalculous cholecystitis, large gallbladder polyps, gallbladder dyskinesia, gallbladder malignant neoplasms, and trauma.⁹⁻¹¹ Contraindications to the procedure are uncommon but typically relate to an inability to tolerate general anesthesia, intractable bleeding disorders, or end-stage liver disease or cirrhosis.^{12,13}

Traditionally, LC has been performed with four incisions (four-port LC; Fig. 81-1A). A 1-cm incision is made adjacent to the umbilicus, and a blunt trocar is inserted into the abdominal cavity, with the subsequent establishment of pneumoperitoneum (10-12 mm Hg) by the insufflation of carbon dioxide through a Veress needle. After the establishment of pneumoperitoneum, a laparoscope is inserted through this first incision. Next, three additional smaller incisions are made in the right lateral upper abdomen and to the left of the falciform ligament, and three trocars are inserted through these sites (Fig. 81-1B). Specialized grasping instruments are then inserted through these trocars to grasp the fundus and infundibulum of the gallbladder, to expose the surgical field, to dissect and clip the cystic artery and duct (with placement of a surgical clip), to remove the gallbladder through the periumbilical port, and to coagulate the gallbladder fossa (Fig. 81-1C, D).^{10,13,14}

Increasingly, however, as a result of patient cosmetic concerns and a desire to reduce operative trauma to the abdominal wall, there has been a trend toward the use of fewer incisions and ports. The newest operative technique, known as single-port laparoscopic surgery, entails the creation of a single periumbilical incision, with the subsequent use of a specialized single port that contains four openings: one for gas insufflation and three for trocars to perform the surgical procedure.¹⁴ Whereas data on these new single-port techniques are still forthcoming, early studies have suggested improved cosmesis and decreased postoperative pain.¹⁴

NORMAL IMAGING FINDINGS AFTER UNCOMPLICATED LAPAROSCOPIC CHOLECYSTECTOMY

In most cases, the imaging findings after LC should be relatively minimal.

- A small amount of pneumoperitoneum is an expected finding.^{15,16} The volume of free air after laparoscopic procedures is generally smaller and lasts for a shorter time compared with open surgery, largely as a result of the relatively small incisions in the anterior abdominal

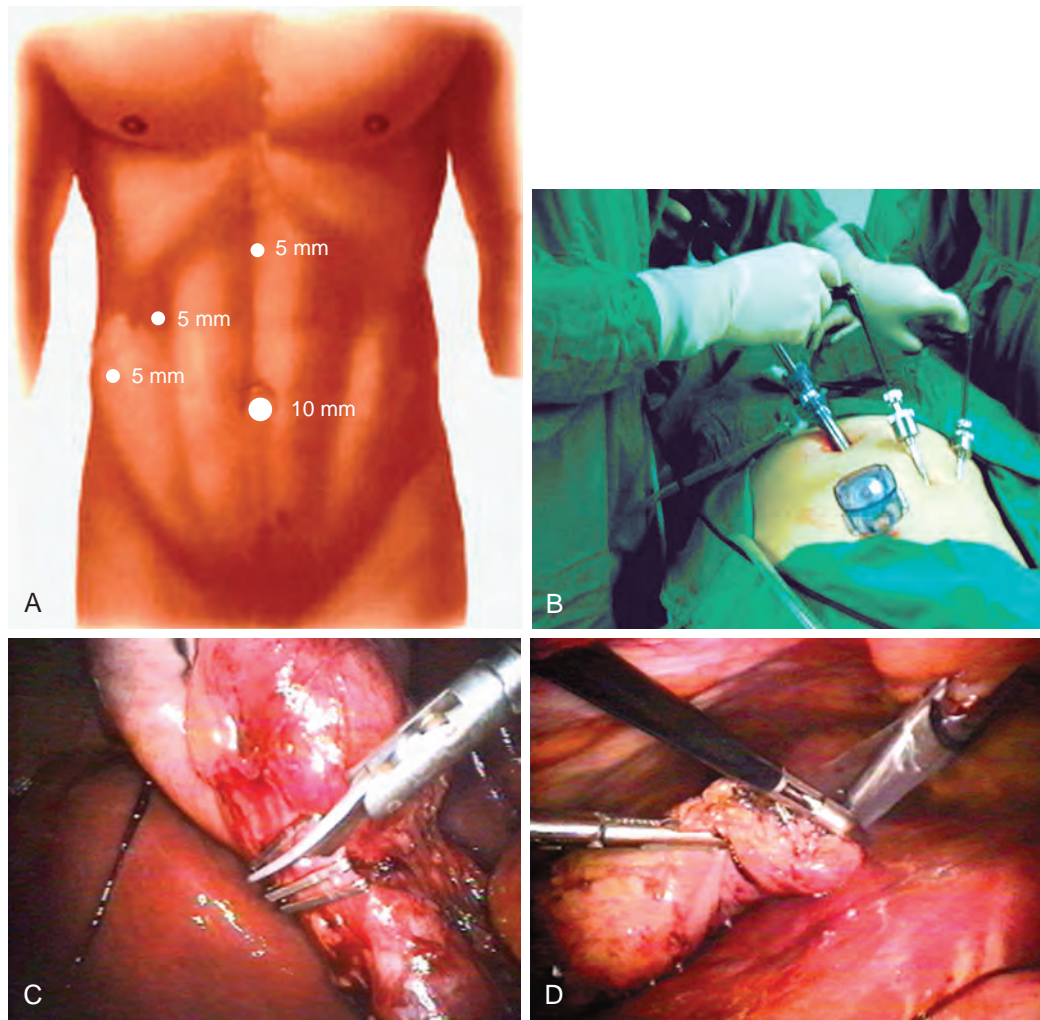


Figure 81-1 Laparoscopic surgery. **A.** The four trocar insertion sites during laparoscopic cholecystectomy. **B.** Trocars in place during surgery. **C.** Clips are applied to cystic duct. **D.** Gallbladder is prepared for removal.

wall and the use of carbon dioxide for insufflation (which is rapidly absorbed).¹⁷⁻¹⁹ As with other abdominal surgeries, the presence of a large amount of pneumoperitoneum after surgery, or pneumoperitoneum that persists for a longer than expected duration (10-14 days), should raise concern for bowel injury or perforation during the procedure.

- A small amount of subcutaneous emphysema at the incision site is not uncommon, usually resulting from the dissection of insufflated carbon dioxide around the trocars into the subcutaneous soft tissues. This finding is common in the first 24 to 48 hours after surgery but should not be seen in significant amounts thereafter.^{16,20}
- Small densities in the subcutaneous fat surrounding the trocar insertion sites can develop over time and probably represent sites of fat necrosis or scarring related to the surgical intervention.²⁰
- Small postoperative fluid collections in the gallbladder fossa are a common finding immediately after surgery and may be associated with a tiny amount of free fluid in the pelvis.²⁰⁻²³ These fluid collections are almost always asymptomatic and should resolve spontaneously.²¹

Nevertheless, if there are clinical signs of infection, reimaging may be helpful as these collections can rarely become superinfected and develop into abscesses.

- Permanent surgical materials, such as surgical clips, are a common finding in the gallbladder fossa. Potentially confusing, however, is the presence of absorbable hemostatic sponges, occasionally used intraoperatively to control bleeding, which should gradually be absorbed over time. The most commonly used of these materials is gelatin sponge (Gelfoam; Pharmacia and Upjohn, Kalamazoo, Mich) or oxidized absorbable cellulose (Sur-gicel; Ethicon, Somerville, NJ). The appearance of these absorbable agents on computed tomography (CT) is typically as a discrete mass with mixed or low attenuation and with central or peripheral gas collections (Fig. 81-2). In the absence of a reliable clinical history, such an appearance can be extremely difficult to distinguish from a postoperative abscess or fluid collection, and a discussion with the surgeon may be necessary to arrive at the correct diagnosis.²⁴ If not, this absorbable material should disappear in a period of weeks on serial CT examinations.

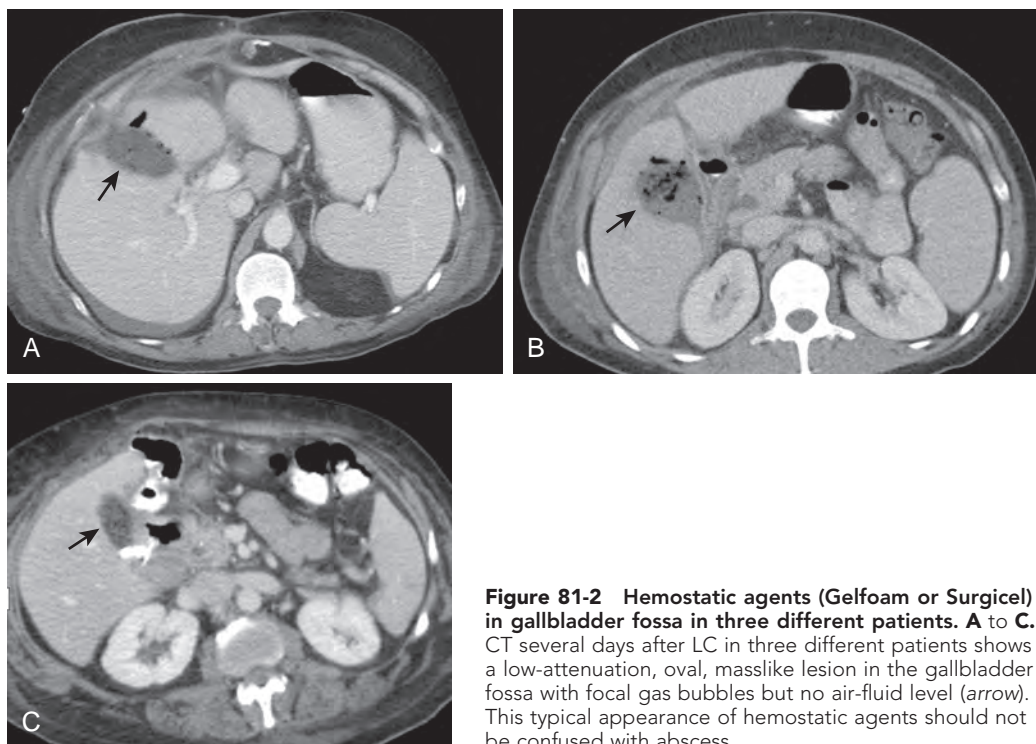


Figure 81-2 Hemostatic agents (Gelfoam or Surgicel) in gallbladder fossa in three different patients. A to C. CT several days after LC in three different patients shows a low-attenuation, oval, masslike lesion in the gallbladder fossa with focal gas bubbles but no air-fluid level (arrow). This typical appearance of hemostatic agents should not be confused with abscess.

GENERAL POSTSURGICAL COMPLICATIONS

Postsurgical complications after LC are relatively rare. Overall, there is no evidence in the literature that the transition from open to laparoscopic surgical technique has resulted in any appreciable increases in morbidity or mortality. A Cochrane Database review that examined 38 different studies in the literature (with 2338 patients) found no difference in mortality between open cholecystectomy and LC, and although there was the suggestion of a lower overall complication rate with laparoscopic technique, this could not be validated in the highest quality studies. Moreover, laparoscopic technique is clearly associated with a shorter hospital stay, better cosmetic results, less postoperative pain, and faster return to work.^{13,25}

Nevertheless, postsurgical complications are not infrequently encountered regardless of the surgical technique used. Complications are thought to be more likely in patients with active (or prior bouts of) cholecystitis, longer time (typically > 72 hours) between the onset of cholecystitis symptoms and surgery, male gender, prior upper abdominal surgery, significant pericholecystic fluid, high body mass index, diabetes, and advanced age, all of which are factors that may render LC more technically difficult.^{9,13,26,27} Notably, these same patient factors represent the most common risk factors for conversion of LC into an open procedure, and the conversion rate is thought to be as high as 12%.^{3,28,29} As one would expect, patients with significant gallbladder inflammation (including gangrenous and emphysematous cholecystitis) are also at higher risk for complications and conversion to an open procedure.³⁰

Complications of LC include those associated with the laparoscopic component of the procedure as well as those related to the cholecystectomy itself.¹⁰ The most common complications related to laparoscopy include abdominal wall or omental bleeding, intraperitoneal or retroperitoneal vessel injury, bowel

injury or perforation, and solid visceral organ injury. The most common complications related to cholecystectomy include gallbladder fossa bleeding, bile duct injury, bile leakage, gallbladder perforation (with stone spillage), retained biliary stones, and biliary strictures.¹⁰ Less commonly, laparoscopic cholecystectomies can be complicated by vascular injuries, with an incidence ranging between 0.05% and 0.25%. Vascular injury is the second leading cause of death in patients undergoing laparoscopic procedures (of any kind), and the hepatic artery is the most frequently injured vessel during LC. Given that the mortality rate for patients suffering vascular injuries during laparoscopy can be as high as 9%, careful evaluation of the hepatic artery along its entire course is critically important in evaluating multidetector CT (MDCT) studies in patients who have recently undergone LC.³¹

The majority of complications are manifested in the early postoperative period, but others may appear weeks or even months after the procedure.^{10,21,32} Most patients undergoing LC experience an uneventful, straightforward postoperative course, but a high index of suspicion is essential for those patients who demonstrate any concerning symptoms, including fevers, persistent abdominal pain, tachycardia, vomiting, or high degrees of bile output from a drain or wound site.

BILIARY TRACT COMPLICATIONS

Biliary tract complications are the most important complications of cholecystectomy and represent a major source of litigation.³³ Biliary tract complications can be encountered with both open and laparoscopic cholecystectomies, and there is little evidence of any increase in biliary tract complications with laparoscopic technique. Many of these complications are often not recognized at the time of surgery and are not uncommonly diagnosed after a significant delay, resulting in considerable

patient morbidity and mortality.^{26,27,33,34} The most important biliary complications for the radiologist to recognize are bile duct injury, bile leak, retained stones, bile duct strictures, and spilled stones in the peritoneal cavity.²¹

Bile Duct Injury and Bile Leak

There are more than 2500 bile duct injuries related to LC in the United States each year, and many of these injuries are attributable to acute or chronic inflammation obscuring fat planes surrounding the gallbladder or intraoperative misidentification of the common bile duct (CBD) by the surgeon.³⁵ Other risk factors include inadequate exposure, patient obesity, congenital anatomic anomalies of the bile ducts, emergent surgery, and failed cholangiography.³⁶⁻³⁸ The incidence of bile duct injury after LC is 0.1% to 1.3%, and although there does not appear to be a significant difference in the incidence of bile duct injuries compared with open procedures, injuries after LC may possibly be more severe.^{13,26,33,37,39-47}

Bile duct injuries encompass a wide range of different lesions, including tears, transections, and ligations.⁴⁸ The most common injury results in a defect of the CBD due to a portion of the CBD having been mistaken for the cystic duct and, as a result, being partially or completely transected.⁴⁶ Many minor bile duct injuries (perhaps seen in up to 1.2% of patients) are now successfully treated with endoscopic management (usually internal drainage), allowing bile flow away from the site of injury into the duodenum and consequently allowing the injured bile duct segment to heal. On the other hand, complex or severe bile duct injuries (i.e., common hepatic duct, CBD, right hepatic duct, or transection of the right posterior sectoral duct) are almost always treated with surgical biliary reconstruction.^{37,49}

There is debate within the surgical literature as to whether the routine use of intraoperative cholangiography (IOC) can help reduce the incidence of bile duct injury, and some surgeons

advocate that cholangiography should constitute a routine component of every LC. Proponents argue that IOC can help better define biliary anatomy, thereby reducing the incidence of biliary injuries. Moreover, in those cases in which injuries occur, proponents argue that IOC allows earlier discovery of these injuries.⁵⁰ However, those who argue against routine cholangiography suggest that instead of reducing the incidence of bile duct injury, surgeons performing IOC may actually cause a bile duct injury while attempting to cannulate the cystic duct or by inadvertently cannulating the CBD.⁵¹ Moreover, IOC undoubtedly increases operative time and surgical costs.^{44,47}

Depending on its severity, bile duct injury can result in a frank bile leak (Figs. 81-3 to 81-9). Whereas bile leaks can theoretically occur at any site of bile duct injury, the most common locations are the cystic duct stump, the duct of Luschka, and the gallbladder bed.³⁹ When leaks occur at the cystic duct stump (the most common site of bile leak), causes can include a misplaced surgical clip, resulting in inadequate closure of the cystic duct; necrosis of the cystic duct after placement of a clip; elevated CBD pressures (often due to a distally impacted CBD stone) transmitted to the cystic duct, resulting in cystic duct "blow-out"; and operative injury to the cystic duct.^{46,52} In those cases attributable to operative injury, leaks may occur because of difficulty in dissecting the cystic duct and common hepatic duct, particularly when adhesions are present, and as a result of unrecognized aberrant ducts.^{20,46} The second most common site of bile leak is from the duct of Luschka, an accessory duct in the right hepatic lobe that traverses the gallbladder fossa and can drain into either the right or common hepatic duct. This bile duct is uniquely vulnerable to injury and leak as a result of its variable course and location within the operative field.³⁹

Bile leaks carry a high risk of morbidity and mortality and should be suspected in any patient who presents with fever, jaundice, abdominal pain, peritonitis, or elevated liver function test results in the first week after surgery.^{39,53,54} In particular, a

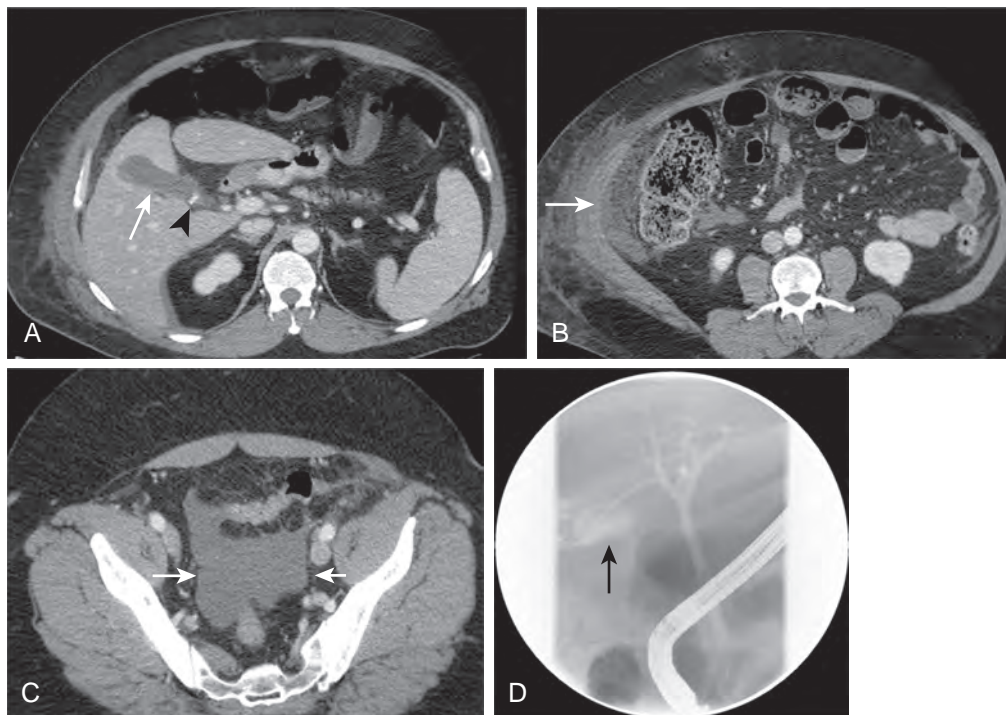


Figure 81-3 Bile leakage resulting in a biloma, biliary ascites, and peritonitis. **A.** CT 6 days after LC shows an oval fluid collection, a biloma, in the gallbladder fossa (arrow) adjacent to a surgical clip (arrowhead). The leaking bile assumes a pear-shaped configuration resembling the gallbladder. There is some free fluid in Morison's pouch. **B.** Inflammatory changes induced by leaking bile seen as marked omental infiltration (arrow), displacing the ascending colon medially. **C.** Large amount of fluid in pelvis (arrows); its clear density, although nonspecific, is compatible with bile. **D.** Subsequent ERCP shows active extravasation of contrast material, probably from the cystic duct remnant (arrow).

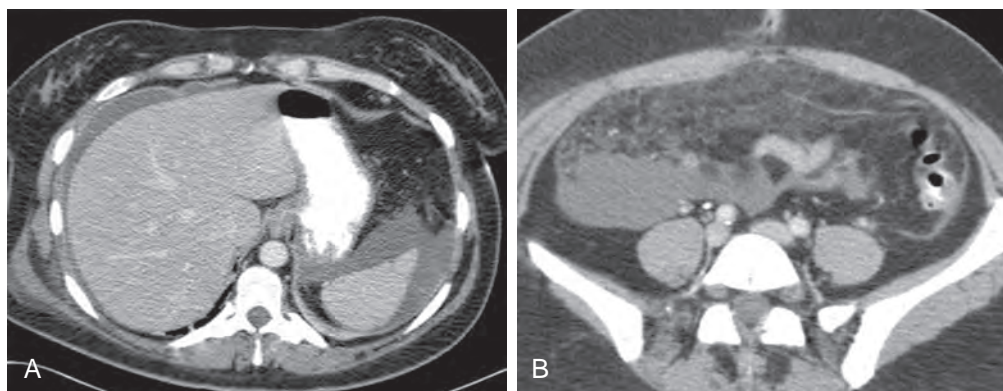


Figure 81-4 Bile leakage inducing bile peritonitis **A.** Ten days after LC, CT shows free fluid, compatible with bile, around the spleen and the liver. **B.** Pelvic CT shows a large amount of free fluid and marked infiltration of the mesentery and omentum, indicating infected bile.

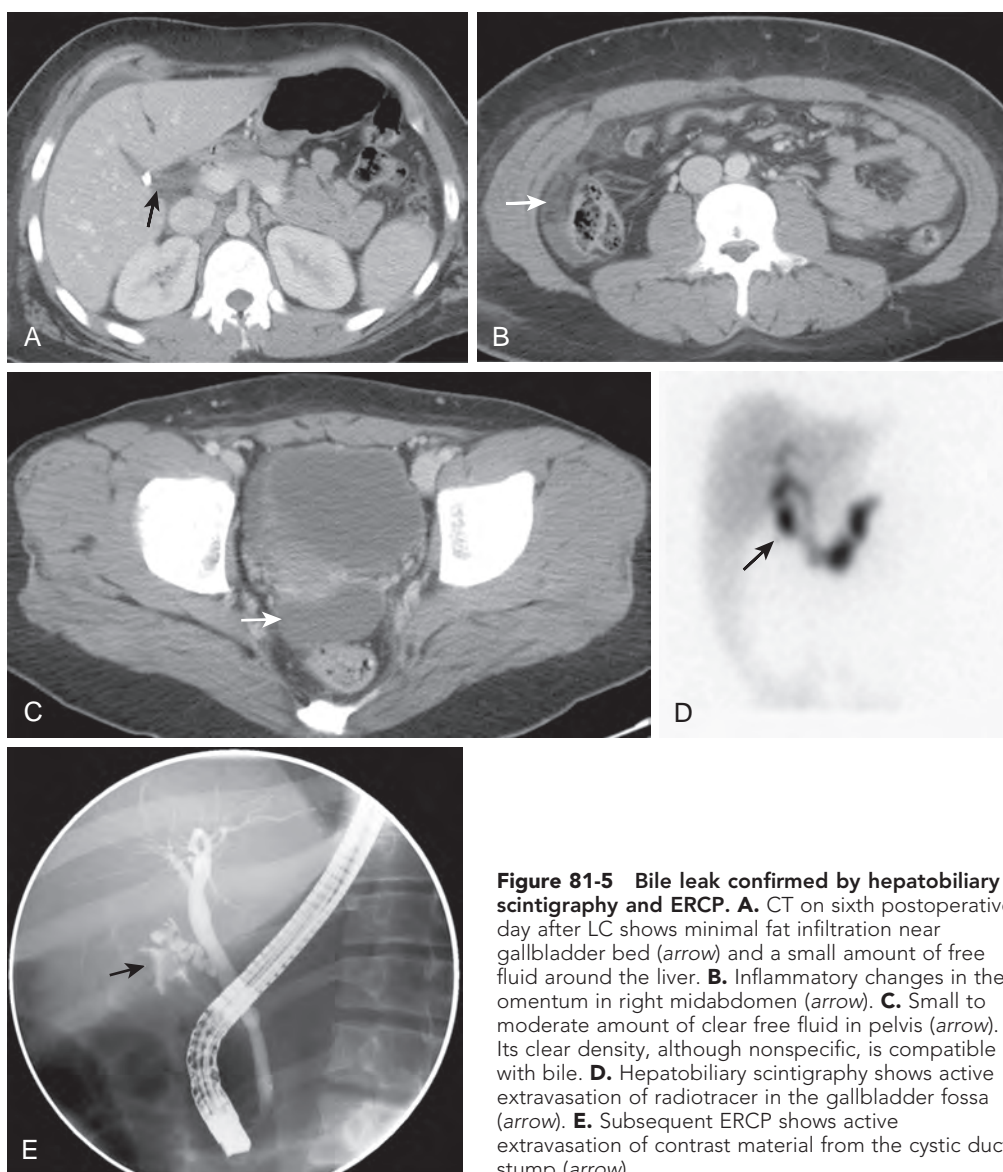


Figure 81-5 Bile leak confirmed by hepatobiliary scintigraphy and ERCP. **A.** CT on sixth postoperative day after LC shows minimal fat infiltration near gallbladder bed (arrow) and a small amount of free fluid around the liver. **B.** Inflammatory changes in the omentum in right midabdomen (arrow). **C.** Small to moderate amount of clear free fluid in pelvis (arrow). Its clear density, although nonspecific, is compatible with bile. **D.** Hepatobiliary scintigraphy shows active extravasation of radiotracer in the gallbladder fossa (arrow). **E.** Subsequent ERCP shows active extravasation of contrast material from the cystic duct stump (arrow).

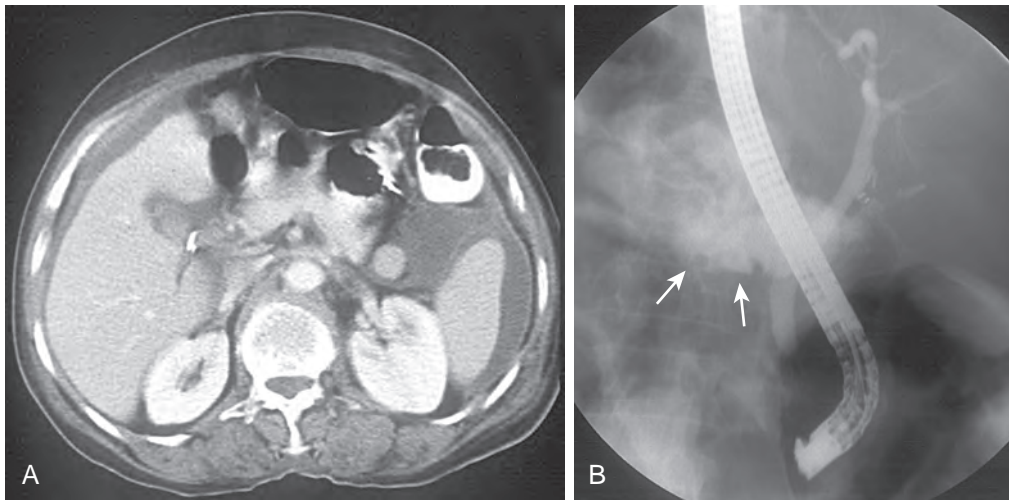


Figure 81-6 Bile leak confirmed by ERCP. **A.** CT obtained 5 days after LC shows free fluid in the upper abdomen mainly around the spleen and the liver and some fluid also in the gallbladder fossa, adjacent to a surgical clip. **B.** ERCP after the CT study shows extensive extravasation, probably from the cystic duct remnant (arrows).

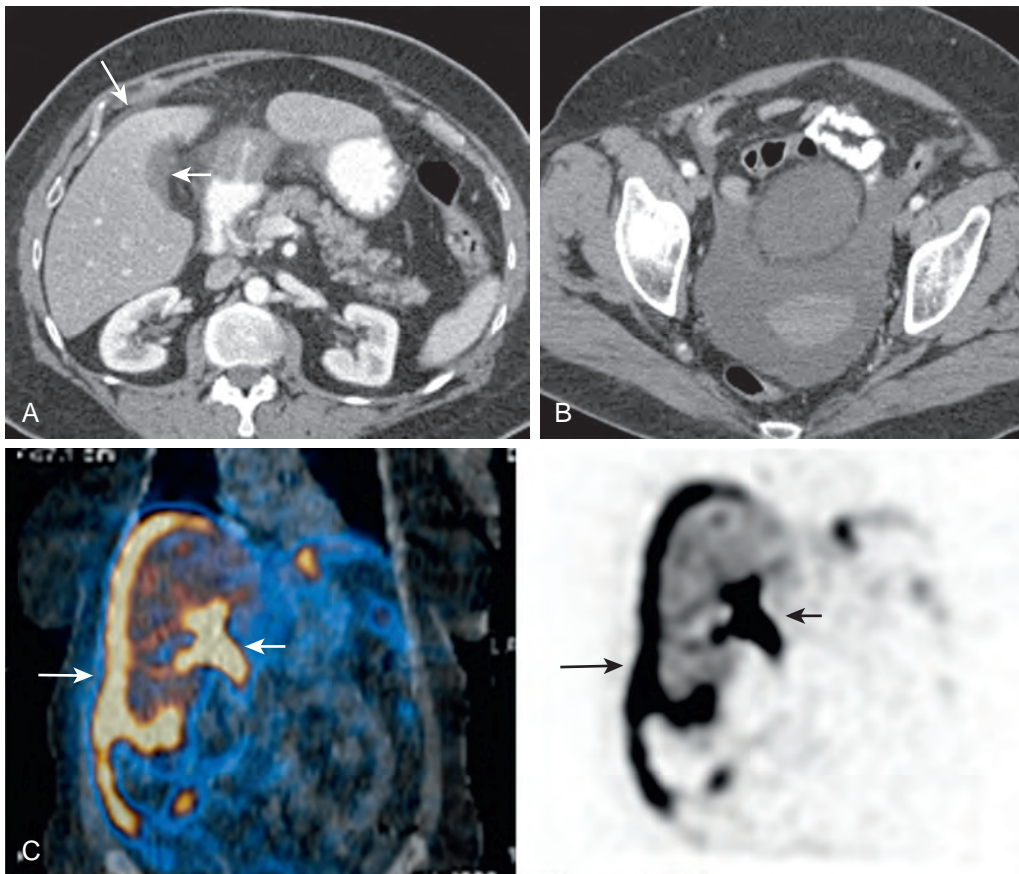


Figure 81-7 Bile leak confirmed by hepatobiliary scintigraphy. **A.** CT on second postoperative day after LC in 63-year-old woman with leukocytosis shows minute amount of free fluid around liver (long arrow) and in gallbladder fossa (short arrow); however, a large amount of clear fluid is seen in the pelvis (**B**). **C.** ^{99m}Tc -labeled iminodiacetic acid (HIDA) by single photon emission computed tomography (SPECT) on twelfth postoperative day shows active extravasation of radiotracer in the gallbladder fossa (short arrow) and biliary ascites around liver and in right paracolic gutter (long arrow).

markedly elevated serum bilirubin level and, alternatively, the presence of significant bile output from an abdominal drain are both features highly suggestive of a large biloma, although the absence of bile output from an abdominal drain cannot exclude a bile leak.³³ Bile can leak freely into the peritoneal cavity, resulting in either sterile or infected biliary ascites (see Figs. 81-3 to 81-7 and 81-9), or accumulate into a loculated fluid collection, resulting in a sterile biloma (see Figs. 81-3A and 81-8) or an infected abscess (Fig. 81-10).^{38,55}

The treatment of bile duct injuries and leaks remains controversial, and there are a number of different management algorithms in use. In general, patients with a suspected bile leak and a single fluid collection or biloma on CT are initially treated with placement of a percutaneous drainage catheter. Although it is uncommon, in a small subset of patients with a minor leak and minimal bile duct injury, there is the possibility of spontaneous resolution of the leak after placement of the drainage catheter. If the leak then fails to resolve, patients typically

proceed to endoscopic retrograde cholangiopancreatography (ERCP), in which minor leaks are treated with placement of a biliary stent. The biliary stent diverts bile away from the site of biliary injury into the duodenum, giving the injured segment time to heal (see Fig. 81-9B). Notably, whereas sphincterotomy has traditionally been thought to be useful in these patients, there is now little consensus in the literature on its utility; some studies suggest that this procedure raises the risk of perforation, bleeding, and mortality, and there are few data to suggest that sphincterotomy provides benefit in terms of leak resolution.³⁴ If a major bile leak or significant biliary injury is detected on ERCP, patients undergo operative repair and biliary reconstruction.^{37,56,57}

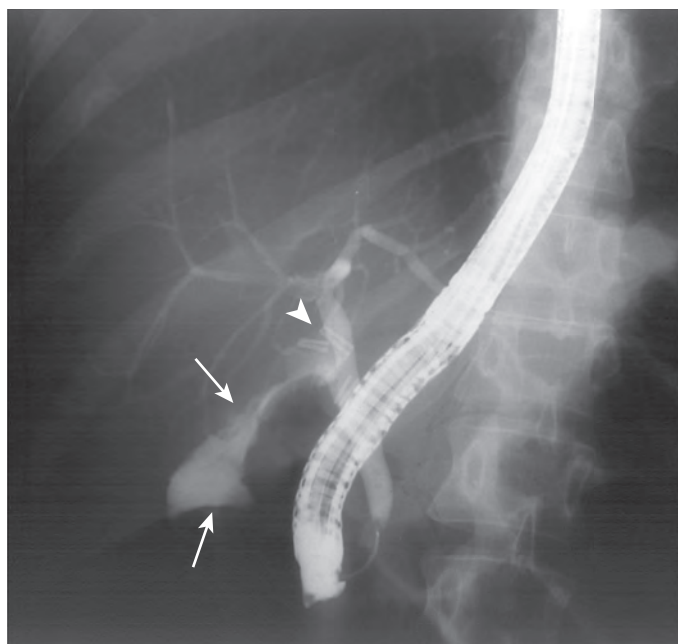
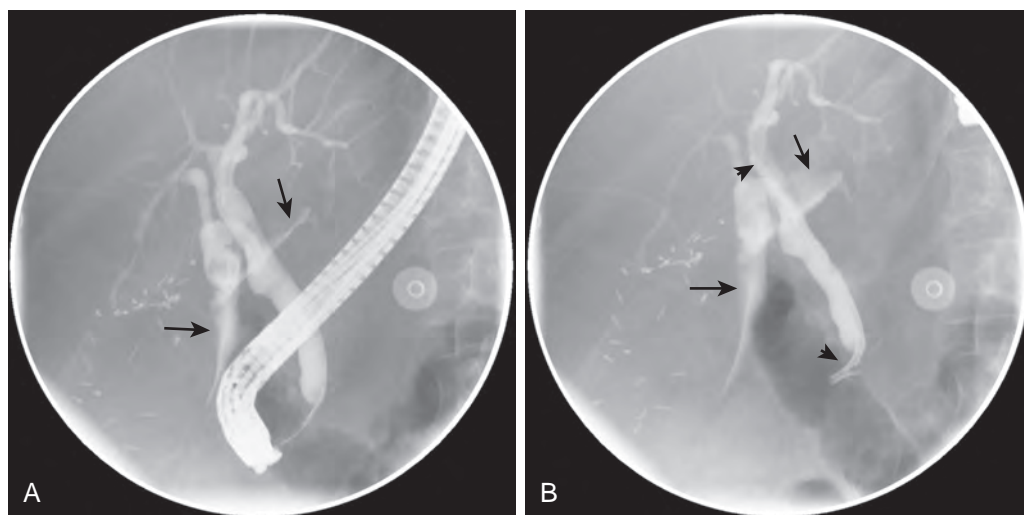


Figure 81-8 Bile leak from cystic duct stump. Endoscopic retrograde cholangiography 9 days after LC shows leak of contrast material originating adjacent to surgical clips (arrowhead) at the cystic duct stump. The leaking contrast material assumes a pear-shaped configuration, a biloma, resembling the gallbladder (arrows).

Figure 81-9 Bile leak after cholecystectomy. A and B. ERC 10 days after cholecystectomy (for gallbladder cancer) shows active extravasation of contrast material (arrows). This was considered a “minor” leak and treated with ERCP-guided stent placement (arrowheads in B).



Retained Biliary Stones

Small biliary stones occasionally remain after LC, often within the intrahepatic or extrahepatic biliary tract.⁹ Moreover, in some cases in which LC is technically challenging as a result of difficulty in identifying anatomic landmarks, adhesions, marked bleeding, or severe gallbladder inflammation, portions of the gallbladder infundibulum may be inadvertently left behind (subtotal cholecystectomy), and this gallbladder remnant may contain stones.^{41,58} Such incomplete resection of the gallbladder is relatively common, occurring in up to 13.3% of cholecystectomies.⁵⁹ For the same reasons, particularly in patients with an unusually long cystic duct, portions of the cystic duct containing stones may also be left behind after surgery.⁵⁸

These retained stones, regardless of whether they reside within the intrahepatic biliary tree, CBD, cystic duct stump, or gallbladder remnant, may subsequently migrate distally into the CBD, resulting in biliary obstruction (Fig. 81-11). The overall incidence of retained stones, regardless of location, after LC is 0.5%; the most common location for retained stones is within the CBD, with an incidence ranging between 5% and 15%.⁶⁰⁻⁶⁵ There is some debate in the literature as to the necessity of defining the presence of biliary tract stones (outside the gallbladder) by preoperative magnetic resonance cholangiopancreatography (MRCP), and some surgeons advocate performing intraoperative cholangiography for the purpose of detecting biliary stones in the highest risk patients during cholecystectomy.^{65,66}

It is thought that retained stones in the biliary system after cholecystectomy may be a common cause for postcholecystectomy syndrome, a term used to describe the recurrent biliary colic symptoms suffered by 10% to 40% of patients after cholecystectomy.^{41,58} Symptoms of retained biliary stones can include jaundice and right upper quadrant pain, and the diagnosis is usually made in the first 2 months postoperatively.^{27,44} Rarely, retained distally impacted stones in the CBD may secondarily result in biliary leakage from the cystic duct remnant by causing increased biliary pressure that displaces the cystic duct clips, a phenomenon often referred to as cystic duct blow-out.⁹ Retained stones can usually be extracted by ERCP and sphincterotomy. Open or laparoscopic CBD exploration is only rarely necessary.^{27,44}

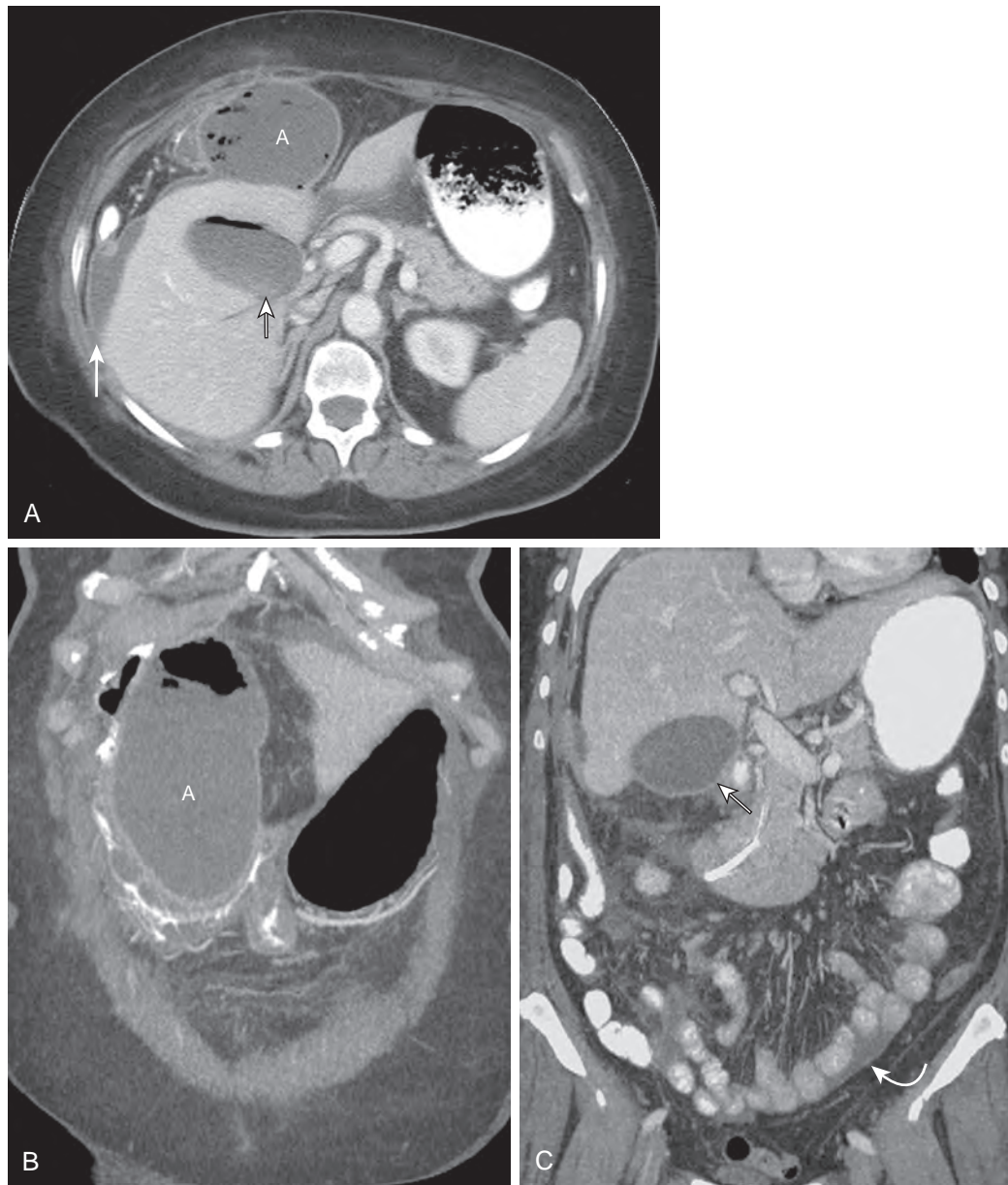


Figure 81-10 Postoperative abscess after LC. **A.** Contrast-enhanced CT shows gas-containing abscess anterior to liver (A). Fluid and gas in gallbladder fossa (short arrow). Fluid around liver (long arrow). **B.** Coronal reformat shows full extent of abscess cavity (A). **C.** Coronal reformat shows fluid in gallbladder fossa (straight arrow) and pelvis (curved arrow).

Bile Duct Strictures

Postoperative biliary strictures are not uncommon with both open and laparoscopic cholecystectomies. Several different causes have been proposed, including focal bile duct ischemia due to intraoperative damage and thermal injury during surgical dissection, intense connective tissue response with fibrosis and scarring as a result of bile duct manipulation, inadvertent clipping or ligation of the bile duct, and scarring as a result of T-tube placement (Figs. 81-12 and 81-13).^{38,54,59,67}

Biliary stricture after cholecystectomy is relatively rare, occurring in 0.2% to 0.5% of patients. In many cases, these strictures are not recognized for months or years after the patient's surgery, with a mean time to stricture of 3 to 6 months.⁶⁷ Many patients are not overtly symptomatic, and the

diagnosis is often made on the basis of progressive biliary dilation on cross-sectional imaging. In other cases, patients can present with painless jaundice, cholangitis, or sepsis. Patients with a markedly delayed diagnosis may ultimately present with advanced biliary cirrhosis and its complications.³⁸

Whereas surgical treatment (usually in the form of a Roux-en-Y hepaticojejunostomy) has traditionally been the treatment of choice for iatrogenic biliary strictures related to LC, endoscopic treatment is increasingly becoming the first-line treatment of choice.^{54,68} In addition to being safer and better tolerated (with lesser degrees of associated morbidity and mortality), endoscopic balloon dilation with stent placement has been associated with a lesser risk of recurrent strictures and cholangitis, although patients may require multiple sessions of balloon dilation with periodic replacement of bile duct stents.⁶⁹ In

particular, endoscopic approaches appear to be more effective for strictures in the distal CBD, whereas surgery may still be the preferred option for complex strictures in the more proximal CBD.⁶⁷

Imaging of Postoperative Bile Duct Injuries

Ultrasound and Multidetector Computed Tomography. In most patients with a suspected bile duct injury or leak after LC, ultrasound and contrast-enhanced CT are the most common initial imaging studies performed. Both studies can be completed quickly and efficiently, even in the most critically ill patients, and ultrasound can be performed at the bedside in the

critical care setting. In most cases, both studies will demonstrate an intra-abdominal fluid collection, most often in the right upper quadrant (often the subhepatic space or gallbladder fossa) close to the surgical bed (see Figs. 81-1 and 81-3 to 81-7). CT, in particular, can better delineate peripheral enhancement and complexity and distinguish free bile fluid from a loculated biloma. Notably, however, neither imaging modality can distinguish a biloma from other common causes of a postoperative fluid collection, including a seroma, abscess, hematoma, or lymphocele; the distinction between these different entities is often based on the analysis of fluid obtained from surgical drains or the direct aspiration of a fluid collection under image guidance

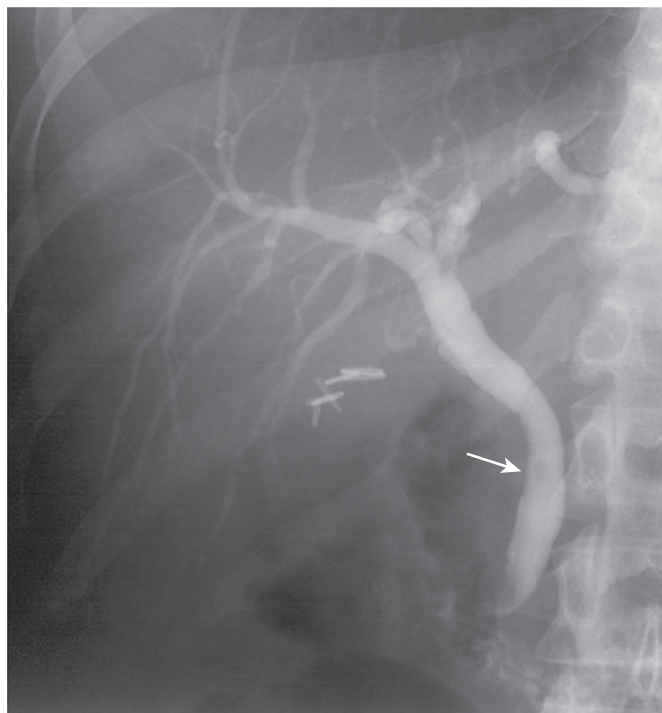


Figure 81-11 Retained stone in CBD. ERCP 16 days after LC shows a calculus (arrow) in distal part of the CBD. Sphincterotomy was performed and the stone was removed.

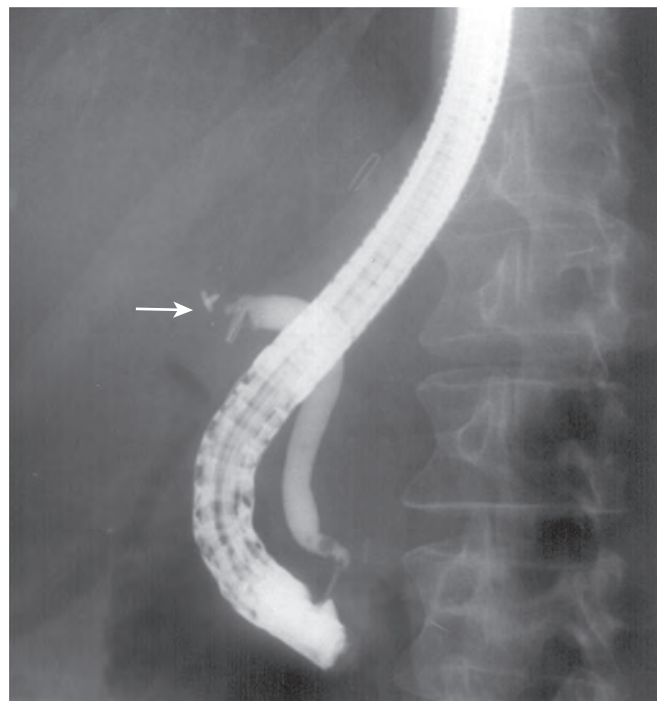


Figure 81-12 Inadvertent ligation of CBD. ERCP shows CBD filling to level of surgical clips (arrow), indicating the site where the cystic duct had originated. No contrast material is identified proximally in the bile duct.

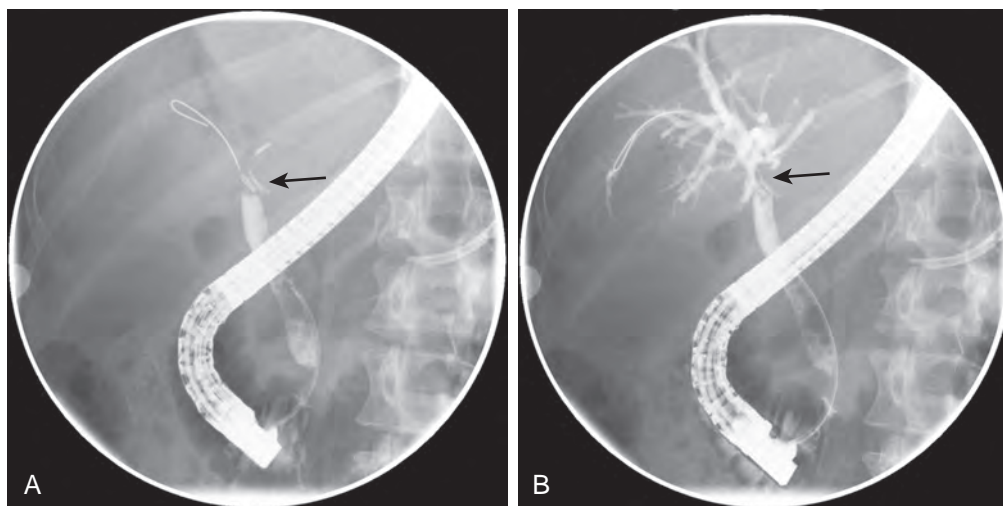


Figure 81-13 Bile duct injury during LC resulting in CBD stricture. A. ERCP shows abrupt narrowing (arrow) of CBD at level of cholecystectomy clips. **B.** Subsequent ERCP, with wire advanced proximal to stricture, better delineates site of stricture (arrow).

(CT or ultrasound). In addition, the location of a collection may not be helpful in distinguishing these entities; bile fluid can potentially disperse widely throughout the peritoneal cavity (see Figs. 81-1 and 81-3 to 81-7) and become loculated relatively distant to the site of bile leak, whereas lymphoceles, abscesses, seromas, and hematomas can develop in close contiguity with the biliary tree (i.e., gallbladder fossa or subhepatic space; see Fig. 81-10).^{33,34,53} In addition, neither ultrasound nor CT can accurately define the source of a leak, and cholangiography may be necessary to differentiate leaks originating from different sites in the biliary tree (see Figs. 81-3D, 81-5E, 81-6B, 81-8, and 81-9).

Both CT and ultrasound are also important tools in identifying evidence of biliary dilation, often before there is biochemical evidence of obstruction. New biliary dilation after a cholecystectomy should suggest either the presence of a retained CBD stone (with associated obstruction) or, alternatively, the development of a bile duct stricture. At the same time, a mild degree of biliary dilation after cholecystectomy is a normal finding and should not be overinterpreted as obstruction. Although the presence of bowel gas will often obscure the distal CBD and ampulla (perhaps in a majority of cases), in certain rare cases, ultrasound may be able to define a distal CBD stone as a highly echogenic focus with posterior acoustic shadowing.⁹ Alternatively, although the diagnosis can be difficult on CT, the use of multiplanar reformations and three-dimensional reconstructions can help define the course of the CBD along its entire length and may demonstrate a meniscus sign at the site of obstruction by a CBD stone. Depending on the calcium content of a stone, an obstructing retained stone may be radiodense and calcified or of soft tissue attenuation. Whereas bile duct injury or stricture is the other diagnostic possibility when one is confronted with progressive dilation of the biliary tree after cholecystectomy, the absence of bile duct dilation on CT or ultrasound does not exclude bile duct injury, and further investigations will often be necessary if these entities are strongly suspected clinically.^{33,38,53}

Hepatobiliary Scintigraphy. Hepatobiliary scintigraphy, most often performed with technetium Tc 99m mebrofenin (or a number of other technetium-based agents) has proved to be an extremely sensitive method for detecting both bile leaks and biliary obstruction (see Figs. 81-5D and 81-7C).^{32,70,71} In particular, hepatobiliary scintigraphy has proved to be extremely accurate in identifying bile leaks in the setting of a recent cholecystectomy, with a sensitivity that may approach 100%, even including leaks into diagnostically difficult locations, such as the lesser sac.⁷² Not only can the extravasation of radiotracer from the biliary system during scintigraphy reliably identify the presence of a leak, the absence of a leak can allow the clinician to confidently proceed with conservative management.^{33,70}

Nevertheless, hepatobiliary scintigraphy has certain key limitations, which can diminish its utility. Most important, whereas scintigraphy can identify the presence of leak, it cannot accurately delineate the site of leak, limiting its ability to guide further intervention. Moreover, although the modality can identify the leak, it provides no information about the severity of the leak or bile duct injury, again somewhat limiting its usefulness in terms of guiding subsequent therapy and intervention.³³ For example, scintigraphy cannot differentiate between the complete transection of a duct (which would typically require surgery) and a minimal tear of a duct (which could potentially be treated endoscopically).

Percutaneous Transhepatic Cholangiography. Whereas evaluation of the biliary system after a suspected bile duct injury almost always begins with ERCP, this modality struggles in certain situations; specifically, in performing ERCP, occlusion or transection of a large central bile duct is visualized as only a “stump” of the CBD, and the more proximal biliary tract cannot be visualized. This is of critical importance as the more proximal biliary tract must be visualized to facilitate surgical planning as well as to evaluate for other sites of potential bile duct injury. Moreover, injuries to the right posterior segmental bile duct draining segments VI and VII will often be missed on ERCP, and this is a commonly underdiagnosed and underappreciated site of bile duct injury during cholecystectomy.⁷³ As a result, percutaneous transhepatic cholangiography (PTC) is considered to be the “gold standard” radiographic examination in the evaluation of patients with suspected biliary injuries or strictures as it allows evaluation of the entire proximal biliary tree (even in cases with a significant distal bile duct injury) and the reliable identification of injuries to the right posterior segmental bile duct.

In most institutions, ERCP is typically performed first in the setting of a suspected bile duct injury to differentiate patients with a cystic duct leak or incomplete tear of a duct from those with a complete duct transection. Those patients with a completely transected duct then undergo PTC for evaluation of the proximal ductal system.⁷³ In addition to its valuable diagnostic role, PTC also serves as the first step in the placement of a percutaneous transhepatic catheter, allowing decompression of the biliary system either to treat or to prevent cholangitis resulting from biliary obstruction. Moreover, PTC can also facilitate the percutaneous treatment of biliary strictures, usually with balloon dilation.^{21,34,44}

Endoscopic Retrograde Cholangiopancreatography. ERCP is an excellent modality for both the diagnosis and management of many biliary complications after LC. In almost all cases, ERCP will be the first diagnostic study performed in the setting of a suspected leak, and in many cases, it may be the only required study.

With regard to biliary leaks, ERCP can identify the site of bile leak in more than 95% of cases, a clear advantage relative to other diagnostic studies, such as contrast-enhanced magnetic resonance imaging (MRI) and hepatobiliary scintigraphy, which cannot reliably identify the exact site of leakage (see Figs. 81-3D, 81-5E, 81-6B, 81-8, and 81-9). Compared with PTC, ERCP has a generally lower rate of complications and carries a lesser risk of iatrogenic bile duct injury, bile leak, cholangitis, and sepsis. ERCP is also a highly effective means of treating bile duct leaks as these complications can be managed endoscopically in more than 80% of cases (biliary stents with or without sphincterotomy).^{53,74} Nevertheless, ERCP is an invasive modality with an associated risk of postprocedural complications and the need for patient sedation.⁹

Whereas ERCP alone is sufficient in the diagnosis of low-grade strictures and injuries to the major central bile ducts, it is insufficient in patients with complete obstruction of the extrahepatic bile tree or with high ductal injuries as the intrahepatic bile ducts more proximally cannot be visualized. In these cases, PTC is needed to evaluate the intrahepatic ducts and to fully define the exact length of a patient's stricture.^{34,44,74} When both studies are performed, a gap of several centimeters may be present between a blind-ending distal duct demonstrated on ERCP and the proximal bile ducts opacified on PTC,

precluding percutaneous transhepatic stricture dilation.⁴⁴ As mentioned previously, the treatment for bile duct strictures is gradually moving away from surgical reconstruction and toward endoscopic management (usually balloon dilation and stenting; see Fig. 81-9), although surgery continues to play a major role in certain lesions.

Magnetic Resonance Cholangiopancreatography. During the last several years, the introduction of a number of different hepatobiliary contrast agents for MRI, the most important of which is gadoxetate disodium (Eovist; Bayer HealthCare Pharmaceuticals), has made MRI a highly valuable option for the detection of bile leaks. These agents, which are excreted into the biliary system in varying amounts, allow the acquisition of normal contrast-enhanced images in the arterial, venous, and delayed phases, followed by excellent opacification of the biliary system in the delayed hepatobiliary phase (usually at 10 to 20 minutes). This opacification of the biliary system has been improved with the introduction of gadoxetate disodium, 50% of which is excreted through the hepatobiliary system, compared with 3% to 5% of older hepatobiliary contrast agents, allowing faster and more avid enhancement of the bile ducts. A number of studies, conducted with a variety of different hepatobiliary agents, have suggested that contrast-enhanced MRI does very well in the identification of bile leaks, with a sensitivity up to 95% and a specificity up to 100%.⁷⁵⁻⁸⁰ Bile leaks on these images appear as areas of active extravasation of contrast material from the involved segment of the biliary tree into the peritoneum and perihepatic space. In the more chronic setting, contrast-enhanced MRI with hepatobiliary agents can also be potentially helpful in terms of identifying sites of biliary narrowing or obstruction as a result of biliary strictures. Although it is not completely necessary, conventional MRCP images (highly T2 weighted volumetric images) may be helpful as an ancillary imaging sequence to identify obstructing stones as well as to provide high-resolution volumetric images of the biliary tree to identify subtle sites of stricture or narrowing.⁷⁷

However, the use of these agents is limited in patients with cirrhosis, jaundice, or significant hepatobiliary disease as excretion of the contrast agent into the biliary system may be significantly impaired in such patients.⁷⁵⁻⁸⁰ This can be a significant obstacle to the use of this technique in patients with bile duct

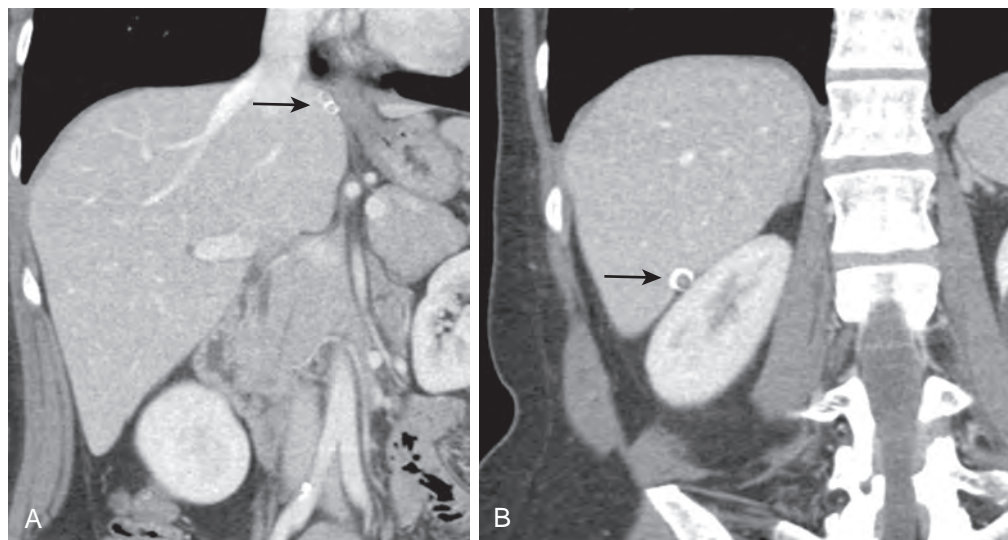
injury or bile leak after cholecystectomy as many of these patients present with hepatobiliary dysfunction and jaundice. Moreover, as with other MRI examinations, the quality of images depends heavily on the patient's ability to adequately perform a breath-hold maneuver, a necessity that can be a problem in critically ill patients.⁹

Spilled Gallstones

Whereas LC has proved extremely effective during the last two decades, largely obviating the need for open cholecystectomy except in the most complicated cases, the use of this technique has resulted in an increased incidence of "spilled," "dropped," or "retained" gallstones during the procedure.⁸¹ Spilled gallstones result from perforation of the gallbladder during cholecystectomy, with subsequent spillage of stones into the intraperitoneal space. Unlike in open cholecystectomy, in which these stones are relatively easy to identify and to retrieve during the course of the procedure itself, surgeons performing LC may not realize that stones have been spilled or alternatively may not have adequate surgical exposure to retrieve the stones laparoscopically.⁸¹⁻⁸⁶ The incidence of gallbladder perforation during LC may be as high as 36%, and the rate of gallstone spillage may reach 19%.⁸⁷ Moreover, when spillage occurs, one series found that up to 50% of stones were lost and not retrieved during the procedure.^{82,88} If spilled stones are noted intraoperatively, the surgeon will often attempt to retrieve as many stones as possible. Nevertheless, given the low rate of associated complications, most surgeons will not convert the procedure to an open cholecystectomy to retrieve every possible stone, and some stones will undoubtedly be left behind.⁸⁹

Whereas spilled gallstones are common, the incidence of complications related to these stones is relatively rare, occurring in 8.5% of patients.^{82,84,85,87,89} Most patients are asymptomatic, and in many cases, stones are simply discovered as an incidental finding on an imaging examination (usually CT or MRI) (Figs. 81-14 to 81-16).⁸¹ Complications are thought to be more likely with infected stones (in the setting of acute cholecystitis), larger stone size (>1.5 cm), pigment stones, and increased age of the patient.^{83,90} The most common complication related to spilled stones is the development of an abscess surrounding the stones, either within the abdominal cavity (usually the subhepatic

Figure 81-14 Spilled gallstones, incidentally seen on CT 10 years after LC. **A.** Two small peripherally calcified gallstones medial to liver, adjacent to gastroesophageal junction (arrow). **B.** Slightly larger peripherally calcified gallstone caudal to liver (arrow).



space or in the retroperitoneum inferior to the subhepatic space) or within the anterior abdominal wall itself (Figs. 81-17 and 81-18).^{81,85,91,92} These abscesses can develop months or even years after surgery, and radiologists should always consider this a potential cause when confronted with a patient who develops an abdominal abscess of unknown etiology.⁸² The delay between cholecystectomy and abscess presentation can be considerable, probably as a result of the indolent nature of the inflammatory process and the often unusual sites of these abscesses.⁸⁶ In one review, the time interval between cholecystectomy and the onset of symptoms was 5.5 months (range, 0-36 months).^{85,86}

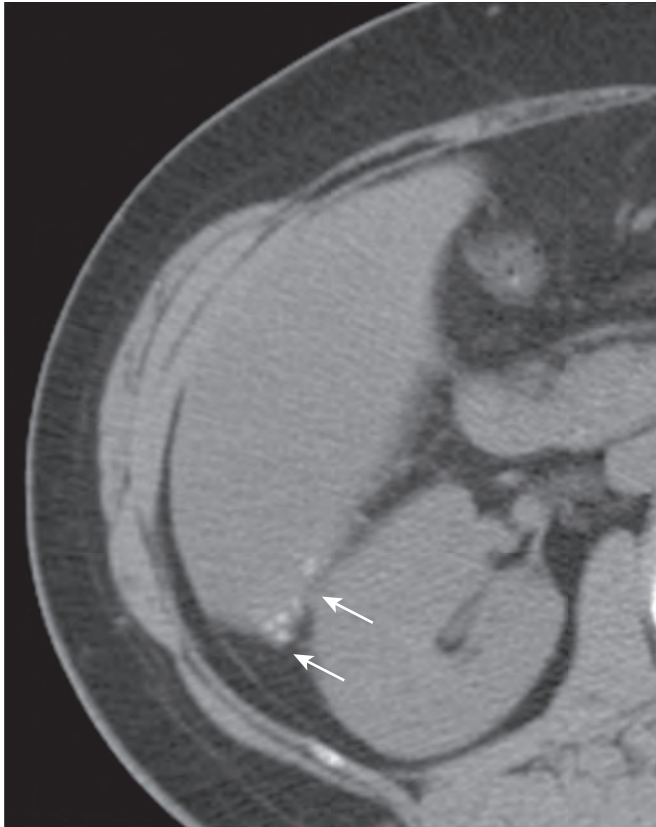


Figure 81-15 Spilled gallstones. Innumerable tiny dropped gallstones along Morison's pouch (arrows) in an asymptomatic patient several years after LC. Similar appearance of innumerable tiny gallstones was seen on preoperative ultrasound (not shown).

Other more rare complications include fistula formation, pain as a result of stones lodged in unusual locations (i.e., a hernia sac, ovary, fallopian tube), liver abscesses, bacteremia, adhesions, bowel obstruction, and even transdiaphragmatic migration of stones. Stones can migrate into the thorax either secondary to the erosion of gallstones through the diaphragm or from the formation of a subphrenic abscess, which subsequently connects supradiaphragmatically into the pleural space, lung, or bronchial tree.^{88,90} This can result in cholelithoptysis (expectoration of gallstones) or pleurolithiasis.^{46,85,93}

Imaging of Spilled Gallstones. Ultrasound, CT, and MRI may demonstrate spilled stones lying freely in the abdomen, often primarily around the liver.⁸⁶ On CT, the conspicuity of stones will vary dramatically, depending on their composition; pigment stones (with a high calcium content) usually are readily recognizable as calcified high-density nodules, whereas cholesterol stones and other stones with low calcium content can be difficult to identify or appear as small soft tissue nodules. Notably, when there is little or no calcium content on CT, spilled gallstones can very much mimic the appearance of peritoneal tumor implants or carcinomatosis.⁸¹ Stones, regardless of their type, are relatively easy to identify on MRI as most gallstones are highly hypointense on T2-weighted images.⁸²

Perhaps most important, when they are associated with infection, spilled stones likely serve as the nidus of an abscess, and the identification of a stone at the center of such a collection is critical in terms of management (see Figs. 81-17C and 81-18C). These collections are not treated with simple percutaneous drainage, but instead the stone (which represents the cause of the infection) must be retrieved either surgically (either open or laparoscopically) or percutaneously by an interventional radiologist.^{81,86} The majority of these abscesses are confined to the subhepatic space or the retroperitoneum inferior to the subhepatic space. Several unusual locations, however, have been described, including the thorax, subphrenic space, within the abdominal wall at trocar sites, and at the sites of incisional hernias.⁸⁶ These abscesses appear on CT as one or more fluid collections containing small opacities, ranging in density (based on their calcium content and stone type) from hypodense nodules to nodules that are partially or completely calcified.^{84,86,94} On ultrasound, echogenic shadowing foci within a fluid collection are typical of dropped stones, and the presence of calculi within a collection is virtually diagnostic of spilled stones complicated by abscess formation.⁸⁶

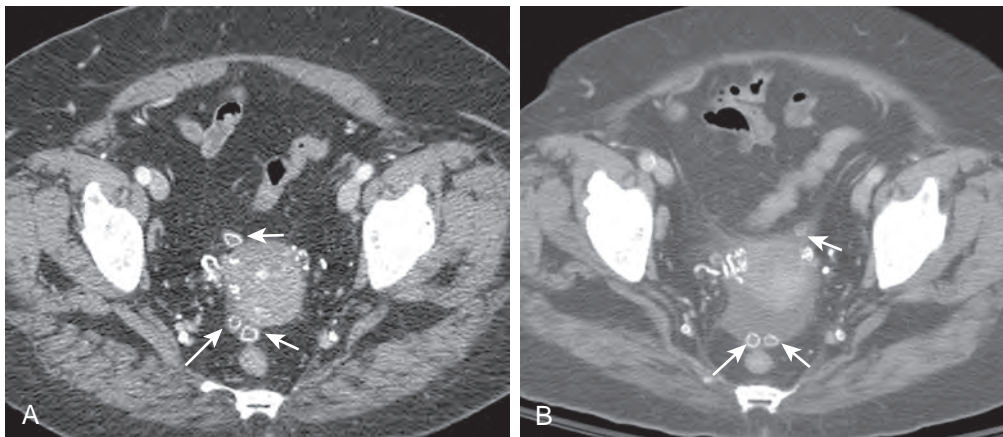


Figure 81-16 Spilled gallstones.

A. Several spilled gallstones incidentally detected in pelvis (arrows) adjacent to uterus.
B. Patient subsequently developed ascites; the spilled gallstones are more conspicuous (arrows).

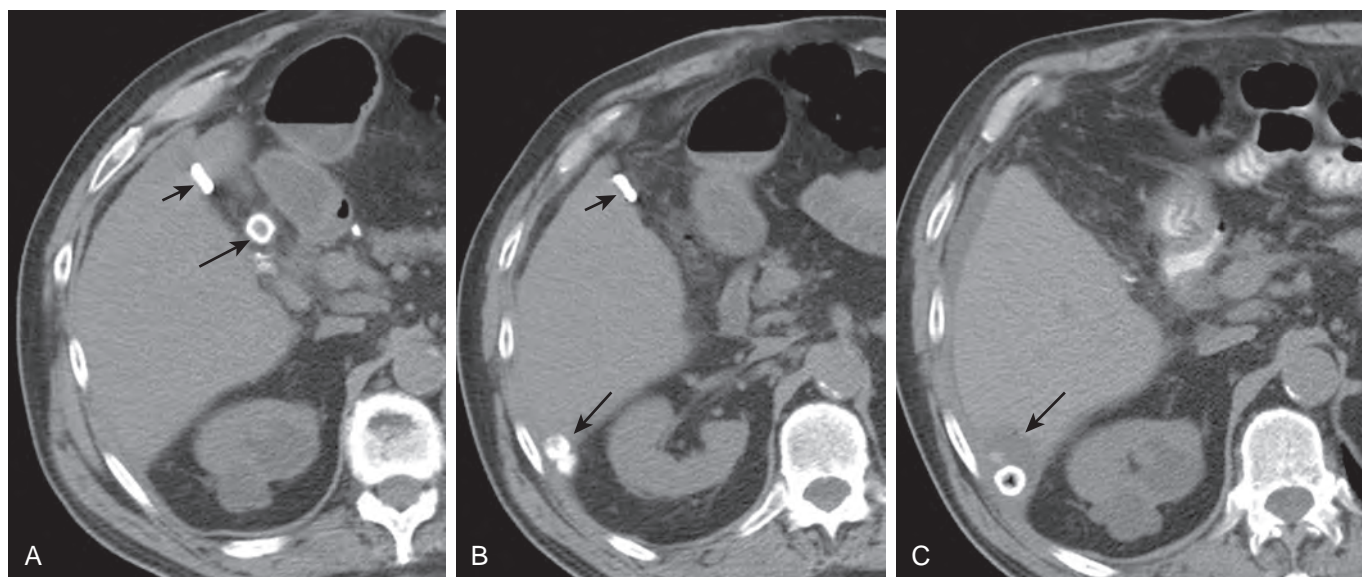


Figure 81-17 Spilled gallstones resulting in perihepatic abscess. **A** and **B.** Noncontrast CT 3 days after LC shows a dropped gallstone in the porta hepatis (*long arrow, A*) and two dropped gallstones in Morison's pouch (*arrow, B*). Note surgical clip (*short arrow*) in gallbladder fossa. **C.** Patient presented 4 weeks after LC with fever and abdominal pain. Noncontrast CT shows interval development of an abscess surrounding the two dropped gallstones in Morison's pouch (*arrow*) and free fluid around the liver.

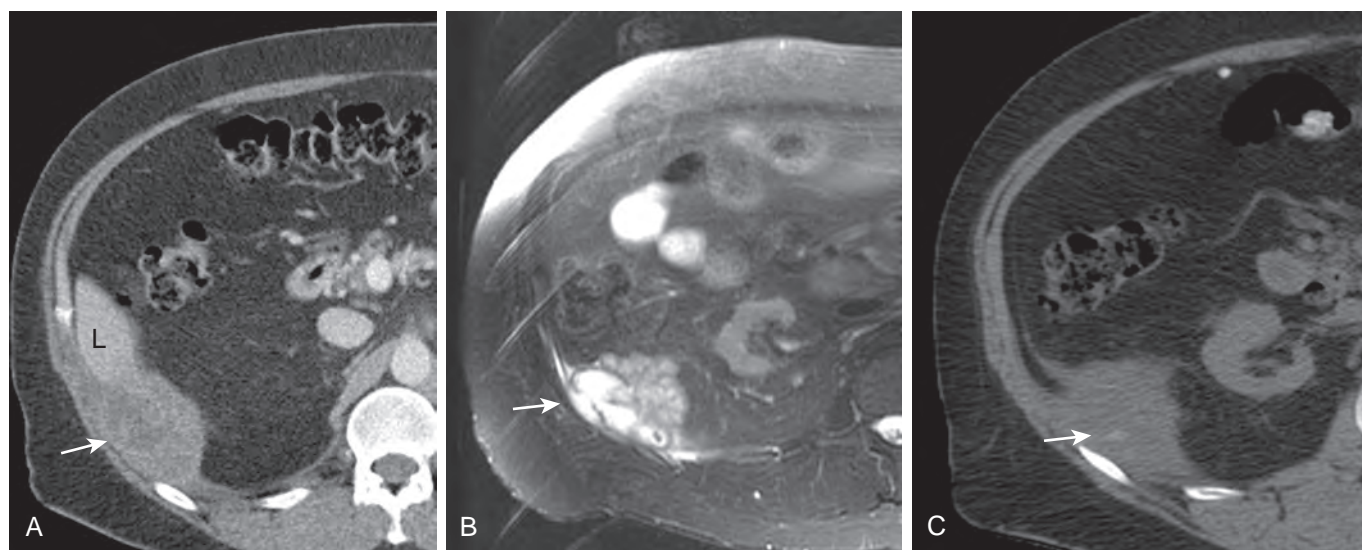


Figure 81-18 Spilled gallstones resulting in a large perihepatic abscess. Patient presented 9 months after LC with low-grade fever, fatigue, and lack of appetite. Contrast-enhanced CT (**A**) and axial T2-weighted MR (**B**) demonstrate a multiseptate abscess (*arrow*) caudal to right lobe of liver (L). The small calcified spilled gallstone within it, the nidus of the abscess, is seen only on noncontrast CT (**C**, *arrow*).

Biliary-Enteric Anastomosis

BACKGROUND, INDICATIONS, AND TECHNICAL CONSIDERATIONS

The creation of a biliary-enteric anastomosis has become a common component of multiple different surgical procedures and can be performed for a number of different reasons. The most common indications for the creation of such an anastomosis include liver transplantation; the resection of tumors involving the biliary tree, duodenum, or pancreatic head (often as part of a pancreaticoduodenectomy); benign or malignant biliary obstruction; biliary stones, biliary strictures, choledochal

cysts, or bile duct injuries; and inflammatory conditions of the biliary tree, such as primary sclerosing cholangitis.^{4,5}

Over time, reconstruction of the biliary system by a biliary-enteric anastomosis has most commonly been performed through the creation of a hepaticojejunostomy. Although choledochoduodenostomy and hepaticoduodenostomy are also viable alternatives, both have clear downsides. The use of the duodenum carries a significant risk of bile gastritis due to duodenogastric reflux.⁹⁵ Whereas a direct duct-to-duct anastomosis is also a possible option and is sometimes still used in liver transplantation, the creation of such an anastomosis is more technically difficult and carries much higher risks of anastomotic strictures and leaks (perhaps as high as 40%).⁹⁶ In

contrast, hepaticojejunostomy has proved to be safe and effective, with a much lower risk of bile leak (2.4%-5.6%).⁹⁶

There are minor variations in how a hepaticojejunostomy is created, depending on the presence or absence of a malignant neoplasm or a bile duct stricture and the exact site of this tumor or stricture. However, the surgical procedure usually includes the following. Once the abdomen is entered and the hepatoduodenal ligament is dissected free, the common duct must be identified. The common duct is usually the most anterior structure as it enters the liver, with the hepatic artery and portal vein running immediately posterior. This arrangement provides the surgeon with free access to the anterior aspect of the common duct. Importantly, the right hepatic duct typically will have a very short extrahepatic course, whereas the left hepatic duct is nearly entirely intrahepatic, features that have great significance as the surgeon dissects the ducts and prepares to create the anastomosis. Once the common duct is identified and dissected free, it is usually ligated distally, traction sutures are placed proximally, and the common duct is divided in between. In general, the common duct is carefully handled and dissected to avoid injury to its vascular supply, which would predispose the patient to strictures. If there is any pathologic process (i.e., stricture, malignant neoplasm) more proximally in the common duct near the confluence, the common duct may need to be resected in its entirety.^{96,97}

The jejunum is then transected 20 cm distal to the ligament of Treitz, and this limb of jejunum is brought up to the liver hilum in a retrocolic fashion. An anastomotic orifice is then created in the jejunal limb, and the proximal common duct (or the confluence of the ducts) is anastomosed to the jejunum. In those cases in which the common duct has been entirely sacrificed and the right and left hepatic ducts cannot be approximated for a common anastomosis, two separate anastomoses with the jejunum may be necessary. Notably, the anastomosis is almost always created by side-to-side technique, and depending on the surgeon, a transanastomotic stent may or may not be used.^{96,97}

The biliary-enteric anastomosis is usually best visualized on MDCT in the coronal or sagittal planes and can be difficult to identify on the source axial images. Pneumobilia is a common finding after the surgery, and this can be used to the radiologist's advantage in identifying the anastomosis as gas can sometimes be directly traced from the hepatic ducts into the jejunal limb. As mentioned earlier, some surgeons use a transanastomotic stent, and this can also be a valuable means of identifying the hepaticojejunostomy in the immediate perioperative period. In many cases, the right upper quadrant jejunal limb may be nondistended, further increasing the difficulty in adequately evaluating the anastomosis.⁹⁸

Hepaticojejunostomy may be associated with a number of different complications, including cholangitis, sepsis, liver abscesses, bile leaks, anastomotic strictures, hemorrhage, and pancreatitis. In addition, patients can present with a number of complications common to other major hepatobiliary surgeries, including delayed gastric emptying, bleeding, abscess formation, fistulas, and wound infections.⁹⁹

COMPLICATIONS

Biliary Leak

The rate of bile leaks after hepaticojejunostomy varies by the type of surgery performed. In general, the rate of bile leaks after

pancreaticoduodenectomy, pancreatectomy, and repair for bile duct injury ranges between 0% and 5%, whereas the incidence of bile leaks after liver transplantation (1%-25%) and biliary resection for cholangiocarcinoma (11%) is higher. A study by Antolovic and colleagues,⁴ looking at 519 patients who underwent hepaticojejunostomy in the setting of a number of different surgeries, found an overall leak rate of 5.6%.

Bile leaks are more commonly seen in the setting of liver transplantation as the jejunum is often not anastomosed to the common duct but rather to the right or left hepatic duct (or even smaller ducts). Bile leak rates also increase with cholangiocarcinoma resection because of the need for a concomitant liver resection, which often results in a bile leak from the liver surface rather than from the hepaticojejunostomy itself. Other risk factors include the use of preoperative chemotherapy (in patients with an underlying malignant neoplasm), high body mass index, diabetes, and lack of experience on the part of the surgeon (technical failure).⁴ However, one should note that the "bile leak rate" in many of these studies includes not simply bile leak from the hepaticojejunostomy anastomosis but also bile leak from the cut surface of the liver (if hepatic resection was performed) or leakage after the removal of a T tube.¹⁰⁰

In general, many minor bile leaks that do not involve the anastomosis can generally be managed conservatively, often with placement of a percutaneous drainage catheter into a collection identified on CT. In those patients with a minor leak for whom intervention is necessary, ERCP-guided stent placement can be difficult or impossible (particularly if there is associated anastomotic stricture), and PTC-guided treatment may be the best option. In cases of major leaks from the anastomosis itself, reoperation is often considered, although this can be extraordinarily difficult technically as the ductal tissue is often broken down and no longer suitable for reanastomosis.¹⁰¹

There are no imaging findings on MDCT that are absolutely specific for the diagnosis of anastomotic leak, although the presence of a fluid collection adjacent to the hepaticojejunostomy should certainly suggest this diagnosis. Nevertheless, a postoperative biloma due to anastomotic failure cannot be differentiated from a seroma, abscess, evolving hematoma, or lymphocele. As mentioned earlier, hepatobiliary scintigraphy can identify the presence of a leak but cannot definitively identify the source of a leak as originating from the anastomosis, whereas MRI with hepatobiliary contrast agents may be able to more precisely localize a leak to the anastomosis itself.

Biliary Stricture

The reported rate of stricture formation at the hepaticojejunostomy ranges from 5% to 17%, depending on the series.^{99,102,103} Hepaticojejunostomy strictures can be associated with the development of cholangitis and sepsis, and in a series by Schmidt and coworkers,¹⁰³ five of nine patients with a hepaticojejunostomy stricture ultimately developed biliary cirrhosis and one patient developed a cholangiocarcinoma at the stricture site. Risk factors for the development of a significant stricture include associated vascular injuries, active peritonitis at the time of repair, injury above or at the level of the biliary bifurcation, and prior biliary tract surgery or intervention.^{99,102}

A mild degree of intrahepatic biliary dilation after hepaticojejunostomy is not uncommon and should not automatically be assumed to represent an anastomotic stricture (or anastomotic tumor recurrence if the patient has a primary malignant neoplasm). However, the biliary system should be carefully

observed over sequential studies, and any significant or increasing biliary dilation should certainly raise suspicion for a stricture.⁹⁸ The treatment of hepaticojunostomy strictures is usually nonoperative and tends to rely on balloon dilation under PTC or ERCP guidance. Despite this, the recurrence rate after balloon dilation is relatively high (up to 20%), and multiple rounds of dilation may be necessary. However, in certain cases that are refractory to balloon dilation, surgical revision may be necessary.¹⁰⁴

Post-Traumatic Lesions of the Biliary Tree

Traumatic injury to the biliary tree and gallbladder is rare, with an incidence of less than 0.1%. In most cases, biliary tract injuries tend to be associated with significant injuries elsewhere in the abdomen and pelvis, including pancreatic, duodenal, hepatic, splenic, and vascular injuries.^{6,7}

Injury to the intrahepatic bile ducts is relatively common in the setting of hepatic trauma. In most cases, particularly when the injury is to a small peripheral intrahepatic duct, these injuries are self-limited, and bile leakage from these ducts is usually insignificant.³³ Only in rare cases is intervention or drainage required. Extrahepatic biliary tract injuries are more rare but may occur after both blunt and penetrating abdominal trauma.^{6,7} These injuries may be difficult to detect, and a high clinical index of suspicion is needed to avoid diagnostic delay as they are associated with high morbidity and mortality.⁸ Unlike injuries to the intrahepatic bile ducts, extrahepatic duct injuries are not typically self-limited and usually require intervention (often biliary stenting or surgical biliary diversion). Injuries to the extrahepatic bile duct, as a result of its anatomic location, have a high association with injuries to the hepatic artery and portal vein.³³

The most common location of traumatic biliary injury is the gallbladder, which is involved in up to 3% of patients after blunt abdominal trauma.¹⁰⁵⁻¹⁰⁹ Isolated injury to the gallbladder is rare as a result of the protective effects of the rib cage and liver. Accordingly, there are almost always concomitant injuries to adjacent organs, most notably the liver.* Not surprisingly, injury is most likely in a thin-walled or distended gallbladder, and alcohol intake may increase the likelihood of injury by raising pressures at the sphincter of Oddi. Alternatively, any thickening of the gallbladder wall, or even the presence of gallstones, is thought to have a protective effect.^{107-108,111}

Traumatic injuries to the gallbladder can be classified along a spectrum by the degree of severity: contusions, laceration/perforation, and gallbladder avulsion.^{8,105,107,108} In most cases, gallbladder injuries result from a direct blow to the right upper abdomen in a blunt trauma, although gallbladder avulsion can result from severe shear injuries as well.^{107,111} In many cases, contusion injuries, which represent hemorrhage into the gallbladder wall and lumen, go undiagnosed, and the majority of these patients probably never demonstrate clinical symptoms.¹¹² Gallbladder laceration, on the other hand, will often be manifested with frank perforation, resulting in a gallbladder leak.^{107,113} In rare cases, a laceration may not be manifested with perforation at initial clinical presentation, and patients may

subsequently develop delayed perforation after several days.¹¹⁴ Gallbladder avulsions, the most severe injuries, represent frank tearing of the gallbladder from the hepatic bed and are usually associated with a wide spectrum of other traumatic injuries in the abdomen.¹⁰⁷ The degree of separation of the gallbladder from the gallbladder fossa can vary, and the complete disruption of the gallbladder from all its attachments, including the cystic duct and artery, is termed a total avulsion.^{108,111,112}

IMAGING OF POST-TRAUMATIC LESIONS

Gallbladder injuries can be identified by a number of different radiologic modalities, including CT, ultrasound, hepatobiliary scintigraphy, and MRCP. However, in the acute setting, CT is certainly the most practical and effective means of making the diagnosis. Whereas many of the CT imaging features of gallbladder injury are nonspecific, there are several imaging findings that can be highly suggestive of the diagnosis, particularly when multiple findings are seen in conjunction. The presence of high-density blood products within the lumen of the gallbladder should raise strong suspicion for gallbladder injury (Fig. 81-19), although high-density stones, milk of calcium bile, vicarious excretion of contrast material into the gallbladder from a prior imaging study, and hyperdense biliary sludge could potentially mimic this finding. Other ancillary features that can also suggest the diagnosis include pericholecystic free fluid and hemorrhage (see Fig. 81-19), gallbladder hydrops (dilation), gallbladder wall thickening, irregularity and poor definition of the gallbladder wall, active extravasation of contrast material into the gallbladder lumen on arterial phase images, and even a focal defect or nonenhancement of a portion of the gallbladder wall (Fig. 81-20). One must be careful, however, as injury to the adjacent liver or right kidney could potentially account for some of these findings (especially pericholecystic

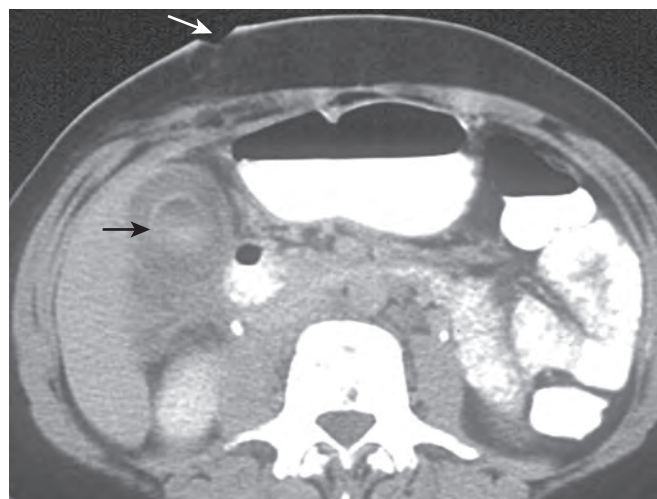


Figure 81-19 Trauma to gallbladder. CT 2 days after stab wound to the right upper quadrant shows gallbladder wall thickening with an intraluminal bile-blood level and infiltration of the pericholecystic tissue (black arrow). A subcutaneous right upper quadrant defect (white arrow) indicates the location of the penetrating knife. At surgery, two lacerations were found in the anterior and posterior aspect of the gallbladder with mild biliary peritonitis. (From Zissin R, Osadchy A, Shapiro-Feinberg M, et al: CT of a thickened-wall gall-bladder. *Br J Radiol* 76:137-143, 2003.)

*References 6, 8, 107, 108, 110, 111.

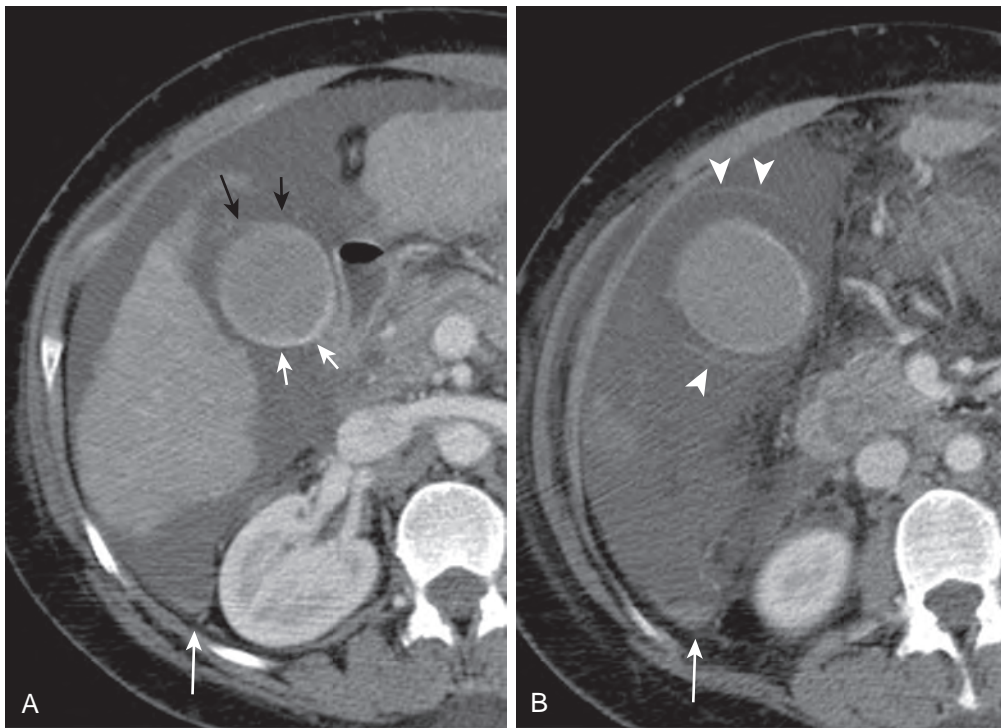


Figure 81-20 Gallbladder avulsion. Alcoholic patient with cirrhosis after motor vehicle accident. **A.** Contrast-enhanced CT shows inhomogeneous enhancement of the gallbladder, with hypoenhancing (black arrows) and hyperenhancing areas (short white arrows). **B.** A thin membrane (arrowheads) surrounds the gallbladder, strongly suggesting the diagnosis of gallbladder avulsion, a finding confirmed at laparotomy. Moderate ascites, primarily secondary to cirrhosis. The hematocrit effect (long white arrow, **A** and **B**) in right paracolic gutter reflects component of hemoperitoneum.

hemorrhage and free fluid) and spuriously suggest the diagnosis of gallbladder injury.^{8,105,107,108}

Whereas CT is certainly the first-line imaging modality in the setting of trauma, other imaging modalities may be helpful if the CT findings of gallbladder injury are equivocal. Ultrasound may be able to detect subtle amounts of layering blood products within the gallbladder lumen that are not detectable

on CT; MRI, with its superior soft tissue resolution, may be able to identify subtle disruption or nonenhancement of the gallbladder wall that is beyond the resolution of CT. Ultimately, in those cases in which there is a strong clinical suspicion, or alternatively, when the CT findings are suggestive but not completely definitive, hepatobiliary scintigraphy may help identify leakage of bile from the injured segment of the biliary tree.¹⁰⁷

REFERENCES

- Ferreres AR, Asbun HJ: Technical aspects of cholecystectomy. *Surg Clin North Am* 94:427–454, 2014.
- Mulvihill SJ: Surgical management of gallstone disease and postoperative complications. *Semin Gastrointest Dis* 14:237–244, 2003.
- Livingston EH, Rege RV: A nationwide study of conversion from laparoscopic to open cholecystectomy. *Am J Surg* 188:205–211, 2004.
- Antolovic D, Koch M, Galindo L, et al: Hepaticojejunostomy—analysis of risk factors for postoperative bile leaks and complications. *J Gastrointest Surg* 11:555–561, 2007.
- Zafar SN, Khan MR, Raza R, et al: Early complications after biliary enteric anastomosis for benign disease: A retrospective analysis. *BMC Surg* 11:19, 2011.
- Burgess P, Fulton RL: Gallbladder and extrahepatic biliary duct injury following abdominal trauma. *Injury* 23:413–414, 1992.
- Carrillo EH, Lottenberg L, Saridakis A: Blunt traumatic injury of the gallbladder. *J Trauma* 57:408–409, 2004.
- Gupta A, Stuhlfaut JW, Fleming KW, et al: Blunt trauma of the pancreas and biliary tract: A multimodality imaging approach to diagnosis. *Radiographics* 24:1381–1395, 2004.
- Lohan D, Walsh S, McLoughlin R, Murphy J: Imaging of the complications of laparoscopic cholecystectomy. *Eur Radiol* 15:904–912, 2005.
- Wright TB, Bertino RB, Bishop AF, et al: Complications of laparoscopic cholecystectomy and their interventional radiologic management. *Radiographics* 13:119–128, 1993.
- Bittner R: The standard of laparoscopic cholecystectomy. *Langenbecks Arch Surg* 389:157–163, 2004.
- de Goede B, Klitsie PJ, Hagen SM, et al: Meta-analysis of laparoscopic cholecystectomy versus open cholecystectomy for patients with liver cirrhosis and symptomatic cholelithiasis. *Br J Surg* 100:209–216, 2013.
- Strasberg S, Drebin J: Calculous biliary disease. In Greenfield LJ, editor: *Surgery, Scientific Principles and Practice*, Philadelphia, 2001, Lippincott Williams & Wilkins, pp 1011–1033.
- Steinemann DC, Raptis DA, Lurje G, et al: Cosmesis and body image after single-port laparoscopic or conventional laparoscopic cholecystectomy: A multicenter double blinded randomised controlled trial (SPOCC-trial). *BMC Surg* 11:24, 2011.
- McAllister JD, D'Altorio RA, Rao V: CT findings after uncomplicated and complicated laparoscopic cholecystectomy. *Semin Ultrasound CT MR* 14:356–367, 1993.
- McAllister JD, D'Altorio RA, Snyder A: CT findings after uncomplicated percutaneous laparoscopic cholecystectomy. *J Comput Assist Tomogr* 15:770–772, 1991.
- Schauer PR, Page CP, Ghiatas AA, et al: Incidence and significance of subdiaphragmatic air following laparoscopic cholecystectomy. *Am Surg* 63:132–136, 1997.
- Millitz K, Moote DJ, Sparrow RK, et al: Pneumoperitoneum after laparoscopic cholecystectomy: Frequency and duration as seen on upright chest radiographs. *AJR Am J Roentgenol* 163:837–839, 1994.
- Gayer G, Jonas T, Apter S, et al: Postoperative pneumoperitoneum as detected by CT: Prevalence, duration, and relevant factors affecting its possible significance. *Abdom Imaging* 25:301–305, 2000.
- Moran J, Del Grosso E, Wills J, et al: Laparoscopic cholecystectomy: Imaging of complications and normal postoperative CT appearance. *Abdom Imaging* 19:143–146, 1994.
- McGahan JP, Stein M: Complications of laparoscopic cholecystectomy: Imaging and intervention. *AJR Am J Roentgenol* 165:1089–1097, 1995.

22. Kang EH, Middleton WD, Balfé DM, Soper NJ: Laparoscopic cholecystectomy: Evaluation with sonography. *Radiology* 181:439–442, 1991.
23. Hakansson K, Leander P, Ekberg O, Hakansson HO: MR imaging of upper abdomen following cholecystectomy. Normal and abnormal findings. *Acta Radiol* 42:181–186, 2001.
24. O'Connor AR, Coakley FV: Retained surgical materials in the postoperative abdomen and pelvis. *Semin Ultrasound CT MR* 25:290–302, 2004.
25. Keus F, de Jong JA, Gooszen HG, et al: Laparoscopic versus open cholecystectomy for patients with symptomatic cholelithiasis. *Cochrane Database Syst Review* (4):CD006231, 2006.
26. Deziel DJ, Millikan KW, Economou SG, et al: Complications of laparoscopic cholecystectomy: A national survey of 4,292 hospitals and an analysis of 77,604 cases. *Am J Surg* 165:9–14, 1993.
27. Konstadoulakis MM, Antonakis PT, Karatzikos G, et al: Intraoperative findings and postoperative complications in laparoscopic cholecystectomy: The Greek experience with 5,539 patients in a single center. *J Laparoendosc Adv Surg Tech A* 14:31–36, 2004.
28. Fathy O, Zeid MA, Abdallah T, et al: Laparoscopic cholecystectomy: A report on 2000 cases. *Hepatogastroenterology* 50:967–971, 2003.
29. Lee NW, Collins J, Britt R, Britt LD: Evaluation of preoperative risk factors for converting laparoscopic to open cholecystectomy. *Am Surg* 78:831–833, 2012.
30. Eldar S, Eitan A, Bickel A, et al: The impact of patient delay and physician delay on the outcome of laparoscopic cholecystectomy for acute cholecystitis. *Am J Surg* 178:303–307, 1999.
31. Parthenis DG, Skevis K, Stathopoulos V, et al: Post-laparoscopic iatrogenic pseudoaneurysms of the arteries of the peritoneal and retroperitoneal space: Case report and review of the literature. *Surg Laparosc Endosc Percutan Tech* 19:90–97, 2009.
32. Trerotola SO, Savader SJ, Lund GB, et al: Biliary tract complications following laparoscopic cholecystectomy: Imaging and intervention. *Radiology* 84:195–200, 1992.
33. Thomson BN, Cullinan MJ, Banting SW, Collier NA: Universities of Melbourne Hepatobiliary Group: Recognition and management of biliary complications after laparoscopic cholecystectomy. *ANZ J Surg* 73:183–188, 2003.
34. Stewart L: Iatrogenic biliary injuries: Identification, classification, and management. *Surg Clin North Am* 94:297–310, 2014.
35. Sahajpal AK, Chow SC, Dixon E, et al: Bile duct injuries associated with laparoscopic cholecystectomy. *Arch Surg* 145:757–763, 2012.
36. Lau KN, Sindram D, Agee N, et al: Bile duct injury after single incision laparoscopic cholecystectomy. *JSL* 14:587–591, 2010.
37. Hii MW, Gyorki DE, Sakata K, et al: Endoscopic management of post-cholecystectomy biliary fistula. *HPB (Oxford)* 13:699–705, 2011.
38. Lillemoe KD: Biliary strictures and sclerosing cholangitis. In Greenfield LJ, editor: *Surgery, Scientific Principles and Practice*, Philadelphia, 2001, Lippincott Williams & Wilkins, pp 1046–1061.
39. Vitale GC, Davis BR: Evaluation and treatment of biliary leaks after gastrointestinal surgery. *J Gastrointest Surg* 15:1323–1324, 2011.
40. Deziel DJ: Complications of cholecystectomy. Incidence, clinical manifestations, and diagnosis. *Surg Clin North Am* 74:809–823, 1994.
41. Walsh RM, Henderson JM, Vogt DP, et al: Trends in bile duct injuries from laparoscopic cholecystectomy. *J Gastrointest Surg* 2:458–462, 1998.
42. Slater K, Strong RW, Wall DR, Lynch SV: Iatrogenic bile duct injury: The scourge of laparoscopic cholecystectomy. *ANZ J Surg* 72:83–88, 2002.
43. Mahatharadol V: Bile duct injuries during laparoscopic cholecystectomy: An audit of 1522 cases. *Hepatogastroenterology* 51:12–14, 2004.
44. Ward EM, LeRoy AJ, Bender CE, et al: Imaging of complications of laparoscopic cholecystectomy. *Abdom Imaging* 18:150–155, 1993.
45. MacFadyen BV, Jr, Vecchio R, Ricardo AE, Mathis CR: Bile duct injury after laparoscopic cholecystectomy. The United States experience. *Surg Endosc* 12:315–321, 1998.
46. Shamiyeh A, Wayand W: Laparoscopic cholecystectomy: Early and late complications and their treatment. *Langenbecks Arch Surg* 389:164–171, 2004.
47. Z'graggen K, Wehrli H, Metzger A, et al: Complications of laparoscopic cholecystectomy in Switzerland. A prospective 3-year study of 10,174 patients. *Swiss Association of Laparoscopic and Thoracoscopic Surgery. Surg Endosc* 12:1303–1310, 1998.
48. Seeliger H, Furst A, Zulke C, Jauch KW: Surgical management of bile duct injuries following laparoscopic cholecystectomy: Analysis and follow-up of 28 cases. *Langenbecks Arch Surg* 387:286–293, 2002.
49. Zerem E, Omerovic S: Minimally invasive management of biliary complications after laparoscopic cholecystectomy. *Eur J Intern Med* 20:686–689, 2009.
50. Pesce A, Portale TR, Minutolo V, et al: Bile duct injury during laparoscopic cholecystectomy without intraoperative cholangiography: A retrospective study on 1100 selected patients. *Dig Surg* 29:310–314, 2012.
51. Hammad MA, Nada AA, Abdel-Atty MY, et al: Major biliary complications in 2714 cases of laparoscopic cholecystectomy without intraoperative cholangiography: A multicenter retrospective study. *Surg Endosc* 25:3747–3751, 2011.
52. Sinha R, Chandra S: Cystic duct leaks after laparoscopic single-site cholecystectomy. *J Laparoendosc Adv Surg Tech A* 22:533–537, 2012.
53. Dexter SP, Miller GV, Davides D, et al: Relaparoscopy for the detection and treatment of complications of laparoscopic cholecystectomy. *Am J Surg* 179:316–319, 2000.
54. Lillemoe KD: Benign post-operative bile duct strictures. *Baillieres Clin Gastroenterol* 11:749–779, 1997.
55. Braithwaite BM, Cabanilla LT, Lilly M: Hepatic subcapsular biloma: A rare complication of laparoscopic cholecystectomy and common bile duct exploration. *Curr Surg* 60:196–198, 2003.
56. Barton JR, Russell RC, Hatfield AR: Management of bile leaks after laparoscopic cholecystectomy. *Br J Surg* 82:980–984, 1995.
57. Stewart L, Way LW: Bile duct injuries during laparoscopic cholecystectomy. Factors that influence the results of treatment. *Arch Surg* 130:1123–1128, 1995.
58. Demetriades H, Pramateftakis MG, Kanellos I, et al: Retained gallbladder remnant after laparoscopic cholecystectomy. *J Laparoendosc Adv Surg Tech A* 18:276–279, 2008.
59. Greenfield NP, Azziz AS, Jung AJ, et al: Imaging late complications of cholecystectomy. *Clin Imaging* 36:763–767, 2012.
60. Scientific Committee for the European Association for Endoscopic Surgery (EAES): Diagnosis and treatment of common bile duct stones (CBDs): Results of a consensus development conference. *Surg Endosc* 12:856–886, 1998.
61. Barkun JS, Fried GM, Barkun AN, et al: Cholecystectomy without operative cholangiography. *Ann Surg* 218:371–379, 1993.
62. Flowers JL, Zucker KA, Graham SM, et al: Laparoscopic cholangiography: Results and indications. *Ann Surg* 215:209–216, 1992.
63. Sackier JM, Berci G, Phillips E, et al: The role of cholangiography in laparoscopic cholecystectomy. *Arch Surg* 126:1021–1026, 1991.
64. Lillemoe KD, Yeo CJ, Talamini MA, et al: Selective cholangiography: Current role in laparoscopic cholecystectomy. *Ann Surg* 215:269–276, 1992.
65. Shapey IM, Jaunoo SS, Arachchilage KM, Tan LC: Biliary tract imaging for retained calculi after laparoscopic cholecystectomy: Is risk stratification useful? *Surg Laparosc Endosc Percutan Tech* 22:459–462, 2012.
66. Ford JA, Soop M, Loveday BPT, Rogers M: Systematic review of intraoperative cholangiography in cholecystectomy. *Br J Surg* 99:160–167, 2012.
67. Shimada H, Endo I, Shimada K, et al: The current diagnosis and treatment of benign biliary stricture. *Surg Today* 42:1143–1153, 2012.
68. Redwan AA: Complex post-cholecystectomy biliary injuries: Management with 10 years' experience in a major referral center. *J Laparoendosc Adv Surg Tech A* 22:539–549, 2012.
69. Costamagna G, Shah SK, Tringali A: Current management of postoperative complications and benign biliary strictures. *Gastrointest Endosc Clin N Am* 13:635–648, ix, 2003.
70. Tripathi M, Chandrashekar N, Kumar R, et al: Hepatobiliary scintigraphy: An effective tool in the management of bile leak after laparoscopic cholecystectomy. *Clin Imaging* 28:40–43, 2004.
71. Ray CE, Jr, Hibbeln JF, Wilbur AC: Complications after laparoscopic cholecystectomy: Imaging findings. *AJR Am J Roentgenol* 160:1029–1032, 1993.
72. Balakrishnan VB, Kumar R, Dhanpathi H, et al: Hepatobiliary scintigraphy in detecting lesser sac bile leak in post-cholecystectomy patients: The need to recognize as a separate entity. *Clin Nucl Med* 33:161–167, 2008.
73. Fidelman N, Kerlan RK, Laberge JM, Gordon RL: Accuracy of percutaneous cholangiography in predicting the location and nature of major bile duct injuries. *J Vasc Interv Radiol* 22:884–892, 2011.
74. Goenka MK, Kochhar R, Nagi B, et al: Endoscopic retrograde cholangiopancreatography in postcholecystectomy syndrome. *J Assoc Physicians India* 44:119–122, 1996.
75. Vitellas KM, El-Dieb A, Vaswani K, et al: Using contrast-enhanced MR cholangiography with IV mangafodipir-trisodium (Teslascan) to evaluate bile duct leaks after cholecystectomy:

- A prospective study of 11 patients. *AJR Am J Roentgenol* 179:409–416, 2002.
76. Park MS, Kim KW, Yu JS, et al: Early biliary complications of laparoscopic cholecystectomy: Evaluation on T2-weighted MR cholangiography in conjunction with mangafodipir trisodium-enhanced 3D T1-weighted MR cholangiography. *AJR Am J Roentgenol* 183:1559–1566, 2004.
 77. Aduna M, Larena JA, Martin D, et al: Bile duct leaks after laparoscopic cholecystectomy: Value of contrast-enhanced MRCP. *Abdom Imaging* 30:480–487, 2005.
 78. Pilleul F, Billaud Y, Gautier G, et al: Mangafodipir-enhanced magnetic resonance cholangiography for the diagnosis of bile duct leaks. *Gastrointest Endosc* 59:818–822, 2004.
 79. Akin EB, Vitellas KM, Rajab A, et al: Magnetic resonance cholangiography with mangafodipir trisodium (Teslascan) to evaluate bile duct leaks after T-tube removal in liver transplantation. *J Comput Assist Tomogr* 28:613–616, 2004.
 80. Marin D, Bova V, Agnello F, et al: Gadoxetate disodium-enhanced magnetic resonance cholangiography for the noninvasive detection of an active bile leak after laparoscopic cholecystectomy. *J Comput Assist Tomogr* 34:213–216, 2010.
 81. Khalid M, Rashid M: Gallstone abscess: A delayed complication of spilled gallstone after laparoscopic cholecystectomy. *Emerg Radiol* 16:227–229, 2009.
 82. Karabulut N, Tavasli B, Kiroglu Y: Intra-abdominal spilled gallstones simulating peritoneal metastasis: CT and MR imaging features. *Eur Radiol* 18:851–854, 2008.
 83. Arishi AR, Rabie E, Khan SH, et al: Spilled gallstones: The source of an enigma. *JSL* 12:321–325, 2008.
 84. Bennett AA, Gilkeson RC, Haaga JR, et al: Complications of “dropped” gallstones after laparoscopic cholecystectomy: Technical considerations and imaging findings. *Abdom Imaging* 25:190–193, 2000.
 85. Brockmann JG, Kocher T, Senninger NJ, Schürmann GM: Complications due to gallstones lost during laparoscopic cholecystectomy. *Surg Endosc* 16:1226–1232, 2002.
 86. Morrin MM, Kruskal JB, Hochman MG, et al: Radiologic features of complications arising from dropped gallstones in laparoscopic cholecystectomy patients. *AJR Am J Roentgenol* 174:1441–1445, 2000.
 87. Sarli L, Pietra N, Costi R, Grattarola M: Gallbladder perforation during laparoscopic cholecystectomy. *World J Surg* 23:1186–1190, 1999.
 88. Zehetner J, Shamiyeh A, Wayand W: Lost gallstone in laparoscopic cholecystectomy: All possible complications. *Am J Surg* 193:73–78, 2007.
 89. Tumer AR, Yuksek YN, Yasti AC, et al: Dropped gallstones during laparoscopic cholecystectomy: The consequences. *World J Surg* 29:437–440, 2005.
 90. Helme S, Samdani T, Sinha P: Complications of spilled gallstones following laparoscopic cholecystectomy: A case report and literature overview. *J Med Case Rep* 3:8626, 2009.
 91. Patterson EJ, Nagy AG: Don't cry over spilled stones? Complications of gallstones spilled during laparoscopic cholecystectomy: Case report and literature review. *Can J Surg* 40:300–304, 1997.
 92. Zamir G, Lyass S, Pertsemliadis D, Katz B: The fate of the dropped gallstones during laparoscopic cholecystectomy. *Surg Endosc* 13:68–70, 1999.
 93. Hanna SJ, Barakat O, Watkin S: Cholelithoptysis: An unusual delayed complication of laparoscopic cholecystectomy. *J Hepatobiliary Pancreat Surg* 11:190–192, 2004.
 94. Koc E, Suher M, Oztugut SU, et al: Retroperitoneal abscess as a late complication following laparoscopic cholecystectomy. *Med Sci Monit* 10:CS27–CS29, 2004.
 95. Machado NO: Biliary complications post-laparoscopic cholecystectomy: Mechanism, preventive measures, and approach to management: A review. *Diagn Ther Endosc* 2011:967017, 2011.
 96. Hirano S, Tanaka E, Tsuchikawa T, et al: Techniques of biliary reconstruction following bile duct resection (with video). *J Hepatobiliary Pancreat Sci* 19:203–209, 2012.
 97. Sarmiento JM: Hepaticojunostomy: Indications and surgical technique. *Oper Tech Gen Surg* 2:295–303, 2000.
 98. Raman SP, Horton KM, Fishman EK: Computed tomography after pancreaticoduodenectomy: Spectrum of normal findings and complications. *AJR Am J Roentgenol* 201:2–13, 2013.
 99. Kucukay F, Okten RS, Yurdakul M, et al: Long-term results of percutaneous biliary balloon dilation treatment for benign hepaticojunostomy structures: Are repeated balloon dilations necessary? *J Vasc Interv Radiol* 23:1347–1355, 2012.
 100. Akamatsu N, Sugawara Y, Hashimoto D: Biliary reconstruction, its complications and management of biliary complications after adult liver transplantation: A systematic review of the incidence, risk factors, and outcome. *Transplant Int* 24:379–392, 2011.
 101. Kim JH, Ko G, Sung K, et al: Bile leak following living donor liver transplantation: Clinical efficacy of percutaneous transhepatic treatment. *Liver Transplant* 14:1142–1149, 2008.
 102. Rothlin MA, Lopfe M, Schlumpf R, et al: Long-term results of hepaticojunostomy for benign lesions of the bile ducts. *Am J Surg* 175:22–26, 1998.
 103. Schmidt SC, Langrehr JM, Hintze RE, et al: Long-term results and risk factors influencing outcomes of major bile duct injuries following cholecystectomy. *Br J Surg* 92:76–82, 2005.
 104. Reid-Lombardo KM, Ramos-Dela Medina A, Thomsen K, et al: Long-term anastomotic complications after pancreaticoduodenectomy for benign diseases. *J Gastrointest Surg* 11:1704–1711, 2007.
 105. Erb RE, Mirvis SE, Shanmuganathan K: Gallbladder injury secondary to blunt trauma: CT findings. *J Comput Assist Tomogr* 18:778–784, 1994.
 106. Chen X, Talner LB, Jurkovich GJ: Gallbladder avulsion due to blunt trauma. *AJR Am J Roentgenol* 177:822, 2001.
 107. Birn J, Jung M, Dearing M: Isolated gallbladder injury in a case of blunt abdominal trauma. *J Radiol Case Rep* 6:25–30, 2012.
 108. Lyles AD, Rexroad JT: Isolated traumatic gallbladder avulsion: A case report. *Emerg Radiol* 17:419–421, 2010.
 109. Ball CG, Dixon E, Kirkpatrick AW, et al: A decade of experience with injuries to the gallbladder. *J Trauma Manag Outcomes* 4:3, 2010.
 110. Sharma O: Blunt gallbladder injuries: Presentation of twenty-two cases with review of the literature. *J Trauma* 39:576–580, 1995.
 111. Jaggard MKJ, Johal NS, Choudhry M: Blunt abdominal trauma resulting in gallbladder injury: A review with emphasis on pediatrics. *J Trauma* 70:1005–1010, 2011.
 112. Pavlidis TE, Lalountas MA, Psarras K, et al: Isolated complete avulsion of the gallbladder (near traumatic cholecystectomy): A case report and review of the literature. *J Med Case Rep* 5:392, 2011.
 113. Zissin R, Osadchy A, Shapiro-Feinberg M, et al: CT of a thickened-wall gall bladder. *Br J Radiol* 76:137–143, 2003.
 114. Kim HH, Ryu SH, Lee JH, et al: Delayed isolated gallbladder rupture after blunt abdominal trauma. *Intern Med J* 41:799–800, 2011.

Gallbladder and Biliary Tract: Differential Diagnosis

RICHARD M. GORE

CHAPTER OUTLINE

Gallbladder Imaging

- Table 82-1. Gallbladder Filling Defects
- Table 82-2. Enlarged Gallbladder
- Table 82-3. Small Gallbladder
- Table 82-4. Gallbladder Wall Thickening
- Table 82-5. Pericholecystic Fluid
- Table 82-6. Multiseptate Gallbladder
- Table 82-7. Gas in the Gallbladder or Biliary Tract
- Table 82-8. Cholecystenteric and Biliary-Enteric Fistula

Ultrasound

- Table 82-9. Focal, Mobile, Shadowing Gallbladder Reflectors
- Table 82-10. Focal, Mobile, Nonshadowing Gallbladder Reflectors
- Table 82-11. Focal, Nonmobile, Shadowing Gallbladder Reflectors
- Table 82-12. Hyperechoic Foci in Gallbladder Wall
- Table 82-13. Nonvisualization of the Gallbladder by Ultrasound
- Table 82-14. Artifacts That Mimic Gallstones
- Table 82-15. Structures That Sonographically Mimic the Gallbladder

Computed Tomography

- Table 82-16. Increased Attenuation of Gallbladder Lumen

Nuclear Medicine

- Table 82-17. Nonvisualization of the Gallbladder by Scintigraphy
- Table 82-18. Delayed Visualization of the Gallbladder
- Table 82-19. Nonvisualization of the Isotope in Bowel
- Table 82-20. Delayed Bowel Activity
- Table 82-21. Rim Sign

Biliary Tract Imaging

- Table 82-22. Filling Defects or Segmental Lesions of Bile Ducts
- Table 82-23. Bile Duct Narrowing or Obstruction
- Table 82-24. Biliary Dilation
- Table 82-25. Biliary Dilation Without Jaundice
- Table 82-26. Biliary Obstruction Without Dilation
- Table 82-27. Cystic Dilation of the Bile Ducts

Imaging Findings in Specific Gallbladder and Biliary Diseases

- Table 82-28. Acute Cholecystitis
- Table 82-29. Chronic Cholecystitis
- Table 82-30. Sclerosing Cholangitis
- Table 82-31. Primary Biliary Cirrhosis
- Table 82-32. Cholangiocarcinoma
- Table 82-33. Gallbladder Carcinoma
- Table 82-34. Cystic Biliary Disease: Caroli's Disease, Choledochal Cyst, Choledochocoele

Gallbladder Imaging

TABLE 82-1 Gallbladder Filling Defects

COMMON

Gallstones
Sludge
Mucosal folds
Partial volume artifact (ultrasound, CT)
Adenomyomatosis
Cholesterosis
Pseudomass-duodenal impression (ultrasound)
Air volume averaging with adjacent bowel (CT, MR)

UNCOMMON

Carcinoma
Metastases, especially melanoma, lung, kidney, esophagus
Adenoma
Papilloma

Villous hyperplasia
Epithelial cyst
Mucus retention cyst
Worms and parasites: *Ascaris*, *Paragonimus*, *Clonorchis*, *Filaria*, *Schistosoma*, *Fasciola*
Fibrinous debris
Desquamated mucosa
Metachromatic leukodystrophy
Ectopic pancreatic, gastric, hepatic, intestinal, prostatic tissue
Varices
Inflammatory polyp
Food through enterobiliary fistula
Fibroadenoma
Neurinoma
Hemangioma

TABLE 82-2 Enlarged Gallbladder**COMMON**

Cystic duct or common bile duct obstruction
 Hyperalimentation
 Post surgery
 Prolonged fasting
 Vagotomy
 Diabetes mellitus
 AIDS
 Mucocele
 Empyema
 Hydrops
 Hepatitis
 Pancreatitis
 Alcoholism
 Narcotic analgesia
 Anticholinergics

UNCOMMON

Kawasaki's syndrome
 Leptospirosis
 Scarlet fever
 Acromegaly

TABLE 82-3 Small Gallbladder

Chronic cholecystitis
 Congenital multiseptate gallbladder
 Postprandial study
 Cystic fibrosis
 Congenital hypoplasia
 Congenital multiseptate gallbladder
 Hypoplastic gallbladder

TABLE 82-4 Gallbladder Wall Thickening**COMMON**

Acute cholecystitis
 Chronic cholecystitis
 Hyperplastic cholecystosis
 Hepatitis
 Portal hypertension
 Right-sided heart failure
 Hypoproteinemia or hypoalbuminemia
 Gallbladder carcinoma
 Renal failure
 Total parenteral nutrition
 Cirrhosis
 Sepsis
 Infectious mononucleosis
 Acute pancreatitis
 AIDS
 Postprandial study
 Pyelonephritis of right kidney

UNCOMMON

Sclerosing cholangitis
 Schistosomiasis
 Xanthogranulomatous cholecystitis
 Extrahepatic portal vein obstruction
 Lymphatic obstruction
 Gallbladder wall varices
 Multiple myeloma
 Lymphoma
 Obstructed gallbladder lymphatics
 Acute myelogenous leukemia
 Brucellosis
 Graft-versus-host disease

TABLE 82-5 Pericholecystic Fluid

Pericholecystic abscess
 Pancreatitis
 Acute cholecystitis
 Pericholecystic abscess
 Ascites
 AIDS
 Peritonitis

TABLE 82-6 Multiseptate Gallbladder

Desquamated gallbladder mucosa
 Congenital malformation
 Normal folded gallbladder
 Cholesterosis
 Adenomyomatosis

TABLE 82-7 Gas in the Gallbladder or Biliary Tract**COMMON**

Postoperative (e.g., status post sphincterotomy or Whipple's procedure)
 Biliary-enteric fistula (see Table 82-8)
 Pancreatitis
 Emphysematous cholecystitis

UNCOMMON

Common duct entry into duodenal diverticulum
 Crohn's disease
 Incompetent sphincter
 Carcinoma of the gallbladder, ampulla, duodenum, bile ducts, stomach, colon
 Metastases
 Lymphoma
 Trauma
 Status post intubation or ERCP
 Parasites: *Strongyloides*, *Clonorchis*, *Ascaris*, ruptured amebic abscess of liver

TABLE 82-8 Cholecystenteric and Biliary-Enteric Fistula**COMMON**

Gallstone fistula from gallbladder or bile ducts
 Postoperative (e.g., Whipple's procedure)

UNCOMMON

Carcinoma of the gallbladder, bile ducts, duodenum, colon, stomach
 Peptic ulcer perforation into biliary tract
 Crohn's disease
 Diverticulitis of the duodenum or hepatic flexure
 Actinomycosis
 Tuberculosis
 Trauma
 Lymphoma
 Perforating cholecystitis

Ultrasound**TABLE 82-9** Focal, Mobile, Shadowing Gallbladder Reflectors

Gallstones
 Intraluminal gas
 Calcified parasites: *Ascaris*, *Clonorchis*, *Fasciola*

TABLE 82-10 Focal, Mobile, Nonshadowing Gallbladder Reflectors

Small stones not in transducer focal zone
 Blood clots
 Pus
 Sludge balls
 Parasites: *Ascaris*, *Clonorchis*, *Fasciola*
 Precipitated contrast material from ERCP
 Fibrinous debris
 Desquamated mucosa

TABLE 82-11 Focal, Nonmobile, Shadowing Gallbladder Reflectors

Stone or crystal in Rokitsky-Aschoff sinus
 Impacted gallstone
 Spiral valve folds
 Polyp-containing cholesterol
 Adherent gallstone

TABLE 82-12 Hyperechoic Foci in Gallbladder Wall

Polyps
 Adherent stones
 Intramural gas in emphysematous cholecystitis
 Intramural microabscesses
 Rokitsky-Aschoff sinuses

TABLE 82-13 Nonvisualization of the Gallbladder by Ultrasound**COMMON**

Postprandial contraction
 Post cholecystectomy
 Chronic cholecystitis
 Technical factors: obese patient or thin patient with superficial gallbladder
 Ectopic gallbladder
 Gallbladder obscured by gas

UNCOMMON

Carcinoma of the gallbladder
 "Porcelain" gallbladder
 Gangrenous cholecystitis
 Emphysematous cholecystitis
 Metastases to the gallbladder
 Acute hepatic dysfunction (e.g., hepatitis)
 Congenital absence (0.03% of population)

TABLE 82-14 Artifacts That Mimic Gallstones

Partial volume artifact with duodenal impression
 Refraction from folds in gallbladder neck
 Inspissated sludge
 Any cause of intraluminal defect

TABLE 82-15 Structures That Sonographically Mimic the Gallbladder

Fluid-filled duodenal bulb
 Dilated cystic duct remnant
 Hepatic cyst
 Renal cyst
 Omental cyst
 Ligamentum teres abscess
 Choledochal cyst

Computed Tomography

TABLE 82-16 Increased Attenuation of Gallbladder Lumen

Gallstones
 Sludge
 Debris
 Vicarious excretion of contrast medium
 Hemobilia
 Milk of calcium bile
 Mucinous adenocarcinoma of the gallbladder
 Volume averaging with adjacent structures
 Hydrops
 Hemorrhagic cholecystitis
 Prior ERCP or oral cholecystography

Nuclear Medicine

TABLE 82-17 Nonvisualization of the Gallbladder by Scintigraphy**COMMON**

Acute cholecystitis

UNCOMMON

Prolonged fasting
 Carcinoma of the gallbladder
 Chronic cholecystitis
 Severe hepatocellular disease
 Complete common bile duct obstruction
 Acute pancreatitis
 Nonfasting patient
 Gallbladder hydrops
 Post cholecystectomy
 Hyperalimentation

RARE

Alcoholism
 Choledochal cyst
 Dubin-Johnson syndrome
 Kawasaki's syndrome
 Mirizzi syndrome

TABLE 82-18 Delayed Visualization of the Gallbladder**COMMON**

Chronic cholecystitis

UNCOMMON

Acalculous cholecystitis
 Pancreatitis
 Hepatocellular disease
 Total parenteral nutrition
 Carcinoma of the gallbladder
 Dubin-Johnson syndrome

TABLE 82-19 Nonvisualization of the Isotope in Bowel**COMMON**

Cholelithiasis

UNCOMMON

Obstructive pancreatic carcinoma
 Drug-induced cholestasis
 Sphincter of Oddi spasm secondary to morphine
 Severe hepatocellular disease
 Biliary atresia

RARE

Pancreatitis
 Cholangiocarcinoma
 Sepsis
 Choledochal cyst with complete obstruction
 Portal vein thrombosis
 Surgical ligation of common bile duct

TABLE 82-20 Delayed Bowel Activity**COMMON**

Cholelithiasis with incomplete obstruction
 Severe hepatocellular disease

UNCOMMON

Acute and chronic cholecystitis
 Sphincter of Oddi spasm, stricture, or tumor
 Ascending cholangitis
 Choledochal cyst with incomplete obstruction

TABLE 82-21 Rim Sign**COMMON**

Acute cholecystitis
 Gangrenous cholecystitis
 Emphysema of the gallbladder
 Gallbladder perforation

UNCOMMON

Chronic cholecystitis
 Adjacent hepatic inflammatory process
 Hepatic amebic abscess

Biliary Tract Imaging**TABLE 82-22 Filling Defects or Segmental Lesions of Bile Ducts****COMMON**

Gallstone
 Air bubble
 Blood clot
 Sphincter of Oddi or Boyden spasm (pseudocalculus)
 Ampullary edema
 Sludge or debris
 Cholangiocarcinoma
 Carcinoma of the ampulla, duodenum, or pancreas
 Stricture
 Postoperative defect
 Dilated crossing vessel
 Mirizzi syndrome

UNCOMMON

Metastases
 Neoplasms: adenoma, papilloma, spindle cell, hamartoma, polyp, sarcoma
 Parasites: *Ascaris lumbricoides*, *Clonorchis sinensis*, *Fasciola hepatica*, *Echinococcus granulosus*
 Enlarged lymph node
 Hydatid cyst eroding into biliary tree

TABLE 82-23 Bile Duct Narrowing or Obstruction**MALIGNANT STRICTURES**

Cholangiocarcinoma
 Hepatoma
 Ampullary carcinoma
 Lymphoma
 Metastasis from neoplasms of pancreas, gallbladder, stomach, lymph nodes, hepatic parenchyma, hepatoduodenal ligament

BENIGN STRICTURES**Acquired**

Cholangitis
 Cholelithiasis
 Papillary stenosis
 Sclerosing cholangitis
 Cholangiolytic hepatitis
 Mirizzi syndrome
 Duodenal diverticulum

Iatrogenic or Traumatic

Surgical injury
 Hepatic artery chemotherapy
 Trauma
 Radiation therapy
 Hepatic artery embolization

Infectious

AIDS
Clonorchis sinensis
Fasciola hepatica
Ascaris lumbricoides
Echinococcus
 Tuberculous adenitis
 Cytomegalovirus

Extrinsic

Acute pancreatitis
 Chronic pancreatitis
 Tuberculous lymphadenitis
 Sarcoid lymphadenitis
 Cirrhosis
 Hepatitis
 Perforated duodenal ulcer
 Abscess

Congenital

Biliary atresia
 Membranous diaphragm
 Congenital hepatic fibrosis
 Complicated Caroli's disease

TABLE 82-24 Biliary Dilation**COMMON**

Calculus
Advanced age
Carcinoma of pancreas, bile duct, ampulla
Cholangitis
Pancreatitis
Distal ductal stricture: postoperative, inflammatory
Sclerosing cholangitis
Adenopathy with extrinsic compression

UNCOMMON

Papillitis or fibrosis of ampulla
Caroli's disease
Choledochal cyst, choledochoceles
Mirizzi syndrome
Parasites: *Ascaris*, *Clonorchis*, *Fasciola*, *Echinococcus*, *Opisthorchis*
Liver abscess
Extrinsic compression from duodenal or ductal diverticulum
Liver infarcts after transcatheter embolization of hepatic artery
Metastasis
Penetrating duodenal ulcer
Biliary diaphragm or web
Extrinsic compression from aneurysm of the hepatic artery or aorta
Extrahepatic biliary atresia
Hepatic fibrosis with ductal ectasia
Retroperitoneal fibrosis

TABLE 82-25 Biliary Dilation Without Jaundice

Post cholecystectomy
Sequelae of common duct exploration
Early obstruction
Post obstruction
Advanced age
Worms or parasites
Nonobstructive gallstone
Normal variant
Intestinal hypomotility

TABLE 82-26 Biliary Obstruction Without Dilation

Acute severe biliary obstruction (first 3 days)
Cholangitis
Sclerosing cholangitis
Ascending cholangitis
Debris-filled ducts
Pancreatitis
Hemobilia
Cholangiocarcinoma with tumor encasement

TABLE 82-27 Cystic Dilation of the Bile Ducts

Oriental cholangiohepatitis
Papillomatosis of intrahepatic bile ducts
Choledochal cyst
Choledochoceles
Caroli's disease
Congenital hepatic fibrosis

Imaging Findings in Specific Gallbladder and Biliary Diseases**TABLE 82-28** Acute Cholecystitis**SONOGRAPHIC FINDINGS**

Gallbladder wall thickening >3 mm
Gallbladder wall lucency (halo sign): three-layer configuration with sonolucent middle layer
Striated wall thickening: alternating echogenic and hypodense mural bands
Gallbladder distention >5 cm in anteroposterior diameter
Sonographic Murphy sign
Pericholecystic fluid
Pseudomembrane formation
Gallstones

NUCLEAR SCINTIGRAPHY

Nonvisualization of the gallbladder despite the presence of isotope in the bile ducts and duodenum
Rim sign: increased activity in the gallbladder fossa conforming to the inferior hepatic edge

COMPUTED TOMOGRAPHY

Gallstones, mural thickening, pericholecystic fluid
Increased gallbladder wall enhancement
Focal or nonuniform contrast-enhanced thickening
Mural nodularity, loss of crisp demarcation between gallbladder and liver, mild infiltration of pericholecystic fat
Elevated attenuation of gallbladder bile because of hemorrhage or empyema
Low-density edema in the hepatocholecystic space
Transient hepatic attenuation difference in adjacent liver

MR IMAGING

Gallstones, mural thickening, pericholecystic fluid
Gallbladder wall and adjacent tissues demonstrate increased enhancement on gadolinium-enhanced, fat-suppressed images
Transient hepatic intensity difference in adjacent liver

TABLE 82-29 Chronic Cholecystitis**SONOGRAPHIC FINDINGS**

Gallstones
Smooth irregular gallbladder wall thickening >3 mm
Noncontractility or decreased response after cholecystokinin injection

NUCLEAR SCINTIGRAPHY

Normal, delayed, or absent gallbladder visualization
Visualization of bowel before gallbladder
Noncontractility or decreased response after cholecystokinin injection

COMPUTED TOMOGRAPHY

Mural thickening and gallstones
Lack of contrast enhancement of gallbladder bile
Small, contracted gallbladder

MR IMAGING

Small, irregularly shaped gallbladder with a thickened, mildly enhancing wall on gadolinium-enhanced, fat-suppressed images

TABLE
82-30**Sclerosing Cholangitis****LOCATION**

Intrahepatic and extrahepatic ducts involved (90%)
 Intrahepatic ducts only (1%-5%)
 Extrahepatic ducts only (5%-10%)
 Cystic duct involved (18%)

CHOLANGIOGRAPHY

Multifocal strictures with predilection for bifurcations
 Small saccular outpouchings
 Beaded appearance with alternating segments of dilation and stenosis
 "Pruned tree" appearance with opacification of central ducts and nonfilling of more peripheral ducts
 Intrahepatic ductal dilation
 Coarse, nodular mural irregularities
 Gallbladder irregularities

COMPUTED TOMOGRAPHY

Skip dilation, stenosis, pruning, beading of intrahepatic bile ducts
 Dilation, stenosis, enhancing mural nodularity, thickening, and contrast enhancement of the bile ducts
 Mural thickening of the gallbladder
 Periportal adenopathy
 Caudate lobe hypertrophy
 Atrophy of lateral segment of left lobe of liver

ULTRASOUND

Brightly echogenic portal triads
 Mural thickening of the gallbladder and extrahepatic bile ducts
 Focal areas of intrahepatic biliary dilation
 Periportal adenopathy
 Caudate lobe hypertrophy
 Atrophy of lateral segment of left lobe of liver

MR IMAGING

Mild duct wall thickening, beading, skip dilations
 Periportal inflammation with mural and periportal enhancement on gadolinium-enhanced T1-weighted imaging
 Peripheral, wedge-shaped zones of hyperintense signal on T2-weighted imaging
 Increased signal intensity in liver on T1-weighted imaging not corresponding to fat
 Patchy, segmental, peripheral parenchymal enhancement on immediate postgadolinium injection images
 Periportal adenopathy
 Caudate lobe hypertrophy
 Atrophy of lateral segment of left lobe of liver

HEPATOBILIARY SCINTIGRAPHY

Multiple focal areas of isotope retention in the intrahepatic biliary tree
 Prolongation of hepatic clearance
 Gallbladder visualized in only 70% of cases

TABLE
82-31**Primary Biliary Cirrhosis****CHOLANGIOGRAPHY**

Only intrahepatic ducts are involved
 Tortuous intrahepatic ducts with narrowing, caliber variation, decreased arborization—the "tree in winter" appearance

HEPATOBILIARY SCINTIGRAPHY

Marked prolongation of hepatic isotope clearance
 Uniform hepatic isotope retention
 Normal visualization of the gallbladder and bile ducts

COMPUTED TOMOGRAPHY AND ULTRASOUND

Gallstones (40%)
 Hepatomegaly (50%)
 Periportal adenopathy
 Caudate lobe hypertrophy

MR IMAGING

Periportal halo sign due to periportal fibrosis
 Periportal adenopathy
 Caudate lobe hypertrophy

TABLE 82-32 Cholangiocarcinoma**LOCATION**

Distal common bile duct (30%-50%)
 Proximal common bile duct (15%-30%)
 Common hepatic duct (14%-37%)
 Confluence of hepatic ducts (10%-26%)
 Left or right hepatic duct (8%-13%)
 Cystic duct (6%)

CHOLANGIOGRAPHY

Long, or rarely short, concentric focal stricture with wall irregularities
 Exophytic intraductal tumor mass, 2 to 4 mm in diameter
 Prestenotic diffuse focal biliary dilation
 Progression of ductal strictures

ULTRASOUND

Biliary dilation
 Hyperechoic (75%), hypoechoic (14%), or isoechoic mass (14%)

COMPUTED TOMOGRAPHY

Predominantly homogeneous, hypodense mass with irregular borders
 No enhancement or mild ring enhancement on portal venous phase
 Diffuse contrast enhancement seen on delayed (10-15 minutes) image because of the nature of the vascularity of this tumor
 Ancillary findings: hepatic lobar atrophy associated with crowding of ducts; asymmetric, intrahepatic bile duct dilation; segmental or lobar attenuation abnormalities

MR IMAGING

High-grade biliary obstruction and bile duct wall thickness >5 mm
 Tumor is isointense or low signal relative to liver on T1-weighted images
 Tumor signal intensity on T2-weighted images ranges from markedly increased to mildly increased relative to liver
 Tumor enhances moderately on gadolinium-enhanced T1-weighted images
 Ductal tumors arising in intrapancreatic portion of common bile duct are well delineated as low signal intensity masses highlighted by the high signal intensity of the pancreatic head on fat-suppressed T1-weighted images

SCINTIGRAPHY

Biliary obstruction on hepatobiliary scan
 Intrahepatic tumors are cold on sulfur colloid and hepatobiliary scans
 Mass may show focal uptake on gallium scan

ANGIOGRAPHY

Hypervascular tumor with neovascularity (50%)
 Poor or absent tumor stain
 Arterioarterial collaterals along the course of the bile ducts associated with arterial obstruction
 Displacement, encasement, or occlusion of the hepatic artery and portal vein

TABLE 82-34 Cystic Biliary Disease: Caroli's Disease, Choledochal Cyst, Choledochocoele**CAROLI'S DISEASE**

Multiple cystic structures that converge toward the porta hepatis as either localized or diffusely scattered cysts communicating with bile ducts
 Segmental saccular or beaded appearance of the intrahepatic ducts
 Extrahepatic ducts frequently ectatic
 Sludge and calculi often present in these dilated ducts

CHOLEDOCHAL CYST**Location**

Intrahepatic and extrahepatic ducts (73%)
 Extrahepatic ducts alone (27%)
 Dilated left and right main intrahepatic ducts (45%); bilateral (58%); unilateral (42%), left lobe only

Cholangiography

Dilated duct diameter (2-15 cm)
 Abrupt change in ductal caliber at site of cyst

Computed Tomography and Ultrasound

Large, fluid-filled structure beneath the porta hepatis separate from the gallbladder, which communicates with the hepatic ducts
 Abrupt caliber change at junction of dilated segment and normal ducts
 Intrahepatic biliary dilation

Hepatobiliary Scintigraphy

Late filling and stasis of isotope within cyst
 Dilation of intrahepatic biliary system

Upper Gastrointestinal Tract Series

Soft tissue mass in right upper quadrant
 Anterior displacement of the second portion of the duodenum and distal stomach
 Widening of the duodenal sweep
 Inferior displacement of the duodenum
 Extrinsic compression of the proximal duodenum

CHOLEDOCHOCOELE

Smooth clublike or saclike dilation of the intramural segment of the common bile duct
 Smooth, well-defined intraluminal duodenal filling defect in the region of the papilla on barium studies that changes shape with compression and peristalsis

TABLE 82-33 Gallbladder Carcinoma

Replacement of gallbladder by tumor (40%-65%)
 Focal or diffuse, asymmetric, irregular thickening of the gallbladder wall (20%-30%)
 Bulky tumor involving the gallbladder fossa, adjacent liver, and hepatoduodenal ligament
 Granular punctate calcifications with mucinous adenocarcinoma
 Liver metastases; enlarged regional lymph nodes; intraperitoneal seeding; invasion of adjacent duodenum, colon, right kidney, stomach
 Mass has increased signal intensity on T2-weighted MR sequences

SUGGESTED READINGS

1. Dähnert W: Radiology Review Manual, ed 7, Baltimore, 2011, Williams & Wilkins.
2. Reeder MM: Reeder and Felson's Gamuts in Radiology, ed 4, New York, 2003, Springer-Verlag.
3. Eisenberg RL: Gastrointestinal Radiology—A Pattern Approach, ed 4, New York, 2004, Lippincott-Raven.
4. Chapman S, Nakielnny R: Aids to Radiological Differential Diagnosis, London, 1990, Baillière Tindall.
5. Baker SR: The Abdominal Plain Film, East Norwalk, CT, 1990, Appleton & Lange.
6. Lee JKT, Sagel SS, Stanley RJ, Heiken J, editors: Computed Body Tomography with MRI Correlation, New York, 2006, Raven.
7. Rumack CM, Nilson SR, Charboneau JW, editors: Diagnostic Ultrasound, ed 4, St. Louis, 2011, CV Mosby.
8. Semelka RC: Abdominal-Pelvic MRI, ed 2, New York, 2010, Wiley-Liss.
9. Datz FL: Gamuts in Nuclear Medicine, ed 3, St. Louis, 1995, CV Mosby.
10. Lamps LW: Diagnostic Pathology: Hepatobiliary and Pancreas, Salt Lake City, Utah, 2012, Amirsys.
11. Odze RD, Goldblum JR: Surgical Pathology of the GI Tract, Liver, Biliary Tract and Pancreas: Expert Consult, ed 2, Philadelphia, 2009, Elsevier.
12. Federle MP, Jeffrey RB, Jr, Tublin M, et al: Specialty Imaging: Hepatobiliary and Pancreas, Salt Lake City, Utah, 2013, Amirsys.

SECTION

X

Liver

Liver: Normal Anatomy and Examination Techniques

ALEXANDER DING | NAVEEN KULKARNI | FLORIAN J. FINTELMANN |
SANJAY SAINI

CHAPTER OUTLINE

Normal Anatomy

Hepatic Blood Supply
Lobar and Segmental Hepatic Anatomy
Porta Hepatis
Bile Ducts
Hepatic Lymphatics
Nerve Supply

Radiologic Techniques

Plain Radiography
Ultrasound
Computed Tomography
Magnetic Resonance Imaging
Selecting an Appropriate Imaging Technique

Normal Anatomy

The liver is the largest abdominal organ and occupies the majority of the upper right quadrant of the abdomen. The diaphragm borders the liver superiorly, laterally, and anteriorly. The stomach, duodenum, and transverse colon border the liver medially; the hepatic colonic flexure, inferiorly; and the right kidney and adrenal gland, posteriorly. The liver is encapsulated by a dense layer of connective tissue, eponymously named Glisson's capsule. Peritoneum covers the liver, except in the regions of the gallbladder fossa, the fossa for the inferior vena cava (IVC), and the bare area. The surface morphology of the liver features a convex diaphragmatic surface and a concave visceral surface. The bare area abuts the diaphragmatic surface posteriorly and is demarcated by the coronary ligament. The coronary ligament itself is formed by folds of parietal and visceral peritoneum. The superior and inferior limbs of the coronary ligament fuse to form the right and left triangular ligaments laterally (Fig. 83-1). The right and left limbs of the coronary ligament fuse ventrally and extend as the falciform ligament that contains the ligamentum teres, which extends from the umbilicus to the superior surface of the liver.¹

The porta hepatis is a transverse slit in the hilum of the liver that is perforated by the right and left hepatic ducts, hepatic artery, and portal vein. The common bile duct, hepatic artery, portal vein, nerves of the liver, and lymphatics lie enclosed within the layers of the hepatoduodenal ligament (free edge of lesser omentum). The gastrohepatic ligament, which forms the superior aspect of the lesser omentum, attaches the liver to the lesser curvature of the stomach.

HEPATIC BLOOD SUPPLY

The liver has a dual blood supply from the hepatic artery, which provides systemic arterial circulation, and the portal vein, which returns blood from the gastrointestinal tract and spleen.² Hepatic arterial flow provides about 25% of the hepatic blood supply. The majority of the blood supply of the liver comes from mesenteric portal drainage because of the liver's role in gastrointestinal physiologic activity.³ Factors that influence the relative contribution of arterial and portal venous blood flow include hormonal, autonomic neural, and nutritional factors. The balance of blood supply may also become dysregulated by disease, such as hepatic parenchymal disease.^{1,4}

Portal Vein

The portal vein arises from the confluence of the superior mesenteric and splenic veins and is located posterior to the neck of the pancreas (Figs. 83-2 and 83-3). The portal vein courses superiorly and toward the right, just posterior to the common bile duct and hepatic artery, within the hepatoduodenal ligament. At the porta hepatis, the portal vein divides into left and right branches. The right branch courses horizontally and bifurcates into anterior and posterior branches. The left branch is horizontal initially but then courses cranially and terminates into ascending and descending branches. The left portal vein joins the obliterated umbilical vein within the fissure of the ligamentum teres hepatis.^{2,4-6} In embryonic life, the umbilical vein is patent and blood from the umbilical vein drains into the left portal vein, where much of it is shunted through the ductus venosus.

Many anatomic variations of the portal vein exist. Most common is absence of the right portal vein with anomalous branches from the main portal vein and the left portal vein. Absence of the horizontal segment of the left portal vein is more rare.

Hepatic Artery

The celiac axis divides into the common hepatic, splenic, and left gastric arteries at the level of T12-L1. The common hepatic artery courses along the upper border of the pancreatic head, anteriorly and to the right, behind the posterior layer of peritoneum of the lesser sac. After giving off the gastroduodenal artery, the common hepatic artery becomes the proper hepatic artery. The proper hepatic artery enters the subperitoneal space of the hepatoduodenal ligament at the upper margin of the duodenum.⁴ The proper hepatic artery ascends to the liver, anterior to the portal vein and medial to the common bile duct. After entering the porta hepatis, the proper hepatic artery divides into the right, left, and occasionally middle hepatic arteries. The right and left hepatic arteries supply the right and

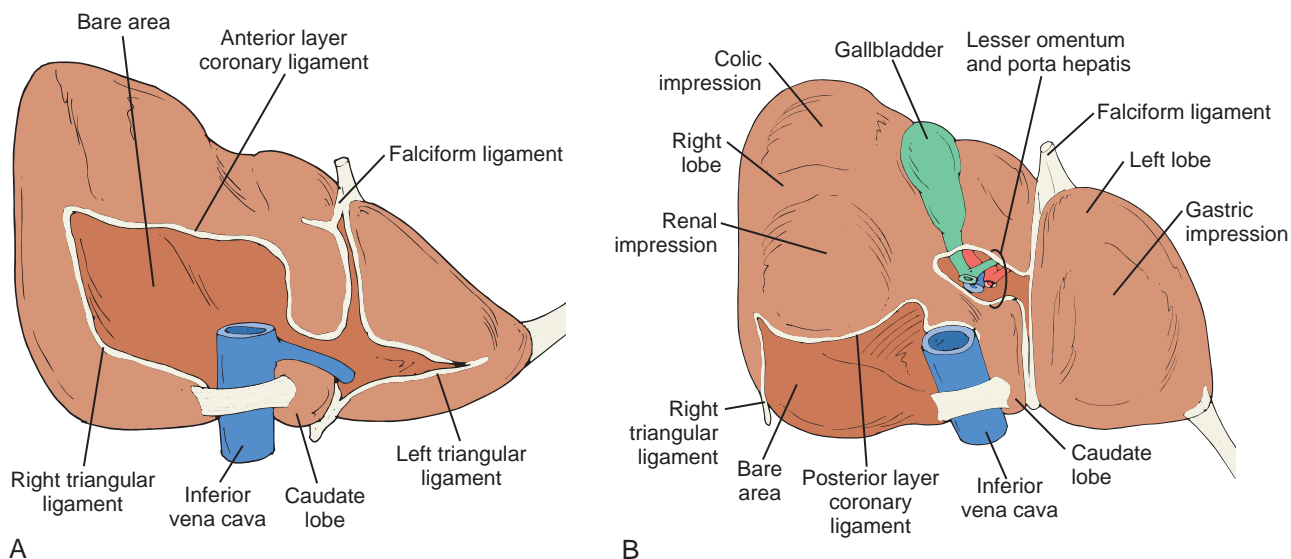


Figure 83-1 Peritoneal and visceral relationships of the liver. Diaphragmatic (A) and visceral (B) surfaces of the liver from a radiologic perspective.

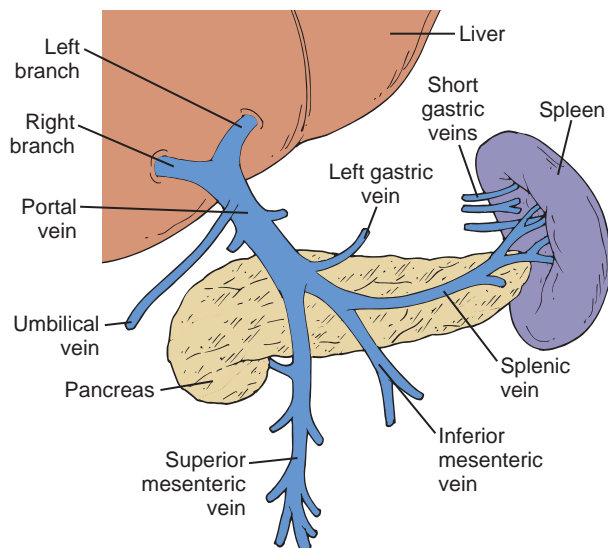


Figure 83-2 Origin of the portal vein. (From Sherlock S: *The portal venous system and portal hypertension*. In Sherlock S [ed]: *Diseases of the Liver and Biliary System*. Oxford, Blackwell Scientific, 1985, pp 134–181.)

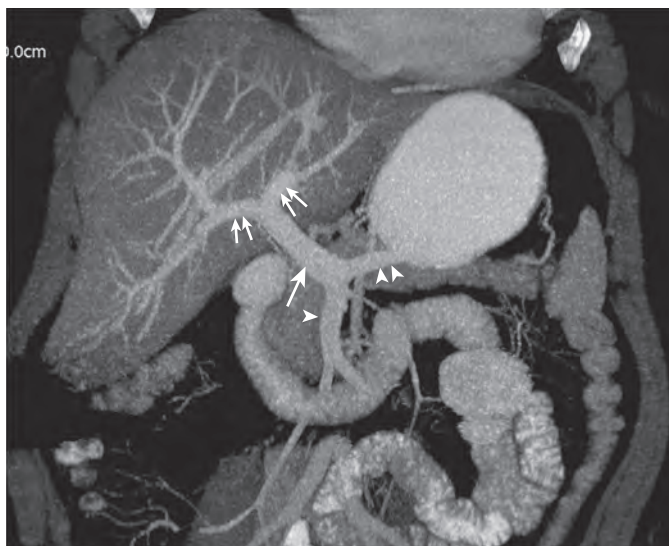


Figure 83-3 Portal venous anatomy. Maximum intensity projection image of CT of upper abdomen demonstrates confluence of superior mesenteric vein (single arrowhead) and splenic vein (double arrowheads) forming main portal vein (arrow). The main portal vein divides into right and left branches (double arrows) at the porta.

left lobes of the liver, respectively. The middle hepatic artery, if present, supplies the medial segment of the left lobe, augmented by branches of the left hepatic artery. Branches of the right hepatic artery supply the caudate lobe; but in some variations, the left or middle hepatic artery may make perfusional contributions.^{2,5} The right hepatic artery also gives off the cystic artery to the gallbladder.

This classic arrangement of the hepatic arterial anatomy is seen in only 55% of patients (Figs. 83-4 and 83-5).² Common variants include the right hepatic artery partially (18%) or completely (14%) replaced by a branch from the superior mesenteric artery, the entire hepatic artery arising from the superior mesenteric artery (2%-4%), a partially or completely replaced

origin of the left hepatic artery from the left gastric artery (18%-25%), and the left hepatic artery giving rise to the middle hepatic artery (45%).^{4,5}

Hepatic Veins

The right, middle, and left hepatic veins lie within the postero-superior aspect of the liver. These veins course through the liver superiorly and obliquely and drain into the IVC. Several small emissary hepatic veins drain the caudate lobe independently into the IVC. The diameter of the hepatic veins is variable and may increase transiently with the Valsalva maneuver. Persistent dilation of the IVC and hepatic veins may be seen with right-sided congestive heart failure.

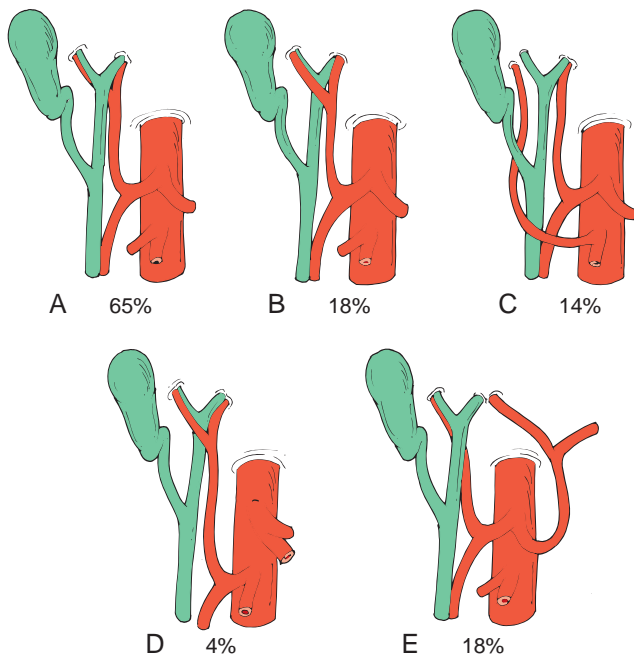


Figure 83-4 Variations in the anatomy of the hepatic arteries.

A. Normal pattern. Right hepatic artery posterior to common hepatic duct. **B.** Right hepatic artery anterior to common hepatic duct. **C.** Right hepatic artery from superior mesenteric artery (sole or accessory). **D.** Common hepatic artery from superior mesenteric artery. **E.** Left hepatic artery from left gastric artery.



Figure 83-5 Hepatic arterial anatomy. Maximum intensity projection image of CT of upper abdomen demonstrates left gastric artery (arrow), splenic artery (double arrows), and common hepatic artery (small arrow) arising from the celiac axis. The common hepatic artery continues as the proper hepatic artery (double arrowheads) after giving off the gastroduodenal artery (double small arrows). The proper hepatic artery divides into right and left branches (arrowheads) at the porta.

Duplication of the right, middle, and left hepatic veins is seen in 20%, 5%, and 15% of subjects, respectively.⁷ Absence of the main hepatic veins occurs in 8% of subjects.⁸ Accessory hepatic veins may also be seen in the liver. In one third of the population, the most common accessory hepatic vein drains the anterosuperior segment of the right hepatic lobe, which empties into the middle hepatic vein or occasionally into the right hepatic vein. Rarely, a separate inferior right hepatic vein drains directly into the IVC.⁷

LOBAR AND SEGMENTAL HEPATIC ANATOMY

The liver can be divided into the right, left, and caudate lobes. The interlobar fissure separating the right and left lobes is oriented along a line passing through the gallbladder fossa inferiorly and the middle hepatic vein superiorly. Although this fissure is well formed in some patients, it may be incomplete in others. The fissure for the ligamentum teres forms the left intersegmental fissure, which divides the left lobe into medial and lateral segments. The fissure for the ligamentum venosum separates the left lateral hepatic segment from the caudate lobe.

Advances in surgical techniques of liver lesion resection have made conventional hepatic lobar anatomy obsolete, however. Surgeons need precise localization of liver lesions in the functional segments rather than in lobes for planning resection. The functional segmentation of the liver is based on surgical definition of feasible intrahepatic boundaries for resection. The segmental anatomy of the liver is primarily based on vascular anatomy that can be illustrated on cross-sectional imaging (Fig. 83-6).⁹⁻¹³ Each segment has an independent vascular supply and biliary drainage. The portal venous, hepatic arterial, and bile duct branches course through the segments (intrahepatic). The main hepatic veins course in between the segments (intersegmental).⁹⁻¹³ The segmental nomenclature most commonly followed is the Bismuth-Couinaud system (Fig. 83-7).^{14,15}

The Bismuth-Couinaud system serves as the anatomic basis for localizing focal hepatic lesions. In this system, the liver is divided into one segment and eight subsegments. The vertical divisions along planes of the main hepatic veins are maintained and are further divided by a horizontal plane passing through the right and left portal veins. The plane through the middle hepatic vein separates the right lobe from the left lobe. By these vascular landmarks, segmental localization of liver lesions can be performed with cross-sectional imaging.^{16,17}

Segment I is the caudate lobe. The caudate lobe is a pedunculated portion of the liver extending medially from the right lobe between the portal vein and the IVC (Fig. 83-8). It has some unique features.^{18,19} Functionally, the caudate lobe is an autonomous part of the liver, with a separate blood supply, bile drainage, and venous drainage. The right border of the caudate lobe is continuous with the parenchyma of the right hepatic lobe by an isthmus. Posteriorly, the IVC borders the caudate lobe. Inferiorly, the caudate lobe forms the superior margin of the foramen of Winslow and divides into a left-sided anterior prominence called the papillary process and a transverse caudate process that protrudes laterally to join the right hepatic lobe. The papillary process can be prominent and penetrate the lesser sac behind the gastric antrum close to the hepatic artery and the portal vein.^{18,19} In some cases, it may simulate a pseudolesion, misinterpreted as an enlarged lymph node or pancreatic mass on cross-sectional images.²⁰

The next consecutive segment numbers are given to segments of the left lobe, followed by the right lobe, in a clockwise fashion as seen in the frontal projection, with the exception of segment IVa. The lateral segments II and III of the left lobe lie lateral and to the left of the left hepatic vein. Segment II lies above and segment III lies below the plane of the portal vein. Segment IV lies between the middle and left hepatic veins. Segment IVa and segment IVb lie above and below the plane of the portal vein, respectively. In the right lobe, the right hepatic vein separates the anterior segments (V and VIII) from the posterior segments (VI and VII). The superior segments (VII

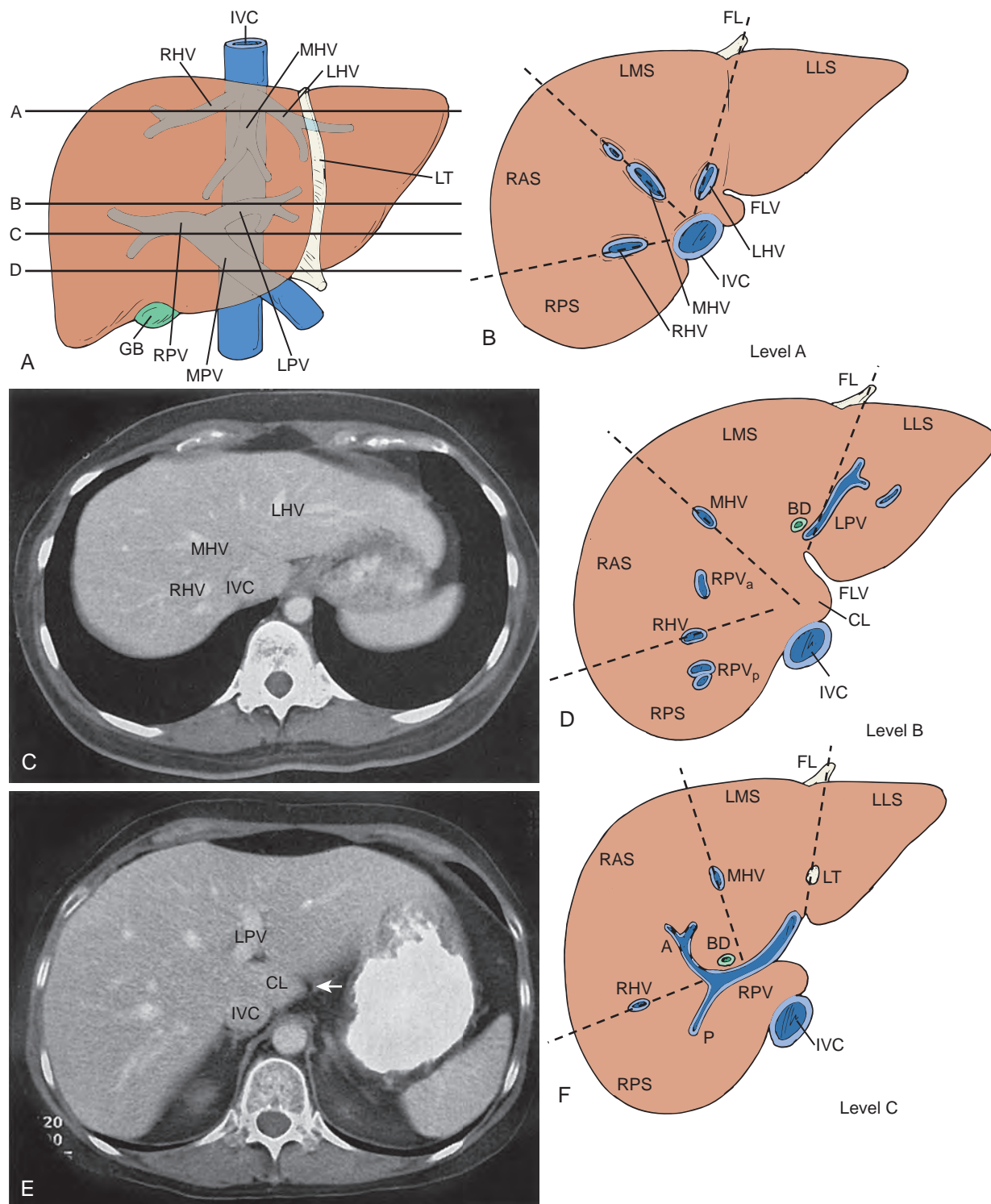


Figure 83-6 Segmental anatomy of the liver. **A.** Anteroposterior “see-through” diagram of the liver demonstrates the major venous anatomy and the levels of multiple axial sections used to depict segmental hepatic anatomy. IVC, Inferior vena cava; RHV, right hepatic vein; MHV, middle hepatic vein; LHV, left hepatic vein; LT, ligamentum teres; LPV, left portal vein; MPV, main portal vein; RPV, right portal vein; GB, gallbladder. **B.** Axial anatomy, level A. The RHV, MHV, and LHV drain into the IVC. The RHV separates the anterior segment right lobe (RAS) from the posterior segment right lobe (RPS). The MHV separates the medial segment left lobe (LMS) from the RAS. The LHV acts as a boundary between the LMS and the lateral segment left lobe (LLS) and lies in the same plane as the falciform ligament (FL). FLV, Fissure for the ligamentum venosum. Dashed lines, Segmental hepatic boundaries. **C.** Axial anatomy, level A. Axial CT. **D.** Axial anatomy, level B. At this level, the ascending portion of the LPV courses between the LLS and LMS of the left lobe. The anterior and posterior segments of the right portal vein (RPV_a, RPV_p) are bisected by the RHV. BD, Bile duct; CL, caudate lobe. **E.** Corresponding CT scan. **F.** Axial anatomy, level C. This is at the level of the horizontal portion of the RPV and its bifurcation into anterior (A) and posterior (P) branches. The RHV lies midway between the portal venous branches. The LT and FL serve as a border between the LLS and LMS.

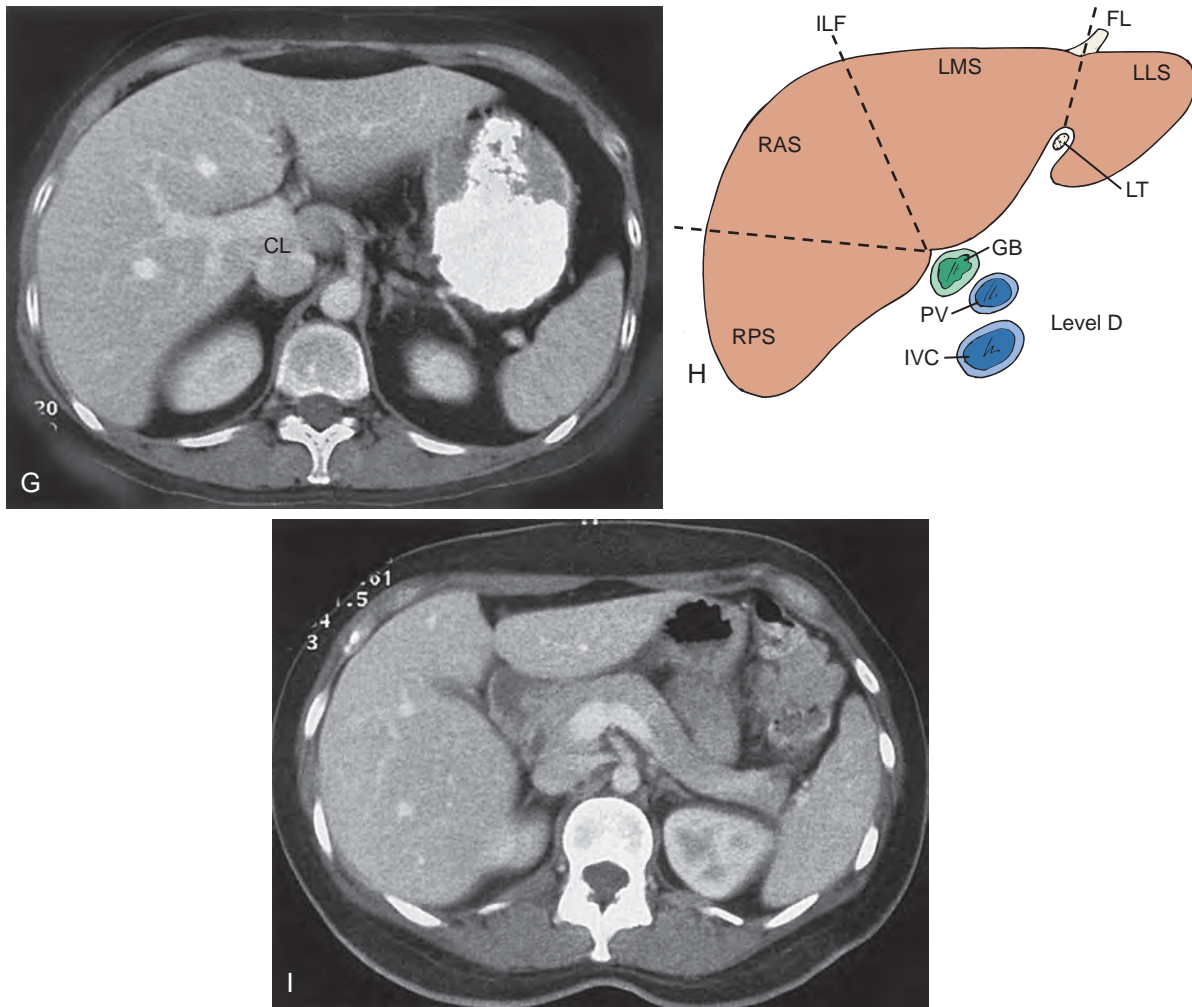


Figure 83-6, cont'd **G.** Corresponding CT section. **H.** Axial anatomy, level D. The right and left hepatic lobes are separated by a line drawn through the IVC and the gallbladder fossa–interlobar fissure (ILF). This fissure extends superiorly from the neck of the gallbladder and is often incompletely visualized on CT. The LLS and LMS are separated by the LT. **I.** Corresponding CT scan.

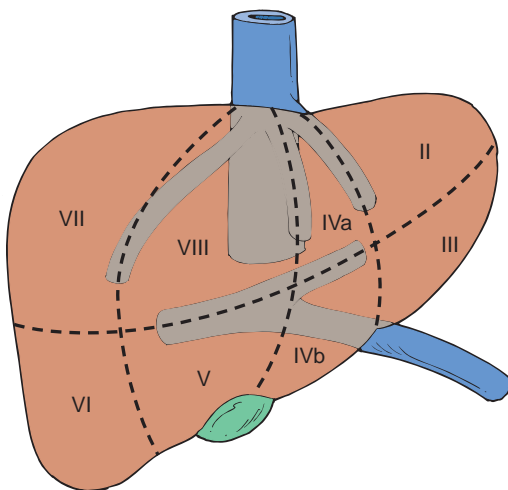


Figure 83-7 Subsegmental liver anatomy: Bismuth-Couinaud nomenclature. Frontal projection. Segments II and III compose the lateral segment of the left lobe and segments IVa and IVb the medial segment. Segments V and VI compose the anterior segment of the right lobe and segments VI and VII the posterior. Segment I (the caudate lobe) is not shown.

and VIII) and the inferior segments (V and VI) lie above and below the plane of the portal vein, respectively. Segmental localization, however, is difficult in patients with variant hepatic vascular anatomy. Hepatic vein landmarks may be unreliable in patients with duplication of hepatic veins. The dorsal portion of segment IV is supplied by a branch from the right hepatic artery in 8% of subjects. Accessory portal segments with independent blood supply from the main portal vein or its right branch may be seen in 30% of subjects. Riedel's lobe is an inferiorly positioned portion of the right hepatic lobe extending below the expected confines of the liver. After segmental hepatic resection, the remaining segments hypertrophy and distort the segmental anatomy by displacing the vessels.

PORTA HEPATIS

The porta hepatis is the hilum of the liver through which the portal vein, hepatic artery, common hepatic duct, nerves, and lymphatics enter the liver (Fig. 83-9). The portal vein is the most consistent anatomic landmark. The common hepatic duct is a 3- to 5-mm thin-walled structure that lies anterior to the portal vein and lateral to the common hepatic artery.²¹⁻²³ The

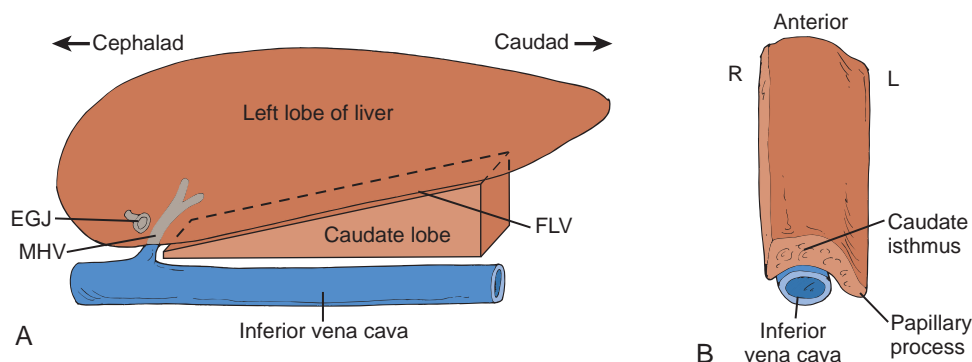


Figure 83-8 Caudate lobe of the liver. **A.** Diagram depicting the relationships of the caudate lobe of the liver. The caudate lobe is wedge shaped, and its posterior border abuts the inferior vena cava (IVC). The anterior border of the caudate lobe is separated from the left lobe of the liver by the fissure for the ligamentum venosum (FLV). The inferior margin of the caudate lobe forms the superior margin of the foramen of Winslow, which leads to the lesser sac. The superior margin of the caudate lobe is the cephalic portion of the right hepatic lobe, where the middle hepatic vein (MHV) enters the IVC. This corresponds to the level of the esophagogastric junction (EGJ). **B.** Schematic representation of the caudate lobe view frontally. The right margin of the caudate lobe connects to the right hepatic lobe by an isthmus. Its anterior border is formed by the fissure of the ligament venosum. The papillary process projects from the caudal margin of the caudate lobe. R, Right; L, left. (A and B from Dodds WJ, Erickson SJ, Taylor AJ, et al: Caudate lobe of the liver: Anatomy, embryology, and pathology. *AJR Am J Roentgenol* 154:87–93, 1990. © by American Roentgen Ray Society.)

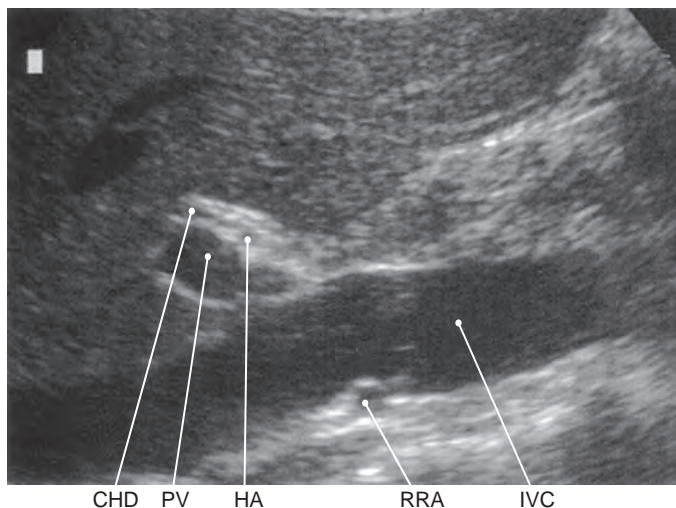


Figure 83-9 Porta hepatis. Oblique sagittal sonogram demonstrates a branch of the portal vein (PV), common hepatic duct (CHD), hepatic artery (HA), inferior vena cava (IVC), and right renal artery (RRA).

right hepatic artery lies posterior to the common hepatic duct in 75% of patients and anterior in 25% of patients.

BILE DUCTS

The segmental distribution of bile ducts closely follows the course of hepatic arterial branches (Fig. 83-10A). The ducts draining the right and left lobes communicate only at the porta hepatis. There is no communication between the bile ducts of the anterior and posterior segments of the right lobe.²⁴

HEPATIC LYMPHATICS

Superficial lymphatics originate from subperitoneal tissue of the liver surface. The visceral surface drains into lymph nodes at the porta hepatis. The diaphragmatic surface drains toward the IVC and aortic lymph nodes near the celiac axis

(Fig. 83-10B). Some lymphatics penetrate the diaphragm to enter retrosternal, cardiohepatic nodes that ascend as high as the neck along the right thoracic artery.² The deep lymphatics of the liver form a major and a smaller trunk. The major trunk passes through the porta hepatis nodes, through the cisterna chyli, and, finally, into the thoracic duct. The smaller trunk courses along with hepatic veins and terminates in lymph nodes near the IVC. Lymphatics of the liver dilate secondary to cirrhosis, portal hypertension, veno-occlusive disease, right-sided heart failure, pericardial effusion, hypoproteinemia, liver transplant rejection, and glycogenesis.²

NERVE SUPPLY

The anterior hepatic nerve plexus surrounds the hepatic artery. It consists primarily of branches of the left celiac plexus, the right and left vagus nerves, and the right phrenic nerve. The posterior hepatic nerve plexus is located around the portal vein and the bile ducts. The hepatic arteries are innervated by the sympathetic nervous system. Pain from the gallbladder and the liver capsule may be referred to the right shoulder by the third and fourth cervical nerves.^{2,25,26}

Radiologic Techniques

PLAIN RADIOGRAPHY

Plain abdominal radiography has a limited role in the evaluation of the liver, both grossly and for focal lesions, because of the homogeneous soft tissue density of the liver.^{27–29} The superior border of the liver is outlined by the lung and the diaphragm. Other borders are seen only if they are outlined by intra-abdominal fat, gas-filled bowel loops, or free air. The lateral border of the liver is outlined by extraperitoneal fat continuous within the posterior pararenal space. This fat is also interposed between the inferior surface of the right hemidiaphragm and the parietal peritoneum. It may appear as a thick black line between the diaphragm and the hepatic dome radiographically.^{27,28,30} Retroperitoneal fat in the anterior pararenal space outlines the posteroinferior margin of the liver. Fluid in

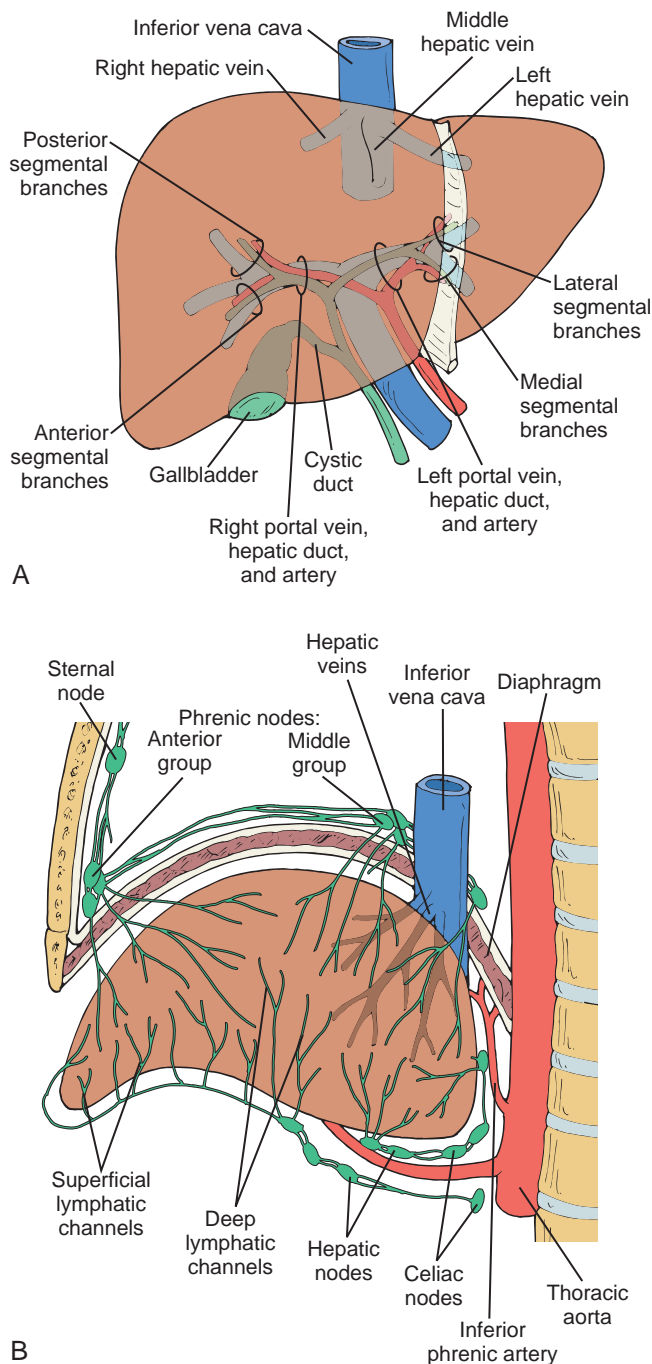


Figure 83-10 Hepatic bile ducts and lymphatics. **A.** Usual branching pattern of bile ducts (green), hepatic artery (red), and portal vein (blue). **B.** Diagram depicting the lymphatic drainage of the liver. (**B** from Woodburne RT, Burkell WE: *Essentials of Human Anatomy*. New York, Oxford University Press, 1988, pp 461 and 466.)

Morison's pouch may obscure this interface, resulting in non-visualization of the edge of the liver. The anteroinferior liver edge is less commonly seen because the amount of omental and pericolic fat that outlines the margin is more variable.³¹ The left hepatic lobe extends to the left of midline, ventral to the stomach and superior to the transverse colon.

Radiographic estimation of liver size is highly unreliable because of inconsistent visualization of borders, although it is more accurate than clinical palpation.³² Radiography may aid

in detection of portal or hepatic venous and biliary tract air or calcified liver lesions, although sensitivity for these indications remains low.^{30,33} Plain abdominal radiography has become obsolete for evaluation of liver lesions with the advent and availability of cross-sectional imaging modalities like magnetic resonance imaging (MRI), computed tomography (CT), and ultrasound.

ULTRASOUND

The liver has a broad area of contact with the abdominal wall, making it an ideal organ for evaluation with real-time ultrasonography. Sonography is a safe, noninvasive, quick, and relatively inexpensive means of evaluating the liver and can be performed at the bedside, requiring little cooperation of the patient.

Evaluation Techniques

The liver is ideally examined after a 6-hour fast so that the gallbladder is not contracted. The highest possible transducer frequency should be chosen while maintaining the penetration through the posterior aspect of the liver. Near and far gain settings should be adjusted for uniform representation of echotexture of the liver parenchyma.³⁴ A small footprint transducer may improve visualization of liver for an intercostal approach. Both supine and right anterior oblique views with the patient rotated on the left side should be used. Breath hold after deep inspiration causes caudal displacement of the liver and improves the visualization of the dome of the liver. Sagittal, transverse, coronal, and subcostal oblique views complete the examination. Focal lesions are easily identified on the real-time study and may be less well appreciated on the hard copy films or static images.³⁵⁻³⁹

Sonography is an excellent modality for evaluating the course of the hepatic and portal veins. The portal vein divides at the porta hepatis into the right and left main branches. The portal veins are anechoic structures with echogenic walls. The bile ducts run with the portal veins and are too small to be seen except at the hilum, unless they are dilated.⁴⁰ Contrary to common belief, there is no constant anteroposterior relationship between the intrahepatic bile ducts and the corresponding portal veins. The hepatic arteries also run with these structures but are usually too small to be seen except with the aid of color flow Doppler imaging.⁴¹⁻⁴⁵

The hepatic veins course posteriorly and superiorly through the liver to the IVC. They are intersegmental, whereas portal veins are intrasegmental with the exception of the ascending segment of the left portal vein. The walls of the hepatic veins are usually less echogenic than those of the portal veins.

Size and Architecture

Ultrasound of the liver is commonly used for evaluation of size of the liver. However, no single measurement of the liver reflects true size because of its variable shape.^{46,47} On longitudinal scans obtained through the midhepatic line, if the liver measures 13 cm or less, it is normal in 93% of individuals. If this measurement is 15.5 cm or more, the liver is enlarged in 75% of cases.⁴⁸ Liver size should be evaluated in at least two planes to compensate for variable hepatic configuration. In the midclavicular line, the normal liver measures 10.5 ± 1.5 cm in longitudinal diameter and 8.1 ± 1.9 cm in the anteroposterior projection, with 12.6 cm and 11.3 cm being the 95th percentile.

In the midline, the normal liver measures 8.3 ± 1.7 cm (95th percentile = 10.9 cm) and 5.7 ± 1.5 cm (95th percentile = 8.2 cm) in longitudinal and anteroposterior dimensions.⁴⁹ Subjective evaluation of the configuration of the inferior border of the liver can be used to predict liver enlargement.³⁹ An inferior angle of more than 45 degrees in the left lobe and more than 90 degrees in the right lobe indicates hepatic enlargement. When the liver is enlarged, its area of contact with the anterior border of the right kidney extends below the superior two thirds of the right kidney.

The normal liver is homogeneous with fine echoes that appear as moderately small dots or lines.^{50,51} The liver has an even brightness and texture interrupted only by the hepatic veins, portal vein, and fissures. The echogenicity of hepatic parenchyma depends on the equipment, transducer, and gain settings. Hence, the parenchymal echogenicity is judged by comparison with internal references. The right renal cortex, body of the pancreas, and portal vein walls are used for internal reference. The liver is either minimally hyperechoic or isoechoic compared with the adjacent normal right renal cortex in parasagittal or lateral coronal scans (Fig. 83-11A). Compared with the liver, the pancreas is hypoechoic in the young, isoechoic in adults, and hyperechoic in the elderly because of increasing fatty infiltration of the pancreas with age (Fig. 83-11B). The liver is hypoechoic to the spleen. The lateral segment of the left hepatic lobe may extend to the left and abut the spleen, mimicking a subphrenic or subcapsular splenic fluid collection (Fig. 83-11C).⁵² The portal vein wall is echogenic in the normal liver. All these architectural comparisons assume that the kidney and pancreas are normal. When these structures are diseased, internal sonographic references are less useful. In acute hepatitis, the parenchyma is hypoechoic to the right renal cortex, and the portal vein walls appear exceptionally bright.⁵³ Conversely, in

fatty infiltration and cirrhosis, the liver is markedly hyperechoic to the right renal cortex, and the portal vein walls are “silhouetted out” by the echogenic hepatic parenchyma.⁵⁴

Artifacts

Sonographic artifacts observed in the liver can mimic abnormalities.⁵⁵⁻⁶⁰ Focal fatty infiltration and focal fat sparing of the liver can appear as hyperechoic and hypoechoic pseudolesions, respectively. These lesions commonly involve the periportal region of the medial segment of the left lobe. Focal subcapsular fat infiltration may occur in diabetic patients treated with insulin in the intraperitoneal dialysate.⁶¹ The caudate lobe may appear as a hypoechoic mass because of attenuation of the sound beam by the fissure for the ligamentum venosum. The ligamentum teres, surrounded by collagen and fat of the falciform ligament, can simulate an echogenic mass. However, this can be recognized by its typical location. Ascites can increase sound transmission to a nodular portion of the liver, simulating an echogenic mass. Accessory fissures and folding of the diaphragm into the liver can also cause echogenic pseudolesions.⁵⁵⁻⁶⁰

Intraoperative Ultrasound

Transabdominal ultrasound of the liver is limited by scattering and attenuation of the sound beam by subcutaneous fat and bowel gas. A high-frequency probe directly placed on the liver surface is without any beam scattering interfaces. Hence, with intraoperative ultrasound, high-resolution images of the liver can be obtained. Intraoperative ultrasound is an expanding field that can provide critical information to the surgeon and enable the surgeon to choose the appropriate surgical technique. The examination should be tailored to the specific needs of the surgeon to avoid undue prolongation of total duration

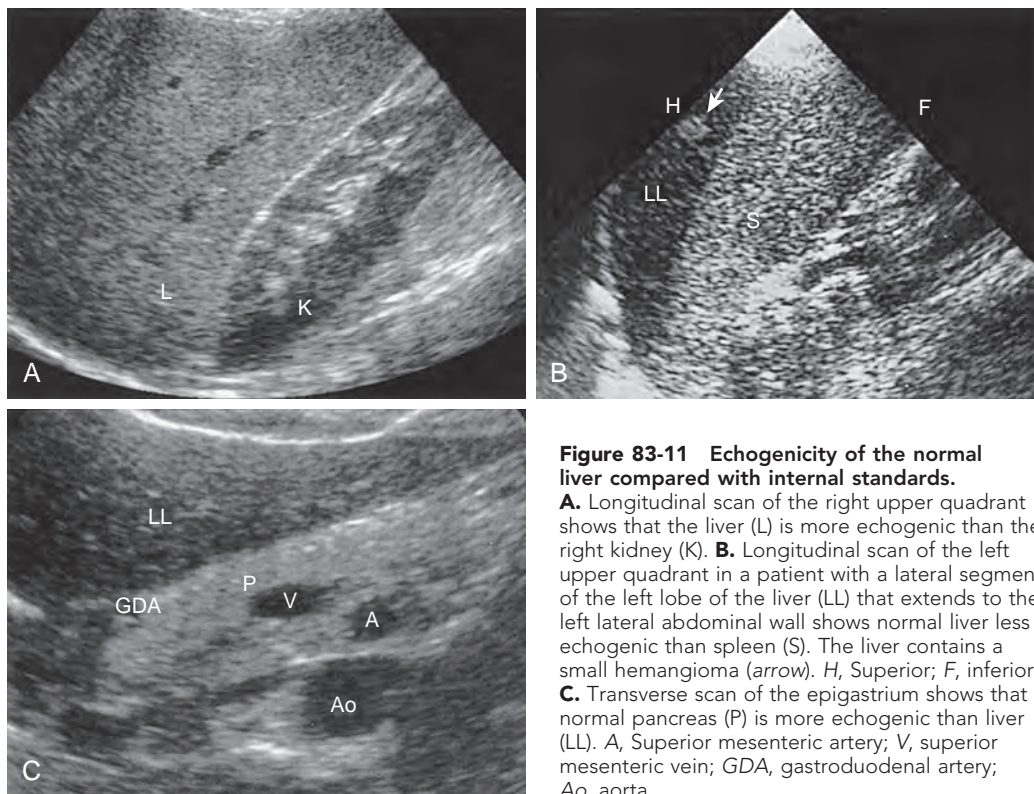


Figure 83-11 Echogenicity of the normal liver compared with internal standards.

A. Longitudinal scan of the right upper quadrant shows that the liver (L) is more echogenic than the right kidney (K). **B.** Longitudinal scan of the left upper quadrant in a patient with a lateral segment of the left lobe of the liver (LL) that extends to the left lateral abdominal wall shows normal liver less echogenic than spleen (S). The liver contains a small hemangioma (arrow). H, Superior; F, inferior. **C.** Transverse scan of the epigastrium shows that normal pancreas (P) is more echogenic than liver (LL). A, Superior mesenteric artery; V, superior mesenteric vein; GDA, gastroduodenal artery; Ao, aorta.

of the surgical procedure. Intraoperative ultrasound can be performed during open laparotomy as well as during laparoscopy. Small, superficially focused, high-frequency, linear array transducers are used for ultrasound during laparotomy. These transducers have a wide field of view in the near field with improved near-field resolution. Intraoperative ultrasound can be employed for diagnostic evaluation as well as for imaging guidance for intraoperative ablation of focal hepatic masses (Fig. 83-12).⁶²⁻⁷⁰

The most common application of intraoperative ultrasound is during surgery in patients undergoing segmental resection for hepatic metastases from colorectal carcinoma. Intraoperative ultrasound can provide information about the relationship of normal vascular anatomy to pathologic masses, vascular invasion or thrombosis caused by tumors, and small, nonpalpable lesions that are difficult to detect on preoperative imaging studies.^{63,70} Intraoperative ultrasound can accurately detect cysts as small as 1 to 3 mm and solid focal lesions of 3 to 5 mm. Brower and colleagues reported that the sensitivity, specificity, and accuracy of intraoperative ultrasound (78%, 100%, and 84%, respectively) are superior to those of arteriography, CT, preoperative ultrasound, and palpation for detection of liver lesions.⁷¹

Intraoperative ultrasound can detect additional liver lesions and modify the surgical management of patients with liver metastases from colorectal carcinoma.^{72,73} Intraoperative ultrasound has also been extended to use in identifying primary hepatic tumors during resection, in particular, hepatocellular carcinoma.⁷⁴ Multiple studies have now shown that intraoperative ultrasound has increased sensitivity for detection of lesions compared with contrast-enhanced CT and MRI.^{61,75-77} Some have even advocated for intraoperative ultrasound as an imaging “gold standard” for focal hepatic lesion detection.⁷⁸ Intraoperative ultrasound can be used to guide interstitial radiotherapy and cryotherapy for the treatment of liver metastases.⁷⁹⁻⁸¹ The combination of intraoperative ultrasound and ultrasound contrast agents has also been shown to increase sensitivity for

metastases not otherwise seen on preoperative CT or MRI.⁸²⁻⁸⁵ One study showed that the operative course of more than a quarter of patients was changed because of additional findings with intraoperative ultrasound.⁸⁶ The combination, however, of preoperative imaging and intraoperative ultrasound remains of highest detection value.⁸⁷

During laparoscopic ultrasound, the transducer is introduced through the laparoscopic port, usually periumbilical or right lower quadrant. A multifrequency 5-, 6.5-, or 7.5-MHz curvilinear laparoscopic ultrasound probe with a flexible tip is used. A substantial pitfall in visualization during laparoscopic ultrasound has been poor near-field visualization. Laparoscopic ultrasound can demonstrate more liver lesions compared with CT⁸⁸ and CT portography.⁸⁹ Laparoscopic ultrasound identified liver tumors not seen at laparoscopy in 33% and provided additional staging information to laparoscopy alone in 42% in a study of patients with potentially resectable liver lesions by preoperative imaging.⁹⁰

Doppler Ultrasound

Duplex and color flow Doppler imaging improve the diagnostic capabilities of ultrasound by enabling the evaluation of complex circulatory dynamics of the liver.^{33,91-96} Thrombosis, reversal of flow, aneurysms, and fistulas are better demonstrated with duplex and color flow Doppler sonography than with gray-scale ultrasound.^{33,92,96,97} Doppler settings need to be optimized to achieve the greatest sensitivity to allow the detection of low flow, and power Doppler may be helpful in this setting. Color gain must be increased to a level just below the level that would create artifacts. In addition, Doppler imaging can be used for detection of vascularity and vascular invasion of focal lesions of the liver. Color and spectral Doppler are unable to detect the vascularity of the majority of focal lesions of the liver because of low intensity of the signals. Tumor vascularity is better evaluated with power Doppler and ultrasound contrast agents.

Doppler tracing of the hepatic artery demonstrates a high diastolic flow that indicates low impedance (Fig. 83-13A).

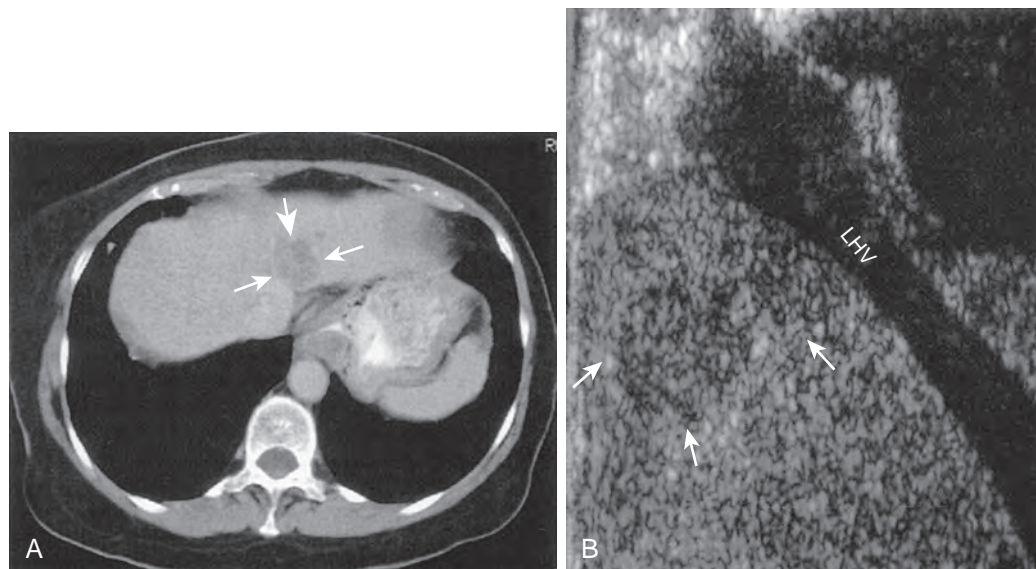


Figure 83-12 Hepatocellular carcinoma: intraoperative ultrasound and CT. **A.** CT demonstrates a low-attenuation lesion (arrows) adjacent to combined confluence of left and middle hepatic veins. **B.** Sagittal ultrasound image during laparotomy confirms that the lesion (arrows) cannot be resected free of the left hepatic vein (LHV). (Courtesy Helena Gabriel, MD, Chicago, IL.)

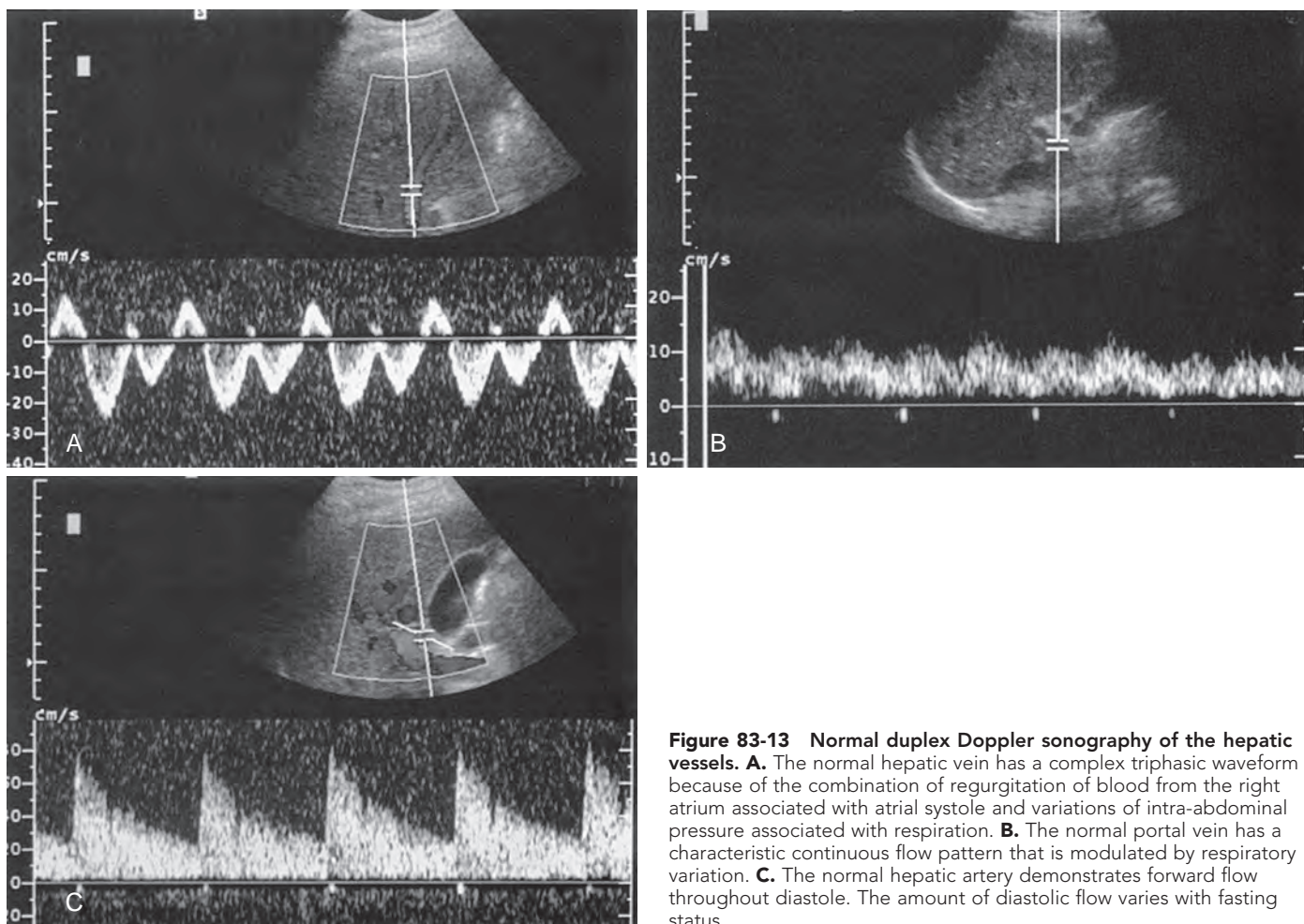


Figure 83-13 Normal duplex Doppler sonography of the hepatic vessels. **A.** The normal hepatic vein has a complex triphasic waveform because of the combination of regurgitation of blood from the right atrium associated with atrial systole and variations of intra-abdominal pressure associated with respiration. **B.** The normal portal vein has a characteristic continuous flow pattern that is modulated by respiratory variation. **C.** The normal hepatic artery demonstrates forward flow throughout diastole. The amount of diastolic flow varies with fasting status.

Doppler sonography is most often used to differentiate the hepatic artery from a bile duct in the porta hepatis. Color flow images may be needed to localize the hepatic artery.⁹⁸ The intrahepatic branches of the hepatic artery are usually not visualized on gray-scale ultrasound. When there is compensatory dilation of intrahepatic branches of the hepatic artery in cirrhosis, Doppler ultrasound can differentiate this from dilation of intrahepatic biliary radicals.

In liver transplant recipients, survival of the allograft depends on patency of the hepatic artery. Changes in the normal hepatic artery waveform may suggest stenosis or thrombosis in these patients.^{99,100} These changes include slow rise to peak systole, diminished amplitude, and prominent diastolic flow, referred to as a *tardus-parvus* waveform. The normal marked increase in postprandial hepatic artery resistive index seen in normal individuals is generally not seen with severe liver disease.¹⁰¹

The flow pattern of the hepatic veins (Fig. 83-13B) is similar to that of the IVC and other large systemic veins, undulating with cardiac and respiratory motion. Normal hepatic venous flow is directed toward the vena cava. With tricuspid regurgitation, there is a pronounced systolic reversal of hepatic venous blood flow.¹⁰² The triphasic pattern is lost in cirrhosis as the liver, which encases the hepatic veins, becomes less compliant.¹⁰³

The portal vein has a characteristic continuous flow pattern (Fig. 83-13C) modulated by respiratory variations. This normal

respiratory variation is either attenuated or lost in portal hypertension.¹⁰³ Portal vein pulsatility is increased in patients with right-sided heart failure, as cardiac pulsations are transmitted to the portal vein.

Tissue Harmonic Imaging

Conventional gray-scale ultrasound transmits and receives the sound beam at the same frequency. In tissue harmonic imaging (THI), the second harmonic signal is received by filtering out the fundamental echoes from the tissue being evaluated. Body wall artifacts, side lobes, and scatter are minimized and signal-to-noise ratio is improved with THI as the harmonic signals are generated in the tissues.¹⁰⁴ The shorter wavelength of the sound beam used in THI results in improved axial resolution. THI can detect additional liver lesions and alter the clinical management compared with conventional ultrasound.¹⁰⁵

Ultrasound Contrast Agents

The availability of ultrasound contrast agents has extended the clinical applications of sonography to primarily aid in the display of parenchymal microvasculature.¹⁰⁶ An ultrasound contrast agent is defined as an exogenous substance that can be administered either in the blood pool or in a cavity to enhance sonographic signals. Contrast agents increase the backscattered signal intensity, resulting in improved gray-scale echogenicity on sequences such as harmonic imaging and pulse inversion as

well as increased color and spectral Doppler signal strength. Agents are injected intravenously, and imaging proceeds immediately thereafter. The advantages of contrast-enhanced ultrasound are the ability to assess contrast enhancement in real time and the excellent temporal resolution. Contrast agents generally also have a strong safety profile. The limitations of contrast-enhanced ultrasound include a relatively narrow time window available for scanning after administration of the contrast agent and limited evaluation if the baseline ultrasound is also limited.

Ultrasound contrast agents for evaluation of the liver are microbubbles stabilized by a shell. The most prevalently used include SonoVue (Bracco SpA, Milan, Italy), a sulfur hexafluoride encased in a phospholipid shell, introduced in 2001 and available in Europe, China, India, Korea, Hong Kong, New Zealand, Singapore, and Brazil; Definity (Lantheus Medical, Billerica, MA), a perflutren in a lipid shell, introduced in 2001 and available in Canada and Australia; Sonazoid (Daiichi-Sankyo, GE, Tokyo, Japan), a perfluorobutane in a phospholipid shell, introduced in 2007 and available in Japan and South Korea; and Levovist (Bayer Schering AG, Germany), a granule of galactose and palmitic acid, for which production is halted.¹⁰⁶ At the time of this writing, none of these agents or any ultrasound contrast agent has been approved by the Food and Drug Administration for clinical use in the United States.

Most agents have similar vascular behavior, with rapid enhancement of the vasculature after injection and slow dissipation during 5 to 10 minutes. Sonazoid is an exception and has an extended late phase, known as the post-vascular phase, and can persist up to a couple of hours in the liver because of phagocytosis by Kupffer cells.^{107,108}

Harmonic imaging detects microbubbles as they resonate at their characteristic frequencies. Microbubble contrast agents are better demonstrated and detected longer in various organs as well as in tumor vessels with harmonic imaging than with color Doppler imaging.¹⁰⁹ Quaia and associates¹¹⁰ reported that pulse inversion harmonic imaging with ultrasound contrast agents detected additional liver metastases in 47% of patients compared with conventional gray-scale ultrasound. Liver metastases even as small as 2 mm can be detected by pulse inversion harmonic imaging with ultrasound contrast enhancement.¹¹¹ Tissue canceling ultrasound techniques can provide a microbubble-only image that can be helpful for making lesions more prominent than by superimposition of microbubble and B-mode images; however, users must be careful about understanding unique artifacts in this mode.¹¹²

Ultrasound contrast agents generally have a good safety profile. Unlike with CT and MR agents, there is no associated known nephrotoxicity. The risk of severe allergic and anaphylactic response is similarly low to that of MR contrast agents.¹¹³ Although the risks are low, emergency response and a trained clinician should be immediately available, just as with all administrations of contrast agents.

COMPUTED TOMOGRAPHY

Advances in multidetector CT (MDCT) technology have revolutionized liver imaging. MDCT enables fast scan coverage and acquisition of submillimeter section thickness images of isotropic volume resolution. Faster image acquisition enables multiphasic CT acquisition through the liver with injection of a single bolus of contrast material, and the isotropic image data set improves the conspicuity of small lesions and the quality of

three-dimensional (3D) reformations.¹¹⁴⁻¹¹⁷ The multiplanar reformations can better demonstrate the anatomic relationship of hepatic focal lesions with the blood vessels, which can help surgeons plan segmental resection of the liver. The 3D reformations enable illustration of hepatic vascular anatomy for evaluation of liver donors. Emerging techniques like dual-energy CT (DECT) and CT perfusion imaging have added new horizons of capabilities to CT with lesion detection, characterization, and treatment monitoring.

Unenhanced Computed Tomography

Noncontrast CT scans of the liver are inferior to contrast-enhanced studies for lesion detection and thus are not routinely performed except in certain specific situations.¹¹⁸⁻¹²⁰ Liver disorders that diffusely alter hepatic attenuation, such as fatty change, hemochromatosis, glycogen storage diseases, chemotherapy, amiodarone administration, and gold therapy, should be evaluated with noncontrast CT. Patients with cirrhosis should also undergo noncontrast scans to search for iron in dysplastic and siderotic nodules. Noncontrast liver CT may be indicated for evaluation of lesion calcification, hemorrhage (in lesions like hepatocellular adenomas; Fig. 83-14), and metastases from hypervascular tumors like carcinoid, renal, thyroid, insulinoma, pheochromocytoma, and breast.¹²¹⁻¹²⁴ These hypervascular metastases may become isodense after contrast enhancement.^{125,126} However, DECT with the capability to reconstruct virtual unenhanced images similar to true noncontrast CT can preclude acquisition of separate noncontrast series as further discussed later.¹²⁷

Contrast-Enhanced Computed Tomography

Iodinated Contrast Dynamics. The goal of contrast enhancement is to improve lesion visibility by increasing the relative attenuation difference between the lesion and normal hepatic parenchyma. This difference is a fundamental factor in lesion conspicuity and characterization.¹²³ Many factors affect the timing and degree of hepatic enhancement and thus the contrast difference between normal hepatic parenchyma and lesions. Hepatic enhancement is most dependent on the phase



Figure 83-14 Hemorrhage in hepatocellular adenoma. Noncontrast CT of upper abdomen of a 28-year-old woman with hepatocellular adenoma reveals a central hyperdense area (arrow) within the hypodense mass suggestive of hemorrhage.

of the contrast delivery during which scanning occurs. These phases can be divided into vascular, redistribution, and equilibrium.¹²⁸ During the vascular phase, there is a rapid increase in aortic enhancement and a slow increase in hepatic enhancement. This phase is short because iodinated contrast material diffuses rapidly from the vascular blood pool to the extravascular or interstitial space of the liver, thus beginning the redistribution phase. During this time, there is a rapid decrease in aortic enhancement and an increase in hepatic enhancement. This represents the ideal time for detecting most lesions (Fig. 83-15). In the equilibrium phase, there is decline in aortic and hepatic enhancement. Hence, lesions may become isoattenuating to hepatic parenchyma.

Helical CT technology allows multiphase CT acquisition with the administration of a single bolus of contrast material. An initial acquisition can be obtained during the hepatic arterial phase, so that highly vascular lesions are highlighted against a background of nonenhanced normal liver parenchyma. These lesions may become isodense with remaining liver if scanning is performed later. A later, portal venous (redistribution) phase scan is obtained when most of the contrast material bolus enhances the normal hepatic parenchyma. Because metastases receive primarily arterial blood supply, most metastases are hypodense compared with normal liver (see Fig. 83-15). These phases are further discussed in the section on biphasic scanning.

The timing of these different phases and peak enhancement is directly affected by the way in which contrast material is delivered. The volume, type, concentration, and rate of injection of contrast material used affect the time to peak enhancement. Several studies suggest that the time to peak contrast enhancement is dependent on the duration of contrast material injection.¹²⁹⁻¹³¹ Higher injection rate or lower volume injections produce an earlier peak enhancement because of the short duration of the injection.

The amount of hepatic enhancement is determined by technical and patient-related factors. Technical factors include concentration of the contrast material, volume, and injection rate. These factors have interdependent effects.¹²⁹ Hepatic enhancement increases with higher volume, injection rate, and concentration of the contrast material.¹³²⁻¹³⁸ Increasing the injection rate from 2 to 3 mL/s results in 16% increase in peak hepatic enhancement.¹³⁹ However, increasing the injection rate above 4

to 5 mL/s does not result in substantial increase in peak hepatic enhancement.¹⁴⁰

Patient-related factors that affect enhancement include weight and cardiac output. There is decreasing hepatic enhancement with increasing weight.¹³⁰ In thin patients undergoing spiral CT, the dose of the contrast agent may be reduced by up to 40%.¹³⁶ Megibow and associates¹³⁴ reported that a weight-based dose of 1.5 mL/kg of 300 mg I/mL contrast material can provide acceptable contrast enhancement in most patients, with a significant cost savings. Although faster image acquisition with MDCT has enabled considerable reduction of the dose of the contrast agent for CT angiography studies,¹⁴¹ enthusiastic reduction of the contrast material dose for CT evaluation of the liver is limited by the minimum iodine dose required for optimum liver enhancement. The iodine dose required to achieve a hepatic enhancement of 50 HU has been reported to be 521 mg I/mL.^{142,143} Decreased cardiac output delays hepatic enhancement.

Faster image acquisition with MDCT mandates high iodine influx rate for optimum enhancement. High-concentration contrast material is a valuable option for this because of the limited range of possible fast injection rates. Increased enhancement of hepatocellular carcinoma in arterial phase CT and improved lesion conspicuity with high-concentration contrast material (370 mg I/mL) have been reported.¹⁴⁴ This improved enhancement with high-concentration contrast material is visually significant in patients weighing more than 65 kg.¹⁴⁵ The use of a chaser bolus of 20 mL of saline has been reported to increase the enhancement of liver, portal vein, and aorta.¹⁴⁶

Automated methods of timing delivery of the contrast material have been advocated to achieve a greater and more consistent level of hepatic enhancement from patient to patient than with the use of a conventional fixed delay time.^{147,148} These methods make use of a region of interest placed on the aorta, portal vein, or liver parenchyma. During delivery of the contrast material, multiple images are obtained at a fixed level at 3- to 5-second intervals. When a preselected threshold of 50 HU is reached, the scan is initiated.¹⁴⁹ Automated bolus tracking can increase the mean liver parenchymal enhancement substantially compared with empirical time delay scanning.¹⁵⁰⁻¹⁵² In addition, automated bolus tracking can improve the liver-to-lesion conspicuity.¹⁵³

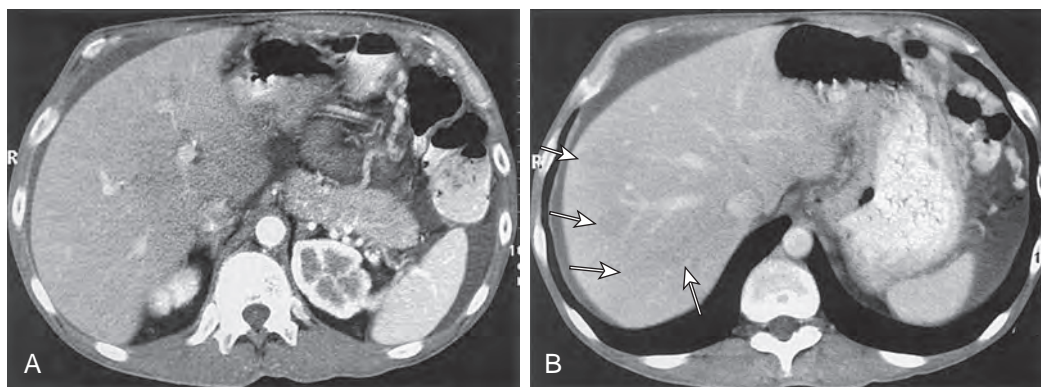


Figure 83-15 Importance of timing of contrast material bolus in liver lesion detection on CT. To evaluate a possible pancreatic mass, a thin-collimation spiral was obtained from the inferior pancreas upward, with a second spiral covering the cranial portion of the liver. Although present on subsequent ultrasound, no metastases were detected on the lower image (A) because scanning occurred during the arterial phase. The more cranial portal venous phase image (B) demonstrates multiple metastases (arrows) from a nonhypervascular carcinoid tumor.

Helical Portal Venous Phase Scan (Single-Phase Scan). This is the preferred CT technique for routine hepatic evaluation. With helical CT, the entire liver can be scanned during peak parenchymal enhancement, further improving diagnostic accuracy.¹⁵⁴ This is accomplished by imaging the liver beginning at about 55 to 70 seconds after the start of the contrast material bolus, depending on injection rate. Reduced cardiac output can delay the peak hepatic enhancement. Most centers use 100 to 150 mL of 300 to 370 mg I/mL contrast material injected at a rate of 3 mL/s or more.

Biphasic Helical Scan. Biphasic CT using a hepatic artery dominant phase technique and a portal venous phase technique is more efficacious than conventional CT using a single portal venous phase technique to detect hypervascular lesions, including hepatocellular carcinoma and metastases from renal, breast, carcinoid, and pancreatic islet cell tumors. Attenuation differences between an intensely enhancing hypervascular metastasis supplied by hepatic arterial flow and the remainder of the liver are maximized during the arterial phase scan (Fig. 83-16A). Portal vein flow would render the hypervascular metastases isoattenuating (Fig. 83-16B). Arterial phase images are acquired by scanning 20 to 30 seconds after the start of injection of the contrast material. The time at onset of arterial phase is dependent on the injection rate of the contrast material.¹⁵⁵ With a fixed injection rate, small changes in volume do not affect the duration of the arterial phase.¹⁵⁶ Faster injection rates increase the amount of arterial enhancement as well as the length of time between peak aortic enhancement and the end of the arterial phase, which might increase detection of hypervascular tumors.¹⁵⁵ A second acquisition is then obtained during the portal venous phase, after a delay of 55 to 65 seconds from the

beginning of the injection of the contrast material. Contrast material is delivered at a faster rate of 4 to 5 mL/s for biphasic CT study, instead of 3 mL/s, which is used for single-phase CT study.

Biphasic helical scanning has been found especially helpful in hepatocellular carcinoma, in which the addition of an arterial phase scan improves lesion detection compared with portal phase scans alone or CT arterial portography.¹⁵⁷⁻¹⁵⁹ In addition, arterial phase data enable vascular road mapping for oncologic liver surgery planning.¹⁶⁰ Detection of a hypervascular hepatic lesion in a patient with cirrhosis is suggestive of hepatocellular carcinoma. Biphasic technique for the detection of hypervascular metastases has had more mixed results. Several studies have found that 21% to 37% of lesions 2 cm or smaller either are visible only or are more conspicuous on arterial phase images.^{161,162} Another study, however, found that nonenhanced and portal venous phase images detected significantly more hypervascular metastases than did hepatic arterial phase and portal venous phase or portal venous phase images alone.¹⁶³ Hepatic arterial phase scanning does not need to be performed for evaluation of hypovascular hepatic lesions as they do not show enhancement during the hepatic arterial phase.¹⁶⁴ Although multiphase liver imaging with MDCT improves sensitivity and specificity of liver imaging, the risk of radiation exposure increases with this.¹⁶⁵ Application of automatic exposure control may result in substantial reduction of radiation dose to the patient while maintaining acceptable image quality.^{166,167}

Delayed Iodine Scanning. Delayed scanning has been employed to improve detection of intrahepatic cholangiocarcinoma (Fig. 83-17) and metastases.¹⁶⁸⁻¹⁷³ Cholangiocarcinoma

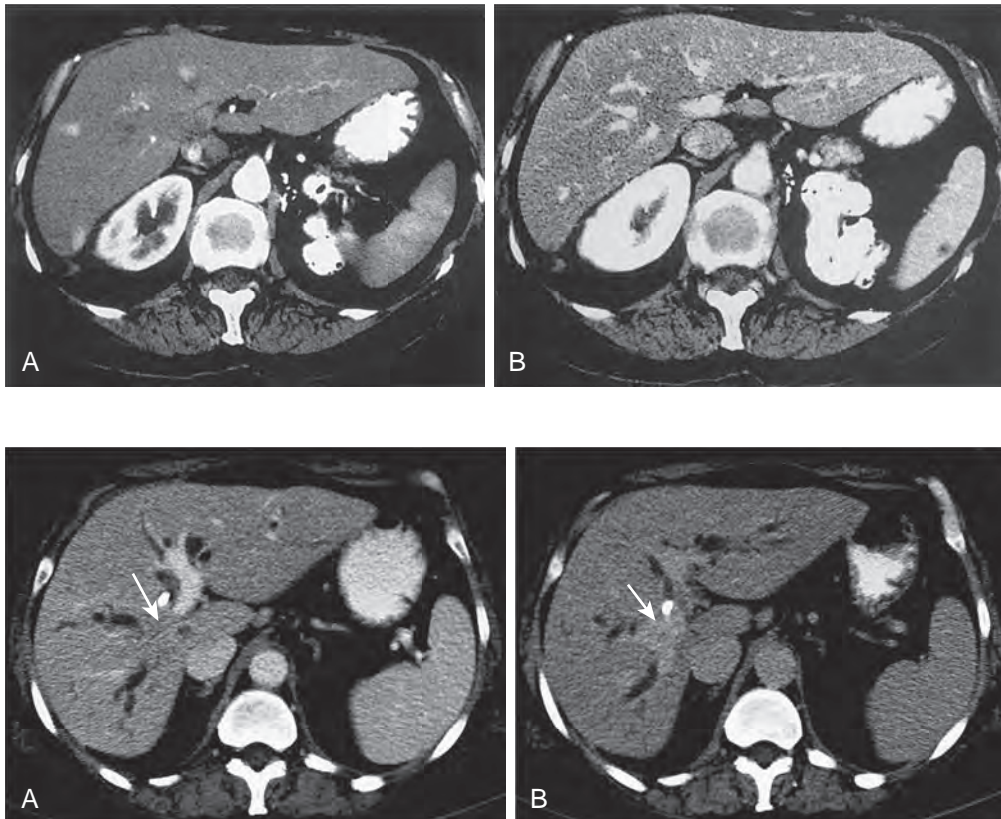


Figure 83-16 Hypervascular metastases: biphasic CT demonstrating carcinoid metastases only on arterial phase images. Arterial phase CT image (A) demonstrates multiple brightly enhancing metastases that are invisible on portal venous phase scan (B). Images are displayed at narrow (liver) windows.

Figure 83-17 Delayed enhancement of hilar cholangiocarcinoma. Portal venous phase CT image (A) of 55-year-old woman with hilar cholangiocarcinoma causing biliary obstruction demonstrates isodense mass (arrow) at porta hepatis with intrahepatic biliary dilation. Delayed image (B) obtained after 10 minutes reveals enhancement of this mass (arrow). Images are displayed at narrow (liver) windows.

appears hyperdense on delayed scans in 74% of patients.¹⁶⁸ Studies assessing whether delayed scanning is helpful in detecting hepatocellular carcinoma have produced conflicting results.^{157,159} In one study, the sensitivity of detection of hepatocellular carcinoma increased by 4% by addition of delayed phase scanning (180 seconds) to the hepatic arterial and portal venous phase scanning.¹⁷⁴ In addition, the filling in of hemangioma with contrast material can be demonstrated on delay phase scans.

Computed Tomography Angiography and Portography. In this technique, an arterial catheter is placed selectively in the hepatic, splenic, or superior mesenteric artery in the angiography suite and contrast material is injected through this catheter.^{123,175,176} Hence, during CT arterial portography (CTAP), there is dense enhancement of liver parenchyma receiving portal venous blood.¹⁷⁷⁻¹⁷⁹ Liver lesions that receive primarily arterial rather than portal venous blood supply appear as hypodense defects on CTAP.^{176,177,180}

Perfusion defects and other artifacts diminish the specificity of CTAP.^{181,182} CTAP has a false-positive rate of 15% to 17%.¹⁸³ An additional delayed phase acquisition can improve the specificity of CTAP.¹⁸⁴ CTAP is seldom performed now because of its invasive nature and increasing use of noncatheter CT angiography and intraoperative ultrasound.

Computed Tomography Liver Protocol Optimization and Radiation Dose Reduction

Protocol Optimization. When it is necessary to perform CT, the radiologist should aim to reduce the CT dose but yet maintain diagnostic image quality. To achieve this, the single most important step is protocol optimization. Optimization of CT technique involves careful selection of scan length and manipulation of several modifiable parameters during the scan, including slice thickness, pitch, tube current, peak tube potential, gantry rotation speed, and noise reduction reconstruction algorithms.

Adjustments to tube current and peak tube potential are among the most common strategies in optimizing CT protocol. Tube potential should be optimized more carefully because unlike tube current, it affects not only the image noise but also the tissue contrast. For a given image noise, higher peak kilovoltage techniques require lower tube current and vice versa. The patient's size should serve as an appropriate guide. Most routine adult abdomen CTs performed at 120 kVp rather than at 140 kVp achieve 20% to 40% reduction in radiation dose. For patients with a larger body habitus, however, 140 kVp tube potential should be employed to avoid loss of diagnostic quality. For smaller subjects, such as pediatric patients, peak kilovoltage may be decreased to 100 or 80 as smaller body habitus leads to minimal attenuation of the x-ray beam, allowing adequate image quality without significant increase in tube currents. A low peak kilovoltage approach at 100 kVp for CT hepatic angiography in organ donor patients may be used; this has been shown to achieve 30% to 35% dose reduction compared with 120 kVp, without affecting diagnostic quality¹⁸⁵⁻¹⁸⁷ (Fig. 83-18).

The tube current on modern CT scanners is determined by automatic modulation of tube current (ATCM). Many studies have shown that ATCM can significantly decrease radiation dose. The basic principle behind the ATCM techniques is to customize the tube current on the basis of the patient's thickness along the z-axis or axial plane derived by orthogonal scout

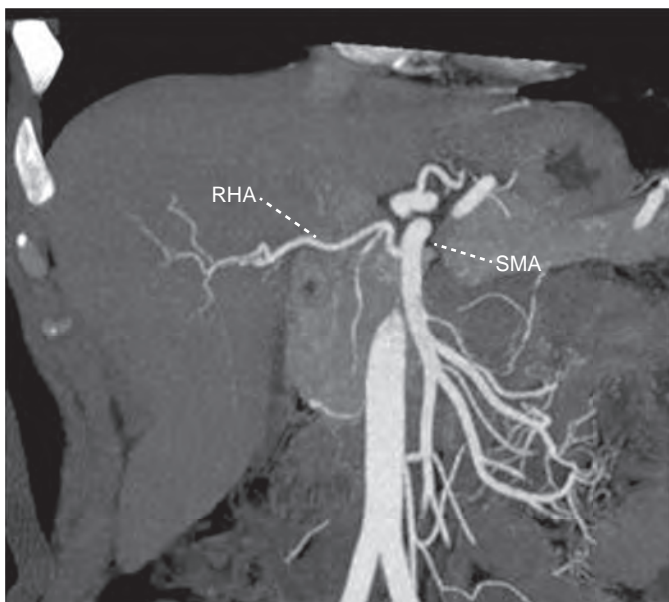


Figure 83-18 CT angiogram of a liver donor patient (body weight, 74 kg) at 100 kVp tube potential still provides good delineation of arterial mapping. Use of a low peak kilovoltage approach over the standard 120 kVp can attain dose reduction of up to 20% to 30%. RHA, Right hepatic artery; SMA, superior mesenteric artery.

projections. This reduces the radiation dose compared with a fixed tube current across the entire rotation. ATCM relies on user-specified image quality in terms of image noise or tube current–time product value. In scanning younger patients, particularly children, lower tube currents with radiation doses as low as reasonably achievable and lower than those for most adult patients should be employed. One may also consider lower fixed tube current settings, based on patient weight or body girth. Because there is wide variation in weight, varying from less than 5 kg up to 100 kg, selection of tube current as well as peak tube potential factors should be carefully done by categorizing into different weight groups. A prospective study exhibited that a mean dose reduction in the abdomen and liver of 38% with angular modulation and 18% with z-axis modulation can be achieved with no compromise in image noise or quality. The selection of image noise level is based on the clinical indication of the liver CT. For example, CT angiography should be undertaken at a relatively higher image noise level compared with portal phase CT for detection of low-contrast liver metastases. Automatic selection of peak tube potential, which functions on the basis of the patient's tissue attenuation profile, has also been implemented recently.¹⁸⁶⁻¹⁹²

Although it is possible to achieve submillimeter imaging on current MDCT scanners, thinner slice images require an increase in radiation dose to maintain an adequate signal-to-noise ratio. In clinical practice, typically 2.5- to 5-mm prospective slices are reconstructed. When thinner slice images are required, for example, in hepatic CT angiography requiring 1-mm slice especially for 3D reconstruction, a reasonable approach would be to obtain thicker slice images but then to retrospectively reconstruct at the desired thickness from the volumetric data. This is a feature that is available on most modern MDCT scanners.¹⁹³

Keeping other CT parameters constant, faster table speed, for a given collimation, results in higher pitch with reduced

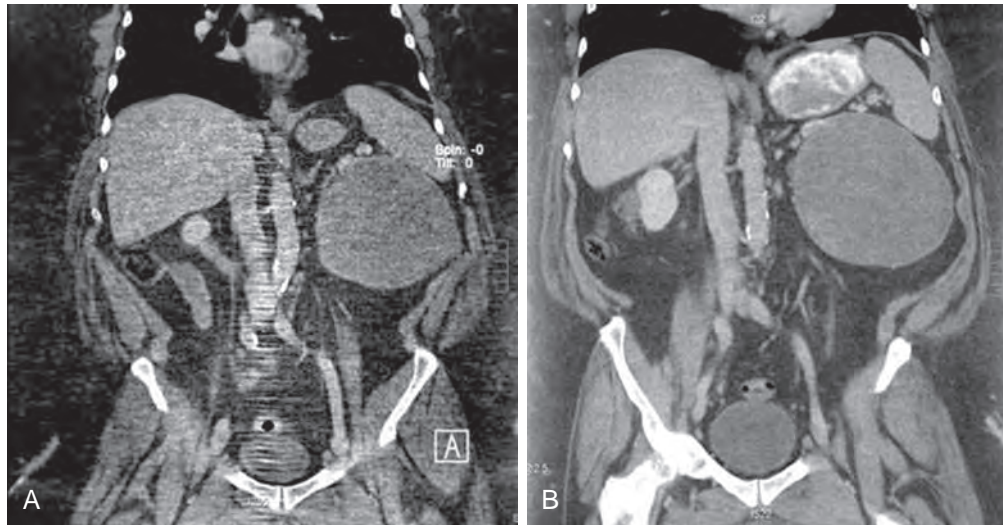


Figure 83-19 **A.** Coronal CT images of 56-year-old patient (body weight, 91 kg) with routine contrast-enhanced CT in portal venous phase (120 kVp; noise index, 15; automatic tube current, 150-550 mA) performed with filtered back projection technique shows increased image noise and artifact. **B.** In the same patient, CT done at different time point using ASIR reconstruction (120 kVp; noise index, 19; automatic tube current, 150-450 mA) shows improved image noise and image quality and substantially reduced artifacts.

radiation dose and vice versa. Modern MDCT scanners have mechanisms to automatically recommend the appropriate tube current to maintain a given image noise level when the pitch is changed. A pitch factor of approximately 1.0 to 1.3 can be used for CT of the abdomen and pelvis in patients weighing up to 300 pounds and a lower pitch of 0.7 for large patients (>300 pounds). Higher pitches should be avoided because they are associated with worsening helical artifacts and may also potentially miss some data.^{188,194}

Noise Reduction Techniques. Filtered back projection algorithms are inherently sensitive to low-dose examinations, resulting in increased image noise. Image noise reduction algorithms include conventional noise reduction filters and newer techniques based on iterative reconstruction. These techniques primarily do not decrease radiation dose but enhance image quality by decreasing image noise and improving contrast from low-dose CT. On the other hand, noise reduction filters, popularly the adaptive CT filters using linear processing techniques, result in homogeneous decrease in image noise across all pixels, thereby reducing image contrast and conspicuity of smaller lesions. This potential drawback limits the dose-saving capability of CT image filters.^{195,196}

By using nonlinear processing, iterative reconstruction techniques have been able to avoid an unacceptable tradeoff between image contrast/resolution and image noise, especially at substantially reduced doses. Because conventional iterative reconstruction methods required long computational times, shorter partial reconstruction algorithms applied in projection or the image space domain were initially introduced by different vendors. More recently, robust full iterative reconstruction algorithms have been made available for clinical use by different vendors. Such techniques include adaptive statistical iterative reconstruction (ASIR) and model-based iterative reconstruction (MBIR) by GE HealthCare and iterative reconstruction in image space (IRIS) and sinogram-affirmed iterative reconstruction (SAFIRE) by Siemens Medical Solutions. Investigators have tested and validated the utility of such techniques, which

have enabled dose reduction to as much as 40% to 60% lower than with standard-dose CT (Fig. 83-19). By synergistic use of these described strategies with noise reduction filters with iterative reconstruction methods, CT protocols at significantly lower dose can be implemented while minimizing compromising diagnostic capability.^{193,197-199}

Computed Tomography Perfusion Imaging

CT perfusion imaging is a functional tool based on temporal changes in tissue density on dynamic contrast-enhanced image acquisition. By dynamic contrast-enhanced imaging, tumor perfusion parameters can be captured and quantified by applying certain mathematical models. Owing to increasing use of targeted therapy like antiangiogenic drugs directed at tumor vascularity, perfusion imaging has received increased attention. Because of its ability to detect early changes in tumor microenvironment, which precede morphologic changes within tumor, CT perfusion is suited to monitor early effects of antiangiogenic therapies. CT perfusion has the advantage of excellent spatial resolution and simpler quantification of tissue vascularity due to a linear relationship between iodine concentration and tissue density. Improved scanner technology in current MDCT with faster scanning time and wider coverage makes this technique feasible for various abdominal applications, including evaluation of liver lesions.^{200,201}

CT perfusion technique typically involves an initial noncontrast scan to localize a lesion followed by a contrast-enhanced dynamic acquisition using 40 to 70 mL of intravenous contrast material at a rate ranging from 3.5 to 10 mL/s. Typically, a first-pass phase (usually 45-60 seconds) is followed by a delayed phase (usually 2-10 minutes) for optimal assessment of tumor perfusion and permeability measurement. Postprocessing of dynamic data is performed with perfusion software to generate color-coded maps of blood flow, blood volume, mean transit time, and surface permeability. Quantitative assessment of the lesion is performed with region-of-interest analysis. Analyzed perfusion parameters of the perfusion software may vary by commercial vendors (Fig. 83-20).

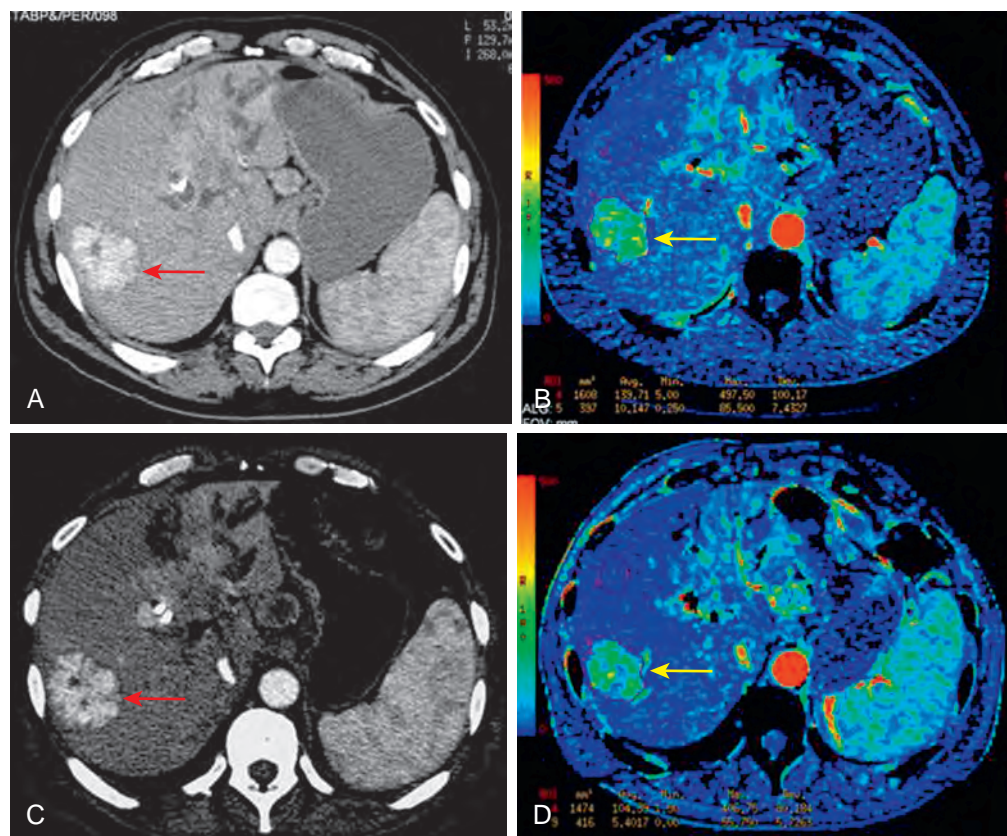


Figure 83-20 Liver metastasis. **A** and **C**. CT perfusion images before and after antiangiogenic treatment in a 53-year-old man with liver cancer (arrow). **B**. Colored perfusion map of blood flow (arrow) at baseline before antiangiogenic treatment shows a high tumor blood flow (140 mL per 100 g/min). **D**. Colored perfusion map after treatment shows a reduction in tumor blood flow (104 mL per 100 g/min). On contrast-enhanced CT images (**A** and **C**), the lesion appears stable by size.

In oncologic imaging, the role of CT perfusion has been investigated and found useful in evaluation of liver tumors. Many studies have found CT perfusion effective to characterize and to assess biologic aggressiveness of hepatocellular carcinoma and in monitoring response to treatment. In treated metastasis, higher perfusion parameters have been shown to be a good prognostic indicator suggesting desired response to treatment. Among nononcologic applications, CT perfusion can be used for quantification of liver perfusion. There is evidence that this may be helpful for earlier evaluation of liver cirrhosis.^{202,203}

Use of CT perfusion, however, is limited because of high radiation dosage and limited coverage (2–4 cm), although the latter limitation is addressed by recent improvement in technology, enabling larger coverage of up to 40 cm. Another limitation is lack of standardized guidelines on image acquisition and data analysis, thereby limiting reproducibility.

Dual-Energy Computed Tomography

DECT is an evolving modality with specific capacities beyond single-energy CT that can translate into improved liver imaging. The two different energy settings acquired allow the differentiation of materials on the basis of their energy-related attenuation characteristics and have the potential to provide better lesion detection, characterization, and monitoring than with single-energy CT. The basic concept of DECT is based on the principle that different elements absorb x-rays with different attenuation, depending on the electronic configuration of atoms.

DECT is performed with two concurrent x-ray beams at different kilovoltage peaks, usually 80 and 140 kVp, during

the same study. Depending on the vendors, different approaches are used to perform dual-energy scanning. In one design, this is achieved by mounting two x-ray tubes in the gantry that are set at different energy levels. In another design, a single x-ray tube capable of rapidly switching between differing energy levels is used. A third approach, which is yet to be commercially available, involves two layered sandwich detectors that can absorb lower and higher energy photons. The DECT technology provides advanced postprocessing applications, including virtual noncontrast (VNC), monochromatic (at different energy levels), and iodine images, which have wide potential applications.²⁰⁴

For most hepatic applications, dual-energy scanning is performed in the arterial phase at the tube potentials of 80 and 140 kVp for patients weighing less than 200 pounds and 100 and 140 kVp in patients weighing more than 200 pounds for optimal material and tissue characterization. Dual-energy imaging has been found useful to improve lesion detection and characterization. In oncology, detection and quantification of iodine can help assess tumor viability and monitor therapy response.²⁰⁵

Improved Lesion Detection. Because of the k-edge proximity, in comparison to standard 120 kVp images, increased conspicuity of hypervascular liver lesions can be attained on 80/100 kVp and low-energy monochromatic images (40–70 keV) to increase the conspicuity of enhancing lesions. Such an application can improve diagnosis and management of hepatocellular carcinoma as well as of metastasis from hyperenhancing primary tumors (e.g., renal cell carcinoma, melanoma)

(Fig. 83-21). Low-kiloelectron volt or low-energy monochromatic images can also be used for 3D vascular mapping and reconstruction in liver donor subjects.^{206,207}

Improved Characterization. DECT imaging can be used to determine presence of fat, iron, calcium, or hemorrhage within the tumor, which can help narrow a differential diagnosis. For example, detection of fat within a hepatic tumor is suggestive of adenoma or hepatocellular carcinoma, whereas calcium indicates prior infection or mucinous metastasis. It may also help in differentiating simple cysts and hypodense metastatic lesions by analyzing internal iodine uptake, which can be positive in metastasis. Currently published data on DECT for characterization of hepatic lesions have demonstrated variable results and continue to evolve.²⁰⁴ Further studies are needed for validation.

Virtual Noncontrast Imaging. VNC images reconstructed from DECT acquisition may provide information similar to that of a true noncontrast CT image. Although on first-generation DECT the VNC images were not exactly equivalent to true noncontrast CT images, several studies have confirmed that VNC images on second-generation DECT provide attenuation values close to those of true noncontrast CT and are sufficient to assess and quantify the enhancement of focal liver lesions. When contrast-enhanced phase alone is performed, VNC images may be used to distinguish calcification (e.g., mucinous metastases) from contrast enhancement. This can

obviate the need for a separate unenhanced phase, thus limiting CT phases and radiation burden to the patient.^{204,208,209}

Therapy Monitoring. Image biomarkers of tumor biology are desired for predicting response to treatment and for follow-up of lesions during and after treatment. After radiofrequency ablation and cryoablation of hepatic lesions and in patients who undergo antiangiogenic therapies, the tumor dimensions may remain stable but change in vascularity, representing the earliest marker of treatment response. Iodine images are a new method and an alternative for monitoring response to treatment. A study has shown better lesion conspicuity and internal homogeneity of the ablation zone on iodine maps, providing an additional benefit for assessing the safety margin after radiofrequency ablation²¹⁰ (Fig. 83-22).

MAGNETIC RESONANCE IMAGING

MRI allows tissue characterization without ionizing radiation. Given the proximity of the liver to the heart and lungs, a tailored protocol is required to minimize motion artifact. Only since the development of rapid acquisition techniques with excellent image quality and tissue-specific contrast agents has MRI become the most accurate imaging modality for the evaluation of liver disease.²¹¹ In many instances, with the appropriate combination of sequences, MRI can diagnose and characterize diffuse liver disease accurately and obviate the need for invasive procedures.²¹² MRI therefore plays an important role in the

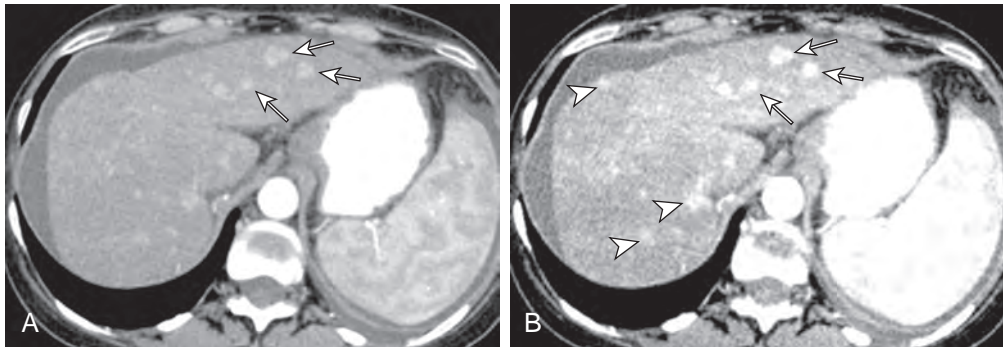


Figure 83-21 **A.** Dual-energy contrast-enhanced CT in a patient with known hepatocellular carcinoma shows hypervascular lesions in the liver (arrows) on weighted 120 kVp image. **B.** However, on monochromatic spectral image at 40 keV reconstructed from the same acquisition, the same lesions (arrows) have improved conspicuity, and some additional lesions are better detected (arrowheads).

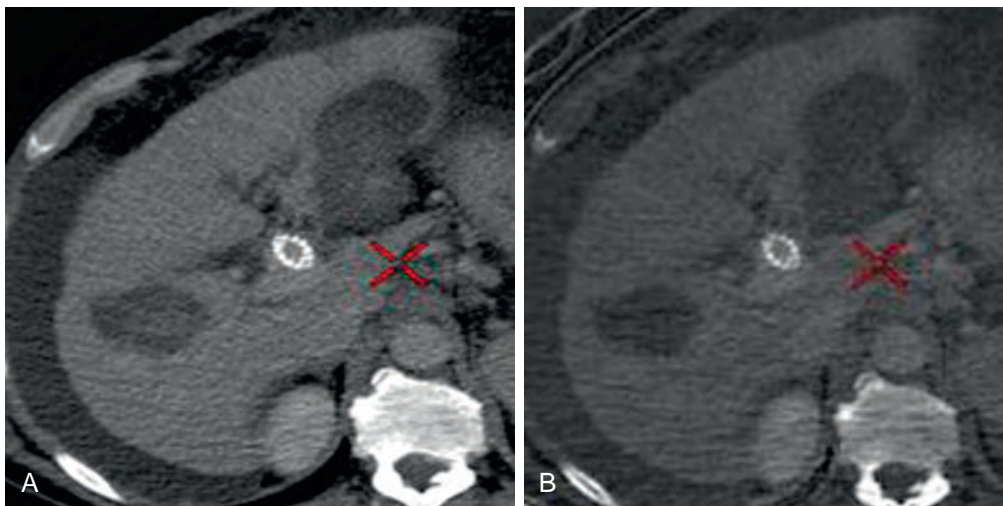


Figure 83-22 **Hepatocellular carcinoma after radiofrequency ablation.** **A.** On weighted 140 kV image, there is hyperdensity within the radiofrequency ablation bed, which may represent enhancement, suggesting local recurrence, or hemorrhage. **B.** On iodine image, there is no enhancement, confirming it to be hemorrhage, demonstrating better tissue characterization.

evaluation of complications and in the follow-up of diffuse hepatic disease, and it is an invaluable tool for characterization of focal lesions.

Many different pulse sequences can be used in hepatic MRI. Choice of sequence and performance depend on magnetic field strength, software, and gradients. The advent of 3T systems has increased available options, but more experience still exists with 1.5T magnets.

In general, T1- and T2-weighted sequences are performed, and contrast agents are added in most situations. Use of torso phased-array surface coils instead of body coils increases signal-to-noise ratio by at least a factor of 2, thereby providing increased lesion-to-liver contrast, lesion detection, and image definition.^{213,214}

T1-Weighted Sequences

The purpose of obtaining T1-weighted images is twofold. First, T1-weighted images provide basic tissue characterization, such as the detection of fat and blood products. Second, T1-weighted images are the mask to which subsequently acquired contrast-enhanced images will be compared to determine tissue enhancement characteristics.

Fast spoiled gradient-echo sequences with short repetition time and echo time and low flip angles are most frequently used to obtain T1-weighted images. Examples include fast low-angle shot (FLASH) on Siemens and spoiled gradient recalled acquisition in the steady state (GRASS, SPGR) on GE systems (Fig. 83-23).

These sequences allow imaging of the entire liver during a single 15- to 25-second breath hold, a prerequisite for dynamic contrast-enhanced imaging when the same area is acquired at multiple time points after intravenous administration of contrast material.²¹⁵⁻²²⁴

On T1-weighted images, the signal intensity of normal liver is greater than that of spleen, muscle, and kidney and less than that of surrounding fat. Bile, ascites, and fluid-filled gut have the lowest signal intensities.²²⁵ Bile within the gallbladder

may have a layering of signal intensities related to the state of fasting and relative lipid, aqueous, proteinaceous, and calcified contents.²²⁶ Most hepatic tumors and abscesses have a long T1 and thus appear as hypointense lesions on T1-weighted images. Most blood vessels appear as dark structures because of flow void phenomena.^{12,227} Portions of the hepatic or portal venous system and IVC may appear hyperintense or isointense with the liver because of inflow phenomena and even echo rephasing.²²⁸

T2-Weighted Sequences

Spin-echo, segmented spin-echo (such as fast or turbo spin-echo), and short tau inversion recovery (STIR) sequences can be used to obtain T2-like information (Fig. 83-24). When spin-echo techniques with a long repetition time (>2000 ms) and long echo time (80-120 ms) are used, T2 differences predominate^{229,230} (see Fig. 83-24). Signal intensity increases with increasing T2 values, and structures with long T2 values, such as gallbladder, fluid-filled bowel, ascites, spleen, and kidney, become bright. Fat is somewhat less bright, and liver and muscle are relatively hypointense. The lung and air-filled bowel are black.

Segmented (fast) spin-echo sequences with fat saturation are commonly used in place of conventional spin-echo images to achieve T2-weighted images. In these sequences, a series of seven or more spin echoes is typically acquired after an initial 90-degree excitation. This enables substantial scan time reduction.^{223,231,232} Fast spin-echo techniques have shown consistently sharper anatomic detail with fewer respiratory and cardiac motion artifacts than in conventional spin-echo sequences.²³³ Segmented spin-echo sequences can also be performed as a breath-hold technique to reduce motion and aortic pulsation artifacts further.²³⁴ These sequences are thought to be at least equivalent to conventional spin-echo sequences.²³⁵ Half-Fourier acquisition single-shot turbo spin-echo (HASTE) is a modification of turbo spin echo allowing a further reduction in scan time by use of a slab acquisition mode.²³⁶

Figure 83-23 Liver MRI: T1-weighted gradient-echo image. This axial T1-weighted gradient-echo image (142/4.4/80 degrees) has excellent anatomic detail. The signal intensity of the liver is greater than that of spleen and muscle. Note the peripheral bright signal intensity from the torso phased-array coil.





Figure 83-24 Liver MRI: rapid T2-weighted image. This axial T2-weighted turbo spin-echo image (2118/80 degrees) exploits differences in T2 relaxation between normal liver and masses. Spleen, kidneys, gallbladder, and bile become brightest. Liver and muscle become relatively hypointense. This image was obtained in a body coil.

STIR imaging can be performed to acquire T2-like information. These sequences suppress fat signal, relying on its short T1 relaxation time. When the TI of inversion recovery sequences is reduced to 80 to 120 ms, the signal from fat is suppressed because it is near the null point (inversion point) of magnetization recovery. Because fat in the body wall and mesentery is a major source of motion artifact, this sequence increases signal-to-noise and contrast-to-noise ratios.²³⁷⁻²⁴⁰ The sequence yields excellent lesion-to-liver contrast, which helps confirm the presence of a lesion or increase confidence in its absence. It also has a high sensitivity for fatty infiltration, periportal changes, and biliary dilation but suffers from a relatively low signal-to-noise ratio. A short inversion time makes the image both T1 and T2 dependent, so that structures with long T1 and T2 values, such as tumors, are conspicuously bright. The STIR sequence is usually not used by itself but is useful in confirming the presence of a lesion or increasing confidence in its absence.

Fat Suppression Techniques

Fat suppression allows the detection and suppression of signal from adipose tissue. This can be achieved in three ways: frequency-selective fat saturation, inversion recovery imaging, and opposed-phase imaging.²⁴¹

Frequency-selective fat saturation relies on the application of a saturation radiofrequency pulse with the same resonance frequency as that of lipids to each slice-selection radiofrequency pulse. A homogeneity spoiling gradient pulse is applied immediately after the saturation pulse to dephase the lipid signal. The signal excited by the subsequent slice-selection pulse contains no contribution from lipid.²⁴¹ Frequency-selective fat suppression can be used with both gradient-echo and spin-echo sequences. It helps suppress the fat signal on fast spin-echo T2-weighted images, on which fat is relatively bright because of the application of the multiple 180-degree pulses. Fatty liver may diminish conspicuity of focal high signal intensity lesions. Application of frequency-selective fat suppression to contrast-enhanced T1-weighted images helps minimize this effect. In the presence of magnetic field or radiofrequency inhomogeneities and imperfect radiofrequency profiles, the homogeneity of the frequency-selective fat saturation is appreciably compromised.

Fat saturation with inversion recovery imaging is based on differences in the T1 of tissues. The T1 of adipose tissue is shorter than the T1 of water. Therefore, the longitudinal magnetization of adipose tissue will recover faster than that of water after a 180-degree inversion pulse. If a 90-degree pulse is applied at the null point of adipose tissue, adipose tissue will produce no signal, whereas water will continue to produce a signal.²⁴¹

Opposed-phase imaging works best to detect small amounts of fat on T1-weighted gradient-echo images.²⁴²⁻²⁴⁴ Fat protons resonate at a slightly lower frequency than water protons, such that the two constantly fall in and out of phase with each other. When fat and water exist in the same voxel (as in fatty transformation), choosing an echo time when their signals are out of phase results in signal loss.²⁴⁵ Normal liver and most cancers do not contain an observable amount of triglycerides, so that the image intensity remains the same on in-phase and opposed-phase images. In the presence of fatty change, the signal intensity of the liver decreases on opposed-phase images compared with in-phase images. Likewise, fat within lesions can be detected, improving lesion characterization.²⁴⁶ Instead of merely suppressing the signal from fat, opposed-phase imaging can also be used to decompose fat and water proton signals by use of their resonant frequency difference and to isolate these two components into two separate images. Such water-fat separation methods are based on work by Dixon.²⁴⁷ Modifications of the Dixon technique, such as IDEAL, have been developed to overcome local magnetic field (B_0) or radiofrequency (B_1) inhomogeneities at higher field strengths.²⁴⁸

Magnetic Resonance Contrast Agents

MR contrast agents can improve liver lesion detection and characterization.^{249,250} They can be categorized on the basis of their distribution into extracellular fluid agents, hepatobiliary-specific agents, reticuloendothelial agents, and blood pool agents.²⁵¹

Extracellular Fluid Agents. This class of agents includes the gadolinium chelates gadopentetate dimeglumine (Gd-DTPA) and gadoteridol (Gd-HP-DO3A). These paramagnetic agents act by shortening T1 relaxation times.^{252,253} These agents function in a manner analogous to iodinated CT contrast agents by

rapidly diffusing from the intravascular space to the extracellular space. Thus, they require rapid imaging to exploit perfusion differences between liver lesions and normal hepatic parenchyma. Rapid breath-hold 3D fat-saturated spoiled gradient-echo T1-weighted techniques are most frequently used, allowing the entire liver to be imaged in a single breath hold (15–25 seconds). Although the signal-to-noise ratio is less than that of higher resolution sequences, such as spin-echo sequences, this technique allows faster imaging in multiple phases of contrast enhancement, analogous to multiphasic spiral CT. Images are obtained before the administration of contrast material, in the arterial predominant phase, in the portal predominant phase (Fig. 83-25), and then during equilibrium. The arterial dominant phase is usually 25 seconds after injection, and the portal venous phase is 70 seconds after injection. Some institutions use a test bolus or bolus tracking instead of relying on fixed time delays, especially in patients with poor cardiac status.

Dynamic contrast enhancement has proved useful in characterizing hemangiomas, detecting hypervascular metastases or small hepatocellular lesions, and detecting enhancement in the central scar of focal nodular hyperplasia.^{254–256} It has been shown not only to improve the distinction between benign and malignant lesions but also to achieve a specific diagnosis in many focal lesions.²⁵⁷ Gadolinium chelate-enhanced 3D rapid gradient-echo images have been found superior to T2-weighted fast spin-echo images (with or without fat suppression and breath holding) for the detection of focal liver masses.²⁵⁸

Hepatobiliary-Specific Agents. The gadolinium-based agents gadoxetic acid (Gd-EOB-DTPA) and gadobenate dimeglumine (Gd-BOPTA) and the no longer commercially available manganese-based mangafodipir trisodium (Mn-DPDP) are taken up to varying degrees by functioning hepatocytes and are excreted in the bile. Whereas hepatic uptake is approximately 50% for gadoxetic acid, it is only 5% for gadobenate dimeglumine. The resulting T1 shortening of the liver, biliary tree, and hepatocyte-containing lesions (Fig. 83-26) results in an increased contrast-to-noise and signal-to-noise ratio for non-hepatocellular lesions.²⁵⁹ Secretion in the biliary tract enables

diagnostic imaging of the bile ducts, such as evaluation for bile leaks. Because the hepatobiliary phase of enhancement is relatively prolonged, the imaging in this phase does not have to be precisely timed (as it does in dynamic imaging with extracellular fluid agents), and high spatial resolution sequences in separate breath holds can be used. Because gadoxetic acid and gadobenate dimeglumine are in part excreted through the kidneys, the vascularity of a lesion can also be assessed, like an extracellular agent.^{260,261} Liver MRI after administration of gadobenate dimeglumine can increase the detection of liver lesions in patients with primary malignant hepatic neoplasm, especially for lesions smaller than 1 cm.²⁶² A 56% increased detection of liver metastases has been demonstrated with the use of these contrast agents.^{259–261} Decreased hepatic blood flow and liver dysfunction diminish hepatic enhancement.²⁶³

Reticuloendothelial Agents. This class of agents includes superparamagnetic iron oxide particles coated with dextran, ferumoxide (AMI-25), and ultrasmall superparamagnetic iron oxide agents like SHU-555A and AMI-227.^{264–266} Uptake occurs in endothelial and Kupffer cells of the liver. On T2* weighted imaging, areas of normal liver containing Kupffer cells that have taken up superparamagnetic iron oxide particles appear dark, whereas lesions without hepatocytes will remain bright. The effect depends on the strength of the applied magnetic field.²⁶⁷ Reticuloendothelial system agents are used primarily for lesion detection but are no longer available in the U.S. market.

Blood Pool Agents. Gadofosveset trisodium is an intravascular gadolinium-based contrast agent available in both the United States and Europe. Its high degree of albumin binding slows the renal excretion and therefore greatly increases its relaxivity. The approved indication in the United States is vascular imaging, and there are few publications on the use of intravascular contrast agents for liver imaging. It has potential for high-resolution steady-state arterial, portal venous, and hepatic venous imaging in the liver as well as quantitative perfusion imaging.

Diffusion-Weighted Magnetic Resonance Imaging

The advent of echoplanar imaging techniques enabled diffusion-weighted MRI of the abdomen.^{268–270} Diffusion-weighted imaging can be performed relatively quickly (as short as two breath-hold acquisitions) and allows lesion detection without contrast agent injection, which makes it attractive in patients with decreased renal function. Low b values (below 100 s/mm²) provide black-blood images, with high inherent tissue contrast and robust image quality. In the liver, diffusion-weighted imaging provides higher sensitivity for lesion detection than T2-weighted images and has inferior to equivalent sensitivity compared with contrast-enhanced T1-weighted images.^{271,272}

Higher b values (≥ 500 s/mm²) are used for lesion characterization by comparing lesion signal intensity and lesion signal intensity changes with liver parenchyma as well as by quantitative assessment of the apparent diffusion coefficient (ADC). Malignant lesions (which are usually more cellular) typically demonstrate restricted diffusion, which is manifested as high residual signal intensity on images obtained with high b values compared with background liver parenchyma, as opposed to benign nonsolid lesions, such as liver cysts and hemangiomas, with ADC of malignant lesions visually equal to or lower than that of surrounding liver parenchyma.²⁷³ Quantitative ADC threshold values have been investigated for

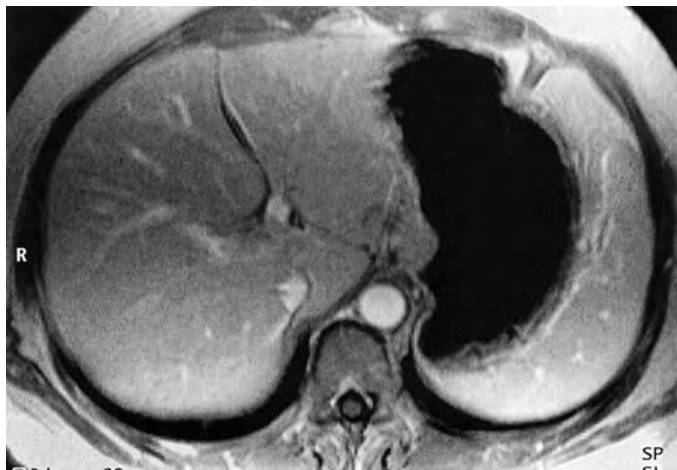


Figure 83-25 Liver MRI: T1-weighted gradient-echo image after administration of gadolinium. The aorta, IVC, and hepatic parenchyma are brightly enhanced. Gadolinium enhancement affords improved characterization of focal lesions.

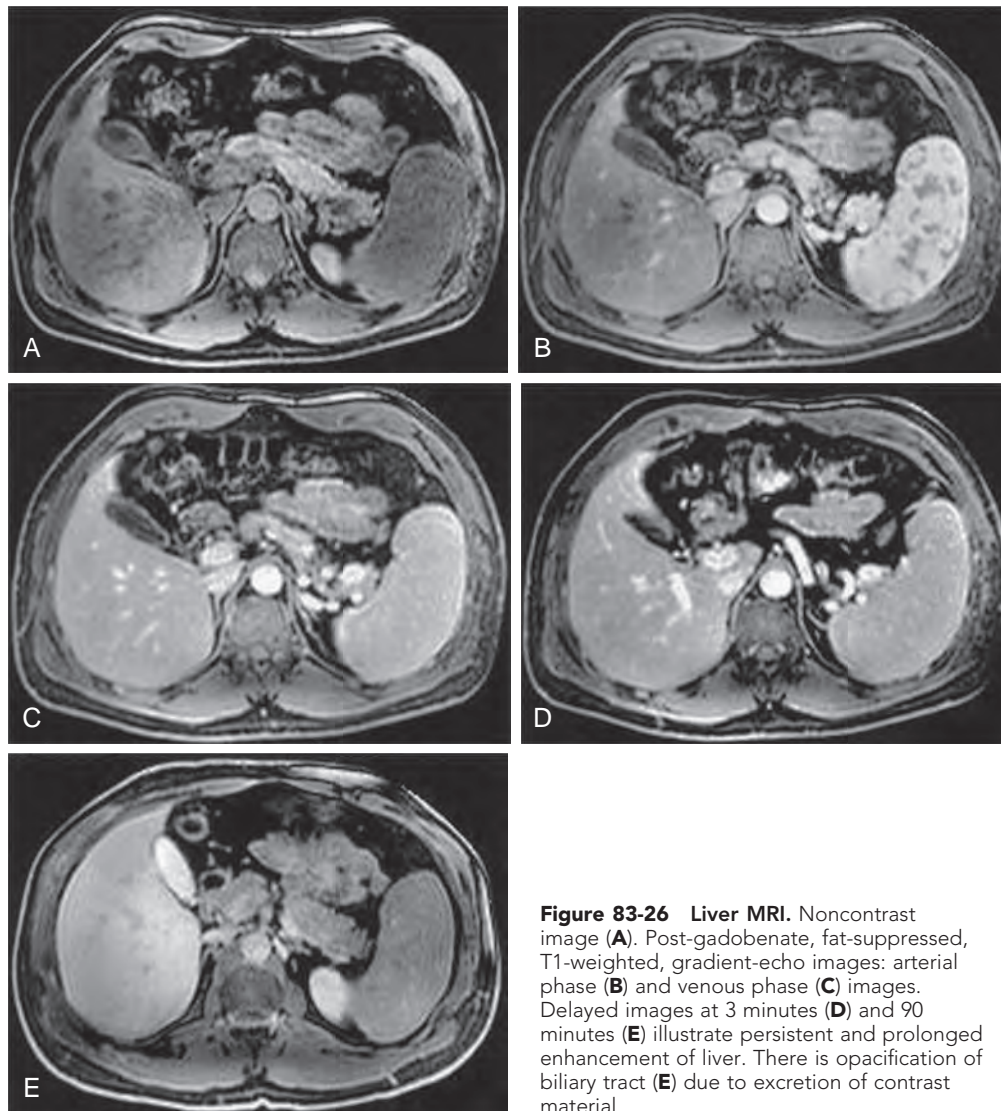


Figure 83-26 Liver MRI. Noncontrast image (A). Post-gadobenate, fat-suppressed, T1-weighted, gradient-echo images: arterial phase (B) and venous phase (C) images. Delayed images at 3 minutes (D) and 90 minutes (E) illustrate persistent and prolonged enhancement of liver. There is opacification of biliary tract (E) due to excretion of contrast material.

lesion characterization, with variable accuracy, depending on the patient population and lesion type.

A major limitation to the widespread use of diffusion-weighted imaging has been the fact that the proposed ADC cutoffs depend on the b values used for acquisition. A meta-analysis by Xia and colleagues²⁷⁴ documented significantly higher ADC values for benign lesions compared with malignant lesions, with variable overlap. Of note, the accuracy decreases when benign hepatocellular lesions such as focal nodular hyperplasia and hepatocellular adenomas are included.²⁷²

Elastography

MRI techniques have become available to noninvasively diagnose and grade hepatic fibrosis by analyzing the propagation of mechanical waves through tissue.²⁷⁵ Stiffness of the hepatic parenchyma as an indicator of fibrosis is derived from gradient-echo images acquired as externally generated shear waves propagate through the liver. Motion-sensitizing gradients similar to those used in phase contrast MR angiography are applied during the image acquisition. The resulting phase contrast images, which depict propagating mechanical waves, are processed to generate quantitative stiffness maps, also known as

elastograms. These maps depict tissue stiffness as the elastic shear modulus on a per-pixel basis (in units of kilopascals) and are often displayed with a color scale.²⁷⁶

Because elastography has been shown to differentiate between low- and high-grade fibrosis, it could be used for non-invasive longitudinal monitoring of hepatic fibrosis.²⁷⁷ However, MR elastographic assessment of liver fibrosis conceivably may be confounded by a variety of factors expected to alter liver stiffness, including hepatic inflammation, steatosis, hepatic vascular congestion, cholestasis, and portal hypertension, and the technique has yet to be validated in large clinical trials.

Spectroscopy

Spectroscopy is being investigated to quantify the degree of steatohepatitis and to reveal a necroinflammatory response in the setting of chronic liver disease.²⁷⁸ Although it is largely restricted to research protocols, this technique has been applied in a general population to establish the prevalence of hepatic steatosis. The good correlation of values obtained with spectroscopy with the results of liver biopsy makes spectroscopy a promising method for estimating the hepatic triglyceride content.²⁷⁹ However, MR spectroscopy is not widely used for

these purposes and has not been validated for routine clinical applications.

Magnetic Resonance Perfusion Imaging

Perfusion MRI represents a useful alternative to CT perfusion imaging for surveillance of hepatocellular carcinoma. Jackson and coworkers²⁶⁰ reported 3D dynamic contrast-enhanced perfusion MRI in humans for lesion-specific permeability mapping. Perfusion characteristics of lesions with dual blood supply were unreliable because they used only the hepatic arterial supply as input function.²⁸⁰ Annet and colleagues^{261,268} reported increased fractional arterial perfusion and decreased mean transit time when they evaluated humans with cirrhosis by dual-input, single-compartment perfusion MRI with a standard low-molecular-weight contrast material. Further technical improvements are required.

Artifact Minimization

Several techniques to minimize artifact have been used, including obtaining multiple signal averages, respiratory compensation, fat suppression, and saturation pulses for abdominal wall fat. Strategies depend on the magnet at hand because 3T systems require an approach different from that for 1.5T systems.²⁸¹

Selecting an Appropriate Imaging Technique

Technologic advances in radiology offer several imaging tools for evaluation of focal liver lesions. These include ultrasound, CT, and MRI. Choosing the most appropriate imaging modality

for evaluating the liver lesion under question depends on the information required from imaging for clinical management decisions. Although ultrasound might be an appropriate examination for a patient with no prior medical history and increased alkaline phosphatase and bilirubin levels, ultrasound is not an adequate screening test for hepatocellular carcinoma in a patient with cirrhosis and increased α -fetoprotein. Although MDCT serves as the first-line imaging modality for evaluation of the liver, MRI offers an attractive alternative to radiation-based CT examination. The clinical applications of MRI for evaluation of the liver are rapidly expanding because of availability of faster sequences and newer contrast agents. Indeed, in some centers, MRI is being used as the imaging modality of choice for evaluation of liver disease.²⁸²⁻²⁸⁴ However, in most centers, MRI is still reserved for certain clinical situations, such as further characterization of liver lesions detected on CT, patients with allergy to iodinated contrast agents, and work-up for hepatic resection.²¹¹ Intraoperative ultrasound has become a standard liver imaging tool for resection of liver metastases from colorectal carcinoma.²⁸⁵ The choice of appropriate imaging modality should be made on an individual case basis, depending on the lesion under question, availability of imaging facilities, and cost issues.

Acknowledgment

We would like to thank Drs. Saravanan Namasivayam, Mannudeep K. Kalra, and William C. Small, the authors of this chapter in the third edition, whose manuscript this chapter is built on, and Dr. Diego Martin, Department of Radiology, Emory University Hospital, Atlanta, for contributing some of the MR images for this chapter.

REFERENCES

- McCuskey RM: Anatomy of the liver. In Boyer TD, Manns MP, Sanyal AJ, editors: *Zakim & Boyer's Hepatology*, ed 6, Philadelphia, 2012, Saunders, pp 3-19.
- Schneck CD: Embryology, histology, gross anatomy, and normal imaging anatomy of the liver. In Friedman A, Dachman A, editors: *Radiology of the Liver, Biliary Tract, and Pancreas*, St. Louis, 1994, Mosby, pp 1-24.
- Raytch RE, Smith GW: Anatomy and physiology of the liver. In Zuidema GD, editor: *Shackelford's Surgery of the Alimentary Tract*, vol IV, Philadelphia, 1996, WB Saunders, pp 257-273.
- Reuter SR, Redman HC, Cho KJ: *Gastrointestinal Angiography*, ed 3, Philadelphia, 1986, WB Saunders.
- Wanless IR: Anatomy and developmental anomalies of the liver. In Feldman M, Scharschmidt BF, Sleisenger MH, editors: *Sleisenger and Fordtran's Gastrointestinal and Liver Disease*, Philadelphia, 1998, WB Saunders, pp 1055-1060.
- Sherlock S, Dooley J: *Diseases of the Liver and Biliary System*, ed 9, Oxford, 1993, Blackwell Scientific.
- Makuuchi M, Hasegawa H, Yamazaki S, et al: The inferior right hepatic vein: Ultrasonic demonstration. *Radiology* 148:213-217, 1983.
- Cosgrove DO, Arger PH, Coleman BG: Ultrasonic anatomy of hepatic veins. *J Clin Ultrasound* 15:231-235, 1987.
- Mukai JK, Stack CM, Turner DA, et al: Imaging of surgically relevant hepatic vascular and segmental anatomy: Part 2. Extent and resectability of hepatic neoplasms. *AJR Am J Roentgenol* 149:293-297, 1987.
- Mukai JK, Stack CM, Turner DA, et al: Imaging of surgically relevant hepatic vascular and segmental anatomy: Part 1. Normal anatomy. *AJR Am J Roentgenol* 149:287-292, 1987.
- Gazelle GS, Haaga J: Hepatic neoplasms: Surgically relevant segmental anatomy and imaging techniques. *AJR Am J Roentgenol* 158:1015-1018, 1992.
- Waggenspack GA, Tabb DR, Tiruchelvam V, et al: Three-dimensional localization of hepatic neoplasms with computer-generated scissurae recreated from axial CT and MR images. *AJR Am J Roentgenol* 160:307-309, 1993.
- Silverman PM, Zeman RK: Normal anatomy of the liver and biliary system. In Silverman PM, Zeman RK, editors: *CT and MRI of the Liver and Biliary System*, New York, 1990, Churchill Livingstone, pp 1-20.
- Couinaud C: *Le foie: Études anatomiques et chirurgicales*, Paris, 1957, Masson.
- Bismuth H, Houssin D, Castaing D: Major and minor segmentectomies "régliées" in liver surgery. *World J Surg* 6:10-24, 1982.
- Soyer P, Bluemke DA, Bliss DF, et al: Surgical segmental anatomy of the liver: Demonstration with spiral CT during arterial portography and multiplanar reconstruction. *AJR Am J Roentgenol* 163:99-103, 1994.
- Lafortune M, Madore F, Patriquin H, et al: Segmental anatomy of the liver: A sonographic approach to the Couinaud nomenclature. *Radiology* 181:443-448, 1991.
- Dodds WJ, Erickson SJ, Taylor AJ, et al: Caudate lobe of the liver: Anatomy, embryology, and pathology. *AJR Am J Roentgenol* 154:87-93, 1990.
- Auh YH, Rosen A, Rubenstein WA, et al: CT of the papillary process of the caudate lobe of the liver. *AJR Am J Roentgenol* 142:535-538, 1984.
- Donoso L, Martinez-Noguera A, Zidan A, et al: Papillary process of the caudate lobe of the liver: Sonographic appearance. *Radiology* 173:631-633, 1989.
- Balfe DM, Mauro MA, Koehler RE, et al: Gastrohepatic ligament: Normal and pathologic CT anatomy. *Radiology* 150:485-490, 1984.
- Zirinsky K, Auh YH, Rubenstein WA, et al: The portacaval space: CT with MR correlation. *Radiology* 156:453-458, 1985.
- Weinstein JB, Heiken JP, Lee JKT, et al: High resolution CT of the porta hepatis and hepatoduodenal ligament. *Radiographics* 6:1-37, 1986.
- Russell E, Yrizzary JM, Montalvo BM, et al: Left hepatic duct anatomy: Implications. *Radiology* 174:353-356, 1990.
- Meyers WC, Jones RS: *Textbook of Liver and Biliary Surgery*, Philadelphia, 1990, JB Lippincott.
- Taylor HM, Ros PR: Hepatic imaging. *Radiol Clin North Am* 36:237-246, 1998.
- Gelfand DW: The liver: Plain film diagnosis. *Semin Roentgenol* 10:177-187, 1975.

28. Gore RM, Goldberg HI: Plain film and cholangiographic findings in liver tumors. *Semin Roentgenol* 12:87–93, 1983.
29. Rogers JV, Torres WE, Clements J, et al: Plain film diagnosis of the liver. In Bernardino ME, Sones PJ, editors: *Hepatic Radiography*, New York, 1984, Macmillan, pp 1–49.
30. Baker SR: *The Abdominal Plain Film*, East Norwalk, CT, 1990, Appleton & Lange.
31. Love L, Demos TC, Reynes CJ, et al: Visualization of the lateral edge of the liver in ascites. *Radiology* 122:619–622, 1977.
32. Fleischner FG, Sayegh V: Assessment of the size of the liver. *N Engl J Med* 259:271–274, 1985.
33. Darlak JJ, Moskowitz M, Kattan K: Calcifications in the liver. *Radiol Clin North Am* 18:209–220, 1980.
34. Cooperberg PL, Rowley VA: Abdominal sonographic examination technique. In Taveras J, Ferrucci J, editors: *Radiology: Diagnosis-Imaging-Intervention*, Philadelphia, 1990, JB Lippincott, pp 1–11.
35. Parulekar SG, Bree RL: Liver. In McGahan JP, Goldberg BB, editors: *Diagnostic Ultrasound—A Logical Approach*, Philadelphia, 1998, Lippincott-Raven, pp 599–692.
36. Withers CE, Wilson SR: The liver. In Rumack CM, Wilson SR, Charboneau JW, editors: *Diagnostic Ultrasound*, ed 2, St. Louis, 1998, Mosby, pp 87–154.
37. Shkolnik ML: *Guide to the Ultrasound Examination of the Abdomen*, New York, 1986, Springer-Verlag.
38. Chan V, Hanbidge A, Wilson S, et al: Case for active physician involvement in US practice. *Radiology* 199:555–560, 1996.
39. Grant EG: Liver. In Mittelstaedt C, editor: *General Ultrasound*, New York, 1992, Churchill Livingstone, pp 173–249.
40. Wing VW, Laing FC, Jeffrey RB, et al: Sonographic differentiation of enlarged hepatic arteries from dilated intrahepatic bile ducts. *AJR Am J Roentgenol* 145:57–61, 1985.
41. Berland LL, Lawson TL, Foley WD: Porta hepatis: Sonographic discrimination of bile ducts from arteries with pulsed Doppler with new anatomic detail. *AJR Am J Roentgenol* 138:833–840, 1987.
42. Bret P, de Stempel JV, Atri M, et al: Intrahepatic bile duct and portal vein anatomy revisited. *Radiology* 169:405–407, 1988.
43. Fraser-Hill MA, Atri M, Bret PM, et al: Intrahepatic portal venous system: Variations demonstrated with duplex and color Doppler US. *Radiology* 177:523–526, 1990.
44. Lim JH, Ryuk N, Ko YT, et al: Anatomic relationship of intrahepatic bile ducts to portal veins. *J Ultrasound Med* 9:137–143, 1990.
45. Lauth WW, Greenway CV: Conceptual review of the hepatic vascular bed. *Hepatology* 7:952–963, 1987.
46. Skrainka B, Stahlut J, Fulbeck CL, et al: Measuring liver span: Bedside examination versus ultrasound and scintiscan. *J Clin Gastroenterol* 8:267–270, 1990.
47. Meire HB: Ultrasound of the liver. In Wilkins R, Nunnerly H, editors: *Imaging of the Liver, Pancreas and Spleen*, Oxford, 1990, Blackwell Scientific, pp 10–24.
48. Gosink BB, Leymaster CE: Ultrasonic determination of hepatosplenomegaly. *J Clin Ultrasound* 9:37–41, 1981.
49. Niederau C, Sonnenberg AM, Muller JE, et al: Sonographic measurements of the normal liver, spleen, pancreas, and portal vein. *Radiology* 149:537–540, 1983.
50. Needleman L: Diffuse benign liver disease. In Kurtz A, Goldberg B, editors: *Gastrointestinal Ultrasonography*, New York, 1988, Churchill Livingstone, pp 57–74.
51. Leung NWY, Farrant P, Peters TJ: Liver volume measurement by ultrasonography in normal subjects and alcoholic patients. *J Hepatol* 2:157–164, 1986.
52. Aube C, Oberti F, Korali N, et al: Ultrasonographic diagnosis of hepatic fibrosis or cirrhosis. *J Hepatol* 30:472–478, 1999.
53. Simonousky V: The diagnosis of cirrhosis by high resolution ultrasound of the liver surface. *Br J Radiol* 72:29–34, 1999.
54. Makuuchi M, Hasegawa H, Yamazaki S, et al: The use of operative ultrasound as an aid to liver resection in patients with hepatocellular carcinoma. *World J Surg* 11:615–623, 1987.
55. Tochio H, Kudo M, Okabe Y, et al: Association between a focal spared area in the fatty liver and intrahepatic efferent blood flow from the gallbladder wall: Evaluation with color Doppler sonography. *AJR Am J Roentgenol* 172:1249–1253, 1999.
56. Auh YH, Rubenstein WA, Zirinsky K, et al: Accessory fissures of the liver: CT and sonographic appearance. *AJR Am J Roentgenol* 143:565–572, 1984.
57. Hillman BJ, D'Orsi CJ, Smith EH, et al: Ultrasonic appearance of the falciform ligament. *AJR Am J Roentgenol* 132:205–206, 1979.
58. Sones PJ, Jr, Torres WE: Normal ultrasonic appearance of the ligamentum teres and falciform ligament. *J Clin Ultrasound* 6:392–394, 1978.
59. Parulekar SG: Ligaments and fissures of the liver: Sonographic anatomy. *Radiology* 130:409–411, 1979.
60. Taylor KJW, Carpenter DA: The anatomy and pathology of the porta hepatis demonstrated by gray scale ultrasonography. *J Clin Ultrasound* 3:117–119, 1975.
61. Kallio T, Nevalainen PI, Lahtela JT, et al: Hepatic subcapsular steatosis in diabetic CAPD patients treated with intraperitoneal insulin: Description of a typical pattern. *Acta Radiol* 42:323–325, 2001.
62. Machi J, Isomoto H, Yamashita Y, et al: Intraoperative ultrasonography in screening for liver metastases from colorectal cancer: Comparative accuracy with traditional procedures. *Surgery* 104:678–685, 1987.
63. Castainy D, Edmond J, Bismuth H, et al: Utility of operative ultrasound in the surgical management of liver tumors. *Ann Surg* 204:600–605, 1986.
64. Gozzetti G, Angelini L: The use of intraoperative ultrasonography in hepatic surgery. In Kurtz A, Goldberg B, editors: *Gastrointestinal Ultrasonography*, New York, 1988, Churchill Livingstone, pp 237–251.
65. Parker GA, Lawrence W, Horsley JS, et al: Intraoperative ultrasound of the liver affects operative decision making. *Ann Surg* 209:569–577, 1989.
66. Igawa S, Sakai K, Kihoshita H, et al: Intraoperative sonography: Clinical usefulness in liver surgery. *Radiology* 156:473–478, 1985.
67. Glen PM, Noseworthy J, Babcock DS: Use of intraoperative ultrasonography to localize a hepatic abscess. *Arch Surg* 119:347–348, 1984.
68. el Mouaouy A, Naruhn M, Becker HD: Diagnosis of liver metastases from malignant gastrointestinal neoplasms: Results of preoperative and intraoperative ultrasound examinations. *Surg Endosc* 5:209–213, 1991.
69. Simeone JF: Intraoperative ultrasonography of liver. In Ferrucci J, Stark D, editors: *Liver Imaging*. Boston, Andover Medical, 1990, pp 247–255.
70. Soyer P, Levesque M, Elias D, et al: Detection of metastases from colorectal cancer: Comparison of intraoperative US and CT during arterial portography. *Radiology* 183:541–544, 1992.
71. Brower ST, Schwartz M, Miller C: Intraoperative ultrasound and liver tumors. *Cancer Treat Res* 69:197–220, 1994.
72. Sahani DV, Kalva SP, Tanabe KK, et al: Intraoperative US in patients undergoing surgery for liver neoplasms: Comparison with MR imaging. *Radiology* 232:810–814, 2004.
73. Ravikumar TS, Kane R, Cady B, et al: Hepatic cryosurgery with intraoperative ultrasound monitoring for metastatic colon carcinoma. *Arch Surg* 122:403–404, 1987.
74. Torzilli G: Intraoperative ultrasound in surgery for hepatocellular carcinoma. *Ann Ital Chir* 79:99–106, 2008.
75. Onik G, Kane R, Steele G, et al: Monitoring hepatic cryosurgery with sonography. *AJR Am J Roentgenol* 147:665–669, 1986.
76. Dritschio A, Grant EG, Harter KW, et al: Interstitial radiation therapy for hepatic metastases: Sonographic guidance for applicator placement. *AJR Am J Roentgenol* 146:275–278, 1986.
77. Wagnetz U, Atri M, Massey C, et al: Intraoperative ultrasound of the liver in primary and secondary hepatic malignancies: Comparison with preoperative 1.5-T MRI and 64-MDCT. *AJR Am J Roentgenol* 196:562–568, 2011.
78. Berger-Kulemann V, Schima W, Baroud S, et al: Gadolinium-enhanced 3.0 T MR imaging versus multidetector-row CT in the detection of colorectal metastases in fatty liver using intraoperative ultrasound and histopathology as a standard of reference. *Eur J Surg Oncol* 38:670–676, 2012.
79. Marchesa P, Milsom JW, Hale JC, et al: Intraoperative laparoscopic liver ultrasonography for staging of colorectal cancer: Initial experience. *Dis Colon Rectum* 39(Suppl):S73–S78, 1996.
80. Feld RI, Liu JB, Nazarian L, et al: Laparoscopic liver sonography: Preliminary experience in liver metastases compared with CT portography. *J Ultrasound Med* 15:288–295, 1996.
81. John TG, Greig JD, Crosbie JL, et al: Superior staging of liver tumors with laparoscopy and laparoscopic ultrasound. *Ann Surg* 220:711–719, 1994.
82. Schulz A, Dormagen JB, Drolsum A, et al: Impact of contrast-enhanced intraoperative ultrasound on operation strategy in case of colorectal liver metastasis. *Acta Radiol* 53:1081–1087, 2012.
83. Ruzzenente A, Conci S, Iacono C, et al: Usefulness of contrast-enhanced intraoperative ultrasonography (CE-IIOUS) in patients with colorectal liver metastases after preoperative chemotherapy. *J Gastrointest Surg* 17:281–287, 2013.
84. Shah AJ, Callaway M, Thomas MG, Finch-Jones MD: Contrast-enhanced intraoperative ultrasound improves detection of liver metastases during surgery for primary colorectal cancer. *HPB (Oxford)* 12:181–187, 2010.
85. Mitsunori Y, Tanaka S, Nakamura N, et al: Contrast-enhanced intraoperative ultrasound for hepatocellular carcinoma: High sensitivity

- of diagnosis and therapeutic impact. *J Hepato-biliary Pancreat Sci* 20:234–242, 2013.
86. Pazaiti A, Toutouzas KG, Papadimitriou DI, et al: Change in preoperative strategy based on intraoperative ultrasound findings. *Int Surg* 94:58–62, 2009.
 87. Lordan JT, Stenson KM, Karanjia ND: The value of intraoperative ultrasound and preoperative imaging, individually and in combination, in liver resection for metastatic colorectal cancer. *Ann R Coll Surg Engl* 93:246–249, 2011.
 88. Koslin DB, Mulligan SA, Berland LL: Duplex assessment of the portal venous system. *Semin Ultrasound CT MR* 13:22–33, 1992.
 89. Grant EG, Tessler FN, Perrella RR: Clinical Doppler imaging. *AJR Am J Roentgenol* 152:707–717, 1989.
 90. Foley WD, Erickson SJ: Color Doppler flow imaging. *AJR Am J Roentgenol* 156:3–13, 1991.
 91. Zweibel WJ, Fruechte D: Basics of abdominal and pelvic duplex: Instrumentation, anatomy and vascular Doppler signatures. *Semin Ultrasound CT MR* 13:3–21, 1992.
 92. Carlisle KM, Halliwell M, Read AE, et al: Estimation of total hepatic blood flow by duplex ultrasound. *Gut* 3:92–97, 1992.
 93. Parvey HR, Eisenberg RL, Giyanani V, et al: Duplex sonography of the portal venous system: Pitfalls and limitations. *AJR Am J Roentgenol* 152:765–770, 1989.
 94. Foley WD: Abdominal color-flow ultrasound imaging. *Ultrasound Q* 7:271–291, 1989.
 95. Ralls PW: Color Doppler sonography of the hepatic artery and portal venous system. *AJR Am J Roentgenol* 155:517–525, 1990.
 96. Dodd GD, 3rd, Memel DS, Zajko AB, et al: Hepatic artery stenosis and thrombosis in transplant recipients: Doppler diagnosis with resistive index and systolic acceleration time. *Radiology* 192:657–661, 1994.
 97. Platt JF, Yutzy GG, Bude RO, et al: Use of Doppler sonography for revealing hepatic artery stenosis in liver transplant recipients. *AJR Am J Roentgenol* 168:473–476, 1997.
 98. Joynt LK, Platt JF, Rubin JM, et al: Hepatic artery resistance before and after standard meal in subjects with diseased and healthy livers. *Radiology* 196:489–492, 1995.
 99. Lafortune M, Patriquin H: Doppler sonography of the liver and splanchnic veins. *Semin Interv Radiol* 7:27–38, 1990.
 100. Koslin DB, Mulligan SA, Berland LL: Duplex assessment of splanchnic vasculature. *Semin Ultrasound CT MR* 13:34–39, 1992.
 101. Madrazo BL, Jafri SZ, Shirkhoda A, et al: Portosystemic collaterals: Evaluation with color Doppler imaging and correlation with CT and MRI. *Semin Interv Radiol* 7:169–184, 1990.
 102. Buonamico P, Sabba C: Echo Doppler duplex scanner and color in the study of portal hypertension. *J Clin Gastroenterol* 13:342–347, 1991.
 103. Van Leeuwen MS: Doppler ultrasound in the evaluation of portal hypertension. In Taylor K, Strandness D, editors: *Duplex Doppler Ultrasound*, New York, 1990, Churchill Livingstone, pp 53–76.
 104. Hann LE, Bach AM, Cramer LD, et al: Hepatic sonography: Comparison of tissue harmonic and standard sonography techniques. *AJR Am J Roentgenol* 173:201–206, 1999.
 105. Harvey CJ, Albrecht T: Ultrasound of focal liver lesions. *Eur Radiol* 11:1578–1593, 2001.
 106. Claudon M, Dietrich CF, Choi BI, et al: Guidelines and good clinical practice recommendations for contrast enhanced ultrasound (CEUS) in the liver—update 2012; a WFUMB-EFSUMB initiative in cooperation with representatives of AFSUMB, AIUM, FLAUS and ICUS. *Ultraschall Med* 34:11–29, 2013.
 107. Robbin ML: Ultrasound contrast agents: A promising future. *Radiol Clin North Am* 39:399–414, 2001.
 108. Goldberg BB, Liu J-B, Forsberg F: Ultrasound contrast agents: A review. *Ultrasound Med Biol* 20:319–333, 1994.
 109. Rawool NM, Forsberg F, Liu J, et al: US contrast enhancement in conventional and harmonic imaging modes. *Radiology* 201(P):514, 1996.
 110. Quiaia E, Bertolotto M, Forgacs B, et al: Detection of liver metastases by pulse inversion harmonic imaging during Levovist late phase: Comparison with conventional ultrasound and helical CT in 160 patients. *Eur Radiol* 13:475–483, 2003.
 111. Esteban JM, Molla MA, Tomas C, Maldonado L: Improved detection of liver metastases with contrast-enhanced wideband harmonic imaging: Comparison with CT findings. *Eur J Ultrasound* 15:119–126, 2002.
 112. Dietrich CD, Ignee A, Hocke M, et al: Pitfalls and artefacts using contrast enhanced ultrasound. *Z Gastroenterol* 49:350–356, 2011.
 113. Piscaglia F, Bolondi L: The safety of Sonovue in abdominal applications: Retrospective analysis of 23188 investigations. *Ultrasound Med Biol* 32:1369–1375, 2006.
 114. Maher MM, Kalra MK, Sahani DV, et al: Techniques, clinical applications and limitations of 3D reconstruction in CT of the abdomen. *Korean J Radiol* 5:55–67, 2004.
 115. Paushter DM, Zeman RK, Scheibler ML, et al: CT evaluation of suspected hepatic metastases: Comparison of techniques for i.v. contrast enhancement. *AJR Am J Roentgenol* 152:267–271, 1989.
 116. Mayo-Smith WW, Gupta H, Ridler MS, et al: Detecting hepatic lesions: The added utility of CT liver window settings. *Radiology* 210:601–604, 1999.
 117. Zeman RK, Clements LA, Silverman PM, et al: CT of the liver: A survey of prevailing methods for administration of contrast material. *AJR Am J Roentgenol* 150:107–109, 1988.
 118. Mathieu D, Runeton JN, Drouillard J, et al: Hepatic adenomas and focal nodular hyperplasia: Dynamic CT study. *Radiology* 160:53–57, 1986.
 119. Berland LL, Lawson TL, Foley WD, et al: Comparison of pre- and postcontrast CT in hepatic masses. *AJR Am J Roentgenol* 138:853–858, 1982.
 120. Dodd GD, III, Baron RL: Investigation of contrast enhancement in CT of the liver: The need for improved methods. *AJR Am J Roentgenol* 160:643–646, 1993.
 121. Dubrow RA, David CL, Libshitz HI, et al: Detection of hepatic metastases in breast cancer: The role of nonenhanced and enhanced CT scanning. *J Comput Assist Tomogr* 14:366–369, 1990.
 122. Bressler EL, Alpern MB, Glazer GM, et al: Hypervascular hepatic metastases: CT evaluation. *Radiology* 162:49–54, 1987.
 123. Patten RM, Byun JY, Freeny PC: CT of hypervascular hepatic tumors: Are unenhanced scans necessary for diagnosis? *AJR Am J Roentgenol* 161:979–984, 1993.
 124. Uchida M, Ishibashi M, Abe T, et al: Three-dimensional imaging of liver tumors using helical CT during intravenous injection of contrast material. *J Comput Assist Tomogr* 23:435–440, 1999.
 125. Chambers TP, Baron RL, Lush RM: Hepatic CT enhancement: Part I. Alterations in the volume of contrast material within the same patients. *Radiology* 193:513–517, 1994.
 126. Heiken JP, Brink JA, McClennan BL, et al: Dynamic incremental CT: effect of volume and concentration of contrast material and patient weight on hepatic enhancement. *Radiology* 195:353–357, 1995.
 127. Heye T, Nelson RC, Ho LM, et al: Dual-energy CT applications in the abdomen. *AJR Am J Roentgenol* 199(Suppl):S64–S70, 2012.
 128. Garcia PA, Bonaldi VM, Bret PM, et al: Effect of rate of contrast medium injection on hepatic enhancement at CT. *Radiology* 199:185–189, 1996.
 129. Irie T, Kusano S: Contrast-enhanced spiral CT of the liver: Effect of injection time on time to peak hepatic enhancement. *J Comput Assist Tomogr* 20:633–637, 1996.
 130. Freeny PC, Gardner JC, vonIngersleben G, et al: Hepatic helical CT: Effect of reduction of iodine dose of intravenous contrast material on hepatic contrast enhancement. *Radiology* 197:89–93, 1995.
 131. Baker ME, Beam C, Leder R, et al: Contrast material for combined abdominal and pelvic CT: Can cost be reduced by increasing the concentration and decreasing the volume? *AJR Am J Roentgenol* 160:637–641, 1993.
 132. Heiken JP: Liver. In Lee J, Sagel S, Stanley R, et al, editors: *Computed Body Tomography with MRI Correlation*, ed 3, Philadelphia, 1998, Lippincott-Raven, pp 701–777.
 133. Brink JA, Heiken JP, Forman HP, et al: Hepatic spiral CT: Reduction of dose of intravenous contrast material. *Radiology* 197:83–88, 1995.
 134. Megibow AJ, Jacob G, Heiken JP, et al: Quantitative and qualitative evaluation of volume of low osmolality contrast medium needed for routine helical abdominal CT. *AJR Am J Roentgenol* 176:583–589, 2001.
 135. Birnbaum BA, Jacobs JE, Yin D: Hepatic enhancement during helical CT: A comparison of moderate rate uniphasic and biphasic contrast injection protocols. *AJR Am J Roentgenol* 165:853–858, 1995.
 136. Foley WD, Hoffmann RG, Quiroz FA, et al: Hepatic helical CT: Contrast material injection protocol. *Radiology* 192:367–371, 1994.
 137. Chambers TP, Baron RL, Lush RM: Hepatic CT enhancement: Part II. Alterations in contrast material volume and rate of injection within the same patients. *Radiology* 193:518–522, 1994.
 138. Heiken JP: Liver. In Lee JKT, Sagel SS, Stanley RJ, Heiken JP, editors: *Computed Body Tomography with MRI Correlation*, Philadelphia, 1998, Lippincott-Raven, pp 701–778.
 139. Foley WD, Karcaaltincaba M: Computed tomography angiography: Principles and clinical applications. *J Comput Assist Tomogr* 27:S23–S30, 2003.
 140. Yagyu Y, Awai K, Inoue M, et al: MDCT of hypervascular hepatocellular carcinomas: A prospective study using contrast materials with different iodine concentrations. *AJR Am J Roentgenol* 184:1535–1540, 2005.
 141. Hanninen EL, Vogl TJ, Relfe R, et al: Detection of focal liver lesions at biphasic spiral CT: Randomized double-blind study of the effect of iodine concentration in contrast materials. *Radiology* 216:403–409, 2000.

142. Sultana S, Morishita S, Awai K, et al: Evaluation of hypervascular hepatocellular carcinoma in cirrhotic liver by means of helical CT: Comparison of different contrast medium concentrations within the same patient. *Radiat Med* 21:239–245, 2003.
143. Schoellnast H, Tillich M, Deutschmann HA, et al: Improvement of parenchymal and vascular enhancement using saline flush and power injection for multiple-detector-row abdominal CT. *Eur Radiol* 14:659–664, 2004.
144. Silverman PM, Roberts S, Tefft MC, et al: Helical CT of the liver: Clinical application of an automated computer technique, SmartPrep, for obtaining images with optical contrast enhancement. *AJR Am J Roentgenol* 165:73–78, 1995.
145. Kopka L, Funke M, Fischer U, et al: Parenchymal liver enhancement with bolus-triggered helical CT: Preliminary clinical results. *Radiology* 195:282–284, 1995.
146. Paulson EK, Fisher AJ, DeLong DM, et al: Helical liver CT with computer-assisted bolus-tracking technology: Is it possible to predict which patients will not achieve a threshold of enhancement? *Radiology* 209:787–792, 1998.
147. Silverman PM, Roberts SC, Ducic J, et al: Assessment of technology that permits individualized scan delays on helical hepatic CT: A technique to improve efficiency in use of contrast material. *AJR Am J Roentgenol* 167:79–84, 1996.
148. Dinkel HP, Fieger M, Knupffer J, et al: Optimizing liver contrast in helical liver CT: Value of a real-time bolus-triggering technique. *Eur Radiol* 8:1608–1612, 1998.
149. Kopka L, Funke M, Fischer U, et al: Parenchymal liver enhancement with bolus-triggered helical CT: Preliminary clinical results. *Radiology* 195:282–284, 1995.
150. Mehnert F, Pereira PL, Trubenbach J, et al: Automatic bolus tracking in monophasic spiral CT of the liver: Liver-to-lesion conspicuity. *Eur Radiol* 11:580–584, 2001.
151. Nelson RC, Moyers JH, Chezmar JL, et al: Hepatic dynamic sequential CT: Section enhancement profiles with a bolus of ionic and nonionic contrast agents. *Radiology* 178:499–502, 1991.
152. Kim T, Murakami T, Tsuda K, et al: Effects of injection rates of contrast material on arterial phase hepatic CT. *AJR Am J Roentgenol* 171:429–432, 1998.
153. Kopka L, Rodenwaldt J, Fischer U, et al: Dual-phase helical CT of the liver: Effects of bolus tracking and different volumes of contrast material. *Radiology* 201:321–326, 1996.
154. Choi BI, Lee HJ, Han JK, et al: Detection of hypervascular nodular hepatocellular carcinomas: Value of triphasic helical CT compared with iodized-oil CT. *AJR Am J Roentgenol* 168:219–224, 1997.
155. Kanematsu M, Oliver JH, 3rd, Carr B, et al: Hepatocellular carcinoma: The role of helical biphasic contrast-enhanced CT versus CT during arterial portography. *Radiology* 205:75–80, 1997.
156. Hwang GJ, Kim MJ, Yoo HS, et al: Nodular hepatocellular carcinomas: Detection with arterial-, portal-, and delayed-phase images at spiral CT. *Radiology* 202:383–388, 1997.
157. Sahani D, Mehta A, Blake M, et al: Preoperative hepatic vascular evaluation with CT and MR angiography: Implications for surgery. *Radiographics* 24:1367–1380, 2004.
158. Hollett MD, Jeffrey RB, Jr, Nino-Murcia M, et al: Dual-phase helical CT of the liver: Value of arterial phase scans in the detection of small (≤ 1.5 cm) malignant hepatic neoplasms. *AJR Am J Roentgenol* 164:879–884, 1995.
159. Miller FH, Butler RS, Hoff FL, et al: Using triphasic helical CT to detect focal hepatic lesions in patients with neoplasms. *AJR Am J Roentgenol* 171:643–649, 1998.
160. Oliver JH, 3rd, Baron RL, Federle MP, et al: Hypervascular liver metastases: Do unenhanced and hepatic arterial phase CT images affect tumor detection? *Radiology* 205:709–715, 1997.
161. Federle MP, Blachar A: CT evaluation of the liver: Principles and techniques. *Semin Liver Dis* 21:135–146, 2001.
162. Kalra MK, Maher MM, Rizzo S, Saini S: Radiation exposure and projected risks with multi-detector row computed tomography scanning: Clinical strategies and technologic developments for dose reduction. *J Comput Assist Tomogr* 28:S46–S49, 2004.
163. Kalra MK, Maher MM, Toth TL, et al: Comparison of z-axis automatic tube current modulation technique with fixed tube current CT scanning of abdomen and pelvis. *Radiology* 232:347–353, 2004.
164. Kalra MK, Prasad S, Saini S, et al: Clinical comparison of standard-dose and 50% reduced-dose abdominal CT: Effect on image quality. *AJR Am J Roentgenol* 179:1101–1106, 2002.
165. Lacomis JM, Baron RL, Oliver JH, 3rd, et al: Cholangiocarcinoma: Delayed CT contrast enhancement patterns. *Radiology* 203:98–104, 1997.
166. Keogan MT, Seabourn JT, Paulson EK, et al: Contrast-enhanced CT of intrahepatic and hilar cholangiocarcinoma: Delay time for optimal imaging. *AJR Am J Roentgenol* 169:1493–1499, 1997.
167. Bernardino ME, Erwin BC, Steiberg HV, et al: Delayed hepatic CT scanning: Increased confidence and improved detection of hepatic metastases. *Radiology* 159:71–74, 1986.
168. Miller DL, Simmons JT, Chang R, et al: Hepatic metastasis detection: Comparison of three CT contrast enhancement methods. *Radiology* 165:785–790, 1987.
169. Perkerson RB, Erwin BC, Baumgartner BR, et al: CT densities in delayed iodine hepatic scanning. *Radiology* 155:445–446, 1985.
170. Phillips VM, Erwin BC, Bernardino ME: Delayed iodine scanning of the liver: A promising CT technique. *J Comput Assist Tomogr* 9:415–419, 1985.
171. Iannaccone R, Laghi A, Catalano C, et al: Hepatocellular carcinoma: Role of unenhanced and delayed phase multi-detector row helical CT in patients with cirrhosis. *Radiology* 234:460–467, 2005.
172. Nelson RC, Moyers JH, Chezmar JL, et al: Hepatic dynamic sequential CT: Section enhancement profiles with a bolus of ionic and nonionic contrast agents. *Radiology* 178:499–502, 1991.
173. Heiken JP, Weyman PJ, Lee JKT, et al: Detection of focal hepatic masses: Prospective evaluation with CT, delayed CT, CT during arterial portography, and MR imaging. *Radiology* 171:47–51, 1989.
174. Bluemke DA, Soyer PA, Chan BW, et al: Spiral CT during arterial portography: Technique and applications. *Radiographics* 15:623–637, 1995.
175. Nghiem HV, Dimas CT, McVicar JP, et al: Impact of double helical CT and three-dimensional CT arteriography on surgical planning for hepatic transplantation. *Abdom Imaging* 24:278–284, 1999.
176. Freeny PC, Nghiem HV, Winter TC: Helical CT during arterial portography: Optimization of contrast enhancement and scanning parameters. *Radiology* 194:83–90, 1995.
177. Soyer P, Roche A, Gad M, et al: Preoperative segmental localization of hepatic metastases: Utility of three-dimensional CT during arterial portography. *Radiology* 180:653–658, 1991.
178. Freeny PC, Marks WM: Hepatic perfusion abnormalities during CT angiography: Detection and interpretation. *Radiology* 159:685–691, 1986.
179. Fernandez MDP, Bernardino ME: Hepatic pseudolesion: Appearance of focal low attenuation in the medial segment of the left lobe at CT arterial portography. *Radiology* 181:809–812, 1992.
180. DeSanctis JT, Gazelle GS, Saini S: CT techniques. In Gazelle GS, Saini S, Mueller PR, editors: *Hepatobiliary and Pancreatic Radiology Imaging and Intervention*, New York, 1998, Thieme, pp 38–61.
181. Li L, Liu LZ, Xie ZM, et al: Multi-phasic CT arterial portography and CT hepatic arteriography improving the accuracy of liver cancer detection. *World J Gastroenterol* 10:3118–3121, 2004.
182. Pandharipande PV, Krinsky GA, Rusinek H, et al: Perfusion imaging of the liver: Current challenges and future goals. *Radiology* 234:661–673, 2005.
183. Van Beers BE, Leconte I, Materne R, et al: Hepatic perfusion parameters in chronic liver disease: Dynamic CT measurements correlated with disease severity. *AJR Am J Roentgenol* 176:667–673, 2001.
184. Kemmerer SR, Mortele KS, Ros PR: CT scan of the liver. *Radiol Clin North Am* 36:247–262, 1998.
185. Sahani DV, Kalva SP, Hahn PE, Saini S: 16-MDCT angiography in living kidney donors at various tube potentials: Impact on image quality and radiation dose. *AJR Am J Roentgenol* 188:115–120, 2007.
186. Kalra MK, Prasad S, Saini S, et al: Clinical comparison of standard-dose and 50% reduced-dose abdominal CT: Effect on image quality. *AJR Am J Roentgenol* 179:1101–1106, 2002.
187. Mahesh M: Advances in CT technology and application to pediatric imaging. *Pediatr Radiol* 41(Suppl 2):493–497, 2011.
188. McCollough CH, Bruesewitz MR, Kofler JM, Jr: CT dose reduction and dose management tools: Overview of available options. *Radiographics* 26:503–512, 2006.
189. Rizzo S, Kalra M, Schmidt B, et al: Comparison of angular and combined automatic tube current modulation techniques with constant tube current CT of the abdomen and pelvis. *AJR Am J Roentgenol* 186:673–679, 2006.
190. Kalra MK, Maher MM, Toth TL, et al: Comparison of Z-axis automatic tube current modulation technique with fixed tube current CT scanning of abdomen and pelvis. *Radiology* 232:347–353, 2004.
191. Eller A, May MS, Scharf M, et al: Attenuation-based automatic kilovolt selection in abdominal computed tomography: Effects on radiation exposure and image quality. *Invest Radiol* 47:559–565, 2012.

192. Gnannt R, Winklehner A, Eberli D, et al: Automated tube potential selection for standard chest and abdominal CT in follow-up patients with testicular cancer: Comparison with fixed tube potential. *Eur Radiol* 22:1937–1945, 2012.
193. Kulkarni NM, Uppot RN, Eisner BH, Sahani DV: Radiation dose reduction at multidetector CT with adaptive statistical iterative reconstruction for evaluation of urolithiasis: How low can we go? *Radiology* 265:158–166, 2012.
194. Lezzi R, Santoro M, Marano R, et al: Low-dose multidetector CT angiography in the evaluation of infrarenal aorta and peripheral arterial occlusive disease. *Radiology* 263:287–298, 2012.
195. Kalra MK, Maher MM, Blake MA, et al: Detection and characterization of lesions on low-radiation-dose abdominal CT images postprocessed with noise reduction filters. *Radiology* 232:791–797, 2004.
196. Silva AC, Lawder HJ, Hara A, et al: Innovations in CT dose reduction strategy: Application of the adaptive statistical iterative reconstruction algorithm. *AJR Am J Roentgenol* 194:191–199, 2010.
197. Hara AK, Paden RG, Silva AC, et al: Iterative reconstruction technique for reducing body radiation dose at CT: Feasibility study. *AJR Am J Roentgenol* 193:764–771, 2009.
198. Han BK, Grant KL, Garberich R, et al: Assessment of an iterative reconstruction algorithm (SAFIRE) on image quality in pediatric cardiac CT datasets. *J Cardiovasc Comput Tomogr* 6:200–204, 2012.
199. Prakash P, Kalra MK, Kambadakone AK, et al: Reducing abdominal CT radiation dose with adaptive statistical iterative reconstruction technique. *Invest Radiol* 45:202–210, 2010.
200. Miles KA: Tumour angiogenesis and its relation to contrast enhancement on computed tomography: A review. *Eur J Radiol* 30:198–205, 1999.
201. Miles KA: Perfusion CT for the assessment of tumour vascularity: Which protocol? *Br J Radiol* 76(Spec1):S36–S42, 2003.
202. Miles KA, Hayball MP, Dixon AK: Functional images of hepatic perfusion obtained with dynamic CT. *Radiology* 188:405–411, 1993.
203. Spira D, Schulze M, Sauter A, et al: Volume perfusion-CT of the liver: Insights and applications. *Eur J Radiol* 81:1471–1478, 2012.
204. Graser A, Johnson TRC, Hecht EM, et al: Dual-energy CT in patients suspected of having renal masses: Can virtual nonenhanced images replace true nonenhanced images? *Radiology* 252:433–440, 2009.
205. Heye T, Nelson RC, Ho LM, et al: Dual-energy CT applications in the abdomen. *AJR Am J Roentgenol* 199(Suppl):S64–S70, 2012.
206. Marin D, Nelson RC, Samei E, et al: Hypervascular liver tumors: Low tube voltage, high tube current multidetector CT during late hepatic arterial phase for detection—initial clinical experience. *Radiology* 251:771–779, 2009.
207. Robinson E, Chandarana H, Macari M: Dual source dual energy MDCT: Comparison of 80 kVp and weighted average 120 kVp data for conspicuity of hypo-vascular liver metastases. *Invest Radiol* 45:413–418, 2010.
208. Coursey CA, Nelson RC, Boll DT, et al: Dual-energy multidetector CT: How does it work, what can it tell us, and when can we use it in abdominopelvic imaging? *Radiographics* 30:1037–1055, 2010.
209. Song KD, Kim CK, Park BK, Kim B: Utility of iodine overlay technique and virtual unenhanced images for the characterization of renal masses by dual-energy CT. *AJR Am J Roentgenol* 197:W1076–W1082, 2011.
210. Lee SH, Lee JM, Kim KW, et al: Dual-energy computed tomography to assess tumor response to hepatic radiofrequency ablation: Potential diagnostic value of virtual noncontrast images and iodine maps. *Invest Radiol* 46:77–84, 2011.
211. Urhahn R, Drobnitzky M, Klose K-C, et al: Incremental flip angle snapshot FLASH MRI of hepatic lesions: Improvement of signal-to-noise and contrast. *J Comput Assist Tomogr* 16:219–225, 1992.
212. Taupitz M, Hamm B, Speidel A, et al: Multisection FLASH: Method for breath-hold MR imaging of the entire liver. *Radiology* 183:73–79, 1992.
213. Gehl HB, Bohnndorf KC, Klose KC, et al: Two-dimensional MR angiography in the evaluation of abdominal veins with gradient refocused sequences. *J Comput Assist Tomogr* 14:619–624, 1990.
214. Raval B, Mehta S, Narayana P, et al: Feasibility of fast MR imaging of the liver at 1.5 T. *Magn Reson Imaging* 7:203–210, 1989.
215. Semelka RC, Hricak H, Bis KG: Liver lesion detection: Comparison between excitation-spoiling fat suppression and regular spin-echo at 1.5T. *Abdom Imaging* 18:56–60, 1993.
216. Vassiliades VCG, Bernardino ME: Magnetic resonance imaging of the liver. *Top Magn Reson Imaging* 2:1–16, 1990.
217. Semelka RC, Simm FC, Recht M, et al: T1-weighted sequences for MR imaging of the liver: Comparison of three techniques for single-breath whole-volume acquisition at 1.0 and 1.5 T. *Radiology* 180:629–635, 1991.
218. Meyer CA, Colon E, Provost T, et al: Delineation of surgical segmental anatomy: Value of PRIDE, and MR fast-scanning technique. *AJR Am J Roentgenol* 158:299–301, 1992.
219. Nghiem HV, Herfkens RJ, Francis IR, et al: T2-weighted fast spin echo MR imaging of the abdomen and pelvis. *Radiology* 185:213–217, 1992.
220. Chien D, Atkinson DJ, Edelman RR: Strategies to improve contrast in turbo FLASH imaging: Reordered phase encoding and K-space segmentation. *J Magn Reson Imaging* 1:63–70, 1991.
221. Haacke EM, Tkach JA: Fast MR imaging: Techniques and clinical applications. *AJR Am J Roentgenol* 155:951–964, 1990.
222. Low RN, Francis IR, Herfkens RJ, et al: Fast multiplanar spoiled gradient-recalled imaging of the liver: Pulse sequence optimization and comparison with spin-echo imaging. *AJR Am J Roentgenol* 160:501–509, 1993.
223. Kanematsu M, Hoshi H, Itoh K, et al: Focal hepatic lesion detection: Comparison of four fat-suppressed T2-weighted MR imaging pulse sequences. *Radiology* 211:363–371, 1999.
224. McCarthy S, Hricak H, Cohen M, et al: Cholecystitis: Detection with MR imaging. *Radiology* 158:333–336, 1986.
225. Foley WD, Kneeland JB, Cates JD, et al: Contrast optimization for the detection of focal hepatic lesions by MR imaging at 1.5 T. *AJR Am J Roentgenol* 149:1155–1160, 1987.
226. Henkelman RM, Hardy P, Poon PY, et al: Optimal pulse sequence for imaging hepatic metastases. *Radiology* 161:727–730, 1986.
227. Jolesz FA, Higuchi N, Oshio K, et al: Clinical implementation of fast spin-echo imaging. *Radiology* 181:164–165, 1991.
228. Melki PS, Mulkern RV, Panych LS, et al: Comparing the FAISE method with conventional dual-echo sequences. *J Magn Reson Imaging* 1:319–326, 1991.
229. Low RN, Francis IR, Sigeti JS, et al: Abdominal MR imaging: Comparison of T2-weighted fast and conventional spin-echo, and contrast enhanced fast multiplanar spoiled gradient-recalled imaging. *Radiology* 186:803–811, 1993.
230. Soyer P, Le Normand S, Clement de Givry S, et al: T2-weighted spin-echo MR imaging of the liver: Comparison of breath-hold fast spin-echo with non-breath-hold fast spin-echo with and without fat suppression. *AJR Am J Roentgenol* 166:593, 1996.
231. Siegelman ES, Outwater EK: MR imaging techniques of the liver. *Radiol Clin North Am* 36:263–284, 1998.
232. Semelka RC, Kelekis NL, Thomasson D, et al: HASTE MR imaging: Description of technique and preliminary results in the abdomen. *J Magn Reson Imaging* 6:698–699, 1996.
233. Bydder GM, Steiner RE, Blumgart CH, et al: MR imaging of the liver using short T1 inversion recovery sequences. *J Comput Assist Tomogr* 9:1084–1089, 1985.
234. Bydder GM, Young IR: MRI: Clinical uses of the inversion recovery sequence. *J Comput Assist Tomogr* 9:659–675, 1985.
235. Dousset M, Weissleder R, Hendrick RE, et al: Short T1 inversion recovery imaging of the liver: Pulse sequence optimization and comparison spin echo imaging. *Radiology* 171:327–333, 1989.
236. Shuman WP, Baron RL, Peters MJ, et al: Comparison of STIR and spin echo MR imaging at 1.5 T in 90 lesions of the chest, liver, and pelvis. *AJR Am J Roentgenol* 152:853–859, 1989.
237. Schertz D, Lee JKT, Heiken JP, et al: Proton spectroscopic imaging (Dixon method) of the liver: Clinical utility. *Radiology* 173:401–406, 1989.
238. Lee JKT, Dixon NT, Ling D, et al: Fatty infiltration of the liver: Demonstration by proton spectroscopic imaging: Preliminary observations. *Radiology* 153:195–199, 1984.
239. Brateman L: Chemical shift imaging: A review. *AJR Am J Roentgenol* 146:971–980, 1986.
240. Wehrli FW, Perkins TG, Shimakawa A, et al: Chemical shift-induced amplitude modulations in images obtained with gradient refocusing. *Magn Reson Imaging* 5:157–158, 1987.
241. Delfaut EM, Beltran J, Johnson G, et al: Fat suppression in MR imaging: Techniques and pitfalls. *Radiographics* 19:373–382, 1999.
242. Martin J, Sentis M, Zidan A, et al: Fatty metamorphosis of hepatocellular carcinoma: Detection with chemical shift gradient-echo MR imaging. *Radiology* 195:125, 1995.
243. Mitchell DG, Stolpen AH, Siegelman ES, et al: Fatty tissue on opposed-phase MR images: Paradoxical suppression of signal intensity by paramagnetic contrast agents. *Radiology* 198:351–357, 1996.
244. Semelka RC, Helmberger TKG: Contrast agents for MR imaging of the liver. *Radiology* 218:27–38, 2001.
245. Harisinghani MG, Jhaveri KS, Weissleder R, et al: MRI contrast agents for evaluating focal hepatic lesions. *Clin Radiol* 56:714–725, 2001.
246. Edelman RR, Siegel JB, Singer A, et al: Dynamic MR imaging of the liver with Gd-DTPA: Initial clinical results. *AJR Am J Roentgenol* 153:1213–1219, 1989.

247. Dixon WT: Simple proton spectroscopic imaging. *Radiology* 153:189–194, 1984.
248. Reeder SB, McKenzie CA, Pineda AR, et al: Water-fat separation with IDEAL gradient-echo imaging. *J Magn Reson Imaging* 25:644–652, 2007.
249. Brancatelli G, Federle MP, Baron RL, et al: Arterially enhancing liver lesions: Significance of sustained enhancement on hepatic venous and delayed phase with magnetic resonance imaging. *J Comput Assist Tomogr* 31:116–122, 2007.
250. Kelekis NL, Semelka RC, Worawattanakul S, et al: Hepatocellular carcinoma in North America: A multiinstitutional study of appearance on T1-weighted, T2-weighted, and serial gadolinium-enhanced gradient-echo images. *AJR Am J Roentgenol* 170:1005–1013, 1998.
251. Gandhi SN, Brown MA, Wong JG, et al: MR contrast agents for liver imaging: What, when, how. *Radiographics* 26:1621–1636, 2006.
252. Mahfouz A-E, Hamm B: Contrast agents. *MRI Clin North Am* 5:223–240, 1997.
253. Soyer P, de Givry SC, Gueye C, et al: Detection of focal hepatic lesions with MR imaging: Prospective comparison of T2-weighted fast spin-echo with and without fat suppression, T2-weighted breath-hold fast spin-echo, and gadolinium chelate-enhanced 3D gradient-recalled imaging. *AJR Am J Roentgenol* 166:1115–1121, 1996.
254. Namkung S, Zech CJ, Helmberger T, et al: Superparamagnetic iron oxide (SPIO)-enhanced liver MRI with ferucarbotran: Efficacy for characterization of focal liver lesions. *J Magn Reson Imaging* 25:755–765, 2007.
255. Saini S, Edelman RR, Sharma P, et al: Blood-pool MR contrast material for detection and characterization of focal hepatic lesions: Initial clinical experience with ultrasmall superparamagnetic iron oxide (AMI-227). *AJR Am J Roentgenol* 164:1147–1152, 1995.
256. Saini S, Sharma R, Baron RL, et al: Multicenter dose-ranging study on the efficacy of USPIO ferumoxtran-10 for liver MR imaging. *Clin Radiol* 55:690–695, 2000.
257. Ward J, Naik KS, Guthrie JA, et al: Hepatic lesion detection: Comparison of MR imaging after the administration of superparamagnetic iron oxide with dual-phase CT by using alternative-free response receiver operating characteristic analysis. *Radiology* 210:459–466, 1999.
258. Savranoglu P, Obuz F, Karasu S, et al: The role of SPIO-enhanced MRI in the detection of malignant liver lesions. *Clin Imaging* 30:377–381, 2006.
259. Chan JHM, Tsui EYK, Luk SH, et al: Diffusion-weighted MR imaging of the liver: Distinguishing hepatic abscess from cystic or necrotic tumor. *Abdom Imaging* 26:161–165, 2001.
260. Jackson A, Haroon H, Zhu XP, et al: Breath-hold perfusion and permeability mapping of hepatic malignancies using magnetic resonance imaging and a first-pass leakage profile model. *NMR Biomed* 15:164–173, 2002.
261. Annet L, Materne R, Danse E, et al: Hepatic flow parameters measured with MR imaging and Doppler US: Correlations with degree of cirrhosis and portal hypertension. *Radiology* 229:409–414, 2003.
262. Vogl TJ, Pegios W, McMahon C, et al: Gadobenate dimeglumine, a new contrast agent for MR imaging: Preliminary evaluation in healthy volunteers. *AJR Am J Roentgenol* 158:887–892, 1992.
263. Cruite I, Schroeder M, Merkle EM, Sirlin CB: Gadoxetate disodium-enhanced MRI of the liver: Part 2, protocol optimization and lesion appearance in the cirrhotic liver. *AJR Am J Roentgenol* 195:29–41, 2010.
264. Poeckler-Schoeniger C, Koepke J, Gueckel F, et al: MRI with superparamagnetic iron oxide: Efficacy in the detection and characterization of focal hepatic lesions. *Magn Reson Imaging* 17:383–392, 1999.
265. Yamashita Y, Yamamoto H, Hirai A, et al: MR imaging enhancement with superparamagnetic iron oxide in chronic liver disease: Influence of liver dysfunction and parenchymal pathology. *Abdom Imaging* 21:318–323, 1996.
266. Sahani DV, O'Malley ME, Bhat S, et al: Contrast-enhanced MRI of the liver with mangafodipir trisodium: Imaging technique and results. *J Comput Assist Tomogr* 26:216–222, 2002.
267. Murakami T, Baron RL, Peterson MS, et al: Hepatocellular carcinoma: MR imaging with mangafodipir trisodium (Mn-DPDP). *Radiology* 200:69–77, 1996.
268. Mannelli L, Bhargava P, Osman SP, et al: Diffusion-weighted imaging of the liver: A comprehensive review. *Curr Prob Diagn Radiol* 42:77–83, 2013.
269. Wallis F, Gilbert FJ: Magnetic resonance imaging in oncology: An overview. *J R Coll Surg Edinb* 44:117–125, 1999.
270. Glockner JF: Hepatobiliary MRI: Current concepts and controversies. *J Magn Reson Imaging* 25:681–695, 2007.
271. Shimada K, Isoda H, Hirokawa Y, et al: Comparison of gadolinium-EOB-DTPA-enhanced and diffusion-weighted liver MRI for detection of small hepatic metastases. *Eur Radiol* 20:2690–2698, 2010.
272. Parikh T, Drew SJ, Lee VS, et al: Focal liver lesion detection and characterization with diffusion-weighted MR imaging: Comparison with standard breath-hold T2-weighted imaging. *Radiology* 246:812–822, 2008.
273. Taouli B: Diffusion-weighted MR imaging for liver lesion characterization: A critical look. *Radiology* 262:378–380, 2012.
274. Xia D, Jing J, Shen H, Wu J: Value of diffusion-weighted magnetic resonance images for discrimination of focal benign and malignant hepatic lesions: A meta-analysis. *J Magn Reson Imaging* 32:130–137, 2010.
275. Manduca A, Oliphant TE, Dresner MA, et al: Magnetic resonance elastography: Non-invasive mapping of tissue elasticity. *Med Image Anal* 5:237–254, 2001.
276. Talwalkar JA, Yin M, Fidler JL, et al: Magnetic resonance imaging of hepatic fibrosis: Emerging clinical applications. *Hepatology* 47:332–342, 2008.
277. Rouvière O, Yin M, Dresner MA, et al: MR elastography of the liver: Preliminary results. *Radiology* 240:440–448, 2006.
278. Cho SG, Kim MY, Kim HJ, et al: Chronic hepatitis: In vivo proton MR spectroscopic evaluation of the liver and correlation with histopathologic findings. *Radiology* 221:740–746, 2001.
279. Szczepaniak LS, Nurenberg P, Leonard D, et al: Magnetic resonance spectroscopy to measure hepatic triglyceride content: Prevalence of hepatic steatosis in the general population. *Am J Physiol Endocrinol Metab* 288:E462–E468, 2005.
280. Paley MR, Ros PR: MR imaging of the liver—a practical approach. *MRI Clin North Am* 5:415–430, 1997.
281. Barth MM, Smith MP, Pedrosa I, et al: Body MR Imaging at 3.0 T: Understanding the opportunities and challenges. *Radiographics* 27:1445–1462, 2007.
282. Hamer OW, Schlottmann K, Sirlin CB, et al: Technology insight: Advances in liver imaging. *Nat Clin Pract Gastroenterol Hepatol* 4:215–228, 2007.
283. Kanematsu M, Goshima S, Kondo H, et al: Gadolinium-enhanced multiphasic 3D MRI of the liver with prospective navigator correction: Phantom study and preliminary clinical evaluation. *AJR Am J Roentgenol* 188:W309–W316, 2007.
284. Zizka J, Klzo L, Ferda J, et al: Dynamic and delayed contrast enhancement in upper abdominal MRI studies: Comparison of gadoxetic acid and gadobutrol. *Eur J Radiol* 62:186–191, 2007.
285. Tan-Tam C, Chung SW: Minireview on laparoscopic hepatobiliary and pancreatic surgery. *World J Gastrointest Endosc* 6:60–67, 2014.

Interventional Radiology of the Liver

MICHAEL A. WOODS | DOUGLAS R. KITCHIN | ORHAN S. OZKAN |
FRED T. LEE, JR

CHAPTER OUTLINE

Liver Biopsy

Percutaneous Liver Biopsy

Transjugular Liver Biopsy

Liver Aspiration and Drainage

Hepatic Abscess

Hepatic Venous Pressure Gradient

Brief Rationale and Indications

Guidance and Technique

Results and Complications

Transjugular Intrahepatic Portosystemic Shunt

Brief Rationale and Indications

Relative and Absolute Contraindications

Guidance and Technique

Results

Complications

Follow-up and TIPS Revision

Interventional Oncology in the Liver

Preoperative Portal Vein Embolization

Tumor Ablation

Endovascular Intra-Arterial Therapies

Combination Interstitial and Endovascular Therapy

Liver Biopsy

PERCUTANEOUS LIVER BIOPSY

Random

Brief Rationale. The first percutaneous liver aspiration was performed by German physician Paul Ehrlich in 1883, but the technique became widely accepted only after the landmark publication by Menghini in 1958.¹ It is likely that the intensive efforts to characterize and to quantify diffuse liver disease through magnetic resonance (MR) elastography, MR spectroscopy, and ultrasound elastography will at some point obviate the need for liver biopsy in many patients. However, liver biopsy currently remains the “gold standard” for parenchymal evaluation in the setting of diffuse hepatic disease.²⁻⁴ Current indications for nonfocal liver biopsy include the diagnosis and staging of cirrhosis, cholestatic liver disease, metabolic storage disease, and other infiltrative diseases.⁵

Preprocedural Evaluation and Contraindications. Patients should have nothing by mouth for 4 to 6 hours before a liver biopsy if intravenous sedatives are to be administered. Although there is wide variation in individual practices, the Society of Interventional Radiology has provided a consensus set of guidelines for periprocedural management of laboratory coagulation

parameters and medications that recommends checking preprocedural international normalized ratio (INR) in all patients and activated partial thromboplastin time (aPTT) in patients receiving unfractionated heparin with subsequent correction to INR below 1.5 and aPTT of less than 1.5 times the control value. Although these guidelines do not recommend checking platelets before the procedure, they do recommend correcting platelets to more than 50,000 in patients with known thrombocytopenia. Warfarin as well as antiplatelet agents such as clopidogrel should be discontinued for at least 5 days before biopsy.⁶ Although there is no consensus, many practices restart antiplatelet therapy such as clopidogrel 48 to 72 hours and warfarin 24 hours after the biopsy.⁵ There also is no consensus addressing the alteration of heparin therapy, although others have suggested holding heparin for between 2 and 6 hours before the procedure and restarting heparin 12 hours after the procedure.⁷

Although no absolute contraindications to liver biopsy exist, relative contraindications, such as the patient's cooperation, extrahepatic biliary obstruction, and severe coagulopathy, may warrant consideration of transjugular liver biopsy in specific cases. However, correction of coagulation abnormalities can also be performed to proceed safely with percutaneous liver biopsy.

Guidance and Technique. Percutaneous liver biopsy is a safe procedure that can be performed on an outpatient basis. Imaging guidance is becoming increasingly prevalent and has multiple advantages over palpation- or percussion-guided techniques, including a decreased complication rate and superior diagnostic yield.⁸ Ultrasound is the preferred imaging modality in most cases because of low cost, real-time guidance, multiplanar imaging, portability, visualization and avoidance of major blood vessels and lung, and lack of ionizing radiation. Imaging guidance with ultrasound has also been shown to decrease the number of major and minor complications.^{9,10} Although ultrasound-guided liver biopsies are slightly more costly on a per-procedure basis than biopsies guided by palpation, cost-effectiveness analyses have suggested that the other benefits of ultrasound guidance may reduce the overall cost of liver biopsy.^{11,12}

Ultrasound-guided biopsies can be performed through a subcostal or intercostal approach. A subcostal approach is generally favored over an intercostal puncture because of a lower risk of pneumothorax or intercostal artery injury.¹³ Sonographically guided interventions can be performed either by a free-hand technique (which provides for greater freedom in needle placement) or with an attached biopsy guide (which provides greater accuracy). Local anesthetic should be liberally applied from the skin entry site down through the subcutaneous fat and peritoneum directly onto the liver capsule. If possible, the biopsy needle should be placed during a breath hold to reduce



Figure 84-1 Random liver biopsy. Ultrasound image demonstrates real-time percutaneous needle placement for a random liver biopsy in the evaluation of a patient with known hepatitis C through a subcostal approach.

the risk of capsule laceration and to facilitate biopsy at the site of local anesthetic administration.¹⁴ Although the American Association for the Study of Liver Diseases (AASLD) recommends a 16-gauge biopsy needle of 2 or 3 cm in length for the diagnosis, grading, and staging of diffuse parenchymal liver diseases, the use of 18-gauge cutting needles is common in many institutions.⁵ The patients should be monitored for 2 to 4 hours after the procedure in a recovery unit before discharge (Fig. 84-1).

Complications. The most common complication after liver biopsy is pain, the exact cause of which is unknown but may be due to a small bile leak or subcapsular hematoma. Most post-biopsy pain is readily managed with intravenous or oral analgesics.¹⁵ Bleeding is the most important complication after liver biopsy. Subclinical bleeding not requiring specific intervention occurs in up to 23% of liver biopsies, and severe hemorrhage requiring transfusion or other intervention occurs in 0.35% to 0.5%.^{8,16-18} Other potential complications include damage to adjacent organs, pneumothorax, hemothorax, peritonitis, and death. The reported mortality rate after liver biopsy is approximately 0.01%.⁵

Image-Guided Percutaneous Liver Mass Biopsy

Indications

Hepatocellular Carcinoma. The recommendations for hepatocellular cancer screening have recently been updated by the AASLD, and surveillance for patients at high risk for the development of hepatocellular carcinoma (HCC) is recommended with ultrasound every 6 months.¹⁹ Routine serum α -fetoprotein is no longer recommended for screening or diagnosis because of lack of sensitivity and specificity.^{20,21} If a nodule larger than 1 cm is identified on screening ultrasound, contrast-enhanced multiphasic computed tomography (CT) or magnetic resonance imaging (MRI) is performed. Liver biopsy is rarely indicated in the evaluation for HCC, particularly in the setting of cirrhosis, because of the ability to diagnose most cases of HCC with imaging alone. In addition, the small but real risk of bleeding and tumor seeding generally outweighs the benefit of histologic diagnosis, given the extremely high pretest probability of HCC with imaging. The risk of tumor seeding along a biopsy

track is estimated at 0.9% per patient per year.²² At most institutions, HCC is predominantly an imaging diagnosis, and patients are managed without histologic confirmation.^{23,24} There are currently two sets of imaging criteria for the diagnosis of HCC on CT or MRI, the Liver Imaging Reporting and Data System (LI-RADS) and the United Network for Organ Sharing (UNOS)/Organ Procurement and Transplant Network (OPTN) criteria.^{25,26} Both sets of criteria incorporate the presence or absence of arterial enhancement, washout, capsule, and growth to diagnose HCC. Percutaneous image-guided liver biopsy is reserved for lesions that do not meet strict imaging characteristics by MRI and CT.¹⁶ However, even biopsy is not 100% accurate for the diagnosis of small HCCs.²⁷

Other Focal Liver Lesions. Targeted liver biopsies are frequently performed in the evaluation of focal hepatic abnormalities not suspected of being HCC. CT and MRI are often used for first-line characterization of focal hepatic abnormalities because of the ability to definitively diagnose many HCCs, hemangiomas, adenomas, and focal hepatic steatosis. Other lesions have a less characteristic imaging appearance and typically require biopsy for tissue diagnosis.²⁸ As metastatic lesions are more common than primary hepatic malignant disease, the majority of targeted hepatic biopsies are performed in an effort to evaluate focal liver lesions in the setting of a known primary malignant neoplasm. Sampling the metastatic lesions in the liver (or elsewhere) can serve both to make a diagnosis and to stage the disease concurrently. Thus, liver biopsy is often performed, even when the site of extrahepatic primary malignant disease is suspected or known (Fig. 84-2).

Preprocedural Evaluation. The preprocedural evaluation for patients undergoing percutaneous liver biopsy for a focal mass lesion in the liver is similar to that described for image-guided random liver biopsy.

Guidance and Technique. Most image-guided liver biopsies are performed under either ultrasound or CT guidance. Ultrasound is the preferred imaging modality worldwide for liver biopsy guidance for the reasons described in the preceding section. However, CT guidance has been proved to be effective and safe for experienced operators.²⁹ The advantages of ultrasound include less expense, lack of radiation, and real-time imaging as well as ability to access lesions at the hepatic dome. The disadvantages of ultrasound include user dependence and difficulty of imaging large patients. The lack of inherent tissue contrast often makes identification of targets difficult by non-contrast CT. Both core needle and fine-needle aspiration techniques can be used for liver biopsy, but most studies favor obtaining a core needle specimen because of increased specificity and accuracy in diagnosis and subtyping of tumors, superiority in diagnosis of benign lesions, decreased biologic sampling errors, and preservation of tissue architecture.³⁰⁻³² In biopsy of a focal liver lesion, every attempt should be made to perform the biopsy through a cuff of normal liver parenchyma to decrease the risk of bleeding.³³ With larger masses, core samples should be taken from the periphery of the lesion to avoid central necrosis.³⁴

Results and Complications. Image-guided biopsy of focal liver lesions has been shown to have a high diagnostic accuracy (94.5%-100%), even for lesions between 0.5 and 1.0 cm.^{29,34-36} In patients with a known primary malignant neoplasm with a

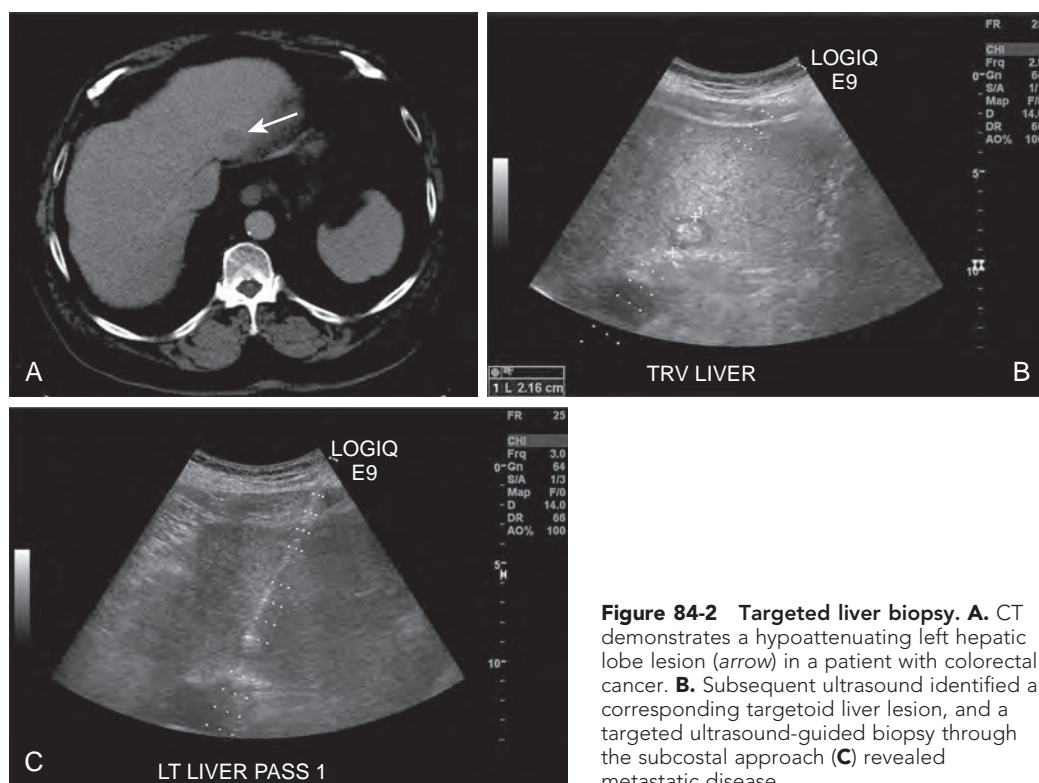


Figure 84-2 Targeted liver biopsy. **A.** CT demonstrates a hypoattenuating left hepatic lobe lesion (arrow) in a patient with colorectal cancer. **B.** Subsequent ultrasound identified a corresponding targetoid liver lesion, and a targeted ultrasound-guided biopsy through the subcostal approach (**C**) revealed metastatic disease.

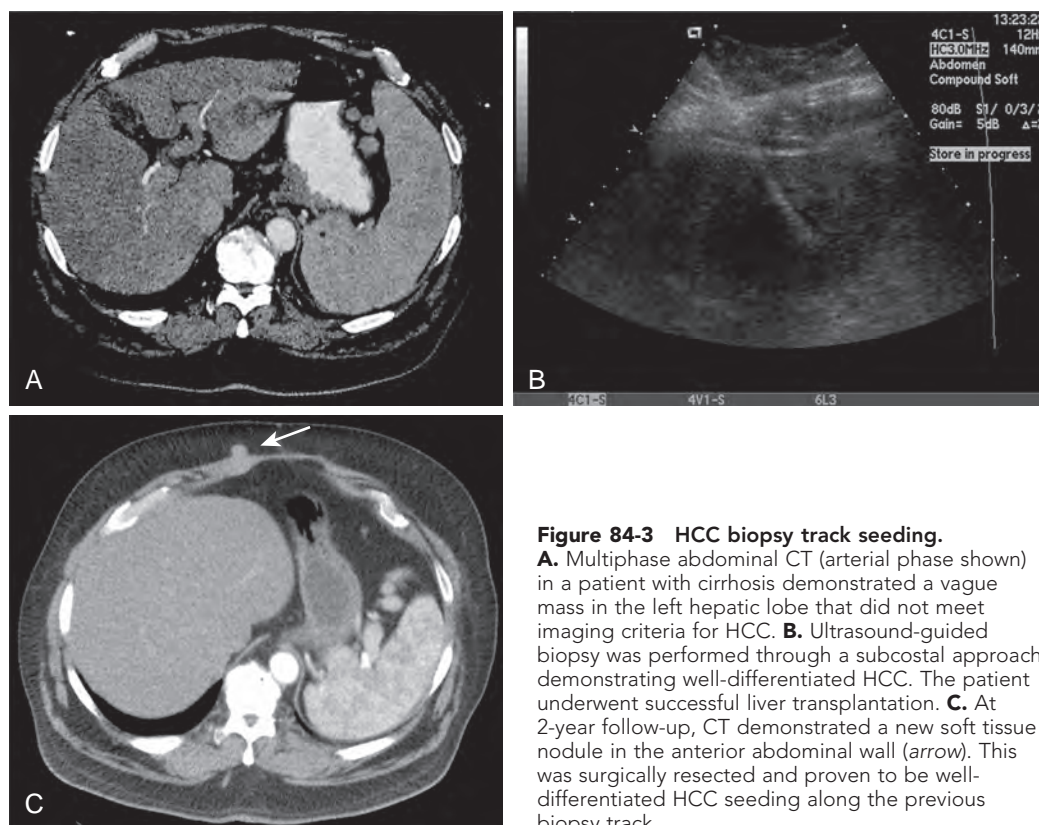


Figure 84-3 HCC biopsy track seeding.

A. Multiphase abdominal CT (arterial phase shown) in a patient with cirrhosis demonstrated a vague mass in the left hepatic lobe that did not meet imaging criteria for HCC. **B.** Ultrasound-guided biopsy was performed through a subcostal approach, demonstrating well-differentiated HCC. The patient underwent successful liver transplantation. **C.** At 2-year follow-up, CT demonstrated a new soft tissue nodule in the anterior abdominal wall (arrow). This was surgically resected and proven to be well-differentiated HCC seeding along the previous biopsy track.

focal liver lesion, a second malignant neoplasm was diagnosed in 5% of cases, and a benign entity was identified in another 3.4%.³⁶ The complications associated with liver biopsy of a focal liver lesion are similar to those for random liver biopsy. The risk of tumor seeding after biopsy of HCC is high (0.76%-2.7%)

and is a catastrophic complication, potentially causing removal from the transplant list^{22,37,38} (Fig. 84-3).

Because most HCCs can be diagnosed on the basis of imaging findings without the need for tissue, biopsy of masses in cirrhotic patients should be rare and reserved for atypical cases

that do not meet LI-RADS or AASLD criteria. Tumor seeding after biopsy of metastatic liver lesions is rare and is usually associated with a generalized rapid growth in all tumor sites.^{39,40}

TRANSJUGULAR LIVER BIOPSY

Brief Rationale and Indication

Transjugular liver biopsy was first described in humans in 1970 and is the preferred technique for obtaining random tissue samples of the liver in patients with uncorrectable coagulopathies.⁴¹ The most common indications for performing transjugular liver biopsy are coagulopathy, massive ascites, and in conjunction with other procedures such as measurement of hepatic venous pressure gradient or hepatic/caval venography.⁴² Acute liver failure, early postoperative liver transplants, and congenital clotting disorders are also scenarios in which transjugular liver biopsy has been shown to be of benefit.⁴³⁻⁴⁵

Guidance and Technique

The right internal jugular vein is accessed under ultrasound guidance, and the right hepatic vein is cannulated through the inferior vena cava with an angled catheter. Continuous electrocardiographic monitoring throughout the procedure is recommended to detect arrhythmias induced by passage of the catheter through the heart. The right hepatic vein is preferred because of its angle with the inferior vena cava and the larger size of the right hepatic lobe. Hepatic venography is performed to confirm appropriate positioning. Peripheral punctures should be avoided because of the risk of capsular puncture.⁴⁶ The number of biopsy passes is operator dependent; however, an increased number of passes (four vs. three) has been shown to produce longer specimens and a greater number of complete portal tracts for histologic interpretation.⁴⁷

Results and Complications

Transjugular liver biopsy has been shown to have a high success rate with a tissue adequacy rate of approximately 96%. Technical failures are most commonly due to failure to cannulate the hepatic veins. Minor and major complication rates have been reported as 6.5% and 0.56%, respectively. The most common major complication is intraperitoneal hemorrhage secondary to perforation of the liver capsule. Mortality after transjugular liver biopsy is reported as approximately 0.1% and in most cases is due to intraperitoneal hemorrhage or ventricular arrhythmia.⁴⁸

Liver Aspiration and Drainage

HEPATIC ABSCESS

Epidemiology and Symptoms

The mortality from pyogenic liver abscess has decreased from approximately 40% to 6% in the modern era as a result of advances in cross-sectional imaging, antibiotic therapy, and percutaneous image-guided therapy.⁴⁹⁻⁵¹ The incidence of pyogenic liver abscesses has increased in Western countries and is now at a rate of 1.1 to 3.6 per 100,000 people. In Eastern countries such as Taiwan, a higher rate of liver abscesses (17.6 per 100,000) is due to increased rates of cholangitis and parasitic infections.⁵² Clinically, patients often present with vague signs and symptoms such as fever, chills, nausea, abdominal pain, and

leukocytosis. Most liver abscesses are diagnosed and monitored with CT, MRI, or ultrasound.

Most pyogenic liver abscesses in Western countries are due to biliary disease. Although pyogenic abscesses historically were most commonly due to *Escherichia coli*, more recent data suggest that *Klebsiella pneumoniae* is now the most common pathogen causing pyogenic liver abscesses in Western countries.⁵³ Other causative organisms in the West commonly include *Streptococcus* and *Staphylococcus* species, although polymicrobial infections are common. Culture and antimicrobial sensitivity results should always assist in guiding antimicrobial coverage.^{51,54,55} Other potential causes include septic pylephlebitis related to appendicitis, diverticulitis, and other inflammatory conditions of the intestine that are transmitted to the liver through the portal vein as well as postsurgical or post-traumatic injury, direct extension from contiguous organs, and after interventional oncologic treatments in patients with incompetent sphincters of Oddi.⁴⁹⁻⁵¹ Primary or metastatic liver malignant neoplasms can also rarely be manifested as liver abscesses.⁵²

Guidance and Technique

Minimally invasive image-guided percutaneous treatments such as needle aspiration and catheter drainage have supplanted surgical therapy for the treatment of liver abscesses, with significant decreases in hospital stay, overall cost, and morbidity.^{56,57} Surgery still plays an important role for the treatment of recalcitrant abscesses and in the setting of malignant disease. Abscesses smaller than 3 cm are usually treated successfully with parenteral antibiotics alone; however, aspiration may be requested for microbial identification.⁵⁸ Image-guided needle aspiration has been shown to be highly effective for unilocular abscesses smaller than 5 cm.^{56,59,60} Multiple aspiration sessions may be required for complete success. Image-guided percutaneous catheter drainage is preferred for abscesses larger than 5 cm, multiloculated abscesses, or those in direct continuity with bile ducts or bowel.^{56,57,60,61}

Preprocedural assessment should include evaluation of coagulation parameters with a target INR below 1.5, aPTT of less than 1.5 times the control value, and platelet count above 50,000/ μ L.⁶ Ultrasound or CT guidance can be used for aspiration or catheter drainage on the basis of the operator's preference. In choosing a puncture path, the least amount of hepatic parenchyma should be traversed, and care should be taken to avoid damaging adjacent organs or traversing the pleura because of the risk of empyema. Needle aspiration is usually performed with an 18-gauge needle; catheter drainage may be performed by the Seldinger or trocar technique with placement of a multi-side hole, locking catheter. Drainage is usually continued until the patient demonstrates clinical improvement and drainage output is less than 10 to 20 mL/day.⁶² A fluoroscopic sinogram can be obtained before catheter removal to assess the residual size of the cavity and the presence of fistulization to the bowel or biliary system (Fig. 84-4).

Results and Complications

Success rates for image-guided needle aspiration of simple pyogenic liver abscesses smaller than 5 cm approach 100% with minimal complications.^{56,59,60} Catheter drainage success rates have varied significantly in the literature from 66% to 100%, probably secondary to abscess and patient factors. Higher failure rates have been associated with the presence of advanced malignant disease, particularly necrotic infected tumors, and

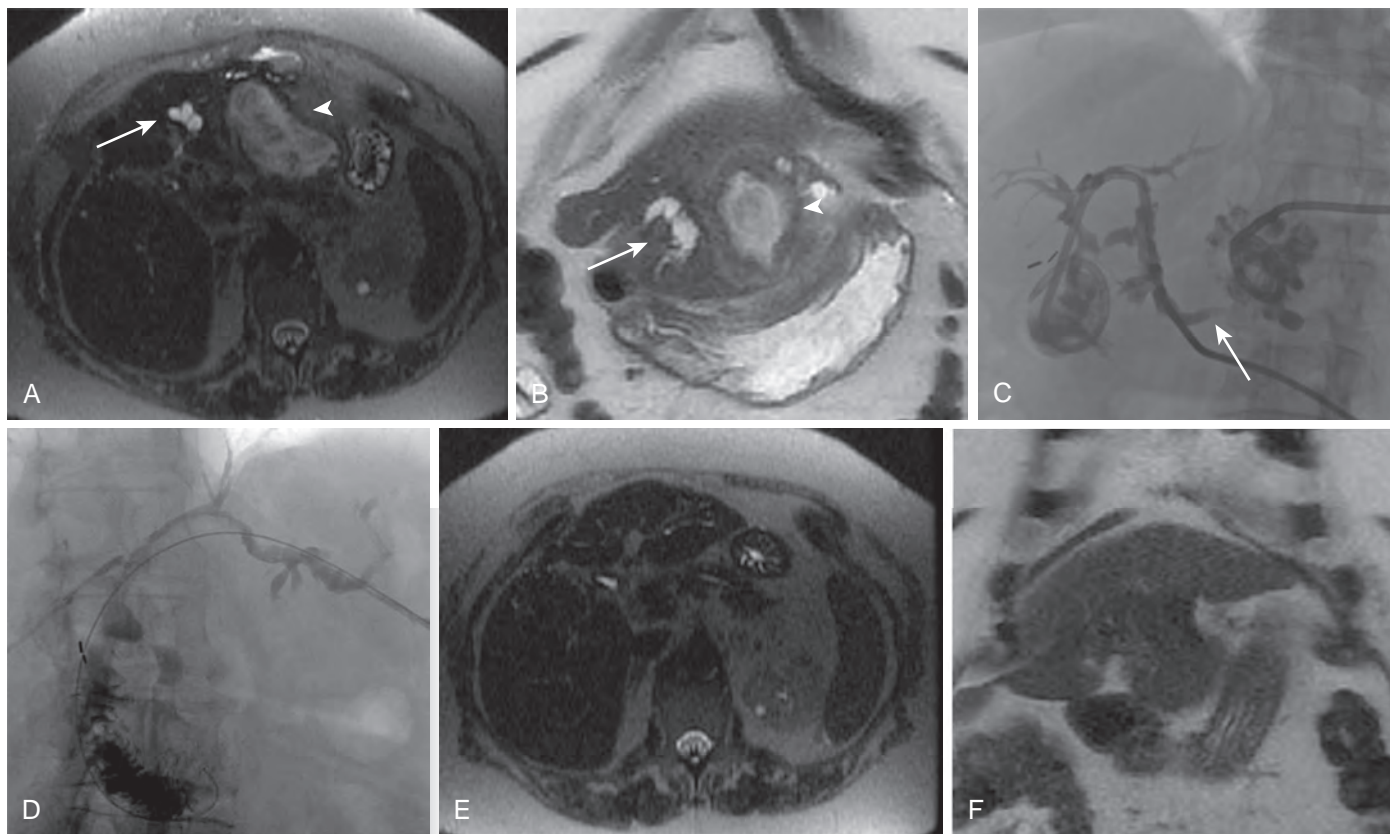


Figure 84-4 Hepatic abscess drainage. **A** and **B**. Initial axial T2 and coronal T2 single-shot fast spin-echo MR cholangiopancreatography images from a patient who presented with a hepatic abscess demonstrate a large heterogeneous T2 intense lesion in segment III of the liver (arrowhead) with adjacent intrahepatic biliary dilation (arrow). The patient was treated with a multi-side hole pigtail drain in the abscess, an internal/external biliary drain through the peripheral dilated biliary radicles of segment III, and intravenous antibiotics for a polymicrobial infection. **C**. Fluoroscopic image after drain placement with injection of contrast material into the abscess cavity demonstrates communication to the biliary system (arrow). The abscess developed secondary to a benign intrahepatic stricture that was treated with repeated balloon dilation (images not shown). **D**. Follow-up pullback cholangiogram demonstrates no residual stricture and resolution of the intrahepatic abscess. **E** and **F**. Follow-up axial T2 and coronal T2 single-shot fast spin-echo MR cholangiopancreatography images 3 months later demonstrate complete resolution of the intrahepatic abscess and biliary dilation in segment III.

the presence of fistulization to an obstructed biliary system.^{57,61} The risk of complications is minimal; complications such as pneumothorax, intraperitoneal hemorrhage, and mild pain are the most frequently reported.

Hepatic Venous Pressure Gradient

BRIEF RATIONALE AND INDICATIONS

Portal hypertension is a complication of chronic liver diseases and is responsible for many of the most severe clinical consequences of cirrhosis. Whereas noninvasive measurements of portal pressure such as elastography are currently being developed, direct measurement of the hepatic venous pressure gradient is the current gold standard for estimating the degree of portal hypertension.⁶³⁻⁶⁵

First described in 1951, hepatic venous pressure gradients can aid in the diagnosis and classification of portal hypertension; assessment of prognosis in patients with cirrhosis and portal hypertension-related clinical events including ascites, spontaneous bacterial peritonitis, hepatic encephalopathy, and variceal bleeding; monitoring of response to pharmacologic therapy; and preoperative evaluation in patients with cirrhosis

selected for hepatic resection.^{66,67} The hepatic venous pressure gradient is obtained by introducing a balloon occlusion catheter into a hepatic vein and measuring the difference between the occluded venous pressure and free venous pressure. The occlusion of a hepatic vein blocks blood flow in the distal hepatic veins and in the sinusoids; thus catheter pressure measured in this position reflects the pressure in the sinusoids, which in turn reflects portal pressure in sinusoidal or post-sinusoidal portal hypertension. Pressure changes within the central venous system are corrected for by subtracting the free hepatic venous pressure from the wedged hepatic venous pressure. This results in a hepatic venous pressure gradient, with clinically significant portal hypertension defined as more than 12 mm Hg.⁶⁷

$$\begin{aligned} \text{Hepatic vein pressure gradient (HVPG)} \\ &= \text{Wedged hepatic venous pressure (WHVP)} \\ &\quad - \text{Free hepatic venous pressure (FHVP)} \end{aligned}$$

GUIDANCE AND TECHNIQUE

By use of a transjugular approach and fluoroscopic guidance, a mean pressure measurement is first recorded in the

retrohepatic inferior vena cava. All pressure measurements should be recorded with the transducer in a fixed position in the midaxillary line at the level of the right atrium. An occlusion balloon catheter is then advanced into either the right or middle hepatic vein, and the free hepatic venous pressure is measured in the hepatic vein 2 to 4 cm from its opening into the inferior vena cava. The balloon catheter should then be positioned in the middle third or at the transition zone between the middle and distal thirds of the hepatic vein and inflated until complete occlusion is observed by deformation of the balloon. The pressure recording should be allowed to stabilize for 45 to 60 seconds, and then a mean pressure is recorded for the wedged hepatic venous pressure. This process should be repeated at least three times, and finally a wedged hepatic venogram is obtained to evaluate for any venous-to-venous shunting to another hepatic vein that would result in underestimation of the wedged hepatic venous pressure. If venous shunting is identified, the balloon catheter should be placed distal to the shunting; if this is not technically feasible, another hepatic vein should be selected for interrogation.^{68,69}

RESULTS AND COMPLICATIONS

The use of balloon occlusion catheters has been shown to correlate more accurately with directly measured portal pressures during placement of transjugular intrahepatic portosystemic shunts (TIPS) compared with the use of an end-hole catheter wedged into a hepatic venule.⁷⁰ Technical success rates have been reported above 95%, and failure is usually the result of hepatic venous occlusion. Severe postprocedure complications are exceedingly uncommon.⁶⁷

Transjugular Intrahepatic Portosystemic Shunt

BRIEF RATIONALE AND INDICATIONS

TIPS is a percutaneous image-guided procedure that has proved to be beneficial for the treatment of complications of portal hypertension. First described in an animal model by Rösch and coworkers⁷¹ in 1969, a TIPS is a constructed channel within the liver connecting a portal vein branch to a hepatic vein with the goal of creating a portosystemic shunt to decrease portal venous pressure. A TIPS is created under fluoroscopic guidance by placing a stent graft from a hepatic vein (most commonly the right hepatic vein) through the liver parenchyma into an intrahepatic portal venous branch (most commonly the right portal vein). Another variation is a direct intrahepatic portosystemic shunt, which was first described in 2001.⁷² A direct intrahepatic portosystemic shunt is created with use of intravascular ultrasound, passing a needle from the inferior vena cava through the caudate lobe into the portal vein. Subsequent stent placement is performed under fluoroscopic guidance in a fashion similar to TIPS placement. The strongest evidence of TIPS efficacy has been established for secondary prevention of variceal bleeding and treatment of refractory ascites.⁷³ Other indications for TIPS creation include refractory acute variceal bleeding, portal hypertensive gastropathy, hepatorenal syndrome (types 1 and 2), Budd-Chiari syndrome, hepatic hydrothorax, hepatic veno-occlusive disease, and hepatopulmonary syndrome.⁷⁴⁻⁸⁰

RELATIVE AND ABSOLUTE CONTRAINDICATIONS

Absolute contraindications to TIPS placement include congestive heart failure, severe tricuspid regurgitation, severe pulmonary hypertension (mean pulmonary pressure >45 mm Hg), uncontrolled systemic infection or sepsis, and unrelieved biliary obstruction. Relative contraindications include anatomic issues that can reduce the technical success of shunt placement, such as polycystic liver disease, extensive primary or metastatic malignant disease (especially centrally near the porta hepatis), and obstruction of the hepatic veins or thrombosis of the portal venous system. Hepatic artery thrombosis, severe coagulopathy or thrombocytopenia, and the presence of hepatic encephalopathy may also significantly increase the risk of postprocedure complications.⁷³

Preprocedure evaluation includes complete laboratory work-up consisting of a complete blood count, coagulation panel, and comprehensive metabolic panel. Significant thrombocytopenia (platelet count <50,000 cells/ μ L), anemia (hematocrit <25%), or coagulopathy (INR > 1.5) should be corrected and arrangements made for crossmatched blood products. Recent cross-sectional imaging within 1 month should be reviewed to assess for vascular patency and anatomic considerations. If recent imaging is unavailable or an abrupt deterioration of hepatic function occurs, an urgent or emergent ultrasound with Doppler evaluation of the hepatic vasculature may be warranted to assess vascular patency. Echocardiography is also recommended to assess cardiac function and to specifically assess for pulmonary arterial hypertension.⁷³

GUIDANCE AND TECHNIQUE

TIPS procedures are mostly performed by use of general anesthesia with endotracheal intubation. The right hepatic vein is accessed through the right internal jugular vein, and balloon occlusion hepatic venography using carbon dioxide can be performed to visualize the course and flow in the portal venous system. Fluoroscopically guided needle passes are then made to achieve portal venous access. Direct portal venous pressure is measured, and a portosystemic pressure gradient is calculated as the pressure difference between the main portal vein and right atrium. A stent graft is deployed so that the uncovered caudal portion of the stent remains in the portal vein, with the cranial end terminating near the junction of the hepatic vein and inferior vena cava. Polytetrafluoroethylene (PTFE)-covered stent grafts have become the standard of care for de novo TIPS placement compared with bare metal stents because of a lower rate of TIPS dysfunction, higher rate of primary patency, lower rate of clinical relapse, and decreased incidence of hepatic encephalopathy.⁸¹ After deployment, trans-TIPS portal venography and pressure measurements in the main portal vein and right atrium are repeated. In patients with variceal bleeding, a post-TIPS portosystemic gradient below 12 mm Hg should be achieved to prevent rebleeding.⁸² Retrospective studies have shown that variceal embolization with coils, cyanoacrylate, or sclerosing agents such as sodium tetradecyl sulfate in addition to TIPS placement significantly decreases the risk for recurrent variceal bleeding.^{83,84} For patients with refractory ascites, the Society of Interventional Radiology and the AASLD guidelines recommend reducing the portosystemic gradient to below 8 mm Hg.⁸⁵ A portosystemic gradient below 5 mm Hg has been

associated with an increase in the risk of liver failure and severe hepatic encephalopathy requiring an intervention such as TIPS reduction⁸⁶ (Fig. 84-5).

RESULTS

Success after TIPS placement can be classified as technical, hemodynamic, and clinical. Technically successful creation of a shunt from the hepatic vein to the portal vein and hemodynamic success in reduction of a portosystemic gradient to below 12 mm Hg with nonfilling of gastroesophageal varices should be achieved in more than 95% of cases.⁸⁷ Clinical success for the separate indications for TIPS placement varies among studies because of different inclusion and evaluation criteria. Meta-analyses evaluating TIPS for secondary prevention of variceal bleeding compared with various forms of endoscopic therapy found a threefold decrease in the risk of recurrent bleeding after TIPS with similar all-cause mortality rates. However, a more than twofold increased risk for development of hepatic encephalopathy was noted after TIPS.^{88,89} A multicenter randomized controlled trial in high-risk patients with acute variceal bleeding demonstrated a statistically significant decrease in treatment failure and mortality for patients undergoing TIPS placement compared with those treated with repeated endoscopy and pharmacotherapy.⁷⁴

In the treatment of refractory ascites, a meta-analysis of randomized controlled trials demonstrated a 7.1-fold reduction in the risk of recurrent ascites, with rates of improvement ranging from 38% to 84% after TIPS compared with 0% to 43% after large-volume paracentesis.⁹⁰ No significant survival advantage for TIPS was found in early studies. A more recent randomized controlled trial in a select group of patients with preserved hepatic and renal function did demonstrate a significant survival advantage after TIPS placement.⁹¹ The rate of hepatic encephalopathy in this group of patients was 2.2-fold higher after TIPS.⁹⁰ TIPS also is likely to lead to survival prolongation

in patients with Budd-Chiari syndrome, with 1- and 5-year liver transplant-free survival of 88% and 78%, respectively, with a median Model for End-Stage Liver Disease (MELD) score of 17.⁷⁵ At least partial improvement in clinical symptoms is experienced in 68% to 82% of patients with hepatic hydrothorax, and complete resolution of the hydrothorax occurs in 57% to 71% after TIPS creation.⁷⁸

COMPLICATIONS

Patients with a MELD score above 18 have a significantly higher mortality 3 months after TIPS than that of patients with a MELD score of 18 or less.⁷² Technical complications such as transcapsular puncture may occur in up to 33% of cases but result in significant intraperitoneal hemorrhage in only 1% to 2%.⁸⁵ Stent migration or misplacement into the inferior vena cava or portal vein may occur in up to 10% to 20% of cases. Creation of the shunt results in diversion of portal blood flow past the metabolic filtering effect of the hepatic parenchyma, which can lead to new or worsening hepatic encephalopathy in 10% to 44% of patients. Patients of advanced age, with a past history of encephalopathy, and with advanced liver disease are at increased risk for development of hepatic encephalopathy. However, encephalopathy usually responds to medical treatment, and only rarely is TIPS reduction or occlusion necessary.⁸⁵ Other potential complications, such as hepatic infarction, creation of a biliary-venous or hepatic artery–portal vein fistula, hemolysis, sepsis, and TIPS infection, are much rarer.

The introduction and widespread use of PTFE-covered stent grafts for TIPS creation has led to a dramatic improvement in long-term TIPS patency. The incidence of shunt dysfunction with bare metal stents ranges from 18% to 78%, probably secondary to intimal hyperplasia protruding through the stent interstices.⁸⁵ Primary patency rates at 1 year with PTFE-covered stent grafts have been reported at 81% to 86%^{81,92} (Fig. 84-6).



Figure 84-5 TIPS placement. **A.** Dual iodinated contrast material injection through the sheath in the right hepatic vein and the pigtail catheter in the main extrahepatic portal vein. **B.** Post-stent deployment injection in the main portal vein. Note the metallic ring on the distal portion of the stent (white arrow). The stent proximal to the ring is covered and intraparenchymal. The stent distal to the ring is uncovered and intravascular in the right portal vein. Also note the proximal aspect of the stent at the confluence of the right hepatic vein and inferior vena cava (arrowhead). Post-stent venogram also demonstrates nonfilling of the coronary vein (black arrow).

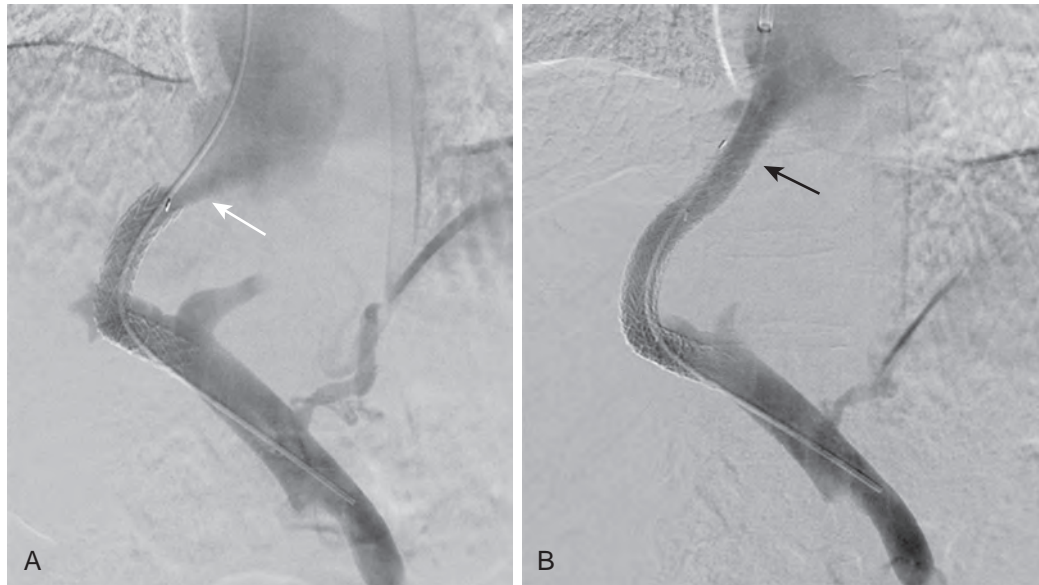


Figure 84-6 Hepatic venous stenosis after TIPS placement. Fluoroscopic images from TIPS revision in a patient with recurrent ascites after original TIPS placement. Doppler ultrasound before the procedure demonstrated temporal increase in the velocity in the hepatic venous end of the shunt (images not shown). **A.** A portal venogram demonstrates hepatic venous stenosis with the proximal portion of the stent in the hepatic parenchyma short of the confluence of the right hepatic vein and inferior vena cava (arrow). **B.** A second PTFE-covered stent was placed and extended to the inferior vena cava (arrow). Portal systemic gradient decreased from 13 to 7 mm Hg after stent deployment, and the patient's ascites resolved.

FOLLOW-UP AND TIPS REVISION

Despite the decrease in TIPS dysfunction after implementation of PTFE-covered stent grafts, regular shunt surveillance is recommended. One protocol for surveillance uses Doppler ultrasound at 1, 3, 6, and 12 months after TIPS creation and every 6 to 12 months thereafter, depending on the patient's clinical status.⁹³ A significant degree of variability regarding the sensitivity and specificity of Doppler ultrasound for detection of TIPS dysfunction has been reported. Measured velocities throughout the course of the shunt should range between 90 and 190 cm/s.⁹⁴ Direction of flow within the left portal vein should be hepatofugal (toward the shunt) after TIPS placement. Left portal vein hepatopetal flow (toward the liver) is therefore indicative of shunt dysfunction.⁹⁵ Temporal changes in the peak velocity greater than 50 cm/s have also been recommended as an indication for venography and pressure measurements, which are the gold standard for assessing TIPS dysfunction.⁹⁶ Patients with symptoms suggestive of recurrent portal hypertension in the setting of normal findings on Doppler ultrasound also warrant further investigation with venography. In the setting of TIPS dysfunction secondary to stenosis, repeated stenting has been shown to lead to better patency than angioplasty alone. Patients with a bare metal stent requiring reintervention should be revised with a PTFE-covered stent graft.^{85,97}

Interventional Oncology in the Liver

Liver-directed locoregional therapies for unresectable primary and metastatic malignant neoplasms continue to evolve with advances in ablative and endovascular technologies and techniques. The goal of liver-directed therapy in patients with hepatic malignant neoplasms can be multifaceted and vary from allowing a patient with unresectable disease to become

a resection or transplant candidate to curative treatment in nonsurgical candidates or improvement of survival and quality of life in a palliative setting. The choice of treatment modality depends on multiple factors including the presence of underlying liver dysfunction, tumor type, overall tumor burden, number and location of tumors, and patient factors such as performance status and functional liver reserve. The most common locoregional therapies currently being used are portal vein embolization (PVE), radiofrequency (RF) and microwave (MW) ablation, transarterial chemoembolization with or without drug-eluting beads (TACE and DEB-TACE), and transarterial radioembolization. Other liver-directed therapies, such as percutaneous ethanol ablation, cryoablation, and other ablative technologies such as laser-induced interstitial thermotherapy, high-intensity focused ultrasound, irreversible electroporation, hepatic arterial infusion chemotherapy, and transarterial bland embolization, have also been reported and play a lesser role in current treatment algorithms. The latter techniques either are still in development or are of historical interest and are beyond the scope of this chapter.

PREOPERATIVE PORTAL VEIN EMBOLIZATION

Brief Rationale

Surgical resection of both primary malignant neoplasms and liver metastases remains the mainstay of curative therapy. Continued advances in surgical techniques have led to improved overall patient outcomes; however, major hepatic resection places patients at risk for liver insufficiency. Determination of the volume of liver that remains after surgery, the future liver remnant (FLR), has been shown to be a strong independent predictor of postoperative complications.⁹⁸ In patients with an inadequate FLR, PVE of the lobe to be removed can cause hypertrophy to the FLR and atrophy of the embolized

segment. PVE has been most commonly used in patients with colorectal metastatic disease, intrahepatic cholangiocarcinoma, and HCC.⁹⁹ Whereas the exact mechanisms of hepatocyte regeneration are unknown, studies have demonstrated that in addition to redistribution of portal venous blood flow, PVE also induces an increase in hepatic growth factor and transforming growth factors α and β .¹⁰⁰ FLR hypertrophy rates have been noted to be impaired in patients with underlying cirrhosis or fibrosis and in diabetic patients.⁹⁹

Indications

Patients undergoing major hepatic resection may benefit from preoperative determination of the FLR. CT volumetry is used to measure the volume of the FLR. Calculations with either the measured total liver volume minus the tumor burden volume or the estimated total liver volume by use of body surface area are performed to assess percentage of FLR after resection. PVE is recommended in patients with preserved liver function and an FLR of less than 20%, patients with either hepatic steatosis or significant exposure to hepatotoxic chemotherapy and an FLR of less than 30%, and patients with well-compensated cirrhosis and an FLR of less than 40%.¹⁰¹⁻¹⁰³ Relative contraindications to PVE include extrahepatic metastases, uncorrectable coagulopathy, extensive tumor burden precluding safe access into the portal vein, and tumoral invasion into the portal vein.

Guidance and Technique

Multiple different approaches and techniques have been described for PVE. Historically, PVE was performed through an intraoperative transileocolic approach. Currently, the most commonly used approach is the percutaneous ipsilateral approach. This approach is favored over the contralateral approach because of the avoidance of potential damage to the FLR during access and catheter manipulation. However, if there is no safe route through the ipsilateral liver because of tumor burden, a contralateral approach remains an acceptable alternative. With use of either conscious sedation or general anesthesia, a peripheral branch of the portal venous system to be embolized, most commonly the right, is accessed with a micropuncture needle under ultrasound guidance. Once access is secured, portal venography is performed, and the portal venous system is embolized, depending on the planned surgery. Most commonly, this involves embolizing segments V to VIII of the liver for a right hepatectomy. For an extended right hepatectomy, some authors have advocated embolizing segment IV as well to obtain a greater hypertrophy rate in segments II and III, although the risk of nontarget embolization to the FLR is theoretically greater.¹⁰⁴ The choice of embolic agent is at the discretion of the operator and includes *n*-butyl cyanoacrylate mixed with Lipiodol and polyvinyl alcohol particles or gelatin sponge and coils. A meta-analysis suggested that the use of *n*-butyl cyanoacrylate results in a higher percentage of FLR volume increase.⁹⁹ After embolization is complete, the sheath track is embolized with either gelatin sponge or coils.

Results and Complications

Technical success rates of PVE are approximately 99%. Most technical failures result from an inability to cannulate the portal system because of altered anatomy or unexpected thrombosis of the portal system due to tumor progression or invasion.⁹⁹ After embolization, follow-up CT is performed at 4 weeks for recalculation of the FLR as liver regeneration tends to plateau

after 3 weeks.⁹⁸ The clinical success rate (defined as sufficient FLR hypertrophy to allow resection) is 96.1% with a mean increase in the FLR volume of 37.9%, with a range of 20.5% to 69.4%⁹⁹ (Fig. 84-7). However, approximately 20% of patients do not undergo the originally planned liver resection secondary to local intrahepatic tumor progression, new tumor in the FLR, extrahepatic tumor spread, insufficient hypertrophy of the FLR, complications of PVE leading to nonresectability, or refusal of the patient for further treatment. Some select patients may benefit from combination treatment with either transarterial or ablative treatments to achieve curative resection.

Minor complications, including postembolization syndrome consisting of fevers and abdominal pain, occur in 25% to 35% of patients. Transient elevation of liver transaminases is seen in 37% of patients. Major complications, such as portal thrombosis, embolization of nontarget vessels, intraperitoneal hemorrhage or liver hematoma, abscess, and intraperitoneal bile leakage, are rare, occurring in less than 1% of patients.⁹⁹

TUMOR ABLATION

Image-guided ablation therapy of hepatic tumors is a rapidly growing aspect of the field of interventional oncology. Whereas there are many new technologies with relatively few outcomes data, the focus of this discussion is primarily on the most widely used techniques, RF and MW ablation.

Chemical Ablation

Chemical ablation has long been used percutaneously for the treatment of HCC and has the longest clinical follow-up studies of any percutaneous ablation technique. Absolute ethanol is the most commonly used agent, although the use of acetic acid has been described. Ethanol is percutaneously injected into the hepatic tumor and results in tumor destruction by both coagulation and ischemic necrosis. Chemical ablation is most effective for small tumors (<2 cm) and often requires repeated treatments for complete tumor treatment. Ethanol ablation is more effective for treatment of HCC than for metastatic disease, presumably because the tumor capsule or pseudocapsule typical of many HCCs prevents diffusion of ethanol into surrounding parenchyma. In addition, diffusion of ethanol in cirrhotic liver is limited. Studies have demonstrated the superiority of thermal ablation techniques over ethanol for complete tumor destruction. Ethanol is currently reserved for cases in which thermal ablation is contraindicated because of the proximity of adjacent vulnerable structures or in developing countries where cost is the most important selection criterion. Chemical ablation is not recommended for metastatic disease.¹⁰⁵

Thermal Ablation

Cryoablation. Cryoablation involves placement of cryoprobes into a tumor to induce freeze-thaw cycles. Argon gas is the most common cryogen in modern cryoablation systems. The mechanism of cell death is primarily cellular membrane disruption, but tissue ischemia and direct damage to intracellular organelles are also present. After initial enthusiasm, cryoablation is less frequently used to treat malignant hepatic tumors because of the lengthy ablation cycles, the lack of ability to cauterize the applicator track (increasing the risk of hemorrhage), a risk of hepatic fracture, and the risk of multiorgan failure termed cryoshock, particularly in cirrhotics.¹⁰⁶

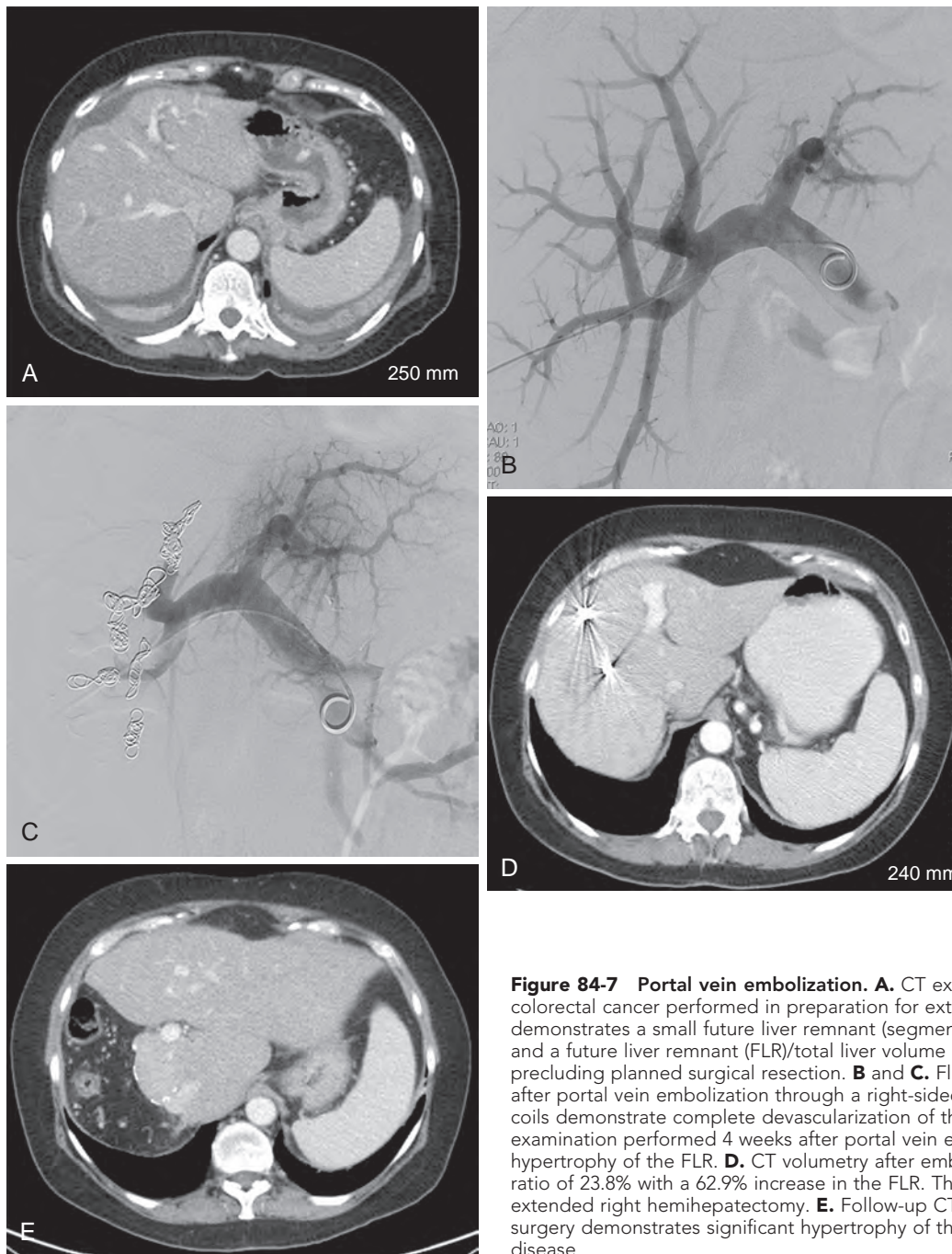


Figure 84-7 Portal vein embolization. **A.** CT examination in a patient with metastatic colorectal cancer performed in preparation for extended right hepatectomy demonstrates a small future liver remnant (segments I-III). CT volumetry was performed, and a future liver remnant (FLR)/total liver volume (TLV) ratio was calculated at 15.2%, precluding planned surgical resection. **B** and **C.** Fluoroscopic images before and after portal vein embolization through a right-sided approach with particles and coils demonstrate complete devascularization of the right hemiliver. Follow-up CT examination performed 4 weeks after portal vein embolization demonstrates significant hypertrophy of the FLR. **D.** CT volumetry after embolization demonstrated an FLR/TLV ratio of 23.8% with a 62.9% increase in the FLR. The patient underwent the planned extended right hemihepatectomy. **E.** Follow-up CT examination performed 2 years after surgery demonstrates significant hypertrophy of the liver remnant without recurrent disease.

Radiofrequency Ablation. Heat-based ablation techniques can result in coagulation necrosis when tissue is heated to a temperature threshold for a specific time. Tissue heating to 50°C for approximately 5 minutes typically results in cell death, whereas temperatures above 60°C cause cell death within seconds. RF ablation is currently the most frequently used thermal ablation technique in the treatment of hepatic tumors. In monopolar RF systems, a generator is used to create alternating electrical current that oscillates between the electrode placed in the tumor and grounding pads, resulting in cellular agitation and tissue heating. Standard electrodes include single-needle or multiple-needle arrays (sometimes

cooled to prevent charring) and multiple tines emanating from one needle. Multiple tines improve heating efficiency and energy deposition but typically require larger diameter, more invasive needles. Multiple-probe RF systems are now available that take advantage of thermal synergy to create larger and more confluent ablation zones. However, because of electrical interactions between simultaneously activated electrodes, a switching system is necessary.¹⁰⁷ In bipolar RF systems, two electrodes are placed within or adjacent to the tumor and current oscillates between them, without the need for grounding pads. In all RF configurations, saline can be instilled to decrease charring and to reduce impedance, thus

resulting in more energy deposition but potentially less control of the ablation zone.¹⁰⁵

Microwave Ablation. MW ablation technology is based on tissue heating by dielectric hysteresis, requiring molecules with an intrinsic dipole moment to continuously realign with an applied field, resulting in increased kinetic energy and tissue heating. MW technology has multiple advantages over RF ablation. Because MW energy readily penetrates even those tissues with high impedance (such as charred tissues), it can be applied at much higher temperatures than RF energy. MW ablation does not require grounding pads, and multiple antennas can be used simultaneously without switching to create both electrical and thermal synergy. Despite these advantages, MW energy is a more complicated technology to apply in tissue. For example, reflected power at the tissue-antenna interface can cause antenna shaft heating and result in thermal injury along the puncture track. More recent MW systems use a cooling jacket with circulating water or gas to obviate this problem. To date, MW ablation technology has been used most extensively in Asia, although it is becoming much more frequently used worldwide.¹⁰⁵

In general, RF technology suffers in areas of high blood flow because of the heat sink effect and also struggles in tissues with high impedance because of decreased power distribution. MW technology is faster, more efficient, less sensitive to heat sink effect, and not sensitive to differences in tissue impedance. Despite being less well studied than RF technology, early clinical results demonstrate that MW is at least as effective as RF ablation, resulting in rapid replacement of RF because of the overall physical advantages listed before.¹⁰⁵

Indications

HCC is the most common indication worldwide for hepatic tumor ablation. The treatment strategy of HCC is generally shaped by the Barcelona Clinic Liver Cancer (BCLC) guidelines.^{19,108} Although studies have shown that surgical tumor resection provides the best survival outcome, only 20% of patients are resection candidates, generally defined as patients without portal hypertension and with a normal bilirubin level. Liver transplantation is also a curative treatment for patients with HCC. However, orthotopic liver transplantation is often available only for patients who meet Milan criteria (up to three tumors smaller than 3 cm or one tumor larger than 5 cm) and is limited by organ availability.¹⁰⁹ For those patients who are not resection candidates because of poor hepatic function and who are poor transplantation candidates, tumor ablation is a potentially curative alternative therapy. Ablation is also used as a bridge to transplantation in the setting of either local tumor control during the waiting period for liver transplantation or downstaging the tumor so that the patient meets Milan criteria. Although there have been some excellent results with downstaging into Milan criteria, this remains a controversial topic because of the limited number of donor livers available and the large numbers of patients on the waiting list.¹¹⁰⁻¹¹²

The second most common indication for liver tumor ablation is unresectable colorectal cancer metastasis. In general, surgical resection is first-line therapy for hepatic colorectal metastatic disease in eligible patients. However, many patients are not resection candidates because of comorbidities, recent surgery, or anatomic considerations. Percutaneous ablation can often achieve excellent local tumor control, particularly for

tumors smaller than 3 cm.^{113,114} Patients who are not resection or ablation candidates because of either the location or the number of metastases are typically treated with either TACE/radioembolization or systemic chemotherapy.

Although less well studied, tumor ablation has also been used for hepatic metastatic disease from sites other than colorectal primary tumors, including breast, renal cell, and neuroendocrine primary tumors, for both local disease control and symptomatic relief in patients who are not surgical candidates.¹¹⁵⁻¹¹⁸ Both RF ablation and MW ablation have also been used successfully to treat benign hepatic tumors, such as symptomatic hepatic hemangiomas.¹¹⁹

Contraindications

Patients with severe liver failure are poor ablation candidates for fear of worsening hepatic function. Tumors close to vital structures, such as main portal venous branches, large segmental bile ducts, gallbladder, and bowel, may not be amenable to percutaneous ablation. However, nontarget structures such as the gallbladder, diaphragm, and bowel can often be displaced by hydrodissection, and many tumors can then be successfully treated.^{120,121} Uncorrectable coagulopathies have traditionally been considered contraindications to tumor ablation. With the ability to perform intraprocedural cautery with heat-based ablation, many centers are adopting more liberal coagulation parameter guidelines. Extrahepatic metastatic disease is typically a contraindication to ablation therapy unless the goal is tumor debulking in the setting of an indolent malignant neoplasm.¹⁰⁶ Finally, 40% to 50% of patients who have undergone prior biliary sphincterotomy or surgery will develop a postablation abscess, despite prophylactic antibiotic therapy.¹²²

Coagulation parameters should be evaluated before hepatic tumor ablation is performed. The most widely accepted guidelines suggest that the patient have an INR below 1.5 and a platelet count of more than 50,000/ μ L before undergoing percutaneous hepatic tumor ablation.¹²³ Anticoagulant and antiplatelet medication therapies are typically held for 5 to 7 days before the procedure, although the risk of complications from withholding of these medications must also be considered, particularly in patients with recently placed coronary artery stents.

Guidance and Technique

Most hepatic tumor ablation procedures are performed under general anesthesia, given the pain resulting from tissue heating. General anesthesia also provides for more reliable breath holding, which is essential for accurate probe placement. Continuous sonographic guidance is most frequently used for both probe placement and monitoring of the ablation zone, although CT guidance is occasionally necessary for lesions that are sonographically occult. At the completion of the ablation procedure, many centers elect to perform a contrast-enhanced CT examination to ensure that the ablation zone appropriately encompasses the tumor (Fig. 84-8). Whereas a margin of 5 mm is acceptable for HCC, margins of at least 1 cm are suggested for hepatic metastases because of the high prevalence of metastatic tumor cells beyond the visible tumor margin.^{124,125}

Fluid injected into the peritoneal space (artificial ascites) or other body cavities can be used to decrease postprocedural body wall pain or to displace bowel or other nontarget collateral organs.^{120,121,126} Dextrose in water is the preferred fluid for use with RF ablation as the nonionic nature prevents electrical current conduction. Saline is an ionic medium that allows the

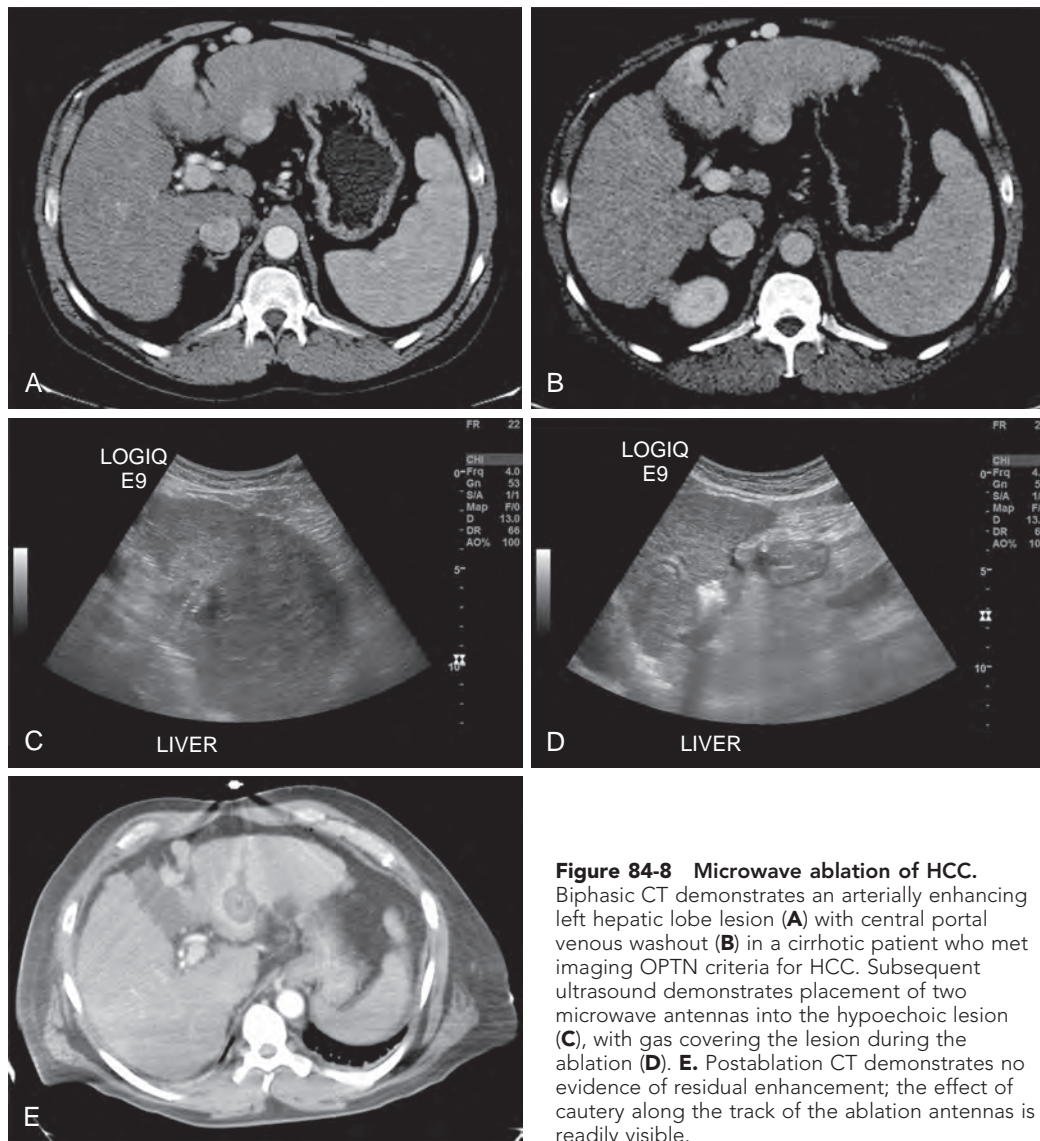


Figure 84-8 Microwave ablation of HCC.

Biphasic CT demonstrates an arterially enhancing left hepatic lobe lesion (**A**) with central portal venous washout (**B**) in a cirrhotic patient who met imaging OPTN criteria for HCC. Subsequent ultrasound demonstrates placement of two microwave antennas into the hypoechoic lesion (**C**), with gas covering the lesion during the ablation (**D**). **E**. Postablation CT demonstrates no evidence of residual enhancement; the effect of cautery along the track of the ablation antennas is readily visible.

propagation of electricity. Either fluid is acceptable for use with MW ablation. Iodinated contrast material can be added to any fluid for improved visualization on intraprocedural CT.¹²⁷

Results

HCC. The results after treatment of HCC with RF or MW ablation are dependent primarily on tumor diameter. Treatment of tumors smaller than 3 cm is associated with excellent local tumor control, with survival equivalent to that of surgical resection.¹²⁸⁻¹³⁰ Local tumor control decreases for tumors larger than 3 cm. Recent work exploring the combination thermal ablation and intra-arterial therapies (such as TACE) demonstrates promising results for local control for intermediate-size tumors (3-5 cm in diameter).¹³¹ Local therapy must be performed with the understanding that it is not only HCC but also the patient's underlying liver disease that is life limiting. Many patients die of underlying liver failure rather than of HCC.

Metastatic Disease. Survival after treatment of metastases with RF ablation is superior to that with chemotherapy alone but

may be slightly worse than with liver resection. However, no randomized controlled trials have been performed comparing ablation and resection for patients who are candidates for either treatment, and most ablation series include patients who are not surgical candidates with substantial comorbidities.^{132,133} Similar to the results with HCC, smaller tumors (<3-4 cm) are associated with lower local tumor progression than larger tumors. Survival after RF ablation of colorectal liver metastases ranges from 91% to 93% at 1 year, 28% to 69% at 3 years, and 25% to 46% at 5 years.¹³⁴⁻¹³⁶

Complications

Mortality rates after hepatic tumor ablation are low and range from 0.1% to 0.5%, most commonly resulting from liver failure, sepsis, or portal venous thrombus. Major complications are seen in approximately 2% to 3% and include hemorrhage, hepatic abscess, liver failure, and bile duct injury. As mentioned previously, patients who have undergone prior biliary sphincterotomy or stent placement are at much higher risk of hepatic abscess formation after the procedure. Tumor applicator track

seeding is uncommon but can be an important complication in the setting of HCC. The incidence of track seeding varies, but a median risk is approximately 0.6% after HCC ablation.^{137,138} When tumor does seed along the ablation track, it should have the same enhancement characteristics as the primary tumor. Either follow-up imaging or biopsy is necessary to differentiate between postablation inflammatory soft tissue and applicator track seeding.¹³⁹

Postablation syndrome is manifested by influenza-like symptoms beginning 48 hours after the procedure, generally resolving by 7 days after the procedure. Although uncomfortable, it is generally not a serious complication and can be managed with anti-inflammatory medications and supportive care. Cryoshock can be a severe complication related to release of intracellular contents into the circulation, which can result in disseminated intravascular coagulation, hepatic and renal failure, and death.¹³⁸ This syndrome is seen almost exclusively in cirrhotic patients treated with cryoablation.

Follow-up

The timing of follow-up imaging examinations is specific to individual institutions, but follow-up scans should be performed several times in the first year after ablation to evaluate for local tumor progression, development of new disease, and postablation complications. CT and MRI are the most common methods of imaging follow-up, although positron emission tomography (PET)/CT has been shown to be useful for certain tumors. CT or MRI performed 1 to 3 months after ablation typically demonstrates a nonenhancing ablation zone, usually larger than the original tumor because of the ablative margin. A thin rim of peripheral enhancement is commonly seen secondary to inflammation or hyperemia and should not be misconstrued as local tumor progression. The central ablation zone will demonstrate a high-attenuation T1 hyperintense center corresponding to desiccated tissues and blood products. The ablation zone should progressively decrease in size during 6 to 12 months but may remain visible for several years. If track cautery was used during withdrawal of the ablation applicator, the track is often seen with characteristics similar to those of the ablation zone.¹⁴⁰ Local tumor progression, if present, will generally be seen as irregular nodular enhancement at the periphery of the ablation zone and will have imaging findings similar to residual disease. MRI is typically more sensitive than CT in identifying residual disease or local progression. Residual tumor at MRI demonstrates T2 hyperintensity (in contrast to the T2 hypointensity of the ablation zone). Diffusion-weighted images can be helpful to identify small residual tumor nodules.¹⁴¹

A variety of postablation complications are possible. Biliary duct injury typically is manifested with focal biliary ductal dilation due to a more central stricture. Bilomas are also possible. Gallbladder injury is manifested with gallbladder wall thickening and pericholecystic fluid. Hepatic abscess is common after ablation in patients with previous biliary manipulation and is manifested as enlargement of the ablation zone or an intrahepatic collection. Gas is common within the ablation zone immediately after the procedure, but if the amount of gas increases on subsequent examinations, this is concerning for ablation zone infection. Bowel injury is manifested with focal bowel wall thickening and mucosal hyperenhancement. Finally, the hepatic vasculature should be evaluated on follow-up imaging as portal vein thrombosis, hepatic arterial

pseudoaneurysm, and hepatic infarction have been reported¹⁴¹ (Fig. 84-9).

ENDOVASCULAR INTRA-ARTERIAL THERAPIES

Transcatheter intra-arterial therapies have been developed for the treatment of both primary and secondary hepatic malignant neoplasms. The goal of intra-arterial therapy is to selectively deliver anticancer treatment to tumors with the hope of achieving reduced toxicity profiles and tumor response. The basis for intra-arterial therapy of liver tumors stems from the dual blood supply to the liver. Hepatic neoplasms preferentially receive most of their blood flow from the hepatic arterial system, whereas normal liver parenchyma derives approximately 70% of its blood flow from the portal vein. This duality allows catheter-based therapies such as transarterial embolization, hepatic intra-arterial chemoinfusion, TACE and DEB-TACE, and transarterial radioembolization to selectively target tumors and to spare normal parenchyma.

Transarterial Chemoembolization

Brief Rationale. TACE with the use of anticancer drugs followed by Gelfoam embolization for unresectable HCC was introduced in the late 1970s by Yamada and associates.¹⁴² TACE is defined as the infusion of a mixture of chemotherapeutic agents with or without iodized oil followed by embolization with particles. The goal of chemoembolization is to expose tumors to high concentrations of a local chemotherapeutic agent in a hypoxic environment with minimal systemic drug bioavailability. Ischemia induced by embolization may result in failure of transmembrane pumps, thus allowing increased absorption of the agents by the cells with decreased washout.

There is no consensus on the type or concentration of chemotherapeutic agents used in TACE. The most common multidrug combination used in the United States is a mixture of mitomycin C, doxorubicin, and cisplatin. Doxorubicin is the most commonly used single-agent regimen worldwide. Regardless of the chemotherapeutic regimen, the drugs are emulsified in Lipiodol, an oily contrast agent that acts as a carrier of the chemotherapeutic agents and accumulates selectively within the neovasculature and extravascular spaces of liver tumors.^{143,144} Multiple different agents have also been used for embolization of the target vessel after infusion of the Lipiodol chemotherapeutic agent mixture, including absorbable gelatin sponge, polyvinyl alcohol particles, and trisacryl gelatin microspheres.

Indications and Contraindications. The indications for TACE for HCC have become more standardized as described before. Currently, TACE is recommended for unresectable intermediate-stage HCC (BCLC stage B or Child-Pugh class A/B with large or multifocal HCC and no vascular invasion or extrahepatic spread).^{19,108} It has recently been reported that TACE may also be safely performed in select patients with portal vein thrombosis with no increase in morbidity or mortality.^{145,146} TACE may also be considered in combination therapies with ablation, in patients with recurrence after curative therapy, and in potential transplant recipients to avoid progression of disease and subsequent removal from the transplant waiting list. TACE has also demonstrated an effective role for the palliative treatment of multiple hepatic malignant neoplasms, including cholangiocarcinoma as well as neuroendocrine, colorectal, uveal melanoma, and breast metastases.¹⁴⁷⁻¹⁵² General exclusion criteria

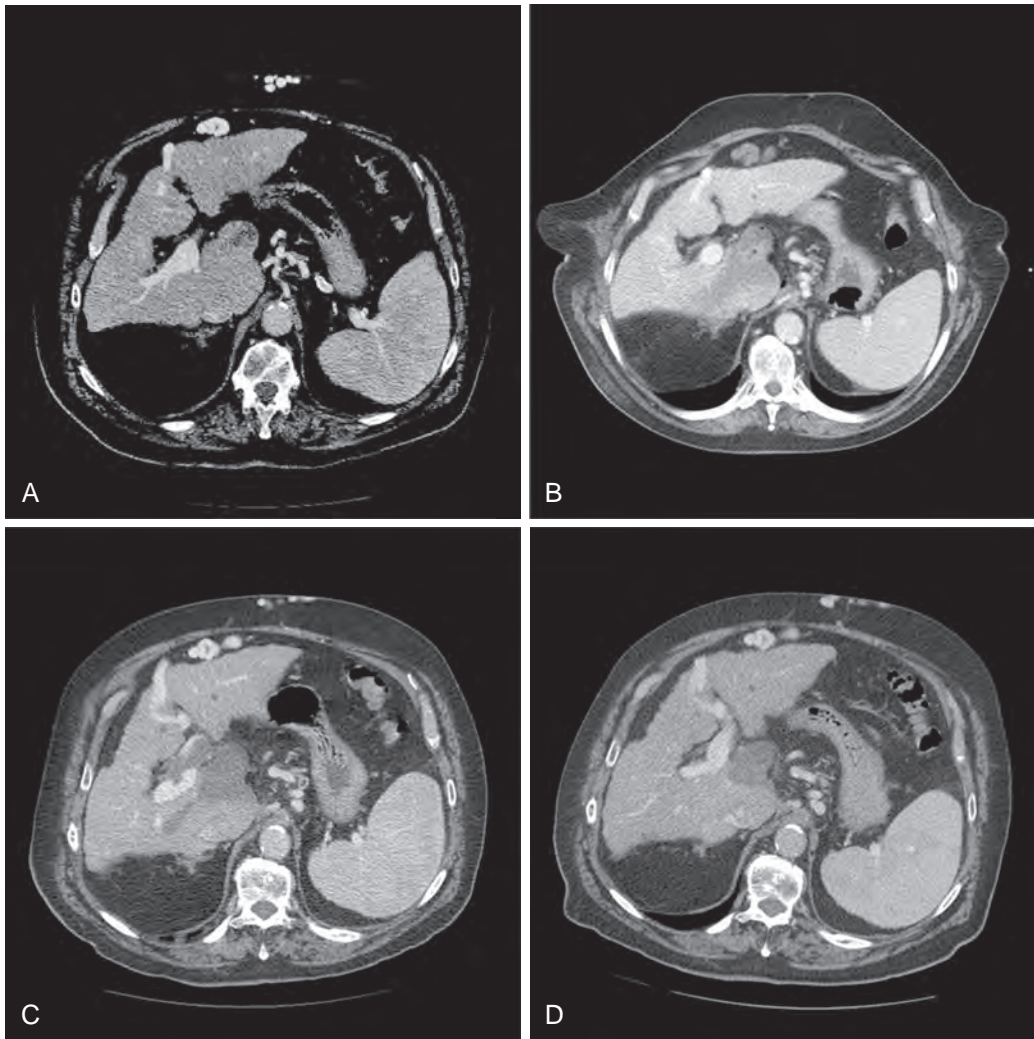


Figure 84-9 Portal vein thrombosis after microwave ablation. **A.** Portal venous phase CT demonstrates an exophytic lesion arising from the caudate lobe that met imaging criteria for HCC, which underwent percutaneous microwave ablation. **B.** Subsequent CT demonstrates the immediate postablation appearance. **C.** CT performed at 1 month after the procedure demonstrates nonocclusive portal venous thrombus, a complication of the ablation procedure. **D.** The patient was prescribed warfarin and the thrombus resolved, as seen on the CT performed at 1 year after the procedure.

for TACE have not been well defined. Multiple factors are associated with increased periprocedure mortality, including the combination of elevated bilirubin levels above 2 mg/dL, more than 50% tumor burden, lactate dehydrogenase levels greater than 425 mg/dL, and aspartate aminotransferase levels greater than 100 IU/L.¹⁵³ Child-Pugh class C liver disease, elevated bilirubin levels above 3 mg/dL, and elevated MELD (>10) or CLIP (>2) scores also are relative contraindications.¹⁵⁴

Guidance and Technique. After proper patient selection based on imaging and clinical findings, TACE is performed with standard endovascular techniques. Review of preoperative imaging is imperative for comprehensive evaluation of possible variant hepatic arterial anatomy, presence of extrahepatic tumoral blood supply, and portal vein patency. Selective angiography of the celiac and superior mesenteric arteries is performed to assess for variant hepatic arterial anatomy with imaging through the portal venous phase to confirm patency of the portal venous system. Various microcatheters are available for subsequent superselective angiography of the intrahepatic arterial vasculature. TACE can be performed from the subsegmental to the lobar level, depending on the type and number of tumors to be treated. The use of cone-beam CT during TACE procedures has been shown to be associated with

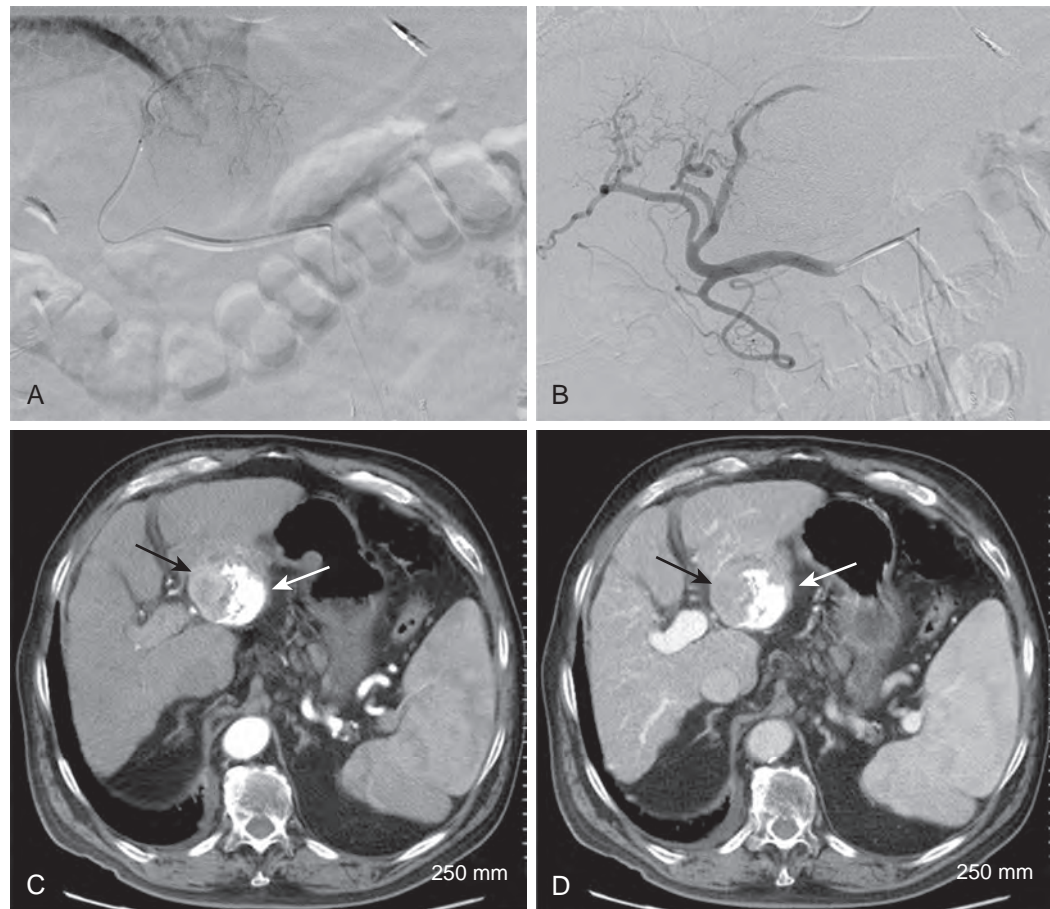
improved survival outcomes, identification of extrahepatic tumoral blood supply, and decreased risk of nontarget chemoembolization.¹⁵⁵ Intermittent infusion of 1% lidocaine between aliquots of the chemotherapy/Ethiodol slurry can decrease postembolization pain. After the procedure, patients are admitted to the hospital for overnight observation and pain control. Some centers recommend antibiotic treatment for 3 to 7 days after TACE to cover gram-negative enteric pathogens, with prolonged treatment of 2 weeks for patients with a disrupted sphincter of Oddi; however, the data regarding this practice are inconclusive.¹⁵⁴ Repeated treatment with TACE for new or residual disease is evaluated on a patient-by-patient basis, with planned consecutive treatments at least 3 weeks apart (Fig. 84-10).

Results

HCC. Multiple large case series have been reported showing the efficacy of conventional TACE for carefully selected patients with HCC. Randomized controlled trials have demonstrated that TACE provides a statistically significant benefit in survival and tumor response over the best supportive care measures.^{156,157} A large systematic review showed survival rates for patients with HCC undergoing TACE after the year 2000 at 1, 3, and 5 years of 71% ± 18%, 34% ± 13%, and 14% ± 10%.¹⁵⁸ Another large

Figure 84-10 Transarterial chemoembolization of HCC.

A. Selective angiography of the left hepatic artery demonstrates a 5-cm hypervascular mass consistent with hepatocellular carcinoma. **B.** Angiogram of the common hepatic artery after transarterial chemoembolization demonstrates no evidence of arterial enhancement within the treated lesion. **C and D.** Follow-up CT examination in the late arterial and portal venous phases demonstrates dense Lipiodol uptake within the left lateral aspect of the lesion (*white arrow*). At the right lateral aspect, there is persistent arterial enhancement and portal venous washout with rim enhancement consistent with residual untreated tumor (*black arrow*).



prospective cohort study of 8510 patients showed an overall median survival of 34 months with 1-, 3-, and 5-year survival rates of 82%, 47%, and 26%, respectively.¹⁵⁹ Currently, studies are investigating the effect of the combination of TACE with systemic molecular targeted therapies such as sorafenib, a multikinase inhibitor with antiangiogenic and antiproliferative effects that has shown survival benefit in patients with advanced HCC. An interim analysis of one of these studies has shown that this combination results in increased tumor response and time to progression.¹⁶⁰

Metastatic Disease and Cholangiocarcinoma. Overall median survival for patients with unresectable intrahepatic cholangiocarcinoma treated with TACE has been reported at 13 months with 1-, 3-, and 5-year survival rates of 52%, 29%, and 10%.¹⁴⁷ Child-Pugh class A liver dysfunction, hypervascular tumors, and initial tumor response were found to be factors associated with statistically significant increase in patient survival. TACE not only has shown a survival benefit in patients with metastatic neuroendocrine disease to the liver but also has a significant symptomatic benefit for patients suffering from carcinoid syndrome, with a symptomatic response rate of 60% to 95% for 20 to 85 months and a 5-year survival of between 50% and 65%. Bland transarterial embolization has shown similar response rates.¹⁴⁸ A median survival time of 9 to 14 months has been reported for patients undergoing TACE for unresectable colorectal liver metastases after failure of standard chemotherapy protocols, with a significant increase in median survival when TACE was implemented after first- or

second-line systemic therapy compared with third- to fifth-line therapies.^{149,150}

Complications. Postembolization syndrome, consisting of transient fever, pain, elevation of hepatic transaminases, and increased white blood cell count, can be seen in 60% to 80% of patients undergoing TACE. This is not considered a complication but rather an expected procedural outcome. The incidence of major complications after TACE ranges from 1% to 7.5%; these include liver failure, abscess, cholecystitis, biloma requiring percutaneous drainage, pulmonary arterial oil embolus, gastrointestinal hemorrhage or ulceration from nontarget embolization, renal dysfunction, and iatrogenic hepatic artery injury preventing treatment. The 30-day mortality after TACE is approximately 1% to 2.5% and has been most commonly reported secondary to acute liver failure but also can be secondary to acute renal failure, upper gastrointestinal bleeding, tumor rupture, and sepsis.¹⁵⁸

Follow-up. Follow-up imaging after TACE is usually performed 4 to 6 weeks after all tumor-bearing areas have been treated; however, some physicians may perform imaging studies between staged bilobar treatments. Assessment of tumor response after TACE is generally based on iodized oil deposition on unenhanced CT and tumor enhancement and size on postcontrast CT or MR images. High concentrations of iodized oil within a lesion after TACE may make assessment of enhancing tumor difficult. MRI may have advantages over CT for assessing tumor

viability after TACE as iodized oil does not affect MR signal intensity.^{161,162} One early study has shown that dual-energy CT can be used to improve evaluation for residual disease after TACE.¹⁶³ Hypovascular tumors, such as cholangiocarcinoma and various metastatic lesions such as breast cancer, may also demonstrate a decrease in overall tumor enhancement after TACE.

Drug-Eluting Bead Chemoembolization

Brief Rationale. Chemoembolization with drug-eluting beads is a recent advance in transarterial oncologic therapies with the goal of enhancing the delivery of potent chemotherapeutic agents to the site of tumor. Chemotherapeutic agents are loaded into polyvinyl alcohol-based microspheres, which allows fixed dosing and controlled and sustained release of the agents locally after embolization. Significant reductions in peak plasma concentrations of chemotherapeutic agents after DEB-TACE compared with conventional TACE have been shown, which may suggest a higher concentration of the drug in the tumoral microenvironment compared with the systemic circulation.^{164,165} This may result in more potent tumoricidal effect with a decrease in systemic side effects. Currently, the two most common chemotherapeutic agents being used for DEB-TACE are doxorubicin for HCC and irinotecan for metastatic colorectal cancer.

Indications and Contraindications. The indications for and contraindications to DEB-TACE in the setting of primary or metastatic liver disease are similar to those reported for conventional TACE.¹⁶⁶

Guidance and Technique. The endovascular approach to DEB-TACE is similar to conventional TACE. The dose of doxorubicin administered during a single treatment for HCC can vary on the basis of individual patient- and tumor-related factors but usually consists of either 75 mg of doxorubicin loaded into one vial of microspheres or 150 mg of doxorubicin loaded into two vials of microspheres.¹⁶⁷ The administered dose of irinotecan for metastatic colorectal cancer usually is 100 mg loaded into one vial of microspheres.¹⁶⁸ The size of microspheres used for DEB-TACE varies; 100- to 300- μ m beads are recommended on the basis of the expected distribution inside the tumor or close to the tumor margin.¹⁶⁹ Loaded microspheres should be mixed with a nonionic contrast medium before injection to aid in visualization during treatment. Similar to conventional TACE, treatment with drug-eluting beads can be performed from a subsegmental to a lobar level, depending on the type and number of tumors to be treated. Injection should be performed at a slow, controlled rate and continued until near stasis is observed or the entire dose has been administered. Meticulous attention to technique should be observed to avoid nontarget extrahepatic embolization. After the procedure, patients are admitted to the hospital for pain control. Repeated treatment with DEB-TACE for bilobar disease can be performed 2 to 4 weeks after the original treatment in the absence of complications, whereas a 4- to 8-week interval for re-treatment is recommended for residual disease.¹⁶⁷

Results. A large, multicenter randomized controlled trial comparing conventional TACE to DEB-TACE with doxorubicin for patients with unresectable HCC in BCLC classes A and B showed no statistically significant differences with respect to

tumor response. However, patients treated with DEB-TACE demonstrated improved tolerability with a statistically significant decrease in serious liver toxicity and a lower rate of doxorubicin-related side effects.¹⁷⁰ A randomized controlled trial comparing DEB-TACE to bland embolization demonstrated a significant difference in time to progression, with lower rates of recurrences and higher rate of complete response at 9 and 12 months.¹⁷¹ Survival rates at 1, 3, and 5 years have been reported at 90% to 94%, 62% to 66%, and 23% to 38%, respectively, for patients with BCLC class A and B disease, with an overall median survival ranging from 44 to 49 months.^{172,173}

The efficacy of DEB-TACE with irinotecan for the treatment of metastatic colorectal cancer refractory to systemic chemotherapy has been reported by a multicenter single-arm study, with overall survival of 19 months and progression-free survival of 11 months.¹⁶⁸

Complications. The incidence of postembolization syndrome with DEB-TACE is similar to that with conventional TACE; mild symptoms are reported in up to 86.5% of patients. Minor complications after DEB-TACE include cholecystitis, pleural effusion, and skin erythema after embolization of extrahepatic collateral vessels, with reported rates of less than 5%. Major complications include acute liver failure, abscess formation, and upper gastrointestinal tract bleeding, with 30-day mortality rates reported from 0% to 3.6%.^{174,175}

Follow-up Imaging. Follow-up imaging protocols are similar to those for conventional TACE. Initial imaging is performed 4 to 6 weeks after treatment with dynamic CT or MRI. Assessment of tumor response is based on size and enhancement characteristics.

Transarterial Radioembolization

Brief Rationale, Indications, and Contraindications. Whole liver external beam radiation therapy has had a limited role in the treatment of both primary and metastatic liver malignant neoplasms because of the relative radiosensitivity of normal hepatic tissue. Radiation-induced hepatitis has been observed in doses exceeding 35 Gy, which is below the estimated tumoricidal dose of 50 to 70 Gy.^{176,177} Transarterial radioembolization has been developed as a method of selectively administering microspheres loaded with a radioisotope, yttrium 90 (⁹⁰Y), into the hepatic arteries supplying the tumor to achieve radiation doses as high as 150 Gy without development of the clinical complications seen with external beam therapy.¹⁷⁷ ⁹⁰Y is a pure beta emitter with a half-life of 64.2 hours that decays to stable zirconium 90. The emissions have a mean tissue penetration of 2.5 mm with a maximum reach of 11 mm. Radioembolization results in localized generation of oxygen free radicals of water molecules near to the tumor cell's DNA. In the presence of normal oxygen tension, permanent DNA damage is caused and results in apoptosis.¹⁷⁶

There are currently two commercially available radioembolic agents. Theraspheres (MDS Nordion, Ottawa, Ontario, Canada) are glass microspheres ranging in diameter from 20 to 30 μ m. SIR-spheres (Sirtex Medical, North Ryde, Australia) are resin microspheres ranging in diameter from 20 to 60 μ m. Radioembolization with ⁹⁰Y has been shown to have clinical benefit in HCC, intrahepatic cholangiocarcinoma, and metastatic disease from colorectal, neuroendocrine, breast, and uveal melanoma primary malignant neoplasms.¹⁷⁸⁻¹⁸⁶ Patients considered for

radioembolization therapy should have unresectable hepatic primary or metastatic cancer with liver-dominant tumor burden and a life expectancy of more than 3 months.¹⁸⁷ Patients presenting with branch portal vein invasion and good liver function may also be considered for radioembolization as hepatic arterial inflow is maintained after treatment.¹⁸⁸ Contraindications to radioembolization therapy include a pretreatment technetium Tc 99m macroaggregated albumin scan demonstrating the potential for 30 Gy or more of radiation exposure to the lung or flow to the gastrointestinal tract that cannot be corrected by catheter embolization techniques, a limited hepatic reserve, a bilirubin level of more than 2 mg/dL without a reversible cause, and a history of prior radiotherapy involving the liver.¹⁸⁷

Guidance and Technique. After careful patient selection, preferably by multidisciplinary consensus involving medical oncology, surgical oncology, radiation oncology, and interventional radiology, treatment with ⁹⁰Y microspheres involves at least a two-stage process. Patients undergo a vascular mapping procedure by standard endovascular techniques to delineate the mesenteric and hepatic arterial blood supply to the intended targeted treatment area and to identify any variant hepatic arterial anatomy that may require separate treatment sessions. Prophylactic embolization of extrahepatic arteries, such as the gastroduodenal and right gastric arteries, may be performed to isolate the hepatic arterial circulation and to decrease the risk of nontarget radioembolization to the gastrointestinal tract. Finally, ^{99m}Tc-macroaggregated albumin is injected with the catheter position and flow rate that mimics the anticipated ⁹⁰Y

injection, with subsequent scintigraphic imaging to evaluate for hepatopulmonary shunting or gastrointestinal tract uptake. The dose of ⁹⁰Y microspheres to be delivered is then calculated on the basis of the chosen particles (glass vs. resin microspheres), the intended treatment volume (whole vs. lobar vs. segmental treatment), and the percentage of pulmonary shunting. The treatment session should take place 1 to 3 weeks after the vascular mapping procedure, and arteriography is performed before ⁹⁰Y microsphere injection to evaluate for revascularization of extrahepatic branches that may result in nontarget radioembolization. If bilobar treatment is planned, the second treatment is usually performed 4 to 6 weeks after the first treatment.

Results. The results of treatment of HCC with ⁹⁰Y microspheres depends on multiple clinical factors including clinical stage at presentation, presence of portal vein thrombosis, performance status, hepatic reserve, and presence of extrahepatic disease. Two large studies demonstrated median survival of 24.4 to 26.9 months for BCLC class A, 16.9 to 17.2 months for BCLC class B, and 7.3 to 10.0 months for BCLC class C.^{178,179} Patients with Child-Pugh class A liver disease and branch portal vein thrombosis demonstrated a median survival of 16.6 months compared with 7.7 months in Child-Pugh class A with main portal vein thrombosis, 6.5 months in Child-Pugh class B with branch portal vein thrombosis, and 4.5 months in Child-Pugh class B with main portal vein thrombosis.¹⁷⁸ Treatment of HCC with ⁹⁰Y microspheres has also been reported as a measure for downstaging patients to more curative therapies, such as ablation, resection, and liver transplantation^{178,179} (Fig. 84-11).

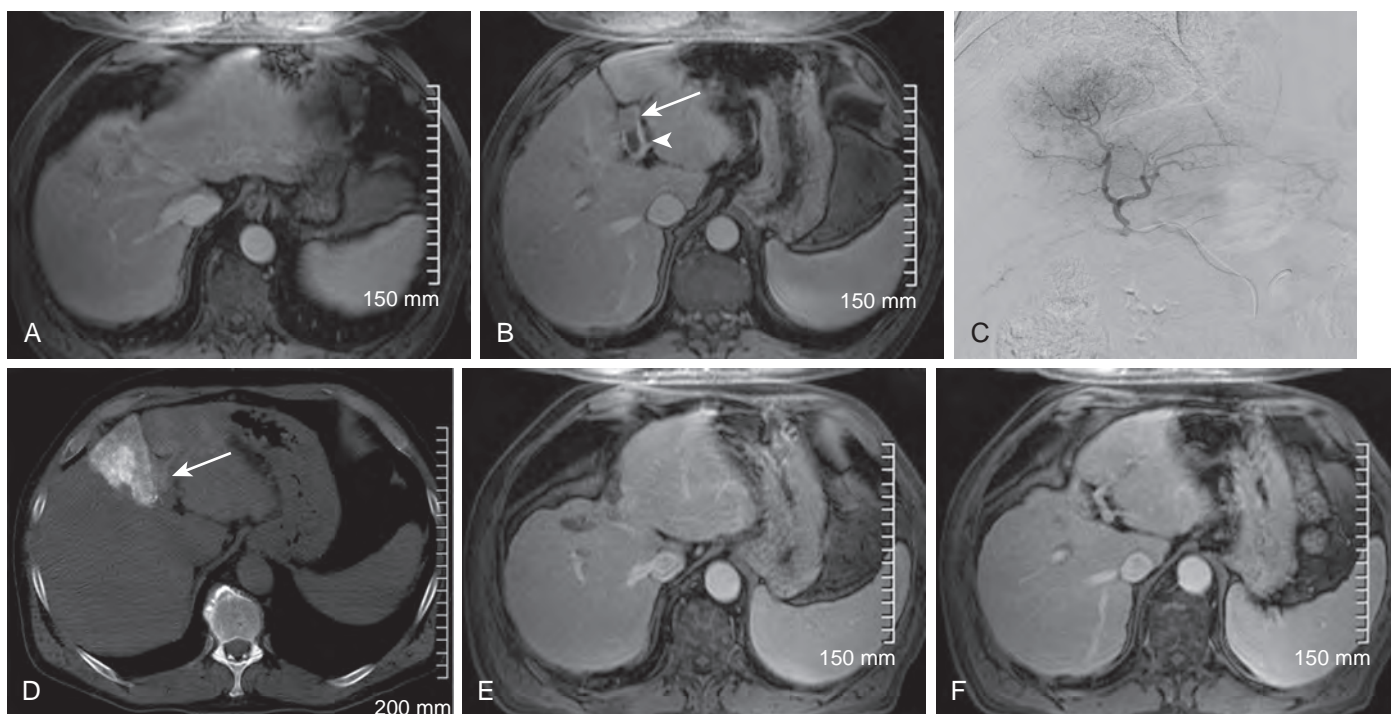


Figure 84-11 HCC with tumor thrombus treated with ⁹⁰Y transarterial radioembolization. **A** and **B**. Portal venous phase MRI demonstrates an infiltrative lesion with central portal venous washout and rim enhancement. Enhancing tumor thrombus (arrow) as well as nonenhancing bland thrombus (arrowhead) is identified in the left main portal vein. **C**. Selective left hepatic angiography demonstrates a hypervascular mass in segment IV. **D**. Intraprocedural CT after direct injection of iodinated contrast material into the left hepatic artery confirms tumor thrombus (arrow) in the left main portal vein. ⁹⁰Y glass microspheres were administered into the left hepatic artery. **E** and **F**. Portal venous phase imaging 3 years after ⁹⁰Y injection demonstrates complete response to therapy, changes of radiation segmentectomy, and a widely patent left portal vein.

Response rates for patients with unresectable intrahepatic cholangiocarcinoma vary significantly on the basis of preprocedure performance status, with a median survival of 18.3 to 29.4 months for patients with Eastern Cooperative Oncology Group (ECOG) 0 performance status compared with 7 to 10 months for ECOG 1 and 3 to 5.1 months for ECOG 2.^{180,181} In the setting of salvage treatment of colorectal metastatic disease after failure of at least three lines of chemotherapy, patients who responded to radioembolization treatment (by imaging or biochemical tumor assay) demonstrated a median survival of 10.5 months compared with 4.5 months for nonresponders and historical controls.¹⁸² With regard to neuroendocrine liver metastases, a large multicenter retrospective series demonstrated stable disease in 22.7%, partial response in 60.5%, complete response in 2.7%, and progressive disease in 4.9%, with an overall median survival of 70 months.¹⁸⁴

Complications. The most common minor complication is postradioembolization syndrome, which can affect 20% to 55% of patients and is characterized by clinical symptoms of fatigue, nausea, vomiting, anorexia, fever, abdominal discomfort, and cachexia.¹⁸⁹ Other potential complications include radiation-induced liver disease (0%-4%); biliary sequelae, such as biliary stricture, necrosis, or radiation cholecystitis (<10%); radiation pneumonitis (<1%); and gastrointestinal ulceration (<4%).¹⁸⁹ The mild adverse events and constitutional symptoms secondary to ⁹⁰Y microsphere radioembolization rarely require hospitalization, whereas the serious adverse events can be mitigated by proper patient selection, appropriate dosimetry methods, and meticulous technique.

Follow-up. Patients are usually followed up clinically 2 weeks after treatment with a review of systems, physical examination, and routine laboratory tests.¹⁸⁷ Routine imaging performed with CT or MRI at 4 to 6 weeks after treatment is common at many centers. Early imaging after ⁹⁰Y microsphere radioembolization often demonstrates hepatic parenchymal edema, and lesions may mildly increase in size but usually show signal intensity or attenuation differences. Assessment of enhancement at early imaging by the modified response evaluation criteria in solid tumors (mRECIST) or the European Association for the Study of the Liver (EASL) criteria correlates with response on follow-up imaging. Full treatment response by size criteria is usually evident by 3 months after treatment with resolution of the acute radiation changes. PET/CT may show earlier decreases in metabolic activity for FDG-avid lesions at 6 weeks after treatment, but PET/CT has limited sensitivity for detecting activity in small lesions.

COMBINATION INTERSTITIAL AND ENDOVASCULAR THERAPY

Ablation and TACE

Brief Rationale and Indications. Ablative therapies for HCC have shown promising results and may be equivalent to surgical resection for some cases, particularly when tumors are smaller than 3 cm.¹⁹⁰ For tumors larger than 3 cm, it is difficult to ablate all viable tumor tissue and to create an adequate tumor-free margin. Also, the presence of satellite nodules is more commonly seen in larger tumors. Combination therapy consisting of TACE followed by ablation has been increasingly used to obtain larger ablation zones and to achieve better local control in patients with tumors larger than 3 cm.¹⁹¹ The synergistic effect of combination therapy results from the occlusion of hepatic arterial flow by embolization, which reduces the cooling effect of hepatic blood flow on thermal coagulation. In addition, Lipiodol fills the peripheral portal veins surrounding the tumor through multiple arteriportal communications and thus reduces portal flow. The tumoricidal effect of anticancer agents is enhanced by hyperthermia, which may result in cell death in marginal areas of the ablation zone that reach sublethal temperatures. Finally, TACE may also help control the small satellite microlesions not encompassed in the ablation zone.

Results. Multiple studies have demonstrated that combination therapy of TACE followed by RF ablation results in significantly lower local tumor progression rates with improved survival rates for tumors larger than 3 cm compared with RF ablation alone.¹⁹²⁻¹⁹⁴ A randomized study comparing combination therapy with RF ablation alone for recurrent HCC also demonstrated significantly decreased local tumor progression rates and improved overall survival at 1, 3, and 5 years for combination therapy compared with RF ablation alone for lesions larger than 3 cm; however, these differences were found not to be significant in patients with recurrences smaller than 3 cm.¹⁹⁵ A randomized study of patients with HCCs smaller than 3 cm also failed to show a benefit of combination therapy compared with RF ablation alone, with equivocal rates of local tumor progression and overall survival at 1, 2, 3, and 4 years.¹⁹⁶ Combination therapy may also prove useful for lesions in anatomically difficult locations (i.e., subcapsular or caudate lobe lesions), residual disease after primary ablation not amenable to re-treatment, and lesions difficult to identify on ultrasound imaging alone.¹⁹⁷⁻²⁰⁰ Complication rates for combination therapy have been reported to be similar to those of the treatments separately without additive effect.

REFERENCES

- Menghini G: One-second needle biopsy of the liver. *Gastroenterology* 35:190-199, 1958.
- Godfrey EM, Mannelli L, Griffin N, Lomas DJ: Magnetic resonance elastography in the diagnosis of hepatic fibrosis. *Semin Ultrasound CT MR* 34:81-88, 2013.
- Yada N, Kudo M, Morikawa H, et al: Assessment of liver fibrosis with real-time tissue elastography in chronic viral hepatitis. *Oncology* 84(Suppl 1):13-20, 2013.
- Lee Y, Jee HJ, Noh H, et al: In vivo ¹H-MRS hepatic lipid profiling in nonalcoholic fatty liver disease: An animal study at 9.4 T. *Magn Reson Med* 2012. [Epub ahead of print.]
- Rockey DC, Caldwell SH, Goodman ZD, et al: Liver biopsy. *Hepatology* 49:1017-1044, 2009.
- Patel IJ, Davidson JC, Nikolic B, et al: Consensus guidelines for periprocedural management of coagulation status and hemostasis risk in percutaneous image-guided interventions. *J Vasc Interv Radiol* 23:727-736, 2012.
- O'Connor SD, Taylor AJ, Williams EC, Winter TC: Coagulation concepts update. *AJR Am J Roentgenol* 193:1656-1664, 2009.
- Gilmore IT, Burroughs A, Murray-Lyon IM, et al: Indications, methods, and outcomes of percutaneous liver biopsy in England and Wales: An audit by the British Society of Gastroenterology and the Royal College of Physicians of London. *Gut* 36:437-441, 1995.
- Lindor KD, Bru C, Jorgensen RA, et al: The role of ultrasonography and automatic-needle biopsy in outpatient percutaneous liver biopsy. *Hepatology* 23:1079-1083, 1996.
- Farrell RJ, Smiddy PF, Pilkington RM, et al: Guided versus blind liver biopsy for chronic

- hepatitis C: Clinical benefits and costs. *J Hepatol* 30:580–587, 1999.
11. Younossi ZM, Teran JC, Ganiats TG, Carey WD: Ultrasound-guided liver biopsy for parenchymal liver disease: An economic analysis. *Dig Dis Sci* 43:46–50, 1998.
12. Pasha T, Gabriel S, Therneau T, et al: Cost-effectiveness of ultrasound-guided liver biopsy. *Hepatology* 27:1220–1226, 1998.
13. Papini E, Pacella CM, Rossi Z, et al: A randomized trial of ultrasound-guided anterior subcostal liver biopsy versus the conventional Menghini technique. *J Hepatol* 13:291–297, 1991.
14. Grant A, Neuberger J: Guidelines on the use of liver biopsy in clinical practice. *British Society of Gastroenterology. Gut* 45(Suppl 4):IV1–IV11, 1999.
15. Caldwell SH: Controlling pain in liver biopsy, or “we will probably need to repeat the biopsy in a year or two to assess the response”. *Am J Gastroenterol* 96:1327–1329, 2001.
16. McGill DB, Rakela J, Zinsmeister AR, Ott BJ: A 21-year experience with major hemorrhage after percutaneous liver biopsy. *Gastroenterology* 99:1396–1400, 1990.
17. Piccinino F, Sagnelli E, Pasquale G, Giusti G: Complications following percutaneous liver biopsy. A multicentre retrospective study on 68,276 biopsies. *J Hepatol* 2:165–173, 1986.
18. Minuk GY, Sutherland LR, Wiseman DA, et al: Prospective study of the incidence of ultrasound-detected intrahepatic and subcapsular hematomas in patients randomized to 6 or 24 hours of bed rest after percutaneous liver biopsy. *Gastroenterology* 92:290–293, 1987.
19. Bruix J, Sherman M: American Association for the Study of Liver Diseases: Management of hepatocellular carcinoma: An update. *Hepatology* 53:1020–1022, 2011.
20. Singal A, Volk ML, Waljee A, et al: Meta-analysis: Surveillance with ultrasound for early-stage hepatocellular carcinoma in patients with cirrhosis. *Aliment Pharmacol Ther* 30:37–47, 2009.
21. Lok AS, Sterling RK, Everhart JE, et al: Des-gamma-carboxy prothrombin and alpha-fetoprotein as biomarkers for the early detection of hepatocellular carcinoma. *Gastroenterology* 138:493–502, 2010.
22. Silva MA, Hegab B, Hyde C, et al: Needle track seeding following biopsy of liver lesions in the diagnosis of hepatocellular cancer: A systematic review and meta-analysis. *Gut* 57:1592–1596, 2008.
23. Forner A, Vilana R, Ayuso C, et al: Diagnosis of hepatic nodules 20 mm or smaller in cirrhosis: Prospective validation of the noninvasive diagnostic criteria for hepatocellular carcinoma. *Hepatology* 47:97–104, 2008.
24. Sangiovanni A, Manini MA, Iavarone M, et al: The diagnostic and economic impact of contrast imaging techniques in the diagnosis of small hepatocellular carcinoma in cirrhosis. *Gut* 59:638–644, 2010.
25. Wald C, Russo MW, Heimbach JK, et al: New OPTN/UNOS policy for liver transplant allocation: Standardization of liver imaging, diagnosis, classification, and reporting of hepatocellular carcinoma. *Radiology* 266:376–382, 2013.
26. American College of Radiology: Liver Imaging Reporting and Data System, Version 2013.1. <http://www.acr.org/Quality-Safety/Resources/LIRADS/>.
27. International Consensus Group for Hepatocellular Neoplasia: Pathologic diagnosis of early hepatocellular carcinoma: A report of the international consensus group for hepatocellular neoplasia. *Hepatology* 49:658–664, 2009.
28. Simard EP, Ward EM, Siegel R, Jemal A: Cancers with increasing incidence trends in the United States: 1999 through 2008. *CA Cancer J Clin* 2012. [Epub ahead of print.]
29. Thanos L, Zormpala A, Papaioannou G, et al: Safety and efficacy of percutaneous CT-guided liver biopsy using an 18-gauge automated needle. *Eur J Intern Med* 16:571–574, 2005.
30. Dusenbery D, Ferris JV, Thaete FL, Carr BI: Percutaneous ultrasound-guided needle biopsy of hepatic mass lesions using a cytohistologic approach. Comparison of two needle types. *Am J Clin Pathol* 104:583–587, 1995.
31. Pagani JJ: Biopsy of focal hepatic lesions. Comparison of 18 and 22 gauge needles. *Radiology* 147:673–675, 1983.
32. Martino CR, Haaga JR, Bryan PJ, et al: CT-guided liver biopsies: Eight years' experience. Work in progress. *Radiology* 152:755–757, 1984.
33. Ch Yu S, Metreweli C, Lau WY, et al: Safety of percutaneous biopsy of hepatocellular carcinoma with an 18 gauge automated needle. *Clin Radiol* 52:907–911, 1997.
34. Appelbaum L, Kane RA, Kruskal JB, et al: Focal hepatic lesions: US-guided biopsy—lessons from review of cytologic and pathologic examination results. *Radiology* 250:453–458, 2009.
35. Yu SC, Liew CT, Lau WY, et al: US-guided percutaneous biopsy of small (< or = 1-cm) hepatic lesions. *Radiology* 218:195–199, 2001.
36. Elsayes KM, Ellis JH, Elkhoully T, et al: Diagnostic yield of percutaneous image-guided tissue biopsy of focal hepatic lesions in cancer patients: Ten percent are not metastases from the primary malignancy. *Cancer* 117:4041–4048, 2011.
37. Chang S, Kim SH, Lim HK, et al: Needle tract implantation after sonographically guided percutaneous biopsy of hepatocellular carcinoma: Evaluation of doubling time, frequency, and features on CT. *AJR Am J Roentgenol* 185:400–405, 2005.
38. Herrero JJ, Sangro B, Pardo F, et al: Liver transplantation in patients with hepatocellular carcinoma across Milan criteria. *Liver Transpl* 14:272–278, 2008.
39. Robertson EG, Baxter G: Tumour seeding following percutaneous needle biopsy: The real story! *Clin Radiol* 66:1007–1014, 2011.
40. Cresswell AB, Welsh FK, Rees M: A diagnostic paradigm for resectable liver lesions: To biopsy or not to biopsy? *HPB (Oxford)* 11:533–540, 2009.
41. Weiner M, Hanafee WN: A review of transjugular cholangiography. *Radiol Clin North Am* 8:53–68, 1970.
42. McAfee JH, Keefe EB, Lee RG, Rosch J: Transjugular liver biopsy. *Hepatology* 15:726–732, 1992.
43. Blasco A, Fornis X, Carrion JA, et al: Hepatic venous pressure gradient identifies patients at risk of severe hepatitis C recurrence after liver transplantation. *Hepatology* 43:492–499, 2006.
44. Miraglia R, Luca A, Gruttadauria S, et al: Contribution of transjugular liver biopsy in patients with the clinical presentation of acute liver failure. *Cardiovasc Intervent Radiol* 29:1008–1010, 2006.
45. Shin JL, Teitel J, Swain MG, et al: A Canadian multicenter retrospective study evaluating transjugular liver biopsy in patients with congenital bleeding disorders and hepatitis C: Is it safe and useful? *Am J Hematol* 78:85–93, 2005.
46. Gamble P, Colapinto RF, Stronell RD, et al: Transjugular liver biopsy: A review of 461 biopsies. *Radiology* 157:589–593, 1985.
47. Vibhakorn S, Cholongitas E, Kalambokis G, et al: A comparison of four- versus three-pass transjugular biopsy using a 19-G Tru-Cut needle and a randomized study using a cassette to prevent biopsy fragmentation. *Cardiovasc Intervent Radiol* 32:508–513, 2009.
48. Kalambokis G, Manousou P, Vibhakorn S, et al: Transjugular liver biopsy—indications, adequacy, quality of specimens, and complications—a systematic review. *J Hepatol* 47:284–294, 2007.
49. Kaplan GG, Gregson DB, Laupland KB: Population-based study of the epidemiology of and the risk factors for pyogenic liver abscess. *Clin Gastroenterol Hepatol* 2:1032–1038, 2004.
50. Jepsen P, Vilstrup H, Schonheyder HC, Sorensen HT: A nationwide study of the incidence and 30-day mortality rate of pyogenic liver abscess in Denmark, 1977–2002. *Aliment Pharmacol Ther* 21:1185–1188, 2005.
51. Meddings L, Myers RP, Hubbard J, et al: A population-based study of pyogenic liver abscesses in the United States: Incidence, mortality, and temporal trends. *Am J Gastroenterol* 105:117–124, 2010.
52. Tsai FC, Huang YT, Chang LY, Wang JT: Pyogenic liver abscess as endemic disease, Taiwan. *Emerg Infect Dis* 14:1592–1600, 2008.
53. Rahimian J, Wilson T, Oram V, Holzman RS: Pyogenic liver abscess: Recent trends in etiology and mortality. *Clin Infect Dis* 39:1654–1659, 2004.
54. Mezhir JJ, Fong Y, Fleischer D, et al: Pyogenic abscess after hepatic artery embolization: A rare but potentially lethal complication. *J Vasc Interv Radiol* 22:177–182, 2011.
55. Law ST, Li KK: Is hepatic neoplasm-related pyogenic liver abscess a distinct clinical entity? *World J Gastroenterol* 18:1110–1116, 2012.
56. Ferraioli G, Garlaschelli A, Zanaboni D, et al: Percutaneous and surgical treatment of pyogenic liver abscesses: Observation over a 21-year period in 148 patients. *Dig Liver Dis* 40:690–696, 2008.
57. Mezhir JJ, Fong Y, Jacks LM, et al: Current management of pyogenic liver abscess: Surgery is now second-line treatment. *J Am Coll Surg* 210:975–983, 2010.
58. Hope WW, Vrochides DV, Newcomb WL, et al: Optimal treatment of hepatic abscess. *Am Surg* 74:178–182, 2008.
59. Giorgio A, de Stefano G, Di Sarno A, et al: Percutaneous needle aspiration of multiple pyogenic abscesses of the liver: 13-year single-center experience. *AJR Am J Roentgenol* 187:1585–1590, 2006.
60. Zerem E, Hadzic A: Sonographically guided percutaneous catheter drainage versus needle aspiration in the management of pyogenic liver abscess. *AJR Am J Roentgenol* 189:W138–W142, 2007.
61. Liu CH, Gervais DA, Hahn PF, et al: Percutaneous hepatic abscess drainage: Do multiple abscesses or multiloculated abscesses preclude drainage or affect outcome? *J Vasc Interv Radiol* 20:1059–1065, 2009.
62. Rajak CL, Gupta S, Jain S, et al: Percutaneous treatment of liver abscesses: Needle aspiration versus catheter drainage. *AJR Am J Roentgenol* 170:1035–1039, 1998.

63. Vizzutti F, Arena U, Romanelli RG, et al: Liver stiffness measurement predicts severe portal hypertension in patients with HCV-related cirrhosis. *Hepatology* 45:1290–1297, 2007.
64. Bureau C, Metivier S, Peron JM, et al: Transient elastography accurately predicts presence of significant portal hypertension in patients with chronic liver disease. *Aliment Pharmacol Ther* 27:1261–1268, 2008.
65. Lemoine M, Katsahian S, Zioli M, et al: Liver stiffness measurement as a predictive tool of clinically significant portal hypertension in patients with compensated hepatitis C virus or alcohol-related cirrhosis. *Aliment Pharmacol Ther* 28:1102–1110, 2008.
66. Friedman EW, Weiner RS: Estimation of hepatic sinusoid pressure by means of venous catheters and estimation of portal pressure by hepatic vein catheterization. *Am J Physiol* 165:527–531, 1951.
67. Merkel C, Montagnese S: Hepatic venous pressure gradient measurement in clinical hepatology. *Dig Liver Dis* 43:762–767, 2011.
68. Cavaluzzi JA, Sheff R, Harrington DP, et al: Hepatic venography and wedge hepatic vein pressure measurements in diffuse liver disease. *AJR Am J Roentgenol* 129:441–446, 1977.
69. Chelliah ST, Keshava SN, Moses V, et al: Measurement of hepatic venous pressure gradient revisited: Catheter wedge vs balloon wedge techniques. *Indian J Radiol Imaging* 21:291–293, 2011.
70. Maleux G, Willems E, Fieus S, et al: Prospective study comparing different indirect methods to measure portal pressure. *J Vasc Interv Radiol* 22:1553–1558, 2011.
71. Rösch J, Hanafee WN, Snow H: Transjugular portal venography and radiologic portacaval shunt: An experimental study. *Radiology* 92:1112–1114, 1969.
72. Petersen B, Uchida BT, Timmermans H, et al: Guided direct intrahepatic portacaval shunt with a PTFE-covered stent-graft: Feasibility study in swine and initial clinical results. *J Vasc Interv Radiol* 12:475–486, 2001.
73. Fidelman N, Kwan SW, LaBerge JM, et al: The transjugular intrahepatic portosystemic shunt: An update. *AJR Am J Roentgenol* 199:746–755, 2012.
74. Garcia-Pagan JC, Caca K, Bureau C, et al: Early use of TIPS in patients with cirrhosis and variceal bleeding. *N Engl J Med* 362:2370–2379, 2010.
75. Garcia-Pagan JC, Heydtmann M, Raffa S, et al: TIPS for Budd-Chiari syndrome: Long-term results and prognostic factors in 124 patients. *Gastroenterology* 135:808–815, 2008.
76. Hernandez-Guerra M, Turnes J, Rubinstein P, et al: PTFE-covered stents improve TIPS patency in Budd-Chiari syndrome. *Hepatology* 40:1197–1202, 2004.
77. Azoulay D, Castaing D, Lemoine A, et al: Transjugular intrahepatic portosystemic shunt (TIPS) for severe veno-occlusive disease of the liver following bone marrow transplantation. *Bone Marrow Transplant* 25:987–992, 2000.
78. Dhanasekaran R, West JK, Gonzales PC, et al: Transjugular intrahepatic portosystemic shunt for symptomatic refractory hepatic hydrothorax in patients with cirrhosis. *Am J Gastroenterol* 105:635–641, 2010.
79. Spencer EB, Cohen DT, Darcy MD: Safety and efficacy of transjugular intrahepatic portosystemic shunt creation for the treatment of hepatic hydrothorax. *J Vasc Interv Radiol* 13:385–390, 2002.
80. Martinez-Palli G, Drake BB, Garcia-Pagan JC, et al: Effect of transjugular intrahepatic portosystemic shunt on pulmonary gas exchange in patients with portal hypertension and hepatopulmonary syndrome. *World J Gastroenterol* 11:6858–6862, 2005.
81. Bureau C, Pagan JC, Layrargues GP, et al: Patency of stents covered with polytetrafluoroethylene in patients treated by transjugular intrahepatic portosystemic shunts: Long-term results of a randomized multicentre study. *Liver Int* 27:742–747, 2007.
82. Garcia-Tsao G, Groszmann RJ, Fisher RL, et al: Portal pressure, presence of gastroesophageal varices and variceal bleeding. *Hepatology* 5:419–424, 1985.
83. Tesdal IK, Filser T, Weiss C, et al: Transjugular intrahepatic portosystemic shunts: Adjunctive embolotherapy of gastroesophageal collateral vessels in the prevention of variceal rebleeding. *Radiology* 236:360–367, 2005.
84. Gaba RC, Omene BO, Podczewinski ES, et al: TIPS for treatment of variceal hemorrhage: Clinical outcomes in 128 patients at a single institution over a 12-year period. *J Vasc Interv Radiol* 23:227–235, 2012.
85. Boyer TD, Haskal ZJ: American Association for the Study of Liver Diseases Practice Guidelines: The role of transjugular intrahepatic portosystemic shunt creation in the management of portal hypertension. *J Vasc Interv Radiol* 16:615–629, 2005.
86. Chung HH, Razavi MK, Sze DY, et al: Portosystemic pressure gradient during transjugular intrahepatic portosystemic shunt with Viatorr stent graft: What is the critical low threshold to avoid medically uncontrolled low pressure gradient related complications? *J Gastroenterol Hepatol* 23:95–101, 2008.
87. Haskal ZJ, Martin L, Cardella JF, et al: Quality improvement guidelines for transjugular intrahepatic portosystemic shunts. *J Vasc Interv Radiol* 14(Pt 2):S265–S270, 2003.
88. Burroughs AK, Vangeli M: Transjugular intrahepatic portosystemic shunt versus endoscopic therapy: Randomized trials for secondary prophylaxis of variceal bleeding: An updated meta-analysis. *Scand J Gastroenterol* 37:249–252, 2002.
89. Zheng M, Chen Y, Bai J, et al: Transjugular intrahepatic portosystemic shunt versus endoscopic therapy in the secondary prophylaxis of variceal rebleeding in cirrhotic patients: Meta-analysis update. *J Clin Gastroenterol* 42:507–516, 2008.
90. D'Amico G, Luca A, Morabito A, et al: Uncovered transjugular intrahepatic portosystemic shunt for refractory ascites: A meta-analysis. *Gastroenterology* 129:1282–1293, 2005.
91. Narahara Y, Kanazawa H, Fukuda T, et al: Transjugular intrahepatic portosystemic shunt versus paracentesis plus albumin in patients with refractory ascites who have good hepatic and renal function: A prospective randomized trial. *J Gastroenterol* 46:78–85, 2011.
92. Hausegger KA, Karnel F, Georgieva B, et al: Transjugular intrahepatic portosystemic shunt creation with the Viatorr expanded polytetrafluoroethylene-covered stent-graft. *J Vasc Interv Radiol* 15:239–248, 2004.
93. Darcy M: Evaluation and management of transjugular intrahepatic portosystemic shunts. *AJR Am J Roentgenol* 199:730–736, 2012.
94. Kanterman RY, Darcy MD, Middleton WD, et al: Doppler sonography findings associated with transjugular intrahepatic portosystemic shunt malfunction. *AJR Am J Roentgenol* 168:467–472, 1997.
95. Feldstein VA, Patel MD, LaBerge JM: Transjugular intrahepatic portosystemic shunts: Accuracy of Doppler US in determination of patency and detection of stenoses. *Radiology* 201:141–147, 1996.
96. Dodd GD, 3rd, Zajko AB, Orons PD, et al: Detection of transjugular intrahepatic portosystemic shunt dysfunction: Value of duplex Doppler sonography. *AJR Am J Roentgenol* 164:1119–1124, 1995.
97. Jirkovsky V, Fejfar T, Safka V, et al: Influence of the transjugular deployment of expanded polytetrafluoroethylene-covered stent grafts on maintenance of transjugular intrahepatic portosystemic shunt patency. *J Vasc Interv Radiol* 22:55–60, 2011.
98. Ribero D, Abdalla EK, Madoff DC, et al: Portal vein embolization before major hepatectomy and its effects on regeneration, resectability and outcome. *Br J Surg* 94:1386–1394, 2007.
99. van Lienden KP, van den Esscher JW, de Graaf W, et al: Portal vein embolization before liver resection: A systematic review. *Cardiovasc Intervent Radiol* 36:25–34, 2013.
100. Hayashi H, Beppu T, Sugita H, et al: Serum HGF and TGF-beta1 levels after right portal vein embolization. *Hepatol Res* 40:311–317, 2010.
101. Dixon E, Abdalla E, Schwarz RE, Vauthey JN: AHPBA/SSO/SSAT sponsored Consensus Conference on Multidisciplinary Treatment of Hepatocellular Carcinoma. HPB (Oxford) 12:287–288, 2010.
102. May BJ, Talenfeld AD, Madoff DC: Update on portal vein embolization: Evidence-based outcomes, controversies, and novel strategies. *J Vasc Interv Radiol* 24:241–254, 2013.
103. Farges O, Belghiti J, Kianmanesh R, et al: Portal vein embolization before right hepatectomy: Prospective clinical trial. *Ann Surg* 237:208–217, 2003.
104. Kishi Y, Madoff DC, Abdalla EK, et al: Is embolization of segment 4 portal veins before extended right hepatectomy justified? *Surgery* 144:744–751, 2008.
105. Ahmed M, Brace CL, Lee FT, Jr, Goldberg SN: Principles of and advances in percutaneous ablation. *Radiology* 258:351–369, 2011.
106. McCarley JR, Soulen MC: Percutaneous ablation of hepatic tumors. *Semin Interv Radiol* 27:255–260, 2010.
107. Brace CL, Sampson LA, Hinshaw JL, et al: Radiofrequency ablation: Simultaneous application of multiple electrodes via switching creates larger, more confluent ablations than sequential application in a large animal model. *J Vasc Interv Radiol* 20:118–124, 2009.
108. de Lope CR, Tremosini S, Forner A, et al: Management of HCC. *J Hepatol* 56(Suppl 1):S75–S87, 2012.
109. Mazzaferro V, Bhoori S, Sposito C, et al: Milan criteria in liver transplantation for hepatocellular carcinoma: An evidence-based analysis of 15 years of experience. *Liver Transpl* 17(Suppl 2):S44–S57, 2011.
110. Heckman JT, Devera MB, Marsh JW, et al: Bridging locoregional therapy for hepatocellular carcinoma prior to liver transplantation. *Ann Surg Oncol* 15:3169–3177, 2008.
111. DuBay DA, Sandroussi C, Kachura JR, et al: Radiofrequency ablation of hepatocellular carcinoma as a bridge to liver transplantation. HPB (Oxford) 13:24–32, 2011.

112. Hoyer DP, Paul A, Lauenstein T, et al: [Relevance of ablation therapies for HCC: "A real bridging" for liver transplantation?] *Zentralbl Chir* 2013. [Epub ahead of print.]
113. Gervais DA, Goldberg SN, Brown DB, et al: Society of Interventional Radiology position statement on percutaneous radiofrequency ablation for the treatment of liver tumors. *J Vasc Interv Radiol* 20(Suppl):S342-S347, 2009.
114. Solbiati L, Ahmed M, Cova L, et al: Small liver colorectal metastases treated with percutaneous radiofrequency ablation: Local response rate and long-term survival with up to 10-year follow-up. *Radiology* 265:958-968, 2012.
115. Sofocleous CT, Nascimento RG, Gonen M, et al: Radiofrequency ablation in the management of liver metastases from breast cancer. *AJR Am J Roentgenol* 189:883-889, 2007.
116. Gunabushanam G, Sharma S, Thulker S, et al: Radiofrequency ablation of liver metastases from breast cancer: Results in 14 patients. *J Vasc Interv Radiol* 18(Pt 1):67-72, 2007.
117. Langan RC, Ripley RT, Davis JL, et al: Liver directed therapy for renal cell carcinoma. *J Cancer* 3:184-190, 2012.
118. Mazzaglia PJ, Berber E, Milas M, Siperstein AE: Laparoscopic radiofrequency ablation of neuroendocrine liver metastases: A 10-year experience evaluating predictors of survival. *Surgery* 142:10-19, 2007.
119. Hinshaw JL, Laeseke PJ, Weber SM, Lee FT, Jr: Multiple-electrode radiofrequency ablation of symptomatic hepatic cavernous hemangioma. *AJR Am J Roentgenol* 189:W146-W149, 2007.
120. Levit E, Bruners P, Gunther RW, Mahnken AH: Bile aspiration and hydrodissection to prevent complications in hepatic RFA close to the gallbladder. *Acta Radiol* 53:1045-1048, 2012.
121. Tsoumakidou G, Buy X, Garnon J, et al: Percutaneous thermal ablation: How to protect the surrounding organs. *Tech Vasc Interv Radiol* 14:170-176, 2011.
122. Elias D, Di Pietroantonio D, Gachot B, et al: Liver abscess after radiofrequency ablation of tumors in patients with a biliary tract procedure. *Gastroenterol Clin Biol* 30:823-827, 2006.
123. Patel IJ, Davidson JC, Nikolic B, et al: Consensus guidelines for periprocedural management of coagulation status and hemostasis risk in percutaneous image-guided interventions. *J Vasc Interv Radiol* 23:727-736, 2012.
124. Nakazawa T, Kokubu S, Shibuya A, et al: Radiofrequency ablation of hepatocellular carcinoma: Correlation between local tumor progression after ablation and ablative margin. *AJR Am J Roentgenol* 188:480-488, 2007.
125. Wang X, Sofocleous CT, Erinjeri JP, et al: Margin size is an independent predictor of local tumor progression after ablation of colon cancer liver metastases. *Cardiovasc Intervent Radiol* 36:166-175, 2013.
126. Hinshaw JL, Laeseke PF, Winter TC, 3rd, et al: Radiofrequency ablation of peripheral liver tumors: Intraperitoneal 5% dextrose in water decreases postprocedural pain. *AJR Am J Roentgenol* 186(Suppl):S306-S310, 2006.
127. Campbell C, Lubner MG, Hinshaw JL, et al: Contrast media-doped hydrodissection during thermal ablation: Optimizing contrast media concentration for improved visibility on CT images. *AJR Am J Roentgenol* 199:677-682, 2012.
128. Lu MD, Kuang M, Liang LJ, et al: [Surgical resection versus percutaneous thermal ablation for early-stage hepatocellular carcinoma: A randomized clinical trial.] *Zhonghua Yi Xue Za Zhi* 86:801-805, 2006.
129. Chen MS, Li JQ, Zheng Y, et al: A prospective randomized trial comparing percutaneous local ablative therapy and partial hepatectomy for small hepatocellular carcinoma. *Ann Surg* 243:321-328, 2006.
130. Tohme S, Geller DA, Cardinal JS, et al: Radiofrequency ablation compared to resection in early-stage hepatocellular carcinoma. *HPB (Oxford)* 15:210-217, 2013.
131. Crocetti L, de Baere T, Lencioni R: Quality improvement guidelines for radiofrequency ablation of liver tumours. *Cardiovasc Intervent Radiol* 33:11-17, 2010.
132. Wu YZ, Li B, Wang T, et al: Radiofrequency ablation vs hepatic resection for solitary colorectal liver metastasis: A meta-analysis. *World J Gastroenterol* 17:4143-4148, 2011.
133. Ruers T, Punt C, Van Coevorden F, et al: Radiofrequency ablation combined with systemic treatment versus systemic treatment alone in patients with non-resectable colorectal liver metastases: A randomized EORTC Intergroup phase II study (EORTC 40004). *Ann Oncol* 23:2619-2626, 2012.
134. Gillams AR, Lees WR: Radio-frequency ablation of colorectal liver metastases in 167 patients. *Eur Radiol* 14:2261-2267, 2004.
135. Oshowo A, Gillams A, Harrison E, et al: Comparison of resection and radiofrequency ablation for treatment of solitary colorectal liver metastases. *Br J Surg* 90:1240-1243, 2003.
136. Solbiati L, Livraghi T, Goldberg SN, et al: Percutaneous radio-frequency ablation of hepatic metastases from colorectal cancer: Long-term results in 117 patients. *Radiology* 221:159-166, 2001.
137. Livraghi T, Solbiati L, Meloni MF, et al: Treatment of focal liver tumors with percutaneous radio-frequency ablation: Complications encountered in a multicenter study. *Radiology* 226:441-451, 2003.
138. Bertot LC, Sato M, Tateishi R, et al: Mortality and complication rates of percutaneous ablative techniques for the treatment of liver tumors: A systematic review. *Eur Radiol* 21:2584-2596, 2011.
139. Lee JK, Baek SY, Kim Y: Extrahepatic soft tissue mimicking applicator-tract implantation after percutaneous radiofrequency ablation of hepatic malignancy. *AJR Am J Roentgenol* 199:453-457, 2012.
140. Sainani NI, Gervais DA, Mueller PR, Arellano RS: Imaging after percutaneous radiofrequency ablation of hepatic tumors: Part 1, normal findings. *AJR Am J Roentgenol* 200:184-193, 2013.
141. Sainani NI, Gervais DA, Mueller PR, Arellano RS: Imaging after percutaneous radiofrequency ablation of hepatic tumors: Part 2, abnormal findings. *AJR Am J Roentgenol* 200:194-204, 2013.
142. Yamada R, Sato M, Kawabata M, et al: Hepatic artery embolization in 120 patients with unresectable hepatoma. *Radiology* 148:397-401, 1983.
143. Bhattacharya S, Dhillion AP, Winslet MC, et al: Human liver cancer cells and endothelial cells incorporate iodised oil. *Br J Cancer* 73:877-881, 1996.
144. Terayama N, Matsui O, Gabata T, et al: Accumulation of iodized oil within the nonneoplastic liver adjacent to hepatocellular carcinoma via the drainage routes of the tumor after transcatheter arterial embolization. *Cardiovasc Intervent Radiol* 24:383-387, 2001.
145. Kothary N, Weintraub JL, Susman J, Rundback JH: Transarterial chemoembolization for primary hepatocellular carcinoma in patients at high risk. *J Vasc Interv Radiol* 18:1517-1526, quiz 1527, 2007.
146. Luo J, Guo RP, Lai EC, et al: Transarterial chemoembolization for unresectable hepatocellular carcinoma with portal vein tumor thrombosis: A prospective comparative study. *Ann Surg Oncol* 18:413-420, 2011.
147. Vogl TJ, Naguib NN, Nour-Eldin NE, et al: Transarterial chemoembolization in the treatment of patients with unresectable cholangiocarcinoma: Results and prognostic factors governing treatment success. *Int J Cancer* 131:733-740, 2012.
148. Vogl TJ, Naguib NN, Zangos S, et al: Liver metastases of neuroendocrine carcinomas: Interventional treatment via transarterial embolization, chemoembolization and thermal ablation. *Eur J Radiol* 72:517-528, 2009.
149. Albert M, Kiefer MV, Sun W, et al: Chemoembolization of colorectal liver metastases with cisplatin, doxorubicin, mitomycin C, ethiodol, and polyvinyl alcohol. *Cancer* 117:343-352, 2011.
150. Vogl TJ, Gruber T, Balzer JO, et al: Repeated transarterial chemoembolization in the treatment of liver metastases of colorectal cancer: Prospective study. *Radiology* 250:281-289, 2009.
151. Gupta S, Bedikian AY, Ahrar J, et al: Hepatic artery chemoembolization in patients with ocular melanoma metastatic to the liver: Response, survival, and prognostic factors. *Am J Clin Oncol* 33:474-480, 2010.
152. Vogl TJ, Naguib NN, Nour-Eldin NE, et al: Transarterial chemoembolization (TACE) with mitomycin C and gemcitabine for liver metastases in breast cancer. *Eur Radiol* 20:173-180, 2010.
153. Berger DH, Carrasco CH, Hohn DC, Curley SA: Hepatic artery chemoembolization or embolization for primary and metastatic liver tumors: Post-treatment management and complications. *J Surg Oncol* 60:116-121, 1995.
154. Brown DB, Nikolic B, Covey AM, et al: Quality improvement guidelines for transhepatic arterial chemoembolization, embolization, and chemotherapeutic infusion for hepatic malignancy. *J Vasc Interv Radiol* 23:287-294, 2012.
155. Iwazawa J, Ohue S, Hashimoto N, et al: Survival after C-arm CT-assisted chemoembolization of unresectable hepatocellular carcinoma. *Eur J Radiol* 81:3985-3992, 2012.
156. Llovet JM, Real MI, Montana X, et al: Arterial embolisation or chemoembolisation versus symptomatic treatment in patients with unresectable hepatocellular carcinoma: A randomised controlled trial. *Lancet* 359:1734-1739, 2002.
157. Lo CM, Ngan H, Tso WK, et al: Randomized controlled trial of transarterial lipiodol chemoembolization for unresectable hepatocellular carcinoma. *Hepatology* 35:1164-1171, 2002.
158. Marelli L, Stigliano R, Triantos C, et al: Transarterial therapy for hepatocellular carcinoma: Which technique is more effective? A systematic review of cohort and randomized studies. *Cardiovasc Intervent Radiol* 30:6-25, 2007.

159. Takayasu K, Arai S, Ikai I, et al: Prospective cohort study of transarterial chemoembolization for unresectable hepatocellular carcinoma in 8510 patients. *Gastroenterology* 131:461–469, 2006.
160. Chung YH, Han G, Yoon JH, et al: Interim analysis of START: Study in Asia of the combination of TACE (transcatheter arterial chemoembolization) with sorafenib in patients with hepatocellular carcinoma trial. *Int J Cancer* 132:2448–2458, 2013.
161. Hunt SJ, Yu W, Weintraub J, et al: Radiologic monitoring of hepatocellular carcinoma tumor viability after transhepatic arterial chemoembolization: Estimating the accuracy of contrast-enhanced cross-sectional imaging with histopathologic correlation. *J Vasc Interv Radiol* 20:30–38, 2009.
162. Kloeckner R, Otto G, Biesterfeld S, et al: MDCT versus MRI assessment of tumor response after transarterial chemoembolization for the treatment of hepatocellular carcinoma. *Cardiovasc Intervent Radiol* 33:532–540, 2010.
163. Lee JA, Jeong WK, Kim Y, et al: Dual-energy CT to detect recurrent HCC after TACE: Initial experience of color-coded iodine CT imaging. *Eur J Radiol* 82:569–576, 2013.
164. Varela M, Real MI, Burrell M, et al: Chemoembolization of hepatocellular carcinoma with drug eluting beads: Efficacy and doxorubicin pharmacokinetics. *J Hepatol* 46:474–481, 2007.
165. Poon RT, Tso WK, Pang RW, et al: A phase I/II trial of chemoembolization for hepatocellular carcinoma using a novel intra-arterial drug-eluting bead. *Clin Gastroenterol Hepatol* 5:1100–1108, 2007.
166. Martin RC, 2nd, Scoggins CR, Tomalty D, et al: Irinotecan drug-eluting beads in the treatment of chemo-naïve unresectable colorectal liver metastasis with concomitant systemic fluorouracil and oxaliplatin: Results of pharmacokinetics and phase I trial. *J Gastrointest Surg* 16:1531–1538, 2012.
167. Lencioni R, de Baere T, Burrell M, et al: Transcatheter treatment of hepatocellular carcinoma with Doxorubicin-loaded DC Bead (DEBDOX): Technical recommendations. *Cardiovasc Intervent Radiol* 35:980–985, 2012.
168. Martin RC, Joshi J, Robbins K, et al: Hepatic intra-arterial injection of drug-eluting bead, irinotecan (DEBIR) in unresectable colorectal liver metastases refractory to systemic chemotherapy: Results of multi-institutional study. *Ann Surg Oncol* 18:192–198, 2011.
169. Lee KH, Liapi E, Vossen JA, et al: Distribution of iron oxide-containing Embosphere particles after transcatheter arterial embolization in an animal model of liver cancer: Evaluation with MR imaging and implication for therapy. *J Vasc Interv Radiol* 19:1490–1496, 2008.
170. Lammer J, Malagari K, Vogl T, et al: Prospective randomized study of doxorubicin-eluting-bead embolization in the treatment of hepatocellular carcinoma: Results of the PRECISION V study. *Cardiovasc Intervent Radiol* 33:41–52, 2010.
171. Malagari K, Pomoni M, Kelekis A, et al: Prospective randomized comparison of chemoembolization with doxorubicin-eluting beads and bland embolization with BeadBlock for hepatocellular carcinoma. *Cardiovasc Intervent Radiol* 33:541–551, 2010.
172. Burrell M, Reig M, Forner A, et al: Survival of patients with hepatocellular carcinoma treated by transarterial chemoembolisation (TACE) using drug eluting beads. Implications for clinical practice and trial design. *J Hepatol* 56:1330–1335, 2012.
173. Malagari K, Pomoni M, Moschouris H, et al: Chemoembolization with doxorubicin-eluting beads for unresectable hepatocellular carcinoma: Five-year survival analysis. *Cardiovasc Intervent Radiol* 35:1119–1128, 2012.
174. Malagari K, Pomoni M, Spyridopoulos TN, et al: Safety profile of sequential transcatheter chemoembolization with DC Bead: Results of 237 hepatocellular carcinoma (HCC) patients. *Cardiovasc Intervent Radiol* 34:774–785, 2011.
175. Martin RC, Howard J, Tomalty D, et al: Toxicity of irinotecan-eluting beads in the treatment of hepatic malignancies: Results of a multi-institutional registry. *Cardiovasc Intervent Radiol* 33:960–966, 2010.
176. Lawrence TS, Robertson JM, Anscher MS, et al: Hepatic toxicity resulting from cancer treatment. *Int J Radiat Oncol Biol Phys* 31:1237–1248, 1995.
177. Kennedy AS, Nutting C, Coldwell D, et al: Pathologic response and microdosimetry of ⁹⁰Y microspheres in man: Review of four explanted whole livers. *Int J Radiat Oncol Biol Phys* 60:1552–1563, 2004.
178. Salem R, Lewandowski RJ, Mulcahy ME, et al: Radioembolization for hepatocellular carcinoma using yttrium-90 microspheres: A comprehensive report of long-term outcomes. *Gastroenterology* 138:52–64, 2010.
179. Sangro B, Carpanese L, Cianni R, et al: Survival after yttrium-90 resin microsphere radioembolization of hepatocellular carcinoma across Barcelona clinic liver cancer stages: A European evaluation. *Hepatology* 54:868–878, 2011.
180. Saxena A, Bester L, Chua TC, et al: Yttrium-90 radiotherapy for unresectable intrahepatic cholangiocarcinoma: A preliminary assessment of this novel treatment option. *Ann Surg Oncol* 17:484–491, 2010.
181. Hoffmann RT, Paprottka PM, Schon A, et al: Transarterial hepatic yttrium-90 radioembolization in patients with unresectable intrahepatic cholangiocarcinoma: Factors associated with prolonged survival. *Cardiovasc Intervent Radiol* 35:105–116, 2012.
182. Kennedy AS, Coldwell D, Nutting C, et al: Resin ⁹⁰Y-microsphere brachytherapy for unresectable colorectal liver metastases: Modern USA experience. *Int J Radiat Oncol Biol Phys* 65:412–425, 2006.
183. Mulcahy ME, Lewandowski RJ, Ibrahim SM, et al: Radioembolization of colorectal hepatic metastases using yttrium-90 microspheres. *Cancer* 115:1849–1858, 2009.
184. Kennedy AS, Dezarn WA, McNeillie P, et al: Radioembolization for unresectable neuroendocrine hepatic metastases using resin ⁹⁰Y-microspheres: Early results in 148 patients. *Am J Clin Oncol* 31:271–279, 2008.
185. Coldwell DM, Kennedy AS, Nutting CW: Use of yttrium-90 microspheres in the treatment of unresectable hepatic metastases from breast cancer. *Int J Radiat Oncol Biol Phys* 69:800–804, 2007.
186. Gonsalves CF, Eschelman DJ, Sullivan KL, et al: Radioembolization as salvage therapy for hepatic metastasis of uveal melanoma: A single-institution experience. *AJR Am J Roentgenol* 196:468–473, 2011.
187. Kennedy A, Nag S, Salem R, et al: Recommendations for radioembolization of hepatic malignancies using yttrium-90 microsphere brachytherapy: A consensus panel report from the radioembolization brachytherapy oncology consortium. *Int J Radiat Oncol Biol Phys* 68:13–23, 2007.
188. Kulik LM, Carr BI, Mulcahy ME, et al: Safety and efficacy of ⁹⁰Y radiotherapy for hepatocellular carcinoma with and without portal vein thrombosis. *Hepatology* 47:71–81, 2008.
189. Riaz A, Lewandowski RJ, Kulik LM, et al: Complications following radioembolization with yttrium-90 microspheres: A comprehensive literature review. *J Vasc Interv Radiol* 20:1121–1130, quiz 1131, 2009.
190. Huang GT, Lee PH, Tsang YM, et al: Percutaneous ethanol injection versus surgical resection for the treatment of small hepatocellular carcinoma: A prospective study. *Ann Surg* 242:36–42, 2005.
191. Yan S, Xu D, Sun B: Combination of radiofrequency ablation with transarterial chemoembolization for hepatocellular carcinoma: A meta-analysis. *Dig Dis Sci* 58:2107–2113, 2013.
192. Peng ZW, Zhang YJ, Chen MS, et al: Radiofrequency ablation with or without transcatheter arterial chemoembolization in the treatment of hepatocellular carcinoma: A prospective randomized trial. *J Clin Oncol* 31:426–432, 2013.
193. Kim JH, Won HJ, Shin YM, et al: Medium-sized (3.1–5.0 cm) hepatocellular carcinoma: Transarterial chemoembolization plus radiofrequency ablation versus radiofrequency ablation alone. *Ann Surg Oncol* 18:1624–1629, 2011.
194. Morimoto M, Numata K, Kondou M, et al: Midterm outcomes in patients with intermediate-sized hepatocellular carcinoma: A randomized controlled trial for determining the efficacy of radiofrequency ablation combined with transcatheter arterial chemoembolization. *Cancer* 116:5452–5460, 2010.
195. Peng ZW, Zhang YJ, Liang HH, et al: Recurrent hepatocellular carcinoma treated with sequential transcatheter arterial chemoembolization and RF ablation versus RF ablation alone: A prospective randomized trial. *Radiology* 262:689–700, 2012.
196. Shibata T, Isoda H, Hirokawa Y, et al: Small hepatocellular carcinoma: Is radiofrequency ablation combined with transcatheter arterial chemoembolization more effective than radiofrequency ablation alone for treatment? *Radiology* 252:905–913, 2009.
197. Morimoto M, Numata K, Kondo M, et al: Radiofrequency ablation combined with transarterial chemoembolization for subcapsular hepatocellular carcinoma: A prospective cohort study. *Eur J Radiol* 82:497–503, 2013.
198. Fujimori M, Takaki H, Nakatsuka A, et al: Combination therapy of chemoembolization and radiofrequency ablation for the treatment of hepatocellular carcinoma in the caudate lobe. *J Vasc Interv Radiol* 23:1622–1628, 2012.
199. Lencioni R, Crocetti L, Petruzzi P, et al: Doxorubicin-eluting bead-enhanced radiofrequency ablation of hepatocellular carcinoma: A pilot clinical study. *J Hepatol* 49:217–222, 2008.
200. Park BJ, Byun JH, Jin YH, et al: CT-guided radiofrequency ablation for hepatocellular carcinomas that were undetectable at US: Therapeutic effectiveness and safety. *J Vasc Interv Radiol* 20:490–499, 2009.

Anomalies and Anatomic Variants of the Liver

ALI SHIRKHODA | RICHARD M. GORE

CHAPTER OUTLINE

Hepatic Embryology

Normal Anatomic Variants

Accessory Fissures and Diaphragmatic Slips

Sliver of Liver

Papillary Process of the Caudate Lobe

Anatomic Anomalies

Riedel's Lobe

Pedunculated Accessory Hepatic Lobes

Agenesis and Hypoplasia of the Right Hepatic Lobe

Agenesis and Hypoplasia of the Left Hepatic Lobe

The diagnostic pitfalls in cross-sectional imaging studies of the liver include variants of normal anatomy, developmental anomalies, and postsurgical changes. Others are often related to intravenous contrast material and scanning at various hepatic phases. This chapter focuses on anatomic variants and anomalies and describes how they can be recognized because they may simulate pathologic processes.

Whereas congenital abnormalities of human liver are rare, hepatic anatomic variants are relatively common and represent normal interindividual variation of liver morphology. Such variants include diaphragmatic slips, “sliver of liver” (a leftward extension of the lateral segment of the left lobe), and variants related to the papillary process of the caudate lobe.

There are many kinds of congenital hepatic abnormalities that result from disturbed development of the liver. There are many variations of the hepatic vascular anatomy that may affect liver morphology.¹⁻³ The anomalies that result from excessive development of hepatic tissue occur as a lobar anomaly and include Riedel's lobe as well as other accessory lobes. Those resulting from defective development of the liver include agenesis, hypoplasia, and aplasia of the right or left hepatic lobes. Agenesis refers to complete absence of a lobe, whereas hypoplasia represents a small hepatic lobe that is diminutive but otherwise normal. Aplasia is defined as a small lobe that is structurally abnormal and contains abundant connective tissue, scattered hepatic parenchyma, numerous bile ducts, and abnormal blood vessels.^{4,5}

The position and orientation of the liver may also be altered during embryologic development, resulting in situs inversus, situs ambiguus, and liver herniation. Bipartite liver is extremely rare and occurs when the right and left hepatic lobes are in their respective upper quadrants and are connected by a bridge of tissue.

Hepatic Embryology

During the third week of fetal life, the liver primordium appears as an outgrowth of endodermal epithelium at the distal end of the foregut. This outgrowth, known as the hepatic diverticulum or liver bud, consists of rapidly proliferating cell strands that penetrate the septum transversum, which is the mesodermal plate between the primitive heart and the stalk of the yolk sac. While the hepatic cell strands continue to penetrate into the septum transversum, the connection between the hepatic diverticulum and the distal foregut narrows, thus forming the bile duct.

With further development, the epithelial liver cords intermingle with the vitelline and umbilical veins, forming the hepatic sinusoids (Fig. 85-1). The liver cords differentiate in the hepatocytes and form the lining of the biliary ducts. The Kupffer cells and connective tissue cells of the liver are derived from the mesoderm of the septum transversum.⁶

Normal Anatomic Variants

ACCESSORY FISSURES AND DIAPHRAGMATIC SLIPS

The two main fissures of the liver are the fissures for the falciform ligament and the ligamentum venosum. However, the liver may also contain accessory and pseudoaccessory fissures. True accessory fissures are rare and are the result of an inward folding of the peritoneum, usually involving the undersurface of the liver. The most common one is the inferior accessory fissure, which divides the posterior segment of the right hepatic lobe into lateral and medial portions.⁷⁻¹⁰

Pseudoaccessory fissures are common anatomic variants that result from invaginations of diaphragmatic muscle fibers, usually along the superior surface of the liver (Fig. 85-2). They are more frequently seen involving the right hepatic lobe, but they can occur on the left as well.⁶ These infoldings of the diaphragm often seen in elderly patients can give the liver a scalloped or a lobular appearance and should not be mistaken for macronodular liver in cirrhosis. They can also be a cause of hypodense peripheral pseudomasses on CT (Fig. 85-3). On ultrasound, they may occasionally appear as an echogenic focus in one plane; however, on scanning in the orthogonal plane, the true linear morphology of a fissure is revealed.

SLIVER OF LIVER

Leftward extension of the lateral segment of the left hepatic lobe is referred to as sliver of the liver. It is a common anatomic variant and appears as a crescentic density that wraps around

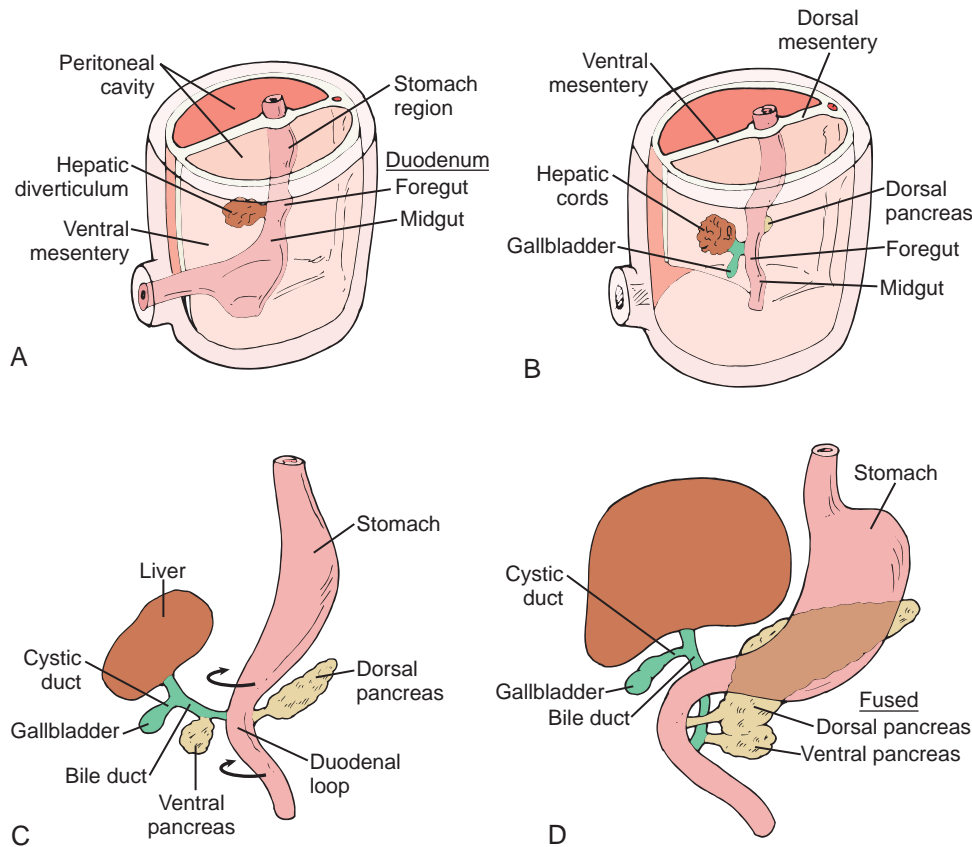


Figure 85-1 Embryonic development of the liver, pancreas, extrahepatic biliary apparatus, and duodenum. Appearance at 4 weeks (A), 5 weeks (B and C), and 6 weeks (D). (A–D from Gray SW, Skandalakis JE: *Embryology for Surgeons*. Philadelphia, WB Saunders, 1972.)

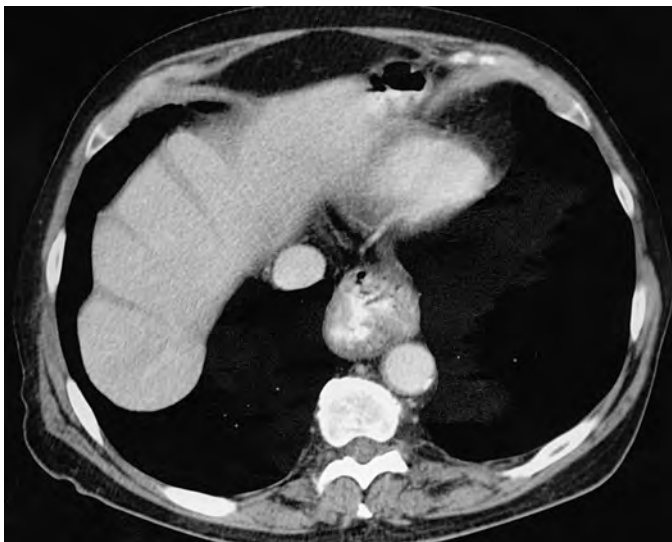


Figure 85-2 Diaphragmatic invagination in the liver. As a result of invagination of the diaphragmatic slips along the superior aspect of the liver, pseudoaccessory fissures are formed.

the spleen (Fig. 85-4) and may lie lateral, medial, and even posterior to the spleen. It is important not to confuse this variant with either perisplenic or perigastric disease. On ultrasound, this variant can mimic perisplenic hypoechoic collections, and the correct diagnosis is achieved by using color Doppler imaging and documenting continuity with the remainder of the left hepatic lobe.^{7,11}

PAPILLARY PROCESS OF THE CAUDATE LOBE

The caudate lobe is a portion of the liver that extends medially from the right lobe between the inferior vena cava and the fissure for the ligamentum venosum. On occasion, it is divided into two processes. The anterior medial extension of the caudate lobe is known as the papillary process, which extends anteriorly and to the left in the region of the lesser sac. The posterior extension is referred to as the caudate process. Below the porta hepatis, this papillary process can appear separate from the caudate process by a cleft in its inferior margin and can mimic a periportal node or a mass near the head of the pancreas or near the inferior vena cava^{6,7} (Fig. 85-5). However, on multidetector computed tomography (CT) and by use of multiplanar reformation, this anatomic variant is easily recognizable.

Anatomic Anomalies

RIEDEL'S LOBE

Described by Bernhard Moritz Carl Ludwig Riedel, a German surgeon (1846-1916), Riedel's lobe is the most common accessory lobe of the liver, and it is seen most frequently in asthenic women. It is a tongue-like projection from the anterior aspect of the right lobe of the liver that can extend quite inferiorly in some patients. It usually extends along the right paracolic gutter into the iliac fossa (Fig. 85-6) and can be 20 cm or more in length. On physical examination, this anomaly can be mistaken for an enlarged liver or a right renal mass. Riedel's lobe may be connected to the liver by a pedicle consisting of hepatic

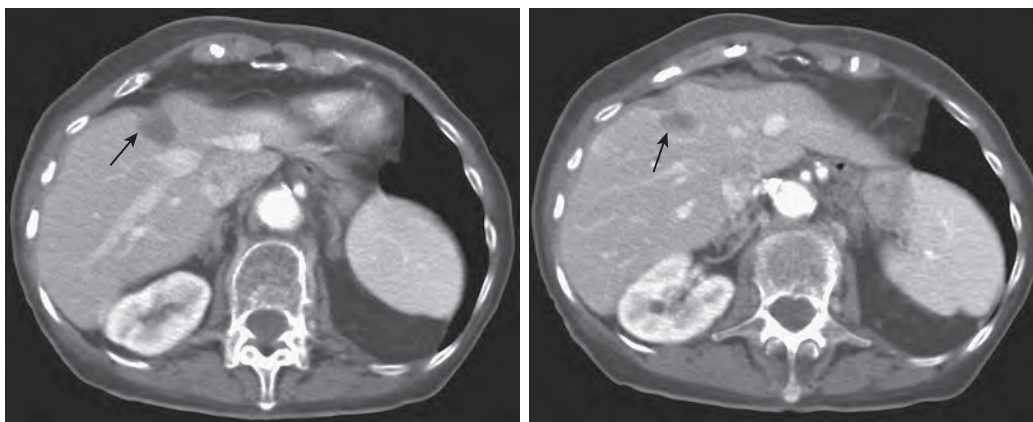


Figure 85-3 Diaphragmatic invagination mimicking hepatic nodule. As a result of diaphragmatic invagination, a small, round, low-density mass (arrows) may be suspected in the right hepatic lobe.

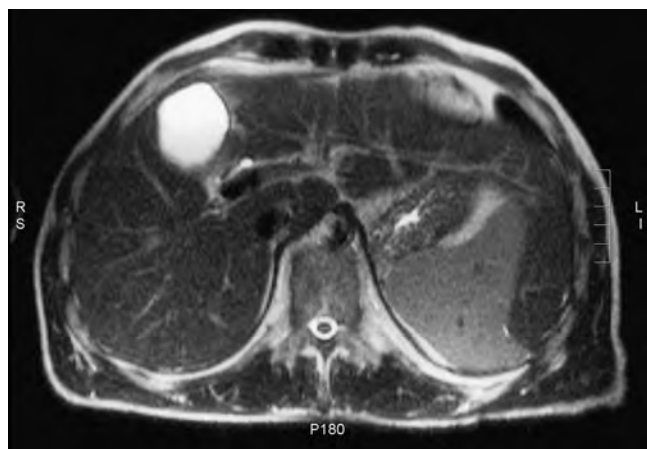


Figure 85-4 Sliver of liver. The T2-weighted image of the upper abdomen reveals leftward lateral extension of the left lobe of the liver, which appears as a crescentic low-intensity structure wrapping around the lateral aspect of the spleen.

parenchyma or fibrous tissue. It is usually asymptomatic and is discovered incidentally; however, it may be complicated by torsion with gangrenous changes.⁵ On occasion, the left lobe can behave like a Riedel lobe and extend inferiorly in the abdomen.⁷

PEDUNCULATED ACCESSORY HEPATIC LOBES

Accessory lobe of the liver is an uncommon anatomic variation that is usually asymptomatic. In this condition, the liver tissue is in communication with the main liver (Fig. 85-7), whereas in ectopic liver, the liver tissue lies in the vicinity of the liver without communication with the liver. When an accessory lobe loses its continuity with the liver, it becomes an ectopic liver nodule, which may be attached to the gallbladder, umbilical cord, or pancreas or may lie within the gastrohepatic ligament or thoracic cavity. Ectopic liver has a higher incidence of malignancy.¹² Sato and coworkers,¹³ in a series of 1800 laparoscopic studies, found congenital anomalies of the liver in 19% of the cases, with the incidence of ectopic liver lobe and accessory liver lobe being 0.7%. Other anomalies that were found in this study included fissure formation with anomalous lobation in

4.3%, lobar fusion in 0.5%, left deviation of the round ligament in 3.6%, and high insertion of the round ligament in 2.8%. The accessory lobe is composed of normal hepatic tissue and contains its own hepatic blood vessels and bile ducts. It is connected to the rest of the liver by either normal hepatic parenchyma or a mesentery^{13,14} (see Fig. 85-7). Most accessory lobes are attached to the inferior surface of the liver and have been found in the vicinity of several anatomic sites, including the gallbladder fossa, gastrohepatic ligament, umbilicus, adrenal gland, pancreas, esophagus, and rarely the thoracic cavity. These accessory lobes, particularly when the liver is infiltrated by fat, may be spared and therefore can occasionally mimic masses or adenopathy in these regions.¹⁵ Multiplanar reconstruction and review of continuous thin-slice images are often the key to their diagnosis.

Although most accessory lobes of the liver are asymptomatic, some are pedunculated and suspended from a mesentery that may undergo torsion,¹⁶⁻¹⁸ causing both acute and recurrent abdominal pain. There is an increased incidence of accessory lobes in patients with abdominal wall defects, such as omphalocele.

AGENESIS AND HYPOPLASIA OF THE RIGHT HEPATIC LOBE

Agenesis and hypoplasia of the right lobe of the liver are rare entities diagnosed by noting absence or hypoplasia of liver tissue to the right of the main interlobar fissure.¹⁹⁻²¹ This disorder is thought to be a developmental abnormality that results from either failure of the right portal vein to develop or an error in the mutual induction between the septum transversum (primitive liver).^{21,22} This entity is usually seen in asymptomatic individuals and is discovered incidentally when imaging studies are being performed for unrelated reasons (Fig. 85-8). On occasion, a segment such as an anterior segment of the right lobe may be absent. Postnecrotic cirrhosis, biliary obstruction, and venous occlusive disease have been associated with atrophy or hypoplasia of a hepatic lobe or segment and should be differentiated from congenital absence or hypoplasia.¹⁹

Agenesis of the right lobe of the liver alters the normal anatomy of the upper abdomen. This is due in part to absence of the right lobe as well as to compensatory hypertrophy of the left lobe. Colonic interposition, high position of the

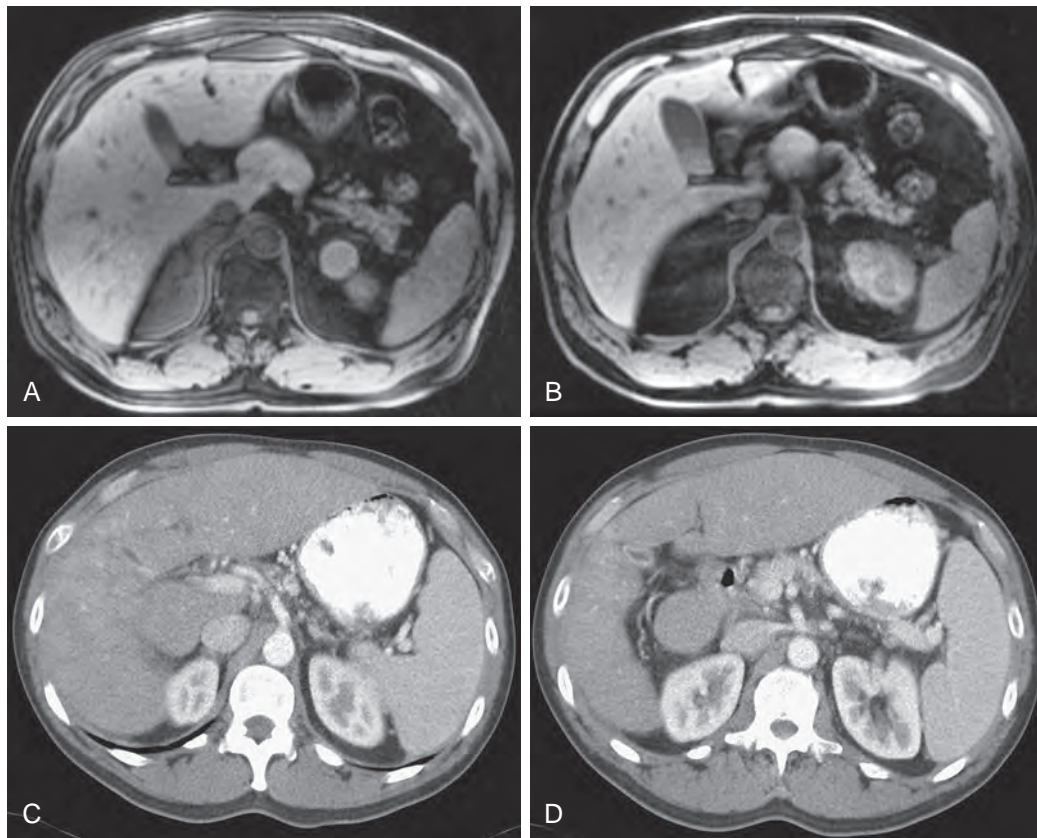


Figure 85-5 Papillary and caudate process pseudomass. **A** and **B.** The T1-weighted fat suppression images reveal medial extension of the papillary process near the head of the pancreas. Notice that the signal characteristics of this mass are similar to the remainder of the liver and not to the pancreas. **C** and **D.** Contrast-enhanced CT scan of the upper abdomen in a different patient reveals inferior extension of an enlarged caudate process mimicking a mass anterior and lateral to the inferior vena cava.

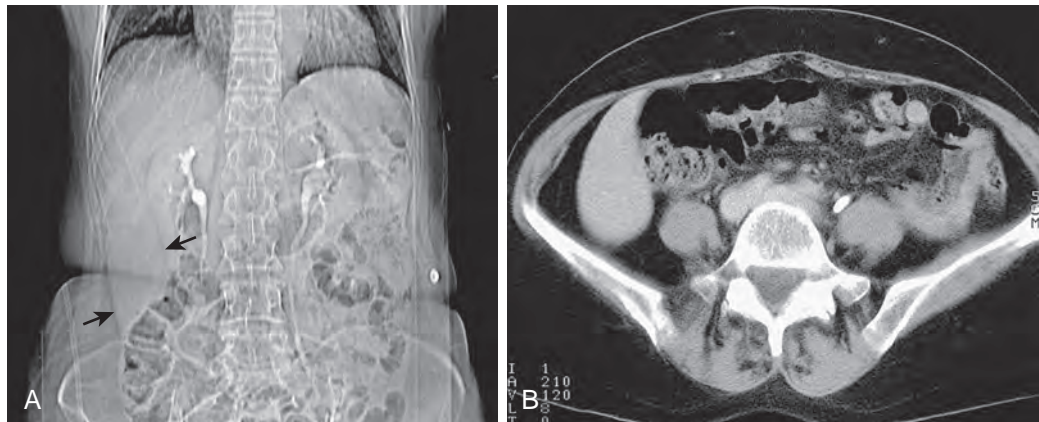


Figure 85-6 Riedel's lobe. Coronal reformatted CT scan displays an elongated inferior extension of the right lobe of the liver (arrows) characteristic of Riedel's lobe.

right kidney, ectopy of the gallbladder (which can be suprahepatic, subdiaphragmatic, or infrahepatic in location), and U- or hammock-shaped stomach can be seen in individuals with agenesis of the right lobe. The caudate lobe may be absent, normal, or hypertrophied.²²⁻²⁴ This entity may also be associated with partial or complete absence of the right hemidiaphragm, intestinal malrotation, choledochal cysts, and agenesis of the gallbladder. Other, more common conditions

can mimic agenesis of the right lobe of the liver, including cirrhosis, atrophy secondary to biliary obstruction, hepatic surgery (Fig. 85-9), and trauma.²⁵ A careful clinical history as well as any associated imaging findings will help to arrive at the correct diagnosis.^{22,26}

Even though a retrohepatic gallbladder and a severely distorted hepatic appearance due to compensatory hypertrophy of the left and caudate lobes may suggest agenesis of the right lobe

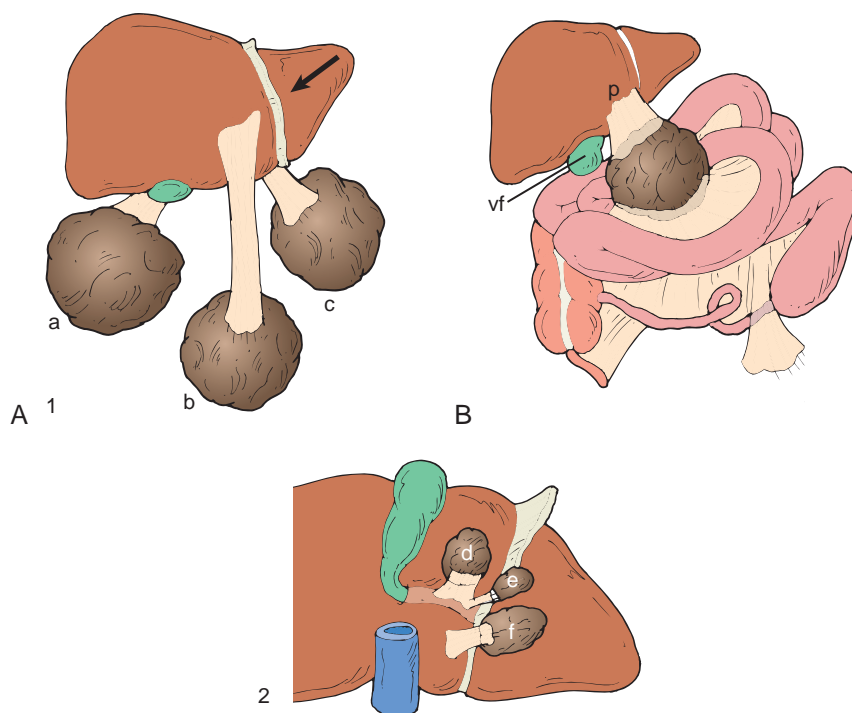
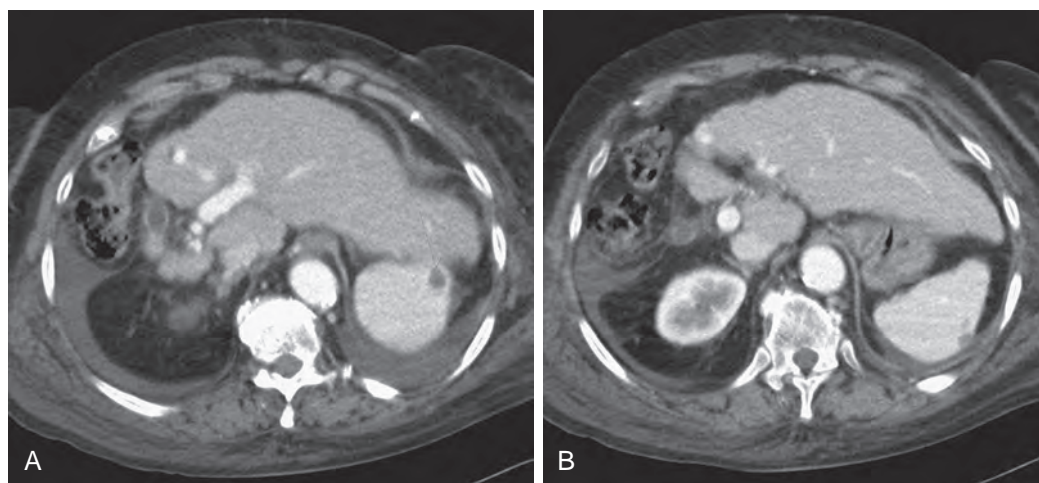


Figure 85-7 Pedunculated accessory hepatic lobes. **A.** Frontal (1) and caudal (2) diagrams depict a variety of pedunculated hepatic lobulations (a-f). **B.** They are usually asymptomatic unless they obstruct the gut with their pedicle (p). vf, Gallbladder. **C.** Axial image of the contrast-enhanced CT scan reveals pedunculated accessory left hepatic lobe that mimics a mass in the gastrohepatic ligament. (**A** and **B** from Champetier J, Yver R, Letoublon C, et al: A general review of anomalies of hepatic morphology and their clinical implications. *Anat Clin* 7:285-299, 1985.)



Figure 85-8 Atrophic right lobe of the liver. **A** and **B.** Contrast-enhanced CT study of the upper abdomen reveals atrophy of the right lobe with hypertrophy of the left lobe and prominence of the caudate lobe. Notice that there is only a left portal vein opacified. The fissure for the ligamentum venosum is seen anterior to the caudate lobe.



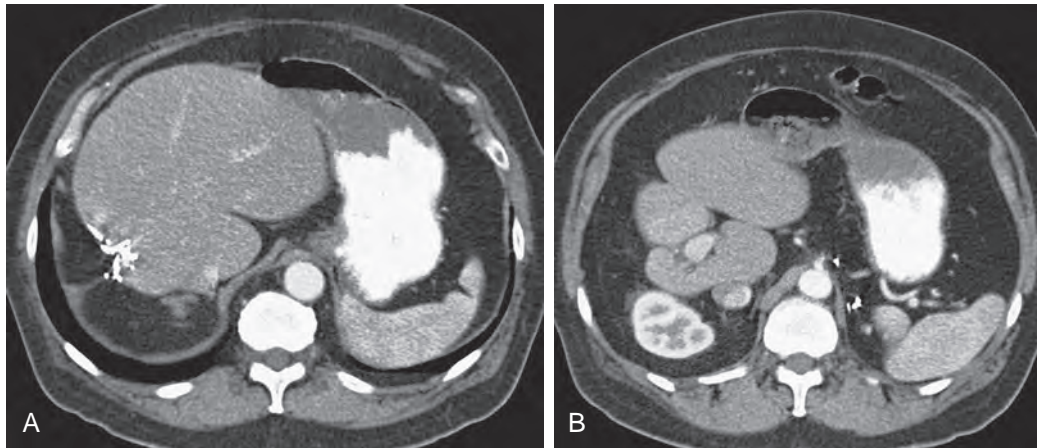


Figure 85-9 Post-right hepatic lobectomy. **A** and **B.** Hypertrophy of the medial and lateral segments of the left lobe and the caudate lobe is seen in this patient who has total right hepatic lobectomy for metastatic colon carcinoma. Notice marked deviation of the left hepatic lobe to the right upper quadrant.

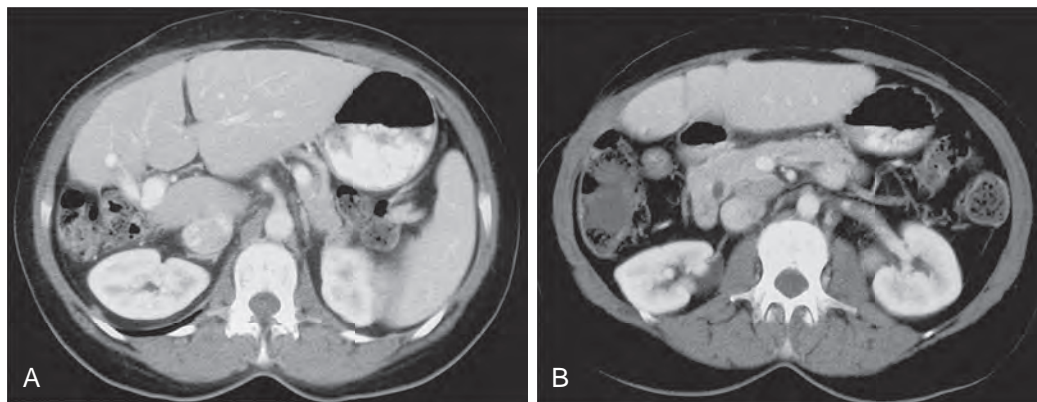


Figure 85-10 Agenesis of the right hepatic lobe. **A.** CT reveals agenesis of the right lobe of the liver with compensatory hypertrophy of the left lobe. **B.** On a more inferior image, only the left lobe of the liver is identified. The colon occupies the bed of the right hepatic lobe.

of the liver (Fig. 85-10), absence of visualization of all of the right hepatic vein, right portal vein and its branches, and occasionally dilated left intrahepatic ducts is a prerequisite for the diagnosis of agenesis of the right hepatic lobe on CT. In severe lobar atrophy, at least one of these structures is recognizable.¹⁹

AGENESIS AND HYPOPLASIA OF THE LEFT HEPATIC LOBE

Agenesis and hypoplasia of the left hepatic lobe are rare but slightly more common than the right-sided anomalies; however, these are still rare occurrences.²⁷ The diagnosis is made by noting absence or hypoplasia of liver tissue to the left of the main interlobar fissure. Failure to visualize the falciform ligament or ligamentum teres is supportive evidence of agenesis (Fig. 85-11). This disorder is believed to result from the extension of the obliterative process that closes the ductus venosus to the left branch of the portal vein.

Hann and colleagues²⁸ described 13 cases of hepatic lobar atrophy that were evaluated for vascular patency and bile duct obstruction. Hepatic lobar atrophy usually occurs in the setting of combined biliary and portal vein obstruction. A correlation exists between lobar atrophy and ipsilateral portal vein obstruction. Ishida and associates²⁹ reported six cases of lobar atrophy

and investigated the relationship between lobar atrophy and portal flow disturbance. In their report, atrophy of the right lobe was always associated with marked enlargement of the left lobe, but obstruction of flow to the left lobe did not universally result in hypertrophy of the right lobe. As in agenesis of the right lobe of the liver, left lobe agenesis is usually asymptomatic and is discovered incidentally when imaging studies are being performed for other unrelated reasons.^{22,27}

Agenesis of the left lobe of the liver also alters the normal topography of the upper abdomen.²⁷ The stomach and splenic flexure of the colon migrate superiorly and medially to fill the area normally occupied by the left hepatic lobe (Fig. 85-12). Associated findings include a high position of the duodenal bulb, a U-shaped stomach, and a low-lying hepatic flexure of the colon secondary to compensatory hypertrophy of the right lobe of the liver.^{22,30} This anomaly may also be associated with partial or complete absence of the left hemidiaphragm and gastric volvulus.

Before a diagnosis of agenesis of the left lobe of the liver is made, it is important to exclude other causes of acquired atrophy of the left hepatic lobe, such as cirrhosis, malignant disease, malnutrition, or rarely vascular compromise.^{31,32} In these disorders, at least some liver tissue is found left of the main lobar fissure.³³

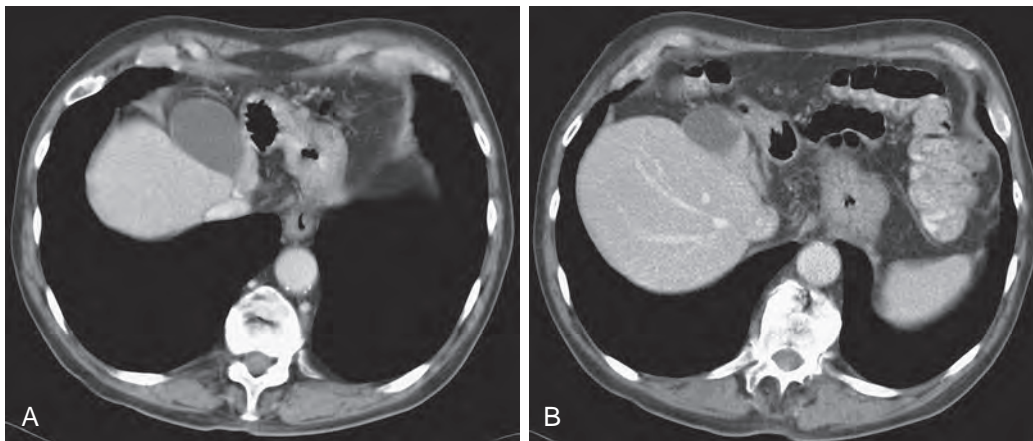


Figure 85-11 Agenesis of the left lobe. **A.** In this contrast-enhanced CT study of the upper abdomen, there is total agenesis of the left lobe with the gallbladder being seen anterior and medial to the right lobe. The gastric fundus is displaced medially. **B.** Notice absence of the left hepatic vein, while the middle and right hepatic veins are opacified.

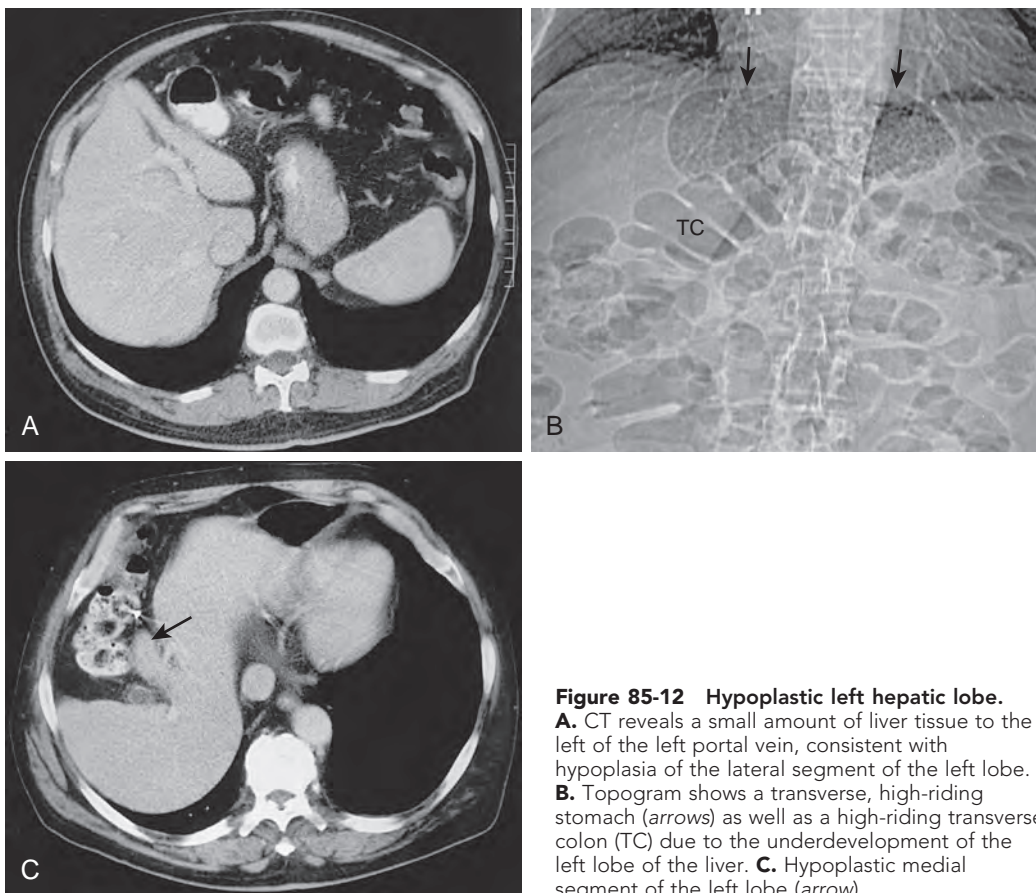


Figure 85-12 Hypoplastic left hepatic lobe. **A.** CT reveals a small amount of liver tissue to the left of the left portal vein, consistent with hypoplasia of the lateral segment of the left lobe. **B.** Topogram shows a transverse, high-riding stomach (arrows) as well as a high-riding transverse colon (TC) due to the underdevelopment of the left lobe of the liver. **C.** Hypoplastic medial segment of the left lobe (arrow).

REFERENCES

1. Keplinger KM: Anatomy and embryology of the biliary tract. *Surg Clin North Am* 94:203–217, 2014.
2. Ramanadham S, Toomay SM, Yopp AC, et al: Rare hepatic arterial anatomic variants in patients requiring pancreatoduodenectomy and review of the literature. *Case Rep Surg* 2012: 953195, 2012.
3. Ugurel MS, Battal B, Bozlar U, et al: Anatomical variations of hepatic arterial system, coeliac trunk and renal arteries: An analysis with multidetector CT angiography. *Br J Radiol* 83:661–667, 2010.
4. Champetier J, Yuer R, Letoublon C, et al: A general review of anomalies of hepatic

- morphology and their clinical implications. *Anat Clin* 7:285–299, 1985.
5. White M: Hepatic anatomic variations and developmental anomalies. In Ferrucci J, editor: *Radiology*, Philadelphia, 1997, Lippincott-Raven.
 6. Sadler T: *Medical Embryology*, ed 5, Baltimore, 1985, Williams & Wilkins, pp 230–232.
 7. Kasales CJ, Patel S, Hopper KD: Imaging variants of the liver, pancreas, and spleen. *Crit Rev Diagn Imaging* 35:485–543, 1994.
 8. Farah M, Shirkhoda A: The diaphragm. In Shirkhoda A, editor: *Variants and Pitfalls in Body Imaging*, Philadelphia, 2000, Lippincott Williams & Wilkins, pp 133–151.
 9. Krebs C, Giyanani V, Eisenberg R: *Ultrasound Atlas of Disease Processes*, Norwalk, CT, 1993, Appleton & Lange, p 19.
 10. Martinoli C, Cittadini G, Conzi R: Sonographic characterization of an accessory fissure of the left hepatic lobe determined by omental infolding. *J Ultrasound Med* 11:103–107, 1992.
 11. Dunlop D, Evans R: Congenital abnormality of the liver initially misdiagnosed as splenic haematoma. *J R Soc Med* 89:702–704, 1996.
 12. Caygill CP, Gatenby PA: Ectopic liver and hepatocarcinogenesis. *Eur J Gastroenterol Hepatol* 16:727–729, 2004.
 13. Sato N, Kawakami K, Matsumoto S, et al: Agenesis of the right lobe of the liver. *Surg Today* 18:643–646, 1998.
 14. Bedda S, Bataille N, Montariol T, Zareski E: Accessory liver lobe torsion mimicking a pancreatic tumor. *Ann Chir* 128:53–54, 2003.
 15. Hashimoto M, Oomachi K, Watarai J: Accessory lobe of the liver mimicking a mass in the left adrenal gland. A case report. *Acta Radiol* 38:309–310, 1997.
 16. Sanguesa C, Esteban M, Gomez J, et al: Liver accessory lobe torsion in the infant. *Pediatr Radiol* 25:153–154, 1995.
 17. Koumandidou C, Nasi E, Koutrouveli E, et al: Torsion of an accessory hepatic lobe in a child: Ultrasound, computed tomographic, and magnetic resonance imaging findings. *Pediatr Surg Int* 13:526–527, 1998.
 18. Ladurner R, Brandacher G, Mark W, et al: Complete hepatic ischemia due to torsion of a large accessory liver lobe: First case to require transplantation. *Transpl Int* 18:467, 2005.
 19. Chou CK, Mak CW, Lin MB, et al: CT of agenesis and atrophy of the right hepatic lobe. *Abdom Imaging* 23:603–607, 1998.
 20. Mankanjuola D, al-Smayer S, al-Orainy I, et al: Radiographic features of lobar agenesis of the liver. *Acta Radiol* 37:255–258, 1996.
 21. Cesani F, Walser E, Goodacre B, et al: Agenesis of the right lobe of the liver. *Clin Nucl Med* 21:1001–1002, 1996.
 22. Kakitsubata Y, Kakitsubata S, Asada K, et al: MR imaging of anomalous lobes of the liver. *Acta Radiol* 34:417–419, 1993.
 23. Karamen C, Ozek T, Urhan M, et al: Agenesis of the right lobe of the liver. Case report. *Acta Radiol* 38:428–430, 1997.
 24. Kakitsubata Y, Kakitsubata S, Asada K, et al: Anomalous right lobe of the liver. CT appearance. *Gastrointest Radiol* 16:326–328, 1991.
 25. Couanet D, Shirkhoda A, Wallace S: Computed tomography after partial hepatectomy. *J Comput Assist Tomogr* 8:453–457, 1984.
 26. Kakitsu Y, Kakitsubata S, Watanabe K: Hypoplasia of the right hepatic lobe with ectopy of the gallbladder. *Clin Imaging* 19:85–87, 1995.
 27. Sener R, Yorulmaz I, Oyar O, et al: Hypoplasia of the left lobe of the liver. *AJR Am J Roentgenol* 158:213–214, 1992.
 28. Hann IE, Getrajdman GI, Brown KT, et al: Hepatic lobar atrophy: Association with ipsilateral portal vein obstruction. *AJR Am J Roentgenol* 167:1017–1021, 1996.
 29. Ishida H, Naganuma H, Konno K, et al: Lobar atrophy of the liver. *Abdom Imaging* 23:150–153, 1998.
 30. Ozgun B, Warshauer D: Absent medial segment of the left hepatic lobe. CT appearance. *J Comput Assist Tomogr* 16:666–668, 1992.
 31. Hiroshi Y, Masahiko O, Takashi T, et al: Extreme left hepatic lobar atrophy in a case with hilar cholangiocarcinoma. *J Nippon Med Sch* 69:278–281, 2002.
 32. Lupescu IG, Grasu M, Capsa R, et al: Hepatic perfusion disorders: Computer-tomographic and magnetic resonance imaging. *Gastrointest Liver Dis* 15:273–279, 2006.
 33. Saba L, Mallarini G: Anatomic variations of arterial liver vascularization: An analysis by using MDCTA. *Surg Radiol Anat* 33:559–568, 2011.

Benign Tumors of the Liver

PABLO R. ROS | SUKRU MEHMET ERTURK

CHAPTER OUTLINE

Imaging Evaluation of Focal Liver Lesions

Hemangioma

Pathologic Findings
Incidence and Clinical Presentation
Plain Radiographic Findings
Nuclear Medicine
Ultrasound
Computed Tomography
Angiography
Magnetic Resonance Imaging
Diagnostic Work-up

Focal Nodular Hyperplasia

Pathologic Findings
Incidence and Clinical Presentation
Plain Radiographic Findings
Nuclear Medicine
Ultrasound
Computed Tomography
Angiography
Magnetic Resonance Imaging
Telangiectatic Focal Nodular Hyperplasia

Hepatocellular Adenoma

Pathologic Findings
Incidence and Clinical Presentation
Plain Radiographic Findings
Nuclear Medicine
Ultrasound
Computed Tomography
Angiography
Magnetic Resonance Imaging
Multiple Hepatocellular Adenomatosis

Nodular Regenerative Hyperplasia

Pathologic Findings
Incidence and Clinical Presentation
Plain Radiographic Findings
Nuclear Medicine
Ultrasound
Computed Tomography

Angiography
Magnetic Resonance Imaging
Summary

Lipomatous Tumors

Pathologic Findings
Radiologic Findings
Pseudolipoma

Cysts and Cystic Tumors

Simple Cyst
Bile Duct Hamartomas (von Meyenberg Complexes)
Congenital Hepatic Fibrosis and Polycystic Liver Disease
Cystadenoma

Infantile Hemangioendothelioma

Pathologic Findings
Incidence and Clinical Presentation
Plain Radiographic Findings
Ultrasound
Computed Tomography
Angiography
Magnetic Resonance Imaging
Summary

Mesenchymal Hamartoma

Pathologic Findings
Incidence and Clinical Presentation
Plain Radiographic Findings
Ultrasound
Computed Tomography
Angiography
Magnetic Resonance Imaging
Summary

Miscellaneous Benign Tumors

Bile Duct Adenoma
Lymphangiomatosis
Leiomyoma
Fibroma (Fibrous Mesothelioma)
Adrenal Rest Tumor
Pancreatic Heterotopia
Inflammatory Pseudotumor

Each of the cellular components of the liver can give rise to both benign and malignant tumors. Epithelium can degenerate into cystadenomas and cholangiocarcinoma, and mesenchymal tissue may produce hemangiomas or angiosarcomas. In this chapter, the benign primary hepatic neoplasms are discussed (Box 86-1).

Imaging Evaluation of Focal Liver Lesions

The liver is a large and homogeneous organ and therefore is well suited for evaluation by many imaging techniques. The study of liver neoplasms is particularly challenging. In many cases, a

BOX 86-1 BENIGN LIVER TUMORS AND TUMOR-LIKE CONDITIONS**HEPATOCELLULAR ORIGIN**

- Hepatocellular adenoma
- Hepatocellular hyperplasia
- Focal nodular hyperplasia
- Nodular regenerative hyperplasia
- Macroregenerative nodule (adenomatous hyperplasia)

CHOLANGIOCELLULAR ORIGIN

- Hepatic cysts
- Simple hepatic cysts
- Congenital hepatic fibrosis or polycystic liver disease
- Biliary cystadenoma
- Bile duct adenoma

MESENCHYMAL ORIGIN

- Mesenchymal hamartoma
- Hemangioma
- Infantile hemangioendothelioma
- Lymphangioma
- Lipoma, angiomyolipoma, myelolipoma
- Leiomyoma
- Fibroma
- Heterotopic tissue
- Adrenal rests
- Pancreatic rests
- Primary hepatic carcinoma

preoperative diagnosis may be achieved with the appropriate combination of imaging techniques in a purely noninvasive fashion. This is important because many adults have benign, nonsurgical hepatic lesions, such as hemangioma or simple cyst. For many tumors, each imaging technique provides a piece of information that, like a puzzle, must be combined with findings from other imaging techniques as well as clinical information for a diagnosis to be achieved.

The study of focal liver lesions by imaging can be likened to a game in which different “players” (imaging techniques) must be used appropriately to achieve the diagnosis.¹ In evaluation of focal liver diseases, the following imaging techniques are available:

- Plain abdominal radiography;
- Nuclear medicine: positron emission tomography (PET), red blood cells (RBCs) tagged with technetium Tc 99m;
- Ultrasonography: gray-scale and color Doppler sonography, contrast-enhanced examinations;
- Multidetector computed tomography (MDCT): nonenhanced scans and contrast-enhanced dynamic scans including arterial, portal venous, and delayed phases;
- Angiography; and
- Magnetic resonance imaging (MRI): nonenhanced, vascular enhanced with gadolinium, reticuloendothelial enhanced with small and ultrasmall superparamagnetic iron oxide particles (SPIOs and USPIOs), hepatocyte enhanced with gadolinium benzyloxypropionictetraacetate (Gd-BOPTA), and gadolinium ethoxybenzyl diethylenetriaminepentaacetic acid (gadoxetate; Gd-EOB-DTPA).

The “plays” that the foregoing players can offer are listed in Box 86-2.

With the widespread use of new cross-sectional imaging techniques such as MDCT and the development of

BOX 86-2 IMAGING TECHNIQUES IN LIVER NEOPLASMS**TO ASSESS VASCULARITY**

- Contrast-enhanced CT
- Gadolinium-enhanced MR
- Contrast-enhanced ultrasound
- Angiography
- Blood pool studies (^{99m}Tc-labeled red blood cells)

TO ASSESS HEPATOCYTE FUNCTION OR BILIARY EXCRETION

- MR imaging enhanced with hepatocyte-specific contrast agents

TO ASSESS METABOLIC ACTIVITY OF NEOPLASMS

- ¹⁸F-FDG PET imaging

TO ASSESS KUPFFER CELL ACTIVITY

- MR imaging enhanced with intravenous superparamagnetic iron oxide

TO ASSESS TUMORAL CALCIFICATION

- CT
- Ultrasound
- Plain radiographs

TO ASSESS CAPSULE PRESENCE

- CT (enhanced/nonenhanced)
- Ultrasound (enhanced/nonenhanced)
- MR (enhanced/nonenhanced)

TO ASSESS INTERNAL NATURE OF NEOPLASMS (E.G., SOLID VERSUS CYSTIC, HEMORRHAGE, FIBROSIS)

- CT
- MR
- Ultrasound

reticuloendothelial and hepatocyte-specific MRI contrast agents, the role of older techniques such as angiography and nuclear medicine has become more limited. The majority of liver lesions can now be detected and characterized noninvasively, and angiography is required only in exceptional circumstances. Although conventional scintigraphic techniques are only exceptionally used for the evaluation of focal liver lesions, PET and PET/CT are effective techniques, especially for detection of hepatic metastatic disease. Today, most focal liver lesions are diagnosed by ultrasound, CT, and MRI.

As mentioned before, two main groups of liver-specific contrast agents are used in MRI.^{2,3} Superparamagnetic iron oxide particles (SPIOs) are the first group. These particles are taken up by the reticuloendothelial system or Kupffer cells of the liver by phagocytosis.⁴ By causing magnetic field inhomogeneities with shortening of T2 relaxation time, these substances decrease the signal intensity of the normal liver parenchyma on T2-weighted images, which is best seen on T2* or gradient recalled echo sequences for lesion detection. However, to evaluate signal intensity loss for lesion characterization, T2-weighted turbo spin-echo sequences or HASTE (half-Fourier acquisition single-shot turbo spin-echo) sequences are more sensitive. Benign hepatocellular lesions show uptake of these contrast agents, depending on the content of the Kupffer cells.^{4,5} Being an exception for this although lacking Kupffer cells, hemangiomas show a decrease in signal on T2-weighted images because of their relatively large, slow-flowing blood pool that allows the effect of the SPIO particles to occur.^{2,4}

Lesions lacking Kupffer cells, such as malignant lesions or metastases, do not take up SPIO contrast agents, so they appear bright in the dark liver parenchyma on T2-weighted post-SPIO sequences. This increased contrast between the liver and a lesion of nonhepatic origin allows an easy distinction from benign hepatic lesions.⁵

The second group consists of gadolinium-based contrast material, gadobenate dimeglumine (MultiHance; Bracco Diagnostics, Princeton, NJ) and gadoxetate (Primovist; Bayer Schering Pharma, Berlin, Germany). Gadobenate dimeglumine (Gd-BOPTA) and gadoxetate disodium (Gd-EOB-DTPA) are hepatobiliary contrast agents that allow evaluation of the vascularity of the lesion and hepatocellular function within the lesion.³ These contrast agents are taken up by hepatocytes and excreted in the biliary tract.⁶ The administered doses of Gd-BOPTA and Gd-EOB-DTPA are excreted in the bile at a rate of approximately 5% and 50%, respectively (Fig. 86-1). Both act as nonspecific extracellular contrast agents on the early postcontrast phase, whereas they act as hepatocyte-specific agents on the delayed contrast-enhanced phases (40 to 120 minutes for Gd-BOPTA and 10 to 20 minutes for Gd-EOB-DTPA).^{6,7} These contrast agents will be taken up by normal hepatocytes on delayed post-contrast phases.⁸

They increase the signal intensity of the normal liver parenchyma on T1-weighted images. Because malignant lesions do not take up hepatocyte-specific contrast agents during the hepatobiliary phase, they appear hypointense and become more conspicuous.⁹

Hemangioma

PATHOLOGIC FINDINGS

A hemangioma is defined microscopically as a tumor composed of multiple vascular channels lined by a single layer of endothelial cells supported by a thin, fibrous stroma¹⁰ (Fig. 86-2). The

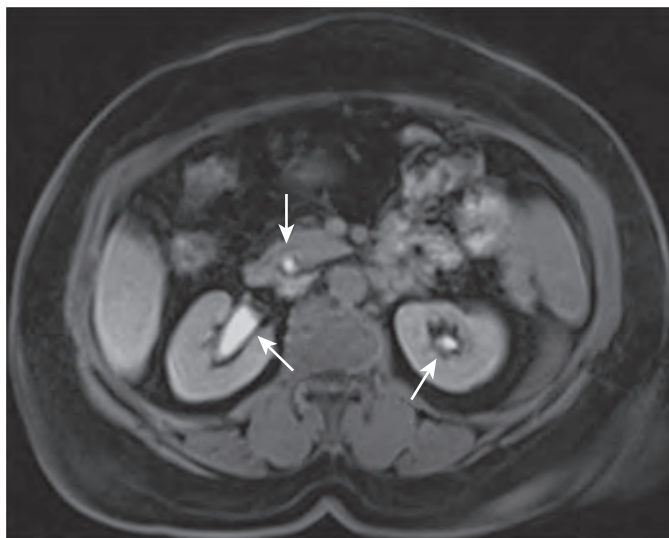


Figure 86-1 Gd-EOB-DTPA elimination: MR image. Gd-EOB-DTPA is eliminated through the biliary system (50%) and kidneys (50%).

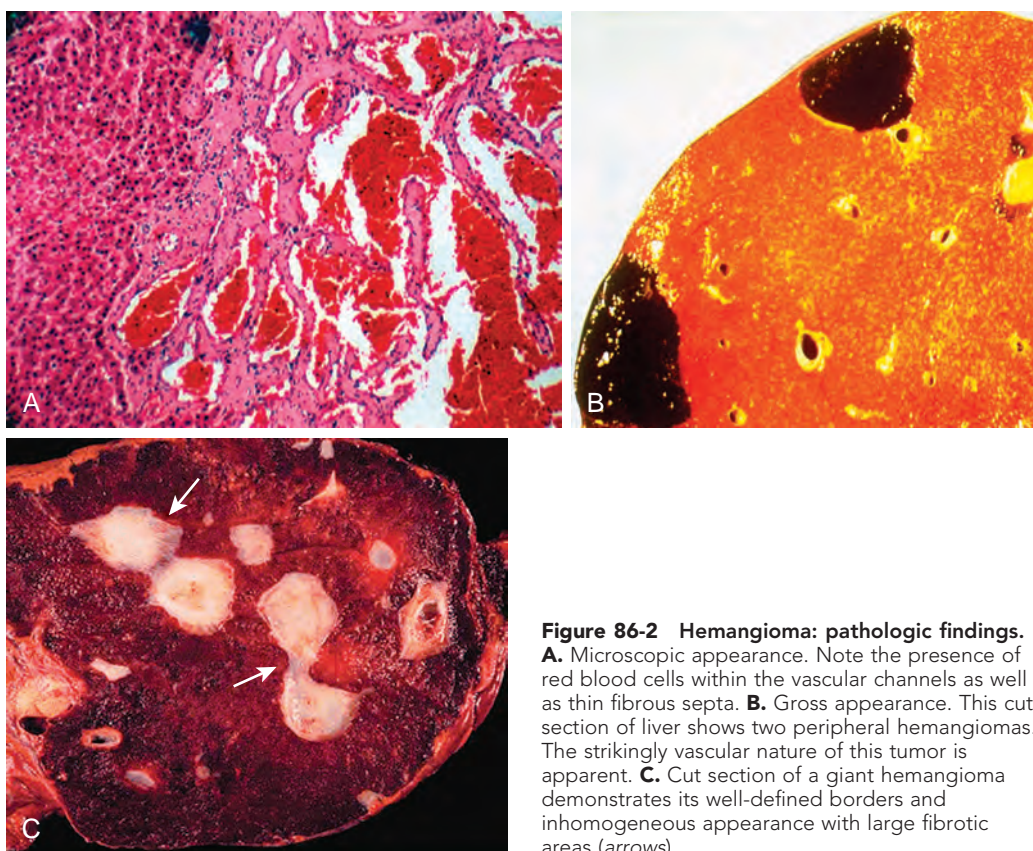


Figure 86-2 Hemangioma: pathologic findings. **A.** Microscopic appearance. Note the presence of red blood cells within the vascular channels as well as thin fibrous septa. **B.** Gross appearance. This cut section of liver shows two peripheral hemangiomas. The strikingly vascular nature of this tumor is apparent. **C.** Cut section of a giant hemangioma demonstrates its well-defined borders and inhomogeneous appearance with large fibrotic areas (arrows).

TABLE 86-1 Hemangioma

Pathologic Features	Radiologic Features
Vascular channels	Echogenic mass: ultrasound
Blood-filled cavity	Hyperintense mass: T2-weighted image (MR)
No arteriovenous shunting	Early globular peripheral enhancement on contrast-enhanced helical CT, dynamic Gd-DTPA-enhanced T1-weighted MR and USPIO-enhanced T1-weighted MR
	Delayed-persistent filling on red blood cell scan, enhanced conventional CT, Gd-DTPA-enhanced MR, angiography
Fibrosis	Hypodense region: CT
	Hypointense region: MR
	Hypoechoic region: ultrasound
Calcification	Dense region: plain films, CT
	Absent signal: MR
	Hyperechoic shadowing region: ultrasound

*See text for full names of imaging agents.

channels are separated by thin fibrous septa, which may form finger-like protrusions into the channels. In gross appearance, it is frequently solitary, well circumscribed, and blood filled and ranges in size from a few millimeters to more than 20 cm.¹⁰ Hemangiomas may be multiple in up to 50% of cases.

Hemangiomas larger than 10 cm are defined as giant hemangiomas. On cut sections, hemangiomas are almost always heterogeneous with areas of fibrosis, necrosis, and cystic change.^{11,12} The radiologic-pathologic correlates of hemangioma are listed in Table 86-1.

INCIDENCE AND CLINICAL PRESENTATION

Hemangioma is the most common benign tumor of the liver, with a reported incidence ranging from 1% to 20%.¹³ The latter figure is the result of a prospective autopsy study in which a dedicated search for this lesion was performed.¹²

Hemangiomas occur primarily in women (female-to-male ratio of 5:1). Although hemangiomas may be present at all ages, they are seen more commonly in postmenopausal women. The worldwide prevalence of this tumor is fairly uniform. In a study of Vilgrain and associates,¹⁴ it was reported that there was a significant association between focal nodular hyperplasia and hemangioma in the liver. Whereas each of these lesions is found commonly as an isolated hepatic mass, in 20% of patients in the study group of Vilgrain and associates, both lesions were present together.

PLAIN RADIOGRAPHIC FINDINGS

Calcification is rare in this tumor; less than 10% of hemangiomas have calcification detectable by plain radiographs.¹⁵ Calcification can be either large and coarse (amorphous calcification within zones of fibrosis) or phlebolith-like thrombi within the vascular channels of hemangioma.

NUCLEAR MEDICINE

Radionuclide scintigraphy for identification of hemangiomas is not performed routinely in all centers, especially outside the United States.¹⁴ With tagged RBC pool scans, there is a defect in the early phases that shows prolonged and persistent “filling

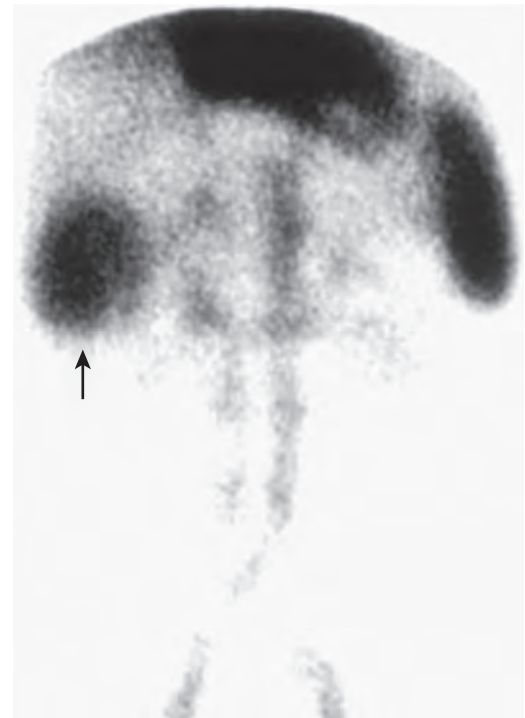


Figure 86-3 Hemangioma: ^{99m}Tc-labeled red blood cell scintiscan. Two-hour delayed scintiscan shows persistent uptake of the isotope within the tumor (arrow).

in” on delayed scans^{16,17} (Fig. 86-3). Many vascular tumors, such as hepatocellular carcinoma, adenoma, and focal nodular hyperplasia, may have persistent uptake, but all exhibit early uptake rather than a defect. Rarely, angiosarcomas can demonstrate the hemangioma pattern of early defect and late isotope uptake.¹⁸ In this context, new hybrid single photon emission computed tomography (SPECT)/CT systems may further aid diagnosis of hemangiomas by means of a more accurate anatomic localization of the lesions. In a study, SPECT/CT increased the accuracy of RBC scintigraphy in classifying the hepatic lesions as hemangiomas and nonhemangiomas from 70.8% to 87.5%.¹⁹

ULTRASOUND

On sonography, hemangiomas are typically hyperechoic and well demarcated and exhibit faint acoustic enhancement^{20,21} (Fig. 86-4). The echogenicity may vary because these tumors may contain cystic and fibrotic regions. Color Doppler ultrasound demonstrates filling vessels in the periphery of the tumor but no significant color Doppler flow deep within the hemangioma itself. Power Doppler, however, may detect minimal flow within hemangiomas, but the pattern is nonspecific and may be seen in hepatocellular carcinomas and metastases.²²

Hemangiomas, like other focal lesions of the liver, are detected and characterized with ultrasound not only by an analysis of echogenicity and vascularity but also by the changes occurring in inflow kinetics of ultrasound contrast agents.²³ In general, ultrasound contrast agents consist of microbubbles of air or perfluorocarbon gas stabilized by a protein, lipid, or polymer shell.²⁴ The small size (approximately the same as RBCs) and stability of the bubbles allow them to traverse the pulmonary and cardiac circulations after intravenous injection.

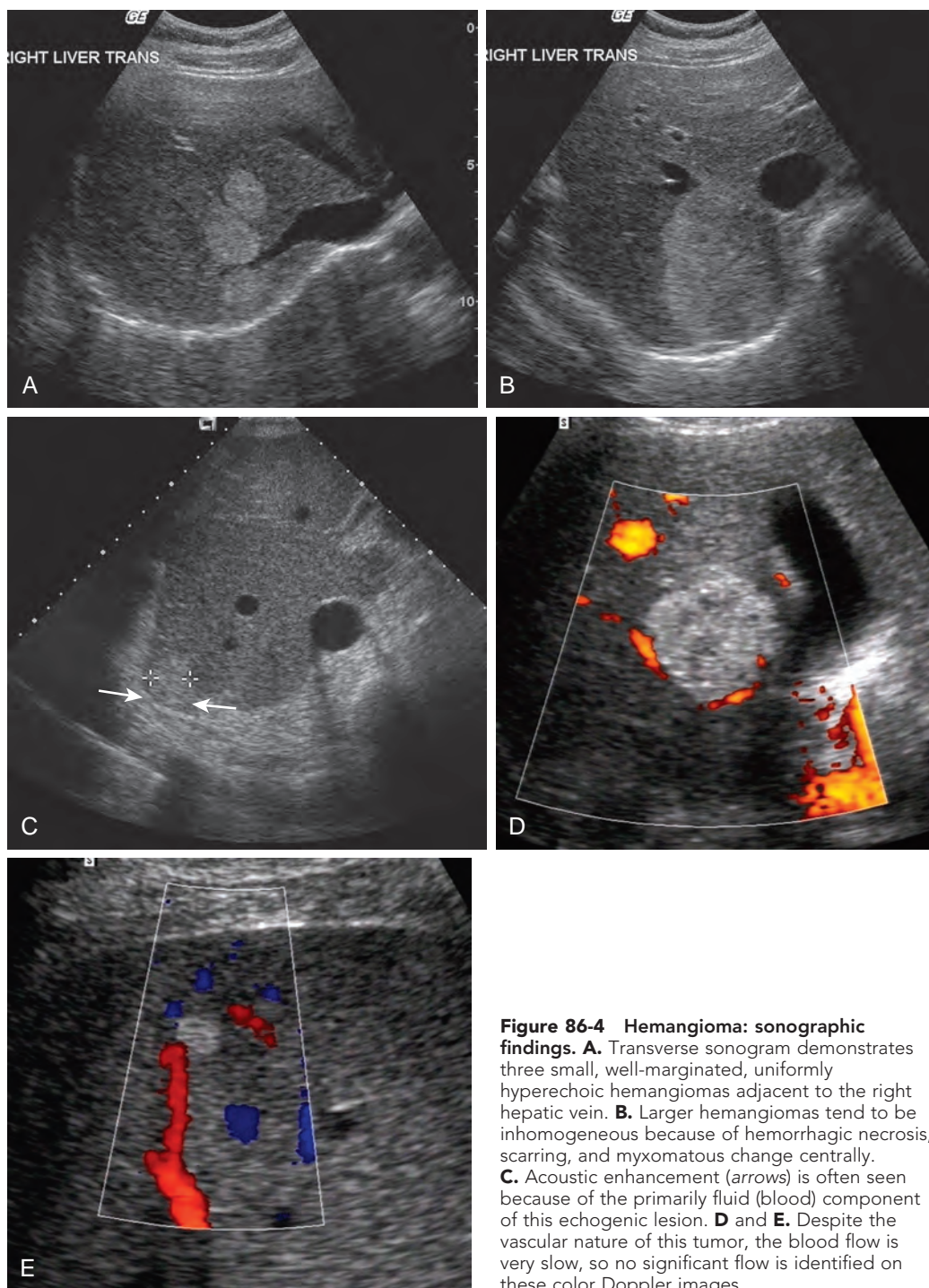


Figure 86-4 Hemangioma: sonographic findings. **A.** Transverse sonogram demonstrates three small, well-margined, uniformly hyperechoic hemangiomas adjacent to the right hepatic vein. **B.** Larger hemangiomas tend to be inhomogeneous because of hemorrhagic necrosis, scarring, and myxomatous change centrally. **C.** Acoustic enhancement (arrows) is often seen because of the primarily fluid (blood) component of this echogenic lesion. **D** and **E.** Despite the vascular nature of this tumor, the blood flow is very slow, so no significant flow is identified on these color Doppler images.

The bubbles cannot move through the vascular endothelium into the interstitium and remain within the vessel until they disappear by the diffusion of the gas through their thin shell. Therefore, they are true blood pool agents and have a typical half-life of a few minutes in the circulation. Bubbles respond to sound emitted by the imaging transducer by oscillating and returning detectable echoes to the transducer.

On contrast-enhanced ultrasonography, hemangiomas demonstrate a typical specific peripheral nodular contrast enhancement and centripetal fill in. Whereas the “filling in” of the lesion

can take several minutes with CT and iodinated contrast material, the kinetics of ultrasound contrast agents is different, and with them, the process can last even less than a minute.^{23,24} Therefore, imaging in the first 60 seconds is critical in characterizing hemangiomas at ultrasound.

COMPUTED TOMOGRAPHY

Hemangiomas appear as low-density masses with well-defined, lobulated borders on nonenhanced CT scans. Calcification is

observed in 10% to 20% of cases.¹³ After intravenous administration of contrast material, both arterial phase and portal venous phase CT scans show early, peripheral, globular enhancement of the lesion. The attenuation of the peripheral nodules is equal to that of aorta.^{25,26} In a study of Leslie and colleagues,²⁷ the presence of globular enhancement isodense with the aorta was found to be 67% sensitive and 100% specific in differentiating hemangiomas from hepatic metastases. Therefore, if this pattern is visualized, no further evaluation is required. If venous phase CT is obtained, centripetal enhancement that progresses to uniform filling persists on delayed phase images (Fig. 86-5). Although small lesions often fill in completely, large tumors may not show central nonenhancing zones during venous and delayed phases, corresponding to scar tissue or cystic cavities.²⁸ On the other hand, approximately 16% of all hemangiomas and 42% of small ones (<1 cm in diameter) show immediate homogeneous enhancement at arterial phase CT imaging.^{25,29} This feature is relatively challenging for the differential diagnosis because other hypervascular tumors, including hepatocellular carcinoma, also may enhance rapidly during this phase of imaging. In such cases, accurate diagnosis can be made with

delayed phase CT imaging because hemangiomas remain hyperattenuating, whereas hypervascular metastases do not.²⁵ Another important and helpful imaging finding in diagnosis of this type of hemangiomas is that their attenuation is equal to that of the aorta during all phases of dynamic CT imaging.³⁰ Hemangiomas may also be a cause of transient hepatic attenuation differences (THADs).

ANGIOGRAPHY

Although angiography is not routinely used in the diagnostic evaluation of hepatic hemangiomas, knowledge of the characteristic appearances is important because hemangiomas may coexist with metastases. In this scenario, correct identification of the lesions is vital because therapeutic options such as hepatic resection depend on the number and distribution of metastases. On angiography, there is pooling of contrast medium within the hemangioma, producing a characteristic “cotton wool” appearance, without evidence of arteriovenous shunting or tumor neovascularity.³¹ Hemangiomas typically retain contrast medium well beyond the venous phase.

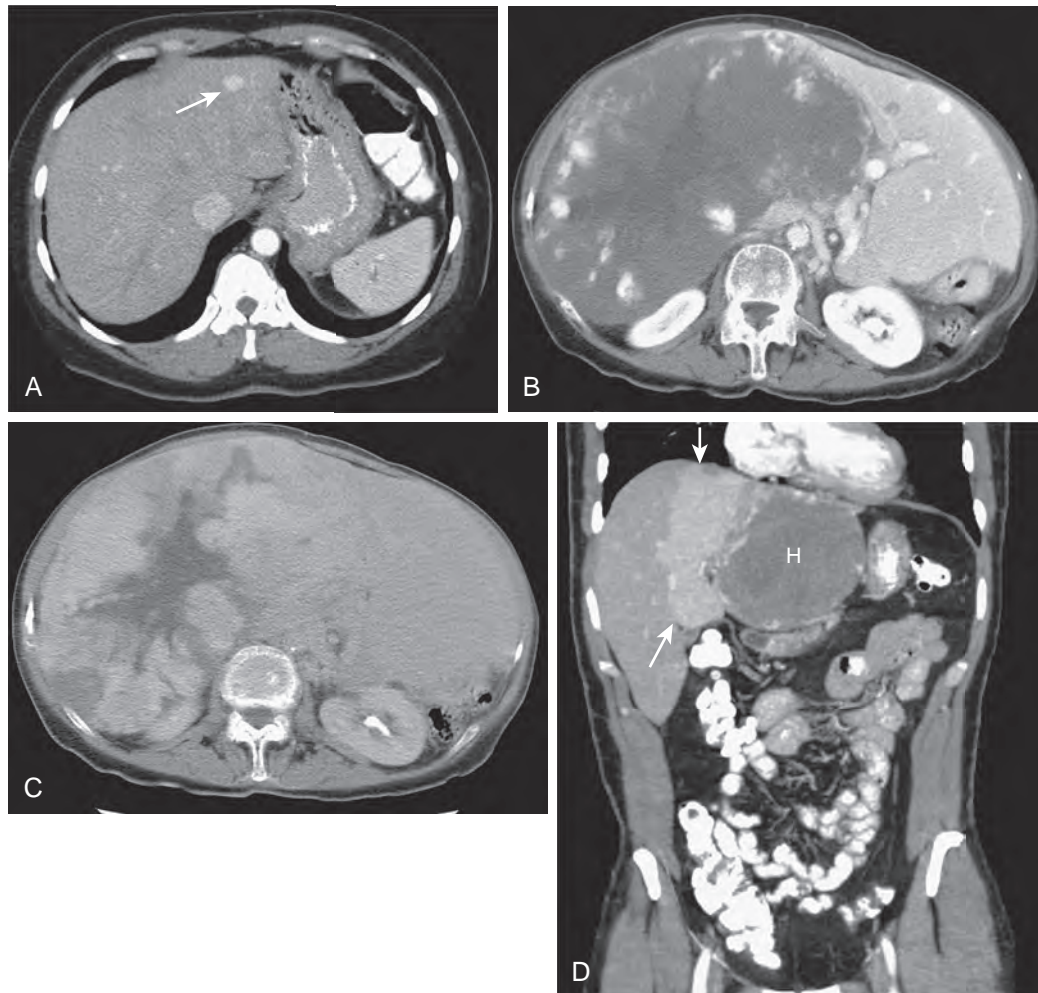


Figure 86-5 Hepatic hemangioma: CT features. **A.** Small hemangiomas (arrow) may demonstrate “flash filling” after intravenous administration of contrast material. The lesion, however, remains isodense with the blood pool, unlike focal nodular hyperplasia, adenoma, hepatoma, and hypervascular metastases, which may also show flash filling. **B** and **C.** Giant hemangioma, which replaces the right lobe, shows peripheral nodular enhancement that progresses in a centripetal fashion. The attenuation of the enhanced portions of the mass is isodense with the blood pool. The central portion of the lesion is a low-attenuation region of central fibrosis. **D.** This hemangioma (H) in the lateral segment of the left lobe is causing a transient hepatic attenuation difference (THAD) in the medial segment of the left hepatic lobe (arrows).

MAGNETIC RESONANCE IMAGING

The study of hemangiomas of the liver is one of the major applications of abdominal MRI (Figs. 86-6 to 86-8). Hemangiomas generally have moderately low signal intensity on T1-weighted images and characteristically demonstrate marked hyperintensity on T2-weighted images, which may contain low-intensity areas correlating with zones of fibrosis.^{11,32-37} They maintain high signal intensity on longer echo time (>120 milliseconds) T2-weighted sequences.³⁸ Nevertheless, the signal characteristics of other masses and neoplasms may overlap with those of hemangioma owing to their similar T2 values, and because of this overlap, characteristics at contrast-enhanced MRI are used for further evaluation.³⁹ Suspected hemangiomas should be evaluated by a dynamic breath-hold sequence, in a manner similar to contrast-enhanced dynamic CT protocol. After intravenous administration of a contrast agent, a fast gradient-echo T1-weighted sequence (20-30 seconds) is repeatedly acquired once per minute until the lesion has filled in completely or nearly completely. In fact, three patterns of enhancement may be seen, depending on the size of the lesion.⁴⁰ The majority of small (<1.5 cm) lesions show uniform early enhancement or peripheral nodular enhancement progressing centripetally to uniform enhancement. This second pattern is commonly seen in medium-sized lesions (1.5-5 cm) and in a few large (>5 cm) lesions.⁴⁰ Most large hemangiomas exhibit peripheral nodular enhancement while the center of the lesion

remains hypointense.⁴⁰ Peripheral nodular enhancement is a useful discriminating feature in the differential diagnosis between hemangiomas and metastases.⁴¹ However, small lesions can be a diagnostic problem because a uniform pattern of enhancement is seen in both hemangiomas and vascular metastases.⁴⁰ Flash-filling hemangiomas may also cause a serious problem regarding their differentiation from hypervascular metastases (e.g., those of malignant neuroendocrine tumors) because of a similar appearance in unenhanced and contrast-enhanced imaging.⁴² In the majority of cases, the combination of T2-weighted images and serial dynamic postgadolinium images allows a confident diagnosis of hemangioma to be made.⁴³ The role of USPIOs has also been evaluated in the characterization of hemangiomas.⁴⁴ This agent is ultimately cleared by the reticuloendothelial system but resides in the intravascular compartment ("blood pool") immediately after injection.⁴⁴ On T1-weighted images, hemangiomas enhance immediately because of their vascularity and become isointense with normal liver. On T2-weighted scans, hemangiomas demonstrate decreased signal intensity and may become isointense to the liver at higher doses of USPIOs.⁴⁴ Hemangiomas do not demonstrate uptake of SPIOs because they do not contain Kupffer cells or normal hepatocytes.¹

Hemangiomas appear isointense or hypointense in the late dynamic phase and hepatocyte phase with use of Gd-EOB-DTPA. The reasons for this are marked hepatocyte uptake of Gd-EOB-DTPA in the surrounding liver, substantially low

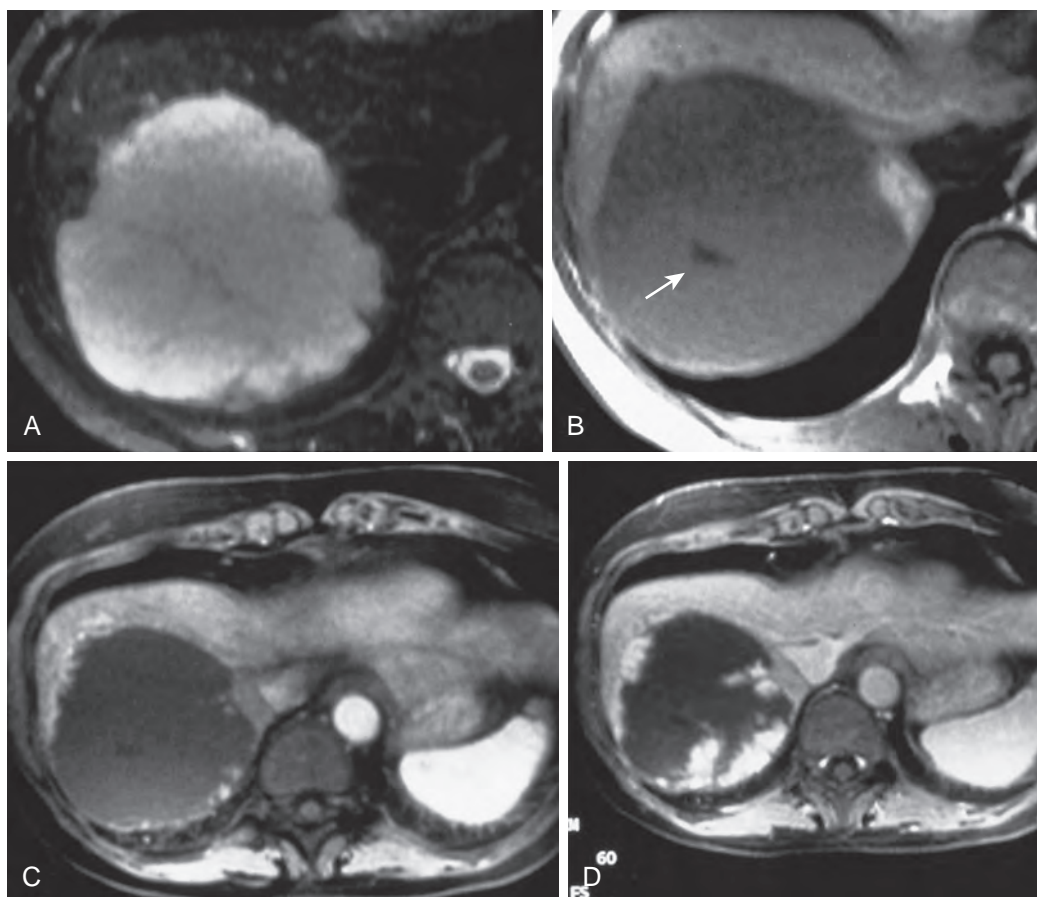


Figure 86-6 Hepatic hemangioma: MRI findings. **A.** Nonenhanced T2-weighted MR image shows a large hyperintense hepatic mass. **B.** Nonenhanced T1-weighted image shows low signal intensity. There is a central scar (arrow) that is often seen in large hemangiomas. **C** and **D.** Gadolinium enhancement demonstrates the characteristic peripheral nodular enhancement pattern that shows centripetal progression.

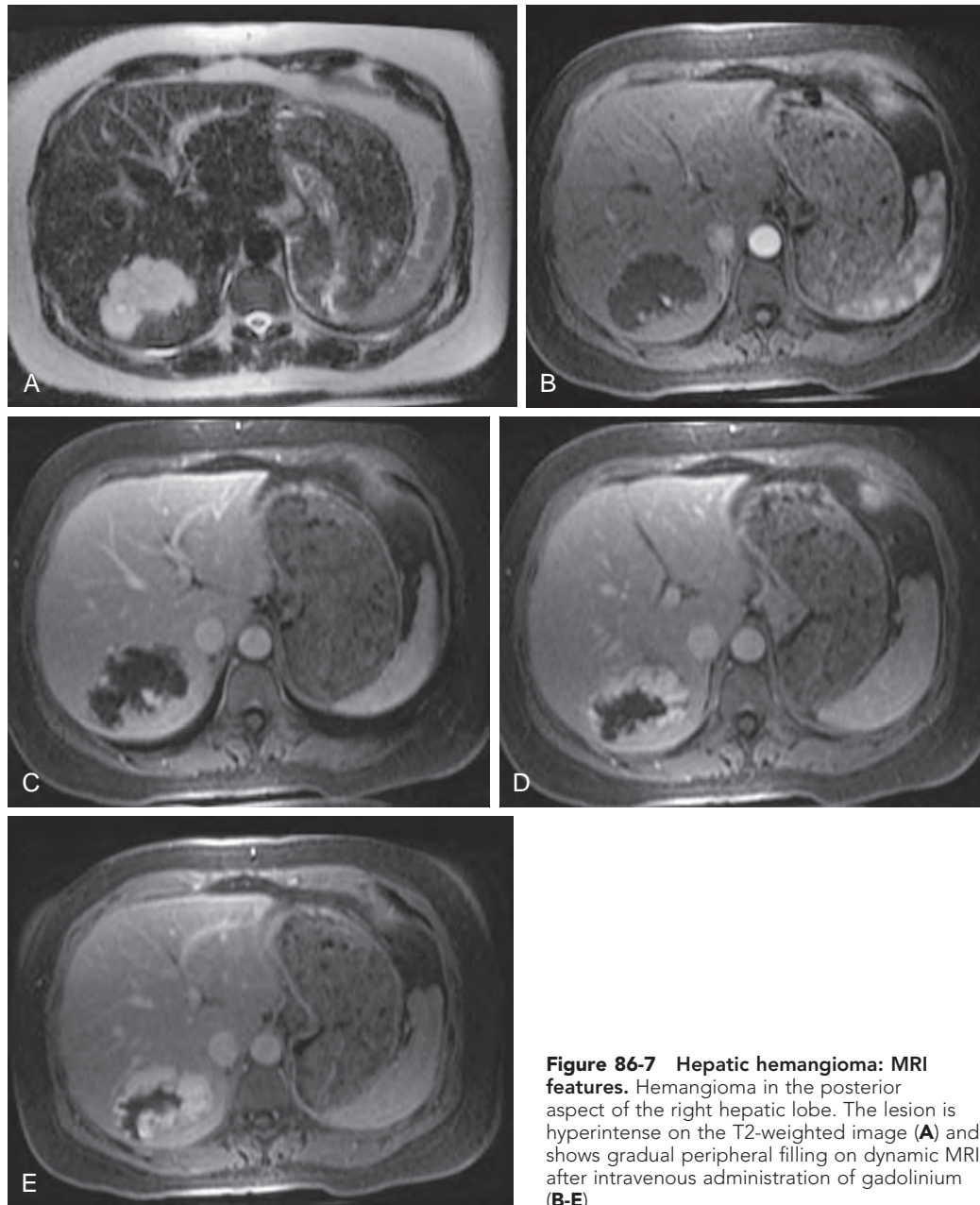


Figure 86-7 Hepatic hemangioma: MRI features. Hemangioma in the posterior aspect of the right hepatic lobe. The lesion is hyperintense on the T2-weighted image (A) and shows gradual peripheral filling on dynamic MRI after intravenous administration of gadolinium (B-E).

overall administered dose of Gd-EOB-DTPA, and substantially short plasma half-life of Gd-EOB-DTPA (Fig. 86-9).⁴²

On diffusion-weighted imaging, hemangiomas show low signal intensity with increased b values and have high apparent diffusion coefficient (ADC) values like simple cysts (Fig. 86-10). However, differentiation between cystic metastases and hemangioma or small flash-filling hemangiomas and hypervascular metastases cannot be achieved solely with this single-pulse sequence, and it should be interpreted in conjunction with contrast-enhanced images.⁴⁵⁻⁴⁷

DIAGNOSTIC WORK-UP

Differentiation of hepatic hemangiomas from other benign and malignant focal liver lesions is one of the most common problems in abdominal imaging.⁴⁸ Most authorities believe that if a

focal liver lesion has the classic appearance of a hemangioma on ultrasound, CT, or MRI examinations, it should be left alone. We believe that in patients with known malignant disease or abnormal liver function test results, one of the tests with high accuracy should be performed, such as multiphasic MDCT or gadolinium-enhanced dynamic MRI, for confirmation. In atypical cases, biopsy should be considered.⁴⁹

Focal Nodular Hyperplasia

PATHOLOGIC FINDINGS

Focal nodular hyperplasia (FNH) is defined microscopically as a tumor-like condition characterized by a central fibrous scar with surrounding nodules of hyperplastic hepatocytes and small bile ductules.¹⁰ The nodules seen in FNH lack normal

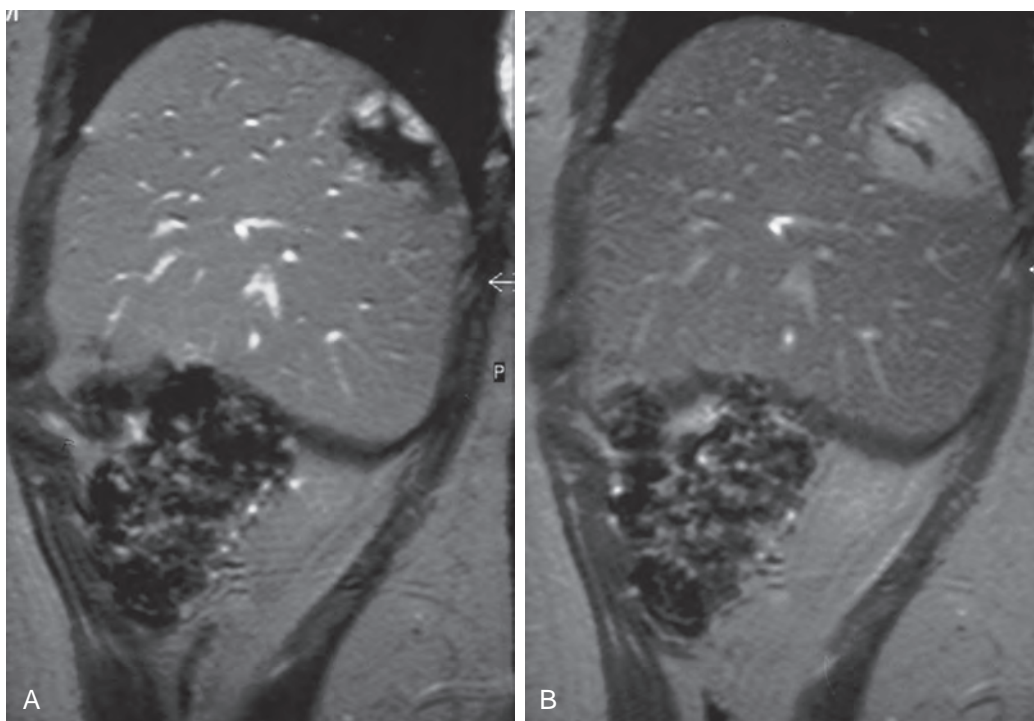


Figure 86-8 Hepatic hemangioma: MRI features. **A** and **B.** Sagittal gadolinium-enhanced images show a lesion with a central scar. Although central scars are generally associated with focal nodular hyperplasia, the contrast retention in this lesion establishes the diagnosis of a hemangioma.

central veins and portal tracts. The bile ductules seen in the central scar do not connect to the biliary tree. Vessels course through the tumor and are most abundant in the fibrous scar⁵⁰ (Fig. 86-11A).

In gross appearance, FNH is a well-circumscribed, solitary mass (95%) that is often located on the surface of the liver or pedunculated.¹⁰ On cut section, the majority of these tumors have an obvious central fibrous scar, and although the margin is sharp, there is no capsule (Fig. 86-11B). Hemorrhage and necrosis are rare because this tumor has excellent vascularity. The majority of FNHs are smaller than 5 cm and have a mean diameter of 3 cm at the time of diagnosis. On occasion, FNH replaces an entire lobe of the liver (lobar FNH).¹⁰ The consistency is firm to rubbery, and the color is always paler than that of the surrounding liver. When an FNH is sectioned, it bulges from the cut surface with the stellate scar depressed and forming stellate fibrous septa that course through the tumor. Multiple FNHs have been reported in association with vascular malformations of various organs and neoplasia of the brain.⁵¹ FNH is believed to be a hyperplastic response to an underlying “spider-like” arterial malformation.⁵² It has to be emphasized that on microscopic examination, particularly by needle biopsy, the appearance of FNH resembles that of a cirrhotic process; however, acinar landmarks are not present.⁵³

Radiologic-pathologic correlates of this tumor are listed in Table 86-2.

INCIDENCE AND CLINICAL PRESENTATION

FNH is the second most common benign hepatic tumor, constituting 8% of primary hepatic tumors in autopsy series.¹⁰

FNH is more common in women, predominating in the third to fifth decades of life. Oral contraceptives have a trophic effect on FNH, but there is debate as to whether these agents actually cause this tumor.

Clinically, FNH is usually an incidental finding at autopsy, elective surgery, or cross-sectional imaging. Fewer than one third of cases are discovered because of clinical symptoms, usually right upper quadrant or epigastric pain.

PLAIN RADIOGRAPHIC FINDINGS

Plain radiograph calcification is almost never present. On occasion, a pedunculated FNH lesion may project to the margin of the liver and compress the adjacent stomach or hepatic flexure.⁵⁴

NUCLEAR MEDICINE

In the past, sulfur colloid scintigraphy was the preferred imaging technique in the diagnosis of FNH because of normal tracer uptake in approximately 50%, and a defect is seen in 40% of FNH cases. “Hot spots,” present in 10% of lesions, indicate an increased number of Kupffer cells.⁵⁵ Hepatobiliary scans show tracer uptake in the majority of cases, and isotope excretion can be observed in 50% of delayed scans.⁵⁶ Tagged RBC pool studies show early isotope uptake and late defect. There is no gallium uptake in FNH.

There are only a few studies about PET imaging of FNH. In one study, it was reported that in contrast to liver metastases, there is no increased glucose metabolism in FNH in vivo. Also, the imaging features of FNH on ¹⁸F-fluorodeoxyglucose (FDG) PET imaging are not specific.⁵⁷

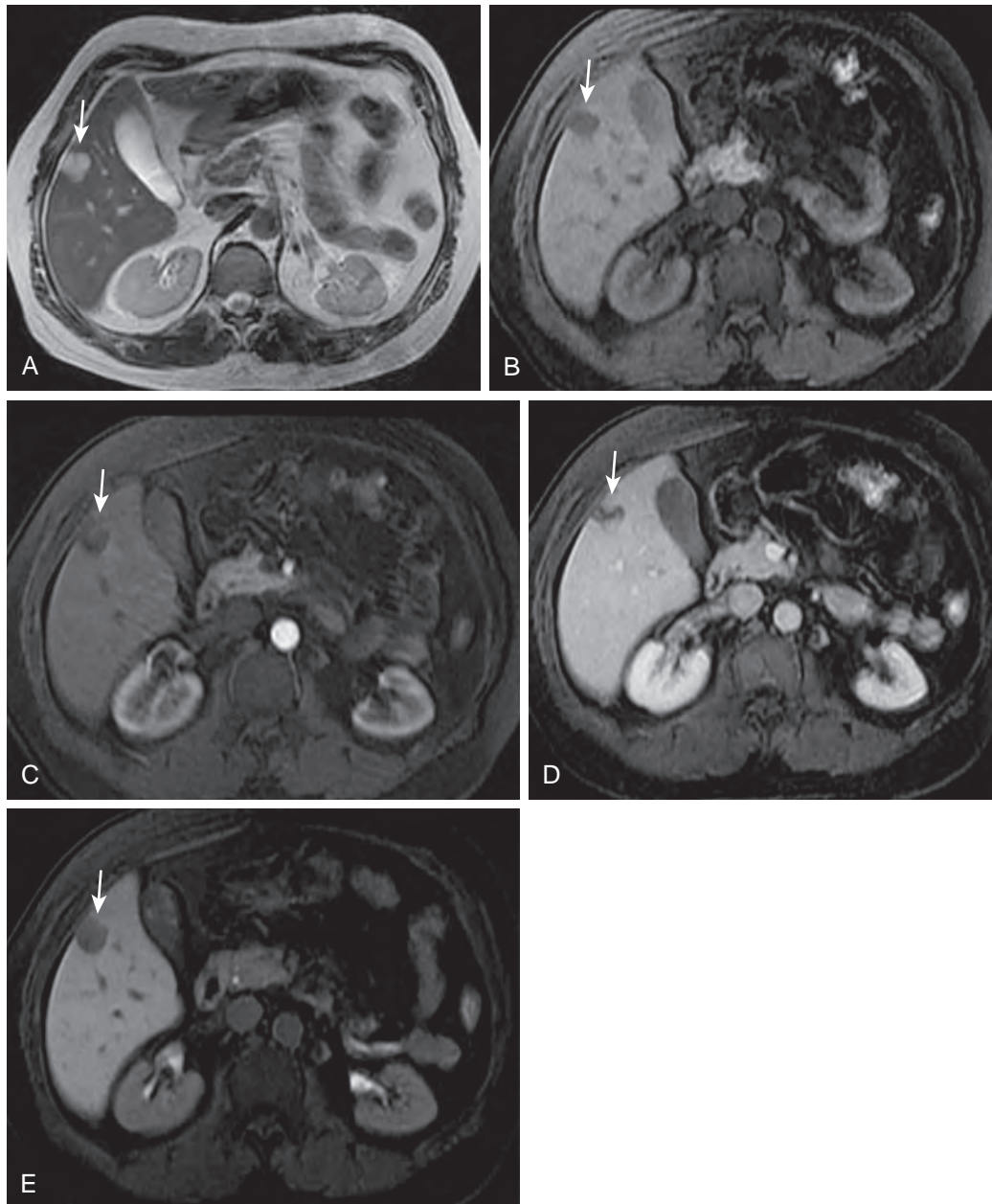


Figure 86-9 Hepatic hemangioma: MRI features. A patient with a typical hemangioma in the right lobe of the liver (arrow). The hemangioma is hyperintense on the T2-weighted image (A) and hypointense on the T1-weighted image (B). It shows progressive nodular enhancement on the arterial phase (C) and late phase (D) images. As expected, it does not show any uptake of the hepatobiliary contrast agent and becomes hypointense on the hepatocellular phase image (E).

Today, CT and MRI are used in the diagnostic work-up of FNH. Nuclear medicine studies are reserved for exceptional circumstances.

ULTRASOUND

On gray-scale ultrasound studies, FNH typically appears as a well-demarcated, hypoechoic mass that is homogeneous in tissue texture except for a central scar^{56,58} (Fig. 86-12). Rarely (1.4%), calcifications may be seen within FNH, and the lesion may resemble fibrolamellar hepatocellular carcinoma.⁵⁹ On color Doppler sonography (Fig. 86-13), FNH shows increased

blood flow, and a pattern of blood vessels radiating peripherally from a central feeding artery may be seen, similar to the findings at conventional angiography.⁶⁰ In a contrast-enhanced examination, like hepatocellular carcinoma, FNH in the early arterial phase appears typically as a hyperperfused structure relative to the adjacent liver tissue. However, the specific morphologic features of these two entities are different. FNH typically enhances uniformly without the necrosis and heterogeneity often seen in hepatocellular carcinoma. The stellate lesion vascularity, a central nonenhancing scar, and a tortuous feeding artery are the other typical features of FNH. Nevertheless, portal venous phase imaging is critical for an accurate diagnosis

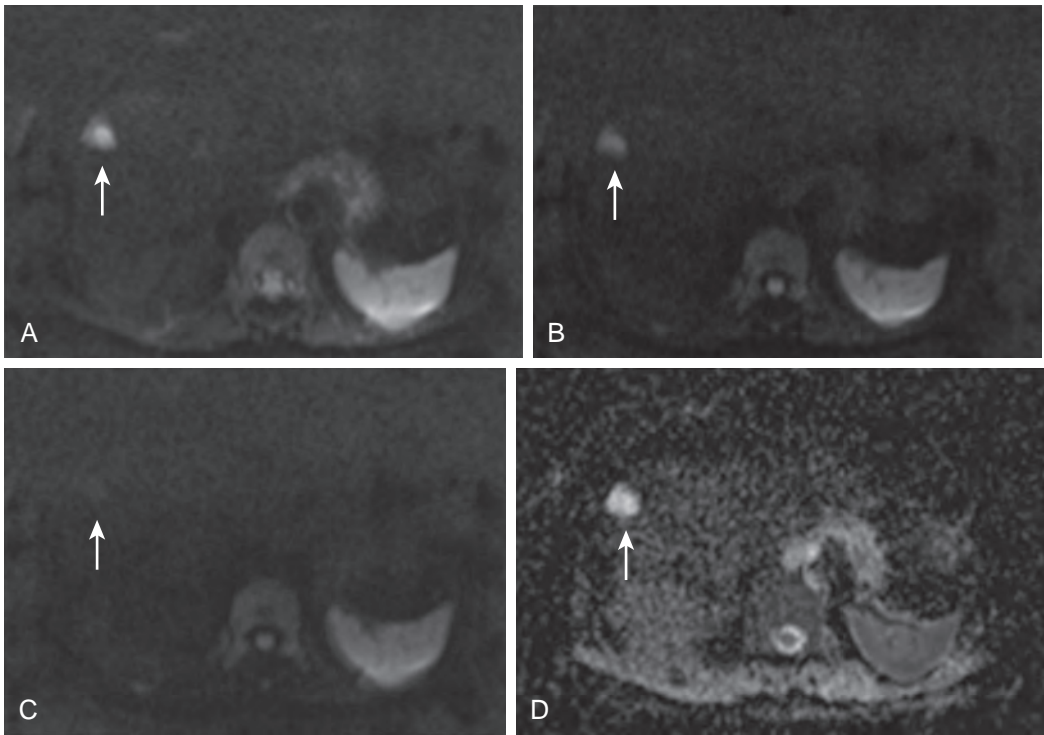


Figure 86-10 Simple cyst: diffusion-weighted MRI features with different b values. A simple cyst in the right lobe of the liver (arrow). The cyst is markedly hyperintense on the diffusion-weighted image with a b value of 50 (A). With increasing b values (B and C, 400 and 800, respectively), the cyst loses signal intensity. It has a high ADC value (D).

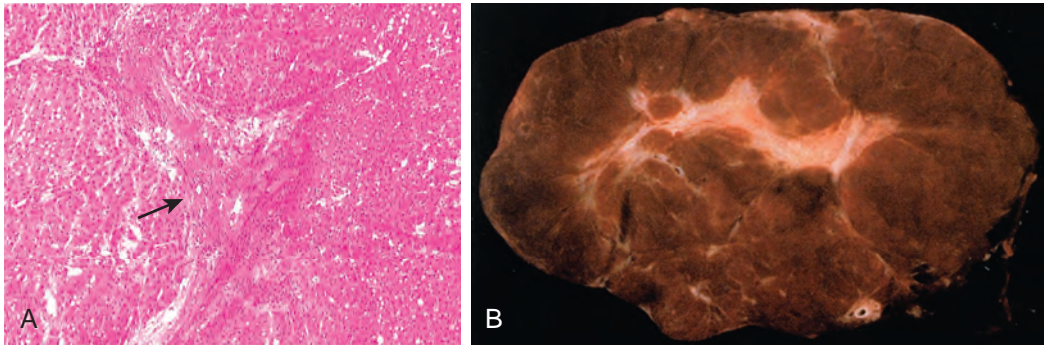


Figure 86-11 Focal nodular hyperplasia: pathology. A. Normal hepatocytes are arranged in incomplete nodules that are partially separated by fibrous tissue (arrow). B. This lesion is usually lighter brown than the adjacent liver. It has a central fibrous scar that consists of fibrovascular tissue, which explains its enhancement pattern after the intravenous administration of contrast medium.

TABLE 86-2 Focal Nodular Hyperplasia	
Hyperplasia of normal liver Uptake of SPIO results in loss of signal	
Pathologic Features	Radiologic Features
Central scar with vessels and bile ducts	Hyperintense region: T2-weighted images (MR) Spoke-wheel pattern: angiography Calcification rare
Hyperplasia of normal liver (Kupffer cells, portal spaces, bile ductules)	Sulfur colloid uptake (80%) Iminodiacetic acid uptake and excretion Homogeneous mass: CT, ultrasound, MR, angiography Hyperdense relative to live on arterial phase of contrast-enhanced helical CT, becoming isodense during portal venous phase of enhancement Uptake of SPIO results in loss of signal on T2-weighted MR Uptake of hepatobiliary contrast agents (e.g., mangafodipir, Gd-EOB-DTPA) results in hyperintensity relative to liver on T1-weighted images

*See text for full names of imaging agents.

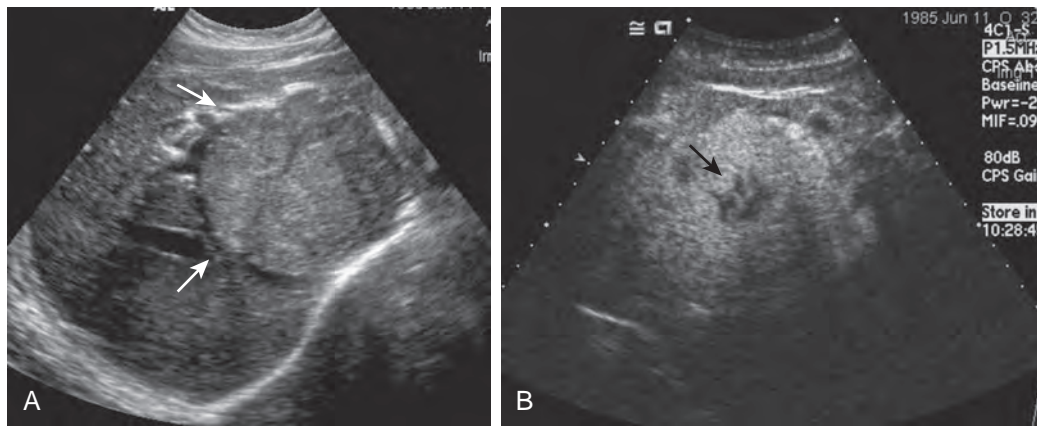


Figure 86-12 Focal nodular hyperplasia: ultrasound findings. **A.** Sonogram demonstrates a large lesion in the right lobe of the liver (arrows). **B.** Contrast-enhanced sonogram demonstrates early arterial enhancement of FNH; note that central scar shows no enhancement (arrow).

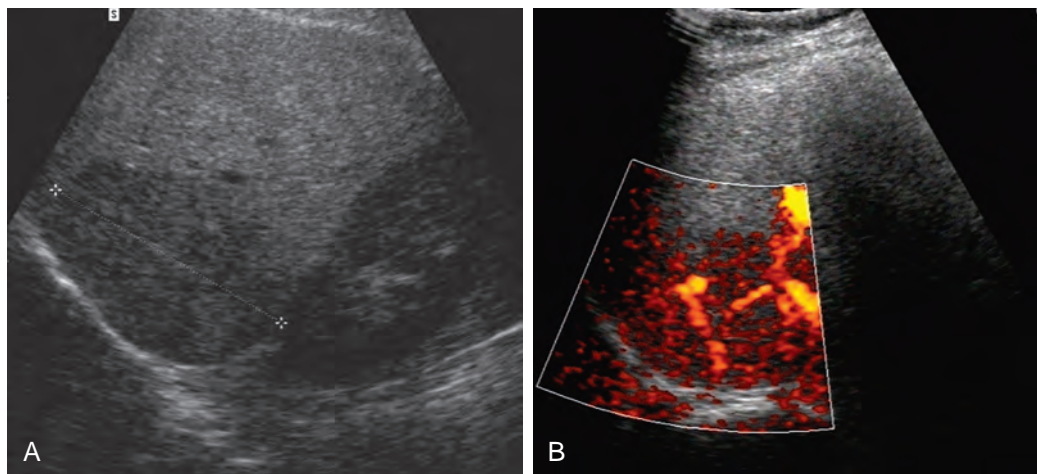


Figure 86-13 Focal nodular hyperplasia: color Doppler ultrasound. **A.** There is a large hypoechoic mass in the right lobe of the liver. **B.** It is quite vascular on color Doppler imaging.

to be reached. During this phase, as opposed to hepatocellular carcinoma, in which washout is generally seen, FNH remains isoechogenic with the portal vein and later with the liver parenchyma.^{23,24}

COMPUTED TOMOGRAPHY

On nonenhanced scans, FNH usually appears as a homogeneous, hypodense mass (Fig. 86-14). In a third of cases, a low-density central area is seen, corresponding to the scar.^{61,62} During the arterial phase of contrast-enhanced CT, FNH enhances rapidly and becomes hyperdense relative to normal liver⁶³ (Fig. 86-15). The low-attenuation scar appears conspicuous against the hyperdense tissue, and foci of enhancement representing arteries may be seen within the scar⁶³ (see Fig. 86-14B). In the portal venous phase and later phases of enhancement, the difference in attenuation between FNH and normal liver decreases and the FNH may become isodense with normal liver.⁶³⁻⁶⁵ Ten-minute delayed images can show increased uptake of contrast material in the scar relative to surrounding liver.²⁶

ANGIOGRAPHY

On angiography, FNH is a hypervascular tumor with a centrifugal blood supply creating a “spoke-wheel” pattern⁶⁶ in 70% of cases. The scar is usually hypovascular. During the capillary phase, an intense and inhomogeneous stain without avascular zones is characteristic. During the venous phase, large veins draining the hypervascular FNH are noted. Angiography is no longer primarily used to diagnose FNH.

MAGNETIC RESONANCE IMAGING

MRI has higher sensitivity (70%) and specificity (98%) for FNH than CT and ultrasound.⁶² On nonenhanced MRI studies, FNH is an isointense tumor on T1-weighted images that becomes slightly hyperintense to isointense on T2-weighted images (Figs. 86-16 and 86-17). The central scar is hypointense on T1-weighted images and hyperintense on T2-weighted images.^{67,68} However, there is overlap in the appearance of FNH and malignant lesions on nonenhanced T1-weighted and

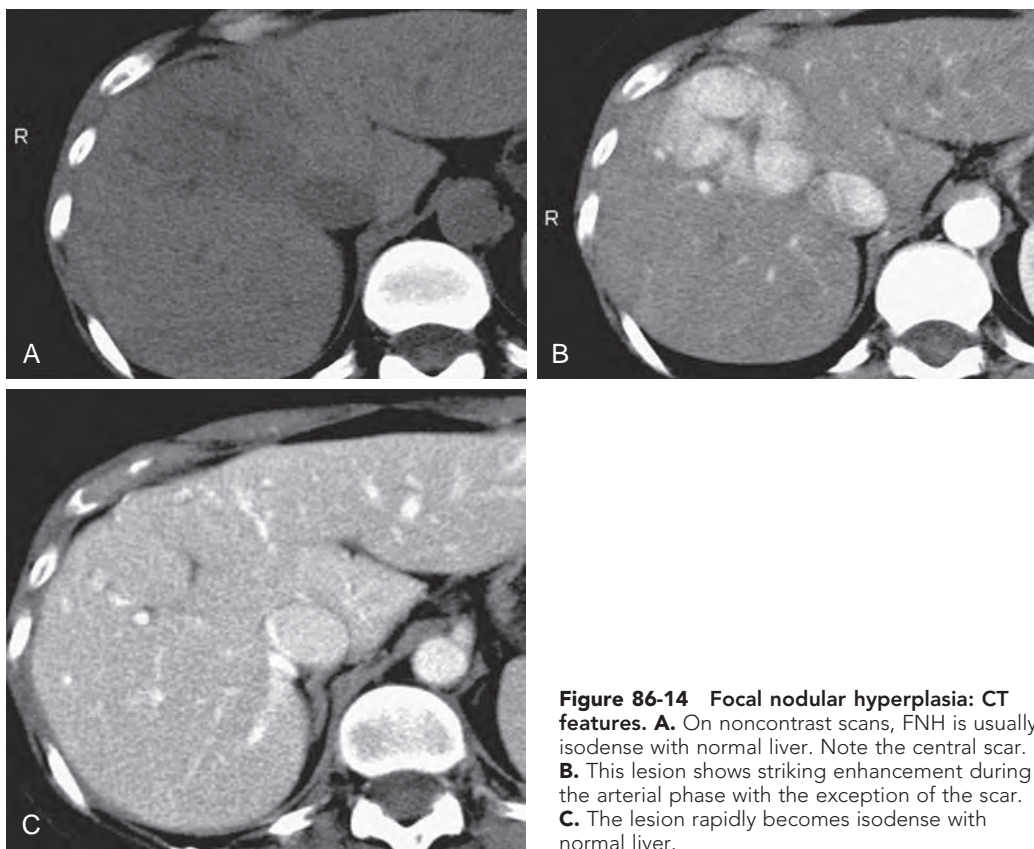


Figure 86-14 Focal nodular hyperplasia: CT features. **A.** On noncontrast scans, FNH is usually isodense with normal liver. Note the central scar. **B.** This lesion shows striking enhancement during the arterial phase with the exception of the scar. **C.** The lesion rapidly becomes isodense with normal liver.

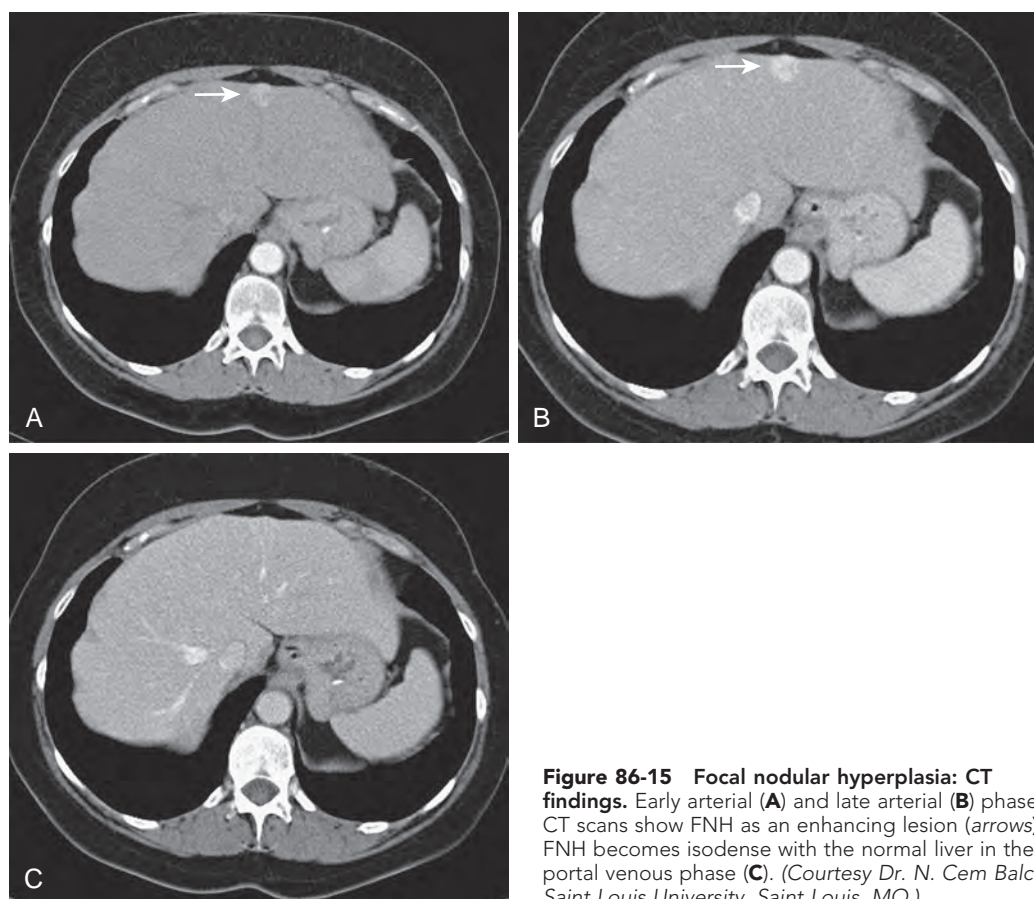


Figure 86-15 Focal nodular hyperplasia: CT findings. Early arterial (**A**) and late arterial (**B**) phase CT scans show FNH as an enhancing lesion (arrows). FNH becomes isodense with the normal liver in the portal venous phase (**C**). (Courtesy Dr. N. Cem Balci, Saint Louis University, Saint Louis, MO.)

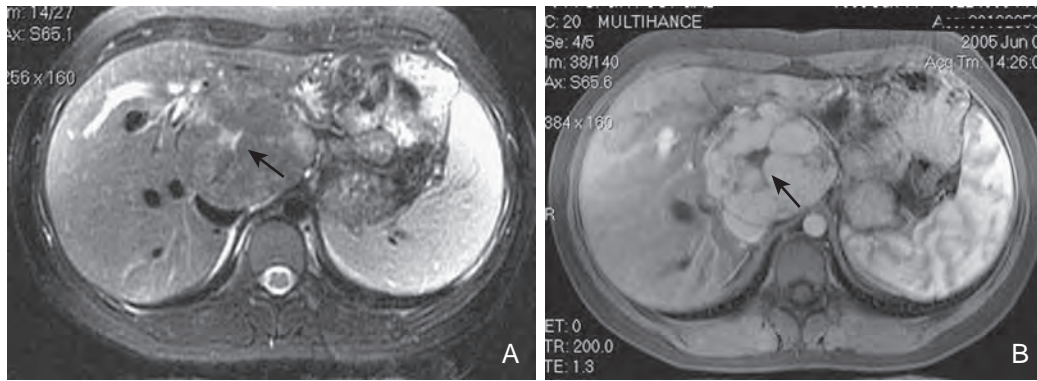


Figure 86-16 Focal nodular hyperplasia: MRI features. **A.** A large lesion is seen on this T2-weighted image obtained with fat suppression. The lesion is isointense to the normal liver, and the central scar is hyperintense (arrow). **B.** Gadolinium-enhanced early arterial phase demonstrates homogeneous enhancement of the lesion. The central scar (arrow) does not enhance early.

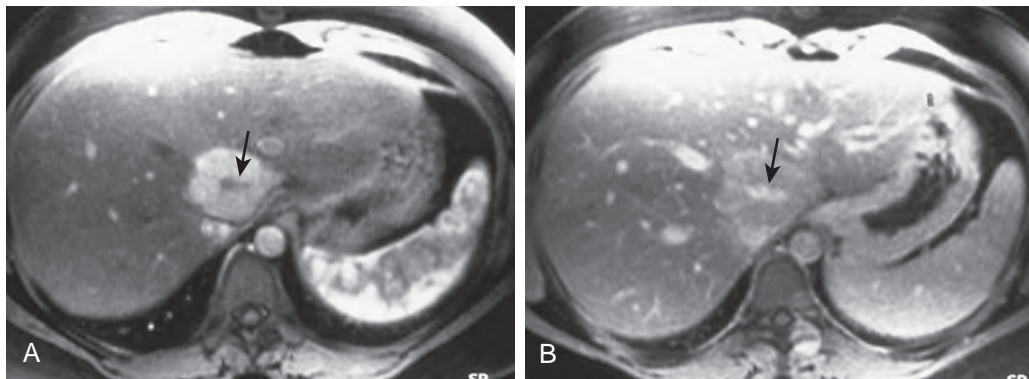


Figure 86-17 Focal nodular hyperplasia: MRI features. **A.** During the arterial phase of enhancement, the lesion shows robust enhancement with the exception of the central scar (arrow). **B.** The mass rapidly de-enhances, and there is enhancement of the central scar (arrow).

T2-weighted images, and further characterization with contrast-enhanced dynamic studies may be necessary.

FNH, which is a hypervascular tumor, enhances robustly and homogeneously in the arterial phase, with the exception of late-enhancing central scar (see Figs. 86-16 and 86-17).^{38,64,67} Hepatocellular adenomas show less intense enhancement and lack a central scar.

Although other focal liver lesions, such as giant hemangiomas and hepatocellular carcinomas, may also have a central scar, MRI findings can help establish a specific diagnosis. The central scar in giant hemangiomas is typically larger and brighter on T2-weighted images. Because of the presence of scar tissue, calcifications, or necrosis, the central scar in hepatocellular carcinoma tends to show low signal intensity on T2- and T1-weighted images and typically does not enhance that much on contrast-enhanced images. Nevertheless, in some cases, FNH may show atypical features, such as very high signal intensity on T2-weighted images and a central scar with a low signal intensity that causes difficulty in differential diagnosis. In such cases, application of more sophisticated contrast media, such as SPIOs, or hepatobiliary agents, such as Gd-EOB-DTPA, may be necessary to demonstrate the hepatocellular origin of the lesion. On T2-weighted images with SPIO administration, FNH shows loss of signal due to uptake of iron oxide particles by Kupffer cells within the lesion.⁶⁷ The degree of signal loss seen in FNH

with use of SPIOs is significantly greater than in other focal liver lesions, such as metastases and hepatocellular adenoma.⁶⁸

Hepatobiliary agents can also be helpful in characterization of FNH. FNH contains hepatocytes, which take up these agents, resulting in hyperintensity of the lesion relative to the liver on T1-weighted images.⁶⁹⁻⁷¹ On hepatocyte phase images, FNH usually appears isointense or hyperintense relative to the surrounding liver parenchyma and shows the classic popcorn-like enhancement pattern as a result of the accumulation of Gd-EOB-DTPA and poor biliary drainage.^{72,73} Similar to hemangiomas, the central scar appears hyperintense on delayed phase imaging with extracellular agents and hypointense on hepatocyte phase images with Gd-EOB-DTPA.⁴²

Hepatobiliary-specific contrast agents can be useful for differentiation of FNH from adenomas. FNH shows hyperintensity or isointensity except for a central scar in the hepatobiliary-specific phase (typically 20-minute delay for Gd-EOB-DTPA), whereas adenoma usually shows hypointensity (Fig. 86-18).⁷⁴

FNH does not have a true tumor capsule. A pseudocapsule may be present because of compression of the adjacent liver parenchyma and surrounding inflammation. The pseudocapsule is typically a few millimeters thick and hyperintense on T2-weighted images. It may also show some enhancement on delayed postcontrast images.⁶⁴

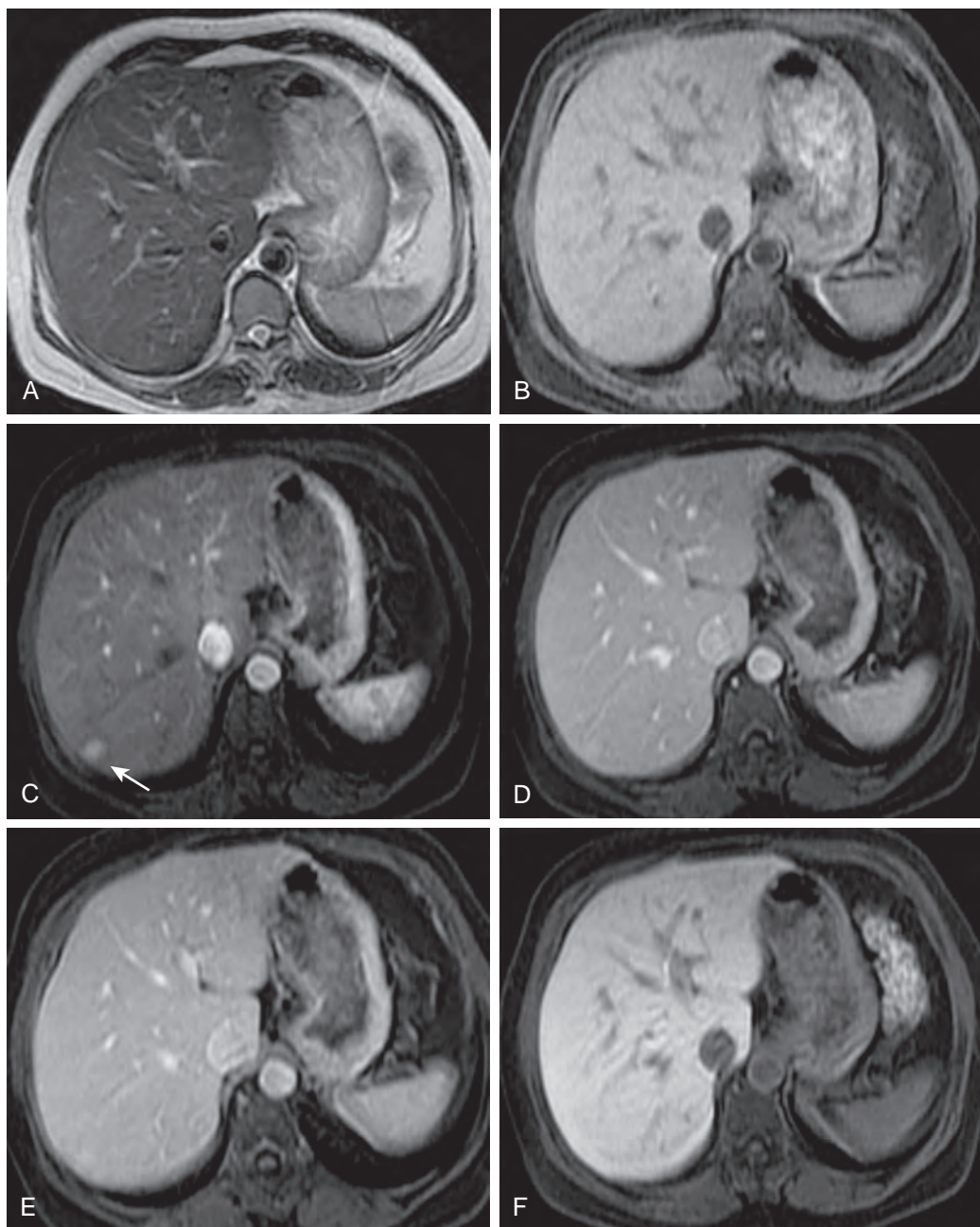


Figure 86-18 Focal nodular hyperplasia: MRI features. A small FNH in the right lobe of the liver. The lesion is isointense with the liver parenchyma on the T2- and T1-weighted images (**A** and **B**). It shows strong arterial enhancement and becomes visible on the arterial phase image (arrow, **C**). On the portal venous and hepatic venous phase images (**D** and **E**), FNH becomes isointense with the liver. Because it shows uptake of the hepatobiliary contrast agent, it remains isointense with the liver on the hepatocellular phase image (**F**).

Fatty change in the liver parenchyma is not uncommon in patients with FNH. The lesion may tend to show mildly low signal intensity on in-phase gradient-echo T1-weighted images and high signal intensity on out-of-phase images.

As a solid tumor, FNH shows slightly high signal intensity with increasing b values on diffusion-weighted imaging and low signal intensity on ADC mapping, with a reported ADC value between 1 and $1.40 \times 10^{-3} \text{ mm}^2/\text{s}$. However, the ADC values cannot be relied on for lesion characterization because of the overlap with other solid lesions, including adenoma and malignant lesions.^{45,46}

TELANGIECTATIC FOCAL NODULAR HYPERPLASIA

The uncommon telangiectatic subtype of FNH is characterized by the presence of centrally located, multiple dilated blood-filled spaces and is commonly associated with multiple FNH syndrome. In telangiectatic FNH, arteries have hypertrophied muscle media but no intimal proliferation in contrast to the classic form. Furthermore, these abnormal vessels drain directly into the adjacent sinusoids, whereas in classic FNH, connections to the sinusoids are almost never seen.^{47,75} Besides these

histologic differences, there are also reported imaging differences of telangiectatic FNH. Telangiectatic subtype of FNH may be hyperintense on T1-weighted images and strongly hyperintense on T2-weighted images and show persistent lesion enhancement on delayed phase images. All of these features are extremely rare in classic FNH and relatively common in telangiectatic subtype. Furthermore, absence of a central scar is not an uncommon finding in this subentity.⁷⁶

Hepatocellular Adenoma

PATHOLOGIC FINDINGS

Hepatocellular adenoma (HCA) should be considered a spectrum of lesions that are associated with a number of diseases and etiologic factors and that demonstrate a variety of histologic appearances. Accordingly, a new classification of adenomas (Table 86-3) has been proposed in which, in addition to the typical adenoma, anabolic steroid-associated HCA is described separately.¹⁰ This is due to its distinctive histologic appearance, which often resembles that of hepatocellular carcinoma. In addition, multiple hepatocellular adenomatosis should be considered separately from typical HCA.

Typical HCA is defined as a tumor composed of hepatocytes arranged in cords that occasionally form bile¹⁰ (Fig. 86-19). The tumor lacks portal tracts and terminal hepatic veins; consequently, necrosis, hemorrhage, and rupture commonly occur in large tumors.³⁶

In gross appearance, a typical HCA is a large tumor (usually 8-10 cm in diameter at discovery), readily seen from the external surface of the liver.⁴⁰ Pedunculation is seen in approximately 10% of cases. On cut section, its surface is tan and irregular and frequently has large areas of hemorrhage or infarction. However, homogeneous adenomas without rupture can be seen with

numerous blood vessels throughout the tumor and occasionally fibrous septa. Large vessels run through the surface of adenomas.⁴⁰ Most adenomas are solitary.⁵³

On microscopic examination, the tumor is composed of neoplastic cells that are separated by compressed sinusoidal spaces, resulting in a sheetlike pattern.¹⁰ The sinusoids are lined by endothelial cells, and enzymatically active Kupffer cells have been demonstrated in adenomas.⁷⁷ Fatty hepatocytes are frequently present as well. Adenomas rarely undergo malignant transformation to hepatocellular carcinoma, even after years of maintaining a stable appearance.⁷⁸

Radiologic-pathologic correlates of HCA are given in Table 86-4.

INCIDENCE AND CLINICAL PRESENTATION

The majority of HCAs are related to the use of oral contraceptives, with an overall estimated incidence of four adenomas per 100,000 users.^{79,80} Withdrawal of estrogen compounds may result in regression of the HCA, which can require a period of several months.⁸¹

PLAIN RADIOGRAPHIC FINDINGS

When they are sufficiently large, HCAs can cause a right upper quadrant mass on plain radiographs.²³ When these lesions

TABLE 86-3 Hepatocellular Adenoma: Classification

Typical hepatocellular adenoma	
Type I	Estrogen-associated hepatocellular adenoma
Type II	Spontaneous hepatocellular adenoma in women
Type III	Spontaneous hepatocellular adenoma in men
Type IV	Spontaneous hepatocellular adenoma in children
Type V	Metabolic disease-associated hepatocellular adenoma
Anabolic steroid-associated hepatocellular adenoma	
Multiple hepatocellular adenomas (adenomatosis)	

TABLE 86-4 Hepatocellular Adenoma

Pathologic Features	Radiologic Features
Rich in fat	Hyperechoic mass: ultrasound Hypodense mass: CT Hyperintense mass: MR
No stroma, internal hemorrhage	Anechoic, potentially cystic mass: ultrasound Hyperdense area: CT Hyperintense area: T1-weighted images (MR) Avascular areas: angiography
Peripheral "feeders" Kupffer cells	Peripheral enhancement: angiography, contrast-enhanced MDCT, and MR Sulfur colloid uptake (20%), SPIO uptake resulting in reduced signal on T2-weighted MR images
Hepatocytes, no ductules	Iminodiacetic acid uptake, no excretion

*See text for full names of imaging agents.

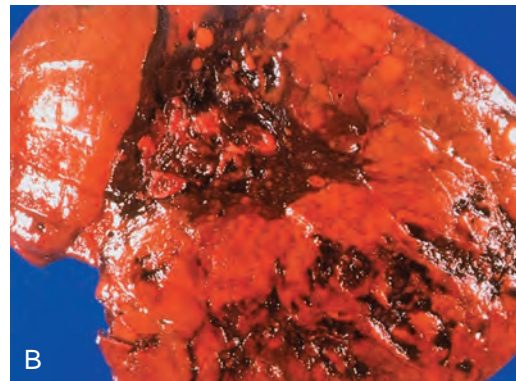
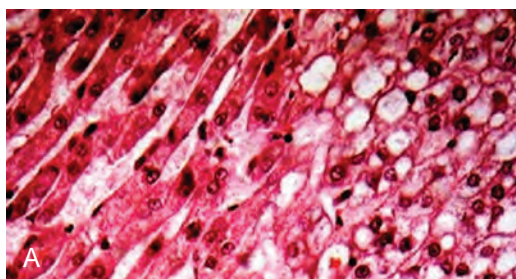


Figure 86-19 Adenoma: pathology. **A.** Normal hepatocytes are identified on the left side of this histologic image. On the right, fat-containing hepatocytes are present. **B.** Gross section shows hemorrhage within a large adenoma.

rupture, free intraperitoneal hemorrhage can occur, producing the typical “ground glass” appearance of free intraperitoneal fluid.

NUCLEAR MEDICINE

As in hemangioma and FNH, nuclear medicine is no longer routinely used in the diagnostic work-up of HCA. There are also no studies reporting usefulness of PET imaging in this context. Sulfur colloid scintigraphy demonstrates a defect in 80% of cases, although tracer uptake can be present in up to 20% of tumors.⁵⁵ Uptake is found in adenomas with a vascular supply sufficient to deliver the isotope to the prominent sinusoids.

Hepatobiliary scans show tracer uptake in the majority of cases; however, no excretion is seen on delayed scans because of lack of bile ductules.⁵⁶ Tagged RBC scintigraphy demonstrates early uptake and a delayed defect, indicating the vascular nature of this tumor.

ULTRASOUND

Sonography typically demonstrates a large hyperechoic lesion with central anechoic areas, corresponding to zones of internal hemorrhage if it is present⁵⁸ (Fig. 86-20). These findings are nonspecific. On occasion, adenomas may undergo massive necrosis and hemorrhage, and the ultrasound appearance is that of a complex mass with large cystic components. Color Doppler ultrasound demonstrates peripheral arteries and veins, correlating well with both gross and angiographic findings. In addition, color Doppler may identify intratumoral veins.⁸² This finding is absent in FNH and may be a useful discriminating feature for HCA.⁸²

On contrast-enhanced ultrasound, adenomas show homogeneous contrast enhancement, typically as a rapid (1-2 seconds) complete centripetal filling in arterial phase. In the early portal venous phase, adenomas become isoechoic or, more rarely, remain slightly hyperechoic relative to liver parenchyma.⁸³ The typical peritumoral arteries with centripetal or diffuse filling of intratumoral enhancement of adenoma in early arterial phase

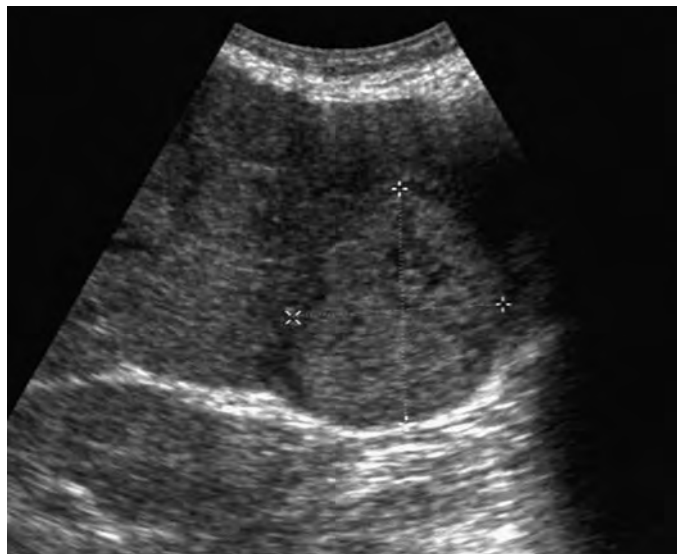


Figure 86-20 Adenoma: ultrasound findings. There is a large, solid echogenic mass in the right lobe of the liver. Note the fairly well defined hypoechoic rim.

is different from the centrifugal enhancement of FNH.⁸⁴ Hypoechoic nonenhancing areas in the lesion may be seen, possibly representing necrosis or previous hemorrhage. Therefore, in some instances, clear differentiation from FNH cannot be made adequately with the help of the contrast-enhanced ultrasound pattern alone. A correct diagnosis can be achieved only when the spoke-wheel pattern of arterial vessels and a central scar are observed in FNH or intralesional venous signals or nonperfused areas, indicating previous hemorrhage, are present in adenoma.⁸³

COMPUTED TOMOGRAPHY

Nonenhanced CT usually demonstrates a hypodense mass due to the presence of fat and glycogen within the tumor⁵¹ (Fig. 86-21). However, hyperdense areas corresponding to fresh hemorrhage can be noted (Fig. 86-22).

On MDCT, small HCAs enhance rapidly after intravenous administration of contrast medium.⁸⁵ The enhancement does not persist in adenomas because of arteriovenous shunting,¹³ and the lesions become nearly isodense to normal liver on portal venous and delayed scans. A peripheral and centripetal enhancement pattern, reflecting the presence of the large subcapsular feeding vessels, may also be seen.⁷⁸ Larger HCAs may be more heterogeneous than smaller lesions, and the CT appearance is nonspecific.⁸⁵

ANGIOGRAPHY

HCA is manifested angiographically as a hypervascular mass with centripetal flow and large peripheral vessels.^{86,87} Frequently, avascular areas resulting from internal hemorrhage are seen.¹⁵

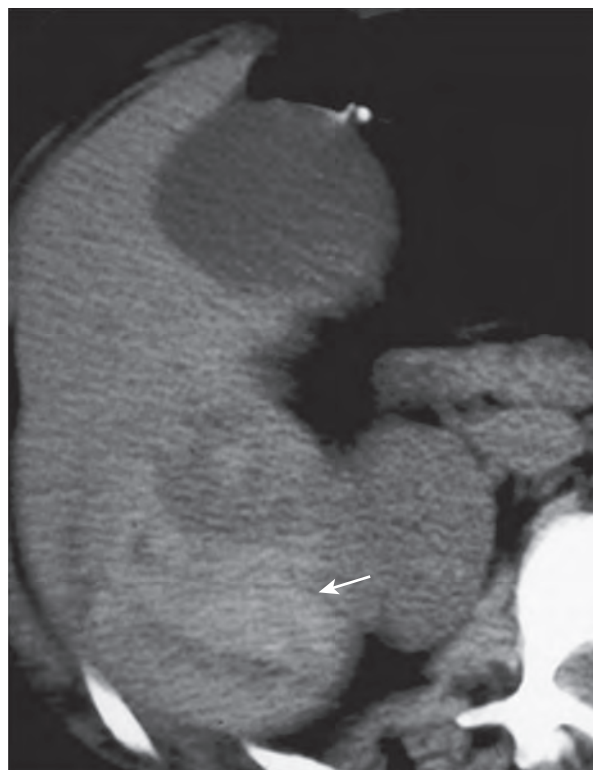


Figure 86-21 Adenoma: noncontrast CT features. Hyperdense hemorrhage (arrow) is present within the right lobe of the liver.

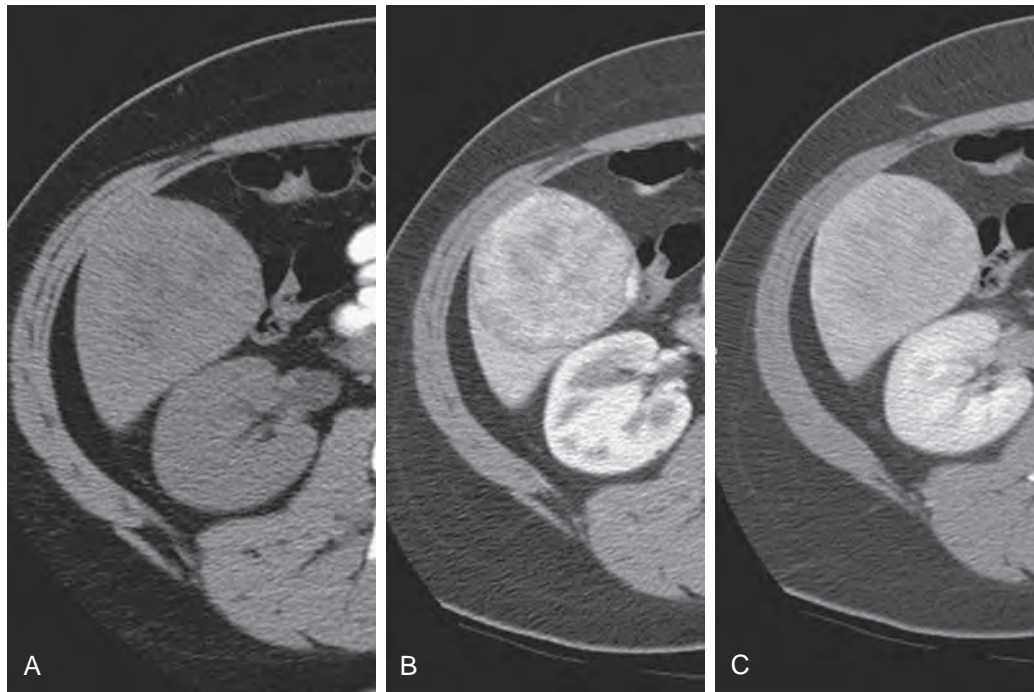


Figure 86-22 Adenoma: CT features. **A.** Noncontrast scan shows an inhomogeneous mass with areas of low density. **B** and **C.** A mosaic, inhomogeneous enhancement pattern is seen after intravenous administration of contrast material.

MAGNETIC RESONANCE IMAGING

On MRI, adenomas are heterogeneous in appearance (Fig. 86-23). They contain areas of increased signal intensity on T1-weighted images resulting from the presence of fat and hemorrhage and low signal areas corresponding to necrosis⁸⁸ (Fig. 86-24). HCAs are predominantly hyperintense relative to liver on T2-weighted images. As on T1-weighted images, they contain areas of heterogeneous signal intensity reflecting the presence of hemorrhage and necrosis. One third of HCAs have a peripheral rim corresponding to a fibrous capsule.⁸⁹ In most cases, this rim has a low signal intensity on both T1- and T2-weighted images.⁸⁹ Hepatic adenomas typically demonstrate decreased signal intensity on out-of-phase T1-weighted gradient-echo images or fat-suppressed T1-weighted images because of their fat content.³⁸

On contrast-enhanced dynamic studies, the adenomas show early enhancement during the arterial phase and a rapid washout (Fig. 86-25). Hepatic adenomas show a more uniform and moderate enhancement on arterial phase images compared with intense homogeneous and peripheral nodular enhancement patterns of focal nodular hyperplasias and hemangiomas, respectively.

With the use of SPIO contrast agents (ferucarbotran or ferumoxime), adenomas may show an isointense signal intensity relative to healthy liver parenchyma or remain hyperintense on T2-weighted images. A variable number of Kupffer cells within adenomas causes the extent of signal intensity loss with SPIO contrast agents, and iron oxide uptake typically is moderate at best.⁹⁰

After administration of hepatocyte-specific contrast agents, such as gadoxetate (Gd-EOB-DTPA), hepatic adenomas typically appear hypointense relative to normal liver (see Fig.

86-25). Several explanations have been postulated for the signal hypointensity seen in hepatic adenomas in the hepatocellular phase. One explanation holds that hepatic adenomas contain functioning hepatocytes but no bile ductules, and bilirubin and hepatocyte-specific contrast agents therefore cannot be excreted. A more plausible explanation is that the expression of OATP1 or similar membrane transporters is reduced in hepatic adenomas.⁹¹

Although adenomas are uncommon, it is clinically important to differentiate them from FNH because an adenoma may undergo malignant degeneration into hepatocellular carcinoma and have a higher potential for bleeding compared with FNH, possibly resulting in life-threatening hemoperitoneum. Increased hormonal levels during pregnancy or exogenous therapy with estrogen or an anabolic steroid may cause a rapid increase in the size of hepatic adenomas that is associated with an increased risk of rupture. For these reasons, a solitary hepatic adenoma is often resected. However, it may be difficult to recognize a hepatic adenoma at dynamic MRI performed with extracellular gadolinium chelates.⁹²

In hepatocellular phase, the enhancement patterns of adenomas may overlap with those of atypical FNH lesions, including heterogeneous enhancement and rimlike enhancement. It is even reported that adenomas may demonstrate such marked uptake of hepatocyte-specific contrast agents that they appear hyperintense in the hepatocellular phase. The difference in the levels of membrane transporter expression appears likely to be the reason for the disparate appearances of FNH lesions and hepatic adenomas at hepatocellular phase imaging.⁹¹

On diffusion-weighted imaging, as a solid tumor, hepatic adenoma shows slight signal intensity increase with increasing b values and appears hypointense on ADC mapping. The ADC value ranges between 1 and $1.40 \times 10^{-3} \text{ mm}^2/\text{s}$. However, the

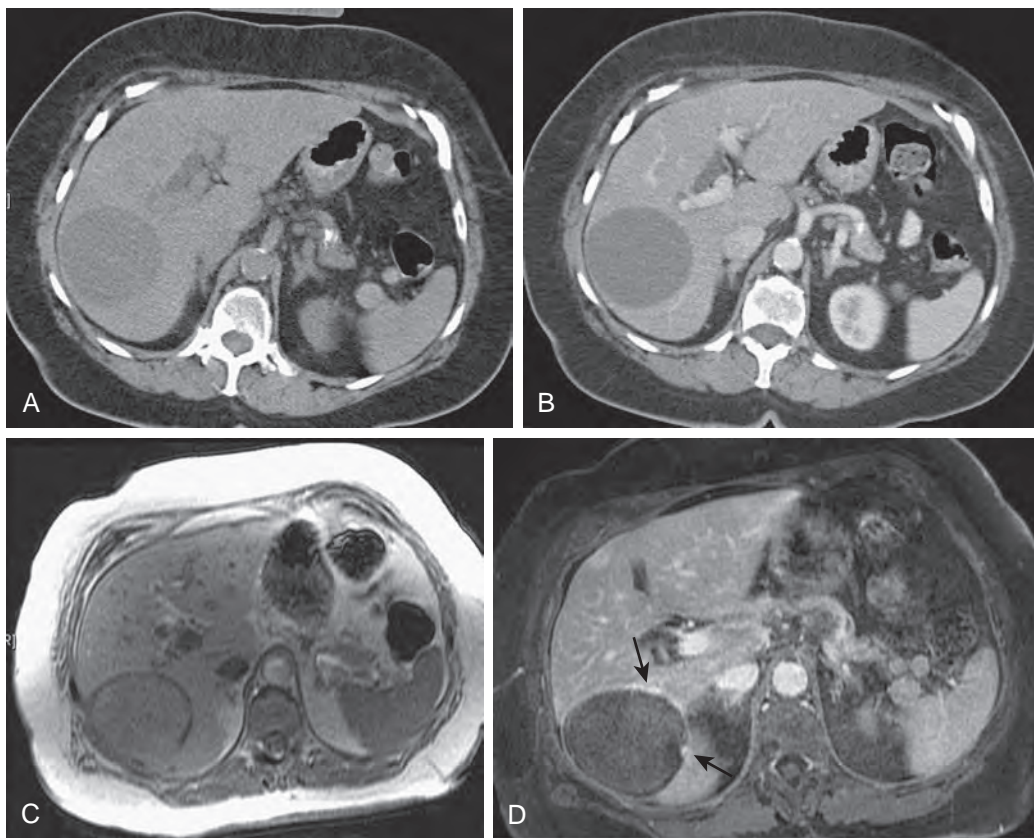


Figure 86-23 Adenoma: CT and MRI features. **A.** Nonenhanced CT scan shows a hypodense mass. **B.** On contrast-enhanced CT scan, the lesion shows no enhancement. **C.** On T1-weighted MR image, adenoma is slightly hypointense in comparison with the normal liver, and the fibrous capsule is isointense. **D.** Contrast-enhanced T1-weighted image demonstrates the subcapsular feeding vessels (arrows).

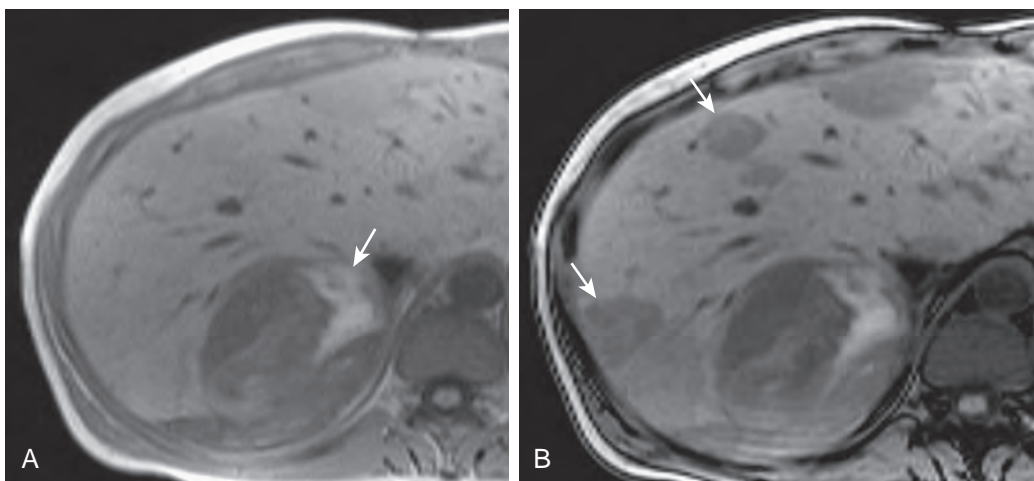


Figure 86-24 Adenoma: MRI features. **A.** In-phase image shows high signal intensity hemorrhage (arrow) within this mass. **B.** Opposed-phase image shows loss of signal intensity of the mass indicating fat. There are multiple areas of focal fatty infiltration (arrows).

ADC values may overlap with FNH and malignant solid lesions like hepatocellular carcinoma.⁹³

MULTIPLE HEPATOCELLULAR ADENOMATOSIS

Multiple hepatocellular adenomatosis is a rare entity characterized by the presence of multiple (more than four) HCAs, usually

present in both hepatic lobes.^{94,95} This entity should not be confused with other hyperplastic hepatocellular conditions, such as nodular regenerative hyperplasia, macroregenerative nodules of cirrhosis, or adenomatous hyperplastic nodules (Table 86-5).

Hepatic adenomatosis can be associated with metabolic disorders such as glycogen storage disease.⁹¹

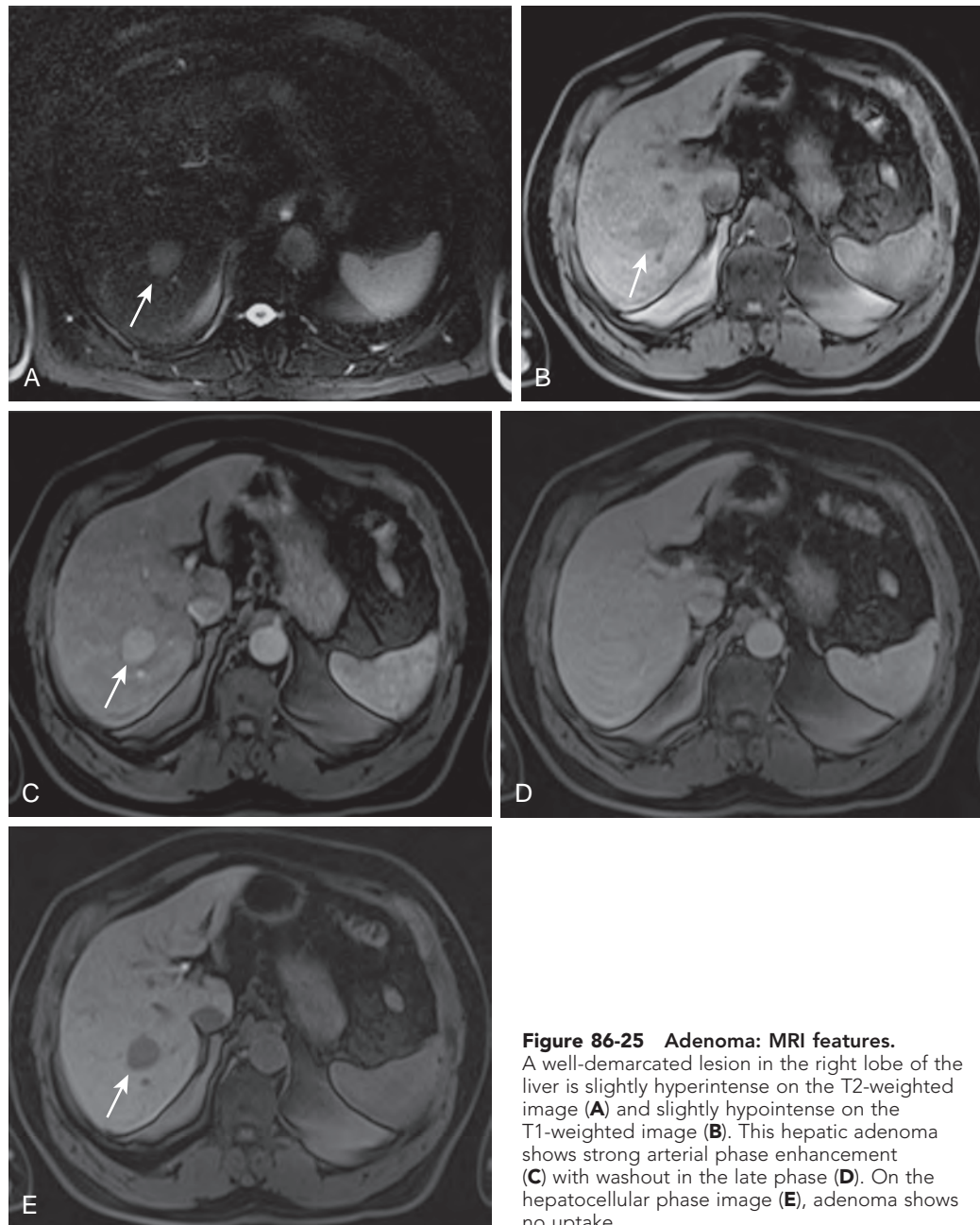


Figure 86-25 Adenoma: MRI features. A well-demarcated lesion in the right lobe of the liver is slightly hyperintense on the T2-weighted image (A) and slightly hypointense on the T1-weighted image (B). This hepatic adenoma shows strong arterial phase enhancement (C) with washout in the late phase (D). On the hepatocellular phase image (E), adenoma shows no uptake.

TABLE 86-5 Comparison of Hyperplastic Hepatocellular Conditions

Criteria	Focal Nodular Hyperplasia	Hepatocellular Adenoma	Nodular Regenerative Hyperplasia	Multiple Hepatocellular Adenoma	Macroregenerative Nodule
Gross number of lesions	Scar 1 (90%)	Hemorrhage, necrosis 1 (90%)	Bulging nodules Many	Bulging nodules Many	Bulging nodules Many or few
Size (average range)	1-6 cm	4-12 cm	>1.5 cm	2-9 cm	1-6 cm
Key feature	Pseudoductules	Neohepatocytes	Small nodules	Normal cords	Portal tracts
Prior liver disease	None	None	None	None	Submassive hepatic necrosis or cirrhosis
Associated etiology	None	Estrogen, anabolic steroids	Vascular disease	None	None

Modified from Craig GR, Peters RL, Edmonson HA: Tumors of the liver and intrahepatic bile ducts. *Atlas of Tumor Pathology, Second Series*. Washington, DC, Armed Forces Institute of Pathology, 1989.

Nodular Regenerative Hyperplasia

PATHOLOGIC FINDINGS

Nodular regenerative hyperplasia (NRH) is defined as diffuse nodularity of the liver produced by many regenerative nodules that are not associated with fibrosis.⁹⁶ In gross appearance, NRH is characterized by the presence of multiple bulging nodules on the external surface of the liver that on cut surface appear as discrete, round, flat nodules resembling diffuse involvement with metastatic carcinoma (Fig. 86-26A). The nodules vary in size from a few millimeters to several centimeters and are diffusely scattered.

On microscopic examination, the nodules are composed of cells resembling normal hepatocytes, and no fibrosis is noted.⁹⁷ This is an important difference between NRH and regenerative nodules of cirrhosis.

INCIDENCE AND CLINICAL PRESENTATION

NRH is known by numerous synonyms, including nodular transformation of the liver, partial nodular transformation, miliary hepatocellular adenomatosis, adenomatous hyperplasia, diffuse nodular hyperplasia, and noncirrhotic nodulation.¹⁰ NRH is rare, although autopsy series have shown a prevalence as high as 0.6%.⁹⁸ Approximately one third of cases were initially considered cases of FNH. Clinically, NRH is discovered

either incidentally on autopsy or in the work-up of portal hypertension and its complications.

Various systemic diseases and drugs are often associated with NRH⁹⁹⁻¹⁰¹: myeloproliferative syndromes (polycythemia vera, chronic myelogenous leukemia, and myeloid metaplasia), lymphoproliferative syndromes (Hodgkin's and non-Hodgkin's lymphoma, chronic lymphocytic leukemia, and plasma cell dysplasias), chronic vascular disorders (rheumatoid arthritis), Felty's syndrome, polyarteritis nodosa, scleroderma, calcinosis cutis, Raynaud's phenomenon, sclerodactyly and telangiectasia, lupus erythematosus, steroids, and anti-neoplastic medication.⁹⁷

As described earlier, the appearance grossly and therefore at laparotomy is that of a cirrhotic liver with diffuse nodularity.¹⁰²

PLAIN RADIOGRAPHIC FINDINGS

Plain abdominal radiographs may demonstrate splenomegaly, ascites, and other signs of portal hypertension.

NUCLEAR MEDICINE

Because NRH nodules are composed of abnormal hepatocytes with Kupffer cells, they take up ^{99m}Tc-sulfur colloid. The appearance of the liver may be normal if the nodules are small. Large nodules, measuring up to several centimeters, take up sulfur

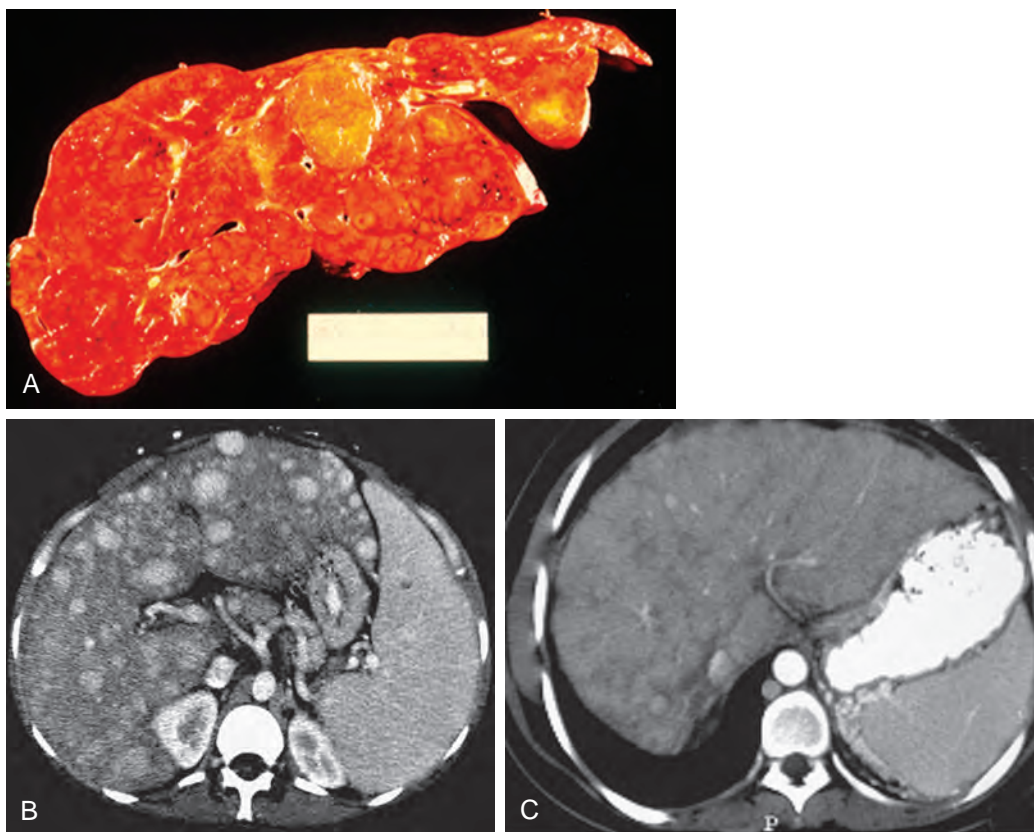


Figure 86-26 Nodular regenerative hyperplasia. **A.** This rare condition is characterized by small regenerative nodules composed of hepatocytes that compress the surrounding parenchyma and are not surrounded by fibrous tissue. This lack of fibrosis differentiates nodular regenerative hyperplasia from cirrhosis. **B and C.** Multiple robustly enhancing hepatic masses are identified on these contrast-enhanced CT scans in two patients with the Budd-Chiari syndrome. (**A and B** courtesy Michael P. Federle, MD, Palo Alto, CA.)

colloid as well.¹⁰¹ There are no studies reporting the usefulness of PET imaging in this context.

ULTRASOUND

The sonographic appearance of NRH ranges from that of a normal liver to that of a liver with focal nodules that vary in echogenicity. Central hemorrhage within a large nodule may occur and produce a complex mass.

COMPUTED TOMOGRAPHY

On CT scans, the appearance of NRH ranges from that of a normal liver to that of a liver with focal nodules of varying attenuation that are primarily hypodense.¹⁰¹ Central hemorrhage within a large nodule may produce a complex mass with variable density. On contrast-enhanced MDCT scans, arterial phase imaging shows hypervascular lesions (Fig. 86-26B, C) that may become almost imperceptible on portal venous examination.²⁶

ANGIOGRAPHY

On angiography, the typical findings of portal hypertension with esophageal varices, portal collaterals, and splenomegaly are demonstrated.¹⁰¹ On occasion, individual nodules of NRH can be distinguished; they are vascular and fill from the periphery.

MAGNETIC RESONANCE IMAGING

Lesions are isointense to normal liver on T2-weighted images and contain foci of high signal on T1-weighted scans.¹⁰³ These lesions may show robust enhancement after the intravenous administration of Gd-DTPA.

SUMMARY

NRH is an underdiagnosed disease, frequently related to chronic illnesses or prolonged therapy. NRH can be manifested as tiny nodules diffusely involving the liver or as focal larger nodules producing a spectrum of radiologic findings ranging from a normal-appearing liver with associated portal hypertension to multiple hepatic masses.

NRH must be differentiated from other hepatocellular hyperplasias. Currently, hepatocellular hyperplasia is divided into several categories, and some groups overlap with prior concepts of these conditions. FNH, HCA, NRH, multiple HCAs (hepatocellular adenomatosis), and macroregenerative nodules are considered separate entities, and their differences are included in Table 86-5.

Lipomatous Tumors

PATHOLOGIC FINDINGS

Benign hepatic tumors composed of fat cells include lipoma, hibernoma, and combined tumors such as angiomyolipoma (fat and blood vessels), myelolipoma (fat and hematopoietic tissue), and angiomyelolipoma.⁵⁰

In gross appearance, lipomatous tumors are usually solitary, well circumscribed, and round and usually occur in a noncirrhotic liver.¹⁰⁴ The microscopic features are similar to those of lipomatous tumors of soft tissues. There is no sex predilection, and they have been reported in a broad age range (24-70 years).¹⁰ Approximately 10% of patients with tuberous sclerosis and renal angioliipomas have hepatic fatty tumors, either lipoma (Fig. 86-27) or angiomyolipoma (Fig. 86-28).¹⁰⁵ Most lipomatous tumors of the liver are asymptomatic and are incidental findings. These tumors occasionally bleed, causing abdominal pain.

RADIOLOGIC FINDINGS

Angiomyolipomas are highly echogenic on sonography and indistinguishable from hemangiomas.¹⁰⁵ On CT scans, lipomas and angiomyolipomas appear as well-defined masses with attenuation values in the range of those of fat (see Fig. 86-28).^{105,106} On angiography, angiomyolipomas are hypervascular and may show large aneurysms, as in angiomyolipomas of the kidneys.¹⁰⁷ On MRI scans, the fatty component of angiomyolipomas is of high signal on T1- and T2-weighted images.¹⁰⁸ However, hepatocellular carcinomas containing fat deposits may have a similar appearance. The early phase of contrast-enhanced dynamic CT or MRI may be useful in discriminating between angiomyolipomas and hepatocellular carcinomas with fat because the fatty areas of angiomyolipomas are well vascularized and enhance early.¹⁰⁸ Conversely, the areas of fatty

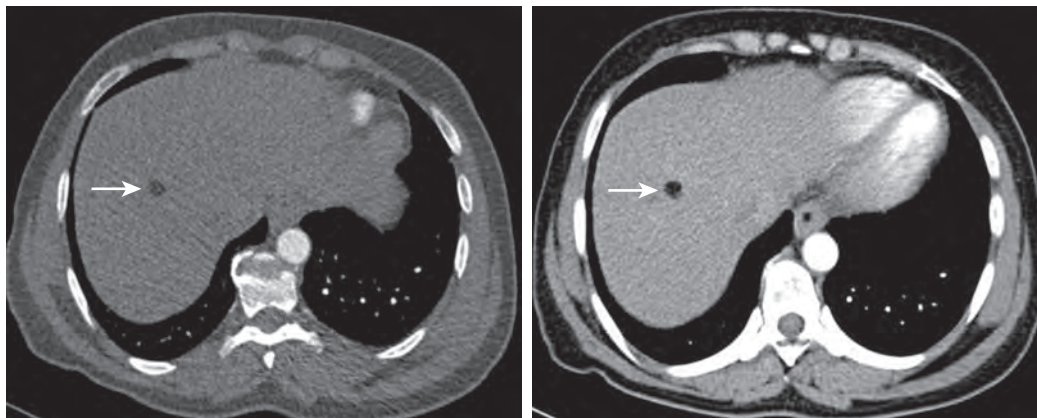


Figure 86-27 Lipoma: CT findings. A hepatic lipoma (arrows) that appears hypodense (fat density) on this contrast-enhanced scan.

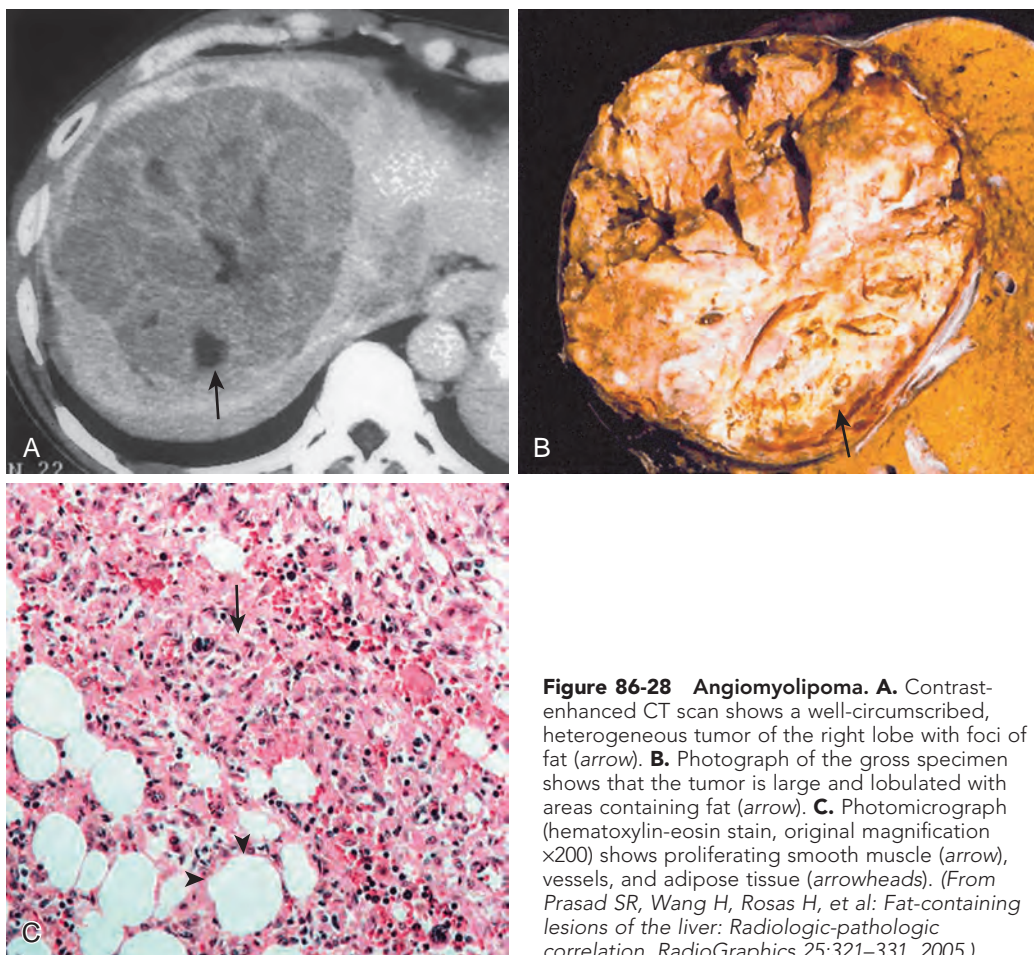


Figure 86-28 Angiomyolipoma. **A.** Contrast-enhanced CT scan shows a well-circumscribed, heterogeneous tumor of the right lobe with foci of fat (arrow). **B.** Photograph of the gross specimen shows that the tumor is large and lobulated with areas containing fat (arrow). **C.** Photomicrograph (hematoxylin-eosin stain, original magnification $\times 200$) shows proliferating smooth muscle (arrow), vessels, and adipose tissue (arrowheads). (From Prasad SR, Wang H, Rosas H, et al: Fat-containing lesions of the liver: Radiologic-pathologic correlation. *RadioGraphics* 25:321–331, 2005.)

change in hepatocellular carcinoma are relatively avascular, and enhancement is less obvious.¹⁰⁸ MRI with fat suppression is a useful technique in the characterization of hepatic angiomyolipomas.¹⁰⁹ The lesions have high signal intensity on T1- and T2-weighted images and appear hypointense to liver on images obtained with fat suppression.¹⁰⁹ The presence of large intratumoral vessels (“macroaneurysms”) is a classic feature of large angiomyolipomas. Color Doppler ultrasound, CT, and MRI are useful techniques in the detection of macroaneurysms.¹¹⁰

Other focal fatty lesions of the liver include pseudolipoma and focal fatty change.

PSEUDOLIPOMA

Pseudolipoma is usually due to fat ectopia within Glisson’s capsule. It represents epiploic appendices that become attached to or embedded in the liver parenchyma.¹¹¹

Cysts and Cystic Tumors

The classification of hepatic cysts is somewhat confusing because of varying criteria and incomplete histologic evaluation. Hepatic cysts should be distinguished from other cystic masses of the liver determined by radiologic as well as gross characteristics.¹¹² The following is a discussion of the “true” cyst of the liver, or bile duct cyst, defined by the presence of an epithelial lining.

SIMPLE CYST

Pathologic Findings

A simple hepatic (bile duct) cyst (Fig. 86-29A, B) is defined as a single, unilocular cyst lined by a single layer of cuboidal, bile duct epithelium. The wall is a thin layer of fibrous tissue, and the adjacent liver is normal. In gross appearance, the wall is 1 mm or less in thickness and typically occurs just beneath the surface of the liver, although some may occur deeper. The simple hepatic cyst is considered to be of congenital, developmental origin, although it is usually discovered in the fifth through seventh decades of life.¹¹³

Incidence and Clinical Presentation

Simple hepatic (bile duct) cysts range in incidence from 1% to 14% in autopsy series and appear to occur more commonly in women than in men (5:1).¹⁰ Simple cysts are usually found incidentally, although up to 20% have been reported in surgical series of patients who presented with symptoms caused by a mass effect (abdominal pain, jaundice, intra-abdominal mass).¹¹⁴ Asymptomatic cysts are not usually treated unless they are complicated by hemorrhage or infection. The treatment for symptomatic cysts is wide incision and drainage.

Radiologic Findings

Simple cysts cause a nonspecific photopenic defect on hepatobiliary scans with sulfur colloid and iminodiacetic acid

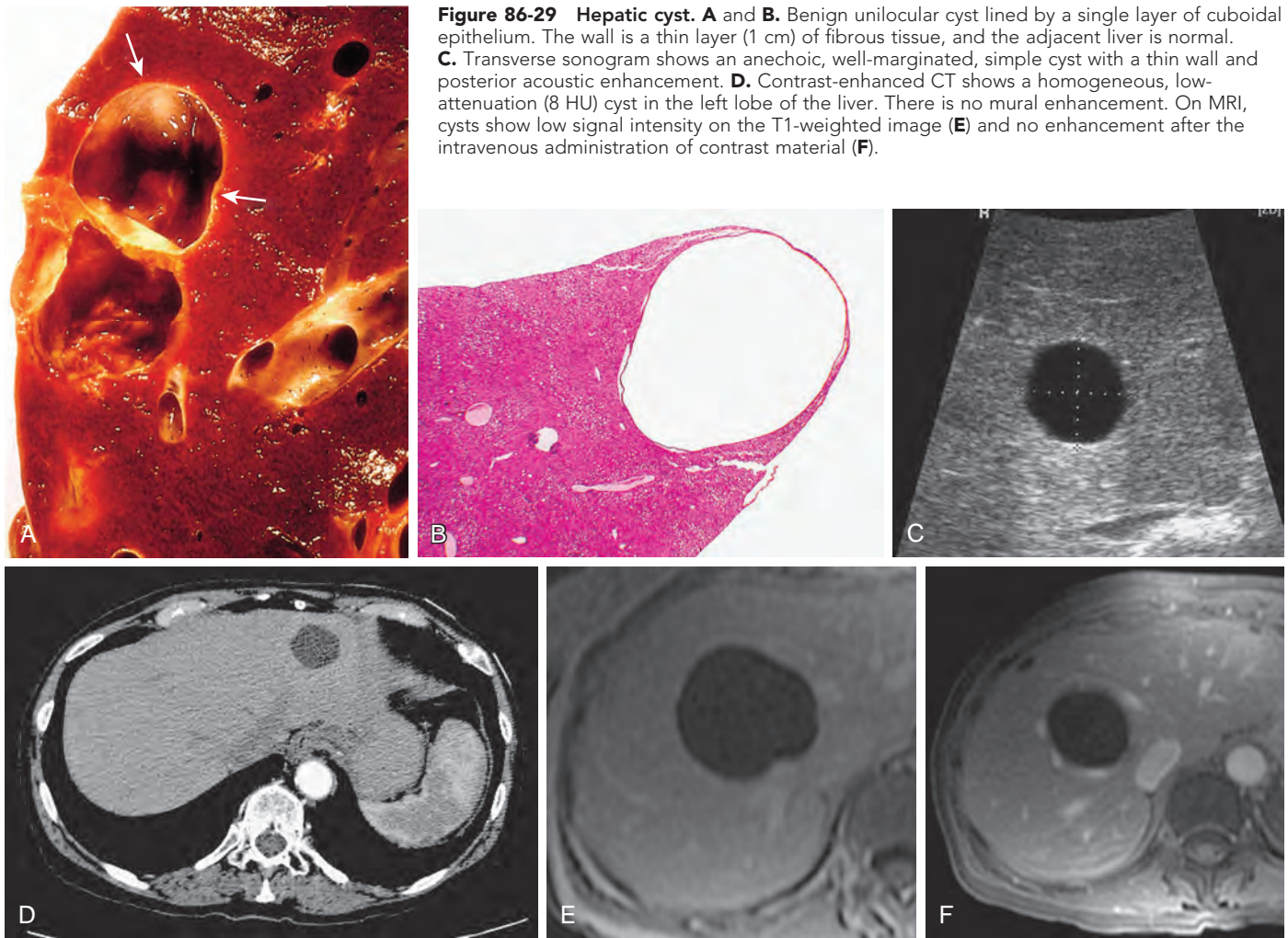


Figure 86-29 Hepatic cyst. **A** and **B.** Benign unilocular cyst lined by a single layer of cuboidal epithelium. The wall is a thin layer (1 cm) of fibrous tissue, and the adjacent liver is normal. **C.** Transverse sonogram shows an anechoic, well-margined, simple cyst with a thin wall and posterior acoustic enhancement. **D.** Contrast-enhanced CT shows a homogeneous, low-attenuation (8 HU) cyst in the left lobe of the liver. There is no mural enhancement. On MRI, cysts show low signal intensity on the T1-weighted image (**E**) and no enhancement after the intravenous administration of contrast material (**F**).

derivatives. On sonography (Fig. 86-29C), uncomplicated simple (bile duct) cysts are manifested as anechoic masses, with smooth borders, lateral shadowing, posterior echo enhancement, nondetectable walls, no septations, and no mural calcification.

The CT features (Fig. 86-29D) of an uncomplicated hepatic cyst are a well-defined intrahepatic mass; water attenuation; round or oval shape; smooth, thin walls; absence of internal structures; and no enhancement after administration of contrast material.¹¹²

As implied in the definition, simple cysts of the liver are usually solitary but can number fewer than 10. When more than 10 cysts are seen, one of the fibropolycystic diseases should be considered.¹¹⁵

On MRI studies (Fig. 86-29E, F), simple cysts are extremely hyperintense on T2-weighted images and hypointense on T1-weighted images (Fig. 86-30). They usually have a homogeneous, well-defined, oval appearance.³⁸ Cysts with intracystic hemorrhage may show high signal intensity on both T1-weighted and T2-weighted images.¹¹⁶ No enhancement is seen after administration of gadolinium chelates.

Summary

Ultrasound is the best way to confirm the cystic nature of a hepatic mass. Cysts complicated by infection or hemorrhage

may have septations or internal debris as well as enhancement of the wall. Percutaneous aspiration and sclerotherapy with alcohol are useful for treatment of symptomatic hepatic cysts.^{117,118}

BILE DUCT HAMARTOMAS (VON MEYENBERG COMPLEXES)

Bile duct hamartomas (BDHs) are a focal disorderly collection of bile ducts that is due to failure of involution of embryonic bile ducts. With extreme dilation, these ducts become visible on imaging. These lesions are 1 to 5 mm in size (Fig. 86-31). There can be 50,000 to 100,000 BDHs in a normal-sized liver.

Nearly all individuals with adult polycystic liver disease (APLD) have multiple BDHs, and 11% of patients with multiple BDHs have APLD. It is postulated that the larger cysts of APLD result from gradual dilation of the hamartomas. BDHs have a 0.69% to 5.6% incidence at autopsy.

On CT, innumerable cystic lesions less than 5 mm in diameter are present. They show no contrast enhancement. On MRI, BDHs have low signal intensity on T2-weighted images and high signal intensity on T2-weighted images.

Biliary hamartomas do not show uptake of liver-specific contrast agents because of their lack of communication with the bile ducts. On diffusion-weighted imaging, biliary

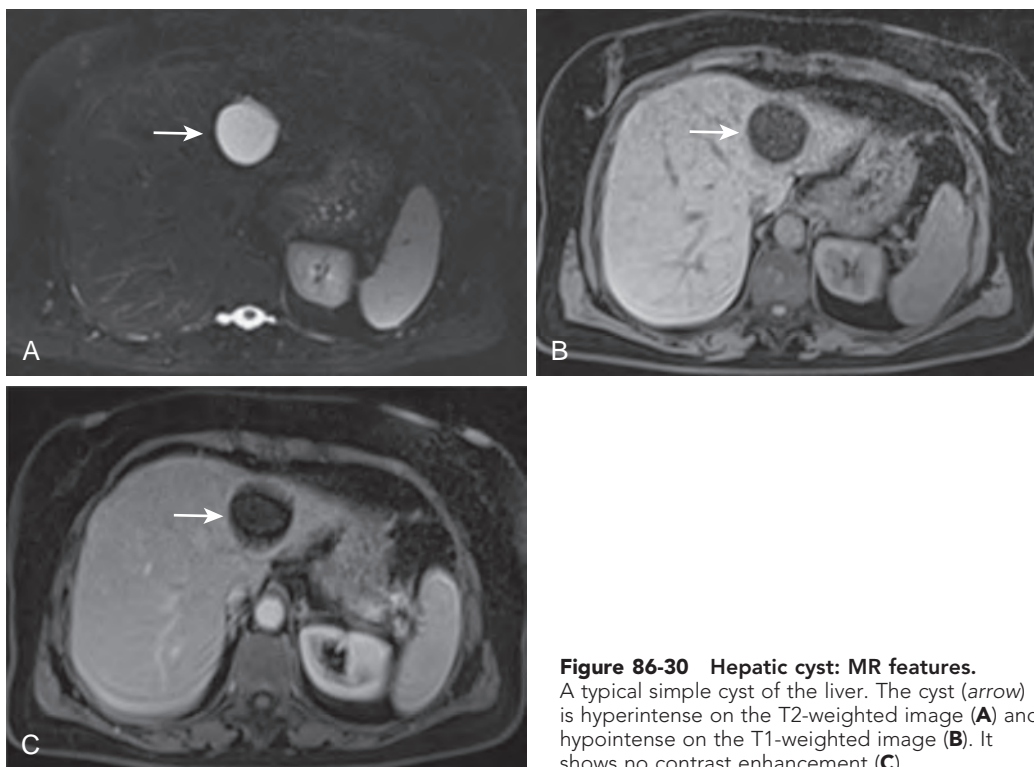


Figure 86-30 Hepatic cyst: MR features.

A typical simple cyst of the liver. The cyst (arrow) is hyperintense on the T2-weighted image (A) and hypointense on the T1-weighted image (B). It shows no contrast enhancement (C).

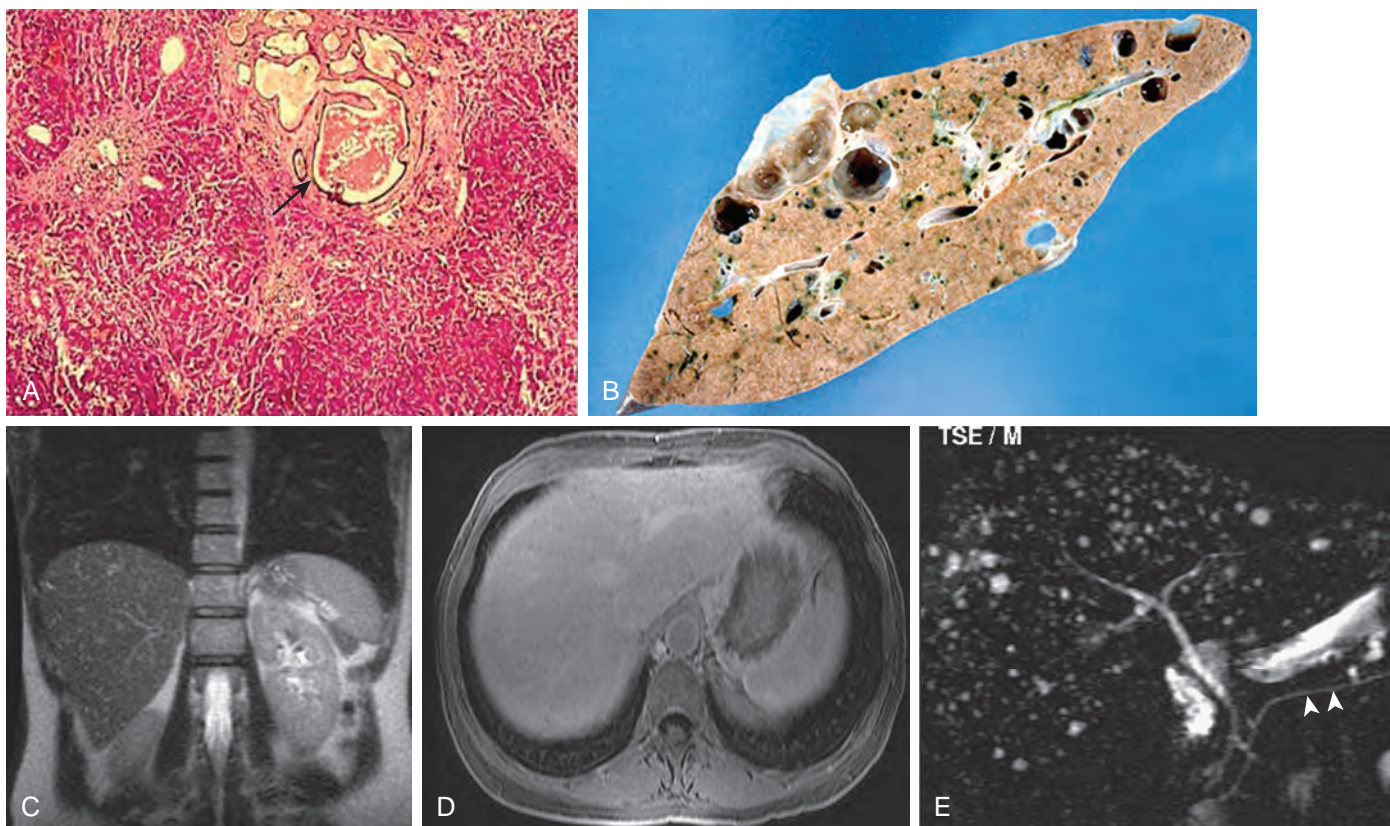


Figure 86-31 Multiple bile duct hamartomas (von Meyenberg complexes). A. These are small bile ductules embedded in a fibrous, sometimes hyalinized stroma. Each lumen may contain inspissated bile concretions (arrow), and the lumina may interconnect. These are usually incidental findings at autopsy and cross-sectional imaging. B. They are usually small and multiple, located in the subcapsular region and distributed in both lobes. C. Coronal, T2-weighted MRI scan shows multiple, tiny hyperintense lesions in the liver. D. MRCP images show these hyperintense lesions. They have fluid (bile) signal intensity. E. MRCP image demonstrates innumerable tiny hyperintense cysts typical of this disorder. Arrowheads point to pancreatic duct.

hamartomas, like cystic lesions, show signal intensity loss with increasing b values and appear strongly hyperintense on ADC mapping.⁹

CONGENITAL HEPATIC FIBROSIS AND POLYCYSTIC LIVER DISEASE

Pathologic Findings

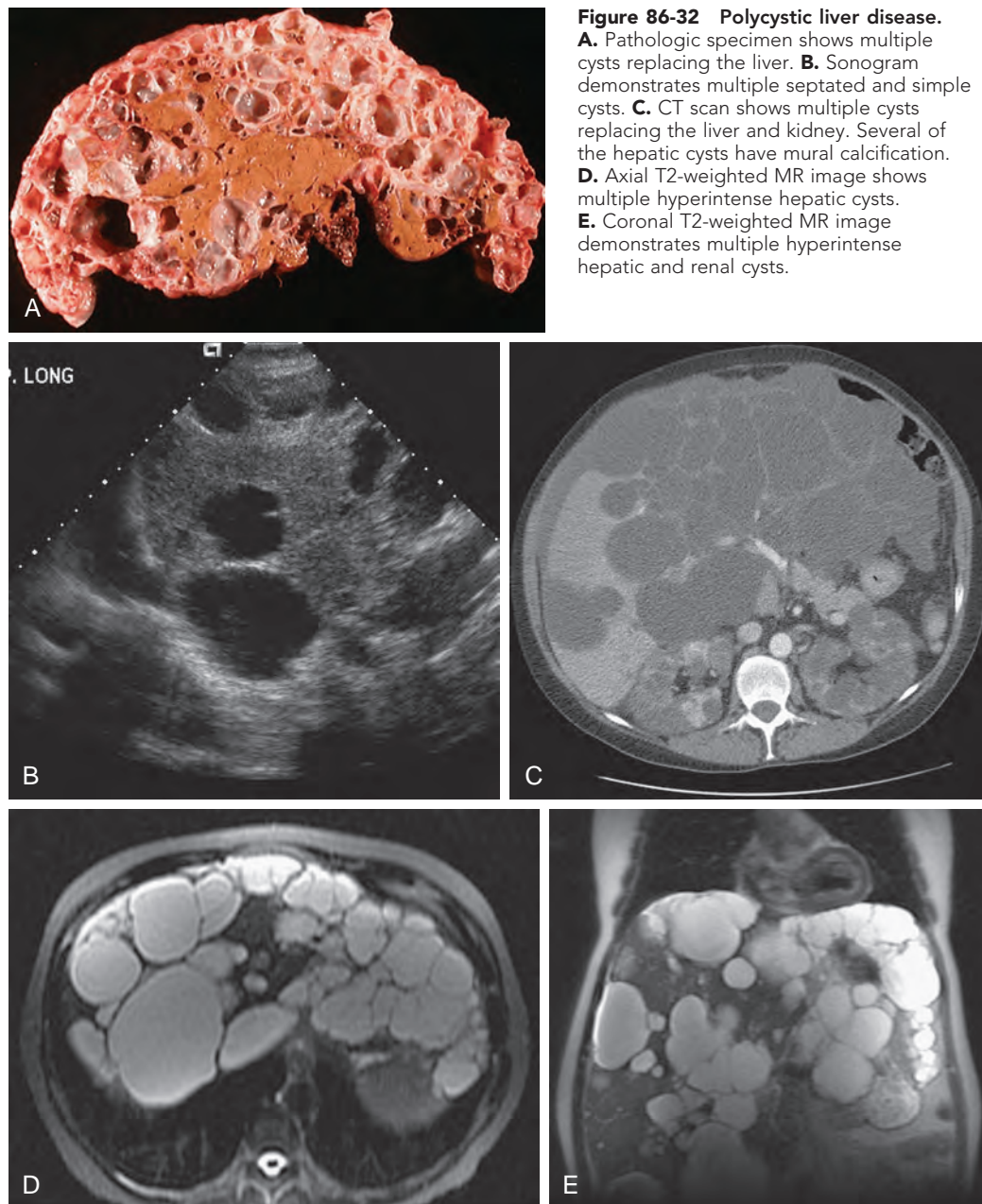
Congenital hepatic fibrosis is part of the spectrum of hepatic cystic diseases. Congenital hepatic fibrosis is characterized by aberrant bile duct proliferation and periductal fibrosis.¹⁰ In typical congenital hepatic fibrosis, cysts are not visible without a hand lens. However, in the polycystic liver disease variant, numerous large and small cysts coexist with fibrosis (Fig. 86-32A). In cases of polycystic liver or kidney disease, the liver surrounding the cysts is not normal, frequently containing

von Meyenburg complexes and increased fibrous tissue.¹⁰ In patients with adult polycystic kidney disease, there is hepatic involvement in approximately 30% to 40%.¹¹⁷ On occasion, hepatic cysts occur without radiographically identifiable renal involvement.¹¹⁵

Incidence and Clinical Presentation

The incidence of congenital hepatic fibrosis and polycystic liver disease is difficult to determine because of the various degrees of expression.¹¹⁹ Clinically, the majority of patients present in childhood, when congenital hepatic fibrosis predominates, with bleeding varices and other manifestations of portal hypertension.¹²⁰

In patients with polycystic liver disease predominance, the lesions are usually identified incidentally at radiologic examination. Approximately 70% of patients with polycystic liver disease



also have adult polycystic kidney disease. Congenital hepatic fibrosis is also related to Caroli's disease, which is discussed in Chapter 76.

Radiologic Findings

Cross-sectional imaging shows multiple cysts in the liver (Fig. 86-32B), frequently associated with multiple renal cysts.¹¹⁵ Hypoattenuating cystic lesions demonstrate regular outlines on nonenhanced CT scans and no wall or content enhancement on contrast-enhanced images (Fig. 86-32C). At MRI, cysts show a very low signal intensity on T1-weighted images and do not enhance after administration of gadolinium. Because of their fluid content, on T2-weighted MR images, they show high signal intensity (Fig. 86-32D, E). Signal intensity alterations indicating intracystic hemorrhage are commonly seen.¹¹⁶ Calcification in the cyst wall is occasionally seen, and the cysts may contain blood and fluid levels.¹¹² These hepatic cysts are pathologically identical to simple or bile duct cysts.

CYSTADENOMA

Biliary cystadenoma is a cystic tumor of the liver with a recognized propensity to undergo malignant transformation. It is considered a premalignant lesion and is discussed with cystadenocarcinoma in Chapter 87.

Infantile Hemangioendothelioma

PATHOLOGIC FINDINGS

Infantile hemangioendothelioma (IHE) is a vascular tumor derived from endothelial cells that proliferate and form vascular channels. In gross appearance, IHEs are usually multiple and diffuse; a solitary lesion is an uncommon variant.¹²¹ The nodules of IHEs vary from a few millimeters to 15 cm or more in size. Lesions are usually multiple, nodular, round, red-brown, and spongy to white-yellow with fibrotic predominance in mature cases.¹⁵ Calcification may be present.

On microscopic examination, IHEs are composed of a proliferation of small vascular channels lined by endothelial cells. Cavernous areas as well as zones of hemorrhage, thrombosis, fibrosis, and calcification are common. The cavernous areas noted in some lesions correspond to the areas of puddling of contrast material seen angiographically. The multinodular type may involve other organs and the skin, in which angiomas are also present. The solitary variant has no associated skin hemangiomas.¹⁰

INCIDENCE AND CLINICAL PRESENTATION

IHE is the most common benign vascular tumor of infancy and accounts for 12% of all childhood hepatic tumors.^{122,123} Eighty-five percent of patients with IHE present as young infants between 1 and 6 months of age, with less than 5% of cases detected beyond 1 year of age and females affected more often than males. Clinical findings include hepatomegaly, congestive heart failure (present in up to 25% of cases), thrombocytopenia caused by trapping of platelets by the tumor, and occasional rupture with hemoperitoneum.^{124,125} Most tumors continue to grow during the first year of life and then spontaneously regress, probably because of thrombosis and scar formation.¹²⁶ Cutaneous hemangiomas, as described earlier, are

more commonly present in the multinodular form of IHE, occurring in up to 40% of patients.

PLAIN RADIOGRAPHIC FINDINGS

On plain radiographs of the abdomen, IHE appears as an upper abdominal mass or as hepatomegaly if the liver is diffusely involved. Speckled calcifications may be present.¹²⁷ Chest radiographs may show signs of congestive heart failure in 30% of cases.¹²⁷

ULTRASOUND

Ultrasonographic features of IHE are varied. There is typically a complex liver mass with large draining hepatic veins.¹²⁸ Single or multiple lesions may be seen, and the lesions may range from hypoechoic to hyperechoic. During a period of months, these lesions tend to involute slowly and develop increased echogenicity.^{127,129} Dilated hepatic vasculature with prominent blood flow is typical at Doppler ultrasound if significant arteriovenous shunting is present.

COMPUTED TOMOGRAPHY

On precontrast CT scans, IHE appears as single or multiple hypodense masses with or without calcifications¹³⁰ (Fig. 86-33A). Contrast-enhanced CT shows an enhancement pattern that may resemble an adult giant hemangioma, with "nodular" peripheral early enhancement and delayed progression to the center of the lesion (Fig. 86-33B). In larger tumors, the central portion of the tumor remains hypodense because of fibrosis, hemorrhage, or necrosis.^{126,131}

ANGIOGRAPHY

On angiography, enlarged tortuous feeding arteries as well as draining vessels and large vascular lakes are seen with prolonged pooling of the contrast agent. The aorta typically has a decreased caliber distal to the origin of the hepatic mass, indicating the large blood supply to the tumor.^{132,133}

MAGNETIC RESONANCE IMAGING

On MRI, IHE has a nonspecific appearance and is predominantly hypointense on T1-weighted images and hyperintense on T2-weighted images.¹³⁰ Foci of hyperintense or hypointense signal on T1-weighted scans correspond to areas of hemorrhage and fibrosis.^{130,134} In tumors with arteriovenous shunting and high blood flow, flow voids may be seen on T2-weighted images. On contrast-enhanced dynamic MRI (Fig. 86-33C), the lesions usually demonstrate an enhancement pattern similar to that on MDCT. In some cases, however, the lesion may show a complete "rimlike" enhancement at dynamic imaging, which may simulate other childhood tumors.¹²³

SUMMARY

IHE is the most common liver tumor during the first 6 months of life. These lesions are usually multiple and markedly hypervascular and may be associated with cutaneous angiomas. Although IHE may grow to a large size, producing cardiac failure, it involutes spontaneously with time. The radiologic

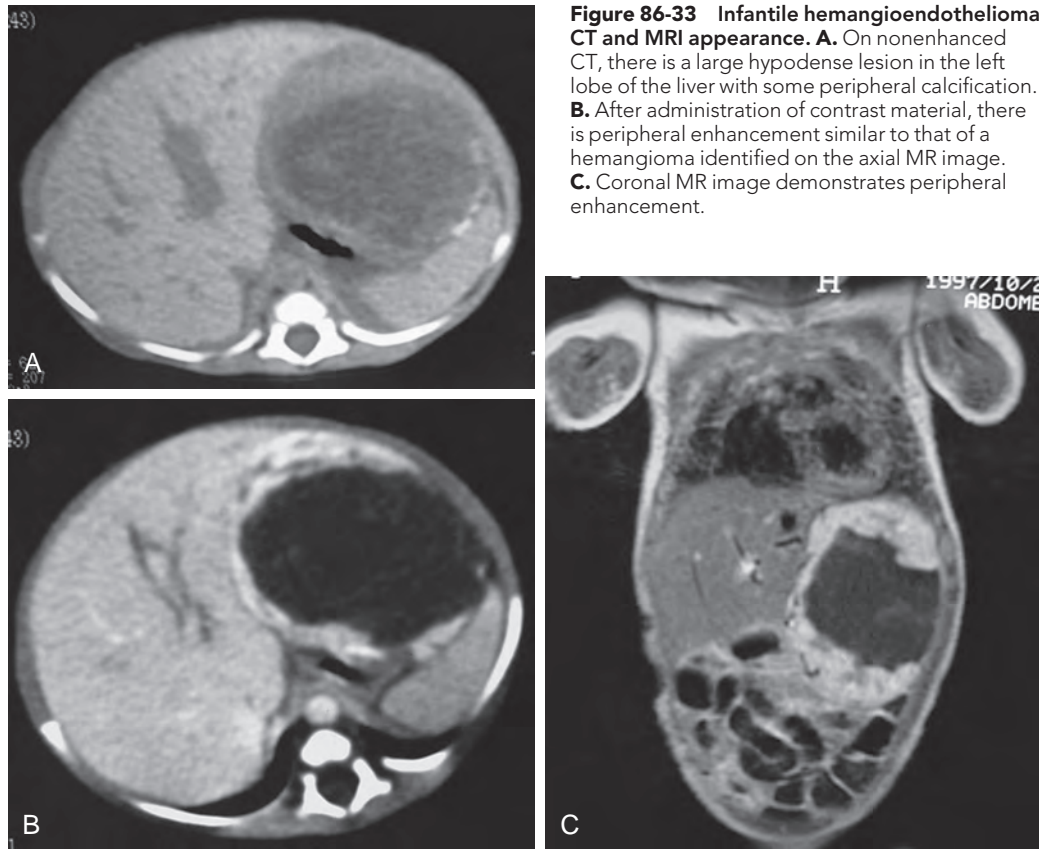


Figure 86-33 Infantile hemangioendothelioma: CT and MRI appearance. **A.** On nonenhanced CT, there is a large hypodense lesion in the left lobe of the liver with some peripheral calcification. **B.** After administration of contrast material, there is peripheral enhancement similar to that of a hemangioma identified on the axial MR image. **C.** Coronal MR image demonstrates peripheral enhancement.

findings for IHE are similar to those for multiple hemangiomas of the liver in the adult.

Mesenchymal Hamartoma

PATHOLOGIC FINDINGS

Mesenchymal hamartoma is a benign cystic developmental lesion and is not considered a true neoplasm. It is composed of gelatinous mesenchymal tissue with cyst formation as well as remnants of normal hepatic parenchyma.^{135,136} In gross appearance, mesenchymal hamartoma is a large, soft, predominantly cystic mass measuring 15 cm or more in largest diameter at the time of diagnosis.¹³⁷ These tumors are well defined and encapsulated or pedunculated.¹³⁸ Cysts are present grossly in 80% of cases. On cut section, mesenchymal hamartomas can have either mesenchymal predominance (a solid appearance) or cystic predominance (the bulk of the tumor appears as multiloculated cystic masses). On histologic evaluation, the tumor consists of cysts, remnants of portal triads, hepatocytes, and fluid-filled mesenchyme.

INCIDENCE AND CLINICAL PRESENTATION

Mesenchymal hamartoma is an uncommon lesion, accounting for 8% of all childhood liver tumors.¹³⁷ The majority of cases occur during the first 3 years of life, and there is a slight male predominance.¹³⁶ Clinically, slow, progressive, painless abdominal enlargement is seen. Sometimes rapid enlargement may occur because of rapid accumulation of fluid in the cyst. This enlargement may occasionally cause respiratory distress and edema of the lower extremities.¹³⁹

PLAIN RADIOGRAPHIC FINDINGS

This large tumor is manifested as a noncalcified right upper quadrant soft tissue mass on radiographs.

ULTRASOUND

Sonography demonstrates either large cysts within internal septa (cystic predominance) or, less commonly, smaller cysts with thick septa (mesenchymal predominance).¹³⁸

COMPUTED TOMOGRAPHY

On CT, these tumors appear as well-defined masses with central hypodense areas and internal septa (Fig. 86-34A). Both solid and cystic components may be distinguished.^{138,140} After the administration of contrast media, enhancement of the solid areas may be detectable.¹³¹

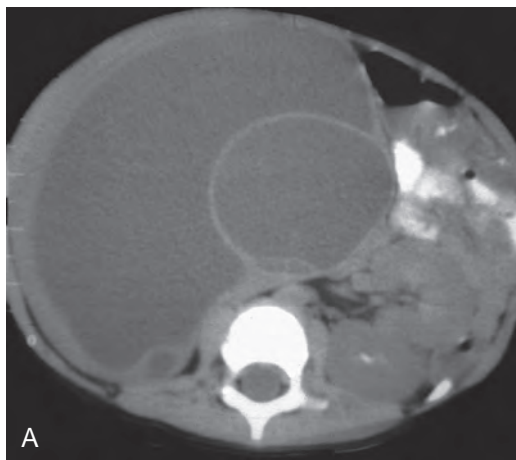
ANGIOGRAPHY

Angiography shows a hypovascular or avascular mass causing displacement of vessels. Hypervascularity has been described in the solid portions.^{140,141}

MAGNETIC RESONANCE IMAGING

The MRI appearance of mesenchymal hamartoma depends on whether an individual lesion is predominantly stromal or cystic. For lesions with stromal predominance, the intensity on T1-weighted images is lower than that of the normal liver because of increased fibrosis. Conversely, if there is cystic

Figure 86-34 Mesenchymal hamartoma. CT (A) and MRI (B) appearance. The lesion is markedly cystic and has septa.



predominance, the mesenchymal hamartoma is predominantly hypointense on T1-weighted images and markedly hyperintense on T2-weighted images (Fig. 86-34B). On T2-weighted images, multiple septa can be seen traversing the tumor, indicating that the mass is not a simple cyst.¹³⁴ The stromal components may enhance after the administration of gadolinium-chelate agents.¹⁴²

SUMMARY

Mesenchymal hamartoma is a rare liver tumor that occurs in the first 2 years of life. Hepatoblastoma and IHE have a similar age presentation but are solid, whereas mesenchymal hamartomas are predominantly cystic.

Mesenchymal hamartoma is not a neoplasm but a failure of normal development. Therefore, it does not require extensive surgery; single excision, marsupialization, or incisional drainage may be sufficient therapy.

Mesenchymal hamartoma should not be confused with other cystic-appearing masses that may occur in the liver of toddlers, such as abscesses or hematomas.

Miscellaneous Benign Tumors

BILE DUCT ADENOMA

This benign, solitary, small (<1 cm) mass is composed of small bile ducts and is discovered incidentally at autopsy.¹⁰

LYMPHANGIOMATOSIS

Hepatic lymphangiomas are defined by the presence of multiple masses composed of prominent lymphatic channels that compress the normal hepatic architecture.¹⁰ Usually, it is part of a systemic syndrome in which other organs, including the spleen, skeleton, soft tissues, lung, and brain, are also involved.

LEIOMYOMA

This extremely rare lesion is a well-circumscribed smooth muscle tumor arising in the liver with nonspecific radiologic characteristics.¹⁴³ Several cases of leiomyoma have recently been reported in adults and children infected with human immunodeficiency virus, suggesting that there may be a clinical association between these two entities.¹⁴⁴⁻¹⁴⁶ On ultrasound examination, the lesion may appear solid or hypoechoic with internal echoes.^{145,146} Leiomyomas are of low attenuation relative to the liver on noncontrast CT scans and display two distinct enhancement patterns: peripheral rim enhancement similar to abscesses or homogeneous enhancement resembling hemangioma.¹⁴⁴⁻¹⁴⁶ On MRI, leiomyomas are hypointense relative to the liver on T1-weighted images and hyperintense on T2-weighted images.^{145,146}

FIBROMA (FIBROUS MESOTHELIOMA)

Fibrous mesotheliomas are rare tumors that localize on the surface of the liver.^{53,147} They are usually large and consist histologically of spindle cells and collagen.

ADRENAL REST TUMOR

Adrenal rest tumors are derived from ectopic adrenal tissue that is histologically identical to that in adrenocortical tumors. They are extremely rare.¹⁴⁸

PANCREATIC HETEROTOPIA

Ectopic pancreas in the liver has been rarely described.^{149,150}

INFLAMMATORY PSEUDOTUMOR

Inflammatory pseudotumor is a rare uncommon space-occupying lesion. It is characterized by proliferating

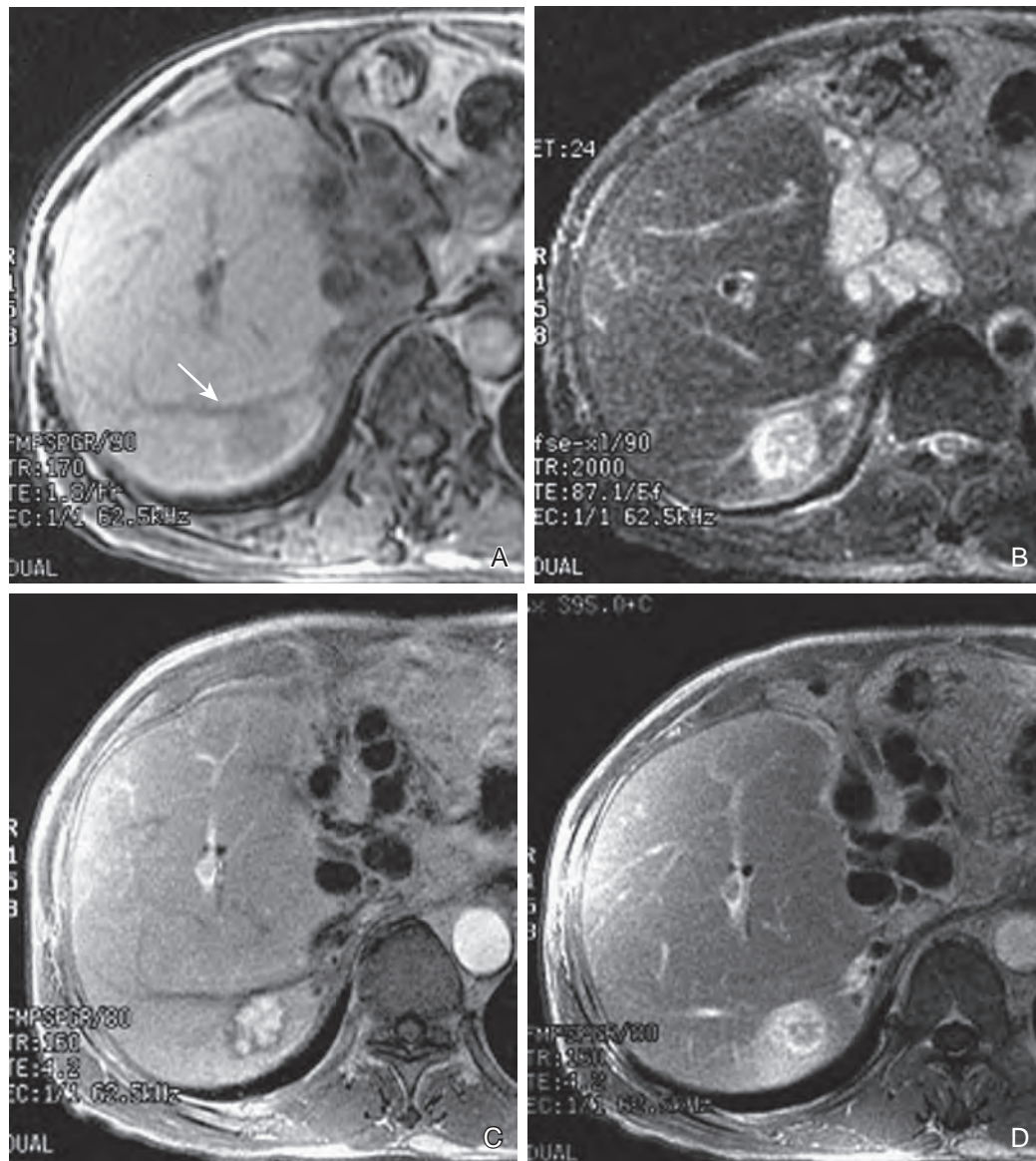


Figure 86-35 Inflammatory pseudotumor. **A.** T1-weighted MR image shows a hypointense lesion in the posterior aspect of the right hepatic lobe (arrow). **B.** The lesion is hyperintense on T2-weighted images. Note the dilated biliary ducts due to cholangitis. **C.** Gadolinium-enhanced arterial phase T1-weighted MR image shows enhancing inflammatory pseudotumor. **D.** On the delayed phase images, the enhancement of the liver parenchyma surrounding the tumor indicates inflammation. (Courtesy Dr. Tomoaki Ichikawa, Yamanashi University, Yamanashi, Japan.)

fibrovascular tissue mixed with inflammatory cells. The exact etiology of this entity is uncertain, but it has been stated that inflammatory pseudotumors have been associated with lymphoma or inflammatory processes, including inflammatory bowel disease and primary sclerosing cholangitis. Interestingly, they appear to be more common in non-European populations, such as Southeast Asians.¹⁵¹ Inflammatory pseudotumors do not require surgical resection and typically resolve completely.²⁶ On the other hand, it may be challenging to differentiate them from malignant liver neoplasms or abscesses.

Inflammatory pseudotumor is usually large (>3 cm) at presentation. The ultrasound appearance may be hypoechoic, isoechoic, or hyperechoic. On nonenhanced CT images, the

lesion is hypodense or isodense with the liver. At contrast-enhanced dynamic CT imaging, pseudotumors show early arterial enhancement, and they are almost isodense or slightly hyperdense in portal venous phase.²⁶ Delayed phase images may show increased contrast retention within the lesion relative to normal liver parenchyma. The signal intensity on both precontrast T1- and T2-weighted images varies from hypointense to hyperintense. The most common although nonspecific precontrast MRI finding is hyperintensity on T2-weighted images¹⁵² (Fig. 86-35). Contrast enhancement patterns on MRI are similar to those observed on CT. Because of the nonspecific imaging characteristics of this entity, a core biopsy is usually required for accurate diagnosis.¹⁵³

REFERENCES

- Wills M, Harvey CJ, Kuzmich S, et al: Characterizing benign liver lesions with ultrasound. *Br J Hosp Med* 75:91–95, 2014.
- Cogley JR, Miller FH: MR imaging of benign liver tumors. *MR imaging of benign focal liver lesions*. *Radiol Clin North Am* 52:657–682, 2014.
- Donati OF, Hunziker R, Fisher MA, et al: MRI for characterization of primary tumors in the non-cirrhotic liver. *Eur J Radiol* 83:1075–1079, 2014.
- Ba-Ssalamah A, Heinz-Peer G, Schima W, et al: Detection of focal hepatic lesions: Comparison of unenhanced and SHU 555 A-enhanced MR imaging versus biphasic helical CTAP. *J Magn Reson Imaging* 11:665–672, 2000.
- Ba-Ssalamah A, Fakhrai N, Matzek WK, et al: Magnetic resonance imaging of liver malignancies. *Top Magn Reson Imaging* 18:445–455, 2007.
- Bartolozzi C, Crocetti L, Lencioni R, et al: Biliary and reticuloendothelial impairment in hepatocarcinogenesis: The diagnostic role of tissue-specific MR contrast media. *Eur Radiol* 17:2519–2530, 2007.
- Lupescu IG, Capsa RA, Gheorghe L, et al: Tissue specific MR contrast media role in the differential diagnosis of cirrhotic liver nodules. *J Gastrointest Liver Dis* 17:341–345, 2008.
- Khatri G, Merrick L, Miller FH: MR imaging of hepatocellular carcinoma. *Magn Reson Imaging Clin N Am* 18:421–450, 2010.
- Ba-Ssalamah A, Baroud S, Bastati N, Qayyum A: MR imaging of benign focal liver lesions. *Magn Reson Imaging Clin N Am* 18:403–419, 2010.
- Terkivatan T, Hussain SM, De Man RA, Ijzermans JN: Diagnosis and treatment of benign focal liver lesions. *Scand J Gastroenterol Suppl* 243:102–115, 2006.
- Ros PR, Lubbers PR, Olmsted WW, et al: Hemangioma of the liver: Magnetic resonance-gross morphologic correlation. *AJR Am J Roentgenol* 149:1167–1170, 1987.
- Dimitroulis D, Charalampoudis P, Lainas P, et al: Focal nodular hyperplasia and hepatocellular adenoma: Current views. *Acta Chir Belg* 113:162–169, 2013.
- Ros PR: Computed tomography: Pathologic correlations in hepatic tumors. In Ferrucci JT, Mathieu DG, editors: *Advances in Hepatobiliary Radiology*. St. Louis, 1990, CV Mosby, pp 75–108.
- Vilgrain V, Uzan F, Brancatelli G, et al: Prevalence of hepatic hemangioma in patients with focal nodular hyperplasia: MR imaging analysis. *Radiology* 229:75–79, 2003.
- Ros PR, Rasmussen JF, Li KCP: Radiology of malignant and benign liver tumors. *Curr Probl Diagn Radiol* 18:95–155, 1989.
- Moihuddin M, Allison JR, Montgomery JH, et al: Scintigraphic diagnosis of hepatic hemangioma: Its role in the management of hepatic mass lesions. *AJR Am J Roentgenol* 145:223–228, 1985.
- Schillaci O, Filippi L, Danieli R, et al: Single-photon emission computed tomography/computed tomography in abdominal diseases. *Semin Nucl Med* 37:48–61, 2007.
- Buetow PR, Buck JL, Ros PR, et al: Malignant vascular tumors of the liver: Radiologic-pathologic correlation. *Radiographics* 14:153–166, 1994.
- Schillaci O, Danieli R, Manni C, et al: Technetium-99m-labelled red blood cell imaging in the diagnosis of hepatic haemangiomas: The role of SPECT/CT with a hybrid camera. *Eur J Nucl Med Mol Imaging* 31:1011–1015, 2004.
- Heiken JP: Liver. In Lee JKT, Sagel SS, Stanley RJ, et al, editors: *Computed Body Tomography with MRI Correlation*, ed 3, Philadelphia, 1998, Lippincott-Raven, pp 701–778.
- Celli N, Gaiani S, Piscaglia F, et al: Characterization of liver lesions by real-time contrast-enhanced ultrasonography. *Eur J Gastroenterol Hepatol* 19:3–14, 2007.
- Kim SH, Lee JM, Kim KG, et al: Comparison of fundamental sonography, tissue-harmonic sonography, fundamental compound sonography, and tissue-harmonic compound sonography for focal hepatic lesions. *Eur Radiol* 16:2444–2453, 2006.
- Dietrich CF: Characterisation of focal liver lesions with contrast enhanced ultrasonography. *Eur J Radiol* 51(Suppl):S9–S17, 2004.
- Brannigan M, Burns PN, Wilson SR: Blood flow patterns in focal liver lesions at microbubble-enhanced US. *Radiographics* 24:921–935, 2004.
- Vilgrain V, Boulos L, Vullierme MP, et al: Imaging of atypical hemangiomas of the liver with pathologic correlation. *Radiographics* 20:379–397, 2000.
- Ibrahim S, Chen CL, Wang SH, et al: Liver resection for benign liver tumors: Indications and outcome. *Am J Surg* 93:5–9, 2007.
- Leslie DF, Johnson CD, Johnson CM, et al: Distinction between cavernous hemangiomas of the liver and hepatic metastases on CT: Value of contrast enhancement patterns. *AJR Am J Roentgenol* 164:625–629, 1995.
- Yamashita Y, Ogata I, Urata J, et al: Cavernous hemangioma of the liver: Pathologic correlation with dynamic CT findings. *Radiology* 203:121–125, 1997.
- Kim T, Federle MP, Baron RL, et al: Discrimination of small hepatic hemangiomas from hypervascular malignant tumors smaller than 3 cm with three-phase helical CT. *Radiology* 219:699–706, 2001.
- Quinn SE, Benjamin GG: Hepatic cavernous hemangiomas: Simple diagnostic sign with dynamic bolus CT. *Radiology* 182:545–548, 1992.
- Mergo PJ, Ros PR: Benign lesions of the liver. *Radiol Clin North Am* 36:319–332, 1998.
- Semelka RC: Liver. In Semelka RC, Ascher SM, Reinhold C, editors: *MRI of the Abdomen and Pelvis*, New York, 1997, Wiley-Liss, pp 19–136.
- Siegelman ES, Outwater EK: MR imaging techniques of the liver. *Radiol Clin North Am* 36:263–287, 1998.
- Schima W, Saini S, Echeverri JA, et al: Focal liver lesions: Characterization with conventional spin-echo T2-weighted MR imaging. *Radiology* 202:389–394, 1997.
- Soyer P, Bluemke DA, Rymer R: MR imaging of the liver: Technique. *Magn Reson Imaging Clin N Am* 5:205–222, 1997.
- Yoshida H, Itai Y, Ohtomo K, et al: Small hepatocellular carcinoma and cavernous hemangioma: Differentiation with dynamic FLASH MR imaging with Gd-DTPA. *Radiology* 171:339–342, 1989.
- Ohtomo K, Itai Y, Yoshikawa K, et al: Hepatic tumors: Dynamic MR imaging. *Radiology* 163:27–31, 1987.
- Motohara T, Semelka RC, Nagase L: MR imaging of benign hepatic tumors. *Magn Reson Imaging Clin N Am* 10:1–14, 2002.
- Kamel IR, Bluemke DA: MR imaging of liver tumors. *Radiol Clin North Am* 41:51–65, 2003.
- Semelka RC, Brown ED, Ascher SM, et al: Hepatic hemangiomas: A multi-institutional study of appearance on T2-weighted and serial gadolinium-enhanced gradient-echo MR images. *Radiology* 192:401–406, 1994.
- Whitney WS, Herfkens RJ, Jeffrey RB, et al: Dynamic breath-hold multiplanar spoiled gradient-recalled MR imaging with gadolinium enhancement for differentiating hepatic hemangiomas from malignancies at 1.5T. *Radiology* 189:863–870, 1993.
- Ringe KI, Husarik DB, Sirlin CB, Merkle EM: Gadotetate disodium-enhanced MRI of the liver: Part 1, protocol optimization and lesion appearance in the noncirrhotic liver. *AJR Am J Roentgenol* 195:13–28, 2010.
- Caseiro-Alves F, Brito J, Araujo AE, et al: Liver haemangioma: Common and uncommon findings and how to improve the differential diagnosis. *Eur Radiol* 17:1544–1554, 2007.
- Saini S, Edelman RR, Sharma P, et al: Blood-pool MR contrast material for detection and characterization of focal hepatic lesions: Initial clinical experience with ultrasmall superparamagnetic iron oxide (AMI-227). *AJR Am J Roentgenol* 164:1147–1152, 1995.
- Qayyum A: Diffusion-weighted imaging in the abdomen and pelvis: Concepts and applications. *Radiographics* 29:1797–1810, 2009.
- Koike N, Cho A, Nasu K, et al: Role of diffusion-weighted magnetic resonance imaging in the differential diagnosis of focal hepatic lesions. *World J Gastroenterol* 15:5805–5812, 2009.
- Nguyen BN, Flejou JF, Terris B, et al: Focal nodular hyperplasia of the liver: A comprehensive pathologic study of 305 lesions and recognition of new histologic forms. *Am J Surg Pathol* 23:1441–1454, 1999.
- Kim MJ, Kim JH, Chung JJ, et al: Focal hepatic lesions: Detection and characterization with combination gadolinium- and superparamagnetic iron oxide-enhanced MR imaging. *Radiology* 228:719–726, 2003.
- Klotz T, Montoriol PF, Da Ines D, et al: Hepatic haemangioma: Common and uncommon imaging features. *Diagn Interv Imaging* 9:849–859, 2013.
- Goodman ZD: Benign tumors of the liver. In Okuda K, Ishak KG, editors: *Neoplasms of the Liver*, Tokyo, 1987, Springer-Verlag, pp 105–125.
- Wanless IR, Albrecht S, Bilbow J, et al: Multiple focal nodular hyperplasia associated with vascular malformation of various organs and neoplasia of the brain: A new syndrome. *Mod Pathol* 2:456–462, 1989.
- Wanless IR, Mawdsley C, Adams R: On the pathogenesis of focal nodular hyperplasia of the liver. *Hepatology* 5:1194–1200, 1985.
- Ishak KG: Benign tumors and pseudotumors of the liver. *Appl Pathol* 6:82–104, 1988.
- Bioulac-Sage P, Balabaud C, Bedossa P, et al: Pathological diagnosis of liver cell adenoma and focal nodular hyperplasia: Bordeaux update. *J Hepatol* 46:521–527, 2007.
- Welch TJ, Sheedy PF, II, Johnson CM, et al: Focal nodular hyperplasia and hepatic

- adenoma: Comparison of angiography, CT, US and scintigraphy. *Radiology* 156:593–595, 1985.
56. Shen YH, Fan J, Wu ZQ, et al: Focal nodular hyperplasia of the liver in 86 patients. *Hepatobiliary Pancreat Dis Int* 6:52–57, 2007.
 57. Kurtaran A, Becherer A, Pfeffel F, et al: ¹⁸F-fluorodeoxyglucose (FDG)-PET features of focal nodular hyperplasia (FNH) of the liver. *Liver* 20:487–490, 2000.
 58. Kamel IR, Liapi E, Fishman EK: Focal nodular hyperplasia: Lesion evaluation using 16-MDCT and 3D CT angiography. *AJR Am J Roentgenol* 186:1587–1596, 2006.
 59. Caseiro-Alves F, Zins M, Mahfouz A-E, et al: Calcification in focal nodular hyperplasia: A new problem for differentiation from fibrolamellar hepatocellular carcinoma. *Radiology* 198:889–892, 1996.
 60. Huang-Wei C, Bleuzen A, Bourlier P, et al: Differential diagnosis of focal nodular hyperplasia with quantitative parametric analysis in contrast-enhanced sonography. *Invest Radiol* 41:363–368, 2006.
 61. Huang-Wei C, Bleuzen A, Olar M, et al: Role of parametric imaging in contrast-enhanced sonography of hepatic focal nodular hyperplasia. *J Clin Ultrasound* 34:367–373, 2006.
 62. Mortelet KJ, Praet M, Van Vlierberghe H, et al: CT and MR imaging findings in focal nodular hyperplasia of the liver: Radiologic-pathologic correlation. *AJR Am J Roentgenol* 175:687–692, 2000.
 63. Buetow PC, Pantongrag-Brown L, Buck JL, et al: Focal nodular hyperplasia of the liver: Radiologic-pathologic correlation. *Radiographics* 16:369–388, 1996.
 64. Hussain SM, Terkivatan T, Zondervan PE, et al: Focal nodular hyperplasia: Findings at state-of-the-art MR imaging, US, CT, and pathologic analysis. *Radiographics* 24:3–17, 2004.
 65. Brancatelli G, Federle MP, Grazioli L, et al: Focal nodular hyperplasia: CT findings with emphasis on multiphasic helical CT in 78 patients. *Radiology* 219:61–68, 2001.
 66. Lizardi-Cervera J, Cuellar-Gamboa L, Motola-Kuba D: Focal nodular hyperplasia and hepatic adenoma: A review. *Ann Hepatol* 5:206–211, 2006.
 67. Mahfouz A-E, Hamm B, Taupitz M, et al: Hypervascular liver lesions: Differentiation of focal nodular hyperplasia from malignant tumors with dynamic gadolinium-enhanced MR imaging. *Radiology* 186:133–138, 1993.
 68. Terkivatan T, van den Bos IC, Hussain SM, et al: Focal nodular hyperplasia: Lesion characteristics on state-of-the-art MRI including dynamic gadolinium-enhanced and superparamagnetic iron-oxide-uptake sequences in a prospective study. *J Magn Reson Imaging* 24:864–872, 2006.
 69. Marin D, Iannaccone R, Laghi A, et al: Focal nodular hyperplasia: Intraindividual comparison of dynamic gadobenate dimeglumine- and ferucarbotran-enhanced magnetic resonance imaging. *J Magn Reson Imaging* 25:775–782, 2007.
 70. Paley MR, Mergo PJ, Ros PR: Characterization of focal liver lesions with SPIO-enhanced T2WI: Patterns of signal intensity and liver lesion contrast change. *Radiology* 205:455–456, 1997.
 71. Cha DI, Yoo SI, Kim JH, et al: Clinical and imaging features of focal nodular hyperplasia in children. *AJR* 202:960–965, 2014.
 72. Zech CJ, Grazioli L, Breuer J, et al: Diagnostic performance and description of morphological features of focal nodular hyperplasia in Gd-EOBTPA-enhanced liver magnetic resonance imaging: Results of a multicenter trial. *Invest Radiol* 43:504–511, 2008.
 73. Marin D, Brancatelli G, Federle MP, et al: Focal nodular hyperplasia: Typical and atypical MRI findings with emphasis on the use of contrast media. *Clin Radiol* 63:577–585, 2008.
 74. Grazioli L, Morana G, Kirchin MA, et al: Accurate differentiation of focal nodular hyperplasia from hepatic adenoma at gadobenate dimeglumine-enhanced MR imaging: Prospective study. *Radiology* 236:166–177, 2005.
 75. Wanless IR, Albrecht S, Bilbao J, et al: Multiple focal nodular hyperplasia of the liver associated with vascular malformations of various organs and neoplasia of the brain: A new syndrome. *Mod Pathol* 2:456–462, 1989.
 76. Attal P, Vilgrain V, Brancatelli G, et al: Telangiectatic focal nodular hyperplasia: US, CT, and MR imaging findings with histopathologic correlation in 13 cases. *Radiology* 228:465–472, 2003.
 77. Brancatelli G, Federle MP, Vullierme MP, et al: CT and MR imaging evaluation of hepatic adenoma. *J Comput Assist Tomogr* 30:745–750, 2006.
 78. Grazioli L, Federle MP, Brancatelli G, et al: Hepatic adenomas: Imaging and pathologic findings. *Radiographics* 21:877–892, 2001.
 79. Rooks JB, Ory HW, Ishak KG, et al: Epidemiology of hepatocellular adenoma: The role of contraceptive steroid use. *JAMA* 242:644–648, 1979.
 80. Christopherson WM, Mays ET, Barrows G: A clinicopathologic study of steroid-related tumors. *Am J Surg Pathol* 1:31–41, 1977.
 81. Anderson PH, Packer JT: Hepatic adenoma: Observations after estrogen withdrawal. *Arch Surg* 111:898–900, 1976.
 82. Golli M, Nhieu JTV, Mathieu D, et al: Hepatocellular adenoma: Color Doppler US and pathologic correlations. *Radiology* 190:741–744, 1994.
 83. Piscaglia F, Lencioni R, Sagrini E, et al: Characterization of focal liver lesions with contrast-enhanced ultrasound. *Ultrasound Med Biol* 36:531–550, 2010.
 84. Kim TK, Jang HJ, Burns PN, et al: Focal nodular hyperplasia and hepatic adenoma: Differentiation with low-mechanical-index contrast-enhanced sonography. *AJR Am J Roentgenol* 190:58–66, 2008.
 85. Bluemke DA, Soyer P, Fishman EK: Helical (spiral) CT of the liver. *Radiol Clin North Am* 33:863–886, 1995.
 86. Goldstein HM, Neiman HL, Mena E, et al: Angiographic findings in benign liver cell tumors. *Radiology* 110:339–343, 1974.
 87. Freeny PC: Angiography of hepatic neoplasms. *Semin Roentgenol* 18:114–122, 1983.
 88. Hussain SM, van den Bos IC, Dwarkasing RS, et al: Hepatocellular adenoma: Findings at state-of-the-art magnetic resonance imaging, ultrasound, computed tomography and pathologic analysis. *Eur Radiol* 16:1873–1886, 2006.
 89. Arrive L, Flejou J-F, Vilgrain V, et al: Hepatic adenoma: MR findings in 51 pathologically proved lesions. *Radiology* 193:507–512, 1994.
 90. Vogl TJ, Hammerstingl R, Schwarz W, et al: Superparamagnetic iron oxide-enhanced versus gadolinium-enhanced MR imaging for differential diagnosis of focal liver lesions. *Radiology* 198:881–887, 1996.
 91. Goodwin MD, Dobson JE, Sirlin CB, et al: Diagnostic challenges and pitfalls in MR imaging with hepatocyte-specific contrast agents. *Radiographics* 31:1547–1568, 2011.
 92. Grazioli L, Morana G, Kirchin MA, Schneider G: Accurate differentiation of focal nodular hyperplasia from hepatic adenoma at gadobenate dimeglumine-enhanced MR imaging: Prospective study. *Radiology* 236:166–177, 2005.
 93. Schmid-Tannwald C, Dahi F, Jiang F, et al: DW-MRI of liver lesions: Can a single ADC-value represent the entire lesion? *Clin Radiol* 69:492–498, 2014.
 94. Chen KT, Bocian JJ: Multiple hepatic adenomas. *Arch Pathol Lab Med* 107:274–275, 1983.
 95. Lewin M, Handra-Luca A, Arrive L, et al: Liver adenomatosis: Classification of MR imaging features and comparison with pathologic findings. *Radiology* 241:433–440, 2006.
 96. Steiner PE: Nodular regenerative hyperplasia of the liver. *Am J Pathol* 49:943–953, 1959.
 97. Ghabril M, Vuppalanchi R: Drug-induced nodular regenerative hyperplasia. *Semin Liver Dis* 34:240–245, 2014.
 98. Wanless IR, Todtwin TA, Allen F, et al: Nodular regenerative hyperplasia of the liver in hematologic disorders, a possible response to obliterative portal venopathy: A morphometric study of nine cases with an hypothesis on the pathogenesis. *Medicine (Baltimore)* 49:367–379, 1980.
 99. Wanless IR, Solt LC, Kortan P, et al: Nodular regenerative hyperplasia of the liver associated with macroglobulinemia. *Am J Med* 170:1203–1209, 1981.
 100. Nakanuma Y, Ohta G, Sasaki K: Nodular regenerative hyperplasia of the liver associated with polyarteritis nodosa. *Arch Pathol Lab Med* 108:133–135, 1984.
 101. Dachman AH, Ros PR, Goodman ZD, et al: Nodular regenerative hyperplasia of the liver: Clinical and radiologic observations. *AJR Am J Roentgenol* 148:717–722, 1987.
 102. Mones JM, Saldana MJ: Nodular regenerative hyperplasia of the liver in a 4-month-old infant. *Am J Dis Child* 138:79–81, 1984.
 103. Siegelman ES, Outwater EK, Furth EE, et al: MR imaging of hepatic nodular regenerative hyperplasia. *J Magn Reson Imaging* 5:730–732, 1995.
 104. Goodman ZD, Ishak KG: Angiomyolipomas of the liver. *Am J Surg Pathol* 8:745–750, 1984.
 105. Roberts JL, Fishman EK, Hartman DS, et al: Lipomatous tumors of the liver: Evaluation with CT and US. *Radiology* 158:613–617, 1986.
 106. Prayer LM, Schurawitzki HJ, Wimberger DM: Case report: Lipoma of the liver: Ultrasound, CT and MR imaging. *Clin Radiol* 45:353–354, 1992.
 107. Dai CL, Xue LP, Li YM: Multi-slice computed tomography manifestations of hepatic epithelioid angiomyolipoma. *World J Gastroenterol* 20:3364–3368, 2014.
 108. Murakami T, Nakamura H, Hori S, et al: Angiomyolipoma of the liver. *Ultrasound, CT, MR imaging and angiography. Acta Radiol* 34:392–394, 1993.
 109. Hooper LD, Mergo PJ, Ros PR: Multiple hepatorenal angiomyolipomas: Diagnosis with fat suppression, gadolinium-enhanced MRI. *Abdom Imaging* 19:549–551, 1994.
 110. Ros PR: Hepatic angiomyolipoma: Is fat in the liver friend or foe? *Abdom Imaging* 19:552–553, 1994.

111. Valls C, Iannaccone R, Alba E, et al: Fat in the liver: Diagnosis and characterization. *Eur Radiol* 16:2292–2308, 2006.
112. Murphy BJ, Casillas J, Ros PR, et al: The CT appearance of cystic masses of the liver. *Radiographics* 9:307–322, 1989.
113. Litwin DE, Taylor BR, Langer B, et al: Non-parasitic cysts of the liver: The case for conservative surgical management. *Ann Surg* 205:405–408, 1991.
114. Kelly K, Weber SM: Cystic diseases of the liver and bile ducts. *J Gastrointest Surg* 18:627–634, 2014.
115. Bosniak MA, Ambros MA: Polycystic kidney disease. *Semin Roentgenol* 10:133–143, 1975.
116. Mortelet KJ, Ros PR: Cystic focal liver lesions in the adult: Differential CT and MR imaging features. *Radiographics* 21:895–910, 2001.
117. Kairaluoma M, Leinonen A, Stahlberg MM, et al: Percutaneous aspiration and alcohol sclerotherapy for symptomatic hepatic cysts. *Ann Surg* 210:208–215, 1989.
118. Bean WJ, Rodan BA: Hepatic cysts: Treatment with alcohol. *AJR Am J Roentgenol* 144:237–241, 1985.
119. Levine E, Cook LT, Grantham JJ: Liver cysts in autosomal-dominant polycystic kidney disease: Clinical and computed tomographic study. *AJR Am J Roentgenol* 145:229–233, 1985.
120. Kerr DN, Harrison CV, Sherlock S, et al: Congenital hepatic fibrosis. *Q J Med* 30:91–133, 1961.
121. McLean RH, Moller JH, Warwick WJ: Multinodular hemangiomatosis of the liver in infancy. *Pediatrics* 49:563–573, 1972.
122. Dehner LP: Hepatic tumors in the pediatric age group: A distinctive clinicopathologic spectrum. *Perspect Pediatr Pathol* 4:217–268, 1978.
123. Mortelet KJ, Vanzieleghem B, Mortelet B, et al: Solitary hepatic infantile hemangioendothelioma: Dynamic gadolinium-enhanced MR imaging findings. *Eur Radiol* 12:862–865, 2002.
124. Earnest F, 4th, Johnson CD: Hepatic epithelioid hemangioendothelioma. *Radiology* 240:295–298, 2006.
125. Braun P, Ducharme JC, Riopelle JL, et al: Hemangiomatosis of the liver in infants. *J Pediatr Surg* 10:121–126, 1975.
126. Roos JE, Pfiffner R, Stallmach T, et al: Infantile hemangioendothelioma. *Radiographics* 23:1649–1655, 2003.
127. Alomari AI: The lollipop sign: A new cross-sectional sign of hepatic epithelioid hemangioendothelioma. *Eur J Radiol* 59:460–464, 2006.
128. Weiner SN, Parulekar SG: Scintigraphy and ultrasonography of hepatic hemangioma. *Radiology* 132:149–153, 1979.
129. Pardes JG, Bryan PJ, Gauderer MWL: Spontaneous regression of infantile hemangioendotheliomatosis of the liver. *J Ultrasound Med* 1:349–353, 1982.
130. Pobielski RS, Bisset GS, III: Pictorial essay: Imaging of liver tumors in the infant and child. *Pediatr Radiol* 25:495–506, 1995.
131. Helmberger TK, Ros PR, Mergo PJ, et al: Pediatric liver neoplasms: A radiologic-pathologic correlation. *Eur Radiol* 9:1339–1347, 1999.
132. Slovis TL, Berdon WE, Haller JO, et al: Hemangiomas of the liver in infants. *AJR Am J Roentgenol* 123:791–801, 1975.
133. Moss AA, Clark RE, Palubinskas AJ, et al: Angiographic appearance of benign and malignant hepatic tumors in infants and children. *AJR Am J Roentgenol* 113:61–69, 1971.
134. O'Neil J, Ros PR: Knowing hepatic pathology aids MRI of liver tumors. *Diagn Imaging* 19:58–67, 1989.
135. Dehner LP, Ewing SL, Sumner HW: Infantile mesenchymal hamartoma of the liver. *Histologic and ultrastructural observations. Arch Pathol Lab Med* 99:379–382, 1975.
136. Stocker JT, Ishak KG: Mesenchymal hamartoma of the liver: Report of 30 cases and review of the literature. *Pediatr Pathol* 1:245–267, 1983.
137. Molina EG, Schiff ER: Benign solid lesions of the liver. In Schiff ER, Sorrell MF, Maddrey WC, editors: *Diseases of the Liver*, ed 8, Philadelphia, 1999, Lippincott Williams & Wilkins, pp 1245–1268.
138. Ros PR, Goodman ZD, Ishak KG, et al: Mesenchymal hamartoma of the liver: Radiologic-pathologic correlation. *Radiology* 158:619–624, 1986.
139. Stringer MD: The role of liver transplantation in the management of paediatric liver tumours. *Ann R Coll Surg Engl* 89:12–21, 2007.
140. Stanley P, Hall TR, Woolley MM, et al: Mesenchymal hamartomas of the liver in childhood: Sonographic and CT findings. *AJR Am J Roentgenol* 147:1035–1039, 1986.
141. Kaude JV, Felman AH, Hawkins IF: Ultrasonography in primary hepatic tumors in early childhood. *Pediatr Radiol* 9:77–83, 1980.
142. Siegel MJ, Hoffer FA: Magnetic resonance imaging of nongynecologic pelvic masses in children. *Magn Reson Imaging Clin N Am* 10:325–344, 2002.
143. Hawkins EP, Jordan GL, McGavran MH: Primary leiomyoma of the liver. Successful treatment by lobectomy and presentation of criteria for diagnosis. *Am J Surg Pathol* 4:301–304, 1980.
144. Mueller BU, Butler KM, Higham MC, et al: Smooth muscle tumors in children with human immunodeficiency virus infection. *Pediatrics* 90:460–463, 1992.
145. Reinertson TE, Fortune JB, Peters JC, et al: Primary leiomyoma of the liver: A case report and review of the literature. *Dig Dis Sci* 37:622–627, 1992.
146. Wachsberg RH, Cho KC, Adekoso A: Two leiomyomas of the liver in an adult with AIDS: CT and MR appearance. *J Comput Assist Tomogr* 18:156–157, 1994.
147. Saul SH: Masses of the liver. In Sternberg SS, editor: *Diagnostic Surgical Pathology*, ed 3, Philadelphia, 1999, Lippincott Williams & Wilkins, pp 1553–1628.
148. Wilkins L, Ravich MM: Adrenocortical tumor arising in the liver of a three-year-old boy with signs of virilism and Cushing's syndrome. Report of a case with cure after partial resection of the right lobe of the liver. *Pediatrics* 9:671–680, 1952.
149. Mobini J, Krouse TB, Cooper DR: Intrahepatic pancreatic heterotopia. Review and report of a case presenting as an abdominal mass. *Am J Dig Dis* 19:64–70, 1974.
150. Wanless IR: Anatomy and developmental anomalies of the liver. In Feldman M, Scharschmidt BF, Sleisenger MH, editors: *Sleisenger and Fordtran's Gastrointestinal and Liver Disease*, ed 6, Philadelphia, 1998, WB Saunders, pp 1055–1060.
151. Koea JB, Broadhurst GW, Rodgers MS, McCall JL: Inflammatory pseudotumor of the liver: Demographics, diagnosis, and the case for nonoperative management. *J Am Coll Surg* 196:226–235, 2003.
152. Mortelet KJ, Wiesner W, de Hemptinne B, et al: Multifocal inflammatory pseudotumor of the liver: Dynamic gadolinium-enhanced, ferumoxides-enhanced, and mangafodipir trisodium-enhanced MR imaging findings. *Eur Radiol* 12:304–308, 2002.
153. Park JY, Choi MS, Lim YS, et al: Clinical features, imaging findings, and prognosis of the liver. *Gut Liver* 8:58–63, 2014.

Malignant Tumors of the Liver

PABLO R. ROS | SUKRU MEHMET ERTURK

CHAPTER OUTLINE

Hepatocellular Carcinoma

Pathologic Findings
Incidence and Clinical Presentation
Radiologic Findings

Fibrolamellar Carcinoma

Pathologic Findings
Incidence and Clinical Presentation
Radiologic Findings
Differential Diagnosis

Hepatoblastoma

Pathologic Findings
Incidence and Clinical Presentation
Radiologic Findings

Intrahepatic Cholangiocarcinoma

Pathologic Findings
Incidence and Clinical Presentation
Radiologic Findings

Cystadenoma and Cystadenocarcinoma

Pathologic Findings
Incidence and Clinical Presentation
Radiologic Findings

Angiosarcoma

Pathologic Findings
Incidence and Clinical Presentation
Radiologic Findings

Undifferentiated (Embryonal) Sarcoma

Pathologic Findings
Incidence and Clinical Presentation
Radiologic Findings

Epithelial Hemangioendothelioma

Pathologic Findings
Incidence and Clinical Presentation
Radiologic Findings

Other Mesenchymal Sarcomas (Leiomyosarcoma, Malignant Fibrous Histiocytoma)

Pathologic Findings
Incidence and Clinical Presentation
Radiologic Findings

LYMPHOMA

Pathologic Findings
Incidence and Clinical Presentation
Radiologic Findings

Metastases

Pathologic Findings
Incidence and Clinical Presentation
Radiologic Findings

Differential Diagnosis—Incidental Mass

Practical Approach to Liver Masses

Primary malignant neoplasms of the liver are classified by the cell of origin (Box 87-1). Secondary malignant liver tumors are metastases and lymphomas. Overall, metastases are the most frequent malignant tumors of the liver, except in patients with preexisting cirrhosis, in whom primary malignant neoplasms are more frequent.¹

In this chapter, primary malignant liver tumors of hepatocyte origin are discussed first: hepatocellular carcinoma, fibrolamellar carcinoma, and hepatoblastoma. Intrahepatic carcinoma and cystadenocarcinoma that arise from biliary cells are then considered. Angiosarcoma, undifferentiated (embryonal) sarcoma, epithelial hemangioendothelioma, and other mesenchymal sarcomas that originate in the mesenchymal tissue are reviewed. Finally, the secondary liver tumors, lymphomas and metastases, are discussed.

Hepatocellular Carcinoma

PATHOLOGIC FINDINGS

Hepatocellular carcinoma (HCC) is the most common primary hepatic tumor and one of the most common visceral malignant

neoplasms worldwide.² Terms such as *hepatoma* and *primary liver cancer* are often used synonymously with HCC, but they should be avoided in the interest of clarity and the term *hepatocellular carcinoma* should be encouraged.³

HCC is a malignant lesion composed of cells that attempt to differentiate into normal liver, mimicking hepatocyte cords. However, their abnormal growth prevents the malignant hepatocytes from forming normal hepatic acini. Several clinical and histologic patterns occur, and the prognosis differs according to the associated condition (e.g., cirrhosis) and the extent of the tumor at diagnosis.²

In gross appearance, there are three major patterns of growth (Fig. 87-1): single or massive HCC characterized by the presence of a solitary, often large, mass; nodular or multifocal HCC, in which multiple well-separated nodules are seen throughout the liver, mimicking the appearance of metastases; and diffuse or cirrhotomimetic HCC, in which multiple small foci are seen throughout the liver in a diffuse manner.

A gross variant, encapsulated HCC, has a better prognosis because of its greater resectability^{4,5} (Fig. 87-2). Regardless of its gross appearance, HCC is a soft tumor that frequently undergoes necroses and hemorrhages because of lack of stroma.

BOX 87-1 MALIGNANT LIVER TUMORS**HEPATOCELLULAR ORIGIN**

Hepatocellular carcinoma
Atypical hepatocellular carcinoma
Clear cell carcinoma
Giant cell carcinoma
Childhood hepatocellular carcinoma
Carcinosarcoma
Fibrolamellar carcinoma
Hepatoblastoma
Sclerosing hepatic carcinoma

CHOLANGIOCELLULAR ORIGIN

Cholangiocarcinoma
Cystadenocarcinoma

MESENCHYMAL ORIGIN

Angiosarcoma
Epithelioid hemangioendothelioma
Leiomyosarcoma
Fibrosarcoma
Malignant fibrous histiocytoma
Primary lymphoma
Primary hepatic osteosarcoma

Vascular invasion of perihepatic vessels is common.⁶ Conversely, biliary invasion is uncommon.⁶

On microscopic examination, the cells of HCC resemble normal liver cells, and it is often difficult to distinguish normal hepatocytes from cells of HCC or hepatocellular adenoma.⁷ This is of considerable importance in planning an aspiration biopsy of a focal liver lesion. In some cases, the malignant hepatocytes are so well differentiated that they even produce bile, which is seen in tumor cells and in biliary canaliculi. A variety of products can be produced by the abnormal hepatocytes of HCC: Mallory bodies, α -fetoprotein, α_1 -antitrypsin, and other serum proteins. Fat and glycogen are often present in the cytoplasm of HCC hepatocytes. If there are large amounts of fat, the tumor is called clear cell carcinoma of the liver.

The most frequent HCC histologic growth pattern is trabecular, in which the tumor cells attempt to recapitulate the cords seen in normal liver.⁸ The trabeculae are separated by vascular spaces with no stroma or supportive connective tissue. On occasion, the center of the trabeculae contains tumor secretions, giving the tumor a pseudoglandular or acinar pattern. In other cases, the trabeculae grow together, producing a solid pattern (Fig. 87-3).

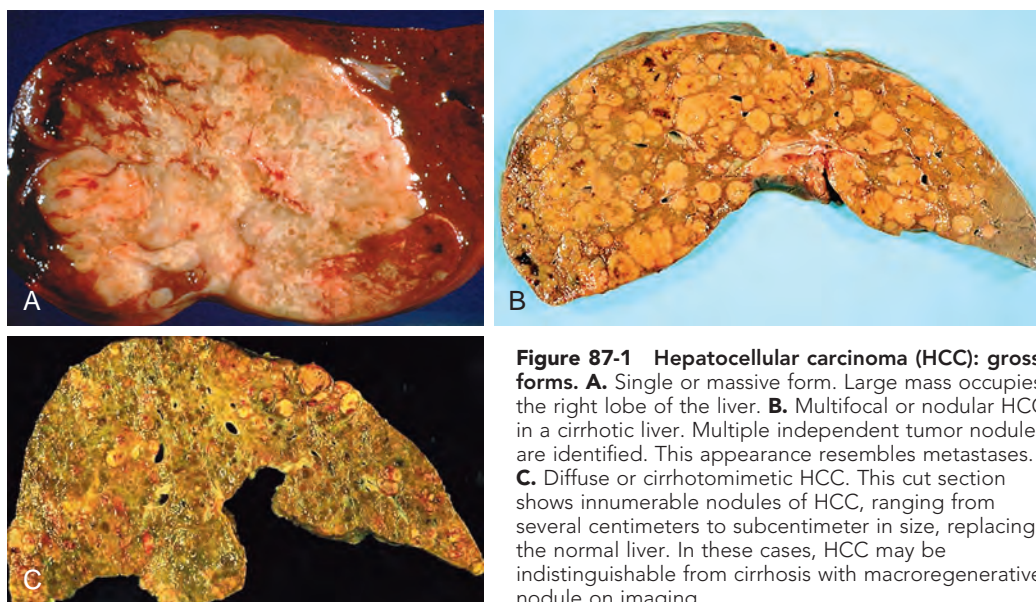


Figure 87-1 Hepatocellular carcinoma (HCC): gross forms. **A.** Single or massive form. Large mass occupies the right lobe of the liver. **B.** Multifocal or nodular HCC in a cirrhotic liver. Multiple independent tumor nodules are identified. This appearance resembles metastases. **C.** Diffuse or cirrhotomimetic HCC. This cut section shows innumerable nodules of HCC, ranging from several centimeters to subcentimeter in size, replacing the normal liver. In these cases, HCC may be indistinguishable from cirrhosis with macroregenerative nodule on imaging.

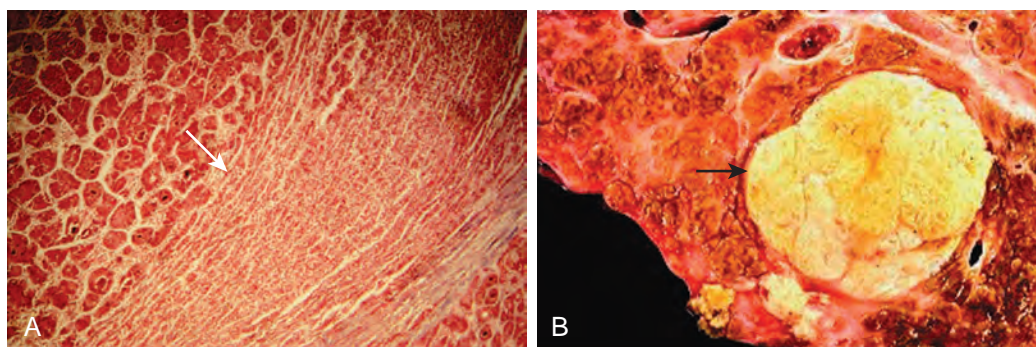


Figure 87-2 Encapsulated HCC. **A.** Photomicrograph demonstrates a capsule (arrow) that demarcates the HCC. **B.** Gross specimen demonstrates bands of fibrous tissue (arrow) that surround this HCC.

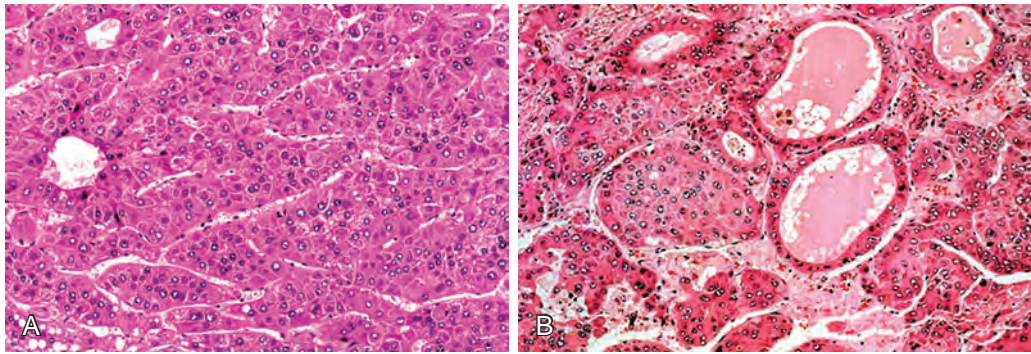


Figure 87-3 HCC: histologic appearance. **A.** Photomicrograph of a solid or cellular histologic pattern. In solid HCC, the imaging appearance of the tumor is similar to that of normal liver because of its marked cellularity. **B.** Photomicrograph of a well-differentiated HCC with an acinar pattern. Large amounts of tumor secretions are seen within HCC cells (arrow). HCCs with large intratumoral secretions have a lower CT density than normal liver. The spectrum of microscopic findings explains the spectrum of radiologic appearances in HCC.

BOX 87-2 IMAGING TECHNIQUES IN LIVER NEOPLASMS

TO ASSESS VASCULARITY

Contrast-enhanced computed tomography
Gadolinium-enhanced magnetic resonance imaging
Contrast-enhanced ultrasound
Angiography
Blood pool studies (^{99m}Tc -labeled red blood cells)

TO ASSESS HEPATOCYTE FUNCTION OR BILIARY EXCRETION

Magnetic resonance imaging enhanced with hepatocyte-specific contrast agents

TO ASSESS METABOLIC ACTIVITY OF NEOPLASMS

^{18}F -FDG positron emission tomography

TO ASSESS KUPFFER CELL ACTIVITY

Magnetic resonance imaging enhanced with intravenous superparamagnetic iron oxide

TO ASSESS TUMORAL CALCIFICATION

Computed tomography
Ultrasound
Plain radiography

TO ASSESS CAPSULE PRESENCE

Computed tomography (enhanced or unenhanced)
Ultrasound (enhanced or unenhanced)
Magnetic resonance imaging (enhanced or unenhanced)

TO ASSESS INTERNAL NATURE OF NEOPLASMS (e.g., solid versus cystic, hemorrhage, fibrosis)

Computed tomography
Magnetic resonance imaging
Ultrasound

These microscopic variations are important for the radiologist to appreciate because cellular HCCs may appear similar to normal liver, so that only subtle changes in density or echogenicity may be present. However, if there is fat deposition or pseudogland formation, the HCC may appear hyperechoic on ultrasound studies, hypodense on computed tomography (CT) scans, and hyperintense on magnetic resonance imaging (MRI).⁹

The radiologic correlates of the pathology of HCCs are listed in [Box 87-2](#).

An important challenge for radiologists and pathologists lies in the early diagnosis of HCC, particularly within a cirrhotic

liver. Successful treatment of HCCs with any of the available therapies, such as surgical resection, liver transplantation, percutaneous ethanol injection, and transcatheter embolization, is most likely if the lesion is small, so early detection is critical.¹⁰ With this aim, an attempt has been made to standardize the terminology of nodular liver lesions, thereby clarifying the pathogenesis of HCC in the cirrhotic liver and enhancing the early diagnosis of premalignant nodules and small HCCs.¹¹ A cirrhotic nodule is defined as a regenerative nodule composed of hepatocytes and is largely or completely surrounded by fibrous septa. A “dysplastic” nodule, which is an intermediate stage between a cirrhotic nodule and HCC, is at least 1 mm in diameter and contains areas of dysplasia but no histologic evidence of malignancy.^{11,12} Synonyms for dysplastic nodule include adenomatous hyperplasia and macroregenerative nodule.¹¹ Dysplastic nodules are subdivided into low-grade and high-grade types on the basis of findings at light microscopy.¹¹ It is widely accepted that dysplastic nodules are premalignant, although the exact mechanisms of transformation of cirrhotic nodule to dysplastic nodule to HCC have yet to be defined.¹³

INCIDENCE AND CLINICAL PRESENTATION

Although HCC has a similar histologic appearance worldwide, it has a bimodal geographic distribution in terms of incidence and clinical presentation. It is rare in the Western hemisphere (low-incidence areas) and relatively frequent in sub-Saharan Africa and Asia (high-incidence areas).¹⁴

Even in the United States, the incidence varies. According to the World Health Organization, the incidence ranges from 0.9 per 100,000 in women in New York to 30.9 per 100,000 in men of Chinese origin in San Francisco.² Worldwide, the highest incidence is in Japan, where it is reported to be as high as 4.8%.¹⁵

Clinically, in the low-incidence areas, symptoms are insidious in onset and include malaise, fever, and abdominal pain.^{2,6} Jaundice is rare. Liver function test results are normal and indistinguishable from those in cirrhosis, except for elevation of the α -fetoprotein level. Other proteins produced by HCC may give rise to numerous paraneoplastic syndromes, such as erythrocytosis, hypercalcemia, hypoglycemia, hypercholesterolemia, and hirsutism. The usual age at presentation in the low-incidence areas is 70 to 80 years, and the male/female ratio is 2.5:1.^{2,14} Most patients have a long history of alcoholic cirrhosis, hemochromatosis, or steroid use.

In the high-incidence areas, the age at presentation is younger (30-45 years), and men are affected eight times more frequently than women.¹⁴ The primary etiologic factors in high-incidence areas are hepatitis B and C viruses and exposure to aflatoxins. In these areas, HCC is aggressive and may be manifested with hepatic rupture and massive hemoperitoneum.¹⁶

RADIOLOGIC FINDINGS

Plain Radiography

When it is sufficiently large, HCC may appear as a nonspecific upper abdominal mass on plain abdominal radiographs. Calcification is rare in the typical HCC but more common in other hepatocellular neoplasms, such as fibrolamellar carcinoma. In patients with hemochromatosis, plain radiographs of the extremities demonstrate degenerative changes with calcium pyrophosphate deposition disease in cartilages.

Nuclear Medicine

Nuclear medicine is only occasionally used for the detection of HCC. On sulfur colloid studies of Western patients, HCC is manifested as a defect in a cirrhotic liver. Hepatomegaly with heterogeneous uptake of the radionuclide and colloid shift to the spleen and bone marrow are frequently noted.¹⁶ It is reported that 30% to 50% of HCCs are not ¹⁸F-fluorodeoxyglucose (¹⁸F-FDG) avid or are only mildly avid^{17,18} because of the abundant amount of the enzyme glucose-6-phosphatase in certain types of HCC. Glucose-6-phosphatase dephosphorylates FDG-6-phosphatase, and as a result of this, FDG “leaks back” into the circulation. However, the use of ¹¹C-acetate as a positron emission tomography (PET) tracer for detection of kinetics and uptake characteristics of fatty acid synthesis in HCC has shown promising results. Well-differentiated HCC, which tends to show negative uptake for FDG because of glucose-6-phosphatase, has uptake of ¹¹C. Unfortunately, ¹¹C has a short half-life of 20 minutes, which leads to the need for an on-site cyclotron. Therefore, in routine situations, there is little role of PET or PET/CT in the diagnosis or staging of HCC.

The soft tissue contrast of liver MRI is far more superior to that of PET for the detection of small primary HCC (<2 cm), especially when liver-specific contrast agents are used. Furthermore, functional MRI techniques, such as diffusion-weighted MRI, have been demonstrated to significantly improve the detection rate of subcentimeter-sized intrahepatic metastasis of HCC compared with conventional MRI alone.¹⁹ If the high sensitivity of liver MRI and the potential of functional MRI can be transferred to combined PET/MRI, it can show a performance no less than that of MRI for the primary diagnosis of HCC. The major advantage of PET/MRI scanners is that MRI evaluation of primary tumor extent and PET evaluation for whole body staging can be performed with a single examination.²⁰

PET/MRI unites the high soft tissue contrast of MRI, the data of functional MRI, and the metabolic information of PET in the evaluation of tumor volume and viability. PET can serve as a tool for differentiating HCCs with low biologic behavior and highly aggressive biologic behavior by measuring tumor ¹⁸F-FDG uptake (standardized uptake value). The aggressiveness of biologic behavior is related to the volume doubling time of HCC and thus is predictive for survival rate, with an inverse relation between the standardized uptake value and survival rate.²¹

Furthermore, ¹⁸F-FDG PET imaging has been proved to be useful for the detection of tumor recurrence in HCC patients after liver transplantation and interventional therapy.²² Although there are studies outlining the high potential of functional MRI techniques, such as dynamic contrast-enhanced MRI and diffusion-weighted MRI, as partners in combination with PET, the exact sensitivity and specificity of PET/MRI for tumor recurrence are still in question.

Ultrasound

The sonographic appearance of HCC is varied (Fig. 87-4). These lesions are frequently hyperechoic, particularly if there is fatty change or marked sinusoidal dilation.²³⁻²⁵ Ultrasonography can detect extremely small tumors and, in combination with serum α -fetoprotein assays, serves as an excellent screening method for high-risk patients with long-standing cirrhosis.^{26,27} This approach to patients has been successful in Asia but has been found to be far less accurate in the United States because of differences in patient body habitus and sonography expertise.

Some authors explain the varied sonographic appearance of HCC on the basis of size. Small HCCs (<3 cm) often appear hypoechoic and are associated with posterior acoustic enhancement; tumors larger than 3 cm more often have a mosaic or mixed pattern.²⁸⁻³⁰ Ultrasound is also capable of demonstrating the capsule in encapsulated HCC, which appears as a thin, hypoechoic band.⁴

Sonography, in conjunction with color and duplex Doppler imaging, can diagnose tumor thrombus in the portal and hepatic veins as well as in the inferior vena cava.^{31,32}

Color Doppler ultrasound has been used to assess the vascularity of HCC.³³ These data plus the resistive index of tumor vessels have been used to differentiate HCC from other tumors.^{34,35} Color Doppler ultrasound demonstrates an intralesional tangle of vessels, the “basket” pattern, in up to 15% of cases, indicating hypervascularity and tumor shunting.^{36,37} Power Doppler has also been assessed in the characterization of HCCs. Although most HCCs show a central pattern of vascularity, so do some hemangiomas and metastases, and the clinical usefulness of this technique is therefore limited.³⁸

The introduction of intravascular contrast agents has improved the ability of ultrasound to diagnose HCC. An HCC typically demonstrates an early hyperperfusion compared with the adjacent normal liver tissue. A chaotic vessel dysmorphism and washout during the portal venous phase are the other characteristics of the tumor.^{39,40}

Computed Tomography

Unenhanced CT scans demonstrate a large, hypodense mass with central areas of lower attenuation that correspond to the tumor necrosis frequently seen in HCC (Figs. 87-5 and 87-6). In North American and European patients, the remainder of the liver shows cirrhosis (60%) or hemochromatosis (20%)^{3,5} (Fig. 87-7).

Multiphasic multidetector computed tomography (MDCT) including nonenhanced, hepatic arterial, portal venous, and delayed phase images is an efficient technique for determination of HCC and preoperative staging of HCC.^{41,42} Because HCC derives most of its blood supply from the hepatic artery, the tumor demonstrates early enhancement during arterial phase and is relatively hypodense on the delayed phase images because of the early washout of contrast medium by arterial blood (see

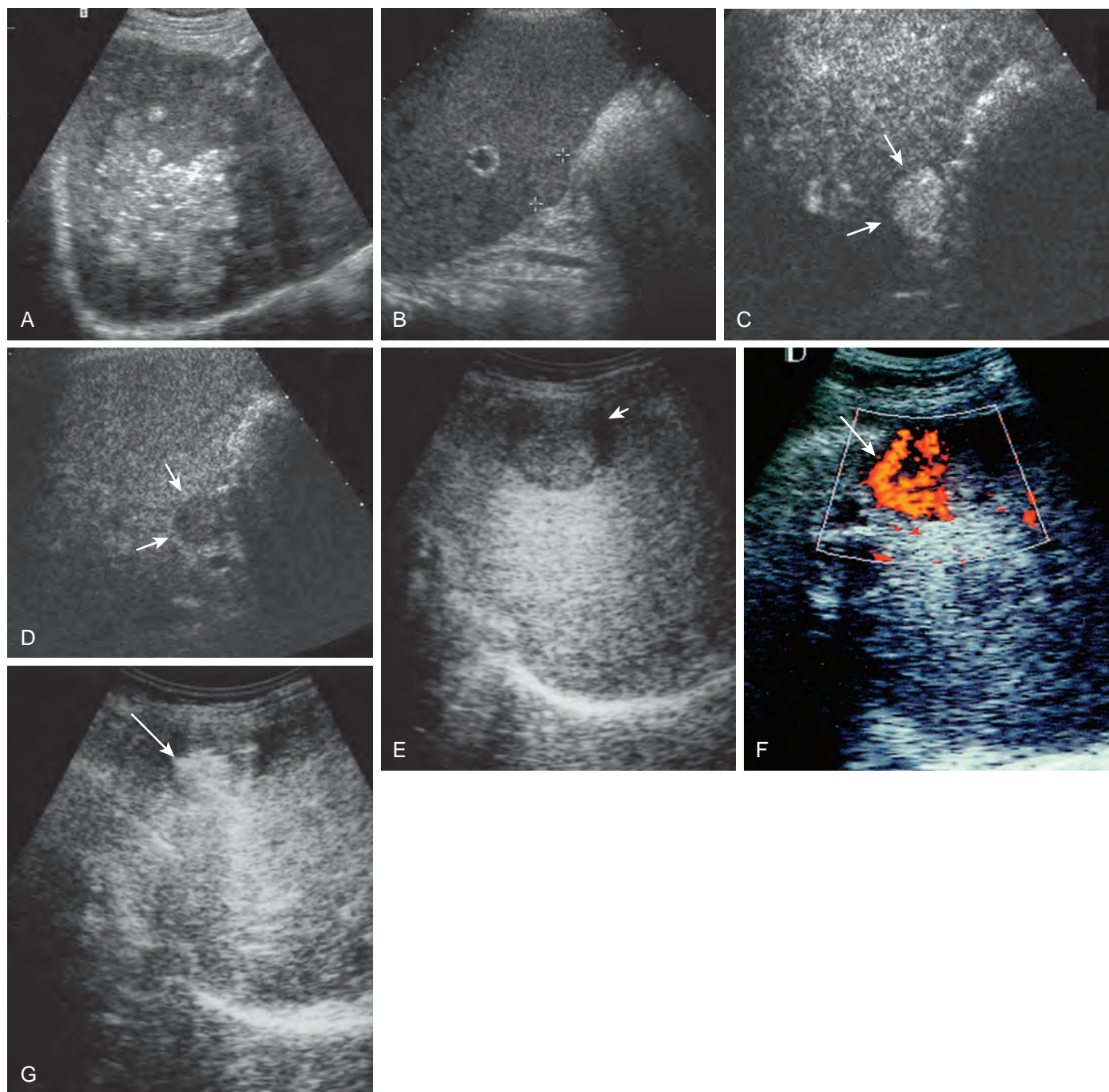


Figure 87-4 HCC: sonographic features. **A.** The neoplasm is strikingly echogenic in this patient. Because of variable amounts of hemorrhage and necrosis, this tumor can have a variety of sonographic appearances. **B-D.** Dynamic contrast-enhanced sonographic images of the liver of 70-year-old man with segment V hepatocellular carcinoma (diameter, 2.3 cm). Baseline sonographic image (**B**) shows focal hypoechoic hepatocellular carcinoma in right hepatic lobe (cursors delineate margins of the tumor). Arterial phase image after the injection of microbubbles (**C**) shows homogeneous enhancement of the lesion (arrows point to margins of the tumor). Late portal phase image (**D**) obtained at 180 seconds shows that the HCC is clearly hypoechoic with respect to surrounding liver. **E-G.** Hepatocellular carcinoma in 59-year-old man. Unenhanced gray-scale sonogram (**E**) shows peripheral halo sign (arrow). Power Doppler sonogram (**F**) shows heterogeneous vascularity (arrow). Early-phase carbon dioxide-enhanced sonogram (**G**) shows vascularity (arrow) similar to that seen in **F**. (**B-D** from Nicolau V, Vilana R, Catalá V, et al: Importance of evaluating all vascular phases on contrast-enhanced sonography in the differentiation of benign from malignant focal liver lesions. *AJR Am J Roentgenol* 186:158–167, 2006. **E-G** from Chen R-C, Chen W-T, Tu H-Y, et al: Assessment of vascularity in hepatic tumors: Comparison of power Doppler sonography and intraarterial CO₂-enhanced sonography. *AJR Am J Roentgenol* 178:67–73, 2002. Reprinted with permission from the American Journal of Roentgenology.)

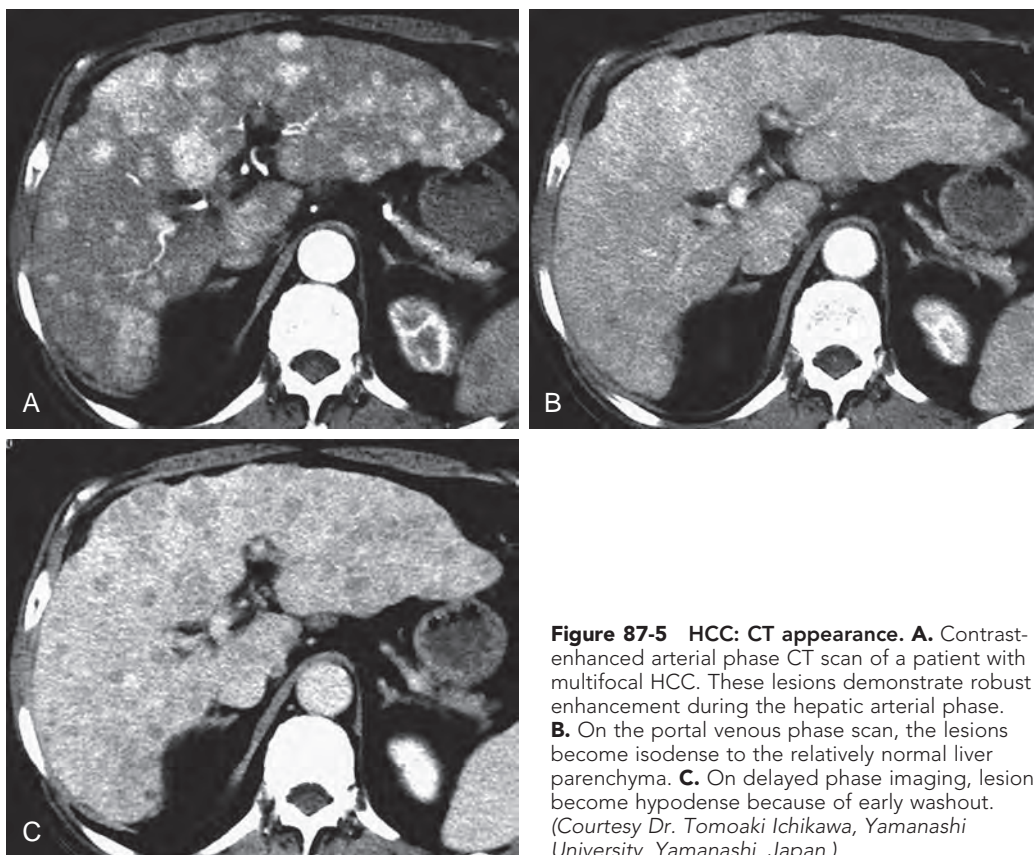


Figure 87-5 HCC: CT appearance. **A.** Contrast-enhanced arterial phase CT scan of a patient with multifocal HCC. These lesions demonstrate robust enhancement during the hepatic arterial phase. **B.** On the portal venous phase scan, the lesions become isodense to the relatively normal liver parenchyma. **C.** On delayed phase imaging, lesions become hypodense because of early washout. (Courtesy Dr. Tomoaki Ichikawa, Yamanashi University, Yamanashi, Japan.)

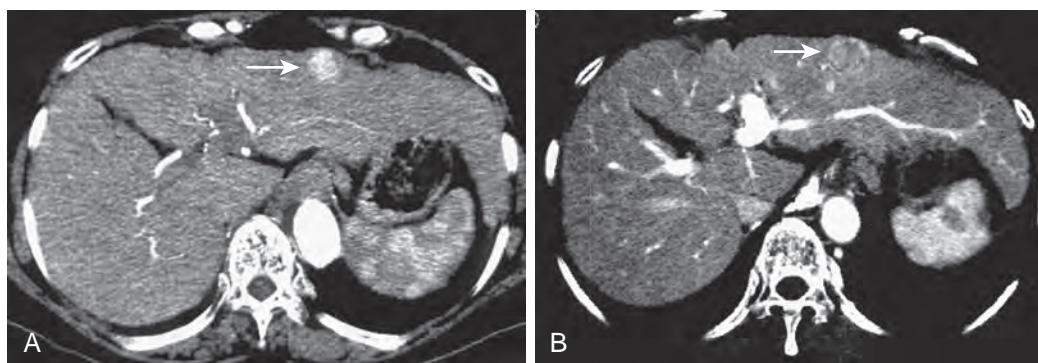


Figure 87-6 HCC: CT findings. **A.** Early arterial phase (25 seconds) contrast-enhanced CT scan shows a rapidly enhancing lesion in the left lobe of the liver (arrow). **B.** On late arterial phase image (40 seconds), HCC becomes less conspicuous because of early washout (arrow). (Courtesy Dr. Tomoaki Ichikawa, Yamanashi University, Yamanashi, Japan.)

Figs. 87-5 and 87-6). The tumor has a variable appearance on the portal phase images.⁴³ Small tumors may appear as lesions of different attenuation, whereas larger ones almost always demonstrate central necrosis (see Fig. 87-7). The capsule appears isodense or hypodense relative to the liver during the hepatic arterial phase and enhances on delayed CT images (see Fig. 87-7).

HCC has a tendency to invade the portal and hepatic veins so that an enlarged venous segment that exhibits intraluminal low attenuation is highly suggestive of tumor thrombus. Differential diagnosis of tumor thrombus can be made through demonstration of the expansion of the main portal

vein diameter (≥ 23 mm) and intrathrombus neovascularity on arterial phase images.⁴⁴ Hepatic venous tumor thrombus may extend into the inferior vena cava and even to the right atrium in some cases. CT can also depict complications of HCC, such as hemoperitoneum associated with rupture of HCC and vascular invasion.^{5,45} Ruptured tumors tend to be located in the periphery of the liver and have a protruding contour.⁴⁶ On arterial phase images, a ruptured tumor appears as a nonenhancing hypodense lesion with focal discontinuity and peripheral rim enhancement. This finding is termed the enucleation sign because of its similarity to an enucleated orbital globe with the remaining intact sclera.⁴³

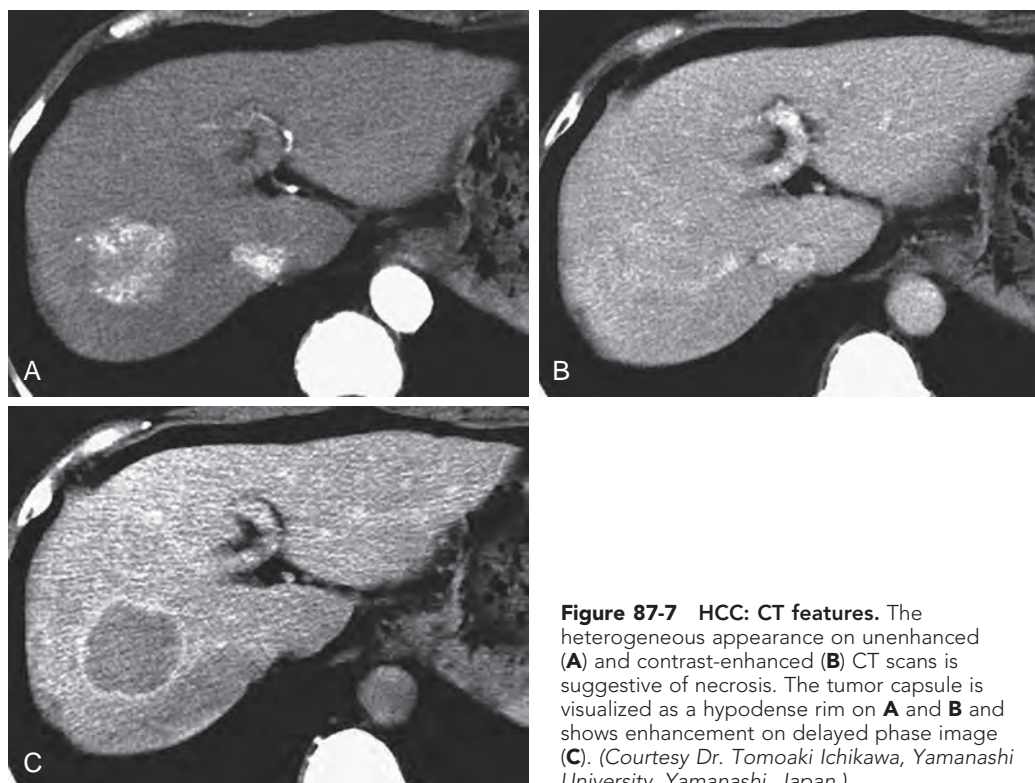


Figure 87-7 HCC: CT features. The heterogeneous appearance on unenhanced (**A**) and contrast-enhanced (**B**) CT scans is suggestive of necrosis. The tumor capsule is visualized as a hypodense rim on **A** and **B** and shows enhancement on delayed phase image (**C**). (Courtesy Dr. Tomoaki Ichikawa, Yamanashi University, Yamanashi, Japan.)



Figure 87-8 HCC: coronal reformatted CT image. Arterial phase CT image shows the tumor (arrow) and feeding artery (arrowhead) branching from the inferior branch of the left hepatic artery. (Courtesy Dr. Tomoaki Ichikawa, Yamanashi University, Yamanashi, Japan.)

An additional role for CT lies in the noninvasive evaluation of hepatic arterial anatomy in potential candidates for liver transplantation.⁴⁷ In the majority of cases, three-dimensional (3D) CT arteriography is comparable to conventional arteriography and surgical findings in the delineation of the major hepatic arteries. The technique of 3D CT angiography is safe, convenient, and less invasive than conventional arteriography (Fig. 87-8).⁴⁷

In patients with underlying hemochromatosis, a dense liver resulting from iron deposition is identified on unenhanced CT scans.³

Angiography

On angiography, HCC is a hypervascular tumor with marked neovascularity and arteriovenous shunting. A large hepatic artery, abnormal vessels, and vascular invasion are usually present.⁴⁸ Avascular or hypovascular areas may be present as a result of necrosis or hemorrhage. Extension of the tumor into the porta hepatis and other perihepatic veins is frequently detected.⁴⁹ Hepatic venous tumor thrombus has been described in 6% of cases.⁵⁰ The presence of the “threads and streaks” sign is characteristic of this intravenous tumor thrombus.⁴⁹

Although biliary invasion by HCC is rare, percutaneous or retrograde cholangiography and magnetic resonance cholangiopancreatography (MRCP) may occasionally demonstrate that the tumor is causing obstruction or a mass within the biliary tree.

Magnetic Resonance Imaging

On MRI, HCC has a variable appearance (Figs. 87-9 to 87-11) with low-intensity, isointensity, and high-intensity patterns seen on T1-weighted images, depending on the degree of fatty change, the presence of internal fibrosis, and the dominant histologic pattern.⁵¹⁻⁵³ The capsule of encapsulated HCCs is visualized as a hypointense rim in T1-weighted images.

MRI has also been used to differentiate small HCCs from regenerative nodules of cirrhosis.^{54,55} Cirrhotic nodules are usually of high signal intensity on T1-weighted images.⁵⁶ On T2-weighted images, cirrhotic nodules are isodense or hypointense to the liver.⁵⁶ The relative hypointensity is due to greater accumulation of iron within the nodule than in surrounding liver.⁵⁶ Also, the inflammatory fibrous septa within the liver demonstrate increased signal on T2-weighted images, and consequently cirrhotic nodules appear relatively hypointense.⁵⁶ In contrast, HCCs are often hyperintense on T2-weighted images

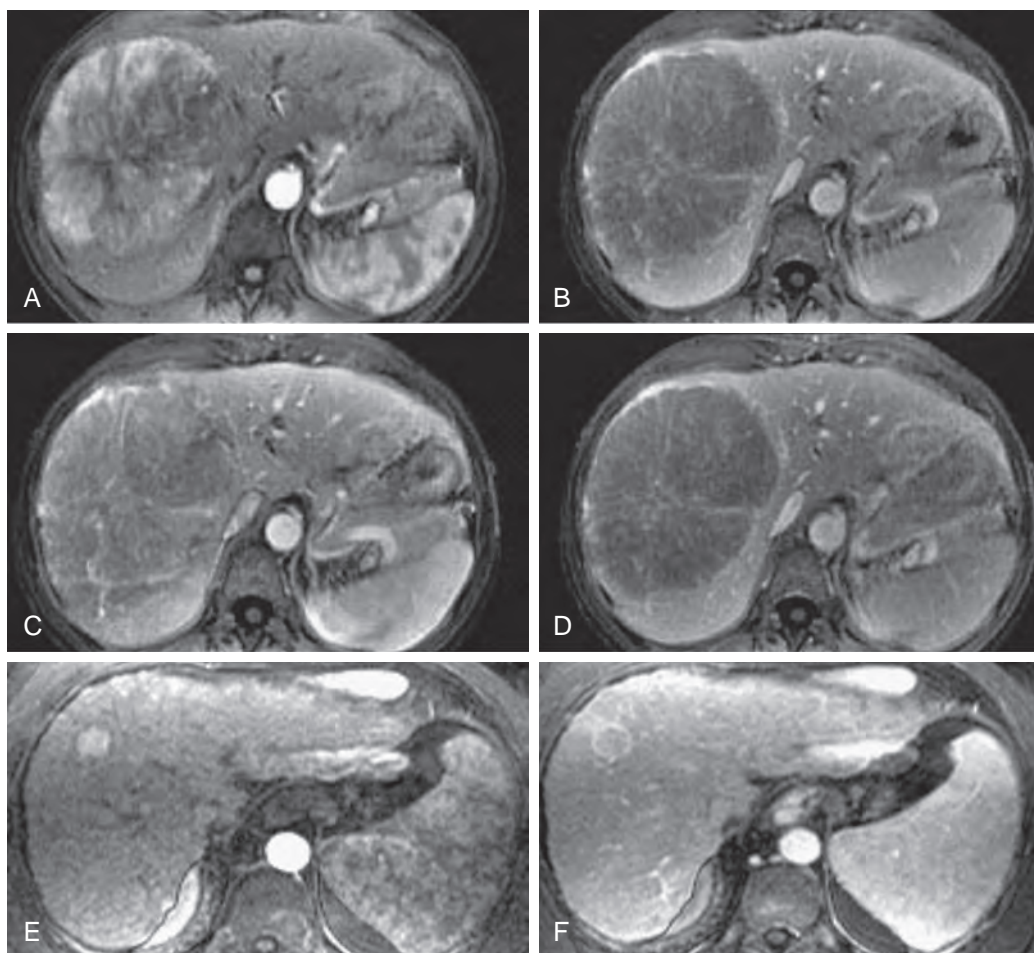


Figure 87-9 HCC: MRI contrast enhancement patterns. Hypervascular HCC shows robust contrast enhancement during the hepatic arterial phase (**A**), which rapidly becomes isointense during the portal venous phase (**B**). This tumor rapidly becomes hypointense relative to the normal liver on delayed phase imaging (**C** and **D**). In a different patient with cirrhosis, this small HCC shows uniform enhancement during the hepatic arterial phase (**E**) and washout with ring enhancement on the portal venous phase image (**F**).

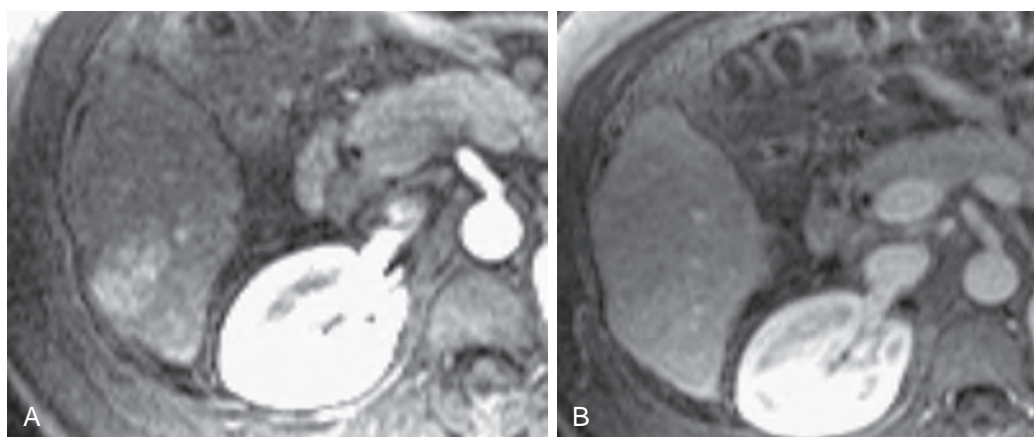


Figure 87-10 HCC: the importance of hepatic arterial phase imaging on MRI. The tumor enhances during the hepatic arterial phase (**A**) and becomes isodense with the adjacent parenchyma during the portal venous phase (**B**). Thus this lesion would not be detected if scans were obtained only during the portal venous phase.

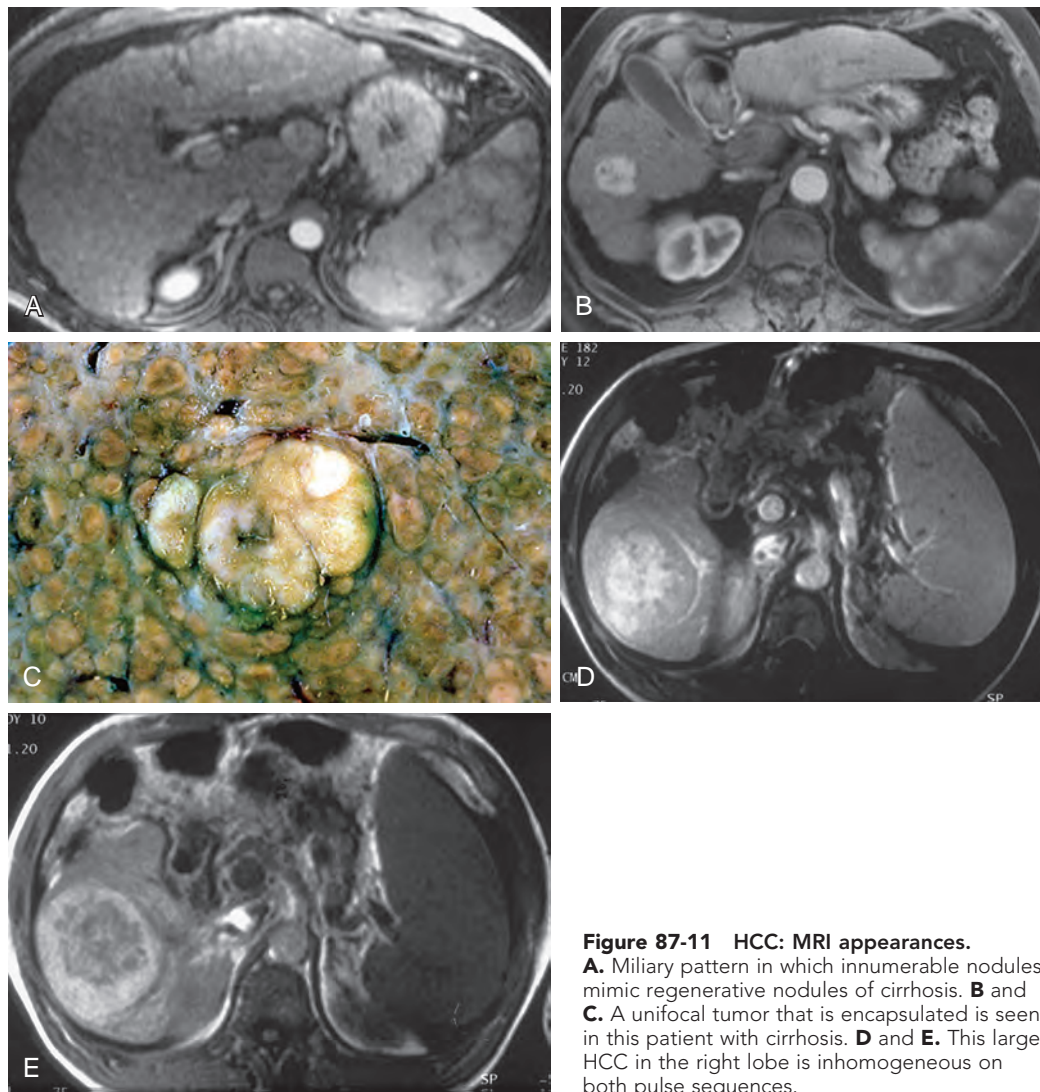


Figure 87-11 HCC: MRI appearances.

A. Miliary pattern in which innumerable nodules mimic regenerative nodules of cirrhosis. **B** and **C.** A unifocal tumor that is encapsulated is seen in this patient with cirrhosis. **D** and **E.** This large HCC in the right lobe is inhomogeneous on both pulse sequences.

and can be distinguished from hypointense nodules.⁵⁶ However, some well-differentiated HCCs have signal characteristics similar to cirrhotic nodules, and diagnosis is less straightforward.⁵⁶ HCC arising within a siderotic nodule has a characteristic “nodule within a nodule” appearance on MRI. The HCC appears as a small focus of high signal intensity within the low signal intensity nodule.⁵⁶ These lesions are often demonstrated only at MRI, and MR-guided biopsy is now being performed at many centers.⁵⁷ However, biopsy may be technically difficult because the lesions are small; direct referral for surgery may be a better option if the patient is a good surgical candidate.^{56,57}

As with CT, HCC during dynamic gadolinium-enhanced MRI (Fig. 87-12; see also Fig. 87-9) shows early enhancement in the hepatic arterial phase. In the portal venous phase, the tumor is usually isointense; in delayed phase, it becomes hypointense because of the washout of contrast medium. However, some tumors may show progressive enhancement in the dynamic imaging.⁴³ HCCs larger than 1.5 cm tend to have a fibrous capsule that may be demonstrated as a hypointense band on delayed phase images.⁵⁸ MRI depicts vascular invasion, which is seen in 30% to 50% of patients, as a lack of signal

void on multislice T1-weighted gradient recalled echo and flow-compensated T2-weighted fast spin-echo images.⁵⁹ On gadolinium-enhanced images, the tumor thrombus shows a typical early arterial enhancement.

Intravenous administration of superparamagnetic iron oxide (SPIO) also increases the detection sensitivity of MRI.⁶⁰ MRI with SPIO is especially helpful in the detection of small HCCs in cirrhotic livers. In a study, more HCCs were detected on images acquired with SPIO-enhanced fast low-angle shot and long repetition time sequences (2000/70 and 2000/28) than on unenhanced scans.⁶¹ A potential limitation of this technique is that early HCCs may accumulate iron because of the presence of reticuloendothelial cells and will therefore mimic normal liver parenchyma on SPIO-enhanced sequences.⁶¹ In these cases, unenhanced MR images may provide valuable information concerning the internal morphology of these lesions, enabling the correct diagnosis of HCCs.⁶¹ Hepatobiliary contrast agents such as gadoxetate (Gd-EOB-DTPA) may be useful in the characterization of questionable lesions. Use of hepatobiliary contrast agents may allow differentiation of hepatocellular tumors such as HCC from nonhepatocellular tumors.⁶²

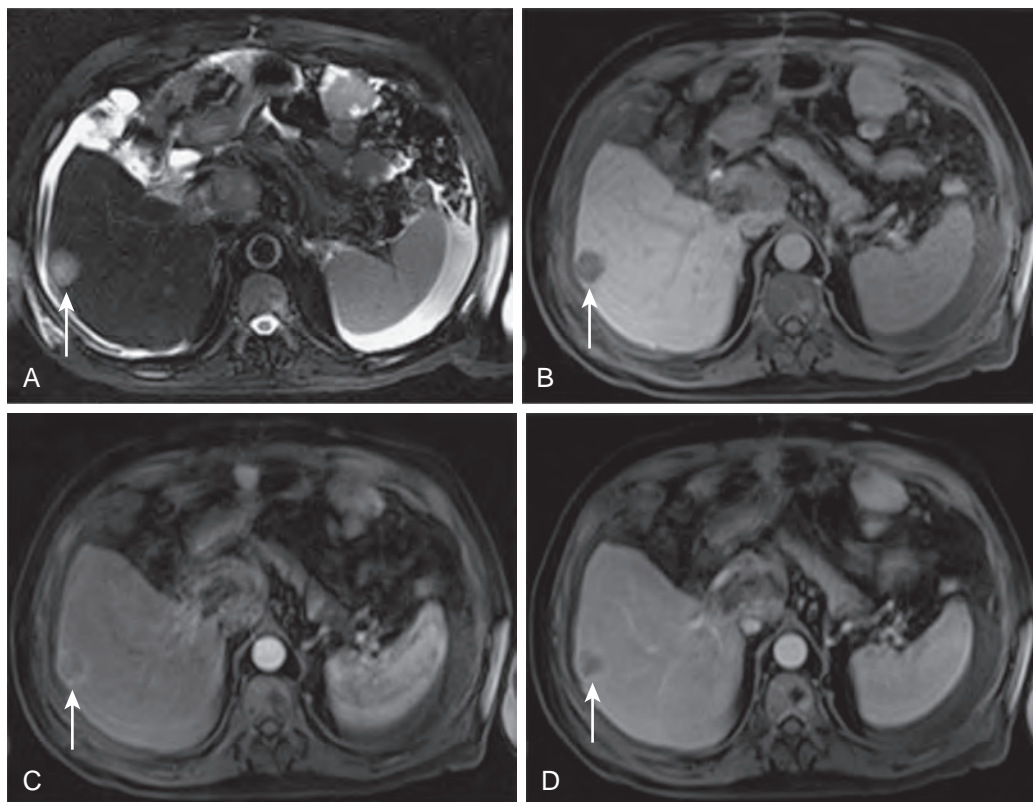


Figure 87-12 HCC (arrows): MRI findings. HCC in the right lobe of the liver that is hyperintense on the T2-weighted image (A) and hypointense on the T1-weighted image (B). It shows arterial enhancement and then washout on the arterial phase (C) and portal venous phase (D) images, respectively.

Preliminary studies suggest that on delayed images with a hepatobiliary contrast agent, well-differentiated HCCs often behave like hepatocytes, appearing isointense or sometimes hyperintense, whereas poorly differentiated HCCs typically do not accumulate the contrast agent and appear relatively hypointense.^{63,64} Although accumulation of contrast material in a lesion does not exclude HCC, if HCC accumulates a hepatobiliary contrast agent, it is postulated to be well differentiated.^{63,64}

Approximately 15 to 20 minutes after the injection Gd-EOB-DTPA, in the hepatocytic phase, hepatocytes take up contrast agent by transporter of organic anion-transporting polypeptides 1B3 (OATP1B3).⁶⁵ Gd-EOB-DTPA works as a T1-shortening agent at the hepatocytic phase, and malignant liver lesions, such as HCC and metastases, are spared from the uptake of contrast material that occurs in the background liver parenchyma.^{66,67}

HCC usually appears hypointense relative to background liver signal intensity in the hepatocellular phase, probably owing to impaired expression of the membrane cotransporters necessary for uptake of the contrast agent. A minority of HCCs appear isointense or hyperintense relative to the background liver signal intensity, demonstrating hepatocellular phase uptake. It is reported that there is a significant correlation between the level of expression of OATP1B3 and the enhancement ratio within the tumors.⁶⁵ On the basis of the data published to date, it appears that HCCs with uniform signal hyperintensity in the hepatocellular phase may be well or moderately differentiated but are rarely if ever poorly differentiated.⁶⁸

Many small hypovascular HCCs can be detected only on hepatocytic phase images, showing no arterial enhancement and only mild washout in the portal venous and equilibrium phases of dynamic MDCT and dynamic MRI with Gd-DTPA (Fig. 87-13).⁶⁹

Gd-EOB-DTPA-enhanced MRI can reveal HCC as a nodule appearing hypointense relative to the background liver parenchyma regardless of its histologic differentiation (Figs. 87-14 and 87-15).^{70,71} Gd-EOB-DTPA-enhanced MRI has higher sensitivity for detection of hypovascular and hypervascular HCCs compared with either dynamic MDCT or dynamic MRI with Gd-DTPA. Gd-EOB-DTPA-enhanced MRI also has higher sensitivity for detection of hypovascular HCC or hypervascular HCC compared with SPIO-enhanced MRI.⁷¹

Regenerative nodules and dysplastic nodules are the two key cirrhotic nodular lesions that are important to identify and differentiate from HCC. Regenerative nodules have primarily portal venous blood supply with mild contribution from hepatic artery blood.⁵⁸ Therefore, they typically do not show early enhancement during the arterial phase of dynamic MRI while enhancing with the rest of the liver in the portal phase. Regenerative nodules are usually isointense on both T1- and T2-weighted images, with the exception of some “siderotic” nodules that contain iron and therefore have a low signal intensity on T1- and T2-weighted MRI.⁵⁸

Dysplastic nodules develop from regenerative nodules and are present in 15% to 25% of cirrhotic livers.⁷² Although they contain atypical hepatocytes, they do not have definite features of malignancy on histology.¹⁰ Depending on the degree of

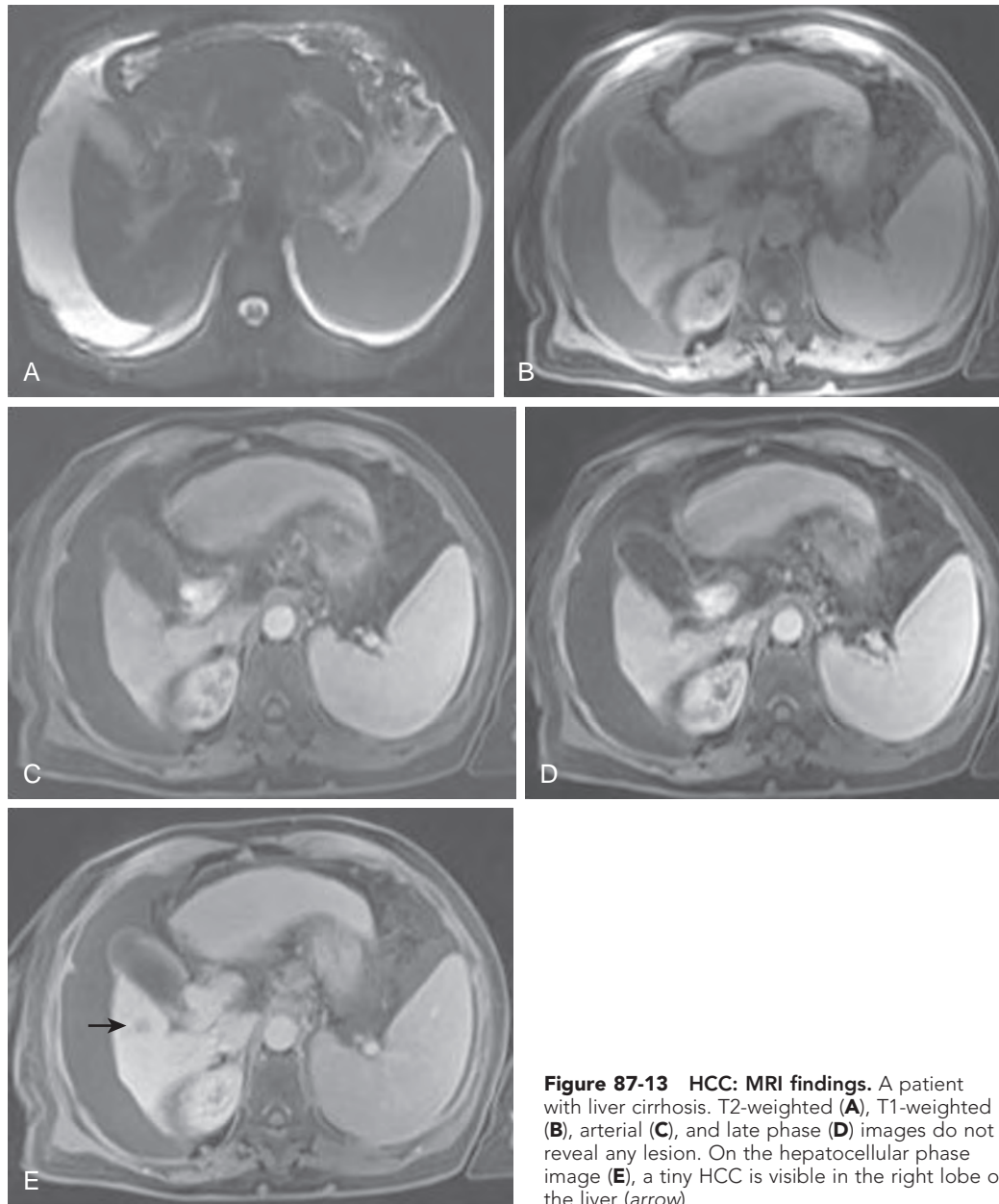


Figure 87-13 HCC: MRI findings. A patient with liver cirrhosis. T2-weighted (A), T1-weighted (B), arterial (C), and late phase (D) images do not reveal any lesion. On the hepatocellular phase image (E), a tiny HCC is visible in the right lobe of the liver (arrow).

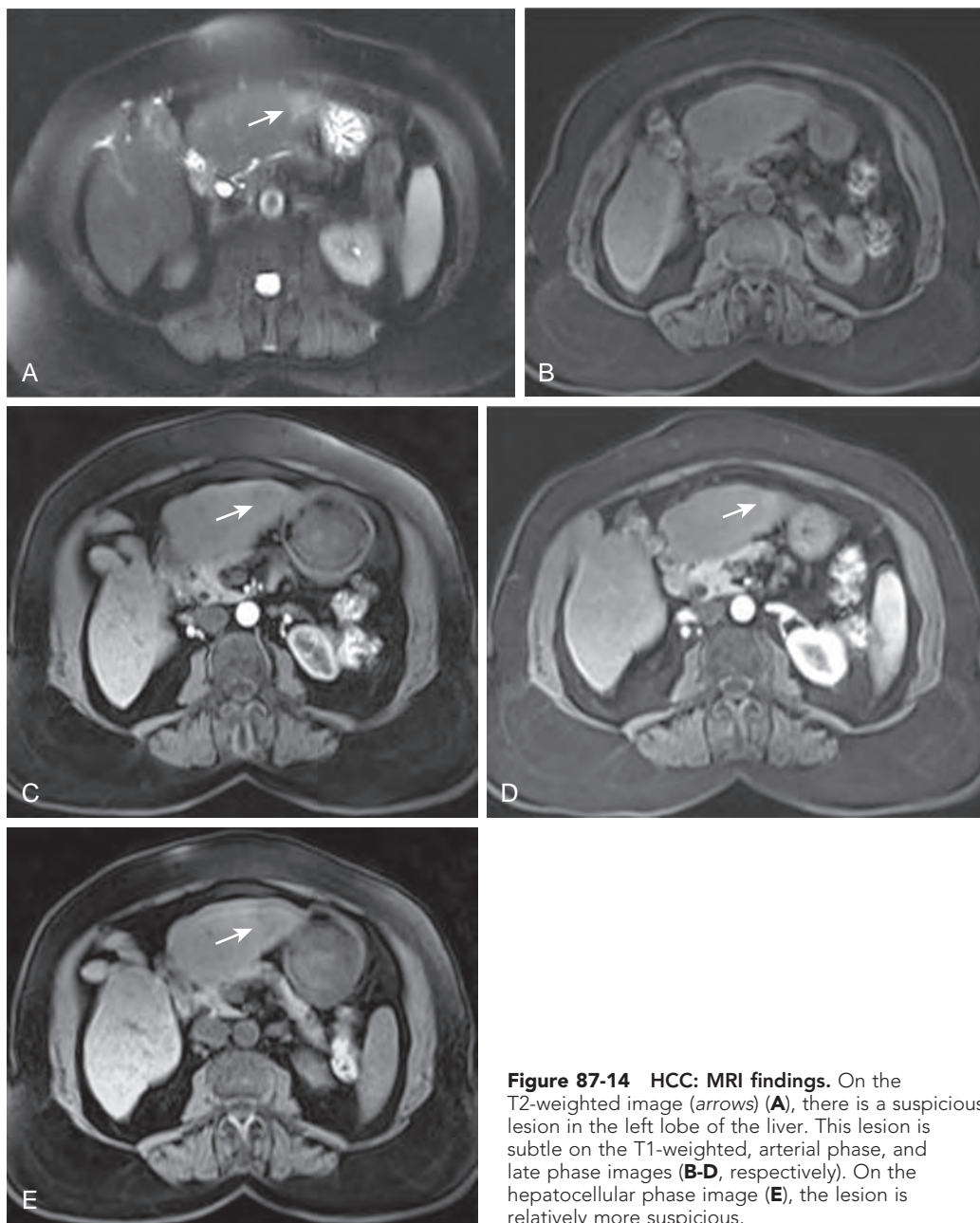


Figure 87-14 HCC: MRI findings. On the T2-weighted image (arrows) (A), there is a suspicious lesion in the left lobe of the liver. This lesion is subtle on the T1-weighted, arterial phase, and late phase images (B-D, respectively). On the hepatocellular phase image (E), the lesion is relatively more suspicious.

differentiation, they are histologically classified as low grade or high grade. Although high-grade ones may develop arterial hypervascularity, dysplastic nodules receive their blood supply mainly from the portal vein.⁷³ High-grade dysplastic nodules are considered premalignant⁷⁴ and can undergo malignant transformation within a short time like 4 months (Fig. 87-16).⁷⁵ Nevertheless, the clinical significance of dysplastic nodules is unclear, and current management guidelines do not advocate aggressive workup of suspected dysplastic nodules.⁷⁶

Their usual MR appearance is that of homogeneous hyperintensity on T1-weighted images and hypointensity on T2-weighted images. A high signal intensity focus within a low signal intensity nodule on T2-weighted images is the nodule within a nodule appearance of a dysplastic nodule with a focus of HCC.^{58,77}

After administration of Gd-EOB-DTPA, in the hepatocyte phase, regenerative nodules generally take up and excrete contrast material because of preserved hepatocellular function and intact organic ion transporters, showing signal intensity similar to liver parenchyma. The number of expressed organic ion transporters decreases with progression of atypia in dysplastic nodules, reducing their ability to take up Gd-EOB-DTPA. Dysplastic nodules that retain their ability to take up but not to excrete the contrast media appear homogeneously or heterogeneously hyperintense because of intracellular cholestasis, whereas nodules that lost their ability to take up contrast media appear hypointense in the hepatocyte phase of Gd-EOB-DTPA.⁷⁸ Such hypointense nodules can be mistaken for HCCs in the hepatocyte phase, and their interpretation is not fully understood.⁷⁸

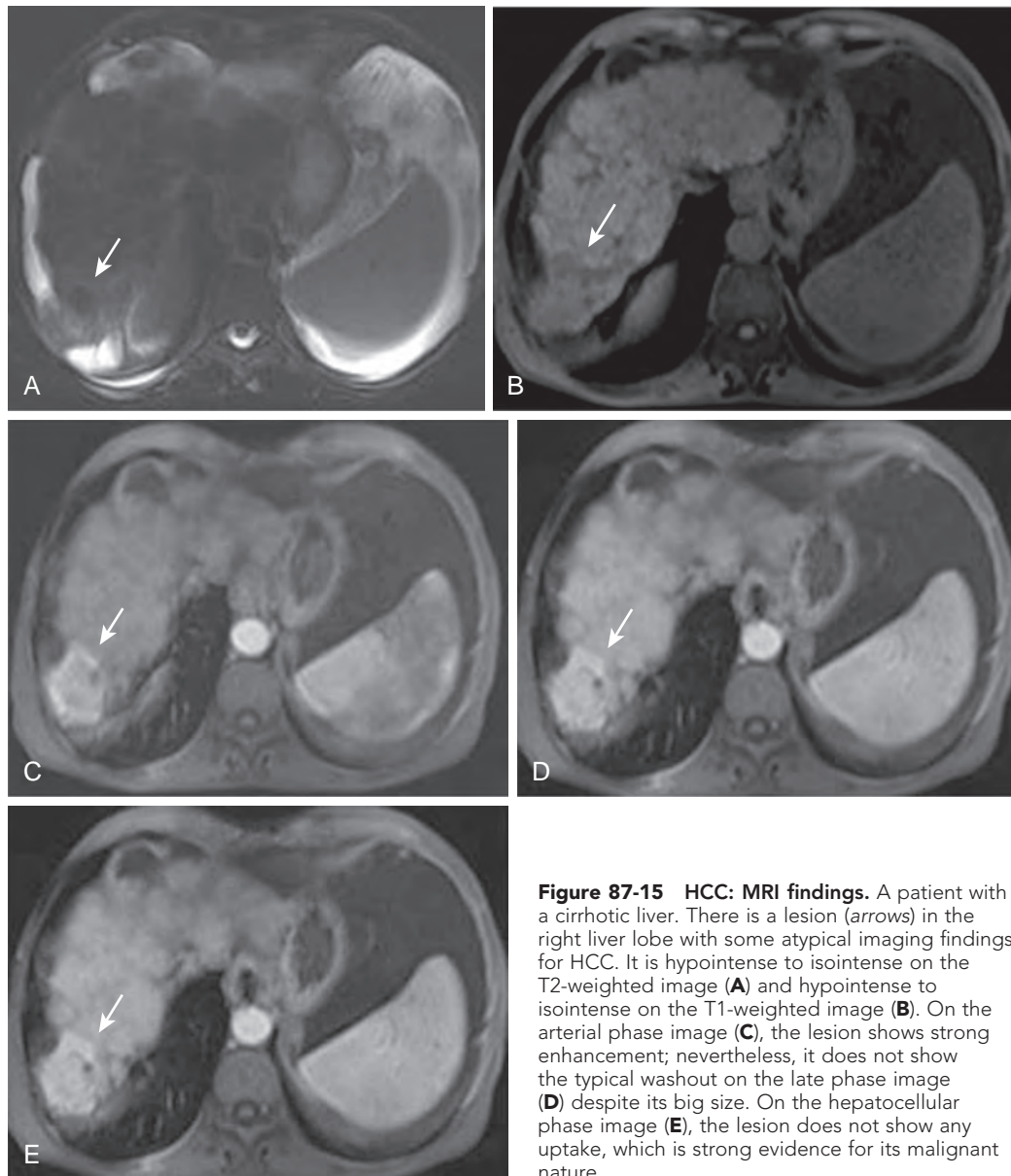


Figure 87-15 HCC: MRI findings. A patient with a cirrhotic liver. There is a lesion (arrows) in the right liver lobe with some atypical imaging findings for HCC. It is hypointense to isointense on the T2-weighted image (A) and hypointense to isointense on the T1-weighted image (B). On the arterial phase image (C), the lesion shows strong enhancement; nevertheless, it does not show the typical washout on the late phase image (D) despite its big size. On the hepatocellular phase image (E), the lesion does not show any uptake, which is strong evidence for its malignant nature.

Studies have shown that diffusion-weighted imaging can be helpful in differentiating cysts and hemangiomas from solid lesions, but differentiation among different solid lesions such as HCC, focal nodular hyperplasia (FNH), and adenoma may be challenging on the basis of apparent diffusion coefficient (ADC) values alone.^{79,80} A mass in a cirrhotic liver that shows restricted diffusion favors a solid lesion and is more likely to be HCC, especially when other supporting MRI features are present. Conversely, not all HCCs show restricted diffusion on diffusion-weighted imaging. A hepatic mass demonstrating MRI features of hepatoma even with the absence of restricted diffusion can still be HCC. Diffusion-weighted imaging has also been used for monitoring of response to therapies such as transarterial chemoembolization and radioembolization; however, the utility of diffusion-weighted imaging in differentiation of tumor grades is not clearly established.^{81,82}

Fibrolamellar Carcinoma

PATHOLOGIC FINDINGS

Fibrolamellar carcinoma (FLC) is a slow-growing tumor that arises in normal liver. It is composed of neoplastic hepatocytes separated into cords by lamellar fibrous strands.² These lesions have a distinctive microscopic pattern with eosinophilic, malignant hepatocytes containing prominent nuclei⁸³ (Fig. 87-17). Some of the markers usually present in typical HCC, such as inclusions of α -fetoprotein bodies, are not present. The fibrous component accounts for half of the tumor distributed in multilamellate strands, except in larger tumors containing large central scars.²

FLC usually arises in a normal liver, with only 20% of patients having underlying cirrhosis.⁸³ Satellite nodules are often present. The gross appearance of FLC is somewhat similar to that of

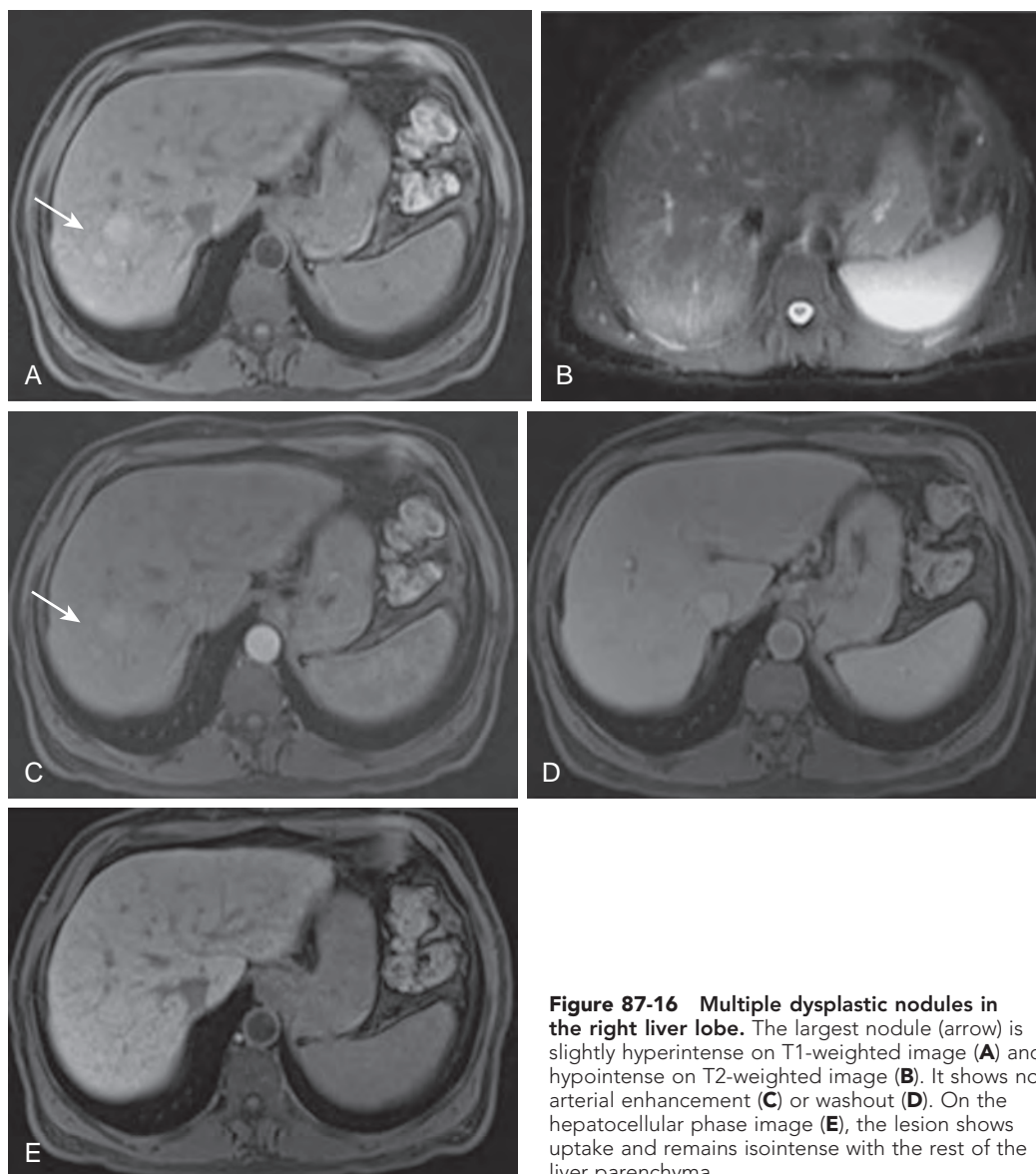


Figure 87-16 Multiple dysplastic nodules in the right liver lobe. The largest nodule (arrow) is slightly hyperintense on T1-weighted image (A) and hypointense on T2-weighted image (B). It shows no arterial enhancement (C) or washout (D). On the hepatocellular phase image (E), the lesion shows uptake and remains iso-intense with the rest of the liver parenchyma.

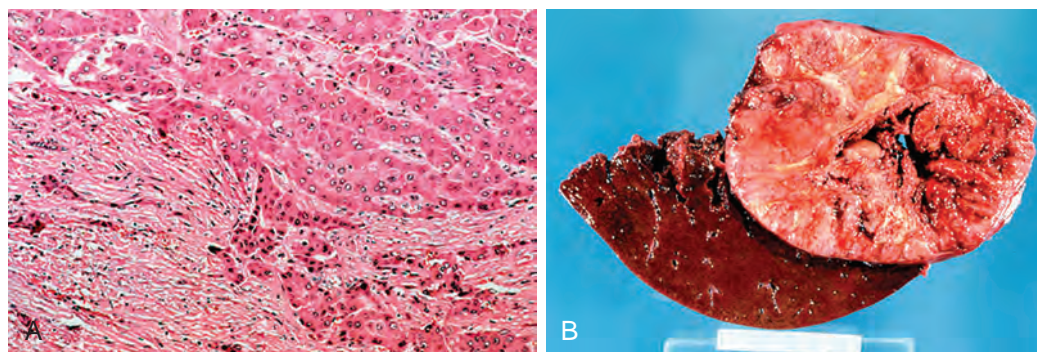


Figure 87-17 Fibrolamellar carcinoma (FLC): pathology. A. Coarse lamellar fibrosis is characteristic of FLC. B. Cut section demonstrates a central scar with radiating septa.

TABLE 87-1
Fibrolamellar Carcinoma

Pathologic Features	Radiologic Features
Lamellar fibrosis (septa), "true scar"	Hypovascular: CT, angiography Hypointense: T2-weighted MRI Calcification: CT, plain radiography, ultrasound
No necrosis or hemorrhage	Homogeneous mass: CT, ultrasound, MRI
No underlying cirrhosis	Normal hepatic morphology except for mass: CT, ultrasound, MRI

FNH in that both tumors have a central scar and multiple fibrous septa. Hemorrhage and necrosis are rare. Radiologic-pathologic correlates are given in Table 87-1.

INCIDENCE AND CLINICAL PRESENTATION

There is some confusion in the literature about the incidence and clinical presentation of FLC because it was not recognized as a biologic entity until the 1980s.⁸⁴ FLC usually occurs in adolescents and adults younger than 40 years and without underlying cirrhosis or other predisposing risk factors.⁸³ There is no sex predominance, and the mean survival is considerably better than that for other types of HCC (45-60 months vs. 6 months), with a high likelihood of cure (40%) if the tumor is surgically resectable.^{85,86}

Clinically, patients with HCC usually present with pain, malaise, and weight loss; jaundice occurs only occasionally, when FLC invades the biliary tree. A palpable mass is seen in two thirds of patients.⁸⁷ α -Fetoprotein levels are usually normal.

RADIOLOGIC FINDINGS

Plain Radiography

On plain abdominal radiographs, FLC frequently appears as a partially calcified upper abdominal mass.

Nuclear Medicine

Nuclear medicine is no longer routinely used in the detection of FLC. Sulfur colloid scintiscans usually demonstrate a defect in a liver that has no evidence of underlying cirrhosis. Multiple defects can be seen in cases of multifocal FLC.

Ultrasound

Sonography typically demonstrates a large, well-defined, lobulated mass (Fig. 87-18) with variable echotexture. FLC usually is of mixed echogenicity (60% of cases) and predominantly contains hyperechoic or isoechoic components.⁸⁸ If the central scar is present, it may be visualized as a central area of hyperechogenicity.

Computed Tomography

On unenhanced CT scans, FLC appears as a hypodense mass with a well-defined contour (Figs. 87-19 and 87-20). Areas of decreased density within the tumor correspond to the central scar or necrosis and hemorrhage.⁸⁹ Stellate calcification within the central scar can also occur.^{87,89} During the arterial and portal phases of dynamic enhanced CT, the "nonscar" portion of FLC enhances heterogeneously. This heterogeneous enhancement

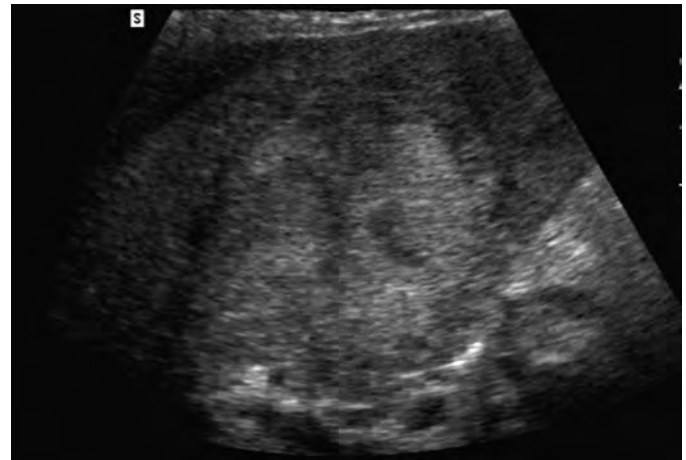


Figure 87-18 FLC: ultrasound findings. The extensive fibrosis present within this neoplasm accounts for the echogenic appearance of this mass.

pattern during the arterial and portal phases probably corresponds to the more vascular, cellular portions of the tumor in comparison with the fibrous (lamellae and scar) and necrotic portions.⁸⁸ On the other hand, the relative delayed phase homogeneity of the tumor probably reflects the washout of the contrast material from its more vascular portions together with delayed enhancement of the fibrous lamellae. In some cases, central scar may also demonstrate delayed enhancement, and the appearance of the tumor, on delayed images, may closely simulate that of FNH. Although FLC is a tumor not characteristically encapsulated, the compressed liver tissue adjacent to it may demonstrate delayed enhancement.⁸⁸ Features that determine the resectability of FLCs, such as portal vein invasion and lymphadenopathy, are well seen on CT scans.⁸⁹⁻⁹¹

Angiography

On angiography, FLC is a hypervascular tumor with compartmentalization in the capillary phase resulting from multiple fibrous septa.⁷⁵ Daughter nodules or secondary lesions may be noted in the capillary phase of arteriography.

Magnetic Resonance Imaging

FLC is hypointense or isointense with normal liver on T1-weighted images and isointense or slightly hyperintense on T2-weighted images.^{92,93} Because of its purely fibrous nature, the scar is hypointense on both T1- and T2-weighted images (Fig. 87-21). However, hyperintensity of the central scar on T2-weighted images has been described in a biopsy-proved FLC that was initially diagnosed as FNH on the basis of imaging findings alone.⁹⁴ The enhancement pattern of FLC seen with gadolinium-enhanced dynamic MRI parallels the enhancement seen with dynamic contrast-enhanced CT. The tumor demonstrates heterogeneous enhancement in the arterial and portal phases and progressively becomes more homogeneous on delayed images (Fig. 87-22).⁹³

On hepatocyte phase images, fibrolamellar HCC appears predominantly hypointense, but components of the tumor may show some uptake of Gd-EOB-DTPA, indicative of a primary liver lesion. FNH, on the other hand, shows intense uptake of hepatocyte-specific (hepatobiliary) contrast agents during the hepatobiliary phase.^{95,96}

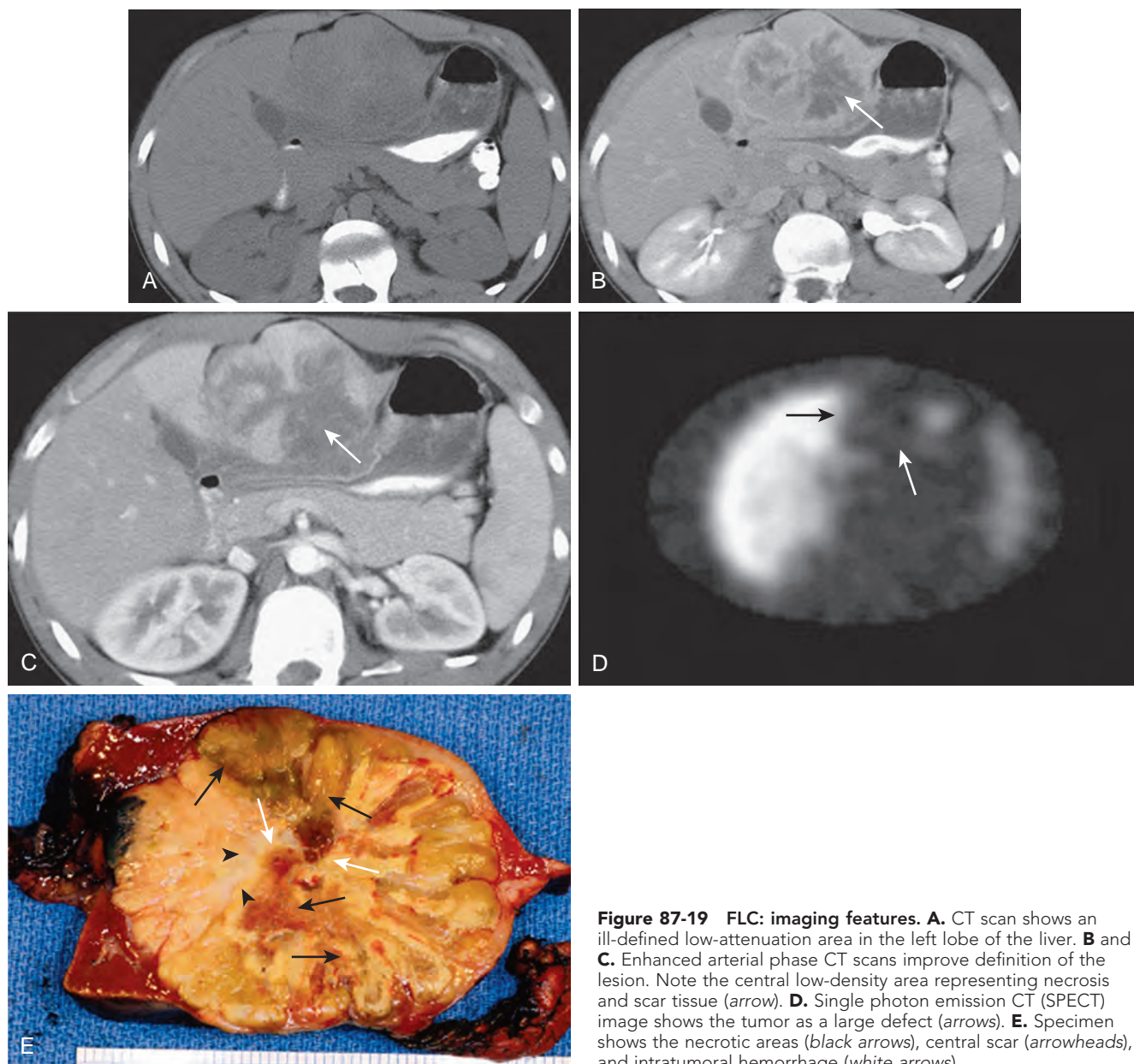


Figure 87-19 FLC: imaging features. **A.** CT scan shows an ill-defined low-attenuation area in the left lobe of the liver. **B** and **C.** Enhanced arterial phase CT scans improve definition of the lesion. Note the central low-density area representing necrosis and scar tissue (arrow). **D.** Single photon emission CT (SPECT) image shows the tumor as a large defect (arrows). **E.** Specimen shows the necrotic areas (black arrows), central scar (arrowheads), and intratumoral hemorrhage (white arrows).

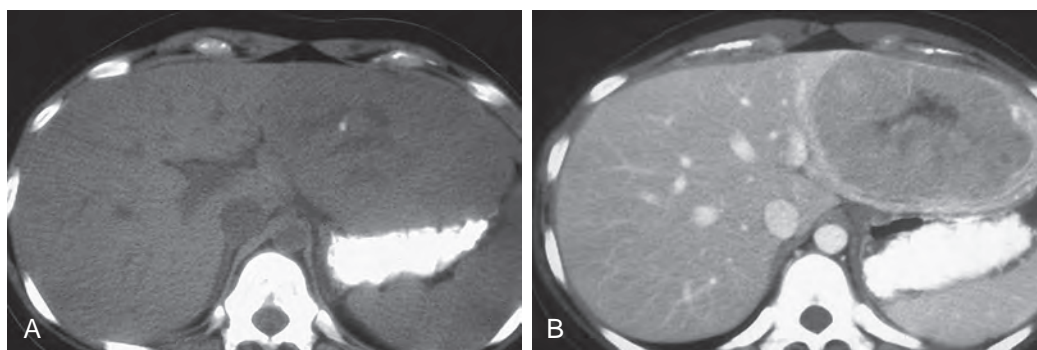


Figure 87-20 FLC: CT findings. **A.** This noncontrast scan shows calcification of the central scar. **B.** The central scar is better appreciated on this contrast-enhanced scan.

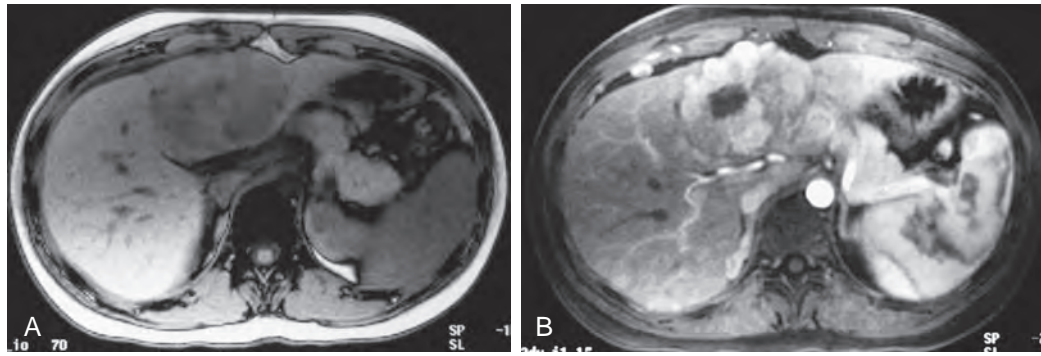


Figure 87-21 FLC: MRI findings. Unenhanced scan of a low signal intensity mass (A) that showed striking enhancement with the exception of the central scar on the contrast-enhanced image (B).

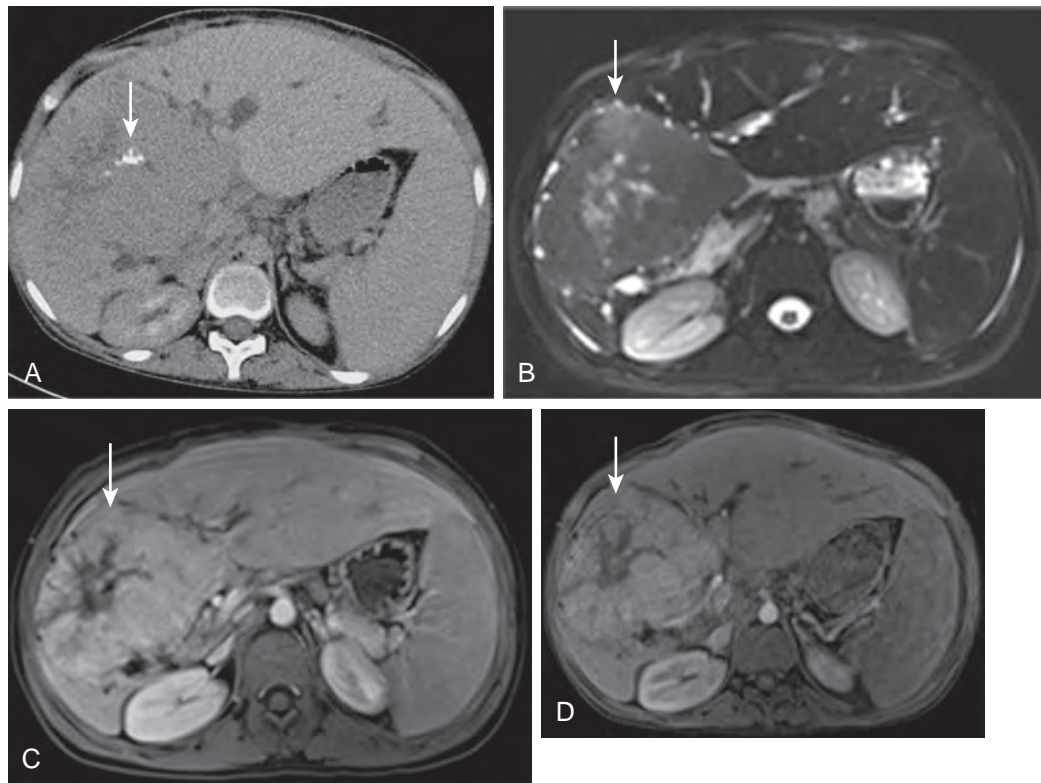


Figure 87-22 FLC: CT and MRI findings. A patient with a large fibrolamellar carcinoma (arrows). Note the central calcification as depicted on the nonenhanced CT image (A). The lesion is slightly hyperintense on the T2-weighted image (B), with areas of central necrosis. It shows strong enhancement on the arterial and portal venous images (C-D, respectively).

DIFFERENTIAL DIAGNOSIS

The major differential diagnosis with FLC is FNH. FNH can be differentiated from FLC in the majority of cases because the central scar of FNH is hyperintense on T2-weighted images. FNH rarely has calcification within the scar (<1.5% of cases compared with up to 55% of FLC).^{89,97} FNH is usually asymptomatic, whereas patients with FLC usually present with some symptoms. FNH shows strong uptake of hepatobiliary contrast agents. Biopsy demonstrates malignant, eosinophilic hepatocytes in FLC and normal hepatocytes with bile ductules in FNH (Table 87-2).

Hepatoblastoma

PATHOLOGIC FINDINGS

Hepatoblastoma is a malignant tumor of hepatocyte origin that often contains mesenchymal elements.⁹⁸ On microscopic examination, it can be classified as epithelial or mixed (epithelial-mesenchymal).²

Epithelial hepatoblastoma consists of fetal or embryonal malignant hepatocytes. Mixed hepatoblastoma has both an epithelial (hepatocyte) component and a mesenchymal component consisting of primitive mesenchymal tissue and osteoid

material or cartilage⁹⁹ (Fig. 87-23). This histologic classification has prognostic implications; the epithelial type, particularly if it has fetal hepatocyte predominance, has a better prognosis than the other forms. Embryonal epithelial cells are more primitive than fetal epithelial and mesenchymal cells, and tumors with this histologic type have a worse prognosis.^{99,100} A rare anaplastic form of hepatoblastoma has an even poorer prognosis than the mixed form of hepatoblastoma.²

In gross appearance, hepatoblastoma is usually a large, well-circumscribed solitary mass that has a nodular or lobulated surface; 20% are multifocal.² On cut section, the appearance varies according to the histologic type. Epithelial hepatoblastomas are more homogeneous; mixed hepatoblastomas with osteoid and cartilage have large calcifications, fibrotic bands, and overall a more heterogeneous appearance.¹⁰¹

INCIDENCE AND CLINICAL PRESENTATION

Hepatoblastoma is the most common primary liver neoplasm in childhood. It usually develops in the first 3 years of life. Although it may be present at birth or develop in adolescents and young adults,¹⁰² this tumor has a peak incidence between 18 and 24 months of age. Hepatoblastoma is more frequent in males than in females.

Clinically, children with hepatoblastoma present with abdominal swelling that may be accompanied by anorexia or weight loss. More rarely, children may present with precocious puberty due to secretion of gonadotropins or testosterone by the tumor.¹⁰³ The serum α -fetoprotein level is markedly elevated in most patients. This tumor is aggressive, and lung metastases are frequently encountered at the time of diagnosis.¹⁰⁴ Conditions associated with hepatoblastoma include Beckwith-Wiedemann syndrome, hemihypertrophy, familial polyposis coli, and Wilms' tumor.¹⁰³

RADIOLOGIC FINDINGS

Plain Radiography

Because hepatoblastoma is usually a large solitary tumor, a large right upper quadrant mass may be detected on plain abdominal radiographs. Extensive coarse, dense calcification is often present because of osteoid formation.¹⁰⁴

Nuclear Medicine

Hepatoblastoma appears as a large defect on sulfur colloid scans. It may take up gallium and FDG and excrete iminodiacetic acid derivative agents.

Ultrasound

On sonography, hepatoblastoma appears as an echogenic mass that may have shadowing echogenic foci corresponding to intratumor calcification.¹⁰⁴ Hyperechoic or cystic areas, corresponding to hemorrhage within the tumor, or necrotic areas may be present as well.^{105,106} Hepatoblastoma is associated with high Doppler frequency shifts that correlate with the neovascularity typical of this tumor.¹⁰⁷

Computed Tomography

On unenhanced CT scans, hepatoblastoma appears as a solid hypodense mass, with or without calcification, that may occupy large portions of the liver. A lobulated pattern caused by bands of fibrosis can frequently be seen.¹⁰⁴ Calcification and a heterogeneous appearance are particularly extensive in mixed hepatoblastoma. After intravenous administration of a contrast agent, the tumor appears hyperdense, in keeping with its hypervascular nature. In the early arterial phase, enhancement of a thick peripheral rim, corresponding to the viable portion of the tumor, may be seen.¹⁰⁸ Invasion of perihepatic vessels or other structures can be demonstrated.¹⁰⁴ The 3D reconstruction of helical CT data provides important information

TABLE 87-2 Focal Nodular Hyperplasia versus Fibrolamellar Carcinoma		
Features	Focal Nodular Hyperplasia	Fibrolamellar Carcinoma
Hepatobiliary	Shows uptake of contrast agent	No uptake
Scar	Hyperintense on T2-weighted images High signal intensity (flow) on GRE images	Hypointense on T2-weighted images No signal on GRE images
Calcification	No	Frequent
Symptoms	No (usually incidental finding)	Symptomatic
Biopsy	Normal hepatocytes Portal branches Biliary ductules	Malignant eosinophilic hepatocytes No portal branches No biliary ductules

GRE, gradient-recalled echo.

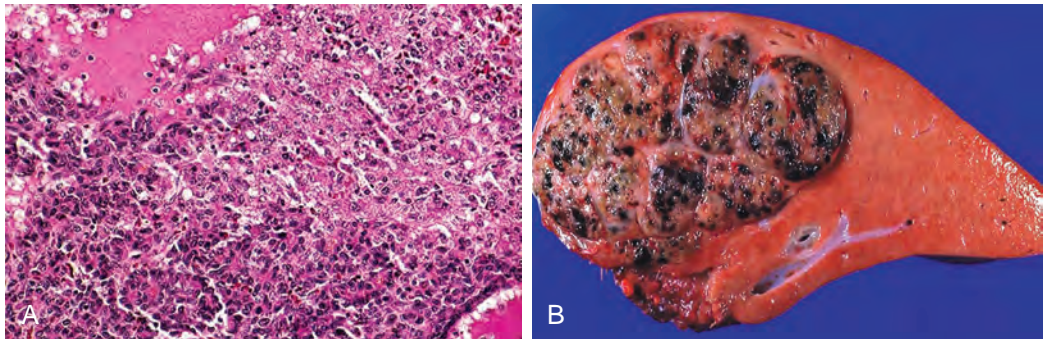


Figure 87-23 Hepatoblastoma: pathologic findings. **A.** Small tumor cells with fairly round to oval nuclei form tubular, acinar, or ribbon-like arrangements. **B.** This tumor typically is a large, solitary mass that is often multinodular because of foci of hemorrhage and necrosis.

in the preoperative assessment of patients with hepatoblastoma¹⁰⁹ (Fig. 87-24). For example, when tumor impinges on the portal vein, the initial treatment is chemotherapy to reduce the size of the lesion. If shrinkage of the tumor away from the vessel is seen on follow-up 3D CT, surgery is indicated.¹⁰⁹

Angiography

On angiography, hepatoblastoma is hypervascular and occasionally has a “spoke-wheel” pattern, reminiscent of FNH, that is due to the presence of multiple fibrous septa and bands. Arteriovenous shunting is uncommon, and invasion of the vessels is rare.¹¹⁰ Hypovascular or avascular zones resulting from hemorrhage can occur within the tumor.

Magnetic Resonance Imaging

Hepatoblastoma is hyperintense on T2-weighted images and hypointense on T1-weighted images. Foci of high signal due to hemorrhage may be seen on T1-weighted images.¹¹¹ On T2-weighted images, internal septa corresponding to fibrosis within the tumor appear as hypointense bands.¹¹² The mixed type may demonstrate a more heterogeneous appearance on T1- and T2-weighted images because of the necrosis, hemorrhage, fibrosis, calcification, cartilage, and fibrous septa contents. After intravenous administration of gadolinium, hepatoblastoma shows immediate diffuse (homogeneous or

heterogeneous) enhancement followed by a rapid washout. On the hepatocellular phase of an MR scan with hepatobiliary contrast agents, the lesion does not show uptake of the agent. MRI also demonstrates the presence of perihepatic vascular invasion. MRI can be more accurate than conventional CT in both assessing preoperative tumor extension and detecting postoperative tumor recurrence.¹¹³ However, CT has an important advantage over MRI in the evaluation of the pediatric abdomen; shorter scanning times result in less motion artifact, obviating the need for sedation.¹⁰⁹

Intrahepatic Cholangiocarcinoma

PATHOLOGIC FINDINGS

Intrahepatic cholangiocarcinoma (ICAC), or adenocarcinoma of biliary duct origin, originates in the small intrahepatic ducts and represents only 10% of all cholangiocarcinomas.² Hilar (Klatskin's) and bile duct cholangiocarcinomas account for the remaining 90%.^{2,114}

In gross appearance, these neoplasms are large, firm masses (Fig. 87-25). On cut section, they are characterized by large amounts of whitish, fibrous tissue. They rarely have internal areas of necrosis and hemorrhage.¹¹⁵

On microscopic examination, the tumor is an adenocarcinoma with a glandular appearance and cells resembling biliary

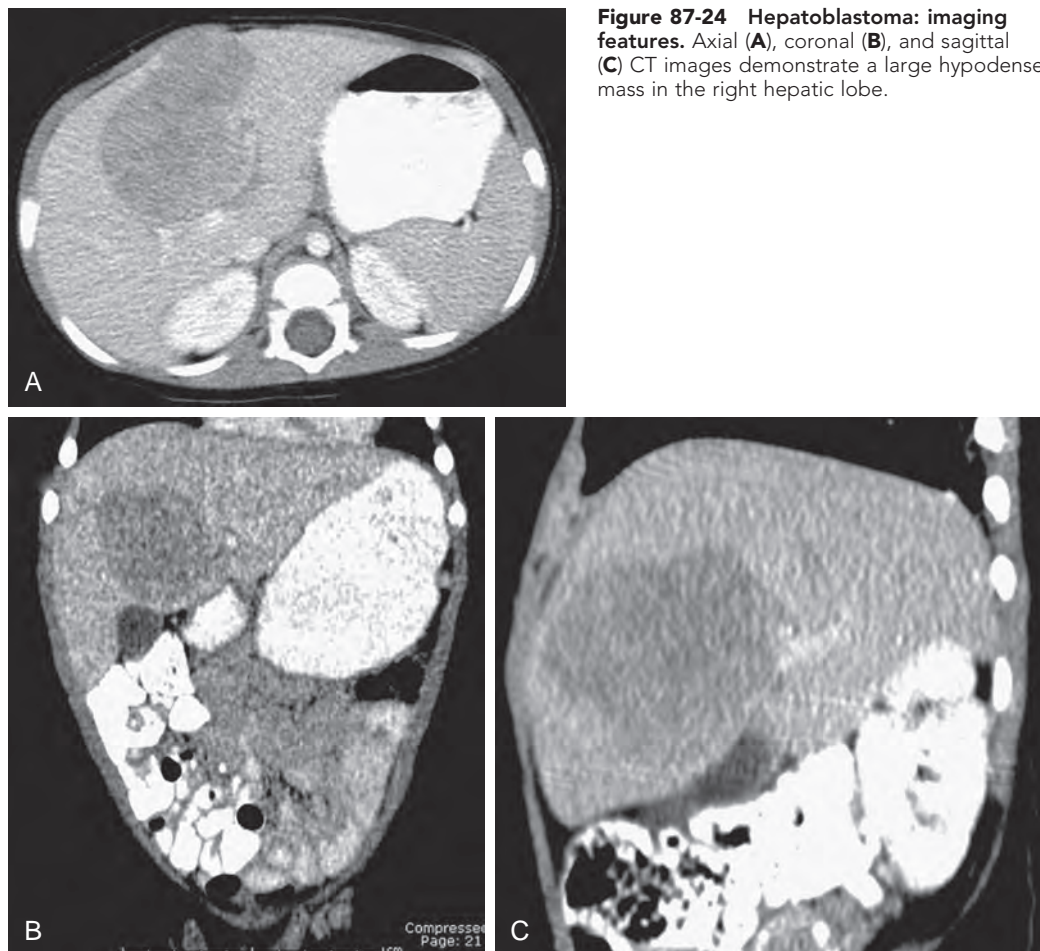


Figure 87-24 Hepatoblastoma: imaging features. Axial (A), coronal (B), and sagittal (C) CT images demonstrate a large hypodense mass in the right hepatic lobe.

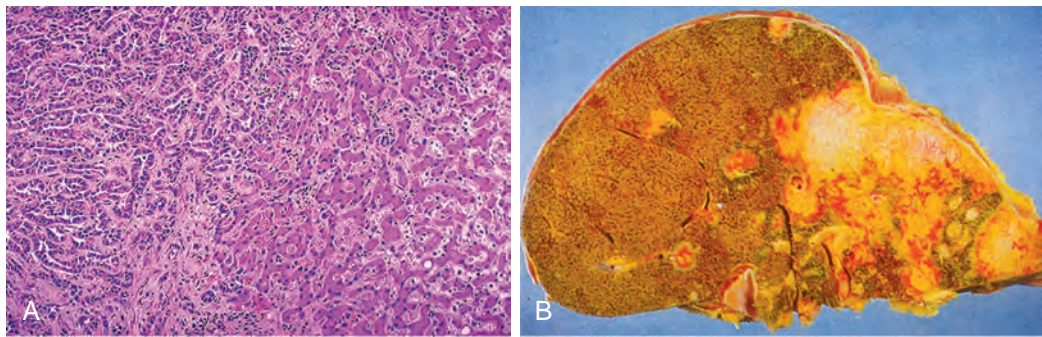


Figure 87-25 Intrahepatic cholangiocarcinoma (ICAC): pathology. **A.** Photomicrograph demonstrates cuboidal cells resembling biliary epithelium with pseudogland formation. **B.** The gross specimen shows a large, whitish, homogeneous lesion within a cirrhotic liver. The tumor extends to the liver capsule. The whitish, homogeneous nature is indicative of the large amount of fibrosis and relative hypovascularity of these neoplasms.

TABLE 87-3 Intrahepatic Cholangiocarcinoma	
Pathologic Features	Radiologic Features
Fibrosis	Calcification: CT, ultrasound Hypodense areas: CT Hypointense areas: MRI Hyperechoic areas: ultrasound
No necrosis or hemorrhage	Homogeneous mass: CT, ultrasound, MRI
Vascular encasement	Hypovascular mass: angiography, contrast CT, MRI Encasement: angiography, Doppler ultrasound, contrast CT, MRI

epithelium.¹¹⁶ Mucin and calcification can often be demonstrated. A large amount of desmoplastic reaction is typical of cholangiocarcinoma.

Pathologic-radiologic correlates of this lesion are given in Table 87-3.

INCIDENCE AND CLINICAL PRESENTATION

ICAC is the second most common primary hepatic malignant neoplasm in adults. It is usually seen in the seventh decade of life, and there is a slight male predominance.²

Clinical signs and symptoms are related to the site of origin of the tumor. Symptoms are vague until the tumor is far advanced, and patients present with abdominal pain and a palpable mass in the upper abdomen. Jaundice is rarely a presenting symptom in ICAC, whereas it is common with hilar or ductal cholangiocarcinoma.

RADIOLOGIC FINDINGS

Plain Radiography

On plain radiographs, ICAC may appear as a large upper abdominal mass. Calcification is frequently seen and results from mucous secretions or amorphous calcification in sclerotic areas.¹¹⁵

Nuclear Medicine

Sulfur colloid and hepatobiliary scans demonstrate a large defect; signs of cirrhosis are present in 20% of patients with ICAC.¹¹⁵ There is no accumulation of gallium in ICAC. Red

blood cell scans demonstrate a defect without late filling, reflecting the markedly hypovascular nature of this tumor.

Ultrasound

On sonograms, ICAC appears as a homogeneous mass that is usually hypoechoic.¹¹⁷ Satellite nodules may be seen. Calcified foci can be seen as high-level echoes with acoustic shadowing. Although the majority of the tumors appear slightly hyperperfused in color Doppler ultrasound studies, Doppler imaging findings vary widely.³⁶ In the arterial phase of contrast-enhanced sonography, the perfusion picture of ICAC is variable but mainly hyperperfused. In the late portal venous phase, the tumor is contrasted as punched-out defects.

Computed Tomography

On unenhanced CT, this lesion usually is manifested as a homogeneous, hypodense mass. After injection of contrast material, there is early peripheral enhancement with delayed, persistent central enhancement that may take 5 to 15 minutes to be manifested¹¹⁵⁻¹²⁰ (Fig. 87-26). Retraction of the overlying liver capsule is a feature suggestive of ICAC.¹¹⁷ A central scar may be seen in 30% of cases.¹¹³ Small areas of necrosis, hemorrhage, mucin, and calcification can also be present within the tumor. Biliary dilation adjacent to the tumor is another finding seen in 20% of the cases.

Extension through the hepatic capsule and invasion of organs adjacent to the liver are common in ICAC but rare in HCC. Invasion of vascular structures around the liver is uncommon but may be seen with ICAC.

Angiography

On angiography, ICAC is predominantly hypovascular with small, thin vessels corresponding to the fibrous nature of this tumor.¹²¹ Encasement of hepatic arteries and other major vessels is associated with the degree of sclerosis resulting from the tumor.

Magnetic Resonance Imaging

On MRI, ICAC appears as a large mass of decreased signal intensity on T1-weighted images and increased signal on T2-weighted images.^{122,123} A central area of hypointensity is seen in some cases on T2-weighted images and corresponds to the central scar. The pattern of enhancement on Gd-DTPA-enhanced scans depends on the size of the lesion (Fig. 87-27).¹²³

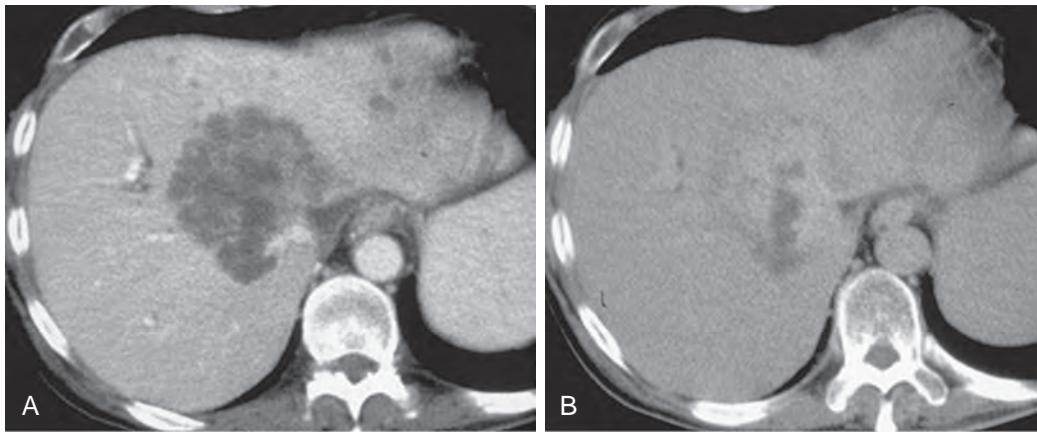


Figure 87-26 ICAC: CT features. **A.** This lesion does not enhance on the portal venous phase image. **B.** Significant contrast enhancement, with the exception of the central scar, is present on the 10-minute delayed scan.

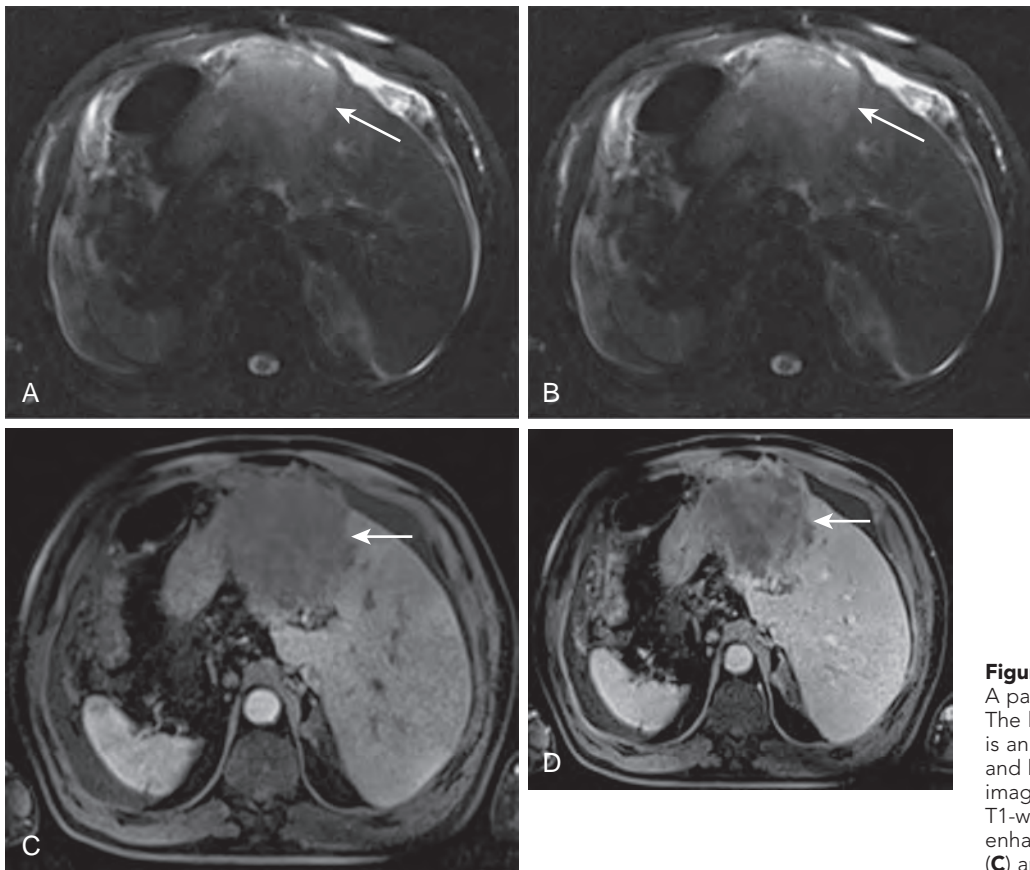


Figure 87-27 ICAC: MRI findings. A patient with situs inversus (arrows). The lesion is in the "left" liver lobe and is an ICAC. It is poorly demarcated and hyperintense on the T2-weighted image (**A**). ICAC is hypointense on the T1-weighted image (**B**) and shows late enhancement as depicted on the arterial (**C**) and late phase (**D**) images.

Larger ICACs (>4 cm) show peripheral enhancement that progresses centripetally and spares the central scar (Fig. 87-28). Smaller lesions (2-4 cm) enhance homogeneously.¹²³ These patterns of enhancement may also be seen in hemangiomas. However, the degree of enhancement of hemangiomas is greater.^{122,123} In addition, ICACs may have other features, such as satellite nodules, invasion of the portal vein, and dilation of intrahepatic bile ducts distal to the lesion, that are not associated with hemangiomas.¹²² ICACs do not show uptake of hepatobiliary contrast agents during the hepatocellular phase scans. On diffusion-weighted imaging with increasing b values, ICACs show high signal intensity and low ADC values, indicating their malignant character.

Cystadenoma and Cystadenocarcinoma

PATHOLOGIC FINDINGS

Biliary cystadenoma and cystadenocarcinoma are currently considered forms of the same disease, with cystadenocarcinoma being overtly malignant and cystadenoma having malignant potential. Transformation of cystadenoma to cystadenocarcinoma is a recognized complication.^{124,125}

On microscopic examination (Fig. 87-29), cystadenomas and cystadenocarcinomas are commonly mucinous, but a serous variety is also recognized. The locules of these tumors

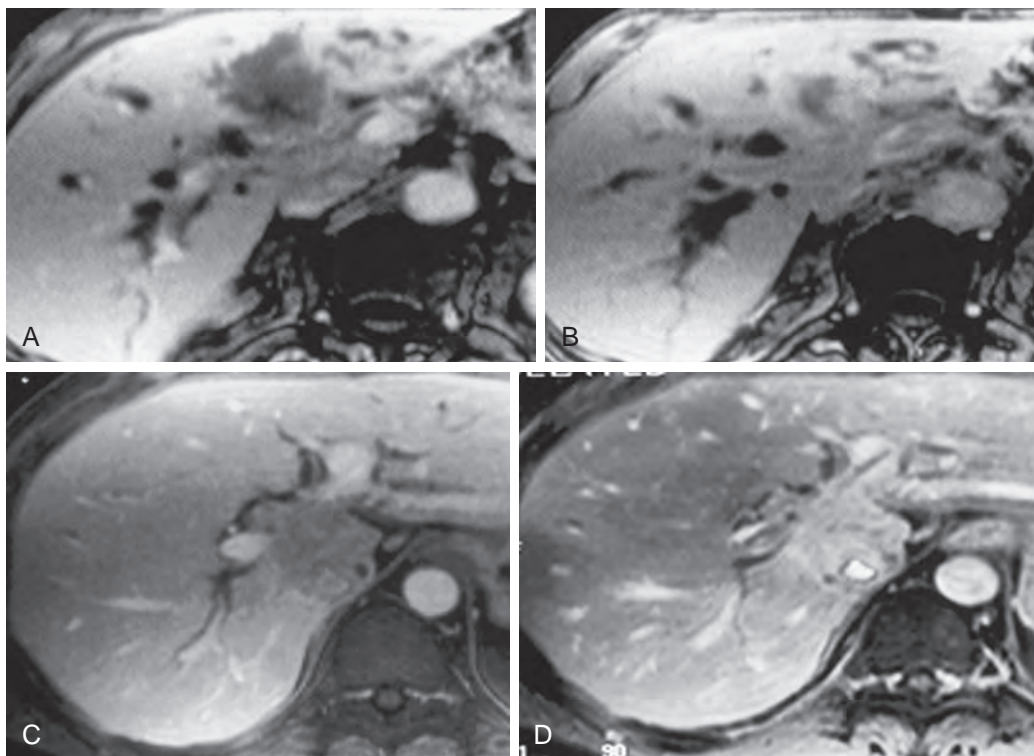


Figure 87-28 ICAC: MRI findings. No significant enhancement of the tumor is noted on the early phase scan (**A**), but on the 10-minute delayed scan (**B**), there is enhancement with the exception of the central scar. In a different patient, the lesion in the caudate lobe does not enhance on early scan (**C**) but does on delayed scan (**D**).

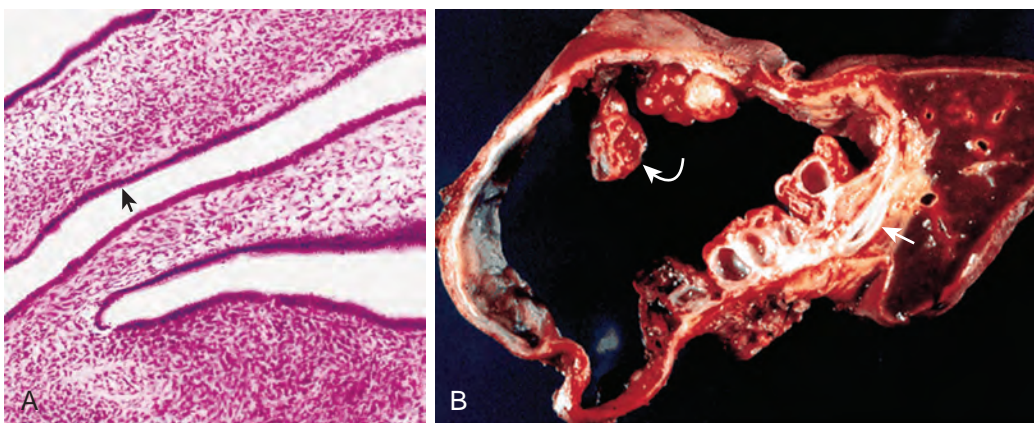


Figure 87-29 Biliary cystadenoma: pathology. **A.** Photomicrograph shows the cyst wall lined by benign cuboidal epithelium (arrow) with a subepithelial mesenchymal "ovarian-like" stroma. **B.** The cut resected left lobe shows the fibrous wall of the tumor, multiple tumor nodules (curved arrow), and loculi. The mass arises from the compressed bile duct (straight arrow). (From Levy AD, Murakata LA, Abbott RM, Rohrmann CA Jr: Benign tumors and tumorlike lesions of the gallbladder and extrahepatic bile ducts: Radiologic-pathologic correlation. *RadioGraphics* 22:387–413, 2002.)

are lined by columnar, cuboidal, or even flattened epithelium.² Polypoid projections and papillary areas are frequently present. There is a well-formed wall, and focal calcification within the wall is rare. Biliary-type epithelium lines the cysts. In cystadenocarcinoma, malignant epithelial cells line the cysts. Pathologists have categorized biliary cystadenocarcinoma by whether ovarian stroma is present or absent.¹²⁶ Cystadenocarcinoma with ovarian stroma is found in women and has an indolent course and a good prognosis, whereas tumors without ovarian stroma are found in both sexes and have an aggressive clinical course and a poor prognosis.¹²⁶

In gross appearance, these tumors are usually solitary and may become up to 30 cm in size.² The surface is shiny, smooth, or bosselated. On cut section, multiple communicating locules of variable size have a smooth and glistening lining. Papillary excrescences or mural nodules are seen in the tumor wall.

INCIDENCE AND CLINICAL PRESENTATION

Cystadenomas and cystadenocarcinomas are rare and represent only 5% of all intrahepatic cysts of bile duct origin.¹²⁷ They are probably congenital in origin because of the presence of

aberrant bile ducts. There are no associated pathogenic factors, and these tumors usually occur in middle-aged women.²

A “microcystic” cystadenoma variant is composed of multiple small cysts lined by a single layer of cuboidal epithelial cells that are rich in glycogen.¹²⁸ The papillary features and the cellular mesenchymal stroma typical of the mucinous variety of cystadenoma or cystadenocarcinoma are not seen in microcystic, glycogen-rich cystadenoma. No radiologic descriptions of microcystic cystadenoma of the liver have been published.

RADIOLOGIC FINDINGS

Endoscopic retrograde cholangiopancreatography (ERCP) can show communication of the tumor with the bile duct (Fig. 87-30). Cystadenoma or cystadenocarcinoma of the liver usually appears as a large, unilocular or multilocular mass on cross-sectional imaging. Ultrasound nicely demonstrates the septa as well as the mural nodules in the wall of these tumors (Fig. 87-31). Good correlation is seen between the nodularity and septation on ultrasound scans and gross specimens.¹²⁶

On CT scans, these tumors are large, unilocular or multilocular low-attenuation intrahepatic masses¹²⁶ with well-defined thick fibrous capsules, mural nodules, and internal septa¹²⁹ (Fig. 87-32). Calcification may be seen within the wall and septa in a minority of cases.¹²⁶

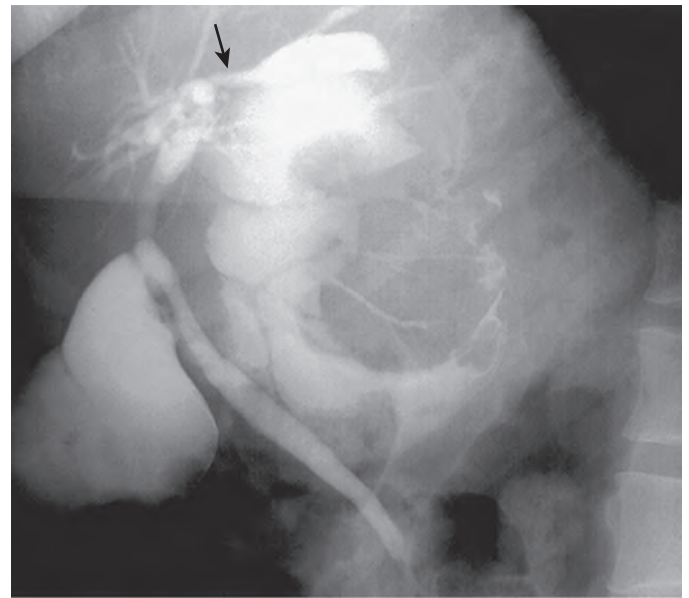


Figure 87-30 Biliary cystadenoma: ERCP. Lateral radiograph of the abdomen obtained after ERCP shows communication of the tumor (arrow) with the biliary system. The gallbladder has an anterior location. (From Levy AD, Murakata LA, Abbott RM, Rohrmann CA Jr: Benign tumors and tumorlike lesions of the gallbladder and extrahepatic bile ducts: Radiologic-pathologic correlation. *RadioGraphics* 22:387–413, 2002.)

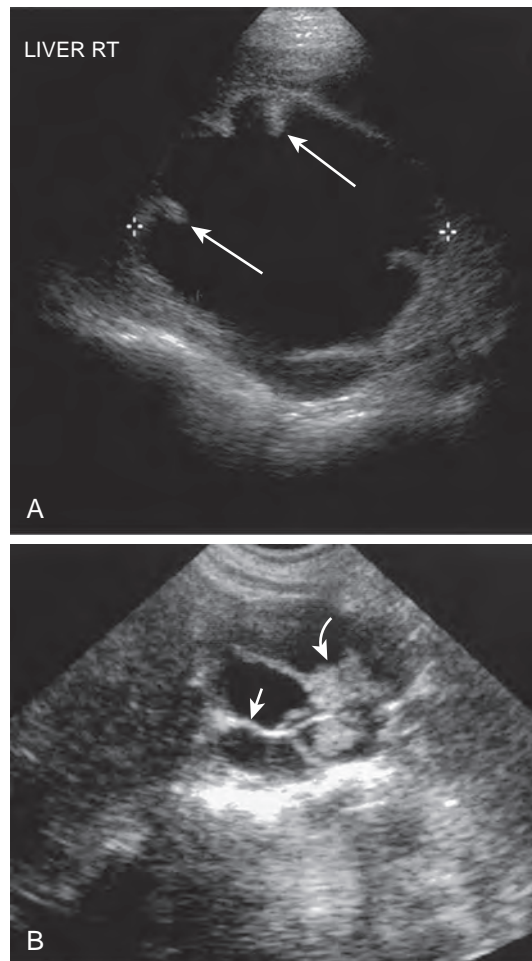
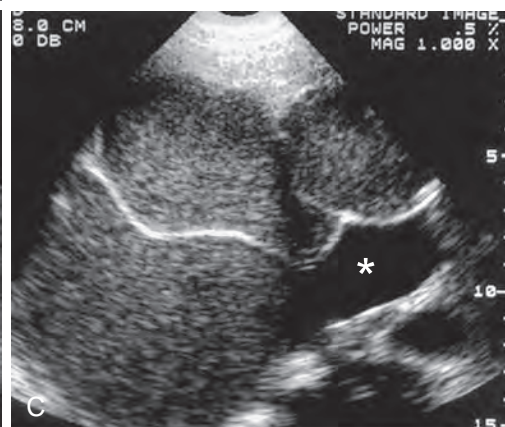
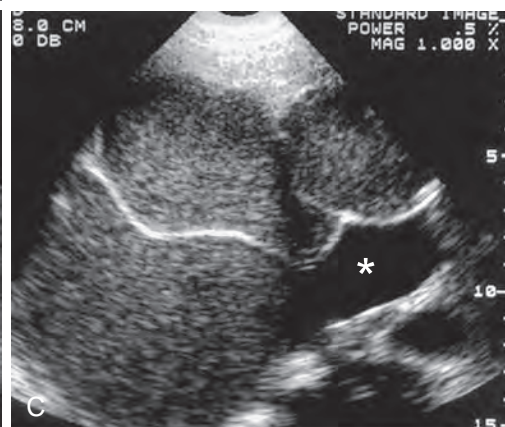


Figure 87-31 Biliary cystadenoma: sonographic findings. **A.** Transverse image of the liver shows a well-defined anechoic cystic structure with enhanced through-transmission. There are multiple echogenic tumor excrescences extending into the cyst lumen (arrows). **B.** Transverse image of the left hepatic lobe in a different patient reveals a complex anechoic cyst containing echogenic septa (straight arrow) and tumor nodules (curved arrow). **C.** Transverse image of the liver in a different patient shows a biliary cystadenoma composed of complex fluid containing diffuse low-level internal echoes. Echogenic septa course through the complex fluid. A portion of the tumor (asterisk) contains simple anechoic fluid. (From Levy AD, Murakata LA, Abbott RM, Rohrmann CA Jr: Benign tumors and tumorlike lesions of the gallbladder and extrahepatic bile ducts: Radiologic-pathologic correlation. *RadioGraphics* 22:387–413, 2002.)



On angiography, most cystadenomas and cystadenocarcinomas are avascular, although a small peripheral vascular blush may be seen in a few cases.¹²⁶

On MRI, the tumors are multiseptate and have predominantly high signal on T2-weighted images and mixed or low signal on T1-weighted images (Fig. 87-33). The areas of high signal on T1-weighted images represent hemorrhagic fluid components.¹²⁶ A low signal rim on T2-weighted images may be due to hemorrhage in the wall of the lesion.¹²⁶ Variable signal intensity within the locules of biliary cystadenoma and cystadenocarcinoma on both T1- and T2-weighted images was reported as a new sign.¹³⁰ This feature may prove extremely useful in the characterization of a multiseptate hepatic lesion as cystadenoma or cystadenocarcinoma.

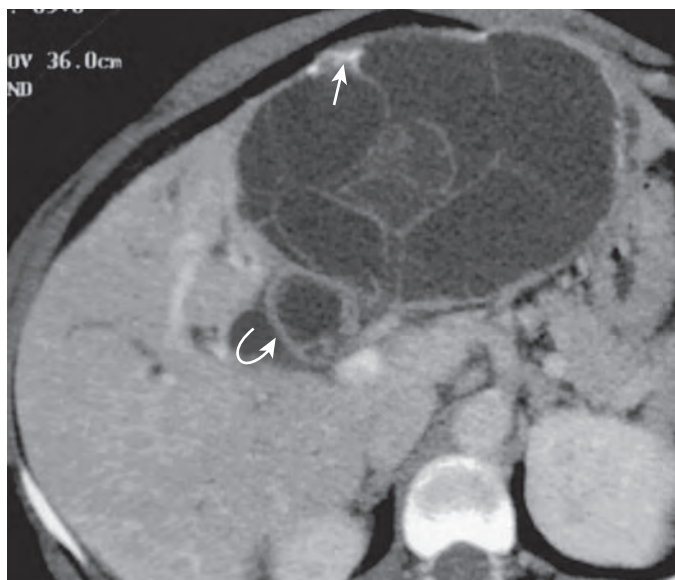


Figure 87-32 Biliary cystadenoma: CT. Contrast-enhanced scan shows a multilocular cyst with septations and mural calcifications (straight arrow) in the left hepatic lobe. There is duct dilation and extension of the cyst into the left hepatic and common bile ducts (curved arrow). (From Levy AD, Murakata LA, Abbott RM, Rohrmann CA Jr: Benign tumors and tumorlike lesions of the gallbladder and extrahepatic bile ducts: Radiologic-pathologic correlation. *RadioGraphics* 22:387–413, 2002.)

It is impossible to distinguish cystadenomas from cystadenocarcinomas radiologically. However, the combination of septation and nodularity is suggestive of cystadenocarcinoma (Fig. 87-34), whereas septation without nodularity is seen only in cystadenoma.¹²⁶ In addition, the presence of distant metastases, adenopathy, or other signs of widespread malignancy are consistent with cystadenocarcinoma.¹²⁶ It is also difficult to distinguish between cystadenoma or cystadenocarcinoma, hydatid disease, and abscess on cross-sectional imaging.^{126,131} However, use of clinical and laboratory findings should enable identification of an infectious cause.¹²⁶

Angiosarcoma

PATHOLOGIC FINDINGS

Angiosarcoma of the liver is a malignant tumor derived from endothelial lining cells that occurs primarily in adults with exposure to a variety of chemical agents and radiation (thorium oxide administration).^{2,132,133}

On microscopic examination, angiosarcomas are composed of malignant endothelial cells lining vascular channels of variable size from cavernous to capillary. These vascular channels try to form sinusoids. Thorotrast particles can be found within the malignant endothelial cells in cases of Thorotrast-induced angiosarcoma.

In gross appearance, the majority of angiosarcomas are multiple and have areas of internal hemorrhage.¹³² When angiosarcoma appears as a single, large mass, it does not have a capsule and frequently contains large cystic areas filled with bloody debris.

The radiologic correlates of the pathology of angiosarcoma are given in Table 87-4.

INCIDENCE AND CLINICAL PRESENTATION

Angiosarcoma is a rare neoplasm that occurs most frequently in men (2:1 to 4:1 more often than in women) in the seventh decade of life. It is 30 times less common than HCC.¹³⁴ Angiosarcoma is associated with previous exposure to toxins such as Thorotrast, vinyl chloride, arsenicals, and steroids. It has also been found in association with hemochromatosis.

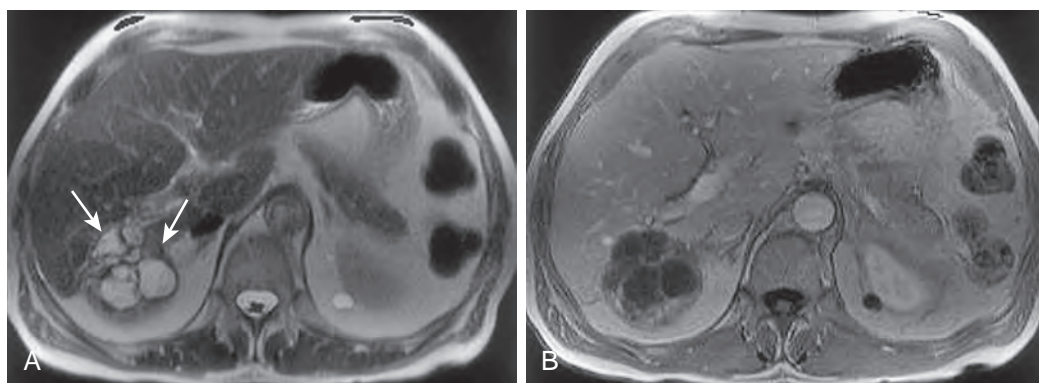


Figure 87-33 Biliary cystadenoma on MRI. A. Fast spin-echo T2-weighted MR image shows a multilocular, septated mass (arrows) in segment VII of the liver, with high signal intensity within the tumor. **B.** Corresponding portal venous phase gadolinium-enhanced T1-weighted image shows enhancement of the capsule and septa. (From Mortelet KJ, Ros PR: Cystic focal liver lesions in the adult: Differential CT and MR imaging features. *RadioGraphics* 21:895–910, 2001.)

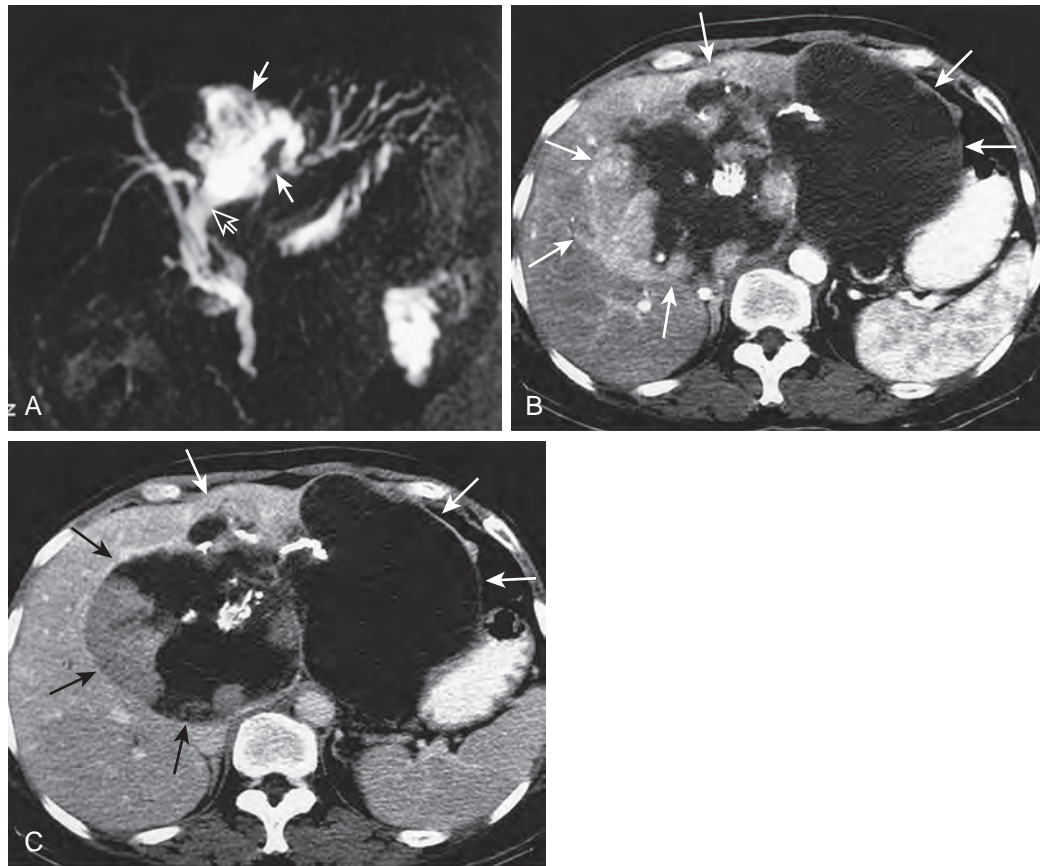


Figure 87-34 Biliary cystadenocarcinoma: imaging features. **A.** MRCP. Biliary cystadenocarcinoma in a 65-year-old woman with abdominal pain. Single-shot fast spin-echo MRCP image shows a large, fluid-filled mass in the left hepatic lobe (solid arrows), with proximal dilation of the left intrahepatic bile ducts. The low signal intensity filling defects in the mass are related to polypoid masses of the wall, and the low signal intensity filling defect in the common hepatic duct (open arrow) is related to mucin secreted by the mass. In a different patient, arterial (**B**) and equilibrium phase (**C**) CT scans show a large, bilobular, cystic mass with internal septation and calcification (arrows) that involves the left hepatic lobe. Papillary excrescences and mural nodules along the cyst wall enhance well during the arterial phase. (**A** from Vitellas KM, Keogan MT, Spritzer CE, et al: MR cholangiopancreatography of bile and pancreatic duct abnormalities with emphasis on the single-shot fast spin-echo technique. *RadioGraphics* 20:939–957, 2000. **B** and **C** from Lee WJ, Lim HK, Jangy KM, et al: Radiologic spectrum of cholangiocarcinoma: Emphasis on unusual manifestations and differential diagnoses. *RadioGraphics* 21:S97–S116, 2001.)

TABLE 87-4
Angiosarcoma

Pathologic Features	Radiologic Features
Multiple nodules	Hyperechoic nodules: ultrasound Hypodense nodule (central): CT Hypointense nodule: MRI
Thorium oxide (Thorotrast) deposition	Metallic density: CT
Areas of hemorrhage	Heterogeneous mass: CT, ultrasound Hyperdense regions: CT Hyperechoic regions: ultrasound Hyperintense regions: T1-weighted MRI
Vascular channels	Persistence of contrast medium: red blood cell scintigraphy, contrast-enhanced CT and MRI

Clinically, patients with angiosarcoma frequently present with generalized weakness, weight loss, abdominal pain, hepatomegaly, and ascites. Thrombocytopenia caused by platelet sequestration within a large angiosarcoma may be present. Rupture and acute hemoperitoneum are rare.^{135,136}

RADIOLOGIC FINDINGS

Plain Radiography

The plain abdominal radiographic findings depend on the presence or absence of prior Thorotrast exposure. If there is no history of Thorotrast exposure, the findings of angiosarcoma are nonspecific. A soft tissue density mass in the upper abdomen may be detected if there is a large predominant angiosarcoma nodule.

If there is a history of Thorotrast exposure, localized areas of increased density, in a network fashion, are visualized in the liver and spleen as well as in the mesenteric and celiac lymph nodes. Circumferential displacement of the Thorotrast by nodules of angiosarcoma can be identified on plain films.¹³⁷

Nuclear Medicine

Sulfur colloid scans demonstrate either solitary or multiple filling defects in an often diffusely abnormal liver. A defect is also noted on hepatobiliary and gallium scans. Tagged red blood cell pool studies may show early as well as late uptake. Angiosarcoma, therefore, can mimic the appearance of hemangiomas on red blood cell studies, with persistent uptake of the tracer.¹³⁸

The retention of the tagged red blood cells by this tumor is not as prolonged as that by hemangiomas, however.

Ultrasound

On ultrasound studies, angiosarcomas appear as either single or multiple hyperechoic masses. The echo architecture is heterogeneous because of hemorrhage of various ages.

Computed Tomography

CT scans show the reticular pattern of deposition of Thorotrast extremely well in both the liver and the spleen. Circumferential displacement of Thorotrast in the periphery of a nodule has been described as a characteristic finding of angiosarcoma.¹³⁸

When there is no evidence of Thorotrast deposition, angiosarcomas are manifested with single or multiple masses that are hypodense on unenhanced CT scans except for hyperdense areas of fresh hemorrhage. In case of rupture of the hepatic angiosarcoma, the diagnosis is made by demonstrating free intraperitoneal fluid and focal high-density area adjacent to the tumor representing acute blood clot.¹³⁹ Centripetal enhancement with contrast material can be seen mimicking the hemangioma pattern.¹⁴⁰ However, in most cases, angiosarcomas have additional imaging features that are atypical for hemangiomas, such as focal areas of enhancement that show less attenuation than the aorta or peripheral ring-shaped enhancement.

Angiography

On angiography, these moderately hypervascular tumors show diffuse puddling of contrast medium that persists into the venous phase.¹⁴¹ Angiosarcomas are fed by large peripheral vessels, and centripetal flow can be recorded angiographically. Avascular areas corresponding to central hemorrhage can be seen within the tumors. On occasion, angiosarcomas may rupture, and angiography and CT can demonstrate the bleeding as well as the presence of hemoperitoneum.¹³⁶

Magnetic Resonance Imaging

Angiosarcoma (Fig. 87-35) is of low signal intensity on T1-weighted images and of predominantly high signal on T2-weighted images with central areas of low signal.^{121,142} Imaging features that have been described on T2-weighted

images include fluid-fluid levels reflecting the hemorrhagic nature of the tumor and marked heterogeneity with focal areas of high intensity along with septum-like or rounded areas of low intensity. On T1-weighted imaging, areas of hyperintensity are related to hemorrhage. During dynamic scanning after intravenous administration of Gd-DTPA, peripheral nodular enhancement is seen, which progresses centripetally.¹⁴² On delayed postcontrast images, the peripheral enhancement persists while the center of the lesion remains unenhanced and may represent fibrous tissue or deoxyhemoglobin.^{121,142} Although the pattern of enhancement mimics hemangiomas, the inhomogeneity of angiosarcomas on T2-weighted images is not seen in hemangiomas.^{121,142} Because Thorotrast does not produce a recognizable MR signal, it, like the presence of calcification, may easily be missed.

Undifferentiated (Embryonal) Sarcoma

PATHOLOGIC FINDINGS

Undifferentiated (embryonal) sarcoma (UES), or mesenchymal sarcoma, is a malignant tumor occurring primarily in children. It is composed of primitive, undifferentiated spindle cells, with frequent mitoses and myxoid stroma, that resemble primitive (embryonal) cells.¹⁴³ In gross appearance, UES is a large, usually solitary, spherical mass with well-defined margins (Fig. 87-36). On occasion, a pseudocapsule is present. On cut surface, it has a variegated, glistening appearance with cystic areas of variable size that contain necrotic debris, hemorrhagic fluid, blood, or gelatinous material.^{143,144} Cystic tumors are seen more frequently than solid ones.

INCIDENCE AND CLINICAL PRESENTATION

UES is the fourth most common hepatic neoplasm in children, after hepatoblastoma, infantile hemangioendothelioma, and HCC.¹⁴³ It usually occurs in older children, 6 to 10 years of age, and 90% of patients are younger than 15 years.¹⁴⁵ The incidence is almost the same in males and females.

The usual presenting symptoms are pain and abdominal mass, with fever, jaundice, weight loss, and gastrointestinal

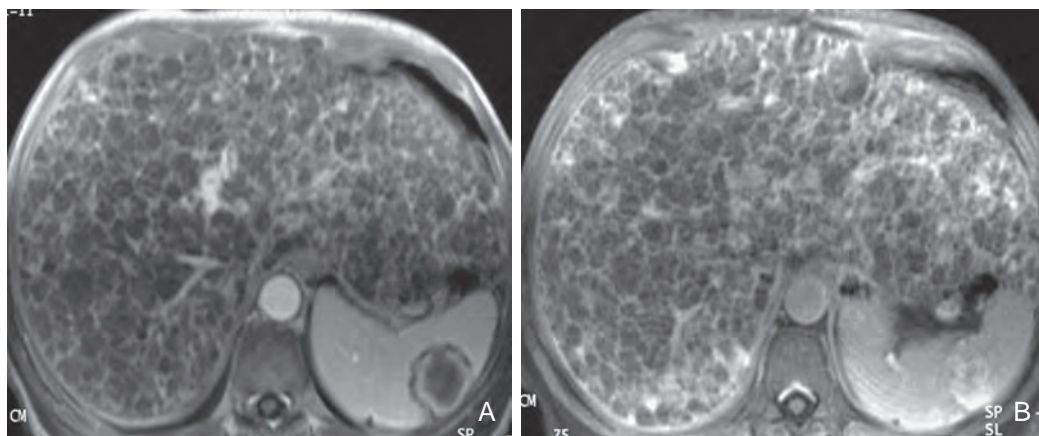


Figure 87-35 Angiosarcoma. Gadolinium-enhanced MR images obtained in the arterial (A) and portal venous (B) phases demonstrate the replacement of the liver parenchyma with numerous nodules. There is also an angiosarcoma in the spleen.

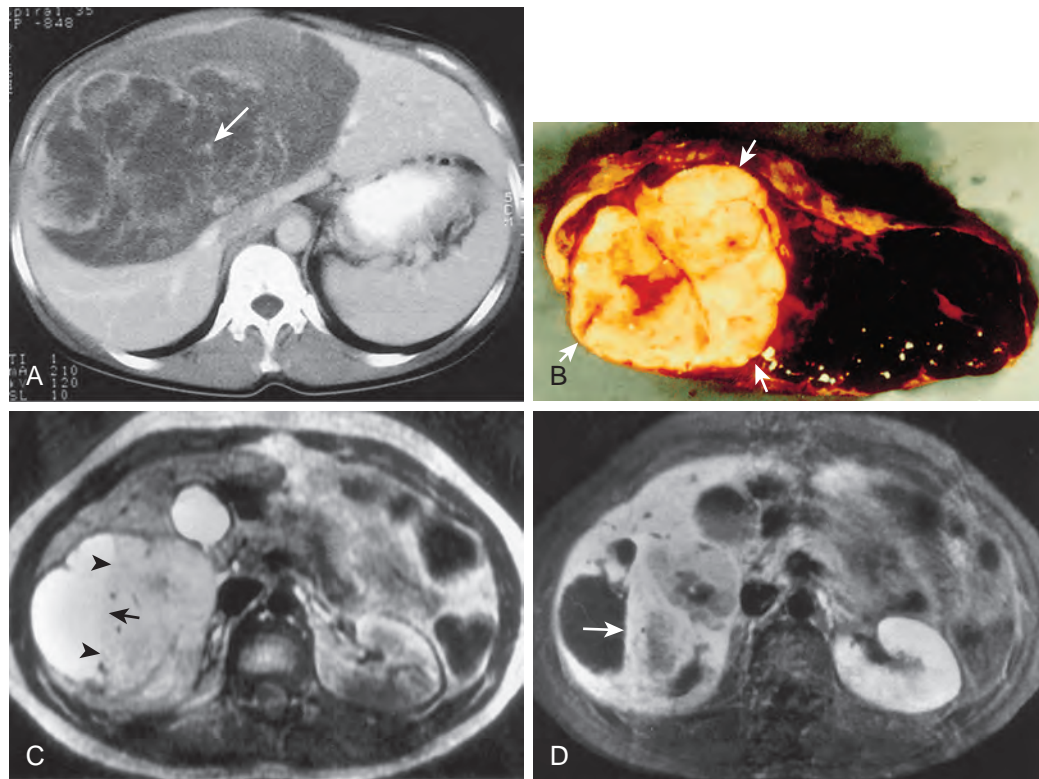


Figure 87-36 Undifferentiated embryonal sarcoma. **A** and **B.** Undifferentiated embryonal sarcoma in a 22-year-old woman. Portal venous phase contrast-enhanced CT scan (**A**) shows a 10-cm-diameter cystic lesion with septa in the right lobe of the liver. Note the calcifications (arrow) within the mass. Specimen photograph (**B**) shows that the mass has predominantly solid components (arrows) with coexisting hemorrhagic areas. **C** and **D.** Undifferentiated embryonal sarcoma in a 36-year-old woman. T2-weighted MR image (**C**) shows a mass in the right lobe of the liver. The solid portions of the mass (arrowheads) are hyperintense relative to normal liver tissue, and the cystic portions (arrow) have signal intensity similar to that of water. Delayed phase gadolinium-enhanced T1-weighted MR image (**D**) shows heterogeneous enhancement of the solid portions of the lesion (arrow). (From Koenraad J, Mortelet KJ, Ros PR: Cystic focal liver lesions in the adult: Differential CT and MR imaging features. *RadioGraphics* 21:895–910, 2001.)

complaints found less commonly. α -Fetoprotein levels are usually not elevated.

RADIOLOGIC FINDINGS

Plain Radiography

Abdominal radiographs demonstrate a large, usually noncalcified mass in the upper abdomen associated with displacement of adjacent structures and elevation of the diaphragm on the right side. Calcification, although rare, may occur, with small, punctate chunks of calcium seen within the solid portions of this tumor.¹⁴⁵

Nuclear Medicine

On liver sulfur colloid scans, UES is usually a well-defined intrahepatic defect. Blood pool studies demonstrate no early uptake or delayed filling, corresponding to the hypovascular nature of this tumor.¹⁴⁵ Bone scintigraphy and gallium scans demonstrate no uptake by UES.¹⁴⁵

Ultrasound

On sonograms, the appearance of UES ranges from a multiseptate cystic mass to an inhomogeneous, predominantly

echogenic solid mass. The cysts range in size from a few millimeters to several centimeters, corresponding to the cystic changes seen grossly.¹⁴⁵ In a review of 28 cases of UES, all tumors were predominantly solid.¹⁴⁶

Computed Tomography

On CT scans, UES appears as a hypodense mass resembling old intrahepatic hemorrhage or a biloma¹⁴⁷ (see Fig. 87-36A). Calcification is a rare feature.¹⁴⁶ Septa are seen as dense bands within the cystic tumor, corresponding to solid portions. If there is a pseudocapsule, a thin rim of dense tissue may surround the predominantly cystic tumor. On contrast-enhanced CT images, heterogeneous enhancement is present in the solid, usually peripheral portions of the mass, especially on delayed images.^{108,129}

Angiography

Angiographic studies demonstrate a large hypovascular to avascular mass. Abnormal vessels as well as hypervascular portions can be seen in the solid component of UES. Intratumoral aneurysms, arteriovenous shunting, pooling of contrast medium, and arterial encasement can be found in tumors with a sizable solid component.

Magnetic Resonance Imaging

On MRI, UES has signal characteristics similar to cerebrospinal fluid, with high signal on T2-weighted images and low signal on T1-weighted images.¹⁴⁶ In addition, foci of high signal intensity are seen on T1-weighted images corresponding to hemorrhage.¹⁴⁶ If present, the pseudocapsule and septations are of low signal intensity on both T1- and T2-weighted images. The enhancement pattern of UES on postcontrast MR images is parallel to that on CT images (see Fig. 87-36D).

Epithelial Hemangioendothelioma

PATHOLOGIC FINDINGS

Epithelial hemangioendothelioma (EHE) is a rare malignant hepatic neoplasm of vascular origin that develops in adults. It should not be confused with infantile hemangioendothelioma, which occurs predominantly in young children.

INCIDENCE AND CLINICAL PRESENTATION

EHE is usually discovered incidentally, although jaundice, liver failure, and occasionally rupture with hemoperitoneum may be present.¹⁴⁸ It is more common in women than in men.

In gross appearance, the tumors are often multiple and are composed of neoplastic cells that infiltrate the sinusoids and intrahepatic veins. The prognosis of EHE is much more favorable than that of angiosarcoma; extrahepatic metastases occur in only one third of the reported cases.¹⁴⁸ It appears that the biologic behavior of this tumor is related to its matrix, including inflammation, sclerosis, and calcification.

RADIOLOGIC FINDINGS

EHEs appear as multiple nodules that grow and coalesce, forming large confluent masses. This lesion usually develops in the periphery of the liver and commonly shows calcifications corresponding to the fibrotic nature of this tumor.¹⁴⁹ The calcifications are visible on plain radiographs in 15% of cases.¹³⁸

On sonography, EHE is primarily hypoechoic.^{138,150} On CT scans, the full spectrum of growth may be seen from multiple nodules to large confluent masses.¹³⁸ On unenhanced CT scans, EHE is of low attenuation, corresponding to myxoid stroma.¹³⁸ Portions of these large, low-attenuation masses become isodense after administration of contrast material, so it is often easier to identify the extent of the disease on unenhanced scans. With extensive involvement, compensatory enlargement of the uninvolved portions of the liver is seen.¹³⁸ On angiographic examination, the tumor may be hypervascular, hypovascular, or avascular, depending on the extent of hyalinization and sclerosis within the tumor.^{138,150} Invasion of hepatic veins may be seen.¹³⁸

The MRI features of EHEs are similar to the CT appearances, and either peripheral nodules or larger confluent lesions are seen.^{151,152} The tumors are hypointense on T1- and hyperintense on T2-weighted images, although a hypointense center may be seen on both sequences corresponding to calcification, necrosis, and hemorrhage.¹⁵² After intravenous administration of Gd-DTPA, moderate peripheral enhancement and delayed

central enhancement are seen.¹⁵² MRI also demonstrates invasion of the portal veins by the tumor.¹⁵² With the exception of calcification, MRI demonstrates the internal architecture of EHE better than CT does.¹⁵²

Other Mesenchymal Sarcomas (Leiomyosarcoma, Malignant Fibrous Histiocytoma)

PATHOLOGIC FINDINGS

Primary tumors arising in mesenchymal elements of the adult liver are extremely rare. They include angiosarcoma, fibrous sarcoma, rhabdomyosarcoma, leiomyosarcoma, and malignant fibrous histiocytoma.¹⁵³⁻¹⁵⁵ These sarcomas of the liver are usually large, solid, smoothly lobulated tumors and on cut surface show fibrous septa or central necrosis and hemorrhage.

INCIDENCE AND CLINICAL PRESENTATION

Primary leiomyosarcoma of the liver is rare, with few cases reported in the literature.¹⁵³ The majority of patients are adults with an average age at discovery of 57 years. Leiomyosarcomas grow slowly, with slowly evolving clinical abnormalities present for several months. Survival ranges from several months to years.

RADIOLOGIC FINDINGS

On CT scans, both leiomyosarcoma and malignant fibrous histiocytoma have a similar appearance: a large, noncalcified, hypodense, homogeneous mass that exhibits inhomogeneous peripheral enhancement after administration of the contrast agent.^{156,157} Ultrasound demonstrates a variable appearance from hyperechoic to isoechoic and hypoechoic patterns.

Lymphoma

PATHOLOGIC FINDINGS

Hepatic lymphoma can be either primary or secondary and can occur in both Hodgkin's lymphoma (HL) and non-Hodgkin's lymphoma (NHL). The majority of lymphomas of the liver are secondary; primary lymphoma is rare.¹⁵⁸ However, secondary lymphoma of the liver is found in more than 50% of patients with HL or NHL.^{159,160}

Nodular and diffuse forms of hepatic lymphoma are seen. HL occurs more often as miliary lesions than as masses. Early in the disease, liver involvement is microscopic, but with time, small nodules a few millimeters to several centimeters in size develop.¹⁶¹ HL of the liver is almost invariably associated with splenic involvement, and the likelihood of hepatic disease is greater if there is extensive splenic disease.^{162,163}

In patients with HL, a Reed-Sternberg variant type of cell is accepted as evidence for liver involvement. Typical Reed-Sternberg cells are rarely identified, particularly in biopsy specimens. In NHL, the lymphocytic form tends to be miliary whether the large cell or histiocytic varieties are nodular or tumoral.¹⁶⁴ In both HL and NHL, initial involvement is seen in

the portal areas because this is where the majority of the scant lymphatic tissue of the liver is found.

INCIDENCE AND CLINICAL PRESENTATION

Primary hepatic lymphoma occurs most commonly in middle-aged white men.¹⁶⁵ Organ transplant recipients and patients with acquired immunodeficiency syndrome are at high risk for development of hepatic lymphoma. Patients usually present with right upper quadrant pain, hepatomegaly, or a tender upper abdominal mass. Hepatomegaly may be present in an uninvolved liver, and a diffusely infiltrated liver can be of normal size.¹⁶⁶

RADIOLOGIC FINDINGS

Plain Abdominal Radiography

Plain abdominal radiography may demonstrate hepatomegaly in cases in which the liver is markedly enlarged. Calcifications are not detected in untreated hepatic lymphoma. Barium studies may demonstrate other involved areas in the gut.

Nuclear Medicine

Lymphomas may be manifested as focal defects on technetium Tc 99m sulfur colloid scans or with diffusely inhomogeneous hepatic uptake. Gallium citrate is taken up by normal liver tissue and lymphoma, and the usefulness of the technique in the diagnosis of hepatic lymphoma is therefore questionable. However, it may help confirm areas of liver involvement seen by other imaging techniques and may have a role in assessing response to therapy.^{165,167} On occasion, areas of increased uptake in relation to normal liver can be identified.

Ultrasound

On ultrasound studies, hepatic lymphoma appears as a hypoechoic mass or masses in the tumoral form of the disease. In the diffuse form, the echogenicity of the hepatic parenchyma may be normal or the overall architecture of the liver may be altered.¹⁶⁵ If there is bleeding within the lymphoma deposit, true cystic ultrasonographic characteristics may be detected.¹⁶⁸

Computed Tomography

CT is currently the preferred imaging method for evaluating lymphoma of the liver, with a specificity of almost 90% and a sensitivity of almost 60%.^{169,170}

Secondary hepatic lymphoma most commonly is manifested as multiple well-defined, large, homogeneous low-density masses (Fig. 87-37). Areas of diffuse infiltration by lymphoma causing hepatomegaly may not be distinguishable from normal liver tissue by CT. Frequently, additional areas of involvement may be noted in the spleen, lymph nodes (para-aortic, celiac, and periportal), and kidneys.¹⁷⁰

Angiography

On angiography, primary and secondary lymphomatous liver masses are usually hypovascular or avascular. There may be arterial displacement; however, encasement is not noted. In the capillary phase, the tumor mass is relatively hypolucent.



Figure 87-37 Hepatic lymphoma. Contrast-enhanced CT scan shows a lesion with heterogeneous low attenuation in the right hepatic lobe.

Magnetic Resonance Imaging

Hepatic lymphoma is hypointense compared with normal liver on T1-weighted images and hyperintense on T2-weighted images. After intravenous administration of contrast material, transient perilesional enhancement of focal hepatic lymphoma deposits has been reported. However, these tumors generally remain hypointense during the dynamic study as a result of their poor vascularity.^{58,171} Although it is easy to distinguish normal liver, the difference in relaxation times of lymphoma and metastases is not significant. Diffuse hepatic lymphoma is more readily detectable by CT than by MRI. Although some authors indicate that MRI may be slightly more sensitive than CT for all forms of hepatic involvement, this has not been completely proved.¹⁷²

Metastases

PATHOLOGIC FINDINGS

Gross Pathology

Metastases vary in size, consistency, uniformity of growth, stromal response, and vascularity (Fig. 87-38). They can be infiltrative or expansive. All these factors depend on the primary source and mode of metastasis. The gross morphologic patterns of the major liver metastases are described in Table 87-5.^{173,174}

Metastatic adenocarcinomas from the gallbladder and colon often have a slimy cut surface because of mucin production. Tumors that are expanding and massive, such as colon cancer metastases, often have central liquefactive necrosis. Metastases that have significant necrosis or fibrosis can umbilicate the surface of the liver capsule, which is a helpful diagnostic feature because HCCs rarely cause umbilication.^{173,174}

Poorly differentiated tumors such as seminomas, oat cell carcinomas, NHLs, and undifferentiated sarcomas tend to have a uniformly soft, “fish flesh–like” consistency. Squamous cell carcinomas have a granular and caseous central portion that lacks the shiny appearance of most adenocarcinomas.^{173,174}

Individual metastases in the same liver can vary greatly in appearance because of differences in blood supply, hemorrhage,

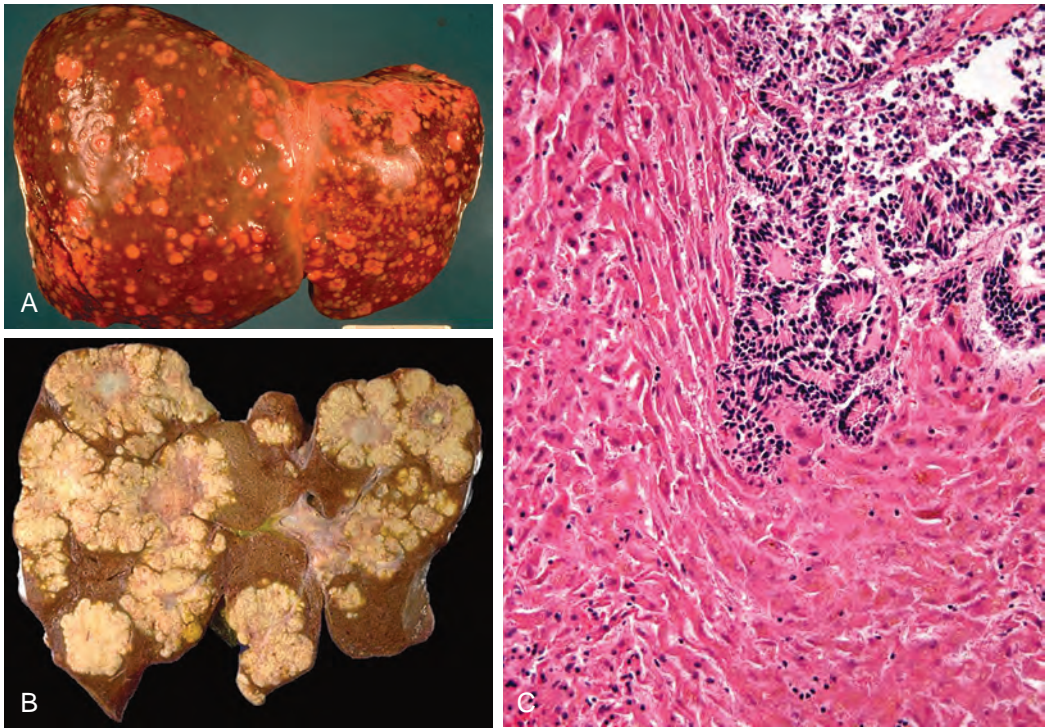


Figure 87-38 Hepatic metastases: pathology. **A.** Multiple metastases from breast cancer are present in both lobes of the liver. **B.** Cut section shows multiple large metastases from lung cancer. **C.** Photomicrograph shows normal liver on the left and gastric cancer metastases on the right side of the image.

TABLE 87-5	Morphologic Patterns of Metastatic Tumors to Liver	
Pattern	Site	
Expanding massive (solitary with satellites or multiple foci)	Colon, gallbladder, testis	
Uniformly nodular	Lung, melanoma, pancreas	
Infiltrative massive	Lung, breast, pancreas, bladder, melanoma	
Uniformly multifocal	Breast, pancreas, lung, melanoma	
Diffuse	Breast, pancreas, lymphomas	
Surface spreading	Colon, ovary, occasionally stomach	
Miliary	Prostate, occasionally any	
Mixed or indeterminate	Any	

Modified from Edmondson HA, Craig JR: *Neoplasms of the liver*. In Schiff L, Schiff ER (eds): *Diseases of the Liver*, 8th ed. Philadelphia, JB Lippincott, 1987, pp 1109–1158.

cellular differentiation, fibrosis, and necrosis. This variable pattern is particularly common in the vascular metastases carcinoid, renal cell carcinoma, choriocarcinoma, and bronchogenic carcinoma.^{173,174}

An unusual zone of venous stasis up to 1 cm in size is observed in approximately 25% of affected livers. This zone is uniformly circumferential, and either all or none of the metastatic foci have this finding. This phenomenon is seen most commonly with bronchogenic cancer and least commonly with colon cancer and has important implications for imaging and enhancement with contrast material.^{173,174}

Microscopic Pathology

Most metastases maintain the microscopic features of the primary tumor, including the degree of stromal growth. Metastatic carcinomas of the pancreas and breast incite an intense fibrous or sclerosing reaction around the tumor acini, leading to fibrous scar formation. Oat cell carcinoma intermingles with the liver plates, blending in with the hepatocytes. In fact, some tumors with no organoid pattern at the primary site (e.g., bronchogenic carcinoma, bladder carcinoma) may retain the pattern of the sinusoidal bed and simulate a ductal liver neoplasm. In colon cancer metastases, a thin collagenous pseudocapsule is often situated between the tumor margin and compressed liver but does not surround individual tumor glands.^{173,174}

Approximately 7% to 15% of patients with metastatic liver disease have tumor thrombi that occlude the portal or hepatic veins. Metastases that penetrate the large portal veins disseminate throughout peripheral portal branches. When the hepatic veins are penetrated, pulmonary metastases can develop.^{173,174}

In the presence of mucin, necrosis, and phosphatase activity, metastases can develop calcification that is detectable radiographically.^{175,176} This is particularly common in metastases from mucinous adenocarcinomas of the colon, pancreas, and stomach.

INCIDENCE AND CLINICAL PRESENTATION

Metastases (Table 87-6) are by far the most common cause of malignant focal liver lesions, outnumbering primary malignant tumors by a factor of 18 : 1. The liver is second only to regional lymph nodes as a site of metastatic disease, and approximately 25% to 50% of all patients who die of cancer have liver

TABLE 87-6 Most Common Nonlymphoma Hepatic Metastases

Tumor	No. of Primary Tumors	No. with Metastases	Percentage with Metastases
Lung	682	285	41.8
Colon	323	181	56.0
Pancreas	179	126	70.4
Breast	218	116	53.2
Stomach	159	70	44.0
Unknown primary	102	59	57.0
Ovary	97	47	48.0
Prostate	333	42	12.6
Gallbladder	49	38	77.6
Cervix	107	34	31.7
Kidney	142	34	23.9
Melanoma	50	25	50.0
Bladder and ureter	66	25	37.9
Esophagus	66	20	30.3
Testis	45	20	44.4
Endometrium	54	17	31.5
Thyroid	70	12	17.1

Modified from Edmondson HA, Craig JR: *Neoplasms of the liver*. In Schiff L, Schiff ER (eds): *Diseases of the Liver*, 8th ed. Philadelphia, JB Lippincott, 1987, pp 1109–1158.

metastases at autopsy. Colon (42%), stomach (23%), pancreas (21%), breast (14%), and lung (13%) are the most common primary neoplasms. A silent primary with hepatic metastasis most often occurs in carcinoma of the pancreas, stomach, and lung. The highest percentage of liver metastases occurs in primary carcinoma of the gallbladder, pancreas, colon, and breast; the lowest percentage occurs in prostate cancer.

Approximately 50% of patients who die with metastatic carcinoma of the liver have some hepatic signs or symptoms. Hepatomegaly (31%) is the most common finding, followed by ascites (18%), jaundice (14.5%), and varices (1%). Liver function tests are notoriously unreliable for detection of metastases; results are normal in 25% to 50% of patients with metastases and can be abnormal in any number of conditions, such as parenchymal tumor replacement, tumor obstructing the intrahepatic or extrahepatic bile ducts, or chemotherapy hepatotoxicity. For this reason, imaging is the key to both the diagnosis and serial follow-up of liver metastases.^{175,177} In addition, cross-sectional imaging techniques now have a unique and important role in the management of patients with hepatic metastases from colorectal cancer. Many of these patients have good survival rates of 20% to 40% at 5 years if resection of liver metastases is performed. However, the preoperative evaluation of these patients is vital in selecting those who will benefit from surgery. Accurate assessment of the presence, extent, and number of liver metastases and the delineation of extrahepatic disease are requirements of any imaging technique.¹⁷⁸

RADIOLOGIC FINDINGS

Plain Radiography

Plain abdominal radiographs in patients with metastatic disease most commonly show normal findings. Nonspecific findings include hepatomegaly, ascites, and splenomegaly, which may be due to humoral factors, tumor, or portal hypertension.^{179,180}

BOX 87-3 METASTATIC LIVER TUMORS THAT MAY CALCIFY

Mucinous carcinoma of the colon, stomach, and pancreas
Islet cell pancreatic tumor
Leiomyosarcoma, osteogenic sarcoma, rhabdomyosarcoma, chondrosarcoma
Papillary serous ovarian cystadenocarcinoma
Malignant melanoma
Pleural mesothelioma
Neuroblastoma
Embryonal tumor of the testis
Bronchogenic carcinoma
Breast cancer

Calcification (Box 87-3) is a more specific sign but is insensitive (<1%) except in small children with metastatic neuroblastoma, in whom the sensitivity approaches 25%. Colloid carcinomas of the colon or stomach most commonly cause calcification that has been described as stippled, amorphous, flaky, punctate, granular, or poppy seed-like. The pattern of calcification, however, seldom indicates whether the tumor is primary or metastatic, and even differentiation from benign disease may be difficult. When there is a progressive increase in the size and number of calcifications accompanied by hepatomegaly, the diagnosis of neoplasm is nearly certain. Calcification may also occur in focal areas of metastasis after radiation therapy or chemotherapy.

Nuclear Medicine

Metastases typically are manifested as focal defects on both sulfur colloid and hepatobiliary scintiscans.¹⁸¹⁻¹⁸⁴ They are, in fact, the most common cause of focal “cold” liver lesions. Most often, multiple round focal defects of relatively uniform size are seen. The scintigraphic pattern, however, depends on the primary tumor type, stage of disease, and presence of underlying hepatic disease, such as cirrhosis, acute or chronic hepatitis, or steatosis. When only a single defect is seen, it must be differentiated from a normal variant, cyst, abscess, or intrahepatic gallbladder. Multiple defects make the diagnosis of metastases likely, but multiple cysts, hemangiomas, or abscesses may occasionally have the appearance.^{185,186}

Some tumors (leukemia, lymphoma) may infiltrate the liver diffusely, whereas others (breast and oat cell carcinoma) cause numerous small focal nodules. In both of these circumstances, hepatomegaly or diffuse heterogeneity of uptake or both may be seen. Colon cancers commonly produce large, often solitary defects.^{185,186}

Whereas nuclear medicine is no longer routinely used for the detection of hepatic metastatic lesions, PET with ¹⁸F-FDG has emerged as a sensitive tool for the detection of liver metastases from colorectal primaries (Fig. 87-39).¹⁸⁷ ¹⁸F-FDG is a glucose analogue that is metabolized more rapidly in tumor cells than in normal cells, resulting in increased uptake in malignant lesions.¹⁸⁷ However, PET has important limitations. The spatial resolution is poor, so complementary anatomic information from cross-sectional imaging techniques such as CT is necessary for evaluation of PET findings.¹⁷⁸ PET/CT is an efficient tool to solve this problem by means of combining the metabolic imaging and spatial localization advantages of PET and CT. A

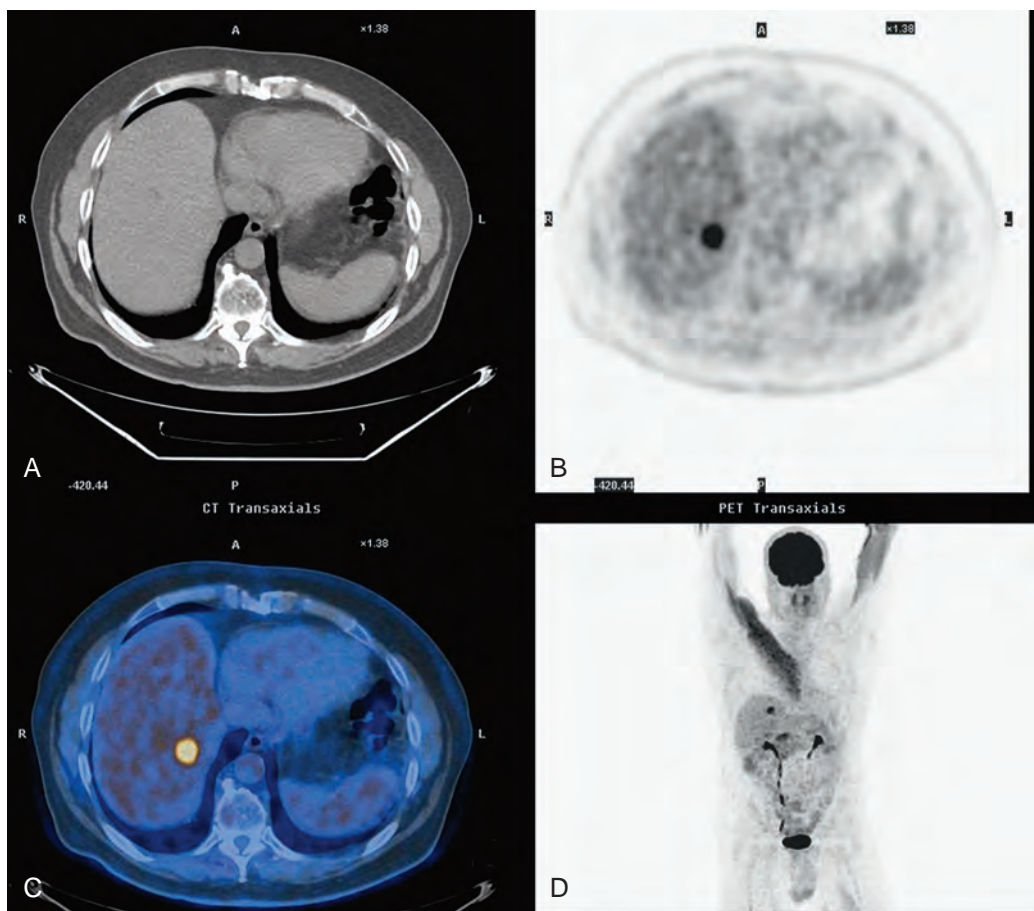


Figure 87-39 Hepatic metastases: PET/CT. **A.** Axial, unenhanced CT shows no mass. **B.** PET image at the same level shows uptake of ^{18}F -FDG in the right lobe. **C.** Fused image provides precise localization of the colon cancer metastasis. **D.** Whole body PET image shows the solitary hepatic metastasis.

second limitation is the ^{18}F -FDG uptake by inflammation, which makes clinical correlation necessary to assess the significance of PET findings.¹⁸⁸

^{18}F -FDG PET has been shown to be valuable in the response assessment of liver metastases undergoing systemic or local interventional therapy. ^{18}F -FDG PET is superior to CT in the assessment of radiofrequency ablation response by being able to distinguish between a marginal zone of reactive hyperperfusion, which is frequently seen at the rim of metastases on contrast-enhanced CT after radiofrequency ablation, and residual viable tumor tissue.¹⁸⁹⁻¹⁹²

After radiofrequency ablation treatment, most metastases that were persistently ^{18}F -FDG PET positive recurred within the follow-up time of 16 months, whereas metastases that were found to be ^{18}F -FDG PET negative within 3 weeks after treatment were less likely to relapse.¹⁹³ Recently, regarding the patients with liver metastases from breast cancer, the only independent predictive factor for patient survival was identified as a change in maximal standardized uptake value between the preinterventional stage and 3 months after selective internal radiation therapy.¹⁹⁴ In respect to this, it can be said that after therapy, functional MRI and PET can be useful for providing complementary information on tumor tissue viability. A study comparing diagnostic performance of fused ^{18}F -FDG PET and Gd-EOB-DTPA-enhanced MRI retrospectively versus

stand-alone Gd-EOB-DTPA-enhanced MRI and integrated PET/CT for liver lesion detection revealed that PET/MRI was significantly more accurate than PET/CT, providing significantly greater confidence for discrimination between benign and malignant liver lesions and representing a perfect test for the detection of hepatic lesions larger than 1 cm.¹⁹⁵ According to the same study, comparison of stand-alone Gd-EOB-DTPA-enhanced MRI and PET/MRI did not reveal significant change in sensitivity or specificity. Interestingly, the performances of both PET/MRI and Gd-EOB-DTPA-enhanced MRI were better than PET/CT in the detection and characterization of lesions smaller than 1 cm.¹⁹⁵

It seems that especially for detection of small hepatic lesions, compared with CT, MRI compensates for the drawbacks in PET better (Figs. 87-40 and 87-41)¹⁹⁶ and enhances lesion discrimination.¹⁹⁵ However, PET/MRI does not seem to have any benefits over MRI alone.²⁰

Ultrasound

Ultrasound has a diagnostic sensitivity of more than 90% in the detection of metastases.¹⁹⁷ In the absence of complications, such as hemorrhage, infection, or necrosis, focal metastatic liver disease is manifested with five basic sonographic patterns (Fig. 87-42): hypoechoic, bull's-eye or target pattern, calcified, cystic, and diffuse. Although there is no consistent correlation between

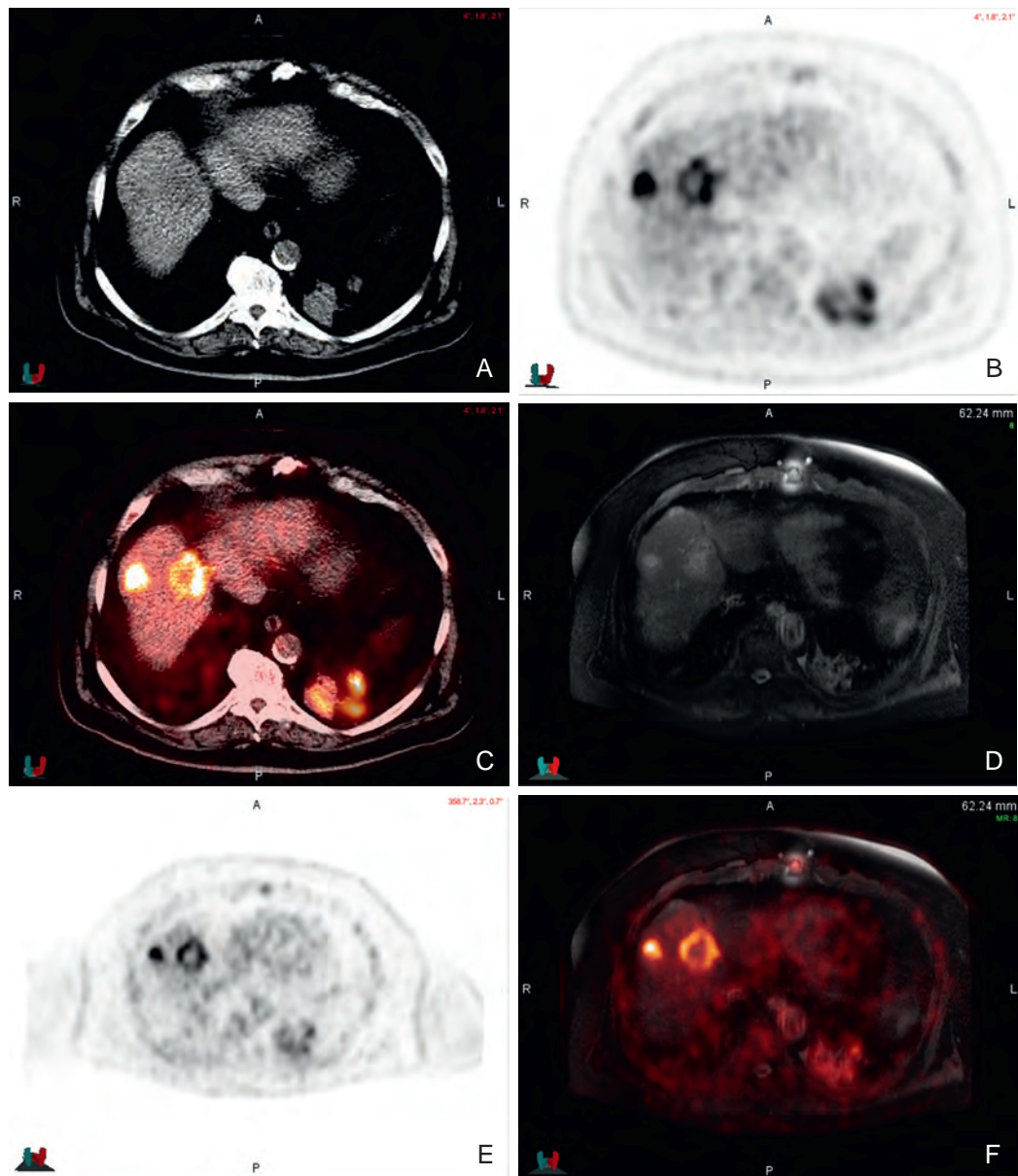


Figure 87-40 Hepatic metastases: PET/CT and PET/MRI. Metastatic colon cancer in a 76-year-old man. Axial CT (A), ^{18}F -FDG PET (B), and fused PET/CT (C) images demonstrate two hypermetabolic low-attenuation lesions in the dome of the liver. The metastatic lesions are well appreciated on T2-weighted spectral attenuated inversion recovery image (D). ^{18}F -FDG PET image (E) and fused PET/MRI axial image (F) delineate the hypermetabolic activity.

sonographic appearance and primary tumor type, certain generalities can be made (Box 87-4).¹⁹⁷⁻²⁰³

Hyperechoic Metastases. These usually arise from colon cancers and other gastrointestinal neoplasms. Vascular metastases from islet cell tumors, carcinoid, choriocarcinoma, and renal cell carcinoma tend to be echogenic as well.¹⁹⁸ They are echogenic because of numerous interfaces arising from the abnormal vessels.

Bull's-Eye or Target Pattern. The anechoic, thin, poorly defined halo that often surrounds solid liver metastases is most often a result of peritumoral compression of normal parenchyma and less often a result of tumor infiltrating into

the surrounding parenchyma. Its presence usually indicates an aggressive tumor.^{204,205} This is frequently seen in metastases from bronchogenic carcinoma.

Hypoechoic Metastases. These lesions tend to be hypovascular and highly cellular with few internal interfaces. Lymphoma, particularly when it is associated with acquired immunodeficiency syndrome, can be manifested with multiple hypoechoic deposits. More commonly, lymphoma is diffusely infiltrating.^{198,199}

Cystic Metastases. Cystic metastases usually develop in patients with primary neoplasms that have a cystic component: cystadenocarcinoma of the pancreas and ovary and mucinous

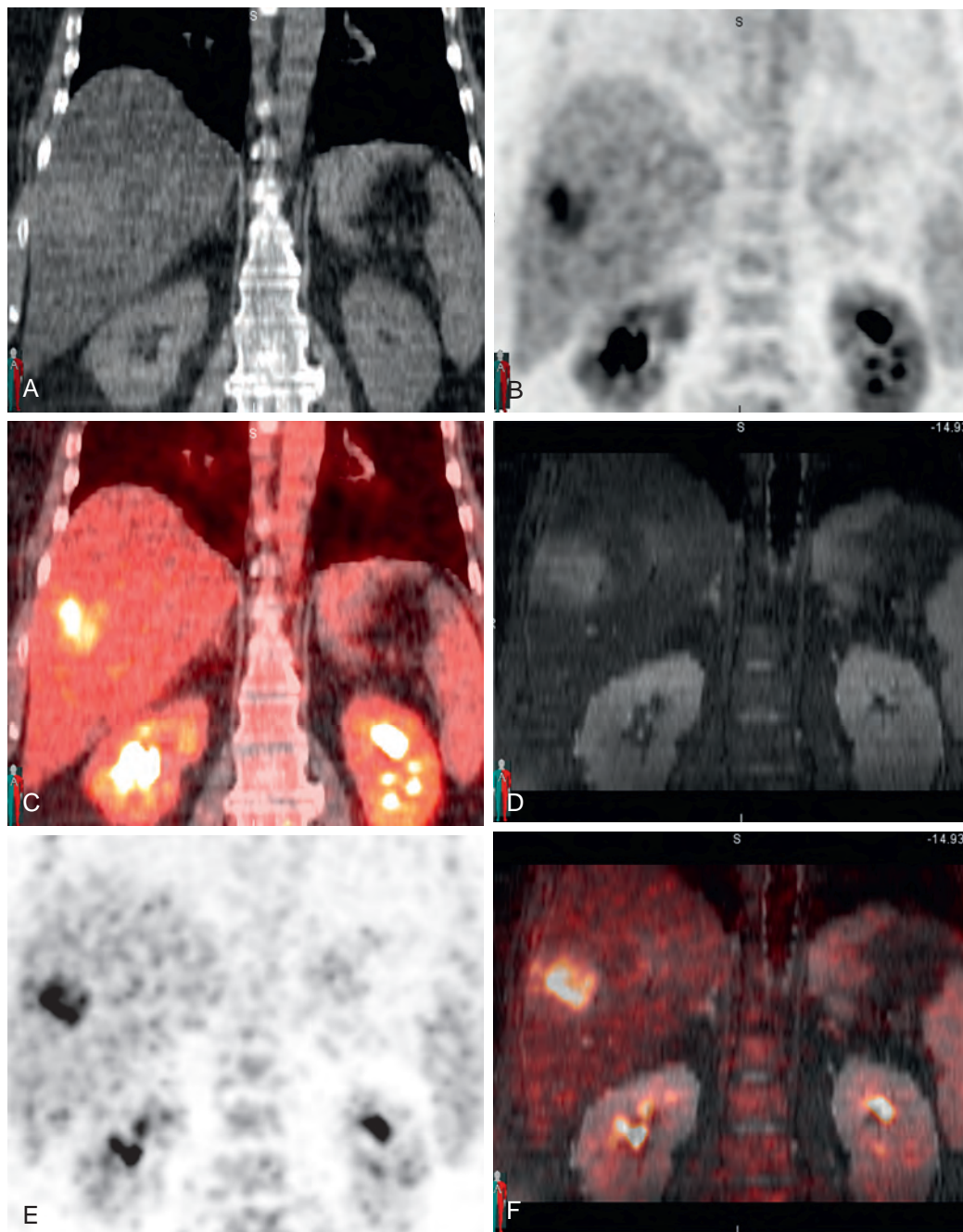


Figure 87-41 Hepatic metastasis: PET/CT and PET/MRI. Metastatic colon cancer in a 60-year-old man. Coronal CT image (A) demonstrates a subtle segment V lesion, further depicted on ^{18}F -FDG PET (B) and fused PET/CT (C) images. T2-weighted spectral attenuated inversion recovery image (D) better delineates the metastasis, with associated hypermetabolic uptake seen on ^{18}F -FDG PET (E) and fused PET/MRI (F) images.

carcinoma of the colon.²⁰⁵ Indeed, these lesions may resemble benign cysts on CT scans. Ultrasound, however, can usually reveal certain differentiating features: septa, mural nodules, debris, fluid-fluid levels, and mural thickening. When the central portion of a liver metastasis undergoes extensive necrosis, sonolucent metastases with low-level echoes and an irregularly thickened wall may be seen.²⁰⁶

Calcified Metastases. These metastases are relatively distinctive because of their marked echogenicity and acoustic shadowing (see Box 87-3). Mucinous adenocarcinoma of the colon is the

most common primary neoplasm associated with calcified liver metastases.^{207,208}

Diffuse Infiltration. This diffuse permeative infiltration is the most difficult sonographic pattern to be appreciated because the tissue texture is diffusely inhomogeneous, without the presence of well-defined masses. Diagnosis is further compromised in the presence of cirrhosis and fatty infiltration.^{198,209}

Contrast-enhanced ultrasound shows lesion blood flow in metastases as a reflection of the vascularity of the primary

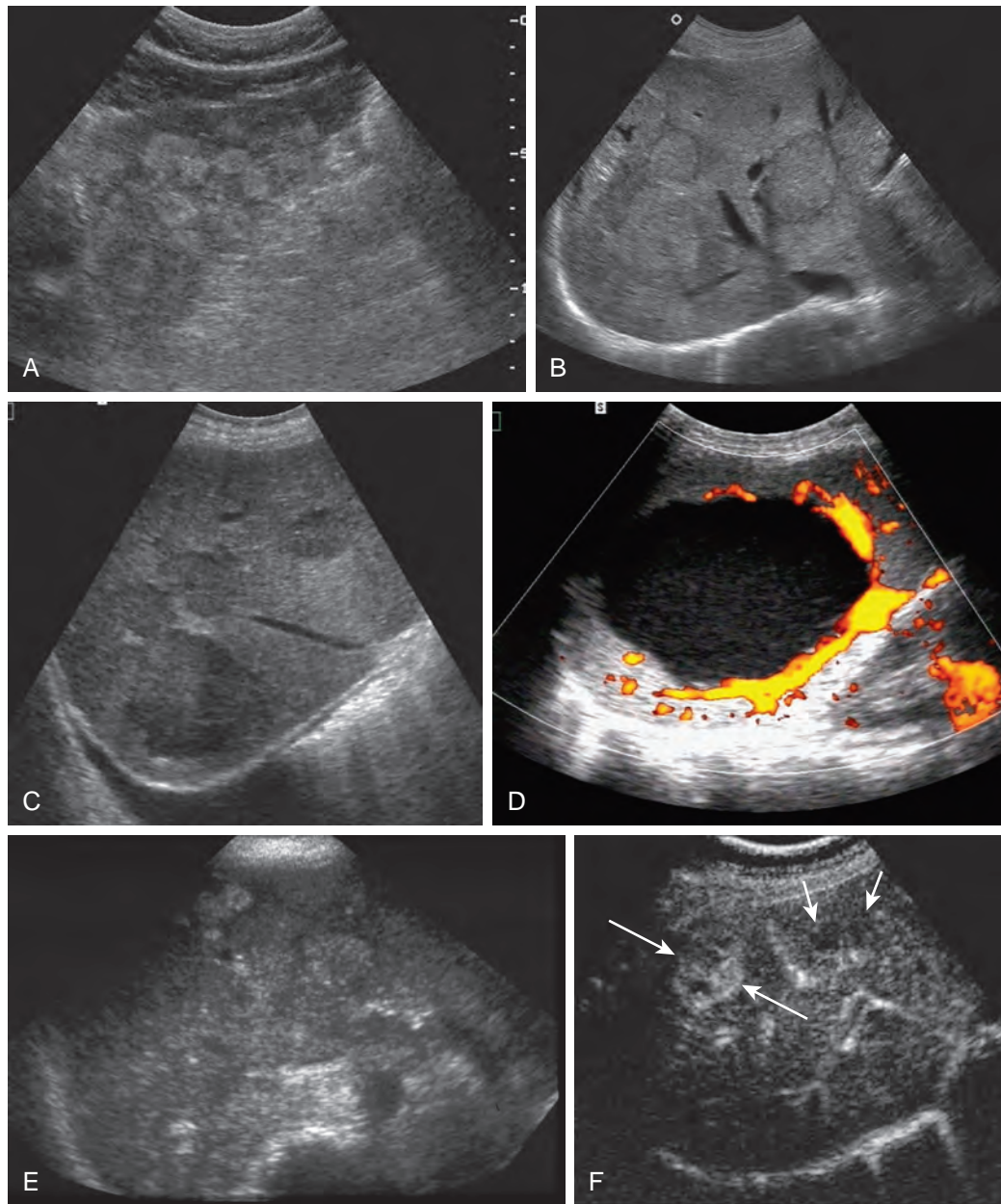


Figure 87-42 Hepatic metastases: spectrum of sonographic findings. **A.** Hyperechoic metastases are seen on this sagittal scan of the left hepatic lobe in a patient with carcinoid tumor. **B.** Bull's-eye lesions are present on this axial scan in a patient with metastatic lung cancer. **C.** Hypoechoic metastases are demonstrated in this patient with pancreatic cancer. There is a pleural effusion as well. **D.** Cystic metastasis with multiple fine internal echoes is present in this patient with mucinous ovarian carcinoma. **E.** Calcified metastases are seen in this patient with mucinous colon carcinoma. **F.** Hypervascular liver metastases in a 60-year-old man with previously resected retroperitoneal sarcoma. Early arterial phase ultrasound image (**F**) obtained 20 seconds after contrast material injection shows a large lesion with heterogeneous and mostly peripheral (nonglobular) enhancement (large arrows). Two small lesions remain hypoechoic (small arrows). (**F** from Catalano O, Nunziata A, Lobianco R, et al: *Real-time harmonic contrast material-specific US of focal liver lesions*. *RadioGraphics* 25:333–349, 2005.)

tumor.³⁹ Because of this, considerable variation is seen during the arterial phase enhancement. Hypervascular metastases may reveal enhancement features that overlap with those of HCC. Hypovascular metastases mostly show a slight signal enhancement with a marginal emphasis (halo sign, rim sign).⁴⁰ Fortunately, regardless of their appearance during the arterial phase, metastases have consistently shown less enhancement than the liver during the portal venous phase of contrast-enhanced ultrasound.

Computed Tomography

On CT scans, metastases can be hyperdense, isodense, hypodense, hypodense with peripheral enhancement, cystic, complex, calcified, or diffusely infiltrating (Figs. 87-43 to 87-46). The CT appearance depends on tumor size and vascularity, the degree of hemorrhage and necrosis, and the quality of the intravenous contrast material bolus. Thus, individual metastatic lesions within the liver can have

different CT findings, and metastases from different cell types can appear identical.²¹⁰⁻²¹⁴

Hyperdense metastases (see Fig. 87-44) are uncommon. These lesions are usually hypervascular (Box 87-5) and enhance rapidly and diffusely, becoming isodense with normal liver. These lesions may be difficult to visualize on contrast-enhanced CT scans obtained during the portal venous phase of enhancement. Hypervascular lesions may also occasionally be seen as hypoattenuating lesions on portal venous phase images.²¹⁵

Islet cell tumors are among the most common of the very hypervascular metastases. Breast carcinoma, carcinoid,

melanoma, thyroid carcinoma, and renal cell carcinoma also result in hypervascular metastases.²¹⁶

The majority of metastases are hypodense (see Fig. 87-45) with an attenuation between that of water and that of normal liver. These lesions are usually hypovascular, and intravenous contrast medium increases their conspicuity by increasing the density of normal liver. These lesions are best depicted during the portal phase of enhancement (60 seconds after intravenous administration of contrast material).^{215,217} Colon, lung, prostate, gastric, and transitional cell carcinoma are the most common tumors that appear as hypovascular liver metastases.²¹⁸

On the delayed phase images, metastases are often isoattenuating. Some metastases will show hypoattenuating peripheral areas surrounding an enhanced center on delayed images. This appearance is thought to represent contrast material washing out of the viable tumor periphery while remaining in the extracellular space of the center.²¹⁹

BOX 87-4 SONOGRAPHIC PATTERNS OF LIVER METASTASES

HYPOECHOIC

- Lymphoma
- Pancreas
- Cervical carcinoma
- Adenocarcinoma of the lung
- Nasopharyngeal cancer

MIXED ECHOGENICITY

- Breast cancer
- Lung cancer
- Stomach cancer
- Anaplastic cancer
- Cervical cancer
- Carcinoid

HYPERECHOIC

- Colon cancer
- Hepatoma
- Treated breast cancer

CYSTIC

- Mucinous ovarian carcinoma
- Colorectal carcinoma
- Sarcoma
- Melanoma
- Lung cancer
- Carcinoid



Figure 87-43 Calcified liver metastases on CT. This patient has mucinous adenocarcinoma of the colon.

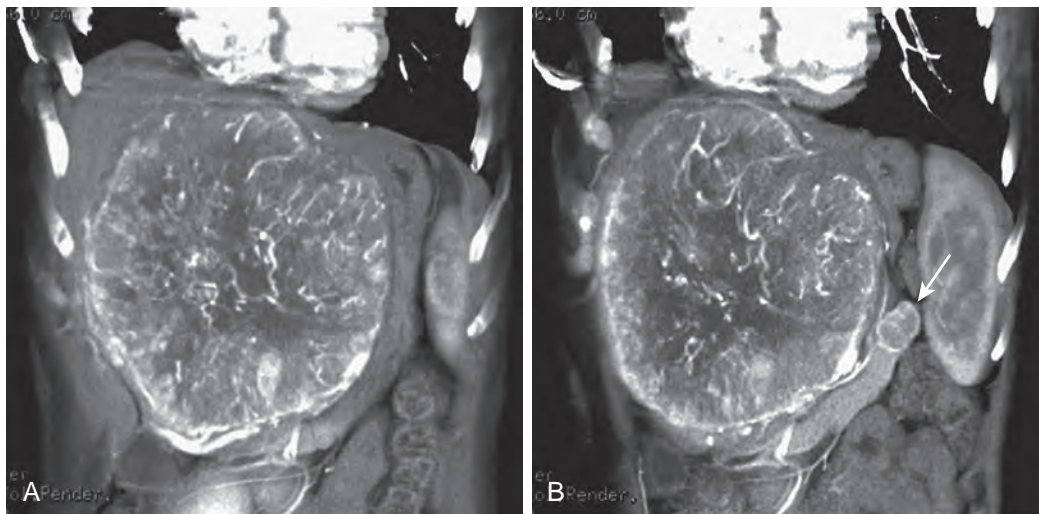


Figure 87-44 Hypervascular liver metastases on CT. **A** and **B**. A dominant, strikingly hypervascular mass from metastatic leptomeningeal hemangiopericytoma is demonstrated on these two coronal volume rendered images. Arrow, Pancreatic tail metastasis.

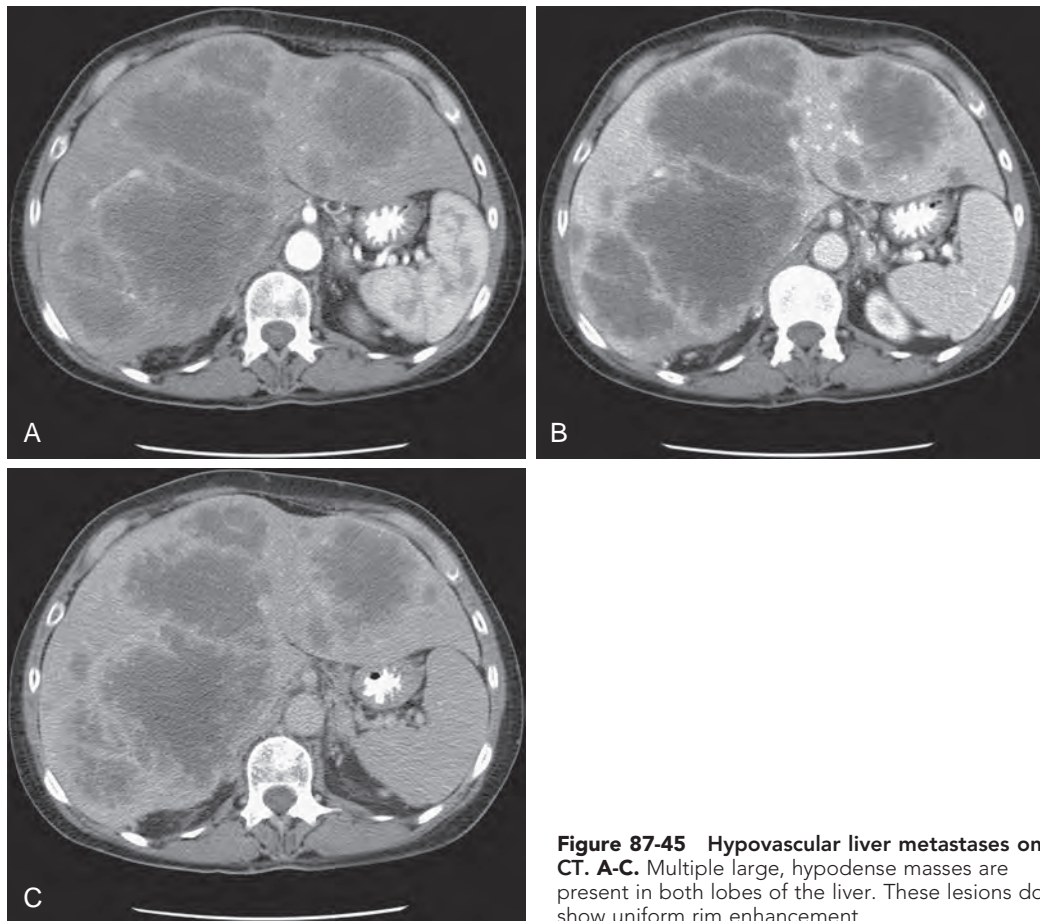


Figure 87-45 Hypovascular liver metastases on CT. A-C. Multiple large, hypodense masses are present in both lobes of the liver. These lesions do show uniform rim enhancement.

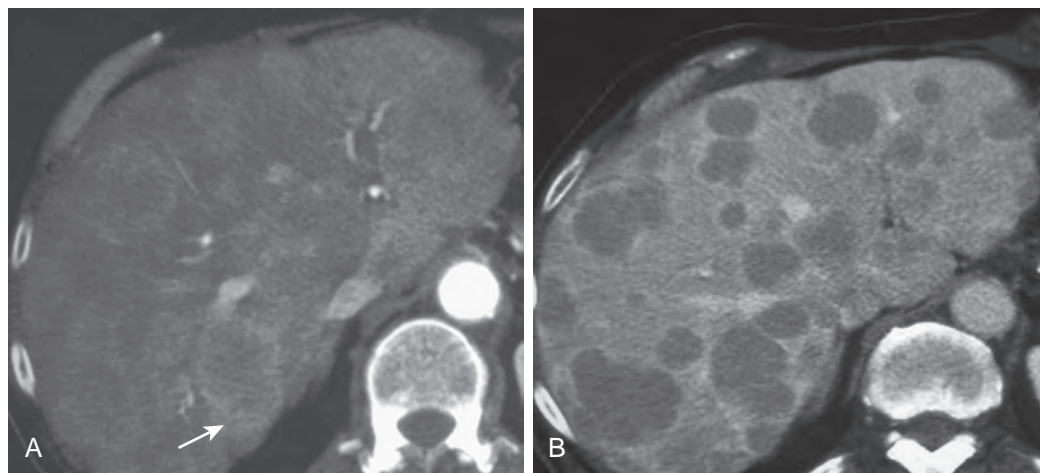


Figure 87-46 Ring enhancement of liver metastases on CT. Arterial (A) and portal venous (B) phase images show a hypervascular ring of enhancement (arrow). This complete ring of enhancement is typical of metastases but can also be seen in hepatic abscesses.

BOX 87-5 HYPERVASCULAR LIVER METASTASES

Melanoma
 Carcinoid
 Pancreatic islet cell tumor
 Choriocarcinoma
 Pheochromocytoma
 Breast cancer
 Thyroid carcinoma
 Renal cell carcinoma

Certain metastases may be cystic, having an attenuation less than 20 HU. Ultrasound may be needed to differentiate these lesions from simple cysts. Calcifications are also well demonstrated on CT scans.

Rim enhancement (see Fig. 87-46) of a hypodense metastasis represents a vascularized viable tumor periphery contrasted with a hypovascular or necrotic center.^{210,213}

Unless the size or contour of the liver is altered, diffusely infiltrating metastases can be difficult to appreciate. Diagnosis is also difficult in patients with cirrhosis and hepatic steatosis.

In these cases, MRI can be useful in appreciating the tumor nodules.

The borders of hepatic metastases can be sharp, ill-defined, or nodular, and their shape may be ovoid, round, or irregular.

Magnetic Resonance Imaging

The T1 and T2 relaxation times of liver metastases vary considerably, depending on the primary tumor, degree of necrosis, hemorrhage, and vascularity. Nevertheless, the T1 and T2 relaxation times of most liver metastases (Fig. 87-47) are longer than those of normal liver and shorter than those of simple cysts or hemangiomas.²²⁰⁻²²⁸ Five major morphologic patterns have been described for metastases on MR images.²²⁹

Doughnut. On T1-weighted images, metastases, because of their long T1 relaxation time, are manifested as a low signal intensity mass containing a distinct central region of even lower signal intensity. This pattern is usually seen with larger lesions and those that are prone to undergo necrosis. Metastases that contain considerable mucin, fat, subacute hemorrhage, or melanin, however, may have a relatively high signal intensity on T1-weighted images. High signal intensity has also been observed in carcinoids with hemorrhage.²²⁹

Target. On T2-weighted images, some metastases are manifested with a central smooth or irregularly rounded area of high signal intensity surrounded by a ring of tissue with a somewhat

weaker signal intensity. This pattern is also seen in lesions that are large and tend to undergo necrosis.²²⁹⁻²³¹

Amorphous. These metastases have variable increased signal intensity with inhomogeneous and featureless contents. The outer margins tend to be round and indistinct.

Halo. These masses have a distinct but not necessarily smooth circumferential rim of high signal intensity. The rim varies in thickness from 2 to 10 mm and encircles a lesion of somewhat lower signal intensity. The lower signal intensity may reflect the presence of fibrosis, coagulative necrosis, and mucin. This halo is probably a manifestation of greater water content than in adjacent normal liver parenchyma, perhaps reflecting an edematous reaction incited by tumor cell infiltration. Alternatively, it may reflect a viable tumor. Therefore, the peripheral zone of hyperintensity should be assumed to represent tumor for the purposes of surgical planning and estimating tumor volume. Some 50% of colon cancer metastases have some central hypointensity.²²⁹⁻²³¹

Light Bulb. These lesions are smooth, sharply defined, and round or elliptic. The contents have high signal intensity, similar to that of gallbladder, cerebrospinal fluid, cysts, and hemangiomas. In these cases, the high signal intensity on T2-weighted images is attributed to either fluid contents or considerable blood flow. In metastases, this may be due to complete tumor necrosis and liquefaction or a hypervascular mass. The light

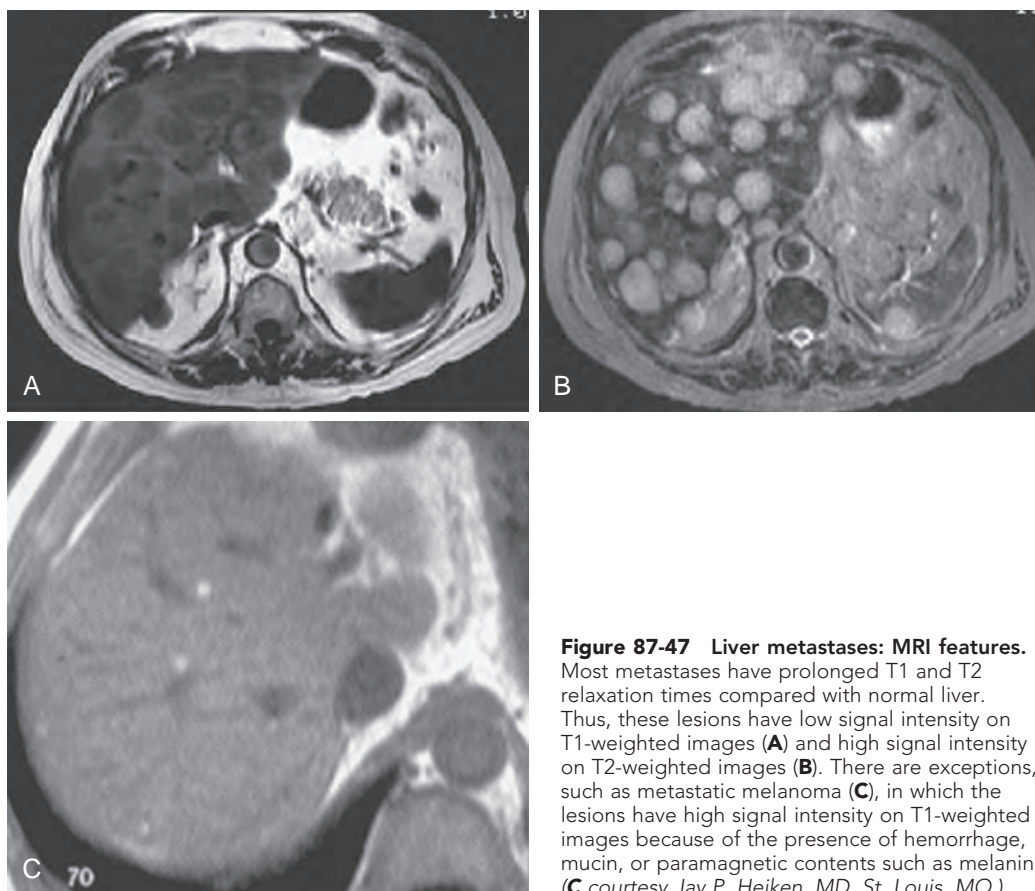


Figure 87-47 Liver metastases: MRI features.

Most metastases have prolonged T1 and T2 relaxation times compared with normal liver. Thus, these lesions have low signal intensity on T1-weighted images (A) and high signal intensity on T2-weighted images (B). There are exceptions, such as metastatic melanoma (C), in which the lesions have high signal intensity on T1-weighted images because of the presence of hemorrhage, mucin, or paramagnetic contents such as melanin. (C courtesy Jay P. Heiken, MD, St. Louis, MO.)

bulb sign has been described in cystic neoplastic metastases, pheochromocytoma, carcinoid, and islet cell tumor.²²⁹⁻²³²

Role of Magnetic Resonance Imaging

The introduction of hepatic resection as a potentially curative treatment for patients with liver metastases from colorectal primaries has created major challenges for MRI. The preoperative assessment of these patients requires accurate delineation of the precise number and location of metastases and their relationship to adjacent vascular structures. Also, because benign liver lesions such as cysts and hemangiomas are relatively common, imaging techniques must be able to distinguish between benign and malignant lesions with a high degree of specificity.²³³ For the performance of MRI to be improved in this clinical context, numerous different sequences and contrast agents have been evaluated. The use of Gd-DTPA in the detection of liver metastases has been disappointing, and no clear benefit of using dynamic gadolinium-enhanced sequences over unenhanced T1-weighted images has been demonstrated at 1.5T.²³⁴ After the intravenous administration of contrast material with dynamic imaging (Fig. 87-48), enhancement patterns of the hepatic metastases are similar to those on CT. Hypervascular metastases show marked early enhancement as a continuous ring that on later images fills in centrally, or they may show early uniform enhancement (Fig. 87-49). During the portal venous phase, hypervascular metastases may become isointense or hypointense (Fig. 87-50). Hypovascular metastases are seen as hypointense masses that may have an enhancing peripheral rim best seen during the arterial phase. Progressive centripetal fill-in may occur on delayed phases.

Several studies have evaluated the accuracy of SPIO-enhanced MRI in the detection of liver metastases by use of findings at intraoperative ultrasound and pathologic examination as the "gold standard."²³⁵⁻²³⁷ With use of SPIO, metastatic lesions should appear unenhanced against a negatively enhanced liver.²¹⁹ SPIO-enhanced MRI detected more lesions than unenhanced MRI, percutaneous ultrasound, and contrast-enhanced CT and was comparable to CT arterial portography.^{235,236} Important advantages of SPIO-enhanced MRI are its lack of invasiveness compared with CT arterial portography and the availability of an extended imaging window, allowing greater flexibility in scanning times (Fig. 87-51).²³⁸

With use of hepatobiliary contrast agents such as Gd-EOB-DTPA, hepatic metastases from extrahepatic malignant neoplasms do not enhance in the hepatocellular phase because of

lack of functioning hepatocytes or bile ducts, and they typically appear uniformly hypointense relative to normal liver (Fig. 87-52). On occasion, at the interface between a metastasis and normal liver parenchyma, a thin rim of hyperintensity can be seen that presumably represents a perilesional biliary reaction, compressed normal hepatic parenchyma, or a combination of the two.⁶⁸

Gd-EOB-DTPA appears to be suitable not only for detecting very small metastases less than 1 cm but also in differentiating them from FNH and simple cysts.^{239,240} In several studies, it is reported that with the use of Gd-EOB-DTPA, more liver metastases are depicted, and also lesion characterization and diagnostic confidence are improved.^{240,241}

The usefulness of diffusion-weighted imaging in the detection of liver metastases compared with unenhanced and dynamic liver-specific contrast-enhanced MRI has been demonstrated by several studies. Lesion conspicuity of hemangiomas and metastases is significantly higher with respiratory triggered diffusion-weighted imaging at low b values compared with conventional unenhanced MRI because of an excellent lesion-to-liver contrast and suppression of background signals from vessels.²⁴² However, diffusion-weighted imaging alone is not useful because it is susceptible to motion artifacts that obscure lesions, and difficulty arises for image interpretation.²⁴³ Breath-hold or respiratory triggered diffusion-weighted imaging has a significantly higher overall lesion detection rate compared with conventional T2-weighted MRI.²⁴⁴ Especially in considering small metastases less than 10 mm, respiratory echo planar diffusion-weighted imaging is more sensitive in detection compared with conventional MRI with and without contrast.²⁴⁵ Low lesion-to-liver contrast and the interfering bright signal from intrahepatic vessels hinder lesion detection on T2 turbo spin-echo sequences. Lesion conspicuity with diffusion-weighted imaging is excellent, and limitation of the diffusion-weighted imaging sequence is predominantly referred to lesion characterization rather than to lesion detectability.²⁴⁶

Angiography

Angiography is no longer used to diagnose liver metastases but is performed to provide a vascular road map for the surgeon and to guide intra-arterial therapy.²⁴⁷ Because metastases are almost completely supplied by the hepatic artery, injection of the celiac or superior mesenteric artery may show hypervascular tumor circulation early and

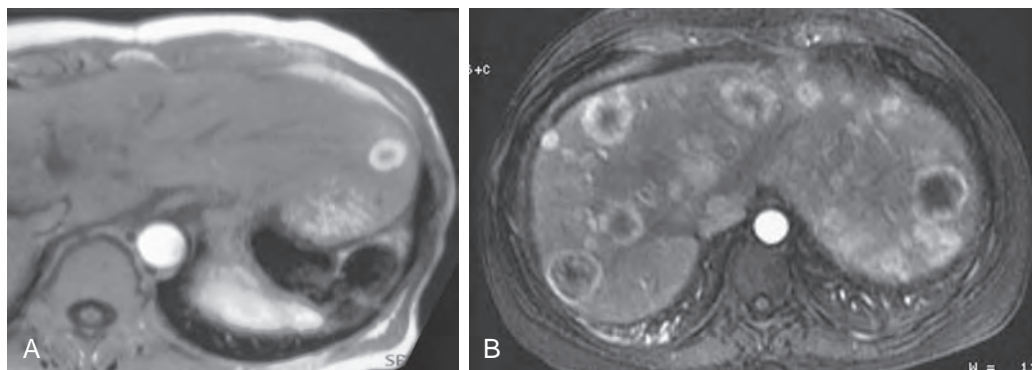


Figure 87-48 Liver metastases: ring enhancement on MRI. There are complete rings of lesion enhancement seen in this patient with breast cancer and a solitary metastasis in the left lobe (A) and in a different patient with multiple carcinoid metastases (B).

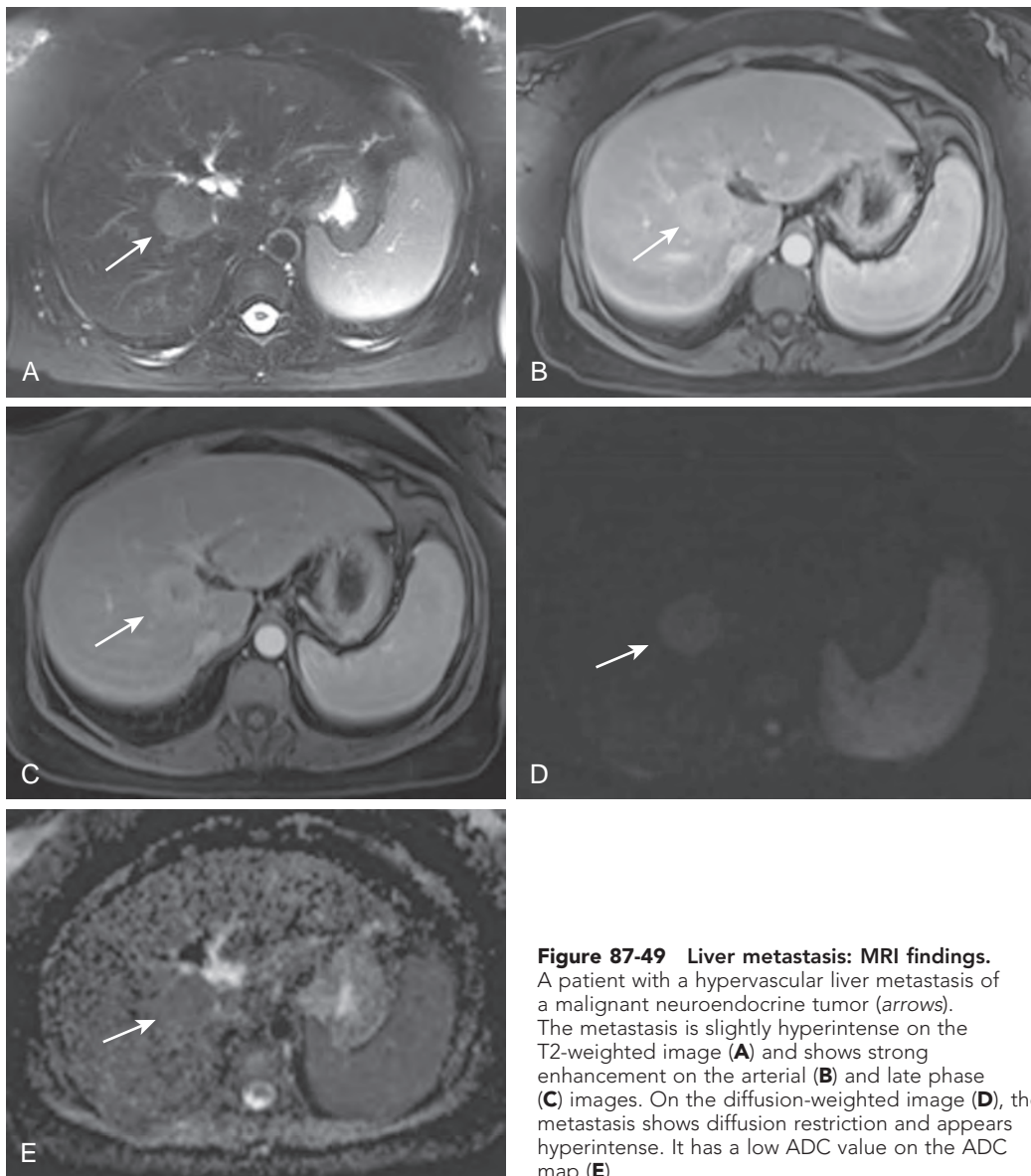


Figure 87-49 Liver metastasis: MRI findings.

A patient with a hypervascular liver metastasis of a malignant neuroendocrine tumor (arrows). The metastasis is slightly hyperintense on the T2-weighted image (A) and shows strong enhancement on the arterial (B) and late phase (C) images. On the diffusion-weighted image (D), the metastasis shows diffusion restriction and appears hyperintense. It has a low ADC value on the ADC map (E).

hypovascularity during the venous phase as portal blood containing contrast medium perfuses the surrounding normal hepatic parenchyma.²⁴⁷⁻²⁴⁹

Differential Diagnosis— Incidental Mass

Improvements in cross-sectional imaging have led to the detection of more and smaller hepatic lesions. Detection of lesions smaller than 15 mm can be a problem because of their uncertain clinical significance. In one study using CT, a single small (<1.5 cm) lesion was benign in 65% of patients, and two to four tiny lesions were benign in 59% of cases. When the number of lesions increases or an additional large lesion is present, the likelihood of malignancy increases. Even in the presence of extrahepatic malignant disease, 51% of these small lesions are benign. This has important implications for patients with dominant metastases who are being considered for hepatic resection.

The possibility that the other lesions are benign should be considered.²⁵⁰

Metastases are not the only causes of multiple hepatic masses. Abscess, cyst, extramedullary hematopoiesis, multifocal or diffuse HCC, ICAC, angiosarcoma, nodular regenerative hyperplasia, and hemangioma can all be multiple.

Practical Approach to Liver Masses

The evaluation of focal liver masses should be systematic and include both radiologic appearance and clinical information to help narrow the differential diagnosis. The three most important pieces of clinical information in evaluating liver neoplasms are the age and sex of the patient and the presence of extrahepatic malignant disease. In adults, metastases, FLC, FNH, and hepatocellular adenoma are seen in patients younger than 40 years. Metastases, typical HCC, ICAC, angiosarcoma, and hemangioma are most frequently seen in patients older than 50 years. In pediatric patients, the vascular tumors infantile

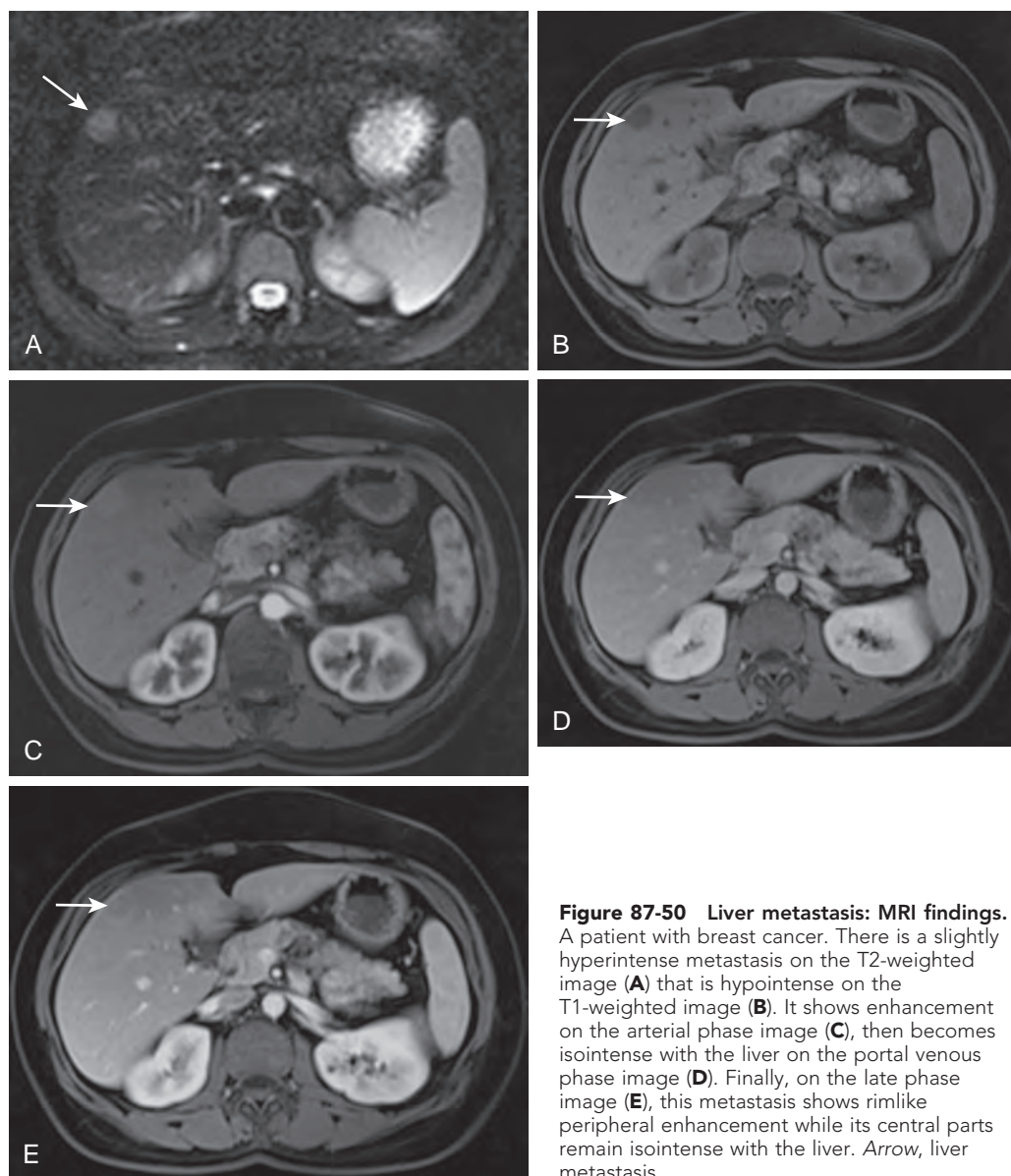


Figure 87-50 Liver metastasis: MRI findings. A patient with breast cancer. There is a slightly hyperintense metastasis on the T2-weighted image (**A**) that is hypointense on the T1-weighted image (**B**). It shows enhancement on the arterial phase image (**C**), then becomes isointense with the liver on the portal venous phase image (**D**). Finally, on the late phase image (**E**), this metastasis shows rimlike peripheral enhancement while its central parts remain isointense with the liver. Arrow, liver metastasis.

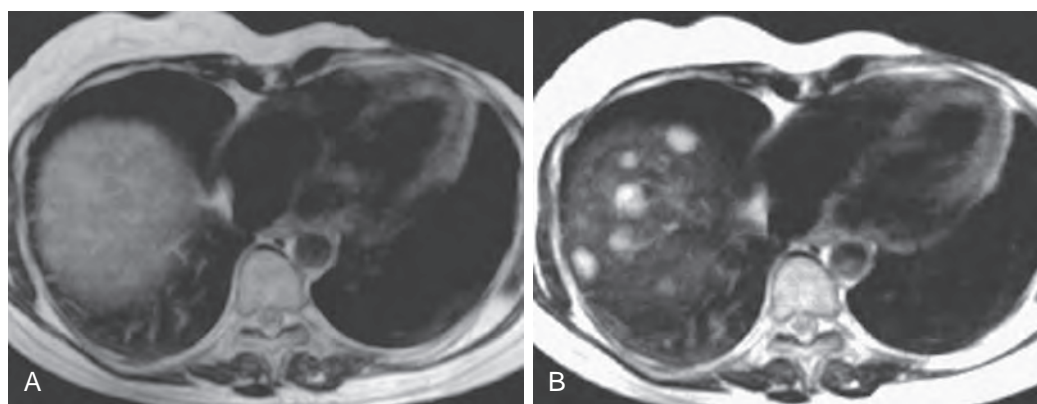


Figure 87-51 MRI of liver metastases with SPIO-enhanced scan. Metastases that are barely visualized on T2-weighted MR image (**A**) can be easily detected after the administration of SPIO (**B**). (Courtesy Dr. Tomoaki Ichikawa, Yamanashi University, Yamanashi, Japan.)

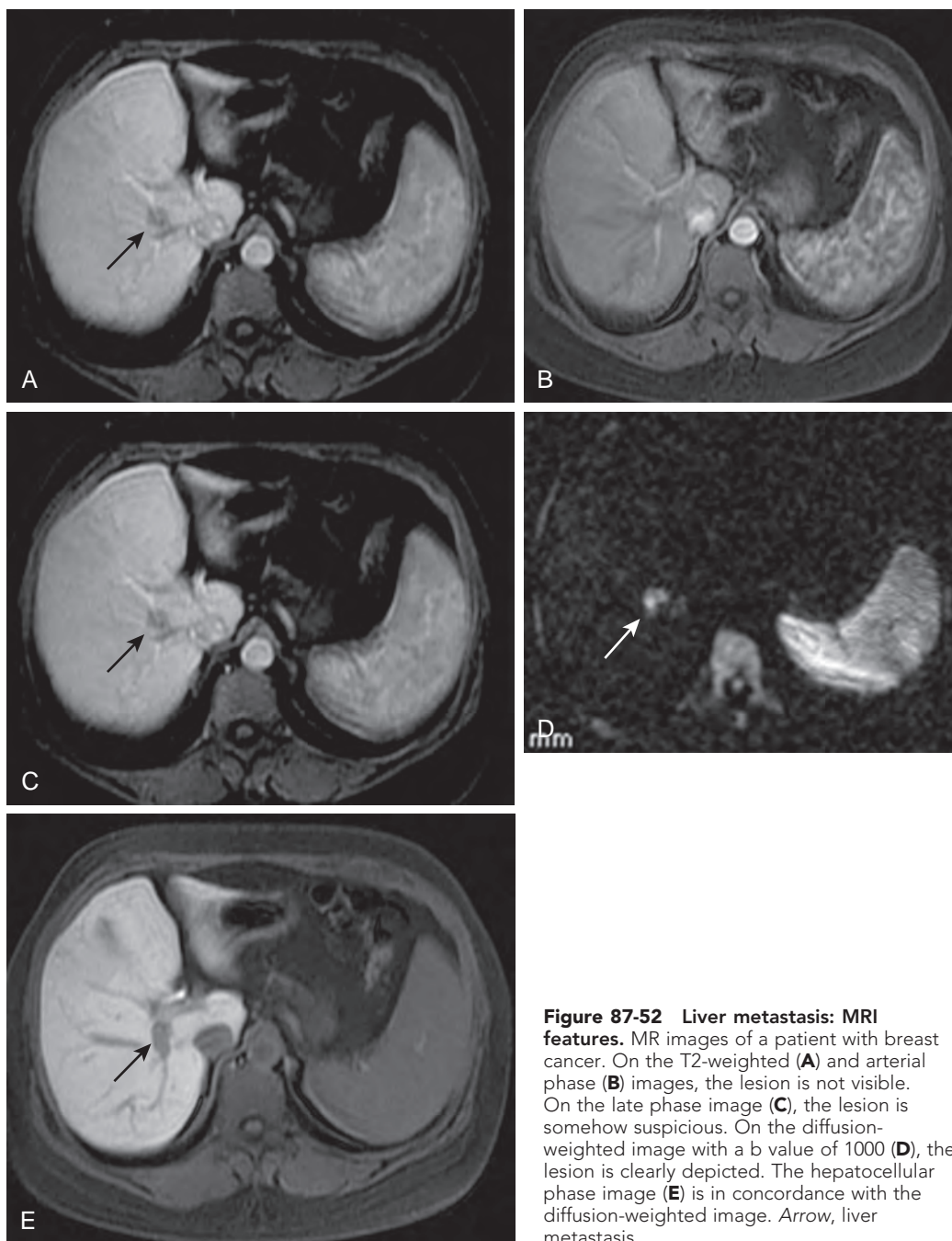


Figure 87-52 Liver metastasis: MRI features. MR images of a patient with breast cancer. On the T2-weighted (A) and arterial phase (B) images, the lesion is not visible. On the late phase image (C), the lesion is somehow suspicious. On the diffusion-weighted image with a b value of 1000 (D), the lesion is clearly depicted. The hepatocellular phase image (E) is in concordance with the diffusion-weighted image. Arrow, liver metastasis.

hemangioendothelioma and hemangioma are seen in the first 6 months of life. Hepatoblastoma usually is manifested in the first 3 years of life, and although it may be present at birth, the peak incidence is at 18 months. Benign mesenchymal hamartoma has an incidence similar to that of hepatoblastoma. Tumors that occur in older children and adolescents include HCC and UES. With regard to sex, malignant primary liver tumors are generally more frequent in men and benign primary tumors in women. Metastases are overwhelmingly more frequent than primary liver neoplasms in both the pediatric and the adult populations. Other significant clinical data include a history of chronic steroid and contraceptive use. Neoplasms related to steroid use include hepatocellular adenoma and, to a

lesser degree, FNH, nodular regenerative hyperplasia, hemangioma, and HCC.

Multiple imaging tests are available for evaluating hepatic neoplasms. Contrast-enhanced dynamic MR and CT imaging and sonography provide important diagnostic clues that can help establish a final diagnosis. In interpreting a hepatic imaging study, the parameters to consider are the presence of single versus multiple masses; calcification; sharpness of contour; presence, absence, or persistence of enhancement; patency of vessels; and extrahepatic extension.

After all these considerations, the radiologist must determine whether a hepatic mass is a nonsurgical lesion. In the adult, the two most common nonsurgical primary tumors

are hemangioma and FNH. All other primary neoplasms of the liver are surgical lesions if they are resectable. Therefore, the two most important determinations the radiologist must make are whether the mass in the liver is hemangioma or FNH and, if it is not, whether the mass is resectable for cure. Metastases, HCC, FLC, ICAC, angiosarcoma, and hepatocellular adenoma are all potentially resectable in the adult. In children, hepatoblastoma, UES, HCC, and mesenchymal hamartoma are all surgical lesions. Infantile hemangioendothelioma does not require surgery if the patient can survive with supportive therapy or embolization until the tumor regresses spontaneously.

Hemangioma has a highly suggestive appearance on ultrasound, CT, MRI, and scintigraphic studies. However, the optimal imaging techniques are dynamic MRI with gadolinium enhancement and contrast-enhanced CT (see Chapter 83). The appearance of FNH on ultrasound, CT, and unenhanced MRI is nonspecific, unless a central scar is present, and overlaps with FLC and hepatocellular adenoma. However, gadolinium-enhanced dynamic MRI and T2-weighted MRI enhanced with SPIO may demonstrate imaging features of FNH that aid in narrowing of the differential diagnosis. FNH shows characteristically dramatic signal loss. The degree of signal loss is greater than in other focal liver lesions, such

as hepatocellular adenoma and metastases, and is a useful diagnostic feature for FNH.²⁵¹

Hepatobiliary contrast agents also play a major role in the diagnostic work-up of liver masses. They can be used to differentiate benign lesions from the malignant ones and most probably to estimate the differentiation degree of HCCs. Nevertheless, hepatocellular phase images are not enough for a correct diagnosis to be made. The extracellular phases (arterial, portal venous, and hepatic venous phases) of MRI with hepatobiliary contrast agents, T2-weighted images, diffusion-weighted images, and in-phase and out-of-phase images are all crucial for a definite diagnosis of the liver masses to be reached.

Finally, the use of percutaneous needle biopsies should be considered for exceptional cases, when noninvasive imaging studies have yielded atypical or inconclusive findings. In general, liver biopsies are devoid of significant risk when they are performed with CT or ultrasound guidance. The material obtained by percutaneous biopsy is sometimes not sufficient for a diagnosis, and an open biopsy should be done.

In summary, the differential diagnosis of a liver neoplasm can be narrowed significantly by use of different imaging and clinical features. In addition, percutaneous biopsy may be useful in further defining tumors without a characteristic imaging appearance.

REFERENCES

1. Ayuso C, Rimola J, García-Criado A: Imaging of HCC. *Abdom Imaging* 37:215–230, 2012.
2. Ros PR, Rasmussen JF, Li KCP: Radiology of malignant and benign liver tumors. *Curr Probl Diagn Radiol* 11:95–99, 1989.
3. Roth GG, Mitchell DG: Hepatocellular carcinoma and other hepatic malignancies: MR imaging. *Radiol Clin North Am* 52:683–707, 2014.
4. Freeny PC, Baron RL, Teefey SA: Hepatocellular carcinoma: Reduced frequency of typical findings with dynamic contrast-enhanced CT in a non-Asian population. *Radiology* 182:143–148, 1992.
5. Catala V, Nicolau C, Vilana R, et al: Characterization of focal liver lesions: Comparative study of contrast-enhanced ultrasound versus spiral computed tomography. *Eur Radiol* 17:1066–1073, 2007.
6. Noguchi S, Yamamoto R, Tatsuta M, et al: Cell features and patterns in fine-needle aspirates of hepatocellular carcinoma. *Cancer* 58:321–328, 1986.
7. Knudsen ES, Gopal P, Singal AG: The changing landscape of hepatocellular carcinoma: Etiology, genetics, and therapy. *Am J Pathol* 184:574–583, 2014.
8. Ros PR: Focal liver masses other than metastases. In Gore RM, editor: *Syllabus for Categorical Course on Gastrointestinal Radiology*, Reston, VA, 1991, American College of Radiology, pp 159–169.
9. Sadek AG, Mitchell DG, Siegelman ES, et al: Early hepatocellular carcinoma that develops within macrorregenerative nodules: Growth depicted at serial MR imaging. *Radiology* 195:753–756, 1995.
10. Salgia R, Singal AG: Hepatocellular carcinoma and other liver lesions. *Med Clin North Am* 1981:103–118, 2014.
11. Hecht EM, Holland AE, Israel GM, et al: Hepatocellular carcinoma in the cirrhotic liver: Gadolinium-enhanced 3D T1-weighted MR imaging as a stand-alone sequence for diagnosis. *Radiology* 239:438–447, 2006.
12. Salgia R, Singal AG: Hepatocellular carcinoma and other liver lesions. *Med Clin North Am* 98:103–118, 2014.
13. Kew MC: Hepatic tumors and cysts. In Feldman M, Schar Schmidt BF, Sleisinger MH, editors: *Sleisinger & Fordtran's Gastrointestinal and Liver Disease*, ed 6, Philadelphia, 1998, WB Saunders, pp 1364–1387.
14. Nakashima T, Okuda K, Kojiro M, et al: Pathology of HCC in Japan: 232 consecutive cases autopsied in ten years. *Cancer* 51:863–877, 1983.
15. Kanematsu M, Imaeda T, Yamawaki Y, et al: Rupture of hepatocellular carcinoma: Predictive value of CT findings. *AJR Am J Roentgenol* 158:1247–1250, 1992.
16. Kudo M, Hirasa M, Takakuwa H, et al: Small hepatocellular carcinomas in chronic liver disease: Detection with SPECT. *Radiology* 159:697–703, 1986.
17. Ho CL: Clinical PET imaging—an Asian perspective. *Ann Acad Med Singapore* 33:155–165, 2004.
18. Cottone M, Mareceno MP, Maringhini A, et al: Ultrasound in the diagnosis of hepatocellular carcinoma associated with cirrhosis. *Radiology* 147:517–519, 1983.
19. Yu JS, Chung JJ, Kim JH, et al: Detection of small intrahepatic metastases of hepatocellular carcinomas using diffusion-weighted imaging: Comparison with conventional dynamic MRI. *Magn Reson Imaging* 29:985–992, 2011.
20. Buchbender C, Heusner TA, Lauenstein TC, et al: Oncologic PET/MRI, part 1: Tumors of the brain, head and neck, chest, abdomen, and pelvis. *J Nucl Med* 53:928–938, 2012.
21. Shiomi S, Nishiguchi S, Ishizu H, et al: Usefulness of positron emission tomography with fluorine-18-fluorodeoxyglucose for predicting outcome in patients with hepatocellular carcinoma. *Am J Gastroenterol* 96:1877–1880, 2001.
22. Sun L, Guan YS, Pan WM, et al: Metabolic restaging of hepatocellular carcinoma using whole-body F-FDG PET/CT. *World J Hepatol* 1:90–97, 2009.
23. Tanaka S, Kitamura T, Imaoka S, et al: Hepatocellular carcinoma: Sonographic and histologic correlation. *AJR Am J Roentgenol* 140:701–707, 1983.
24. Kudo M, Ikekubo K, Yamamoto K, et al: Distinction between hemangioma of the liver and hepatocellular carcinoma: Value of labeled RBC-SPECT scanning. *AJR Am J Roentgenol* 152:977–983, 1989.
25. Shapiro RS, Katz R, Mendelson DS, et al: Detection of hepatocellular carcinoma in cirrhotic patients: Sensitivity of CT and ultrasonography. *J Ultrasound Med* 15:497–502, 1996.
26. Solmi L, Primareno AM, Gondolfi L: Ultrasound follow-up of patients at risk for hepatocellular carcinoma: Results of a prospective study of 360 cases. *Am J Gastroenterol* 91:1189–1194, 1996.
27. Takayasu K, Moriyama N, Muramatsu Y, et al: The diagnosis of small hepatocellular carcinomas: Efficacy of various imaging procedures in 100 patients. *AJR Am J Roentgenol* 155:49–54, 1990.
28. DeSantis M, Romagnoli R, Cristani A, et al: MRI of small hepatocellular carcinoma: Comparison with US, CT, DSA and Lipiodol-CT. *J Comput Assist Tomogr* 16:189–197, 1992.
29. Catalano O, Nunziata A, Lobianco R, et al: Real-time harmonic contrast material-specific US of focal liver lesions. *Radiographics* 25:333–349, 2005.

30. Lencioni R, Pinto F, Armilotta N, et al: Assessment of tumor vascularity in hepatocellular carcinoma: Comparison of power Doppler US and color Doppler US. *Radiology* 201:353–358, 1996.
31. Tanaka S, Kitamura T, Fujita M, et al: Small hepatocellular carcinoma: Differentiation from adenomatous hyperplastic nodule with color Doppler flow imaging. *Radiology* 182:161–165, 1992.
32. Wilson SR, Burns PN, Muradali D, et al: Harmonic hepatic US with microbubble contrast agent: Initial experience showing improved characterization of hemangioma, hepatocellular carcinoma, and metastasis. *Radiology* 215:153–184, 2000.
33. Tarantino L, Francica G, Sordelli I, et al: Diagnosis of benign and malignant portal vein thrombosis in cirrhotic patients with hepatocellular carcinoma: Color Doppler US, contrast-enhanced US, and fine-needle biopsy. *Abdom Imaging* 31:537–544, 2006.
34. Zheng SG, Xu HX, Liu LN: Management of hepatocellular carcinoma: The role of contrast-enhanced ultrasound. *World J Radiol* 6: 7–14, 2014.
35. Brannigan M, Burns PN, Wilson SR: Blood flow patterns in focal liver lesions at microbubble-enhanced US. *Radiographics* 24: 921–935, 2004.
36. Dietrich CF: Characterisation of focal liver lesions with contrast enhanced ultrasonography. *Eur J Radiol* 51(Suppl):S9–S17, 2004.
37. Brannigan M, Burns PN, Wilson SR: Blood flow patterns in focal liver lesions at microbubble-enhanced US. *Radiographics* 24: 921–935, 2004.
38. Jang HJ, Lim JH, Lee SJ, et al: Hepatocellular carcinoma: Are combined CT during arterial portography and CT hepatic arteriography in addition to triple-phase helical CT all necessary for preoperative evaluation? *Radiology* 215:373–380, 2000.
39. Doyle DJ, O'Malley ME, Jang HJ, et al: Value of the unenhanced phase for detection of hepatocellular carcinomas 3 cm or less when performing multiphase computed tomography in patients with cirrhosis. *J Comput Assist Tomogr* 31:86–92, 2007.
40. Yu SC, Yeung DT, So NM: Imaging features of hepatocellular carcinoma. *Clin Radiol* 59:145–156, 2004.
41. Tublin ME, Dodd GD, 3rd, Baron RL: Benign and malignant portal vein thrombosis: Differentiation by CT characteristics. *Am J Roentgenol* 168:719–723, 1997.
42. Iannaccone R, Piacentini F, Murakami T, et al: Hepatocellular carcinoma in patients with nonalcoholic fatty liver disease: Helical CT and MR imaging findings with clinical-pathologic comparison. *Radiology* 43:422–430, 2007.
43. Choi BG, Park SH, Byun JY, et al: The findings of ruptured hepatocellular carcinoma on helical CT. *Br J Radiol* 74:142–146, 2001.
44. Winter TC, III, Freeny PC, Nghiem HV, et al: Hepatic arterial anatomy in transplantation candidates: Evaluation with three-dimensional CT arteriography. *Radiology* 195:363–370, 1995.
45. Sumida M, Ohto M, Ebara M, et al: Accuracy of angiography in the diagnosis of small hepatocellular carcinoma. *AJR Am J Roentgenol* 147:531–536, 1986.
46. Kanazawa S, Yusui K, Doke T, et al: Hepatic arteriography in patients with hepatocellular carcinoma. *AJR Am J Roentgenol* 147:531–536, 1995.
47. Mathieu D, Guinet C, Bouklia-Hassane A, et al: Hepatic vein involvement in hepatocellular carcinoma. *Gastrointest Radiol* 13:55–60, 1988.
48. Fujita T, Honjo K, Ito K, et al: High-resolution dynamic MR imaging of hepatocellular carcinoma with a phased-array body coil. *Radiographics* 17:315–331, 1997.
49. Li CS, Chen RC, Lii JM, et al: Magnetic resonance imaging appearance of well-differentiated hepatocellular carcinoma. *J Comput Assist Tomogr* 30:597–603, 2006.
50. Ohtomo K, Matsuoka Y, Abe O, et al: High-resolution MR imaging evaluation of hepatocellular carcinoma. *Abdom Imaging* 22: 182–186, 1997.
51. Murakami T, Kim T, Nakamura H, et al: Hepatitis, cirrhosis, and hepatoma. *J Magn Reson Imaging* 8:346–358, 1998.
52. Mitchell DG, Rubin R, Siegelman ES, et al: Hepatocellular carcinoma within siderotic regenerative nodules: Appearance as a nodule within a nodule on MR images. *Radiology* 178:101–103, 1991.
53. Mitchell DG: Focal manifestations of diffuse liver disease at MR imaging. *Radiology* 185:1–11, 1992.
54. Brown JJ, Naylor MJ, Yagan N, et al: Imaging of hepatic cirrhosis. *Radiology* 202:1–16, 1997.
55. Harisinghani MG, Hahn PF: Computed tomography and magnetic resonance imaging evaluation of liver cancer. *Gastroenterol Clin North Am* 31:759–776, 2002.
56. Hussain SM, Zondervan PE, IJzermans JN, et al: Benign versus malignant hepatic nodules: MR imaging findings with pathologic correlation. *Radiographics* 22:1023–1036, 2002.
57. Shimamoto K, Sakuma S, Ishigaki T, et al: Hepatocellular carcinoma: Evaluation with color Doppler US and MR imaging. *Radiology* 182:149–153, 1992.
58. Yamamoto H, Yamashita Y, Yoshimatsu S, et al: Hepatocellular carcinoma in cirrhotic livers: Detection with unenhanced and iron-oxide enhanced MR imaging. *Radiology* 195:106–112, 1995.
59. Ganeshan D, Szklaruk J, Kundra V, et al: Imaging features of fibrolamellar hepatocellular carcinoma. *AJR* 202:544–552, 2014.
60. Yu JS, Cho ES, Kim KH, et al: Newly developed hepatocellular carcinoma (HCC) in chronic liver disease: MR imaging findings before the diagnosis of HCC. *J Comput Assist Tomogr* 30:765–771, 2006.
61. Mitchell DG, Rubin R, Mitchell DG, et al: Hepatocellular carcinoma within siderotic regenerative nodules: Appearance as a nodule within a nodule on MR images. *Radiology* 178:101–103, 1991.
62. Becker CD, Grossholz M, Mentha G, et al: Ablation of hepatocellular carcinoma by percutaneous ethanol injection: Imaging findings. *Cardiovasc Intervent Radiol* 20:204–209, 1997.
63. Bartolozzi C, Crocetti L, Lencioni R, et al: Biliary and reticuloendothelial impairment in hepatocarcinogenesis: The diagnostic role of tissue-specific MR contrast media. *Eur Radiol* 17:2519–2530, 2007.
64. Lupescu IG, Capsa RA, Gheorghe L, et al: Tissue specific MR contrast media role in the differential diagnosis of cirrhotic liver nodules. *J Gastrointest Liver Dis* 17:341–345, 2008.
65. Narita M, Hatano E, Arizono S, et al: Expression of OATP1B3 determines uptake of Gd-EOB-DTPA in hepatocellular carcinoma. *J Gastroenterol* 44:793–798, 2009.
66. Lim KS: Diffusion-weighted MRI of hepatocellular carcinoma cirrhosis. *Clin Radiol* 69:1–10, 2014.
67. Brasch RC: New directions in the development of MR imaging contrast media. *Radiology* 183:1–11, 1992.
68. Goodwin MD, Dobson JE, Sirlin CB, et al: Diagnostic challenges and pitfalls in MR imaging with hepatocyte-specific contrast agents. *Radiographics* 31:1547–1568, 2011.
69. Murakami T, Okada M, Hyodo T: CT versus MR imaging of hepatocellular carcinoma: Toward improved treatment decisions. *Magn Reson Med Sci* 11:75–81, 2012.
70. Kogita S, Imai Y, Okada M, et al: Gd-EOB-DTPA-enhanced magnetic resonance images of hepatocellular carcinoma: Correlation with histological grading and portal blood flow. *Eur Radiol* 20:2405–2413, 2010.
71. Okada M, Imai Y, Kim T, et al: Comparison of enhancement patterns of histologically confirmed hepatocellular carcinoma between gadoxetate- and ferucarbotran-enhanced magnetic resonance imaging. *J Magn Reson Imaging* 32:903–913, 2010.
72. Bartolozzi C, Battaglia V, Bozzi E: HCC diagnosis with liver-specific MRI: Close to histopathology. *Dig Dis* 27:125–130, 2009.
73. Matsui O, Kadoya M, Kameyama T, et al: Benign and malignant nodules in cirrhotic livers: Distinction based on blood supply. *Radiology* 178:493–497, 1991.
74. Coleman WB: Mechanisms of human hepatocarcinogenesis. *Curr Mol Med* 3:573–588, 2003.
75. Byam J, Renz J, Millis JM: Liver transplantation for hepatocellular carcinoma. *Hepatobiliary Surg Nutr* 2:22–30, 2013.
76. Cruite I, Schroeder M, Merkle EM, Sirlin CB: Gadaxetate disodium-enhanced MRI of the liver: Part 2, protocol optimization and lesion appearance in the cirrhotic liver. *AJR Am J Roentgenol* 195:29–41, 2010.
77. Okazaki M, Higashihara H, Koganemaru F, et al: Intraoperative hemorrhage from hepatocellular carcinoma: Emergency chemoembolization or embolization. *Radiology* 180: 647–651, 1991.
78. Saito K, Kotake F, Ito N, et al: Gd-EOB-DTPA enhanced MRI for hepatocellular carcinoma: Quantitative evaluation of tumor enhancement in hepatobiliary phase. *Magn Reson Med Sci* 4:1–9, 2005.
79. Sandrasegaran K, Akisik FM, Lin C, et al: The value of diffusion-weighted imaging in characterizing focal liver masses. *Acad Radiol* 16: 1208–1214, 2009.
80. Miller FH, Hammond N, Siddiqi AJ, et al: Utility of diffusion-weighted MRI in distinguishing benign and malignant hepatic lesions. *J Magn Reson Imaging* 32:138–147, 2010.
81. Nasu K, Kuroki Y, Tsukamoto T, et al: Diffusion-weighted imaging of surgically resected hepatocellular carcinoma: Imaging characteristics and relationship among signal intensity, apparent diffusion coefficient, and histopathologic grade. *AJR Am J Roentgenol* 193:438–444, 2009.
82. Muhi A, Ichikawa T, Motosugi U, et al: High-b-value diffusion-weighted MR imaging of hepatocellular lesions: Estimation of grade of malignancy of hepatocellular carcinoma. *J Magn Reson Imaging* 30:1005–1011, 2009.

83. Berman MA, Burnham JA, Sheahan DG: Fibrolamellar carcinoma of the liver: An immunohistochemical study of nineteen cases and a review of the literature. *Hum Pathol* 19:784–794, 1988.
84. Friedman AC, Lichtenstein JE, Goodman Z, et al: Fibrolamellar hepatocellular carcinoma. *Radiology* 157:583–587, 1985.
85. McLarney JK, Rucker PT, Bender GN, et al: Fibrolamellar carcinoma of the liver: Radiologic-pathologic correlation. *Radiographics* 19:453–471, 1999.
86. Buetow PC, Midkiff RB: Primary malignant neoplasms in the adult. *MRI Clin North Am* 5:289–318, 1997.
87. Francis IR, Agha FP, Thompson NW, et al: Fibrolamellar hepatocarcinoma: Clinical, radiologic and pathologic features. *Gastrointest Radiol* 11:67–72, 1986.
88. Ross Stevens W, Johnson CD, Stephens DH, et al: Fibrolamellar hepatocellular carcinoma: Stage at presentation and results of aggressive surgical management. *AJR Am J Roentgenol* 164:1153–1158, 1995.
89. Mattison GR, Glazer GM, Quint LE, et al: MR imaging of hepatic focal nodular hyperplasia: Characterization and distinction from primary malignant hepatic tumors. *AJR Am J Roentgenol* 148:711–715, 1987.
90. Corrigan K, Semelka RC: Dynamic contrast-enhanced MR imaging of fibrolamellar hepatocellular carcinoma. *Abdom Imaging* 20:122–125, 1995.
91. Hamrick-Turner JE, Shipkey FH, Cranston PE: Fibrolamellar hepatocellular carcinoma: MR appearance mimicking focal nodular hyperplasia. *J Comput Assist Tomogr* 18:301–304, 1994.
92. Caseiro-Alves F, Zins M, Mahfouz A-E: Calcification in focal nodular hyperplasia: A new problem for differentiation from fibrolamellar hepatocellular carcinoma. *Radiology* 198:889–892, 1996.
93. Fernandez-Pineda I, Cabello-Laureano R: Differential diagnosis and management of liver tumors in infants. *World J Hepatol* 6:486–495, 2014.
94. Honeyman JN, La Quaglia MP: Malignant liver tumors. *Semin Pediatr Surg* 21:245–254, 2012.
95. Bartolozzi C, Battaglia V, Bozzi E: HCC diagnosis with liver-specific MRI: Close to histopathology. *Dig Dis* 27:125–130, 2009.
96. Ringe KI, Husarik DB, Sirlin CB, Merkle EM: Gadoxetate disodium-enhanced MRI of the liver: Part 1, protocol optimization and lesion appearance in the noncirrhotic liver. *AJR Am J Roentgenol* 195:13–28, 2010.
97. Karski EE, Dvorak CC, Leung W, et al: Treatment of hepatoblastoma with high-dose chemotherapy and stem cell rescue: The Pediatric Blood and Marrow Transplant Consortium experience and review of the literature. *J Pediatr Hematol Oncol* 36:362–368, 2014.
98. Murakami T, Baron RL, Peterson MS, et al: Hepatocellular carcinoma: MR imaging with mangafodipir trisodium (MnDPDP). *Radiology* 200:69–77, 1996.
99. Stringer MD: The role of liver transplantation in the management of paediatric liver tumours. *Ann R Coll Surg Engl* 89:12–21, 2007.
100. Davey MS, Cohen MD: Imaging of gastrointestinal malignancy in childhood. *Radiol Clin North Am* 34:717–742, 1996.
101. Dachman AH, Parker RL, Ros PR, et al: Hepatoblastoma: A radiologic-pathologic correlation in 50 cases. *Radiology* 164:15–19, 1987.
102. Kaude JV, Felman AH, Hawkins IF, Jr: Ultrasonography in primary hepatic tumors in early childhood. *Pediatr Radiol* 9:77–83, 1980.
103. Miller JH: The ultrasonographic appearance of cystic hepatoblastoma. *Radiology* 138:141–143, 1981.
104. Bates SM, Keller MS, Ramos IM, et al: Hepatoblastoma: Detection of tumor vascularity with duplex Doppler US. *Radiology* 176:505–507, 1990.
105. Helmberger TK, Ros PR, Mergo PJ, et al: Pediatric liver neoplasms: A radiologic-pathologic correlation. *Eur Radiol* 9:1339–1347, 1999.
106. Plumley DA, Grosfeld JL, Kopecky KK, et al: The role of spiral (helical) computerized tomography with three-dimensional reconstruction in pediatric solid tumors. *J Pediatr Surg* 30:317–321, 1995.
107. Smith WL, Franken EA, Mitros FA: Liver tumors in children. *Semin Roentgenol* 18:136–148, 1983.
108. Powers C, Ros PR, Stoupis C, et al: Primary liver neoplasms: MR imaging with pathologic correlation. *Radiographics* 14:459–482, 1994.
109. Lu M, Greer ML: Hypervascular multifocal hepatoblastoma: Dynamic gadolinium-enhanced MRI findings indistinguishable from infantile hemangioendothelioma. *Pediatr Radiol* 37:587–591, 2007.
110. Boechat MI, Kangaroo H, Ortega J, et al: Primary liver tumors in children: Comparison of CT and MR imaging. *Radiology* 169:727–732, 1988.
111. Klatskin G: Adenocarcinoma of the hepatic duct at its bifurcation within the porta hepatis. *Am J Med* 38:241–256, 1965.
112. Ros PR, Buck JL, Goodman ZD, et al: Intrahepatic cholangiocarcinoma: Radiologic-pathologic correlation. *Radiology* 167:689–693, 1988.
113. Welzel TM, Mellema L, Gloria G, et al: Risk factors for intrahepatic cholangiocarcinoma in a low-risk population: A nationwide case-control study. *Int J Cancer* 120:638–641, 2007.
114. Soyer P, Bluemke DA, Reichle R, et al: Imaging of cholangiocarcinoma: 1. Peripheral cholangiocarcinoma. *AJR Am J Roentgenol* 165:1427–1431, 1995.
115. Choi BI, Han JK, Kim TK: Diagnosis and staging of cholangiocarcinoma by computed tomography. In Meyers MA, editor: *Neoplasms of the Digestive Tract: Imaging, Staging, and Management*, Philadelphia, 1998, Lippincott-Raven, pp 503–516.
116. Imai Y, Araki T, Furui S, et al: Computed tomography of primary intrahepatic biliary malignancy. *Radiology* 147:485–490, 1983.
117. Meyers MA: Cholangiocarcinoma: Imaging, staging, and management. In Meyers MA, editor: *Neoplasms of the Digestive Tract: Imaging, Staging, and Management*, Philadelphia, 1998, Lippincott-Raven, pp 150–183.
118. Fan ZM, Yamashita Y, Harada M, et al: Intrahepatic cholangiocarcinoma: Spin-echo and contrast-enhanced dynamic MR imaging. *AJR Am J Roentgenol* 161:313–317, 1993.
119. Adjei ON, Tamura S, Sugimura H, et al: Contrast-enhanced MR imaging of intrahepatic cholangiocarcinoma. *Clin Radiol* 50:6–10, 1995.
120. Brown KM, Geller DA: Proximal biliary tumors. *Surg Clin North Am* 94:311–323, 2014.
121. Teoh AY, Ng SS, Lee KF, et al: Biliary cystadenoma and other complicated cystic lesions of the liver: Diagnostic and therapeutic challenges. *World J Surg* 30:1560–1566, 2006.
122. Buetow PC, Buck JL, Pantongrag-Brown L, et al: Biliary cystadenoma and cystadenocarcinoma: Clinical-imaging-pathologic correlation with emphasis on the importance of ovarian stroma. *Radiology* 196:805–810, 1995.
123. Murphy BJ, Casillas J, Ros PR, et al: The CT appearance of cystic masses of the liver. *Radiographics* 9:307–322, 1989.
124. Ishak KG: Benign tumors and pseudotumors of the liver. *Appl Pathol* 6:82–104, 1988.
125. Mortele KJ, Ros PR: Cystic focal liver lesions in the adult: Differential CT and MR imaging features. *Radiographics* 21:895–910, 2001.
126. Stoupis C, Ros PR, Dolson DJ: Recurrent biliary cystadenoma: MR imaging appearance. *J Magn Reson Imaging* 4:99–101, 1994.
127. Seidel R, Weinrich M, Pistorius G, et al: Biliary cystadenoma of the left intrahepatic duct. *Eur Radiol* 17:1380–1383, 2007.
128. Kojiro M, Nakashima T, Ito Y, et al: Thorium dioxide-related angiosarcoma of the liver. Pathomorphologic study of 29 autopsy cases. *Arch Pathol Lab Med* 109:853–857, 1985.
129. Ito Y, Kojiro M, Nakashima T, et al: Pathomorphologic characteristics of 102 cases of Thorotrast-related hepatocellular carcinoma, cholangiocarcinoma, and hepatic angiosarcoma. *Cancer* 62:1153–1162, 1988.
130. Ishak KG: Mesenchymal tumors of the liver. In Okuda K, Peter RL, editors: *Hepatocellular Carcinoma*, New York, 1976, John Wiley & Sons, pp 228–257.
131. Ishak KG: Pathogenesis of liver diseases. In Farber E, Phillips MJ, Kaufman N, editors: *International Academy of Pathology Monograph*, No. 28, Baltimore, 1987, Williams & Wilkins, pp 314–315.
132. Heo SH, Jeong YY, Shin SS, et al: Solitary small hepatic angiosarcoma: Initial and follow-up imaging findings. *Korean J Radiol* 8:180–183, 2007.
133. Levy DW, Rindsberg S, Friedman AC, et al: Thorotrast-induced hepatosplenic neoplasia: CT identification. *AJR Am J Roentgenol* 146:997–1004, 1986.
134. Buetow PC, Buck JL, Ros PR, et al: Malignant vascular tumors of the liver: Radiologic-pathologic correlation. *Radiographics* 14:153–166, 1994.
135. Weitz J, Klimstra DS, Cymes K, et al: Management of primary liver sarcomas. *Cancer* 109:1391–1396, 2007.
136. Azodo MVU, Gutierrez OH, Greer T: Thorotrast-induced ruptured hepatic angiosarcoma. *Abdom Imaging* 18:78–81, 1993.
137. Zheng YW, Zhang XW, Zhang JL, et al: Primary hepatic angiosarcoma and potential treatment options. *J Gastroenterol Hepatol* 29:906–911, 2014.
138. Worawattanakul S, Semelka RC, Kelekis NL, et al: Angiosarcoma of the liver: MR imaging pre- and post-chemotherapy. *Magn Reson Imaging* 15:613–617, 1997.
139. Stocker JT, Ishak KG: Undifferentiated (embryonal) sarcoma of the liver. Report of 31 cases. *Cancer* 42:336–348, 1978.
140. Horowitz ME, Etcubanas E, Webber BL, et al: Hepatic differentiated (embryonal) sarcoma and rhabdomyosarcoma in children. Results of therapy. *Cancer* 59:396–402, 1987.
141. Ros PR, Olmsted WW, Dachman AH, et al: Undifferentiated (embryonal) sarcoma of the liver: Radiologic-pathologic correlation. *Radiology* 160:141–145, 1986.

142. Buetow PC, Buck JL, Pantongrag-Brown L, et al: Undifferentiated (embryonal) sarcoma of the liver: Pathologic basis of imaging findings in 28 cases. *Radiographics* 203:779–783, 1997.
143. Vermess M, Collier NA, Mutum SS, et al: Misleading appearance of a rare malignant liver tumor on computed tomography. *Br J Radiol* 57:262–265, 1984.
144. Zhao XY, Rakhda MI, Habib S, et al: Hepatic epithelioid hemangioendothelioma. *Oncol Lett* 7:977–983, 2014.
145. Miller WJ, Dodd GD, Federle MP, et al: Epithelioid hemangioendothelioma of the liver: Imaging findings with pathologic correlation. *AJR Am J Roentgenol* 159:53–57, 1992.
146. Radin DR, Craig JR, Colletti PM: Hepatic epithelioid hemangioendothelioma. *Radiology* 169:145–148, 1988.
147. Ohtomo K, Araki T, Itai Y, et al: MR imaging of malignant mesenchymal tumors of the liver. *Gastrointest Radiol* 17:58–62, 1992.
148. Van Beers B, Roche A, Mathieu D, et al: Epithelioid hemangioendothelioma of the liver: MR and CT findings. *J Comput Assist Tomogr* 16:420–424, 1992.
149. Ferrozzi F, Bova D, Zangrandi A, et al: Primary liver leiomyosarcoma: CT appearance. *Abdom Imaging* 21:157–160, 1996.
150. Yao D, Dai C: Clinical characteristics of the primary hepatic malignant fibrous histiocytoma in China: Case report and review of the literature. *World J Surg Oncol* 10:2, 2012.
151. Conran RM, Stocker JT: Malignant fibrous histiocytoma of the liver: A case report. *Am J Gastroenterol* 80:813–815, 1985.
152. Reed RG, Goodman P, Soloway RD: Primary malignant fibrous histiocytoma of the liver: MRI findings. *Magn Reson Imaging* 11:139–143, 1993.
153. Soyer P, Bluemke DA, Riopel M, et al: Hepatic leiomyosarcomas: CT features with pathologic correlation. *Eur J Radiol* 19:177–182, 1995.
154. Loddenkemper C, Longerich T, Hummel M, et al: Frequency and diagnostic patterns of lymphomas in liver biopsies with respect to the WHO classification. *Virchows Arch* 450:493–502, 2007.
155. Levitan R, Diamond HD, Graver LF: The liver in Hodgkin disease. *Gut* 2:60–71, 1971.
156. Ohsawa M, Aozasa K, Horiuchi K, et al: Malignant lymphoma of the liver. *Dig Dis Sci* 37:1105–1109, 1992.
157. Sherlock S, Dooley J: *Diseases of the Liver and Biliary System*, ed 9, Oxford, 1993, Blackwell Scientific, pp 44–61.
158. Gowing NFC: Modes of death and post mortem studies. In Smithers D, editor: *Hodgkin Disease*, Edinburgh, 1973, Churchill Livingstone, pp 163–166.
159. Bruneton JN, Schnider M: *Radiology of Lymphoma*, New York, 1986, Springer-Verlag.
160. Cerban R, Gheorghe L, Becheanu G, et al: Primary focal T-cell lymphoma of the liver: A case report and review of the literature. *J Gastrointest Liver Dis* 21:213–216, 2012.
161. Shirkhoda A, Ros PR, Farah J, et al: Lymphoma of the solid abdominal viscera. *Radiol Clin North Am* 28:785–799, 1990.
162. Ben Haim S, Bar-Shalom R, Israel O, et al: Liver involvement in lymphoma: Role of gallium-67 scintigraphy. *J Nucl Med* 36:900–904, 1995.
163. Ginaldi S, Bernardino ME, Jing BS: Patterns of hepatic lymphoma. *Radiology* 136:427–431, 1980.
164. Zornoza J, Ginaldi S: Computed tomography in hepatic lymphoma. *Radiology* 138:405–410, 1981.
165. Castellino RA, Hoppe RT, Blank N, et al: Computed tomography, lymphography and staging laparotomy in colon: Correlations in staging of Hodgkin disease. *AJR Am J Roentgenol* 143:37–41, 1984.
166. Kelekis NL, Semelka RC, Siegelman ES, et al: Focal hepatic lymphoma: Magnetic resonance demonstration using current techniques including gadolinium enhancement. *Magn Reson Imaging* 15:625–636, 1997.
167. Weissleder R, Stark DD, Elizondo G: MRI of hepatic lymphoma. *Magn Reson Imaging* 6:675–681, 1988.
168. Le Brecque DR: Neoplasia of the liver. In Kaplowitz N, editor: *Liver and Biliary Disease*, ed 2, Baltimore, 1996, Williams & Wilkins, pp 391–438.
169. Goodman ZD: Nonparenchymal and metastatic malignant tumors of the liver. In Haubrich WS, Schaffner F, Berk JE, editors: *Bockus Gastroenterology*, Philadelphia, 1995, WB Saunders, pp 2488–2500.
170. Golding SJ, Fletcher EWL: The radiology of secondary malignant neoplasms of the liver. In Wilkins RA, Nunnerley HB, editors: *Imaging of the Liver, Pancreas and Spleen*, Oxford, 1990, Blackwell Scientific, pp 198–219.
171. Wilson MA: Metastatic disease of the liver. In Wilson MA, Ruzicka FF, editors: *Modern Imaging of the Liver*, New York, 1989, Marcel Dekker, pp 631–659.
172. Weiss L, Gilbert HA: *Liver Metastases*, Boston, 1992, GK Hall.
173. Baker ME, Pelley R: Hepatic metastases: Basic principles and implications for radiologists. *Radiology* 197:329–337, 1995.
174. Gore RM, Goldberg HI: Plain film and cholangiographic findings in liver tumors. *Semin Roentgenol* 18:87–93, 1983.
175. Baker SR: *The Abdominal Plain Film*, East Norwalk, CT, 1990, Appleton & Lange, pp 243–298.
176. Darlak JJ, Moskowitz M, Kattan KR: Calcifications in the liver. *Radiol Clin North Am* 18:209–219, 1980.
177. Paley M, Ros PR: Hepatic calcification. *Radiol Clin North Am* 36:391–398, 1998.
178. Dolan PA: Tumor calcification following therapy. *AJR Am J Roentgenol* 89:166–168, 1963.
179. Rogers JV, Torres WE, Clements J: Plain film diagnosis of the liver. In Bernardino ME, Sones PJ, editors: *Hepatic Radiography*, New York, 1984, Macmillan, pp 1–49.
180. Drane WE: Nuclear medicine techniques for the liver and biliary system. *Radiol Clin North Am* 29:1129–1149, 1991.
181. Kinnard MF, Alavi A, Rubin RP, et al: Nuclear imaging of solid hepatic masses. *Semin Roentgenol* 30:375–395, 1995.
182. Delbeke D, Vitola JV, Sandler MP, et al: Staging recurrent metastatic colorectal carcinoma with PET. *J Nucl Med* 38:1196–1201, 1997.
183. Goldberg MA, Lee MJ, Fischman AJ, et al: Fluorodeoxyglucose PET of abdominal and pelvic neoplasms: Potential role in oncologic imaging. *Radiographics* 13:1047–1062, 1993.
184. Rapoport ED, Loft A, Berthelsen AK, et al: Contrast-enhanced FDG-PET/CT vs. SPIO-enhanced MRI vs. FDG-PET vs. CT in patients with liver metastases from colorectal cancer: A prospective study with intraoperative confirmation. *Acta Radiol* 48:369–378, 2007.
185. Findlay M, Young H, Cunningham D, et al: Noninvasive monitoring of tumor metabolism using fluorodeoxyglucose and positron emission tomography in colorectal cancer liver metastases: Correlation with tumor response to fluorouracil. *J Clin Oncol* 14:700–708, 1997.
186. Marn CS, Bree RL, Silver TM: Ultrasonography of liver: Technique and focal and diffuse disease. *Radiol Clin North Am* 29:1151–1170, 1991.
187. Withers CE, Wilson SR: The liver. In Rumack CM, Wilson SR, Charboneau JW, editors: *Diagnostic Ultrasound*, St. Louis, 1992, Mosby-Year Book, pp 45–86.
188. Parulekar SG, Bree RL: The liver. In McGahan JP, Goldberg BB, editors: *Diagnostic Ultrasound: A Logical Approach*, Philadelphia, 1998, Lippincott-Raven, pp 599–692.
189. Niesenbaum HL, Rowling SE: Ultrasound of focal hepatic lesions. *Semin Roentgenol* 30:324–346, 1995.
190. Hillman BJ, Smith EH, Gammelgaard J, et al: Ultrasonic-pathologic correlation of malignant hepatic masses. *Gastrointest Radiol* 4:361–365, 1979.
191. Antoch G, Vogt FM, Veit P, et al: Assessment of liver tissue after radiofrequency ablation: Findings with different imaging procedures. *J Nucl Med* 46:520–525, 2005.
192. Veit P, Antoch G, Stergar H, et al: Detection of residual tumor after radiofrequency ablation of liver metastasis with dual-modality PET/CT: Initial results. *Eur Radiol* 16:80–87, 2006.
193. Choi J: Imaging of hepatic metastases. *Cancer Control* 13:6–12, 2006.
194. Haug AR, Tiega Donfack BP, Trumm C, et al: ¹⁸F-FDG PET/CT predicts survival after radioembolization of hepatic metastases from breast cancer. *J Nucl Med* 53:371–377, 2012.
195. Donati OF, Hany TF, Reiner CS, et al: Value of retrospective fusion of PET and MR images in detection of hepatic metastases: Comparison with ¹⁸F-FDG PET/CT and Gd-EOB-DTPA-enhanced MRI. *J Nucl Med* 51:692–699, 2010.
196. Schreiter NF, Nogami M, Steffen I, et al: Evaluation of the potential of PET-MRI fusion for detection of liver metastases in patients with neuroendocrine tumours. *Eur Radiol* 22:458–467, 2012.
197. Li R, Guo Y, Hua X, et al: Characterization of focal liver lesions: Comparison of pulse-inversion harmonic contrast-enhanced sonography with contrast-enhanced CT. *J Clin Ultrasound* 35:109–117, 2007.
198. Marchal G, Tshibwabwa-Tumba E, Oyen R, et al: Correlation of sonographic patterns in liver metastases with histology and microangiography. *Invest Radiol* 20:79–84, 1985.
199. Marchal GJ, Pylyser K, Tshibwabwa-Tumba EA: Anechoic halo in solid liver tumors: Sonographic, microangiographic, and histologic correlation. *Radiology* 156:479–483, 1985.
200. Larsen LP, Rosenkilde M, Christensen H, et al: The value of contrast enhanced ultrasonography in detection of liver metastases from colorectal cancer: A prospective double-blinded study. *Eur J Radiol* 62:302–307, 2007.
201. Federle MP, Filly RA, Moss AA: Cystic hepatic neoplasms: Complementary roles of computed tomography and sonography. *AJR Am J Roentgenol* 136:345–348, 1981.
202. Bruneton JN, Ladree D, Caramella E, et al: Ultrasonographic study of calcified hepatic metastases: A report of 13 cases. *Gastrointest Radiol* 7:61–63, 1982.
203. Catala V, Nicolau C, Vilana R, et al: Characterization of focal liver lesions: Comparative

- study of contrast-enhanced ultrasound versus spiral computed tomography. *Eur Radiol* 17: 1066–1073, 2007.
204. Yukisawa S, Ohto M, Masuya Y, et al: Contrast-enhanced three-dimensional fusion sonography of small liver metastases with pathologic correlation. *J Clin Ultrasound* 35:1–8, 2007.
 205. Heiken JP: Liver. In Lee JKT, Sagel SS, Stanley RJ, et al, editors: *Computed Body Tomography with MRI Correlation*, ed 3, Philadelphia, 1998, Lippincott-Raven, pp 701–778.
 206. Stephens DH: The liver. In Haaga JR, Alfidi RJ, editors: *Computed Tomography of the Whole Body*, St. Louis, 1988, CV Mosby, pp 792–853.
 207. Garrett R: Solid liver masses: Approach to management from the standpoint of a radiologist. *Curr Gastroenterol Rep* 15:359, 2013.
 208. Baron RL, Freeny PC, Moss AA: The liver. In Moss AA, Gamsu G, Genant HK, editors: *Computed Tomography of the Whole Body*, ed 2, Philadelphia, 1992, WB Saunders, pp 735–822.
 209. Foley WD, Jochem RJ: Computed tomography: Focal and diffuse disease. *Radiol Clin North Am* 29:1213–1233, 1991.
 210. Oliver JH, III, Baron RL, Federle MP, et al: Detecting hepatocellular carcinoma: Value of unenhanced or arterial phase CT imaging or both used in conjunction with conventional portal venous phase contrast-enhanced CT imaging. *AJR Am J Roentgenol* 167:71–77, 1996.
 211. Oliver JH, 3rd, Baron RL, Federle MP, et al: Hypervascular liver metastases: Do unenhanced and hepatic arterial phase CT images affect tumor detection? *Radiology* 205:709–715, 1997.
 212. Tresoldi S, Sardanelli F, Borzani I, et al: Liver metastases on serial contrast-enhanced multidetector computed tomography examinations: Was the detection possible on previous examinations? *J Comput Assist Tomogr* 30:378–385, 2006.
 213. Pedro MS, Semelka RC, Braga L: MR imaging of hepatic metastases. *Magn Reson Imaging Clin N Am* 10:15–29, 2002.
 214. Sica GT, Ji H, Ros PR: CT and MR imaging of hepatic metastases. *AJR Am J Roentgenol* 174:691–698, 2000.
 215. Kim YK, Ko SW, Hwang SB, et al: Detection and characterization of liver metastases: 16-slice multidetector computed tomography versus superparamagnetic iron oxide-enhanced magnetic resonance imaging. *Eur Radiol* 16:1337–1345, 2006.
 216. Semelka RC: Liver. In Semelka RC, Ascher SM, Reinhold C, editors: *MRI of the Abdomen and Pelvis*, New York, 1997, Wiley-Liss, pp 19–136.
 217. Siegelman ES, Outwater Ek: MR imaging techniques of the liver. *Radiol Clin North Am* 36:263–287, 1998.
 218. Hahn PF: Liver specific MR imaging contrast agents. *Radiol Clin North Am* 36:287–298, 1998.
 219. Palmucci S: Focal liver lesions detection and characterization: The advantages of gadoxetic acid-enhanced liver MRI. *World J Hepatol* 7:477–485, 2014.
 220. Semelka RA, Mitchell DG: Liver and biliary system. In Edelman RR, Hesselink JR, Zlatkin MB, editors: *Clinical Magnetic Resonance Imaging*, ed 2, Philadelphia, 1996, WB Saunders, pp 1466–1512.
 221. Gandhi SN, Brown MA, Wong JG, et al: MR contrast agents for liver imaging: What, when, how. *Radiographics* 26:1621–1636, 2006.
 222. Reinig JW: Differentiation of hepatic lesions with MR imaging: The last word? *Radiology* 179:601–602, 1991.
 223. Paling MR, Abbitt PL, Mugler JP, et al: Liver metastases: Optimization of MR imaging pulse sequences at 1.0 T. *Radiology* 167:695–699, 1988.
 224. Schnall M: Magnetic resonance imaging. *Semin Roentgenol* 30:347–361, 1995.
 225. Lee MJ, Saini S, Compton CC: MR demonstration of edema adjacent to a liver metastasis: Pathologic correlation. *AJR Am J Roentgenol* 157:499–501, 1991.
 226. Outwater E, Tomaszewski JE, Daly JM, et al: Hepatic colorectal metastases: Correlation of MR imaging and pathologic appearance. *Radiology* 180:327–332, 1991.
 227. Goldberg MA, Saini S, Hahn PF, et al: Differentiation between hemangiomas and metastases of the liver with ultrafast MR imaging: Preliminary results with T2 calculations. *AJR Am J Roentgenol* 157:727–730, 1991.
 228. Onishi H, Murakami T, Kim T, et al: Hepatic metastases: Detection with multidetector row CT, SPIO-enhanced MR imaging, and both techniques combined. *Radiology* 239:131–138, 2006.
 229. Hamm B, Mahfouz A-E, Taupitz M, et al: Liver metastases: Improved detection with dynamic gadolinium-enhanced MR imaging. *Radiology* 202:677–682, 1997.
 230. Bipat S, van Leeuwen MS, Comans EFI, et al: Colorectal liver metastases: CT, MR imaging, and PET for diagnosis: Meta-analysis. *Radiology* 237:123–131, 2005.
 231. Seneterre E, Taourel P, Bouvier Y, et al: Detection of hepatic metastases: Ferumoxides-enhanced MR imaging versus unenhanced MR imaging and CT during arterial portography. *Radiology* 200:785–792, 1996.
 232. Oudkerk M, van den Heuvel AG, Wielopolski PA, et al: Hepatic lesions: Detection with ferumoxide-enhanced T1-weighted MR imaging. *Radiology* 203:449–456, 1997.
 233. Soyer P: Will ferumoxides-enhanced MR imaging replace CT in the detection of hepatic metastases? Prologue to a promising future. *Radiology* 201:610–611, 1996.
 234. Caudana R, Morana G, Pirovano GP, et al: Focal malignant hepatic lesions: MR imaging enhanced with gadolinium benzyloxypropionictetra-acetate (BOPTA)—preliminary results of phase II application. *Radiology* 199:513–520, 1996.
 235. Vogl TJ, Kummel S, Hammerstingl R, et al: Liver tumors: Comparison of MR imaging with Gd-EOB-DTPA and Gd-DTPA. *Radiology* 200:59–67, 1996.
 236. del Frate C, Bazzocchi M, Morteale KJ, et al: Detection of liver metastases: Comparison of gadobenate dimeglumine-enhanced and ferumoxides-enhanced MR imaging examinations. *Radiology* 225:766–772, 2002.
 237. Freeny PC: Angiography of hepatic neoplasm. *Semin Roentgenol* 18:114–122, 1983.
 238. Sainani NI, Gervais DA, Mueller PR, et al: Imaging after percutaneous ablation of hepatic tumors. *AJR* 200:194–204, 2013.
 239. Hammerstingl R, Huppertz A, Breuer J, et al: Diagnostic efficacy of gadoxetic acid (Primovist)-enhanced MRI and spiral CT for a therapeutic strategy: Comparison with intraoperative and histopathologic findings in focal liver lesions. *Eur Radiol* 18:457–467, 2008.
 240. Zech CJ, Herrmann KA, Reiser MF, et al: MR imaging in patients with suspected liver metastases: Value of liver-specific contrast agent Gd-EOB-DTPA. *Magn Reson Med* 6:43–52, 2007.
 241. Bartolozzi C, Donati F, Cioni D, et al: Detection of colorectal liver metastases: A prospective multicenter trial comparing unenhanced MRI, MnDPDP-enhanced MRI, and spiral CT. *Eur Radiol* 14:14–20, 2004.
 242. Maurea S, Mainenti PP, Tambasco A, et al: Diagnostic accuracy of MR imaging to identify and characterize focal liver lesions. *Quant Imaging Med Surg* 4:181–189, 2014.
 243. Koh DM, Scurr E, Collins DJ, et al: Colorectal hepatic metastases: Quantitative measurements using single-shot echo-planar diffusion-weighted MR imaging. *Eur Radiol* 16: 1898–1905, 2006.
 244. Parikh T, Drew SJ, Lee VS, et al: Focal liver lesion detection and characterization with diffusion-weighted MR imaging: Comparison with standard breath-hold T2-weighted imaging. *Radiology* 246:812–822, 2008.
 245. Bruegel M, Rummeny EJ: Hepatic metastases: Use of diffusion-weighted echo-planar imaging. *Abdom Imaging* 35:454–461, 2010.
 246. Kele PG, van der Jagt EJ: Diffusion weighted imaging in the liver. *World J Gastroenterol* 16:1567–1576, 2010.
 247. Sandrasegaran K: Functional imaging of the abdomen. *Radiol Clin North Am* 52:883–903, 2014.
 248. Taylor HM, Ros PR: Hepatic imaging: An overview. *Radiol Clin North Am* 36:237–246, 1998.
 249. Namasivayam S, Martin DR, Saini S: Imaging of liver metastases: MRI. *Cancer Imaging* 7:2–9, 2007.
 250. Rapoport ED, Loft A, Berthelsen AK, et al: Contrast-enhanced FDG-PET/CT vs. SPIO-enhanced MRI vs. FDG-PET vs. CT in patients with liver metastases from colorectal cancer: A prospective study with intraoperative confirmation. *Acta Radiol* 48:369–378, 2007.
 251. Catala V, Nicolau C, Vilana R, et al: Characterization of focal liver lesions: Comparative study of contrast-enhanced ultrasound versus spiral computed tomography. *Eur Radiol* 17:1066–1073, 2007.

Focal Hepatic Infections

PABLO R. ROS | SUKRU MEHMET ERTURK | ABDULLAH MAHMUTOGLU

CHAPTER OUTLINE

Bacterial (Pyogenic) Hepatic Abscesses

Incidence
Pathogenesis
Pathology
Clinical Findings
Radiologic Findings
Treatment

Amebic Abscesses

Incidence
Pathogenesis
Pathology
Clinical Findings
Radiologic Findings
Complications
Treatment

Hepatic Echinococcal Disease

Epidemiology
Pathophysiology
Pathology
Clinical Findings
Radiologic Findings
Complications
Treatment

Fasciola hepatica

Candidiasis and Fungal Infections

Schistosomiasis

Epidemiology
Pathophysiology
Pathology
Clinical Findings
Radiologic Findings
Treatment

Pneumocystis carinii (*Pneumocystis jiroveci*) Infection

Tuberculosis

Technologic advances have significantly enhanced the role of radiology in the detection, characterization, and management of focal infectious diseases of the liver. Today, all cross-sectional techniques allow highly accurate detection of focal hepatic infections. Computed tomography (CT) is particularly helpful in revealing the presence of calcifications and gas and in detailing the enhancement pattern.¹ With its multiplanar capacity and sensitivity to small differences in tissue composition, magnetic resonance imaging (MRI) is a useful tool to diagnose and to characterize lesions such as hepatic abscess,

hydatid cyst, and candidiasis. The impact of imaging is particularly dramatic for pyogenic abscess; early diagnosis and imaging-guided percutaneous drainage have markedly reduced both the mortality rates (from 40% to 2% of cases) and the need for surgery.¹ This chapter is a review of the radiologic and pathologic findings in a variety of focal hepatic infections, including abscesses, parasitic diseases, and fungal diseases.

Bacterial (Pyogenic) Hepatic Abscesses

INCIDENCE

Pyogenic liver abscesses are uncommon in Western countries, accounting for 0.1% of hospital admissions and having a prevalence at autopsy series of nearly 1%. There is a slight female predominance, and individuals between 40 and 60 years of age are most often affected.²⁻⁶

PATHOGENESIS

Hepatic abscess can develop by five major routes: biliary—ascending cholangitis from benign or malignant biliary obstruction, choledocholithiasis; portal vein—pyelephlebitis from appendicitis, diverticulitis (Fig. 88-1A), necrotic colon cancer, inflammatory bowel disease, proctitis, infected hemorrhoids, pancreatitis; hepatic artery—septicemia from bacterial endocarditis, pneumonitis, osteomyelitis; direct extension from contiguous organs—perforated gastric or duodenal ulcer, lobar pneumonia, pyelonephritis, subphrenic abscess; and traumatic, from blunt or penetrating injuries. Metastatic tumor nodules can also become abscesses.⁷⁻¹⁴

Before the antibiotic era, pyelephlebitis of the portal vein from seeding by appendicitis and diverticulitis was the most common cause of hepatic abscess.¹⁵ Indeed, appendicitis, which was once responsible for 34% of all pyogenic abscesses, now accounts for less than 2%.¹³⁻¹⁶ Biliary tract disease is now the most common source of pyogenic liver abscess.¹⁵ Obstruction of bile flow allows bacterial proliferation. Through pressurization and distention of canaliculi, portal tributaries and lymphatics are invaded, with subsequent pyelephlebitic abscess formation. Cholecystitis, stricture (benign or malignant), malignant neoplasms, and congenital diseases are common inciting conditions. Approximately 50% of pyogenic abscesses are caused by an anaerobic organism, mixed anaerobic organisms, or mixed anaerobic and aerobic organisms. Facultative gram-negative enteric bacilli, anaerobic gram-negative bacilli, and microaerophilic streptococci are the organisms most often responsible for liver abscesses. *Escherichia coli* is the organism most commonly isolated in culture in adults (Fig. 88-1B).

Staphylococci organisms are most often isolated from hepatic abscesses in children.⁵

PATHOLOGY

Abscesses of biliary tract origin are multiple and in 90% of cases involve both hepatic lobes. Abscesses of portal origin are usually solitary; 65% occur in the right lobe, 12% occur in the left lobe, and 23% are bilateral. This distribution is explained by the streaming effect of mesenteric blood flow in the portal vein.²

CLINICAL FINDINGS

The high morbidity and mortality of hepatic abscesses (50%-70%) before the era of cross-sectional imaging attest to the difficulty of establishing a diagnosis of pyogenic liver abscess on clinical grounds alone. The most common symptoms are fever, malaise, pain, rigors, nausea and vomiting, and weight loss. Tender hepatomegaly is the most common clinical sign, and leukocytosis, elevated serum alkaline phosphatase levels, hypoalbuminemia, and prolonged prothrombin time are the most common laboratory abnormalities. Clearly, these findings are nonspecific, and cross-sectional imaging has proved vital in the prompt diagnosis and management of hepatic abscess, resulting in improved survival.^{2,5,6,17}

RADIOLOGIC FINDINGS

Cholangiography

Ascending cholangitis is the most common cause of pyogenic hepatic abscess, and cholangiography has become an important aid to diagnosis in many cases. Percutaneous transhepatic cholangiography and endoscopic retrograde cholangiography can accurately define the level and cause of biliary obstruction; they are a first step in biliary drainage procedures and can accurately define biliary anatomy for the surgeon. These procedures increase intrabiliary pressure and can precipitate deterioration of a patient who is already septic. Accordingly, biliary drainage procedures should be anticipated.¹⁸ Magnetic resonance cholangiopancreatography is an important tool in diagnosis of obstructive biliary tract lesions.

Ultrasound

Real-time ultrasound can detect hepatic abscesses as small as 1.5 cm with a sensitivity of 75% to 90%. Pyogenic hepatic abscesses are extremely variable in shape and echogenicity. They are usually spherical (Fig. 88-2) or ovoid but may be lobulated or lentiform. Mural thickness is variable, and the wall typically is irregular and hypoechoic. On sonography, abscesses appear anechoic (50%), hyperechoic (25%), or hypoechoic (25%). Septa, fluid-fluid levels, internal debris, and posterior acoustic

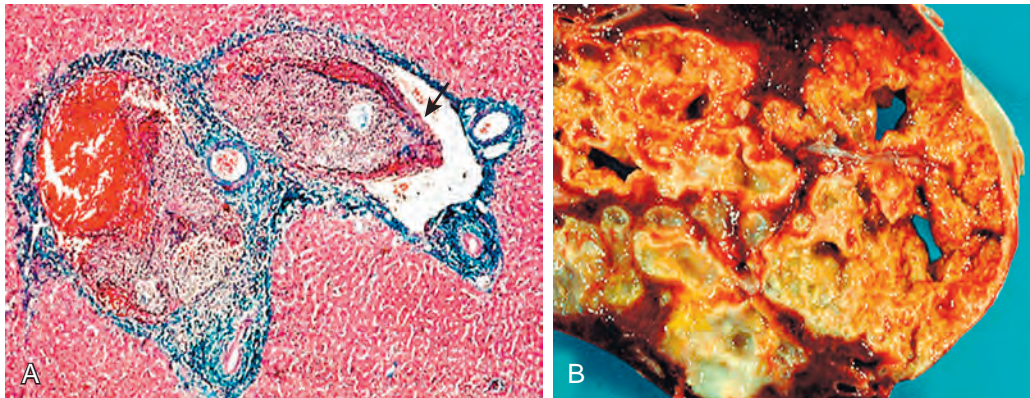


Figure 88-1 *Escherichia coli* pyogenic liver abscess: pathologic findings. This 76-year-old woman died of sigmoid diverticulitis and pylephlebitis of the inferior mesenteric vein and portal vein, causing a liver abscess. **A.** Infected material is present within a portal vein (arrow). **B.** A multicompartmental suppurative liver abscess is present.

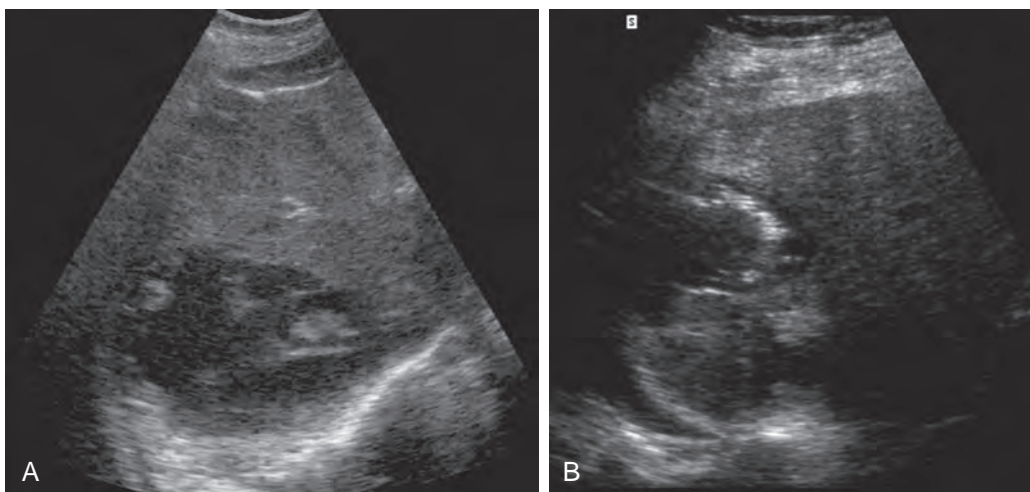


Figure 88-2 Pyogenic liver abscess: sonographic features. **A.** Transverse sonogram of the liver shows a complex, predominantly hypoechoic mass with posterior acoustic enhancement containing coarse, clumpy debris. **B.** Longitudinal sonogram of the liver in a different patient shows bright reflectors within the abscess due to gas.

enhancement may also be seen. Early lesions tend to be echogenic and poorly demarcated; they may evolve into well-demarcated, nearly anechoic lesions. If gas is present in an abscess, brightly echogenic reflectors with posterior reverberation artifact may be noted.¹⁹⁻²⁵

The sonographic differential diagnosis includes amebic or hydatid infection, necrotic or cystic neoplasm, hematoma, complicated biloma, and simple cyst with infection.

Nuclear Scintigraphy

Pyogenic liver abscesses appear as rounded, cold areas on technetium Tc 99m sulfur colloid and hepatobiliary scintiscans. On occasion, communication between the abscess cavity and the biliary system can be demonstrated on the ^{99m}Tc-sulfur colloid study.²⁶⁻²⁸

Gallium citrate Ga 67 scintigraphy and imaging with leukocytes labeled with indium In 111 are the two nuclear medicine techniques that were used for the detection of pyogenic abscess in the past but are abandoned today.

Magnetic Resonance Imaging

Hepatic abscesses, like most other focal hepatic processes, prolong T1 and T2 relaxation times.²⁹ At MRI, air within the abscess appears as a signal void and is therefore more difficult to differentiate from calcifications. However, the shape and location (air-fluid level) should enable the correct diagnosis. After administration of gadopentetate dimeglumine (Gd-DTPA), abscesses typically show rim enhancement (Fig. 88-3), which is secondary to increased capillary permeability in the surrounding liver parenchyma (the double target sign). Small lesions (<1 cm) may enhance homogeneously, mimicking hemangiomas.²⁹ Abscess wall enhancement on dynamic postgadolinium images may be considered a distinctive feature of pyogenic liver abscesses. Abscess wall shows a fast and intense enhancement that persists on portal venous and late-phase images. Some of the lesions may contain internal septations, which also reveal persistent enhancement on late-phase images.³⁰ Perilesional edema, shown as high signal on T2-weighted images, is associated with 50% of abscesses. However, it may also be seen in 20% to 30% of patients with

primary or secondary hepatic malignant neoplasms. Therefore, the presence of perilesional edema can be used only to differentiate a hepatic abscess from a benign cystic hepatic lesion.¹ Resolution of perilesional edema may indicate response to therapy.²⁹ Limitations of MRI in the investigation of patients with abscesses include the relatively high cost and the lack of easy access for drainage procedures.¹⁷

Computed Tomography

By virtue of its good spatial and contrast resolution, CT is the single best method for detecting hepatic abscess, with a sensitivity as high as 97% (Fig. 88-4). On CT scans, abscesses appear as generally rounded masses that are hypodense on both contrast and noncontrast scans. The attenuation ranges between 0 and 45 HU and thus overlaps with the appearance of cysts, bilomas, and hypodense neoplasms. Most have a peripheral rim or capsule that shows contrast enhancement in a pattern similar to that seen on MRI (see Fig. 88-2). Most abscesses are sharply defined, but a minority have a grossly lobular contour and circumferential “transition zones” of intermediate attenuation.^{24,31}

Another helpful finding is the transient segmental or wedge-shaped enhancement of the hepatic parenchyma surrounding an abscess on the arterial dominant phase of a contrast-enhanced dynamic CT scan.³²

Some abscesses show the cluster sign (see Fig. 88-4C-E), in which small, pyogenic abscesses appear to cluster or aggregate in a pattern suggesting coalescence into a single large cavity.

All of these findings are nonspecific and require aspiration for diagnosis. Central gas (see Fig. 88-4A), as either air bubbles or an air-fluid level, is a specific sign, but it is present in less than 20% of cases. A large air-fluid or fluid-debris level is often associated with communication with the gut.³³

TREATMENT

Effective treatment of pyogenic liver abscess entails elimination of both the abscess and its underlying source. Current therapeutic options include surgical drainage, antibiotics alone, percutaneous aspiration in conjunction with antibiotics, and percutaneous catheter drainage.^{2,5,34-49}

As a rule, aspiration alone is sufficient if the fluid collection is unilocular, well demarcated, and less than 5 cm in diameter and shows no communication with the gut or biliary tree. Unless the abscess is chronic and the cavity walls are fibrotic or calcified, small intrahepatic abscess cavities quickly collapse when aspirated, unlike abscesses in other organs and peritoneal spaces. In a retrospective study of 115 patients, excellent results were obtained with ultrasound-guided percutaneous needle aspiration of pyogenic abscesses followed by injection of antibiotics into the abscess cavity.⁴⁸ Cure was achieved in 98% of cases, with no deaths, complications, or recurrences at 3-year follow-up.⁴⁸ Fluid drainage usually requires introduction of a 16- or 18-gauge Teflon-sheathed needle into the collection and, if the fluid is extremely viscous, temporary insertion of a 5F to 8F pigtail catheter. All fluid is aspirated, and the cavity is irrigated with normal saline or an antiseptic solution.^{37,42}

Before removal of the catheter, the collection is injected with contrast medium to rule out communication with surrounding organs. Intravenous antibiotics are given before, during, and after the procedure and are changed accordingly when the infecting organism is identified.^{37,42}

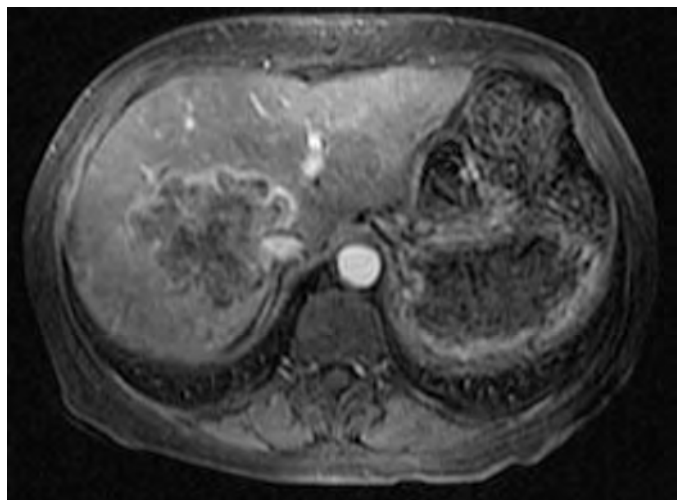


Figure 88-3 Pyogenic liver abscess: MRI findings. Gadolinium-enhanced, fat-suppressed T1-weighted image shows a predominantly low signal intensity mass with enhancing wall and septations.

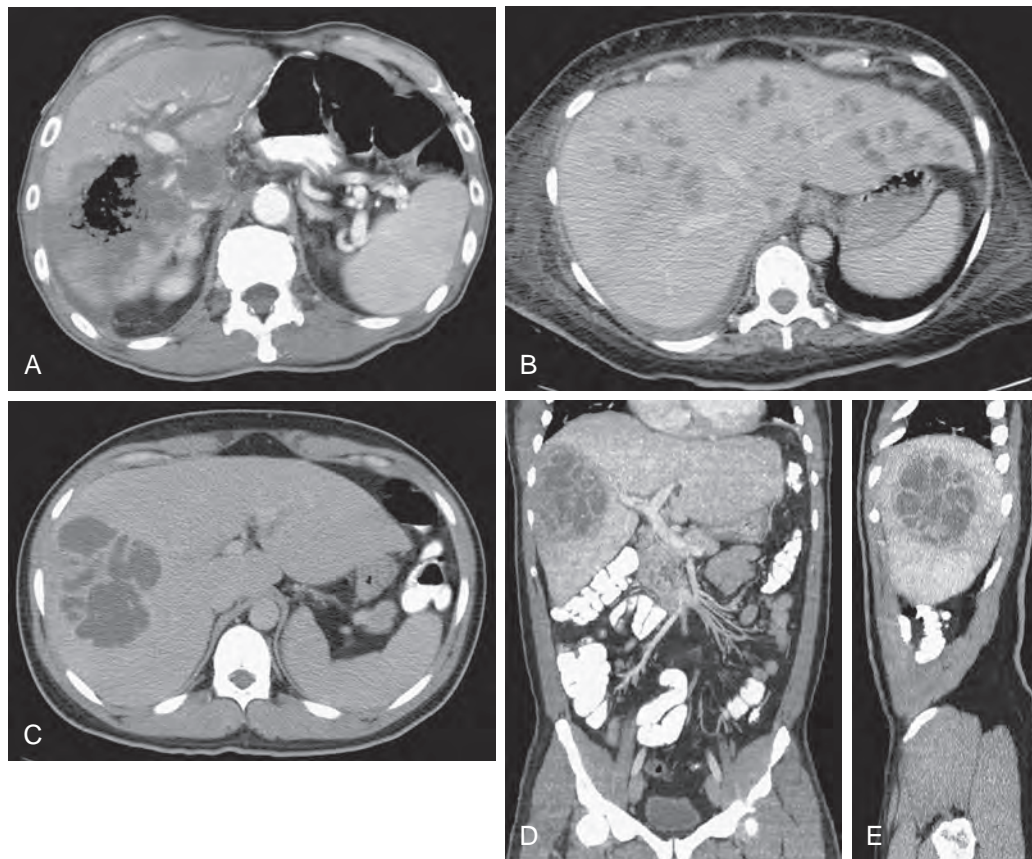


Figure 88-4 Pyogenic liver abscess: CT findings. **A.** Mottled gas collection is present in this right lobe abscess. **B.** A multifocal abscess is identified in this patient with cholangitis. Axial (**C**), coronal (**D**), and sagittal (**E**) images show the classic cluster sign of a multiloculated pyogenic liver abscess. Note the peripheral lobulations and thin enhancing wall.

An indwelling drainage catheter is usually required when the fluid collection is ill-defined, multiloculated, or more than 5 cm in diameter or when communication with the gut or biliary tree is suspected. A variety of drainage catheter styles (single lumen, double lumen, sump type) and sizes (8.3F–16F) are available.^{34,39} Most are made of a flexible Silastic material with a pigtail curve containing multiple side holes. Smaller catheters (8.3F–10F) are usually sufficient to adequately drain thin fluid collections or extremely small abscesses; large abscesses require larger catheters (12F–16F), especially if they contain particulate material. The catheter can be inserted under CT, ultrasound, or fluoroscopic guidance by the Seldinger or trocar technique. Other chapters contain complete discussions of imaging guidance and abscess catheterization. The catheter is left in place until drainage volume has decreased to less than 20 mL/day. If there is a known or suspected fistula, a fluoroscopic sinogram is obtained before catheter removal to rule out communication with bowel, bile duct, or pancreatic duct. If no fistula is present, most hepatic abscesses require only 2 to 14 days of drainage.^{37,42,49}

The failure and recurrence rates of catheter therapy are 8.4% and 8%, respectively. They are most often associated with complicated abscesses caused by fistula, phlegmons, or infected tumors.^{37,42,49}

Surgery is reserved for patients for whom percutaneous drainage has failed, those with associated intra-abdominal perforation of hepatic abscess, and those with fistula formation (e.g., biliary, colonic).

The mortality rate for pyogenic hepatic abscess has declined from 80% to less than 10% owing to earlier diagnosis, antibiotics, and advances in surgical and percutaneous drainage techniques.^{44,47}

Amebic Abscesses

INCIDENCE

Approximately 10% of the world's population is infected with *Entamoeba histolytica*, which causes more deaths than any other parasite with the exceptions of malaria-causing plasmodia and schistosomes. Less than 10% of infected individuals, however, are symptomatic. Amebic liver abscess is the most common extraintestinal manifestation, occurring in 3% to 7% of this population.^{50–56}

Although amebiasis is usually considered a disease of developing countries, certain groups are at high risk in Western nations: recent immigrants, institutionalized patients, and homosexual persons. Indeed, *E. histolytica* has been isolated in the stool of up to 30% of sexually active homosexual men; its clinical significance is unclear.⁵⁰ Worldwide, some 85% to 90% of amebic liver abscesses occur in men.

In the United States, the overall mortality rate for hepatic amebic abscess is 3%. It is less than 1% when the abscess is confined to the liver, 6% with extension into the chest, and 30% with extension into the pericardium.⁵⁷

PATHOGENESIS

The cystic form of *E. histolytica* gains access to the body by oral ingestion of infected material, usually contaminated water (Fig. 88-5A). The mature cysts are resistant to gastric acid and pass unchanged into the intestine. The cyst wall is then digested by trypsin; four invasive trophozoites are released, which live and multiply in the colon, particularly the cecum. The trophozoites exist in two forms, small (10-20 mm) and large (20-60 mm). The large form usually occurs in invasive amebiasis when the mucosa is invaded. This can cause minute superficial mucosal ulcerations. With further invasion, hemorrhage, perforation, enterocolic or cutaneous fistulas, amebic appendicitis, or ameboma formation can occur. Amebic trophozoites can also enter the mesenteric venules and lymphatics and be carried to the liver, lungs, and other organs. The liver can be invaded in one of three ways: through the portal vein (most common); through lymphatics; or by direct extension through the colon wall into the peritoneum and then through the liver capsule.^{2,4,52}

When a sufficient number of trophozoites become lodged in small hepatic venules, thrombosis and infarction of small areas of hepatic parenchyma occur (amebic hepatitis). The host's nutritional and immune status determine whether the initial infestation heals or progresses to a macroabscess. A visible abscess results from the coalition of multiple small areas of ischemic necrosis and amebic destruction of hepatic parenchymal cells.

Trophozoites that pass into the distal colon may change into round, resistant cysts (Fig. 88-5B) that pass into the feces. Indeed, human carriers who pass amebic cysts into their stool are the primary source of infection.^{2,4,54}

PATHOLOGY

The fluid of an amebic abscess is usually dark reddish brown and has the consistency of anchovy paste (Fig. 88-5C). This material is usually sterile, consisting of a mixture of blood and destroyed hepatocytes. Rarely, the trophozoites are found centrally within the paste, but they are often found in the zone of necrotic tissue adjacent to the outer abscess wall. The wall of connective tissue becomes better developed with age, and leukocyte infiltration and inflammatory reaction are characteristically absent. If the abscess is not treated, it may rupture into the peritoneum, pleural cavity, lung, or pericardium.^{2,4,54}

Amebic abscesses are most often solitary (85%) and affect the right lobe more often (72%) than the left lobe (13%). Solitary liver abscesses and right lobe predominance are more marked in amebic than in pyogenic abscesses because most infestations are transmitted through the portal vein. Amebiasis most often affects the right colon, which drains into the superior mesenteric vein, which preferentially streams into the right lobe. Flow from the inferior mesenteric vein (left colon) and splenic vein streams preferentially into the left lobe.^{2,4,54}

CLINICAL FINDINGS

Most patients with amebic liver abscess present with a tender liver and right upper quadrant pain. Compared with persons who have pyogenic liver abscess, they are more likely to have diarrhea and hepatomegaly and less likely to have jaundice or sepsis. Amebae are not found in the stool of most patients with an amebic liver abscess.⁵⁰⁻⁵²

Because clinical features and findings of stool examination for amebae usually are nonspecific or negative, serologic tests are particularly helpful when hepatic amebic abscess is suspected. The indirect hemagglutination test result is positive in more than 90% of these patients.⁵⁰⁻⁵²

RADIOLOGIC FINDINGS

Nuclear Scintigraphy

Amebic abscesses appear as cold defects on sulfur colloid scans. They often show "rim enhancement" on hepatobiliary scintiscans, presumably owing to inflammation of the adjacent parenchyma. A cold lesion with a hot periphery is suggestive of the diagnosis. Nevertheless, nuclear medicine techniques are not routinely used for detection of hepatic amebic abscess.

Ultrasound

Amebic abscess on ultrasound studies is usually a round or oval, sharply defined hypoechoic mass (Fig. 88-6) that abuts the liver capsule with homogeneous, fine, low-level echoes and distal acoustic enhancement.¹⁵ In comparison of amebic and pyogenic abscesses, amebic abscess is more likely to have a round or oval shape (82% vs. 60%) and a hypoechoic appearance with fine, low-level internal echoes at high gain settings (58% vs. 36%).^{20,58-63} On contrast-enhanced ultrasonography, pyogenic abscess appears as a partially enhancing lesion with a thin or thick rim of dense opacification and persistently hypoechoic center.⁶⁴

Computed Tomography

The CT appearance of amebic abscess is variable and nonspecific. The lesions are usually peripheral, round or oval areas of low attenuation (10-20 HU). A peripheral rim of slightly higher attenuation can be seen on noncontrast scans and shows marked enhancement after administration of contrast material (Fig. 88-7). A peripheral zone of edema around the abscess is also common and somewhat characteristic for this lesion.¹ Lesions may appear unilocular or multilocular and demonstrate nodularity of the margins. Concomitant extrahepatic abnormalities include right-sided pleural effusion, perihepatic fluid, and gastric or colonic involvement.^{65,66}

Magnetic Resonance Imaging

On MRI (Fig. 88-8), amebic liver abscesses are spherical and usually solitary lesions with a hyperintense center on T2-weighted images and a hypointense center on T1-weighted images. The abscess wall is thick, and on gadolinium-enhanced images, the enhancement pattern is similar to that of pyogenic abscess.^{1,30} Diffuse central inhomogeneity is often seen on T2-weighted images. Edema in otherwise normal surrounding parenchyma may be appreciated on T2-weighted images.^{67,68}

After treatment, abscesses become more homogeneously hypointense on T2-weighted images. Successful treatment may show concentric rings of different signal intensity surrounding the lesion on T2-weighted images.^{67,68}

COMPLICATIONS

Pleuropulmonary amebiasis is the most frequent complication of amebic liver abscess, occurring in 20% to 35% of patients. This may be manifested as pulmonary consolidation or abscess, serous effusion, empyema, or hepatobronchial fistula.^{50-52,69}

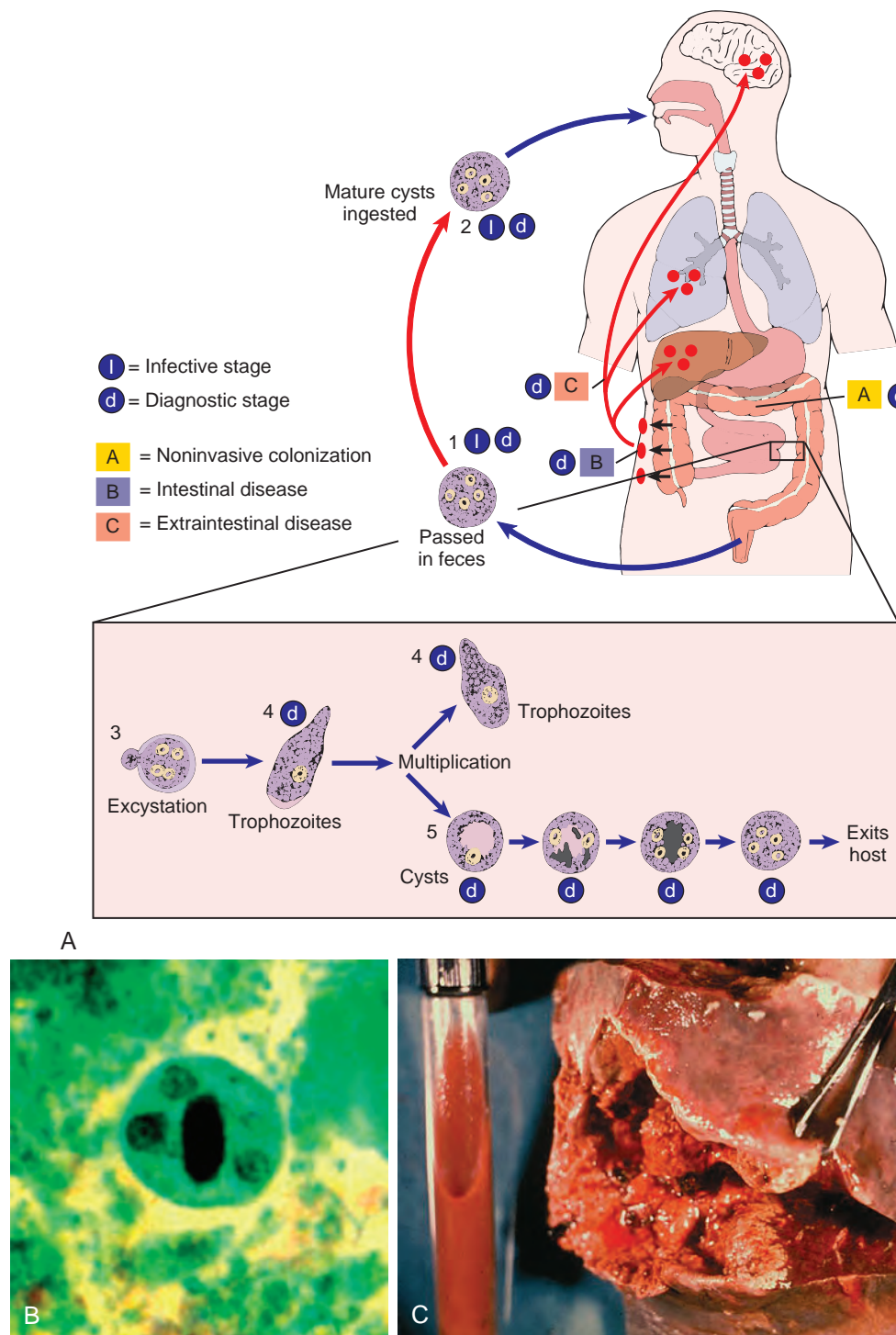


Figure 88-5 Amebiasis: pathologic findings. A. Life cycle. Cysts are passed in feces (1). Infection by *Entamoeba histolytica* occurs by ingestion of mature cysts (2) in fecally contaminated food, in water, or on hands. Excystation (3) occurs in the small intestine and trophozoites (4) are released, which migrate to the large intestine. The trophozoites multiply by binary fission and produce cysts (5), which are passed in the feces (1). Because of the protection conferred by their walls, the cysts can survive days to weeks in the external environment and are responsible for transmission. (Trophozoites can also be passed in diarrheal stools but are rapidly destroyed once outside the body and if ingested would not survive exposure to the gastric environment.) In many cases, the trophozoites remain confined to the intestinal lumen (A, noninvasive infection) of individuals who are asymptomatic carriers, passing cysts in their stool. In some patients, the trophozoites invade the intestinal mucosa (B, intestinal disease) or, through the bloodstream, extraintestinal sites such as the liver, brain, and lungs (C, extraintestinal disease), with resultant pathologic manifestations. It has been established that the invasive and noninvasive forms represent two separate species, respectively, *E. histolytica* and *E. dispar*; however, not all persons infected with *E. histolytica* will have invasive disease. These two species are morphologically indistinguishable. Transmission can also occur through fecal exposure during sexual contact (in which case not only cysts but also trophozoites could prove infective). **B.** Cyst of *E. histolytica*, permanent preparation stained with trichrome. **C.** Typical anchovy paste-like material drained from an amebic abscess. (A source: Centers for Disease Control and Prevention. <http://www.cdc.gov/parasites/amebiasis/biology.html>.)

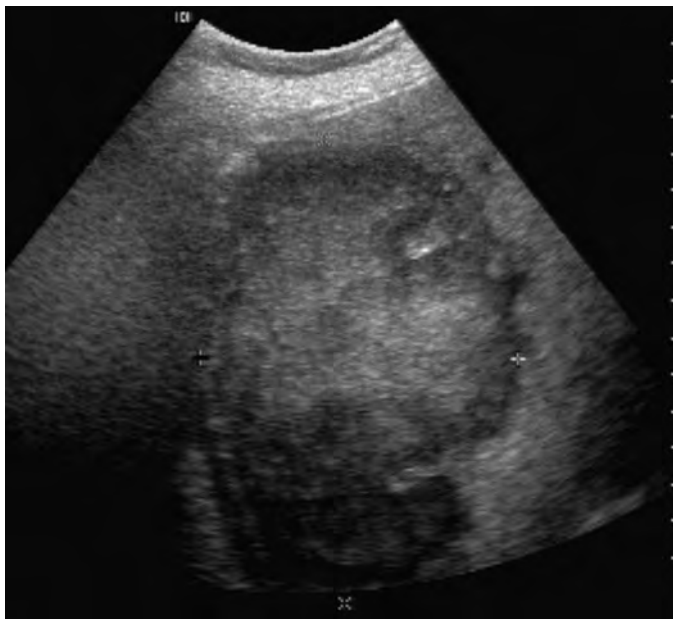


Figure 88-6 Amebic abscess: sonographic features. A large, well-defined abscess is identified in the right lobe of the liver.

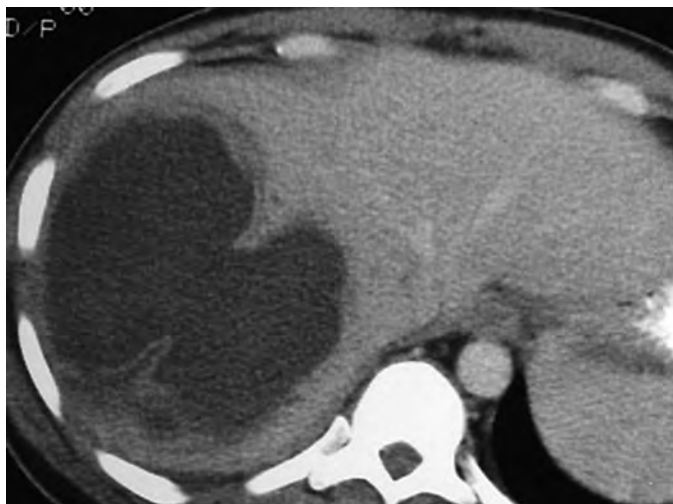


Figure 88-7 Amebic abscess: CT features. A large unilocular mass with an enhancing wall demonstrates a thin peripheral hypodense rim of surrounding edema that is typical of amebic abscesses.

Peritoneal amebiasis occurs in 2% to 7.5% of patients with amebic liver abscess. Sudden rupture is manifested dramatically, in the manner of a perforated viscus. Pericardial amebiasis is the most serious complication of amebic liver abscess because it can lead to progressive tamponade or sudden development of shock. Most abscesses responsible for this complication are located in the left hepatic lobe. Renal amebiasis is a rare complication that can result from abscess rupture.^{50-52,69,70}

TREATMENT

The complications of amebic liver abscess just mentioned are becoming less frequent because of earlier diagnosis, improved

imaging and serologic techniques, and effective medical, percutaneous, and surgical management.⁷¹ More than 90% of hepatic amebic abscesses respond to antimicrobial (metronidazole or chloroquine) therapy alone. The efficacy of these amebicidal agents has reduced the mortality rate of hepatic amebic abscesses from 81% to 4%.^{50-52,72,73}

There are, nevertheless, some circumstances in which aspiration and drainage of amebic abscess are indicated: to differentiate pyogenic from amebic abscess; for a large symptomatic abscess in which rupture is imminent; after poor response to medical therapy; with suspected bacterial superinfection; in pregnancy; for noncompliance with medical treatment; and as an alternative to surgery when an abscess ruptures. Drainage can be accompanied by intralesional delivery of drug, which can increase mean intralesional drug levels up to 246-fold.⁷⁴⁻⁷⁸

Confirmation of an amebic abscess may not always be possible by percutaneous aspiration. In one series, only 50% of patients had the classic “anchovy paste” appearance, and positive diagnoses based on fluid evaluation were established in only 5% of cases. Therefore, the primary role of percutaneous aspiration and drainage in these patients is the diagnosis and treatment of superimposed bacterial infection.⁷⁴⁻⁷⁸

Hepatic Echinococcal Disease

EPIDEMIOLOGY

Hydatid disease is prevalent throughout much of the world, and the two main forms that affect humans are *Echinococcus granulosus* and *Echinococcus multilocularis*. The disease flourishes in rural areas where dogs are used for herding livestock, especially sheep. Greece, Uruguay, Argentina, Australia, and New Zealand are the countries with the highest incidence of hydatid disease.⁷⁹

PATHOPHYSIOLOGY

E. granulosus is a small tapeworm, 3 to 6 mm long, that lives in the intestine of the definitive host, usually the dog. The life cycle (Fig. 88-9A) depends on a primary host harboring the adult worm and an intermediate (human) host harboring the larval stage. The adult parasite sheds eggs, which may infect humans when contaminated, unwashed vegetables are ingested or through contact with infected dogs, which may carry ova on their fur or shed them onto soil where children play.⁷⁹⁻⁸¹

In humans, the external shell of the egg is digested in the duodenum and the embryo is freed. The embryo actively penetrates the intestinal mucosa until it enters a blood vessel, from which it is transported until trapped by narrowing of the capillaries. Most are carried by the portal vein and trapped in the liver, but the lungs, spleen, kidneys, bone, and central nervous system can also be involved.⁷⁹⁻⁸¹

Although most embryos are destroyed by host defenses, surviving embryos (Fig. 88-9B) develop into the hydatid stage in 4 to 5 days while trapped within a capillary. After 3 months, this cyst measures 5 mm in diameter. The life cycle is complete when the infected intermediate host (sheep or other ruminant) dies and its viscera, which contain the larval form, are consumed by a definitive host.⁷⁹⁻⁸¹

E. multilocularis (*alveolaris*) is a less common but more aggressive form of echinococcus. The disease is endemic in central Europe, the former Soviet Union, Japan, and central

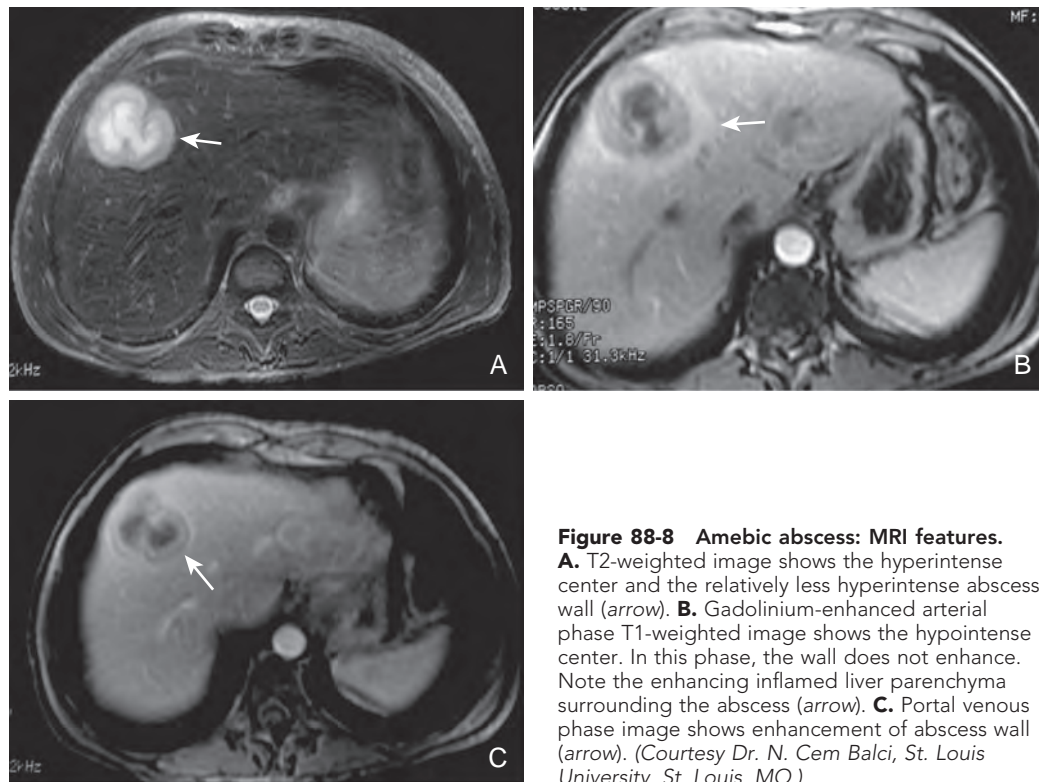


Figure 88-8 Amebic abscess: MRI features.

A. T2-weighted image shows the hyperintense center and the relatively less hyperintense abscess wall (arrow). **B.** Gadolinium-enhanced arterial phase T1-weighted image shows the hypointense center. In this phase, the wall does not enhance. Note the enhancing inflamed liver parenchyma surrounding the abscess (arrow). **C.** Portal venous phase image shows enhancement of abscess wall (arrow). (Courtesy Dr. N. Cem Balci, St. Louis University, St. Louis, MO.)

and northern North America.⁸²⁻⁸⁵ The main host of the adult parasite is the fox, although less commonly domestic dogs and cats may serve as hosts.⁸² The intermediate hosts, usually wild rodents, acquire infection by eating contaminated wild berries. Humans become infected either by eating wild fruits contaminated with fox feces or by direct contact with infected animals.⁸²⁻⁸⁴ The larvae reach the liver through the portal vein. Here they proliferate and penetrate surrounding tissue, which causes a diffuse and infiltrative process that simulates a malignant neoplasm. *E. multilocularis* organisms induce a brisk granulomatous reaction with central necrosis, cavitation, and calcification.⁷⁹⁻⁸¹

PATHOLOGY

The hydatid cyst has three layers composed of both host and parasite tissue (Fig. 88-9C). The outer pericyst is composed of modified host tissue that forms a rigid protective zone only several millimeters thick. As the cyst expands, the vessels and ductal structures of the liver become incorporated in the cyst wall; this explains enhancement of the wall on contrast CT and MR studies and angiography.

The two internal layers are formed by the parasite. The middle layer is a thicker (1-2 mm) laminated membrane that resembles the white of a hard-boiled egg and is easily ruptured with manipulation. It permits the passage of nutrients but is impervious to bacteria. Disruption of this layer predisposes to bacterial infection. The innermost or germinal layer (endocyst) is the living parasite, which is one cell thick. It produces the laminated membrane and scolices that represent the larval stage. Brood capsules are small spheres of disrupted germinal membrane that produce scolices (Fig. 88-9D). Free-floating

brood capsules and scolices form a white sediment of barely visible particles known as hydatid sand.

Cyst fluid is secreted by the germinal lining and normally is crystal clear. It is a transudate of serum that contains protein and is antigenic. The high secretion pressure is responsible for progressive cyst enlargement. Up to 60% of cysts are multiple.

In contrast to *E. granulosus*, the alveolar form has daughter cysts that arise on the outer surface of the original cyst with invasion of adjacent liver parenchyma.⁸⁶ On histologic examination, the cysts have a thick lamellated wall.^{86,87} Surrounding this is the marked granulomatous reaction with hepatic necrosis, collagenous tissue, multinucleated giant cells, and lymphocytes.⁷⁸ In contrast to the cysts of *E. granulosus*, the *E. alveolaris* cysts rarely contain scolices in human infestation.^{87,88}

CLINICAL FINDINGS

Most patients acquire hydatid disease in childhood but are not diagnosed until the third or fourth decade of life. Echinococcal cysts enlarge at a rate of approximately 1 cm/year. Most cysts are initially asymptomatic and remain so until they grow large enough to cause pain; erode into a moderate-sized bile duct, allowing cyst fluid to enter the bile (and vice versa), causing fever and jaundice; or induce an allergic reaction because of leakage of cyst fluid. Large cysts can obstruct blood and bile flow, leading to portal hypertension and jaundice.⁷²

Routine blood analysis is usually not helpful in establishing the diagnosis of hydatid disease. Results of serologic tests are positive in more than 80% of cases and are diagnostic of echinococcoses.⁷² The clinical manifestations of *E. multilocularis* may occur 5 to 20 years after the inciting event.⁸⁶⁻⁸⁸ Abdominal discomfort, jaundice, and hepatomegaly may be present, and

eosinophilia is frequently observed.^{86,89} Although the serum levels of the transaminases usually remain normal, alkaline phosphatase and γ -glutamyl transpeptidase values are elevated.^{86,88} Serologic titers are elevated in alveolar echinococcosis and aid in diagnosis.⁸⁹

RADIOLOGIC FINDINGS

Plain Radiographic Findings

Calcification is visible on 20% to 30% of abdominal plain radiographs (Fig. 88-10). The calcification is usually curvilinear or ringlike and lies in the pericyst. Daughter cysts may calcify, creating rings of calcification. Calcification does not always indicate death of the parasite, and small irregular areas of calcification may be secondary to dystrophic calcification in old blood clots.⁹⁰ *E. multilocularis* can cause faint or dense punctate calcification scattered throughout necrotic and granulomatous tissue.

Ultrasound

Hepatic hydatid disease is manifested sonographically in several different fashions (Fig. 88-11), depending on the stage of evolution and maturity: a well-defined anechoic cyst; an anechoic cyst except for hydatid sand; a multiseptate cyst with daughter cysts and echogenic material between the cysts (characteristic); a cyst with a floating, undulating membrane with a detached endocyst, the characteristic “water lily” sign; or a densely calcified mass. Daughter cysts usually cause mural thickening as well.^{15,91}

Ultrasound has been used to monitor the efficacy of medical antihydatid therapy. Findings suggesting a positive response include reduction in cyst size, membrane detachment, progressive increase in cyst echogenicity, and mural calcification.^{20,92-99} When hydatid cysts become infected, they lose their characteristic sonographic appearance and become diffusely hyperechoic.^{20,82,92-99}

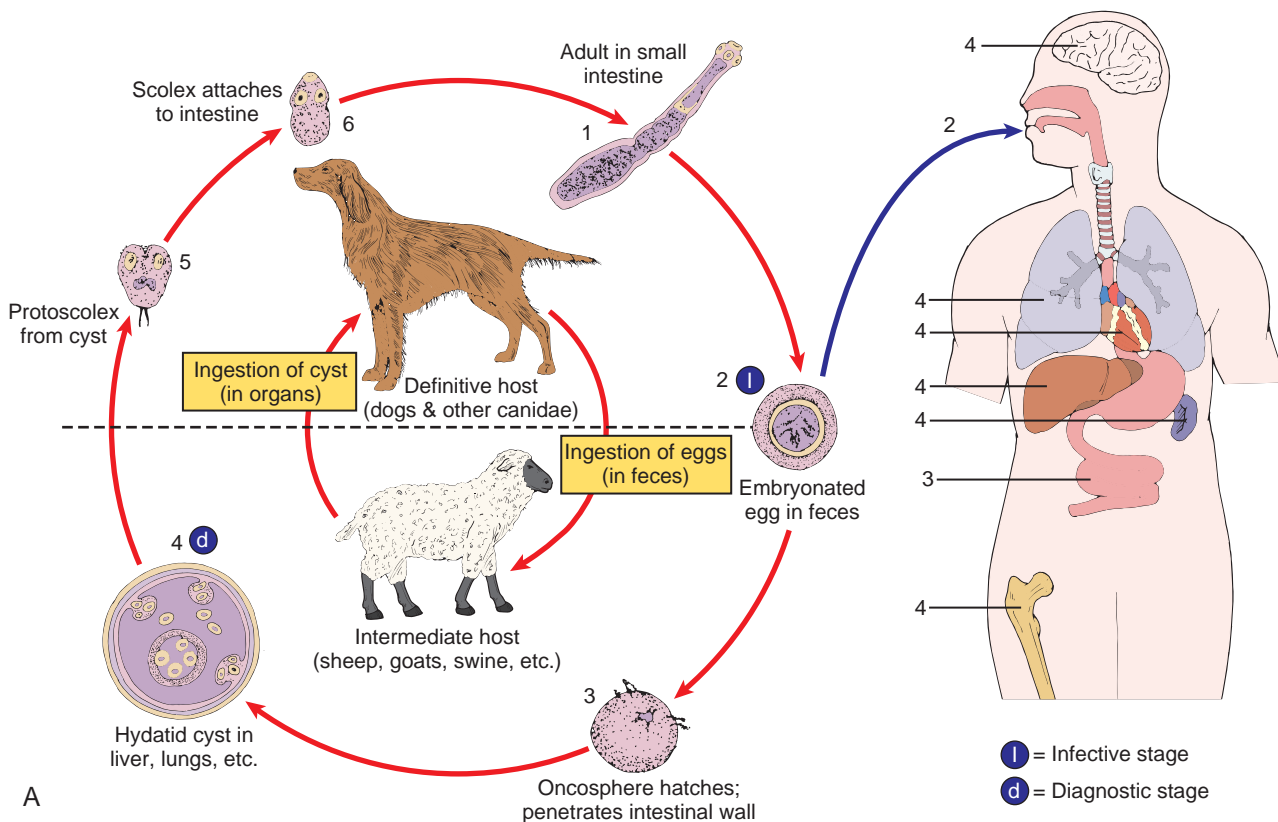


Figure 88-9 Hydatid disease: pathologic findings. A. Life cycle. The adult *Echinococcus granulosus* (3-6 mm long) (1) resides in the small bowel of the definitive hosts, dogs or other canids. Gravid proglottids release eggs (2) that are passed in the feces. After ingestion by a suitable intermediate host (under natural conditions: sheep, goat, swine, cattle, horses, camel), the egg hatches in the small bowel and releases an oncosphere (3) that penetrates the intestinal wall and migrates through the circulatory system into various organs, especially the liver and lungs. In these organs, the oncosphere develops into a cyst (4) that enlarges gradually, producing protoscolices and daughter cysts that fill the cyst interior. The definitive host becomes infected by ingesting the cyst-containing organs of the infected intermediate host. After ingestion, the protoscolices (5) evaginate, attach to the intestinal mucosa (6), and develop into adult stages (1) in 32 to 80 days. The same life cycle occurs with *E. multilocularis* (1.2-3.7 mm), with the following differences: the definitive hosts are foxes and to a lesser extent dogs, cats, coyotes, and wolves; the intermediate hosts are small rodents; and larval growth (in the liver) remains indefinitely in the proliferative stage, resulting in invasion of the surrounding tissues. With *E. vogeli* (up to 5.6 mm long), the definitive hosts are bush dogs and dogs; the intermediate hosts are rodents; and the larval stage (in the liver, lungs, and other organs) develops both externally and internally, resulting in multiple vesicles. *E. oligarthrus* (up to 2.9 mm long) has a life cycle that involves wild felids as definitive hosts and rodents as intermediate hosts. Humans become infected by ingesting eggs (2), with resulting release of oncospheres (3) in the intestine and the development of cysts (4) in various organs.

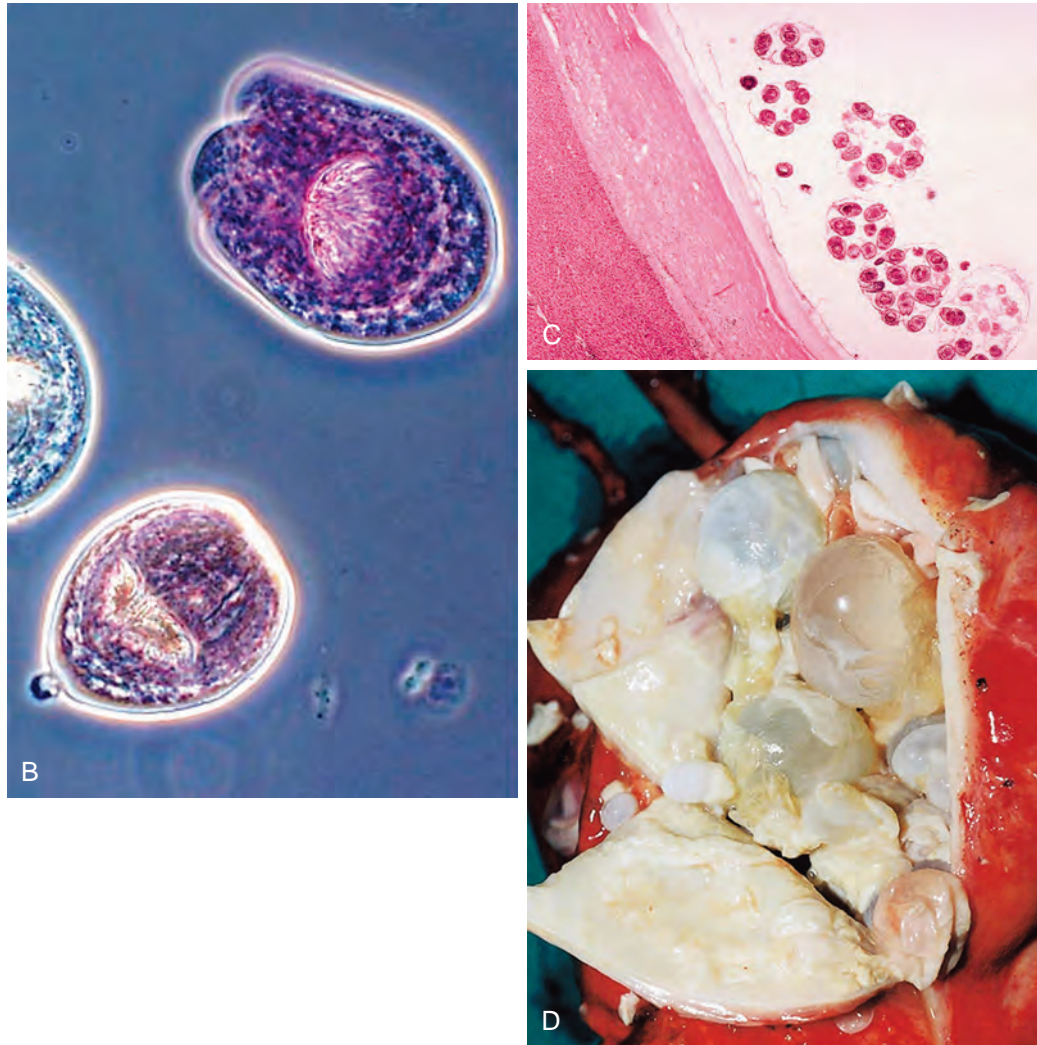


Figure 88-9, cont'd B to D. Hydatid cysts are typically spherical and have the ability to achieve large sizes. The insides of the cysts are filled with fluid, brood capsules, daughter cysts, and protoscolices that have the capability to grow into adult worms if consumed by a definitive host. If a cyst is ruptured, which may occur through a sharp blow or during surgery, each protoscolex released may form a new cyst. Also, the fluid within the hydatids is highly allergenic and may cause anaphylactic shock and rapid death if it is freed inside the body. (A source: Centers for Disease Control and Prevention. <http://www.cdc.gov/parasites/echinococcosis/biology.html>.)

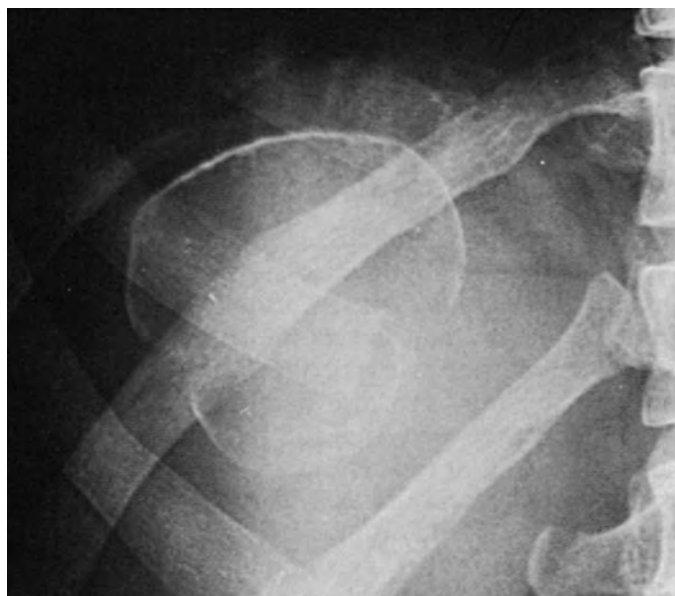


Figure 88-10 Hydatid cyst: plain radiographic findings. Curvilinear calcification of the pericyst is present in 20% to 30% of abdominal radiographs in patients with hydatid cysts.

E. multilocularis produces echogenic lesions that can be single or multiple and are usually situated in the right lobe.⁸² Irregular necrotic regions can be seen.^{82,100} Microcalcifications have been described in about 50% of cases.⁸² Intrahepatic biliary dilation is a common sonographic finding.⁸² *E. multilocularis* lesions are infiltrative with a propensity to spread to the liver hilum.⁸²

Computed Tomography

On CT scans, hydatid disease appears as unilocular or multilocular, well-defined cysts with either thick or thin walls.^{1,30} (Fig. 88-12). Daughter cysts are usually seen as areas of lower attenuation than the mother cyst and are usually oriented in the periphery of the lesion (see Fig. 88-12). Daughter cysts can also float free in the lumen of the mother cyst, so altering the patient's position may change the position of these cysts, confirming the diagnosis of echinococcal disease (Fig. 88-13). Curvilinear ringlike calcification is also a common feature.¹⁰¹⁻¹⁰⁷

E. multilocularis causes geographic, infiltrating lesions without sharp margins or high-attenuation rims. These low-density (14-40 HU) lesions are solid masses rather than cysts. There is little if any enhancement with intravenous administration of contrast material.⁸²⁻⁸⁸ These are invasive

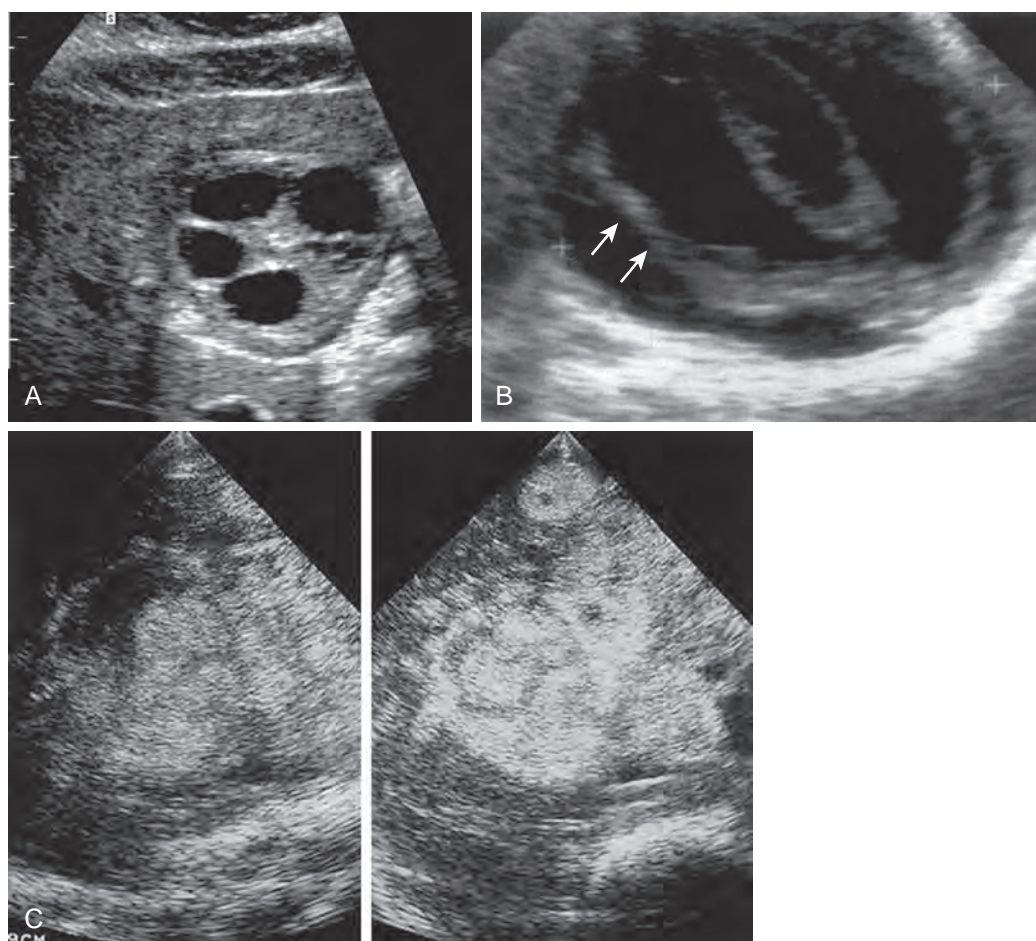


Figure 88-11 Hydatid disease: sonographic features. **A.** Longitudinal scan shows a rounded, well-defined, multilocular hypoechoic lesion with echogenic internal septa due to *E. granulosus*. **B.** Hydatid cyst in the right lobe with wavy bands of delaminated endocyst (water lily sign, arrows). **C.** *E. multilocularis* cysts. Transverse ultrasound images obtained at different levels of the liver show *E. multilocularis* infection with the typical hailstorm pattern, characterized by multiple echogenic nodules with irregular and indistinct margins. (**B** and **C** from Mortelet, KJ, Segatto E, Ros PR: The infected liver: Radiologic-pathologic correlation. *RadioGraphics* 24:937-955, 2004.)

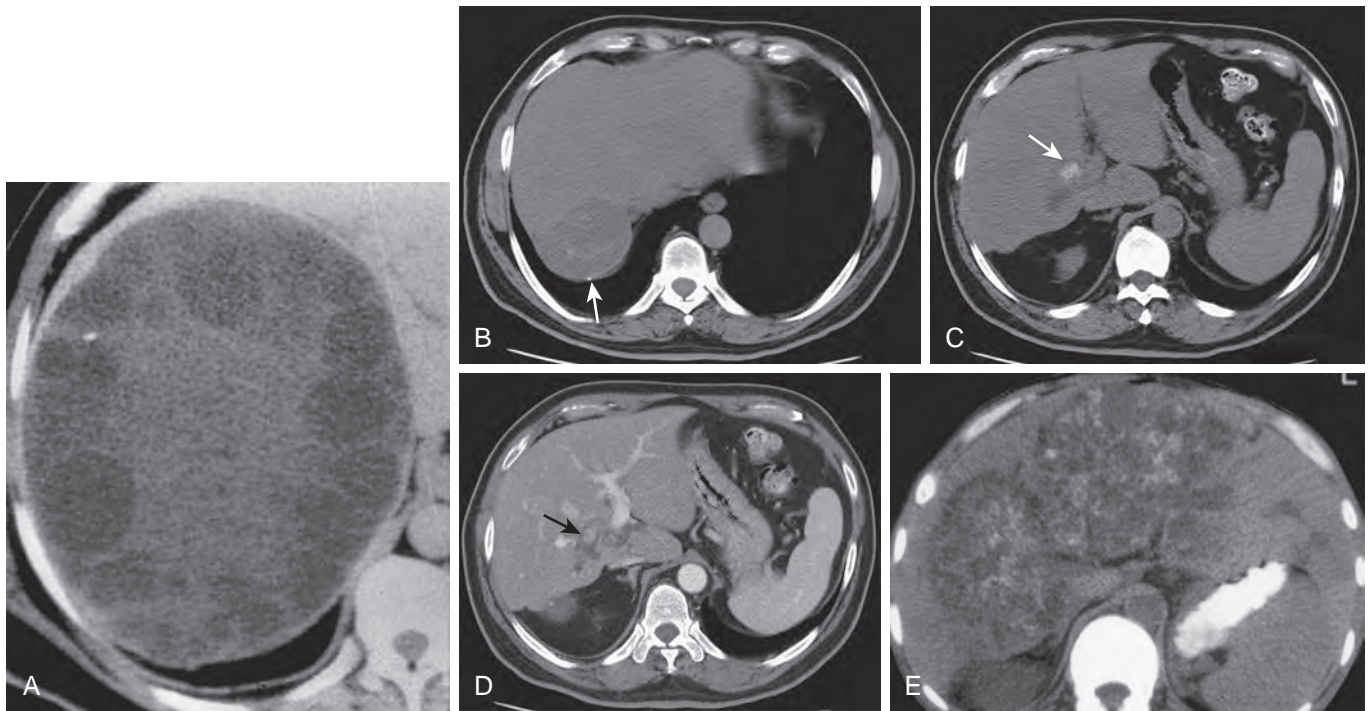


Figure 88-12 Hydatid disease: CT findings. **A.** CT scan shows a large multilocular cyst with a thick wall. Multiple daughter cysts line the periphery of the mass. **B.** Calcification is seen within the dominant cyst in the right lobe on this noncontrast scan. **C.** More caudal scan shows intrabiliary passage of hyperdense cyst contents (arrow). **D.** Contrast-enhanced scan at the same level as **C** demonstrates filling defects (arrow) within dilated intrahepatic bile duct. **E.** Precontrast scan in a patient with *E. alveolaris* demonstrates an extensive, infiltrative lesion with calcifications in the right lobe.

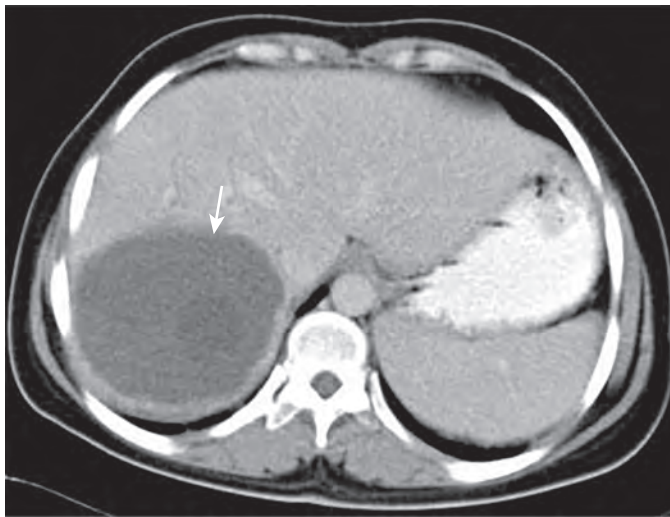


Figure 88-13 Hydatid disease: CT findings. Contrast-enhanced CT image of a patient with hydatid cyst (arrow).

rather than expansile lesions whose nonspecific appearance can simulate a primary or secondary hepatic tumor. Calcification, when it is present, is usually amorphous rather than ringlike. When the alveolar lesion is located centrally, it may cause hepatic lobar atrophy.⁸⁵

Magnetic Resonance Imaging

On MRI studies, the cyst component of echinococcal cysts is similar to that of other cysts, with long T1 and T2 relaxation

times (Fig. 88-14). However, because of its superb contrast resolution, MRI best demonstrates the pericyst, the matrix or hydatid sand (debris consisting of freed scolices), and the daughter cysts (Fig. 88-15).¹ The pericyst usually has low signal intensity on T1- and T2-weighted images because of its fibrous component. This rim and a multiloculated or multicystic appearance are distinctive features. The hydatid matrix appears hypointense on T1-weighted images and markedly hyperintense on T2-weighted images. When present, daughter cysts are hypointense relative to the matrix on both T1- and T2-weighted images.¹⁰⁸ Floating membranes have low signal intensities on T1- and T2-weighted images.

MRI with its multiplanar capabilities is useful in displaying extrahepatic extension of *E. multilocularis*, such as transdiaphragmatic spread to the pleura, lung, pericardium, and heart.^{83,109} The relationship between the hepatic lesions and vessels such as the hepatic veins and inferior vena cava is well delineated on MRI.⁸³ The regions of fibrous and parasitic tissue are of low signal intensity on T1- and T2-weighted sequences and correspond to areas of nonenhancement on CT scans.⁸³ Small cystic extensions from the main lesion are shown as peripheral areas of increased signal on T2-weighted images and are thought to represent the active portions of the disease.⁸³ Large regions of necrosis do not have a characteristic signal pattern.⁸³ Calcifications display low signal but are more difficult to identify on MRI than on CT.⁸³

COMPLICATIONS

Rupture, the major complication of echinococcal disease, can be classified into three types: contained, when only the endocyst



Figure 88-14 Hydatid disease: MRI features. **A.** Axial gradient-echo T1-weighted image shows a hydatid cyst with a hypointense fibrous pericyst (arrow). The hydatid matrix has intermediate signal intensity, and peripheral daughter cysts that are hypointense relative to the matrix are seen. **B.** On an axial T2-weighted image, the matrix is hyperintense and the daughter cysts again are relatively hypointense. (From Mortelet, KJ, Segatto E, Ros PR: *The infected liver: Radiologic-pathologic correlation*. *RadioGraphics* 24:937–955, 2004.)

ruptures and the cyst contents are confined by the host-derived pericyst; communicating, when cyst contents escape into biliary or bronchial radicles that are incorporated into the pericyst; and direct, when both the endocyst and pericyst tear, spilling cyst contents into the pleural, peritoneal, or pericardial cavity.¹¹⁰

When cyst contents enter the biliary tract (see Fig. 88-12B and C), the cyst becomes echogenic. Intrabiliary hydatid material, including echogenic or nonechogenic daughter cysts and echogenic fragmented membranes, may fill the biliary system. Cyst–bile duct communication may be manifested as interruption of the cyst wall adjacent to a bile duct wall. On CT scans, there is interruption of the cyst wall and higher attenuation hydatid material in the biliary system. On MRI studies, cyst rupture is recognized as an area of discontinuity of the low-intensity wall.^{111–116} A fat–fluid level within hepatic hydatid cysts has been described on CT and MRI studies of two patients with communicating rupture of the cysts into the biliary tree.¹¹⁷ Laboratory analysis of the contents of the hydatid cysts revealed elevated levels of bile, confirming that the fat seen in the cysts on CT and MRI scans represented lipid material within bile.¹¹⁷

This intrabiliary hydatid material can lead to obstructive jaundice. Passage of hydatid sand or hydatid liquid can also lead to inflammation and spasm of the sphincter of Oddi.^{118–121} Until surgery can be performed, endoscopic retrograde sphincterotomy can be used as a temporizing measure to decompress the obstructed biliary system. Some 25% of cysts become infected and are manifested clinically as abscess.

If *E. multilocularis* is left untreated, the outcome is invariably fatal within 10 to 15 years as the cyst continues to slowly grow and destroy hepatic tissue.^{84,86–93} In some cases with Budd-Chiari syndrome or inferior vena cava thrombosis, death may be sudden due to embolic events to the heart or pulmonary

arteries.⁸⁴ Another serious complication is hemorrhage from esophageal varices secondary to portal hypertension. Metastasis to the brain is a less common cause of death in patients with *E. multilocularis*.⁸⁹

TREATMENT

Hepatic hydatid cysts require drainage because medical therapy with mebendazole and albendazole is usually ineffective. There are two surgical approaches: radical, in which a pericystectomy and hepatic resection are performed; and conservative, with injection of scolicalid agents followed by evacuation of the cyst, removal of the germinal lining and laminated membrane, and closure, capitonnage, drainage, or omentoplasty of the remaining cyst cavity. Surgical complications are high, including a 4% mortality rate and a 50% complication rate. The recurrence rate is high for the conservative approach, and both procedures require approximately 3 weeks of hospitalization.^{122,123}

Hydatid disease of the liver has been treated percutaneously in an effort to obviate surgery and its attendant morbidity and mortality. At one time, percutaneous drainage or even diagnostic aspiration of these cysts was discouraged because of potential complications, such as anaphylactic shock and spread of daughter cysts into the peritoneum. This has not proved to be the case, particularly when a transhepatic approach is used. A new cutting device has been described that can percutaneously extract laminated membranes and all daughter cysts with little chance of fluid leakage.^{124–128} A single aspiration and drainage procedure with this instrument resulted in successful evacuation of cyst contents in 90% of patients, with few major complications and no recurrence.¹²⁹

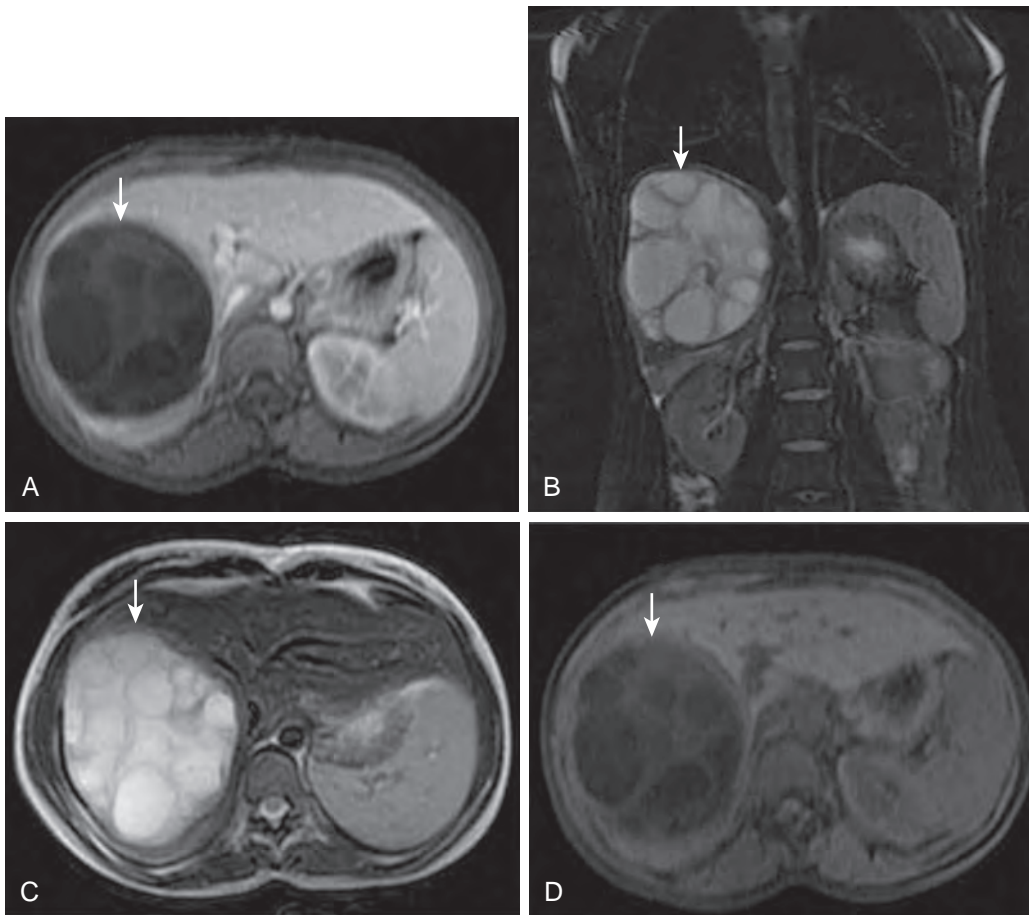


Figure 88-15 Hydatid disease: MRI features. A patient with hydatid cyst. On the coronal (A) and axial (B) T2-weighted images, the lesion (arrow) appears hyperintense and includes daughter cysts. On the T1-weighted image (C), the lesion (arrow) is hypointense and does not show any enhancement after the injection of gadolinium (D). Note that the daughter cysts are darker (arrow) on the T1-weighted images.

A number of scolical agents have been used; hypertonic (20%) saline and alcohol are effective percutaneous therapies for hepatic hydatid cysts and are associated with low complication rates.^{130,131} Percutaneous therapy should be attempted only with an accessible, dominant cyst that is truly cystic and uncomplicated. Infected cysts and cysts that communicate with the biliary system require surgical drainage (Fig. 88-16).¹³²

The treatment of choice for patients with *E. multilocularis* is complete excision with partial hepatectomy where possible.^{83,84,88,89} In patients with extensive disease, palliative procedures including hepaticojejunostomy, portosystemic shunts, and drainage of necrotic areas or abscesses in combination with benzimidazole therapy may be undertaken to prolong survival.^{84,88} Prolonged mebendazole therapy may slow disease progression and suppress metastasis.⁸⁷⁻⁸⁹ More recent treatment strategies include hepatectomy with orthotopic liver transplantation to effect a cure.^{83,84,86} However, the disease can recur after liver transplantation.⁸⁶

Fasciola hepatica

Fasciola hepatica is a trematode liver fluke. Contaminated water or vegetables are causes of human infestations.¹³³ First, the metacercariae encyst in the stomach; by perforating the duodenal wall, they migrate into the peritoneal cavity; and after perforating the hepatic capsule, they reach the liver parenchyma, where they browse for approximately 6 weeks.¹³³ As soon as the parasites spread into the biliary system, they start to mature into adult parasites and begin to produce eggs. CT

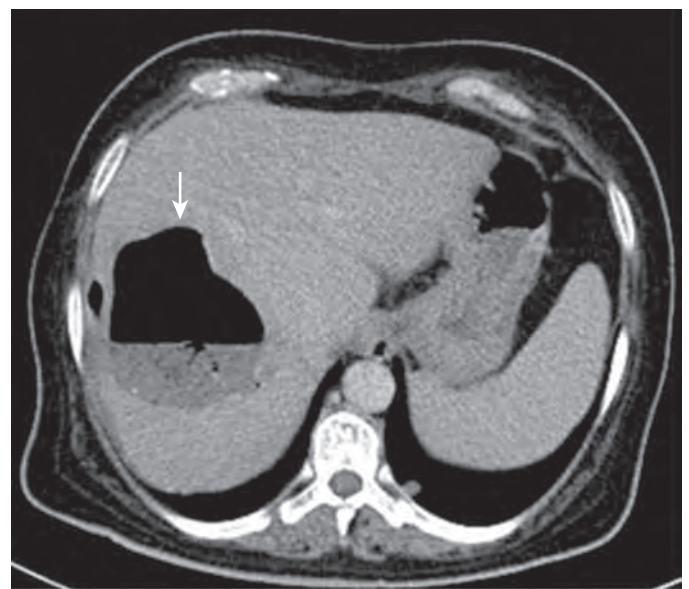


Figure 88-16 Hydatid disease: CT findings. A large infected hydatid cyst (arrow) that shows an air-fluid level on the contrast-enhanced CT image.

is the best imaging modality to detect fascioliasis, which typically is manifested as multiple clustered hypoattenuating nodules and multiple branching, hypoattenuating subcapsular peripheral lesions pointing toward the hilum of the liver (Fig. 88-17).¹³³

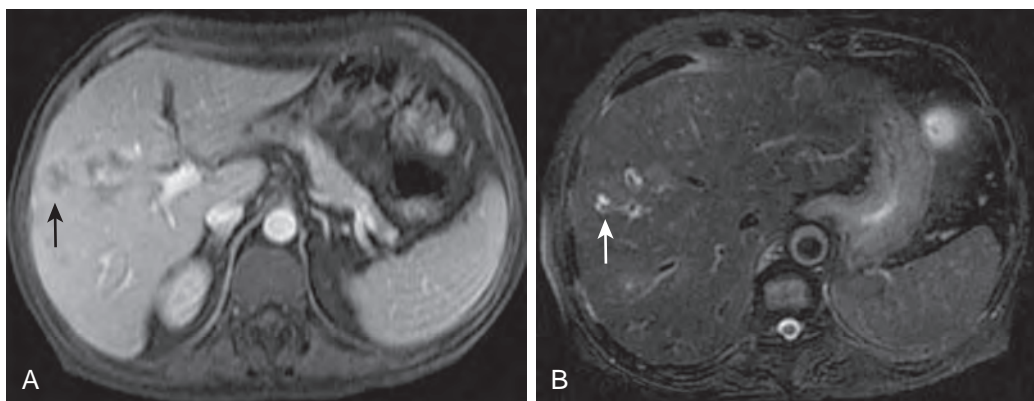


Figure 88-17 Fasciola hepatica: MRI findings. A patient with *Fasciola hepatica* (arrow). Note the branching subcapsular peripheral lesions on T2-weighted (A) and portal venous phase (B) images.

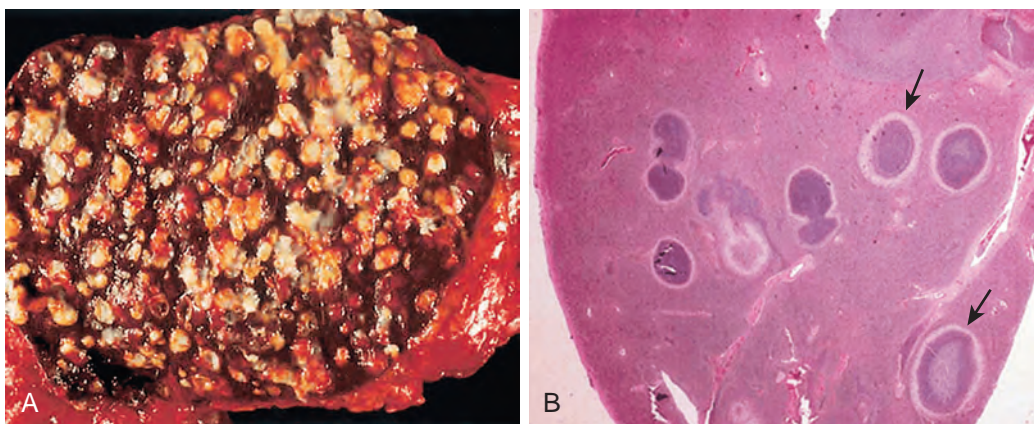


Figure 88-18 Candidiasis: pathology. A. Gross specimen of the spleen shows multiple small, white nodules representing involvement by candidiasis throughout the parenchyma. B. Low-power photomicrograph shows multiple candidiasis microabscesses with a peripheral zone of fibrosis and a central area of necrosis (arrows). (From Mortelet, KJ, Segatto E, Ros PR: *The infected liver: Radiologic-pathologic correlation*. RadioGraphics 24:937–955, 2004.)

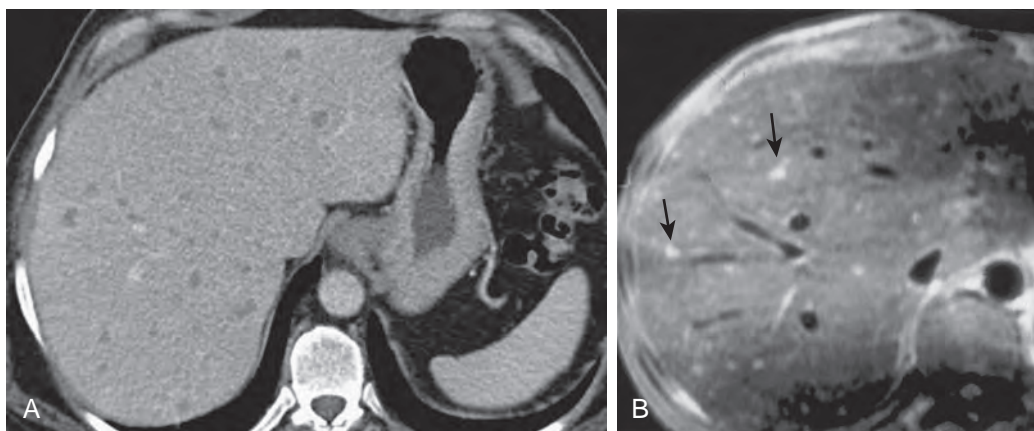


Figure 88-19 Candidiasis on CT and MRI. A. Contrast-enhanced CT scan of the liver shows multiple hypoattenuating microabscesses less than 1 cm in diameter disseminated throughout the hepatic parenchyma. B. Axial T1-weighted MR image reveals relatively hyperintense lesions less than 1 cm in diameter in the liver (arrows). (From Mortelet, KJ, Segatto E, Ros PR: *The infected liver: Radiologic-pathologic correlation*. RadioGraphics 24:937–955, 2004.)

Candidiasis and Fungal Infections

Candidiasis (Figs. 88-18 and 88-19) is the most frequently encountered systemic fungal infection in immunocompromised hosts. It is becoming more common with the acquired immunodeficiency syndrome (AIDS) epidemic and with

increasingly intensive chemotherapy. Indeed, hepatic candidiasis is found in 50% to 70% of patients with acute leukemia and 50% of those with lymphoma at the time of autopsy. Diagnosis is difficult on clinical grounds because blood cultures are positive in only 50% of affected patients, so cross-sectional imaging is necessary for diagnosis.¹³⁴⁻¹³⁶

On sonography, four major patterns of hepatic candidiasis are seen: wheel within a wheel, in which a peripheral zone surrounds an inner echogenic wheel, which in turn surrounds a central hypoechoic nidus that represents focal necrosis in which fungal elements are found early in the disease; bull's-eye, a 1- to 4-mm lesion with a hyperechoic center that surrounds a hypoechoic rim, present when the neutrophil count returns to normal; uniformly hypoechoic, the most common appearance attributable to progressive fibrosis; and echogenic, caused by scar formation.^{15,136-139} After antifungal therapy, the lesions increase in echogenicity and decrease in size, often disappearing altogether, although in some cases sonographic inhomogeneity of the liver may persist for up to 3 years after treatment.¹⁴⁰

On CT scans, the most common pattern is multiple small, rounded areas of decreased attenuation that may require both precontrast and postcontrast scans to be appreciated. Areas of scattered increased attenuation representing calcification can be seen on noncontrast scans. Periportal areas of increased attenuation, correlating with fibrosis, may be seen as well.¹⁴¹⁻¹⁴³

On the basis of available evidence, CT is more sensitive than ultrasound in detecting hepatic candidal lesions¹⁴⁴ (see Fig. 88-19). Although CT and ultrasound appearances may be suggestive of candidiasis, they are not specific, and a definitive diagnosis is necessary before treatment because antifungal drugs may have significant side effects. Percutaneous needle biopsy achieves a definitive diagnosis in the majority of cases.¹³⁴

On MRI, untreated nodules are minimally hypointense on T1-weighted pregadolinium and postgadolinium images and markedly hyperintense on T2-weighted images.¹ In the subacute presentation after treatment, lesions appear mildly to moderately hyperintense on T1- and T2-weighted images and also demonstrate enhancement after intravenous administration of contrast material. A dark ring is usually seen around these lesions with all sequences. Completely treated lesions are minimally hypointense on T1-weighted images, isointense to mildly hyperintense on T2-weighted images, and moderately hypointense on early postcontrast images. They become minimally hypointense in delayed phase images.^{145,146}

Candida microabscesses have been reported as cold lesions on both sulfur colloid and gallium scans.¹³⁸

Schistosomiasis

EPIDEMIOLOGY

Schistosomiasis is one of the most common and serious parasitic infections of humans. This disease affects 200 million people worldwide, and in endemic areas its prevalence is nearly 70%. Some 10% of patients in endemic areas develop hepatosplenic involvement. *Schistosoma japonicum* occurs in the coastal areas of China, Japan, Taiwan, and the Philippines. *Schistosoma mansoni* occurs in parts of Africa, in the Middle East and West Indies, and in the northern part of South America. *Schistosoma haematobium* is seen in North Africa, the Mediterranean, and southwest Asia.¹⁴⁷⁻¹⁴⁹

PATHOPHYSIOLOGY

The schistosomal larvae are shed by snails, the intermediate host, into fresh water (Fig. 88-20A). Human infection occurs

in the course of bathing in or wading through contaminated irrigation canals, streams, and ponds. The schistosomal cercariae penetrate intact skin or mucous membranes and then migrate through venules and lymphatics to the heart. They pass through the pulmonary circulation to enter the mesenteric circulation. All schistosomes die except those that enter the mesenteric arteries, where they pass through capillaries into the portal venous system and mature within intrahepatic portal venous radicles. The host responds to the ova with granulomatous inflammation, which becomes replaced by fibrous tissue, leading to periportal fibrosis. If the trematode infestation is sufficiently chronic and heavy, progressive intrahepatic portal vein occlusion, presinusoidal portal hypertension, varices, and splenomegaly result. Schistosomiasis is the most common cause of portal hypertension worldwide. These parasites (Fig. 88-20B) are also known as blood flukes, and the importance of their vascular location cannot be overemphasized.²¹

The life cycle is completed when the mature female worm, after living within the male in the portal vein for some 10 to 15 years, swims against blood flow to reach the venules of the urinary bladder (*S. haematobium*) or gut (*S. mansoni*, *S. japonicum*) to deposit eggs. The eggs pass through the wall of the intestine or bladder to release miracidia, which infect mollusks. Cercariae emerge after maturing in their intermediate host.

PATHOLOGY

In severe *S. mansoni* and *S. japonicum* infections, the liver is dark colored, showing a bumpy but not nodular surface that is distinct from the appearance of ordinary cirrhosis. Cut section reveals granulomas (Fig. 88-20C) with widespread periportal fibrosis beginning in the porta hepatis and extending peripherally. The intervening parenchyma, however, is not distorted by regenerative nodules. The fibrous triads simulate the cross section of a clay pipe stem. Some portal triads lack a perceptible vein, and latex casts demonstrate widespread distortion and blockage of the portal vascular bed. These features account for the portal hypertension. Jaundice and hepatocellular necrosis usually ensue after variceal hemorrhage.^{146,148}

CLINICAL FINDINGS

Schistosomiasis is an insidious and chronic disease. Because hepatocellular necrosis occurs late in its course, patients may seek medical attention for portal hypertension and variceal bleeding. Patients with *S. haematobium* infection, which affects the liver less severely, typically present with hematuria resulting from urinary tract involvement.²¹

RADIOLOGIC FINDINGS

Conventional Studies

Calcification is usually too faint to be appreciated on abdominal plain radiographs. Splenomegaly is commonly seen, and barium studies may reveal esophageal and gastric varices.

Ultrasound

In patients with severe hepatic disease, thick, densely echogenic bands replace the portal triads. They sometimes reach a

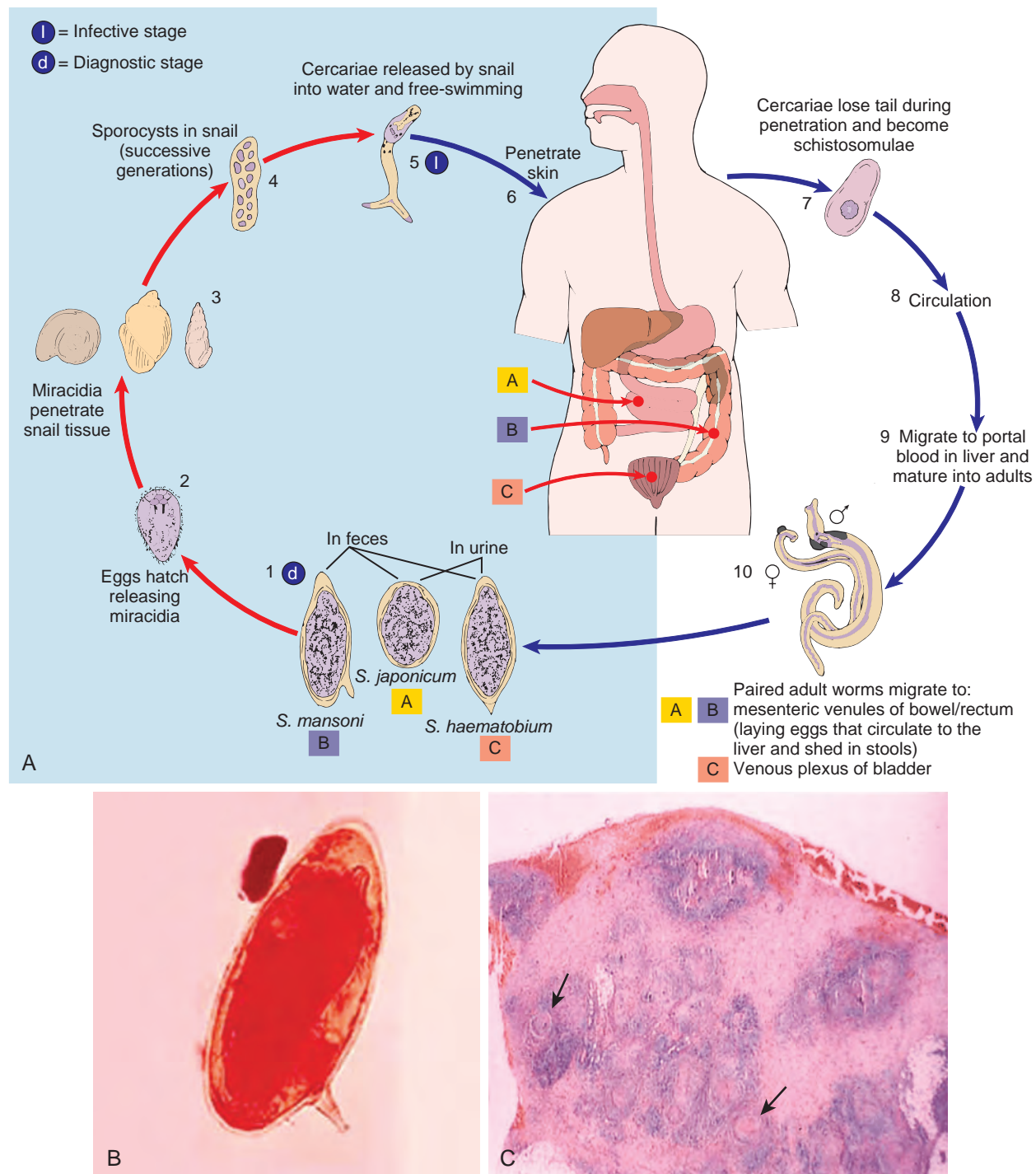


Figure 88-20 Schistosomiasis: pathologic findings. A. Life cycle. Eggs are eliminated with feces or urine (1). Under optimal conditions, the eggs hatch and release miracidia (2), which swim and penetrate specific snail intermediate hosts (3). The stages in the snail include two generations of sporocysts (4) and the production of cercariae (5). On release from the snail, the infective cercariae swim, penetrate the skin of the human host (6), and shed their forked tail, becoming schistosomula (7). The schistosomula migrate through several tissues and stages to their residence in the veins (8, 9). Adult worms in humans reside in the mesenteric venules in various locations, which at times seem to be specific for each species (10). For instance, *S. japonicum* is more frequently found in the superior mesenteric veins draining the small intestine (A), and *S. mansoni* occurs more often in the superior mesenteric veins draining the large intestine (B). However, both species can occupy either location, and they are capable of moving between sites, so it is not possible to state unequivocally that one species occurs only in one location. *S. haematobium* most often occurs in the venous plexus of bladder (C), but it can also be found in the rectal venules. The females (7–20 mm; males slightly smaller) deposit eggs in the small venules of the portal and perivesical systems. The eggs are moved progressively toward the lumen of the intestine (*S. mansoni* and *S. japonicum*) and of the bladder and ureters (*S. haematobium*) and are eliminated with feces or urine, respectively (1). Pathology of *S. mansoni* and *S. japonicum* schistosomiasis includes Katayama fever, presinusoidal egg granulomas, Symmers pipestem periportal fibrosis, portal hypertension, and occasional embolic egg granulomas in brain or spinal cord. Pathology of *S. haematobium* schistosomiasis includes hematuria, scarring, calcification, squamous cell carcinoma, and occasional embolic egg granulomas in brain or spinal cord. **B.** *S. mansoni* egg (iodine stain). **C.** Low-power photomicrograph of a liver specimen reveals calcified eggs (arrows) and fibrosis in the subcapsular region. (A source: Centers for Disease Control and Prevention. <http://www.cdc.org/pdfs/schistosomiasis/biology.html>. C from Morteale, KJ, Segatto E, Ros PR: The infected liver: Radiologic-pathologic correlation. RadioGraphics 24:937–955, 2004.)

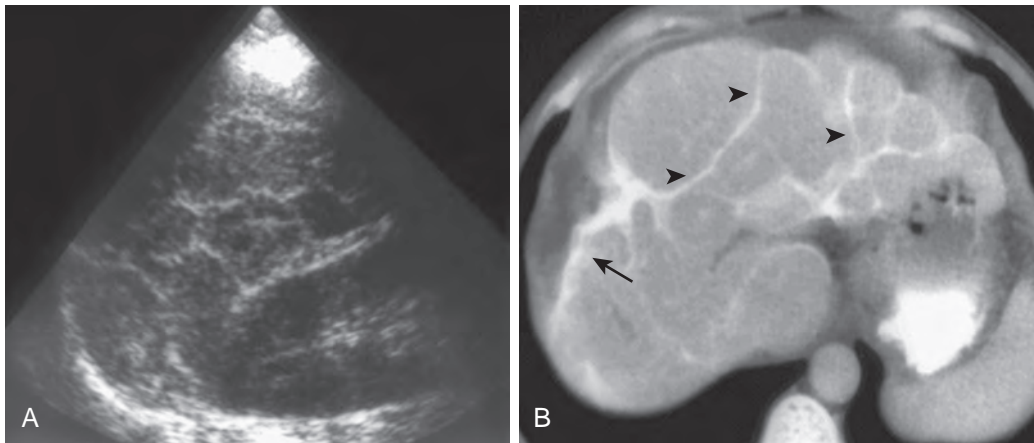


Figure 88-21 Schistosomiasis on CT and ultrasound. Hepatic *Schistosoma japonicum* infection. **A.** Sonogram demonstrates thick and densely echogenic bands producing a network pattern. **B.** Contrast-enhanced CT scan demonstrates capsular calcification (arrow) and gross septations (arrowheads).

thickness of 2 cm, radiating from the porta hepatis to the periphery. When scanning is performed perpendicular to the triad, rounded foci of echogenic material with a hypoechoic rim can be identified. This produces a “network” pattern with echogenic septa outlining polygonal areas of relatively normal liver (Fig. 88-21A).¹⁵⁰ A “bird’s claw” appearance is present at bifurcating points. Early, the liver is enlarged, but as periportal fibrosis progresses, it becomes contracted and the features of portal hypertension (varices, splenomegaly, ascites) become more apparent.¹⁵¹

Computed Tomography

Peripheral hepatic or capsular calcification is the hallmark of *S. japonicum* infection (Fig. 88-21B). The liver also shows gross septations that contain numerous calcified *Schistosoma* eggs resulting in bands of calcification described as a “turtle back” appearance.^{152,153} Prominent periportal low-density areas may also be present. There is an increased incidence of hepatocellular carcinoma in these livers.¹⁵³ In patients with acute schistosomiasis (Katayama syndrome), multiple hypodense nodules may develop.¹⁵³

S. mansoni infection is manifested as low-density, rounded foci with linear branching bands that encompass the portal tracts. These fibrotic bands sometimes show enhancement with contrast material but usually do not calcify.^{137,150}

Magnetic Resonance Imaging

On MRI, the septa are of low signal on T1-weighted scans and are hyperdense on T2-weighted images and reveal enhancement on postgadolinium images.³⁰ The septal calcifications are depicted less well on MRI than on CT.^{150,154}

Angiography

Angiography shows the hemodynamic changes of presinusoidal portal hypertension: normal hepatic venous outflow, decreased portal blood flow, and compensatory increased hepatic arterial flow. Wedged hepatic venous pressure is normal or only slightly elevated compared with portal hypertension resulting from alcoholic cirrhosis.

TREATMENT

Praziquantel, an isoquinoline derivative, and oxamniquine are effective against schistosomal infestation. Colchicine, an antiparasitic agent, has shown encouraging results in the treatment of schistosome-induced hepatic fibrosis.²

Pneumocystis carinii (*Pneumocystis jiroveci*) Infection

Pneumocystis carinii (*P. jiroveci*) is the most common cause of opportunistic infection in patients with AIDS. Nearly 80% of AIDS patients are affected, and extrapulmonary dissemination is becoming increasingly common.^{21,155}

P. jiroveci infection of the liver can be manifested sonographically as diffuse, tiny, nonshadowing echogenic foci or extensive replacement of normal liver parenchyma by echogenic clumps of dense calcification. This pattern, although suggestive, has also been reported in *Mycobacterium avium-intracellulare* and cytomegalovirus infection.¹⁵⁶ On CT scans, these regions are first hypodense but then become characteristically calcified. The calcifications may be punctate, nodular, or rimlike.¹⁵⁷⁻¹⁵⁹

Tuberculosis

Tuberculosis is an infectious disease in which different ways of liver involvement may be seen. Being one of the most common infectious diseases, tuberculosis has two forms of presentation, miliary and local. The local form has two subdivisions as nodular tuberculosis (tuberculoma or abscess) and hepatobiliary tuberculosis.^{1,160,161} Imaging techniques are most frequently not adequate to detect miliary tuberculosis, in which hepatomegaly is usually the only radiologic finding. Tuberculomas may be manifested as hypoechoic round masses at ultrasound, nonenhancing hypodense lesions at CT, and hypointense lesions on T1-weighted images and hypointense to isointense lesions on T2-weighted images at MRI.¹⁶¹

REFERENCES

- Mortele KJ, Segatto E, Ros PR: The infected liver: Radiologic-pathologic correlation. *Radiographics* 24:937-955, 2004.
- Kim AY, Chung RT: Bacterial, parasitic, and fungal infections of the liver, including liver abscess. In Feldman M, Friedman LS, Sleisenger MH, editors: *Sleisenger & Fordtran's Gastrointestinal and Liver Disease*, ed 9, Philadelphia, 2010, WB Saunders, pp 1351-1370.
- Doyle DJ, Hanbridge AE, O'Malley ME: Imaging of hepatic infections. *Clin Radiol* 61: 737-748, 2006.
- Mohan S, Talwar N, Chaudhary A, et al: Liver abscess: A clinicopathological analysis of 82 cases. *Int Surg* 91:228-233, 2006.
- Lamps LW, Washington K: Acute and chronic hepatitis. In Odze RD, Goldblum JR, Crawford JM, editors: *Surgical Pathology of the GI Tract, Liver, Biliary Tract, and Pancreas*, Philadelphia, 2004, Saunders, pp 783-810.
- Albrecht H: Bacterial and miscellaneous infections of the liver. In Zakim D, Boyer TD, editors: *Hepatology*, ed 4, Philadelphia, 2003, WB Saunders, pp 1109-1124.
- Canto MIF: Bacterial infections of the liver and biliary system. In Surawicz C, Owen RL, editors: *Gastrointestinal and Hepatic Infections*, Philadelphia, 1995, WB Saunders, pp 355-390.
- Eisenberg PJ, Mueller PR, Rattner DW: Hepatic abscess. In Pitt HA, Carr-Locke DL, Ferrucci JT, editors: *Hepatobiliary and Pancreatic Disease*, Boston, 1995, Little, Brown, pp 81-90.
- Cook GC: Hepatic involvement in bacterial, protozoan, and helminthic infections. *Curr Opin Gastroenterol* 8:458-465, 1992.
- Block M: Abscesses of the liver (other than amebic). In Haubrich WS, Schaffner F, Berk JE, editors: *Bockus Gastroenterology*, ed 5, Philadelphia, 1995, WB Saunders, p 2405.
- Mueller PR, White EM, Glass-Royal M, et al: Infected abdominal tumors: Percutaneous catheter drainage. *Radiology* 173:627-629, 1989.
- Allard JC, Kuligowska E: Percutaneous treatment of an intrahepatic abscess caused by a penetrating duodenal ulcer. *J Clin Gastroenterol* 95:603-606, 1987.
- Kandel G, Marion NE: Pyogenic liver abscess: New concepts of an old disease. *Am J Gastroenterol* 79:65-71, 1984.
- Altmeir WA, Schowenger DT, Whiteley DH: Abscess of the liver: Surgical considerations. *Arch Surg* 101:258-267, 1982.
- Ralls PW: Inflammatory disease of the liver. *Clin Liver Dis* 6:203-225, 2002.
- Ochsner A, Debaquey M, Murray S: Pyogenic liver abscess. II: An analysis of 47 cases with review of the literature. *Am J Surg* 40:292-319, 1938.
- Huang C-J, Pitt HA, Lipsett PA, et al: Pyogenic hepatic abscess: Changing trends over 42 years. *Ann Surg* 223:600-609, 1996.
- Robert JH, Mirescu D, Ambrosetti P, et al: Critical review of the treatment of pyogenic hepatic abscess. *Surg Gynecol Obstet* 174:97-102, 1992.
- Kanner R, Weinfeld A, Tedesco FJ: Hepatic abscess: Plain film findings as an early aid to diagnosis. *Am J Gastroenterol* 71:432-437, 1979.
- Wilson SR, Withers CE: The liver. In Rumack CM, Wilson SR, Charboneau JW, editors: *Diagnostic Ultrasound*, ed 3, Philadelphia, 2003, Elsevier Mosby, pp 77-146.
- Sherlock S, Dooley J: *Diseases of the Liver and Biliary System*, ed 9, Oxford, 1993, Blackwell Scientific, pp 471-502.
- Newlin N, Silver TM, Stuck KJ, et al: Ultrasonic features of pyogenic liver abscesses. *Radiology* 139:155-159, 1991.
- Kuligowska E, Connors SK, Shapiro JH: Liver abscess: Sonography in diagnosis and treatment. *AJR Am J Roentgenol* 138:253-257, 1982.
- Halvorsen RA, Korobkin M, Foster WL, et al: The variable appearance of hepatic abscesses. *AJR Am J Roentgenol* 141:941-944, 1984.
- Rubinson HA, Isikoff MB, Hill MC: Diagnostic imaging of hepatic abscesses: A retrospective analysis. *AJR Am J Roentgenol* 135:735-740, 1980.
- Fawcett HD, Lantieri RL, Frankel A, McDougall IR: Differentiating hepatic abscess from tumor: Combined ¹¹¹In white blood cell and ^{99m}Tc liver scans. *AJR Am J Roentgenol* 135:53-56, 1980.
- Zaman A, Bramley PN, Wyatt J, et al: Hodgkin's disease presenting as liver abscesses. *Gut* 32:959-962, 1991.
- Moreno AJ, Battafarano NJ, Nelson PM, et al: Multiple anaerobic hepatic abscesses demonstrated on hepatobiliary scintigraphy. *Clin Nucl Med* 11:204-205, 1986.
- Mendez RJ, Schiebler ML, Outwater EK, et al: Hepatic abscesses: MR imaging findings. *Radiology* 190:431-436, 1994.
- Balci NC, Sirvanci M: MR imaging of infective liver lesions. *Magn Reson Imaging Clin N Am* 10:121-135, 2002.
- Heiken JP, Menias CD, Elsayes K: Liver. In Lee JKT, Sagal SS, Stanley RI, et al, editors: *Computed Body Tomography With MRI Correlation*, ed 4, Philadelphia, 2006, Lippincott Williams & Wilkins, pp 829-930.
- Gabata T, Kadoya M, Matsui O, et al: Dynamic CT of hepatic abscesses: Significance of transient segmental enhancement. *AJR Am J Roentgenol* 176:675-679, 2001.
- Jeffrey RB, Tolentino CS, Chang FC, et al: CT of small pyogenic hepatic abscesses: The cluster sign. *AJR Am J Roentgenol* 151:487-489, 1988.
- Kim SB, Je BK, Lee KY, et al: Computed tomographic differences of pyogenic liver abscesses caused by *Klebsiella pneumoniae* and non-*Klebsiella pneumoniae*. *J Comput Assist Tomogr* 31:59-65, 2007.
- Robert JH, Mirescu D, Ambrosetti P, et al: Critical review of the treatment of pyogenic hepatic abscess. *Surg Gynecol Obstet* 174:97-102, 1992.
- Rajak CL, Gupta S, Jain S, et al: Percutaneous treatment of liver abscesses: Needle aspiration versus catheter drainage. *AJR Am J Roentgenol* 170:1035-1039, 1998.
- Bret PM, Ritchie RG: Percutaneous drainage of liver abscesses and fluid collections. In Kadir S, editor: *Current Practice of Interventional Radiology*, Philadelphia, 1991, BC Decker, pp 481-486.
- Do H, Lambiase RE, Deyoe L, et al: Percutaneous drainage of hepatic abscesses: Comparison of results in abscesses with and without intrahepatic biliary communication. *AJR Am J Roentgenol* 157:1209-1212, 1991.
- Gatewood LH, Collins TL, Yrizarry JM: Percutaneous management of multiple liver abscesses. *AJR Am J Roentgenol* 139:390-392, 1982.
- Bernardino ME, Berkman WA, Plemmons M, et al: Percutaneous drainage of multiseptated hepatic abscess. *J Comput Assist Tomogr* 8:38-41, 1984.
- Johnson RD, Mueller PR, Ferrucci JT, et al: Percutaneous drainage of pyogenic liver abscesses. *AJR Am J Roentgenol* 144:463-467, 1985.
- Fernandez MDP, Murphy FB: Hepatic biopsies and fluid drainages. *Radiol Clin North Am* 29:1311-1328, 1991.
- Sheinfeld AM, Steiner AE, Rivkin LB, et al: Transcutaneous drainage of hepatic, intraabdominal, and mediastinal abscesses guided by computerized axial tomography. Successful alternative to open drainage. *Am J Surg* 145: 120-125, 1983.
- Romano G, Agrusa A, Frazzetta G, et al: Laparoscopic drainage of liver abscess: Case report and literature review. *G Chir* 34:180-182, 2013.
- Gerzof SG, Johnson WC, Robbins AH, et al: Intrahepatic pyogenic abscess treatment by percutaneous drainage. *Am J Surg* 149:487-494, 1985.
- Maher JA, Reynolds TB, Yellin AE: Successful medical treatment of pyogenic liver abscess. *Gastroenterology* 77:618-622, 1979.
- Bergamini TM, Larson GM, Malagoni MA, et al: Liver abscess: Review of a 12-year experience. *Am Surg* 53:596-599, 1987.
- Giorgio A, Tarantino L, Mariniello N, et al: Pyogenic liver abscesses: 13 years of experience in percutaneous needle aspiration with US guidance. *Radiology* 195:122-124, 1995.
- Yu SCH, Lo RHG, Kan PS, et al: Pyogenic liver abscess: Treatment with needle aspiration. *Clin Radiol* 52:912-916, 1997.
- Reed SL: Amebiasis: An update. *Clin Infect Dis* 14:385-393, 1992.
- Moenroe LS: Gastrointestinal parasites. In Haubrich WS, Schaffner F, Berk JE, editors: *Bockus Gastroenterology*, ed 5, Philadelphia, 1995, WB Saunders, pp 3113-3198.
- Desoubreux G, Chaussade H, Thellier M, et al: Unusual multiple large abscesses of the liver: Interest of the radiological features and the real-time PCR to distinguish between bacterial and amebic etiologies. *Pathog Glob Health* 108:53-57, 2014.
- Choudhuri G, Rangan M: Amebic infection in humans. *Indian J Gastroenterol* 31:153-162, 2012.
- Cevallos AM, Farthing MJG: Parasitic infections of the gastrointestinal tract. *Curr Opin Gastroenterol* 9:96-102, 1993.
- Remedios PA, Colletti PM, Ralls PW: Hepatic amebic abscess: Cholescintigraphic rim enhancement. *Radiology* 160:395-398, 1986.
- Mokhtari M, Kumar PV: Amebic liver abscess. *Acta Cytol* 58:225-228, 2014.
- McDougall IR: The appearance of amebic abscess of liver on In-111-leukocyte scan. *Clin Nucl Med* 6:67-69, 1981.
- Ralls PW, Colletti PM, Quinn MF, et al: Sonographic findings in hepatic amebic abscess. *Radiology* 145:123-126, 1982.
- Missalek W: Ultrasonography in the diagnosis of amoebic liver abscess and its complications. *Trop Doct* 22:59-63, 1992.
- Withers CE, Wilson SR: The liver. In Rumack CM, Wilson SR, Charboneau JW, editors: *Diagnostic Ultrasound*, ed 2, St Louis, 1998, Mosby-Year Book, pp 87-154.

61. Ralls PW, Meyers HJ, Lapin SA, et al: Gray-scale ultrasonography of hepatic amebic abscesses. *Radiology* 132:125–129, 1979.
62. Ralls PW, Quinn MF, Boswell WP, et al: Patterns of resolution in successfully treated hepatic amebic abscess: Sonographic evaluations. *Radiology* 149:541–543, 1983.
63. Fujihara T, Nagai Y, Kuba T, et al: Amebic liver abscess. *J Gastroenterol* 31:659–663, 1996.
64. Catalano O, Sandomenico F, Raso MM, Siani A: Low mechanical index contrast-enhanced sonographic findings of pyogenic hepatic abscesses. *AJR Am J Roentgenol* 182:447–450, 2004.
65. Radin DR, Ralls PW, Colletti PM, et al: CT of amebic liver abscess. *AJR Am J Roentgenol* 150:1297–1301, 1988.
66. Verhaegen F, Poey C, Lebras Y, et al: CT findings in diagnosis and treatment of amebic liver abscesses. *J Radiol* 77:23–28, 1996.
67. Ralls PW, Henley DS, Colletti PM, et al: Amebic liver abscess: MR imaging. *Radiology* 165:801–804, 1987.
68. Elizondo G, Weissleder R, Stark DD, et al: Amebic liver abscess: Diagnosis and treatment evaluation with MR imaging. *Radiology* 165:795–800, 1987.
69. Greaney GC, Reynolds TB, Donovan AJ: Ruptured amebic liver abscess. *Arch Surg* 120:555–561, 1985.
70. Tandon N, Karak PK, Mukhopadhyay S, et al: Amoebic liver abscess: Rupture into retroperitoneum. *Gastrointest Radiol* 16:240–242, 1991.
71. Filice C, DiPerri G, Strosselli M, et al: Outcome of hepatic amebic abscesses managed with three different therapeutic strategies. *Dig Dis Sci* 37:240–247, 1992.
72. DiazGranados CA, Duffus WA, Albrecht H: Parasitic diseases of the liver. In Zakim D, Boyer TD, editors: *Hepatology*, ed 4, Philadelphia, 2003, WB Saunders.
73. Ralls PW, Barnes PF, Johnson MB, et al: Medical treatment of hepatic amebic abscess: Rare need for percutaneous drainage. *Radiology* 165:805–807, 1987.
74. vanSonnenberg E, Mueller PR, Schiffman HR, et al: Intrahepatic amebic abscesses: Indications for and results of percutaneous catheter drainage. *Radiology* 156:631–635, 1985.
75. Nordestgaard AG, Stapleford L, Worthen N, et al: Contemporary management of amoebic liver abscess. *Am Surg* 58:315–320, 1992.
76. Ken JG, vanSonnenberg E, Casola G, et al: Perforated amebic liver abscesses: Successful percutaneous treatment. *Radiology* 170:195–197, 1989.
77. Van Allen RJ, Katz MD, Johnson MB, et al: Uncomplicated amoebic liver abscess: Prospective evaluation of percutaneous therapeutic aspiration. *Radiology* 183:827–830, 1982.
78. Giorgio A, Amoroso P, Francica G, et al: Echo-guided percutaneous puncture: A safe and valuable therapeutic tool for amebic liver abscess. *Gastrointest Radiol* 13:336–340, 1988.
79. Ammann RW, Eckert J: Cestodes-echinococcus. *Gastroenterol Clin North Am* 25:655–689, 1996.
80. Bakoyiannis A, Delis S, Triantopoulou C, Dervenis C: Rare cystic liver lesions: A diagnostic and managing challenge. *World J Gastroenterol* 19:7603–7719, 2013.
81. Rinaldi F, Brunetti E, Neumayr A, et al: Cystic echinococcosis of the liver: A primer for hepatologists. *World J Hepatol* 6:293–305, 2014.
82. Didier D, Weiler S, Rohmer P, et al: Hepatic alveolar echinococcosis: Correlative US and CT study. *Radiology* 154:179–186, 1985.
83. Claudon M, Bessieres M, Regent D, et al: Alveolar echinococcosis of the liver: MR findings. *J Comput Assist Tomogr* 14:608–614, 1990.
84. Bresson-Hadni S, Franza A, Miquet JP, et al: Orthotopic liver transplantation for incurable alveolar echinococcosis of the liver: Report of 17 cases. *Hepatology* 13:1061–1070, 1991.
85. Rozanes I, Acunas B, Celik L, et al: CT in lobar atrophy of the liver caused by alveolar echinococcosis. *J Comput Assist Tomogr* 16:216–218, 1992.
86. Filippou D, Tselepis D, Filippou G, et al: Advances in liver echinococcosis: Diagnosis and treatment. *Clin Gastroenterol Hepatol* 5:152–159, 2007.
87. Maoz D, Greif F, Chen J: Operative treatment of hepatic hydatid cysts: A single center experience in Israel, a nonendemic country. *ISRN Surg* 2013:276807, 2013.
88. Gourgoutis S, Stratopoulos C, Moustafellos P, et al: Surgical techniques and treatment for hepatic hydatid cysts. *Surg Today* 37:389–395, 2007.
89. Lewall DB, Nyak P: Hydatid cysts of the liver: Two cautionary signs. *Br J Radiol* 71:37–41, 1998.
90. Lewall DB: Hydatid disease: Biology, pathology, imaging and classification. *Clin Radiol* 53:863–874, 1998.
91. Friedman AC, Frazier S, Hendrix TM, et al: Focal disease. In Friedman AC, Dachman AH, editors: *Radiology of the Liver, Biliary Tract, Pancreas, and Spleen*, St. Louis, 1994, Mosby-Year Book, pp 169–328.
92. Gharbi HA, Hassine W, Brauner MW, et al: Ultrasound examination of hydatid liver. *Radiology* 139:459–463, 1981.
93. Mendez Montero JV, Arrazola Garcia JA, Lopez Lafuente JL, et al: Fat-fluid level in hepatic hydatid cyst: A new sign of rupture into the biliary tree? *AJR Am J Roentgenol* 167:91–94, 1996.
94. Bezzi M, Teggi A, De Rosa F, et al: Abdominal hydatid disease: US findings during medical treatment. *Radiology* 162:91–95, 1987.
95. Choji K, Fujita N, Chen M, et al: Alveolar hydatid disease of the liver: Computed tomography with transabdominal ultrasound with histopathologic correlation. *Clin Radiol* 46:97–103, 1992.
96. Gürses N, Sungur R, Gürses B, et al: Ultrasound diagnosis of liver hydatid disease. *Acta Radiol* 28:161–163, 1987.
97. Ceramanai M, Benci A, Maestrini R, et al: Abdominal cystic hydatid disease (CHD): Classification of sonographic appearance and response to treatment. *J Clin Ultrasound* 24:491–500, 1996.
98. Lewall DB, McCorkell SJ: Hepatic echinococcal cysts: Sonographic appearance and classification. *Radiology* 155:773–775, 1985.
99. Kornaros SE, Aboul-Nour TA: Frank intrabiliary rupture of hydatid hepatic cyst: Diagnosis and treatment. *J Am Coll Surg* 183:466–470, 1996.
100. Czermak BV, Unsinn KM, Gotwald T, et al: *Echinococcus multilocularis* revisited. *AJR Am J Roentgenol* 176:1207–1212, 2001.
101. Pandolfo I, Blandino G, Scribano E, et al: CT findings in hepatic involvement by *Echinococcus granulosus*. *J Comput Assist Tomogr* 8:839–845, 1984.
102. Murphy BJ, Casillas J, Ros PR, et al: The CT appearance of cystic masses of the liver. *Radiographics* 9:307–322, 1989.
103. Kalovidouris A, Pissiotis C, Pontifex G, et al: CT characterization of multivesicular hydatid cysts. *J Comput Assist Tomogr* 8:839–845, 1984.
104. Acunas B, Rozanes I, Acunas G, et al: Hydatid cyst of the liver: Identification of detached cyst lining on CT scans obtained after cyst puncture. *AJR Am J Roentgenol* 156:751–752, 1991.
105. Gonzalez LR, Marcos J, Illanas M, et al: Radiologic aspects of hepatic echinococcosis. *Radiology* 130:21–27, 1979.
106. Scherer U, Weinzerl M, Sturm R, et al: Computed tomography of hydatid disease of the liver: A report on 13 cases. *J Comput Assist Tomogr* 2:612–617, 1978.
107. Lewall DB, Bailey TM, McCorkell SJ: Echinococcal matrix: Computed tomographic, sonographic, and pathologic correlation. *J Ultrasound Med* 5:33–35, 1986.
108. Cogley JR, Miller FH: MR imaging of benign focal liver lesions. *Radiol Clin North Am* 52:657–682, 2014.
109. Proietti S, Abdelmoumene A, Genevay M, et al: Echinococcal cyst. *Radiographics* 24:861–865, 2004.
110. Lewall DB, McCorkell SJ: Rupture of echinococcal cysts: Diagnosis classification, and clinical implications. *AJR Am J Roentgenol* 146:391–394, 1986.
111. Marti-Bonmati L, Serrano FM: Complications of hepatic hydatid cysts: Ultrasound, computed tomography, and magnetic resonance diagnosis. *Gastrointest Radiol* 15:119–125, 1990.
112. Frei P, Misselwitz B, Prakash MK, et al: Late biliary complications in human alveolar echinococcosis are associated with high mortality. *World J Gastroenterol* 20:5881–5888, 2014.
113. Marti-Bonmati L, Menor F, Ballesta A: Hydatid cyst of the liver: Rupture into the biliary tree. *AJR Am J Roentgenol* 150:1051–1053, 1988.
114. Camunez F, Simo G, Robledo R, et al: Ultrasound diagnosis of ruptured hydatid cyst of the liver with biliary obstruction. *Gastrointest Radiol* 11:330–333, 1986.
115. Cockeram AW, Baker RJ, Sullivan SN: The echogenic echinococcal cyst. A diagnostic trap. *J Clin Gastroenterol* 8:100–102, 1986.
116. Grande D, Ruiz JC, Elizagary E, et al: Hepatic echinococcosis complicated with transphrenic migration and bronchial fistula: CT demonstration. *Gastrointest Radiol* 15:115–118, 1990.
117. Mendez Montero J, Arrazola Garcia J, Lopez J, et al: Fat-fluid level in hepatic hydatid cyst: A new sign of rupture into the biliary tree? *AJR Am J Roentgenol* 167:91–94, 1996.
118. Hesse AA, Nouri A, Hassan HS, Hashish AA: Parasitic infestations requiring surgical interventions. *Semin Pediatr Surg* 21:142–150, 2012.
119. Alkharawi MA, Yasawy MI, Mohamed ARE: Endoscopic management of biliary hydatid disease: Report on six cases. *Endoscopy* 23:278–281, 1992.
120. Magistrelli P, Masetti R, Coppola R, et al: Value of ERCP in the diagnosis and management of pre- and postoperative biliary complications in hydatid disease of the liver. *Gastrointest Radiol* 14:315–320, 1989.
121. Zargar SA, Khuroo MS, Khan BA, et al: Intra-biliary rupture of hepatic hydatid cyst: Sonographic and cholangiographic appearances. *Gastrointest Radiol* 17:14–45, 1992.

122. Langer JC, Rose DB, Keystone JS, et al: Diagnosis and management of hydatid disease of the liver. *Ann Surg* 199;412-417, 1984.
123. Ozmen V, Igci A, Kebudi A, et al: Surgical treatment of hepatic hydatid disease. *Can J Surg* 35:423-427, 1992.
124. Saremi F: Percutaneous drainage of hydatid cysts: Use of a new cutting device to avoid leakage. *AJR Am J Roentgenol* 158:83-85, 1992.
125. Men S, Hekimoglu B, Yucesoy C, et al: Percutaneous treatment of hepatic hydatid cysts: An alternative to surgery. *AJR Am J Roentgenol* 172:83-89, 1999.
126. Akhan O, Dincer A, Gököz A, et al: Percutaneous treatment of abdominal hydatid cysts with hypertonic saline and alcohol. *Invest Radiol* 28:121-127, 1993.
127. Khuroo MS, Zargar SA, Mahajan R: *Echinococcus granulosus* cysts in the liver: Management with percutaneous drainage. *Radiology* 180: 141-145, 1991.
128. Acunas B, Rozanes I, Celik L, et al: Purely cystic hydatid disease of the liver: Treatment with percutaneous aspiration and injection of hypertonic saline. *Radiology* 182:541-543, 1992.
129. Saremi F, McNamara TO: Hydatid cysts of the liver: Long-term results of percutaneous treatment using a cutting instrument. *AJR Am J Roentgenol* 165:1163-1167, 1995.
130. Simonetti G, Profili S, Sergiacomi GL, et al: Percutaneous treatment of hepatic cysts by aspiration and sclerotherapy. *Cardiovasc Intervent Radiol* 16:81-84, 1993.
131. Ustunsoz B, Akhan O, Kamiloglu MA, et al: Percutaneous treatment of hydatid cysts of the liver: Long-term results. *AJR Am J Roentgenol* 172:91-96, 1999.
132. Giorgio A, Tarantino L, Francica G, et al: Unilocular hydatid liver cysts: Treatment with US-guided, double percutaneous aspiration and alcohol injection. *Radiology* 184:705-710, 1992.
133. Catalano OA, Sahani DV, Forcione DG, et al: Biliary infections: Spectrum of imaging findings and management. *Radiographics* 29: 2059-2080, 2009.
134. Thaler M, Pastakia B, Shawker TH, et al: Hepatic candidiasis in cancer patients: The evolving picture of the syndrome. *Ann Intern Med* 108:88-100, 1988.
135. Francis IR, Glazer GM, Amendola MA, et al: Hepatic abscesses in the immunocompromised patient: Role of CT in detection, diagnosis, management, and follow-up. *Gastrointest Radiol* 11:257-262, 1986.
136. Gordon SC, Watts JC, Vener RJ, et al: Focal hepatic candidiasis with perihepatic adhesions: Laparoscopic and immunohistologic diagnosis. *Gastroenterology* 88:214-217, 1990.
137. Pastakia B, Shawker TH, Thaler M, et al: Hepatosplenic candidiasis: Wheels within wheels. *Radiology* 166:417-421, 1988.
138. Miller JH, Greenfield LD, Wald BR: Candidiasis of the liver and spleen in childhood. *Radiology* 142:375-380, 1982.
139. Callen PW, Filly RA, Marcus FS: Ultrasonography and computed tomography in the evaluation of hepatic microabscesses in the immunosuppressed patient. *Radiology* 136: 433-434, 1980.
140. Gorg C, Weide R, Schwerek WB, et al: Ultrasound evaluation of hepatic and splenic microabscesses in the immunocompromised patient: Sonographic patterns, differential diagnosis, and follow-up. *J Clin Ultrasound* 22:525-529, 1994.
141. Shirkhoda A, Lopez-Berestein G, Holbert JM, et al: Hepatosplenic fungal infection: CT and pathologic evaluation after treatment with liposomal amphotericin B. *Radiology* 159:349-353, 1986.
142. Shirkhoda A: CT findings in hepatosplenic and renal candidiasis. *J Comput Assist Tomogr* 11:795-798, 1987.
143. Berlow ME, Spirt BA, Weil L: CT follow-up of hepatic and splenic fungal microabscesses. *J Comput Assist Tomogr* 8:42-45, 1984.
144. Anttila VJA, Ruutu P, Bondestam S, et al: Hepatosplenic yeast infection in patients with acute leukemia: A diagnostic problem. *Clin Infect Dis* 18:979-981, 1994.
145. Semelka RC, Shoenut JP, Greenberg HM, et al: Detection of acute and treated lesions of hepatosplenic candidiasis: Comparison of dynamic contrast-enhanced CT and MR imaging. *J Magn Reson Imaging* 2:341-345, 1992.
146. Semelka RC, Kelekis N, Sallah S, et al: Hepatosplenic fungal disease: Diagnostic accuracy and spectrum of appearances on MR imaging. *AJR Am J Roentgenol* 169:1311-1316, 1997.
147. Marcial MA, Marcial-Rojas RA: Parasitic diseases of the liver. In Schiff L, Schiff ER, editors: *Diseases of the Liver*, ed 6, Philadelphia, 1987, JB Lippincott, pp 1171-1196.
148. Palmer PES: Schistosomiasis. *Semin Roentgenol* 33:6-25, 1998.
149. Patel SA, Castillo DF, Hibbeln JF, et al: Magnetic resonance imaging appearance of hepatic schistosomiasis, with ultrasound and computed tomography correlation. *Am J Gastroenterol* 88:113-116, 1993.
150. Monzawa S, Uchiyama G, Ohtomo K, et al: Schistosomiasis japonica of the liver: Contrast-enhanced CT findings in 113 patients. *AJR Am J Roentgenol* 161:323-327, 1993.
151. Pereira LM, Domingues AL, Spinelli V, et al: Ultrasonography of the liver and spleen in Brazilian patients with hepatosplenic schistosomiasis and cirrhosis. *Trans R Soc Trop Med Hyg* 92:639-642, 1998.
152. Araki T, Hayakawa K, Okada J, et al: Hepatic schistosomiasis japonica identified by CT. *Radiology* 157:757-760, 1985.
153. Cheung H, Lai YM, Loke TK, et al: The imaging diagnosis of hepatic schistosomiasis japonicum sequelae. *Clin Radiol* 51:51-55, 1996.
154. Monzawa S, Ohtomo K, Oba H, et al: Septa in the liver of patients with chronic hepatic schistosomiasis japonica: MR appearance. *AJR Am J Roentgenol* 162:1347-1351, 1994.
155. Koziel MJ, Peters MG: Viral hepatitis in HIV infection. *N Engl J Med* 356:1445-1454, 2007.
156. Mathieson JR, Smith FJ: Hepatobiliary and pancreatic ultrasound in AIDS. In Reeders JWAJ, Mathieson JR, editors: *AIDS Imaging: A Practical Approach*, Philadelphia, 1998, WB Saunders, pp 188-202.
157. Sansom H, Seddon B, Padley SP: Clinical utility of abdominal CT scanning in patients with HIV disease. *Clin Radiol* 52:698-703, 1997.
158. Radin DR: Hepatopancreatic and biliary imaging in AIDS: Computed tomography. In Reeders JWAJ, Mathieson JR, editors: *AIDS Imaging: A Practical Approach*, Philadelphia, 1998, WB Saunders, pp 203-213.
159. Gore RM, Miller FH, Yaghamai V: Acquired immunodeficiency syndrome (AIDS) of the abdominal organs: Imaging features. *Semin Ultrasound CT MR* 9:175-189, 1998.
160. Sonika U, Kar P: Tuberculosis and liver disease: Management issues. *Trop Gastroenterol* 33: 102-106, 2012.
161. Shastri M, Kausadikar S, Jariwala J, et al: Isolated hepatic tuberculosis. *Australas Med J* 7:247-250, 2014.

Diffuse Liver Disease

TARA MORGAN | ALIYA QAYYUM | RICHARD M. GORE

CHAPTER OUTLINE

Hepatic Steatosis

Clinical Findings
Pathologic Findings
Radiologic Findings

Hepatitis

Viral Hepatitis
Alcoholic Hepatitis

Toxin- and Drug-Induced Liver Disease

Chemotherapy Toxicity
Amiodarone Toxicity

Radiation-Induced Liver Disease

Clinical Findings
Pathologic Findings
Radiologic Findings

Hemosiderosis and Hemochromatosis

Clinical Findings
Pathologic Findings
Radiologic Findings

Glycogen Storage Disease

Clinical and Pathologic Findings
Radiologic Findings

Amyloidosis

Clinical and Pathologic Findings
Radiologic Findings

Wilson's Disease

Clinical and Pathologic Findings
Radiologic Findings

Gaucher's Disease

Clinical and Pathologic Findings
Radiologic Findings

Sarcoidosis

Clinical and Pathologic Findings
Radiologic Findings

Biliary Hamartomas

Clinical and Pathologic Findings
Radiologic Findings

Primary Biliary Cirrhosis

Clinical and Pathologic Findings
Radiologic Findings

Secondary Biliary Cirrhosis

Acquired Immunodeficiency Syndrome

Clinical Findings
Pathologic Findings
Radiologic Findings

Cirrhosis

Epidemiology
Pathophysiology
Portal Hypertension
General Radiologic Findings: Cirrhosis
Ultrasound: Cirrhosis
Computed Tomography: Cirrhosis
Magnetic Resonance Imaging: Cirrhosis
Ultrasound: Portal Hypertension
Computed Tomography: Portal Hypertension
Magnetic Resonance Imaging: Portal Hypertension
Transjugular Intrahepatic Portosystemic Shunt

The liver has quite accurately been called the custodian of the *milieu intérieur*, and as such, it is vulnerable to a variety of metabolic, vascular, toxic, infectious, and neoplastic insults. Diffuse liver disease can be diagnostically challenging because of nonspecific and overlapping clinical signs and symptoms or even asymptomatic disease. The ability to assess liver and spleen size and the presence of ascites is limited on physical examination. Liver function tests also lack diagnostic specificity, are affected by nonhepatic factors, and in general poorly correlate with physiologic hepatic function.¹⁻⁴

Imaging plays a critical role in the diagnosis and treatment of diffuse liver disease by detecting its presence, determining its distribution and severity, and identifying associated complications, such as cirrhosis, portal hypertension, and malignant disease. Dramatic advances, particularly in magnetic

resonance imaging (MRI), have led to novel techniques to noninvasively diagnose and to characterize patterns of diffuse hepatic disease.

Hepatic Steatosis

The excessive accumulation of intracellular fat within hepatocytes, known as hepatic steatosis, occurs as a metabolic complication of a variety of hepatic exposures (Table 89-1). Common causes include alcohol abuse and viral hepatitis (discussed separately), obesity and metabolic disorders, toxins, human immunodeficiency virus (HIV) infection, genetic lipodystrophies, and chemotherapy. This abnormal intracellular accumulation of fat within hepatocytes is now recognized as an important causative factor in liver injury. Although it is initially reversible,

TABLE 89-1 Causes of Hepatic Steatosis

TOXIN OR MEDICATION RELATED
Alcohol
Chemotherapy
Carbon tetrachloride
Corticosteroids
Phosphorus
Tetracycline
Reye's syndrome
INFECTIOUS
Viral hepatitis
Tuberculosis
METABOLIC
Obesity
Malnutrition
Total parenteral nutrition
Small bowel bypass surgery
Glycogen storage disease
Hyperlipidemia
CHRONIC DISEASE
Congestive heart failure
Inflammatory bowel disease
Cystic fibrosis
Obstructive sleep apnea
OTHER
Pregnancy
Trauma

the process may also progress and can result in cirrhosis and increased risk for hepatocellular carcinoma (HCC).⁵⁻¹⁰

Nonalcoholic fatty liver disease (NAFLD) is a disease spectrum extending from simple steatosis to the more severe form with inflammation and fibrosis known as nonalcoholic steatohepatitis (NASH), the result of hepatic metabolic disturbance in the absence of alcohol abuse. Steatosis is the hallmark feature of NAFLD. NASH is established histopathologically by the presence of steatosis with evidence of hepatitis (centrilobular inflammation, hepatocyte ballooning degeneration, and spotty necrosis) and variable degrees of fibrosis (stages 0-3). Advanced or stage 4 fibrosis is indicative of cirrhosis. Severity of NASH is based on grading of inflammation and different stages of fibrosis.¹¹ As a result of the current epidemic of obesity and metabolic syndrome, NAFLD is reported to occur in 20 to 80 million Americans and is the most common chronic liver disease in the United States. Recent research suggests that NAFLD is an independent risk factor for cardiovascular disease and contributes to the development of diabetes by impairment of insulin regulation within the liver.¹²⁻¹⁴

The development of HCC is common in steatohepatitis; up to 7% of patients with NAFLD-related cirrhosis develop HCC within 10 years. The population of patients with chronic liver disease is growing, particularly from NAFLD, and it is anticipated to become an increasingly significant burden on the health care system as well as the number one cause of cirrhosis and HCC.⁹

CLINICAL FINDINGS

Hepatic steatosis from any cause is often clinically asymptomatic, which clinically increases the challenge for early

intervention and treatment of the patient. In NAFLD, liver chemistry values are often normal. On physical examination, liver size may be normal or slightly enlarged and potentially difficult to evaluate in the obese patient. Alcohol-related steatosis can be manifested with vague right upper quadrant pain, with or without hepatomegaly, and is more often associated with liver function test abnormalities. One third of patients with alcoholism, however, have a fatty liver and are asymptomatic. Hepatic steatosis is also commonly seen in oncology patients as a result of chemotherapy administration, and its presence can impair imaging detection of concurrent metastatic disease. Hepatic steatosis with concomitant viral hepatitis can accelerate cellular damage and also decreases the effectiveness of antiviral therapies. Less commonly, hepatic steatosis can develop acutely secondary to pregnancy, carbon tetrachloride exposure, or binge drinking and can be manifested with jaundice, acute hepatic failure, or encephalopathy.^{2,6,15}

Hepatic steatosis is a potentially reversible disease treatable by removal of the insulting agent such as alcohol, other drug cessation, or treatment of infection. NAFLD can be treated by weight loss; however, it is often difficult for patients to achieve the recommended amount (5%-10% of body weight)¹⁶ without intervention, such as gastric bypass or banding surgery.^{17,18} Bariatric surgery patients have an incidental rate of 91% with NAFLD and 37% with steatohepatitis.¹⁹ Cellular damage from inflammation and the development of fibrosis and cirrhosis are irreversible, however, and the definitive treatment to prevent liver failure is transplantation. The early reversibility of this disease obviates the need for effective screening and treatment in a largely asymptomatic population.

PATHOLOGIC FINDINGS

Fat is deposited in the liver as a result of a number of metabolic derangements. These include increased hepatic synthesis of fatty acids (alcohol), decreased hepatic oxidation or utilization of fatty acids (carbon tetrachloride, high-dose tetracycline), impaired release of hepatic lipoproteins, and excessive mobilization of fatty acids from adipose tissue (starvation, steroids, alcohol).^{2,20,21}

On pathologic examination, lipid accumulates within the cytoplasm of the hepatocyte, predominantly in the centrilobular zone (Fig. 89-1). As lipid accumulation progresses, these small vacuoles coalesce, creating large, clear, macrovesicular spaces that peripherally displace the cell nucleus and virtually transform the hepatocyte into a lipocyte. Retention of water and protein adds to cellular enlargement. The liver may weigh 4 to 6 kg (normal, 1.5-2.5 kg) and at gross pathologic examination has a soft, yellow, greasy cut surface.²²

Segmental areas of fatty infiltration of the liver may develop as a result of a variety of traumatic and ischemic insults that reduce the amount of nutrients and insulin normally necessary to produce glycogen, culminating in a “metabolic infarct” of the involved region. Fatty replacement occurs where glycogen is depleted from the liver. This occurs primarily in regions where portal venous blood is reduced secondary to tumor, Budd-Chiari syndrome, or vascular thrombus. There is a difference in hormonal balance between the right and left lobes; pancreatic and splenic venous blood contains higher concentrations of insulin, and glycogen preferentially supplies the left portal vein.^{2,21,22} Accordingly, fat often infiltrates the right lobe of the liver before involvement of the left.

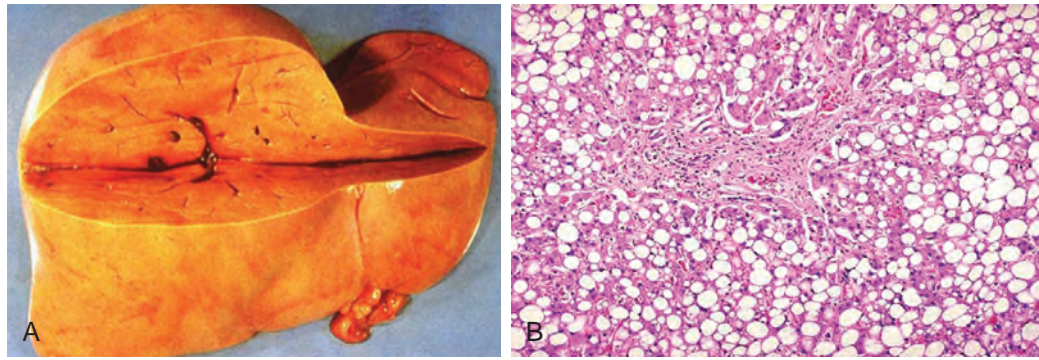


Figure 89-1 Hepatic steatosis: pathologic findings. **A.** Gross specimen shows a yellow, greasy liver that has undergone diffuse fatty metamorphosis. **B.** Pathologic specimen shows lipid accumulation within the hepatocytes, primarily in the centrilobular zone.

Focal fat sparing of the parenchyma in an otherwise fatty liver can also present as a diagnostic challenge. This occurs in characteristic locations, including the inferior medial portion of the liver, along the gallbladder fossa adjacent to the interlobar fissure, subcapsular portions of the liver, and adjacent to the porta hepatis. Direct vascular communications to the portal system from aberrant gastric venous flow or accessory cystic veins are found in certain areas of these spared regions, and it is postulated that these areas are perfused by systemic blood rather than by splanchnic venous blood from the portal veins. The posterior aspect of segment IV, a common area to be spared in diffuse fatty infiltration, has been shown to have aberrant direct gastric venous flow when focal fat sparing is present. Consequently, a “third blood supply” to these areas may help spare them the adverse effects of toxic agents entering through the portal circulation.^{23,24}

RADIOLOGIC FINDINGS

Several major patterns of fat deposition can be visualized at cross-sectional imaging: diffuse deposition; focal deposition and focal sparing; multifocal deposition; perivascular deposition; and subcapsular deposition.²⁵ Diffuse deposition is the most common pattern and is associated with homogeneous involvement and hepatomegaly. Focal deposition or diffuse deposition with focal sparing is a less common pattern that characteristically occurs adjacent to the falciform ligament, fissure for the ligamentum venosum, porta hepatis, and gallbladder fossa. This probably relates to variant arterial supply or venous drainage as described before. A true mass can be differentiated from focal regions of fat deposition and focal sparing because these occur in characteristic locations and typically have a geographic shape (but may appear nodular), poorly delineated margins, and, importantly, absence of mass effect on blood vessels.²⁵ Multifocal deposition of fat may simulate true masses such as metastases. In these patients, differentiation can be made by measurement of the tissue density on computed tomography (CT) or specific sequences performed with MRI to evaluate for the presence of fat. With perivascular fat deposition, halos of fat surround the hepatic or portal veins. This fat is tramlike or tubular in appearance when the course is in the imaging plane and ringlike or round for vessels with a course perpendicular to the imaging plane.²⁵ Subcapsular fat deposition can be seen in patients with renal failure and insulin-dependent diabetes in which insulin is added to the peritoneal

dialysate. The dialysate exposes the subcapsular hepatocytes to a higher concentration of insulin than in the remainder of the liver and promotes the esterification of free fatty acids into triglycerides. This in turn results in subcapsular deposition of fat.²⁵

Plain Radiographs

Plain film radiography is relatively insensitive to the presence of fat in the liver unless marked degrees of infiltration are present. In these cases, the liver may appear hyperlucent and blend imperceptibly with the right retroperitoneal fat stripe. This produces a visible interface between the combined radiolucency of the fatty liver and flank stripe and the relatively radiodense abdominal musculature. A fat-fluid interface may be present if the patient has ascites. The outer wall of the gut may produce a viscus wall sign as the soft tissue density of the bowel wall is contrasted with the fatty liver. These changes, however, are most commonly seen in pediatric patients.

Ultrasound

Ultrasound is the most common modality used to evaluate the liver and is often the first imaging examination performed. It is low in cost, fast, and readily available. The positive predictive value for the presence of steatosis is low, however, at 62% to 77%.^{26,27} It is also operator dependent and difficult in obese patients, who represent a large population of those patients requiring assessment.

On sonographic evaluation, in diffuse hepatic steatosis, there is increased hepatic echogenicity roughly proportional to the histopathologic grade of steatosis²⁸⁻³¹ (Fig. 89-2). Sonographic changes also tend to correlate with the severity of biochemical and clinical dysfunction. The key ultrasound findings are accentuation of the brightness of parenchymal echoes and an increased number of echogenic foci resulting from the proliferation of fat-nonfat interfaces. These small echogenic foci increase attenuation of the ultrasound beam, resulting in poor visualization of deep hepatic structures and of the hepatic venous system.

Normally, four to six portal and hepatic veins are seen per longitudinal section of the right lobe. With fatty infiltration, fewer vessels are seen, and the smaller vascular structures may be nonvisible. This dropout of vessels is due to physical vascular compression by parenchymal swelling, decreased sound penetration, and loss of contrast between echogenic vascular walls

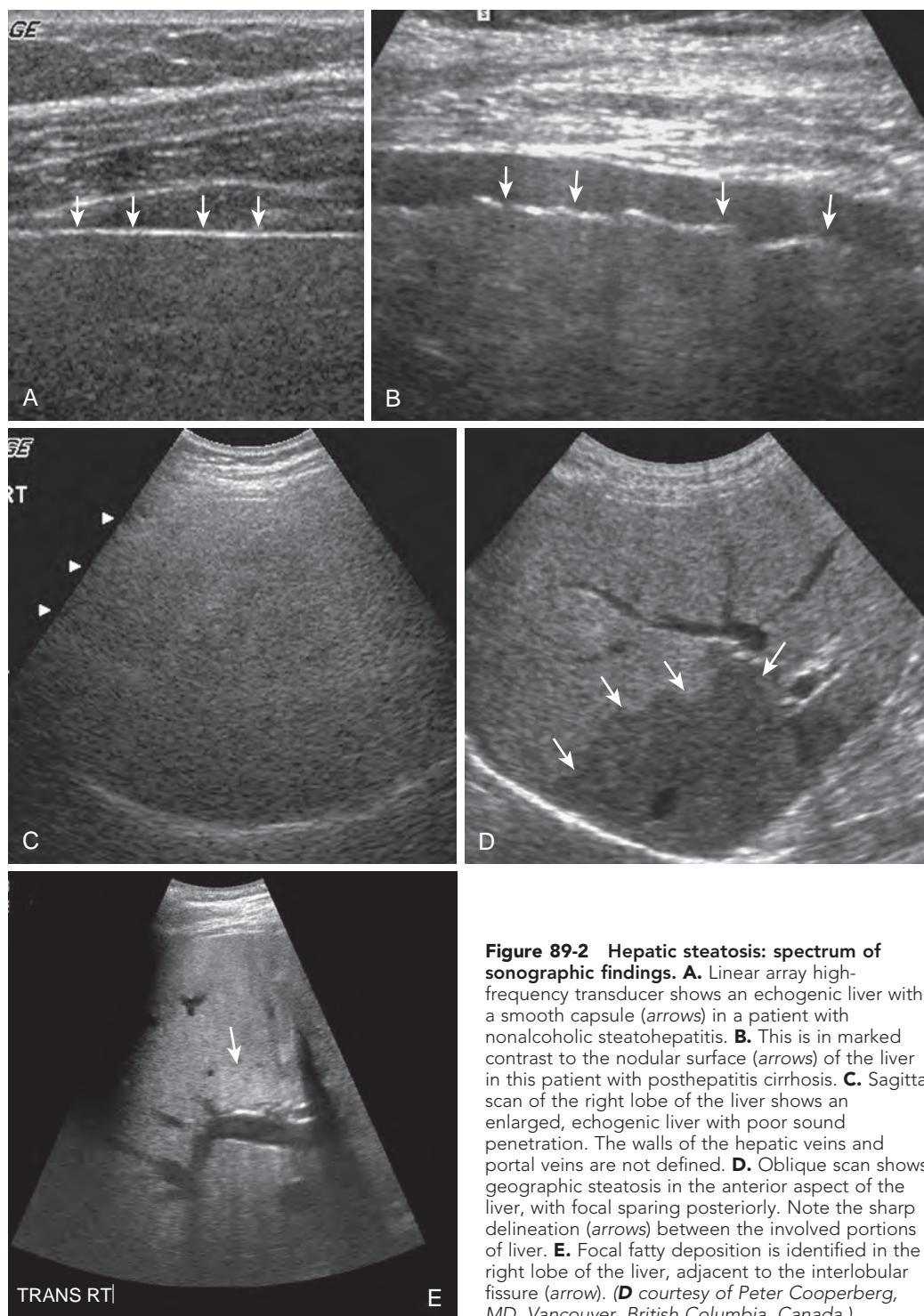


Figure 89-2 Hepatic steatosis: spectrum of sonographic findings. **A.** Linear array high-frequency transducer shows an echogenic liver with a smooth capsule (arrows) in a patient with nonalcoholic steatohepatitis. **B.** This is in marked contrast to the nodular surface (arrows) of the liver in this patient with posthepatitis cirrhosis. **C.** Sagittal scan of the right lobe of the liver shows an enlarged, echogenic liver with poor sound penetration. The walls of the hepatic veins and portal veins are not defined. **D.** Oblique scan shows geographic steatosis in the anterior aspect of the liver, with focal sparing posteriorly. Note the sharp delineation (arrows) between the involved portions of liver. **E.** Focal fatty deposition is identified in the right lobe of the liver, adjacent to the interlobular fissure (arrow). (*D* courtesy of Peter Cooperberg, MD, Vancouver, British Columbia, Canada.)

and abnormally increased echogenicity of the surrounding parenchyma.²⁸⁻³⁰

Four sonographic patterns of focal fatty infiltration have been described: (1) hyperechoic nodule, (2) multiple confluent hyperechoic lesions, (3) hypoechoic skip nodules, and (4) irregular hyperechoic and hypoechoic areas. On occasion, a focal area of liver parenchyma may be spared from fatty metamorphosis and appear as an ovoid, spherical, or sheetlike hypoechoic mass in an otherwise echogenic liver. The characteristic

location, lack of mass effect on surrounding vessels, straight linear interface between normal and fatty parenchyma, and increased echogenicity of the liver compared with the cortex of the right kidney are useful diagnostic criteria. Hepatic hemangiomas, most often sonographically hyperechoic, in the presence of fat may appear hypoechoic compared with the adjacent liver and simulate a suspicious mass. Focal fatty infiltration in an otherwise normal-appearing liver may also produce a hyperechoic space-occupying mass. An angular or interdigitating

geometric margin, when present, is characteristic of focal fat.²⁸⁻³¹ Hepatic steatosis and fibrosis appear similar on ultrasound and often coexist. Differentiation of hepatic steatosis from a mass or other liver pathologic process may necessitate confirmation with CT or MRI, both of which have an increased sensitivity.

Technical considerations are important in the sonographic diagnosis of focal fat. The operator should take care not to erroneously change the time-gain-compensation curve, which can cause fatty parenchyma to have normal rather than increased echogenicity, whereas the spared, normal liver appears abnormally hypoechoic, simulating focal disease.

Computed Tomography

CT is an imaging technique that is also fast and widely available (Fig. 89-3). It is a strong diagnostic tool for hepatic steatosis because of the excellent correlation between the hepatic parenchymal CT attenuation value and the amount of hepatic triglycerides found on liver biopsy specimens.^{23,24}

On non-contrast-enhanced scans, the normal liver appears homogeneous with an attenuation value ranging from 50 to 70 Hounsfield units (HU), which is 8 to 10 HU greater than the attenuation of the spleen.^{23,24} The diffusely steatotic liver has a reduced attenuation value of less than 40 HU and appears and measures less dense than the spleen. The accumulation of other substances, such as iron, copper, glycogen, drugs (including amiodarone and gold therapy), and even cirrhosis or edema, can increase the attenuation value of the liver and underestimate the presence of fat. CT is also insensitive for mild steatosis, which makes it a poor screening tool for early disease. In a study of potential liver donors, unenhanced CT was able to provide an accurate diagnosis of macrovesicular steatosis of 30% or greater.^{23,24} A meta-analysis from 2011 compared CT with histopathologic examination with an overall sensitivity of 46.1% to 77%.³²

The rapid intravenous administration of contrast medium causes transiently increased attenuation of the spleen in comparison with the liver secondary to differences in vascularity that vary with rate of contrast agent administration and scan acquisition time, particularly early (<100 seconds) after the infusion, which can mimic the presence of fat in a normal liver.³³ Hepatic steatosis can be suggested on postcontrast images, with confirmation needed, preferably, on noncontrast or delayed phase postcontrast imaging. A recent publication on assessment of hepatic steatosis with contrast-enhanced CT found this technique 100% specific but only 60.5% sensitive.³³

In patients with NASH, the mean liver-to-spleen attenuation ratio is 0.66.^{23,24} The craniocaudal span of the liver has a mean of 21.4 cm; hepatomegaly is present in 92% of patients.^{23,24} The caudate lobe-to-left lobe ratio is usually normal (mean, 0.43), as is the preportal space (mean, 4.5 mm). Mildly prominent lymph nodes are present in the porta hepatis in 58.3% of patients. In mild but visible steatosis, the diagnosis can be made by comparing the relative CT attenuation of the liver and spleen, which appear and measure nearly equal. In more severe steatosis, the liver appears less dense than the spleen as well as the portal and hepatic veins, simulating the appearance of intravascular contrast material on a noncontrast examination.^{23,24}

Hepatic steatosis is manifested with a wide spectrum of CT appearances (see Fig. 89-3). Although diffuse parenchymal involvement is commonly seen, similar to the ultrasound appearance, fat may also be deposited in a focal, lobar,

segmental, or nonpattern-like distribution. Fatty infiltration of the liver can obscure the detection of focal liver lesions, such as neoplasm or abscess, by lowering the background liver attenuation to a level similar to that of an otherwise hypoattenuating mass or fluid collection.

When fatty infiltration is lobar, segmental, or wedge shaped, differentiation from other focal hepatic disease is straightforward. In such cases, it usually has a straight-line margin, typically extending to the liver capsule without associated bulging of the contour to suggest an underlying mass. When the steatosis is focal or nodular, differentiation from metastatic disease can be challenging. Absolute attenuation values are affected by multiple parameters other than fat as previously described and alone are not diagnostically reliable. The previously mentioned differentiating features of focal fat, including characteristic location, lack of contour abnormality, and normal course of the hepatic vessels, are helpful and are only rarely simulated in metastatic tumor lesions. On occasion, discrete focal areas of fatty replacement have a central core of normal-appearing tissue, the reverse of the typical tumor necrosis pattern.^{23,24}

Because of its unique ability to characterize the presence of fat, MRI is often required. It is the most reliable diagnostic tool in differentiating any geographic pattern of hepatic steatosis or fatty sparing from metastatic disease.³⁴

Magnetic Resonance Imaging

MRI is the most sensitive modality for hepatic steatosis and has the highest correlation with histopathologic evaluation with a sensitivity of 76.1% to 95.3%.³² In addition, MRI can be used to quantify the amount of fat present. Severity of liver fat or steatosis is categorized by a 4-point grading system for histopathologic liver fat of 0 to 3, representing less than 5%, 6% to 33%, 34% to 66%, and more than 66%, respectively.³⁵ The grading system incorporates the accepted normal value of liver fat, which is less than 5%. Limitations of MRI include increased cost, longer time to be performed, and less widespread availability. MRI also requires the patient's cooperation, such as the ability to lie still and breath-hold.

Proton chemical shift imaging, also termed opposed-phase gradient-echo imaging, is a rapidly acquired, high-resolution, and commonly used sequence to confirm the presence of microscopic fat within multiple organs including the liver, kidney, and adrenal gland (Fig. 89-4A, B). This technique capitalizes on the difference in precession frequency between fat and water protons (3.7 ppm). Imaging is performed when their signals are additive (in-phase) and opposite or subtractive (opposed-phase). The presence of water alone in a solid organ will have the same signal intensity on both the in-phase and opposed-phase images. When fat and water are present, signal will be lost in the corresponding area on the opposed-phase image only because of cancellation of the contribution of signal from both water and fat in opposite phases or direction.³⁶ At 1.5T, water and fat are in-phase every 4.6 ms (2.3 ms at 3T), with signal acquired at 4.6 ms, 9.2 ms, 13.4 ms, and so on (2.3 ms, 4.6 ms, 6.9 ms, and so on at 3T). Opposed-phase imaging occurs at 2.3 ms and every subsequent interval of 4.6 ms (6.9 ms, 11.5 ms, and so on). At 3T, opposed-phase imaging starts at 1.15 ms and is performed at every multiple of 2.3 ms (3.5 ms, 5.8 ms, and so on). A fat signal fraction can be calculated to quantify fat by the equation $(IP - OP)/(2IP)$, where IP is the signal of the liver with in-phase divided by the signal of the spleen with in-phase and OP is the signal of the

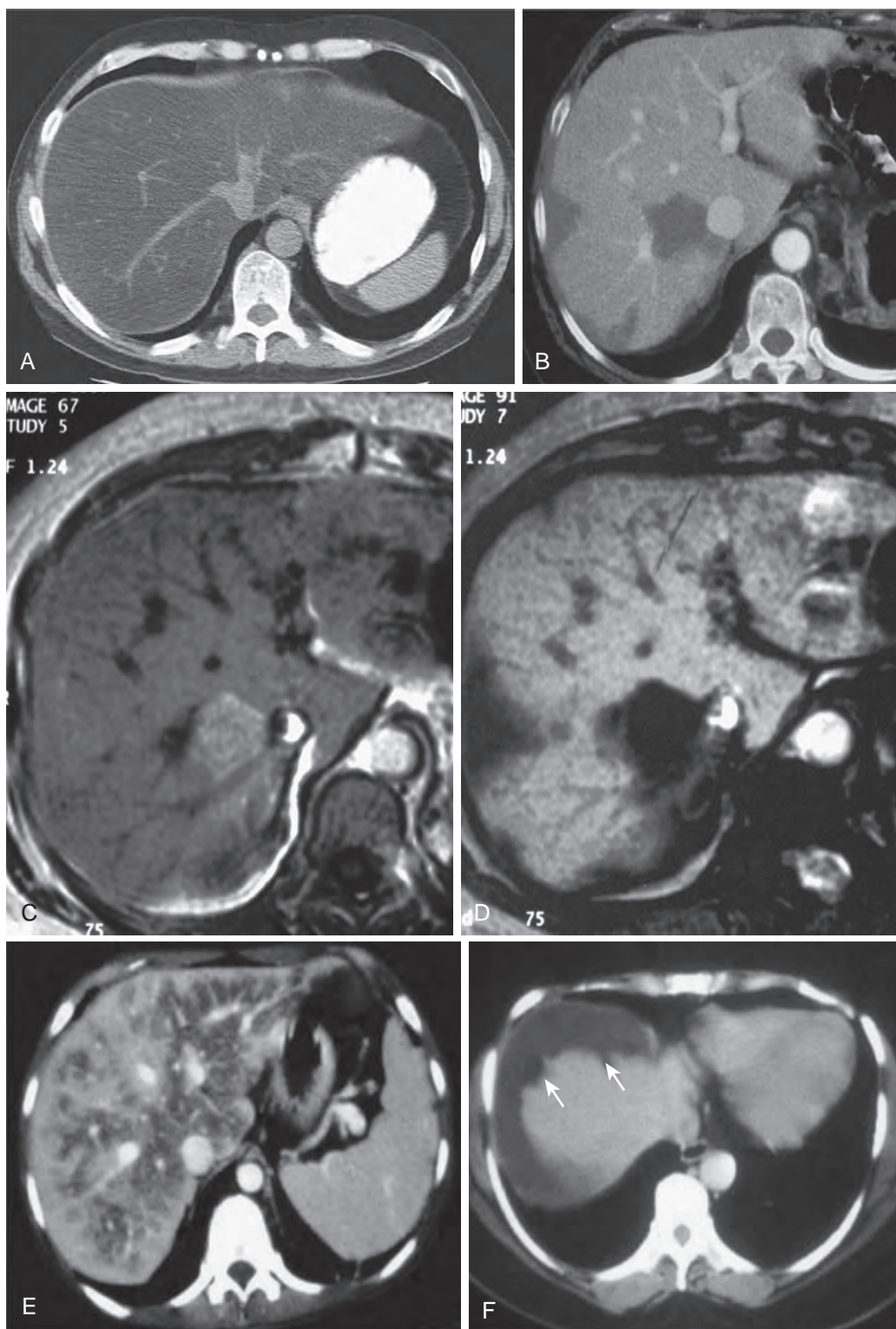


Figure 89-3 Hepatic steatosis: spectrum of CT findings. **A.** Diffuse hepatic steatosis. The density of the liver parenchyma is lower than that of the spleen on this unenhanced CT scan. Note how the intrahepatic blood vessels stand out as hyperattenuating structures. **B.** CT scan shows several hypodense masses in a patient with colon cancer. In-phase (**C**) and opposed-phase (**D**) MR images show that these hypodense areas represent fat. **E.** Perivascular steatosis in a patient with cystic fibrosis. Notice the fat highlighting the hepatic blood vessels. **F.** Capsular steatosis (arrows) is identified in this diabetic patient with renal failure and peritoneal dialysis who had received insulin in the dialysis fluid. (**E** and **F** courtesy of Pablo Ros, MD, Boston, MA.)

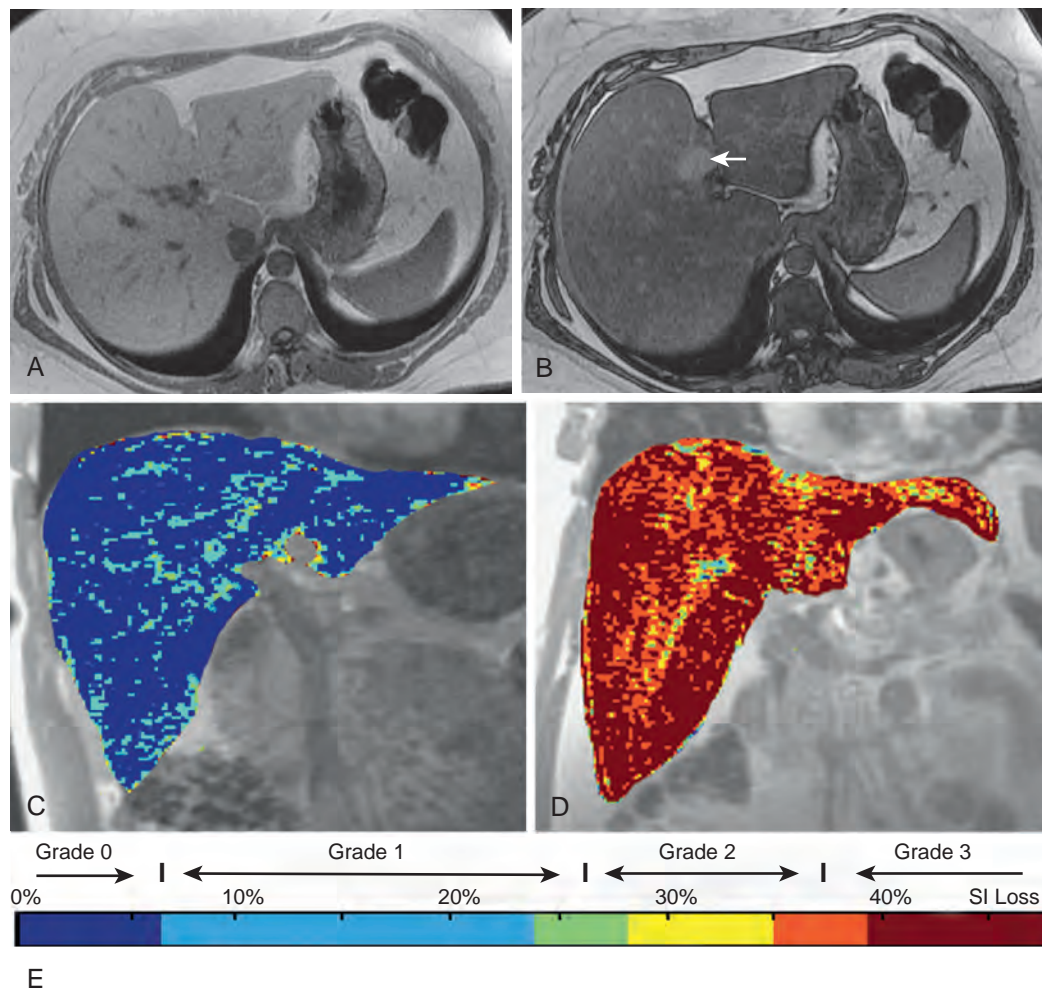


Figure 89-4 Hepatic steatosis: spectrum of MR findings. **A.** In-phase T1-weighted spoiled gradient-echo image demonstrates normal hepatic signal intensity. **B.** Opposed-phase image shows diffuse loss of hepatic signal intensity indicating diffuse hepatic steatosis. Note the focal region of sparing (arrow) adjacent to the falciform ligament in the medial segment of the left hepatic lobe. **C** and **D.** Color maps of the liver show signal intensity loss in a healthy subject corresponding with grade 0 steatosis (**C**) and in a subject with grade 3 steatosis (**D**). **E.** Corresponding color scale for signal intensity loss by steatosis grade.

liver with opposed-phase divided by the signal of the spleen with opposed-phase. Inclusion of the spleen signal is used to normalize inherent imaging inhomogeneities. In normal liver, the lipid fraction is less than 10% and is without significant signal loss on opposed-phase imaging. Clinically significant hepatic steatosis is often greater than 20%³⁷ and can be detected with proton chemical shift imaging qualitatively with a visualized signal loss or quantitatively by creation of a fat signal fraction map (Fig. 89-4C-E). Chemical shift imaging is limited in the detection of a low amount of fat (<10%); at higher levels, fat amount is detected but ambiguous, with 40% fat appearing the same as 60%, reducing accurate quantification at these levels. Additional methods to detect fat include fat suppression with either T1 or T2, which performs as well as or better than chemical shift imaging, and MR spectroscopy, which is sensitive to small amounts of fat and has high accuracy but with limitations of difficulty to perform and to analyze, limited availability, high cost, small spatial sample region, and sampling error with repeated examinations.^{14,38}

When signal loss is present with chemical shift imaging, the presence of fat is confirmatory. The technique is limited,

however, secondary to several confounders, including magnet field inhomogeneities such as in the presence of iron, T2* decay, T1 bias (which refers to the different T1 weighting for fat versus water), and inclusion of only one spectral peak for fat when multiple smaller peaks exist and add to the fat signal. These confounders result in underestimation or lack of detection of fat. These effects are most dramatic at low fat levels, the range where screening for early disease would be important.^{37,39}

New MRI techniques continue to be developed to correct for these cofounders and also to better quantify the presence of fat to accurately grade steatosis. The benefit of these techniques is the potential to replace the “gold standard” for fat quantification, which currently is percutaneous biopsy, an invasive technique that samples only a small portion of the liver. These techniques may also serve as an early and accurate screening tool for asymptomatic but high-risk patients. These techniques result in accurate separation of signal created by mobile fat protons from all other mobile protons by calculating a proton density fat fraction.³⁷⁻³⁹ This fraction can be used to create a fat map of the entire liver that can be viewed with a color scale to demonstrate the variability of fat fractions throughout the

parenchyma. These maps are also useful in monitoring changes over time with treatment. Early results have demonstrated high correlation of these methods with MR spectroscopy and improved ability to detect smaller amounts of fat (<5%) where the transition lies from normal to clinically significant steatosis (>5.56%).^{40,41}

Hepatitis

Hepatitis is a general term used to describe acute or chronic inflammation of the liver. In general medical parlance, *hepatitis* refers to viral hepatitis, but diffuse parenchymal inflammation can result from numerous hepatic infectious or inflammatory processes. It can also be seen after inhalation, ingestion, or parenteral administration of a number of agents, including alcohol, acetaminophen, carbon tetrachloride, halothane, isoniazid, chlorpromazine, oral contraceptives, α -methyldopa, methotrexate, azathioprine, and 6-mercaptopurine.⁴²⁻⁴⁴

VIRAL HEPATITIS

The liver is almost invariably involved in all hematogenous viral infections. These include mononucleosis; herpes simplex; cytomegalovirus infection in patients with acquired immunodeficiency syndrome (AIDS); yellow fever in tropical countries; and rubella, adenovirus infection, and enterovirus infection in children. The term *viral hepatitis* is usually reserved for hepatic infections caused by a small group of hepatotropic viruses known as hepatitis A, B, C, D, and E. Viral hepatitis is the etiology for 60% of cases of fulminant hepatic failure in the United States.⁴²⁻⁴⁴

Clinical Findings

Viral hepatitis type A is an acute infection that occurs sporadically or epidemically and is transmitted by a fecal-oral route. Its incubation period is 15 to 50 days, and it most often has a benign self-limited course that does not cause chronic hepatitis and only rarely causes fulminant hepatitis.⁴²⁻⁴⁴

Viral hepatitis type B is the most common of the hepatotropic viruses worldwide. It is also the most versatile in its presentation and can cause an asymptomatic carrier state, acute hepatitis, chronic hepatitis, cirrhosis, fulminant hepatitis with massive hepatocyte necrosis, or HCC. Viral hepatitis type B is manifested within 30 to 180 days of infection by parenterally administered infected blood or by vertical transmission from mother to child at birth. There are more than 240 million carriers of the virus worldwide and 1.4 million in the United States.⁴²⁻⁴⁶

Hepatitis B viral infection is closely linked to the global distribution of HCC. In endemic areas, the annual incidence of HCC is 387 per 100,000 for men and 63 per 100,000 for women. In Europe and the United States, the carrier rate of hepatitis B virus is less than 1%. In Africa and Southeast Asia, the carrier rate is up to 10%. In high-incidence locales, HCC accounts for almost 40% of all cancers, as opposed to 2.3% in the West. Vertical transmission of the virus from infected mothers is the most common means of disease spread in these regions.⁴²⁻⁴⁴ Vaccination has been available since 1982 and is 95% effective.

Hepatitis C is caused by a parenterally transmitted RNA virus that affects 0.5% to 1% of normal volunteer blood donors in the United States. It now accounts for 90% of the cases of

hepatitis as a result of contaminated blood transfusions before standard screening. A routine blood test for anti-hepatitis C antibody has been developed, greatly improving transfusion safety. The use of unclean needles is also a major mode of transmission. Approximately 150 million people are chronically infected with hepatitis C worldwide.⁴⁵ The mean delay of the onset of symptoms and seropositivity is 22 weeks.⁴²⁻⁴⁴ Hepatitis C can cause either acute or chronic hepatitis; at least 50% of acute cases progress to chronic hepatitis. Chronic hepatitis C tends to be a silent, insidious disease; 10% to 20% of patients eventually develop cirrhosis.⁴²⁻⁴⁴

The hepatitis D virus (HDV), a defective virus that requires the presence of the hepatitis B virus (HBV) to exist, can be acquired either as a coinfection (occurs simultaneously) with HBV or as a superinfection in persons with existing chronic HBV infection. HBV-HDV coinfection has a more severe acute disease and a higher risk (2%-20%) for development of acute liver failure compared with those infected with HBV alone. Chronic HBV carriers who acquire HDV superinfection usually develop chronic HDV infection. Progression to cirrhosis is believed to be more common with HBV-HDV chronic infections than with HBV infection alone.⁴²⁻⁴⁴

Hepatitis E is a single-stranded RNA virus that is waterborne and transmitted by the fecal-oral route; it has an incubation period of 6 weeks. There is no chronic carrier state, and the disease is usually self-limited with a rate of fulminant hepatic failure of about 2%. The mortality and morbidity are significantly higher in pregnant women, with a mortality rate of 20%.

Patients with viral hepatitis typically present subacutely with fatigue, anorexia, nausea and vomiting, malaise, mild pyrexia, myalgias, photophobia, pharyngitis, cough, and coryza. These constitutional symptoms precede the onset of jaundice by 1 to 2 weeks. When jaundice appears, the patient's clinical condition improves, but the liver becomes enlarged and tender in 70% of cases. Splenomegaly is present in 20%. Complete clinical and biochemical recovery is usually seen in 3 to 4 months.⁴²⁻⁴⁴ If the inflammatory changes persist for more than 6 months, the patient is considered to have chronic hepatitis. The prognosis is often poor for these patients, who have jaundice and hepatosplenomegaly associated with an immune-mediated multisystem disease.

Pathologic Findings

On pathologic examination, the changes of acute viral hepatitis are virtually the same regardless of the offending agent. The entire liver is acutely inflamed, with centrilobular necrosis, hepatocyte necrosis, periportal infiltration by leukocytes and histiocytes, and reactive changes in the Kupffer cells and sinusoidal lining cells (Fig. 89-5). Centrilobular cholestasis and bile duct proliferation also occur.²

In chronic active hepatitis, the chronic periportal inflammatory changes extend into the liver parenchyma, producing necrosis and formation of intralobular fibrous septa. Chronic persistent hepatitis is a relatively benign condition characterized histologically by cellular infiltrates within the necrosis. In both disorders, definitive diagnosis is made by liver biopsy.²

Radiologic Findings

The diagnosis of viral hepatitis can usually be made on the basis of history, serologic markers, and liver function test abnormalities. Imaging is usually done to ensure that there is no obstructive component of the patient's hepatic dysfunction, to assess

for cirrhosis and its complications, to exclude focal hepatic abnormalities such as HCC, and to assess hepatic vascular patency.

Ultrasound

Ultrasound findings in acute hepatitis, although often present, are nonspecific. The major role of ultrasound in hepatitis is to exclude biliary obstruction as the cause of liver disease and to diagnose other major complications, such as ascites or vascular occlusion. In chronic viral hepatitis, ultrasound is also used to screen for the development of cirrhosis or HCC. Although its

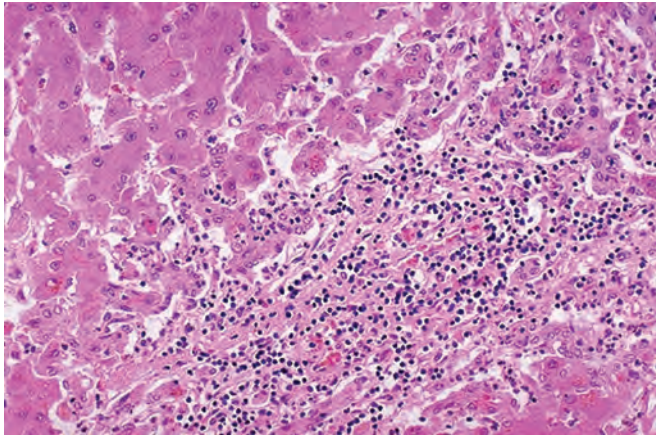


Figure 89-5 Hepatitis: pathologic findings. Liver biopsy specimen shows so-called piecemeal necrosis typical of viral hepatitis.

sensitivity for both lags in comparison to CT and MRI, ultrasound is less expensive and more readily available.

In acute viral hepatitis, the liver and spleen are frequently enlarged. When parenchymal damage is severe, the parenchymal echogenicity is decreased and the portal venule walls are “brighter” than normal (Fig. 89-6). The increased sonographic contrast between the parenchyma and the periportal collagenous tissue is probably due to increased hepatic water, hydropic swelling of hepatocytes, and inflammatory cell infiltration. The increased hepatic water (periportal edema) accentuates the acoustic mismatch between the hepatocytes and the portal tracts.^{3,30,31} Also, the decreased attenuation of the liver allows greater sound penetration to “highlight” these vessels, with increased echogenicity of the walls of peripheral portal veins. This has been termed the centrilobular pattern or “starry sky” appearance. It has been observed in up to 60% of patients with acute hepatitis and is best appreciated in thin patients.^{3,31} This pattern is nonspecific and has also been reported in toxic shock syndrome, cytomegalovirus infection, idiopathic neonatal jaundice, leukemia, diabetic ketoacidosis, and lymphoma. Hepatomegaly is another nonspecific finding in patients with acute hepatitis.

When it is severe, chronic hepatitis produces increased parenchymal echogenicity and loss of mural definition of the portal veins. This is attributed to “silhouetting out” of the portal vein walls by the echogenic fibrotic and inflammatory process surrounding the lobules that abut the portal triads. These findings are nonspecific and can also be seen in patients with fatty infiltration and cirrhosis. One useful differentiating feature is the presence of adenopathy in the hepatoduodenal ligament in

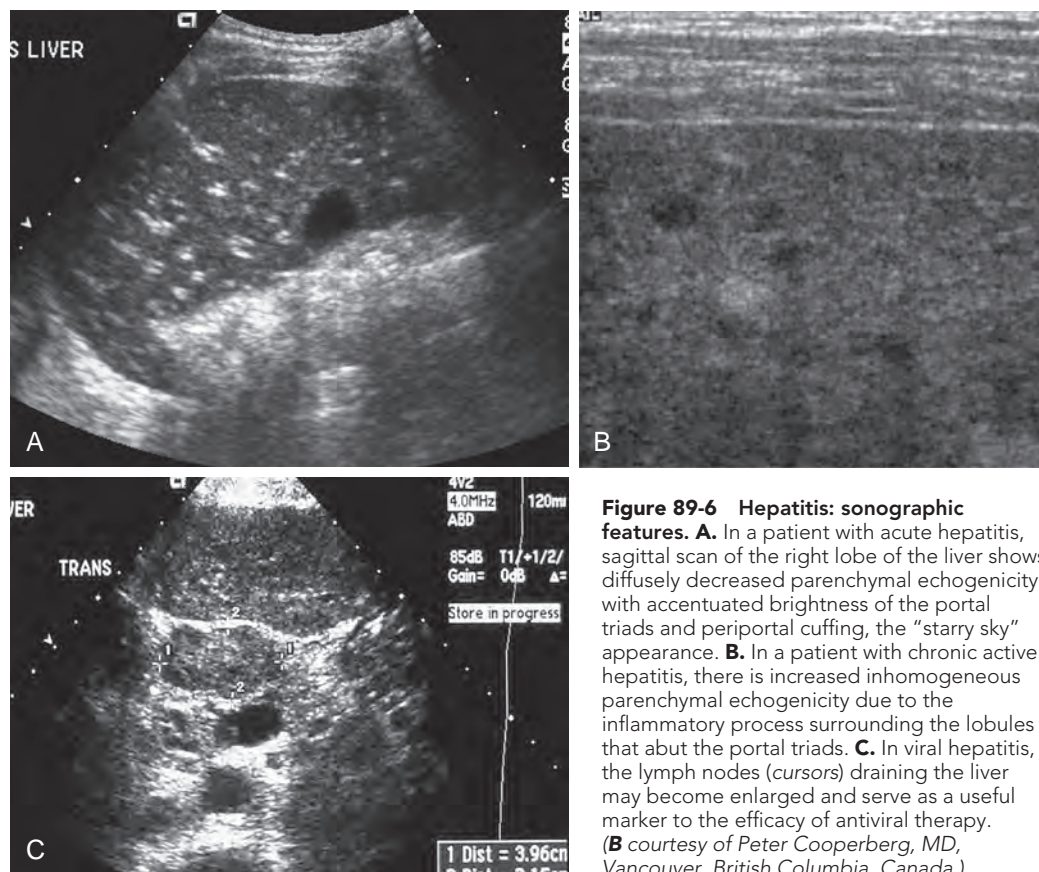


Figure 89-6 Hepatitis: sonographic features. **A.** In a patient with acute hepatitis, sagittal scan of the right lobe of the liver shows diffusely decreased parenchymal echogenicity with accentuated brightness of the portal triads and periportal cuffing, the “starry sky” appearance. **B.** In a patient with chronic active hepatitis, there is increased inhomogeneous parenchymal echogenicity due to the inflammatory process surrounding the lobules that abut the portal triads. **C.** In viral hepatitis, the lymph nodes (cursors) draining the liver may become enlarged and serve as a useful marker to the efficacy of antiviral therapy. (B courtesy of Peter Cooperberg, MD, Vancouver, British Columbia, Canada.)

chronic active hepatitis, which has been attributed to direct spread of the hepatic inflammatory process.

Acute viral hepatitis can also be associated with thickening of the gallbladder wall. In early hepatitis, the gallbladder is hypertonic, whereas in patients more than 9 days after disease onset, the gallbladder is hypokinetic with a large volume and demonstrates a diminished response to a fatty meal.^{3,31}

Computed Tomography

The primary role of CT in patients with hepatitis is to assess for the development of cirrhosis and associated sequelae, including HCC. CT findings in hepatitis are usually nonspecific. Hepatomegaly, gallbladder wall thickening, and hepatic periportal lucency (Fig. 89-7) are the major CT findings in patients with acute viral hepatitis. This lucency is due to periportal fluid and lymphedema surrounding the portal veins and has also been reported in patients with AIDS, trauma, neoplasm, liver transplants, liver transplant rejection, and congestive heart failure. Early in the disease, the liver is enlarged and heterogeneous. Multiple regenerative nodules may be seen, and the liver becomes smaller and nodular with time as fibrosis increases and progresses to cirrhosis. CT has shown that hepatic necrosis is repaired by hypertrophy of regenerative nodules rather than by an increase in the number of nodules. These nodules give rise to the macronodular pattern of postnecrotic cirrhosis. Rarely, the nodules may be hypodense and simulate metastases on CT. Cirrhosis is discussed in detail later in this chapter.

In patients with chronic active hepatitis, lymphadenopathy is commonly found in the porta hepatis, gastrohepatic ligament, and retroperitoneum; it may be the only CT abnormality in a patient with severe hepatic dysfunction. CT can also follow the course of antiviral therapy by observing a reduction in lymph node size.

Magnetic Resonance Imaging

On MRI, acute hepatitis may show nonspecific findings such as heterogeneous signal intensity, most apparent on T2-weighted sequences, and a heterogeneous pattern of enhancement on

arterial-dominant phase spoiled gradient-echo images. This abnormal enhancement becomes more marked and can persist into the venous and delayed phases as the severity of disease increases. High signal intensity periportal edema can be seen on T2-weighted images. In both acute and chronic hepatitis, adenopathy in the lesser omentum may be the only abnormality identified.⁴⁷⁻⁵¹

In chronic hepatitis, MRI can provide information on the degree of histologic activity of disease and help monitor the response to therapy. Homogeneous or heterogeneous increase in signal intensity has been described on T2-weighted images and reflects the presence of inflammation or necrosis of the liver parenchyma. Early patchy enhancement patterns in patients with chronic hepatitis have been shown to be associated with significant parenchymal inflammatory reaction. Absence of this early patchy enhancement correlates with low inflammatory reaction.⁴⁸

In patients with chronic fibrosis associated with cirrhosis, there is progressive enhancement on delayed images due to leakage of gadolinium contrast from the intravascular into the interstitial space.⁴⁹

ALCOHOLIC HEPATITIS

Clinical Findings

Alcoholic liver disease is manifested as three distinct but overlapping entities: fatty liver, alcoholic hepatitis, and cirrhosis. The first is reversible with abstinence; the last two are progressive and shorten life expectancy. Alcoholic hepatitis is part of the spectrum of alcoholic liver disease in which a major drinking binge produces acute liver cell necrosis. These changes are usually superimposed with steatosis or already developing cirrhosis from chronic alcohol use. In most cases, cessation of alcohol consumption and adequate nutrition may ameliorate the patient clinically and histologically. Repeated bouts of acute alcoholic hepatitis are associated with a 10% to 20% risk of death and a 35% risk for development of cirrhosis. Patients usually have fever and neutrophil leukocytosis and may present with malaise, anorexia, weight loss, upper abdominal pain, tender hepatomegaly, and jaundice.⁵²⁻⁵⁶

Pathologic Findings

The specific mechanism of alcohol-induced hepatotoxicity is uncertain despite extensive research on both biochemical and immunologic models of hepatocyte damage. Theories range from peroxidation of cell membranes to modification of membrane permeability to sensitized T cells directed against hepatocytes. The histologic hallmark of alcoholic hepatitis consists of Mallory bodies, which are eosinophilic cytoplasmic inclusions that take the form of “candle droppings” in ballooned, degenerating hepatocytes. In most cases, alcoholic hepatitis is accompanied by pericellular and perivenular fibrosis, again suggesting that this is a precursor to cirrhosis.⁵²⁻⁵⁶

Radiologic Findings

In patients with alcoholic hepatitis, imaging is done to exclude obstructive biliary disease and neoplasm and to evaluate parenchymal damage noninvasively.

Ultrasound

In acute alcoholic hepatitis, the liver is hyperechoic secondary to fatty infiltration. The liver may be enlarged early in the

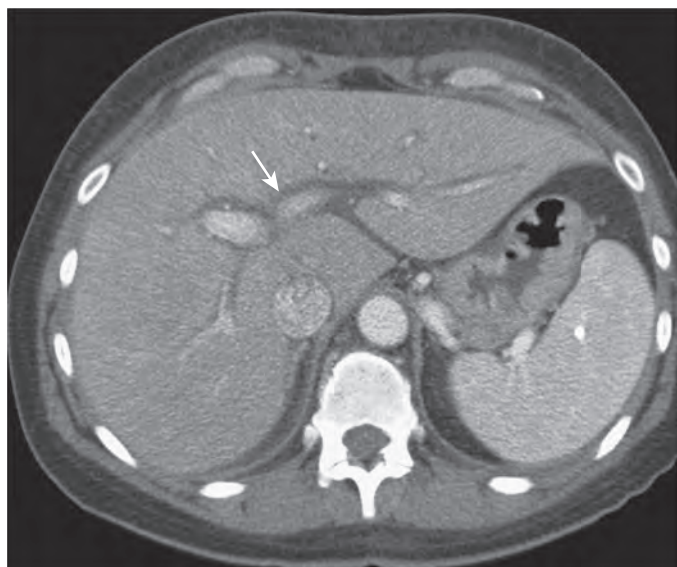


Figure 89-7 Acute hepatitis: CT findings. CT scan shows periportal edema (arrow) highlighting the intrahepatic blood vessels.

disease process, but it becomes atrophic as cirrhosis ensues. Because cirrhosis and fatty infiltration appear similar sonographically, both with heterogeneous echotexture, increased echogenicity, and sound attenuation, CT and MRI are more sensitive in their differentiation.^{3,31}

Computed Tomography

CT may show fatty infiltration in a normal-sized, enlarged, or atrophic liver, depending on the extent of prior liver injury.⁵⁷ As hepatitis progresses to cirrhosis, alcoholic cirrhosis characteristically demonstrates a micronodular pattern as well as enlargement of the caudate lobe and of the right posterior hepatic lobe notch of greater proportion than in other causes of hepatitis. HCC develops at a 5-year cumulative rate of 8%.⁵⁸ Biliary stasis and development of gallstones as well as periportal lymphadenopathy are common in alcoholic hepatitis.

Magnetic Resonance Imaging

Similar to CT, MRI depicts hepatic size and morphology and can be useful in depicting hepatic fibrosis, steatosis, and cirrhosis. MRI is also the most sensitive modality for detection of HCC. Phosphorus 31 MR spectroscopy has shown that livers of patients with alcoholic hepatitis and cirrhosis can be differentiated from normal liver and from each other on the basis of intracellular pH and absolute molar concentration of adenosine triphosphate. Hepatocytes are more alkaline than normal in alcoholic hepatitis and more acidic than normal in cirrhosis.⁴⁷

Toxin- and Drug-Induced Liver Disease

Although drug-induced liver disease represents a small proportion of all adverse drug effects, it accounts for 2% to 5% of hospital admissions for jaundice in the United States and up to 43% of admissions for “acute hepatitis.”

Anesthetics (halothane, enflurane), anticonvulsants (phenytoin), anti-inflammatory agents (gold, clometacin, sulindac), analgesics (acetaminophen), hormonal derivatives (danazol), antidepressant or anti-anxiety drugs (amitriptyline, amineptine), antimicrobials (isoniazid, amoxicillin, sulfamethoxazole-trimethoprim), antiulcer drugs (cimetidine, ranitidine), hypolipidemic agents (nicotinic acid, gemfibrozil), drugs for inflammatory bowel disease (sulfasalazine), and cardiovascular drugs (quinidine, amiodarone) have all been associated with parenchymal liver disease.⁵⁶ Liver damage may be severe, exemplified by 20% to 50% of cases of fulminant hepatic failure being attributed to drugs such as halothane, acetaminophen, α -methyldopa, and phenytoin.⁵⁶

Certain drugs and other chemical agents are capable of producing a wide variety of clinical consequences ranging from very mild liver disease to hepatic failure. The spectrum of hepatotoxicity varies from acute, dose-related, predictable, hepatocellular necrosis to chronic inflammatory disorders ranging from mild chronic persistent hepatitis to severe chronic active hepatitis. In addition, vascular disorders, such as peliosis hepatis and the Budd-Chiari syndrome, and neoplastic lesions, such as angiosarcomas and benign hepatic adenomas, are associated with certain naturally occurring toxins such as “bush teas” and aflatoxins in peanuts, oral contraceptives and anabolic steroids, industrial toxins such as vinyl chloride (Thorotrast), and organic arsenic found in pesticides.⁵⁶

CHEMOTHERAPY TOXICITY

The liver plays a key role in the metabolism of most medications that are either parenterally administered or gastrointestinally absorbed into the portal venous system and therefore is vulnerable to possible injury as a result of exposure. Hepatic deterioration resulting from chemical toxicity can be a diagnostic dilemma in oncology patients with known liver metastases. It is often clinically difficult to differentiate chemotherapy-induced parenchymal injury from other processes, including tumor progression, tumor necrosis, portal and hepatic venous thrombosis, hepatic ischemia and infarction, transfusion reactions, viral hepatitis, and segmental biliary obstruction by tumor. Radiology plays a key role in elucidating the cause of hepatic dysfunction in these patients.

Clinical or subclinical hepatotoxicity is common during systemic chemotherapy. A large series of patients with breast cancer demonstrated that 77% of those receiving systemic adjuvant chemotherapy and 82% of those being treated for metastatic breast cancer, all with normal pretreatment liver function test results, developed abnormal hepatic laboratory values during and after therapy.⁵⁴⁻⁵⁶ The mechanism of chemotherapy agents often involves prevention or retardation of cell division, which can also damage liver cells and diminish immune response. Methotrexate is often associated with steatosis, fibrosis of the portal triads, and eventually cirrhosis. Corticosteroids and L-asparaginase may produce steatosis. Dacarbazine and 6-thioguanine can cause thrombosis of intrahepatic portal veins, producing a Budd-Chiari-like appearance. Azathioprine and 6-mercaptopurine therapy may result in intrahepatic cholestasis and variable degrees of parenchymal cell necrosis. Intra-arterial infusion of floxuridine may cause chemical hepatitis and biliary strictures simulating sclerosing cholangitis. Mithramycin is perhaps the most hepatotoxic drug used in chemotherapy and is associated with acute parenchymal necrosis. Bevacizumab (Avastin) has been associated with hepatic veno-occlusive disease.⁵⁴

On cross-sectional images, the findings are fairly nonspecific and identical to those seen in other liver injuries: hepatomegaly, cirrhosis, and fatty infiltration. Cross-sectional imaging, however, is vital in excluding biliary obstruction or worsening liver metastases as the cause of the patient's hepatic dysfunction. MRI and MR spectroscopy may be helpful in evaluating parenchymal injury. In vitro and laboratory MR experiments have shown that carbon tetrachloride produces water and sodium retention, which can be detected by sodium 23 and proton imaging. Cellular damage is most prominent in the periportal regions, which may be seen as a high signal intensity on T2-weighted images and high sodium signal intensity on spectroscopy.⁴⁷

AMIODARONE TOXICITY

Hepatotoxicity caused by amiodarone is well documented and is usually manifested by mild asymptomatic elevation of serum transaminase levels. When more severe injury occurs, it can simulate alcoholic liver disease with steatosis, Mallory bodies, and cirrhosis. The length of treatment with amiodarone before recognition of hepatic damage can range from several weeks to several years.⁵⁶

The sonographic findings in this disorder are nonspecific and related to steatosis or cirrhosis. The CT appearance

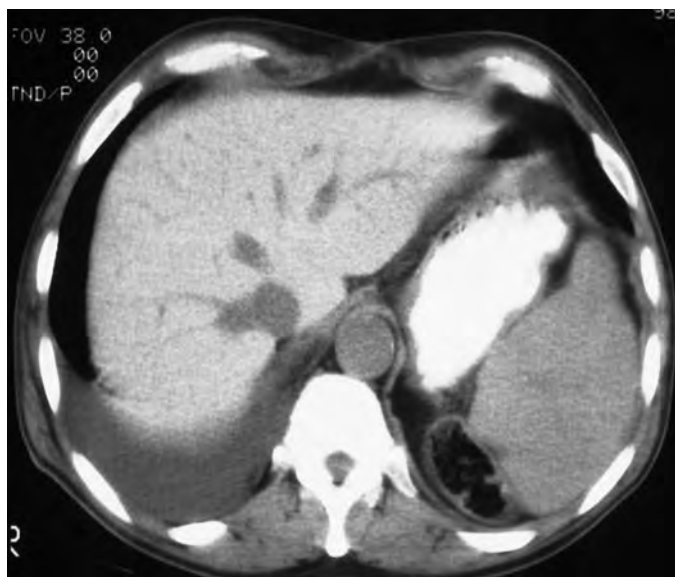


Figure 89-8. Amiodarone hepatotoxicity. Non-contrast-enhanced CT scan of a cardiac patient who had been taking amiodarone demonstrates a liver with an abnormally high attenuation compared with the spleen. Note how the hepatic blood vessels are highlighted by the dense parenchyma. The appearance is indistinguishable from that of hepatic iron overload. There is a right-sided pleural effusion.

(Fig. 89-8), however, is distinctive. When this drug or its metabolites, which contain iodine, accumulate in sufficient quantities in the liver, increased parenchymal attenuation simulating hemochromatosis can be identified.

Radiation-Induced Liver Disease

CLINICAL FINDINGS

Although the liver was once believed to be relatively radioresistant, hepatic morphologic and functional alterations have been observed after radiation therapy since the 1960s and are now established as a complication.

The liver is usually not the intended target for radiation treatment; its exposure occurs when it is unavoidably included in the treatment portal for primary malignant neoplasms of the breast, esophagus, stomach, pancreas, and lymphoma. Patients who receive greater than 30 Gy of total liver radiation are at risk of developing radiation-induced hepatitis.^{56a} Nearly 75% of patients receiving whole liver irradiation have liver function test abnormalities.^{1,2} The classic signs and symptoms of acute hepatic radiation injury are hepatomegaly and ascites. Such effects are not observed when the area of irradiated hepatic tissue is small. High doses of radiation to the liver during childhood can result in hepatic atrophy. In children, restricted development can occur in other structures included in the radiation field, such as the kidney or vertebral bodies.

Radiation damage can also occur from local effects of targeted radiation therapy to the liver with yttrium 90. These microspheres are delivered angiographically to treat either a primary malignant neoplasm or metastatic disease to the liver and inflict a combination of local intense radiation and embolic devascularization. Although local radiation effects can occur, a

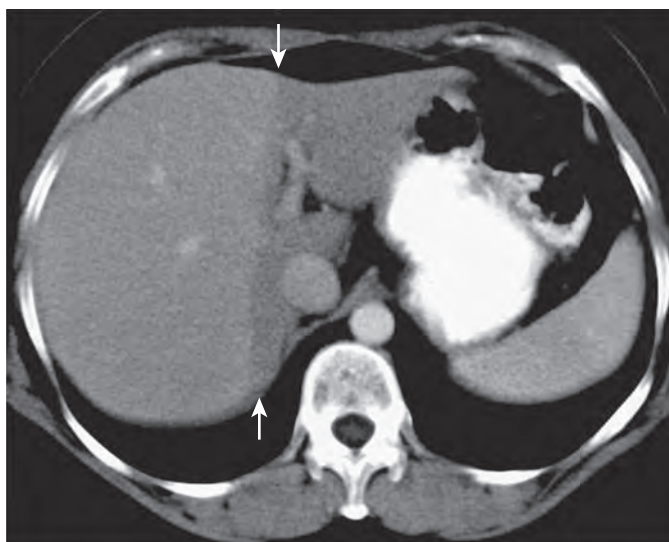


Figure 89-9. Radiation-induced hepatic injury. Contrast-enhanced CT scan shows a sharply defined region (arrows) of hepatic hypoattenuation near the dome of the liver. This patient had received external beam radiation therapy for lung carcinoma.

major advantage of targeted radiation is that radiation-induced diffuse liver disease with hepatomegaly and ascites is extremely rare.⁵⁹

PATHOLOGIC FINDINGS

Radiation hepatitis is characterized by massive panlobular congestion, hyperemia, hemorrhage, and mild proliferative change in the sublobular central veins. Most of the acute findings are sequelae of blood flow stasis secondary to injury of these veins. Complete clinical recovery is typically seen within 60 days, but there may be irreversible hepatocyte loss, fat deposition, fibrosis, or obliteration of the central veins.^{1,2}

RADIOLOGIC FINDINGS

With ultrasonography, geographic areas of radiation injury are hypoechoic relative to the remainder of the liver. This is likely the result of localized hepatic congestion or edema. These changes are more easily detected sonographically in patients with a background of hepatic steatosis resulting from chemotherapy or other causes, which accentuates the hypoechoic areas of radiation injury.^{28,31}

CT performed within several months of the radiation therapy shows a sharply defined band of low attenuation corresponding to the treatment port (Fig. 89-9). This is due to edema or fatty infiltration of the involved area. If hepatic congestion is severe, it may appear heterogeneous and possibly simulate other processes, such as malignant neoplasms. In patients with a background of diffuse hepatic steatosis, the irradiated hepatic area may appear as a region of relatively increased attenuation. This may be due to loss of fat accumulation in the irradiated hepatocytes or regional edema, with the water content demonstrating higher attenuation in comparison with the steatotic parenchyma. During a period of weeks, the initially sharp borders of the irradiated zone become more irregular and indistinct as the peripheral areas of parenchyma begin to regenerate.

Eventually, the irradiated area may become atrophic, demonstrated by volume loss. Radiation effects from yttrium 90 therapy can be manifested with hyperenhancement or hypoenhancement of a portion of the liver and chronically result in atrophy, similar to external beam radiation. The difference is that the distribution of the changes occurs in a hepatic arterial territory distribution rather than along a sharply marginated line. Extensive fibrosis from any radiation source can also potentially cause portal hypertension. Biliary strictures and radiation-induced cholecystitis can rarely occur.⁵⁹

Radiation hepatitis on MRI is manifested as geographic areas of low signal intensity on T1-weighted images and high signal intensity on T2-weighted images secondary to increased water content as determined by proton spectroscopic imaging.⁴⁷ Similar to CT, a distinctly sharp margin between the normal and abnormal liver parenchyma and appropriate clinical history are useful in making the specific diagnosis of postradiation changes.

Hemosiderosis and Hemochromatosis

The body normally contains 2 to 6 g of iron, 80% of which is functional iron in the form of hemoglobin, myoglobin, and iron-containing enzymes. The other 20% is in the storage form as either hemosiderin or ferritin and is normally stored within the reticuloendothelial system, which includes Kupffer cells within the liver and macrophages within the spleen and bone marrow. When it is present in excess amounts, iron is deposited into additional organs, where it can potentially cause dysfunction. Increased iron deposition without parenchymal organ damage is called hemosiderosis and is usually seen with body iron stores between 10 and 20 g.⁶⁰⁻⁶⁴

Hemochromatosis is an iron overload disorder that results in structural and functional impairment of the involved organs. In these cases, body iron accumulation may reach 50 to 60 g. Primary hemochromatosis is an inherited disorder characterized by abnormally increased iron absorption by the mucosa of the duodenum and jejunum that leads to excessive delivery of iron into the portal venous system. Iron accumulates within the liver; once it is saturated, the iron spills into the systemic circulation, where it binds to transferrin. Iron is then deposited preferentially into organs with a high transferrin receptor density, including the pancreas, heart, thyroid, gonads, pituitary gland, and skin, and generally spares the reticuloendothelial system. Secondary hemochromatosis develops in three groups of patients: those with high iron intake (e.g., prolonged consumption of medicinal iron, iron-laden wine, kaffir beer, multiple blood transfusions); anemic patients with ineffective erythropoiesis and multiple blood transfusions (e.g., thalassemia major, sideroblastic anemia); and patients with liver disease in alcoholic cirrhosis and after portacaval shunts.⁶⁰⁻⁶⁴ Iron liberated from red blood cells as a result of multiple transfusions or hemolytic anemias is taken up primarily by phagocytes within the liver, spleen, bone marrow, and lymph nodes, and organ function is generally preserved (hemosiderosis).⁶⁰⁻⁶⁴ Unlike in primary hemochromatosis, reticuloendothelial cell iron overload resulting from transfusions and rhabdomyolysis is usually of little clinical consequence; however, if it is prolonged or severe, such as in thalassemia or sickle cell disease, iron overload can cause a similar pattern of organ dysfunction and is then referred to as secondary hemochromatosis.

CLINICAL FINDINGS

The classic triad of hemochromatosis consists of micronodular pigment cirrhosis, diabetes mellitus, and hyperpigmentation. Patients with primary hemochromatosis usually present in the fourth or fifth decade of life because it takes many years to accumulate sufficient iron (20-40 g) to result in symptoms. There is a 10:1 male predominance in fully developed hemochromatosis. Women are protected from this disorder by the iron loss that occurs during normal menstruation, pregnancy, and lactation.⁶⁰⁻⁶⁴

The liver is the first organ damaged in hemochromatosis, and hepatomegaly is present in 95% of symptomatic cases. Splenomegaly is present in nearly 50% of cases. Arthropathy of the small joints of the hands develops in 25% to 50% of cases and may antedate other symptoms. Cardiac involvement is the presenting complaint in about 15% of cases and is most commonly manifested as congestive heart failure in young adults. Loss of libido, loss of body hair, and testicular atrophy resulting from failure of gonadotropin production are also common. Increased melanin deposition in the basal layers of the epidermis leads to hyperpigmentation, resulting in so-called bronze diabetes in these patients.⁶⁰⁻⁶⁴

The life expectancy of untreated patients with idiopathic hemochromatosis after the disease becomes clinically manifested is 4.4 years. The most common causes of death in these patients are cardiac failure (30%), hepatic coma (15%), hematemesis (14%), HCC (14%), and pneumonia (12%). Removal of iron by repeated phlebotomy and use of iron chelators increases the 5-year survival from 33% to 89%. The liver and spleen decrease in size, liver function test results return to normal, pigmentation decreases, glucose tolerance normalizes, and cardiac function improves with successful therapy. Once cirrhosis occurs, liver injury is irreversible, and about one third of patients develop HCC as a late sequela despite adequate therapy. The risk for development of HCC is increased more than 200-fold in patients with hereditary hemochromatosis. It is therefore important to diagnose this disorder early, in the pre-cirrhotic stage.⁶⁰⁻⁶⁴ Early diagnosis, however, is often difficult because there may be considerable hepatic iron accumulation before the patient becomes symptomatic. CT and MRI may fortuitously detect iron overload, and these modalities are useful in confirming the diagnosis in patients with equivocal laboratory data. Classically, the serum iron level is greater than 250 mg/dL (normal, 50-150 mg/dL), serum ferritin value is above 500 ng/dL (normal, below 150 ng/dL), and transferrin saturation approaches 100% (normal, 25%-30%) in patients with hemochromatosis. Transferrin saturation is the earliest and most sensitive indicator of increased iron stores. Virtually all patients older than 20 years have levels greater than 50%.⁶⁰⁻⁶⁴ Serum ferritin levels, however, are nonspecific and influenced by the presence of inflammatory states, neoplastic disorders, and other hepatocellular diseases. Imaging or biopsy helps clarify the results of these sensitive but somewhat nonspecific tests.⁶⁰⁻⁶⁴

PATHOLOGIC FINDINGS

The principal features of classic primary hemochromatosis are excessive intracellular ferritin and hemosiderin aggregates as the result of excessive intestinal absorption of iron. Iron first accumulates in periportal hepatocytes and then in the lobular

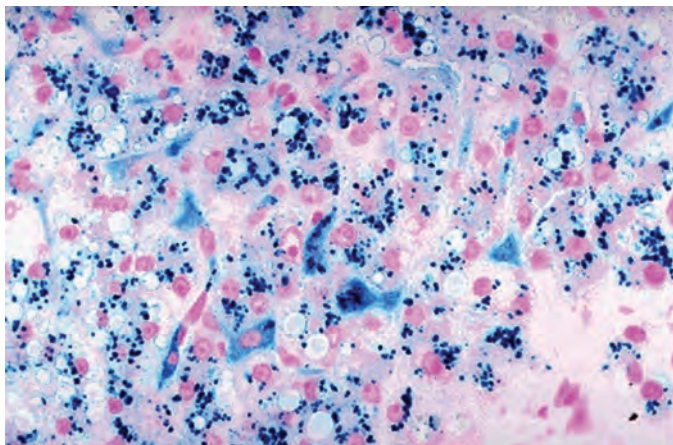


Figure 89-10 Iron overload: histologic findings. Prussian blue stain showing extensive iron deposition.



Figure 89-11 Iron overload: gross pathologic findings. Autopsy specimens show iron deposition in the liver, pancreas, and a lymph node in a patient who died with hemochromatosis. Note the dark brown hue of these organs.

hepatocytes, Kupffer cells, and biliary epithelium. When the liver becomes overwhelmed, iron enters the systemic circulation bound to transferrin and subsequently is deposited into organs with high transferrin-binding receptors including the pancreas, heart, joints, endocrine glands, and skin, in decreasing order of severity (Figs. 89-10 and 89-11). Free iron within cells causes formation of free radicals and results in cell damage leading to inflammation, cell death, and fibrosis. Because the liver contains up to one third of the total body store of iron, it is the organ most profoundly damaged in hemochromatosis. At gross pathologic examination, early in the disease, the liver is slightly larger than normal, dense, and chocolate brown due to ferritin with focal golden yellow granules of hemosiderin. Progressive deposition leads to slowly evolving liver damage and development of fibrous septa similar to those in alcoholic cirrhosis, ultimately producing micronodular cirrhosis. Late in disease, the liver size is only slightly diminished, and fat is usually absent. Liver biopsy can be used to provide an objective measurement of hepatic iron concentration (normal, 7 to 100 pg/100 mg). With primary hemochromatosis, the pancreas is intensely pigmented and demonstrates diffuse interstitial fibrosis resulting



Figure 89-12 Iron overload: CT findings. The attenuation of the liver is diffusely increased secondary to intraparenchymal iron deposition.

in a deficiency of exocrine and, to a greater extent, endocrine function. Hemosiderin is found in both acinar and islet cells, and some correlation is reported between the degree of iron deposition in pancreatic islets and the severity of endocrine dysfunction.⁶⁰⁻⁶⁴

RADIOLOGIC FINDINGS

Plain Radiographs

Rarely, diffuse, homogeneously increased density of the liver may be seen on plain abdominal radiographs in patients with hemochromatosis. Skeletal abnormalities include chondrocalcinosis and degenerative arthritis in the second and third metacarpal heads. Chondrocalcinosis occurs in two thirds of patients and is associated with cartilage narrowing.

Ultrasound

The sonographic appearance of hemochromatosis is nonspecific and related to fibrosis and cirrhosis. Parenchymal iron deposits are too small to be reflective, so ultrasound has no role in the early diagnosis of hepatic iron overload.

Computed Tomography

CT has had a significant impact on the noninvasive diagnosis of excess hepatic iron deposition, although it has a limited sensitivity (63%) and high specificity (96%).⁶⁵ The normal density of the liver is between 45 and 65 HU on noncontrast scans obtained at 120 kVp. On CT, in patients with hemochromatosis, the liver demonstrates homogeneously increased density with an attenuation of greater than 72 HU (Fig. 89-12). The increased attenuation highlights the lower attenuation hepatic and portal veins on unenhanced CT. As discussed elsewhere in this chapter, a similar, diffuse pattern of increased attenuation can be seen in patients treated with amiodarone and in patients with glycogen storage disease that can be indistinguishable from iron overload with CT. Other causes of high parenchymal attenuation that are usually inhomogeneous or focal include calcification resulting from shock liver, exposure to Thorotrast, prior

intravasation of enteric barium, gold therapy administration for treatment of rheumatoid arthritis, and, rarely, Wilson's disease and chronic arsenic poisoning. Clinical history and the lack of homogeneity in these entities are useful in differentiating these from iron accumulation.⁶⁶ High density may also be seen on noncontrast CT in siderotic nodules of cirrhosis.

Measurement of the liver attenuation with CT is confounded by the presence of other diffuse liver processes, particularly hepatic steatosis. The fat decreases the attenuation value, which masks the increase in density seen from iron accumulation. The use of dual-energy CT has been proposed as a method with accuracy similar to that of MRI for the detection of iron in the setting of hepatic steatosis.⁶⁷

For accurate assessment for malignant disease in patients with iron accumulation, it is particularly important to obtain a noncontrast sequence. The high attenuation of the background liver parenchyma can decrease the conspicuity of contrast-enhancing masses, and the noncontrast images may best demonstrate the attenuation difference between a hypoattenuating mass and high-attenuation background parenchyma. Nonspecific changes of cirrhosis and portal hypertension with end-stage hemochromatosis can also be readily depicted with CT.

Magnetic Resonance Imaging

MRI is the most sensitive and specific imaging test for the demonstration of hepatic iron overload and for follow-up of patients undergoing treatment (Figs. 89-13 and 89-14). In primary hemochromatosis, MRI shows dramatic reduction in the signal intensity of the liver (90%). This signal loss is due to the large paramagnetic susceptibility of ferritin and hemosiderin-iron-oxyhydroxide crystals, which contain ferric ions (Fe^{3+}), that profoundly shortens both the T1 and T2 relaxation times of the adjacent protons within the liver. This paramagnetic effect is more conspicuous on T2-weighted images and is most profound on T2*-weighted images, both clinically used to assess for iron. When iron concentrations within the liver are elevated, the T2-shortening effect predominates, accounting for the diminished hepatic signal intensity. Iron overload can sometimes be recognized in the heart and pancreas by diminished signal intensity, as seen in the liver.^{25-27,42} In reticuloendothelial overload, decreased signal intensity is seen on T2 within the spleen and bone marrow. In hemolytic anemias, the renal cortex also occasionally has decreased T2-weighted signal intensity. The paramagnetic effect increases as the echo time increases.

On T1 in-phase and opposed-phase gradient-echo sequences, signal loss is greater on the T1 in-phase imaging because of its longer echo time in comparison with the opposed-phase imaging. This is opposite to the pattern of signal loss seen in the presence of microscopic fat, when signal loss occurs on the opposed-phase sequence. Focal iron deposition may also be demonstrated by MRI, such as in siderotic nodules seen in cirrhosis.

The normal hepatic parenchyma has a slightly increased T2- and T2*-weighted MR signal intensity compared with that of the kidney and paraspinal musculature, which can be used for comparison both qualitatively and quantitatively. MRI can be helpful to distinguish the parenchymal overload that occurs in primary hemochromatosis from reticuloendothelial cell iron overload (see Figs. 89-13 and 89-14). Whereas abnormally decreased T2 signal intensity is seen in both, in primary hemochromatosis, decreased signal intensity is observed within the pancreas and heart; in reticuloendothelial cell iron overload, decreased signal intensity of the spleen, bone marrow, and occasionally lymph nodes is observed with normal signal intensity of the other organs.^{47-49,68}

MRI can also be used to diagnose and to monitor treatment of patients with parenchymal iron overload. Quantitative assessment can be performed with two techniques, signal intensity ratio and relaxometry. The signal intensity ratio method uses T2- and T2*-weighted imaging at multiple different echo times or flip angles and measures the signal intensity of the liver and of a reference tissue that will not accumulate iron, usually the paraspinal muscle.⁶⁹ The mean signal intensity of the liver is divided by the mean signal intensity of the reference tissue. For estimated concentration of more than 85 $\mu\text{mol/g}$, the positive predictive value for hemochromatosis is 100%; for less than 40 $\mu\text{mol/g}$, the negative predictive value for hemochromatosis is 100%.⁶⁸ Complete signal loss at concentrations above 300 $\mu\text{mol/g}$ precludes accurate measurements with iron overload above these levels. Other limitations of this technique include the need for breath holding and inhomogeneity of signal intensity resulting from the presence of fat or minor variations in the location of selected regions of interest between sequences. In the relaxometry method, the signal intensity of the liver is measured as a function of increasing echo time, which is used to calculate a signal decay constant. Iron concentration is inversely proportional to these values.⁷⁰ Technical factors include calibration for the field strength and choosing a

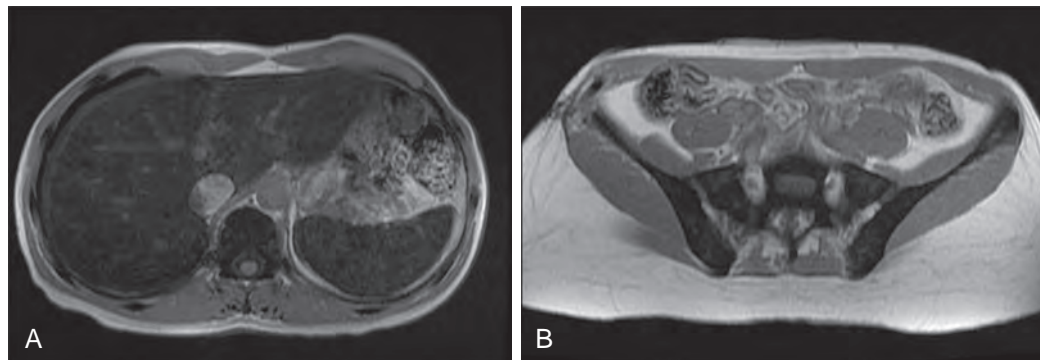


Figure 89-13 Hemosiderosis: MR findings. **A.** Axial T1-weighted image shows marked decrease in signal intensity of the liver and spleen due to iron deposition into the Kupffer cells of the liver and the reticuloendothelial cells of the spleen. **B.** Axial T1-weighted image of the pelvis in the same patient shows markedly decreased signal intensity within the pelvic bones due to the deposition of iron into bone marrow reticuloendothelial cells.

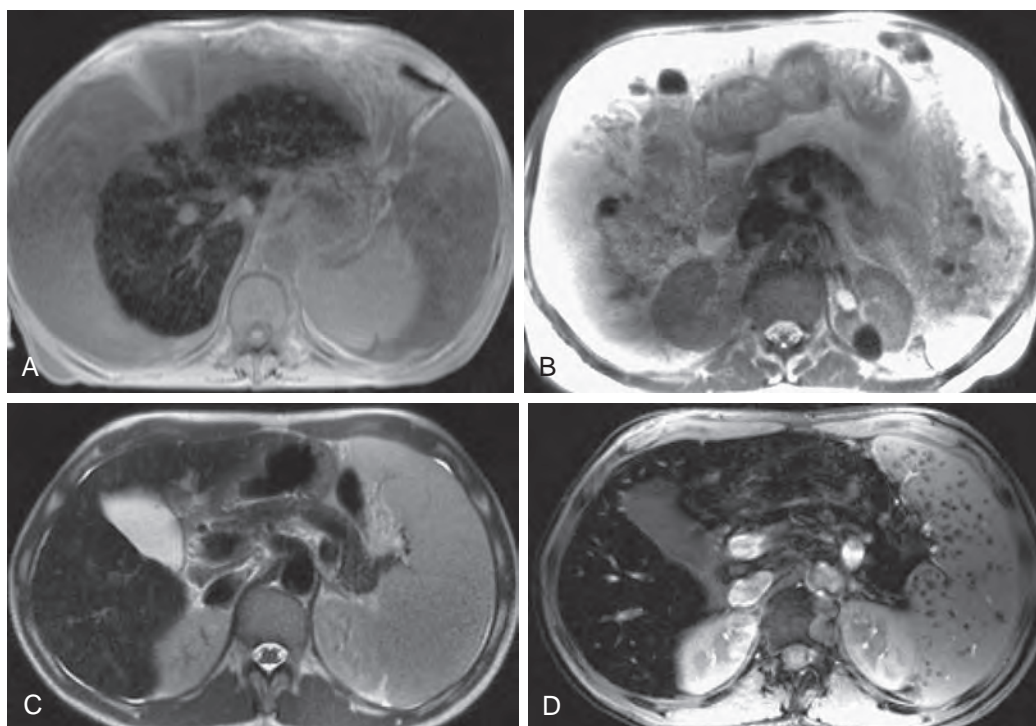


Figure 89-14 Hemochromatosis: MR findings. Two different patients with hemochromatosis. **A.** MR scan shows a cirrhotic, markedly hypointense liver surrounded by ascites. The spleen is spared because it is composed primarily of reticuloendothelial cells, which do not accumulate iron in hemochromatosis, an important differentiating feature from hemosiderosis. **B.** Scan obtained caudal to **A** shows low signal intensity of the pancreas; the acinar cells do accumulate iron. In a different patient, T1-weighted (**C**) gradient-echo (**D**) images of the upper abdomen show marked hypointensity of the liver and spleen due to the deposition of iron in the hepatocytes of the liver and the acinar cells of the pancreas. Notice the low signal intensity Gamna-Gandy bodies in the spleen, secondary to hemosiderin deposition, a finding seen in portal hypertension with microhemorrhages into the splenic parenchyma.

clinical range of echo time values. The choice of parameters used for measurement and the pulse sequence design also affect the calculated result. For both methods, normal variability within tissues, concurrent processes such as steatosis and fibrosis, choice of voxel size and location, technical factors related to MRI hardware and technique, and mathematical models used for data calculation all potentially limit the accuracy of iron quantification.⁷¹⁻⁷⁵

Glycogen Storage Disease

CLINICAL AND PATHOLOGIC FINDINGS

The liver has a major role in the synthesis and storage of glycogen as well as its ultimate catabolism into glucose. Among inherited disorders of glycogen metabolism, types Ia, Ib, II, III, IV, VI, and IX affect the liver and are manifested with hepatomegaly.⁷⁶ Type Ia (von Gierke's disease) is the most common subtype to affect the liver. It is due to a deficiency of glucose-6-phosphatase in the liver and kidneys, which results in excessive glycogen deposition in the hepatocytes and proximal renal tubules. On pathologic examination, intracytoplasmic accumulations of glycogen and small amounts of lipid are found. Patients clinically demonstrate failure to thrive, hypoglycemia, hyperlipidemia, hyperuricemia, stunted growth, hepatomegaly, and nephromegaly. Hepatic adenomas are much more common than in the normal population, and the presence of more than 10 hepatic adenomas, known as adenomatosis, is seen in up to 60% of patients with type Ia glycogen storage disease.

Adenomas are also seen in glycogen storage disease types Ib and III. Increase in the size and number of adenomas increases the risk for associated hemorrhage. Much less commonly, HCCs can occur from malignant degeneration of an adenoma. Both processes are thought to result from hepatic exposure to chronic hormonal stimulation resulting from the chronic hypoglycemia. Types III and IV glycogen storage disease can progress to cirrhosis. Imaging surveillance of these patients is useful to evaluate for complications of the disease, including hemorrhage and malignant transformation.

RADIOLOGIC FINDINGS

Ultrasound

On sonographic evaluation, the liver is enlarged with increased echogenicity and beam attenuation, presumably from fatty infiltration and possibly contributed to by the excess glycogen deposition. Adenomas are common and can appear well circumscribed and may be hypoechoic, isoechoic, or hyperechoic in relation to the remainder of the liver. Increased sound transmission with refractile shadowing at the tumor margins is commonly seen. These findings are related to the paucity of fat and glycogen in the adenomas compared with the rest of the involved liver. These sonographic features are unique to adenomas in patients with glycogen storage disease, whereas adenomas from other causes tend to contain more fat in comparison to the background liver parenchyma. Change in the sonographic appearance of adenomas over time may reflect malignant degeneration or hemorrhagic necrosis.^{28,30} HCC can occur, and

any new or significantly changing mass should be further evaluated with contrast-enhanced CT or MRI.

Computed Tomography

The CT density of the liver in glycogen storage disease is altered by two processes with conflicting imaging effects: hepatic attenuation is increased by glycogen storage and decreased by fatty infiltration (Fig. 89-15A, B). Which appearance predominates within the liver depends, therefore, on the predominant underlying pathologic process. In addition to the liver, the spleen and kidneys are typically enlarged and the renal cortex may appear dense secondary to glycogen deposition. On noncontrast CT, hepatic adenomas are hypodense compared with normal liver and spuriously hyperdense if there is concomitant fatty infiltration. Unenhanced CT may also demonstrate hemorrhage within an adenoma. Adenomas are also usually well circumscribed and rarely have calcification. After the administration of contrast material, adenomas usually are hypervascular to the liver parenchyma on arterial phase imaging and nearly isoattenuating during the portal venous phase. Adenomas should remain stable in size or show slow growth on follow-up examination. Although distinction of adenomas from HCCs may be challenging on the basis of imaging morphology alone, malignant degeneration should be suspected if there is rapid growth or density change with a focal mass. Clinical assessment with surveillance of α -fetoprotein can also be used to detect development of malignancy and should not be elevated with the presence of adenomas alone.⁷⁷

Magnetic Resonance Imaging

On MRI, the appearance of adenomas varies but in general is heterogeneously hyperintense on T1- and T2-weighted imaging.

Focal areas of hypointensity may represent old hemorrhage or calcification. The presence of microscopic fat demonstrates focal signal intensity loss on the T1 opposed-phase sequence in comparison with the in-phase sequence⁷⁷ (Fig. 89-15C). Enhancement on hepatobiliary phase imaging with liver-specific gadolinium agents is not expected, which, however, does not help differentiate an adenoma from a dysplastic or malignant mass.⁷⁸

Amyloidosis

CLINICAL AND PATHOLOGIC FINDINGS

Amyloidosis is a systemic process whereby insoluble protein aggregates accumulate in various organs throughout the body. Several categories of amyloidosis exist, all of which can affect the liver. Primary amyloidosis results from overproduction by the bone marrow, such as in multiple myeloma. Secondary amyloidosis is due to chronic inflammatory disease. A rare familial form of amyloidosis also exists. Hepatic infiltration and enlargement are frequently found in patients with systemic amyloidosis, but significant liver disease is rare. Amyloid within the liver is deposited within spaces of Disse and then progressively encroaches on adjacent hepatic parenchymal cells and sinusoids. Cellular replacement of large areas of liver parenchyma may occur, giving the liver at gross pathologic examination a pale, waxy gray, firm appearance. Hepatic function is usually preserved despite marked amyloid infiltration. When amyloidosis is severe, it may be clinically symptomatic, manifested with right upper quadrant pain caused by stretching of Glisson's capsule, pruritus, ascites, malaise, weight loss, intrahepatic cholestasis, or portal hypertension.⁷⁹⁻⁸²

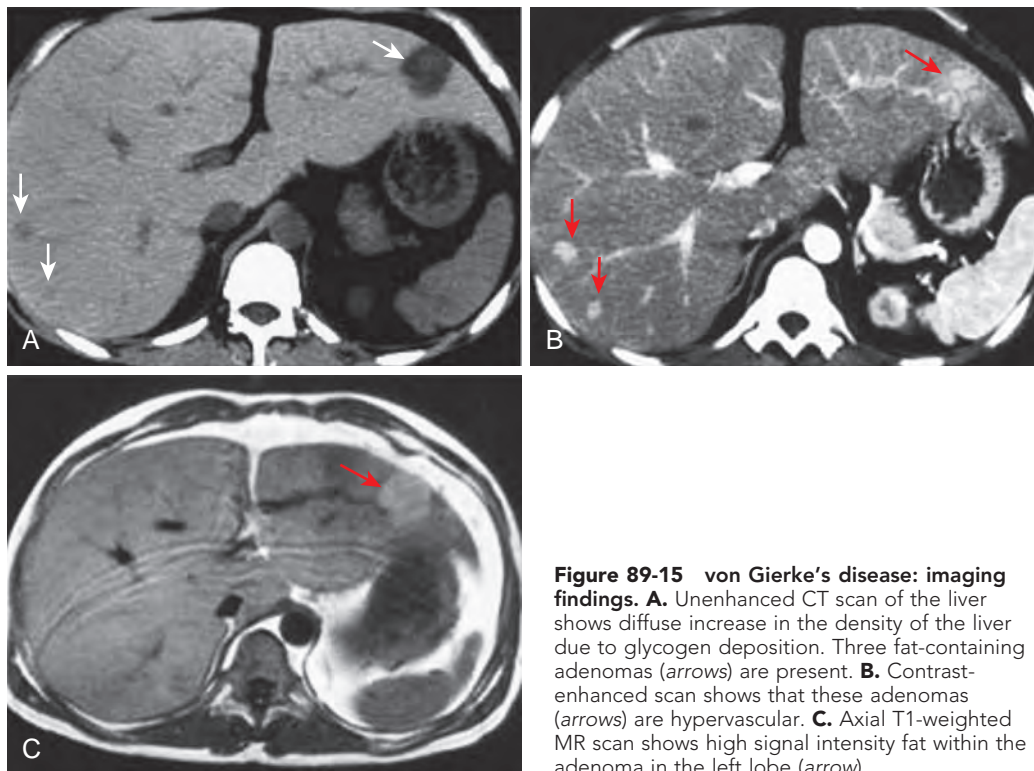


Figure 89-15 von Gierke's disease: imaging findings. **A.** Unenhanced CT scan of the liver shows diffuse increase in the density of the liver due to glycogen deposition. Three fat-containing adenomas (arrows) are present. **B.** Contrast-enhanced scan shows that these adenomas (arrows) are hypervascular. **C.** Axial T1-weighted MR scan shows high signal intensity fat within the adenoma in the left lobe (arrow).

RADIOLOGIC FINDINGS

Radiologic findings of amyloidosis are mostly nonspecific. On sonographic evaluation, the liver is enlarged and inhomogeneous in echotexture.^{83,84} On CT, findings also include hepatomegaly, and areas of low attenuation can occasionally be seen in focal areas of amyloid deposition. Calcification, also nonspecific, can also be present. Delayed contrast enhancement may be seen in the involved areas because of vascular and sinusoidal infiltration. A specific pattern of hepatomegaly with focal triangular enlargement near the falciform ligament and pointed surface anteriorly has been suggested.⁸⁵ Concomitant abnormalities seen in the spleen, including enlargement, decreased attenuation, and possible calcification, are helpful in differentiating amyloid deposition from hepatic neoplasm and fatty infiltration but are not often present.

On MRI, patients with primary amyloidosis demonstrate decreased T2 signal intensity within the spleen and adrenal glands and increased T2 signal intensity of the pancreas in comparison with normal individuals. Signal intensity within the liver may appear normal or increased on T1 (etiology unknown); however, T2 intensity is not significantly changed within the liver.^{84,85} Suggestion of delayed or absent contrast enhancement with liver-specific contrast agents has been suggested as a way to identify focal areas of amyloid deposition.⁸⁶

Wilson's Disease

CLINICAL AND PATHOLOGIC FINDINGS

Wilson's disease, also called hepatolenticular degeneration, is an autosomal recessive inherited disorder of copper metabolism. Copper is balanced within the body by regulation of its excretion and is protein bound within the serum. In Wilson's disease, there is a copper-transporting enzyme mutation that is manifested with decreased biliary excretion of copper, excessive absorption of copper from the gastrointestinal tract, abnormal urinary excretion of copper, and decreased levels of ceruloplasmin, the serum protein to which 95% of body copper is bound. Copper accumulates in hepatocytes until all the binding sites are used, at which point unbound copper causes oxidative damage. Accumulation then occurs in other organs, including the basal ganglia, renal tubules, cornea, bones, joints, and parathyroid glands.⁸⁷⁻⁸⁹

Clinical presentation can vary secondary to different mutations and degree of dysfunction of the copper-transporting adenosine triphosphatase; onset of the disease occurs as early as 5 years to as late as 40 years of age. Liver disease with a completely nonfunctioning enzyme most often is manifested in childhood or early adolescence with signs and symptoms including fatigue, hepatosplenomegaly, variceal bleeding, ascites, and encephalopathy. Hemolytic anemia can occur by a mechanism thought to be due to hemoglobin damage secondary to serum copper accumulation. This can result in acute fulminant hepatic failure.

The onset of neurologic symptoms usually occurs later, in early adulthood after cirrhosis is present. If hepatic changes remain subclinical, the patient may present with an asymmetric tremor, ataxia, speech disturbance, personality changes, and Parkinson-like symptoms including decreased movement and facial expression.⁹⁰ Kayser-Fleischer rings are green to brown copper deposits in the cornea, and their presence is a helpful

diagnostic finding in 98% of untreated patients. A slit-lamp examination is warranted in any patient with this suspected diagnosis of Wilson's disease.⁸⁷⁻⁸⁹

Laboratory diagnostic tests can be helpful in differentiating Wilson's disease from other hepatic diseases. Low serum ceruloplasmin concentration (<50 mg/100 mL) is present in 95% of cases and highly suggestive of Wilson's disease. Urinary copper (>100 µg/day) is elevated and can be useful in diagnosis and treatment monitoring. Liver aspartate transaminase, although nonspecific, is also elevated early in the disease. Genetic testing in patients with a family history can be performed.

On pathologic examination, electron microscopy of liver biopsy specimens shows fat droplets, nuclear glycogen deposits, and cellular necrosis. Inflammatory cells accumulate, and eventually fibrosis, loss of hepatic architecture, and cirrhotic changes are seen. Hepatic copper content is high (>250 µg/g dry weight; normal is <55 µg/g),⁹¹ which is concentrated in the sinusoidal and periportal distribution. Copper initially accumulates in the cytoplasm, followed by lysosomes. Morphologic abnormalities of the mitochondria are also seen. Marked elevation of hepatic copper can also be seen in the setting of chronic cholestasis but can usually be differentiated from Wilson's disease with clinical information and biliary obstruction seen with imaging.^{92,93}

The difficulty in the early recognition of this disease is its infrequency and subtlety of its early manifestations. Early diagnosis is crucial to the prognosis; effective treatment is available with copper chelators, such as penicillamine, to prevent toxic copper deposition. Dietary intake of copper should also be limited. According to the American Association for the Study of Liver Diseases, the diagnosis of Wilson's disease should be considered in patients aged 3 to 55 years with liver disease of uncertain etiology, in acute hepatic failure, and in NAFLD.⁹⁴ Treatment of asymptomatic patients prevents manifestations of the disease; however, treated symptomatic patients also often improve, sometimes dramatically.⁹³ Acute hepatic failure, end-stage cirrhosis, and failure of chelation therapy are indications for liver transplantation, which is curative.

RADIOLOGIC FINDINGS

Imaging findings of Wilson's disease are predominantly nonspecific, although more specific features have been suggested. The natural history of Wilson's disease is similar to that of other diffuse liver diseases and includes fatty infiltration, acute hepatitis, chronic active hepatitis, cirrhosis, and sequelae of portal hypertension.

Ultrasound, CT, and MRI can show heterogeneous hepatic parenchyma, contour irregularity, and macronodularity (nodules >3 mm). Ultrasound can demonstrate these macronodules, which are predominantly hypoechoic. A publication evaluating 28 patients suggests that unique imaging features of Wilson's disease, which include a normal caudate lobe-to-right hepatic lobe ratio (normal, <0.6)⁹⁵ and a perihepatic layer of fat, can be demonstrated with all three modalities.⁹⁶ HCC can occur but is reported almost exclusively in patients who have developed cirrhosis.⁹⁷

Copper has a high atomic number and can increase hepatic attenuation on CT. This can be seen diffusely or focally within hepatic nodules. This finding is not often seen, however, probably secondary to coexistent hepatic steatosis, lowering the overall hepatic density and diminishing this effect.

Copper also has a paramagnetic effect and shortens T1 relaxation time, which would be expected to result in T1 hyperintensity. Copper, however, has low magnetic susceptibility⁹⁸ and does not significantly alter the local magnetic field in comparison to other metals, such as iron and titanium. MRI signal is therefore not visibly altered in the presence of copper and cannot be used to differentiate Wilson's disease from other diffuse liver diseases. Regenerative nodules are often present and as in other forms of cirrhosis can contain iron, resulting in T1/T2 hypointensity, also nonspecific.⁹⁵

Phosphorus 31 MR spectroscopy is a technique that can be used to assess the severity of hepatic injury and provide a non-invasive baseline to assess treatment response as an alternative to percutaneous biopsy (Fig. 89-16). This technique may have limited availability and practicality.⁹⁹

Bone changes occur in up to 85% of patients and may be incidentally seen with liver imaging. These include osteomalacia, chondrocalcinosis, premature degenerative joint disease with fragmentation, cystic changes and sclerosis of subchondral bone, and anterior compression of the dorsal vertebral bodies.⁸⁷ In addition, copper accumulation in the brain results in possible cortical atrophy and mixed abnormal signal intensity within the thalami and basal ganglion.

Gaucher's Disease

CLINICAL AND PATHOLOGIC FINDINGS

Gaucher's disease is an autosomal recessive inherited disease and is the most common lysosomal storage disease caused by deficiency of the enzyme glucosylceramidase. Type I Gaucher's disease is the subtype that can involve the liver and has an incidence of 1 in 2500 births, most commonly among the Ashkenazi Jewish ethnic population. Accumulation of the enzyme's substrate, glucosylceramide, occurs within the reticuloendothelial system and, when there is hepatic involvement, within Kupffer cells. Symptoms are manifested in either childhood or early adulthood and include bone pain and fractures from bone marrow involvement and hepatosplenomegaly. The degree of liver involvement correlates with the severity of extrahepatic disease. Rarely there can be extensive replacement of the liver by Gaucher cells (lipid-laden Kupffer cells), and cirrhosis and portal hypertension can develop.^{100,101}

RADIOLOGIC FINDINGS

All imaging modalities may show hepatosplenomegaly and occasionally multiple hepatic calcifications. Bone changes are common and include modeling deformities of the lower femoral shafts ("Erlenmeyer flask" appearance), pathologic fractures, and vertebral body collapse.

In a study of 500 symptomatic patients with Gaucher's disease, 7.8% had hepatic abnormalities seen on ultrasound. Findings included hepatomegaly, fatty infiltration, heterogeneous echotexture, and focal hypoechoic or hyperechoic lesions. These focal lesions are most often the accumulation of Gaucher cells and are small and slow growing. More rapid changes should prompt evaluation for malignant disease.¹⁰² CT and MRI show similar findings, which are nonspecific; however, the presence or absence of liver abnormalities in patients with known Gaucher's disease may help triage patients who could benefit from enzyme replacement therapy.

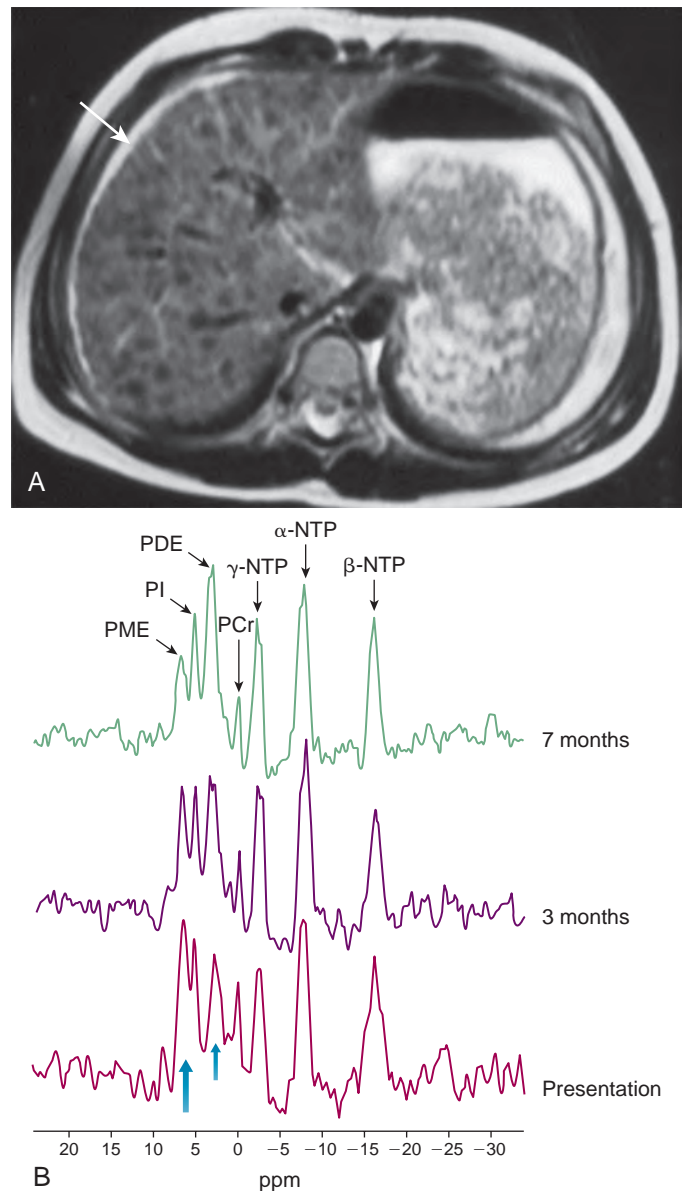


Figure 89-16 Wilson's disease: imaging findings. **A.** A 9-year-old girl with Wilson's disease. T2-weighted axial MR image (TR/TE, 1800/90) of the liver shows numerous tiny hypointense nodules at presentation before medical treatment. Note hyperintense ascitic fluid (arrow) around edge of liver. **B.** Graph shows representative serial phosphorus 31 MR liver spectra before and after 3 and 7 months of medical treatment. Elevation in phosphomonoester (PME) resonance (long blue arrow) is concurrent with reduction in phosphodiester (PDE) resonance (short blue arrow) at presentation, followed by gradual reversal change in subsequent 3- and 7-month spectra. NTP, Nucleotide triphosphate; PI, inorganic phosphate; PCr, phosphocreatine. (From Chu WCW, Leung TF, Chan KF, et al: *Wilson's disease with chronic active hepatitis: Monitoring by in vivo 31-phosphorus MR spectroscopy before and after medical treatment.* *AJR Am J Roentgenol* 183:1339–1342, 2004. Reprinted with permission from the American Journal of Roentgenology.)

Sarcoidosis

CLINICAL AND PATHOLOGIC FINDINGS

Sarcoidosis is a systemic granulomatous disorder that commonly affects the liver; reported series show 24% to 79% of patients with hepatic involvement.⁶⁰⁻⁶⁵ As in the lungs and other

organs, hepatic granulomas can form. These are most often clinically unapparent, although a surrounding fibrotic and possibly immune-mediated process can occur and rarely can lead to chronic inflammation, chronic hepatitis, and cirrhosis. Three patterns of disease presentation are cholestatic liver disease with jaundice, Budd-Chiari syndrome, and cirrhosis and portal hypertension. Biopsy of the liver will reveal diffuse, small, non-caseating granulomas, usually less than 2 mm in size. The differential diagnosis for this finding on histopathologic evaluation also includes primary biliary cirrhosis. A mitochondrial antibody test can be used to differentiate these two entities; the result is negative in sarcoidosis and usually positive in primary biliary cirrhosis.¹⁰³⁻¹⁰⁸

RADIOLOGIC FINDINGS

The most prevalent CT finding (Fig. 89-17) of sarcoidosis in the liver is hepatomegaly, and hypoattenuating nodules varying in size up to 2 cm will occasionally be seen on both non-contrast and contrast-enhanced images. Because most granulomas at pathologic examination are small, imaging studies depict nodular changes in only approximately one third of affected patients. At ultrasound examination, larger granulomas can be seen as hypoechoic nodules; at MRI, when nodules are visualized, they appear hypointense on both T1-weighted and T2-weighted sequences (Fig. 89-18) compared with adjacent liver parenchyma. Associated upper abdominal lymphadenopathy, as elsewhere in the body, is often present. The

presence of hepatic nodules at imaging does not correlate with severity of pulmonary disease.¹⁰³⁻¹⁰⁸ Also unlike in pulmonary disease, resolution of imaging findings within the liver after treatment does correlate with a positive treatment response.



Figure 89-17 Sarcoidosis: CT findings. Contrast-enhanced CT scan shows hepatomegaly with innumerable small hypodense nodules. Portal adenopathy is also present (arrows). (From Warshaw DM, Lee JKT: Imaging manifestations of abdominal sarcoidosis. *AJR Am J Roentgenol* 182:15–28, 2004. Reprinted with permission from the American Journal of Roentgenology.)

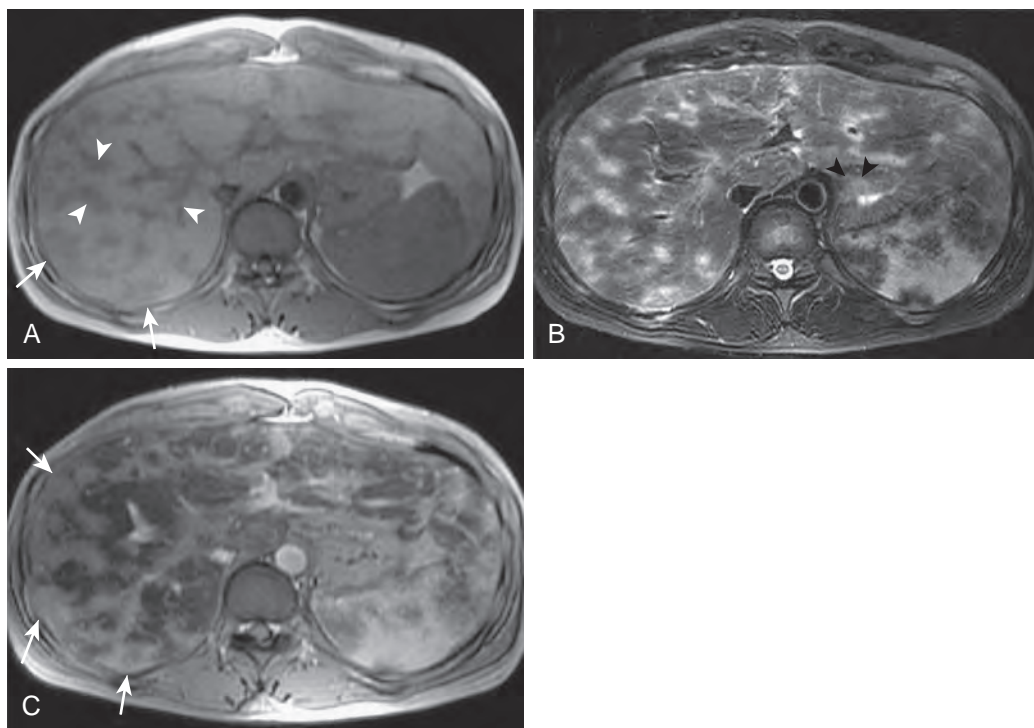


Figure 89-18 Sarcoidosis: MR findings. **A.** Unenhanced gradient-echo T1-weighted MR image of the upper abdomen demonstrates irregularly shaped, low signal intensity nodules peripherally in the liver (arrows) and widening of the periportal tract (arrowheads). **B.** On a T2-weighted MR image of the upper abdomen, the peripheral liver nodules demonstrate increased signal intensity. Multiple hypointense nodules in the spleen create a heterogeneous appearance. The area of focal hyperintensity (arrowheads) represents gastric mucosal involvement. **C.** Ferumoxides-enhanced gradient-echo T2*-weighted MR image shows multiple hyperintense nodules scattered throughout the periphery of the liver (arrows) and a hyperintense, widened periportal tract. (From Koyama T, Ueda H, Togashi K, et al: Radiologic manifestations of sarcoidosis in various organs. *RadioGraphics* 24:87–104, 2004.)

Biliary Hamartomas

CLINICAL AND PATHOLOGIC FINDINGS

Biliary hamartomas, also known as von Meyenburg complexes, are benign malformations of the biliary tract characterized by irregular bile ducts, surrounded by fibrous stroma. These malformations are incidental findings at pathologic examination (in approximately 2.6% of the population) or imaging and almost always produce no clinical symptoms.¹⁰⁹⁻¹²¹ There are also reported associations with both polycystic liver and polycystic kidney disease. Gross pathologic specimens show small gray-white nodules. Malignant transformation is exceedingly rare, with only a few cases reported.

RADIOLOGIC FINDINGS

Biliary hamartomas are near fluid density on all modalities with some variability and appear as multiple small cysts measuring 0.5 to 1.5 cm without a capsule. Their small size helps differentiate them from simple hepatic cysts. There is no communication with the biliary tree, which can be nicely demonstrated with magnetic resonance cholangiopancreatography (MRCP). The larger lesions may be detected at imaging as multiple focal lesions, often simulating a multifocal or diffuse process. On sonographic evaluation, these lesions appear small, hypoechoic, heterogeneous, and well circumscribed. CT may show numerous small, hypoattenuating lesions on unenhanced scans that persist and may be more conspicuous as hypoattenuating lesions on postcontrast imaging. MRI (Fig. 89-19) reveals small nodules as hypointense on T1-weighted and hyperintense on T2-weighted images compared with normal parenchyma. Contrast enhancement is usually not present on CT or MRI, with the exception of some reported cases demonstrating thin peripheral enhancement.¹⁰⁹⁻¹²¹

Primary Biliary Cirrhosis

Primary biliary cirrhosis is a chronic, usually progressive liver disease characterized by inflammation and destruction of

interlobular and septal bile ducts, leading to chronic cholestasis, cirrhosis, and ultimately hepatic failure (Fig. 89-20). This is a relentless process in which the initial destructive cholangitis is followed by proliferation of atypical bile ductules, scarring, and septum formation. The etiology of this disorder is unknown, and autoimmune, genetic, and endocrine abnormalities have been postulated.¹²²⁻¹²⁷

CLINICAL AND PATHOLOGIC FINDINGS

Patients afflicted with primary biliary cirrhosis are more than 90% female and between the ages of 30 and 65 years. Pruritus and fatigue are often the first clinical symptoms, followed by jaundice months to years later. Physical findings include hepatomegaly (50%), hyperpigmentation (50%), and xanthomas

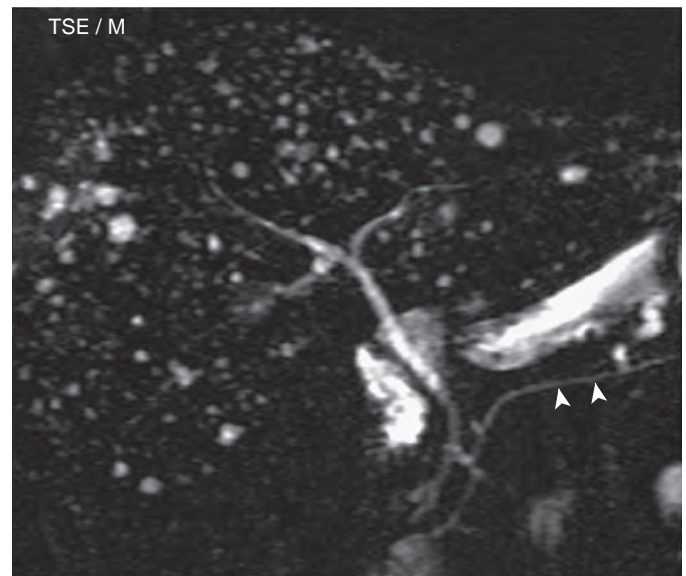


Figure 89-19 Multiple bile duct hamartomas. Magnetic resonance cholangiopancreatography image demonstrates multiple high signal intensity bile duct hamartomas. Arrowheads, Pancreatic duct.

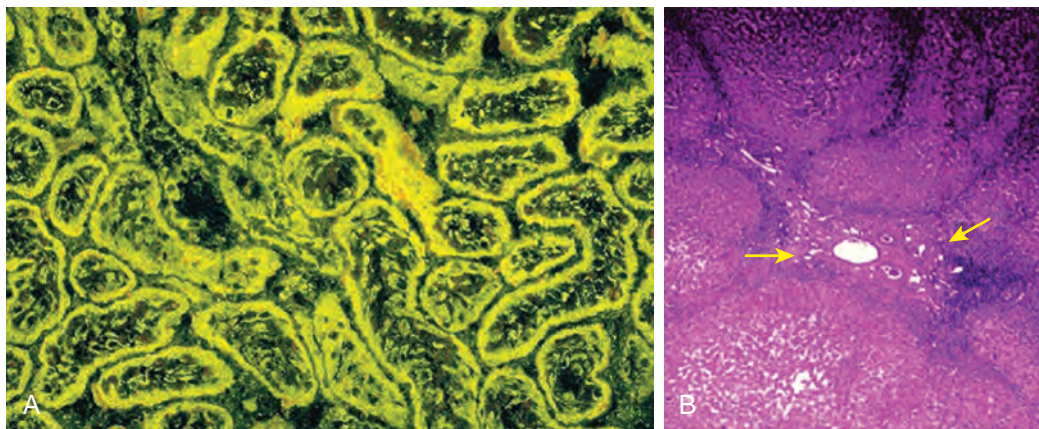


Figure 89-20 Primary biliary cirrhosis: pathologic findings. **A.** Immunofluorescent stain shows antimitochondrial antibodies, typical of this disease. **B.** Photomicrograph of liver tissue from a 41-year-old woman with primary biliary cirrhosis with MR periportal halo sign. Stellate areas of hepatocellular parenchymal extinction (arrows) around portal triads can be seen. Larger and more variably sized regenerative nodules encircle periportal halo sign. *AJR Am J Roentgenol* 176:885-889, 2001. Reprinted with permission from the American Journal of Roentgenology.)

(25%).¹²²⁻¹²⁷ Other commonly associated autoimmune disorders are Hashimoto's thyroiditis, scleroderma, lupus, the sicca complex, celiac disease, and even other hepatic disorders, including autoimmune hepatitis and primary sclerosing cholangitis.¹²²⁻¹²⁷ Other organ systems are affected late in the disease; findings of osteomalacia with pathologic fractures, muscle wasting, palmar erythema, and clubbing are observed.

The first abnormality detected at routine checkup in an asymptomatic individual may be increased serum alkaline phosphatase and elevated cholesterol concentration. Bilirubin and transaminase levels may be normal or slightly elevated. Diagnosis of primary biliary cirrhosis is serologic and based on detection of high titers of antimitochondrial antibody and cryoproteins composed of immunoglobulins M and G (90%-95%), which are pathognomonic. The presence of antinuclear antibody (30%-50%), anti-smooth muscle antibody (30%-90%), rheumatoid factor (25%-60%), and antithyroid antibody (15%-26%) can also be seen.¹²²⁻¹²⁷ As the disease evolves, conjugated bilirubin becomes progressively elevated and may reach 30 mg/dL.¹²²⁻¹²⁷

Untreated, patient survival ranges between 7.5 and 16 years.¹²⁸ Treatment consists of anti-inflammatory agents; immunosuppressants, such as steroids, methotrexate, cyclosporine, and azathioprine; and D-penicillamine, which lowers the hepatic copper concentration and reduces circulating immune complexes and autoantibodies. Cholestyramine and rifampicin are given to treat the pruritus.¹²²⁻¹²⁷ Liver transplantation is definitive treatment in patients with advanced disease. Primary biliary cirrhosis is the third most common indication for hepatic transplantation in adults, following viral and alcohol-induced cirrhosis. Primary biliary cirrhosis can recur after transplantation within 30% within 10 years and usually with a milder course.¹²⁸

Liver biopsy is often unnecessary but can be performed when the diagnosis is equivocal. Four pathologic stages of primary biliary cirrhosis based on location of inflammatory and fibrotic changes are described. Stage 1 disease is associated with portal

inflammation; in stage 2, inflammation extends periportal, and there is bile duct proliferation; in stage 3, there is fibrosis, which extends into the septal region; and in stage 4, disease cirrhosis is present. All four stages may occur simultaneously, and the distribution may be nonuniform.¹²⁸

RADIOLOGIC FINDINGS

Endoscopic retrograde cholangiopancreatography (ERCP) is the primary radiographic technique for imaging evaluation of primary biliary cirrhosis, and cross-sectional imaging should be used to exclude extrahepatic causes of biliary obstruction and biliary cirrhosis. On ERCP, there is pruning of the peripheral bile ducts, which results in a "tree in winter" appearance. The cross-sectional imaging findings in primary biliary cirrhosis are discussed in detail in Chapter 80. Briefly, early in the course of the disease, the liver is enlarged and remains smooth in contour. Regenerative nodules later develop with hepatic atrophy, distortion, and progression to cirrhosis. Gallstones and lymphadenopathy are also frequently present. On ultrasound, the liver is heterogeneous and hyperechoic as in other forms of cirrhosis. Nodules are hyperdense on CT, isointense on T1-weighted MRI, and hypointense on T2-weighted MRI. Lacelike fibrosis surrounds the nodules and is T1 hypointense, T2 hyperintense. A reportedly specific finding (present within 43%) for primary biliary cirrhosis is the MRI "periportal halo" sign, multiple T1- and T2-weighted regions of low signal intensity measuring 5 to 10 mm surrounding small portal vein branches without mass effect in both lobes. This finding is thought to be a result of fibrosis or focal cellular depletion¹²⁹ (Fig. 89-21).

Secondary Biliary Cirrhosis

Secondary biliary cirrhosis results from long-standing partial or complete obstruction of the common bile duct

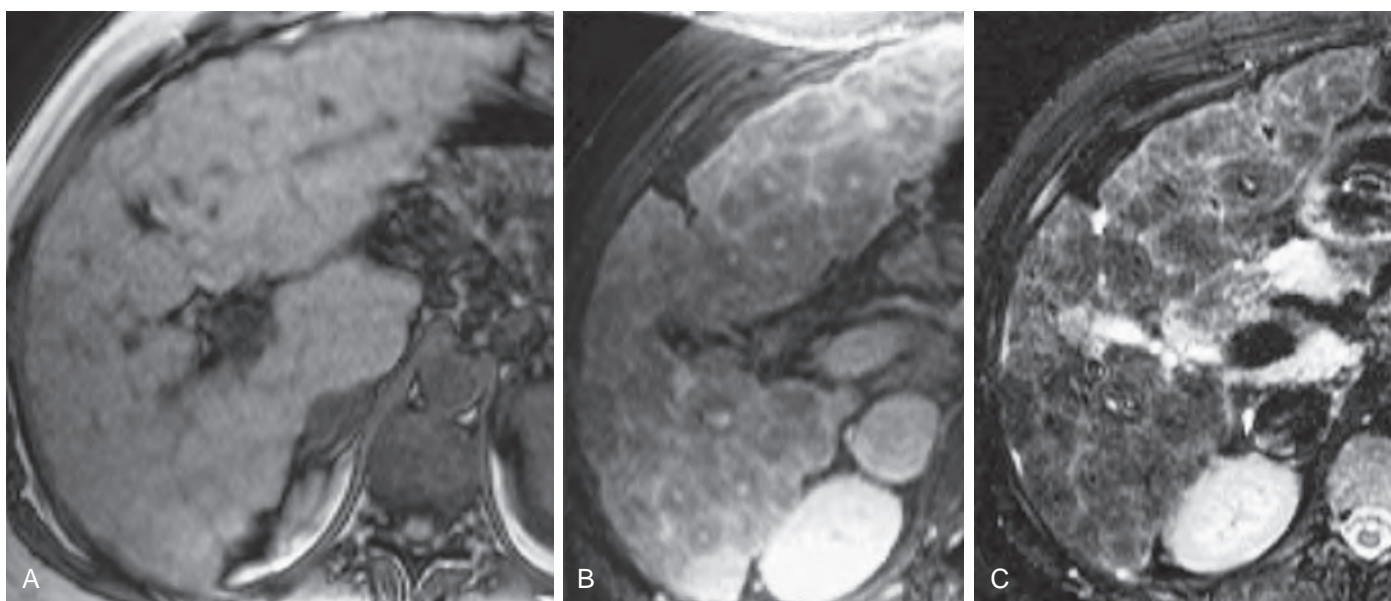


Figure 89-21 Primary biliary cirrhosis: MR findings. **A.** T1-weighted, unenhanced MR image shows numerous small regenerative nodules. **B.** T1-weighted MR image obtained 3 minutes after infusion shows conspicuous areas of low signal intensity around portal veins. **C.** T2-weighted single-shot fast spin-echo MR image reveals round areas of low signal intensity encircling portal veins.

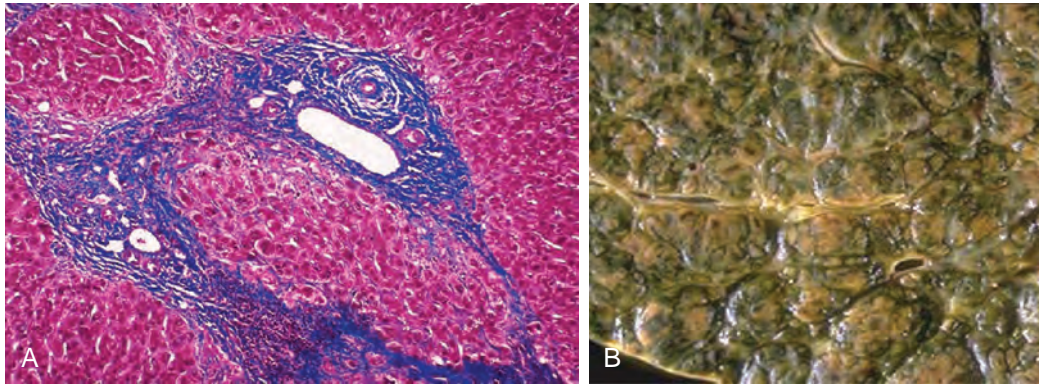


Figure 89-22 Secondary biliary cirrhosis due to primary sclerosing cholangitis: pathologic findings. **A.** Trichrome histologic stain shows fibrosis surrounding the bile ducts. **B.** End-stage macronodular cirrhosis is seen in this specimen. Note the greenish hue of the liver.

or its major branches. Causes include postoperative strictures or choledocholithiasis often with superimposed infectious cholangitis, chronic pancreatitis, primary sclerosing cholangitis, pericholangitis of ulcerative colitis, and cystic fibrosis. Congenital atresia of the intrahepatic or extrahepatic bile ducts induces rapidly advancing periportal fibrosis in infants.

Primary sclerosing cholangitis is an idiopathic disease of chronic cholestasis of the extrahepatic and large intrahepatic bile ducts (discussed in detail in Chapters 74, 75, and 80). Similar to primary biliary cirrhosis, it is of unknown etiology with evidence for autoimmune and genetic components. Histologic grading of primary sclerosing cholangitis is similar to that of primary biliary cirrhosis (Fig. 89-22).

Cirrhosis as a result of primary sclerosing cholangitis is associated with pronounced lobulation of the liver contour, atrophy of the posterior right lobe and left lateral segment of the left lobe, and hypertrophy of the caudate lobe. Atrophy of the lateral segment of the left lobe is distinctive (Fig. 89-23) because hypertrophy rather than atrophy of the lateral segment of the left lobe is typical in most other forms of cirrhosis. The caudate lobe may have a higher attenuation than the remainder of the liver on noncontrast scans, producing a pseudotumor appearance. Enlarged lymph nodes in the lesser omentum are also common.¹²⁹⁻¹³⁷

On MRI (Fig. 89-24), peripheral wedge-shaped zones of hyperintense signal can be seen on T2-weighted images. These triangular areas range in size from 1 to 5 cm. On T1-weighted images, areas of increased signal intensity in the liver that do not correspond to fat may be seen. After the administration of contrast material, areas of increased enhancement that are patchy or segmental are frequently seen. These areas often remain mildly or markedly hyperintense on delayed images. Primary sclerosing cholangitis often produces large regenerative nodules that may cause obstruction of bile ducts and ultimately segmental atrophy of the peripheral liver.¹²⁹⁻¹³⁷

Clinical history is important in differentiating between causes of secondary biliary cirrhosis. Evidence of cholecystectomy, chronic pancreatitis, or biliary stones may be helpful. The treatment approach is the same as in primary biliary cirrhosis for end-stage disease and is curative only with liver transplantation.

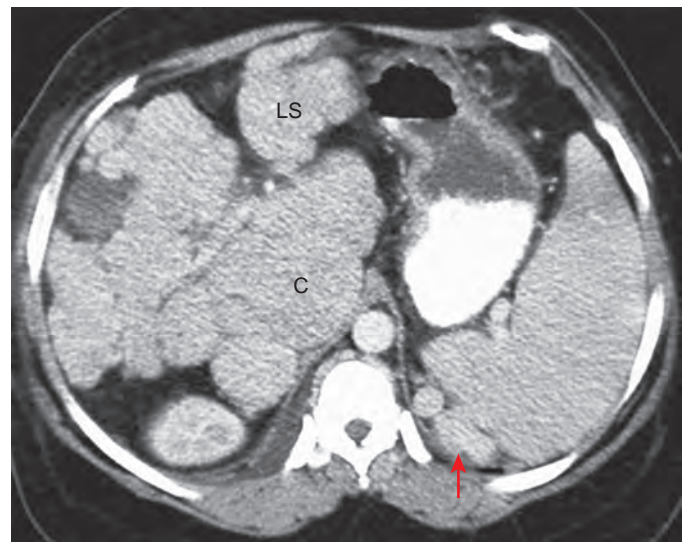


Figure 89-23 Secondary biliary cirrhosis due to primary sclerosing cholangitis: CT findings. Advanced cirrhotic changes are present with a markedly lobulated liver, enlargement of the caudate lobe (C), and widening of the fissures. There is atrophy of the lateral segment (LS) of the left lobe, which is a key differentiating feature from alcoholic and posthepatic cirrhosis. Note the splenomegaly and retroperitoneal varices (arrow).

Acquired Immunodeficiency Syndrome

CLINICAL FINDINGS

With improved survival of AIDS patients since the introduction of antiretroviral therapy, hepatic manifestations of AIDS have increased in prevalence and are now the leading cause of death (14%-18%). The hepatobiliary disease profile affecting AIDS patients, which includes infection, malignant neoplasm, autoimmune abnormalities, and drug toxicity, has also changed.¹³⁸⁻¹⁴¹

A long list of opportunistic infections including viral, bacterial, and fungal that can be a result of the immunocompromised state of HIV infection and AIDS can cause primary or disseminated infection of the liver. Before antiretroviral therapy, the most common infectious organisms were cytomegalovirus and

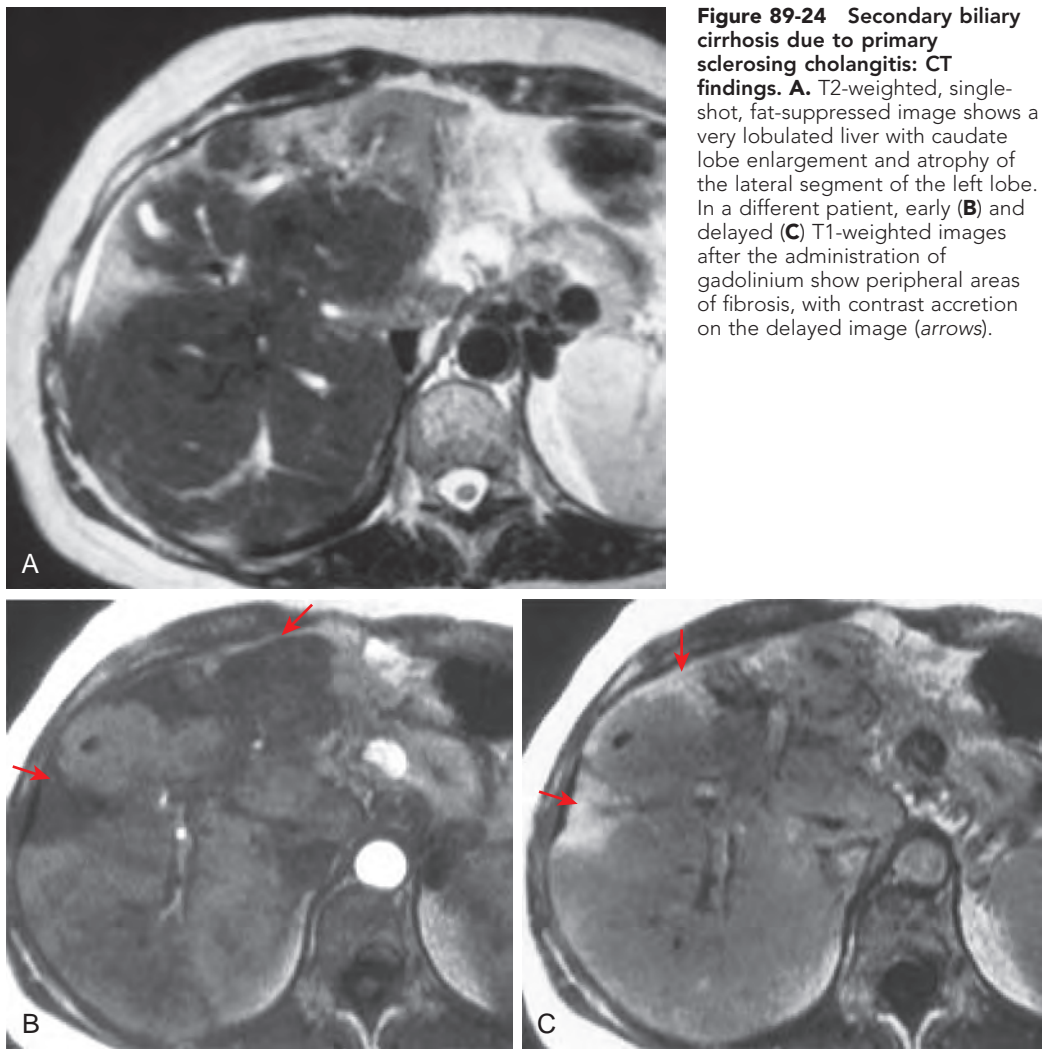


Figure 89-24 Secondary biliary cirrhosis due to primary sclerosing cholangitis: CT findings. **A.** T2-weighted, single-shot, fat-suppressed image shows a very lobulated liver with caudate lobe enlargement and atrophy of the lateral segment of the left lobe. In a different patient, early (**B**) and delayed (**C**) T1-weighted images after the administration of gadolinium show peripheral areas of fibrosis, with contrast accretion on the delayed image (arrows).

non-tuberculosis *Mycobacterium*. Although these and other infectious agents (Table 89-2) continue to affect AIDS patients, currently the most clinically significant coinfection with HIV infection is viral hepatitis. Concurrent hepatitis B is present in 25% and hepatitis C in 10% of HIV-infected patients because of a similar route of transmission. The increased life span of AIDS patients receiving antiretroviral therapy can result in adequate time for chronic viral hepatitis to progress to cirrhosis. This progression is also accelerated in the setting of coinfection with HIV infection in comparison to patients with viral hepatitis alone. Cirrhosis and its comorbidities, including HCC, are now a significant cause of death in the AIDS population. *Mycobacterium avium* complex and cytomegalovirus remain the most common hepatic infections in AIDS. Interestingly, *Pneumocystis jiroveci* can preferentially involve the liver when inhaled prophylactics protect the lungs. Another entity known as bacillary peliosis hepatitis, a rare process in which blood-filled cavities form in the liver, replacing the parenchyma, is associated with *Bartonella* infection.¹³⁸⁻¹⁴¹

AIDS patients are at increased risk for malignant disease including AIDS-related lymphoma and Kaposi's sarcoma. Non-Hodgkin's lymphoma involves the liver in 33% of cases and can be manifested nonspecifically with pain or jaundice and with

TABLE 89-2 Hepatic Infections in AIDS

VIRAL
Hepatitis A, B, C, D, E
Cytomegalovirus
Herpes simplex virus
Human herpes virus 6
Varicella-zoster virus
Epstein-Barr virus
Adenovirus
FUNGAL
<i>Cryptococcus neoformans</i>
<i>Histoplasma capsulatum</i>
<i>Coccidioides immitis</i>
<i>Candida albicans</i>
<i>Aspergillus fumigatus</i>
OTHER
<i>Mycobacterium avium</i>
<i>Mycobacterium tuberculosis</i>
<i>Pneumocystis</i>
<i>Toxoplasma gondii</i>
<i>Strongyloides stercoralis</i>
Microsporidia
<i>Bartonella henselae</i>

nonspecific increase in liver function test results. Kaposi's sarcoma involves the liver in 9% of cases and clinically is most often asymptomatic. HCC, as mentioned before, and other malignant neoplasms, such as anal and cervical cancers, are other important malignant neoplasms to consider in the AIDS patient.

Drug therapies commonly used to treat AIDS patients, including antimycobacterial agents, acyclovir, and sulfonamides, can unfortunately be hepatotoxic.¹⁴¹ This can be manifested with mild symptoms and elevation of liver function test results to fulminant hepatic failure. The hepatotoxic effect of these drugs is increased when there is concurrent viral hepatitis and HIV infection. The mechanisms for hepatic damage include direct drug toxicity, hypersensitivity reactions, mitochondrial toxicity, and immune reconstitution inflammatory syndrome.

Biliary disease in AIDS patients encompasses AIDS cholangiopathy and acalculous cholecystitis, both attributed to infectious causes, most commonly cryptosporidium and cytomegalovirus. Other infectious agents as well as autoimmune diseases as mentioned before can also affect the biliary system. AIDS cholangiopathy results in biliary obstruction, which can clinically be manifested with right upper quadrant pain, fever, nausea, and vomiting. There is marked elevation in alkaline phosphatase, with less increase in bilirubin and normal or slight increase in liver function test results. This is manifested most commonly in patients with low CD4 count and therefore is less common since implementation of antiretroviral therapy, which is also the preferred therapy. Cholecystectomy is preferred in cases of acalculous cholecystitis.¹³⁸⁻¹⁴¹

Other causes of hepatobiliary disease in AIDS patients include NAFLD, alcoholic hepatitis, and autoimmune diseases such as autoimmune hepatitis, primary biliary cirrhosis, and primary sclerosing cholangitis.

PATHOLOGIC FINDINGS

Therapeutic decisions seldom require liver biopsy, nor does biopsy significantly correlate with improved survival. Liver biopsy should be reserved for patients with unexplained fever, patients with an elevated serum alkaline phosphatase level, and those with focal mass lesions seen on imaging studies. The list of opportunistic infections in AIDS patients is long (see [Table 89-2](#)). Organisms can be isolated from biopsy specimens for tailored therapy.

AIDS hepatic disease is histologically nonspecific. Macrovesicular steatosis and portal inflammation represent the most common findings. Hepatic granulomas have been reported in 16% to 100% of biopsy and autopsy specimens. These granulomas are most frequently associated with mycobacterial infection, usually *Mycobacterium avium-intracellulare*. In AIDS cholangiopathy, recovered infectious agents include cryptosporidium and cytomegalovirus. On pathologic examination, there is periductal inflammation. Targeted biopsy of a hepatic mass may be used to diagnose Kaposi's sarcoma or AIDS-related lymphoma.¹³⁸⁻¹⁴¹

RADIOLOGIC FINDINGS

Ultrasound

On ultrasound studies, hepatic parenchymal abnormalities in AIDS patients include hyperechoic parenchyma (45.5%), hepatomegaly (41%), and focal masses (9%). Hepatic steatosis and

granulomatous hepatitis are responsible for increased echogenicity of the liver.^{12,141} It is postulated that the tiny aggregates of histiocytes found in granulomas act as multiple reflective interfaces that produce the hyperechoic pattern. Metastatic Kaposi's sarcoma, lymphoma, pyogenic abscess, fungal or mycobacterial abscess, and preexisting benign lesions such as hemangiomas can also be seen sonographically as focal masses.^{28,141}

On ultrasound, AIDS cholangiopathy is manifested with periportal hyperechoic and hypoechoic regions associated with mural thickening of the gallbladder, cystic duct, and bile ducts and can simulate primary sclerosing cholangitis. Acalculous cholecystitis is manifested with gallbladder wall thickening and distention without cholelithiasis and can be manifested acutely with a sonographic Murphy sign, pain, and fever. The biliary manifestations of AIDS are also illustrated in Chapter 80.

Kaposi's sarcoma is uncommonly seen on ultrasound; however, when present, these lesions may appear as small (5- to 12-mm) hyperechoic nodules with associated dense periportal bands. The presence of hepatomegaly does not predict Kaposi's sarcoma involvement because the liver is commonly enlarged in patients with AIDS or AIDS-related complex even when there is no specific pathologic process.^{28,47,141}

Hepatic lymphoma with ultrasound is usually hypoechoic compared with the normal liver parenchyma and may be anechoic and septate, mimicking a fluid collection. Associated adenopathy in the porta hepatis and retroperitoneum can be present but is nonspecific; it may also be present as a result of AIDS alone, chronic hepatitis, infection, or other neoplasm.^{28,47,141}

Computed Tomography

On CT scans, patients with AIDS generally demonstrate hepatomegaly that is often associated with focal or diffuse fatty infiltration. Patients with long-standing hepatitis and postnecrotic change may also present with cirrhosis. Periportal lymphedema seen as low attenuation surrounding the large portal branches is also common and reflects lymphadenitis, hepatitis, or malnutrition.¹⁴¹

Cirrhosis can occur in an accelerated fashion when both HIV infection and viral hepatitis are present; they are indistinguishable from other causes of cirrhosis at imaging, other than possibly by a more rapidly progressive disease course. Screening for HCC with multiphase contrast-enhanced CT is also necessary.

Lymphoma is particularly aggressive in AIDS patients, and hepatic involvement is manifested on CT scans by focal hypodense lesions because of the high cellular content. CT abnormalities are more commonly found in affected livers in AIDS-associated lymphoma than in those with lymphoma and without AIDS.

Parenchymal calcifications in the liver, spleen, lymph nodes, and kidneys can be seen in patients with healed disseminated *P. jiroveci* infection. Kaposi's sarcoma can involve the liver in AIDS, but the lesions are usually not seen on CT. When present, they appear as small low-attenuation masses often located near the portal triads, which may simulate the appearance of intrahepatic bile ducts or fungal microabscesses. Masses in Kaposi's sarcoma show enhancement on delayed scans, helping to differentiate them from cystic lesions.¹³⁸⁻¹⁴¹

AIDS cholangiopathy is manifested with mural thickening of the gallbladder; gallbladder distention; and intrahepatic and extrahepatic biliary strictures, irregularity, and dilation.¹⁴¹

Endoscopic Retrograde Cholangiopancreatography

ERCP is useful in demonstrating the findings of AIDS cholangiopathy. Irregularity of the intrahepatic and extrahepatic bile duct walls with intervening strictures and dilation simulating primary sclerosing cholangitis is the cholangiographic corollary of biliary abnormalities seen with ultrasound and CT. Specific findings of ampullary stenosis, common bile duct enlargement, and ulcerations of the common bile duct mucosa combined with intrahepatic strictures can help differentiate these entities. ERCP also has the advantage of offering therapeutic relief in these patients by performance of a papillary sphincterotomy.¹³⁸

MRI and MRCP

MRI is most useful to assess AIDS cholangiopathy and demonstrates the dilated and irregular bile ducts, which are hypointense on T1-weighted and hyperintense on T2-weighted imaging. Fat-suppressed T1-weighted dynamic images after the administration of contrast material can demonstrate enhancement along the bile ducts as a result of periportal inflammation. MRI with contrast enhancement is also useful in demonstrating hepatic abscesses, whether bacterial or fungal, and is more sensitive than ultrasound and CT. MRI can also help differentiate abscesses from malignant disease. Another advantage of MRI is the large field of view permitting assessment for concurrent disease of other abdominal organs, particularly the spleen. Cirrhosis and other nonspecific findings in AIDS-related hepatic disease, including lymphadenopathy, focal masses, and fatty infiltration, can also be seen at MRI with high sensitivity.

MRCP, a heavily T2-weighted, high-resolution sequence that is similar to ERCP, can noninvasively demonstrate enlargement and focal irregularities from strictures of the intrahepatic and extrahepatic biliary tree. These appear hyperintense because of the fluid content and may be subtracted from the surrounding

hepatic parenchyma and other background with the use of a long echo time. Enlargement of the common bile duct from ampullary stenosis can also readily be seen.¹³⁸⁻¹⁴¹

Cirrhosis

EPIDEMIOLOGY

Cirrhosis is the end response of the liver to chronic inflammation complicated by parenchymal necrosis and fibrosis. Nodular regeneration also occurs; as a result, there is disorganization of the hepatic lobular and vascular architecture coupled with deteriorating hepatic function. Cirrhosis can result from a variety of causes. The most common worldwide is hepatitis B, closely followed by alcohol abuse, NAFLD, and hepatitis C.

Cirrhosis is one of the leading causes of death in the Western world and was the ninth leading cause in the United States in 2012. Age-adjusted mortality is 2.3 times higher in males than in females and 1.7 times higher in black than in white persons. The mortality rate from cirrhosis has also shown a major increase in the United States during the past 25 years; it is a significant cause of premature death, the fifth leading cause of death in the 45- to 64-year age group, and the third leading cause of death for men 34 to 54 years of age. One third of deaths related to cirrhosis are consequent to hemorrhage, usually from esophageal varices.¹⁴²⁻¹⁴⁵

PATHOPHYSIOLOGY

Although no completely satisfactory scheme for the classification of cirrhosis (Fig. 89-25) has been developed, the disorder has traditionally been divided into several categories: (1) micronodular cirrhosis, in which equal-sized nodules up to 3 mm in diameter involve every lobule; (2) macronodular (postnecrotic) cirrhosis, characterized by variable-sized nodules (3 mm to 3 cm) that are focal and do not involve every lobule;



Figure 89-25 Cirrhosis: pathologic findings.

A. Photomicrograph shows a regenerative nodule (RN) with surrounding fibrosis, the key pathologic finding in cirrhosis. This patient had hepatitis C cirrhosis. **B.** Micronodular cirrhosis is evident in this specimen image of a patient with alcoholic cirrhosis. **C.** Larger nodules are present in this specimen image of macronodular cirrhosis.

and (3) mixed cirrhosis. Alcoholic cirrhosis is associated with the micronodular pattern. Viral hepatitis is associated with the macronodular pattern. Other causes include primary and secondary biliary cirrhosis and hemochromatosis.¹⁴²⁻¹⁴⁵ A more complete listing of the causes of cirrhosis can be found in Table 89-3.

On pathologic examination, all forms of cirrhosis share the following characteristics: (1) the entire parenchymal architecture is disorganized by interconnecting fibrous scars formed in response to hepatocyte injury and death; (2) the fibrosis may appear as delicate portal-central or portal-portal bands or constitute broad scars replacing multiple adjacent lobules; (3) the micronodules or macronodules are created by regenerative activity with the intervening network of scars; and (4) the vascular architecture of the liver is reorganized by the parenchymal damage and scarring with formation of abnormal arteriovenous interconnections.

Regenerative nodules have been further classified as siderotic or nonsiderotic, with a greater tendency for siderotic nodules to undergo malignant transformation. The increased incidence of HCC in patients with cirrhosis has been shown in part to be a progression of dysplasia within regenerative nodules, with the precursor to HCC being dysplastic nodules.¹⁴²⁻¹⁴⁵ HCC may be seen in patients infected with hepatitis B virus without development of cirrhosis. The presence of dysplastic nodules confers an increased risk of HCC through dedifferentiation not only of the dysplastic nodule itself but also in other regions of the liver. Longitudinal studies indicate that dysplastic nodules remain stable in size unless there is progression to HCC.^{146,147} Dysplastic nodules have been reported to occur in 15% to 25% of patients with cirrhosis (usually less than 10 per liver) on the basis of histopathology data,^{146,147} although typically not all dysplastic nodules are identified at imaging.

Life-threatening complications of cirrhosis are related to decline in hepatic function and development of portal hypertension.¹⁴²⁻¹⁴⁵ Ascites is the most common complication of cirrhosis and is associated with nearly 50% of deaths. Variceal hemorrhage in patients with ascites accounts for nearly 25% of deaths; 10% are due to renal failure resulting from the hepatorenal syndrome, 5% result from spontaneous bacterial peritonitis in patients with massive ascites, and 10% are due to the complications of interventions for ascites.¹⁴²⁻¹⁴⁵

A third potentially life-threatening sequela of cirrhosis is the development of HCC. Its incidence varies with the underlying

etiology, with an increased incidence in cirrhosis caused by alcoholism and a 2.5-fold greater occurrence in cirrhosis with hepatitis B surface antigen positivity. HCC has also been reported in patients with various other types of cirrhosis, including primary biliary cirrhosis, NASH, Wilson's disease, and hemochromatosis.¹⁴²⁻¹⁴⁵

PORTAL HYPERTENSION

The fibrosis of the liver that occurs with cirrhosis can result in dramatic changes in the hepatic circulation. The scarred parenchyma causes an increase in intrahepatic vascular resistance that decreases portal venous liver perfusion. This leads to increased pressure within the portal system, normally between 5 and 10 mm Hg; portal hypertension is defined as a portal venous pressure of more than 10 mm Hg.

The hepatic artery, with a higher systemic pressure and muscle support of its wall, increases its flow and contribution of blood supply to the liver, allowing partial compensation. In addition, capillarization of the sinusoids is observed in the form of endothelial defenestration, deposition of collagen in the extravascular spaces of Disse, and formation of basal laminae. The transit time of large and small molecules, including contrast material, is significantly affected by the sinusoidal capillarization.¹⁴⁵

Portal hypertension may develop in a variety of clinical conditions but is most often secondary to cirrhosis. The causes of portal hypertension (Table 89-4) have been classically divided

TABLE 89-3 Etiology of Cirrhosis

Alcoholic cirrhosis (60%-70%)
Postnecrotic: viral hepatitis (10%)
Biliary cirrhosis: primary and secondary (5%-10%)
Pigment cirrhosis: hemochromatosis (5%)
Cardiac failure
Constrictive pericarditis
Hepatic vein obstruction
Malnutrition
Hereditary: Wilson's disease, α_1 -antitrypsin deficiency, galactosemia, tyrosinemia, hereditary tetany, hereditary fructose intolerance, type IV glycogen storage disease, Osler-Weber-Rendu syndrome
Drug induced: methotrexate, oxyphenisatin, α -methyl dopa, nitrofurantoin, isoniazid, mithramycin, 6-mercaptopurine, azathioprine

TABLE 89-4 Classification of Portal Hypertension

PREHEPATIC

Portal vein thrombosis
Splenic vein thrombosis
Node or tumor extrinsic compression of portal vein

Intrahepatic

Presinusoidal
Schistosomiasis
Biliary cirrhosis
Congenital hepatic fibrosis
Neoplasm
Arteriovenous portal fistula
Hyperkinetic portal hypertension

Sinusoidal

Laënnec's cirrhosis
Postnecrotic cirrhosis
Fatty liver
Hepatitis
Sickle cell anemia and sinus thrombosis

Postsinusoidal

Alcoholic cirrhosis
Hepatic vein obstruction
Neoplasm
Veno-occlusive disease

POSTHEPATIC

Congestive heart failure
Constrictive pericarditis
Inferior vena cava webs or thrombosis
Rheumatic heart disease
Neoplasm

into three major groups according to the level of obstruction: presinusoidal, postsinusoidal, and sinusoidal (intrahepatic). In most of these disorders, increased resistance to portal flow is found. In several diseases, there is increased flow into the portal system, so-called hyperkinetic portal hypertension.

Cirrhosis is the most common cause of sinusoidal portal hypertension. It occurs secondary to the mechanical effect of the regenerative nodules and scar tissue that distort the hepatic vascular tree and impedes hepatic drainage and ultimately produces backpressure in the portal system. This alteration in the microcirculatory route leads to portal hypertension.

Presinusoidal obstruction can be caused by schistosomiasis, the leading cause of portal hypertension worldwide. The ova of the schistosomes travel through the mesenteric venous circulation into the portal venous system and implant on small portal radicles within the liver, where they induce inflammation and granuloma formation, resulting in destruction of the portal venules. Other major presinusoidal causes of portal hypertension are portal or splenic vein thrombus, primary biliary cirrhosis, sarcoidosis, myeloproliferative disease, and congenital hepatic fibrosis.^{145,148}

Posthepatic obstruction occurs in patients with veno-occlusive disease (Budd-Chiari syndrome), right-sided heart failure, and constrictive pericarditis (discussed in Chapter 90).

Increased portal flow is an infrequent cause of portal hypertension and is usually secondary to either congenital (hereditary hemorrhagic telangiectasia) or acquired (post-traumatic or aneurysm rupture) arteriovenous fistulas. Hyperkinetic portal hypertension involves increased portal flow without fistulas, splenomegaly, and increased flow in the splenic artery and vein.

Varices

With increasing portal hypertension, portal venous blood flow seeks a pathway of less resistance and can change direction, resulting in the formation of portosystemic collateral vessels known as varices. These can be classified into two groups: varices that drain toward the superior vena cava and varices that drain toward the inferior vena cava.¹⁴⁸

Varices That Drain into the Superior Vena Cava. The left gastric (coronary) vein is the most common visible varix in portal hypertension. It is located in the gastrohepatic ligament and drains into the superior vena cava. The normal left gastric vein drains both the anterior and posterior surfaces of the stomach, and it ascends the lesser curvature within the lesser omentum to the esophageal hiatus, where it anastomoses with the esophageal veins. The left gastric vein divides into anterior branches draining to the esophageal veins and posterior branches draining to the paraesophageal veins. Left gastric varices typically are accompanied by esophageal or paraesophageal varices. Esophageal and paraesophageal varices usually drain into the azygos-hemiazygos venous system but may also enter the subclavian-brachiocephalic system through the left pericardiophrenic vein or the inferior vena cava through the inferior phrenic vein. When the left gastric vein is larger than 5 to 6 mm in diameter, portal hypertension should be considered. A left gastric vein larger than 7 mm in diameter is associated with a portohepatic gradient greater than 10 mm Hg.¹⁴⁸

Short gastric veins are present in the gastrosplenic ligament and drain the gastric fundus. They communicate with the splenic vein or one of its large tributaries along the greater

curvature of the stomach. These vessels can be dilated in isolation with splenic vein thrombosis.¹⁴⁸

Varices That Drain into the Inferior Vena Cava. The splenic vein and left and short gastric veins communicate with the left renal vein through the splenorenal and gastrosplenic ligaments, respectively. Reversal of blood flow in these veins from portal hypertension can cause preferential drainage into the left renal vein and a splenorenal or gastrosplenic shunt. Normally, four or five short gastric veins drain the gastric fundus and the left part of the greater curvature, traversing the gastrosplenic ligament to reach the splenic vein. Short gastric veins should be smaller than 5 mm in diameter. Gastrosplenic and splenorenal shunts are seen as varices in the region of the splenic and left renal hilum that drain into an enlarged left renal vein. This may cause fusiform dilation of the inferior vena cava at the level of the left renal vein.¹⁴⁸

Small veins normally found in the ligamentum teres and falciform ligament can enlarge and form paraumbilical varices arising from the left portal vein. These vessels may also course through the medial segment of the liver rather than the ligamentum teres. Paraumbilical varices can anastomose either with the superior epigastric or internal thoracic veins and drain into the superior vena cava or with the inferior epigastric vein and then drain into the inferior vena cava through the external iliac vein. Varices in the anterior abdominal wall surrounding the umbilicus produce the “Medusa’s head” appearance.¹⁴⁸

Collateral vessels may also arise from the superior and inferior mesenteric veins within the subperitoneal space of the small bowel mesentery. These usually drain into the retroperitoneal or pelvic veins. A retroperitoneal shunt may develop between the mesenteric vessels and the renal vein or inferior vena cava. Veins of Retzius are communications between the inferior vena cava and intestinal or retroperitoneal tributaries of the superior or inferior mesenteric veins and systemic veins.¹⁴⁸

The intrahepatic portal veins can form collateral pathways with hepatic venous branches or direct communication with the left gastric vein. There is a loose collateral plexus over the hepatic surface, and it is sometimes widely distributed over the parietal peritoneum with branches piercing the diaphragm to join pericardial, pleural, and pulmonary veins, the so-called pleuropericardial collaterals. The intercostal veins may also dilate and help drain hepatofugal blood flow through the azygos-hemiazygos system.¹⁴⁸

GENERAL RADIOLOGIC FINDINGS: CIRRHOSIS

Liver Morphology

Many of the morphologic changes that occur in cirrhosis can be appreciated with multiple modalities, including ultrasound, CT, and MRI. These include gross changes in the hepatic size, vascular changes, and extrahepatic findings (Table 89-5).

Changes in the hepatic parenchyma in cirrhosis occur in a predictable pattern with asymmetric atrophy of the right lobe and medial left lobe and preservation or increase in size of the lateral left lobe and caudate lobe. These changes can often be qualitatively observed but can also be demonstrated quantitatively with comparative measurements. The normal size ratio of the right lobe to the left lobe is 1.44. In cirrhosis, this ratio decreases to less than 1.3, most prominent in viral hepatitis-associated cirrhosis (mean, 1.17) and less

TABLE 89-5 Cirrhosis: Morphologic Features

Nodular hepatic contour
Enlarged caudate lobe
Enlarged lateral segment of left lobe
Atrophy of the right and quadrate lobes
Prominence of the fissures and porta hepatis
Portal hypertension: varices, ascites, splenomegaly
Fatty infiltration
Colonic interposition
Altered gallbladder angle
Increased density of mesenteric fat
Regenerative nodules
Intrahepatic arterial-portal fistulas
Fibrosis (focal confluent or lacy network surrounding nodules)

pronounced in non-hepatitis-related cirrhosis (mean, 1.25). A ratio of 1.40 reportedly excludes cirrhosis in 100% of cases; a ratio of 1.35 has 90% sensitivity, 82% specificity, and 81% accuracy; a ratio of 1.3 has 74% sensitivity, 100% specificity, and 93% accuracy.¹⁴⁸⁻¹⁵⁵

Hepatic segment IV also undergoes atrophy in patients with cirrhosis. Compared with a normal mean diameter of 43 ± 8 mm (standard deviation), the mean diameter of segment IV is 28 ± 9 mm in patients with cirrhosis. The cause or severity of cirrhosis had no influence on the size of segment IV.¹⁵⁴ Lafortune and colleagues¹⁵⁴ found that measurement at ultrasound of the transverse diameter of segment IV had a sensitivity of 74% for the diagnosis of cirrhosis, with a specificity of 100%.¹⁵⁴ The transverse diameter was obtained from a measurement between the left wall of the gallbladder and the ascending portion of the left portal vein at the point where it gives rise to the segment IV branch. These results were obtained by use of a lower limit of normal diameter of 30 mm, with atrophy below that indicative of cirrhosis.

Measurements of the ratio of the caudate lobe size to that of the right lobe have been reported to be accurate in diagnosing the presence or absence of cirrhosis. To determine the caudate lobe-to-right lobe ratio, the caudate lobe is measured transversely from its most medial aspect to the right lateral wall of the main portal vein, just caudal to its bifurcation. The right lobe is measured from the same portion of the main portal vein to the right lateral margin of the liver. If the caudate lobe-to-right lobe ratio exceeds 0.65, the diagnosis of cirrhosis can be made with 96% confidence. By use of this sole criterion, the diagnosis can be made with a sensitivity of 84%, specificity of 100%, and accuracy of 94%. The normal caudate lobe-to-right lobe ratio is 0.37, and the mean ratio in cirrhotic livers is 0.83. An alternative measurement uses the right portal venous bifurcation rather than the bifurcation of the main portal vein to mark the lateral boundary of the hypertrophied caudate lobe and central liver from the atrophied right lobe.¹⁵⁶

The gallbladder and interlobar fissure also undergo counter-clockwise rotation in patients with cirrhotic liver morphology. These topographic alterations may be quantified by measuring the gallbladder angle. This angle is determined by drawing a line through the interlobar fissure, gallbladder neck, or medial aspect of the anterior segment of the right hepatic lobe (whichever is visible) and the inferior vena cava. Another line is drawn coronally through the inferior vena cava parallel to the patient's back. The gallbladder angle subtended by these lines is a useful marker of gallbladder position. In normal patients, the angle is

46 degrees, but in cirrhosis, the angle is reduced to 35 degrees. Thus, the gallbladder becomes a more lateral and superficial structure in cirrhosis, prone to inadvertent injury during "blind" liver biopsy, surgery, and percutaneous transhepatic procedures.¹⁵⁶⁻¹⁵⁹

The alterations in segmental hepatic anatomy described previously produce profound changes in the topography of the right upper quadrant. Colonic interposition between the liver and the anterior lateral abdominal wall or diaphragm is seen in 25% of cirrhotic patients as opposed to 3% of control subjects on CT scans.¹⁵⁶⁻¹⁵⁹ Although these measurements do reflect the underlying morphologic changes and are documented in peer-reviewed literature, they are infrequently needed in clinical practice to diagnose cirrhosis.¹⁵⁶⁻¹⁵⁹

A vascular corollary of the changes in the segmental morphology of the liver has been described. Normally, the diameter of the right portal vein is greater than that of the left portal vein because the right hepatic lobe is larger than the left lobe. When the lateral segment of the left lobe hypertrophies and the right lobe atrophies, the left portal vein diameter becomes equal to or greater than the right portal vein diameter. The sensitivity and specificity of this finding are 85% and 88%, respectively, for alcoholics without recanalization of the umbilical vein.¹⁴²⁻¹⁵⁸

The cirrhotic liver is defined by the presence of both nodules and fibrosis. A spectrum of nodules (Figs. 89-26 and 89-27) ranging from benign regenerative nodules to HCC can be visualized on pathologic examination and cross-sectional imaging.¹⁶⁰⁻¹⁷⁰ Regenerative nodules are a benign process that is the liver's response to cellular injury and attempt at parenchymal repair. Dysplastic nodules are thought to be an evolutionary process from a dominant large regenerative nodule associated with increased iron content, the siderotic nodule. These nodules are at risk for malignant transformation.

At the time of transplantation, approximately 20% of patients with hepatitis B or C and 10% of patients with alcohol-induced cirrhosis will harbor an occult HCC. For detection, noncontrast, late arterial, portal venous, and delayed phase imaging sequences after administration of a large bolus of contrast material are important. Even with optimum technique, 35% to 40% of lesions will not be detected.¹⁶⁰⁻¹⁷⁰ The cirrhotic liver also demonstrates pseudotumors, such as focal confluent fibrosis, and vascular anomalies, including arteriportal shunts, small arteriovenous malformations, and hemangiomas.¹⁶⁰⁻¹⁷⁰

The fibrosis seen in cirrhosis is usually a diffuse, lacy process that surrounds and increases the conspicuity of regenerative nodules throughout the liver parenchyma. In patients with advanced cirrhosis, approximately 30% will develop collapse of normal hepatic architecture and replacement of liver parenchyma with massive, confluent regions of fibrosis, termed focal confluent fibrosis (see Fig. 89-27). This can simulate a mass. Fortunately, associated morphologic changes are often present that allow characterization of focal confluent fibrosis. These lesions most commonly affect the anterior segment of the right lobe and the medial segment of the left lobe, usually with a wedge-shaped appearance radiating from the porta hepatis. Another key differentiating feature is associated focal capsular retraction over the abnormal region due to atrophy in the fibrotic region. Most untreated tumors, by comparison, cause a bulge in the overlying liver contour. When focal confluent fibrosis has an atypical appearance or location, it can be difficult to differentiate from tumor.¹⁵⁶⁻¹⁵⁹ Contrast enhancement of focal

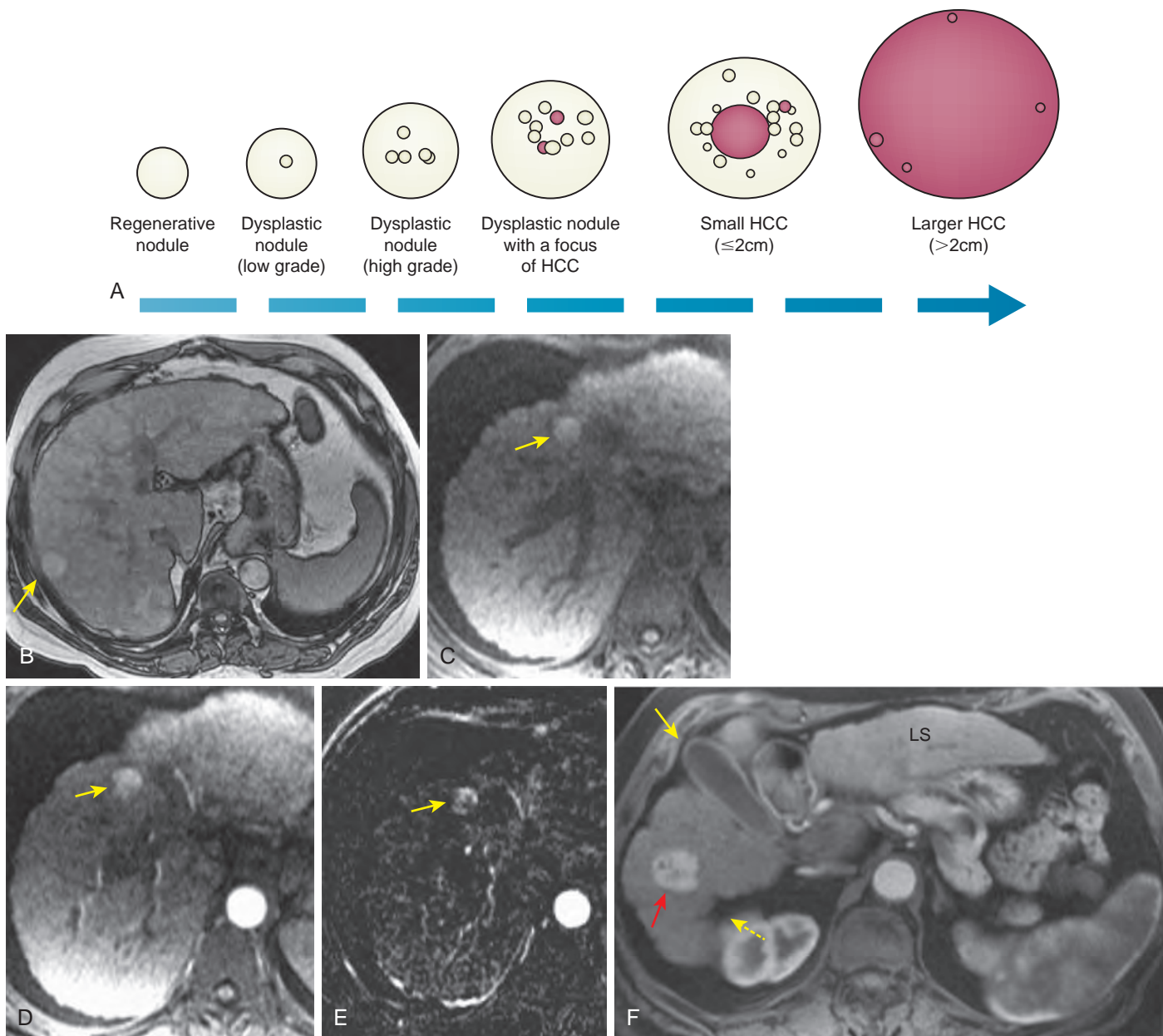


Figure 89-26 Hepatocellular nodules in cirrhosis: MR features. **A.** Stepwise pathway of carcinogenesis for hepatocellular carcinoma (HCC) in cirrhosis. One or more regenerative nodules may show signs of atypia and change into dysplastic nodules. Atypia indicates a number of changes in the shape and size of the nuclei and the cytoplasm of the hepatocytes. These changes often result in an increased number of cells (increased cellularity), which may be present in groups of small cells (small cell dysplasia) or large cells (large cell dysplasia). Atypia within dysplastic nodules can progress further and give rise to small and large HCCs. In addition to the cellular changes, the hepatic parenchymal structure will often be distorted in HCC. **B.** Opposed-phase MR image shows hyperintense dysplastic nodule in the right lobe of the liver (arrow). Precontrast (**C**), postcontrast (**D**), and subtraction (**E**) images show enhancement of a dysplastic nodule (arrow) that had a subfocus of HCC pathologically. **F.** Small HCC (red arrow) is present within a cirrhotic liver showing a nodular hepatic contour, right lobe notch (broken yellow arrow), enlarged lateral segment (LS) of the left lobe, and superficial gallbladder (solid yellow arrow). (A from Hussain SM, Zondervan PE, Ijzermans JN, et al: Benign versus malignant nodules: MR imaging findings with pathologic correlation. *RadioGraphics* 22:1023–1039, 2002.)

hepatic fibrosis with either CT or MRI most commonly demonstrates delayed enhancement only, a key differentiation from a typical HCC.

Etiology of Specific Findings

Although the imaging findings for cirrhosis are most often non-specific in regard to the underlying etiology, some disease-specific alterations can be observed.

The volume of the caudate lobe is often significantly larger in alcoholic cirrhosis than in other causes of cirrhosis, including viral hepatitis. In addition, a notch in the right posterior hepatic lobe is more commonly seen in alcoholic cirrhosis. Regenerative nodules are significantly greater in size in hepatitis B-related cirrhosis than in alcoholic cirrhosis.¹⁷¹

Patients with biliary cirrhosis (see Fig. 89-21B), particularly secondary to chronic changes from sclerosing cholangitis (see

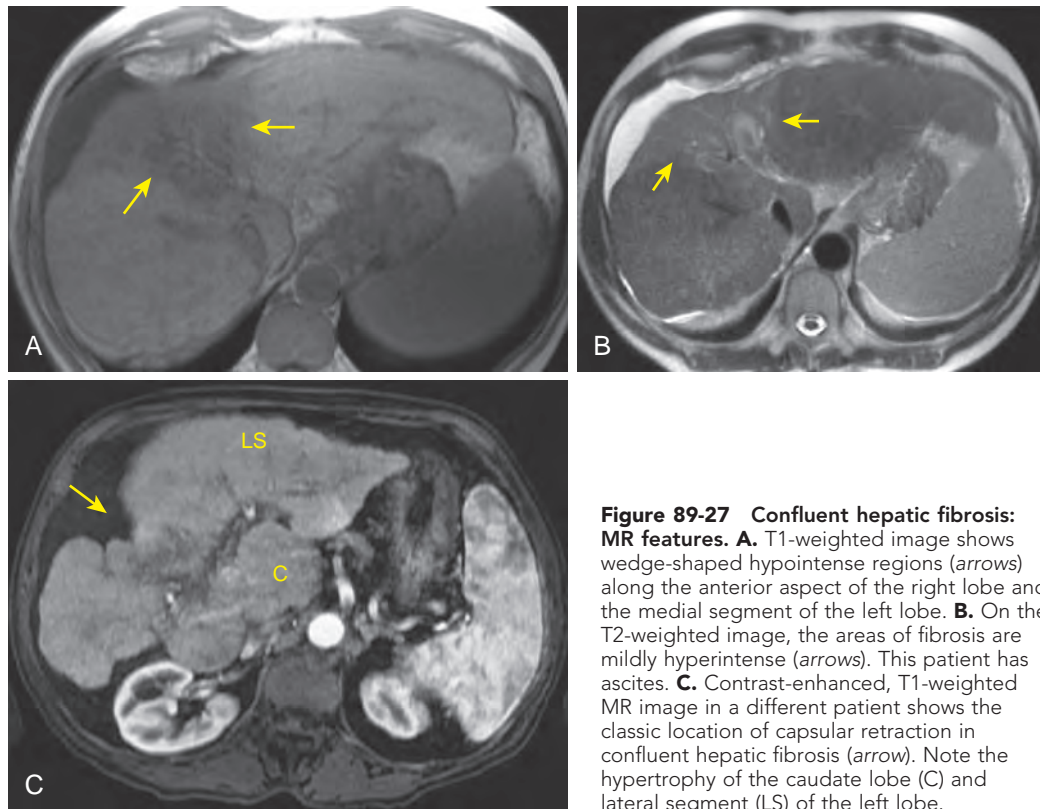


Figure 89-27 Confluent hepatic fibrosis: MR features. **A.** T1-weighted image shows wedge-shaped hypointense regions (arrows) along the anterior aspect of the right lobe and the medial segment of the left lobe. **B.** On the T2-weighted image, the areas of fibrosis are mildly hyperintense (arrows). This patient has ascites. **C.** Contrast-enhanced, T1-weighted MR image in a different patient shows the classic location of capsular retraction in confluent hepatic fibrosis (arrow). Note the hypertrophy of the caudate lobe (C) and lateral segment (LS) of the left lobe.

Figs. 89-23 and 89-24), in addition to the marked atrophy of the right lobe often characteristically have marked atrophy of the lateral segment of the liver. These changes, coupled with marked caudate lobe hypertrophy, result in a squared or rounded appearance to the liver. The atrophy of the more distal parts of the liver to a greater degree in these patients is thought to be due to the effects of chronic biliary obstruction. In addition, zones of focal fibrosis in these patients can appear as peripheral bands of low attenuation.

Extrahepatic Findings

Mesenteric, omental, and retroperitoneal edema can be seen in patients with cirrhosis and portal hypertension. The increased hydrostatic pressure within the mesenteric veins causes fluid to seep into the mesentery. Liver dysfunction also produces a state of water overload due to hypoalbuminemia and decreased aldosterone catabolism. These features also play a role in the development of mesenteric edema, ascites, pleural effusion, and subcutaneous edema. With increasing severity, mesenteric edema can develop a more diffuse distribution and masslike appearance associated with recruitment of omental and retroperitoneal sites. The degree of edema correlates with other findings of severe ascites, subcutaneous edema, pleural effusions, and low mean serum albumin concentration.¹⁴²⁻¹⁵⁸

Siderotic nodules, or Gamna-Gandy bodies, may rarely be identified as masses in the spleen.¹⁵³ Siderotic nodules are seen in patients with portal hypertension and are caused by focal hemorrhage into the spleen. The nodules are composed of fibrous tissue encrusted with hemosiderin and calcium. Presumably, the fibrous tissue and calcium account for these echogenic splenic masses. The incidence of gallstones is also increased in patients with cirrhosis regardless of etiology or gender. A

number of mechanisms make stones more prevalent in the cirrhotic population. Ingestion of alcohol may cause spasm of the sphincter of Oddi and edema of the papilla of Vater, thus interfering with bile duct and gallbladder emptying. Bile stasis and calculus formation may result from poor food intake and excessive alcohol consumption. Indeed, ascites, encephalopathy, and varices are more common in cirrhotic patients with stones than in those without stones. Chronic hemolysis is perhaps the most significant factor in pigment stone formation. Hypersplenism is another major contributing factor. Because of functional damage to the liver, cholesterol stones are uncommon in cirrhotic patients.¹⁴²⁻¹⁵⁸

As with hepatitis, the chronic inflammation present in cirrhosis results in enlargement of abdominal lymph nodes in multiple upper abdominal locations. Such enlarged nodes range in size up to 4 cm in maximal diameter and can be found in patients with cirrhosis from all causes. Although they are most common in patients with primary biliary cirrhosis and primary sclerosing cholangitis, enlarged nodes have been reported with high frequency in patients with alcoholic cirrhosis (37%) and hepatitis B or C (45%-49%). The affected lymph node chains reported include (in order of frequency of involvement) the portacaval space, porta hepatis and hepatoduodenal ligament, gastrohepatic ligament, cardiophrenic angle, and celiac axis as well as other lesser, more remote abdominal chains.¹⁵⁶⁻¹⁵⁹

ULTRASOUND: CIRRHOSIS

Liver Morphology

The sonographic features of fibrosis and fatty infiltration can also overlap significantly. Both demonstrate decreased beam penetration of the hepatic parenchyma, decreased

conspicuity of intrahepatic vessels, and increased parenchymal echogenicity¹⁴⁸⁻¹⁵⁵ (see Table 93-11). Some authors have shown that the attenuation of sound can be normal in cirrhotic patients without fatty deposition. Cirrhosis should be suspected if on ultrasound there are alterations in liver size as detailed before, nodularity of the liver surface, accentuation of the fissures, heterogeneity and coarsening of the hepatic architecture, nodules, or signs of portal hypertension (Fig. 89-28). Specifically, contour nodularity of the undersurface of the liver has a high sensitivity of 86% versus 53% along the superior surface.¹⁷²

The reported sensitivity of ultrasound in the diagnosis of cirrhosis based on hepatic architecture varies between 65% and 95%.¹⁴⁸⁻¹⁵⁵ Although ultrasound has up to a 98% positive predictive value in the diagnosis of diffuse parenchymal disease, it cannot reliably differentiate the underlying etiology. Irregularity of the liver surface has been suggested as a fairly sensitive sign (88%) of cirrhosis. It is detected by use of a high-frequency (9 MHz) linear probe.¹⁴⁸⁻¹⁵⁵ Surface nodularity correlates pathologically with sinusoidal obstruction to portal flow and the development of portal hypertension. It has a higher correlation with severe fibrosis or cirrhosis on histopathologic evaluation than with caudate lobe hypertrophy or hepatic venous flow abnormalities.⁹⁶ In one series, high-resolution sonography was found to be useful in assessing the severity of hepatic scarring and differentiating macronodular and micronodular cirrhosis.^{28,141-155}

Regenerative nodules that are 2 to 3 mm or larger in diameter can occasionally be appreciated sonographically as hypoechoic areas with echogenic borders resulting from fibrous and fatty connective tissue surrounding and separating the nodules. They can usually be seen only with high-frequency transducers unless they are quite large, in which case they may simulate a malignant neoplasm. For these reasons, ultrasound can be a difficult tool to use for screening in cirrhotic patients to detect HCC. Some studies have reported that ultrasound sensitivity for detection of HCC in screening of cirrhotic patients is only approximately 50%. The current lack of an ultrasound contrast agent to detect the vascularity indicative of tumor makes ultrasound a less reliable tool than CT or MRI for screening of cirrhotic patients.¹⁴⁸⁻¹⁵⁵

Ultrasound contrast with microbubbles, currently used in Europe and Asia, can characterize vascular patterns to differentiate cirrhotic nodules from small tumors and may be particularly useful in patients who cannot receive iodinated or gadolinium contrast agents.¹⁷³ Ultrasound elastography can also be used to assess mechanical tissues in both cirrhosis and focal tumors that have increased liver stiffness.^{174,175}

Vascular Changes

On Doppler ultrasound, phasicity is normally seen in the hepatic vein waveform from the transmission of pressure changes within the right atrium throughout the cardiac cycle. This phasicity may be decreased or absent in cirrhosis because of decreased compliance of the fibrotic liver.¹⁴⁸⁻¹⁵⁵ Narrowing of the hepatic veins from extrinsic compression can result in spectral broadening in cirrhosis. Early in cirrhosis, the portal vein flow remains hepatopetal. In more advanced cirrhosis with the development of portal hypertension, the portal vein size increases to 1.4 cm or greater, and flow can become reversed to hepatofugal (discussed later). High resistance in the hepatic artery is a nonspecific finding that can be seen in cirrhosis and

other forms of diffuse liver disease and is suggestive of but usually not used to diagnose cirrhosis. Alternatively, low arterial resistance can be present if there is significant arteriovenous or arterioportal shunting.¹⁷⁶

Extrahepatic Findings

Lymph nodes and gallstones are commonly seen on ultrasound in cirrhosis. When present, Gamna-Gandy bodies within the spleen are hyperechoic on ultrasound. Ascites, pleural effusions, and sequelae of portal hypertension can also be demonstrated.

COMPUTED TOMOGRAPHY: CIRRHOSIS

Liver Morphology

In the United States, CT¹⁵⁶⁻¹⁵⁹ is the primary noninvasive imaging modality in the evaluation of cirrhosis. Early parenchymal changes may not be visible on CT scans; however, fatty infiltration, which is the initial feature of alcoholic liver disease, is well displayed. The density of the liver is less than that of the spleen, and there is often initially hepatomegaly. Alcoholic hepatitis and hepatic steatosis are discussed more fully in other sections of this chapter.

In the later stages of cirrhosis (Fig. 89-29), the overall liver volume is diminished with the characteristic changes detailed before. Whereas all patients pathologically demonstrate regenerative nodules, these are infrequently demonstrated at CT. Nodularity of the liver contour caused by regenerative nodules, fibrous scarring, and nonuniform lobar atrophy or hypertrophy may be demonstrated, particularly in the presence of ascites. Regenerative nodules, although present pathologically in all cirrhotic livers, are visualized on multidetector CT (MDCT) in only approximately 25% of patients. Regenerative nodules, however, are most commonly isoattenuating with liver parenchyma before and after contrast material administration. Uncommonly, regenerative nodules can appear as hypoattenuating small nodules on contrast-enhanced liver CT, simulating tumor. This is most commonly seen in primary biliary cirrhosis. Siderotic nodules will appear of higher attenuation than the normal liver because of hemosiderin content; they are most apparent on unenhanced CT and appear hyperdense but usually become isoattenuating with contrast-enhanced liver parenchyma. Because of the insensitivity of CT to depict regenerative nodules, it is not able to depict or to differentiate the transformation process of regenerative nodules to dysplastic nodules. On occasion, large dysplastic nodules can be identified on unenhanced CT with increased attenuation, perhaps owing to increased iron composition or packed cellular material with increased glycogen content. Most often, however, these nodules go undetected by CT.¹⁵⁶⁻¹⁵⁹

Cirrhotic liver parenchyma often demonstrates less contrast enhancement than normal liver and appears inhomogeneous because of the underlying regeneration, fibrosis, and altered portal venous blood flow. The hepatic and portal vein radicles in the liver are often compressed and difficult to visualize. The porta hepatis and intrahepatic fissures are also unusually prominent because of the hepatic atrophy.¹⁵⁶⁻¹⁵⁹

Focal confluent fibrosis can appear at CT imaging as a focal mass, in some ways simulating tumor. It appears most conspicuous on noncontrast CT and usually either becomes isoattenuating with contrast-enhanced CT or remains slightly hypoattenuating. In some cases, the fibrosis will show irregular

contrast enhancement, making it difficult to differentiate from HCC.

These underlying parenchymal changes distort the liver parenchyma and can simulate other masses, such as HCC. In addition, the parenchymal changes can obscure subtle findings of HCC. Before the development of MDCT, it was difficult to detect even large foci of HCC in cirrhotic patients. The advent of MDCT gained the ability to optimally time contrast administration and scanning and to detect arterial phase enhancement and delayed washout, which is critical in the diagnosis of HCC and has substantially increased the ability to detect small tumors in cirrhotic patients. The appearance of HCC is discussed more fully in Chapter 87.

Vascular Findings

Small vascular shunts can be seen as focal hyperenhancement without delayed washout. The arteries may also appear tortuous with a “corkscrew” appearance in cirrhosis because of the surrounding fibrosis. The hepatic artery and portal vein may both enlarge. Intrahepatic arterial-portal fistulas are occasionally seen on CT scans in patients with cirrhosis. They cause early

opacification of the portal vein, which is best appreciated on dynamic scans by measuring the time-density curve in the aorta and the intrahepatic portal vein or hepatic hilum. In addition, the lobe that contains the arterial-portal fistula has higher density in the later arterial phase (transient hepatic attenuation difference) than the contralateral lobe.¹⁵⁶⁻¹⁵⁹

Extrahepatic Findings

Patients with cirrhosis and portal hypertension also show an increase in the density of the mesenteric fat compared with the retroperitoneal fat (56 vs 107 HU). The CT density of the mesenteric fat is also significantly higher in these patients (56 HU) than in normal subjects (107 HU).¹⁵⁶⁻¹⁵⁹ Pericaval fat collections are seen in up to 25% of patients with chronic liver disease. They are located along the posterior aspect of the IVC in most cases. The rightward angulation and narrowing of the intrahepatic IVC that occur in cirrhosis can cause the pericaval fat collections to appear intraluminal on axial CT scans.

Other findings commonly seen on CT are gallstones, lymphadenopathy, varices and other sequelae of portal hypertension, and cirrhosis-related colopathy. Gamna-Gandy bodies are often

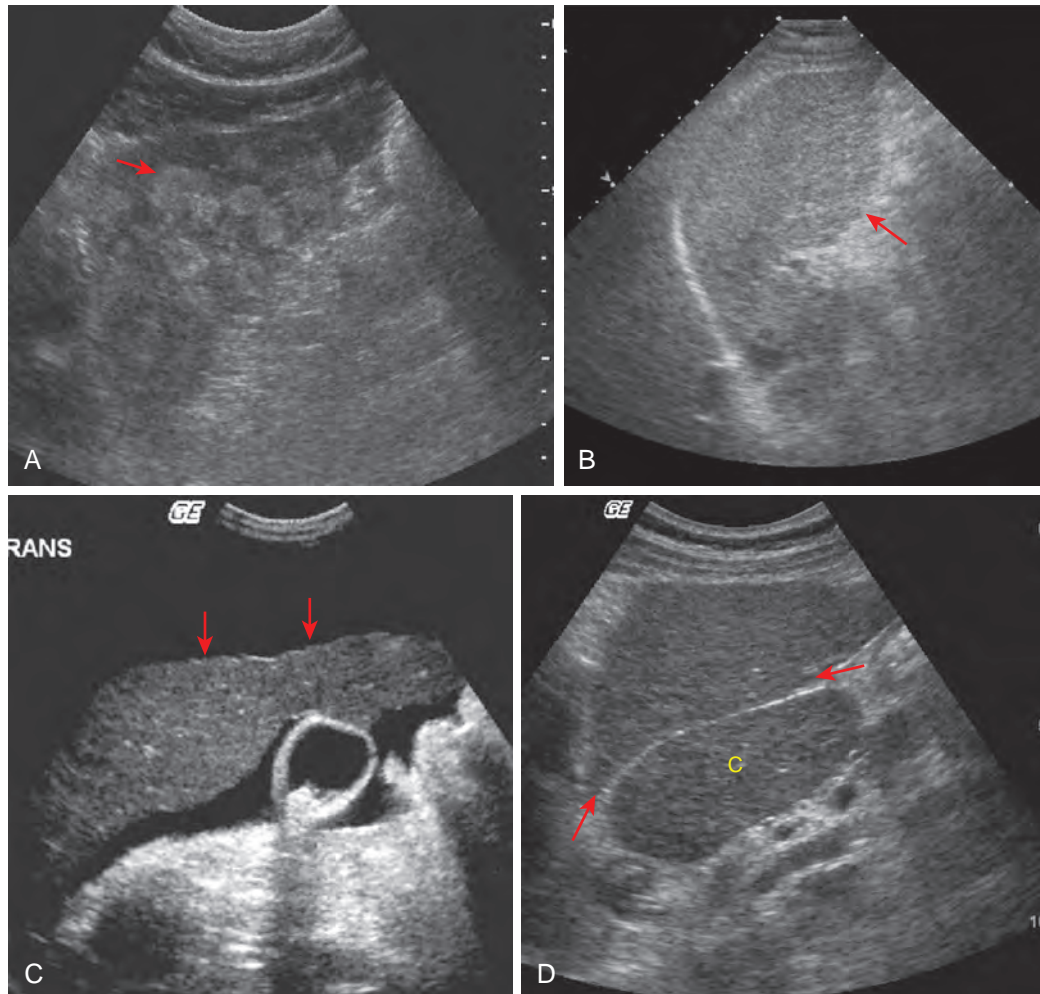


Figure 89-28 Cirrhosis: sonographic findings. **A.** Sagittal scan of the left lobe of the liver shows multiple echogenic nodules (arrow) simulating metastases. They proved to be macroregenerative nodules. **B.** Sagittal scan of the right lobe demonstrates nodularity of the undersurface of the liver (arrow). **C.** A nodular hepatic surface (arrows) is highlighted by ascites. Note the thick gallbladder wall and gallstones. **D.** Sagittal sonogram showing enlargement of the caudate lobe (C) in a patient with cirrhosis. Arrows, Fissure for the ligamentum venosum.

Continued

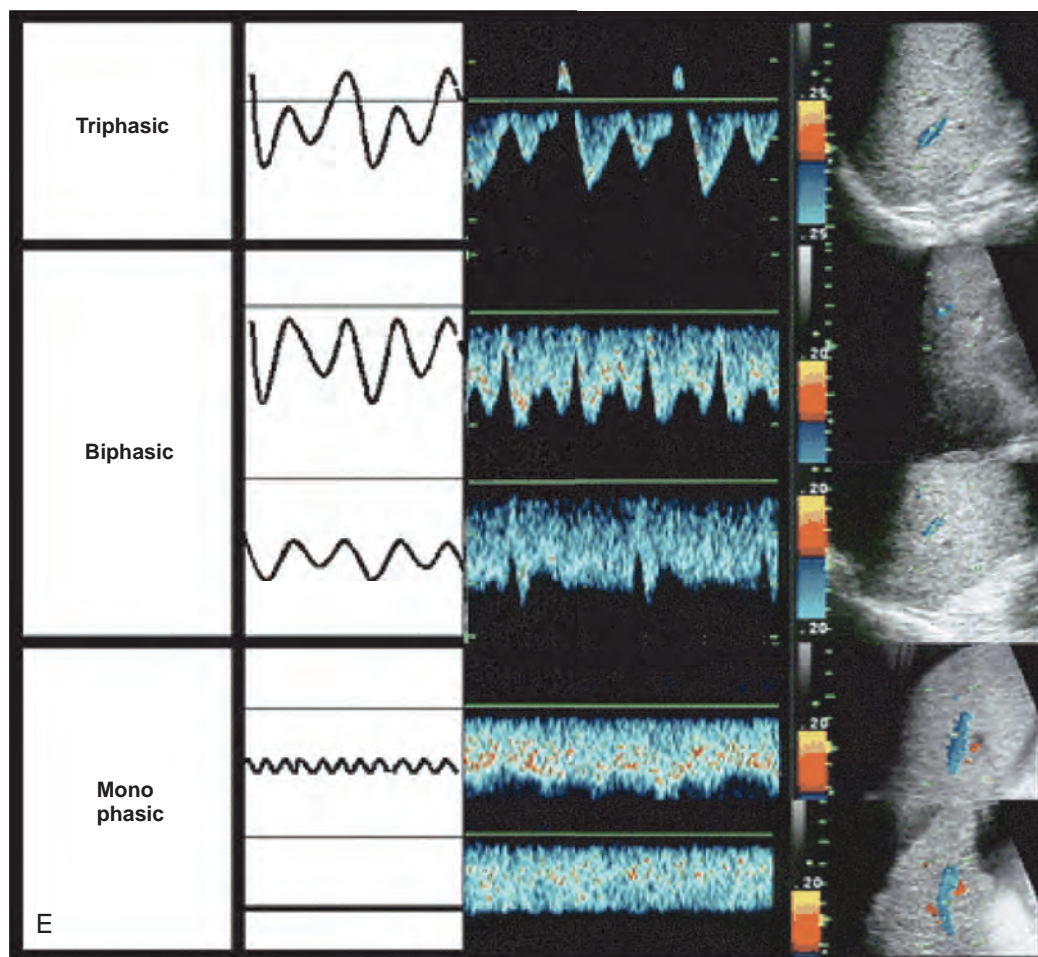


Figure 89-28, cont'd E. A combination of schematic drawings and Doppler waveforms shows classification of hepatic vein Doppler waveforms in patients with cirrhosis and portal hypertension. (A courtesy of Peter Cooperberg, MD, Vancouver, British Columbia, Canada. E from Baik SKB, Kim JW, Kim HS, et al: Recent variceal bleeding: Doppler US hepatic vein waveform in assessment of severity of portal hypertension and vasoactive drug response. *Radiology* 240:574–580, 2006.)

poorly seen on CT; when present, they can appear as faint areas of increased attenuation on noncontrast CT from focal calcification.

MAGNETIC RESONANCE IMAGING: CIRRHOSIS

The role of MRI in the cirrhotic patient is to assess liver size, to evaluate the effects of portal hypertension, to screen for HCC, and to better characterize masses detected in the liver by other techniques.

Liver Morphology

MRI (Fig. 89-30; see also Figs. 89-26 and 89-27) can often detect cirrhosis at an earlier stage than CT and ultrasound can.¹⁷⁷⁻¹⁸⁷ Early in the evolution of cirrhosis, MRI can demonstrate subtle changes, such as fine strands of fibrosis and enlargement of the hilar and periportal spaces. Opposed-phase spoiled gradient-echo images, which are heavily T1 weighted, are sensitive to the depiction of subtle fibrotic change that is manifested as a lace-like hypointense network of abnormal signal intensity.⁴⁷ Linear enhancement is seen on the interstitial phase of enhancement, reflecting the distribution of gadolinium in the large extracellular spaces of the fibrotic septal tissue. There is also

enlargement of the hilar periportal space that lies anterior to the right portal vein. This is due to atrophy of segment IV and is visible in most patients with early cirrhosis.¹⁷⁷⁻¹⁸⁷

MRI is the most sensitive imaging modality for demonstration of regenerative nodules. They appear as isointense to hyperintense on T2-weighted imaging surrounded by a thin network of fibrotic change forming a hypointense background. Regenerative nodules are isointense to hypointense on T1 compared with the liver parenchyma. When hemosiderin deposits are present, these nodules may have low signal intensity on both T1- and T2-weighted imaging from magnetic susceptibility effects.¹⁷⁷⁻¹⁸⁷ These also enhance similarly to or slightly more than the background liver parenchyma during the portal venous phase of contrast administration, which is explained by their predominant portal venous blood supply. On MRI, these lesions are brightly hyperintense on T1-weighted images and hypointense to liver on T2-weighted images, although a wide variety of signal intensity combinations have been reported.¹⁶⁰⁻¹⁷⁰

Dysplastic nodules are premalignant and have a spectrum of increased cellular density and cellular atypia, which is usually classified as low or high grade. Most small dysplastic nodules are not visualized as distinct masses on MRI. Similar to regenerative nodules, surrounding fibrosis makes them distinct from

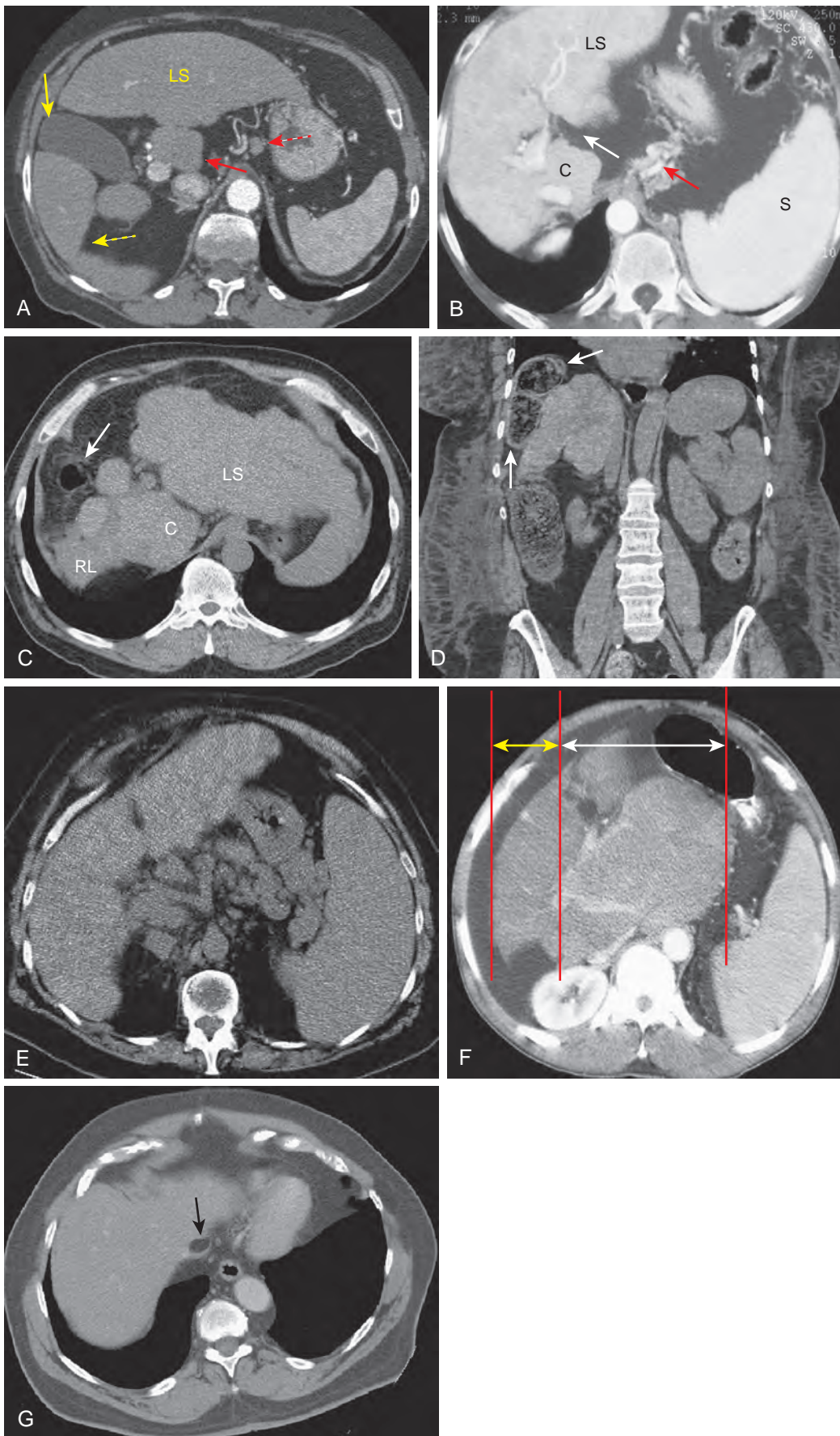


Figure 89-29 Cirrhosis: CT features. **A.** Contrast-enhanced CT scan demonstrates enlargement of the lateral segment (LS) of the left lobe, atrophy of the medial segment (solid red arrow) of the left lobe, and atrophy of the right lobe with a characteristic notch (broken yellow arrow) on the right posterior surface of the liver. Note that the gallbladder (solid yellow arrow) is in a more superficial and lateral position as a result of these morphologic changes. Several borderline size lymph nodes (broken red arrow) are present within the gastrohepatic ligament. **B.** Contrast-enhanced CT scan demonstrates widening of the gallbladder fossa (white arrow), enlargement of the lateral segment (LS) of the left lobe and caudate lobe (C) of the liver, ascites, varices (red arrow), and splenomegaly (S). **C.** Non-contrast-enhanced CT scan shows diffuse nodularity of the hepatic contour associated with enlargement of the lateral segment (LS) of the left hepatic lobe and caudate lobe (C). Note the interposition of the colon (arrow) between the liver and lateral abdominal wall. RL, Right lobe. **D.** Coronal reformatted MDCT image shows interposition of colon (arrows) between liver and right diaphragm (Chilaiditi's syndrome), which is much more common in cirrhosis due to atrophy of the right lobe. **E.** Non-contrast-enhanced CT scan shows diffuse regenerative nodules that are hyperdense due to the presence of iron. **F.** Diagram depicting method of determining the presence of caudate lobe hypertrophy and right lobe atrophy. White arrow shows transverse diameter of the caudate lobe; yellow arrow depicts diameter of right lobe. If the caudate lobe-to-right lobe ratio is larger than 0.9, the diagnosis of cirrhosis can be predicted with a fairly good accuracy. **G.** Changes in the topography of the right upper quadrant commonly highlight pericaval fat in patients with cirrhosis, often simulating a fatty mass (arrow) in the inferior vena cava.

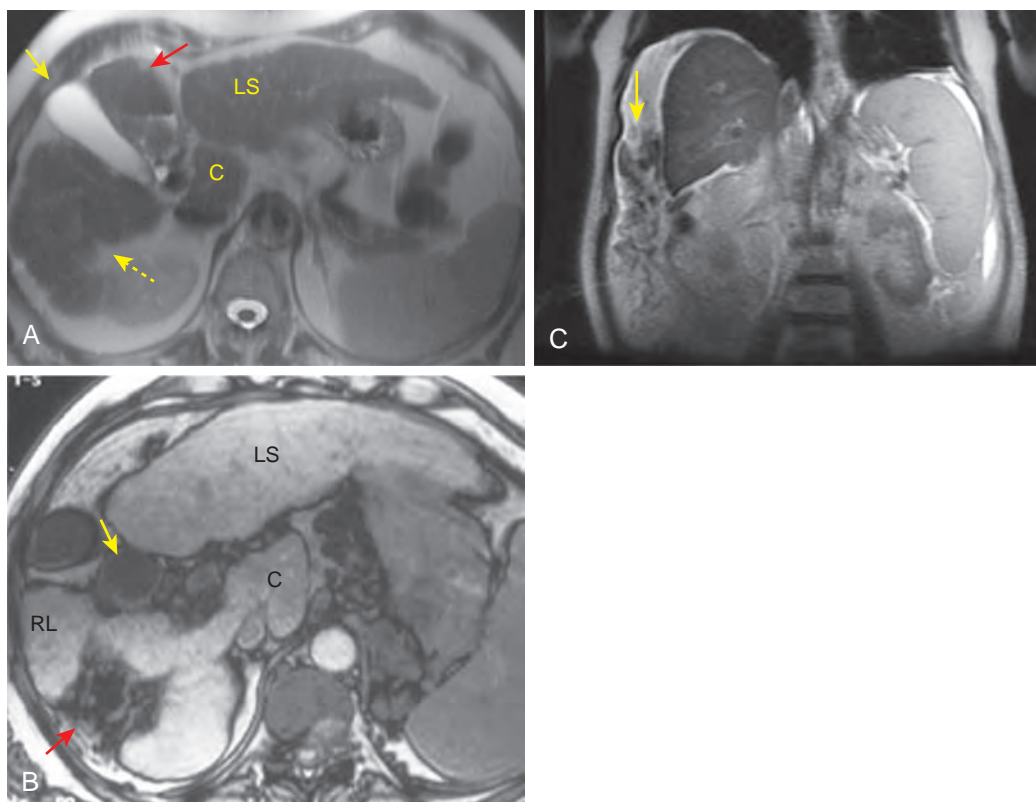


Figure 89-30 Cirrhosis: MR features. **A.** T2-weighted MR image demonstrates enlargement of the lateral segment (LS) of the left lobe, atrophy of the medial segment (solid red arrow) of the left lobe, and atrophy of the right lobe with a characteristic notch (broken yellow arrow) on the right posterior surface of the liver. Note that the gallbladder (solid yellow arrow) is in a more superficial and lateral position as a result of these morphologic changes. C, caudate lobe. **B.** Marked atrophy of the right lobe (RL) of the liver is seen in association with enlargement of the lateral segment (LS) of the left lobe and caudate lobe (C). The gallbladder fossa is widened, and the gallbladder (yellow arrow) and hepatic flexure (red arrow) of the colon are in a superficial location. **C.** Coronal T2-weighted image shows marked hepatic atrophy associated with ascites and interposition of colon (arrow) between the liver and lateral abdominal wall. Splenomegaly is also present.

the remaining liver parenchyma. Signal characteristics of dysplastic nodules are variable and can overlap with both regenerative nodules and HCC. Dysplastic nodules are often hypointense on T2, and as dysplasia increases, the signal intensity can increase, appearing more similar to the increased T2 signal intensity of malignant disease (see Fig. 89-26). Dysplastic nodules classically appear hyperintense on T1, which does not vary with the degree of dysplasia. Dysplastic nodules are hypovascular and predominantly supplied by the portal system. Less commonly, they have an increase in hepatic arterial supply (approximately 12%), which can overlap with the appearance of HCC. When a small focus of HCC is present within a dysplastic nodule, it has been called a “nodule within a nodule” appearance with central high signal intensity of T2 with surrounding hypointensity of the dysplastic tissue. The MR characteristics of hepatic lesions during dynamic arterial, venous, and delayed phases in conjunction with serum α -fetoprotein level and number of lesions are predictors of hepatic malignant disease.¹⁸²

Liver-specific MR contrast agents (Gd-EOB-DTPA) can also help differentiate nodules from malignant changes. Regenerative nodules contain Kupffer cells and appear similar to the hepatic parenchyma during the hepatobiliary phase of imaging. With increasing dysplasia, the amount of normal hepatic function within nodules decreases and uptake is decreased with these contrast agents. However, well-differentiated HCC, which

retains some hepatocyte function, can retain these contrast agents, creating a false negative and pitfall of this technique.

Early fibrosis on MRI appears as a thin lacelike network with hyperintense T2 and hypointense T1 signal. As fibrosis progresses, these areas thicken, coalesce, and can demonstrate enhancement on delayed phase imaging. These findings are most prominent along the periphery and associated with capsular retraction and can form focal confluent fibrosis as previously described. Liver-specific contrast agents can also help demonstrate fibrosis, which will not enhance during the hepatobiliary phase, differentiating it from the liver background. Unfortunately, these signal characteristics are similar to most HCCs. As with CT, the diagnosis rests with identifying the characteristic location and capsular retraction of this lesion. When focal confluent fibrosis appears round on axial images, the high signal intensity lesions on T2-weighted images replicate findings of HCC.¹⁷⁷⁻¹⁸⁷

Several new techniques allow further assessment of hepatic fibrosis at MRI. MR elastography has shown promise as a non-invasive means of determining the degree of hepatic fibrosis. Patients with liver fibrosis have elevated MR elastographic liver stiffness measurements, which increase as fibrosis progresses, and higher stages of fibrosis can be differentiated with this technique.¹⁸⁷

Diffusion-weighted MRI may help detect cirrhosis, particularly assessment of multi-b value-generated apparent diffusion

coefficient values, which are decreased in cirrhosis. Analysis of phosphorus-based MR spectroscopy has also been investigated and has been reported to show alterations in the ratio of phosphorus-based liver metabolites.

Extrahepatic Findings

MRI is also useful in depicting Gamna-Gandy bodies (see Fig. 89-14D) in the spleen in patients with portal hypertension. These siderotic nodules are composed of hemosiderin and calcification adjacent to thickened bundles of collagen fibers and result from repeated hemorrhages in the splenic follicles or adjacent to trabeculae. These tiny nodules have low signal intensity at virtually all pulse sequences because of their paramagnetic effect but are best seen on gradient-echo or fast low-angle shot images.¹⁷⁷⁻¹⁸⁷ Other extrahepatic findings described on ultrasound and CT can also be appreciated with MRI.

ULTRASOUND: PORTAL HYPERTENSION

Sonography (Figs. 89-31 and 89-32) plays a key role in the management of patients with cirrhosis in the detection of portal hypertension and the noninvasive evaluation of the portosystemic collateral circulation. The sonographic features of portal hypertension depend on changes in size and blood flow in the portal system, congestive splenomegaly, and development of collateral pathways. Sonography is also useful in differentiating presinusoidal causes of portal hypertension from obstruction at the sinusoidal or postsinusoidal level.^{28,188,189}

Measuring portal vein size and observing respiratory variations in the superior mesenteric and splenic veins are simple and sensitive methods for detection of portal hypertension. The diameter of the portal vein in normal individuals ranges from 0.64 to 1.21 cm; the mean diameter is 1.2 cm in cirrhotic patients. There is a significant correlation between the diameter of the portal vein and maximal spleen length and the magnitude of varices seen endoscopically. A patent portal vein larger than 1.3 cm is 100% specific for portal hypertension but is seen in only 75% of cases. Other signs of portal hypertension are patency of the umbilical vein (58%); splenomegaly with dilation of splenic vein radicles (91.3%); and disappearance of normal splenic and mesenteric vessel caliber variation with respiration, which occurs in 78.5% and 88.4% of patients, respectively. Lack of distensibility of the portal vessels with respiration is an important sign. In normal individuals, the portal venous system distends with deep inspiration and breath holding because of diaphragmatic descent and compression of hepatic venous outflow. The diameter of the splenic or superior mesenteric veins may increase 50% to 100%. Ninety percent of patients with manometrically proved portal hypertension fail to show this distensibility because the portal venous system is already maximally distended and respiration-induced pressure changes are poorly transmitted through the scarred liver. The caliber of these veins decreases and respiratory variation returns if therapy with various vasoconstrictors is successful.^{28,188,189}

The size of the superior mesenteric and left gastric veins is also affected in portal hypertension. If the superior mesenteric

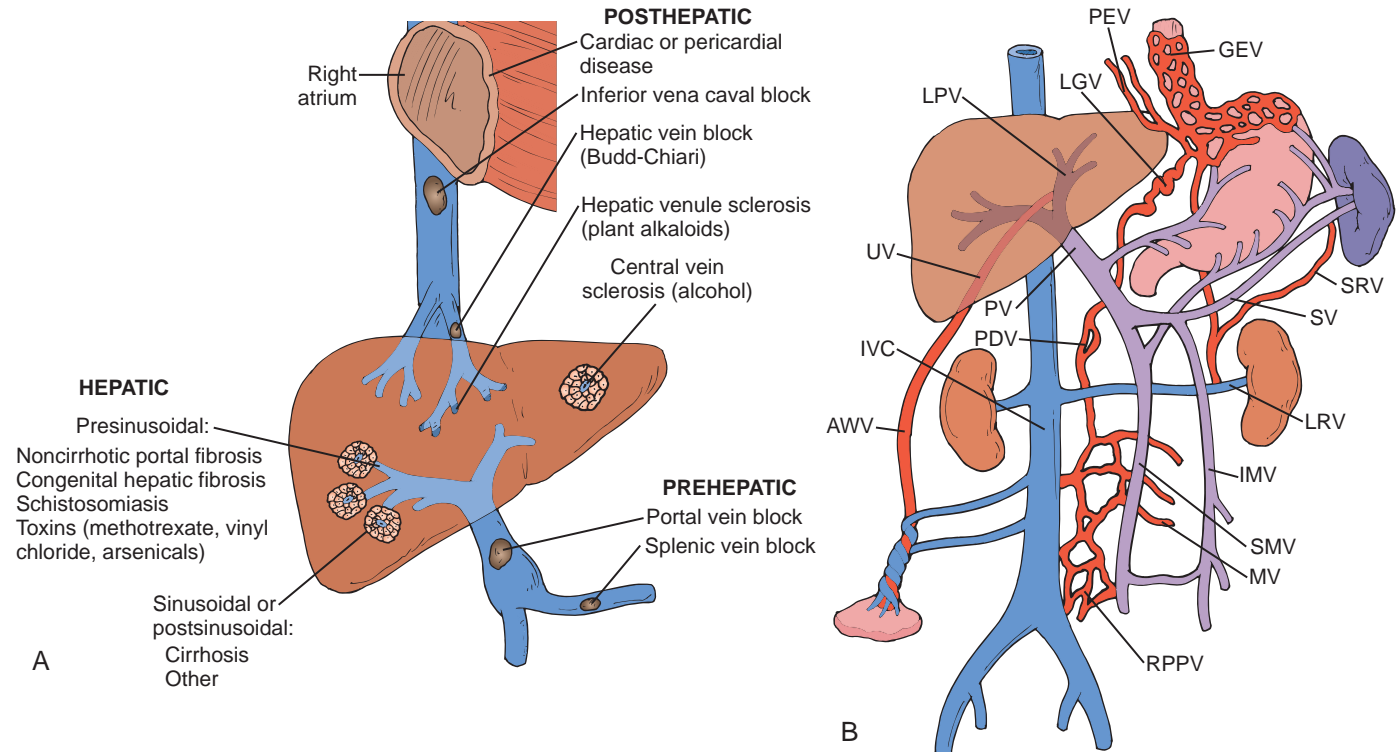


Figure 89-31 Portal hypertension: diagrammatic depictions of causes and decompressive pathways. A. Causes of portal hypertension. **B.** Drawing illustrates the collateral vessels in portal hypertension: AWW, abdominal wall vein; GEV, gastroesophageal vein; IMV, inferior mesenteric vein; IVC, inferior vena cava; LGV, left gastric vein; LPV, left portal vein; LRV, left renal vein; MV, mesenteric vein; PDV, pancreaticoduodenal vein; PEPV, paraesophageal vein; PV, portal vein; RPPV, retroperitoneal-paravertebral vein; SMV, superior mesenteric vein; SRV, splenorenal vein; SV, splenic vein; UV, umbilical vein.

Continued

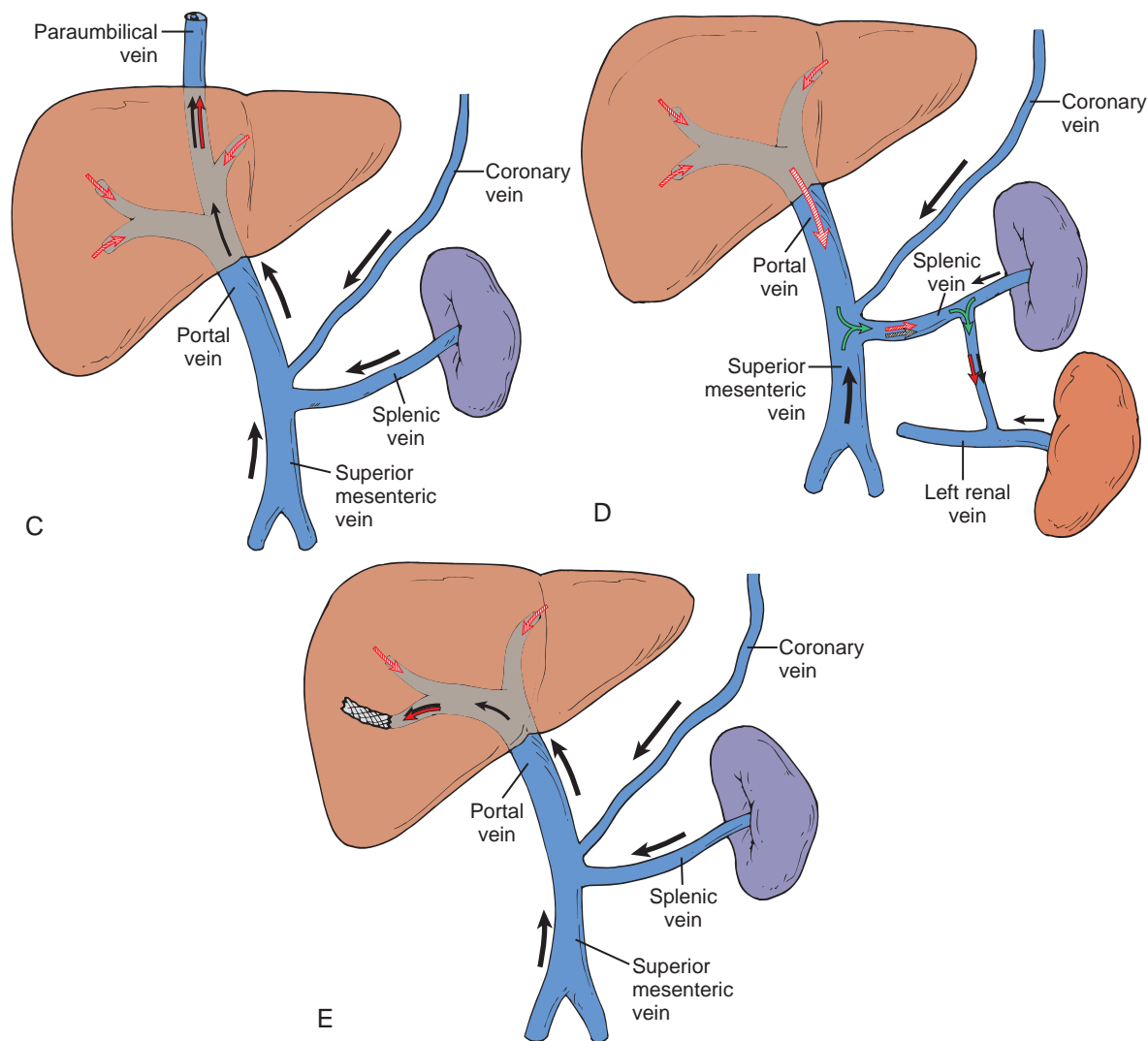


Figure 89-31, cont'd **C.** Prominent paraumbilical vein in a patient with cirrhosis. Diagram shows a large paraumbilical vein associated with hepatopetal flow in the main portal vein but hepatofugal flow (striped red arrows) in intrahepatic portal vein branches. Both splanchnic venous blood (black arrows) and hepatic artery blood are shunted to the systemic venous circulation through the paraumbilical vein. Despite hepatopetal flow in the portal vein, the hepatic parenchyma is not perfused by splanchnic venous blood because portal venous inflow is completely shunted to the paraumbilical vein. Solid red arrow, hepatic artery blood shunted through the paraumbilical vein. **D.** Splenorenal shunt. Diagram shows diffuse intrahepatic arterioportal shunting that drains through a portosystemic connection between the splenic and left renal veins. Note the hepatofugal flow (striped red arrow) in the intrahepatic portal vein branches, the main portal vein, and the retropancreatic segment of the splenic vein. Superior mesenteric vein flow is also shunted through this pathway. Note that both hepatic artery flow and splanchnic venous flow are shunted to the systemic circulation through the splenorenal pathway, whereas only splanchnic venous blood is shunted through this pathway as shown here. Green arrows, sites of flow diversion; solid black arrows, normally directed venous flow; solid red arrow, hepatic artery flow shunted through the splenorenal pathway. **E.** Transjugular intrahepatic portosystemic shunt in a patient with cirrhosis. Diagram shows hepatofugal flow in the intrahepatic portal veins (striped red arrows) and hepatopetal flow in the main portal vein. Note the similarity to the hemodynamics seen with a large paraumbilical vein. Black arrows, splanchnic venous blood; solid red arrow, hepatic artery blood shunted through a transjugular intrahepatic portosystemic shunt. (A reprinted from Losowsky MS: *The physician's viewpoint*. In Herlinger H, Lunderquist A, Wallace S [eds]: *Clinical Radiology of the Liver. Part B*. New York, Marcel Dekker, 1983, pp 581–594, by courtesy of Marcel Dekker, Inc. B from Kang HK, Jeong YY, Choi JH, et al: Three-dimensional multi-detector row CT portal venography in the evaluation of portosystemic collateral vessels in liver cirrhosis. *RadioGraphics* 22:1053–1061, 2002. C, D, and E from Wachsberg RH, Bahramipour P, Sofocleous CT, et al: Hepatofugal flow in the portal venous system: Pathophysiology, imaging findings, and diagnostic pitfalls. *RadioGraphics* 22:123–140, 2002.)

vein is larger than the portal vein or the left gastric vein is larger than 4 mm, portal hypertension is present. The superior mesenteric vein and splenic veins should be no larger than 11 and 12 mm, respectively. A left gastric vein larger than 7 mm indicates a portohepatic gradient larger than 10 mm Hg, which makes variceal bleeding likely.^{28,188,189}

Collateral vessels can be seen sonographically in up to 88% of patients with portal hypertension. The most important varices involve the left gastric vein and associated esophageal varices. These varices can be identified as circular and tubular sonolucencies in the region of the gastroesophageal junction and lesser curvature of the stomach. These vessels are normally

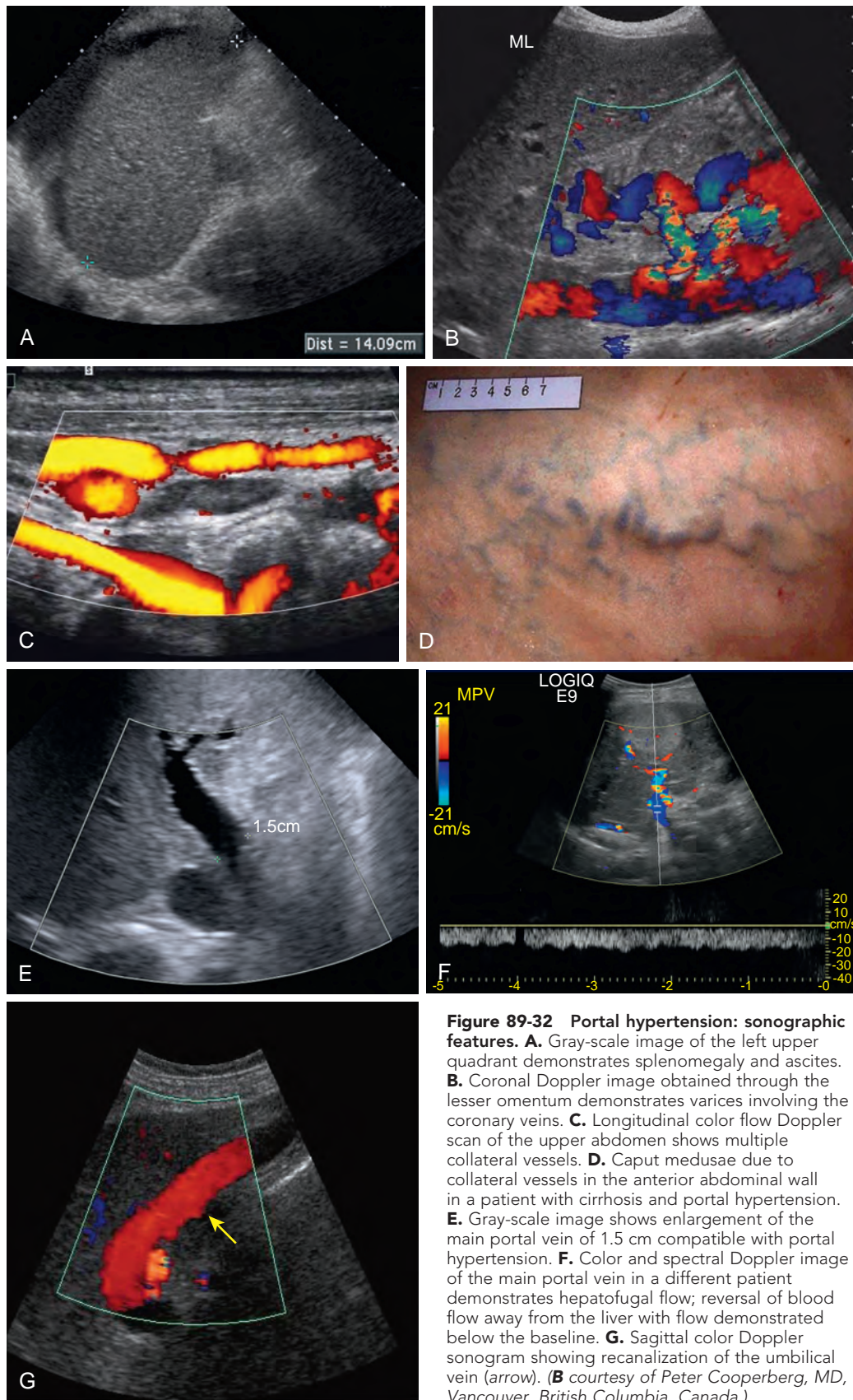


Figure 89-32 Portal hypertension: sonographic features. **A.** Gray-scale image of the left upper quadrant demonstrates splenomegaly and ascites. **B.** Coronal Doppler image obtained through the lesser omentum demonstrates varices involving the coronary veins. **C.** Longitudinal color flow Doppler scan of the upper abdomen shows multiple collateral vessels. **D.** Caput medusae due to collateral vessels in the anterior abdominal wall in a patient with cirrhosis and portal hypertension. **E.** Gray-scale image shows enlargement of the main portal vein of 1.5 cm compatible with portal hypertension. **F.** Color and spectral Doppler image of the main portal vein in a different patient demonstrates hepatofugal flow; reversal of blood flow away from the liver with flow demonstrated below the baseline. **G.** Sagittal color Doppler sonogram showing recanalization of the umbilical vein (arrow). (**B** courtesy of Peter Cooperberg, MD, Vancouver, British Columbia, Canada.)

no larger than 4 mm. CT, however, more reliably depicts varices in this location.^{28,188,189} The portal circulation commonly decompresses through paraumbilical veins in the ligamentum teres. This usually echogenic structure becomes sonolucent centrally, producing a “bull’s-eye” appearance in the transverse plane. A central vascular channel exceeding 3 mm in diameter is a specific sign of portal hypertension. On longitudinal scans, these paraumbilical varices can be followed caudally toward the umbilicus as a tubular lucency. A patent umbilical vein excludes an extrahepatic cause of portal hypertension because the umbilical vein arises from the intrahepatic portion of the left portal vein. This vein enables the formation of an anastomosis between the left branch of the portal vein and the veins of the anterior abdominal wall, creating a portal-systemic bypass circuit known as the Cruveilhier-Baumgarten syndrome. The vein may sometimes become aneurysmally dilated and simulate a fluid collection, emphasizing the importance of Doppler assessment of cystic structures in patients with cirrhosis before biopsy. Doppler sonography can also be used to assess the hemodynamic significance of flow in the paraumbilical vein. When hepatofugal flow in the umbilical vein exceeds hepatopetal flow in the portal vein, patients are less likely to have esophageal varices and bleeding. Although it occurs more commonly in patients with severe functional impairment, it may play a protective role against variceal bleeding.^{28,188,189}

The inferior mesenteric vein also dilates in patients with portal hypertension. It provides a conduit for portosystemic shunting through two major pathways: communication with the left gonadal vein and with the middle and inferior hemorrhoidal veins. The inferior mesenteric vein is considered dilated when it is larger than 6 mm in diameter.

Duplex sonography and color flow Doppler sonography are extremely useful in patients with portal hypertension. Doppler sonography provides more precise identification and characterization of vessels and flow direction than conventional sonography does. It is particularly useful in patients with patent paraumbilical veins because patency of these channels can also be seen in normal patients but blood flow is hepatopetal, not hepatofugal as in cirrhosis. Doppler sonography can also suggest the likelihood of a spontaneous splenorenal shunt by demonstrating hepatofugal flow and dilated splenic and renal veins. The normal hepatic vein waveform (see Fig. 89-28) is triphasic because of central venous pressure variations that occur in the cardiac cycle. In patients with cirrhosis and portal hypertension, the waveforms become biphasic and ultimately monophasic. Monophasic waveforms are associated with severe portal hypertension with a sensitivity of 74% and specificity of 95%.¹⁷⁹

Other changes in the splanchnic circulation in cirrhosis and portal hypertension can also be observed with Doppler ultrasound. Superior mesenteric, splenic, and portal venous flows are significantly increased in patients with chronic cirrhosis. This is a result of increased portal inflow in cirrhosis because of a hyperdynamic circulatory state in the splanchnic circulation of the intestine and spleen in patients with portal hypertension. Not surprisingly, splenic and superior mesenteric artery blood flow also significantly increases in patients with cirrhosis compared with normal subjects and patients with chronic hepatitis. The resistive index of hepatic arterial flow is elevated (>0.78) in patients with hepatic fibrosis and portal hypertension. Although it is specific for a large portal pressure gradient, the resistive index is not sensitive. Portal venous velocity is diminished in cirrhotic patients with (7.1 ± 2.3 cm/s) and

without (12.0 ± 3.4 cm/s) spontaneous splenorenal shunts compared with normal subjects (16.5 ± 4.9 cm/s).^{28,188,189} Flow can also become reversed (hepatofugal) in the main portal vein. Decreased flow within the portal venous system in either direction increases the risk for portal venous thrombosis, another potential complication in cirrhosis and portal hypertension.

There is a correlation sonographically between hepatic venous pressure gradient and renovascular impedance. High renovascular impedance, as evidenced by elevated pulsatility and resistive indices, indicates renal vasoconstriction, which in turn indicates severe portal hypertension.¹⁷⁸

Duplex Doppler sonography should be the initial screening examination in patients with a transjugular intrahepatic portosystemic shunt (TIPS) who present with new or recurring variceal bleeding or increasing ascites when there is a question of shunt patency. It is also ideal for routine serial follow-up. Color Doppler sonography is a superb means of guiding TIPS procedures.^{28,188,189}

COMPUTED TOMOGRAPHY: PORTAL HYPERTENSION

CT (Fig. 89-33) is also excellent in demonstrating portal hypertension with its attendant varices, splenomegaly, and ascites. On CT scans, portosystemic collaterals appear as tortuous, tubular, or round soft tissue masses that may be mistaken for lymph nodes on noncontrast scans. Enhancement after intravenous administration of contrast agent confirms their vascular origin. By demonstrating selective vessel collateralization, CT also has the ability to diagnose and to differentiate their cause. Whereas short gastric and coronary collateral vessels are seen in both portal hypertension and splenic vein occlusion, enlargement of the gastroepiploic vein is seen only in splenic vein occlusion and paraumbilical varices only in portal hypertension.¹⁹⁰⁻²⁰³ Esophageal and gastric varices can be inferred from CT scans when marked enhancement is seen in association with mural thickening. Varices can also create intraluminal esophageal protrusions, giving a scalloped appearance. Liver MDCT is useful for grading of esophageal varices as well. It appears that a diameter of 3 mm for the varix is useful in identifying high-risk patients who benefit most from endoscopy and prophylactic therapy.¹⁹⁴

Although duplex Doppler sonography can provide information concerning variceal flow and direction, CT is superior in demonstrating retroperitoneal varices and in depicting azygos, hemiazygos, pericardial, and periesophageal varices that can simulate mediastinal masses.¹⁹⁰⁻²⁰³

Hepatofugal portal venous flow in patients with cirrhosis indicates the presence of advanced portal hypertension placing the patient at increased risk for hepatic dysfunction, hepatic encephalopathy, variceal bleeding, and poorer response of the varices to endoscopic ligation compared with cirrhotic patients with hepatopetal flow.²⁰¹ A portal vein diameter of less than 1 cm in the presence of cirrhosis is a highly specific but less sensitive sign of hepatofugal portal venous flow in cirrhotic patients. This implies that the liver is being almost exclusively supplied by the hepatic artery. This has important prognostic and therapeutic implications in planning chemoembolization of tumors or placement of a TIPS.

The splenic index is a good indicator of the severity of esophageal varices and hepatic functional reserve in cirrhotic patients. A splenic index (= length \times width \times thickness of

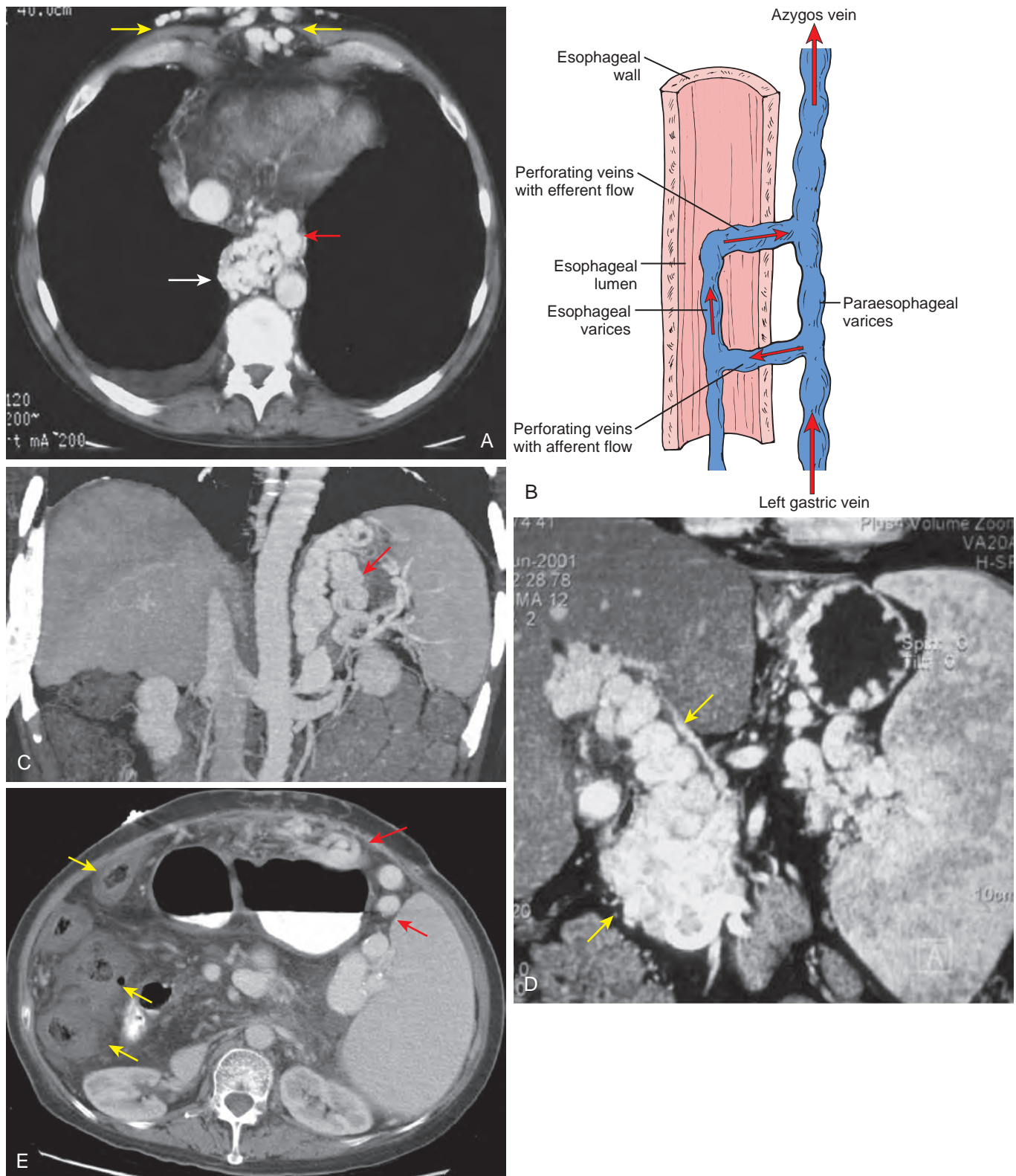


Figure 89-33 Portal hypertension: CT features. **A.** Axial CT scan showing esophageal (white arrow) and paraesophageal (red arrow) varices. Superficial collateral vessels are also present (yellow arrows). **B.** Diagram shows connections between esophageal and paraesophageal varices through perforating veins with afferent or efferent blood flow. Paraesophageal varices are formed by union of groups of dilated perforating veins, and varices connect with left gastric veins inferiorly and with azygos vein superiorly. Throughout their length, esophageal varices form connections with paraesophageal varices through perforating veins. **C.** Coronal reformatted MDCT image shows short gastric and perigastric varices (arrow). **D.** Cavernous transformation of the portal vein (arrows) is identified in this patient with portal vein thrombosis, hepatic steatosis, and splenomegaly. Note also the gastric wall varices. In the following patient, CT demonstrates colonic disease associated with cirrhosis and portal hypertension. **E.** Axial CT with contrast enhancement shows mural thickening of the right colon (yellow arrows); the left colon (not shown) was uninvolved. Note the perisplenic and gastrocolic ligament varices (red arrows). Splenomegaly is also noted. (**B** from Matsuo M, Kanematsu M, Kim T, et al: Esophageal varices: Diagnosis with gadolinium enhanced MR imaging of the liver for patients with chronic liver damage. *AJR Am J Roentgenol* 180:461–466, 2003. Reprinted with permission from the American Journal of Roentgenology. **C** and **D** courtesy of Elliot Fishman, MD, Baltimore, MD.)

spleen) greater than 963 cm³ is a good indicator of the presence of esophageal varices at risk for bleeding.²⁰²

Thickening of the wall of the small bowel and colon is common in patients with cirrhosis due to the presence of portal hypertension and low protein states. There is, however, a specific right-sided colitis (see Fig. 89-33) that can be due specifically to the portal hypertension. The increased pressure within the superior mesenteric vein leads to the release of a number of inflammatory mediators, including interleukin-1 and nitrous oxide. This can lead to a colitis that simulates inflammatory bowel disease. Vascular ectasias that have a propensity to bleed may also develop. The presence of this right-sided colitis is associated with an increased risk of spontaneous bacterial peritonitis as bacteria more readily translocate through the diseased colonic wall. The imaging differential diagnosis of the colonic submucosal edema includes inflammatory bowel disease, ischemia, and infections including pseudomembranous colitis.

MAGNETIC RESONANCE IMAGING: PORTAL HYPERTENSION

MRI (Fig. 89-34) is uniquely suited for the depiction of large vascular collaterals because of the natural contrast between flowing blood and surrounding soft tissues. The most successful

MRI techniques for delineation of abdominal blood vessels are MR angiographic techniques that can be used with or without gadolinium injection. Collateral pathways are demonstrated as tortuous structures of high signal intensity on MR angiograms. Direct sagittal scans are particularly useful for imaging of the paraumbilical vein, and coronal scans are helpful for esophageal and mesenteric varices.^{47,204,205}

Increased blood supply from the hepatic artery can cause heterogeneous increased arterial enhancement of the parenchyma. Vascular shunts and occlusions can be seen similarly with MRI as with CT and MRI.

Other findings of portal hypertension, including ascites, splenomegaly, and colitis, can also be seen with MRI.

TRANSJUGULAR INTRAHEPATIC PORTOSYSTEMIC SHUNT

The TIPS has become the mainstay of nonsurgical treatment of portal hypertension due to cirrhosis. This procedure is discussed in detail in Chapter 84. The goal of this procedure is to reduce the portal vein–hepatic vein gradient to 12 mm Hg or less. Doppler ultrasound is most commonly used to assess the TIPS and can determine patency and directionality of flow. CT and MRI can also be used to assess patency of the TIPS²⁰⁵⁻²¹¹ (Fig. 89-35).

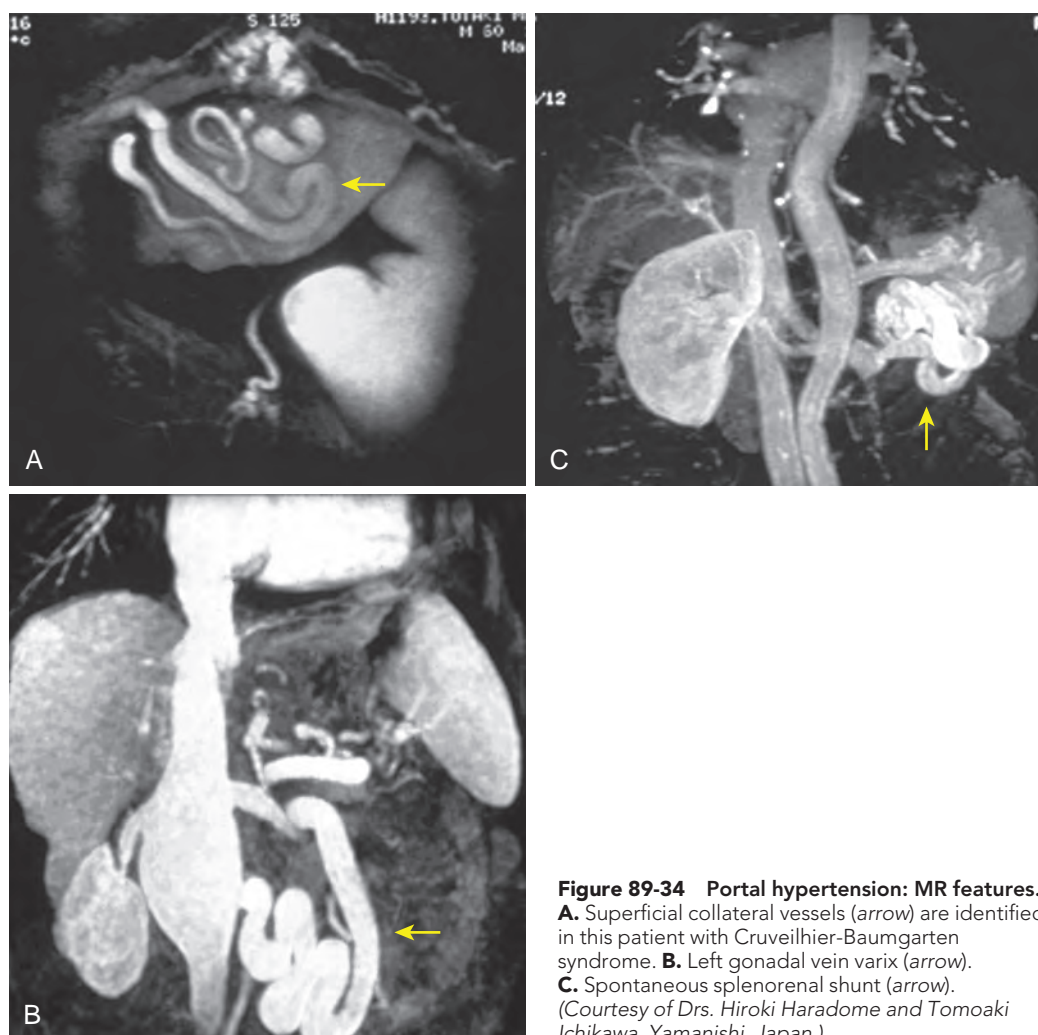


Figure 89-34 Portal hypertension: MR features.
A. Superficial collateral vessels (arrow) are identified in this patient with Cruveilhier-Baumgarten syndrome. **B.** Left gonadal vein varix (arrow). **C.** Spontaneous splenorenal shunt (arrow).
 (Courtesy of Drs. Hiroki Haradome and Tomoaki Ichikawa, Yamanishi, Japan.)

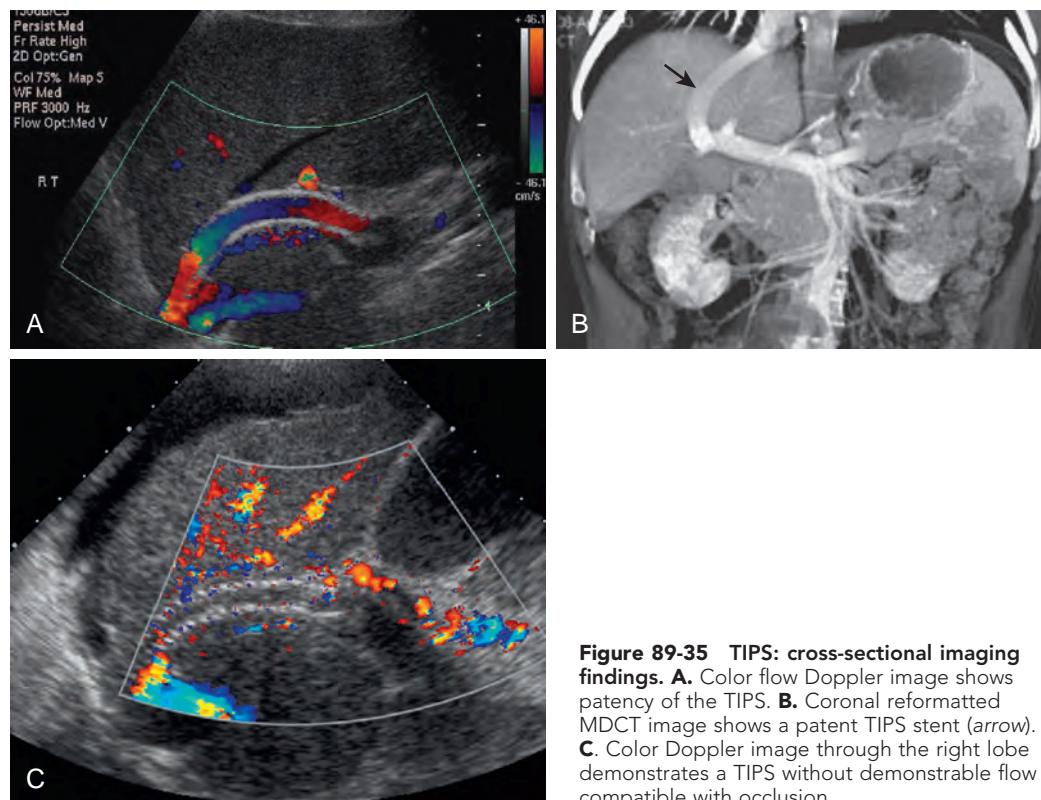


Figure 89-35 TIPS: cross-sectional imaging findings. **A.** Color flow Doppler image shows patency of the TIPS. **B.** Coronal reformatted MDCT image shows a patent TIPS stent (arrow). **C.** Color Doppler image through the right lobe demonstrates a TIPS without demonstrable flow compatible with occlusion.

REFERENCES

- Schuppan D, Kim YO: Evolving therapies for liver fibrosis. *J Clin Invest* 123:1887–1901, 2013.
- Blachier M, Leleu H, Peck-Radosavljevic M, et al: The burden of liver disease in Europe: A review of available epidemiological data. *J Hepatol* 58:593–608, 2013.
- Stolz A: Liver physiology and metabolic function. In Feldman M, Friedman LS, Sleisenger MH, editors: *Gastrointestinal and Liver Disease*, ed 7, Philadelphia, 2002, Saunders, pp 1202–1226.
- Chrostek L, Panasiuk A: Liver fibrosis markers in alcoholic liver disease. *World J Gastroenterol* 20:8018–8023, 2014.
- Lok AS, Everhart JE, Chung RT, et al: Evolution of hepatic steatosis in patients with advanced hepatitis C: Results from the hepatitis C antiviral long-term treatment against cirrhosis (HALT-C) trial. *Hepatology* 49:1828–1837, 2009.
- Dyson JK, Anstee QM, McPherson S: Non-alcoholic fatty liver disease: A practical approach to diagnosis and staging. *Frontline Gastroenterol* 5:211–218, 2014.
- Adams LA, Waters OR, Knuiam MW, et al: NAFLD as a risk factor for the development of diabetes and the metabolic syndrome: An eleven-year follow-up study. *Am J Gastroenterol* 104:861–867, 2009.
- Dunn W, Xu R, Wingard DL, et al: Suspected nonalcoholic fatty liver disease and mortality risk in a population-based cohort study. *Am J Gastroenterol* 103:2263–2271, 2008.
- Sanyal AJ, Banas C, Sargeant C, et al: Similarities and differences in outcomes of cirrhosis due to nonalcoholic steatohepatitis and hepatitis C. *Hepatology* 43:682–689, 2006.
- Ekstedt M, Franzen LE, Mathiesen UL, et al: Long-term follow-up of patients with NAFLD and elevated liver enzymes. *Hepatology* 44:865–873, 2006.
- Batts K, Ludwig J: Chronic hepatitis: An update on terminology and reporting. *Am J Surg Pathol* 19:1409–1419, 1995.
- Koo SH: Nonalcoholic fatty liver disease: Molecular mechanisms for the hepatic steatosis. *Clin Mol Hepatol* 19:210–215, 2013.
- Verbeek J, Cassiman D, Lannoo M, et al: Treatment of non-alcoholic fatty liver disease: Can we already face the epidemic? *Acta Gastroenterol Belg* 76:200–209, 2013.
- Szczepaniak LS, Nurenberg P, Leonard D, et al: Magnetic resonance spectroscopy to measure hepatic triglyceride content: Prevalence of hepatic steatosis in the general population. *Am J Physiol Endocrinol Metab* 288:E462–E468, 2005.
- Moscattello S, Manini R, Marchesini G: Diabetes and liver disease: An ominous association. *Nutr Metab Cardiovasc Dis* 17:63–70, 2007.
- Attar BM, Van Thiel DH: Current concepts and management approaches in nonalcoholic fatty liver disease. *Scientificworldjournal* 2013: 481893, 2013.
- Heath ML, Kow L, Slavotinek JP, et al: Abdominal adiposity and liver fat content 3 and 12 months after gastric banding surgery. *Metabolism* 58:753–758, 2009.
- Phillips ML, Boase S, Wahlroos S, et al: Associates of change in liver fat content in the morbidly obese after laparoscopic gastric banding surgery. *Diabetes Obes Metab* 10:661–667, 2008.
- Machado M, Marques-Vidal P, Cortez-Pinto H: Hepatic histology in obese patients undergoing bariatric surgery. *J Hepatol* 45:600–606, 2006.
- Day CP: From fat to inflammation. *Gastroenterology* 130:207–210, 2006.
- Hubscher SG: Histological assessment of non-alcoholic fatty liver disease. *Histopathology* 49:450–465, 2006.
- Hoofnagle JH, Heller T: Hepatitis C. In Zakim D, Boyer TD, editors: *Hepatology: A Textbook of Liver Disease*, Philadelphia, 2003, Saunders, pp 3–31.
- Park SH, Kim PN, Kim KW, et al: Macrovesicular hepatic steatosis in living liver donors: Use of CT for quantitative and qualitative assessment. *Radiology* 239:105–112, 2006.
- Merkle EM, Nelson RC: Dual gradient-echo in-phase and opposed-phase hepatic MR imaging: A useful tool for evaluating more than fatty infiltration or fatty sparing. *Radiographics* 26:1409–1418, 2006.
- Hamer OW, Aguirre DA, Casola G, et al: Imaging features of perivascular fatty infiltration of the liver: Initial observations. *Radiology* 237:159–169, 2005.
- Saadeh S, Younossi ZM, Remer EM, et al: The utility of radiological imaging in nonalcoholic fatty liver disease. *Gastroenterology* 123:745–750, 2002.
- Graif M, Yanuka M, Baraz M, et al: Quantitative estimation of attenuation in ultrasound

- video images: Correlation with histology in diffuse liver disease. *Invest Radiol* 35:319–324, 2000.
28. Wilson SR, Withers CE: The liver. In Rumack C, Wilson SR, Charboneau WR, et al, editors: *Diagnostic Ultrasound*, ed 3, Philadelphia, 2005, Elsevier-Mosby.
 29. Oliva MR, Mortelet KJ, Segatto E, et al: Computed tomography features of nonalcoholic steatohepatitis with histopathologic correlation. *J Comput Assist Tomogr* 30:37–46, 2006.
 30. Cobbald JF, Wylezinska M, Cunningham C, et al: Non-invasive evaluation of hepatic fibrosis using magnetic resonance imaging and ultrasound techniques. *Gut* 55:1670–1672, 2006.
 31. Tchelepi H, Ralls PW, Radin R, et al: Sonography of diffuse liver disease. *J Ultrasound Med* 21:1023–1032, 2002.
 32. Bohte AE, van Werven JR, Bipat S, Stoker J: The diagnostic accuracy of US, CT, MRI and ¹H-MRS for the evaluation of hepatic steatosis compared with liver biopsy: A meta-analysis. *Eur Radiol* 21:87–97, 2011.
 33. Lawrence DA, Oliva IB, Israel GM: Detection of hepatic steatosis on contrast-enhanced CT images: Diagnostic accuracy of identification of areas of presumed focal fatty sparing. *AJR Am J Roentgenol* 199:44–47, 2012.
 34. Hamer OW, Aguirre DA, Casola G, et al: Fatty liver: Imaging patterns and pitfalls. *Radiographics* 26:1637–1653, 2006.
 35. Brunt E: Nonalcoholic steatohepatitis: Definition and pathology. *Semin Liver Dis* 21:3–16, 2001.
 36. Dixon WT: Simple proton spectroscopic imaging. *Radiology* 153:189–194, 1984.
 37. Hussain HK, Chenevert TL, Londy FJ, et al: Hepatic fat fraction: MR imaging for quantitative measurement and display—early experience. *Radiology* 237:1048–1055, 2005.
 38. Qayyum A, Goh JS, Kakar S, et al: Accuracy of liver fat quantification at MR imaging: Comparison of out-of-phase gradient-echo and fat-saturated fast spin-echo techniques—initial experience. *Radiology* 237:507–511, 2005.
 39. Hamilton G, Yokoo T, Bydder M, et al: In vivo characterization of the liver fat ¹H MR spectrum. *NMR Biomed* 24:784–790, 2011.
 40. Yokoo T, Bydder M, Hamilton G, et al: Nonalcoholic fatty liver disease: Diagnostic and fat-grading accuracy of low-flip-angle multiecho gradient-recalled-echo MR imaging at 1.5 T. *Radiology* 251:67–76, 2009.
 41. Meisamy S, Hines CD, Hamilton G, et al: Quantification of hepatic steatosis with T1-independent, T2-corrected MR imaging with spectral modeling of fat: Blinded comparison with MR spectroscopy. *Radiology* 258:767–775, 2011.
 42. Hoofnagle JH, Heller T: Hepatitis C. In Zakim D, Boyer TD, editors: *Hepatology: A Textbook of Liver Disease*, Philadelphia, 2003, Saunders, pp 3–31.
 43. Thimme R, Spangenberg HC, Blum HE: Acute viral hepatitis. In Weinstein WM, Hawkey CJ, Bosch J, editors: *Clinical Gastroenterology and Hepatology*, Philadelphia, 2005, Elsevier-Mosby, pp 583–594.
 44. Yee HF, Lidofsky SD: Acute liver failure. In Feldman M, Friedman LS, Sleisenger MH, editors: *Gastrointestinal and Liver Disease*, ed 7, Philadelphia, 2002, Saunders, pp 1202–1226.
 45. World Health Organization: Hepatitis B: Fact Sheet 204. <www.who.int/mediacentre/factsheets/fs204/en/>. Updated July 2013. Accessed September 13, 2013.
 46. Centers for Disease Control and Prevention: Hepatitis B. Publication 21-1073. <www.cdc.gov/hepatitis/HBV/PDFs/HepBGeneralFactSheet.pdf>. 2010. Accessed September 13, 2013.
 47. Semelka RC, Braga L, Armao D: Liver. In Semelka RC, editor: *Abdominal-Pelvic MRI*, New York, 2002, Wiley-Liss, pp 33–318.
 48. Danet I-M, Semelka RC, Braga L: MR imaging in diffuse liver disease. *Radiol Clin North Am* 41:67–87, 2003.
 49. Martin DR, Semelka RC: Magnetic resonance imaging of the liver: Review of techniques and approach to common diseases. *Semin Ultrasound CT MR* 26:116–131, 2005.
 50. Lee V: Can MR imaging replace liver biopsy for the diagnosis of early fibrosis? *Radiology* 239:309–310, 2006.
 51. Ly JN, Miller FH: Periportal contrast enhancement and abnormal signal intensity on state-of-the-art MR images. *AJR Am J Roentgenol* 176:891–897, 2001.
 52. Russmann S, Reichen J: Drug-induced and toxic liver disease. In Weinstein WM, Hawkey CJ, Bosch J, editors: *Clinical Gastroenterology and Hepatology*, Philadelphia, 2005, Elsevier-Mosby, pp 677–686.
 53. Mookerjee RP, Jalan R: Alcoholic liver disease. In Weinstein WM, Hawkey CJ, Bosch J, editors: *Clinical Gastroenterology and Hepatology*, Philadelphia, 2005, Elsevier-Mosby, pp 637–646.
 54. Farrell GC: Liver disease caused by drugs, anesthetics, and toxins. In Feldman M, Friedman LS, Sleisenger MH, editors: *Gastrointestinal and Liver Disease*, ed 7, Philadelphia, 2002, Saunders, pp 1403–1447.
 55. Maher JJ: Alcoholic liver disease. In Feldman M, Friedman LS, Sleisenger MH, editors: *Gastrointestinal and Liver Disease*, ed 7, Philadelphia, 2002, Saunders, pp 1375–1386.
 56. Lee WM: Drug-induced hepatotoxicity. *N Engl J Med* 349:474–484, 2003.
 - 56a. Russell AH, Clyde C, Wasserman TH, et al: Accelerated hyperfractionated hepatic irradiation in the management of patients with liver metastases: results of the RTOG dose escalating protocol. *Int J Radiat Oncol Biol Phys* 27:117–123, 1993.
 57. Colli A, Massironi S, Faccioli P, et al: “Pseudotumoral” hepatic areas in acute alcoholic hepatitis: A computed tomography and histological study. *Am J Gastroenterol* 100:831–836, 2005.
 58. Fattovich G, Stroffolini T, Zagni I, Donato F: Hepatocellular carcinoma in cirrhosis: Incidence and risk factors. *Gastroenterology* 127 (Suppl 1):S35–S50, 2004.
 59. Ibrahim SM, Nikolaidis P, Miller FH, et al: Radiologic findings following Y90 radioembolization for primary liver malignancies. *Abdom Imaging* 34:566–581, 2009.
 60. Crownover BK, Covey CJ: Hereditary hemochromatosis. *Am Fam Physician* 87:183–190, 2013.
 61. Bacon B, Britton RS: Hereditary hemochromatosis. In Feldman M, Friedman LS, Sleisenger MH, editors: *Gastrointestinal and Liver Disease*, ed 7, Philadelphia, 2002, Saunders, pp 1261–1268.
 62. Tavill AS, Bacon DR: Hemochromatosis and iron overload syndromes. In Zakim D, Boyer TD, editors: *Hepatology: A Textbook of Liver Disease*, Philadelphia, 2003, Saunders, pp 3–31.
 63. Kowdley KV: Iron, hemochromatosis, and hepatocellular carcinoma. *Gastroenterology* 127:S79–S86, 2004.
 64. Sharma N, Butterworth J, Cooper BT, et al: The emerging role of the liver in iron metabolism. *Am J Gastroenterol* 100:201–206, 2005.
 65. Queiroz-Andrade M, Blasbalg R, Ortega CD, et al: MR imaging findings of iron overload. *Radiographics* 29:1575–1589, 2009.
 66. Ben Salem D, Cercueil J-P, Ricolfi F, et al: Erythropoietic hemochromatosis. *Radiology* 233:116–119, 2004.
 67. Joe E, Kim SH, Lee KB, et al: Feasibility and accuracy of dual-source dual-energy CT for noninvasive determination of hepatic iron accumulation. *Radiology* 262:126–135, 2012.
 68. Alustiza JM, Artetxe J, Agirre A, et al: MR quantification of hepatic iron concentration. *Radiology* 230:479–484, 2004.
 69. Olthoff AW, Sijens PE, Kreeftenberg HG, et al: Non-invasive liver iron concentration measurement by MRI: Comparison of two validated protocols. *Eur J Radiol* 71:116–121, 2009.
 70. Alexopoulou E, Stripeli F, Baras P, et al: R2 relaxometry with MRI for the quantification of tissue iron overload in beta-thalassemic patients. *J Magn Reson Imaging* 23:163–170, 2006.
 71. Bulte JW, Miller GF, Vymazal J, et al: Hepatic hemosiderosis in non-human primates: Quantification of liver iron using different field strengths. *Magn Reson Med* 37: 530–536, 1997.
 72. Clark PR, Chua-anusorn W, St Pierre TG: Bi-exponential proton transverse relaxation rate (R2) image analysis using RF field intensity-weighted spin density projection: potential for R2 measurement of iron-loaded liver. *Magn Reson Imaging* 21:519–530, 2003.
 73. Ghugre NR, Coates TD, Nelson MD, Wood JC: Mechanisms of tissue-iron relaxivity: Nuclear magnetic resonance studies of human liver biopsy specimens. *Magn Reson Med* 54:1185–1193, 2005.
 74. Taouli B, Chouli M, Martin AJ, et al: Chronic hepatitis: role of diffusion-weighted imaging and diffusion tensor imaging for the diagnosis of liver fibrosis and inflammation. *J Magn Reson Imaging* 28:89–95, 2008.
 75. Chebrolu VV, Hines CD, Yu H, et al: Independent estimation of T2* for water and fat for improved accuracy of fat quantification. *Magn Reson Med* 63:849–857, 2010.
 76. Boll DT, Merkle EM: Diffuse liver disease: Strategies for hepatic CT and MR imaging. *Radiographics* 29:1591–1614, 2009.
 77. Grazioli L, Federle MP, Brancatelli G, et al: Hepatic adenomas: Imaging and pathologic findings. *Radiographics* 21:877–892, 2001.
 78. Giovanoli O, Heim M, Terracciano L, et al: MRI of hepatic adenomatosis: Initial observations with gadoteric acid contrast agent in three patients. *AJR Am J Roentgenol* 190: W290–W293, 2008.
 79. Mieli-Vergani G, Thompson R: Genetic and metabolic liver disease. In Weinstein WM, Hawkey CJ, Bosch J, editors: *Clinical Gastroenterology and Hepatology*, Philadelphia, 2005, Elsevier-Mosby, pp 687–692.
 80. Thiele DL: Hepatic manifestations of systemic disease and other disorders of the liver. In Feldman M, Friedman LS, Sleisenger MH, editors: *Gastrointestinal and Liver Disease*,

- ed 7, Philadelphia, 2002, Saunders, pp 1603–1619.
81. Mainetti PP, D'Agostino L, Socia E, et al: Hepatic and splenic amyloidosis: Dual-phase spiral CT findings. *Abdom Imaging* 28:688–690, 2003.
82. Campbell-Washburn AE, Price AN, Ellmerich S, et al: Monitoring systemic amyloidosis using MRI measurements of the extracellular volume fraction. *Amyloid* 20:93–98, 2013.
83. Monzawa S, Tsukamoto T, Omata K, et al: A case of primary amyloidosis of the liver and spleen: Radiologic findings. *Eur J Radiol* 41:237–241, 2002.
84. Georgiades CS, Neyman EG, Fishman EK: Cross-sectional imaging of amyloidosis: An organ system based approach. *J Comput Assist Tomogr* 26:1035–1041, 2002.
85. Kim SH, Han JK, Lee KH, et al: Abdominal amyloidosis: Spectrum of radiological findings. *Clin Radiol* 58:610–620, 2003.
86. Möller JM, Santoni-Rugiu E, Chabanova E, et al: Magnetic resonance imaging with liver-specific contrast agent in primary amyloidosis and intrahepatic cholestasis. *Acta Radiol* 48:145–149, 2007.
87. Gitlin JD: Wilson's disease. In Zakim D, Boyer TD, editors: *Hepatology: A Textbook of Liver Disease*, ed 6, Philadelphia, 2011, Elsevier, pp 1273–1288.
88. Ferenci P: Wilson's disease. *Clin Gastroenterol Hepatol* 3:726–733, 2005.
89. Medici V, Trevisan CP, D'Inca R, et al: Diagnosis and management of Wilson's disease: Results of a single center experience. *J Clin Gastroenterol* 40:936–941, 2006.
90. Walshe JM: Copper: Its role in the pathogenesis of liver disease. *Semin Liver Dis* 4:252–263, 1984.
91. Smallwood RA, Williams HA, Rosenoer VM, Sherlock S: Liver-copper levels in liver disease: Studies using neutron activation analysis. *Lancet* 292:1310–1313, 1968.
92. Mehta A: Epidemiology and natural history of Gaucher's disease. *Eur J Intern Med* 17 (Suppl):S2–S5, 2006.
93. Purchase R: The treatment of Wilson's disease, a rare genetic disorder of copper metabolism. *Sci Prog* 96(Pt 1):19–32, 2013.
94. Roberts EA, Schilsky ML: American Association for Study of Liver Diseases (AASLD): Diagnosis and treatment of Wilson disease: An update. *Hepatology* 47:2089–2111, 2008.
95. Akhan O, Akpınar E, Karcaaltincaba M, et al: Imaging findings of liver involvement of Wilson's disease. *Eur J Radiol* 69:147–155, 2009.
96. Awaya H, Mitchell DG, Kamishima T, et al: Cirrhosis: Modified caudate-right lobe ratio. *Radiology* 224:769–774, 2002.
97. Xu R, Hajdu CH: Wilson disease and hepatocellular carcinoma. *Gastroenterol Hepatol (N Y)* 4:438–439, 2008.
98. Bennett LH: Artifacts in magnetic resonance imaging from metals. *J Appl Phys* 79:4712–4714, 1996.
99. Chu WCW, Leung TF, Chan KF, et al: Wilson's disease with chronic active hepatitis: Monitoring by in vivo 31-phosphorus MR spectroscopy before and after medical treatment. *AJR Am J Roentgenol* 183:1339–1342, 2004.
100. Poll LW, Koch JA, vom Dahl S, et al: Extraosseous manifestation of Gaucher's disease type I: MR and histological appearance. *Eur Radiol* 10:1660–1663, 2000.
101. Rosenbloom BE, Weinreb NJ: Gaucher disease: A comprehensive review. *Crit Rev Oncog* 18:163–175, 2013.
102. Hadas-Halpern I, Deeb M, Abrahamov A, et al: Gaucher disease: Spectrum of sonographic findings in the liver. *J Ultrasound Med* 29:727–733, 2010.
103. Karagiannidis A, Karavalaki M, Koulaouzidis A: Hepatic sarcoidosis. *Ann Hepatol* 5:251–256, 2006.
104. Bakker GJ, Haan YC, Maillette de Buy Wenniger LJ, et al: Sarcoidosis of the liver: To treat or not to treat? *Neth J Med* 70:349–356, 2012.
105. Koyama T, Ueda H, Togashi K, et al: Radiologic manifestations of sarcoidosis in various organs. *Radiographics* 24:87–104, 2004.
106. Warshauer DM, Lee JKT: Imaging manifestations of abdominal sarcoidosis. *AJR Am J Roentgenol* 182:15–28, 2004.
107. Nguyen BD: F-18 FDG PET imaging of disseminated sarcoidosis. *Clin Nucl Med* 32:53–54, 2007.
108. Jung G, Brill N, Poll LW, et al: MRI of hepatic sarcoidosis: Large confluent lesions mimicking malignancy. *AJR Am J Roentgenol* 183:171–173, 2004.
109. Lalosević D, Milosević P, Vucković N, et al: Von Meyenburg complex associated with adult polycystic liver disease. *Med Pregl* 58:191–195, 2005.
110. Wei SC, Huang GT, Chen CH, et al: Bile duct hamartomas: A report of two cases. *J Clin Gastroenterol* 25:608–611, 1997.
111. Zheng RQ, Zhang B, Kudo M, et al: Imaging findings of biliary hamartomas. *World J Gastroenterol* 11:6354–6359, 2005.
112. Mortelet B, Mortelet K, Seynaeve P, et al: Hepatic bile duct hamartomas (von Meyenburg complexes): MR and MR cholangiography findings. *J Comput Assist Tomogr* 26:438–443, 2002.
113. Lev-Toaff AS, Bach AM, Wechsler RJ, et al: The radiologic and pathologic spectrum of biliary hamartomas. *AJR Am J Roentgenol* 165:309–313, 1995.
114. Krause D, Cercueil JP, Dransart M, et al: MRI for evaluating congenital bile duct abnormalities. *J Comput Assist Tomogr* 26:541–552, 2002.
115. Mortelet KJ, Ros PR: Cystic focal liver lesions in the adult: Differential CT and MR imaging features. *Radiographics* 21:895–910, 2001.
116. Brancatelli G, Federle MP, Vilgrain V, et al: Fibropolycystic liver disease: CT and MR imaging findings. *Radiographics* 25:659–670, 2005.
117. Martinoli C, Cittadini G, Jr, Rollandi GA, Conzi R: Case report: Imaging of bile duct hamartomas. *Clin Radiol* 45:203–205, 1992.
118. Wohlgemuth WA, Böttger J, Bohndorf K: MRI, CT, US and ERCP in the evaluation of bile duct hamartomas (von Meyenburg complex): A case report. *Eur Radiol* 8:1623–1626, 1998.
119. Slone HW, Bennett WF, Bova JG: MR findings of multiple biliary hamartomas. *AJR Am J Roentgenol* 161:581–583, 1993.
120. Maher MM, Dervan P, Keogh B, Murray JG: Bile duct hamartomas (von Meyenburg complexes): Value of MR imaging in diagnosis. *Abdom Imaging* 24:171–173, 1999.
121. Semelka RC, Hussain SM, Marcos HB, Woosley JT: Biliary hamartomas: Solitary and multiple lesions shown on current MR techniques including gadolinium enhancement. *J Magn Reson Imaging* 10:196–201, 1999.
122. Bowlus CL, Gershwin ME: The diagnosis of primary biliary cirrhosis. *Autoimmun Rev* 13:441–444, 2014.
123. Kummern M, Schrupf E, Boberg KM: Liver abnormalities in bowel diseases. *Best Pract Res Clin Gastroenterol* 27:531–542, 2013.
124. Neuberger J: Primary biliary cirrhosis. In Weinstein WM, Hawkey CJ, Bosch J, editors: *Clinical Gastroenterology and Hepatology*, Philadelphia, 2005, Elsevier-Mosby, pp 659–664.
125. Batts KP: Autoimmune and cholestatic disorders of the liver. In Odze RD, Goldblum JR, Crawford JM, editors: *Surgical Pathology of the GI Tract, Liver, Biliary Tract, and Pancreas*, Philadelphia, 2004, Saunders, pp 863–885.
126. Jacob DA, Neumann UP, Bahra M, et al: Long-term follow-up after recurrence of primary biliary cirrhosis after liver transplantation in 100 patients. *Clin Transplant* 20:211–220, 2006.
127. Khettry U, Anand N, Faul PN, et al: Liver transplantation for primary biliary cirrhosis: A long-term pathologic study. *Liver Transpl* 9:87–96, 2006.
128. Hohenester S, Oude-Elferink RP, Beuers U: Primary biliary cirrhosis. *Semin Immunopathol* 31:283–307, 2009.
129. Knowlton JQ, Taylor AJ, Reichelderfer M, Stang J: Imaging of biliary tract inflammation: An update. *AJR Am J Roentgenol* 190:984–992, 2008.
130. Dodd GD, 3rd, Baron RL, Oliver JH, 3rd, et al: End-stage primary sclerosing cholangitis: CT findings of hepatic morphology in 36 patients. *Radiology* 211:357–362, 1999.
131. Elsayes KM, Oliveira EP, Narra VR, et al: MR and MRCP in the evaluation of primary sclerosing cholangitis: Current applications and imaging findings. *J Comput Assist Tomogr* 30:398–404, 2006.
132. Berstad AE, Aabakken L, Smith HJ, et al: Diagnostic accuracy of magnetic resonance and endoscopic retrograde cholangiography in primary sclerosing cholangitis. *Clin Gastroenterol Hepatol* 4:514–520, 2006.
133. Dusunceli E, Erden A, Erden I, et al: Primary sclerosing cholangitis: MR cholangiopancreatography and T2-weighted MR imaging findings. *Diagn Interv Radiol* 11:213–218, 2005.
134. Bader TR, Beavers KL, Semelka RC: MR imaging features of primary sclerosing cholangitis: Patterns of cirrhosis in relationship to clinical severity of disease. *Radiology* 226:675–685, 2003.
135. Revelon G, Rashid A, Kawamoto S, et al: Primary sclerosing cholangitis: MR imaging findings with pathologic correlation. *AJR Am J Roentgenol* 173:1037–1042, 1999.
136. Johnson KJ, Olliff JE, Olliff SP: The presence and significance of lymphadenopathy detected by CT in primary sclerosing cholangitis. *Br J Radiol* 71:1279–1282, 1998.
137. Bader TR, Beavers KL, Semelka RC: MR imaging features of primary sclerosing cholangitis: Patterns of cirrhosis in relationship to clinical severity of disease. *Radiology* 226:675–685, 2003.
138. Koenraad J, Mortelé KJ, Segatto E, Ros PR: The infected liver: Radiologic-pathologic correlation. *Radiographics* 24:937–955, 2004.
139. National Institutes of Health: Action Plan for Liver Disease Research. NIH Publication number 04-5491. <www2.niddk.nih.gov/NR/>

- rdonlyres/38C08EFA-D0A3-49CF-952F-AB6CB673CFA6/0/ldrb_chapter6.pdf>. December 2004. Accessed September 28, 2013.
140. Price JC, Thio CL: Liver disease in the HIV-infected individual. *Clin Gastroenterol Hepatol* 8:1002–1012, 2010.
 141. Carucci LR, Halvorsen RA: Abdominal and pelvic CT in HIV-positive population. *Abdom Imaging* 29:631–642, 2004.
 142. D'Amico G, Malizia G: Cirrhosis of the liver. In Weinstein WM, Hawkey CJ, Bosch J, editors: *Clinical Gastroenterology and Hepatology*. Philadelphia, 2005, Elsevier-Mosby, pp 699–706.
 143. Bass NM, Yao FY: Portal hypertension and variceal bleeding. In Feldman M, Friedman LS, Sleisenger MH, editors: *Gastrointestinal and Liver Disease*, ed 7. Philadelphia, 2002, Saunders, pp 1487–1516.
 144. Wanless IR, Crawford JM: Cirrhosis. In Odze RD, Goldblum JR, Crawford JM, editors: *Surgical Pathology of the GI Tract, Liver, Biliary Tract, and Pancreas*. Philadelphia, 2004, Saunders, pp 863–885.
 145. Van Beers BE, Leconte I, Materne R, et al: Hepatic perfusion parameters in chronic liver disease. *AJR Am J Roentgenol* 176:667–673, 2001.
 146. Hytiroglou P, Theise ND, Schwartz M, et al: Macroregenerative nodules in a series of adult cirrhotic liver explants: Issues of classification and nomenclature. *Hepatology* 21:703–708, 1995.
 147. Borzio M, Borzio F, Croce A, et al: Ultrasonography-detected macroregenerative nodules in cirrhosis: A prospective study. *Gastroenterology* 112:1617–1623, 1997.
 148. Kim M, Mitchell DG, Ito K: Portosystemic collaterals of the upper abdomen: Review of anatomy and demonstration on MR imaging. *Abdom Imaging* 25:462–470, 2006.
 149. Colli A, Fraquelli M, Andreoletti M, et al: Severe liver fibrosis or cirrhosis: Accuracy of US for detection—analysis of 300 cases. *Radiology* 227:89–94, 2003.
 150. Nishura T, Watanabe H, Ito M, et al: Ultrasound evaluation of the fibrosis stage in chronic liver disease by the simultaneous use of low and high frequency probes. *Br J Radiol* 78:189–197, 2005.
 151. Caturelli E, Castellano L, Fusilli S, et al: Coarse nodular US pattern in hepatic cirrhosis: Risk for hepatocellular carcinoma. *Radiology* 226: 691–697, 2003.
 152. Nicolau C, Bianchi L, Vilana R: Grey-scale ultrasound in hepatic cirrhosis and chronic hepatitis: Diagnosis, screening, and intervention. *Semin Ultrasound CT MR* 23:3–18, 2002.
 153. Martinez-Noguera A, Montserrat E, Torrubia S, et al: Doppler in hepatic cirrhosis and chronic hepatitis. *Semin Ultrasound CT MR* 23:19–36, 2002.
 154. Lafortune M, Matricardi L, Denys A, et al: Segment 4 (the quadrate lobe): A barometer of cirrhotic liver disease. *Radiology* 206:157–160, 1998.
 155. Lim AKP, Patel N, Eckersley RJ, et al: Can Doppler sonography grade the severity of hepatitis C-related liver disease? *AJR Am J Roentgenol* 184:1848–1853, 2005.
 156. Awaya H, Mitchell DG, Kamishima T, et al: Cirrhosis: Modified caudate-right lobe ratio. *Radiology* 224:769–774, 2002.
 157. Valls C, Andia E, Roca Y, et al: CT in hepatic cirrhosis and chronic hepatitis. *Semin Ultrasound CT MR* 23:37–91, 2002.
 158. Gibo M, Murata S, Kuroki S: Pericaval fat collection mimicking an intracaval lesion on CT in patients with chronic liver disease. *Abdom Imaging* 26:492–495, 2001.
 159. Nakagawa H, Toda N, Taniguchi M, et al: Prevalence and sonographic detection of Childlaiditi's sign in cirrhotic patients without ascites. *AJR Am J Roentgenol* 187:W589–W593, 2006.
 160. Lim JH, Kim MJ, Park CK, et al: Dysplastic nodules in liver cirrhosis: Detection with triple phase helical dynamic CT. *Br J Radiol* 77:911–916, 2004.
 161. Lim JH, Choi BI: Dysplastic nodules in liver cirrhosis: Imaging. *Abdom Imaging* 27:117–128, 2002.
 162. Krinsky G: Terminology of hepatocellular nodules in cirrhosis: Plea for consistency. *Radiology* 224:638–639, 2002.
 163. Shimizu A, Ito K, Kioke S, et al: Cirrhosis or chronic hepatitis: Evaluation of small (≤ 2 -cm) early-enhancing hepatic lesions with serial contrast-enhanced dynamic MR imaging. *Radiology* 226:550–555, 2003.
 164. Jeong YY, Mitchell DG, Kamishima T: Small (< 20 mm) enhancing hepatic nodules seen on arterial phase MR imaging of the cirrhotic liver: Clinical implications. *AJR Am J Roentgenol* 178:1327–1334, 2002.
 165. Yu J-S, Cho E-S, Kim K-H, et al: Newly developed hepatocellular carcinoma (HCC) in chronic liver disease: MR imaging findings before the diagnosis of HCC. *J Comput Assist Tomogr* 30:765–771, 2006.
 166. Shimura R, Matsui O, Kobayashi S, et al: Cirrhotic nodules: Association between MR imaging signal intensity and intranodular blood supply. *Radiology* 237:512–519, 2005.
 167. Ito K, Fujita T, Shimizu A, et al: Multiarterial phase dynamic MRI of small early enhancing hepatic lesions in cirrhosis or chronic hepatitis: Differentiating between hypervascular hepatocellular carcinomas and pseudolesions. *AJR Am J Roentgenol* 183: 699–705, 2004.
 168. Krinsky GA, Lee VS, Theise ND: Focal lesions in the cirrhotic liver: High resolution ex vivo MRI with pathologic correlation. *J Comput Assist Tomogr* 24:189–196, 2000.
 169. Kim YK, Kwak HS, Kim CS, et al: Hepatocellular carcinoma in patients with chronic liver disease. *Radiology* 238:531–542, 2006.
 170. Takayasu K, Muramatsu Y, Misuguchi Y, et al: CT evaluation for the progression of hypotenuating nodular lesions in virus-related chronic liver disease. *AJR Am J Roentgenol* 187:454–463, 2006.
 171. Okazaki H, Ito K, Fujita T, et al: Discrimination of alcoholic from virus-induced cirrhosis on MR imaging. *AJR Am J Roentgenol* 175:1677–1681, 2000.
 172. Filly RA, Reddy SG, Nalbandian AB, et al: Sonographic evaluation of liver nodularity: Inspection of deep versus superficial surfaces of the liver. *J Clin Ultrasound* 30:399–407, 2002.
 173. Leoni S, Piscaglia F, Granito A, et al: Characterization of primary and recurrent nodules in liver cirrhosis using contrast-enhanced ultrasound: Which vascular criteria should be adopted? *Ultraschall Med* 34:280–287, 2013.
 174. Lee YJ, Lee JM, Lee JE, et al: MR elastography for noninvasive assessment of hepatic fibrosis: Reproducibility of the examination and reproducibility and repeatability of the liver stiffness value measurement. *J Magn Reson Imaging* 2013. [Epub ahead of print.]
 175. Gheorghe L: Real time elastography—a non-invasive diagnostic method of small hepatocellular carcinoma in cirrhosis. *J Gastrointest Liver Dis* 18:439–446, 2009.
 176. McNaughton DA, Abu-Yousef MM: Doppler US of the liver made simple. *Radiographics* 31:161–188, 2011.
 177. Ito K, Mitchell DG, Gabata T, et al: Expanded gallbladder fossa: Simple MR imaging sign of cirrhosis. *Radiology* 211:723–726, 1999.
 178. Berzigotti A, Casadei A, Magalotti D, et al: Renovascular impedance correlates with portal pressure in patients with cirrhosis. *Radiology* 240:581–586, 2006.
 179. Baik SKB, Kim JW, Kim HS, et al: Recent variceal bleeding: Doppler US hepatic vein waveform in assessment of severity of portal hypertension and vasoactive drug response. *Radiology* 240:574–580, 2006.
 180. Lipson JA, Qayyum A, Avrin DE, et al: CT and MRI of hepatic contour abnormalities. *AJR Am J Roentgenol* 184:75–81, 2005.
 181. Yang DM, Kim HS, Cho SW, et al: Various causes of hepatic capsular retraction: CT and MR findings. *Br J Radiol* 75:994–1002, 2002.
 182. Carlos RC, Kin HM, Hussain HK, et al: Developing a prediction rule to assess hepatic malignancy with cirrhosis. *AJR Am J Roentgenol* 180:893–900, 2003.
 183. Vitellas KM, Tzalonikou MT, Bennett WF, et al: Cirrhosis: Spectrum of findings on unenhanced and dynamic gadolinium-enhanced MR imaging. *Abdom Imaging* 26:601–615, 2001.
 184. Hussain HK, Syed I, Nghiem HV, et al: T2-weighted MR imaging in the assessment of the cirrhotic liver. *Radiology* 230:637–644, 2004.
 185. Mortelet KJ, Ros PR: MR imaging in chronic hepatitis and cirrhosis. *Semin Ultrasound CT MR* 23:79–100, 2002.
 186. Aguirre DA, Behling CA, Alpert E, et al: Liver fibrosis: Noninvasive diagnosis with double contrast material-enhanced MR imaging. *Radiology* 239:425–437, 2006.
 187. Rouviere O, Yin M, Drsnar MA, et al: MR elastography of the liver: Preliminary results. *Radiology* 240:440–673, 2006.
 188. Wachsberg RH: Inferior mesenteric vein: Gray-scale and Doppler sonographic findings in normal subjects and in patients with portal hypertension. *AJR Am J Roentgenol* 184:481–486, 2005.
 189. Farber E, Fischer D, Eliakim R, et al: Esophageal varices: Evaluation with esophagography with barium versus endoscopic gastroduodenoscopy in patients with compensated cirrhosis. *Radiology* 237:535–540, 2005.
 190. Kang HK, Jeong YY, Choi JH, et al: Three-dimensional multi-detector row CT portal venography in the evaluation of portosystemic collateral vessels in liver cirrhosis. *Radiographics* 22:1053–1061, 2002.
 191. Groves AM, Dixon AK: Superficial collateral veins on abdominal CT: Findings in cirrhosis and systemic venous obstruction. *Br J Radiol* 75:645–657, 2002.
 192. Kamel IR, Liapi E, Fishman EK: Liver and biliary system: Evaluation by multidetector CT. *Radiol Clin North Am* 43:977–998, 2005.
 193. Wachsberg RH, Bahramipour P, Sofocleous CT, et al: Hepatofugal flow in the portal venous system: Pathophysiology, imaging findings,

- and diagnostic pitfalls. *Radiographics* 22:123–140, 2002.
194. Kim YJ, Raman SS, Yu NC, et al: Esophageal varices in cirrhotic patients: Evaluation with liver CT. *AJR Am J Roentgenol* 188:139–144, 2007.
 195. Lonjedo E, Ripolles T: Vascular imaging and interventional procedures in hepatic cirrhosis. *Semin Ultrasound CT MR* 23:130–140, 2002.
 196. Van Beers BE, Leconte I, Materne R, et al: Hepatic perfusion parameters in chronic liver disease: Dynamic CT measurements correlated with disease severity. *AJR Am J Roentgenol* 176:667–673, 2001.
 197. Merkle EM, Gilkeson RC: Remnants of fetal circulation: Appearance on MDCT in adults. *AJR Am J Roentgenol* 185:541–549, 2005.
 198. Fritz GA, Schoellnast H, Deutshmann HA, et al: Density histogram analysis of unenhanced hepatic computed tomography in patients with diffuse liver diseases. *J Comput Assist Tomogr* 30:201–205, 2006.
 199. Annet L, Peeters F, Horsmans Y, et al: Esophageal varices: Evaluation with transesophageal MR imaging: Initial experience. *Radiology* 238:167–175, 2006.
 200. Annet L, Materne R, Danse E, et al: Hepatic flow parameters measured with MR imaging and Doppler US: Correlations with the degree of cirrhosis and portal hypertension. *Radiology* 229:409–414, 2003.
 201. Bryce TJ, Yeh BJ, Qayyum A, et al: CT signs of hepatofugal venous flow in patients with cirrhosis. *AJR Am J Roentgenol* 181:1629–1633, 2003.
 202. Watanabe S, Hosimo N, Kitade Y, et al: Assessment of the presence and severity of esophagogastric varices by splenic index in patients with liver cirrhosis. *J Comput Assist Tomogr* 24:788–794, 2000.
 203. Kamel IR, Lawler LP, Corl FM, et al: Patterns of collateral pathways in extrahepatic portal hypertension as demonstrated by multidetector row computed tomography and advanced image processing. *J Comput Assist Tomogr* 28:469–477, 2004.
 204. Matsuo M, Kanematsu M, Kim T, et al: Esophageal varices: Diagnosis with gadolinium enhanced MR imaging of the liver for patients with chronic liver damage. *AJR Am J Roentgenol* 180:461–466, 2003.
 205. Kim M-J, Mitchell DG, Ito K: Portosystemic collaterals of the upper abdomen: Review of anatomy and demonstration on MR imaging. *Abdom Imaging* 25:462–470, 2000.
 206. Tesdal IK, Filser T, Weiss C, et al: Transjugular intrahepatic portosystemic shunts: Adjunctive embolotherapy of gastroesophageal collateral vessels in the prevention of variceal rebleeding. *Radiology* 236:36–37, 2005.
 207. Henderson JM: Surgery versus transjugular intrahepatic portal systemic shunt in the treatment of severe variceal bleeding. *Clin Liver Dis* 10:599–612, 2006.
 208. Laberge JM: Transjugular intrahepatic portosystemic shunt: Role in treating intractable variceal bleeding, ascites, and hepatic hydrothorax. *Clin Liver Dis* 10:583–598, 2006.
 209. Centers for Disease Control and Prevention: National Vital Statistics Reports, vol 61, no 6. www.cdc.gov/nchs/data/nvsr/nvsr61/nvsr61_06.pdf. October 10, 2012. Accessed October 2, 2013.
 210. Rahimi RS, Rockey DC: End-stage liver disease complications. *Curr Opin Gastroenterol* 29: 257–263, 2013.
 211. Qi XS, Bai M, Yang ZP, Fan DM: Selection of TIPS stent for management of portal hypertension in liver cirrhosis: An evidence-based review. *World J Gastroenterol* 20:6470–6480, 2014.

Vascular Disorders of the Liver and Splanchnic Circulation

RICHARD M. GORE | AHMED BA-SSALAMAH

CHAPTER OUTLINE

Transient Hepatic Attenuation Differences (THADs) and Transient Hepatic Intensity Differences (THIDs)

THADs and THIDs Associated with a Mass Lesion
THADs and THIDs Not Associated with a Mass Lesion

Budd-Chiari Syndrome and Sinusoidal Obstruction Syndrome

Clinical Findings
Etiology
Pathologic Findings
Radiologic Findings
Treatment

Liver in Cardiac Disease

Clinical Findings
Radiologic Findings

Peliosis Hepatis

Pathophysiology
Radiologic Findings

Portal Vein Thrombosis

Clinical Findings
Pathophysiology
Radiologic Findings
Treatment

Cavernous Transformation of the Portal Vein

Superior Mesenteric Vein Thrombosis

Clinical Findings
Pathophysiology
Radiologic Findings
Treatment

Splenic Vein and Inferior Mesenteric Vein Thrombosis

Hepatic Infarction

Clinical Findings
Pathologic Findings
Radiologic Findings

Hemolysis, Elevated Liver Enzymes, Low Platelets (HELLP) Syndrome

Visceral Artery Aneurysms

Clinical Findings
Radiologic Findings

Splanchnic Vein Aneurysms

Osler-Weber-Rendu Disease

Hepatopulmonary Syndrome

Pathophysiology
Imaging of Intrapulmonary Vascular Dilations
Treatment

The liver has a unique, dual blood supply in which 25% of the flow comes from the hepatic artery and 75% through the portal vein (Fig. 90-1). There is an inverse relationship between these two blood supplies. If portal flow decreases, arterial flow will increase as if an impedance has been removed. In addition, there are several communications between these vessels that open in response to nervous and humoral factors: trans-sinusoidal, transvasal, and transplexal. When vascular compromise develops, the volume and direction of blood flow of an individual vessel will be altered. Multidetector computed tomography (MDCT), Doppler ultrasound, and magnetic resonance imaging (MRI) are sensitive in the diagnosis of these perfusion disorders and are discussed in this chapter.

Transient Hepatic Attenuation Differences (THADs) and Transient Hepatic Intensity Differences (THIDs)

Intraparenchymal perfusion disorders such as transient hepatic attenuation differences (THADs) and transient hepatic

intensity differences (THIDs) are epiphenomena of alterations of the dual vascular supply of the liver.¹⁻⁹ There is a compensatory relationship between hepatic arterial and portal venous blood supply so that arterial flow increases when portal flow decreases (Fig. 90-2). This is made possible by communication among the main vessels, sinusoids, and peribiliary venules that dilate in response to autonomic nervous system and humoral factors activated by hepatic demand for oxygen and metabolites. THADs and THIDs are areas of parenchymal enhancement visible during the hepatic arterial phase after the intravenous administration of contrast media. These lesions can be classified by morphology, etiology (Figs. 90-3 to 90-6), and pathogenesis.¹⁻⁴

THADS AND THIDS ASSOCIATED WITH A MASS LESION

Benign and malignant masses produce two morphologic types of THADs and THIDs by four pathophysiologic mechanisms: directly, by siphoning effect of the mass (lobar multisegmental shape); indirectly, by means of portal hypoperfusion (sectorial

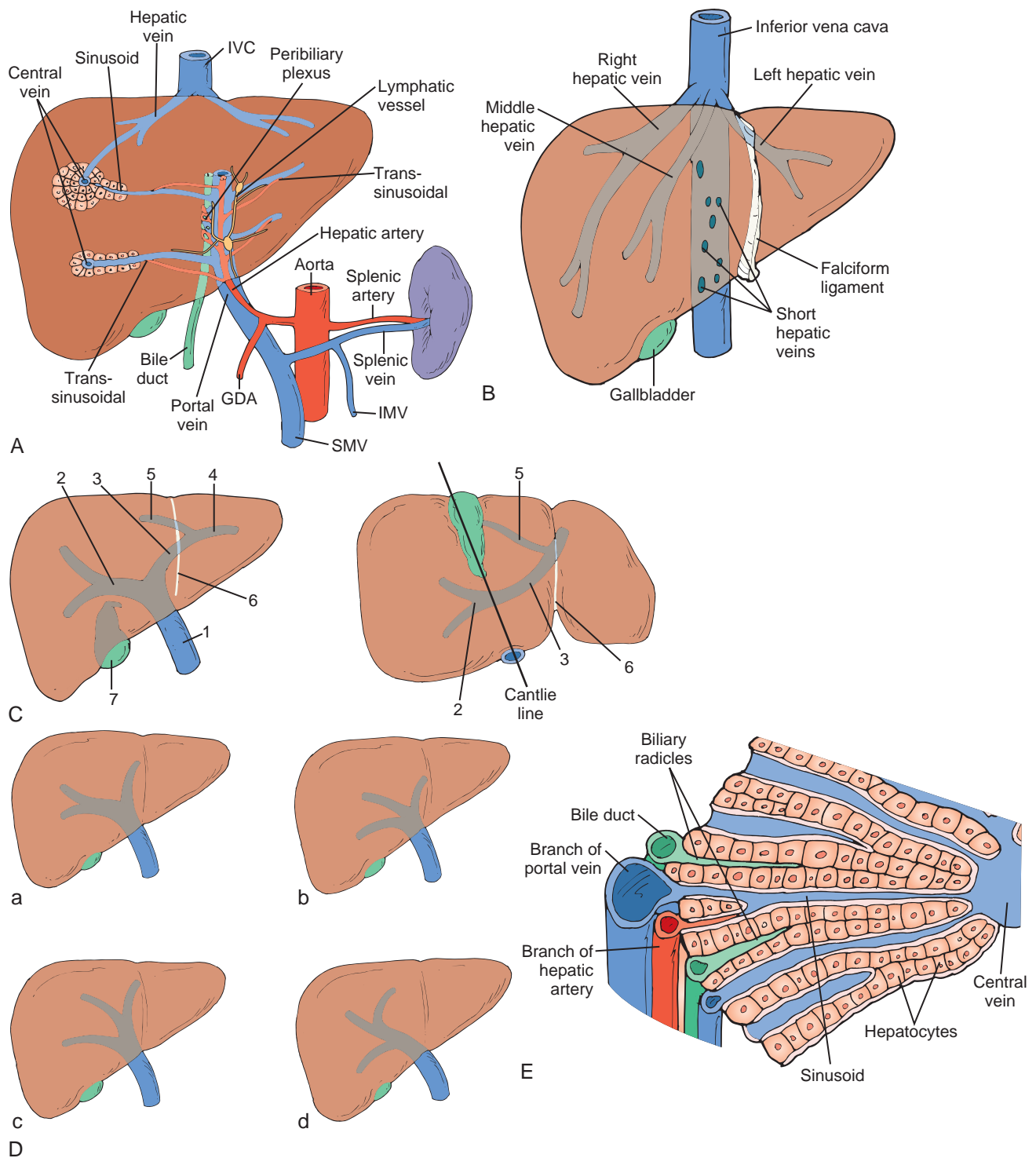


Figure 90-1 Hepatic blood supply. **A.** Diagram shows that the arterial and venous supplies to the liver are not independent systems. There are numerous communications between them, including the trans-sinusoidal route (between the interlobular arterioles and portal venules or sinusoids) and the transplexal route (peribiliary plexus), which play an important role when portal venous inflow is compromised. GDA, Gastroduodenal artery; IMV, inferior mesenteric vein; IVC, inferior vena cava; SMV, superior mesenteric vein. **B.** Normal hepatic venous anatomy. Drawing shows major hepatic veins and short hepatic vein orifices. **C.** Normal branching pattern of the portal vein. Coronal (left) and axial (right) diagrams show that the main portal vein (1) divides into the right (2) and left portal veins. The left portal vein first courses horizontally (horizontal portion [3]), then turns anteriorly (umbilical portion [4]) toward the ligamentum teres [6]). The Cantlie line corresponds to the median fissure and extends from the gallbladder (7) to the inferior vena cava. It is located to the right of the umbilical ligament and divides the liver into right and left lobes. 5, Branch to segment IV. **D.** Four most common branching patterns of the intrahepatic portal vein. **a.** Coronal diagram shows the normal branching pattern. **b.** Coronal diagram shows trifurcation of the main portal vein. The right portal vein is not present, and the main portal vein divides into the right anterior, right posterior, and left portal veins at the same level. **c.** Coronal diagram shows the right anterior branch arising from the left portal vein. The main portal vein divides into the right posterior and left portal veins, and the right anterior portal vein arises from the left portal vein. **d.** Coronal diagram shows the right posterior branch arising from the main portal vein. The first branch to split off is the right posterior branch. The main portal vein then continues to the right for a variable distance and bifurcates into the right anterior and left portal veins. **E.** Diagram shows anatomic relationship between hepatic arterial and portal venous branches and bile duct (portal triad), biliary radicles, cords of hepatocytes, intervening sinusoid, and central draining hepatic vein. Hepatic blood supply is depicted at the sinusoidal level. Note that the bile ducts primarily derive their blood supply from the hepatic arteries.

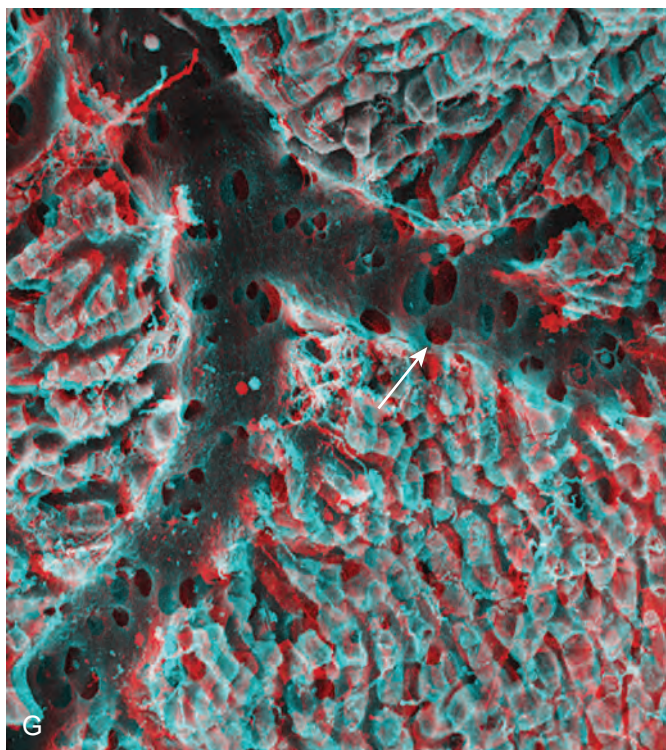
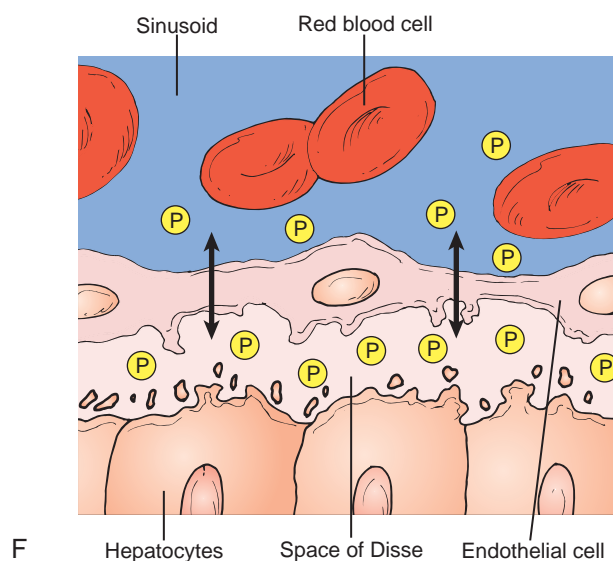


Figure 90-1, cont'd F. Diagram of microanatomic relationship of red blood cells within sinusoid, fenestrated endothelial cells, plasma (P), space of Disse, and hepatocyte. The communication through the sinusoids of the hepatic veins and portal veins is shown. **G.** Photomicrograph showing the fenestrated walls of the sinusoids (arrow). (**A** from Quiroga S, Sebastia C, Pallisa E, et al: Improved diagnosis of hepatic perfusion disorders: Value of hepatic arterial phase imaging during helical CT. *RadioGraphics* 21:65–81, 2001. **B** from Desser TS, Sze DY, Jeffrey RB: Imaging and intervention in the hepatic veins. *AJR Am J Roentgenol* 180:1583–1591, 2003. **C** and **D** from Gallego C, Velasco M, Marcuello P, et al: Congenital and acquired anomalies of the portal venous system. *RadioGraphics* 22:141–159, 2002. **E** and **F** from Pandharipande PV, Krinsky GA, Rusinek H, Lee VS: Perfusion imaging of the liver: Current challenges and future goals. *Radiology* 234:661–673, 2005.)

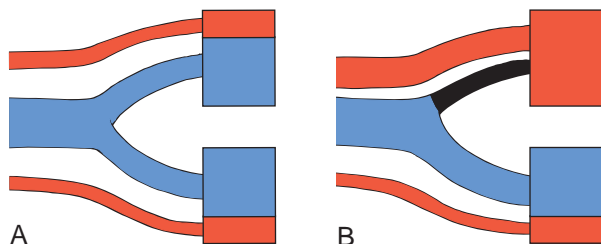


Figure 90-2 The inverse relationship of portal venous and hepatic blood flow: the origin of THADs (transient hepatic attenuation differences) and THIDs (transient hepatic intensity differences). **A.** In the normal situation, a segment of liver derives most of its blood supply from the portal vein (blue) and a minority from the hepatic artery (red). **B.** If the portal vein flow is compromised (black) by obstruction or extrinsic compression or if intraparenchymal pressure exceeds portal venous pressure, that segment of liver will derive its blood supply almost exclusively from the hepatic artery (red). The normal liver will be perfused by both the hepatic artery (red) and the portal vein (blue). This has important implications for contrast-enhanced MDCT and MRI studies. (Courtesy Dennis M. Balfe, MD, St. Louis, Mo.)

shape) due to portal branch compression or infiltration; by thrombus, resulting in a portal branch blockade; or by flow diversion caused by an arteriportal shunt.¹⁻⁴

Lobar multisegmental THADs and THIDs occur when a benign hypervascular lesion or an abscess induces an increase

in the primary arterial inflow, which leads to surrounding parenchyma perfusion, the so-called siphoning effect. These THADs and THIDs do not assume a triangular shape, but a straight border may be present between the arterial phenomena from adjacent parenchyma.¹⁻⁴

Sectorial THADs and THIDs follow hepatic vessel dichotomy and appear as triangular areas that result from the strict relationship between the portal hypoperfused area and the arterial reaction. These can be seen in benign and malignant tumors as well as in abscesses due to the spread of inflammatory mediators. The THADs and THIDs can be wedge or fan shaped.¹⁻⁴

THADs AND THIDs NOT ASSOCIATED WITH A MASS LESION

THIDs and THADs can be seen in the absence of a focal lesion as a result of three mechanisms: portal hypoperfusion due to portal branch compression or thrombosis; flow diversion by arteriportal or an anomalous blood supply; or inflammation of the bile ducts or gallbladder.¹⁻⁴

Sectorial THIDs and THADs are usually caused by portal hypoperfusion due to portal vein or hepatic vein thrombosis, long-standing biliary obstruction, or arteriportal shunt that may be congenital, traumatic, or due to cirrhosis. These THIDs and THADs can have a globular shape, especially when they are adjacent to Glisson's capsule.¹⁻⁴

Polymorphous THADs and THIDs have four major causes: external compression by a rib or subcapsular collection;

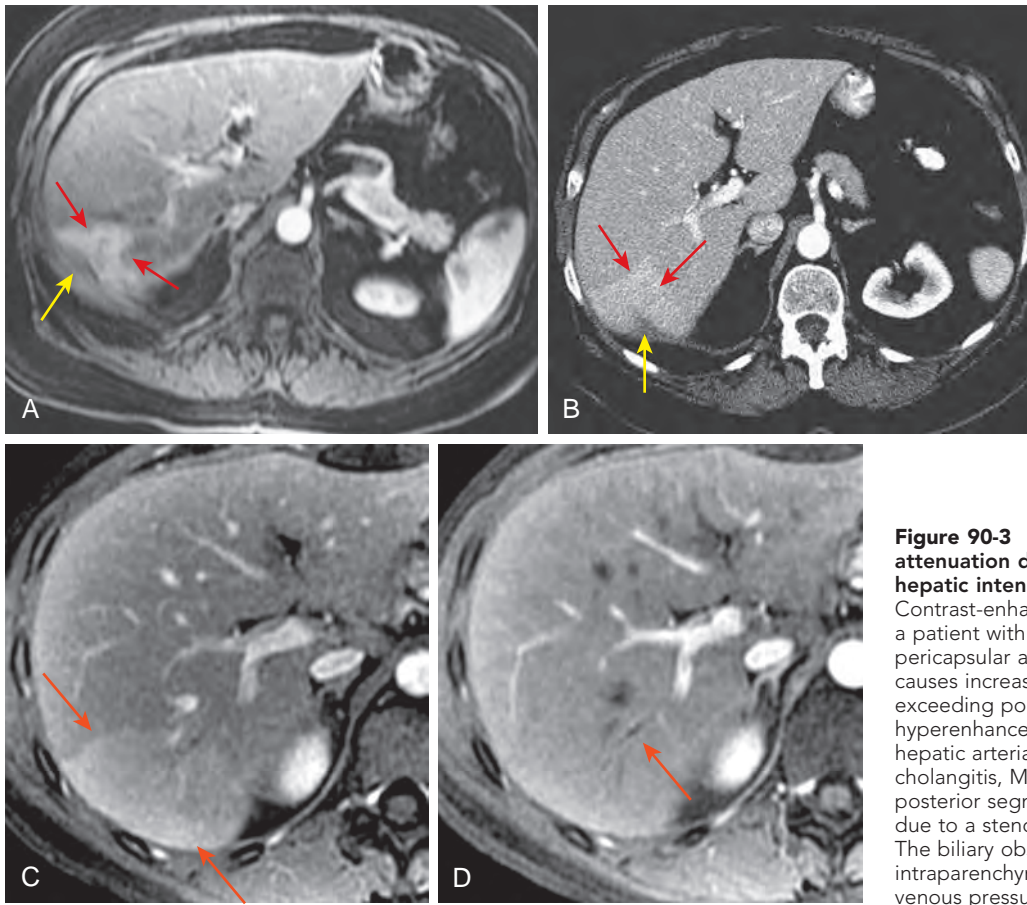


Figure 90-3 THADs (transient hepatic attenuation differences) and THIDs (transient hepatic intensity differences): benign causes. Contrast-enhanced MRI (A) and MDCT (B) in a patient with a dropped gallstone and pericapsular abscess. The abscess (yellow arrow) causes increased intraparenchymal pressure exceeding portal venous pressure, leading to hyperenhancement (red arrows) from compensatory hepatic arterial flow. In a patient with sclerosing cholangitis, MR shows a THID (C, arrows) in the posterior segment of the right lobe of the liver due to a stenotic intrahepatic bile duct (D, arrow). The biliary obstruction leads to increased intraparenchymal hepatic pressure exceeding portal venous pressure, leading to the hyperenhancement.

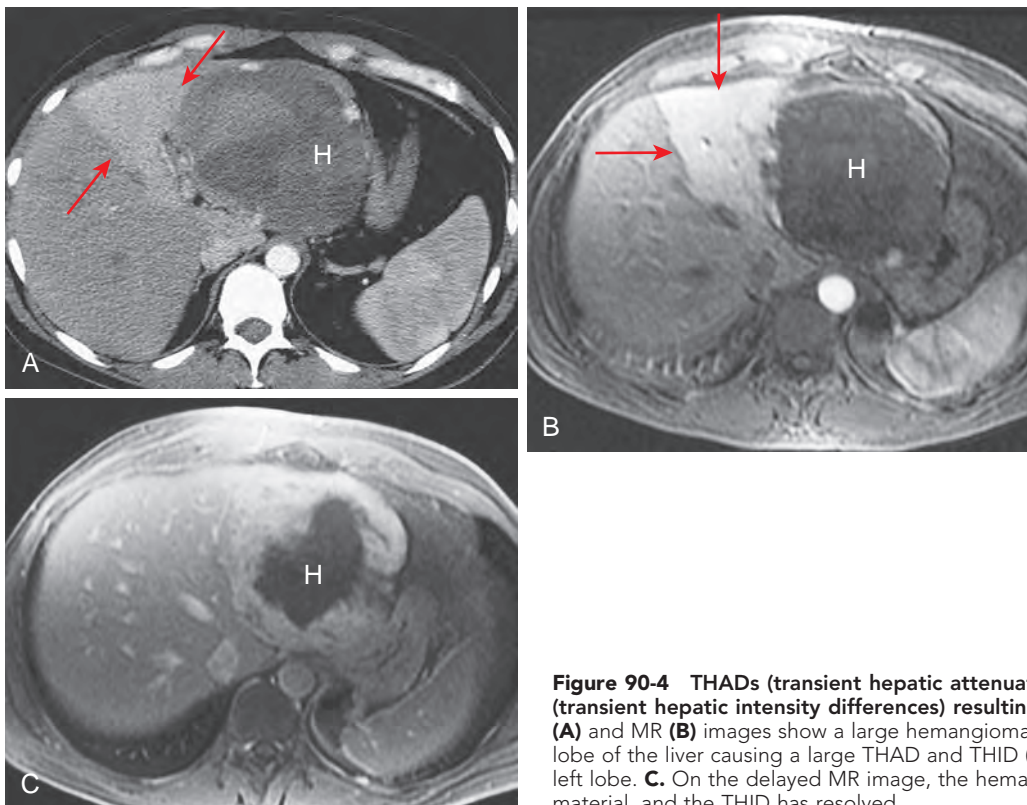


Figure 90-4 THADs (transient hepatic attenuation differences) and THIDs (transient hepatic intensity differences) resulting from a hemangioma. Axial CT (A) and MR (B) images show a large hemangioma (H) in the lateral segment of the left lobe of the liver causing a large THAD and THID (arrows) in the medial segment of the left lobe. C. On the delayed MR image, the hemangioma (H) has filled in with contrast material, and the THID has resolved.

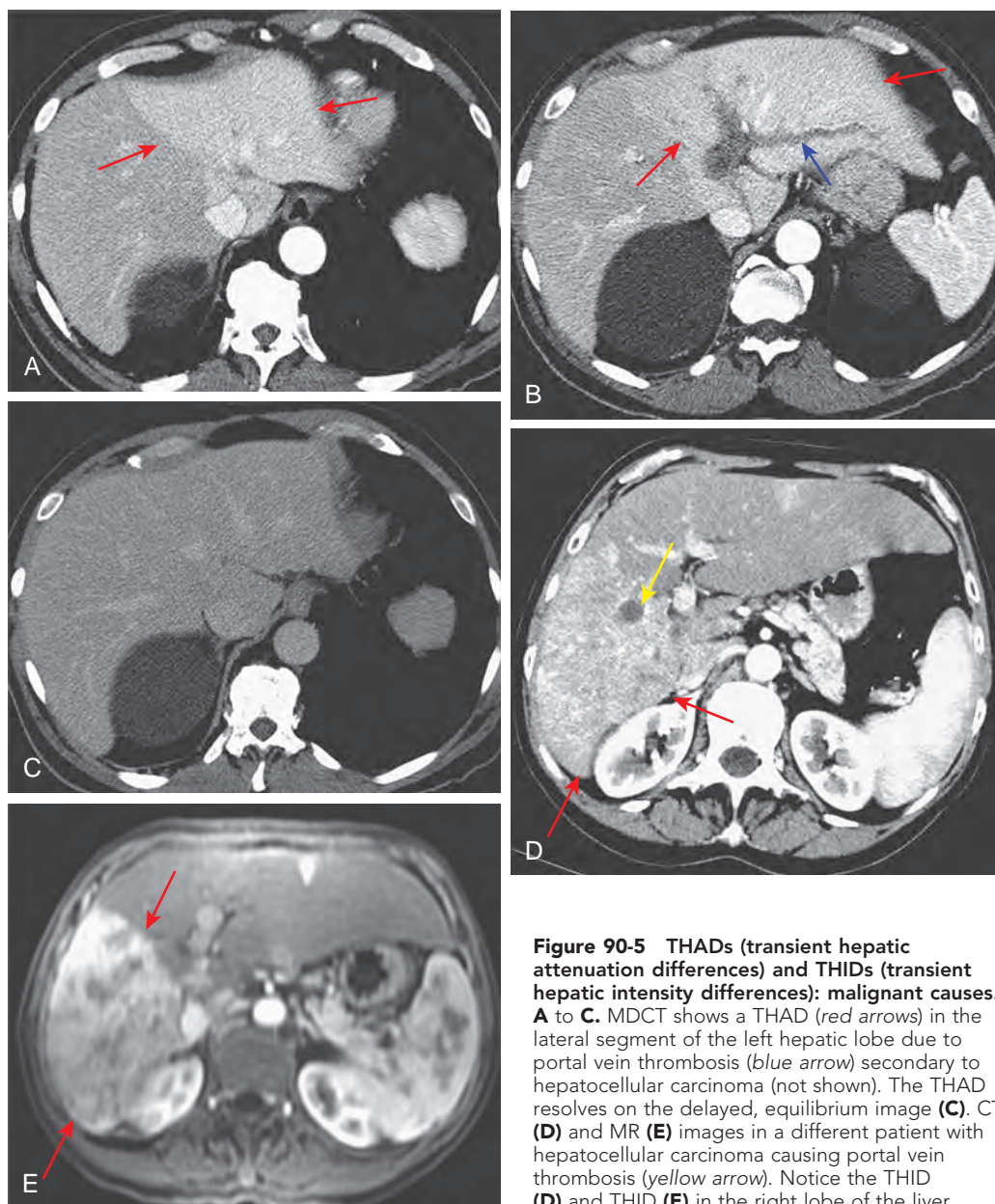


Figure 90-5 THADs (transient hepatic attenuation differences) and THIDs (transient hepatic intensity differences): malignant causes. **A to C.** MDCT shows a THAD (red arrows) in the lateral segment of the left hepatic lobe due to portal vein thrombosis (blue arrow) secondary to hepatocellular carcinoma (not shown). The THAD resolves on the delayed, equilibrium image (**C**). **CT (D)** and **MR (E)** images in a different patient with hepatocellular carcinoma causing portal vein thrombosis (yellow arrow). Notice the THID (**D**) and THID (**E**) in the right lobe of the liver.

anomalous blood supply from atypical arteries, collateral venous vessels, or accessory veins, especially in segment IV of the liver; inflammation of adjacent organs, such as cholecystitis and pancreatitis that spread inflammatory mediators and reduce portal inflow because of interstitial edema; and trauma, biopsy, or radiofrequency ablation of hepatic tumors.¹⁻⁴

In patients with obstruction of the superior vena cava, the medial segment of the left lobe (segment IV) of the liver will hyperenhance because of collateral veins. The internal mammary vein connects to the left portal vein by the paraumbilical vein.

Diffuse THADs and THIDs can be seen in right-sided heart failure (see later), Budd-Chiari syndrome (see later), and biliary obstruction, leading to abnormal attenuation and signal intensity adjacent to the portal triads.

Budd-Chiari Syndrome and Sinusoidal Obstruction Syndrome

The term *Budd-Chiari syndrome* is applied to a diverse group of conditions associated with hepatic venous outflow obstruction, at the level of either the large hepatic veins or the suprahepatic segment of the inferior vena cava. Diagnosis of this disorder is frequently difficult because of its protean causes and clinical manifestations. Sinusoidal obstruction syndrome is a subset of the Budd-Chiari syndrome in which nonthrombotic occlusion of the small pre-sinusoidal venules occurs. This usually develops in the setting of chemotherapy, radiation therapy, and immunosuppressive therapy.¹⁰⁻²¹

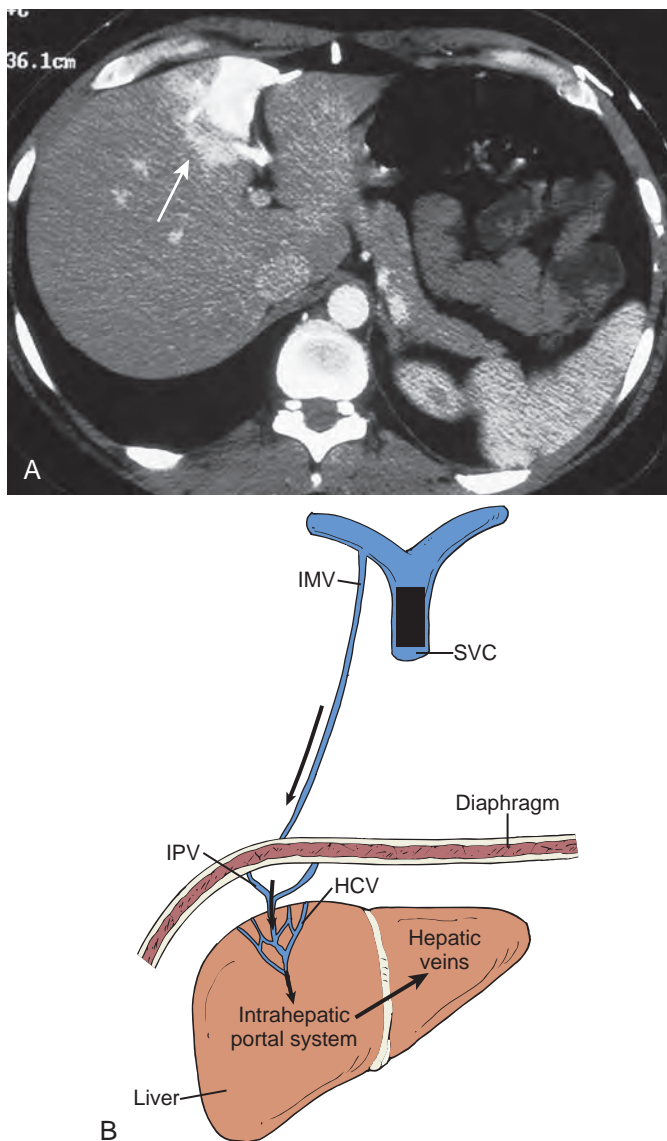


Figure 90-6 THADs (transient hepatic attenuation differences) due to superior vena cava obstruction by lung cancer. A. Axial CT scan shows robust enhancement of the medial segment of the left lobe of the liver (arrow). **B.** Diagram depicting the decompression pathways responsible for this THAD. HCV, Hepatic central veins; IMV, internal mammary vein; IPV, inferior phrenic vein; SVC, superior vena cava. (B from Cihangiroglu M, Lin BH, Dachman AH: Collateral pathways in superior vena caval obstruction as seen on CT. *J Comput Assist Tomogr* 25:1–8, 2001.)

CLINICAL FINDINGS

The two major clinical presentations of Budd-Chiari syndrome are determined by the extent and speed of onset of venous occlusion. The acute form follows simultaneous obstruction of all three hepatic veins or, more frequently, obstruction of the last patent hepatic vein after previous, clinically occult thrombosis of the others. These patients experience rapid onset of abdominal pain, tender hepatomegaly, vomiting, ascites, and arterial hypotension. This constellation of findings is associated with mild or marked increase of serum bilirubin level, marked elevation of the transaminase values, and decreased clotting factors resulting from hepatocellular failure.¹⁰⁻²¹

BOX 90-1 CAUSES OF BUDD-CHIARI SYNDROME

HYPERCOAGULABLE STATES

- Antiphospholipid syndrome
- Antithrombin III deficiency
- Essential thrombocytosis
- Factor V Leiden
- Lupus anticoagulant
- Myeloproliferative disorder
- Paroxysmal nocturnal hemoglobinuria
- Polycythemia rubra vera
- Postpartum thrombocytopenic purpura
- Protein C deficiency
- Protein S deficiency
- Sickle cell disease

INFECTION

- Amebic liver abscess
- Aspergillosis
- Filariasis
- Hepatic abscess
- Hydatid cysts
- Pelvic cellulitis
- Schistosomiasis
- Syphilis
- Tuberculosis

CANCER

- Adrenal cancer
- Bronchogenic carcinoma
- Fibrolamellar cancer
- Hepatoma
- Leiomyosarcoma
- Leukemia
- Renal cell cancer
- Rhabdomyosarcoma

MISCELLANEOUS

- Behçet's disease
- Celiac disease
- Crohn's disease
- Laparoscopic cholecystectomy
- Membranous obstruction of vena cava
- Oral contraceptives
- Polycystic disease
- Pregnancy
- Sarcoidosis
- Trauma

Patients with the chronic form of Budd-Chiari syndrome present with ascites of insidious onset, right upper quadrant pain, hepatomegaly, normal or moderately increased transaminase values, decreased albumin and clotting factors, mild jaundice, and splenomegaly or variceal bleeding if cirrhosis develops. The diagnosis is seldom made on clinical grounds alone because clinicians tend to ignore the abdominal pain and ascribe the hepatomegaly and ascites to cirrhosis. The correct diagnosis may be inferred from the absence of a cause for the cirrhosis; episodes of abdominal pain during the preceding month; or, uncommonly, a palpable caudate lobe.¹⁰⁻²¹

ETIOLOGY

Budd-Chiari syndrome is classified as either primary or secondary, depending on the cause and pathophysiologic manifestations (Box 90-1). In the primary type, there is total or incomplete membranous obstruction of hepatic venous blood, either above the entrance of the hepatic veins into the inferior vena cava or

between the ostium of the right hepatic vein, which remains patent, and the more superior middle and left hepatic veins. Membranous obstruction, although uncommon in Europe and North America, is the most common cause of Budd-Chiari syndrome in Japan, India, Israel, and South Africa. These membranes vary greatly in size, from wafer thin to several centimeters thick. The origin of this lesion is controversial; most are believed to be congenital malformations that result from deviations of the complex embryologic process by which the inferior vena cava is formed. Other theories suggest that some of these lesions are acquired secondary to mechanical injury, infection, phlebitis, or organization of a preexisting thrombus. This origin would explain the adult presentation of the disorder.⁶⁻²¹

Membranous obstruction of the inferior vena cava is complicated by hepatocellular carcinoma in 20% to 40% of cases in South African and Japanese series. It is postulated that the obstruction renders the hepatocytes more susceptible to the action of one or more environmental carcinogens or that perhaps long-standing venous obstruction induces formation of hyperplastic nodules, which may undergo malignant transformation.⁶⁻²¹

Secondary Budd-Chiari syndrome can be classified on the basis of the site of hepatic venous obstruction. Obstruction at the level of the central and sublobular veins may follow chemotherapy with thioguanine, vincristine, cytarabine, 6-mercaptopurine, or dacarbazine; internal or external hepatic radiation; chemoradiation therapy before bone marrow transplantation; azathioprine for immunosuppression; arsenic poisoning; pregnancy (particularly in the postpartum period); and oral contraceptive use. Naturally occurring toxins, such as the pyrrolizidine alkaloids found in herbal teas containing senecio and aflatoxins, have been implicated as well. Nonthrombotic occlusion of small central and sublobular veins is termed sinusoidal obstruction syndrome.⁶⁻²¹

Sinusoidal obstruction syndrome (also known as hepatic veno-occlusive disease) is a distinctive and potentially fatal form of hepatic injury that occurs after drug and toxin exposure. Obstruction of the sinusoids occurs in central areas with hepatocyte necrosis and hemorrhage. Endothelial injury is the initiating event. Sinusoidal obstruction syndrome produces a hypercoagulable state. The venular and sinusoidal lumens are reduced because of edema and partial to complete fibrosis of venular lumens. Cyclophosphamide is the most common agent.

Obstruction of the major hepatic veins may occur in the setting of polycythemia vera, paroxysmal nocturnal hemoglobinuria, myeloproliferative disorders, thrombocytosis, hyper-eosinophilic syndrome, sickle cell anemia, Behçet's disease, anticardiolipin antibodies, lupus anticoagulant, protein S or C deficiency, antithrombin III deficiency, antiphospholipid antibodies, mixed connective tissue disease, and Sjögren's syndrome.⁶⁻²¹

A variety of hepatic and extrahepatic masses can also compress the inferior vena cava and hepatic veins. These masses are the second most common mechanism of hepatic venous outflow block in Western countries. Hepatocellular carcinoma, hypernephroma, adrenal and bronchial carcinomas, leiomyosarcoma of the inferior vena cava, and hepatic adenoma or cystadenoma are the most common neoplasms associated with Budd-Chiari syndrome. Benign masses, such as hydatid cysts, intrahepatic hematoma, Caroli's disease, large simple cysts, and amebic abscesses, can also cause obstruction.⁶⁻²¹

PATHOLOGIC FINDINGS

In acute Budd-Chiari syndrome, the liver is markedly enlarged and reddish (Fig. 90-7A-C). On histologic examination, sinusoidal dilation is evident, and parenchymal damage ranges from mild atrophy to marked hemorrhagic necrosis in the centrilobular areas.

In chronic Budd-Chiari syndrome, the liver is nodular and irregular in shape, often with caudate lobe hypertrophy. Centrilobular fibrosis is the hallmark of this disorder, and the centrally scarred areas may link to form connective tissue bridges. Sinusoidal dilation also predominates around hepatic venules and is associated with liver cell atrophy and perisinusoidal fibrosis.

In sinusoidal obstruction syndrome, the venular and sinusoidal lumens are reduced because of edema and partial to complete fibrosis of venular lumens (Fig. 90-7D).

Regenerative nodules are often seen in Budd-Chiari syndrome and are usually multiple, measuring between 5 and 40 mm. They develop in the setting of insufficient blood supply to the liver, leading to atrophy along with compensatory nodular hyperplasia in areas of hepatic parenchyma that have an adequate blood supply. The nodules are composed of hyperplastic hepatocytes arranged in plates of one or two cells in width. The nodules grow in an expansile fashion, compressing the surrounding liver and obliterating the central vein. There is no evidence that these nodules degenerate into malignancy.⁶⁻²¹

RADIOLOGIC FINDINGS

Traditionally, the radiographic "gold standard" for the diagnosis of Budd-Chiari syndrome has been hepatic venography and cavography. However, these invasive angiographic procedures are not suitable for screening of patients with nonspecific signs and symptoms. The cross-sectional imaging modalities have proved successful in the diagnosis of this disorder, and such studies can usually obviate angiography or venography.

Ultrasound

Because of its excellent sensitivity, high specificity, noninvasiveness, relatively low cost, availability, lack of contrast requirements, and multiplanar imaging ability, sonography can be the initial screening study for the Budd-Chiari syndrome. The sonographic features (Fig. 90-8) of the Budd-Chiari syndrome are stenosis of hepatic veins (which often have thick, echogenic walls and proximal dilation), echogenic intravenous thrombi, intrahepatic collaterals or extrahepatic anastomoses, and large inferior right hepatic vein.²²⁻²⁴

In chronic cases, the hepatic veins may not be visible. The inferior vena cava may also be narrowed by a grossly swollen liver. Ascites, abnormal hepatic shape with enlargement of the caudate lobe, and atrophy of the right lobe are present in most cases except in disease of acute onset. When both the left lobe and the caudate lobe are enlarged, confusion with cirrhosis can occur. Membranous webs are identified as echogenic or focal oblations of the lumen.²²⁻²⁴

In patients with hepatomegaly, evaluation of the hepatic veins can be difficult because they are often compressed and may not be visible. In these patients, an abdomen distended by ascites can further interfere with sonography. Similarly, in cirrhotic livers, patent hepatic veins may be difficult to identify, which precludes placement of the duplex Doppler cursor.

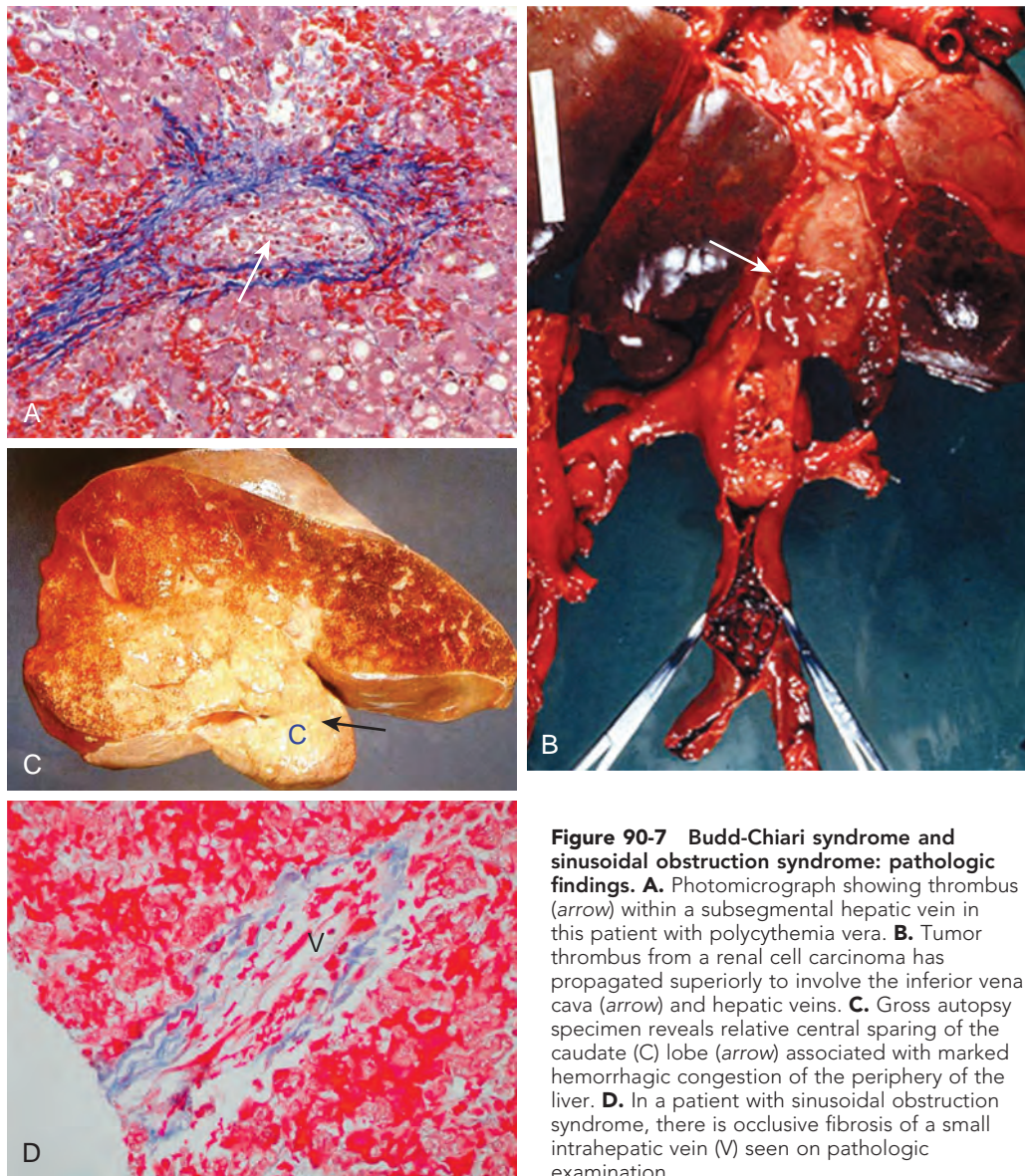


Figure 90-7 Budd-Chiari syndrome and sinusoidal obstruction syndrome: pathologic findings. **A.** Photomicrograph showing thrombus (arrow) within a subsegmental hepatic vein in this patient with polycythemia vera. **B.** Tumor thrombus from a renal cell carcinoma has propagated superiorly to involve the inferior vena cava (arrow) and hepatic veins. **C.** Gross autopsy specimen reveals relative central sparing of the caudate (C) lobe (arrow) associated with marked hemorrhagic congestion of the periphery of the liver. **D.** In a patient with sinusoidal obstruction syndrome, there is occlusive fibrosis of a small intrahepatic vein (V) seen on pathologic examination.

Visualization of hepatic webs is also a problem. Color flow Doppler examination may be helpful in these cases.²²⁻²⁴

Absent or reversed flow in the hepatic veins or flat flow in the hepatic veins associated with reversed flow in the inferior vena cava as demonstrated by duplex Doppler ultrasound is diagnostic of Budd-Chiari syndrome. The flow in the portal vein may be slow or reversed.

Color Doppler sonography overcomes some of the limitations of real-time sonography by demonstrating reversed flow in the retrohepatic inferior vena cava, documenting the presence of intrahepatic venous collaterals, and confirming the absence of flow in presumably thrombosed vessels. Color flow imaging rapidly and accurately determines the status of the hepatic veins and inferior vena cava and the direction of flow. Areas of occlusion are also clearly depicted, as are areas of narrowing, tortuosity, and reversal of flow direction.²²⁻²⁴

In sinusoidal obstruction syndrome, there is nonthrombotic occlusion of small hepatic veins and terminal hepatic venules, the major hepatic veins show normal hepatofugal flow

direction, and the inferior vena cava is patent with flow toward the heart. Decreased, reversed, or to-and-fro flow (flow demodulation) may be seen in the main portal vein. Other Doppler criteria include decrease in spectral density, reversed flow or maximum flow in the main portal vein of 210 cm/s, portal vein congestion index (cross-sectional area of vein divided by average velocity), hepatic artery resistive index of 0.75 or greater, monophasic flow in the hepatic veins, and flow recorded in paraumbilical veins. Gray-scale criteria include hepatic vein diameter of less than 3 mm, portal vein diameter of more than 8 mm in children and more than 12 mm in adults, and mural thickening of the gallbladder of more than 6 mm. Nonspecific findings include hepatosplenomegaly, ascites, and visualization of paraumbilical veins.²²⁻²⁴

Computed Tomography

The CT features of Budd-Chiari syndrome depend on the age and extent of the obstruction and the presence of coexisting changes in portal venous blood flow.^{25,26} On noncontrast scans,

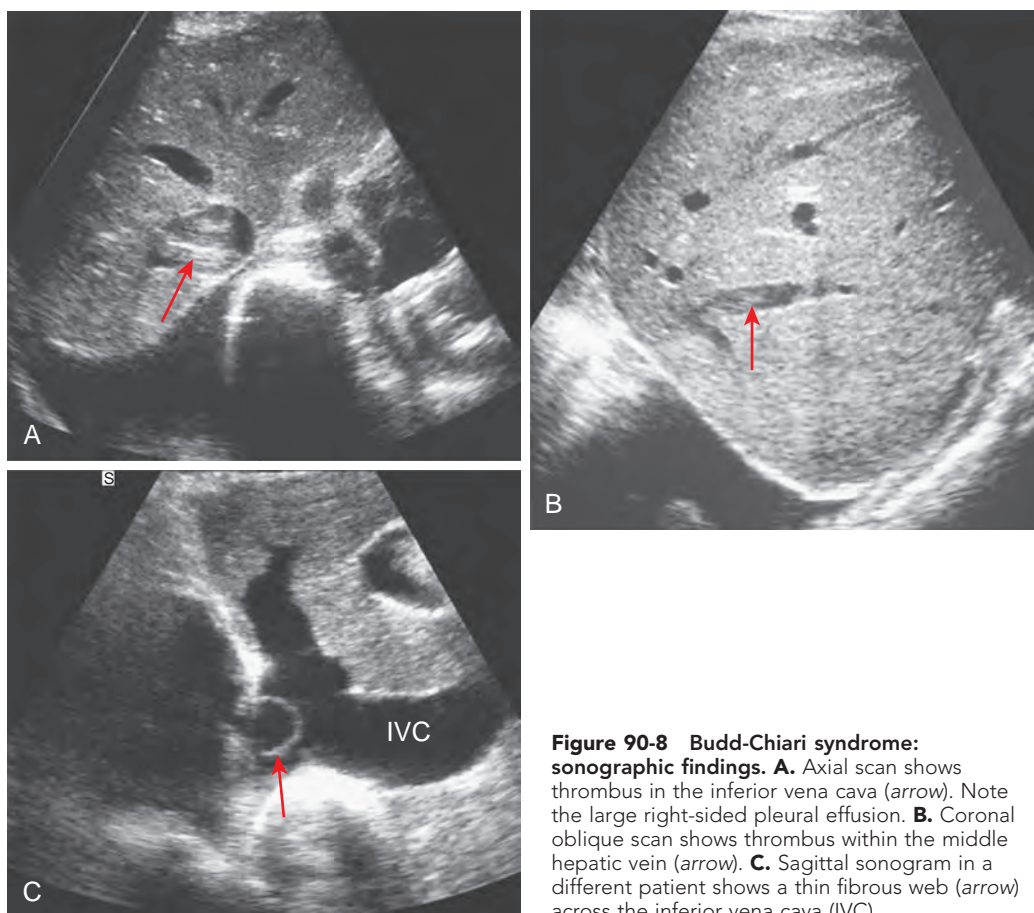


Figure 90-8 Budd-Chiari syndrome: sonographic findings. **A.** Axial scan shows thrombus in the inferior vena cava (arrow). Note the large right-sided pleural effusion. **B.** Coronal oblique scan shows thrombus within the middle hepatic vein (arrow). **C.** Sagittal sonogram in a different patient shows a thin fibrous web (arrow) across the inferior vena cava (IVC).

in the acute phase of the disease, diffuse hepatic hypodensity is associated with global liver enlargement and ascites. The hepatic hypodensity is presumably due to hepatic parenchymal congestion. Hyperdense thrombus with an attenuation of 38 to 42 HU may be seen in the inferior vena cava and hepatic veins. Rarely, a calcified caval membrane is identified. After the injection of contrast material, the liver typically shows patchy enhancement; this is due to the hepatic congestion, which causes portal and sinusoidal stasis. In most patients, the central regions of the liver, including the caudate lobe and part of the left lobe, may enhance normally and appear hyperdense compared with the more peripheral parts of the liver, which show decreased enhancement. Later, a classic “flip-flop” pattern may develop (Fig. 90-9), in which the contrast material from the normally enhanced central liver washes out so that this region becomes relatively hypodense compared with the peripheral zones, which are slowly accreting contrast material. The subcapsular portions of the liver may enhance normally because they have independent venous drainage through systemic subcapsular veins. These differences in hepatic attenuation and morphologic changes are closely related to regional disturbances in portal flow. In segments of the liver in which venous drainage is obstructed (the hepatic periphery), portal blood flow is diminished, if not reversed. Portal venous flow is normal in the central portion of the liver, where hepatic venous egress is uninterrupted.^{25,26}

Intravascular thrombus is best seen in the acute phase of the Budd-Chiari syndrome as a low-density mass in the lumen of

the hepatic veins and inferior vena cava. The wall of the thrombosed vessel may appear dense relative to the thrombus secondary to the enhancement of the vasa vasorum. The involved vessel also is often enlarged. Portal vein thrombus may be seen in 20% of cases. Compression of the inferior vena cava is also demonstrated²⁴⁻²⁶ (Fig. 90-10).

In more chronic cases of Budd-Chiari syndrome, the thrombi and the hepatic veins are often difficult to visualize. Intravascular thrombus density, which is high for the first 3 weeks, also diminishes over time. As the obstruction becomes more chronic, the liver undergoes morphologic changes that are due to diminished or reversed portal blood flow in the involved hepatic segments. Portal venous blood carries certain hepatotropic agents, mainly insulin, and segments deprived of these agents experience nutritional ischemia and eventually atrophy. Accordingly, the caudate lobe exhibits hypertrophy, and the periphery of the liver tends to exhibit atrophy. These changes may take 2 to 4 months to appear. Unless the membranes are calcified, membranous obstruction of the inferior vena cava is more difficult to visualize.

On MDCT, large regenerative nodules robustly and homogeneously enhance during the arterial dominant phase and remain slightly hyperdense on the portal venous dominant phase images as well.

Magnetic Resonance Imaging

MRI is a useful screening modality for Budd-Chiari syndrome by virtue of its ability to display directly the portal veins, hepatic

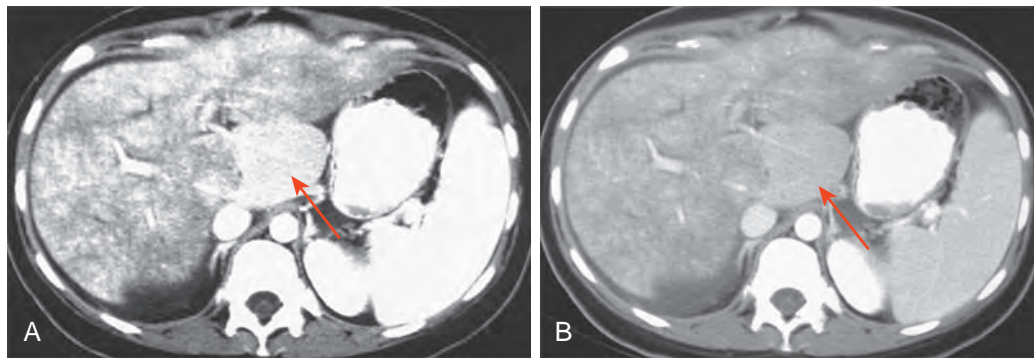


Figure 90-9 Budd-Chiari syndrome: flip-flop pattern on MR. The classic CT flip-flop pattern of hepatic contrast enhancement is shown in this patient with Budd-Chiari syndrome. **A.** Contrast-enhanced MR image of the liver shows rapid enhancement (arrow) of the unobstructed central portion of the liver with a delayed peripheral hepatogram. **B.** Delayed image shows that the central, unobstructed portion of the liver (arrow) has washed out, while the periphery is slowly accreting contrast material.

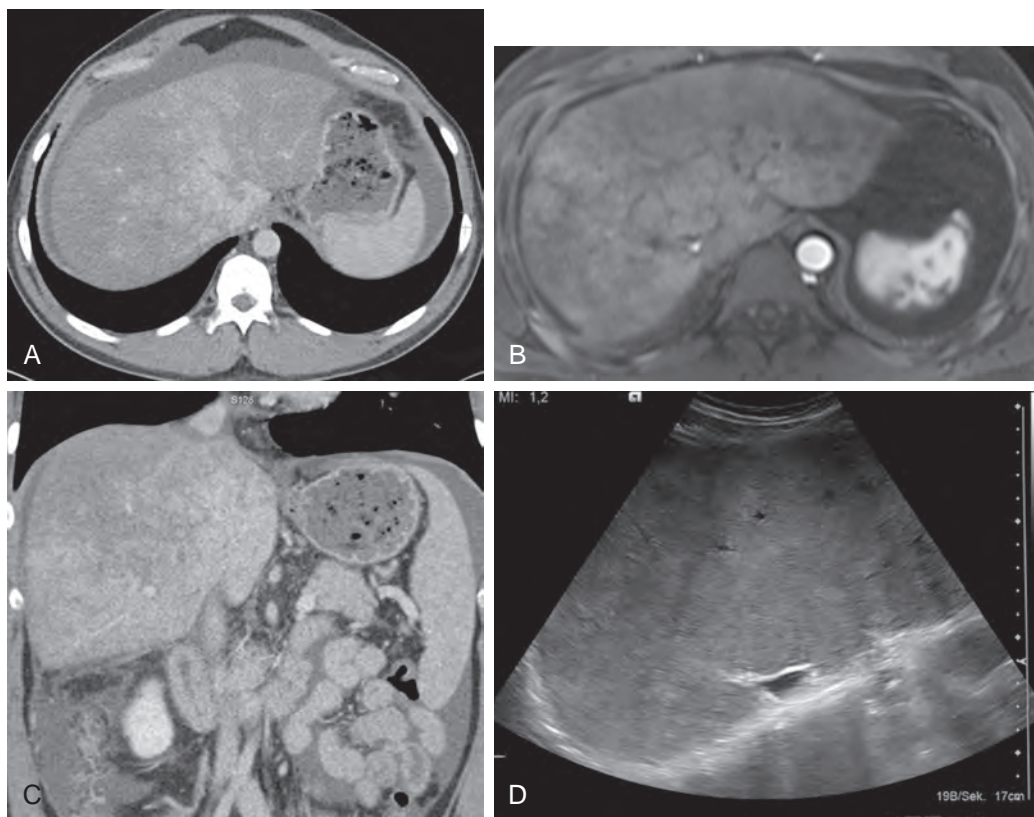


Figure 90-10 Budd-Chiari syndrome: CT features with MR and ultrasound correlation. CT (**A**), MR (**B** and **C**), and sonographic (**D**) images of the liver show a mottled contrast enhancement pattern and narrowing of the inferior vena cava and no discernible hepatic veins.

veins, and inferior vena cava in numerous planes. A number of specific MRI abnormalities²⁷⁻²⁹ are associated with this syndrome (Figs. 90-11 to 90-15): complete absence of hepatic veins or striking attenuation of their caliber, demonstration of thrombus or absent vascular flow in hepatic veins, comma-shaped intrahepatic collateral vessels, and marked constriction of the inferior vena cava. Less specific findings include enlargement of the caudate lobe, ascites, and inhomogeneity of the hepatic parenchyma. Vascular patency can confidently be confirmed when the vessel has no signal.

The multiplanar capabilities of MRI are of great value in depicting tumor thrombus in patients with Budd-Chiari

syndrome secondary to neoplasm. Bland and tumor thrombus can be distinguished by the administration of gadolinium. Tumor thrombus may show contrast enhancement.²⁷⁻²⁹

The degree of enhancement of the liver parenchyma supplied by a thrombosed hepatic vein depends on the acuteness and duration of the thrombosis. Involved parenchyma enhances less than surrounding liver in acute thrombosis. In chronic thrombosis, enhancement is more variable and may be increased. In patients with acute Budd-Chiari syndrome, the congested liver may have a higher water content and longer T2 relaxation time than the spared caudate lobe. Also, the peripheral liver enhances less than the central liver after intravenous

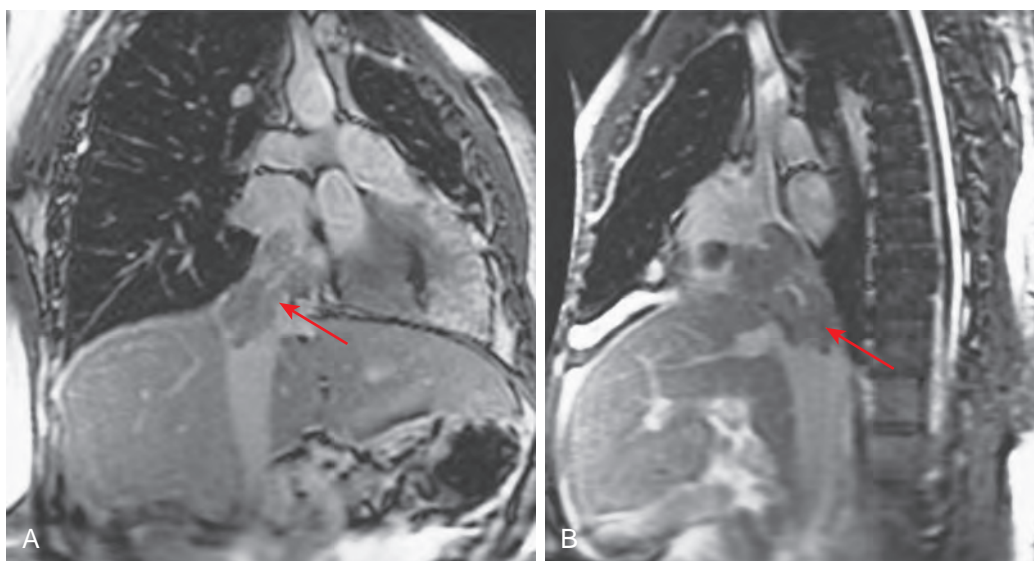


Figure 90-11 Budd-Chiari syndrome: MRI findings in a patient with hepatocellular carcinoma invading the hepatic veins and inferior vena cava. Coronal (A) and parasagittal (B) images shows tumor thrombus (arrows) invading the inferior vena cava and right atrium.

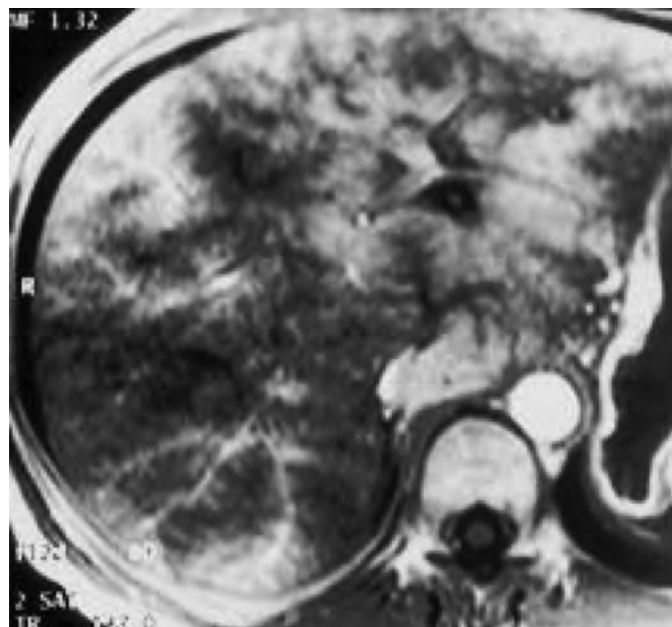


Figure 90-12 Acute Budd-Chiari syndrome: MR findings. The liver is edematous and inhomogeneous in signal intensity on this MR image.

administration of gadolinium because of increased parenchymal pressure with resultant diminished blood supply from both the hepatic artery and the portal vein.

Large regenerative nodules are bright on T1-weighted MR images and show the same enhancement pattern after the intravenous administration of gadopentetate dimeglumine (Gd-DTPA). They are predominantly isointense or hypointense relative to the liver on T2-weighted images.²⁷⁻²⁹

Angiography

Angiography (Fig. 90-16) has traditionally been the radiographic gold standard for the evaluation of patients with Budd-Chiari syndrome. Now it is seldom performed for diagnosis but

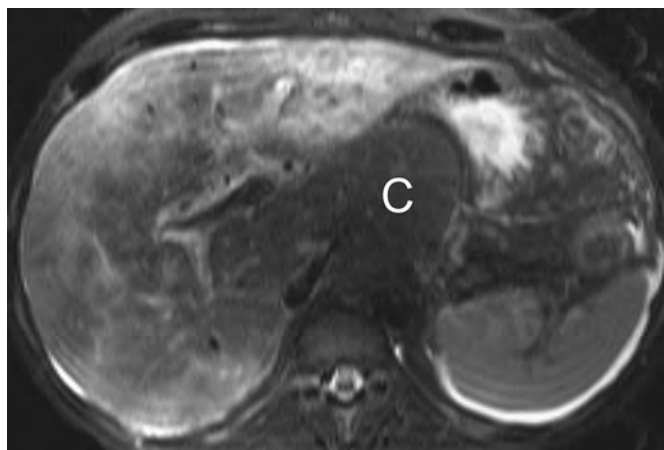


Figure 90-13 Subacute Budd-Chiari syndrome: MRI findings. T2-weighted MR image shows caudate lobe (C) hypertrophy. The periphery of the liver is hyperintense, indicating edema. There is a small amount of ascites.

as a preliminary procedure to radiologic interventions, such as transjugular intrahepatic portosystemic shunt (TIPS) creation, balloon angioplasty, or stricture stenting.

Nodular Regenerative Hyperplasia

On contrast-enhanced CT and MRI studies, multiple enhancing nodules are identified that are usually 5 to 7 mm in diameter³⁰⁻³³ (Fig. 90-17).

TREATMENT

The treatment and prognosis of Budd-Chiari syndrome are determined by the rate and degree of hepatic outflow obstruction. In acute Budd-Chiari syndrome, survival time may be short because of acute liver failure or extension of thrombus into the inferior vena cava with resulting pulmonary emboli. Patients with chronic Budd-Chiari syndrome generally succumb to variceal bleeding secondary to severe cirrhosis and portal

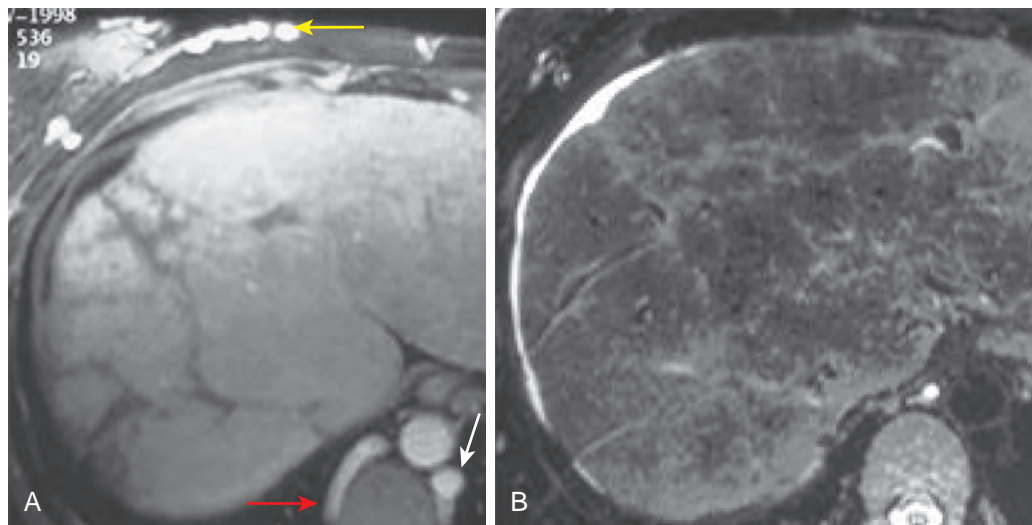


Figure 90-14 Chronic Budd-Chiari syndrome: MRI findings. **A.** Postgadolinium image shows no demonstrable inferior vena cava or hepatic veins. Note the dilated azygos vein (red arrow), hemiazygos vein (white arrow), and superficial collateral (yellow arrow) blood vessels. **B.** T2-weighted image shows inhomogeneous, coarsened hepatic parenchyma. Ascites is present.

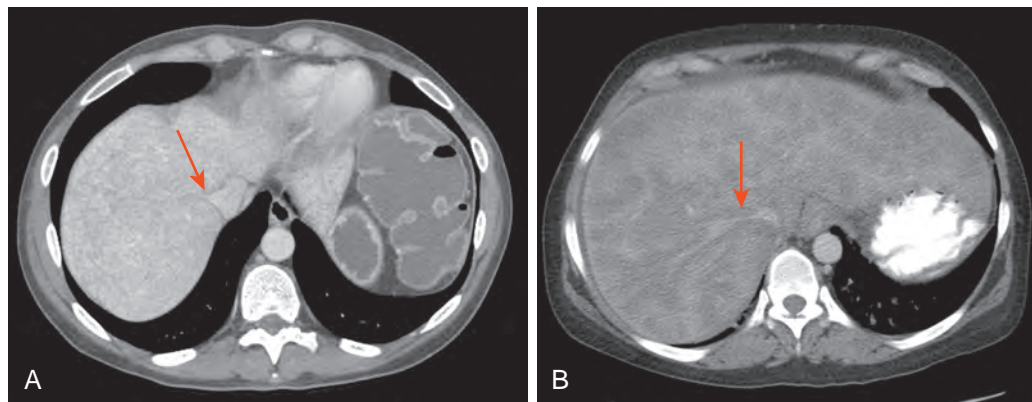


Figure 90-15 Sinusoidal obstruction syndrome: CT findings. Axial CT images in two different patients (**A** and **B**) show a mottled contrast enhancement pattern and narrowing of the right hepatic vein (arrows). This latter finding is suggestive of sinusoidal obstruction syndrome in the appropriate clinical setting.

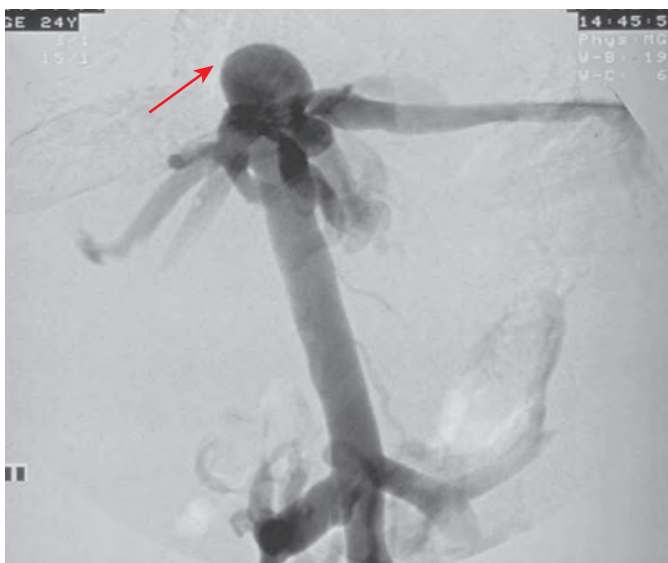


Figure 90-16 Budd-Chiari syndrome: angiographic features. Digital subtraction angiogram shows a web (arrow) obstructing the inferior vena cava.

hypertension. Most patients require portal decompression to prevent liver failure and to resolve the ascites.³⁴⁻⁴²

Treatment of Budd-Chiari syndrome depends on the cause. In some cases, medical management with large doses of steroids (for idiopathic granulomatous venulitis) or nutritional therapy (for an acutely enlarged, fatty liver compressing the inferior vena cava) may suffice. However, in most cases, medical therapy is limited and is directed toward anticoagulation and the control of ascites with diuretics.

Membranous obstructions of the inferior vena cava (see Fig. 90-16) and the hepatic veins are amenable to angioplasty with balloons or lasers and stent insertion. Before any intervention, these patients should receive anticoagulants because of the danger of pulmonary emboli from venous thrombi proximal to the membranes. This danger is the major risk of thrombolytic therapy as well. Angioplasty is more difficult in patients with extensive thrombus, but clinical improvement may accompany dilation and recanalization of only one hepatic vein.³⁴⁻⁴²

Reports suggest the utility of expandable metal stents in the treatment of Budd-Chiari syndrome resulting from tumor compression or from idiopathic obstruction of the inferior vena

cava. The TIPS procedure is useful in treating Budd-Chiari syndrome as well.³⁴⁻⁴²

The surgical alternatives in Budd-Chiari syndrome are as follows: direct repair by membranotomy, membranectomy, or cavoplasty; portosystemic decompression by side-to-side portacaval or mesoatrial shunt; transplantation; and peritoneo-jugular shunt.

Liver in Cardiac Disease

Passive hepatic congestion is caused by stasis of blood within the liver parenchyma as a result of compromise of hepatic venous drainage. It is a common complication of congestive heart failure and constrictive pericarditis, wherein elevated central venous pressure is directly transmitted from the right atrium to the hepatic veins because of their close anatomic relationship. The liver becomes tensely swollen as the hepatic sinusoids engorge and dilate with blood (Fig. 90-18). These changes may be transient, and full recovery follows once the patient's congestive heart failure is corrected. In chronic right atrial failure, cardiac cirrhosis may ensue.⁴³⁻⁴⁹

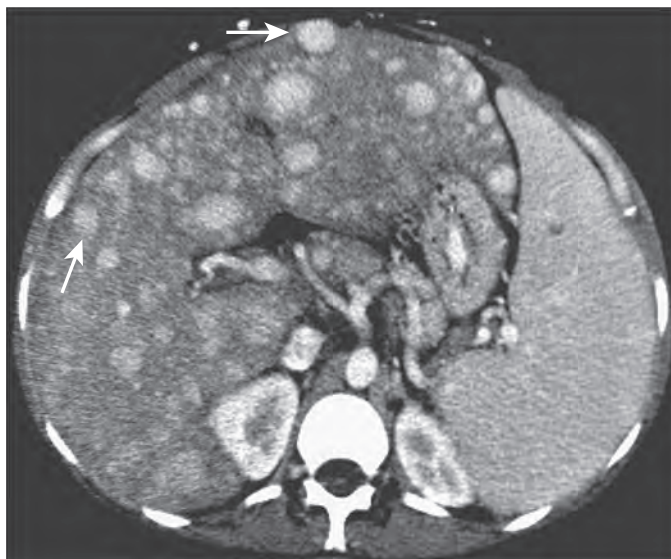


Figure 90-17 Budd-Chiari syndrome: nodular regenerative hyperplasia. Multiple hypervascular lesions (arrows) are identified on contrast-enhanced CT. (Case courtesy Michael P. Federle, MD, Stanford University.)

CLINICAL FINDINGS

With acute congestion, the liver is enlarged and tender, and the patient may have severe right upper quadrant pain that is due to stretching of Glisson's capsule. Patients typically have hepa-tojugular reflux on physical examination. Liver function abnormalities are often mild, but florid hepatic dysfunction simulating acute viral hepatitis may be seen. The diagnosis is usually not made clinically because the signs and symptoms of cardiac failure overshadow those of liver disease. In rare cases of cardiomyopathy, the patient may present with hepatic failure before cardiac disease is recognized as the cause of the hepatic dysfunction.

RADIOLOGIC FINDINGS

Ultrasound

Ultrasound demonstrates hepatic enlargement and dilation of the inferior vena cava and hepatic veins in the early stages of this disorder (Fig. 90-19). Normally, the maximal diameter of the main trunk of the right hepatic vein is 5.6 to 6.2 mm. In patients with congestive heart failure, the mean diameter is 8.8 mm, and it increases to 13.3 mm if there is associated pericardial effusion. Respiratory variations in the caliber of the inferior vena cava and hepatic veins are diminished.

The spectral Doppler waveform of the hepatic vein is also altered. Normally, the inferior vena cava and hepatic veins show a triphasic flow pattern: the first two peaks are toward the heart and are reflections of right atrial and ventricular diastole; the third peak is a short period of reversed blood flow, which accompanies atrial systole (the p wave of the electrocardiogram). In patients with elevated central venous pressure, the hepatic veins lose their triphasic pattern. The spectral signal may have an M shape, and ultimately, in cardiac cirrhosis, a unidirectional, low-velocity continuous flow pattern may be seen.⁴³⁻⁴⁹

In tricuspid regurgitation, the normally triphasic hepatic vein demonstrates a decrease in the size of the antegrade systolic wave and a systolic/diastolic flow velocity ratio less than 0.6 (normal >4.0). The high systolic pressure of the right atrium is transmitted to the inferior vena cava and hepatic veins.⁴³⁻⁴⁹

In patients with severe congestive heart failure, the portal venous Doppler signal may also be altered by the mechanical events in the right side of the heart. Normally, the portal vein shows almost continuous flow except for some increase during inspiration. In passive hepatic congestion, the energy of the

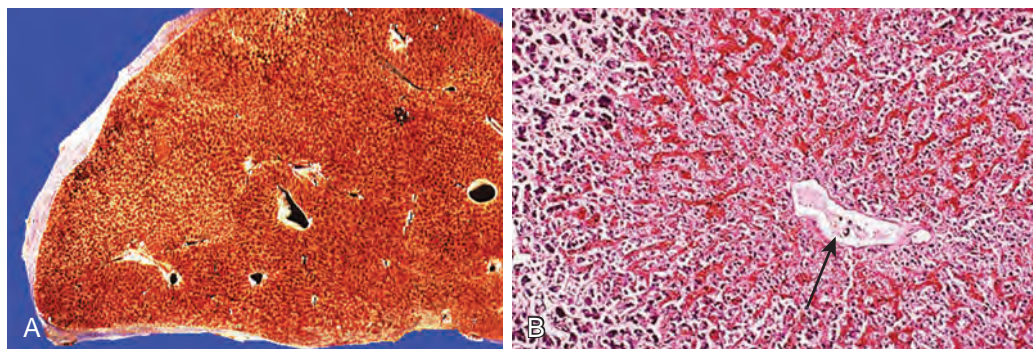


Figure 90-18 Passive hepatic congestion: pathologic findings. A. Classic "nutmeg liver" in a patient with chronic passive hepatic congestion. **B.** Dilated sinusoids are seen surrounding a dilated central hepatic vein (arrow).

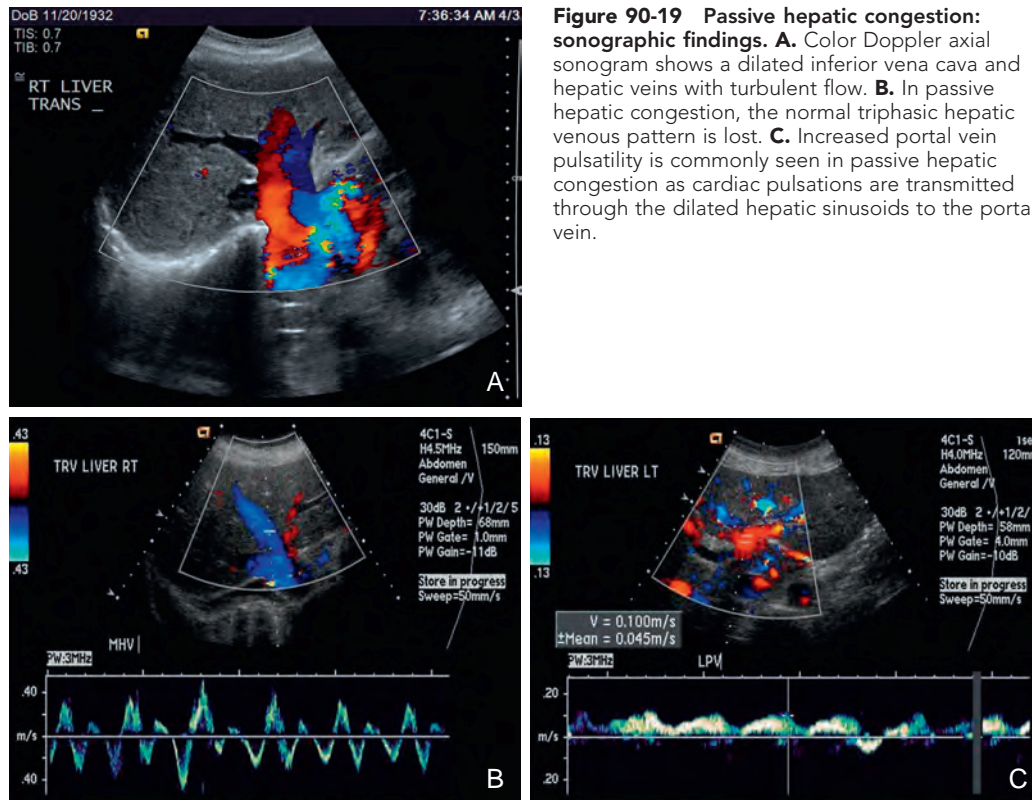


Figure 90-19 Passive hepatic congestion: sonographic findings. **A.** Color Doppler axial sonogram shows a dilated inferior vena cava and hepatic veins with turbulent flow. **B.** In passive hepatic congestion, the normal triphasic hepatic venous pattern is lost. **C.** Increased portal vein pulsatility is commonly seen in passive hepatic congestion as cardiac pulsations are transmitted through the dilated hepatic sinusoids to the portal vein.

elevated pressure from the right atrium and hepatic vein is transmitted directly through the dilated hepatic sinusoids into the portal vein. This energy transmission causes increased pulsatility of the portal venous Doppler signal because the liver no longer prevents changes in central venous pressure from reaching the portal circulation. This pulsatility is manifested by monophasic forward flow with peak velocity at ventricular diastole and gradual diminution of velocity throughout ventricular systole, a reversal of flow during ventricular systole, or vena cava–like biphasic forward velocity peaks during each cardiac cycle.⁴³⁻⁴⁹

As cardiac cirrhosis develops, the morphology of the liver becomes similar to that observed with cirrhosis resulting from other causes. Patients with other forms of cirrhosis may also show flattening of the Doppler waveform in the hepatic veins because of impaired mural compliance of these vessels.

Computed Tomography

The CT findings (Fig. 90-20) of passive hepatic congestion include dilation of the cava and the hepatic veins. When a bolus of contrast material injected intravenously through an arm vein reaches the failing right atrium, it may flow directly into the inferior vena cava and hepatic veins rather than flow normally into the right ventricle. The elevated central venous pressure permits retrograde opacification and enhancement of the inferior vena cava and hepatic veins. Contrast-enhanced CT scans may show an inhomogeneous, mottled, reticulated-mosaic pattern of parenchymal contrast enhancement. The abnormal hepatogram is presumably due to impaired venous outflow leading to altered hepatic hemodynamics and hepatic parenchymal distortion. Linear and curvilinear regions of poor

enhancement may be due to delayed enhancement in regions of small and medium-sized hepatic veins. Larger patchy regions of poor or delayed enhancement in the periphery of the liver probably are a manifestation of the stagnant blood flow in these regions in patients with hepatic venous hypertension. This stagnant blood most likely affects inflow from hepatic arterial and portal venous circulations. Ancillary findings include cardiomegaly, hepatomegaly, intrahepatic periportal lucency resulting from perivascular lymphedema, pleural effusions, ascites, and pericardial effusions.⁴³⁻⁴⁹

Magnetic Resonance Imaging

On early MRI contrast-enhanced images, the liver may enhance in a mosaic fashion with a reticulated pattern of low signal intensity linear markings. The signal intensity of the liver becomes more homogeneous by 1 minute. There is often dilation of the hepatic veins and suprahepatic inferior vena cava. As on CT, contrast material injected into an arm vein may reflux into the hepatic veins and suprahepatic inferior vena cava, enhancing these structures before the portal vein. On gradient-echo MR images, slow or even absent antegrade flow within the inferior vena cava may be identified.⁴³⁻⁴⁹

Peliosis Hepatis

Peliosis hepatis is a rare disorder characterized by cystic hepatic sinusoidal dilation and the presence of multiple blood-filled lacunar spaces of various sizes (1 mm to 3 cm) throughout the liver. These peliotic lesions can also occur in the spleen, bone marrow, lymph nodes, and lungs. The blood-filled spaces freely communicate with the sinusoids and are lined by a thin band

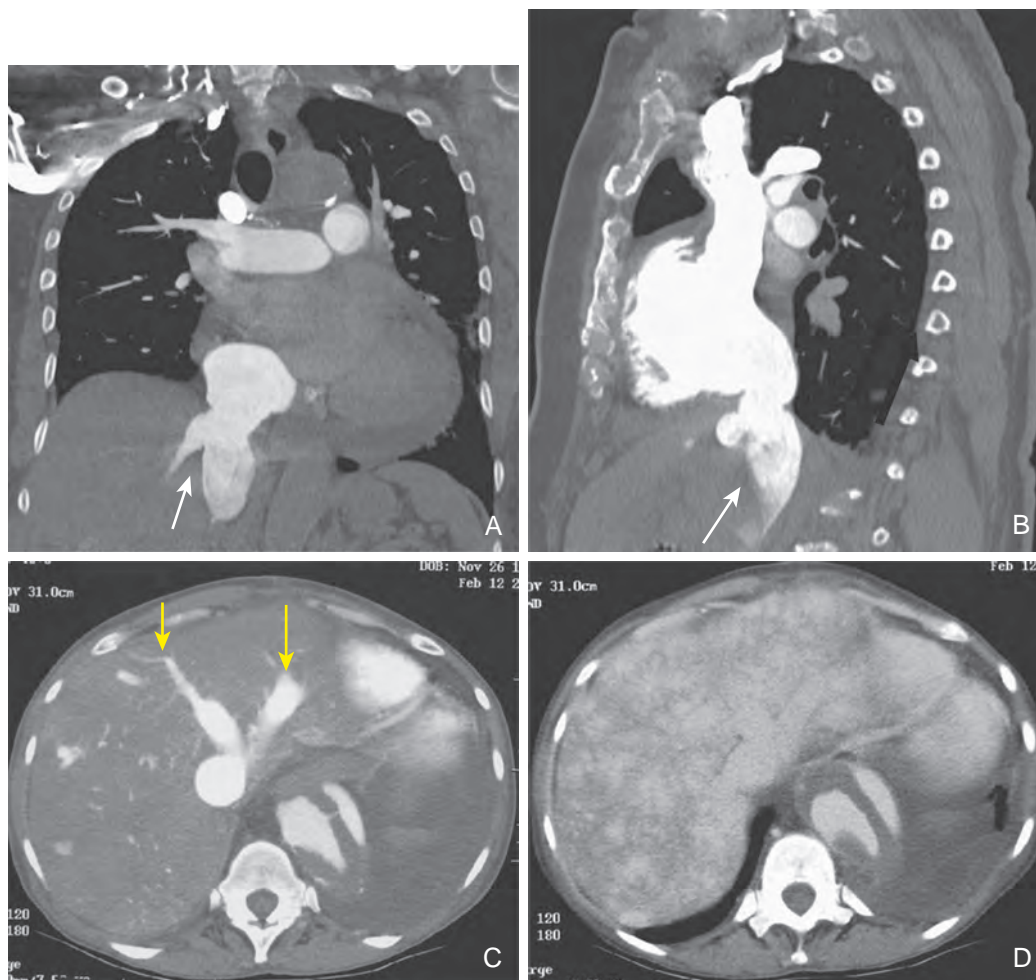


Figure 90-20 Passive hepatic congestion: CT features. Coronal (A) and sagittal (B) reformatted MDCT images demonstrate reflux of contrast material into a dilated inferior vena cava (arrows) and hepatic veins. C. Axial scan in a different patient with a dissecting thoracoabdominal aortic aneurysm shows a dilated inferior vena cava and hepatic veins (arrows). D. Delayed image of patient shown in C reveals a mottled enhancement pattern typical of passive hepatic congestion.

of collagenous tissue and endothelial cells. Peliosis lesions can be differentiated from hemangiomas by the presence of portal tracts within the fibrous stroma of the blood spaces.⁵⁰⁻⁵⁷

PATHOPHYSIOLOGY

Numerous theories have been proposed for the cause of peliosis hepatitis, including outflow obstruction at the sinusoid wall and hepatocellular necrosis leading to cyst formation. There is dilation of a portion of the central vein of the hepatic lobule. Peliosis hepatitis develops in the following settings: with use of anabolic steroids, corticosteroids, tamoxifen, oral contraceptives, or diethylstilbestrol; after renal or cardiac transplantation; in association with a chronic wasting disease, such as tuberculosis, leprosy, malignant disease, or acquired immunodeficiency syndrome (AIDS); in association with celiac diseases, diabetes, necrotizing vasculitis, or Hodgkin's lymphoma; and after exposure to polyvinyl chloride or arsenic.⁵⁰⁻⁵⁷

Peliosis hepatitis is usually found incidentally at autopsy, but it can cause hepatic failure or liver rupture with hemoperitoneum and shock. Patients sometimes present with hepatomegaly, portal hypertension, esophageal varices, and ascites.

RADIOLOGIC FINDINGS

The diagnosis of peliosis hepatitis requires a high degree of suspicion because the radiographic and sonographic findings are nonspecific. On sonographic evaluation, the hepatic echo pattern is inhomogeneous, with hyperechoic and hypoechoic regions, predominantly in the right lobe.

Detecting lesions on CT scans is difficult unless there is associated fatty infiltration to contrast the higher density aggregation of blood-filled spaces (Fig. 90-21). After bolus administration of contrast material, these lesions may appear hypodense early and isodense with time. On angiography, the peliotic lesions are manifested as multiple small accumulations of contrast material on the late arterial phase that become more prominent on the parenchymal and venous phases.⁵⁰⁻⁵⁷

Portal Vein Thrombosis

Portal vein thrombosis is the leading cause of presinusoidal hypertension in the United States. The patency of this vessel is of major concern in the following groups of patients: newborn infants with umbilical catheters who present with ascites,



Figure 90-21 Peliosis hepatis. Multiple small lakes of contrast material are present on this CT scan. The patient also has ascites.

cirrhosis patients who experience sudden decompensation of their disease and exacerbation of ascites, and liver transplant recipients. In some patients, portal vein obstruction is often a diagnosis of exclusion, whereas in others, it is first manifested as a major variceal hemorrhage or vascular emergency. In many cases, splanchnic vein thrombosis is found incidentally in patients with mild, nondescript abdominal pain.⁵⁸⁻⁶⁰

CLINICAL FINDINGS

The clinical presentation of portal vein thrombosis depends on how acutely the obstruction develops and its underlying cause. In most cases, the disease is manifested insidiously, with nonspecific abdominal pain and other manifestations of portal hypertension, including splenomegaly, varices, and massive, intractable ascites, which is a poor prognostic sign. If the thrombosis is due to septic pyelophlebitis, the patient may present with hepatomegaly, pyrexia, leukocytosis, and liver abscesses. In some cases, the disease is manifested catastrophically, with intestinal infarction or massive variceal hemorrhage.⁵⁸⁻⁶⁰

PATHOPHYSIOLOGY

The portal vein may develop a thrombus in its intrahepatic or extrahepatic course, and in 50% of cases, no cause may be apparent (Box 90-2). The most common extrahepatic causes of portal vein occlusion in the West are cancer of the stomach or pancreas and cholangiocarcinoma; acute diverticulitis or appendicitis initiating pyelophlebitis in the portal vein or mesenteric veins; pancreatitis or carcinoma of the pancreas that initiates thrombosis of the splenic vein followed by propagation into the main portal vein; postsurgical thrombosis after upper abdominal procedures, such as splenectomy, endoscopic injection sclerotherapy, and liver transplantation; and trauma. Worldwide, schistosomiasis is the most common cause of portal vein obstruction and the leading cause of portal hypertension.⁵⁸⁻⁶⁰

BOX 90-2 CAUSES OF PORTAL VEIN THROMBOSIS

HYPERCOAGULABLE STATES

- Antiphospholipid syndrome
- Factor V mutations
- Paroxysmal nocturnal hemoglobinuria
- Myeloproliferative diseases
- Oral contraceptives
- Polycythemia rubra vera
- Pregnancy
- Protein S deficiency
- Sickle cell disease

INFLAMMATORY DISEASE

- Behçet's disease
- Crohn's disease
- Pancreatitis
- Ulcerative colitis

COMPLICATIONS OF MEDICAL INTERVENTION

- Alcohol injection
- Ambulatory dialysis
- Chemoembolization
- Islet cell injection
- Liver transplantation
- Partial hepatectomy
- Sclerotherapy
- Splenectomy
- Transjugular intrahepatic portosystemic shunt
- Umbilical catheterization

INFECTIONS

- Actinomycosis
- Appendicitis
- Candida albicans* infection
- Diverticulitis

MISCELLANEOUS

- Cirrhosis
- Bladder cancer
- Nodular regenerative hyperplasia

Cirrhosis is the most common intrahepatic cause of portal vein thrombosis. It is estimated that 10% of patients with cirrhosis of the liver have portal vein thrombosis because stagnant intrahepatic flow predisposes to thrombus formation. These patients are more likely to bleed earlier in the course of their disease than are cirrhosis patients without portal vein thrombosis. Cirrhosis patients with portal vein thrombosis also tolerate portosystemic shunting better than most others do because the hepatic artery supplies virtually all of their hepatic blood flow so that their hepatic hemodynamics are unaffected by portal venous diversion surgery. Less common causes of portal vein thrombosis are Budd-Chiari syndrome, congestive heart failure, intravascular invasion by primary or secondary neoplasms of the liver, cytomegalovirus infection, and Behçet's disease. The incidence of portal vein thrombosis in hepatocellular carcinoma is 26% to 34%, but at autopsy, tumor invasion of portal vein branches is seen in 70% and hepatic vein involvement in 13% of cases. Portal vein thrombosis has been detected sonographically in 8% of patients with liver metastases. For detection of venous invasion in patients with hepatocellular carcinoma, sonography has a sensitivity of 64% and specificity of 98% compared with arterial portography.⁵⁸⁻⁶⁰

Myeloproliferative disorders and blood dyscrasias account for approximately 12% to 48% of cases of portal vein

thrombosis. Portal hypertension, from whatever cause, is also a major risk factor in the development of portal vein thrombosis.⁵⁸⁻⁶⁰

RADIOLOGIC FINDINGS

Plain Radiography

Calcification can occasionally be seen on plain abdominal radiographs in either the portal vein thrombus or the wall of the portal vein. The calcium is deposited diffusely in the clot, whereas mural calcifications are seen as parallel, discontinuous, radiodense lines directed along the course of the portal vein. Plain radiographs may reveal ileus, a localized sentinel loop, or, if the gut is ischemic or infarcted, thumbprinting caused by submucosal edema and hemorrhage.

Ultrasound

Failure to identify the portal vein is a significant finding and virtually diagnostic of portal vein occlusion. Ultrasound is the primary imaging modality for diagnosis and follow-up of portal vein thrombosis because of its ease of execution, sensitivity (particularly combined with color Doppler studies), lower cost, and availability and because it does not require use of intravenous contrast material. On sonographic evaluation (Fig. 90-22), portal vein thrombosis is manifested as an intraluminal echogenic reflector that can partially or completely fill the vein, obscuring normal portal vein landmarks. The portal vein may be expanded in acute thrombosis or when a neoplasm is present. Small sonolucencies may be present within tumor thrombus, but in most cases, bland thrombus cannot be differentiated from tumor thrombus. Tumor thrombosis can be differentiated from bland thrombus by demonstrating color Doppler flow and arterial waveforms (often hepatofugal in direction) within the tumor thrombus on duplex Doppler examination. Lack of flow does not exclude tumor thrombus. Pulsatile flow is fairly specific for malignant thrombus. In these patients, the hepatic artery is dilated with increased systolic central streamline flow.

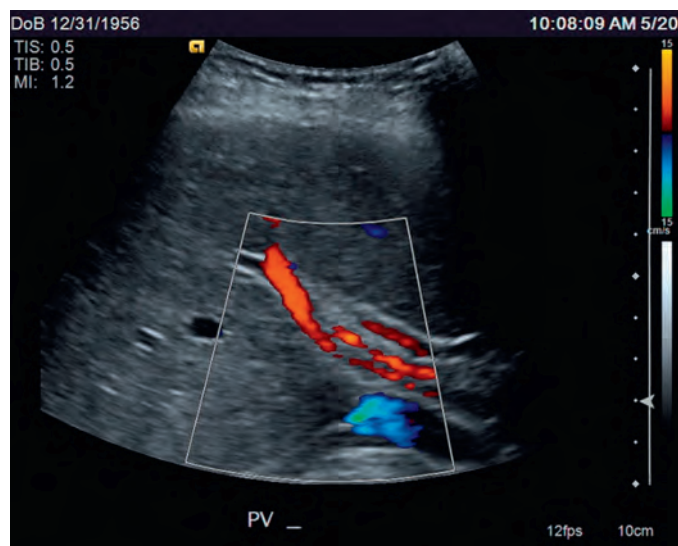


Figure 90-22 Portal vein thrombosis: sonographic findings.

Tumor thrombus is present in the main portal vein in this patient with hepatocellular carcinoma. Arterial color flow signal is identified within the thrombus.

In these cases, fine-needle aspiration under sonographic guidance identifies or excludes tumor. The superior mesenteric and splenic veins may dilate proximal to the thrombus as well. Although the sonographic appearance of tumor thrombus is nonspecific, neoplastic obstruction is often fairly obvious because the offending hepatic or pancreatic mass is usually quite large.⁶¹⁻⁶⁶

Duplex Doppler imaging has a sensitivity of 100% and specificity of 93% in detecting thrombus of the main portal vein.⁶¹⁻⁶⁶ The diagnosis of intrahepatic portal vein thrombus is more difficult to establish confidently because of the high background echogenicity of the liver. Color flow Doppler sonography offers several distinct advantages over conventional spectral Doppler: it passively and automatically depicts blood flow in real time; it permits quick diagnosis of abnormal hepatofugal flow; it can reveal flow and collaterals that are invisible on gray-scale images; and it can allow diagnosis of potentially confusing helical blood flow.

In chronic thrombosis, the portal vein can be normal sized or small, and bridging collaterals may develop in the porta hepatis, particularly when thrombus occurs early in life. These vessels are often prominent in cavernous transformation of the portal vein, which occurs in 30% of patients with portal vein occlusion.⁶¹⁻⁶⁶ Doppler examination shows a typical continuous, low-frequency portal venous flow pattern in these vessels. Secondary sonographic signs of portal vein thrombosis include splenomegaly, ascites, venous collaterals, and mesenteric vein thrombosis causing intestinal congestion or infarction. Serial scans are useful in these patients to determine the efficacy of therapy or to monitor the development of cavernous transformation after acute portal vein thrombosis.

Sonographic demonstration of normal portal and splenic vein diameter and normal vascular caliber variation during respiration excludes the diagnosis of portal vein occlusion with a high level of certainty. Ultrasound can also distinguish between tumor extension into the portal vein and extrinsic portal compression in cases of malignant disease.

Computed Tomography

Portal vein thrombosis appears as a low-density central zone surrounded by an intensely enhanced periphery on contrast-enhanced scans (Figs. 90-23 and 90-24). It is not entirely clear whether this peripheral enhancement is due to flow around the clot or enhancement of the vasa vasorum of the portal vein wall. There is also transient inhomogeneous enhancement of the periportal hepatic parenchyma. Enlargement of the occluded vein increases the likelihood of the presence of tumor thrombus. There may also be streaky enhancement of the clot, which correlates with the angiographic finding of “threads” with septic thrombophlebitis and “streaks” seen in tumor thrombus (Fig. 90-25; see also Fig. 90-22). On precontrast scans, the portal vein contents may be high in attenuation because of the high protein content of concentrated red blood cells.⁶¹⁻⁶⁶

A number of indirect signs of portal vein thrombosis are related to alterations in segmental hepatic blood supply. Portions of liver that experience segmental portal vein occlusion appear atrophic and have decreased attenuation on noncontrast scans. This appearance is caused by fatty infiltration secondary to nutritional ischemia. Decreased parenchymal enhancement is also identified in the lobe involved by portal vein thrombosis. Increased arterial flow may be identified when scans are obtained during the arterial phase.⁶¹⁻⁶⁶

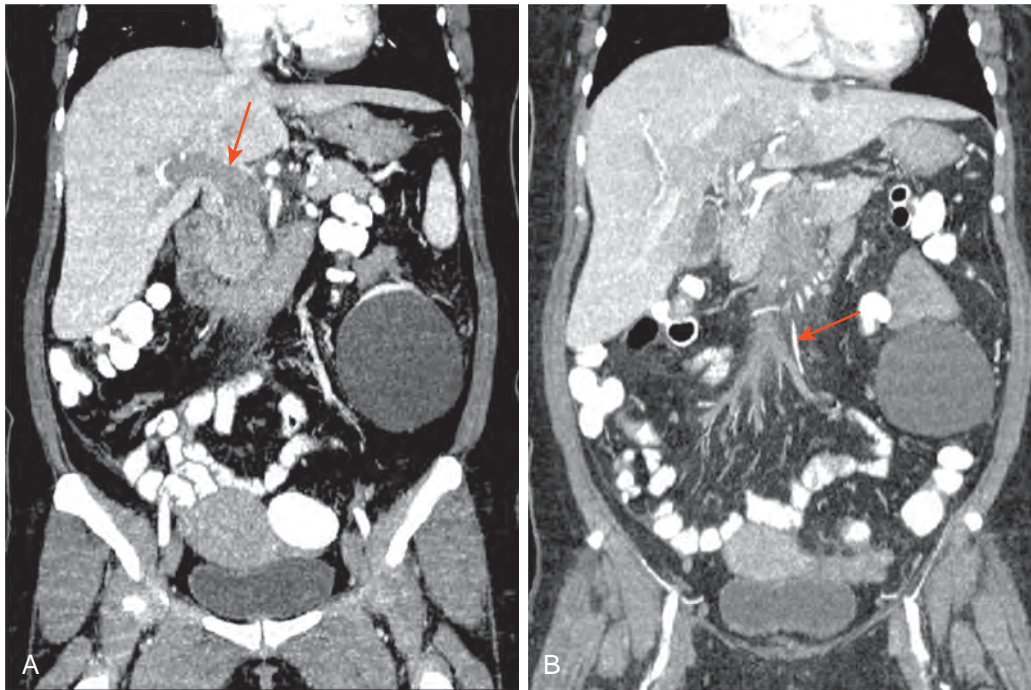


Figure 90-23 Portal and superior mesenteric vein thrombosis: CT findings. **A.** Coronal, reformatted MDCT image shows thrombus (arrow) in the main portal vein in this patient with a coagulopathy. **B.** Coronal reformatted image, anterior to **A**, demonstrates the thrombus extending into the superior mesenteric vein and its branches.

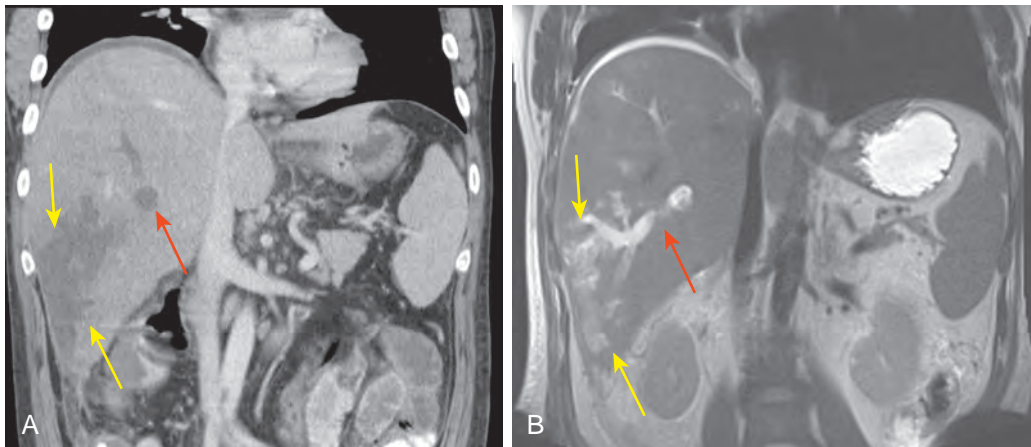


Figure 90-24 Septic intrahepatic portal vein thrombosis: CT and MR findings. Coronal CT (**A**) and MR (**B**) reformatted images show thrombus (red arrow) within an intrahepatic right portal vein. Infection in the liver (yellow arrows) peripheral to this infected thrombus is also present. There is a small amount of ascites.

Arterioportal shunting is another indirect sign of portal vein obstruction. In these cases, enhancement of the involved portal vein branch occurs early in the arterial phase. Calcification of the portal vein thrombus is also readily detected by CT.

On CT scans, portal vein thrombosis may simulate other disorders: gas in a collateral periportal vein can mimic an abscess; expansion of a thrombus-filled inferior mesenteric vein may resemble a pancreatic neoplasm or pseudocyst; segmentally occluded portal veins may simulate dilated bile ducts; and multiple intrahepatic stones may mimic calcified portal vein thrombus.

Magnetic Resonance Imaging

MRI is another excellent means of demonstrating portal vein thrombosis (Figs. 90-26 and 90-27).⁶¹⁻⁶⁶ The appearance of the

clot on MR images depends on its age, oxidation state of hemoglobin, thrombus composition, organization in the thrombus, and field strength. Acute thrombus (<5 weeks old) appears hyperintense relative to muscle and liver on both T1-weighted and T2-weighted images. Older thrombi (between 2 and 18 months) appear hyperintense relative to liver but only on T2-weighted images. Tumor and bland thrombus can be distinguished by the fact that tumor thrombus has a higher signal intensity on T2-weighted images, is soft tissue signal intensity on time-of-flight gradient-echo images, and enhances with gadolinium. Bland thrombus, by contrast, has a low signal intensity on T2-weighted and time-of-flight gradient-echo images and does not enhance with gadolinium. In patients with infected bland thrombus, increased enhancement of the vein wall may be identified.

Intrahepatic portal vein occlusion can produce triangular, wedge-shaped regions in the liver that show high signal intensity on T2-weighted images and on immediate postgadolinium spoiled gradient-echo images. The apex of this region is central, and the base abuts the liver capsule. These changes are presumably due to infarction or edema of the involved hepatic segment.⁶¹⁻⁶⁶

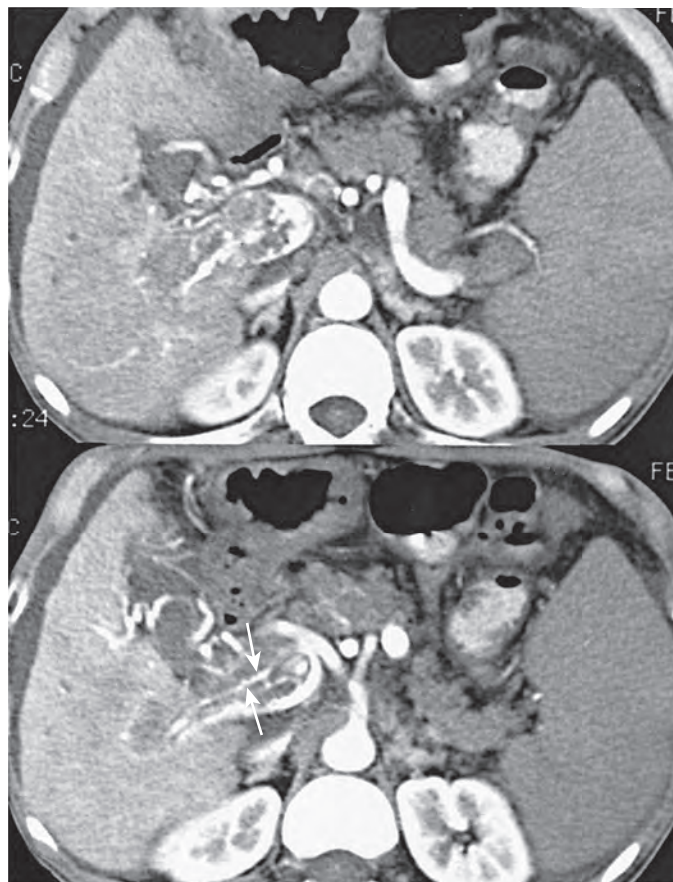


Figure 90-25 Portal vein tumor thrombus: CT features. There is direct visualization of arterial neovascularity in tumor thrombus, producing a "streaks and threads" (arrows) appearance. (Case courtesy Richard L. Baron, MD, Chicago, Ill.)

As noted with CT, after the intravenous administration of gadolinium, transient increased enhancement of hepatic parenchyma may become evident in areas of decreased portal perfusion during the capillary phase of enhancement. Regions with absent or diminished portal blood supply have a commensurate increase in hepatic arterial blood supply. This autoregulatory mechanism provides that areas affected by portal vein thrombosis and increased arterial blood supply enhance intensely because the gadolinium delivered in the first phase is more concentrated in hepatic arteries than in portal veins and is delivered earlier by hepatic arteries than by portal veins. As the concentration of gadolinium in the hepatic arteries and portal veins equilibrates, this differential enhancement disappears.

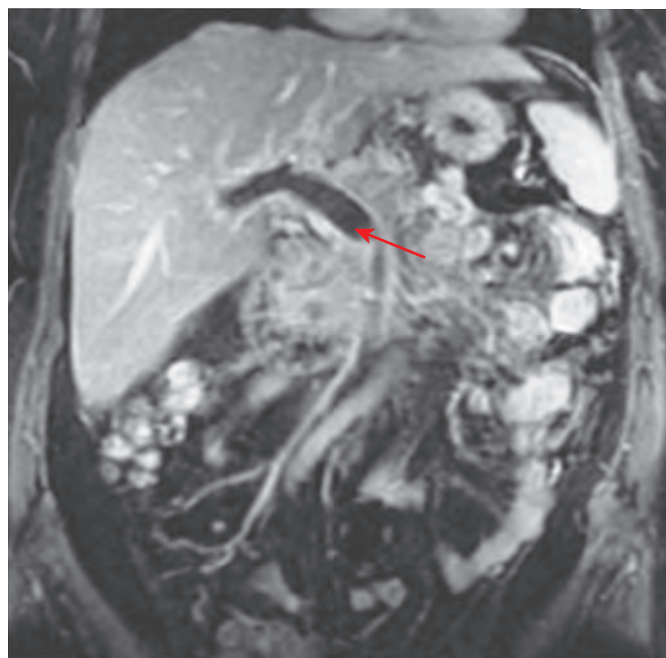


Figure 90-27 Portal vein thrombosis: MRI findings. Coronal image shows thrombus (arrow) in the main portal vein.

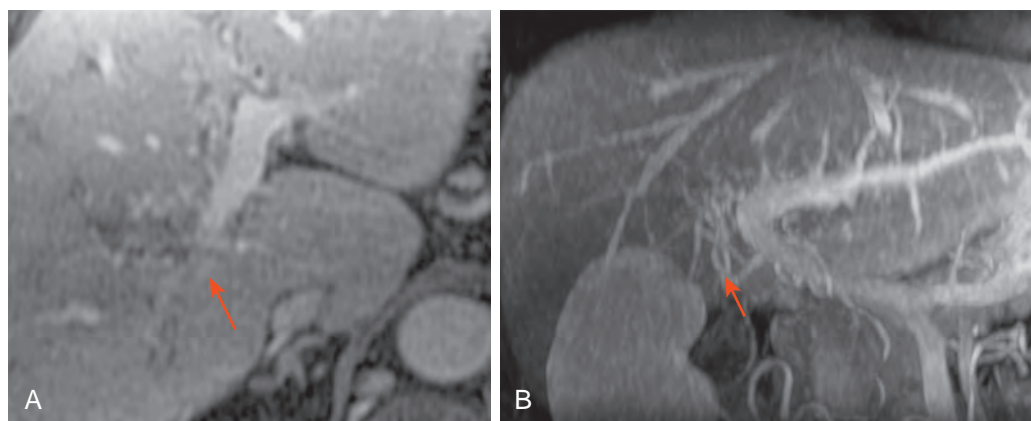


Figure 90-26 Intrahepatic portal vein thrombosis: MRI findings. **A.** Contrast-enhanced multiplanar reconstruction of SD-LAVA sequence shows thrombosis of the intrahepatic portion of the right hepatic vein (arrow). **B.** Thin-slab maximum intensity projection three-dimensional gradient-echo image shows the portal vein thrombus and early venous recanalization (arrow). (Case courtesy Roberto Schuman, MD.)

TREATMENT

Traditionally, the treatment of portal vein thrombosis has been based on early surgical and anticoagulant therapy. A number of percutaneous procedures in which the thrombosis is treated by angioplasty or is lysed by direct urokinase infusion have been reported.

The surgical approach has two major difficulties: the collateral veins are often not sufficiently large to allow a bypass procedure to be performed, and there is an increased incidence of shunt thrombosis and obstruction when a bypass procedure is performed. Therefore, medical management is preferred unless hemorrhage cannot be controlled or there are repeated life-threatening bleeds.⁶¹⁻⁶⁶

Cavernous Transformation of the Portal Vein

Cavernous transformation of the portal vein (CTPV) develops when small collateral veins near the edge of the portal vein dilate, expand, and effectively replace the obliterated portal vein as the major hepatopetal venous conduit. These numerous wormlike vessels at the porta hepatis represent periportal collateral circulation. This transformation develops in long-standing thrombosis, requiring 12 months to occur, and thus more commonly is found in benign disease. This remarkable collateral development reflects the body's effort to maintain hepatopetal portal flow to the liver in the face of occlusion of the extrahepatic portal veins. Collaterals of this magnitude do not typically develop in cirrhotic patients because intrahepatic portal resistance is high in cirrhosis.⁶⁷⁻⁶⁹

In patients with CTPV, sonograms show a mass of tubular anechoic collaterals (Fig. 90-28). Normal portal venous landmarks are obliterated. Doppler evaluation of these collaterals shows a slightly turbulent low-velocity venous signal with little or no respiratory or cardiac variation. It is hepatopetal in direction and has portal venous waveform. Associated findings include splenomegaly, thickening and varices of the lesser omentum, spontaneous splenorenal shunts, and gallbladder varices.

On CT (Fig. 90-29) and MRI (Fig. 90-30), CTPV appears as contrast medium-filled portal collaterals in the hepatoduodenal ligament. In addition, compensatory arterial blood flow in these patients may produce a peculiar enhancement pattern.

CTPV induces morphologic changes in the liver, the most common being atrophy of the right hepatic lobe and left lateral segment and hypertrophy of liver segment IV and the caudate lobe. It is postulated that segment IV and the caudate lobe become hypertrophic with CTPV because of their proximity to the cavernous transformation, which results in maintained portal inflow. Similarly, the right liver lobe and the left lateral segment become atrophic with CTPV because of their greater distance from the cavernous transformation, which leads to compromised portal venous flow.⁶⁸

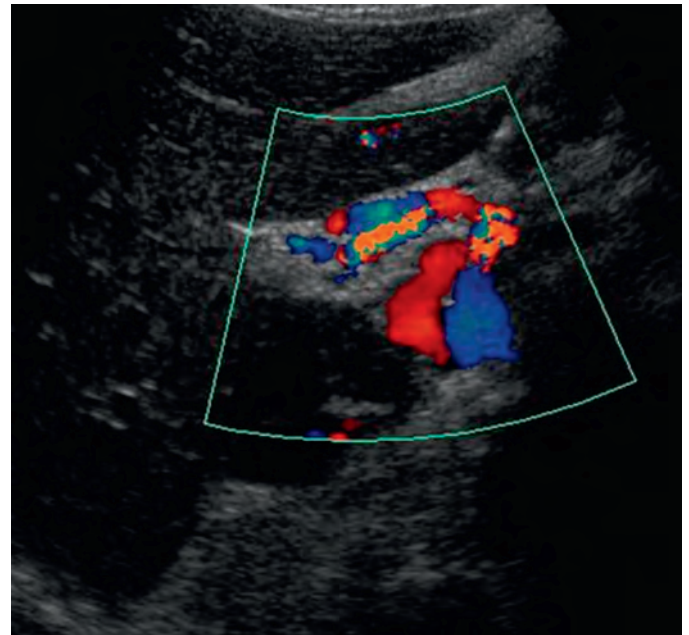


Figure 90-28 Cavernous transformation of the portal vein: sonographic features. Color Doppler scan shows multiple collateral vessels in the portal vein.

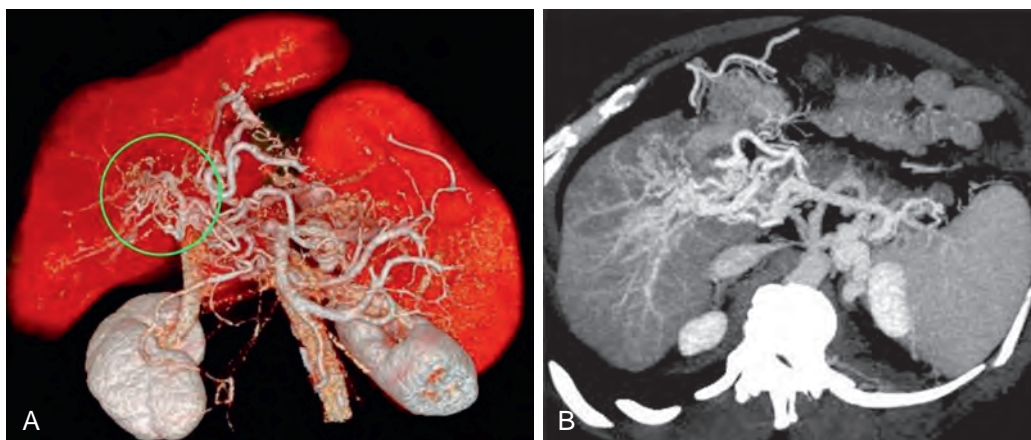


Figure 90-29 Cavernous transformation of the portal vein: CT features. Three-dimensional shaded surface coronal (A) and axial (B) MDCT images show multiple enhancing tubular structures (circle) in the hepatoduodenal ligament.

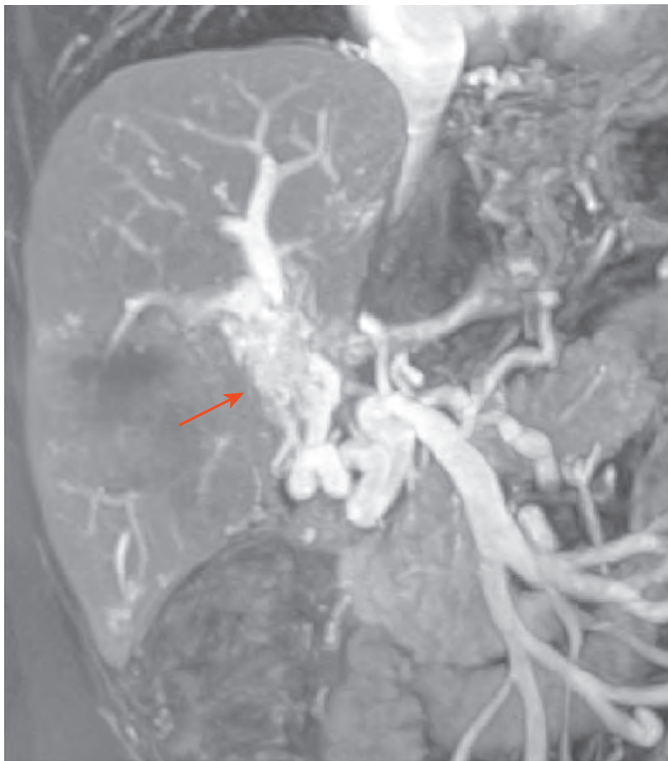


Figure 90-30 Cavernous transformation of the portal vein: MRI features. Coronal MR portogram shows multiple dilated collaterals (arrow) in the hepatoduodenal ligament and dilation of the superior mesenteric vein.

Superior Mesenteric Vein Thrombosis

Isolated superior mesenteric vein (SMV) thrombosis accounts for only 5% to 15% of all intestinal vascular thromboses, being less common than arterial occlusion. It is most common in patients in their 50s and 60s, and 81% of patients have associated illnesses.⁷⁰⁻⁷³

CLINICAL FINDINGS

SMV thrombosis can be classified into acute and chronic presentations for the purposes of management. In acute thrombosis, the patients present with symptoms of less than 4 weeks' duration. The patient has pain out of proportion to the physical findings, nausea, and vomiting, with or without bloody diarrhea. Most cases are associated with metabolic acidosis and mild to moderate leukocytosis. Venous thrombosis occurs in patients younger than those with arterial thrombosis.⁷⁰⁻⁷³

Chronic mesenteric thrombosis is difficult to detect as the onset is insidious and patients are asymptomatic until late complications occur, such as variceal bleeding due to portal hypertension. The patients may present with weight loss, food avoidance, postprandial pain, or distention.⁷⁰⁻⁷³

PATHOPHYSIOLOGY

The causes of isolated SMV thrombosis include myeloproliferative disorders, peritonitis and inflammatory disorders of the abdomen, tumor compression, portal hypertension, the postoperative state, hypercoagulable states (antithrombin III and

protein C and protein S deficiencies), Weber-Christian disease, blood dyscrasias, and pancreatic neoplasms. Extensive venous collaterals in the gut prevent infarction in most cases of SMV thrombosis, so that the mortality rate is only 20%, lower than the 40% to 60% rate for arterial occlusion.⁷⁰⁻⁷³

RADIOLOGIC FINDINGS

Plain film findings are usually noncontributory and may show only ileus. Pneumatosis intestinalis can be seen if the bowel is infarcted, and ascites may develop in patients with chronic SMV thrombosis. Bowel wall thickening and mucosal irregularity indicate intestinal ischemia. On CT scans, the SMV thrombus (Fig. 90-31) appears as a low-density intraluminal mass with a hyperdense periphery, as is seen in portal vein thrombosis. If there is intestinal ischemia as well, mural thickening of the gut may also be seen. Selective angiography usually shows spasm of the superior mesenteric artery (SMA) and no opacification of the affected veins in the venous phase.

Ultrasound is effective in allowing diagnosis of splanchnic vein thrombosis, but if there is no associated portal vein thrombus, the diagnosis of SMV thrombosis is much more difficult, particularly in patients with a gassy abdomen. The gray-scale and Doppler characteristics of SMV thrombus are similar to those seen in the portal vein. Similarly, the CT and MRI findings are identical to those of portal vein thrombosis.

TREATMENT

Small bowel resection in patients with SMV thrombosis is associated with high rates of morbidity and mortality, so that conservative management is indicated when there are no signs of intestinal ischemia or infarction. Direct infusion of fibrinolytic agents into the mesenteric-portal system has been suggested as an alternative treatment in mesenteric vein occlusion. In this procedure, access to the portal system is gained under sonographic guidance, as in percutaneous transhepatic portography, and a large dose of urokinase is infused.⁷⁰⁻⁷³

Splenic Vein and Inferior Mesenteric Vein Thrombosis

Splenic vein occlusion is usually a result of pancreatitis, pancreatic carcinoma, lymphoma, or propagation of clot from the portal vein. Chronic pancreatitis accounts for 65% of all cases of splenic vein thrombosis.⁷⁴⁻⁷⁷ This condition is often clinically silent, but it may cause localized venous hypertension that can result in splenomegaly and bleeding gastric varices. Splenic vein thrombosis should be suspected in patients with splenomegaly and a history of gastrointestinal hemorrhage with normal liver function test results. Other causes include sclerotherapy, splenectomy, and the causes of portal vein and SMA thrombosis.

Splenic vein occlusion produces rerouting of venous flow through the short gastric veins and gastroepiploic vein, causing "left-sided" portal hypertension. Gastric varices in the cardia and fundus are seen in 74% to 83% of patients with splenic vein occlusion.⁷⁴⁻⁷⁷ They appear as broad, serpentine, redundant filling defects or clusters of polypoid defects, simulating thickened rugal folds. These represent the short gastric, gastroepiploic, and left gastric veins that drain retrogradely into the portal vein. Diagnosis is difficult because they are located

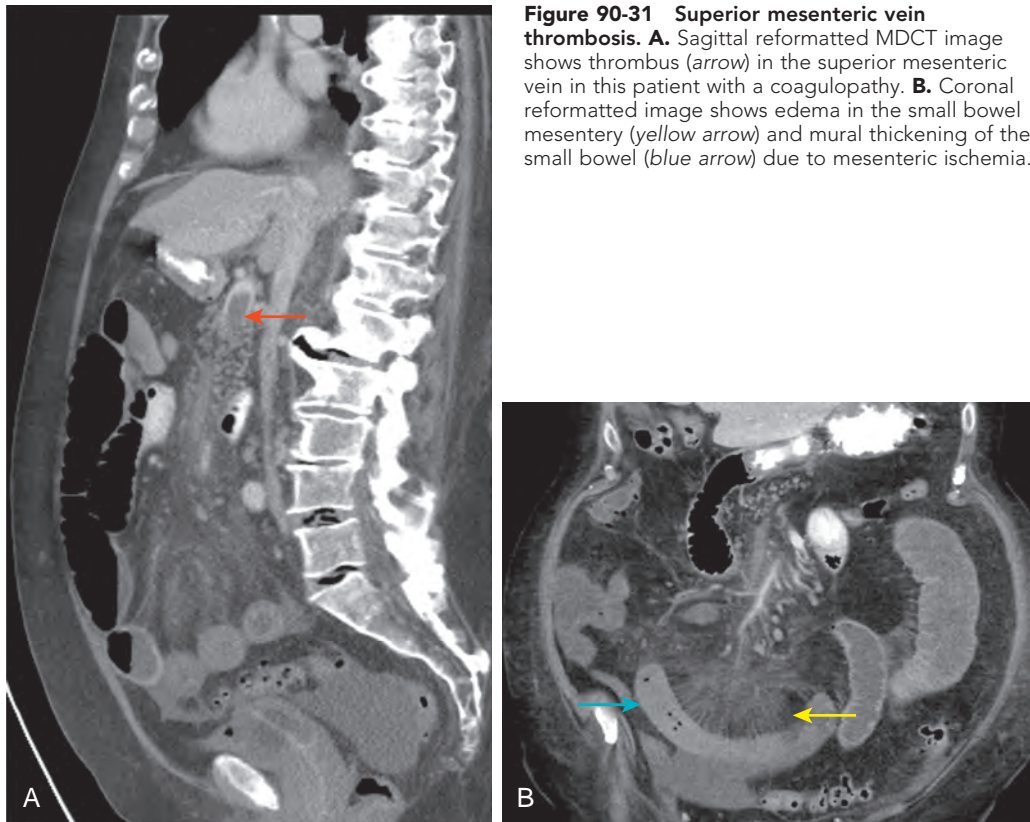


Figure 90-31 Superior mesenteric vein thrombosis. **A.** Sagittal reformatted MDCT image shows thrombus (arrow) in the superior mesenteric vein in this patient with a coagulopathy. **B.** Coronal reformatted image shows edema in the small bowel mesentery (yellow arrow) and mural thickening of the small bowel (blue arrow) due to mesenteric ischemia.

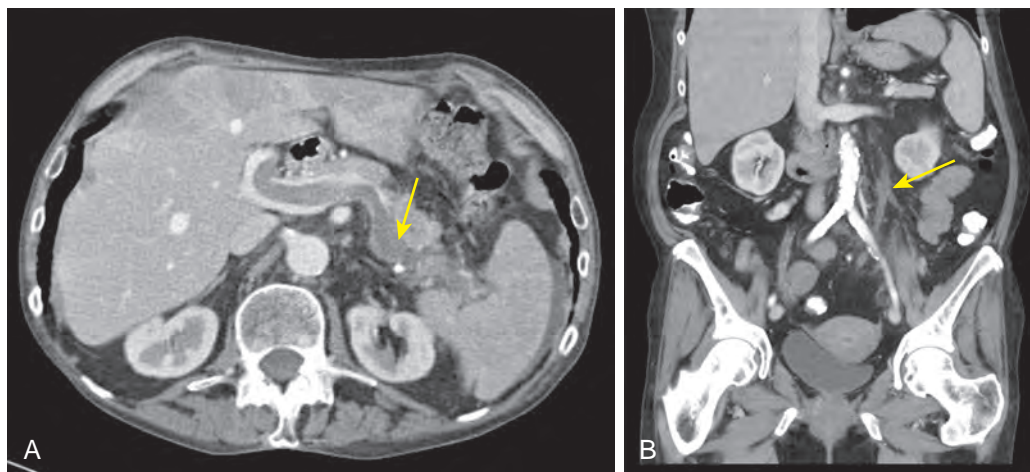


Figure 90-32 Splanchnic venous thrombosis. **A.** Low-density thrombus (arrow) is present within the splenic vein propagating into the portal vein in this patient with a coagulopathy. **B.** Inferior mesenteric vein thrombus (arrow) is depicted on this coronal reformatted CT image in a patient with diverticulitis.

primarily in the subserosa. The appearance of thrombus on CT (Fig. 90-32A), ultrasound, and MRI studies in splenic vein thrombosis is identical to that observed in portal vein or SMV thrombosis. Isolated gastric varices of the short gastric and coronary vessels without esophageal varices were thought to be highly suggestive of splenic vein obstruction; however, one study has demonstrated that portal hypertension is still the most common underlying cause.⁷⁴⁻⁷⁷ Dilation of the gastroepiploic veins is seen only in splenic vein thrombosis.

Splenic vein thrombosis secondary to pancreatitis is now recognized as a fairly common cause of upper gastrointestinal hemorrhage in these patients. For this problem, splenectomy and gastrotomy with oversewing of bleeding varices is sufficient treatment.⁷⁴⁻⁷⁷ Isolated gastric varices caused by splenic vein occlusion can be cured in 90% of cases, and the incidence of recurrent bleeding is low.⁷⁴⁻⁷⁷

Thrombus in the inferior mesenteric vein (Fig. 90-32B) is usually seen in the setting of diverticulitis.

Hepatic Infarction

CLINICAL FINDINGS

Hepatic infarction is a relatively uncommon occurrence because of the liver's dual blood supply and the tolerance of hepatocytes for low oxygen saturation. Hepatic infarction has been associated with shock (Fig. 90-33), sepsis, anesthesia, oral contraceptives, sickle cell disease or trait, polyarteritis nodosa, eclampsia, metastatic carcinoma, bacterial endocarditis, arterial emboli in rheumatic heart disease, trauma, and intra-arterial hepatic chemotherapy. The incidence of ischemic hepatitis in cirrhotic patients admitted to the intensive care unit with variceal bleeding is reported to be as high as 9% with a 60% mortality.⁷⁸⁻⁸⁰

The clinical diagnosis is problematic. Patients usually present with the nonspecific findings of abdominal or back pain (or both), fever, leukocytosis, and abnormal liver function test results, but they may be relatively asymptomatic.

PATHOLOGIC FINDINGS

Ischemic hepatitis is usually diagnosed on the basis of characteristic hepatic histopathologic appearance: minimal centrilobular necrosis and seronegativity for viral hepatitis.

RADIOLOGIC FINDINGS

It is difficult to detect hepatic infarction during its early stages by cross-sectional imaging. The region becomes sonographically hypoechoic when there is sufficient edema and round cell infiltration with indistinct margins. As the necrotic tissue is resorbed, small bile duct cysts or lakes may form. These lakes have the same microscopic appearance as the cysts seen in Caroli's disease, suggesting that the cause of Caroli's disease may actually be neonatal hepatic infarction. On occasion, large bile duct lakes can be seen on CT and ultrasound studies. Infarcts are usually well-circumscribed, peripheral, wedge-shaped lesions, but they can be round or oval and centrally located. With time, areas of infarction develop a more distinct margin and may undergo considerable atrophy. Not all wedge-shaped areas of decreased attenuation on CT scans are due to infarction; decreased portal flow from thrombus, tumor compression,

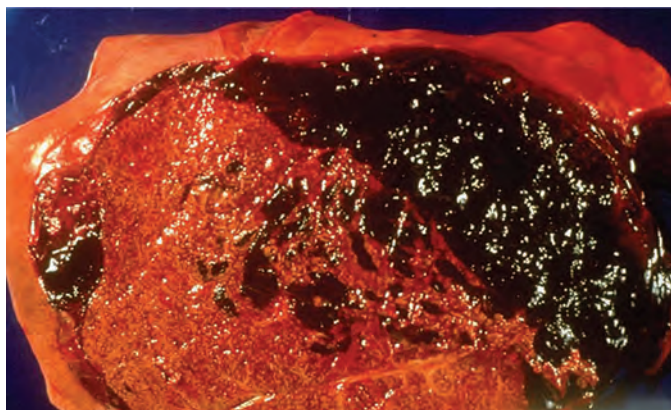


Figure 90-33 Hepatic infarction: pathologic findings. Autopsy specimen from a patient who died of septic shock shows multiple regions of hemorrhage within the liver.

or segmental hepatic vein obstruction may produce a similar picture. Gas formation within a sterile infarct can also be seen on CT (Fig. 90-34) and ultrasound studies. On MR images, the edema of infarction lengthens T1 and T2 relaxation times, causing lower signal intensity on T1-weighted images and higher signal intensity on T2-weighted images of the involved liver.⁷⁸⁻⁸⁰

Hemolysis, Elevated Liver Enzymes, Low Platelets (HELLP) Syndrome

Hepatic ischemia, hemorrhage, and infarction are well-known complications of pregnancy-related HELLP (hemolysis, elevated liver enzymes, low platelets) syndrome. It is a variant of toxemia that occurs either ante partum or post partum and develops in 4% to 12% of patients with severe preeclampsia.⁸¹⁻⁸³

The pathophysiologic mechanism of HELLP syndrome is related to endothelial damage in the placental bed, resulting in activation of the platelets, which causes them to aggregate, and the coagulation cascade, which leads to disseminated intravascular coagulation. The hemolytic anemia is due to passage of red blood cells through small vessels with damaged endothelium covered by fibrin. Fibrin deposition in the liver leads to hepatocellular damage, necrosis, and hemorrhage.

Epigastric or right upper quadrant pain is found in 90% of patients and may be associated with malaise, nausea, vomiting, headache, and nasal bleeding.⁸¹⁻⁸³ Confirmatory laboratory data include hemolytic anemia (hemoglobin <11 g/dL), elevated liver enzymes (lactate dehydrogenase >400 IU/L), and thrombocytopenia (<100,000/mL).⁸¹⁻⁸³

The clinical course of HELLP syndrome is variable. Important complications include massive liver cell necrosis, severe



Figure 90-34 Hepatic infarction: CT features. Gas secondary to infarction is present within the lateral segment of the left lobe of the liver in this patient who had undergone a Whipple procedure 5 days before this study.

disseminated intravascular coagulation, abruptio placentae, renal failure, pulmonary edema, maternal hypoglycemia, and rupture of subcapsular hematoma, with a maternal mortality rate of 3.3%. Standard treatment consists of expeditious delivery of the fetus.⁸¹⁻⁸³

Imaging studies are usually performed in these patients to determine the cause of the abdominal complaints. On sonographic evaluation, the portions of the liver undergoing necrosis have increased echogenicity. CT scan reveals well-defined hypodense, nonenhancing areas or multiple peripheral wedge-shaped areas of low attenuation (Fig. 90-35). The CT and ultrasound appearance in these patients is nonspecific and can mimic focal areas of fatty infiltration.^{84,85}

The MRI appearance in the HELLP syndrome depends on the degree of hemorrhage, necrosis, and steatosis. When edema or cellular necrosis predominates, the affected areas have a low signal intensity on T1-weighted images and high signal intensity on T2-weighted images.^{84,85}

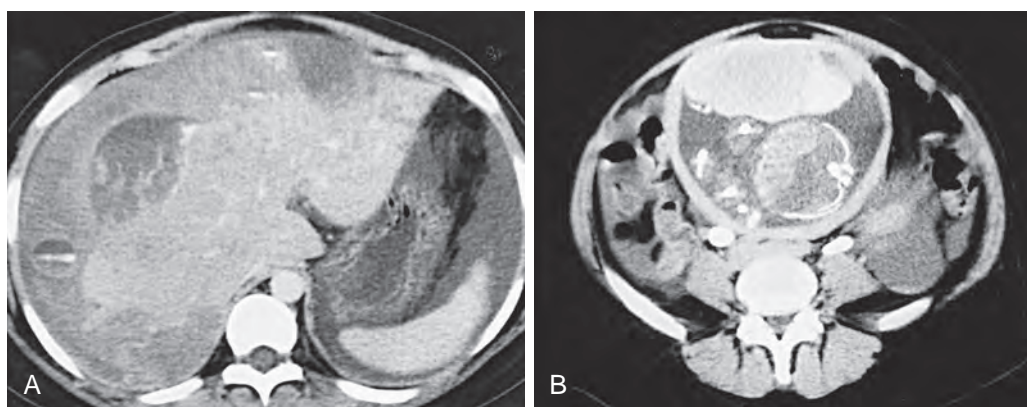


Figure 90-35 HELLP syndrome. This pregnant patient presented with acute abdominal pain, hemolysis, elevated liver enzymes, and low platelets (HELLP). **A.** CT scan shows hepatic hemorrhage with active extravasation of contrast material from multiple sites. Hypodense areas are also present, suggesting thrombosis. **B.** CT scan obtained at a lower level shows the fetus.

Visceral Artery Aneurysms

CLINICAL FINDINGS

Splenic artery aneurysms (Fig. 90-36A) account for 60% of visceral artery aneurysms, followed by the hepatic artery (20%), SMA (5.5%), celiac artery (4%) (Fig. 90-36B), gastric and gastropiploic arteries (4%), jejunal, ileal, and colic arteries (4%), pancreaticoduodenal and pancreatic arteries (2%), gastroduodenal artery (1.5%), and inferior mesenteric artery (<1%).⁸⁶⁻⁹⁵

The splenic artery is a tortuous structure because of the movement of the spleen and differing volumes of blood needed to supply it. The pulsatile nature of the blood flow causes excess stretching of the artery, thereby causing the loops and bends seen angiographically and on cross-sectional imaging; and various branches of the splenic artery that supply the pancreas anchor and prevent the elongating splenic artery from forming one large loop instead of multiple, small excursions from the



Figure 90-36 Visceral artery aneurysms. **A.** CT angiogram shows an aneurysm (arrow) of the superior mesenteric artery. **B.** Aneurysm (circle) of the splenic artery.



direct path. The dilated, tortuous splenic artery protects the delicate splenic pulp so that pressures are less forceful and more indirect.⁸⁷

Splenic artery aneurysms are four times more common in women than in men, and most are small (2-4 cm), asymptomatic, solitary, saccular, and located in the middle to distal splenic artery. There is also an association of splenic artery aneurysm and pregnancy, parity, and portal hypertension. This female predilection likely relates to the hormonal effect of estrogen and progesterone, both with receptor sites in the arterial wall. The hormone relaxin, which is responsible for elasticity of the symphysis pubis in late pregnancy, may also alter the elasticity of the arterial wall. The high flow rate associated with pregnancy and portal hypertension contributes to the deleterious effects on the arterial wall.⁸⁶⁻⁹⁵

Rupture is a catastrophic event that is manifested with pain and hypotension. Impending rupture of a splenic artery aneurysm can produce left upper quadrant pain that radiates to the left subcapsular region. In 20% to 30% of patients, there is double rupture: the initial rupture is contained within the lesser sac, followed by penetration of the lesser sac and free rupture into the peritoneal cavity. Rupture of a splenic artery aneurysm, most common during the third trimester, is a catastrophic event, with reported maternal and fetal mortality rates of 70% and 90%, respectively.⁸⁶⁻⁹⁵

Ruptured and symptomatic splenic artery aneurysms require treatment, as do those found in pregnant women and women of childbearing age. Patients with portal hypertension or those who undergo liver transplantation are also candidates for treatment. Enlarging aneurysms and those larger than 2.5 to 3.0 cm typically require treatment.⁸⁶⁻⁹⁵

Hepatic artery aneurysms show a male predilection of 2:1. Most are solitary and involve the extrahepatic artery, in which case they are most often degenerative or dysplastic. Intrahepatic hepatic artery aneurysms are most frequently the result of trauma, iatrogenic injury from biopsy or intervention, infection, or vasculitis. The use of MDCT has resulted in an increased detection of post-traumatic false aneurysms of the intrahepatic arterial branches. Approximately 60% of hepatic artery aneurysms are symptomatic, and patients most often present with epigastric or right upper quadrant pain, followed in frequency by gastrointestinal hemorrhage and jaundice.⁸⁶⁻⁹⁵ The classic triad of abdominal pain, hemobilia, and obstructive jaundice is observed in only 30% of cases.⁸⁶⁻⁹⁵ When these findings are accompanied by an abdominal bruit or pulsatile mass, the diagnosis of hepatic artery aneurysm should be suspected. The aneurysm may rupture into the peritoneal cavity, extrahepatic bile duct, duodenum, gallbladder, portal vein, or stomach. Obstructive jaundice may result from intrabiliary clots or from extrinsic compression. The mean age at diagnosis is 38 years, and a twofold to threefold male predominance is observed. Extrahepatic aneurysms are four times more common than intrahepatic aneurysms. It is essential to diagnose and to treat hepatic artery aneurysms because of the high incidence of rupture and an associated mortality of up to 82% when this occurs.⁸⁶⁻⁹⁵

Aneurysms and pseudoaneurysms of the gastroduodenal and pancreaticoduodenal arteries are often complications of acute and chronic pancreatitis and pancreatic surgery. Most of these aneurysms are symptomatic and are manifested with gastrointestinal, intraperitoneal, or retroperitoneal hemorrhage.

Aneurysms of the SMA account for 5.5% of all visceral artery aneurysms and can be saccular or fusiform. Most occur within

the proximal 5 cm of this vessel. Most occur in men and are most often diagnosed in the fifth decade of life. These aneurysms may be mycotic in origin or secondary to inflammation, vasculitis, trauma, arterial dissection, and dysplasia and degeneration. These aneurysms are often symptomatic, presenting with acute and colicky upper abdominal pain, nausea, and vomiting.⁸⁶⁻⁹⁵

Celiac artery aneurysms account for 4% of all visceral artery aneurysms and are associated with abdominal aortic aneurysms in 20% of cases and other visceral artery aneurysms in 40%. There is no gender predilection, and most present in the fifth decade of life. The risk of rupture is approximately 13% with high mortality.

In early studies, rupture of visceral artery aneurysm was reported in 22% of cases.⁸⁶⁻⁹⁵ Now a large number are discovered incidentally when the patient is being scanned for other reasons. Indeed, the routine use of MDCT and MRI has led to the increased diagnosis of both symptomatic and asymptomatic aneurysms. Most are degenerative, demonstrating deficiency of the arterial media. Pancreatitis with the escape of pancreatic enzymes may promote destruction of the arterial wall, resulting in pseudoaneurysms of the splenic, hepatic, gastroduodenal, and pancreaticoduodenal arteries. These aneurysms can be treated with surgical or endovascular approaches.

RADIOLOGIC FINDINGS

Hepatic artery aneurysms may produce curvilinear calcification of the right upper quadrant and, when large, produce a mass effect on adjacent viscera on barium studies or on the bile ducts on cholangiograms. Duplex and color flow Doppler studies are the noninvasive screening methods of choice for hepatic artery aneurysm. A pulsatile, cystic mass with arterial flow or a sonolucent or mixed echogenic mass with dilation of ducts proximally suggests the diagnosis. Noncontrast CT may show aneurysm wall calcification. After the bolus administration of contrast material, the residual lumen demonstrates intense enhancement. A low-density thrombus is often seen peripherally. MRI demonstrates a tubular structure that has flow void or strong signal intensity, depending on the imaging sequence used. These aneurysms must be differentiated from pancreatic pseudocysts and cystic pancreatic neoplasms.

Treatment of these lesions is either surgical (ligation or vein grafting) or angiographic (absorbable gelatin foam plugs for small aneurysms and Gianturco coils for larger ones). Invasive radiographic methods are becoming increasingly popular because of the high morbidity and mortality associated with surgery. Reconstructive or ablative surgery is indicated for extrahepatic aneurysms, whereas interventional techniques are favored for those in intrahepatic sites.

Aneurysms of the SMA are rare and may be congenital or associated with pancreatitis, trauma, neoplasm, mycoses, or atherosclerotic disease. They are manifested clinically as a pulsatile mass with a systolic bruit. SMA aneurysms may be saccular or fusiform and are also always located within the first 5 cm of the SMA. The SMA is the most common site for infection of a peripheral muscle artery, which most often occurs secondary to subacute bacterial endocarditis caused by nonhemolytic streptococcal infection. Almost all patients are younger than 50 years. During the previous four decades, infected aneurysms accounted for 58% to 63% of all SMA aneurysms. In the past decade, this has decreased to 33% of reported aneurysms.⁸⁶⁻⁹⁵

This decrease has been accompanied by an increase in the incidence of true aneurysms in the elderly as well as an increase in the incidence of false aneurysms associated with inflammatory processes of the pancreas and biliary tract seen in 12% of SMA aneurysms. Dissection, although uncommon, affects the SMA more than any other visceral artery. Atherosclerosis is present in 25% of reported SMA aneurysms.⁸⁶⁻⁹⁵

In contrast to other visceral artery aneurysms, most SMA aneurysms are symptomatic, presenting with moderate to severe abdominal pain that is usually progressive in its course. A palpable mass is present in 50% of patients, who may also experience nausea, vomiting, gastrointestinal hemorrhage, hemobilia, or jaundice.⁸⁶⁻⁹⁵

Splanchnic Vein Aneurysms

Aneurysms of the portal venous system are uncommon. They represent only 3% of all aneurysms of the venous system but are the most common visceral aneurysms.⁹⁶⁻¹⁰⁴ Because there are variations in the diameters in normal and cirrhotic livers, an aneurysm of the portal venous system is present if the vessel diameter is larger at that point (usually 2 cm) than in the remainder of the vessel. They are usually secondary to pancreatitis and trauma but may be congenital in origin and are seen increasingly in patients with cirrhosis and portal hypertension.

The clinical features of portal vein aneurysms vary. Large aneurysms can cause duodenal compression, common bile duct obstruction, or chronic portal hypertension. Complete obstruction of the portal vein by thrombosis or aneurysm rupture can also occur. Patients who have no symptoms and no signs of portal hypertension should be observed by serial ultrasound scans. Complications of portal vein aneurysms include rupture, thrombosis, complete occlusion of the portal vein, portosystemic shunts, and biliary tract compression.

On ultrasound (Fig. 90-37) and CT studies, a dilated portal vein can usually be identified and distinguished from other lesions. The aneurysm is anechoic, but if thrombus is present, Doppler studies are necessary for confirmation. On Doppler ultrasound, constantly rotating blood is found in an aneurysm of the splenic vein and SMV. Contrast-enhanced CT and MRI will show robust enhancement of the aneurysm.

Osler-Weber-Rendu Disease

Osler-Weber-Rendu disease or hereditary hemorrhagic telangiectasia (HHT) is a rare (incidence of 1 to 2 : 100,000) autosomal dominant disorder characterized by multiple mucocutaneous telangiectasias that may involve most organ systems.¹⁰⁵⁻¹¹¹ Hepatic involvement is frequent and is usually diagnosed 10 to 20 years after the first appearance of mucocutaneous telangiectasias. The typical pathologic features are angiodyplastic vascular changes, including telangiectases, cavernous hemangiomas, aneurysms of the intraparenchymal branches of the hepatic artery, and both hepatoportal and hepatohepatic arteriovenous fistulas. Many patients develop high-output heart failure as a result of left-to-right intrahepatic shunts.

On Doppler ultrasound examinations in patients with HHT, the spectral waveforms show high-velocity flow (153 cm/s) in the dilated and tortuous hepatic artery and its branches. Hepatic artery-to-portal vein shunts cause pulsatility of portal flow with phasic or continuous reversal. Hepatic artery-to-hepatic

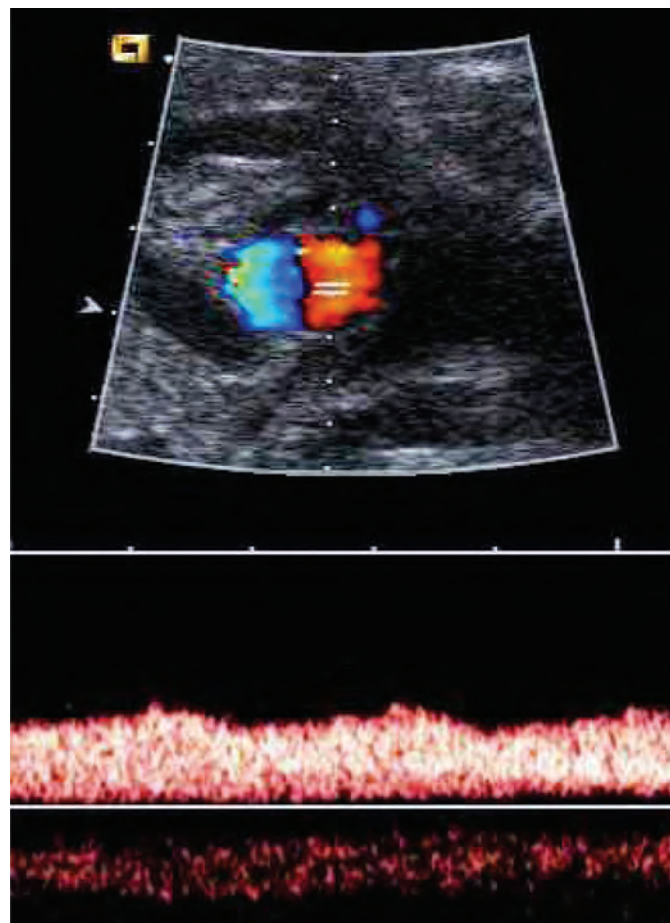


Figure 90-37 Umbilical vein aneurysm. Color Doppler ultrasound shows flow in this venous aneurysm.

vein shunts cause significant changes in the Doppler waveform of the hepatic vein only in severe stages of the disease. Color Doppler sonography demonstrates a large arteriovenous malformation or tangled masses of enlarged tortuous arteries or multiple aneurysms of the hepatic arterial branches within the liver.¹⁰⁵⁻¹¹¹

Contrast-enhanced CT (Fig. 90-38) shows a prominent extrahepatic or both extrahepatic and intrahepatic hepatic artery that is often associated with dilated hepatic or portal veins. Early filling of the portal venous or hepatic venous trunks on helical CT indicates the presence of an arteriovenous shunt. The intrahepatic arteriovenous fistulas are being visualized with increased frequency with the use of MDCT. Other abnormalities include telangiectasias, large confluent vascular masses, and transient hepatic attenuation differences.¹⁰⁵⁻¹¹¹

MR angiograms can provide a map of the anomalous vessels. Dynamic gradient-echo imaging obtained after the injection of Gd-DTPA allows analysis of filling kinetics.

Angiograms in HHT show tortuous dilated hepatic arteries, diffuse telangiectases with a diffuse mottled capillary blush, hemangiomas, and early filling of hepatic or portal veins indicating a shunt. The angiographic appearance depends on the stage of development of the hepatic arteriovenous shunt. All findings are present if the shunting is severe, whereas isolated parenchymal modifications are found only in the case of a mild intrahepatic shunt.

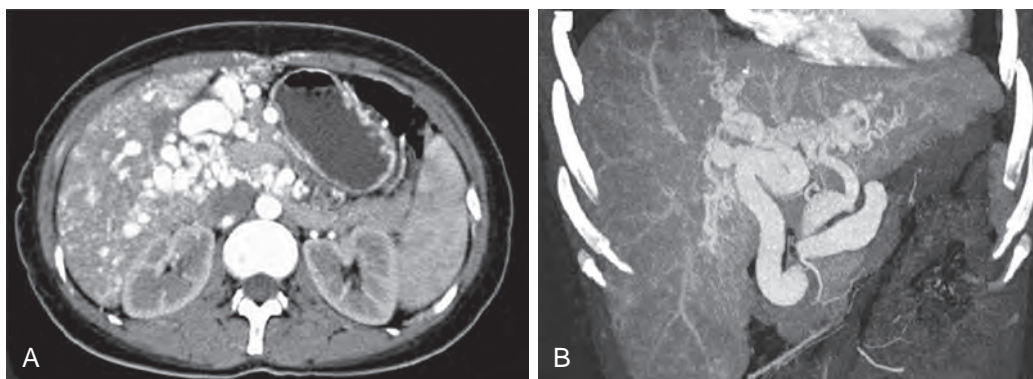


Figure 90-38 Osler-Weber-Rendu disease: CT features. **A.** Arterial phase axial CT image shows irregular and tortuous arteries in the liver parenchyma and porta hepatis. **B.** Coronal maximum intensity projection reconstructed image in arterial phase demonstrates tortuous and irregular arteries in liver and porta hepatis.

Hepatopulmonary Syndrome

The hepatopulmonary syndrome (HPS) describes the clinical relationship between hepatic dysfunction and the presence of pulmonary vascular dilations, which can result in a range of arterial oxygenation abnormalities. HPS can be defined as a triad characterized by severe parenchymal liver disease, hypoxemia (an increased alveolar-arterial gradient on breathing of room air), and evidence of intrapulmonary vascular dilations.¹¹²⁻¹¹⁵

PATHOPHYSIOLOGY

A number of mechanisms underlying the impaired gas exchange in HPS have been proposed: intrapulmonary and porto-pulmonary shunts, pleural spiders, pulmonary hypertension, ventilation-perfusion mismatch, and changes in the affinity of hemoglobin for oxygen.¹¹²⁻¹¹⁵ It now appears that vascular abnormalities known as intrapulmonary vascular dilations are the major cause of severe hypoxemia and are the defining features of HPS (Fig. 90-39A).

IMAGING OF INTRAPULMONARY VASCULAR DILATIONS

Contrast-Enhanced Echocardiography

Contrast-enhanced echocardiography, although generally used to assess intracardiac right-to-left shunts, is valuable for demonstrating the presence of intrapulmonary vascular dilations in patients with hypoxemia and liver disease. Indocyanine green dye and agitated saline are used to provide a stream of microbubbles 60 to 90 μ m in diameter that usually opacify only the right chambers of the heart. The normal pulmonary capillary bed filters these microbubbles so that they do not appear in the left side of the heart. In the presence of an intracardiac or intrapulmonary shunt, microbubbles and indocyanine dye opacify the left-sided heart chambers.

Intracardiac intrapulmonary shunts can be differentiated by the timing of the appearance of left-sided bubbles after injection of the contrast agent. With intracardiac right-to-left shunts, microbubbles and dye are visualized within three heartbeats after the appearance of bubbles in the right-sided heart chambers. In intrapulmonary shunts, the appearance of contrast

material in the left-sided heart chambers is delayed, occurring four to six heartbeats after the initial appearance of contrast material in the right side of the heart.¹¹²⁻¹¹⁵

Perfusion Lung Scanning

The perfusion lung scan (Fig. 90-39B) with technetium Tc 99m-labeled macroaggregated albumin is the second major method for detecting intrapulmonary vascular dilation. The normal pulmonary capillary bed (diameter, 8-15 μ m) traps the albumin macroaggregates, which generally exceed 20 μ m in diameter. The presence of isotope in the brain or kidneys indicates a right-to-left shunt through either an intracardiac or an intrapulmonary shunt. The shunt magnitude is calculated by taking the ratio of the systemic to total body activity of the isotope. Approximately 3% to 6% of the macroaggregated albumin passes through the normal pulmonary vasculature. Shunts ranging from 10% to 71% have been documented in patients with HPS.¹¹²⁻¹¹⁵

Chest Radiography

Patients with HPS usually display the same abnormalities on the chest radiograph that may be seen in all cirrhotic patients: decreased lung volumes, pleural effusions, increased interstitial markings, and increased pulmonary vascular markings. Increased bilateral basilar interstitial markings attributed to intrapulmonary vascular dilations and increased pulmonary vascular markings may be seen as well. These findings are nonspecific.

CT and Angiography

On CT and angiography, the vascular dilations are depicted as enlarged vessels that do not taper normally, extend to the pleural surface, and are most numerous at the lung bases. The ratio of the segmental arterial diameter to bronchial diameter in the right lower lobe is significantly higher in patients with HPS than in cirrhotic patients with normoxemic liver cirrhosis.¹¹²⁻¹¹⁵

TREATMENT

Treatment of HPS is liver transplantation.^{116,117} If the lungs are irreversibly damaged, a liver-lung transplant is in order. The TIPS procedure has been used as a temporizing measure in patients awaiting transplantation.

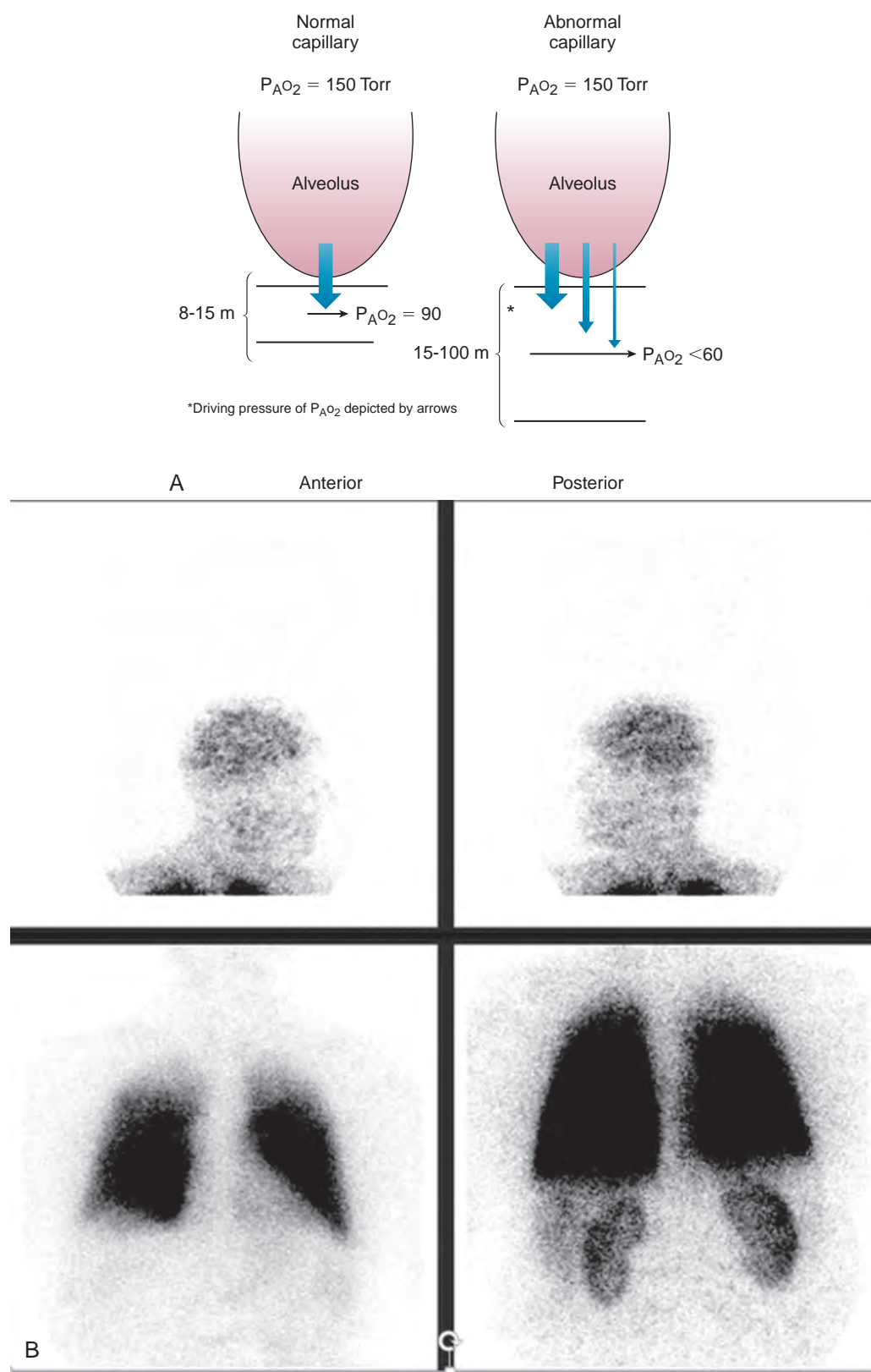


Figure 90-39 Hepatopulmonary syndrome: pathophysiology. **A.** Schematic diagram of the precapillary vascular abnormality seen in both acute and chronic liver disorders. The driving pressure of $P_{A_{O_2}}$ is depicted by the arrows. **B.** Pulmonary perfusion images obtained with technetium Tc 99m-labeled macroaggregated albumin show extrapulmonary uptake in the kidneys and brain. This indicates right-to-left shunting.

REFERENCES

- Colegrande S, Centi N, Galdiero R, et al: Transient hepatic intensity differences: Part 1. Those associated with focal lesions. *AJR Am J Roentgenol* 188:154–159, 2007.
- Colagrande S, Centi N, Galdiero R, et al: Transient hepatic intensity differences: Part 2. Those not associated with focal lesions. *AJR Am J Roentgenol* 188:160–166, 2007.
- Kim HJ, Kim AY, Kim TK, et al: Transient hepatic attenuation differences in focal hepatic lesions: Dynamic CT features. *AJR Am J Roentgenol* 184:83–90, 2005.
- Colagrande S, Centi N, La Villa G, et al: Transient hepatic attenuation differences. *AJR Am J Roentgenol* 183:459–464, 2004.
- Desser TS: Understanding transient hepatic attenuation differences. *Semin Ultrasound CT MR* 30:408–417, 2009.
- Choi SH, Lee JM, Lee KH, et al: Relationship between various patterns of transient hepatic attenuation on CT and portal vein thrombosis related to acute cholecystitis. *AJR Am J Roentgenol* 183:437–442, 2004.
- Yoshimitsu K, Honda H, Kuroiwa T, et al: Unusual hemodynamics and pseudolesions of the noncirrhotic liver at CT. *Radiographics* 21:881–896, 2001.
- Quiroga S, Sebastia C, Pallisa E, et al: Improved diagnosis of hepatic perfusion disorders: Value of hepatic arterial phase imaging during helical CT. *Radiographics* 21:65–81, 2001.
- Haskal ZJ, Potosky DR, Twaddell WS: Percutaneous endovascular creation of an inferior vena cava in a patient with caval agenesis, Budd-Chiari syndrome, and iliofemorocaval thrombosis. *J Vasc Interv Radiol* 25:63–69, 2014.
- MacNicholas R, Olliff S, Elias E, et al: An update on the diagnosis and management of Budd-Chiari syndrome. *Expert Rev Gastroenterol Hepatol* 6:731–744, 2012.
- Ferral H, Behrens G, Lopera J: Budd-Chiari syndrome. *AJR Am J Roentgenol* 199:737–745, 2012.
- Erden A: Budd-Chiari syndrome: A review of imaging findings. *Eur J Radiol* 61:44–56, 2007.
- Fidelman N, Kwan SW, LaBerge JM, et al: The transjugular intrahepatic portosystemic shunt: An update. *AJR Am J Roentgenol* 199:746–755, 2012.
- Li K, Jiang Q, Tian Y, et al: Management of Budd-Chiari: A single-center experience of 280 cases. *Hepatogastroenterology* 61:460–462, 2014.
- Wei X, Hao X, Da-Hai Y, et al: Analysis of interventional treatments of Budd-Chiari syndrome and the related complications: A study of 1006 cases. *Panminerva Med* 55:371–376, 2013.
- Cazals-Hatem D, Vilgrain V, Genin P, et al: Arterial and portal circulation and parenchymal changes in Budd-Chiari syndrome: A study in 17 explanted livers. *Hepatology* 37:510–519, 2003.
- Valla DC: Hepatic vein thrombosis (Budd-Chiari syndrome). *Semin Liver Dis* 22:5–14, 2002.
- Kage M: Budd-Chiari syndrome and hepatocellular carcinoma. *J Gastroenterol* 39:706–707, 2004.
- Bogin V, Marcos A, Shaw-Stiffel T: Budd-Chiari syndrome: In evolution. *Eur J Gastroenterol Hepatol* 17:33–35, 2005.
- England RA, Wells IP, Gutteridge CM: Benign external compression of the inferior vena cava associated with thrombus formation. *Br J Radiol* 78:553–557, 2005.
- Kelleher T, Staunton M, Malone D, et al: Budd-Chiari syndrome associated with angiolipoma of the liver. *J Hepatol* 40:1048–1049, 2004.
- Bargallo X, Gilabert R, Nicolau C, et al: Sonography of the caudate vein: Value in diagnosing Budd-Chiari syndrome. *AJR Am J Roentgenol* 181:1641–1645, 2003.
- Chaubal N, Dighe M, Hanchate V, et al: Sonography in Budd-Chiari syndrome. *J Ultrasound Med* 25:373–379, 2006.
- Bargallo X, Gilabert R, Nicolau C, et al: Sonography of Budd-Chiari syndrome. *AJR Am J Roentgenol* 187:W33–W41, 2006.
- Camera L, Mainenti PP, Di Giacomo A, et al: Triphasic helical CT in Budd-Chiari syndrome: Patterns of enhancement in acute, subacute and chronic disease. *Clin Radiol* 61:331–337, 2006.
- Noone TC, Semelka RC, Siegelman ES, et al: Budd-Chiari syndrome: Spectrum of appearances of acute, subacute, and chronic disease with magnetic resonance imaging. *J Magn Reson Imaging* 11:44–50, 2000.
- Erden A, Erden I, Krayalcin S, et al: Budd-Chiari syndrome: Evaluation with multiphase contrast enhanced three dimensional MR angiography. *AJR Am J Roentgenol* 179:1287–1292, 2002.
- Mortele KJ, Van Vliergerhe H, Wiesner W, et al: Hepatic veno-occlusive disease: MRI findings. *Abdom Imaging* 27:523–526, 2002.
- Erden A, Erden I, Yurdaydin C, et al: Hepatic outflow obstruction: Enhancement patterns of the liver on MR angiography. *Eur J Radiol* 48:203–208, 2003.
- Brancatelli G, Federle MP, Grazioli L, et al: Large regenerative nodules in Budd-Chiari syndrome and other vascular disorders of the liver: CT and MR findings with clinicopathologic correlation. *AJR Am J Roentgenol* 178:873–877, 2002.
- Maetani Y, Itoh K, Egawa H, et al: Benign hepatic nodule in Budd-Chiari syndrome: Radiologic-pathologic correlation with emphasis on the central scar. *AJR Am J Roentgenol* 178:869–875, 2002.
- Brancatelli G, Federle M, Grazioli L, et al: Benign regenerative nodules in Budd-Chiari syndrome and other vascular disorders of the liver: Radiologic-pathologic and clinical correlation. *Radiographics* 22:847–862, 2002.
- Rha SE, Lee MG, Lee YS, et al: Nodular regenerative hyperplasia of the liver in Budd-Chiari syndrome: CT and MR feature. *Abdom Imaging* 25:255–258, 2000.
- Shirai Y, Yoshiji H, Fujimoto M, et al: Successful treatment of acute Budd-Chiari syndrome with percutaneous transluminal angioplasty. *Abdom Imaging* 29:685–687, 2004.
- Hefaidh R, Cheikh M, Marsaoui L, et al: The Budd-Chiari syndrome. *Tunis Med* 91:376–381, 2013.
- Quateen A, Pech M, Berg T, et al: Percutaneous transjugular direct portocaval shunt in patients with Budd-Chiari syndrome. *Cardiovasc Intervent Radiol* 29:565–570, 2006.
- Gandini R, Kondra D, Simonetti G: Transjugular intrahepatic portosystemic shunt patency and clinical outcome in patients with Budd-Chiari syndrome. *Radiology* 241:298–305, 2006.
- Shirai Y, Yoshiji H, Fujimoto M, et al: Successful treatment of acute Budd-Chiari syndrome with percutaneous transluminal angioplasty. *Abdom Imaging* 29:685–687, 2004.
- Rossle M, Oschewski M, Siegerstetter V, et al: The Budd-Chiari syndrome: Outcome after treatment with the transjugular intrahepatic portosystemic shunt. *Surgery* 135:394–403, 2004.
- Klein AS, Molmenti EP: Surgical treatment of Budd-Chiari syndrome. *Liver Transpl* 9:891–896, 2003.
- Mancuso A, Fung K, Mela M, et al: TIPS for acute and chronic Budd-Chiari syndrome: A single-centre experience. *J Hepatol* 38:751–754, 2003.
- Gieling RG, Ruijter JM, Maas AAW, et al: Hepatic response to right ventricular overload. *Gastroenterology* 127:1210–1221, 2004.
- Giallourakis CC, Rosenberg PM, Friedman LS: The liver in heart failure. *Clin Liver Dis* 6:947–967, 2002.
- Gore RM, Mathieu DG, White EM, et al: Passive hepatic congestion: Cross-sectional imaging features. *AJR Am J Roentgenol* 162:71–75, 1994.
- Holley HC, Koslin DB, Berland LL, et al: Inhomogeneous enhancement of liver parenchyma secondary to passive congestion: Contrast-enhanced CT. *Radiology* 170(Pt 1):795–800, 1989.
- Moulton JS, Miller BL, Dodd GD, 3rd, et al: Passive hepatic congestion in heart failure: CT abnormalities. *AJR Am J Roentgenol* 151:939–942, 1988.
- Barakat M: Non-pulsatile hepatic and portal vein waveforms in patients with liver cirrhosis: Concordant and discordant relationships. *Br J Radiol* 77:547–550, 2004.
- Morrin MM, Pedrosa I, Rofsky NM: Magnetic resonance imaging for disorders of liver vasculature. *Top Magn Reson Imaging* 13:177–190, 2002.
- Hiorns MP, Rossi UG, Roebuck DJ: Peliosis hepatis using inferior vena cava compression in a 3-year-old child. *Pediatr Radiol* 35:209–211, 2005.
- Fidelman N, LaBerge JM, Kerlan RK: Massive intraperitoneal hemorrhage caused by peliosis hepatis. *J Vasc Interv Radiol* 13:542–545, 2002.
- Ferrozzi F, Tognini G, Zucconi G, et al: Peliosis hepatis with pseudo-tumoral and hemorrhagic evolution: CT and MR findings. *Abdom Imaging* 26:197–199, 2001.
- Iannaccone R, Federle MP, Brancatelli G, et al: Peliosis hepatis: Spectrum of imaging findings. *AJR Am J Roentgenol* 187:W43–W52, 2006.
- Sandrasegaran K, Hawes DR, Matthew G: Hepatic peliosis (bacillary angiomatosis) in AIDS: CT findings. *Abdom Imaging* 30:738–740, 2005.
- Savastano S, San Bortolo O, Velo E, et al: Pseudotumoral appearance of peliosis hepatis. *AJR Am J Roentgenol* 185:558–559, 2005.
- Steinke K, Terraciano L, Wiesner W: Unusual cross-sectional imaging findings in hepatic peliosis. *Eur Radiol* 13:1916–1919, 2003.
- Gouya H, Vignaux O, Legmann P, et al: Peliosis hepatis: Triphasic helical CT and dynamic MRI findings. *Abdom Imaging* 26:507–509, 2001.

58. Webster GJ, Burroughs AK, Riordan SM: Review article: Portal vein thrombosis—new insights into aetiology and management. *Aliment Pharmacol Ther* 21:1–9, 2005.
59. Sheen CL, Lamparelli H, Milne A, et al: Clinical features, diagnosis, and outcome of acute portal vein thrombosis. *Q J Med* 93:531–534, 2000.
60. Singal AK, Kamath PS, Tefferi A: Mesenteric venous thrombosis. *Mayo Clin Proc* 88:285–294, 2013.
61. Gallego C, Velasco M, Marcuello P, et al: Congenital and acquired anomalies of the portal venous system. *Radiographics* 22:141–159, 2002.
62. Bradbury MS, Kavanaugh PV, Bechtold RE, et al: Mesenteric venous thrombosis: Diagnosis and noninvasive imaging. *Radiographics* 22:527–541, 2002.
63. Rossi S, Rosa L, Ravetta V, et al: Contrast-enhanced versus conventional and color Doppler sonography for the detection of thrombosis of the portal and hepatic venous systems. *AJR Am J Roentgenol* 186:763–773, 2006.
64. Raab BW: The thread and streak sign. *Radiology* 236:284–285, 2005.
65. Janssen HLA, Wijnhoud A, Iwatsuki S, et al: Extrahepatic portal vein thrombosis aetiology and determinants of survival. *Gut* 49:720–724, 2001.
66. Ikeda M, Sekimoto M, Takiguchi S, et al: High incidence of thrombosis of the portal venous system after laparoscopic splenectomy: A prospective study with contrast-enhanced CT scan. *Ann Surg* 241:208–216, 2005.
67. Cellich PP, Crawford M, Kaffes AJ, et al: Portal biliopathy: multidisciplinary management and outcomes of treatment. *ANZ J Surg* 2013 Nov 18. [Epub ahead of print.]
68. Vilgrain V, Condat B, Bureau C, et al: Atrophy-hypertrophy complex in patients with cavernous transformation of the portal vein. *Radiology* 241:149–155, 2006.
69. Song B, Min P, Oudkerk M, et al: Cavernous transformation of the portal vein secondary to tumor thrombosis of hepatocellular carcinoma: Spiral CT visualization of the collateral vessels. *Abdom Imaging* 25:385–396, 2000.
70. Bradbury MS, Kavanagh PV, Bechtold RE, et al: Mesenteric venous thrombosis: Diagnosis and noninvasive imaging. *Radiographics* 22:527–541, 2002.
71. Hatoum OA, Spinelli KS, Abu-Hajir M, et al: Mesenteric venous thrombosis in inflammatory bowel disease. *J Clin Gastroenterol* 39:27–31, 2005.
72. Joh JH, Kim DL: Mesenteric and portal vein thrombosis: Treated with early initiation of anticoagulation. *Eur J Vasc Endovasc Surg* 29: 204–208, 2005.
73. Ibukuro K, Ishii R, Fukuda H, et al: Collateral venous pathways in the transverse mesocolon and greater omentum in patients with pancreatic disease. *AJR Am J Roentgenol* 182:1187–1204, 1825.
74. Ikeda M, Sekimoto M, Takiguchi S, et al: Total splenic vein thrombosis after laparoscopic splenectomy: A possible candidate for treatment. *Am J Surg* 193:21–25, 2007.
75. Kang CM, Chung YE, Jung MJ, et al: Splenic vein thrombosis and pancreatic fistula after minimally invasive distal pancreatectomy. *Br J Surg* 101:114–119, 2014.
76. Morteale KJ, Mergo PJ, Taylor HM, et al: Peripancreatic vascular abnormalities complicating acute pancreatitis: Contrast-enhanced helical CT findings. *Eur J Radiol* 52:67–72, 2004.
77. Morteale KJ, Mergo PJ, Taylor HM, et al: Splenic and perisplenic involvement in acute pancreatitis: Determination of prevalence and morphologic helical CT features. *J Comput Assist Tomogr* 25:50–54, 2001.
78. Tuvia J, Lebwohl O, Lefkowitz J: Hepatic infarction due to thrombotic angiitis; MR appearance. *Clin Radiol* 55:803–805, 2000.
79. Khong SY, James M, Smith P: Diagnosis of liver infarction postpartum. *Obstet Gynecol* 105 (Pt 2):1271–1273, 2005.
80. Giovine S, Pinto A, Crispino S, et al: Retrospective study of 23 cases of hepatic infarction: CT findings and pathological correlations. *Radiol Med (Torino)* 111:11–21, 2006.
81. Boregowda G, Shehata HA: Gastrointestinal and liver disease in pregnancy. *Best Pract Res Clin Obstet Gynaecol* 27:835–853, 2013.
82. Van Runnard Heimel PJ, Franx A, Schobben AE, et al: Corticosteroids, pregnancy, and HELLP syndrome: A review. *Obstet Gynecol Surg* 60:57–70, 2005.
83. Abildgaard U, Heimdal K: Pathogenesis of the syndrome of hemolysis, elevated liver enzymes, and low platelet count (HELLP): A review. *Eur J Obstet Gynecol Reprod Biol* 166:117–123, 2013.
84. Zissin R, Yaffe D, Fejgin M, et al: Hepatic infarction in preeclampsia as part of the HELLP syndrome: CT appearance. *Abdom Imaging* 24:594–596, 1999.
85. Nunes JO, Turner MA, Fulcher MA: Abdominal imaging features of HELLP syndrome: A 10-year retrospective review. *AJR Am J Roentgenol* 185:1205–1210, 2005.
86. Kalko Y, Ugurlucan M, Basaran M, et al: Visceral artery aneurysms. *Heart Surg Forum* 10:E24–E29, 2007.
87. Javors BR: Tortuosity of the splenic artery. *Abdom Imaging* 24:313–314, 1999.
88. Sachdev U, Baril DT, Ellozy SH, et al: Management of aneurysms involving branches of the celiac and superior mesenteric arteries: A comparison of surgical and endovascular therapy. *J Vasc Surg* 44:718–724, 2006.
89. Chiesa R, Astore D, Guzzo G, et al: Visceral artery aneurysms. *Ann Vasc Surg* 11:440–445, 2005.
90. Carr SC, Mahvi DM, Hoch JR, et al: Visceral artery aneurysm rupture. *J Vasc Surg* 33:806–811, 2001.
91. Overhaus M, Lauschke H, Schafer N, et al: The coeliac aneurysm: A rare cause of abdominal pain. *Vasa* 35:201–205, 2006.
92. Singh CS, Giri K, Gupta R, et al: Successful management of hepatic artery pseudoaneurysm complicating chronic pancreatitis by stenting. *World J Gastroenterol* 12:5733–5734, 2006.
93. Sessa C, Tinelli G, Poren P, et al: Treatment of visceral artery aneurysm: Description of a retrospective series of 42 aneurysms in 34 patients. *Ann Vasc Surg* 18:695–703, 2004.
94. Grego FG, Lepidi S, Ragazzi R, et al: Visceral artery aneurysms. *Cardiovasc Surg* 11:19–25, 2005.
95. Sachdev U, Baril DT, Ellozy SH, et al: Management of aneurysms involving branches of the celiac and superior mesenteric arteries: A comparison of surgical and endovascular therapy. *J Vasc Surg* 44:718–724, 2006.
96. De Gaetano AM, Andrisani MC, Gui B, et al: Thrombosed portal vein aneurysm. *Abdom Imaging* 31:545–548, 2006.
97. Okur N, Inal M, Akgul E, et al: Spontaneous rupture and thrombosis of an intrahepatic portal vein aneurysm. *Abdom Imaging* 28: 675–677, 2003.
98. Kocakoc E, Kiris A, Bozgeyik Z, et al: Splenic vein aneurysm with calcification of splenic and portal veins. *J Clin Ultrasound* 33:251–253, 2005.
99. Laumonier H, Montaudon M, Corneloup O, et al: CT angiography of intrahepatic portal aneurysm. *Abdom Imaging* 30:755–757, 2005.
100. Karcaaltincaba M, Haliloglu M, Akpınar E, et al: Multidetector CT and MRI findings in periportal space pathologies. *Eur J Radiol* 61:3–10, 2007.
101. Hayashi S, Yi SQ, Naito M, et al: A case of spontaneous splenorenal shunt associated with splenic artery aneurysm. *Surg Radiol Anat* 28:311–315, 2006.
102. Alabousi A, Patlas MN, Scaglione M, et al: Cross-sectional imaging of nontraumatic emergencies of the spleen. *Curr Probl Diagn Radiol* 43:254–267, 2014.
103. Wolosker N, Zerati AE, Nishinari K, et al: Aneurysm of superior mesenteric vein: Case report with 5-year follow-up and review of the literature. *J Vasc Surg* 39:459–461, 2004.
104. Billaud Y, Pilleul F, Meyer X, et al: Aneurysm of the superior mesenteric vein: Imaging findings. *J Radiol* 84(Pt 1):857–860, 2003.
105. Jaskolka J, Wu L, Chan RP, et al: Imaging of hereditary hemorrhagic telangiectasia. *AJR Am J Roentgenol* 183:307–314, 2004.
106. Wu JS, Saluja S, Garcia-Tsao G, et al: Liver involvement in hereditary hemorrhagic telangiectasia: CT and clinical findings do not correlate in symptomatic patients. *AJR Am J Roentgenol* 187:W399–W405, 2006.
107. Schabel C, Schweinzer K, Ketelsen D, et al: Hereditary hemorrhagic telangiectasia. *Rofo* 184:83–86, 2012.
108. Ravard G, Soyer P, Boudiaf M, et al: Hepatic involvement in hereditary hemorrhagic telangiectasia. *J Comput Assist Tomogr* 28:488–495, 2004.
109. Guttmacher AE, Marchuk DA, White RI: Hereditary hemorrhagic telangiectasia. *N Engl J Med* 333:918–924, 1995.
110. Nozaki T, Nosaka S, Miyazaki O, et al: Syndromes associated with vascular tumors and malformations: A pictorial review. *Radiographics* 33:175–195, 2013.
111. Memeo M, Ianora AAS, Scaradapne A, et al: Hepatic involvement in hemorrhagic telangiectasia: CT finding. *Abdom Imaging* 29:211–230, 2004.
112. Leung AN: Hepatopulmonary syndrome. *Radiology* 229:64–67, 2003.
113. Hansell DM: Small-vessel diseases of the lung: CT-pathologic correlates. *Radiology* 225:639–653, 2002.
114. Engleke C, Schaefer-Prokop C, Schirg E, et al: High-resolution CT and CT angiography of peripheral pulmonary vascular disorders. *Radiographics* 22:739–764, 2002.
115. Meyer CA, White CA, Sherman KE: Diseases of the hepatopulmonary axis. *Radiographics* 20:687–698, 2000.
116. Fritz JS, Fallon MB, Kawut SM: Pulmonary vascular complications of liver disease. *Am J Respir Crit Care Med* 187:133–143, 2013.
117. Koch DG, Fallon MB: Hepatopulmonary syndrome. *Curr Opin Gastroenterol* 30:260–264, 2014.

Hepatic Trauma, Surgery, and Liver-Directed Therapy

HELENA GABRIEL | NANCY A. HAMMOND | MARK TALAMONTI |
RIAD SALEM | RICHARD M. GORE

CHAPTER OUTLINE

Hepatic Trauma

Epidemiology
Clinical Findings
Classification of Hepatic Trauma
Pathophysiology
Radiologic Findings
Treatment
Complications

Hepatic Surgery

Radiology in Surgical Planning
Intraoperative Ultrasound
Indications
Types of Hepatic Resection

Liver-Directed Therapy

Cryosurgery
Radiofrequency Ablation
Chemoembolization
Combination Chemoembolization and Radiofrequency Ablation
Radioembolization
Postoperative Radiologic Appearance of the Liver
Complications
Postprocedural Radiologic Appearance of the Liver

Hepatic Trauma

Hepatic trauma was first graphically described in the *Iliad*, when Achilles “stabbed with his sword at the liver, the liver was torn from its place, and from it the black blood drenched the fold of his tunic and he was shrouded in darkness as the light went out.” The liver is not faring much better 2600 years later, with the increasing violence of urban life, our society’s passion for high-speed travel, and the gastroenterologist and interventional radiologist constantly invading the liver.¹⁻³ The cross-sectional imaging modalities have dramatically improved the promptness and certainty of diagnosis in patients with hepatic trauma and have proved useful in the triage of patients to surgical or conservative management.⁴⁻⁶ The single most important factor allowing nonoperative management of blunt hepatic trauma has been the evolution of computed tomography (CT) scanning.⁷⁻¹¹

EPIDEMIOLOGY

The types of hepatic injury encountered in practice depend to a large degree on the location of the trauma center. In suburban and rural areas, hepatic injury is usually due to blunt trauma sustained in motor vehicle accidents and falls. In the setting of blunt abdominal trauma, the liver and spleen are the most commonly injured solid organs. The reported prevalence of liver injury in patients who have sustained blunt trauma ranges from 1% to 8%.¹² Other associated injuries are present in 80% of people. In large city hospitals, penetrating injuries from firearms and stabbings predominate. In this setting, the liver is the most frequently injured viscus owing to its anterior and partially subcostal location.^{13,14} Iatrogenic hepatic injuries are becoming increasingly common in all hospitals. Indeed, liver biopsy is the most common cause of subcapsular hematoma in the United States today. Because of their markedly different management paradigms and prognoses, blunt, iatrogenic, and penetrating traumatic injuries are discussed separately in this chapter.

CLINICAL FINDINGS

Clinical features associated with hepatic trauma include right upper quadrant pain and tenderness with guarding and rebound tenderness, falling hematocrit, and hypotension. Delayed manifestations of biliary trauma, such as bilomas, are usually accompanied by right upper quadrant pain and jaundice.^{15,16} Trauma is the most frequent cause of hemobilia, which is manifested by hematemesis or melena associated with right upper quadrant pain. Because of the difficulty of identifying hepatic injury by physical examination, CT is often required to avoid missing a significant injury. The mortality rate reported secondary to blunt liver trauma ranges from 4.1% to 11.7%.^{13,17,18} The American College of Surgeons state a mortality rate of 16.8%, taking all hepatic injuries into account on the basis of the National Trauma Data Bank.^{19,20}

Diagnostic peritoneal lavage was one of the most common clinical modalities used in the diagnostic evaluation for blunt abdominal trauma in the mid-20th century.²¹ This procedure is sensitive for hemoperitoneum but led to a high rate (30%) of nontherapeutic, unnecessary laparotomies. Diagnostic peritoneal lavage has largely been replaced with CT or screening ultrasound for the evaluation of hemoperitoneum.²²⁻²⁴

CLASSIFICATION OF HEPATIC TRAUMA

The management of hepatic trauma patients has evolved significantly during the last three decades and is now based on well-defined treatment algorithms. This has highlighted the need for an accurate classification system as a basis for the clinical decision-making process.²⁵ Fundamental to the development of these classification schemes and the subsequent treatment algorithms based on them is the widespread availability of rapid acquisition CT imaging in most major trauma centers. This has also led to a diminution in the role of diagnostic peritoneal lavage in the management of the trauma patient. Diagnostic peritoneal lavage has multiple limitations: lack of specificity regarding the source of bleeding; high sensitivity to detection of small quantities of blood, leading to nontherapeutic laparotomy; and inaccuracy for retroperitoneal injuries. Diagnostic peritoneal lavage fails most importantly in its ability to identify the location and extent of intra-abdominal organ injury. Diagnostic peritoneal lavage is valuable mainly in patients in whom ultrasonography or CT scanning is inappropriate or unavailable.⁸

Previous attempts to categorize hepatic injury were mostly anatomic in design and did not incorporate the mechanism of injury or physiologic changes associated with more severe injuries. In 1987, the Organ Injury Scaling Committee of the American Association for the Surgery of Trauma was organized for the purpose of devising injury severity scales for individual organs. These injury severity scales incorporated etiology, anatomy, and extent of injury and correlated it with subsequent clinical management and outcome. The most recently revised clinical classification is listed in Table 91-1.²⁶ It has been demonstrated that the CT grade of hepatic injury is not predictive of the need for surgery and that the majority of injuries can be safely managed nonoperatively.²⁶⁻³¹ The hemodynamic status of the patient may be the most important

predictor of injury severity; however, patients with higher grade injuries (IV or V) are more likely to be unstable and to require surgery, and increasing organ injury severity scale grade in patients with isolated hepatic injuries is associated with increasing mortality.⁹ In contrast, patients who are stable may be managed conservatively with close observation in intensive care units.^{8,9,32} Mechanism of injury, radiologic classification, and clinical assessment of hemodynamic stability must all be correlated by the trauma surgeon to guide management decisions.

PATHOPHYSIOLOGY

Blunt Trauma

Approximately 1% to 8% of patients who sustain blunt abdominal trauma have a liver injury.¹² Severe compressive trauma to the liver from a steering wheel injury or direct blow can produce satellite fractures that often involve an entire lobe.³³ Rapid deceleration in motor vehicle accidents produces shearing forces that cause different degrees of parenchymal tears. The hepatic lobes may be torn from each other, or the tears may involve the supporting ligaments, hepatic veins, and inferior vena cava. The most frequent site of hepatic injury is the posterior segment of the right lobe of the liver because of its size and proximity to the ribs and spine. Although they are less common, left lobe injuries are more often associated with retroperitoneal injuries (duodenum and pancreas) and transverse colon injuries.^{30,34} There is a high incidence of associated extrahepatic injury, including splenic rupture, head injuries, rib fractures, facial fractures, and pelvic fractures.³⁵

Major hepatic venous injuries occur in 13% of patients with liver trauma. These are most often a result of blunt trauma. They include, in decreasing order of frequency, right hepatic vein avulsion from the inferior vena cava, upper branch right hepatic vein avulsion, avulsion of accessory veins, avulsion of the left hepatic vein, and avulsion of the middle hepatic vein. The right hepatic vein is at greater risk for sudden acceleration-deceleration injury because it has a relatively long extrahepatic segment before it enters the inferior vena cava. The course is shorter for the middle and left hepatic veins, which usually merge to form a common channel and thus are less frequently injured.^{36,37} Venous injuries can be suggested by multiple lacerations around the inferior vena cava or porta hepatis.^{10,11} It is important to identify these findings because they may help prepare the surgeons to expect significant bleeding when the liver is lifted off the inferior vena cava.¹¹ Multiplanar CT reconstruction and three-dimensional rendering can be helpful in the assessment of vascular involvement, especially the portal vein, hepatic veins, and retrohepatic vena cava.³⁸ Injuries of the bare area of the liver may not demonstrate peritoneal signs or findings on diagnostic peritoneal lavage or screening sonography for hemoperitoneum but may show retroperitoneal blood on CT examination.³⁹

Penetrating Injuries

Penetrating wounds are most commonly caused by stabbing, gunshot, or shotgun injury.^{40,41} Knife stabbings usually cause superficial lacerations, whereas high-velocity projectiles generally cause injury from capsule to capsule, with massive parenchymal damage.⁵

TABLE 91-1
Classification of Hepatic Trauma

Grade	Injury
I	Hematoma Subcapsular, <10% surface area
II	Laceration Capsular tear, <1 cm parenchymal depth
III	Hematoma Subcapsular, 10%-50% surface area Intraparenchymal, <10 cm diameter
IV	Laceration 1-3 cm parenchymal depth, <10 cm in length
V	Hematoma Subcapsular, >50% surface area or expanding; ruptured subcapsular or parenchymal hematoma Intraparenchymal hematoma >10 cm or expanding
VI	Laceration Parenchymal fracture >3 cm deep
V	Laceration Parenchymal disruption involving 25%-75% of hepatic lobe or 1-3 Couinaud segments within a single lobe
V	Laceration Parenchymal disruption involving >75% of hepatic lobe or >3 Couinaud segments within a single lobe
VI	Vascular Juxtahepatic venous injuries (i.e., retrohepatic vena cava/central major hepatic veins)
VI	Vascular Hepatic avulsion

From Moore EE, Cogbill TH, Jurkovich GS, et al: Organ injury scaling: Spleen and liver (1994 revision). *J Trauma* 38:323-324, 1995.

Iatrogenic Injuries

The liver is subject to a number of iatrogenic misadventures that may be caused by any of the various needles, wires, canulas, and catheters placed by gastroenterologists and interventional radiologists.^{15,42,43} The liver can also be damaged by external cardiac compression during the course of resuscitation and by inappropriately low insertion of a chest tube.⁴⁴

Diagnostic and interventional procedures can produce a tear of the liver capsule, subcapsular hematoma, bile leak, arteriovenous fistula, pseudoaneurysm, arteriohepatic or venobiliary fistula, hepatic hematoma, hemoperitoneum, and biloma.⁴⁵ The prevalence of this problem was well documented in one study in which intrahepatic (77%) and subcapsular (23%) hematomas were found sonographically in 23% of asymptomatic patients evaluated after liver biopsy.⁴⁶

Spontaneous Rupture

Hepatic rupture and hemorrhage can occur in eclamptic or preeclamptic women during the third trimester due to hemolysis, elevated liver enzymes, and low platelets, the HELLP syndrome.⁴⁷ The maternal mortality rate approaches 60% with hepatic rupture. Because surgery is difficult in these friable livers, hepatic artery transcatheter embolization offers a therapeutic alternative. One report showed good results with absorbable gelatin foam (Gelfoam) embolization in four eclamptic patients.^{48,49} Bleeding from the liver may also immediately follow delivery in noneclamptic women.

Spontaneous hemorrhage can occur in patients who have sickle cell anemia, peliosis, hepatomas, hepatic adenoma, coagulopathies, B-cell lymphoma, metastases, organophosphate toxicity, or collagen-vascular disease and in patients who receive long-term hemodialysis.⁵⁰

RADIOLOGIC FINDINGS

Imaging can make a major contribution to the management of trauma patients who are hemodynamically stable and to the postoperative assessment of these patients.*

Computed Tomography of Hepatic Injuries

Multidetector computed tomography (MDCT) is the imaging technique of choice for hepatic trauma and has had an enormous impact on the detection and management of liver injuries.[†] It can reliably diagnose and stage significant hepatic and extrahepatic injuries, document interval healing of hepatic injuries, and diagnose early and delayed complications.⁵⁷ It can also detect associated and unsuspected injuries to other organs (Fig. 91-1). Patients who are hemodynamically unstable require immediate surgery; surgical delay secondary to imaging can be fatal. Hemodynamically stable patients can be scanned in a matter of seconds, with better resolution and with multiplanar imaging capabilities, given our current CT technology.

With any type of abdominal trauma, the first finding that should be evaluated is the presence or absence of blood, either parenchymal or intraperitoneal (hemoperitoneum). Immediately after injury, hematomas on noncontrast scans are hyperdense relative to normal hepatic parenchyma (Fig. 91-2). After

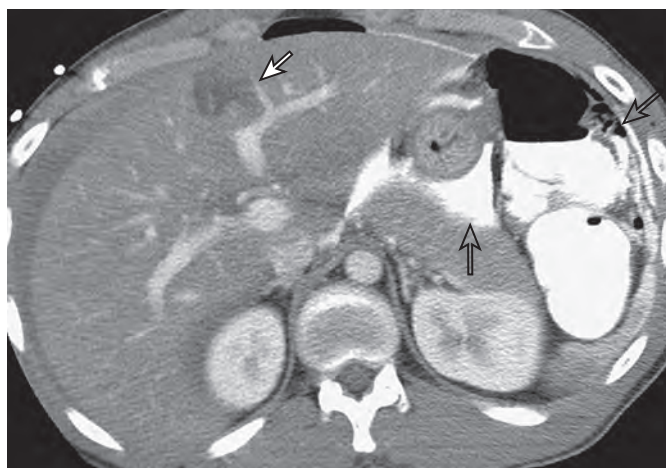


Figure 91-1 Unsuspected hepatic laceration secondary to a gunshot to the left upper abdomen resulting in colonic perforation. CT demonstrates a low-density laceration in the left hepatic lobe (solid arrow). Free air and extravasated rectal contrast material are also seen, indicating bowel perforation (open arrows).



Figure 91-2 Noncontrast appearance of hepatic laceration and hematoma. Noncontrast CT demonstrates a heterogeneous masslike region in the right hepatic lobe with central hyperdensity consistent with hematoma.

intravenous administration of contrast medium, unclotted blood is usually hypodense compared with enhancing normal parenchyma but still usually has an attenuation (20-40 HU) greater than that of simple fluid (0-20 HU).

Active hemorrhage is identified as extravasation of contrast material on contrast-enhanced CT. The attenuation values of extravasated contrast material (155 HU, mean value) and hematoma (54 HU, mean value) help distinguish active bleeding from clotted blood.^{10,58-60} If the liver is involved by focal or diffuse fatty infiltration, a common finding in intoxicated drivers, parenchymal hematomas may appear isodense on contrast-enhanced examinations but can usually be distinguished with narrow CT window settings. In addition, the attenuation and the distribution of fluid can serve as a clue to the site of injury. This phenomenon has been termed the sentinel clot sign.⁶¹ The sentinel clot is the highest density blood collection seen and usually lies adjacent to the injured organ

*References 5, 10, 11, 14, 15, 51-53.

†References 5, 10, 11, 14, 15, 54-56.

(Fig. 91-3). The evaluation of hepatic trauma should also search for other fluid collections, such as bile, as seen in bile leaks and bilomas, which have low attenuation because of their high cholesterol content.

In interpreting CT scans in patients with hepatic trauma, it is important to describe the anatomic site and extent of injury (superficial, deep, lobar, segmental, perihilar), the complexity of the lesion (simple or stellate laceration), and the type of hepatic injury (parenchymal laceration or subcapsular hematoma).^{10,11,62,63}

The major CT findings in blunt hepatic injuries are lacerations, subcapsular and parenchymal hematomas, active hemorrhage, and juxtahepatic venous injuries.¹⁷ Lacerations are the most common injury and appear as branching or linear low-attenuation areas. Lacerations can be classified into superficial (<3 cm from the liver surface) and deep (>3 cm from the surface) (Fig. 91-4). Deep central parenchymal injuries seen on

CT may be unrecognized at laparotomy, especially if the liver surface appears intact, and as a result, the true extent of involvement may be underestimated at surgery.¹⁰ It is imperative to describe any potential laceration extension to the hepatic or portal veins or to the inferior vena cava (Fig. 91-5; see also Fig. 91-3). Hematomas can also occur in hepatic trauma and may be subcapsular or parenchymal in nature. Subcapsular hematomas can be distinguished from free hemoperitoneum by mass effect on the liver surface, creating a contour deformity. Parenchymal hematomas follow the same attenuation values of blood as described before. Again, on contrast-enhanced CT, they may appear relatively lower in attenuation than enhancing liver parenchyma, but their attenuation values are often higher than simple fluid (Fig. 91-6). Yet another type of hepatic injury, contusion, often appears as low-attenuation, sometimes ill-defined areas with intermixed areas of high attenuation representing blood.

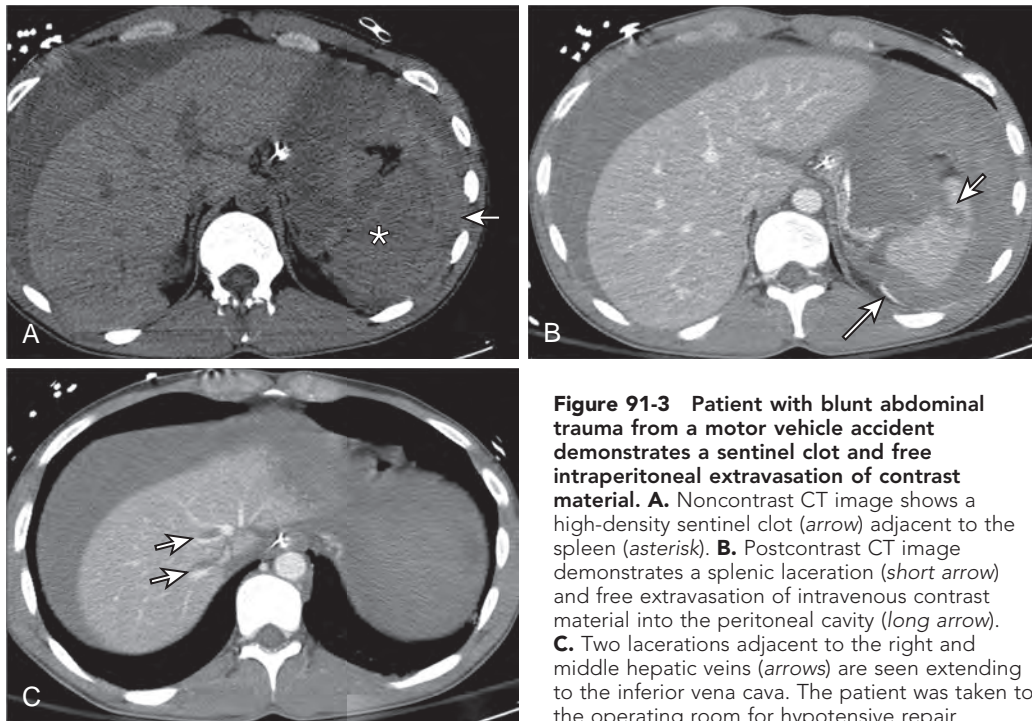


Figure 91-3 Patient with blunt abdominal trauma from a motor vehicle accident demonstrates a sentinel clot and free intraperitoneal extravasation of contrast material. **A.** Noncontrast CT image shows a high-density sentinel clot (arrow) adjacent to the spleen (asterisk). **B.** Postcontrast CT image demonstrates a splenic laceration (short arrow) and free extravasation of intravenous contrast material into the peritoneal cavity (long arrow). **C.** Two lacerations adjacent to the right and middle hepatic veins (arrows) are seen extending to the inferior vena cava. The patient was taken to the operating room for hypotensive repair.

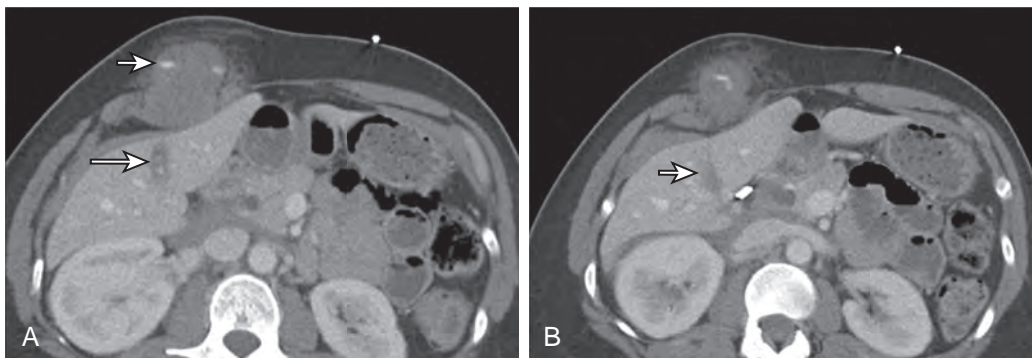


Figure 91-4 Patient with a penetrating injury from a stab wound with a 5-inch steak knife while in the shower. **A.** Within the abdominal wall, a hematoma from the stab wound is seen with a blush of contrast material, suggesting active extravasation (short arrow). A liver laceration is also identified (long arrow). **B.** CT image demonstrates the extent of the laceration through the left lobe of the liver (arrow).

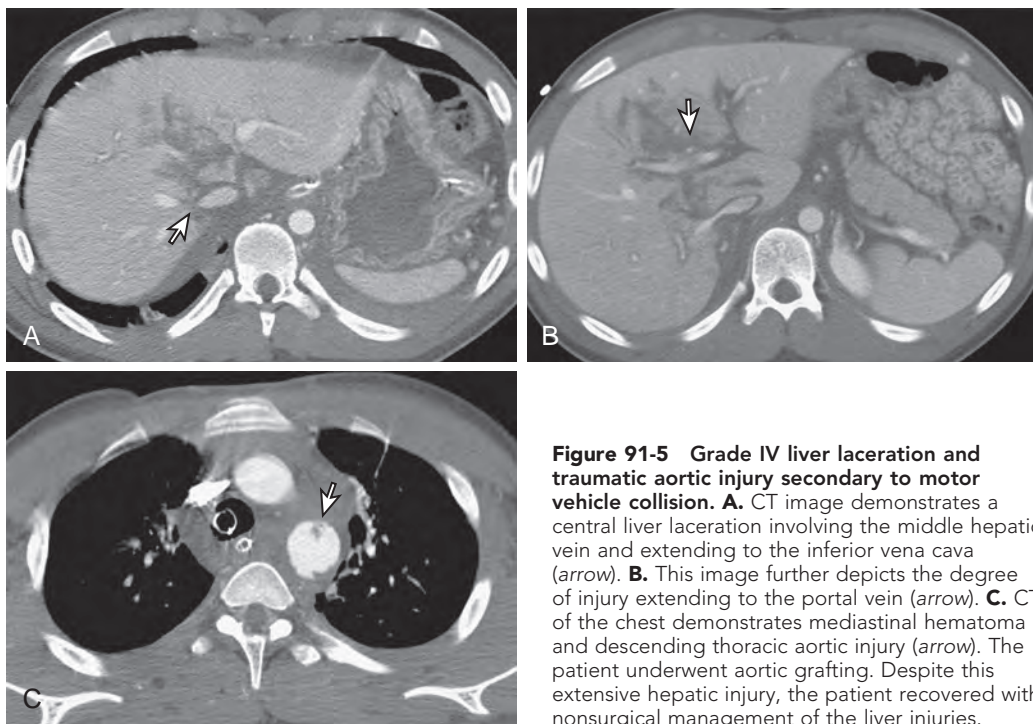


Figure 91-5 Grade IV liver laceration and traumatic aortic injury secondary to motor vehicle collision. **A.** CT image demonstrates a central liver laceration involving the middle hepatic vein and extending to the inferior vena cava (arrow). **B.** This image further depicts the degree of injury extending to the portal vein (arrow). **C.** CT of the chest demonstrates mediastinal hematoma and descending thoracic aortic injury (arrow). The patient underwent aortic grafting. Despite this extensive hepatic injury, the patient recovered with nonsurgical management of the liver injuries.



Figure 91-6 Liver laceration with intraparenchymal hematoma. Contrast-enhanced CT demonstrates a low-density hepatic laceration in the right lobe of the liver with a centrally located high-density collection consistent with an intraparenchymal hematoma (arrow).

Active extravasation on contrast-enhanced CT represents one of the more severe CT features of hepatic injury and can herald life-threatening, active bleeding (Figs. 91-7 and 91-8). On CT, this appears as very high attenuation approximating that of aorta (91–274 HU; mean, 155 HU) compared with the density of clotted blood (28–82 HU; mean, 54 HU).⁶⁰ At times, active extravasation of contrast material may be difficult to distinguish from a pseudoaneurysm. Delayed contrast images are helpful in this instance, demonstrating “washout of contrast attenuation” with pseudoaneurysms (approximating the blood

pool density at that time) and persistence of high density with active bleeding.⁶⁴ Active extravasation of contrast material has been shown to be a strong predictor of potential cardiovascular collapse and failure of nonsurgical management.^{65,66} Treatment of active extravasation is best performed through angiographic embolization.⁶⁷

Vascular injuries of the liver, although relatively rare, can be fatal as well. When these occur, they are usually due to lacerations extending to the inferior vena cava, hepatic veins, and portal veins; thus, it is imperative to identify and to relay this extension to the clinicians (see Fig. 91-3). Alternatively, avulsion of the vessels can occur as well. Inferior vena cava injuries carry a particularly high mortality rate and should be suspected when there is a laceration extending to the proximal hepatic veins and inferior vena cava and when there is a large amount of retrohepatic blood.⁶⁸ If bleeding occurs at the bare area of the liver, there may be extension of blood into the retroperitoneum as well.

Periportal zones of decreased density may be the only manifestation of hepatic trauma. These may represent linear collections of blood in the periportal regions or dilated periportal lymphatics.^{69–71} Periportal low density was previously thought to be an important sign of liver injury but is actually most commonly due to rapid fluid resuscitation, elevating central venous pressure, as suggested by a distended inferior vena cava (Fig. 91-9).^{69–72} Periportal low density may also be seen in nontraumatic causes, including in patients with congestive heart failure, patients with hepatitis, liver transplant recipients, and those with AIDS. The lucency is due to a dilation of the intrahepatic lymphatics caused by obstruction of drainage. Intraparenchymal gas, in the absence of infection, has also been reported in patients with blunt abdominal trauma, but an abscess must always be excluded when extraluminal gas collections are present.^{73,74}

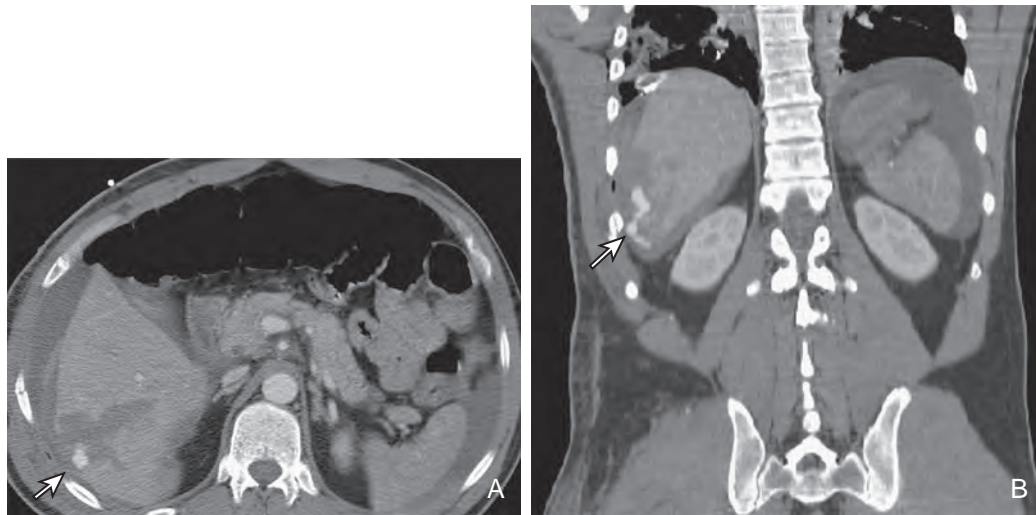


Figure 91-7 Hepatic laceration with active extravasation. **A.** CT shows a low-density laceration in the posterior segment of the right hepatic lobe. Focal hyperdensity consistent with active extravasation of contrast material and active hemorrhage is seen (arrow). **B.** A coronal reformatted image further reveals the extent of active extravasation (arrow). High-density fluid in the peritoneal cavity is consistent with hemoperitoneum.

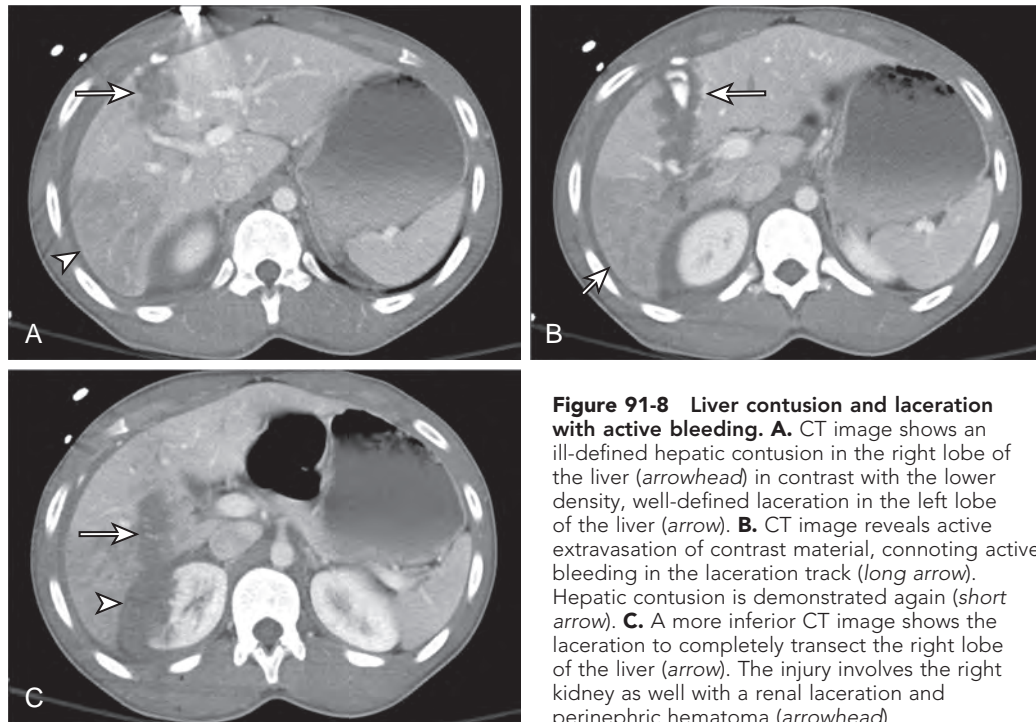


Figure 91-8 Liver contusion and laceration with active bleeding. **A.** CT image shows an ill-defined hepatic contusion in the right lobe of the liver (arrowhead) in contrast with the lower density, well-defined laceration in the left lobe of the liver (arrow). **B.** CT image reveals active extravasation of contrast material, connoting active bleeding in the laceration track (long arrow). Hepatic contusion is demonstrated again (short arrow). **C.** A more inferior CT image shows the laceration to completely transect the right lobe of the liver (arrow). The injury involves the right kidney as well with a renal laceration and perinephric hematoma (arrowhead).

A CT-based classification has been formulated from these findings (Table 91-2). This CT classification system grades the injuries; however, this grading system and the CT features may not correlate with the need for surgery.^{75,76} It is not the grade of the injury but rather the hemodynamic parameters of the patient that often dictate conservative versus operative management decisions.²² Even major hepatic injuries up to and including grade IV can usually be managed conservatively if the patient is hemodynamically stable.^{28-31,63,75} CT findings associated with increased morbidity, mortality, and need for operation include deep perihilar lacerations, failure of the hemoperitoneum to be significantly resorbed within 1 week,

rapid progression of hepatic injuries within hours or days of injury, and major vascular trauma (especially injury to the confluence of hepatic veins).^{13,77} It has been noted that many hemodynamically stable patients can avoid operation despite significant injuries seen on CT examination. Although the CT-based injury grading system may not correlate with the need for surgery, it serves as a consistent means of describing and communicating injuries to surgeons. Radiologists should therefore be familiar with this grading system.

The need for follow-up CT examination to detect delayed complications is favored by some⁷⁸⁻⁸⁰ and opposed by others.^{28,81,82} Patients with persistent or worsening symptoms should have



Figure 91-9 Periportal edema secondary to aggressive hydration in a patient with a stab wound. Periportal lucency extending along both sides of the intrahepatic portal veins indicates periportal edema. This is a nonspecific finding that is most commonly seen with rapid intravenous hydration.

TABLE 91-2 CT-Based Classification of Blunt Hepatic Trauma	
Grade	Criteria
1	Capsular avulsion, superficial laceration(s) <1 cm deep, subcapsular hematoma <1 cm maximal thickness, periportal blood tracking only
2	Laceration(s) 1-3 cm deep, central/subcapsular hematoma(s) 1-3 cm diameter
3	Laceration(s) >3 cm deep, central/subcapsular hematoma(s) >3 cm diameter
4	Massive central/subcapsular hematoma >10 cm, lobar tissue destruction (maceration) or devascularization
5	Bilobar tissue destruction (maceration) or devascularization

From Mirvis SE, Whitley NO, Vainwright JR, et al: Blunt hepatic trauma in adults: CT-based classification and correlation with prognosis and treatment. *Radiology* 171:27–32, 1989.

follow-up examinations.⁸¹ Patients with more severe, complex hepatic injuries may also benefit from repeated CT to evaluate injury status and possible complications.^{9,21,83,84} Meredith and colleagues²⁸ found that hemodynamic stability and lack of peritoneal findings were more predictive than the CT findings of which patients could undergo nonoperative management.

Post-traumatic complications are not uncommon after hepatic injury and are best demonstrated by CT as well.^{78,79} Delayed hemorrhage can occur and can have a high mortality rate. This may be due to several causes, including an expanding injury, a biloma-induced pseudoaneurysm, a misinterpretation of contrast material extravasation on the initial CT scan, and mismanagement of the patient's hemodynamic status (Fig. 91-10).⁸³ This should be suspected if there is a delayed drop in the hematocrit level. Post-traumatic pseudoaneurysms of the hepatic artery and its branches may occur weeks to months after the initial injury. These patients present with delayed hemorrhage and hemobilia (if the pseudoaneurysm decompresses into the biliary system) and should be evaluated with hepatic angiography, at which time the aneurysm can be embolized to

minimize the risk of frank rupture.⁸⁵⁻⁹¹ Bilomas (Fig. 91-11) and intrahepatic and perihepatic abscesses are other major post-traumatic complications. Bilomas are seen in 0.5% to 20% of patients managed nonoperatively.^{8,29,53,92} These fluid collections usually resolve or can be managed successfully by percutaneous drainage.⁹² Aspiration, biliary scintigraphy, or magnetic resonance imaging (MRI) may be necessary for differentiation of these fluid collections.^{35,85} Endoscopic retrograde cholangiopancreatography (ERCP) can identify the bile leak and guide the insertion of a biliary endoprosthesis.

Ultrasound

Ultrasound is being more frequently performed in the emergency department by surgeons, radiologists, and emergency department physicians. The advantages of sonography include portability, ability to rapidly detect intraperitoneal blood, and relative inexpense. Problems include the operator-dependent nature of ultrasound and limitations in demonstrating the extent of injury.

The use of ultrasound was pioneered years ago in the European literature.⁹³ Ultrasound can be used either to identify parenchymal injury directly or to detect intraperitoneal fluid that in the acute setting is presumed to represent hemoperitoneum.^{94,95} Ultrasound is much more accurate in the detection of hemoperitoneum than in the diagnosis of specific parenchymal or hollow viscus injury. The recent interest in ultrasound is primarily in its utility as a rapid screening test for significant injury, the so-called focused abdominal sonogram for trauma (FAST).^{96,97} FAST simply entails sonographic interrogation of sites in which free intraperitoneal fluid most often accumulates: Morison's pouch, the left subphrenic and subsplenic areas, and the pouch of Douglas. It also involves evaluation for the presence of hemopericardium. According to Ma and coworkers,⁹⁸ the suprapubic view is the single view most sensitive for hemoperitoneum (68%), but the sensitivity dramatically increases when multiple views are obtained. The best use of FAST is to triage patients. A hemodynamically stable patient with an abnormal finding on FAST should undergo CT scanning, whereas an unstable patient with an abnormal ultrasound finding should go to surgery emergently. Clinical management in cases with a normal finding on FAST is more nebulous, but at a minimum, those patients should at least be observed for a time.

Multiple studies have been published looking at the accuracy of ultrasound and comparing it with other modalities. In general, ultrasound is relatively sensitive for the detection of free intraperitoneal fluid, but it is far from perfect. There are a wide range of values in the literature for sensitivity (81%-94%), specificity (88%-100%), and accuracy (86%-98%) for free intraperitoneal fluid.⁹⁹⁻¹⁰⁹ This type of variability suggests inconsistent reproducibility of the method. In addition, for these values to be attained, some studies required repetitive sonographic scanning to detect developing fluid. Another confounding factor is that not all blunt abdominal trauma causes free fluid, with false-negative results. In some studies, 26% to 34% of patients with abdominal organ injuries did not have hemoperitoneum.¹⁰⁹⁻¹¹¹ Therefore, although ultrasound is very good in detecting hemoperitoneum, there are false-negative and false-positive findings. Diagnostic peritoneal lavage is a method to detect hemoperitoneum that was used commonly before the advent of ultrasound and CT. Diagnostic peritoneal lavage is known to be more sensitive than ultrasound in the detection of

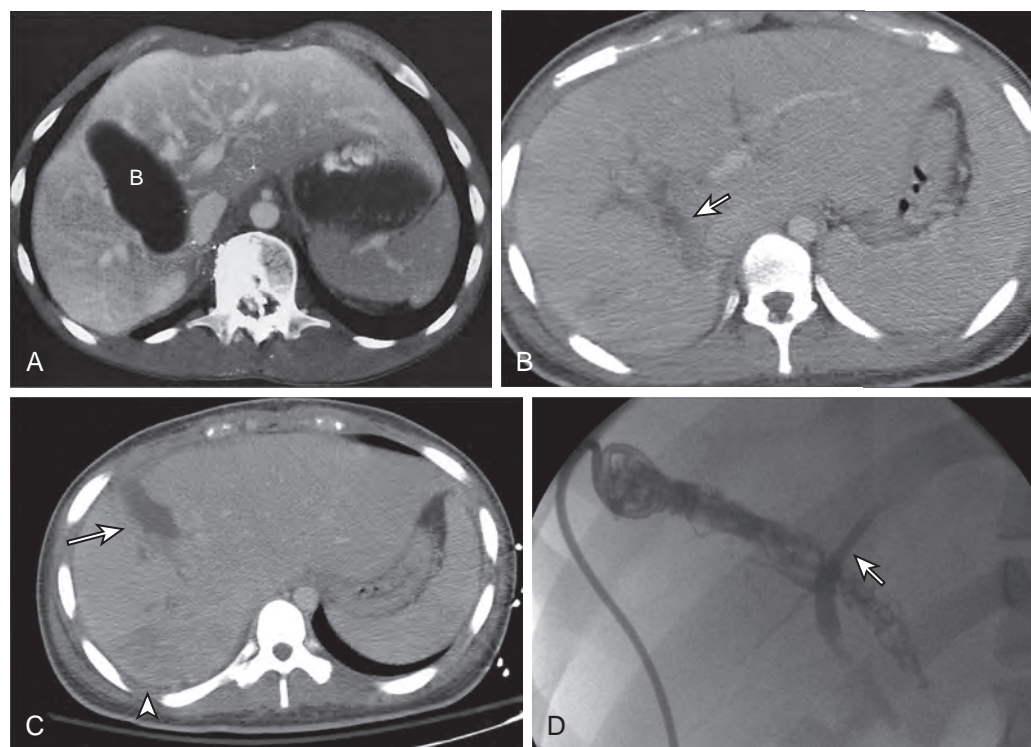
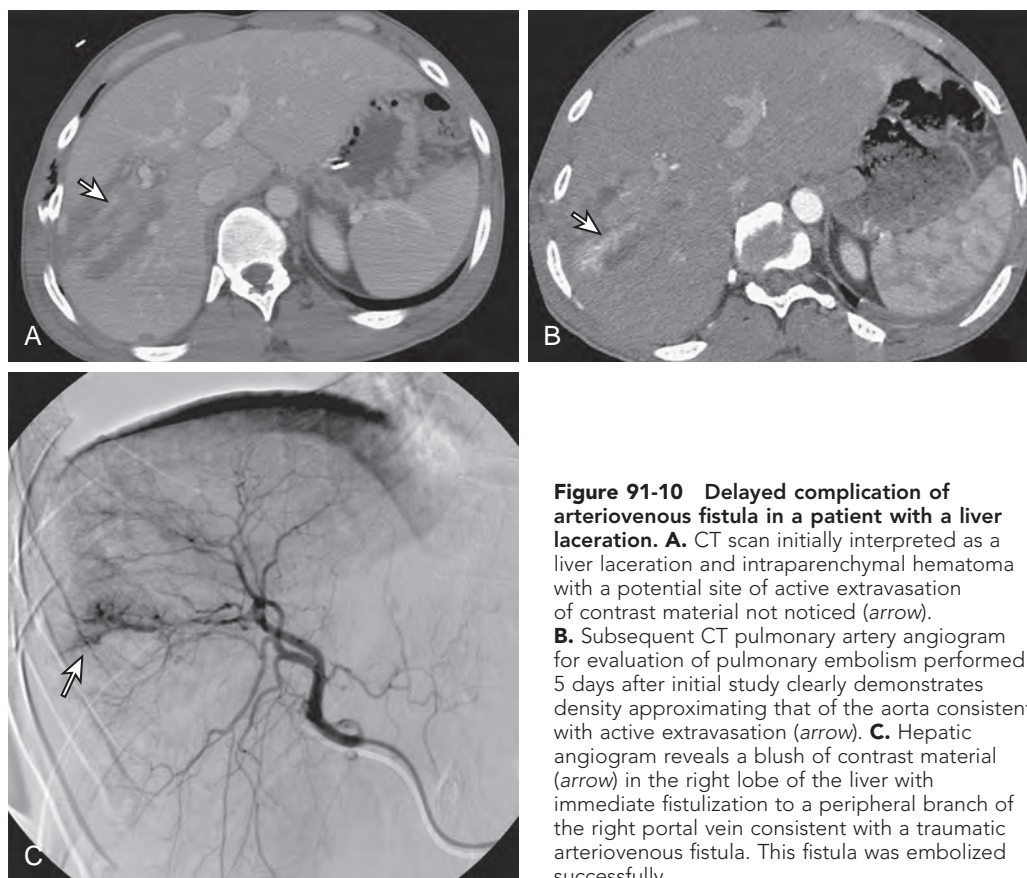


Figure 91-11 Bilomas. **A.** Biloma (B) after a gunshot wound to the liver. The large low-attenuation (5 HU) collection in the liver was aspirated and proved to be a biloma. **B.** Different patient who is status post gunshot wound with a large liver laceration (arrow) that extends posteriorly to involve the right adrenal gland. **C.** CT performed a few days later shows a collection in the right lobe of the liver (arrow). Contusion is also seen (arrowhead). **D.** A drain was placed by interventional radiology and contrast material administered through the tube, demonstrating communication with the biliary tract (arrow) consistent with a biliary injury and biloma.

fluid and injury; however, positive diagnostic peritoneal lavage results led to a 30% rate of nontherapeutic, unnecessary laparotomies.^{23,24} Diagnostic peritoneal lavage has been largely replaced with ultrasound and CT. In addition to the evaluation for hemoperitoneum, ultrasound can be used to detect other injuries. Ultrasound can demonstrate a number of traumatic lesions: subcapsular hematomas, parenchymal tears, contusions, and bilomas. A subcapsular hematoma appears as a lentiform or curvilinear fluid collection with echogenic properties that vary with the age of the lesion (Fig. 91-12). Hematomas are initially anechoic, but as clotting proceeds, they become progressively echogenic by 24 hours. As time passes, the hematoma's echogenicity begins to decrease again.^{112,113} Internal echoes and septations develop within these collections in 1 to 4 weeks. The frequency of the transducer also determines the sonographic characteristics of the hematoma. The complexity and echogenicity of the hematoma can appear greater at higher frequencies as a result of higher spatial resolution.^{5,112-114}

Parenchymal contusions are normally hypoechoic at initial presentation, transiently become hyperechoic, and then become hypoechoic. Lesions that occur posteriorly in the right lobe or over the spine within the left lobe are usually not sonographically demonstrable unless the patient has a slender body habitus.⁸⁹ Parenchymal tears, with or without hematoma, are manifested as irregular defects with abnormal echotexture relative to the surrounding normal tissue. Intraparenchymal hematomas as small as 3.5 mL can be visualized as rounded, echogenic foci.¹¹⁵

Bilomas appear as rounded or ellipsoid, anechoic, loculated structures with sharply defined margins close to the liver and bile ducts.¹¹⁶⁻¹¹⁸ Scintigraphy is an important adjunct in these

cases to show communication of the lesions with the normal biliary tract. Fluid aspiration may be helpful to demonstrate bile.^{119,120} Ultrasound is particularly helpful diagnostically when the collections no longer communicate with the biliary tract. Percutaneous drainage with CT or sonographic guidance may be helpful when fluid collections are symptomatic or infected.

Many studies have evaluated the accuracy of ultrasound for detection of parenchymal hepatic and other solid organ injuries. Sensitivity for detection of all injuries ranges from 43.6% to 93%. This wide range of numbers is due to many factors, including study design, technique, and experience. Papers with very low sensitivities often include small bowel and mesenteric injuries, which are extremely difficult to detect by ultrasound. With respect to liver parenchymal injury specifically, an article by Sato and Yoshii⁹⁹ comparing ultrasound examination with both the clinical outcome and CT revealed a sensitivity for hepatic injury of 87.5% among experts and 46.2% among non-expert sonographers. This suggests that detection of injuries sonographically is more difficult than simply scanning for hemoperitoneum and can be variable. Other pitfalls of ultrasound, however, include limitations in the evaluation of retroperitoneal injuries, diaphragmatic injuries, and hollow viscus perforations.

Some authors have experimented with contrast-enhanced ultrasound in the evaluation of hepatic trauma. These contrast agents use stabilized, encapsulated microbubbles that are small enough to pass through the pulmonary circulation to reach the systemic circulation and ultimately parenchymal tissue. Contrast agents have many potential uses in the heart and vascular system as well as in the detection of focal lesions. In the trauma setting, Catalano and associates¹²¹ have demonstrated that

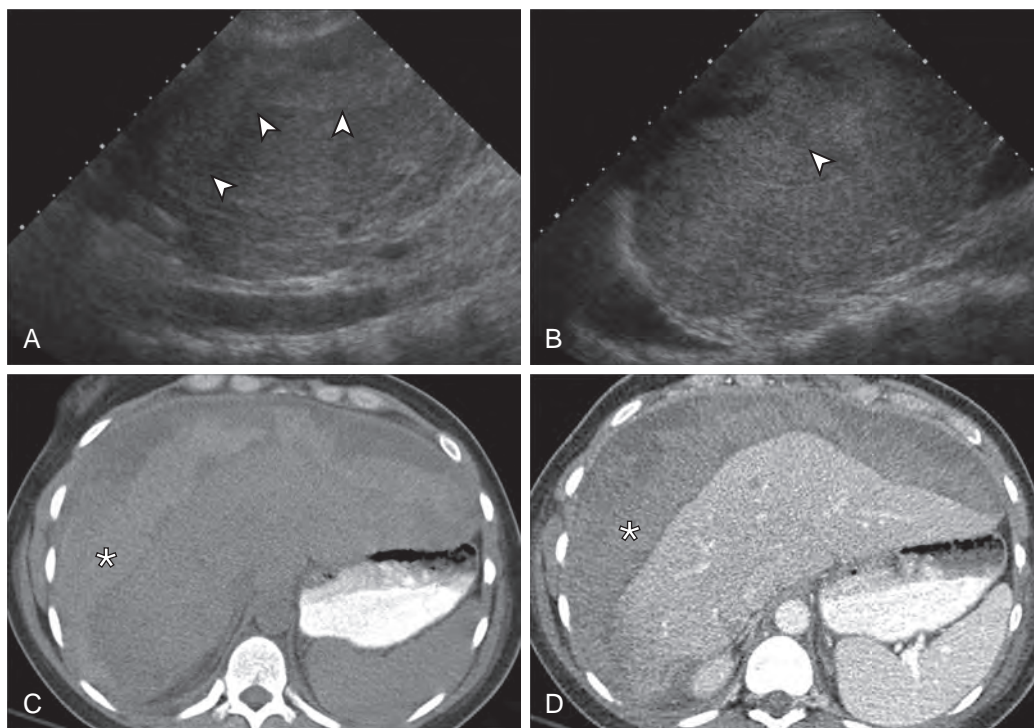


Figure 91-12 Subcapsular hematoma on ultrasound in a pregnant patient with HELLP syndrome. **A.** Extensive subcapsular hematoma is subtly delineated adjacent to the left lobe of the liver on this longitudinal ultrasound scan (arrowheads). **B.** Subcapsular hematoma is also seen adjacent to the right lobe of the liver (arrowhead). **C.** Noncontrast CT shows the corresponding CT appearance of sentinel clot in the subcapsular hematoma (asterisk). **D.** Contrast-enhanced CT also shows the subcapsular hematoma (asterisk).

contrast-enhanced sonography is a promising tool that better depicts hepatic lacerations and hematomas as echo-poor areas against a background of enhanced parenchyma. It also appears to demonstrate the extent of lesions better than conventional sonography.¹²² In addition, it may also have a role in detecting active extravasation of contrast material and therefore active bleeding, which cannot be done with conventional ultrasound. In their study, contrast-enhanced sonography had a higher sensitivity for hepatic injury detection compared with routine ultrasound, 87% versus 65%.¹²¹ This may potentially be a powerful tool in the emergency department setting in the future.

Nuclear Scintigraphy

Bile leaks are rare in blunt hepatic trauma. They more often follow cholecystectomy and partial hepatectomy. Hepatobiliary scans, the most sensitive means of detecting bile leakage, may identify the leak before the onset of clinical symptoms.¹²³ With bile leakage, the tracer may appear as a subcapsular collection or may pool freely in the peritoneal cavity. Parenchymal injuries such as lacerations and hematomas are easily identified on early hepatic phase images.¹²⁰

Magnetic Resonance Imaging

Gadolinium-enhanced MRI can depict complex hepatic injuries in patients with contraindications to iodinated contrast material.¹²⁴ Contrast-enhanced MRI has been shown to demonstrate traumatic hepatic injuries equal to and, occasionally, better than contrast-enhanced CT.¹²⁴ MRI, however, requires a longer imaging time as well as the need to accommodate metallic life support and monitoring equipment, which is more difficult than with CT. In addition, the MR screening process, which is necessary for the safety of the patient, is a timely process that is often not possible in a trauma setting where immediate decisions need to be made. Furthermore, images are compromised by motion to a greater extent than with CT as well as by limited evaluation of the bowel. MRI can help differentiate bilomas from subacute hematomas.¹¹ Despite these limitations, MRI may have a role in imaging of the trauma patient, although its use has not been thoroughly evaluated.¹²⁵ With the advent of gadolinium-based hepatobiliary agents such as gadobenate dimeglumine (MultiHance; Bracco Diagnostics) and gadoxetate (Eovist; Bayer HealthCare), the biliary tree can be evaluated in a functional way.¹²⁶ These hepatobiliary agents have dual excretion through the kidneys and liver. The contrast

agent is taken up by the hepatocytes and excreted through the biliary tree. Approximately 50% of gadoxetate is excreted through the liver, whereas 5% of gadobenate has hepatobiliary excretion. This biliary excretion allows visualization of the bile ducts and any bile leaks or bilomas on T1-weighted MR sequences, on which the gadolinium portion of these agents will cause T1-weighted shortening and increased signal on T1-weighted images. Imaging for the hepatobiliary phase of biliary excretion is done in a delayed fashion after routine images. With Eovist, a delay of approximately 20 to 30 minutes is used; with MultiHance, a delay of 60 minutes is optimal. The few studies performed for the evaluation of bile duct injury have been in iatrogenic injuries after surgery. In this setting, MR has been shown to find and to characterize bilomas with a sensitivity of 80% to 96%.^{127,128} Many other types of biliary abnormalities, including strictures, leaks, obstructions, and anatomic anomalies, can be depicted with these agents (Fig. 91-13). Although it is still a Food and Drug Administration off-label application of these agents, functional biliary imaging with these contrast agents is extremely promising. Apart from identifying biliary injury, MRI may also have a role in follow-up of previously detected hepatic injuries. In severe hepatic injury in which follow-up imaging is warranted, the use of MRI over CT may save a significant radiation dose to often young patients, particularly if multiple follow-up examinations may be needed.

Angiography

Once the mainstay of hepatic trauma diagnosis, angiography is now usually performed to investigate and to treat severe and active hemorrhage, post-traumatic fistulas, and pseudoaneurysms.⁸⁶ Angiography, however, plays a pivotal role in the conservative management of hepatic injury. One of angiography's main roles is to treat active bleeding, which appears as extravasation of contrast material on CT.¹²⁹ In this capacity, angioembolization has a reported efficacy of 83% in controlling bleeding after blunt hepatic injury according to Carrillo and associates.¹³⁰ Numerous other studies have shown even greater success of angioembolization in the control of bleeding, minimizing transfusions and need for surgery.¹³¹⁻¹³⁴ Traumatic pseudoaneurysms, arteriobiliary fistulas, arteriovenous fistulas, and portobiliary fistulas are the major sources of occult or delayed hemorrhage in the traumatized liver. These vascular abnormalities are amenable to transarterial embolization with either

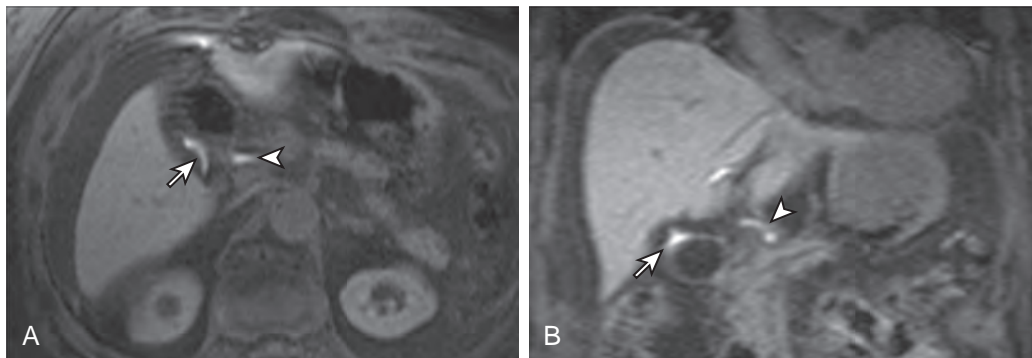


Figure 91-13 Use of MRI in demonstrating biliary leak with Eovist contrast agent. **A.** Axial T1-weighted fat-saturated MR image in the delayed hepatobiliary phase of enhancement reveals excretion of contrast material in the bile duct (arrowhead). A second area of excretion is seen in the gallbladder fossa, which is nonanatomic (arrow). **B.** Coronal T1-weighted fat-saturated image from the same examination shows the biliary excretion into the common bile duct (arrowhead) and the other area of excretion (arrow) that represents a biliary leak.

Gianturco coils or detachable balloons. Gelfoam and Ivalon usually produce only transient hemostasis in patients who have had multiple blood transfusions.^{14,86-92} Transcatheter arterial embolization has been demonstrated to be an effective alternative to surgery in patients with high-grade (Mirvis classification 3 or 4) injuries to the liver and, in one series, was successful in all patients.⁹² Interventional radiologists can manage some of the most lethal venous injuries, including lacerations of the inferior vena cava, with stenting.¹³⁵

Plain Radiographs

Plain radiographic findings are neither sensitive nor specific in patients with hepatic trauma. Nearly 50% of patients with hepatic trauma have fractures of the right lower ribs. When hemoperitoneum is present, there may be loss of the inferior liver-fat interface. Hepatomegaly, irregularity of the liver margin, and caudal displacement of the hepatic flexure all suggest liver injury. Pulmonary contusion, pneumothorax, elevation of the right hemidiaphragm, pleural effusion, hemothorax, and diaphragmatic irregularity frequently accompany hepatic trauma as well.^{4,14,89,136,137}

TREATMENT

Management of blunt abdominal trauma has undergone a complete paradigm shift in the past two decades.^{138,139} Whereas 80% to 90% of injuries were treated operatively in the 1990s, the majority of patients with blunt hepatic trauma and penetrating liver injuries are now managed nonoperatively if they are hemodynamically stable.^{7-9,27,28} As previously stated, it is not the grade of the liver injury but rather the hemodynamic parameters of the patient that determine operative versus conservative management.⁸⁴ Validation of conservative management has been substantiated by lower acute mortality rates and acceptable short-term morbidity and complications relative to exploratory surgery and emergent hepatic resections.^{12,140-142} In patients with American Association for the Surgery of Trauma grade I to grade III liver injuries, the need for surgical exploration after initial resuscitation and observation is usually less than 10% to 20%.^{12,140,141} If patients with grade IV to grade VI injuries can be nonoperatively stabilized, a period of resuscitation and CT imaging may improve the ultimate outcome of emergent surgery by preoperatively defining the extent and location of specific hepatic injuries. Any nonoperative management, however, requires capabilities for close monitoring and operating room availability for potential urgent intervention. Also, adjunctive therapies including embolization by interventional radiology, percutaneous drainage, endoscopy, ERCP, and laparoscopy need to be readily available.¹³⁴

In patients with severe trauma in whom there is massive bleeding, large amounts of devitalized tissue, or massive bile leak and in the clinical scenario of rebleeding, persistent decline of hemoglobin, or failure of embolization, operative intervention is considered.¹⁴³ First, treatment of shock and of head and thoracic injuries has priority; next, abdominal injuries should be addressed.¹⁴⁴ For severe liver injury (grade IV or V), three main surgical principles are control of hemorrhage, drainage of infection, and repair of the biliary system. Bleeding is controlled by specific ligation or direct control of bleeding points; débridement and ligation; hepatic artery ligation; more extensive hepatic resection; tamponade with perihepatic packing; and in

extreme cases of venous avulsion, vena cava occlusion, with or without shunting, or cava resection with graft replacement. Injuries to the hepatic veins are the major cause of immediate death from hepatic trauma and are difficult to repair. In patients who decompensate during surgery, damage control surgery can be done; this consists of perihepatic packing and partial closure of the abdominal incision to allow the patient to go to the intensive care unit for resuscitation and correction of any metabolic derangements and then to return to the operating room when the condition is more stable.²² In patients with extreme uncontrolled bleeding, liver transplantation has been performed in rare cases. Patients with a cerebral intraparenchymal bleed demonstrated on head CT scans are difficult to manage because they may be harmed by the effects of general anesthesia and the fluid shifts that accompany laparotomy, evacuation of hemoperitoneum, and repair of the liver injury.⁷⁷ Operative hemostasis and adequate débridement may be difficult, and hepatic surgery carries the risk of postoperative sepsis.⁷⁹ After operative control of hemorrhage, the liver is drained externally. Finally, biliary injury must be recognized and repaired as it will not heal spontaneously.¹⁴⁵ In patients with penetrating injury, nonoperative management is attempted for stab wounds and low-velocity gunshot wounds in stable patients in the absence of other injuries. If the patient is unstable or has associated bowel injury, surgery is then mandated.²²

COMPLICATIONS

Although the need for surgery is not dependent on the CT grade of injury, the grade of injury and CT findings can prognosticate the chance for the development of complications. Patients with higher grade injuries (grades III-V) are more likely to experience complications. According to Kozar and coworkers, 21% of patients with a grade IV injury and 63% of patients with a grade V injury developed hepatic complications.^{30,138,146} Therefore, with high-grade injuries that undergo nonoperative management, complications should be anticipated, and access to means of treating and monitoring these complications should be readily available.

Bleeding

Bleeding is the most common complication that occurs after trauma.^{29,143} The majority of the time, this can be managed successfully with angioembolization, but rarely surgery is required. Most episodes of bleeding occur early, either on the day of the injury or shortly thereafter. There can be cases of delayed hemorrhage that are due to either delayed rupture of a hematoma or pseudoaneurysm formation. Angioembolization is a vital tool in the management of bleeding at any time during treatment.

Infection

Sepsis and hepatic abscess are serious complications that are far more common with operative than with nonoperative management. Hematomas and bilomas are excellent media for the development of infection. In traumatized patients, bacteria may enter the body through intravenous sites, various indwelling catheters, surgical drains, and other injured areas and by translocation from the gastrointestinal tract.^{63,80} In patients with a suspected intra-abdominal source of sepsis, all intrahepatic or perihepatic fluid collections seen on imaging studies should be viewed with suspicion as a source of infection.⁶³

Biliary Tract Complications

Intrahepatic or extrahepatic biliary tract complications, including biliary leaks, biloma, and bile peritonitis, are being detected with increasing frequency in patients with hepatic trauma because of the increased sensitivity of cross-sectional imaging and hepatobiliary scintigraphy.^{35,63,112,116,118} These lesions may take days to weeks to become manifested clinically owing to the slow rate of leakage from the injured bile duct. Most bilomas are asymptomatic and detected by imaging. CT scans and sonography demonstrate nonspecific fluid collections. Most often, bilomas and bile duct injury can be adequately treated by percutaneous drainage or ERCP stenting, but in rare cases, surgery may be needed.¹³⁸

Hepatic Surgery

Hepatic surgery has been likened to an exercise in hemostasis.^{147,148} No bloodless planes exist, as the liver's complex inflow

and outflow tracts course at right angles. The liver parenchyma is also friable and soft and has few landmarks.¹⁴⁹ These factors had hindered the evolution of hepatic surgery to such a degree that before the 1950s, segmental hepatectomy was reserved almost exclusively for trauma.¹⁴⁹ With advances in surgical techniques and anesthesia and a better understanding of internal vascular anatomy (Fig. 91-14) and hepatic physiology, partial hepatectomy has become a safe and accepted mode of therapy for selected patients with primary and metastatic liver tumors as well as certain benign disorders (Table 91-3).¹⁵⁰⁻¹⁵⁴

Two major principles are fundamental to planning of hepatic resection.¹⁵⁵⁻¹⁵⁸ First, there must be a sufficient amount of hepatic parenchyma to sustain life after surgery. The liver possesses a remarkable capacity to regenerate itself; up to 80% can be safely removed in many patients. Regeneration of liver volume is an efficient, progressive process that in animal studies requires approximately 4 months after an 80% to 85% resection.^{155,157} Coexisting hepatocellular diseases such as cirrhosis decrease the amount of hepatic reserve so much that some

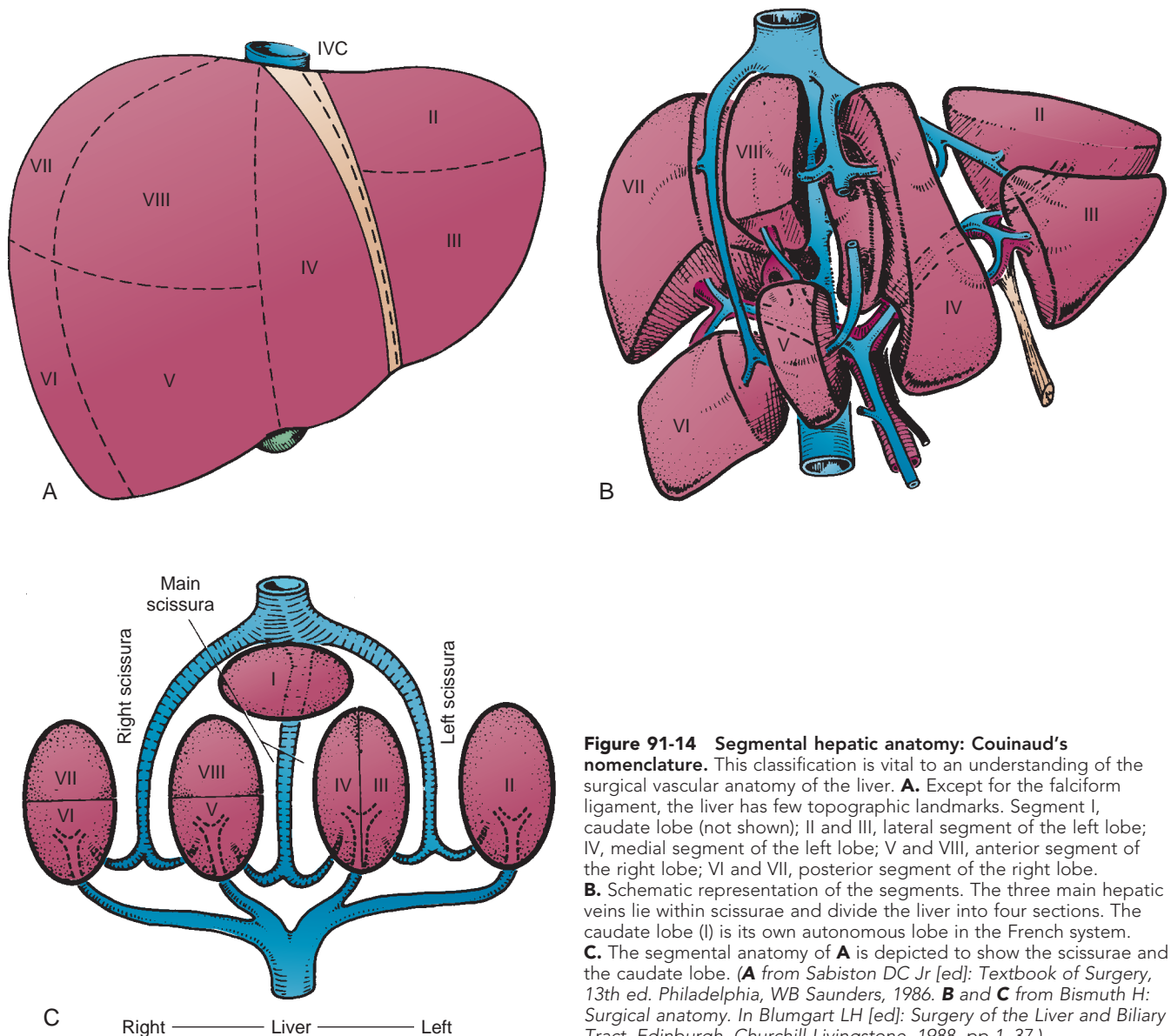


Figure 91-14 Segmental hepatic anatomy: Couinaud's nomenclature. This classification is vital to an understanding of the surgical vascular anatomy of the liver. **A.** Except for the falciform ligament, the liver has few topographic landmarks. Segment I, caudate lobe (not shown); II and III, lateral segment of the left lobe; IV, medial segment of the left lobe; V and VIII, anterior segment of the right lobe; VI and VII, posterior segment of the right lobe. **B.** Schematic representation of the segments. The three main hepatic veins lie within scissurae and divide the liver into four sections. The caudate lobe (I) is its own autonomous lobe in the French system. **C.** The segmental anatomy of **A** is depicted to show the scissurae and the caudate lobe. (**A** from Sabiston DC Jr [ed]: *Textbook of Surgery*, 13th ed. Philadelphia, WB Saunders, 1986. **B** and **C** from Bismuth H: *Surgical anatomy*. In Blumgart LH [ed]: *Surgery of the Liver and Biliary Tract*. Edinburgh, Churchill Livingstone, 1988, pp 1–37.)

TABLE 91-3 Indications for Hepatic Resection

Indication	Frequency (%)
Metastatic tumor	60
Primary malignant neoplasm	15
Undiagnosed mass	8
Benign tumor or cyst	7
Trauma	5
Localized biliary abnormality	3
Infection	2

Modified from Meyers WC, Jones RS: *Textbook of Liver and Biliary Surgery*. Philadelphia, JB Lippincott, 1990, pp 391–402.

patients are unable to tolerate removal of any tissue. Indeed, total hepatectomy and liver transplantation may be the best way to treat patients with small hepatomas or severe cirrhosis.¹⁵⁹⁻¹⁶¹

The second major principle of hepatic resection is preservation of blood supply to the liver tissue left in situ. Adherence to this principle is difficult because the vascular supply is not apparent to the surgeon on inspection of the hepatic surface. In addition, hepatic veins and arteries do not lie in parallel courses, as they generally do in other organs.

RADIOLOGY IN SURGICAL PLANNING

Imaging studies play an important role in identifying the extent of disease that is important for prognosis and therapy. For example, the number and size of hepatic metastases from colorectal neoplasms and extrahepatic involvement determine long-term survival in patients with hepatic resection.¹⁶²⁻¹⁶⁴ The radiologist can help the surgeon adhere to these principles by providing the following information before hepatic resection^{155,157,164-167}:

- Anatomic location of the lesion in relationship to the portal and hepatic veins, fissures, coronary and falciform ligaments, and fissure for the ligamentum venosum
- Presence of vascular invasion of the hepatic vessels by a neoplasm
- Bland or tumor thrombus in portal and hepatic veins distant from the lesion of interest
- Involvement and patency of the inferior vena cava
- Spread of tumor into adjacent structures (e.g., diaphragm, colon, duodenum, lymph nodes)
- Confirmation to the maximal extent possible that the lobe of liver to remain in situ is free of tumor

Preoperative studies should include a chest radiograph and chest CT scan to exclude extrahepatic metastases. MDCT or MRI of the liver and the remainder of the abdomen should also be obtained. Removal of multiple liver metastases is possible in some patients.

A common anomaly, the replaced right hepatic artery arising from the superior mesenteric artery, is important for the surgeon to appreciate preoperatively. Other vascular and biliary variations should be noted as well. The placement of a hepatic artery infusion catheter for chemotherapy may require CT arterial portography to better demonstrate the arterial anatomy and lesions; however, the quality of CT and MRI has improved to such a degree that CT arterial portography is less commonly performed. Because aberrant vessels may course laterally and

more posteriorly in the porta hepatis, dissection of the porta hepatis may be modified if an anatomic anomaly is noted preoperatively.¹⁶⁸

INTRAOPERATIVE ULTRASOUND

Intraoperative ultrasound of the liver can function as both a diagnostic and a therapeutic tool. As a diagnostic aid, intraoperative ultrasound has proved successful for the following indications: to detect small (1-5 cm), nonpalpable, parenchymal liver lesions not detected by preoperative imaging studies; to precisely define the topography of liver tumors and their relationship to the vessels, allowing segmental resections to be performed; to guide intraoperative biopsy or ablative treatments of impalpable lesions; and to differentiate liver neoplasms from certain benign lesions, such as cysts and hemangiomas¹⁶⁹⁻¹⁷⁵ (Figs. 91-15 and 91-16). Several studies have documented the utility of this technique, particularly with its initial use. In the study of Conlon and coworkers,¹⁷⁶ the information provided by intraoperative ultrasound changed the preoperative surgical plan in 18% of patients and provided additional useful information not available preoperatively in 47%, including detection of subcentimeter lesions, lesion characterization, and anatomy of hepatic vasculature. In another study, the sensitivity of intraoperative ultrasound for lesion depiction was 94.3% compared with 86.7% for MRI. However, in this study, in only 4% of the patients did intraoperative ultrasound alter surgical management secondary to additional lesion detection.¹⁷⁷ Another study demonstrated intraoperative ultrasound to change surgical management in only 7% of patients.¹⁷⁸ Wagnetz and colleagues¹⁷⁹ compared intraoperative ultrasound with 1.5T MRI and 64-MDCT and found that the sensitivity of ultrasound for lesion detection was 95.1% compared with 96.8% for MDCT and 94.4% for MRI. Furthermore, MDCT and MRI had a slightly higher negative predictive value than intraoperative ultrasound for identifying disease-free segments in the liver. In only 2.7% of cases was management changed after intraoperative ultrasound. An article by Mui and associates evaluating intraoperative sonography in detection of liver metastases in pancreatic adenocarcinoma found that ultrasound changed management in only 1% of cases. In comparison to initial studies, these more recent studies demonstrate a decreased percentage of cases in which intraoperative ultrasound alters surgical management. This is thought to be partly attributed to technologic advances in preoperative studies such as MRI, resulting in improved selection of patients.¹⁷⁸

Recent interest has arisen in the use of intraoperative contrast-enhanced ultrasound for liver lesion detection, citing increased lesion detection rates relative to noncontrast ultrasound and CT.^{180,181} Despite somewhat conflicting data, intraoperative ultrasound continues to be an important component of hepatic resection for purposes of lesion localization and relationship to hepatic vasculature and biliary structures, segmental localization, and further evaluation for incompletely characterized subcentimeter lesions identified on preoperative imaging studies. Intraoperative ultrasound also helps detect occult extension of hepatic tumors into vascular structures and assists in intraoperative biopsy of liver lesions.¹⁷⁷ Intraoperative ultrasound has also proved useful in guiding intraoperative cryotherapy and radiofrequency ablation in the treatment of liver tumors.¹⁸²⁻¹⁸⁴



Figure 91-15 Utility of intraoperative ultrasound in a patient with rectal cancer and concern for a liver metastasis. **A.** Axial postcontrast CT image reveals a small low-attenuation lesion (arrow) that was new from the prior CT examination and interpreted as suspicious for metastasis, given its interval development. **B** and **C.** Intraoperative ultrasound reveals the questioned lesion on CT to represent a cyst (arrows).

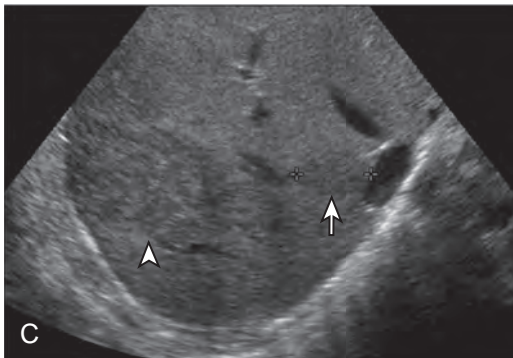
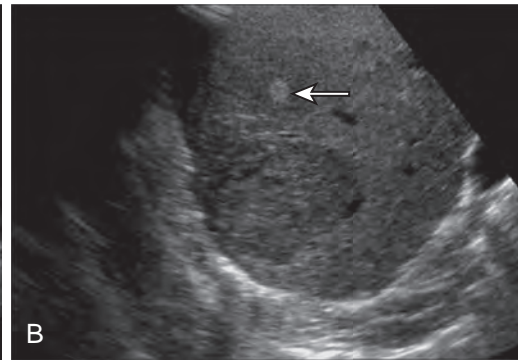
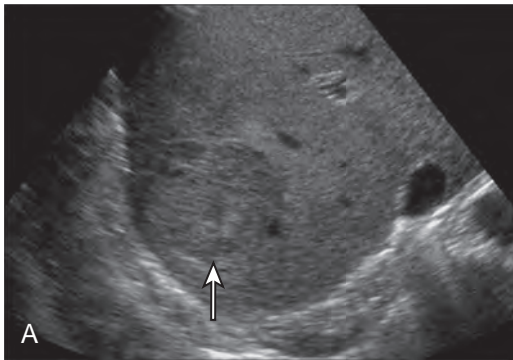
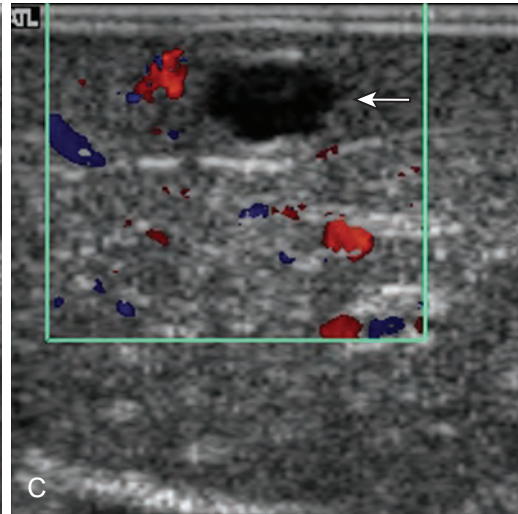


Figure 91-16 Use of intraoperative ultrasound in detecting more lesions in a 36-year-old woman with a hepatic lesion thought to represent an adenoma but with symptoms of pain. **A.** Intraoperative ultrasound reveals the large hypoechoic mass (arrow). **B.** An echogenic lesion characteristic of a hemangioma was also seen (arrow). **C.** An additional unsuspected small hypoechoic mass was also identified (arrow). The dominant lesion is again seen (arrowhead). The hypoechoic lesions were resected and found to represent hepatic adenomas removed because of the patient's symptoms.

INDICATIONS

As surgical techniques become safer, the indications for hepatic surgery are broadening (see Table 91-3).

Benign Lesions

The indications for resection of a benign tumor or cyst include risk of rupture or hemorrhage, symptoms, risk of malignant transformation, and enlargement of the mass so that it is causing pressure on bile ducts, the liver capsule, or adjacent organs. Fenestration-resection is rarely required for cosmetic or symptomatic improvement in patients with adult polycystic liver disease.^{185,186}

Localized biliary abnormalities, such as hepatolithiasis and segmental Caroli's disease, are other indications for resection. Hepatic abscesses that do not respond to medication or percutaneous drainage may also require surgical resection.

Malignant Lesions

Resection of liver metastases is the most common indication for partial hepatectomy in the United States. Liver metastases are an enormous clinical problem in view of the fact that approximately 25% of all malignant neoplasms eventually spread to the liver (Table 91-4). It is the most common site of blood-borne metastasis and more often than not is a major contributor to the patient's demise.¹⁸⁷ Neoplasms grow five to seven times faster in the liver than in most other organs.¹⁶⁶ This is precisely why untreated liver metastases augur such poor survival. Colorectal metastasis is the most commonly resected hepatic tumor in the United States. Five-year survival rates of 25% to 40% for solitary metastases confined to one lobe have been reported.^{178,182-184} In a recent meta-analysis, the overall median survival for all colorectal metastases resected was 3.6 years.¹⁸⁸ Hepatoma is the most commonly resected tumor worldwide owing to its prevalence in portions of the Far East and Africa. Technical improvements in hepatic resection and earlier diagnosis have increased the resectability rates. Patient selection is paramount in the success of hepatic resection for hepatocellular carcinoma. In fact, according to the Barcelona Clinic Liver Cancer group staging system, which has been integrated into the American Association for the Study of the Liver guidelines, hepatic resection has a marginal role in the treatment of hepatocellular carcinoma and is indicated in patients with early-stage hepatocellular carcinoma.¹⁸⁹ Early-stage hepatoma is defined by the Milan criteria,¹⁹⁰ normal clinical performance status, and preserved liver function. Liver resection in such

patients (as well as higher stage) yields favorable 3- and 5-year survival rates of 78% and 39%.^{191,192}

Hepatic Resection for Liver Metastases

With the knowledge that patients with limited metastatic disease may benefit from liver resection, there has been a marked increase in the number of hepatic resections performed during the 1980s and 1990s.

Advances in the techniques of liver resection and extensive preoperative evaluation with careful patient selection have reduced operative mortality rates to less than 5%.¹⁹³⁻²⁰² This improvement in operative morbidity and mortality is attributed to several different factors. Our improved understanding of the segmental anatomy of the liver and specifically of its intrahepatic blood supply has made for safer hepatic resections with minimized blood loss. In addition, improved preoperative diagnostic imaging has excluded patients from operation in whom the operative risks due to major vascular involvement would have resulted in major complications. Resection techniques including vascular inflow occlusion, minimized parenchymal destruction, decreased intraoperative blood loss, and successful management of postoperative complications have improved the safety of this operation. As a result, the operative morbidity and mortality associated with hepatic surgery have significantly decreased, with most current studies reporting operative mortality rates between 2% and 7%.¹⁹³⁻²⁰²

Improved long-term results after hepatic resection are due not only to decreased perioperative mortality and morbidity but also to an improved understanding of the biology of liver metastases and thus the selection criteria for surgery.

Selection of Patients for Resection

If we accept that certain patients with limited hepatic disease will benefit from surgical resection, then careful analysis of the survivors will allow us to identify specific prognostic factors useful in selecting appropriate patients for resection. Much of our knowledge regarding prognostic variables affecting patient outcome after hepatic resection is derived from the collected data of the registry of hepatic metastases by Hughes and associates.¹⁹⁸ This retrospective series analyzed 862 patients from multiple institutions who had undergone hepatic resection for metastatic colorectal cancer. In addition to data from the registry of hepatic metastases, other single-institution reviews have helped identify prognostic features related to the patient, primary tumor characteristics, and features of the liver metastases.

Patient characteristics not thought to influence survival include gender and age of the patient. Currently, a patient's physiologic performance status rather than chronologic age or gender is the major determinant excluding the patient from consideration for resection. Patients with poor hepatic function due to advanced cirrhosis are also considered poor candidates for liver resection.²⁰²

A number of prognostic factors related to the tumor can affect survival of the patient.¹⁸⁸ The *stage and histologic grade of the primary tumor* are thought to be important prognostic factors. In the Hughes registry, patients presenting with regional lymph node metastases (stage III) had a 5-year survival rate of 23% compared with 47% for patients without regional lymph node involvement (stage II).¹⁹⁸ In addition, other retrospective studies have suggested that patients with poorly differentiated, high-grade primary tumors have a shorter survival benefit after

TABLE 91-4 Incidence of Liver Metastases at Autopsy

Primary Tumor	Percentage with Liver Metastases
Pancreas	56
Colon	53
Breast	50
Melanoma	44
Stomach	42
Lung	30
Esophagus	24
Kidney	13
Prostate	70

From Foster JH: *Surgical treatment of metastatic liver tumors. Hepatogastroenterology* 37:182-187, 1990.

resection of liver metastases.²⁰³ Finally, patients with primary tumors originating in the rectum may derive less benefit from resection of hepatic metastases. None of these primary tumor characteristics should exclude a patient from consideration for surgical resection; however, they do identify patients who will be at increased risk for hepatic or extrahepatic recurrence.

The most important prognostic factors determining survival after hepatic resection appear to be those related to the *features and characteristics of the liver metastases*. These were examined in detail in the Hughes registry and by other institutional series.¹⁸⁸ Fong and colleagues²⁰⁴ have analyzed and summarized these characteristics thoroughly in their review of the literature. Although controversy exists as to the influence of tumor size, disease-free interval, and number of metastases on survival, most authorities agree that the ability to achieve a pathologic-negative margin of resection and the absence of extrahepatic metastases are clearly the most important survival determinants.²⁰⁵ Some studies have shown that patients with large (>5 cm) metastases appear to have a worse prognosis than patients with smaller tumors. Survival benefit has been seen in resection of these large lesions predicated on the ability to achieve tumor-free margins of resection. Thus, size in and of itself does not preclude resection but may make the ability to achieve free vascular or parenchymal margins problematic. Similarly, it was previously thought that patients with multiple metastases should not undergo liver resection. In their review, Fong and colleagues²⁰⁴ suggested that patients with three or fewer liver metastases may have a survival advantage compared with patients undergoing resection of four or more metastatic deposits. Survival differences between patients undergoing resection of a solitary metastasis and those with two or three lesions is not as clear-cut. Similar to the argument regarding tumor size, the actual number of liver metastases does not appear to be the major factor limiting resection; however, as the number of metastatic deposits within the liver increases, the ability to achieve a margin-negative resection becomes impaired, as does the ability to preserve enough normally functioning liver.^{198,202}

Because of these concerns, the location and distribution of multiple lesions and the extent of liver resection have been examined as prognostic variables. In the Hughes registry, the distribution of metastases comparing unilobar versus bilobar disease was not thought to be a significant predictor of survival. This has become an important factor with the advances in nonanatomic liver resections. With a greater understanding of hepatic segmental anatomy, more limited liver resections are now being performed. This allows a reduction in the amount of normal liver resected as well as resection of disease from both lobes. In treatment of lesions less than 4 cm in diameter, no differences in survival are seen between more limited segmental resections and formal hepatic lobectomies. Formal lobectomy may be required to obtain tumor-free margins in patients with large tumors. In patients with smaller tumors undergoing segmental resection, no difference in survival has been seen as long as clear pathologic margins are obtained.¹⁹³⁻²⁰²

The time interval between resection of the primary cancer and appearance of liver metastases seems to be a significant variable for survival. The 5-year survival rate for patients presenting with synchronous liver metastases was 27% in the Hughes registry.¹⁹⁸ Similarly, patients developing liver metastases within 12 months after resection of the primary colorectal cancer had a 5-year survival rate of 31%. This difference was

not significant. However, in patients developing hepatic metastases at an interval longer than 12 months, the 5-year survival rate after resection was 42%. This difference was significant and may reflect a biologically less aggressive tumor. Despite the adverse impact on survival, patients with otherwise resectable synchronous lesions should be considered for surgery.²⁰³

Another important variable affecting prognosis is the presence or absence of extrahepatic metastatic disease. Patients with celiac or hepatic lymph node metastases should not be considered for hepatic resection. The presence of such nodal disease is an indicator of systemic dissemination. Hughes and associates reported no 5-year survivors in 24 patients undergoing liver resection who were found to have positive intra-abdominal lymph node metastases.¹⁹⁸ More controversial is the role of resection of non-nodal extrahepatic metastases. Usually, this is thought to mean isolated pulmonary disease in the face of limited hepatic metastases. Although the number of patients who present with such limited pulmonary and hepatic metastases is small, there may be a role for resection in highly selected patients who demonstrate slow disease progression. In general, the presence of extrahepatic visceral metastases is a contraindication to liver resection. Despite our improved understanding of the prognostic variables related to long-term survival after liver resection, still the majority of patients will ultimately succumb to metastatic cancer. Most retrospective series demonstrate 5-year survival rates between 20% and 40% after resection for hepatic colorectal metastases.¹⁹³⁻²⁰⁴ Kanas's meta-analysis of numerous studies found 3-, 5-, and 10-year survival rates to be 57.5%, 38%, and 20%, respectively.¹⁸⁸

TYPES OF HEPATIC RESECTION

Wedge Excision

Wedge excision, the simplest hepatic resection, consists of non-anatomic removal of a small amount of superficial tissue. It is considered nonanatomic because the tissue does not correspond to any hepatic segment or subsegment.¹⁶⁸ The benefit of wedge resection is that it provides hepatic sparing, which is particularly important in patients who have decreased hepatic reserve.²⁰⁶

Subsegmentectomy

Subsegmentectomy is often difficult to perform because of the difficulty of exposure and vascular variability. For example, a solitary lesion in the caudate lobe is usually resected by removal of the medial and lateral segments of the left lobe to gain access to the lesion.^{168,203}

Right Hepatic Lobectomy

In this procedure (Figs. 91-17 and 91-18), the liver is mobilized, a cholecystectomy is performed, and the right branches of the bile duct, hepatic artery, and portal vein are dissected, ligated, and divided while avoiding injury to branches of the left lobe. The surgical plane is lateral to the middle hepatic vein, which must be left intact to provide drainage for the medial segment of the left lobe.^{168,207}

Right Trisegmentectomy

The entire right lobe and medial segment of the left lobe are removed by hilar dissection with ligation and division of the right lobe vessels plus the vessels to the medial segment. The right and middle hepatic veins are removed in this resection.

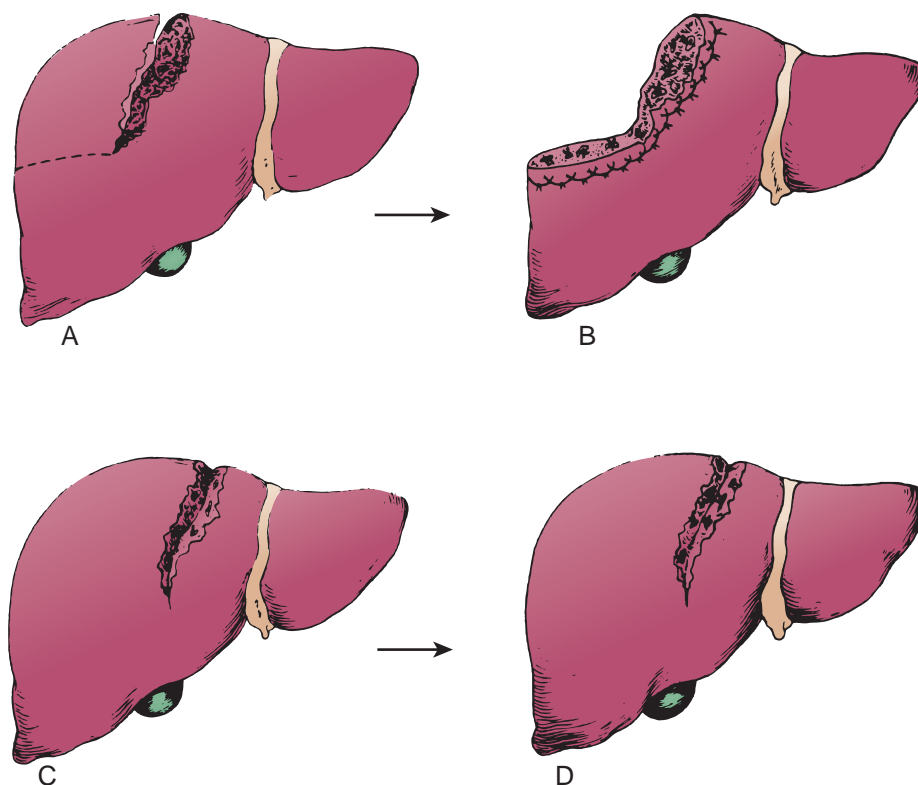


Figure 91-17 Traumatic hepatic injuries: types and treatment. **A.** Blunt injury in which a large defect involves the full thickness of the dome of the liver. **B.** This is treated by resectional débridement and individual vessel ligation. A less severe injury (**C**) requires only control of individual bleeders (**D**). (**A-D** from Madding GF, Kennedy PA: *Trauma to the Liver*, 2nd ed. Philadelphia, WB Saunders, 1971.)

The line of resection is just to the right of the falciform ligament, ensuring that the ascending portion of the portal vein is preserved. This extensive resection, although relatively safe for younger patients, should be used with caution in patients older than 65 years as the associated operative mortality rate is 30.7%.¹⁶⁰

Left Hepatic Lobectomy

During left hepatic lobectomy, the left lobar branches of the hepatic artery are ligated and divided in the hilum. The left hepatic veins are usually resected as well. The caudate lobe may be removed along with the left lobe or left in place. The surgical plane is just to the left of the middle hepatic vein, which must remain intact to drain the anterior segment of the right lobe.^{168,208}

Left Lateral Segmentectomy

This procedure is technically easier than the other forms of hepatic resection because hilar dissection is usually not needed. The surgical plane is just to the left of the umbilical fissure, so that the ascending portion of the portal vein is left intact. Much of the left hepatic vein can be resected because the medial segment of the left lobe is drained by the middle hepatic vein.

Left Trisegmentectomy

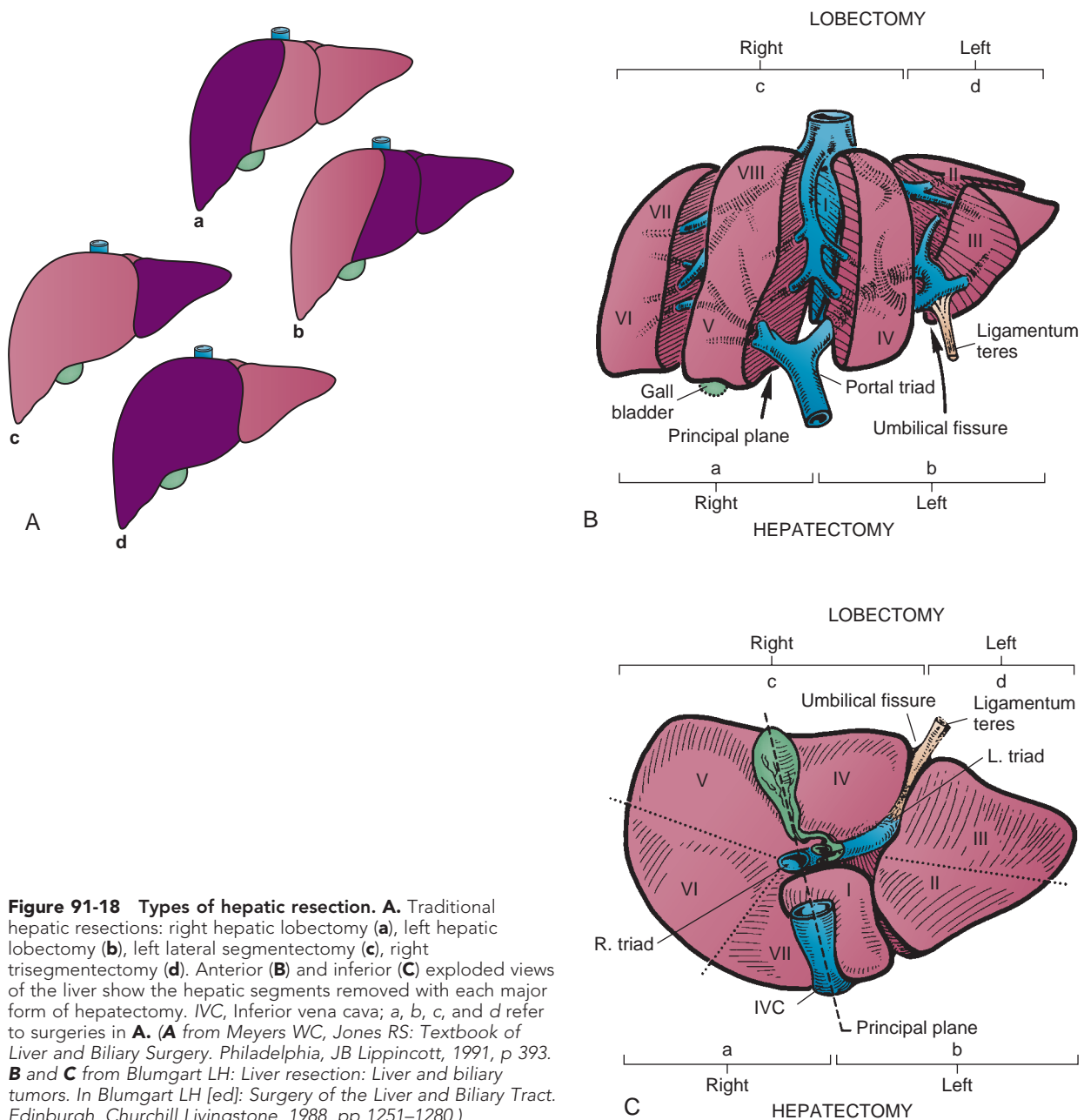
Left trisegmentectomy is a technically difficult procedure in which both segments of the left lobe and the anterior segment of the right lobe are resected. The right hepatic vein needs to be preserved to drain the remaining posterior segment.

Right Posterior Segmentectomy

This procedure is also technically difficult. The posterior segment of the right lobe is resected, leaving the right hepatic vein intact to drain the anterior segment.²⁰⁹

Minimally Invasive Hepatic Resection

The first laparoscopic procedure was performed 25 years ago. For years, laparoscopy in the abdomen was confined to cholecystectomy, but its role has greatly expanded thanks to technological advances, and it can now be used for numerous indications. The use of minimally invasive surgery in the liver has also soared. Minimally invasive surgery in the liver includes pure laparoscopic resection, hand-assisted laparoscopic resection, laparoscopy-assisted open resection (hybrid), and most recently robotic surgery. There are now numerous studies that have validated the use of laparoscopy in benign and malignant liver resections.²¹⁰⁻²¹⁴ Laparoscopically assisted resections generally result in lower operative times, less blood loss and less transfusion requirement, decreased length of stay in the hospital, and decrease in overall operative complications and recurrence of local malignant disease. Robotic surgery is the newest of the minimally invasive techniques and may be the most promising, allowing surgeons to compensate for inherent limitation of conventional laparoscopy by providing better ergonomics, visibility, and more articulating arms. Initial results demonstrate its feasibility in resection of benign and malignant hepatic lesions; however, further study is needed to validate outcomes relative to conventional laparoscopy as well as long-term oncologic follow-up outcomes.^{215,216}



Liver-Directed Therapy

Although hepatic resection and liver transplantation have good 5-year survival rates, more than 80% of patients are not surgical candidates and are deemed unresectable.²¹⁷ Liver-directed therapies offer viable treatment options for these patients. The most commonly used techniques currently are cryoablation, radiofrequency ablation, and intra-arterial therapies, including transarterial chemoembolization and radioembolization.

CRYOSURGERY

Cryosurgery refers to the in situ destruction of liver tumors by precise and rapid cooling of the tumor and a zone of normal hepatic parenchyma to extreme subzero temperatures. By circulation of a coolant such as liquid nitrogen through the core

of the tumor, temperatures as low as 100°C can be achieved. The effect of such profound hypothermia on tissue results in both indirect and direct mechanisms of cell destruction. Details of the lethal effects of cryosurgery have been well described by Ravikumar and colleagues²¹⁸ but essentially involve the formation of intracellular ice crystals leading to protein denaturation and rupture of cell membranes. Indirectly, subzero temperatures result in microvascular thrombosis and tissue anoxia. Further damage occurs if the cells are allowed to slowly thaw and are then rapidly refrozen. Clinical studies have suggested that two such freeze-thaw cycles may be necessary for optimal tissue destruction. Fundamental to the implementation of cryosurgery as a viable treatment option for patients with unresectable liver metastases has been the development of intraoperative ultrasound and refinement of equipment used to deliver the coolant to the tumor.

Early reports demonstrated the feasibility and safety of treating liver metastases by cryosurgery, whereas follow-up series have now helped define the indications for this modality.²¹⁸ The most significant clinical limitation of surgical resection is usually the number of lesions that can be safely removed while sparing sufficient hepatic parenchyma to avoid postoperative liver failure. Thus, the major indications for cryosurgery are either primary or metastatic lesions that are not amenable to resection because of cirrhosis or bilobar involvement in which either the number of lesions or the location of the tumors would risk sufficient postoperative hepatic function after resection.²¹⁸ For colorectal metastases, most centers with sufficient cryosurgical experience will limit this technique to patients with six or fewer metastases (generally <40% of the liver volume) and tumors smaller than 6 to 8 cm in greatest diameter and avoid large central tumors near the hilum of the liver. Similar to other forms of liver-directed therapy, cryosurgery probably offers little advantage to patients with extrahepatic metastatic disease. Operative technique currently involves intraoperative ultrasound localization and monitoring of the cryoprobe placement into the tumor.²¹⁹ In addition, intraoperative ultrasound allows detection of tumors not recognized on preoperative scans and is essential for monitoring of the freeze margins of the ice ball. The cryoprobes are vacuum-insulated devices that circulate supercooled liquid nitrogen through the probe's tip. A 3-mm blunt-tipped probe creates a freeze zone up to 4 cm, and the 8-mm trocar point probe creates a freeze zone of up to 6 cm. A single probe or combination of probes can be used to achieve complete freezing of the tumor and an additional 1 cm beyond the margin to ensure complete cryoablation. The entire process of probe introduction, freeze-thaw cycles, and probe extraction is monitored with real-time intraoperative ultrasound. Major complication rates are reportedly between 10% and 20%, and mortality rates are less than 2%.²¹⁸⁻²²⁰ Complications may

include hemorrhage, biliary fistula, hepatic or subphrenic abscess, and, more rarely, hepatic failure, coagulopathy, and cardiac arrest.²¹⁹⁻²²¹ Disease-free survival rates and patterns of failure have now been reported from several centers. With median follow-up times between 18 and 36 months, most series report 5-year actuarial disease-free survival rates between 15% and 28%.^{219,220}

RADIOFREQUENCY ABLATION

Radiofrequency ablation (RFA) refers to the direct thermal (heat) application (>80°C) to tumors with the intent of achieving cellular kill. The mechanisms of action of RFA include tissue heating, protein denaturation, release of water vapor, mechanical tissue destruction, breakdown of cellular membranes, and vascular thrombosis.²²³

Several studies have been performed demonstrating the effectiveness of RFA in achieving local tissue destruction, and it is now an accepted means of liver-directed therapy in those patients who have been excluded from surgical resection.^{222,224} The limitation continues to be disease progression at the margin of the ablated zone as well as outside the treatment field.^{225,226}

RFA can be accomplished by percutaneous, laparoscopic, or intraoperative means. Intraoperative ultrasound is an essential tool in the live identification of lesions intraoperatively that might not have been seen by standard cross-sectional imaging techniques. Indications for RFA include primary and metastatic liver tumors, renal tumors, osteoid osteoma, painful bone metastases, and lung tumors as well as adjunct to surgery in cases of surgical debulking for neuroendocrine tumors. Complications include bleeding, pneumothorax, biliary and vascular injury, and track seeding^{223,227,228} (Figs. 91-19 and 91-20).

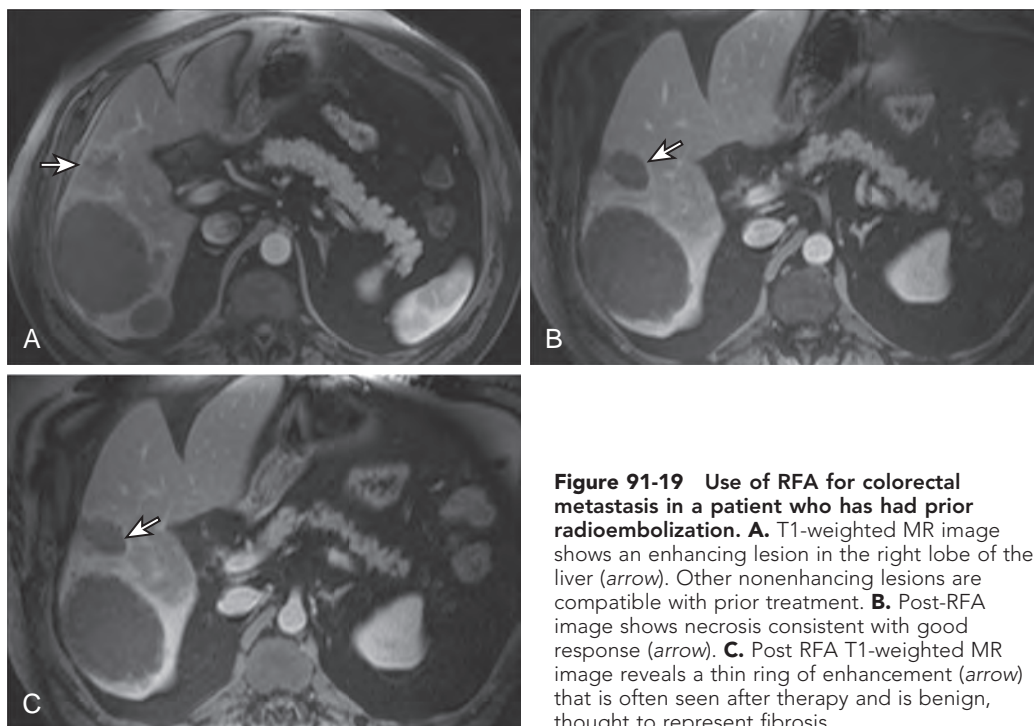


Figure 91-19 Use of RFA for colorectal metastasis in a patient who has had prior radioembolization. A. T1-weighted MR image shows an enhancing lesion in the right lobe of the liver (arrow). Other nonenhancing lesions are compatible with prior treatment. **B.** Post-RFA image shows necrosis consistent with good response (arrow). **C.** Post RFA T1-weighted MR image reveals a thin ring of enhancement (arrow) that is often seen after therapy and is benign, thought to represent fibrosis.

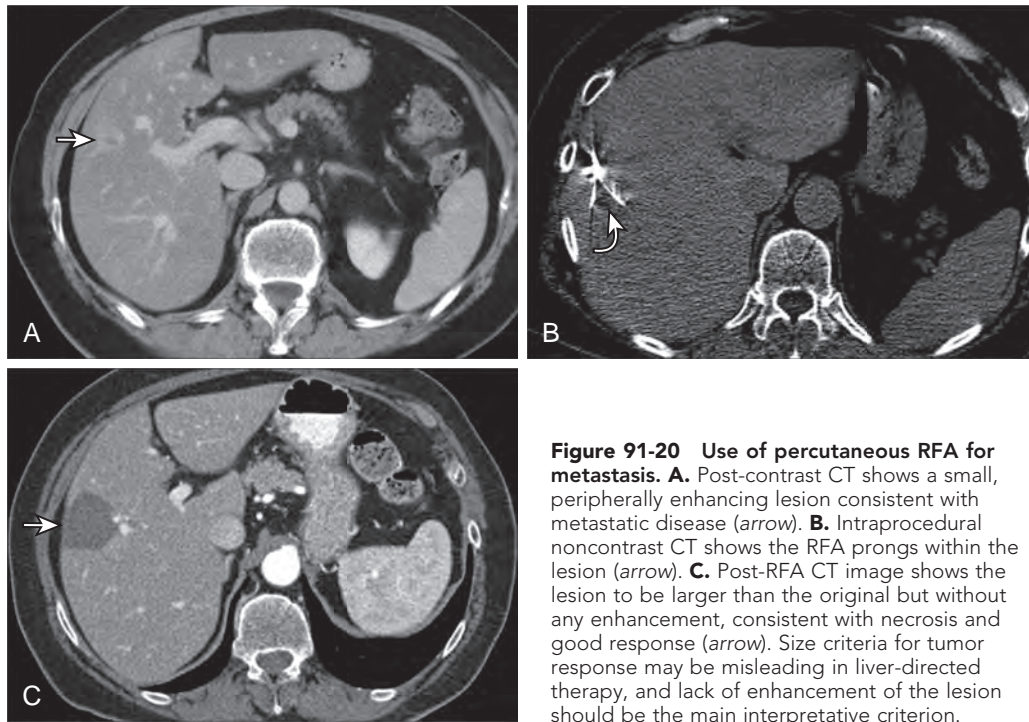


Figure 91-20 Use of percutaneous RFA for metastasis. **A.** Post-contrast CT shows a small, peripherally enhancing lesion consistent with metastatic disease (arrow). **B.** Intraprocedural noncontrast CT shows the RFA prongs within the lesion (arrow). **C.** Post-RFA CT image shows the lesion to be larger than the original but without any enhancement, consistent with necrosis and good response (arrow). Size criteria for tumor response may be misleading in liver-directed therapy, and lack of enhancement of the lesion should be the main interpretative criterion.

CHEMOEMBOLIZATION

Chemoembolization exploits the preferential blood supply provided by the hepatic artery to neoplastic lesions.²²⁹⁻²³¹ Initial attempts at ligation of the hepatic artery resulted in temporary regression of hepatic tumors. The effect was transient because of the rapid development of collateral vessels distal to the ligated vessels.²³² Chemoembolization is performed by placing a catheter into the hepatic artery, followed by concomitant local delivery of chemotherapy and a vascular occlusion agent. The dual injection results in theoretical benefits above those obtained with either procedure alone. In addition to the ischemic damage created by the embolization agent, the vascular occlusion results in more confined and prolonged exposure of the chemotherapeutic agent.^{233,234} Anoxic damage also causes increased vascular permeability with increased infiltration of the tumor with chemotherapy.²³³ Finally, cytotoxic irritation of the vessel may result in an irritant vasculitis, leading to further occlusion and ischemia.²³³ Although there is increased local toxicity with the combination of treatments, systemic toxicity is minimized by drug metabolism during first passage through the liver.²³⁵ Clinical trials have demonstrated significant and sustained responses to chemoembolization in the treatment of unresectable primary hepatomas, metastatic colorectal cancers, and neuroendocrine tumors. In 2002, two landmark publications demonstrated the survival advantage incurred by chemoembolization in patients with intermediate-stage hepatoma. These papers helped establish chemoembolization as the worldwide “gold standard” for treatment of hepatoma.^{236,237} In 2006, Takayasu and colleagues²³⁸ published data from 8510 hepatoma patients treated with chemoembolization and found 1-, 3-, 5-, and 7-year survival rates of 82%, 47%, 26%, and 16%. In summary, the mechanisms of action of chemoembolization include application of chemotherapy directly into the tumor bed and reduction of the blood

supply to the tumor. These have the additive effect of increasing chemotherapeutic concentration within the applied area, increasing dwell time, and reducing systemic toxicity.

Embolization is accomplished by use of a viscous liquid, such as Lipiodol,²³⁹⁻²⁴⁶ or particulate matter, such as Ivalon polyvinyl particles,^{247,248} collagen particles,^{249,250} starch microspheres,²⁵¹⁻²⁵⁵ or steel coils.²⁵⁶ Although some of these agents have special properties, they have not been directly compared. Lipiodol, for example, has been shown to be taken up preferentially by hepatocellular carcinoma tumor cells. Chemotherapeutic agents that have been used for this procedure include 5-fluorouracil, floxuridine, mitomycin C, cisplatin, and doxorubicin. The independent relative effectiveness of these agents has not been determined.

Complications of chemoembolization include postembolization syndrome (pain, nausea, fever), elevated liver function test results, liver infarction, abscess formation, cholecystitis, renal and cardiac failure, and death. The likelihood of hepatic infarction is particularly elevated in patients undergoing chemoembolization in the presence of portal vein thrombosis. Hepatic abscess formation is of particular concern in patients with an incompetent ampulla of Vater (e.g., biliary stents) or in patients with a hepaticocenterostomy.^{257,258}

Conventional radiologic techniques may actually not be adequate to assess response to therapy. Although changes that are consistent with liquefaction necrosis may be seen up to 1 month after chemoembolization, maximal decrease in tumor volume is obtained with scans performed 2 to 3 months after the procedure.²⁵⁰ Carcinoembryonic antigen and α -fetoprotein measurements for colorectal cancers and hepatoma may be used for clinical follow-up.

The goals of chemoembolization are to improve symptom control and to increase disease-free and overall survival. Chemoembolization in conjunction with systemic chemotherapy

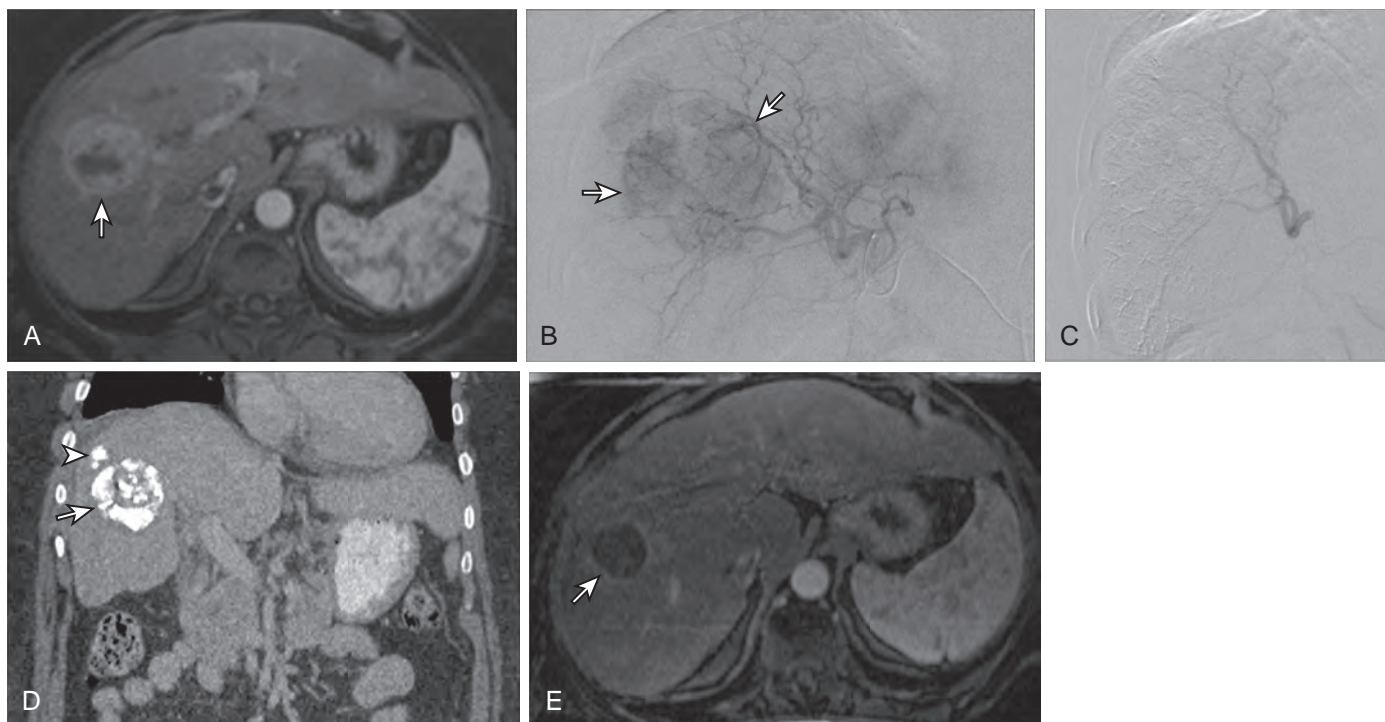


Figure 91-21 Use of chemoembolization in hepatic metastases. **A.** T1-weighted fat-saturated postcontrast MR image reveals an enhancing lesion in the right lobe of the liver (arrow). **B** and **C.** Intraprocedural angiogram reveals tumor blush in two lesions that is then obliterated after embolization (arrows). **D.** CT scan shows high-density material that is typically seen after chemoembolization, representing Lipiodol (arrow, arrowhead) in the dominant and smaller satellite lesions. This should not be confused with enhancement. **E.** Postcontrast T1-weighted fat-saturated MR image shows lack of enhancement consistent with tumor necrosis (arrow).

may yield better results than either modality alone. Clinical parameters that predict response to treatment and survival, such as tumor vascularity and extent of liver involvement, can be used to select patients most likely to benefit from regional chemotherapy. Earlier detection and referral of patients with low-volume hepatic disease may improve outcome (Fig. 91-21).

COMBINATION CHEMOEMBOLIZATION AND RADIOFREQUENCY ABLATION

Given the effectiveness of chemoembolization and RFA as single therapeutic modalities, there has been recent interest in combining the two in an attempt to further improve efficacy. The theory of applying both in combination is analogous to the surgical Pringle maneuver: impairing blood flow to tumor (chemoembolization) with the simultaneous application of ablative heat (RFA). Results combining these therapies have been promising, with recurrence-free time of 12.5 months, more than 70% improvement in tumor markers, and complete necrosis in more than 90% of tumors.²⁵⁹

RADIOEMBOLIZATION

Radioembolization represents a newer transarterial therapy for liver malignant neoplasms. It is defined as the intra-arterial administration of radiation by an embolization vehicle. This technology capitalizes on the fact that hepatic tumors derive their blood supply from the hepatic artery rather than from the portal vein. Hence, radioembolization allows the administration of microscopic radiation particles to be delivered

preferentially to the tumor with concomitant embolization of the feeding artery.²⁶⁰

Although there have been some preliminary case reports on the use of rhenium and holmium microspheres, the most common radioembolic microsphere clinically in use is yttrium 90. Yttrium 90 is a beta emitter with a half-life of 64.2 hours. The microspheres are carried by glass or resin as the embolic carrier and range between 20 and 60 μm . They are preferentially carried by hypervascularity to tumor, where they exert their local radiation effect. This technique of radioembolization allows the administration of high absorbed doses to hepatic tissue (>200–300 Gy). This dose would not be tolerated well systemically, but the transarterial administration allows this level of radiation. The microspheres are selectively administered by percutaneous access to the hepatic artery on a whole liver, lobar, segmental, or subsegmental level.^{261–263} The use of yttrium 90 microspheres has been studied in primary and secondary metastatic tumors to the liver. With hepatoma, radioembolization has been shown to be safe and effective and, as well, to permit downstaging to resection and liver transplantation. Survival in patients with hepatoma is reported to be approximately 700 days for Okuda stage I patients. In patients with metastatic disease to the liver, survival rates range between 7 and 10 months in patients who have failed to respond to standard of care polychemotherapies.^{263–271} Sato and colleagues²⁷² studied radioembolization in patients with unresectable chemorefractory liver metastases who had few treatment options left and found that 87% of lesions demonstrated a halting or reversal of progression. Salem and coworkers²⁷³ published their experience with 463 patients with hepatocellular

carcinoma and found that compared with chemoembolization, radioembolization resulted in longer time to progression and less toxicity. These promising data are quickly making radioembolization the liver-directed therapy of choice in some institutions (Fig. 91-22).

POSTOPERATIVE RADIOLOGIC APPEARANCE OF THE LIVER

CT and MRI are the preferred means of postoperative evaluation of the liver.²⁷⁴ The appearance of the postoperative liver depends on what segment is resected, what operation is performed, the degree of hepatic regeneration, and the

presence and nature of postoperative complications. Baseline postoperative scans are essential for future evaluation of recurrent hepatic malignant disease.²⁷⁴

After resection of the right lobe, hypertrophy of the left lobe occurs with displacement of the ligamentum teres and falciform ligament to the right (Fig. 91-23). The caudate lobe also modestly enlarges, with the portal vein displaced posteriorly, so that the porta hepatis is exposed dorsally to the anterior aspect of the right renal fascia. Other common findings include migration of the colon and the small bowel into the hepatic fossa, elevation of the right kidney, posterior displacement of the inferior vena cava, and elliptical enlargement of the remaining liver.²⁷⁵

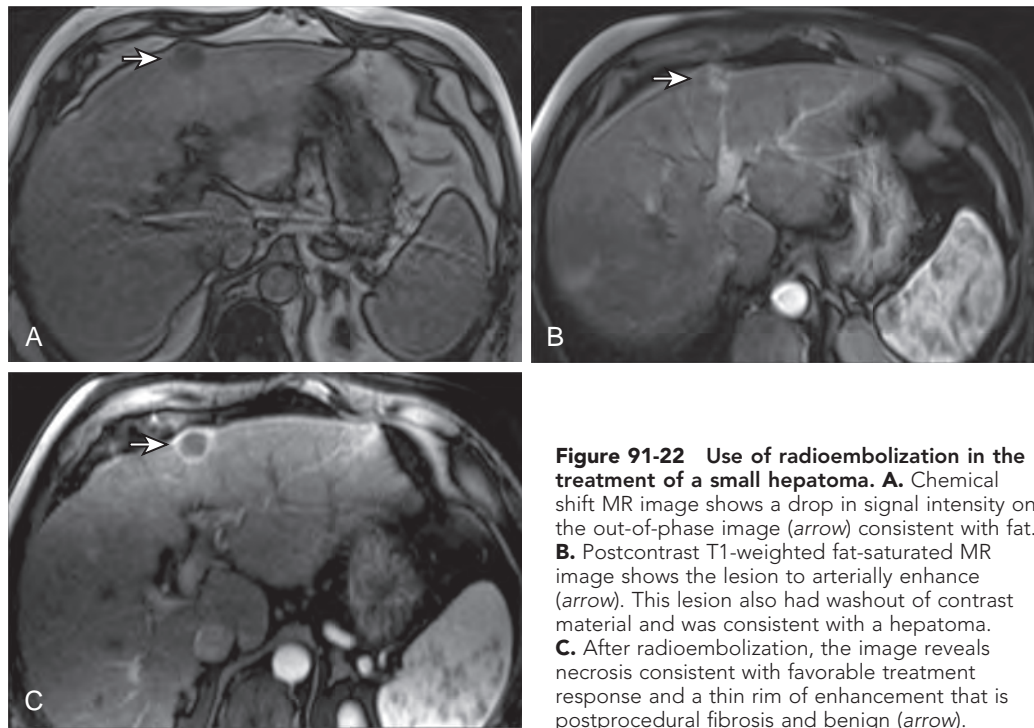


Figure 91-22 Use of radioembolization in the treatment of a small hepatoma. **A.** Chemical shift MR image shows a drop in signal intensity on the out-of-phase image (arrow) consistent with fat. **B.** Postcontrast T1-weighted fat-saturated MR image shows the lesion to arterially enhance (arrow). This lesion also had washout of contrast material and was consistent with a hepatoma. **C.** After radioembolization, the image reveals necrosis consistent with favorable treatment response and a thin rim of enhancement that is postprocedural fibrosis and benign (arrow).

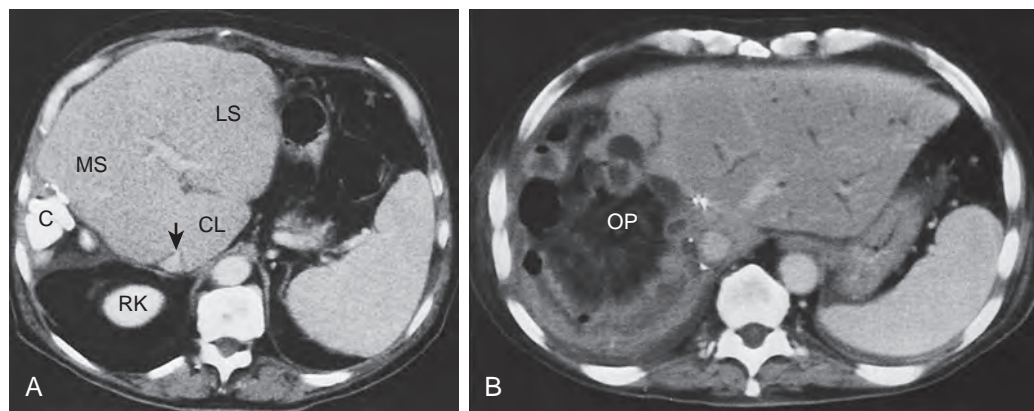


Figure 91-23 Postoperative liver: CT findings. **A.** Typical CT appearance after right hepatic lobectomy. There is hypertrophy of the medial segment (MS) and lateral segment (LS) of the left lobe and caudate lobe (CL). Elevation of the right kidney (RK), posterior displacement of the inferior vena cava (arrow), and migration of colon (C) into the hepatic fossa are seen. **B.** This patient had a trisegmentectomy with construction of a greater omental pack (OP) along the lateral aspect of the remaining lateral segment of the lobe. The patient developed a recurrent tumor, accounting for the intrahepatic biliary dilation.

After left lobectomy, the right lobe enlarges in a rounded shape, with displacement of the porta hepatis and portal vein to the left and inferior displacement of the right kidney. The stomach or colon occupies the left hepatic fossa.²⁷⁵

Partial hepatectomy is often accompanied by a small region of low attenuation near the plane of dissection, which is due to fatty infiltration, fibrous tissue, and hepatocytes laden with bile pigment, presumably representing the sequelae of local trauma.²⁷⁴⁻²⁷⁶ These changes are transient and must be differentiated from abscess and hematoma. Hypertrophy of the hepatic parenchyma can be seen on CT scans as a progressive change in contour of the hepatic parenchyma during a period of 6 months to 1 year.²⁷⁵

The greater omentum is often swung up to the operative site to provide natural “packing” material that helps diminish the frequency of postoperative complications (see Fig. 91-23). The fat in the omentum can simulate a low-density mass lesion, so knowledge of the operative technique is useful in its identification.²⁷⁷ In the early postoperative period, there can be transient fluid that accumulates between the omental pack and the resection margin. This fluid contours with the liver margin and can be differentiated from a focal collection such as a biloma or abscess.²⁷⁴ MR can be particularly useful when CT is limited by streak artifacts caused by surgical clips or is contraindicated because of inability to intravenously administer iodinated contrast material. Regenerated liver has the same signal intensity as normal liver. Diffuse inhomogeneity of the hepatic parenchymal signal can be seen after chemotherapy and may be related to fatty infiltration or vascular damage. These irregular, ill-defined areas are in contrast to recurrent tumor, which generally has more sharply margined regions of high signal intensity on T2-weighted images.²⁷⁸ MR may be helpful in differentiating postoperative hematoma from other focal fluid collections on the basis of the signal intensity of methemoglobin.²⁷⁹

Most hepatic regeneration occurs within 6 months, but the process may take more than 1 year.

Complications

Complications resulting from hepatic surgery are similar to those of other major abdominal operations: abscess, hemorrhage and hematoma, and pleural effusions.²⁸⁰ Biloma and hematoma are fairly common owing to the nature of the surgery and the biliary and vascular structures transected. Surgical complications occur in 25% to 30% of hepatic operations and are best diagnosed and nonoperatively treated with CT.^{274,281,282} Hepatobiliary scintigraphy (Fig. 91-24) and Doppler ultrasound may be needed to help clarify biliary and vascular complications.

POSTPROCEDURAL RADIOLOGIC APPEARANCE OF THE LIVER

Imaging of the liver after liver-directed therapy is critical in assessing response to treatment. This imaging is best performed with either CT or MRI. The normal post-therapy appearance of the liver can be confusing. An understanding of the appearance of hepatic tumors treated with liver-directed therapies is crucial in differentiating normal postprocedural changes from residual and recurrent tumor.

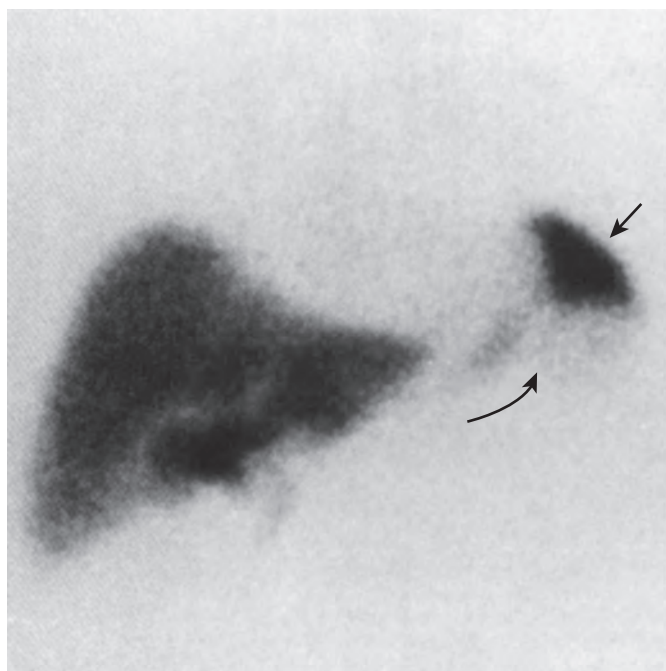


Figure 91-24 Postsurgical bile leak. Bile leak followed focal excision of a hepatic mass in the left lobe. This diisopropyliminodiacetic acid-enhanced hepatobiliary scan shows leakage of bile-containing isotope (curved arrow) that extends into the left subphrenic space (straight arrow).

The conventional means of assessing tumor response by a size decrease according to the World Health Organization or RECIST (Response Evaluation Criteria in Solid Tumors) assessment often does not accurately predict response. Although, with time, the lesions treated with liver-directed therapies decrease in size on early post-therapy scans, there is often an increase in size that should not be construed as progressive disease.²⁸³⁻²⁸⁵ It is the intermediately timed post-therapy scans performed at 2 to 3 months that often begin to show the greatest reduction in tumor volume.²⁸³⁻²⁸⁵ The hallmark of positive response to chemoembolization, radiofrequency ablation, and any of the liver-directed therapies is loss of enhancement on postcontrast imaging. This absence of enhancement correlates with tumor necrosis and can be seen on imaging shortly after therapy (less than 1 month). At times, a thin, peripheral rim of enhancement may be visualized normally, which does not represent residual tumor but is likely to relate to inflammatory or fibrotic response. Areas of nodular peripheral enhancement or a thick rim of enhancement in a treated lesion should be viewed as suspicious for residual or recurrent malignant disease.²⁸⁶ In fact, the modified RECIST criteria incorporate assessment of residual viable tumor by measurement of the longest diameter of only the enhancing part of the tumor, not the necrotic portion.²⁸⁷ In addition, global enhancement assessment of the entire lesion should be performed to determine if there is significant enhancement. As enhancement is one of the main determinants of tumor response, it is important to perform contrast-enhanced CT or MR examinations with precontrast imaging in patients who have undergone chemoembolization. On the precontrast images, the lesion often has high density. This should not be

confused with calcification but actually represents the density of the chemoembolization agents (see Fig. 91-21D). Without precontrast images, this finding could potentially be confused with contrast enhancement. In addition, chemoembolization can cause changes in the adjacent normal liver parenchyma, resulting in low-attenuation regions corresponding to areas of ischemia or infarction.²⁸⁸

The appearance of the liver after cryosurgery can vary slightly from the appearance with other therapies. Here, because the freeze zone is often larger than the original lesion, the resultant post-therapy low-attenuation lesion is often significantly larger. These lesions can appear rounded, oval, or wedge shaped. They can contain foci of air and hemorrhage as well. As in the other liver-directed therapies, a thin peripheral rim of enhancement may be seen.²⁸⁹

The newest liver-directed therapy, radiotherapy with yttrium 90 microspheres, can cause some unique post-procedural imaging changes.²⁹⁰ As with the other therapies, the lack of enhancement reflects the positive response consistent with tumor necrosis (Fig. 91-25). The lesion may initially be unchanged in size or perhaps even slightly increased, but lesion volume usually decreases on subsequent imaging. Again, lack of enhancement suggesting necrosis is the hallmark of positive response, but this can occur more slowly with radioembolization than with other techniques. In this scenario, diffusion-weighted MRI can sometimes predict a favorable response before the visualization of necrosis on imaging²⁹¹ (Fig. 91-26). Whereas solid tumors demonstrate increased cellularity and restricted diffusion, treated lesions contain necrotic tissue with

compromised cell membrane integrity and decreased cellularity. This will result in less diffusion restriction and can predate the loss of enhancement and necrosis seen on MR. Thus, diffusion-weighted MR can sometimes predict a favorable response before the hallmark of necrosis on MR, which can be an invaluable tool in the MR armamentarium of the radiologist. As with other liver-directed therapies, a thin ring of enhancement surrounding the lesion often occurs and should not be interpreted as viable tumor but instead likely represents inflammatory or fibrous tissue.

Within the adjacent tumor-free liver parenchyma, attenuation changes can occur.²⁹² These areas often appear hypointense or hypodense and prominent and heterogeneous. These attenuation alterations can be confused with tumor, but they do not typically enhance. They are thought to represent perivascular edema, congestion, and microinfarction from the radiation exposure. These hypoattenuation areas have been found to be more heterogeneous with lower radiation doses and more diffuse with higher doses. These changes tend to dissipate on later scans (4 months), suggesting that they are reversible.²⁹³ More chronic findings of capsular retraction, parenchymal enhancement, and hepatic fibrosis can occur and are thought to arise from radiation effect on the hepatic parenchyma (Fig. 91-27). There can also be extrahepatic effects of the yttrium radioembolization on the biliary tree, hepatic vessels, gallbladder, duodenum, and stomach, causing radiation ischemia and necrosis (Fig. 91-28). Biliary sequelae can include biliary necrosis, resulting in strictures and bilomas, as well as cholecystitis.^{294,295}

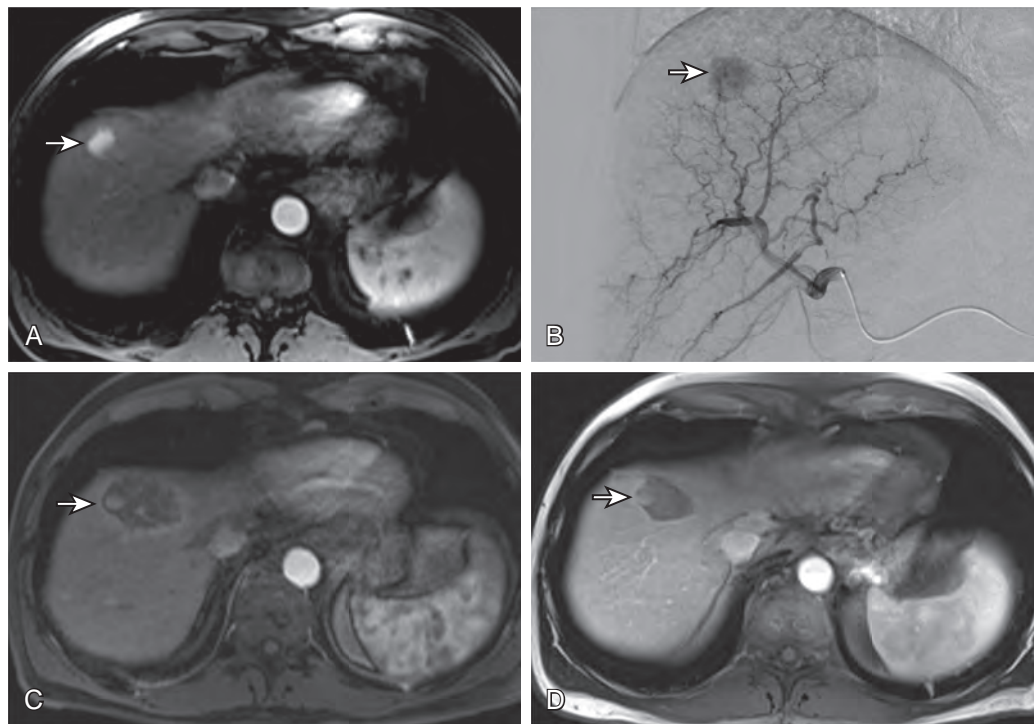


Figure 91-25 Effect of yttrium treatment on hepatocellular carcinoma. **A.** T1-weighted postcontrast MR image reveals a small enhancing hepatocellular carcinoma (arrow). **B.** Radioembolization shows a tumor blush (arrow). **C.** Image after radioembolization reveals the lesion to be larger with minimal enhancement (arrow). Full effect of radioembolization may take longer than in other liver-directed therapies. **D.** Follow-up MRI demonstrates complete nonenhancement compatible with tumor necrosis (arrow).

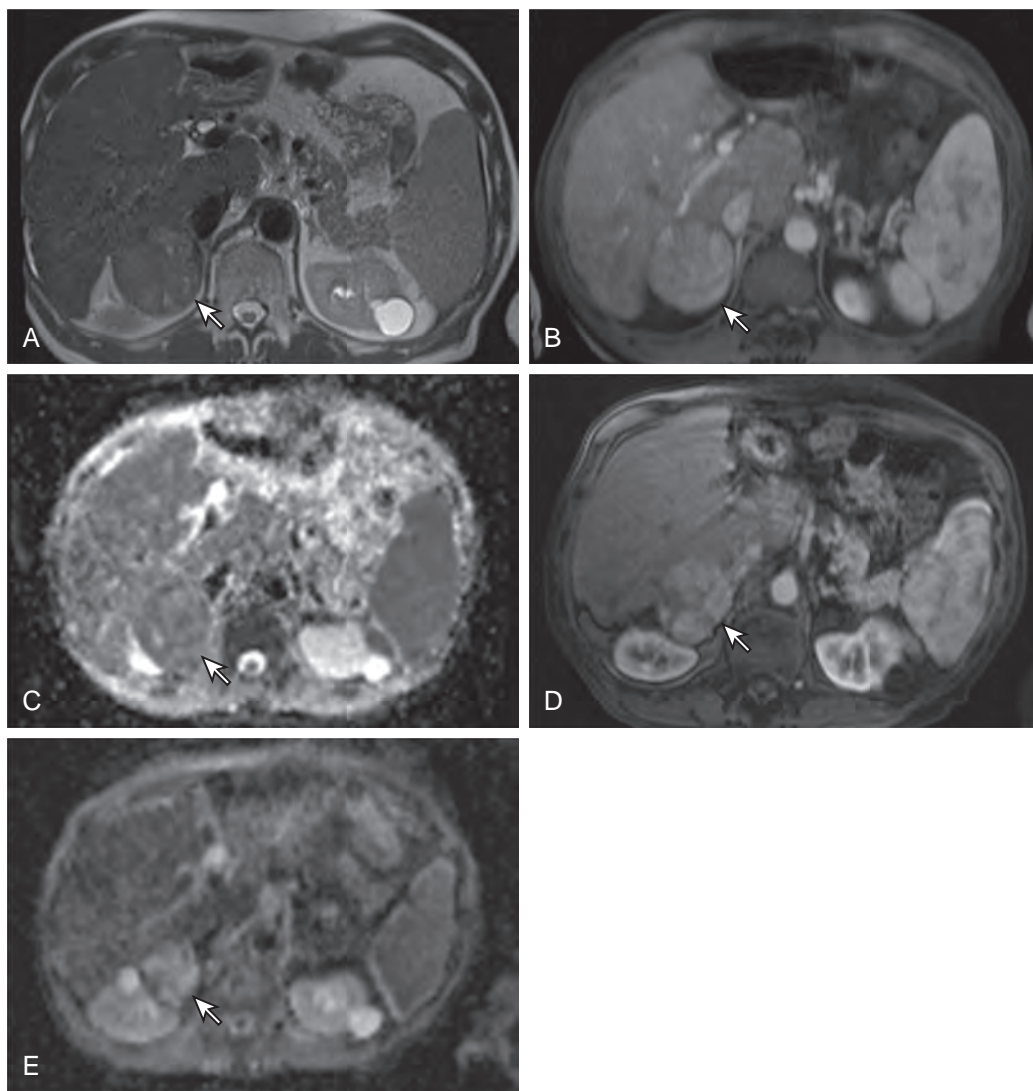


Figure 91-26 Use of diffusion-weighted MRI to predict treatment response. **A.** T2-weighted image shows an exophytic mass from the right lobe of the liver (arrow). **B.** T1-weighted postcontrast image reveals that this mass enhances; it was found to be a hepatoma (arrow). **C.** Diffusion-weighted MRI reveals low signal, suggesting restricted diffusion (arrow). **D.** MR image early after radioembolization shows some persistent enhancement (arrow). **E.** Diffusion-weighted MR, however, reveals increased signal and less restricted diffusion (arrow), which suggests a favorable response to radioembolization despite the persistent enhancement. The diffusion images were able to predict a positive response before the contrast images.

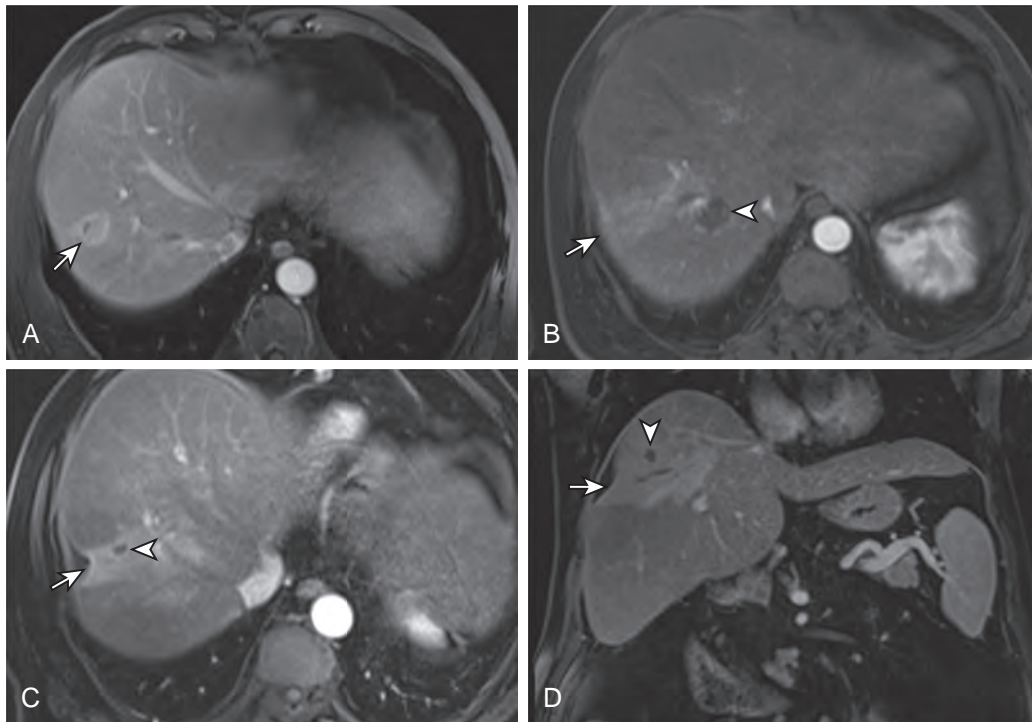


Figure 91-27 Effect of radioembolization on the adjacent hepatic parenchyma. **A.** MR image shows a small enhancing hepatoma (arrow). **B.** Close follow-up post-therapy image shows ill-defined enhancement of adjacent parenchyma in a vascular distribution (arrow), suggesting perivascular edema and inflammation. An incidental hemangioma is seen (arrowhead). **C** and **D.** Follow-up MR images reveal the lesion as a much smaller nonenhancing focus, suggesting excellent treatment response (arrowheads). The adjacent parenchyma enhances in a delayed fashion with capsular retraction (arrows), suggesting hepatic fibrosis from radiation effect.

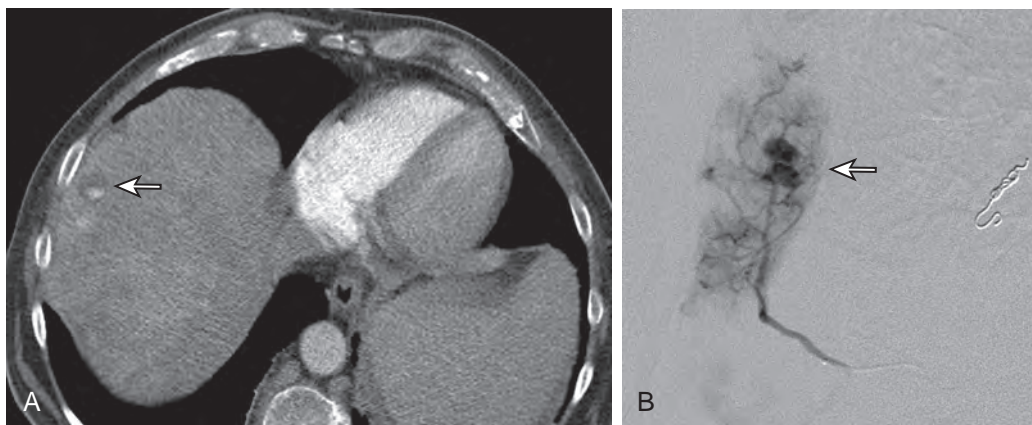


Figure 91-28 Complication of radioembolization. **A.** A postcontrast chest CT of a patient who was status post radioembolization reveals pooling of contrast material, suggesting a pseudoaneurysm (arrow). **B.** Angiogram confirms several small pseudoaneurysms (arrow), which were thought to be radiation induced. They were successfully embolized.

REFERENCES

- Thapar PM, Ghawat RM, Dalvi AN, et al: Massive liver trauma—multidisciplinary approach and minimal invasive surgery can salvage patients. *Indian J Surg* 75(Suppl 1): 449–452, 2013.
- Intravia JM, DeBerardino TM: Evaluation of blunt abdominal trauma. *Clin Sports Med* 32:211–218, 2013.
- Pachter HL: Hepatic trauma. In Taylor MB, editor: *Gastrointestinal Emergencies*, 2nd ed, Baltimore, 1997, Williams & Wilkins, pp 1001–1014.
- McNulty JG: *Radiology of the Liver*, Philadelphia, 1977, WB Saunders, pp 195–213.
- Ralls PW: The liver. In Jeffrey RB, Ralls PW, editors: *CT and Sonography of the Acute Abdomen*, 2nd ed, Philadelphia, 1996, Lippincott-Raven, pp 17–73.
- Jin W, Deng L, Lv H, et al: Mechanisms of blunt liver trauma patterns: An analysis of 53 cases. *Exp Ther Med* 5:395–398, 2013.
- Acker SN, Stovall RT, Moore EE, et al: Trauma remains a surgical disease from cradle to grave. *J Trauma Acute Care Surg* 77:219–225, 2014.
- Pachter HL, Feliciano DV: Complex hepatic injuries. *Surg Clin North Am* 76:763–773, 1996.
- Raza M, Abbas Y, Devi V, et al: Nonoperative management of abdominal trauma—a 10 years review. *World J Emerg Surg* 8:14, 2013.
- Shanmuganathan K, Mirvis SE: CT evaluation of the liver with acute blunt trauma. *Crit Rev Diagn Imaging* 36:73–113, 1995.
- Shuman WP: CT of blunt abdominal trauma in adults. *Radiology* 205:297–306, 1997.
- Matthes G, Stengel D, Seifert J, et al: Blunt liver in polytrauma: Results from a cohort study

- with the regular use of whole-body helical computed tomography. *World J Surg* 27:1124–1130, 2003.
13. Yaniv G, Portnoy O, Simon D, et al: Revised protocol for whole-body CT for multi-trauma patients applying triphasic injection followed by a single-pass scan on a 64-MDCT. *Clin Radiol* 68:668–675, 2013.
 14. Venbrux AC, Savader SJ, Friedman AC: Hepatic trauma. In Friedman AC, Dachman AH, editors: *Radiology of the Liver, Biliary Tract, and Pancreas*. St. Louis, 1994, Mosby, pp 329–344.
 15. Janes CH, Lindor KD: Outcome of patients hospitalized for complications after outpatient liver biopsy. *Ann Intern Med* 118:96–98, 1993.
 16. Bilgic I, Gelecek S, Akgun AE, et al: Predictive value of liver transaminases levels in abdominal trauma. *Am J Emerg Med* 32:705–708, 2014.
 17. Yoon W, Jeong YJ, Kim JK, et al: CT in blunt liver trauma. *Radiographics* 25:87–104, 2005.
 18. Richardson JD: Changes in the management of injuries to the liver and spleen. *J Am Coll Surg* 200:648–669, 2005.
 19. Tinkoff G, Esposito TJ, Reed J, et al: American Association for the surgery of trauma organ injury scale 1: Spleen, liver, and kidney, validation based on the national trauma data bank. *J Am Coll Surgeons* 207:646–655, 2008.
 20. Committee on Trauma, American College of Surgeons: National Trauma Data Bank. www.ntdb.org.
 21. Trunkey DD: Hepatic trauma: Contemporary management. *Surg Clin North Am* 84:437–450, 2004.
 22. Ahmed N, Vernick JJ: Management of liver trauma in adults. *J Emerg Trauma Shock* 4:114–119, 2011.
 23. Olson WR, Redman HC, Hildreth DC: Quantitative peritoneal lavage in blunt abdominal trauma. *Arch Surg* 104:536–543, 1972.
 24. Nagy KK, Roberts RR, Joseph KT, et al: Experience with over 2500 diagnostic peritoneal lavage for suspected intra-abdominal injury following blunt trauma. *Injury* 31:479–482, 2000.
 25. Oniscu GC, Parks RW, Garden OJ: Classification of liver and pancreatic trauma. *HPB (Oxford)* 8:4–9, 2006.
 26. Moore EE, Cogbill TH, Jurkovich GJ, et al: Organ injury scaling: Spleen and liver (1994 revision). *J Trauma* 38:323–324, 1995.
 27. Sherman HF, Savage BA, Jones LM: Nonoperative management of blunt hepatic injuries: Safe at any grade? *J Trauma* 37:616–621, 1994.
 28. Meredith JW, Young JS, Bowling J, et al: Non-operative management of blunt hepatic trauma: The exception or the rule? *J Trauma* 36:529–534, 1994.
 29. Croce MA, Fabian TC, Menke PG, et al: Non-operative management of blunt hepatic trauma is the treatment of choice for hemodynamically stable patients. Results of a prospective trial. *Ann Surg* 221:744–755, 1995.
 30. Boone DC, Federle M, Billiar TR, et al: Evolution of management of major hepatic trauma: Identification of patterns of injury. *J Trauma* 39:344–350, 1995.
 31. Archer LP, Frederick BR, Shackford SR: Selective nonoperative management of liver and spleen injuries in neurologically impaired adult patients. *Arch Surg* 131:309–315, 1996.
 32. Moore EF: Critical decisions in the management of hepatic trauma. *Am J Surg* 148:712–716, 1984.
 33. Federico JA, Horner WR, Clark DE, et al: Blunt hepatic trauma. *Arch Surg* 125:905–909, 1990.
 34. Jeffrey RB, Olcott EW: Imaging of blunt hepatic trauma. *Radiol Clin North Am* 29:1299–1310, 1991.
 35. Zeman RK, Burrell MI: *Gallbladder and Bile Duct Imaging*. New York, 1987, Churchill Livingstone, pp 677–704.
 36. Hollands MJ, Little JM: Hepatic venous injury after blunt abdominal trauma. *Surgery* 107:149–152, 1990.
 37. Trunkey DD: Torso trauma. *Curr Probl Surg* 24:209–265, 1987.
 38. Goodman DA, Tiruchelvam V, Tabb DR, et al: 3D CT reconstruction in the surgical management of hepatic injuries. *Ann R Coll Surg Engl* 77:7–11, 1995.
 39. Patten RM, Spear RP, Vincent LM, et al: Traumatic laceration of the liver limited to the bare area: CT findings in 25 patients. *AJR Am J Roentgenol* 160:1019–1022, 1993.
 40. Hollerman JJ, Fackler ML, Coldwell DM, et al: Gunshot wounds: 2. Radiology. *AJR Am J Roentgenol* 155:691–702, 1990.
 41. Hollerman JJ, Fackler ML, Coldwell DM, et al: Gunshot wounds: 1. Bullets, ballistics, and mechanisms of injury. *AJR Am J Roentgenol* 155:685–690, 1990.
 42. Evers K, Gohel VK: Gastrointestinal system. In Schwartz EE, editor: *The Radiology of Complications in Medical Practice*. Baltimore, 1984, University Park Press, pp 231–288.
 43. Perrault J, McGill DB, Ott BJ, et al: Liver biopsy: Complications in 1000 inpatients and outpatients. *Gastroenterology* 74:103–106, 1978.
 44. McGrath FP, Lee SH, Gibney RG, et al: Hepatic subcapsular hematoma: An unusual complication of biliary lithotripsy. *AJR Am J Roentgenol* 154:1015–1016, 1990.
 45. Davidson B, Carratta R, Paccione F, et al: Surgical emergencies in liver disease. *Baillieres Clin Gastroenterol* 5:737–758, 1991.
 46. Minur GY, Sutherland LR, Wiseman DA, et al: Prospective study of the incidence of ultrasound-detected intrahepatic and subcapsular hematomas in patients randomized to 6 or 24 hours of bedrest after percutaneous liver biopsy. *Gastroenterology* 90:127–138, 1986.
 47. Van Dyke RW: The liver in pregnancy. In Zakim D, Boyer TD, editors: *Hepatology*, 3rd ed, Philadelphia, 1996, WB Saunders, pp 1734–1758.
 48. Riely CA, Portis MC: Pregnancy-related hepatic and gastrointestinal disorders. In Feldman MA, Scharschmidt BE, Sleisenger MH, editors: *Gastrointestinal and Liver Disease*, 6th ed, Philadelphia, 1998, WB Saunders, pp 1253–1264.
 49. Terasaki KK, Quinn ME, Lundell CE, et al: Spontaneous hepatic hemorrhage with pre-eclampsia: Treatment with hepatic arterial embolization. *Radiology* 174:1039–1041, 1990.
 50. Lubner M, Menias C, Rucker C, et al: Blood in the belly: CT findings of hemoperitoneum. *Radiographics* 27:109–125, 2007.
 51. Jeffrey RB: CT diagnosis of blunt hepatic and splenic injuries: A look to the future. *Radiology* 171:17–18, 1989.
 52. Farnell MB, Spencer MP, Thompson E, et al: Nonoperative management of blunt hepatic trauma in adults. *Surgery* 104:748–756, 1988.
 53. Morales Uribe CH, López CA, Cote JC, et al: Surgical treatment of blunt liver trauma, indications for surgery and results. *Cir Esp* 92:23–29, 2014.
 54. Federle MP: CT of upper abdominal trauma. *Semin Roentgenol* 19:269–280, 1984.
 55. Goldstein AS, Sclafani SJA, Kupferstein NH, et al: Diagnostic superiority of computed tomography in the evaluation of acute abdominal trauma. *J Trauma* 25:938–946, 1985.
 56. Wolfman NT, Bechtold RE, Meredith JW: Blunt upper abdominal trauma: Evaluation by CT. *AJR Am J Roentgenol* 158:493–501, 1992.
 57. Moon KL, Federle MP: Computed tomography in hepatic trauma. *AJR Am J Roentgenol* 141:309–314, 1983.
 58. Shanmuganathan K, Mirvis SE, Sover ER: Value of contrast-enhanced CT in detecting active hemorrhage in patients with blunt abdominal or pelvic trauma. *AJR Am J Roentgenol* 161:65–69, 1993.
 59. Jeffrey RB, Jr, Cardoza JD, Olcott EW: Detection of active intraabdominal arterial hemorrhage: Value of dynamic contrast-enhanced CT. *AJR Am J Roentgenol* 156:725–729, 1991.
 60. Willmann JK, Roos JE, Platz A, et al: Multidetector CT: Detection of active hemorrhage in patients with blunt abdominal trauma. *AJR Am J Roentgenol* 179:437–444, 2002.
 61. Orwig D, Federle MP: Localized clotted blood as evidence of visceral trauma on CT: The sentinel clot sign. *AJR Am J Roentgenol* 153:747–750, 1989.
 62. Federle MP: Computed tomography of blunt abdominal trauma. *Radiol Clin North Am* 21:461–465, 1983.
 63. Mirvis SE, Whitley NO: Computed tomography in hepatobiliary trauma. In Ferrucci JT, Mathieu DG, editors: *Advances in Hepatobiliary Radiology*. St. Louis, 1990, CV Mosby, pp 239–274.
 64. Shanmuganathan K: Multidetector row CT imaging of blunt abdominal trauma. *Semin Ultrasound CT MR* 2:180–204, 2004.
 65. Fang JF, Chen RJ, Wong YC, et al: Pooling of contrast material on computed tomography mandates aggressive management of blunt hepatic injury. *Am J Surg* 176:315–319, 1998.
 66. Fang JF, Chen RJ, Wong YC, et al: Classification and treatment of pooling of contrast material on computed tomographic scan of blunt hepatic trauma. *J Trauma* 49:1083–1088, 2000.
 67. Boyd-Kranis R: Solid organ trauma. *Semin Intervent Radiol* 20:71–80, 2003.
 68. Buckman RF, Jr, Miraliakbari R, Badellino MM: Juxtahepatic venous injuries: A critical review of reported management strategies. *J Trauma* 48:978–984, 2000.
 69. Shanmuganathan K, Mirvis S, Amoroso M: Periportal low density on CT in patients with blunt trauma: Association with elevated venous pressure. *AJR Am J Roentgenol* 160:279–283, 1993.
 70. Patrick LE, Ball TI, Atkinson GO, et al: Pediatric blunt abdominal trauma: Periportal tracking at CT. *Radiology* 183:689–691, 1992.
 71. Cox SF, Friedman AC, Radecki PD, et al: Periportal lymphedema in trauma patients. *AJR Am J Roentgenol* 154:1124–1125, 1990.
 72. Macrander SJ, Lawson TL, Foley WD, et al: Periportal tracking in hepatic trauma: CT features. *J Comput Assist Tomogr* 13:952–957, 1989.
 73. Panicek DM, Paquet DJ, Clark KG, et al: Hepatic parenchymal gas after blunt trauma. *Radiology* 159:343–344, 1986.
 74. Abramson SJ, Berdon WE, Kaufman RA, et al: Hepatic parenchymal and subcapsular gas after hepatic laceration caused by blunt abdominal

- trauma. *AJR Am J Roentgenol* 153:1031–1032, 1989.
75. Mirvis SE, Whitley NO, Vainwright JR, et al: Blunt hepatic trauma in adults: CT-based classification and correlation with prognosis and treatment. *Radiology* 171:27–32, 1989.
 76. Ahmed N, Vernick JJ: Management of liver trauma in adults. *J Emerg Trauma Shock* 4:114–119, 2011.
 77. Zago TM, Pereira BM, Nascimento B, et al: Hepatic trauma: A 21-year experience. *Rev Col Bras Cir* 40:318–322, 2013.
 78. Meyer AA, Crass RA, Lim RC, et al: Selective nonoperative management of blunt liver injury using computed tomography. *Arch Surg* 120:550–554, 1985.
 79. Foley WD, Cates JD, Kellman GM, et al: Treatment of blunt hepatic injuries: Role of CT. *Radiology* 164:635–638, 1987.
 80. Olsen WR: Late complications of central liver injuries. *Surgery* 97:733–743, 1982.
 81. Davis KA, Brody JM, Cioffi WG: Computed tomography in blunt hepatic trauma. *Arch Surg* 131:255–260, 1996.
 82. Allins A, Ho T, Nguyen TH, et al: Limited value of routine follow-up CT scans in nonoperative management of blunt liver and splenic injuries. *Am Surg* 62:883–886, 1996.
 83. Carrillo EH, Richardson JD: The current management of hepatic trauma. *Adv Surg* 35:39–59, 2001.
 84. Pachter HL, Khudsen MM, Esrig B, et al: Status of nonoperative management of blunt hepatic injuries in 1995: A multicenter experience with 404 patients. *J Trauma* 40:31–38, 1996.
 85. Haney PJ, Whitley ND, Brotman S, et al: Liver injury and complications in the postoperative trauma patient: CT evaluation. *AJR Am J Roentgenol* 139:271–275, 1982.
 86. Casarella WJ, Martin EC: Angiography in the management of abdominal trauma. *Semin Roentgenol* 15:321–327, 1980.
 87. Janer HP, Laws HL, Kogutt MS, et al: Emergency embolization in blunt hepatic trauma. *AJR Am J Roentgenol* 129:249–252, 1977.
 88. Sclafani SJA, Shaftan GW, McAuley J, et al: Interventional radiology in the management of hepatic trauma. *J Trauma* 24:256–262, 1984.
 89. McIlrath EM, Thomas PS: Trauma of the upper abdomen. In Wilkins RA, Nunnerly HB, editors: *Imaging of the Liver, Pancreas and Spleen*, Oxford, 1990, Blackwell Scientific, pp 489–524.
 90. Hagiwara A, Yukioka T, Ohta S, et al: Nonsurgical management of patients with blunt hepatic injury: Efficacy of transcatheter arterial embolization. *AJR Am J Roentgenol* 169:1151–1156, 1997.
 91. Schwartz RA, Teitelbaum GP, Katz MD, et al: Effectiveness of transcatheter embolization in the control of hepatic vascular injuries. *J Vasc Intervent Radiol* 4:359–365, 1993.
 92. Howdieshell TR, Purvis J, Bates WB, et al: Biloma and biliary fistula following hepatorrhaphy for liver trauma: Incidence, natural history, and management. *Am Surg* 61:165–168, 1995.
 93. Ascher WM, Parvin S, Virgilio RW, et al: Echographic evaluation after blunt trauma. *Radiology* 118:411–415, 1976.
 94. Lentz KA, McKenney MG, Nunez DB, et al: Evaluating blunt abdominal trauma: Role for ultrasonography. *J Ultrasound Med* 15:447–451, 1996.
 95. Wherett LJ, Boulanger BR, McLellan BA, et al: Hypotension after blunt abdominal trauma: The role of emergent abdominal sonography in surgical triage. *J Trauma* 41:815–820, 1996.
 96. Rozycki GS: Abdominal ultrasonography in trauma. *Surg Clin North Am* 75:175–190, 1995.
 97. Rozycki GS, Stackford SR: US, what every trauma surgeon should know. *J Trauma* 40:1–4, 1996.
 98. Ma OJ, Mateer JR, Ogata M, et al: Prospective analysis of a rapid trauma ultrasound examination performed by emergency physicians. *J Trauma* 38:879–885, 1995.
 99. Sato M, Yoshii H: Reevaluation of ultrasonography for solid-organ injury in blunt abdominal trauma. *J Ultrasound Med* 23:1583–1596, 2004.
 100. Sofia S: Bedside US imaging in multiple trauma patients. Part 1: US findings and techniques. *J Ultrasound* 16:147–159, 2013.
 101. Kimura A, Otsuka T: Emergency center ultrasonography in the evaluation of hemoperitoneum: A prospective study. *J Trauma* 31:20–23, 1991.
 102. Hoffmann R, Nerlich M, Muggia-Sullam M, et al: Blunt abdominal trauma in cases of multiple trauma evaluated by ultrasonography: A prospective analysis of 291 patients. *J Trauma* 32:452–458, 1992.
 103. Tso P, Rodriguez A, Cooper C, et al: Sonography in blunt abdominal trauma: A preliminary progress report. *J Trauma* 33:39–44, 1992.
 104. Liu M, Lee CH, P'eng FK: Prospective comparison of diagnostic peritoneal lavage, computed tomographic scanning, and ultrasonography for the diagnosis of blunt abdominal trauma. *J Trauma* 35:267–270, 1993.
 105. McKenney M, Lentz K, Nunez D, et al: Can ultrasound replace diagnostic peritoneal lavage in the assessment of blunt trauma? *J Trauma* 37:439–441, 1994.
 106. Boulanger BR, Brennenman FD, McLellan BA, et al: A prospective study of emergent abdominal sonography after blunt trauma. *J Trauma* 39:325–330, 1995.
 107. Rozycki GS, Ochsner MG, Schmidt JA, et al: A prospective study of surgeon-performed ultrasound as the primary adjuvant modality for injured patient assessment. *J Trauma* 39:492–500, 1995.
 108. Lingawi SS, Buckley AR: Focused abdominal US in patients with trauma. *Radiology* 217:426–429, 2000.
 109. Chiu WC, Cushing BM, Rodriguez A, et al: Abdominal injuries without hemoperitoneum: A potential limitation of focused abdominal sonography for trauma (FAST). *J Trauma* 42:617–625, 1997.
 110. Shanmuganathan K, Mirvis SE, Sherbourne CD, et al: Hemoperitoneum as the sole indicator of abdominal visceral injuries: A potential limitation of screening abdominal US from trauma. *Radiology* 212:423–430, 1999.
 111. Brown MA, Casola G, Sirlin CB, Hoyt DB: Importance of evaluating organ parenchyma during screening abdominal ultrasonography after blunt trauma. *J Ultrasound Med* 20:577–583, 2001.
 112. Kuligowska E, Mueller PR, Simeone JF, et al: Ultrasound in upper abdominal trauma. *Semin Roentgenol* 19:281–295, 1984.
 113. Visconti GN, Gonzalez R, Taylor KJW, et al: Ultrasonic evaluation of hepatic and splenic trauma. *Arch Surg* 115:320–321, 1981.
 114. Wicks JD, Silver TM, Bree RL: Gray scale features of hematomas: An ultrasonic spectrum. *AJR Am J Roentgenol* 131:977–980, 1978.
 115. vanSonnenberg E, Simeone JF, Mueller PR, et al: Sonographic appearance of hematoma in liver, spleen and kidney: A clinical pathologic and animal study. *Radiology* 147:507–510, 1983.
 116. Esensten M, Ralls PW, Colletti P, et al: Post-traumatic intrahepatic biloma: Sonographic diagnosis. *AJR Am J Roentgenol* 140:303–305, 1983.
 117. Ralls PW, Eto R, Quinn M, et al: Gray-scale ultrasonography of a traumatic biliary cyst. *J Trauma* 21:176–177, 1981.
 118. Gould L, Patel A: Ultrasound detection of extrahepatic encapsulated bile: "Biloma." *AJR Am J Roentgenol* 132:1014–1015, 1979.
 119. Weissman HS, Byun KJ, Freeman LM: Role of Tc-99m IDA scintigraphy in the evaluation of hepatobiliary trauma. *Semin Nucl Med* 8:199–222, 1983.
 120. Zeman RK, Lee CH, Stahl RS, et al: Strategy for the use of biliary scintigraphy in non-traumatic biliary trauma. *Radiology* 151:771–776, 1984.
 121. Catalano O, Lobianco R, Raso MM, et al: Blunt hepatic trauma: Evaluation with contrast-enhanced sonography: Sonographic findings and clinical application. *J Ultrasound Med* 24:299–310, 2005.
 122. McGahon JP, Horton S, Gerscovich EO, et al: Appearance of solid organ injury with contrast-enhanced sonography in blunt abdominal trauma: Preliminary experience. *AJR Am J Roentgenol* 187:658–666, 2006.
 123. Caride VJ, Gibson DW: Noninvasive evaluation of bile leakage. *Surg Gynecol Obstet* 154:517–520, 1982.
 124. Terk MR, Rozenberg D: Gadolinium-enhanced MR imaging of traumatic hepatic injury. *AJR Am J Roentgenol* 171:665–669, 1998.
 125. Gupta N, Stuhlfaut JW, Fleming KW, et al: Blunt trauma of the pancreas and biliary tract: A multimodality imaging approach to diagnosis. *Radiographics* 24:1381–1395, 2004.
 126. Gupta RT, Brady CM, Lotz J, et al: Dynamic MR Imaging of the biliary system using hepatocyte-specific contrast agents. *AJR Am J Roentgenol* 195:405–413, 2010.
 127. Kantarci M, Primmoglu B, Karabulut N, et al: Noninvasive detection of biliary leaks using Gd-EOB-DTPA-enhanced MR cholangiography: Comparison with T2-weighted MR cholangiography. *Eur Radiol* 23:2713–2722, 2013.
 128. Cieszanowski A, Stadnik A, Lezak A, et al: Detection of active bile leak with Gd-EOB-DTPA enhanced MR cholangiography: Comparison of 20–25 min delayed and 60–180 min delayed images. *Eur J Radiol* 82:2176–2182, 2013.
 129. Yao DC, Jeffrey RB, Mirvis SE, et al: Using contrast-enhanced helical CT to visualize arterial extravasation after blunt abdominal trauma: Incidence and organ distribution. *AJR Am J Roentgenol* 178:17–20, 2002.
 130. Carrillo EH, Spain DA, Wohltmann CD, et al: Interventional techniques are useful adjuncts in nonoperative management of hepatic injuries. *J Trauma* 46:619–624, 1999.
 131. Velmahos GC, Toutouzas KG, Radin R, et al: High success with nonoperative management of blunt hepatic trauma. *Arch Surg* 138:475–481, 2003.
 132. Wahl WI, Ahms KS, Brandy MM, et al: The need for early angiographic embolization in blunt liver injuries. *J Trauma* 52:1097–1101, 2002.
 133. Wallis A, Kelly MD, Jones L: Angiography and embolization for solid abdominal organ injury

- in adults—a current perspective. *World J Emerg Surg* 5:18, 2010.
134. Stassen MA, Bhullar I, Cheng JD, et al: Nonoperative management of blunt hepatic injury: An Eastern Association for the Surgery of Trauma practice management guideline. *J Trauma Acute Care Surgery* 73:S288–S293, 2012.
 135. Burch JM: New concepts in trauma. *Am J Surg* 173:44–46, 1997.
 136. Mindelzun RE, McCort JJ: Upper abdominal trauma: Conventional radiology. *Semin Roentgenol* 19:259–265, 1984.
 137. Baker SR: *The Abdominal Plain Film*, East Norwalk, CT, 1990, Appleton & Lange, pp 243–298.
 138. Hurtuk M, Reed L, Esposito TJ, et al: Trauma surgeons practice what they preach: The NTDB story on solid organ injury management. *J Trauma* 61:243–255, 2006.
 139. Peitzman AB, Richardson JD: Surgical treatment of injuries to the solid abdominal organs: A 50-year perspective from the *Journal of Trauma*. *J Trauma* 69:1011–1022, 2010.
 140. Jiang H, Wang J: Emergency strategies and trends in the management of liver trauma. *Front Med* 6:225–233, 2012.
 141. Gur S, Orsel A, Atahan K, et al: Surgical treatment of liver trauma (analysis of 244 patients). *Hepatogastroenterology* 50:2109–2111, 2003.
 142. Shafi S, Parks J, Ahn C, et al: More operations, more deaths? Relationship between operative intervention rates and risk-adjusted mortality at trauma centers. *J Trauma* 69:70–77, 2010.
 143. Polanco P, Leon S, Pineda J, et al: Hepatic resection in the management of complex injury to the liver. *J Trauma* 65:1264–1270, 2008.
 144. Federle MP, Goldberg HI, Kaiser JA, et al: Evaluation of abdominal trauma by computed tomography. *Radiology* 138:637–644, 1981.
 145. Hollands MJ, Little JM: The role of hepatic resection in the management of blunt liver trauma. *World J Surg* 14:478–482, 1990.
 146. Kozar RA, Moore JB, Niles SE, et al: Complications of nonoperative management of high-grade blunt hepatic injuries. *J Trauma* 59:1066–1071, 2005.
 147. Wigham A, Alexander Grant L: Radiologic assessment of hepatobiliary surgical complications. *Semin Ultrasound CT MR* 34:18–31, 2013.
 148. Jones RS: The liver: Malignant and benign tumors, nonparasitic cysts, parasitic cysts, abscess, liver anatomy, technique of liver resection. In Moody FG, Carey LC, Jones RS, et al, editors: *Surgical Treatment of Digestive Disease*, Chicago, 1986, Year Book Medical, pp 377–397.
 149. Foster JH: History of liver surgery. *Arch Surg* 126:381–388, 1991.
 150. Suc B, Panis Y, Belghiti J, et al: Natural history of hepatectomy. *Br J Surg* 79:39–42, 1992.
 151. Lambert CJ, Meydrech EF, Scott-Conner CE, et al: Major hepatic resections: A 10-year experience with emphasis on special problems. *Am J Gastroenterol* 85:786–790, 1990.
 152. Scheele J, Stangl R, Alterdorf-Hofman A: Hepatic metastases from colorectal carcinoma: Impact of surgical resection on the natural history. *Br J Surg* 77:1241–1246, 1990.
 153. Farid SG, Morris-Stiff G, Prasad R: Postoperative management after hepatic surgery. *Br J Hosp Med (Lond)* 74:C89–C93, 2013.
 154. Vetto JT, Hughes KS, Rosenstein R, et al: Morbidity and mortality of hepatic resection for metastatic colorectal carcinoma. *Dis Colon Rectum* 33:408–413, 1990.
 155. Turner DA, Doolas A, Silver B, et al: The role of cross-sectional imaging in hepatic resections. In Ferrucci JF, Mathieu DG, editors: *Advances in Hepatobiliary Radiology*, St. Louis, 1990, CV Mosby, pp 209–228.
 156. Soyer P, Roche A, Elias D, et al: Hepatic metastases from colorectal cancer: Influence of hepatic volumetric analysis on surgical decision making. *Radiology* 184:695–697, 1992.
 157. Soyer P, Roche A, Gad M, et al: Preoperative segmental localization of hepatic metastases: Utility of three-dimensional CT during arterial portography. *Radiology* 180:653–658, 1991.
 158. Gazelle GS, Haaga JR: Hepatic neoplasms: Surgically relevant segmental anatomy and imaging techniques. *AJR Am J Roentgenol* 158:1015–1018, 1992.
 159. Salgia R, Singal AG: Hepatocellular carcinoma and other liver lesions. *Med Clin North Am* 98:103–118, 2014.
 160. Sherlock S, Dooley J: *Diseases of the Liver and Biliary System*, 9th ed, Oxford, 1993, Blackwell Scientific, pp 460–471.
 161. Lin S, Hoffmann K, Schemper P: Treatment of hepatocellular carcinoma: A systematic review. *Liver Cancer* 1:144–158, 2012.
 162. Baker ME, Pelley R: Hepatic metastases: Basic principles and implications for radiologists. *Radiology* 197:329–337, 1995.
 163. Taylor HM, Ros PR: Hepatic imaging: An overview. *Radiol Clin North Am* 36:237–245, 1998.
 164. Sugarbaker PH: Surgical decision making for large bowel cancer metastatic to the liver. *Radiology* 174:621–626, 1990.
 165. Malt RA: Surgery for hepatic neoplasms. *N Engl J Med* 313:1591–1595, 1985.
 166. Bergmark S: The surgeon's viewpoint. In Herlinger H, Lunderquist A, Wallace S, editors: *Clinical Radiology of the Liver*, New York, 1983, Marcel Dekker, pp 574–585.
 167. Minton JP, Hamilton WB, Sardi A, et al: Results of surgical excision of one to 13 hepatic metastases in 98 consecutive patients. *Arch Surg* 124:46–48, 1989.
 168. Hodgson WJB, Morgan J, Byrne D, et al: Hepatic resections for primary and metastatic tumors using the ultrasonic surgical dissector. *Am J Surg* 163:246–250, 1992.
 169. Simeone JF: Intraoperative ultrasonography of the liver. In Ferrucci JT, Stack DD, editors: *Liver Imaging*, Boston, 1990, Andover Medical, pp 247–255.
 170. Simeone JF: Intraoperative ultrasonography of liver tumors. In Ferrucci JT, Mathieu DG, editors: *Advances in Hepatobiliary Radiology*, St. Louis, 1990, CV Mosby, pp 229–238.
 171. Bismuth H, Castaing D, Graden OJ: The use of operative ultrasound in surgery of primary liver tumors. *World J Surg* 11:610–614, 1987.
 172. Machi J, Isomotoh I, Yamashita Y, et al: Intraoperative ultrasonography in screening for liver metastases from colorectal cancer: Comparative accuracy with traditional procedures. *Surgery* 105:678–684, 1987.
 173. Makuuchi M: Applications of intraoperative ultrasonography to hepatectomy. In Makuuchi M, editor: *Abdominal Intraoperative Ultrasonography*, Tokyo, 1987, Igaku-Shoin, pp 142–161.
 174. Gozzetti G, Mazziotti A: Intraoperative ultrasound during liver surgery. In Gozzetti G, Mazziotti A, Bolondi L, et al, editors: *Intraoperative Ultrasonography in Hepatobiliary and Pancreatic Surgery*, Boston, 1989, Kluwer Academic, pp 137–154.
 175. Makuuchi M, Hasegawa H, Yamazaki S, et al: The use of operative ultrasound as an aid to liver resection in patients with hepatocellular carcinoma. *World J Surg* 11:615–621, 1987.
 176. Conlon R, Jacobs M, Dasgupta D, et al: The value of intraoperative ultrasound during hepatic resection compared with improved preoperative magnetic resonance imaging. *Eur J Ultrasound* 16:211–216, 2003.
 177. Sahani D, Kalva S, Tanabe K, et al: Intraoperative US in patients undergoing surgery for liver neoplasms: Comparison with MR imaging. *Radiology* 232:810–814, 2004.
 178. Mui L, Pursell LJ, Botwinick IC, et al: Routine intraoperative hepatic sonography does not affect staging of postsurgical hepatic recurrence in pancreatic adenocarcinoma. *J Ultrasound Med* 33:47–51, 2014.
 179. Wagnetz U, Atri M, Massey C, et al: Intraoperative ultrasound of the liver in primary and secondary hepatic malignancies: Comparison with preoperative 1.5-T MRI and 64-MDCT. *AJR Am J Roentgenol* 196:562–568, 2011.
 180. Leen E, Ceccotti P, Moug SJ, et al: Potential value of contrast-enhanced intraoperative ultrasonography during partial hepatectomy for metastases. *Ann Surg* 243:236–240, 2006.
 181. Shah AJ, Callaway M, Thomas MG, et al: Contrast-enhanced intraoperative ultrasound improves detection of liver metastases during surgery for primary colorectal cancer. *HPB (Oxford)* 12:181–187, 2010.
 182. Kane RA, Hughes LA, Cua EJ, et al: The impact of intraoperative ultrasonography on surgery for liver neoplasms. *J Ultrasound Med* 13:1–6, 1994.
 183. Onik G, Kane R, Steele G, et al: Monitoring hepatic cryosurgery with sonography. *AJR Am J Roentgenol* 147:665–671, 1986.
 184. Weaver ML, Atkinson D, Zemel R: Hepatic cryosurgery in the treatment of unresectable metastases. *Surg Oncol* 4:231–236, 1995.
 185. Vauthey JN, Maddern GJ, Kolbinger P, et al: Clinical experience with adult polycystic liver disease. *Br J Surg* 79:562–565, 1992.
 186. Que F, Nagorney DM, Gross JB, et al: Liver resection and cyst fenestration in the treatment of severe polycystic liver disease. *Gastroenterology* 108:487–494, 1995.
 187. Foster JH: Surgical treatment of metastatic liver tumor. *Hepatogastroenterology* 37:182–187, 1990.
 188. Kanas GP, Taylor A, Primrose JN, et al: Survival after liver resection in metastatic colorectal cancer: Review and meta-analysis of prognostic factors. *Clin Epidemiol* 4:283–301, 2012.
 189. Bruix J, Sherman M: Management of hepatocellular carcinoma. *Hepatology* 42:1208–1236, 2005.
 190. Mazzaferro V, Regalia E, Doci R, et al: Liver transplantation for the treatment of small hepatocellular carcinoma in patients with cirrhosis. *N Engl J Med* 334:693–699, 1996.
 191. Ng KK, Vauthey JN, Pawlik TM, et al: Is hepatic resection for large or multinodular hepatocellular carcinoma justified? Results from a multi-institutional database. *Ann Surg Oncol* 12:364–373, 2005.
 192. Torzilli G, Donadon M, Marconi M, et al: Hepatectomy for hepatocellular carcinoma in stage B and C of BCLC classification: A feasible, safe and effective treatment. *Ann Surg Oncol* 14:5, 2007.

193. Adson MA, van Heerden JA, Adson MH, et al: Resection of hepatic metastases from colorectal cancer. *Arch Surg* 119:647–651, 1984.
194. Doci R, Gennari L, Bignami P, et al: One hundred patients with hepatic metastases from colorectal cancer treated by resection: Analysis of prognostic determinants. *Br J Surg* 78:797–801, 1991.
195. Rosen CB, Nagorney DM, Taswell HF, et al: Perioperative blood transfusion and determinants of survival after liver resection for metastatic colorectal carcinoma. *Ann Surg* 216:493–504, 1992.
196. Sugihara K, Hojo K, Moriya Y, et al: Pattern of recurrence after hepatic resection for colorectal metastases. *Br J Surg* 80:1032–1035, 1993.
197. Gayowski TJ, Iwatsuki S, Madariaga JR, et al: Experience in hepatic resection for metastatic colorectal cancer: Analysis of clinical and pathologic risk factors. *Surgery* 116:703–711, 1994.
198. Hughes KS, Simon RM, Songhorabodi S, et al: Resection of the liver for colorectal carcinoma metastases: A multi-institutional study of indications for resection. *Surgery* 103:278–288, 1988.
199. Nordlinger B, Jaeck D, Guiguet M, et al: Surgical resection of hepatic metastases. Multicentric retrospective study by the French Association of Surgery. In Nordlinger B, Jaeck D, editors: *Treatment of Hepatic Metastases of Colorectal Cancer*, Paris, 1992, Springer-France, pp 129–146.
200. Van Ooigen B, Wiggers T, Meijer S, et al: Hepatic resections for colorectal metastases in The Netherlands: A multi-institutional 10-year study. *Cancer* 70:28–34, 1992.
201. Fong Y, Blumgart LH, Cohen A, et al: Repeat hepatic resection for metastatic colorectal cancer. *Ann Surg* 220:657–662, 1994.
202. Wanebo HJ, Chu LD, Veziridis MP, et al: Patient selection for hepatic resection of colorectal metastases. *Arch Surg* 131:322–329, 1996.
203. Adson MA: Resection of liver metastases: When is it worthwhile? *World J Surg* 11:511–520, 1996.
204. Fong Y, Kemeny N, Paty P, et al: Treatment of colorectal cancer: Hepatic metastasis. *Semin Surg Oncol* 12:219–252, 1996.
205. Hasegawa H, Yamazaki S, Makuuchi M: Ultrasonographically guided segmentectomy and subsegmentectomy: Application in the cirrhotic liver. In Blumgart LH, editor: *Pediatric Surgery of the Liver and Biliary Tract*, New York, 1988, Churchill Livingstone, pp 1289–1298.
206. Aragon RJ, Solomon NL: Techniques of hepatic resection. *J Gastrointest Oncol* 3:29–40, 2012.
207. Silen W: Hepatic resection for metastases from colorectal carcinoma is of dubious value. *Arch Surg* 124:1021–1022, 1989.
208. Bucher NLR: Liver regeneration: An overview. *J Gastroenterol Hepatol* 6:615–628, 1991.
209. Shin DS, Ingraham CR, Dighe MK, et al: Surgical resection of a malignant liver lesion: What the surgeon wants the radiologist to know. *AJR* 203:W21–W33, 2014.
210. Koffron AJ, Auffenberg G, Kung R, et al: Evaluation of 300 minimally invasive liver resections at a single institution. Less is more. *Ann Surg* 246:385–394, 2007.
211. Daher I, O'Rourke N, Geller DA, et al: Laparoscopic major hepatectomy: An evolution in standard of care. *Ann Surg* 250:856–860, 2009.
212. Nguyen KT, Gamblin TC, Geller DA: World review of laparoscopic liver resection—2,804 patients. *Ann Surg* 250:831–841, 2009.
213. Lai EC, Tang CN, Yang GP, et al: Multimodality laparoscopic liver resection for hepatic malignancy—from conventional total laparoscopic approach to robot-assisted laparoscopic approach. *Int J Surg* 9:324–328, 2011.
214. Kazaryan AM, Marangos P, Rosseland AR, et al: Laparoscopic liver resection for malignant and benign lesions: Ten-year Norwegian single-center experience. *Arch Surg* 145:34–40, 2010.
215. Reggiani P, Antonelli B, Rossi G: Robotic surgery of the liver: Italian experience and review of the literature. *Ecancermedicalscience* 7:358, 2013.
216. Kitisin K, Packiam V, Bartlett DL, et al: A current update on the evolution of robotic liver surgery. *Minerva Chir* 66:281–293, 2011.
217. Marcos-Alvarez A, Jenkins RL, Washburn WK, et al: A multimodality treatment of hepatocellular carcinoma in a hepatobiliary specialty center. *Arch Surg* 131:292–298, 1996.
218. Ravikumar TS, Kane R, Cady B, et al: A 5-year study of cryosurgery in the treatment of liver tumors. *Arch Surg* 126:1520–1524, 1991.
219. Ravikumar TS: Interstitial therapies for liver tumors. *Surg Oncol Clin North Am* 5:365–377, 1996.
220. Morris DL, Ross WB: Australian experience of cryoablation of liver tumors. *Surg Oncol Clin* 5:391–397, 1996.
221. Daniels JR, Katz M, Wallman M: Retrospective analysis of percutaneous cryoablation of hepatocellular carcinoma (HCC) in liver. *J Vasc Interv Radiol* 24:S44, 2013.
222. Lencioni R, Cioni D, Crocetti L, et al: Early-stage hepatocellular carcinoma in patients with cirrhosis: Long-term results of percutaneous image-guided radiofrequency ablation. *Radiology* 234:961–967, 2005.
223. Weber SM, Lee FT, Jr: Expanded treatment of hepatic tumors with radiofrequency ablation and cryoablation. *Oncology (Williston Park)* 19(Suppl 4):27–32, 2005.
224. Lencioni R, Crocetti L: Radiofrequency ablation of liver cancer. *Tech Vasc Interv Radiol* 10:38–46, 2007.
225. Huo TI, Huang YH, Wu JC: Percutaneous ablation therapy for hepatocellular carcinoma: Current practice and future perspectives. *J Chin Med Assoc* 68:155–159, 2004.
226. Pompili M, Mirante VG, Rondinara G, et al: Percutaneous ablation procedures in cirrhotic patients with hepatocellular carcinoma submitted to liver transplantation: Assessment of efficacy at explant analysis and of safety for tumor recurrence. *Liver Transpl* 11:1117–1126, 2005.
227. Scaife CL, Curley SA: Complication, local recurrence, and survival rates after radiofrequency ablation for hepatic malignancies. *Surg Oncol Clin North Am* 12:243–255, 2003.
228. Hoffman AL, Wu SS, Obaid AK, et al: Histologic evaluation and treatment outcome after sequential radiofrequency ablation and hepatic resection for primary and metastatic tumors. *Am Surg* 68:1038–1043, 2002.
229. Breedis C, Young C: The blood supply of neoplasms in the liver. *Am J Pathol* 30:969–985, 1954.
230. Sigurdson ER, Ridge JA, Kemeny N, et al: Tumor and liver drug uptake following hepatic artery and portal vein infusion. *J Clin Oncol* 5:1936–1940, 1987.
231. Healey JE, Sheena KS: Vascular patterns in metastatic liver tumors. *Surg Forum* 14:121–122, 1963.
232. Murray-Lyon IM, Parsons VA, Blendis LM: Treatment of secondary hepatic tumors by ligation of hepatic artery and infusion of cytotoxic drugs. *Lancet* 2:172–175, 1970.
233. Wallace S, Carrasco CH, Charnsagavej C, et al: Hepatic artery infusion and chemoembolization in the management of liver metastasis. *Cardiovasc Intervent Radiol* 13:153–160, 1990.
234. Chen HSG, Gross JF: Intraarterial infusion of anticancer drugs: Theoretic aspects of drug delivery and review of responses. *Cancer Treat Rep* 64:31–40, 1980.
235. Collins JM: Pharmacologic rationale for regional drug delivery. *J Clin Oncol* 2:498–504, 1984.
236. Llovet JM, Real MI, Montana X, et al: Arterial embolisation or chemoembolisation versus symptomatic treatment in patients with unresectable hepatocellular carcinoma: A randomised controlled trial. *Lancet* 359:1734–1739, 2002.
237. Lo CM, Ngan H, Tso WK, et al: Randomized controlled trial of transarterial lipiodol chemoembolization for unresectable hepatocellular carcinoma. *Hepatology* 35:1164–1171, 2002.
238. Takayasu K, Arai S, Ikai I, et al: Prospective cohort study of transarterial chemoembolization for unresectable hepatocellular carcinoma in 8510 patients. *Gastroenterology* 131:461–469, 2006.
239. Chuang VP, Wallace S, Soo CS: Therapeutic Ivalon embolization of hepatic tumors. *AJR Am J Roentgenol* 138:289–294, 1982.
240. Kobayashi H, Inoue H, Shimada J, et al: Intraarterial injection of adriamycin/mitomycin C lipiodol suspension in liver metastases. *Acta Radiol* 28:275–280, 1986.
241. Inoue H, Kobayashi H, Itoh Y, et al: Treatment of liver metastasis by arterial injection of adriamycin/mitomycin C lipiodol suspension. *Acta Radiol* 30:603–608, 1989.
242. Taniguchi H, Takahashi T, Yamaguchi T, et al: Intraarterial infusion chemotherapy for metastatic liver tumors using multiple anticancer agents suspended in a lipid contrast medium. *Cancer* 64:2001–2006, 1989.
243. Yamashita Y, Takahashi M, Bussaka H, et al: Intraarterial infusion of 5-fluoro-2-deoxyuridine-C8 dissolved in a lymphographic agent in malignant liver tumors. *Cancer* 64:2437–2444, 1989.
244. Kameyama M, Imaoka S, Fukuda I, et al: Delayed washout of intratumor blood flow is associated with good response to intraarterial chemoembolization for liver metastasis of colorectal cancer. *Surgery* 114:97–101, 1992.
245. Lang EK, Brown CL: Colorectal metastases to the liver: Selective chemoembolization. *Radiology* 189:417–422, 1993.
246. Feun LG, Reddy KR, Yrizarry JM, et al: A phase I study of chemoembolization with cisplatin and lipiodol for primary and metastatic liver cancer. *Am J Clin Oncol* 17:405–410, 1994.
247. Fischbach R, Gross-Fengels W, Heindel W, et al: Transcatheter hepatic artery chemoembolization of primary and secondary liver neoplasms: Response rates and survival times. *Cardiovasc Intervent Radiol* 15:417–422, 1992.
248. Martinelli DJ, Wadler S, Bakal CW, et al: Utility of embolization or chemoembolization as second line treatment in patients with

- advanced or recurrent colorectal carcinoma. *Cancer* 74:706–712, 1994.
249. Daniels S, Pentecost M, Reitelbaum G, et al: Hepatic artery chemoembolization for carcinoma of colon using Angiostat collagen and cisplatin, mitomycin and doxorubicin: Response, survival and serum drug levels. *Proc Am Soc Clin Oncol* 11:171–172, 1992.
 250. Meakem TJ, Unger EC, Pond GD, et al: CT findings after hepatic chemoembolization. *J Comput Assist Tomogr* 16:916–920, 1992.
 251. Bester L, Meteling B, Boshell D, et al: Transarterial chemoembolisation and radioembolisation for the treatment of primary liver cancer. *J Med Imaging Radiat Oncol* 58:341–352, 2014.
 252. Hunt TM, Flowerdew ADS, Birch SJ, et al: Prospective randomized controlled trial of hepatic arterial embolization of infusion chemotherapy with 5-fluorouracil and degradable starch microspheres for colorectal liver metastases. *Br J Surg* 77:779–782, 1990.
 253. Aronsen KF, Hellkant C, Holmberg J, et al: Controlled blocking of hepatic artery flow with enzymatically degradable microspheres combined with oncolytic drugs. *Eur Surg Res* 11:99–106, 1979.
 254. Starkhammar H, Hakansson L, Morales O, et al: Intraarterial mitomycin C treatment of unresectable liver tumors. Preliminary results on the effect of degradable starch microspheres. *Acta Oncol* 26:295–300, 1987.
 255. Wollner IS, Walker-Andrews SC, Smith JE, et al: Phase II study of hepatic arterial degradable starch microspheres and mitomycin. *Cancer Drug Deliv* 4:279–284, 1986.
 256. Allison OJ, Booth A: Arterial embolization in the management of liver metastasis. *Cardiovasc Intervent Radiol* 13:153–160, 1990.
 257. Geschwind JF, Kaushik S, Ramsey DE, et al: Influence of a new prophylactic antibiotic therapy on the incidence of liver abscesses after chemoembolization treatment of liver tumors. *J Vasc Interv Radiol* 13:1163–1166, 2002.
 258. Kim W, Clark TW, Baum RA, et al: Risk factors for liver abscess formation after hepatic chemoembolization. *J Vasc Interv Radiol* 12:965–968, 2001.
 259. Yamakado K, Nakatsuka A, Ohmori S, et al: Radiofrequency ablation combined with chemoembolization in hepatocellular carcinoma: Treatment response based on tumor size and morphology. *J Vasc Interv Radiol* 13:1225–1232, 2002.
 260. Lewandowski RJ, Geschwind J, Liapi E, et al: Transcatheter intraarterial therapies: Rationale and overview. *Radiology* 259:641–657, 2011.
 261. Rhee TK, Omary RA, Gates V, et al: The effect of catheter-directed CT angiography on yttrium-90 radioembolization treatment of hepatocellular carcinoma. *J Vasc Interv Radiol* 16:1085–1091, 2005.
 262. Salem R, Lewandowski RJ, Atassi B, et al: Treatment of unresectable hepatocellular carcinoma with use of ⁹⁰Y microspheres (TheraSphere): Safety, tumor response, and survival. *J Vasc Interv Radiol* 16:1627–1639, 2005.
 263. Kennedy AS, Coldwell D, Nutting C, et al: Resin ⁹⁰Y-microsphere brachytherapy for unresectable colorectal liver metastases: Modern USA experience. *Int J Radiat Oncol Biol Phys* 65:412–425, 2006.
 264. Lewandowski RJ, Salem R: Yttrium-90 radioembolization of hepatocellular carcinoma and metastatic disease to the liver. *Semin Intervent Radiol* 23:64–72, 2006.
 265. Lewandowski RJ, Thurston KG, Goin JE, et al: ⁹⁰Y microsphere (TheraSphere) treatment for unresectable colorectal cancer metastases of the liver: Response to treatment at targeted doses of 135–150 Gy as measured by [¹⁸F]fluorodeoxyglucose positron emission tomography and computed tomographic imaging. *J Vasc Interv Radiol* 16:1641–1651, 2005.
 266. Kulik L, Atassi B, van Holsbeeck L, et al: Yttrium-90 microsphere (TheraSphere) treatment of unresectable hepatocellular carcinoma: Downstaging to resection, RFA and bridge to transplantation. *J Surg Oncol* 94:572–586, 2006.
 267. Kulik LM, Mulcahy MF, Hunter RD, et al: Use of yttrium-90 microspheres (TheraSphere) in a patient with unresectable hepatocellular carcinoma leading to liver transplantation: A case report. *Liver Transpl* 11:1127–1131, 2005.
 268. Gray B, Van Hazel G, Hope M, et al: Randomised trial of SIR-Spheres plus chemotherapy vs. chemotherapy alone for treating patients with liver metastases from primary large bowel cancer. *Ann Oncol* 12:1711–1720, 2001.
 269. Van Hazel G, Blackwell A, Anderson J, et al: Randomised phase 2 trial of SIR-Spheres plus fluorouracil/leucovorin chemotherapy versus fluorouracil/leucovorin chemotherapy alone in advanced colorectal cancer. *J Surg Oncol* 88:78–85, 2004.
 270. Van Hazel G, Price D, Bower G, et al: Selective internal radiation therapy (SIRT) plus systemic chemotherapy with FOLFOX4: A phase I dose escalation study, Miami, Fla, 2005, American Society of Clinical Oncology Gastrointestinal Cancers Symposium.
 271. Van Hazel G, Price D, Bower G, et al: Selective internal radiation therapy (SIRT) for liver metastases with concomitant systemic oxaliplatin, 5-fluorouracil and folinic acid: A phase I/II dose escalation study, Miami, Fla, 2005, American Society of Clinical Oncology Gastrointestinal Cancers Symposium.
 272. Sato KT, Lewandowski RJ, Mulcahy MF, et al: Unresectable chemorefractory liver metastases: Radioembolization with ⁹⁰Y microspheres—safety, efficacy, and survival. *Radiology* 247:507–515, 2008.
 273. Salem R, Lewandowski RJ, Kulik L, et al: Radioembolization results in longer time-to-progression and reduced toxicity compared with chemoembolization in patients with hepatocellular carcinoma. *Gastroenterology* 140:497–507, 2011.
 274. Letourneau JG, Steely JW, Crass JR, et al: Upper abdomen: CT findings following partial hepatectomy. *Radiology* 166:139–141, 1988.
 275. Covanet D, Shirkhoda A, Wallace S: Computed tomography after partial hepatectomy. *J Comput Assist Tomogr* 8:453–457, 1984.
 276. Quinn SF, Bodne DJ, Clark RA: Upper abdomen: CT findings following partial hepatectomy. *Radiology* 168:879–880, 1988.
 277. Sefczek RJ, Lupetin AR, Beckman I, et al: CT appearance of omental packs. *Radiology* 156:472–476, 1985.
 278. Arrive L, Hricak H, Goldberg HI, et al: MR appearance of the liver after partial hepatectomy. *AJR Am J Roentgenol* 152:1215–1220, 1989.
 279. Greco A, Stipa F, Huguet C, et al: Early MR follow-up of partial hepatectomy. *J Comput Assist Tomogr* 17:277–282, 1993.
 280. Anderson R, Saarela A, Tranberg KG, et al: Intraabdominal abscess formation after major liver resection. *Acta Chir Scand* 156:707–710, 1990.
 281. Cole DJ, Ferguson CM: Complication of hepatic resection for colorectal carcinoma metastasis. *Am Surg* 58:88–91, 1992.
 282. Vauthey JN: Liver imaging: A surgeon's perspective. *Radiol Clin North Am* 36:445–458, 1998.
 283. Yaghamai V, Miller FH, Rezaei P, et al: Response to treatment series: Part 2, tumor response assessment—using new and conventional criteria. *AJR Am J Roentgenol* 197:18–27, 2011.
 284. Gonzalez-Guindalini F, Botelho MP, Harmath CB, et al: Assessment of liver tumor response to therapy: Role of quantitative imaging. *Radiographics* 33:1781–1800, 2013.
 285. Guo Y, Yaghamai V, Salem R, et al: Imaging tumor response following liver-directed intraarterial therapy. *Abdom Imaging* 38:1286–1299, 2013.
 286. Nghiem HV, Francis IR, Fontana R: Computed tomography appearances of hypervascular hepatic tumors after percutaneous radiofrequency ablation therapy. *Curr Probl Diagn Radiol* 31:105–111, 2002.
 287. Lencioni R, Llovet JM: Modified RECIST (mRECIST) assessment for hepatocellular carcinoma. *Semin Liver Dis* 30:52–60, 2010.
 288. Meakem TJ, 3rd, Unger EC, Pond GD: CT findings after hepatic chemoembolization. *J Comput Assist Tomogr* 16:916–920, 1992.
 289. Niu LZ, Li JL, Zeng JY, et al: Combination treatment with comprehensive cryoablation and immunotherapy in metastatic hepatocellular cancer. *World J Gastroenterol* 19:3473–3480, 2013.
 290. Murthy R, Nunez R, Szklaruk J, et al: Yttrium-90 microsphere therapy for hepatic malignancy: Devices, indications, technical considerations, and potential complications. *Radiographics* 25:S41–S55, 2005.
 291. Deng J, Miller FH, Rhee TK, et al: Diffusion-weighted MR imaging for determination of hepatocellular carcinoma response to yttrium-90 radioembolization. *J Vasc Interv Radiol* 17:1195–1200, 2006.
 292. Atassi B, Bangash AK, Bahrani A, et al: Multimodality imaging following ⁹⁰Y radioembolization: A comprehensive review and pictorial essay. *Radiographics* 28:81–99, 2008.
 293. Kucuk ON, Soydal C, Lacin S, et al: Selective intraarterial radionuclide therapy with yttrium-90 (Y-90) microspheres for unresectable primary and metastatic liver tumors. *World J Surg Oncol* 9:8, 2011.
 294. Atassi B, Bangash AK, Lewandowski RJ, et al: Biliary sequelae following radioembolization with yttrium-90 microspheres. *J Vasc Interv Radiol* 19:691–697, 2008.
 295. Morsbach F, Sah BR, Spring L, et al: Perfusion CT best predicts outcome after radioembolization of liver metastases. *Eur Radiol* 24:1455–1465, 2014.

Liver Transplantation Imaging

LAUREN F. ALEXANDER | MARK D. LITTLE | RUPAN SANYAL

CHAPTER OUTLINE

Indications for Liver Transplantation

Hepatitis C
Alcoholic Liver Disease
Malignant Disease
Nonalcoholic Steatohepatitis
Cholestatic Liver Disease
Acute Hepatic Necrosis
Metabolic Disease

Patient Evaluation for Liver Transplantation

Listing and Timing of Liver Transplantation
Model for End-Stage Liver Disease (MELD) Score
Hepatocellular Carcinoma and Liver Transplantation
Milan Criteria
MELD Exception Points for Hepatocellular Carcinoma

Preoperative Imaging

Exclusion of Hepatocellular Carcinoma
OPTN Classification System for Nodules Seen on
Imaging of Cirrhotic Livers
Portal Vein Evaluation
Hepatic Artery Evaluation
Portosystemic Shunt and Variceal Evaluation

Locoregional Bridging Therapy for Hepatocellular Carcinoma

Surgical Technique

Living Donor Liver Transplantation

Imaging Evaluation of the Potential Living Related Liver Donor
Parenchymal Assessment
Vascular Assessment
Biliary Assessment

Postoperative Complications

Hepatic Arterial Complications
Portal Venous Complications
Hepatic Vein and Inferior Vena Cava Complications
Biliary Complications
Rejection
Fluid Collections
Post-transplantation Malignant Disease

Summary

Orthotopic liver transplantation (OLT) is the only definitive treatment of end-stage liver disease. About 6000 liver transplants are performed annually in the United States. Lack of donors remains a huge challenge for liver transplantation programs. Of the 15,641 patients on the waiting list for liver transplantation in 2009, 2396 patients died waiting for a transplant.¹ The first human liver transplant was performed in 1963 by

Thomas Starzl. The surgical technique and management of patients with liver transplant significantly improved during the next few decades. Increasing experience has resulted in current 1-, 3-, and 5-year survival rates of 87%, 78%, and 73%, respectively. Early graft failure within 6 weeks of transplantation in deceased donors has decreased from 6.9% in 1998 to 3.0% in 2009.¹

In 1987, Congress passed the National Organ Transplant Act, which established the Organ Procurement and Transplantation Network (OPTN) and the Scientific Registry of Transplant Recipients. OPTN links all professionals involved in the organ donation and transplantation system. The United Network for Organ Sharing (UNOS) is the OPTN contractor that coordinates the nation's transplant system. UNOS maintains the national organ transplant waiting list, increases awareness of organ donation, develops policies and standards for transplantation, and monitors members for compliance.

Indications for Liver Transplantation

The indications for OLT are presented in [Table 92-1](#).

HEPATITIS C

Chronic liver disease caused by hepatitis C virus infection is the leading cause of liver transplantation. Unfortunately, reinfection of the allograft by the hepatitis C virus is universal. Reinfection results in faster progression to fibrosis and cirrhosis compared with the nontransplant population. Cirrhosis develops in 25% of recipients within 5 to 10 years of transplantation.² Graft failure rate at 10 years is higher in patients with hepatitis C (45%) compared with the rate for all deceased donors (51.3%).

ALCOHOLIC LIVER DISEASE

Patients who undergo liver transplantation for alcoholic liver disease have outcome similar to that of patients receiving transplants for nonalcoholic disease. However, studies have shown that 10% to 15% of patients receiving transplants for alcoholic liver disease resume heavy drinking, which can harm the transplant. UNOS suggests at least 6 months of abstinence before transplantation (6-month rule). This effectively eliminates patients with acute alcoholic hepatitis from receiving transplants.³

MALIGNANT DISEASE

Hepatocellular carcinoma (HCC) occurring in the setting of cirrhosis is a common indication for transplantation. Cholangiocarcinoma, hemangioendothelioma, and hepatoblastoma are much rarer indications for transplantation.

TABLE 92-1
Indications for Orthotopic Liver Transplantation in the United States (2009)

Primary Cause of Disease	Percentage
Hepatitis C	25.6
Malignant disease	18.7
Alcoholic liver disease	17.4
Cholestatic disease	7.9
Acute hepatic necrosis	4.3
Metabolic liver disease	2.5
Others (nonalcoholic steatohepatitis most common)	23.6

NONALCOHOLIC STEATOHEPATITIS

Nonalcoholic fatty liver disease represents a spectrum of liver disease due to triglyceride accumulation in the hepatocytes ranging from benign steatosis to nonalcoholic steatohepatitis (NASH), fibrosis, and cirrhosis. As a consequence of the growing epidemic of obesity, nonalcoholic fatty liver disease and NASH have a prevalence of 30% and 12%, respectively, in the U.S. population. NASH represents a rapidly growing indication for liver transplantation in the last decade.⁴ It is currently the third most common cause of transplantation. In 2009, NASH was listed as the primary indication for 8.5% of liver transplants compared with 1% in 2001.⁵ These numbers are likely to underestimate the true incidence of NASH as underlying steatosis often dissipates after the development of cirrhosis. A substantial portion of patients with cryptogenic cirrhosis listed as the indication for transplantation probably had NASH.⁵

CHOLESTATIC LIVER DISEASE

Primary biliary cirrhosis and primary sclerosing cholangitis are the most frequent cholestatic conditions in adults, and liver transplantation is an excellent option for patients who progress to end-stage disease. Transplantation for cholestatic disease has better survival rates than many other indications. Biliary atresia, cystic fibrosis, and Alagille's syndrome are cholestatic conditions in children that can be treated with transplantation.⁶

ACUTE HEPATIC NECROSIS

Acute hepatic necrosis or acute liver failure is characterized by sudden massive necrosis of hepatocytes and has very high mortality. Liver transplantation provides the most definitive treatment of acute liver failure. Viral hepatitis and drug toxicity (including acetaminophen) are common causes.⁷

METABOLIC DISEASE

Wilson's disease, hereditary hemochromatosis, and α_1 -antitrypsin deficiency are metabolic diseases that can cause irreversible hepatic damage.

Patient Evaluation for Liver Transplantation

LISTING AND TIMING OF LIVER TRANSPLANTATION

The demand-supply situation for liver transplantation is such that a large number of patients are waitlisted for a small number

of available organs. Before 2002, patients received transplants on a first-come, first-served basis. However, the sickest patients in the most urgent need of transplantation were not always the first on the list, and death on the wait list increased. The optimal timing of liver transplantation should be such that a patient must be sick enough to require a transplant but not be so sick as to be unable to withstand the transplantation. Comorbid conditions (like HCC) should not be allowed to advance so much that survival of the graft or of the patient is affected. The MELD score and Milan criteria are used to evaluate the need of transplantation.

MODEL FOR END-STAGE LIVER DISEASE (MELD) SCORE

The MELD score is a predictor of short-term mortality in patients with chronic liver disease. It is calculated from serum creatinine concentration, international normalized ratio, and bilirubin concentration. Since 2002, UNOS has used the MELD score to assess the acuity of need for liver transplantation. Patients with high MELD scores have more urgent need of transplantation and are placed higher in the list irrespective of their time of listing.

HEPATOCELLULAR CARCINOMA AND LIVER TRANSPLANTATION

HCC commonly arises in cirrhotic livers, particularly in patients with hepatitis B and C. Liver transplantation can potentially treat the underlying liver disease as well as the HCC. The selection of patients with HCC for liver transplantation is complicated. Patients with advanced HCC who undergo transplantation have shown disease recurrence and poor survival.⁸ In view of donor liver shortage, transplantation for patients with advanced HCC is not advisable as scarce organs could be directed to patients more likely to benefit from the transplant.

Patients with HCC may not have such poor synthetic function (or high MELD score) to qualify for a liver transplant. As these patients wait for their liver function to deteriorate enough to qualify for transplantation, the underlying HCC may advance such that the patient is no longer a good candidate for transplantation because of the risk of HCC recurrence.

To deal with this problem, UNOS/OPTN does not allow transplantation in patients with advanced HCC by the Milan criteria and gives exception points (based on certain criteria) to patients with limited HCC for additional priority for liver transplantation.

MILAN CRITERIA

The Milan criteria (Table 92-2) are used to identify patients with HCC in whom the tumor burden is small enough to allow good outcome after liver transplantation. The Milan criteria state that transplantation should be performed in those with a single tumor of 5 cm or less or three tumors that are each 3 cm or less, no macrovascular invasion, and no metastasis. Patients who do not meet the Milan criteria are not considered eligible candidates for liver transplantation. Some authors have suggested that the Milan criteria are too restrictive and that acceptable outcomes can be obtained with more liberal tumor criteria (e.g., University of California, San Francisco, criteria).⁹

MELD EXCEPTION POINTS FOR HEPATOCELLULAR CARCINOMA

For patients within the Milan criteria, UNOS/OPTN grants exception points to stage T2 HCC (one tumor ≥ 2 cm and ≤ 5 cm or two or three tumors ≥ 1 cm and ≤ 3 cm). This allows these patients to undergo transplantation earlier in the course of their disease in an attempt to achieve better long-term survival after transplantation. The goal is to prevent the patient from reaching an HCC tumor burden that exceeds the Milan criteria, which would necessitate the patient's being removed from the transplantation waiting list.

Preoperative Imaging

The main objective of preoperative imaging is to provide the surgeon with the necessary information needed to plan and perform liver transplantation and to exclude patients for whom surgery either is not feasible or would be of no benefit. Preoperative radiologic evaluation is used to detect HCC or other malignant disease, to determine the size and patency of the

portal vein and superior mesenteric vein, to assess hepatic arterial inflow, and to evaluate surgical portosystemic shunts and location of varices.

EXCLUSION OF HEPATOCELLULAR CARCINOMA

Patients awaiting liver transplantation undergo contrast-enhanced computed tomography (CT) or magnetic resonance imaging (MRI) to screen for HCC. Ultrasound is used for routine screening of cirrhotics for HCC, but patients being considered for a transplant usually undergo CT or MRI. A multiphase technique with late arterial, portal venous, and delayed phases is used. HCCs derive their blood supply from the hepatic arteries and show hyperenhancement in the arterial phase. They "washout" or become hypoattenuating to the hepatic parenchyma in the portal venous and delayed phases. A peripheral rim of enhancement or "pseudocapsule" may be present on the portal venous or delayed phase (Fig. 92-1). Any hepatic lesion identified is classified by the OPTN classification system. The number and size of each HCC and the presence of any vascular invasion or metastatic disease are noted (Fig. 92-2).

TABLE 92-2 Description of OPTN Class 5 Nodules That Qualify as Hepatocellular Carcinoma for Exception Points		
Class	Size	
5A	≥ 1 cm but < 2 cm	Increased arterial enhancement and washout and pseudocapsule
5A-g	Same as 5A	Increased arterial enhancement and growth by 50% in 6 months
5B	≥ 2 cm but ≤ 5 cm	Increased arterial enhancement and either washout or pseudocapsule or growth by 50% in 6 months
5T	Prior locoregional therapy for HCC	Describes any residual lesion or perfusion defect at prior UNOS class 5 lesion
5X	> 5 cm	Meets criteria for HCC but outside stage T2 and not eligible for exception points

HCC, Hepatocellular carcinoma; OPTN, Organ Procurement and Transplantation Network; UNOS, United Network for Organ Sharing.

OPTN CLASSIFICATION SYSTEM FOR NODULES SEEN ON IMAGING OF CIRRHOTIC LIVERS

OPTN/UNOS has strict radiologic criteria for classification of nodules in cirrhotic livers as HCC. Only class 5 nodules are considered to meet radiologic criteria for HCC and may qualify for automatic exception, depending on stage (see Table 92-2).

PORTAL VEIN EVALUATION

The portal venous system can be assessed by Doppler ultrasound, CT, or MRI. Liver transplantation in patients with extrahepatic portal venous thrombosis or a small-caliber vein is difficult or sometimes impossible. The normal diameter of the extrahepatic portal vein is 8 to 12 mm. The extrahepatic portal vein usually needs to be at least 4 to 5 mm in diameter for a successful portal vein anastomosis. On Doppler examination, portal vein thrombosis is usually depicted as echogenic material within the portal vein. The extent of thrombus should be determined, and the entire extrahepatic portal vein and superior

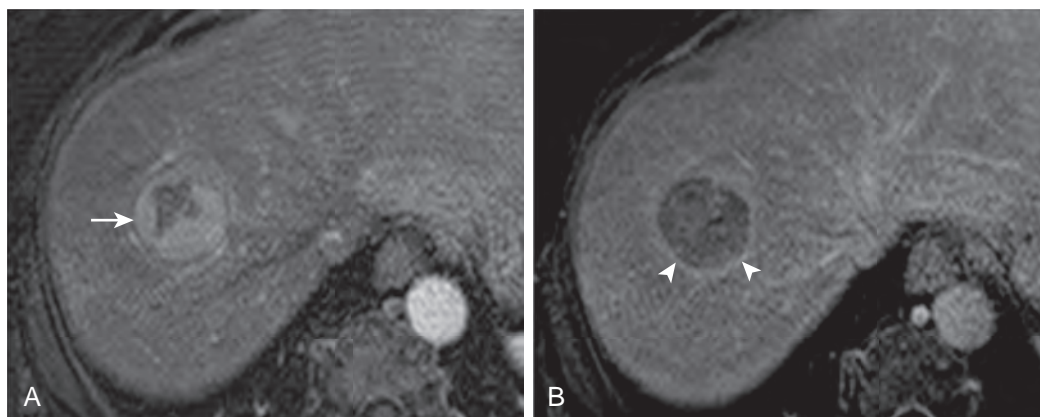


Figure 92-1 HCC identified during pretransplantation evaluation. **A.** Arterial phase of contrast-enhanced MRI shows a hyperenhancing right hepatic lesion (arrow). **B.** A delayed image shows washout of contrast material from the tumor. A peripheral pseudocapsule is noted (arrowheads).

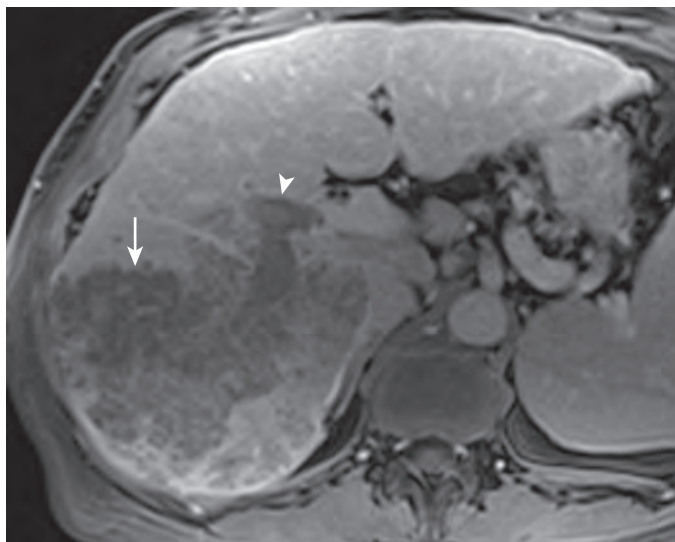


Figure 92-2 Infiltrating HCC with portal venous invasion. Venous phase MR image shows a large infiltrating HCC (arrow) with invasion of the portal vein (arrowhead). The large size and portal venous invasion exclude this patient from liver transplantation (Milan criteria).

mesenteric vein should be evaluated. Although extensive portal vein thrombus was considered a contraindication to OLT in the past, many patients can successfully undergo liver transplantation with modified surgical techniques. In these patients, evaluation of the superior mesenteric vein is critical. If the superior mesenteric vein is patent, placement of an interposition graft or venous jump graft from the superior mesenteric vein to the portal vein is a feasible option.¹⁰ The hepatic veins and inferior vena cava (IVC) also should be evaluated for patency.

HEPATIC ARTERY EVALUATION

Preoperative assessment of recipient hepatic arterial supply is important to ensure adequate hepatic arterial inflow to the transplanted liver. The arterial patency can be assessed on preoperative ultrasound, CT, or MRI. Inadequate hepatic arterial inflow usually results from compression of the celiac trunk by the arcuate ligament or from atherosclerosis. In patients with arcuate ligament compression, simple division of the ligament improves blood flow. Compromised arterial inflow resulting from atherosclerosis usually requires creation of either a supraceliac or an infrarenal aorto–hepatic artery bypass graft.

PORTOSYSTEMIC SHUNT AND VARICEAL EVALUATION

CT and MRI can precisely locate surgical and spontaneous portosystemic shunts and varices that may be encountered. In patients with cirrhosis, surgical portosystemic shunts are often created to decompress portal hypertension and varices to diminish the chance of gastrointestinal hemorrhage. When transplantation is performed, these surgical portosystemic shunts are often ligated so that portal flow to the allograft is not compromised. Likewise, the presence and location of varices are helpful to the surgeon. Varices that are encountered may be ligated. Alternatively, the surgeon may choose to avoid rather

than to ligate certain varices, thereby reducing the potential for hemorrhagic complications.

Locoregional Bridging Therapy for Hepatocellular Carcinoma

Locoregional therapies are used to treat HCC in patients on the transplant waitlist. These are used as bridge strategies with the primary goal of reducing tumor progression to allow patients to be longer on the waitlist. Although bridge strategies are widely used, it is not clear whether they are effective in maintaining patients on the list or improving disease-free survival.^{11,12}

Image-guided transcatheter delivery of therapeutic agents through vessels feeding the HCC is a commonly used bridge therapy that allows more focused delivery of therapeutic material within the tumor. Conventional transcatheter arterial chemoembolization consists of intra-arterial infusion of a drug, such as doxorubicin or cisplatin with or without a viscous emulsion, followed by embolization of the blood vessel with gelatin sponge particles or other embolic agents. Recent advances include use of drug-eluting beads for more controlled and sustained drug release. Radioembolization by transcatheter infusion of microspheres coated with yttrium 90, a beta particle–emitting isotope, into feeding vessels allows delivery of high-energy, low-penetration radiation to the tumor.

Local ablation is a commonly used bridge therapy for small HCCs (single or few) that are accessible either percutaneously or laparoscopically. Multiple ablative techniques, including radiofrequency ablation, microwave ablation, cryoablation, and ethanol injection, are available. In patients with good hepatic function, surgical resection of a solitary HCC is also used as bridge therapy.¹³

Surgical Technique

The main steps of an OLT procedure consist of donor hepatectomy, recipient hepatectomy, hemostasis, and vascular anastomoses followed by biliary anastomosis. The caval anastomosis is the first vascular anastomosis performed. The standard and piggyback techniques are different methods to perform the caval anastomosis (Figs. 92-3 and 92-4). In the standard technique, the recipient's retrohepatic IVC is removed with the recipient's liver. End-to-end anastomosis is then performed twice between the donor and recipient IVC above and below the liver. In the newer piggyback technique, the recipient's IVC is not removed with the recipient's liver. The donor's suprahepatic IVC is anastomosed to the common orifice of the recipient's hepatic veins. The main advantage of the piggyback technique is that it preserves caval flow and reduces hemodynamic instability during the procedure.¹⁴

The portal venous and hepatic arterial anastomoses are done after the caval anastomosis. The portal venous anastomosis is an end-to-end anastomosis. The arterial anastomosis is often performed with a Carrel patch. In this, the donor hepatic artery is harvested at the level of the celiac axis with a patch of the aorta. The aortic patch is then anastomosed to the recipient hepatic artery near the gastroduodenal artery takeoff.

The biliary anastomosis is usually an end-to-end choledochocholedochostomy. A biliary–enteric anastomosis (choledochojejunostomy) is performed in recipients with bile duct

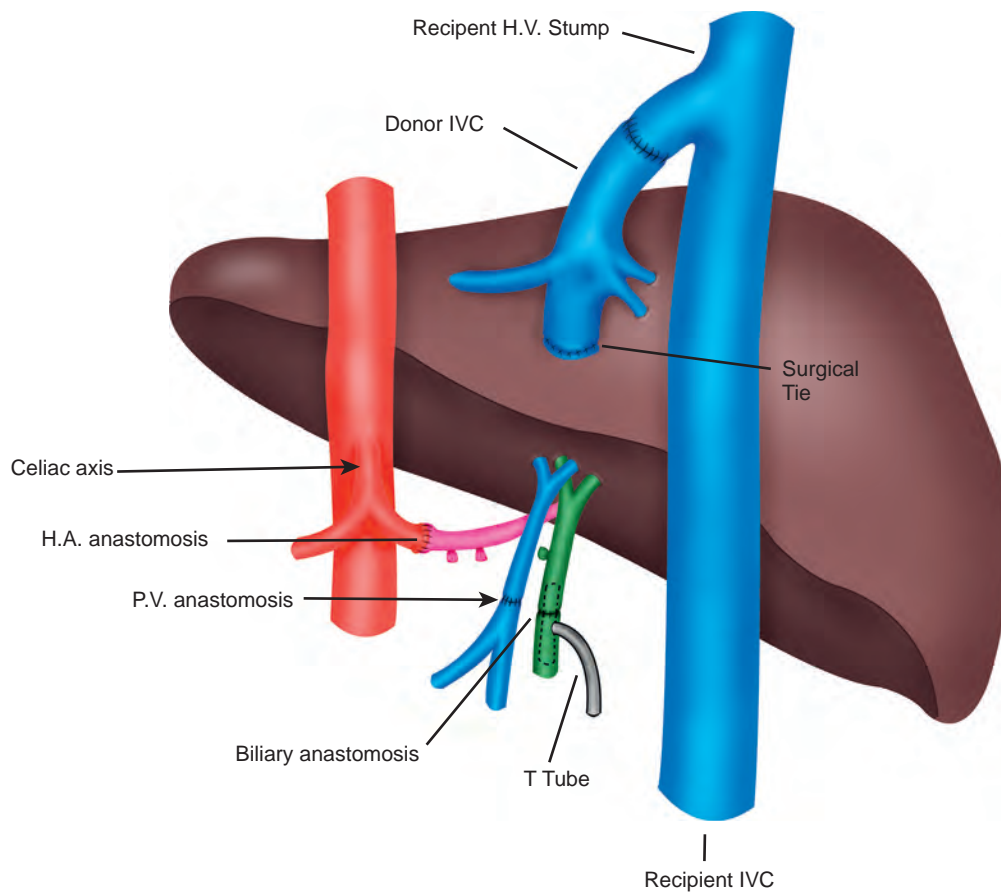


Figure 92-3 Diagram shows surgical anatomy of OLT by piggyback IVC anastomotic technique. The donor's suprahepatic inferior vena cava (IVC) is anastomosed to the common orifice of the recipient's hepatic vein (H.V.). There is an end-to-end hepatic arterial (H.A.) anastomosis of the recipient's hepatic artery near the gastroduodenal artery takeoff with the donor hepatic artery, which is harvested at the level of the celiac axis with a patch of the aorta. An end-to-end portal venous (P.V.) anastomosis and an end-to-end choledochobiliary anastomosis over a T tube are shown.

disease. Traditionally, biliary anastomosis has been performed with T-tube drainage, but some institutions have now moved away from routine use of T-tube drainage for deceased donors.¹⁵ Presence of a T tube allows monitoring of biliary output, supports the anastomosis, and allows access for cholangiography. Other than patient discomfort from prolonged presence of a percutaneous tube, the main limitation of T-tube placement is biliary leakage after its removal.

Shortage of donor organs, primarily in children awaiting a suitable liver for transplantation, has driven the development of reduced size, split liver, and living related donor transplantation techniques. These techniques increase the available supply of donor organs to younger recipients. Reduced size liver transplantation uses a portion of the liver as a graft but is an inefficient use of donor organs. Split liver transplantation, whereby the whole liver is used for transplantation for two recipients, is an attractive means of increasing the use of a limited supply of donor organs to both children and adults.¹⁶ Living related donor transplantation uses a portion of the donor liver. The lateral segment may be used successfully for small or pediatric patients with end-stage liver disease. A larger graft is needed for adult living donor transplantation, and whole right hepatic lobe grafts have been used successfully in many transplantation centers.¹⁷

Living Donor Liver Transplantation

The number of cadaveric donors available for liver transplantation has remained constant for several years. As thousands of patients are on the waiting list, living donor liver transplantation (LDLT) can be a solution for these patients. However, LDLT requires balancing donor risk relative to the recipient outcome and has not become popular in the United States. Only 219 LDLTs were performed in the United States in 2009, probably because of the risk of donor morbidity and mortality.¹ LDLT is more popular in countries with scarcity of deceased donors.

LDLT was initially performed in the 1990s for small or pediatric patients with end-stage liver disease. Procedures using the left lobe or lateral segment were performed at the University of Chicago.¹⁸ Although these techniques were attempted in adult recipients, the smaller left hepatic lobe provided insufficient hepatic mass for most adult patients. The first adult-to-adult right hepatic lobe transplantation was reported in 1993 by Yamaoka and colleagues.¹⁹ The first successful donor right hepatic lobe transplantation was performed in the United States in 1997.²⁰

Other than increasing the pool of potential donors, LDLT has some other advantages. Patients can undergo timely transplantation without waiting for a deceased donor organ. This

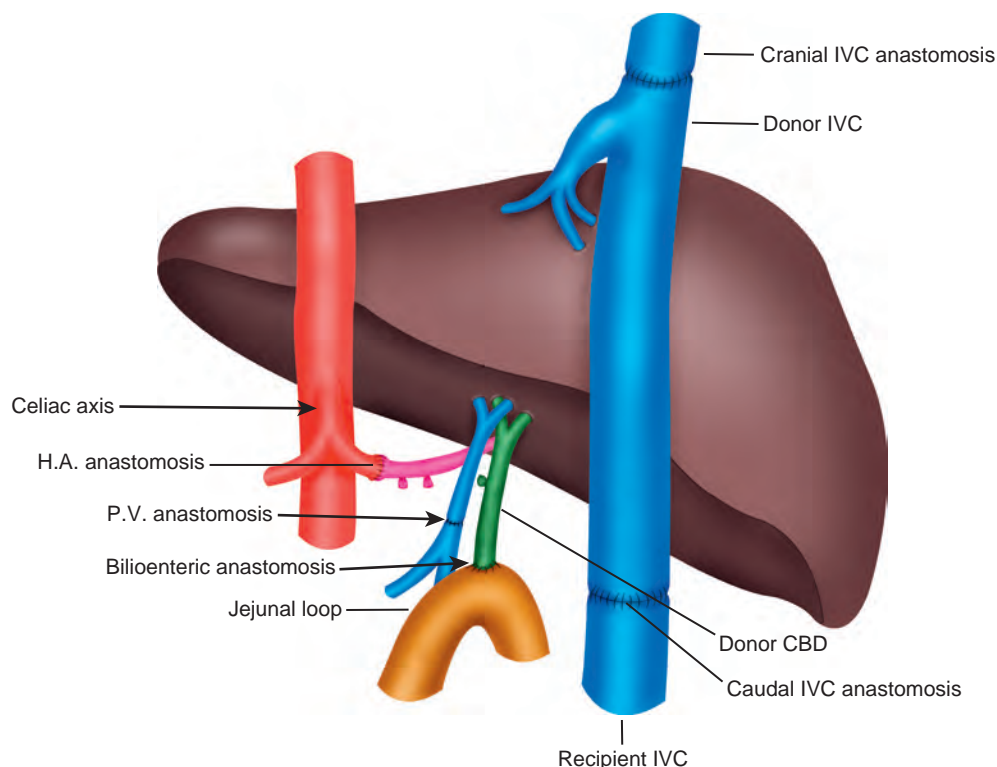


Figure 92-4 Diagram shows surgical anatomy of OLT by standard end-to-end IVC anastomotic technique. End-to-end anastomosis between the donor and recipient inferior vena cava (IVC) is performed cranial and caudal to the liver. A choledochojejunal anastomosis is also demonstrated. CBD, common bile duct; H.A., hepatic arterial; P.V., portal venous.

may confer survival benefit to LDLT, which has been shown to be higher compared with deceased donor transplantation.²¹ A detailed preoperative assessment and clinical management of often critically ill potential recipients are possible. Finally, living donor grafts are obtained from healthy donors who have been extensively screened for disease. Despite these advantages, there are unique risks of LDLT. The risk of donor death is 1.7 per 1000 in the United States.²² Clavien grade 3 or 4 complications are seen in 2.8% of the donors.²²

IMAGING EVALUATION OF THE POTENTIAL LIVING RELATED LIVER DONOR

The ideal screening modality for potential living liver donors would accurately evaluate hepatic parenchyma, provide data for split liver volume assessment, and depict intrahepatic and extrahepatic vascular anatomy before potential partial hepatectomy.²³ MRI is used to depict the vascular variants, hepatic volume issues, and fatty infiltration that may preclude right hepatic lobe donation. Conventional or hepatocyte-specific contrast agent-enhanced MRI can be performed to demonstrate problems with biliary anatomy.²⁴⁻²⁷ Hepatocyte- and biliary-specific contrast agents (e.g., gadobenate dimeglumine, gadoxetate disodium [Gd-EOB-DTPA], mangafodipir trisodium) not only allow dynamic contrast-enhanced scanning but also are differentially taken up by functioning hepatocytes and excreted into the biliary tree. This allows excellent delineation of the biliary anatomy.²⁸

The exquisite spatial resolution of multidetector CT has made it the most widely used modality for the preoperative evaluation of living donors.^{24,29} Rapid scanning makes bolus

timing even more critical; either test boluses or automated triggering is crucial for obtaining images during peak hepatic arterial enhancement. The 2.5-mm collimated images are then obtained during a portal venous (“hepatic”) phase so that portal and hepatic venous anatomy may be displayed. Both the source and reconstructed images should be meticulously reviewed. Volume rendered images are helpful for displaying global anatomy, but many radiologists rely heavily on sliding thick-slab maximum intensity images.

PARENCHYMAL ASSESSMENT

The size of the potential right lobe graft is a crucial determinant of graft viability. A sufficiently large right lobe is needed to prevent the “small for size” syndrome; transplantation of insufficient hepatic mass may result in poor allograft function, graft failure, or the death of the recipient.³⁰ Small grafts are also more prone to sinusoidal injury from increased portal pressures.³¹ Several approaches to assessment of sufficient liver volume for transplantation have been applied; graft weight/recipient standard liver volumes of less than 40% or graft-to-recipient weight ratios of less than 85% are associated with poor outcomes.^{30,32} Both MRI and CT can be used to accurately calculate split liver volumetric measurements of potential donors.

Unenhanced CT or in-phase/out-of-phase MRI is also used to detect fatty infiltration in the potential donor graft.²³ It has been well shown that steatosis increases the likelihood of graft dysfunction and reduces hepatic regenerative function.³³⁻³⁵ Several centers still routinely perform liver donor biopsies to better quantify steatosis.

VASCULAR ASSESSMENT

Anatomic variations of extrahepatic vascular anatomy (e.g., replaced left or right hepatic arteries) are common, well known, and easily demonstrated by CT angiography. The unique contribution of multidetector CT to the evaluation of the prospective right liver donor is its ability to detect variations in arterial and venous anatomy that may traverse the hepatectomy plane.^{36,37} Although adequate hepatic mass may be procured with several techniques (left donor hepatectomy, extended right donor hepatectomy), a traditional right hepatectomy along Cantlie's line, a relatively avascular plane immediately lateral to the middle hepatic vein, is preferred in most institutions. Parenchymal dissection to the hilar plate is performed by ultrasonic dissection. Accurate definition of vascular structures traversing this plane is needed to prevent inadvertent vessel injury and ischemic injury to either the graft or remaining donor liver.

Traditional hepatic arterial anatomy, in which the proper hepatic artery branches into right and left hepatic branches, is seen in only 55% of patients. Although many variants are easily shown at CT, a crucial consideration for donor graft retrieval is the blood supply to segment IV. A middle hepatic artery branch that arises from the right hepatic artery will be disrupted during donor hepatectomy. Inadvertent ligation of this branch during graft retrieval may cause biliary ischemic damage to the remaining donor medial segment. Other significant vascular variants that may affect donor selection include a short right hepatic artery, trifurcation of the common hepatic artery into the gastroduodenal artery and right and left hepatic arteries, and origination of the right or left hepatic arteries before the gastroduodenal artery. Replaced hepatic arteries in the recipient are not absolute contraindications to transplantation, although arterial reconstructions can be more technically demanding. Finally, recipient celiac artery stenosis from atherosclerotic disease or a median arcuate ligament may predispose to graft infarction and biliary complications.²³ Sliding thick-slab maximum intensity projection images obtained from a second portal venous (hepatic) phase are used to display potentially significant hepatic venous variants. Variations in branching of the middle hepatic vein are particularly important because they may necessitate an altered hepatectomy plane. For example, inadvertent ligation of a prominent early branch (>3 mm) of the middle hepatic vein draining segment VIII may result in

segmental hepatic venous congestion in the transplanted liver (Fig. 92-5). The early branch may be spared with a more lateral hepatectomy plane (although this may decrease the volume of the graft), or the surgeon may maintain outflow drainage to segment VIII by directly anastomosing the branch to the recipient IVC. Inferior accessory right hepatic veins are also common variants that may have an impact on graft retrieval; most transplant surgeons will try to preserve inferior accessory veins larger than 3 to 5 mm. If the distance between the vein and the hepatic venous confluence is less than 4 cm, it may be possible to implant both the main and accessory right veins with a single partially occluding clamp on the IVC.²³

Variations in portal venous anatomy also need to be considered before right hepatic lobe donation. Early right portal vein bifurcation or main portal vein trifurcation may make transplantation difficult. The portal vein may be reconstructed on the back table, and vein or interposition grafts may be employed, but this increases the risk of portal vein thrombosis (Fig. 92-6). Portal venous flow to segment IV should also be carefully delineated; flow to the medial segment can arise from either the right or left portal vein; inadvertent disruption of portal venous inflow during donor hepatectomy may result in remaining donor liver ischemic injury. Flow to the entire left lobe through a branch from the right portal vein is an absolute contraindication to organ donation.²³

BILIARY ASSESSMENT

Postoperative biliary leaks and strictures are the most common complication after LDLT. MRI is used to identify aberrant biliary anatomy as inadvertent transection of biliary radicals increases the risk of biliary leak.³⁸ Drainage of the right posterior bile duct into the left hepatic duct and biliary trifurcation are common variants that can lead to bile duct injury in the donor.²⁴

Postoperative Complications

HEPATIC ARTERIAL COMPLICATIONS

Hepatic artery complications include stenosis, thrombosis, pseudoaneurysm, and arteriovenous fistula formation. Arterial complications place the patient at risk for biliary ischemia as

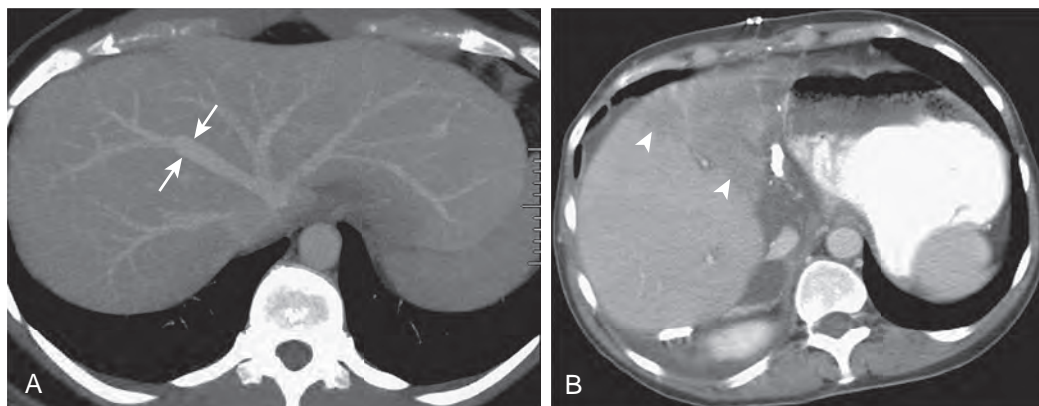


Figure 92-5 Preoperative evaluation of the potential living liver donor. **A.** Thick-slab axial maximum intensity projection CT image shows drainage of segment VIII by a prominent early branch of the middle hepatic vein (arrows). **B.** Enhanced CT shows segmental hepatic venous congestion of the transplanted liver (arrowheads).



Figure 92-6 CT evaluation of the potential living liver donor. Coronal thick-slab maximum intensity projection CT image shows portal venous trifurcation (arrow).

the bile ducts in the transplanted liver receive blood supply only from the hepatic arteries.³⁹ Biliary ischemia results in strictures, abscesses, sepsis, allograft failure, and death.⁴⁰

Normal Postoperative Hepatic Arterial Doppler Findings

After transplantation, hepatic arterial assessment is routinely performed with color and spectral Doppler ultrasound. A baseline study is usually obtained within the first 24 hours after transplantation; additional follow-up imaging is dictated by the patient's clinical course.⁴¹ Careful inspection should assess for any arterial narrowing or focal dilation. Color and spectral Doppler evaluation documents appropriate flow direction and waveform appearance.⁴² The normal main hepatic artery has continuous antegrade flow with a rapid upstroke and resistive index (RI) of 0.55 to 0.8^{39,42-45} (Fig. 92-7). The right and left hepatic arteries should have a similar appearance.⁴²

In the first 72 hours after transplantation, arterial peak systolic velocity and RI may be variable. Median peak systolic velocity is 103 cm/s; however, values range from 13 to 367 cm/s in the first 48 hours.⁴⁶ Early elevated peak systolic velocity with normal RI and waveforms may be due to postoperative edema, variations in the arterial internal diameter, or vessel redundancy.⁴⁶ Gray-scale ultrasound can be used to identify kinks due to vascular redundancy causing spuriously elevated velocities and help differentiate them from stenosis. Adjustment of the Doppler interrogation angle is necessary to accurately measure the velocity at such sites.

High-resistance flow (RI > 0.8, absent or reversed diastolic flow) can be seen in the first 72 hours in almost half the patients and usually returns to normal within 7 to 15 days.⁴⁷ This transient elevation has not been associated with any clinical deterioration or shortened survival time and may be due to postoperative allograft edema or vessel spasm.^{48,49} Low-resistance flow is a good indicator of hepatic arterial complications but can be a normal transient finding in the immediate postoperative period, probably due to anastomotic edema.

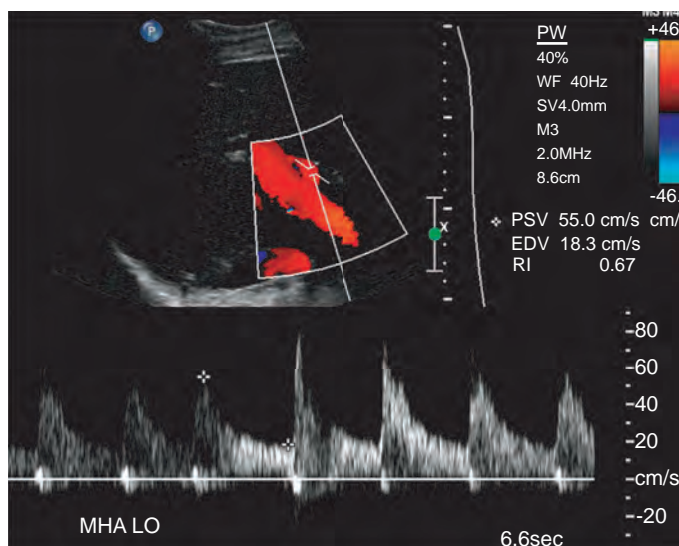


Figure 92-7 Normal main hepatic arterial waveform in a transplant liver with rapid systolic upstroke and normal diastolic flow (RI, 0.67; normal range, 0.55-0.8).

Transient postoperative findings will resolve on follow-up studies, whereas findings due to arterial complications will persist or deteriorate.⁵⁰

Hepatic Artery Thrombosis

Hepatic artery thrombosis (HAT) is the most common vascular complication after liver transplantation with mortality rates of 20% to 60%.^{39,40,51} Occurrence varies in the literature from 3% to 6% in adults,⁵²⁻⁵⁵ with reported occurrence in the pediatric population as high as 12%.^{51,52} Risk of HAT is associated with surgical technique, including arterial conduits, prolonged operation time, variant hepatic arterial anatomy, and retransplantation.^{53,56} The high mortality rate and resultant complications of HAT have led to routine surveillance with ultrasound in the early postoperative period to assess for thrombus.⁴¹

HAT can be divided into early and late categories; early HAT occurs within the first 15 to 30 days after transplantation.^{39,56} Complications of early HAT include fulminant necrosis, liver abscess, sepsis, and graft failure.⁵³ Patients present with massive hepatic necrosis and rapid clinical deterioration, delayed biliary leak and bilomas, or relapsing bacteremia^{51,52} (Fig. 92-8). Development of HAT more than 1 month after transplantation may have a less fulminant course and more variable presenting symptoms.^{57,58}

Ultrasound is diagnostic in up to 92% of cases⁵⁹ by showing absent flow in the main hepatic artery. In some cases of late HAT, development of collaterals can cause tardus-parvus waveforms in the intrahepatic right and left branches.⁵⁸ In general, demonstration of tardus-parvus waveform in the hepatic arteries should raise concern for upstream HAT or hepatic artery stenosis (Fig. 92-9). Causes of false-positive Doppler ultrasound diagnosis of HAT include severe hepatic edema, hypotension, and hepatic artery stenosis.⁶⁰ Evaluation of the main hepatic artery with ultrasound may be limited by body habitus, overlying bowel gas, or bandages, limiting sonographic windows. Confirmation with CT angiography or digital subtraction angiography (DSA) should be considered in any suspicious case (Fig. 92-10).

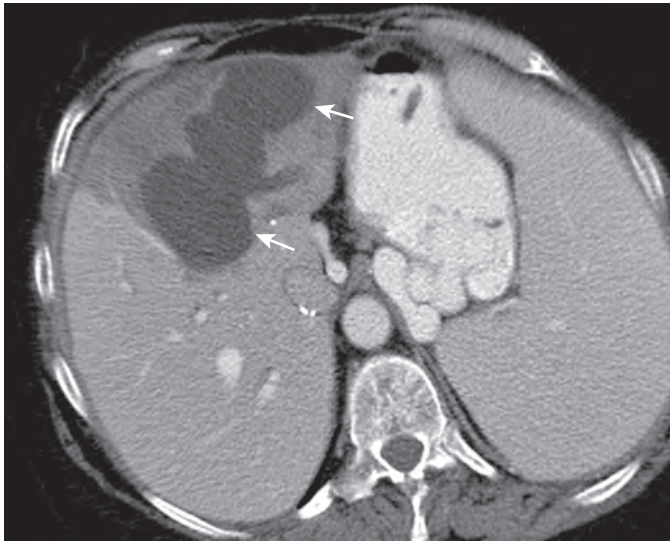


Figure 92-8 Hepatic necrosis after hepatic artery thrombosis. Ischemia has caused biliary and hepatic necrosis in the left hepatic lobe with formation of a large biloma (arrows).

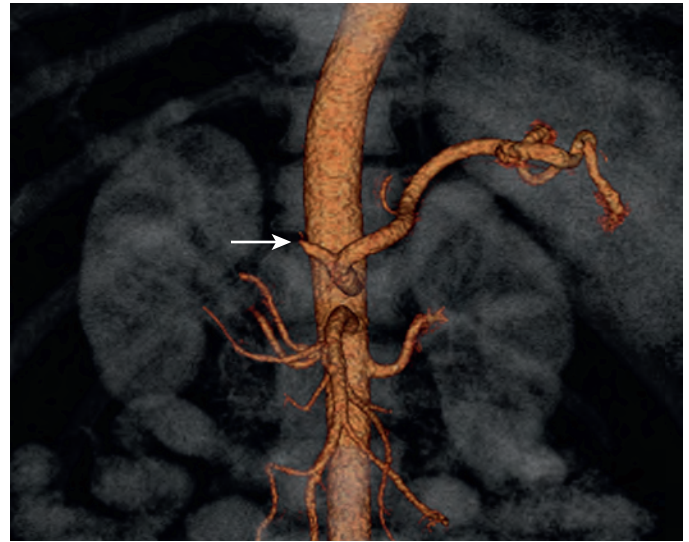


Figure 92-10 Hepatic artery thrombosis. CT angiogram of a patient after OLT shows occlusion of the main hepatic artery (arrow).

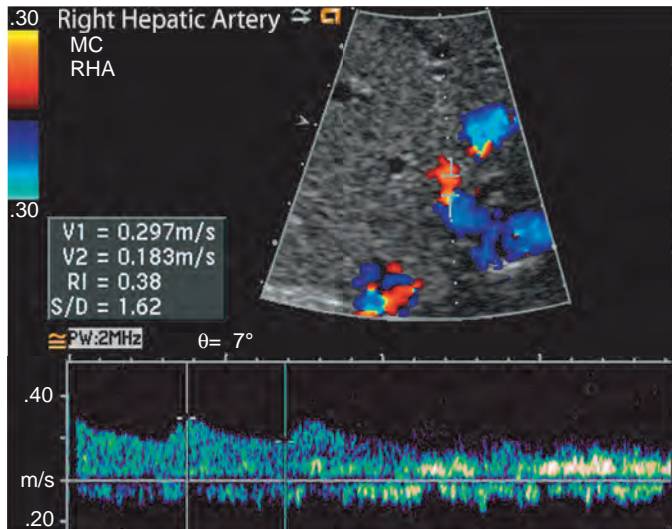


Figure 92-9 Hepatic artery thrombosis. Tardus-parvus waveform (delayed upstroke and decreased RI) in an intrahepatic collateral vessel after hepatic arterial thrombosis.

Treatment of HAT requires retransplantation in up to 75% of cases, often emergent because of massive necrosis.^{51,61,62} Percutaneous or surgical thrombectomy can be considered, particularly in cases with early diagnosis. Early endovascular or surgical revascularization can lead to graft salvage or serve as a bridge to retransplantation.^{63,64}

Hepatic Artery Stenosis

Hepatic artery stenosis (HAS) occurs less often than HAT.^{51,65,66} It is more common at the anastomosis⁴³ but may occur within the graft artery. HAS can lead to complications similar to those of HAT but often has a more insidious course, with symptoms developing during days to weeks. Patients may present with abnormal serum liver enzymes or biliary complications such as nonanastomotic strictures, which occur in up to 22%.⁶⁵ HAS may also be detected without symptoms during routine Doppler ultrasound screening.⁶⁵

As with HAT, color and spectral Doppler ultrasound is the most common screening test for HAS. Direct findings of HAS include turbulent flow and elevated peak systolic velocity of more than 2 m/s in the main hepatic artery at the site of the stenosis⁴³ (Fig. 92-11A). However, the site of stenosis may not be directly visualized, and secondary Doppler findings downstream from the stenosis are useful in diagnosis of HAS. Secondary findings are due to decreased arterial resistance distal to the stenosis and include increased diastolic flow (RI < 0.55) and delayed systolic upstroke (systolic acceleration time > 0.08), with sensitivity and specificity ranges of 73% to 83% and 60% to 73%^{43,45} (Fig. 92-11B). A tardus-parvus waveform may be seen distal to the anastomosis. False positives can occur as RI may be low in the first 72 hours after transplantation.⁴³ The transient postoperative Doppler findings should resolve in a few days, whereas changes due to arterial stenosis or thrombosis will persist or deteriorate. Deterioration of a previously documented normal hepatic arterial waveform in the postoperative period is concerning for arterial complication (HAT or HAS). CT angiography or DSA can confirm findings (Fig. 92-11C, D). DSA allows therapeutic interventions to be performed at the time of diagnosis.

Treatment of HAS includes percutaneous transarterial angioplasty or stent placement, surgical revision with various arterial or venous graft reconstructions, and retransplantation. Patients with biliary complications require retransplantation more often than those without do.⁶⁵ Surgical revision was more common in the earlier literature,⁶⁵ but management with percutaneous angioplasty without or with stent placement is frequently performed with high success rates⁶⁷ and survival rates similar to those of surgical reconstruction⁶⁸ (Fig. 92-11E). Untreated or recurrent HAS after intervention can progress to HAT, and patients with HAS are more likely to develop biliary complications even with HAS treatment.^{51,65-68}

Hepatic Arterial Pseudoaneurysm

Hepatic artery contained rupture or pseudoaneurysm is a rare arterial complication (Fig. 92-12). Pseudoaneurysm can occur at the arterial anastomotic site as a result of infection or be

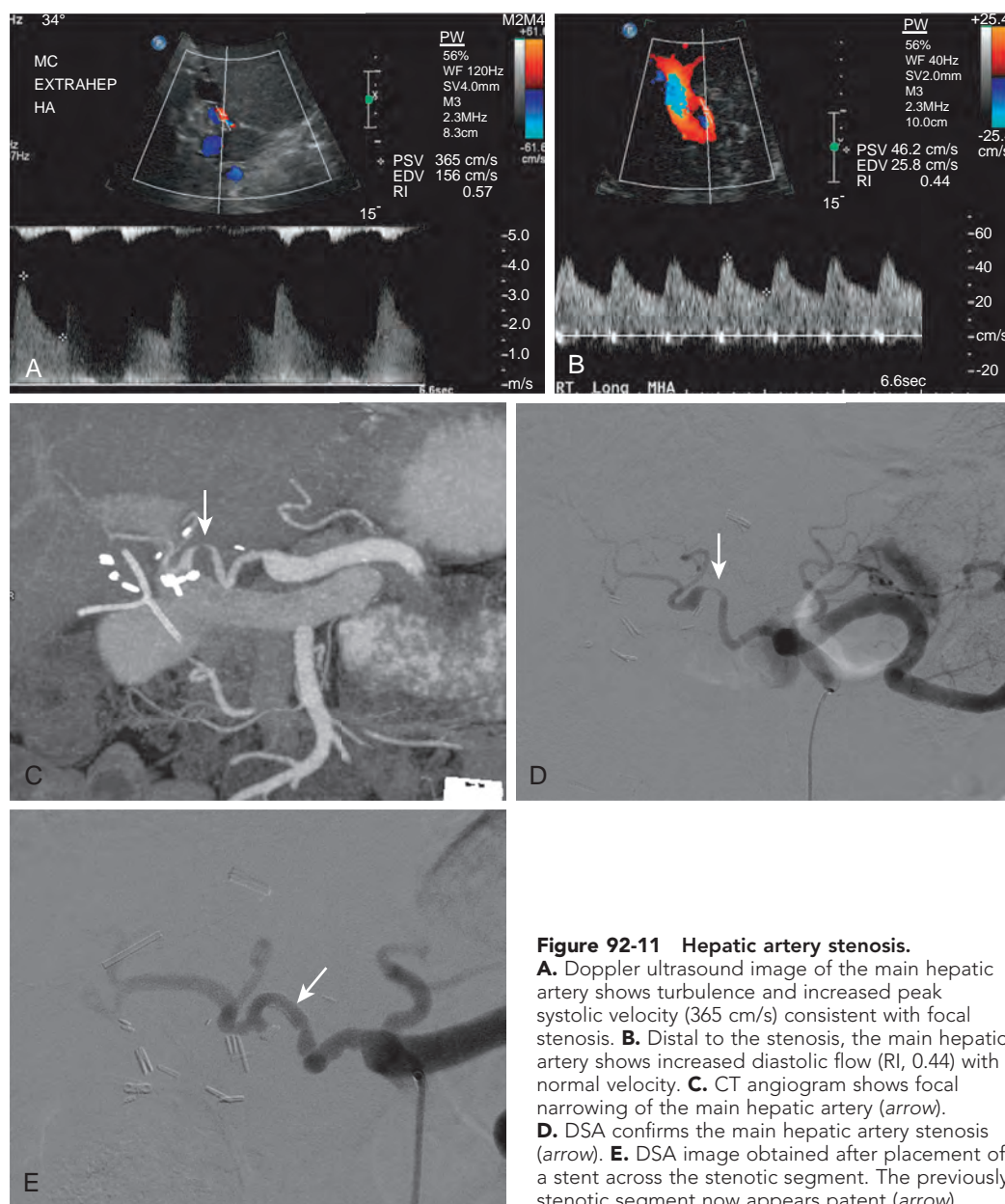


Figure 92-11 Hepatic artery stenosis.

A. Doppler ultrasound image of the main hepatic artery shows turbulence and increased peak systolic velocity (365 cm/s) consistent with focal stenosis. **B.** Distal to the stenosis, the main hepatic artery shows increased diastolic flow (RI, 0.44) with normal velocity. **C.** CT angiogram shows focal narrowing of the main hepatic artery (arrow). **D.** DSA confirms the main hepatic artery stenosis (arrow). **E.** DSA image obtained after placement of a stent across the stenotic segment. The previously stenotic segment now appears patent (arrow).

related to hepatic artery angioplasty procedures. Pseudoaneurysm may be found within the hepatic parenchymal arterial branches as a complication of intervention, such as biopsy or biliary drainage.^{69,70} Pseudoaneurysm rupture can be manifested with gastrointestinal bleeding from hemobilia or hemo-peritoneum and shock.

Ultrasound examination shows a cystic structure along the course of the hepatic artery or within the hepatic parenchyma. With color Doppler assessment, there is disorganized color flow filling the structure.³⁹ Contrast-enhanced CT or MRI can also aid in diagnosis. The pseudoaneurysm will follow blood pool on multiphasic examination, with avid arterial phase enhancement that washes out similar to aortic intensity on later phases.^{40,71} Treatment of hepatic artery pseudoaneurysm depends on location and severity of clinical symptoms. Surgical management with resection is the routine treatment, particularly in mycotic pseudoaneurysm because endovascular material may serve as an infectious nidus. Intravascular hepatic

artery occlusion may serve as a temporizing measure to stabilize patients with active bleeding before surgery. Extrahepatic pseudoaneurysm may be excluded with stent placement across the location, although long-term patency of these stents in small arteries is unknown. Intrahepatic pseudoaneurysm can be treated with coil embolization.^{40,71}

PORTAL VENOUS COMPLICATIONS

Normal Postoperative Portal Venous Doppler Findings

The normal post-transplantation portal vein has smooth walls and an anechoic lumen with mild anastomotic narrowing up to 0.5 cm, probably of no significance in the absence of clinical abnormalities. The anastomosis may be visible as an echogenic shelllike ring in the portal vein wall (Fig. 92-13). Doppler analysis shows continuous forward flow toward the liver with mild respiratory variation. Flow velocity in the main portal vein is

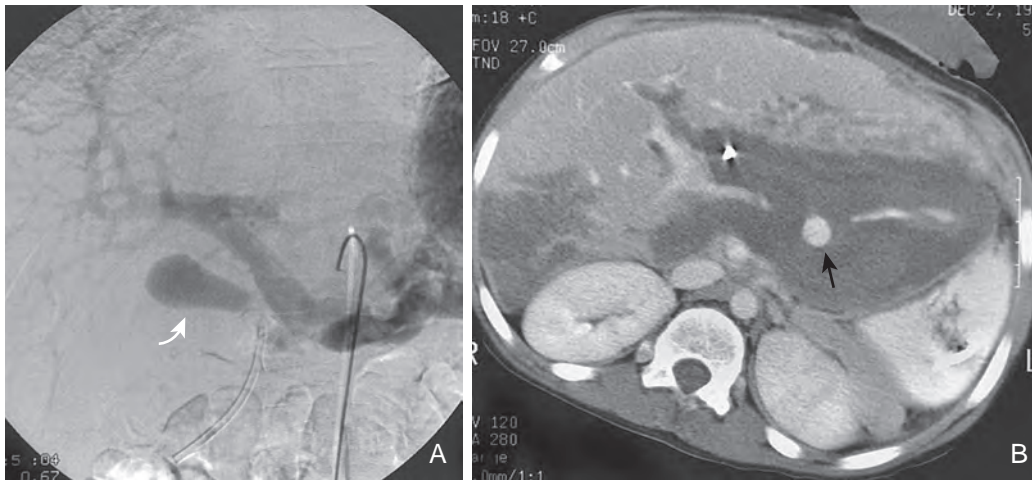


Figure 92-12 Hepatic artery pseudoaneurysm. **A.** Celiac arteriogram demonstrates a hepatic arterial pseudoaneurysm (arrow) that was surgically repaired. **B.** Another patient with a ruptured hepatic arterial pseudoaneurysm. Note the large left subhepatic space hematoma. The pseudoaneurysm (arrow) is depicted as a focally enhanced enlargement of the artery.

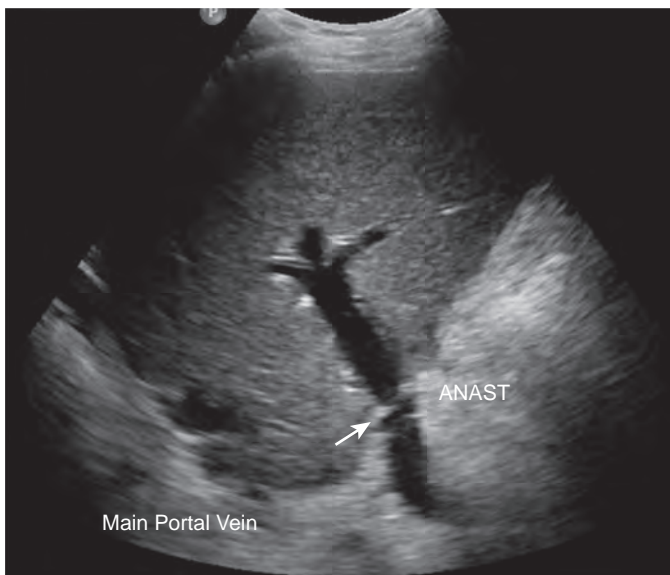


Figure 92-13 Normal ultrasound appearance of the main portal vein after OLT. An indentation is noted at the anastomotic site (arrow).

variable, with velocities decreasing over time after transplantation on serial examinations.³⁹

Portal Venous Stenosis and Thrombosis

Portal vein complications include stenosis and thrombosis. They occur in 1% to 2% of transplant patients, particularly in the pediatric and living related donor population because of small or short graft vein size.^{51,55,64} Causes include misalignment or size discrepancy between the donor and recipient, hypercoagulable state of the recipient, thrombus from portal venous bypass catheter, or prior portal vein surgery.⁵¹ Patients present with signs of portal hypertension or hepatic failure. Portal vein stenosis is seen at ultrasound examination with narrowing at the anastomosis and color aliasing. Velocity in the stenotic area is three to four times greater than velocity upstream from the stenosis^{72,73} (Fig. 92-14).

Treatment options for portal vein stenosis include percutaneous thrombolysis, angioplasty or stent placement, and surgical thrombectomy or stenosis with anastomotic revision or

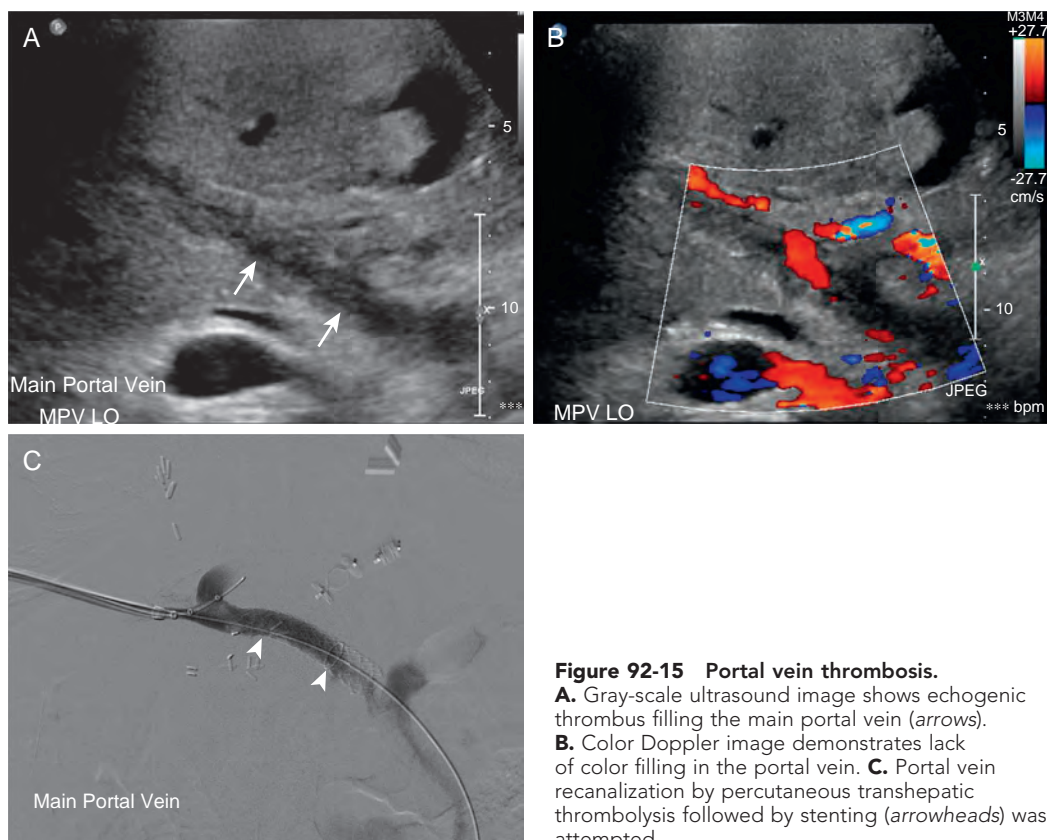
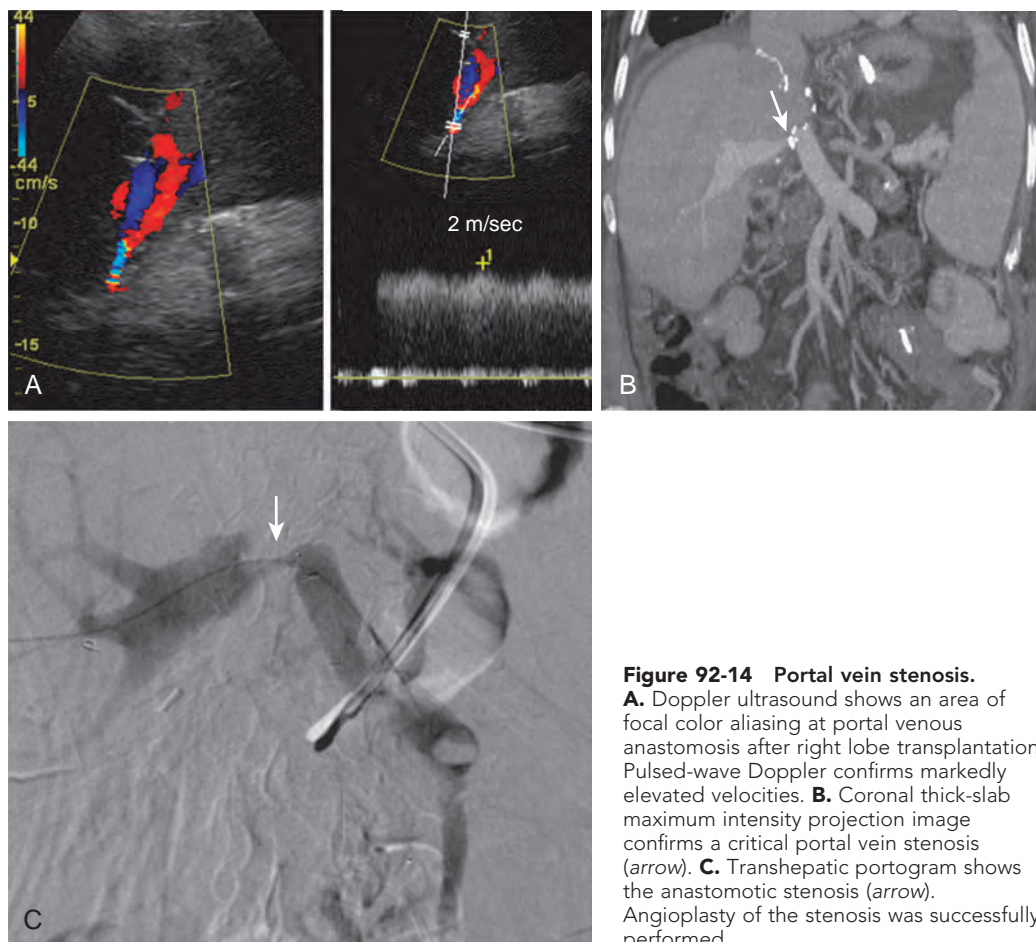
venous jump graft.^{39,51} Percutaneous balloon angioplasty is performed through a peripheral portal vein branch. The right portal vein is preferred because of its straight course. The stenosis is treated with balloon angioplasty until the pressure gradient is less than 5 mm Hg. Patients with persistent pressure gradient after angioplasty or recurrent stenosis after treatment are usually treated with stent placement. Balloon angioplasty has 50% patency at 6 months, with stent patency of 100% in 47 months.⁷⁴

Portal vein thrombus is seen at ultrasound examination as hypoechoic or heterogeneous thrombus within the vessel and little or no color or power Doppler flow³⁹ (Fig. 92-15). Treatment of acute portal vein thrombus includes thrombolysis, thrombectomy, anastomotic revision, and retransplantation.⁷⁵

HEPATIC VEIN AND INFERIOR VENA CAVA COMPLICATIONS

IVC and hepatic vein complications of OLT are rare, occurring in less than 1% to 2% of transplants, and generally are due to stenosis or thrombosis.^{51,76} Knowledge of the type of venous reconstruction is often critical for imaging interpretation as IVC and hepatic vein stenosis and thrombosis typically occur near the anastomosis.⁷² End-to-end caval reconstruction produces suprahepatic and infrahepatic anastomoses, each of which should be evaluated for stenosis. The piggyback technique joins the donor IVC with the recipient's hepatic vein confluence while maintaining a blind-ended stump of the donor's retrohepatic IVC (Fig. 92-16).

Normal hepatic veins and IVC have triphasic spectral waveform due to transmitted cardiac pulsation (Fig. 92-17). In patients with IVC stenosis, the cardiac pulsations are not transmitted to the hepatic veins, which results in monophasic waveforms within the hepatic veins, IVC, or both^{76,77} (Fig. 92-18). Of note, in the postoperative period, it is not uncommon to see abnormal monophasic waveforms or turbulence within the hepatic veins or IVC. This is often secondary to anastomotic edema or compression from hematoma or fluid and should resolve over time.⁵⁰ The IVC anastomosis may be focally narrowed, and color aliasing from increased turbulent flow may be visualized (Fig. 92-19). A threefold or fourfold velocity gradient with the prestenotic segment can be seen in IVC stenosis.⁴⁰ Hepatic vein stenosis is more common in living donor transplants, and sixfold increases in velocity have been reported.⁷⁶



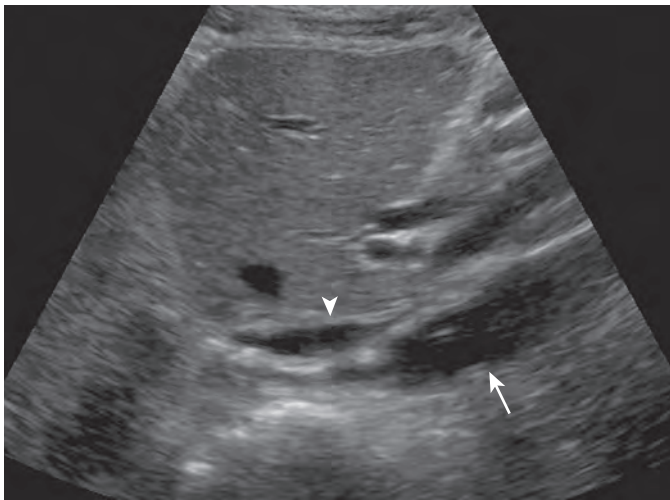


Figure 92-16 Piggyback IVC anastomosis. Sagittal ultrasound image shows ligated donor infrahepatic IVC (arrowhead) and recipient IVC (arrow).

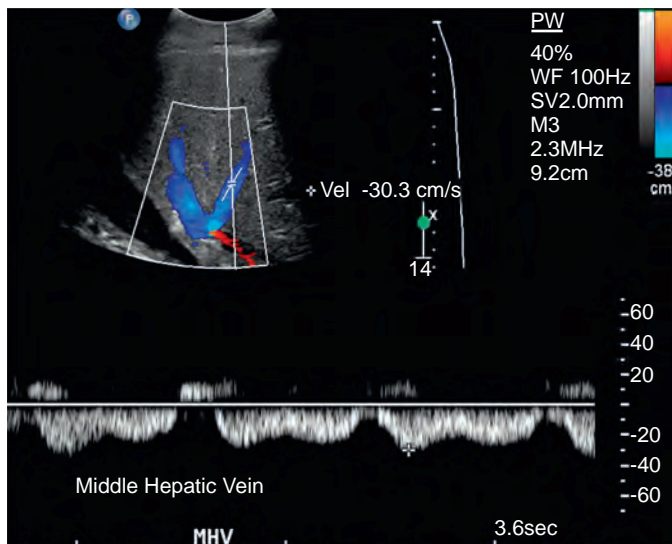


Figure 92-17 Normal hepatic venous waveform. Normal triphasic hepatic venous waveform with a peak above the baseline representing flow away from the heart and two peaks below the baseline indicating flow toward the heart.

Remembering that IVC and hepatic vein complications are rare, abnormal ultrasound findings should always be correlated with the patient's clinical presentation. Clinical presentation varies on the basis of the location and severity of obstruction, but symptoms include hepatomegaly, ascites, pleural effusions, and edema.⁷⁸ In clinically suspected cases, multiplanar CT or MRI may demonstrate focal IVC or anastomotic narrowing, hepatic vein enlargement, and abnormal liver perfusion typical of Budd-Chiari syndrome or hepatic congestion.⁴⁰ Venography is the "gold standard" but is invasive and usually reserved for cases in which there is a high index of suspicion. Angioplasty and expandable stents have proved useful to treat IVC and hepatic vein stenosis.^{40,79}

IVC or hepatic vein thrombosis may have imaging findings similar to those of stenosis. Echogenic intraluminal filling defects and decreased color Doppler flow are demonstrated on

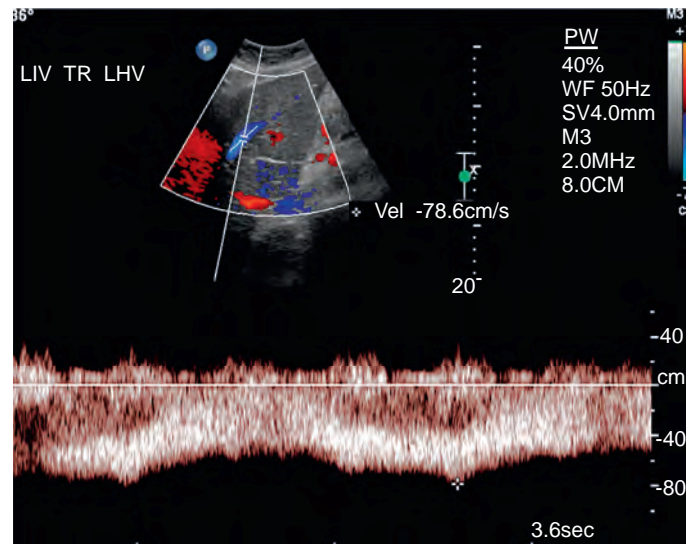


Figure 92-18 Monophasic hepatic venous waveform. Monophasic hepatic venous waveform is seen in patients with hepatic venous outflow obstruction but is nonspecific and can be present without obstruction.

ultrasound⁴⁰ (Fig. 92-20). Multiplanar contrast-enhanced CT or MRI can usually better illustrate the extent of thrombus. An important thing to know is that thrombus normally develops in the piggyback retrohepatic IVC stump, and this finding should not be misdiagnosed as IVC thrombosis.⁸⁰

BILIARY COMPLICATIONS

Biliary complications are a significant cause of morbidity and mortality in OLT.⁸¹ However, with better patient and organ selection and improvement in immunosuppression and surgical techniques, the incidence of these complications has significantly decreased. Nevertheless, biliary complications are still seen in 5% to 25% of patients.⁸² Most occur early, typically within the first 3 months.^{39,78} However, exceptions include stones and strictures, which may develop months to years after transplantation.⁸⁰ In general, biliary complications can be classified as due to obstruction or leak.

Normal Postoperative Cholangiography Findings

In patients with end-to-end choledochocholedochostomy, the donor and recipient ducts should be smooth and uniform in caliber. Mild smooth anastomotic narrowing is common and usually insignificant in asymptomatic patients. On occasion, size discrepancies can exist between the respective ducts, mimicking anastomotic obstruction or stenosis.⁸³ Residual cystic ducts may be present in the donor or recipient system, or both, and should not be confused with leaks. If a T tube is used, it is typically inserted in the recipient duct, more than 5 mm distal to the anastomosis to minimize the risk of ischemia, with the proximal limb bridging the anastomosis. Direct cholangiography should show no extravasation with drainage of contrast material distally into duodenum (Fig. 92-21).

Biliary Obstruction

Biliary obstruction is most often secondary to stricture formation and may be classified as anastomotic or nonanastomotic.

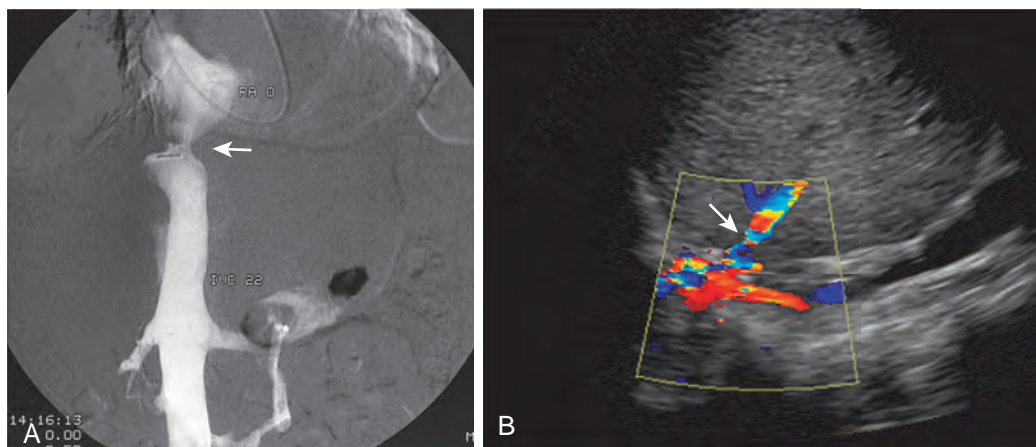


Figure 92-19 Suprahepatic caval stenosis. **A.** Color Doppler image shows focal aliasing at piggyback anastomosis. Hepatic venous flow (not shown) was monophasic. **B.** Venacavography in another patient shows significant narrowing at the suprahepatic caval anastomosis (arrow). This was successfully treated with balloon angioplasty.

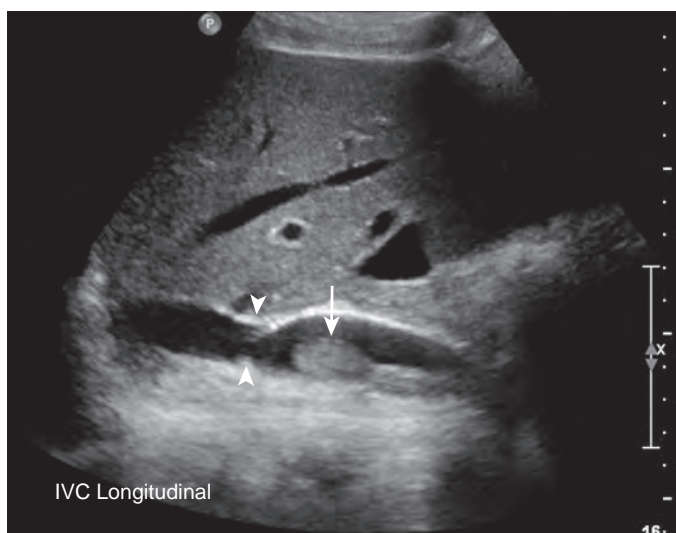


Figure 92-20 IVC thrombosis. Gray-scale ultrasound image shows nonocclusive echogenic caval thrombus (arrow) adjacent to the caudal IVC anastomosis (arrowheads) in a patient who had end-to-end IVC anastomosis.

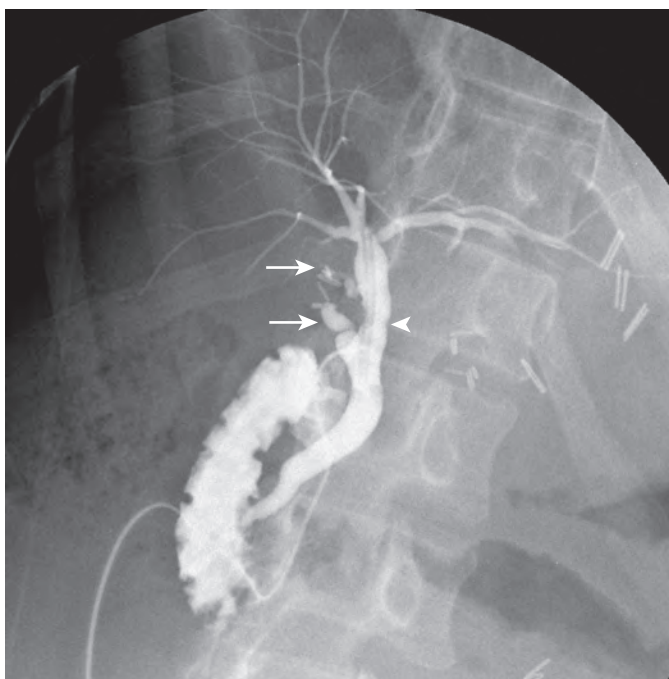


Figure 92-21 Normal postoperative T-tube cholangiogram. T-tube insertion is a few millimeters distal to the anastomosis in the recipient duct (arrowhead). Injected contrast material outlines the biliary tree without any narrowing or filling defect and flows into the duodenum without obstruction. Both donor and recipient cystic duct stumps are present in this patient (arrows). This should not be confused with a leak.

The incidence of biliary stricture is 12% for deceased donors and 19% for living donors.¹⁵ OLT patients with biliary obstruction present clinically with signs of graft dysfunction and abnormal biliary enzymes (total bilirubin, alkaline phosphatase). However, clinical findings are often ambiguous and can be confused with rejection, and imaging is often necessary for diagnosis.⁸³ In postoperative patients with a T tube, direct cholangiography through the existing T tube is the preferred method of evaluating the biliary system. Magnetic resonance cholangiopancreatography and ultrasound can be used in patients without a T tube or who have a biliary-enteric anastomosis.

Anastomotic Biliary Stricture

Anastomotic strictures are due to the surgical technique or fibrosis at the anastomotic site.⁸⁴ Although most anastomotic strictures are manifested within the first 3 months, they can become evident years after transplantation.^{85,86}

Clinically significant anastomotic stenosis is usually characterized by smooth proximal biliary ductal dilation to the

level of the anastomosis (Fig. 92-22). With contrast cholangiography, filling defects corresponding to biliary debris, sludge, or stones may be seen proximal to the stenosis. Ultrasound shows proximal biliary ductal dilation and echogenic debris or stones. Ultrasound is not as reliable as MR cholangiography, which appears more sensitive at detecting biliary complications, including stenosis.⁸⁷⁻⁸⁹ Nevertheless, ultrasound or MR cholangiography may be inconclusive, demonstrating no significant biliary dilation or abnormality, even in patients with clinically significant obstruction. Therefore, when no T tube is present, direct cholangiography with endoscopic retrograde



Figure 92-22 Biliary anastomotic stricture. Endoscopic retrograde cholangiopancreatography image shows a tight biliary anastomotic stricture (arrow). Endoscopic stenting was performed.

cholangiopancreatography or percutaneous transhepatic cholangiography may be required for diagnosis and can facilitate treatment with balloon angioplasty or stenting. On occasion, surgical revision, usually to a choledochojejunostomy, must be performed.⁸⁶

Nonanastomotic Strictures

Compared with anastomotic strictures, nonanastomotic strictures are more menacing because of their high association with biliary ischemia. Acceptance of older donors, donors with cardiac death, and donors with extended criteria has resulted in an increase in incidence of nonanastomotic strictures.^{90,91} Patients with bilioenteric reconstruction or history of primary sclerosing cholangitis are also prone to development of nonanastomotic strictures.⁷¹

Nonanastomotic biliary strictures are manifested clinically as cholestasis or episodes of cholangitis. About half the cases present within the first year; the rest gradually present during several years after transplantation.⁹² The strictures are typically hilar but can be intrahepatic and involve multiple sites. Intrahepatic peripheral biliary involvement is more common with late presentation of nonanastomotic stricture.⁹² Nonanastomotic strictures are often due to biliary ischemia or necrosis caused by hepatic arterial thrombosis or stenosis (macroangiopathic form). A microangiopathic form is due to injury to peribiliary vascular plexus by ischemia-reperfusion or immunologic injury.⁹¹ Recurrent primary sclerosing cholangitis can also cause nonanastomotic strictures.

In patients with nonanastomotic strictures, direct cholangiography demonstrates irregular narrowing or obstruction with focal areas of biliary dilation (Fig. 92-23). There may be focal collections of contrast material pooling within the liver parenchyma, consistent with bilomas. Filling defects due to stone or debris may be present. MRI can show biliary



Figure 92-23 Biliary nonanastomotic stricture. Endoscopic retrograde cholangiopancreatography image shows an irregular hilar stricture (arrow). Multiple filling defects are present in the proximal dilated biliary radicals (arrowheads), representing debris.

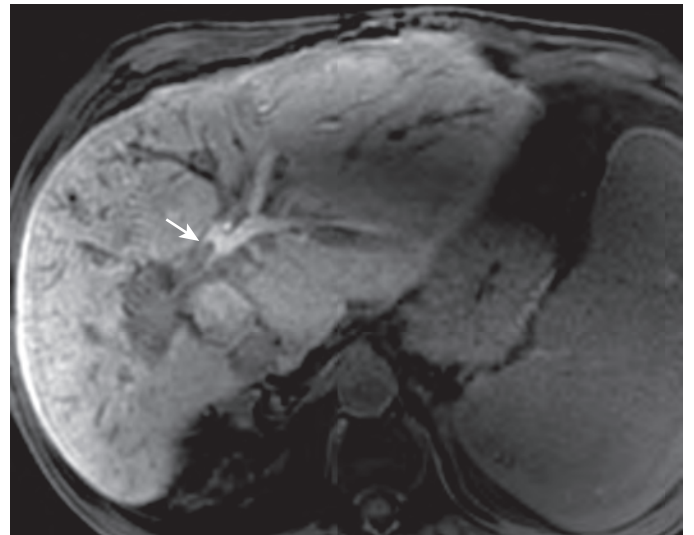


Figure 92-24 Biliary nonanastomotic stricture. Delayed hepatocyte phase MRI with use of hepatobiliary contrast agent (Gd-EOB-DTPA). Excreted contrast material in the biliary duct shows an ischemic biliary hilar stricture (arrow).

dilation and sloughed mucosal casts within the biliary tree, but normal-appearing ducts are not uncommon in the acute setting (Fig. 92-24).

Color Doppler ultrasound should be used to exclude ischemia in all patients with nonanastomotic strictures. Biliary ischemia can be manifested as a spectrum of findings reflecting the location and severity of vascular compromise. Arterial stenosis can result in fibrotic strictures or obstructing casts of sloughed mucosa or sludge. Alternatively, severe ischemia or infarction

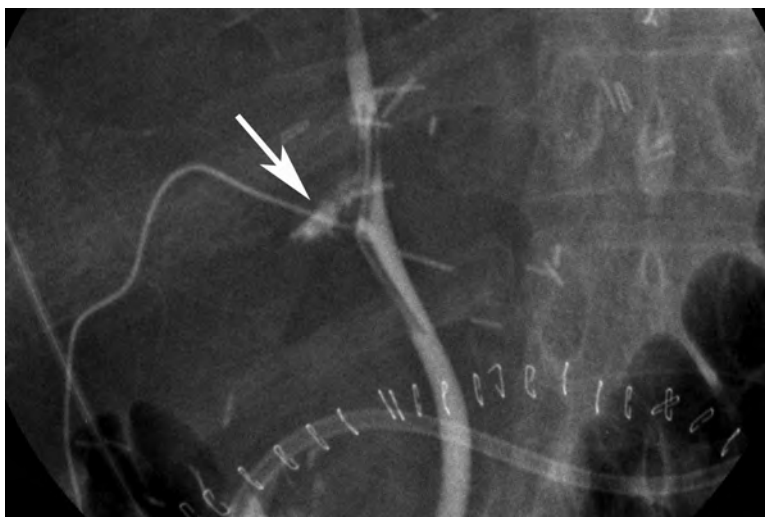


Figure 92-25 Biliary anastomotic leak. Cholangiography through an existing T tube shows biliary leak at the anastomosis (arrow).

can result in biliary necrosis, obstruction, or leak. Careful sonographic interrogation of the hepatic artery and its branches should be performed, although contrast-enhanced CT or MRI is occasionally required. Typically, hepatic arterial abnormalities precede biliary abnormalities by 1 to 3 weeks. Because biliary dilation is minimal in the early stages of stricture formation, sonography is inadequate to examine the intrahepatic bile ducts.⁹³

Ischemic strictures may temporarily respond to balloon angioplasty or stenting, but repeated intervention is usually necessary.⁹⁴ Ultimately, surgical revision or retransplantation is required in many cases.

Biliary Leak

The incidence of biliary leak is about 7.8% for deceased donors and 9.5% for living donors.¹⁵ Biliary leaks are manifested either in the first month after OLT or later immediately after removal of the T tube.⁹¹ The common locations of biliary leak after OLT are the biliary anastomosis (Fig. 92-25), the cystic duct stump (Fig. 92-26), and the T-tube insertion site. Leaks can also occur along the resection margin in partial living donor transplants. Because biliary ischemia may lead to necrosis and leak, non-anastomotic leaks should raise concern for hepatic arterial injury and indicate emergent sonographic evaluation. Most bile leaks are managed by biliary stenting.^{95,96} Small leaks may close spontaneously. Repeated surgery may be required for large leaks. Large leaks can be a significant cause of morbidity or death owing to increased risk of infection in immunocompromised patients, and large bilomas associated with biliary leaks have to be drained.

REJECTION

Hepatic allograft rejection is the most common cause of late allograft failure. Acute cellular rejection usually occurs in the first 2 weeks after transplantation and affects 50% to 100% of the allografts.⁹⁷ It is usually treated by added immunosuppression. Chronic ductopenic rejection occurs in about 8% of the patients and is manifested 6 weeks to 6 months after transplantation.⁹⁷ Ductopenic rejection causes a spectrum of abnormalities ranging from mild loss of bile ducts and mild

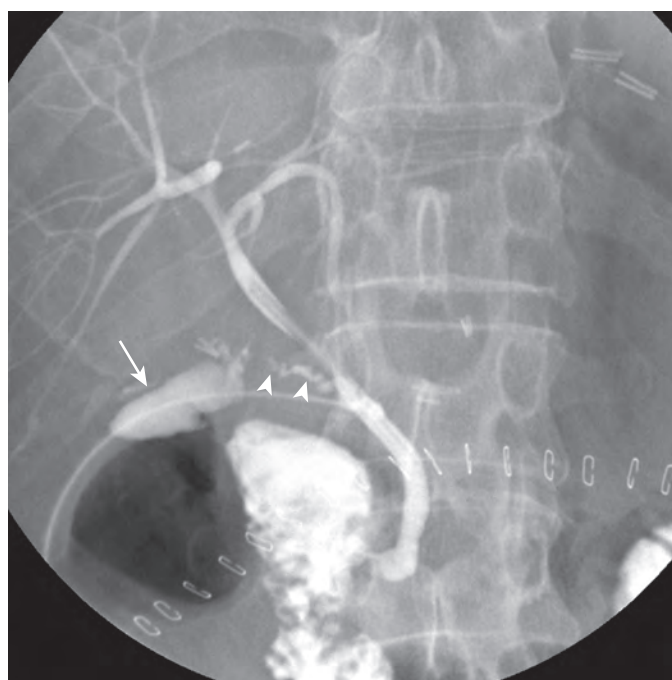


Figure 92-26 Cystic duct stump leak. Cholangiography through an existing T tube shows biliary leak (arrow) at the cystic duct stump (arrowheads).

cholestasis, which is potentially reversible, to a severe form in which most interlobular and septal bile ducts are lost, resulting in severe cholestasis that is unresponsive to therapy. Severe ductopenic rejection is often associated with an arteriopathy of medium-sized hepatic artery branches.

The role of imaging in patients with rejection is largely to exclude other vascular or biliary causes of graft dysfunction. Imaging is neither sensitive nor specific for detection of rejection. The diagnosis of rejection is established by histopathologic evaluation after liver biopsy. Cholangiography may show variable degrees of poor filling, narrowing, or stretching of the bile ducts. Arteriography may show varying degrees of narrowing, stretching, or slow flow in intrahepatic arteries.⁹⁸ Loss of hepatic

artery diastolic flow on Doppler examination is neither a specific nor sensitive finding of allograft rejection.⁴⁸

FLUID COLLECTIONS

Hematomas, seromas, and bilomas are common postoperative fluid collections. Hematomas are identified by their high attenuation on CT. Hematomas change in character over time and become low attenuation. Most collections do not cause any symptoms and resolve spontaneously. Development of wall enhancement or gas in a fluid collection suggests infection. Infected collections and bilomas need to be drained. This can be done percutaneously with imaging guidance.

POST-TRANSPLANTATION MALIGNANT DISEASE

Solid organ transplant recipients are at a higher risk for development of malignant disease. Long-term exposure to immunosuppressive agents and increased risk of oncogenic viral infection are probable causes. Nonmelanoma skin cancer, post-transplantation lymphoproliferative disorder (PTLD), Kaposi's sarcoma, and anogenital tumors are the most common post-transplantation tumors.

PTLD is a cause of morbidity and mortality in post-transplantation patients. It represents a spectrum of diseases ranging from indolent polyclonal proliferation to aggressive lymphoma. Infection by Epstein-Barr virus (EBV) in an immunosuppressed host induces diffuse polyclonal B-lymphocyte proliferation, which results in PTLD. The risk factors include recipient EBV seronegativity, younger recipient age, older donors, high levels of immunosuppression, and antilymphocyte therapies.⁹⁹ EBV infection-associated PTLD occurs in the first 1 to 2 years after liver transplantation, whereas non-EBV-related PTLD occurs later.

PTLD occurs more frequently in the pediatric transplant population because of the higher likelihood of pretransplantation EBV seronegativity. The changes in immunosuppression regimens with lower levels of tacrolimus and cyclosporine and less steroid use has decreased the incidence of PTLD.⁹⁹ Recent data indicate that the incidence of PTLD is now 1.7% for pediatric liver transplants, which is lower than in earlier reports.⁹⁹

Virtually any body tissue can be involved, but the abdominal cavity is the most common site of PTLD. Extranodal disease

(80%) is more common than nodal disease (20%) in the abdominal cavity.¹⁰⁰ The gastrointestinal tract and liver are most often involved in the abdomen. The distal small bowel and proximal colon are the most common sites in the gastrointestinal tract.^{100,101} On imaging, bowel involvement can be manifested with wall thickening, eccentric mass, or luminal ulceration. Liver involvement can be in the form of low-attenuation hypovascular nodules, diffuse infiltration, or porta hepatis mass.¹⁰⁰⁻¹⁰² Splenomegaly or diffuse low-attenuation nodules (less common) can be manifested with splenic involvement.¹⁰⁰⁻¹⁰² Opportunistic infections can have a similar appearance in solid organs and need to be considered in the differential diagnosis. CT/PET is a useful imaging examination for the detection of multifocal PTLD and for assessment of responses to therapy (Fig. 92-27).

PTLD is initially treated with reduction in immunosuppression. Chemotherapy and rituximab (a monoclonal antibody) are used in unresponsive cases.¹⁰³ The mortality of PTLD is high despite treatment.

Patients undergoing liver transplantation for HCC are at risk for recurrence related to initial tumor stage. Poor prognostic indicators for recurrent HCC include vascular invasion, spread to extrahepatic lymph nodes, bilobar tumor, and size larger than 3 cm. Patients undergoing liver transplantation with an incidentally detected HCC found at sectioning of the explant have a low incidence of recurrence. In patients undergoing liver transplantation for HCC, recurrent tumor most commonly involves the lungs, allograft, local and distant lymph nodes, adrenal gland, and bone.¹⁰⁴ Patients with cholangiocarcinoma also have a high recurrence rate after transplantation, and cholangiocarcinoma is considered a contraindication to liver transplantation.¹⁰⁵

Summary

Liver transplantation has become the standard treatment of many patients with end-stage liver disease. Long-term patient and graft survival has continued to improve as a result of improved surgical techniques and improved immunosuppressive therapy. Radiologic imaging has an important role in proper patient selection and providing information that may alter the surgical technique. Most important, early radiologic recognition and treatment of postoperative complications are necessary to lower postoperative morbidity and mortality.

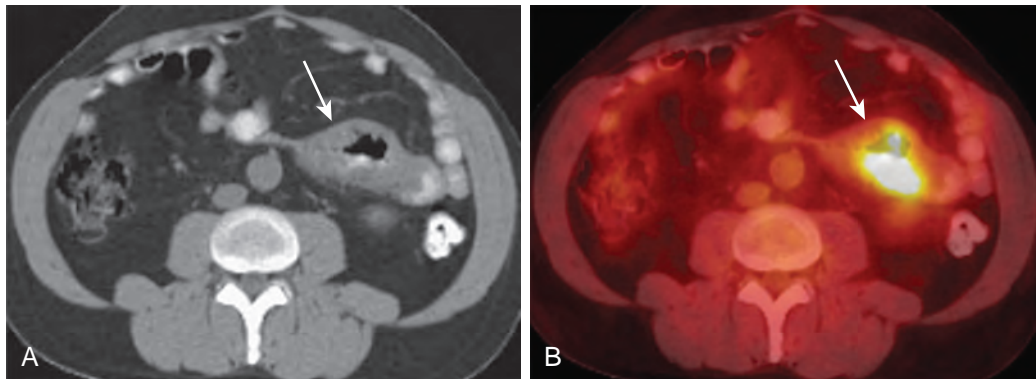


Figure 92-27 Post-transplantation lymphoproliferative disease. A. CT shows focal thickening of proximal jejunum 3 years after transplantation (arrow). The patient presented with melena. **B.** CT/PET shows that the segment is markedly FDG avid (arrow).

REFERENCES

- Organ Procurement and Transplantation Network (OPTN) and Scientific Registry of Transplant Recipients (SRTR): OPTN/SRTR 2010 Annual Data Report, Rockville, Md, 2011, Department of Health and Human Services, Health Resources and Services Administration, Healthcare Systems Bureau, Division of Transplantation.
- Akamatsu N, Sugawara Y: Liver transplantation and hepatitis C. *Int J Hepatol* 2012;68:6135, 2012.
- Leong J, Im GY: Evaluation and selection of the patient with alcoholic liver disease for liver transplant. *Clin Liver Dis* 16:851–863, 2012.
- Agopian VG, Kaldas FM, Hong JC, et al: Liver transplantation for nonalcoholic steatohepatitis: The new epidemic. *Ann Surg* 256:624–633, 2012.
- Charlton MR: Improving long-term outcomes after liver transplantation. *Clin Liver Dis* 18: 717–730, 2014.
- Milkiewicz P, Wunsch E, Elias E: Liver transplantation in chronic cholestatic conditions. *Front Biosci* 17:959–969, 2012.
- Lee WM: Acute liver failure. *N Engl J Med* 329:1862–1872, 1993.
- Iwatsuki S, Gordon RD, Shaw BW, et al: Role of liver transplantation in cancer therapy. *Ann Surg* 202:401–407, 1985.
- Yao FY, Ferrell L, Bass NM, et al: Liver transplantation for hepatocellular carcinoma: Expansion of the tumor size limits does not adversely impact survival. *Hepatology* 33: 1394–1403, 2001.
- Stieber AC, Zetti G, Todo S, et al: The spectrum of portal vein thrombosis in liver transplantation. *Ann Surg* 213:199–206, 1991.
- Chua TC, Liauw W, Saxena A, et al: Systematic review of neoadjuvant transarterial chemoembolization for resectable hepatocellular carcinoma. *Liver Int* 30:166–174, 2010.
- Cescon M, Cucchetti A, Ravaioli M, et al: Hepatocellular carcinoma locoregional therapies for patients in the waiting list. Impact on transplantability and recurrence rate. *J Hepatol* 58:609–618, 2013.
- Lencioni R: Loco-regional treatment of hepatocellular carcinoma. *Hepatology* 52:762–773, 2010.
- Tzakis A, Todo S, Starzl TE: Orthotopic liver transplantation with preservation of the inferior vena cava. *Ann Surg* 210:649–652, 1989.
- Akamatsu N, Sugawara Y, Hashimoto D: Biliary reconstruction, its complications and management of biliary complications after adult liver transplantation: A systematic review of the incidence, risk factors and outcome. *Transpl Int* 24:379–392, 2011.
- Emre S, Umman V: Split liver transplantation: An overview. *Transplant Proc* 43:884–887, 2011.
- Roll GR, Parekh JR, Parker WF, et al: Left hepatectomy versus right hepatectomy for living donor liver transplantation: Shifting the risk from the donor to the recipient. *Liver Transpl* 19:472–481, 2013.
- Kelly D, Wray J: The adolescent liver transplant patient. *Clin Liver Dis* 18:618–632, 2014.
- Yamaoka Y, Washida M, Honda K, et al: Liver transplantation using a right lobe graft from a living related donor. *Transplantation* 57:1127–1130, 1994.
- Wachs ME, Bak TE, Karrer FM, et al: Adult living donor liver transplantation using a right hepatic lobe. *Transplantation* 66:1313–1316, 1998.
- Berg CL, Merion RM, Shearon TH, et al: Liver transplant recipient survival benefit with living donation in the model for endstage liver disease allocation era. *Hepatology* 54:1313–1321, 2011.
- Quintini C, Hashimoto K, Uso TD, et al: Is there an advantage of living over deceased donation in liver transplantation? *Transpl Int* 26:11–19, 2013.
- Sahani D, D'souza R, Kadavigere R, et al: Evaluation of living liver transplant donors: Method for precise anatomic definition by using a dedicated contrast-enhanced MR imaging protocol. *Radiographics* 24:957–967, 2004.
- Catalano OA, Singh AH, Uppot RN, et al: Vascular and biliary variants in the liver: Implications for liver surgery. *Radiographics* 28: 359–378, 2008.
- Lim JS, Kim MJ, Kim JH, et al: Preoperative MRI of potential living-donor-related liver transplantation using a single dose of gadobenate dimeglumine. *AJR Am J Roentgenol* 185:424–431, 2005.
- Lee VS, Krinsky GA, Nazzaro CA, et al: Defining intrahepatic biliary anatomy in living liver transplant donor candidates at mangafodipir trisodium-enhanced MR cholangiography versus conventional T2-weighted MR cholangiography. *Radiology* 233:659–666, 2004.
- Lee NK, Kim S, Lee JW, et al: Biliary MR imaging with Gd-EOB-DTPA and its clinical applications. *Radiographics* 29:1707–1724, 2009.
- Burke C, Alexander Grant L, Goh V, et al: The role of hepatocyte-specific contrast agents in hepatobiliary magnetic resonance imaging. *Semin Ultrasound CT MR* 34:44–53, 2013.
- Pannu HK, Maley WR, Fishman EK: Liver transplantation: Preoperative CT evaluation. *Radiographics* 21(Spec No):S133–S146, 2001.
- Ben-Haim M, Emre S, Fishbein TM, et al: Critical graft size in adult-to-adult living donor liver transplantation: Impact of the recipient's disease. *Liver Transpl* 7:948–953, 2001.
- Emond JC, Renz JE, Ferrell LD, et al: Functional analysis of grafts from living donors. Implications for the treatment of older recipients. *Ann Surg* 224:544–552, discussion 552–554, 1996.
- Sugawara Y, Makuuchi M, Takayama T, et al: Small-for-size grafts in living-related liver transplantation. *J Am Coll Surg* 192:510–513, 2001.
- Hayashi M, Fujii K, Kiuchi T, et al: Effects of fatty infiltration of the graft on the outcome of living-related liver transplantation. *Transplant Proc* 31:403, 1999.
- Selzner M, Clavien PA: Fatty liver in liver transplantation and surgery. *Semin Liver Dis* 21:105–113, 2001.
- Iwasaki M, Takada Y, Hayashi M, et al: Noninvasive evaluation of graft steatosis in living donor liver transplantation. *Transplantation* 78:1501–1505, 2004.
- Guiney MJ, Kruskal JB, Sosna J, et al: Multi-detector row CT of relevant vascular anatomy of the surgical plane in split-liver transplantation. *Radiology* 229:401–407, 2003.
- Erbay N, Raptopoulos V, Pomfret EA, et al: Living donor liver transplantation in adults: Vascular variants important in surgical planning for donors and recipients. *AJR Am J Roentgenol* 181:109–114, 2003.
- Low G, Wiebe E, Walji AH, et al: Imaging evaluation of potential donors in living-donor liver transplantation. *Clin Radiol* 63:136–145, 2008.
- Crossin JD, Muradali D, Wilson SR: US of liver transplants: Normal and abnormal. *Radiographics* 23:1093–1114, 2003.
- Singh AK, Nachiappan AC, Verma HA, et al: Postoperative imaging in liver transplantation: What radiologists should know. *Radiographics* 30:339–351, 2010.
- Jamieson LH, Arys B, Low G, et al: Doppler ultrasound velocities and resistive indexes immediately after liver transplantation: Normal ranges and predictors of failure. *AJR* 203:W110–W116, 2014.
- Rumack CM, Wilson SR, Charboneau JW: *Diagnostic Ultrasound*, ed 3, St. Louis, 2005, Elsevier Mosby.
- Dodd GD, Memel DS, Zajko AB, et al: Hepatic artery stenosis and thrombosis in transplant recipients: Doppler diagnosis with resistive index and systolic acceleration time. *Radiology* 192:657–661, 1994.
- Stavros AT, Parker SH, Yakes WF, et al: Segmental stenosis of the renal artery: Pattern recognition of tardus and parvus abnormalities with duplex sonography. *Radiology* 184:487–492, 1992.
- Platt JF, Yutzy GG, Bude RO, et al: Use of Doppler sonography for revealing hepatic artery stenosis in liver transplant recipients. *AJR Am J Roentgenol* 168:473–476, 1997.
- Stell D, Downey D, Marotta P, et al: Prospective evaluation of the role of quantitative Doppler ultrasound surveillance in liver transplantation. *Liver Transpl* 10:1183–1188, 2004.
- García-Criado A, Gilabert R, Berzigotti A, et al: Doppler ultrasound findings in the hepatic artery shortly after liver transplantation. *AJR Am J Roentgenol* 193:128–135, 2009.
- García-Criado A, Gilabert R, Salmeron JM, et al: Significance of and contributing factors for a high resistive index on Doppler sonography of the hepatic artery immediately after surgery: Prognostic implications for liver transplant recipients. *AJR Am J Roentgenol* 181:831–838, 2003.
- García-Criado A, Gilabert R, Berzigotti A, et al: Doppler ultrasound findings in the hepatic artery shortly after liver transplantation. *AJR Am J Roentgenol* 193:128–135, 2009.
- Sanyal R, Lall CG, Lamba R, et al: Orthotopic liver transplantation: Reversible Doppler US findings in the immediate postoperative period. *Radiographics* 32:199–211, 2012.
- Wozney P, Zajko AB, Bron KM, et al: Vascular complications after liver transplantation: A 5-year experience. *AJR Am J Roentgenol* 147:657–663, 1986.
- Tzakis AG, Gordon RD, Shaw BW, Jr, et al: Clinical presentation of hepatic artery thrombosis after liver transplantation in the cyclosporine era. *Transplantation* 40:667–671, 1985.
- Warner P, Fusai G, Glantzounis GK, et al: Risk factors associated with early hepatic artery thrombosis after orthotopic liver transplantation—univariable and multivariable analysis. *Transpl Int* 24:401–408, 2011.
- Pascual M, Thadhani R, Laposata M, et al: Anticardiolipin antibodies and hepatic artery

- thrombosis after liver transplantation. *Transplantation* 64:1361–1364, 1997.
55. Pungpaong S, Manzarbeitia C, Ortiz J, et al: Cigarette smoking is associated with an increased incidence of vascular complications after liver transplantation. *Liver Transpl* 8:582–587, 2002.
 56. Bekker J, Ploem S, de Jong KP: Early hepatic artery thrombosis after liver transplantation: A systematic review of the incidence, outcome and risk factors. *Am J Transplant* 9:746–757, 2009.
 57. Gunsar F, Rolando N, Pastacaldi S, et al: Late hepatic artery thrombosis after orthotopic liver transplantation. *Liver Transpl* 9:605–611, 2003.
 58. De Gaetano AM, Cotroneo AR, Maresca G, et al: Color Doppler sonography in the diagnosis and monitoring of arterial complications after liver transplantation. *J Clin Ultrasound* 28:373–380, 2000.
 59. Flint EW, Sumkin JH, Zajko AB, et al: Duplex sonography of hepatic artery thrombosis after liver transplantation. *AJR Am J Roentgenol* 151:481–483, 1988.
 60. Nghiem HV: Imaging of hepatic transplantation. *Radiol Clin North Am* 36:429–443, 1998.
 61. Itri JN, Heller MT, Tublin ME: Hepatic transplantation. *Abdom Imaging* 38:1300–1333, 2013.
 62. Shaw BW, Gordon RD, Iwatsuki S, et al: Hepatic retransplantation. *Transplant Proc* 17:264–271, 1985.
 63. Singhal A, Stokes K, Sebastian A, et al: Endovascular treatment of hepatic artery thrombosis following liver transplantation. *Transpl Int* 23:245–256, 2010.
 64. Denys A, Chevallier P, Doenz F, et al: Interventional radiology in the management of complications after liver transplantation. *Eur Radiol* 14:431–439, 2004.
 65. Abbasoglu O, Levy MF, Vodapally MS, et al: Hepatic artery stenosis after liver transplantation—incidence, presentation, treatment, and long term outcome. *Transplantation* 63:250–255, 1997.
 66. Orons PD, Sheng R, Zajko AB: Hepatic artery stenosis in liver transplant recipients: Prevalence and cholangiographic appearance of associated biliary complications. *AJR Am J Roentgenol* 165:1145–1149, 1995.
 67. Saad WE, Davies MG, Sahler L, et al: Hepatic artery stenosis in liver transplant recipients: Primary treatment with percutaneous transluminal angioplasty. *J Vasc Interv Radiol* 16:795–805, 2005.
 68. Ueno T, Jones G, Martin A, et al: Clinical outcomes from hepatic artery stenting in liver transplantation. *Liver Transpl* 12:422–427, 2006.
 69. Kim HJ, Kim KW, Kim AY, et al: Hepatic artery pseudoaneurysms in adult living-donor liver transplantation: Efficacy of CT and Doppler sonography. *AJR Am J Roentgenol* 184:1549–1555, 2005.
 70. Zajko AB, Tobben PJ, Esquivel CO, et al: Pseudoaneurysms following orthotopic liver transplantation: Clinical and radiologic manifestations. *Transplant Proc* 21:2457–2459, 1989.
 71. Caiado AH, Blasbalg R, Marcelino AS, et al: Complications of liver transplantation: Multimodality imaging approach. *Radiographics* 27:1401–1417, 2007.
 72. Nghiem HV, Tran K, Winter TC, 3rd, et al: Imaging of complications in liver transplantation. *Radiographics* 16:825–840, 1996.
 73. Woo DH, Laberge JM, Gordon RL, et al: Management of portal venous complications after liver transplantation. *Tech Vasc Interv Radiol* 10:233–239, 2007.
 74. Funaki B, Rosenblum JD, Leef JA, et al: Percutaneous treatment of portal venous stenosis in children and adolescents with segmental hepatic transplants: Long-term results. *Radiology* 215:147–151, 2000.
 75. Vaidya S, Dighe M, Kolokythas O, et al: Liver transplantation: Vascular complications. *Ultrasound Q* 23:239–253, 2007.
 76. Tamsel B, Demirpolat G, Killi R, et al: Vascular complications after liver transplantation: Evaluation with Doppler US. *Abdom Imaging* 32:339–347, 2007.
 77. Ko EY, Kim TK, Kim PN, et al: Hepatic vein stenosis after living donor liver transplantation: Evaluation with Doppler US. *Radiology* 229:806–810, 2003.
 78. Quiroga S, Sebastia MC, Margarit C, et al: Complications of orthotopic liver transplantation: Spectrum of findings with. *Radiographics* 21:1085–1102, 2001.
 79. Wang SL, Sze DY, Busque S, et al: Treatment of hepatic venous outflow obstruction after piggyback liver transplantation. *Radiology* 236:352–359, 2005.
 80. Federle MP, Kapoor V: Complications of liver transplantation: Imaging and intervention. *Radiol Clin North Am* 41:1289–1305, 2003.
 81. Greif F, Bronsther OL, Van Thiel DH, et al: The incidence, timing, and management of biliary tract complications after. *Ann Surg* 219:40–45, 1994.
 82. Gastaca M: Biliary complications after orthotopic liver transplantation: A review of incidence and risk factors. *Transplant Proc* 44:1545–1549, 2012.
 83. Fulcher AS, Turner MA: Orthotopic liver transplantation: Evaluation with MR cholangiography. *Radiology* 211:715–722, 1999.
 84. Campbell WL, Sheng R, Zajko AB, et al: Intrahepatic biliary strictures after liver transplantation. *Radiology* 191:735–740, 1994.
 85. Akamatsu N, Sugawara Y, Hashimoto D: Biliary reconstruction, its complications and management of biliary complications. *Transpl Int* 24:379–392, 2011.
 86. Weber A, Prinz C, Gerngross C, et al: Long-term outcome of endoscopic and/or percutaneous transhepatic therapy in patients with biliary stricture after orthotopic liver transplantation. *J Gastroenterol* 44:1195–1202, 2009.
 87. Boraschi P, Donati F, Gigoni R, et al: MR cholangiography in orthotopic liver transplantation: Sensitivity and specificity in detecting biliary complications. *Clin Transplant* 24:E82–E87, 2010.
 88. Letourneau JG, Day DL, Ascher NL, et al: Abdominal sonography after hepatic transplantation: Results in 36 patients. *AJR Am J Roentgenol* 149:299–303, 1987.
 89. Beswick DM, Miraglia R, Caruso S, et al: The role of ultrasound and magnetic resonance cholangiopancreatography for the diagnosis of biliary stricture after liver transplantation. *Eur J Radiol* 81:2089–2092, 2012.
 90. Sundaram V, Jones DT, Shah NH, et al: Post-transplant biliary complications in the pre- and post-model for end-stage liver disease era. *Liver Transpl* 17:428–435, 2011.
 91. Seehofer D, Eurich D, Veltzke-Schlieker W, et al: Biliary complications after liver transplantation: Old problems and new challenges. *Am J Transplant* 13:253–265, 2013.
 92. Buis CI, Verdonk RC, Van der Jagt EJ, et al: Nonanastomotic biliary strictures after liver transplantation, part 1: Radiological features and risk factors for early vs. late presentation. *Liver Transpl* 13:708–718, 2007.
 93. Zemel G, Zajko AB, Skolnick ML, et al: The role of sonography and transhepatic cholangiography in the diagnosis of biliary complications after liver transplantation. *AJR Am J Roentgenol* 151:943–946, 1988.
 94. Vandenbroucke F, Plasse M, Dagenais M, et al: Treatment of post liver transplantation bile duct stricture with self-expandable. *HPB (Oxford)* 8:202–205, 2006.
 95. Osorio RW, Freise CE, Stock PG, et al: Non-operative management of biliary leaks after orthotopic liver transplantation. *Transplantation* 55:1074–1077, 1993.
 96. Girometti R, Cereser L, Bazzocchi M, et al: Magnetic resonance cholangiography in the assessment and management of biliary complications after OLT. *World J Radiol* 6:424–436, 2014.
 97. Rodríguez-Perálvarez M, De la Mata M, Burroughs AK: Liver transplantation: Immunosuppression and oncology. *Curr Opin Organ Transplant* 19:253–260, 2014.
 98. White RM, Zajko AB, Demetris AJ, et al: Liver transplant rejection: Angiographic findings in 35 patients. *AJR Am J Roentgenol* 148:1095–1098, 1987.
 99. Narkewicz MR, Green M, Dunn S, et al: Decreasing incidence of symptomatic Epstein-Barr virus disease and posttransplant lymphoproliferative disorder in pediatric liver transplant recipients: Report of the studies of pediatric liver transplantation experience. *Liver Transpl* 19:730–740, 2013.
 100. Borhani AA, Hosseinzadeh K, Almusa O, et al: Imaging of posttransplantation lymphoproliferative disorder after solid organ transplantation. *Radiographics* 29:981–1000, discussion 1000–1002, 2009.
 101. Pickhardt PJ, Siegel MJ: Posttransplantation lymphoproliferative disorder of the abdomen: CT evaluation in 51 patients. *Radiology* 213:73–78, 1999.
 102. Dhillon MS, Rai JK, Gunson BK, et al: Post-transplant lymphoproliferative disease in liver transplantation. *Br J Radiol* 80:337–346, 2007.
 103. Al-Mansour Z, Nelson BP, Evens AM: Post-transplant lymphoproliferative disease (PTLD): Risk factors, diagnosis, and current treatment strategies. *Curr Hematol Malig Rep* 8:173–183, 2013.
 104. Ferris JV, Baron RL, Marsh JW, et al: Recurrent hepatocellular carcinoma after liver transplantation: Spectrum of CT findings and recurrence patterns. *Radiology* 198:233–238, 1996.
 105. DeOliveira ML: Liver transplantation for cholangiocarcinoma: Current best practice. *Curr Opin Organ Transplant* 19:245–252, 2014.

Liver: Differential Diagnosis

RICHARD M. GORE

CHAPTER OUTLINE

General Imaging Abnormalities

- Table 93-1. Diffuse Hepatomegaly
- Table 93-2. Hepatomegaly in the Neonate
- Table 93-3. Focal Hepatic Enlargement
- Table 93-4. Liver Atrophy with Compensatory Hypertrophy
- Table 93-5. Hepatic Capsular Retraction
- Table 93-6. Hepatic Calcification
- Table 93-7. Neonatal Liver Calcification
- Table 93-8. Portal Venous Gas
- Table 93-9. Gas in the Biliary Tract
- Table 93-10. Hepatic Vein Dilation

Ultrasound

- Table 93-11. Diffusely Increased Hepatic Echogenicity ("Bright Liver")
- Table 93-12. Focally Increased Hepatic Echogenicity
- Table 93-13. Diffusely Decreased Hepatic Echogenicity
- Table 93-14. Hepatic Pseudolesions on Ultrasound Studies
- Table 93-15. Intrahepatic Acoustic Shadowing
- Table 93-16. Hypoechoic or Anechoic Focal Masses
- Table 93-17. Multiseptate Cystic Masses
- Table 93-18. Hyperechoic Masses with Acoustic Enhancement
- Table 93-19. Anechoic, Smooth-Walled Masses with Acoustic Enhancement
- Table 93-20. Complex Masses
- Table 93-21. Prominent Periportal Echoes
- Table 93-22. Echo Patterns of Hepatic Metastases
- Table 93-23. Dampening of Hepatic Vein Doppler Waveform
- Table 93-24. Transjugular Intrahepatic Portosystemic Shunt Malfunction

Computed Tomography

- Table 93-25. Focal Hypodense Lesion: Precontrast and Postcontrast Scan Appearance
- Table 93-26. Diffusely Dense Liver
- Table 93-27. Focal Hypodense Lesion: Noncontrast Scans
- Table 93-28. Focal Hyperdense Lesion: Postcontrast Scans
- Table 93-29. Patchy Hepatogram
- Table 93-30. Hyperperfusion Abnormalities of Liver (THADs)

- Table 93-31. Low-Density Mass in Porta Hepatis
- Table 93-32. Fat-Containing Liver Mass
- Table 93-33. Vascular "Scar" Tumor
- Table 93-34. Periportal Lucency
- Table 93-35. Fluid-Fluid Levels Within Focal Hepatic Lesions

Magnetic Resonance

- Table 93-36. Multiple Hypointense Liver Masses: T2-Weighted Images
- Table 93-37. Diffusely Decreased Liver Intensity
- Table 93-38. Increased Periportal Signal Intensity
- Table 93-39. Hepatic Lesions with Fat Signal: T1-Weighted Images
- Table 93-40. Wedge-Shaped Signal Alterations
- Table 93-41. Liver Lesions with Circumferential Rim
- Table 93-42. Central Scars in Primary Liver Tumors

Nuclear Scintigraphy

- Table 93-43. Early or Increased Flow to the Liver: Hepatic Scintiangiography
- Table 93-44. Focally Decreased Flow (Solitary or Multiple): Hepatic Scintiangiography
- Table 93-45. Nonvisualization of Liver: Indium-Labeled Leukocyte Scan
- Table 93-46. Focal Liver Uptake: PET Scan
- Table 93-47. Decreased Hepatic Uptake: PET Scan
- Table 93-48. Liver Rim Sign: Gallium Scan
- Table 93-49. Halo Sign in Gallbladder Fossa: Indium-Labeled Leukocyte Scan

Arteriography

- Table 93-50. Single or Multiple Vascular Hepatic Lesions
- Table 93-51. Single or Multiple Avascular Hepatic Lesions

Imaging Findings in Specific Hepatic Diseases

- Table 93-52. Cirrhosis and Portal Hypertension
- Table 93-53. Fatty Infiltration
- Table 93-54. Viral Hepatitis
- Table 93-55. Budd-Chiari Syndrome
- Table 93-56. Hemochromatosis
- Table 93-57. Hepatocellular Adenoma
- Table 93-58. Cavernous Hemangioma
- Table 93-59. Hepatocellular Carcinoma
- Table 93-60. Focal Nodular Hyperplasia

General Imaging Abnormalities

TABLE
93-1

Diffuse Hepatomegaly

NEOPLASTIC DISEASES Metastases Hepatoma Lymphoma	STORAGE DISEASES Steatosis Amyloidosis Hemochromatosis Gaucher's disease Glycogen storage disease Niemann-Pick disease Histiocytosis Weber-Christian disease Wilson's disease GM ₁ gangliosidosis
INFECTIOUS DISEASES Viral Hepatitis Mononucleosis AIDS Bacterial Pyogenic abscess Tuberculosis, miliary Histoplasmosis, miliary Syphilis <i>Pneumocystis</i> infection Protozoan Amebic abscess Malaria Leptospirosis Trypanosomiasis Kala-azar Parasitic Echinococcosis Schistosomiasis Fungal Candidiasis	MYELOPROLIFERATIVE DISORDERS Myelofibrosis Polycythemia rubra vera Extramedullary hematopoiesis Myeloid metaplasia Thalassemia Sickle cell anemia
DEGENERATIVE DISEASES Cirrhosis Fatty infiltration	CONGENITAL DISORDERS Riedel's lobe Polycystic disease Wolman's disease Reye's syndrome Rubella syndrome Pyruvate kinase deficiency Osteopetrosis Lipoatrophic diabetes Hyperlipoproteinemia Homocystinuria Hepatic fibrosis–renal cystic disease Farber's syndrome Chédiak-Higashi syndrome Zellweger's syndrome Beckwith-Wiedemann syndrome Granulomatous disease of childhood
ELEVATED VENOUS PRESSURE Congestive heart failure Constrictive pericarditis Tricuspid stenosis Budd-Chiari syndrome	MISCELLANEOUS DISORDERS Sarcoid Hematoma Felty's syndrome

TABLE
93-2

Hepatomegaly in the Neonate

Nutritional disorder Heart failure Infection Biliary atresia Metabolic defect Primary neoplasm Metastases

TABLE
93-3

Focal Hepatic Enlargement

COMMON Anomalous lobes (Riedel) Metastasis Cirrhosis Regenerative nodules or lobes Hemangioma Cysts Adenoma Focal nodular hyperplasia Hepatoma Lymphoma Cholangiocarcinoma
UNCOMMON Hemangioendothelioma Actinomycosis Abscess (fungal or pyogenic) Biliary cystadenoma Hamartoma Hepatoblastoma Sarcoma Spindle cell neoplasm Teratoma Cholangioma

TABLE
93-4**Liver Atrophy with Compensatory Hypertrophy**

Cirrhosis
 Hepatic vein obstruction (segmental)
 Portal vein obstruction (segmental)
 Intrahepatic biliary obstruction (segmental)
 Budd-Chiari syndrome
 Radiation therapy
 After chemotherapy for hepatic tumor
 Surgical resection
 Liver metastases
 Lobar agenesis

TABLE
93-7**Neonatal Liver Calcification**

Calcified venous thrombi (e.g., after umbilical vein catheterization)
 Hematoma
 Cytomegalovirus infection
 Herpesvirus infection
 Toxoplasmosis
 Abscess
 Biliary calcification
 Hemangioma
 Hamartoma
 Hepatoblastoma
 Hepatocellular carcinoma
 Metastatic neuroblastoma
 Ischemic infarct
 Rubella

TABLE
93-5**Hepatic Capsular Retraction****ADJACENT TO A HEPATIC TUMOR**

Primary malignant tumors
 Hepatocellular carcinoma
 Fibrolamellar hepatocellular carcinoma
 Intrahepatic cholangiocarcinoma
 Epithelioid hemangioendothelioma
 Metastatic tumors
 Adenocarcinoma of the colon, stomach, breast, lung, pancreas, and gallbladder
 Postembolization of hepatocellular carcinoma
 Postchemotherapy of malignant tumors
 Benign tumor
 Hemangioma

WITHOUT AN ADJACENT HEPATIC TUMOR

Confluent hepatic fibrosis
 Oriental cholangiohepatitis
 Bile duct necrosis
 Pseudoretraction
 Accessory fissure
 Normal liver parenchyma between the protruded masses

TABLE
93-8**Portal Venous Gas**

Mesenteric infarction
 Air intravasation during double-contrast barium enema
 Acute gastric dilation
 Percutaneous abscess drainage
 Necrotizing enterocolitis
 Umbilical vein catheterization
 Erythroblastosis fetalis
 Diverticulitis
 Inflammatory bowel disease
 Corrosive ingestion
 Diabetic coma
 Hemorrhagic pancreatitis
 Hydrogen peroxide enema
 Emphysematous cholecystitis
 Mechanical bowel obstruction with ischemia
 Necrotic colon cancer
 Perforation of gastric ulcer into mesenteric vein
 Abscess
 Closed-loop obstruction
 Pseudomembranous colitis
 Gastric emphysema
 Toxic megacolon
 Sepsis
 Corrosive gastritis
 Catheterization of umbilical artery or mesenteric vein
 After hepatic artery embolization

TABLE
93-6**Hepatic Calcification****INFECTIONS**

Histoplasmosis
 Tuberculosis
 Coccidioidomycosis
 Brucellosis
 Gumma
 Echinococcal cyst, *Armillifer* infestation
 Chronic amebic or pyogenic abscess
 Cytomegalovirus or *Toxoplasma* infection
 Chronic granulomatous disease of childhood
Clonorchis sinensis infection, cysticercosis, filariasis, paragonimiasis

VASCULAR LESIONS

Hepatic artery aneurysm
 Portal vein thrombosis
 Hematoma

BENIGN TUMORS

Cyst
 Cavernous hemangioma
 Capsule of regenerative nodules
 Infantile hemangioendothelioma

PRIMARY MALIGNANT TUMORS

Hepatoma, especially fibrolamellar
 Hepatoblastoma
 Cholangiocarcinoma

METASTATIC TUMORS

Mucinous carcinoma of the colon, breast, or stomach
 Ovarian carcinoma
 Melanoma
 Mesothelioma
 Osteosarcoma
 Carcinoid
 Leiomyosarcoma
 Teratoma
 Thyroid carcinoma
 Chondrosarcoma
 Neuroblastoma

BILIARY TREE

Calculus
 Cholangiocarcinoma
 Ascariasis

TABLE 93-9 Gas in the Biliary Tract

Sphincterotomy
 Gallstone erosion
 Patulous sphincter in elderly patient
 Cholecystoenterostomy
 Choledochenterostomy
 Spontaneous biliary fistula to the colon or duodenum by gallstones
 Perforating duodenal ulcer
 Trauma
 Carcinoma of the gallbladder, colon, stomach, pancreas, duodenum, ampulla, bile duct
 Diverticulitis
 Crohn's disease fistula
 Emphysematous cholecystitis
 Cholecystojejunostomy
 Pancreatitis
Strongyloides infection
 Incompetent sphincter of Oddi
Ascariasis lumbricoides infection
Clonorchis sinensis infection
 Ruptured amebic abscess
 Common duct entry into duodenal diverticulum
 Metastases
 Lymphoma

TABLE 93-12 Focally Increased Hepatic Echogenicity**COMMON**

Hemangioma
 Metastases
 Focal steatosis
 Adenoma
 Focal nodular hyperplasia
 Abscess
 Hematoma or laceration
 Hepatocellular carcinoma
 Fissures

UNCOMMON

Cytomegalovirus or *Candida* infection
 α_1 -Antitrypsin deficiency
 Lipoma
 Angiomyolipoma
 Infarct
 Regenerative nodules of cirrhosis
 Radiation therapy
 Omentum inserted into bed of hepatic resection
Echinococcus multilocularis infection
 Hemangioendothelioma

TABLE 93-10 Hepatic Vein Dilation**COMMON**

Right-sided heart failure
 Constrictive pericarditis
 Hepatic venous thrombus
 Inferior vena cava obstruction or thrombus
 Tricuspid atresia or stenosis
 With Valsalva maneuver in normal young patient

UNCOMMON

Right atrial tumor

TABLE 93-13 Diffusely Decreased Hepatic Echogenicity**COMMON**

Acute viral hepatitis
 Schistosomiasis (early)
 Malignant infiltration

UNCOMMON

Leukemia
 Lymphoma

APPARENT

End-stage renal disease
 Amyloid
 Nephrocalcinosis
 Myoglobinuric renal failure

Ultrasound

TABLE 93-11 Diffusely Increased Hepatic Echogenicity ("Bright Liver")**COMMON**

Fatty infiltration
 Cirrhosis
 Acute alcoholic hepatitis
 Severe viral or drug-induced hepatitis
 Diffuse malignant infiltration
 Chronic right-sided heart failure
 AIDS
 Technical artifact

UNCOMMON

Glycogen storage disease
 Gaucher's disease
 Miliary tuberculosis
 Mononucleosis
 Portal tract fibrosis
 Wilson's disease
 Lymphoma
 Sarcoidosis

TABLE 93-14 Hepatic Pseudolesions on Ultrasound Studies

Diaphragmatic leaflets: peripheral echogenic pseudolesion may simulate mass
 Falciform ligament: echogenic "mass" (pseudolesion) in left lobe
 Focal fatty infiltration: echogenic pseudolesion may simulate metastases
 Focal hepatic sparing in steatosis: hypoechoic pseudolesion often seen in porta
 Perihepatic fat may invaginate liver, causing hyperechoic masses
 Ligamentum venosum: fibrous tissue attenuates sound, causing hypoechoic pseudolesion in caudate lobe
 Gallbladder inflammation: hypoechoic hepatic pseudolesion in adjacent parenchyma

TABLE 93-15 Intrahepatic Acoustic Shadowing**LINEAR OR BRANCHING SHADOWING**

Intrabiliary air
Portal venous air
Intraductal stones

FOCAL SHADOWING

Gas: abscess, necrotic tumor, sequela of tumor embolization or of biopsy
Calcification: metastases, granulomas, abscess, aneurysm, parasites
Refractile artifacts: junction of vessels, gallbladder neck
Foreign material: surgical clips, drains, catheters, stents, sponges

TABLE 93-16 Hypoechoic or Anechoic Focal Masses**COMMON**

Cysts
Polycystic liver disease
Bilomas
Focal sparing in steatosis
Abscesses
Hematomas (early)
Metastases, especially colon, ovary, melanoma, sarcoma
Primary hepatic tumors
Post-traumatic cysts
Hydatid cysts

UNCOMMON

Caroli's disease
Extramedullary hematopoiesis
Focal hepatitis
Focal hepatic necrosis
Radiation therapy (early)
Cavernous hemangiomas
Hepatomas
Intrahepatic gallbladder

TABLE 93-17 Multiseptate Cystic Masses**COMMON**

Metastases
Simple cysts complicated by infection or hemorrhage

UNCOMMON

Teratoma
Cystic hepatoblastoma
Infantile peliosis hepatis
Hepatic hamartoma
Biliary cystadenoma

TABLE 93-18 Hyperechoic Masses with Acoustic Enhancement

Hemangioma
Hepatoma
Carcinoid metastases
Adenoma or hepatoma in glycogen storage disease

TABLE 93-19 Anechoic, Smooth-Walled Masses with Acoustic Enhancement

Cyst
Polycystic disease
Caroli's disease
Choledochal cyst
Hydatid cyst

TABLE 93-20 Complex Masses**SEPTATE**

Hydatid cyst
Biliary cystadenoma
Ovarian carcinoma metastases

NO SEPTA

Abscess
Tumor

BULL'S-EYE LESIONS

Metastases
Abscess
Primary neoplasm

TABLE 93-21 Prominent Periportal Echoes**COMMON**

Acute cholecystitis
Chronic cholecystitis
Cholangitis
Oriental cholangiohepatitis
Cholangiocarcinoma
Sclerosing cholangitis
Hepatocellular carcinoma
Air in biliary tree

UNCOMMON

Cystic fibrosis
Schistosomiasis
Lymphoma
Infectious mononucleosis

IN NEONATES

Biliary atresia
Acute hepatitis
Cytomegalovirus infection
Nesidioblastosis
 α_1 -Antitrypsin deficiency
Idiopathic neonatal jaundice

TABLE 93-22 Echo Patterns of Hepatic Metastases

ECHOGENIC LESIONS
Any carcinoma but especially from the gastrointestinal tract, pancreas, hepatoma, breast, and vascular primaries (islet cell, carcinoid, choriocarcinoma, renal cell carcinoma)
HYPOECHOIC LESIONS
Homogeneous tumor-like lymphomas, some breast and lung cancers
CYSTIC METASTASES
Mucin-secreting metastases from neoplasms of the ovary, colon, pancreas, or stomach
Central necrosis of any lesion, especially sarcomas
DENSELY ECHOGENIC LESIONS, WITH SHADOWING
Mucinous carcinoma of the colon
Adenocarcinoma of the stomach
Pseudomucinous cystadenocarcinoma of the ovary
Cystadenocarcinoma of the pancreas
Adenocarcinoma of the breast
Melanoma
BULL'S-EYE OR TARGET PATTERN
Lung cancer
INFILTRATIVE PATTERN
Breast cancer
Lung cancer
Melanoma

TABLE 93-23 Dampening of Hepatic Vein Doppler Waveform

Cirrhosis
Passive hepatic congestion
Budd-Chiari syndrome
Various parenchymal abnormalities of liver
Extrinsic compression of hepatic veins

TABLE 93-24 Transjugular Intrahepatic Portosystemic Shunt Malfunction

DIRECT SIGNS
No flow—consistent with shunt occlusion or thrombosis
Low-velocity flow—especially at portal venous end of shunt
Change in peak shunt velocity—increase or decrease from baseline of 50 cm/s
Reversal of flow in hepatic vein
Hepatopetal intrahepatic portal venous flow
SECONDARY SIGNS
Reappearance of varices
Reaccumulation of ascites
Reappearance of recanalized paraumbilical vein

Computed Tomography

TABLE 93-25 Focal Hypodense Lesion: Precontrast and Postcontrast Scan Appearance

Lesion	Appearance after Contrast Medium Administration
Metastases	Irregular enhancement or none
Malignant primary tumors	
Hepatoma	
Hemangioendothelioma	
Hemangiosarcoma	
Intrahepatic cholangiocarcinoma	
Lymphoma	
Cholangiocarcinoma	Irregular enhancement
Benign tumors	
Hemangioma	75% Peripheral enhancement 10% Central enhancement 74% Progressively isodense on delayed scans 24% Partially isodense on delayed scans 2% Hypodense on delayed scans
Adenoma	85% Hyperdense during arterial phase but rapidly becomes isodense or hypodense (1 minute)
Focal nodular hyperplasia	Most hyperdense during arterial phase but rapidly becomes isodense or hyperdense (1 minute); a low-density central scar may be present, but it is also seen in fibrolamellar hepatomas and hemangiomas
Cysts	Margins of cyst are more clearly defined
Benign simple cysts	
Polycystic liver disease	
von Hippel-Lindau disease	
Abscesses	Often show peripheral enhancement
Pyogenic	May show a "spoke-wheel" enhancement pattern
Fungal	
Amebic	May show peripheral enhancement
Radiation injury	No change
Focal fatty infiltration	No change
Infarction	No change
Laceration	No change
Old hematoma	No change
Biloma	No change
Caroli's disease	No change
Choledochal cyst	No change
Focal biliary dilation	No change
Intrahepatic extension of pseudocyst	No change

TABLE 93-26 Diffusely Dense Liver

Hemochromatosis
Hemosiderosis
Glycogen storage disease
Amiodarone treatment
Gold therapy
Chronic arsenic poisoning

TABLE 93-27 Focal Hypodense Lesion: Noncontrast Scans

Mucinous metastases: colon, ovary, stomach, pancreas (primary)
 Primary hepatic tumors: hepatoma (especially fibrolamellar),
 hepatoblastoma, hemangioendothelioma
 Benign hepatic tumors: hemangiomas
 Infections

ACUTE HEMORRHAGE

Hematoma

VASCULAR

Budd-Chiari syndrome with spared parenchyma
 Portal vein thrombosis with spared parenchyma
 Fatty infiltration
 Malignant infiltration
 Portal vein thrombosis
 Amyloidosis

TABLE 93-28 Focal Hyperdense Lesion: Postcontrast Scans**HYPERVASCULAR METASTASES**

Carcinoid tumor
 Renal cell carcinoma
 Islet cell tumor
 Pheochromocytoma
 Melanoma

HYPERVASCULAR BENIGN MASSES

Adenoma
 Focal nodular hyperplasia (dense only during arterial phase, then hypodense)

ARTERIOPORTAL SHUNTS**TABLE 93-29 Patchy Hepatogram**

Cirrhosis
 Hepatitis
 Congestive heart failure
 Tricuspid atresia
 Portal vein thrombosis
 Budd-Chiari syndrome
 Lymphomatous infiltration
 Sarcoidosis
 Thyrotoxicosis

TABLE 93-30 Hyperperfusion Abnormalities of Liver (THADs)**LOBAR-SEGMENTAL**

Portal vein obstruction or thrombosis
 Mass effect due to tumor, cyst, abscess within liver
 Cirrhosis with arterial portal shunt
 Ligation of portal vein
 Hypervascular gallbladder disease

SUBSEGMENTAL

Obstruction of peripheral portal branches
 Percutaneous needle biopsy, ethanol ablation
 Acute cholecystitis

GENERALIZED HETEROGENEOUS

Cirrhosis
 Budd-Chiari syndrome

TABLE 93-31 Low-Density Mass in Porta Hepatis

Choledochal cyst
 Hepatic cyst
 Pancreatic pseudocyst
 Biloma
 Hepatic artery aneurysm
 Enteric duplication

TABLE 93-32 Fat-Containing Liver Mass

Hepatoma
 Angiomyolipoma
 Lipoma
 Metastatic liposarcoma or myxoid liposarcoma
 Hepatic adenoma

TABLE 93-33 Vascular "Scar" Tumor

Focal nodular hyperplasia
 Hepatic adenoma
 Giant cavernous hemangioma
 Fibrolamellar hepatocellular carcinoma
 Hypervascular metastases
 Intrahepatic cholangiocarcinoma

TABLE 93-34 Periportal Lucency

Bile duct dilation
 Periportal tracking of edema fluid or blood
 Cardiac failure
 Hepatitis
 Traumatic disruption or neoplasm invasion of hepatic lymphatics
 Bone marrow transplantation
 Liver transplantation
 Non-Hodgkin's lymphoma
 Peribiliary cysts in cirrhosis
 von Meyenburg complexes of the liver

TABLE 93-35 Fluid-Fluid Levels Within Focal Hepatic Lesions

Simple hepatic cyst
 Biliary cystadenoma
 Cavernous hemangioma
 Cystic hepatocellular carcinoma
 Hepatic metastasis (carcinoid, ovarian, lung primaries)

THADs, transient hepatic attenuation differences.

Magnetic Resonance

TABLE 93-36 Multiple Hypointense Liver Masses: T2-Weighted Images

COMMON

Regenerative nodules
Multiple calcified granulomas

UNCOMMON

Gamna-Gandy bodies
Periportal vascular collaterals
Multifocal acute intrahepatic hemorrhages
Biliary duct gas

Rare

Portal vein gas
Osler-Weber-Rendu disease
Multiple calcified parasitic cysts

TABLE 93-37 Diffusely Decreased Liver Intensity

Hemosiderosis
Hemochromatosis
Superparamagnetic contrast medium
Wilson's disease

TABLE 93-38 Increased Periportal Signal Intensity

Cholangitis
Obstructive jaundice
Cholangiocarcinoma
Acute hepatitis
Cirrhosis
AIDS
Vigorous hydration

TABLE 93-39 Hepatic Lesions with Fat Signal: T1-Weighted Images

COMMON

Focal fatty infiltration
Hepatoma
Hepatic adenoma

UNCOMMON

Cavernous hemangioma

RARE

Metastatic liposarcoma or myxoid liposarcoma

TABLE 93-40 Wedge-Shaped Signal Alterations

T1 HYPERINTENSITY

Irregular fatty infiltration

T2 HYPERINTENSITY

Hepatocellular carcinoma with peripheral ischemia or infarction
Metastases with wedge pattern of edema
Primary or secondary portal infarction
THID (transient hepatic intensity difference)

TABLE 93-41 Liver Lesions with Circumferential Rim

HYPOINTENSE RIM ON T1-WEIGHTED IMAGE

Chronic hematoma (hemosiderin)
Hepatocellular carcinoma (pseudocapsular rim is thin)
Hydatid cyst (thick, homogeneous rim, no perilesional edema)
Amebic liver abscess (concentric rims; rim of collagen)

HYPOINTENSE RIM ON T2-WEIGHTED IMAGE

Metastases (peritumoral edema with double ring pattern)
Liver abscess (one or two concentric rings of mixed signal intensity)
Subacute to chronic parenchymal hematoma (white rim also seen on T1-weighted images)

NO RIM

Simple cyst
Cavernous hemangioma
Adenoma
Focal nodular hyperplasia

TABLE 93-42 Central Scars in Primary Liver Tumors

Cavernous hemangioma: hypointense or hyperintense T2-weighted image (can be either inflammatory or fibrous scar)
Hepatic adenoma: variable signal
Focal nodular hyperplasia: hypointense T1-weighted image, hyperintense T2-weighted image (inflammatory scar)
Fibrolamellar hepatocellular carcinoma: hypointense T1-weighted image, hyperintense T2-weighted image (fibrotic repair of scar)

Nuclear Scintigraphy

TABLE 93-43 Early or Increased Flow to the Liver: Hepatic Scintiangiography

COMMON

Metastatic disease
Chronic liver disease
Hepatoma
Lymphoma

UNCOMMON

Hemangioma or hemangioendothelioma
Abscess
Adenoma
Focal nodular hyperplasia
Sequela of radiation therapy

Rare

Dilated portal vein
Massive breast shielding

TABLE
93-44**Focally Decreased Flow (Solitary or Multiple):
Hepatic Scintiangiography****COMMON**

Abscess, amebic or pyogenic
Cyst, of any cause
Extrinsic mass
Hemangioma
Hematoma
Hepatoma
Some metastases

UNCOMMON AND RARE

Fatty infiltration
Lymphoma
Regenerative nodule

TABLE
93-48**Liver Rim Sign: Gallium Scan**

Acute cholecystitis
Pyogenic abscess
Amebic abscess
Necrotic liver metastases
Primary liver cell carcinoma

TABLE
93-49**Halo Sign in Gallbladder Fossa:
Indium-Labeled Leukocyte Scan**

Cholecystitis
Acute acalculous cholecystitis

TABLE
93-45**Nonvisualization of Liver: Indium-Labeled
Leukocyte Scan**

Alcoholic liver disease
Neutropenia

TABLE
93-46**Focal Liver Uptake: PET Scan****COMMON**

Metastases
Abscess, pyogenic or amebic
Hepatoma

UNCOMMON

Cirrhosis (pseudotumor)
Budd-Chiari syndrome
Acute cholecystitis
Cholangiocarcinoma
Sarcoidosis

TABLE
93-47**Decreased Hepatic Uptake: PET Scan**

Chemotherapy
Liver failure
Bile peritonitis

ArteriographyTABLE
93-50**Single or Multiple Vascular Hepatic Lesions****COMMON**

Cavernous hemangioma
Hepatocellular carcinoma
Hemangioendothelioma
Metastases (especially islet cell, carcinoid, renal, breast)
Focal nodular hyperplasia
Adenoma

UNCOMMON

Hamartoma
Hemangiosarcoma
Arteriovenous fistula, congenital, iatrogenic, or traumatic
True or false aneurysm of hepatic artery

TABLE
93-51**Single or Multiple Avascular Hepatic Lesions****COMMON**

Abscess
Hydatid cyst
Cholangiocarcinoma
Metastasis
Cyst

UNCOMMON

Lymphoma
Hematoma
Hamartoma
Biloma
Polycystic disease

Imaging Findings in Specific Hepatic Diseases

TABLE
93-52

Cirrhosis and Portal Hypertension

MORPHOLOGIC CHANGES SEEN ON ULTRASOUND, CT, AND MRI STUDIES

Large liver early
Shrunken liver late, prominent fissures
Enlarged caudate lobe and lateral segment of left lobe
Caudate-to-right lobe ratio >0.65 on transverse images
Surface nodularity and indentations (regenerative nodules)
Altered gallbladder angle
Colonic and omental interposition
Signs of portal hypertension: varices, splenomegaly, ascites

ULTRASOUND

Increased echogenicity
Increased sound attenuation
Heterogeneous echo architecture
Decreased definition of portal and hepatic veins
Dilated hepatic arteries, portal vein, coronary veins, superior mesenteric vein
Thick lesser omentum in children
Increased incidence of gallstones
Regenerative nodules: hypoechoic areas with echogenic borders (rare)
Siderotic nodules in spleen: hyperechoic masses (rare)

Doppler Findings in Portal Hypertension

Dilated portal vein with decreased respiratory variation
Hepatofugal flow in portal system
Varices
Recanalized umbilical vein
Decreased variability of hepatic venous flow
Increased flow in superior mesenteric, splenic, and portal veins
Increased splenic and superior mesenteric artery flow
Resistive index of hepatic arterial flow >0.78

Computed Tomography

Fatty infiltration in early cirrhosis
Dense liver in hemochromatosis
Inhomogeneous enhancement
Portal and hepatic veins possibly compressed and difficult to visualize
Intrahepatic arterial-portal fistulas
Regenerative nodules
Portal hypertension
Varices
Increased density mesenteric fat

MR Imaging

Regenerative nodules: low-intensity areas on T2-weighted images (hemosiderin)
No appreciable change in hepatic signal in fibrosis
Siderotic nodules in spleen

ANGIOGRAPHY

Stretched hepatic artery branches
Corkscrewing: enlarged, tortuous hepatic arteries
Mottled parenchymal phase
Shunting between hepatic artery and portal vein
Delayed emptying into venous phase
Pruned hepatic vein branches

TABLE
93-53

Fatty Infiltration

COMPUTED TOMOGRAPHY

Liver less dense than spleen; spleen normally 6-12 HU less dense than liver
Rapid appearance and disappearance of fat
"Hyperdense" intrahepatic vascular structures
Possible fat deposition in a focal, lobar, segmental, or bizarre geographic distribution
Spared areas: caudate lobe, quadrate lobe, subcapsular, gallbladder fossa

ULTRASOUND

Increased hepatic echogenicity and increased number of echogenic foci in liver
Increased attenuation of sound with poor penetration of the posterior liver
Poor visualization of hepatic and portal veins and diaphragm
Focal fat presentations: multiple confluent hypoechoic lesions; hypoechoic ("skip") nodules; irregular hyperechoic and hypoechoic skip areas may show rapid change in time; do not produce contour abnormalities; do not alter course or caliber of regional vessels

MR IMAGING

No significant change in T1-weighted or T2-weighted images
On opposed-phase images, spin-echo (Dixon's technique), fat suppression techniques, and short T1 inversion recovery images, low signal intensity of fat

TABLE
93-54

Viral Hepatitis

ULTRASOUND

Acute Hepatitis

Hepatosplenomegaly
Decreased hepatic echogenicity
Increased brightness of portal vein walls ("starry sky" pattern)
Mural thickening of gallbladder; hypotonic and dilated gallbladder

Chronic Hepatitis

Increased hepatic echogenicity
Coarsened parenchymal texture
Loss of definition of portal vein walls
Adenopathy in hepatoduodenal ligament in chronic active hepatitis

COMPUTED TOMOGRAPHY

Hepatosplenomegaly
Periportal lucency
Mural thickening of gallbladder
Adenopathy in hepatoduodenal ligament in chronic active hepatitis

MR IMAGING

Hepatosplenomegaly
Periportal hyperintensity on T2-weighted images
Increased T1 and T2 relaxation times of parenchyma

NUCLEAR SCINTIGRAPHY

Hepatosplenomegaly
Colloid shift
Heterogeneous uptake
Delayed parenchymal clearance and blood pool tracer retention on iminodiacetic acid scans

TABLE
93-55**Budd-Chiari Syndrome****MR IMAGING**

Constriction or loss of a signal void in the intrahepatic or suprahepatic inferior vena cava
 Loss in caliber or absence of the hepatic vein signal void
 Comma-shaped, intrahepatic, hypointense collateral vessels
 Nodular liver, with or without hypointense regenerative nodules
 Intrahepatic portal vein thrombosis
 Enlarged caudate lobe, ascites, inhomogeneous hepatic parenchyma

ULTRASOUND

Stenosis, thrombosis, or nonvisualization of hepatic veins
 Thick, echogenic hepatic vein walls
 Narrowed inferior vena cava
 Intrahepatic collateral vessels or extrahepatic anastomoses
 Ascites, enlarged caudate lobe

COMPUTED TOMOGRAPHY**Noncontrast Scans**

Diffuse hypodensity associated with global liver enlargement and ascites
 Caudate lobe may appear hyperdense
 Hyperdense thrombus in inferior vena cava

Contrast Scans

Patchy contrast enhancement because of hepatic congestion
 Central liver (caudate, portions of left lobe) hyperdense; periphery hypodense
 Later ("flip-flop" pattern), center washes out, becomes hypodense relative to liver periphery, which slowly accumulates contrast medium
 Portal vein thrombus
 Nodular regenerative hyperplasia

ANGIOGRAPHY

Absence of main hepatic veins
 "Spider web" appearance of collateral intrahepatic veins or lymphatics
 Inhomogeneous, dense, prolonged, intense hepatogram with fine mottling
 Stretching and draping of intrahepatic arteries with hepatomegaly
 Large lakes of sinusoidal contrast medium accumulation
 Bidirectional or hepatofugal portal vein flow
 Thrombus in hepatic veins or inferior vena cava
 Impairment of caval flow because of diffuse hepatomegaly
 Membranous obstruction of the cava at the ostia of the hepatic veins
 Diminished or hepatofugal flow to involved segments during arterial portography

NUCLEAR SCINTIGRAPHY

Enlarged caudate lobe with increased uptake
 Diffusely decreased uptake in remainder of liver
 Hepatosplenomegaly
 Wedge-shaped focal peripheral defects
 Colloid shift to spleen and bone marrow

TABLE
93-56**Hemochromatosis****COMPUTED TOMOGRAPHY**

Diffuse increase in density up to 80-140 HU
 Hepatic veins and portal veins stand out on noncontrast scans

MR IMAGING

Shortened T1 and T2 relaxation times, T2 shortening effect predominating, with significant signal loss in liver

ULTRASOUND

Nonspecific findings that relate to secondary fibrosis and cirrhosis

NUCLEAR SCINTIGRAPHY

Discordant sulfur colloid and iminodiacetic acid scans early: iminodiacetic acid scan normal; sulfur colloid scan with diffuse parenchymal damage

TABLE
93-57**Hepatocellular Adenoma****COMPUTED TOMOGRAPHY**

Round masses of decreased density, necrotic areas (30%-40%)
 Hyperdense areas of fresh intratumor hemorrhage (22%-55%)
 Variable patterns of enhancement; not enhanced to the same degree as normal liver

ULTRASOUND

When small, well-demarcated and solid echogenic structure
 Well-defined perilesional and intralesional blood vessels with 2- to 4-kHz shifts
 When large, complex hyperechogenic and hypoechogenic heterogeneous mass with anechoic areas

MR IMAGING

Inhomogeneous on all pulse sequences
 Fat within mass, producing hyperintense areas on T1-weighted images
 Sheets of hepatocytes isointense on T2-weighted images
 Areas of necrosis and hemorrhage hyperintense on T2-weighted images

NUCLEAR SCINTIGRAPHY

No gallium uptake
 Photopenic area on sulfur colloid and hepatobiliary scans surrounded by rim of increased uptake

ANGIOGRAPHY

Hypervascular mass that is homogeneous but does not stain intensely in capillary phase
 Hypovascular or avascular regions because of hemorrhage or necrosis
 Enlarged hepatic artery with feeders at tumor periphery (50%)
 Neovascularity

TABLE
93-58**Cavernous Hemangioma****ULTRASOUND**

Hyperechoic, homogeneous mass with discrete margins, usually <3 cm
 When larger, possible hypoechoic center, which may appear lacelike or granular
 Possible acoustic enhancement
 Stable size and appearance

COMPUTED TOMOGRAPHY

Well-circumscribed, spherical to ovoid, low-density mass on noncontrast scans
 Peripheral enhancement with vascular nodules, progressive centripetal flow, complete fill-in on delayed images 3-30 minutes after bolus (55%-89%)
 Complete (75%), partial (24%), or no (2%) fill-in isodensity in delayed phase

MR IMAGING

Well marginated
 Isointense or minimally hypointense signal on T1-weighted images
 T2 relaxation time longer than 80 ms
 No fibrous pseudocapsule
 Peak enhancement >2 minutes after injection of gadolinium diethylenetriaminepentaacetic acid
 Marked hyperintensity at 5-minute delay on T1-weighted image after contrast medium administration
 Variable central scar signal intensity on T1-weighted and T2-weighted images because of clot or fibrous tissue
 Progressive signal hyperintensity with increased T2 weighting
 No daughter nodules
 Intratumoral septa uncommon
 No hepatic venous, portal, or caval tumor thrombi

NUCLEAR SCINTIGRAPHY

Cold region during scintigraphic angiography on technetium Tc 99m-labeled erythrocyte scans
 Increased activity on delayed images at 1-2 hours
 Cold defect on sulfur colloid scans

ANGIOGRAPHY

Dense opacification of dilated, well-circumscribed, irregular, punctate vascular lakes and puddles in late arterial and parenchymal phase, beginning at the periphery
 Normal-sized feeders without arteriovenous shunting
 Contrast medium persistence late into venous phase

TABLE
93-59**Hepatocellular Carcinoma****ULTRASOUND**

Large tumor hyperechoic (59%)
 Small tumor hypoechoic (26%); often see thin, peripheral hypoechoic halo corresponding to fibrous capsule
 Mixed echogenicity in diffuse form (15%)
 Portal vein invasion (25%-40%)
 Hepatic vein invasion (16%)
 Invasion of inferior vena cava
 Hepatomegaly and ascites
 Characteristic high-flow Doppler signals, with shifts ≥ 4.5 kHz
 Fine blood flow network (branching pattern)

COMPUTED TOMOGRAPHY

Hypodense mass
 Circular zone of radiolucency surrounding mass
 Enhancement during arterial phase (80%)
 If sufficient arteriovenous shunting, early visualization of hepatic veins and cava
 Isodense on delayed scans (10%)

MR IMAGING

Poorly marginated
 Isointense to minimally hyperintense (50%) on T1-weighted images because of fat content
 T2 relaxation time <80 ms
 Pseudocapsule hypointense on T1-weighted and T2-weighted images
 Moderate peak enhancement
 Faint enhancement at 5-minute delay after contrast agent administration
 Hypointense central scar on T1-weighted and T2-weighted images
 Less pronounced hyperintensity with progressive T2 weighting
 Daughter nodules present
 Intratumoral septa common
 Intermediate signal intensity tumor thrombi in cava, portal vein, or hepatic vein on T1-weighted images

ANGIOGRAPHY

Enlarged arterial feeders, coarse neovascularity, vascular lakes, arterioportal shunts, and dense tumor stain in differentiated hepatocellular carcinoma
 Vascular encasement, fine neovascularity, displacement, and corkscrewing of vessels in cirrhosis and anaplastic hepatomas
 With tumor invasion of portal vein, "thread and streaks" appearance, linear parallel vascular channels

NUCLEAR SCINTIGRAPHY

On sulfur colloid scan, single cold spot (70%), multiple defects (15%-20%), or heterogeneous distribution (10%)
 Cold nodule on iminodiacetic acid scan
 On gallium scan, avid accumulation in 70%-90%

TABLE 93-60 Focal Nodular Hyperplasia

COMPUTED TOMOGRAPHY Homogeneous mass of slightly decreased attenuation on noncontrast scans Isodense or hypodense on bolus injection of contrast material Markedly hyperdense on arterial phase; may be isodense on portal venous phase because of rapid washout Central scar may be hyperdense or hypodense on arterial phase, hyperdense on delayed images because of delayed washout within myxomatous stroma	MR IMAGING Isointense on T1-weighted and T2-weighted images (80%) Isointense on T1-weighted images and slightly hyperintense on T2-weighted images (20%) Margins poorly defined or invisible Central scar is hypointense on T1-weighted images and hyperintense on T2-weighted images (95%) (compare fibrolamellar hepatoma, in which central scar is hypointense on T1-weighted and T2-weighted images, and hepatoma, in which central scar is rare)
ULTRASOUND Hypoechoic or hyperechoic homogeneous mass, often isoechoic, subtle, difficult to differentiate in echogenicity from adjacent liver Central scar appears as a hypoechoic linear or stellate area within the central portion of the mass Well-developed peripheral and central blood vessels creating a spoke-wheel appearance Predominant arterial signals centrally with a midrange (2-4 kHz) shift	ANGIOGRAPHY Hypervascular mass (90%) with intense capillary blush Enlarged main feeding artery with central blood supply (spoke-wheel pattern, 33%) Decreased vascularity in central stellate fibrous scar NUCLEAR SCINTIGRAPHY Normal sulfur colloid scan (30%-55%), cold spot (40%), or hot spot (10%) Iminodiacetic acid scan: normal or increased uptake (40%-70%) or cold spot (60%)

SUGGESTED READINGS

- Dähnert W: Radiology Review Manual, ed 7, Baltimore, 2011, Williams & Wilkins.
- Reeder MM: Reeder and Felson's Gamuts in Radiology, ed 4, New York, 2003, Springer-Verlag.
- Eisenberg RL: Gastrointestinal Radiology—A Pattern Approach, ed 4, New York, 2004, Lippincott-Raven.
- Chapman S, Nakielnny R: Aids to Radiological Differential Diagnosis, London, 1990, Baillière Tindall.
- Baker SR: The Abdominal Plain Film, East Norwalk, CT, 1990, Appleton & Lange.
- Lee JKT, Sagel SS, Stanley RJ, Heiken J, editors: Computed Body Tomography with MRI Correlation, New York, 2006, Raven.
- Rumack CM, Nilson SR, Charboneau JW, editors: Diagnostic Ultrasound, ed 4, St. Louis, 2011, CV Mosby.
- Semelka RC: Abdominal-Pelvic MRI, ed 2, New York, 2010, Wiley-Liss.
- Datz FL: Gamuts in Nuclear Medicine, ed 3, St. Louis, 1995, CV Mosby.
- Lamps L: Diagnostic Pathology: Hepatobiliary and Pancreas, Salt Lake City, 2012, Utah, Amirsys.
- Odze RD, Goldblum JR: Surgical Pathology of the GI Tract, Liver, Biliary Tract and Pancreas: Expert Consult, ed 2, Philadelphia, 2009, Elsevier.
- Federle MP, Jeffrey RB, Jr, Tublin M, et al: Specialty Imaging: Hepatobiliary and Pancreas, Salt Lake City, 2013, Utah, Amirsys.

SECTION
XI

Pancreas

Pancreas: Normal Anatomy and Examination Techniques

NANCY A. HAMMOND | FREDERICK L. HOFF | RAVI GUTTIKONDA |
HELENA GABRIEL | RICHARD M. GORE

CHAPTER OUTLINE

Historical Perspective

Normal Anatomy

Topography
Common Bile Duct
Pancreatic Duct
Arterial Supply
Venous Drainage
Lymphatics
Nerve Supply

Radiologic Techniques

Plain Radiographs
Contrast Studies
Ultrasound
Computed Tomography
Magnetic Resonance Imaging
Magnetic Resonance Cholangiopancreatography
Endoscopic Retrograde Cholangiopancreatography

Historical Perspective

The pancreas was one of the last organs in the abdomen to receive the attention of anatomists, physiologists, physicians, and surgeons. Located in the “straggling mesenchyme” of the retroperitoneum, the pancreas has in the past been called the hermit or hidden organ of the abdomen.¹ The pancreas was first described in the Talmud and depicted as the “finger of the liver” between 200 BC and AD 200. Ruphos named this organ the pancreas (Greek: *pan*, meaning “all”; *kreas*, meaning “flesh”) shortly thereafter.² More than a millennium passed before anatomic descriptions were completed.

Wirsung of Padua demonstrated the pancreatic duct in 1642, and Santorini of Venice described the accessory duct in 1724. The papilla of Vater was described by A. Vater in 1720. In 1887, Oddi described the complex musculature of the sphincter bearing his name. The histologic structure of the pancreas was described by Langerhans in 1869. The role of the pancreas in digestion was first suggested by Bernard in 1850, and the connection between diabetes and the pancreas was established in the 1890s. Surgery for pancreatic disease was not popular until the pioneering work of Whipple in the 1930s.³

The pancreas also remained a hidden organ for the radiologist for decades. Indirect signs of pancreatic disease on plain films and barium studies were usually present only in advanced disease. The 1970s brought endoscopic retrograde cholangiopancreatography (ERCP) and angiography to the

fore. Computed tomography (CT), ultrasound, and magnetic resonance imaging (MRI) now routinely provide superb visualization of the gland noninvasively.⁴ Endoscopic ultrasound is a useful adjunct to cross-sectional imaging in evaluating for pancreatic disease and allows pancreatic biopsy when it is indicated.

Normal Anatomy

The pancreas is an unpaired accessory digestive gland that has both exocrine and endocrine functions. It is a slender, soft, lobulated organ that in the adult measures approximately 15 to 25 cm in length, 3 to 5 cm in height, and 1.5 to 3.5 cm in thickness and weighs 70 to 110 g.^{5,6} It has a pale, yellow-tan surface that is finely nodular and firm to palpation.

TOPOGRAPHY

The pancreas lies within the anterior pararenal space (Fig. 94-1). The pancreatic head has a constant relationship with the duodenum, with its right lateral border nestled in the duodenal sweep.⁷ The head is the thickest portion of the gland; it gives rise to the uncinate process, which projects like a hook, dorsal to the superior mesenteric vein. The pancreatic neck lies immediately anterior to the confluence of the splenic and superior mesenteric veins. The neck narrows behind the pylorus, then widens as it becomes the body. The body arches anteriorly and laterally to cross the spine and may be thinner than the pancreatic head and tail as it does.^{8,9} The body bulges up in the pancreatic tubercle almost to the level of the celiac axis. The tail is not well demarcated from the body as it extends to the splenic hilum.¹⁰

The shape, position, and axis of the pancreas are variable and are influenced by age, body habitus, previous surgery, and organomegaly.⁹ The head usually lies at the level of L1-L2, and the body crosses the spine at L1; the tail is located more superiorly in the region of the splenic hilum. The longitudinal axis of the pancreas is about 20 degrees in relationship to the transverse plane¹⁰ (Fig. 94-2). The axis of the pancreas is occasionally transverse, and even less commonly the tail may lie caudal to the head. If the left kidney is congenitally or surgically absent, the tail often lies in a posteromedial position, adjacent to the spine. The pancreas can be shaped like an L, S, or inverted V.¹⁰

The gastric body and antrum lie anterior to the body and tail of the pancreas, and the pylorus is located ventral to the pancreatic neck. The duodenum lies along the right lateral border of the pancreatic head; it also passes inferior to the head, body, and tail. The spleen lies along the lateral and superior aspect of the pancreatic tail. The right kidney and adrenal gland are located posterior to the pancreatic head, and the left kidney

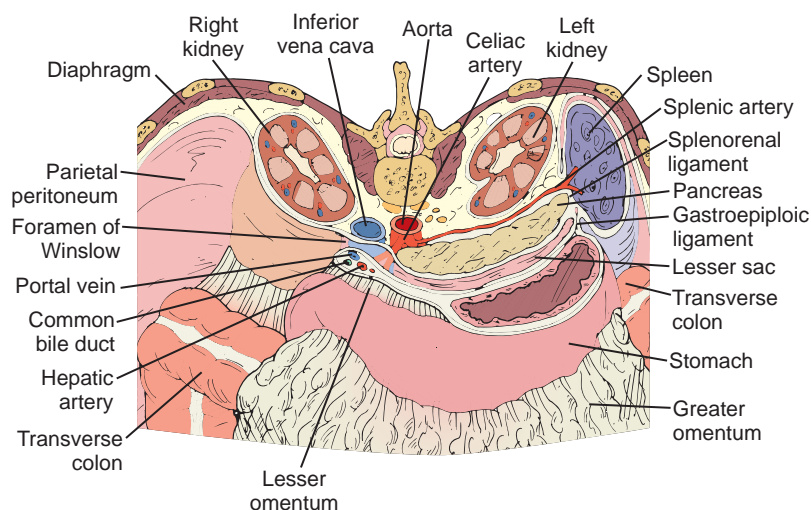


Figure 94-1 Anatomic relationships of the pancreas. (From Meyers MA: *Dynamic Radiology of the Abdomen*. New York, Springer-Verlag, 1988, p 57.)

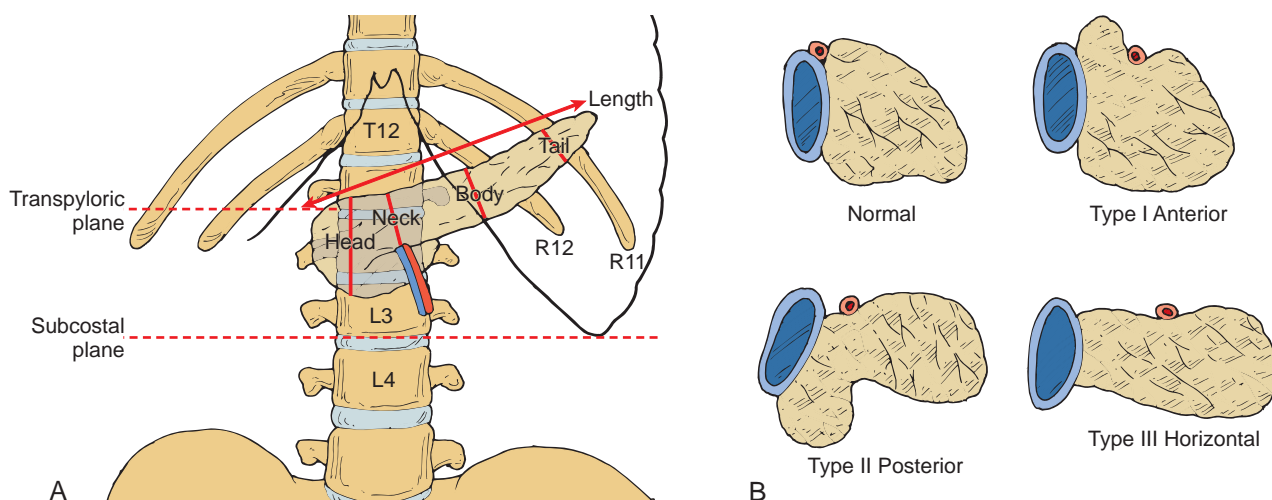


Figure 94-2 Normal pancreatic orientation and appearances of the pancreatic head. **A.** Normal pancreatic dimensions. **B.** Normal pancreatic head configurations. (**A** from Zylak CJ, Pallie W: *Correlative anatomy and computed tomography: A module on the pancreas and posterior abdominal wall*. *RadioGraphics* 1:61–84, 1981. **B** from Mortelet KR, Rocher TC, Stretter JL, et al: *Multimodality imaging of pancreatic and biliary congenital anomalies*. *RadioGraphics* 26:715–731, 2006.)

and adrenal gland are dorsal and occasionally caudal to the tail. Depending on its size, the left lobe of the liver may lie anterior to the pancreatic body. The gallbladder is positioned ventral to the pancreatic head. The transverse colon lies anterior and generally inferior to the pancreas. The small bowel usually lies inferior to the level of the pancreas but occasionally can lie ventral to the tail.^{11,12}

Nearly all of the pancreas is retroperitoneal; a nonperitonealized bare area results from the reflection of the posterior parietal peritoneum to form the two leaves of the transverse mesocolon and the posterior inferior margin of the lesser sac (Fig. 94-3). The transverse mesocolon originates where the hepatic flexure of the colon crosses ventral to the second portion of the duodenum. The bare area begins as a broad strip across the infra-ampullary portion of the descending duodenum and continues across the head, body, and tail of the pancreas. The pancreatic tail, after extending across the left kidney, is actually an intraperitoneal structure incorporated within the leaves of

the splenorenal ligament. The root of the small bowel mesentery originates inferior to the pancreatic body and is contiguous with the transverse mesocolon.^{7,13} Therefore, pancreatic processes may affect the stomach and duodenum by direct spread and the small bowel loops and colon through the small bowel mesentery and transverse mesocolon (see Fig. 94-3).

COMMON BILE DUCT

The common bile duct enters the head of the pancreas after it passes posterior to the first part of the duodenum in the hepatoduodenal ligament. It passes inferiorly and dorsally, embedded in the posterior surface of the pancreatic head, to join the pancreatic duct of Wirsung. This segment runs a short intramural course before it enters the posteromedial aspect of the duodenum through the major papilla of Vater (Fig. 94-4). The common bile duct is 7 cm long and has an average diameter of 7.4 mm.^{8,14,15}

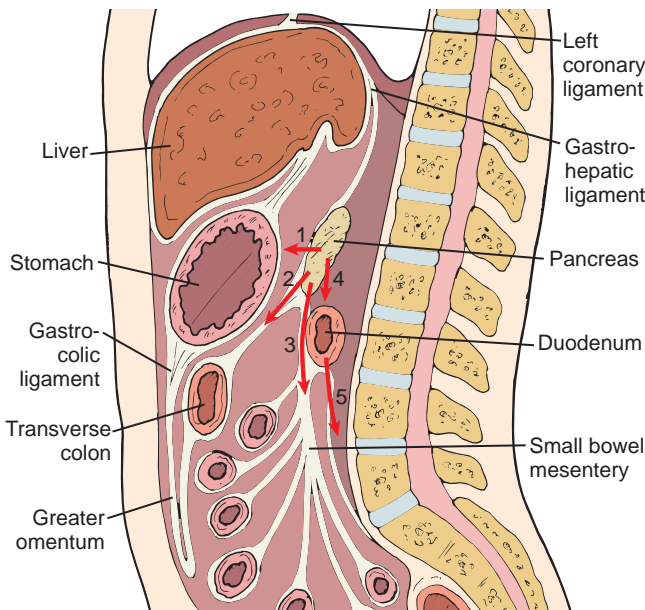


Figure 94-3 The mesenteric, omental, retroperitoneal, and subperitoneal relationships of the pancreas: sagittal perspective. Pancreatic disease may spread into the lesser sac (1), transverse mesocolon (2), root of the small bowel mesentery (3), duodenum (4), and anterior pararenal space (5).

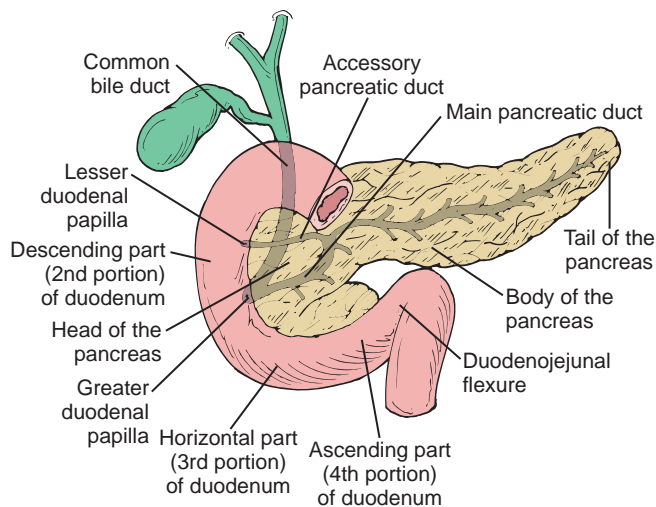


Figure 94-4 Extrahepatic biliary and pancreatic duct system. (From Tersingni R, Toledo-Pereyra LH: *Surgical anatomy of the pancreas*. In Toledo-Pereyra LH [ed]: *The Pancreas: Principles of Medical and Surgical Practice*. New York, Churchill Livingstone, 1985, pp 31–50.)

PANCREATIC DUCT

The pancreatic duct arises from the pancreatic tail and receives 20 to 35 short tributaries entering at right angles to its long axis as it courses toward the head. The duct lies midway between the superior and inferior margins of the pancreas and slightly more dorsally than ventrally. At the level of the major papilla, the main pancreatic duct (duct of Wirsung) courses horizontally to join the caudal surface of the common bile duct, forming the ampulla of Vater. The accessory pancreatic duct of Santorini drains the anterior and superior portion of the head of the pancreas either into the duodenum

at the minor papilla or into the main pancreatic duct (see Fig. 94-4). The minor papilla is often not patent, and the accessory duct may be partially or completely obliterated or have an anomalous connection with the duct of Wirsung.^{16,17} These anatomic variants in ductal anatomy are discussed more fully in Chapter 96.

ARTERIAL SUPPLY

Although the pancreatic parenchyma is well visualized on cross-sectional imaging, it is important to recognize and to define the major pancreatic vascular landmarks¹⁸ (Fig. 94-5). The arterial blood supply of the pancreas arises from the celiac trunk and the superior mesenteric artery. After originating from the celiac artery, the common hepatic artery courses to the right in proximity to the neck and subsequently the head of the pancreas. At this point, it divides into the proper hepatic artery, which enters the free edge of the hepatoduodenal ligament, and the gastroduodenal artery, which courses caudally to lie ventral and lateral to the pancreatic head. The gastroduodenal artery gives rise to the anterior and posterior superior pancreaticoduodenal arteries, which supply the head of the pancreas. These vessels help form the pancreatic arcade when they join the anterior and posterior inferior mesenteric arteries that arise separately or as a common trunk from the proximal portion of the superior mesenteric artery.^{5,11,14,19}

The splenic artery arises from the celiac artery and loops like a snake above and below the superior margin of the pancreas. It becomes more tortuous with age and occasionally becomes embedded within the pancreatic parenchyma. The pancreatic body and tail are supplied by the dorsal pancreatic artery, which arises from the splenic artery or as a fourth branch of the celiac trunk, as well as by the splenic, hepatic, or superior mesenteric arteries. The pancreatica magna is the largest of the series of superior pancreatic branches of the splenic artery.^{19,20}

The superior mesenteric artery arises from the anterior surface of the aorta, 1 to 2 cm below the celiac trunk. It courses caudal and dorsal to the neck of the pancreas, passing anterior to the uncinate process, where it serves as a major landmark for cross-sectional imaging. Displacement of the artery to the right of the aorta is a normal variant.²¹

The most frequent arterial anomaly of the upper abdomen is partial or complete replacement of either the right hepatic or the proper hepatic artery to the superior mesenteric artery. In these patients, the replaced hepatic artery passes cephalad and ventral to the pancreas, then anterior or posterior to the portal vein to reach the liver.²²

VENOUS DRAINAGE

The venous drainage of the pancreas is constant; the portal system serves as an essential landmark for localizing the pancreas on cross-sectional imaging.^{11,19} In general, the veins of the pancreas parallel the arteries and lie inferior to them (Fig. 94-6). Four pancreaticoduodenal veins form venous arcades that drain the pancreatic head and the duodenum. The inferior pancreaticoduodenal veins drain into the first jejunal branch of the superior mesenteric vein. The inferior pancreaticoduodenal veins are smaller than their superior counterparts; they are not commonly visualized on cross-sectional imaging. The posterior superior pancreaticoduodenal vein extends cephalad to join the

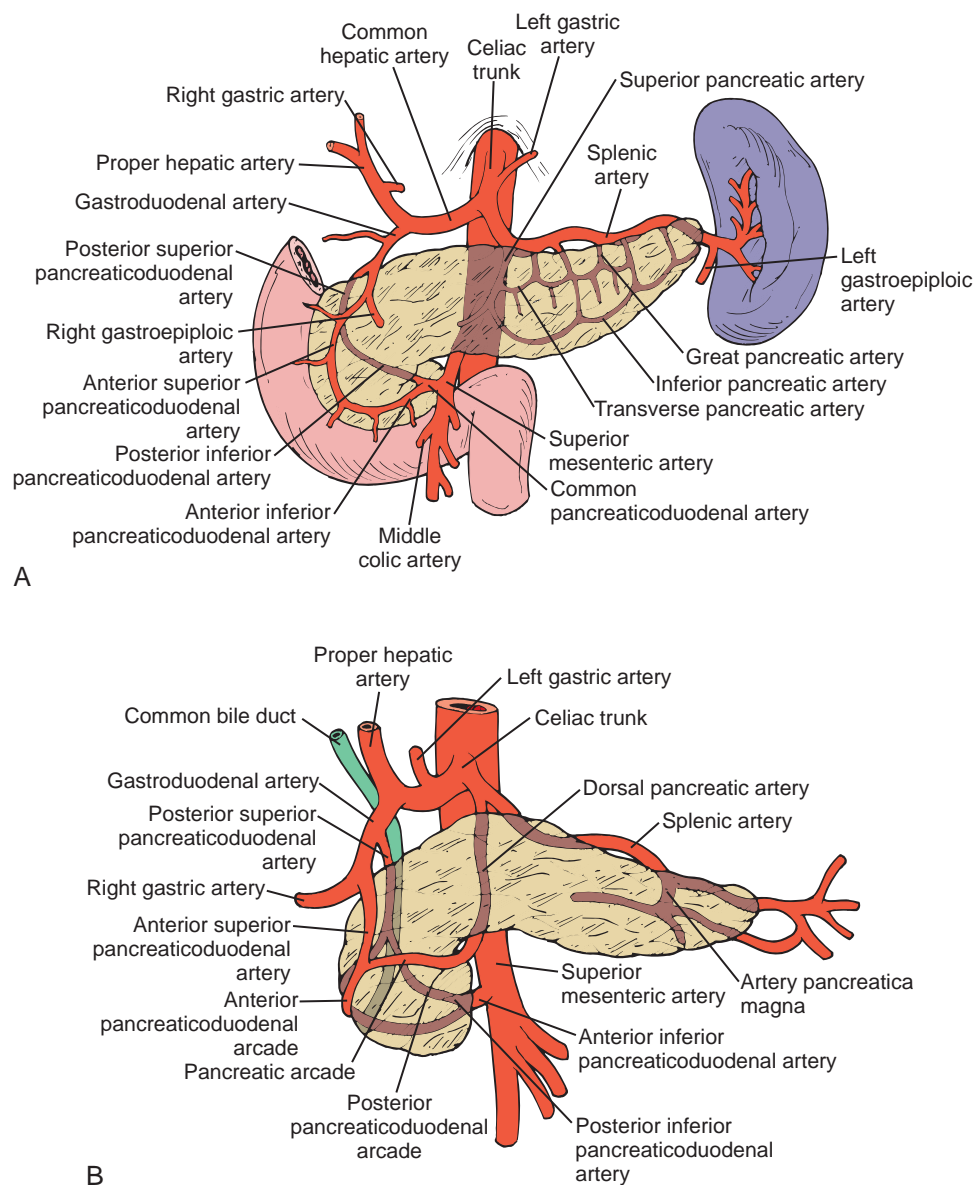


Figure 94-5 Schematic views of the arterial blood supply of the pancreas. (A and B from Tersingni R, Toledo-Pereyra LH: *Surgical anatomy of the pancreas*. In Toledo-Pereyra LH [ed]: *The Pancreas: Principles of Medical and Surgical Practice*. New York, Churchill Livingstone, 1985, pp 31–50.)

caudal aspect of the portal vein directly.^{21,22} The anterior superior pancreaticoduodenal vein runs horizontally to drain into either the gastroduodenal vein or the right gastroepiploic vein, both of which extend to the superior mesenteric vein.²³ Three to 13 small veins from the body and tail empty directly into the splenic vein, which follows a smooth arching course from the spleen to its junction with the superior mesenteric vein. The splenic vein parallels the splenic artery and lies in a groove along the dorsal and superior margin of the pancreas. It is a superb landmark for the posterior aspect of the pancreas, and long segments of this vessel can be seen on CT and ultrasound studies on a single image.²⁴ Rarely, the distal tip of the pancreatic tail can lie posterior to the vein, adjacent to the adrenal gland.²⁵

The splenic vein joins the superior mesenteric vein posterior to the neck of the pancreas and is seen as a round or oval

dilation to the right of the midline, posterior to the neck of the pancreas. The superior mesenteric vein courses anterior to the uncinate process just to the right of the superior mesenteric artery^{11,22} (see Fig. 94-6).

The portal vein is formed behind the pancreatic neck by the union of the splenic and superior mesenteric veins and continues superiorly and laterally toward the porta hepatis as the main extrahepatic portal vein, dorsal to the common bile duct and hepatic artery. In one third of the population, the inferior mesenteric vein enters at the confluence; in another third, it joins the splenic vein close to the junction; and in the remainder, it joins the superior mesenteric vein.⁸

LYMPHATICS

The lymph nodes of the pancreas are distributed along the major vascular pathways (Fig. 94-7). The lymphatic channels of the pancreas form a richly branched plexus that empties

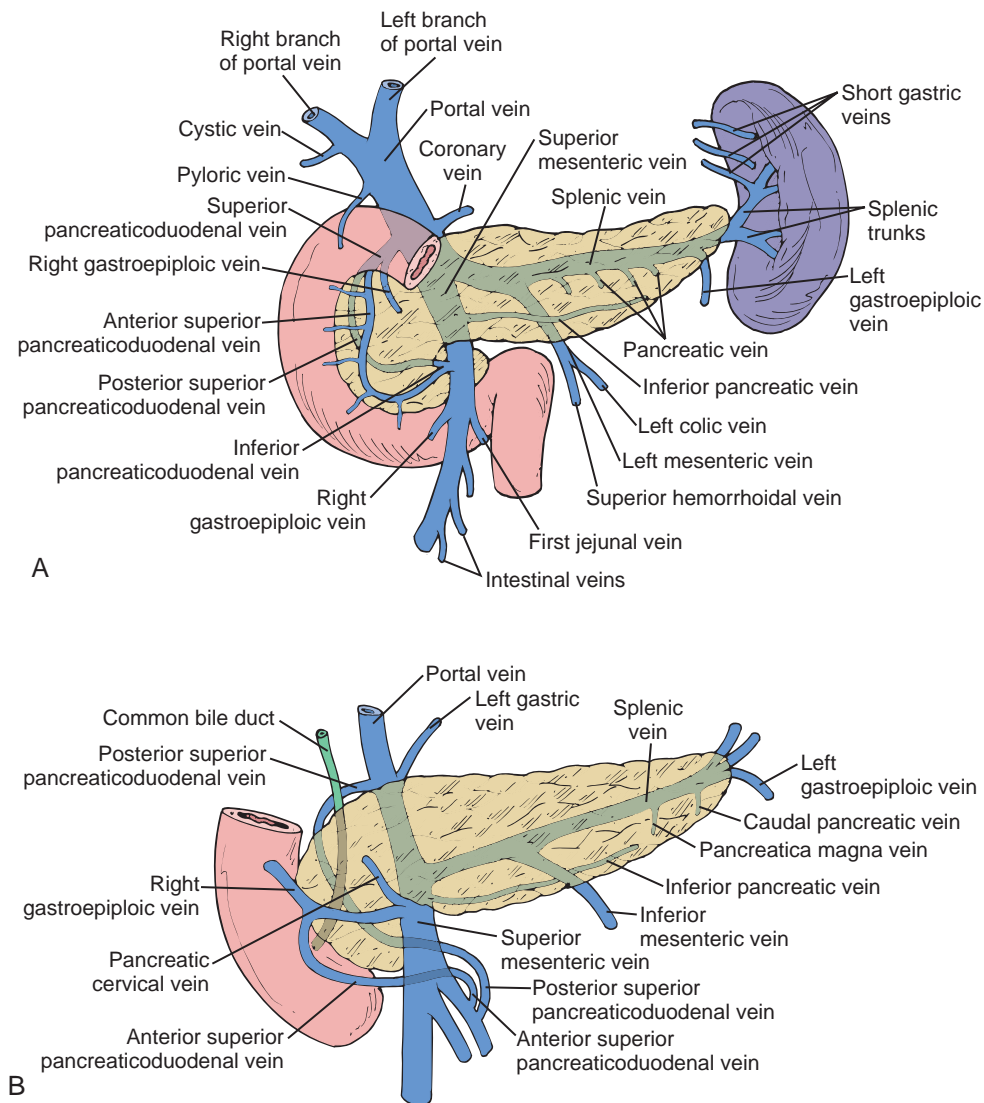


Figure 94-6 Schematic views of the venous drainage of the pancreas. (A and B from Tersingni R, Toledo-Pereyra LH: *Surgical anatomy of the pancreas*. In Toledo-Pereyra LH [ed]: *The Pancreas: Principles of Medical and Surgical Practice*. New York, Churchill Livingstone, 1985, pp 31–50.)

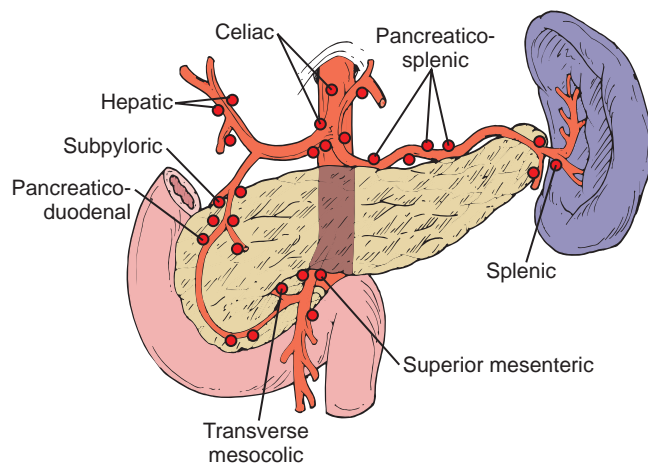


Figure 94-7 Major regional nodal groups of the pancreas. (From Tersingni R, Toledo-Pereyra LH: *Surgical anatomy of the pancreas*. In Toledo-Pereyra LH [ed]: *The Pancreas: Principles of Medical and Surgical Practice*. New York, Churchill Livingstone, 1985, pp 31–50.)

in multiple directions. The extensive network of lymphatic vessels and lymph nodes draining the pancreas provides egress to tumor cells arising from the pancreas and contributes to the fact that pancreatic cancer often presents with positive lymph nodes and a high incidence of local recurrence after resection. The anatomy of the lymphatics suggests that partial removal of the pancreas for cancer may not be sufficient because of the direct connections between different lymphatic chains.^{5,8,15,19,20}

The suprapancreatic and intrapancreatic lymphatic chains receive branches from the neck, body, and portions of the pancreatic tail. Branches from the posterior surface of the head and neck drain into the pancreaticoduodenal and juxta-aortic nodes. The posterior surface of the pancreatic body drains into the suprapancreatic and intrapancreatic nodes. The pancreatic tail drains into the nodes of the splenic hilum and gastropancreatic fold. Some drainage from the pancreatic head and proximal body enters the nodes in the porta hepatis and may extend inferiorly toward the superior mesenteric, mesocolic, and para-aortic nodal chains. The suprapancreatic nodes are closely related to the splenic artery and vein; the intrapancreatic chain is adjacent to the leaves of the transverse mesocolon.

NERVE SUPPLY

It is important to appreciate the nerve supply of the pancreas (Fig. 94-8) in planning celiac nerve blocks for control of pain resulting from pancreatic carcinoma or chronic pancreatitis.²⁶ The pancreas receives sympathetic innervation by way of the splanchnic nerves and parasympathetic innervation from the vagus nerve. The sympathetic nerves carry the pain (visceral afferent) fibers. They pierce the diaphragmatic crura to enter the celiac plexus and celiac ganglion that surround the celiac artery. The superior mesenteric ganglia and plexus surround the superior mesenteric artery. Chemical extirpation of the celiac ganglion interrupts afferent pain fibers from both the sympathetic and the parasympathetic systems and can be accomplished by injection of the chemical agent between the celiac artery and the superior mesenteric artery either antecrurally or retrocrurally.²⁶⁻²⁸

Radiologic Techniques

PLAIN RADIOGRAPHS

In patients with suspected pancreatic disease, plain radiographs are obtained chiefly to exclude other conditions, such as obstruction or a perforated duodenal ulcer that may simulate pancreatitis.²⁹⁻³² Oblique views are often helpful in patients with chronic pancreatitis to detect calcifications that may be obscured by the spine on the anteroposterior view.^{30,32,33}

CONTRAST STUDIES

Before the advent of cross-sectional imaging, angiography, ERCP, and barium studies were the major means of evaluating the pancreas. Although barium studies are less important now in evaluation of the pancreas, the following areas should still be carefully evaluated in patients with suspected pancreatic disease. The posterior gastric wall, the distal duodenum, and the duodenojejunal junction can be abnormal with lesions of the

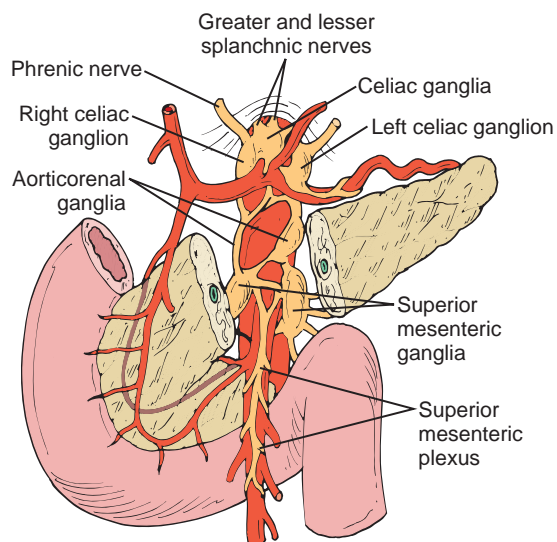


Figure 94-8 Nerve supply of the pancreas. (From Tersingni R, Toledo-Pereyra LH: *Surgical anatomy of the pancreas*. In Toledo-Pereyra LH: *The Pancreas: Principles of Medical and Surgical Practice*. Churchill Livingstone, New York, 1985, pp 31-50.)

pancreatic tail and body; the greater curvature of the gastric antrum and medial aspect of the descending duodenum can provide clues for lesions arising in the pancreatic head and neck. Barium enema examination may reveal abnormalities of the colon caused by disease spread through the transverse mesocolon or at the splenic flexure caused by disease carried by the phrenicocolic ligament.^{13,30,31}

ULTRASOUND

Sonography is a means of noninvasively evaluating the pancreas, particularly in thin patients. It is fast, safe, and inexpensive; it can be done portably; and it requires little preparation or cooperation of the patient and no administration of contrast medium.³⁴ However, ultrasound can be limited by patient body habitus and is dependent on the level of experience of the operator. Ultrasound examination of the pancreas is best performed on the fasting patient to reduce the amount of gas and food in overlying bowel. Real-time equipment with the highest frequency transducer (5-8 MHz) possible should be used.

Examination Techniques

Scans of the pancreas should first be performed with the patient supine and the transducer turned into a modified transverse plane angled cephalad toward the spleen (Fig. 94-9). The long axis of the pancreas is seen anterior to the splenic vein and confluence of the superior mesenteric and splenic veins. The pancreatic head and neck sweep around the superior mesenteric vein, forming the retrovenous, hooklike uncinate process. The common bile duct is often imaged axially within the pancreatic head, and the gastroduodenal artery may be seen along the anterolateral aspect of the pancreatic head. The gas-filled or fluid-filled duodenum, stomach, colon, aorta, inferior vena cava, superior mesenteric artery, and left renal vein are interrogated in this projection as well. The lesser sac, which lies between the posterior gastric wall and pancreas, is best seen in this plane and should be scanned for fluid, masses, or calcifications.³⁵⁻³⁸

Parasagittal scans of the pancreas should begin where the portal vein merges with the longitudinally oriented superior mesenteric vein. The neck of the pancreas in transverse section is seen anterior to this confluence. The uncinate process lies posterior to the superior mesenteric vein. The pancreatic head can be seen to the right of the superior mesenteric vein, with the common bile duct located posteriorly and the gastroduodenal artery sometimes visualized anteriorly. To the left of the superior mesenteric vein, the pancreatic body and proximal portion of the tail are found anterior to the splenic vein and slightly inferior to the splenic artery.³⁹⁻⁴³

With meticulous technique and attention to detail, diagnostic scans of the pancreas can be obtained in 90% of cases. Several maneuvers can improve sonographic visualization of the pancreas.⁴⁴⁻⁴⁹ Deep inspiration causes the liver to move inferiorly over the pancreas, caudally displacing gas-filled bowel. Having the patient drink four 6-oz cups of degassed water can provide a sonographic window for improved visualization of the body and tail.

Normal Findings on Ultrasound

Three morphologic shapes of the pancreas have been described: tadpole shaped (44%), dumbbell shaped (33%), and sausage shaped (23%). Absolute measurements of pancreatic size are controversial, but the maximal normal anteroposterior

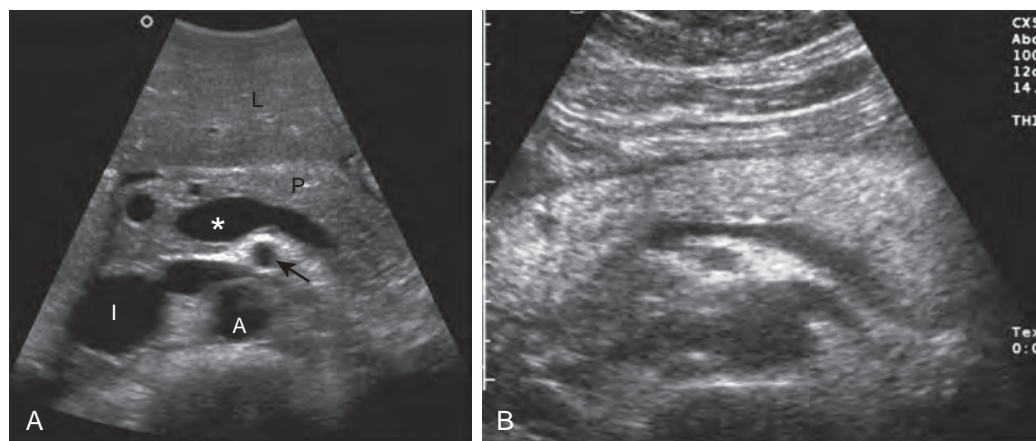


Figure 94-9 Normal pancreatic anatomy on ultrasound.

A. Transverse sonogram demonstrating the majority of the pancreas. The echogenicity of the pancreas (P) is greater than that of the liver (L). A, Aorta; I, inferior vena cava; arrow, superior mesenteric artery; asterisk, confluence of superior mesenteric vein and splenic vein. **B.** Transverse sonogram of a very echogenic pancreas due to fatty infiltration.

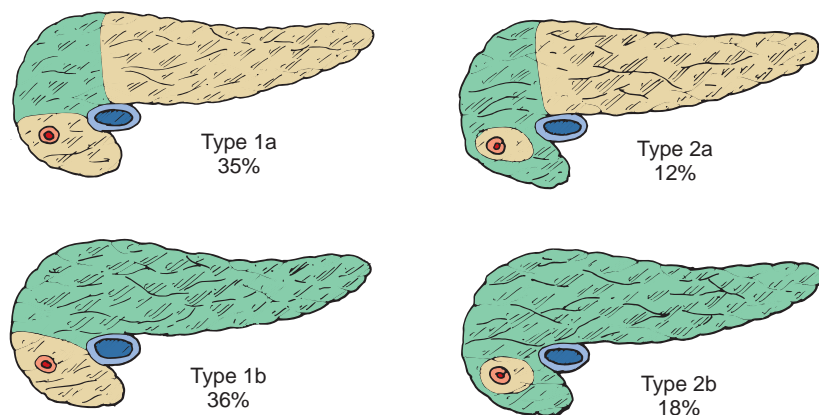


Figure 94-10 Uneven fatty replacement of the pancreas. Drawings illustrate the four different patterns of fatty replacement of the pancreas (green areas). The percentage of cases of uneven pancreatic lipomatosis represented by each type is also indicated. (From Mortelet KR, Rocher TC, Stretter JL, et al: Multimodality imaging of pancreatic and biliary congenital anomalies. *RadioGraphics* 26:715-731, 2006.)

diameters of the pancreatic head and body are 2.6 cm and 2.2 cm.⁵⁰ The tail is much more variable in shape and size and is not measured for diagnostic purposes. In a dumbbell-shaped pancreas, the tail may be 3.5 cm; when the pancreas is sausage shaped, the pancreatic head can be normal up to 3.5 cm.⁵¹ The pancreatic body is usually the narrowest part of the pancreas. In general, the pancreas is proportionately larger in young people; it decreases in relative size with age.^{52,53} The borders of the pancreas are usually smooth in youth and become somewhat irregular with age. Analysis of the shape of the uncinate process is particularly important because any rounding or enlargement implies disease.^{50,54}

The echogenicity of the pancreas is high throughout its substance. The pancreatic tissue texture or echo size is usually coarser, more inhomogeneous, and more echogenic than that of the liver (see Fig. 94-9). It is important to compare the echo patterns and amplitudes of the liver and pancreas at the same depth because dot size and echo amplitude are closely related to the transducer beam profile.^{55,56} The tissue texture of the pancreas is related to the extent of fatty infiltration.^{57,58} As the pancreas ages, it undergoes progressive fatty infiltration, and consequently it becomes more echogenic. Pancreatic parenchyma should be less echogenic than surrounding retroperitoneal fat. When the pancreas is completely replaced by fat in older individuals, it may be difficult to differentiate from the retroperitoneal fat.⁵⁹

Certain caveats apply in scanning the pancreas. Gas within the stomach and duodenum can cause subtle shadowing, artifactually decreasing the echogenicity of the adjacent pancreas.^{50,52} Different amounts of fat may be deposited in the

ventral (head and uncinate process) and dorsal (body and tail) pancreas, making the head appear hypoechoic. In some cases, demarcation of the different echogenicities can be seen to correspond to the expected fusion line of the dorsal and ventral embryologic moieties⁵³ (Fig. 94-10).

On occasion, prepancreatic fat between the stomach and pancreas can be prominent in some patients. It is usually somewhat less echogenic than pancreas and must be differentiated from fluid in the lesser sac, lymphadenopathy, and mural thickening of the stomach.^{60,61} The main pancreatic duct (duct of Wirsung) is identified sonographically in approximately two thirds of patients as an anechoic space surrounded by two parallel hypoechoic lines resembling trolley tracks.⁶² The maximal inner diameter is less than 2 mm; when it is larger, an obstructing mass, stricture, or stone must be suspected. The diameter of the pancreatic duct normally increases with age.⁶³⁻⁶⁷

A number of normal structures may simulate the pancreatic duct, so it is important to image the duct within the substance of the gland. The posterior wall of the stomach can mimic a dilated pancreatic duct, with normal pancreas dorsal and echogenic gastric lumen ventral, sandwiching the relatively hypoechoic gastric wall. The ingestion of water resolves this problem. A tortuous splenic artery can also simulate a dilated pancreatic duct or cystic pancreatic mass when it lies close to the pancreatic parenchyma. Doppler examination can easily resolve the confusion.^{68,69}

In patients with suspected choledocholithiasis or biliary obstruction, every effort should be made to visualize the distal common bile duct. It often is not visualized because it lies posterior to the second portion of the duodenum, which may be

gas filled. This is especially true if the duct is scanned in the supine or left posterior oblique position. A superior method for visualizing the distal common bile duct sonographically is to scan the patient in an erect right posterior oblique position and to rely primarily on transverse rather than parasagittal images. The erect right posterior oblique position minimizes gas within the antrum and duodenum; the transverse scanning plane optimizes identification of the course of the intrapancreatic distal duct.^{70,71} The posterior superior pancreaticoduodenal vein can mimic the distal common bile duct; color Doppler examination can easily differentiate the two structures.⁷²⁻⁷⁷

Intraoperative Ultrasound

Intraoperative sonography is a time-consuming but accurate means of localizing small islet cell tumors of the pancreas. It can also be used to guide open biopsy and aspiration.⁷⁸⁻⁸² With the increased use of laparoscopic techniques, probes for use during this procedure have also been introduced.⁸³

Endoscopic Ultrasound

Ultrasound transducers have been modified so that they can be incorporated into the tip of flexible endoscopes. These transducers have the advantage of higher frequency and spatial resolution, which may be of use in diagnosing small pancreatic tumors, in demonstrating subtle pancreatitis, and in evaluating islet cell tumors preoperatively.⁸⁴⁻⁸⁶ The proximity of the stomach and duodenum to the pancreas allows high-resolution imaging of the pancreas and eliminates the limits of overlying

bowel gas seen in transabdominal ultrasound. When indicated, pancreatic biopsies can also be performed by endoscopic ultrasound.

COMPUTED TOMOGRAPHY

CT is the best single technique for the noninvasive imaging of the pancreas. It is unaffected by bowel gas or large body habitus, is widely available, and is relatively easily performed. CT has greatly diminished the need for diagnostic ERCP and angiography.⁸⁷⁻⁸⁹ Multidetector CT techniques have improved CT examination of the pancreas, allowing thinner contiguous images, overlapping images without increased radiation exposure, and freedom from respiratory misregistration. The rapidity of scanning allows several acquisitions to be made through the pancreas during different phases of a single bolus of contrast material.⁹⁰⁻¹⁰⁸

Size, Shape, and Density on Computed Tomography

The morphologic appearance of the pancreas on CT depends on the amount of fat within the intralobular septa that separates the acinar lobules of the gland. In younger patients, the contour of the gland is smooth; the parenchyma is homogeneous, with an attenuation similar to that of spleen and muscle but less than that of liver on noncontrast scans (Fig. 94-11). With age and progressive fatty deposition, the pancreas becomes lobulated, irregular, and inhomogeneous.^{90,109}

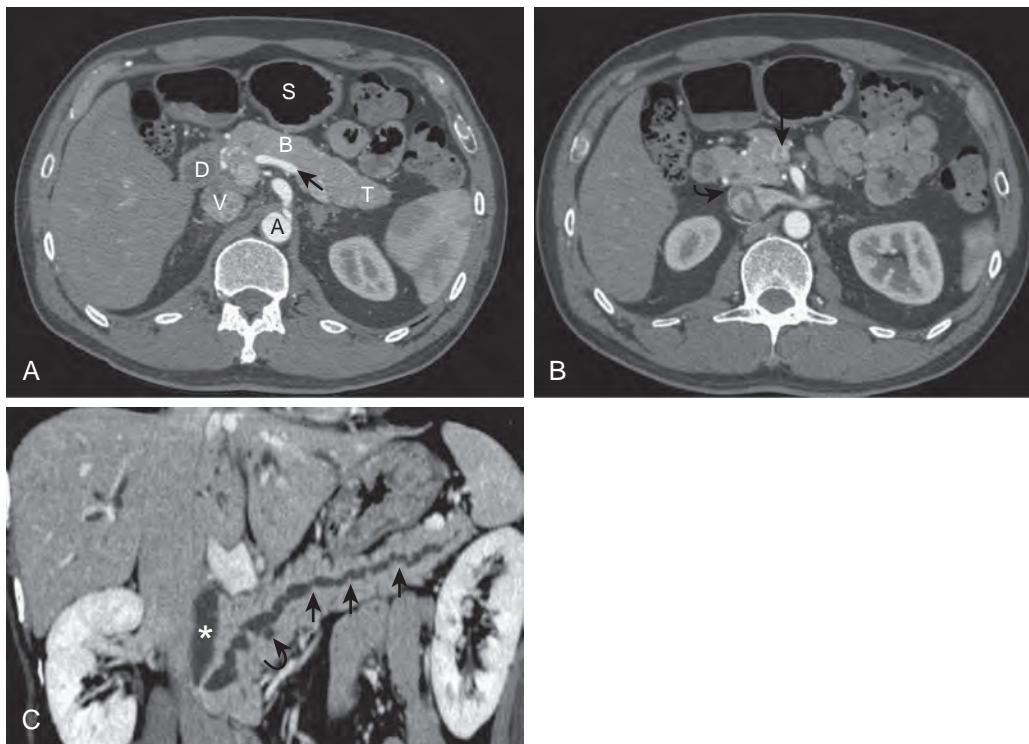


Figure 94-11 Normal pancreas on CT. Because of the oblique line of the pancreas, the entire organ is seldom seen on a single image. **A.** Image through the body (B) and tail (T) of the pancreas. The splenic vein (arrow), which lies immediately dorsal to the body of the pancreas, is an excellent landmark. A, Aorta; D, duodenum; S, stomach; V, inferior vena cava. **B.** Image from the same patient obtained 1 cm caudal to **A** demonstrates the uncinus process of the pancreas. The superior mesenteric vein (arrow) is difficult to visualize on this image that was obtained early in the administration of the contrast material bolus. However, the arterial anatomy is well demonstrated. Curved arrow, Dorsal pancreatic artery. **C.** Coronal curved multiplanar reconstruction image of the pancreas demonstrates a small, side branch, intraductal papillary mucinous neoplasm (curved arrow). This technique is useful in imaging of the pancreatic duct in one image (straight arrows); asterisk, common bile duct.

Although the size of the pancreatic head, neck, body, and tail generally correspond to normal measurements found sonographically, absolute numbers should not be used alone in diagnosing pancreatic enlargement. It is important to observe symmetry within the gland, with the head (maximal normal diameter of 3 cm) being slightly larger in anterior-posterior dimension than the body (2.2 cm) and tail (2.8 cm). The pancreatic tail can be bulbous in some normal patients and measure larger than the head. The thickness of the head of the pancreas should be less than the transverse diameter of the adjacent vertebral body; the body and tail should be less than two thirds of the size. The pancreatic body may be thinner where it crosses the spine. The lateral contour of the pancreatic head may have discrete lobulations lateral to the gastroduodenal or anterior superior pancreaticoduodenal artery in approximately one third of normal examinations.¹¹⁰ The uncinate process has a triangular appearance on cross section as it projects behind the mesenteric vessels.¹¹¹⁻¹¹³ The pancreas moves an average of 3.2 cm craniocaudally between phases of respiration on CT scans.¹¹⁴

In patients with a surgically or congenitally absent left kidney, the pancreatic tail lies dorsomedial, adjacent to the spine, and occupies the empty renal fossa along with bowel and spleen. The entire pancreas may rarely lie to the left of the aorta.

The pancreatic vascular anatomy is well demonstrated by multidetector CT. The thinner slices and overlapping reconstructions allowed by helical technique visualize many of the small named vessels. The splenic vein makes an excellent landmark for the body and tail of the pancreas. The anterior and posterior superior pancreaticoduodenal veins are seen on 98% and 88% of scans, and the gastocolic trunk may be visualized on 89% of scans.¹¹⁵ Frequently visualized are the gastroduodenal, anterior and posterior superior pancreaticoduodenal, and right gastroepiploic arteries. Occasionally visualized are the dorsal pancreatic, pancreatica magna, and anterior and posterior inferior pancreaticoduodenal arteries.¹¹⁶

Pancreatic Duct on Computed Tomography

The normal pancreatic duct appears as a thin, tubular region of low attenuation coursing in the center of the pancreas on CT scans. The duct can be seen at least partially in 70% of normal

patients; usually, short segments are visualized on a limited number of scans. The duct is most frequently seen in the region of the pancreatic body as it arches over the spine and mesenteric vessels or in the region of the head.¹¹⁷

The normal pancreatic duct should be no wider than 2 to 3 mm, but it can occasionally be larger in older individuals. The normal fat plane between the splenic vein and pancreatic parenchyma should not be mistaken for the pancreatic duct.¹¹⁸

Common Bile Duct on Computed Tomography

The internal diameter of the distal common bile duct is less than 6 to 7 mm. In older patients or those with a history of previous biliary tract disease or surgery, the duct may be as large as 10 mm in the absence of obstruction. Thus, the diagnostic significance of ducts 7 to 10 mm in size is often difficult to assess.¹¹⁹ On contrast scans, the vasa vasorum of the duct may enhance.

MAGNETIC RESONANCE IMAGING

The pancreas had been one of the most difficult organs to image reliably on MRI until the development of techniques such as breath-hold imaging, chemically selective fat saturation, and dynamic gadolinium enhancement.¹²⁰ Now the routine use of fast sequences including three-dimensional gradient-echo T1-weighted and MR cholangiopancreatography (MRCP) sequences has resulted in excellent diagnostic quality when MRI is used as a problem-solving tool in patients with elevated liver function test results, acute pancreatitis, and pancreatic cancer. It is used as the primary imaging modality for suspected pancreaticobiliary pain, staging of chronic pancreatitis, and diagnosis and follow-up of cystic pancreatic tumors. The inability to demonstrate small calcifications remains a relative drawback.¹²¹

Normal Pancreas on Magnetic Resonance Imaging

On MRI studies (Figs. 94-12 and 94-13), the pancreas can appear smooth or lobulated and may blend in with the surrounding retroperitoneal fat if there is fatty infiltration.¹²²⁻¹³⁰ The pancreas may be isointense to slightly hyperintense compared with the liver on T1-weighted spin-echo sequences, isointense or slightly hyperintense on T1-weighted spoiled gradient-echo sequences, and slightly brighter on T2-weighted

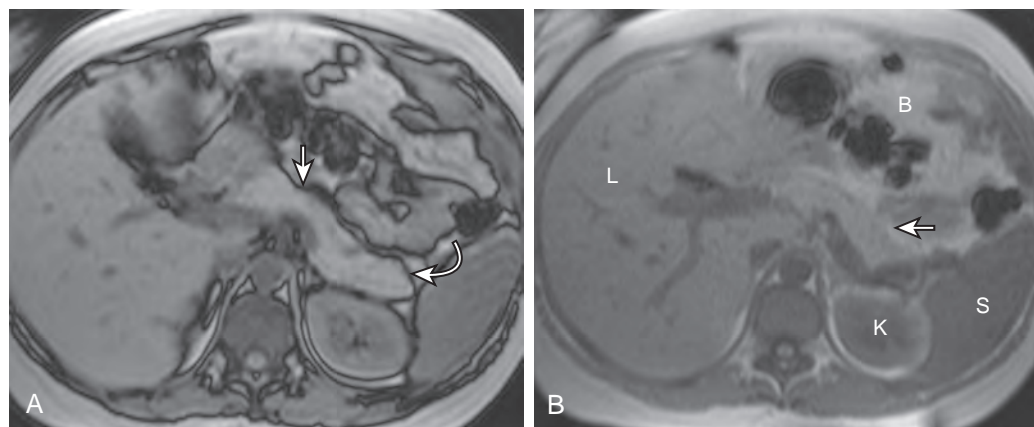


Figure 94-12 Normal pancreatic anatomy on MRI T1-weighted images. **A.** T1-weighted out-of-phase gradient-echo image (239/2.4/70) shows the normal appearance of the pancreatic body (arrow) and tail (curved arrow). **B.** T1-weighted in-phase gradient-echo image (239/4.76/70) similarly shows the pancreas (arrow) without the chemical shift artifact. B, bowel; K, kidney; L, liver; S, spleen.

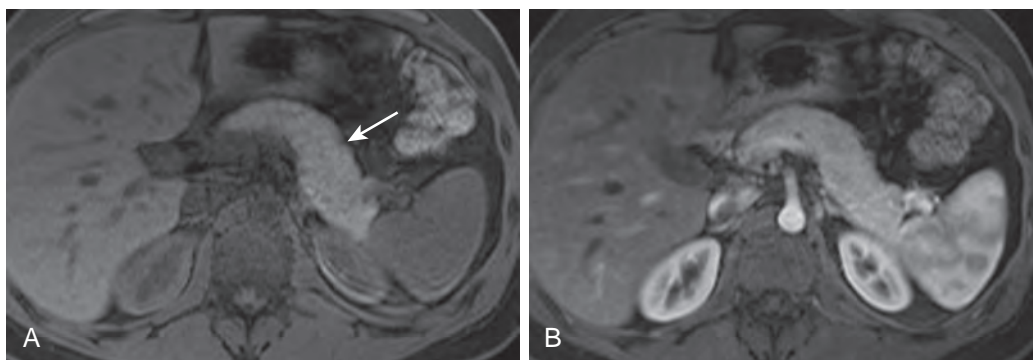


Figure 94-13 Normal MR images of the pancreas before and after gadolinium administration. **A.** T1-weighted fat-saturated breath-hold spoiled gradient-echo image (3.99/1.93/10) before the administration of contrast material demonstrates the normal high signal of the pancreas relative to the rest of the parenchymal organs (arrow) due to proteinaceous material within the glandular elements of the pancreas. This sequence is often the single best noncontrast sequence with which to evaluate the pancreas. **B.** T1-weighted postcontrast imaging with the same parameters shows an early phase of enhancement of the pancreas. Postcontrast images are routinely obtained at 60, 90, and 120 seconds after the administration of gadolinium.

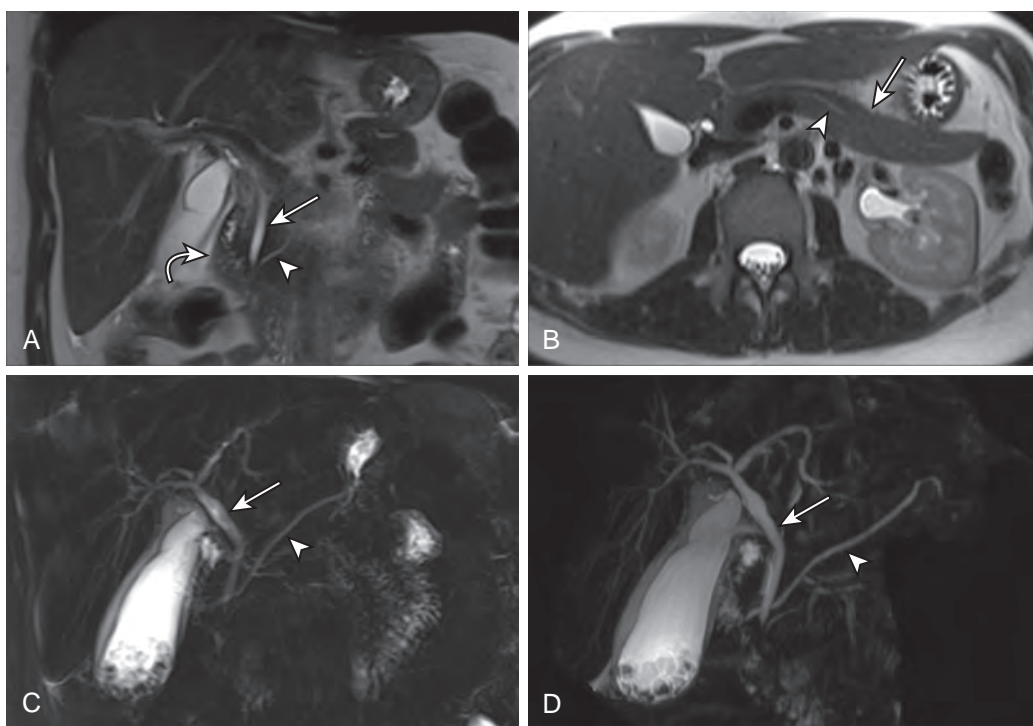


Figure 94-14 Normal MRCP. **A.** Coronal thin-section 3-mm T2-weighted half-Fourier acquisition single-shot turbo spin-echo (HASTE) image (1200/92/154) shows the common duct (arrow) and the pancreatic duct (arrowhead). Nondilated duodenum is also seen (curved arrow). **B.** Axial thin-section 3-mm T2-weighted HASTE image (1300/900/120) shows the normal appearance of the pancreatic body and tail (arrow). A nondilated pancreatic duct is partially visualized (arrowhead). **C.** Coronal thick-slab rapid acquisition and relaxation enhancement (RARE) image (3000/735/180) shows the common bile duct (arrow) and pancreatic duct (arrowhead). There is the suggestion of pancreatic divisum on this image. Filling defects in the gallbladder are compatible with gallstones. Gallbladder wall thickening is also present. **D.** Maximum intensity projection T2-weighted navigator sequence (3517/696/120) is able to locate the position of the diaphragm and thus correct for diaphragmatic motion to minimize respiratory motion and artifact. This maximum intensity projection image nicely displays the common bile duct (arrow) and pancreatic duct (arrowhead). Gallstones are again noted in the gallbladder lumen, and the presence of pancreatic divisum is confirmed on this image.

images. It is relatively high in signal on T1-weighted fat-saturated sequences and enhances rapidly with gadolinium administration. The normal pancreatic duct is occasionally visualized, particularly when torso coils are used. On axial T2-weighted images, the common bile duct can be seen as a bright dot in the pancreatic head, and the gastroduodenal artery appears as a rounded, black structure as a result of flow void phenomena.^{90,130}

MAGNETIC RESONANCE CHOLANGIOPANCREATOGRAPHY

An important technique to examine the pancreatic and biliary tree is MRCP.^{131,132} The normal and abnormal pancreatic duct can be visualized without the invasiveness of ERCP¹³³ (Fig. 94-14). Several variations of the technique have emerged.¹³⁴⁻¹³⁶ All have in common a heavily T2-weighted pulse sequence in

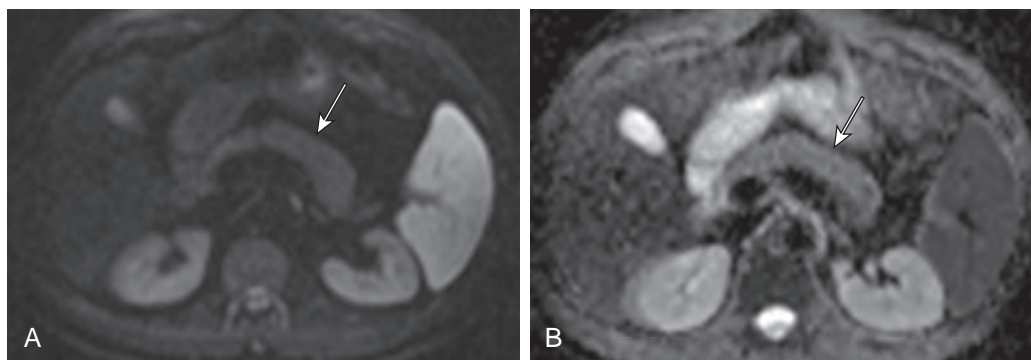


Figure 94-15 Normal diffusion-weighted MR image of the pancreas. **A.** Axial diffusion weighting ($b = 500 \text{ s/mm}^2$) shows normal homogeneous bright signal of the pancreas (arrow). **B.** Axial apparent diffusion coefficient map shows the normal appearance of the pancreas (arrow). The pancreas is homogeneous, and there are no areas of restricted diffusion.

which the fluid-filled ducts stand out from the surrounding low signal intensity tissues.¹³⁷ Many of these are breath-hold sequences that can easily be added to routine pancreatic imaging with little increase in overall examination time. Postprocessing with a maximum intensity profile technique allows visualization from multiple perspectives, giving an appearance similar to that of ERCP. Secretin administered before the dynamic acquisition of images has been used to improve visualization of the pancreatic duct, to diagnose papillary stenosis or dysfunction, and to evaluate reduced pancreatic exocrine reserve.¹³⁸ MRCP may be particularly valuable in postoperative patients in whom ERCP is technically impossible. This technique is discussed more fully in Chapter 75.

Diffusion-Weighted Magnetic Resonance Imaging of the Pancreas

Diffusion-weighted MRI of the pancreas is an emerging technique that is complementary to conventional MRI (Fig. 94-15). Diffusion-weighted MRI uses the differences in the motion of water molecules in extracellular and intracellular fluid and vascular fluids to produce image contrast. Restricted diffusion is observed in tissues with high cellularity, such as tumors, abscesses, and fibrosis. Unimpeded diffusion is found in tissues with low cellularity or disrupted cell membranes, such as cysts and necrotic tissues. Tissues with restricted diffusion will demonstrate hyperintensity on higher b values and hypointensity on the corresponding calculated apparent diffusion coefficient map. Diffusion-weighted MRI has been shown to be highly sensitive and specific for the detection of pancreatic adenocarcinoma and may be useful in detecting small or non-contour-deforming adenocarcinomas. Diffusion-weighted MRI is also useful to improve detection of liver and peritoneal metastatic lesions, which may provide more accurate staging in pancreatic cancer. The inability to differentiate mass-forming pancreatitis from poorly differentiated adenocarcinomas and to distinguish non-neoplastic cysts from cystic neoplasms remains a challenge. Diffusion-weighted MRI of the abdomen is further discussed in Chapter 69.

ENDOSCOPIC RETROGRADE CHOLANGIOPANCREATOGRAPHY

ERCP affords opacification of both the pancreatic and the bile ducts. In addition, the endoscopist can inspect and perform a biopsy of suspicious periampullary lesions, perform a sphincterotomy with or without stone extraction, and place internal biliary stents.¹³⁹⁻¹⁴² A more complete discussion of ERCP can

be found in Chapter 74. The indications for ERCP include the following: to determine the cause of idiopathic pancreatitis (i.e., pancreas divisum); to provide a road map for the surgeon in patients with dilated ducts and chronic pancreatitis before the Puestow procedure; to identify communication of the pancreatic duct with pseudocysts and fistulas; to detect small intraductal pancreatic neoplasms that distort ductal anatomy but do not yet cause a mass effect that can be detected by CT and ultrasound; and to identify the cause of extrahepatic biliary obstruction (e.g., stone, tumor, benign stricture, or inflammation).¹⁴³⁻¹⁴⁵

The upper limits of normal pancreatic duct diameter on ERCP are 6.5, 5.0, and 3.0 mm for the head, body, and tail, respectively. The normal duct gently tapers from the major papilla to its origin in the pancreatic tail. Slight narrowing of the pancreatic duct can be seen at the junction of the ducts of Wirsung and Santorini and at the point at which the superior mesenteric artery crosses ventral to the pancreas. Normally, 20 to 30 side branches of the pancreatic duct, which measure 0.2 mm in diameter, are filled. The duct of Santorini is opacified in about 50% of pancreatograms. A patent accessory duct orifice is present in one third to two thirds of patients but is difficult to cannulate. With aging, the diameter of the pancreatic duct increases, the number of side branches filled decreases, and cystic dilation of the side branches may occur. The pancreatic duct moves significantly with various phases of respiration, particularly within the tail. Contrast material empties from the normal pancreatic duct in 2 to 7 minutes, but this figure increases in elderly patients to 10 minutes.

Injection of contrast material should be performed under fluoroscopic guidance at a pressure insufficient to cause parenchymal filling (acinarization). Injection should be terminated when acinarization occurs, if a pseudocyst is filled, if the patient complains of severe pain, or if contrast material is seen entering the duodenal lumen or wall. When a stricture or abrupt termination of the duct is encountered, heroic attempts to fill the duct upstream should be avoided. Spot films are obtained in the prone and oblique positions. On occasion, lateral and supine views may be needed to complete the examination and to fill the duct in the tail. Pancreatic emptying should be evaluated in this position as well.¹⁴⁶

Positron emission tomography/computed tomography (PET/CT) shows great promise in the staging of pancreatic carcinoma.¹⁴⁷⁻¹⁵⁴ The applications of PET/CT in pancreatic and other abdominal malignant neoplasms are discussed in Chapter 68.

REFERENCES

- Cunningham SC, Demirjau AN, Schulick RD: Pancreaticobiliary surgery: General considerations. In Lillemoe KD, Jarnagin WR, editors: *Hepatobiliary and Pancreatic Surgery*, Philadelphia, 2013, Wolters Kluwer, pp 1–13.
- Barth BA, Burdick JS: Anatomy, histology, embryology, and developmental anatomy of the pancreas. In Feldman M, Friedman LS, Brandt LS, editors: *Gastrointestinal and Liver Disease*, ed 9, Philadelphia, 2010, WB Saunders, pp 761–770.
- Reid-Lombardo KM, Barton J, Sarr MG: Operative palliation of pancreatic cancer. In Lillemoe KD, Jarnagin WR, editors: *Hepatobiliary and Pancreatic Surgery*, Philadelphia, 2013, Wolters Kluwer, pp 59–76.
- El-Gohary YB, Gilles GK: Anatomy, physiology, and embryology of the pancreas. In Yeo CJ, editor: *Surgery of the Alimentary Tract*, vol III, ed 7, Philadelphia, 2013, WB Saunders, pp 1110–1122.
- Drake RL, Vogl AW, Mitchell AWM: The pancreas. In Williams PL, Warwick R, editors: *Gray's Anatomy*, 36th British, Philadelphia, 2010, WB Saunders, pp 1368–1374.
- Gartner LP, Hiatt JL: *Color Textbook of Histology*, ed 3, Philadelphia, 2010, WB Saunders, pp 726–742.
- Meyers MA: *Dynamic Radiology of the Abdomen*, ed 6, New York, 2010, Springer-Verlag, pp 32–42.
- Skandalakis JR, Gray SW, Skandalakis LJ: Surgical anatomy of the pancreas. In Howard JM, Jordan GL, Reber HA, editors: *Surgical Diseases of the Pancreas*, Philadelphia, 1987, Lea & Febiger, pp 11–36.
- Eaton SB, Jr, Ferrucci JT, Jr: Anatomic considerations. In Eaton SB, Jr, Ferrucci JT, Jr, editors: *Radiology of the Pancreas and Duodenum*, Philadelphia, 1973, WB Saunders, pp 1–19.
- Zylak CJ, Pallie W: Correlative anatomy and computed tomography: A module on the pancreas and posterior abdominal wall. *Radiographics* 1:61–83, 1981.
- Nichols MT, Russ PD, Chen YK: Pancreatic imaging: Current and emerging technologies. *Pancreas* 33:211–220, 2006.
- Schneck CD, Dabiez MA, Friedman AC: Embryology, histology, gross anatomy, and normal imaging of the pancreas. In Friedman AC, Dachman AH, editors: *Radiology of the Liver, Biliary Tract, and Pancreas*, St. Louis, 1994, CV Mosby, pp 715–747.
- Meyers MA: *Dynamic Radiology of the Abdomen*, ed 5, New York, 2010, Springer-Verlag.
- Mahour H, Wakim KG, Ferris DO: The common bile duct in man: Its diameter and circumference. *Ann Surg* 165:415–419, 1967.
- Tersigni R, Toledo-Pereyra LH: Surgical anatomy of the pancreas. In Toledo-Pereyra LH, editor: *The Pancreas: Principles of Medical and Surgical Practice*, New York, 1985, Churchill Livingstone, pp 31–50.
- Claussen M, Hellwig H, Rosch W: Anatomy of the pancreatic duct: A duodenoscopic-radiologic study. *Endoscopy* 5:14–17, 1973.
- Klertsch WB: Anatomy of the pancreas: A study with special reference to the duct system. *Arch Surg* 71:795–802, 1955.
- Del Frate C, Zanardi R, Morteale K, et al: Advances in imaging for pancreatic disease. *Curr Gastroenterol Rep* 4(2):140–148, 2002.
- Kalra MK, Maher MM, Sahani DV, et al: Current status of imaging in pancreatic disease. *J Comput Assist Tomogr* 26:661–675, 2002.
- Woodburne RT: *Essentials of Human Anatomy*, ed 5, New York, 1973, Oxford University Press, pp 409–443.
- Kahl S, Malfetherheimer P: Rule of endoscopic ultrasound in the diagnosis of patients with solid pancreatic masses. *Dig Dis* 22:26–31, 2004.
- Reuter SR, Redman HC, Cho KJ: *Gastrointestinal Angiography*, ed 3, Philadelphia, 1986, WB Saunders, pp 32–77.
- Crabo LG, Conley DM, Graney DO, et al: Venous anatomy of the pancreatic head: Normal CT appearance in cadavers and patients. *AJR Am J Roentgenol* 160:1039–1045, 1993.
- Moncada RA, Reynes C, Churchill R, et al: Normal vascular anatomy of the abdomen on computed tomography. *Radiol Clin North Am* 17:25–37, 1979.
- Abiri MM, Kirpekar M: An unusual anatomic location of pancreatic masses. *J Ultrasound Med* 5:703–705, 1986.
- Haaga JR: CT-guided procedures. In Haaga JR, Alfidi RJ, editors: *Computed Tomography of the Whole Body*, St. Louis, 1988, CV Mosby, pp 1200–1320.
- Buy JN, Moss AA, Singler RC: CT guided celiac plexus and splanchnic nerve neurolysis. *J Comput Assist Tomogr* 6:315–319, 1982.
- Seicean A: Celiac plexus neurolysis in pancreatic cancer: The endoscopic ultrasound approach. *World J Gastroenterol* 20:110–117, 2014.
- Brand M, Götz A, Zeman F, et al: Acute necrotizing pancreatitis: Laboratory, clinical, and imaging findings as predictors of patient outcome. *AJR* 202:1215–1231, 2014.
- Côté GA, Smith J, Sherman S, et al: Technologies for imaging the normal and diseased pancreas. *Gastroenterology* 144:1262–1271, 2013.
- Gooding GAW: Conventional radiography of the pancreas. In Howard JM, Jordan GL, Reber HA, editors: *Surgical Diseases of the Pancreas*, Philadelphia, 1987, Lea & Febiger, pp 67–77.
- Krabbenhoft KL: Radiologic evaluation. In Toledo-Pereyra LH, editor: *The Pancreas: Principles of Medical and Surgical Practice*, New York, 1985, Churchill Livingstone, pp 117–142.
- Eaton SB, Ferrucci JT: *Radiology of the Pancreas and Duodenum*, Philadelphia, 1973, WB Saunders, pp 20–50.
- Fried AM: Spleen and retroperitoneum. *Ultrasound Q* 21:275–286, 2003.
- Fleischer AC: Abdominal sonography. In Fleischer AC, James AE, editors: *Diagnostic Sonography*, Philadelphia, 1989, WB Saunders, pp 341–433.
- Cooperberg PL, Rowley VA: Abdominal sonographic examination technique. In Taveras J, Ferrucci JT, editors: *Radiology: Diagnosis, Imaging, Intervention*, Philadelphia, 1990, JB Lippincott, pp 1–11.
- Bertolotto M, D'Onofrio M, Martone E, et al: Ultrasonography of the pancreas. 3. Doppler imaging. *Abdom Imaging* 32:161–170, 2007.
- Zerem E, Imamović G, Latić F, et al: Prognostic value of acute fluid collections diagnosed by ultrasound in the early assessment of severity of acute pancreatitis. *J Clin Ultrasound* 41:203–209, 2013.
- Fried AM: Retroperitoneum, pancreas, spleen, and lymph nodes. In McGahan JP, Goldberg BB, editors: *Diagnostic Ultrasound: A Logical Approach*, Philadelphia, 1998, Lippincott-Raven, pp 761–786.
- Sample WF: Techniques for improved delineation of normal anatomy of the upper abdomen and high retroperitoneum with gray-scale ultrasound. *Radiology* 124:197–202, 1980.
- Weill F, Schraub A, Eiserscher A, et al: Ultrasonography of the normal pancreas. *Radiology* 123:417–423, 1977.
- Weinstein BJ, Weinstein DP: Sonographic anatomy of the pancreas. *Semin Ultrasound* 1:156–165, 1980.
- Taylor KJW, Buchin PJ, Viscomi GN, et al: Ultrasonographic scanning of the pancreas. *Radiology* 138:211–213, 1981.
- Crade M, Taylor KJW, Rosenfield AT: Water distention of the gut in the evaluation of the pancreas by ultrasound. *AJR Am J Roentgenol* 131:348–349, 1978.
- Goldstein HM, Katragadda CS: Prone view ultrasonography for pancreatic tail neoplasms. *AJR Am J Roentgenol* 131:231–234, 1978.
- Jacobson P, Crade M, Taylor KJW: The upright position while giving water for the evaluation of the pancreas. *J Clin Ultrasound* 6:353–354, 1978.
- MacMahon H, Bowie JD, Beezhold C: Erect scanning of pancreas using a gastric window. *AJR Am J Roentgenol* 132:587–591, 1979.
- Warren PS, Garrett WJ, Phil D, et al: The liquid-filled stomach: An ultrasonic window to the upper abdomen. *J Clin Ultrasound* 6:295–302, 1978.
- Gooding GAW, Laing FC: Rapid water infusion: A technique in ultrasonic discrimination of gas-free stomach from a mass in pancreatic tail. *Gastrointest Radiol* 4:139–142, 1979.
- Mittelstaedt CA: *Abdominal Ultrasound*, New York, 1987, Churchill Livingstone, pp 163–220.
- Johnson ML, Mack LA: Ultrasonographic evaluation of the pancreas. *Gastrointest Radiol* 3:257–266, 1978.
- Mark WM, Filly RA, Callen PW: Ultrasound evaluation of normal pancreatic echogenicity and its relationship to fat deposition. *Radiology* 137:475–479, 1980.
- Worthen NJ, Beaubeau D: Normal pancreatic echogenicity: Relation to age and body fat. *AJR Am J Roentgenol* 139:1095–1098, 1982.
- Kreel L, Sandin B, Slavin G: Pancreatic morphology: A combined radiological and pathological study. *Clin Radiol* 24:154–161, 1973.
- Filly RA, London SS: The normal pancreas: Acoustic characteristics and frequency of imaging. *J Clin Ultrasound* 7:121–124, 1979.
- Jaffe CC, Harris DJ: Sonographic tissue texture: Influence of transducer focusing pattern. *AJR Am J Roentgenol* 135:343–347, 1980.
- Marchal G, Verbecken E, Van Steenberghe W, et al: Uneven lipomatosis: A pitfall in pancreatic sonography. *Gastrointest Radiol* 14:233–237, 1989.
- So CB, Cooperberg PL, Glibney RG, et al: Sonographic findings in pancreatic lipomatosis. *AJR Am J Roentgenol* 149:67–68, 1987.
- Taylor KJW, Pollock D, Crade M: Pancreatic ultrasonography: Techniques, artifacts, and clinical results. In Moss AA, Goldberg HI, editors: *Computed Tomography, Ultrasound and X-ray: An Integrated Approach*, San

- Francisco, 1980, University of California Press, pp 81–87.
60. Chatzkel SL, Kurtz AB, Wechsler RJ: Fatty infiltration of the peripancreatic space: CT confirmation of a normal variant. *Gastrointest Radiol* 8:33–36, 1983.
 61. Op den Orth JO: Prepancreatic fat deposition: A possible pitfall in pancreatic sonography. *AJR Am J Roentgenol* 146:1017–1018, 1986.
 62. Bryan PJ: Appearance of normal pancreatic duct: A study using real-time ultrasound. *J Clin Ultrasound* 10:63–66, 1982.
 63. Lawson TL, Berland LL, Foley WD, et al: Ultrasonic visualization of the pancreatic duct. *Radiology* 144:865–871, 1982.
 64. Parulekar SG: Ultrasonic evaluation of the pancreatic duct. *J Clin Ultrasound* 8:457–463, 1980.
 65. Ohto M, Saotome N, Saishott R, et al: Real-time sonography of the pancreatic duct: Application to percutaneous pancreatic ductography. *AJR Am J Roentgenol* 134:647–652, 1980.
 66. Sirli R, Sporea I: Ultrasound examination of the normal pancreas. *Med Ultrason* 12:62–65, 2010.
 67. Hadid A: Pancreatic duct diameter: Sonographic measurement in normal subjects. *J Clin Ultrasound* 11:1722–1724, 1983.
 68. Sanders RC, Chang R: A variant position of the splenic artery mimicking the pancreatic duct. *J Clin Ultrasound* 10:391–393, 1982.
 69. Suramo J, Lobela P, Labde S, et al: The “ghost tail” of the pancreas in ultrasonography. *Eur J Radiol* 2:139–149, 1982.
 70. Laing FC, Jeffrey RB, Wing VW: Improved visualization of choledocholithiasis by sonography. *AJR Am J Roentgenol* 143:949–952, 1984.
 71. Laing FC, Jeffrey RB, Wing VW, et al: Biliary dilatation: Defining the level and cause by real-time US. *Radiology* 160:39–42, 1986.
 72. Wachsberg RH: Posterior superior pancreaticoduodenal vein: Mimic of distal common bile duct at sonography. *AJR Am J Roentgenol* 160:1033–1037, 1993.
 73. Bolondi L, Gaiani S, Casanova P, et al: Improvement of pancreatic ultrasound imaging after secretin administration. *Ultrasound Med Biol* 9:497–501, 1983.
 74. Glaser J, Hogemann B, Schneider M, et al: Significance of a sonographic secretin test in the diagnosis of pancreatic disease. *Scand J Gastroenterol* 24:179–185, 1989.
 75. Glaser J: Clinical perspectives of a sonographic secretin test. *Gastroenterology* 35:579–583, 1997.
 76. Glaser J, Hogemann B, Krummeier T, et al: Sonographic imaging of the pancreatic duct: New diagnostic possibilities using secretin stimulation. *Dig Dis Sci* 10:1075–1081, 1987.
 77. Barbara L, Bolondi L: Functional ultrasonography in gastroenterology. *Ultrasound Q* 6:181–227, 1988.
 78. Laing FC: Sonography of the hepatobiliary tract. In Ghahremani GG, editor: *Categorical Syllabus on Gastrointestinal Radiology*, Reston, Va, 1987, American Roentgen Ray Society, pp 35–43.
 79. Bowerman RA, McCracken S, Silver TM, et al: Abdominal and miscellaneous applications of the intraoperative ultrasound. *Radiol Clin North Am* 23:107–113, 1985.
 80. Smith SJ, Vogelzang RL, Donovan J, et al: Intraoperative sonography of the pancreas. *AJR Am J Roentgenol* 144:557–562, 1985.
 81. Marcal LP, Patnana M, Bhosale P, et al: Intraoperative abdominal ultrasound in oncologic imaging. *World J Radiol* 5:51–60, 2013.
 82. Charboneau JW, Gorman B, Reading CC, et al: Intraoperative ultrasonography of the pancreas. *Clin Diagn Ultrasound* 21:121–150, 1987.
 83. Bezzi M, Merlino P, Orsi F, et al: Laparoscopic sonography during abdominal laparoscopic surgery: Technique and imaging findings. *AJR Am J Roentgenol* 165:1193–1198, 1995.
 84. Zerbey AL, Lee MJ, Brugge WR, et al: Endoscopic sonography of the upper gastrointestinal tract and pancreas. *AJR Am J Roentgenol* 166:45–50, 1996.
 85. Caletti G, Fusaroli P: Endoscopic ultrasonography. *Endoscopy* 31:95–102, 1999.
 86. Itoi T, Kasuya K, Sofuni A, et al: Endoscopic ultrasonography-guided pancreatic duct access: Techniques and literature review of pancreatography, transmural drainage and rendezvous techniques. *Dig Endosc* 25:241–252, 2013.
 87. Hessel SJ, Siegelman SS, McNeil BJ, et al: A prospective evaluation of computed tomography and ultrasound of the pancreas. *Radiology* 143:129–133, 1982.
 88. Freeny PC: Radiology of the pancreas. *Curr Opin Radiol* 3:440–442, 1991.
 89. Choi YH, Rubenstein WA, De Arellano ER, et al: CT and US of the pancreas. *Clin Imaging* 21:414–440, 1997.
 90. Stanley RJ, Semelka RC: Pancreas. In Lee JKT, Sagel SS, Stanley RJ, editors: *Computed Body Tomography with MRI Correlation*, Philadelphia, 1998, Lippincott-Raven, pp 873–959.
 91. Haaga JR: The pancreas. In Haaga JR, Lanzieri CF, Sartoris DJ, et al, editors: *Computed Tomography and Magnetic Resonance Imaging of the Whole Body*, ed 3, St. Louis, 1994, Mosby-Year Book, pp 1037–1130.
 92. Smith SL, Basu A, Rae DM, Sinclair M: Preoperative staging accuracy of multi-detector CT in pancreatic head carcinoma. *Pancreas* 34:180–184, 2007.
 93. Zeman RK, Baron RL, Jeffrey RB, et al: Helical body CT: Evolution of scanning protocols. *AJR Am J Roentgenol* 170:1427–1438, 1998.
 94. Saito S, Yamamoto H, Takai S, et al: Clinical impact of multidetector row computed tomography on patients with pancreatic cancer. *Pancreas* 34:175–179, 2007.
 95. Graf O, Boland GW, Warshaw AL, et al: Arterial versus portal venous helical CT for revealing pancreatic adenocarcinoma: Conspicuity of tumor and critical vascular anatomy. *AJR Am J Roentgenol* 169:119–123, 1997.
 96. Kanji ZS, Gallinger S: Diagnosis and management of pancreatic cancer. *CMAJ* 185:1219–1226, 2013.
 97. Diehl SJ, Lehmann KJ, Sadick M, et al: Pancreatic cancer: Value of dual-phase helical CT in assessing resectability. *Radiology* 206:373–378, 1998.
 98. Kala Z, Valek V, Hiavsa J, et al: The role of CT and endoscopic ultrasound in pre-operative staging of pancreatic cancer. *Eur J Radiol* 62:166–169, 2007.
 99. Yovino S, Darwin P, Daly B, et al: Predicting unresectability in pancreatic cancer patients: The additive effects of CT and endoscopic ultrasound. *J Gastrointest Surg* 11:36–42, 2007.
 100. Bonaldi VM, Bret PM, Atri M, et al: Helical CT of the pancreas: A comparison of cine display and film-based viewing. *AJR Am J Roentgenol* 170:373–376, 1998.
 101. Kuroda C, Mihara N, Hosomi N, et al: Spiral CT during phacoangiography CT using angiotensin II in patients with pancreatic disease: Technique and diagnostic efficacy. *Acta Radiol* 39:138–143, 1998.
 102. Hemmy DC, Zonneveld FW, Lobregt S, et al: A decade of clinical three-dimensional imaging: A review. Part 1. Historical development. *Invest Radiol* 29:489–496, 1993.
 103. Zonneveld FW, Fukuta K: A decade of clinical three-dimensional imaging: A review. Part 2. Clinical applications. *Invest Radiol* 29:574–589, 1994.
 104. Rubin GD, Napel S, Leung AN: Volumetric analysis of volumetric data: Achieving a paradigm shift. *Radiology* 200:312–317, 1996.
 105. Li XH, Zhang JL, Liu YF: Localization of small sized insulinoma by means of combining arteriography with CT: A case report and review of the literature. *Hepatogastroenterology* 57:1579–1583, 2010.
 106. Novick SL, Fishman EK: Three-dimensional CT angiography of pancreatic carcinoma: Role in staging extent of disease. *AJR Am J Roentgenol* 170:139–143, 1998.
 107. Zeman RK, Davros WJ, Berman PM, et al: Three-dimensional models of abdominal vasculature based on helical CT: Usefulness in patients with pancreatic neoplasms. *AJR Am J Roentgenol* 162:1425–1429, 1994.
 108. Raptopoulos V, Prassopoulos P, Chuttani R, et al: Multiplanar CT pancreatography and distal cholangiography with minimum intensity projections. *Radiology* 207:317–324, 1998.
 109. Heuck A, Maubach PA, Reiser M, et al: Age-related morphology of the normal pancreas on computed tomography. *Gastrointest Radiol* 12:18–22, 1987.
 110. Ross BA, Jeffrey RB, Mindelzun RE: Normal variations in the lateral contour of the head and neck of the pancreas mimicking neoplasm: Evaluation with dual-phase helical CT. *AJR Am J Roentgenol* 166:799–801, 1997.
 111. Saisho H, Yamaguchi T: Diagnostic imaging for pancreatic cancer. *Pancreas* 28:273–278, 2004.
 112. Dupuy DE, Costello P, Ecker CP: Spiral CT of the pancreas. *Radiology* 183:815–818, 1992.
 113. Weyman PJ, Stanely RJ, Levitt RG: Computed tomography in evaluation of pancreas. *Semin Roentgenol* 16:301–311, 1981.
 114. Kivisaari L, Makela P, Aarimaa M: Pancreatic mobility: An important factor in pancreatic computed tomography. *J Comput Assist Tomogr* 6:854–856, 1982.
 115. Crabo LG, Conley DM, Graney DO, et al: Venous anatomy of the pancreatic head: Normal CT appearance in cadavers and patients. *AJR Am J Roentgenol* 160:1039–1045, 1993.
 116. Sim JS, Choi BI, Han JK, et al: Helical CT anatomy of pancreatic arteries. *Abdom Imaging* 21:517–521, 1996.
 117. Callen PW, London SS, Moss AA: Computed tomographic evaluation of the dilated pancreatic duct: The value of thin-section collimation. *Radiology* 134:253–255, 1980.
 118. Seidelman FE, Cohen WN, Bryan PJ, et al: CT demonstration of the splenic vein–pancreatic relationship: The pseudodilated pancreatic duct. *AJR Am J Roentgenol* 129:17–21, 1977.
 119. Donovan PJ: Technique of examination and normal pancreatic anatomy. In Siegelman SS, editor: *Computed Tomography of the Pancreas*, New York, 1983, Churchill Livingstone, pp 1–32.

120. Mitchell DG: Fast MR imaging techniques: Impact on the abdomen. *J Magn Reson Imaging* 6:812–821, 1996.
121. Ajaykumar CM, Elsaye KM, Liu PS, et al: Abdominal applications of diffusion-weighted magnetic resonance imaging: Where do we stand *World J Radiol* 28(5):68–80, 2013.
122. Gohde SC, Toth J, Krestin GP, et al: Dynamic contrast-enhanced FMPSPGR of the pancreas: Impact on diagnostic performance. *AJR Am J Roentgenol* 168:689–696, 1997.
123. Burton SS, Liebig T, Frazier SD, et al: High-density oral barium sulfate in abdominal MRI: Efficacy and tolerance in a clinical setting. *Magn Reson Imaging* 15:147–153, 1997.
124. Mehmet Erturk S, Ichikawa T, Sou H, et al: Pancreatic adenocarcinoma: MDCT USMRI in the detection and assessment of locoregional extension. *J Comput Assist Tomogr* 30:583–590, 2006.
125. Schima W: MRI of the pancreas: Tumours and tumour-simulating processes. *Cancer Imaging* 6:199–203, 2006.
126. Miller FH, Rini NJ, Keppke AL: MRI of adenocarcinoma of the pancreas. *AJR Am J Roentgenol* 187:W365–W374, 2006.
127. Wang C, Gordon PB, Hustvedt SO, et al: MR imaging properties and pharmacokinetics of MNDPDP in healthy volunteers. *Acta Radiol* 38:665–676, 1997.
128. Wang Y, Miller FH, Chen ZE, et al: Diffusion-weighted MR imaging of solid and cystic lesions of the pancreas. *Radiographics* 31:E47–E64, 2011.
129. Kettritz U, Warshawer DM, Brown ED, et al: Enhancement of the normal pancreas: Comparison of manganese-DPDP and gadolinium chelate. *Eur Radiol* 6:14–18, 1996.
130. Perez-Johnston R, Sainani NI, Sahani DV: Imaging of chronic pancreatitis (including groove and autoimmune pancreatitis). *Radiol Clin North Am* 50:447–466, 2012.
131. Verma D, Kapadia A, Eisen GM, et al: EUS vs MRCP for detection of choledocholithiasis. *Gastrointest Endosc* 64:248–254, 2006.
132. Asbach P, Dewey M, Klessen C, et al: Respiratory-triggered MRCP applying parallel acquisition techniques. *J Magn Reson Imaging* 24:1095–1100, 2006.
133. Akisik MF, Sandrasegaran K, Aisen AA, et al: Dynamic secretin-enhanced MR cholangiopancreatography. *Radiographics* 26:665–677, 2006.
134. Fulcher AS, Turner MA, Capps GW, et al: Half-Fourier RARE MR cholangiopancreatography: Experience in 300 subjects. *Radiology* 207:21–32, 1998.
135. Barish MA, Yucel EK, Ferrucci JT: Magnetic resonance cholangiopancreatography. *N Engl J Med* 341:258–264, 1999.
136. Tonolini M, Ravelli A, Villa C, et al: Urgent MRI with MR cholangiopancreatography (MRCP) of acute cholecystitis and related complications: Diagnostic role and spectrum of imaging findings. *Emerg Radiol* 19:341–348, 2012.
137. Jara H, Barish MA, Yucel EK, et al: MR hydrography: Theory and practice of static fluid imaging. *AJR Am J Roentgenol* 170:873–882, 1998.
138. Schneider AR, Hammerstingl R, Heller M, et al: Does secretin-stimulated MRCP predict exocrine pancreatic insufficiency? *J Clin Gastroenterol* 40:851–855, 2006.
139. Hyodo T, Kumano S, Kushihata F, et al: CT and MR cholangiography: Advantages and pitfalls in perioperative evaluation of biliary tree. *Br J Radiol* 85:887–896, 2012.
140. Taylor AJ, Bohorfoush AG, III: Interpretation of ERCP. New York, 1997, Lippincott-Raven.
141. Classen M, Phillip J: Endoscopic retrograde cholangiopancreatography and endoscopic therapy in pancreatic disease. *Clin Gastroenterol* 13:819–842, 1984.
142. May G, Gardiner R: Indications for examination. In May G, Gardiner R, editors: *Clinical Imaging of the Pancreas*, New York, 1987, Raven, pp 11–15.
143. Balmadrid B, Kozarek R: Prevention and management of adverse events of endoscopic retrograde cholangiopancreatography. *Gastrointest Endosc Clin N Am* 23:385–403, 2013.
144. Goldberg HI, Bilbao MK, Stewart ET, et al: Endoscopic retrograde cholangiopancreatography (ERCP): Radiographic technique. *Am J Dig Dis* 21:270–278, 1976.
145. Jacobson IM: *ERCP and Its Applications*, New York, 1998, Lippincott-Raven.
146. Bilbao MK, Dotter CT, Lee TG, et al: Complications of endoscopic retrograde cholangiopancreatography (ERCP): A study of 10,000 cases. *Gastroenterology* 70:314–320, 1976.
147. Mun J: Radiofluorinated carbohydrates for positron emission tomography. *Curr Top Med Chem* 13:944–950, 2013.
148. Henkin RE: Selected topics in intra-abdominal imaging via nuclear medicine techniques. *Radiol Clin North Am* 17:39–54, 1987.
149. Sundin A: Radiological and nuclear medicine imaging of gastroenteropancreatic neuroendocrine tumours. *Best Pract Res Clin Gastroenterol* 26:803–818, 2012.
150. Heinrich S, Goerres GW, Schafer M, et al: Positron emission tomography/computed tomography influences on the management of resectable pancreatic cancer and its cost effectiveness. *Ann Surg* 242:235–243, 2005.
151. Nguyen VX, Nguyen CC, Nguyen BD: ¹⁸F-FDG PET/CT imaging of the pancreas: Spectrum of diseases. *JOP* 12:557–566, 2011.
152. De Gaetano AM, Rufini V, Castaldi P, et al: Clinical applications of ¹⁸F-FDG PET in the management of hepatobiliary and pancreatic tumors. *Abdom Imaging* 37:983–1003, 2012.
153. Ansari D, Keussen I, Andersson R: Positron emission tomography in malignancies of the liver, pancreas and biliary tract—indications and potential pitfalls. *Scand J Gastroenterol* 48:259–265, 2013.
154. Rijkers AP, Valkema R, Duivenvoorden HJ, et al: Usefulness of F-18-fluorodeoxyglucose positron emission tomography to confirm suspected pancreatic cancer: A meta-analysis. *Eur J Surg Oncol* 40:794–804, 2014.

Interventional Radiology of the Pancreas

KOENRAAD J. MORTELE | STUART G. SILVERMAN

CHAPTER OUTLINE

Role of Interventional Radiology in the Management of Pancreatic Neoplasms

Background
Indications for Pancreatic Mass Biopsy
Technical Considerations
Diagnostic Effectiveness
Complications

Role of Interventional Radiology in the Management of Acute Necrotizing Pancreatitis

Background
Image-Guided Catheter Drainage: Technique
Management of Sterile Pancreatic Necrosis
Management of Infected Pancreatic Necrosis
Complications
Catheter Care
Ancillary Procedures

Role of Interventional Radiology in the Management of Pancreatic Pseudocysts

Indications
Outcome

Conclusions

Historically, percutaneous biopsy has played only a limited role in the evaluation and management of pancreatic masses.¹ In the past, percutaneous biopsy was reserved mostly for tissue confirmation in tumors that appeared unresectable at the time of diagnosis, for diagnosis of lymphoma or metastatic disease (in which surgery typically would be unnecessary), and for differentiation of inflammatory pseudotumors from true pancreatic neoplasms.² In recent years, however, advanced multidetector computed tomography (MDCT) and magnetic resonance imaging (MRI) techniques have improved the detection of cystic pancreatic neoplasms, and as a result, the role of percutaneous pancreatic mass biopsy has steadily increased.^{3,4}

Similarly, although the mainstay for treatment of patients with acute necrotizing pancreatitis has traditionally been surgical débridement, percutaneous image-guided catheter drainage has been proposed as a safe and alternative treatment option.⁵ Many patients with pancreatic necrosis undergo fine-needle aspiration to differentiate between infected and sterile pancreatic necrosis and, if deemed necessary to control systemic toxicity, percutaneous image-guided catheter drainage of pancreatic necrosis.⁶

In this chapter, we review the specific clinical indications for pancreatic mass biopsy, summarize the reported diagnostic

efficacy of percutaneous pancreatic mass biopsy, discuss the technical factors that contribute to results and failures, and highlight the possible limitations and complications of this procedure. Finally, we emphasize the current status of therapeutic radiology in patients with complicated pancreatitis so that the practicing radiologist can understand the current role of percutaneous image-guided aspiration and catheter drainage in the diagnosis and management of patients with necrotizing pancreatitis and pancreatic pseudocysts.

Role of Interventional Radiology in the Management of Pancreatic Neoplasms

BACKGROUND

Pancreatic ductal adenocarcinoma, accounting for approximately 85% of all pancreatic neoplasms, is the fourth leading cause of cancer-related deaths in the United States; approximately 28,000 new cases of pancreatic cancer are diagnosed each year.^{7,8} Percutaneous biopsy is performed typically to diagnose the cause of a pancreatic mass identified by CT scan, MRI, or sonography.⁹ Biopsy is useful both to diagnose malignant disease and to determine the type of malignant neoplasm.¹⁰ For example, among malignant pancreatic tumors, including ductal adenocarcinomas, islet cell carcinomas, and lymphomas, each carries a different prognosis and is treated differently.

Percutaneous image-guided biopsy is an established means of diagnosing the cause of pancreatic masses.^{8,11,12} The procedure may be performed on an outpatient basis, and complication rates are low, ranging from 3% to 6.7%.^{13,14} A diagnostic rate of 97.7% was recently reported for CT-guided fine-needle aspiration biopsy of pancreatic masses.¹⁵ Endoscopic sonography-guided fine-needle aspiration biopsy is an increasingly used alternative technique for pancreatic mass biopsy.¹⁶

INDICATIONS FOR PANCREATIC MASS BIOPSY

Patients with Imaging Findings That Suggest Unresectable Pancreatic Cancer

Percutaneous pancreatic mass biopsy is mainly indicated in patients with no known malignant neoplasm but whose imaging findings suggest an unresectable pancreatic tumor.¹³ In these patients, biopsy provides a tissue diagnosis that allows appropriate nonsurgical treatment to ensue (Fig. 95-1). Important to realize is that in patients with unresectable pancreatic cancer and other extrapancreatic lesions, such as hepatic or peritoneal/omental masses, biopsy of the extrapancreatic mass could potentially result in less morbidity than biopsy of the pancreatic tumor. For example, in a patient presenting with both a

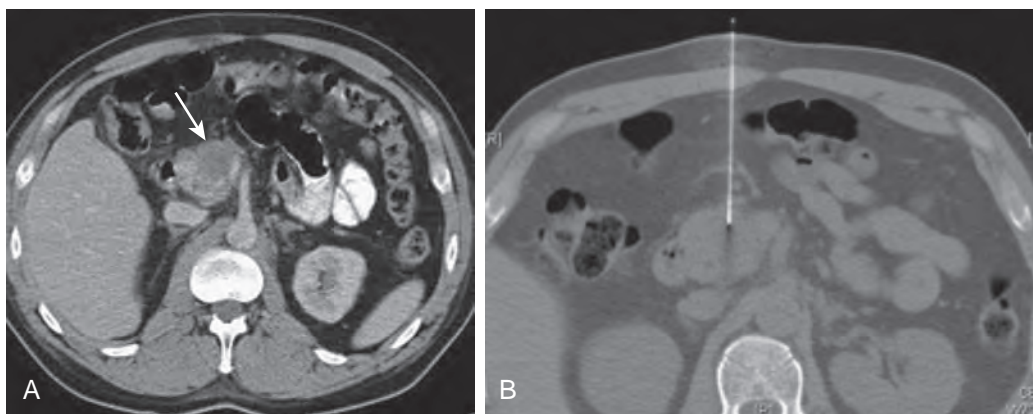


Figure 95-1 Percutaneous biopsy of unresectable pancreatic ductal adenocarcinoma. **A.** Axial contrast-enhanced CT image shows hypovascular mass (arrow) in the head of the pancreas with invasion of the portal venous confluence (indicating unresectability). **B.** Axial noncontrast CT image shows needle sampling (25 gauge) of pancreatic mass; cytology revealed ductal adenocarcinoma.

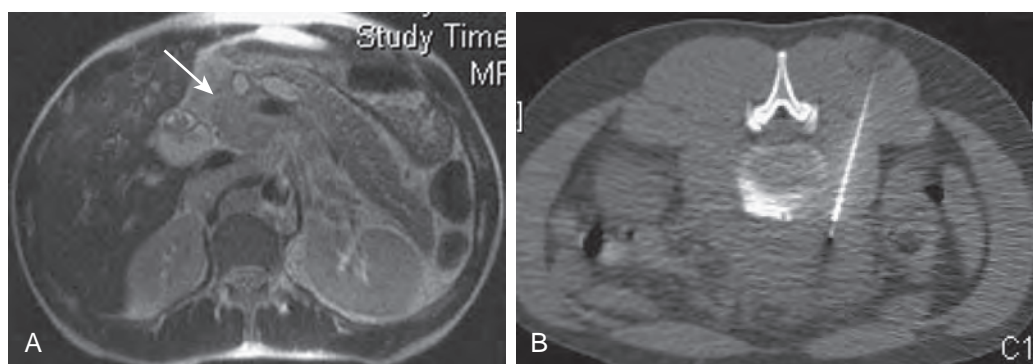


Figure 95-2 Percutaneous biopsy of pancreatic lymphoma. **A.** Axial T2-weighted MR image shows hyperintense mass (arrow) in the head of the pancreas with associated ductal dilation. Also note extensive portocaval and retrocaval lymphadenopathy. **B.** Axial noncontrast CT image (patient in prone position) shows needle sampling (25 gauge through 20 gauge) of pancreatic mass by coaxial technique and a posterior approach; cytology revealed pancreatic lymphoma.

pancreatic mass and a hepatic mass, if biopsy of the hepatic mass revealed a metastasis of pancreatic cancer, it would obviate subsequent biopsy of the pancreatic mass.

Patients with a Known Extrapancreatic Primary Cancer

Another indication for percutaneous biopsy of a pancreatic mass is in a patient with a pancreatic mass and a known extrapancreatic primary malignant neoplasm.¹⁷ Percutaneous pancreatic mass biopsy is indicated in these patients to differentiate a surgically resectable pancreatic ductal adenocarcinoma from a metastasis. A pretreatment diagnosis is needed because virtually all metastases are treated medically, whereas resectable pancreatic carcinomas are treated surgically.¹⁸ The importance of a pretreatment tissue diagnosis in these patients is especially emphasized in patients with lymphoma, renal cell carcinoma, and lung cancer, three tumors that spread not uncommonly to the pancreas.¹⁹ Therefore, when a pancreatic mass is detected in a patient with an extrapancreatic primary malignant neoplasm, the mass should not be presumed to represent a metastasis; biopsy should be performed (Fig. 95-2).

Patients with a Pancreatic Mass That May Be Caused by Inflammation

Chronic pancreatitis (including autoimmune and groove pancreatitis subtypes) can appear masslike and mimic a pancreatic

neoplasm.²⁰ Therefore, an inflammatory etiology should be considered to prevent a patient with a benign mass from going to surgery unnecessarily. Prior history and signs and symptoms of chronic pancreatitis are usually present. However, not infrequently, a pancreatic neoplasm with postobstructive pancreatitis induces overlapping symptoms. Therefore, if there is still the possibility of an inflammatory cause after a careful history and laboratory evaluation, percutaneous biopsy can be used to confirm the diagnosis of cancer or to identify an inflammatory cause.²¹

Patients with a Cystic Pancreatic Mass

The precise role of percutaneous biopsy in the evaluation of cystic pancreatic masses is still controversial.²²⁻²⁵ In the past, the majority of these masses have been considered “surgical lesions” because, with the exception of the benign serous microcystic pancreatic adenoma, cystic neoplasms typically are malignant or have malignant potential (mucinous cystic tumors, intraductal papillary mucinous neoplasm, solid pseudopapillary tumor of the pancreas); they cannot be characterized confidently as benign on the basis of imaging alone, and they can be diagnosed as benign with certainty only if they are removed completely and examined fully at pathology.²⁶ As a result, biopsy specimens obtained from the cyst’s wall or fluid typically contain only scant epithelial cells, inflammatory cells, and fibrous tissue, material that cannot be used to render a specific

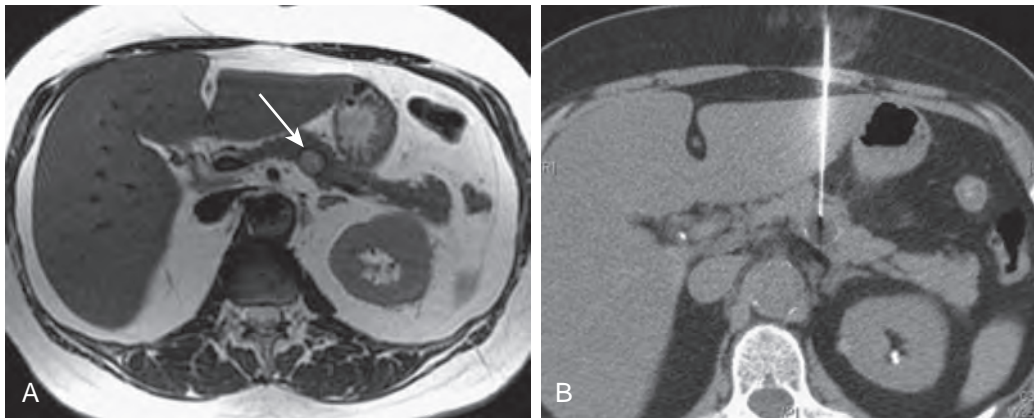


Figure 95-3 Percutaneous biopsy of cystic pancreatic neoplasm. **A.** Axial T2-weighted MR image shows hyperintense cystic mass (arrow) in the body of the pancreas with surrounding rim of calcifications. **B.** Axial noncontrast CT image shows needle sampling (22 gauge) of pancreatic mass through a transhepatic approach; cytology and subsequent fluid analysis plus molecular marking revealed benign mucinous cystic tumor with indolent cytogenetics.

benign diagnosis. Retrieval of no malignant cells still leaves the interventional radiologist, referring physician, and patient with the possibility that the lesion was improperly sampled or missed.^{27,28}

Recently, helped by important advances in cyst fluid tumor marker analysis, immunohistochemistry, and molecular techniques, some authors have argued that percutaneous biopsy can be helpful in identifying patients with benign subtypes of cystic pancreatic masses, obviating surgery in these patients.^{27,29,30} Indeed, new advanced MDCT and MRI techniques have dramatically increased the detection of cystic pancreatic neoplasms, and although resection of all pancreatic cystic tumors would ensure that cancers are not missed, most small cystic pancreatic neoplasms grow slowly or not at all,^{3,4} and up to 87% of patients would undergo surgery unnecessarily.⁴ As a result, percutaneous biopsy may be advocated in selected circumstances, such as in symptomatic patients who have cystic pancreatic neoplasms smaller than 3 cm, patients who have comorbidities that increase the risk of surgical exploration, and patients with a cystic pancreatic mass diagnosed in the setting of acute or chronic pancreatitis (Fig. 95-3). In these patients, biopsy results can simply serve as additional data that can be combined with imaging data to render a probable clinical diagnosis.

Multiple Solid Pancreatic Masses

As pancreatic ductal adenocarcinoma is solitary in more than 95% of cases, patients without a known primary malignant neoplasm who present with multiple, solid pancreatic masses are also good candidates for pancreatic biopsy.²⁶ The differential diagnosis includes metastatic disease, but this is not likely if a primary tumor is not known. Primary lymphoma is another possibility, although lymphoma more commonly involves the pancreas secondarily, and associated lymphadenopathy is usually present at time of presentation. Other differential diagnostic possibilities include multifocal nonhyperfunctioning endocrine tumors and multifocal solid-appearing microcystic pancreatic adenomas. A diagnosis of lymphoma or multifocal solid-appearing microcystic pancreatic adenomas would lead to medical treatment (Fig. 95-4). A diagnosis of multifocal nonhyperfunctioning endocrine tumors would allow the surgical treatment of each tumor to be planned such that the maximum amount of functioning pancreatic tissue can be left remaining.

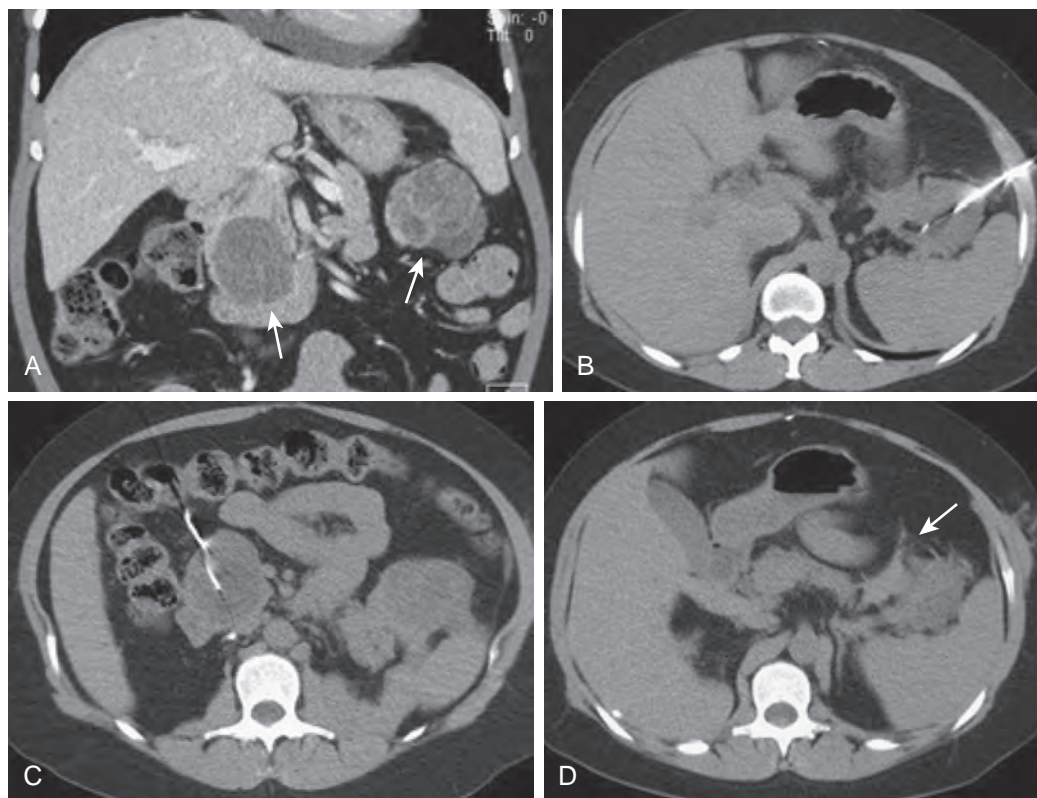
TECHNICAL CONSIDERATIONS

Percutaneous biopsy of pancreatic masses is now most often guided by ultrasound, CT, and, rarely, MRI. To our knowledge, there are no data to support use of one modality for all masses.^{31,32} Ultrasound is widely available, multiplanar, portable, and free of ionizing radiation; it provides real-time imaging and is less expensive than CT or MRI. However, not all pancreatic masses are visible with ultrasound. Because of its posterior location in the anterior pararenal space, the pancreas cannot always be seen in patients with intervening bowel gas or excessive abdominal fat, and it may be difficult to visualize the location of the needle tip.³¹ CT can be used to visualize almost all pancreatic masses (although intravenous contrast material may be needed rarely) and is excellent in depicting surrounding normal pancreas, the hypodense/hypovascular tumor, and the needle tip.³² MRI is typically reserved for the unusual mass that is not visualized well with CT or ultrasound. In general, we recommend using the imaging modality that depicts the mass best and that modality with which the radiologist is most familiar.

Percutaneous biopsy of pancreatic masses can be performed with a wide range of needle sizes.³³ Percutaneous pancreatic mass biopsy refers to a procedure during which imaging is used to guide any needle into a pancreatic mass percutaneously for the purpose of obtaining a tissue diagnosis.³³ This includes biopsies that use fine needles (20 gauge or thinner) or large needles (19 gauge or larger). Some authors distinguish between fine-needle aspirations, during which only fine needles are used and the tissue is examined cytologically, and biopsies, during which large needles are used to procure fragments of tissue, sometimes referred to as cores, which are examined histologically.³³ In general, fine-needle aspiration biopsy specimens are analyzed cytologically, and large-needle biopsy specimens are analyzed histologically. Needles may also differ by type; some are end cutting, others are side cutting.

There are no data to suggest that pancreatic masses are better biopsied with fine needles (20 gauge or thinner) or large needles (19 gauge or larger). Diagnostic sensitivities for percutaneous biopsy procedures using only fine needles vary from 71% to 94.7%.³⁴⁻³⁶ The reason for this range of diagnostic sensitivity might be that some studies included cystic and solid pancreatic masses, whereas others focused on solid pancreatic masses only. As mentioned before, the diagnostic work-up of most cystic

Figure 95-4 Percutaneous biopsy of multiple pancreatic masses. **A.** Coronal contrast-enhanced CT image shows two heterogeneous masses (arrows) in the head and tail of the pancreas. **B.** Axial noncontrast CT image shows large-needle sampling (18-gauge side-cutting device) of pancreatic mass in the tail. **C.** Axial noncontrast CT image shows fine-needle sampling (22 gauge) of pancreatic mass in the head; cytology and surgical pathology assessment of both masses revealed serous microcystic pancreatic adenoma. **D.** Axial noncontrast CT image shows small retroperitoneal hemorrhage (arrow) around the pancreatic tail that was self-limited.



pancreatic masses involves analysis of cystic fluid for biochemical and tumor markers rather than tissue sampling; thus, the accuracy of fine-needle aspiration biopsy is related to both the ability to position a needle in a mass and the accuracy of the biochemical analysis of the cystic fluid.²⁸

Biopsies performed with large (typically 18 gauge) needles have yielded similar sensitivities.^{37,38} These series showed that sensitivities for detection of malignant neoplasms range from 69% to 93%. Therefore, although there has been no statistically valid comparison study for any definitive conclusions to be drawn, on the basis of current available data, it is reasonable to conclude that fine needles are adequate by themselves to biopsy the majority of pancreatic masses. Although use of large needles may increase accuracy in selected circumstances, we believe that they increase the risk of complications, particularly bleeding and pancreatitis. Therefore, in our practice, we begin with fine needles and ask our cytologists to examine one or two specimens intraprocedurally. If the preliminary cytology impression is that the specimen is adequate, the procedure is completed with fine needles alone. If there is any question as to the specimen's adequacy, we obtain large-needle specimens for histologic analysis.³³

The pancreas is located in the anterior pararenal space, and access routes that avoid traversal of liver, stomach, colon, small bowel, spleen, or kidney are preferentially selected to minimize the risk of bacterial contamination and hemorrhage. If possible, an approach avoiding traversal of normal pancreatic tissue is also preferred to minimize the risk of pancreatitis. Anterior routes through the liver or stomach can be used if no other routes are available. Transgressing the stomach theoretically increases the risk of infection in patients who are receiving H1 receptor blockers or any other medications that raise gastric pH

because the gastric fluid is not sterile. Moreover, percutaneous biopsy of cystic pancreatic lesions by a transgastric route may impair the diagnostic accuracy of the biopsy because gastric mucin-producing cells may contaminate the smear.

DIAGNOSTIC EFFECTIVENESS

Several studies have evaluated the sensitivity, specificity, and overall accuracy of biopsy of pancreatic masses. These studies vary considerably with respect to patient population, tumor type, guidance modalities, and needle size.¹⁵ Overall, the sensitivity of biopsy for diagnosis of malignant disease is 71% to 97% regardless of needle size used or whether the specimens were examined by cytology, histology, or both.¹⁵ False-negative results are most often due to failure to place the needle tip accurately in a small mass or to sampling of coexistent desmoplastic reaction or pancreatitis adjacent to the mass. Even in experienced hands, false negatives do occur, suggesting that negative results should be viewed with caution in patients with a radiologically suspicious mass.

Tillou and associates¹³ reported a diagnostic rate of 96.5% for diagnosis of pancreatic masses by CT- and transabdominal ultrasound-guided fine-needle aspiration biopsy. In a retrospective study, Qian and Hecht³⁶ showed that CT-guided biopsies had sensitivity of 71%. In the study by Mallery and coworkers,⁹ CT- and transabdominal ultrasound-guided pancreatic biopsies (80%) had a higher sensitivity than endoscopic sonography-guided biopsies (74%). In one study, we also found higher sensitivity for CT guidance (94.9%) compared with endoscopic sonographic guidance (85%).¹⁵ However, the difference did not reach statistical significance. In the study of Qian and Hecht,³⁶ the negative predictive values of CT- and

endoscopic sonography-guided fine-needle aspiration biopsies were similar, 41% and 45%, respectively. Mallery and coworkers⁹ reported negative predictive values of 23% and 27% for fine-needle aspiration biopsies performed under CT and endoscopic sonographic guidance, respectively. We found negative predictive values of 60% and 57.1% for CT- and endoscopic sonography-guided fine-needle aspiration biopsy, respectively. Also in our study, the frequency of small masses biopsied under endoscopic sonographic guidance (81.5%) was significantly higher than the frequency of those biopsied under CT guidance (32.6%).¹⁵ In fact, since the first report of the use of endoscopic sonography-guided fine-needle aspiration biopsy for the diagnosis of pancreatic cancer in 1994,³⁹ it has been reported that endoscopic sonography-guided fine-needle aspiration biopsy is more accurate than CT-guided fine-needle aspiration biopsy, especially for small pancreatic masses.³⁴ To evaluate the effect of mass size on biopsy performance, we stratified results by mass size. There were no significant differences in test characteristics between the guidance groups after the data were stratified by mass size; small masses were not more effectively biopsied under endoscopic sonography guidance.¹⁵

Because cytology is a relatively insensitive test in the diagnosis of cystic pancreatic neoplasms, advances in cyst fluid tumor markers analysis, immunohistochemistry, and molecular techniques have been used to improve the sensitivity for detection of malignant changes in these lesions. Cyst fluid carcinoembryonic antigen (CEA) values are uniformly low in serous pancreatic adenomas, higher in mucinous lesions, and markedly elevated in mucinous cystadenocarcinomas.²⁷ A pooled analysis of 12 studies in 450 patients on the role of cyst fluid analysis in the differential diagnosis of pancreatic cystic lesions showed that a CEA level greater than 800 ng/mL is strongly suggestive of a mucinous tumor.⁴⁰ Other studies confirmed that of all tested markers (e.g., amylase, mucicarmine staining, carbohydrate antigen 19-9), cyst fluid CEA is the most accurate test available for the diagnosis of mucinous cystic lesions of the pancreas.⁴¹⁻⁴³ Finally, studies have revealed specific roles of molecular analysis of clusterin- β and *MUC4* to help distinguish reactive ductal epithelial cells from the cells of pancreatic adenocarcinoma in fine-needle aspiration samples,⁴⁴ of mutational analysis for *K-ras* point mutations and loss of heterozygosity in differentiating benign from malignant cystic neoplasms,³⁰ and of immunohistochemical staining for *MUC1* overexpression as a specific marker of invasive carcinoma in intraductal papillary mucinous neoplasm.²⁹

COMPLICATIONS

Percutaneous pancreatic mass biopsy is a safe procedure, and reported complication rates are low for both CT-guided and sonography-guided fine-needle aspiration biopsy of the pancreas.¹⁵ In a meta-analysis, Chen and associates¹⁸ reported a complication rate of 4% for CT-guided procedures. Bleeding is the most frequent complication, but it is usually subclinical, detected only with a postprocedural CT scan, and self-limited because of the retroperitoneal location of the pancreas. Although there are no direct comparison data, we believe that peripancreatic hemorrhage is more likely with large needles.

The second most common complication is acute pancreatitis due to inadvertent transgression or biopsy of normal pancreatic parenchyma. It is almost always self-limited but may be prolonged because of pancreatic ductal disruption.⁴⁵

Seeding of the needle track with tumor is a theoretical consequence of percutaneous biopsy of a malignant pancreatic mass, but it is extremely rare and therefore should not be a deterrent to biopsy when there is an appropriate indication. To our knowledge, only one case of needle track seeding associated with pancreatic mass biopsies has been reported.⁴⁶

Role of Interventional Radiology in the Management of Acute Necrotizing Pancreatitis

BACKGROUND

The International Symposium on Acute Pancreatitis held in 1992 in Atlanta defined acute pancreatitis as inflammation of the pancreas with variable secondary involvement of remote organs.⁴⁷ Acute necrotizing pancreatitis is a severe form of the disease associated with significant morbidity and mortality. Percutaneous image-guided catheter drainage is an important treatment option that can be lifesaving when it is used alone or as an adjunct to surgery.⁵ Successful treatment outcomes depend on close cooperation and teamwork among gastroenterologists, surgeons, and interventional radiologists.⁵

Pancreatic necrosis is defined as a diffuse or focal area of nonviable pancreatic tissue.⁴⁸ Infection of the necrotic portion of the pancreas results in infected necrosis. Infected pancreatic necrosis is an "intermediate" complication of acute pancreatitis, usually occurring between the third and eighth weeks after onset of symptoms.⁴⁹ Infected necrosis and sterile necrosis both carry a high mortality rate.⁵ Mortality rates of 30% to 35% have been reported in patients with infected necrosis and 10% to 15% in patients with sterile necrosis.⁷ Although the presence of infection increases the mortality rate in patients with pancreatic necrosis, a review of 1110 cases of acute pancreatitis demonstrated that mortality is more strongly linked to the presence of organ failure than to the presence of infection itself.⁵⁰

Although no universally accepted treatment algorithm exists, a general consensus of indications for the interventional approach to patients with acute pancreatitis has been described.^{5,7,51-61} Some percutaneous drainage procedures are performed to stabilize the seriously ill patient before surgical débridement, whereas others are done with the intent to cure. In some cases, percutaneous drainage follows surgical therapy that has been only partially successful.⁶² Treatment algorithms vary among medical centers and are sometimes based on expertise of both the interventional radiologist and the surgeon. The clinical status of the patient, for instance, the presence of sepsis, also influences which approach is best in any given clinical situation.^{5,7}

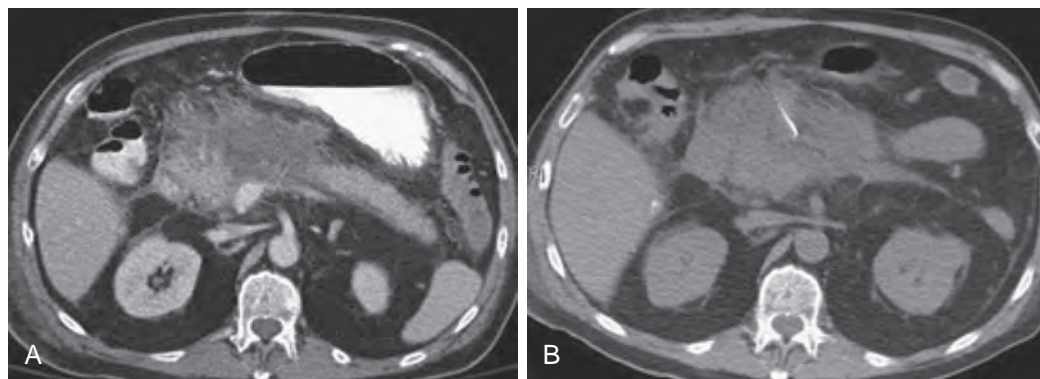
IMAGE-GUIDED CATHETER DRAINAGE: TECHNIQUE

Access Route

Most pancreatic fluid collections are located in the lesser sac, the anterior pararenal space, or other parts of the retroperitoneum.⁴⁸ Access routes that avoid traversal of colon, small bowel, stomach, spleen, and kidney are preferred to minimize the risk of bacterial contamination and hemorrhage. If possible, a retroperitoneal approach through the lateral flank is chosen over an anterior approach through the peritoneum.⁷ Some authors

Figure 95-5 Percutaneous fine-needle aspiration of sterile necrotizing pancreatitis.

A. Axial contrast-enhanced CT image shows hypovascular area in the body of the pancreas consistent with pancreatic necrosis. **B.** Axial noncontrast CT image shows needle sampling (20 gauge) of pancreatic necrotic collection through a right anterior approach. The fluid was analyzed and found to be sterile.



suggest that anterior routes involve the theoretical disadvantage of antigravity flow of fluid through the catheter.^{5,7} Anterior routes through the liver or stomach can be used if no other routes are available.^{5,7} Transgressing the liver theoretically increases the risk of bleeding but in practice is generally safe. Transgressing the stomach is also safe, but peristalsis in the stomach may result in catheter dislodgment several days after its placement. Moreover, caution should be taken in patients who are receiving H1 receptor blockers or any other medications that raise gastric pH because the gastric fluid may not be sterile. Fluid collections involving the pancreatic tail can be drained through the left anterior pararenal space, avoiding the descending colon posteriorly.^{5,7} Similarly, pancreatic head collections can be drained through the right anterior pararenal space.⁶ Typically, the patient's position on the interventional CT table should be adjusted to a slight posterior oblique position to optimize access to the region of interest.

Catheter Selection and Placement

The fluid contained in collections caused by pancreatic necrosis is often viscous. Therefore, adequate drainage of pancreatic and peripancreatic collections typically requires catheters with multiple side holes and a minimum diameter of 12F to 14F.⁵²⁻⁶¹ Multiple catheters may be required to drain large or multiloculated necrotic collections. If the fluid is not viscous, 12F to 14F drainage catheters may be satisfactory.^{5,7} Either the tandem trocar technique or Seldinger technique can be used, depending on the operator's experience. If the Seldinger technique is used, the catheter track should be sequentially dilated over a guide-wire. If the necrotic material is viscous and the collection is not drained completely, catheters larger than 14F may be exchanged several days after a 14F catheter is placed initially. An attempt should be made to place as much length of the catheter containing side holes as possible transversely into the necrotic pancreatic collection from the lateral flank approach to maximize drainage.^{5,7}

MANAGEMENT OF STERILE PANCREATIC NECROSIS

In general, in patients with sterile pancreatic necrosis, CT scans of the abdomen are repeated every 7 to 10 days to follow the evolution of pancreatic necrosis and to look for complications.³ Patients who persistently show clinical instability with tachycardia, fever, leukocytosis, or organ failure may require image-guided percutaneous needle sampling to evaluate for infected pancreatic necrosis.⁵¹ It is important that the access route avoid

small and large bowel so as not to contaminate the collection or the aspiration sample^{5,7} (Fig. 95-5).

If sampled pancreatic fluid is sterile, the patient is considered to have sterile pancreatic necrosis. Some of these patients recover rapidly without additional intervention, whereas others remain persistently toxic because of pancreatic duct disruption with extravasation and accumulation of noxious pancreatic juice into peripancreatic spaces; they usually require continuous support in an intensive care unit.⁶³ Several years ago, patients with persistent toxicity underwent urgent surgical débridement; however, now these patients are managed nonsurgically because early surgical débridement contributes to morbidity and mortality.⁶³⁻⁶⁵ A combination of percutaneous catheter drainage and supportive care offers an alternative to surgery.⁵²

Some suggest that persistently toxic patients should undergo percutaneous image-guided needle sampling every 7 to 10 days to assess for infected necrosis.⁵¹ Instead of performing regular needle sampling, the necrotic fluid may be drained percutaneously.⁶⁶ One or more catheters may be placed and irrigated per standard radiologic protocol to provide a "radiologic necrosectomy" and to reduce systemic toxicity.⁶⁶ Percutaneous catheter drainage of sterile necrosis is, however, still controversial. Only one clinical study is currently available that has compared the results of therapy using weekly percutaneous needle sampling to assess for infection versus indwelling catheter drainage of sterile necrosis.⁶⁶

The main rationale for not using percutaneous catheter drainage is the potential of infecting a sterile pancreatic collection.⁶⁷ Although indwelling catheter colonization is common, serious clinical infection is unlikely to occur if all the fluid and material are drained within 2 or 3 days of the intervention.^{5,7,66} This requires vigilant attention to follow-up CT scans and placement of additional or larger catheters to drain the residual fluid. Adequate drainage is achieved when no residual necrotic fluid is present on follow-up CT scans.

MANAGEMENT OF INFECTED PANCREATIC NECROSIS

Although contrast-enhanced CT scan is excellent in assessing for pancreatic necrosis, it cannot distinguish between infected and sterile necrosis with certainty.⁴⁸ Intrapancreatic, retroperitoneal, or lesser sac gas is a rare finding on CT; however, if it is present, it typically indicates infection.⁴⁸ Bacterial infection of necrotic pancreatic tissue is common and associated with high morbidity and mortality. The risk of infection may or may not increase with the amount of pancreatic necrosis.⁵⁰

Infected pancreatic necrosis has traditionally been managed with surgical necrosectomy and antibiotics.⁶⁵ Percutaneous catheter drainage is often ineffective because of blockage of the catheter by necrotic tissue fragments and viscous fluid.⁶⁵ However, when patients are too unstable to undergo surgery, percutaneous catheter drainage may be successful in draining liquefied pus and minimizing the systemic manifestations of sepsis, thereby preparing patients for surgery.⁶⁸⁻⁷¹

Percutaneous catheter drainage may also be successful alone.⁶⁹ In a study of 23 patients with 38 infected pancreatic fluid collections who were drained percutaneously, 65% were cured without surgery and 35% required some type of surgical intervention after drainage.⁶⁹ Catheter drainage time averaged 29 days for patients with isolated collections and 96 days for patients with pancreatic duct fistulas.⁶⁹ Success largely depends on the following factors: all the collections must be drained; if they are persistent after 2 or 3 days of drainage, additional catheters should be placed and large-bore catheters are often required; vigorous bedside catheter irrigation should be done at least three times a day with 20 mL of sterile saline injected; and follow-up CT scans must be obtained frequently to assess for treatment response^{69,72} (Fig. 95-6).

COMPLICATIONS

Reported major complications of CT-guided catheter drainage are hemorrhage and injury to adjacent organs, such as bowel.^{5,7} Hemorrhage is uncommon and may be due to pancreatitis itself rather than to the drainage procedure^{5,7} (Fig. 95-7). After all percutaneous drainage procedures, CT scan of the abdomen should be done to assess for retroperitoneal hemorrhage. Venous bleeding is usually self-limited. Arterial

pseudoaneurysm or active arterial hemorrhage due to injury of adjacent vessels, such as the splenic artery, requires angiographic embolization. Fistulization to adjacent bowel is almost always due to the pancreatitis itself rather than to catheter drainage.^{5,7} Inadvertent insertion of the catheter through the bowel may occur when bowel loops are collapsed or unopacified. In most cases, the bowel heals without the need for surgical repair.^{5,7}

CATHETER CARE

Daily rounds should be performed by the interventional radiologist with assessment of the patient's vital signs, white blood cell count, and clinical status.⁷² Catheters should be irrigated with sterile saline at least three times a day with a technique that involves aspirating and discarding all the fluid that can be withdrawn from the catheter, followed by forward flushing into the abscess cavity with 20 mL of sterile saline.^{5,7} The process is repeated until the fluid is clear, typically two or three times. Finally, 10 mL of sterile saline is instilled into the catheter toward the patient and an additional 10 mL toward the bag to prevent catheter plugging. The stopcock between the catheter and the drainage bag connecting tube should be left in the open position. It is important to document accurate drainage output amounts by subtracting the instilled volume of saline from the total drainage volume. The nurses should be familiar with drainage catheters placed by interventional radiology so that flushes are done promptly.

Abdominal CT scans should be obtained periodically on the basis of the clinical status and amount of drainage to check for residual or undrained fluid collections.^{5,7} This helps determine whether drainage is adequate or additional catheters should be

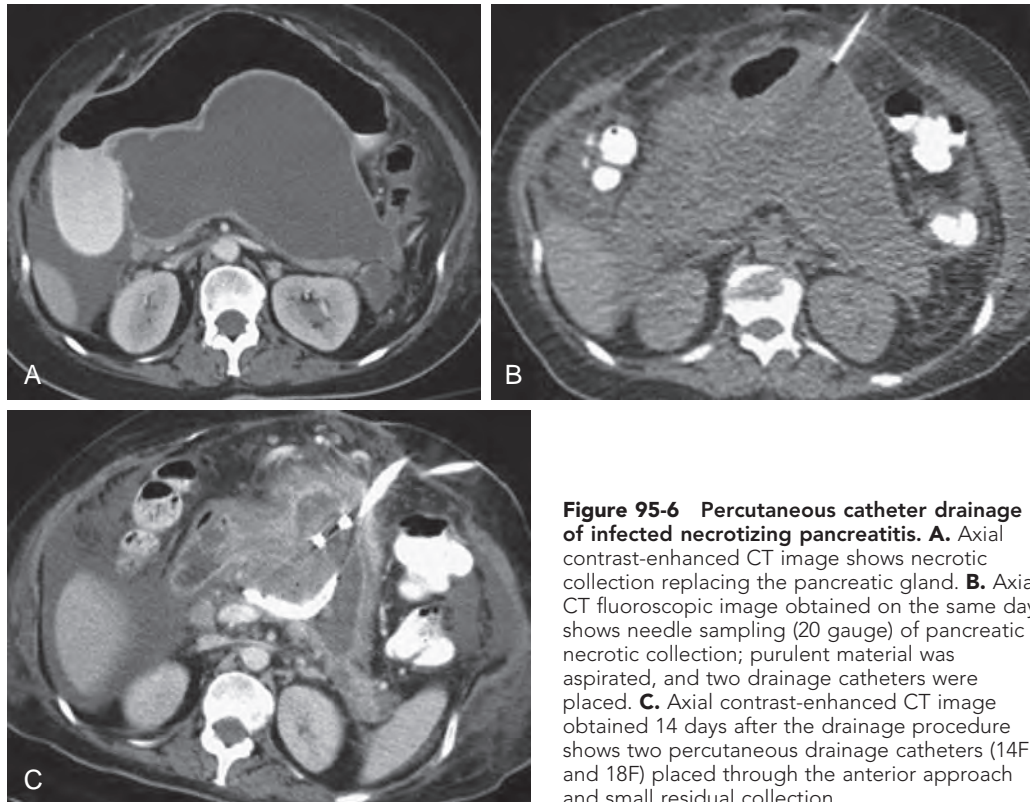
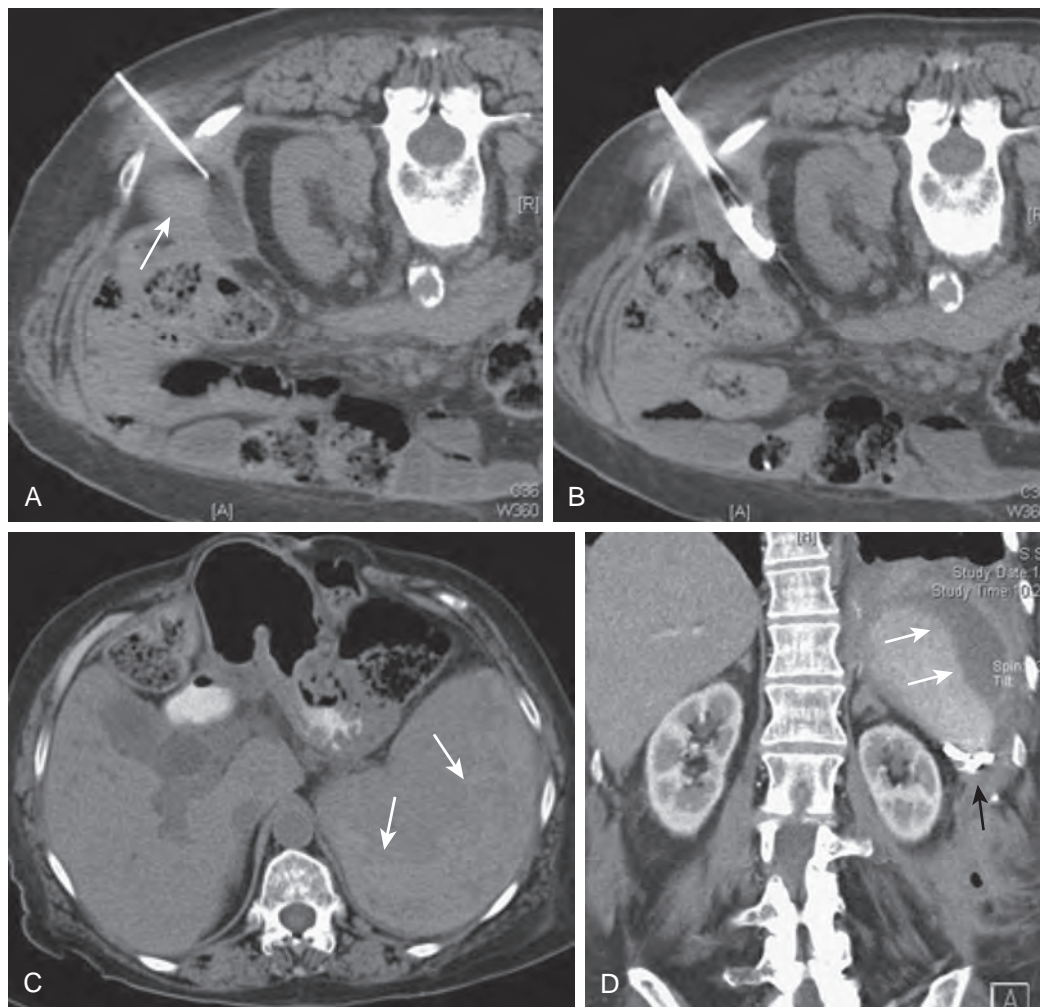


Figure 95-6 Percutaneous catheter drainage of infected necrotizing pancreatitis. **A.** Axial contrast-enhanced CT image shows necrotic collection replacing the pancreatic gland. **B.** Axial CT fluoroscopic image obtained on the same day shows needle sampling (20 gauge) of pancreatic necrotic collection; purulent material was aspirated, and two drainage catheters were placed. **C.** Axial contrast-enhanced CT image obtained 14 days after the drainage procedure shows two percutaneous drainage catheters (14F and 18F) placed through the anterior approach and small residual collection.

Figure 95-7 Procedure-related perisplenic hematoma after percutaneous catheter drainage of infected necrotizing pancreatitis.

A. Axial contrast-enhanced CT image (patient prone) shows well-defined fluid collection around the tail of the pancreas consistent with organized pancreatic necrosis. Note proximity of the collection to the spleen (arrow) and needle sampling (20 gauge) of pancreatic necrotic collection.

B. Axial nonenhanced CT image (patient prone) shows percutaneous drainage catheter (14F) placed through the intercostal approach. **C.** Axial noncontrast CT image obtained 5 days later shows large subcapsular splenic hematoma (arrows). **D.** Coronal contrast-enhanced CT image obtained 3 weeks later shows near-resolution and liquefaction of splenic hematoma (white arrows) and presence of percutaneous drainage catheter (black arrow).



placed. If a catheter is not draining and abdominal CT shows residual collection, the catheter may be blocked or the side holes may not be contiguous with the collection. In such cases, the catheter should be exchanged over a guidewire and repositioned appropriately within the collection or removed and a new catheter placed (Fig. 95-8).

Our criteria for catheter removal include no residual collection on a follow-up CT scan and catheter output of no more than 10 mL/day of nonpurulent fluid for 2 consecutive days. It is important not to remove the catheter solely on the basis of imaging results without assessing the amount of drainage.^{5,7} Likewise, it is important not to remove catheters solely because they stopped draining; catheters may become plugged or be pulled out from the collection. As a result, a CT scan will show residual fluid. In some cases, CT scan may show complete resolution of the collection; however, if there is communication with the pancreatic duct or its branches, the catheter may still be draining significant amounts of fluid daily.^{5,7} Similarly, catheter output may be scant, but a fistula may still be present. Pancreatic duct fistulas usually close over time if the collection is completely drained.⁷³

Patient communication and catheter education must be established as the catheters may have to remain in place for weeks to months.^{5,7} Once stabilized, patients can be discharged home with the catheter in situ and observed as outpatients.

Periodic visits with the interventional radiologist are scheduled for inspection of the catheter insertion site.

ANCILLARY PROCEDURES

Patients with acute pancreatitis may need additional supportive procedures performed by the interventional radiologist.⁵ These include image-guided thoracentesis and paracentesis, fluoroscopically guided nasojejunal or percutaneous jejunal feeding tube placement, and angiographic embolization of pseudoaneurysms or hemorrhaging vessels.^{5,7} Several studies support the use of enteral nutrition rather than parenteral nutrition in patients with acute pancreatitis.⁷⁴⁻⁷⁶ Therefore, nasojejunal or percutaneous jejunal feeding tube placement should be attempted whenever possible.

Some patients with sterile necrotizing pancreatitis remain toxic after 3 to 6 weeks. This is often due to one or more pancreatic duct disruptions with extravasation of noxious pancreatic juice.⁶⁶ Some reports advocate endoscopic placement of a stent across a disruption.^{77,78} However, there are several reasons not to recommend endoscopic pancreatic stent placement in the setting of sterile necrosis.⁵² First, the duct may be obstructed and disruption may not be visualized. Second, if there is no obstruction, the injected contrast material may extravasate and infect the necrotic area. Third, with extensive necrosis of the

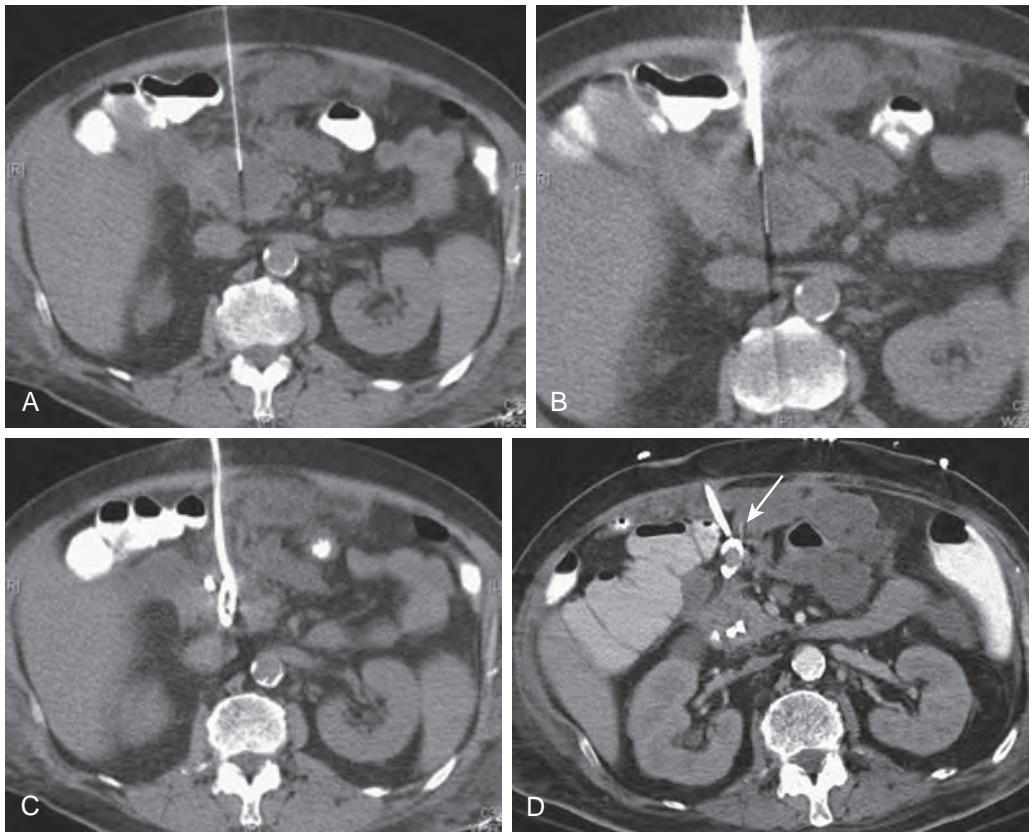


Figure 95-8 Percutaneous drainage catheter dislodgment. **A.** Axial noncontrast CT image shows needle sampling (22 gauge) of pancreatic necrotic collection through an anterior approach. **B.** Axial noncontrast CT image shows percutaneous drainage catheter (14F) insertion by a tandem technique. **C.** Axial noncontrast CT image shows percutaneous drainage catheter in place and complete resolution of pancreatic fluid collection. **D.** Axial contrast-enhanced CT image obtained 14 days after the drainage procedure shows dislodgment of the catheter (arrow) and spillage of pancreatic fluid in the omentum and peripancreatic tissues.

body of the pancreas, the distal portion of the duct cannot be visualized or accessed by a stent. Fourth, even if a stent can be placed across a disruption, it may act as a foreign body and result in superinfection.

If a follow-up CT scan demonstrates complete resolution of the pancreatic collection but the catheter continues to drain significant amounts of fluid daily, there is communication with the pancreatic duct. Fluoroscopic abscessography is then used to visualize the communication and the appearance of the pancreatic duct.⁷³ This communication usually heals over time if the collection is drained completely.

Role of Interventional Radiology in the Management of Pancreatic Pseudocysts

INDICATIONS

Pseudocysts are collections of pancreatic juice enclosed by a wall of granulation tissue.⁷⁹ Typically, they require 4 weeks or more to evolve and result from acute pancreatic fluid collections. Less than 10% of patients with acute pancreatitis will develop pancreatic pseudocysts.⁸⁰ They vary in size and location and are usually asymptomatic. By imaging, pseudocysts are homogeneous fluid collections with attenuation of the fluid content less than 15 HU. The surrounding fibrous pseudocapsule is usually thin (<2 mm). Calcification of the wall, typically curvilinear in shape, is not uncommon. Chronic pseudocysts (i.e., those that do not resolve over time) may point to a persistent communication with the pancreatic duct or its side

branches.^{79,80} When symptomatic, pseudocysts are typically larger than 5 cm and older than 6 weeks. These symptomatic pseudocysts are usually amenable to percutaneous drainage; large nonsymptomatic pseudocysts usually do not need treatment.^{81,82} Secondary complications of pseudocyst formation include infection (resulting in a pancreatic abscess) and erosion into a vessel (resulting in a pseudoaneurysm).

A pancreatic abscess or infected pseudocyst is a circumscribed collection of pus containing little or no necrosis.⁸³ Its incidence is far less (3%) than that of infected pancreatic necrosis; it usually occurs later in the course of the disease, and it is typically multibacterial. Importantly, the mortality of pancreatic abscess is minimal. Among many reasons for this, one is that pancreatic abscesses are typically amenable to percutaneous catheter drainage⁸³ (Fig. 95-9). In most cases, imaging cannot be used to rule in or to rule out the presence of infection in patients with localized fluid collections. Therefore, image-guided percutaneous aspiration is frequently required for diagnosis.

OUTCOME

Percutaneous drainage is an effective frontline treatment for most pancreatic pseudocysts^{84,85}; cure is likely if fluid collections are drained adequately and if sufficient time is allowed for closure of fistulas from the pancreatic duct. In the largest series reported to date,⁸⁴ percutaneous drainage of 101 pancreatic pseudocysts (51 infected, 50 noninfected) in 77 patients is described. In this group of patients, 91 of 101 pseudocysts (90.1%) were cured by means of catheter drainage (noninfected, 43 of 50 [86%]; infected, 48 of 51 [94.1%]). Six patients

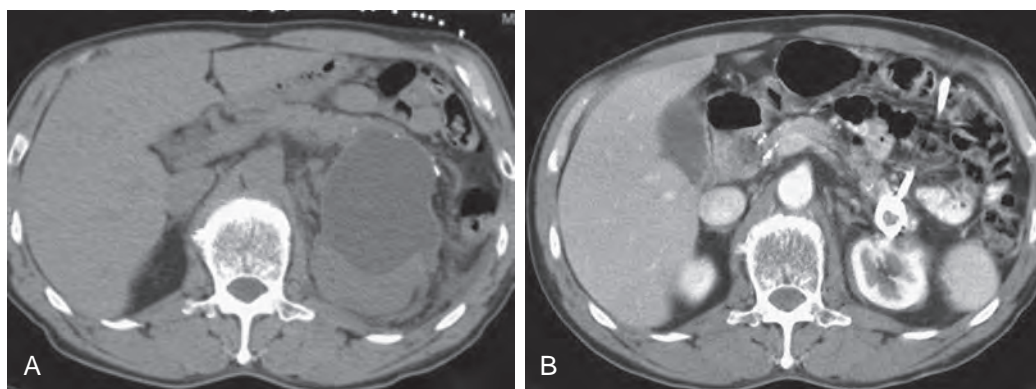


Figure 95-9 Percutaneous catheter drainage of infected pseudocyst (pancreatic abscess). **A.** Axial nonenhanced CT image shows well-defined fluid collection adjacent to the tail of the pancreas with peripheral calcifications consistent with pancreatic pseudocyst. The collection was needle sampled through a left anterior approach; the fluid was analyzed and found to be infected. **B.** Axial contrast-enhanced CT image obtained 3 weeks later shows complete resolution of the infected pseudocyst.

underwent operation after percutaneous treatment because of persistent drainage. In patients with infected pseudocysts, the infection was eradicated by percutaneous drainage before operation. Four pseudocysts recurred and were redrained percutaneously. The mean duration of drainage was 19.6 days (infected pseudocysts, 16.7 days; noninfected, 21.2 days). Four major complications (superinfection of sterile pseudocysts) and six minor complications occurred. Therefore, it can be concluded that percutaneous catheter drainage is a safe and valuable procedure in the management of patients with pancreatic pseudocysts.

Conclusions

Percutaneous biopsy of pancreatic masses is a safe and accurate procedure and can be used to diagnose malignant disease and to guide treatments. In the future, biopsy performance will undoubtedly improve as the field of cytology expands to include

a more sensitive and specific array of immunocytochemical reagents and cytogenetic markers that can be used to improve the analysis of percutaneous needle biopsy specimens.

Image-guided catheter drainage of fluid collections in and around the pancreas in patients with complicated pancreatitis is an important therapeutic option either alone or as an adjunct to surgery.⁸⁶ Successful percutaneous treatment of necrotic collections of the pancreas depends on several important factors. Typically, multiple large-bore catheters are required to drain large or multiloculated collections. Catheters often need to remain in place for several weeks and sometimes months, hence the need for close follow-up. Daily interventional radiology rounds, frequent vigorous bedside catheter irrigations, and willingness to place additional catheters for undrained collections are the norm in the care of these patients. Successful outcomes are best achieved when there is close cooperation among the interventional radiologist, gastroenterologist, and surgeon.

REFERENCES

- Ierardi AM, Lucchina N, Petrillo M, et al: Systematic review of minimally invasive ablation treatment for locally advanced pancreatic cancer. *Radiol Med* 119:483–498, 2014.
- Dodd LG, Mooney EE, Layfield LJ, et al: Fine-needle aspiration of the liver and pancreas: Cytology primer for radiologists. *Radiology* 203:1–7, 1997.
- Walsh RM, Vogt DP, Henderson JM, et al: Natural history of indeterminate pancreatic cysts. *Surgery* 138:665–670, 2005.
- Sahani DV, Soakor A, Hahn PF, et al: Pancreatic cysts 3 cm or smaller: How aggressive should treatment be? *Radiology* 238:912–918, 2006.
- Shankar S, vanSonnenberg E, Silverman SG, et al: Imaging and percutaneous management of acute complicated pancreatitis. *Cardiovasc Intervent Radiol* 27:567–580, 2004.
- Ferrucci JT, Mueller PR: Interventional approach to pancreatic fluid collections. *Radiol Clin North Am* 41:1217–1226, 2003.
- Wallace MB, Woodward T, Raimondo M: EUS and fine-needle aspiration for pancreatic cancer. *Dig Endosc* 16:193–196, 2004.
- Paik WH, Yoon H, Park DH, et al: Utility of endoscopic ultrasound (EUS)-guided fine-needle aspiration for peri-arterial soft tissue cuffs without identifiable pancreas mass on CT and EUS: A prospective comparative study. *Ultrasound Med Biol* 2014. [Epub ahead of print].
- Mallery JS, Centeno BA, Hahn PF, et al: Pancreatic tissue sampling guided by EUS, CT/US, and surgery: A comparison of sensitivity and specificity. *Gastrointest Endosc* 56:218–224, 2002.
- Voss M, Hammel P, Molas G, et al: Value of EUS guided fine needle aspiration biopsy in the diagnosis of solid pancreatic masses. *Gut* 46:244–249, 2000.
- Agarwal B, Abu-Hamda E, Molke KL, et al: Endoscopic ultrasound-guided fine needle aspiration and multidetector spiral CT in the diagnosis of pancreatic cancer. *Am J Gastroenterol* 99:844–850, 2004.
- Edoute Y, Lemberg S, Malberger E: Preoperative and intraoperative fine needle aspiration cytology of pancreatic lesions. *Am J Gastroenterol* 86:1015–1019, 1991.
- Tillou A, Schwartz MR, Jordan PH, Jr: Percutaneous needle biopsy of the pancreas: When should it be performed? *World J Surg* 20:283–286, 1996.
- Brandt KR, Charboneau JW, Stephens DH, et al: CT- and US-guided biopsy of the pancreas. *Radiology* 187:99–104, 1993.
- Erturk SM, Morte KJ, Tuncali K, et al: Fine needle aspiration biopsy of solid pancreatic masses: Comparison of CT and endoscopic sonography guidance. *AJR Am J Roentgenol* 187:1531–1535, 2006.
- Eloubeidi MA, Chen VK, Eltoum IA, et al: EUS-guided fine needle aspiration biopsy of patients with suspected pancreatic cancer: Diagnostic accuracy and acute and 30-day complications. *Am J Gastroenterol* 98:2663–2668, 2003.
- Linder S, Blasjo M, Sundelin P, et al: Aspects of percutaneous fine-needle aspiration biopsy in the diagnosis of pancreatic carcinoma. *Am J Surg* 174:303–306, 1997.
- Chen VK, Arguedas MR, Kilgore ML, et al: A cost-minimization analysis of alternative strate-

- gies in diagnosing pancreatic cancer. *Am J Gastroenterol* 99:2223–2234, 2004.
19. Lee ES, Lee JM: Imaging diagnosis of pancreatic cancer: A state-of-the-art review. *World J Gastroenterol* 20:7864–7877, 2014.
 20. O'Neill E, Hammond N, Miller FH: MR imaging of the pancreas. *Radiol Clin North Am* 52:757–777, 2014.
 21. Yadav D, Lowenfels AB: The epidemiology of pancreatitis and pancreatic cancer. *Gastroenterology* 144:1252–1261, 2013.
 22. MacCarty RL: Cyst fluid analysis and imaging of pancreatic cystic lesions. *AJR Am J Roentgenol* 164:820–821, 1995.
 23. Lewandrowski KB, Southern JF, Pins MR, et al: Cyst fluid analysis in the differential diagnosis of pancreatic cysts. A comparison of pseudocysts, serous cystadenomas, mucinous cystic neoplasms, and mucinous cystadenocarcinoma. *Ann Surg* 217:41–47, 1993.
 24. Hammel P, Levy P, Voitot H, et al: Preoperative cyst fluid analysis is useful for the differential diagnosis of cystic lesions of the pancreas. *Gastroenterology* 108:1230–1235, 1995.
 25. Khalid A, Finkelstein S, McGrath K: Molecular diagnosis of solid and cystic lesions of the pancreas. *Gastroenterol Clin North Am* 33:891–906, 2004.
 26. Ros PR, Morteale KJ: Imaging of pancreatic neoplasms. *JBR-BTR* 84:239–249, 2001.
 27. Brugge WR: Role of endoscopic ultrasound in the diagnosis of cystic tumors of the pancreas. *Pancreatol* 1:637–640, 2001.
 28. Carlson SK, Johnson CD, Brandt KR, et al: Pancreatic cystic neoplasms: The role and sensitivity of needle aspiration and biopsy. *Abdom Imaging* 23:387–393, 1998.
 29. Ueda M, Miura Y, Kunihiro O, et al: MUC1 overexpression is the most reliable marker of invasive carcinoma in intraductal papillary mucinous tumor (IPMN). *Hepatogastroenterology* 52:398–403, 2005.
 30. Schoedel KE, Finkelstein SD, Ohori NP: K-ras and microsatellite marker analysis of fine-needle aspirates from intraductal papillary mucinous neoplasms of the pancreas. *Diagn Cytopathol* 34:605–608, 2006.
 31. Di Stasi M, Lencioni R, Solmi L, et al: Ultrasound-guided fine needle biopsy of pancreatic masses: Results of a multicenter study. *Am J Gastroenterol* 93:1329–1333, 1998.
 32. Amin Z, Theis B, Russell RCG, et al: Diagnosing pancreatic cancer: The role of percutaneous biopsy and CT. *Clin Radiol* 61:996–1002, 2006.
 33. Silverman SG, Gan YU, Morteale KJ, et al: Renal masses in the adult patient: Role of percutaneous biopsy. *Radiology* 240:6–22, 2006.
 34. Rodriguez J, Kasberg C, Nipper M, et al: CT-guided needle biopsy of the pancreas: A retrospective analysis of diagnostic accuracy. *Am J Gastroenterol* 87:1610–1613, 1992.
 35. Edoute Y, Lemberg S, Malberger E: Preoperative and intraoperative fine needle aspiration cytology of pancreatic lesions. *Am J Gastroenterol* 86:1015–1019, 1991.
 36. Qian X, Hecht JL: Pancreatic fine needle aspiration. A comparison of computed tomographic and endoscopic ultrasonographic guidance. *Acta Cytol* 47:723–726, 2003.
 37. Itoi T, Itokawa F, Sofuni A, et al: Puncture of solid pancreatic tumors guided by endoscopic ultrasonography: A pilot study series comparing Trucut and 19-gauge and 22-gauge aspiration needles. *Endoscopy* 37:362–366, 2005.
 38. Storch I, Jorda M, Thurer R, et al: Advantage of EUS Trucut biopsy combined with fine-needle aspiration without immediate on-site cytopathologic examination. *Gastrointest Endosc* 64:505–511, 2006.
 39. Chang KJ, Albers CG, Erickson RA, et al: EUS-guided fine needle aspiration of pancreatic carcinoma. *Am J Gastroenterol* 89:263–266, 1994.
 40. van der Waaij LA, van Dullemen HM, Porte RJ: Cyst fluid analysis in the differential diagnosis of pancreatic cystic lesions: A pooled analysis. *Gastrointest Endosc* 62:383–389, 2005.
 41. Brugge WR, Lewandrowski K, Lee-Lewandrowski E, et al: Diagnosis of pancreatic cystic neoplasms: A report of the cooperative pancreatic cyst study. *Gastroenterology* 126:1330–1336, 2004.
 42. Ryu JK, Woo SM, Hwang JH, et al: Cyst fluid analysis for the differential diagnosis of pancreatic cysts. *Diagn Cytopathol* 31:100–105, 2004.
 43. Frossard JL, Amouyal P, Amouyal G, et al: Performance of endosonography-guided fine needle aspiration in the diagnosis of pancreatic cystic lesions. *Am J Gastroenterol* 98:1516–1524, 2003.
 44. Jhala N, Jhala D, Vickers SM, et al: Biomarkers in diagnosis of pancreatic carcinoma in fine-needle aspirates. *Am J Clin Pathol* 126:572–579, 2006.
 45. Lee LS, Saltzman JR, Bounds BC, et al: EUS-guided fine needle aspiration of pancreatic cysts: A retrospective analysis of complications and their predictors. *Clin Gastroenterol Hepatol* 3:231–236, 2005.
 46. Paquin SC, Garipey G, Lepanto L, et al: A first report of tumor seeding because of EUS-guided FNA of a pancreatic adenocarcinoma. *Gastrointest Endosc* 61:610–611, 2005.
 47. Banks PA, Bollen TL, Dervenis C, et al: Classification of acute pancreatitis—2012. *Gut* 62:102–111, 2013.
 48. Thoeni RF: The revised Atlanta classification of acute pancreatitis: Its importance for the radiologist and its effect on treatment. *Radiology* 262:751–764, 2014.
 49. Schepers NJ, Besseling MG, van Santvoort HC, et al: Early management of acute pancreatitis. *Best Pract Res Clin Gastroenterol* 27:727–743, 2013.
 50. Perez A, Whang EE, Brooks DC, et al: Is severity of necrotizing pancreatitis increased in extended necrosis and infected necrosis? *Pancreas* 3:229–233, 2002.
 51. Banks PA, Gerzof SG, Langevin RE, et al: CT-guided needle aspiration of pancreatic infection: Accuracy and prognostic implications. *Int J Pancreatol* 18:265–270, 1995.
 52. Banks PA: Practice guidelines in acute pancreatitis. *Am J Gastroenterol* 92:377–386, 1997.
 53. Lee MJ, Rattner DW, Legemate DA, et al: Acute complicated pancreatitis: Redefining the role of interventional radiology. *Radiology* 183:171–174, 1992.
 54. Lee MJ, Wittich GR, Mueller PR: Percutaneous intervention in acute pancreatitis. *Radiographics* 18:711–724, 1998.
 55. vanSonnenberg E, Wittich GR, Casola G, et al: Complicated pancreatic inflammatory disease: Diagnostic and therapeutic role of interventional radiology. *Radiology* 155:335–340, 1985.
 56. vanSonnenberg E, Casola G, Varney RR, et al: Imaging and interventional radiology for pancreatitis and its complications. *Radiol Clin North Am* 27:65–72, 1989.
 57. Bollen TL: Imaging of acute pancreatitis: Update of the revised Atlanta classification. *Radiol Clin North Am* 50:429–445, 2012.
 58. vanSonnenberg E, Wing VW, Casola G, et al: Temporizing effect of percutaneous drainage of complicated abscesses in critically ill patients. *AJR Am J Roentgenol* 142:821–826, 1984.
 59. vanSonnenberg E, Wittich GR, Goodacre BW, et al: Percutaneous abscess drainage: Update. *World J Surg* 25:362–369, 2001.
 60. Berzin TM, Morteale KJ, Banks PA: The management of suspected pancreatic sepsis. *Gastroenterol Clin North Am* 35:393–407, 2006.
 61. Thoeni RF: The revised Atlanta classification of acute pancreatitis: Its importance for the radiologist and its effect on treatment. *Radiology* 262:751–764, 2012.
 62. vanSonnenberg E, Ferrucci JT, Mueller PR, et al: Percutaneous drainage of abscesses and fluid collections: Technique, results and applications. *Radiology* 142:1–10, 1982.
 63. Rattner DW, Legermate DA, Lee MJ, et al: Early surgical debridement of symptomatic pancreatic necrosis is beneficial irrespective of infection. *Am J Surg* 163:105–109, 1992.
 64. Bradley EL, III, Allen K: A prospective longitudinal study of observation versus surgical intervention in the management of necrotizing pancreatitis. *Am J Surg* 161:19–24, 1991.
 65. Uhl W, Warshaw A, Imrie C, et al: IAP guideline for the surgical management of acute pancreatitis. *Pancreatol* 2:565–573, 2002.
 66. Walser EM, Nealon WH, Marroquin S, et al: Sterile fluid collections in acute pancreatitis: Catheter drainage versus simple aspiration. *Cardiovasc Intervent Radiol* 29:102–107, 2006.
 67. Isaji S, Takada T, Kawarada Y, et al: JPN guidelines for the management of acute pancreatitis: Surgical management. *J Hepatobiliary Pancreat Surg* 13:48–55, 2006.
 68. Adams DB, Harvey TS, Anderson MC: Percutaneous catheter drainage of infected pancreatic and peripancreatic fluid collections. *Arch Surg* 125:1554–1557, 1990.
 69. Freeny PC, Hauptmann E, Althaus SJ, et al: Percutaneous CT guided drainage of infected acute necrotizing pancreatitis: Techniques and results. *AJR Am J Roentgenol* 170:969–975, 1998.
 70. Freeny PC, Lewis GP, Traverso LW, et al: Infected pancreatic fluid collections: Percutaneous catheter drainage. *Radiology* 167:435–441, 1988.
 71. Endlicher E, Volk M, Feuerbach S, et al: Long-term follow-up of patients with necrotizing pancreatitis treated by percutaneous necrosectomy. *Hepatogastroenterology* 50:2225–2228, 2003.
 72. Goldberg MA, Mueller PR, Saini S, et al: Importance of daily rounds by the radiologist after interventional procedures of the abdomen and chest. *Radiology* 180:767–770, 1991.
 73. Singh AK, Gervais DA, Alhilali LM, et al: Imaging-guided catheter drainage of abdominal collections with fistulous pancreaticobiliary communication. *AJR Am J Roentgenol* 187:1591–1596, 2006.
 74. McClave SA, Greene LM, Snider HL, et al: Comparison of the safety of early enteral vs. parenteral nutrition in mild acute pancreatitis. *J Parenteral Nutr* 21:14–20, 1997.
 75. Windsor AC, Kanwar S, Li AG, et al: Compared with parenteral nutrition, enteral feeding attenuates the acute phase response and improves disease severity in acute pancreatitis. *Gut* 42:431–435, 1998.
 76. Lariño-Noia J, Lindkvist B, Iglesias-Garcia J, et al: Early and/or immediately full caloric diet versus standard refeeding in mild acute pancreatitis. *Pancreatol* 14:167–173, 2014.

77. Thomson DA, Krige JE, Thomson SR, et al: The role of endoscopic retrograde pancreatography in pancreatic trauma. *J Trauma Acute Care Surg* 76:1362–1366, 2014.
78. Chebli JM, Gaburri PD, de Souza AF, et al: Internal pancreatic fistulas: Proposal of a management algorithm based on a case series analysis. *J Clin Gastroenterol* 38:795–800, 2004.
79. Singhal S, Rotman SR, Gaidhane M, et al: Pancreatic fluid collection drainage by endoscopic ultrasound: An update. *Clin Endosc* 46:506–514, 2013.
80. Singhal D, Kakodhar R, Sud R, et al: Issues in management of pancreatic pseudocysts. *JOP* 7:502–507, 2006.
81. Cheruvu CV, Clarke MG, Prentice M, et al: Conservative treatment as an option in the management of pancreatic pseudocyst. *Ann R Coll Surg Engl* 85:313–316, 2003.
82. Wittich GR, vanSonnenberg E: When should radiologists intervene in management of pancreatic pseudocysts and other complications of acute pancreatitis? *AJR Am J Roentgenol* 166:211, 1996.
83. vanSonnenberg E, Wittich GR, Chon KS, et al: Percutaneous radiologic drainage of pancreatic abscesses. *AJR Am J Roentgenol* 168:979–984, 1997.
84. vanSonnenberg E, Wittich GR, Casola G, et al: Percutaneous drainage of infected and noninfected pancreatic pseudocysts: Experience in 101 cases. *Radiology* 170:757–761, 1989.
85. Bhasin DK, Rana SS, Sharma V, et al: Non-surgical management of pancreatic pseudocysts associated with arterial pseudoaneurysm. *Pancreatol* 13:250–253, 2013.
86. Larsen M, Kozarek R: Management of pancreatic ductal leaks and fistulae. *J Gastroenterol Hepatol* 29:1360–1370, 2014.

Anomalies and Anatomic Variants of the Pancreas

ALI SHIRKHODA | PEYMAN BORGHEI | RICHARD M. GORE

CHAPTER OUTLINE

Embryology

Variants of Normal Anatomy

Congenital Anomalies of the Pancreas

Pancreas Divisum

Annular and Semiannular Pancreas

Ectopic Pancreatic Tissue

Agenesis, Hypoplasia, and Hyperplasia of the Pancreas

Ductal Abnormalities

Congenital Cysts

To recognize the anatomic variants of the pancreas and to understand how various pancreatic anomalies develop, it is important to be familiar with pancreatic embryology and development. Errors or variations at several critical periods in the development of the pancreas are responsible for the majority of anomalies. These anomalies can vary in their presentation from being totally asymptomatic to being inconsistent with life.¹⁻⁵ In this chapter, a brief discussion of the important events of pancreatic embryology is followed by presentation of normal variants and various types of pancreatic anomalies.

Embryology

The pancreatic duct develops from two buds originating from the endodermal lining of the duodenum.⁶ One is the dorsal pancreatic bud, which is in the dorsal mesentery and is seen as a diverticulum of the foregut before 28 days. It grows into the dorsal mesentery (Fig. 96-1A). The other is the ventral pancreatic bud located close to the bile duct and appears as an invagination at the biliary-duodenal angle between 30 and 35 days.¹

The dorsal and ventral pancreatic buds soon grow into a pair of branching, arborized ductal systems, each with its own central duct (Fig. 96-1B). At day 37, the ventral pancreas rotates posterior to the duodenum and comes into contact with the dorsal pancreas (Fig. 96-1C). These two anlagen fuse and together with the duodenum fuse with the abdominal wall. In the mature organ, the ventral primordium becomes the inferior portion of the head and the uncinate process, and the dorsal pancreas becomes the body and tail. After the fusion, a new duct connects the distal portion of the dorsal pancreatic duct with the shorter duct of the ventral pancreas to form the main duct or the duct of Wirsung (Fig. 96-2). This main pancreatic duct, which is present in approximately 91% of adults, enters the duodenum together with the bile duct at the major papilla. The proximal portion of the dorsal pancreatic duct is pinched off during fusion and usually atrophies and disappears but may

persist as the small accessory duct of Santorini, which has a variety of appearances (Fig. 96-3). This accessory duct empties into the duodenum at the minor papilla 2 to 3 cm proximal to the ampulla of Vater.^{7,8} In about 10% of all cases, the duct system fails to fuse and the original double system persists.^{1,9}

As the duodenum grows and differentiates, the duodenal wall resorbs the distal bile duct up to its junction with the pancreatic duct. Different degrees of resorption account for variations in the appearance and relationships of the common bile duct and pancreatic duct. If ductal resorption is minimal, a long intramural ampulla is created, and the junction is extramural. The junction becomes intramural with increasing degrees of resorption, which produces a shortened ampulla.¹⁰⁻¹⁵ Maximal resorption produces separate orifices for the pancreatic duct and common bile duct (see Fig. 96-2), which no longer share a common ampulla.^{7,16}

Beginning in the third month of fetal life, the islets of Langerhans develop as clusters of cells from the terminal ductules. They become intimately associated with the capillary plexus and finally separate from the ductules to become the endocrine portion of the pancreas. Insulin secretion begins at approximately the fifth month. The acini develop from terminal ductal cells. The ductal system and the acini collectively become the exocrine portion of the pancreas.⁶ Secretory activity probably becomes established in the pancreas during the second trimester, although this has been disputed.¹ The weight of the pancreas, which is 5 to 5.5 g at birth, will increase to 15 g at the end of the first year.¹¹

The process of pancreatic fusion is complicated, and a wide spectrum of anomalies or anatomic variants related to this process may appear—for example, agenesis, aplasia of the pancreatic anlage, hypoplasia, annular pancreas, and pancreas divisum.¹²

Variants of Normal Anatomy

The lateral aspect of the head and neck of the pancreas can have varieties of shapes and occasionally look prominent (Fig. 96-4). However, many of the contour variations may represent a spectrum of fusion patterns that cannot be attributed to pancreas divisum alone.^{13,14} A deep cleft separating two distinct pancreatic moieties may be identified on computed tomography (CT) scans in the head and neck of the pancreas in patients with pancreas divisum.

The pancreas is surrounded by fat that clearly defines its margin. However, because of the lack of any pancreatic capsule, the pancreatic lobules can be outlined by fat. Such fatty infiltration can be diffuse or focal (Fig. 96-5). Focal fatty infiltration can mimic a mass on CT, particularly if there is associated lobulation (see Fig. 96-4). Therefore, magnetic resonance imaging (MRI) may become necessary to differentiate this benign

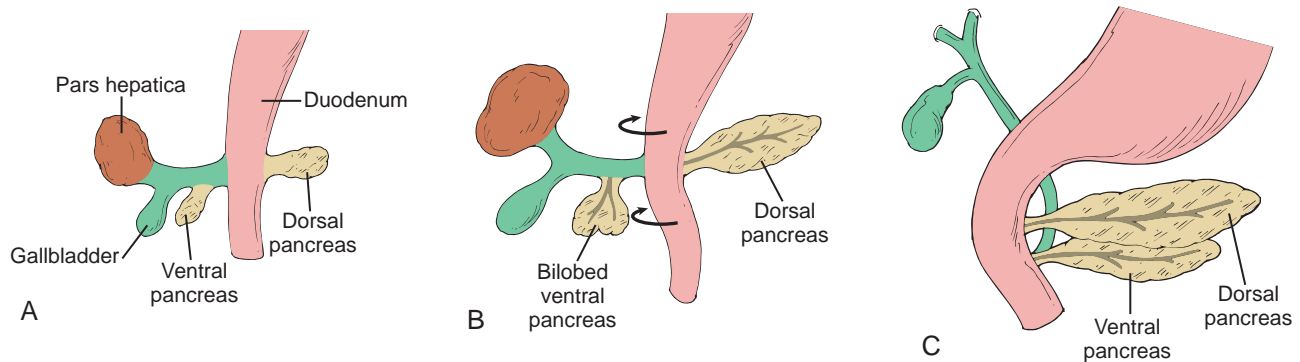


Figure 96-1 Pancreatic duct development. **A.** The dorsal pancreatic segment grows posteriorly into the dorsal mesentery, and the ventral anlage develops as an outpouching from the base of the hepatic diverticulum and grows in the ventral mesentery. **B.** The ventral component transiently develops into a bifid structure. The ventral pancreas and the bile duct system will be carried posteriorly as the duodenum matures. **C.** The final stage of pancreatic duct maturation entails fusion of the two systems. (A–C from Taylor AJ, Bohorfoush AG: *Interpretation of ERCP: With Associated Digital Imaging Correlation*. Philadelphia, Lippincott-Raven, 1996, pp 209–210.)

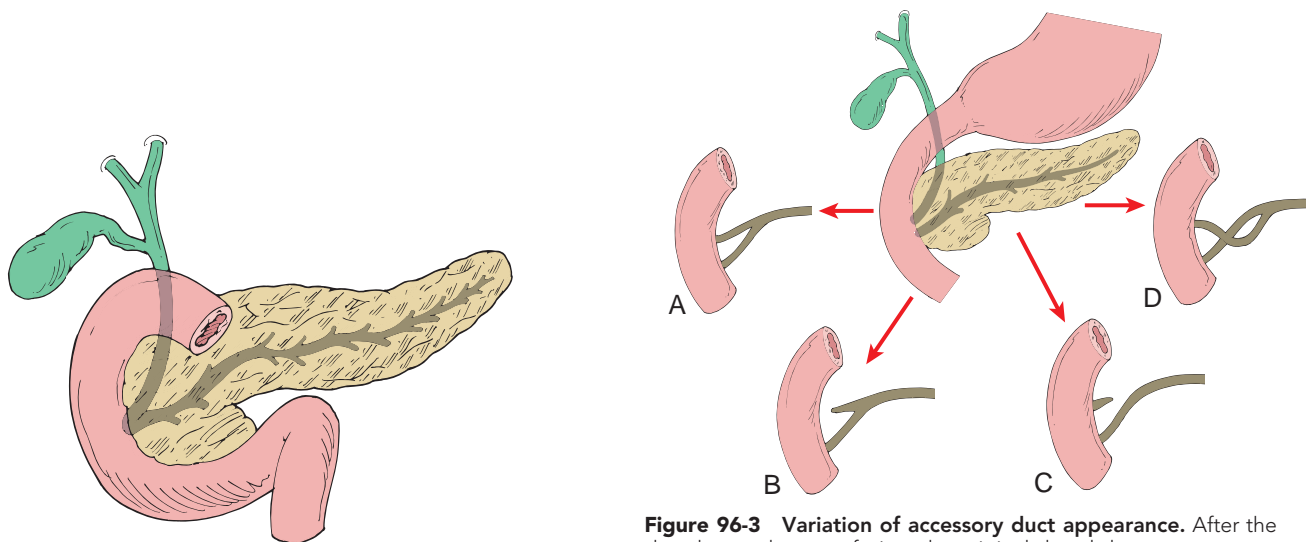
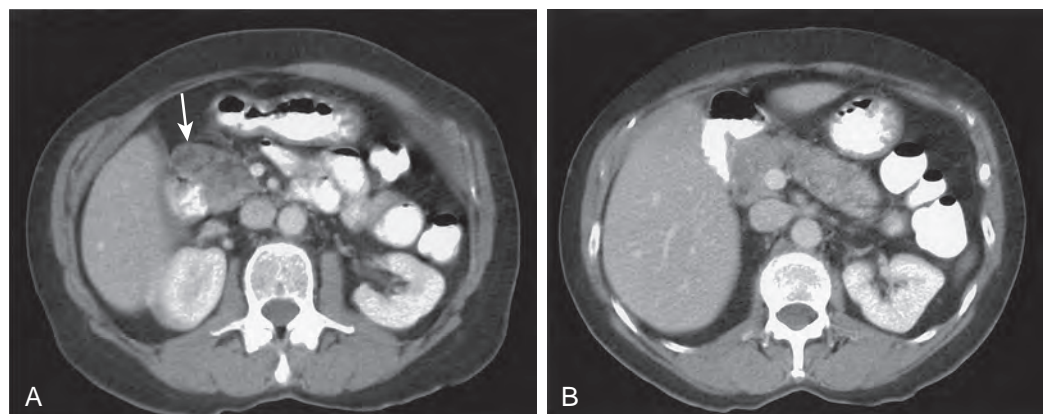


Figure 96-2 Duct of Wirsung. Notice the junction of the ventral duct and common bile duct at the ampulla with total regression of the dorsal duct.

Figure 96-3 Variation of accessory duct appearance. After the dorsal-ventral system fusion, the original dorsal duct segment draining into the duodenum may remain as the duct of Santorini (**A**), serving as a slender, narrowed connection of the main pancreatic duct (MPD) with the duodenum through the minor papilla; maintain connection with the MPD but not drain into the duodenum (**B**), thereby becoming another MPD side branch; maintain communication with the duodenum at the minor papilla but lose connection with the MPD (**C**); or maintain connection with both the duodenum and the MPD but develop a circuitous course forming the ansa pancreatica (**D**). (A–D from Taylor AJ, Bohorfoush AG: *Interpretation of ERCP: With Associated Digital Imaging Correlation*. Philadelphia, Lippincott-Raven, 1996, pp 209–210.)

Figure 96-4 Pancreatic head lobulation and fatty infiltration.

A. Contrast-enhanced CT scan shows lateral lobulation of the pancreatic head (arrow) with heterogeneous density due to fatty infiltration. **B.** Upper portion of the head, body, and tail are spared fatty infiltration.



process from a neoplasm (Fig. 96-6). Fatty infiltration may be associated with focal sparing of pancreatic parenchyma, and that should not be mistaken for tumor.

The position and configuration of the pancreas are variable, and these variations may simulate pathologic conditions. For example, the pancreatic head is not fixed in position, although it almost invariably maintains a fixed relationship medial to the second portion of the duodenum and lateral to the root

of the superior mesenteric vessels, even if these structures are shifted to the left of the midline. Although the splenic vein usually marks the dorsal margin of the body and tail of the pancreas, the tip of the gland may rarely curve dorsal to the splenic vein to simulate adrenal abnormalities (Fig. 96-7). On occasion, even in normal persons, the pancreatic tail may be anterior-lateral to the left kidney, where it may appear as a pseudomass on excretory urography. In patients with prior

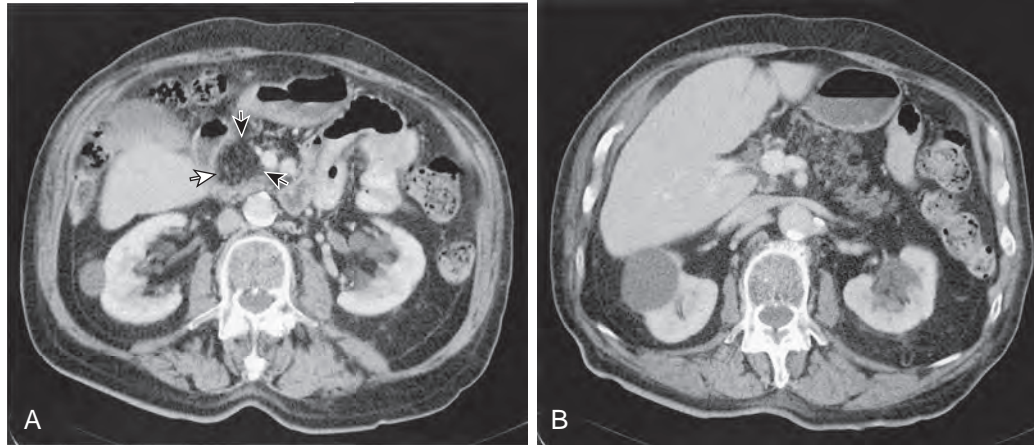


Figure 96-5 Fatty infiltration of the pancreas. **A.** CT of the pancreatic head reveals a large area of fatty infiltration in the head of the pancreas (arrows). A portion of the uncinate process is spared from fat. Notice lack of any mass effect on the adjacent superior mesenteric vein. **B.** Fatty infiltration is also present in the pancreatic body. The tail is spared.

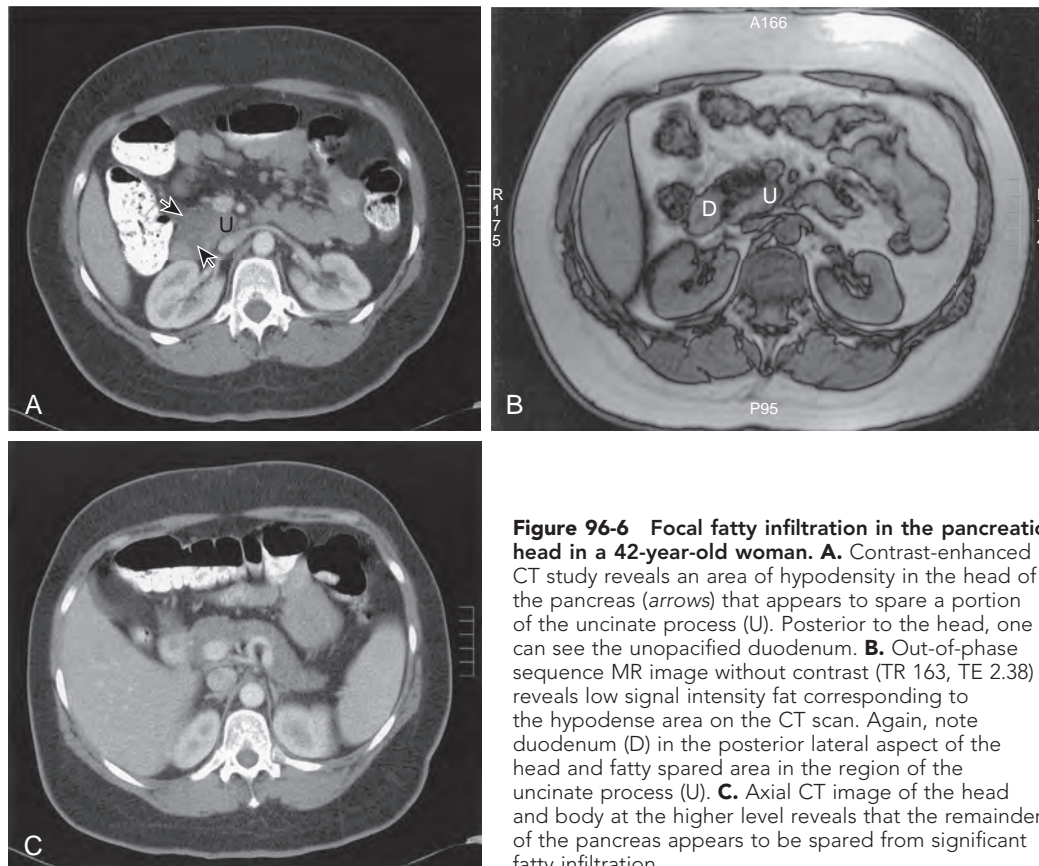


Figure 96-6 Focal fatty infiltration in the pancreatic head in a 42-year-old woman. **A.** Contrast-enhanced CT study reveals an area of hypodensity in the head of the pancreas (arrows) that appears to spare a portion of the uncinate process (U). Posterior to the head, one can see the unopacified duodenum. **B.** Out-of-phase sequence MR image without contrast (TR 163, TE 2.38) reveals low signal intensity fat corresponding to the hypodense area on the CT scan. Again, note duodenum (D) in the posterior lateral aspect of the head and fatty spared area in the region of the uncinate process (U). **C.** Axial CT image of the head and body at the higher level reveals that the remainder of the pancreas appears to be spared from significant fatty infiltration.



Figure 96-7 Extension of the pancreatic tail into the adrenal fossa. Notice as a normal variant, the splenic vein (arrows) no longer serves as the ventral pancreatic landmark. The top and bottom images are continuous 5-mm slices.

left nephrectomy or in those with congenital absence of the left kidney, the pancreatic tail is often displaced into the renal fossa, which may simulate recurrent tumor or a primary retroperitoneal lesion.¹⁵

Kreel and colleagues¹⁶ published a set of in vivo and in vitro measurements of pancreatic dimensions and concluded that the normal diameter of the head is up to 3 cm, that of the neck and body up to 2.5 cm, and that of the tail up to 2 cm. However, the size, shape, and position of the normal pancreas are highly variable (Fig. 96-8), and there is usually a gradual tapering from the head to the tail without abrupt alterations in size or contour. There is gradual decrease in the size of the pancreas with advancing age, sometimes becoming very small beyond the seventh decade. Fatty lobulations are more commonly observed in obese and elderly individuals. Rarely, an accessory spleen can be embedded in the tail of the pancreas, and MRI or a nuclear medicine study may be needed to differentiate this variant from a mass (Fig. 96-9).

Bifid pancreatic duct (Fig. 96-10) is a rare anatomic anomaly in which the main pancreatic duct is bifurcated along its length. It is associated with a high incidence of pancreatitis.¹⁷

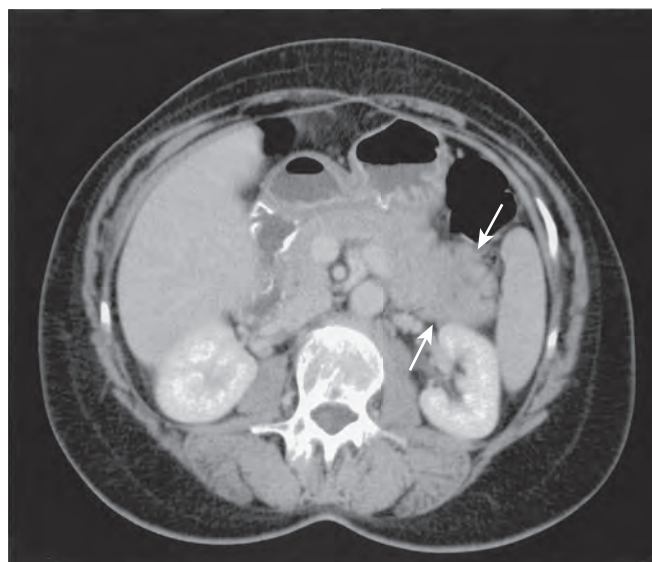


Figure 96-8 Normal variant pancreas in which the tail (arrows) is more prominent than the head and proximal body. Notice homogeneous enhancement of pancreas and normal lobulations of its borders.

Congenital Anomalies of the Pancreas

PANCREAS DIVISUM

In this anomaly, the pancreas is divided in two separate parts as a result of an absent or incomplete fusion of the ventral and dorsal anlagen. As a consequence, the pancreatic head and uncinate process are drained by the duct of Wirsung through the major papilla; the body and tail are drained by the duct of Santorini through the minor papilla^{18,19} (Fig. 96-11). This anomaly is seen in 4% to 11% of autopsy series and 3% to 4% of endoscopic retrograde cholangiopancreatography (ERCP) series.²⁰⁻²³ In an analysis of 650 ERCP studies done by Uomo and coworkers,²⁴ 485 patients had satisfactory imaging of the pancreatic ducts, whereas in 48 cases (9.9%), anatomic variants of the duct were found. These included fusion variants in 26 cases (22 pancreas divisum and 4 functional divisum) and duplication variants in 22 patients (1 bifurcation of the main pancreatic duct, 4 loop, 2 N shaped, and 3 ring).

Clinical Findings

Although the anatomic variant of pancreas divisum has been well known for some time, its clinical significance has become evident with the advent of ERCP. Most cases of pancreas divisum are asymptomatic. This anomaly may contribute to recurrent episodes of idiopathic pancreatitis in younger patients with no risk factors.^{25,26} Between 12% and 26% of patients with idiopathic recurrent pancreatitis have this anomaly, as opposed to 3% to 6% in the general population.^{22,26} The age at presentation varies widely but is most commonly between 30 and 50 years.²⁷ Several reports of pancreatitis associated with pancreas divisum in children have appeared, and there is a report of this anomaly occurring in multiple family members.²⁸

It is postulated that in pancreas divisum, the duct of Santorini and its accessory ampulla are too small to adequately drain the volume of secretions produced by the pancreatic body

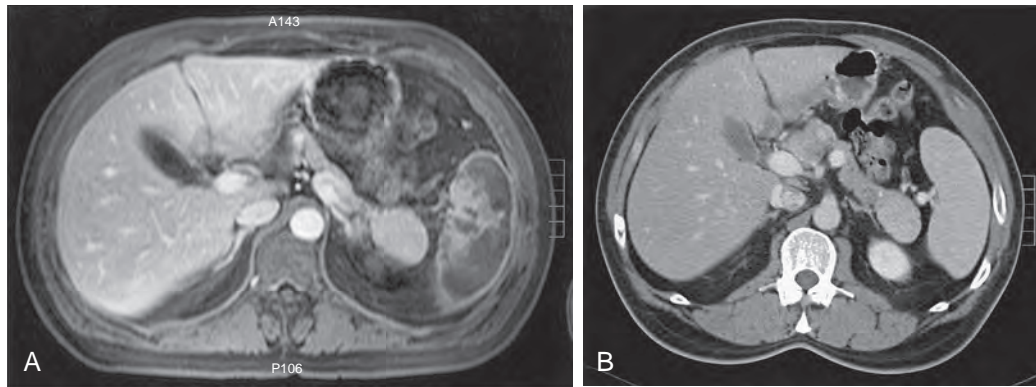


Figure 96-9 Accessory spleen within the tail of the pancreas mimicking a mass. **A.** The contrast-enhanced fat suppression T1-weighted MR image that was obtained because of the patient's left upper quadrant pain reveals areas of infarction of the spleen. There is a well-defined homogeneous mass in the tail of the pancreas displaying signal intensity similar to that of the upper part of the spleen (not shown). **B.** On review of the contrast-enhanced CT scan that was obtained 2 years earlier, the mass has not changed. On a prior study, it was presumed to represent spleen, and a nuclear medicine examination proved the nature of the mass to be accessory spleen in the tail of the pancreas.

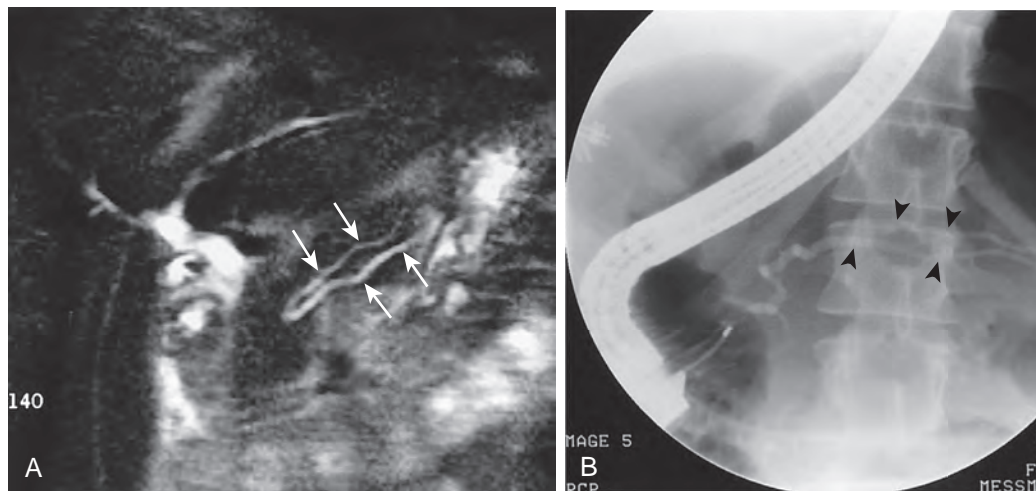


Figure 96-10 Bifid pancreatic duct. **A.** A half-Fourier half-acquisition single-shot turbo spin-echo (HASTE) sequence was used for magnetic resonance cholangiography, which showed a dilated common bile duct due to a distal stone. However, a bifid pancreatic duct (arrows) was incidentally demonstrated. **B.** ERCP clearly demonstrated bifurcation of the pancreatic duct (bifid) throughout the body of the pancreas (arrowheads). (Courtesy Dr. Ann S. Fulcher, Medical College of Virginia, Richmond, VA.)

and tail.²⁹ In a manometer study, patients with pancreas divisum had significantly higher pressure readings of the dorsal duct cannulated through Santorini than of the ventral duct cannulated through Wirsung. The study concluded that in pancreas divisum, there is chronic stasis of pancreatic fluid that, compounded by additional factors such as alcoholism, causes greater viscosity, which increases the risk of pancreatitis.²⁶ Surgical sphincteroplasty of the accessory sphincter has been advocated as an important means of preventing recurrent bouts of pancreatitis in these patients.³⁰⁻³³

Association of pancreatic divisum with pancreatic tumors has been reported.³⁴⁻³⁸ In a limited study, pancreatic tumors were detected in 12.5% of patients with divisum.³⁴ The authors believed that relative stenosis of the minor pancreatic duct and long-standing pancreatic obstruction might be risk factors for development of pancreatic cancer.

There are some other problems associated with divisum, like santorinicele or cystic dilation of the dorsal pancreas at the

minor papillae, that may indicate obstruction at the minor papilla.³⁹ Also, cases of multiple neuroendocrine tumors of the pancreas⁴⁰ and intestinal malrotation⁴¹ have been reported in association with pancreas divisum.

Radiologic Findings

Endoscopic Retrograde Cholangiopancreatography. ERCP is often considered the effective modality for confirming a diagnosis of pancreas divisum.²²⁻²⁴ Often, injection of contrast material into the duct of Wirsung is met with resistance and even pain. However, after opacification, the duct is short and tapered, and acinarization commonly occurs as the endoscopist attempts to fill the "remainder" of the duct. This duct tapers gradually from the orifice, sending branches in the pancreatic head.^{21,42} It must be differentiated from a duct that appears foreshortened secondary to previous trauma, partial pancreatectomy, pseudocyst, or stricture caused by carcinoma or pancreatitis. In these cases, the pancreatic duct typically has an abrupt or irregular

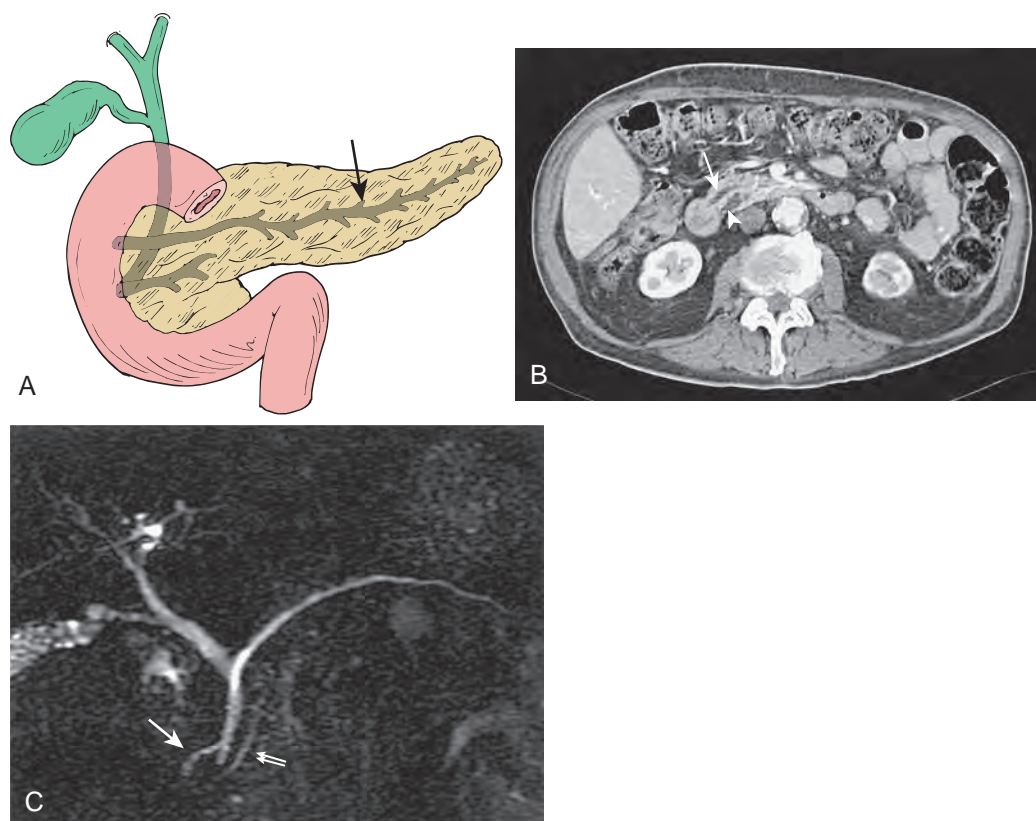


Figure 96-11 Pancreas divisum. **A.** Diagram. Note that the pancreatic head and uncinate process (ventral duct) along with the common bile duct drain into the major papilla, whereas the body and tail (dorsal duct; arrow) drain into the minor papilla. **B.** Axial contrast-enhanced CT study through the head of the pancreas reveals two separate pancreatic ducts draining into the duodenum. Other images prove the separate nature of these ducts, the upper one (arrow) draining the head and body of the pancreas into the minor papilla and the lower one (arrowhead), only from the inferior head and the uncinate process, draining into the major papilla. **C.** Coronal oblique thick-slab MRCP image reveals that the pancreatic duct drains through the minor papilla (single arrow). The duct of Wirsung is also depicted (double arrows) without connection between the two systems. The findings are consistent with complete pancreas divisum. This image was obtained after secretin injection. (Courtesy Dr. Carmen DeJuan, Department of Radiology Hospital Clinic, University of Barcelona, Spain.)

terminus.²¹⁻²³ The duct of Santorini is often not visualized by injection of the major papilla, and if cannulation is successful, the full-length duct of Santorini is seen without communication to the smaller duct. Otherwise, the diagnosis can be made by secretin stimulation and identification of secretions emanating from the minor papilla only. See Chapter 74 for more details.

Linear Array Endoscopic Ultrasonography. Endoscopic ultrasonography (EUS) frequently allows detailed imaging of the pancreatic parenchyma and ductal system. It has been reported that with the use of radial instruments, if the portal vein, common bile duct, and main pancreatic duct could be demonstrated in one image, the diagnosis of pancreatic divisum would be excluded. This is considered an indirect assessment for the evaluation of pancreatic divisum.⁴³ Therefore, with a linear array instrument, if the main pancreatic duct passes from the major papilla to the pancreatic body and tail, or if the duct crosses the border separating the ventral and dorsal anlagen, the diagnosis of pancreatic divisum is excluded. Lai and associates⁴⁴ reported the sensitivity, specificity, and accuracy of this method for diagnosis of pancreas divisum to be 95%, 97%, and 97%, respectively. There are some merits for EUS over magnetic resonance cholangiopancreatography (MRCP), and perhaps ERCP, as it allows direct visualization and fine-needle aspiration biopsy of pancreatic masses that otherwise may lead to the

ductographic phenomenon of pseudodivisum. This could conceivably result from the presence of apparently separate ventral and dorsal ductal systems due to mechanical obstruction near the expected point of connection between these two systems.⁴⁴ Also, EUS seems to be less invasive than ERCP because EUS does not involve pancreatic duct cannulation or injection of contrast material, which is a risk factor for development of iatrogenic pancreatitis.⁴³⁻⁴⁷ Therefore, linear array EUS appears to be a promising, minimally invasive diagnostic imaging modality for the detection of pancreas divisum.^{43,44}

Sonographic Secretin Test. In an attempt to identify patients who will benefit from surgical sphincterotomy, several tests have been proposed to assess the adequacy of the accessory papilla in transmitting pancreatic secretions. In the sonographic secretin test, the main pancreatic duct is sonographically monitored before and after the intravenous administration of secretin (1 unit/kg body weight).⁴⁸ Secretin-induced dilation occurs in 72% of symptomatic patients found to have a stenotic accessory papilla associated with pancreas divisum. The sonographic secretin test is also highly controversial; several authors have demonstrated that dilation of the pancreatic duct can be a normal finding.⁴⁹⁻⁵¹ In addition to surgery, pancreas divisum can be treated by percutaneous dilation and stent placement.^{52,53}

Computed Tomography. Contour abnormalities of the pancreatic head and neck have been identified on CT in some patients with pancreatic divisum.⁵⁴ CT can occasionally suggest this diagnosis when two distinct pancreatic moieties or an unfused ductal system is identified on thin-collimation scans (see Fig. 96-11). The two moieties may cause pancreatic head enlargement or may be separated by a fat cleft. Sometimes, fatty replacement of the dorsal pancreas may delineate it from the ventral moiety.^{30,54} Also, the pancreatic head may be spared from atrophy and pancreatitis affecting the body and tail, which produces a pseudotumor on CT and ultrasound studies.⁵⁵ In alcoholics, isolated ventral pancreatitis may occasionally be observed, which suggests a synergism between the effects of alcohol and bile reflux into the ventral pancreas. The dorsal pancreas is spared this reflux because of the pancreas divisum.⁵⁶ Other ductal anomalies may also produce masses on cross-sectional imaging.^{57,58}

Multidetector CT with high-resolution oblique coronal image reconstruction assists in the depiction of the continuity of pancreatic ducts. The sensitivity and specificity of this method for diagnosis of pancreatic divisum are reported to be 100% and 89%, respectively.⁵⁹

Magnetic Resonance Cholangiopancreatography. Heavily T2-weighted, two-dimensional, fast spin-echo sequences using a body coil can often accurately depict pancreatic ductal anomaly and establish the diagnosis of pancreas divisum.⁶⁰ Gradient sequences using breath hold have been found useful for evaluation of the pancreatic and biliary system. MRCP is superior to ERCP for visualizing the pancreatic ducts, especially with the use of half-Fourier acquisition single-shot turbo spin-echo (HASTE) sequence.⁶¹ However, MRCP with single-shot rapid acquisition with relaxation enhancement may be superior to HASTE for increasing pancreatic duct conspicuity.⁶²

When T1-weighted sequences with fat suppression are performed,^{63,64} MRCP allows visualization of not only the pancreatic ducts but also the pancreatic parenchyma around the duodenum. Indeed, MRCP may be able to replace ERCP in the diagnosis of pancreas divisum.

Secretin-stimulated MRCP has been used in the diagnosis of santorinicele or cystic dilation of dorsal pancreas at the minor papillae and also for pancreas divisum^{39,65,66} (see Fig. 96-11). See Chapter 75 for more detail concerning MRCP.

ANNULAR AND SEMIANNULAR PANCREAS

Annular pancreas is a rare congenital anomaly occurring in 1 of every 12,000 to 15,000 live births. In this anomaly, the

annulus is often a flat band of pancreatic tissue completely encircling the second portion of the duodenum^{21,23} (Figs. 96-12 and 96-13). Unusual locations of annular pancreas have also been reported to be around the third portion of the duodenum.⁶⁷

In normal pancreatic development, the ventral anlage develops as two separate buds from the hepatic diverticulum. The left ventral bud atrophies, and the right ventral bud persists to form the head and uncinate process. The ventral anlage undergoes 180-degree counterclockwise rotation while the duodenum undergoes 90-degree clockwise rotation, so that the ventral anlage occupies a position contiguous with the dorsal anlage, medial to the duodenum. There are three theories concerning the formation of the annular pancreas: hypertrophy of both the dorsal and the ventral ducts, resulting in a complete ring; adherence of the ventral duct to the duodenum before rotation; and hypertrophy or adherence of the left bud of a paired ventral primordium.⁶⁸

Clinical Findings

Annular pancreas is an uncommon congenital anomaly that may be manifested clinically in the neonate (52%) or may be asymptomatic until adulthood (48%). This disorder is not usually manifested clinically until the third to fifth decade of life⁶⁹⁻⁷¹ or even occasionally later.⁷²

Symptoms are usually related to duodenal obstruction. Neonates present with vomiting on the first day of life, and there often is an antecedent history of polyhydramnios and other manifestation of fetal gastrointestinal tract obstruction.^{23,42,73,74} A number of other anomalies, such as intestinal malrotation, duodenal atresias of various forms, and cardiac anomalies, are often present as well.

Annular pancreas may be quiescent and not cause symptoms until adulthood. Kiernan and associates⁷⁵ reviewed 266 patients with symptoms and found that 48% were adults. In older children and adults, nausea, vomiting, and epigastric pain are the chief presenting complaints. The incidence of associated gastric and duodenal ulcers ranges from 26% to 48%, and pancreatitis develops in 15% to 30% of patients. The obstruction of the duodenum in these patients is apparently not sufficient to cause symptoms until there is supervening peptic ulcer disease or pancreatitis.⁷⁶⁻⁷⁸ There are reports of extrahepatic biliary obstruction due to annular pancreas.^{3,5}

In a 10-year review of annular pancreas in children, Jimenez and colleagues⁷⁹ found that among 16 patients, 12 (75%) presented within the first week of life, 5 (31%) had chromosomal anomalies, and 6 had other major congenital problems. In another review of seven cases with annular pancreas, four patients (42.8%) had associated anomalies, including intestinal

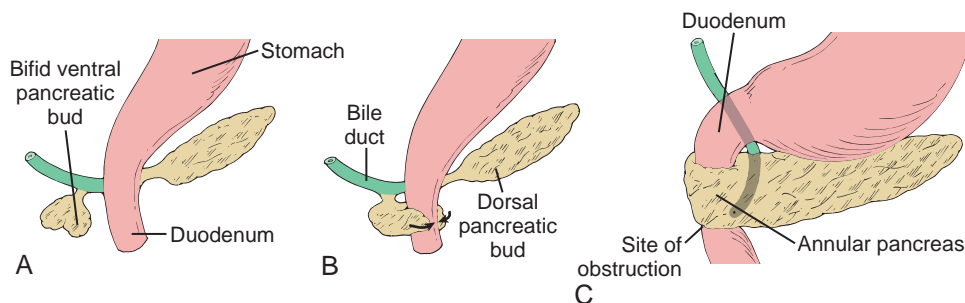


Figure 96-12 Annular pancreas. A and B. Drawings illustrate the probable embryologic basis of annular pancreas. C. An annular pancreas encircles the duodenum. (A and B from Moore KL: *The Developing Human*, 4th ed. Philadelphia, WB Saunders, 1988.)

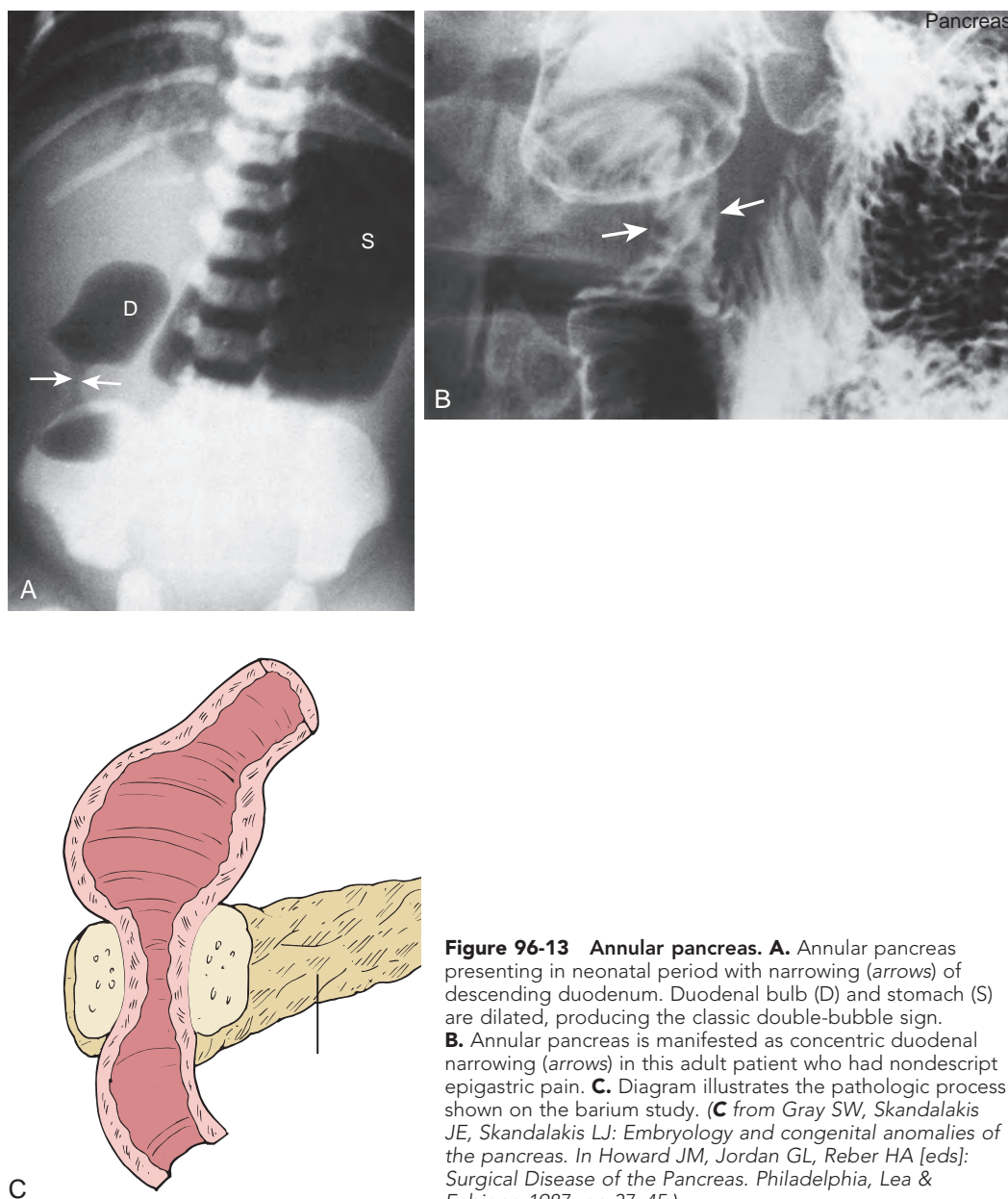


Figure 96-13 Annular pancreas. **A.** Annular pancreas presenting in neonatal period with narrowing (arrows) of descending duodenum. Duodenal bulb (D) and stomach (S) are dilated, producing the classic double-bubble sign. **B.** Annular pancreas is manifested as concentric duodenal narrowing (arrows) in this adult patient who had nondescript epigastric pain. **C.** Diagram illustrates the pathologic process shown on the barium study. (C from Gray SW, Skandalakis JE, Skandalakis LJ: *Embryology and congenital anomalies of the pancreas*. In Howard JM, Jordan GL, Reber HA [eds]: *Surgical Disease of the Pancreas*. Philadelphia, Lea & Febiger, 1987, pp 37–45.)

malrotation (42.8%), intrinsic duodenal obstruction (28.5%), trisomy 21 karyotype (14.2%), cardiac malformation (14.2%), and Meckel's diverticulum (14.2%).⁸⁰ The authors concluded that annular pancreas is most commonly associated with intestinal malrotation.

In the pediatric population, symptomatic annular pancreas is best treated by a bypass procedure such as gastrojejunostomy or duodenojejunostomy.^{17,48} However, in adults, a variety of surgical as well as interventional endoscopic procedures are used therapeutically.

Pancreatic malignant disease in the setting of annular pancreas has been reported, most often arising from the ventral bud.^{81,82} However, involvement of the dorsal bud has also been reported.^{83,84} Evaluation of the pancreas for malignant disease is recommended in cases of annular pancreas presenting with obstructive jaundice.^{85,86}

Radiologic Findings

Plain Radiography and Barium Studies. Pediatric patients with annular pancreas often have diagnostic findings on plain radiographs with the double-bubble sign (see Fig. 96-13A); the proximal bubble is caused by gastric distention and the distal bubble by a dilated duodenal bulb.^{23,25,75}

The radiographic findings on upper gastrointestinal barium studies are often characteristic and are best demonstrated when the duodenum is maximally distended. Stenosis is demonstrated in the periampullary region associated with an extrinsic eccentric defect on the medial margin of the second portion of the duodenum (Fig. 96-13B). The mucosa is intact unless there is associated peptic ulcer.⁸⁷ Peptic ulcer disease is common, so when an ulcer is seen in the periampullary duodenum in an adult, the diagnosis of annular

pancreas as well as Zollinger-Ellison syndrome should be considered.^{23,25}

Endoscopic Retrograde Cholangiopancreatography. Diagnosis of annular pancreas is most commonly suggested by ERCP, which shows typical features in about 85% of cases. In these patients, a normally located main pancreatic duct is seen in the body and tail that communicates with the small duct of the pancreatic head, which encircles the duodenum. This latter duct is seen originating on the right anterior surface of the duodenum, passing posteriorly around the duodenum and entering the main pancreatic or common bile duct near the ampulla. In some patients, biliary obstruction may be seen as well.

Computed Tomography. Findings on CT are often nonspecific, showing enlargement of the pancreatic head that has a central region of high attenuation representing contrast material within the narrowed duodenal segment. If the duodenum is not sufficiently opacified, only pancreatic head enlargement may be noted.⁸⁸ Other CT findings include apparent circumferential thickening of the duodenal wall in association with an enlarged pancreatic head. A peninsular protrusion of pancreatic tissue may also be seen in the duodenal lumen.^{89,90} Review of continuous images on a monitor provides the opportunity to follow the duodenum from above as it enters the encircling pancreatic head and then exits inferiorly. On occasion, the duodenum may not be completely encircled with pancreatic tissue. This anomaly is called semiannular pancreas. Ueki and colleagues⁹¹ reported that three-dimensional CT pancreatography may be useful in clarifying embryogenesis of annular pancreas.

Ultrasound. Nonspecific enlargement of the pancreatic head is the major sonographic abnormality seen in annular pancreas.⁹⁰ EUS is more accurate in making the diagnosis.⁹²

Magnetic Resonance Imaging. Fat-suppressed T1-weighted sequence may show a normal-appearing pancreatic tissue encircling the duodenum.⁹³ MRI as well as CT (Fig. 96-14) may be used as a problem-solving technique to supplement the conventional studies.^{94,95} Because CT may show only an enlarged pancreatic head, MRI is able to clearly discriminate the pancreas from the duodenum.⁹⁶

Angiography. Celiac angiography may demonstrate an anomalous branch from the posterior pancreaticoduodenal artery that courses in a right and inferior direction to supply the annular moiety.^{23,42}

ECTOPIC PANCREATIC TISSUE

Heterotopic pancreas in which glandular acini ducts and well-differentiated islets can be recognized microscopically is rare. It is seen in organs derived, like the normal pancreas, from entoderm. Heterotopic pancreas is the result of heteroplastic differentiation of parts of embryonic entoderm that do not normally produce pancreatic tissue.¹¹ Although the embryonic origins of the pancreas and liver are close anatomically, ectopic pancreas is much more common than heterotopic liver.^{1,10,97,98}

These ectopic rests of pancreatic tissue most commonly occur in the gastric antrum (25.5%) or proximal portion of the duodenum (27.7%). Less frequent sites include jejunum (15.9%), ileum, Meckel's diverticulum, colon, appendix, mesentery, omentum, liver, gallbladder, spleen, bile ducts, esophagus, mediastinal cyst,⁹⁹ fallopian tube, and bronchoesophageal fistula.^{19,22,42,100-103} When it is present in the walls of the duodenum and stomach, heterotopic pancreas is usually composed of normal pancreatic tissue, including islet cells, and a small pancreatic duct. Islet cells are usually absent at other sites. The ectopic pancreatic tissue usually lies submucosally (73%), although it can be located in the muscularis mucosae or on the serosal surface of the gut.^{104,105} Formation of cyst in association with duodenal heterotopic pancreas in pancreas divisum has also been reported.^{104,105}

Ectopic pancreatic tissue is functional and subject to the same inflammatory and neoplastic disorders that afflict the normal pancreas. The majority of cases, however, are asymptomatic and found incidentally.¹⁰³⁻¹⁰⁹ Indeed, many reported cases of pancreatic heterotopia in the duodenum are found incidentally during peptic ulcer surgery. Also, pancreatic tissue was found in the duodenum by careful sectioning in nearly 14% of autopsies, and pancreas-like tissue is also found in 14.1% of postmortem studies of the biliary system. When it is symptomatic, ectopic pancreas may simulate duodenal ulcer, gallbladder disease, or even appendicitis.^{105,108} In the stomach, it may be a component of tumor-like lesions that cause symptoms such as pyloric obstruction.¹⁰⁷ Perivaterian pancreatic tissue may cause

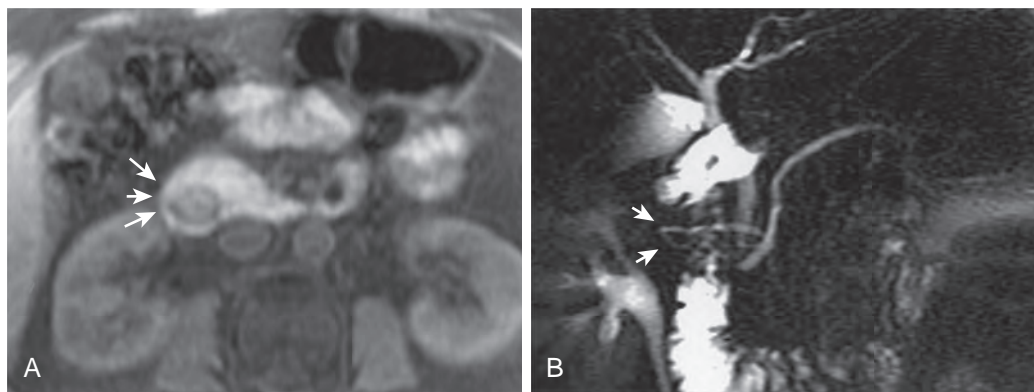


Figure 96-14 Annular pancreas: MR features. **A.** Axial fat saturation T1-weighted image shows the duodenum surrounded by pancreatic tissue (arrows). **B.** Coronal oblique thick-slab MRCP image demonstrates the duct of the annular pancreas (arrows) that forms a complete loop around the duodenum. This examination was performed after secretin administration. (Courtesy Dr. Carmen DeJuan, Department of Radiology Hospital Clinic, University of Barcelona, Spain.)

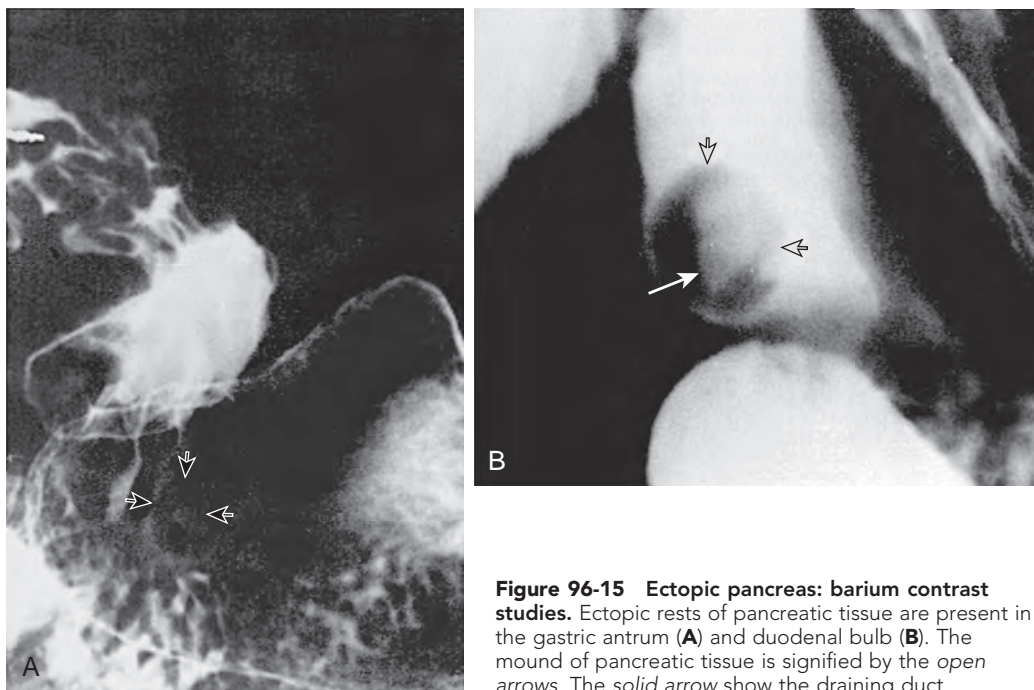


Figure 96-15 Ectopic pancreas: barium contrast studies. Ectopic rests of pancreatic tissue are present in the gastric antrum (**A**) and duodenal bulb (**B**). The mound of pancreatic tissue is signified by the open arrows. The solid arrow shows the draining duct.

biliary obstruction, and if the ectopic tissue is located more distally, it may serve as a lead point for intussusception.¹¹⁰ Symptomatic lesions tend to be larger than 1.5 cm, and malignant tumor has been reported to arise from these tissue rests.^{107,109}

No specific treatment is necessary in this disorder unless the ectopic pancreatic tissue is causing symptoms, such as obstruction or hemorrhage.

Radiologic Findings

Ectopic pancreas characteristically appears as a broad-based, smooth, extramucosal or intramural lesion either along the greater curvature of the gastric antrum or in the proximal duodenum (Fig. 96-15). A small collection of barium appearing as a central niche or umbilication is diagnostic and present in 45% of cases. This represents the orifice of the rudimentary duct into which the ectopic pancreas empties.⁹⁵ This pit may be as large as 5 mm in diameter and 10 mm in length. If this feature is absent, the lesion cannot be differentiated from other submucosal tumors.^{22,23,42} The differential diagnosis includes peptic ulcer disease, gastric polyp, Brunner gland adenoma, gastrointestinal stromal tumor, lymphoma, and metastasis to the stomach such as malignant melanoma or Kaposi's sarcoma.¹¹¹ Rarely, large intramural cystic collections can be seen in the stomach and duodenum on CT scans.¹¹²

AGENESIS, HYPOPLASIA, AND HYPERPLASIA OF THE PANCREAS

Agenesis of the pancreas is rare and typically incompatible with life. A causal relationship with intrauterine growth retardation has been noted and is presumed to be due to the lack of fetal insulin necessary for development.¹¹³ Partial pancreatic agenesis and hypoplasia are also rare; however, cases of agenesis of the

dorsal pancreas have been reported¹¹⁴ along with malrotation. Abnormal rotation of the intestine may interrupt the normal rotation of the pancreatic primordium, with malpositioning of the pancreatic buds resulting in abnormal morphology of the uncinate process.¹¹⁵

DUCTAL ABNORMALITIES

The single main pancreatic duct normally connects with the accessory duct of Santorini, and then they open in conjunction with the common bile duct at the ampulla of Vater. This arrangement is seen in 60% to 70% of normal individuals.^{116,117} The common variations of pancreatic ductal anatomy include junction of the ventral duct and common bile duct at the ampulla with complete regression of the dorsal duct (see Fig. 96-2) (40%-50%); junction of the ventral and common bile ducts at the ampulla but with persistence of the dorsal duct (35%); persistence of both the dorsal and the ventral ducts without communication, or pancreas divisum (5%-10%); common channel with a retroduct entering the common duct 5 to 15 mm from the ampulla (5%-10%); and separate entrance of the ventral duct into the duodenum with variable persistence of the dorsal duct (5%).¹¹⁶⁻¹¹⁹ Variations in ductal configurations include a sigmoid configuration of the duct and descending course of the duct. One may rarely encounter a loop at the point of the embryologic fusion of the ducts.

CONGENITAL CYSTS

The cystic lesions that are congenital and not related to cystic fibrosis of the pancreas are rare. Such cysts do not cause any symptoms, have a thin fibrosed wall, and are lined by a columnar or cubicle type of epithelium. They are not associated with cysts in any other organs.¹¹⁸⁻¹²²

REFERENCES

- Lee NK, Kim S, Jeon TY, et al: Complications of congenital and developmental abnormalities of the gastrointestinal tract in adolescents and adults: Evaluation with multimodality imaging. *Radiographics* 30:1489–1507, 2010.
- Tirkes T, Menias CO, Sandrasegaran K: MR imaging techniques for pancreas. *Radiol Clin North Am* 50:379–393, 2012.
- Etienne D, John A, Menias CO, et al: Annular pancreas: A review of its molecular embryology, genetic basis and clinical considerations. *Ann Anat* 194:422–428, 2012.
- Torra R, Alos L, Ramos J, et al: Renal-hepatic-pancreatic dysplasia: An autosomal recessive malformation. *J Med Genet* 33:409–412, 1996.
- Tolia V, Rao R, Klein M: Annular pancreas. *J Pediatr* 131:14–15, 1997.
- Skandalakis JE, Gray SW, Rowe JS, et al: Anatomic complications of pancreatic surgery. *Contemp Surg* 15:17–36, 1979.
- Faerber EN, Friedman AC, Dabezies MA: Anomalies and congenital disorders. In Feldman AC, Dachman AH, editors: *Radiology of the Liver, Biliary Tract, and Pancreas*, St. Louis, 1994, Mosby, pp 743–762.
- May G, Gardiner R: Clinical Imaging of the Pancreas, New York, 1987, Raven, pp 1–10.
- Schoeffl R, Haefner M, Poetzi R, et al: A case of duplication of the main pancreatic duct. *Endoscopy* 28:401–402, 1996.
- Rutter WJ: Development of the endocrine and exocrine pancreas. In Fitzgerald PJ, Morrison AB, editors: *The Pancreas*, Baltimore, 1980, Williams & Wilkins, pp 30–38.
- Kloppel G, Heitz PU: Pancreatic pathology. In Kloppel G, Heitz PU, editors: *Pancreatic Diseases*, New York, 1984, Churchill Livingstone, pp 225–232.
- Kozu T, Suda K, Toki F: Pancreatic development and anatomical variation. *Gastrointest Endosc Clin North Am* 5:1–30, 1995.
- Ross BA, Jeffrey RB, Jr, Mindelsun RE: Normal variations in the lateral contour of the head and neck of the pancreas mimicking neoplasm: Evaluation with dual-phase helical CT. *AJR Am J Roentgenol* 166:799–801, 1996.
- Dhar A, Chawla Y, Dhiman RK, et al: Bifid pancreas: A case report. *Trop Gastroenterol* 18:75–77, 1997.
- Shirkhoda A: Diagnostic pitfalls in abdominal CT. *Radiographics* 11:969–1002, 1991.
- Kreel L, Haertel M, Katz D: Computed tomography of the normal pancreas. *J Comput Assist Tomogr* 1:290–299, 1977.
- Halpert RD, Shabot JM, Heare BR, et al: The bifid pancreas: A rare anatomical variation. *Gastrointest Endosc* 36:60–61, 1990.
- Phillip J, Koch H, Classen M: Variation and anomalies of the papilla of Vater, the pancreas and the biliary system. *Endoscopy* 6:70–77, 1974.
- Kleitsch WB: Anatomy of the pancreas: A study with special reference to the duct system. *Arch Surg* 71:795–802, 1955.
- Stringer DA: *Pediatric Gastrointestinal Imaging*, Toronto, 1989, BC Decker, pp 585–610.
- DiMaggio MJ, Wamsteker EJ: Pancreas divisum. *Curr Gastroenterol Rep* 13:150–156, 2011.
- May G, Gardiner R: *Clinical Imaging of the Pancreas*, New York, 1987, Raven, pp 50–57.
- Schneck CD, Dabezies MA, Friedman AC: Embryology, histology, gross anatomy, and normal imaging of the pancreas. In Friedman AC, Dachman AH, editors: *Radiology of the Liver, Biliary Tract, and Pancreas*, St. Louis, 1994, Mosby, pp 715–742.
- Uomo G, Manes G, D'Anna L, et al: Fusion and duplication variants of pancreatic duct system. Clinical and pancreatographic evaluation. *Int J Pancreat* 17:23–28, 1995.
- Delhaye M, Engelholm L, Cremer M: Pancreas divisum: Congenital anatomy variant or anomaly? Contribution of endoscopic retrograde dorsal pancreatography. *Gastroenterology* 89:951–958, 1985.
- Staritz M, Hutteroth T, Meyer zum Buschenfelde KH: Pancreas divisum and pancreatitis. *Gastroenterology* 91:525–526, 1986.
- Blair AJ, Russel CG, Cotton PB: Resection for pancreatitis in patients with pancreas divisum. *Ann Surg* 200:590–594, 1984.
- Muzaffar AR, Moyer MS, Dobbins J, et al: Pancreas divisum in a family with hereditary pancreatitis. *J Clin Gastroenterol* 22:16–20, 1996.
- Cotton PB: Pancreas divisum—culprit or curiosity? *Gastroenterology* 89:1431–1435, 1985.
- Lehman GA, Sherman S: Diagnosis and therapy of pancreas divisum. *Gastrointest Endosc Clin North Am* 8:55–77, 1998.
- Lehman GA, Sherman S, Nisi R, et al: Pancreas divisum: Results of minor papilla sphincterotomy. *Gastrointest Endosc* 39:1–8, 1993.
- Warshaw AL, Simeone JF, Schapiro RH, et al: Evaluation and treatment of the dominant dorsal duct syndrome (pancreas divisum redefined). *Am J Surg* 159:59–66, 1990.
- Lehman GA, Sherman S: Pancreas divisum: Diagnosis and therapy. In Jacobson IM, editor: *ERCP and Its Applications*, Philadelphia, 1998, Lippincott-Raven, pp 181–192.
- Kamisawa T, Yoshiike M, Egawa N, et al: Pancreatic tumor associated with pancreas divisum. *J Gastroenterol Hepatol* 20:915, 2005.
- Martin Fernandez J, Ratia T, Gutierrez A, et al: Intraductal pancreatic carcinoma associated with pancreas divisum. *Rev Esp Enferm Dig* 95:358–363, 2003.
- Yarze JC, Chase MP, Herlihy KJ, et al: Pancreas divisum and intraductal papillary mucinous tumor occurring simultaneously in a patient presenting with recurrent acute pancreatitis. *Dig Dis Sci* 48:915, 2003.
- Masatsugu T, Yamaguchi K, Chijiwa K, et al: Serous cystadenoma of the pancreas associated with pancreas divisum. *J Gastroenterol* 37:669–673, 2002.
- Outtas O, Barthet M, De Troyer J, et al: Pancreatic panniculitis with intraductal carcinoid tumor of the pancreas divisum. *Ann Dermatol Venereol* 131:466–469, 2004.
- Peterson MS, Slivka A: Santorinicele in pancreas divisum: Diagnosis with secretin-stimulated magnetic resonance pancreatography. *Abdom Imaging* 26:260–263, 2001.
- Raffel A, Engers R, Cupisti K, et al: Multiple neuroendocrine tumors of the pancreas associated with pancreas divisum. *Eur J Endocrinol* 150:837–840, 2004.
- Bloom C, Hickey N, Haroun J, et al: Pancreatic divisum and intestinal nonrotation diagnosed with magnetic resonance imaging: Case report. *Can Assoc Radiol J* 50:310–313, 1999.
- Freeny PC, Lawson TL: *Radiology of the Pancreas*, New York, 1982, Springer-Verlag, pp 142–168.
- Bhutani MS, Hoffman BJ, Hawes RH: Diagnosis of pancreas divisum by endoscopic ultrasonography. *Endoscopy* 31:167–169, 1999.
- Lai R, Freeman ML, Cass OW, et al: Accurate diagnosis of pancreas divisum by linear-array endoscopic ultrasonography. *Endoscopy* 36:705–709, 2004.
- Wang DB, Yu J, Fulcher AS, Turner MA: Pancreatitis in patients with pancreas divisum: Imaging features at MRI and MRCP. *World J Gastroenterol* 19:4907–4916, 2013.
- Gottlieb K, Sherman S: ERCP and endoscopic biliary sphincterotomy-induced pancreatitis. *Gastrointest Endosc Clin North Am* 8:87–114, 1998.
- Tak WY, Kim DH, Kim H, et al: Risk factors for post-ERCP pancreatitis: A prospective study [abstract]. *Gastroenterology* 118:A206, 2000.
- Wardlaw AL, Simeone J, Schapiro RH, et al: Objective evaluation of ampullary stenosis with ultrasonography and pancreatic stimulation. *Am J Surg* 154:65–72, 1985.
- Barbara L, Bolondi L: Functional ultrasonography in gastroenterology. *Ultrasound Q* 6:181–227, 1988.
- Anis M, Mortelet K: Role of secretin-enhanced magnetic resonance cholangiopancreatography in the evaluation of patients following pancreatojejunostomy. *J Clin Imaging Sci* 3:7, 2013.
- Wathle GK, Tjora E, Ersland L, et al: Assessment of exocrine pancreatic function by secretin-stimulated magnetic resonance cholangiopancreatography and diffusion-weighted imaging in healthy controls. *J Magn Reson Imaging* 39:448–454, 2014.
- Brugge WR: Endoscopic approach to the diagnosis and treatment of pancreatic disease. *Curr Opin Gastroenterol* 29:559–565, 2013.
- Soehendra N, Kempeneers I, Nam VCH, et al: Endoscopic dilation and papillotomy of the accessory papilla and internal drainage in pancreas divisum. *Gastrointest Endosc* 18:129–132, 1986.
- Zeman RK, McVay LV, Silverman PM, et al: Pancreas divisum: Thin section CT. *Radiology* 169:395–398, 1988.
- Silverman PM, McVay L, Zeman RK, et al: Pancreatic pseudotumor in pancreas divisum: CT characteristics. *J Comput Assist Tomogr* 13:140–141, 1989.
- Birnberg DE, Carr MF, Premkumar A, et al: Isolated ventral pancreatitis in an alcoholic with pancreas divisum. *Gastrointest Radiol* 13:323–326, 1988.
- Halpert RD, Shabot JM, Heare BR, et al: The bifid pancreas: A rare anatomical variation. *Gastrointest Endosc* 36:60–61, 1990.
- Siegel JH, Yatto RP, Vender RJ: Anomalous pancreatic ducts causing “pseudomass” of the pancreas. *J Clin Gastroenterol* 5:33–36, 1983.
- Itoh S, Takada A, Satake H, et al: Diagnostic value of multislice computed tomography for pancreas divisum: Assessment with oblique coronal reconstruction images. *J Comput Assist Tomogr* 29:452–460, 2005.
- Rustagi T, Njei B: Magnetic resonance cholangiopancreatography in the diagnosis of pancreas divisum. *Pancreas* 43:823–828, 2014.
- Clores MJ, Thosani A, Buscaglia JM: Multidisciplinary diagnostic and therapeutic approaches to pancreatic cystic lesions. *J Multidiscip Healthc* 7:81–91, 2014.

62. Morrin MM, Farrell RJ, McEntee G, et al: MR cholangiopancreatography of pancreaticobiliary diseases: Comparison of single-shot RARE and multislice HASTE sequences. *Clin Radiol* 55:866–873, 2000.
63. Sandrasegaran K, Patel A, Fogel EL, et al: Annular pancreas in adults. *AJR Am J Roentgenol* 193:455–460, 2009.
64. Hidaka T, Hirohashi S, Uchida H, et al: Annular pancreas diagnosed by single-shot MR cholangiopancreatography. *Magn Reson Imaging* 16: 441–444, 1998.
65. Manfredi R, Costamagna G, Brizi MG, et al: Pancreas divisum and “santorinicele”: Diagnosis with dynamic MR cholangiopancreatography with secretin stimulation. *Radiology* 217: 403–408, 2000.
66. Costamagna G, Ingrosso M, Tringali A, et al: Santorinicele and recurrent acute pancreatitis in pancreas divisum: Diagnosis with dynamic secretin-stimulated magnetic resonance pancreatography and endoscopic treatment. *Gastrointest Endosc* 52:262–267, 2000.
67. Rinnab L, Schulz K, Siech M: A rare localization of annular pancreas at the pars horizontalis duodeni. *Zentralbl Chir* 129:513–516, 2004.
68. Gray SW, Skandalakini JE: Embryology for Surgeons: The Embryological Basis for the Treatment of Congenital Defects, Philadelphia, 1972, WB Saunders, pp 263–282.
69. Ben-David K, Falcone RA, Matthews JB: Diffuse pancreatic adenocarcinoma identified in an adult with annular pancreas. *J Gastrointest Surg* 8:565–568, 2004.
70. Hamm M, Rottger P, Fiedler C: Pancreas annulare as a rare differential diagnosis of duodenal stenosis in adulthood. *Langenbecks Arch Chir* 382:307–310, 1997.
71. Wani AA, Maqsood S, Lala P, Wani S: Annular pancreas in adults: A report of two cases and review of literature. *JOP* 14:277–279, 2013.
72. Whittingham-Jones PM, Riaz AA, Clayton G, et al: Annular pancreas—a rare cause of gastric obstruction in an 82-year-old patient. *Ann R Coll Surg Engl* 87:13–15, 2005.
73. Johnston DWB: Annular pancreas: A new classification and clinical observations. *Can J Surg* 21:241–244, 1978.
74. Stringer DA: Pediatric Gastrointestinal Imaging, Toronto, 1989, BC Decker, pp 235–362.
75. Kiernan PD, ReMine SG, Kiernan PC, et al: Annular pancreas. Mayo Clinic experience from 1957 to 1976 with review of the literature. *Arch Surg* 115:46–50, 1980.
76. Godil A, McCracken GA: Images in clinical medicine. Annular pancreas. *N Engl J Med* 336:1794, 1997.
77. Shenoy KR, Pai US: Annular pancreas in adults—diagnostic difficulties. *J Indian Med Assoc* 94:242–243, 1996.
78. Gilroy JA, Adams AB: Annular pancreas. *Radiology* 75:568–571, 1960.
79. Jimenez JC, Emil S, Podnos Y, Nguyen N: Annular pancreas in children: A recent decade's experience. *J Pediatr Surg* 39:1654–1657, 2004.
80. Sencan A, Mir E, Gunsar C, Alkora B: Symptomatic annular pancreas in newborns. *Med Sci Monit* 8:CR434–CR437, 2002.
81. Kosai YS, Higashi IT, Setoguchi T: Annular pancreas associated with pancreatolithiasis: A case report. *Hepatogastroenterology* 46:527–531, 1999.
82. Shan Y, Sy E, Lin P: Annular pancreas with obstructive jaundice: Beware of underlying neoplasm. *Pancreas* 25:314–316, 2002.
83. Maker V, Gerzenshtein J, Lerner R: Annular pancreas in the adult: Two case reports and review of more than a century of literature. *Am Surg* 69:405–410, 2003.
84. Ben-David K, Falcone RA, Matthews JB: Diffuse pancreatic adenocarcinoma identified in an adult with annular pancreas. *J Gastrointest Surg* 8:565–568, 2004.
85. Shan YS, Sy ED, Lin PW: Annular pancreas with obstructive jaundice: Beware of underlying neoplasm. *Pancreas* 25:314–316, 2002.
86. Urayama S, Kozarek R, Ball T, et al: Presentation and treatment of annular pancreas in an adult population. *Am J Gastroenterol* 90:995–999, 1995.
87. Hamm M, Rottger P, Fiedler C: Pancreas annulare as a rare differential diagnosis of duodenal stenosis in adulthood. *Langenbecks Arch Chir* 382:307–310, 1995.
88. Inamoto K, Ishikawa Y, Itoh N: CT demonstration of annular pancreas: Case report. *Gastrointest Radiol* 8:143–145, 1983.
89. Nguyen KT, Pace R, Groll A: CT appearance of annular pancreas: A case report. *J Can Assoc Radiol* 40:322–323, 1989.
90. Orr LA, Powell RW, Melhem RE: Sonographic demonstration of annular pancreas in the newborn. *J Ultrasound Med* 11:373–375, 1992.
91. Ueki T, Yao T, Beppu T, et al: Three-dimensional computed tomography pancreatography of an annular pancreas with special reference to embryogenesis. *Pancreas* 32:426–429, 2006.
92. Papachristou GI, Topazian MD, Gleeson FC, et al: EUS features of annular pancreas. *Gastrointest Endosc* 65:340–344, 2007.
93. Desai MB, Mitchell DG, Munoz SJ: Asymptomatic annular pancreas: Detection by magnetic resonance imaging. *Magn Reson Imaging* 12:683–685, 1994.
94. Reinhart RD, Brown JJ, Foglia RP, et al: MR imaging of annular pancreas. *Abdom Imaging* 19:301–303, 1994.
95. Lecesne R, Stein L, Reinhold C, et al: MR cholangiopancreatography of annular pancreas. *J Comput Assist Tomogr* 22:85–86, 1998.
96. Mortelet KJ, Rocha TC, Streeter JL, et al: Multimodality imaging of pancreatic and biliary congenital anomalies. *Radiographics* 26:715–731, 2006.
97. Yamagiwa I, Obata K, Ouchi T, et al: Heterotopic pancreas of the esophagus associated with a rare type of esophageal atresia. *Ann Thorac Surg* 65:1143–1144, 1998.
98. Eklof O, Lassrich A, Stanley P, et al: Ectopic pancreas. *Pediatr Radiol* 1:24–27, 1973.
99. Bonnard A, Lagausie P, Malbezin S, et al: Mediastinal pancreatic pseudocyst in a child. A thoracoscopic approach. *Surg Endosc* 15:760, 2001.
100. Ben-Baruch D, Sandbank Y, Wolloch Y: Heterotopic pancreatic tissue in the gallbladder. *Acta Chir Scand* 152:557–558, 1986.
101. Carr MJT, Deiranya AK, Judd PA: Mediastinal cyst containing mural pancreatic tissue. *Thorax* 32:512–516, 1977.
102. Eklof O: Accessory pancreas in the stomach and duodenum: Clinical features, diagnosis, and therapy. *Acta Chir Scand* 121:19–20, 1961.
103. Qizibash AH: Acute pancreatitis occurring in heterotopic pancreatic tissue in the gallbladder. *Can J Surg* 19:413–414, 1976.
104. Mizuta Y, Takeshima F, Yamao T, et al: Cyst formation of duodenal heterotopic pancreas accompanied by pancreas divisum. *Dig Dis Sci* 49:1412–1417, 2004.
105. Ravitch MM: Anomalies of the pancreas. In Carey LC, editor: *The Pancreas*, St. Louis, 1973, CV Mosby, pp 404–416.
106. Yuan Z, Chen J, Zheng Q, et al: Heterotopic pancreas in the gastrointestinal tract. *World J Gastroenterol* 15:3701–3703, 2009.
107. Bedossa P, Millat B, Zrihen E, et al: Adenocarcinoma in heterotopic gastric pancreas. *Gastroenterol Clin Biol* 15:79–82, 1991.
108. Trifan A, Tărcoveanu E, Danciu M, et al: Gastric heterotopic pancreas: An unusual case and review of the literature. *J Gastrointest Liver Dis* 21:209–212, 2012.
109. Ura H, Denno R, Hirata K, et al: Carcinoma arising from ectopic pancreas in the stomach: Endosonographic detection of malignant change. *J Clin Ultrasound* 26:265–268, 1998.
110. Mito T, Nakazawa S, Yoshino J, et al: A case of adult intussusception due to the inverted Meckel's diverticulum with ectopic pancreas which showed characteristic findings of MRI. *Nippon Shokakibyo Gakkai Zasshi* 95:326–332, 1998.
111. Burke GW, Binder SC, Barron AM, et al: Heterotopic pancreas: Gastric outlet obstruction secondary to pancreatitis and pancreatic pseudocyst. *Am J Gastroenterol* 84:52–55, 1989.
112. Claudon M, Verain AL, Bigard MA, et al: Cyst formation in gastric heterotopic pancreas: Report of two cases. *Radiology* 169:659–660, 1988.
113. Lemons JA, Ridenour R, Orsini EN: Congenital absence of the pancreas and intrauterine growth retardation. *Pediatrics* 64:255–257, 1979.
114. Deignan RW, Nizzero A, Malone DE: Case report: Agenesis of the dorsal pancreas: A cause of diagnostic error on abdominal sonography. *Clin Radiol* 51:145–147, 1996.
115. Inoue Y, Nakamura H: Aplasia or hypoplasia of the pancreatic uncinate process: Comparison in patients with and patients without intestinal nonrotation. *Radiology* 205:531–533, 1973.
116. Berman LG, Prior JT, Abramow SM, et al: A study of the pancreatic duct system in man by the use of vinyl acetate casts of postmortem preparations. *Surg Gynecol Obstet* 110:391–403, 1960.
117. Grendell JH: Embryology, anatomy, and anomalies of the pancreas. In Haubrich WS, Schaffner F, Berk JE, editors: *Bockus Gastroenterology*, ed 5, Philadelphia, 1995, WB Saunders, pp 2815–2820.
118. Taylor AJ, Bohorvosh AG: Interpretation of ERCP with Associated Digital Imaging Correlation, Philadelphia, 1997, Lippincott-Raven, pp 207–218.
119. Fulcher AS, Turner MA: MR pancreatography: A useful tool for evaluating pancreatic disorders. *Radiographics* 19:5–24, 1999.
120. Miller JC, Harisinghani M, Richter JM, et al: Magnetic resonance cholangiopancreatography. *J Am Coll Radiol* 4:133–136, 2007.
121. Coté GA, Smith J, Sherman S, et al: Technologies for imaging the normal and diseased pancreas. *Gastroenterology* 144:1262–1271, 2013.
122. O'Neill E, Hammond N, Miller FH: MR imaging of the pancreas. *Radiol Clin North Am* 52:757–777, 2014.

CHAPTER OUTLINE

Classification of Pancreatitis**Acute Pancreatitis**

Etiology

Pathophysiology

Definitions

Clinical Findings

Radiologic Findings

Complications

Chronic Pancreatitis

Etiology

Clinical Findings

Radiologic Findings

Summary

Pancreatitis is one of the most complex and clinically challenging of all abdominal disorders. It remains a major diagnostic challenge because its clinical manifestations are as protean as its causes. Indeed, only one in five severe cases of acute pancreatitis is recognized to be severe at initial presentation,¹⁻³ and 42% of fatal cases of acute pancreatitis do not have a correct diagnosis before autopsy.⁴⁻⁷

Since the late 1970s, cross-sectional imaging and, in particular, high-resolution, bolus contrast-enhanced multidetector helical computed tomography (CT) have dramatically improved the diagnosis and treatment of acute pancreatitis. More recently, magnetic resonance imaging (MRI) has shown that it can have a role in imaging of patients with pancreatitis. The focus of this chapter is on the contribution of radiology to the assessment and management of patients with acute or chronic pancreatitis.

Classification of Pancreatitis

Pancreatitis is classified according to clinical, morphologic, and histologic criteria on the basis of the Marseille and Cambridge symposia and the 1992 International Symposium in Atlanta, Georgia,^{8,9} and more recently the Acute Pancreatitis Classification Working Group in 2008.¹⁰⁻¹²

Acute Pancreatitis

ETIOLOGY

Although the causes of pancreatitis are diverse, alcoholism and biliary tract disease (gallstones) account for approximately 90% of cases in the United States. The relative frequency of these causes varies with the country and population of patients examined. Alcoholic pancreatitis is more common in urban

and Veterans Administration hospitals, whereas gallstone pancreatitis predominates in suburban and rural hospitals. The incidence of acute pancreatitis is 0.005% to 0.01% in the general population.¹³⁻¹⁸ Approximately 10% to 30% of patients with acute pancreatitis will never have the cause of the disorder established and are given the diagnosis of “idiopathic” pancreatitis. Biliary sludge and microlithiasis are probably responsible for the development of pancreatitis in the majority of these cases.^{16,19,20}

Identification of the cause of pancreatitis is important because it helps determine therapy. It may limit further unnecessary examinations and may improve the patient’s long-term outcome.¹⁶

PATHOPHYSIOLOGY

The precise mechanisms of pathogenesis of acute pancreatitis are not completely understood. Alcohol increases the risk for pancreatitis through multiple mechanisms. More than 95% of heavy alcohol users, however, never develop significant pancreatitis, which suggests that this is a complex syndrome, with other risk factors involved.^{21,22} Hypotheses and theories to explain alcoholic pancreatitis include necrosis-fibrosis sequence, duct obstruction, leakage of enzymes from the pancreatic duct, abnormal synthesis of digestive enzymes, toxic metabolites, altered pancreatic blood flow, mitochondrial damage, and activation of pancreatic stellate cells, which produce collagen in the fibrotic pancreas.²²

In alcoholic pancreatitis, the toxic effect and chemical alterations of the exocrine secretions produced by alcohol lead to protein precipitates that obstruct the pancreatic ducts.^{23,24} In addition, alcohol can lead to duodenitis, edema, and spasm of the papilla of Vater, further contributing to ductal obstruction.²³

Alcohol also indirectly stimulates pancreatic secretion by inducing an increase in gastrin and secretin levels and decreases the level of zymogen inhibitor, resulting in the premature activation of trypsin.²⁴ In acute pancreatitis, these activated pancreatic enzymes are extravasated, causing pancreatic autodigestion and necrosis.²⁵ In cholelithiasis-induced pancreatitis, there is obstruction of the common biliopancreatic channel by a stone (Opie stone), with resultant reflux of bile into the pancreatic duct and activation of pancreatic enzymes.^{17,25} Gallstones are found in the stool of most of these patients.²⁶ This is the rationale for emergency cholecystectomy or endoscopic retrograde cholangiopancreatography (ERCP)-directed sphincterotomies in the treatment of gallstone pancreatitis.¹⁶ Reflux of contrast material into the pancreatic duct during intraoperative cholangiography is much more common in patients with gallstone pancreatitis than in patients undergoing cholecystectomy who do not have pancreatitis.^{15,27}

Pancreas divisum, discussed in detail in Chapter 96, is also postulated to induce this disorder by a functional obstruction

at the accessory papilla of Santorini.²⁸ A variety of other causes, such as drugs, calcium, endotoxins, hyperlipidemia, viral infections, ischemia, anoxia, and trauma, can also activate proteolytic enzymes in the pancreas that lead to autodigestion and stimulate other enzymes, such as bradykinin and vasoactive substances, that cause vasodilation, increased vascular permeability, and edema.^{15,29}

Leukocytes attracted by the pancreatic injury release inflammatory mediators called cytokines, which have an important role in disease progression and multisystem complications of acute pancreatitis. Biologically active compounds, such as phospholipase A₂, tumor necrosis factor, polymorphonuclear cell elastase, complement factor, interleukins, and leukotrienes, are released into the systemic circulation, stimulating the production of other mediators and leading to distant organ failure.³⁰⁻³² Some of these mediators, such as tumor necrosis factor, are also toxic to acinar cells and may contribute to pancreatic injury and necrosis.^{32,33} These inflammatory products occur early in the course of the disease and can be used as indicators of severity and prognosis in acute pancreatitis.^{32,34,35}

Pancreatitis has been shown to have an increased prevalence in patients with acquired immunodeficiency syndrome (AIDS), explained either by the effects of medication (pentamidine and 2',3'-dideoxyinosine [DDI]) or by secondary opportunistic infections.^{1,16,36}

No dependable correlation exists between the etiology and the severity of disease. In general, most cases of necrotizing pancreatitis are associated with alcoholism and hyperlipidemia, whereas severe pancreatitis is less commonly noted with other causes.

There are several major pathologic categories of acute pancreatitis. Acute interstitial edematous pancreatitis is the mildest form of pancreatitis. It is characterized by absent or minimal pancreatic and systemic dysfunction and a rapid response to medical therapy without complications. Only pancreatic edema and mild cellular infiltrate are present. The gland may enlarge to three times its normal size and become firm. There may be a few small, scattered foci of necrosis and saponification in the peripancreatic fatty tissue. Other organs generally are not involved. Necrotizing pancreatitis is a far more severe form of pancreatitis in which varying degrees of systemic and distal organ failure and potentially lethal complications can occur. Extensive fat necrosis, hemorrhage, and necrotic liquefaction of the pancreatic parenchyma and adjacent peripancreatic tissues and fascial planes are seen. In addition, a variety of intermediary forms of pancreatitis occur in clinical practice. The degree and extent of injury appear to be related to the quantity, rate of production, and activity of the highly lipolytic and proteolytic extravasated enzymes.¹⁶

DEFINITIONS

Considerable ambiguity and overlap of pathologic features exist in describing the complications of pancreatitis. The following are definitions of commonly encountered sequelae that are discussed in subsequent sections.^{16,37}

Acute pancreatitis is diagnosed when two of the three following criteria are present: (1) abdominal pain related to acute pancreatitis, (2) serum amylase or lipase activity greater than three times the normal level, and (3) imaging findings characteristic of acute pancreatitis.

According to the revised Atlanta classification of acute pancreatitis, acute pancreatitis can be divided into two major types: interstitial edematous pancreatitis and necrotizing pancreatitis.^{10,11}

Interstitial Edematous Pancreatitis. Most patients have diffuse (or less commonly focal) pancreatic enlargement from interstitial edema. The pancreas enhances relatively homogeneously without necrosis, and there is peripancreatic inflammation with mild stranding or fluid. The clinical findings generally resolve within the first week.³⁸ When imaging is performed within the first days after onset of pancreatitis, it may be difficult to distinguish interstitial edematous pancreatitis from patchy necrosis. Follow-up contrast-enhanced CT 3 to 7 days later may be helpful in the distinction.³⁹

Acute Peripancreatic Fluid Collection. Fluid collection in peripancreatic regions typically occurs within 4 weeks of symptom onset, mostly after interstitial edematous pancreatitis. It lacks nonliquefied material and a definable wall.

Necrotizing Pancreatitis. On imaging, necrotizing pancreatitis is defined by lack of enhancement of the pancreatic tissue. Necrosis most commonly involves the pancreas and peripancreatic tissues, followed by the pancreas and, least commonly, the peripancreatic tissues. Necrotizing pancreatitis is quantified on the basis of studies by Balthazar as less than 30%, 30% to 50%, and more than 50%. More recently, it has been graded by modified CT as less than 30% or more than 30%.⁴⁰

Acute Necrotic Collection. Acute necrotic collection refers to a persistent collection containing fluid and necrotic material of various amounts associated with necrotizing pancreatitis. This collection accumulates in the pancreas or peripancreatic tissue and occurs within 4 weeks after development of necrotizing pancreatitis.

Pancreatic Pseudocyst. Pancreatic pseudocysts are localized collections of pancreatic fluid confined by a capsule of fibrous or granulation tissue; they typically develop during 4 weeks after an acute episode or can be associated with stigmata of chronic pancreatitis. Pseudocysts lack a true epithelial lining, which distinguishes this entity from a cyst or cystic neoplasm. They are manifestations of a local complication of acute non-necrotic pancreatitis and should not contain solid material. Current literature estimates that 50% of asymptomatic pseudocysts smaller than 6 cm resolve spontaneously.⁴¹ Pseudocysts larger than 7 cm in diameter are likely to require intervention, particularly in patients with alcoholic pancreatitis.^{37,42} Persistent pseudocysts often communicate with the pancreatic duct and have the potential to rupture, to bleed, to become infected, or to cause a pseudoaneurysm.^{30,43} Infected pseudocysts require drainage.

Walled-off Necrosis. Walled-off necrosis is a persistent collection of necrotic tissue with a thickened wall that lacks a true epithelial lining; it arises in the setting of necrotizing pancreatitis.¹⁰ This collection accumulates in the pancreas or peripancreatic tissue usually 4 weeks or more after onset of necrotizing pancreatitis and may or may not be infected. Unlike a pseudocyst, walled-off necrosis contains necrotic pancreatic parenchyma or fat.¹¹ The liquefied components may be better

characterized by MR or ultrasound, including endoscopic ultrasound (EUS), to guide drainage if it is required.

Phlegmon. Phlegmon is a term formerly used to imply the presence of a heterogeneous masslike enlargement of the pancreas and retroperitoneal tissues. It does not correlate with the presence of infection or necrosis. Because the term has different meanings to gastroenterologists, internists, and surgeons, it should be avoided according to the revised Atlanta criteria.¹⁰⁻¹²

Abscess. Pancreatic abscess develops from infected, extravasated pancreatic secretions. It usually occurs 3 weeks or more after the initial attack or may develop as a secondary infection of a pseudocyst. This term has fallen out of favor with the revised Atlanta classification system, and the term *infected pseudocyst* is used instead.^{10-12,39}

Pseudoaneurysm. A pseudoaneurysm is a focal area of dilation of a splanchnic artery that may occur as a result of inflammatory weakening of the arterial wall by enzymes liberated in acute pancreatitis. Pseudoaneurysms usually are found in the splenic, gastroduodenal, and pancreaticoduodenal arteries and can be freestanding or associated with a pseudocyst. Intermittent or life-threatening hemorrhage into a pseudocyst, retroperitoneum, or peritoneal cavity may occur.

CLINICAL FINDINGS

The clinical diagnosis of pancreatitis is often difficult. Patients' symptoms range from mild abdominal pain, nausea, vomiting, fever, tachycardia, and abdominal distention to severe abdominal pain and shock. Most patients have abdominal tenderness and guarding. These findings are nonspecific, and the differential diagnosis usually includes acute cholecystitis, bowel obstruction or infarction, perforated viscus, renal colic, duodenal diverticulitis, aortic dissection, appendicitis, and ruptured abdominal aortic aneurysm. In very severe cases, flank ecchymosis (Grey Turner's sign) or periumbilical hematoma (Cullen's sign) may be present.

Consequently, a battery of laboratory tests has been developed to diagnose and to grade pancreatitis. These tests include evaluation of serum amylase, lipase, serum/urinary amylase ratio, pancreatic isoamylase, immunoreactive trypsin, chymotrypsin, elastase, serum cyclic adenosine monophosphate, C-reactive protein, urinary trypsinogen-2, and methemalbumin.^{7,34,44} Serum amylase and lipase levels are the most commonly used measures to diagnose pancreatitis. Unfortunately, these values are elevated in only 80% to 90% of patients with acute pancreatitis.⁴⁵ Amylase is rapidly secreted by the kidneys and may return to normal levels during the first 48 to 72 hours.^{37,46} Pancreatitis caused by gallstones, microlithiasis, or drugs is often associated with a greater elevation in amylase than in lipase.^{47,48} The amylase level relative to lipase tends to be lower in alcoholic pancreatitis, hypertriglyceridemia-induced pancreatitis, neoplasia, and chronic pancreatitis.^{20,47,48} There is no correlation between the levels of serum amylase and the severity of acute pancreatitis; patients with mild forms of disease may exhibit levels above 1000 units, whereas patients with severe necrotizing pancreatitis may have normal or low amylase levels.^{49,50} Furthermore, hyperamylasemia may be seen in other acute abdominal conditions, such as bowel obstruction, bowel infarction, gangrenous cholecystitis, and perforated

ulcer.⁵¹ Elevated lipase is more specific for pancreatitis, but the level does not predict the etiology.⁵²

The onset of acute pancreatitis is defined from the time of onset of abdominal pain and not date of hospital admission. The clinical course of acute pancreatitis varies from mild and self-limited disease to shock, overwhelming sepsis, and death. The revised Atlanta classification divides acute pancreatitis into two broad categories: nonsevere acute interstitial edematous pancreatitis; and severe acute pancreatitis, which often involves necrosis of the gland or peripancreatic tissues.¹⁰ Characterization of acute pancreatitis can be considered on the basis of early and late phases of the disease.¹⁰ The early phase of acute pancreatitis appears within the first week and shows systemic reaction of the body to pancreatic enzymatic insults and injuries. This phase usually resolves within a week. The clinical features during this period are commonly the signs of systemic inflammatory response syndrome. The late phase of acute pancreatitis is seen only in moderately severe or severe acute pancreatitis. During this phase, local complications of acute pancreatitis and continuation of systemic signs of inflammation are noted; therefore, both clinical and imaging criteria are important.

Mild acute pancreatitis usually improves within the first week and during the early phase of disease. There is no evidence of organ failure or local or systemic complications of acute pancreatitis, and an imaging examination is often not needed in mild cases. Moderately severe acute pancreatitis is defined by the presence of local or systemic complications of acute pancreatitis or the existence of transient organ failure. By definition, transient organ failure in a patient suffering from acute pancreatitis lasts less than 48 hours. Severe acute pancreatitis determines when organ failure is evident for more than 48 hours.^{53,54}

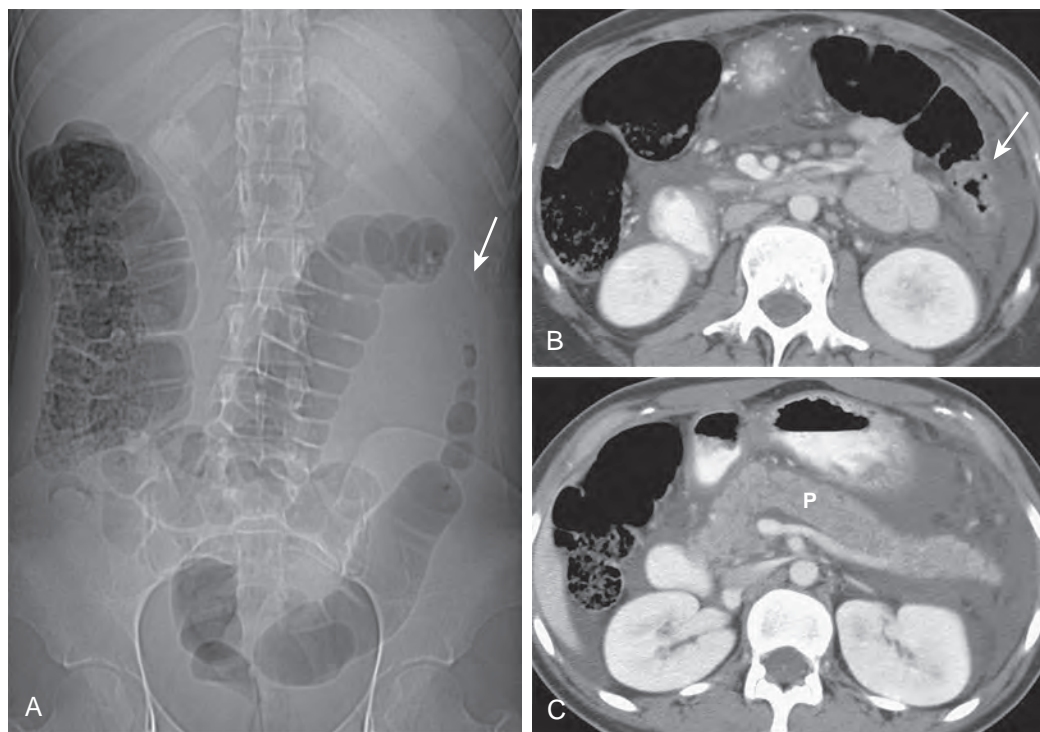
RADIOLOGIC FINDINGS

Cross-sectional imaging has made a significant contribution to the diagnosis and staging of acute pancreatitis. Radiologic imaging of patients with suspected pancreatitis has five major objectives: (1) to exclude other abdominal disorders that can mimic acute pancreatitis; (2) to confirm the clinical diagnosis of acute pancreatitis; (3) to evaluate the extent and nature of pancreatic injury and peripancreatic inflammation in an attempt to stage the severity of disease; (4) to determine the etiology of acute pancreatitis; and (5) to serve as a guide for therapeutic intervention and response to therapy. Although plain films and contrast studies have been used in the past for the diagnosis of pancreatitis, they have been largely replaced by cross-sectional studies, which have significantly greater diagnostic accuracy. Findings and signs indicative of pancreatitis on different imaging modalities are briefly discussed here, with an emphasis on CT and MRI.

Abdominal Plain Films

Abnormalities in the abdominal gas pattern are the most frequent findings on abdominal plain films and range from a gasless abdomen to an ileus pattern. The most common findings are a small bowel ileus (42%), in which an adynamic sentinel loop is seen, and the colon cutoff sign (56%), related to spasm of the splenic flexure with distal paucity of gas caused by spread of the pancreatic inflammation into the phrenocolic ligament.⁵⁵⁻⁵⁹ Although it was originally described in abdominal

Figure 97-1 Colon cutoff sign on MDCT. **A.** Scout topogram for abdominal MDCT shows abrupt interruption (arrow) of colonic gas at splenic flexure in a patient with acute pancreatitis. **B.** Axial contrast-enhanced MDCT image shows narrowing (arrow) of the colonic lumen at the level of the splenic flexure as a result of extension of inflammatory exudate. **C.** Axial contrast-enhanced MDCT image shows pancreas (P) surrounded by inflammatory changes and fluid.



plain films, the colon cutoff sign can also be seen on CT (Fig. 97-1).

Chest Films

Approximately one third of patients with acute pancreatitis demonstrate pulmonary and chest abnormalities: elevated diaphragms, pleural effusions, basal atelectasis, pulmonary infiltrates, and the adult respiratory distress syndrome.⁶⁰⁻⁶⁵ Abnormalities on chest films can be useful to determine the severity of acute pancreatitis.^{66,67}

Barium Studies

Meyers and Evans⁶⁸ have emphasized the importance of the ligaments and mesenteries of the subperitoneal space (Fig. 97-2) in the spread of pancreatitis to understanding of the radiographic findings. Extravasated pancreatic enzymes commonly enter the lesser sac and spread to the transverse mesocolon, phrenocolic ligament, and small bowel mesentery, causing serosal inflammation and irritation of the gastrointestinal tract.^{55,61,68} Thickening and spiculation of mucosal folds in the stomach and duodenum can be seen on CT and barium studies. Varying degrees of atony associated with spastic segments of the duodenum, jejunum, and transverse colon can also be present.⁶⁸⁻⁷¹

Cholangiography

ERCP is generally not performed during an acute episode of pancreatitis because it may exacerbate the inflammation or introduce an infection. The pancreatic duct is usually normal but can be compressed. Some gastroenterologists advocate ERCP with sphincterotomy to alter the course of pancreatitis when it appears that multiple stones are passing through the common bile duct. ERCP can also demonstrate other causes of pancreatitis, such as pancreas divisum, choledochocoele, choledochal cyst, perivaterian duodenal diverticulum, pancreatic or

bile duct carcinoma, and ampullary carcinoma¹⁵ (see Chapter 74). Magnetic resonance cholangiopancreatography (MRCP) is often preferred to investigate the cause of pancreatitis, however, avoiding the complications associated with ERCP.^{72,73}

Angiography

Angiography is usually not performed in patients with acute pancreatitis unless the presence of a pseudoaneurysm that could be treated with transcatheter embolization is suspected. It can also be helpful to elucidate vascular causes of pancreatitis, such as vasculitis, polyarteritis nodosum, post-aortic aneurysm resection, after transplantation, Ortner's syndrome, systemic lupus erythematosus, low-flow states, shock, and diabetes.⁷⁴⁻⁷⁶

Ultrasonography

Abnormal findings are seen at sonography in 33% to 90% of patients with acute pancreatitis.⁷⁷ The classic sonographic appearance in pancreatitis is a diffusely enlarged hypoechoic pancreas.⁷⁸⁻⁸⁰ Less commonly, focal enlargement is present. The echogenicity of the pancreas in acute pancreatitis is extremely variable and depends on a number of factors: the timing of the sonographic study, with maximal decrease in echogenicity occurring 2 to 5 days after the initial episode of acute abdominal pain; the amount of intrapancreatic fat (with age, the pancreas is replaced by fat and hence becomes more echogenic); the presence of hemorrhage; the presence of underlying chronic pancreatitis with calcification; and the degree of extrapancreatic spread of acute pancreatitis.^{78,79,81} Echogenicity is also subjective because the usual internal standard used to gauge pancreatic texture is the liver, which often has altered architecture caused by fatty infiltration, cirrhosis, or alcoholic pancreatitis. Similarly, size changes are difficult to assess without a baseline scan because the overall volume of the gland is variable and diminishes with advanced age.⁸²

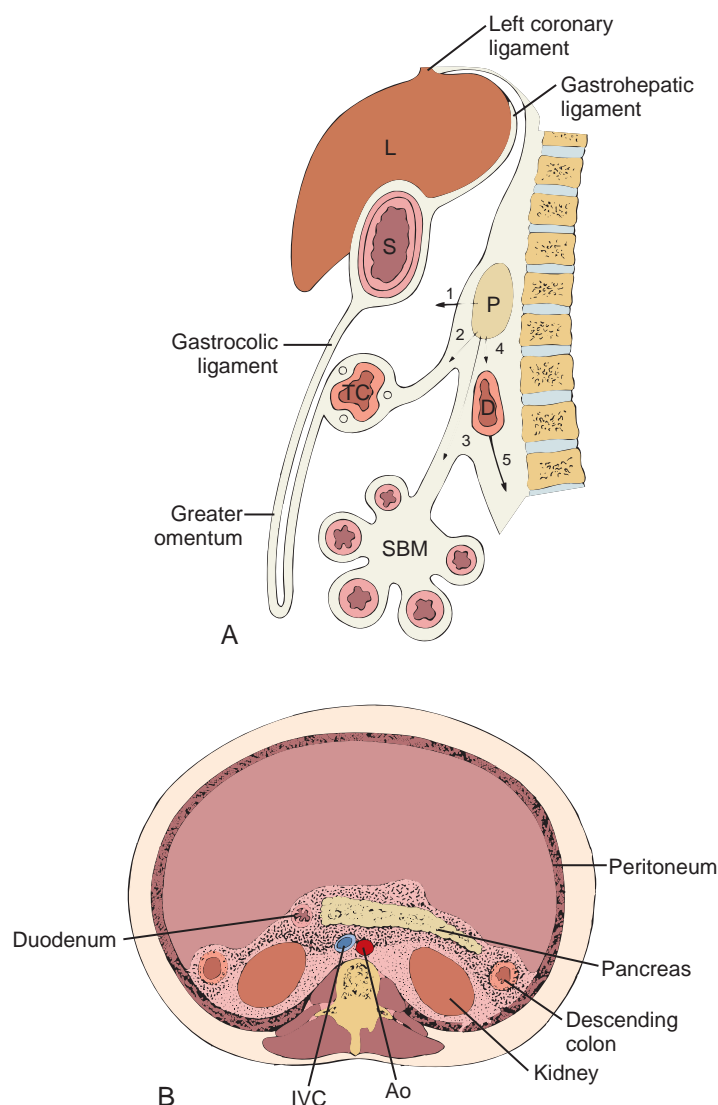


Figure 97-2 Anatomic relationships of the pancreas. These relationships explain the radiographic findings on plain films, barium studies, and cross-sectional images. **A.** Sagittal diagram of the abdomen depicts avenues of spread of the inflammation and fluid of acute pancreatitis: (1) spread into the lesser sac will deform the posterior gastric wall; (2) spread into the transverse mesocolon will cause deformity along the inferior border of the colon; (3) spread into the root of the small bowel mesentery will cause deformity of the small bowel loops; (4) extension into the duodenum will cause deformity and mucosal abnormalities; (5) spread into the remainder of the retroperitoneum will cause changes in the anterior pararenal space. *D*, Duodenum; *L*, lung; *P*, pancreas; *S*, spleen; *SBM*, small bowel mesentery; *TC*, transverse colon. **B.** Axial diagram shows the intimate relationship between the pancreas and other structures in the anterior pararenal space (duodenum, ascending and descending colon). The kidneys lie in the perirenal space. *Ao*, Aorta; *IVC*, inferior vena cava.

The pancreatic duct may dilate, particularly if the inflammation is confined to the pancreatic head. Focal intrapancreatic masses may be due to an acute fluid collection, hemorrhage, or ill-defined and hypoechoic pancreatic enlargement that may sonographically simulate carcinoma. Cystic masses should be scrutinized with Doppler ultrasound studies to exclude pancreatic pseudoaneurysms.⁸³ Lesser sac fluid collections are often seen and may produce a “butterfly” appearance.⁸⁴

The foregoing discussion assumes that the pancreas is well visualized. In acute pancreatitis, bowel gas and other factors will limit visualization of the gland in one fourth to one third of patients. This is one of four major limitations of ultrasound in this clinical setting. The second is the inability of ultrasound to completely define the complex extrapancreatic spread of inflammation along fascial planes and within the peripancreatic compartments. It is particularly limited in visualizing spread into the transverse mesocolon. Third, ultrasound cannot specifically reveal areas of pancreatic necrosis in patients with severe pancreatitis, information that provides important insights into the ultimate prognosis of necrotizing pancreatitis. Finally, only CT, MRI, or angiography can diagnose many gastrointestinal and vascular complications of acute pancreatitis.^{78,79}

What, then, is the role of sonography in acute pancreatitis? It is a good screening test in patients with suspected biliary pancreatitis and a mild clinical course. It is helpful to detect gallstones, for which CT is not effective.⁸⁵⁻⁸⁷ It is also useful in thin patients with mild edematous pancreatitis that promptly responds to conservative therapy. Ultrasound has limitations in the detection of distal common duct stones. It also has limitations in the diagnosis of necrosis. Ultrasound may be used to assess the presence or absence of solid necrotic material and to differentiate it from cystic material to help guide drainage when it is being considered. CT is preferred for patients with clinically severe pancreatitis; those whose disease fails to respond to conservative therapy; acutely ill patients who pose diagnostic dilemmas; and patients with complications, such as infected pseudocyst, hemorrhage, pseudoaneurysm formation, and pancreatic necrosis.^{88,89}

The use of tissue harmonic imaging improves image quality, delineation of the pancreatic tail, lesion conspicuity, and fluid-solid differentiation relative to conventional B-mode sonography.^{90,91} Tissue harmonic sonography was able to detect abnormalities in 91% of patients with acute pancreatitis.⁹² The authors found that the two most useful sonographic findings were extrapancreatic inflammation and parenchymal inhomogeneity. It was difficult, however, to distinguish between fluid collections and extrapancreatic inflammation. Nevertheless, the accuracy of CT is still superior to that of tissue harmonic sonography in the evaluation of acute pancreatitis, as even with tissue harmonics, sonography does not demonstrate necrosis or other complications as well as CT does.

Computed Tomography and Magnetic Resonance Imaging

CT is the premier imaging test in the diagnosis and management of patients with acute pancreatitis. It visualizes the gland, the bowel, the retroperitoneum, the abdominal ligaments, the mesenteries, and the omentum in their entirety. In addition, it may help determine the etiology, stage severity, and detect complications of pancreatitis; it can be used to guide interventional procedures, such as fine-needle aspiration biopsy or catheter placement. However, the radiation dose delivered by CT may be a significant factor for young patients with pancreatitis requiring multiple examinations. MRI may be an option for these patients; however, it is more costly than CT. Other advantages of MRI include its high soft tissue contrast resolution and ability to evaluate the common bile duct, pancreatic duct, and parenchyma in a single examination.⁹³⁻⁹⁶ Before the awareness of nephrogenic systemic fibrosis, contrast-enhanced MRI could be used in patients with renal insufficiency when

contrast-enhanced CT could not be performed. MRI, however, is limited in the more acute setting when the patient is very ill, as patients need to be able to hold the breath and be relatively stable for the longer examination. MRI may be helpful to distinguish peripancreatic fluid collections as solid debris from cystic collections and show the compositions of pseudocysts better than multidetector CT (MDCT).^{39,97-100} Diffusion-weighted MRI can be helpful in the diagnosis of acute pancreatitis.¹⁰¹

CT Technique. The technique used in evaluating patients with pancreatitis should be individualized. The best diagnostic images are obtained with MDCT by achieving optimal vascular and parenchymal enhancement and avoiding respiratory motion. A rapid 5 mL/s intravenous bolus of 150 mL of 60% nonionic contrast material is injected. We routinely use a two-phase imaging technique. Images in the pancreatic and hepatic venous phases are obtained with 2- to 3-mm slice thickness. In addition, unenhanced images may be helpful through the pancreas. Images can be reconstructed into any plane with various thickness and section intervals at any level in the scanned volume.

MRI Technique. The role of MRI has become increasingly more important with the advent of high-field-strength imaging, phased-array surface coils, MR-compatible power injectors, rapid gradient-echo breath-hold techniques, and fat suppression.^{96,102,103} These technologic advances allow faster sequences with high-resolution images that are largely free of artifacts. T1-weighted fat-suppressed sequences before and after gadolinium administration and T2-weighted sequences are essential for pancreatic evaluation. The T1-weighted fat-suppressed sequences are able to detect focal or diffuse abnormalities in the pancreas and to delineate the peripancreatic fat planes. With T1 relaxation time shorter than that of the liver, the normal pancreas has the highest signal intensity of intra-abdominal organs. This is attributed to the abundance of acinar proteins, endoplasmic reticulum, and paramagnetic ions within the pancreas.^{104,105} Contrast-enhanced T1-weighted images in the arterial phase show intense enhancement of the normal pancreas, which becomes less intense on subsequent phases. T2-weighted sequences show fluid as high signal intensity, allowing assessment of the pancreaticobiliary ducts and detection of fluid collections and peripancreatic edema.

Diagnosis. The imaging findings in acute pancreatitis are similar, regardless of etiology, with the exception of traumatic pancreatitis, in which pancreatic lacerations cause high-density (50-90 HU) hematomas. MRI can be helpful in determining the etiology of pancreatitis, including choledocholithiasis, pancreas divisum, and underlying tumors. In the acute setting, however, the etiology may be difficult to determine because of the significant inflammation, which may obscure stones, pancreaticobiliary ducts, or underlying masses.

In mild forms of pancreatitis, CT and MRI may show normal findings or a slight to moderate increase in the size of the pancreas. Mild inflammation may surround an otherwise normal-appearing gland (Fig. 97-3). Alternatively, the pancreas may be diffusely enlarged, with shaggy and irregular contour, and slightly heterogeneous parenchyma, which enhances less than normal (Fig. 97-4). On MRI, there may be decreased pancreatic signal intensity on T1-weighted fat-suppressed sequences before

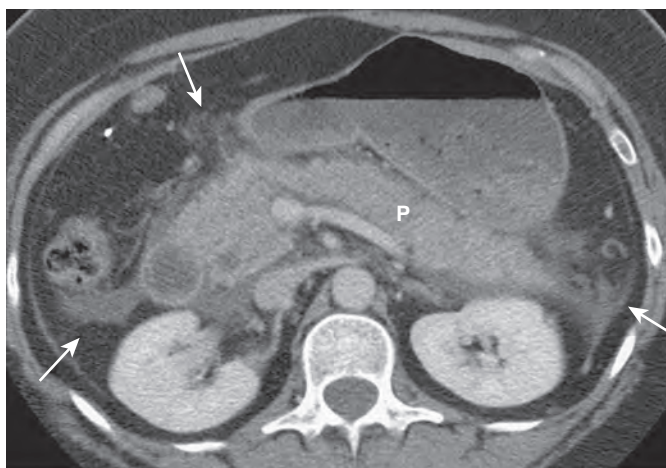


Figure 97-3 Acute pancreatitis. Axial contrast-enhanced MDCT image shows peripancreatic inflammatory changes (arrows) in a patient with abdominal pain and elevated amylase levels. The pancreas (P) has normal size and enhancement.

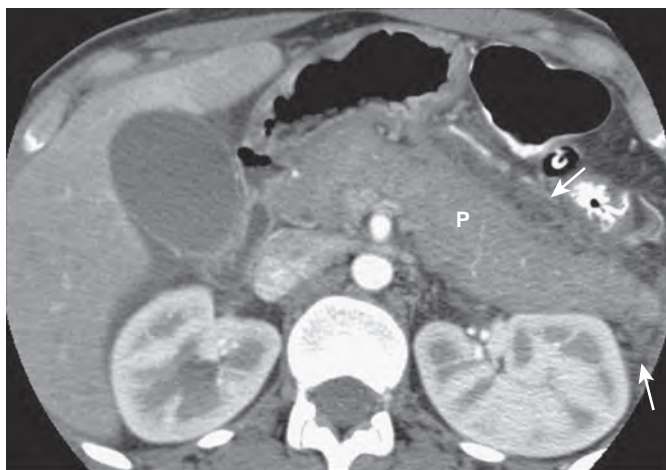


Figure 97-4 Mild acute pancreatitis. Axial arterial phase contrast-enhanced MDCT image shows diffuse enlargement and decreased enhancement of the pancreas. Note peripancreatic inflammatory changes (arrows). P, Pancreas.

and after gadolinium administration, depending on the degree of inflammation and edema (Fig. 97-5).^{96,106}

In more advanced cases, extravasation of pancreatic fluid leads to the formation of intrapancreatic and extrapancreatic fluid collections (Fig. 97-6). Because the pancreas does not have a well-developed fibrous capsule, pancreatic secretions commonly extravasate in the retroperitoneum, most often in the anterior pararenal space (Fig. 97-7; see also Fig. 97-1). CT superbly depicts peripancreatic inflammation, fluid, and occasionally mild thickening of the adjacent fascial planes (see Figs. 97-1 and 97-3). Peripancreatic inflammatory stranding is also well seen on MRI (see Fig. 97-5).

A more unusual segmental form of acute pancreatitis occurs in as many as 18% of patients.^{14,88} The CT findings are similar to those in diffuse pancreatitis; however, only part of the gland is involved either exclusively or predominantly. The segment most often involved is the pancreatic head. This form of pancreatitis is usually mild and is most often associated with stone

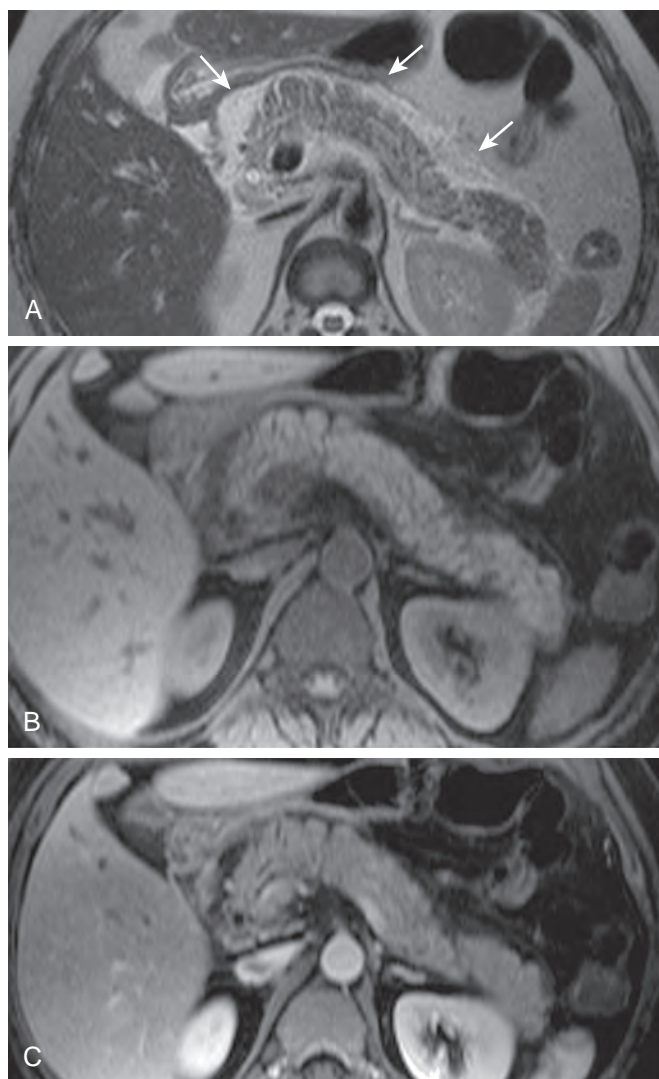


Figure 97-5 Mild ERCP-induced pancreatitis. **A.** Axial T2-weighted half-Fourier acquisition single-shot turbo spin-echo (HASTE) MR image shows peripancreatic fluid (arrows) with high signal intensity. The pancreas also has mildly increased signal intensity due to edema. **B.** Axial T1-weighted fat-suppressed spoiled gradient-echo MR image shows normal high signal intensity of the pancreas in this patient with uncomplicated pancreatitis. The peripancreatic fluid is better seen on T2-weighted images. **C.** The pancreas shows diffusely decreased enhancement during the arterial phase after administration of gadolinium. (A-C from Miller FH, Keppke AL, Dalal K, et al: *MRI of pancreatitis and its complications: Part 1, acute pancreatitis*. AJR Am J Roentgenol 183:1637–1644, 2004. Reprinted with permission from the American Journal of Roentgenology.)

disease.^{6,98,107} However, patients with segmental pancreatitis should be carefully evaluated to exclude the less common possibility of adenocarcinoma simulating pancreatitis or a mass leading to pancreatitis (Figs. 97-8 and 97-9). It may be appropriate to further investigate these patients with EUS, MR, ERCP, or biopsy or to perform short-term follow-up CT or MRI, especially if they are older or do not have risk factors for pancreatitis.¹⁰⁶

In severe forms of necrotizing pancreatitis, the gland may become enlarged, and it is commonly enveloped by high-attenuation heterogeneous fluid collections. Because of

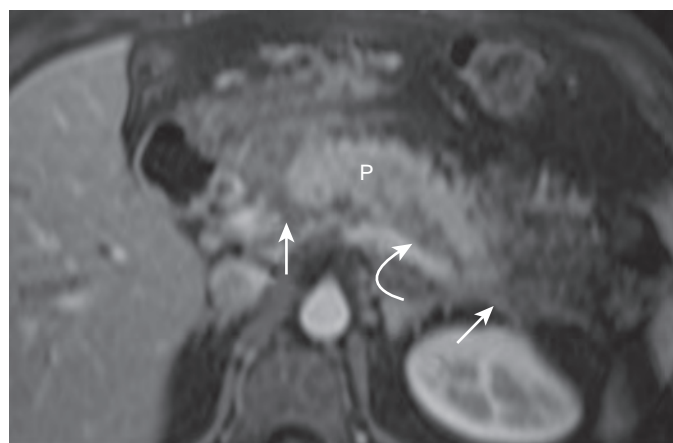


Figure 97-6 ERCP-induced pancreatitis with peripancreatic fluid collections. Axial enhanced T1-weighted fat-suppressed spoiled gradient-echo MR image shows heterogeneous pancreatic enhancement and peripancreatic fluid and inflammation (straight arrows). Fluid (curved arrow) is seen between the pancreas and the splenic vein. P, Pancreas. (From Miller FH, Keppke AL, Dalal K, et al: *MRI of pancreatitis and its complications: Part 1, acute pancreatitis*. AJR Am J Roentgenol 183:1637–1644, 2004. Reprinted with permission from the American Journal of Roentgenology.)

high-attenuation exudates, the presence of pancreatic necrosis cannot be assessed on CT unless the gland is imaged during the late arterial–early portal venous phase of a rapid bolus intravenous injection of contrast medium (Fig. 97-10).⁷⁷ On MRI, peripancreatic high signal intensity may be seen on T1-weighted fat-suppressed sequences related to fat necrosis and hemorrhage (Fig. 97-11). This finding has been associated with a worse prognosis.¹⁰⁸ Patchy areas of absence of enhancement, fragmentation, and liquefaction necrosis can be detected on CT or MRI (Fig. 97-12). Poorly defined peripancreatic exudates obliterate the peripancreatic fat, envelop the pancreas, dissect fascial planes, and penetrate through fascial and peritoneal boundaries and ligaments. These collections most often occur in the anterior pararenal space around the body and tail of the pancreas and within the lesser peritoneal sac (Fig. 97-13).¹⁰⁹ Penetration through Gerota's fascia with involvement of the perirenal fat and kidneys occurs rarely. When fluid collections are massive, they tend to extend inferiorly along the pararenal spaces in the left flank or bilaterally. They can course over the psoas muscle, enter the pelvis (see Fig. 97-13B), and sometimes extend into the groin. Exudates can invade the small bowel mesentery, the transverse mesocolon, and the posterior pararenal spaces (see Fig. 97-7). Fluid can penetrate into solid organs, such as the spleen or the liver, and even the mediastinum. Splenic involvement is most common because of the close anatomic relationship of the pancreatic tail and splenic hilum. Subcapsular or intrasplenic fluid collections or pseudocysts, infarcts, and splenic hemorrhage may be seen with pancreatitis.

In about 7% to 12% of patients with acute pancreatitis, CT or MRI reveals free intraperitoneal fluid, usually in small volumes. Massive pancreatic ascites, caused by communication of a disrupted pancreatic duct with the peritoneal cavity, is rarely seen.^{30,110} This presentation is usually associated with a more severe form of pancreatitis. In most of these patients, characteristic pancreatic and peripancreatic abnormalities are recognized. Rarely, pancreatic ascites can develop in patients

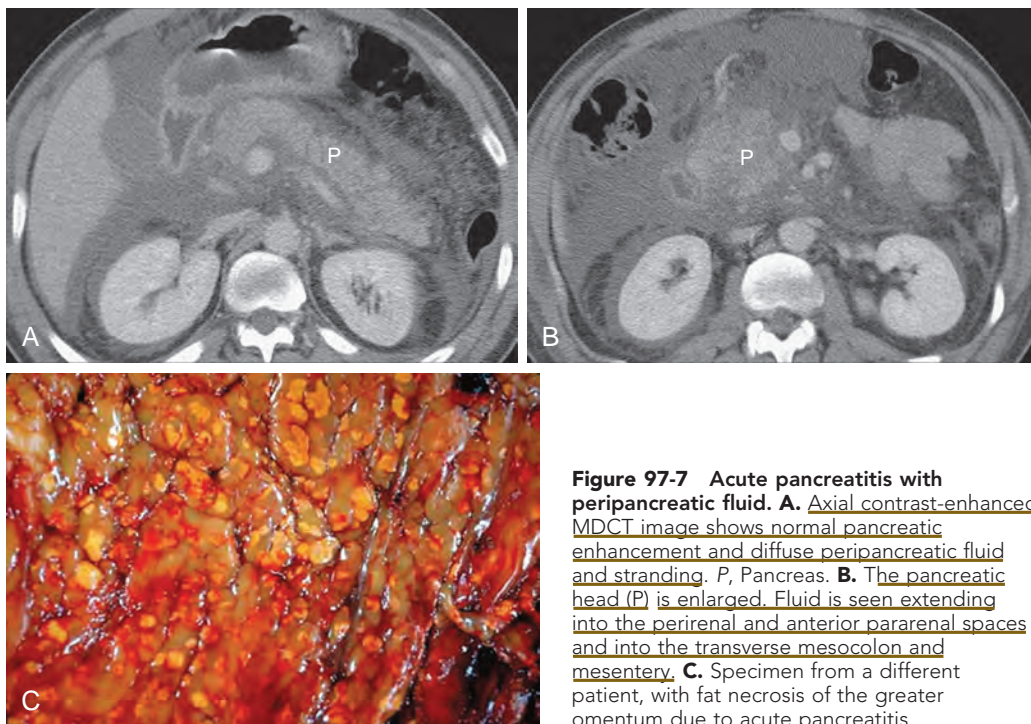


Figure 97-7 Acute pancreatitis with peripancreatic fluid. **A.** Axial contrast-enhanced MDCT image shows normal pancreatic enhancement and diffuse peripancreatic fluid and stranding. P, Pancreas. **B.** The pancreatic head (P) is enlarged. Fluid is seen extending into the perirenal and anterior pararenal spaces and into the transverse mesocolon and mesentery. **C.** Specimen from a different patient, with fat necrosis of the greater omentum due to acute pancreatitis.

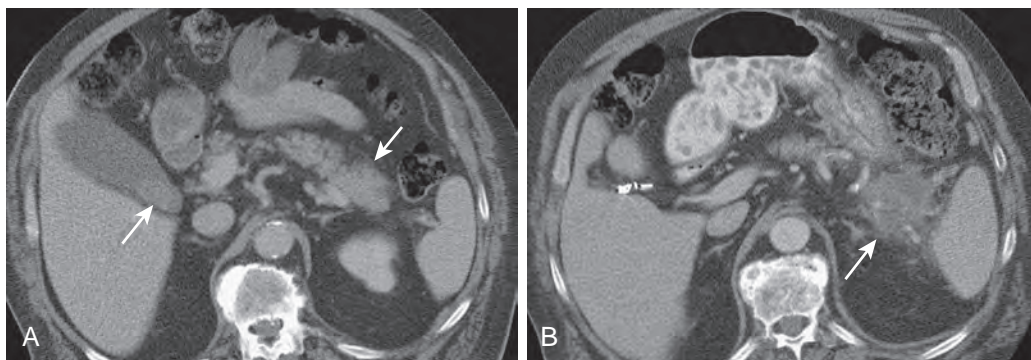


Figure 97-8 Pancreatic cancer mimicking acute pancreatitis. **A.** Axial contrast-enhanced MDCT image shows stranding surrounding pancreatic tail (short arrow) and gallstone (long arrow) in this patient with uncontrollable back pain who was believed to have pancreatitis. **B.** Six months after cholecystectomy, the patient had persistent pain. His amylase and lipase levels were only mildly elevated. Axial contrast-enhanced MDCT image shows a pancreatic tail mass (arrow) that encases vessels and was proved to be adenocarcinoma.

with a normal-appearing gland on CT scans. In these patients, paracentesis with amylase determination is needed to make the diagnosis.¹¹¹ The treatment of pancreatic ascites includes conservative management with nasogastric suction, parenteral nutrition, and repeated paracenteses.^{112,113} If these measures fail, interventional or surgical procedures, including pancreatic duct stenting, pancreaticojejunostomy, and distal pancreatectomy, may be required.

Diagnostic Sensitivity. The accuracy of CT in the diagnosis of acute pancreatitis depends to a large extent on the severity of the disease. The reported CT sensitivity for the diagnosis of acute pancreatitis ranges from 77% to 92%.^{51,114,115} The usefulness of CT is further supported by its high specificity. In most series, there are few false-positive findings, and CT specificity as high as 100% has been reported.¹¹⁴ In addition, by examining

the entire abdomen, CT can reveal a variety of other abdominal conditions in patients clinically suspected of having acute pancreatitis.

Limitations in Diagnosis. Limitations in the CT diagnosis of acute pancreatitis are related to suboptimal examinations resulting from poor technique, lack of intravenous contrast medium, or inability of the patient to cooperate. Motion or streak artifacts and paucity of retroperitoneal fat are limiting factors in some patients. In addition, in mild forms of clinical pancreatitis, morphologic parenchymal or retroperitoneal abnormalities do not develop and the gland may appear normal on CT scans. It occurs in patients with mild symptoms and transitory elevation of serum amylase concentration. The incidence of normal CT scans in these persons is not well established because surgical or pathologic correlation is lacking, but

it has been estimated to be 14% to 28%.^{88,116} Experience has shown that given a good-quality CT scan, all patients with moderate or severe pancreatitis will exhibit some CT abnormality. In patients with normal results of CT examination, pancreatitis is either absent or of minimal clinical significance.

Staging. By virtue of its ability to accurately and rapidly evaluate the pancreas, peritoneum, and retroperitoneum, CT can be used to predict the severity of acute pancreatitis.^{40,117-126} The revision of the Atlanta classification addresses the lack of uniformity between referring physicians and diagnostic radiologists in describing the terms related to acute pancreatitis.^{10,11} The classification addresses fluid collections before and after 4 weeks of the onset of symptoms by the presence or absence of necrosis and by the presence or absence of infection.

Grading System. The CT severity index (CTSI), developed by Balthazar and colleagues, focused on the presence and degree of pancreatic inflammation and necrosis to predict morbidity

and mortality in patients with acute pancreatitis. In 2004, Morte and coworkers⁴⁰ modified the index with improved correlation with patient outcomes. The modified scale ascribes points to degrees of pancreatic inflammation.

Grade A: normal pancreas

Grade B: focal or diffuse enlargement of the gland including contour irregularities and inhomogeneous attenuation but without peripancreatic inflammation

Grade C: intrinsic pancreatic abnormalities associated with inflammatory changes in the peripancreatic fat (see Figs. 97-4 and 97-5)

Grade D: small and usually single, ill-defined fluid collection

Grade E: two or more large fluid collections or the presence of gas in the pancreas or retroperitoneum (Fig. 97-14)^{88,119}

In cases of pancreatic necrosis, points are given for certain degrees of necrosis, with more than 30% necrosis receiving the maximum 4 points. Two points are given for cases that involve extrapancreatic complications. The numerical modified CTSI

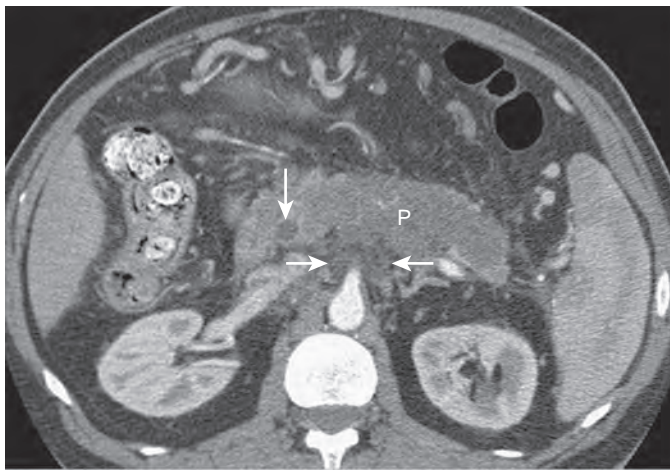


Figure 97-9 Pancreatic cancer mimicking pancreatitis. Axial contrast-enhanced MDCT image shows enlargement and lack of enhancement of the body and tail of the pancreas (P), mimicking pancreatic necrosis. Note peripancreatic stranding and soft tissue density (short arrows) surrounding the celiac artery, raising suspicion for cancer. There was thrombosis of the superior mesenteric vein, splenic vein, and extrahepatic portal vein (long arrow). Histologic examination revealed pancreatic adenocarcinoma.

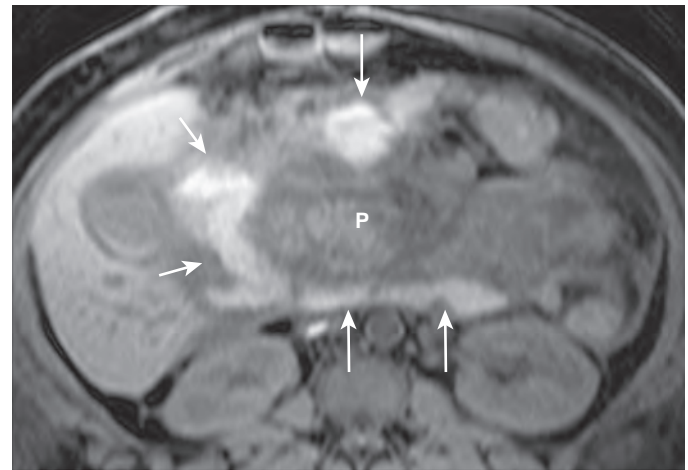


Figure 97-11 Pancreatitis with the development of high signal intensity fluid collections. Axial T1-weighted fat-suppressed spoiled gradient-echo MR image shows complex peripancreatic fluid collection (arrows) with predominantly high signal intensity, which extended inferiorly from the level of the pancreatic head (P). Aspiration biopsy revealed a necrotizing inflammatory process.

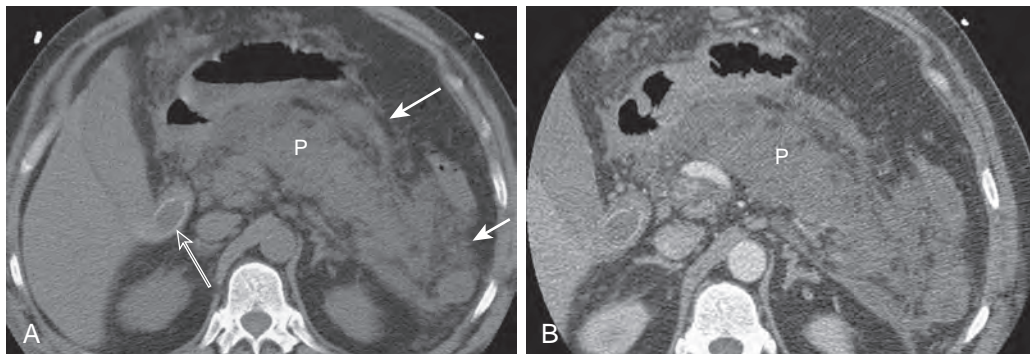


Figure 97-10 Gallstone pancreatitis with necrosis. **A.** Axial nonenhanced MDCT image shows an enlarged pancreas (P) with indistinct borders because of peripancreatic inflammatory changes (solid arrows). Gallstone (open arrow) is seen in the gallbladder neck. **B.** Axial arterial phase contrast-enhanced MDCT image shows lack of enhancement of the pancreas (P), consistent with necrosis.

has a maximum of 10 points and is the sum of inflammation points, pancreatic necrosis points, and extrapancreatic complication points.⁴⁰

Mortele and coworkers⁴⁰ modified the CTSI as the score obtained did not significantly correlate with the development of complications and demonstrated significant interobserver variability in scoring. Moreover, Balthazar and colleagues found no significant difference in morbidity and mortality in differentiating between 30% to 50% necrosis and more than 50% necrosis. The modified CTSI condenses the scoring for necrosis to differentiate above and below 30% and also gives points for extrapancreatic complications.⁴⁰

Delineation of Necrosis. During the arterial phase of bolus intravenous administration of contrast medium, the normal pancreas should enhance homogeneously. Mild inflammation

and interstitial edema do not interfere with the expected homogeneous enhancement of the gland (see Figs. 97-1 and 97-3). When necrosis is present, there is absence of contrast medium enhancement together with liquefaction and a change in the density or signal intensity of the gland (Figs. 97-15 and 97-16). Gadolinium-enhanced T1-weighted gradient-echo MR images demonstrate pancreatic necrosis as low signal areas of nonenhancing parenchyma (Fig. 97-17). The process can be focal or segmental or can affect the entire pancreatic gland and may involve the peripancreatic tissue in combination with the pancreas or separately (see Figs. 97-15 to 97-17).^{122,127,128} In the original series of Kivisaari and associates^{129,130} using CT, mild pancreatitis was associated with a rapid rise in the density of the gland by 40 to 50 HU after administration of contrast material. Pancreatic necrosis was found at surgery in all patients who exhibited absence of enhancement or low enhancing values of

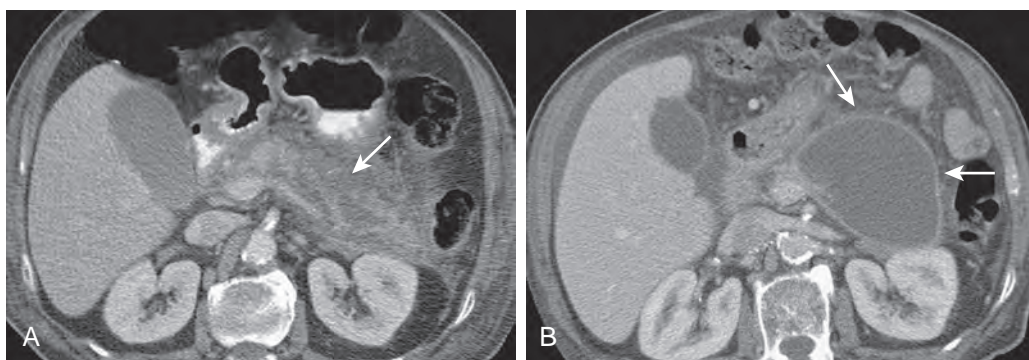


Figure 97-12 Acute pancreatitis with necrosis evolving into walled-off necrosis. **A.** Axial contrast-enhanced MDCT image shows patchy, confluent necrotic areas (arrow) in pancreatic body and tail. Note peripancreatic inflammatory stranding. **B.** Axial contrast-enhanced MDCT image 4 months after the initial episode of pancreatitis shows the development of walled-off necrosis (arrows) in previously necrotic body and tail of pancreas.

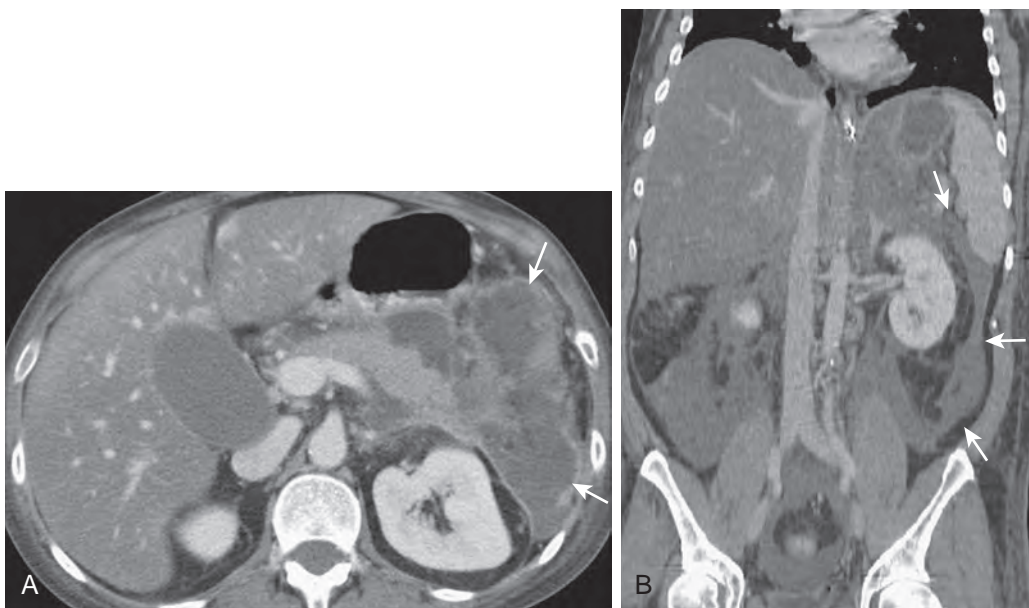


Figure 97-13 Pancreatitis with acute fluid collections. **A.** Axial contrast-enhanced MDCT image shows heterogeneous fluid collection (arrows) in the left anterior pararenal space involving the tail of the pancreas. Note that the fluid collection does not spread beyond Gerota's fascia. This collection extended inferiorly along the left pericolic gutter into the pelvis. **B.** Coronal contrast-enhanced MDCT image from another patient with pancreatitis shows fluid (arrows) extending inferiorly from the pancreatic region along the interfascial planes into the pelvis. The pathway of fluid is better demonstrated on coronal reformatted images.

less than 30 HU (see Figs. 97-15 and 97-16). Other investigators have corroborated the CT-surgical correlation in the detection of pancreatic necrosis.^{131,132} In a series of 93 patients, an overall CT accuracy of 85% with 100% sensitivity for extensive glandular necrosis was found.¹²⁸ At times, MRI may be more

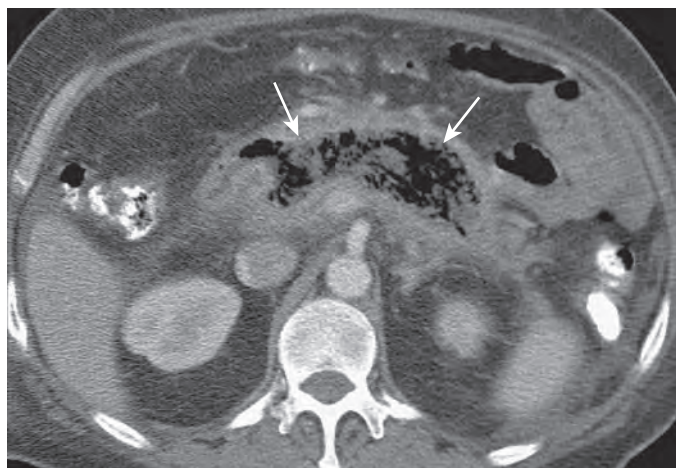


Figure 97-14 Infected necrosis. Axial contrast-enhanced MDCT image shows absence of normal enhancing pancreatic parenchyma. There are air bubbles and debris (arrows) in the pancreatic bed suggesting infected necrosis. The patient underwent pancreatic débridement.



Figure 97-15 Acute necrotizing pancreatitis with acute necrotizing collections in the pancreas and peripancreatic tissues. Axial contrast-enhanced MDCT image shows necrosis of the entire pancreas and peripancreatic necrosis.

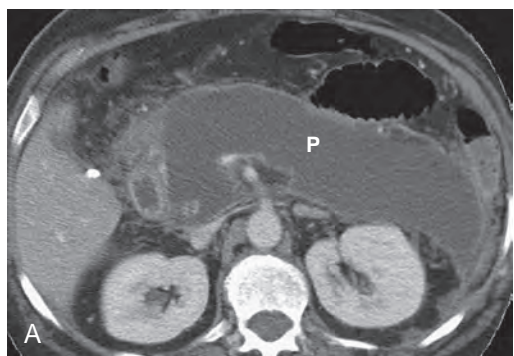


Figure 97-16 Extensive necrotizing pancreatitis. **A.** Axial contrast-enhanced MDCT image shows liquefied necrosis of the entire pancreas (P). Multiple surgical débridements were required. **B.** Autopsy specimen showing necrotizing pancreatitis in a different patient.

sensitive than CT for the detection of pancreatic necrosis because of the greater sensitivity of MRI to gadolinium than of CT to iodinated contrast agents. Many patients with pancreatic necrosis, however, may be seriously ill and may be unable to hold the breath for the required MRI sequences.

In Balthazar's series, there was good correlation between necrosis and length of hospitalization, development of complications, and death; patients without necrosis had no mortality and only 6% morbidity, whereas patients with necrosis exhibited 23% mortality and 82% morbidity.^{119,122} The degree of necrosis also was important. Patients with small areas of necrosis (<30%) showed no mortality and 40% morbidity, whereas large areas of necrosis (≥50%) were associated with 75% to 100% morbidity and 11% to 25% mortality. The combined morbidity of patients with more than 30% necrosis was 94%, and the mortality was 29%. There was no significant difference in prognosis between patients with up to 50% necrosis and those with more than 50% necrosis. Other studies have shown that infected pancreatic necrosis is also a significant predictor of organ failure and mortality in acute pancreatitis.^{90,133,134} Garg⁹⁰ found a mortality rate of 12% for patients with sterile necrosis and 50% for those with infected necrosis.

Indications for Examination. Many patients with acute interstitial edematous pancreatitis have typical clinical presentations and show rapid amelioration with limited supportive therapy. They do not require imaging examinations for diagnosis or management. On the other hand, CT imaging is needed and should be performed early when the clinical diagnosis is in doubt; there is failure to respond to medical treatment within 48 to 72 hours; acute abdominal symptoms (distention, tenderness), leukocytosis, or fever is present; patients have organ failure or signs of severe acute pancreatitis; and there is a change in clinical status suggesting a developing complication. Specific indications for performing MRI over CT include allergy to iodinated contrast agents; to detect the etiology of pancreatitis, such as choledocholithiasis, pancreas divisum, and pancreatic tumors; and to characterize complex fluid collections as liquefied or necrotic and to determine their drainability.

COMPLICATIONS

Local complications after acute pancreatitis include acute peripancreatic fluid collections, pseudocysts, acute necrotic collection, and walled-off necrosis.¹⁰ The prompt detection and treatment of local complications are essential because they are responsible for more than 50% of the mortality associated with acute pancreatitis.^{31,135-137}

Fluid Collections and Pseudocysts

Acute pancreatic fluid collections are generally seen within the first 4 weeks and pseudocysts after 4 weeks. Acute pancreatic fluid collections characteristically do not have a solid component, lack a discrete wall, and are located near the pancreas (see Fig. 97-13). Fluid collections develop in up to 50% of patients with acute pancreatitis within the first few days of pancreatitis. The fluid may be pancreatic juice, serum, or blood. They develop either from actual rupture of the pancreatic duct with liberation of enzymes and pancreatic juice or secondary to exudation of fluid from the surface of the pancreas due to activation of pancreatic enzymes within the gland. The fluid is contained by whatever structures happen to be adjacent to the collection. Most fluid collections are absorbed within 2 to 3 weeks. Drainage or aspiration is generally avoided to prevent introduction of infection unless it is thought to be a rare infected acute pancreatic fluid collection. Unresorbed fluid collections can organize and, within 4 to 6 weeks, develop a fibrous capsule, forming a pseudocyst.^{30,138} The lack of resorption of extravasated secretions and a communicating tract with the pancreatic ductal system are implicated in the development of pseudocysts.

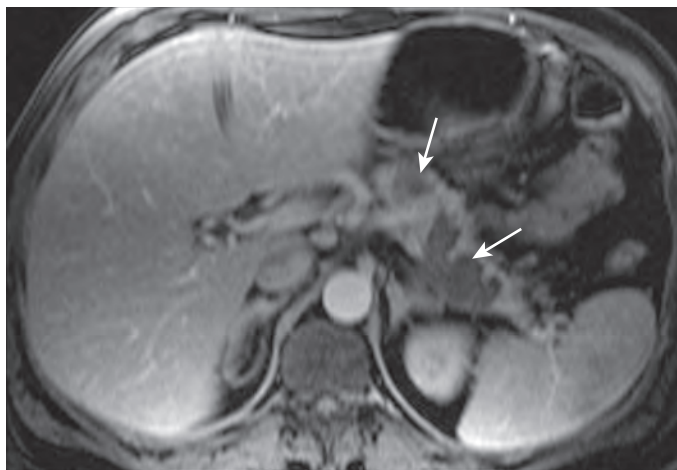


Figure 97-17 Pancreatitis with necrosis involving more than 50% of the gland. Axial gadolinium-enhanced T1-weighted fat-suppressed spoiled gradient-echo MR image shows nonenhancing necrotic areas (arrows) in the body and tail of the pancreas. (From Ly JN, Miller FH: MR imaging of the pancreas: A practical approach. *Radiol Clin North Am* 40:1289–1306, 2002.)

When an acute pancreatic fluid collection becomes encapsulated by a fibrous wall more than 4 weeks after symptom onset, it is referred to as a pseudocyst. Pseudocysts often resolve spontaneously when they lose communication with the pancreatic duct. Pseudocysts develop during the initial attack of pancreatitis in 1% to 3% of patients.^{88,139,140} They have been reported to occur in 12% of patients after several episodes of alcoholic pancreatitis.¹⁶ The main causes of pancreatic pseudocysts are chronic alcoholism (75%) and abdominal trauma (13%), with cholelithiasis, pancreatic carcinoma, and idiopathic causes composing the remainder.¹⁴¹ If the patient with a suspected pseudocyst has no history of pancreatitis, pancreatic trauma, or pancreatic surgery, a follow-up imaging study or aspiration biopsy may be required to exclude a pancreatic cystic neoplasm.¹³⁸

The clinical significance of a pseudocyst is related to its size and the potentially lethal complications that may occur. Pseudocysts displace and compress adjacent abdominal organs and can produce obstruction, pain, and jaundice. Spontaneous rupture in the peritoneal cavity leads to pancreatic ascites or peritonitis. Erosion into an adjacent vessel leads to massive and sudden hemorrhage. Most of these complications, however, occur in pseudocysts larger than 4 to 5 cm. Small pseudocysts, often revealed by CT in asymptomatic patients, have a low incidence of morbidity and can be observed expectantly with clinical and CT examinations.^{30,43} Surgical, endoscopic, or percutaneous drainage is indicated for pseudocysts that increase in size, become symptomatic, or develop complications.^{30,42,142} The development of percutaneous and endoscopic techniques offers an alternative means of drainage of pseudocysts that is less invasive.^{142,143} Success rates of more than 90% have been reported with percutaneous drainage of pseudocysts guided by CT or sonography.^{142,144} Percutaneous drainage techniques of pancreatic fluid collections are discussed in Chapter 95.

Pseudocysts vary greatly in size and are generally round or oval. On CT scans, they are characterized by low fluid density (<15 HU) contents and by a peripheral fibrous capsule. Higher attenuation values are indicative of secondary infection or the presence of necrotic tissue. Hounsfield unit values greater than 40 to 50 are suggestive of intracystic hemorrhage. On MRI, uncomplicated pseudocysts typically show low signal intensity on T1-weighted sequences and high signal intensity on T2-weighted sequences. Complicated pseudocysts may present high signal intensity on T1-weighted images because of hemorrhagic or proteinaceous fluid and may contain solid debris; these are best depicted on T2-weighted images (Figs. 97-18 and 97-19). MRI is superior to other imaging modalities to

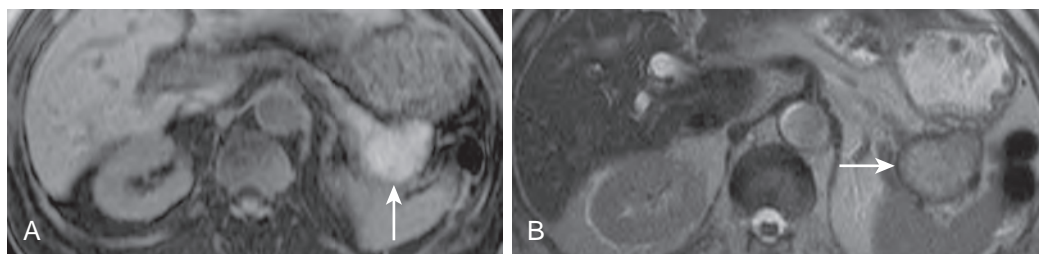


Figure 97-18 Pancreatitis with hemorrhagic pseudocyst. A. Axial T1-weighted fat-suppressed spoiled gradient-echo MR image shows pseudocyst (arrow) in the pancreatic tail with high signal intensity from hemorrhagic content. **B.** Axial T2-weighted HASTE MR image shows low signal intensity rim of hemosiderin in pseudocyst (arrow). The diagnosis of hemorrhage is easily made on MRI because of the hemosiderin rim. (A and B from Miller FH, Keppke AL, Dalal K, et al: MRI of pancreatitis and its complications: Part 1, acute pancreatitis. *AJR Am J Roentgenol* 183:1637–1644, 2004. Reprinted with permission from the American Journal of Roentgenology.)

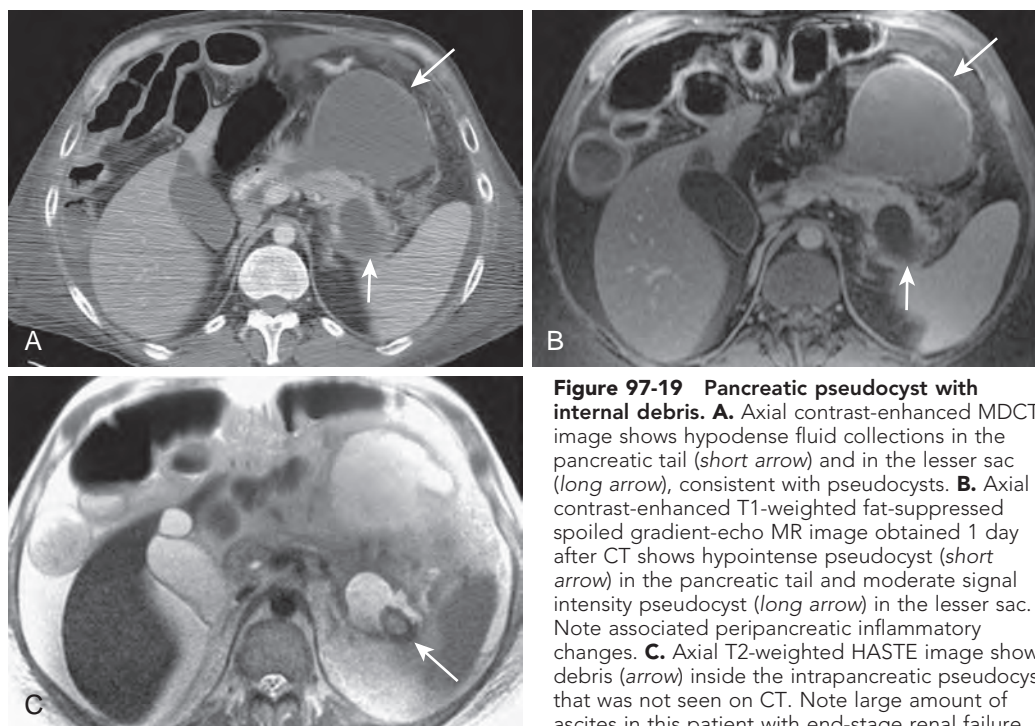


Figure 97-19 Pancreatic pseudocyst with internal debris. **A.** Axial contrast-enhanced MDCT image shows hypodense fluid collections in the pancreatic tail (*short arrow*) and in the lesser sac (*long arrow*), consistent with pseudocysts. **B.** Axial contrast-enhanced T1-weighted fat-suppressed spoiled gradient-echo MR image obtained 1 day after CT shows hypointense pseudocyst (*short arrow*) in the pancreatic tail and moderate signal intensity pseudocyst (*long arrow*) in the lesser sac. Note associated peripancreatic inflammatory changes. **C.** Axial T2-weighted HASTE image shows debris (*arrow*) inside the intrapancreatic pseudocyst that was not seen on CT. Note large amount of ascites in this patient with end-stage renal failure.

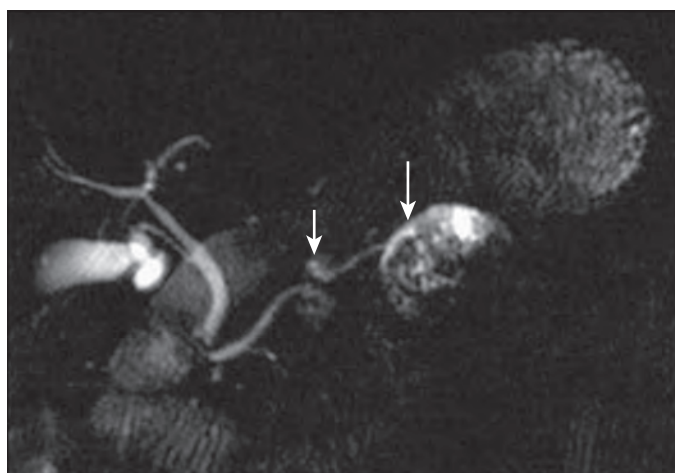


Figure 97-20 Acute pancreatitis with pancreatic duct rupture and pseudocyst. Thick-slab T2-weighted rapid acquisition and relaxation enhancement (RARE) MRCP image shows disrupted pancreatic duct (*short arrow*) and peripancreatic pseudocyst (*long arrow*) containing low signal intensity debris. (From Ly JN, Miller FH: *MR imaging of the pancreas: A practical approach*. Radiol Clin North Am 40:1289–1306, 2002.)

characterize the content of fluid collections, which may have prognostic and therapeutic significance.^{98,145}

ERCP is less effective than CT or MRI in showing pseudocysts as less than 50% of pseudocysts fill with contrast material at ERCP. Conversely, MRCP is able to detect pseudocysts that do not communicate with the pancreatic duct. ERCP, however, may be required to demonstrate communication between a pseudocyst and the pancreatic duct, although sometimes it can be seen on MRI (Fig. 97-20). Communicating pseudocysts may require prolonged catheter drainage until the communication

to the pancreatic duct closes and the cyst collapses. Decompression of concomitant pancreatic duct obstruction may be required.

Although many of the initial poorly defined fluid collections seen in acute pancreatitis resolve spontaneously, the natural history of a pseudocyst is difficult to predict. They may persist, they can resolve, or they can even continue to grow over time. Spontaneous resolution (Fig. 97-21) even of large pseudocysts can occur and is explained by drainage into the pancreatic duct, erosion into an adjacent hollow organ (stomach, small bowel, colon), or rupture with spillage into the peritoneal cavity.

Pancreatic Necrosis

Acute necrotic collection and walled-off necrosis are the terms for local complications of acute necrotizing pancreatitis. Acute necrotic collections, which contain different amounts of fluid and necrotic material, form within 4 weeks of the onset of acute pancreatitis symptoms. They occur only in the setting of acute necrotizing pancreatitis and lack a definable wall. They may be intrapancreatic or extrapancreatic. Walled-off necrosis, a persistent heterogeneous collection (solid and liquefied) with an enhancing thick inflammatory wall, usually develops after 4 weeks of the onset of necrotizing pancreatitis (Figs. 97-22 to 97-24). It may be intrapancreatic or extrapancreatic and may be single or multiple.

The diagnosis of infected necrosis of an acute necrotic collection or walled-off necrosis can be suspected by the patient's clinical findings or presence of gas within a fluid collection. On CT, sterile, partially liquefied pancreatic necrosis cannot be differentiated from infected necrosis unless gas bubbles, seen in about 12% to 18% of cases, are present in the necrotic tissue (see Fig. 97-14).³⁰ In the absence of gas, if required, a percutaneous aspiration for Gram stain and culture could be performed.^{30,140,141,146} Recent series suggest that the large majority of patients do not require fine-needle aspiration, especially if

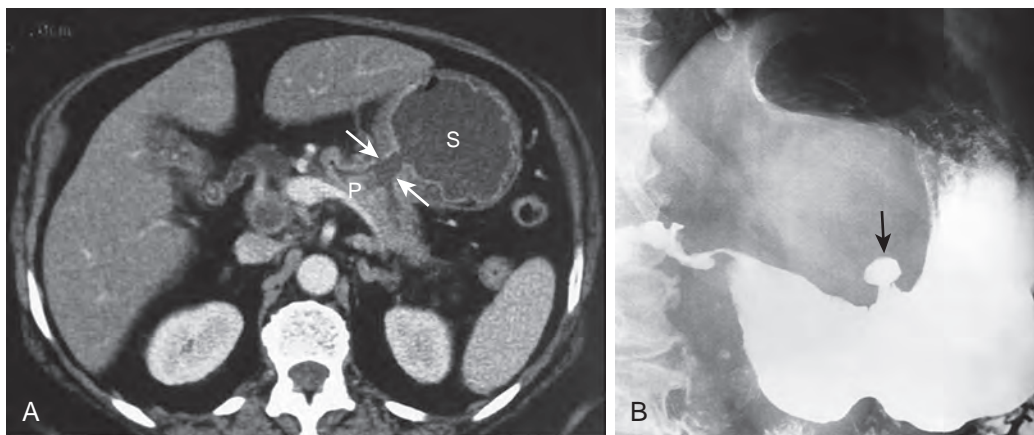


Figure 97-21 Spontaneous rupture of a pseudocyst into the stomach. **A.** The patient had a documented large pseudocyst scheduled to be surgically drained. CT examination before elective surgery shows decompression of the pseudocyst into the stomach (S) (arrows). P, Pancreas. **B.** Upper gastrointestinal examination reveals an ulceration (arrow) consistent with spontaneous drainage of a pseudocyst.

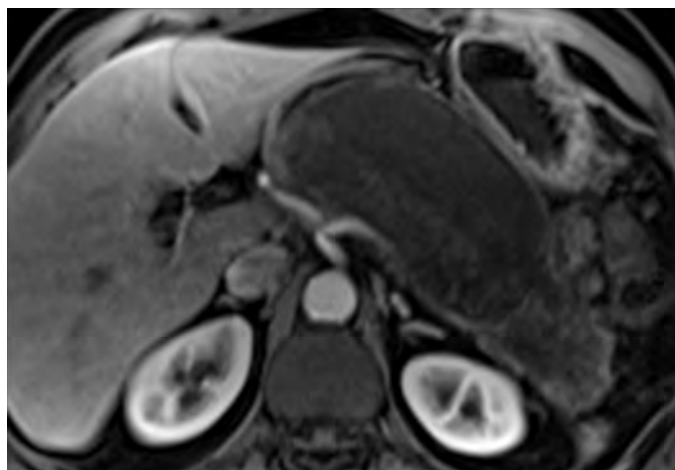


Figure 97-22 Patient with walled-off necrosis. Gadolinium-enhanced T1 fat-suppressed image shows heterogeneous encapsulated collection in the pancreas with nonliquid areas of debris.

percutaneous drainage is part of management.^{10,147} Management of pancreatitis is discussed in Chapter 95.

Infected Pseudocysts

Fluid collections that fail to be resorbed represent an ideal medium for bacterial growth, explaining the development of abscesses, now referred to as infected pseudocysts per the revised Acute Pancreatitis Classification Working Group. In the past, abscesses were considered the major cause of death in acute pancreatitis.^{115,148} The associated high mortality was related mainly to significant delays in diagnosis. They develop within several weeks after the onset of symptoms in patients with severe forms of pancreatitis. Their presence is usually heralded by deterioration in the clinical course with septic systemic symptoms. They may have an inconspicuous clinical presentation initially.¹⁴⁹

Infected pseudocysts are located in the peripancreatic tissues and have different sizes and configurations. On CT scans, they appear as poorly defined or partially encapsulated fluid collections of different densities (20-50 HU) and are often

indistinguishable from residual noninfected fluid collections.⁸⁸ A more characteristic appearance, seen in about 20% of infected pseudocysts, is the presence of gas bubbles produced by gas-forming bacteria. Retroperitoneal gas may be seen in patients with enteric fistulas; however, it is always strongly suggestive of an infection.^{8,13,150} CT is more sensitive than MRI for detection of small gas bubbles, although large collections of gas or gas-fluid levels can be detected on MRI and are best seen on T2-weighted images. CT is accurate in revealing small collections of retroperitoneal fluid and gas and depicting location and extent. This finding quickly identifies a potential life-threatening complication. Infection should be suspected in all patients with pancreatitis in whom poorly encapsulated fluid collections are still present 2 to 4 weeks after the initial attack. MRI may be able to differentiate infected collections with complex internal content from simple collections in these patients (see Fig. 97-24). The use of diffusion-weighted MRI may be helpful. If the diagnosis is in doubt, ultrasound-guided or CT-guided needle aspiration can rapidly and reliably establish the diagnosis, contributing greatly to the early detection, treatment, and decreased mortality in this group of patients.^{142,143,151,152} Percutaneous drainage is the therapeutic procedure of choice for infected pseudocysts.¹⁵³⁻¹⁵⁵

Hemorrhage

Although small patchy areas of hemorrhage combined with necrotic tissue are common findings in acute pancreatitis, massive life-threatening intra-abdominal hemorrhage is seldom reported. This complication may occur within 2 to 3 weeks to several years after an acute episode of pancreatitis.¹⁵⁶⁻¹⁵⁸ It is the result of erosion of peripancreatic vessels with the formation of a pseudoaneurysm and subsequent retroperitoneal bleeding. Commonly, the site of bleeding is along the pancreaticoduodenal arcade or along the splenic vessels adjacent to the tail of the pancreas. Pseudoaneurysms can be located within a pancreatic pseudocyst. Hemorrhage occurs when a slowly enlarging pseudoaneurysm ruptures into the peritoneum or erodes into an adjacent hollow viscus or into the pancreatic duct, producing hemosuccus pancreaticus.¹⁵⁸ CT examination can identify retroperitoneal bleeding by the presence of high-density (50-100 HU) fluid collections. MRI is more sensitive for hemorrhage, which is depicted as high signal intensity on

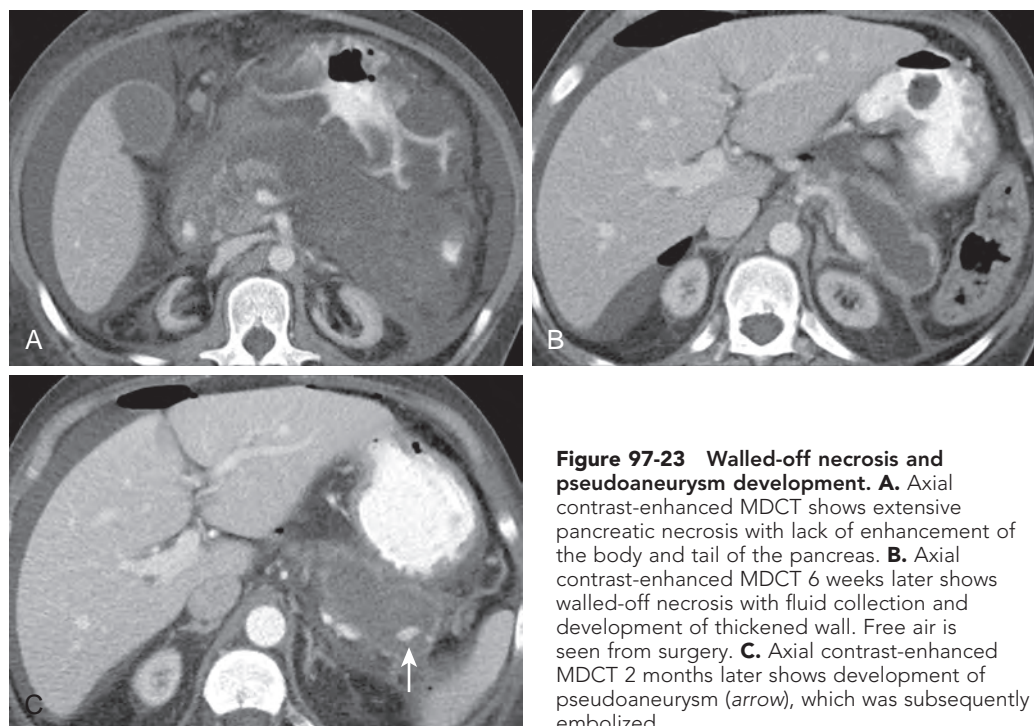


Figure 97-23 Walled-off necrosis and pseudoaneurysm development. **A.** Axial contrast-enhanced MDCT shows extensive pancreatic necrosis with lack of enhancement of the body and tail of the pancreas. **B.** Axial contrast-enhanced MDCT 6 weeks later shows walled-off necrosis with fluid collection and development of thickened wall. Free air is seen from surgery. **C.** Axial contrast-enhanced MDCT 2 months later shows development of pseudoaneurysm (arrow), which was subsequently embolized.

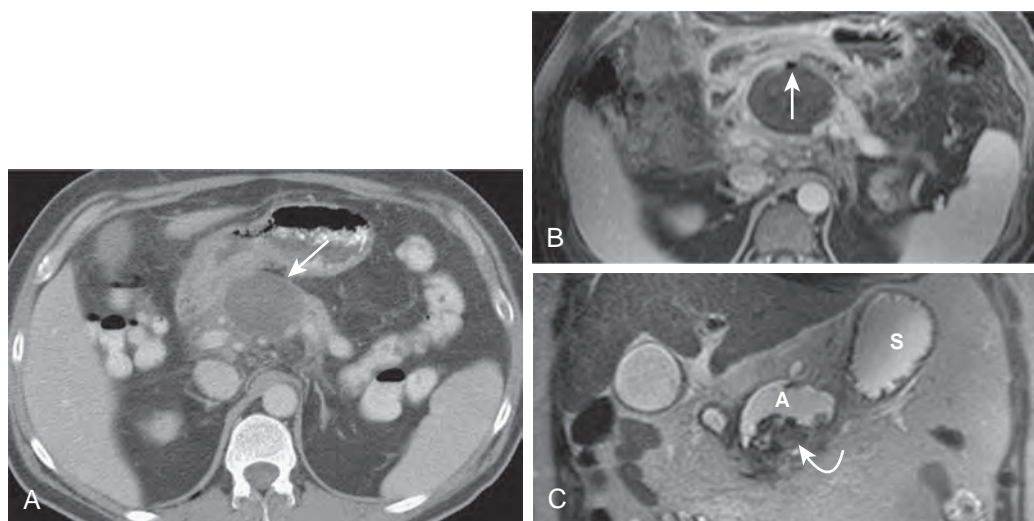


Figure 97-24 Pancreatitis with infected walled-off necrosis. **A.** Axial contrast-enhanced MDCT image shows hypodense fluid collection (arrow) in the pancreatic head suggestive of walled-off necrosis in this patient with pancreatitis. **B.** Axial gadolinium-enhanced T1-weighted fat-suppressed spoiled gradient-echo MR image obtained 11 days after CT shows an air bubble (arrow) within the walled-off necrosis suggestive of infected walled-off necrosis. **C.** Coronal T2-weighted HASTE MR image shows low signal intensity debris (curved arrow) within the pancreatic abscess that was not seen on CT. The presence of necrotic debris was confirmed at surgery. A, Abscess, now referred to as infected walled-off necrosis on the basis of the revised Acute Pancreatitis Classification Working Group. S, Stomach. (B and C from Miller FH, Keppke AL, Dalal K, et al: MRI of pancreatitis and its complications: Part 1, acute pancreatitis. *AJR Am J Roentgenol* 183:1637–1644, 2004. Reprinted with permission from the American Journal of Roentgenology.)

T1-weighted fat-suppressed images because of the presence of methemoglobin. Dynamic enhanced MDCT or T1-weighted gadolinium-enhanced MR images show a pseudoaneurysm as a rapidly enhancing mass similar in contrast density to the adjacent arteries and aorta. Spill of contrast material into the retroperitoneum due to active bleeding, as well as fresh blood in the peritoneal cavity, can also be diagnosed. It is important to have a high index of suspicion for pseudoaneurysm in

patients with history of pancreatitis and a suspected mass in the pancreas or its vicinity and not perform biopsy of these lesions without prior administration of contrast material or Doppler sonography to exclude a pseudoaneurysm (Fig. 97-25; see also Fig. 97-23). If the source of bleeding is obscured by the surrounding hemorrhage, angiography is crucial in identifying the presence and precise location of the bleeding pseudoaneurysm. Therapeutic arterial embolization of the bleeding

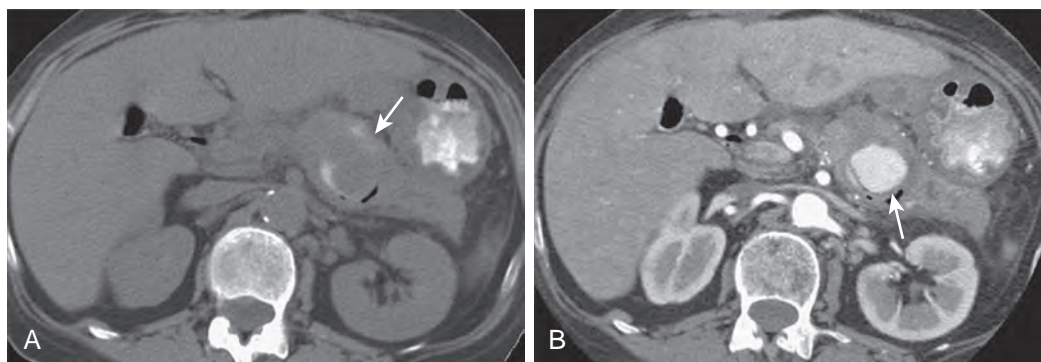


Figure 97-25 Pancreatic pseudoaneurysm. **A.** Axial nonenhanced MDCT image shows expansile lesion (arrow) in pancreatic body, surrounded by contrast material and air from previous ERCP. **B.** Axial arterial phase contrast-enhanced MDCT image clearly shows that the “mass” is a large pseudoaneurysm (arrow). In patients who present with suspected pseudocyst or pancreatic mass for drainage, the intravenous administration of contrast material is critical, as illustrated in this example. This pseudoaneurysm was subsequently embolized.

vessel is required; it is an emergency, lifesaving procedure. Massive hemorrhage from ruptured vessels or pseudoaneurysms requires surgical treatment.

Chronic Pancreatitis

Chronic pancreatitis is a relatively uncommon disease that has been increasing in frequency in the Western world. It is a disease of prolonged pancreatic inflammation characterized by irreversible morphologic and functional damage to the pancreas.¹⁵⁹⁻¹⁶¹

The clinical diagnosis of chronic pancreatitis can be difficult for treating physicians, especially in its early phases, as the findings are nonspecific and imaging features may not be definitive. The diagnosis by imaging relies on morphologic changes of the pancreas that may not be seen in early stages of the disease. The main features include parenchymal atrophy, chronic inflammatory changes, and fibrosis of the pancreas. The incidence of pancreatic cancer is significantly elevated in patients with chronic pancreatitis.^{161,162}

ETIOLOGY

In the United States, approximately 75% of cases of chronic pancreatitis are due to alcoholism. Continued consumption of alcohol for a 3- to 12-year period is necessary before the manifestations of chronic pancreatitis develop.¹⁶² In contrast to their major role in the development of acute pancreatitis, gallstones play little role in the etiology of chronic pancreatitis. Hyperlipidemia, hyperparathyroidism, trauma, and pancreas divisum have been implicated as risk factors for development of chronic pancreatitis.

CLINICAL FINDINGS

Pain is the predominant clinical finding in 95% of patients with chronic pancreatitis. The pain typically radiates from the epigastrium through the back and can be constant or intermittent and extremely difficult to palliate, frequently requiring narcotics or neurolysis. Weight loss often accompanies the pain, and these two findings raise the clinical suspicion of a malignant neoplasm. Endocrine and exocrine deficiencies occur with progressive destruction of the gland. Diabetes and malabsorption with steatorrhea eventually develop in approximately half the patients with chronic pancreatitis.^{162,163}

The clinical diagnosis of chronic pancreatitis, especially in its early stages, is often difficult. Histopathologic diagnosis is rarely available because of the risks associated with pancreatic biopsy, including acute pancreatitis, fistula, and hemorrhage.¹⁶⁴ Therefore, the diagnosis is based on clinical, morphologic, and functional abnormalities. ERCP and pancreatic function tests are considered the “gold standard” diagnostic procedures, but they have limitations, and prolonged clinical follow-up is sometimes required to confirm the diagnosis.

RADIOLOGIC FINDINGS

Plain Films

Typical pancreatic calcifications are diagnostic of chronic pancreatitis. They develop in 40% to 60% of patients with alcoholic pancreatitis, and approximately 90% of calcific pancreatitis is caused by alcoholism. Unfortunately, calcifications occur late in the course of chronic pancreatitis, being associated with severe disease. Most pancreatic calculi are small, irregular calcifications that may be diffuse (Fig. 97-26) or confined to a specific region of the pancreas. Although they can appear on plain films, CT is the most specific and accurate imaging modality to depict pancreatic calcifications.

Ultrasonography

The development of high-resolution linear array scanners has significantly increased the diagnostic accuracy of sonography in patients with pancreatitis. Whereas there have been significant improvements in ultrasound machines and high-frequency and high-resolution transducers, there have not been any recent studies to assess the utility of ultrasound in the diagnosis of chronic pancreatitis. Similar to CT, however, transabdominal sonography is insensitive for the diagnosis of early chronic pancreatitis.

Sonographic findings include abnormalities in gland size, irregular margins, inhomogeneous or heterogeneous echogenicity of parenchyma, and dilation of the pancreatic duct. The classic finding of chronic pancreatitis with sonography is calcifications seen as echogenic foci within the parenchyma or the main pancreatic duct. The calcifications may or may not shadow, depending on their size, and may show color Doppler twinkling artifact.¹⁶⁵ Pseudocysts are often present in chronic pancreatitis, and they are usually unilocular, anechoic, and

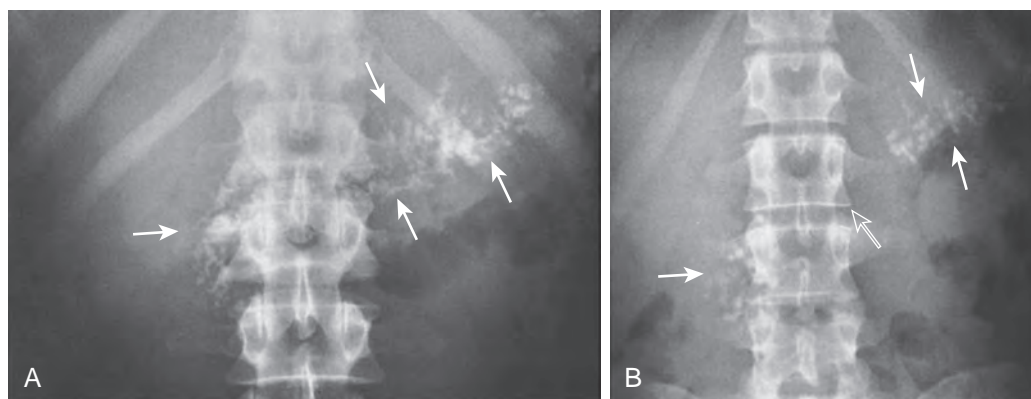


Figure 97-26 Pancreatic calcifications on plain abdominal radiographs. A. The entire gland contains numerous small calcifications located in the main pancreatic duct and its radicles (arrows). **B.** Pancreatic calcifications are located in the head and tail of the pancreas (solid arrows). The lack of calcifications in the body of the pancreas (open arrow) was due to displacement by a pancreatic pseudocyst.

sharply defined.¹⁶⁶⁻¹⁶⁸ Other complications of chronic pancreatitis, such as biliary dilation and splenic vein thrombosis, can also be detected with sonography.

Abnormalities in size and contour of the pancreas are the least sensitive indicators of chronic pancreatitis on ultrasound studies and may be subjective. Diffuse enlargement is often present early in the course of the disease, and atrophy or focal enlargement may be present later. An atrophic gland is usually difficult to appreciate, and some gland atrophy normally occurs with aging.¹⁶⁹

Pancreatic parenchymal echogenicity is also unreliable in the diagnosis of chronic pancreatitis because it can be normal, increased, or decreased. Decreased echogenicity occurs when there are acute exacerbations with parenchymal edema.^{164,169,170}

Dilation of the pancreatic duct is one of the most common sonographic abnormalities of chronic pancreatitis. It is seen in up to 90% of cases as a tubular, anechoic structure in the pancreatic body.

Endoscopic Ultrasound

EUS overcomes many of the limitations of transabdominal sonography because of the proximity of the transducer to the pancreas and the superior image resolution provided by high-frequency transducers. Although EUS is an invasive imaging modality, it has a low risk of complications. In many cases, EUS is helpful to elucidate the cause of pancreatitis, being able to detect small pancreatic tumors and microlithiasis not seen by other imaging modalities.¹⁷¹⁻¹⁷³ EUS can demonstrate biliary sludge and tiny stones that are often masked by the contrast medium on ERCP. In 77% to 92% of cases of idiopathic pancreatitis, EUS is able to diagnose the cause, which is small gallstones in the majority of these patients.^{173,174}

EUS findings indicative of chronic pancreatitis include parenchymal calcifications, hyperechoic foci or strands, pseudocysts, heterogeneous echotexture, and lobular contour of the gland.¹⁷⁵⁻¹⁷⁸ Ductal abnormalities include dilation and irregularity, hyperechoic walls, intraductal stones, and visible branches.^{176,178} Chronic pancreatitis is likely when more than two of these findings are present. With more than six findings, the disease is probably moderate to severe.¹⁷⁸ Unlike ERCP, EUS has the advantage of being able to evaluate simultaneously the pancreatic ductal system and the parenchyma. However, the diagnosis of chronic pancreatitis based on EUS changes alone

is controversial.^{164,175} There is usually a good correlation of EUS with ERCP in patients with moderate or severe chronic pancreatitis, but not in those with mild disease.^{176,179-181} Other studies reported abnormal findings on EUS examinations in patients with normal ERCP findings and pancreatic function test results, suggesting that EUS may overdiagnose chronic pancreatitis, or alternatively, it may be more sensitive than ERCP and function tests to detect subtle pancreatic changes.^{176,182} In a study of patients with suspected chronic pancreatitis, the addition of fine-needle aspiration improved the negative predictive value but did not improve the specificity of EUS findings in patients with normal ERCP findings.¹⁸³ EUS can be especially helpful when it is combined with fine-needle aspiration of a suspicious mass in patients with chronic pancreatitis. Biopsy of regional lymph nodes and assessment of tumor extension and vascular involvement can be performed with EUS to enhance staging in these patients. EUS also has therapeutic applications in chronic pancreatitis, such as to perform celiac plexus blocks to alleviate pain in patients without ductal obstruction and to guide internal stent placement for decompression of pseudocysts.^{184,185} Disadvantages of EUS include its cost, limited availability, long learning curve, and operator dependence.

Endoscopic Retrograde Cholangiopancreatography

Many of the reported findings of chronic pancreatitis are based on ERCP, and because of its relative invasiveness, it is not often used for diagnostic purposes but is used for therapeutic purposes. Less invasive studies, such as CT, MRI, and EUS, are now used mainly for diagnosis of chronic pancreatitis and its complications.^{186,187} In early chronic pancreatitis, the pancreatic duct is often normal, limiting the sensitivity of ERCP. The earliest changes involve the first-order and second-order side branches of the main pancreatic duct and include dilation and contour irregularity, clubbing, stenosis of the side branches, and opacification of small cavities. Some of these changes, however, can be seen in elderly normal patients and must be interpreted with caution in this age group.^{188,189}

With disease progression, the involvement of the main pancreatic duct increases with more dilation, mural irregularities, loss of normal tapering, and areas of stenosis or occlusion. If a solitary stricture is seen in the main pancreatic duct, the differential considerations include neoplasm and pseudocyst. Stenoses are usually shorter, smoother, and more symmetric in

pancreatitis than those associated with neoplasm.^{190,191} Biopsy of suspicious lesions or brushing and collection of pancreatic secretions can be performed with ERCP and may be helpful to diagnose pancreatic carcinoma. In advanced chronic pancreatitis, the dilation is more marked, and intraductal calculi can be seen. The pancreatic duct and side branches may have a “chain of lakes” appearance.

According to the Cambridge classification, chronic pancreatitis is considered mild if the main pancreatic duct is normal but at least three side branches are abnormal. Moderate disease requires abnormalities in the main pancreatic duct and in more than three side branches. Severe disease includes the abnormalities of moderate disease plus one of the following: a large cavity, ductal obstruction, filling defects, severe dilation, or irregularity.¹⁹²

ERCP is able to detect early chronic pancreatitis before morphologic abnormalities can be seen on CT.¹⁶⁴ There is a good correlation between ERCP and histology in chronic pancreatitis. The correlation between pancreatic function tests and ERCP is limited, however, especially in the early stages of chronic pancreatitis.^{164,192,193} ERCP is also helpful in the treatment of complications of pancreatitis, such as pancreatic duct strictures and pseudocysts, avoiding the complications of surgery.¹⁸⁷

Magnetic Resonance Cholangiopancreatography

ERCP used to be the standard imaging modality to evaluate the pancreaticobiliary tract, being a diagnostic and therapeutic procedure. Because of its invasiveness and potentially serious complications, however, ERCP is ideally reserved for patients who need therapeutic intervention. MRCP has been increasingly used in patients with suspected pancreatitis or pancreaticobiliary abnormalities because it lacks ionizing radiation, does not require iodinated contrast material, and is noninvasive, sparing the patient from potential complications. MRCP is also helpful in patients with anatomic abnormalities that impede cannulation of the common bile duct or pancreatic duct. With heavily T2-weighted sequences, MRCP is able to depict fluid-filled structures, such as pseudocysts, and to detect abnormalities of the pancreatic duct, including dilation, irregularity, intraductal stones, and multiple or severe obstructions, which may be a limitation for ERCP.^{194,195} MRCP has the advantage of showing the ductal segments proximal and distal to an obstruction, being able to evaluate its character, extent, location, and cause.

ERCP and more recently MRCP are helpful to evaluate the pancreatic duct for findings of chronic pancreatitis in patients with abdominal pain that is refractory to medical therapy.¹⁹⁵⁻¹⁹⁷ The sensitivity of MRCP to detect ductal abnormalities and dilation ranges from 56% to 100%, and the specificity ranges from 86% to 100%.¹⁹⁵⁻¹⁹⁷ Stricture or obstruction of the pancreatic or bile duct by stones is a major cause of pain and one of the main indications for surgery in chronic pancreatitis.¹⁹⁸ In the presence of ductal dilation, ductal drainage procedures combined with partial resection of the head of the pancreas may result in long-term pain relief in 60% to 80% of patients.

The administration of secretin during MRCP allows evaluation of the exocrine function of the pancreas, improves delineation of the pancreatic duct, and may be useful to detect abnormalities of the side branches in early chronic pancreatitis before morphologic changes seen on imaging.^{72,199,200} Secretin temporarily distends the pancreatic ducts by inducing pancreatic secretions and increasing the tone of the sphincter of Oddi.

Secretin also improves detection of ductal narrowing and endoluminal filling defects in severe chronic pancreatitis.²⁰⁰ Significant correlation between reduced duodenal filling scores during secretin-enhanced MRCP and impaired pancreatic exocrine function has been reported, and it can be performed with semi-quantitative or quantitative measurements.^{199,201-205} Normal quantitative exocrine function consists of complete filling of the duodenum with pancreatic fluid output. Suboptimal quantitative exocrine function consists of filling of only a portion of the duodenum. Diffusion-weighted imaging after secretin may be helpful.^{202,203,206}

Computed Tomography and Magnetic Resonance Imaging

CT imaging is considered by many to currently be the best initial imaging test for the diagnosis of chronic pancreatitis.^{164,207-209} It is widely available and reproducible and allows comprehensive evaluation of the pancreas and adjacent organs to help make the diagnosis of chronic pancreatitis and to exclude other causes of symptoms, such as abdominal pain or weight loss. The diagnostic criteria for chronic pancreatitis on CT and MR examinations are based on assessment of the size and contour of the gland, dilation and shape of the pancreatic duct, and presence of ductal calcifications^{164,190,210} (Fig. 97-27). CT has reported sensitivities of 50% to 90% and specificities of 55% to 85% in the detection of chronic pancreatitis.²⁰⁹ Despite marked improvements in CT technology since this initial study in 1989 by the Mayo Clinic, there have not been any recent studies to evaluate the accuracy of CT in the diagnosis of chronic pancreatitis.

Although CT correctly detects the morphologic alterations of chronic pancreatitis, its ability to evaluate severity of disease is more limited. These shortcomings are related to (1) the inability of CT to accurately diagnose incipient forms of chronic pancreatitis that do not exhibit gross morphologic changes and (2) poor correlation between functional exocrine and endocrine deficit and pancreatic morphology on imaging studies. Compared with ERCP and pancreatic function tests, CT is not sensitive in the diagnosis of early chronic pancreatitis. Some experts^{105,211-213} believe that MRI can detect findings of



Figure 97-27 Chronic pancreatitis. Axial contrast-enhanced MDCT image shows pancreatic atrophy with diffuse calcifications, mild dilation of the pancreatic duct, and a 1.2 × 1-cm pseudocyst (arrow) in the pancreatic body.

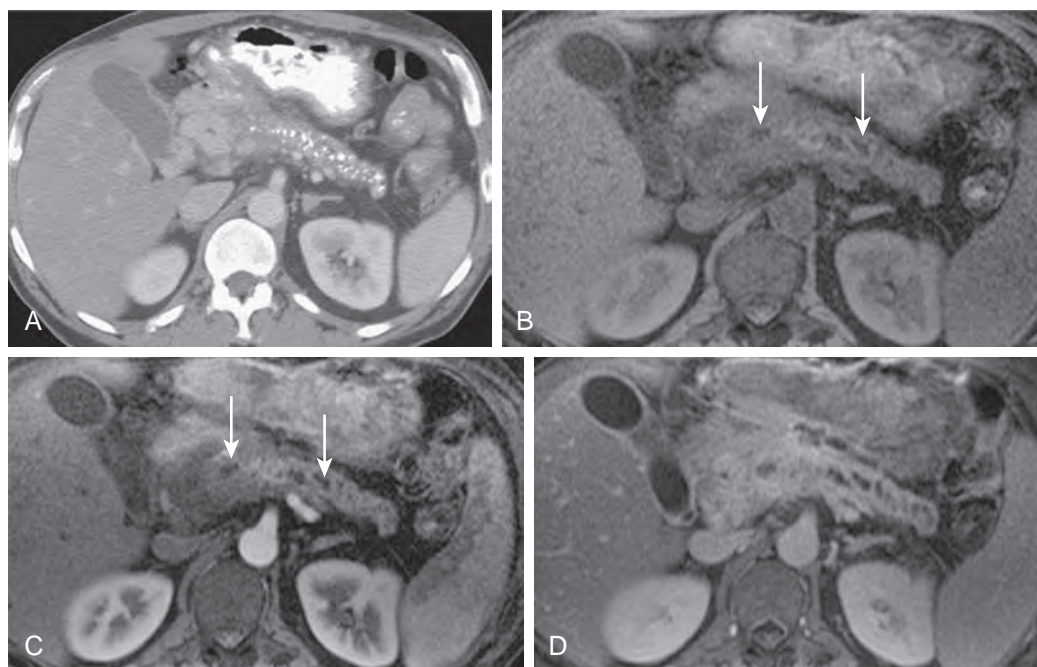


Figure 97-28 Chronic pancreatitis. **A.** Axial contrast-enhanced MDCT image shows pancreatic atrophy with multiple diffuse calcifications in a patient with chronic pancreatitis due to alcohol abuse. **B.** Axial T1-weighted fat-suppressed spoiled gradient-echo MR image shows decreased heterogeneous signal intensity of the pancreas and irregular dilation of the main pancreatic duct (arrows). **C** and **D.** Axial gadolinium-enhanced T1-weighted fat-suppressed spoiled gradient-echo MR images show decreased pancreatic enhancement during the arterial phase (**C**) and delayed enhancement in the venous phase (**D**) related to fibrosis due to chronic pancreatitis. Dilated pancreatic duct (arrows in **C**) is more clearly visualized after gadolinium enhancement. (**B-D** from Miller FH, Kepcke AL, Wadhwa A, et al: MRI of pancreatitis and its complications: Part 2, chronic pancreatitis. *AJR Am J Roentgenol* 183:1645–1652, 2004. Reprinted with permission from the American Journal of Roentgenology.)

chronic pancreatitis before CT on the basis of signal intensity abnormalities of the pancreas, which may be seen before abnormalities involving the pancreatic duct. These changes are best visualized on unenhanced and gadolinium-enhanced T1-weighted fat-suppressed images. The normal pancreas is high signal intensity due to the presence of acinar proteins and enhances markedly after the administration of gadolinium. Chronic pancreatitis and associated fibrosis result in loss of proteinaceous material and decreased signal intensity of the pancreas. Unlike the normal pancreas, the chronically inflamed and fibrotic pancreas shows decreased and heterogeneous enhancement during the arterial phase after administration of contrast material and relatively increased enhancement on later phases.^{105,211,212,214} (Fig. 97-28). Zhang and coworkers²¹³ found a sensitivity of 92% and specificity of 75% for the diagnosis of chronic pancreatitis based on abnormal enhancement pattern, as opposed to 50% diagnostic sensitivity based on morphologic changes of the pancreas.

Alteration in the size of the pancreas with atrophy is often seen in chronic pancreatitis; however, the gland may be normal or only slightly increased in size in 15% to 20% of cases, making the diagnosis more difficult. In one series, focal enlargement was present in 30% and atrophy of the gland in 54% of patients²⁰⁹ (see Fig. 97-27). Significant atrophy of the pancreas may be seen in elderly persons without chronic pancreatitis. Evaluation of the history and clinical and functional findings may be necessary for differential diagnosis. Focal enlargement of the gland produced by a chronic inflammatory mass may simulate a pancreatic neoplasm. In these cases, when CT is inconclusive, MRI may provide additional diagnostic

information; however, regardless of the imaging modality used, this distinction can be difficult.^{215,216} Several studies have demonstrated that focal pancreatitis and pancreatic carcinoma may have similar appearance and pattern of enhancement on CT and MRI because of the presence of fibrosis in both types of lesions.^{212,217-219} As a result, both pancreatic carcinoma and focal chronic pancreatitis may have restricted diffusion from fibrosis with lower apparent diffusion coefficient values. Both conditions may also cause dilation of the pancreatic duct and common bile duct (double duct sign), ductal strictures, and arterial encasement and peripancreatic venous obstruction.²¹⁶ In addition, carcinoma develops in 2% to 3% of cases of chronic pancreatitis, and this malignant degeneration is often difficult to appreciate on CT.²²⁰ A new or rapidly increasing homogeneous and ill-defined pancreatic mass, which can be detected by comparison with previous CT examinations or short-term follow-up, is indicative of malignant disease. Imaging features that favor the diagnosis of inflammatory mass related to chronic pancreatitis over adenocarcinoma include a nondilated or smooth tapering pancreatic duct coursing through the mass (duct penetrating sign), presence of pancreatic calcifications, lower ratio of duct caliber to pancreatic gland width, and irregular ductal dilation.^{212,217,219} The imaging features of adenocarcinoma and focal pancreatitis often overlap, however, and complementary studies including ERCP and EUS with fine-needle aspiration biopsy may be required for definite diagnosis.

Dilation of the pancreatic duct and its secondary radicles (>2 to 3 mm in size) is characteristic of chronic pancreatitis (Figs. 97-29 and 97-30). In advanced disease, the main duct appears

beaded, irregular, or smooth, often containing stones (Fig. 97-31). These pancreatic duct abnormalities are better demonstrated on MRI and MRCP examinations compared with CT scans. Subtle changes in side branches seen in early chronic pancreatitis, however, are best depicted on ERCP. The use of three-dimensional thin-slice MRCP images has improved delineation of the pancreatic duct, and if warranted, secretin can be used to improve pancreatic duct distention. The pancreatic duct should be visualized entirely to the level of the papilla because small tumors of the head of the pancreas may produce similar findings. The pancreatic duct may be dilated in patients with senile atrophy of the pancreas, mimicking chronic pancreatitis.

Pancreatic calcifications (see Figs. 97-27 and 97-28) are seen on CT scans in approximately 50% of patients with chronic pancreatitis.^{209,210} These calcifications are the most reliable imaging indicator of the disease. They can be scattered throughout the gland, isolated, or focal in the head or body of the pancreas. Calcifications vary from innumerable to single and small. The CT findings of chronic calcific pancreatitis are more difficult to visualize on MRI as it is less able to demonstrate calcifications compared with CT. MRI, however, may be helpful

in demonstrating the intraductal nature of stones as T2-weighted images easily show the low signal intensity stone in contrast to the high signal intensity pancreatic fluid in the duct.^{96,214}

Pseudocysts of various sizes may be present within the pancreas or in an extrapancreatic location. They occur in 25% to 60% of patients with chronic pancreatitis and are usually stable.^{13,30}

Pseudoaneurysms and thrombosis of the splenic vein with extensive collateral circulation and gastric varices are sometimes encountered in chronic pancreatitis and can be readily diagnosed by CT and MRI (Fig. 97-32). In addition, patients with repeated episodes of acute exacerbation may present with an acute abdominal catastrophe, dropping hematocrit, and evidence of massive intra-abdominal bleeding.

Pancreaticopleural Fistula

Pancreaticopleural fistula can occur in acute or chronic pancreatitis or as a result of pancreatic trauma. Pancreatic secretions from a ruptured pancreatic duct dissect through the aortic or esophageal hiatus or directly through the diaphragm and reach

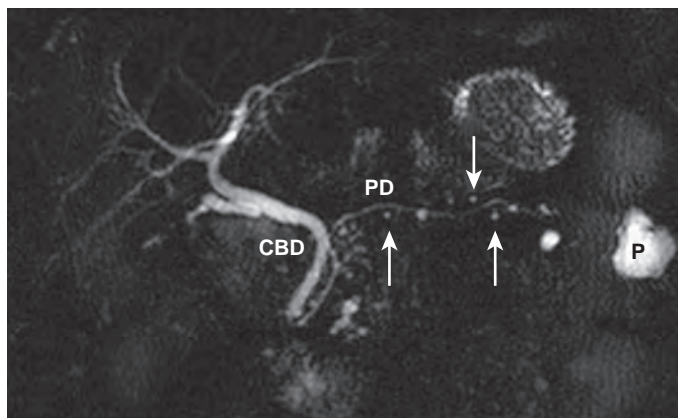


Figure 97-29 Early chronic pancreatitis. Coronal T2-weighted thick-slab RARE MR image shows mild dilation of the secondary branches of the pancreatic duct (arrows) and pseudocyst (P) in the pancreatic tail. The main pancreatic duct (PD) and the common bile duct (CBD) have normal caliber. (From Miller FH, Keppke AL, Wadhwa A, et al: MRI of pancreatitis and its complications: Part 2, chronic pancreatitis. *AJR Am J Roentgenol* 183:1645–1652, 2004. Reprinted with permission from the American Journal of Roentgenology.)

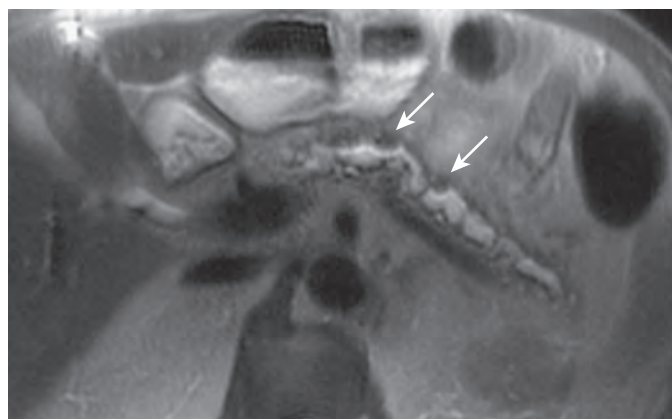


Figure 97-31 Severe chronic pancreatitis. Axial T2-weighted HASTE MR image shows dilation of the main pancreatic duct and side branches, giving a "chain of lakes" appearance. The pancreas is atrophic and contains signal void areas (arrows) related to calcifications from chronic pancreatitis. (From Miller FH, Keppke AL, Wadhwa A, et al: MRI of pancreatitis and its complications: Part 2, chronic pancreatitis. *AJR Am J Roentgenol* 183:1645–1652, 2004. Reprinted with permission from the American Journal of Roentgenology.)

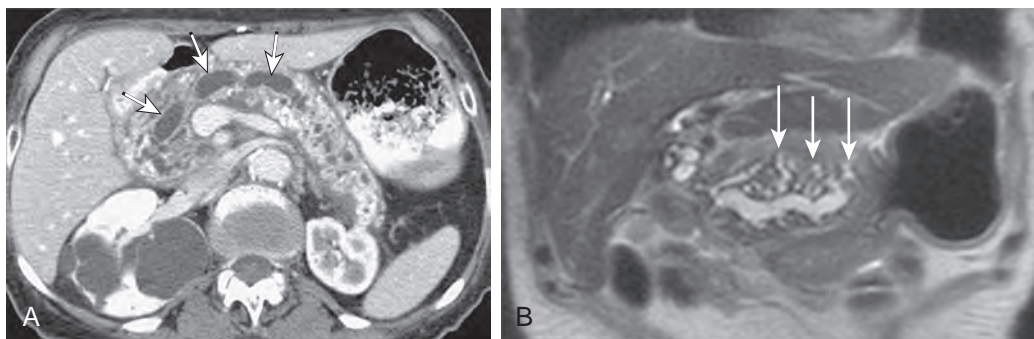


Figure 97-30 Chronic pancreatitis. A. Axial contrast-enhanced MDCT image shows diffuse calcifications in the pancreas with a dilated main pancreatic duct (arrows) measuring 9 mm and dilated side branches. **B.** Coronal T2-weighted MR image shows the dilated pancreatic duct and secondary radicles (arrows) associated with chronic pancreatitis. (B from Miller FH, Keppke AL, Wadhwa A, et al: MRI of pancreatitis and its complications: Part 2, chronic pancreatitis. *AJR Am J Roentgenol* 183:1645–1652, 2004. Reprinted with permission from the American Journal of Roentgenology.)

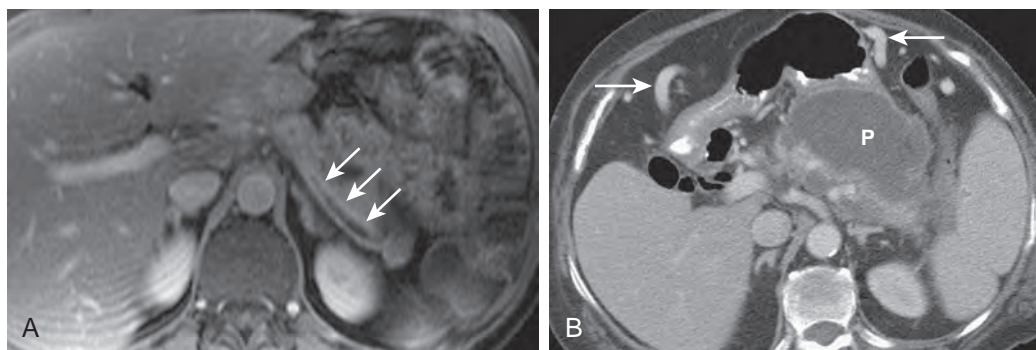


Figure 97-32 Splenic vein thrombosis. **A.** Axial enhanced T1-weighted fat-suppressed spoiled gradient-echo MR image shows low signal intensity thrombus (arrows) in the splenic vein. **B.** Axial contrast-enhanced MDCT image from another patient shows pancreatic pseudocyst (P) and the presence of collateral vessels (arrows), suggesting splenic vein occlusion. (A from Miller FH, Keppke AL, Dalal K, et al: MRI of pancreatitis and its complications: Part 1, acute pancreatitis. *AJR Am J Roentgenol* 183:1637–1644, 2004. Reprinted with permission from the American Journal of Roentgenology.)

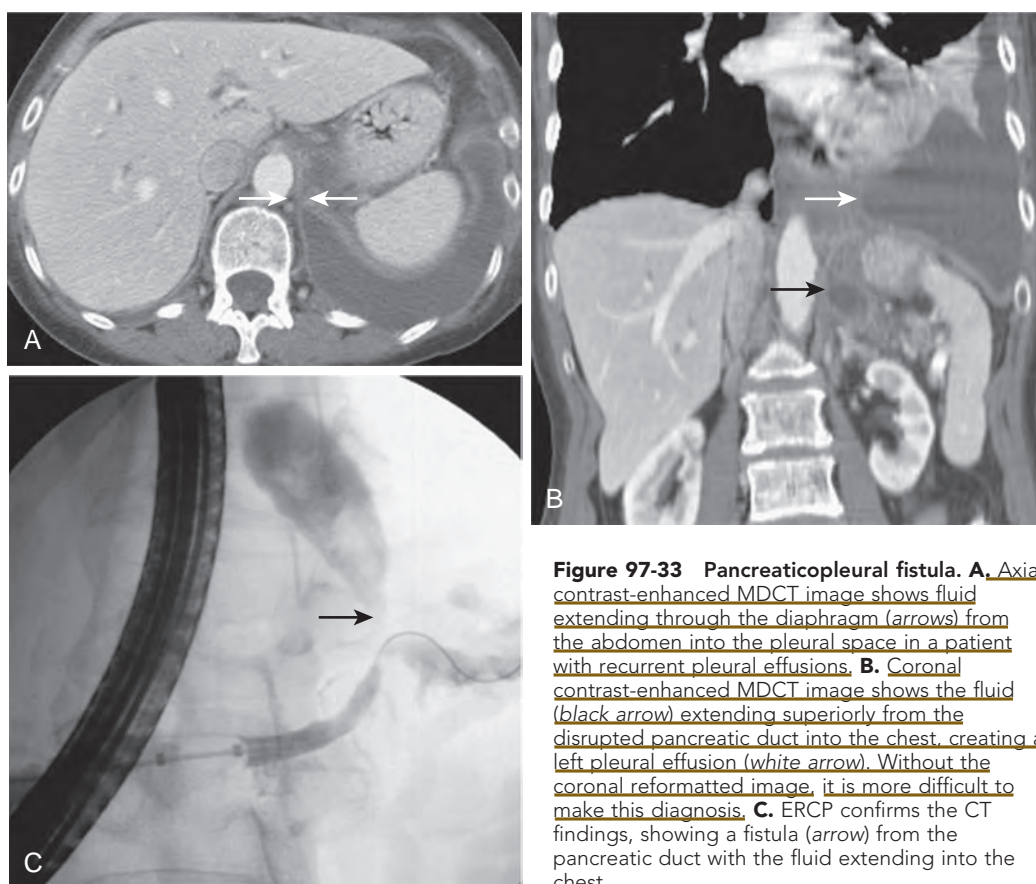


Figure 97-33 Pancreaticopleural fistula. **A.** Axial contrast-enhanced MDCT image shows fluid extending through the diaphragm (arrows) from the abdomen into the pleural space in a patient with recurrent pleural effusions. **B.** Coronal contrast-enhanced MDCT image shows the fluid (black arrow) extending superiorly from the disrupted pancreatic duct into the chest, creating a left pleural effusion (white arrow). Without the coronal reformatted image, it is more difficult to make this diagnosis. **C.** ERCP confirms the CT findings, showing a fistula (arrow) from the pancreatic duct with the fluid extending into the chest.

the mediastinum, pleural cavities, pericardium, or bronchial tree. Patients usually present with large pleural effusions and dyspnea. A high index of suspicion for pancreaticopleural fistula is required. CT and MRI may show the fistula, especially when coronal images are used, as well as the changes of chronic pancreatitis, which are usually present (Fig. 97-33). ERCP has been considered the best imaging modality for evaluation of pancreaticopleural fistulas, but technical failures may result from incomplete opacification of the pancreatic duct or a long fistulous track. MRCP may depict the fistula and the ductal anatomy and can be helpful in the surgical planning of these patients, potentially replacing ERCP.²²¹

Groove Pancreatitis

Patients who suffer repeated episodes of pancreatitis or acute exacerbations of chronic pancreatitis may develop a form of segmental pancreatitis described as groove pancreatitis, in which the inflammatory reaction and fluid collection dissect into the “groove” between the duodenum, the head of the pancreas, and the common bile duct (Fig. 97-34).

Groove pancreatitis has been most frequently reported in young men with a history of alcohol abuse. There is no clear evidence for its exact pathogenesis. Multiple factors have been suggested to play a role in its development. Pancreatic heterotopia, abnormal development of the Santorini duct, pancreas

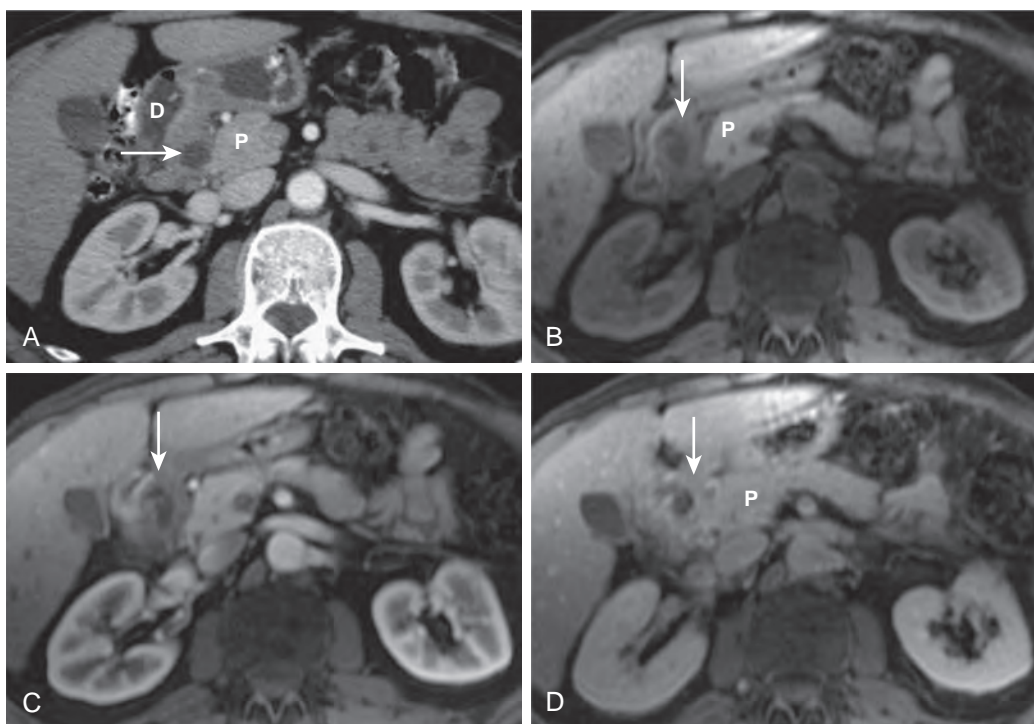


Figure 97-34 Groove pancreatitis. **A.** Axial contrast-enhanced MDCT shows hypoenhancing inflammatory tissue containing low-density cyst (arrow) in the groove between the duodenum (D) and the pancreatic head (P). **B.** Axial T1-weighted fat-suppressed spoiled gradient-echo MR image shows low signal intensity of the inflammatory mass (arrow) between the high signal intensity pancreatic head (P) and the duodenum. **C** and **D.** The mass (arrow) has decreased enhancement in the arterial phase (**C**) and delayed enhancement in the venous phase (**D**) after gadolinium administration because of fibrosis. (**A-D** from Miller FH, Keppke AL, Wadhwa A, et al: MRI of pancreatitis and its complications: Part 2, chronic pancreatitis. *AJR Am J Roentgenol* 183:1645–1652, 2004. Reprinted with permission from the American Journal of Roentgenology.)

divisum, peptic ulcer disease, and alcohol abuse are precipitating risk factors.²²²

Two forms of groove pancreatitis have been described, the pure form and the segmental form. The pure form is associated with scar tissue in the groove without pancreatic involvement; the segmental form includes scar tissue in the groove and involvement of the pancreatic head. Because of the enzymatic action of pancreatic secretions, as many as 50% of patients develop duodenal stenosis or strictures of the common bile duct.¹¹¹ The recognition of groove pancreatitis is important to distinguish it from pancreatic and duodenal carcinoma, which can be challenging.²²³⁻²²⁵ With groove pancreatitis, contrast-enhanced CT shows a poorly enhancing lesion extending between the duodenum and the pancreatic head. Cysts in the groove or duodenal wall and duodenal stenosis are often seen. The head of the pancreas enhances normally. MR findings of groove pancreatitis include a sheetlike fibrotic mass between the pancreatic head and a thickened duodenal wall associated with cystic changes in the duodenal wall.²²⁶ This fibrotic mass is hypointense to the pancreas on T1-weighted images and can be hypointense, isointense, or slightly hyperintense on T2-weighted images. The cystic component is low signal intensity on T1-weighted images and high signal intensity on T2-weighted images and does not enhance because of its fluid content. The fibrotic component demonstrates delayed enhancement after the administration of gadolinium and is easily demarcated from the normal pancreas, which has marked enhancement initially and less intense enhancement on more delayed images (see Fig. 97-34).^{212,227} Similar duodenal changes, referred to as cystic

dystrophy of the duodenal wall, have been reported in patients with acute pancreatitis and heterotopic pancreatic tissue in the duodenum.²²⁸ The cystic lesions in the duodenal wall may compress the common bile duct and main pancreatic duct, causing duct dilation.

MRCP is the imaging modality of choice for evaluation of the biliary and pancreatic ducts in groove pancreatitis.²²³ The main pancreatic duct usually appears normal in the pure form of groove pancreatitis but may have mild dilation in the segmental form, which presents with a focal hypodense lesion in the head of the pancreas and duodenal wall.²²³ In general, groove pancreatitis causes a smooth, long, and medially deviated common duct with stenosis in the distal common bile duct or intrapancreatic portion of the common bile duct.

The distinction of groove pancreatitis from cancer may be difficult (Fig. 97-35). Marked dilation of the main pancreatic duct, encasement and invasion of the peripancreatic vessels and tissues, and associated liver lesions favor malignant adenocarcinoma. In contrast, the characteristic location of a mass near the groove, cysts in the duodenal wall, and lack of encased and invaded peripancreatic vessels are more suggestive of segmental groove pancreatitis. Peripancreatic lymph nodes may also be seen, making the diagnosis difficult to distinguish from malignant disease. The findings may be nonspecific, and the discrimination between an inflammatory pancreatic mass and a malignant neoplasm can be very difficult and require biopsy, especially if the clinical features do not suggest groove pancreatitis.

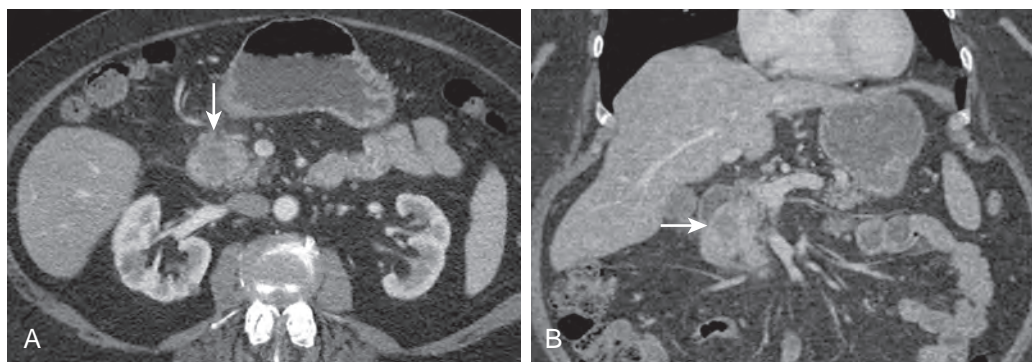


Figure 97-35 Pancreatic adenocarcinoma mimicking groove pancreatitis. Axial (A) and coronal (B) contrast-enhanced MDCT shows hypoenhancing mass (arrow) between the duodenum and pancreatic head from pancreatic cancer.

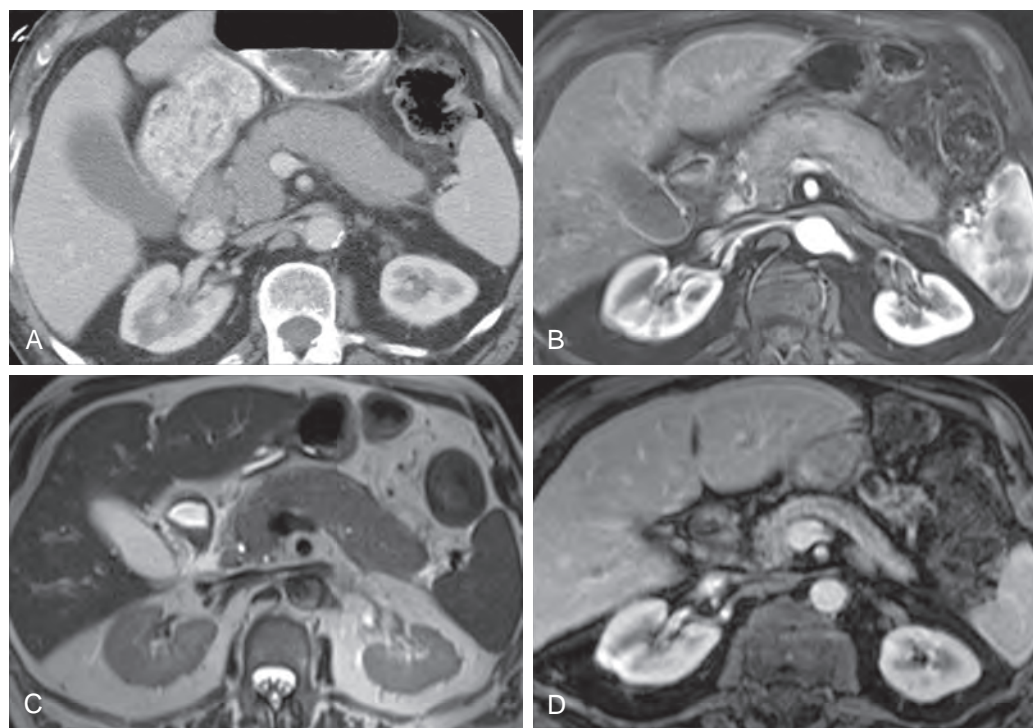


Figure 97-36 Autoimmune pancreatitis. A. Axial contrast-enhanced MDCT shows uniformly enlarged pancreas. Note peripancreatic hypodense rim suggestive but not diagnostic of autoimmune pancreatitis. B. Axial T1-weighted image shows decreased enhancement of the pancreas with hypointense rim. C. T2-weighted image shows sausage-shaped appearance of pancreas. D. Axial contrast-enhanced T1-weighted image after therapy shows atrophy of the pancreas.

Autoimmune Chronic Pancreatitis

Autoimmune chronic pancreatitis (AIP) has unique clinical, histologic, and imaging features.²²⁹ It has an autoimmune mechanism and has been seen as an immunoglobulin G subtype 4 (IgG4) systemic disease; it can affect multiple organs, including the pancreas, bile ducts, kidney, retroperitoneum, lungs, salivary glands, and lymph nodes.^{229,230} It may coexist with diabetes mellitus and autoimmune diseases, such as Sjögren's syndrome, primary sclerosing cholangitis, and primary biliary cirrhosis. AIP may be relatively asymptomatic or be manifested as painless jaundice from an obstructive pancreatic mass. It occurs predominantly in middle-aged or older men and usually shows a remarkable response to steroids.^{231,232} Most of the patients are older than 50 years, and overall prevalence of AIP has been reported to be around 5% to 6% of patients suffering

from chronic pancreatitis.²³¹ Laboratory findings may include increased levels of serum IgG4. Pancreatic fibrosis with infiltration of lymphocytes and plasma cells, characteristically around the periductal area of pancreatic tissue, is seen on histopathologic examination.²³²

Imaging studies show a rare association of diffuse enlargement of the pancreas with irregular narrowing of the pancreatic duct.²³¹ Diffuse hypoechogenicity of the pancreas is seen on transabdominal sonography, which is nonspecific for the diagnosis. On CT and MRI, the pancreas appears diffusely enlarged, with a sausage-like appearance, usually without calcifications or stones.^{231,233,234} Typical findings of AIP on cross-sectional imaging include diffuse enlargement of the pancreas with loss of lobulation of the pancreatic border, narrowing of the main pancreatic duct, and capsule-like rim (Fig. 97-36).^{233,235} On MRI, the involved pancreas is hypointense on T1-weighted

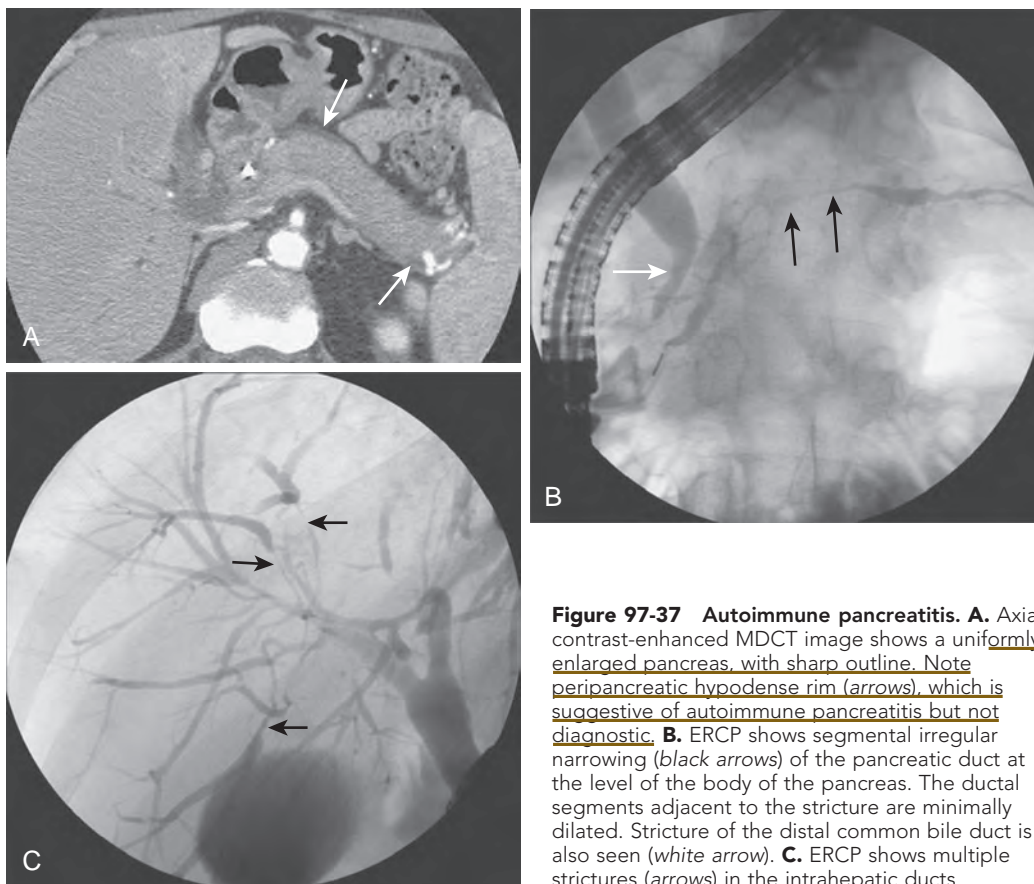


Figure 97-37 Autoimmune pancreatitis. **A.** Axial contrast-enhanced MDCT image shows a uniformly enlarged pancreas, with sharp outline. Note peripancreatic hypodense rim (arrows), which is suggestive of autoimmune pancreatitis but not diagnostic. **B.** ERCP shows segmental irregular narrowing (black arrows) of the pancreatic duct at the level of the body of the pancreas. The ductal segments adjacent to the stricture are minimally dilated. Stricture of the distal common bile duct is also seen (white arrow). **C.** ERCP shows multiple strictures (arrows) in the intrahepatic ducts.

imaging and hyperintense on T2-weighted imaging and shows restricted diffusion.^{233,236,237} As in chronic pancreatitis of other causes, the pancreas shows decreased enhancement in the arterial phase and increased enhancement in delayed phases after administration of contrast material. A characteristic low-density rim, likely composed of fibrous tissue and inflammatory reactions, is often seen surrounding the pancreas.^{227,231} This capsule-like rim shows delayed enhancement on dynamic imaging and low signal intensity on T1- and T2-weighted MR images.²²⁷ Diffuse or segmental irregular narrowing of the main pancreatic duct associated with strictures of the intrahepatic and extrahepatic biliary tract is typically demonstrated on ERCP (Fig. 97-37). Diffuse narrowing of the main pancreatic duct without significant upstream dilation supports the diagnosis, unlike the typical more severe dilation seen with cancer or chronic pancreatitis. Biliary thickening and enhancement or mass and lymphadenopathy may also be seen, mimicking sclerosing cholangitis or cholangiocarcinoma. Gallbladder wall thickening may also be present.²³⁵ MRCP shows the biliary tract abnormalities well but does not show the stenosis of the pancreatic duct as well as ERCP does.^{227,238} Other features of chronic pancreatitis, such as pseudocysts and pancreatic calcifications, are rare with AIP. Segmental involvement can mimic malignant disease. Unlike pancreatic adenocarcinoma, AIP can be distinguished by the lack of vascular invasion or findings to suggest metastases.

AIP has many extrapancreatic manifestations, including most commonly involvement of the biliary tree (up to 80%).^{230,239} Renal (35%) and retroperitoneal (10%) involvement

is common. In the majority of patients, renal involvement is manifested as bilateral multiple round or wedge-shaped renal cortical lesions, but it can also infiltrate kidneys diffusely or show a single masslike lesion arising from the renal parenchyma. Retroperitoneal fibrosis, a soft tissue mass surrounding the aorta and inferior vena cava, is seen in 10% to 20% of patients. Salivary and lacrimal gland enlargement may be seen in 14% to 24% of patients. Gastrointestinal tract abnormalities and pulmonary opacities or lesions have been reported in AIP. These extrapancreatic manifestations should be considered additional clues that can be helpful in diagnosis of AIP, particularly in atypical manifestations of AIP, such as segmental or masslike pancreatic lesions or atrophy of the pancreas due to late stages of AIP.²³⁰

The diagnosis of AIP is highly suspected when these typical imaging features are combined with supportive serology findings. There has been development of several different criteria for the diagnosis, including the Mayo Clinic histology, imaging, serology, other organ involvement, and response to therapy (HISORT) criteria and the Japan Pancreas Society and Asian diagnostic criteria.²⁴⁰⁻²⁴² EUS is most helpful for fine-needle aspiration or biopsy, especially when the diagnosis is not clear and cancer needs to be excluded.^{243,244}

Corticosteroid therapy has been used for diagnostic and therapeutic purposes by gastroenterologists experienced in treating AIP after pancreatic cancer has been excluded, although disease recurrence can be seen in up to 40% of patients.²⁴⁵ After corticosteroid therapy, the pancreatic morphologic abnormalities of the common bile duct and pancreatic

duct usually resolve.²⁴⁶ The two most important expected findings after corticosteroid therapy for AIP are significant decrease in pancreatic size and normalization of the main pancreatic duct appearance. Improvement of biliary tree involvement and other extrahepatic manifestations is also frequently reported. Whereas the diffuse form of AIP may be considered difficult to discriminate from mild acute pancreatitis, significant response to steroid therapy and lack of retroperitoneal fluid and inflammation in AIP can help distinguish these two entities.²⁴⁶

It has been shown that AIP responds well to corticosteroid therapy when some features exist on imaging. This may reflect the presence of various stages of disease evolution from early active inflammation to late sclerosis and fibrosis stages. Diffuse enlargement of the pancreas, the presence of a peripancreatic halo, ductal obliteration, or wall thickening usually responds rapidly to corticosteroid therapy and may relate to active inflammation. In some patients, features of pancreatic tail retraction, persistent ductal stenosis, and focal masslike inflammatory lesions have been reported to be the imaging findings that are suggestive of a reduced or suboptimal response to steroid therapy, probably because of the presence of late-phase fibrosis or sclerosis.²⁴⁶⁻²⁴⁹

Summary

Experience accumulated since the late 1970s has shown that CT is the single most important imaging modality in evaluating patients with pancreatitis. CT has high sensitivity and specificity in diagnosis of moderate and severe pancreatitis as well as in detection of serious complications that are often

clinically unsuspected. In addition, CT plays a valuable role as an early predictive indicator of disease severity. Patients with fluid collections and pancreatic necrosis are at high risk for development of complications. These patients should be closely monitored clinically and with follow-up CT examinations. They require intensive care treatment and percutaneous or surgical drainage procedures when sepsis develops. MRI has also become an accurate imaging modality for assessment of pancreatitis. It is especially helpful in patients with allergy to iodinated contrast agents or poor renal function and to evaluate the pancreaticobiliary tract, to characterize complex fluid collections, and to diagnose early chronic pancreatitis. Sonography is used mainly to exclude a diagnosis of gallstones and biliary obstruction. The role of ERCP has diminished as MRCP emerged as a noninvasive alternative diagnostic tool. ERCP is mainly used for interventional procedures, such as endoscopic therapy for complications of pancreatitis and ductal obstruction, and to perform tissue biopsy to differentiate benign from malignant clinical and imaging features. It is occasionally used to provide a road map of the pancreatic duct before surgical procedures and to diagnose early side branch abnormalities in chronic pancreatitis. Noninvasive imaging, however, has increased in use for the diagnosis, management, and treatment of patients with acute and chronic pancreatitis during the last few decades and has played a major role in these patients.

ACKNOWLEDGMENTS

We would like to thank Dr. Areza Ghasemi and Dr. Elise Saddleton with preparation of this manuscript. We also wish to thank Holly Harper and David Botos for their assistance.

REFERENCES

- Gomatos IP, Xiaodong X, Ghaneh P, et al: Prognostic markers in acute pancreatitis. *Expert Rev Mol Diagn* 14:333–346, 2014.
- Sarr MG, Banks PA, Bollen TL, et al: The new revised classification of acute pancreatitis 2012. *Surg Clin North Am* 93:549–562, 2013.
- Wu BU, Banks PA: Clinical management of patients with acute pancreatitis. *Gastroenterology* 144:1272–1281, 2013.
- Brand M, Götz A, Zeman F, et al: Acute necrotizing pancreatitis: Laboratory, clinical, and imaging findings as predictors of patient outcomes. *AJR* 202:1215–1231, 2014.
- Rau BM: Predicting severity of acute pancreatitis. *Curr Gastroenterol Rep* 9:107–115, 2007.
- Sternby B, O'Brien JF, Zinsmeister AR, DiMagno EP: What is the best biochemical test to diagnose acute pancreatitis? A prospective clinical study. *Mayo Clin Proc* 71:1138–1144, 1996.
- Bradley EL, 3rd.: A clinically based classification system for acute pancreatitis. Summary of the International Symposium on Acute Pancreatitis, Atlanta, Ga, September 11 through 13, 1992. *Arch Surg* 128:586–590, 1993.
- Banks PA: A new classification system for acute pancreatitis. *Am J Gastroenterol* 89:151–152, 1994.
- Rebours V, Lévy P, Bretagne JF, et al: Do guidelines influence medical practice? Changes in management of acute pancreatitis 7 years after the publication of the French guidelines. *Eur J Gastroenterol Hepatol* 24:143–148, 2012.
- Banks PA, Bollen TL, Dervenis C, et al: Classification of acute pancreatitis—2012: Revision of the Atlanta classification and definitions by international consensus. *Gut* 62:102–111, 2013.
- Thoeni RF: The revised Atlanta classification of acute pancreatitis: Its importance for the radiologist and its effect on treatment. *Radiology* 262:751–764, 2012.
- Zaheer A, Singh VK, Qureshi RO, Fishman EK: The revised Atlanta classification for acute pancreatitis: Updates in imaging terminology and guidelines. *Abdom Imaging* 38:125–136, 2013.
- Balthazar EJ, Freeny PC, van Sonnenberg E: Imaging and intervention in acute pancreatitis. *Radiology* 193:297–306, 1994.
- Radecki PD, Friedman AC, Dabiezies M: Pancreatitis. In Friedman AC, Dachman AH, editors: *Radiology of the Liver, Biliary Tract, and Pancreas*, St. Louis, 1994, Mosby—Year Book, pp 763–806.
- May GR, Gardiner R: *Clinical Imaging of the Pancreas*, New York, 1987, Raven Press.
- Karne S, Gorelick FS: Etiopathogenesis of acute pancreatitis. *Surg Clin North Am* 79:699–710, 1999.
- Lerch MM, Gorelick FS: Models of acute and chronic pancreatitis. *Gastroenterology* 144:1180–1193, 2013.
- Russo MW, Wei JT, Thiny MT, et al: Digestive and liver diseases statistics, 2004. *Gastroenterology* 126:1448–1453, 2004.
- Saraswat VA, Sharma BC, Agarwal DK, et al: Biliary microlithiasis in patients with idiopathic acute pancreatitis and unexplained biliary pain: Response to therapy. *J Gastroenterol Hepatol* 19:1206–1211, 2004.
- Levy MJ, Geenen JE: Idiopathic acute recurrent pancreatitis. *Am J Gastroenterol* 96:2540–2555, 2001.
- Hanck C, Whitcomb DC: Alcoholic pancreatitis. *Gastroenterol Clin North Am* 33:751–765, 2004.
- Oruc N, Whitcomb DC: Theories, mechanisms, and models of alcoholic chronic pancreatitis. *Gastroenterol Clin North Am* 33:733–750, v–vi, 2004.
- Kloppel G, Adler G, Kern H: Pathomorphology of acute pancreatitis in relation to its clinical course and pathogenesis. In Malfertheiner P, Ditschuneit H, editors: *Diagnostic Procedures in Pancreatic Disease*, New York, 1997, Springer-Verlag, pp 11–18.
- Singh M, Simsek H: Ethanol and the pancreas. Current status. *Gastroenterology* 98:1051–1062, 1990.
- Kemppainen EA, Hedstrom JJ, Puolakkainen PA, et al: Rapid measurement of urinary trypsinogen-2 as a screening test for acute pancreatitis. *N Engl J Med* 336:1788–1793, 1997.
- Marotta PJ, Gregor JC, Taves DH: Biliary sludge: a risk factor for 'idiopathic' pancreatitis? *Can J Gastroenterol* 10:385–388, 1996.

27. Fogel EL, Sherman S: ERCP for gallstone pancreatitis. *N Engl J Med* 370:150–157, 2014.
28. Kamisawa T, Egawa N, Tsuruta K, et al: Pancreatitis associated with congenital abnormalities of the pancreaticobiliary system. *Hepatogastroenterology* 52:223–229, 2005.
29. Draganov P, Forsmark CE: "Idiopathic" pancreatitis. *Gastroenterology* 128:756–763, 2005.
30. Balthazar EJ: Complications of acute pancreatitis: Clinical and CT evaluation. *Radiol Clin North Am* 40:1211–1227, 2002.
31. Arvanitakis M, Koustiani G, Gantzaru A, et al: Staging of severity and prognosis of acute pancreatitis by computed tomography and magnetic resonance imaging—a comparative study. *Dig Liver Dis* 39:473–482, 2007.
32. Gross V, Leser HG, Heinisch A, Scholmerich J: Inflammatory mediators and cytokines—new aspects of the pathophysiology and assessment of severity of acute pancreatitis? *Hepatogastroenterology* 40:522–530, 1993.
33. Denham W, Norman J: The potential role of therapeutic cytokine manipulation in acute pancreatitis. *Surg Clin North Am* 79:767–781, 1999.
34. Rau B, Schilling MK, Beger HG: Laboratory markers of severe acute pancreatitis. *Dig Dis* 22:247–257, 2004.
35. Jiang CF, Shiao YC, Ng KW, Tan SW: Serum interleukin-6, tumor necrosis factor alpha and C-reactive protein in early prediction of severity of acute pancreatitis. *J Chin Med Assoc* 67:442–446, 2004.
36. Reisler RB, Murphy RL, Redfield RR, Parker RA: Incidence of pancreatitis in HIV-1-infected individuals enrolled in 20 adult AIDS clinical trials group studies: Lessons learned. *J Acquir Immune Defic Syndr* 39:159–166, 2005.
37. Behrman SW, Melvin WS, Ellison EC: Pancreatic pseudocysts following acute pancreatitis. *Am J Surg* 172:228–231, 1996.
38. Singh VK, Bollen TL, Wu BU, et al: An assessment of the severity of interstitial pancreatitis. *Clin Gastroenterol Hepatol* 9:1098–1103, 2011.
39. Bollen TL: Imaging of acute pancreatitis: Update of the revised Atlanta classification. *Radiol Clin North Am* 50:429–445, 2012.
40. Mortelet KJ, Wiesner W, Intriere L, et al: A modified CT severity index for evaluating acute pancreatitis: Improved correlation with patient outcome. *AJR Am J Roentgenol* 183:1261–1265, 2004.
41. Lenhart DK, Balthazar EJ: MDCT of acute mild (necrotizing) pancreatitis: Abdominal complications and fate of fluid collections. *AJR Am J Roentgenol* 190:643–649, 2008.
42. Yeo CJ, Bastidas JA, Lynch-Nyhan A, et al: The natural history of pancreatic pseudocysts documented by computed tomography. *Surg Gynecol Obstet* 170:411–417, 1990.
43. Hjeltnqvist B, Watsgard C, Borgstrom A, et al: Pathobiochemistry and early CT findings in acute pancreatitis. *Digestion* 44:184–190, 1989.
44. Yadav D, Agarwal N, Pitchumoni CS: A critical evaluation of laboratory tests in acute pancreatitis. *Am J Gastroenterol* 97:1309–1318, 2002.
45. Steer M: Acute pancreatitis. In Taylor MB, editor: *Gastrointestinal Emergencies*, ed 2, Baltimore, 1997, Williams & Wilkins, pp 227–238.
46. Agarwal N, Pitchumoni CS: Simplified prognostic criteria in acute pancreatitis. *Pancreas* 1:69–73, 1986.
47. Gumaste VV, Dave PB, Weissman D, Messer J: Lipase/amylase ratio. A new index that distinguishes acute episodes of alcoholic from non-alcoholic acute pancreatitis. *Gastroenterology* 101:1361–1366, 1991.
48. Tenner SM, Steinberg W: The admission serum lipase:amylase ratio differentiates alcoholic from nonalcoholic acute pancreatitis. *Am J Gastroenterol* 87:1755–1758, 1992.
49. Winslet M, Hall C, London NJ, Neoptolemos JP: Relation of diagnostic serum amylase levels to aetiology and severity of acute pancreatitis. *Gut* 33:982–986, 1992.
50. Lankisch PG, Burchard-Reckert S, Lehnich D: Underestimation of acute pancreatitis: Patients with only a small increase in amylase/lipase levels can also have or develop severe acute pancreatitis. *Gut* 44:542–544, 1999.
51. De Sanctis JT, Lee MJ, Gazelle GS, et al: Prognostic indicators in acute pancreatitis: CT vs APACHE II. *Clin Radiol* 52:842–848, 1997.
52. Steinberg WM, Goldstein SS, Davis ND, et al: Diagnostic assays in acute pancreatitis. A study of sensitivity and specificity. *Ann Intern Med* 102:576–580, 1985.
53. Johnson CD, Abu-Hilal M: Persistent organ failure during the first week as a marker of fatal outcome in acute pancreatitis. *Gut* 53:1340–1344, 2004.
54. Mofidi R, Duff MD, Wigmore SJ, et al: Association between early systemic inflammatory response, severity of multiorgan dysfunction and death in acute pancreatitis. *Br J Surg* 93:738–744, 2006.
55. Balthazar EJ, Lutzker S: Radiological signs of acute pancreatitis. *CRC Crit Rev Clin Radiol Nucl Med* 7:199–242, 1976.
56. Brascho DJ, Reynolds TN, Zanca P: The radiographic "colon cut-off sign" in acute pancreatitis. *Radiology* 79:763–769, 1962.
57. Meyers MA: Roentgen significance of the phrenicocolic ligament. *Radiology* 95:539–545, 1970.
58. Schwartz S, Nadelhaft J: Simulation of colonic obstruction at the splenic flexure by pancreatitis: Roentgen features. *Am J Roentgenol Radium Ther Nucl Med* 78:607–616, 1957.
59. Pickhardt PJ: The colon cutoff sign. *Radiology* 215:387–389, 2000.
60. Roseman DM, Kowlessar OD, Sleisenger MH: Pulmonary manifestations of pancreatitis. *N Engl J Med* 263:294–296, 1960.
61. Renert WA, Pitt MJ, Capp MP: Acute pancreatitis. *Sem Roentgenol* 8:405–414, 1973.
62. Ranson JH, Turner JW, Roses DF, et al: Respiratory complications in acute pancreatitis. *Ann Surg* 179:557–566, 1974.
63. Pastor CM, Matthay MA, Frossard JL: Pancreatitis-associated acute lung injury: New insights. *Chest* 124:2341–2351, 2003.
64. Lankisch PG, Droge M, Becher R: Pulmonary infiltrations. Sign of severe acute pancreatitis. *Int J Pancreatol* 19:113–115, 1996.
65. Heller SJ, Noordhoek E, Tenner SM, et al: Pleural effusion as a predictor of severity in acute pancreatitis. *Pancreas* 15:222–225, 1997.
66. Pezzilli R, Billi P, Barakat B, et al: The use of the peripheral leukocyte count and chest X-rays in early assessment of the severity of acute pancreatitis in comparison with the Ranson score system. *Panminerva Med* 41:39–42, 1999.
67. Raghu MG, Wig JD, Kochhar R, et al: Lung complications in acute pancreatitis. *JOP* 8:177–185, 2007.
68. Meyers MA, Evans JA: Effects of pancreatitis on the small bowel and colon: Spread along mesenteric planes. *Am J Roentgenol Radium Ther Nucl Med* 119:151–165, 1973.
69. Lindahl F, Vejsted H, Backer OG: Lesions of the colon following acute pancreatitis. *Scand J Gastroenterol* 7:375–378, 1972.
70. Safrit HD, Rice RP: Gastrointestinal complications of pancreatitis. *Radiol Clin North Am* 27:73–79, 1989.
71. Thompson WM, Kelvin FM, Rice RP: Inflammation and necrosis of the transverse colon secondary to pancreatitis. *AJR Am J Roentgenol* 128:943–948, 1977.
72. Fulcher AS, Turner MA: MR cholangiopancreatography. *Radiol Clin North Am* 40:1363–1376, 2002.
73. Masci E, Toti G, Mariani A, et al: Complications of diagnostic and therapeutic ERCP: A prospective multicenter study. *Am J Gastroenterol* 96:417–423, 2001.
74. Vujic I: Vascular complications of pancreatitis. *Radiol Clin North Am* 27:81–91, 1989.
75. Dreiling DA, Robert J, Toledano AE: Vascular pancreatitis. A clinical entity of growing importance. *J Clin Gastroenterol* 10:3–6, 1988.
76. Pagnoux C, Mahr A, Cohen P, Guillemin L: Presentation and outcome of gastrointestinal involvement in systemic necrotizing vasculitides: Analysis of 62 patients with polyarteritis nodosa, microscopic polyangiitis, Wegener granulomatosis, Churg-Strauss syndrome, or rheumatoid arthritis-associated vasculitis. *Medicine (Baltimore)* 84:115–128, 2005.
77. Balthazar EJ: Acute pancreatitis: Assessment of severity with clinical and CT evaluation. *Radiology* 223:603–613, 2002.
78. Jeffrey RB, Jr: Sonography in acute pancreatitis. *Radiol Clin North Am* 27:5–17, 1989.
79. Jeffrey RB, Jr, Laing FC, Wing VW: Extrapancratic spread of acute pancreatitis: New observations with real-time US. *Radiology* 159:707–711, 1986.
80. Loren I, Lasson A, Fork T, et al: New sonographic imaging observations in focal pancreatitis. *Eur Radiol* 9:862–867, 1999.
81. Hashimoto BE, Laing FC, Jeffrey RB, Jr, Federle MP: Hemorrhagic pancreatic fluid collections examined by ultrasound. *Radiology* 150:803–808, 1984.
82. Merkle EM, Gorich J: Imaging of acute pancreatitis. *Eur Radiol* 12:1979–1992, 2002.
83. Gooding GA: Ultrasound of a superior mesenteric artery aneurysm secondary to pancreatitis: A plea for real-time ultrasound of sonolucent masses in pancreatitis. *J Clin Ultrasound* 9:255–256, 1981.
84. McMahon MJ, Pickford IR, Playforth MJ: Early prediction of severity of acute pancreatitis using peritoneal lavage. *Acta Chir Scand* 146:171–175, 1980.
85. Morgan DE: Imaging of acute pancreatitis and its complications. *Clin Gastroenterol Hepatol* 6:1077–1085, 2008.
86. Anderson SW, Lucey BC, Varghese JC, Soto JA: Accuracy of MDCT in the diagnosis of choledocholithiasis. *AJR Am J Roentgenol* 187:174–180, 2006.
87. Anderson SW, Rho E, Soto JA: Detection of biliary duct narrowing and choledocholithiasis: Accuracy of portal venous phase multidetector CT. *Radiology* 247:418–427, 2008.
88. Balthazar EJ, Ranson JH, Naidich DP, et al: Acute pancreatitis: Prognostic value of CT. *Radiology* 156:767–772, 1985.
89. Fishman M, Talner LB: Pancreatitis causing focal caliectasis. *AJR Am J Roentgenol* 156:1005–1006, 1991.

90. Garg PK, Madan K, Pande GK, et al: Association of extent and infection of pancreatic necrosis with organ failure and death in acute necrotizing pancreatitis. *Clin Gastroenterol Hepatol* 3:159–166, 2005.
91. Hohl C, Schmidt T, Haage P, et al: Phase-inversion tissue harmonic imaging compared with conventional B-mode ultrasound in the evaluation of pancreatic lesions. *Eur Radiol* 14:1109–1117, 2004.
92. Finstad TA, Tchelepi H, Ralls PW: Sonography of acute pancreatitis: Prevalence of findings and pictorial essay. *Ultrasound Q* 21:95–104, quiz 150, 153–104, 2005.
93. Gohde SC, Toth J, Krestin GP, Debatin JF: Dynamic contrast-enhanced FMPSGR of the pancreas: Impact on diagnostic performance. *AJR Am J Roentgenol* 168:689–696, 1997.
94. Stimac D, Miletic D, Radic M, et al: The role of nonenhanced magnetic resonance imaging in the early assessment of acute pancreatitis. *Am J Gastroenterol* 102:997–1004, 2007.
95. Kim MJ, Mitchell DG, Ito K, Outwater EK: Biliary dilatation: Differentiation of benign from malignant causes—value of adding conventional MR imaging to MR cholangiopancreatography. *Radiology* 214:173–181, 2000.
96. Ly JN, Miller FH: MR imaging of the pancreas: A practical approach. *Radiol Clin North Am* 40:1289–1306, 2002.
97. Macari M, Finn ME, Bennett GL, et al: Differentiating pancreatic cystic neoplasms from pancreatic pseudocysts at MR imaging: Value of perceived internal debris. *Radiology* 251:77–84, 2009.
98. Morgan DE, Baron TH, Smith JK, et al: Pancreatic fluid collections prior to intervention: Evaluation with MR imaging compared with CT and US. *Radiology* 203:773–778, 1997.
99. Xiao B, Zhang XM, Tang W, et al: Magnetic resonance imaging for local complications of acute pancreatitis: A pictorial review. *World J Gastroenterol* 16:2735–2742, 2010.
100. Xiao B, Zhang XM: Magnetic resonance imaging for acute pancreatitis. *World J Radiol* 2:298–308, 2010.
101. Thomas S, Kayhan A, Lakadamyali H, Oto A: Diffusion MRI of acute pancreatitis and comparison with normal individuals using ADC values. *Emerg Radiol* 19:5–9, 2012.
102. Kettritz U, Semelka RC: Contrast-enhanced MR imaging of the pancreas. *Magn Reson Imaging Clin N Am* 4:87–100, 1996.
103. Keogan MT, Edelman RR: Technologic advances in abdominal MR imaging. *Radiology* 220:310–320, 2001.
104. O'Neill E, Hammond N, Miller FH: MR imaging of pancreas. *Radiol Clin North Am* 52:757–777, 2014.
105. Hakime A, Giraud M, Vullierme MP, Vilgrain V: [MR imaging of the pancreas]. *J Radiol* 88(Pt 1):11–25, 2007.
106. Miller FH, Keppke AL, Dalal K, et al: MRI of pancreatitis and its complications: Part I, acute pancreatitis. *AJR Am J Roentgenol* 183:1637–1644, 2004.
107. Piironen A, Kivisaari R, Pitkaranta P, et al: Contrast-enhanced magnetic resonance imaging for the detection of acute haemorrhagic necrotizing pancreatitis. *Eur Radiol* 7:17–20, 1997.
108. Martin DR, Karabulut N, Yang M, McFadden DW: High signal peripancreatic fat on fat-suppressed spoiled gradient echo imaging in acute pancreatitis: Preliminary evaluation of the prognostic significance. *J Magn Reson Imaging* 18:49–58, 2003.
109. Siegelman SS, Copeland BE, Saba GP, et al: CT of fluid collections associated with pancreatitis. *AJR Am J Roentgenol* 134:1121–1132, 1980.
110. Johst P, Tsiotos GG, Sarr MG: Pancreatic ascites: A rare complication of necrotizing pancreatitis. A case report and review of the literature. *Int J Pancreatol* 22:151–154, 1997.
111. Balthazar EJ: CT diagnosis and staging of acute pancreatitis. *Radiol Clin North Am* 27:19–37, 1989.
112. Fernandez-Cruz L, Margarona E, Llovera J, et al: Pancreatic ascites. *Hepatogastroenterology* 40:150–154, 1993.
113. Fielding GA, McLatchie GR, Wilson C, et al: Acute pancreatitis and pancreatic fistula formation. *British J Surg* 76:1126–1128, 1989.
114. Clavien PA, Hauser H, Meyer P, Rohner A: Value of contrast-enhanced computerized tomography in the early diagnosis and prognosis of acute pancreatitis. A prospective study of 202 patients. *Am J Surg* 155:457–466, 1988.
115. Ranson JH: Diagnostic standards for acute pancreatitis. *World J Surg* 21:136–142, 1997.
116. Hill MC, Barkin J, Isikoff MB, et al: Acute pancreatitis: Clinical vs. CT findings. *AJR Am J Roentgenol* 139:263–269, 1982.
117. Arvanitakis M, Delhaye M, De Maertelaere V, et al: Computed tomography and magnetic resonance imaging in the assessment of acute pancreatitis. *Gastroenterology* 126:715–723, 2004.
118. Lecesne R, Taourel P, Bret PM, et al: Acute pancreatitis: Interobserver agreement and correlation of CT and MR cholangiopancreatography with outcome. *Radiology* 211:727–735, 1999.
119. Ranson JH, Balthazar E, Caccavale R, Cooper M: Computed tomography and the prediction of pancreatic abscess in acute pancreatitis. *Ann Surg* 201:656–665, 1985.
120. Nordestgaard AG, Wilson SE, Williams RA: Early computerized tomography as a predictor of outcome in acute pancreatitis. *Am J Surg* 152:127–132, 1986.
121. Vernacchia FS, Jeffrey RB, Jr, Federle MP, et al: Pancreatic abscess: Predictive value of early abdominal CT. *Radiology* 162:435–438, 1987.
122. Balthazar EJ, Robinson DL, Megibow AJ, Ranson JH: Acute pancreatitis: Value of CT in establishing prognosis. *Radiology* 174:331–336, 1990.
123. Balthazar EJ: Staging of acute pancreatitis. *Radiol Clin North Am* 40:1199–1209, 2002.
124. Paulson EK, Vitellas KM, Keogan MT, et al: Acute pancreatitis complicated by gland necrosis: Spectrum of findings on contrast-enhanced CT. *AJR Am J Roentgenol* 172:609–613, 1999.
125. Casas JD, Diaz R, Valderas G, et al: Prognostic value of CT in the early assessment of patients with acute pancreatitis. *AJR Am J Roentgenol* 182:569–574, 2004.
126. Vriens PW, van de Linde P, Slotema ET, et al: Computed tomography severity index is an early prognostic tool for acute pancreatitis. *J Am Coll Surg* 201:497–502, 2005.
127. Yassa NA, Agostini JT, Ralls PW: Accuracy of CT in estimating extent of pancreatic necrosis. *Clin Imaging* 21:407–410, 1997.
128. Nichols MT, Russ PD, Chen YK: Pancreatic imaging: Current and emerging technologies. *Pancreas* 33:211–220, 2006.
129. Kivisaari L, Somer K, Standertskjold-Nordenstam CG, et al: A new method for the diagnosis of acute hemorrhagic-necrotizing pancreatitis using contrast-enhanced CT. *Gastrointest Radiol* 9:27–30, 1984.
130. Kivisaari L, Somer K, Standertskjold-Nordenstam CG, et al: Early detection of acute fulminant pancreatitis by contrast-enhanced computed tomography. *Scand J Gastroenterol* 18:39–41, 1983.
131. Nuutinen P, Kivisaari L, Schroder T: Contrast-enhanced computed tomography and microangiography of the pancreas in acute human hemorrhagic/necrotizing pancreatitis. *Pancreas* 3:53–60, 1988.
132. Johnson CD, Stephens DH, Sarr MG: CT of acute pancreatitis: Correlation between lack of contrast enhancement and pancreatic necrosis. *AJR Am J Roentgenol* 156:93–95, 1991.
133. Isenmann R, Rau B, Beger HG: Bacterial infection and extent of necrosis are determinants of organ failure in patients with acute necrotizing pancreatitis. *Br J Surg* 86:1020–1024, 1999.
134. Gotzinger P, Sautner T, Kriwanek S, et al: Surgical treatment for severe acute pancreatitis: Extent and surgical control of necrosis determine outcome. *World J Surg* 26:474–478, 2002.
135. McKay CJ, Evans S, Sinclair M, et al: High early mortality rate from acute pancreatitis in Scotland, 1984–1995. *Br J Surg* 86:1302–1305, 1999.
136. Lowham A, Lavelle J, Leese T: Mortality from acute pancreatitis. Late septic deaths can be avoided but some early deaths still occur. *Int J Pancreatol* 25:103–106, 1999.
137. Mutinga M, Rosenbluth A, Tenner SM, et al: Does mortality occur early or late in acute pancreatitis? *Int J Pancreatol* 28:91–95, 2000.
138. Kim YH, Saini S, Sahani D, et al: Imaging diagnosis of cystic pancreatic lesions: Pseudocyst versus nonpseudocyst. *Radiographics* 25:671–685, 2005.
139. Kaufman J, Waltman A, Fernandez CD: Pancreatic hemorrhage. In Pitt HA, Carr-Locke DL, Ferrucci JT, editors: *Hepatobiliary and Pancreatic Disease: The Team Approach to Management*, Boston, 1995, Little, Brown, pp 377–386.
140. Wilson C: Management of the later complications of severe acute pancreatitis—pseudocyst, abscess and fistula. *Eur J Gastroenterol Hepatol* 9:117–121, 1997.
141. Freeny PC, Hauptmann E, Althaus SJ, et al: Percutaneous CT-guided catheter drainage of infected acute necrotizing pancreatitis: Techniques and results. *AJR Am J Roentgenol* 170:969–975, 1998.
142. vanSonnenberg E, Wittich GR, Casola G, et al: Percutaneous drainage of infected and noninfected pancreatic pseudocysts: Experience in 101 cases. *Radiology* 170(Pt 1):757–761, 1989.
143. Lee MJ, Wittich GR, Mueller PR: Percutaneous intervention in acute pancreatitis. *Radiographics* 18:711–724, discussion 728, 1998.
144. Adams DB, Harvey TS, Anderson MC: Percutaneous catheter drainage of pancreatic pseudocysts. *Am Surg* 57:29–33, 1991.
145. Ward J, Chalmers AG, Guthrie AJ, et al: T2-weighted and dynamic enhanced MRI in acute pancreatitis: Comparison with contrast enhanced CT. *Clin Radiol* 52:109–114, 1997.
146. Vege SS, Baron TH: Management of pancreatic necrosis in severe acute pancreatitis. *Clin Gastroenterol Hepatol* 3:192–196, 2005.
147. van Santvoort HC, Besselink MG, Bakker OJ, et al: A step-up approach or open necrosectomy for necrotizing pancreatitis. *N Engl J Med* 362:1491–1502, 2010.
148. Cui ML, Kim KH, Kim HG, et al: Incidence, risk factors and clinical course of pancreatic

- fluid collections in acute pancreatitis. *Dig Dis Sci* 59:1055–1062, 2014.
149. Alexander ES, Clark RA, Federle MP: Pancreatic gas: Indication of pancreatic fistula. *AJR Am J Roentgenol* 139:1089–1093, 1982.
 150. Working Group IAP/APA Acute Pancreatitis Guidelines: IAP/APA evidence-based guidelines for the management of acute pancreatitis. *Pancreatol* 13(4 Suppl 2):e1–e15, 2013.
 151. Gerzof SG, Banks PA, Robbins AH, et al: Early diagnosis of pancreatic infection by computed tomography-guided aspiration. *Gastroenterology* 93:1315–1320, 1987.
 152. Banks PA, Gerzof SG, Langevin RE, et al: CT-guided aspiration of suspected pancreatic infection: Bacteriology and clinical outcome. *Int J Pancreatol* 18:265–270, 1995.
 153. Baril NB, Ralls PW, Wren SM, et al: Does an infected peripancreatic fluid collection or abscess mandate operation? *Ann Surg* 231:361–367, 2000.
 154. Mithofer K, Mueller PR, Warshaw AL: Interventional and surgical treatment of pancreatic abscess. *World J Surg* 21:162–168, 1997.
 155. vanSonnenberg E, Wittich GR, Chon KS, et al: Percutaneous radiologic drainage of pancreatic abscesses. *AJR Am J Roentgenol* 168:979–984, 1997.
 156. Muller CH, Lahnert U, Schafmayer A, Lankisch PG: Massive intraperitoneal bleeding from tryptic erosions of the splenic vein. Another cause of sudden deterioration during recovery from acute pancreatitis. *Int J Pancreatol* 26:49–52, 1999.
 157. Bretagne JF, Heresbach D, Darnault P, et al: Pseudoaneurysms and bleeding pseudocysts in chronic pancreatitis: Radiological findings and contribution to diagnosis in 8 cases. *Gastrointest Radiol* 15:9–16, 1990.
 158. Balthazar EJ, Fisher LA: Hemorrhagic complications of pancreatitis: Radiologic evaluation with emphasis on CT imaging. *Pancreatol* 1:306–313, 2001.
 159. Chari ST: Chronic pancreatitis: Classification, relationship to acute pancreatitis, and early diagnosis. *J Gastroenterol* 42(Suppl 17):58–59, 2007.
 160. Witt H, Apte MV, Keim V, Wilson JS: Chronic pancreatitis: Challenges and advances in pathogenesis, genetics, diagnosis, and therapy. *Gastroenterology* 132:1557–1573, 2007.
 161. Owyang C, DiMaggio M: Chronic pancreatitis. In Yamada T, editor: *Textbook of Gastroenterology*, ed 5, Philadelphia, 2009, Lippincott, pp 1811–1852.
 162. Sherman S, Lehman G: Chronic pancreatitis. In DiMarino AJ, Benjamin SB, editors: *Gastrointestinal Disease: An Endoscopic Approach*, ed 2, Thorofare, NJ, 2002, Slack, pp 1277–1296.
 163. Clain JE, Pearson RK: Diagnosis of chronic pancreatitis. Is a gold standard necessary? *Surg Clin North Am* 79:829–845, 1999.
 164. Remer EM, Baker ME: Imaging of chronic pancreatitis. *Radiol Clin North Am* 40:1229–1242, v, 2002.
 165. Tsao TF, Kang RJ, Tyan YS, et al: Color Doppler twinkling artifact related to chronic pancreatitis with parenchymal calcification. *Acta Radiol* 47:547–548, 2006.
 166. Otte M: Ultrasound in chronic pancreatitis. In Malfertheiner P, Ditschuneit H, editors: *Diagnostic Procedures in Pancreatic Disease*, New York, 1986, Springer-Verlag, pp 143–148.
 167. Bolondi L, Gaiani S, Casanova P, et al: Critical evaluation and controversial points of ultrasound findings in chronic pancreatitis. In Malfertheiner P, Ditschuneit H, editors: *Diagnostic Procedures in Pancreatic Disease*, New York, 1986, Springer-Verlag, pp 149–154.
 168. Atri M, Finnegan P: The pancreas. In Rumack CM, Wilson S, Charboneau JW, editors: *Diagnostic Ultrasound*, ed 2, Philadelphia, 1998, Elsevier/Mosby, pp 225–278.
 169. Alpern MB, Sandler MA, Kellman GM, Madrazo BL: Chronic pancreatitis: Ultrasonic features. *Radiology* 155:215–219, 1985.
 170. Shawker TH, Linzer M, Hubbard VS: Chronic pancreatitis: The diagnostic significance of pancreatic size and echo amplitude. *J Ultrasound Med* 3:267–272, 1984.
 171. Tandon M, Topazian M: Endoscopic ultrasound in idiopathic acute pancreatitis. *Am J Gastroenterol* 96:705–7609, 2001.
 172. Coyle WJ, Pineau BC, Tarnasky PR, et al: Evaluation of unexplained acute and acute recurrent pancreatitis using endoscopic retrograde cholangiopancreatography, sphincter of Oddi manometry and endoscopic ultrasound. *Endoscopy* 34:617–623, 2002.
 173. Norton SA, Alderson D: Endoscopic ultrasonography in the evaluation of idiopathic acute pancreatitis. *Br J Surg* 87:1650–1655, 2000.
 174. Frossard JL, Sosa-Valencia L, Amouyal G, et al: Usefulness of endoscopic ultrasonography in patients with “idiopathic” acute pancreatitis. *Am J Med* 109:196–200, 2000.
 175. Raimondo M, Wallace MB: Diagnosis of early chronic pancreatitis by endoscopic ultrasound. Are we there yet? *JOP* 5:1–7, 2004.
 176. Catalano MF, Geenen JE: Diagnosis of chronic pancreatitis by endoscopic ultrasonography. *Endoscopy* 30(Suppl 1):A111–A115, 1998.
 177. Kochman ML, Elta GH, Bude R, et al: Utility of a linear array ultrasound endoscope in the evaluation of suspected pancreatic disease. *J Gastrointest Surg* 2:217–222, 1998.
 178. Sahai AV, Zimmerman M, Aabakken L, et al: Prospective assessment of the ability of endoscopic ultrasound to diagnose, exclude, or establish the severity of chronic pancreatitis found by endoscopic retrograde cholangiopancreatography. *Gastrointest Endosc* 48:18–25, 1998.
 179. Nattermann C, Goldschmidt AJ, Dancygier H: [Endosonography in chronic pancreatitis. A comparative study of endoscopic retrograde pancreatography and endoscopic sonography]. *Ultraschall Med* 13:263–270, 1992.
 180. Wiersma MJ, Hawes RH, Lehman GA, et al: Prospective evaluation of endoscopic ultrasonography and endoscopic retrograde cholangiopancreatography in patients with chronic abdominal pain of suspected pancreatic origin. *Endoscopy* 25:555–564, 1993.
 181. Bhutani MS: Endoscopic ultrasound in pancreatic diseases. Indications, limitations, and the future. *Gastroenterol Clin North Am* 28:747–770, xi, 1999.
 182. Wallace MB, Hawes RH: Endoscopic ultrasound in the evaluation and treatment of chronic pancreatitis. *Pancreas* 23:26–35, 2001.
 183. Hollerbach S, Klamann A, Topalidis T, Schmigel WH: Endoscopic ultrasonography (EUS) and fine-needle aspiration (FNA) cytology for diagnosis of chronic pancreatitis. *Endoscopy* 33:824–831, 2001.
 184. Gress F, Schmitt C, Sherman S, et al: A prospective randomized comparison of endoscopic ultrasound- and computed tomography-guided celiac plexus block for managing chronic pancreatitis pain. *Am J Gastroenterol* 94:900–905, 1999.
 185. Giovannini M, Bernardini D, Seitz JF: Cystogastrotomy entirely performed under endosonography guidance for pancreatic pseudocyst: Results in six patients. *Gastrointest Endosc* 48:200–203, 1998.
 186. Malfertheiner P, Buchler M: Correlation of imaging and function in chronic pancreatitis. *Radiol Clin North Am* 27:51–64, 1989.
 187. Bolan PJ, Fink AS: Endoscopic retrograde cholangiopancreatography in chronic pancreatitis. *World J Surg* 27:1183–1191, 2003.
 188. Kasugai T, Tanehiro K, Kurimoto K, et al: Progression of radiological changes in relapsing and chronic pancreatitis. *J Gastroenterol Hepatol* 4:305–311, 1989.
 189. Taylor AJ, Bohorvosh AG: Interpretation of ERCP: With Associated Digital Imaging Correlation, Philadelphia, 1997, Lippincott-Raven.
 190. Lees WR: Critical evaluation and controversial points of computed tomography findings in chronic pancreatitis. In Malfertheiner P, Ditschuneit H, editors: *Diagnostic Procedures in Pancreatic Disease*, New York, 1986, Springer-Verlag, pp 161–168.
 191. Sherman S, Lehman G: Endoscopic therapy of chronic pancreatitis: Stones and strictures. In Jacobson IM, editor: *ERCP and Its Applications*, Philadelphia, 1998, Lippincott-Raven, pp 169–180.
 192. Axon AT: Endoscopic retrograde cholangiopancreatography in chronic pancreatitis. Cambridge classification. *Radiol Clin North Am* 27:39–50, 1989.
 193. Malfertheiner P, Buchler M, Stanescu A, Ditschuneit H: Exocrine pancreatic function in correlation to ductal and parenchymal morphology in chronic pancreatitis. *Hepatogastroenterology* 33:110–114, 1986.
 194. Fulcher AS, Turner MA, Capps GW, et al: Half-Fourier RARE MR cholangiopancreatography: Experience in 300 subjects. *Radiology* 207:21–32, 1998.
 195. Sica GT, Braver J, Cooney MJ, et al: Comparison of endoscopic retrograde cholangiopancreatography with MR cholangiopancreatography in patients with pancreatitis. *Radiology* 210:605–610, 1999.
 196. Calvo MM, Bujanda L, Calderon A, et al: Role of magnetic resonance cholangiopancreatography in patients with suspected choledocholithiasis. *Mayo Clinic Proc* 77:422–428, 2002.
 197. Varghese JC, Masterson A, Lee MJ: Value of MR pancreatography in the evaluation of patients with chronic pancreatitis. *Clin Radiol* 57:393–401, 2002.
 198. Talamonti MS, Denham W: Staging and surgical management of pancreatic and biliary cancer and inflammation. *Radiol Clin North Am* 40:1397–1410, viii, 2002.
 199. Cappeliez O, Delhay M, Deviere J, et al: Chronic pancreatitis: Evaluation of pancreatic exocrine function with MR pancreatography after secretin stimulation. *Radiology* 215:358–364, 2000.
 200. Manfredi R, Costamagna G, Brizi MG, et al: Severe chronic pancreatitis versus suspected pancreatic disease: Dynamic MR cholangiopancreatography after secretin stimulation. *Radiology* 214:849–855, 2000.
 201. Matos C, Metens T, Deviere J, et al: Pancreatic duct: Morphologic and functional evaluation with dynamic MR pancreatography after secretin stimulation. *Radiology* 203:435–441, 1997.

202. Mensel B, Messner P, Mayerle J, et al: Secretin-stimulated MRCP in volunteers: Assessment of safety, duct visualization, and pancreatic exocrine function. *AJR* 202:102–108, 2014.
203. Balci C: MRI assessment of chronic pancreatitis. *Diagn Interv Radiol* 17:249–254, 2011.
204. Sandrasegaran K, Lin C, Akisik FM, Tann M: State-of-the-art pancreatic MRI. *AJR Am J Roentgenol* 195:42–53, 2010.
205. Punwani S, Gillams AR, Lees WR: Non-invasive quantification of pancreatic exocrine function using secretin-stimulated MRCP. *Eur Radiol* 13:273–276, 2003.
206. Erturk SM, Ichikawa T, Motosugi U, et al: Diffusion-weighted MR imaging in the evaluation of pancreatic exocrine function before and after secretin stimulation. *Am J Gastroenterol* 101:133–136, 2006.
207. Siddiqi AJ, Miller F: Chronic pancreatitis: Ultrasound, computed tomography, and magnetic resonance imaging features. *Semin Ultrasound CT MR* 28:384–394, 2007.
208. Kim DH, Pickhardt PJ: Radiologic assessment of acute and chronic pancreatitis. *Surg Clin North Am* 87:1341–1358, viii, 2007.
209. Luetmer PH, Stephens DH, Ward EM: Chronic pancreatitis: Reassessment with current CT. *Radiology* 171:353–357, 1989.
210. Maier W: Computed tomography in chronic pancreatitis. In Malfertheiner P, Ditschuneit H, editors: *Diagnostic Procedures in Pancreatic Disease*, New York, 1986, Springer-Verlag, pp 155–160.
211. Sica GT, Miller FH, Rodriguez G, et al: Magnetic resonance imaging in patients with pancreatitis: Evaluation of signal intensity and enhancement changes. *J Magn Reson Imaging* 15:275–284, 2002.
212. Miller FH, Keppke AL, Wadhwa A, et al: MRI of pancreatitis and its complications: Part 2, chronic pancreatitis. *AJR Am J Roentgenol* 183:1645–1652, 2004.
213. Zhang XM, Shi H, Parker L, et al: Suspected early or mild chronic pancreatitis: Enhancement patterns on gadolinium chelate dynamic MRI. *Magnetic resonance imaging*. *J Magn Reson Imaging* 17:86–94, 2003.
214. Keppke AL, Miller FH: Magnetic resonance imaging of the pancreas: The future is now. *Semin Ultrasound CT MR* 26:132–152, 2005.
215. Semelka RC, Kelekis NL, Molina PL, et al: Pancreatic masses with inconclusive findings on spiral CT: Is there a role for MRI? *J Magn Reson Imaging* 6:585–588, 1996.
216. Balthazar EJ: Pancreatitis associated with pancreatic carcinoma. Preoperative diagnosis: Role of CT imaging in detection and evaluation. *Pancreatol* 5:330–344, 2005.
217. Ichikawa T, Sou H, Araki T, et al: Duct-penetrating sign at MRCP: Usefulness for differentiating inflammatory pancreatic mass from pancreatic carcinomas. *Radiology* 221:107–116, 2001.
218. Kim T, Murakami T, Takamura M, et al: Pancreatic mass due to chronic pancreatitis: Correlation of CT and MR imaging features with pathologic findings. *AJR Am J Roentgenol* 177:367–371, 2001.
219. Johnson PT, Outwater EK: Pancreatic carcinoma versus chronic pancreatitis: Dynamic MR imaging. *Radiology* 212:213–218, 1999.
220. Lankisch PG: Chronic pancreatitis. In Haubrich WS, Schaffner F, Berk JE, Bockus HL, editors: *Bockus Gastroenterology*, ed 5, Philadelphia, 1995, Saunders, pp 2930–2958.
221. Fulcher AS, Capps GW, Turner MA: Thoraco-pancreatic fistula: Clinical and imaging findings. *J Comput Assist Tomogr* 23:181–187, 1999.
222. Becker V, Mischke U: Groove pancreatitis. *Int J Pancreatol* 10:173–182, 1991.
223. Triantopoulou C, Derveniz C, Giannakou N, et al: Groove pancreatitis: A diagnostic challenge. *Eur Radiol* 19:1736–1743, 2009.
224. Castell-Monsalve FJ, Sousa-Martin JM, Carranza-Carranza A: Groove pancreatitis: MRI and pathologic findings. *Abdom Imaging* 33:342–348, 2008.
225. Raman SP, Salari SN, Hruban RH, Fishman EK: Groove pancreatitis: Spectrum of imaging findings and radiology-pathology correlation. *AJR Am J Roentgenol* 201:W29–W39, 2013.
226. Blasbalg R, Baroni RH, Costa DN, Machado MC: MRI features of groove pancreatitis. *AJR Am J Roentgenol* 189:73–80, 2007.
227. Irie H, Honda H, Kuroiwa T, et al: MRI of groove pancreatitis. *J Comput Assist Tomogr* 22:651–655, 1998.
228. Vullierme MP, Vilgrain V, Flejou JF, et al: Cystic dystrophy of the duodenal wall in the heterotopic pancreas: Radiopathological correlations. *J Comput Assist Tomogr* 24:635–643, 2000.
229. Finkelberg DL, Sahani D, Deshpande V, Brugge WR: Autoimmune pancreatitis. *N Engl J Med* 355:2670–2676, 2006.
230. Bodily KD, Takahashi N, Fletcher JG, et al: Autoimmune pancreatitis: Pancreatic and extrapancreatic imaging findings. *AJR Am J Roentgenol* 192:431–437, 2009.
231. Kim KP, Kim MH, Song MH, et al: Autoimmune chronic pancreatitis. *Am J Gastroenterol* 99:1605–1616, 2004.
232. Kamisawa T, Egawa N, Nakajima H, et al: Comparison of radiological and histological findings in autoimmune pancreatitis. *Hepato-gastroenterology* 53:953–956, 2006.
233. Sahani DV, Kalva SP, Farrell J, et al: Autoimmune pancreatitis: Imaging features. *Radiology* 233:345–352, 2004.
234. Nakazawa T, Ohara H, Sano H, et al: Difficulty in diagnosing autoimmune pancreatitis by imaging findings. *Gastrointest Endosc* 65:99–108, 2007.
235. Takahashi N, Fletcher JG, Fidler JL, et al: Dual-phase CT of autoimmune pancreatitis: A multireader study. *AJR Am J Roentgenol* 190:280–286, 2008.
236. Irie H, Honda H, Baba S, et al: Autoimmune pancreatitis: CT and MR characteristics. *AJR Am J Roentgenol* 170:1323–1327, 1998.
237. Kamisawa T, Takuma K, Anjiki H, et al: Differentiation of autoimmune pancreatitis from pancreatic cancer by diffusion-weighted MRI. *Am J Gastroenterol* 105:1870–1875, 2010.
238. Kwon S, Kim MH, Choi EK: The diagnostic criteria for autoimmune chronic pancreatitis: It is time to make a consensus. *Pancreas* 34:279–286, 2007.
239. Vlachou PA, Khalili K, Jang HJ, et al: IgG4-related sclerosing disease: Autoimmune pancreatitis and extrapancreatic manifestations. *Radiographics* 31:1379–1402, 2011.
240. Okazaki K, Kawa S, Kamisawa T, et al: Clinical diagnostic criteria of autoimmune pancreatitis: Revised proposal. *J Gastroenterol* 41:626–631, 2006.
241. Chari ST, Smyrk TC, Levy MJ, et al: Diagnosis of autoimmune pancreatitis: The Mayo Clinic experience. *Clin Gastroenterol Hepatol* 4:1010–1016, quiz 1934, 2006.
242. Otsuki M, Chung JB, Okazaki K, et al: Asian diagnostic criteria for autoimmune pancreatitis: Consensus of the Japan-Korea Symposium on Autoimmune Pancreatitis. *J Gastroenterol* 43:403–408, 2008.
243. Farrell JJ, Garber J, Sahani D, Brugge WR: EUS findings in patients with autoimmune pancreatitis. *Gastrointest Endosc* 60:927–936, 2004.
244. Levy MJ, Reddy RP, Wiersma MJ, et al: EUS-guided trucut biopsy in establishing autoimmune pancreatitis as the cause of obstructive jaundice. *Gastrointest Endosc* 61:467–472, 2005.
245. Sugumar A: Diagnosis and management of autoimmune pancreatitis. *Gastroenterol Clin North Am* 41:9–22, 2012.
246. Manfredi R, Graziani R, Cicero C, et al: Autoimmune pancreatitis: CT patterns and their changes after steroid treatment. *Radiology* 247:435–443, 2008.
247. Sahani DV, Sainani NI, Deshpande V, et al: Autoimmune pancreatitis: Disease evolution, staging, response assessment, and CT features that predict response to corticosteroid therapy. *Radiology* 250:118–129, 2009.
248. Hedgire SS, McDermott S, Borczuk D, et al: The spectrum of IgG4-related disease in the abdomen and pelvis. *AJR Am J Roentgenol* 201:14–22, 2013.
249. O'Reilly DA, Malde DJ, Duncan T, et al: Review of the diagnosis, classification and management of autoimmune pancreatitis. *World J Gastrointest Pathophysiol* 5:71–81, 2014.

Pancreatic Neoplasms

ALEC J. MEGIBOW

CHAPTER OUTLINE

Ductal Adenocarcinoma

- Goals of Imaging
- Multidetector Computed Tomography Protocols
- Magnetic Resonance Imaging Protocols
- Multidetector Computed Tomography Findings
- Magnetic Resonance Imaging Findings
- Endoscopic Ultrasound
- Accuracies of Multidetector Computed Tomography, Magnetic Resonance Imaging, and Endoscopic Ultrasound
- Changes in the Pancreatic Duct
- Other Imaging Modalities

Cystic Neoplasms

- Serous Cystadenoma
- Mucinous Cystic Tumor
- Intraductal Papillary Mucinous Neoplasm
- Other Cystic Tumors

Pancreatic Neuroendocrine Tumors

- Insulinoma
- Gastrinoma
- Nonfunctioning Pancreatic Neuroendocrine Tumor
- Imaging

Secondary Pancreatic Neoplasms

The World Health Organization classification of pancreatic neoplasms is remarkable for the wide variety and type. This is because benign, borderline, and malignant tumors can arise from exocrine, neuroendocrine, intraductal, and stromal elements. In addition, secondary (metastatic) neoplasms and non-neoplastic tumor-like conditions (e.g., mass-forming chronic pancreatitis) affect the pancreas. However, in clinical practice, only a few of these (adenocarcinoma, cystic neoplasms, pancreatic neuroendocrine tumors, and metastases) are encountered with any frequency. This chapter attempts to review the protocol details that are necessary to be used for patients thought to have a pancreatic neoplasm; the roles of additional imaging, such as positron emission tomography (PET) and endoscopic ultrasound (EUS); and the imaging appearances of these tumors.

Ductal Adenocarcinoma

Pancreatic ductal adenocarcinoma (PDA) is the fourth most common cause of cancer deaths for both men and women in the United States. The American Cancer Society estimates approximately 45,000 new cases with 38,000 deaths for 2014.¹ This is a striking increase from the 32,000 expected new cases of ductal cancers predicted in 2005; a true increase in incidence

is documented between 1998 and 2008.² Despite improvements in imaging, surgery, radiation, and chemotherapy and rapidly emerging molecular understanding, mortality remains high; 23% of patients will be alive at 1 year from diagnosis, whereas 4% will be alive at 5 years. Established risk factors for development of PDA include cigarette smoking, male African American, *BRCA2* gene positivity, hereditary pancreatitis, cirrhosis, diabetes mellitus, chronic pancreatitis, hypercholesterolemia, obesity, Peutz-Jeghers syndrome, Lynch syndrome, vitamin D deficiency, certain occupations, and carcinogens.³ Common symptoms include weight loss, jaundice, floating stool, pain, dyspepsia, nausea, and depression. New-onset type 2 diabetes in patients older than 50 years may trigger investigation for PDA.⁴

The American Joint Committee on Cancer has developed a TNM-based staging system for pancreatic adenocarcinoma⁵; however, because only 15% to 20% of patients are candidates for surgery at the time of diagnosis, the majority of patients will not be able to be formally assigned to a stage. For all patients who do not undergo surgery, clinical staging is solely based on imaging.⁶ The quality of imaging can directly affect the accuracy of staging; patients deemed to have unresectable tumor at non-pancreatic-directed imaging have been shown to actually be surgical candidates.⁷

Ductal adenocarcinoma accounts for 85% to 90% of all pancreatic tumors; 60% to 70% arise in the head, 5% to 10% in the body, and 10% to 15% in the tail of the gland.^{8,9} Up to 22% of tumors can affect multiple regions of the gland (diffuse).¹⁰ By the time the tumors are discovered, they usually measure 2 to 3 cm in diameter. Pancreatic adenocarcinoma has scant cellular elements and elicits an intense desmoplastic response within the stroma surrounding the tumor. The stromal reaction encases intrapancreatic blood vessels, explaining why 90% of these masses are hypodense compared with background pancreas. The upstream main pancreatic duct may be obstructed, and the surrounding parenchyma is atrophic. Tumors in the head of the pancreas will also eventually obstruct the common bile duct. The tumor rapidly grows through lymphatics, along peripancreatic vessels, and along nerves; it may also grow along tissue planes into the surrounding duodenum and posterior wall of the stomach. Lesions in the tail of the pancreas infiltrate into the splenic hilum and into the left renal hilum. Distant metastases are most frequently found in the liver and peritoneal cavity. These can be present even in cases in which the tumor does not appear locally advanced.¹¹

The major blood vessels involved by PDA are the superior mesenteric artery, celiac axis, and branches. More frequently, the tumor will involve the superior mesenteric, splenic, and portal veins. Once the major arterial branches are involved with tumor, most surgeons agree that they are unresectable. However, experienced surgeons can achieve a negative-margin resection if the degree of contact between the tumor and the vessel is minimal. Most lymph node disease in pancreatic cancer is

found in unenlarged lymph nodes¹²; lymphadenopathy is unusual. Most surgeons will operate on patients who have lymph node disease within the field of resection. Distant lymph node disease is a contraindication to resection.

GOALS OF IMAGING

A high-quality imaging study is the first part of the evaluation of *all* patients thought to have pancreatic cancer.⁴ In most cases, multidetector computed tomography (MDCT), magnetic resonance imaging (MRI), or EUS, with needle aspiration biopsy, will serve as that procedure.^{13,14} Other imaging modalities, such as transabdominal ultrasound, diagnostic endoscopic retrograde cholangiopancreatography (ERCP), ¹⁸F-fluorodeoxyglucose PET (FDG PET), and receptor (somatostatin)-specific nuclear medicine studies, are secondary procedures. Examinations such as upper gastrointestinal series, hypotonic duodenography, and selective catheter angiography no longer have any role in the diagnostic work-up.

The choice of imaging study must take into account safety, patient comfort, and affordability combined with a sufficient sensitivity, specificity, and accuracy. The protocol for the imaging test is designed to detect the presence of a pancreatic neoplasm and to determine whether an individual patient has truly resectable disease.¹⁵ Timing of the imaging acquisition must be optimized to maximize lesion-to-background pancreas contrast differences, to evaluate the integrity of major peripancreatic arteries and veins, and to detect extrapancreatic metastases (Fig. 98-1). There is a high level of agreement that

high-quality MDCT using a multiphase acquisition protocol is the procedure of choice for these patients.^{4,16,17}

MULTIDETECTOR COMPUTED TOMOGRAPHY PROTOCOLS

Image data from MDCT examination is collected by use of the narrowest detector configuration. From the data acquisition, two sets of image data are reconstructed. The first set is reconstructed at familiar CT slice widths (3 or 4 mm); these images are sent to a picture archiving and communications system (PACS) or film. The second set is reconstructed at the thinnest possible slice width as determined by the detector (e.g., 0.75-mm sections from a 0.6-mm detector configuration).¹⁸ These isotropic data sets are sent to a three-dimensional (3D) workstation, allowing multiplanar reformatting, 3D volume rendering, CT angiography, and CT cholangiopancreatography (CTCP).¹⁹⁻²³ Utility of 3D imaging is enhanced by the use of neutral (close to water density) oral contrast material.²⁴

Proper delivery of intravenous contrast material and timing of the acquisition are critical for successful pancreatic CT. A low-osmolality intravenous contrast agent with high iodine concentration (370 mg I/mL) at a dose of 1.5 mg I/kg provides optimal pancreatic parenchymal and hepatic enhancement.²⁵ The contrast agent should be administered by power injector at a minimum rate of 3 mL but preferably between 4 and 5 mL/s. All investigators use a dual acquisition protocol.²⁶⁻²⁸ The first image set is acquired during the pancreatic phase (approximately 40 to 50 seconds), and a second image set is acquired

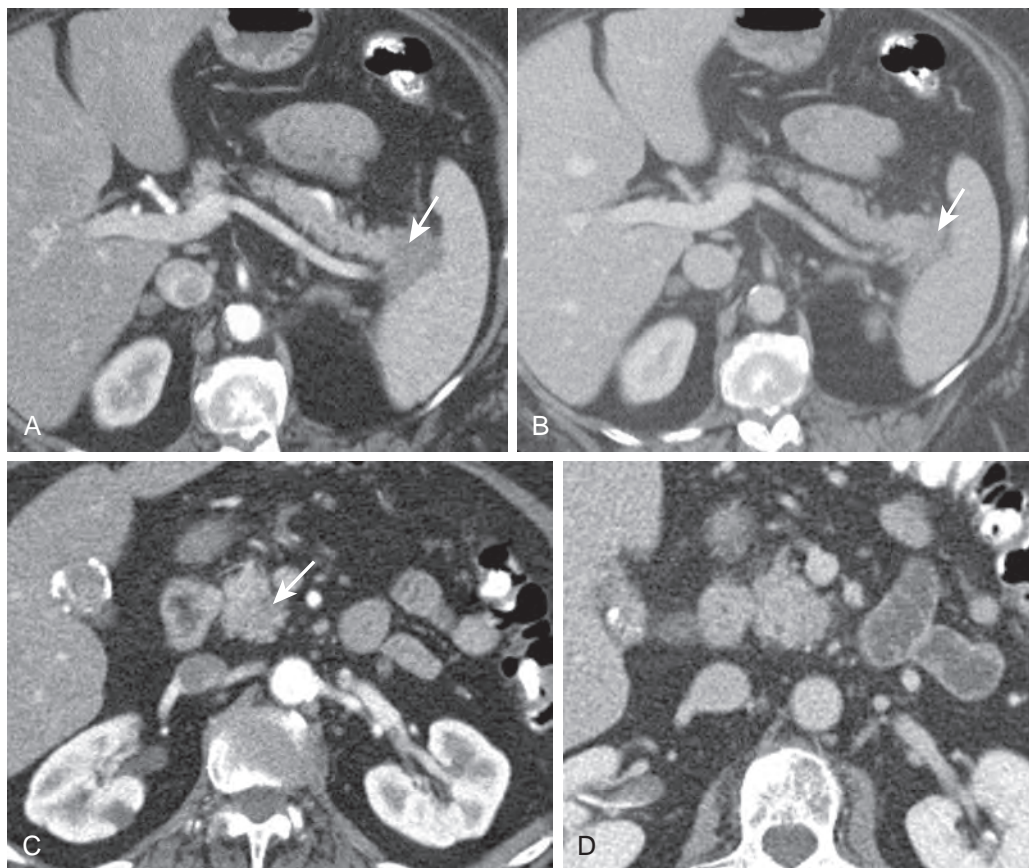


Figure 98-1 Pancreatic adenocarcinoma.

A. Adenocarcinoma of the tail of the pancreas in a 57-year-old man. During the pancreatic phase, the mass in the tail of the pancreas (arrow) is easily recognized. **B.** Adenocarcinoma, tail of pancreas; same patient as in **A**. During the portal phase, the mass is almost isodense with the remainder of the pancreas (arrow). **C.** Adenocarcinoma of the head of the pancreas in a 64-year-old woman. There is a low-attenuation region in the head of the pancreas (arrow). **D.** Adenocarcinoma, head of pancreas and same patient as **C**. The mass is unrecognizable 20 seconds later during the portal phase. Both cases illustrate the critical importance of pancreatic phase imaging.

during the portal venous phase (70 to 80 seconds) (Fig. 98-1).²⁹ Some advocate a three-phase protocol that includes an unenhanced acquisition; in our practice, we incorporate an unenhanced acquisition only when pancreatic neuroendocrine tumor is suspected.

Dual-energy CT acquisitions have the advantage of allowing the radiologist to view images acquired at two different energies (kVp). Viewing the images acquired at the lower energy or by simulating the contrast that might have been acquired at a lower beam energy (monoenergetic imaging) enhances tissue contrast by maximizing photoelectric interactions. This results in an increase in the attenuation of background pancreas with resultant increase in lesion-to-background conspicuity.^{30,31}

MAGNETIC RESONANCE IMAGING PROTOCOLS

A comprehensive (“one-stop shopping”) MRI evaluation of the pancreas and biliary tree can be performed by use of multiple acquisitions at multiple pulse sequences. In our practice, a pancreas-dedicated MRI evaluation includes an axial fat-suppressed fast (turbo) T2 sequence; two-dimensional (2D) axial in-phase and opposed-phase noncontrast T1-weighted sequences; axial and coronal single-shot fast spin-echo (HASTE or spoiled GRASS) T2-weighted acquisition; and multiphasic

gadolinium-enhanced, 3D T1-weighted gradient recalled acquisition with frequency selected fat suppression (VIBE) sequences during the phase of pancreatic enhancement and the portal phase of hepatic enhancement.³²⁻³⁶ Current MRI scanners can obtain diffusion-weighted sequences; however, these have been shown not to be reliable for pancreatic adenocarcinoma.^{37,38}

Magnetic resonance cholangiopancreatography (MRCP) is also performed with a heavily weighted T2 acquisition either in 2D with thick slab or 3D respiratory-triggered acquisition. The 2D pancreaticobiliary duct evaluation can also be obtained from the HASTE acquisitions.

MULTIDETECTOR COMPUTED TOMOGRAPHY FINDINGS

PDA appears as a hypodense mass with poorly defined borders compared with the background parenchyma during the pancreatic phase.³⁹ With current MDCT technology, non-contour-deforming tumors will be frequently encountered, underscoring the critical importance of imaging the pancreas during the phase of maximal background pancreatic enhancement, in which the tumor-to-gland attenuation difference is greatest.⁴⁰ In 11% of cases, pancreatic adenocarcinoma may be isoattenuating (Fig. 98-2).⁴¹ Secondary findings include dilation of the

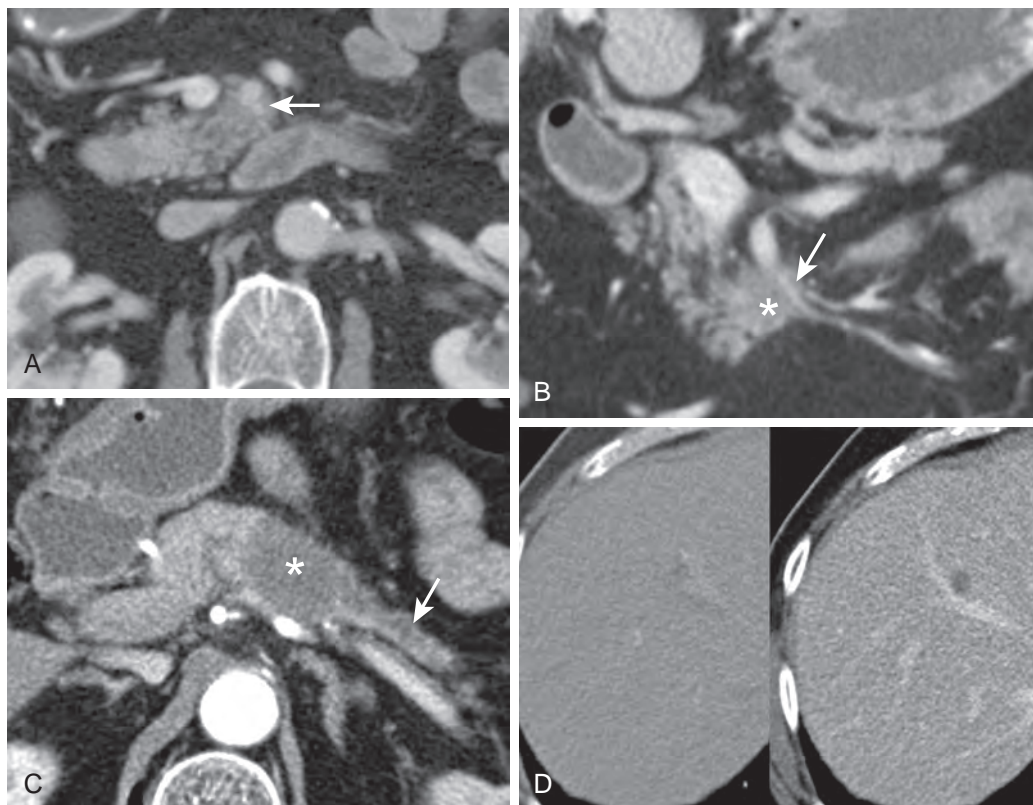


Figure 98-2 Pancreatic adenocarcinoma. **A.** Locally unresectable pancreatic adenocarcinoma in a 78-year-old woman. There is an infiltrating mass projecting medially from the uncinate process appearing to contact the superior mesenteric artery over a greater than 180-degree circumference (arrow). **B.** Locally unresectable pancreatic adenocarcinoma, same patient as in **A.** This volume rendered CT angiographic view more optimally displays the mass (asterisk) and clearly depicts the complete contact of the superior mesenteric artery (arrow). **C.** Locally resectable pancreatic adenocarcinoma in a 68-year-old man. There is a mass (asterisk) in the body of the pancreas that contacts but does not surround the splenic artery. Note the upstream atrophy and main pancreatic duct dilation in the body and tail of the pancreas (arrow). On the basis of local staging, the tumor would be classified as borderline resectable. **D.** Locally resectable pancreatic adenocarcinoma but distant metastasis. Same patient as in **C.** The hepatic metastasis is seen on the portal acquisition; on the pancreatic phase, there is only a vague region of low attenuation. This case illustrates the differing times of peak enhancement of the pancreas and liver. The presence of the hepatic metastasis makes this case unresectable despite the fact that the tumor is locally resectable.

upstream pancreatic duct and dilation of the common bile duct when the tumor is located within the pancreatic head. Use of curved multiplanar reformatting or 3D volume rendering can improve detection of ductal dilation.⁴²

CT findings of major arterial encasement include obliteration of the normal fat between the pancreatic margin and the adjacent vessel; more than 180-degree contact between the tumor and the vessel; and morphologic changes in the artery, including narrowing or encasement of the affected artery.^{43,44} With 3D volume rendering, images of the pancreatic arterial supply can be created that rival conventional catheter angiography, making recognition of the vascular changes straightforward⁴⁵ (Fig. 98-2). CT angiographic images have been shown to be more accurate for detection of arterial involvement from pancreatic adenocarcinoma than by looking at traditional axial slices alone⁴⁶ (Fig. 98-3).

With improving MDCT technology, there is increasing appreciation of local spread of PDA before it actually encases major vessels. Predictable pathways for perilymphatic and perineural tumor infiltration have been correlated with detailed anatomic dissections. High-quality thin-section imaging is needed to view these changes.^{47,48} When spread along these pathways is suspected, the surgeon should be alerted, and neoadjuvant therapy may be appropriate before attempt at resection.⁴⁹

Criteria for venous invasion include more than 180-degree contact with a soft tissue mass and the vein. When the superior

mesenteric vein is involved with tumor, it may display a “tear-drop” configuration⁵⁰ (Fig. 98-4). Although soft tissue contact with the venous system has a high predictive value for nonresectability,⁵¹ significant involvement of the vein may be found at surgery when the imaging study fails to reveal any direct contact with the vein.⁵² It is therefore critical to evaluate the presence and pattern of collateral venous channels surrounding the pancreatic head.^{53,54} In advanced cases, collateral venous channels are easily recognized. Common collateral channels include prominent short gastric varices, gastrohepatic ligament varices, and gastroepiploic to gastroduodenal trunk. It is important to look for the small posterior pancreaticoduodenal veins; when these collaterals are present, there is a high likelihood that the tumor has involved the superior mesenteric vein to a degree that would preclude the ability to obtain a negative tumor margin⁵⁴ (Fig. 98-4).

MAGNETIC RESONANCE IMAGING FINDINGS

The appearance of the pancreatic mass will depend on the acquisition sequence used (Fig. 98-5). As outlined in the preceding section, a multisequence approach is used for a comprehensive evaluation. Because the pancreatic mass elicits a dense desmoplastic stromal response, most masses will have a shorter relaxation time than the surrounding normal parenchyma and therefore appear as a “dark” region. Contrast-enhanced pancreatic phase T1-weighted sequences are most

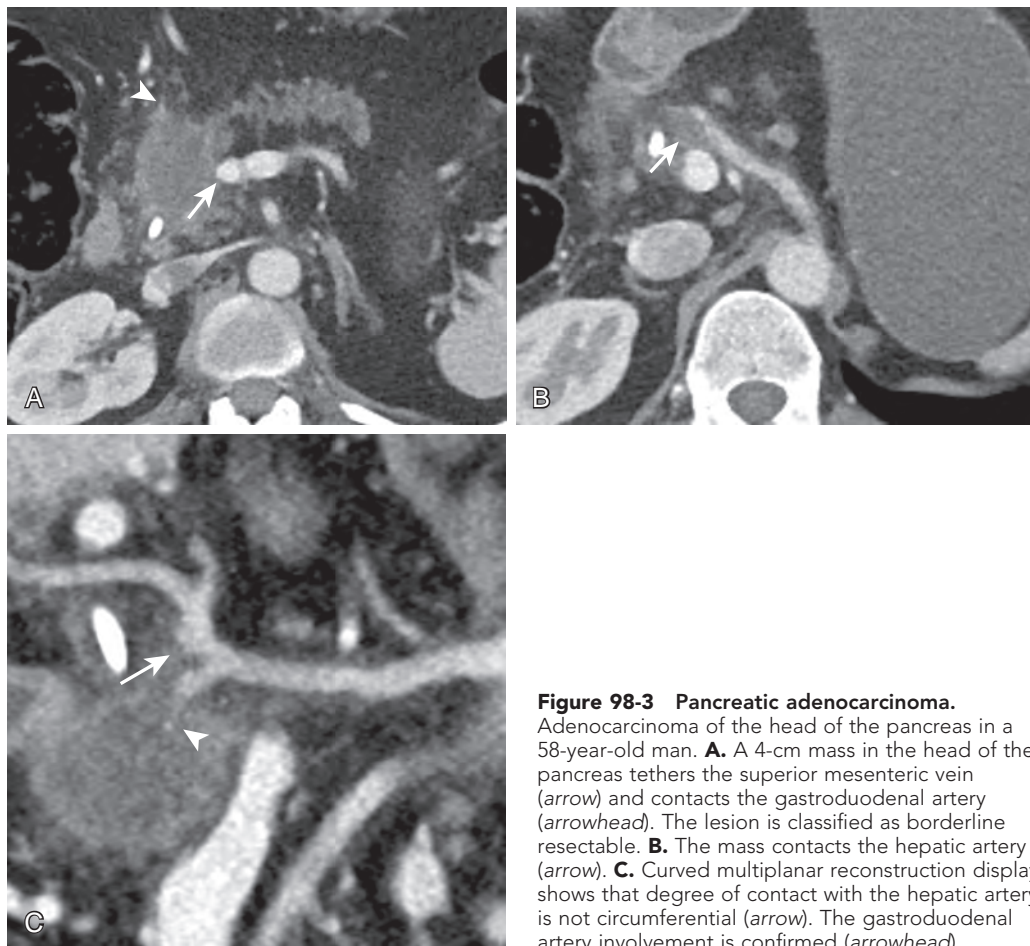


Figure 98-3 Pancreatic adenocarcinoma.

Adenocarcinoma of the head of the pancreas in a 58-year-old man. **A.** A 4-cm mass in the head of the pancreas tethers the superior mesenteric vein (arrow) and contacts the gastroduodenal artery (arrowhead). The lesion is classified as borderline resectable. **B.** The mass contacts the hepatic artery (arrow). **C.** Curved multiplanar reconstruction display shows that degree of contact with the hepatic artery is not circumferential (arrow). The gastroduodenal artery involvement is confirmed (arrowhead).

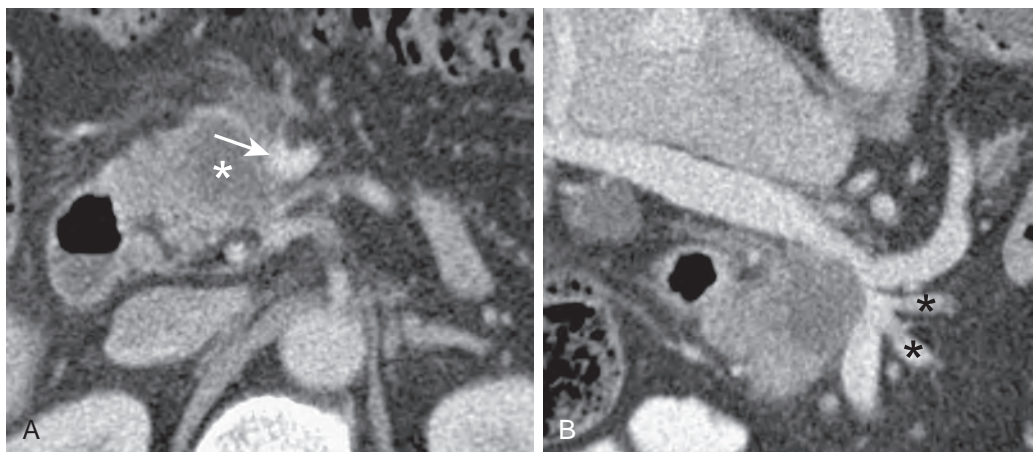


Figure 98-4 Pancreatic adenocarcinoma. Unresectable adenocarcinoma of the head of the pancreas in a 54-year-old man. **A.** The tumor in the head of the pancreas (asterisk) contacts the superior mesenteric vein (arrow). There was no contact with arteries. **B.** Whereas the degree of contact is less than 180 degrees, the intestinal veins (asterisks) join at the confluence with the splenic vein. A venous graft could not be placed because the drainage of intestinal venous branches would be obstructed.

effective in delineating the mass. Fat suppression will increase the conspicuity of the mass by significantly decreasing the signal from intraperitoneal and retroperitoneal fat, thereby increasing the signal from the pancreas, heightening contrast between normal parenchyma, the mass, and the pancreatic duct. PDA is hypointense compared with background pancreatic parenchyma, similar to CT findings. Liver metastases are best seen against a densely enhanced liver as occurs in the portal venous phase. Metastases possess a more rapid relaxation time than the background liver on both T1- and T2-weighted sequences and therefore will appear relatively bright. Detection of liver metastases is improved when diffusion-weighted sequences are obtained in addition to contrast-enhanced acquisitions.⁵⁵

Because the gadolinium-enhanced imaging sequences are acquired as a 3D volume, the arterial and venous anatomy can be displayed as MR angiographic images with imaging features of vascular involvement and tumor extension similar to those displayed on MDCT. Familiar 3D techniques, such as maximum intensity projection and volume rendering, can be used to create displays of the pathologic process in any useful plane.

ENDOSCOPIC ULTRASOUND

The accuracy of EUS in the diagnosis of pancreatic and periampullary neoplasm is well established.⁵⁶ However, with rapid improvement in both MDCT and MRI, EUS use is predominantly complementary to cross-sectional techniques and for case-by-case problem solving.⁵⁷ EUS is an excellent guide for fine-needle aspiration biopsy, with positive results in 75% of cases.⁵⁸ It has been shown that there is a statistically significant lower chance for development of peritoneal carcinomatosis after EUS biopsy as opposed to percutaneous fine-needle aspiration biopsy.⁵⁹

ACCURACIES OF MULTIDETECTOR COMPUTED TOMOGRAPHY, MAGNETIC RESONANCE IMAGING, AND ENDOSCOPIC ULTRASOUND

There is relatively uniform consensus at the time of this writing that MDCT ranges in overall accuracy between 86% and

99%.^{21,40,60-67} The positive predictive value of CT for predicting resectability ranges between 45% and 79% because the criteria for diagnosis of vascular invasion favor specificity over sensitivity.⁶⁸ However, there has been overall improvement coincident with improving technology.⁶⁹ This trend has continued; high-quality MDCT restaged 81 of 88 patients considered unresectable to resectable, with 94% having R0 resections.⁷ Centers that see a high volume of pancreatic cancer patients will obtain a repeated pancreas-dedicated CT study if outside imaging is considered inadequate.⁷⁰

Reported accuracy for MDCT in detection of arterial involvement is reported as high as 99%, with a negative predictive value of 100%.⁷¹ Confirmation of venous involvement is best assessed on hepatic phase images, and the negative predictive value approaches 100%.⁴⁰ Detection of lymph node metastasis is limited. With use of a short-axis diameter of more than 10 mm as the criterion for nodal involvement, CT has a reported sensitivity of 14%, a specificity of 85%, a negative predictive value of 82%, and an overall accuracy of 73%.¹²

Reported accuracies for high-quality multiacquisition MRI range between 76% and 89%.⁷²⁻⁷⁴ A meta-analysis of eight studies found the pooled sensitivity, specificity, and positive and negative likelihood ratio to be identical for CT and MRI for diagnosis of vascular invasion.⁷⁵ Some centers find the improved contrast sensitivity of MRI over CT useful for planning radiation therapy (see Fig. 98-5).

The most frequent cause of understaging of pancreatic adenocarcinoma is the failure of the detection of small metastases in the liver and peritoneal cavity. Imaging is poor in the detection of these small lesions. Small peritoneal implants may be present without ascites or other more flagrant signs of peritoneal carcinomatosis, making them extremely difficult to detect. A combination of CT scanning supplemented by laparoscopic ultrasound immediately before surgery in those patients deemed to have resectable tumor is an imaging strategy that has accuracy as high as that of more expensive tests, with preservation of the highest levels of quality-adjusted life-years.⁷⁶ In most clinical practice, MDCT is the primary imaging modality, with MRI reserved for patients with allergy to contrast material. EUS is used in cases in which ductal obstruction is visualized *without* a mass visible on the cross-sectional study

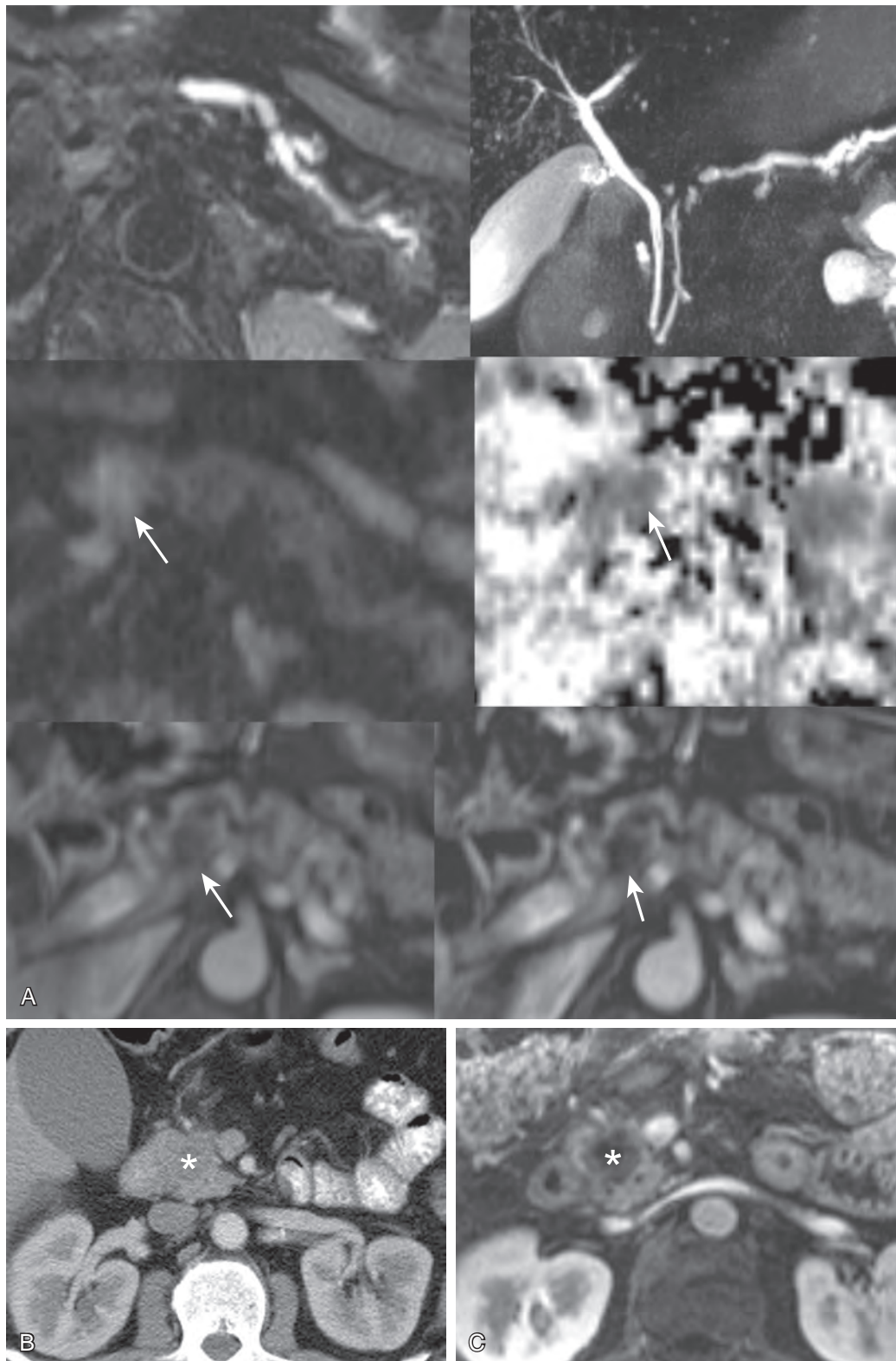


Figure 98-5 Pancreatic adenocarcinoma. **A.** MRI evaluation of a 68-year-old woman. *Top row:* Fat-saturated T2 sequence (left) and long T2 slab MRCP (right) reveal segmental main pancreatic duct dilation. *Middle row:* High b value diffusion-weighted image (left) shows restriction with high signal in region of change in duct caliber (arrow). Corresponding apparent diffusion coefficient map shows decrease in region of interest (arrow). This combination is characteristic of neoplasm. *Bottom row:* Image from gadolinium-enhanced gradient recalled echo sequence (left) reveals focal low signal mass at point of caliber change in pancreatic duct (arrow). Contrast is increased by use of subtraction imaging (right). **B.** Adenocarcinoma, head of pancreas, in a 52-year-old man. An infiltrating mass (asterisk) in the head of the pancreas is seen on pancreatic phase MDCT. **C.** Adenocarcinoma, head of pancreas; same patient as in **B**. The mass (asterisk) is more clearly delineated on the gadolinium-enhanced gradient recalled echo T1-weighted sequence. Radiation therapists find MR useful for more precise definition of tumor margins, resulting in better targeting.

and is the best method for obtaining tissue to confirm malignant disease.⁷⁷

With reported successes of newer neoadjuvant treatment options and increasing skill in surgical removal of tumor, consistent detailed reporting that specifically addresses each of the components of the status of a given tumor around which appropriate therapeutic decisions are made is desirable. Such reports guarantee that the examination has been adequately performed and carefully reviewed. Furthermore, these reports can serve as a record by which institutional accuracy in image interpretation can be measured as well as provide a uniform database for larger interinstitutional trials. The Society of Abdominal Radiology and the American Pancreatic Association called together a panel of experts in imaging, gastroenterology, and surgery to create a template for reporting of imaging findings in patients with pancreatic adenocarcinoma. The results have been published in both the radiology⁷⁸ and gastroenterology literatures.⁷⁹

CHANGES IN THE PANCREATIC DUCT

The main pancreatic duct is routinely visualized on MRCP performed with most current MR systems in clinical use. Rapid T2-weighted sequences and respiratory-gated long T2 3D sequences can show the normal duct in almost all cases. The duct can be visualized on high-quality pancreatic phase MDCT⁴² and with moderate frequency during the portal phase.⁸⁰ Minimum intensity projections and curved multiplanar reformatting facilitate recognition of the duct.

When this finding is observed on an imaging study, patients should undergo an intensive work-up to exclude malignant disease as the cause^{81,82} (Fig. 98-6). In one series, 71 of 86 isolated duct strictures were due to a malignant disease.⁸³ Pancreatic adenocarcinoma⁸⁴ and neuroendocrine tumor⁸⁵ are the most common tumor causes. Differential diagnosis includes main duct intraductal papillary mucinous neoplasm. When the entire duct is dilated, chronic pancreatitis cannot be excluded.

Isolated duct strictures may predate the typical imaging appearance of PDA and can be thought of as a sign of “early” pancreatic cancer. Several studies have documented that retrospective review of prior imaging studies in patients presenting with PDA will reveal abnormalities in the pancreas in nearly half of patients, the most common being segmental dilation of the main pancreatic duct. This finding can predate the clinical appearance of pancreatic neoplasm by as long as 18 months.^{86,87} In our practice, when we detect segmental pancreatic duct obstruction, the patient will be referred for EUS and biopsy; the high sensitivity and specificity for diagnosis of the underlying neoplasm are validated in the literature.⁸⁸ Small cysts (>5 mm) associated with a dilated pancreatic duct appear to be a predictor of future development of PDA.⁸⁹

OTHER IMAGING MODALITIES

Several other imaging modalities are in current use for imaging of pancreatic adenocarcinoma, including transabdominal ultrasound, ERCP, and FDG PET. Several reports have shown promise of FDG PET scanning to detect pancreatic cancer⁹⁰⁻⁹²;

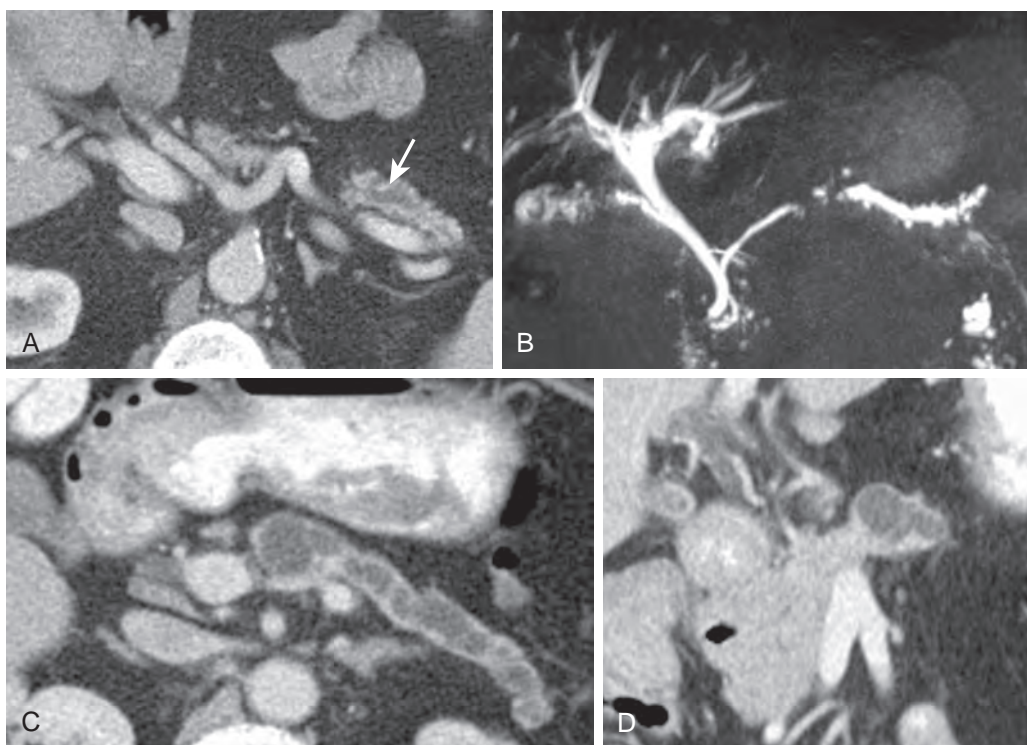


Figure 98-6 Pancreatic adenocarcinoma: importance of main pancreatic duct. **A.** This 84-year-old man, who was being observed for prostate cancer, developed a segmentally dilated main pancreatic duct (arrow). **B.** The finding is confirmed on MRCP. The patient underwent a distal pancreatectomy and is alive 3 years after these imaging studies. **C.** The dilated pancreatic duct in this 69-year-old woman was discovered incidentally during surveillance for known carcinoma of the cervix. **D.** No mass is seen at the transition point. No discrete pancreatic mass was recognized at the time of surgery, but a distal pancreatectomy was performed. Poorly differentiated adenocarcinoma was present.

however, with improved MDCT and MRI balanced against the cost, most believe that PET-CT is complementary and best used on a case-by-case basis.⁹³

Transabdominal ultrasound will often be used in jaundiced patients to rapidly identify a dilated biliary tree. Whereas a dilated intrahepatic biliary tree is easily demonstrated, the specific cause of extrahepatic bile duct dilation is frequently difficult to establish. The most frequent reason for this is bowel gas obscuring the region of the pancreatic head and common bile duct. In selected patients, however, careful transabdominal technique can demonstrate the echogenic mass obstructing either the pancreatic or common bile duct. Contrast-enhanced transabdominal ultrasound has become an established technique to detect pancreatic lesions and to measure organ perfusion.⁹⁴

ERCP is often used preoperatively to place a drainage stent within an obstructed common bile duct. Several studies have shown that this preoperative stent placement should not be performed before surgical resection as there is a clear increase in the complication rate.⁹⁵ Most leading pancreatic surgeons will request common bile duct stenting when surgery will be delayed more than 14 days after diagnostic evaluation. Expandable metallic endoscopically placed endobiliary stents should be reserved for those patients with unresectable disease needing palliation.

Cystic Neoplasms

Cystic pancreatic neoplasms are frequently encountered on imaging studies. Despite a large accumulating clinical and imaging experience with these lesions, their behavior in individual patients is difficult to predict. Therefore, when they are detected on an imaging study, there will be uncertainty about the diagnosis and varying recommendations for follow-up or treatment⁹⁶ despite the fact that there has been improving ability to correctly characterize individual lesions on imaging studies.^{97,98}

Cystic pancreatic neoplasms can be divided into four distinct categories: serous cystadenoma (SCA); mucinous cystic neoplasm; intraductal papillary mucinous neoplasm (IPMN); and “other”⁹⁹ (Fig. 98-7). This classification helps in focusing of the imaging search for diagnostic features that allow differentiation of benign from malignant lesions, paralleling the management that is distinct within each category.

SEROUS CYSTADENOMA

SCA accounts for approximately 1% to 2% of all exocrine pancreatic neoplasms. The World Health Organization classification of pancreatic tumors considers SCA a benign lesion.¹⁰⁰ At the time of diagnosis, 25% to 50% of patients will be

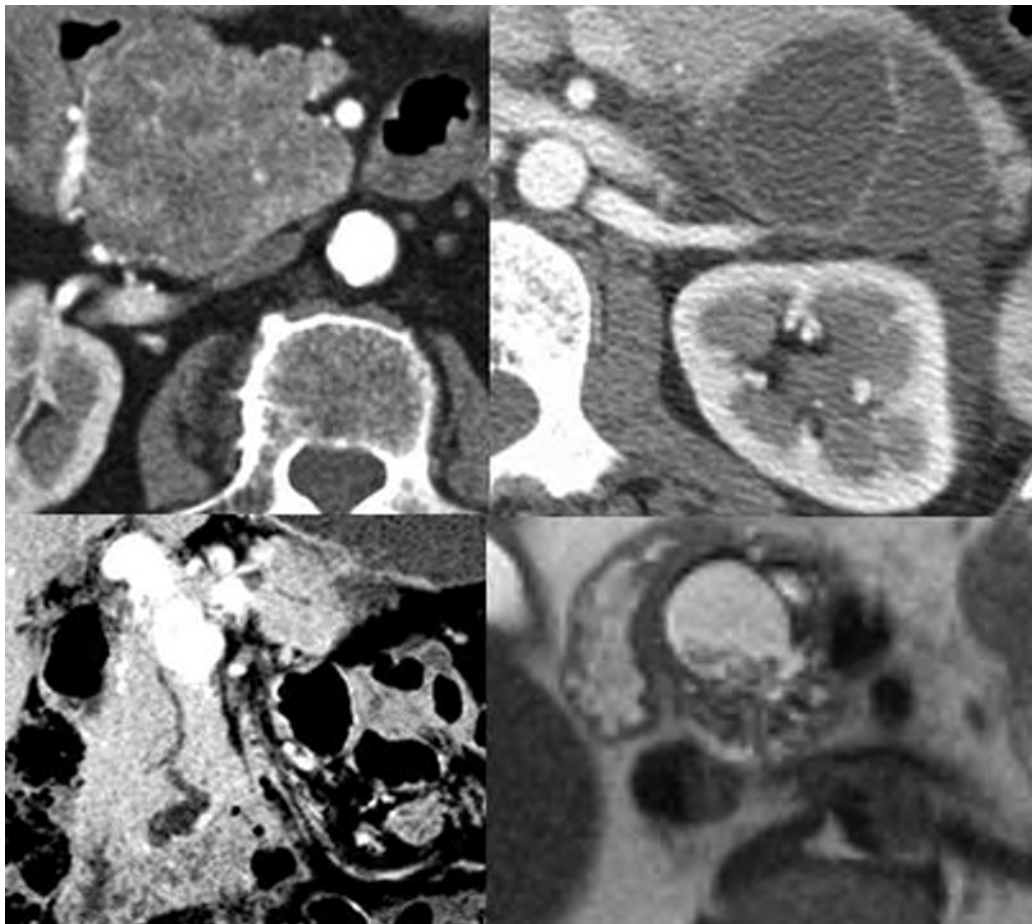


Figure 98-7 Pancreatic cystic neoplasms. Classic imaging findings in four different patients. *Top left:* Serous cystadenoma with radially arrayed dense septa. *Top right:* Mucinous cystic tumor in a 45-year-old woman. Note the scant septa and typical location in the pancreatic tail. *Bottom left:* Branch duct IPMN. The minimum intensity projection CT shows relation to main pancreatic duct. *Bottom right:* Walled off pancreatic necrosis. The presence of dependent debris on the T2-weighted image allows specific diagnosis. With current imaging technology and increasing appreciation of the appearances of pancreatic cysts, specific diagnosis can be made in approximately two thirds of cases.

symptomatic.¹⁰¹ The tumor occurs more frequently in women (mean age of 57 years) and most often in the pancreatic head. The tumor contains glycogen-rich periodic acid–Schiff–positive epithelial cells delimiting cysts separated by variable amounts of fibrous septations. They most frequently occur sporadically; 60% to 80% of patients with von Hippel–Lindau syndrome will have pancreatic SCA.

SCA has two morphologic appearances: the microcystic or classic type, and the macrocystic or oligocystic type. The microcystic form, accounting for two thirds of SCAs, is a spongelike lesion formed from innumerable cysts containing clear watery fluid. The cysts range from 1 to 5 mm in the center of the mass; larger cysts (up to 2 cm) are present in the periphery. A central fibrous stellate nidus is present giving rise to radially oriented fibrous bands. This central nidus frequently calcifies. The oligocystic type has scant locules or can be unilocular. There is no central scar; the fluid may be clear but often is hemorrhagic.¹⁰² Because of the recognition of the oligocystic type of SCA, the term *microcystic serous cystadenoma* is no longer used to describe these lesions.

The imaging features of SCA reflect the morphologic appearance of the mass. The classic variety is manifested as a solitary mass that displays central calcification and a radial arrangement of dense fibrous tissue delimiting a variable number of cysts (Fig. 98-8). In some tumors, the cysts are so small and the fibrous component so dense that the lesion may actually appear “solid.”¹⁰³ As one might imagine, on MDCT, the cysts are near water density, and the surrounding fibrous network appears dense; on MRI, the appearance is dependent on the pulse sequence of the acquisition. Central calcification establishes the diagnosis of SCA, but it is present, at most, in 30% of cases,⁹⁷ best detected by MDCT. The tumors may encase vessels and

obstruct the pancreatic or biliary duct system. Nevertheless, even these seemingly aggressive tumors may remain indolent.

On T1-weighted fat-suppressed sequences, the fluid component is darker than the fibrous matrix; on T2-weighted acquisitions, the fluid component becomes more conspicuous, appearing bright because of the longer T2 relaxation time. EUS may be particularly useful in displaying the honeycombed internal structure in lesions smaller than 2 cm. EUS provides an excellent means by which to sample cyst fluid.¹⁰⁴

The oligocystic variety can be suspected when there is a unilocular nonenhancing cystic mass in the pancreatic head with a lobulated contour.¹⁰⁵ Despite the high reported specificity of this constellation of findings, differentiation of this lesion from mucinous cystic tumor or pseudocyst may be impossible.

MUCINOUS CYSTIC TUMOR

These rare neoplasms are thought to be potentially malignant; therefore, the terms *mucinous cystadenoma* and *mucinous cystadenocarcinoma* should not be used; rather, the lesion is properly referred to as mucinous cystic tumor. Mucinous cystic tumors are formed from variably atypical epithelial cells that produce mucin and are supported by an ovarian-type stroma, which does *not* communicate with the pancreatic duct system. They account for 2% to 6% of all exocrine pancreatic neoplasms.¹⁰⁶ These tumors occur almost exclusively in women, with peak incidence in the fifth decade. The female preponderance is similar to that of mucinous tumors of the hepatobiliary system, retroperitoneum, and ovary. The stromal component of the mucinous cystic tumor stains for cytokeratin markers, indicative of cellular luteinization,¹⁰² the ovarian-type stroma

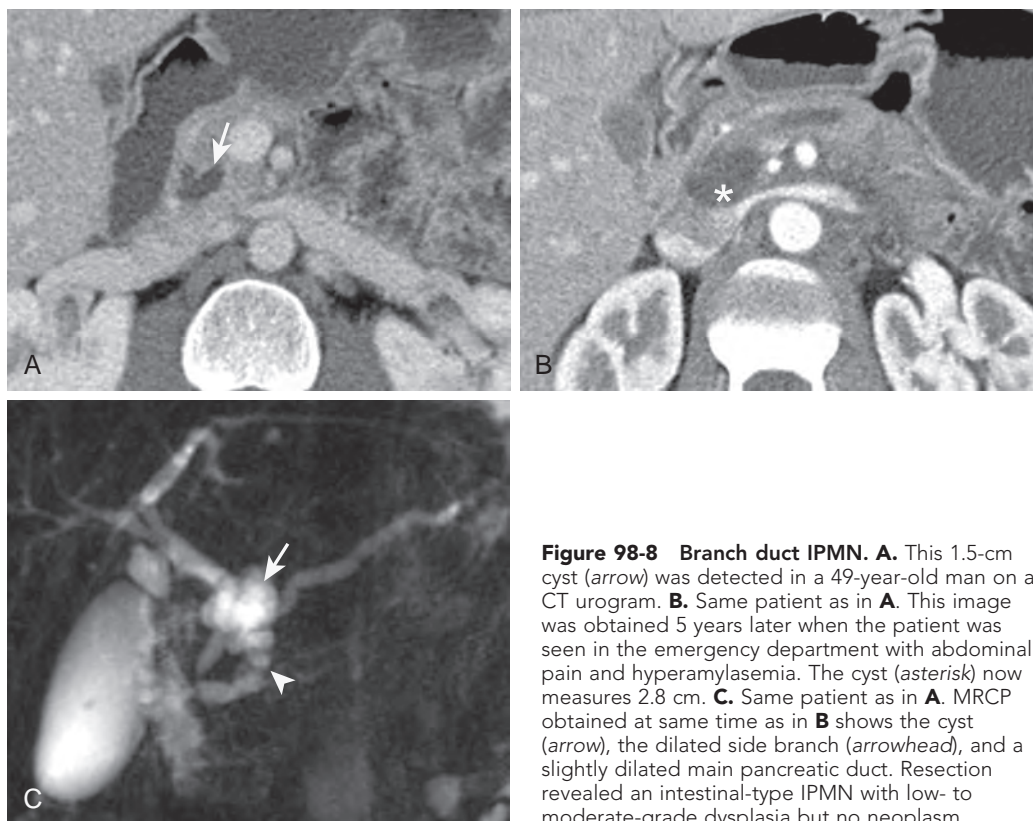


Figure 98-8 Branch duct IPMN. **A.** This 1.5-cm cyst (arrow) was detected in a 49-year-old man on a CT urogram. **B.** Same patient as in **A.** This image was obtained 5 years later when the patient was seen in the emergency department with abdominal pain and hyperamylasemia. The cyst (asterisk) now measures 2.8 cm. **C.** Same patient as in **A.** MRCP obtained at same time as in **B** shows the cyst (arrow), the dilated side branch (arrowhead), and a slightly dilated main pancreatic duct. Resection revealed an intestinal-type IPMN with low- to moderate-grade dysplasia but no neoplasm.

characteristic of these lesions. It is important to remember this fact because the diagnosis of mucinous cystic tumor should probably not be considered in a male patient.

At MDCT, the lesions will display large cysts with thin septa, best seen after intravenous administration of contrast material. When calcification occurs, it is lamellated (as opposed to the starburst pattern seen in SCA) and in the periphery of the lesion (as opposed to the central location of calcification in SCA). Lesions with a higher degree of epithelial atypia will display nodules on the wall, peripheral calcification, and a more disorganized internal architecture (Fig. 98-9). Malignant lesions tend to be larger than benign lesions.¹⁰⁷ On MRI, the lesion will appear bright on T2-weighted sequences. On T1-weighted sequences, intravenous administration of gadolinium is necessary to image the septations, which become more apparent the longer the imaging sequence is carried out^{107,108} (Fig. 98-10). Mucin itself can produce decreased signal

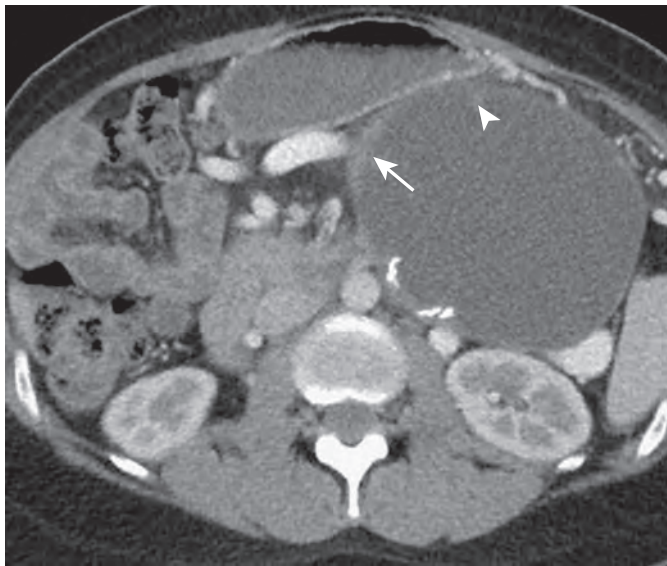


Figure 98-9 Pancreatic mucinous cystic tumor with features of malignancy. This cyst in a 43-year-old woman has three features that must raise the suspicion that portions of the lesion will have neoplastic histologic features, including peripheral calcification, variable wall thickness (arrow), and mural nodule (arrowhead). Foci of atypia and noninvasive malignant change were confirmed at resection.

within the center of the lesion that should not be confused with the radiating septa seen in SCA. On EUS, the mural nodularity is easily recognized and can be differentiated from the honeycombed appearance of SCA. EUS is particularly valuable for aspiration of cyst fluid.¹⁰⁹ Presence of carcinoembryonic antigen in aspirated cyst fluid has a high predictive value for mucinous cystic tumor.¹¹⁰

INTRADUCTAL PAPILLARY MUCINOUS NEOPLASM

The IPMN was first described at ERCP by Ohhashi in 1982¹¹¹; the first report in the imaging literature was by Itai and colleagues in 1986.¹¹² The entity has been reported under a wide variety of names, including ductectatic mucinous cystadenoma, villous adenoma of the main pancreatic duct, and intraductal mucinous hypersecreting neoplasm, to name a few; at this time, the term *intraductal papillary mucinous neoplasm* (IPMN) is most frequently used. The prevalence of this lesion is high among patients with pancreatic cysts. Currently, most cysts detected at imaging are assumed to be IPMN until proven otherwise.^{113,114} IPMN occurs with a slight increased frequency in male patients compared with other pancreatic cysts. The pathologic hallmarks of the lesion are diffuse or segmental dilation of the main or side branch pancreatic ducts, intraductal growth of the mucin-producing epithelial lining cells, and protrusion and dilation of the major and minor papilla with mucus excretion.¹¹⁵ In slightly more than 50% of the cases, the pancreatic duct bulges into the ampulla of Vater, with marked hypersecretion of mucus seen pouring into the duodenum at endoscopy.

Two morphologic forms are distinguished: those involving the main pancreatic duct with or without side branch involvement (Fig. 98-11), and those exclusively within the branch ducts (see Fig. 98-8). Within both of these varieties, there are five histologic types: intestinal, pancreaticobiliary, gastric, intraductal tubulopapillary, and intraductal oncocytic.¹¹⁶ Cases in which the main duct is involved have a significantly higher likelihood of harboring more malignant epithelium than those restricted to the branch ducts,^{117,118} but malignant change is not invariably found (Fig. 98-11). The different histologic types cannot be differentiated on imaging; however, the risk of malignancy varies significantly between them. Branch duct IPMNs can arise anywhere within the pancreas, although

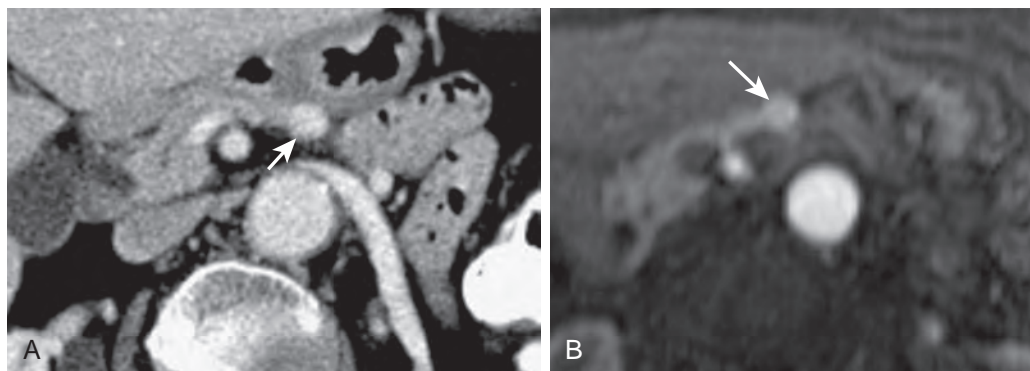


Figure 98-10 Insulinoma. **A.** MDCT of insulinoma in a 58-year-old male patient. CT in arterial phase reveals a hyperdense mass (arrow) in the body of the pancreas. The mass appears as bright as the surrounding vessels. **B.** MRI of insulinoma in the same patient as in **A.** Arterial phase image from gadolinium-enhanced gradient recalled VIBE sequence again demonstrates the mass in the body of the pancreas (arrow). An insulin-secreting PNET was resected.

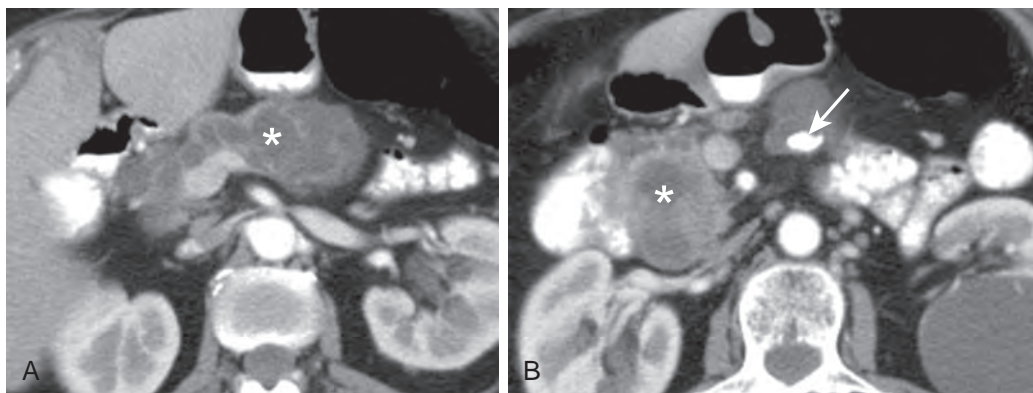


Figure 98-11 Main duct IPMN with adenocarcinoma. A. The main pancreatic duct in this 74-year-old woman is diffusely dilated (asterisk). **B.** Same patient as in **A.** A soft tissue attenuation mass is present in the pancreatic head (asterisk). Note the calcification in the more proximal portion of the main pancreatic duct (arrow). Peripheral calcifications are frequently present in these lesions.

the uncinate process, head, and neck are the most common locations. Individual lesions contain a wide spectrum of epithelial dysplasia; however, an individual lesion's biologic behavior is variable (see Fig. 98-8). Factors correlating with malignancy include advanced age, main duct involvement, concurrent diabetes or other pancreas-related abdominal symptoms, lesion size (>3 cm) and multiplicity, and presence of visible mural nodules or any other solid elements.¹¹⁹ Malignancy in main duct IPMN is more frequently encountered but not always present; patients who are symptomatic and have duct dilation of more than 8 mm are more likely to have malignant tumors than are those with less duct dilation.¹²⁰

At imaging, the lesion is characterized by increased diameter of a portion of the pancreatic duct system. Visualization is optimal with use of intravenous contrast-enhanced thin-section MDCT or T2-weighted MRI. The diagnosis is confirmed by demonstration of communication with the pancreatic duct, best determined by 3D techniques including CTCP⁴² and MRCP^{118,121} (see Fig. 98-8). Careful attention to protocol will allow the radiologist to demonstrate the bulging papilla into the duodenal lumen, a finding that when present allows distinction from chronic pancreatitis.¹¹⁹ Mural nodules or mucinous accretions can be seen on both MDCT¹²² and T2-weighted MRI¹²³ (see Fig. 98-9). EUS is particularly useful for evaluating main duct tumors, particularly the longitudinal extent of main duct involvement, aiding surgical planning.¹²⁴

A complex analytic process of the imaging findings is necessary. Despite this, considerable uncertainty about recommending additional interventions or follow-up still exists. Furthermore, the frequency and interval of the follow-up periods are not universally agreed on. First, the size of the lesion must be determined. In multiple studies, there appears to be a significant change in the risk of malignancy in tumors smaller than 3 cm (low) or larger than 3 cm.^{125,126} Current recommendations advocate aggressive characterization of lesions larger than 3 cm. Lesions smaller than 1 cm are usually observed. Uncertainty exists in deciding how to handle cysts that range between 1 and 3 cm in size. In our practice, we will attempt to characterize cysts of this size by pancreas-dedicated imaging (usually by MRI) with the explicit purpose of visualizing the cyst in relation to the main pancreatic duct. If the cyst can be characterized as an IPMN, 6-month follow-up for a 4-year period is recommended for younger patients; for asymptomatic patients with other comorbidities, the follow-up regimen is determined on a

case-by-case basis. If the cyst is uncharacterized, it is assumed to be an IPMN. EUS may be performed for larger cysts (closer to 3 cm) as opposed to 6-month follow-up for smaller cysts. Factors that influence the decisions include the age of the patient and the presence or absence of pancreas-related symptoms.¹²⁷ Regardless of the size of the cyst, we advocate cyst fluid aspiration before any cyst is resected¹²⁸; an elevated carcinoembryonic antigen level in the cyst has high predictive value for mucin content.¹²⁹

The strongest predictor of a malignant cyst is the presence of mural nodules, particularly those larger than 6 mm.¹³⁰ These may be difficult to detect on cross-sectional imaging studies; EUS is much better suited to see them. Virtually all consensus recommendations concerning pancreatic cysts agree that mural nodules are a highly significant finding in terms of risk stratification for an individual cyst. Their presence has been shown to be a more reliable independent predictor of malignancy than cyst size, septa, or mural thickness.¹³⁰

Nonoperative surveillance has become widely accepted when pancreatic cysts are initially detected. Because many will be small, the morphologic features of malignancy may not be easily recognized.¹³¹ Follow-up allows some estimate of the growth rate of an individual cyst. Branch duct IPMN that grows at a rate of more than 2 mm per year has a significantly higher rate of malignancy than that of tumor with a slower growth rate (45.6% vs 1.8%).¹³²

There are increasing numbers of case reports of metachronous development of pancreatic adenocarcinoma at sites distant to the branch duct IPMN. The incidence of metachronous tumor development is consistently reported in the range of 6% to 11%.¹³³⁻¹³⁵ This substantiates speculation that branch duct IPMN arises as a field defect in a whole pancreas that is at risk for development of malignancy. Newer molecular pathology studies have shown that metachronous tumors develop more frequently in patients with gastric-type IPMN.¹³⁶ Knowledge of molecular markers within a given lesion therefore may have significant implication in developing a follow-up schedule for an individual patient.

OTHER CYSTIC TUMORS

The solid and pseudopapillary epithelial neoplasm, also known as the Hamoudi tumor, deserves mention. This tumor is most frequently found in female patients at a mean age consistently

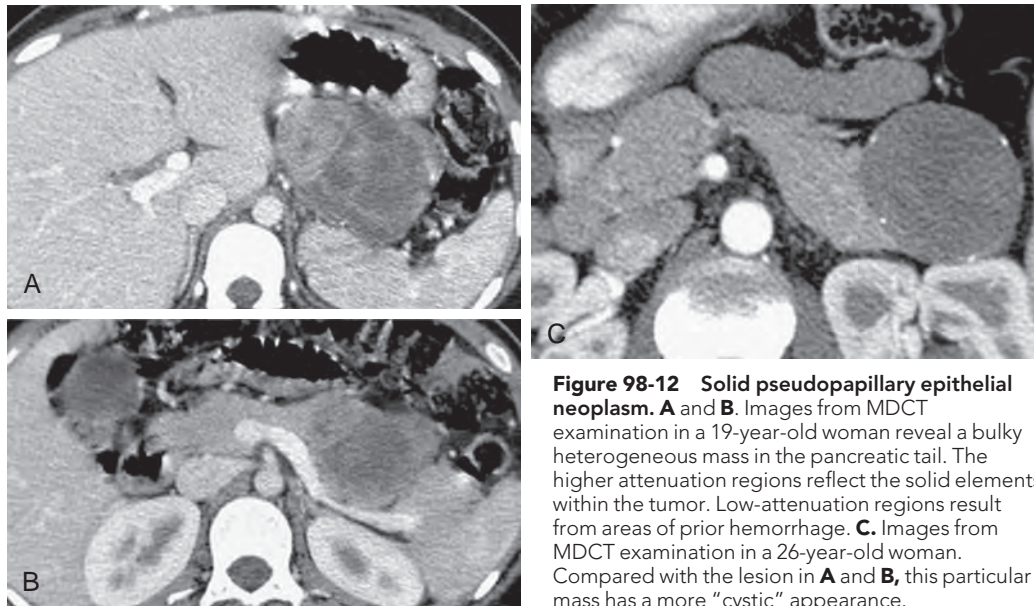


Figure 98-12 Solid pseudopapillary epithelial neoplasm. **A** and **B.** Images from MDCT examination in a 19-year-old woman reveal a bulky heterogeneous mass in the pancreatic tail. The higher attenuation regions reflect the solid elements within the tumor. Low-attenuation regions result from areas of prior hemorrhage. **C.** Images from MDCT examination in a 26-year-old woman. Compared with the lesion in **A** and **B**, this particular mass has a more “cystic” appearance.

reported in the mid-20s,¹³⁷ but the lesion has been reported in patients as young as 10 years and as old as 79 years. Review of the literature suggests that approximately 15% of these tumors are malignant, with the likelihood of malignancy increasing with the patient's age.¹³⁸

The proportion of solid and cystic elements within the tumor is directly related to the degree of hemorrhage the tumor has undergone. The lesion appears as a round, encapsulated mass with variable amounts of necrotic and soft tissue foci (Fig. 98-12). The presence of blood products within the tumor results in hyperintense signal on T1-weighted MR sequences.¹³⁹ No septations are visualized; central and rim calcifications have been reported in 29% of patients.¹³⁷ The recommended treatment is surgery; localized lesions are treated as low-grade neoplasms. Median survival rates of 5.2 years are reported for patients with metastatic disease.¹⁴⁰

Any pancreatic neoplasm can display a “cystic morphology.” Cystic islet cell tumor and cystic ductal adenocarcinoma have been reported. True epithelial pancreatic cysts are extremely rare in the absence of systemic cystic disease, such as adult polycystic liver and kidney disease or von Hippel–Lindau disease. When a cystic tumor of the pancreas is recognized, every effort should be made to exclude a history of acute or chronic pancreatitis because pancreatic pseudocysts remain the single most common cystic pancreatic mass.¹⁴¹

Pancreatic Neuroendocrine Tumors

Pancreatic neuroendocrine tumors (PNETs) are a heterogeneous group of tumors, some of which are associated with secretion of hormones that produce clinically recognizable syndromes. The current World Health Organization classification divides PNETs into the subcategories of well-differentiated endocrine tumor, well-differentiated endocrine carcinoma, and poorly differentiated endocrine carcinoma. The well-differentiated PNETs are further divided into those with benign behavior (confined to pancreas, nonaggressive, <2 cm in size, functional or nonfunctional) and uncertain behavior (confined

to pancreas, >2 cm in size or with angioinvasion, functional or nonfunctional). All well-differentiated PNETs are thought to be low-grade malignant neoplasms and are categorized on the basis of size, mitotic rate, cell proliferation (as measured by Ki-67 labeling index), and evidence of invasion.¹⁴²

PNETs account for 1% to 10% of all pancreatic neoplasms. Their overall prevalence is reported at 1 per 100,000, with an annual incidence of 1 to 4 cases/million persons per year. Nonfunctioning PNETs account for 14% to 30% of PNETs, although they have been reported in as high as 80%.¹⁴³ PNETs occurs with equal frequency in men and women, with peak age in the 50s and 60s. PNETs are found with equal frequency throughout the pancreas.¹⁴⁴ Increased frequency is well documented in patients with four inherited disorders: autosomal dominant multiple endocrine neoplasia (MEN 1), von Hippel–Lindau disease, tuberous sclerosis, and neurofibromatosis 1.¹⁴⁵

The most widely expected imaging appearance of PNET is a hypervascular mass best seen in the pancreatic phase of enhancement on MDCT (Fig. 98-13) or a briskly enhancing focus on fat-suppressed, gadolinium-enhanced T1-weighted MRI.^{146,147} Five percent to 10% of PNETs will be cystic; the thick enhancing peripheral rim may allow differentiation from other pancreatic cysts. On occasion, they will be manifested with an isolated duct stricture.⁸⁵

INSULINOMA

Insulinoma is the most common functioning PNET (see Fig. 98-10). Patients may present with Whipple's triad (neuromuscular disorders, hypoglycemia, and symptom reversal with administration of glucose). Fifty percent of the lesions are found in the head of the pancreas, the remainder elsewhere within the gland; 85% are solitary, and 0.5% of the lesions are extrapancreatic. Most lesions are 1 to 2 cm, and metastases occur in less than 15% of cases; however, 10% of the lesions are malignant. Malignant insulinomas are larger (measuring up to 8 cm) and produce extremely high levels of insulin or

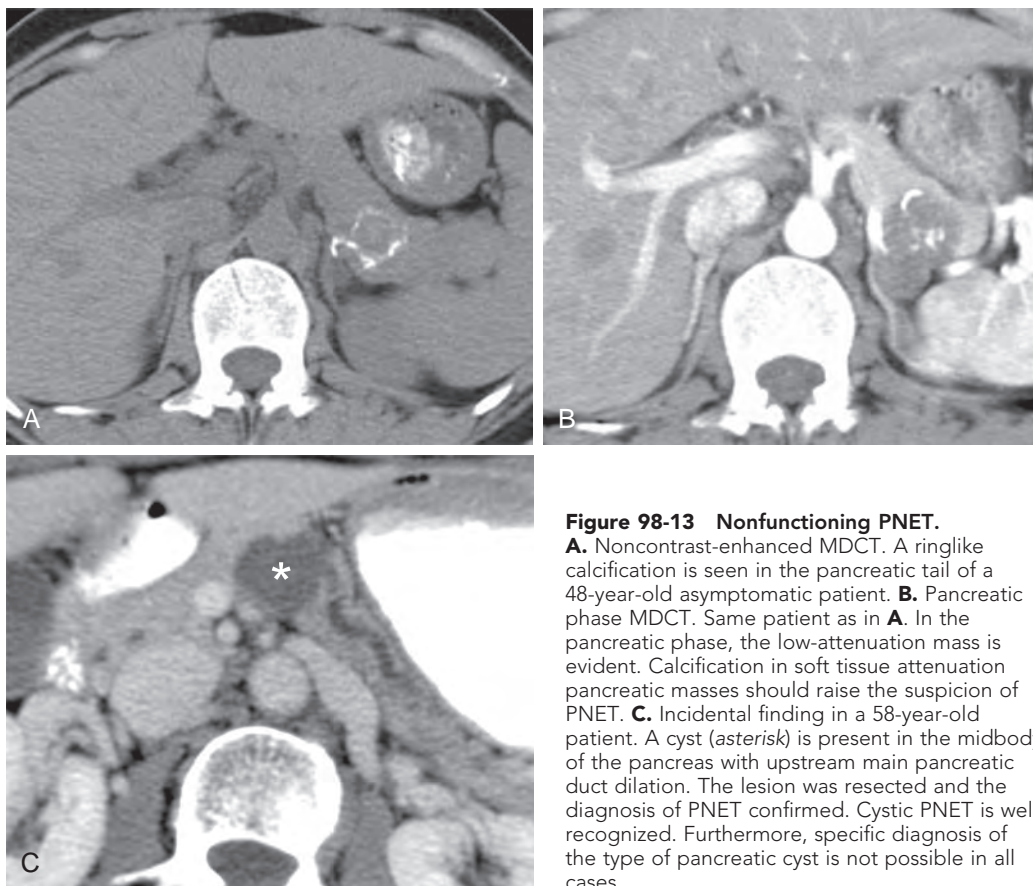


Figure 98-13 Nonfunctioning PNET.

A. Noncontrast-enhanced MDCT. A ringlike calcification is seen in the pancreatic tail of a 48-year-old asymptomatic patient. **B.** Pancreatic phase MDCT. Same patient as in **A**. In the pancreatic phase, the low-attenuation mass is evident. Calcification in soft tissue attenuation pancreatic masses should raise the suspicion of PNET. **C.** Incidental finding in a 58-year-old patient. A cyst (asterisk) is present in the midbody of the pancreas with upstream main pancreatic duct dilation. The lesion was resected and the diagnosis of PNET confirmed. Cystic PNET is well recognized. Furthermore, specific diagnosis of the type of pancreatic cyst is not possible in all cases.

proinsulin, and metastases are present at the time of diagnosis.¹⁴⁸ When the lesion is solitary and localized, simple excision or enucleation is sufficient for treatment.

GASTRINOMA

Gastrinoma is the second most functioning PNET. Most are located in the anatomic region between the pancreatic head and common bile duct and within the first or second portion of the duodenum, the so-called gastrinoma triangle¹⁴⁹ (Fig. 98-14). The excessive gastrin production leads to the Zollinger-Ellison syndrome either as a sporadic entity or as a manifestation of MEN 1. Fifty percent to 70% of sporadic cases of Zollinger-Ellison syndrome are usually the result of tumors within the pancreas; the remaining cases are secondary to tumors located within the duodenum. Most of the gastrinomas found in MEN 1 are located within the duodenum. At diagnosis, 60% of gastrinomas already have metastasized to peripancreatic lymph nodes or, less frequently, the liver.¹⁴⁸

NONFUNCTIONING PANCREATIC NEUROENDOCRINE TUMOR

Nonfunctioning PNET has a peak incidence in the 50s and 60s with an equal distribution between men and women. The masses are usually large; 60% to 83% of lesions are malignant at the time of diagnosis, usually with liver metastases. They are frequently hypervascular at imaging. Internal calcifications are frequent; nonfunctioning PNET is the most likely etiology of a

solid-appearing pancreatic mass with dense calcifications (see Fig. 98-13). The 5-year survival rates are excellent compared with ductal carcinoma; 5-year survival rates approach 70%, and 10-year survival rates approach 50% of patients.^{150,151}

IMAGING

MDCT has been shown to increase the detection of insulinomas to 94% compared with the single-slice CT success rate of 29%.^{152,153} The median sensitivity of tumor detection for all subtypes is on the order of 84%. The overall detection rate of 85% is similar to that of MRI. MRI results reach 100% sensitivity for lesions larger than 3 cm, but MRI has extremely poor performance for smaller lesions.¹⁵⁴ On MRI, PNET displays significantly higher signal intensity than normal pancreas on T2-weighted images and will demonstrate a ringlike enhancement after intravenous administration of contrast material.¹⁵⁵ EUS and molecular methods are widely used and provide a statistically incremental improvement in the imaging assessment of these patients. Most believe that MDCT can be a first-line study, but if the findings are normal, EUS can be performed. EUS may be the better first-line test for the evaluation of suspected insulinoma.¹⁵⁶

Utility of molecular agents that target specific metabolic pathways or receptors is directly related to the specific tumor subtype. Somatostatin receptor scintigraphy is widely performed; [¹¹¹In]-pentetate (Octreoscan) is widely available for clinical use. This agent is useful only in tumors with somatostatin receptor sites. Newer agents, particularly those that

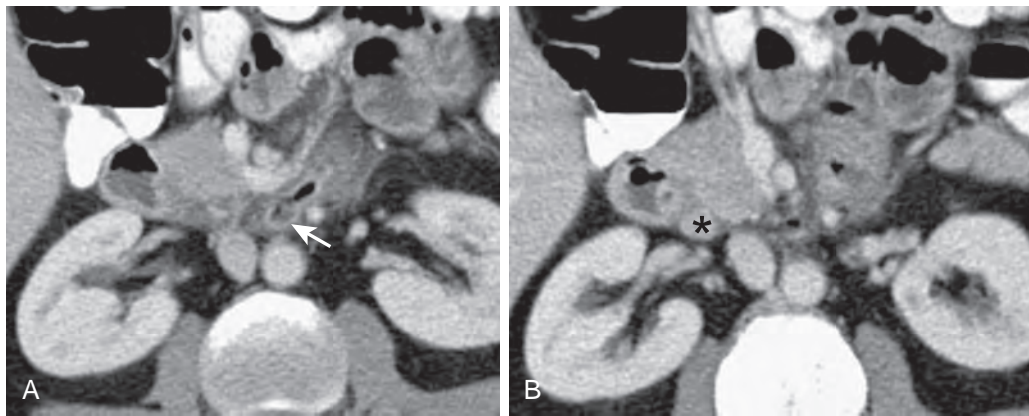


Figure 98-14 Zollinger-Ellison syndrome. **A.** MDCT scan in a 44-year-old male patient with severe upper abdominal pain. An ulcer (arrow) is present in the third portion of the duodenum. Note the mural edema. **B.** Same patient as in **A.** There is a slightly hyperdense mass (asterisk) in the groove between the undersurface of the pancreas and the medial wall of the duodenum. A well-differentiated neuroendocrine tumor (gastrinoma) was resected in this lymph node.

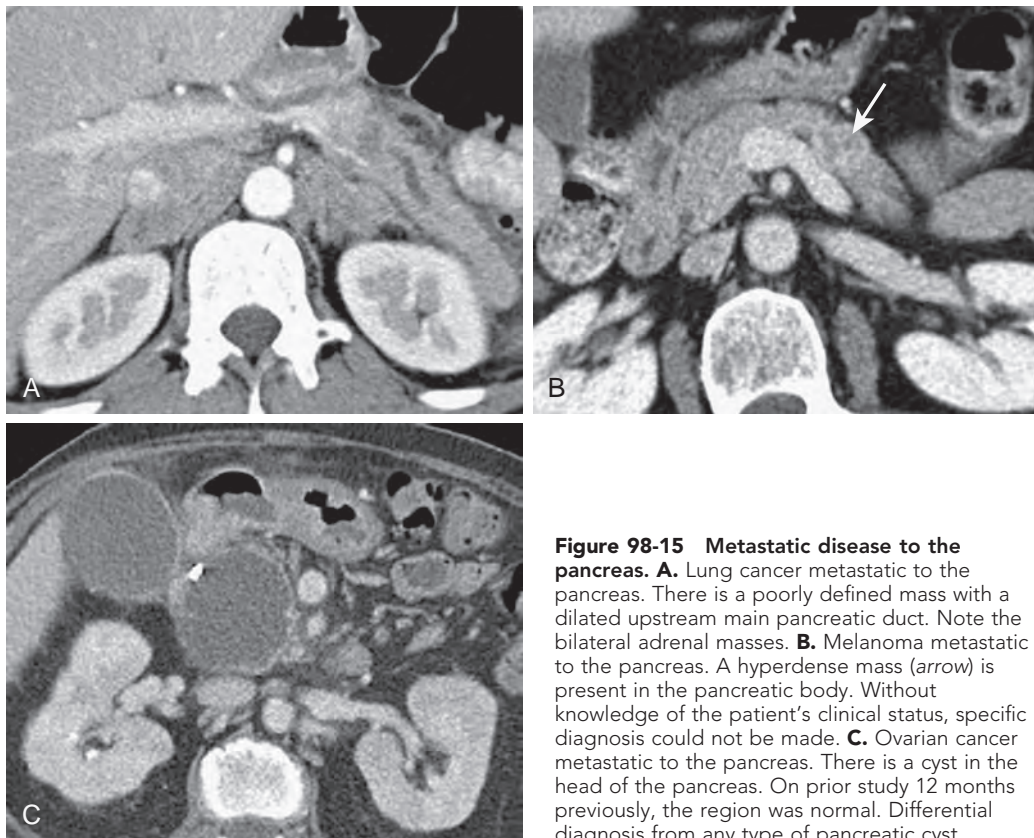


Figure 98-15 Metastatic disease to the pancreas. **A.** Lung cancer metastatic to the pancreas. There is a poorly defined mass with a dilated upstream main pancreatic duct. Note the bilateral adrenal masses. **B.** Melanoma metastatic to the pancreas. A hyperdense mass (arrow) is present in the pancreatic body. Without knowledge of the patient's clinical status, specific diagnosis could not be made. **C.** Ovarian cancer metastatic to the pancreas. There is a cyst in the head of the pancreas. On prior study 12 months previously, the region was normal. Differential diagnosis from any type of pancreatic cyst.

can be used with CT-PET scanning, such as 68-DOTA-NOC, display more true-positive tumor foci than [^{111}In]-DTPA octreotide.¹⁵⁷ The major utility of these and other newly developed molecular agents is increased detection of sites of unsuspected metastases.

Continuous improvements in MDCT and MRI technology also have resulted in improved detection and analysis of PNET. Using dual-energy spectral CT, Lin and coworkers¹⁵⁸ reported a 95.7% sensitivity compared with a 68.8% sensitivity with MDCT, the improvement being directly related to the ability to combine a monochromatic and iodine density image. Apparent diffusion coefficient values show an inverse correlation with Ki-67 labeling index and may help predict biologic behavior of an individual tumor.

Secondary Pancreatic Neoplasms

The pancreas can be secondarily involved by neoplasm by direct extension from a contiguous primary tumor (e.g., gastric carcinoma), invasion from local metastatic lymph nodes (e.g., invasion of the pancreatic head by metastatic peripancreatic lymph nodes draining a primary tumor of the right colon), and hematogenous metastases. Renal cell carcinoma is the most common primary neoplasm to metastasize to the pancreas. The lesions appear as hypervascular foci within the pancreatic parenchyma.¹⁵⁹ Other common sources of metastases to the pancreas include melanoma and lung cancer; however, metastases to the pancreas can be present from virtually any primary neoplasm¹⁶⁰ (Fig. 98-15).

REFERENCES

1. Siegel R, Ma J, Zou Z, et al: Cancer statistics, 2014. *CA Cancer J Clin* 64:9–29, 2014.
2. Simard EP, Ward EM, Siegel R, Jemal A: Cancers with increasing incidence trends in the United States: 1999 through 2008. *CA Cancer J Clin* 2012. [E-pub ahead of print.]
3. Raimondi S, Maisonneuve P, Lowenfels AB: Epidemiology of pancreatic cancer: An overview. *Nat Rev Gastroenterol Hepatol* 6:699–708, 2009.
4. Tempero MA, Arnoletti JP, Behrman SW, et al: Pancreatic adenocarcinoma, version 2.2012: Featured updates to the NCCN Guidelines. *J Natl Compr Canc Netw* 10:703–713, 2012.
5. Byrd SB, Compton CC, Fritz AG, et al, editors: *AJCC Cancer Staging Manual*, ed 7, New York, 2010, Springer.
6. Bilimoria KY, Bentrem DJ, Ko CY, et al: Validation of the 6th edition AJCC Pancreatic Cancer Staging System: Report from the National Cancer Database. *Cancer* 110:738–744, 2007.
7. Mohammed S, Van Buren G, Fisher WE: Pancreatic cancer advances in treatment. *World J Gastroenterol* 20:9354–9360, 2014.
8. Fernandez-del Castillo C, Jimenez RE: Pancreatic cancer, cystic pancreatic neoplasms, and other nonendocrine pancreatic tumors. In Feldman M, Friedman LS, Schlessenger MH, editors: *Sleisenger and Fordtran's Gastrointestinal and Liver Disease*, ed 7, Philadelphia, 2002, Elsevier, pp 970–987.
9. Cubilla AL, Fitzgerald P: *Tumors of the Exocrine Pancreas*, Washington, DC, 1984, Armed Forces Institute of Pathology.
10. Cubilla A, Fitzgerald PJ: Pancreas cancer. I. Duct adenocarcinoma. A clinical-pathologic study of 380 patients. *Pathol Annu* 1:241–289, 1978.
11. Bogoevski D, Strate T, Yekebas EF, Izbicki JR: Pancreatic cancer: A generalized disease—prognostic impact of cancer cell dissemination. *Langenbecks Arch Surg* 393:911–917, 2008.
12. Roche CJ, Hughes ML, Garvey CJ, et al: CT and pathologic assessment of prospective nodal staging in patients with ductal adenocarcinoma of the head of the pancreas. *AJR Am J Roentgenol* 180:475–480, 2003.
13. Lee ES, Lee JM: Imaging diagnosis of pancreatic cancer: A start-of-the-art review. *World J Gastroenterol* 20:7864–7877, 2014.
14. Kalra MK, Maher MM, Mueller PR, Saini S: State-of-the-art imaging of pancreatic neoplasms. *Br J Radiol* 76:857–865, 2003.
15. Megibow AJ: Pancreatic adenocarcinoma: Designing the examination to evaluate the clinical questions. *Radiology* 183:297–303, 1992.
16. Simianu VV, Zyromski NJ, Nakeeb A, Lillemoe KD: Pancreatic cancer: Progress made. *Acta Oncol* 49:407–417, 2010.
17. Callery MP, Chang KJ, Fishman EK, et al: Pretreatment assessment of resectable and borderline resectable pancreatic cancer: Expert consensus statement. *Ann Surg Oncol* 16:1727–1733, 2009.
18. Dalrymple NC, Prasad SR, El-Merhi FM, Chintapalli KN: Price of isotropy in multidetector CT. *Radiographics* 27:49–62, 2007.
19. Scaglione M, Pinto A, Romano S, et al: Using multidetector row computed tomography to diagnose and stage pancreatic carcinoma: The problems and the possibilities. *JOP* 6:1–5, 2005.
20. Tunaci M: Multidetector row CT of the pancreas. *Eur J Radiol* 52:18–30, 2004.
21. Prokesch RW, Schima W, Chow LC, Jeffrey RB: Multidetector CT of pancreatic adenocarcinoma: Diagnostic advances and therapeutic relevance. *Eur Radiol* 13:2147–2154, 2003.
22. Horton KM, Fishman EK: Adenocarcinoma of the pancreas: CT imaging. *Radiol Clin North Am* 40:1263–1272, 2002.
23. Bashir MR, Gupta RT: MDCT evaluation of the pancreas. *Radiol Clin North Am* 50:365–377, 2012.
24. Winter TC, Ager JD, Nghiem HV, et al: Upper gastrointestinal tract and abdomen: Water as an orally administered contrast agent for helical CT. *Radiology* 201:365–370, 1996.
25. Ma X, Setty B, Uppot RN, Sahani DV: Multiple-detector computed tomographic angiography of pancreatic neoplasm for presurgical planning: Comparison of low- and high-concentration nonionic contrast media. *J Comput Assist Tomogr* 32:511–517, 2008.
26. Diehl SJ, Lehmann KJ, Sadick M, et al: Pancreatic cancer: Value of dual-phase helical CT in assessing resectability. *Radiology* 206:373–378, 1998.
27. Valls C, Andia E, Sanchez A, et al: Dual-phase helical CT of pancreatic adenocarcinoma: Assessment of resectability before surgery. *AJR Am J Roentgenol* 178:821–826, 2002.
28. Nino-Murcia M, Olcott EW, Jeffrey RB, Jr: Dual-phase helical CT of locally invasive pancreatic adenocarcinoma. *J Comput Assist Tomogr* 22:282–287, 1998.
29. McNulty NJ, Francis IR, Platt JF, et al: Multidetector row helical CT of the pancreas: Effect of contrast-enhanced multiphasic imaging on enhancement of the pancreas, peripancreatic vasculature, and pancreatic adenocarcinoma. *Radiology* 220:97–102, 2001.
30. He YL, Zhang DM, Xue HD, Jin ZY: Clinical value of dual-energy CT in detection of pancreatic adenocarcinoma: Investigation of the best pancreatic tumor contrast to noise ratio. *Chin Med Sci J* 27:207–212, 2013.
31. Macari M, Spieler B, Kim D, et al: Dual-source dual-energy MDCT of pancreatic adenocarcinoma: Initial observations with data generated at 80 kVp and at simulated weighted-average 120 kVp. *AJR Am J Roentgenol* 194:W27–W32, 2010.
32. Martin DR, Semelka RC: MR imaging of pancreatic masses. *Magn Reson Imaging Clin N Am* 8:787–812, 2000.
33. Fayad LM, Mitchell DG: Magnetic resonance imaging of pancreatic adenocarcinoma. *Int J Gastrointest Cancer* 30:19–25, 2001.
34. O'Neill E, Hammond N, Miller FH: MR imaging of the pancreas. *Radiol Clin North Am* 52:757–777, 2014.
35. Keppke AL, Miller FH: Magnetic resonance imaging of the pancreas: The future is now. *Semin Ultrasound CT MR* 26:132–152, 2005.
36. Zhong L, Li L, Yao QY: Preoperative evaluation of pancreaticobiliary tumor using MR multi-imaging techniques. *World J Gastroenterol* 11:3756–3761, 2005.
37. Rosenkrantz AB, Matza BW, Sabach A, et al: Pancreatic cancer: Lack of association between apparent diffusion coefficient values and adverse pathological features. *Clin Radiol* 68:e191–e197, 2013.
38. Fukukura Y, Takumi K, Kamimura K, et al: Pancreatic adenocarcinoma: Variability of diffusion-weighted MR imaging findings. *Radiology* 263:732–740, 2012.
39. Tamm EP, Bhosale PR, Vikram R, et al: Imaging of pancreatic ductal adenocarcinoma: State of the art. *World J Radiol* 5:98–105, 2013.
40. Fletcher JG, Wiersma MJ, Farrell MA, et al: Pancreatic malignancy: Value of arterial, pancreatic, and hepatic phase imaging with multi-detector row CT. *Radiology* 229:81–90, 2003.
41. Prokesch RW, Chow LC, Beaulieu CF, et al: Isoattenuating pancreatic adenocarcinoma at multi-detector row CT: Secondary signs. *Radiology* 224:764–768, 2002.
42. Itoh S, Ikeda M, Ota T, et al: Assessment of the pancreatic and intrapancreatic bile ducts using 0.5-mm collimation and multiplanar reformatted images in multislice CT. *Eur Radiol* 13:277–285, 2003.
43. Lu DS, Reber HA, Krasny RM, et al: Local staging of pancreatic cancer: Criteria for unresectability of major vessels as revealed by pancreatic-phase, thin-section helical CT. *AJR Am J Roentgenol* 168:1439–1443, 1997.
44. Vargas R, Nino-Murcia M, Trueblood W, Jeffrey RB, Jr: MDCT in pancreatic adenocarcinoma: Prediction of vascular invasion and resectability using a multiphasic technique with curved planar reformations. *AJR Am J Roentgenol* 182:419–425, 2004.
45. Fishman EK, Horton KM, Urban BA: Multidetector CT angiography in the evaluation of pancreatic carcinoma: Preliminary observations. *J Comput Assist Tomogr* 24:849–853, 2000.
46. Mehmet Erturk S, Ichikawa T, Sou H, et al: Pancreatic adenocarcinoma: MDCT versus MRI in the detection and assessment of locoregional extension. *J Comput Assist Tomogr* 30:583–590, 2006.
47. Sai M, Mori H, Kiyonaga M, et al: Peripancreatic lymphatic invasion by pancreatic carcinoma: Evaluation with multi-detector row CT. *Abdom Imaging* 35:154–162, 2010.
48. Deshmukh SD, Willmann JK, Jeffrey RB: Pathways of extrapancreatic perineural invasion by pancreatic adenocarcinoma: Evaluation with 3D volume-rendered MDCT imaging. *AJR Am J Roentgenol* 194:668–674, 2010.
49. Heinemann V, Haas M, Boeck S: Neoadjuvant treatment of borderline resectable and non-resectable pancreatic cancer. *Ann Oncol* 24:2484–2492, 2013.
50. Hough TJ, Raptopoulos V, Siewert B, Matthews JB: Teardrop superior mesenteric vein: CT sign for unresectable carcinoma of the pancreas. *AJR Am J Roentgenol* 173:1509–1512, 1999.
51. Nakayama Y, Yamashita Y, Kadota M, et al: Vascular encasement by pancreatic cancer: Correlation of CT findings with surgical and pathologic results. *J Comput Assist Tomogr* 25:337–342, 2001.
52. Hommeyer SC, Freeny PC, Crabo LG: Carcinoma of the head of the pancreas: Evaluation of the pancreaticoduodenal veins with dynamic CT—potential for improved accuracy in staging. *Radiology* 196:233–238, 1995.
53. Vedantham S, Lu DS, Reber HA, Kadell B: Small peripancreatic veins: Improved assessment in pancreatic cancer patients using thin-section pancreatic phase helical CT. *AJR Am J Roentgenol* 170:377–383, 1998.

54. Yamada Y, Mori H, Kiyosue H, et al: CT assessment of the inferior peripancreatic veins: Clinical significance. *AJR Am J Roentgenol* 174:677–684, 2000.
55. Wu LM, Hu J, Gu HY, et al: Can diffusion-weighted magnetic resonance imaging (DW-MRI) alone be used as a reliable sequence for the preoperative detection and characterisation of hepatic metastases? A meta-analysis. *Eur J Cancer* 49:572–584, 2013.
56. Nawaz H, Fan CY, Kloke J, et al: Performance characteristics of endoscopic ultrasound in the staging of pancreatic cancer: A meta-analysis. *JOP* 14:484–497, 2013.
57. Munroe CA, Fehmi SM, Savides TJ: Endoscopic ultrasound in the diagnosis of pancreatic cancer. *Expert Opin Med Diagn* 7:25–35, 2013.
58. Caglar E, Senturk H, Atasoy D, et al: The role of EUS and EUS-FNA in the management of pancreatic masses: Five-year experience. *Hepatogastroenterology* 60:896–899, 2013.
59. Micames C, Jowell PS, White R, et al: Lower frequency of peritoneal carcinomatosis in patients with pancreatic cancer diagnosed by EUS-guided FNA vs. percutaneous FNA. *Gastrointest Endosc* 58:690–695, 2003.
60. Procacci C, Biasiutti C, Carbognin G, et al: Spiral computed tomography assessment of resectability of pancreatic ductal adenocarcinoma: Analysis of results. *Dig Liver Dis* 34:739–747, 2002.
61. Nino-Murcia M, Tamm EP, Charnsangavej C, Jeffrey RB, Jr: Multidetector-row helical CT and advanced postprocessing techniques for the evaluation of pancreatic neoplasms. *Abdom Imaging* 28:366–377, 2003.
62. Brugel M, Link TM, Rummeny EJ, et al: Assessment of vascular invasion in pancreatic head cancer with multislice spiral CT: Value of multiplanar reconstructions. *Eur Radiol* 14:1188–1195, 2004.
63. House MG, Yeo CJ, Cameron JL, et al: Predicting resectability of periampullary cancer with three-dimensional computed tomography. *J Gastrointest Surg* 8:280–288, 2004.
64. Maire F, Sauvanet A, Trivin F, et al: Staging of pancreatic head adenocarcinoma with spiral CT and endoscopic ultrasonography: An indirect evaluation of the usefulness of laparoscopy. *Pancreatol* 4:436–440, 2004.
65. Smith SL, Rajan PS: Imaging of pancreatic adenocarcinoma with emphasis on multidetector CT. *Clin Radiol* 59:26–38, 2004.
66. Imbriaco M, Megibow AJ, Ragozzino A, et al: Value of the single-phase technique in MDCT assessment of pancreatic tumors. *AJR Am J Roentgenol* 184:1111–1117, 2005.
67. He J, Page AJ, Weiss M, et al: Management of borderline and locally advanced pancreatic cancer: Where do we stand? *World J Gastroenterol* 20:2255–2266, 2014.
68. Wong JC, Lu DS: Staging of pancreatic adenocarcinoma by imaging studies. *Clin Gastroenterol Hepatol* 6:1301–1308, 2008.
69. Zhao WY, Luo M, Sun YW, et al: Computed tomography in diagnosing vascular invasion in pancreatic and periampullary cancers: A systematic review and meta-analysis. *Hepatobiliary Pancreat Dis Int* 8:457–464, 2009.
70. Walters DM, Lapar DJ, de Lange EE, et al: Pancreas-protocol imaging at a high-volume center leads to improved preoperative staging of pancreatic ductal adenocarcinoma. *Ann Surg Oncol* 18:2764–2771, 2011.
71. Li H, Zeng MS, Zhou KR, et al: Pancreatic adenocarcinoma: The different CT criteria for peripancreatic major arterial and venous invasion. *J Comput Assist Tomogr* 29:170–175, 2005.
72. Obuz F, Dicle O, Coker A, et al: Pancreatic adenocarcinoma: Detection and staging with dynamic MR imaging. *Eur J Radiol* 38:146–150, 2001.
73. Nishiharu T, Yamashita Y, Abe Y, et al: Local extension of pancreatic carcinoma: Assessment with thin-section helical CT versus with breath-hold fast MR imaging—ROC analysis. *Radiology* 212:445–452, 1999.
74. Hänninen E, Amthauer H, Hosten N, et al: Prospective evaluation of pancreatic tumors: Accuracy of MR imaging with MR cholangiopancreatography and MR angiography. *Radiology* 224:34–41, 2002.
75. Zhang Y, Huang J, Chen M, Jiao LR: Preoperative vascular evaluation with computed tomography and magnetic resonance imaging for pancreatic cancer: A meta-analysis. *Pancreatol* 12:227–233, 2012.
76. McMahon PM, Halpern EF, Fernandez-del Castillo C, et al: Pancreatic cancer: Cost-effectiveness of imaging technologies for assessing resectability. *Radiology* 221:93–106, 2001.
77. Suits J, Frazee R, Erickson RA: Endoscopic ultrasound and fine needle aspiration for the evaluation of pancreatic masses. *Arch Surg* 134:639–642, 1999.
78. Al-Hawary MM, Francis IR, Chari ST, et al: Pancreatic ductal adenocarcinoma radiology reporting template: Consensus statement of the Society of Abdominal Radiology and the American Pancreatic Association. *Radiology* 270:248–260, 2014.
79. Al-Hawary MM, Francis IR, Chari ST, et al: Pancreatic ductal adenocarcinoma radiology reporting template: Consensus statement of the Society of Abdominal Radiology and the American Pancreatic Association. *Gastroenterology* 146:291–304.e1, 2014.
80. Anderson SW, Soto JA: Pancreatic duct evaluation: Accuracy of portal venous phase 64 MDCT. *Abdom Imaging* 34:55–63, 2009.
81. Yoon SH, Lee JM, Cho JY, et al: Small (≤ 20 mm) pancreatic adenocarcinomas: Analysis of enhancement patterns and secondary signs with multiphasic multidetector CT. *Radiology* 259:442–452, 2011.
82. Takeshita K, Kutomi K, Haruyama T, et al: Imaging of early pancreatic cancer on multidetector row helical computed tomography. *Br J Radiol* 83:823–830, 2010.
83. Uehara H, Tatsumi K, Masuda E, et al: Scraping cytology with a guidewire for pancreatic ductal strictures. *Gastrointest Endosc* 70:52–59, 2009.
84. Edge MD, Hoteit M, Patel AP, et al: Clinical significance of main pancreatic duct dilation on computed tomography: Single and double duct dilation. *World J Gastroenterol* 13:1701–1705, 2007.
85. Shi C, Siegelman SS, Kawamoto S, et al: Pancreatic duct stenosis secondary to small endocrine neoplasms: A manifestation of serotonin production? *Radiology* 257:107–114, 2010.
86. Gangi S, Fletcher JG, Nathan MA, et al: Time interval between abnormalities seen on CT and the clinical diagnosis of pancreatic cancer: Retrospective review of CT scans obtained before diagnosis. *AJR Am J Roentgenol* 182:897–903, 2004.
87. Ahn SS, Kim MJ, Choi JY, et al: Indicative findings of pancreatic cancer in prediagnostic CT. *Eur Radiol* 19:2448–2455, 2009.
88. Wang W, Shpaner A, Krishna SG, et al: Use of EUS-FNA in diagnosing pancreatic neoplasm without a definitive mass on CT. *Gastrointest Endosc* 78:73–80, 2013.
89. Tanaka S, Nakao M, Ioka T, et al: Slight dilatation of the main pancreatic duct and presence of pancreatic cysts as predictive signs of pancreatic cancer: A prospective study. *Radiology* 254:965–972, 2010.
90. Rijkers AP, Valkema R, Duivenvoorden HJ, et al: Usefulness of F-18-fluorodeoxyglucose positron emission tomography to confirm suspected pancreatic cancer: A meta-analysis. *Eur J Surg Oncol* 40:794–804, 2014.
91. Kalady MF, Clary BM, Clark LA, et al: Clinical utility of positron emission tomography in the diagnosis and management of periampullary neoplasms. *Ann Surg Oncol* 9:799–806, 2002.
92. Heinrich S, Goerres GW, Schafer M, et al: Positron emission tomography/computed tomography influences on the management of resectable pancreatic cancer and its cost-effectiveness. *Ann Surg* 242:235–243, 2005.
93. Serrano OK, Chaudhry MA, Leach SD: The role of PET scanning in pancreatic cancer. *Adv Surg* 44:313–325, 2010.
94. Faccioli N, Crippa S, Bassi C, D'Onofrio M: Contrast-enhanced ultrasonography of the pancreas. *Pancreatol* 9:560–566, 2009.
95. Erickson RA: ERCP and pancreatic cancer. *Ann Surg Oncol* 11:555–557, 2004.
96. Farrell JJ, Fernandez-del Castillo C: Pancreatic cystic neoplasms: Management and unanswered questions. *Gastroenterology* 144:1303–1315, 2013.
97. Curry CA, Eng J, Horton KM, et al: CT of primary cystic pancreatic neoplasms: Can CT be used for patient triage and treatment? *AJR Am J Roentgenol* 175:99–103, 2000.
98. Sainani NI, Saokar A, Deshpande V, et al: Comparative performance of MDCT and MRI with MR cholangiopancreatography in characterizing small pancreatic cysts. *AJR Am J Roentgenol* 193:722–731, 2009.
99. Sarr MG, Kendrick ML, Nagorney DM, et al: Cystic neoplasms of the pancreas: Benign to malignant epithelial neoplasms. *Surg Clin North Am* 81:497–509, 2001.
100. Kloppel G, Luttges J: WHO-classification 2000: Exocrine pancreatic tumors. *Verh Dtsch Ges Pathol* 85:219–228, 2001.
101. Palmucci S, Cappello G, Trombatore C, et al: Cystic pancreatic neoplasms: Diagnosis and management emphasizing their imaging features. *Eur Rev Med Pharmacol Sci* 18:1259–1268, 2014.
102. Zamboni G, Capelli A, Pesci A, Brighenti A: Pathology of cystic tumors. In Procacci C, Megibow AJ, editors: *Imaging of the Pancreas: Cystic and Rare Tumors*, New York, 2003, Springer.
103. Procacci C, Graziani R, Bicego E, et al: Serous cystadenoma of the pancreas: Report of 30 cases with emphasis on the imaging findings. *J Comput Assist Tomogr* 21:373–382, 1997.
104. Clores MJ, Thosani A, Buscaglia JM: Multidisciplinary diagnostic and therapeutic approaches to pancreatic cystic lesions. *J Multidiscip Healthc* 7:81–91, 2014.
105. Cohen-Scali F, Vilgrain V, Brancatelli G, et al: Discrimination of unilocular macrocystic

- serous cystadenoma from pancreatic pseudocyst and mucinous cystadenoma with CT: Initial observations. *Radiology* 228:727–733, 2003.
106. Solcia E, Capella C, Kloppel G: Tumors of the exocrine pancreas. In Solcia E, Capella C, Kloppel G, editors: *Tumors of the Pancreas*, Washington, DC, 1997, Armed Forces Institute of Pathology, pp 145–210.
 107. Procacci C, Carbognin G, Accordini S, et al: CT features of malignant mucinous cystic tumors of the pancreas. *Eur Radiol* 11:1626–1630, 2001.
 108. Buetow PC, Rao P, Thompson LD: From the Archives of the AFIP. Mucinous cystic neoplasms of the pancreas: Radiologic-pathologic correlation. *Radiographics* 18:433–449, 1998.
 109. Khashab MA, Kim K, Lennon AM, et al: Should we do EUS/FNA on patients with pancreatic cysts? The incremental diagnostic yield of EUS over CT/MRI for prediction of cystic neoplasms. *Pancreas* 42:717–721, 2013.
 110. Brugge WR, Lewandrowski K, Lee-Lewandrowski E, et al: Diagnosis of pancreatic cystic neoplasms: A report of the cooperative pancreatic cyst study. *Gastroenterology* 126:1330–1336, 2004.
 111. Ohhashi K, Murakami Y, Maruyama M, et al: Four cases of mucus secreting pancreatic cancer. *Prog Dig Endosc* 20:348–351, 1982.
 112. Imai Y, Ohhashi K, Nagai H, et al: “Ductectatic” mucinous cystadenoma and cystadenocarcinoma of the pancreas. *Radiology* 161:697–700, 1986.
 113. Correa-Gallego C, Ferrone CR, Thayer SP, et al: Incidental pancreatic cysts: Do we really know what we are watching? *Pancreatol* 10:144–150, 2010.
 114. Valsangkar NP, Morales-Oyarvide V, Thayer SP, et al: 851 resected cystic tumors of the pancreas: A 33-year experience at the Massachusetts General Hospital. *Surgery* 152(Suppl 1):S4–S12, 2012.
 115. Tierney WM, Francis IR, Eckhauser F, et al: The accuracy of EUS and helical CT in the assessment of vascular invasion by peripapillary malignancy. *Gastrointest Endosc* 53:182–188, 2001.
 116. Shi C, Hruban RH: Intraductal papillary mucinous neoplasm. *Hum Pathol* 43:1–16, 2012.
 117. Terris B, Ponsot P, Paye F, et al: Intraductal papillary mucinous tumors of the pancreas confined to secondary ducts show less aggressive pathologic features as compared with those involving the main pancreatic duct. *Am J Surg Pathol* 24:1372–1377, 2000.
 118. Sugiyama M, Izumisato Y, Abe N, et al: Predictive factors for malignancy in intraductal papillary-mucinous tumors of the pancreas. *Br J Surg* 90:1244–1249, 2003.
 119. Procacci C, Megibow AJ, Carbognin G, et al: Intraductal papillary mucinous tumor of the pancreas: A pictorial essay. *Radiographics* 19:1447–1463, 1999.
 120. Abdeljawad K, Vemulapalli KC, Schmidt CM, et al: Prevalence of malignancy in patients with pure main duct intraductal papillary mucinous neoplasms. *Gastrointest Endosc* 79:623–629, 2014.
 121. Fukukura Y, Fujiyoshi F, Sasaki M, et al: Intraductal papillary mucinous tumors of the pancreas: Thin-section helical CT findings. *AJR Am J Roentgenol* 174:441–447, 2000.
 122. Takada A, Itoh S, Suzuki K, et al: Branch duct-type intraductal papillary mucinous tumor: Diagnostic value of multiplanar reformatted images in multislice CT. *Eur Radiol* 15:1888–1897, 2005.
 123. Khouri J, Saif MW: Intraductal papillary mucinous neoplasms of the pancreas (IPMNS): New insights on clinical outcomes and malignant progression. *JOP* 15:310–312, 2014.
 124. Cellier C, Cuillerier E, Palazzo L, et al: Intraductal papillary and mucinous tumors of the pancreas: Accuracy of preoperative computed tomography, endoscopic retrograde pancreatography and endoscopic ultrasonography, and long-term outcome in a large surgical series. *Gastrointest Endosc* 47:42–49, 1998.
 125. Sahani DV, Saokar A, Hahn PF, et al: Pancreatic cysts 3 cm or smaller: How aggressive should treatment be? *Radiology* 238:912–919, 2006.
 126. Allen PJ, D’Angelica M, Gonen M, et al: A selective approach to the resection of cystic lesions of the pancreas: Results from 539 consecutive patients. *Ann Surg* 244:572–582, 2006.
 127. Lee CJ, Scheiman J, Anderson MA, et al: Risk of malignancy in resected cystic tumors of the pancreas < or = 3 cm in size: Is it safe to observe asymptomatic patients? A multi-institutional report. *J Gastrointest Surg* 12:234–242, 2008.
 128. Hawes RH, Clancy J, Hasan MK: Endoscopic ultrasound-guided fine needle aspiration in cystic pancreatic lesions. *Clin Endosc* 45:128–131, 2012.
 129. Cizginer S, Turner BG, Bilge AR, et al: Cyst fluid carcinoembryonic antigen is an accurate diagnostic marker of pancreatic mucinous cysts. *Pancreas* 40:1024–1028, 2011.
 130. Kim KW, Park SH, Pyo J, et al: Imaging features to distinguish malignant and benign branch-duct type intraductal papillary mucinous neoplasms of the pancreas: A meta-analysis. *Ann Surg* 259:72–81, 2014.
 131. Gaujoux S, Brennan MF, Gonen M, et al: Cystic lesions of the pancreas: Changes in the presentation and management of 1,424 patients at a single institution over a 15-year time period. *J Am Coll Surg* 212:590–600, discussion 600–603, 2011.
 132. Kang MJ, Jang JY, Kim SJ, et al: Cyst growth rate predicts malignancy in patients with branch duct intraductal papillary mucinous neoplasms. *Clin Gastroenterol Hepatol* 9:87–93, 2011.
 133. Ingkakul T, Sadakari Y, Ienaga J, et al: Predictors of the presence of concomitant invasive ductal carcinoma in intraductal papillary mucinous neoplasm of the pancreas. *Ann Surg* 251:70–75, 2010.
 134. Tanno S, Nakano Y, Sugiyama Y, et al: Incidence of synchronous and metachronous pancreatic carcinoma in 168 patients with branch duct intraductal papillary mucinous neoplasm. *Pancreatol* 10:173–178, 2010.
 135. Uehara H, Nakaizumi A, Ishikawa O, et al: Development of ductal carcinoma of the pancreas during follow-up of branch duct intraductal papillary mucinous neoplasm of the pancreas. *Gut* 57:1561–1565, 2008.
 136. Ideno N, Ohtsuka T, Kono H, et al: Intraductal papillary mucinous neoplasms of the pancreas with distinct pancreatic ductal adenocarcinomas are frequently of gastric subtype. *Ann Surg* 258:141–151, 2013.
 137. Buetow PC, Buck JL, Pantongrag-Brown L, et al: Solid and papillary epithelial neoplasm of the pancreas: Imaging-pathologic correlation on 56 cases. *Radiology* 199:707–711, 1996.
 138. Ganesham DM, Paulson E, Tamm EP, et al: Solid pseudo-papillary tumors of the pancreas: Current update. *Abdom Imag* 38:1373–1382, 2013.
 139. Savci G, Kilicirgay S, Sivri Z, et al: Solid and papillary epithelial neoplasm of the pancreas: CT and MR findings. *Eur Radiol* 6:86–88, 1996.
 140. Yoon DY, Hines OJ, Bilchik AJ, et al: Solid and papillary epithelial neoplasms of the pancreas: Aggressive resection for cure. *Am Surg* 67:1195–1199, 2001.
 141. Kim YH, Saini S, Sahani D, et al: Imaging diagnosis of cystic pancreatic lesions: Pseudocyst versus nonpseudocyst. *Radiographics* 25:671–685, 2005.
 142. Lewis RB, Lattin GE, Jr, Paal E: Pancreatic endocrine tumors: Radiologic-clinical-pathologic correlation. *Radiographics* 30:1445–1464, 2010.
 143. Kramplitz GW, Norton JA: Pancreatic neuroendocrine tumors. *Curr Probl Surg* 50:509–545, 2013.
 144. Solcia E, Capella C, Kloppel G, editors: *Tumors of the Pancreas*, Washington, DC, 1997, Armed Forces Institute of Pathology.
 145. Arva NC, Pappas JG, Bhatla T, et al: Well-differentiated pancreatic neuroendocrine carcinoma in tuberous sclerosis—case report and review of the literature. *Am J Surg Pathol* 36:149–153, 2012.
 146. Noone TC, Hosey J, Firat Z, Semelka RC: Imaging and localization of islet-cell tumours of the pancreas on CT and MRI. *Best Pract Res Clin Endocrinol Metab* 19:195–211, 2005.
 147. Fidler JL, Johnson CD: Imaging of neuroendocrine tumors of the pancreas. *Int J Gastrointest Cancer* 30:73–85, 2001.
 148. Cirillo F, Falconi M, Bettini R: Clinical manifestations and therapeutic management of hyperfunctioning endocrine tumors. In Procacci C, Megibow AJ, editors: *Imaging the Pancreas: Cystic and Rare Tumors*, New York, 2003, Springer.
 149. Stabile BE, Morrow DJ, Passaro E, Jr: The gastrinoma triangle: Operative implications. *Am J Surg* 147:25–31, 1984.
 150. Minter RM, Simeone DM: Contemporary management of nonfunctioning pancreatic neuroendocrine tumors. *J Gastrointest Surg* 16:435–446, 2012.
 151. Zerbi A, Falconi M, Rindi G, et al: Clinicopathological features of pancreatic endocrine tumors: A prospective multicenter study in Italy of 297 sporadic cases. *Am J Gastroenterol* 105:1421–1429, 2010.
 152. Gouya H, Vignaux O, Augui J, et al: CT, endoscopic sonography, and a combined protocol for preoperative evaluation of pancreatic insulinomas. *AJR Am J Roentgenol* 181:987–992, 2003.
 153. Rapoport ED, Hansen CP, Kjaer A, Knigge U: Multidetector computed tomography and neuroendocrine pancreaticoduodenal tumors. *Acta Radiol* 47:248–256, 2006.
 154. Fiebrich HB, van Asselt SJ, Brouwers AH, et al: Tailored imaging of islet cell tumors of the pancreas amidst increasing options. *Crit Rev Oncol Hematol* 82:213–226, 2012.
 155. Thoeni RF, Mueller-Lisse UG, Chan R, et al: Detection of small, functional islet cell tumors in the pancreas: Selection of MR imaging

- sequences for optimal sensitivity. *Radiology* 214:483–490, 2000.
156. Khashab MA, Yong E, Lennon AM, et al: EUS is still superior to multidetector computerized tomography for detection of pancreatic neuroendocrine tumors. *Gastrointest Endosc* 73: 691–696, 2011.
 157. Shi W, Johnston CF, Buchanan KD, et al: Localization of neuroendocrine tumours with [¹¹¹In] DTPA-octreotide scintigraphy (Octreoscan): A comparative study with CT and MR imaging. *QJM* 91:295–301, 1998.
 158. Lin XZ, Wu ZY, Tao R, et al: Dual energy spectral CT imaging of insulinoma—value in preoperative diagnosis compared with conventional multi-detector CT. *Eur J Radiol* 81: 2487–2494, 2012.
 159. Adler H, Redmond CE, Heneghan HM, et al: Pancreatectomy for metastatic disease: A systematic review. *Eur J Surg Oncol* 40:379–386, 2014.
 160. Ahmed S, Johnson PT, Hruban R, Fishman EK: Metastatic disease to the pancreas: Pathologic spectrum and CT patterns. *Abdom Imaging* 38:144–153, 2013.

Pancreatic Trauma and Surgery

PAUL NIKOLAIDIS | JOSEPH MERANDA | FRANK H. MILLER |
ALLISON L. SUMMERS | HELENA GABRIEL | MARK TALAMONTI |
RICHARD M. GORE

CHAPTER OUTLINE

Pancreatic Trauma

Epidemiology and Pathophysiology

Clinical Findings

Surgical Classification

Radiologic Findings

Treatment

Pancreatic Surgery

Indications for Pancreatic Surgery

Role of Radiology

Types of Pancreatic Operations and Postoperative

Radiologic Findings

Postoperative Complications

Pancreatic Trauma

Traumatic injury to the pancreas is rare and difficult to diagnose. The retroperitoneal location of the pancreas is a mixed anatomic blessing in patients with abdominal trauma. Its fixed position anterior to the vertebral column provides excellent protection against deceleration injury and posterior stab wounds.¹⁻³ This protected environment, however, can be breached by bullets and more severe deceleration forces that may cause life-threatening pancreatic injury. Because of its rarity and nonspecific symptoms, the diagnosis of pancreatic injury is often delayed.⁴ The retroperitoneal location is detrimental to prompt diagnosis because signs and symptoms of pancreatic injury often evolve slowly and may be misleading.⁵ Delay in diagnosis and initiation of treatment in large part contributes to the potentially significant complications of pancreatic injury, including pseudocyst, abscess and fistula formation, sepsis, and chronic pancreatitis.⁶ There is considerable truth to the surgical aphorism that “the pancreas is not your friend” in terms of the unforgiving nature of pancreatic injuries.^{1,7} Because of the retroperitoneal location of the pancreas, pancreatic injuries are not easily diagnosed by diagnostic peritoneal lavage, which has a high false-negative rate. Furthermore, the classic presentation of upper abdominal pain, leukocytosis, and hyperamylasemia common in acute pancreatitis is far less reliable in the setting of pancreatic trauma.^{4,8,9} Multidetector computed tomography (MDCT), ultrasound, magnetic resonance imaging (MRI) with magnetic resonance cholangiopancreatography (MRCP), and endoscopic retrograde cholangiopancreatography (ERCP) can expedite the diagnosis and management of these patients.¹⁰

EPIDEMIOLOGY AND PATHOPHYSIOLOGY

Pancreatic injuries are relatively rare, found in only 72 (0.4%) of more than 16,000 trauma patients.¹¹ The pancreas is involved in only 2% of penetrating injuries and 5% to 12% of blunt abdominal injuries. The incidence of pancreatic trauma is increasing, however, because of the rising number of high-speed automobile injuries and gunshot wounds. Approximately three quarters of pancreatic injuries are due to penetrating trauma caused by gunshot or stab wounds. The remainder are secondary to blunt trauma caused by a sudden localized force to the upper abdomen as a result of a direct blow from a fall, a kick, or a steering wheel or bicycle handlebar injury. These forces compress the neck or body of the pancreas against the spine just to the left of the mesenteric vessels, causing crushing injury or transection.^{3,12} Blows to the left of midline may injure the pancreatic tail or distal body and may be associated with concurrent splenic, gastric, left renal, or descending colonic injury.⁹ Blows to the right of midline may injure the pancreatic head or uncinate process along with the bile ducts and may be associated with additional hepatic, duodenal, right renal, or ascending colonic injury.⁹

Although pancreatic injuries are relatively infrequent, they have an overall mortality rate of 16% to 20%, which increases substantially when they are associated with other abdominal injuries.^{3,11,13} The mortality rate is independent of the mechanism or grade of injury.¹¹ The mortality rates vary on the basis of the location of pancreatic injury, with rates of 22%, 18%, and 10% for the head, body, and tail, respectively.¹⁴ Approximately 90% of patients with pancreatic damage have concomitant visceral injuries because of the intimate relationship between the pancreas and the duodenum, biliary tract, colon, spleen, stomach, and major systemic and splanchnic blood vessels.¹⁵ Indeed, there are an average of 3.5 associated intra-abdominal injuries in patients with pancreatic trauma.³ In patients with combined pancreatic and duodenal injuries, the mortality rates are 5% for stab wounds, 15% for blunt injuries, 20% for gunshot wounds, and more than 50% for shotgun wounds.¹⁶ Most of the deaths occur within the first 48 hours of injury and are due to hypovolemic shock and major hemorrhage that result from vascular injury. The main source of delayed morbidity and mortality is disruption of the pancreatic duct, as isolated pancreatic injuries that spare the pancreatic duct rarely result in a poor outcome.⁸ Multiple organ failure and infection account for the remaining deaths. One third of survivors have major complications, such as chronic pancreatitis, pancreatic fistula, pseudocyst, pancreatic abscess, delayed massive hemorrhage, focal necrosis, hypocalcemic tetany, diabetes, and steatorrhea.¹⁷ Fistula formation after pancreatic trauma is seen in 7% to 20%.^{18,19} A delay in diagnosis is a major contributing factor to the high morbidity and mortality associated with pancreatic

injury. Although the need for surgical exploration is obvious in patients with penetrating trauma, pancreatic injury may be clinically occult, and a high index of suspicion must be maintained.^{17,20} With the current emphasis on nonoperative management of blunt trauma with established solid organ injuries, the risk of missed pancreatic injury becomes even more important.⁴

Rarely, the pancreas is injured during CT- or ultrasound-guided pancreatic biopsy, leading to pancreatitis or major hemorrhage.^{21,22} Even more uncommon is the possibility of pancreatic injury during laparoscopic urologic surgery, with an incidence of 0.44%, exclusively reported in left-sided procedures.²³

CLINICAL FINDINGS

The classic clinical triad of acute pancreatic trauma of upper abdominal pain, leukocytosis, and hyperamylasemia is of limited value in the diagnosis of pancreatic injury. The serum amylase level is often elevated in patients with pancreatic trauma, but it may initially be normal in a large percentage of patients, especially if it is obtained within 3 hours of trauma.^{7,24,25} Elevated serum amylase and lipase levels may be seen in only 73% to 82% of cases, respectively.⁸ Hyperamylasemia is a non-specific finding and can be seen with bowel injuries and salivary gland contusion from head injuries. The degree of serum hyperamylasemia does not correlate with the severity of pancreatic injury and may actually be greater in patients with contusions than in those with frank transections.^{7,26} The retroperitoneal location of the pancreas often masks symptoms of significant injury. In some cases, the patient may be asymptomatic initially, with pain, tenderness, and abdominal distention developing gradually in a 12- to 24-hour period. Peritoneal lavage results are usually negative if the peritoneum overlying the pancreas remains intact.^{5,7} Another clinical sign recently shown to correlate with the presence of pancreatic injury in children is the “seat belt sign.” Pancreatic injury was 22 times more commonly present in children with this sign (erythema, ecchymoses, and abrasions across the patient’s abdominal wall resulting from the vehicle’s seat belt restraint).²⁷

SURGICAL CLASSIFICATION

Box 99-1 details the classification system proposed by the American Association for the Surgery of Trauma that describes

pancreatic injuries.^{9,28,29} This remains the most recent classification system and is still in use. It addresses key issues that are of importance to both the surgeon and the radiologist: the depth and location of the pancreatic injury, the degree of parenchymal disruption, and the integrity of the ampulla and main pancreatic duct. It acknowledges the significance of more complex injuries to the pancreas, particularly injuries that affect the pancreatic duct and the head of the gland; it also allows correlation with other organ injury scales.²⁸

RADIOLOGIC FINDINGS

Computed Tomography

CT is the preferred means of evaluating patients with blunt abdominal trauma.^{4,10,30-36} Pancreatic lacerations are often subtle relative to injuries involving the liver, spleen, or kidneys and difficult to visualize on imaging studies immediately after trauma. With continued improvements in MDCT technology, near-isotropic CT data sets with three-dimensional postprocessing techniques may improve detection and characterization of pancreatic lacerations. Focal pancreatic enlargement and peripancreatic fluid are suggestive of pancreatic injury, and faint lacerations or fracture lines may be seen on closer inspection¹⁰ (Figs. 99-1 and 99-2). The radiologist must rely on secondary findings because many injuries are manifested as pancreatitis with diffuse or focal swelling of the pancreas.^{10,30,31} Minor thickening of the anterior limb of Gerota’s fascia and fluid or increased attenuation in the anterior pararenal space, small bowel mesentery, or transverse mesocolon may be the only CT abnormalities.³² Fluid between the pancreas and the splenic vein was initially thought to be a useful sign of pancreatic injury.³³ This sign was subsequently found to be neither sensitive nor specific in a later study.³⁴ Fluid in this location, however, should direct the radiologist to a closer examination of the pancreas.^{10,29} A list of CT findings suggestive of pancreatic injury is shown in Box 99-2.^{9,10}

A major limitation of CT in pancreatic injury is that it often cannot reliably assess the integrity of the pancreatic duct. Several postprocessing techniques, including curved planar

BOX 99-1 THE AMERICAN ASSOCIATION FOR THE SURGERY OF TRAUMA PANCREATIC INJURY GRADING SCALE

Grade	Injury Description
I Hematoma	Minor contusion without ductal injury
Laceration	Superficial laceration without ductal injury
II Hematoma	Major contusion without ductal injury or tissue loss
Laceration	Major laceration without ductal injury or tissue loss
III Laceration	Distal transection or pancreatic parenchymal injury with ductal injury
IV Laceration	Proximal transection or pancreatic parenchymal injury involving the ampulla
V Laceration	Massive disruption of the pancreatic head

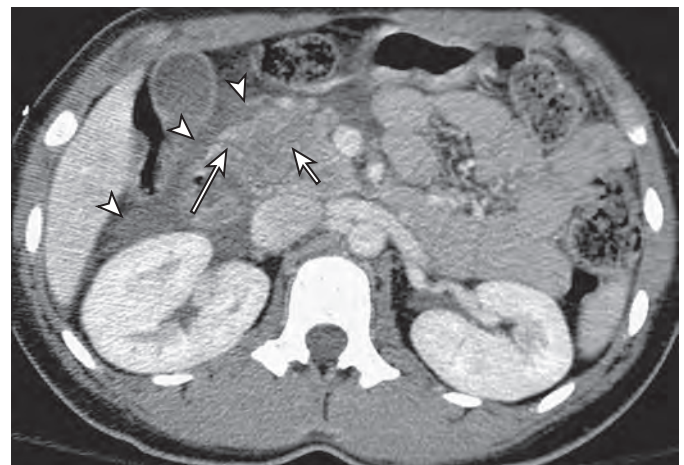


Figure 99-1 CT findings in pancreatic contusion. Axial MDCT scan of a 44-year-old woman involved in a motor vehicle accident shows a contusion of the pancreatic head (short arrow) and a subtle laceration of the head of the pancreas (long arrow). Note the presence of fluid outlining the duodenum and portion of the pancreatic head (arrowheads).

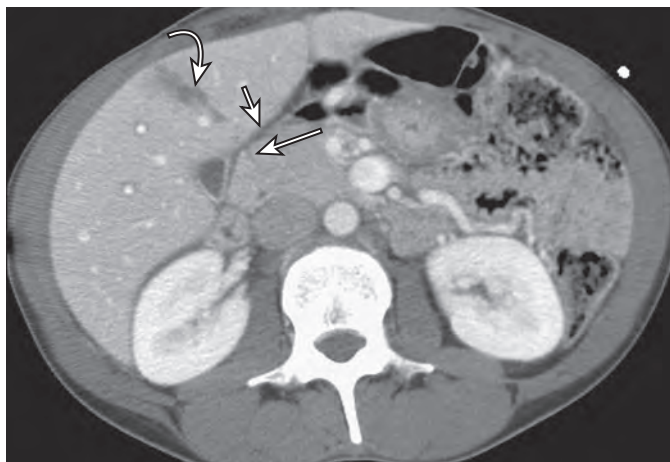


Figure 99-2 CT of superficial pancreatic laceration. CT scan of a 27-year-old patient with a stab wound to the abdomen shows a laceration through the hepatic parenchyma (curved arrow), with concomitant superficial laceration of the pancreatic head (long arrow). A small amount of fluid is seen between the pancreas and liver (short arrow). Subsequent endoscopic retrograde pancreatogram was negative.

BOX 99-2 FINDINGS SUGGESTIVE OF PANCREATIC INJURY ON COMPUTED TOMOGRAPHY

- Pancreatic laceration or fracture
- Focal (or diffuse) pancreatic enlargement
- Pancreatic contusion or hematoma
- Areas of diminished or heterogeneous enhancement
- Fluid between the splenic vein and pancreas
- Fluid in the peripancreatic fat, mesocolon, and mesentery
- Peripancreatic or mesenteric fat stranding
- Fluid in the anterior and posterior pararenal spaces or lesser sac
- Thickening of the left anterior pararenal fascia
- Dilation or discontinuity of the pancreatic duct
- Peripancreatic fluid collections, including pseudocyst formation
- Abscess or fistula formation
- Injuries to adjacent structures, including the duodenum, liver, and spleen

reformats and minimum intensity projection images, that are now feasible with isotropic or near-isotropic data sets have resulted in improvements in the visualization of the pancreatic duct by MDCT, but they still require validation in the trauma setting. As CT still may not directly show the pancreatic duct injury, such injury may be suspected on the basis of the degree of parenchymal injury.¹⁰ In addition, the pancreas may appear relatively normal on initial examinations. It has been reported that in 20% to 40% of patients with acute blunt pancreatic trauma, the pancreas can appear normal, especially within 12 hours after the injury.

Later examinations may demonstrate injuries not seen on the initial examination; however, this may relate to the characteristic evolution of pancreatic injury rather than an inaccurate initial examination. The tear progressively increases in size and becomes more well defined, often associated with extrapancreatic fluid collections.³⁷⁻⁴¹ Repeated scanning in 12 to 24 hours can be helpful if there is a strong suspicion for fracture in the face of a negative CT result.⁴² Some of the prior reports of poor

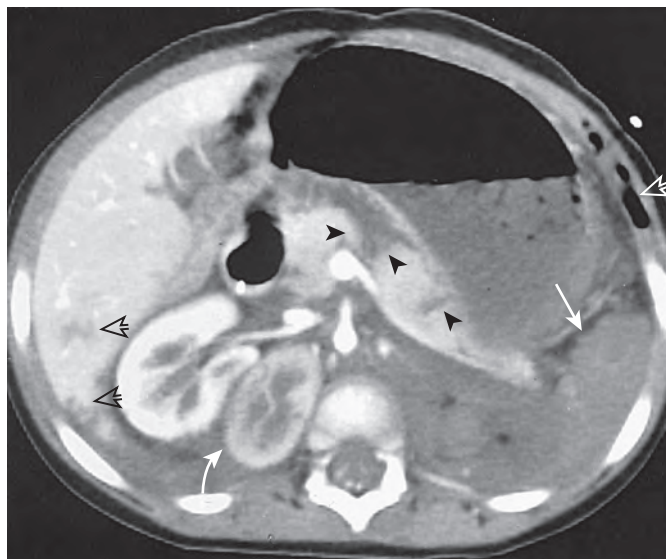


Figure 99-3 Pancreatic lacerations and multiorgan injury. A 16-month-old toddler was involved in a minivan accident. Contrast-enhanced CT demonstrates multiple pancreatic lacerations (black arrowheads), devitalized spleen (white arrow), a vascular injury of an ectopic unfused kidney (curved white arrow), right hepatic laceration (open black arrows), and subcutaneous emphysema (open white arrow) from a pneumothorax. The patient also had a spinal compression fracture. (Courtesy Andrew J. Fisher, MD, Mallinckrodt Institute of Radiology, St. Louis, Mo.)

results with CT examination may in part relate to the studies being performed without helical or MDCT scanners, thin slices, and optimal intravenous contrast material or with lack of oral contrast material.²⁶ Sensitivity and specificity of CT in pancreatic injury have improved with the use of MDCT and thinner collimation.⁴³

MDCT findings of pancreatic duct injury are either highly sensitive and nonspecific or insensitive and specific. For example, in a study aimed at evaluation of blunt pancreatic trauma with MDCT, it was determined that the finding of low-attenuation peripancreatic fluid was 100% sensitive and only 4.9% specific. Alternatively, identification of pancreatic laceration involving more than 50% of the parenchymal width had a sensitivity of 50% and a specificity of 95.1%.

Pancreatic contusions most often are isodense but occasionally may present as hyperdense masses because of intraparenchymal hemorrhage or may be hypodense due to edema (Fig. 99-1). A laceration through the pancreas is usually manifested by a thin linear lucency (Fig. 99-2). Pancreatic fractures may be seen as well-demarcated lucent defects traversing the gland, generally involving the neck of the pancreas perpendicular to its long axis (Figs. 99-3 and 99-4). There is often little or no separation of the pancreatic fragments, and the density change can be subtle but may be obscured by surrounding hematomas and fluid collections or streak artifacts.⁴⁴ Dynamic scanning after bolus injection of contrast medium is important in fracture detection because it improves visualization of normal enhancing pancreatic parenchyma.^{31,32} Pseudocysts may form within a few days after pancreatic duct laceration and appear similar on CT to pseudocysts from pancreatitis (Fig. 99-5).

Ultrasound

Although ultrasound is sensitive to demonstrate intra-abdominal fluid (hemoperitoneum), it has limited value to demonstrate pancreatic injuries.⁴⁵ Ultrasound in pancreatic injury can miss associated hemorrhage because of the retroperitoneal location of the pancreas. The actual pancreatic parenchymal injury may be difficult to visualize sonographically. In addition, many of these patients have an associated ileus, limiting sonographic evaluation of the pancreas. The sonographic findings may be relatively subtle, usually demonstrating nonspecific gland enlargement caused by pancreatitis or contusion.⁴⁵⁻⁴⁸ The sensitivity of conventional ultrasound in the diagnosis of pancreatic trauma is reported to be low (45.7%-63%).

Even with these limitations, ultrasound is usually the first-choice screening test in the pediatric patient. Contrast-enhanced ultrasound is an imaging modality that has shown promise for the assessment of hepatic, splenic, and renal trauma. Although little research has focused on contrast-enhanced evaluation for

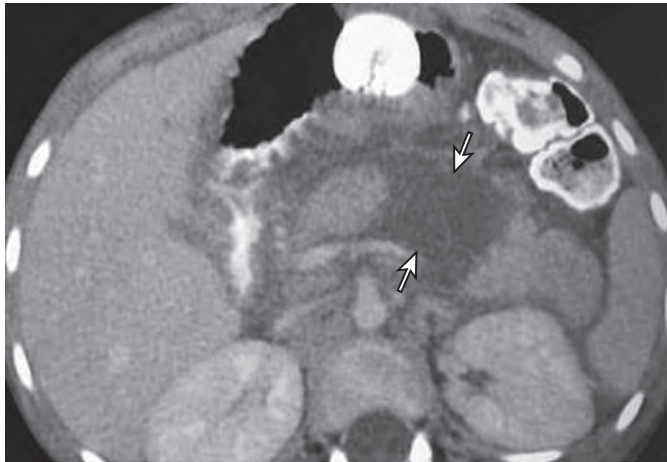


Figure 99-4 CT findings in pancreatic transection. CT scan of a pediatric patient, victim of child abuse, shows a large, well-demarcated lucent defect representing a pancreatic fracture with transection of the pancreas (arrows). (Courtesy Christine Menias, Mallinckrodt Institute of Radiology, St. Louis, Mo.)

pancreatic trauma, there are a few animal-based studies that show promise. Similar to conventional ultrasonography, the portability and cheaper cost are major benefits.

Magnetic Resonance Pancreatography

MR pancreatography (MRCP) has recently been established as a superb alternative for direct imaging of the pancreatic duct.^{49,50} Advantages of MRCP over ERCP include its noninvasiveness, decreased cost, and wider availability. Furthermore, MRCP allows assessment of the whole pancreatic anatomy, including not only the pancreatic duct but also the parenchyma. In addition, this imaging modality allows assessment of any peripancreatic collections and of the pancreatic duct beyond a site of disruption^{10,51} (Fig. 99-5). MRCP may also reveal ductal abnormalities, such as pancreas divisum, important information for the endoscopist to know before ERCP.¹⁰ MRI has been shown to accurately detect disruption of the pancreatic duct.

Newer refinements and technical advances in MRCP, including secretin-enhanced MRCP, provide additional information. Dynamic assessment improves detection of pancreatic ductal anatomy and presence of leak after trauma.

Pancreatic injuries rarely occur in isolation, and MRI also allows assessment of additional organs in the upper abdomen, including the liver, kidneys, and spleen.

The exact role of MRCP in the setting of acute pancreatic injury has not yet been established. Controversy exists about its usefulness as a screening tool in the acute setting. As MRI becomes more widely available and technology continues to improve, more studies and clinical experience are needed to establish the exact role of MRCP in acute pancreatic injury.

Conventional Pancreatography

The main pancreatic duct is a rigid and brittle structure compared with the pancreatic parenchyma. Accordingly, the duct may be lacerated without producing cross-sectional imaging abnormalities or surgically detectable peripancreatic hemorrhage or capsular disruption. The diagnosis can be missed at the time of surgical exploration, and this has led some surgeons to advocate routine intraoperative or preoperative pancreatography to avoid the morbidity and mortality of an unsuspected or a misdiagnosed ductal disruption.⁵²⁻⁵⁷ ERCP is not an appropriate screening test for pancreatic trauma; furthermore, the role of MRCP in this setting has not yet been firmly established.

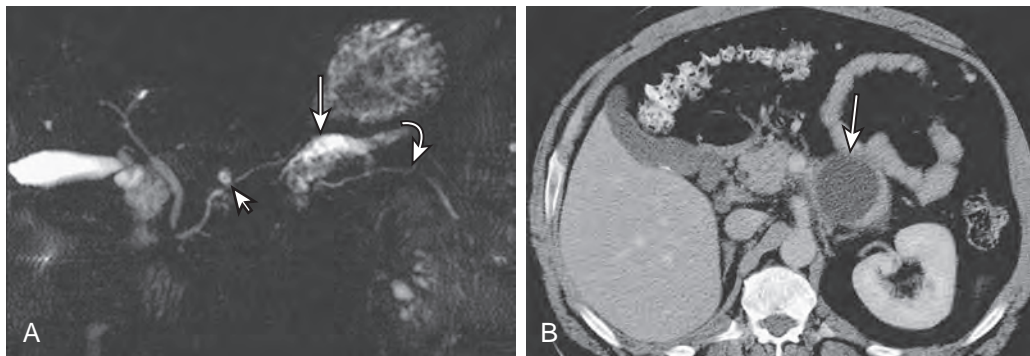


Figure 99-5 Pancreatic duct injury and subsequent pseudocyst formation. The initial CT scan showed no abnormality in the pancreas, but the patient returned with severe abdominal pain. **A.** Thick-slab rapid acquisition and relaxation enhancement (RARE) MRCP image shows the disrupted duct (short arrow) and the resulting peripancreatic fluid collection (long arrow). Note how it is feasible with MRCP to evaluate the pancreatic duct distal to the site of injury and extravasation (curved arrow). **B.** Short-term follow-up axial MDCT scan shows a more organized pancreatic pseudocyst (arrow), which was subsequently successfully drained.

However, in cases in which the CT scan or MRCP study is equivocal or technically inadequate, emergent ERCP is useful in identifying the presence and location of pancreatic duct disruption. Demonstration of a normal duct can obviate the need for exploratory surgery in these patients. The technique is not universally available, especially on an emergent basis. In addition, patients must be clinically stable for the examination. The ductal transection appears as either duct obstruction or extravasation of contrast material from the pancreatic duct. ERCP is also useful in detecting post-traumatic pancreatic ductal strictures and pseudocyst communication.⁵³⁻⁵⁷

Gastrointestinal Studies

Pancreatic trauma is often associated with duodenal injury. When coexisting pancreatic and duodenal injuries are suspected, water-soluble agents can disclose duodenal perforation or mass effect involving the duodenum from acute pancreatitis or pseudocysts.⁵⁸

TREATMENT

The first priority in pancreatic trauma is to control hemorrhage and to contain bacterial contamination. The other main management priority is the identification of specific pancreatic injury with special attention to the integrity of the ductal system. Ductal injury is the single most important factor in late morbidity and mortality. Most pancreatic injuries can be managed with closed external drainage.⁹ Débridement of devitalized pancreatic tissue adjacent to the fracture site is essential in severe pancreatic injuries. It is important, however, to preserve at least 20% to 50% of functional pancreatic tissue whenever possible. Resection should be accompanied by drainage and duodenal diversion for concurrent pancreatic head and duodenal injuries. If there is only a contusion or laceration without evidence of major duct disruption, suture closure and external drainage usually suffice. Severe injuries of the pancreatic head can be managed according to their appearance on intraoperative pancreatography. If the duct is intact, wide-bore drainage should suffice. If duct injury is demonstrated, a Roux-en-Y diversion may be considered.⁵⁹ However, increased complication rates of up to 60% have been reported in patients with high-grade injuries treated with pancreaticojejunostomy, suggesting that distal pancreatectomy, when feasible, is a superior operative treatment for these patients.⁶⁰

Controversy exists about the optimal management of grade III injury of the left pancreas. Drainage alone was effective in 54 of 63 patients with gunshot wounds, with low mortality, but many complications were seen, generally related to the large number of associated organ injuries.⁶¹ Another group performed distal pancreatectomy and splenectomy in 48 of 57 patients with gunshot wounds to the left aspect of the pancreas, also with a low mortality rate but many complications due to associated organ injury.⁶² Patients who had distal pancreatectomy with splenic preservation had a significantly lower complication rate (22% vs 73%); however, this is probably due to increased comorbidities, such as associated visceral or splenic injury and the emergent nature of the surgery.⁶⁰ The decision about whether to salvage all or part of the spleen is based on both patient hemodynamics and age. Again, overlooked or underestimated pancreatic injury can lead to potentially disastrous complications.²⁶ Pancreatic abscesses may develop owing

to inadequately drained fluid collections that become infected from intestinal spillage or bacteremia.³⁷

Endoscopic pancreatic duct stent placement has been described in the literature, with good results.^{6,60,63} Case reports have described good short-term results and a potential role in the delayed management of traumatic pancreatic duct disruption with endoscopic pancreatic duct stenting.⁶ Successful outcomes with pancreatic duct stenting were described in partially disrupted ducts with placement of a bridging stent.⁶³ However, whereas good short-term results have been reported with duct stenting, later complications, including stricture formation, inability to subsequently remove the stent, and stent migration, raise questions about the utility of this procedure in the acute phase.⁶⁰ More important, pancreatic duct stenting in the acute phase may delay timely operative intervention and definitive repair of life-threatening injuries. Therefore, it has been proposed that pancreatic duct stenting be used later to treat post-traumatic pancreatic fistulas.⁶⁰

The optimal management of pancreatic injuries in children has remained controversial. Similar to nonoperative management of splenic and hepatic injuries, there has been a trend toward nonoperative management of pancreatic injuries in children without major ductal injuries or clinical deterioration.^{64,65} ERCP has been advocated for management of these children; demonstration of a transected pancreatic duct typically requires exploratory laparotomy with a spleen-preserving distal pancreatectomy.⁶⁶ There is limited experience of endoscopic treatment with stent placement in the pediatric population. In a small series of nine children with main duct injury treated by an endoscopically placed stent, all children managed with therapeutic ERCP avoided pancreatic resection, although most (66%) developed pancreatic fluid collections requiring drainage.

Pancreatic Surgery

INDICATIONS FOR PANCREATIC SURGERY

Benign Disease

Most attacks of acute pancreatitis are self-limited and respond to conservative management not requiring any radiologic imaging or management.⁶⁷ The role of surgery during an episode of acute pancreatitis is limited to débridement of infected necrotic tissue, drainage of abscesses that cannot be satisfactorily drained percutaneously, and control of massive hemorrhage from ruptured vessels or pseudoaneurysms.⁶⁸ Infected pancreatic necrosis, pancreatic abscess, severe hemorrhagic pancreatitis, and pseudoaneurysm formation are the few remaining indications for open surgery in acute pancreatitis. Even when it is indicated, surgery is frequently delayed or even replaced by minimally invasive surgical techniques.⁶⁹ Simple abscesses and acute pseudocysts can be drained percutaneously with use of CT for diagnosis and CT or sonographic guidance during percutaneous catheter management.^{70,71} Sterile necrosis is managed nonsurgically.^{72,73} The term *walled-off pancreatic necrosis* was introduced to describe the evolution of a postnecrotic pancreatic fluid collection by the 2007 revision of the Atlanta classifications. In walled-off pancreatic necrosis, a thick wall develops without an epithelial lining, mimicking a pseudocyst; however, it can be differentiated on CT images by the presence of internal debris (typically fat in attenuation), larger size, extension to paracolic space, irregular wall definition, and

pancreatic deformity or discontinuity. It can be treated conservatively if it is sterile. However, infected or symptomatic collections are usually treated with direct endoscopic necrosectomy, conventional transmural endoscopic drainage, or percutaneous drainage. Overall, more than 90% of patients with sterile necrosis can be successfully treated without surgical intervention.⁷⁴⁻⁷⁶ Persistent sepsis caused by infected, necrotic pancreatic tissue requires surgical drainage and débridement because the necrotic tissue cannot be removed by percutaneous drainage. Differentiation between sterile and infected necrosis is possible by CT- or ultrasound-guided aspiration of necrotic foci.^{72,73}

Severe hemorrhagic pancreatitis or hemorrhage from pseudoaneurysm formation also requires prompt intervention. Operative débridement of the necrotic tissue and aneurysm repair can be more safely and effectively accomplished if they are preceded by preoperative angiographic identification and embolization.^{77,78} With embolization, conservative therapy may be attempted instead of surgery. Some surgeons advocate emergent cholecystectomy and common duct exploration in patients with presumed gallstone pancreatitis in the hope that removal of the offending stones will ameliorate the severity of pancreatitis.⁷⁹⁻⁸¹ Most surgeons prefer to wait until the acute episode of pancreatitis resolves because of the high operative mortality associated with early aggressive intervention.⁸⁰ The role of early endoscopic removal of stones by ERCP is generally accepted in acute biliary pancreatitis with biliary obstruction or cholangitis but is still controversial in cases lacking such clear findings.^{72,73,82-85} One study recommended that MRCP be used as an initial diagnostic tool; if stones are visualized in the common bile duct, urgent ERCP is recommended. Conversely, if there are no common bile duct stones, the patient can be spared the invasive ERCP.⁸⁶ Most cases of gallstone pancreatitis resolve without complication.

The management of patients with chronic pancreatitis remains a challenging problem. Main indications for surgery remain intractable pain, suspicion of malignant disease, and involvement of adjacent organs. Less frequent indications for operative treatment include complications such as pseudocysts, nonresolving biliary or duodenal obstruction, internal pancreatic fistulas, and left-sided portal hypertension resulting from splenic vein thrombosis. The surgical approach usually involves proximal pancreatic resection, but lateral pancreaticojejunal drainage may be used for large-duct disease. The duodenum-preserving head resections of Beger and Frey provide overall good pain control and preservation of pancreatic function. Thoracoscopic splanchnicectomy and the endoscopic approach await trials to confirm their efficiency in the management of chronic pancreatitis. Newer advances in endoscopic management, including the use of fully covered self-expandable metal stents, have been recently explored in chronic pancreatitis-related biliary duct strictures for which conventional treatment with plastic stents has failed. Furthermore, endoscopic ultrasound-guided transmural drainage of the main pancreatic duct with a duct-gastrostomy has been introduced as a newer alternative treatment option in selected cases. Further studies are needed to validate these techniques.

Common bile duct obstruction is surgically addressed by distal Roux-en-Y choledochojejunostomy; but in combination with duodenal obstruction, it must be treated by pancreatic head resection. Pancreatic ascites due to disrupted pancreatic duct should be treated by internal drainage.⁸⁷⁻⁹⁴ Obstruction of

the pancreatic or bile duct by a stricture, calculus, or series of strictures is a major cause of pain. Ductal drainage procedures often result in pain relief and improved pancreatic function.⁹⁵⁻¹⁰² If there is no ductal dilation, decompressive procedures usually will not ameliorate the patient's pain. Nerve ablation (celiac nerve block) has been advocated before consideration of extirpative procedures because these operations are associated with exocrine and endocrine pancreatic insufficiency.¹⁰³⁻¹⁰⁵

Acute and chronic pseudocysts can be managed surgically, but radiographically guided or endoscopic management should be attempted first.¹⁰⁶⁻¹¹³

Malignant Disease

Surgical management of ductal adenocarcinoma of the pancreas was previously considered to be controversial.¹¹⁴⁻¹²⁰ Most controversies, however, such as whether to perform extended lymph node dissection and standard versus pylorus-preserving resections, have been addressed by randomized, prospective clinical trials.^{121,122} From a surgical perspective, the first objective in the management of pancreatic carcinoma is to determine the potential for resection.¹²² Factors contraindicating resection include the presence of distant metastases; major venous thrombosis; and superior mesenteric, celiac, or hepatic artery encasement.¹²¹ Pancreatoduodenectomy (the Whipple procedure) is the only proved cure for carcinoma of the pancreatic head. Unfortunately, success is modest, with an overall 5-year survival rate between 15% and 25% in patients who have undergone resection.¹²³ The Whipple procedure is one of the most complex of all surgical procedures, with significant associated morbidity and mortality. A better technical success rate and fewer overall complications have been described in high-volume regional referral centers that perform many such surgeries.¹²² Surgery is effective in palliating certain symptoms: relief of jaundice with biliary-enteric bypass; relief of duodenal obstruction with gastrojejunostomy; and relief of pain by chemical splanchnicectomy.¹¹⁷ Biliary bypass and celiac nerve block can be performed percutaneously.

The management of pancreatic cystic neoplasms depends on the presence of symptoms, malignant potential of the lesion, and surgical risk. Serous cystadenomas do not require resection unless the patient is symptomatic or the diagnosis is uncertain. In contrast, mucinous cystic neoplasms should be resected because of their higher malignant potential.^{124,125} When these lesions are aspirated preoperatively, in addition to the presence of malignant cells, the cystic fluid carcinoembryonic antigen level has been shown to accurately predict the presence of a mucinous neoplasm.¹²⁶ Cystic neoplasms of the pancreas have a much better prognosis than ductal adenocarcinomas. In fact, nearly half of patients with cystadenocarcinomas can be cured by surgical therapy.^{127,128}

The results of surgical intervention are similarly encouraging with pancreatic neuroendocrine tumors. Insulinomas are the most frequent functional neuroendocrine tumors and are characterized by inappropriately high levels of insulin. They are typically small and multiple in 10% to 15% of patients. Preoperative angiography, MRI, and CT and intraoperative ultrasound reduce the need for "blind" pancreatic resection when the tumor is not palpable.¹²⁹⁻¹³¹ The management of gastrinomas is more complicated due to the advent of more effective medical therapy that reduces the complications of peptic ulcer disease. Excision of gastrinomas is still recommended because of the lower rate of hepatic metastasis in

surgically treated patients.¹³² Furthermore, more than 60% of gastrinomas are malignant, and more than half have metastasized by the time of operation. As many as 75% of patients have multiple lesions, and many of these tumors cannot be localized by preoperative studies or by surgical palpation. The preferred course for these tumors is surgical exploration in all good-risk patients. If the disease appears localized, primary surgical excision is undertaken.¹¹⁸ Proton pump inhibitors are indicated in patients with unresectable lesions, rendering gastrectomy unnecessary.¹³³

ROLE OF RADIOLOGY

In patients with pancreatic neoplasms, the radiologist should provide the surgeon with information concerning the extent of the tumor and the presence of local or distant tumor spread. Because surgery for pancreatic carcinoma is extensive with significant associated morbidity, patient selection is extremely important so that a patient who is a candidate for potentially curative surgery is not excluded while at the same time someone is not subjected to an unnecessary operation. The goal of staging through imaging, therefore, is to distinguish resectable from unresectable disease.

The extent of testing necessary to determine resectability has historically been controversial in the surgical literature but is becoming less so with the advent of the high-quality imaging abilities of MDCT and MRI. Advocates of limited preoperative evaluation followed by surgical exploration in all patients with nonmetastatic pancreatic tumors believe that intraoperative evaluation is the most sensitive method of determining resectability. They suggest that if the tumor is found to be unresectable, operative palliation is the best way to provide sustained relief of symptomatic jaundice or gastric outlet obstruction.^{134,135} Others argue that direct intraoperative assessment of the extent of retroperitoneal tumor growth in relation to the superior mesenteric artery origin is not completed until the final step in tumor transection, after gastric and pancreatic transection, when the surgeon is committed to resection even if all of the tumor cannot be safely removed.¹³⁶ The need for accurate preoperative assessment is substantiated by the large number of positive-margin resections reported and the high incidence of local recurrence after resection.^{137,138} Other series suggest that for most patients with unresectable disease, laparotomy for palliation may be avoided owing to the advances in endoscopic, percutaneous, and laparoscopic methods of biliary decompression.¹³⁹

In pancreatitis, imaging has two major roles: staging of the severity of the inflammatory process and detection of complications, such as fluid exudation, vascular compromise, pancreatic necrosis, pancreatic abscess, and pseudocyst formation.

Computed Tomography

With MDCT, it is now possible to attain better spatial resolution along the z-axis as well as to further improve temporal resolution. MDCT permits rapid thin-section acquisition of regional body anatomy with multipass multiplanar data obtained during defined circulatory phases to best outline the vasculature and to detect and characterize focal parenchymal lesions. Typical imaging protocols include multiphasic imaging with unenhanced pancreatic parenchymal phase and venous phase imaging.¹⁴⁰⁻¹⁴³ The detection and characterization of benign or malignant pancreatic tumors and imaging of inflammatory

pancreatic disease with its associated complications can be successfully performed by MDCT.^{140,144}

The extent and severity of pancreatitis can be assessed by evaluating the degree of pancreatic enlargement in addition to the number, size, and location of pseudocysts and peripancreatic fluid collections and the presence of pancreatic necrosis. Associated complications include vascular thrombosis and gastrointestinal fistula formation. In patients with acute pancreatitis, a double-pass helical imaging technique that includes pancreatic and hepatic phase acquisitions is potentially beneficial for outlining focal areas of pancreatic necrosis.^{145,146}

In up to 30% of patients with definite clinical and laboratory signs of acute pancreatitis, the pancreas may appear completely normal on CT. Similarly, in 10% of patients with clinically diagnosed chronic pancreatitis, there are no abnormalities seen on CT.^{144,147}

MDCT currently plays a vital role in pancreatic cancer staging as imaging before surgery most often determines whether the surgery is performed. CT is often considered to be the optimal imaging modality for pancreatic cancer staging. Continued advancements in computers, scanner technology, and three-dimensional software have improved CT detection of smaller masses and staging by greatly improving the visualization of the pancreas and adjacent vasculature. Another potential advantage is anecdotal evidence that the ability to obtain thinner slices can improve detection of small peritoneal metastases.^{140-143,148}

The major finding shown by MDCT is a hypoattenuating pancreatic mass on early arterial (pancreatic) phase imaging, with associated pancreatic duct dilation. In tumors located in the pancreatic head, biliary duct dilation is expected. An important feature for determining potential tumor resectability is perivascular tumor invasion, particularly in relation to the celiac and mesenteric arteries, the splenic and superior mesenteric veins, and the portal confluence.¹⁴⁵ Curved multiplanar reformatted images and high-quality, volume rendered, three-dimensional reconstructions may help depict excellent vascular detail. Invasion of the root of the mesentery and transverse mesocolon associated with ascites is an ominous finding that suggests peritoneal carcinomatosis. Local extrapancreatic extension on CT is suggested by contiguous organ involvement except for the duodenum, which is included in the resection in a Whipple procedure. CT signs suggesting that the lesion is unresectable include hepatic, omental, or peritoneal metastases; locally advanced extension into the peripancreatic and retroperitoneal soft tissues; thrombosis of the portal vein–superior mesenteric vein confluence; and encasement of the celiac trunk or superior mesenteric artery.¹⁴⁹⁻¹⁵⁵ Vascular invasion, lymph node metastasis, liver metastasis, and peritoneal carcinomatosis are generally accepted reasons for unresectability.¹⁵⁶⁻¹⁵⁸ Positive predictive values of CT for surgical unresectability have been excellent, ranging from 89% to 95%.¹⁵⁹⁻¹⁶¹ Among patients with tumors judged potentially resectable on the basis of CT criteria, however, surgical results show that 60% to 91% of the tumors are truly resectable. The most frequent reasons for tumor unresectability found at surgery are small (<1 cm) hepatic, peritoneal, or omental metastases, lymph node metastases, and vascular invasion.^{122,144,158,160,162-164}

If a CT examination considers a tumor resectable, this should be considered potential resectability because CT can miss subtle spread of disease. Literature, including a study by Vargas and associates,¹⁶⁵ reported an accuracy of 99% and a negative

predictive value of 100% for prediction of vascular invasion by tumor with MDCT. Various grading systems for vascular involvement have been described; some suggest that different criteria may be necessary in evaluating arteries and veins. Vascular involvement is confirmed by the presence of tumor thrombus or vascular occlusion (nonvisualization, vessel cutoff, or abrupt changes in vessel caliber).^{144,166,167} Nonetheless, other adjunct studies, including endoscopic ultrasound and staging laparoscopy, may provide additional information before major pancreatic surgery is undertaken. CT is also important in the evaluation of other solid pancreatic neoplasms. A major advantage of multiple phase postcontrast CT in patients with islet cell or carcinoid tumors is the detection and localization of hypervascular metastases. Islet cell tumors and metastases are most typically hypervascular. If tumor ablation therapy is being considered, MDCT is important in the pretreatment planning.¹⁴⁵ CT and MRI are also effective in the evaluation of cystic tumors of the pancreas, including serous and mucinous tumors, as well as intraductal papillary mucinous neoplasms.

In summary, the importance of CT in pancreatic imaging has been further enhanced by the advent of MDCT technology, which is highly reliable in assessing pancreatitis and staging pancreatic neoplasms. It has become the “gold standard” in the work-up and continued surveillance for the majority of these patients.

FDG PET/CT

Fluorodeoxyglucose (FDG) positron emission tomography/computed tomography (PET/CT) has been shown to have a role in the diagnosis of the postoperative recurrence of pancreatic adenocarcinoma. In one study, PET/CT correctly detected local recurrence in all cases of recurrence in patients who had surgery, whereas MDCT alone detected the recurrence in 64% of cases, suggesting that PET/CT is superior in these patients.^{166,167}

Magnetic Resonance Imaging

Several reports have compared the efficacy of MRI with CT, with variable results. The earliest studies, which were generally performed with low-field-strength magnets and without gadolinium, showed either a superiority of CT or equivalent results.¹⁶⁸ Later studies using dynamic contrast enhancement with gadolinium suggested a superiority of MRI.^{169,170} A large prospective study comparing state-of-the-art helical CT and MRI examinations needs to be performed.

MRI, magnetic resonance angiography, and cholangiopancreatography are comparable to CT in evaluating a suspected pancreatic mass and may be particularly valuable when CT findings are indeterminate. Evaluation of acute and chronic pancreatitis as well as of their complications can be successfully accomplished with MRI. In addition, MRI is a viable alternative to CT when there is a history of allergy to iodinated contrast material or when examination of the biliary tree is requested.^{171,172}

Multiple recent advances in abdominal MRI, including the development of high-gradient systems and the advent of parallel imaging, allow optimal imaging of the pancreas. The most important sequences for the evaluation of the pancreatic parenchyma are precontrast T1-weighted spoiled gradient-echo with fat suppression and dynamic imaging after intravenous administration of gadolinium. On precontrast T1 fat-suppressed sequences, the normal pancreas has high signal intensity relative to the liver because of the presence of acinar proteins.^{171,172} More recently, advances in MR gradient technology and fast imaging

techniques have permitted diffusion-weighted imaging and measurement of the apparent diffusion coefficient, which has become another important tool in MRI of the pancreas. Diffusion-weighted imaging is a relatively quick sequence to obtain and provides great tissue contrast. In addition, diffusion-weighted imaging requires no contrast material administration. Studies have shown that diffusion-weighted imaging and apparent diffusion coefficients not only are helpful in detecting pancreatic tumors but also can assist in detecting tumor spread and response to therapy.

T2-weighted sequences are especially useful for the evaluation of the biliary tract and pancreatic duct. These sequences can accurately depict pseudocysts, fluid collections, gallstones, and choledocholithiasis. MRCP, which is based on heavily T2-weighted sequences, has been increasingly used as the first-line modality for diagnostic purposes, with ERCP ensuing when necessary, thereby avoiding potential complications related to endoscopic technique, particularly when it is used for screening and in asymptomatic individuals. The ability to perform dynamic imaging, functional evaluation of the pancreas, and overall excellent diagnostic yield, even in rare pathologic processes, render MRCP an indispensable diagnostic tool in modern gastroenterology.^{173,174}

MRCP is excellent for the evaluation of changes in the anatomy of patients after pancreaticobiliary surgery, particularly with biliodigestive anastomoses and nondilated bile ducts.¹⁷⁴ It is reliable, fast, safe, and noninvasive and can be used to screen symptomatic patients for treatment, to help guide further therapeutic procedures, or for follow-up.¹⁷³

Other techniques that can aid in the preoperative assessment of resectability are endoscopic ultrasound and laparoscopy.¹⁷⁵ Laparoscopy and limited staging surgery and laparoscopy with laparoscopic ultrasound are routinely used at some centers before definitive laparotomy in an attempt to decrease unnecessary surgeries.¹²² In a recently published meta-analysis, it was reported that on average, performing diagnostic laparoscopy with biopsy and histopathologic confirmation of suspicious lesions before laparotomy would avoid 23 unnecessary laparotomies per 100 patients in whom pancreatic surgery with curative intent is planned on the basis of findings on CT.

Intraoperative Ultrasound

Intraoperative ultrasound is helpful in the detection of small and elusive pancreatic neuroendocrine tumors. In patients with carcinoma of the pancreas, intraoperative sonography is useful in locating a nonpalpable neoplasm, staging the extent of disease, defining its relationship to adjacent structures, and providing guidance for a variety of procedures.¹⁷⁵⁻¹⁷⁸ The exact stage of disease and potential resectability can be determined immediately after laparotomy but before tissue dissection. Tumor invasion, particularly in the portal venous system but also hepatic metastatic disease and regional adenopathy, is easily assessed with intraoperative sonography.¹⁷⁵

Intraoperative ultrasound is also useful in patients with pancreatitis for localizing and characterizing pseudocysts and other fluid collections. These collections are often difficult to localize by direct visualization and palpation during surgery owing to the presence of dense surrounding inflammatory tissue and necrosis.^{175,178-181} In patients with chronic pancreatitis, the dilated pancreatic duct can be localized sonographically for intraoperative pancreatography, surgical decompression, or other surgical procedures^{175,181} (Fig. 99-6).

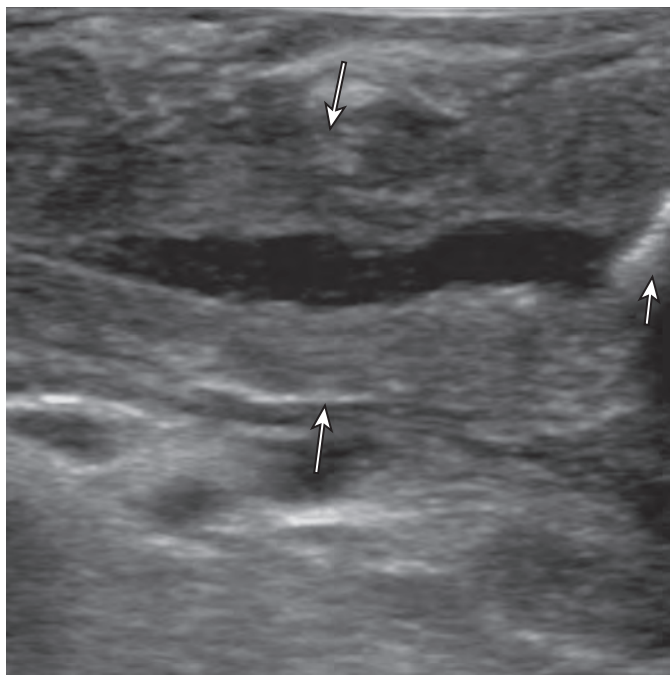


Figure 99-6 Intraoperative ultrasound of the pancreas for localization of the pancreatic duct before decompressive surgery. The pancreas is well visualized with intraoperative sonography (long arrows). Note the dilated pancreatic duct, measuring 6 mm in diameter. The needle tip is seen entering the pancreatic duct (short arrow).

TYPES OF PANCREATIC OPERATIONS AND POSTOPERATIVE RADIOLOGIC FINDINGS

Sphincterotomy

Surgical sphincterotomy is one therapeutic approach to patients with sphincter of Oddi spasm and pancreas divisum. After surgery, CT, ultrasound, and plain films may show intrabiliary and, more rarely, pancreatic ductal gas. On upper gastrointestinal studies, reflux of barium into the bile duct is common. Because the barium quickly empties into the duodenum, the reflux is usually not clinically significant.^{52,116,182,186}

Puestow Procedure

A Puestow procedure may be considered in patients with severe abdominal pain associated with chronic pancreatitis and pancreatic duct dilation (>6 mm) associated with obstruction and strictures.^{187,188} In these patients, an extended longitudinal incision is made throughout the length of the duct until all the strictures are opened (Fig. 99-7). The duct is then anastomosed to a Roux-en-Y loop of jejunum, which provides drainage at the obstructed regions. The procedure allows good postoperative pain relief in 60% to 80% of patients and maintains pancreatic function by providing wide ductal drainage without pancreatic resection.¹⁸⁹⁻¹⁹² These patients usually do not show any abnormalities of the stomach, duodenum, or upper jejunum on gastrointestinal studies unless barium or air refluxes into the afferent loop. On rare occasions when barium does reflux, it is of no significance unless there is prolonged retention of contrast material by the afferent loop or fistula formation.¹⁸²⁻¹⁸⁶ On CT examination, when the anastomosis contains fluid or air, it may mimic a pancreatic or peripancreatic abscess. In addition, soft tissue seen normally anterior

to the pancreatic body or tail from the jejunal anastomosis to the pancreas can mimic a tumor or an internal hernia if the radiologist is not aware that the patient has undergone a Puestow procedure.^{188,189}

Frey Procedure

This procedure has been gaining in popularity recently as it is the simpler of the surgeries for chronic pancreatitis and has fewer associated complications.¹⁹³ It entails partial resection of the pancreatic head and a longitudinal pancreaticojejunostomy with a Roux loop (Fig. 99-8). This procedure should not be performed in the presence of a pancreatic or biliary stricture.¹⁸⁸ There is a reduced rate of postoperative complications, most notably, anastomotic leaks, compared with the Beger procedure.¹⁹⁴ In a study comparing this procedure with the Beger procedure, there was a tendency for better pain control with the Frey procedure. The functional outcomes of the two procedures in that study were almost identical. After this surgical procedure, a large cavity may be seen in the pancreatic head on CT; this should not be mistaken for a cystic fluid collection or neoplasm.¹⁸⁸

Beger Procedure

This procedure is less radical than a Whipple operation but is technically much more complex to perform; it is also significantly more complex than the Frey procedure.¹⁸⁸ The Beger procedure involves a complex extensive surgical resection, whereas the Frey procedure is a simpler decompressive surgery.¹⁹⁴ The Beger procedure is also associated with a higher percentage of complications.^{193,195} The pancreatic body and large part of the pancreatic head are resected. The duodenum is left intact along with a small portion of the adjacent pancreas with the intrapancreatic, choledochal, and ampullary structures; that preserves blood flow through the posterior branch of the gastroduodenal artery to the duodenum. As a result, there are two pancreaticojejunostomy sites with the Roux loop¹⁸⁸ (Fig. 99-8). In a study comparing this procedure with the Whipple procedure, improved pain tolerance and glucose control were noted with the Beger procedure.¹⁹⁶

Central Pancreatectomy

This procedure is mainly used in patients with traumatic pancreatic transection and intractable chronic pancreatitis. It has also been proposed for selective management of benign and low malignant potential lesions of the pancreatic neck. It consists of resection of part of the neck or body of the pancreas, followed by a Roux-en-Y pancreaticojejunostomy to the distal pancreatic remnant. The distal pancreatic end can also be anastomosed to the stomach. The proximal cut edge is sutured.

Whipple Operation

This procedure, also known as pancreaticoduodenectomy, is considered to be the standard procedure for resection of head lesions and carcinoma of the periampullary region; it entails resection of the distal stomach, duodenum, and either part or all of the pancreas.¹²² Total pancreatectomy (double Whipple) has the theoretical advantage of preventing local recurrence of the tumor but results in permanent diabetes and exocrine insufficiency. Also, this radical operation has not been proved to be associated with significantly increased survival.

The gastrointestinal tract must be reconstructed, which requires anastomosis of the jejunum to the pancreas

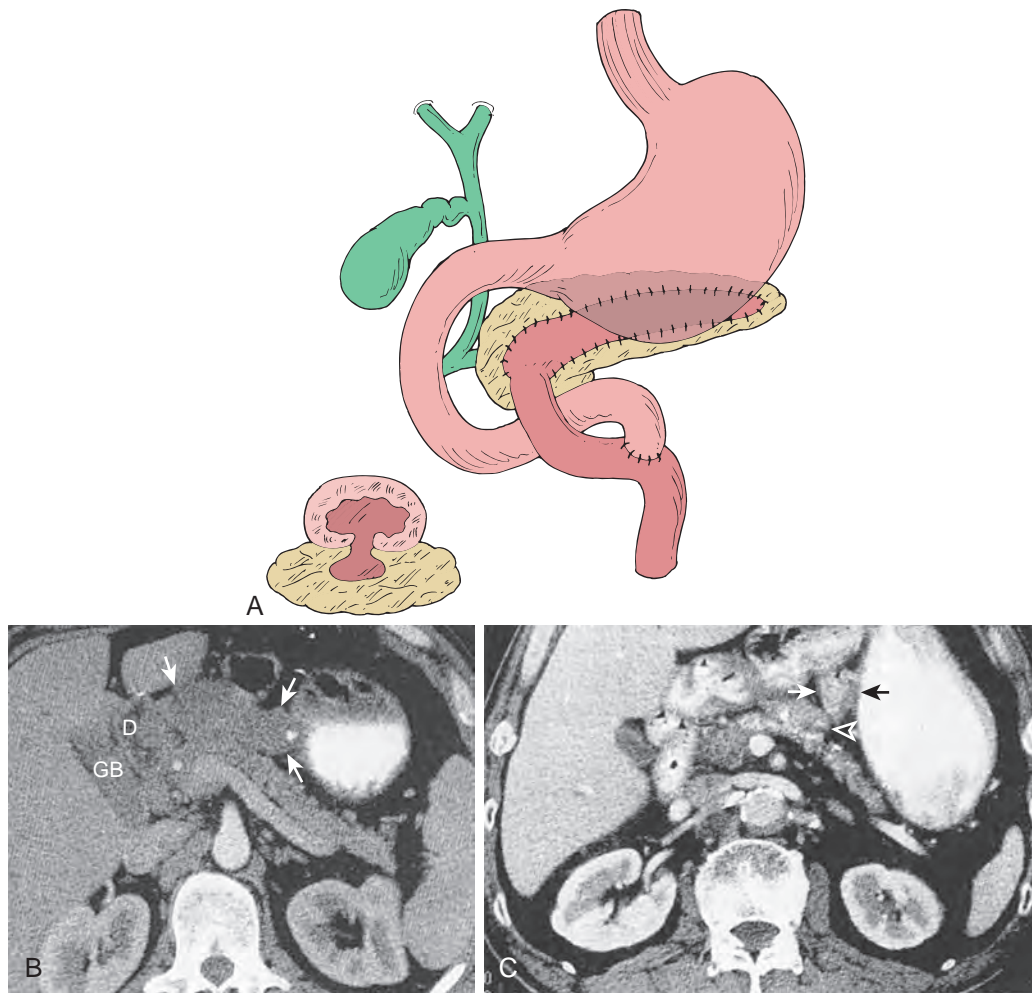


Figure 99-7 Puestow procedure. **A.** Color diagram of the expected anatomy after Puestow procedure. A long longitudinal incision throughout the main pancreatic duct is performed with anastomosis to a similarly opened Roux-en-Y loop of jejunum to create the longitudinal pancreaticojejunal anastomosis. Inset shows the anastomosis in cross section. **B.** CT scan obtained in a 41-year-old man during the arterial phase of contrast material enhancement shows the expected alterations in normal anatomy after a Puestow procedure. The collapsed pancreaticojejunal anastomosis (arrows) is immediately anterior to the body of the pancreas. D, Duodenum; GB, gallbladder. **C.** CT scan of the pancreatic tail in a 70-year-old man shows the Roux-en-Y loop (arrows) distal to the pancreaticojejunal anastomosis (arrowhead). The loop contains a small amount of oral contrast material and gas. (B and C from Freed KS, Paulson EK, Frederick MG, et al: Abdomen after a Puestow procedure: Postoperative CT appearance, complications and potential pitfalls. Radiology 203:790-794, 1997.)

(pancreaticojejunostomy), the biliary tract (usually the common hepatic duct; hepaticojejunostomy), and the stomach (gastrojejunostomy). This reconstruction also requires that the inflow of alkaline bile and pancreatic juice be inserted proximal to the gastrojejunostomy to further protect against marginal ulceration.^{122,182-189} Potential technical modifications of this procedure include performing a pancreaticogastrostomy instead of pancreaticojejunostomy along with the pancreaticoduodenectomy and the pyloric-preserving Whipple operation. In comparing pancreaticogastrostomy with pancreaticojejunostomy, overall postoperative complications and pancreatic fistulas occurred at the same rate; however, biliary fistula, postoperative collections, and delayed gastric emptying were reduced with pancreaticogastrostomy.¹⁹⁷ Another study, comparing the standard and pyloric-preserving Whipple procedure, showed similar overall outcomes including complication and survival rates in both patient groups.¹⁹⁸

On CT examinations, there are several findings related to the three surgical anastomoses of a Whipple operation that can serve as potential pitfalls in the interpretation of these postoperative scans.^{199,200} Accurate interpretation of these complex postoperative examinations requires knowledge of the type of surgery performed, including surgical anastomoses, the interval between surgery and imaging, and whether the patient has received any ancillary treatment such as radiation therapy or chemotherapy. Optimizing scanning techniques and a strong familiarity with the expected postoperative imaging findings are essential to the early detection of recurrent and metastatic disease and to avoid false-positive or false-negative interpretations²⁰¹ (Figs. 99-9 and 99-10).

The hepaticojejunostomy often will reflux air and sometimes contrast material in 80% of patients. The duodenojejunostomy or gastrojejunostomy can have a confusing appearance, depending on its position determined by the surgeon, generally

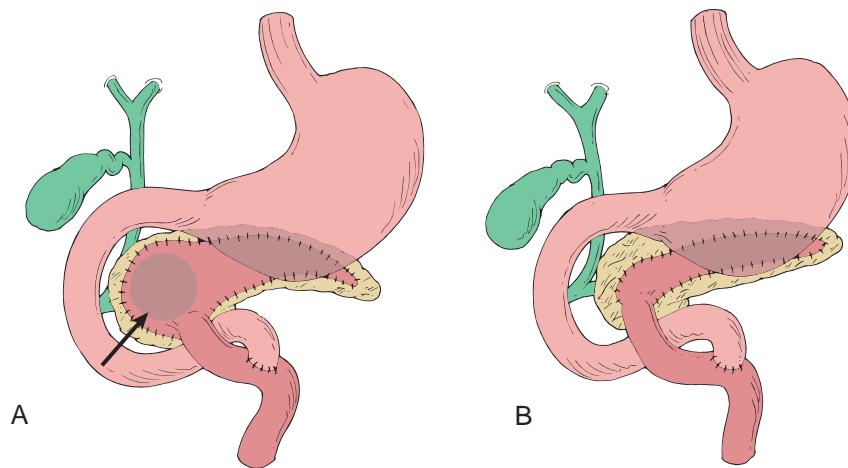


Figure 99-8 Frey and Beger procedures. **A.** Color diagram shows expected postsurgical changes after a Frey procedure. Partial resection of the pancreatic head is performed with a longitudinal pancreaticojejunostomy of the main pancreatic duct and Roux-en-Y jejunal loop. The arrow indicates the area of pancreatic head resection, which may appear as a large cavity on imaging. **B.** Color diagram shows the postsurgical anatomy after a Beger procedure. The pancreatic body and a smaller portion of the pancreatic head are resected. A portion of the pancreatic head, along with the duodenum, is left intact. This preserves the adjacent intrapancreatic choledochal and ampullary structures. Two separate pancreaticojejunostomy sites with the Roux-en-Y jejunal loop are created. (Medical illustration by David Botos, Northwestern University.)

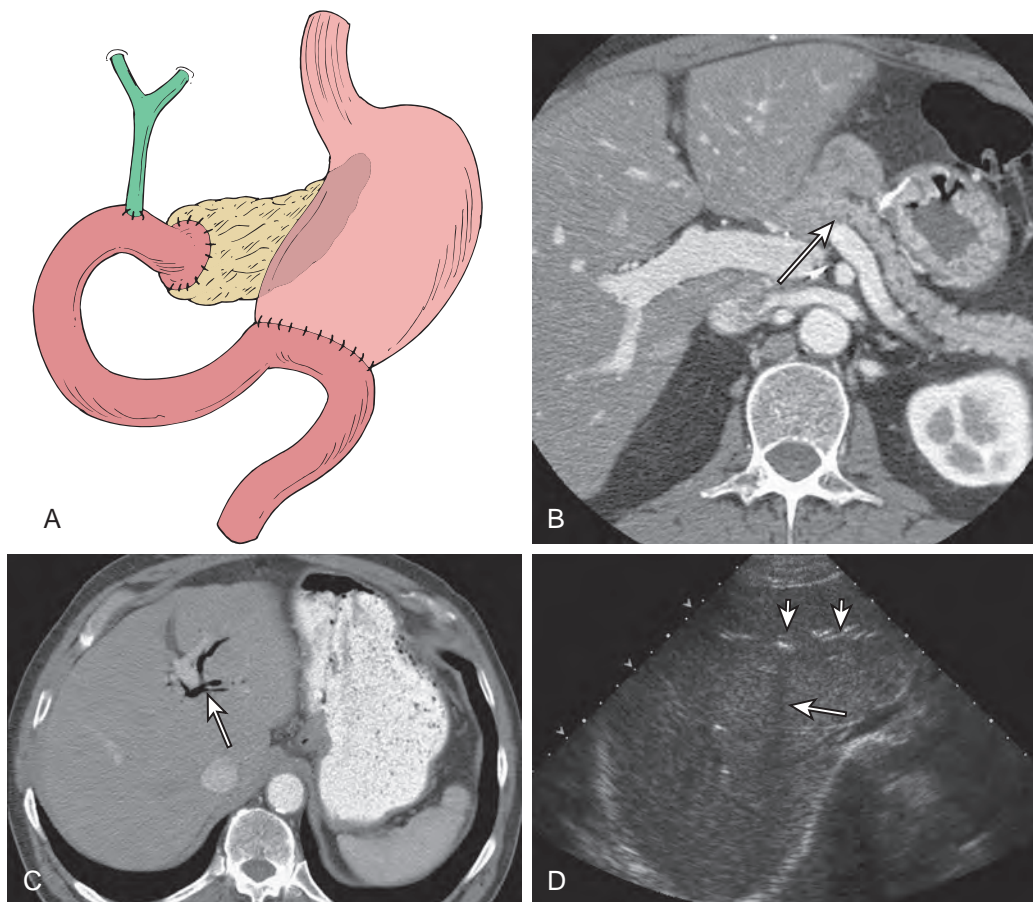


Figure 99-9 Whipple procedure. **A.** Color illustration showing postoperative changes of the Whipple procedure. The duodenum, distal stomach, and pancreatic head are resected. Subsequent anastomosis of jejunum to the pancreas, biliary tree, and stomach is performed with the resultant afferent loop. **B.** Postoperative appearance after Whipple procedure on CT. Contrast-enhanced CT appearance of the pancreaticojejunostomy (arrow) in a 52-year-old woman who underwent Whipple operation for pancreatic cancer. Surgical clips are also seen in the gastric antrum, related to partial resection of the distal stomach. The gastrojejunostomy is not seen on this image. **C.** Normal pneumobilia after biliary-enteric anastomosis on CT. Air (arrow) is identified in nondependent left hepatic ducts on the contrast-enhanced CT scan. **D.** Normal pneumobilia after biliary-enteric anastomosis on ultrasound. Biliary air is seen as bright intrahepatic specular reflectors (short arrows) that cast an acoustic shadow (long arrow).

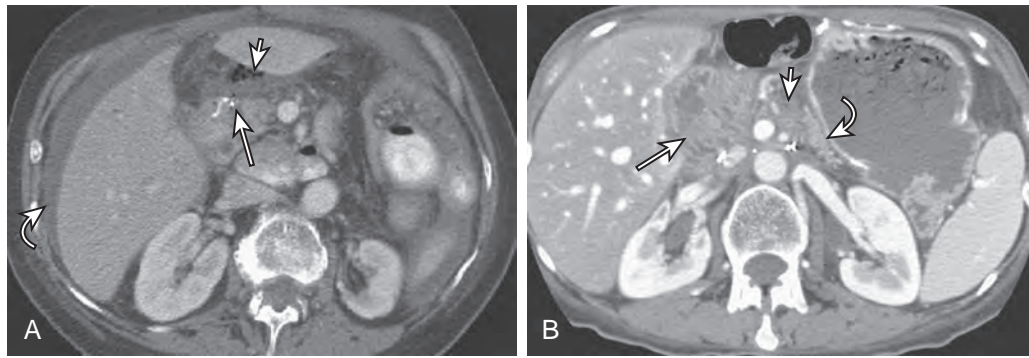


Figure 99-10 Follow-up imaging after Whipple procedure. **A.** Anastomotic breakdown. Contrast-enhanced CT in a 67-year-old woman on postoperative day 10 after Whipple procedure. There is dehiscence of the anastomosis at the afferent loop (*long arrow*) with a small collection of air (*short arrow*) and early abscess formation. Perihepatic free fluid is also present (*curved arrow*). **B.** Recurrent pancreatic cancer. Contrast-enhanced CT in a 57-year-old woman 8 months after Whipple procedure for pancreatic cancer. There is a soft tissue mass encasing the mesenteric vasculature (*short arrow*). The afferent loop (*long arrow*) has a normal appearance. Expected pancreatic body and tail atrophy is seen (*curved arrow*).

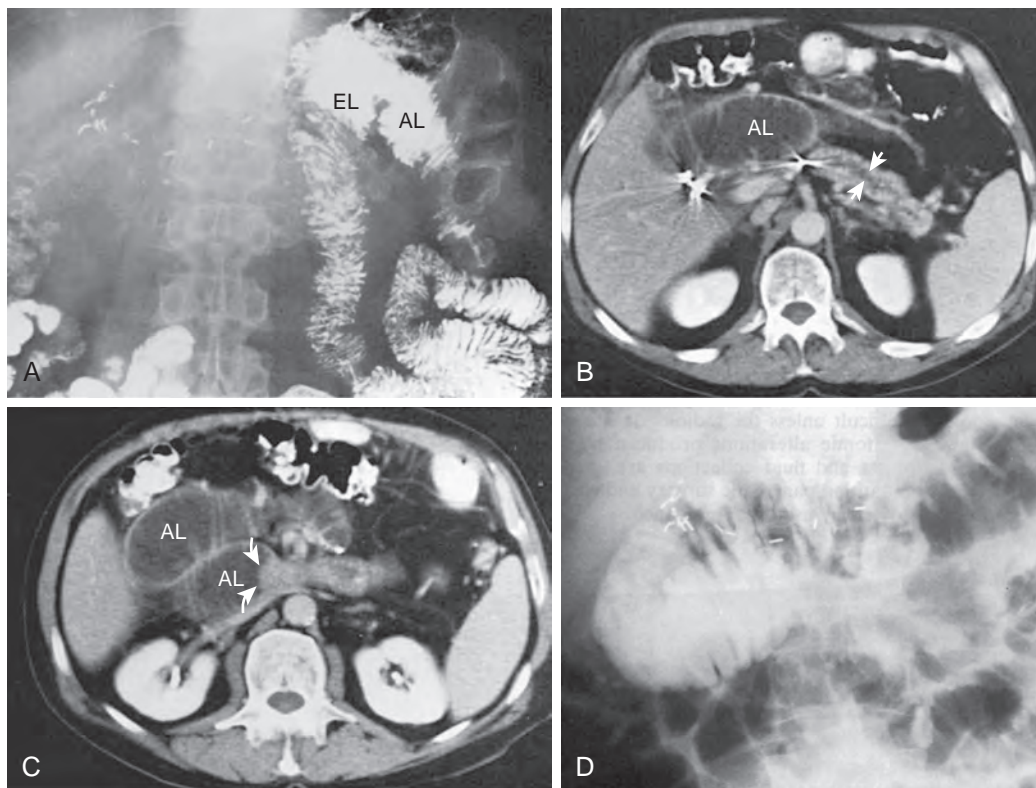


Figure 99-11 Afferent loop obstruction. Obstructed afferent loop caused by tumor recurrence after Whipple procedure for carcinoma of the pancreatic head. **A.** Barium study shows an antiperistaltic Billroth II gastrojejunostomy. The efferent loop (EL) fills normally. The distal portion of the afferent loop (AL) is also opacified. **B.** CT scan at the level of the pancreas shows the dilated afferent loop. The pancreatic duct (*arrows*) is dilated as well. **C.** More caudal scan shows the dilated afferent loop and tumor recurrence (*arrows*). **D.** Afferent loop dilation and retention of contrast medium were confirmed by endoscopic retrograde pancreatography.

antecolic in the left upper quadrant. Sometimes, the anastomosis can be positioned in a retrocolic fashion that lies adjacent to the superior mesenteric vein, simulating the duodenum, a lymph node, or recurrent tumor. The pancreaticojejunostomy may cause a soft tissue prominence that is secondary to surgical invagination of the pancreas into the bowel loop.¹⁹⁹ The pancreatic remnant usually atrophies to some degree, and the pancreatic duct becomes slightly prominent. Reactive lymph nodes and streakiness of the peripancreatic fat surrounding the superior mesenteric artery can simulate recurrent tumor. Common postradiation effects include thickening of the gastric antrum

or gastrojejunostomy; fatty infiltration of the liver; stranding of the mesenteric fat within the radiation port; and occasionally decreased function within the medial portions of the kidneys, depending on the depth of the radiation port.²⁰¹

It appears that the serum marker cancer antigen 19-9 is expressed by the majority of pancreatic cancers, and it may be able to suggest recurrences.^{202,203} Thus, serial postoperative CT scans should be obtained at 3- to 6-month intervals in conjunction with laboratory values because pancreatic neoplasms can recur quickly.²⁰⁴⁻²⁰⁶ Furthermore, PET/CT may have an important role in assessing the post-Whipple cancer patient.

In one study, PET/CT correctly detected local recurrence in all cases of recurrence in patients who had surgery, whereas MDCT alone detected the recurrence in 64% of cases. This was a relatively small study, and larger, more conclusive studies are needed.

Bypass Procedures

Cholecystojejunostomy or choledochojejunostomy is performed to bypass unresectable pancreatic head neoplasms. Contrast medium and intestinal gas (Fig. 99-9) will reflux into the biliary system as a result.²⁰⁷

POSTOPERATIVE COMPLICATIONS

Definitive or palliative surgery for pancreatic disease is fraught with the same complications that attend other abdominal operations: abscess, anastomotic leaks or strictures, and recurrent disease. Interpretation of imaging studies is difficult unless the radiologist is aware of the specific anatomic alterations produced by the surgery (Fig. 99-11). Pseudocysts and fluid collections are specific complications that may occur with pancreatic surgery, and they can be diagnosed and treated with ultrasound, CT, and MRI.²⁰⁸⁻²¹¹

REFERENCES

- Debi U, Kaur R, Prasad KK, et al: Pancreatic trauma: A concise review. *World J Gastroenterol* 19:9003-9011, 2013.
- Lahiri R, Bhattacharya S: Pancreatic trauma. *Ann R Coll Surg Engl* 95:241-245, 2013.
- Iqbal CW, St Peter SD, Tsao K, et al: Operative vs nonoperative management for blunt pancreatic transection in children. *J Am Coll Surg* 218:157-162, 2014.
- Ilahi O, Bochicchio GV, Scalea TM: Efficacy of computed tomography in the diagnosis of pancreatic injury in adult blunt trauma patients: A single-institutional study. *Am Surg* 68:704-707, 2002.
- Jordan GL: Pancreatic trauma. In Howard JM, Jordan FL, Reber HA, editors: *Surgical Diseases of the Pancreas*, Philadelphia, 1987, Lea & Febiger, pp 3-10.
- Cattaneo SM, Sedlack JD, Kalloo AN, et al: Management of a pancreatic duct injury with an endoscopically placed stent. *Surgery* 135:690-692, 2004.
- Jobst MA, Canty TG, Lynch FP: Management of pancreatic injury in pediatric blunt abdominal trauma. *J Pediatr Surg* 34:818-823, 1999.
- Bradley EL, 3rd, Young PR, Jr, Chang MC, et al: Diagnosis and initial management of blunt pancreatic trauma: Guidelines from a multi-institutional review. *Ann Surg* 227:861-869, 1998.
- Cirillo RL, Jr, Koniaris LG: Detecting blunt pancreatic injuries. *J Gastrointest Surg* 6:587-598, 2002.
- Gupta A, Stuhlfaut JW, Flemming KW, et al: Blunt trauma of the pancreas and biliary tract: A multimodality imaging approach to diagnosis. *Radiographics* 24:1381-1395, 2004.
- Scollay JM, Yip VS, Garden OJ, et al: A population-based study of pancreatic trauma in Scotland. *World J Surg* 30:2136-2141, 2006.
- Martin JK, van Heerden JA, Bess MA: Surgical management of acute pancreatitis. *Mayo Clin Proc* 59:259-267, 1984.
- Buck JR, Sorensen VJ, Fath VJ, et al: Severe pancreaticoduodenal injuries: The effectiveness of pyloric exclusion with vagotomy. *Am Surg* 58:557-561, 1992.
- Lahiri R, Bhattacharya S: Pancreatic trauma. *Ann R Coll Surg Engl* 95:241-245, 2013.
- Wilson RH, Moorehead RJ: Current management of trauma to the pancreas. *Br J Surg* 78:1196-1202, 1991.
- Biffi WL, Moore EE, Croce M, et al: Western Trauma Association critical decisions in trauma: Management of pancreatic injuries. *J Trauma Acute Care Surg* 75:941-946, 2013.
- Johanet H, Fasan JJ, Marmuse A, et al: Pancreatic trauma: Diagnostic and therapeutic emergency. *J Chir* 128:337-342, 1991.
- Madiba TE, Mokoena TR: Favourable prognosis after surgical drainage of gunshot, stab or blunt trauma of the pancreas. *Br J Surg* 82:1236-1239, 1995.
- Farrell RJ, Krige JEJ, Bornman PC, et al: Operative strategies in pancreatic trauma. *Br J Surg* 83:934-937, 1996.
- Carrel T, Lerut J, Niederhauser U, et al: Diagnosis and treatment of traumatic injuries of the duodenum and pancreas: 21 cases. *J Chir* 127:438-444, 1990.
- Mueller PR, Miketic LM, Simeone JF, et al: Severe acute pancreatitis after percutaneous biopsy of the pancreas. *AJR Am J Roentgenol* 151:493-494, 1988.
- Evans WK, Ho CS, McLaughlin MJ, et al: Fatal necrotizing pancreatitis following fine needle aspiration biopsy of the pancreas. *Radiology* 141:61-62, 1981.
- Varkarakis IM, Allaf ME, Bhayani SB, et al: Pancreatic injuries during laparoscopic urologic surgery. *Urology* 64:1089-1093, 2004.
- Takishima T, Sugimoto K, Hirata M, et al: Serum amylase level on admission in the diagnosis of blunt injury to the pancreas: Its significance and limitations. *Ann Surg* 226:70-76, 1997.
- Olsen WR: The serum amylase in blunt abdominal trauma. *Trauma* 13:200-204, 1973.
- Arkovitz MS, Johnson N, Garcia VF: Pancreatic trauma in children: mechanisms of injury. *J Trauma* 42:49-53, 1997.
- Sokolove PE, Kuppermann N, Holmes JF: Association between the "seat belt sign" and intra-abdominal injury in children with blunt torso trauma. *Acad Emerg Med* 12:808-813, 2005.
- Oniscu GC, Parks RW, Garden JO: Classification of liver and pancreatic trauma. *HPB (Oxford)* 8:4-9, 2006.
- Linsenmaier U, Wirth S, Reiser M, et al: Diagnosis and classification of pancreatic and duodenal injuries in emergency radiology. *Radiographics* 28:1591-1602, 2008.
- Lane MJ, Mindelzun RE, Jeffrey RB: Diagnosis of pancreatic injury after blunt abdominal trauma. *Semin Ultrasound CT MR* 17:177-182, 1996.
- Sivit CJ, Eichelberger MR, Taylor GA, et al: Blunt pancreatic trauma in children: CT diagnosis. *AJR Am J Roentgenol* 158:1097-1100, 1992.
- Patel SV, Spencer JA, el-Hasani S, et al: Imaging of pancreatic trauma. *Br J Radiol* 71:985-990, 1998.
- Lane MJ, Mindelzun RE, Sandhu JS, et al: CT diagnosis of blunt pancreatic trauma: Importance of detecting fluid between the pancreas and splenic vein. *AJR Am J Roentgenol* 163:833-835, 1994.
- Sivit CJ, Eichelberger MR: CT diagnosis of pancreatic injury in children: Significance of fluid separating the splenic vein and the pancreas. *AJR Am J Roentgenol* 165:921-924, 1995.
- Shuman WP: CT of blunt abdominal trauma in adults. *Radiology* 205:297-306, 1997.
- Fabian TC, Croce MA, Minard G, et al: Current issues in trauma. *Curr Probl Surg* 39:1160-1224, 2002.
- Lahiri R, Bhattacharya S: Pancreatic trauma. *Ann R Coll Surg Engl* 95:241-245, 2013.
- Debi U, Kaur R, Prasad KK, et al: Pancreatic trauma: A concise review. *World J Gastroenterol* 19:9003-9011, 2013.
- Debi U, Kaur R, Prasad KK, et al: Pancreatic trauma: A concise review. *World J Gastroenterol* 19:9003-9011, 2013.
- Smith DR, Stanley RJ, Rue LW, III: Delayed diagnosis of pancreatic transection after blunt abdominal trauma. *J Trauma* 40:1009-1013, 1996.
- Procacci C, Graziani R, Bicego E, et al: Blunt pancreatic trauma: Role of CT. *Acta Radiol* 38:543-549, 1997.
- Soto JA, Anderson SW: Multidetector CT of blunt abdominal trauma. *Radiology* 265:678-693, 2012.
- Shanmuganathan K: Multi-detector row CT imaging of blunt abdominal trauma. *Semin Ultrasound CT MR* 25:180-204, 2004.
- Schonfeld D, Lee LK: Blunt abdominal trauma in children. *Curr Opin Pediatr* 24:314-318, 2012.
- Nnamonu MI: Diagnostic value of abdominal ultrasonography in patients with blunt abdominal trauma. *J Emerg Trauma Shock* 6:308, 2013.
- Dreizin D, Bordegaray M, Tirada N, et al: Evaluating blunt pancreatic trauma at whole body CT: Current practices and future directions. *Emerg Radiol* 20:517-527, 2013.
- Hersman MJ, Maxwell R, Rosin RD: Pancreatic pseudocyst due to fractured pancreas. *J R Soc Med* 85:295-296, 1992.
- Kaude JV, McInnis AN: Pancreatic ultrasound following blunt abdominal trauma. *Gastrointest Radiol* 7:53-56, 1982.

49. Fulcher AS, Turner MA, Yelon JA, et al: Magnetic resonance cholangiopancreatography (MRCP) in the assessment of pancreatic duct trauma and its sequelae: Preliminary findings. *J Trauma* 48:1001–1007, 2000.
50. Ragozzino A, Manfredi R, Scaglione M, et al: The use of MRC in the detection of pancreatic injuries after blunt trauma. *Emerg Radiol* 10:14–18, 2003.
51. Soto JA, Alvarez O, Múnera F, et al: Traumatic disruption of the pancreatic duct: Diagnosis with MR pancreatography. *AJR Am J Roentgenol* 176:175–178, 2001.
52. Berni GA, Bandyk DF, Oreskovich MR: Role of intraoperative pancreatography in patients with injury to the pancreas. *Am J Surg* 143: 602–605, 1982.
53. Wind P, Turet E, Cunningham C, et al: Contribution of endoscopic retrograde pancreatography in management of complications following distal pancreatic trauma. *Am Surg* 65:777–783, 1999.
54. Rescorla FJ, Plumley DA, Sherman S, et al: The efficacy of early ERCP in pediatric pancreatic trauma. *J Pediatr Surg* 30:336–340, 1995.
55. Barkin JS, Ferstenberg RM, Panullo W, et al: Endoscopic retrograde cholangiopancreatography in pancreatic trauma. *Gastrointest Endosc* 34:102–105, 1988.
56. Bosboom D, Braam AW, Blickman JG, et al: The role of imaging studies in pancreatic injury due to blunt abdominal trauma in children. *Eur J Radiol* 59:3–7, 2007.
57. Whittwell AE, Gomez GO, Byers P, et al: Blunt pancreatic trauma: Prospective evaluation of early endoscopic retrograde pancreatography. *South Med J* 82:586–591, 1989.
58. Dodds WJ, Taylor AJ, Erickson SJ, et al: Traumatic fracture of the pancreas: CT characteristics. *J Comput Assist Tomogr* 14:375–378, 1990.
59. Johnson CD: Pancreatic trauma. *Br J Surg* 82: 1153–1154, 1995.
60. Lin BC, Chen RJ, Fang JF, et al: Management of blunt major pancreatic injury. *J Trauma* 56:774–778, 2004.
61. Madib TE, Mokoena TR: Favourable prognosis after surgical drainage of gunshot, stab or blunt trauma of the pancreas. *Br J Surg* 82: 1236–1239, 1995.
62. Degiannis E, Levy RD, Potkor T, et al: Distal pancreatectomy for gunshot injuries of the distal pancreas. *Br J Surg* 82:1240–1242, 1995.
63. Varadarajulu S, Noone T, Tutuian R, et al: Predictors of outcome in pancreatic duct disruption managed by endoscopic transpapillary stent placement. *Gastrointest Endosc* 61:568–575, 2005.
64. Keller MS, Stafford PW, Vane DW: Conservative management of pancreatic trauma in children. *J Trauma* 42:1097–1100, 1997.
65. Takishima T, Sugimoto K, Asari Y, et al: Characteristics of pancreatic injury in children: A comparison with such injury in adults. *J Pediatr Surg* 31:896–900, 1996.
66. McGahren ED, Magnuson D, Schaller RT, et al: Management of transected pancreas in children. *Aust N Z J Surg* 65:242–246, 1995.
67. Balthazar EJ, Freeny PC, vanSonnenberg E: Imaging and intervention in acute pancreatitis. *Radiology* 193:297–306, 1994.
68. Sarr MG, Banks PA, Bollen TL, et al: The new revised classification of acute pancreatitis 2012. *Surg Clin North Am* 93:549–562, 2013.
69. Mayerle J, Hlouschek V, Lerch MM: Current management of acute pancreatitis. *Nat Clin Pract Gastroenterol Hepatol* 2:473–483, 2005.
70. vanSonnenberg E, Wittich GR, Chon KS, et al: Percutaneous drainage of pancreatic abscesses. *AJR Am J Roentgenol* 168:979–984, 1997.
71. Ranson JHC, Balthazar EJ, Caccavale R, et al: Computed tomography and the prediction of pancreatic abscess in acute pancreatitis. *Ann Surg* 201:656–665, 1985.
72. UK Working Party on Acute Pancreatitis: UK guidelines for the management of acute pancreatitis. *Gut* 54(Suppl 3):iii1–iii9, 2005.
73. Yousaf M, McCallion K, Diamond T: Management of severe acute pancreatitis. *Br J Surg* 90:407–420, 2003.
74. Connor S, Neoptolemos JP: Surgery for pancreatic necrosis: “Whom, when and what.” *World J Gastroenterol* 10:1697–1698, 2004.
75. Ashley SW, Perez A, Pierce EA, et al: Necrotizing pancreatitis: Contemporary analysis of 99 consecutive cases. *Ann Surg* 234:572–580, 2001.
76. Lee JK, Kwak KK, Park JK, et al: The efficacy of nonsurgical treatment of infected pancreatic necrosis. *Pancreas* 34:399–404, 2007.
77. Barge JU, Lopera JE: Vascular complications of pancreatitis: Role of interventional therapy. *Korean J Radiol* 13(Suppl 1):S45–S55, 2012.
78. Bergert H, Hinterseher I, Kersting S, et al: Management and outcome of hemorrhage due to arterial pseudoaneurysms in pancreatitis. *Surgery* 137:323–328, 2005.
79. Oria A, Cimmino D, Ocampo C, et al: Early endoscopic intervention versus early conservative management in patients with acute gallstone pancreatitis and biliopancreatic obstruction: A randomized clinical trial. *Ann Surg* 245:10–17, 2007.
80. Martin RF, Hein AR: Operative management of acute pancreatitis. *Surg Clin North Am* 93:595–610, 2013.
81. Bahr MH, Davis BR, Vitale GC: Endoscopic management of acute pancreatitis. *Surg Clin North Am* 93:563–584, 2013.
82. Bahr MH, Davis BR, Vitale GC: Endoscopic management of acute pancreatitis. *Surg Clin North Am* 93:563–584, 2013.
83. Fan S-T, Lai ECS, Mok FPT, et al: Early treatment of acute biliary pancreatitis by endoscopic papillotomy. *N Engl J Med* 328:228–232, 1993.
84. Folsch UR, Nitsche R, Ludtke R, et al: German study group on acute biliary pancreatitis. *N Engl J Med* 336:237–242, 1997.
85. Aiyer MK, Burdick JS, Sonnenberg A: Outcome of surgical and endoscopic management of biliary pancreatitis. *Dig Dis Sci* 44:1684–1690, 1999.
86. Makary MA, Duncan MD, Harmon JW, et al: The role of magnetic resonance cholangiography in the management of patients with gallstone pancreatitis. *Ann Surg* 241:119–124, 2005.
87. Traverso LW, Kozarek RA: Pancreatoduodenectomy for chronic pancreatitis. Anatomic selection criteria and subsequent long-term outcome analysis. *Ann Surg* 226:429–438, 1997.
88. Howard JM, Zhang Z: Pancreaticoduodenectomy (Whipple resection) in the treatment of chronic pancreatitis. *World J Surg* 14:77–82, 1990.
89. Rossi RL: Pancreatic resections for chronic pancreatitis. *Hepatogastroenterology* 37:227–232, 1990.
90. Cooperman AM: Surgery and chronic pancreatitis. *Surg Clin North Am* 81:431–455, 2001.
91. Cunha JEM, Penteado S, Jukemura J, et al: Surgical and interventional treatment of chronic pancreatitis. *Pancreatol* 4:540–550, 2004.
92. Pitchumoni CS, Agarwal N: Pancreatic pseudocysts: When and how should drainage be performed? *Gastroenterol Clin North Am* 28:615–639, 1999.
93. Vijungco JD, Prinz RA: Management of biliary and duodenal complications of chronic pancreatitis. *World J Surg* 27:1258–1270, 2003.
94. Cunha JE, Machado M, Bacchella T, et al: Surgical treatment of pancreatic ascites and pancreatic pleural effusions. *Hepatogastroenterology* 42:748–751, 1995.
95. Warshaw AL: Chronic pancreatitis: Drainage procedures. In Najarian JS, Delaney JP, editors: *Progress in Hepatic, Biliary, and Pancreatic Surgery*, Chicago, 1990, Year Book Medical, pp 289–304.
96. Poulsen JL, Olesen SS, Malver LP, et al: Pain and chronic pancreatitis: A complex interplay of multiple mechanisms. *World J Gastroenterol* 19:7282–7291, 2013.
97. Gall FP, Zirngibl H, Gebhardt C, et al: Duodenal pancreatectomy with occlusion of the pancreatic duct. *Hepatogastroenterology* 37: 290–294, 1990.
98. Rebibo L, Yzet T, Cosse C, et al: Frey procedure for the treatment of chronic pancreatitis associated with common bile duct stricture. *Hepatobiliary Pancreat Dis Int* 12:637–644, 2013.
99. Inui K, Yoshino J, Miyoshi H, et al: New developments in diagnosis and non-surgical treatment of chronic pancreatitis. *J Gastroenterol Hepatol* 28(Suppl 4):108–112, 2013.
100. Prinz RA, Greenlee HB: Pancreatic duct drainage in chronic pancreatitis. *Hepatogastroenterology* 37:295–300, 1990.
101. Dumonceau JM, Macias-Gomez C: Endoscopic management of complications of chronic pancreatitis. *World J Gastroenterol* 19:7308–7315, 2013.
102. Stable BE, Calabria R, Wilson SE, et al: Stricture of the common bile duct from chronic pancreatitis. *Surgery* 165:121–126, 1987.
103. Haaga JR: Image-guided micro procedures: CT and MRI interventional procedures. In Haaga JR, editor: *CT and MR Imaging of the Whole Body*, ed 4, St. Louis, 2003, Mosby, pp 2123–2258.
104. Haaga JR, Kori SH, Eastwood DW, et al: Improved technique for CT-guided celiac ganglia block. *AJR Am J Roentgenol* 142:1201–1204, 1984.
105. Buy JN, Moss AA, Singler RC: CT guided celiac plexus and splanchnic nerve neurolysis. *J Comput Assist Tomogr* 6:315–319, 1982.
106. Aranha GV, Prinz RA, Freeark RJ, et al: Evaluation of the therapeutic options for pancreatic pseudocysts. *Arch Surg* 117:717–721, 1982.
107. Nunez D, Yrizarry JM, Russell E, et al: Transgastric drainage of pancreatic fluid collections. *AJR Am J Roentgenol* 145:815–818, 1985.
108. Bernardino ME, Amerson JR: Percutaneous gastrocystostomy: A new approach to pancreatic pseudocyst drainage. *AJR Am J Roentgenol* 143:1096–1097, 1984.
109. Song TJ, Le SS: Endoscopic drainage of pseudocysts. *Clin Endosc* 47:222–226, 2014.

110. da Costa DW, Boerma D, van Santvoort HC, et al: Staged multidisciplinary step-up management for necrotizing pancreatitis. *Br J Surg* 101:e65–e79, 2014.
111. Walt AJ, Bouwan DL, Weaver DW, et al: The impact of technology on the management of pancreatic pseudocyst. *Arch Surg* 125:759–763, 1990.
112. vanSonnenberg E, Wittich GR, Casola G, et al: Percutaneous drainage of infected and noninfected pancreatic pseudocysts: Experience in 101 cases. *Radiology* 170:757–761, 1989.
113. Grosso M, Gandini G, Cassinis AC, et al: Percutaneous treatment (including pseudocystogastrostomy) of 74 pancreatic pseudocysts. *Radiology* 173:493–497, 1989.
114. Tran Cao HS, Lopez N, Chang DC, et al: Improved perioperative outcomes with minimally invasive distal pancreatectomy: Results from a population-based analysis. *JAMA Surg* 149:237–243, 2014.
115. Spanheimer PM, Cyr AR, Liao J, et al: Complications and survival associated with operative procedures in patients with unresectable pancreatic head adenocarcinoma. *J Surg Oncol* 109:697–701, 2014.
116. Moosa AR: Tumors of the pancreas. In Moosa AR, Schimpff SC, Robson MC, editors: *Comprehensive Textbook of Oncology*, ed 2, Baltimore, 1991, Williams & Wilkins, pp 958–988.
117. Watanapa P, Williamson RCN: Surgical palliation for pancreatic cancer: Developments during the past two decades. *Br J Surg* 79:8–20, 1992.
118. Norton JA, Doppmann JL, Jensen RT: Curative resection in Zollinger-Ellison syndrome. *Ann Surg* 215:8–18, 1992.
119. Van Heerden JA, McIlrath DC, Ilstrup DM, et al: Total pancreatectomy for ductal adenocarcinoma of the pancreas: An update. *World J Surg* 12:658–662, 1988.
120. Hartwig W, Werner J, Jäger D, et al: Improvement of surgical results for pancreatic cancer. *Lancet Oncol* 14:e476–e485, 2013.
121. Alexakis N, Halloran C, Raraty M, et al: Current standards of surgery for pancreatic cancer. *Br J Surg* 91:1410–1427, 2004.
122. Ujiki MB, Talamonti MS: Surgical management of pancreatic cancer. *Semin Radiat Oncol* 15:218–225, 2005.
123. Sener SF, Fremgen A, Menck HR, et al: Pancreatic cancer: A report of treatment and survival trends for 100,313 patients diagnosed from 1985–1995, using the national cancer database. *J Am Coll Surg* 189:1–7, 1999.
124. Sahani DV, Kambadakone A, Macari M, et al: Diagnosis and management of cystic pancreatic lesions. *AJR Am J Roentgenol* 200:343–354, 2013.
125. Gore RM, Wenzke DR, Thakrar KH, et al: The incidental cystic pancreas mass: A practical approach. *Cancer Imaging* 12:414–421, 2012.
126. Lim SJ, Alasadi R, Wayne JD, et al: Preoperative evaluation of pancreatic cystic lesions: Cost-benefit analysis and proposed management algorithm. *Surgery* 138:672–680, 2005.
127. Karatzas T, Dimitroulis D, Charalampoudis P, et al: Management of cystic and solid pancreatic incidentalomas: A review analysis. *J BUON* 18:17–24, 2013.
128. Atiq M, Suzuki R, Khan AS, et al: Clinical decision making in the management of pancreatic cystic neoplasms. *Expert Rev Gastroenterol Hepatol* 7:353–360, 2013.
129. Karakaxas D, Gazouli M, Liakakos T, et al: Pancreatic neuroendocrine tumors: Current opinions on a rare, but potentially curable neoplasm. *Eur J Gastroenterol Hepatol* 26:826–835, 2014.
130. Semelka RC, Cumming MJ, Shoenut JP, et al: Islet cell tumors: Comparison of dynamic contrast-enhanced CT and MR imaging with dynamic gadolinium enhancement and fat suppression. *Radiology* 186:799–802, 1993.
131. Pavone P, Mitchell DG, Leonetti F, et al: Pancreatic B-cell tumors: MRI. *J Comput Assist Tomogr* 17:403–407, 1993.
132. Azimuddin K, Chamberlain RS: The surgical management of pancreatic neuroendocrine tumors. *Surg Clin North Am* 81:511–525, 2001.
133. Thompson JC, Townsend CM: *Endocrine pancreas*. In Townsend CM, Beauchamp RD, Evers BM, et al, editors: *Sabiston Textbook of Surgery: The Biological Basis of Modern Surgical Practice*, ed 17, Philadelphia, 2004, Elsevier, pp 1001–1022.
134. Kanji ZS, Gallinger S: Diagnosis and management of pancreatic cancer. *CMAJ* 185:1219–1226, 2013.
135. Lillemoe KD, Sauter PK, Pitt HA, et al: Current status of surgical palliation of periampullary carcinoma. *Surg Gynecol Obstet* 176:1–10, 1993.
136. Fuhrman GM, Charnsangavej C, Abbruzzese JL, et al: Thin-section contrast-enhanced computed tomography accurately predicts the resectability of malignant pancreatic neoplasms. *Am J Surg* 167:104–113, 1994.
137. Katz MH, Marsh R, Herman JM, et al: Borderline resectable pancreatic cancer: Need for standardization and methods for optimal clinical trial design. *Ann Surg Oncol* 20:2787–2795, 2013.
138. Ishikawa O, Ohigashi H, Sasaki Y, et al: Practical usefulness of lymphatic and connective tissue clearance for carcinoma of the pancreatic head. *Ann Surg* 208:215–220, 1988.
139. Warshaw AL, Gu Z, Wittenberg J, et al: Preoperative staging and assessment of resectability of pancreatic cancer. *Arch Surg* 125:230–233, 1992.
140. Paspulati RM: Multidetector CT of the pancreas. *Radiol Clin North Am* 43:999–1020, 2005.
141. Harris JP, Nelson RC: Abdominal imaging with multidetector computed tomography: State of the art. *J Comput Assist Tomogr* 28(Suppl 1):S17–S19, 2004.
142. Foley WE, Kerimoglu U: Abdominal MDCT: Liver, pancreas, and biliary tract. *Semin Ultrasound CT MR* 25:122–144, 2004.
143. McNulty NJ, Francis IR, Platt JF, et al: Multidetector row helical CT of the pancreas: Effect of contrast-enhanced multiphasic imaging on enhancement of the pancreas, peripancreatic vasculature, and pancreatic adenocarcinoma. *Radiology* 220:3–4, 2001.
144. Tunaci M: Multidetector row CT of the pancreas. *Eur J Radiol* 52:18–30, 2004.
145. Foley DW: Multidetector CT: Abdominal visceral imaging. *Radiographics* 22:701–719, 2002.
146. Paulson EK, Vitellas KM, Keogan MT, et al: Acute pancreatitis complicated by gland necrosis: Spectrum of findings on contrast-enhanced CT. *AJR Am J Roentgenol* 172:609–613, 1999.
147. Otsuki M, Takeda K, Matsuno S, et al: Criteria for the diagnosis and severity stratification of acute pancreatitis. *World J Gastroenterol* 19:5798–5805, 2013.
148. Horton KM, Fishman EK: Adenocarcinoma of the pancreas: CT imaging. *Radiol Clin North Am* 40:1263–1272, 2002.
149. Nghiem HV, Freene PC: Radiologic staging of pancreatic adenocarcinoma. *Radiol Clin North Am* 32:71–79, 1994.
150. Coley SC, Strickland NH, Walker JD: Spiral CT and the pre-operative assessment of pancreatic adenocarcinoma. *Clin Radiol* 52:24–30, 1997.
151. Bluemke DA, Cameron JC, Hruban RH: Potentially resectable pancreatic adenocarcinoma: Spiral CT assessment with surgical and pathologic correlation. *Radiology* 197:381–385, 1995.
152. McCarthy MJ, Evans J, Sagar G: Prediction of resectability of pancreatic malignancy by computed tomography. *Br J Surg* 85:320–325, 1998.
153. Al-Hawary MM, Francis IR, Chari ST, et al: Pancreatic ductal adenocarcinoma radiology reporting template: Consensus statement of the Society of Abdominal Radiology and the American Pancreatic Association. *Radiology* 270:248–260, 2014.
154. Loizou L, Albiin N, Anson C, et al: Computed tomography staging of pancreatic cancer: A validation study addressing interobserver agreement. *Pancreatol* 13:570–575, 2013.
155. Feng XY, Wang W, Luo GY, et al: Comparison of endoscopic ultrasonography and multislice spiral computed tomography for the preoperative staging of gastric cancer—results of a single institution study of 610 Chinese patients. *PLoS ONE* 8:e78846, 2013.
156. Valls C, Andia E, Sanchez A, et al: Dual-phase helical CT of pancreatic adenocarcinoma: Assessment of resectability before surgery. *AJR Am J Roentgenol* 178:821–826, 2002.
157. Al-Hawary MM, Francis IR, Chari ST, et al: Pancreatic ductal adenocarcinoma radiology reporting template: consensus statement of the Society of Abdominal Radiology and the American Pancreatic Association. *Gastroenterology* 146:291–304, 2014.
158. Sahani DV, Shah ZK, Catalano OA, et al: Radiology of pancreatic adenocarcinoma: Current status of imaging. *J Gastroenterol Hepatol* 23:23–33, 2008.
159. Kinney T: Evidence-based imaging of pancreatic malignancies. *Surg Clin North Am* 90:235–249, 2010.
160. Megibow AJ, Zhou XH, Rotterdam H, et al: Pancreatic adenocarcinoma: CT versus MR imaging in the evaluation of respectability—report of the Radiology Diagnostic Oncology Group. *Radiology* 195:327–332, 1995.
161. Bluemke DA, Cameron JL, Hruban RH, et al: Potentially resectable pancreatic adenocarcinoma: Spiral CT assessment with surgical and pathologic correlation. *Radiology* 197:381–385, 1995.
162. O'Malley ME, Boland GW, Wood BJ, et al: Adenocarcinoma of the head of the pancreas: Determination of surgical unresectability with thin section pancreatic-phase CT. *AJR Am J Roentgenol* 173:1513–1518, 1999.
163. Diehl SJ, Lehmann KJ, Sadick M, et al: Pancreatic cancer: Value of dual-phase helical CT in assessing resectability. *Radiology* 206:373–378, 1998.
164. Muniraj T, Jamidar PA, Aslanian HR: Pancreatic cancer: A comprehensive review and update. *Dis Mon* 59:368–402, 2013.
165. Vargas R, Nino-Murcia M, Trueblood W, et al: MDCT in pancreatic adenocarcinoma: Prediction of vascular invasion and resectability

- using a multiphasic technique with curved planar reformations. *AJR Am J Roentgenol* 182:419–425, 2004.
166. Horton KM, Fishman EK: Multidetector CT angiography of pancreatic carcinoma: Part 1, evaluation of venous involvement. *AJR Am J Roentgenol* 178:827–831, 2002.
 167. Horton KM, Fishman EK: Multidetector CT angiography of pancreatic carcinoma: Part 2, evaluation of venous involvement. *AJR Am J Roentgenol* 178:833–836, 2002.
 168. Sharma J, Ng J, Goodman MD, et al: New developments in the management of borderline resectable pancreatic cancer. *JOP* 14:123–125, 2013.
 169. Kim JH, Eun HW, Kim YJ, et al: Staging accuracy of MR for pancreatic neuroendocrine tumor and imaging findings according to the tumor grade. *Abdom Imaging* 38:1106–1114, 2013.
 170. Ichikawa T, Haradome H, Hachiya J, et al: Pancreatic ductal adenocarcinoma: Preoperative assessment with helical CT versus dynamic MR imaging. *Radiology* 202:655–662, 1997.
 171. Tamm EP, Balachandran A, Bhosale PR, et al: Imaging of pancreatic adenocarcinoma: Update on staging/resectability. *Radiol Clin North Am* 50:407–428, 2012.
 172. Miller FH, Keppke AL, Dalal K, et al: MRI of pancreatitis and its complications: Part 1, acute pancreatitis. *AJR Am J Roentgenol* 183:1637–1644, 2004.
 173. Tang Y, Yamashita Y, Arakawa A, et al: Pancreaticobiliary ductal system: Value of half-Fourier rapid acquisition with relaxation enhancement MR cholangiopancreatography for postoperative evaluation. *Radiology* 215: 81–88, 2000.
 174. Becker CD, Grossholz M, Mentha G, et al: MR cholangiopancreatography: Technique, potential indications, and diagnostic features of benign, postoperative and malignant conditions. *Eur Radiol* 7:865–874, 1997.
 175. Machi J, Oishi AJ, Furumoto NL, et al: Intraoperative ultrasound. *Surg Clin North Am* 84:1085–1111, 2004.
 176. Ganguli S, Kruskal JB, Brennan DD, et al: Intraoperative laparoscopic ultrasound. *Radiol Clin North Am* 44:925–935, 2006.
 177. Galiber AK, Reading CC, Charboneau JW, et al: Localization of pancreatic insulinoma: Comparison of pre- and intraoperative ultrasonography with CT and angiography. *Radiology* 166:405–408, 1988.
 178. Smith J, Vogelzang RL, Donovan J, et al: Intraoperative sonography of the pancreas. *AJR Am J Roentgenol* 144:557–561, 1985.
 179. Gooding GAW, Linkowski DG, Deveney C, et al: Intraoperative sonography of perisplenic pseudocysts. *AJR Am J Roentgenol* 145:1013–1015, 1985.
 180. Charboneau JW, Gorman B, Reading CC, et al: Intraoperative ultrasonography of the pancreas. *Clin Diagn Ultrasound* 21:121–150, 1987.
 181. Marcal LP, Patnana M, Bhosale P, et al: Intraoperative abdominal ultrasound in oncologic imaging. *World J Radiol* 5:51–60, 2013.
 182. Jordan GL: Pancreatic resection for pancreatic surgery. In Howard JM, Jordon GL, Reber HA, editors: *Surgical Diseases of the Pancreas*, Philadelphia, 1987, Lea & Febiger, pp 3–10.
 183. Beazley RM: Pancreatic cancer: Surgical aspects. In Toledo-Pereyra LH, editor: *The Pancreas: Principles of Medical and Surgical Practice*, New York, 1985, Churchill Livingstone, pp 1–30.
 184. Moosa AR, Davies R: Pancreatic cancer. In Moody FG, Carey LC, Jones RS, et al, editors: *Surgical Treatment of Digestive Disease*, ed 2, Chicago, 1990, Year Book Medical, pp 528–544.
 185. Gomez-Rivera F, Stewart AE, Amoletti JP, et al: Surgical treatment of pancreatic endocrine neoplasms. *Am J Surg* 193:460–465, 2007.
 186. Michelassi F, Erroi F, Dawson PF, et al: Experience with 467 consecutive tumors of the duodenum, ampulla, head of the pancreas, and distal common bile duct. *Ann Surg* 210:544–556, 1989.
 187. Howell JG, Johnson LW, Sehon JK, et al: Surgical management of chronic pancreatitis. *Am Surg* 67:487–490, 2001.
 188. Sandrasegaran K, Maglinte D, Howard T, et al: Surgery for chronic pancreatitis: Cross-sectional imaging of postoperative anatomy and complications. *AJR Am J Roentgenol* 184: 1118–1127, 2005.
 189. Freed KS, Paulson EK, Frederick MG, et al: Abdomen after a Puestow procedure: Postoperative CT appearance, complications, and potential pitfalls. *Radiology* 203:790–794, 1997.
 190. Karagianni VT, Papalois AE, Triantafyllidis JK: Nutritional status and nutritional support before and after pancreatectomy for pancreatic cancer and chronic pancreatitis. *Indian J Surg Oncol* 3:348–359, 2012.
 191. Hakaim AG, Broughan TA, Vogt DP, et al: Long-term results of the surgical management of chronic pancreatitis. *Am Surg* 60:306–308, 1994.
 192. Traverso LW, Kozarek RA: Pancreatoduodenectomy for chronic pancreatitis: Anatomic selection criteria and subsequent long-term outcome analysis. *Ann Surg* 226:429–438, 1997.
 193. Frey CF, Mayer KL: Comparison of local resection of the head of the pancreas combined with longitudinal pancreaticojejunostomy (Frey procedure) and duodenum-preserving resection of the pancreatic head (Beger procedure). *World J Surg* 27:1217–1230, 2003.
 194. Andersen DK, Topazian MD: Pancreatic head excavation: A variation of the theme of duodenum-preserving pancreatic head resection. *Arch Surg* 139:375–379, 2004.
 195. Izbicki JR, Bloechle C, Broering DC: Extended drainage versus resection in surgery for chronic pancreatitis: A prospective randomized trial comparing the longitudinal pancreaticojejunostomy combined with local pancreatic head excision with the pylorus-preserving pancreatoduodenectomy. *Ann Surg* 228:771–779, 1998.
 196. Alberts SR, Gross GJ, Kim GP, et al: Treatment options for hepatobiliary and pancreatic cancer. *Mayo Clin Proc* 82:628–637, 2007.
 197. Bassi C, Falconi M, Molinari E, et al: Reconstruction by pancreaticojejunostomy versus pancreaticogastrostomy following pancreatectomy: Results of a comparative study. *Ann Surg* 242:767–773, 2005.
 198. Tran KTC, Smeenk HG, van Eick CHJ, et al: Pylorus preserving pancreaticoduodenectomy versus standard Whipple procedure. A prospective, randomized, multicenter analysis of 170 patients with pancreatic and peripapillary tumors. *Ann Surg* 240:738–745, 2004.
 199. Cameron K, Golan S, Simpson W, et al: Recurrent pancreatic carcinoma and cholangiocarcinoma: ¹⁸F-fluorodeoxyglucose positron emission tomography/computed tomography (PET/CT). *Abdom Imaging* 36:463–471, 2011.
 200. Lepanto L, Gianfelice D, Dery R, et al: Postoperative changes, complications, and recurrent disease after Whipple's operation: CT features. *AJR Am J Roentgenol* 163:841–846, 1994.
 201. Johnson PT, Curry CA, Urban BA, et al: Spiral CT following the Whipple procedure: Distinguishing normal postoperative findings from complications. *J Comput Assist Tomogr* 26: 956–961, 2002.
 202. Poruk KE, Gay DZ, Brown K, et al: The clinical utility of CA 19-9 in pancreatic adenocarcinoma: Diagnostic and prognostic updates. *Curr Mol Med* 13:340–351, 2013.
 203. Fong ZV, Winter JM: Biomarkers in pancreatic cancer: Diagnostic, prognostic, and predictive. *Cancer J* 18:530–538, 2012.
 204. Heiken JP, Balfe DM, Picus D, et al: Radical pancreatectomy: Post-operative evaluation by CT. *Radiology* 153:211–215, 1984.
 205. Coombs RJ, Zeiss J, Howard JM, et al: CT of the abdomen after the Whipple procedure: Value in depicting postoperative anatomy, surgical complications, and tumor recurrence. *AJR Am J Roentgenol* 154:1011–1014, 1990.
 206. Bhosale P, Fleming J, Balachandran A, et al: Complications of Whipple surgery: Imaging analysis. *Abdom Imaging* 38:273–284, 2013.
 207. Morgan DE: Imaging after pancreatic surgery. *Radiol Clin North Am* 50:529–545, 2012.
 208. Hartwig W, Werner J, Jäger D, et al: Improvement of surgical results for pancreatic cancer. *Lancet Oncol* 14:e476–e485, 2013.
 209. Yamauchi FI, Ortega CD, Blasbalg R, et al: Multidetector CT evaluation of the postoperative pancreas. *Radiographics* 32:743–764, 2012.
 210. Thomson DA, Krige JE, Thomson SR, et al: The role of endoscopic retrograde pancreatography in pancreatic trauma: A critical appraisal of 48 patients treated at a tertiary institution. *J Trauma Acute Care Surg* 76: 1362–1366, 2014.
 211. Raman SP, Horton KM, Cameron JL, et al: CT after pancreaticoduodenectomy: Spectrum of normal findings and complications. *AJR Am J Roentgenol* 201:2–13, 2013.

Pancreatic Transplantation Imaging

FAUZIA Q. VANDERMEER | MARIA A. MANNING | ALETTA A. FRAZIER |
JADE J. WONG-YOU-CHEONG

CHAPTER OUTLINE

Types of Pancreas Transplantation

Pancreas Transplant Anatomy

Pancreas Procurement

Pancreas Transplant Imaging: Normal Appearances

Ultrasound

Computed Tomography

Magnetic Resonance Imaging and Angiography

Pancreas Transplant Imaging: Postoperative Complications

Vascular Complications

Graft Rejection

Graft Pancreatitis

Hemorrhage

Bowel Complications

Intra-Abdominal Fluid Collections

Post-Transplantation Lymphoproliferative Disease

Conclusion

Pancreas transplantation offers patients with severe type 1 diabetes mellitus the ability to restore normoglycemia and to halt or reverse the progression of diabetic complications, such as nephropathy, retinopathy, and vasculopathy.^{1,2} The standard procedure is transplantation of a whole-organ cadaveric pancreas while the recipient's native pancreas is left in place. Surgical techniques are varied and have evolved during the last four decades. Despite improvements during this period in both patient and graft survival rates, graft loss occurs with high prevalence. Early detection of graft-related complications is fundamental for graft survival and often relies on multiple imaging modalities. Imaging after pancreas transplantation poses a special challenge to the radiologist because it requires knowledge of the transplantation procedure, the complex postsurgical anatomy, and a wide spectrum of postoperative complications. Ultrasound (US), computed tomography (CT), and magnetic resonance imaging (MRI) offer specific advantages and limitations in this setting, and a multimodality approach is often required to optimally evaluate the pancreas transplant. In this chapter, we review the spectrum of surgical procedures, postoperative anatomy, and complications of pancreas transplantation with emphasis on the normal and abnormal findings seen at US, CT, and MRI.

Types of Pancreas Transplantation

According to the International Pancreas Transplant Registry, more than 26,000 pancreas transplantations have been

performed in the United States since 1988; 1042 were performed in 2012.³ Three types of pancreas transplantation procedures are typically performed. Most commonly, the pancreas is transplanted from a deceased donor together with a kidney transplantation occurring at the same time (simultaneous pancreas-kidney [SPK] transplantation); this accounts for 75% of pancreas transplants performed in the United States today.⁴ Less commonly (18% of cases), a patient receives a pancreas transplant after having already undergone successful kidney transplantation from a live or a deceased donor (pancreas after kidney [PAK] transplantation).⁴ Pancreas transplantation alone (PTA) is performed least commonly, accounting for 7% of cases.⁴

SPK transplants allow patients to be free of both insulin therapy and dialysis and result in higher 1-year graft survival rates (86%) than PAK or PTA transplants (80% and 78%, respectively).⁴ This difference persists in the long term, with SPK transplants demonstrating a graft function rate of 45% at 20 years compared with 16% for PAK and 12% for PTA transplants.⁵ The advantages of pancreas transplantation must be balanced against short-term surgical complications and long-term immunosuppressive regimens. However, with recent advances in surgical technique, human leukocyte antigen matching, and immunosuppressive regimens, all types of pancreas transplants have shown significant improvements in both patient and graft survival rates during the last two decades.^{4,6,7} Living donor pancreas transplants account for a small minority of cases (0.5%) and are not discussed.⁸

Pancreas Transplant Anatomy

PANCREAS PROCUREMENT

The pancreas allograft is harvested with its vascular support and a segment of the donor duodenum containing the ampulla of Vater. The donor's iliac artery bifurcation is also procured for reconstruction of the arterial conduit. Surgical techniques have evolved over time to deal with arterial inflow, venous outflow (endocrine secretions), and pancreatic duct exocrine drainage, with the most variability in the venous and duodenal attachments.

Arterial Supply

The pancreas transplant receives arterial inflow from two sources: the donor superior mesenteric artery, which supplies the head through the inferior pancreaticoduodenal artery; and the donor splenic artery, which supplies the body and tail.⁸⁻¹⁰ The internal and external iliac arteries of the donor iliac bifurcation are attached in an end-to-end fashion to the donor superior mesenteric artery and splenic arteries, forming a Y graft (Figs. 100-1 and 100-2). The common iliac portion is then anastomosed to the recipient common iliac artery or external

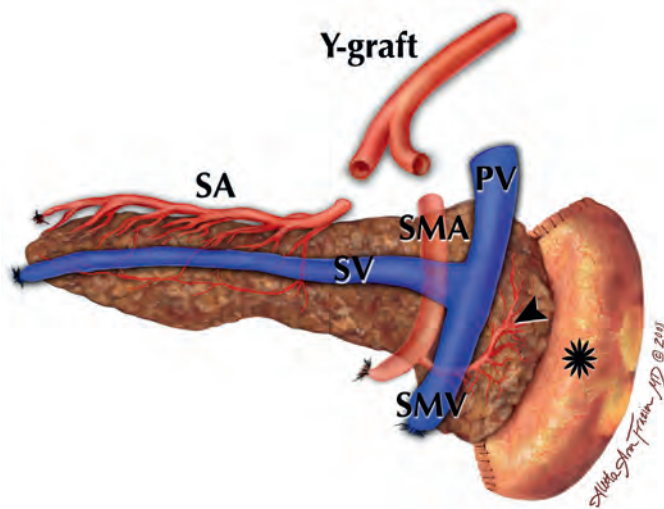


Figure 100-1 Posterior view of donor pancreas demonstrating vascular reconstruction. The donor iliac Y graft is attached to the donor splenic artery (SA) to supply the body of the pancreas and to the donor superior mesenteric artery (SMA) to supply the head of the pancreas through the inferior pancreaticoduodenal artery (arrowhead). The donor portal vein (PV) functions as the main graft vein and drains the donor splenic vein (SV) and donor superior mesenteric vein (SMV). The donor duodenal stump is harvested along with the pancreas (asterisk). (Copyright © 2015 Aletta Ann Frazier, MD. Published by Elsevier Inc. All rights reserved.)

iliac artery, with a variable graft length depending on the venous and duodenal attachments.

Venous Drainage

Venous outflow from the graft may be drained to the recipient's portal or systemic venous system. Pancreas transplantations were originally performed with systemic venous drainage. However, pancreatic endocrine secretions contained in the venous outflow raised concerns about systemic hyperinsulinemia causing accelerated atherosclerosis, hypertension, and hypercholesterolemia and resulted in a change to the more physiologic state of portal venous drainage.^{8,11-14} This is accomplished by grafting the donor portal vein, which functions as the main graft vein, to the recipient superior mesenteric vein (see Figs. 100-1 and 100-2A). Systemic venous drainage involves an anastomosis of the graft vein to the recipient iliac vein (see Fig. 100-2B) or, rarely, to the inferior vena cava. These techniques are currently equivalent in terms of patient and short-term graft survival, and although systemic drainage is currently predominant, portal venous drainage is still widely used.^{4,8,15}

Exocrine Secretions

Pancreatic exocrine secretions drain into the donor duodenal stump that is harvested with the pancreas. This can be attached side-to-side to the recipient's small bowel for enteric drainage or to the recipient's bladder. Enteric exocrine drainage is used

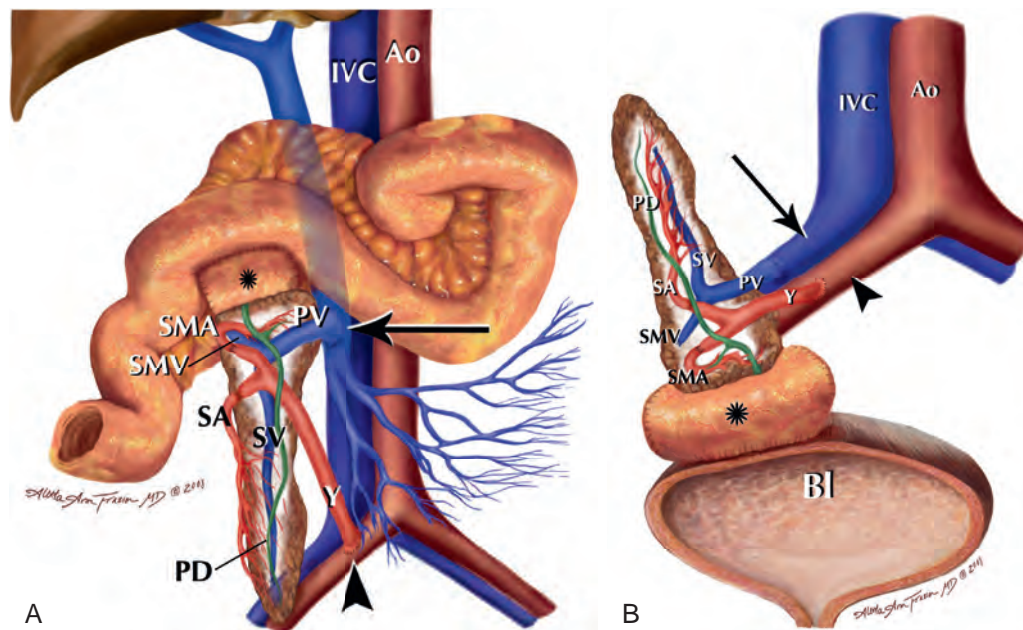


Figure 100-2 Anterior view of two types of pancreas transplants as seen through the overlying pancreas. **A.** Portal venous and enteric exocrine drainage. The graft artery (Y) is attached to the common iliac artery (arrowhead) proximally; the distal limbs are connected to the donor splenic artery (SA) and donor superior mesenteric artery (SMA). The graft vein (PV) is attached to the recipient superior mesenteric vein (arrow) for portal venous drainage. The donor splenic vein (SV) and donor superior mesenteric vein (SMV) are demonstrated as well. Exocrine drainage is achieved through the pancreatic duct (PD) draining to the duodenal stump (asterisk), which is anastomosed to the jejunum. IVC, Inferior vena cava; Ao, aorta. **B.** Systemic venous and bladder exocrine drainage. The graft artery (Y) is attached to the common iliac artery (arrowhead) proximally; the distal limbs are connected to the donor splenic artery (SA) and donor superior mesenteric artery (SMA). The graft vein (PV) is anastomosed to the recipient external iliac vein (arrow), providing systemic venous drainage of the donor splenic vein (SV) and the donor superior mesenteric vein (SMV). Exocrine secretions are drained through the pancreatic duct (PD) to the duodenal stump (asterisk), which is anastomosed to the bladder (Bl). (Copyright © 2015 Aletta Ann Frazier, MD. Published by Elsevier Inc. All rights reserved.)

most commonly (91% of SPK, 89% of PAK, 85% of PTA), with or without the creation of a Roux-en-Y loop (see Fig. 100-2A).⁴ Enterically drained transplants are usually located in the midabdomen to the right of midline, with the head of the pancreas situated cranially for portal venous drainage or caudally for systemic venous drainage. Bladder drainage of exocrine secretions is achieved by an anastomosis between the donor duodenal stump and the superior aspect of the bladder (see Fig. 100-2B). Bladder-drained allografts are usually located in the right pelvis, superior to the bladder, with the head of the pancreas directed caudally. One advantage of bladder drainage is that urinary amylase may be used to monitor graft function. However, in many centers, enteric drainage is preferred to bladder drainage because it is associated with fewer metabolic complications and lower rates of hematuria and recurrent urinary infections.¹⁶ Enteric conversion may be successfully performed after initial bladder drainage; up to 25% of patients undergo this procedure.⁸

Pancreas Transplant Imaging: Normal Appearances

ULTRASOUND

US is the most commonly used imaging modality to evaluate the transplanted pancreas; it is routinely used in its initial evaluation.¹⁰ Gray-scale imaging can demonstrate the allograft and peripancreatic fluid collections; color and duplex Doppler imaging can document perfusion and evaluate the arterial and venous vasculature.^{9,10} The well-known advantages of US include availability, repeatability, and portability for ill and unstable patients in the postoperative setting. US can also be used to guide percutaneous biopsy of the transplant pancreas. Sonographic evaluation is, however, operator dependent, and anatomic challenges, such as obscuration by bowel, are not uncommon. Unless it is abnormally dilated, the duodenal component most often cannot be separately evaluated. When direct visualization of the transplant pancreas is difficult, color and power Doppler imaging can help in identifying parenchymal and graft vessel flow, thereby localizing the pancreas.

The normal pancreas transplant is a homogeneous soft tissue structure hypoechoic relative to surrounding mesenteric fat on gray-scale US (Fig. 100-3A).^{10,17} Because it lacks a capsule, its borders may be indistinct, and it may be difficult to distinguish the allograft from adjacent structures. Color and power Doppler are essential to demonstrate pancreas transplant perfusion and vascular anatomy; the Y arterial graft, graft vein, and splenic artery and vein are usually visible (Fig. 100-3B-D). Arterial waveforms normally show a rapid systolic upstroke and continuous diastolic blood flow, whereas venous structures demonstrate a monophasic waveform within an anechoic lumen (Fig. 100-3E). Arterial resistive indices are variable within the graft and are not useful in distinguishing normal from abnormal grafts.^{18,19}

COMPUTED TOMOGRAPHY

CT is most often performed when there is concern for abdominal infection, bowel complication, or pancreatitis or its complications. It is better suited to evaluate fluid collections and bowel complications because of its wider field of view and intrinsic properties.¹⁷ CT can reliably demonstrate the pancreas, the

duodenal stump, and the recipient small bowel, which can be useful when the transplant cannot be visualized sonographically because of overlying bowel gas. This may be particularly helpful in guiding percutaneous biopsy.

Positive enteric contrast agents should be used to differentiate bowel from fluid collections and from the transplant. Because most allografts are SPK transplants, CT is usually performed without intravenous contrast material to avoid further renal injury in patients with impaired renal function. This limits evaluation of the vasculature and parenchymal enhancement. On unenhanced CT, the allograft appears as a homogeneous soft tissue structure that may be isodense to and difficult to distinguish from unopacified and nondistended bowel, although surgical staples on either side of the duodenal stump are helpful for localization (Fig. 100-4A). The donor duodenum is often collapsed and thick walled but can be misinterpreted as a fluid collection when it is distended. It inconsistently opacifies with oral contrast material even when the adjacent jejunum is contrast filled. Contrast-enhanced CT, especially with multiplanar reformations, can demonstrate the vascular anatomy and parenchymal enhancement well (Fig. 100-4B, C).

MAGNETIC RESONANCE IMAGING AND ANGIOGRAPHY

MRI and magnetic resonance angiography (MRA) are used less frequently in the evaluation of the transplanted pancreas. They are most commonly performed to confirm the diagnosis of a vascular complication, after an abnormal or nondiagnostic US or CT study. High-resolution, three-dimensional (3D), contrast-enhanced MRA provides an accurate diagnostic technique for evaluation of the arterial and venous anatomy of the pancreas transplant.^{17,20-22} Unenhanced MRI sequences readily separate the pancreatic allograft from adjacent structures and are superior to CT without intravenous contrast material. MR is particularly useful when US is limited by overlying bowel gas or by body habitus. Given the increased risk for nephrogenic systemic fibrosis in patients with end-stage renal disease, the risk/benefit ratio of intravenous gadolinium-based contrast agents should be carefully assessed. Unenhanced MRA is unlikely to perform as well as contrast-enhanced MRA, but it has not been formally evaluated in this setting.

On T1-weighted images, the pancreatic parenchyma is homogeneous and hyperintense relative to the liver. On T2-weighted images, the normal pancreas allograft will show signal intensity between fluid and muscle (Fig. 100-5A). T2-weighted images are most sensitive to abnormalities of the pancreatic transplant because the majority of pathologic processes increase glandular water content. We typically use a coronal 3D fat-suppressed breath-hold gradient-echo T1-weighted dynamic enhanced sequence to demonstrate the arterial and venous anatomy and parenchymal enhancement (Fig. 100-5B). The data set can be used to generate 3D maximum intensity projection or volume-rendered images to optimally evaluate the vasculature (Fig. 100-5C).

Pancreas Transplant Imaging: Postoperative Complications

Despite steady improvements in patient and graft survival rates, graft failure remains a problem after pancreas transplantation.

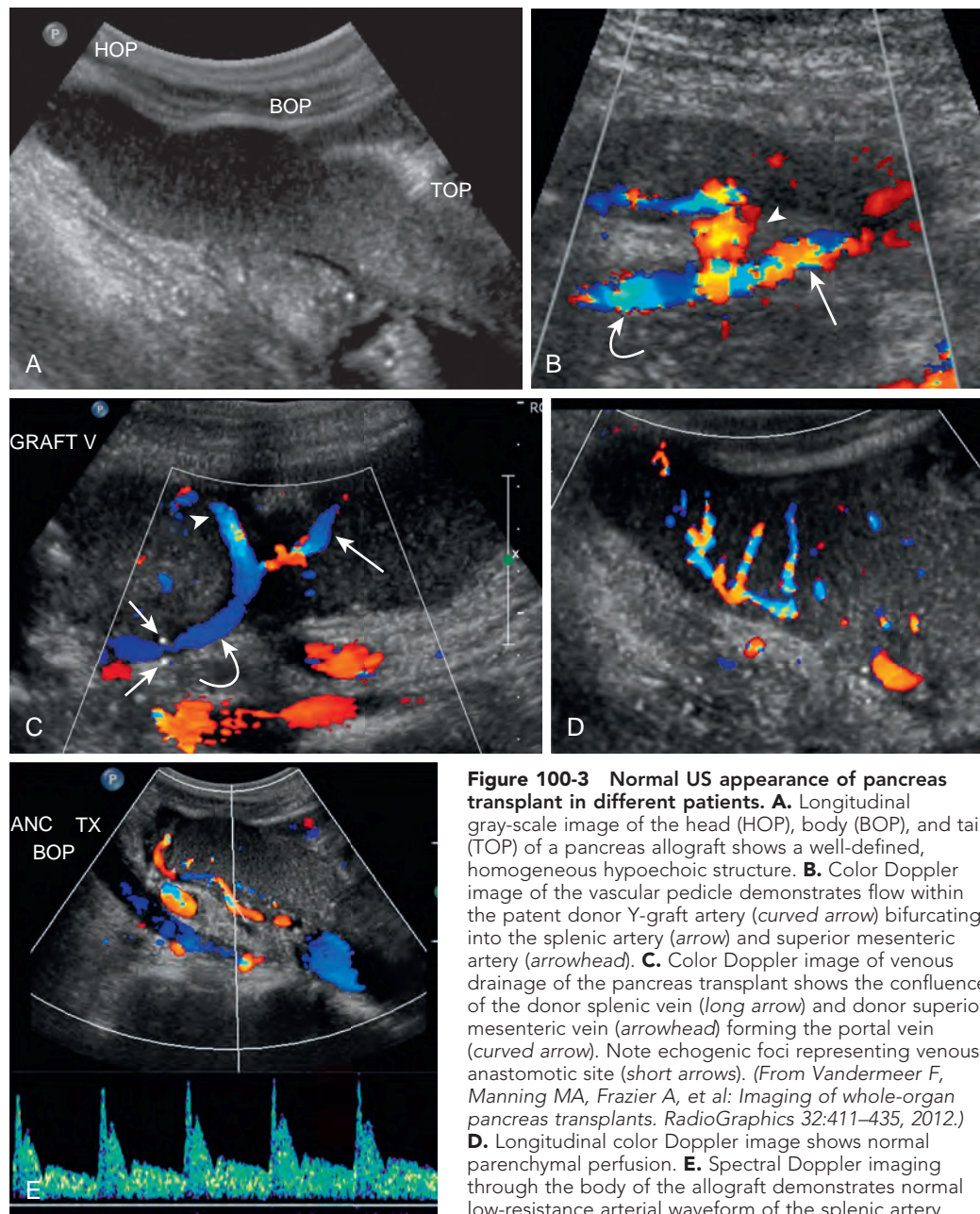


Figure 100-3 Normal US appearance of pancreas transplant in different patients. **A.** Longitudinal gray-scale image of the head (HOP), body (BOP), and tail (TOP) of a pancreas allograft shows a well-defined, homogeneous hypoechoic structure. **B.** Color Doppler image of the vascular pedicle demonstrates flow within the patent donor Y-graft artery (curved arrow) bifurcating into the splenic artery (arrow) and superior mesenteric artery (arrowhead). **C.** Color Doppler image of venous drainage of the pancreas transplant shows the confluence of the donor splenic vein (long arrow) and donor superior mesenteric vein (arrowhead) forming the portal vein (curved arrow). Note echogenic foci representing venous anastomotic site (short arrows). (From Vandermeer F, Manning MA, Frazier A, et al: *Imaging of whole-organ pancreas transplants*. *RadioGraphics* 32:411–435, 2012.) **D.** Longitudinal color Doppler image shows normal parenchymal perfusion. **E.** Spectral Doppler imaging through the body of the allograft demonstrates normal low-resistance arterial waveform of the splenic artery.

The causes of graft failure vary by the time since transplantation and the type of transplant. In the first 6 months after transplantation, most complications are due to surgical or technical failure, more than 55% in all categories of transplants.²³ Technical failure occurs in 7% to 9% of cases and includes thrombosis, infection, pancreatitis, anastomotic leak, and bleeding leading to removal.²⁴ Repeated laparotomy rates remain high for all types of transplants, up to 35%.^{24,25} Nonsurgical complications are usually immunologic, with rejection being the single most common cause of graft loss. Acute rejection peaks between 3 and 12 months, whereas graft loss due to chronic rejection increases at a constant rate over time.^{23,26} Primary nonfunction occurs in 0.5% to 1% and is defined by the exclusion of other causes of early graft failure.²⁴

VASCULAR COMPLICATIONS

Graft Thrombosis

Acute graft thrombosis is the most frequent and serious technical cause of graft failure in the early postoperative period, occurring in 2% to 10% of patients, typically in the first 6 weeks after surgery.^{24,25} Venous thrombosis is more common than arterial and accounts for the second most common cause of overall graft failure after rejection.^{27,28} Acute vascular thrombosis can be manifested with hyperglycemia, abnormal levels of amylase, graft tenderness, and swelling with hematuria, if the transplant is bladder drained. Thrombectomy and thrombolysis have a limited role in management, confined to short-segment thrombosis without necrosis.²⁴ Prompt pancreatectomy is

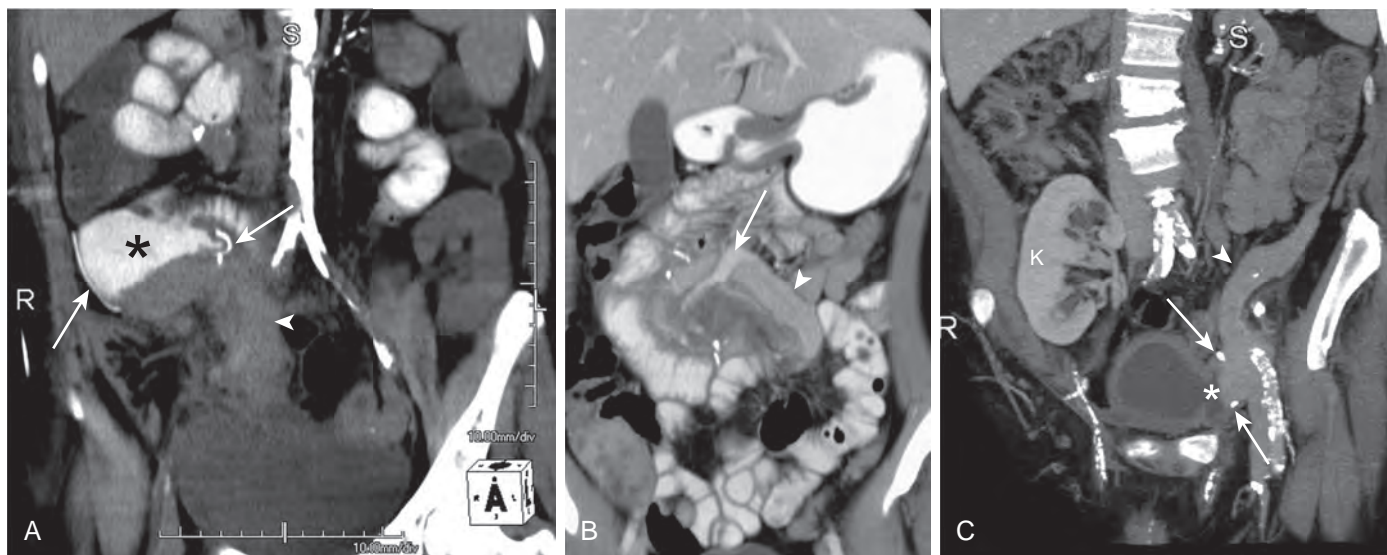


Figure 100-4 Normal CT appearance of pancreas transplant in different patients. **A.** Coronal maximum intensity projection image from unenhanced CT shows surgical staple lines (arrows) along the duodenal stump (asterisk), aiding localization of the pancreas transplant (arrowhead). **B.** Coronal multiplanar reconstruction image shows a patent graft vein (arrow) with normal parenchymal enhancement of the pancreatic body and tail (arrowhead). **C.** Coronal anterior oblique 8-mm maximum intensity projection image from an enhanced CT study of a bladder-drained left lower quadrant pancreas allograft transplanted after a renal transplant (K) shows surgical staple lines (arrows) along the lateral margins of the duodenal stump, which aids in the identification of the duodenocystostomy (asterisk). The pancreas transplant (arrowhead) is readily identified with normal parenchymal enhancement. (From Vandermeer F, Manning MA, Frazier A, et al: *Imaging of whole-organ pancreas transplants*. *RadioGraphics* 32:411–435, 2012.)

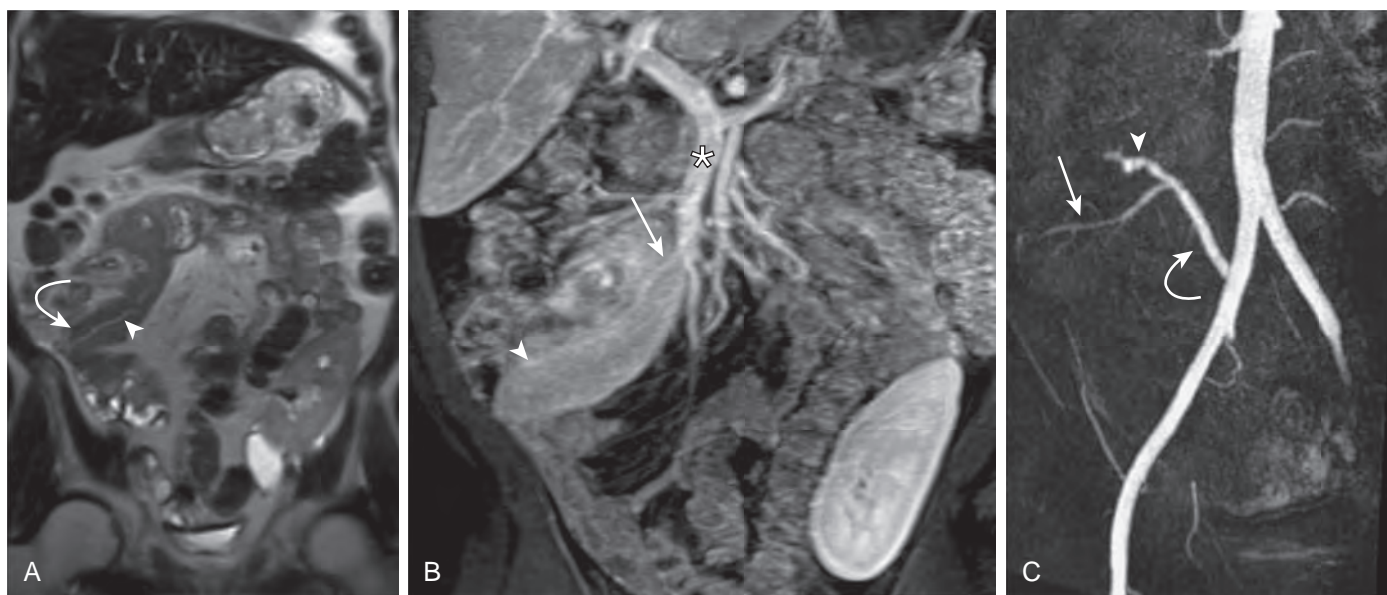


Figure 100-5 Normal MR appearance of pancreas transplant in different patients. **A.** Coronal half-Fourier acquisition single-shot turbo spin-echo (HASTE) T2-weighted MR image shows the pancreas transplant (curved arrow), which has signal intensity between that of muscle and fluid. A nondilated segment of pancreatic duct is visible (arrowhead). **B.** Coronal dynamic volume-interpolated breath-hold examination (VIBE) shows normal enhancement of the pancreas transplant (arrowhead), with a patent graft vein (arrow) draining into the recipient's superior mesenteric vein (asterisk). Note the normally enhancing left lower quadrant renal transplant. **C.** Maximum intensity projection shows a patent Y-graft artery (curved arrow) anastomosed to the right common iliac artery. Note the splenic (arrow) and superior mesenteric (arrowhead) branches. (From Vandermeer F, Manning MA, Frazier A, et al: *Imaging of whole-organ pancreas transplants*. *RadioGraphics* 32:411–435, 2012.)

usually required because early pancreatectomy decreases infectious complications and mortality.

The etiology of thrombosis is multifactorial. The pancreas has a smaller microcirculatory blood flow than other allografts, resulting in an increased propensity to thrombosis. Contributory donor factors include donor obesity and cardiovascular disease, back-table preparation, and cold ischemia time.²⁷ Thrombosis occurs more often in PAK and PTA grafts than in SPK transplants and more often with enteric than with bladder drainage.^{8,26} Severe pancreatitis, arterial wall injury, and development of stump thrombi also place the patient at risk.^{20,29,30} When the pancreas is harvested, vascular stumps are created within the peripheral superior mesenteric and splenic arterial and venous segments (see Figs. 100-1 and 100-2). Stagnant blood may clot in these low-flow areas and result in stump thrombi. Short-segment peripheral splenic vein thrombi can be seen incidentally and may not interfere with graft functioning. Full anticoagulation is usually instituted to prevent clot propagation; thrombolysis has also been attempted. Many centers use prophylactic anticoagulation perioperatively with attendant increased risks of bleeding.²⁴

Graft thrombosis after the early postoperative period may also be the result of acute or chronic graft rejection, in which an autoimmune vasculitis and fibrosis cause the gradual occlusion of small and large vessels. Extensive thrombosis usually causes parenchymal necrosis, requiring urgent pancreatectomy.²⁷ Rarely, after total arterial Y-graft thrombosis, collateral vasculature may preserve some pancreatic function and parenchyma.

US findings of vascular thrombosis depend on the degree and location of the clot.^{17,30} These include echogenic intraluminal thrombus on gray-scale imaging and absence of vascular flow in the vessel and possibly throughout the parenchyma at color and pulsed Doppler imaging (Figs. 100-6A and 100-7A). With venous thrombosis, arterial waveforms typically show a high-resistance pattern with reversal of diastolic flow (Fig. 100-6B). If pancreatic infarction results, the transplant will appear enlarged and hypoechoic without color flow (Fig. 100-6A). With chronic thrombosis, the allograft may be

atrophic and difficult to see with US. It is typically increased in echogenicity with decreased perfusion.

Thrombosis cannot be excluded with CT unless intravenous iodinated contrast material is used. However, acute thrombus may be suspected on unenhanced CT as a subtle, high-density tubular abnormality, typically prompting confirmation with US, MRI, or MRA. Conventional angiography has a limited role in the diagnosis of graft thrombosis but may be combined with thrombolysis in highly selected cases.

Multiphasic 3D contrast-enhanced MRA can be used after nondiagnostic or inconclusive sonography; MRA is a reliable method for identifying vascular complications of occlusion, stenosis, and infarction.²⁰⁻²² After contrast enhancement, thrombus may be visualized as a hypointense intraluminal filling defect, and the degree of pancreatic enhancement can be assessed (Figs. 100-7B, 100-8, and 100-9A,B). In complete infarction, the pancreas transplant shows high T2 signal intensity and absence of enhancement. T1 signal intensity may also be increased in hemorrhagic infarction.

In the much less common setting of chronic thrombosis, collateral vessels may produce peripheral rim enhancement around the otherwise nonenhancing pancreas (see Fig. 100-8B).

In patients with renal failure and decreased creatinine clearance, in whom gadolinium-based contrast agents are avoided because of the risk for nephrogenic systemic fibrosis, unenhanced MRI may be adequate for vascular evaluation. Although parenchymal enhancement cannot be evaluated without contrast material, thrombus may be detected as increased T1 signal or lack of flow void in the vessels (Fig. 100-9C). TrueFISP (true fast imaging with steady-state free precession) or gradient-echo/time-of-flight sequences can be particularly useful in demonstrating abnormal low signal intensity in the thrombosed vessel (Fig. 100-9D).

Graft Stenosis

Stenoses can develop at any anastomotic site but are not common.³¹ Many recipients have peripheral vascular disease, and vascular inflow to the allograft may become compromised

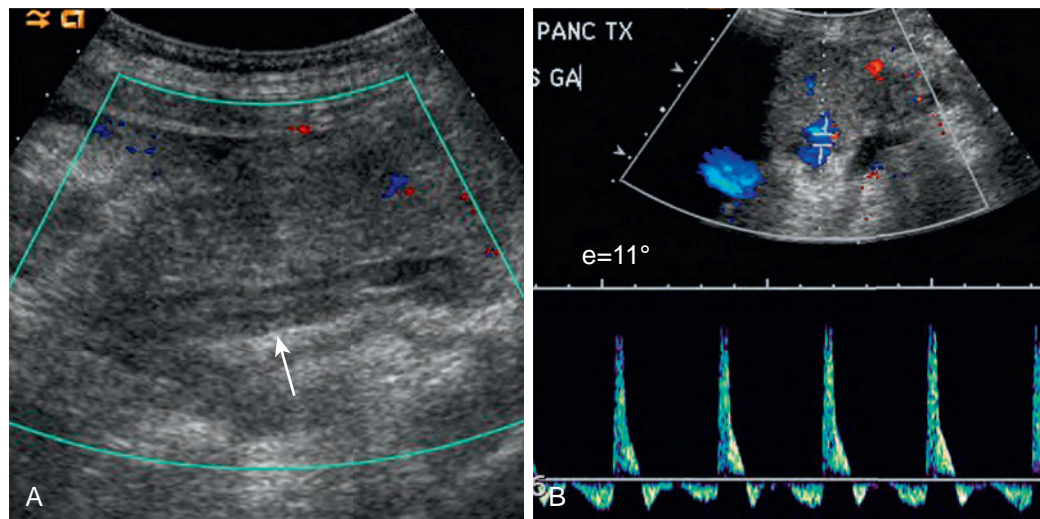


Figure 100-6 Splenic vein thrombosis, requiring explantation on postoperative day 3, in a 35-year-old man after SPK transplantation.

A. Color Doppler US shows striated echogenic material distending the splenic vein (arrow) with no blood flow in the vessel or within the pancreatic allograft. **B.** Arterial waveforms obtained in the graft artery demonstrate a very high resistance waveform with reversal of diastolic flow. (From Vandermeer F, Manning MA, Frazier A, et al: Imaging of whole-organ pancreas transplants. *RadioGraphics* 32:411–435, 2012.)

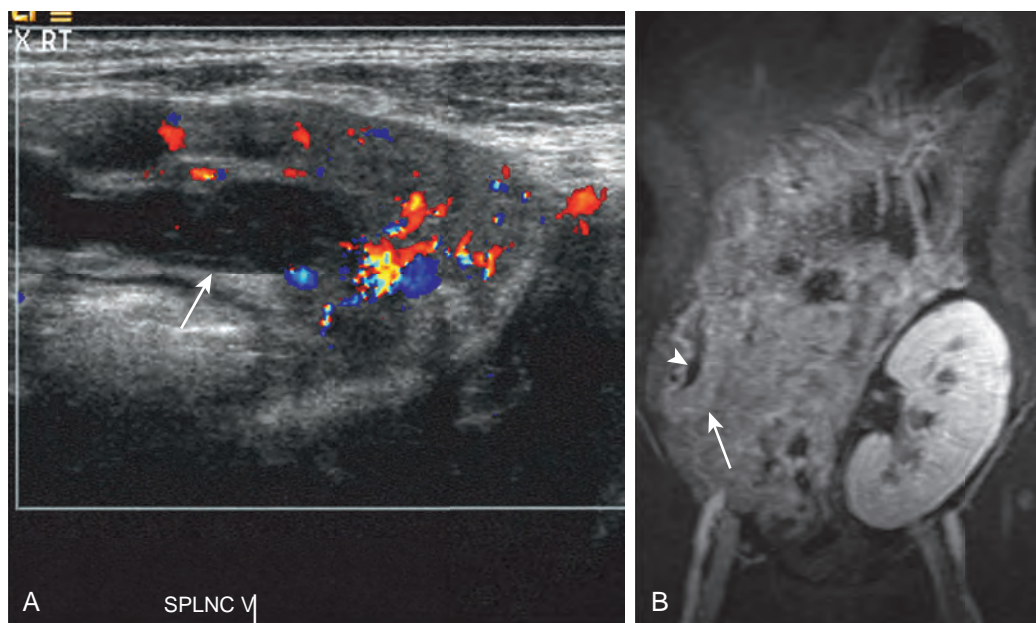


Figure 100-7 Splenic vein thrombosis in a 48-year-old man after SPK transplantation. **A.** Longitudinal color Doppler US of the pancreatic tail shows a distended splenic vein containing intraluminal thrombus (arrow). **B.** Postcontrast fat-suppressed T1-weighted coronal MR image confirms the splenic vein thrombus (arrowhead) but also demonstrates normal gland enhancement (arrow). (From Vandermeer F, Manning MA, Frazier A, et al: *Imaging of whole-organ pancreas transplants*. *RadioGraphics* 32:411–435, 2012.)

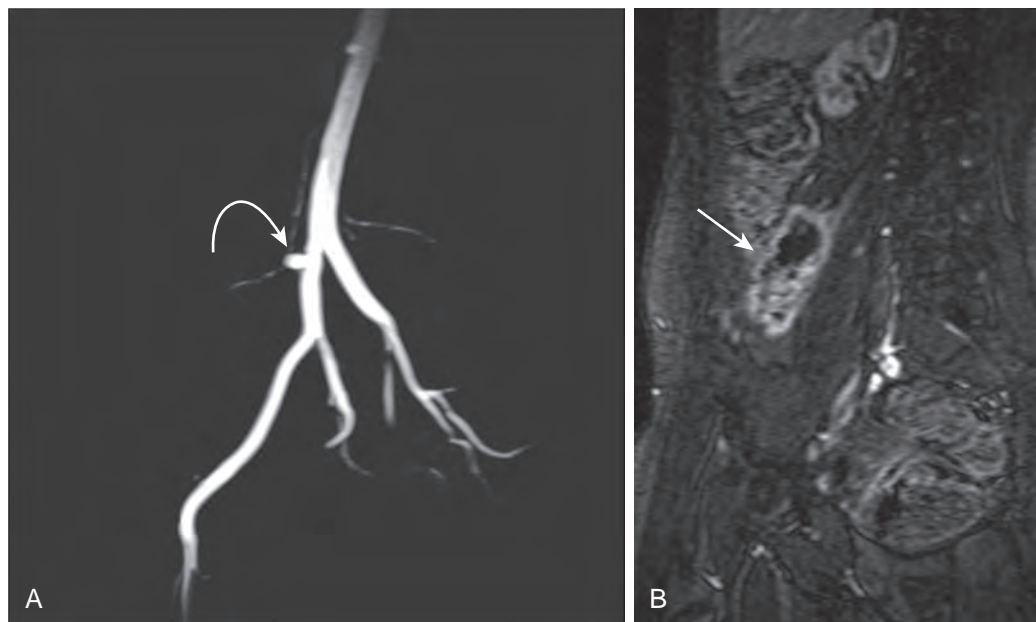


Figure 100-8 Chronic arterial graft thrombosis due to chronic rejection in a 53-year-old woman. **A.** Subtracted MRA shows the stump (arrow) of the occluded graft artery. **B.** Coronal postcontrast fat-suppressed T1-weighted MR image shows that the pancreas (arrow) is largely infarcted with rim enhancement. (From Vandermeer F, Manning MA, Frazier A, et al: *Imaging of whole-organ pancreas transplants*. *RadioGraphics* 32:411–435, 2012.)

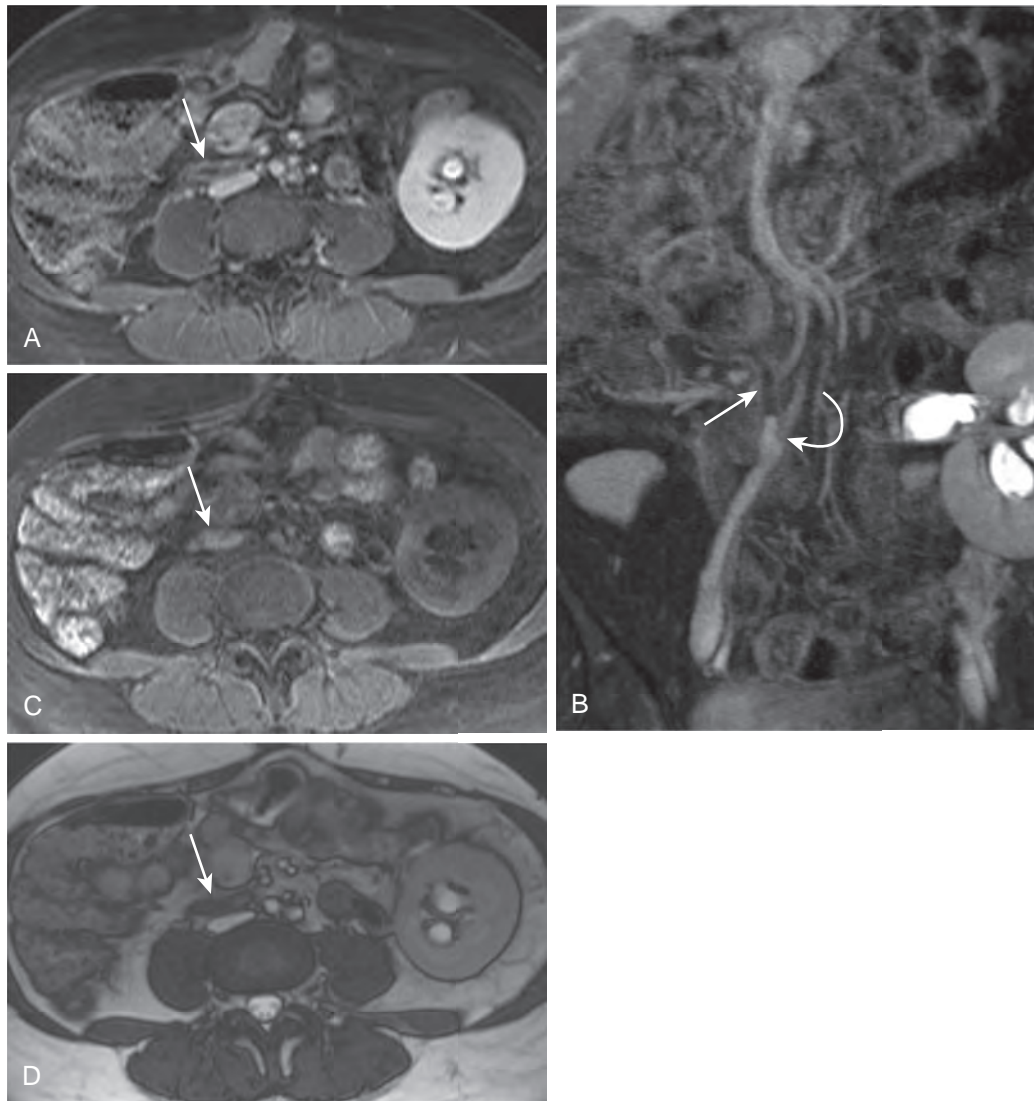


Figure 100-9 Chronic arterial graft thrombosis in a 45-year-old woman after two failed pancreas transplants. **A.** Axial gadolinium-enhanced fat-suppressed T1-weighted MR image demonstrates no intraluminal opacification in the graft artery (arrow). **B.** Coronal oblique maximum intensity projection image derived from data acquired 3 minutes after the initial injection shows loss of intraluminal signal within the graft artery (arrow) just distal to the anastomosis with the right common iliac artery (curved arrow). Note the normally enhancing left lower quadrant renal transplant. **C.** Axial fat-suppressed T1-weighted image demonstrates high signal thrombus (arrow) in the graft artery. **D.** Axial TrueFISP MR image shows absence of normal high signal in the graft artery compatible with occlusion (arrow). (From Vandermeer F, Manning MA, Frazier A, et al: *Imaging of whole-organ pancreas transplants*. *RadioGraphics* 32:411–435, 2012.)

by atherosclerotic plaques. Stenoses may be detected at US by finding high velocity or turbulence at an anastomosis but are generally confirmed with MRA or conventional angiography.^{20,22} These may be suitable for endoluminal therapy.

Extrinsic compression or kinking of a vascular segment may mimic thrombosis on imaging. This can be seen when longer Y grafts are required to appropriately position portal-enteric transplants higher in the abdomen; these may kink or twist, resulting in another cause of vascular stenosis (Fig. 100-10).²² This condition may be identified only intraoperatively during planned explantation for presumed thrombosis.¹⁷

Pseudoaneurysm and Arteriovenous Fistula

Pseudoaneurysms or arteriovenous fistulas are uncommon postsurgical complications after pancreas transplantation. They may arise at a vascular anastomosis or biopsy site or in the

setting of infection or pancreatitis.¹⁷ Although usually asymptomatic, they are associated with a high risk of hemorrhage and a high incidence of graft loss.³² Pseudoaneurysms can mimic a postoperative fluid collection with gray-scale US. Duplex Doppler imaging and MRA best demonstrate these vascular complications.^{10,17,21,22,30}

US of a pseudoaneurysm shows a rounded structure on gray-scale imaging, with internal swirling blood flow on color Doppler imaging and a characteristic to-and-fro waveform in the neck, communicating with an adjacent artery.^{10,17,30} On contrast-enhanced MRA, the pseudoaneurysm fills with contrast material and may be variable in size.³³ Arteriovenous fistulas are variable in size and may not be visible on gray-scale images. Color Doppler imaging shows color aliasing and a characteristic high-velocity low-resistance Doppler waveform with pulsatile flow in the draining vein if it is large (Figs. 100-11 and



Figure 100-10 Pancreas transplant with portal venous–enteric drainage, initially placed in the right abdomen with the head of the pancreas directed cephalad, in a 25-year-old woman. Coronal gadolinium-enhanced T1-weighted VIBE MR image demonstrates twisting of the elongated graft artery (arrow), which is anastomosed to the right common iliac artery. Thrombosis (arrowhead) is seen just distal to the twisted segment. The tail of the pancreas allograft (curved arrow) has migrated from the right lower quadrant into the left upper quadrant. Note persistent but decreased enhancement of the allograft; areas of pancreatic infarction were identified during surgical exploration, necessitating explantation. Incidentally shown is normal arterial and venous supply of the normally enhancing left lower quadrant renal transplant. (From Vandermeer F, Manning MA, Frazier A, et al: *Imaging of whole-organ pancreas transplants*. *RadioGraphics* 32:411–435, 2012.)

100-12).³⁰ Contrast-enhanced CT or MRI may show early opacification of donor venous structures during arterial phase imaging. Management of these vascular complications depends on the anatomy and size; small fistulas after biopsy may be self-limited and managed conservatively. Endovascular or surgical approaches are required otherwise.^{32,33}

GRAFT REJECTION

Rejection continues to be the overall primary cause of graft loss, with rates between 5% and 25%, depending on immunosuppressive regimen.⁸ Acute rejection has decreased dramatically with recent immunosuppressive advances, although less so with PTA transplants than with SPK or PAK grafts.³⁴ Because chronic rejection has been less affected by these advancements, this remains the major long-term cause of graft failure after the first 6 months, with little long-term improvement in pancreas survivability.³⁵

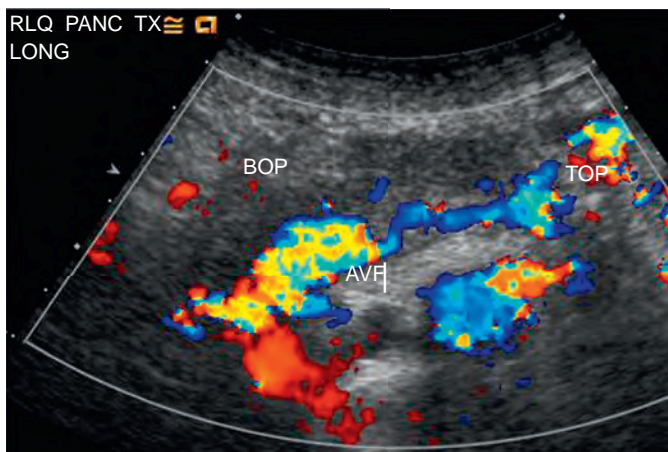


Figure 100-11 Iatrogenic arteriovenous fistula following biopsy in a 42-year-old woman after PTA. Longitudinal color Doppler sonogram shows a dilated tubular structure with turbulent flow closely associated with the transplant splenic vein and graft artery compatible with an arteriovenous fistula (AVF) within the proximal body of the pancreas (BOP). TOP, Tail of pancreas. (From Vandermeer F, Manning MA, Frazier A, et al: *Imaging of whole-organ pancreas transplants*. *RadioGraphics* 32:411–435, 2012.)

Graft rejection can occur at any time after pancreas transplantation. Hyperacute rejection, a rare occurrence, develops immediately after transplantation in response to the presence of preformed circulating cytotoxic antibodies in the recipient's blood. It causes thrombosis and immediate graft loss. Acute rejection usually develops 1 week to 3 months after transplantation and results in a peak in graft loss between 3 and 12 months.³⁶ Early detection is essential to institute antirejection treatment and to avert graft failure. Acute rejection is an autoimmune vasculitis that results in small-vessel occlusion and decreased perfusion, leading to infarction if it is severe and untreated. Multiple episodes of undiagnosed or partially treated acute rejection may culminate in chronic rejection with fibrosis and atrophy of the gland, resulting in insidious, progressive loss of graft function.¹⁸ The clinical diagnosis of rejection is difficult as elevation of serum glucose, amylase, and lipase levels correlates poorly with the presence or degree of rejection. Graft tenderness may be present. In bladder-drained pancreas transplants, urinary amylase and lipase levels may be abnormal. Percutaneous biopsy is therefore the cornerstone for diagnosis and grading of rejection. With a simultaneous pancreas and kidney transplant from the same donor, rejection of the kidney transplant may be used as a surrogate for pancreas rejection and monitored by serum creatinine concentration and renal biopsy.

US has a limited role in detecting acute rejection. Sonographic findings of graft enlargement and increased heterogeneity of the parenchymal echotexture lack specificity and may also be seen with acute pancreatitis and ischemia (Fig. 100-13).^{10,17} Color Doppler US usually demonstrates major vessel patency, which excludes graft thrombosis as a cause of poor function but cannot differentiate pancreatitis from rejection. Resistive indices have not been useful in diagnosis of acute rejection.^{18,37} In practice, the major role of US is to exclude thrombosis and to guide biopsy (Fig. 100-14). Severe acute rejection or hyperacute rejection may culminate in vascular thrombosis and infarction and be mistaken for primary

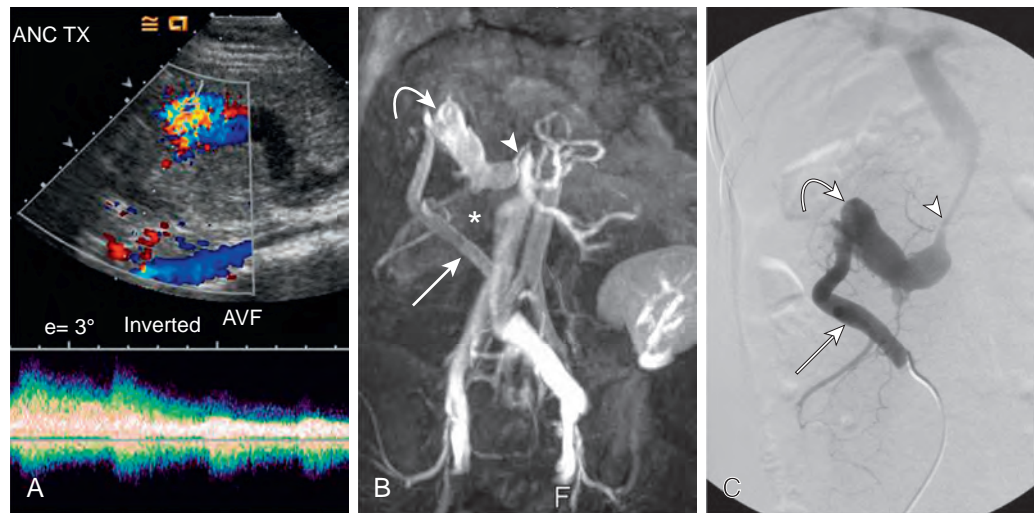


Figure 100-12 Iatrogenic arteriovenous fistula between donor superior mesenteric artery and donor portal vein in a 29-year-old woman 2 weeks after SPK transplantation. **A.** Duplex Doppler US image of a large vessel in the head of the pancreas shows a high-velocity, low-resistance waveform typical of an arteriovenous fistula (AVF). **B.** MRA demonstrates a dilated graft artery (arrow) and superior mesenteric vein (curved arrow). Focal narrowing of the distal vein graft (arrowhead) proximal to the anastomosis is also seen (asterisk, pancreas transplant). **C.** Selective arteriography confirms the fistula and better demonstrates an associated venous outflow stenosis (arrowhead). The fistula was embolized, but explantation of the allograft was subsequently performed for sepsis (arrow, dilated graft artery; curved arrow, dilated graft vein). (From Vandermeer F, Manning MA, Frazier A, et al: *Imaging of whole-organ pancreas transplants*. *RadioGraphics* 32:411–435, 2012.)

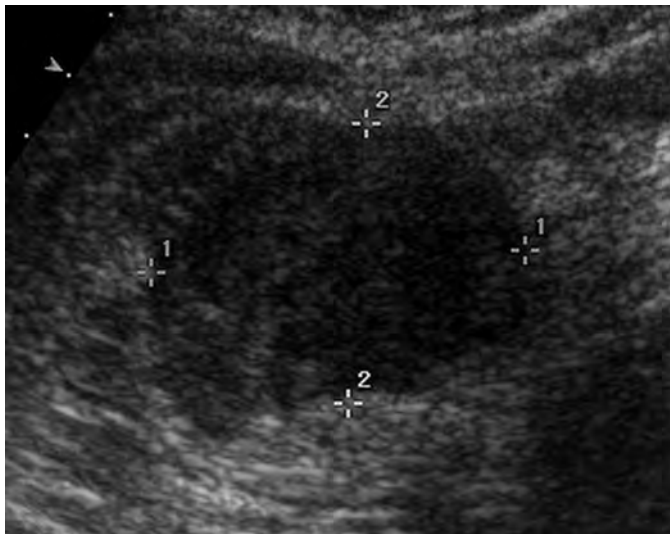


Figure 100-13 Acute rejection in a 30-year-old woman 7 months after PTA. Gray-scale US image shows an enlarged, hypoechoic allograft reflecting nonspecific edema that could be due to acute rejection, acute pancreatitis, or ischemia.

thrombosis. However, irrespective of the cause of thrombosis, management is surgical in these instances.

Unenhanced CT also offers limited utility in the diagnosis of acute rejection, demonstrating nonspecific gland enlargement, sometimes with peripancreatic fluid and duodenal edema, identical to findings seen with acute pancreatitis (Fig. 100-15). With iodinated contrast agents, the allograft is much more conspicuous and the vascular supply is optimally demonstrated, excluding thrombosis. However, decreased or heterogeneous enhancement resulting from occlusion of small graft vessels may be present.

At MRI, allograft edema from acute rejection can be recognized by increased T2 signal intensity; but this is nonspecific, and other causes of increased T2 signal include acute pancreatitis and ischemia. There may be a significant difference in enhancement between rejecting and normal pancreas allografts; however, this finding is only moderately specific.³⁸

With no reliable imaging modality to confirm or to grade acute rejection, image-guided percutaneous biopsy is the “gold standard.”³⁹ Although biopsy is most often performed with US guidance, CT-guided biopsy may be necessary when bowel obscures the anterior approach.

Chronic rejection occurs in 4% to 10% of patients.⁸ It is manifested as progressive loss of exocrine and then endocrine function secondary to small-vessel endarteritis, acinar atrophy, and interstitial fibrosis. This causes marked pancreatic atrophy, with the end result being a shrunken or disappearing pancreas transplant (Fig. 100-16). The demonstration of a small enhancing structure with patent graft vasculature at contrast-enhanced MRA confirms the diagnosis. Severe chronic rejection may ultimately result in infarction and necrosis from long-standing small-vessel occlusion with high signal seen on T2-weighted imaging (Fig. 100-17).

GRAFT PANCREATITIS

Mild, self-limited, and subclinical pancreatitis is common in the immediate postoperative setting; prolonged elevation of serum amylase occurs in up to 35% of patients.^{24,25} This usually results from reperfusion injury related to impaired microcirculation. Risk factors relate to donor age and preservation methods, including solution volumes, cold ischemia preservation time, and handling of the organ during surgery.^{24,40} Clinically significant pancreatitis occurs in 10% of patients.³¹ Symptoms include graft tenderness, abdominal pain, nausea,



Figure 100-14 US-guided percutaneous biopsy of the pancreas transplant. Transverse image obtained during a biopsy shows the 18-gauge core biopsy needle within the tail of the pancreas transplant.

vomiting, and ileus. Increased rates are seen with the bladder drainage technique.²⁴

The imaging appearance of the pancreatic graft may be normal with mild pancreatitis. More severe episodes may result in nonspecific enlargement and heterogeneity of the graft (Figs. 100-18 and 100-19). There may be perigraft fluid or mural thickening of adjacent bowel loops. Doppler US should demonstrate parenchymal flow in the transplant, unless the complication of pancreatic necrosis develops. US can demonstrate complications of pancreatitis, including pseudocyst or abscess formation and pancreatic infarction or necrosis. However, CT and MRI are more sensitive for peritransplant collections (see Fig. 100-19). The higher contrast resolution capability of MRI may best demonstrate the graft edema and potential complications, including vascular thrombosis.

HEMORRHAGE

Intra-abdominal hemorrhage is one of the most common reasons for relaparotomy after pancreas transplantation; however, it is an infrequent cause of graft loss.^{4,24} Bleeding may develop after any intra-abdominal surgery as a result of perioperative anticoagulation. If significant hemoperitoneum persists after correction of the coagulation profile, surgical evacuation is necessary to clear out potential medium for infection and can be therapeutic in itself.²⁴ Hemorrhage can also occur at vascular, bladder, or enteric anastomoses or secondary to an arterioenteric fistula.²⁴ Intravesical hemorrhage can be seen in bladder-drained transplants and may be early or late, potentially requiring enteric conversion.²⁴ Expedient evaluation should include CT and possibly conventional angiography. Unenhanced CT can best demonstrate intra-abdominal hemorrhage as a hyperdense collection.

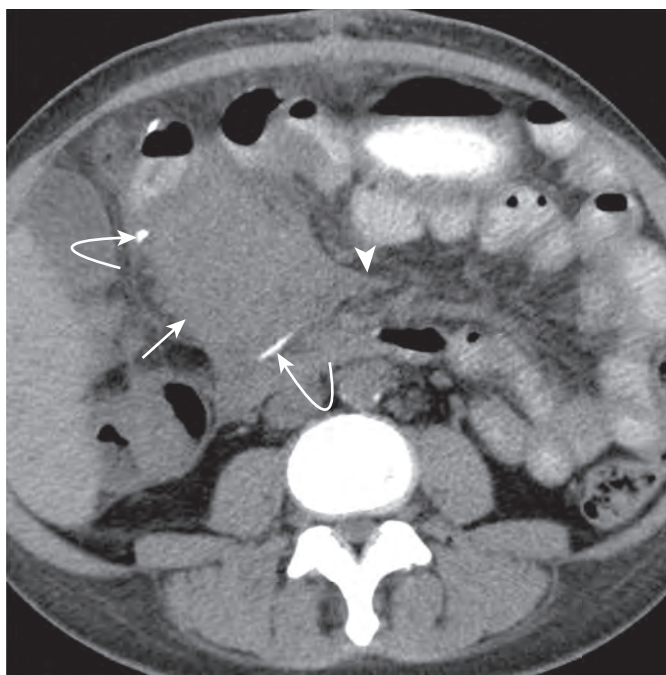


Figure 100-15 CT appearance of nonspecific pancreas transplant edema, later shown to be acute rejection on biopsy. Unenhanced axial CT image demonstrates the pancreas transplant (arrow) as an ill-defined soft tissue structure in the right lower quadrant, difficult to distinguish from unopacified small bowel in the absence of intravenous contrast material but identified by duodenal stump suture lines (curved arrows). There is a small amount of adjacent free fluid (arrowhead). (From Vandermeer F, Manning MA, Frazier A, et al: *Imaging of whole-organ pancreas transplants*. *RadioGraphics* 32:411–435, 2012.)

BOWEL COMPLICATIONS

A review of bowel complications after pancreas transplantation showed a rate of 19.4%.⁴¹ These include small bowel obstruction, anastomotic leak, abscess, and pseudomembranous or cytomegalovirus colitis. CT should be performed when clinical findings suggest a bowel complication or abdominal infection. Early diagnosis is important in these immunosuppressed recipients to decrease mortality and morbidity.

Small Bowel Obstruction

Small bowel obstruction can occur as a result of adhesions after any major abdominal procedure; however, the intra-peritoneal placement of an enterically drained pancreas allograft through a mesenteric defect adds an additional risk factor for internal herniation. The rate of strangulation is higher with an internal hernia than with an adhesive small bowel obstruction. Therefore, internal herniation should be suspected in the context of obstruction. An internal hernia can be detected at CT by finding distended loops of distal small bowel posterior to the transplant or donor duodenum.⁴¹ Contrast opacification of the duodenal stump may indicate more distal bowel obstruction or may be normal. Small bowel obstruction resulting from adhesions tends to occur in the anterior abdomen and is usually low grade.⁴¹ CT with multiplanar reformations is the best imaging modality for this complication.

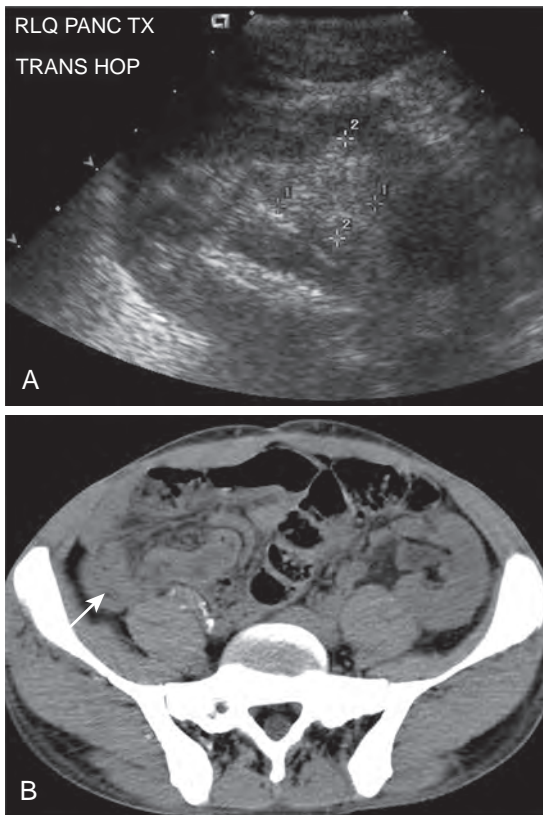


Figure 100-16 Chronic rejection in a 40-year-old man, 10 years after PAK transplantation. **A.** Transverse gray-scale US shows an atrophic echogenic pancreatic head (calipers) difficult to distinguish from mesenteric fat. **B.** Unenhanced CT image obtained before a CT-guided biopsy. Because the pancreas transplant (arrow) was small and difficult to separate from bowel, a biopsy could not be performed. **C.** Contrast-enhanced MRA showed a patent graft artery (not shown) and enhancing parenchyma (arrow) in the right lower quadrant. Note the enhancing left lower quadrant renal transplant. (From Vandermeer F, Manning MA, Frazier A, et al: *Imaging of whole-organ pancreas transplants*. *RadioGraphics* 32:411–435, 2012.)

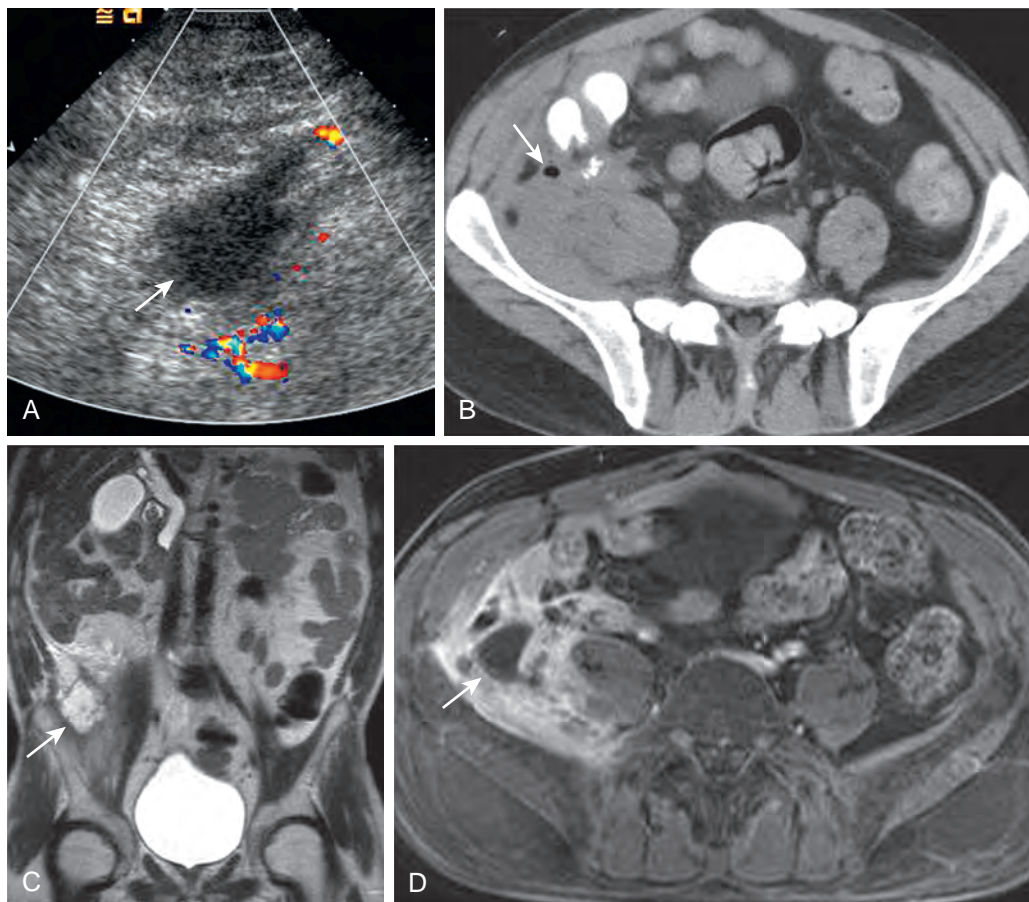


Figure 100-17 Chronic rejection and necrosis in a 42-year-old man after PTA 8 years earlier. **A.** Color Doppler US over an area of tenderness in the right iliac fossa shows a nonvascular ill-defined fluid collection (arrow) with no identifiable pancreatic tissue. **B.** Unenhanced CT shows loss of definition of tissue planes with fluid and gas (arrow) in the same area. **C.** Coronal HASTE T2-weighted MR image shows a high signal fluid collection (arrow) in the right lower quadrant and edema of the subjacent musculature. **D.** Postcontrast fat-suppressed T1-weighted axial MR image shows the rim-enhancing fluid collection (arrow) and inflammation of the iliacus and psoas muscles. At surgery, there was a purulent phlegmon and no recognizable pancreatic tissue. (From Vandermeer F, Manning MA, Frazier A, et al: *Imaging of whole-organ pancreas transplants*. *RadioGraphics* 32:411–435, 2012.)

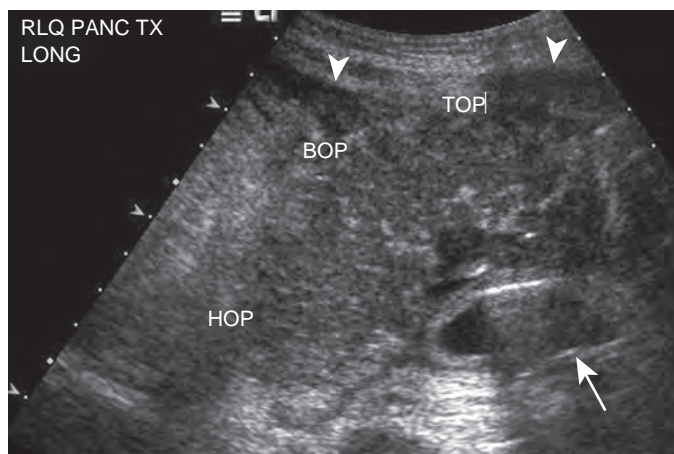


Figure 100-18 Postoperative pancreatitis after SPK transplantation in a 27-year-old woman. Longitudinal ultrasound image demonstrates an enlarged, hypoechoic transplant with surrounding fluid (arrowheads) and thickening of an adjacent bowel loop (arrow). HOP, head of pancreas; BOP, body of pancreas; TOP, tail of pancreas. (From Vandermeer F, Manning MA, Frazier A, et al: *Imaging of whole-organ pancreas transplants*. *RadioGraphics* 32:411–435, 2012.)

Anastomotic Exocrine Leak

Presenting symptoms and signs of an anastomotic leak include abdominal pain, fever, leukocytosis, peritonitis, and sepsis. Early leaks may be attributed to surgical factors, whereas late leaks are thought to result from infection, rejection, pancreatitis, or duodenitis.⁴²

Leaks occur in 2% to 10% of transplant patients after enteric drainage and predispose to intra-abdominal infection, which is the second most common cause of technical failure after vascular thrombosis.^{4,25} However, early recognition and appropriate management can minimize the impact of this complication on the patient's postoperative course. Anastomotic leaks are responsible for less than 0.5% of all graft losses,⁴³ with higher rates of loss for enterically drained grafts than for bladder-drained transplants.²⁴

Leaks in enterically drained transplants result in greater patient morbidity and mortality because of peritonitis and sepsis, which may result from the spillage of bowel contents from the leakage site, often the duodenojejunal anastomosis. Immediate surgical intervention with revision of the anastomosis is required.²⁴ For bladder-drained allografts, early leaks occur at the anastomosis to the bladder, and later leaks occur at the oversewn duodenal stump.^{24,25} Bladder leaks are less serious and may be managed by bladder catheterization. However, in the setting of peritonitis, repeated laparotomy is required, and conversion to enteric drainage is often necessary.

CT with oral contrast material is the modality of choice for diagnosis, although gas-containing collections may be detected at US (Fig. 100-20A, B). Leaks of duodenal secretions can be difficult to separate from other pancreatitis-related collections unless they contain gas. Oral contrast material should be administered to increase diagnostic confidence in distinguishing a leak from a collection. However, this can be of variable utility, given inconsistent filling of the duodenal bulb. An enterocutaneous fistula can result if a leak is not promptly diagnosed and treated (Fig. 100-20C). Leaks from bladder-

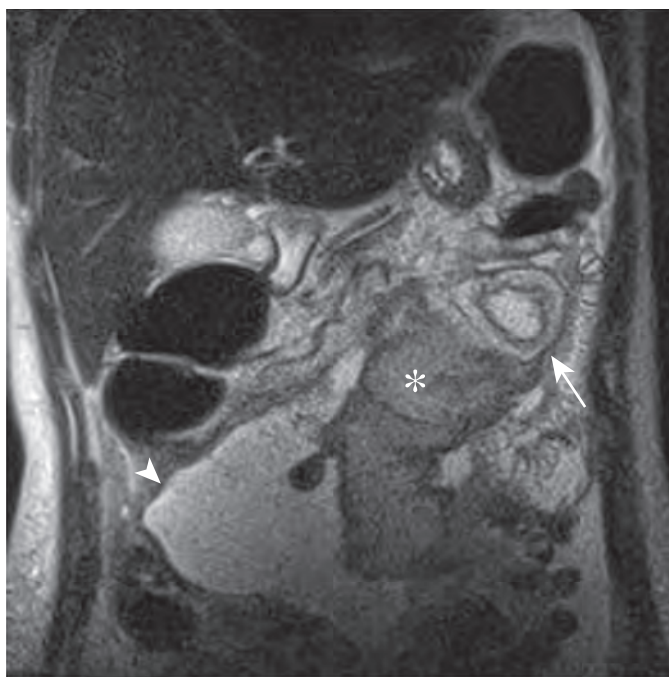


Figure 100-19 Pancreatitis with peripancreatic fluid collections in a 45-year-old woman after PAK transplantation. Coronal HASTE T2-weighted MR image shows a high signal fluid collection (arrowhead) surrounding and displacing the edematous transplant (asterisk) to the left and extending into the right lower quadrant. Note the wall thickening and edema of the adjacent bowel loop (arrow). The fluid collections eventually caused venous thrombosis and ultimately required explantation of the graft. (From Vandermeer F, Manning MA, Frazier A, et al: *Imaging of whole-organ pancreas transplants*. *RadioGraphics* 32:411–435, 2012.)

drained transplants may be diagnosed by conventional cystography or CT cystography (Fig. 100-21).

Colitis

Pseudomembranous or cytomegalovirus colitis may be seen uncommonly after pancreas transplantation. CT with oral contrast material is the preferred imaging modality. However, appearances are not specific, and correlation with stool and blood evaluation is necessary.

INTRA-ABDOMINAL FLUID COLLECTIONS

Fluid collections are commonly seen after pancreas transplantation in the early and late postoperative course and can be detected by US, CT, or MRI. These may be clinically insignificant or associated with intra-abdominal infection. Ascites is not uncommon but usually low in volume. Surgical site infection may occur in up to 50% of patients, and most are superficial and managed with antibiotics and local care.²⁵ Deep infections are associated with higher morbidity, graft loss, and mortality, and after vascular thrombosis, they are the second leading cause of technical failure in the early postoperative period.⁴ Organisms include bacterial and fungal, and 50% of infections are diffuse. The clinical presentation and imaging findings are similar to those of an enteric leak, and in 30% there is an associated leak (see Fig. 100-20).²⁴ Localized abscesses may be managed by percutaneous drainage, but the threshold for laparotomy and washout is low (see Figs. 100-17 and 100-19).

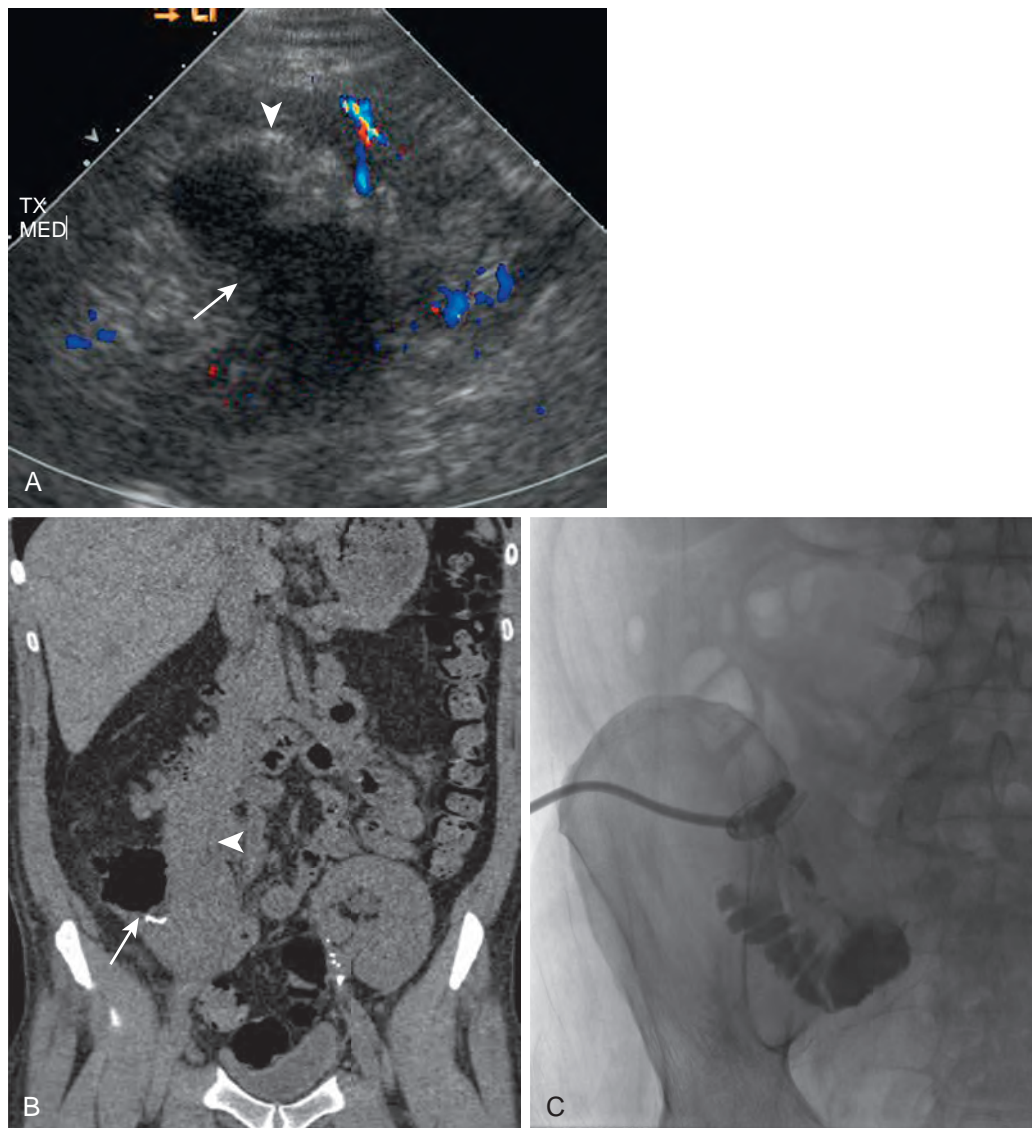


Figure 100-20 Duodenal anastomotic leak in a 53-year-old man after systemic venous–enteric PAK transplantation. **A.** Color Doppler US image shows an avascular complex fluid collection lateral to the pancreas transplant (arrow) with echogenic foci (arrowhead) in the nondependent portion, suggesting the presence of gas. **B.** Unenhanced CT better shows the gas-containing complex peripancreatic fluid collection, closely associated with the duodenal suture line (arrow), which aids in localizing the pancreas transplant (arrowhead). **C.** Sinogram obtained after injection of contrast material through the existing pigtail drainage catheter shows opacification of a loop of small bowel compatible with a duodenal anastomotic leak. (From Vandermeer F, Manning MA, Frazier A, et al: *Imaging of whole-organ pancreas transplants*. *RadioGraphics* 32:411–435, 2012.)

Intra-abdominal collections could also represent seroma, hematoma, lymphocele, urinoma, or pseudocyst. Hematomas may be suspected by their internal echoes at US and higher density at CT (Figs. 100-22A, B and 100-23). MRI can also be helpful in identifying peripancreatic hematoma or hemorrhagic necrosis because of its bright T1 signal (Fig. 100-22C). However, the character of the fluid most often cannot be determined by the imaging appearance alone. Percutaneous US- or CT-guided aspiration is useful in diagnosis and therapeutic intervention. It is important to consider that a fluid collection adjacent to the head of the pancreas may be associated with the duodenum, possibly representing a dilated duodenal bulb or hematoma (see Fig. 100-23).

POST-TRANSPLANTATION LYMPHOPROLIFERATIVE DISEASE

Post-transplantation lymphoproliferative disease (PTLD) is a rare late complication after pancreas transplantation, occurring with an incidence of between 2.3% and 6%.^{34,44} PTA recipients experience a higher incidence of PTLD than SPK or PAK recipients do, probably related to their increased immunosuppressive requirements and higher rates of acute rejection.³⁴ Although the majority of cases are related to primary Epstein-Barr virus infection, cytomegalovirus infection and immunosuppression regimens are contributory. PTLD after pancreas transplantation may be more aggressive than

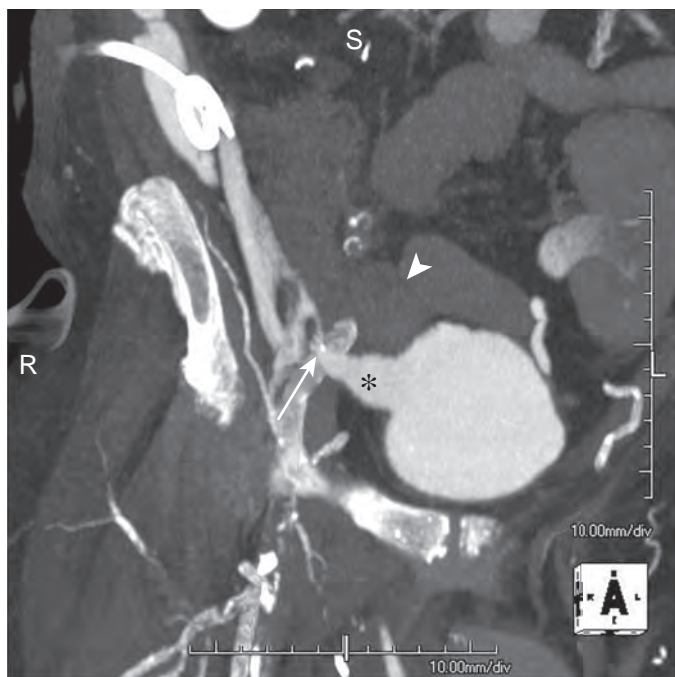


Figure 100-21 Anastomotic leak at the duodenocystostomy in a 53-year-old man 17 years after SPK transplantation with systemic venous–bladder drainage. Retrograde CT cystogram demonstrates leakage from the lateral margin of the duodenocystostomy (asterisk) adjacent to the duodenal suture line (arrow). The pancreas transplant (arrowhead) is more difficult to visualize because of lack of intravenous contrast material. Note the percutaneous pigtail drain in the right lower quadrant. (From Vandermeer F, Manning MA, Frazier A, et al: *Imaging of whole-organ pancreas transplants*. *RadioGraphics* 32:411–435, 2012.)

in other solid organ transplants.⁴⁵ The mean time to diagnosis is 1.5 ± 0.5 years. Extranodal and widespread involvement is the hallmark of PTLD in pancreas transplant recipients and is present in 69%.⁴⁴ Lymph nodes and liver are the most frequent sites of involvement, in 39% to 40% of all PTLD patients, followed by the gastrointestinal tract in 33%.⁴⁵ The allograft is involved in 10%.⁴⁴

Disease extent is best imaged by CT or MR (Fig. 100-24), which may demonstrate solid masses in the liver and allograft and distribution of lymphadenopathy.⁴⁶ Hepatic involvement can be diffuse or multifocal. Bowel manifestations include focal masses, wall thickening, and dilation.

Conclusion

Diagnosis of postoperative complications after pancreas transplantation is often a complex process involving a multimodality approach and knowledge of the common surgical techniques and the spectrum of postoperative complications. US should be the first-line modality in evaluation of the pancreas allograft and vasculature. CT is useful in the evaluation of extra-allograft processes, particularly in ruling out abscess formation or evaluating for suspected bowel complication. MRI and MRA are reserved for transplants that cannot be completely evaluated by US or CT and for accurate assessment of vascular abnormalities.

The authors of this chapter published a comprehensive review of this topic with supplemental online material.⁴⁷ Images are reproduced from this article with permission from RadioGraphics.

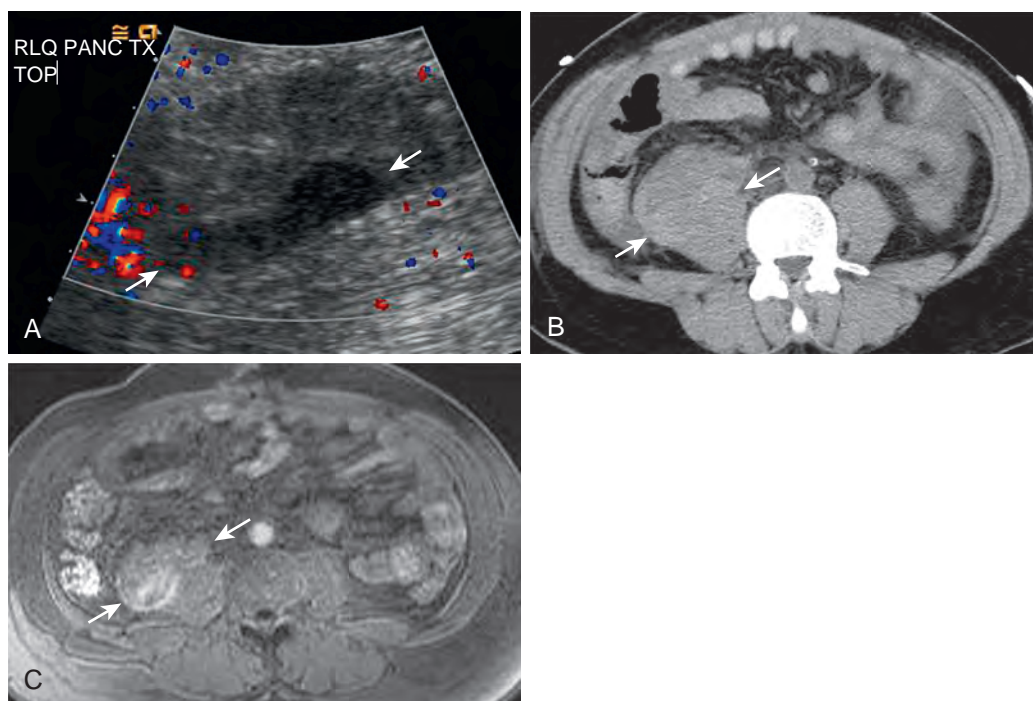


Figure 100-22 Peripancreatic hematoma in a 44-year-old man after anticoagulation for partial splenic and superior mesenteric vein thrombosis in PAK transplantation. **A.** Longitudinal US shows a nonspecific hypoechoic avascular collection (arrows) with internal echoes posterior to the transplant pancreas and anterior to the right psoas muscle. **B.** Axial unenhanced CT demonstrates hyperdensity within the collection (arrows), suggestive of hematoma. **C.** On fat-suppressed T1-weighted MR image, there is characteristic high signal within the collection (arrows), confirming presence of blood products. (From Vandermeer F, Manning MA, Frazier A, et al: *Imaging of whole-organ pancreas transplants*. *RadioGraphics* 32:411–435, 2012.)

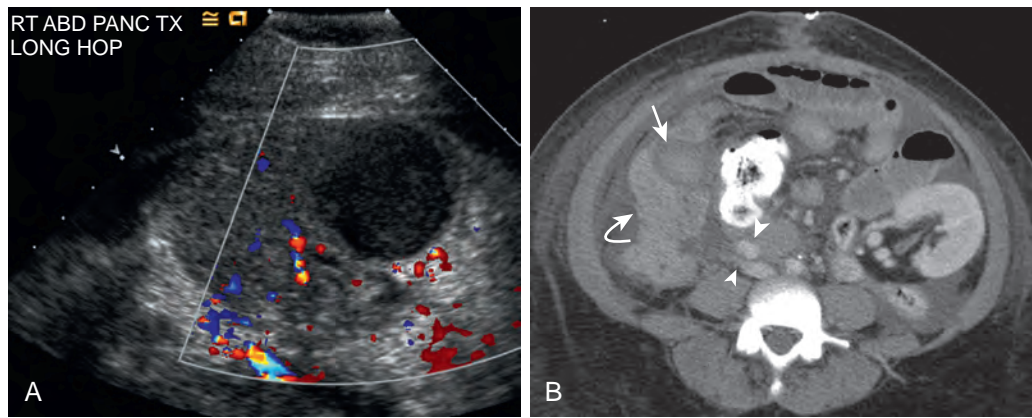


Figure 100-23 Duodenal hematoma in a 31-year-old woman after systemic venous–enteric exocrine pancreas transplantation.

A. Longitudinal color Doppler image through the head of the pancreas demonstrates a focal avascular fluid collection containing internal echoes. **B.** Subsequent axial contrast-enhanced CT shows high-density material within the fluid collection (arrow), compatible with hematoma. Note normal enhancement of the pancreatic head (curved arrow) and patency of the graft artery (arrowhead) and graft vein (small arrowhead), which is anastomosed to the inferior vena cava. Given the location, adjacent to the pancreatic head, this was described as probable duodenal hematoma. On surgical exploration, the duodenum was found to be grossly necrotic, and although the pancreas was normally perfused and graft vessels were patent, the allograft was explanted. (From Vandermeer F, Manning MA, Frazier A, et al: *Imaging of whole-organ pancreas transplants*. *RadioGraphics* 32:411–435, 2012.)

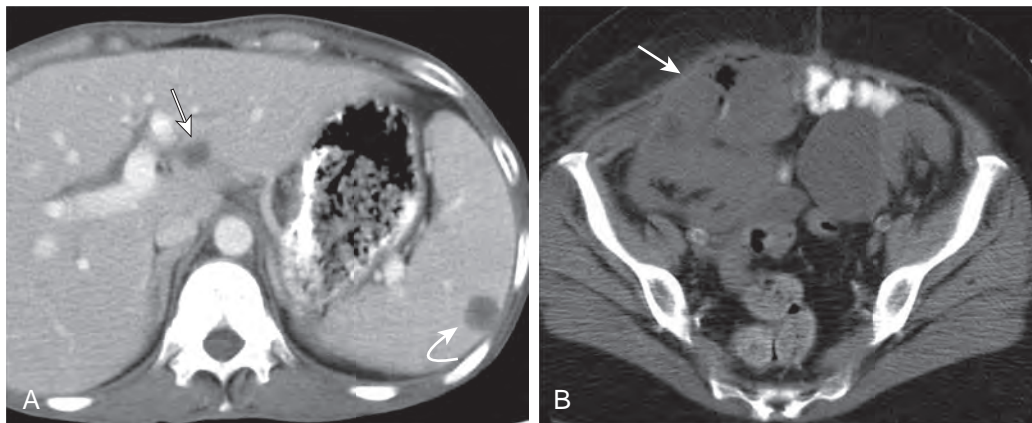


Figure 100-24 PTLD in two pancreas transplant recipients. **A.** Contrast-enhanced CT demonstrates rounded hypodense lesions in the liver (arrow) and spleen (curved arrow). **B.** Unenhanced CT in a different patient demonstrates a large necrotic mass arising from the small bowel and growing into the anterior abdominal wall (arrow). The pancreas transplant is not shown. Note bilateral renal transplants. (From Vandermeer F, Manning MA, Frazier A, et al: *Imaging of whole-organ pancreas transplants*. *RadioGraphics* 32:411–435, 2012.)

REFERENCES

- Fourtounas C: Transplant options for patients with type 2 diabetes and chronic kidney disease. *World J Transplant* 4:102–110, 2014.
- Fioretto P, Steffes MW, Sutherland DE, et al: Reversal of lesions of diabetic nephropathy after pancreas transplantation. *N Engl J Med* 339:69–75, 1998.
- Health Resources and Services Administration Organ Procurement and Transplantation Network: Data posted online September 27, 2013. <<http://optn.transplant.hrsa.gov/>>. Accessed October 3, 2013.
- Gruessner AC: 2011 Update on pancreas transplantation: Comprehensive trend analysis of 25,000 cases followed up over the course of twenty-four years at the International Pancreas Transplant Registry (IPTR). *Rev Diabet Stud* 8:6–16, 2011.
- Gruessner AC, Sutherland DER, Gruessner RW: Long-term outcome after pancreas transplantation. *Curr Opin Organ Transplant* 17:100–105, 2012.
- Gruessner RW, Gruessner AC: Pancreas transplant alone: A procedure coming of age. *Diabetes Care* 36:2440–2447, 2013.
- Gruessner RW, Gruessner AC: The current state of pancreas transplantation. *Nat Rev Endocrinol* 9:555–562, 2013.
- White SA, Shaw JA, Sutherland DER: Pancreas transplantation. *Lancet* 373:1808–1817, 2009.
- Pozniak MA, Propeck PA, Kelcz F, Sollinger H: Imaging of pancreas transplants. *Radiol Clin North Am* 33:581–594, 1995.
- Nikolaïdis P, Amin RS, Hwang CM, et al: Role of sonography in pancreatic transplantation. *Radiographics* 23:939–949, 2003.
- Diem P, Abid M, Redmon JB, et al: Systemic venous drainage of pancreas allografts as independent causes of hyperinsulinemia in type I diabetic recipients. *Diabetes* 39:534–540, 1990.
- Stratta RJ, Gaber AO, Shokouh-Amiri MH, et al: A prospective comparison of systemic-bladder versus portal-enteric drainage in vascularized pancreas transplantation. *Surgery* 127:217–226, 2000.
- Lo A, Stratta RJ, Hathaway DK, et al: Long-term outcomes in simultaneous kidney-pancreas transplant recipients with portal-enteric versus systemic-bladder drainage. *Am J Kidney Dis* 38: 132–143, 2001.
- Philosophie B, Farney AC, Schweitzer EJ, et al: Superiority of portal venous drainage over systemic venous drainage in pancreas

- transplantation: A retrospective study. *Ann Surg* 234:689–696, 2001.
15. Ming CS, Chen ZH: Progress in pancreas transplantation and combined pancreas-kidney transplantation. *Hepatobiliary Pancreat Dis Int* 6:17–23, 2007.
 16. Sanchez EQ, Melton LB, Chinnakotla S, et al: Whole-organ transplantation at Baylor Regional Transplant Institute: A chance to cure diabetes. *Proc (Bayl Univ Med Cent)* 23:3–6, 2010.
 17. Dillman JR, Elsayes KM, Bude RO, et al: Imaging of pancreas transplants: Postoperative findings with clinical correlation. *J Comput Assist Tomogr* 33:609–617, 2009.
 18. Audeyan QA, Foshager MC, Benedetti E, et al: Correlation of the arterial resistive index in pancreas transplants of patients with transplant rejection. *AJR Am J Roentgenol* 168:1445–1447, 1997.
 19. Kubota K, Billing H, Kelter U, et al: Duplex-Doppler ultrasonography for evaluating pancreatic grafts. *Transplant Proc* 22:183, 1990.
 20. Hagspiel KD, Nandalur K, Burkholder B, et al: Contrast-enhanced MR angiography after pancreas transplantation: Normal appearance and vascular complications. *AJR Am J Roentgenol* 184:465–473, 2005.
 21. Dobos N, Roberts DA, Insko EK, et al: Contrast-enhanced MR angiography for evaluation of vascular complications of the pancreas transplant. *Radiographics* 25:687–695, 2005.
 22. Hagspiel KD, Nandalur K, Pruett TL, et al: Evaluation of vascular complications of pancreas transplantation with high-spatial-resolution contrast-enhanced MR angiography. *Radiology* 242:590–599, 2007.
 23. International Pancreas Transplant Registry. www.iptr.umn.edu/annual_reports/2004_annualreport/9_panc_graft_fail_cat/home.html. Accessed Aug 4, 2013.
 24. Vincent M, Moria O, Branchereau J: Multi detector computed tomography (MDCT) for the diagnosis of early complications after pancreas transplantation. *Abdom Imaging* 2014 May 23. [Epub ahead of print].
 25. Goodman J, Becker YT: Pancreas surgical complications. *Curr Opin Organ Transplant* 14:85–99, 2009.
 26. Gruessner AC, Sutherland DER, Gruessner RW: Pancreas transplantation in the United States: A review. *Curr Opin Organ Transplant* 15:93–101, 2010.
 27. Muthusamy AS, Giangrande PL, Friend PJ: Pancreas allograft thrombosis. *Transplantation* 90:705–707, 2010.
 28. Ionescu C, Wolf P, Eller B, Mihaescu G: The venous thrombosis of the pancreatic graft. *J Gastrointest Liver Dis* 16:287–292, 2007.
 29. Eubank WB, Schmiedl UP, Levy AE, Marsh CL: Venous thrombosis and occlusion after pancreas transplantation: Evaluation with breath-hold gadolinium-enhanced three-dimensional MR imaging. *AJR Am J Roentgenol* 175:381–385, 2000.
 30. Finlay DE, Letourneau JG, Longley DG: Assessment of vascular complications of renal, hepatic, and pancreatic transplantation. *Radiographics* 12:981–996, 1992.
 31. Sandrasegaran K, Lall C, Berry WA, et al: Enteric drainage pancreatic transplantation. *Abdom Imaging* 31:588–595, 2006.
 32. Barth MM, Khwaja K, Faintuch S, Rabkin D: Transarterial and transvenous embolotherapy of arteriovenous fistulas in the transplanted pancreas. *J Vasc Interv Radiol* 19:1231–1235, 2008.
 33. Orsenigo E, De Cobelli F, Salvioni M, et al: Successful endovascular treatment for gastroduodenal artery pseudoaneurysm with an arteriovenous fistula after pancreas transplantation. *Transpl Int* 16:694–696, 2003.
 34. Kandaswamy R, Stock PG, Skeans MA, et al: OPTN/SRTR 2011 annual data report: Pancreas. *Am J Transplant* 13:47–72, 2013.
 35. Waki K, Sugawara Y, Kokudo N, et al: Long-term pancreas allograft survival in simultaneous pancreas-kidney transplantation by era. *Clin Transpl* 13–22, 2012.
 36. Drachenberg CB, Papadimitriou JC: Spectrum of histopathological changes in pancreas allograft biopsies and relationship to graft loss. *Transplant Proc* 39:2326–2328, 2007.
 37. Wong JJ, Krebs TL, Klassen DK, et al: Sonographic evaluation of acute pancreatic transplant rejection: Morphology-Doppler analysis versus guided percutaneous biopsy. *AJR Am J Roentgenol* 166:803–807, 1996.
 38. Krebs TL, Daly B, Wong-You-Cheong JJ, et al: Acute pancreatic transplant rejection: Evaluation with dynamic contrast-enhanced MR imaging compared with histopathologic analysis. *Radiology* 210:437–442, 1999.
 39. Klassen DK, Hoen-Saric EW, Weir MR, et al: Isolated pancreas rejection in combined kidney pancreas transplantation. *Transplantation* 61:974–977, 1996.
 40. Benz S, Bergt S, Obermaier R, et al: Impairment of microcirculation in the early reperfusion period predicts the degree of graft pancreatitis in clinical pancreas transplantation. *Transplantation* 71:759–763, 2001.
 41. Lall CG, Sandrasegaran K, Maglinte DT, Fridell JA: Bowel complications seen on CT after pancreas transplantation with enteric drainage. *AJR Am J Roentgenol* 187:1288–1295, 2006.
 42. Nath DS, Gruessner A, Kandaswamy R, et al: Late anastomotic leaks in pancreas transplant recipients—clinical characteristics and predisposing factors. *Clin Transplant* 19:220–224, 2005.
 43. Gruessner AC, Sutherland DER: Pancreas transplant outcomes for United States (US) cases as reported to the United Network for Organ Sharing (UNOS) and the International Pancreas Transplant Registry (IPTR). *Clin Transpl* 45–56, 2008.
 44. Issa N, Amer H, Dean PG, et al: Posttransplant lymphoproliferative disorder following pancreas transplantation. *Am J Transplant* 9:1894–1902, 2009.
 45. Paraskevas S, Coad JE, Gruessner A, et al: Posttransplant lymphoproliferative disorder in pancreas transplantation: A single-center experience. *Transplantation* 80:613–622, 2005.
 46. Borhani AA, Hosseinzadeh K, Almusa O, et al: Imaging of posttransplantation lymphoproliferative disorder after solid organ transplantation. *Radiographics* 29:981–1000, 2009.
 47. Vandermeer FQ, Manning MA, Frazier AA, Wong-You-Cheong JJ: Imaging of whole-organ pancreas transplants. *Radiographics* 32:411–435, 2012.

Pancreas: Differential Diagnosis

RICHARD M. GORE

CHAPTER OUTLINE

Imaging Abnormalities

- Table 101-1. Pancreatic Calcification
- Table 101-2. Focal Pancreatic Mass
- Table 101-3. Dilated Pancreatic Duct
- Table 101-4. Gas in Pancreatic Duct
- Table 101-5. Cystic Pancreatic Masses Within and Adjacent to Pancreas Pseudocyst
- Table 101-6. Pseudocysts Versus Cystic Pancreatic Neoplasms: Differentiating Features
- Table 101-7. Pancreatic Lipomatosis

Ultrasound

- Table 101-8. Hypoechoic Pancreatic Masses
- Table 101-9. Focal Shadowing Pancreatic Masses

Computed Tomography and Magnetic Resonance Imaging

- Table 101-10. Hypervascular Pancreatic Masses
- Table 101-11. Magnetic Resonance Pattern Recognition: Focal Pancreatic Lesions

Cholangiography

- Table 101-12. Pancreatic Duct Stricture: ERCP or MRCP

Imaging Findings in Specific Pancreatic Diseases

- Table 101-13. Acute Pancreatitis
- Table 101-14. Chronic Pancreatitis
- Table 101-15. Pancreatic Ductal Adenocarcinoma
- Table 101-16. Cystic Pancreatic Neoplasms
- Table 101-17. Incidental Cystic Pancreatic Lesions

Imaging Abnormalities

TABLE
101-1

Pancreatic Calcification

COMMON

Volume averaging with vascular calcification
Chronic pancreatitis
 Alcoholic (20%-50%)
 Hereditary (35%-60%)
 Biliary (2%)
 Idiopathic
Common bile duct stone

UNCOMMON

Acute pancreatitis with saponification
Serous cystadenoma (sunburst, 33%)
Mucinous cystadenoma or cystadenocarcinoma (rounded)
Pseudocyst
Islet cell tumor
Metastasis
Cystic fibrosis
Kwashiorkor
Cavernous lymphangioma
Adenocarcinoma (2%)
Intraparenchymal hemorrhage
Hyperparathyroidism
After infarct, abscess
After rupture of pancreatic neoplasm
Hemochromatosis

TABLE
101-2

Focal Pancreatic Mass

INFLAMMATORY

Acute pancreatitis
Chronic pancreatitis
Groove pancreatitis
Pseudocyst
Abscess

NEOPLASTIC—PRIMARY

Ductal adenocarcinoma
Intraductal papillary mucinous neoplasm
Islet cell tumors
Serous cystadenoma
Mucinous cystadenoma
Mucinous cystadenocarcinoma
Lymphoma
Metastases
Normal anatomic variant
Peripancreatic disease
Aneurysms
Thrombosed vessels

TABLE 101-3 Dilated Pancreatic Duct

Chronic pancreatitis
Pancreatic or ampullary mass
Distal common duct stone
Intraductal pancreatic mucinous neoplasm
Aging

NATURE OF DILATION**Suggesting Pancreatitis**

Irregular dilation
Calculi
Duct occupies >50% of anteroposterior gland diameter

Suggesting Neoplasm

Smooth and beaded appearance
Duct occupies >50% of anteroposterior gland diameter

TABLE 101-4 Gas in Pancreatic Duct

After endoscopic retrograde cholangiopancreatography
Prior papillotomy
Patulous Vaterian sphincter
Duodenal diverticulum
Enteropancreatic fistula (spontaneous, surgical)
Abscess

TABLE 101-5 Cystic Pancreatic Masses Within and Adjacent to Pancreas Pseudocyst

Cystic biliary and pancreatic duct anomalies
After inflammation
After trauma
After surgery
Idiopathic

CYSTIC NEOPLASMS

Ductal cancer
Cystadenoma
Cystadenocarcinoma
Leiomyosarcoma
Dermoid
Vascular
Lymphangioma
Hemangioma

RETENTION (POSTOBSTRUCTIVE)

Pancreatic cancer
Pancreatic lithiasis
Acute and chronic pancreatitis
Cholelithiasis and cholecystitis
Echinococcus infection
Ascaris infection
Clonorchis sinensis infection

CONGENITAL

Simple
Polycystic diseases
Cystic fibrosis
Duodenal enteric (duplication)
Intrapaneatic choledochal cyst
Cystic biliary and pancreatic duct anomalies

TABLE 101-6 Pseudocysts Versus Cystic Pancreatic Neoplasms: Differentiating Features

Feature	Cystic Neoplasm	Pseudocyst
Number of cysts	Multiple	Single
Common site	Body, tail	Head
Wall calcification	10%	Frequent
Wall thickness	>1 cm	<1 cm

TABLE 101-7 Pancreatic Lipomatosis

Obstruction of the main pancreatic duct
Age—atherosclerosis of elderly
Obesity
Steroid therapy
Cushing's syndrome
Cystic fibrosis
Shwachman-Diamond syndrome
Malnutrition
Hemochromatosis
Viral infection
Obstruction of the main pancreatic duct

Ultrasound

TABLE 101-8 Hypoechoic Pancreatic Masses

Focal pancreatitis
Lymphoma
Carcinoma
Metastases

TABLE 101-9 Focal Shadowing Pancreatic Masses

Gas in pseudocyst communicating with gut
Calcific pancreatitis
Pancreatic calculi
Cystic pancreatic tumor with calcification
Gas in pancreatic abscess
Arterial calcification

Computed Tomography and Magnetic Resonance Imaging

TABLE 101-10 Hypervascular Pancreatic Masses**VASCULAR**

Aneurysm
Pseudoaneurysm

PRIMARY TUMORS

Islet cell tumors

METASTASES

Angiosarcoma
Leiomyosarcoma
Melanoma
Carcinoid
Renal cell carcinoma
Adrenal carcinoma
Thyroid carcinoma

TABLE 101-11 Magnetic Resonance Pattern Recognition: Focal Pancreatic Lesions

Tumor Type	T1WI	T2WI	Early Gadolinium	Late Gadolinium	Imaging Comments
Ductal adenocarcinoma, small	↓	Ø	↓	↓-↑	Usually no background chronic pancreatitis, so tumor is well seen on precontrast T1WI
Ductal adenocarcinoma, large	↓-Ø	Ø-↑	↓	↓	Usually causes background pancreatitis, so tumor not well seen on precontrast T1WI Focal mass with definable margins shown on early postgadolinium images is the most common characteristic
Insulinoma	↓	↑	↑	Ø-↑	Tumors are usually < 1 cm
Gastrinoma	↓	↑	↑, Ring	Ø-↑	Tumors are usually in pancreatic head, and 50% have metastases at time of diagnosis. Liver metastases tend to be uniform, smooth, ring-enhancing tumors on immediate postgadolinium images that show peripheral washout.
Somatostatinoma	↓	↑	↑, Diffuse	Ø	Tumors are usually large at diagnosis, with most having liver metastases. Liver metastases are multiple with irregular ring enhancement and variable size.
Glucagonoma	↓	↑	Homogeneous	Heterogeneous	Primary tumor usually small at initial diagnosis with few varying size liver metastases with irregular ring enhancement
VIPoma	↓	↑	↑	Ø	Small cysts best seen on steady-state T2-weighted (SST2) sequences. Thin and regular septations. Septations may enhance on immediate postgadolinium images of larger tumors with thicker septations. Tumors may show a central scar that shows delayed enhancement.
Microcystic cystadenoma	↓	↑↑	Ø-↑	Ø	Septations of uniform thickness without mural irregularity or nodules
Macrocytic cystadenoma	↓	↑↑	Ø	Ø	Tumor may be locally aggressive with liver metastases. Liver metastases may have high signal on T1W1 due to high mucin content.
Macrocytic cystadenocarcinoma	↓	↑	Ø-↑	Ø-↑	

↓, Mildly decreased signal intensity; Ø, isodense; ↑, mildly increased signal intensity; ↑↑, moderately to markedly increased signal intensity.
 From Semelka RC, Nagase LL, Armao D, et al: *Pancreas*. In Semelka RC (ed): *Abdominal-Pelvic MRI*. Philadelphia, Wiley-Liss, 2002.

Cholangiography

TABLE 101-12 Pancreatic Duct Stricture: ERCP or MRCP

Normal Parenchyma	Abnormal Parenchyma
Vascular compression	Carcinoma
Aneurysm	Chronic pancreatitis
Osteophyte	Duct hyperplasia

Imaging Findings in Specific Pancreatic Diseases

TABLE 101-13 Acute Pancreatitis

ULTRASOUND

Hypoechoic gland—diffuse (80%)
Hypoechoic mass—focal (20%); head or tail, not body
Peripancreatic fluid collection
Pseudocyst formation
Extrapaneatic hypoechoic mass—phlegmon
Dilation of the pancreatic duct if head is focally involved
Thick gallbladder wall

COMPUTED TOMOGRAPHY

Normal (29%)
Enlarged gland—diffuse (80%)
Enlarged gland—focal (20%)
Pancreas diffusely or focally hypodense
Hyperdense areas (50-70 HU) in hemorrhagic pancreatitis
Nonenhancing parenchyma in areas of pancreatic necrosis
Thickening of anterior pararenal fascia
Fluid collections in lesser sac, anterior pararenal space, posterior pararenal space, left subphrenic space, subperitoneal and interfascial spaces
Pseudocyst formation

MR IMAGING

Focal or diffuse enlargement
Heterogeneous appearance on precontrast T1-weighted fat-suppressed images
Heterogeneous diminished enhancement on immediate postgadolinium images
Hemorrhagic pancreatitis—high signal intensity on T1-weighted fat-suppressed images
Simple pseudocysts—low signal intensity on spin-echo and T1-weighted fat-suppressed images; high signal intensity on T2-weighted images

CHOLANGIOGRAPHY

Long, gently tapered narrowing of common bile duct
Prestenotic biliary dilation
Calculus in distal bile duct or common orifice

PLAIN ABDOMINAL RADIOGRAPH

“Colon cutoff” sign—dilated transverse colon with abrupt change to a gasless descending colon
“Sentinel loop”
“Renal halo” sign—water density of inflammation in anterior pararenal space contrasts with perirenal fat
Mottled peripancreatic region because of fat necrosis
Intrapaneatic gas bubbles
Gasless abdomen

UPPER GASTROINTESTINAL SERIES

Frostberg reverse 3 sign—reverse 3 contour to the medial portion of the duodenal sweep
Edematous swelling of papilla of Vater
Widened duodenal sweep with inferior displacement of the ligament of Treitz
Widened retrogastric space
Thick edematous folds of duodenum, gastric antrum, and greater curvature
Thickening of jejunal and ileal folds
Diminished duodenal peristalsis
Gastric and esophagogastric varices

BARIUM ENEMA

Narrowing, nodularity, and distortion along the inferior haustral row of the transverse colon
Stricture in region of hepatic flexure—proximal descending colon

TABLE 101-14 Chronic Pancreatitis

ULTRASOUND

Increased echogenicity of gland
Intraductal calcification
Atrophy
Focal or diffuse glandular enlargement
Pseudoaneurysm formation
Irregular pancreatic contour
Mild biliary ectasia
Splenic vein thrombosis and splenomegaly
Intrapaneatic and peripancreatic pseudocysts

COMPUTED TOMOGRAPHY

Small, atrophic gland
Fatty replacement of the parenchyma
Focal (12%-30%) or diffuse (27%-45%) pancreatic enlargement
Pseudoaneurysm formation
Intraductal calcification
Irregular pancreatic contour
Mild biliary ectasia
Splenic vein thrombosis and splenomegaly
Intrapaneatic and peripancreatic pseudocysts

MR IMAGING

Fibrosis—diminished signal intensity on T1-weighted fat-suppressed images and decreased, heterogeneous enhancement in immediate postgadolinium spin-echo images
Diminished enhancement in postcontrast capillary phase images because of disruption of normal capillary bed and replacement by less vascularized granulation tissue
Calcifications are manifested as a signal void.
Focal enlargement—cancer versus pancreatitis. Both show low signal intensity on noncontrast T1-weighted fat-suppressed and T2-weighted images. Postgadolinium image in focal pancreatitis shows heterogeneous enhancement with signal void cysts and calcifications, without a definable, minimally enhanced mass lesion. A definable, marginated mass suggests tumor.
Diffuse low signal intensity of the entire pancreas, including area of focal enlargement in T1-weighted fat-suppressed and immediate postgadolinium spin-echo images, is typical.
Ten percent show pseudocysts that are low signal intensity or signal void oval structures on T1-weighted images. They have signal intensity that varies on the basis of the presence of blood, protein, infection, and debris.

CHOLANGIOPANCREATOGRAPHY

Early: slight ductal ectasia with clubbing of side branches
Narrowing of the origins of side branches
Tortuosity, dilation, wall rigidity, main ductal stenosis (moderate disease)
“Beading,” “chain of lakes,” “string of pearls” sign in which dilation, stenosis, and obstruction of the main pancreatic duct and side branches (severe disease) are seen
Intraductal protein plugs and calculi
Prolonged retention of contrast material after endoscopic retrograde cholangiopancreatography
Stenosis with proximal dilation of the distal common bile duct

PLAIN RADIOGRAPHS

Numerous irregular calcifications

UPPER GASTROINTESTINAL SERIES

Displacement of the stomach or duodenum by a pseudocyst
Induration of gastric folds
Duodenal stricture

**TABLE
101-15****Pancreatic Ductal Adenocarcinoma****COMPUTED TOMOGRAPHY**

Focal mass (95%), diffuse enlargement (4%), normal scan (1%)
 Hypodense central zone in mass (75%-83%)
 Dilation of common bile duct and pancreatic duct
 Isolated dilation of bile duct or pancreatic duct
 Atrophy of pancreatic body and tail (20%)
 Postobstructive pseudocyst (11%)
 Obliteration of retroperitoneal fat (50%)
 Calcifications (2%)
 Dilation of common bile duct and pancreatic duct without a mass (4%)
 Invasion of perivascular lymphatics of celiac axis or superior mesenteric artery (60%)
 Local tumor extension into splenic hilum, into porta hepatis, or posteriorly (68%)
 Contiguous organ invasion of the stomach, duodenum, colon, greater omentum, mesenteric root, or transverse mesocolon
 Rounding of the uncinate process or other contour defect

ULTRASOUND

Hypoechoic pancreatic mass
 Contour deformity of gland and rounding of uncinate process
 Dilation of the common bile duct, pancreatic duct, or both

Mr Imaging

Low signal intensity on T1-weighted fat-suppressed images
 Rim of enhancement on immediate postgadolinium spin-echo images
 Intermediate signal intensity tumor, which invades low-intensity suppressed fat on gadolinium-enhanced fat-suppressed spin-echo images acquired 1-10 minutes after injection of contrast material
 Involved lymph nodes, which have moderate to high signal intensity in a background of low signal intensity suppressed fat on T2-weighted fat-suppressed spin-echo and interstitial-phase gadolinium-enhanced fat-suppressed T1-weighted images

ANGIOGRAPHY

Serrated, serpiginous, or smooth arterial encasement of the superior mesenteric artery (33%), splenic artery (14%), celiac trunk (11%), hepatic artery (11%), gastroduodenal artery (3%), left renal artery (0.6%)
 Venous obstruction: splenic vein (34%), superior mesenteric vein (10%)
 Venous encasement: superior mesenteric vein (23%), splenic vein (15%), portal vein (4%)
 Hypovascular tumor with neovascularity

CHOLANGIOGRAPHY

Irregular, nodular, "rat tail," eccentric stenosis of pancreatic duct
 Rat-tail or "nipple-like" obstruction of common bile duct
 Single or double obstruction of the common bile duct and duct of Wirsung
 Long, tapering stenosis with loss of lateral branches
 Loss of lateral branches with filling of a necrotic zone
 Abrupt occlusion of the main pancreatic duct
 Nonfilling of branches

UPPER GASTROINTESTINAL SERIES

Frostberg reverse 3 sign—reverse 3 contour to the medial portion of the duodenal sweep
 Antral "padding"—extrinsic indentation of the posteroinferior margin of the antrum
 Nodular mass in region of papilla with ampullary carcinoma
 Traction, spiculation, and fixation of the duodenal wall

BARIUM ENEMA

Serrated, flattened effect along inferior aspect of transverse colon and splenic flexure

**TABLE
101-16****Cystic Pancreatic Neoplasms****SEROUS CYSTADENOMA**

Well-demarcated, lobulated mass 4-25 cm in size (mean, 13 cm)
 Innumerable cysts <2 cm
 Prominent central stellate scar
 Amorphous central calcification (visible on plain film, 33%) in dystrophic area of scar
 Pancreatic and common bile duct that may be displaced, encased, or obstructed

Ultrasound

Complex, echogenic mass with internal echoes resembling a solid lesion; this is due to innumerable tiny cysts and dense radiating septa

Computed Tomography

Stellate septa
 Enhancement in the septa and cyst wall
 Honeycomb appearance

MR Imaging

Lobulated external border, especially on T2-weighted image with grapelike high-intensity cysts
 Multiple compartments with low signal intensity on T1-weighted image and high signal intensity on T2-weighted image
 Tumor septations, which usually enhance minimally to moderately

Angiography

Hypervascular or moderately vascular masses
 Dilated feeding arteries
 Arterial displacement, no encasement
 Neovascularity
 Occasional arteriovenous shunting
 Obstruction or compression of the splenic or superior mesenteric veins in 50%

MUCINOUS CYSTADENOMA OR CYSTADENOCARCINOMA

Well-demarcated, thick-walled mass 5-33 cm in size (mean, 12 cm)
 Large cysts >2 cm
 Unilocular or multilocular with septa
 Curvilinear mural calcification
 85% occur in pancreatic tail

Ultrasound

Multilocular
 Fixed septa with nodular tumor papillary excrescences
 Complex echo pattern at high gain settings

Computed Tomography

No central stellate septa, no honeycomb appearance
 Mural projections and localized thickening of cyst walls
 Central calcifications

MR Imaging

Round or irregularly oval tumors
 Cystic compartments vary in signal intensity on T1-weighted and T2-weighted images
 Shaggy, papillary excrescences

MRA, CTA, and Conventional Angiography

Hypovascular tumors
 Arterial dilation and neovascularity less frequent
 Arterial encasement or obstruction

TABLE 101-17 Incidental Cystic Pancreatic Lesions

UNILOCULAR CYST Intraductal papillary mucinous neoplasm Serous cystadenoma Pseudocyst	MACROCYSTIC LESION WITH SOLID COMPONENTS Malignant transformation of an intraductal papillary mucinous neoplasm Mucinous cystadenocarcinoma Solid pseudopapillary epithelial neoplasm Necrotic islet cell Necrotic metastasis
MICROCYSTIC LESION Serous cystadenoma	
MACROCYSTIC LESION Mucinous cystadenoma Mucinous cystadenocarcinoma Intraductal papillary mucinous neoplasm	

SUGGESTED READINGS

- Dähnert W: Radiology Review Manual, ed 7, Baltimore, 2011, Williams & Wilkins.
- Reeder MM: Reeder and Felson's Gamuts in Radiology, ed 4, New York, 2003, Springer-Verlag.
- Baker SR, Cho KC: Abdominal Plain Film Interpretation with Imaging Correlation, Norwalk, Ct, 1998, Appleton & Lange.
- Rumack CM, Nilson SR, Charboneau JW, editors: Diagnostic Ultrasound, ed 4, Philadelphia, 2011, Elsevier-Mosby.
- Semelka RC, Nagase LL, Armao D, et al: Pancreas. In Semelka RC, editor: Abdominal-Pelvic MRI, Philadelphia, 2010, Wiley-Liss.
- Beger H-G, Buchler M, Kozarek R, et al: The Pancreas: An Integrated Textbook of Basic Science, Medicine, and Surgery, Boston, 2008, Blackwell Publishing.
- Lamps LW: Diagnostic Pathology: Hepatobiliary and Pancreas, Salt Lake City, 2011, Utah, Amirsys.
- Odze RD, Goldblum JR: Surgical Pathology of the GI Tract, Liver, Biliary Tract and Pancreas: Expert Consult, ed 2, Philadelphia, 2009, Elsevier.
- Federle MP, Jeffrey RB, Jr, Tublin M, et al: Specialty Imaging: Hepatobiliary and Pancreas, Salt Lake City, 2013, Utah, Amirsys.
- Campbell F, Verbeke CS: Pathology of the Pancreas: A Practical Approach, New York, 2013, Springer.
- Kalb B, Sarmiento JM, Kooby DA, et al: MR imaging of cystic lesions of the pancreas. Radiographics 29:1749–1765, 2009.
- Palmucci S, Cappello C, Trombatore C, et al: Cystic pancreatic neoplasms: Diagnosis and management emphasizing their imaging features. Eur Rev Med Pharmacol Sci 18:1259–1268, 2014.
- Pinho DF, Rofsky NM, Pedrosa I: Incidental pancreatic cysts: Role of magnetic resonance imaging. Top Magn Reson Imaging 23:117–128, 2014.

SECTION
XII

Spleen

Spleen: Normal Anatomy and Examination Techniques

STEPHEN THOMAS | ABRAHAM H. DACHMAN

CHAPTER OUTLINE

Gross and Microscopic Anatomy

Physiology

Radiologic Anatomy and Technique

Plain Film Radiography

Nuclear Scintigraphy

Positron Emission Tomography

Angiography

Ultrasound

Computed Tomography

Magnetic Resonance Imaging

Gross and Microscopic Anatomy

The spleen is a reticuloendothelial lymphoid organ located in the left upper abdomen, posterolateral to the stomach, tail of the pancreas, and colic flexure. The adult spleen is 10 to 12 cm in length and weighs an average of 168 g in the adult man and 135 g in the adult woman. Splenic weight positively correlates to height, body weight, body mass index, and body surface area.¹ The spleen is most commonly located between the 9th and 12th ribs with its long axis in line with the 11th rib.²

The visceral peritoneum is reflected at its hilum to form two “pedicles”; one is reflected over the gastrosplenic ligament, and the other is reflected posteriorly over the tail of the pancreas and lienorenal ligament³ (Fig. 102-1). The tail of the pancreas lies within the lienorenal ligament together with the splenic vessels, lymphatics, and nerves and extends to the splenic hilum.

The superior convex surface of the spleen abuts the concavity of the diaphragm and is closely related to the posterior costophrenic recess and the left lung base. The posterior aspect of the spleen lies adjacent to the left adrenal gland or left kidney, and in up to one third of normal cases, part of the spleen is retrorenal.⁴ The anterior surface is related to the splenic flexure of the colon and connected to it by the splenocolic ligament. The splenophrenic, splenorenal, and gastrosplenic ligaments also fix the spleen in its position. The visceral or concave surface of the spleen is related to the stomach and tail of the pancreas in addition to the left kidney and the colon. The splenic hilum occupies approximately 25% to 33% of the splenic surface area.

The splenic artery, a branch of the celiac axis, runs a transverse and often tortuous course along the upper border of the pancreas to reach the splenic hilum, where it divides into five or more major branches.⁵ The splenic vein is formed at the splenic hilum and runs in the lienorenal ligament anterior to the left kidney, the left diaphragmatic crus, and the aorta in a groove along the dorsal aspect of the pancreas (Fig. 102-2). It

joins the inferior mesenteric vein and then the superior mesenteric vein behind the head of the pancreas to form the portal vein. The spleen provides 40% of the blood volume of the portal circulation. The lymphatic vessels are subcapsular and are formed by the drainage of large trabecular tributaries. These vessels drain into the pancreaticocolic nodes at the splenic hilum.

The framework of the spleen consists of collagenous fibrous and elastic tissue forming the capsule (which is less than 1.5 mm thick), trabeculae, and reticular fibers (Fig. 102-3). Blood enters the trabeculae through splenic arterial branches and exits through central arteries (in the white pulp) that are surrounded by the periarteriolar lymphoid sheaths, whose enlargements at irregular intervals are known as malpighian bodies.⁶

The lymphatic sheaths and follicles make up the white pulp of the spleen. The blood vessels transport blood to the sinusoids in the red pulp. Capillaries may open directly into sinusoids or may first pass through spaces in the red pulp. The red pulp performs the phagocytic function of the spleen.

The spleen has between two and five arterial segments, with the avascular plane running parallel to the short axis of the spleen. There are typically two polar arteries and variable segmental arteries supplying the interpolar portion.⁷

The splenic nerve supply is derived from the celiac plexus. It is located along the splenic artery and sends postganglionic sympathetic fibers that innervate the splenic white pulp. These fibers distribute with the vascular and trabecular systems and associate mainly with the central artery and its branches, the periarteriolar lymphatic sheath, the marginal sinus, and the parafollicular zone, with occasional fibers in the follicles.⁸

Physiology

About 4% of the cardiac output or 150 mL of blood per minute flows through the spleen. This amounts to 350 L of blood per day.⁹ The normal transit time of blood in the spleen is 20 to 25 seconds.

The spleen discriminates between normal and abnormal cells and selectively sequesters abnormal and aged red or white blood cells and platelets. The microcirculation of the spleen is thought to direct 10% of splenic arterial blood directly into the venous sinuses and 90% through the red pulp, whose endothelial pores and macrophages remove abnormal particles. Abnormal red blood cells, viruses, bacteria, nuclear remnants (Howell-Jolly bodies), and parasites are removed, with normal erythrocytes left intact. It is not certain what factors sensitize an aged blood cell to splenic destruction; however, it has been suggested that aging erythrocytes have stiffened membranes, which slows or halts their passage through the narrow network of splenic cords, making them an easy target for phagocytosis.¹⁰ About 30% of platelets are normally sequestered within the

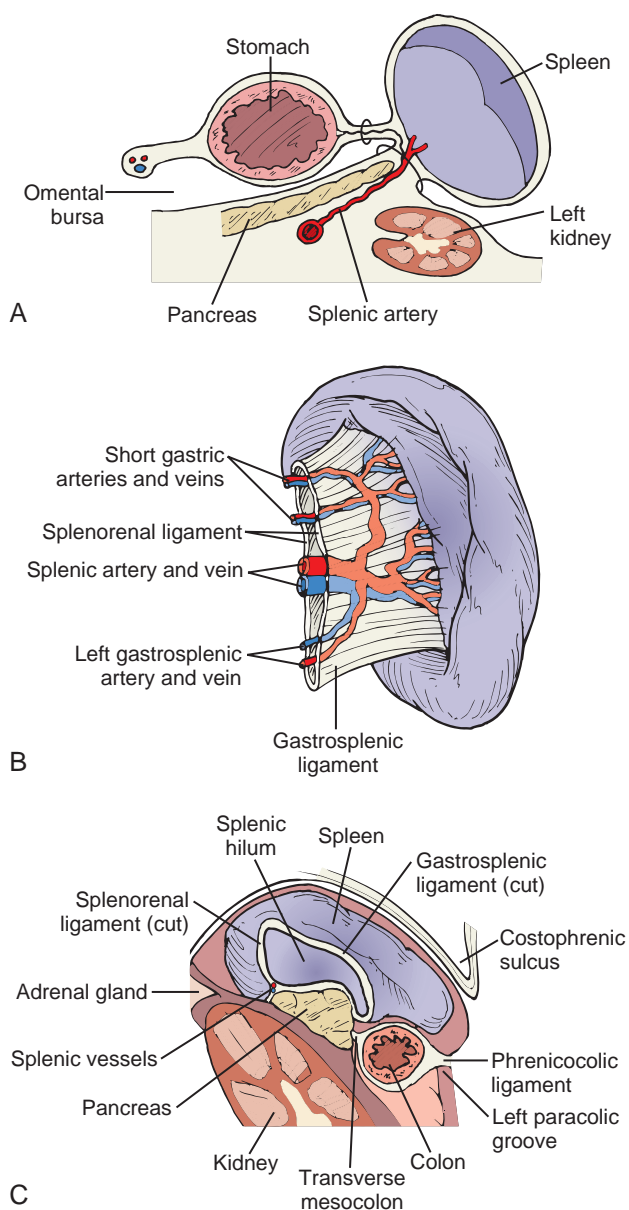


Figure 102-1 Anatomic relationships of the spleen. **A.** Splenic ligaments. The spleen has two pedicles: the gastrosplenic and the splenorenal ligaments. **B.** Splenic vessels within the two pedicles. The diagram depicts the ligaments of the spleen and their relationship to splenic vessels. **C.** Anatomic relationships of the splenic hilum to other abdominal organs. (**A** from Dachman AH: *The spleen: Normal anatomy and radiology*. In Friedman AC [ed]: *Radiology of the Liver, Biliary Tract, Pancreas and Spleen*. Baltimore, Williams & Wilkins, 1987, pp 899-910. **B** from Linder HH: *Clinical Anatomy*. East Norwalk, Ct, Appleton & Lange, 1989, p 438. **C** from Meyers MA: *Dynamic Radiology of the Abdomen*. New York, Springer-Verlag, 1988, p 42.)

spleen. When splenomegaly is present, up to 80% of platelets may be sequestered.

The role of the spleen in the immune response is incompletely understood, but it is important in the initiation of humoral and cellular immune responses. The lymphatic tissue in the spleen is unique in that the white pulp of the spleen is perfused by blood rather than by lymph. Thus, it is able to respond rapidly to antigens introduced into the bloodstream.

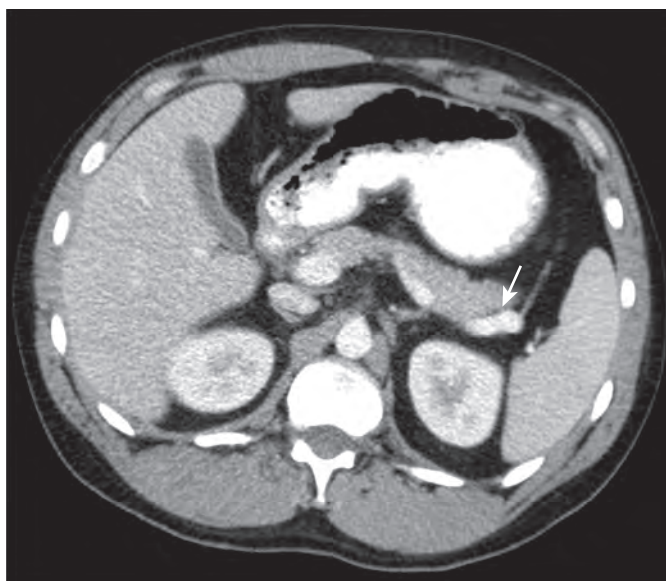


Figure 102-2 Contrast-enhanced CT shows the course of the splenic vein (arrow) posterior to the pancreas and anterior to the left kidney.

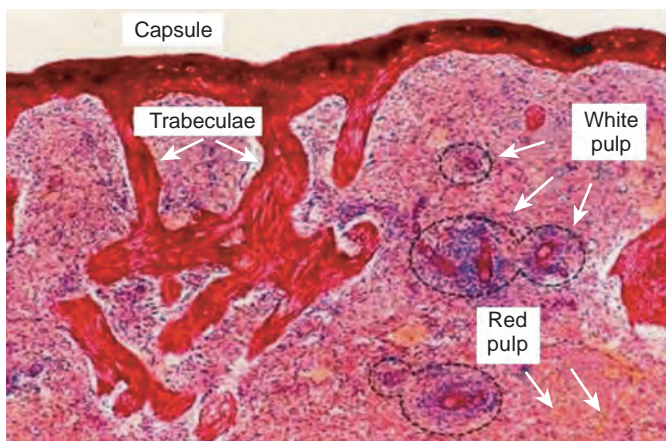


Figure 102-3 Normal trabecular anatomy of the spleen.

The spleen produces a tetrapeptide known as tuftsin that coats leukocytes and facilitates phagocytosis. The absence of tuftsin in splenectomized patients may contribute to the increased incidence of infection reported in these patients by impairing opsonization of bacteria. The spleen is the main site of immunoglobulin M antibody synthesis. Serum immunoglobulin M levels have been shown to decrease significantly after splenectomy.¹¹

Whereas the storage function is not considered to be well developed in the human spleen, it can on average contain 200 to 250 mL of blood and can maintain red blood cell volume in the face of bleeding unless the blood loss is marked.¹² Red blood cells are released into the circulation by splenic contraction, which is controlled by the actions of postganglionic fibers on the capsule and trabeculae. Platelets and white blood cells are also stored within the spleen. In splenomegaly (increased storage), pancytopenia can occur; in asplenia (no storage), one may see pantoctocytopenia.

Radiologic Anatomy and Technique

Splenic size and morphology can be assessed by physical examination or imaging studies. Palpation and percussion of the spleen can be complementary to imaging but are insensitive.¹³ Individuals with a large body habitus and up to 10% of normal children do have palpable spleens. Thus, there is an important role for radiographic imaging in diagnosis of suspected splenic disease.

PLAIN FILM RADIOGRAPHY

The spleen (Fig. 102-4) is often partially outlined on plain films by fat in the greater omentum and distal transverse mesocolon and by the adjacent air-filled stomach or colon.¹⁴ The ventral surface of the spleen may be outlined by fat on lateral views of the chest or abdomen, particularly if the spleen is enlarged. The normal spleen can be visualized in fewer than 100 of 500 (20%) plain films, and the splenic tip can be seen in about 44% of cases.¹⁵ The long axis of the spleen usually parallels the posterior



Figure 102-4 Abdominal radiograph shows spleen outlined by transverse colon (arrows).

ribs and generally does not project significantly below the costal margin.¹⁴ Plain film radiography is useful for detection of moderate or massive splenomegaly and splenic calcifications as commonly seen in granulomatous disease (tuberculosis, histoplasmosis, brucellosis). Curvilinear calcifications may be seen with chronic hematoma, healed abscess, and cysts. Thorotrast deposition, although of historical interest only, is also usually visible on plain films as a fine reticular pattern.

NUCLEAR SCINTIGRAPHY

Splenic scintigraphic evaluation is commonly performed with technetium Tc 99m sulfur colloid (Fig. 102-5). Indications include detection of congenital abnormalities of the spleen and assessment of splenic size, accessory or residual splenic tissue, heterotopic splenic tissue, splenic atrophy, and asplenic states. Splenic lesions larger than 1 cm may be evaluated with planar imaging, but smaller lesions require single photon emission computed tomography (SPECT) or SPECT/CT.¹⁶

POSITRON EMISSION TOMOGRAPHY

Fluorine-18 fluorodeoxyglucose (¹⁸F-FDG) positron emission tomography/computed tomography (PET/CT) is established as a powerful imaging tool for cancer detection and monitoring of response to therapy. There is faint radiotracer uptake in normal splenic tissue (Fig. 102-6). Diffuse increased splenic uptake can be present with the use of marrow-stimulating factors and hematopoietic disorders, as the spleen is a site of extramedullary hematopoiesis.¹⁷ Focal or diffuse pathologic increased ¹⁸F-FDG uptake is present in malignant neoplasms that involve the spleen.¹⁸

ANGIOGRAPHY

The splenic artery is approximately 13 cm in length (range, 8-32 cm). Trifurcation of the celiac trunk into the hepatic, splenic, and left gastric arteries is considered conventional and can be found in 85% of humans.¹⁹ The splenic artery usually originates just distal to the left gastric artery.^{14,20} In 15% of cases, all three branches of the celiac trunk arise at the same point.²¹ Normal variations include origin of the splenic artery from the ventral or right surface of the celiac axis and origin from the aorta or superior mesenteric artery.²⁰ A branch supplying

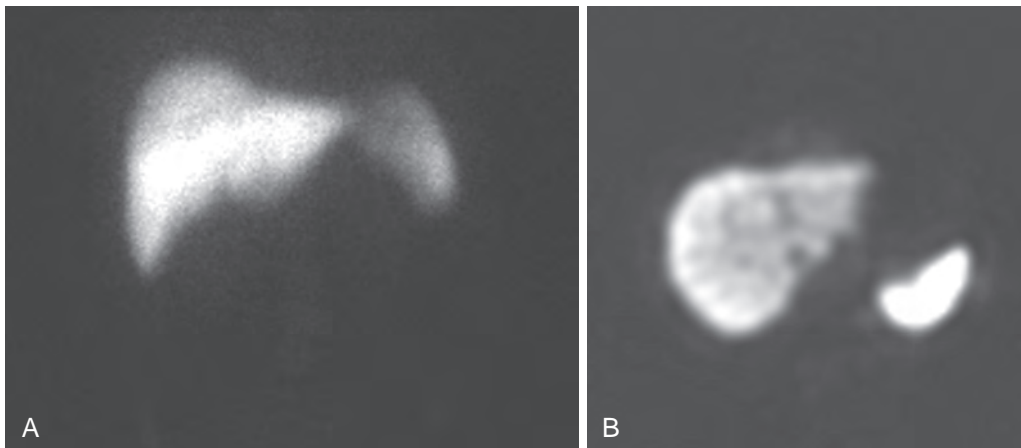
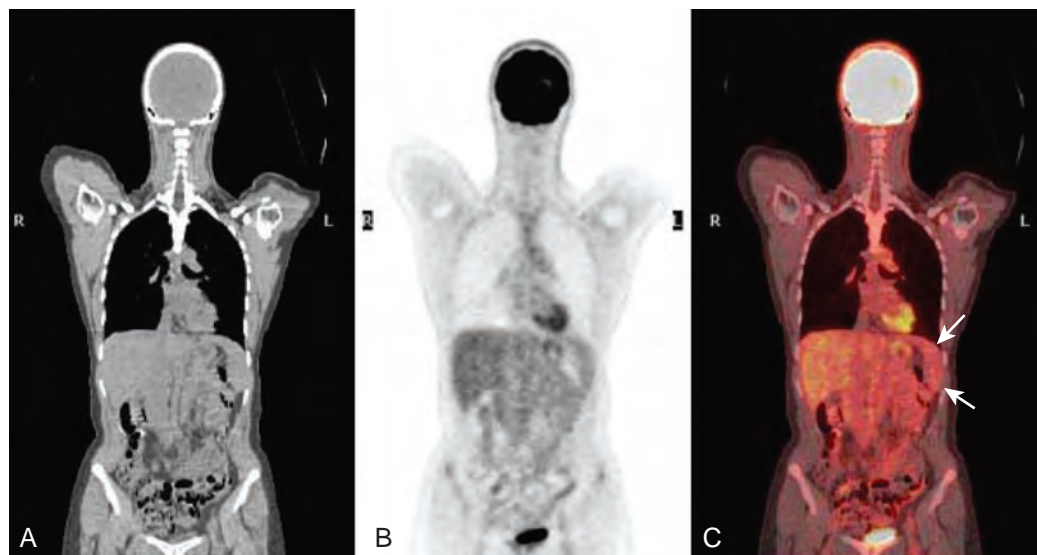


Figure 102-5 ^{99m}Tc-sulfur colloid scan. **A.** Anteroposterior projection planar image shows normal splenic activity in the left upper abdomen. **B.** SPECT image shows greater activity in the spleen compared with the liver.

Figure 102-6 Normal PET/CT scan. **A.** Normal coronal view CT image. **B.** Normal coronal view PET image. **C.** Normal fused PET/CT image. The spleen shows normal activity (arrows).



the upper splenic pole may originate separately from the celiac axis, giving the appearance of a double splenic artery.²² The splenic artery can be divided into suprapancreatic, pancreatic, prepancreatic, and perihilar segments.⁵ Its tortuosity is variable and increases with age. The most tortuous segment is usually the pancreatic segment, which runs along the dorsal surface of the pancreas and gives off small pancreatic branches. The pancreatic tail and the perihilar segment run between the spleen and the tail of the pancreas.

There are two basic splenic shapes based on arterial configuration: the distributed type and the compact type. The distributed configuration (70% of cases) consists of a short splenic artery with numerous small branches that penetrate the splenic hilum in a distributed fashion. The compact configuration (30% of cases) has a narrow hilum in which the arterial branches are few and large.²³

The splenic artery also supplies portions of the pancreatic body and tail. The dorsal pancreatic artery arises from the first 1 to 3 cm (suprapancreatic segment) of the splenic artery and the greater pancreatic artery (arteria pancreatica magna), which arises from the middle segment of the splenic artery and supplies the tail of the pancreas.²⁴ Another branch, the artery of Buhler, may course inferiorly to communicate with the superior mesenteric artery.²² The short gastric arteries and the left gastropiploic artery usually arise just proximal to the first division of the splenic artery.²⁰

In the parenchymal phase of splenic arteriography, splenic density is dependent on the ratio of splenic volume to the volume of contrast material injected. It is often homogeneous or slightly speckled. Venous anatomy is normally visualized about 7 seconds after arterial injection. Splenic venous anatomy can also be demonstrated with splenoportography.

ULTRASOUND

Ultrasound can be useful in evaluating the spleen, which is best scanned in the left anterior oblique, right lateral decubitus, or prone position. Ultrasound evaluation is best performed with a curved array transducer with a median frequency of 3 to 5 MHz. Use of a subcostal or oblique intercostal plane can

increase the sonographic window. An anterior approach is often limited by gastric or colonic gas. Transverse and longitudinal (coronal) imaging should be obtained (Fig. 102-7). Full or varying degrees of inspiration will improve visualization of the paradiaphragmatic portion of the spleen, which is the most difficult to image. It is often helpful to fill the stomach with fluid for scanning in the supine position. The transducer may be moved in an arc along the intercostal space or in a sector motion. A convex transducer may improve visualization of the “blind areas” adjacent to the dome of the diaphragm.²² Care should be taken in differentiating a prominent lateral segment of the left lobe of the liver, which may wrap around the spleen. When there is a paucity of intra-abdominal fat in thin patients, as in children and young women, the lateral segment of the left lobe may give the appearance of a pseudoperisplenic lesion.²⁵ This can simulate a fluid collection superior and lateral to the spleen.²⁵

Normal splenic parenchyma has a homogeneous, mid- to low-level fine tissue echotexture punctuated by occasional bright echoes representing blood vessels. The spleen is slightly more echogenic than normal liver and markedly more echogenic than normal renal parenchyma.²⁶ However, if the liver echogenicity is abnormal, optimization of the time gain control curve and detection of texture abnormalities of the spleen may prove difficult. The size and shape of the spleen and position of the hilum and its relationship to the diaphragm, stomach, pancreas, and left kidney should be identified.

There are multiple methods for splenic size measurement. The spleen is roughly $12 \times 7 \times 4$ cm in an adult, corresponding to a 150-g spleen. In clinical practice, we use 12 to 13 cm as the maximal length of the spleen as seen in the right lateral decubitus position, measured from upper to lower pole.²⁷ Size criteria have also been established for children by this method.²⁸ Estimations of splenic volume have been described by use of a splenic volumetric index with both ultrasound and CT.²⁹ This is the product of the maximal length, width, and anterior-posterior thickness of the spleen divided by 27, with a normal range of 8 to 34.^{27,28} Another method is to multiply the transverse and vertical dimensions of the spleen taken from an image in which the spleen has maximal cross-sectional size.^{27,28}

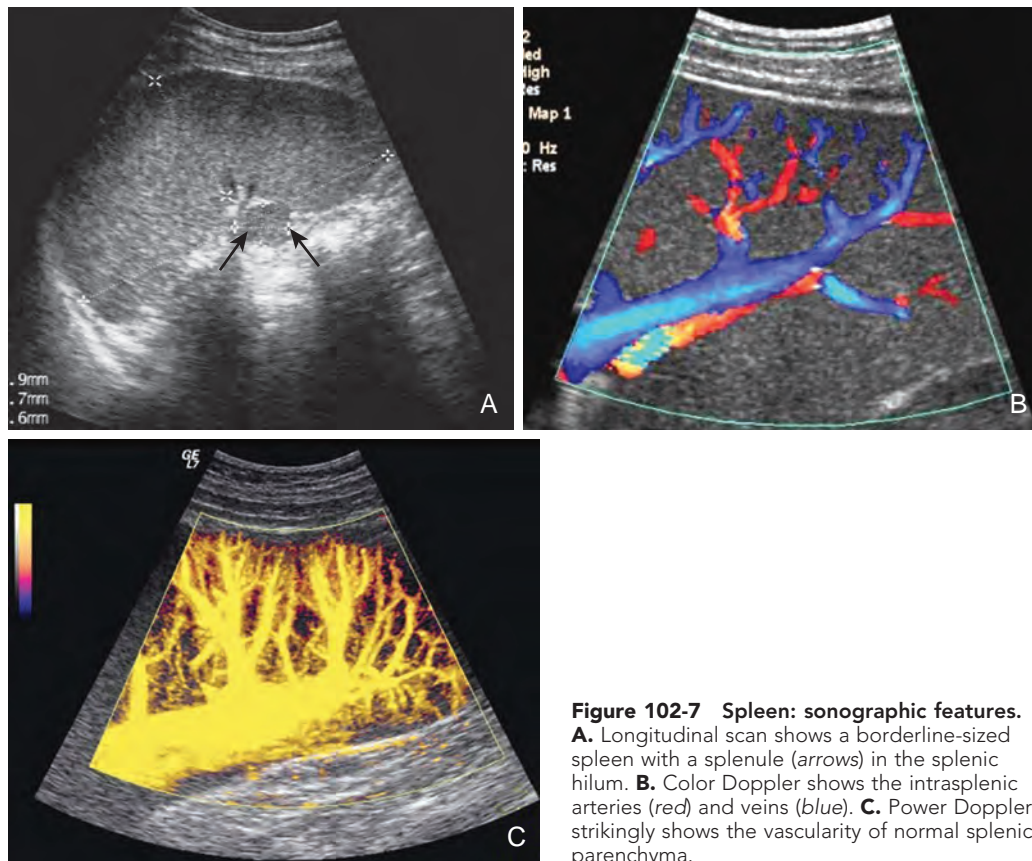


Figure 102-7 Spleen: sonographic features.

A. Longitudinal scan shows a borderline-sized spleen with a splenule (arrows) in the splenic hilum. **B.** Color Doppler shows the intrasplenic arteries (red) and veins (blue). **C.** Power Doppler strikingly shows the vascularity of normal splenic parenchyma.

Ultrasound is useful in detecting and characterizing focal lesions and in estimating splenic size and volume. Color Doppler ultrasound is helpful in interrogating the splenic artery and vein. This can be useful in differentiating vascular structures, such as normal vessels or aneurysms, from non-vascular structures, such as pancreatic pseudocysts.³⁰ Power Doppler may help show blood flow in the spleen, particularly in assessing decreased flow (as in sickle cell crisis or infarction). Splenic elasticity measured with real-time tissue elastography, which measures the parenchymal stiffness, can be used as a marker of portal hypertension in patients with chronic liver disease.³¹

Ultrasound microbubble contrast agents, which have been used to characterize liver lesions, can characterize splenic lesions and improve visualization of splenic infarctions and lacerations.^{32,33}

COMPUTED TOMOGRAPHY

CT superbly demonstrates the size, shape, location, and texture of the normal spleen as well as intrasplenic abnormalities. Technical artifacts may result from motion, beam hardening, or dynamic scanning. The relationship of the spleen to the pancreatic tail, left lobe of the liver, diaphragm, left adrenal gland, left kidney, stomach, splenic flexure, and adjacent mesenteric and omental fat is reliably depicted by CT. The posterior surface of the spleen abutting the left hemidiaphragm is called the bare area and has a constant relation to Gerota's fascia.³⁴ This portion of the spleen is about 2 to 3 cm long and may be outlined by air in the posterior costophrenic

sulcus. The point of reflection of the splenorenal ligament at the bare area is thought to correspond to the intermediate ridge of the spleen.³⁴ The bare area is useful in differentiating ascites from pleural effusion because ascites is excluded from the bare area.³⁴

CT displays variations in the size, shape, and position of the spleen³⁵ (Fig. 102-8). Ventral and caudal shift of both the liver and the spleen is seen when the patient turns from the supine to the prone position.³⁶ This positional change can be significant if CT is used to plan radiation therapy portals. On non-contrast CT, the spleen is homogeneous in attenuation and measures 5 to 10 Hounsfield units (HU) less than a normal liver, between 40 and 60 HU.^{30,37-39} Unenhanced scans are useful for the detection of splenic calcifications, such as those seen in abscesses, granulomas, hematomas, parasitic cysts, congenital cysts, and infarctions.⁴⁰ The omental and mesenteric fat surrounding the spleen sharply demarcates the capsule and hilar vasculature even without contrast enhancement. The splenic artery is often tortuous and may appear curvilinear, round, or oval on axial CT scans. The splenic vein may vary in its relationship with the pancreas, and the peripancreatic fat can mimic a dilated pancreatic duct.⁴¹

The splenic index, described with ultrasound, has also been applied with CT. A simplified CT splenic index uses the product of the maximal length (L), width (W), and anterior-posterior thickness (T) of the spleen, with a normal less than 480. A volume can be calculated from the splenic index $V = 30 \times 0.58 \times L \times W \times T$.⁴² Semiautomated and fully automated methods of detection of splenic volume can be performed by either manual or automated segmentation of the spleen. Studies in children

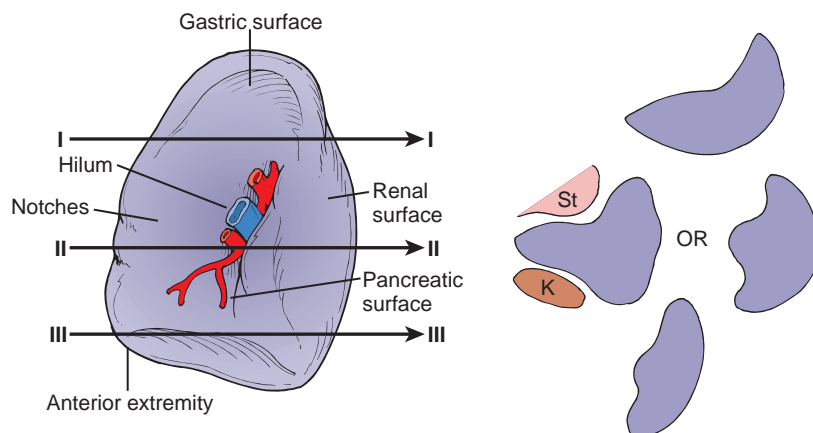


Figure 102-8 Variations of splenic morphology on CT. On axial images, the spleen may have several normal configurations because of prominent lobulation or ridging. K, kidney; St, stomach. (From Piekarski J, Federle MP, Moss AA, London SS: *Computed tomography of the spleen*. Radiology 135:683–689, 1980.)

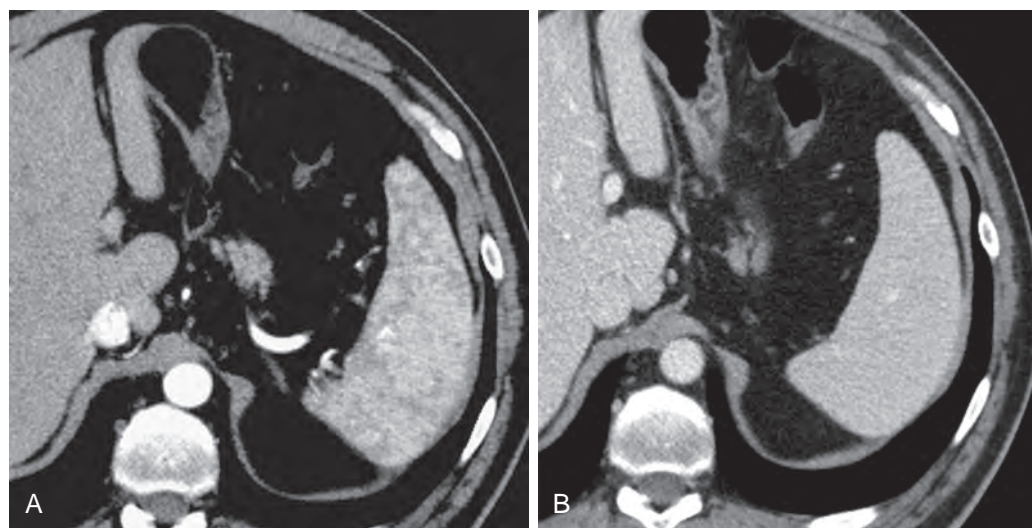


Figure 102-9 Normal pattern of splenic enhancement on multidetector CT. **A.** Arterial phase shows a mottled enhancement pattern due to differential flow of contrast material in the red and white pulp of the spleen. **B.** Portal venous phase shows uniform splenic enhancement.

have shown that the ratio of splenic volume to the body weight decreases exponentially with age from 4.5 cm³/kg at 1 month to 2.4 cm³/kg at 25 years of age.⁴²

Contrast enhancement is generally indicated for the diagnosis of splenic disease and in distinguishing splenic from pancreatic or adrenal abnormalities. Bolus injection of intravenous iodinated contrast material produces dense enhancement of the hilar vasculature and an initial heterogeneous blush, sometimes with striped or mottled patterns (“zebra spleen”)⁴³ (Fig. 102-9). Slow infusion of the contrast agent creates a uniform increase in parenchymal density.^{36,43} This is due to variable rates of flow through the red pulp.^{43,44} A homogeneous splenic blush should be seen within 2 minutes after bolus injection.³⁵ A detailed analysis of the patterns of inhomogeneity after bolus injection suggests that a mottled pattern is due to uneven enhancement in the capillary phase, and curvilinear low densities correspond to intrasplenic veins.⁴⁵ Splenic inhomogeneities lasting longer than 40 seconds after peak aortic enhancement indicate a pathologic process, whereas those lasting less than 40 seconds represent normal, hemodynamically related inhomogeneities.^{45,46}

Splenic perfusion can be calculated with dynamic CT by drawing regions of interest on the spleen and aorta and calculating time-attenuation curves. This technique has been

used to study splenic perfusion in correlation with portal pressures. Splenic arterial perfusion is lower in patients with chronic liver disease (0.92 mL/min) compared with normal controls (1.35 mL/min).⁴⁷ This is similar to values of 0.96 to 1.19 mL/min/g based on rare gas inhalation washout studies.⁴⁸

Splenic parenchyma enhances significantly higher during the arterial phase with 400 mg/mL iodine-containing contrast agents compared with 300 mg/mL, but parenchymal enhancement is similar during the portal venous phase. As portal venous imaging is typically used to assess splenic parenchyma, intravenous contrast agents with a higher concentration of iodine do not improve CT imaging. However, visualization of the splenic artery and its branches may be better achieved with a higher concentration of contrast agent during the arterial perfusion phase.⁴⁹

MAGNETIC RESONANCE IMAGING

New magnetic resonance imaging (MRI) techniques have increased the role of MRI in detection and characterization of splenic diseases. MRI is an excellent tool for the evaluation of focal and diffuse pathologic processes of the spleen. Rapid scanning techniques allowing breath-hold imaging and respiratory

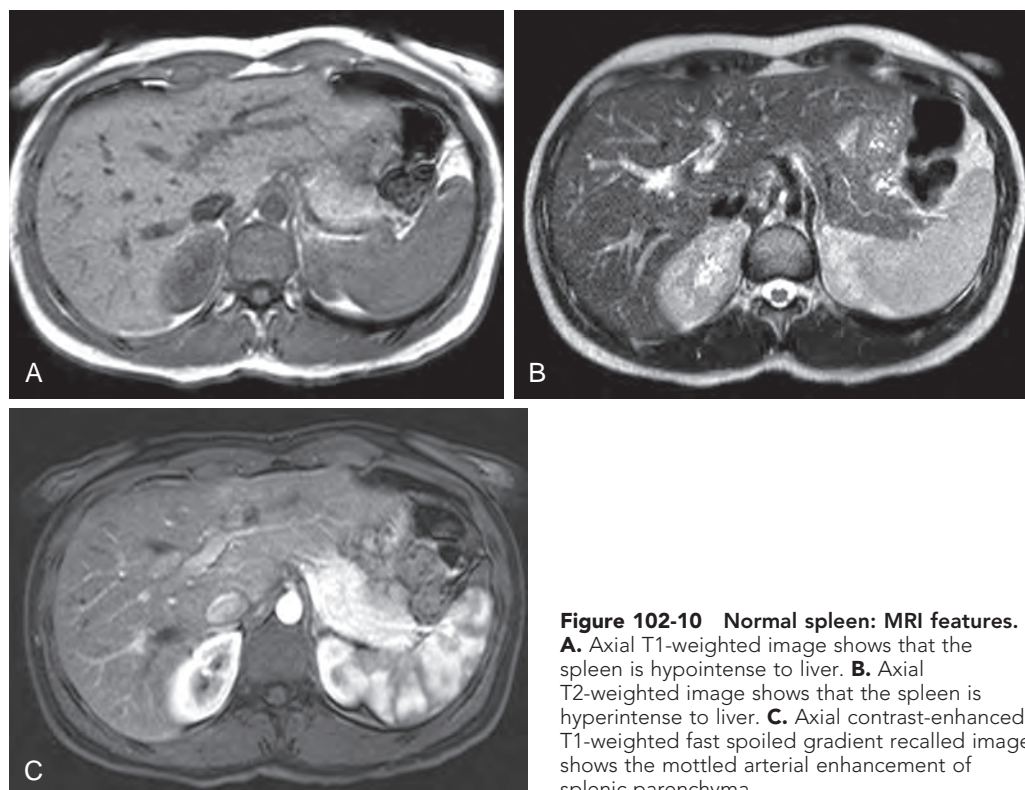


Figure 102-10 Normal spleen: MRI features.

A. Axial T1-weighted image shows that the spleen is hypointense to liver. **B.** Axial T2-weighted image shows that the spleen is hyperintense to liver. **C.** Axial contrast-enhanced T1-weighted fast spoiled gradient recalled image shows the mottled arterial enhancement of splenic parenchyma.

gated techniques have reduced the motion artifacts related to the spleen's proximity to the diaphragm and artifacts due to bowel motion.⁵⁰⁻⁵⁵

The large fractional heme content in the spleen results in long T1 and T2 relaxation times compared with the liver. Thus, on T1-weighted images, the normal MR signal intensity of the spleen is less than that of the liver but slightly greater than that of muscle. On T2-weighted images, the spleen has higher signal intensity relative to liver (Fig. 102-10).^{56,57} The inherent increased T2 signal can result in poor contrast between normal and abnormal spleen.^{50,53,58} In infants, the spleen signal intensity differs from that of children or adults. The T2-weighted signal intensity gradually increases from isointense to hypointense relative to the liver during the first week of life to moderately hyperintense to the liver by 8 months of age.⁵⁴ This may be due

to the relatively large amount of red pulp at birth. The non-thrombosed blood is dark on T2-weighted images. It is important not to mistake this signal characteristic for disease in the neonate.⁵⁴

Imaging of the spleen includes precontrast and postcontrast fast T1-weighted fat-suppressed gradient-echo images for improved lesion detection and characterization. With intravenous gadolinium contrast enhancement, the spleen demonstrates an early striped or arcuate pattern that becomes homogeneous approximately 60 to 90 seconds after the administration of contrast material.^{52,56} Iron deposition or iron-containing lesions in the spleen can be detected from their reduced signal intensity on in-phase T1-weighted (long echo time) gradient recalled echo images compared with that on opposed-phase images (short echo time).^{59,60}

REFERENCES

1. Yildiz AE, Ariyurek MO, Karcaaltincaba M: Splenic anomalies of shape, size, and location: Pictorial essay. *Scientificworldjournal* 2013; 321810, 2013.
2. Mirjalili SA, McFadden SL, Buckenham T, et al: A reappraisal of adult abdominal surface anatomy. *Clin Anat* 25:844–850, 2012.
3. Shrestha BM, Brown PW, Wilkie ME, et al: The anatomy and pathology of the lesser sac: Implications for peritoneal dialysis. *Perit Dial Int* 30:496–501, 2010.
4. Hopper KD, Chantelais AE: The retrorenal spleen. Implications for percutaneous left renal invasive procedures. *Invest Radiol* 24:592–595, 1989.
5. Pandey SK, Bhattacharya S, Mishra RN, et al: Anatomical variations of the splenic artery and its clinical implications. *Clin Anat* 17:497–502, 2004.
6. Polák Š, Gálfiová P, Varga I: Ultrastructure of human spleen in transmission and scanning electron microscope. *Biologia (Bratisl)* 64:402–408, 2009.
7. Garcia-Porrero JA, Lemes A: Arterial segmentation and subsegmentation in the human spleen. *Acta Anat (Basel)* 131:276–283, 1988.
8. Felten DL, Ackerman KD, Wiegand SJ, et al: Noradrenergic sympathetic innervation of the spleen: I. Nerve fibers associate with lymphocytes and macrophages in specific compartments of the splenic white pulp. *J Neurosci Res* 18:28–36, 118–121, 1987.
9. Macpherson AIS, Richmond J, Stuart AE: *The Spleen*, Springfield, Ill, 1973, Charles C Thomas.
10. Bratosin D, Mazurier J, Tissier JP, et al: Cellular and molecular mechanisms of senescent erythrocyte phagocytosis by macrophages. A review. *Biochimie* 80:173–195, 1998.
11. Cadili A, de Gara C: Complications of splenectomy. *Am J Med* 121:371–375, 2008.
12. Stewart IB, McKenzie DC: The human spleen during physiological stress. *Sports Med* 32:361–369, 2002.
13. Yang JC, Rickman LS, Bosser SK: The clinical diagnosis of splenomegaly. *West J Med* 155:47–52, 1991.
14. Sinner WN, Chirasthivat S: Plain film diagnosis of diseases of the liver and spleen. In Serafini AN, Guter M, editors: *Medical Imaging of the Liver and Spleen*, Norwalk, Ct, 1983, Appleton-Century-Crofts, pp 9–21.

15. Brogdon BG, Crow NE: Observations on the normal spleen. *Radiology* 72:412–414, 1959.
16. Middleton ML, Strober MD: Planar scintigraphic imaging of the gastrointestinal tract in clinical practice. *Semin Nucl Med* 42:33–40, 2012.
17. Blodgett TM, Ames JT, Torok FS, et al: Diffuse bone marrow uptake on whole-body F-18 fluorodeoxyglucose positron emission tomography in a patient taking recombinant erythropoietin. *Clin Nucl Med* 29:161–163, 2004.
18. Metser U, Miller E, Kessler A, et al: Solid splenic masses: Evaluation with ¹⁸F-FDG PET/CT. *J Nucl Med* 46:52–59, 2005.
19. Oran I, Yesildag A, Memis A: Aortic origin of right hepatic artery and superior mesenteric origin of splenic artery: two rare variations demonstrated angiographically. *Surg Radiol Anat* 23:349–352, 2001.
20. Reuter SR, Redman HC: *Gastrointestinal Angiography*, ed 2, Philadelphia, 1977, WB Saunders.
21. Vandamme JP, Bonte J: Systematisation of the arteries in the splenic hilus. *Acta Anat (Basel)* 125:217–224, 1986.
22. Abrams HL, Baum S, Pentecost MJ: *Abrams' Angiography: Interventional Radiology*, ed 2, Philadelphia, 2006, Lippincott Williams & Wilkins.
23. Michels NA: The variational anatomy of the spleen and splenic artery. *Am J Anat* 70:21–72, 1942.
24. Madoff DC, Denys A, Wallace MJ, et al: Splenic arterial interventions: Anatomy, indications, technical considerations, and potential complications. *Radiographics* 25(Suppl 1):S191–S211, 2005.
25. Rumack CM: *Diagnostic Ultrasound*, ed 4, St. Louis, 2011, Elsevier Mosby.
26. Benter T, Kluhs L, Teichgraber U: Sonography of the spleen. *J Ultrasound Med* 30:1281–1293, 2011.
27. Ishibashi H, Higuchi N, Shimamura R, et al: Sonographic assessment and grading of spleen size. *J Clin Ultrasound* 19:21–25, 1991.
28. Rosenberg HK, Markowitz RI, Kolberg H, et al: Normal splenic size in infants and children: Sonographic measurements. *AJR Am J Roentgenol* 157:119–121, 1991.
29. Pietri H, Boscaini M: Determination of a splenic volumetric index by ultrasonic scanning. *J Ultrasound Med* 3:19–23, 1984.
30. Mitchell DG, Blum L, Kurtz AB: Case of the day. Splenic artery pseudoaneurysm. *Radiographics* 10:366–368, 1990.
31. Hirooka M, Ochi H, Koizumi Y, et al: Splenic elasticity measured with real-time tissue elastography is a marker of portal hypertension. *Radiology* 261:960–968, 2011.
32. Peddu P, Shah M, Sidhu PS: Splenic abnormalities: A comparative review of ultrasound, microbubble-enhanced ultrasound and computed tomography. *Clin Radiol* 59:777–792, 2004.
33. Yu X, Yu J, Liang P, et al: Real-time contrast-enhanced ultrasound in diagnosing of focal spleen lesions. *Eur J Radiol* 81:430–436, 2012.
34. Vibhakkar SD, Bellon EM: The bare area of the spleen: A constant CT feature of the ascitic abdomen. *AJR Am J Roentgenol* 142:953–955, 1984.
35. Warschauer DM: Spleen. In Lee JKT, Sagel SS, Stanley RJ, et al, editors: *Computed Body Tomography with MRI Correlation*, New York, 2006, Lippincott-Raven, pp 973–1006.
36. Ball WS, Wicks JD, Mettler FA, Jr: Prone-supine change in organ position: CT demonstration. *AJR Am J Roentgenol* 135:815–820, 1980.
37. Mategrano VC, Petasnick J, Clark J, et al: Attenuation values in computed tomography of the abdomen. *Radiology* 125:135–140, 1977.
38. Stephens DH, Sheedy PF, Hattery RR, et al: Computed tomography of the liver. *AJR Am J Roentgenol* 128:579–590, 1977.
39. Piekarski J, Federle MP, Moss AA, et al: Computed tomography of the spleen. *Radiology* 135:683–689, 1980.
40. Wegener OM: *Ganzkörper Computertomographie*, Basel, 1992, Karger, pp 357–366.
41. Seidemann FE, Cohen WN, Bryan PJ, et al: CT demonstration of the splenic vein–pancreatic relationship: The pseudodilated pancreatic duct. *AJR Am J Roentgenol* 129:17–21, 1977.
42. Prassopoulos P, Daskalogiannaki M, Raissaki M, et al: Determination of normal splenic volume on computed tomography in relation to age, gender and body habitus. *Eur Radiol* 7:246–248, 1997.
43. Glazer GM, Axel L, Goldberg HI, et al: Dynamic CT of the normal spleen. *AJR Am J Roentgenol* 137:343–346, 1981.
44. Miles KA, McPherson SJ, Hayball MP: Transient splenic inhomogeneity with contrast-enhanced CT: Mechanism and effect of liver disease. *Radiology* 194:91–95, 1995.
45. Partanen K, Soimakallio S, Kivimäki T, et al: Dynamic topography of the contrast enhancement of the spleen. *Eur J Radiol* 4:101–106, 1984.
46. Blomley MJ, Korman M, Coulton R, et al: Splenic blood flow: Evaluation with computed tomography. *Acad Radiol* 4:13–20, 1997.
47. Tsushima Y, Koizumi J, Yokoyama H, et al: Evaluation of portal pressure by splenic perfusion measurement using dynamic CT. *AJR Am J Roentgenol* 170:153–155, 1998.
48. Huchzermeyer H, Schmitz-Feuerhake I, Reblin T: Determination of splenic blood flow by inhalation of radioactive rare gases. *Eur J Clin Invest* 7:345–349, 1977.
49. Fenchel S, Fleiter TR, Aschoff AJ, et al: Effect of iodine concentration of contrast media on contrast enhancement in multislice CT of the pancreas. *Br J Radiol* 77:821–830, 2004.
50. Torres GM, Terry NL, Mergo PJ, et al: MR imaging of the spleen. *Magn Reson Imaging Clin N Am* 3:39–50, 1995.
51. Ito K, Mitchell DG, Honjo K, et al: MR imaging of acquired abnormalities of the spleen. *AJR Am J Roentgenol* 168:697–702, 1997.
52. Mirowitz SA, Brown JJ, Lee JK, et al: Dynamic gadolinium-enhanced MR imaging of the spleen: Normal enhancement patterns and evaluation of splenic lesions. *Radiology* 179:681–686, 1991.
53. Ito K, Mitchell DG, Honjo K, et al: Gadolinium-enhanced MR imaging of the spleen: Artifacts and potential pitfalls. *AJR Am J Roentgenol* 167:1147–1151, 1996.
54. Soyer P, Scherrer A: Magnetic resonance imaging of the spleen: Influence of the dose of a gadolinium chelate on the degree of parenchymal enhancement. *Acad Radiol* 3:197–201, 1996.
55. Lin W, Guo J, Rosen MA, et al: Respiratory motion–compensated radial dynamic contrast-enhanced (DCE)–MRI of chest and abdominal lesions. *Magn Reson Med* 60:1135–1146, 2008.
56. Semelka RC, Shoenut JP, Lawrence PH, et al: Spleen: Dynamic enhancement patterns on gradient-echo MR images enhanced with gadopentetate dimeglumine. *Radiology* 185:479–482, 1992.
57. Rabushka LS, Kawashima A, Fishman EK: Imaging of the spleen: CT with supplemental MR examination. *Radiographics* 14:307–332, 1994.
58. Bruneton JN, Falewee MN, Francois E, et al: Liver, spleen, and vessels: Preliminary clinical results of CT with perfluorooctylbromide. *Radiology* 170:179–183, 1989.
59. Sohawon D, Lau KK, Lau T, et al: Extramedullary haematopoiesis: A pictorial review of its typical and atypical locations. *J Med Imaging Radiat Oncol* 56:538–544, 2012.
60. Thipphavong S, Duigenan S, Schindera ST, et al: Nonneoplastic, benign, and malignant splenic diseases: Cross-sectional imaging findings and rare disease entities. *AJR* 203:315–322, 2014.

Angiography and Interventional Radiology of the Spleen

J. SATHEESH KRISHNA | NAVEEN KALRA | AJAY K. SINGH

CHAPTER OUTLINE

General Preparation of the Patient

Image-Guided Biopsy

Catheter Drainage

Alcohol Ablation

Radiofrequency Ablation

Splenic Arterial Interventions

Embolization in Splenic Trauma

Embolization in Hypersplenism

Embolization in Portal Hypertension

Embolization of Splenic Artery Aneurysms or Pseudoaneurysms

Embolization in Splenic Arterial Steal Syndrome

Complications of Splenic Arterial Embolization

Transarterial Splenic Irradiation

Interventions in the spleen have not been performed widely because of the perceived increased risk of complications, especially bleeding. A widely prevailing notion is that splenic interventions result in increased morbidity from hemorrhagic complications. This perception partly stems from the fact that splenic interventions are performed infrequently compared with interventions in other abdominal viscera, and if a more accessible lesion is present in another organ, most operators prefer to sample the other lesion rather than the splenic lesion. However, with increased familiarity with these procedures and availability of finer needles, we are now able to perform these procedures more safely and confidently.

The literature reveals that the rates of complications are much lower than anticipated. In fact, mortality is much more common from liver and pancreatic interventional procedures than from splenic interventions, probably because of the higher number of liver and pancreatic procedures performed. The success rate is 91% for splenic biopsy, 100% for splenic fluid aspiration, and 86% for splenic fluid drainage.¹ These high success rates have been the prime impetus for widespread acceptance of splenic interventions in clinical practice.

This chapter covers the entire spectrum of splenic interventions with focus on image-guided biopsy, catheter drainage, alcohol ablation of cysts, radiofrequency ablation (RFA), and splenic artery embolization.

General Preparation of the Patient

Splenic interventions need no special prerequisite or preparation, and the general guidelines for interventions in the other

abdominal viscera apply. However, a more meticulous attention may be given to the clotting and coagulation parameters, and the following laboratory values are generally recommended: platelet count higher than 50,000/ μ L; international normalized ratio below 1.2; and activated partial thromboplastin time, 20 to 33 seconds.

The patients are instructed to fast either overnight or for 8 hours, as applicable. The procedures are usually performed under conscious sedation with midazolam or fentanyl for adults. Typically, 1% lidocaine local anesthetic is injected in the skin and abdominal wall. However, pediatric patients may require general anesthesia with dedicated support by the pediatric anesthetic team. Securing an intravenous access before the procedure is considered mandatory.

The patients are monitored for 3 hours after the percutaneous procedure. Regular monitoring of blood pressure and pulse rate is advisable. We monitor the vital signs every 15 minutes for the first hour and every 30 minutes for the next 2 hours. Patients who remain stable in the observation period with no or only minimal discomfort can be discharged home. The patients are instructed to avoid significant physical exertion and lifting of heavy weights for at least 3 days.

Image-Guided Biopsy

The central theme of biopsy is to obtain tissue diagnosis by minimally invasive means to preclude the need for unnecessary splenectomy. Thus, the prime candidates for biopsy are patients with an indeterminate solid or cystic lesion in whom a definitive diagnosis cannot be established after clinicoradiologic correlation. The most common clinical scenarios requiring biopsy of a focal splenic lesion include patients with a known extrasplenic neoplasm and patients with known or suspected lymphoma.

Depending on the lesion, either computed tomography (CT) or ultrasound (US) guidance can be used. The choice also depends on the comfort level of the radiologist and the visibility of the lesions by either modality. In general, US is the preferred modality because of real-time guidance and quicker access. Moreover, Doppler US can also be performed before and during the biopsy to detect and to avoid large hilar vessels.

General aseptic and guiding principles apply for image-guided biopsy procedures. The biopsy sample is taken in suspended respiration. The most peripheral lesions are preferably sampled to allow a shorter parenchymal needle track and to avoid inadvertent injury to the hilar vasculature. Biopsy is done from the periphery of the lesion to decrease the possibility of obtaining necrotic material from the center. Lesions near the dome of the diaphragm need real-time US guidance or gantry tilt CT technique to avoid puncture of the pleura. US or CT is usually performed at the end of the procedure to rule out hematoma formation.

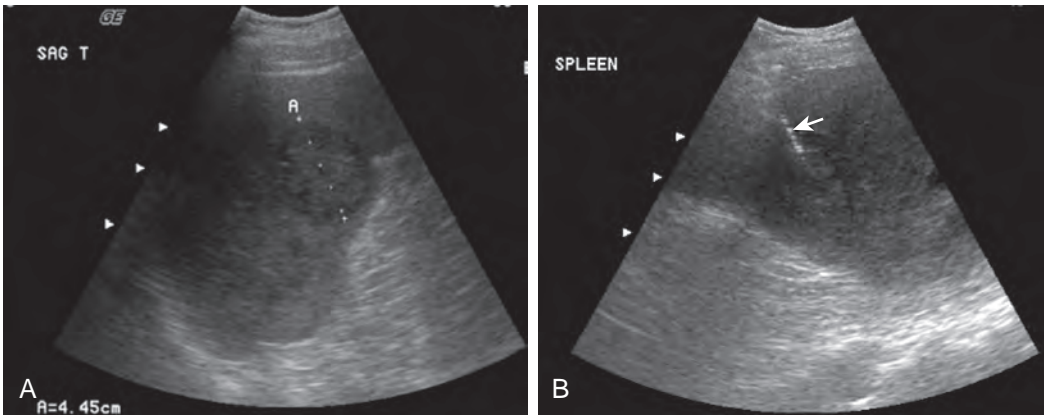


Figure 103-1 US-guided biopsy of focal splenic mass. **A.** A focal, heterogeneously echogenic lesion is seen in the spleen on US measured between the calipers labelled A. **B.** The focal lesion is seen with needle in situ (arrow). The histopathologic evaluation revealed hamartoma.

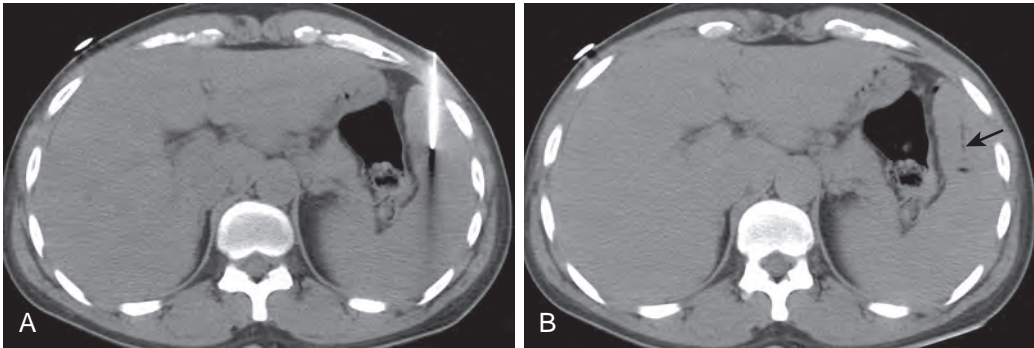


Figure 103-2 CT-guided biopsy of splenic mass. **A.** Axial CT shows a 17-gauge coaxial needle in the splenic parenchyma. **B.** Postprocedural CT shows the biopsy track (arrow). The histopathologic diagnosis was extramedullary hematopoiesis.

One of the more controversial areas in splenic lesion biopsy is the size of the needle used. In general, the sizes range from 18- to 22-gauge for core biopsy and 20- to 23-gauge for fine-needle aspiration (Figs. 103-1 and 103-2). Core needle biopsy has an approximately 88% or better sensitivity in making a diagnosis in varying studies in the literature.¹⁻¹² The success rates, however, are lower with fine-needle aspiration procedures.^{2,5} A spinal needle is used for lesions less than 8 cm in depth, and a Chiba needle is used for lesions situated deeper than 8 cm.

The number of passes obtained is usually at the discretion of the interventional radiologist performing the procedure. Additional passes are obtained in cases of suspected lymphoma to obtain material for immunophenotyping by flow cytometry and cell block. If cytology shows no evidence of malignant transformation, a portion of the aspirate is sent for culture and sensitivity profiling.

The complications that may be encountered include hemorrhage, pneumothorax, pleural effusion, and bowel injury (Table 103-1 and Fig. 103-3). The most dreaded of the complications is uncontrolled non-self-limited hemorrhage, which may require blood transfusion, embolization, or splenectomy. One method to ensure hemostasis along the needle track is to inject gelatin sponge at the end of the procedure. However, if hemorrhage does occur nevertheless, it is then managed with aggressive fluid resuscitation and blood transfusions. Progressive hematomas not responding to conservative management may

TABLE 103-1 Complications of Splenic Biopsy			
Study	Needle (gauge)	Patients	Complications
Tam et al, ¹² 2008	22	147	1.9% major (two splenectomies) 14.7% minor 2%
Liang et al, ⁷ 2007	21, 18	46	None
Kang et al, ⁶ 2007	22	78	None
Muraca et al, ⁴ 2001	18-21	30	None
Keogan et al, ³ 1999	20-22	18	None
Lieberman et al, ² 2003	20-22	20	10% minor (hemorrhage)
Lucey et al, ¹ 2002	18-23	24	10% (two splenectomies and one case of bleeding)

be subjected to catheter angiography with embolization. Splenectomy may be resorted to if all else fails.

In general, these complications occur with increasing frequency with increasing caliber of the biopsy needle. Fine-needle aspiration is generally considered safer than core biopsy. In one series, no complications were reported in 1000 blind

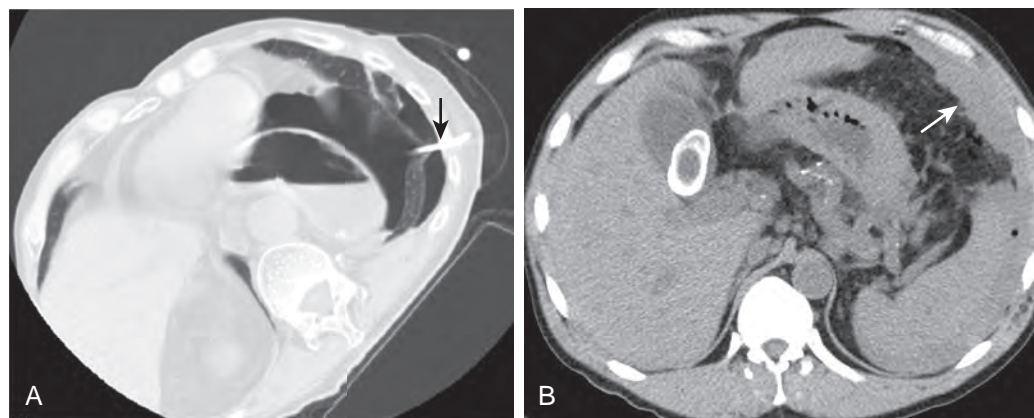


Figure 103-3 Postbiopsy complications. **A.** Postbiopsy CT showed a left-sided pneumothorax that was successfully managed with catheter drainage (arrow). **B.** Postbiopsy CT shows hemorrhage (arrow) in the left upper quadrant, which was conservatively managed.

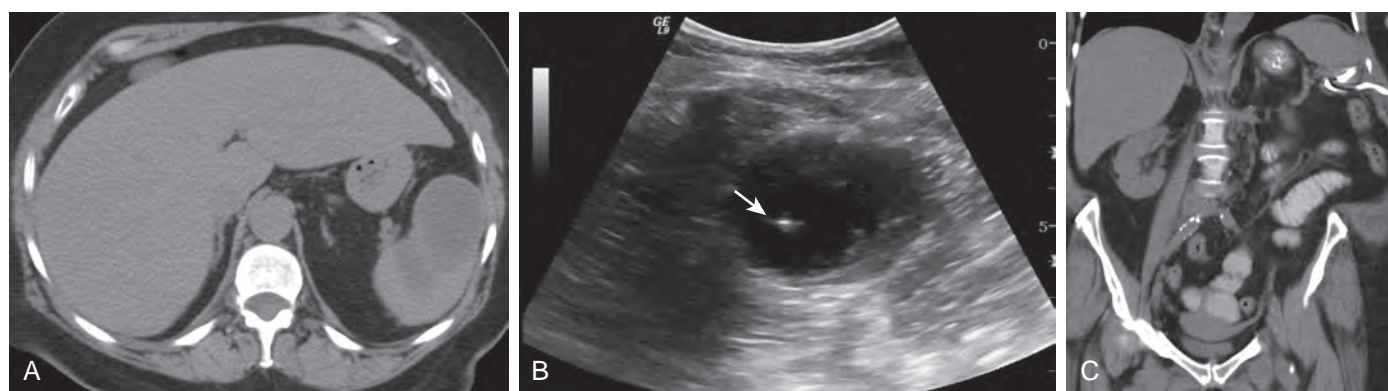


Figure 103-4 Catheter drainage of splenic abscess. **A.** Noncontrast CT demonstrates a focal fluid-density hypodense lesion in the splenic parenchyma. **B.** US revealed that the focal lesion was predominantly anechoic with dependent debris, suggesting an abscess. The echogenic needle tip is seen (arrow) within the abscess cavity. **C.** Follow-up CT after the procedure shows the pigtail catheter in the lower pole of the spleen with collapse of the abscess cavity.

fine-needle aspiration procedures done with 22-gauge needles, whereas another series reported a complication rate of 12% (four of 32 patients) with a 14-gauge core biopsy needle, with one patient needing splenectomy and three needing transfusions^{8,9} (Table 103-1).

Catheter Drainage

Traditionally, splenic abscesses were managed with antibiotics, and splenectomy was resorted to if antibiotic treatment failed. Image-guided aspiration with catheter drainage is an excellent minimally invasive alternative with a high success rate.^{1,13-15} In addition to being less invasive than surgery, it also helps preserve the spleen and avoid the long-term immunologic dysfunctions seen with splenectomy.

The ideal collection amenable to drainage is a unilocular collection with a discrete wall without internal septations or loculations. As with biopsy, collections in the periphery, especially in the middle or lower pole, are easier to drain. A trial aspiration is done, and the catheter is inserted if frank pus is aspirated. The most commonly used catheters are the pigtail catheters in varying sizes ranging from 7F to 12F (Fig. 103-4).^{1,13} In general, more viscous abscesses need larger bore catheters, and the catheter may need to be upgraded to a larger one in case of inadequate drainage.

Although multiloculated abscesses are more difficult to drain, drainage of these abscesses can be done with one or more catheters. The hydrostatic pressure that is created by the drainage can break the septations and drain the entire cavity. The septations can also be broken by injection of urokinase through the catheter.¹⁶

As with biopsy, either US or CT may be used for guidance and navigation. The two commonly used methods are the trocar technique and the Seldinger technique. Whereas the trocar technique is quicker, the Seldinger technique is more precise at the expense of a slightly longer procedure time. There is also a possibility of loss of access in cases of buckling or kinking of the guidewire in the Seldinger technique.

It is mandatory to flush catheters with saline every 8 hours to prevent clogging of the lumen and the side holes. Repeated flushing also makes the collection less viscous and easy to drain. The catheter can be removed when the tube drains less than 10 mL/day for 3 consecutive days. Care should be taken to straighten the hook-shaped curve of the pigtail catheter before pulling it out to minimize pain as well as soft tissue injury.

The drainage catheter is often placed for about 7 to 14 days. The prerequisites for catheter removal are patient improvement clinically (including normal temperature and white blood cell count) and resolution of the cavity. Typically, the catheter is

discontinued when the catheter output is 10 mL/24 hours and no residual cavity is seen on imaging.

Again, as with image-guided biopsy, hemorrhage is a serious complication, and the rate of significant uncontrolled bleeding requiring splenectomy is considerably higher compared with biopsy.^{1,14} Hence, meticulous monitoring for a longer period (24 hours) is advisable versus the shorter (3 hours) monitoring time after biopsies.

Alcohol Ablation

Alcohol ablation sclerotherapy works on the principle of denaturation of proteins in the wall of the cyst, eventually leading to cell death and fibrosis of the cyst wall. It has been extensively used in symptomatic cysts and hydatid cysts in the solid viscera, especially in hepatic and renal cysts.¹⁷⁻¹⁹ Other sclerosants, like tetracycline, have also been used successfully in children.²⁰ The advantages of this therapy are its easy availability, high efficacy, and technical ease compared with surgery.

The symptomatic splenic cysts may be treated by alcohol ablation. These cysts are usually large, and therefore an 8F to 10F pigtail catheter is placed inside the cyst under image guidance (Fig. 103-5). All the fluid is aspirated, which is then sent for cytologic and microbiologic analysis. Contrast material may be injected through the placed pigtail catheter at this point to ensure optimal catheter placement and to rule out any intraperitoneal spillage. An intraperitoneal spillage of contrast material would be a contraindication to alcohol therapy.

Once catheter access has been achieved and the fluid content aspirated, 95% ethyl alcohol is injected into the cyst. The volume injected is generally half the amount of fluid that was aspirated (up to a maximum of 100 mL). After 20 minutes, the entire injected alcohol is reaspirated, and this is confirmed on CT. A follow-up CT scan after 3 months is obtained to look for any recurrences. The ablation therapy may be repeated in case of recurrence.

The complications include pain, bleeding, hypotension, infection, and damage to adjacent structures due to inadvertent spillage of the sclerosant.

Radiofrequency Ablation

RFA is based on the principle of radiofrequency deposition at the needle tip, which leads to ionic agitation and frictional

heating. At temperatures in excess of 50°C, tissue desiccation and protein denaturation result in coagulative necrosis.

RFA has been used for local treatment of splenic neoplasm, especially secondary metastases. Significant shrinkage of the lesion has been demonstrated at 6-month follow-up.²¹ Improvement in platelet count as well as liver function has been documented after ablation of 30% to 40% of splenic volume in patients with hypersplenism.²²⁻²⁴ RFA has also been used to desiccate the splenic tissue surrounding an infected hydatid cyst before surgical removal.²⁵

Although RFA has been successfully used in a variety of body parts for a variety of indications, the literature on splenic RFA is relatively sparse, again likely attributable to the fear associated with bleeding complications in splenic interventions. However, counterintuitively, RFA has been used to treat grade 4 splenic lacerations in pigs.²⁶ Further studies are required before RFA becomes a mainstream interventional tool in managing splenic lesions.

Splenic Arterial Interventions

Arterial interventions in the spleen are increasingly used nowadays and may be substituted for surgery in specific clinical indications. A good knowledge of arterial anatomy is needed for successful embolization as well as prevention of unintended complications.

EMBOLIZATION IN SPLENIC TRAUMA

The spleen is the most commonly injured solid abdominal organ. Because of the risk of fatal sepsis after splenectomy and impaired immunity to organisms, there has been a paradigm shift from surgical to nonsurgical management. This conservative management strategy for splenic trauma has a significant inherent failure rate (from 2% to 52%).^{27,28} Splenic arterial embolization may be used to reduce this failure rate and to preclude the need for secondary splenectomies.

Embolization is especially indicated when there is evidence of arterial injury on CT. In such cases, microcoils are deployed as distally as possible in the bleeding artery to preserve the perfusion to the rest of the spleen. Distal splenic embolizations are associated with higher rates of infarction and intrasplenic air.²⁹ Air, in this setting, is not indicative of abscess formation. Proximal embolization is indicated in patients with a high risk

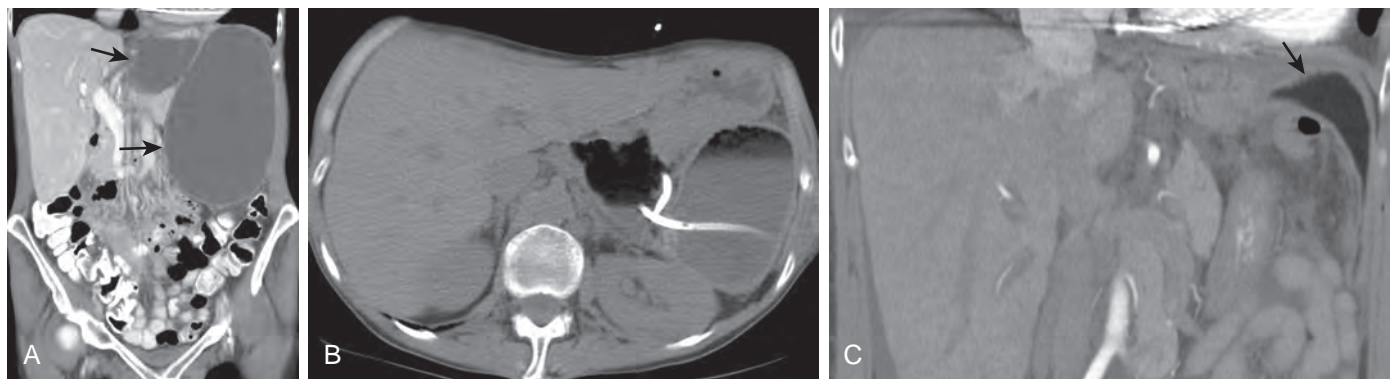


Figure 103-5 Alcohol ablation of splenic cyst. **A.** Contrast enhanced CT shows a large bilobed cyst (arrows) in the spleen that was symptomatic because of the mass effect. **B.** Axial CT shows a drainage catheter placed across the two cysts. The nondependent low-density fluid in the cysts represents the 95% alcohol injected into the cysts for the ablation procedure. **C.** Postablation CT scan shows marked reduction in the size of the cyst (arrow).

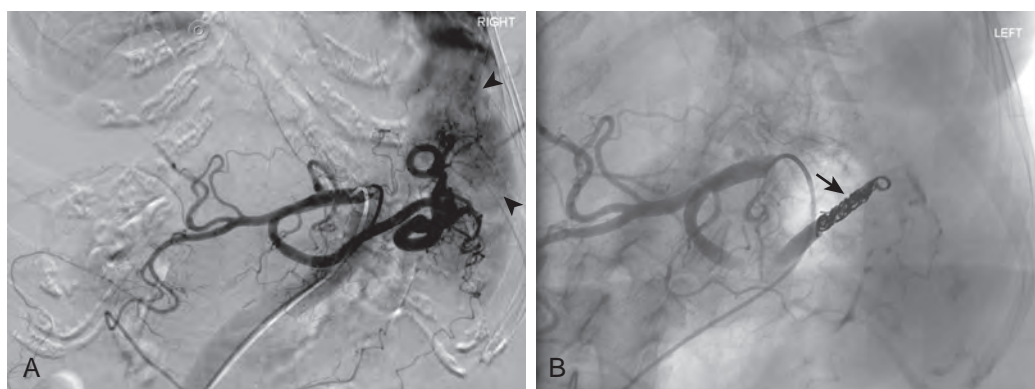


Figure 103-6 Splenic artery embolization for splenic laceration. **A.** Selective celiac artery angiogram demonstrates extravasation of contrast material (arrowheads) in a patient with grade 4 splenic laceration. **B.** Postprocedural angiogram performed after placement of twelve 0.035-inch Tornado coils (arrow) in the main splenic artery shows complete occlusion of the splenic artery.

of secondary rupture to decompress the splenic parenchyma and to reduce the pressure in the system (Fig. 103-6). This allows collateralization, principally through the short gastric and gastroepiploic arteries, to the patent distal splenic, transgastric, and transpancreatic arteries, and the relative hypotension produced allows splenic repair and regeneration without infarction.^{30,31} Also, in patients who have intraprocedural hemodynamic deterioration, a quicker, more proximal embolization can be performed.

EMBOLIZATION IN HYPERSPLENISM

Hypersplenism, seen most commonly in patients with cirrhosis and portal hypertension, is characterized by sequestration as well as destruction of corpuscular elements of blood. Proximal splenic arterial embolization is usually unsuccessful in this setting because of extensive collateral blood flow. Incomplete or partial splenic embolization is advocated in this setting to reduce the amount of viable splenic parenchyma. Ideally, the aim is 60% to 70% splenic parenchymal infarction because the hematologic response correlates with the degree of infarction. The general guideline, usually termed the Spigos technique, is as follows³²:

- Pneumococcal vaccines are administered before the procedure.

- Broad-spectrum antibiotics are administered 8 to 12 hours before the procedure and continued for 2 weeks after the procedure.

- Local antibiotics are suspended in the embolic solution.

- The procedure is performed under strict aseptic precautions.

- Selective catheterization is attained beyond the origin of the major arteries to the pancreas to prevent their embolization.

- Embolization is performed with particulate embolic agents. Avoid excessive embolization (not more than 80% infarction).

- Provide postprocedural pain management and prevent pulmonary complications.

Two methods of embolization include selective partial embolization and nonselective partial embolization. Selective partial embolization involves superselective cannulation and embolization of distal branches of the splenic artery. The rest of the branches are left untreated and provide blood flow to

viable splenic parenchyma. A check angiogram in the parenchymal phase reveals the viable splenic parenchyma with areas of dropout of contrast material that correspond to the degree of infarction.

Nonselective partial embolization involves embolization with the catheter tip in a more proximal position in the main splenic artery, distal to the origin of major pancreatic branches. Generalized reduction of parenchymal blush is the usual endpoint.

Although proximal splenic arterial occlusion is ineffective treatment of hypersplenism, it may be used preoperatively to reduce intraoperative blood loss in patients undergoing splenectomy, especially because most of these patients have thrombocytopenia due to hypersplenism.

EMBOLIZATION IN PORTAL HYPERTENSION

Partial splenic embolization may also have a place in the management of portal hypertension and resistant variceal hemorrhage. Embolization decreases venous return from the spleen, thereby reducing portal pressures.

EMBOLIZATION OF SPLENIC ARTERY ANEURYSMS OR PSEUDOANEURYSMS

Aneurysms of the splenic artery are usually small (<2 cm) and saccular and are commonly located at branch points. They are more commonly found in multiparous women and patients with cirrhosis and portal hypertension. Pseudoaneurysms of the splenic artery most commonly occur as sequelae of pancreatitis. The release of proteolytic enzymes in pancreatitis results in necrotizing arteritis and fragmentation of elastic fibers in the vessel wall with resultant destruction of vessel wall architecture. This results in pseudoaneurysm formation, which may lead to gastrointestinal bleeding.

Splenic artery aneurysms are embolized in cases of symptomatic aneurysms, in women of childbearing age, in portal hypertension, and with size larger than 2.5 cm. It is considered that all splenic artery pseudoaneurysms need treatment regardless of size and symptoms as the natural history of an asymptomatic pseudoaneurysm of the splenic artery is not known. Traditionally, treatment involved surgical ligation. Recently, however, endovascular transcatheter embolization is considered the management of choice.³³⁻³⁵ Coils can be deployed directly

into the aneurysmal sac, or the neck of the aneurysm can be excluded by the "sandwich method" of deploying coils both proximal and distal to the neck. Percutaneous image-guided thrombin injection can also be used in selective cases.³⁶⁻³⁸ Endoscopic US-guided thrombin injection has also been tried.³⁹ A flexible self-expanding covered stent to exclude the aneurysm is an attractive option as it preserves the blood flow through the splenic artery.

EMBOIZATION IN SPLENIC ARTERIAL STEAL SYNDROME

Splenic arterial steal syndrome is a rare complication of liver transplantation, the classic triad being liver failure, reduced hepatic arterial perfusion, and increased blood flow in the splenic circulation after liver transplantation. This is due to decreased splenic arteriolar resistance, which is common in cirrhotics with portal hypertension. Prompt diagnosis and management are essential as it mimics graft failure.⁴⁰

Although hepatic arterial reimplantation into the aorta is the ideal therapeutic option, a minimally invasive procedure is usually preferred because of increased morbidity associated with the second surgery. Splenic arterial embolization is an attractive option to decrease shunting of blood into the splenic circulation.⁴¹

COMPLICATIONS OF SPLENIC ARTERIAL EMBOLIZATION

Potential complications of splenic arterial embolization include hemorrhage, infarction, abscess formation, systemic infection, iatrogenic vascular injury (splenic vein thrombosis), coil migration, necrosis of stomach wall, and pancreatitis. A postembolization syndrome is common; it consists of low-grade fever and left upper quadrant pain with leukocytosis and may require analgesics for relief of symptoms.

Transarterial Splenic Irradiation

External beam radiotherapy has been effective in lymphoma, leukemia, myelofibrosis, idiopathic thrombocytopenic purpura, and polycythemia vera. Intra-arterial irradiation is emerging as an encouraging alternative to decrease complications associated with external beam radiotherapy and to increase the maximum allowable dose. The usual agent is yttrium-90 microspheres.⁴²⁻⁴⁴

A variety of interventional tools and modalities have been used with varying success in management of splenic lesions. Awareness of the indications and limitations of individual techniques is essential to minimize potential complications in splenic interventions.

REFERENCES

- Lucey BC, Boland GW, Maher MM, et al: Percutaneous nonvascular splenic intervention: A 10-year review. *AJR Am J Roentgenol* 179:1591-1596, 2002.
- Lieberman S, Libson E, Maly B, et al: Imaging-guided percutaneous splenic biopsy using a 20- or 22-gauge cutting-edge core biopsy needle for the diagnosis of malignant lymphoma. *AJR Am J Roentgenol* 181:1025-1027, 2003.
- Keogan MT, Freed KS, Paulson EK, et al: Imaging-guided percutaneous biopsy of focal splenic lesions: Update on safety and effectiveness. *AJR Am J Roentgenol* 172:933-937, 1999.
- Muraca S, Chait PG, Connolly BL, et al: US-guided core biopsy of the spleen in children. *Radiology* 218:200-206, 2001.
- Venkataramu NK, Gupta S, Sood BP, et al: Ultrasound guided fine needle aspiration biopsy of splenic lesions. *Br J Radiol* 72:953-956, 1999.
- Kang M, Kalra N, Gulati M, et al: Image guided percutaneous splenic interventions. *Eur J Radiol* 64:140-146, 2007.
- Liang P, Gao Y, Wang Y, et al: US-guided percutaneous needle biopsy of the spleen using 18-gauge versus 21-gauge needles. *J Clin Ultrasound* 35:477-482, 2007.
- Söderström N: How to use cytodiagnostic spleen puncture. *Acta Med Scand* 199:1-5, 1976.
- Lindgren PG, Hagberg H, Eriksson B, et al: Excisional biopsy of the spleen by ultrasonic guidance. *Br J Radiol* 58:853-857, 1985.
- Zeppa P, Vetrani A, Luciano L, et al: Fine needle aspiration biopsy of the spleen: A useful procedure in the diagnosis of splenomegaly. *Acta Cytol* 38:299-309, 1994.
- Cavanna L, Civardi G, Fornari F, et al: Ultrasoundically guided percutaneous splenic tissue core biopsy in patients with malignant lymphomas. *Cancer* 69:2932-2936, 1992.
- Tam A, Krishnamurthy S, Pillsbury EP, et al: Percutaneous image-guided splenic biopsy in the oncology patient: An audit of 156 consecutive cases. *J Vasc Interv Radiol* 19:80-87, 2008.
- Thanos L, Dailiana T, Papaioannou G, et al: Percutaneous CT-guided drainage of splenic abscess. *AJR Am J Roentgenol* 179:629-632, 2002.
- Taşar M, Uğurel MS, Kocaoglu M, et al: Computed tomography-guided percutaneous drainage of splenic abscesses. *Clin Imaging* 28:44-48, 2004.
- Gasparini D, Basadonna PT, Di Donna A: Splenic abscesses: Their percutaneous treatment and the role of the interventional radiologist [in Italian]. *Radiol Med (Torino)* 87:803-807, 1994.
- Lahorra JM, Haaga JR, Stellato T, et al: Safety of intracavitary urokinase with percutaneous abscess drainage. *AJR Am J Roentgenol* 160:171-174, 1993.
- Ustünsöz B, Akhan O, Kamiloğlu MA, et al: Percutaneous treatment of hydatid cysts of the liver: Long-term results. *AJR Am J Roentgenol* 172:91-96, 1999.
- Giorgio A, de Stefano G, Esposito V, et al: Long-term results of percutaneous treatment of hydatid liver cysts: A single center 17 years experience. *Infection* 36:256-261, 2008.
- Etlík O, Arslan H, Bay A, et al: Abdominal hydatid disease: Long-term results of percutaneous treatment. *Acta Radiol* 45:383-389, 2004.
- Moir C, Guttman F, Jequier S, et al: Splenic cysts: Aspiration, sclerosis, or resection. *J Pediatr Surg* 24:646-648, 1989.
- Wood BJ, Bates S: Radiofrequency thermal ablation of a splenic metastasis. *J Vasc Interv Radiol* 12:261-263, 2001.
- Feng K, Ma K, Liu Q, et al: Randomized clinical trial of splenic radiofrequency ablation versus splenectomy for severe hypersplenism. *Br J Surg* 98:354-361, 2011.
- Liu Q, Ma K, Song Y, et al: Two-year follow-up of splenic radiofrequency ablation in patients with cirrhotic hypersplenism: Does increased hepatic arterial flow induce liver regeneration? *Surgery* 143:509-518, 2008.
- Liu Q, Ma K, He Z, et al: Radiofrequency ablation for hypersplenism in patients with liver cirrhosis: A pilot study. *J Gastrointest Surg* 9:648-657, 2005.
- Zacharoulis D, Katsogridakis E, Hatzitheofilou C: A case of splenic abscess after radiofrequency ablation. *World J Gastroenterol* 12:4256-4258, 2006.
- Felekouras E, Kontos M, Pissanou T, et al: A new spleen-preserving technique using radiofrequency ablation technology. *J Trauma* 57:1225-1229, 2004.
- Velmahos GC, Toutouzas KG, Radin R, et al: Nonoperative treatment of blunt injury to solid abdominal organs. *Arch Surg* 138:844-851, 2003.
- Miller PR, Chang MC, Hoth JJ, et al: Prospective trial of angiography and embolization for all grade III to V blunt splenic injuries: Nonoperative management success rate is significantly improved. *J Am Coll Surg* 218:644-648, 2014.
- Killeen KL, Shanmuganathan K, Boyd-Kranis R, et al: CT findings after embolization for blunt splenic trauma. *J Vasc Interv Radiol* 12:209-214, 2001.
- Scalfani SJ, Shaftan GW, Scalea TM, et al: Nonoperative salvage of computed tomography-diagnosed splenic injuries: Utilization of angiography for triage and embolization for hemostasis. *J Trauma* 39:818-825, 1995.
- Link DP, Seibert JA, Gould J, Lantz BM: Online monitoring of sequential blood flow reduction

- during splenic embolization. *Acta Radiol* 30:101–103, 1989.
32. Spigos DG, Jonasson O, Mozes M, Capek V: Partial splenic embolization in the treatment of hypersplenism. *AJR Am J Roentgenol* 132:777–782, 1979.
 33. Golzarian J, Nicaise N, Devière J, et al: Transcatheter embolization of pseudoaneurysms complicating pancreatitis. *Cardiovasc Intervent Radiol* 20:435–440, 1997.
 34. Gambiez LP, Ernst OJ, Merlier OA, et al: Arterial embolization for bleeding pseudocysts complicating chronic pancreatitis. *Arch Surg* 132:1016–1021, 1997.
 35. McDermott VG, Shlansky-Goldberg R, Cope C: Endovascular management of splenic artery aneurysms and pseudoaneurysms. *Cardiovasc Intervent Radiol* 17:179–184, 1994.
 36. Stone P, Lohan JA, Copeland SE, et al: Iatrogenic pseudoaneurysms: Comparison of treatment modalities, including duplex-guided thrombin injection. *W V Med J* 99:230–232, 2003.
 37. Armstrong EM, Edwards A, Kingsnorth AN, et al: Ultrasound guided thrombin injection to treat a pseudoaneurysm secondary to chronic pancreatitis. *Eur J Vasc Endovasc Surg* 26:448–449, 2003.
 38. McErlean A, Looby S, Lee MJ: Percutaneous ultrasound-guided thrombin injection as first-line treatment of pancreatic pseudoaneurysm. *Cardiovasc Intervent Radiol* 30:526–528, 2007.
 39. Robinson M, Richards D, Carr N: Treatment of a splenic artery pseudoaneurysm by endoscopic ultrasound-guided thrombin injection. *Cardiovasc Intervent Radiol* 30:515–517, 2007.
 40. De Carlis L, Sansalone CV, Rondinara GF, et al: Splenic artery steal syndrome after orthotopic liver transplantation: Diagnosis and treatment. *Transplant Proc* 25:2594–2596, 1993.
 41. Uflacker R, Selby JB, Chavin K, et al: Transcatheter splenic artery occlusion for treatment of splenic artery steal syndrome after orthotopic liver transplantation. *Cardiovasc Intervent Radiol* 25:300–306, 2002.
 42. Ariel IM, Padula G: Irradiation of the spleen by the intra-arterial administration of 90 yttrium microspheres in patients with malignant lymphoma: A preliminary report. *Cancer* 31:90–96, 1973.
 43. Becker CD, Rosler H, Biasiutti FD, Baer HU: Congestive hypersplenism: Treatment by means of radioembolization of the spleen with Y-90. *Radiology* 195:183–186, 1995.
 44. Muylle K, Nguyen J, de Wind A, et al: Radioembolization of the spleen: A revisited approach for the treatment of malignant lymphomatous splenomegaly. *Cardiovasc Intervent Radiol* 36:1155–1160, 2013.

Anomalies and Anatomic Variants of the Spleen

STEPHEN THOMAS | ABRAHAM H. DACHMAN

CHAPTER OUTLINE

Embryology

Splenic Clefts, Lobulations, and Bands

Wandering or Ectopic Spleen

Clinical Findings

Radiologic Findings

Diagnostic Approach and Therapy

Accessory Spleen

Clinical Findings

Radiologic Findings

Splenic-Gonadal Fusion

Heterotaxy Syndromes

Asplenia Syndrome

Polysplenia Syndrome

Embryology

Splenic development begins in the fifth week of gestation from a condensation of mesenchymal cells that aggregate between the two leaves of the dorsal mesogastrium. Aggregates from several adjoining areas fuse to form a lobulated embryonic spleen.¹ Rotation of the stomach and growth of the dorsal mesogastrium cause the translocation of the developing spleen from the midline to the upper left side of the abdominal cavity, and the mesogastrium fuses with the peritoneum over the left kidney, forming the splenorenal ligament (Fig. 104-1).² This causes the lienorenal ligament to fuse dorsally, and the splenic artery has a course to the left behind the peritoneum as it enters the splenorenal ligament in the adult.

The capsule, connective tissue framework, and parenchyma of the spleen form from differentiated mesenchymal cells. The spleen serves a hematopoietic function from the fourth to the eighth month of gestation. Lymphocyte and monocyte production, however, continues throughout life.¹

Splenic Clefts, Lobulations, and Bands

In the fetal period, the spleen is lobulated; however, the lobulations normally disappear before birth. Lobulation may persist along the medial (hilar) aspect of the spleen and is considered a normal feature of splenic anatomy. Notches or clefts along the superior border are remnants of the grooves that originally separated fetal lobules.² An abnormally deep fissure may give the appearance of a band. If the fissure traverses the entire

spleen, a waist is created that may mimic a laceration. Peritoneum may be embedded on this waist and may mimic a hematoma, infarction, or laceration.³ Deep fissures tend to occur along the superior border of the spleen. When they occur along the inferior border, a lobule of splenic tissue may extend medially and anteriorly to the left kidney. Less frequently, the lobule may lie posterior to the upper pole of the left kidney and displace it anteriorly.⁴

Wandering or Ectopic Spleen

Wandering or ectopic spleen refers to migration of the spleen from its normal fixed posterolateral location in the left upper abdomen. The reported incidence is 0.16% on the basis of 3853 splenectomies performed for various indications involving all ages.⁵ It usually is manifested between the ages of 20 and 40 years; 70% to 80% of reported cases are in women in the reproductive age. One third of cases are found in children, most (70%) older than 10 years.⁶

The spleen is normally anchored in the left upper abdomen by two ligaments: the gastrosplenic ligament, which connects the spleen to the greater curvature of the stomach; and the splenorenal ligament, which connects the spleen to the left kidney and the posterior body wall.²

The etiology of wandering spleen may be congenital or acquired. Congenitally, the condition is from absence or weakness of one or more of the ligaments that affix the spleen in its normal position in the upper left abdomen. The spleen is instead solely attached by its vascular pedicle and can become a wholly intraperitoneal hypermobile organ. Rarely, a normal spleen may be seen in the left upper quadrant, and an accessory spleen may be mobile and wander.⁷

The pathologic process also may be acquired as a result of splenomegaly or ligamentous laxity, such as in pregnancy or muscular dystrophies.⁸ There is a higher incidence of wandering spleen in multiparous women, which suggests an etiologic role of hormonal effects and abdominal laxity associated with pregnancy.^{9,10} Wandering spleen has been reported in prune-belly syndrome and in cases of diseases causing splenic enlargement, such as splenic cysts, malaria, Hodgkin's disease, and lymphangioma.¹¹

CLINICAL FINDINGS

The clinical presentation of wandering spleen is variable. Affected patients may be asymptomatic and the condition may be detected incidentally. Diagnosis may be made incidentally as a mass on physical examination or imaging. Classically, a firm, movable, notched mass can be palpated. Symptoms occur when there is pressure on the vascular pedicle of the spleen or when torsion develops.⁸

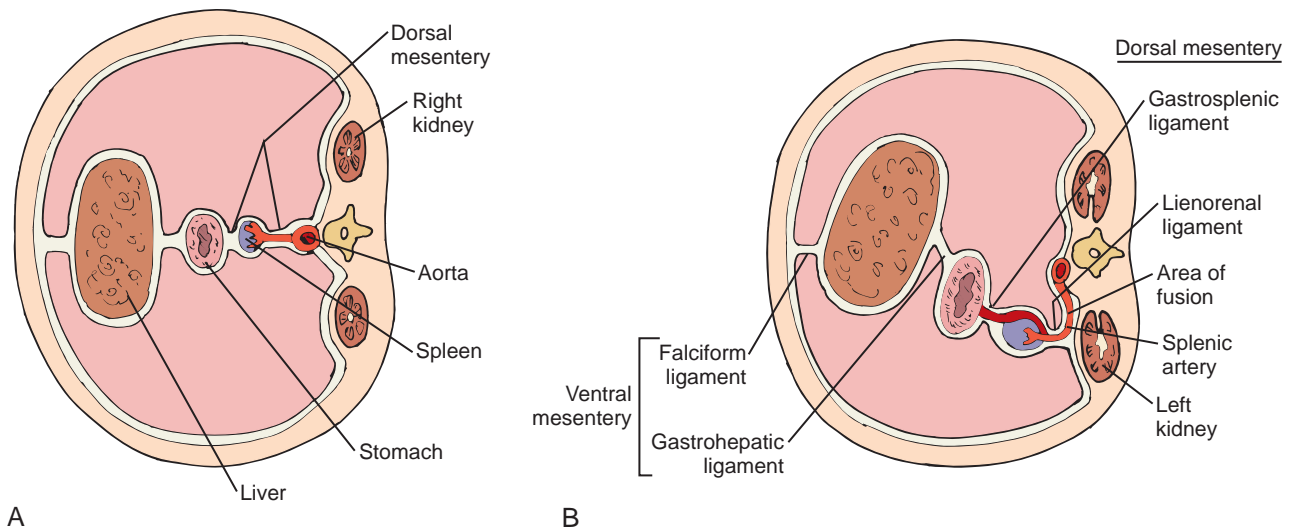


Figure 104-1 Embryology. **A.** Transverse section at the end of the fifth week shows the spleen developing within the dorsal mesogastrium. **B.** As rotation begins, the splenic artery courses to the left in an area of fusion of the dorsal mesogastrium with the posterior peritoneum. (From Dachman AH: *Normal anatomy and radiology*. In Friedman AC [ed]: *Radiology of the Liver, Biliary Tract, Pancreas, and Spleen*. Baltimore, Williams & Wilkins, 1987, pp 899–915.)

The most common presentation in children is acute abdominal pain. Patients may also present clinically with nonspecific symptoms, such as occasional nausea, emesis, or mild, crampy abdominal pain.¹¹ Pain may be vague in cases of chronic intermittent splenic torsion.¹² Wandering spleen with torsion may involve the tail of the pancreas, resulting in pancreatitis, and the splenic venous occlusion may result in splenomegaly and cause hypersplenism.⁹ Less common presentations of wandering spleen include small bowel or colonic obstruction and even duodenal obstruction due to compression by the splenic pedicle.⁶

RADIOLOGIC FINDINGS

Conventional Radiography

Supine and erect abdominal radiographs may show absence of the normal splenic silhouette or a mobile mass in the left or central abdomen. With the spleen absent from its normal location, bowel loops may fill the splenic fossa.¹³ The left kidney may be elevated and lack the usual splenic impression or hump and may cause elevation of the left hemidiaphragm.¹⁴

With the spleen not fixed in the abdomen, the elongated pedicle of the spleen or the displaced spleen can cause gastric outlet obstruction, small bowel obstruction, or colonic obstruction. Abdominal radiographs can show a distended stomach, a small bowel obstruction pattern, or colonic obstruction. The splenic pedicle may cause a linear defect across the involved bowel segment or colon.^{15–17}

Nuclear Scintigraphy

Technetium Tc 99m sulfur colloid scintigraphy can identify reticuloendothelial activity in the liver as well as in the spleen and is useful in identifying ectopic functional splenic tissue in the abdomen.¹⁸ Similarly, heat-denatured ^{99m}Tc-labeled red blood cell imaging, specific for splenic tissue, provides useful information for spleen size and localization as well as for the specific red blood cell sequestration function of the splenic tissue.¹⁹ A wandering spleen is diagnosed by normal uptake of

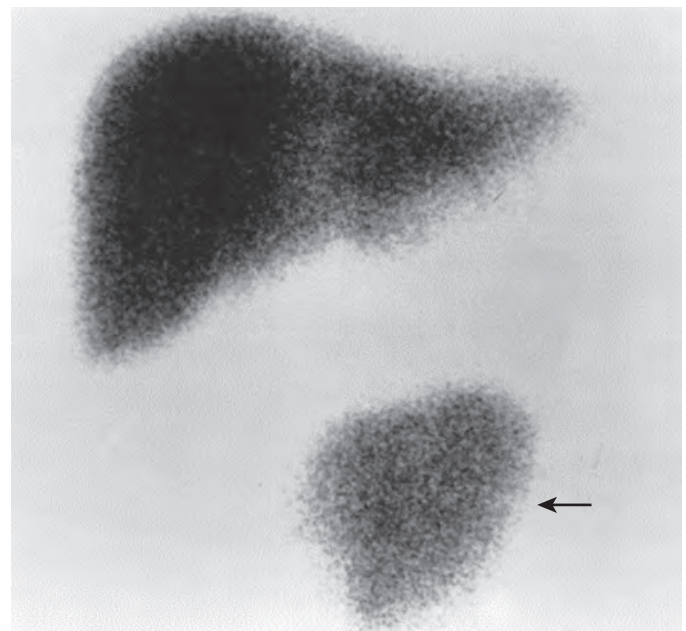


Figure 104-2 Wandering spleen. Anterior ^{99m}Tc-sulfur colloid scintigram shows absence of radiotracer activity in the left upper abdomen and uptake in an abnormally located spleen in the pelvis (arrow). The liver also shows normal radiotracer uptake (top). (From Paterson A, Frush DP, Donnelly LF, et al: *A pattern-oriented approach to splenic imaging in infants and children*. *RadioGraphics* 19:1465–1485, 1999.)

radiotracer by functioning splenic tissue in an abnormal location in the abdomen (Fig. 104-2). The lack of tracer activity in a previously demonstrated wandering spleen indicates torsion.²⁰

Ultrasound

Gray-scale sonography and power Doppler sonography are valuable in the diagnosis of wandering spleen and allow the diagnosis of complications such as torsion and infarction.

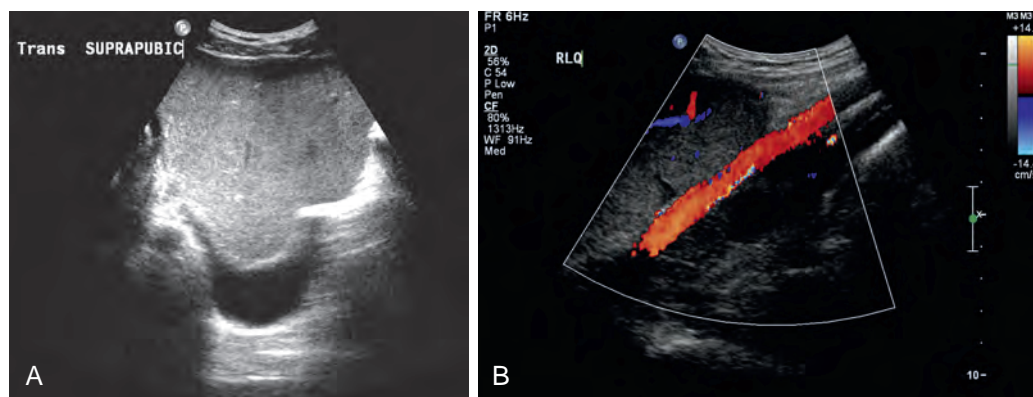


Figure 104-3 Wandering spleen: sonographic features. **A.** Transverse ultrasound image of the pelvis shows the spleen overlying the bladder. **B.** Color Doppler image shows blood flow in the splenic parenchyma adjacent to the iliac artery.

Sonography can confirm the absence of the spleen in its normal position in the left upper abdomen and can identify the ectopic spleen in the abdomen or pelvis (Fig. 104-3). The ectopic spleen is of uniform echotexture with a peripheral indentation on the mass, representing the hilar vasculature. Use of power Doppler, color Doppler, and duplex sonography allows evaluation of blood flow in the splenic parenchyma and in the major splenic vessels.^{21,22}

Real-time sonography can be used to identify splenic hypermobility and twisting of the vascular pedicle, which can increase risk of infarction. The spleen may be enlarged owing to an intermittent twist of the vascular pedicle and venous congestion.²³

Computed Tomography and Magnetic Resonance Imaging

Contrast-enhanced computed tomography (CT) can diagnose an ectopic spleen and its associated complications and is often performed as patients may present with abdominal pain. A pathognomonic CT finding of a wandering spleen is the absence of the spleen in the upper abdomen and the presence of a well-marginated homogeneously enhancing soft tissue mass in the abdomen or pelvis (Fig. 104-4).²⁴

Features of splenic torsion include poor or absent enhancement of splenic parenchyma, hyperdense pedicle indicating thrombosis, and enhancing splenic capsule from peripheral circulation. The whirl appearance of the splenic vascular pedicle is a specific sign of torsion. Splenomegaly, although not specific, is an important sign of torsion in the setting of a wandering spleen.²⁵ A markedly hypodense spleen due to infarction may be misdiagnosed as a mesenteric cyst, a dilated fluid-filled bowel loop, or an abscess.²⁶ Torsion of a wandering spleen may be associated with intestinal obstruction (due to compression of other abdominal organs), abscess formation, necrosis of the pancreatic tail, and recurrent pancreatitis.²⁷

Magnetic resonance imaging (MRI) has gained popularity in diagnosis of wandering spleen.^{28,29} It can locate the ectopic spleen and identify the viability of the splenic parenchyma as well as depict splenic vessel anatomy.³⁰

Angiography

Although it is not usually required for diagnosis, celiac arteriography may show torsion of wandering spleen by demonstrating a tapered and abruptly twisted distal splenic artery. The



Figure 104-4 Wandering spleen. Coronal contrast-enhanced CT shows abnormally located spleen in the pelvis, with small bowel loops in the left upper abdomen.

venous phase may suggest splenic vein obstruction and may show collateral circulation and varices.³¹ MR angiography can be particularly useful in demonstrating the location and length of the splenic artery before surgery.²⁹

DIAGNOSTIC APPROACH AND THERAPY

When wandering spleen is suspected, radiologic imaging should locate the ectopic spleen and evaluate the anatomy and patency of the splenic vessels. Evaluation of the viability of the splenic parenchyma, including any areas of infarction, is important as it guides therapy.

The definitive therapy for a wandering spleen is surgery. Splenopexy with splenic salvage is the preferred treatment in cases in which the spleen is viable after detorsion and the splenic vein is not thrombosed. Splenectomy is the option in cases of splenic infarction.³²

Accessory Spleen

Accessory spleen is a congenital anomaly caused by failure of embryonic splenic buds to unite within the dorsal mesogastrium and extreme lobulation of the spleen with pinching off of splenic tissue. Its reported incidence ranges from 10% to 30% in autopsy series.^{33,34} Accessory spleen is identified in 11% of patients undergoing contrast-enhanced CT³⁵ and 45% to 65% of patients after splenectomy.³⁶

Accessory splenic tissue measures between 1 and 3 cm in diameter but can be as large as the spleen. It is usually located about the splenic hilum or ligaments.³⁵ The tail of the pancreas is the second most common site for an accessory spleen, accounting for 16% of the cases.³⁴ Accessory spleens can be found in the wall of the stomach, the large bowel, the omentum, the mesentery, and rarely even the scrotum.^{37,38}

The morphologic appearance is identical to that of normal spleen, and the accessory tissue is usually supplied by a branch of the splenic artery and drains into splenic veins. Of the patients with an accessory spleen, 88% were solitary, 8% had two, and 3% had three.³⁵

CLINICAL FINDINGS

Accessory spleen is an incidental finding of no clinical significance in most patients. However, it can become symptomatic because of torsion or spontaneous rupture.³⁹ Accessory spleen is important to identify as it may mimic lymph nodes or tumors, especially in the tail of the pancreas.⁴⁰

Identification of all accessory splenic tissue is important in the setting of idiopathic thrombocytopenic purpura, in which all functional splenic tissue should be removed for the treatment of the hematologic disorder.⁴¹

RADIOLOGIC FINDINGS

Nuclear scintigraphy, sonography, CT, and MRI can identify and characterize accessory splenic tissue. The normal accessory spleen has the same echotexture and enhancement as normal spleen. When the tissue is recognized as an accessory spleen, no further work-up is needed. Diagnostic studies are indicated if this tissue simulates a neoplasm or if therapeutic splenectomy is planned in patients with hematologic disorders.⁴¹

On gray-scale ultrasound, accessory spleen is identified as a round or oval mass about the splenic hilum that is identical to spleen in echotexture. On color or power Doppler ultrasound, a vascular hilum entering the lesion is a diagnostic feature of accessory spleen.⁴² Contrast-enhanced ultrasound has been shown to demonstrate accessory spleen with an enhancement pattern paralleling that of the adjacent spleen.⁴³

On multiphase contrast-enhanced CT, an accessory spleen is usually identified as a well-circumscribed mass about the splenic hilum with an inhomogeneous striped arterial enhancement pattern identical to the spleen (Fig. 104-5).³⁵ Intrapane-creatic accessory spleen can mimic pancreatic neoplasms, such as hypervascular islet cell tumors. The attenuation of the spleen is



Figure 104-5 Accessory spleen: CT findings. An accessory spleen (arrow) is seen with a feeding vessel (arrowhead). It has the same attenuation and enhancement as the main spleen.

typically higher than that of the pancreas on the arterial, pancreatic, and portal venous phases, and similarly, intrapancreatic accessory spleen tends to be higher in attenuation than pancreas on all phases of imaging.⁴⁴ Conversely, hypervascular pancreatic tumors, including islet cell tumor, are hyperattenuating on the arterial phase and isoattenuating or lower attenuating to the adjacent pancreas on the venous phase.⁴⁵

On MRI, accessory spleen is isointense to mildly hypointense to spleen on T1 imaging and isointense to spleen on T2 imaging. Its enhancement pattern is identical to that of spleen on arterial, portal, and late phases of contrast enhancement (Fig. 104-6). Accessory spleen is isointense to spleen on diffusion-weighted imaging. The identical MRI features of accessory spleen to spleen allow the discrimination from pancreatic neoplasms.⁴⁶

^{99m}Tc-labeled heat-damaged red blood cell (^{99m}Tc-HDRBC) scintigraphy is a highly specific method for detection of splenic tissue as up to 90% of the injected HDRBCs are trapped by splenic tissue.⁴⁷ ^{99m}Tc-HDRBC scintigraphy allows selective splenic visualization with an excellent spleen-to-liver ratio; splenic visualization may be impaired when minimal functioning splenic tissue is present, as happens in cases of accessory spleens. In addition, ^{99m}Tc-HDRBC planar imaging scintigraphy and even single photon emission computed tomography (SPECT) offer inferior spatial resolution compared with other cross-sectional imaging modalities. ^{99m}Tc-HDRBC SPECT is frequently used in conjunction with other cross-sectional imaging modalities to diagnose and to precisely localize an accessory spleen (see Fig. 104-6).⁴⁸

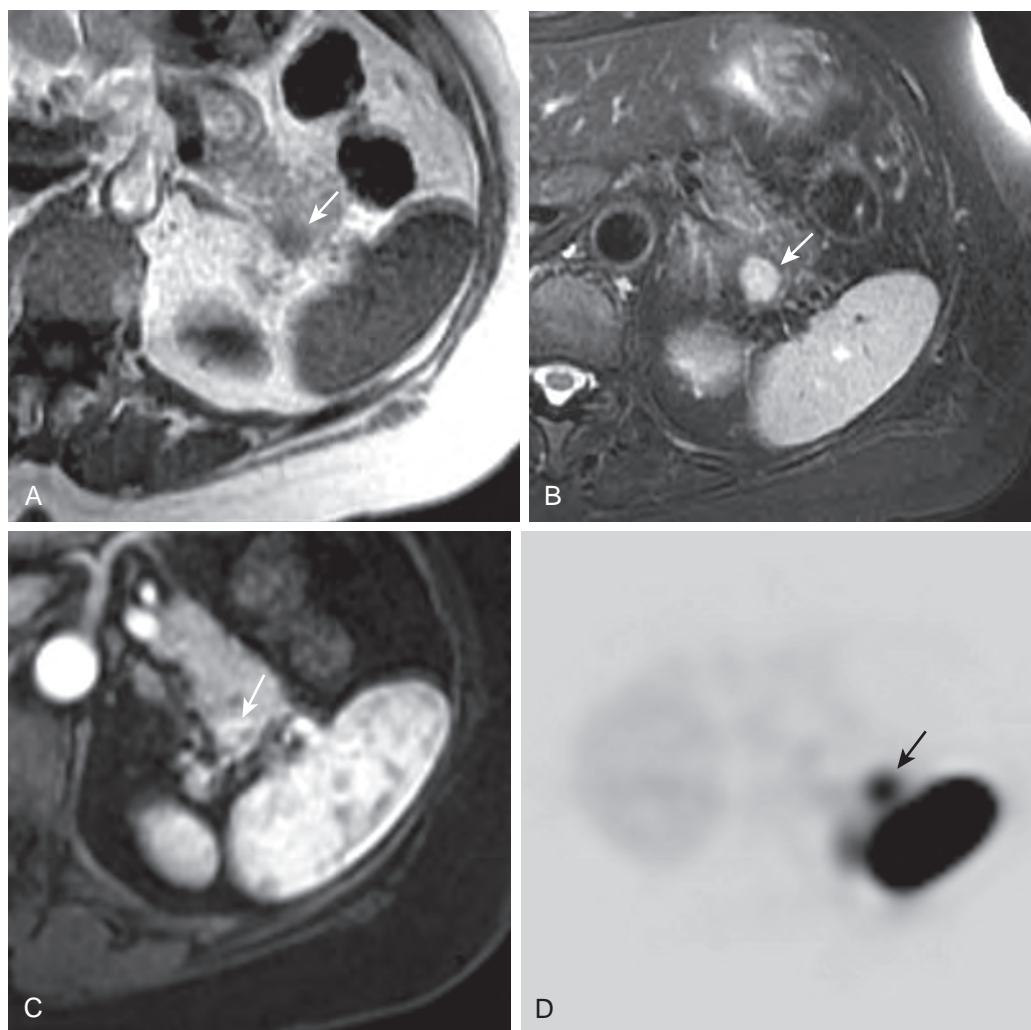


Figure 104-6 Intrapancreatic accessory spleen: MRI findings and ^{99m}Tc -HDRBC SPECT. **A.** T1-weighted axial MRI shows an intrapancreatic tail mass (arrow) that is hypointense to pancreas and mildly hypointense to spleen. **B.** T2 fat-saturated MRI shows the intrapancreatic mass (arrow) to be hyperintense to pancreas but isointense to spleen. **C.** Gadolinium-enhanced fat-saturated T1-weighted fast spoiled gradient recalled MRI shows the pancreatic tail mass (arrow) to have arterial enhancement similar to that of spleen. **D.** ^{99m}Tc -HDRBC SPECT shows focal uptake (arrow) near the splenic hilum in the region of the tail of the pancreas.

Splenic-Gonadal Fusion

This rare congenital anomaly is characterized by an abnormal connection between the gonad and the spleen or by ectopic splenic tissue. The left gonad is virtually always involved; only one case of right-sided involvement has been reported.⁴⁹ Before the sixth week of gestation, the splenic anlage developing in the left dorsal mesogastrium is close to the left urogenital fold that contains gonadal mesoderm during rotation of the embryonic gut. The accepted theory is that splenic-gonadal fusion is the abnormal attachment that occurs during the fifth to eighth week of gestation when both organs are close. Splenic-gonadal fusion occurs with a male-to-female ratio of 16:1 and can interfere with the normal descent of the left testis or can cause failure of closure of the processus vaginalis; it is frequently associated with an ipsilateral inguinal hernia and cryptorchidism.⁵⁰

The continuous form, in which the spleen remains attached to the gonad by a fibrous or splenic cord that traverses the peritoneal cavity, is the most common type, occurring in

about 55% of the published cases. Continuous splenic-gonadal fusion is associated with limb defect syndrome and other congenital malformations, including cardiac malformations, thoracic malformations, cleft palate, micrognathia, anal anomalies, spina bifida, craniosynostosis, diaphragmatic hernia, and pulmonary anomalies.⁵¹ The discontinuous form, representing 45% of the cases, is not associated with other congenital anomalies.^{52,53}

The diagnosis of splenic-gonadal fusion should be suspected if there is chronic swelling or mass in the left gonad, especially if there is an associated undescended testis.⁵⁴ The gonadal mass, if palpable, is firm and rubbery and may be poorly delineated from the testis. The first study is ultrasound, which can show a well-defined scrotal mass that is isoechoic to spleen.⁵³ Malignant disease associated with splenic-gonadal fusion is exceedingly rare and occurs in the undescended testis.⁵⁵

^{99m}Tc -sulfur colloid scintigraphy is useful to confirm ectopic splenic tissue and shows uptake in the inguinal or scrotal area.^{56,57}

Heterotaxy Syndromes

ASPLENIA SYNDROME

Situs ambiguus with asplenia, or Ivemark syndrome, is characterized by an absent spleen and duplication of right-sided structures (bilateral right-sidedness), affecting males twice as commonly as females.⁵⁸ Asplenia syndrome occurs in 1 per 10,000 to 1 per 40,000 live births and is due to defects in multiple genes.⁵⁹ It virtually is always accompanied by a variety of congenital malformations, particularly cardiovascular (Figs. 104-7 and 104-8).⁵⁸⁻⁶³ Congenital heart malformations are present in about 85% to 95% of patients with asplenia (Box 104-1). The isolated form of congenital asplenia lacks other developmental anomalies, particularly those of the cardiovascular system.⁶⁴

Abdominal Radiologic Findings

In asplenia syndrome, the aorta and IVC are in juxtaposition on the same side of the spine, which can be identified by sonography or contrast-enhanced CT (Fig. 104-9). The IVC-atrial communication can be evaluated by either modality.⁶⁵ The spleen will be absent, and the liver is symmetric and midline. The splenic artery is absent, and the celiac axis may arise from the superior mesenteric artery. Malrotation of the bowel occurs with the stomach on the right and an abnormal location of the ligament of Treitz, with the jejunal loops of bowel in the right hemiabdomen and the ileal loops of bowel in the left hemiabdomen. This is associated with inversion of the normal

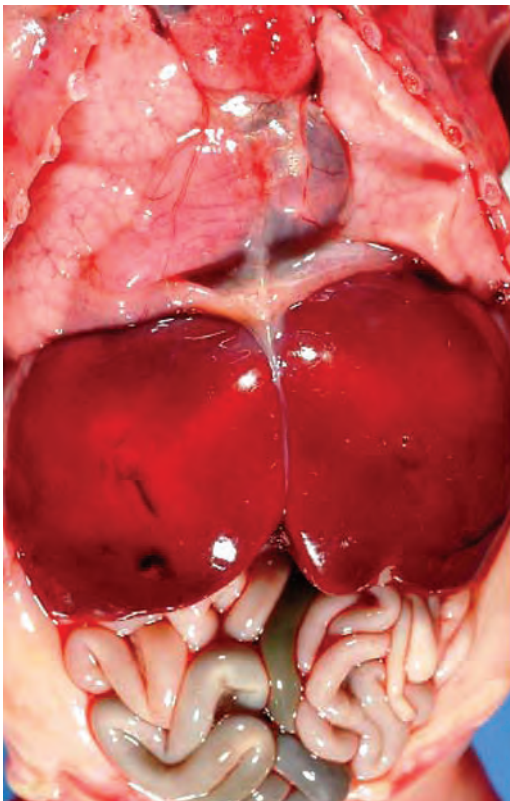


Figure 104-7 Asplenia: gross specimen. Autopsy specimen of a patient with asplenia, infracardiac anomalous pulmonary venous return, atrial septal defect, and pulmonary atresia. The liver straddles the midline. No spleen is identified.

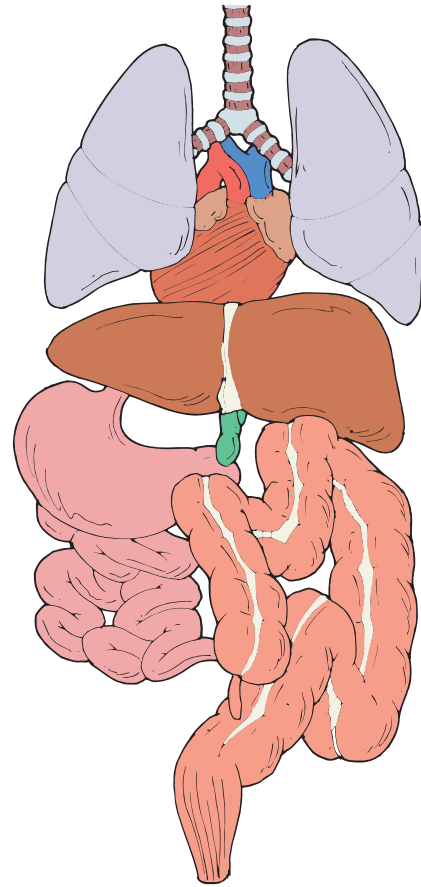


Figure 104-8 Asplenia: associated anomalies. Diagram shows organ positions in situs ambiguus with asplenia. (From Fulcher AS, Turner MA: Abdominal manifestations of situs anomalies in adults. *RadioGraphics* 22:1439–1456, 2002.)

BOX 104-1 DEVELOPMENTAL ANOMALIES WITH ASPLENIA SYNDROME

PULMONARY ANOMALIES

Bilateral trilobed lungs with eparterial bronchi

CONGENITAL HEART MALFORMATIONS

Cardiac malposition

Mesocardia

Dextrocardia

Right-sided aortic arch

Great vessels

Transposition of the great vessels

Pulmonary stenosis or atresia

Venous system

Bilateral superior vena cava

Bilateral inferior vena cava (IVC)

Partial or total anomalous pulmonary venous drainage

Cardiac defects

Hypoplasia or absence of one ventricle

Double-outlet right ventricle

Ventricular septal defect

Atrial septal defect

Absent coronary sinus

Single coronary artery

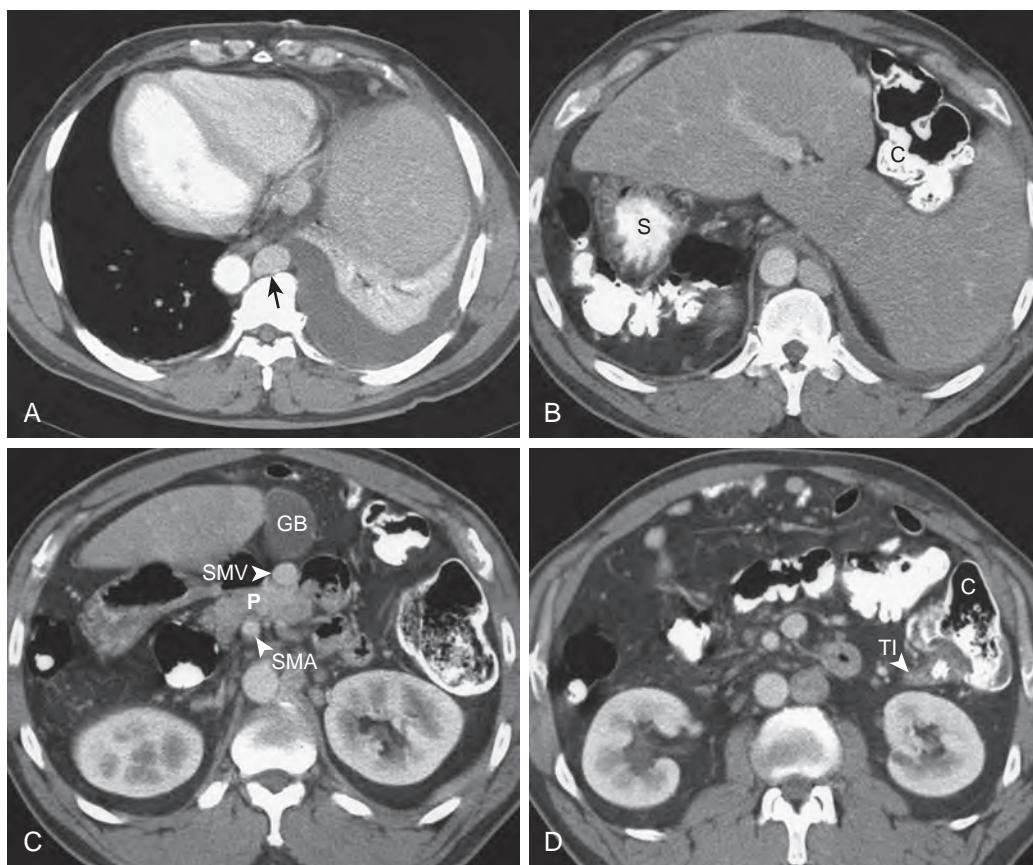


Figure 104-9 Situs ambiguus with asplenia. **A.** Transverse contrast-enhanced CT scan of the lower chest of a 48-year-old man shows dextrocardia and azygos continuation of the inferior vena cava. The aorta is located to the right of the enlarged azygos vein (arrow). The scan also shows left lower lobe collapse and a left pleural effusion. **B.** CT scan obtained 15 mm caudad to **A** shows the stomach (S) and colon (C) in the expected location of the spleen. The hypoplasia of the anterior segment of the right hepatic lobe allows cephalic migration of the colon. **C.** On another CT scan obtained caudad to **B**, the gallbladder (GB) lies in the midline. The superior mesenteric vein (SMV) lies anterior to the truncated pancreas (P), whereas the superior mesenteric artery (SMA) lies posterior to it. **D.** CT scan obtained at the level of the right renal hilum reveals that the cecum (C) is located in the left lower quadrant. Notice the terminal ileum (TI) entering the colon. (From Fulcher AS, Turner MA: *Abdominal manifestations of situs anomalies in adults*. *RadioGraphics* 22:1439–1456, 2002.)

relationship of the superior mesenteric artery and superior mesenteric vein.⁶⁶

^{99m}Tc-labeled, heat-altered, autologous erythrocyte SPECT/CT is a reliable study to evaluate for functioning splenic tissue in the abdomen and pelvis.⁶⁷

POLYSPLENIA SYNDROME

Polysplenia syndrome, a heterotaxy syndrome characterized by multiple small spleens (Figs. 104-10 and 104-11), is referred to as situs ambiguus with left isomerism. In contrast to asplenia, it occurs equally in males and females, with some studies showing a female predilection to polysplenia. The reported incidence is 1 per 250,000 live births.⁵⁹ Polysplenia has a lower prevalence of congenital heart disease (50%-90%) and less severe defects than those with asplenia (Box 104-2).⁶⁸

Abdominal Radiologic Findings

In polysplenia, dextroposition of the stomach is present in approximately 45% of patients, and intestinal malrotation occurs in approximately 27%.⁶⁹ Polysplenia cannot be excluded solely on the basis of situs solitus.

Splenic tissue number and location are varied; 2 to 16 splenic nodules of approximately equal size can be found in the right

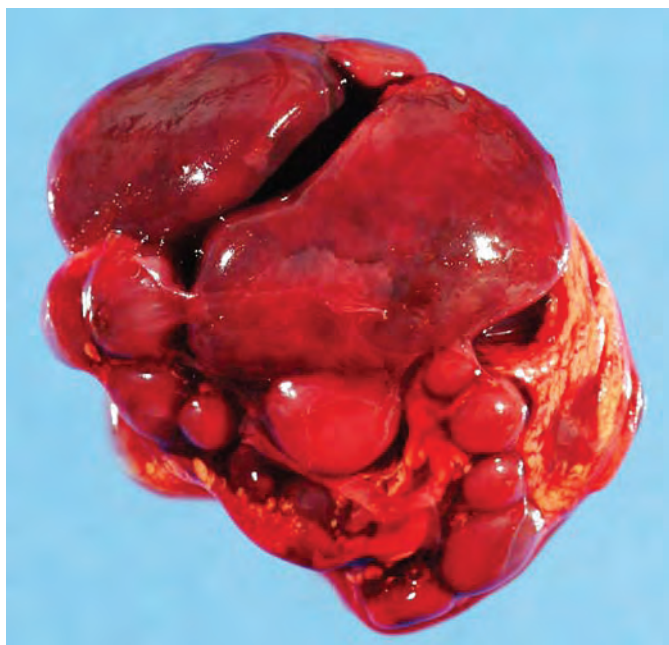


Figure 104-10 Polysplenia: gross specimen. Autopsy specimen of a patient with polysplenia shows multiple spleens.

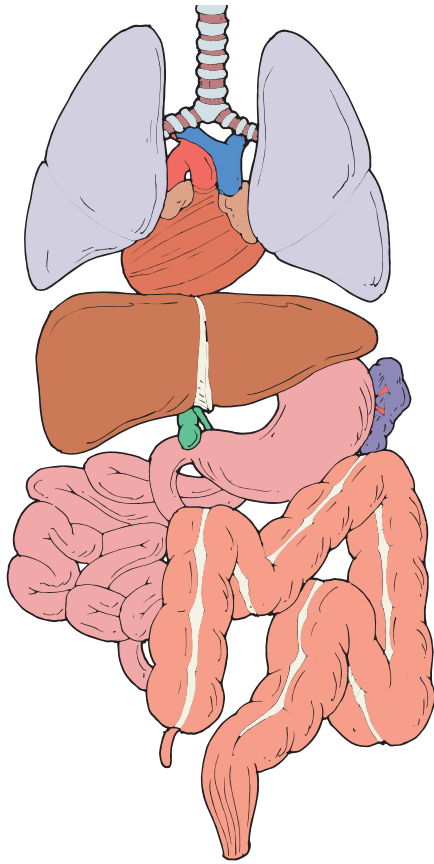


Figure 104-11 Polysplenia: associated anomalies. Diagram shows the organ position in situs ambiguus with polysplenia. (From Fulcher AS, Turner MA: *Abdominal manifestations of situs anomalies in adults*. *RadioGraphics* 22:1439–1456, 2002.)

or left upper quadrant, depending on situs.⁷⁰ Ectopic splenic tissue may be difficult to characterize on a CT scan, and some patients may have poor splenic function. Splenic scintigraphy with ^{99m}Tc-labeled, heat-altered, autologous erythrocyte scintigraphy SPECT/CT is a sensitive method to detect functioning splenic tissue and correctly diagnose polysplenia.⁷¹

Polysplenia is associated with pancreatic abnormalities including short pancreas, dorsal agenesis, pancreas divisum, and annular or semiannular pancreas.⁷² Pancreatic development is closely associated with duodenal jejunal rotation, and pancreatic abnormalities are found to coexist with bowel malrotation and a preduodenal portal vein.⁷³

Biliary atresia is found to coexist with other congenital anatomic abnormalities in 20% of the cases. The most common is biliary atresia splenic malformation syndrome, and up to 90% are associated with polysplenia and gallbladder agenesis.⁷⁴ Magnetic resonance cholangiography with hepatocyte-specific gadolinium contrast agents has been shown to be superior to ^{99m}Tc-disofenin (DISIDA) hepatobiliary scintigraphy in the detection of biliary atresia.⁷⁵

BOX 104-2 DEVELOPMENTAL ANOMALIES WITH POLYSPLENIA SYNDROME

PULMONARY ANOMALIES

Bilateral morphologic left lung (bilobed) with bilateral hyparterial bronchi

CONGENITAL HEART MALFORMATIONS

Cardiac malposition

Dextrocardia

Great vessels

Subvalvar and valvar pulmonary or aortic obstruction or atresia

Cardiac defects

Absent coronary sinus

Absent atrial septum resulting in common atrium

Atrioventricular canal defects

Hypoplasia or absence of one ventricle

Double-outlet right ventricle

Venous system

Bilateral superior vena cava

Interrupted IVC with azygos continuation

Anomalous drainage due to an abnormal position of the atrial septum

Polysplenia is associated with absence (interruption) of the IVC between the renal and the hepatic veins, with independent drainage of the hepatic veins into the right atrium. The renal portion of the IVC receives blood return from both kidneys and passes posterior to the diaphragmatic crura to enter the thorax as the azygos vein (Fig. 104-12). The azygos vein joins the superior vena cava at the normal location in the right paratracheal space. Since the advent of cross-sectional imaging, azygos continuation of the IVC can be seen in otherwise asymptomatic patients without associated severe congenital heart disease and asplenia or polysplenia syndromes.⁷⁶ Sonography, CT, MRI, and angiography can confirm the diagnosis by showing the absence of the IVC between the renal and the hepatic veins with independent drainage of the hepatic veins into the right atrium.⁷⁷

Patients without cardiac anomalies may reach adulthood, accounting for 10% to 15% of cases of polysplenia. Because most adult patients do not exhibit any symptoms, polysplenia syndrome is often diagnosed incidentally during other procedures. Even adult patients can have anomalies in abdominal organs, including visceral heterotaxia with a right-sided stomach, left-sided or large midline liver, right-sided spleen, malrotation of the intestine, short pancreas, and anomalies of the IVC.⁷⁸

Polysplenia syndrome is recognized easily on diagnostic imaging, including a combination of abdominal ultrasonography, CT, and MRI. Identification of splenic tissue and location can serve as a landmark for detection and characterization of the subtypes of heterotaxy.⁷⁹

Multiple other malformations are associated with heterotaxy syndromes (Box 104-3).^{58-63,79-81}

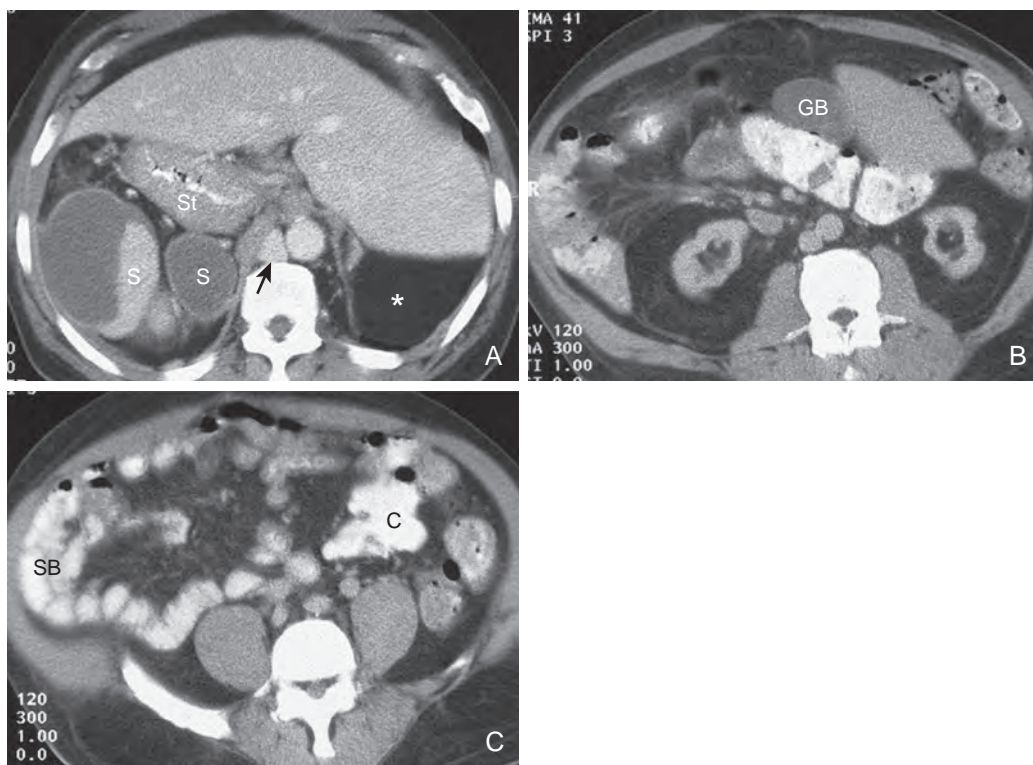


Figure 104-12 Situs ambiguus with polysplenia in a 67-year-old man. **A.** Transverse contrast-enhanced CT scan of the abdomen shows a midline liver, multiple spleens (S) in the right upper quadrant adjacent to the collapsed stomach (St), and inferior vena cava interruption with azygos continuation (arrow). The low attenuation of the spleens is related to infarctions, which cause liquefaction and subcapsular hematomas. Notice the absence of splenic tissue in the left upper quadrant (asterisk). **B.** Transverse CT scan through the midabdomen reveals a midline gallbladder (GB). **C.** Transverse CT scan through the lower abdomen reveals the small bowel (SB) in the right lower quadrant and the colon in the left lower quadrant. The cecum (C) lies near the midline, a finding that indicates incomplete fixation. (From Fulcher AS, Turner MA: *Abdominal manifestations of situs anomalies in adults*. *RadioGraphics* 22:1439–1456, 2002.)

BOX 104-3 MALFORMATIONS ASSOCIATED WITH HETEROTAXY SYNDROMES

GASTROINTESTINAL TRACT

- Omphalocele
- Esophageal atresia and tracheoesophageal fistula
- Intestinal malrotation
- Duplication, hypoplasia, or angiodysplasia of the stomach
- Anal stenosis or atresia
- Aganglionic colon
- Duodenal atresia
- Gallbladder agenesis

PANCREAS

- Pancreas hypoplasia, (polycystic) malformations

LIVER

- Absence of the gallbladder
- Extrahepatic biliary atresia
- Polycystic liver
- Ectopic liver tissue in the adrenal glands

GENITOURINARY TRACT

- Renal agenesis or hypoplasia, cystic malformations
- Horseshoe kidney
- Duplicated collecting system
- Bilobed urinary bladder
- Urethral duplication or urethral valves
- Rectourethral fistula
- Bicornuate uterus
- Agenesis of the ovaries and ovarian cysts
- Duplicated, bicornuate or unicornuate uterus; vaginal atresia or duplication
- Testicular hypoplasia
- Penis duplication, hypospadias

RESPIRATORY TRACT

- Laryngeal cleft or hypoplasia
- Tracheoesophageal fistula, tracheal or esophageal atresia
- Pulmonary hypoplasia

CENTRAL NERVOUS SYSTEM

- Spine malformations, including midline abnormalities
- Dysgenesis or agenesis of the corpus callosum
- Porencephalic, cerebellar, or Dandy-Walker cysts
- Holoprosencephaly, hydranencephaly
- Cerebellar cysts
- Hypoplasia, dysplasia, or agenesis of the cerebellum
- Hydrocephalus
- Septum pellucidum abnormality
- Lumbar myelomeningocele
- Cleft lip or palate

MUSCULOSKELETAL

- Hypoplasia or dysostosis of cranial bones
- Overlapping toes, clubbed hands, polydactyly, absent radii
- Vertebral or rib anomalies
- Caudal regression, bifid sacrum, sacral agenesis

OTHER

- Fused or absent adrenal glands
- Single umbilical artery
- Diaphragmatic hernia

REFERENCES

- Varga I, Galfiova P, Adamkov M, et al: Congenital anomalies of the spleen from an embryological point of view. *Med Sci Monit* 15:RA269–RA276, 2009.
- Moore KL, Persaud TVN, Torchia MG: *The Developing Human: Clinically Oriented Embryology*, ed 9, Philadelphia, 2013, Elsevier/Saunders.
- Brennan TV, Lipshutz GS, Posselt AM, et al: Congenital cleft spleen with CT scan appearance of high-grade splenic laceration after blunt abdominal trauma. *J Emerg Med* 25:139–142, 2003.
- Lee JKT: *Computed Body Tomography with MRI Correlation*, ed 3, Philadelphia, 1998, Lippincott-Raven.
- Heydari MB, Johari HG, Eskandari S: Wandering spleen presenting as small bowel obstruction. *Am J Emerg Med* 31:984–985, 2013.
- Steinberg R, Karmazyn B, Dlugy E, et al: Clinical presentation of wandering spleen. *J Pediatr Surg* 37:E30, 2002.
- Erden A, Karaalp G, Ozcan H, et al: Wandering accessory spleen. *Surg Radiol Anat* 17:89–91, 1995.
- Taori K, Ghonge N, Prakash A: Wandering spleen with torsion of vascular pedicle: Early diagnosis with multiplanar reformation technique of multislice spiral CT. *Abdom Imaging* 29:479–481, 2004.
- Gilman RS, Thomas RL: Wandering spleen presenting as acute pancreatitis in pregnancy. *Obstet Gynecol* 101:1100–1102, 2003.
- Simpson A, Ashby EC: Torsion of wandering spleen. *Br J Surg* 52:344–346, 1965.
- Soleimani M, Mehrabi A, Kashfi A, et al: Surgical treatment of patients with wandering spleen: Report of six cases with a review of the literature. *Surg Today* 37:261–269, 2007.
- Peitgen K, Majetschak M, Walz MK: Laparoscopic splenectomy by peritoneal and omental pouch construction for intermittent splenic torsion (“wandering spleen”). *Surg Endosc* 15:413, 2001.
- Iqbal M, Tareen MA, Sohail U: Torsion of a wandering spleen presenting as a case of acute abdomen. *J Coll Physicians Surg Pak* 19:123–124, 2009.
- Kulkarni ML, Sneharoop B, Vani HN, et al: Eventration of the diaphragm and associations. *Indian J Pediatr* 74:202–205, 2007.
- Sanchez R, Lobert P, Herman R, et al: Wandering spleen causing gastric outlet obstruction and pancreatitis. *Pediatr Radiol* 40(Suppl 1):S89–S91, 2010.
- Yasuda H, Inoue M, Uchida K, et al: Wandering spleen causing intestinal obstruction after repair of congenital diaphragmatic hernia. *Eur J Pediatr Surg* 20:121–123, 2010.
- El Bouhaddouti H, Lamrani J, Louchi A, et al: Torsion of a wandering spleen. *Saudi J Gastroenterol* 16:288–291, 2010.
- Gayer G, Hertz M, Strauss S, et al: Congenital anomalies of the spleen. *Semin Ultrasound CT MR* 27:358–369, 2006.
- Kao PF, Tzen KY, Tsai MF, et al: ^{99m}Tc -sulphur-colloid and heat-denatured ^{99m}Tc -labelled red cell scans demonstrating a giant intrapelvic spleen in a girl after splenectomy. *Pediatr Radiol* 31:283–285, 2001.
- Paterson A, Frush DP, Donnelly LE, et al: A pattern-oriented approach to splenic imaging in infants and children. *Radiographics* 19:1465–1485, 1999.
- Danaci M, Belet U, Yalin T, et al: Power Doppler sonographic diagnosis of torsion in a wandering spleen. *J Clin Ultrasound* 28:246–248, 2000.
- Jones B, Callahan J, Cole A, et al: The case of the wandering spleen. *J Diagn Med Sonogr* 29:130–132, 2013.
- Chen JW, Yeh DM, Peng SH, et al: Sonographic diagnosis of a subclinical wandering spleen: Role of the decubitus position. *J Ultrasound Med* 31:483–487, 2012.
- Bakir B, Poyanli A, Yekeler E, et al: Acute torsion of a wandering spleen: Imaging findings. *Abdom Imaging* 29:707–709, 2004.
- Priyadarshi RN, Anand U, Kumar B, et al: Torsion in wandering spleen: CT demonstration of whirl sign. *Abdom Imaging* 38:835–838, 2013.
- Ben Ely A, Zissin R, Copel L, et al: The wandering spleen: CT findings and possible pitfalls in diagnosis. *Clin Radiol* 61:954–958, 2006.
- Fonseca AZ, Ribeiro M, Jr, Contrucci O: Torsion of a wandering spleen treated with partial splenectomy and splenopexy. *J Emerg Med* 44:e33–e36, 2013.
- Arda K, Kizilkanat K, Celik M, et al: Intermittent torsion of a wandering spleen in a child: The role of MRI in diagnosis. *JBR-BTR* 87:70–72, 2004.
- Deux JF, Salomon L, Barrier A, et al: Acute torsion of wandering spleen: MRI findings. *AJR Am J Roentgenol* 182:1607–1608, 2004.
- Arleo EK, Kovanlikaya A, Mennitt K, et al: Multimodality imaging of a neonatal wandering spleen. *Clin Imaging* 34:302–305, 2010.
- Fujiwara T, Takehara Y, Isoda H, et al: Torsion of the wandering spleen: CT and angiographic appearance. *J Comput Assist Tomogr* 19:84–86, 1995.
- Soleimani M, Mehrabi A, Kashfi A, et al: Surgical treatment of patients with wandering spleen: Report of six cases with a review of the literature. *Surg Today* 37:261–269, 2007.
- Curtis GM, Movitz D: The surgical significance of the accessory spleen. *Ann Surg* 123:276–298, 1946.
- Halpert B, Alden ZA: Accessory spleens in or at the tail of the pancreas. A survey of 2,700 additional necropsies. *Arch Pathol* 77:652–654, 1964.
- Romer T, Wiesner W: The accessory spleen: Prevalence and imaging findings in 1,735 consecutive patients examined by multidetector computed tomography. *JBR-BTR* 95:61–65, 2012.
- Eraklis AJ, Filler RM: Splenectomy in childhood: A review of 1413 cases. *J Pediatr Surg* 7:382–388, 1972.
- Wadham BM, Adams P, Johnson M: Incidence and location of accessory spleens. *N Engl J Med* 304:1111, 1981.
- Altat AM, Sawatzky M, Ellsmere J, et al: Laparoscopic accessory splenectomy: The value of perioperative localization studies. *Surg Endosc* 23:2675–2679, 2009.
- Perez Fontan FJ, Soler R, Santos M, et al: Accessory spleen torsion: US, CT and MR findings. *Eur Radiol* 11:509–512, 2001.
- Kawamoto S, Johnson PT, Hall H, et al: Intrapancratic accessory spleen: CT appearance and differential diagnosis. *Abdom Imaging* 37:812–827, 2012.
- Quah C, Ayiomamitis GD, Shah A, et al: Computed tomography to detect accessory spleens before laparoscopic splenectomy: Is it necessary? *Surg Endosc* 25:261–265, 2011.
- Subramanyam BR, Balthazar EJ, Horii SC: Sonography of the accessory spleen. *AJR Am J Roentgenol* 143:47–49, 1984.
- Catalano O, Sandomenico F, Matarazzo I, et al: Contrast-enhanced sonography of the spleen. *AJR Am J Roentgenol* 184:1150–1156, 2005.
- Kim SH, Lee JM, Han JK, et al: MDCT and superparamagnetic iron oxide (SPIO)-enhanced MR findings of intrapancreatic accessory spleen in seven patients. *Eur Radiol* 16:1887–1897, 2006.
- Muscogiuri E, Scardapane A, Angelelli G: Multislice CT in the study of insulinomas: Preliminary experience. *Radiol Med* 107:325–331, 2004.
- Jang KM, Kim SH, Lee SJ, et al: Differentiation of an intrapancreatic accessory spleen from a small (<3-cm) solid pancreatic tumor: Value of diffusion-weighted MR imaging. *Radiology* 266:159–167, 2013.
- Ota T, Tei M, Yoshioka A, et al: Intrapancratic accessory spleen diagnosed by technetium-99m heat-damaged red blood cell SPECT. *J Nucl Med* 38:494–495, 1997.
- Kim SH, Lee JM, Han JK, et al: Intrapancratic accessory spleen: Findings on MR imaging, CT, US and scintigraphy, and the pathologic analysis. *Korean J Radiol* 9:162–174, 2008.
- Halvorsen JE, Stray O: Splenogonadal fusion. *Acta Paediatr Scand* 67:379–381, 1978.
- Cortes D, Thorup JM, Visfeldt J: The pathogenesis of cryptorchidism and splenogonadal fusion: A new hypothesis. *Br J Urol* 77:285–290, 1996.
- Bonneau D, Roume J, Gonzalez M, et al: Splenogonadal fusion limb defect syndrome: Report of five new cases and review. *Am J Med Genet* 86:347–358, 1999.
- Khairat ABM, Ismail AM: Splenogonadal fusion: Case presentation and literature review. *J Pediatr Surg* 40:1357–1360, 2005.
- Ferrón SA, Arce JD: Discontinuous splenogonadal fusion: New sonographic findings. *Pediatr Radiol* 1–4, 2013.
- Milliken I, Cherian A, Najmaldin A, et al: Splenogonadal fusion: A rare cause of testicular enlargement. *Pediatr Surg Int* 23:365–367, 2007.
- Lopes RI, de Medeiros MT, Arap MA, et al: Splenogonadal fusion and testicular cancer: Case report and review of the literature. *Einstein (São Paulo)* 10:92–95, 2012.
- McLean GK, Alavi A, Ziegler MM, et al: Splenicogonadal fusion: Identification by radionuclide scanning. *J Pediatr Surg* 16:649–651, 1981.
- Guarin U, Dimitrieva Z, Ashley SJ: Splenogonadal fusion—a rare congenital anomaly demonstrated by ^{99m}Tc -sulfur colloid imaging: case report. *J Nucl Med* 16:922–924, 1975.
- Phoon CK, Neill CA: Asplenia syndrome: Insight into embryology through an analysis of cardiac and extracardiac anomalies. *Am J Cardiol* 73:581–587, 1994.
- Rose V, Izukawa T, Moes CA: Syndromes of asplenia and polysplenia. A review of cardiac and non-cardiac malformations in 60 cases with special reference to diagnosis and prognosis. *Br Heart J* 37:840–852, 1975.
- Ivemark BI: Implications of agenesis of the spleen on the pathogenesis of conotruncal anomalies in childhood; an analysis of the heart malformations in the splenic agenesis syndrome, with fourteen new cases. *Acta Paediatr Suppl* 44:7–110, 1955.

61. Wilkinson JL, Holt PA, Dickinson DF, et al: Asplenia syndrome in one of mono-zygotic twins. *Eur J Cardiol* 10:301–304, 1979.
62. Noack F, Sayk F, Ressel A, et al: Ivemark syndrome with agenesis of the corpus callosum: A case report with a review of the literature. *Prenat Diagn* 22:1011–1015, 2002.
63. Balan A, Lazoura O, Padley SP, et al: Atrial isomerism: A pictorial review. *J Cardiovasc Comput Tomogr* 6:127–136, 2012.
64. Mahlaoui N, Minard-Colin V, Picard C, et al: Isolated congenital asplenia: A French nationwide retrospective survey of 20 cases. *J Pediatr* 158:142–148, 148.e1, 2011.
65. Tonkin I, Tonkin A: Visceroatrial situs abnormalities: Sonographic and computed tomographic appearance. *AJR Am J Roentgenol* 138: 509–515, 1982.
66. Fulcher AS, Turner MA: Abdominal manifestations of situs anomalies in adults. *Radiographics* 22:1439–1456, 2002.
67. De Porto A, Lammers A, Bennink R, et al: Assessment of splenic function. *Eur J Clin Microbiol Infect Dis* 29:1465–1473, 2010.
68. Park SS, Min BW, Kim WB, et al: Double cancer of the stomach and oesophagus with situs ambiguus with polysplenia: The importance of preoperative evaluation. *Digest Liver Dis* 37: 799–802, 2005.
69. Ticho BS, Goldstein AM, Van Praagh R: Extracardiac anomalies in the heterotaxy syndromes with focus on anomalies of midline-associated structures. *Am J Cardiol* 85:729–734, 2000.
70. Mortelé KJ, Mortelé B, Silverman SG: CT features of the accessory spleen. *AJR Am J Roentgenol* 183:1653–1657, 2004.
71. Abut E, Akkaya L, Uysal U, et al: Selective spleen scintigraphy in the diagnosis of polysplenia syndrome. *Br J Radiol* 77:698–700, 2004.
72. Ito H, Ohgi S, Kanno T, et al: Heterotaxy syndrome with pancreatic malrotation: CT features. *Abdom Imaging* 28:856–858, 2003.
73. Pickhardt PJ, Bhalla S: Intestinal malrotation in adolescents and adults: Spectrum of clinical and imaging features. *AJR Am J Roentgenol* 179: 1429–1435, 2002.
74. Hartley JL, Davenport M, Kelly DA: Biliary atresia. *Lancet* 374:1704–1713, 2009.
75. Ryeom HK, Choe BH, Kim JY, et al: Biliary atresia: Feasibility of Mangafodipir trisodium-enhanced MR cholangiography for evaluation. *Radiology* 235:250–258, 2005.
76. Bass JE, Redwine MD, Kramer LA, et al: Spectrum of congenital anomalies of the inferior vena cava: Cross-sectional imaging findings. *Radiographics* 20:639–652, 2000.
77. Koc Z, Oguzkurt L: Interruption or congenital stenosis of the inferior vena cava: Prevalence, imaging, and clinical findings. *Eur J Radiol* 62: 257–266, 2007.
78. Seo H-I, Jeon TY, Sim MS, et al: Polysplenia syndrome with preduodenal portal vein detected in adults. *World J Gastroenterol* 14:6418, 2008.
79. Bartram U, Wirbelauer J, Speer CP: Heterotaxy syndrome—asplenia and polysplenia as indicators of visceral malposition and complex congenital heart disease. *Neonatology* 88:278–290, 2005.
80. Tawfik AM, Batouty NM, Zaky MM, et al: Polysplenia syndrome: A review of the relationship with viscero-atrial situs and the spectrum of extra-cardiac anomalies. *Surg Radiol Anat* 35: 647–653, 2013.
81. Hill SJ, Heiss KF, Mittal R, et al: Heterotaxy syndrome and malrotation. *J Pediatr Surg* 49:934–937, 2014.

Benign and Malignant Lesions of the Spleen

PATRICK M. VOS | STUART A. BARNARD | PETER L. COOPERBERG

CHAPTER OUTLINE

Splenunculi, Splenic Ectopia, and Splenosis

Radiologic Findings
Differential Diagnosis

Hemangioma

Epidemiology and Pathogenesis
Clinical Findings
Pathology
Radiologic Findings

Hamartoma

Epidemiology and Pathogenesis
Clinical Findings
Pathology
Radiologic Findings

Lymphangioma

Epidemiology and Pathogenesis
Clinical Findings
Pathology
Radiologic Findings

Inflammatory Pseudotumor

Epidemiology and Pathogenesis
Clinical Findings
Pathology
Radiologic Findings

Peliosis of the Spleen

Epidemiology and Pathogenesis
Clinical Findings
Pathology
Radiologic Findings

Cystic Splenic Lesions

Congenital Cysts and Pseudocysts
Hydatid Disease
Differential Diagnosis of Cystic Splenic Masses

Splenic Infection and Inflammatory Disease

Splenic Nodular Disease
Fungal Abscess and Microabscess
Tuberculosis
Mycobacterium avium Complex Infection
Pneumocystis jiroveci Pneumonia
Cat-Scratch Disease
Sarcoidosis
Lymphoma or Metastatic Disease
Gamna-Gandy Bodies
Pyogenic Abscess

Splenic Infarction

Epidemiology and Pathogenesis
Clinical Findings
Pathology
Radiologic Findings

Nontraumatic Splenic Rupture

Splenomegaly

Miscellaneous Disorders

Sickle Cell Disease
Splenic Involvement in Pancreatitis
Gaucher's Disease
Hemosiderosis
Thorotrast

Primary Malignant Lesions

Angiosarcoma

Secondary Malignant Lesions

Lymphoma
Leukemia and Myeloproliferative Disorders
Metastatic Disease

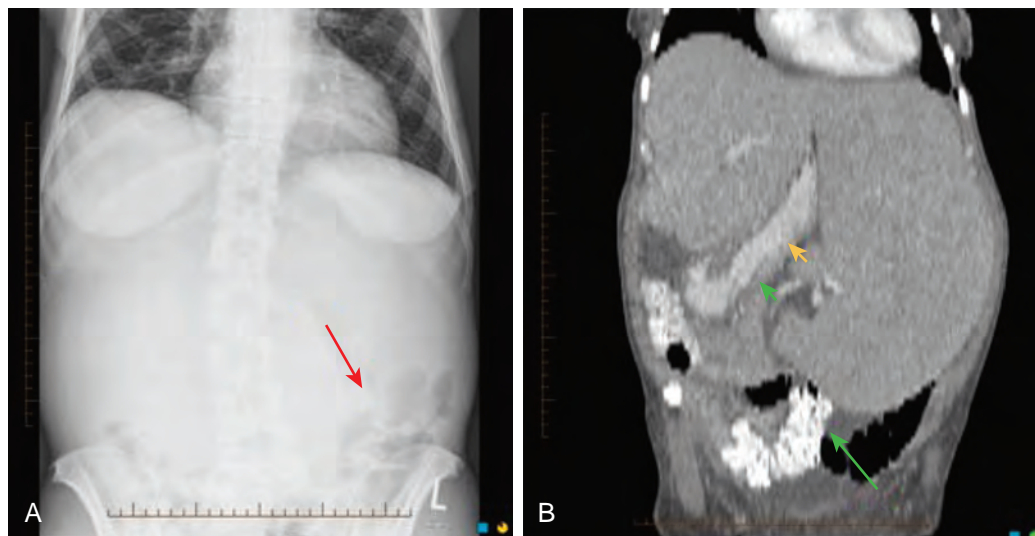
Although it is affected by many diseases, the spleen is not considered a great challenge to the radiologist.¹ In daily practice, the size and shape of the spleen typically are subjectively evaluated, and if there is no obvious splenomegaly or focal abnormality, the spleen usually is ignored. However, when abnormalities are detected, the radiologist plays an important role in providing a diagnosis and directing further clinical management.

Each imaging modality, including ultrasound, computed tomography (CT), magnetic resonance imaging (MRI), and scintigraphy, has specific advantages and limitations in

assessing the spleen. Plain radiographs of the abdomen can detect splenomegaly (Fig. 105-1) and splenic calcifications (Box 105-1) but otherwise do not have a significant diagnostic role. Currently, angiography is used only for therapeutic purposes, such as splenic embolization in trauma, hypersplenism, or rare vascular tumors.² ¹⁸F-fluorodeoxyglucose positron emission tomography (FDG PET) combined with CT (FDG PET/CT) is becoming increasingly useful in the evaluation of malignant disease and has a high negative predictive value in predicting a malignant neoplasm in patients with solid-appearing splenic masses.³ Because of a perceived high risk of bleeding,

Figure 105-1 Massive hepatosplenomegaly.

A. Abdominal radiograph demonstrates a large soft tissue density in the left side of the abdomen that is displacing the splenic flexure of the colon inferiorly (arrow). **B.** The corresponding coronal reformatted CT image demonstrates the massively enlarged spleen that is displacing the stomach medially (short arrows) and the splenic flexure of the colon inferiorly (long arrow).



BOX 105-1 SOURCES OF SPLENIC CALCIFICATIONS

Cysts
Hemangioma
Hamartoma
Lymphangioma
Splenic artery
Granulomas
 Tuberculosis
 Histoplasmosis
 Pneumocystis jiroveci pneumonia
Hydatid disease
Hematomas
Hemosiderosis
Infarcts
Metastases
Sarcoidosis
Sickle cell disease
Gamna-Gandy bodies
Thorotrast (not true calcifications)

BOX 105-2 PATTERNS OF INVOLVEMENT IN SPLENIC PARENCHYMAL DISEASE

SOLITARY LESIONS

Solitary focus of any typically multifocal disease
Benign neoplasms: hemangioma, lymphangioma, hamartoma, inflammatory pseudotumor, peliosis, littoral cell angioma, sclerosing angiomatoid nodular transformation
Solitary pyogenic abscess

MULTIPLE FOCAL ABNORMALITIES

Trauma: lacerations, fractures, intrasplenic and subcapsular hematomas
Splenic rupture
Abscess: bacterial, fungal, granulomatous
Calcified granulomas
Sarcoidosis
Lymphangiomatosis, hemangiomatosis, peliosis
Lymphoma, lymphoproliferative disorders
Gaucher's disease
Metastatic disease
Hemangioma, hemangioendothelioma, peliosis

DIFFUSE DISEASE WITHOUT FOCAL LESIONS

Congestive disease: portal hypertension, splenic vein occlusion, or congestive heart failure
Inflammatory disease: various infections (e.g., tuberculosis) and inflammation (e.g., sarcoid)
Hyperplastic splenomegaly: hypertrophy resulting from removal of abnormal blood cells from the circulation (e.g., polycythemia vera)
Infiltrative (e.g., Gaucher's disease, hemosiderosis, malignant disease)

Modified from Paterson A, Frush DP, Donnelly LF, et al: A pattern-oriented approach to splenic imaging in infants and children. RadioGraphics 19:1465, 1999.

percutaneous biopsies of the spleen are not often performed in general practice. They are, however, relatively safe.⁴⁻⁶

The various imaging appearances and characteristics of benign and malignant splenic lesions are described in this chapter. Recognizing the range of the imaging and pathologic features of splenic abnormalities will narrow the differential diagnosis and help in planning further management.

A unique feature of the spleen on multidetector CT and MRI is the inhomogeneous enhancement pattern during the first minute after the intravenous administration of contrast material, which is most pronounced in the arterial phase (first 25-35 seconds). The enhancement pattern varies with different injection rates and tends to be more prominent in the presence of splenomegaly. These patterns have been described as serpentine, arciform, striped (i.e., zebra spleen), mottled, focal, and diffuse heterogeneity.⁷ This normal phenomenon is probably the result of differential flow through the vascular sinuses and cords of the red and white pulp.⁸ In most patients, this heterogeneity resolves after 60 to 70 seconds and should not be confused with disease.⁷⁻⁹ Keeping this phenomenon in mind, the

normal spleen should be homogeneous on all imaging modalities.

True lesions involving the spleen can be categorized as diseases manifesting with focal lesions, multifocal lesions, or a diffuse infiltrating pattern (Box 105-2).¹⁰ Although often asymptomatic, focal abnormalities must raise the suspicion of a pathologic condition.¹¹ Rarely, when the lesions are large, they may cause symptoms.

If the patient has a known disease, such as metastases, lymphoma, or tuberculosis, a general assumption is made that the focal abnormality represents splenic involvement. Ultimately, it is often the radiologist who has to decide whether further investigations are indicated or follow-up is more appropriate.

Splenunculi, Splenic Ectopia, and Splenosis

Splenunculi, also known as accessory spleens, splenules, and supernumerary spleens, are a common finding. They are found in approximately 10% to 30% of autopsies and in 16% of patients undergoing abdominal CT.^{12,13} The normal spleen is formed after multifocal development of splenic foci and subsequent fusion. Splenunculi are formed when one or more of these splenic foci fail to fuse.¹⁴

Accessory spleens are a few millimeters to several centimeters in the greatest diameter. They are typically supplied by branches of the splenic artery and demonstrate the same imaging and enhancement characteristics as normal splenic tissue. They are most commonly located medial to the spleen in or near its hilum (75%) and adjacent to the tail of the pancreas. Less common locations are within the pancreatic tail (17%), the gastrosplenic or splenorenal ligaments, the wall of the stomach or bowel, the mesentery or omentum, and the pelvis and scrotum (Fig. 105-2).¹⁵⁻¹⁷ Those found in the pancreatic tail are usually small and rarely noticed radiologically; if detected, they are often misdiagnosed as hypervascular tumors.^{18,19}

In patients with heterotaxia, left isomerism, or bilateral left-sidedness, many bilateral spleens or splenunculi may be present.^{20,21} Splenosis is autotransplantation of splenic tissue after disruption of the splenic capsule by trauma or surgery. Splenosis has been described in up to 74% of patients who underwent splenectomy after trauma, and it is often detected years after the initial trauma.²² These splenic implants closely resemble splenunculi on histologic examination, and distinction between these two conditions usually is not possible.^{14,23} Compared with accessory spleens, these implants are more numerous and variable in size and shape, and they are supplied by small perforating vessels arising at the site of implantation. They are typically located in the abdomen but may be found in various locations, including the pelvis, thorax, and scars.²⁴

Splenunculi and splenosis usually have little clinical significance, although there are exceptions.¹³ When splenectomy is

performed to control hematologic disorders such as idiopathic thrombocytopenic purpura or lymphoma, hypertrophy of an accessory spleen may cause or harbor the site of recurrent disease.²⁵ Accessory spleens also may mimic various pathologic conditions, such as lymphadenopathy, tumors associated with surrounding organs (e.g., pancreas, adrenal, kidney), abdominal and pelvic masses, endometriosis, and metastases. Rarely, splenunculi may be manifested with nonspecific abdominal pain or become symptomatic when they undergo torsion, cyst formation, or hemorrhage.²⁶⁻³⁰

RADIOLOGIC FINDINGS

On ultrasound, accessory spleens are well-circumscribed, round or oval nodules with an echogenicity identical or slightly hypoechoic to that of the adjacent spleen (Fig. 105-3A). Seventy-five percent demonstrate acoustic enhancement or an incomplete hyperechoic rim, or both.²²

MR images of accessory spleens demonstrate signal intensity and enhancement similar to those of the normal spleen on all sequences (Fig. 105-3B). On CT, accessory spleens are well-marginated, rounded, homogeneously enhancing lesions (Fig. 105-3C). Attenuation of small accessory spleens (<1 cm) is often somewhat less than that of the spleen because of partial volume effects.¹³

Heat-denatured red blood cell scintigraphy is considered the best study for detection of an accessory spleen because of its high sensitivity and specificity.^{31,32} Denatured red blood cells are labeled with technetium Tc 99m pertechnetate, after which single photon emission CT imaging is performed. On this examination, the round to ovoid foci with avid tracer uptake are seen colocalizing to the nodules seen on CT.

^{99m}Tc-sulfur colloid scans are less commonly used to evaluate splenic disorders, but they are less accurate than heat-denatured red blood cell scans in the detection of splenunculi.³³ Radioimmunoscinigraphy of the spleen provides no additional diagnostic information over heat-denatured red blood cell scintigraphy of the spleen in detecting splenunculi.³²

DIFFERENTIAL DIAGNOSIS

The differential diagnosis of supernumerary spleens includes lymphadenopathy, abdominal and pelvic masses, endometriosis, masses associated with surrounding organs (e.g., pancreas, adrenal, kidney), peritoneal mesothelioma, and metastases. Imaging characteristics similar to those of the normal spleen

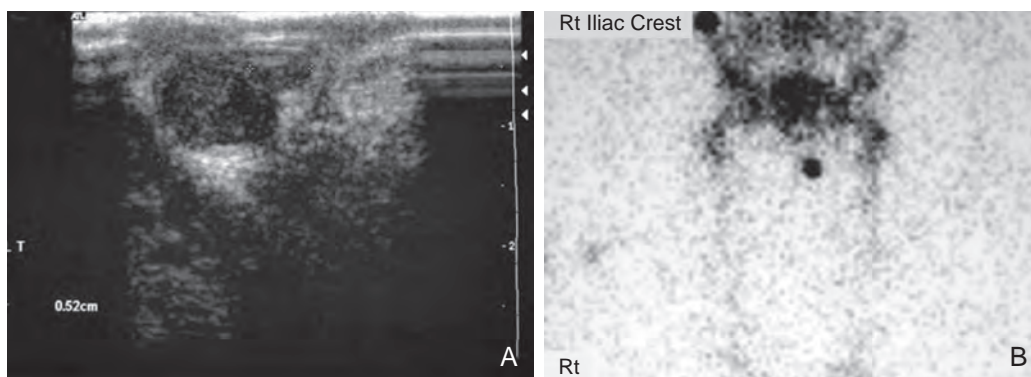


Figure 105-2 Splenogonadal fusion in a 4-year-old boy.

A. Ultrasound demonstrates a 5-mm nodular lesion adjacent to the left testicle. **B.** ^{99m}Tc-sulfur colloid scan of the pelvis demonstrates a focus of uptake into the left side of the scrotum.

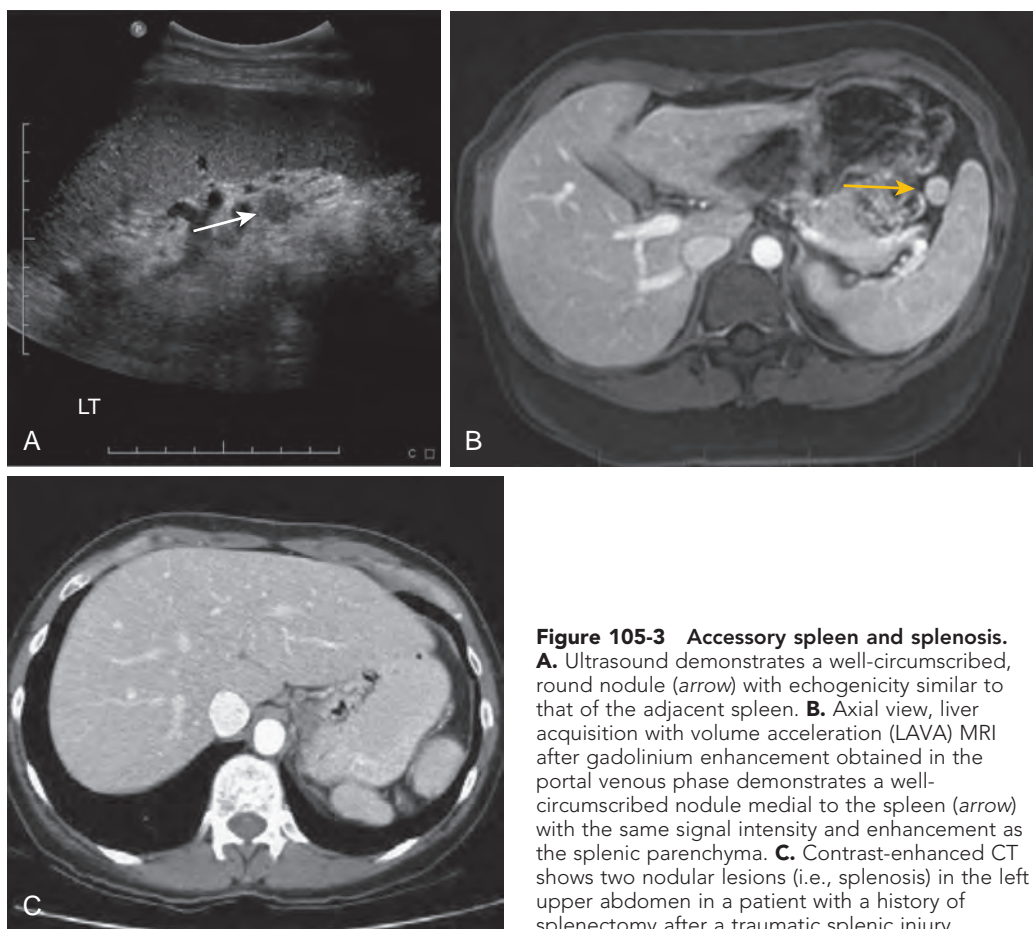


Figure 105-3 Accessory spleen and splenosis.

A. Ultrasound demonstrates a well-circumscribed, round nodule (arrow) with echogenicity similar to that of the adjacent spleen. **B.** Axial view, liver acquisition with volume acceleration (LAVA) MRI after gadolinium enhancement obtained in the portal venous phase demonstrates a well-circumscribed nodule medial to the spleen (arrow) with the same signal intensity and enhancement as the splenic parenchyma. **C.** Contrast-enhanced CT shows two nodular lesions (i.e., splenosis) in the left upper abdomen in a patient with a history of splenectomy after a traumatic splenic injury.

and heat-denatured red blood cell scintigraphy permit differentiation from other disorders.

Hemangioma

EPIDEMIOLOGY AND PATHOGENESIS

Hemangioma is the most common benign neoplasm of the spleen, found in approximately 0.3% to 14% of autopsy specimens.^{34,35} Hemangiomas primarily affect young to middle-aged adults, but they are found in all age groups.³⁵ Some investigators report predominance in males, whereas others did not find a gender predilection.^{34,36-37} Hemangiomas typically are found incidentally on radiologic imaging or pathologic studies. On occasion, they are multiple or diffuse, a condition called hemangiomatosis, or they are part of generalized angiomatosis, such as Klippel-Trénaunay-Weber syndrome.³⁸

CLINICAL FINDINGS

Patients with hemangiomas are generally asymptomatic.³⁷ Rarely, large hemangiomas or hemangiomatosis may be manifested with a palpable mass in the left upper quadrant, pain, or splenomegaly. Kasabach-Merritt syndrome, characterized by hemangiomatosis, thrombocytopenia, and intravascular coagulation, is a rare syndrome resulting from sequestration of red blood cells and platelets and consumption of clotting factors in the hemangiomas typically seen in early infancy.^{39,40}

Spontaneous splenic rupture of splenic hemangiomas is extremely uncommon.⁴¹ Resection should be reserved for the rare situations, such as untreatable pain, diagnostic uncertainty, or compression of adjacent organs.³⁵

PATHOLOGY

On gross examination, hemangiomas appear blue to red and spongy, and they are typically well circumscribed.⁴² Most splenic hemangiomas are cavernous and a few are capillary or may demonstrate both features.³⁴ On histopathologic examination, they are nonencapsulated proliferations of vascular channels of various sizes lined by a single layer of plump endothelial cells with little intervening fibrous tissue filled with red blood cells.^{14,42} Small hemangiomas of the spleen are typically homogeneously solid, although larger ones may demonstrate multiple cystic spaces of various sizes.⁴³ They may contain calcifications.⁴⁴ Diffuse hemangiomatosis is a rare, benign neoplastic condition in which the entire spleen is replaced by neoplastic blood vessels interspersed with sparse connective tissue.^{40,42,45}

RADIOLOGIC FINDINGS

The imaging appearance of splenic hemangiomas depends on the gross morphology and is a spectrum from solid to mixed to purely cystic.⁴⁵ Findings on abdominal radiographs are usually normal, but a large hemangioma may be manifested as a soft

tissue mass in the left upper quadrant. If calcifications are present, they can be punctate or curvilinear.³⁴

On ultrasound, small splenic hemangiomas appear as discrete echogenic lesions similar to those in the liver (Fig. 105-4).⁴⁶ Large hemangiomas may appear as complex masses with both solid and cystic areas.⁴⁷ Acoustic shadowing due to calcifications may be seen.

Hemangiomas may be manifested as solid, homogeneous masses or complex cystic masses with slight hypodensity on nonenhanced CT scans.^{44,47-49} Punctate, peripheral, and curvilinear calcifications may be present. Other splenic hemangiomas may appear cystic or heterogeneous, depending on the

extent of the cystic and solid components. On contrast-enhanced CT, hemangiomas of the spleen may demonstrate a progressive centripetal enhancement pattern and become isodense on the delayed images, as can be seen in liver hemangiomas (Fig. 105-5A, B) although this occurs less frequently in the splenic hemangiomas than with hepatic hemangiomas. This probably reflects the differences in vascular supply of the liver and spleen.^{34,36,50}

On MR studies, splenic hemangiomas are isointense to hypointense on the T1-weighted images and typically hyperintense on the T2-weighted images compared with the normal spleen (Fig. 105-5C).³⁵ Ramani and coworkers³⁶ demonstrated

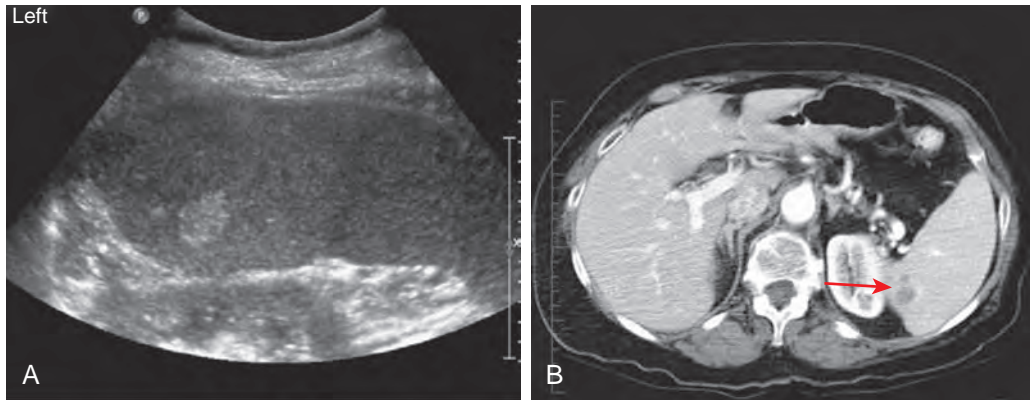


Figure 105-4 Splenic hemangioma. **A.** Longitudinal ultrasound image shows a well-defined, hyperechoic lesion. **B.** Corresponding contrast-enhanced CT demonstrates a hypodense lesion with some faint peripheral enhancement in the portal venous phase (arrow).

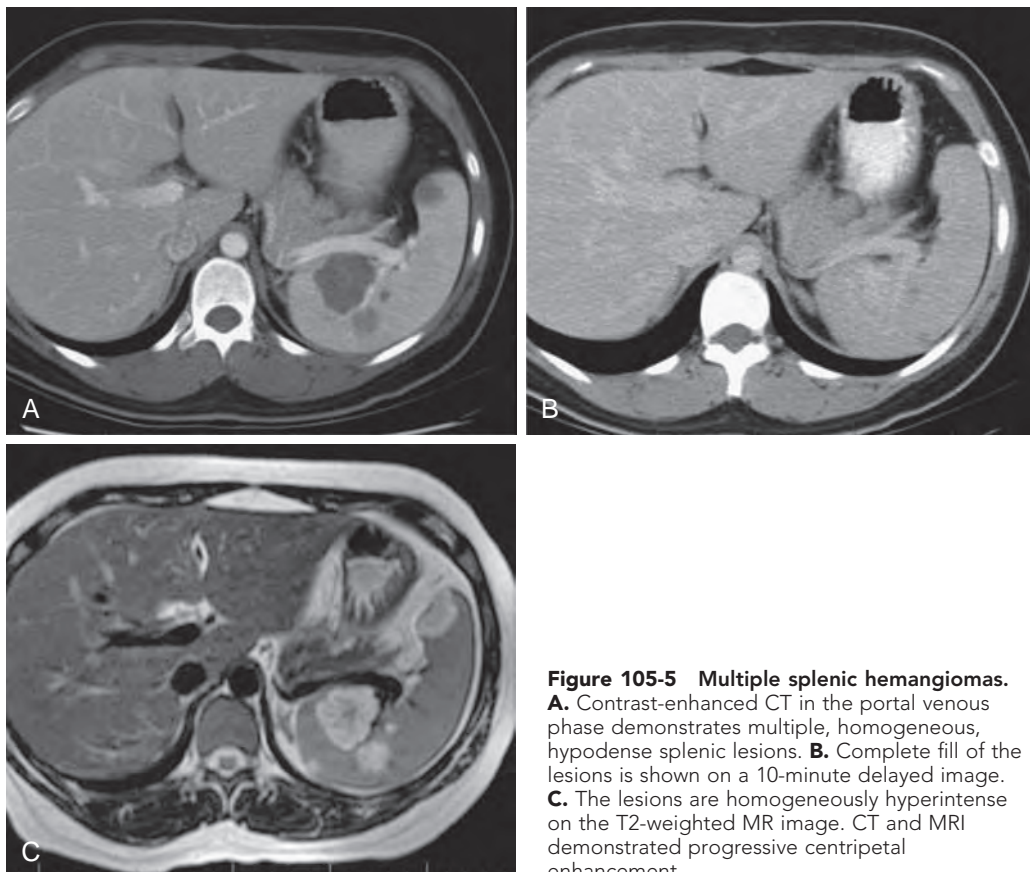


Figure 105-5 Multiple splenic hemangiomas.

A. Contrast-enhanced CT in the portal venous phase demonstrates multiple, homogeneous, hypodense splenic lesions. **B.** Complete fill of the lesions is shown on a 10-minute delayed image. **C.** The lesions are homogeneously hyperintense on the T2-weighted MR image. CT and MRI demonstrated progressive centripetal enhancement.

in a study of 22 hemangiomas that 19 were hyperintense, two were isointense, and one was hypointense relative to the spleen on T2-weighted images. In the same study, a progressive centripetal pattern of enhancement was observed in 19 of 22 hemangiomas on the dynamic gadolinium-enhanced series, and 19 hemangiomas demonstrated uniform enhancement on the delayed images. Other types of enhancement that can be observed are immediate homogeneous and persistent enhancement on the delayed images and a peripheral centripetal enhancement with a persistent lack of central enhancement on delayed images.^{36,51} Sometimes, a central fibrous scar may demonstrate persistent enhancement.⁵² Cavernous hemangiomas typically demonstrate heterogeneous enhancement; the cystic components do not demonstrate enhancement on contrast-enhanced CT and MRI.⁵⁰

There is a paucity of published data regarding scintigraphy of splenic hemangiomas, and the results are often based on criteria used for the liver.⁵³ ^{99m}Tc-sulfur colloid scintigraphy of the liver and spleen may demonstrate a photopenic defect in the spleen.⁴⁴ ^{99m}Tc-labeled red blood cell scans demonstrate a hypovascular area on the blood flow images; early blood pool images may reveal a hypovascular lesion or demonstrate some pooling of tracer activity. Typically, the hemangiomas demonstrate increased activity on the delayed images, giving a perfusion-blood pool mismatch. This phenomenon is considered pathognomonic of hepatic hemangiomas.^{53,54}

Angiographic findings of splenic hemangiomas are variable and nonspecific. They can be hypovascular or hypervascular, with or without pooling of contrast material and with or without abnormal tumor vessels.⁴⁴

Hamartoma

EPIDEMIOLOGY AND PATHOGENESIS

Hamartoma of the spleen is a rare, benign tumor first described by Rokitsansky in 1859 as a splenoma.⁵⁵ Hamartomas are also known as a spleen within a spleen, post-traumatic scars, nodular hyperplasia, and hyperplastic nodules. They are usually discovered incidentally during diagnostic imaging, splenectomy, or autopsy.^{56,57} Most are described in case reports or small series. The reported incidence in large autopsy and splenectomy series varies from 0.12% to 0.17%.⁵⁸⁻⁶⁰ The definitive diagnosis of a splenic hamartoma is rarely made on the basis of imaging. Hamartomas are often confirmed by pathologic evaluation after splenectomy.^{60,61}

No gender predilection has been demonstrated for hamartomas, and they can be found in any age group. Most hamartomas are solitary. Hamartomas of the spleen have been associated with hematologic disorders, tuberous sclerosis, malignant neoplasms, and Wiskott-Aldrich-like syndrome.^{56,57,60,62}

CLINICAL FINDINGS

Hamartomas are usually discovered incidentally, and most patients are asymptomatic, but a large hamartoma may be manifested as a palpable mass or splenomegaly. Rupture of a splenic hamartoma is rare.⁶³ Splenic hamartomas can be associated with hematologic disorders, including pancytopenia, anemia, and thrombocytopenia. This association probably results from sequestration of the hematopoietic cells in the abnormal vascular spaces. Resolution of these hematologic disorders after

hamartoma resection has been reported.^{62,64} Associated growth retardation and recurrent infections have been reported in the pediatric population.⁵⁶ It can be difficult, especially by cytologic analysis, to differentiate a hamartoma from a malignant neoplasm. Resection—partial or total splenectomy—is often performed because of diagnostic uncertainty.^{60,61,65,66}

PATHOLOGY

On gross examination, hamartomas are well-circumscribed, solid lesions that compress the surrounding parenchyma. They vary in size from less than 1 cm to more than 20 cm in diameter.⁵⁶ On histologic examination, splenic hamartomas are composed of disorganized red pulp elements with reticuloendothelial cell proliferation. Normal white pulp is usually absent.^{14,34,42,66} They contain a mixture of unorganized sinus-like structures lined by endothelial cells surrounded by fibrotic cords of predominant splenic red pulp without a true capsule.^{34,42} Cystic spaces and coarse calcifications have been reported.³⁴ Special immunohistochemical techniques can be used to differentiate hamartomas from hemangiomas. The etiology of splenic hamartomas is controversial; some authors consider splenic hamartomas to be congenital in origin, whereas others consider hamartomas to be true neoplasms or to be an acquired proliferative process.^{42,60}

RADIOLOGIC FINDINGS

On sonography, hamartomas are typically well-defined, homogeneous masses (Fig. 105-6A). The reported appearance varies from isoechoic to mildly hyperechoic or hypoechoic.⁶⁷⁻⁶⁹ The mass may contain cystic areas or coarse calcifications.^{68,70} On color Doppler images, the mass often demonstrates increased blood flow.^{67,69} Some investigators report that sonography is more sensitive than CT in depicting hamartomas of the spleen.⁷⁰

A contour abnormality is often the only visible finding on CT (Fig. 105-6B).³⁴ A typical hamartoma is isodense or mildly hypodense on nonenhanced and on intravenously enhanced CT scans (Fig. 105-6C).⁷¹ Heterogeneous enhancement can be observed in larger lesions; uniform and prolonged contrast enhancement is often shown on the delayed images.⁷²

On MRI, hamartomas are well-defined, isointense masses on the T1-weighted images. In a series of five patients, four were imaged with T2 sequences. In three of these, the lesions were heterogeneously hyperintense, and in one, the mass was hypointense relative to the normal spleen.³⁶ In the same series, all hamartomas demonstrated diffuse, heterogeneous enhancement in the early phases and became more uniformly enhanced on delayed images on dynamic contrast-enhanced sequences. Similar MRI characteristics were described by other investigators, including prolonged enhancement on the delayed images after intravenous administration of gadolinium.⁷¹⁻⁷³

Angiography, sometimes performed for preoperative embolization, may demonstrate a hypervascular mass with peripheral tumor vessels and tumor stains.^{56,67,74,75}

The literature describing scintigraphic imaging findings for splenic hamartomas is sparse. Case reports of splenic hamartomas describe hot spots on ^{99m}Tc-sulfur colloid scintigraphy, presumably caused by uptake in reticuloendothelial cells.^{75,76} The dynamic images of radiocolloid scans may show increased flow in the spleen. Other studies have described decreased

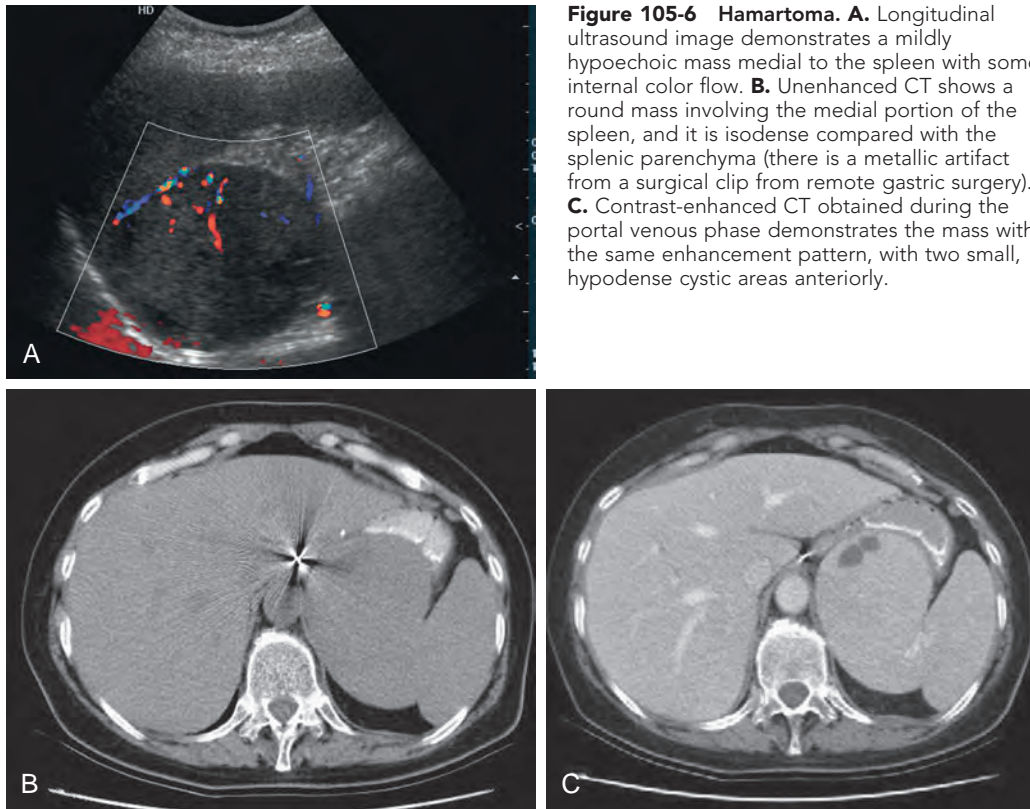


Figure 105-6 Hamartoma. **A.** Longitudinal ultrasound image demonstrates a mildly hypoechoic mass medial to the spleen with some internal color flow. **B.** Unenhanced CT shows a round mass involving the medial portion of the spleen, and it is isodense compared with the splenic parenchyma (there is a metallic artifact from a surgical clip from remote gastric surgery). **C.** Contrast-enhanced CT obtained during the portal venous phase demonstrates the mass with the same enhancement pattern, with two small, hypodense cystic areas anteriorly.

uptake of the radiocolloid tracer compared with the normal spleen.⁷⁰

Although splenic hamartoma may be suspected on the basis of the imaging characteristics, a definitive diagnosis can rarely be made by the imaging findings alone.^{34,60} A definitive diagnosis may be established with a percutaneous biopsy, although this often proves to be a challenge for the pathologist, and more often, splenectomy is needed for a definitive diagnosis.^{4,66,77}

Lymphangioma

EPIDEMIOLOGY AND PATHOGENESIS

Splenic lymphangiomas are rare, benign, slow-growing, congenital neoplasms.⁷⁸⁻⁸⁰ They are typically seen in childhood, with only a few reported cases in adults. Splenic lymphangiomas can be isolated solitary lesions within the spleen, or the entire spleen may be replaced (i.e., splenic lymphangiomatosis).⁷⁸ This may be part of a rare congenital malformation of the lymphatics called lymphangiomatosis.⁸¹ Lymphangiomatosis predominantly affects pediatric patients and typically involves multiple organs and locations, including the neck, mediastinum, and retroperitoneum.^{78,81} Lymphangiomas of the spleen have also been associated with Klippel-Trénaunay-Weber syndrome.⁸²

CLINICAL FINDINGS

In adults, splenic lymphangiomas are often asymptomatic.⁸⁰ When symptoms are present, they are usually related to the increased size of the spleen and include left upper quadrant

pain, nausea, and abdominal distention.^{34,83} Associated coagulopathy, hypersplenism, and portal hypertension have been described.^{84,85} Physical examination may reveal a tender mass in the left upper quadrant.⁸⁰

Management varies from conservative treatment for small, asymptomatic lesions to partial or total splenectomy for large, symptomatic lesions.^{83,86} Subtotal splenic embolization is also described as an effective treatment option.⁷⁸

PATHOLOGY

On gross examination, splenic lymphangiomas typically are subcapsular, multicystic lesions filled with watery pink proteinaceous fluid.¹⁴ On histologic evaluation, they are composed of multiple, thin-walled cysts of various sizes lined with a flat endothelium. Lymphangiomas often involve the capsule and trabeculae, where lymphatic structures are normally present.⁴² Lymphangiomas are traditionally classified as capillary, cavernous, or cystic, depending on the histologic findings.^{81,87}

RADIOLOGIC FINDINGS

Findings on plain radiographs are usually normal, but they may demonstrate splenomegaly with a mass effect on adjacent viscera. Curvilinear calcifications can be present.³⁴

Ultrasound typically shows multiple cysts that are a few millimeters to several centimeters in diameter and are divided by thin septations (Fig. 105-7).^{80,84,88} Splenic lymphangiomas may have calcifications, and the finding of internal echoes depends on the presence of proteinaceous or hemorrhagic fluid.

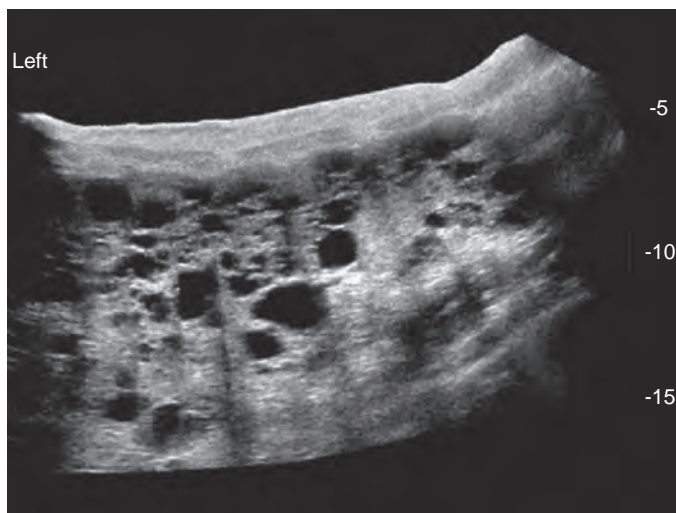


Figure 105-7 Lymphangiomatosis in a young female patient involving multiple organs, including the spleen. Longitudinal image demonstrates an enlarged spleen with numerous cystic lesions; sizes range from a few millimeters to several centimeters.

Vascularity within the walls and the septa can be demonstrated with color Doppler imaging.⁸⁵

CT can reveal subcapsular, low-density, nonenhancing, sharply marginated, thin-walled cysts. Small, curvilinear or punctate calcifications may be observed.^{34,78} After administration of an intravenous contrast agent, the septa may demonstrate enhancement.^{80,88}

MRI reveals multiple, well-defined cysts within the spleen. They appear hypointense on T1-weighted images and hyperintense on the T2-weighted sequences.^{34,88} The cysts may demonstrate high signal intensity on the T1-weighted images if they contain proteinaceous or hemorrhagic fluid.⁴³ The septa appear as hypointense structures on the T2-weighted sequences.⁸⁹ These septa are usually better defined on contrast-enhanced CT and MR images.

When the lymphatic spaces are small, as in capillary lymphangiomas, the lesion may have a solid appearance on radiologic imaging, making a correct preoperative radiologic diagnosis difficult.⁹⁰ The literature on angiographic and scintigraphic findings in splenic lymphangiomas is limited. Lymphangiomas do not demonstrate uptake of the radiopharmaceutical on ^{99m}Tc-sulfur colloid scintigraphy.⁸²

On angiography, splenic lymphangiomas have been observed as round or oval, hypovascular mass lesions displacing the surrounding arterial branches without neovascularity.⁸⁶ With more extensive involvement, many focal lucencies of various sizes can be seen in the venous phase, producing the so-called Swiss cheese appearance.^{86,91}

Inflammatory Pseudotumor

EPIDEMIOLOGY AND PATHOGENESIS

Splenic inflammatory pseudotumor is a rare, benign lesion. Although the cause and pathogenesis are unknown, it is thought that inflammatory pseudotumors result from an unusual, non-specific, inflammatory reparative response to injury such as infection.^{42,92-94}

CLINICAL FINDINGS

Like most other benign splenic tumors, inflammatory pseudotumors are usually asymptomatic. In the typical scenario, this lesion is discovered incidentally, sometimes presumed to represent lymphoma. Fever and leukocytosis are the most commonly described associated symptoms.⁹² If the pseudotumor is large, a palpable mass may be discovered on physical examination.

PATHOLOGY

On gross examination, the lesions are often well defined and white. On histopathologic examination, the lesions are found to be well circumscribed and composed of spindle cells and various proportions of mixed inflammatory cells, including small lymphocytes, plasma cells, and histiocytes. A zonal distribution is characteristic, with central foci of necrosis and hemorrhage, foamy histiocytes, granulomas, and giant cells.^{95,96} Calcifications can be present.

RADIOLOGIC FINDINGS

Unfortunately, radiologic imaging techniques do not permit preoperative diagnosis of these lesions. Splenic inflammatory pseudotumors are typically misdiagnosed as other masses, such as lymphoma or metastatic disease.^{92,94}

Abdominal radiographs are of limited utility. Ultrasound usually demonstrates a well-defined hypoechoic mass and acoustic shadowing when calcifications are present.⁹²

Unenhanced CT scans reveal a rounded mass with low attenuation with or without calcifications. Enhancement can be homogeneous or heterogeneous, and delayed enhancement patterns are often described.⁹³ Central, stellate, low-density areas may persist within the mass, probably corresponding to focal areas of fibrosis.⁹⁷

On MRI, these lesions appear isointense to the splenic parenchyma on T1-weighted images. Both heterogeneously hypointense and hyperintense lesions compared with normal spleen tissue have been described on T2-weighted images.^{93,94} As with CT, most investigators describe a peripheral enhancement pattern with gradual, delayed central enhancement from the periphery to the center on the dynamic sequences.^{93,94,98}

Peliosis of the Spleen

EPIDEMIOLOGY AND PATHOGENESIS

Splenic peliosis is a rare condition characterized by sinusoidal dilation and formation of multiple, cystlike, blood-filled cavities within the parenchyma.⁹⁹ This condition most commonly affects the liver, but any organ, including the spleen, can be affected. Splenic peliosis as an isolated finding is rare; it is usually associated with hepatic peliosis.¹⁰⁰ The pathogenesis of splenic peliosis is unclear. Splenic peliosis has been associated with various conditions, including infection, hematologic malignant neoplasms, use of anabolic steroids, and immunocompromised states.

CLINICAL FINDINGS

Patients with splenic peliosis are often asymptomatic, and the condition is found incidentally on imaging studies or at autopsy.

However, peliosis can be manifested with spontaneous splenic rupture.¹⁰¹ The first well-documented case of peliosis was reported in 1866, when Cohnheim described a spontaneous splenic rupture in a young man with peliosis.¹⁰²

PATHOLOGY

On gross examination, the size of the spleen is often found to be normal. Multiple, blood-filled cavities are round to oval and are 1 mm to several centimeters in diameter. The blood-filled cystic spaces may be arranged sporadically, may occur in clusters, or may be disseminated throughout the spleen.³⁴ Thrombosis may occur in the cystic spaces. On microscopic examination, the cysts located within the red pulp are lined with flattened, sinusoidal endothelium, or they may lack a clear cell lining.^{42,99}

RADIOLOGIC FINDINGS

No large series of splenic peliosis are available. The imaging findings are typically described in publications of hepatic peliosis and in case reports. The imaging findings of peliosis are variable and depend on the size of the cysts and whether there is thrombosis of the cystic contents.¹⁰³

Sonography typically reveals multiple, poorly defined, hypoechoic lesions. The lesions may be hyperechoic if thrombosis is present.³⁴

On unenhanced CT, peliosis lesions usually appear as multiple areas of low attenuation. On contrast-enhanced CT scans, splenic peliosis most commonly is manifested as multiple, small, well-defined, hypoattenuating, cystlike lesions.^{34,101} High-attenuation lesions and fluid-fluid levels, which are thought to reflect a hematocrit effect, demonstrating enhancement in their dependent portions have also been described.^{104,105}

The signal intensities of the lesions on MRI depend on the age and status of the blood components. On T2-weighted sequences, these lesions are usually hyperintense. On T1-weighted sequences, the lesions are typically hypointense or isointense to the normal spleen. After gadolinium injection, peliotic lesions may or may not enhance.¹⁰⁴ Various patterns of enhancement have been described.

Angiography may reveal areas of pooling of contrast material and distortion of the intrasplenic vessels.¹⁰⁶ If the lesions rupture, perisplenic hematoma, splenic laceration, and intraperitoneal hemorrhage may be evident.^{101,106}

Cystic Splenic Lesions

Cystic lesions of the spleen are relatively uncommon compared with the frequency with which cysts are encountered in other solid abdominal organs. The reported incidence of splenic cysts at autopsy is approximately 7.6 per 10,000 people.¹⁰⁷ The true incidence is probably higher; in one series, the incidence was approximately 1% detected with abdominal ultrasound.¹¹

A wide variety of lesions may be manifested as splenic cysts (Table 105-1). In Western countries, most splenic cysts are asymptomatic and discovered incidentally during routine abdominal imaging or autopsy. The most common splenic cysts in the Western world are congenital and traumatic in origin. Worldwide, parasitic cysts (most are echinococcal) are much more common and account for approximately 70% of splenic cysts.¹⁰⁸ The correct cause and pathophysiologic mechanism of

TABLE 105-1 Cystic Lesions of the Spleen

Type of Lesion	Examples
Congenital	Epidermoid cysts (primary, true, mesothelial) Dermoid (rare)
Acquired	Pseudocysts (secondary cysts): postinflammatory, post-traumatic, postinfarction, pancreatic
Infection	Parasitic: echinococcosis Abscess: pyogenic, fungal
Neoplastic	Benign: cystic hemangioma, cystic hamartoma, cystic lymphangioma, peliosis Malignant: angiosarcoma, lymphoma, metastases

a splenic cyst can often be suggested by the medical history, symptoms, and appearance of the cyst on imaging.⁴³

CONGENITAL CYSTS AND PSEUDOCYSTS

Epidemiology and Pathogenesis

Traditionally, nonparasitic, non-neoplastic splenic cysts have been grouped as true cysts and pseudocysts on the basis of a classification system developed in 1940 by Fowler.^{109,110} Congenital cysts, also known as true, primary, epidermoid, or mesothelial cysts, have an epithelial or mesothelial cell lining and are thought to be developmental in origin. Pseudocysts, also known as secondary cysts or false cysts, do not have an epithelial lining.

Congenital cysts are believed to be the result of embryonic inclusions of splenic capsular mesothelial cells into the splenic parenchyma with subsequent gradual growth, although numerous other theories have been postulated.^{14,42,111} Congenital cysts account for approximately 10% of all splenic cysts, and they are not associated with cysts in other organs.^{107,112} Congenital cysts are often discovered in children and young adults, but they are found in all age groups, and they have a female predominance.¹¹³⁻¹¹⁵ A rare familial occurrence of splenic epidermoid cysts has also been reported.^{112,116} Dermoid cysts of the spleen are rare and have been described in only a few case reports.¹¹⁷

Pseudocysts are thought to be the result of an intrasplenic hematoma, infarct, or infection, although a history of trauma or infection is often not apparent. They are more common in females, often discovered in young adults, but they can be found in all age groups.^{113,114} Most primary or secondary splenic cysts are located in the superior portion, but they can be found anywhere in the spleen.¹¹³

Although Fowler's categorization of splenic cysts is widely accepted, Morgenstern has made a case against the traditional classification of true and false cysts and argued that it is much more likely that most cysts are congenital in origin. He reasoned that a history of significant trauma is rarely obtained and that hemorrhagic cystic lesions after a known trauma usually have a different appearance. With the current practice of nonoperative management of splenic injuries, there should have been a significant rise in the incidence of splenic cysts. He stated that it can be difficult to identify an epithelial lining in splenic cysts and that this probably led to the erroneous classification of many reported cysts as pseudocysts.¹¹⁴

The natural history of splenic cysts is unknown. No long-term follow-up reports of patients with splenic cysts have been published.¹¹²

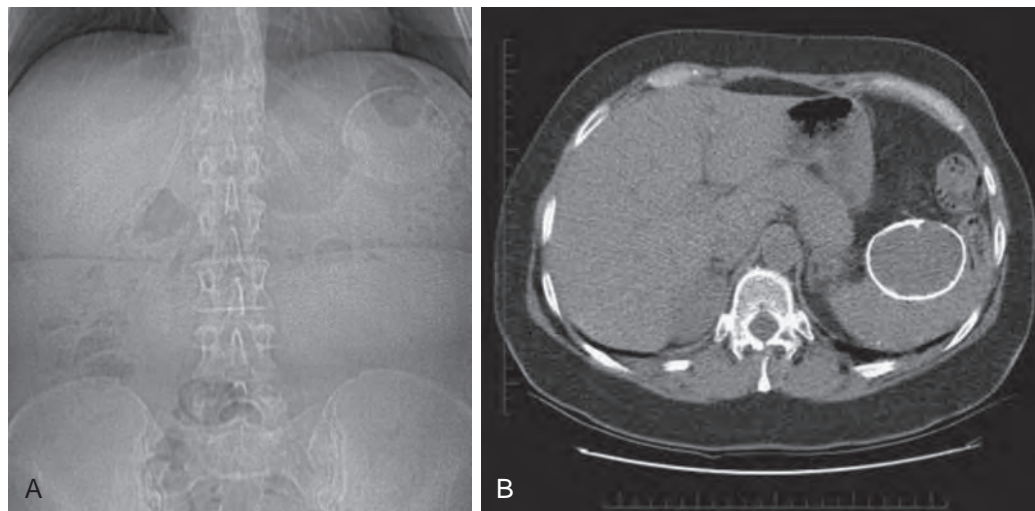


Figure 105-8 Pseudocyst.

A. The abdominal radiograph demonstrates a round, calcified lesion in the left upper abdomen.

B. Unenhanced CT shows a homogeneously hypodense lesion (15 HU) with a thin, calcified wall.

Clinical Findings

In Western countries, virtually all splenic cysts are asymptomatic and found during routine imaging.¹¹⁵ Symptoms may occur when the cysts are large and include left upper quadrant discomfort, fullness, and pain.^{113,114} Complications, such as spontaneous hemorrhage, rupture, or secondary infection, are rare.¹¹⁸⁻¹²⁰ If the cyst is large, physical examination may reveal splenomegaly or a palpable mass with or without tenderness.¹¹² Results of routine laboratory tests usually are normal, although epidermoid cysts of the spleen have been associated with elevated levels of cancer antigen 19-9 and carcinoembryonic antigen.¹²¹

In our opinion, small and asymptomatic cysts are best managed conservatively. Treatment of large and symptomatic cysts includes percutaneous aspiration with or without sclerotherapy and partial splenectomy.^{114,115,122}

Pathology

In the series of Dachman and colleagues,¹¹³ true and false cysts could not be differentiated on the basis of gross appearance. True cysts are typically unilocular, and they have a trabeculated, shiny, pearly white lining. The fluid may be clear or turbid, and the color can be yellow, green, or brown, containing cholesterol or blood degradation products.^{14,42,114} On microscopic examination, the epithelial lining is variable, and a stratified squamous epithelium is the most common finding.¹²³ On occasion, septations or thick, partially calcified walls can be seen.^{42,113} When inflammation or hemorrhage occurs in these cysts, the cellular lining may be replaced by nonspecific fibrous or granulation tissue, and histologic distinction between epidermoid cysts and pseudocysts becomes difficult.

Most pseudocysts are unilocular and have a smooth inner surface. The wall is formed by fibrous tissue with or without calcified components, and these cysts are often filled with serous or hemorrhagic fluid.^{14,42,115}

Radiologic Findings

It is not possible to distinguish between true and false cysts with any imaging technique.^{43,113} The wall of a pseudocyst tends to be thicker. If a cyst is large, it may be identified on plain radiographs. In certain instances, it may be possible to

differentiate a cyst from splenomegaly by the observation of a round mass with a normal, intact splenic tip.¹¹³ Curvilinear calcifications may also help identify the presence of a splenic cyst (Fig. 105-8).

On ultrasound, splenic cysts, like cysts elsewhere in the body, characteristically appear as anechoic lesions with smooth borders and demonstrate increased through-transmission (Fig. 105-9A). Epidermoid cysts and pseudocysts may demonstrate septations, thick walls, trabeculations, internal echoes, and calcified walls.¹¹³

On CT, splenic cysts appear as homogeneous, well-defined, round or oval, low-enhancing or nonenhancing, hypodense lesions (Fig. 105-9B). The attenuation values typically range from 0 to 15 HU. Higher attenuation values are found in the presence of protein or blood degradation products. The cyst wall can be thick or partially calcified, and septations are sometimes observed.^{43,113}

On MRI, splenic cysts demonstrate low signal intensity on the T1-weighted images and high, uniform signal intensity on the T2-weighted images (Fig. 105-9C).^{51,124,125} Complicated cysts, because of the presence of proteinaceous fluid or hemorrhage, may demonstrate high signal intensity on the T1-weighted images and mixed signal intensity on the T2-weighted images. Cysts should not demonstrate any enhancement after the administration of gadolinium.

On scintigraphy, if the cyst is large enough, a solitary photopenic defect may be seen. Splenic cysts are avascular on angiography.¹¹³

HYDATID DISEASE

Epidemiology and Pathogenesis

Hydatid disease, or echinococcosis, is a zoonotic tapeworm infection caused by the species *Echinococcus granulosus*. The larva, known as the hydatid, forms a cyst as it develops in the lung, liver, kidney, or spleen. The disease involves the spleen in approximately 2.5% to 6% of patients with abdominal hydatidosis and typically occurs in patients living in or emigrated from endemic areas.¹²⁶⁻¹²⁹ Splenic hydatid involvement is usually part of more widespread abdominal disease after rupture of a hydatid liver cyst. Primary echinococcal involvement of the spleen is rare.¹⁰⁸ Alveolar echinococcal

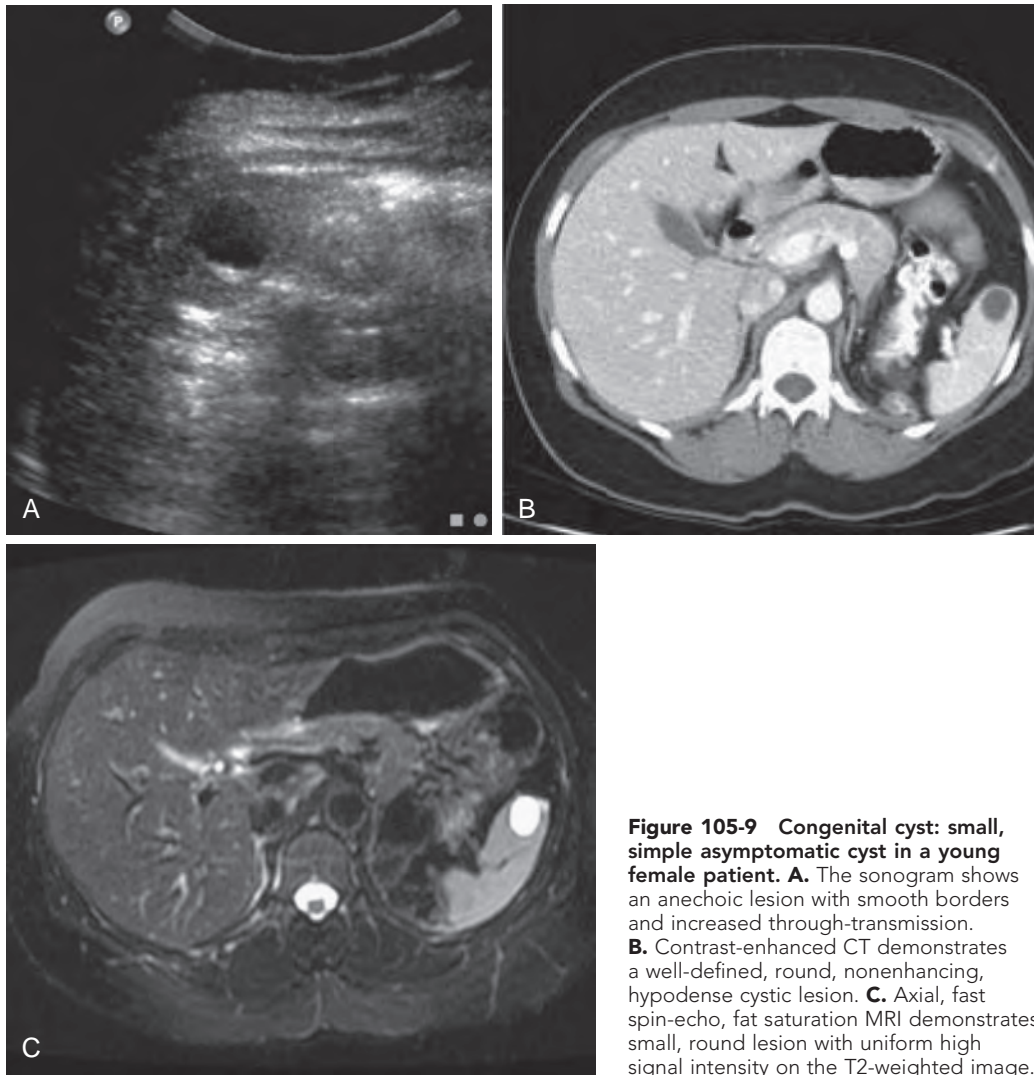


Figure 105-9 Congenital cyst: small, simple asymptomatic cyst in a young female patient. **A.** The sonogram shows an anechoic lesion with smooth borders and increased through-transmission. **B.** Contrast-enhanced CT demonstrates a well-defined, round, nonenhancing, hypodense cystic lesion. **C.** Axial, fast spin-echo, fat saturation MRI demonstrates small, round lesion with uniform high signal intensity on the T2-weighted image.

disease is caused by *Echinococcus multilocularis* and rarely involves the spleen.¹³⁰

Pathology

The hydatid cyst wall has three layers. The larvae of the tapeworm incite an inflammatory host response that forms an outer layer of inflammatory cells and fibrous tissue called the pericyst. The true cyst wall, also called the endocyst, is composed of an outer laminated membrane lined by an inner germinal layer made up of daughter cysts, also called the brood capsules. Scolices develop on the inner aspect of the brood capsules and after separation of the cyst wall form a sandlike material within the cysts.^{42,129,131} When the parasites die, the cysts become inactive, and the cysts may calcify and undergo fibrosis.

Clinical Findings

Splenic hydatidosis is often asymptomatic. Symptoms, if present, include abdominal pain and splenomegaly.^{108,128} More often, the clinical and radiologic findings are nonspecific, and the diagnosis should be suspected in all patients from endemic areas presenting with a splenic cyst.

Large cysts may cause compression of surrounding structures. Complications include infection, cyst rupture, and fistulization to surrounding organs.¹²⁸ Rupture into the abdominal cavity may result in an anaphylactic reaction and the spread of multiple cysts throughout the abdomen.¹³² Serologic tests have a sensitivity of approximately 90% in diagnosis of hydatid disease.¹³³ The imaging findings, combined with the clinical, serologic, and epidemiologic results, usually provide the correct diagnosis.^{134,135}

Albendazole is the mainstay of echinococcal treatment. Splenic hydatid cysts can be treated percutaneously with cyst aspiration and injection of hypertonic saline solution or alcohol, also known as the PAIR technique (i.e., puncture, aspiration, injection, reaspiration).¹³⁵⁻¹³⁷ Splenectomy or partial splenectomy can be performed if other treatment options have failed. Inactive cysts are typically observed and managed conservatively.

Classification

A World Health Organization Working Group on echinococcosis formulated a standardized sonographic classification of echinococcal cysts (Table 105-2).^{134,138}

The classification is intended to follow the natural history of cystic hydatid disease. Type CL cysts are usually seen at an early stage of development and are not fertile. These cysts cannot be differentiated from nonparasitic splenic cysts on the basis of imaging. Because the origin is uncertain, this cyst is not given the designation of a cystic echinococcosis (CE) type of lesion and is recorded as a cystic lesion (CL). The CE 1 and CE 2 types are active, usually fertile cysts containing viable protoscoleces. CE 3 cysts are degenerative and are entering a transitional stage. Most CE 4 and CE 5 cysts are inactive, nonfertile cysts.

Radiologic Imaging

The radiologic appearance of hydatid cysts reflects the natural history of the disease, in which daughter cyst formation is part

of the natural aging process. The imaging findings are variable and range from purely cystic to solid-appearing pseudotumors, depending on the stage of the disease (see Table 105-2). All of these characteristic imaging appearances are lost when the cysts become infected.

Plain radiographs are of limited utility. Curvilinear or ring-like calcifications, representing calcifications of pericysts, could suggest cystic echinococcosis, especially in patients from endemic areas.¹³⁹

Ultrasound is the most popular and readily available technique worldwide for evaluation of abdominal echinococcal disease. Ultrasound is used for diagnosis, therapeutic decision-making, and follow-up. Portable ultrasound is also used in remote areas to screen, to diagnose, and to treat patients.¹³⁵

Fine internal echoes within the cysts may be seen because of shifting of the brood capsules, often called hydatid sand (i.e., the snowflake sign). Wavy bands of detached, laminated endocysts (i.e., the water lily sign) may be observed within the cysts. Daughter cysts may partially or completely fill the mother cyst (Fig. 105-10A). Calcifications, varying from tiny to massive, are often present.

CT and MRI are indicated for patients not suited for ultrasound and for evaluation of widespread or complicated disease. Cross-sectional imaging is helpful in planning percutaneous therapy or surgery. Subtle cyst wall calcifications are best demonstrated with CT.

On CT, a hydatid cyst may be manifested as a well-defined, hypoattenuating cystic lesion with water-attenuation values and a distinguishable wall. Coarse wall calcifications are often present. The hydatid cysts can be hyperdense because of debris, hydatid sand, and inflammatory cells. In CE 2 cysts, the round daughter cysts are arranged at the periphery, or they completely fill the mother cysts. CT attenuation of the daughter cysts is typically lower than that of the mother cysts. Type CE 3 lesions appear as relatively high attenuation, round or oval masses with scattered calcifications and occasional daughter cysts (Fig. 105-10B). Type CE 4 cysts may appear as a complex mass. The septa and cyst wall frequently enhance after the intravenous administration of contrast material.¹²⁹ Type CE 5 cysts are complex cystic or solid-looking lesions, and they can be partially or completely calcified.

On MRI, the simple cysts are hypointense on the T1-weighted images and markedly hyperintense on the T2-weighted images.

Classification	Description
CL	Simple cystic lesion; no cyst wall visible
CE 1	Unilocular simple cyst with visible cyst wall; may exhibit "hydatid sand," fine internal echoes due to shifting of the brood capsules (i.e., snowflake sign)
CE 2	Multivesicular, multiseptate cyst; daughter cysts may partially or completely fill the mother cyst; septations may produce wheel-like structures; contained daughter cysts may produce a rosette-like or honeycomb-like structure
CE 3	Unilocular, anechoic content with detachment of the laminated membrane from the cyst wall, visible as a floating membrane (i.e., water lily sign), or complex masses caused by unilocular cysts containing daughter cysts and echoic areas
CE 4	Heterogeneous hypoechoic or inhomogeneous degenerative contents; no daughter cysts; degenerating membranes may produce a ball of wool sign
CE 5	Cysts with a thick, calcified, arch-shaped wall; lesions are partially or completely calcified

CE, Cystic echinococcosis; CL, undifferentiated, simple cystic lesions. Modified from WHO Informal Working Group: International classification of ultrasound images in cystic echinococcosis for application in clinical and field epidemiological settings. *Acta Trop* 85:253–261, 2003.

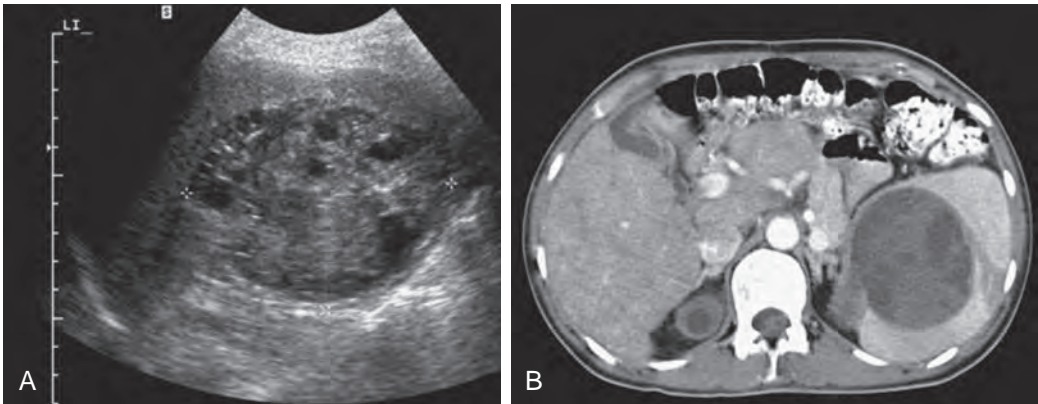


Figure 105-10 Echinococcal cyst: cystic echinococcosis type 3. **A.** Longitudinal ultrasound image of the spleen demonstrates a complex lesion with central hyperechoic areas and small peripheral daughter cysts. **B.** Contrast-enhanced CT during the arterial phase demonstrates an oval mass involving the medial portion of the spleen with relatively high central attenuation and a few peripheral hypodense daughter cysts. There is associated involvement of the right adrenal. (Courtesy M. de Jonge, MD, Amsterdam, The Netherlands.)

A low signal intensity rim (i.e., the rim sign), which is more evident on T2-weighted MR images, has been described as characteristic of hydatidosis.¹³¹ The septa and cyst wall frequently enhance after the intravenous administration of gadolinium. The daughter cysts may appear hypointense or isointense relative to the maternal matrix on T1- and T2-weighted images. The collapsed parasitic membranes may reflect a serpent sign or snake sign. These membranes have low signal intensity on all sequences. Type CE 4 and CE 5 cysts usually are hypointense on T1- and T2-weighted images.

The presence of a cystic lesion in a patient from an endemic area with positive serologic test results most likely indicates hydatid disease. In almost all cases of splenic hydatid cystic disease, hydatid liver disease coexists. The presence of daughter cysts is probably the most helpful imaging feature.

DIFFERENTIAL DIAGNOSIS OF CYSTIC SPLENIC MASSES

The differential diagnosis of cystic splenic masses is extensive (see Box 105-2) and includes true or false splenic cysts, parasitic (hydatid) cysts, pseudocysts related to pancreatitis, pyogenic abscess, benign tumors of the spleen (e.g., hemangiomas, hamartomas, lymphangiomas, lymphoma), and metastatic tumors. The correct diagnosis can usually be suggested by an analysis of clinical findings and symptoms, the medical history, and the appearance of the cyst.

Splenic cysts (true or false) are the most common in Western countries. They are typically well defined, are of homogeneous water density, and have a thin or imperceptible wall. After infection or hemorrhage, the cysts become more complex.

The presence of a cystic lesion with wall calcification and daughter cysts in a patient from an endemic area should raise the suspicion of cystic echinococcosis. Most cases of splenic hydatid cystic disease have coexisting hydatid liver disease.

Patients with a splenic abscess usually are sick or septic, and they present with fever, left upper abdominal pain, and leukocytosis. A cystic splenic mass developing in a patient with pancreatitis is likely to be a pancreatic pseudocyst.

Benign splenic neoplasms (e.g., hemangioma, lymphangioma, hamartoma) may show single or multiple cystic spaces in the mass that rarely fulfill the criteria for a simple cyst. Splenic lymphoma may be manifested as ill-defined, hypoechoic masses with internal echoes on ultrasound or as low-density lesions with or without a thick rim on CT scans, mimicking a cystic lesion.^{140,141} Cystic metastases to the spleen have been reported from melanoma and adenocarcinoma of the breast and ovary, but they usually occur in the setting of widespread metastatic disease and typically have a complex appearance. Isolated splenic metastases are rare.

Splenic Infection and Inflammatory Disease

Inflammation and infection of the spleen are manifested in three distinct patterns: generalized splenomegaly without discerning focal lesions; solitary lesions; and a diffuse, miliary or macronodular pattern with or without splenomegaly.¹⁰ Generalized splenomegaly is a nonspecific finding and can be found in a variety of diseases, including infections and inflammatory diseases (Box 105-3). Multiple splenic nodular lesions, usually

BOX 105-3 COMMON CAUSES OF DIFFUSE SPLENOMEGALY

Congestive splenomegaly
 Portal hypertension
 Splenic vein thrombosis
 Congestive heart failure
 Infectious and inflammatory diseases
 Acute infections (e.g., infectious mononucleosis)
 Chronic infections (e.g., miliary tuberculosis, malaria)
 Sarcoidosis
 Systemic lupus erythematosus
 Hyperplastic splenomegaly (i.e., hypertrophy)
 Hemolytic anemias (e.g., malaria, polycythemia vera)
 Infiltrative splenomegaly
 Lymphomas, leukemias
 Metastases
 Extramedullary hematopoiesis
 Storage diseases (e.g., Gaucher's disease, amyloidosis)
 Splenic neoplasms
 Lymphangiomatosis
 Hemangiomatosis
 Peliosis

BOX 105-4 CAUSES OF SPLENIC NODULAR LESIONS*

Fungal microabscesses
 Bacterial microabscesses
 Protozoal infections
 Tuberculosis
Mycobacterium avium complex infection
Pneumocystis jiroveci pneumonia
 Cat-scratch disease
 Sarcoidosis
 Gamna-Gandy bodies
 Hodgkin's lymphoma
 Non-Hodgkin's lymphoma
 Metastases

*Splenic nodules are less than 2 cm in diameter.

smaller than 2 cm in diameter, are commonly associated with nonbacterial infections, such as fungal and granulomatous infections. An abscess may be manifested as a solitary lesion. The presence of gas in a lesion, although rare, is pathognomonic of a pyogenic infection.

SPLENIC NODULAR DISEASE

Multiple, small, nodular splenic lesions are encountered in a wide variety of diseases (Box 105-4). These consist of bacterial, fungal, and protozoal infections; granulomatous diseases, including mycobacterial infections; and sarcoidosis and malignant neoplasms, such as lymphoma and metastases. Many patients with multiple splenic nodules have an established diagnosis, such as lymphoma, metastases, or tuberculosis. In these cases, the nodules are presumed to represent the same disease, and pathologic confirmation is usually not necessary. Multiorgan involvement is typical, and similar changes are seen in the liver and other organs.

If no diagnosis has been established and the splenic nodules are an isolated finding, the diagnosis can rarely be made on the

imaging findings alone. The different causes are often manifested in a clinically similar fashion, typically with splenomegaly and fever. The history and clinical presentation may narrow the differential diagnosis. Additional investigations, such as laboratory tests (including tumor markers), tuberculosis testing, and bone marrow biopsies, may be indicated. When the underlying disease is successfully treated, the nodules usually resolve or become calcified granulomas.

The imaging characteristics of the various nodular conditions are nonspecific and similar. The nodules are often numerous and are a few millimeters up to 2 cm in diameter. They are hypoechoic on ultrasound and hypoattenuating on CT. The lesions appear hypointense on T1-weighted sequences and vary from hypointense to hyperintense on the T2-weighted sequences. The nodules usually do not enhance or may show ring enhancement after intravenous administration of contrast material. Healed granulomas appear as scattered, discrete, small calcifications in an otherwise normal spleen.

FUNGAL ABSCESS AND MICROABSCESS

Fungal infections of the spleen typically occur in immunocompromised patients with neutropenia. Acquired immunodeficiency syndrome (AIDS), chemotherapy, immunosuppressive agents, and lymphoproliferative disorders are the most common risk factors.¹⁴²⁻¹⁴⁴ Hepatosplenic fungal infection is found in approximately 7% of patients with acute leukemia, and these patients have a poor prognosis.^{143,144} *Candida* is the fungal organism most frequently encountered, followed by *Aspergillus*, *Cryptococcus*, and *Histoplasma*.¹⁴⁵

When the host response improves, the focus of candidiasis becomes encapsulated and walled off by neutrophils and inflammatory cells. As a result, the findings on diagnostic imaging are often normal in patients with chronic disseminated candidiasis because the characteristic changes become visible only when the neutrophil count recovers.¹⁴⁶⁻¹⁴⁸ In an analogous case, the phenomenon of waning of focal hepatic and splenic lesions on imaging during neutropenia was described by Pestalozzi.¹⁴⁹

No single imaging technique has proved to be specific and sensitive in patients with suspected or proven fungal infections, and only serial imaging may be able to detect hepatosplenic involvement.¹⁴⁸ Regardless of the imaging findings, a biopsy may be necessary to establish the final diagnosis because blood cultures are often falsely negative, particularly with *Candida* infections.¹⁵⁰

Pathology

On histologic examination, these lesions are poorly confined, containing pseudohyphae and yeast forms. On microscopic examination, the lesions are multilayered, consisting of an outer ring of fibrosis, a middle area of inflammatory cells, and a central area of necrosis.¹⁴⁷

Clinical Findings

The most common manifestation of systemic candidiasis is persistent fever not responsive to conventional antibiotics.¹⁴⁴⁻¹⁴⁸ The clinical diagnosis of fungal infection is often difficult because the presenting symptoms may be similar to those of the patient's primary disorder: fever and splenomegaly. Unexplained clinical deterioration in an immunosuppressed patient should raise the suspicion of a disseminated fungal infection.

Radiologic Findings

The limitation of all imaging modalities in the diagnosis of hepatosplenic fungal disease is the inability to visualize fungal lesions during the neutropenic phase. It is important to consider repeating the studies after recovery of the neutrophil count, especially if the clinical suspicion is high and the patient is not responding to conventional antibiotic therapy.¹⁵¹

Different sonographic patterns of hepatosplenic candidiasis have been described. Multiple, small, hypoechoic nodules are the most common finding (Fig. 105-11A).¹⁴² A less common appearance can be seen in the early course of infection and has been described as the wheel-within-a-wheel appearance (i.e., the target sign). It is caused by a peripheral hypoechoic zone of fibrosis, the first wheel, and an echogenic second wheel of inflammatory cells around a central echogenic nidus containing necrosis and fungal elements (Fig. 105-11B).^{152,153} This type of

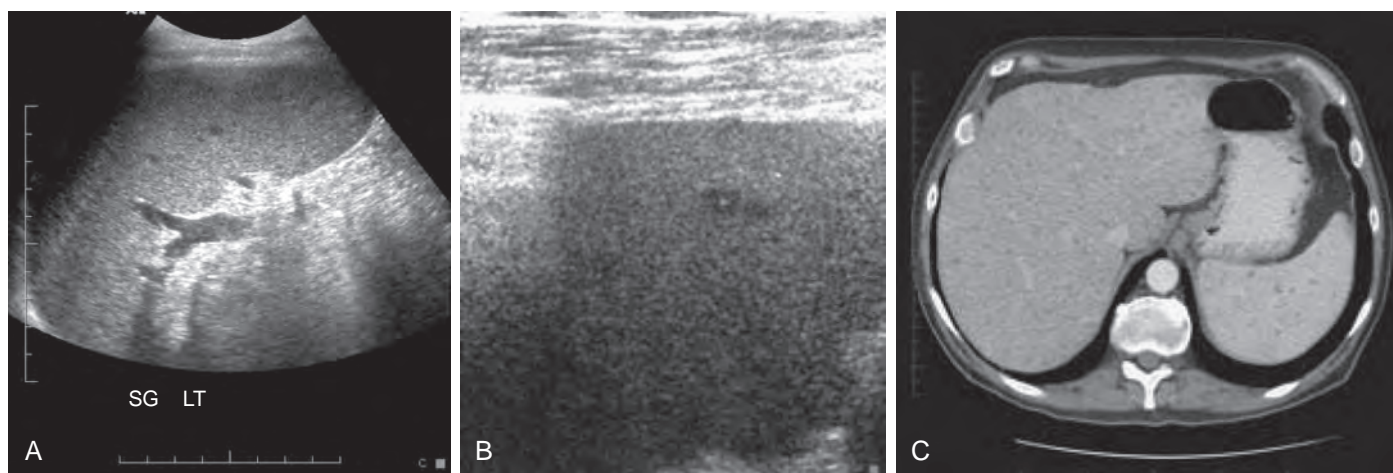


Figure 105-11 Dissemminated *Candida* infection in a patient with acute myelogenous leukemia. **A.** Transverse ultrasound image shows multiple, small, hypoechoic lesions in the splenic parenchyma. **B.** Sonogram with a high-frequency (5-12 MHz) linear transducer demonstrates a small, hypoechoic nodule with a central echogenic nidus. **C.** Contrast-enhanced CT shows numerous, subcentimeter, hypodense nodular lesions throughout the liver and spleen.

lesion may evolve into a bull's-eye lesion, which histologically corresponds to inflammatory cells surrounded by fibrosis. Late in the disease with healing, lesions usually become small and hyperechoic with various degrees of posterior acoustic shadowing, with or without calcification, or they may disappear.^{142,152} The use of higher frequency, linear array transducers significantly improves lesion detection.¹⁵⁴

On CT, fungal microabscesses are typically 5- to 10-mm, hypodense, nodular lesions (Fig. 105-11C). The detection rate is low (30%) on noncontrast scans.¹⁵⁵ In the arterial phase (25-35 seconds), most lesions (70%) demonstrate an enhancing peripheral ring that typically disappears in the portal venous phase.¹⁵⁶ In the study by Metser and associates,¹⁵⁵ the detection rate of about 90% was not significantly different between the arterial phase and portal venous phase. Similar findings are typical for the liver and sometimes for the kidneys.¹⁵³

Rudolph and colleagues¹⁵⁶ demonstrated another appearance in approximately 30% of patients. In the arterial phase, these lesions showed an inhomogeneous central enhancement surrounded by a double target ring consisting of a hypodense inner ring surrounded by a hyperdense outer ring. Over time, contrast enhancement is in a centrifugal direction, and the lesions appear smaller or disappear in the portal venous phase.

MRI is superior to CT and ultrasound for identification of hepatosplenic fungal disease, with a reported sensitivity of 100% and specificity of 96%.^{144,151} MRI is especially useful for following the course of infection during antifungal therapy and for evaluating the response to treatment.¹⁴⁵

On MRI, in the acute phase of hepatosplenic fungal disease, the lesions are small, measuring less than 1 cm in diameter. They are mildly hypointense on the T1-weighted images and markedly hyperintense on the T2-weighted images.

In the subacute phase, the lesions tend to be mildly hyperintense on both T1- and T2-weighted sequences.^{151,153} A peripheral ring of very low signal intensity is typical on all sequences in the subacute phase.¹⁵¹ The central region of the lesions may demonstrate enhancement after gadolinium administration, with the peripheral ring continuing to have low signal intensity, making them more visible. The time for transformation from acute to subacute lesions is 2 weeks to 3 months.¹⁴⁵

After successful antifungal treatment, the 1- to 3-cm lesions become irregular, and the central area disappears. The time to appearance of healed fungal foci on MRI ranges from 3 months to more than 1 year.¹⁵⁷

^{99m}Tc-sulfur colloid liver-spleen, indium In 111-labeled leukocyte, and gallium Ga 67 scans usually are not helpful in detecting microabscesses because normal uptake of the radio-tracer obscures the small lesions. Results of ⁶⁷Ga scans are variable and may show multifocal areas of increased or decreased uptake in the spleen.¹⁵⁸

FDG PET scans show increased ¹⁸F-fluorodeoxyglucose uptake. This represents a promising imaging technique in patients at high risk for infections, although published data regarding fungal infections are still limited.¹⁵⁹

TUBERCULOSIS

Mycobacterium tuberculosis is an important health problem in developing countries; in Western countries, it is typically seen in immunocompromised patients.¹⁶⁰ Splenic tuberculosis usually occurs in the setting of disseminated, miliary infection and is manifested as multiple splenic nodules between 0.2 and

1 cm in diameter. Macronodular presentation is rare.¹⁶¹ In cases of disseminated, miliary pulmonary tuberculosis, splenic involvement has been found in 80% to 100% at autopsy. Associated findings include lymphadenopathy and a hypoechoic pattern on ultrasound or central low attenuation on CT, which is more commonly seen in patients with *Mycobacterium avium* complex infection (Fig. 105-12).¹⁶²

MYCOBACTERIUM AVIUM COMPLEX INFECTION

Mycobacterium avium complex infections of the spleen, also called *Mycobacterium avium-intracellulare* infections, are typically seen in immunocompromised patients, such as those with AIDS. Splenomegaly with multiple, low-attenuation nodules can be seen on imaging (Fig. 105-13). Associated findings, such

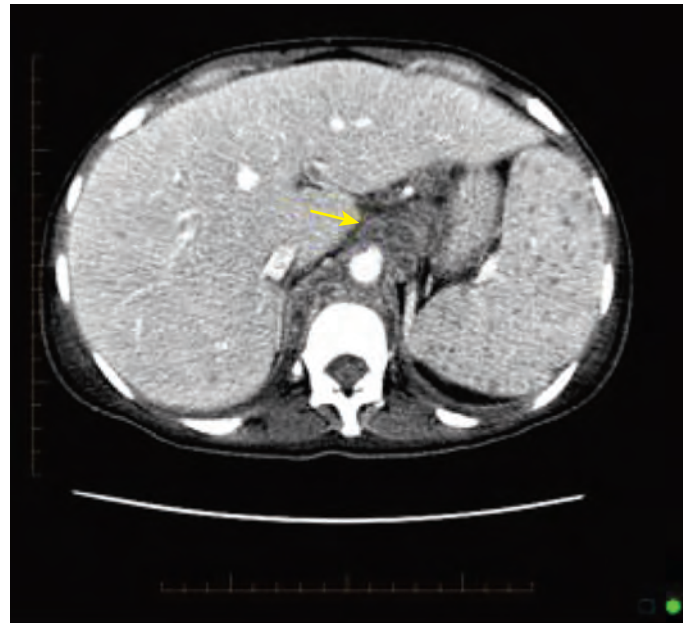


Figure 105-12 Disseminated miliary tuberculosis. Contrast-enhanced CT demonstrates multiple hypodense nodules. Notice the associated para-aortic and retrocrural hypodense lymphadenopathy (arrow).



Figure 105-13 *Mycobacterium avium* complex infection. Longitudinal sonogram demonstrates splenomegaly with multiple, small, hypoechoic nodules.

as marked hepatic and splenic enlargement, diffuse jejunal wall thickening, and enlarged lymph nodes, suggest disseminated *M. avium* complex infection.^{163,164} Patients with *M. avium* complex infection tend to have more homogeneous lymph nodes compared with those with tuberculosis, but a tissue diagnosis is mandatory.

PNEUMOCYSTIS JIROVECI PNEUMONIA

Pneumocystis jiroveci pneumonia, formerly known as *Pneumocystis carinii* pneumonia, is the most common opportunistic infection in patients with AIDS. Extrapulmonary involvement causes necrotizing granulomas. Intrasplenic *P. jiroveci* infection is often discovered incidentally in patients with AIDS undergoing diagnostic imaging for a fever of unknown origin.¹⁶⁵ When it is treated successfully, the nodules may enlarge and become progressively calcified in a rimlike or a punctate fashion.^{166,167} On ultrasound, the findings include splenomegaly with small, hypoechoic lesions with cystic components or tiny, highly reflective, nonshadowing foci or calcified granulomas (Fig. 105-14).¹⁶⁵ The nodules are hypodense on CT or manifested as calcified granulomas in the later stages of disease.^{168,169}

CAT-SCRATCH DISEASE

Cat-scratch disease is a self-limited infection by *Bartonella henselae* that occurs after being scratched by a domestic cat. It affects an estimated 22,000 people in the United States each year, and most are children and adolescents.¹⁷⁰ Hepatosplenic involvement is uncommon, but *B. henselae* infection should be considered in a patient with fever of unknown origin, abdominal pain, and multiple hypodense lesions in the liver and spleen.^{171,172}

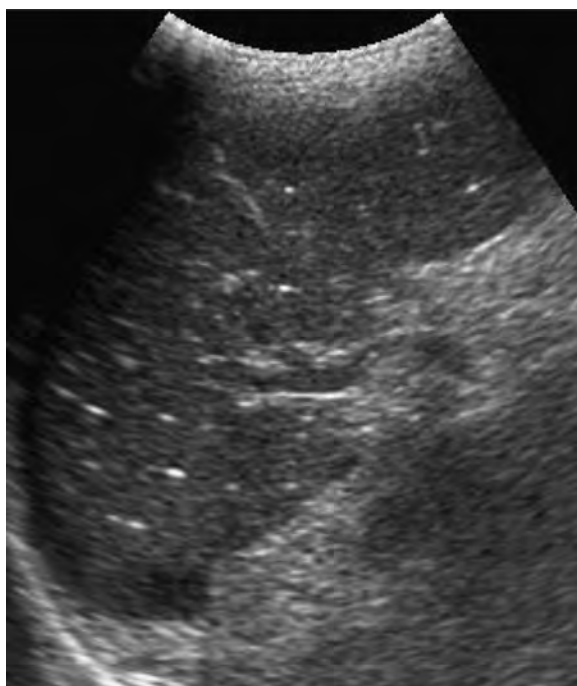


Figure 105-14 *Pneumocystis jiroveci* pneumonia. Longitudinal ultrasound image demonstrates multiple, punctate calcifications after successful treatment.

SARCOIDOSIS

Sarcoidosis is a systemic disease of unknown cause characterized by formation of noncaseating, epithelioid granulomas. Sarcoidosis most commonly affects the lungs and intrathoracic lymph nodes, but any organ system can be involved.¹⁷³ Splenomegaly, typically associated with hepatomegaly and abdominal lymphadenopathy, is usually mild and seen in 25% to 60% of these patients.¹⁷⁴⁻¹⁷⁶ Massive splenomegaly (>18 cm long) is seen in approximately 6% of patients with sarcoidosis.¹⁷⁷

Histologic evidence of liver and spleen involvement is seen in up to 77% at autopsy, but it is a relatively uncommon finding at diagnostic imaging.¹⁷⁷ On imaging, splenic nodules are seen in 6% to 33% of patients with sarcoid.¹⁷⁴⁻¹⁷⁶ In one study, these patients typically presented with hepatosplenomegaly, abdominal lymphadenopathy, and symptoms such as abdominal pain, fatigue, and malaise.¹⁷⁷ In the same study, the nodules were not associated with advanced lung disease and did not indicate a change in chest radiographic stage. The infradiaphragmatic adenopathy in sarcoidosis tends to be small and discrete, and retrocrural adenopathy is uncommon in these patients compared with patients with lymphoma. There is, however, a significant overlap in appearance and distribution of the lymph nodes in lymphoma and sarcoidosis, and these criteria cannot be used for accurate disease characterization.¹⁷⁶

The nodules in sarcoid are 0.1 to 3.0 cm in diameter.¹⁷⁸⁻¹⁸⁰ On ultrasound, the nodules have been described as hypoechoic to slightly hyperechoic or inhomogeneous.^{177,180} On CT, the nodules are hypodense relative to adjacent normal spleen after intravenous administration of a contrast agent (Fig. 105-15).^{178,179} The nodules are hypointense on all MR sequences and best seen on early-phase, gadolinium-enhanced, T2-weighted, fat-suppressed images or on T1-weighted sequences.¹⁷⁷ The nodules do not enhance after intravenous administration of contrast material on CT or MRI.

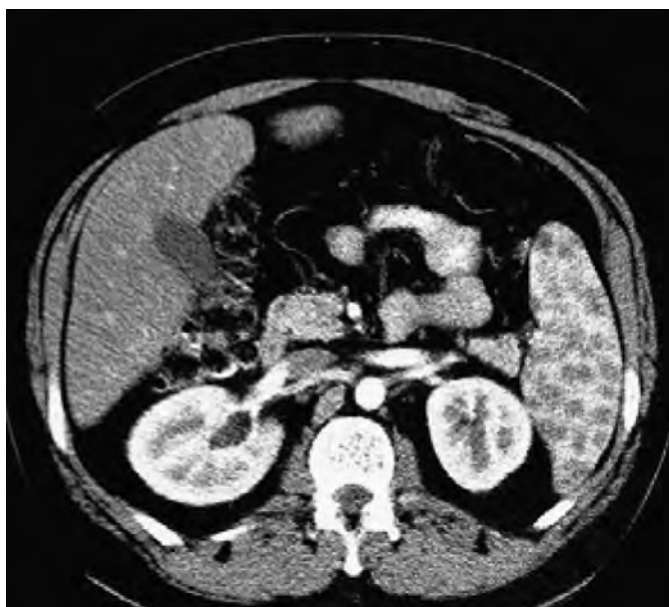


Figure 105-15 Sarcoidosis. Contrast-enhanced CT obtained in the portal venous phase shows numerous hypodense nodules.

LYMPHOMA OR METASTATIC DISEASE

Lymphomas—typically small cell lymphomas and mantle cell lymphomas and, less frequently, Hodgkin's lymphoma—can be manifested with multiple, nodular splenic lesions or with a miliary pattern. Nodules resembling those found in sarcoidosis have been described in patients with Hodgkin's lymphoma.^{42,181} This finding is usually part of disseminated disease including lymphadenopathy. Isolated splenic lymphoma is rare.^{14,42}

Metastatic disease to the spleen may be manifested as solitary or multiple nodules, rarely in a miliary pattern. This typically occurs in patients with advanced disease and widespread involvement of other organs.

GAMNA-GANDY BODIES

Gamna-Gandy bodies are siderotic nodules caused by focal organized hemorrhagic infarcts. They are typically seen in patients with congestive splenomegaly and sickle cell disease. They were also described in patients with hemolytic anemia, leukemia, lymphoma, or acquired hemochromatosis and in patients receiving multiple blood transfusions.^{182,183} The siderotic nodules occur in 9% to 12% of patients with portal hypertension and are not related to the degree of splenomegaly.^{182,184} On histologic examination, the nodules are small, yellow or brown, fibrotic lesions containing hemosiderin and calcium and sometimes containing foreign body giant cells.

Gamna-Gandy bodies are best seen by MRI as multiple, 3- to 8-mm, markedly hypointense nodules on T1-weighted and T2-weighted images.¹⁸² The gradient recalled echo sequence is the most sensitive for detection of hemosiderin and these nodules.¹⁸²⁻¹⁸⁴ Nodule conspicuity increases after gadolinium enhancement on the T1-weighted, gradient recalled echo images (Fig. 105-16). Gamna-Gandy bodies do not enhance.

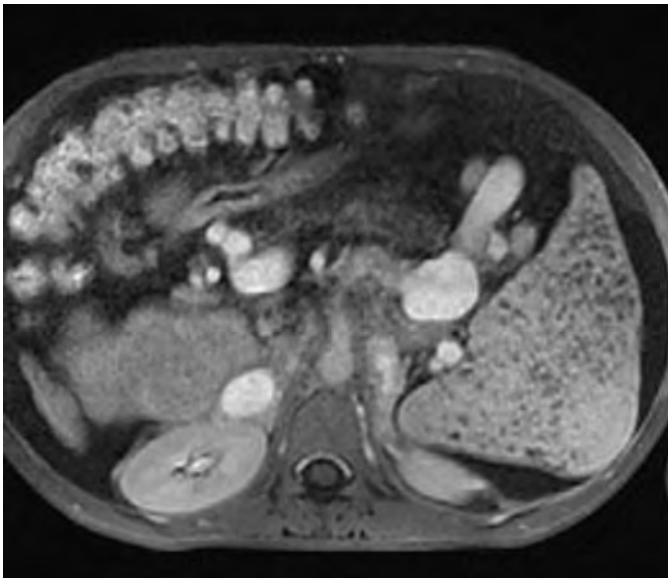


Figure 105-16 Gamna-Gandy bodies in a patient with cirrhosis and portal hypertension. Portal venous phase, axial, T1-weighted FAME (fast acquisition with multiphase enhanced fast gradient recalled echo with three-dimensional Fourier transformation) MR image after gadolinium enhancement demonstrates numerous, small, hypointense nodules throughout the spleen.

Ultrasound is less accurate than MRI. In a study by Chan and associates,¹⁸⁵ ultrasound detected the nodules in 24 of 34 patients, with a sensitivity of 70.6% and a specificity of 78.9%. Gamna-Gandy bodies appear as multiple, punctate, hyperechoic foci.

Unenhanced CT may detect Gamna-Gandy bodies as multiple, faint, hyperdense nodules shown by the calcifications within them.¹⁸⁶ However, the nodules often are not detected on CT.¹⁸⁴

PYOGENIC ABSCESS

Epidemiology and Pathogenesis

An isolated splenic abscess is a rare entity, with a reported incidence in autopsy series between 0.14% and 0.7%.¹⁸⁷⁻¹⁸⁹ However, splenic abscesses are becoming more common as a result of an increasing number of immunosuppressed patients, patients with AIDS, and injection drug abusers.¹⁹⁰ Pyogenic splenic abscesses are usually solitary and unilocular or multilocular, but they can also be multifocal.

Most abscesses are caused by disseminated infection and are seen in patients with sepsis and septic emboli.^{190,191} Less common routes are contiguous infection (e.g., infected pancreatitis, perinephric abscess) and superinfection after an underlying splenic injury (e.g., trauma, infarct). In approximately 20% of cases, no source or cause is discovered.¹⁹¹ Roughly one third of patients have other concurrent extrasplenic abscesses. The reported mortality rate for splenic abscess in the literature is about 10%.^{191,192} Multiple splenic abscesses, gas-containing abscesses, and gram-negative bacillus infection are poor prognostic factors.^{191,193} Depending on the underlying disease, a variety of microorganisms may be encountered, including gram-negative bacilli (e.g., *Klebsiella pneumoniae*), gram-positive cocci, fungi, polybacteria, and mycobacteria.^{192,193}

Clinical Findings

The most common clinical presentations in patients with splenic abscesses are fever (92%), left upper abdominal pain (77%), and leukocytosis (66%).¹⁹⁴ Other symptoms include left pleural effusion and splenomegaly. Diabetes, immunosuppression, or immunodeficiency is often a contributing factor.¹⁹⁵

Early diagnosis of a splenic abscess with identification of organisms and determination of sensitivity is essential for effective antibiotic treatment. In small abscesses, percutaneous diagnostic aspiration can be performed. For larger abscesses, percutaneous drainage procedures have become the treatment of choice, allowing preservation of the spleen.^{4,5,196,197} Splenectomy is reserved for complicated cases. Complications of splenic abscesses include rupture and peritonitis with potential life-threatening results.

Radiologic Findings

The appearance of a splenic abscess depends on the stage of development. In the early phase, there is an ill-defined mass that later develops into a complex collection with septations and debris and that sometimes contains gas.¹⁹⁴ When a capsule has developed, the lesion becomes well defined. Splenic abscesses can be solitary and unilocular, solitary and multilocular, or multifocal.¹⁸⁷ The infecting organism cannot be predicted on the basis of imaging appearances.

The most frequent plain radiographic finding in splenic abscess is a left pleural effusion (42%), followed by an infiltrate

in the left lung base (20%) and splenomegaly.¹⁹¹ A splenic abscess is rarely identified by extraluminal gas or air-fluid levels in the left upper quadrant on plain films.

Ultrasound has a sensitivity of 75% to 98% in detecting a splenic abscess.^{187,191,198} Sonography is especially useful as a screening examination for bedridden patients, for patients with renal impairment, and for evaluation of small splenic lesions. In some patients, the examination may be technically difficult because of overlying gas from the bowel or lung. The sonographic appearance of a splenic abscess depends on the stage of development, and a typical pattern is encountered in only 44% of cases.¹⁹³ In the early phase, there is an ill-defined, hypoechoic lesion mimicking a mass. Later, the abscess may develop into an anechoic cysts or a complex cystic lesion with septa, debris, and acoustic shadowing caused by gas (Fig. 105-17A).¹⁹⁴ When a capsule has developed, the lesion is typically well defined with a thin, hyperechoic rim.

On CT, a splenic abscess typically is manifested as a unilocular or multilocular, hypodense collection or complex cystic lesion with an enhancing rim after intravenous administration of contrast material (Fig. 105-17B). CT can be diagnostic if the collection contains gas, but this is a rare finding.¹⁹⁶

The advantages of CT are high sensitivity (92%-98%), non-invasiveness, and speed.^{187,191} CT aids in differentiating unilocular from multilocular abscesses, is excellent for exact localization, and provides better anatomic information about the perisplenic area. This information can then be used to guide further management (Fig. 105-17C). CT may reveal concurrent areas of infection and can help detect the underlying source of disease.

MRI is not often performed in the work-up of patients with splenic abscesses because CT is highly sensitive, and many patients are not clinically stable. Splenic abscesses are hypointense on the T1-weighted images and mildly to moderately hyperintense on the T2-weighted images compared with the normal spleen; they demonstrate minimal to intense peripheral enhancement after intravenous administration of gadolinium.^{51,124}

Nuclear medicine plays a limited role in the detection and localization of splenic abscesses. If the abscess is more than 2 cm in diameter, ^{99m}Tc-sulfur colloid scans of the liver and spleen may demonstrate a nonspecific splenic filling defect. The ⁶⁷Ga scan and the ¹¹¹In-labeled leukocyte scan may show increased accumulation of radionuclide in the spleen. However, normal, inherent splenic activity on ⁶⁷Ga scans and ¹¹¹In-labeled leukocyte scans typically obscures an inflammatory focus within or near the spleen, resulting in a false-negative examination finding. A ⁶⁷Ga scan is nonspecific because tracer uptake is also seen in neoplastic lesions, particularly in lymphomas.¹⁸⁸ A ^{99m}Tc-sulfur colloid scan of the liver and spleen before injection of ¹¹¹In-labeled leukocytes appears to improve detection and characterization compared with performing ¹¹¹In-tagged leukocyte scans alone.^{188,199} FDG PET/CT is helpful in detecting a site of infection; however, its role in diagnosis of a focal splenic abscess has not been evaluated.^{3,159}

Angiography is sometimes used for management of vascular complications. Intrasplenic mycotic aneurysms are rare and described only in case reports.²⁰⁰ If angiography is performed,

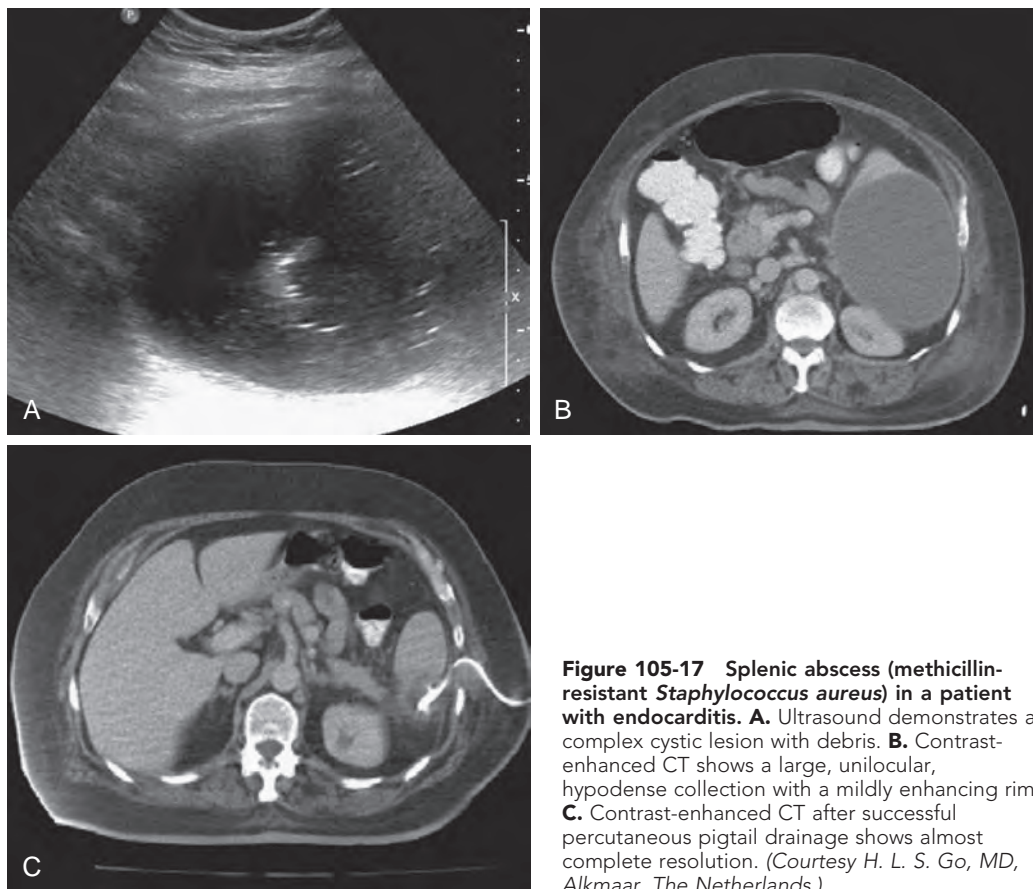


Figure 105-17 Splenic abscess (methicillin-resistant *Staphylococcus aureus*) in a patient with endocarditis. **A.** Ultrasound demonstrates a complex cystic lesion with debris. **B.** Contrast-enhanced CT shows a large, unilocular, hypodense collection with a mildly enhancing rim. **C.** Contrast-enhanced CT after successful percutaneous pigtail drainage shows almost complete resolution. (Courtesy H. L. S. Go, MD, Alkmaar, The Netherlands.)

the abscess appears as a mass with attenuated vessels and a hypervascular rim.

Splenic Infarction

EPIDEMIOLOGY AND PATHOGENESIS

Splenic infarction, the result of arterial or venous compromise, has many potential causes, including hematologic disorders, thromboembolic disease, vascular diseases, and trauma (Box 105-5). Although splenic infarction is a relatively common finding, only a few larger series have been published, and most of the literature consists of case reports.²⁰¹⁻²⁰³

The cause of splenic infarcts tends to vary with age. Patients younger than 40 years most often have an associated hematologic disorder, and those older than 41 years more often have an embolic event.²⁰¹ Overall, hematologic disorders, including sickle cell disease, are probably the most common cause of splenic infarction.

Infarcts may be segmental or massive, involving the entire organ. Because the branches of the splenic artery are end arteries, occlusion leads to focal splenic infarction.¹⁰ Complications of splenic infarction occur in 7% to 20% of patients and include abscesses, pseudocysts, hemorrhage, subcapsular hematoma, and rupture.²⁰⁴⁻²⁰⁶

CLINICAL FINDINGS

The most common manifestation is pain in the left upper abdomen and fever.²⁰⁷ Associated findings include pleuritic chest pain, referred pain to the left shoulder, and

leukocytosis.^{201,202,207} However, 30% to 50% of patients remain asymptomatic.^{207,208} Symptoms may develop when complications occur, such as abscess formation or hemorrhage.

PATHOLOGY

All infarcts are initially hemorrhagic; over time, they become pale with hyperemic borders; and finally, they become fibrotic.⁴² On histologic examination, most infarcts caused by emboli have a wedge-shaped, pale appearance, with the base at the capsular surface.¹⁴ In the course of healing, the infarcts may completely resolve or leave atrophic, fibrotic tissue with or without calcifications. Small emboli may produce a miliary or nodular pattern, resulting in a spotted spleen. Infarcts in patients with massive splenomegaly or caused by an infiltrative process often do not have the typical wedge-shaped appearance.

RADIOLOGIC FINDINGS

The classic radiologic appearance of a splenic infarct is a wedge-shaped area with the base at the splenic capsule and the apex pointing toward the hilum (Fig. 105-18). However, the radiologic appearance of splenic infarcts varies and includes a multinodular or mottled appearance and a masslike appearance with irregular margins (Fig. 105-19).²⁰⁹ In the subacute phase, when the infarct organizes, the affected area usually becomes better defined. In time, the changes may completely resolve, or the infarcted area may show atrophic changes with or without calcifications.²¹⁰ In rare cases, the entire spleen may undergo infarction, leaving only a thin rim of normal, enhancing parenchyma along the outer margin because of preserved capsular vessels.^{10,211}

The sonographic findings reflect the variable anatomic-pathologic manifestations, and a wide range of appearances can be seen, including single or multiple, wedge-shaped or round, and hypoechoic, anechoic, and hyperechoic lesions (Fig. 105-20A).^{208,212} In the acute phase, the infarct tends to be hypoechoic, peripheral, and wedge shaped or round. The lesion may become better defined during the course of several days. In the chronic

BOX 105-5 CAUSES OF SPLENIC INFARCTION

- Embolic sources
 - Thromboembolic diseases
 - Septic emboli
 - Atherosclerosis
 - Therapeutic transcatheter embolization
- Splenic sources
 - Massive splenomegaly
 - Hematologic diseases
 - Sickle cell disease
 - Myelofibrosis with myeloid metaplasia
 - Polycythemia vera
 - Neoplasms
 - Leukemia
 - Lymphoma
 - Vasculitis
 - Polyarteritis nodosa
 - Systemic lupus erythematosus
 - Rheumatoid arthritis (e.g., Felty's syndrome)
 - Pancreatic disease
 - Pancreatitis
 - Storage disease
 - Gaucher's disease
 - Amyloid
- Splenic artery
 - Trauma
 - Acute splenic torsion
 - Pancreatic masses causing splenic arterial occlusion or extrinsic compression
- Splenic vein
 - Portal hypertension
 - Splenic vein thrombosis



Figure 105-18 Chronic splenic infarct. Contrast-enhanced CT demonstrates a classic wedge-shaped, peripherally nonenhancing, hypodense area. The base of the infarct is at the splenic capsule, and the apex points toward the hilum. Some volume loss and capsular retraction indicate a chronic infarct.

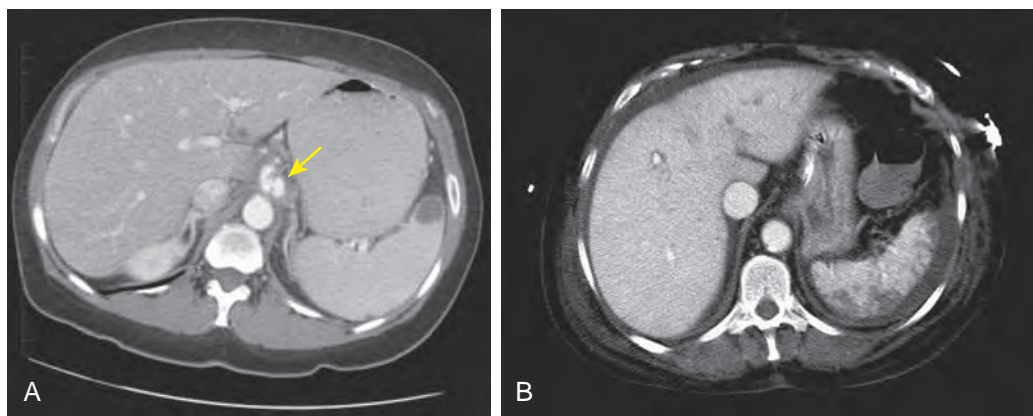


Figure 105-19 Acute splenic infarct. **A.** Contrast-enhanced CT demonstrates a round infarct in a patient with a mycotic aneurysm of the celiac axis (arrow). Many similar lesions throughout the spleen were seen (not shown). **B.** Contrast-enhanced CT in a different patient demonstrates a mottled appearance of the splenic infarcts with associated perisplenic fluid.

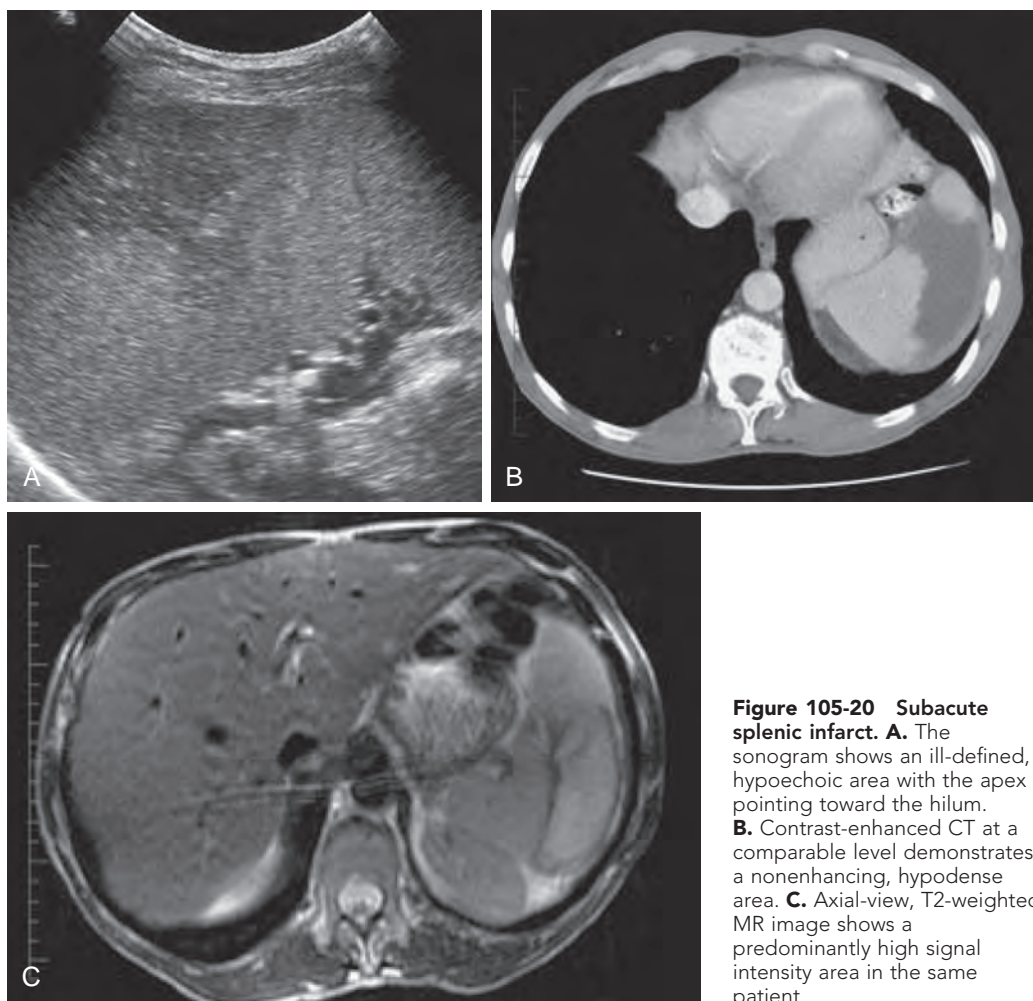


Figure 105-20 Subacute splenic infarct. **A.** The sonogram shows an ill-defined, hypoechoic area with the apex pointing toward the hilum. **B.** Contrast-enhanced CT at a comparable level demonstrates a nonenhancing, hypodense area. **C.** Axial-view, T2-weighted MR image shows a predominantly high signal intensity area in the same patient.

stage, splenic infarcts appear as areas of increased echogenicity that represent fibrotic scar.

Although the infarcts can sometimes be detected on noncontrast CT scans, enhanced CT markedly improves visualization. On CT, the findings vary from the classic wedge-shaped, peripherally nonenhancing, hypodense area (Fig. 105-20B) to the heterogeneously hypodense, ill-defined, masslike lesion.^{206,209,213} In the hyperacute phase, CT may show areas of mottled increased

attenuation, representing hemorrhagic areas. In the subacute phase, infarcts tend to become better demarcated. In time, the findings vary and include complete resolution, persistent changes, and progressive volume loss with capsular retraction due to focal fibrosis.²⁰⁶

On MRI, the signal intensity of infarcted areas depends on the age of the infarct and the degree of the hemorrhagic component.²¹⁴ Acute and subacute infarcted areas usually appear as

diffuse low signal intensity on the T1-weighted images and as inhomogeneously high signal intensity on the T2-weighted images (Fig. 105-20C). The area does not enhance after intravenous administration of contrast material, although similar to what can be visualized on enhanced CT, capsular enhancement can be seen on MRI.^{214,215}

An infarct is manifested as a focal area of diminished activity on splenic scintigraphy, but this is a nonspecific finding.²¹⁵ No uptake of the radiotracer in the spleen may be observed with massive infarction.²¹⁶ Alternatively, a ^{99m}Tc-labeled, heat-denatured red blood cell scan may be used to demonstrate viable splenic tissue that is not evident on CT, MRI, or ^{99m}Tc-sulfur colloid scintigraphy.²¹⁷

Angiography demonstrates wedge-shaped regions of decreased perfusion or nonvisualization of the spleen in cases of complete infarction.²⁰⁶

The imaging findings of complicated splenic infarction include progressive liquefaction necrosis with outward expansion, subcapsular hemorrhage, splenic rupture with free blood in the peritoneal cavity, and locules of intraparenchymal gas, indicating a superimposed infection.^{208,218} Intraparenchymal splenic gas may be found after therapeutic splenic embolization, and only 17% of these patients prove to have an infection.²¹⁹

Nontraumatic Splenic Rupture

Nontraumatic splenic rupture, also called spontaneous splenic rupture or pathologic splenic rupture, is a rare but potentially life-threatening condition. Nontraumatic splenic rupture has been described in a wide variety of medical conditions (Box 105-6). The diseased spleen is often enlarged, and there is no history of trauma. However, insignificant activities, such as coughing, sneezing, or vomiting, have been described as possible triggers in splenic rupture.²²⁰ Spontaneous rupture of a normal spleen is even more uncommon.²²¹ In patients with splenic disease, the spleen is more prone to rupture because of the altered consistency and the splenomegaly that extends the spleen below the rib cage.²²² Other than the apparent mechanism, the clinical, pathologic, and imaging findings are the same as those seen in traumatic rupture of the spleen (Fig. 105-21).

BOX 105-6 CAUSES OF PATHOLOGIC SPLENIC RUPTURE

- Infection
- Infectious mononucleosis
- Malaria
- Abscess
- Splenic cyst
- Storage diseases
- Amyloid
- Sickle cell disease
- Splenic infarction
- Vasculitis
- Polyarteritis nodosa
- Systemic lupus erythematosus
- Rheumatoid arthritis (e.g., Felty's syndrome)
- Pancreatitis
- Splenic peliosis
- Angiosarcoma
- Leukemia
- Lymphoma
- Hemangioma
- Peliosis

Splenomegaly

There are numerous causes of diffuse splenic enlargement, and there are various ways of classifying splenomegaly (see Box 105-3). Splenomegaly can be categorized on the basis of pathogenesis. Congestive splenomegaly is the result of portal hypertension, splenic vein occlusion, or congestive heart failure. Inflammatory splenomegaly develops in association with various infections and inflammatory processes and results from an increase in the immune response with resultant lymphoid hyperplasia (e.g., infectious mononucleosis). Hyperplastic splenomegaly is caused by hypertrophy resulting from the removal of abnormal blood cells from the circulation (e.g., polycythemia vera). Infectious splenomegaly, the result of splenic filtering of blood-borne pathogens, may lead to microabscess formation (e.g., mycobacterial infection). Infiltrative splenomegaly is the result of engorgement of macrophages with indigestible materials (e.g., Gaucher's disease, amyloidosis, malignant disease).

On imaging, the average adult spleen is less than 11 cm long, less than 7 cm wide, and less than 5 cm thick. The spleen has an average weight of 150 g, with a range between 80 and 300 g. The normal spleen decreases in size and weight with advancing age.^{223,224} On radiographs, splenomegaly can be detected as a soft tissue mass in the left upper quadrant, displacing the stomach medially and the splenic flexure of the colon inferiorly (see Fig. 105-1). Ultrasound, CT, and MRI are accurate in determining the size and volume of the spleen.²²⁵⁻²²⁷ The length of the spleen (on ultrasound in the right lateral decubitus position) can be used to accurately diagnose splenomegaly.^{225,228}

Miscellaneous Disorders

SICKLE CELL DISEASE

Epidemiology and Pathogenesis

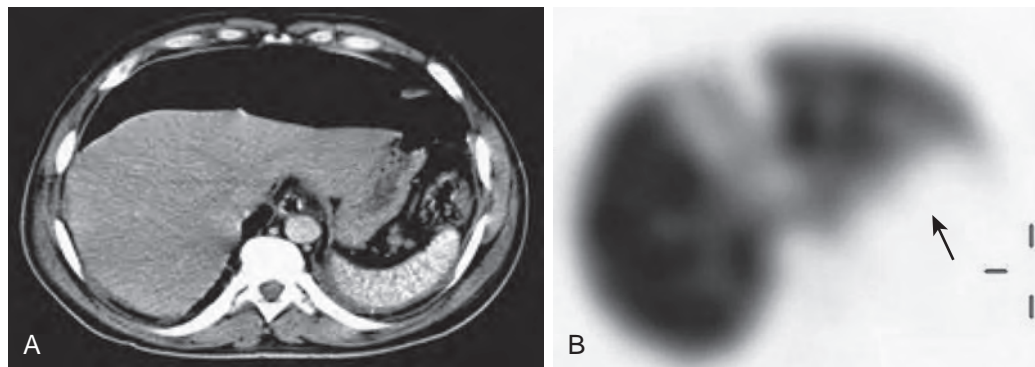
Sickle cell disease, also called sickle cell anemia, is an autosomal recessive disorder affecting red blood cells. A mutation in the hemoglobin A (HbA) gene leads to formation of an abnormal hemoglobin molecule (HbS). Patients may be heterozygotes



Figure 105-21 Spontaneous splenic rupture in a patient with malaria. Contrast-enhanced CT demonstrates a subcapsular hematoma (short arrows) and a linear, hypodense parenchymal defect (long arrow).

Figure 105-22 End-stage spleen in a patient with homozygous sickle cell disease.

A. Unenhanced CT shows a small and densely calcified spleen.
B. ^{99m}Tc -sulfur colloid scan of the liver and spleen demonstrates no uptake of the radiotracer, which is consistent with functional asplenia (arrow). (Courtesy R. Attariwala, MD, PhD, Vancouver, Canada.)



(i.e., sickle cell trait), with one normal HbA gene (*HBA1* or *HBA2*) and one abnormal HbS gene, or homozygotes, with two abnormal hemoglobin genes (HbSS). Carrier frequency of sickle cell disease varies significantly around the world, with high rates in areas with a high incidence of malaria.²²⁹ It is believed that the high frequency of the HbS variant is maintained in these populations by an increased resistance to malaria infection in heterozygous carriers. Sickle cell disease is the most common inherited blood disorder in the United States. About 8% of the African American population are carriers, and the homozygous form of sickle cell disease affects approximately 1 in every 396 African Americans.²³⁰ Less common forms of sickle cell disease include sickle cell–hemoglobin C disease and sickle cell– β -thalassemia.

When deoxygenated, the abnormal hemoglobin molecules form viscous polymers that aggregate with other hemoglobin molecules, distorting the red blood cells into an abnormal (sickle) shape. The tendency to form sickle cells is exacerbated by stressful conditions, such as illness, fever, cold temperature, and high altitude. The sickle shape results in less flexible red blood cells that obstruct the microcirculation, causing tissue hypoxia and infarction, which promote further sickling. Sickle-shaped red blood cells have a short life span of only 10 to 20 days, resulting in chronic anemia (i.e., sickle cell anemia). The complications of vascular occlusion are usually much more troublesome than the anemia, which is typically well tolerated.²³¹

The spleen usually is affected in patients with sickle cell disease. The most common splenic complications are autosplenectomy, splenic sequestration crisis, hypersplenism, massive splenic infarction, and splenic abscess.²³² In homozygous sickle cell disease, multiple infarcts during infancy usually result in a small, scarred, fibrotic spleen and complete loss of function, resulting in an end-stage spleen (i.e., autosplenectomy). By the age of 5 years, 94% of patients with homozygous sickle cell disease are asplenic.²³¹ In patients with heterozygous sickle cell disease, splenomegaly usually persists into adulthood.

On histologic examination, the end-stage spleen is replaced by fibrosis with calcium and hemosiderin deposits.⁴² On radiography, a small, heterogeneously dense spleen with punctate or amorphous calcifications can be seen. Patients with heterozygous sickle cell disease often present with splenomegaly and may demonstrate the sequelae of infarction.

The spleen is usually small, making it more difficult to visualize, with diffuse enhanced echogenicity demonstrated on sonography. Sometimes, hypoechoic foci are seen on ultrasound scans.²³³ CT usually shows a small and densely calcified

spleen (Fig. 105-22A).²³¹ The focal calcifications may be as small as 0.5 to 1.0 cm in diameter. MRI reveals diffuse, diminished signal intensity of the spleen relative to skeletal musculature on all sequences, representing calcifications and hemosiderin deposits.²³⁴ Diminished or no uptake of radiotracer, indicating loss of function, is seen on ^{99m}Tc -sulfur colloid scans of the liver and spleen (Fig. 105-22B).

Intrasplenic areas of preserved normal splenic tissue are sometimes present in an otherwise small and fibrotic spleen, and they should not be mistaken for an abscess or mass. These areas are hypoechoic relative to the echogenic spleen on ultrasound, are hypodense on CT, have the imaging characteristics of normal spleen on MRI, and demonstrate uptake of radiotracer on ^{99m}Tc -sulfur colloid imaging.²³⁵

Acute splenic sequestration is a life-threatening complication of sickle cell disease; it typically occurs in infants and children with homozygous sickle cell disease. It represents sudden trapping of a large amount of blood in the spleen, resulting in sudden splenic enlargement.²²⁹ A rapid fall in the hematocrit, hypovolemic shock, and death may occur within hours.²³⁶ On histologic examination, the splenic sinusoids are clogged with sickle erythrocytes, and there are areas of infarction, hemorrhage, and necrosis.

On imaging, the spleen is larger than expected. An apparently normal size may indicate an enlarged spleen because most patients have small spleens.²³¹ The spleen is heterogeneous with multiple hypoechoic areas on ultrasound. CT shows an enlarged spleen with heterogeneous enhancement and hypodense areas that may be interspersed with areas of higher attenuation. MRI of the spleen demonstrates areas of high signal intensity on the T1- and T2-weighted sequences, which is compatible with hemorrhage.²³⁶

The loss of splenic function is the pathophysiologic basis for increased susceptibility to aggressive, generalized infections, occurring in 10% of patients with homozygous sickle cell disease. Infections caused by encapsulated bacteria, including *Streptococcus pneumoniae*, *Haemophilus influenzae* type b, and *Salmonella*, are an important cause of morbidity and death.²³¹ A focal splenic abscess is a relatively uncommon complication. *Salmonella* was the most common causative organism identified in one series.²³⁷

SPLenic INVOLVEMENT IN PANCREATITIS

Epidemiology and Pathogenesis

Splenic involvement in pancreatitis occurs in 1% to 5% of patients and includes splenic vein thrombosis, infarction,

intrasplenic pseudocyst, subcapsular hematoma, splenic rupture, and hemorrhage from splenic artery pseudoaneurysm.^{238,239} Approximately 6% of patients with pancreatic pseudocysts have splenic parenchymal involvement.²⁴⁰

Complications usually result from direct extension of a pancreatic pseudocyst, caused by the digestive effects of pancreatic enzymes on splenic vessels or parenchyma, or from the liquefaction of splenic infarcts.²⁴¹ Most splenic parenchymal complications of pancreatitis regress spontaneously and can be managed conservatively.²⁴² However, potential complications, such as splenic rupture, infection, and hemorrhage, are life-threatening events.²⁴⁰

Radiologic Findings

CT is the most useful imaging technique for detection and follow-up of acute pancreatitis with or without splenic complications.²⁴³ Imaging typically reveals pancreatitis and its sequelae. Subcapsular splenic fluid collections or hematomas appear as lentiform collections that flatten or indent the splenic contour (Fig. 105-23). The appearance of the fluid collections depends on the amount of necrosis, infection, and hemorrhage.²⁴⁴ Evidence of fluid-fluid levels within a splenic pseudocyst favors the diagnosis of hemorrhage. Gas in a collection, although rare, confirms infection. Focal, wedge-shaped, or diffuse areas of decreased attenuation in the spleen are most likely to represent infarction. Portal vein thrombosis and pseudoaneurysms are typically detected with contrast-enhanced CT.

Percutaneous drainage of collections within or around the spleen may be considered to prevent splenic rupture and to treat infection. However, percutaneous drainage of splenic pancreatic pseudocysts has been associated with significant complications.²⁴⁰

GAUCHER'S DISEASE

Gaucher's disease is inherited in an autosomal recessive manner. The lipid storage disease is caused by a lack of the enzyme glucocerebrosidase.²⁴⁵ It is characterized by the deposition of



Figure 105-23 Pancreatic pseudocyst. Contrast-enhanced CT demonstrates an oval collection involving the splenic hilum in a patient with pancreatitis.

glucocerebroside in cells of the reticuloendothelial system. Three clinical subtypes have been described; type 1 is the most common. Gaucher's disease often is manifested in childhood with hepatosplenomegaly, pancytopenia, and skeletal disease, although striking clinical variability occurs in the severity of the disease. Glucosylceramide accumulation in the liver and spleen leads to pancytopenia and massive hepatosplenomegaly in most cases.

Histologic examination reveals a diffusely infiltrated spleen or focal clusters of glycolipid-laden macrophages (i.e., Gaucher cells). Fibrosis, infarction, and foci of extramedullary hematopoiesis may also be present.⁴²

Diagnostic imaging studies typically show massive splenomegaly. Nodular changes and infarcts are often present. The nodules are 0.5 to 7 cm in diameter.²⁴⁶ In a series of 46 patients with Gaucher's disease studied by MRI, 100% had hepatosplenomegaly, 33% had splenic infarcts, and 30% had splenic nodules.²⁴⁷

On sonographic evaluation, most patients with Gaucher's disease have multiple, discrete, hypoechoic lesions that correspond pathologically to focal, homogeneous clusters of Gaucher cells (Fig. 105-24A).^{246,247} Some patients have discrete, hyperechoic lesions that are composed of Gaucher cells and fibrosis or infarction.²⁴⁷

CT is useful in depicting splenomegaly and the hypodense nodules (Fig. 105-24B, C).²⁴⁶ On T1-weighted MRI, the signal intensity of the spleen tends to be lower than for normal spleens because of the accumulation of glucocerebroside.^{248,249} Nodules are isointense on T1-weighted imaging and variably hypointense or hyperintense on the T2-weighted images.²⁴⁹

HEMOSIDEROSIS

Hemosiderosis, or iron overload of the spleen, is usually caused by secondary hemochromatosis. It is most commonly seen in transfusion-dependent patients. After hemolysis of the transfused erythrocytes, excess iron is deposited in the reticuloendothelial system of the liver, spleen, and bone marrow.^{249,250} Abnormal iron accumulation in the reticuloendothelial system does not damage the parenchymal cells of the affected organ; it is usually of little clinical significance. There is often associated splenomegaly, depending on the underlying disease.²⁵¹

Splenic hemosiderosis should be differentiated from primary (idiopathic) hemochromatosis, an inherited autosomal recessive disorder. Primary hemochromatosis is characterized by inappropriately high iron absorption, resulting in progressive iron overload in the parenchymal cells.²⁵² Unless this condition is treated, it will lead to cellular and organ damage. The organs most commonly involved are the liver, causing cirrhosis and hepatic malignant neoplasms, and the heart and pancreas. The spleen usually is not affected or becomes involved only with advanced disease.

Ultrasound has a limited role because diffuse excess iron in the liver and spleen usually does not change the echogenicity. The increased iron deposition may cause diffuse increased attenuation of the liver and spleen on noncontrast CT examinations. However, CT is of limited value in the evaluation of increased iron deposition in the liver because of its poor sensitivity.²⁵²

MRI is the most helpful imaging technique to detect and to quantify iron storage disease.²⁵³ Iron causes increased magnetic susceptibility, which leads to increased T2* decay due

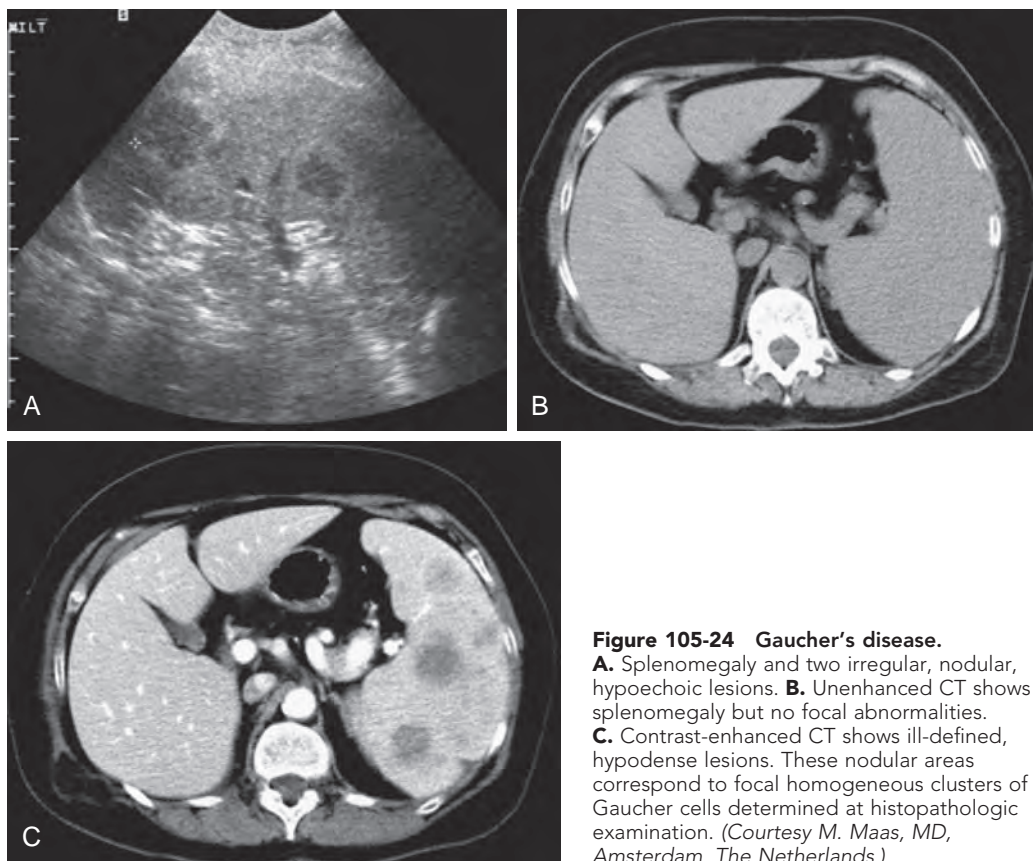


Figure 105-24 Gaucher's disease.

A. Splenomegaly and two irregular, nodular, hypoechoic lesions. **B.** Unenhanced CT shows splenomegaly but no focal abnormalities.

C. Contrast-enhanced CT shows ill-defined, hypodense lesions. These nodular areas correspond to focal homogeneous clusters of Gaucher cells determined at histopathologic examination. (Courtesy M. Maas, MD, Amsterdam, The Netherlands.)

to spin dephasing. The dephasing results in decreased signal intensity on MR images. In determining whether the signal intensity of the liver or spleen is abnormally low, muscle can be used as a control because skeletal muscle usually is spared. If the liver or spleen demonstrates signal intensity equal to or lower than that of skeletal muscle on the T2-weighted gradient-echo or T2-weighted spin-echo images (less sensitive), increased iron accumulation in the spleen can be suspected (Fig. 105-25).²⁵⁰⁻²⁵³

The dual gradient-echo technique is also helpful in the visualization of T2* effects. The splenic parenchymal signal intensity decreases on the image with the longer echo time because of continued decay of the transverse magnetization. Hepatic iron overload is discussed in Chapter 89.

THOROTRAST

Thorotrast is the trade name of a colloidal suspension of thorium dioxide and dextrin. It was used as a contrast agent from the 1920s through the mid-1950s. Thorium dioxide is radioactive, predominantly emitting alpha particles with a biologic half-life of 400 years.²⁵³ When it is used as an intravascular contrast agent, it is retained by the reticuloendothelial system and can be found in the liver, spleen, lymph nodes, and bone marrow years after it is administered.

Its former use has been reported in relation to its long-term effects. The alpha radiation causes a wide range of complications, primarily of the liver, and the major causes of mortality are cirrhosis and hepatobiliary and hematologic malignant neoplasms.^{254,255} Thorotrast increases the risk of

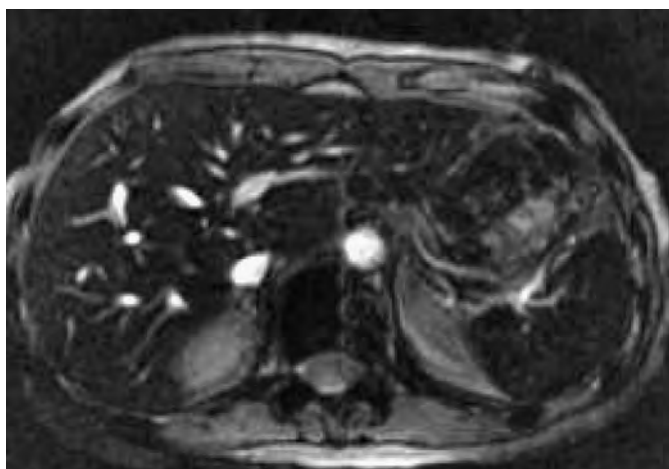


Figure 105-25 Hemosiderosis in a patient with transfusion-dependent thalassemia. There is marked decreased signal intensity of the liver and spleen compared with the skeletal muscles on axial, gradient recalled echo, T2-weighted MRI.

liver angiosarcomas, but this phenomenon has not been observed in the spleen, possibly because of the marked fibrosis and atrophy that typically develop.²⁵⁶

Splenic changes due to Thorotrast depend on the amount administered and exposure time. Thorotrast particles are phagocytosed by the reticuloendothelial cells, resulting in splenic pulp fibrosis and atrophy. Consequently, the spleen is small or has a normal size.

Abdominal radiographs show patchy, high-density, or punctate densities in the left upper quadrant. Sonography shows high-density areas in the liver, spleen, and abdominal lymph nodes. On CT, Thorotrast deposition in the spleen is demonstrated as homogeneous, high-density areas or punctate densities with or without atrophy. Similar high-attenuation changes are usually seen in the liver and abdominal lymph nodes. On MRI, the deposits may be seen as low signal intensity areas or signal voids on all sequences. In one study, the Thorotrast deposits were not detected on MRI.²⁵⁶

Primary Malignant Lesions

ANGIOSARCOMA

Epidemiology and Pathogenesis

Angiosarcoma, although rare, is the most common primary nonhematopoietic malignant tumor of the spleen (Table 105-3).²⁵⁷⁻²⁵⁹ The estimated annual incidence is 0.14 to 0.25 case per 1 million persons.²⁵⁸⁻²⁶⁰ Angiosarcomas are aggressive tumors, usually manifested with widespread metastatic disease, and they have a poor prognosis, with most patients dying within a year of diagnosis.²⁶⁰ The average age at presentation is older than 55 years, although angiosarcomas have been reported in all age groups, including children.²⁶¹ No apparent gender predilection is demonstrated.^{258,260} Unlike with angiosarcomas of the liver, correlation with exposure to toxins such as Thorotrast or vinyl chloride has not been documented. Rarely, angiosarcomas have been associated with previous chemotherapy for malignant lymphoma or radiotherapy for breast cancer.^{257,262}

Clinical Findings

The most common symptoms are abdominal pain (70%), fever (10%), fatigue, and weight loss.^{257,259,260} Splenomegaly is found in 70% of patients; spontaneous splenic rupture is relatively common at presentation and is reported in approximately 25% of patients.²⁵⁸⁻²⁶⁰ Anemia, thrombocytopenia, and coagulopathy are often encountered. Metastatic disease is common, usually widespread, and often rapidly progressive. The most common metastatic sites are liver, lungs, and bones.²⁵⁸

Special care should be taken before performing a percutaneous biopsy of a possible angiosarcoma of the spleen

or its metastases because of the high risk of massive hemorrhage.^{263,264}

Pathology

Macroscopic examination commonly reveals splenomegaly with hemorrhagic nodular changes.²⁵⁸ The cut specimens typically demonstrate multiple nodules of various sizes that are associated with hemorrhage, infarction, and necrosis.^{257,258,260} An unusual manifestation is a solitary mass.^{257,259} The microscopic appearance of splenic angiosarcomas is varied, and different growth patterns are observed, including sarcomatous solid, papillary, and epithelioid types.^{260,262} Hemorrhage and necrosis are frequently identified within the tumor.^{259,260,262} The main histologic features include irregular vascular channels lined by atypical endothelial cells. The well-differentiated areas appear as splenic sinus-like structures.²⁵⁷ In the more poorly differentiated areas, the tumors have a sarcomatous appearance. The solid areas may resemble an undifferentiated spindle cell sarcoma.^{258,260,262,265} With immunohistochemical techniques, it has been demonstrated that splenic angiosarcoma probably arises from the splenic sinus endothelial cells.²⁶⁶ On occasion, the histologic features suggest a mixed origin from blood capillaries and lymphatic endothelium.²⁶⁷

Radiologic Findings

The usual imaging appearance of splenic angiosarcoma is an aggressive splenic mass or masses associated with metastatic disease.²⁵⁷ Ultrasound examination often reveals splenomegaly and numerous, solid, ill-defined masses with a heterogeneous architecture (Figs. 105-26 and 105-27).²⁵⁹ Cystic areas are frequently encountered and probably represent necrosis, hemorrhage, or vascular lakes.^{257,259} Increased Doppler flow may be visualized in the solid areas and in the vascular lake areas (see Fig. 105-26B).

On CT, the most common presentation is an enlarged spleen containing multiple, ill-defined, hypervascular masses with heterogeneous contrast enhancement and areas of necrosis (see Figs. 105-26C, D and 105-27B).^{257,259} Intraspinal, subcapsular, or perisplenic hemorrhage is another frequently encountered manifestation.^{268,269} Calcifications are rare, but punctate and massive calcifications in a radial pattern have been reported.^{257,270}

MRI usually demonstrates splenomegaly with heterogeneous areas of increased and decreased signal intensity on the T1- and T2-weighted sequences, which is consistent with the presence of blood products and necrosis (see Fig. 105-27C, D).^{271,272} Low signal intensity lesions on MR images have been determined to represent siderotic nodules.²⁷³ Contrast-enhanced MRI demonstrates diffuse, heterogeneous, intense enhancement within the areas of the tumor, similar to the CT findings and corresponding to the pathologic changes (see Fig. 105-27E).^{257,259,268,271,272}

Angiography, occasionally performed for chemoembolization, demonstrates patchy accumulations of contrast material and irregular pooling of contrast material in the arterial and venous phases, which is consistent with vascular lakes (see Fig. 105-27F). Tumor vessels usually are not present.²⁷⁴ In our experience, early portal venous enhancement during angiography was observed, indicating arterial venous shunts.

Differential Diagnosis

The differential diagnosis includes benign lesions, such as hemangiomas, hemangioepitheliomas, abscesses, and littoral cell

TABLE 105-3 Malignant Tumors of the Spleen

Tumor Type	Focal	Multifocal	Diffuse
PRIMARY SPLENIC LESIONS			
Primary lymphoma	+	+	(+)
Angiosarcoma		(+)	+
Hemangioendothelioma		+	
Littoral cell angiosarcoma			+
SECONDARY SPLENIC LESIONS			
Secondary lymphoma			
Non-Hodgkin's lymphoma	+	+	+
Hodgkin's lymphoma	+	+	(+)
Leukemia	(+)	(+)	(+)
Metastases	+	+	(+)
Kaposi's sarcoma	(+)	+	

+, Most common presentation; (+), uncommon presentation.

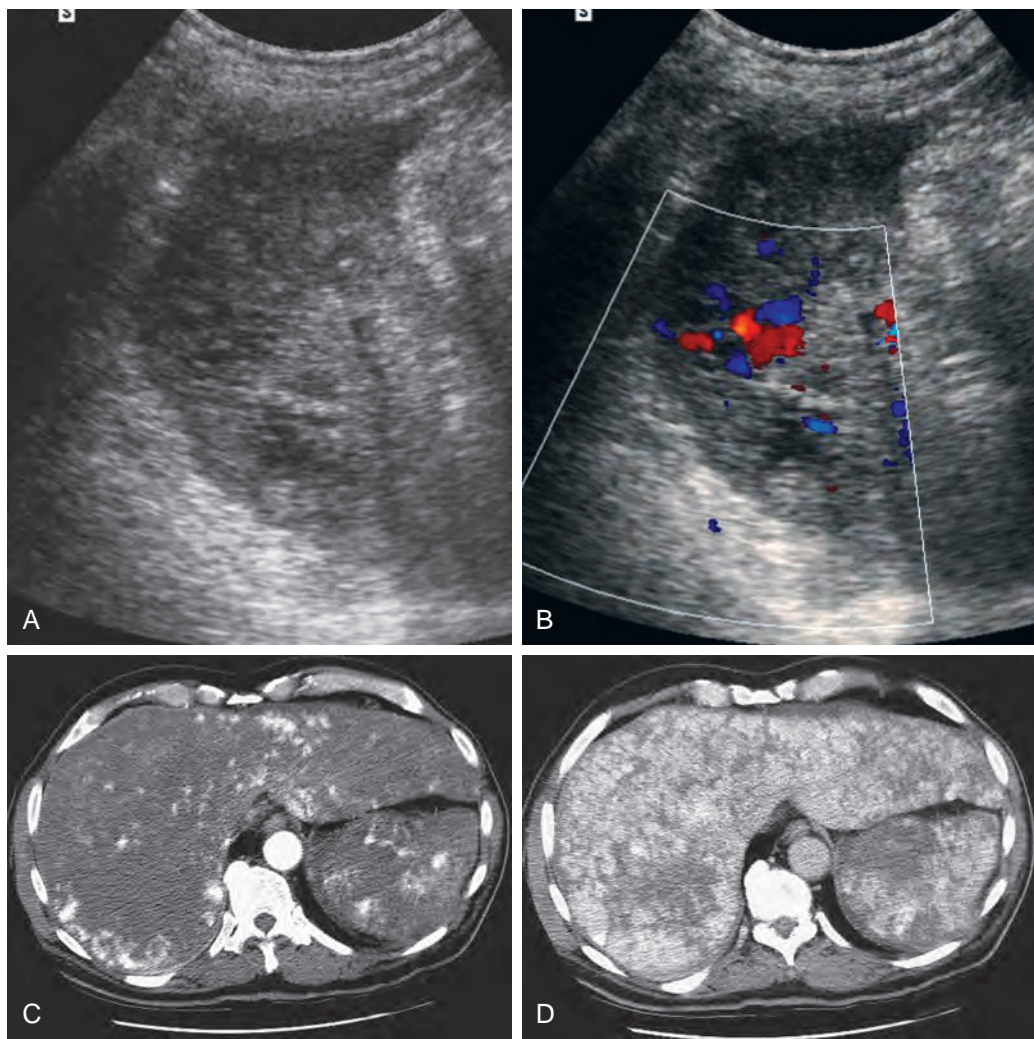


Figure 105-26 Angiosarcoma of liver and spleen. **A.** Ultrasound demonstrates a normal-sized, inhomogeneous spleen with a few “cystic” areas. **B.** Color flow is demonstrated in some of these areas, consistent with vascular lakes. **C** and **D.** CT after intravenous administration of contrast material in the arterial phase (**C**) and portal venous phase (**D**) shows many irregular areas of enhancement in the liver and spleen and areas of relatively low attenuation in the spleen. Autopsy revealed multiple angiosarcomas involving the spleen and liver. It was not possible to determine whether the spleen or the liver was the primary site.

angiomas, and malignant lesions, such as lymphomas, metastases, Kaposi’s sarcomas, and hemangioendotheliomas. All have similar imaging findings.^{257,259}

Secondary Malignant Lesions

LYMPHOMA

Epidemiology and Pathogenesis

Lymphoma is a malignant proliferation of lymphocytes arising in lymph nodes (nodal) or in lymphoid tissue of various organs, including the spleen (extranodal). Lymphoma is the fifth most common malignant neoplasm in the United States. Non-Hodgkin’s lymphoma (NHL) accounts for approximately 88%, and Hodgkin’s lymphoma (HL) accounts for 12%.^{275,276} Overall, NHL accounts for 5% of new cancers in men and 4% in women. NHL is responsible for approximately 5% of cancer deaths in the United States and is the leading cause of death from cancer in men between the ages of 20 and 39 years. The

World Health Organization classification recognizes more than 30 types of NHL, and there has been an increase in incidence and mortality rates of NHL worldwide during the past few decades.²⁷⁷

In general, the incidence of NHL increases with age. In contrast, a bimodal peak of presentation is seen for HL, with a peak between the ages of 20 and 29 years, a plateau between 30 and 55 years, and a second rise after 55 years. The incidence of lymphoma is higher among men than among women (1.5:1) for HL and NHL.²⁷⁵⁻²⁷⁷

There is an increased risk of lymphoma in immunocompromised patients, including patients with human immunodeficiency virus infection (HIV) and post-transplantation patients.²⁷⁸⁻²⁸⁰ Before the era of highly active antiretroviral therapy (HAART), the relative risk of AIDS-related lymphoma was more than 100.²⁸¹ In the HAART era, the risk of AIDS-related lymphoma remains increased relative to that for the general population, although it is lower than in the pre-HAART era.²⁸² AIDS-related lymphomas include NHL and HL, and they are usually highly aggressive. One of the diagnostic challenges

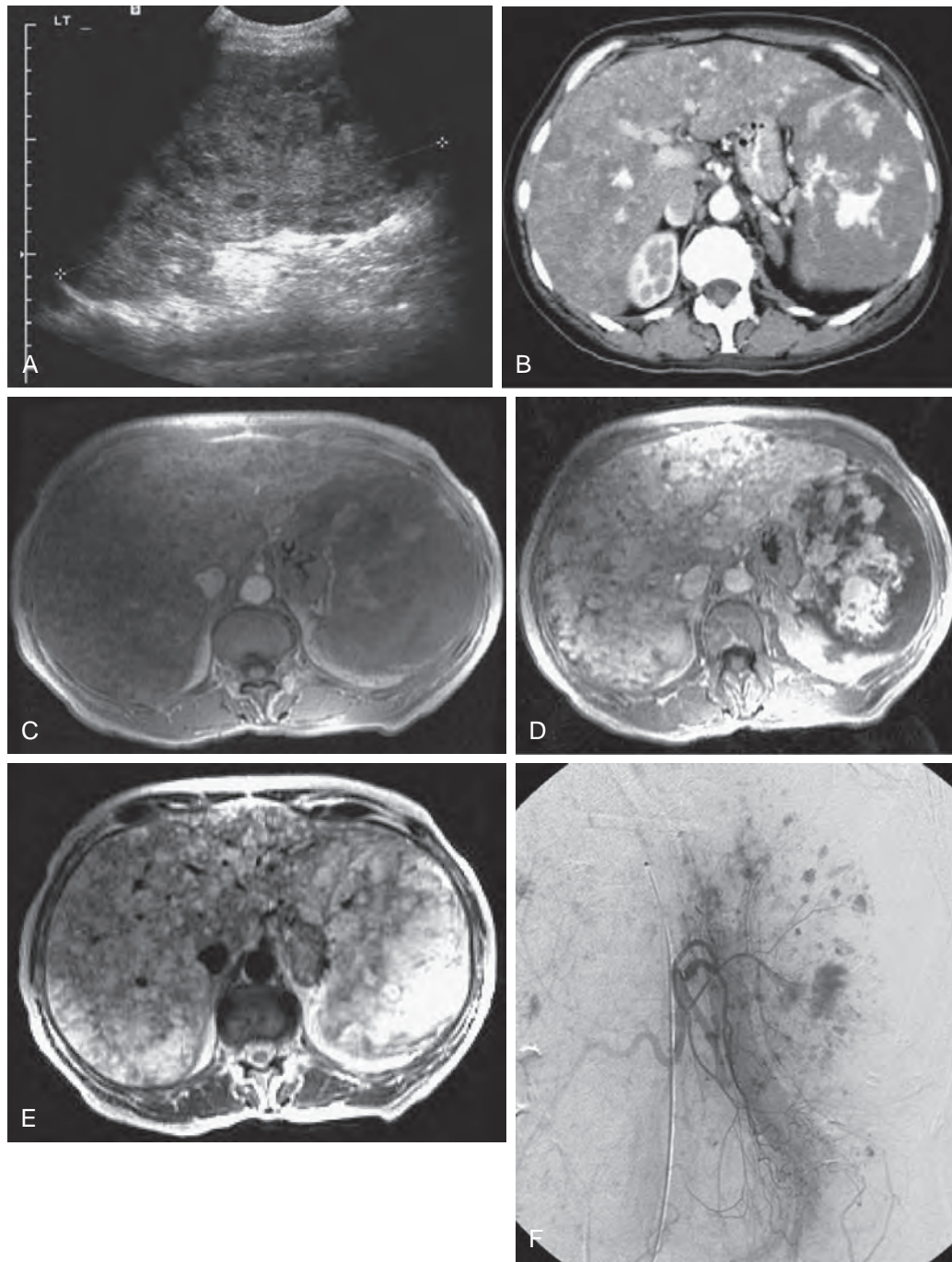


Figure 105-27 Angiosarcoma of the liver and spleen. A 62-year-old woman had a history of increasing upper abdominal pain on the left side, hepatosplenomegaly, pleural effusions, and coagulopathy. **A.** Ultrasound demonstrates a markedly enlarged spleen containing many ill-defined echogenic masses and hypoechoic areas. **B.** CT after intravenous administration of contrast material in the arterial phase shows a large, hypodense spleen with multiple areas of irregular enhancement and smaller similar lesions in the liver. **C.** T1-weighted image (FAME technique) at the same level reveals an enlarged spleen with ill-defined areas of decreased signal intensity relative to the surrounding spleen and areas of increased signal intensity (presumably hemorrhage). Multiple, small, hypointense lesions in the liver are also seen. **D.** Gadolinium-enhanced, T1-weighted MR image (FAME technique) at the corresponding level demonstrates an irregular central enhancement pattern and numerous enhancing lesions throughout the liver. **E.** The corresponding T2-weighted image (fast relaxation fast spin-echo = 3050/100 ms) demonstrates intrasplenic and intrahepatic masses with increased signal intensity. **F.** Pre-embolization angiogram during the early arterial phase shows splenomegaly, multiple hypervascular splenic masses, and vascular lakes.

of lymphoma in HIV-infected patients is that splenomegaly and lymphadenopathy are frequently also encountered in immunocompromised patients with nonmalignant conditions.²⁸³ The clinical and radiologic manifestations of AIDS-related lymphomas vary and may mimic Kaposi's sarcoma, mycobacterial

infections, fungal infections, and immune reconstitution inflammatory syndrome (Fig. 105-28).²⁸⁴⁻²⁸⁸

Splenic involvement is often observed in patients with malignant lymphomas, and lymphoma is the most common malignant disease that involves the spleen. Splenic involvement

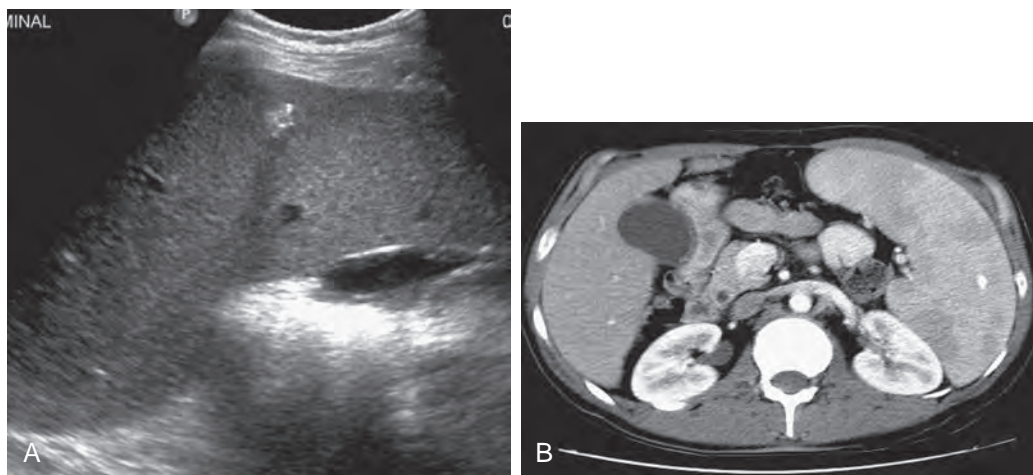


Figure 105-28 Burkitt's lymphoma in a 32-year-old man with AIDS. **A.** The sagittal sonogram demonstrates marked splenomegaly and parenchymal calcification. **B.** Enhanced helical CT scan during the portal venous phase demonstrates marked splenomegaly with inhomogeneous splenic texture and a calcification. The CT appearance suggests diffuse lymphomatous infiltration.

usually occurs as part of a generalized systemic disease. Lymphoma confined to the spleen, called primary splenic lymphoma, is an uncommon manifestation that is encountered in less than 1% of patients; it usually is an NHL of B-cell origin.²⁸⁹⁻²⁹³

Routine staging for lymphoma includes laboratory investigations, bone marrow aspirate and biopsy, and cross-sectional imaging, including CT scans and often FDG PET imaging. Accurate staging is essential for patients with lymphoma in guiding their management and optimizing outcomes, and it includes evaluation of potential splenic involvement.²⁹⁴ Staging laparotomy with splenectomy, done before the routine availability of CT scanning, revealed splenic involvement in approximately 45% of patients with HL.²⁹⁵ Approximately 30% to 40% of patients with known NHL have splenic involvement at presentation.²⁹⁴

In general, splenic size correlates with the risk of lymphomatous involvement, and the presence of massive splenomegaly indicates a high probability of splenic involvement. However, marked splenomegaly may occur without lymphomatous involvement, and conversely, a normal size and appearance of the spleen do not exclude lymphomatous involvement.²⁹⁵⁻²⁹⁷

Definitive diagnosis of malignant lymphoma requires histopathologic analysis. Accurate diagnosis of the many subtypes of NHL usually requires an evaluation of the tissue's architecture. At minimum, this requires a core-needle biopsy and often requires an excisional biopsy. In HL, the malignant cells (i.e., Reed-Sternberg cells) are a minority of cells occurring in a background majority of polyclonal inflammatory cells, and tissue diagnosis is essential. With these caveats, in selected cases, percutaneous splenic biopsy can provide a diagnosis and possibly avoid splenectomy in cases with no other sites of involvement amenable to biopsy.^{264,298-301} Splenectomy may still be beneficial for patients with primary splenic lymphoma to provide a diagnosis and partial treatment.³⁰²

Clinical Findings

Lymphoma most commonly is manifested as a painless enlargement of one or more peripheral lymph nodes. Fever, night sweats, and weight loss often accompany the lymphadenopathy.^{289,290} Other nonspecific findings are abdominal pain,

abdominal masses, and splenomegaly. Primary splenic lymphoma may be manifested with left upper quadrant pain and splenomegaly.³⁰³ Lymphomatous involvement of the spleen is usually confined within the splenic capsule, but extracapsular extension and local invasion into adjacent organs can occur. Nontraumatic splenic rupture in lymphoma is a rare presentation.^{304,305} The combination of splenomegaly, focal splenic lesions, and associated lymphadenopathy should raise the suspicion of lymphoma (see Table 105-3). The prognosis depends on the histologic type and stage of the lymphoma.

Pathology

Classification of splenic involvement by lymphoma is based on the cell type and the architectural growth pattern. The white pulp is most commonly involved in primary and secondary lymphomas, followed by the marginal zone and the red pulp.³⁰⁶ Different macroscopic patterns of splenic involvement in lymphoma can be seen¹: homogeneous enlargement without masses²⁵⁸; miliary masses (<5 mm)²⁵⁹; multiple solid masses of various sizes²⁶⁰; and a large, solitary mass (>5 cm).^{290,306,307} HL is rarely extranodal in the immunocompetent patient, whereas extranodal involvement is common in NHLs. Large cell lymphomas usually are manifested as solitary or multiple tumor masses. The miliary nodules are more often caused by small cell lymphomas, such as follicular lymphomas of the small cleaved and mixed cell types and mantle cell lymphoma.^{262,265} Primary splenic lymphoma usually is manifested with a solid mass or masses, and it often represents NHL of B-cell origin.^{292,303} When HL involves the spleen, it commonly is manifested as solitary or multiple tumor masses (Fig. 105-29).^{262,308}

Radiologic Findings

Radiography. Radiography plays a limited role nowadays. When splenomegaly is present, it can be demonstrated on plain films of the upper abdomen with elevation of the left hemidiaphragm, deviation of the stomach and splenic flexure of the colon, and displacement of the left kidney.

Ultrasound. Although the specificity of ultrasound in detecting lymphomatous involvement of the spleen approaches 100%, the

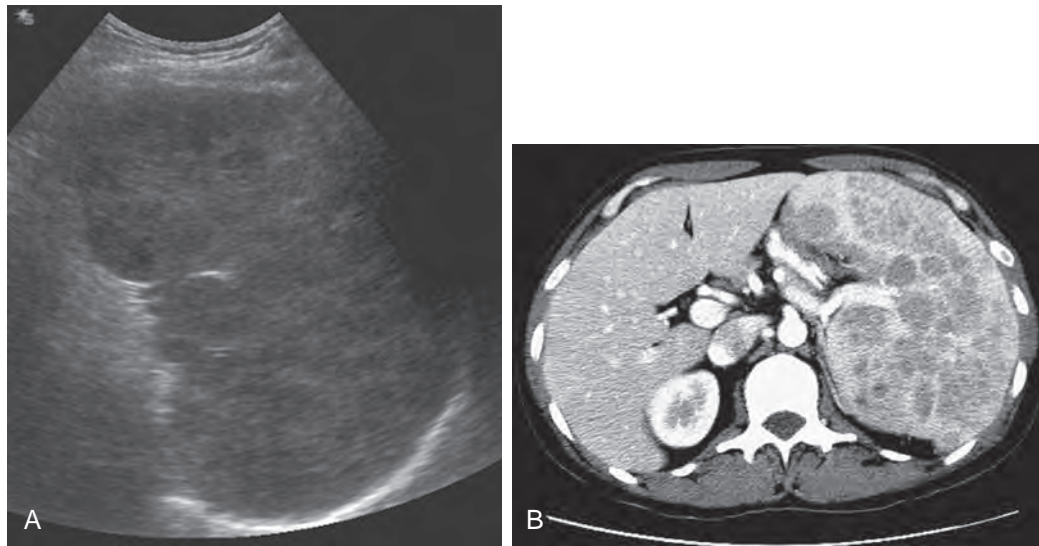


Figure 105-29 Hodgkin's lymphoma in a 42-year-old man. **A.** The sagittal sonogram reveals an enlarged spleen containing multiple ill-defined, hypoechoic lesions. **B.** The CT scan of the upper abdomen demonstrates multiple low-density masses.

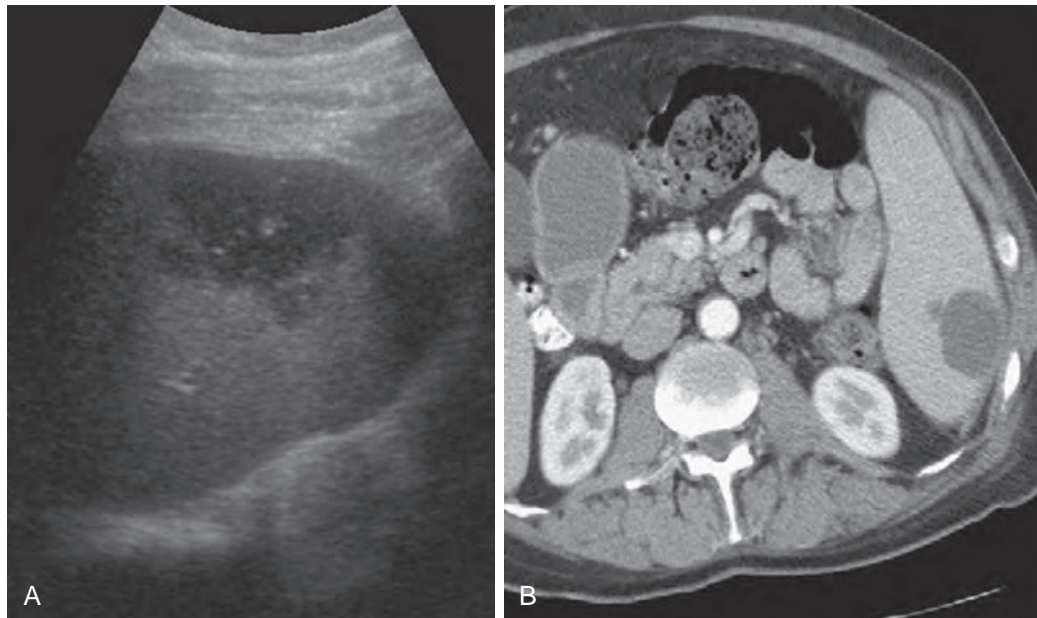


Figure 105-30 Malignant B-cell lymphoma in a 46-year-old man with subacute abdominal pain in the left upper abdomen. **A.** Focused sonography of the spleen demonstrates an anechoic peripheral area with some internal echoes. **B.** The enhanced helical CT scan during the portal venous phase shows a hypodense peripheral lesion and splenomegaly. Similar lesions were demonstrated in the liver (not shown).

sensitivity is low (63%). This may be explained by a poor sensitivity in detecting diffuse involvement.^{309,310} Sonography is possibly more sensitive than CT, especially in detecting inhomogeneities or small, nodular infiltrates.^{309,310}

Four different sonographic patterns are described in patients with lymphomatous involvement of the spleen corresponding with the pathologic findings²⁵⁷: diffuse involvement (37%)²⁵⁸, focal, small nodular lesions (39%)²⁵⁹; focal, large nodular lesions (23%)²⁶⁰; and bulky, solid mass lesions (2%).³¹¹ Diffuse involvement usually is manifested as splenomegaly with a normal echotexture. Focal lesions are hypoechoic and lack acoustic enhancement (see Fig. 105-29A).³¹¹⁻³¹³ A diffuse, small, nodular

pattern is predominantly visualized in cases of low-grade NHL and in HL.³¹¹ On occasion, after central necrosis occurs with subsequent liquefaction, lesions may be manifested as anechoic masses with or without septations, mimicking cystic lesions of the spleen or even abscesses (Fig. 105-30A).³¹⁴⁻³¹⁷

Computed Tomography. CT is the established radiologic technique for staging of lymphomas.^{318,319} New-generation multidetector CT scanners allow rapid imaging of the entire body during a single breath hold with a high spatial resolution. Both nodal and extranodal involvement can be detected with CT. CT is used to evaluate tumor location and volume

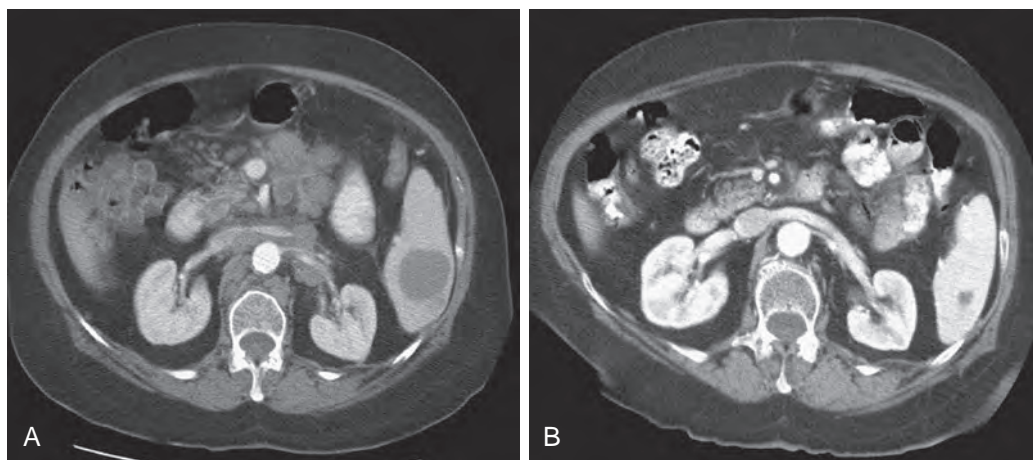


Figure 105-31 B-cell non-Hodgkin's lymphoma. A 74-year-old woman had a 2-month history of increasing general fatigue and low-grade fever. **A.** The enhanced CT scan during the portal venous phase shows an ill-defined, solitary, hypodense lesion in the inferior portion of the spleen. The spleen was moderately enlarged, and extensive para-aortic, paracaval, and abdominal lymphadenopathy is also visible. **B.** The enhanced CT scan of the upper abdomen 3 months after chemotherapy demonstrates marked improvement of the lymphadenopathy and decreased size of the splenic lesion.

and to monitor response to therapy (Fig. 105-31).^{320,321} CT also is helpful in planning surgical or percutaneous biopsy procedures and for planning radiotherapy. The most important limitation of CT is the inability to identify the involvement of disease in normal-sized lymph nodes and the relatively poor sensitivity in the detection of splenic, brain, and bone marrow infiltration.^{322,323} Furthermore, CT is not able to evaluate disease activity in residual tissue after treatment.³²⁴

The combined use of FDG PET imaging and CT (hybrid PET/CT) offers the advantages of excellent anatomic resolution of CT and the biologic characterization provided by FDG PET. The combination improves overall accuracy in staging of the disease.^{325,326}

Splenomegaly with hypodense lesions may be observed on the noncontrast CT scan. However, intravenous administration of contrast material is usually required to demonstrate focal splenic involvement (Fig. 105-32). The physician should be careful when evaluating the images in the arterial phase because variable contrast enhancement of the normal spleen resulting from differential flow through the vascular sinuses and cords of red and white pulp is common. In almost all patients, this heterogeneity resolves after 60 to 70 seconds.³²⁷⁻³²⁹

Different CT appearances of splenic lymphoma have been described²⁵⁷: normal size and appearance²⁵⁸; enlarged with no focal defects²⁵⁹; diffuse, miliary, hypodense lesions (Fig. 105-33)²⁶⁰; multiple, focal masses of various sizes (see Fig. 107-29B)²⁶¹; and a solitary, large mass (>5 cm; Fig. 105-34).³⁰³ The spleen may be bulky in patients with primary or secondary splenic lymphoma. The focal splenic masses caused by lymphoma usually demonstrate minimal enhancement and have a hypodense appearance compared with the surrounding spleen (see Fig. 105-32).

Rim-enhancing lesions with central necrosis may mimic splenic abscesses. Wedge-shaped, hypodense areas in patients with lymphoma and leukemia are sometimes observed and probably reflect secondary splenic infarction.

Large masses demonstrating capsular involvement and perisplenic infiltration into adjacent organs may be observed.

Splenic calcifications after treatment of lymphoma are occasionally seen; calcifications before treatment of splenic lymphoma are rare (Fig. 105-35; see also Fig. 105-28).^{303,330}

Magnetic Resonance Imaging. MRI is superior to CT in assessing lymphomatous involvement of extranodal disease in the brain, spinal cord, and bone marrow.³³¹ However, MRI has the same limitations as CT in detecting lymphomatous involvement in normal-sized lymph nodes and in residual tumor masses after therapy. The main disadvantages of MRI compared with CT include higher costs, longer scan time, and respiratory artifacts. For staging of abdominal lymphomas, MRI with a T2-weighted, turbo spin-echo sequence demonstrated results similar to those of spiral CT in detecting lymphadenopathy and demonstrating focal abdominal organ lesions.³³² In an older study, MRI and ultrasound were better than CT in revealing HL infiltrates in the spleen. However, most lymphomatous involvement of the spleen by NHL was not revealed with any of these modalities, except when the size of the spleen was considered.³³³ With the development of new and faster imaging techniques and the addition of diffusion-weighted imaging, excellent results have been reported in staging of lymphoma with MRI.³³⁴

Lymphoma involving the spleen usually has T1 and T2 imaging characteristics similar to the normal splenic parenchyma, making adequate staging challenging. If focal lesions are identified, they tend to have variable signal intensity on the T1- and T2-weighted images. Dynamic gadolinium-enhanced sequences usually are required for better evaluation of splenic lymphomatous involvement.³³⁵ T1-weighted, spoiled gradient-echo images immediately after administration of gadolinium and with a delay of approximately 20 seconds provide the best sensitivity.^{336,337} Diffuse involvement may be demonstrated as splenomegaly with irregularly enhancing regions of high and low signal intensity. Focal lesions can be demonstrated in the normal, enhancing spleen. Multifocal disease can be seen as many focal, hypointense lesions relative to the surrounding spleen. Nodular lesions may have low signal intensity on the T2-weighted images compared with the normal spleen, and this feature can be used to differentiate lymphoma from metastatic

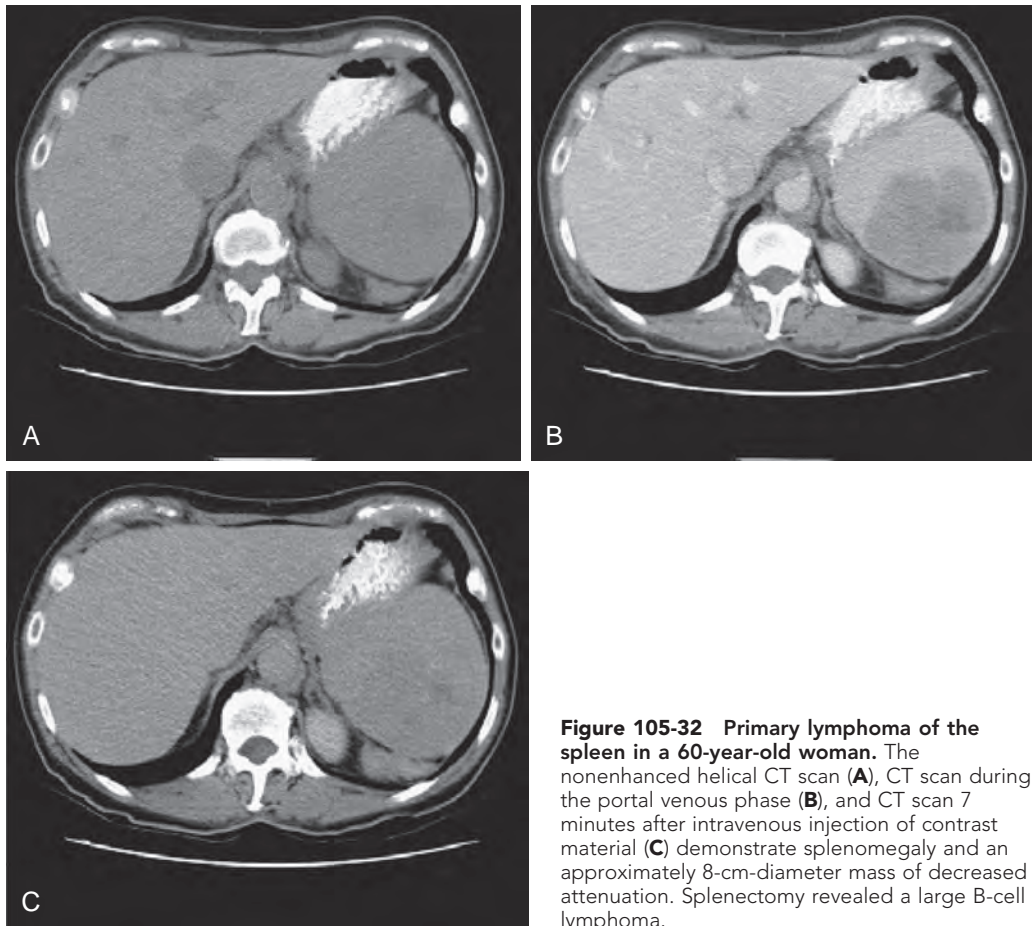


Figure 105-32 Primary lymphoma of the spleen in a 60-year-old woman. The nonenhanced helical CT scan (**A**), CT scan during the portal venous phase (**B**), and CT scan 7 minutes after intravenous injection of contrast material (**C**) demonstrate splenomegaly and an approximately 8-cm-diameter mass of decreased attenuation. Splenectomy revealed a large B-cell lymphoma.

solid organ tumors because metastases rarely have low signal intensity on T2-weighted images (Fig. 105-36).^{337,338}

Secondary cystic, necrotic, or hemorrhagic changes may be helpful in detecting splenic involvement on MRI.³³⁹ The use of MR contrast agents, such as reticuloendothelial system–specific superparamagnetic iron oxide, appeared to be a promising approach for the evaluation of focal splenic lesions, as demonstrated in a few small series.^{340,341} There is normal uptake of the superparamagnetic particles in the reticuloendothelial system, causing decreased signal intensity on T2-weighted images. There is no uptake of the superparamagnetic particles in the malignant cells, and these areas do not change in signal intensity, making them more conspicuous.^{337,342} However, use of these specific contrast materials in general radiologic practice remains limited, and not much has been published recently.

Nuclear Imaging. FDG PET is a functional imaging technique based on glucose metabolism in tissue. In most lymphomas, the involved tissue is hypermetabolic, with resultant increased intracellular glucose accumulation. FDG PET demonstrates increased uptake of the radiopharmaceutical in affected tissue (Fig. 105-37).

FDG PET has had higher sensitivity and specificity than CT and all other imaging modalities in many comparative series. In several circumstances, FDG PET may change the primary staging, planning, and monitoring of therapy for lymphoma patients.³⁴³ Whether FDG PET can change clinical management and consequently affect survival (outcomes) is

a subject of ongoing investigation.^{344,345} FDG PET can be performed at the same time as CT imaging in the form of hybrid or fusion PET/CT. PET/CT already has become the preferred initial staging tool for patients with lymphoma at some institutions.³²²

Limitations of FDG PET are its lack of availability, high operating expenses, and false-positive and false-negative results for patients with lymphoma. For example, false-positive results may occur for metabolizing tissue such as muscle or inflammatory tissue, and indolent (low-grade) NHL may fail to take up FDG, yielding false-negative results. The role of FDG PET imaging in certain types of lymphoma, such as T-cell NHL and highly aggressive NHL, is still uncertain. ^{99m}Tc-sulfur colloid and ⁶⁷Ga-citrate forms of scintigraphy have low sensitivity, specificity, and accuracy in detecting splenic lymphoma.³⁴⁶ Since the introduction of FDG PET, these two imaging modalities have played a limited role in the evaluation of splenic lymphoma.³⁴⁷

LEUKEMIA AND MYELOPROLIFERATIVE DISORDERS

The spleen often is involved in myeloproliferative disorders and in acute and chronic leukemias.²⁶⁵ Unlike lymphoma, these disorders mainly affect the red pulp, although the white pulp eventually may be infiltrated.^{262,265} Splenomegaly is often encountered, but the frequency and severity depend on the type and duration of the disease. Diffuse involvement and focal, solid lesions



Figure 105-33 Mantle cell lymphoma in a 70-year-old woman. Coronal, multiplanar reformat reconstruction CT scan during the late venous phase demonstrates massive splenomegaly displacing the surrounding organs. The spleen has an inhomogeneous, miliary appearance.



Figure 105-34 Diffuse small cell lymphoma. CT demonstrates a hypodense mass with capsular invasion. There is lymphadenopathy surrounding the celiac axis and splenic artery.

(solitary or multiple) have been described.³⁴⁸ Unlike lymphoma, the focal lesions are often hyperechoic on ultrasound.³⁴⁹ Extramedullary hematopoiesis may cause echogenic lesions in these patients.³⁴⁸ Splenic rupture is an uncommon manifestation of leukemic disorders and may be caused by infiltration of the splenic capsule and trabecular framework or by infarction (Fig.

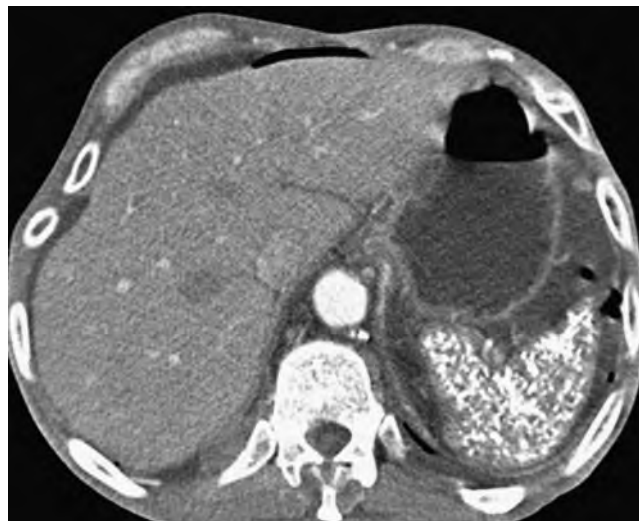


Figure 105-35 Punctate calcifications throughout the spleen 5 years after successful treatment of non-Hodgkin's lymphoma. Calcified lymph nodes (not shown) were also demonstrated in other locations. (Courtesy M. de Jonge, Amsterdam, The Netherlands.)

105-38).^{350,351} Fine-needle biopsy can be performed for definitive diagnosis.²⁹⁸⁻³⁰¹

METASTATIC DISEASE

Epidemiology and Pathogenesis

Splenic involvement by metastases is relatively uncommon and occurs with a frequency of 0.6% to 7.1% in autopsy series.^{352,353} Different types of splenic involvement can be encountered; patients most commonly present with solitary or multiple nodules. On occasion, a miliary pattern, diffuse infiltration of the parenchyma, serosal implants, or direct tumor invasion from adjacent organs is encountered.^{262,352} Tumors that most commonly metastasize to the spleen are melanoma (34%), breast (12%), ovary (12%), colon (10%), and lung (9%).³⁵³ In a study of an Asian population, the lung was the most common primary tumor site (21%), followed by the stomach (16%), pancreas (12%), liver (9%), and colon (9%).³⁵² Kaposi's sarcoma can involve the spleen, usually in AIDS patients with disseminated Kaposi's sarcoma. Isolated metastases to the spleen are very rare, with approximately 40 cases reported in the literature.^{352,354,355}

Several theories have been proposed for the relatively uncommon occurrence of splenic metastases. The absence of afferent lymphatic vessels in the splenic parenchyma is the most likely explanation.^{262,265,353} Hematogenous spread through the splenic artery is considered the most probable origin of metastases, and the frequency of splenic metastases is comparable to that of the kidney.³⁵³ Much less common pathways are metastases through the splenic vein in patients with portal hypertension and retrograde lymphatic spread from nodes in the splenic hilum.^{353,356}

Implants on the serosal surface of the spleen are seen in patients with peritoneal carcinomatosis from ovarian cancer, gastrointestinal adenocarcinoma, and pancreatic cancer. The implants cause indentation and scalloping of the surface of the spleen with solid and cystic components, and these features are typically well demonstrated by CT (Fig. 105-39).

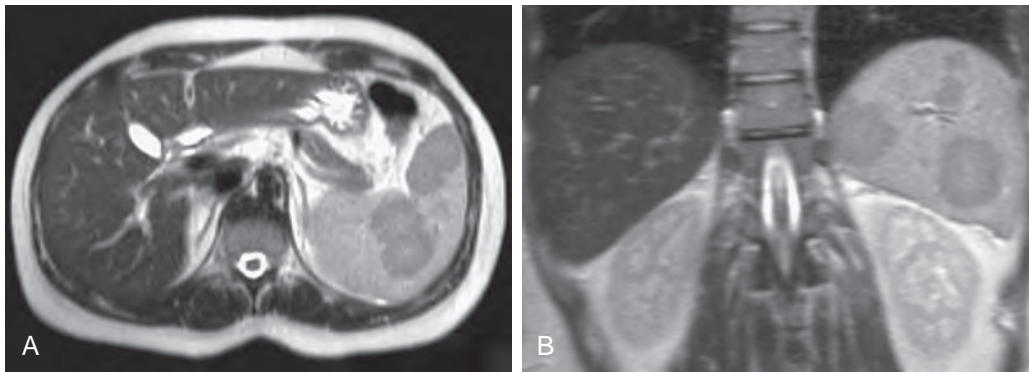


Figure 105-36 Lymphoma. Axial (A) and coronal (B) half-Fourier acquisition single-shot turbo spin-echo (HASTE) MR images demonstrate low signal intensity masses in the spleen of a 32-year-old pregnant woman with a low-grade lymphoma. (Courtesy D. Vanbeckevoort, MD, Leuven, Belgium.)

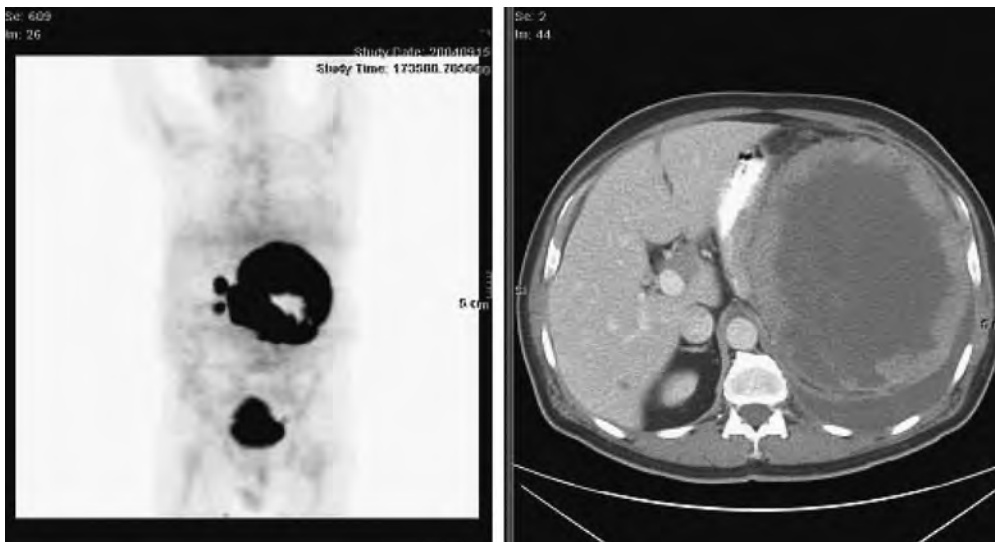


Figure 105-37 Large B-cell lymphoma. Left, PET maximum intensity projection image demonstrates a large peripheral area of increased fluorine-18-deoxyglucose (FDG) uptake with a central hypometabolic region involving the spleen. Right, Corresponding CT image after intravenous administration of contrast material demonstrates a large, hypodense, necrotic mass involving the central spleen. (Courtesy R. Attariwala, MD, PhD, Vancouver, Canada.)



Figure 105-38 Spontaneous splenic rupture. In a 69-year-old man with acute lymphoblastic leukemia, the enhanced helical CT scan demonstrates splenomegaly and multiple hypoechoic areas, subcapsular and pericapsular dense fluid, and free fluid around the liver. Laparotomy and splenectomy confirmed a ruptured subcapsular hematoma and diffuse leukemic involvement of the spleen.



Figure 105-39 Splenic metastasis from colon cancer. In a 56-year-old woman, enhanced helical CT scan shows large splenic lesions with capsular invasion and subcapsular and intrahepatic metastases. CT also demonstrated diffuse tumor infiltration of the abdomen, peritoneal and omental nodules, and subcapsular and intrahepatic metastases. Laparotomy confirmed these findings and showed a cecal adenocarcinoma. (Courtesy C. Keogh, MD, Vancouver, Canada.)

Psammomatous or dense calcifications can be seen in cases of metastatic mucinous adenocarcinoma. Pseudomyxoma peritonei, characterized by extensive spread of a mucin-secreting neoplasm along the peritoneal surfaces, often also involves the spleen.

Direct tumor invasion of the spleen is uncommon. Spread may occur from adjacent organs, such as lymph nodes at the hilum, stomach, colon, pancreatic tail, or left kidney, or from tumors in the retroperitoneum (Figs. 105-40 and 105-41).³⁵⁷



Figure 105-40 Direct invasion of the spleen by a pancreatic adenocarcinoma. In a 63-year-old man, the enhanced CT scan of the upper abdomen shows a partially solid and partially cystic mass involving the tail of the pancreas that is invading the spleen. Percutaneous biopsy from the pancreatic tail mass revealed a pancreatic adenocarcinoma.

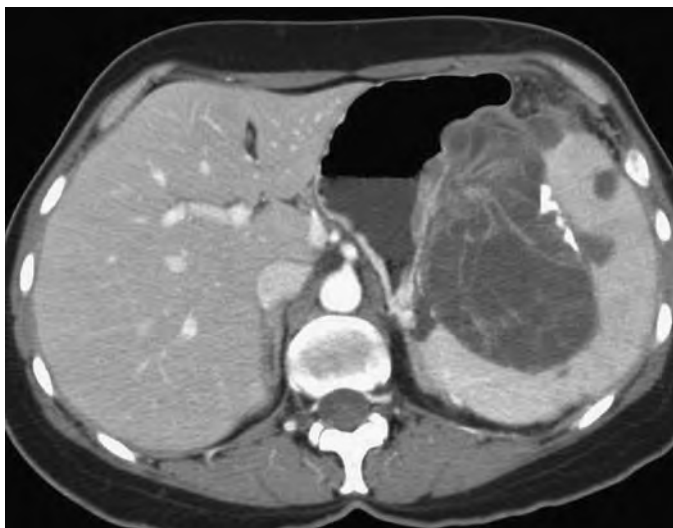


Figure 105-41 Direct invasion of the spleen by a pancreatic mucinous cystadenocarcinoma. In a 52-year-old woman, the enhanced CT scan of the upper abdomen demonstrates a septate cystic mass with some coarse calcifications involving the tail of the pancreas (not shown) that is invading and displacing the splenic hilum. A few small, hypodense lesions in the spleen are consistent with metastatic disease.

Clinical Findings

Splenic metastases usually are seen in patients with advanced disease and widespread involvement of other organs. Solitary splenic metastasis in the absence of other metastases is rare, and splenectomy may be beneficial in these isolated cases.^{355,358,359}

Most splenic metastases do not cause symptoms and are found during routine staging. Splenomegaly is rarely encountered.³⁵⁴

Few patients are symptomatic, and they may present with an abdominal mass, left upper quadrant discomfort due to splenomegaly, and acute pain due to splenic infarcts caused by tumor emboli. More often, patients present with symptoms of disseminated metastatic disease, such as anorexia and cachexia. When there is diffuse parenchymal involvement, the patient may present with hematologic abnormalities and thrombocytopenia. Splenic rupture caused by nonhematologic malignant neoplasms is rare, with approximately 22 cases reported in the literature.³⁶⁰

Pathology

Approximately 80% of splenic metastases can be identified macroscopically.^{352,353} Different types of splenic involvement can be encountered, including solitary metastases, multiple metastases, metastases to the splenic capsule, and diffuse infiltration of the splenic red pulp.^{262,265,352} Most metastatic tumors are manifested as solitary or multiple nodules, and diffuse infiltration is a rare phenomenon.

Radiologic Findings

Ultrasound. The sonographic appearance of splenic metastases varies. Focal lesions can be hypoechoic, mixed, or cystic, or they can have a target or halo appearance (i.e., echogenic lesion with hypoechoic rim).³⁶¹ Approximately 50% of focal splenic metastases are hypoechoic; the larger lesions tend to be more complex. Hyperechoic metastases are rare but can be seen in patients with melanoma, nasopharyngeal carcinoma, and colon and gastric cancers (Fig. 105-42).^{362,363} No correlation between the sonographic features of the metastases and the type of the primary tumor has been demonstrated.³⁶¹

Computed Tomography. Splenic metastases are typically ill-defined, hypodense, rounded lesions (Fig. 105-43). Noncontrast scans are usually not helpful in depicting splenic metastases. In most cases, tumor conspicuity is best in the portal venous phase 60 to 70 seconds after intravenous administration of contrast material because of the normally inhomogeneous early enhancement pattern of the spleen. Splenic metastases occasionally may appear cystic or necrotic.³¹⁷ Cystic metastases may be unilocular or multilocular, and the septations and the periphery may show enhancement.^{317,327} Differentiation of cystic metastases from true splenic cysts may prove difficult.

Splenic metastases with calcifications are rare. Calcifications may be seen in metastases from a mucinous adenocarcinoma (Fig. 105-44).³⁶⁴

Magnetic Resonance Imaging. Splenic metastases are often isointense or slightly hypointense on T1-weighted images and are usually slightly hyperintense on T2-weighted images. Metastases are rarely hypointense on T2-weighted images, and this fact can be used to differentiate splenic metastases from lymphoma.^{337,338} Melanoma metastases may demonstrate

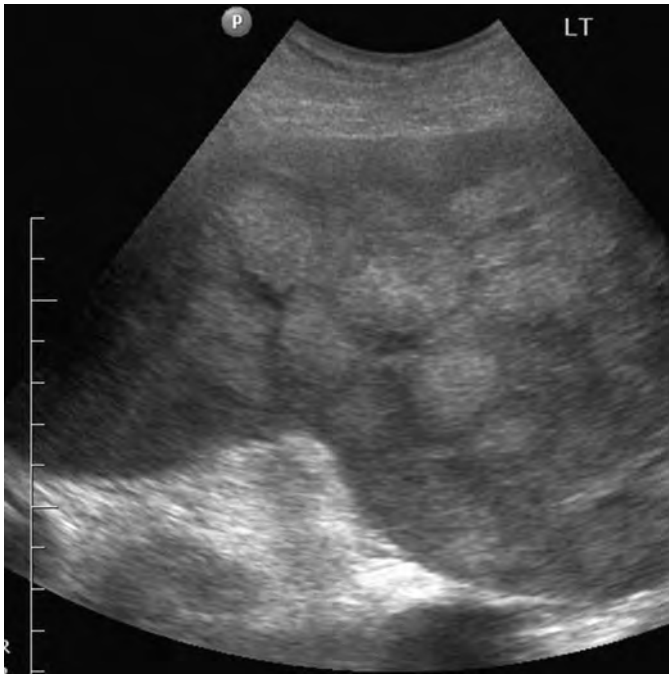


Figure 105-42 Hyperechoic splenic metastasis from melanoma. Ultrasound demonstrates multiple hyperechoic masses throughout the spleen. Multiple similar lesions were present throughout the liver (not shown).

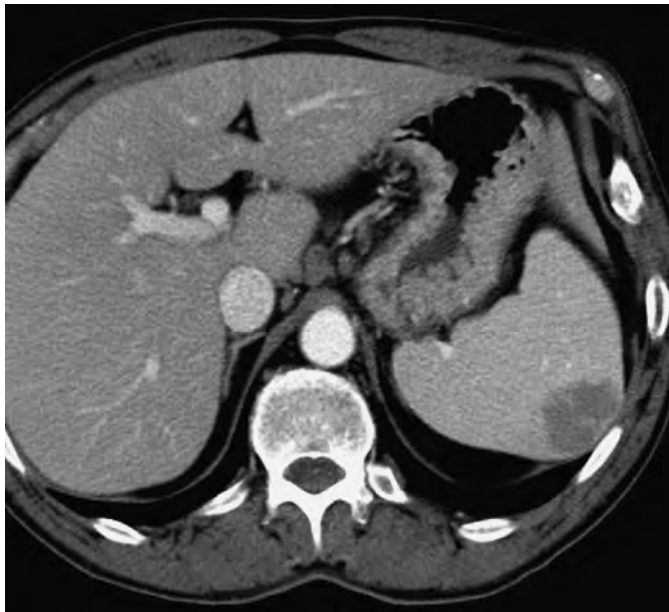


Figure 105-43 Splenic metastasis from lung cancer. The enhanced CT scan of the upper abdomen during the portal venous phase reveals an ill-defined, hypodense mass in the spleen 6 months after resection of a lung cancer (i.e., confirmed squamous cell cancer).

high signal intensity on the T1-weighted images because of the T1 shortening effect of melanin.³⁶⁵ MRI can easily detect necrotic or cystic components. The degree and characteristics of enhancement depend on the nature and type of the primary neoplasm.³³⁸ Metastases are usually hypointense on

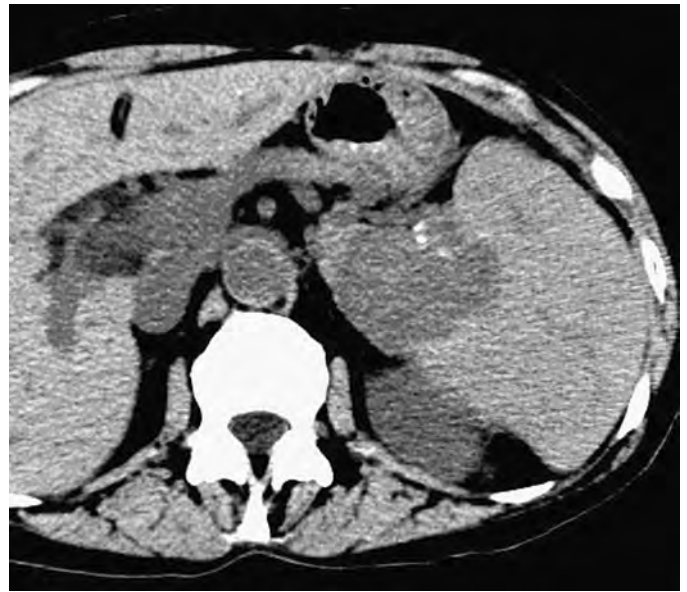


Figure 105-44 Splenic metastasis and peritoneal carcinomatosis from ovarian cancer. Noncontrast CT of the upper abdomen reveals an ill-defined mass containing a few small calcifications invading the hilum of the spleen.

T1-weighted images after the administration of gadolinium. Early (20 seconds) dynamic gadolinium-enhanced imaging is essential because the metastases typically become isointense with the splenic parenchyma after approximately 30 seconds.³³⁷ After treatment, metastases usually demonstrate decreased enhancement and diminished signal intensity on T2-weighted images. The use of specific contrast agents (e.g., superparamagnetic iron oxide) increases lesion conspicuity and decreases the threshold size for lesion detection.^{342,366} However, the use of these agents remains limited in a general radiologic practice.

Nuclear Scintigraphy. FDG PET is becoming the imaging modality of choice for the diagnosis and follow-up of malignant neoplasms, and growing evidence supports its use.^{367,368} The strength of PET imaging is in detecting both nodal and extra-nodal metastases. FDG PET demonstrates focal increased uptake of the radiopharmaceutical in affected locations (Fig. 105-45). The role and accuracy of FDG PET in diagnosis and staging of different malignant neoplasms are being studied, but the accuracy in detection of metastases to the spleen has not been evaluated.³⁶⁹ The combined use of FDG PET imaging and multidetector CT (PET/CT) produces an integrated examination for functional and anatomic imaging.³⁷⁰⁻³⁷⁴ PET/MR also combines functional imaging with the superb contrast resolution of MR.³⁷⁵

Since the introduction of FDG PET, there is no longer a clinical use for ^{99m}Tc-sulfur colloid and ⁶⁷Ga imaging to detect splenic metastases. ^{99m}Tc-sulfur colloid scintigraphy has low sensitivity and specificity for screening of splenic metastases. When abnormalities are detected on these scans, focal defects are demonstrated in the spleen, but the findings are nonspecific. ⁶⁷Ga imaging of splenic metastases is unreliable and of limited clinical use in detecting metastases.

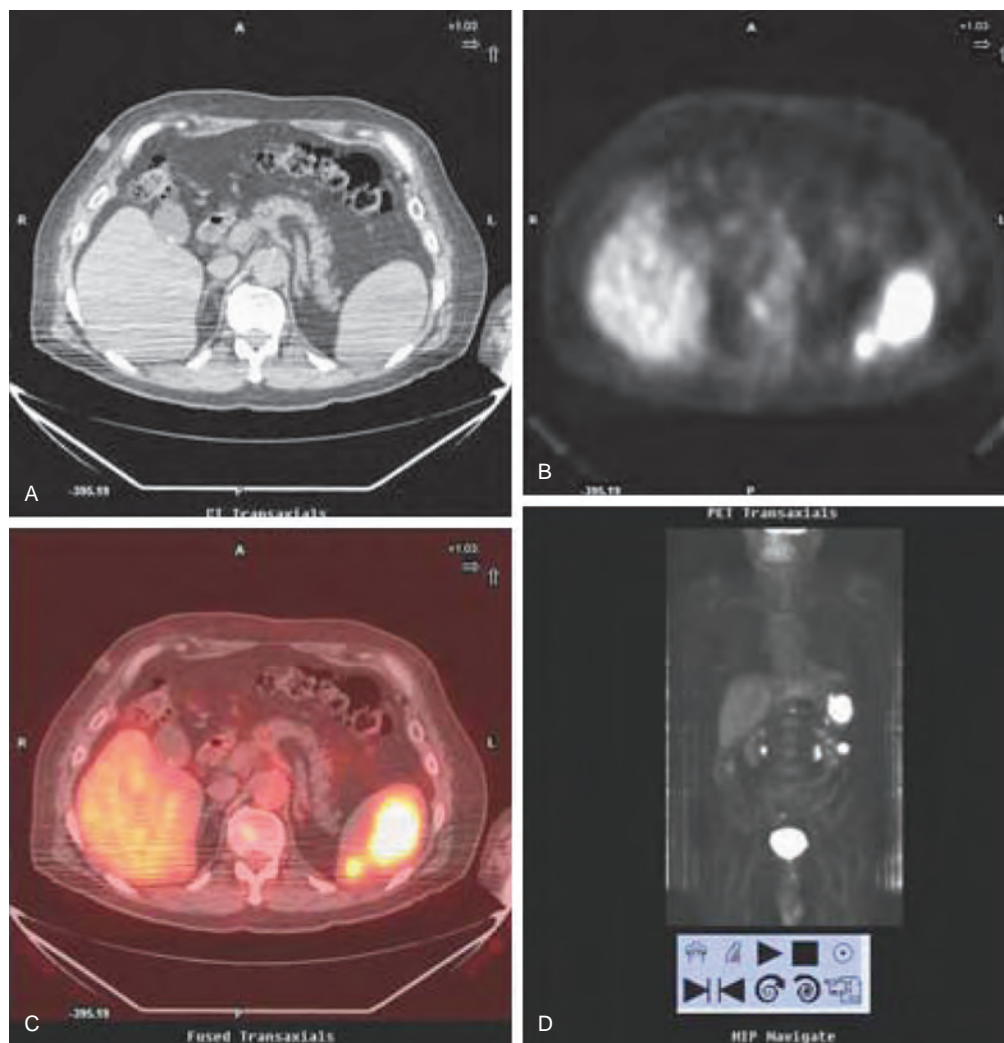


Figure 105-45 Splenic metastases from a malignant melanoma as imaged by PET/CT. **A.** The nonenhanced CT scan of the upper abdomen demonstrates a hypodense area centrally in the spleen. **B.** The axial PET image demonstrates two areas of increased ^{18}F -fluorodeoxyglucose (FDG) activity. **C.** The fused PET/CT image demonstrates the two FDG-avid lesions localized anatomically within the spleen. **D.** The maximum intensity projection image demonstrates the large and small (medial) splenic lesions and another lesion inferior to the largest lesion, which projects lateral to the kidney. (Courtesy Terence Z. Wong, MD, PhD, Duke University Medical Center, Durham, NC.)

REFERENCES

- Robertson F, Leander P, Ekberg O: Radiology of the spleen. *Eur Radiol* 11:80–95, 2001.
- Sammon J, Twomey M, Crush L, et al: Image-guided percutaneous splenic biopsy and drainage. *Semin Intervent Radiol* 29:301–310, 2012.
- Metser U, Miller E, Kessler A, et al: Solid splenic masses: Evaluation with ^{18}F -FDG PET/CT. *J Nucl Med* 46:52–59, 2005.
- Keogan MT, Freed KS, Paulson EK, et al: Imaging-guided percutaneous biopsy of focal splenic lesions: Update on safety and effectiveness. *AJR Am J Roentgenol* 172:933–937, 1999.
- Lucey BC, Boland GW, Maher MM, et al: Percutaneous nonvascular splenic intervention: A 10-year review. *AJR Am J Roentgenol* 179:1591–1596, 2002.
- Siniluoto T, Paivansalo M, Tikkakoski T, Apaja-Sarkkinen M: Ultrasound-guided aspiration cytology of the spleen. *Acta Radiol* 33:137–139, 1992.
- Urban BA, Fishman EK: Helical CT of the spleen. *AJR Am J Roentgenol* 170:997–1003, 1998.
- Donnelly LF, Foss JN, Frush DP, Bisset GS, 3rd: Heterogeneous splenic enhancement patterns on spiral CT images in children: Minimizing misinterpretation. *Radiology* 210:493–497, 1999.
- Semelka RC, Shoenut JB, Lawrence PH, et al: Spleen: Dynamic enhancement patterns on gradient-echo MR images enhanced with gadopentetate dimeglumine. *Radiology* 185:479–482, 1992.
- Paterson A, Frush DP, Donnelly LF, et al: A pattern-oriented approach to splenic imaging in infants and children. *Radiographics* 19:1465–1485, 1999.
- Klee FE, Osswald BR, Wysocki S: Splenic cyst—a “classic incidental” finding. *Zentralbl Chir* 121:805–816, 1996.
- Gayer G, Hertz M, Strauss S, et al: Congenital anomalies of the spleen. *Semin Ultrasound CT MR* 27:358–369, 2006.
- Mortele KJ, Mortele B, Silverman SG: CT features of the accessory spleen [erratum in *AJR Am J Roentgenol* 184:348, 2005]. *AJR Am J Roentgenol* 183:1653–1657, 2004.
- Wilkins BS, Wright DH: *Illustrated Pathology of the Spleen*, New York, 2000, Cambridge University Press.
- Gayer G, Zissin R, Apter S, et al: CT findings in congenital anomalies of the spleen. *Br J Radiol* 74:767–772, 2001.
- Li WF, Luan MX, Ma Z, et al: Splenogonadal fusion: Report of four cases and review of the literature. *Exp Ther Med* 6:816–818, 2013.
- Halpert B, Gyorkey F: Lesions observed in accessory spleens of 311 patients. *Am J Clin Pathol* 32:165–168, 1959.
- Sica GT, Reed MF: Case 27: Intrapancreatic accessory spleen. *Radiology* 217:134–137, 2000.
- Ota T, Ono S: Intrapancreatic accessory spleen: Diagnosis using contrast enhanced ultrasound. *Br J Radiol* 77:148, 2004.
- Applegate KE, Goske MJ, Pierce G, Murphy D: Situs revisited: Imaging of the heterotaxy syndrome. *Radiographics* 19:837–852, 1999.
- Fulcher AS, Turner MA: Abdominal manifestations of situs anomalies in adults. *Radiographics* 22:1439–1456, 2002.
- Lake ST, Johnson PT, Kawamoto S, et al: CT of splenosis: Patterns and pitfalls. *AJR Am J Roentgenol* 199:W686–W693, 2012.
- Carr NJ, Turk EP: The histological features of splenosis. *Histopathology* 21:549–553, 1992.
- Moon C, Choi YJ, Kim EY, et al: Combined intrathoracic and intraperitoneal splenosis after splenic injury: Case report and review of the literature. *Tuberc Respir Dis (Seoul)* 74:134–139, 2013.
- Gigot JF, Jamar F, Ferrant A, et al: Inadequate detection of accessory spleens and splenosis with laparoscopic splenectomy. A shortcoming

- of the laparoscopic approach in hematologic diseases. *Surg Endosc* 12:101–106, 1998.
26. Perez Fontan FJ, Soler R, Santos M, Facio I: Accessory spleen torsion: US, CT and MR findings. *Eur Radiol* 11:509–512, 2001.
 27. Lehtinen SJ, Schammel CM, Devane M, et al: Intrapaneatic accessory spleen presenting as a pancreatic mass. *J Gastrointest Oncol* 4:E23–E26, 2013.
 28. Tasci Y, Kayikcioglu F, Cavusoglu D, Gokcin H: Splenosis mimicking pelvic mass. *Obstet Gynecol* 106(Pt 2):1167–1169, 2005.
 29. Zitzer P, Pansky M, Maymon R, et al: Pelvic splenosis mimicking endometriosis, causing low abdominal mass and pain. *Hum Reprod* 13:1683–1685, 1998.
 30. Sikov WM, Schiffman FJ, Weaver M, et al: Splenosis presenting as occult gastrointestinal bleeding. *Am J Hematol* 65:56–61, 2000.
 31. Nielsen JL, Ellegaard J, Marquers J, Hansen HH: Detection of splenosis and ectopic spleens with ^{99m}Tc-labelled heat damaged autologous erythrocytes in 90 splenectomized patients. *Scand J Haematol* 27:51–56, 1981.
 32. Phom H, Kumar A, Tripathi M, et al: Comparative evaluation of Tc-99m–heat-denatured RBC and Tc-99m–anti-D IgG opsonized RBC spleen planar and SPECT scintigraphy in the detection of accessory spleen in postsplenectomy patients with chronic idiopathic thrombocytopenic purpura. *Clin Nucl Med* 29:403–409, 2004.
 33. Massey MD, Stevens JS: Residual spleen found on denatured RBC scan following negative colloid scan. *J Nucl Med* 32:2286–2287, 1991.
 34. Abbott RM, Levy AD, Aguilera NS, et al: From the archives of the AFIP: Primary vascular neoplasms of the spleen: Radiologic-pathologic correlation. *Radiographics* 24:1137–1163, 2004.
 35. Husni EA: The clinical course of splenic hemangioma: With emphasis on spontaneous rupture. *Arch Surg* 83:681–688, 1961.
 36. Ramani M, Reinhold C, Semelka RC, et al: Splenic hemangiomas and hamartomas: MR imaging characteristics of 28 lesions. *Radiology* 202:166–172, 1997.
 37. Willcox TM, Speer RW, Schlinkert RT, Sarr MG: Hemangioma of the spleen: Presentation, diagnosis, and management. *J Gastrointest Surg* 4:611–613, 2000.
 38. Pakter RL, Fishman EK, Nussbaum A, et al: CT findings in splenic hemangiomas in the Klippel-Trenaunay-Weber syndrome. *J Comput Assist Tomogr* 11:88–91, 1987.
 39. Schulz AS, Urban J, Gessler P, et al: Anaemia, thrombocytopenia, and coagulopathy due to occult diffuse infantile haemangiomatosis of spleen and pancreas. *Eur J Pediatr* 158:379–383, 1999.
 40. Dufau JP, le Tourneau A, Audouin J, et al: Isolated diffuse hemangiomatosis of the spleen with Kasabach-Merritt-like syndrome. *Histopathology* 35:337–344, 1999.
 41. Norris PM, Hughes SC, Strachan CJ: Spontaneous rupture of a benign cavernous haemangioma of the spleen following thrombolysis. *Eur J Vasc Endovasc Surg* 25:476–477, 2003.
 42. Neiman RS, Orazi A: Disorders of the Spleen, ed 2, Philadelphia, 1999, WB Saunders. Major Problems in Pathology Series, vol 38.
 43. Urrutia M, Mergo PJ, Ros LH, et al: Cystic masses of the spleen: Radiologic-pathologic correlation. *Radiographics* 16:107–129, 1996.
 44. Ros PR, Moser RPJ, Dachman AH, et al: Hemangioma of the spleen: Radiologic-pathologic correlation in ten cases. *Radiology* 162:73–77, 1987.
 45. Steininger H, Pfofe D, Marquardt L, et al: Isolated diffuse hemangiomatosis of the spleen: Case report and review of literature. *Pathol Res Pract* 200:479–485, 2004.
 46. Goerg C, Schwerk WB, Goerg K: Splenic lesions: Sonographic patterns, follow-up, differential diagnosis. *Eur J Radiol* 13:59–66, 1991.
 47. Duddy MJ, Calder CJ: Cystic hemangioma of the spleen: Findings on ultrasound and computed tomography. *Br J Radiol* 62:180–182, 1989.
 48. Moss CN, Van Dyke JA, Koehler RE, et al: Multiple cavernous hemangiomas of the spleen: CT findings. *J Comput Assist Tomogr* 10:338–340, 1986.
 49. Disler DG, Chew FS: Splenic hemangioma. *AJR Am J Roentgenol* 157:44, 1991.
 50. Ferrozzi F, Bova D, Draghi F, Garlaschi G: CT findings in primary vascular tumors of the spleen. *AJR Am J Roentgenol* 166:1097–1101, 1996.
 51. Martin DR, Brown MA, Semelka RC: Spleen. In Martin DR, Brown MA, Semelka RC, editors: *Primer on MR Imaging of the Abdomen and Pelvis*, New York, 2005, Wiley-Liss, pp 125–152.
 52. Morteale KJ: Imaging of tumoral conditions of the spleen. *JBR-BTR* 83:213–215, 2000.
 53. Wijaya J, Kapoor R, Roach P: Tc-99m–labeled RBC scintigraphy and splenic hemangioma. *Clin Nucl Med* 26:1022–1023, 2001.
 54. Phillpott J, Ali SA, Briscoe EG, et al: Three-phase Tc-99m labeled RBC scintigraphy of a splenic hemangioma. *Clin Nucl Med* 22:158–160, 1997.
 55. Lehrbuch der Pathologischen Anatomie. Dritter Band. Carl Rokitski. Wien 1861.
 56. Wang JH, Ma XL, Ren FY, et al: Multi-modality imaging findings of splenic hamartoma: A report of nine cases and review of the literature. *Abdom Imaging* 38:154–162, 2013.
 57. Steinberg JJ, Suhrland M, Valensi Q: The spleen in the spleen syndrome: The association of splenoma with hematopoietic and neoplastic disease—compendium of cases since 1864. *J Surg Oncol* 47:193–202, 1991.
 58. Berge T: Splenoma. *Acta Pathol Microbiol Scand* 63:333–339, 1965.
 59. Silverman ML, LiVolsi VA: Splenic hamartoma. *Am J Clin Pathol* 70:224–229, 1978.
 60. Lam KY, Yip KH, Peh WC: Splenic vascular lesions: Unusual features and review of the literature. *Aust N Z J Surg* 69:422–425, 1999.
 61. Zissin R, Lishner M, Rathaus V: Case report: Unusual presentation of splenic hamartoma: Computed tomography and ultrasonic findings. *Clin Radiol* 45:410–411, 1992.
 62. Kassarian A, Patenaude YG, Bernard C, Bell L: Symptomatic splenic hamartoma with renal, cutaneous, and hematological abnormalities. *Pediatr Radiol* 31:111–114, 2001.
 63. Dong A, Wang Y, Lu J, Zuo C: Enhanced CT and FDG PET/CT findings of splenic hamartoma. *Clin Nucl Med* 2013. [Epub ahead of print].
 64. Compton CN, McHenry CR, Aijazi M, Chung-Park M: Thrombocytopenia caused by splenic hamartoma: Resolution after splenectomy. *South Med J* 94:542–544, 2001.
 65. Havlik RJ, Touloukian RJ, Markowitz RI, Buckley P: Partial splenectomy for symptomatic splenic hamartoma. *J Pediatr Surg* 25:1273–1275, 1990.
 66. Cheuk W, Lee AK, Arora N, et al: Splenic hamartoma with bizarre stromal cells. *Am J Surg Pathol* 29:109–114, 2005.
 67. Tang S, Shimizu T, Kikuchi Y, et al: Color Doppler sonographic findings in splenic hamartoma. *J Clin Ultrasound* 28:249–253, 2000.
 68. Nakanishi S, Shiraki K, Yamamoto K, et al: Basket pattern blood flow signals discovered in a case of splenic hamartoma by power Doppler ultrasonography. *World J Gastroenterol* 11:5235–5238, 2005.
 69. Chou YH, Chiou HJ, Tiu CM, et al: Splenic hamartoma: Presentation on contrast-enhanced sonography. *J Clin Ultrasound* 32:425–428, 2004.
 70. Thompson SE, Walsh EA, Cramer BC, et al: Radiological features of a symptomatic splenic hamartoma. *Pediatr Radiol* 26:657–660, 1996.
 71. Yu RS, Zhang SZ, Hua JM: Imaging findings of splenic hamartoma. *World J Gastroenterol* 10:2613–2615, 2004.
 72. Wang JH, Ma XL, Ren FY, et al: Multi-modality imaging findings of splenic hamartoma: A report of nine cases and review of the literature. *Abdom Imaging* 38:154–162, 2013.
 73. Fernandez-Canton G, Capelastegui A, Merino A, et al: A typical MRI presentation of a small splenic hamartoma. *Eur Radiol* 9:883–885, 1999.
 74. Caremani M, Occhini U, Caremani A, et al: Focal splenic lesions: US findings. *J Ultrasound* 16:65–74, 2013.
 75. Shimizu K, Suga K, Matsunaga N, et al: Splenic hamartoma presenting as a “hot spot” on Tc-99m phytate SPECT imaging. *Clin Nucl Med* 23:370–373, 1998.
 76. Okada J, Yoshikawa K, Uno K, et al: Increased activity on radiocolloid scintigraphy in splenic hamartoma. *Clin Nucl Med* 15:112–115, 1990.
 77. Lee SH: Fine-needle aspiration cytology of splenic hamartoma. *Diagn Cytopathol* 28:82–85, 2003.
 78. Wadsworth DT, Newman B, Abramson SJ, et al: Splenic lymphangiomatosis in children. *Radiology* 202:173–176, 1997.
 79. Chang WC, Liou CH, Kao HW, et al: Solitary lymphangioma of the spleen: Dynamic MR findings with pathological correlation. *Br J Radiol* 80:4–6, 2007.
 80. Solomou EG, Patriarheas GV, Mpadra FA, et al: Asymptomatic adult cystic lymphangioma of the spleen: Case report and review of the literature. *Magn Reson Imaging* 21:81–84, 2003.
 81. Wunderbaldinger P, Paya K, Partik B, et al: CT and MR imaging of generalized cystic lymphangiomatosis in pediatric patients. *AJR Am J Roentgenol* 174:827–832, 2000.
 82. Nusser CA, Tuggle DW, McLanahan KB, Leonard JC: Splenic lymphangioma: An unusual manifestation of the Klippel-Trenaunay-Weber syndrome. *Clin Nucl Med* 20:844–845, 1995.
 83. Morgenstern L, Bello JM, Fisher BL, Verham RP: The clinical spectrum of lymphangiomas and lymphangiomatosis of the spleen. *Am Surg* 58:599–604, 1992.
 84. Caremani M, Occhini U, Caremani A, et al: Focal splenic lesions: US findings. *J Ultrasound* 16:65–74, 2013.
 85. Komatsuda T, Ishida H, Konno K, et al: Splenic lymphangioma: US and CT diagnosis and clinical manifestations. *Abdom Imaging* 24:414–417, 1999.

86. Kwon AH, Inui H, Tsuji K, et al: Laparoscopic splenectomy for a lymphangioma of the spleen: Report of a case. *Surg Today* 31:258–261, 2001.
87. Bader TR, Ranner G, Klimpfinger M: Case report: CT appearance of capillary and cavernous lymphangiomatosis of the spleen in an adult. *Clin Radiol* 53:379–381, 1998.
88. Bezzi M, Spinelli A, Pierleoni M, Andreoli G: Cystic lymphangioma of the spleen: US-CT-MRI correlation. *Eur Radiol* 11:1187–1190, 2001.
89. Ito K, Murata T, Nakanishi T: Cystic lymphangioma of the spleen: MR findings with pathologic correlation. *Abdom Imaging* 20:82–84, 1995.
90. Takayama A, Nakashima O, Kobayashi K, Kojiro M: Splenic lymphangioma with papillary endothelial proliferation: A case report and review of the literature. *Pathol Int* 53:483–488, 2004.
91. Tuttle RJ, Minielly JA: Splenic cystic lymphangiomatosis: A usual cause of massive splenomegaly. *Radiology* 126:47–48, 1978.
92. Inada T, Yano T, Shima S, et al: Inflammatory pseudotumor of the spleen. *Intern Med* 931:941–945, 1992.
93. Irie H, Honda H, Kaneko K, et al: Inflammatory pseudotumors of the spleen: CT and MRI findings. *J Comput Assist Tomogr* 20:244–248, 1996.
94. Hegde N: Inflammatory pseudotumour of the spleen: A diagnostic dilemma. *J Clin Diagn Res* 7:1460–1462, 2013.
95. Celebi A, Kayacan SM, Keskin S, et al: A case of inflammatory pseudotumor in the spleen. *South Med J* 99:774–776, 2006.
96. Alimoglu O, Cevikbas U: Inflammatory pseudotumor of the spleen: Report of a case. *Surg Today* 33:960–964, 2003.
97. Franquet T, Montes M, Aizcorbe M, et al: Inflammatory pseudotumor of the spleen: Ultrasound and computed tomographic findings. *Gastrointest Radiol* 14:181–183, 1989.
98. Wu WC, Lin ZY, Chuang WL, Chang WY: Multiple inflammatory pseudotumors of the spleen: Case report. *Abdom Imaging* 28:691–693, 2003.
99. Tsokos M, Erbersdobler A: Pathology of peliosis. *Forensic Sci Int* 149:25–33, 2005.
100. Tsokos M, Puschel K: Isolated peliosis of the spleen: Report of 2 autopsy cases. *Am J Forensic Med Pathol* 25:251–254, 2004.
101. Lashbrook DJ, James RW, Phillips AJ, et al: Splenic peliosis with spontaneous splenic rupture: Report of two cases. *BMC Surg* 6:9, 2006.
102. Cohnheim J: Tod durch Berstung von Varicen der Milz. *Virchows Arch A Pathol Anat* 37:413–415, 1866.
103. Iannaccone R, Federle MP, Brancatelli G, et al: Peliosis hepatis: Spectrum of imaging findings. *AJR Am J Roentgenol* 187:W43–W52, 2006.
104. Maves CK, Caron KH, Bisset GS, III, et al: Splenic and hepatic peliosis: MR findings. *AJR Am J Roentgenol* 158:75–76, 1992.
105. Shimono T, Yamaoka T, Nishimura K, et al: Peliosis of the spleen: Splenic rupture with intraperitoneal hemorrhage. *Abdom Imaging* 23:201–202, 1998.
106. Tsuda K, Nakamura H, Murakami T, et al: Peliosis of the spleen with intraperitoneal hemorrhage. *Abdom Imaging* 18:283–285, 1993.
107. Robbins FG, Yellin AE, Lingua RW, et al: Splenic epidermoid cysts. *Ann Surg* 187:231–235, 1978.
108. Durgun V, Kapan S, Kapan M, et al: Primary splenic hydatidosis. *Dig Surg* 20:38–41, 2003.
109. Warschauer DM, Hall HL: Solitary splenic lesions. *Semin Ultrasound CT MR* 27:358–369, 2006.
110. Martin JW: Congenital splenic cysts. *Am J Surg* 96:302–308, 1958.
111. Burring KF: Epithelial (true) splenic cysts. Pathogenesis of the mesothelial and so-called epidermoid cyst of the spleen. *Am J Surg Pathol* 12:275–281, 1988.
112. Ragozzino MW, Singletary H, Patrick R: Familial splenic epidermoid cyst. *AJR Am J Roentgenol* 155:1233–1234, 1990.
113. Dachman AH, Ros PR, Murari PJ, et al: Nonparasitic splenic cysts: A report of 52 cases with radiologic-pathologic correlation. *AJR Am J Roentgenol* 147:537–542, 1986.
114. Sinha CK, Agrawal M: Nonparasitic splenic cysts in children: Current status. *Surgeon* 9:49–53, 2011.
115. Labruzzo C, Haritopoulos KN, El Tayar AR, et al: Posttraumatic cyst of the spleen: A case report and review of the literature. *Int Surg* 87:152–156, 2002.
116. Welten CA, Sijbrandij ES: Familial nonparasitic splenic cysts. *Neth J Med* 40:236–239, 1992.
117. Nakao A, Saito S, Yamano T, et al: Dermoid cyst of the spleen: Report of a case. *Surg Today* 29:660–662, 1999.
118. Lam CM, Yuen ST, Yuen WK: Hemoperitoneum caused by spontaneous rupture of a true splenic cyst. *Hepatogastroenterology* 45:1884–1886, 1998.
119. Thorne MT, Chwals WJ: Treatment of complicated congenital splenic cysts. *J Pediatr Surg* 28:1635–1636, 1993.
120. Spencer NJ, Arthur RJ, Stringer MD: Ruptured splenic epidermoid cyst: Case report and imaging appearances. *Pediatr Radiol* 26:871–873, 1996.
121. Gilani SM, Tashjian R, Qu H: Histopathological, histogenetic, and immunohistochemical analysis of epidermoid cyst of spleen. *Acta Chir Belg* 113:325–329, 2013.
122. Goktay AY, Secil M, Ozcan MA, Dicle O: Percutaneous treatment of congenital splenic cysts: Drainage and sclerotherapy with polidocanol. *Cardiovasc Intervent Radiol* 29:469–472, 2005.
123. Burring KF: Epithelial (true) splenic cysts: Pathogenesis of the mesothelial and so-called epidermoid cyst of the spleen. *Am J Surg Pathol* 12:275–281, 1988.
124. Elsayes KM, Narra VR, Mukundan G, et al: MR imaging of the spleen: Spectrum of abnormalities. *Radiographics* 25:967–982, 2005.
125. Ito K, Mitchell DG, Honjo K, et al: MR imaging of acquired abnormalities of the spleen. *AJR Am J Roentgenol* 168:697–702, 1997.
126. Safioleas M, Misiakos E, Manti C: Surgical treatment for splenic hydatidosis. *World J Surg* 21:374–377, 1997.
127. Li Q, Samir AE: Echinococcal cysts of the liver and spleen: Complex hepatic and splenic cystic lesions. *Ultrasound Q* 28:205–207, 2012.
128. Uriarte C, Pomares N, Martin M, et al: Splenic hydatidosis. *Am J Trop Med Hyg* 44:420–423, 1991.
129. Polat P, Kantarci M, Alper F, et al: Hydatid disease from head to toe. *Radiographics* 23:475–494, 2003.
130. Reuter S, Seitz HM, Kern P, Junghans T: Extrahepatic alveolar echinococcosis without liver involvement: A rare manifestation. *Infection* 28:187–192, 2000.
131. Pedrosa I, Saiz A, Arrazola J, et al: Hydatid disease: Radiologic and pathologic features and complications. *Radiographics* 20:795–817, 2000.
132. Li Y, Zheng H, Cao X, et al: Demographic and clinical characteristics of patients with anaphylactic shock after surgery for cystic echinococcosis. *Am J Trop Med Hyg* 85:452–455, 2011.
133. Sbihi Y, Rmiqui A, Rodriguez-Cabezas MN, et al: Comparative sensitivity of six serological tests and diagnostic value of ELISA using purified antigen in hydatidosis. *J Clin Lab Anal* 15:14–18, 2001.
134. WHO Informal Working Group: International classification of ultrasound images in cystic echinococcosis for application in clinical and field epidemiological settings. *Acta Trop* 85:253–261, 2003.
135. Macpherson CN, Bartholomot B, Frider B: Application of ultrasound in diagnosis, treatment, epidemiology, public health and control of *Echinococcus granulosus* and *E. multilocularis*. *Parasitology* 127(Suppl):S21–S35, 2003.
136. Etlik O, Arslan H, Bay A, et al: Abdominal hydatid disease: Long-term results of percutaneous treatment. *Acta Radiol* 45:383–389, 2004.
137. Ormeci N, Soykan I, Palabiyikoglu M, et al: A new therapeutic approach for treatment of hydatid cysts of the spleen. *Dig Dis Sci* 47:2037–2044, 2002.
138. Gharbi HA, Hassine W, Brauner MW, Dupuch K: Ultrasound examination of the hydatid liver. *Radiology* 139:459–463, 1981.
139. Beggs I: The radiology of hydatid disease. *AJR Am J Roentgenol* 145:639–648, 1985.
140. Takabe K, Al-Refaie W, Chin B, et al: Can large B-cell lymphoma mimic cystic lesions of the spleen? *Int J Gastrointest Cancer* 35:83–88, 2005.
141. Ishida H, Konno K, Ishida J, et al: Splenic lymphoma: Differentiation from splenic cyst with ultrasonography. *Abdom Imaging* 26:529–532, 2001.
142. Goerg C, Weide R, Schwerk WB, et al: Ultrasound evaluation of hepatic and splenic microabscesses in the immunocompromised patient: Sonographic patterns, differential diagnosis, and follow-up. *J Clin Ultrasound* 22:525–529, 1994.
143. Chen CY, Chen YC, Tang JL, et al: Hepato-splenic fungal infection in patients with acute leukemia in Taiwan: Incidence, treatment, and prognosis. *Ann Hematol* 82:93–97, 2003.
144. Anttila VJ, Lamminen AE, Bondestam S, et al: Magnetic resonance imaging is superior to computed tomography and ultrasonography in imaging infectious liver foci in acute leukaemia. *Eur J Haematol* 56:82–87, 1996.
145. Sallah S, Semelka R, Kelekis N, et al: Diagnosis and monitoring response to treatment of hepatosplenic candidiasis in patients with acute leukemia using magnetic resonance imaging. *Acta Haematol* 100:77–81, 1998.
146. Chew FS, Smith PL, Barboriak D: Candidal splenic abscesses. *AJR Am J Roentgenol* 156:474, 1991.
147. Von Eiff M, Essink M, Roos N, et al: Hepato-splenic candidiasis, a late manifestation of *Candida* septicemia in neutropenic patients with hematologic malignancies. *Blut* 60:242–248, 1990.
148. Karthaus M, Huebner G, Elser C, et al: Early detection of chronic disseminated *Candida*

- infection in leukemia patients with febrile neutropenia: Value of computer-assisted serial ultrasound documentation. *Ann Hematol* 77:41–45, 1998.
149. Pestalozzi BC, Krestin GP, Schanz U, et al: Hepatic lesions of chronic disseminated candidiasis may become invisible during neutropenia. *Blood* 90:3858–3864, 1997.
 150. Shirkhoda A: CT findings in hepatosplenic and renal candidiasis. *J Comput Assist Tomogr* 11:795–798, 1987.
 151. Semelka RC, Kelekis NL, Sallah S, et al: Hepatosplenic fungal disease: Diagnostic accuracy and spectrum of appearances on MR imaging. *AJR Am J Roentgenol* 169:1311–1316, 1997.
 152. Pastakia B, Shawker TH, Thaler M, et al: Hepatosplenic candidiasis: Wheels within wheels. *Radiology* 166:417–421, 1988.
 153. Mortelet KJ, Segatto E, Ros PR: The infected liver: Radiologic-pathologic correlation. *Radiographics* 24:937–955, 2004.
 154. Murray JG, Patel MD, Lee S, et al: Microabscesses of the liver and spleen in AIDS: Detection with 5-MHz sonography. *Radiology* 197:723–727, 1995.
 155. Metser U, Haider MA, Dill-Mackay M, et al: Fungal liver infection in immunocompromised patients: Depiction with multiphasic contrast-enhanced helical CT. *Radiology* 235:97–105, 2005.
 156. Rudolph J, Rodenwaldt J, Ruhnke M, et al: Unusual enhancement pattern of liver lesions in hepatosplenic candidiasis. *Acta Radiol* 45:499–503, 2004.
 157. Masood A, Sallah S: Chronic disseminated candidiasis in patients with acute leukemia: Emphasis on diagnostic definition and treatment. *Leuk Res* 29:493–501, 2005.
 158. Vasquez TE, Evans DG, Schiffman H, et al: Fungal splenic abscesses in the immunosuppressed patient: Correlation of imaging modalities. *Clin Nucl Med* 12:36–38, 1987.
 159. Gafter-Gvili A, Paul M, Bernstine H, et al: The role of ¹⁸F-FDG PET/CT for the diagnosis of infections in patients with hematological malignancies and persistent febrile neutropenia. *Leuk Res* 37:1057–1062, 2013.
 160. Buckner CB, Leithiser RE, Walker CW, et al: The changing epidemiology of tuberculosis and other mycobacterial infections in the United States: Implications for the radiologist. *AJR Am J Roentgenol* 156:255–264, 1991.
 161. Sheen-Chen SM, Chou FF, Wan YL, Eng HL: Tuberculosis presenting as a solitary splenic tumour. *Tuber Lung Dis* 76:80–83, 1995.
 162. Koh DM, Burn PR, Mathews G, et al: Abdominal computed tomographic findings of *Mycobacterium tuberculosis* and *Mycobacterium avium intracellulare* infection in HIV seropositive patients. *Can Assoc Radiol J* 54:45–50, 2003.
 163. Radin DR: Intraabdominal *Mycobacterium tuberculosis* vs *Mycobacterium avium-intracellulare* infections in patients with AIDS: Distinction based on CT findings. *AJR Am J Roentgenol* 156:487–491, 1991.
 164. Pantongrag-Brown L, Krebs TL, Daly BD, et al: Frequency of abdominal CT findings in AIDS patients with *M. avium* complex bacteraemia. *Clin Radiol* 53:816–819, 1998.
 165. Spouge AR, Wilson SR, Gopinath N, et al: Extrapulmonary *Pneumocystis carinii* in a patient with AIDS: Sonographic findings. *AJR Am J Roentgenol* 155:76–78, 1990.
 166. Lubat E, Megibow AJ, Balthazar EJ, et al: Extrapulmonary *Pneumocystis carinii* infection in AIDS. *Radiology* 174:157–160, 1990.
 167. Radin DR, Baker EL, Klatt EC, et al: Visceral and nodal calcification in patients with AIDS-related *Pneumocystis carinii* infection. *AJR Am J Roentgenol* 154:27–31, 1990.
 168. Feurstein IM, Francis P, Raffeld M, et al: Widespread visceral calcification in disseminated *Pneumocystis carinii* infection: CT characteristics. *J Comput Assist Tomogr* 14:149–151, 1990.
 169. Fishman EK, Magid D, Kuhlman JE: *Pneumocystis carinii* involvement of the liver and spleen: CT demonstration. *J Comput Assist Tomogr* 14:146–148, 1990.
 170. Pelton SI, Kim JY, Kradin RL: Case records of the Massachusetts General Hospital. Case 27-2006. A 17-year-old boy with fever and lesions in the liver and spleen. *N Engl J Med* 355:941–948, 2006.
 171. Hopkins KL, Simoneaux SF, Patrick LE, et al: Imaging manifestations of cat-scratch disease. *AJR Am J Roentgenol* 166:435–438, 1996.
 172. Rappaport DC, Cumming WA, Ros PR: Disseminated hepatic and splenic lesions in cat-scratch disease: Imaging features. *AJR Am J Roentgenol* 156:1227–1228, 1991.
 173. Thanos L, Zorpala A, Broutzos E, et al: Nodular hepatic and splenic sarcoidosis in a patient with normal chest radiograph. *Eur J Radiol* 41:10–11, 2002.
 174. Koyama T, Ueda H, Togashi K, et al: Radiologic manifestations of sarcoidosis in various organs. *Radiographics* 24:87–104, 2004.
 175. Folz SJ, Johnson CD, Swensen SJ: Abdominal manifestations of sarcoidosis in CT studies. *J Comput Assist Tomogr* 19:573–579, 1995.
 176. Warschauer DM: Splenic sarcoidosis. *Semin Ultrasound CT MR* 28:21–27, 2007.
 177. Warschauer DM, Lee JK: Imaging manifestations of abdominal sarcoidosis. *AJR Am J Roentgenol* 82:15–28, 2004.
 178. Scott GC, Berman JM, Higgins JL, Jr: CT patterns of nodular hepatic and splenic sarcoidosis: A review of the literature. *J Comput Assist Tomogr* 21:369–372, 1997.
 179. Kim SL, Gedgaudas-McClees RK, Waring JP: Sarcoidosis with multiple hepatic and splenic nodules on dynamic computed tomography. *Ann Intern Med* 117:399–400, 1992.
 180. Kessler A, Mitchell DG, Israel HL, Goldberg BB: Hepatic and splenic sarcoidosis: Ultrasound and MR imaging. *Abdom Imaging* 18:159–163, 1993.
 181. Pak HY, Friedman NB: Pseudosarcoid granulomas in Hodgkin's disease. *Hum Pathol* 12:832–837, 1981.
 182. Minami M, Itai Y, Ohtomo K, et al: Siderotic nodules in the spleen: MR imaging of portal hypertension. *Radiology* 172:681–684, 1989.
 183. Dobritz M, Nomayr A, Bautz W, et al: Gamna-Gandy bodies of the spleen detected with MR imaging: A case report. *Magn Reson Imaging* 19:1249–1251, 2001.
 184. Sagoh T, Itoh K, Togashi K, et al: Gamna-Gandy bodies of the spleen: Evaluation with MR imaging. *Radiology* 172:685–687, 1989.
 185. Chan YL, Yang WT, Sung JJ, et al: Diagnostic accuracy of abdominal ultrasonography compared with magnetic resonance imaging in siderosis of the spleen. *J Ultrasound Med* 19:543–547, 2000.
 186. Luo TY, Itai Y, Yamaguchi M, et al: Gamna-Gandy bodies of the spleen depicted by unenhanced CT: Report of two cases. *Radiat Med* 16:473–476, 1998.
 187. Ooi LL, Leong SS: Splenic abscesses from 1987 to 1995. *Am J Surg* 174:87–93, 1997.
 188. de Bree E, Tsiftsis D, Christodoulakis M, et al: Splenic abscess: A diagnostic and therapeutic challenge. *Acta Chir Belg* 98:199–202, 1998.
 189. Alonso Cohen MA, Galera MJ, Ruiz M, et al: Splenic abscess. *World J Surg* 14:513–517, 1990.
 190. Phillips GS, Radosevich MD, Lipsett PA: Splenic abscess: Another look at an old disease. *Arch Surg* 132:1331–1335, 1997.
 191. Chang KC, Chuah SK, Changchien CS, et al: Clinical characteristics and prognostic factors of splenic abscess: A review of 67 cases in a single medical center of Taiwan. *World J Gastroenterol* 12:460–464, 2006.
 192. Caslowitz PL, Labs JD, Fishman EK, et al: The changing spectrum of splenic abscess. *Clin Imaging* 13:201–207, 1989.
 193. Changchien CS, Tsai TL, Hu TH, et al: Sonographic patterns of splenic abscess: An analysis of 34 proven cases. *Abdom Imaging* 27:739–745, 2002.
 194. Ng KK, Lee TY, Wan YL, et al: Splenic abscess: Diagnosis and management. *Hepatogastroenterology* 49:567–571, 2002.
 195. Joazlina ZY, Wastie ML, Ariffin N: Computed tomography of focal splenic lesions in patients presenting with fever. *Singapore Med J* 47:37–41, 2006.
 196. Thanos L, Dailiana T, Papaioannou G, et al: Percutaneous CT-guided drainage of splenic abscess. *AJR Am J Roentgenol* 179:629–632, 2002.
 197. Chou YH, Tiu CM, Chiou HJ, et al: Ultrasound-guided interventional procedures in splenic abscesses. *Eur J Radiol* 28:167–170, 1998.
 198. Tikkakoski T, Siniluoto T, Päänsalo M, et al: Splenic abscess: Imaging and intervention. *Acta Radiol* 33:561–565, 1992.
 199. Youssef IM, Milardovic R, Perone RW, et al: Importance of Tc-99m sulfur colloid liver-spleen scans performed before indium-111 labeled leukocyte imaging for localization of abdominal infection. *Clin Nucl Med* 30:87–90, 2005.
 200. Avery GR, Wilsdon JB, Mitchell L: Case report: CT and angiographic appearances of intrasplenic mycotic aneurysm. *Clin Radiol* 44:271–272, 1991.
 201. Jaroch MT, Broughan TA, Hermann RE: The natural history of splenic infarction. *Surgery* 100:743–749, 1986.
 202. O'Keefe JH, Jr, Holmes DR, Jr, Schaff HV, et al: Thromboembolic splenic infarction. *Mayo Clin Proc* 61:967–972, 1986.
 203. Antopolsky M, Hiller N, Salameh S, et al: Splenic infarction: 10 years of experience. *Am J Emerg Med* 27:262–265, 2009.
 204. Romano S, Scaglione M, Gatta G, et al: Association of splenic and renal infarctions in acute abdominal emergencies. *Eur J Radiol* 50:48–58, 2004.
 205. Mahesh B, Muwanga CL: Splenic infarct: A rare cause of spontaneous rupture leading to massive haemoperitoneum. *ANZ J Surg* 74:1030–1032, 2004.
 206. Miller LA, Mirvis SE, Shanmuganathan K, Ohson AS: CT diagnosis of splenic infarction in blunt trauma: Imaging features, clinical significance and complications. *Clin Radiol* 59:342–348, 2004.
 207. Nores M, Phillips EH, Morgenstern L, et al: The clinical spectrum of splenic infarction. *Am Surg* 64:182–188, 1998.

208. Goerg C, Schwerk WB: Splenic infarct: Sonographic patterns, diagnosis, follow-up, and complications. *Radiology* 174:803–807, 1990.
209. Balcar I, Seltzer SE, Davis S, et al: CT patterns of splenic infarction: A clinical and experimental study. *Radiology* 151:723–729, 1984.
210. Emery KH: Splenic emergencies. *Radiol Clin North Am* 35:831–843, 1997.
211. Beckett D, Miller C, Ferrando JR, Banerjee AK: Case report: Polycythemia vera presenting as massive splenic infarction and liquefaction. *Br J Radiol* 77:876–877, 2004.
212. Maresca G, Mirk P, De Gaetana AM, et al: Sonographic patterns in splenic infarct. *J Clin Ultrasound* 14:23–28, 1986.
213. Shirkhoda A, Wallace S, Sokhandan M: Computed tomography and ultrasonography in splenic infarction. *J Can Assoc Radiol* 36:29–33, 1985.
214. Rabushka LS, Kawashima A, Fishman EK: Imaging of the spleen: CT with supplemental MR examination. *Radiographics* 14:307–332, 1994.
215. Wong CP, Auyong TK, Tong CM: Cold splenic lesion on Tc-99m colloid and denatured RBC scintigraphy. *Clin Nucl Med* 29:105–109, 2004.
216. Paknikar S, Singh A: Nonvisualization of spleen on sulfur colloid images: A sequel of massive infarction. *Semin Nucl Med* 28:188–191, 1998.
217. Hikeson M, Derbeyan V, Lisbona R, Novales-Diaz J: Assessment of viable splenic tissue in massive splenic infarction with a Tc-99m heat-damaged RBC scan. *Clin Nucl Med* 26:419–422, 2001.
218. Balthazar EJ, Hilton S, Naidich D, et al: CT of splenic and perisplenic abnormalities in septic patients. *AJR Am J Roentgenol* 144:53–56, 1985.
219. Haan J, Bochicchio G, Kramer M, Scalea T: Air following splenic embolization: Infection or incidental finding? *Am Surg* 69:1036–1039, 2003.
220. Toubia NT, Tawk MM, Potts RM, Kinasewitz GT: Cough and spontaneous rupture of a normal spleen. *Chest* 128:1884–1886, 2005.
221. Choudhury AK: Spontaneous rupture of a normal spleen. *Injury* 35:325–326, 2004.
222. Aubrey-Bassler FK, Sowers N: 613 cases of splenic rupture without risk factors or previously diagnosed disease: A systematic review. *BMC Emerg Med* 12:11, 2012.
223. Loftus WK, Chow LT, Metreweli C: Sonographic measurement of splenic length: Correlation with measurement at autopsy. *J Clin Ultrasound* 27:71–74, 1999.
224. Spielmann AL, DeLong DM, Kliever MA: Sonographic evaluation of spleen size in tall healthy athletes. *AJR Am J Roentgenol* 184:45–49, 2005.
225. Lamb PM, Lund A, Kanagasabay RR, et al: Spleen size: How well do linear ultrasound measurements correlate with three-dimensional CT volume assessments? *Br J Radiol* 75:573–577, 2002.
226. Yetter EM, Acosta KB, Olson MC, Blundell K: Estimating splenic volume: Sonographic measurements correlated with helical CT determination. *AJR Am J Roentgenol* 181:1615–1620, 2003.
227. Farragher SW, Jara H, Chang KJ, et al: Liver and spleen volumetry with quantitative MR imaging and dual-space clustering segmentation. *Radiology* 237:322–328, 2005.
228. Bezerra AS, D'Ippolito G, Faintuch S, et al: Determination of splenomegaly by CT: Is there a place for a single measurement? *AJR Am J Roentgenol* 184:1510–1513, 2005.
229. Gill FM, Sleeper LA, Weiner SJ, et al: Clinical events in the first decade in a cohort of infants with sickle cell disease. Cooperative Study of Sickle Cell Disease. *Blood* 86:776–783, 1995.
230. Lorey FW, Arnopp J, Cunningham GC: Distribution of hemoglobinopathy variants by ethnicity in a multiethnic state. *Genet Epidemiol* 13:501–512, 1996.
231. Lonergan GJ, Cline DB, Abbondanzo SL: Sickle cell anemia. *Radiographics* 21:971–994, 2001.
232. Al-Salem AH, Naserullah Z, Qaisaruddin S, et al: Splenic complications of the sickling syndromes and the role of splenectomy. *J Pediatr Hematol Oncol* 21:401–406, 1999.
233. Gorg C, Zugmaier G: Chronic recurring infarction of the spleen: Sonographic patterns and complications. *Ultraschall Med* 24:245–249, 2003.
234. Adler DD, Glazer GM, Aisen AM: MRI of the spleen: Normal appearance and findings in sickle-cell anemia. *AJR Am J Roentgenol* 147:843–845, 1986.
235. Levin TL, Berdon WE, Haller JO, et al: Intraspinal masses of “preserved” functioning splenic tissue in sickle cell disease: Correlation of imaging findings (CT, ultrasound, MRI, and nuclear scintigraphy). *Pediatr Radiol* 26:646–649, 1996.
236. Roshkow JE, Sanders LM: Acute splenic sequestration crisis in two adults with sickle cell disease: US, CT, and MR imaging findings. *Radiology* 177:723–725, 1990.
237. Al-Salem AH, Qaisaruddin S, Al Jam'a A, et al: Splenic abscess and sickle cell disease. *Am J Hematol* 58:100–104, 1998.
238. Fishman EK, Soyer P, Bliss DF, et al: Splenic involvement in pancreatitis: Spectrum of CT findings. *AJR Am J Roentgenol* 164:631–635, 1995.
239. Malka D, Hammel P, Levy P, et al: Splenic complications in chronic pancreatitis: Prevalence and risk factors in a medical-surgical series of 500 patients. *Br J Surg* 85:1645–1649, 1998.
240. Heider R, Behrns KE: Pancreatic pseudocysts complicated by splenic parenchymal involvement: Results of operative and percutaneous management. *Pancreas* 23:20–25, 2001.
241. Lankisch PG: The spleen in inflammatory pancreatic disease. *Gastroenterology* 98:509–516, 1990.
242. Rypens F, Deviere J, Zalzman M, et al: Splenic parenchymal complications of pancreatitis: CT findings and natural history. *J Comput Assist Tomogr* 21:89–93, 1997.
243. Morteel KJ, Mergo PJ, Taylor HM, et al: Splenic and perisplenic involvement in acute pancreatitis: Determination of prevalence and morphologic helical CT features. *J Comput Assist Tomogr* 25:50–54, 2001.
244. Vyborny CJ, Merrill TN, Reda J, et al: Subacute subcapsular hematoma of the spleen complicating pancreatitis: Successful percutaneous drainage. *Radiology* 169:161–162, 1988.
245. Niederau C, Haussinger D: Gaucher's disease: A review for the internist and hepatologist. *Hepatogastroenterology* 47:984–997, 2000.
246. Poll LW, Koch JA, vom Dahl S, et al: Gaucher disease of the spleen: CT and MR findings. *Abdom Imaging* 25:286–289, 2000.
247. Hill SC, Reinig JW, Barranger JA, et al: Gaucher disease: Sonographic appearance of the spleen. *Radiology* 160:631–634, 1986.
248. Lanir A, Hader H, Cohen I, et al: Gaucher disease: Assessment with MR imaging. *Radiology* 161:239–244, 1986.
249. Hill SC, Damaska BM, Ling A, et al: Gaucher disease: Abdominal MR imaging findings in 46 patients. *Radiology* 184:561–566, 1992.
250. Siegelman ES, Mitchell DG, Semelka RC: Abdominal iron deposition: Metabolism, MR findings, and clinical importance. *Radiology* 199:13–22, 1996.
251. Papakonstantinou O, Drakonaki EE, Maris T, et al: MR imaging of spleen in beta-thalassemia major. *Abdom Imaging* 2006. [Epub ahead of print].
252. Guyader D, Gandon Y, Deugnier Y, et al: Evaluation of computed tomography in the assessment of liver iron overload. A study of 46 cases of idiopathic hemochromatosis. *Gastroenterology* 97:737–743, 1989.
253. Alustiza JM, Artetxe J, Castiella A, et al: MR quantification of hepatic iron concentration. *Radiology* 230:479–484, 2004.
254. Travis LB, Hauptmann M, Gaul LK, et al: Site-specific cancer incidence and mortality after cerebral angiography with radioactive Thorotrast. *Radiat Res* 160:691–706, 2003.
255. Lipshutz GS, Brennan TV, Warren RS: Thorotrast-induced liver neoplasia: A collective review. *J Am Coll Surg* 195:713–718, 2002.
256. Levy DW, Rindsberg S, Friedman AC, et al: Thorotrast-induced hepatosplenic neoplasia: CT identification. *AJR Am J Roentgenol* 146:997–1004, 1986.
257. Abbott RM, Levy AD, Aguilera NS, et al: From the archives of the AFIP: Primary vascular neoplasms of the spleen: Radiologic-pathologic correlation. *Radiographics* 24:1137–1163, 2004.
258. Falk S, Krishnan J, Meis JM: Primary angiosarcoma of the spleen: A clinicopathologic study of 40 cases. *Am J Surg Pathol* 17:959–970, 1993.
259. Thompson WM, Levy AD, Aguilera NS, et al: Angiosarcoma of the spleen: Imaging characteristics in 12 patients. *Radiology* 235:106–115, 2005.
260. Neuhauser TS, Derringer GA, Thompson LD, et al: Splenic angiosarcoma: A clinicopathologic and immunophenotypic study of 28 cases. *Mod Pathol* 13:978–987, 2000.
261. den Hoed ID, Granzen B, Granzen B, et al: Metastasized angiosarcoma of the spleen in a 2-year-old girl. *Pediatr Hematol Oncol* 22:387–390, 2005.
262. Neiman RS, Orazi A: Disorders of the Spleen, ed 2, Philadelphia, 1999, WB Saunders. Major Problems in Pathology Series, vol 38.
263. Drinkovic I, Brkljacic B: Two cases of lethal complications following ultrasound-guided percutaneous fine-needle biopsy of the liver. *Cardiovasc Intervent Radiol* 19:360–363, 1996.
264. Lucey BC, Boland GW, Maher MM, et al: Percutaneous nonvascular splenic intervention: A 10-year review. *AJR Am J Roentgenol* 179:1591–1596, 2002.
265. Wilkins BS, Wright DH: Illustrated Pathology of the Spleen, New York, 2000, Cambridge University Press.
266. Takato H, Iwamoto H, Ikezu M, et al: Splenic hemangiosarcoma with sinus endothelial differentiation. *Acta Pathol Jpn* 43:702–708, 1993.
267. Breiteneder-Geleff S, Soleiman A, Kowalski H, et al: Angiosarcomas express mixed endothelial phenotypes of blood and lymphatic capillaries: Podoplanin as a specific marker for

- lymphatic endothelium. *Am J Pathol* 154:385–394, 1999.
268. Vrachliotis TG, Bennett WF, Vaswani KK, et al: Primary angiosarcoma of the spleen—CT, MR, and sonographic characteristics: Report of two cases. *Abdom Imaging* 25:283–285, 2000.
 269. Ferrozzi F, Bova D, Draghi F, et al: CT findings in primary vascular tumors of the spleen. *AJR Am J Roentgenol* 166:1097–1101, 1996.
 270. Kinoshita T, Ishii K, Yajima Y, et al: Splenic hemangiosarcoma with massive calcification. *Abdom Imaging* 24:185–187, 1999.
 271. Ha HK, Kim HH, Kim BK, et al: Primary angiosarcoma of the spleen: CT and MR imaging. *Acta Radiol* 35:455–458, 1994.
 272. Imaoka I, Sugimura K, Furukawa M, et al: CT and MR findings in splenic angiosarcoma. *Radiat Med* 17:67–70, 1999.
 273. Kaneko K, Onitsuka H, Murakami J, et al: MRI of primary spleen angiosarcoma with iron accumulation. *J Comput Assist Tomogr* 16: 298–300, 1992.
 274. Kishikawa T, Numaguchi Y, Watanabe K, et al: Angiographic diagnosis of benign and malignant splenic tumors. *Radiology* 130:339–344, 1978.
 275. Greenlee RT, Murray T, Bolden S, Wingo PA: Cancer statistics, 2000. *CA Cancer J Clin* 50:7–33, 2000.
 276. Groves FD, Linet MS, Travis LB, Devesa SS: Cancer surveillance series: Non-Hodgkin's lymphoma incidence by histologic subtype in the United States from 1978 through 1995. *J Natl Cancer Inst* 92:1240–1251, 2000.
 277. Jaffe ES, Harris NL, Stein H, Vardiman JW, editors: World Health Organization Classification of Tumours, Pathology and Genetics. Tumours of Haematopoietic and Lymphoid Tissues, Geneva, 2001, International Agency for Research on Cancer Press.
 278. Frisch M, Biggar RJ, Engels EA, et al: AIDS-Cancer Match Registry Study Group: Association of cancer with AIDS-related immunosuppression in adults. *JAMA* 285: 1736–1745, 2001.
 279. Reams BD, McAdams HP, Howell DN, et al: Posttransplant lymphoproliferative disorder: Incidence, presentation, and response to treatment in lung transplant recipients. *Chest* 124:1242–1249, 2003.
 280. Birkeland SA, Hamilton-Dutoit S: Is posttransplant lymphoproliferative disorder (PTLD) caused by any specific immunosuppressive drug or by the transplantation per se? *Transplantation* 76:984–988, 2003.
 281. Goedert JJ: The epidemiology of acquired immunodeficiency syndrome malignancies. *Semin Oncol* 27:390–401, 2000.
 282. Diamond C, Taylor TH, Aboumrat T, Anton-Culver H: Changes in acquired immunodeficiency syndrome-related non-Hodgkin lymphoma in the era of highly active antiretroviral therapy. *Cancer* 106:128–135, 2006.
 283. Radin R: HIV infection: Analysis in 259 consecutive patients with abnormal abdominal CT findings. *Radiology* 197:712–722, 1995.
 284. Levine AM: AIDS-associated lymphoma. *Med Clin North Am* 76:253–268, 1992.
 285. Townsend RR: CT of AIDS-related lymphoma. *AJR Am J Roentgenol* 156:969–974, 1991.
 286. Nyberg DA, Jeffrey RB, Federle MP, et al: AIDS-related lymphomas: Evaluation by abdominal CT. *Radiology* 159:59–63, 1986.
 287. Federle MP, Nyberg DA, Hulnick DH, et al: Malignant neoplasms: Kaposi's sarcoma, lymphoma, and other diseases with similar radiographic features. In Federle MP, Naidich DP, editors: *Radiology of Acquired Immune Deficiency Syndrome*, New York, 1988, Raven Press, pp 107–129.
 288. Powles T, Thirlwell C, Nelson M, Bower M: Immune reconstitution inflammatory syndrome mimicking relapse of AIDS related lymphoma in patients with HIV 1 infection. *Leuk Lymphoma* 44:1417–1419, 2003.
 289. Gobbi PG, Grignani GE, Pozzetti U, et al: Primary splenic lymphoma: Does it exist? *Haematologica* 79:286–293, 1994.
 290. Brox A, Shustik C: Non-Hodgkin's lymphoma of the spleen. *Leuk Lymphoma* 11:165–171, 1993.
 291. Wani NA, Parray FO: Primary lymphoma of the spleen. *Int Surg* 90:279–283, 2005.
 292. Bhatia K, Sahdev A, Reznick RH: Lymphoma of the spleen. *Semin Ultrasound CT MR* 28:12–20, 2007.
 293. Kansal R, Ross CW, Singleton TP, et al: Histopathologic features of splenic small B-cell lymphomas. A study of 42 cases with a definitive diagnosis by the World Health Organization classification. *Am J Clin Pathol* 120:335–347, 2003.
 294. Castellino RA: The non-Hodgkin lymphomas: Practical concepts for the diagnostic radiologist. *Radiology* 178:315–321, 1991.
 295. Rueffer U, Sieber M, Stemberg M, et al: German Hodgkin's Lymphoma Study Group (GHSG): Spleen involvement in Hodgkin's lymphoma: Assessment and risk profile. *Ann Hematol* 82:390–396, 2003.
 296. Hess CF, Kurtz B, Hoffmann W, et al: Ultrasound diagnosis of splenic lymphoma: ROC analysis of multidimensional splenic indices. *Br J Radiol* 66:859–864, 1993.
 297. Hancock SL, Scidmore NS, Hopkins KL, et al: Computed tomography assessment of splenic size as a predictor of splenic weight and disease involvement in laparotomy staged Hodgkin's disease. *Int J Radiat Oncol Biol Phys* 28:93–99, 1994.
 298. Zeppa P, Picardi M, Marino G, et al: Fine-needle aspiration biopsy and flow cytometry immunophenotyping of lymphoid and myeloproliferative disorders of the spleen. *Cancer* 99:118–127, 2003.
 299. Zeppa P, Marino G, Troncone G, et al: Fine-needle cytology and flow cytometry immunophenotyping and subclassification of non-Hodgkin lymphoma: A critical review of 307 cases with technical suggestions. *Cancer* 102:55–65, 2004.
 300. Bonifacio A, Goldberg RE, Patterson BJ, Haider M: Flow-cytometry-enhanced fine-needle aspiration biopsy of the spleen. *Can Assoc Radiol J* 51:158–162, 2000.
 301. Silverman JF, Geisinger KR, Raab SS, Stanley MW: Fine needle aspiration biopsy of the spleen in the evaluation of neoplastic disorders. *Acta Cytol* 37:158–162, 1993.
 302. Musteata VG, Corcimaru IT, Iacovleva IA, et al: Treatment options for primary splenic low-grade non-Hodgkin's lymphomas. *Clin Lab Haematol* 26:397–401, 2004.
 303. Dachman AH, Buck JL, Krishnan J, et al: Primary non-Hodgkin's splenic lymphoma. *Clin Radiol* 53:137–142, 1998.
 304. Giagounidis AA, Burk M, Meckenstock G, et al: Pathologic rupture of the spleen in hematologic malignancies: Two additional cases. *Ann Hematol* 73:297–302, 1996.
 305. Brissette M, Dhru RD: Hodgkin's disease presenting as spontaneous splenic rupture. *Arch Pathol Lab Med* 116:1077–1079, 1992.
 306. Arber DA, Rappaport H, Weiss LM: Non-Hodgkin's lymphoproliferative disorders involving the spleen. *Mod Pathol* 10:18–32, 1997.
 307. Falk S: Malignant lymphoma of the spleen. Histological and immunohistochemical studies of morphology and differential diagnosis. *Veroff Pathol* 136:1–265, 1991.
 308. Falk S, Muller H, Stutte HJ: Hodgkin's disease in the spleen: A morphological study of 140 biopsy cases. *Virchows Arch A Pathol Anat Histopathol* 411:359–364, 1987.
 309. Siniluoto T, Paivansalo M, Alavaikko M: Ultrasonography of spleen and liver in staging Hodgkin's disease. *Eur J Radiol* 13:181–186, 1991.
 310. Munker R, Stengel A, Stabler A, et al: Diagnostic accuracy of ultrasound and computed tomography in the staging of Hodgkin's disease. Verification by laparotomy in 100 cases. *Cancer* 76:1460–1466, 1995.
 311. Goerg C, Weide R, Schwerk WB: Malignant splenic lymphoma: Sonographic patterns, diagnosis and follow-up. *Clin Radiol* 52:535–540, 1997.
 312. Siniluoto TM, Tikkakoski TA, Lahde ST, et al: Ultrasound or CT in splenic diseases? *Acta Radiol* 35:597–605, 1994.
 313. Goerg C, Schwerk WB, Goerg K: Sonography of focal splenic lesions of the spleen. *AJR Am J Roentgenol* 156:949–953, 1991.
 314. Nakashima A, Nakashima K, Seto H, et al: Primary splenic lymphoma presenting as a large cyst. *Radiat Med* 12:42–45, 1994.
 315. Takabe K, Al-Refaie W, Chin B, et al: Can large B-cell lymphoma mimic cystic lesions of the spleen? *Int J Gastrointest Cancer* 35:83–88, 2005.
 316. Ishida H, Konno K, Ishida J, et al: Splenic lymphoma: Differentiation from splenic cyst with ultrasonography. *Abdom Imaging* 26:529–532, 2001.
 317. Urrutia M, Mergo PJ, Ros LH, et al: Cystic masses of the spleen: Radiologic-pathologic correlation. *Radiographics* 16:107–129, 1996.
 318. Gossman A, Eich HT, Engert A, et al: CT and MR imaging in Hodgkin's disease—present and future. *Eur J Haematol Suppl* 66:83–89, 2005.
 319. Caslowitz PL, Labs JD, Fishman EK, et al: Non-traumatic focal lesions of the spleen: Assessment of imaging and clinical evaluation. *Comput Med Imaging Graph* 14:133–141, 1990.
 320. Saboo SS, Krajewski KM, O'Regan KN: Spleen in hematological malignancies: Spectrum of imaging findings. *Br J Radiol* 85:81–92, 2012.
 321. Fishman EK, Kuhlman JE, Jones RJ: CT of lymphoma: Spectrum of disease. *Radiographics* 11:647–669, 1991.
 322. Hicks RJ, Mac Manus MP, Seymour JF: Initial staging of lymphoma with positron emission tomography and computed tomography. *Semin Nucl Med* 35:165–175, 2005.
 323. Vinnicombe SJ, Reznick RH: Computerised tomography in the staging of Hodgkin's disease and non-Hodgkin's lymphoma. *Eur J Nucl Med Mol Imaging* 30(Suppl 1):S42–S55, 2003.
 324. Guppy AE, Tebbutt NC, Norman A, Cunningham D: The role of surveillance CT scans in patients with diffuse large B-cell non-Hodgkin's lymphoma. *Leuk Lymphoma* 44: 123–125, 2003.

325. de Jong PA, van Ufford HM, Baarslag HJ, et al: CT and ¹⁸F-FDG PET for noninvasive detection of splenic involvement in patients with malignant lymphoma. *AJR Am J Roentgenol* 192:745–753, 2009.
326. Macapinlac HA: FDG PET and PET/CT imaging in lymphoma and melanoma. *Cancer J* 10:262–270, 2004.
327. Urban BA, Fishman EK: Helical CT of the spleen. *AJR Am J Roentgenol* 170:997–1003, 1998.
328. Donnelly LF, Foss JN, Frush DP, Bisset GS, 3rd: Heterogeneous splenic enhancement patterns on spiral CT images in children: Minimizing misinterpretation. *Radiology* 210:493–497, 1999.
329. Zeman RK, Baron RL, Jeffrey RB, Jr, et al: Helical body CT: Evolution of scanning protocols. *AJR Am J Roentgenol* 170:1427–1438, 1998.
330. Apter S, Avigdor A, Gayer G, et al: Calcification in lymphoma occurring before therapy: CT features and clinical correlation. *AJR Am J Roentgenol* 178:935–938, 2002.
331. Hoane BR, Shields AE, Porter BA, Borrow JW: Comparison of initial lymphoma staging using computed tomography (CT) and magnetic resonance (MR) imaging. *Am J Hematol* 47:100–105, 1994.
332. Jung G, Heindel W, von Bergwelt-Baildon M, et al: Abdominal lymphoma staging: Is MR imaging with T2-weighted turbo-spin-echo sequence a diagnostic alternative to contrast-enhanced spiral CT? *J Comput Assist Tomogr* 24:783–787, 2000.
333. Nyman R, Rehn S, Glimelius B, et al: Magnetic resonance imaging, chest radiography, computed tomography and ultrasonography in malignant lymphoma. *Acta Radiol* 28:253–262, 1987.
334. Gu J, Chan T, Zhang J, et al: Whole-body diffusion-weighted imaging: The added value to whole-body MRI at initial diagnosis of lymphoma. *AJR Am J Roentgenol* 197:W384–W391, 2011.
335. Semelka RC, Shoenut JP, Lawrence PH, et al: Spleen: Dynamic enhancement patterns on gradient-echo MR images enhanced with gadopentetate dimeglumine. *Radiology* 185:479–482, 1992.
336. Torres GM, Terry NL, Mergo PJ, Ros PR: MR imaging of the spleen. *Magn Reson Imaging Clin North Am* 3:39–50, 1995.
337. Martin DR, Brown MA, Semelka RC, et al: Spleen. In Martin DR, Brown MA, Semelka RC, editors: *Primer on MR Imaging of the Abdomen and Pelvis*, New York, 2005, Wiley-Liss, pp 125–152.
338. Elsayes KM, Narra VR, Mukundan G, et al: MR imaging of the spleen: Spectrum of abnormalities. *Radiographics* 25:967–982, 2005.
339. Ito K, Mitchell DG, Honjo K, et al: MR imaging of acquired abnormalities of the spleen. *AJR Am J Roentgenol* 168:697–702, 1997.
340. Harisinghani MG, Saini S, Weissleder R, et al: Splenic imaging with ultrasmall superparamagnetic iron oxide ferumoxtran-10 (AMI-7227): Preliminary observations. *J Comput Assist Tomogr* 25:770–776, 2001.
341. Weissleder R, Elizondo G, Stark DD, et al: The diagnosis of splenic lymphoma by MR imaging: Value of superparamagnetic iron oxide. *AJR Am J Roentgenol* 152:175–180, 1989.
342. Chen F, Ward J, Robinson PJ: MR imaging of the liver and spleen: A comparison of the effects on signal intensity of two superparamagnetic iron oxide agents. *Magn Reson Imaging* 17:549–556, 1999.
343. Divgi C: Imaging: Staging and evaluation of lymphoma using nuclear medicine. *Semin Oncol* 32(Suppl 1):S11–S18, 2005.
344. Jerusalem G, Hustinx R, Beguin Y, Fillet G: Evaluation of therapy for lymphoma. *Semin Nucl Med* 35:186–196, 2005.
345. Kostakoglu L, Gallamini A: Interim ¹⁸F-FDG PET in Hodgkin lymphoma: Would PET-adapted clinical trials lead to a paradigm shift? *J Nucl Med* 54:1082–1093, 2013.
346. Shen YY, Kao A, Yen RF: Comparison of ¹⁸F-fluoro-2-deoxyglucose positron emission tomography and gallium-67 citrate scintigraphy for detecting malignant lymphoma. *Oncol Rep* 9:321–325, 2002.
347. Even-Sapir E, Israel O: Gallium-67 scintigraphy: A cornerstone in functional imaging of lymphoma. *Eur J Nucl Med Mol Imaging* 30(Suppl 1):S65–S81, 2003.
348. Siniluoto TM, Hyvarinen SA, Paivansalo MJ, et al: Abdominal ultrasonography in myelofibrosis. *Acta Radiol* 33:343–346, 1992.
349. Gorg C, Riera-Knorrenschild J, Gorg K, Zugmaier G: Focal splenic lesions in myeloproliferative disease: Association with fatal outcome. *Ann Hematol* 83:14–17, 2004.
350. Arimura K, Arima N, Kukita T, et al: Fatal splenic rupture caused by infiltration of adult T cell leukemia cells. *Acta Haematol* 113:255–257, 2005.
351. Bernat S, Garcia Boyero R, Guinot M, et al: Pathologic rupture of the spleen as the initial manifestation in acute lymphoblastic leukemia. *Haematologica* 83:760–761, 1998.
352. Lam KY, Tang V: Metastatic tumors to the spleen: A 25-year clinicopathologic study. *Arch Pathol Lab Med* 124:526–530, 2000.
353. Berge T: Splenic metastases: Frequencies and patterns. *Acta Pathol Microbiol Scand* 82:499–506, 1974.
354. Klein B, Stein M, Kuten A, et al: Splenomegaly and solitary spleen metastasis in solid tumors. *Cancer* 60:100–102, 1987.
355. Schmidt BJ, Smith SL: Isolated splenic metastasis from primary lung adenocarcinoma. *South Med J* 97:298–300, 2004.
356. Marymond JH, Gross S: Patterns of metastatic cancer in the spleen. *Am J Clin Pathol* 40:58–66, 1963.
357. Taylor AJ, Dodds WJ, Erickson SJ, et al: CT of acquired abnormalities of the spleen. *AJR Am J Roentgenol* 15:1213–1219, 1991.
358. Hadjileontis C, Amplianitis I, Valsamides C, et al: Solitary splenic metastasis of endometrial carcinoma ten years after hysterectomy. Case report and review of the literature. *Eur J Gynaecol Oncol* 25:233–235, 2004.
359. Lee SS, Morgenstern L, Phillips EH, et al: Splenectomy for splenic metastases: A changing clinical spectrum. *Am Surg* 66:837–840, 2000.
360. Hoar FJ, Chan SY, Stonelake PS, et al: Splenic rupture as a consequence of dual malignant pathology: A case report. *J Clin Pathol* 56:709–710, 2003.
361. Siniluoto T, Paivansalo M, Lahde S: Ultrasonography of splenic metastases. *Acta Radiol* 30:463–465, 1989.
362. Caremani M, Occhini U, Caremani A, et al: Focal splenic lesions: US findings. *J Ultrasound* 16:65–74, 2013.
363. Goerg C, Schwerk WB, Goerg K: Sonography of focal splenic lesions of the spleen. *AJR Am J Roentgenol* 156:949–953, 1991.
364. Williams L, Kumar A, Aggarwal S: Calcified splenic metastasis from gastric carcinoma. *Abdom Imaging* 20:312–314, 1995.
365. Kelekis NL, Semelka RC, Woosley JT: Malignant lesions of the liver with high signal intensity on T1-weighted MR images. *J Magn Reson Imaging* 6:291–294, 1996.
366. Ferrucci JT, Stark DD: Iron oxide-enhanced MR imaging of the liver and spleen: Review of the first 5 years. *AJR Am J Roentgenol* 155:943–950, 1990.
367. Rohren EM, Turkington TG, Coleman RE: Clinical applications of PET in oncology. *Radiology* 231:305–332, 2004.
368. Bomanji JB, Costa DC, Ell PJ: PET in oncology: Will it replace the other modalities? *Semin Nucl Med* 27:94–106, 1997.
369. Bar-Shalom R, Valdivia AY, Blaufox MD: PET imaging in oncology. *Semin Nucl Med* 30:150–185, 2000.
370. Wechalekar K, Sharma B, Cook G: PET/CT in oncology—a major advance. *Clin Radiol* 60:1143–1155, 2005.
371. Metser U, Even-Sapir E: The role of ¹⁸F-FDG PET/CT in the evaluation of solid splenic masses. *Semin Ultrasound CT MR* 27:420–425, 2006.
372. Brepoels L, Stroobants S, Verhoef G: PET and PET/CT for response evaluation in lymphoma: Current practice and development. *Leuk Lymphoma* 48:270–282, 2007.
373. Blodgett TM, Meltzer CC, Townsend DW: PET/CT: Form and function. *Radiology* 242:360–385, 2007.
374. Wong TZ, Paulson EK, Nelson RC, et al: Practical approach to diagnostic CT combined with PET. *AJR Am J Roentgenol* 188:622–629, 2007.
375. Torigian DA, Zaidi H, Kwee TC, et al: PET/MR imaging: Technical aspects and potential clinical applications. *Radiology* 267:26–44, 2013.

CHAPTER OUTLINE

Splenic Trauma

Epidemiology

Clinical Findings

Pathophysiology

Radiologic Findings

Complications of Splenic Injury

Treatment and Outcome

Splenic Surgery

Splenic Trauma

The spleen is the most commonly injured organ in blunt abdominal trauma.^{1,2} It receives 5% of the cardiac output, accounts for 25% of the total reticuloendothelial cell mass, and plays a major role in clearing the plasma antigens.³ Recognition of this fundamental role in the immune response during the last century has led to greater efforts to preserve the spleen after injury. Nonoperative management is now widely accepted in carefully selected, hemodynamically stable patients. Development of sophisticated and accurate diagnostic imaging techniques, such as multislice computed tomography (CT), has been a major driving force behind these changes. The accurate diagnosis of splenic injury has therefore assumed an increasingly important role in the evaluation of the traumatized patient. It is very difficult to exclude solid organ injury in patients with blunt abdominal trauma without CT.⁴ CT greatly facilitates selection of patients who are treated nonoperatively by allowing accurate identification and characterization of splenic injuries as well as of other associated injuries.^{5,6} Both CT and ultrasound are important in the immediate follow-up of these patients, although ultrasound may fail to demonstrate injury in the absence of hemoperitoneum.⁷⁻¹⁰

EPIDEMIOLOGY

The spleen can be injured by various mechanisms, including blunt abdominal trauma, penetrating injuries, and iatrogenic and intraoperative accidents. Splenic injury accounts for approximately 25% of all solid abdominal organ injuries.¹¹ Motor vehicle accidents and motor sports produce most splenic injuries, followed by direct blows and falls.¹¹ Associated injuries of the central nervous system, liver, kidney, and hollow viscera occur in 10% to 40% of blunt splenic injuries, and these may alter therapeutic options.¹²

Penetrating trauma of the chest or abdomen can also result in splenic injury. Whereas penetrating trauma may involve the spleen, the spleen is less frequently injured compared with the small and large intestine. Up to 40% of all splenectomies are performed for iatrogenic injury. The risk of splenic injury is

highest during left hemicolectomy (1%-8%), open antireflux procedures (3%-20%), left nephrectomy (4%-13%), and exposure and reconstruction of the proximal abdominal aorta and its branches (21%-60%); most iatrogenic injuries result from excessive retraction and disruption of ligamentous attachments.¹³ Penetrating iatrogenic splenic injuries during interventional procedures involving the left kidney can occur because of the variable relationship of the spleen and the left kidney.¹⁴⁻¹⁶ Splenic injury is an uncommon complication of colonoscopy that may be unsuspected clinically but evident on CT scans.¹⁷⁻¹⁹

CLINICAL FINDINGS

The clinical diagnosis of splenic injury after blunt abdominal trauma can be difficult. As many as 40% of patients with significant intra-abdominal trauma may have no apparent signs or symptoms on their initial presentation to the emergency department.^{1,20-22} In the setting of blunt abdominal trauma, non-CT criteria can identify only 12% of patients without intra-abdominal injuries and 22% of patients without major injuries.⁴ Laboratory analysis in combination with physical examination findings can contribute significantly to the identification of intra-abdominal injuries after blunt trauma.²³ However, diagnostic clues can be masked in the presence of intracranial or spinal injury, shock, or intoxication.^{22,24-26} One study has shown clinically significant findings on CT in 19% of trauma patients with no obvious signs of chest or abdominal injury.²⁷

The patient's complaints may include left upper quadrant tenderness or referred left shoulder pain (Kehr's sign), which may be elicited best by placing patients in the Trendelenburg position. Rib fractures are found in 7% to 10% of patients with multiple trauma.^{28,29} Hypotension and overt shock occur in approximately 30% to 40% of patients with splenic injuries, although this number continues to decline with advances in field resuscitation and transport. Signs of persistent intraperitoneal hemorrhage or hemodynamic instability are clear indications for surgery. Many surgeons continue to advocate the use of diagnostic peritoneal lavage (DPL) for the evaluation of splenic injuries, especially in the unstable or multiply injured patient. The relative value of DPL compared with CT continues to be debated; however, a major limitation of DPL is its lack of specificity as the injured organ may be difficult to identify and the grade of injury cannot be determined.³⁰⁻³² Care should also be exercised when DPL is performed before abdominal CT as the lavage fluid may reduce attenuation of hemoperitoneum because of dilution.

PATHOPHYSIOLOGY

The spleen is particularly susceptible to injury after blunt trauma because of its complex ligamentous attachments and



Figure 106-1 Splenic arterial anatomy. The arterial anatomy of the spleen follows a predictable segmental anatomy. The arterial branch vessels enter the spleen perpendicular to its long axis, as shown in this maximum intensity projection image from a CT angiogram.

spongy parenchymal consistency. The spleen is firmly attached to the retroperitoneum by the lienorenal and phrenocolical ligaments. It is also attached to the mobile colon and stomach by the gastrosplenic and colosplenic ligaments.³³ The spleen is divided into four or six segments by arterial supply, whereas the venous system is highly anastomotic and does not follow a predictable segmental anatomy. The arterial branch vessels enter the spleen perpendicular to the long axis, allowing segmental resection (Fig. 106-1). The spleen is enclosed within a thin capsule derived from the peritoneum. In pediatric patients, the splenic capsule is relatively thicker and contains more elastic and contractile elements.³⁴

The spleen can be injured by sudden compression or contrecoup mechanisms during rapid deceleration. In deceleration injuries, the mobility of the stomach and the transverse colon is transferred to the spleen, which results in ligamentous-capsular avulsions or vascular injury to the pedicle or short gastric vessels. Blunt compression can occur from a direct blow or transmitted shock wave and usually results in parenchymal injuries and venous bleeding along segmental anatomic lines. With greater energy transfer, blunt injury does not respect segmental anatomy, and stellate fractures occur with extensive arterial and venous bleeding.³³ Injuries that result in parenchymal hematomas with an intact capsule are less common than was originally believed but may account for the 1% to 2% incidence of delayed splenic rupture.³⁵

The sequelae of penetrating splenic injury depend on the wounding instrument and its trajectory. In contrast to blunt trauma, penetrating trauma does not respect segmental anatomy and tends to have more vascular disruption. Penetrating trauma also has a higher incidence of associated organ injury, including

the gut, which typically necessitates exploration. An abnormal spleen is prone to injury by trivial trauma.

The enlarged spleen is more prone to blunt injury and is exposed beneath the rib cage. Splenomegaly can result from a variety of disease states, including portal hypertension, blood dyscrasias, infection, and lymphoproliferative disorders.

RADIOLOGIC FINDINGS

Imaging of patients with abdominal trauma is secondary to initial resuscitation efforts and clinical evaluation. Although plain films are part of most standard trauma protocols, the appropriateness of cross-sectional imaging depends on the clinical situation. Hemodynamically unstable patients or individuals with critical nonabdominal injuries that require immediate attention are not suitable candidates for CT and are typically evaluated by DPL or are explored immediately.^{1,36} However, in hemodynamically stable patients, imaging can play an invaluable role in detecting and staging splenic injury.³⁷⁻³⁹ Imaging can also be useful in the follow-up and postoperative evaluation of these patients.

Computed Tomography

CT has become the “gold standard” for the diagnosis of splenic injuries after trauma.⁴⁰⁻⁴³ CT has an accuracy exceeding 95% in the detection of splenic injuries. However, these impressive results can be obtained only by use of meticulous CT technique. Streak artifacts from the patient’s arms, external wires and hardware, nasogastric tubes, and gastric distention or gastric air-fluid levels should be avoided or minimized. Contrast-enhanced multislice CT is the current method of choice for evaluation of trauma patients with suspected abdominal injury in most institutions. Multislice CT scanning with bolus technique is preferred to optimize injury detection and to minimize delay within the department.^{39,44-46} Multislice scanners with fast tube rotation minimize scanning time and motion artifact.^{39,44,46}

Assessment of splenic injury should include evaluation for hematoma, extent of laceration, active extravasation of contrast material, and associated vascular injuries.⁴⁷ Splenic hematomas are hyperdense relative to the splenic parenchyma on unenhanced CT and generally hypodense on contrast-enhanced CT. Splenic hematomas may be intraparenchymal, subcapsular, or perisplenic. Intrasplenic hematomas (Fig. 106-2) typically appear as hypodense areas within the splenic parenchyma after administration of contrast medium.^{26,37,38,48} These intrasplenic hematomas may be nearly isodense in some cases, particularly after inadequate administration of contrast material.^{26,49,50}

Splenic lacerations on CT appear as linear, low-attenuation foci that may not extend completely across the spleen (Fig. 106-3). Lacerations may be single, multiple, or stellate (Fig. 106-4). Splenic fractures (Fig. 106-5) are defined as lacerations that extend completely across the splenic parenchyma and commonly involve the splenic hilum. Intraparenchymal lacerations become smaller and less dense with smoother margins over time. This healing may take weeks, and follow-up CT, particularly in the setting of an uncomplicated clinical course, is not helpful and does not affect management.^{7,51-53} Follow-up imaging after hospital discharge is not advocated by many centers.⁵²⁻⁵⁴

Subcapsular hematomas follow the splenic contour and compress the parenchyma. Subcapsular hematomas (Fig. 106-6) typically appear as crescentic fluid collections along the lateral

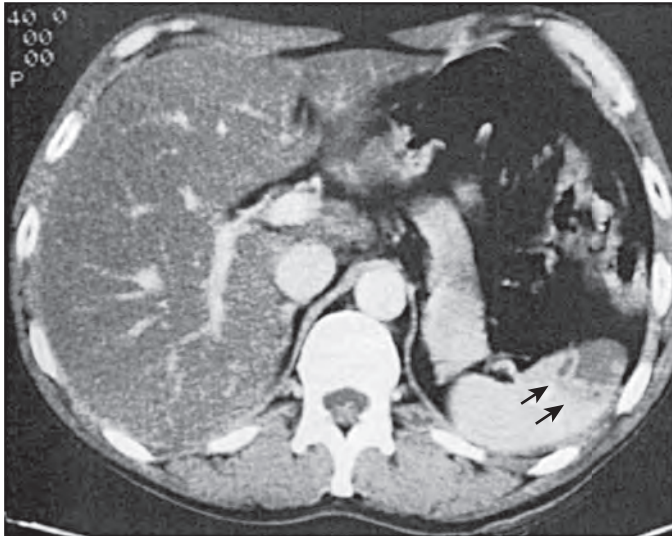


Figure 106-2 Intrasplenic hematoma. Hematoma is demonstrated as a low-density collection of blood (arrows), which can vary in attenuation from hypodense to isodense relative to the spleen.

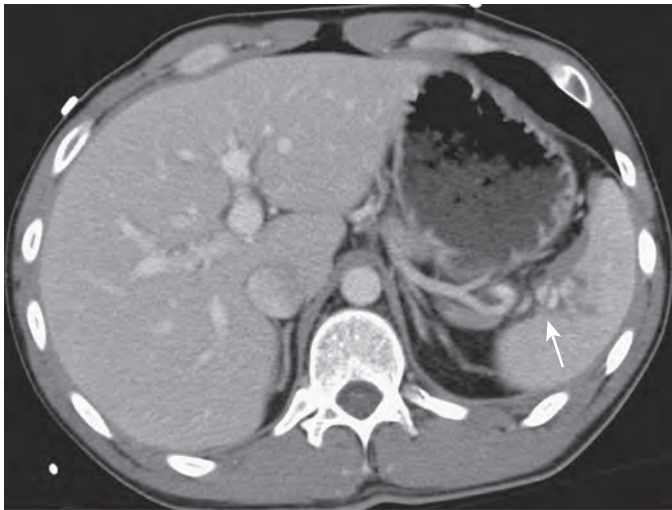


Figure 106-3 Splenic laceration. Laceration (arrow) extends to the splenic hilum and is associated with traumatic pseudoaneurysm with dissection. Notice the small perisplenic hematoma.

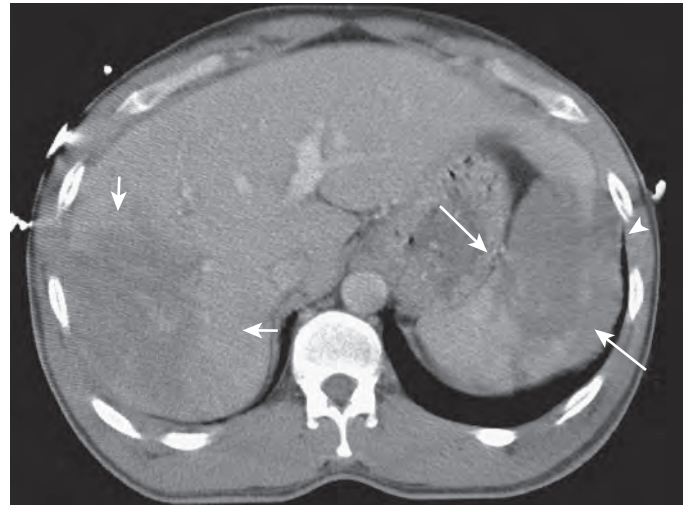


Figure 106-4 Complex splenic laceration. Linear foci of low attenuation (long arrows) are consistent with lacerations. There is segmental ischemia in the anterior aspect of the spleen. A small perisplenic hematoma (arrowhead) and a large hepatic laceration (short arrows) are identified.

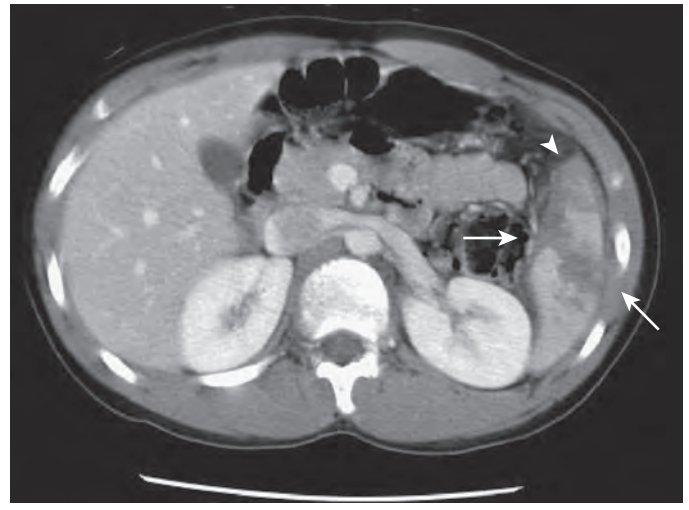


Figure 106-5 Splenic fracture. The lacerations traverse the splenic parenchyma (arrows). A small perisplenic hematoma is identified (arrowhead).

aspect of the spleen, which may be difficult to distinguish from perisplenic fluid (Fig. 106-7). These hematomas become less dense over time and may mimic free intraperitoneal fluid. However, mass effect on the splenic parenchyma and its location between the enhancing capsule and the parenchyma distinguishes it from free fluid. Subcapsular hematomas usually resolve within 4 to 6 weeks. These hematomas are not associated with delayed splenic rupture and are not an indication for splenorrhaphy.⁵⁵

Severe disruption of the splenic parenchyma results in a “shattered” spleen (Fig. 106-8). Vascular pedicle injuries usually result in significant hemorrhage and cardiovascular instability and are usually not referred for CT evaluation. These patients do have a characteristic CT appearance with nonenhancement of the caudal portion of the spleen and preservation of upper pole perfusion through the short gastric arteries.⁴⁷ Active

hemorrhage appears as areas of irregular collection of contrast material that can be distinguished from adjacent clot by its density (Fig. 106-9).^{37,55} Extravasated contrast material has a higher mean attenuation than hematoma (132 HU vs 51 HU).⁵⁶ In general, contrast material extravasation has a higher likelihood of splenic hemorrhage at laparotomy.^{37,56} Laparotomy in these patients may be avoided by prophylactic embolization of the proximal main splenic artery.^{43,57,58}

Splenic injuries may be subtle, and parenchymal or capsular lesions may not be directly visualized. The presence of perisplenic high-attenuation fluid or clot, the so-called sentinel clot (Fig. 106-10), is a useful indicator of splenic injury.^{2,48} In one series, 20% of patients with surgically proven splenic injury demonstrated perisplenic clot as the principal finding. Another subtle sign of limited splenic injury is thickening of the anterior renal fascia and the left lateroconal fascia, presumably from

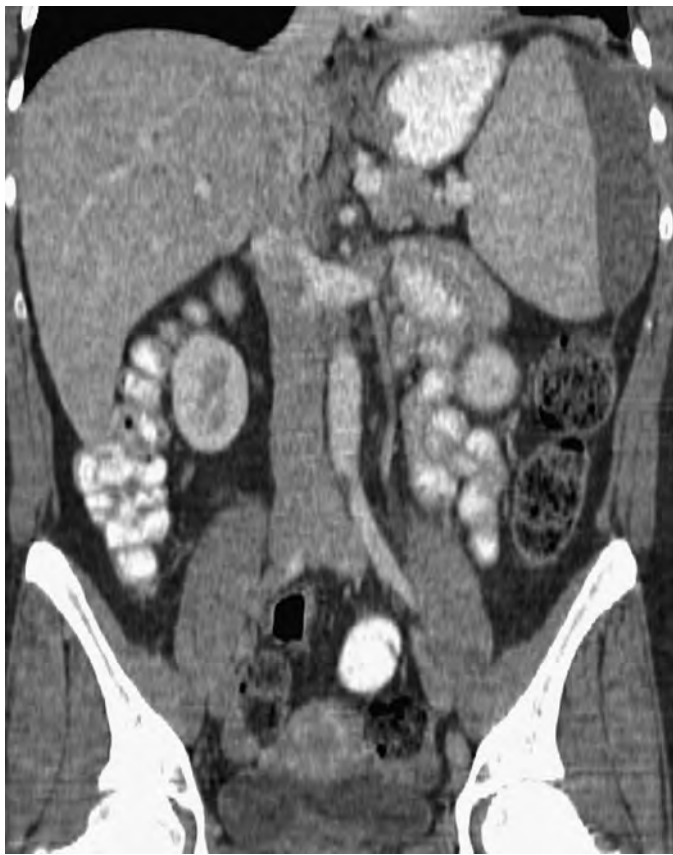


Figure 106-6 Subcapsular hematoma. The low-attenuation fluid collection is located along the lateral surface of the spleen and causes straightening of the lateral margin. The subcapsular hematoma follows the contour of the spleen. Coronal reformations can be particularly helpful for the assessment of the location of intra-abdominal free fluid in the setting of trauma.

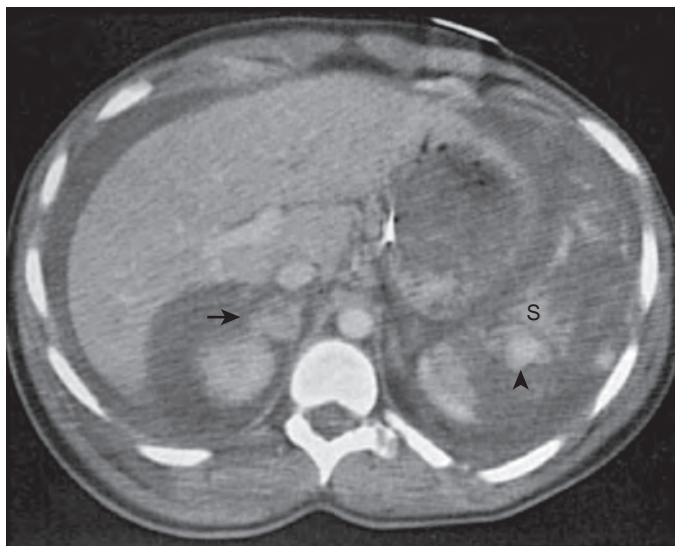


Figure 106-8 Shattered spleen. Severe splenic injury after blunt trauma resulted in fragmentation of the spleen (S). Several islands of enhancement are identified (arrowhead). These focal areas of enhancement may represent pseudoaneurysm formation, which can be a predictor of the need for endovascular or surgical intervention. Splenectomy was required in this patient. Associated injuries of the left kidney and right adrenal gland (arrow) also are identified. Streak artifact from the patient's arms along the abdomen degrades image quality.

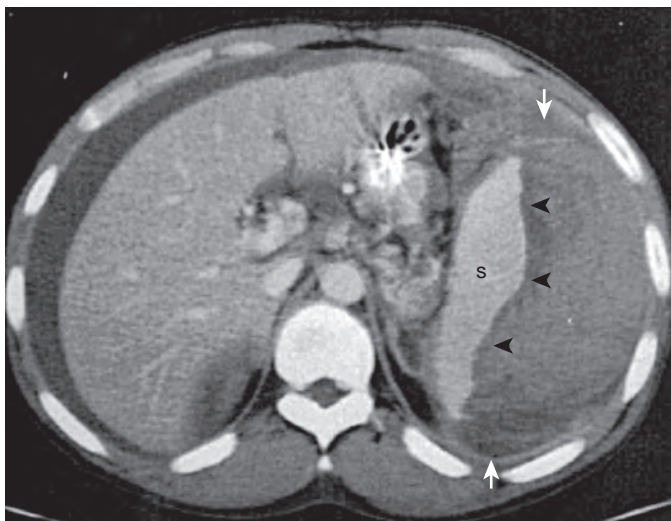


Figure 106-7 Larger subcapsular hematoma. Distinction between subcapsular and perisplenic fluid can be difficult. In this case, the large subcapsular component (arrowheads) is compressing the splenic (S) parenchyma, but it is difficult to separate from perisplenic hematoma (arrows). Notice the blood lateral to the liver.

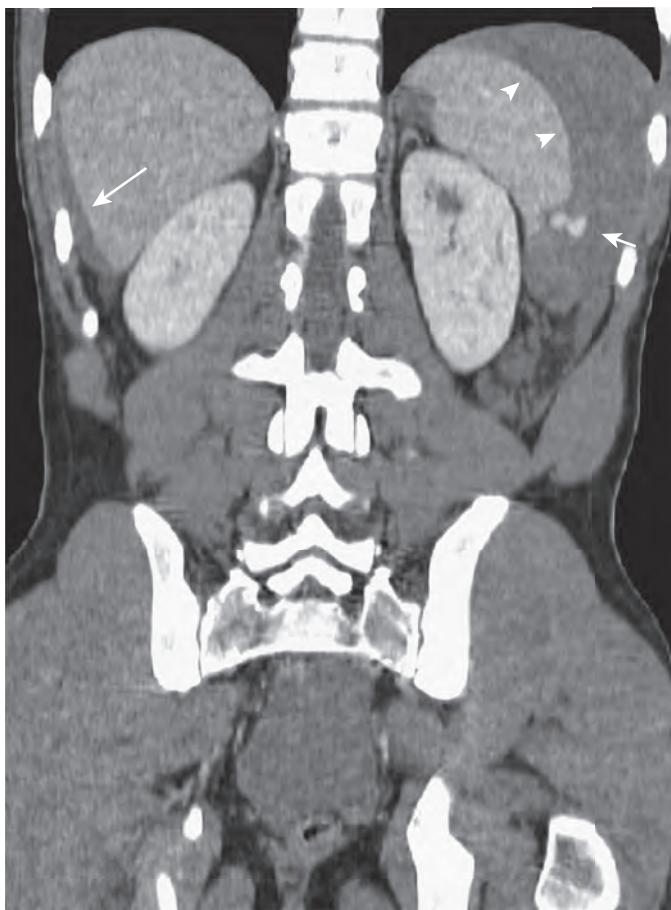


Figure 106-9 Active extravasation of contrast material. There is active extravasation of contrast material from the site of splenic laceration (short arrow). Extravasation of contrast material can be distinguished from the perisplenic hematoma (arrowheads) by its higher density. Notice the extension of the hemoperitoneum to the perihepatic space (long arrow).

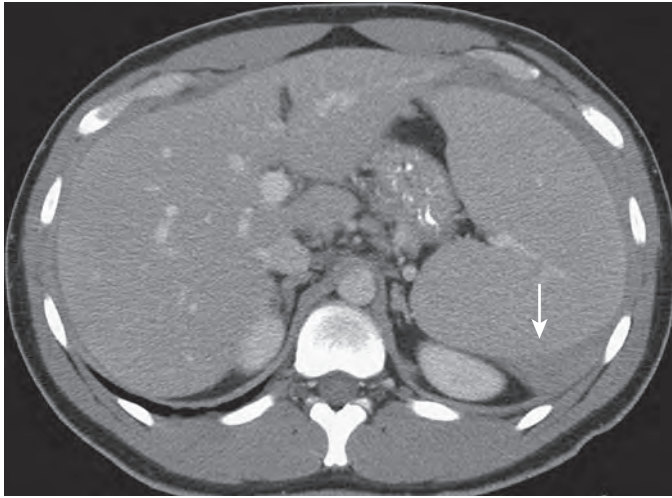


Figure 106-10 The sentinel clot sign. Isolated, perisplenic, high-attenuation hematoma (arrow) indicates a high likelihood of splenic injury. The splenic laceration was not apparent.

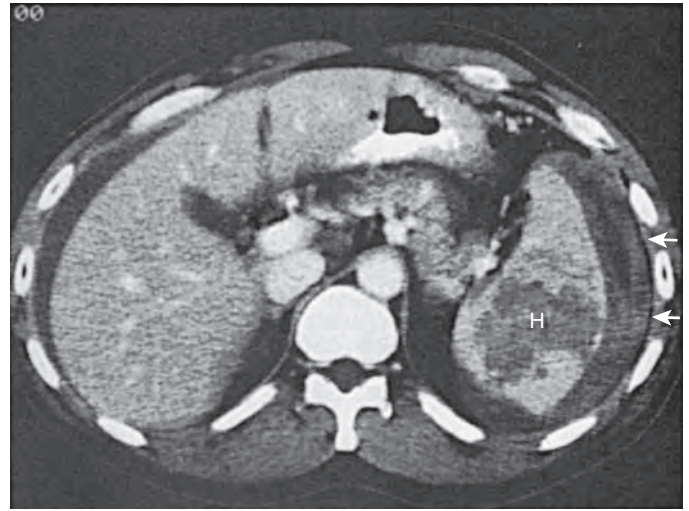


Figure 106-11 Delayed splenic rupture. Enhanced CT scan of a 17-year-old patient who presented with worsening abdominal and left shoulder pain 1 week after being kicked in the abdomen. A low-attenuation splenic hematoma (H) and associated perisplenic fluid and hemorrhage (arrows) are identified. Splenectomy was required.

dissection of hemorrhage through the splenorenal ligament to the retroperitoneal interfascial planes.⁵⁹

Splenic artery pseudoaneurysm is a rare but life-threatening complication of splenic injury after blunt abdominal trauma. Davis and colleagues⁶⁰ reported well-circumscribed focal contrast blush indicative of pseudoaneurysm formation in the CT of 8% of their adult patients with blunt splenic injury. Pseudoaneurysm may also be diagnosed by ultrasound, but it has lower sensitivity than CT.^{61,62} The current management of post-traumatic splenic artery pseudoaneurysm in adults and children diagnosed by CT or ultrasound is not well established and ranges from conservative treatment to immediate confirmation and embolization by angiography.^{43,60,63-66} A pseudoaneurysm may be distinguished from active extravasation of contrast material by examining the arterial and excretory phases of CT; pseudoaneurysm will become isodense to the adjacent vascular structures on delayed images, whereas active hemorrhage demonstrates no significant change in attenuation. Delayed CT may be obtained with reduced radiation setting without significant degradation of image quality.⁶⁷

Significant intimal injury in the splenic artery may lead to splenic infarction. This unusual finding may be associated with splenic or other adjacent organ injury and may not be associated with significant adjacent hemoperitoneum.⁶⁸

Several case reports have described delayed splenic rupture after initial normal findings on CT scan.^{69,70} It is hypothesized that these uncommon delayed ruptures may result from low-grade venous bleeding that eludes detection by initial clinical examination, imaging, and DPL.⁷¹ This phenomenon should always be remembered by radiologists and trauma physicians, but it should not be viewed as a shortcoming of CT alone. CT scanning has been proved useful in the assessment of patients who present with delayed or remote rupture (Fig. 106-11).⁷⁰ The degree of injury by the Splenic Injury Scale as proposed by the American Association for the Surgery of Trauma (see later for grading of splenic injury) as well as the presence of a pseudoaneurysm must be closely evaluated.⁷⁰ Increase in the size of linear foci on follow-up scans should alert the clinician to the possibility of progression of laceration. A hyperdense focus

within the injured parenchyma after intravenous administration of contrast material may indicate pseudoaneurysm formation. As discussed previously, the role of CT in follow-up of patients with splenic injury who are hemodynamically stable and are without evidence of blood loss has not been clearly established. Many institutions obtain follow-up CT within 48 hours of the initial diagnosis to assess for possible progression of injuries.^{60,71} However, most studies have shown that follow-up CT without a clear clinical indication is not necessary.^{52,54,72,73}

Changes in splenic size on follow-up examinations should be interpreted carefully. Splenic enlargement has been observed in stable patients after blunt trauma, which is believed to represent return to normal size after physiologic contraction. Goodman and Aprahamian⁷⁴ reported an average 25% increase in splenic volume on follow-up CT scans in trauma patients, with more than half of their patients manifesting an average increase in splenic volume of 56%.

CT is equally useful in penetrating injuries, particularly stab wounds. CT can reveal commonly associated chest, diaphragmatic, and intra-abdominal injuries (Fig. 106-12). The use of water-soluble oral and rectal contrast agents facilitates the detection of associated visceral injuries. Munera and coworkers emphasized the role of CT with triple contrast in evaluation of patients with gunshot wound injury who are not immediate exploratory laparotomy candidates.^{75,76} However, this approach is controversial and not universally accepted.^{77,78}

It is important to be aware of interpretive pitfalls in diagnosis of splenic injury by CT. Splenic parenchymal enhancement in normal patients usually appears heterogeneous during the early phase of scanning and should be interpreted with caution in trauma patients (Fig. 106-13). Portal venous phase of enhancement optimizes splenic enhancement for evaluation of traumatic injury. Therefore, start of the scanning approximately 65 seconds after the start of contrast material injection improves hepatic and splenic enhancement. Diminished splenic enhancement relative to liver has been reported in trauma patients without splenic injury, possibly related to adrenergic stimulation and splanchnic vasoconstriction, and should not

necessarily be interpreted as indicative of splenic injury or vascular compromise.⁷⁴

Significant artifact from the patient's arms or overlying support lines may simulate splenic injury or limit its evaluation. Close attention to patient positioning is mandatory, and its importance should be communicated to the trauma team. Respiratory motion artifact mimicking subcapsular hematoma, common with older scanners, is uncommon with the latest multislice scanners. Congenital splenic clefts are common and should not be mistaken for lacerations. Clefts typically are found along the medial surface of the spleen (Fig. 106-14),

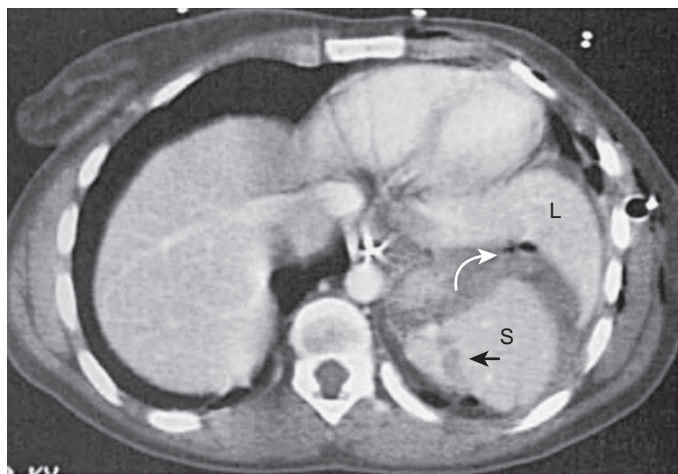


Figure 106-12 Penetrating splenic injury. CT scan of a 22-year-old woman who was stabbed in the anterior chest shows a low-attenuation splenic laceration (black arrow) and gas bubbles (curved white arrow) from gastric perforation. The prominent left hepatic lobe (L) is a variant that can abut the lateral margin of the spleen (S).

whereas most lacerations originate from the lateral surface of the spleen.⁷⁹ However, neither of these generalizations is absolute, and at times, clefts may be difficult to distinguish from a laceration.

Surgical and CT Classification of Splenic Injury. Splenic injuries have been anatomically classified by the Organ Injury Scaling Committee of the American Association for the Surgery of Trauma (Table 106-1) to reflect the impact of specific injuries on the patient's therapy and outcome.^{80,81} The Organ Injury Scaling classification is based on the anatomic disruption of the spleen scaled 1 to 5. These represent increasingly complex injuries that affect surgical management.⁸¹ This anatomic system, currently used by most trauma centers, is limited because it does not account for the presence and volume of hemoperitoneum or other organ injuries. Several CT-based grading systems have been created to incorporate this information.^{5,33,82} A splenic injury grading system that takes these findings into consideration has been proposed by Mirvis and colleagues but awaits prospective trial.^{40,43}

Mirvis and colleagues⁴⁰ found that CT is accurate in identifying splenic injury but is not useful in predicting outcomes. CT grading of blunt splenic trauma has been found to be an unreliable predictor of patient outcome by several other investigators also.⁸³⁻⁸⁵ Studies have shown that evidence of active hemorrhage on contrast-enhanced CT and traumatic splenic pseudoaneurysms and arteriovenous malformations indicate higher likelihood of failed conservative treatment.^{55,86,87} Their influence on grading and patient outcome is being studied at several institutions.* Perhaps a common difficulty in such grading is the influence of nonanatomic factors, such as patient age,

*References 37, 43, 56, 60, 65, 66, 86.

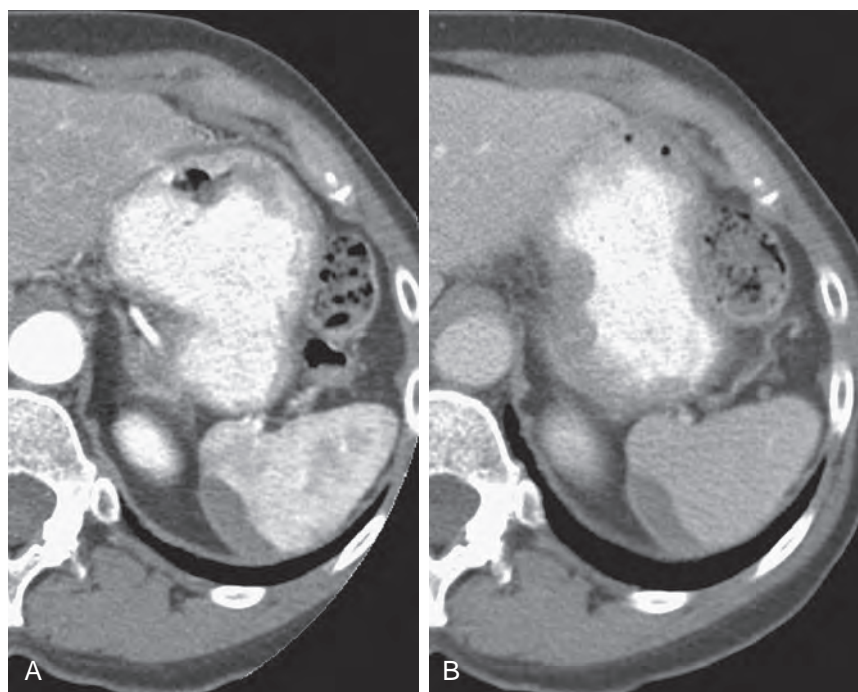


Figure 106-13 Heterogeneous enhancement of the spleen. **A.** The spleen appears heterogeneous during the late arterial and early portal venous phases of enhancement. The heterogeneous enhancement mimics intraparenchymal hematomas in this patient with subcapsular hematoma. **B.** Image obtained during the portal venous phase of hepatic enhancement shows the splenic subcapsular hematoma, but the spleen is otherwise unremarkable.

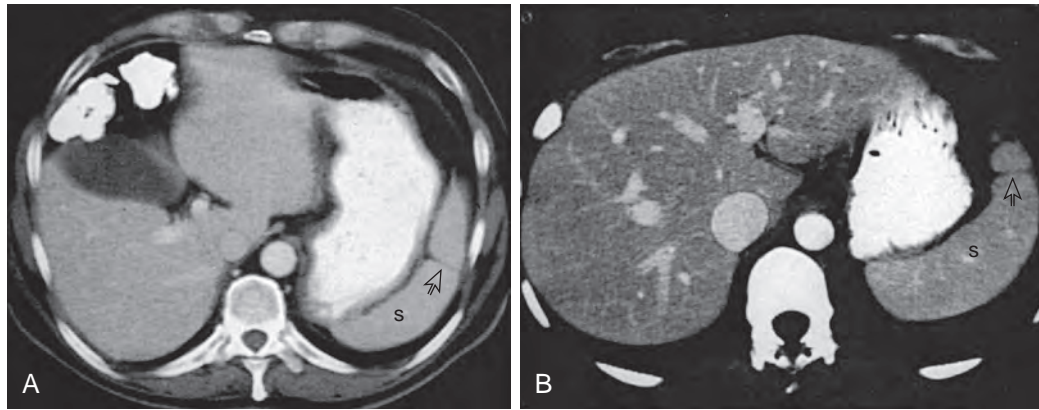


Figure 106-14 Congenital splenic clefts. These commonly observed variants more typically involve the medial aspect of the spleen. When they extend across the spleen, they can be mistaken for splenic laceration or fracture. **A.** A low-attenuation cleft (arrow) is more prominent on the medial aspect of the spleen (S). **B.** A cleft (arrow) traverses the full thickness of the spleen (S).

TABLE 106-1 American Association for the Surgery of Trauma Splenic Injury Scale (1994 Revision)

Grade*	Lesion	Injury Description
I	Hematoma	Subcapsular, nonexpanding, <10% of surface area
	Laceration	Capsular tear, nonbleeding, parenchymal depth <1 cm
II	Hematoma	Subcapsular, nonexpanding, 10%-50% of surface area; intraparenchymal, nonexpanding, <5 cm in diameter
	Laceration	Capsular tear, active bleeding; 1-3 cm parenchymal depth that does not involve a trabecular vessel
III	Hematoma	Subcapsular, >50% of surface area or expanding; ruptured subcapsular hematoma with active bleeding; intraparenchymal hematoma >5 cm or expanding
	Laceration	Parenchymal depth >3 cm or involving trabecular vessels
IV	Hematoma	Ruptured intraparenchymal hematoma with active bleeding
	Laceration	Laceration involving segmental or hilar vessel producing major devascularization (>25% of spleen)
V	Laceration	Completely shattered spleen
	Vascular	Hilar vascular injury that devascularizes spleen

*Advance one grade (up to grade III) for multiple splenic injuries. Modified from Moore EE, Cogbill TH, Malangoni MA, et al: Organ injury scaling. *Surg Clin North Am* 75:293-303, 1995.

overall hemodynamic stability, and preparedness of the trauma center, regardless of the injury grade.* Marmery and associates⁹⁴ incorporated vascular injury and active bleeding in a new grading system for the classification of splenic injury and showed its superiority over the American Association for the Surgery of Trauma system in predicting the need for angiography and embolization or splenic surgery in patients sustaining blunt splenic injury. Further prospective studies are required to validate these results.

Ultrasound

Ultrasound is the primary imaging modality of trauma patients in many centers outside the United States. Its use in the United

States has also increased significantly during the past two decades, with 79% of level I trauma centers currently performing focused assessment with sonography for trauma (FAST).⁹⁵⁻⁹⁷ FAST has two significant advantages over CT: it can be performed at the bedside with hand-held devices and uses no ionizing radiation.⁹⁸ The primary goal of FAST is detection of free intraperitoneal fluid. This is based on the assumption that significant intra-abdominal injury is unlikely without the presence of free intraperitoneal fluid. Its reported sensitivity for detection of free intraperitoneal fluid ranges between 42% and 98%.^{10,97,99-101} Several studies have shown significant false-negative and false-positive rates in both adult and pediatric patients, casting doubt on the utility of FAST.^{8,9,102-104} Investigators have shown decreased sensitivity of FAST when patients are stable.^{26,99,105,106} This may be related to operator dependence of ultrasound as well as lack of free intraperitoneal free fluid with less severe injuries. In addition, ultrasound has limited sensitivity for detection of retroperitoneal injuries.^{103,107-109} Furthermore, patient obesity, subcutaneous emphysema, and limited acoustic window as well as isoechoic clot can limit its sensitivity.¹¹⁰

The detection of intraparenchymal and subcapsular lesions depends on the sonographic appearance of hemorrhage, which in turn is dependent on the age of the blood and frequency of the interrogating transducer. In the acute setting, lacerations and hematomas appear echogenic because of the presence of clotted blood. Both fresh and chronic hemorrhage can appear hypoechoic (Fig. 106-15).^{111,112} Because the liver is usually less echogenic than the spleen, the left hepatic lobe that extends to the left upper quadrant of the abdomen and indents the spleen may simulate a subcapsular hematoma of the spleen sonographically (Fig. 106-16). Scanning should also include a general survey to detect hemoperitoneum within the abdomen. The detection of blood surrounding the gastrosplenic ligament, the “left butterfly” sign, has been reported to indicate hemorrhage within the lesser sac and should direct the sonographer to the possibility of splenic, gastric, or pancreatic injury.¹¹¹ Color Doppler study may help in detection of intrasplenic pseudoaneurysm.⁶¹ Contrast-enhanced sonography for the evaluation of splenic trauma has been reported to be more sensitive than a baseline sonogram, but its wide acceptance awaits larger trials.^{62,113-116}

The relatively lower accuracy of ultrasound compared with CT and DPL for detection of intra-abdominal injury suggests that this modality has a complementary rather than a

*References 6, 40, 43, 57, 63, 72, 80, 88-93.

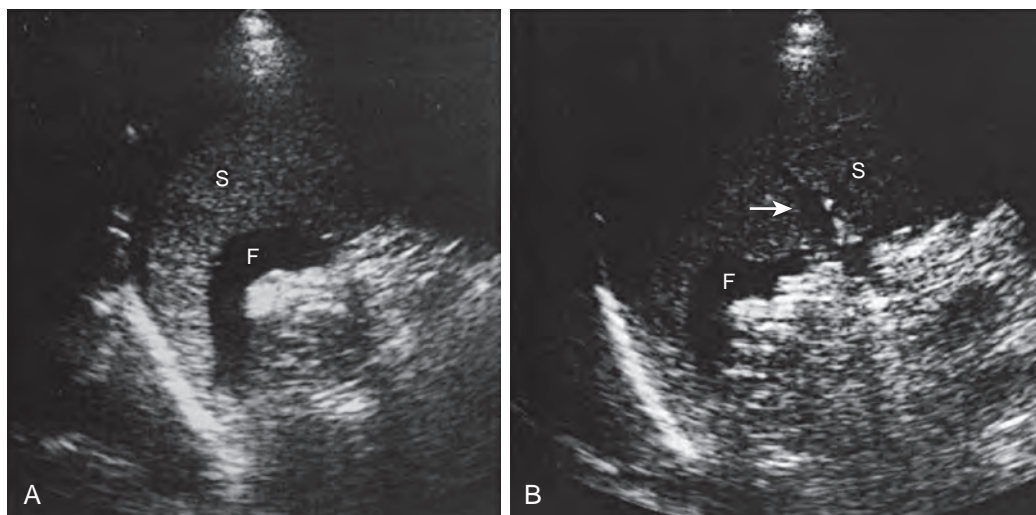


Figure 106-15 Ultrasound diagnosis of splenic injury. Correlative ultrasound scan of a 19-year-old with known splenic laceration, splenic cleft, and perisplenic fluid to diagnose splenic injury. **A.** An oblique coronal image obtained intercostally demonstrates hypoechoic perisplenic fluid (F) adjacent to the spleen (S). **B.** A companion oblique image illustrates the perisplenic fluid (F) and the known splenic cleft (arrow). The patient's CT-diagnosed splenic laceration was not observed sonographically.



Figure 106-16 Splenic vein thrombosis. The patient has extensive splenic and hepatic lacerations and splenic vein thrombosis (arrow).

competing role with CT and DPL.^{96,117-120} All patients with normal findings at the initial FAST should be observed for several hours to avoid missing of significant injuries. In addition, serial ultrasound or CT examinations should be obtained in those with suspected significant injuries.^{110,121,122} A principal role of ultrasound today is in the postoperative patient and for long-term follow-up of patients treated conservatively. Sequential sonograms can be used to document resolution of splenic parenchymal abnormalities and to monitor the volume of hemoperitoneum.

Other Techniques

The technetium Tc 99m sulfur colloid scan has been shown to be a sensitive albeit somewhat nonspecific test in splenic trauma.¹²³ Scintigraphy, however, no longer has a role in assessment of blunt abdominal trauma. Likewise, angiography is no longer appropriate as a screening modality but has been shown

to be effective in identifying specific sites of injury determined by CT and provides access for therapeutic embolization of splenic bleeders.¹²⁴

Plain film findings in traumatized patients are usually non-specific. Abnormal findings suggesting splenic trauma include posterior left rib or upper lumbar transverse process fractures, medial displacement of gastric air bubble, elevation of the left hemidiaphragm, and signs of hemoperitoneum. However, lack of abnormal findings on chest or abdominal films does not obviate the need for further diagnostic evaluation.

COMPLICATIONS OF SPLENIC INJURY

Complications of splenic injury depend on the mechanism of injury and the choice of therapy. In patients treated conservatively or with spleen-preserving surgery, the principal concern is rebleeding. Other sequelae include spontaneous splenic vein thrombosis, splenic abscess formation, pancreatitis, and intra-abdominal or thoracic splenosis.¹²⁵⁻¹²⁷ When splenectomy is required, typical postoperative complications include left lower lobe atelectasis, pneumonia, and pleural effusions. Subphrenic abscess, disseminated intravascular coagulopathy, and pancreatic injury are less commonly observed complications.¹²⁸

The major concern in the postsplenectomy patient is the loss of splenic immune functions and the risk of overwhelming postsplenectomy sepsis.^{129,130} The incidence of overwhelming postsplenectomy sepsis after trauma varies from 0.28% to 1%, and mortality is reported to be as high as 50% to 80%.^{131,132} The syndrome of overwhelming postsplenectomy sepsis is characterized by the systemic symptoms of nausea, vomiting, and malaise that rapidly progress to coma, hypotension, and death within hours of the onset of symptoms. There is usually a sub-clinical focus of infection by encapsulated organisms, such as *Streptococcus*, *Haemophilus*, or *Neisseria*. In addition, postoperative infectious complications are much more frequent in splenectomized patients. The risk of septicemia in asplenic has been estimated to be 140 times greater than in the general population. Patients undergoing splenectomy have longer hospital stays than those conservatively managed.^{31,129,132}

TREATMENT AND OUTCOME

Recognition of the importance of preserving splenic function has led to a dramatic shift in surgical opinion and practice. Nonoperative management of splenic injury in pediatric patients is the norm and is successful in more than 90% of appropriately selected patients.^{133,134} Although the nonoperative approach to pediatric splenic injury is well established, application of this practice to adult trauma patients is still evolving but gaining wider acceptance.^{81,135-138} Although age older than 55 years has been considered a criterion for operative management, Barone and coworkers¹³⁹ and Myers and colleagues⁹² reported a failure rate of 6% and 17% for nonoperative management of patients older than 55 years, respectively. Grade of splenic injury rather than age was reported to play an important role in outcome by Nix and coworkers.⁶ Success rates in adults have ranged from 27% to 90%.^{137,138} Major criticisms directed toward nonoperative management include failure to detect associated injuries, such as bowel perforation or diaphragmatic disruption, and an increase in transfusion requirements. Some authors have suggested that the risk-benefit ratio for nonoperative management is exceeded by transfusion risks posed by administration of more than 2 units of blood or presence of a significant amount of hemoperitoneum on CT.^{140,141} Patients should meet strict criteria for consideration of nonoperative treatment: low-grade and isolated splenic injury, hemodynamic stability, and mental alertness.¹⁴² In this regard, CT evaluation may be useful in selecting patients who are inappropriate for nonoperative treatment and would benefit from early spleen-preserving surgery. Most patients (up to 85%) are now managed nonoperatively as some of the previous expert consensus contraindications mentioned earlier (e.g., advanced age, fear of missing a hollow viscus injury, >2 units of packed red blood cell transfusion) are no longer completely valid.^{143,144}

Splenic artery embolization has been shown to improve outcome of nonoperative management.^{60,64,143,145-149} Haan and associates¹⁵⁰ reported a splenic salvage rate of 87% by embolization. In their series, more than 80% of splenic injury grades 4 and 5 were successfully managed nonoperatively. Patients older than 55 years had outcome similar to that of the younger patients. Complications were seen in 16 of 140 patients, with bleeding and abscess representing the most frequent complications. A more recent study has shown similar outcome for main artery coil embolization versus selective or combined embolization techniques.¹⁵¹ Higher splenic injury score, lower blood pressure, lower pH, and increased number of packed red blood cell transfusions are factors that favor an operation over embolization.¹⁵² However, successful transcatheter arterial embolization for splenic injury has been reported in hemodynamically unstable patients.¹⁵³ CT after embolization is indicated if there is abdominal pain, hypotension, or signs of infection. Gelfoam used in embolization may appear as gas within the infarcted area.¹⁵⁴

An important alternative to nonoperative management is the splenic salvage procedure, in which either a simple splenorrhaphy or more complex segmental resection with repair is performed.³³ These procedures have led to success rates of more than 95%.¹⁴⁰

Splenic Surgery

After splenectomy for traumatic lesions is excluded, most splenectomies are performed for control or evaluation of

hematologic or neoplastic disease. Regardless of the reason for splenectomy, the principal surgical consideration is adequate mobilization of the spleen. Because of the intimate association of the stomach and colon with the spleen, inadvertent injuries can occur intraoperatively, with postoperative abscess being the primary complication. Similarly, the pancreatic tail is usually found to extend into the splenic hilum and can be injured during splenectomy. The significant incidence of postoperative complications, including pancreatitis, pancreatic fistula, and pseudocyst, has led to considerable debate among surgeons as to whether the splenectomy bed should be routinely drained. Laparoscopic splenectomy, now practiced in many centers, has a lower morbidity and hospital stay compared with open splenectomy.¹⁵⁵⁻¹⁵⁷ However, it poses certain technical challenges, such as management of the massive spleen, specimen extraction, and identification of remotely located accessory spleens.^{158,159} Portal or splenic venous thrombosis is a more frequent complication of laparoscopic splenectomy and can be treated safely.¹⁶⁰ In one study, the incidence of portal or splenic venous thrombosis was shown to be around 20% at 1 week on Doppler ultrasound evaluation. The authors recommended ultrasonographic screening for portal or splenic venous thrombosis at postoperative day 7.¹⁶¹ Multidetector CT angiography with volumetric and anatomic evaluation provides accurate and reproducible information for planning of laparoscopic splenectomy.¹⁶²

The radiologic evaluation of the postsplenectomy patient is performed for evaluation of infection, hemorrhage, or pancreatic injury. Because of these indications and the usual limitations of ultrasound in the left upper quadrant, CT is the preferred modality. Adequate oral or rectal contrast material is important for evaluation of the splenectomy bed. The ability of CT to distinguish sterile postoperative collections from abscess is limited, and percutaneous aspiration is important. Subphrenic abscess (Fig. 106-17) can be difficult at times to distinguish from pleural fluid collections. Percutaneous management of subphrenic abscess by CT guidance can be performed.

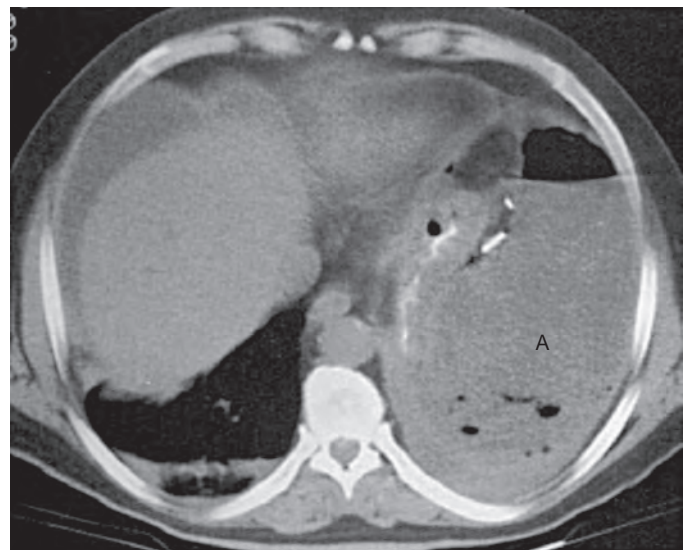


Figure 106-17 Subphrenic abscess after splenectomy. A large, left, upper quadrant air-fluid collection (A) compresses the stomach in a patient after splenectomy for trauma. A large subphrenic abscess was drained at reoperation.

REFERENCES

1. Olthof DC, van der Vlies CH, Joosse P, et al: PYTHIA Collaboration Group: Consensus strategies for the nonoperative management of patients with blunt splenic injury: A Delphi study. *J Trauma Acute Care Surg* 74:1567–1574, 2013.
2. Lubner M, Menias C, Rucker C, et al: Blood in the belly: CT findings of hemoperitoneum. *Radiographics* 27:109–125, 2007.
3. Yildiz AE, Ariyurek MO, Karcaaltincaba M: Splenic anomalies of shape, size, and location: Pictorial essay. *ScientificWorldJournal* 2013: 321810, 2013.
4. Poletti PA, Mirvis SE, Shanmuganathan KM, et al: Blunt abdominal trauma patients: Can organ injury be excluded without performing computed tomography? *J Trauma* 57:1072–1081, 2004.
5. Buntain WL, Gould HR, Maull KI: Predictability of splenic salvage by computed tomography. *J Trauma* 28:24–34, 1988.
6. Nix JA, Costanza MM, Daley BJ, et al: Outcome of the current management of splenic injuries. *J Trauma* 50:835–842, 2001.
7. Minarik L, Slim M, Rachlin S, et al: Diagnostic imaging in the follow-up of nonoperative management of splenic trauma in children. *Pediatr Surg Int* 18:429–431, 2002.
8. Rhea JT, Garza DH, Novelline RA: Controversies in emergency radiology. CT versus ultrasound in the evaluation of blunt abdominal trauma. *Emerg Radiol* 10:289–295, 2004.
9. Brown MA, Casola G, Sirlin CB, et al: Importance of evaluating organ parenchyma during screening abdominal ultrasonography after blunt trauma. *J Ultrasound Med* 20:577–583, 2001.
10. Miller MT, Pasquale MD, Bromberg WJ, et al: Not so FAST. *J Trauma* 54:52–60, 2003.
11. Fink M: *Splenic Trauma*, Baltimore, 1997, Williams & Wilkins.
12. Rappaport W, McIntyre KE, Carmona R: The management of splenic trauma in the adult patient with blunt multiple injuries. *Surg Gynecol Obstet* 170:204–208, 1990.
13. Cassar K, Munro A: Iatrogenic splenic injury. *J R Coll Surg Edinb* 47:731–741, 2002.
14. Hopper KD, Yakes WF: The posterior intercostal approach for percutaneous renal procedures: Risk of puncturing the lung, spleen, and liver as determined by CT. *AJR Am J Roentgenol* 154:115–117, 1990.
15. Kondas J, Szentgyorgyi E, Vaczi L, et al: Splenic injury: A rare complication of percutaneous nephrolithotomy. *Int Urol Nephrol* 26:399–404, 1994.
16. Thomas AA, Pierce G, Walsh RM, et al: Splenic injury during percutaneous nephrolithotomy. *JSL* 13:233–236, 2009.
17. Prowda JC, Trevisan SG, Lev-Toaff AS: Splenic injury after colonoscopy: Conservative management using CT. *AJR Am J Roentgenol* 185: 708–710, 2005.
18. Piccolo G, Di Vita M, Cavallaro A, et al: Presentation and management of splenic injury after colonoscopy: A systematic review. *Surg Laparosc Endosc Percutan Tech* 24:95–105, 2014.
19. Singla S, Keller D, Thirunavukarasu P, et al: Splenic injury during colonoscopy—a complication that warrants urgent attention. *J Gastrointest Surg* 16:1225–1234, 2012.
20. Olsen WR, Hildreth DH: Abdominal paracentesis and peritoneal lavage in blunt abdominal trauma. *J Trauma* 11:824–829, 1971.
21. Rodriguez A, DuPriest RW, Shatney CH: Recognition of intra-abdominal injury in blunt trauma victims. A prospective study comparing physical examination with peritoneal lavage. *Am Surg* 48:457–459, 1982.
22. Yu J, Fulcher AS, Turner MA, et al: Multidetector computed tomography of blunt hepatic and splenic trauma: Pearls and pitfalls. *Semin Roentgenol* 47:352–361, 2012.
23. Holmes JF, Sokolove PE, Brant WE, et al: Identification of children with intra-abdominal injuries after blunt trauma. *Ann Emerg Med* 39:500–509, 2002.
24. Wilson CB, Vidrine A, Rives JD: Unrecognized abdominal trauma in patients with head injuries. *Ann Surg* 161:608–613, 1965.
25. Buduhan G, McRitchie DI: Missed injuries in patients with multiple trauma. *J Trauma* 49:600–605, 2000.
26. Boscak A, Shanmuganathan K: Splenic trauma: What is new? *Radiol Clin North Am* 50:105–122, 2012.
27. Salim A, Sangthong B, Martin M, et al: Whole body imaging in blunt multisystem trauma patients without obvious signs of injury: Results of a prospective study. *Arch Surg* 141:468–475, 2006.
28. Holmes JF, Nguyen H: Do patients with left lower chest injury require abdominal CT? *Acad Emerg Med* 8:516, 2001.
29. Shweiki E, Klena J, Wood GC, et al: Assessing the true risk of abdominal solid organ injury in hospitalized rib fracture patients. *J Trauma* 50:684–688, 2001.
30. Root HD, Hauser CW, McKinley CR, et al: Diagnostic peritoneal lavage. *Surgery* 57:633–637, 1965.
31. Renz BM, Feliciano DV: Unnecessary laparotomies for trauma: A prospective study of morbidity. *J Trauma* 38:350–356, 1995.
32. van der Vlies CH, Olthof DC, Gaakeer M, et al: Changing patterns in diagnostic strategies and the treatment of blunt injury to solid abdominal organs. *Int J Emerg Med* 4:47, 2011.
33. Witte CL, Esser MJ, Rappaport WD: Updating the management of salvageable splenic injury. *Ann Surg* 215:261–265, 1992.
34. Benya EC, Bulas DL: Splenic injuries in children after blunt abdominal trauma. *Semin Ultrasound CT MR* 17:170–176, 1996.
35. Black JJ, Sinow RM, Wilson SE, et al: Subcapsular hematoma as a predictor of delayed splenic rupture. *Am Surg* 58:732–735, 1992.
36. Schauer BA, Nguyen H, Wisner DH, et al: Is definitive abdominal evaluation required in blunt trauma victims undergoing urgent extra-abdominal surgery? *Acad Emerg Med* 12:707–711, 2005.
37. Federle MP, Courcoulas AP, Powell M, et al: Blunt splenic injury in adults: Clinical and CT criteria for management, with emphasis on active extravasation. *Radiology* 206:137–142, 1998.
38. Wolfman NT, Bechtold RE, Scharling ES, et al: Blunt upper abdominal trauma: Evaluation by CT. *AJR Am J Roentgenol* 158:493–501, 1992.
39. Heyer CM, Rduch GJ, Wick M, et al: [Evaluation of multiple trauma victims with 16-row multidetector CT (MDCT): A time analysis]. *Rof* 177:1677–1682, 2005.
40. Mirvis SE, Whitley NO, Gens DR: Blunt splenic trauma in adults: CT-based classification and correlation with prognosis and treatment. *Radiology* 171:33–39, 1989.
41. Smith JS, Jr, Wengrovitz MA, DeLong BS: Prospective validation of criteria, including age, for safe, nonsurgical management of the ruptured spleen. *J Trauma* 33:363–368, discussion 368–369, 1992.
42. Croce MA, Fabian TC, Menke PG, et al: Nonoperative management of blunt hepatic trauma is the treatment of choice for hemodynamically stable patients. Results of a prospective trial. *Ann Surg* 221:744–753, discussion 753–755, 1995.
43. Shanmuganathan K, Mirvis SE, Boyd-Kranis R, et al: Nonsurgical management of blunt splenic injury: Use of CT criteria to select patients for splenic arteriography and potential endovascular therapy. *Radiology* 217:75–82, 2000.
44. Hormann M, Scharitzer M, Philipp M, et al: First experiences with multidetector CT in traumatized children. *Eur J Radiol* 48:125–132, 2003.
45. Gralla J, Spycher F, Pignolet C, et al: Evaluation of a 16-MDCT scanner in an emergency department: Initial clinical experience and workflow analysis. *AJR Am J Roentgenol* 185: 232–238, 2005.
46. Daly KP, Ho CP, Persson DL, et al: Traumatic retroperitoneal injuries: Review of multidetector CT findings. *Radiographics* 28:1571–1590, 2008.
47. Gavatt ML, Schurr M, Flick PA, et al: Predicting clinical outcome of nonsurgical management of blunt splenic injury: Using CT to reveal abnormalities of splenic vasculature. *AJR Am J Roentgenol* 168:207–212, 1997.
48. Federle MP, Griffiths B, Minagi H, et al: Splenic trauma: Evaluation with CT. *Radiology* 162:69–71, 1987.
49. Wolverson MK, Crepps LF, Sundaram M, et al: Hyperdensity of recent hemorrhage at body computed tomography: Incidence and morphologic variation. *Radiology* 148:779–784, 1983.
50. Kelly J, Raptopoulos V, Davidoff A, et al: The value of non-contrast-enhanced CT in blunt abdominal trauma. *AJR Am J Roentgenol* 152: 41–48, 1989.
51. Uecker J, Pickett C, Dunn E: The role of follow-up radiographic studies in nonoperative management of spleen trauma. *Am Surg* 67:22–25, 2001.
52. Rovin JD, Alford BA, McIlhenny TJ, et al: Follow-up abdominal computed tomography after splenic trauma in children may not be necessary. *Am Surg* 67:127–130, 2001.
53. Mizzi A, Shabani A, Watt A: The role of follow-up imaging in paediatric blunt abdominal trauma. *Clin Radiol* 57:908–912, 2002.
54. Sharma OP, Oswanski MF, Singer D: Role of repeat computerized tomography in nonoperative management of solid organ trauma. *Am Surg* 71:244–249, 2005.
55. Willmann JK, Roos JE, Platz A, et al: Multidetector CT: Detection of active hemorrhage in patients with blunt abdominal trauma. *AJR Am J Roentgenol* 179:437–444, 2002.
56. Shanmuganathan K, Mirvis SE, Sover ER: Value of contrast-enhanced CT in detecting active hemorrhage in patients with blunt abdominal or pelvic trauma. *AJR Am J Roentgenol* 161:65–69, 1993.
57. Gross JL, Woll NL, Hanson CA, et al: Embolization for pediatric blunt splenic injury is an alternative to splenectomy when observation

- fails. *J Trauma Acute Care Surg* 75:421–425, 2013.
58. Schnuriger B, Inaba K, Konstantinidis A, et al: Outcomes of proximal versus distal splenic artery embolization after trauma: A systematic review and meta-analysis. *J Trauma* 70:252–260, 2011.
 59. Sutton CS, Haaga JR: CT evaluation of limited splenic trauma. *J Comput Assist Tomogr* 11: 167–169, 1987.
 60. Davis KA, Fabian TC, Croce MA, et al: Improved success in nonoperative management of blunt splenic injuries: Embolization of splenic artery pseudoaneurysms. *J Trauma* 44:1008–1015, 1998.
 61. Goletti OM, Ghiselli GM, Lippolis PV, et al: Intrasplenic posttraumatic pseudoaneurysm: Echo color Doppler diagnosis. *J Trauma* 41: 542–545, 1996.
 62. Poletti PA, Platon A, Becker CD, et al: Blunt abdominal trauma: Does the use of a second-generation sonographic contrast agent help to detect solid organ injuries? *AJR Am J Roentgenol* 183:1293–1301, 2004.
 63. Omert LA, Salyer D, Dunham CM, et al: Implications of the “contrast blush” finding on computed tomographic scan of the spleen in trauma. *J Trauma* 51:272–277, discussion 277–278, 2001.
 64. Yardeni DM, Polley TZ, Coran AG: Splenic artery embolization for post-traumatic splenic artery pseudoaneurysm in children. *J Trauma* 57:404–407, 2004.
 65. Cloutier DR, Baird TB, Gormley P, et al: Pediatric splenic injuries with a contrast blush: Successful nonoperative management without angiography and embolization. *J Pediatr Surg* 39:969–971, 2004.
 66. Lutz N, Mahboubi S, Nance ML, et al: The significance of contrast blush on computed tomography in children with splenic injuries. *J Pediatr Surg* 39:491–494, 2004.
 67. Stuhlfaut JW, Lucey BC, Varghese JC, et al: Blunt abdominal trauma: Utility of 5-minute delayed CT with a reduced radiation dose. *Radiology* 238:473–479, 2006.
 68. Miller LA, Mirvis SE, Shanmuganathan K, et al: CT diagnosis of splenic infarction in blunt trauma: Imaging features, clinical significance and complications. *Clin Radiol* 59:342–348, 2004.
 69. Pappas D, Mirvis SE, Crepps JT: Splenic trauma: False-negative CT diagnosis in cases of delayed rupture. *AJR Am J Roentgenol* 149: 727–728, 1987.
 70. Ruffolo DC: Delayed splenic rupture: Understanding the threat. *J Trauma Nurs* 9:34–40, 2002.
 71. Riezzo I, Di Battista B, De Salvia A, et al: Delayed splenic rupture. *Forensic Sci Int* 234: 64–71, 2014.
 72. Shapiro MJ, Krausz CM, Durham RM, et al: Overuse of splenic scoring and computed tomographic scans. *J Trauma* 47:651, 1999.
 73. Raza M, Abbas Y, Devi V, et al: Non operative management of abdominal trauma—a 10 years review. *World J Emerg Surg* 8:14, 2013.
 74. Goodman LR, Aprahamian C: Changes in splenic size after abdominal trauma. *Radiology* 176:629–632, 1990.
 75. Munera F, Morales C, Soto JA, et al: Gunshot wounds of abdomen: Evaluation of stable patients with triple-contrast helical CT. *Radiology* 231:399–405, 2004.
 76. Shanmuganathan K, Mirvis SE, Chiu WC, et al: Triple-contrast helical CT in penetrating torso trauma: A prospective study to determine peritoneal violation and the need for laparotomy. *AJR Am J Roentgenol* 177: 1247–1256, 2001.
 77. Moore EE, Moore JB, Van Duzer-Moore S, et al: Mandatory laparotomy for gunshot wounds penetrating the abdomen. *Am J Surg* 140:847–851, 1980.
 78. McCarthy MC, Lowdermilk GA, Canal DE, et al: Prediction of injury caused by penetrating wounds to the abdomen, flank, and back. *Arch Surg* 126:962–965, 1991.
 79. Dodds WJ, Taylor AJ, Erickson SJ, et al: Radiologic imaging of splenic anomalies. *AJR Am J Roentgenol* 155:805–810, 1990.
 80. Moore EE, Cogbill TH, Malangoni MA, et al: Organ injury scaling. *Surg Clin North Am* 75:293–303, 1995.
 81. Cocanour CS, Moore FA, Ware DN, et al: Age should not be a consideration for nonoperative management of blunt splenic injury. *J Trauma* 48:606–612, 2000.
 82. Scatamacchia SA, Raptopoulos V, Fink MP, et al: Splenic trauma in adults: Impact of CT grading on management. *Radiology* 171:725–729, 1989.
 83. Kohn JS, Clark DE, Isler RJ, et al: Is computed tomographic grading of splenic injury useful in the nonsurgical management of blunt trauma? [see comment]. *J Trauma* 36:385–389, discussion 390, 1994.
 84. Becker CD, Spring P, Glatli A, et al: Blunt splenic trauma in adults: Can CT findings be used to determine the need for surgery? *AJR Am J Roentgenol* 162:343–347, 1994.
 85. Barquist ES, Pizano LR, Feuer W, et al: Inter- and intrarater reliability in computed axial tomographic grading of splenic injury: Why so many grading scales? *J Trauma* 56:334–338, 2004.
 86. Nwomeh BC, Nadler EP, Meza MP, et al: Contrast extravasation predicts the need for operative intervention in children with blunt splenic trauma. *J Trauma* 56:537–541, 2004.
 87. Olthof DC, van der Vlies CH, Scheerder MJ, et al: Reliability of injury grading systems for patients with blunt splenic trauma. *Injury* 45:146–150, 2014.
 88. Umlas SL, Cronan JJ: Splenic trauma: Can CT grading systems enable prediction of successful nonoperative treatment? *Radiology* 178:481–487, 1991.
 89. Milzman DP, Boulanger BR, Rodriguez A, et al: Pre-existing disease in trauma patients: A predictor of fate independent of age and injury severity score. *J Trauma* 32:236–243, discussion 243–244, 1992.
 90. Moore EE, Cogbill TH, Jurkovich GJ, et al: Organ injury scaling: Spleen and liver (1994 revision). *J Trauma* 38:323–324, 1995.
 91. Starnes S, Klein P, Magagna L, et al: Computed tomographic grading is useful in the selection of patients for nonoperative management of blunt injury to the spleen. *Am Surg* 64:743–748, discussion 748–749, 1998.
 92. Myers JG, Dent DL, Stewart RM, et al: Blunt splenic injuries: Dedicated trauma surgeons can achieve a high rate of nonoperative success in patients of all ages. *J Trauma* 48:801–806, 2000.
 93. McIntyre LK, Schiff M, Jurkovich GJ: Failure of nonoperative management of splenic injuries: Causes and consequences. *Arch Surg* 140: 563–569, 2005.
 94. Marmery H, Shanmuganathan K, Alexander MT, et al: Optimization of selection for nonoperative management of blunt splenic injury: Comparison of MDCT grading systems. *AJR Am J Roentgenol* 189:1421–1427, 2007.
 95. Boulanger BR, Kearney PA, Brenneman FD, et al: Utilization of FAST (focused assessment with sonography for trauma) in 1999: Results of a survey of North American trauma centers. *Am Surg* 66:1049–1055, 2000.
 96. McKenney KL, Nunez DB, Jr, McKenney MG, et al: Sonography as the primary screening technique for blunt abdominal trauma: Experience with 899 patients. *AJR Am J Roentgenol* 170:979–985, 1998.
 97. Pearl WS, Todd KH: Ultrasonography for the initial evaluation of blunt abdominal trauma: A review of prospective trials. *Ann Emerg Med* 27:353–361, 1996.
 98. Kirkpatrick AW, Sirois M, Laupland KB, et al: Prospective evaluation of hand-held focused abdominal sonography for trauma (FAST) in blunt abdominal trauma. *Can J Surg* 48:453–460, 2005.
 99. Nunes LW, Simmons S, Hallowell MJ, et al: Diagnostic performance of trauma US in identifying abdominal or pelvic free fluid and serious abdominal or pelvic injury. *Acad Radiol* 8:128–136, 2001.
 100. McGahan JP, Rose J, Coates TL, et al: Use of ultrasonography in the patient with acute abdominal trauma. *J Ultrasound Med* 16:653–662, quiz 663–664, 1997.
 101. Korner M, Krotz MM, Degenhart C, et al: Current role of emergency US in patients with major trauma. *Radiographics* 28:225–242, 2008.
 102. Shanmuganathan K, Mirvis SE, Sherbourne CD, et al: Hemoperitoneum as the sole indicator of abdominal visceral injuries: A potential limitation of screening abdominal US for trauma. *Radiology* 212:423–430, 1999.
 103. Brown MA, Casola G, Sirlin CB, et al: Blunt abdominal trauma: Screening US in 2,693 Patients. *Radiology* 218:352–358, 2001.
 104. Emery KH, McAneney CM, Racadio JM, et al: Absent peritoneal fluid on screening trauma ultrasonography in children: A prospective comparison with computed tomography. *J Pediatr Surg* 36:565–569, 2001.
 105. Poletti PA, Kinkel K, Vermeulen B, et al: Blunt abdominal trauma: Should US be used to detect both free fluid and organ injuries? *Radiology* 227:95–103, 2003.
 106. Natarajan B, Gupta PK, Cemaj S, et al: FAST scan: Is it worth doing in hemodynamically stable blunt trauma patients? *Surgery* 148:695–700, discussion 700–701, 2010.
 107. Yoshii H, Sato M, Yamamoto S, et al: Usefulness and limitations of ultrasonography in the initial evaluation of blunt abdominal trauma. *J Trauma* 45:45–50, discussion 50–51, 1998.
 108. Williams SR, Perera P, Gharabaghian L: The FAST and E-FAST in 2013: Trauma ultrasonography. *Crit Care Clin* 30:119–150, 2014.
 109. Sirlin CB, Brown MA, Andrade-Barreto OA, et al: Blunt abdominal trauma: Clinical value of negative screening US scans. *Radiology* 230: 661–668, 2004.
 110. McKenney KL: Role of US in the diagnosis of intraabdominal catastrophes. *Radiographics* 19:1332–1339, 1999.
 111. Cagini L, Gravante S, Malaspina CM, et al: Contrast enhanced ultrasound (CEUS) in blunt abdominal trauma. *Crit Ultrasound J* 5 (Suppl 1):S9, 2013.

112. Doody O, Lyburn D, Geoghegan T, et al: Blunt trauma to the spleen: Ultrasonographic findings. *Clin Radiol* 60:968–976, 2005.
113. Catalano O, Lobianco R, Sandomenico F, et al: Splenic trauma: Evaluation with contrast-specific sonography and a second-generation contrast medium: Preliminary experience. *J Ultrasound Med* 22:467–477, 2003.
114. Catalano O, Sandomenico F, Matarazzo I, et al: Contrast-enhanced sonography of the spleen. *AJR Am J Roentgenol* 184:1150–1156, 2005.
115. Catalano O, Lobianco R, Raso MM, et al: Blunt hepatic trauma: Evaluation with contrast-enhanced sonography: sonographic findings and clinical application. *J Ultrasound Med* 24:299–310, 2005.
116. Valentino M, Serra C, Pavlica P, et al: Contrast-enhanced ultrasound for blunt abdominal trauma. *Semin Ultrasound CT MR* 28:130–140, 2007.
117. Sato M, Yoshii H: Reevaluation of ultrasonography for solid-organ injury in blunt abdominal trauma. *J Ultrasound Med* 23:1583–1596, 2004.
118. Boulanger BR, Brenneman FD, McLellan BA, et al: A prospective study of emergent abdominal sonography after blunt trauma. *J Trauma* 39:325–330, 1995.
119. Craig S, Egerton-Warburton D, Mellett T: Ultrasound use in Australasian emergency departments. *Emerg Med Australas* 26:268–273, 2014.
120. Ochsner MG, Knudson MM, Pachter HL, et al: Significance of minimal or no intraperitoneal fluid visible on CT scan associated with blunt liver and splenic injuries: A multicenter analysis. *J Trauma* 49:505–510, 2000.
121. Boulanger BR, Brenneman FD, Kirkpatrick AW, et al: The indeterminate abdominal sonogram in multisystem blunt trauma. *J Trauma* 45:52–56, 1998.
122. Kirkpatrick AW, Sirois M, Ball CG, et al: The hand-held ultrasound examination for penetrating abdominal trauma. *Am J Surg* 187:660–665, 2004.
123. Nebesar RA, Rabinov KR, Potsaid MS: Radionuclide imaging of the spleen in suspected splenic injury. *Radiology* 110:609–614, 1974.
124. Poletti PA, Wintermark M, Schnyder P, et al: Traumatic injuries: Role of imaging in the management of the polytrauma victim (conservative expectation). *Eur Radiol* 12:969–978, 2002.
125. Livingston CD, Sirinek KR, Levine BA, et al: Traumatic splenic injury: Its management in a patient population with a high incidence of associated injury. *Arch Surg* 117:670–674, 1982.
126. Brigden ML: Overwhelming postsplenectomy infection still a problem. *West J Med* 157:440–443, 1992.
127. Ekeh AP, McCarthy MC, Woods RJ, et al: Complications arising from splenic embolization after blunt splenic trauma. *Am J Surg* 189:335–339, 2005.
128. Romano FM, Caprotti RM, Scaini AM, et al: Elective laparoscopic splenectomy and thrombosis of the spleno-portal axis: A prospective study with ecocolordoppler Ultrasound. *Surg Laparosc Endosc Percutan Tech* 16:4–7, 2006.
129. Pachter HL, Guth AA, Hofstetter SR, et al: Changing patterns in the management of splenic trauma: The impact of nonoperative management. *Ann Surg* 227:708–719, 1998.
130. Demetriades D, Scalea TM, Degiannis E, et al: Blunt splenic trauma: Splenectomy increases early infectious complications: A prospective multicenter study. *J Trauma Acute Care Surg* 72:229–234, 2012.
131. Bisharat N, Omari H, Lavi I, et al: Risk of infection and death among post-splenectomy patients. *J Infect* 43:182–186, 2001.
132. Green JB, Shackford SR, Sise MJ, et al: Late septic complications in adults following splenectomy for trauma: A prospective analysis in 144 patients. *J Trauma* 26:999–1004, 1986.
133. Jacobs IA, Kelly K, Valenziano C, et al: Nonoperative management of blunt splenic and hepatic trauma in the pediatric population: Significant differences between adult and pediatric surgeons? *Am Surg* 67:149–154, 2001.
134. Potoka DA, Schall LC, Ford HR: Risk factors for splenectomy in children with blunt splenic trauma. *J Pediatr Surg* 37:294–299, 2002.
135. Krause KR, Howells GA, Bair HA, et al: Nonoperative management of blunt splenic injury in adults 55 years and older: A twenty-year experience. *Am Surg* 66:636–640, 2000.
136. Olthof DC, Joosse P, van der Vlies CH, et al: Prognostic factors for failure of nonoperative management in adults with blunt splenic injury: A systematic review. *J Trauma Acute Care Surg* 74:546–557, 2013.
137. Hartnett KL, Winchell RJ, Clark DE: Management of adult splenic injury: A 20-year perspective. *Am Surg* 69:608–611, 2003.
138. Harbrecht BG: Is anything new in adult blunt splenic trauma? *Am J Surg* 190:273–278, 2005.
139. Barone JE, Burns GM, Svehlak SA, et al: Management of blunt splenic trauma in patients older than 55 years. *J Trauma* 46:87–90, 1999.
140. Lange DA, Zaret P, Merlotti GJ, et al: The use of absorbable mesh in splenic trauma. *J Trauma* 28:269–275, 1988.
141. Velmahos GC, Toutouzas KG, Radin R, et al: Nonoperative treatment of blunt injury to solid abdominal organs: A prospective study. *Arch Surg* 138:844–851, 2003.
142. Peitzman AB, Heil BM, Rivera LM, et al: Blunt splenic injury in adults: Multi-institutional study of the Eastern Association for the Surgery of Trauma. *J Trauma* 49:177–189, 2000.
143. Moore FA, Davis JW, Moore EE, Jr, et al: Western Trauma Association (WTA) critical decisions in trauma: Management of adult blunt splenic trauma. *J Trauma* 65:1007–1011, 2008.
144. Stassen NA, Bhullar I, Cheng JD, et al: Selective nonoperative management of blunt splenic injury: An Eastern Association for the Surgery of Trauma practice management guideline. *J Trauma Acute Care Surg* 73:S294–S300, 2012.
145. Haan JM, Scott JS, Boyd-Kranis RL, et al: Admission angiography for blunt splenic injury: Advantages and pitfalls. *J Trauma* 51:1161–1165, 2001.
146. Hagiwara A, Yukioka T, Ohta S, et al: Nonsurgical management of patients with blunt splenic injury: Efficacy of transcatheter arterial embolization. *AJR Am J Roentgenol* 167:159–166, 1996.
147. Dent DM, Alsabrook G, Erickson BA, et al: Blunt splenic injuries: High nonoperative management rate can be achieved with selective embolization. *J Trauma* 56:1063–1067, 2004.
148. Liu PP, Lee WC, Cheng YF, et al: Use of splenic artery embolization as an adjunct to nonsurgical management of blunt splenic injury. *J Trauma* 56:768–773, 2004.
149. Madoff DC, Denys A, Wallace MJ, et al: Splenic arterial interventions: Anatomy, indications, technical considerations, and potential complications. *Radiographics* 25:S191–S211, 2005.
150. Haan JM, Biffl WM, Knudson MM, et al: Splenic embolization revisited: A multicenter review. *J Trauma* 56:542–547, 2004.
151. Debi U, Kaur R, Prasad KK, et al: Pancreatic trauma: A concise review. *World J Gastroenterol* 19:9003–9011, 2013.
152. Wahl WL, Ahrns KS, Chen S, et al: Blunt splenic injury: Operation versus angiographic embolization. *Surgery* 136:891–899, 2004.
153. Hagiwara A, Fukushima H, Murata A, et al: Blunt splenic injury: Usefulness of transcatheter arterial embolization in patients with a transient response to fluid resuscitation. *Radiology* 235:57–64, 2005.
154. Killen KL, Shanmuganathan K, Boyd-Kranis R, et al: CT Findings after embolization for blunt splenic trauma. *J Vasc Interv Radiol* 12:209–214, 2001.
155. Lechner K: Management of adult immune thrombocytopenia. *Rev Clin Exp Hematol* 5:222–235, discussion 311–312, 2001.
156. Li Y, Cui L, Zhang W, et al: Laparoscopic radiofrequency ablation for traumatic splenic rupture. *J Surg Res* 185:711–716, 2013.
157. Musallam KM, Khalife M, Sfeir PM, et al: Postoperative outcomes after laparoscopic splenectomy compared with open splenectomy. *Ann Surg* 257:1116–1123, 2013.
158. Park A, Targarona EM, Trias M: Laparoscopic surgery of the spleen: State of the art. *Langenbecks Arch Surg* 386:230–239, 2001.
159. Winslow ER, Brunt LM: Perioperative outcomes of laparoscopic versus open splenectomy: A meta-analysis with an emphasis on complications. *Surgery* 134:647–653, 2003.
160. Ikeda M, Sekimoto M, Takiguchi S, et al: High incidence of thrombosis of the portal venous system after laparoscopic splenectomy: A prospective study with contrast-enhanced CT scan. *Ann Surg* 241:208–216, 2005.
161. Tran T, Demyttenaere SV, Polyhronopoulos G, et al: Recommended timing for surveillance ultrasonography to diagnose portal splenic vein thrombosis after laparoscopic splenectomy. *Surg Endosc* 24:1670–1678, 2010.
162. Fisichella PM, Wong YM, Pappas SG, et al: Laparoscopic splenectomy: Perioperative management, surgical technique, and results. *J Gastrointest Surg* 18:404–410, 2014.

Spleen: Differential Diagnosis

RICHARD M. GORE

CHAPTER OUTLINE

Imaging Abnormalities

- Box 107-1. Congenital Syndromes with Splenomegaly
- Box 107-2. Small Spleen

Ultrasound

- Box 107-3. Increased Splenic Echogenicity: Diffuse
- Box 107-4. Decreased Splenic Echogenicity: Diffuse
- Box 107-5. Multifocal Hypoechoic Splenic Masses
- Box 107-6. Echogenic Splenic Masses
- Box 107-7. Solid Heterogeneous Splenic Masses
- Box 107-8. Splenomegaly: Normal Echogenicity
- Box 107-9. Splenomegaly: Hyperechoic Pattern
- Box 107-10. Splenomegaly: Hypoechoic Pattern

Computed Tomography

- Box 107-11. Focal Hypodense Lesion: Noncontrast Scan
- Box 107-12. Focal Hyperdense Lesion: Noncontrast Scan
- Box 107-13. Increased Splenic Density: Diffuse

Magnetic Resonance Imaging

- Box 107-14. Multiple Splenic Hypointensities on T1-Weighted Magnetic Resonance Images
- Box 107-15. Multiple Splenic Hyperintensities on T2-Weighted Magnetic Resonance Images
- Table 107-1. Multiple Splenic Calcifications
- Table 107-2. Solitary Splenic Calcification
- Table 107-3. Splenomegaly
- Table 107-4. Pattern Recognition of Common Splenic Lesions

Imaging Abnormalities

BOX 107-1 CONGENITAL SYNDROMES WITH SPLENOmegaly

Aase-Smith syndrome
 α_1 -Antitrypsin syndrome
 Anemia (e.g., thalassemia, sickle cell, pyruvate kinase deficiency)
 Chédiak-Higashi syndrome
 Cogan's syndrome
 Ethanolamniosis
 Farber's syndrome
 Felty's syndrome
 Fetal infection (e.g., herpes simplex, rubella, cytomegalovirus infection)
 Gaucher's disease, types I and III
 Gangliosidosis (e.g., GM₁, GM₂)
 Hepatic fibrosis and renal cystic disease
 Hyperlipoproteinemia
 Lipoatrophic diabetes
 Mucopolysaccharidosis
 Niemann-Pick disease
 Osteopetrosis
 Rubella syndrome
 Sea-blue histiocyte syndrome
 Vaquez-Osler syndrome

BOX 107-2 SMALL SPLEEN

Inflammatory bowel disease
 Hereditary hypoplasia
 After irradiation
 Infarction
 Polysplenia syndrome
 Sickle cell anemia

Ultrasound

BOX 107-3 INCREASED SPLENIC ECHOGENICITY: DIFFUSE

Polycythemia
 Sarcoidosis
 Leukemia
 Tuberculosis
 Malaria
 Brucellosis

BOX 107-4 DECREASED SPLENIC ECHOGENICITY: DIFFUSE

Congestion from portal hypertension
 Leukemia
 Lymphoma
 Multiple myeloma

BOX 107-5 MULTIFOCAL HYPOECHOIC SPLENIC MASSES

Abscesses (e.g., pyogenic, fungal)
 Metastases
 Septic emboli
 Infarction
 Lymphoma
 Cysts (e.g., simple, epidermoid, hydatid, pancreatic)
 Lymphangiomatosis
 Granulomatous disease (e.g., tuberculosis, *Mycobacterium avium-intracellulare* infection, sarcoidosis, cat-scratch disease)
 Hamartoma, hemangioma
 Splenic artery aneurysm
 Disseminated *Pneumocystis carinii* (*Pneumocystis jiroveci*) infection

BOX 107-6 ECHOGENIC SPLENIC MASSES

Hereditary spherocytosis
 Infarct (chronic)
 Hematoma
 Metastases
 Calcified granulomas
 Plasmacytoma
 Abscess with air bubbles
 Schistosomiasis
 Cholesterol crystals in simple cyst
 Hydatid "sand" in hydatid cyst

BOX 107-7 SOLID HETEROGENEOUS SPLENIC MASSES

Hematoma
Abscess
Infarct
Angiosarcoma
Hemangioma
Hemangiosarcoma

BOX 107-8 SPLENOMEGALY: NORMAL ECHOGENICITY

Congestion from portal hypertension
Myelogenous leukemia
Infection
Sickle cell disease (early)
Hereditary spherocytosis
Hemolysis
Still's disease
Felty's syndrome
Wilson's disease
Polycythemia
Myelofibrosis

BOX 107-9 SPLENOMEGALY: HYPERECHOIC PATTERN

Leukemias (i.e., acute lymphocytic, chronic lymphocytic, or myelogenous after chemotherapy or radiation therapy)
Lymphoma
Malaria
Tuberculosis
Brucellosis
Sarcoidosis
Polycythemia
Hereditary spherocytosis
Portal vein thrombosis
Dysgammaglobulinemia
Myelofibrosis
Hematoma
Metastases

BOX 107-10 SPLENOMEGALY: HYPOECHOIC PATTERN

Noncaseating granulomatous infection
Lymphoma
Multiple myeloma
Chronic lymphocytic leukemia
Congestion from portal hypertension

Computed Tomography**BOX 107-11 FOCAL HYPODENSE LESION: NONCONTRAST SCAN**

Infarction
Hematoma
Dilantin therapy
Abscess
Metastases
Congenital or traumatic cyst
Echinococcal cyst
Primary angiosarcoma
Lymphoma
Extramedullary hematopoiesis
Hamartoma
Lymphangiomatosis
Hemangioma
Fibroma
Dermoid cyst
Epidermoid cyst
Granulomatous disease (e.g., tuberculosis, *M. avium-intracellulare* infection, sarcoidosis, cat-scratch disease)

BOX 107-12 FOCAL HYPERDENSE LESION: NONCONTRAST SCAN

Calcification
Mucinous metastases
Colon, stomach, or pancreas primary tumor
Hydatid, healed *Pneumocystis* infection
Acute hemorrhage (e.g., post-traumatic, spontaneous)
Calcified hematoma
Hemangioma complicated by rupture and hemorrhage
Hemorrhagic acute infarct
Complicated cysts attributable to intracystic hemorrhage or infection

BOX 107-13 INCREASED SPLENIC DENSITY: DIFFUSE

Hemochromatosis
Sickle cell anemia
Fanconi's anemia
Hemosiderosis

Magnetic Resonance Imaging**BOX 107-14 MULTIPLE SPLENIC HYPINTENSITIES ON T1-WEIGHTED MAGNETIC RESONANCE IMAGES**

Infarcts
Metastases
Calcified granulomas
Gamna-Gandy bodies
Cysts
Hemangiomas
Hamartomas
Lymphoma
Pyogenic abscess
Amyloidosis
Dilantin therapy
Fungemia with multifocal abscess formation
Flow void of arteriovenous malformation
Sarcoidosis
Peliosis

BOX 107-15 MULTIPLE SPLENIC HYPERINTENSITIES ON T2-WEIGHTED MAGNETIC RESONANCE IMAGES

Infarcts
 Metastases
 Cysts
 Hemangiomas
 Hamartomas
 Pyogenic abscess
 Fungemia with multifocal abscess formation
 Echinococcal cysts
 Peliosis
 Lymphangioma

TABLE 107-1 Multiple Splenic Calcifications

Common Conditions	Uncommon Conditions
Histoplasmosis	Hematoma
Phleboliths	Infarct
Hemangiomas	Brucellosis
Tuberculosis	<i>Armillifer armillatus</i> infestation
AIDS—healed <i>Pneumocystis</i> infection	Echinococcal cyst
Splenic artery atherosclerosis	Post-traumatic cyst
Splenic artery aneurysm	Congenital cyst
	Hamartomas
	Hydatid cyst
	Sickle cell anemia

TABLE 107-2 Solitary Splenic Calcification

Common Conditions	Uncommon Conditions
Splenic artery aneurysm	Abscess
Splenic artery atherosclerosis	Dermoid cyst
Infarct	Epidermoid cyst
Traumatic hemorrhagic cyst	Hydatid cyst
Hematoma	Tuberculosis
	Metastasis
	Hemangioma
	Phlebolith

TABLE 107-3 Splenomegaly

Possible Disease	Examples
Neoplasms	Lymphoma Leukemia (especially chronic myeloid) Metastases Fibroma, hamartoma, angiosarcoma Hemangioma, lymphangioma
Congestive splenomegaly	Heart failure Portal hypertension Cirrhosis Banti's syndrome Splenic vein occlusion
Infection	Hepatitis Malaria Leishmaniasis Tuberculosis Typhoid Syphilis Echinococcosis Brucellosis Typhus Histoplasmosis AIDS Schistosomiasis Bacterial endocarditis Kala-azar Cytomegalovirus infection
Hemolytic anemias	Hemoglobinopathies Hereditary spherocytosis Primary neutropenia Thrombotic thrombocytopenic purpura
Extramedullary hematopoiesis	Osteopetrosis Myelofibrosis Polycythemia vera Hemochromatosis
Collagen-vascular diseases	Felty's syndrome Systemic lupus erythematosus Juvenile rheumatoid arthritis
Storage diseases	Gaucher's disease Amyloidosis Diabetes Hemochromatosis Histiocytosis Niemann-Pick disease Gargoylism
Miscellaneous conditions	Hematoma Abscess Congenital cyst Post-traumatic cyst Sarcoid

TABLE 107-4 Pattern Recognition of Common Splenic Lesions

Lesion	T1	T2	Early Gd	Late Gd	Other Features
Cyst	↓-∅	↑↑	None	None	Well defined
Hamartoma	∅	∅-↑	Heterogeneous, intense	Homogeneous, isointense	Usually >4 cm; arises from the medial surface of the midspleen
Hemangioma	↓-∅	↑	Peripheral nodular or homogeneous	Centripetal enhancement; retains contrast	Usually <2 cm; lesions often flash fill on immediate post-Gd images, reflecting their small sizes compared with liver hemangiomas, which tend to be larger
Metastases	↓-∅	∅-↓	Focal lesions with minimal enhancement	Isointense	Metastases commonly become isointense by 1 min after Gd
Lymphoma, focal	↓-∅	↑-↓	Focal lesions with minimal enhancement	Isointense	Focal lesions often become isointense by 1 min after Gd; adenopathy usually present elsewhere
Lymphoma, diffuse	↓-∅	∅-↓	Focal lesions with minimal enhancement	Isointense	Lesions often become isointense by 1 min after Gd; adenopathy usually present elsewhere

From Nagase LL, Semelka RC, Armao D: Spleen. In Semelka RC (ed): *Abdominal-Pelvic MRI*. New York, Wiley-Liss, 2002, pp 491-526.

Gd, gadolinium; T1, T1-weighted magnetic resonance image; T2, T2-weighted magnetic resonance image; ↓, mildly decreased; ∅, isointense; ↑, mildly increased; ↑↑, moderately to markedly increased.

SUGGESTED READINGS

1. Dähnert W: Radiology Review Manual, ed 7, Baltimore, 2011, Williams & Wilkins.
2. Reeder MM: Reeder and Felson's Gamuts in Radiology, ed 4, New York, 2003, Springer-Verlag.
3. Baker SR, Cho KC: Abdominal Plain Film Interpretation with Imaging Correlation, Norwalk, CT, 1998, Appleton & Lange.
4. Rumack CM, Nilson SR, Charboneau JW, editors: Diagnostic Ultrasound, ed 4, Philadelphia, 2011, Elsevier-Mosby.
5. Semelka RC, editor: Abdominal-Pelvic MRI, New York, 2010, Wiley-Liss.
6. Caremani M, Occhini U, Caremani A, et al: Focal splenic lesions: US findings. *J Ultrasound* 16:65–74, 2013.
7. Benter T, Klühs L, Teichgräber U: Sonography of the spleen. *J Ultrasound Med* 30:1281–1293, 2011.
8. Thipphavong S, Duigenan S, Schindera ST, et al: Nonneoplastic, benign, and malignant splenic disease: Cross-sectional imaging findings and rare disease entities. *AJR* 203:315–322, 2014.

SECTION
VIII

**General Radiologic
Principles for
Imaging and Intervention
of the Solid Viscera**

Anatomy and Imaging of the Peritoneum and Retroperitoneum

VINCENT M. MELLNICK | DENNIS M. BALFE | CHRISTINE M. PETERSON

CHAPTER OUTLINE

Embryology

Upper Abdominal Embryogenesis

Lower Abdominal and Pelvic Embryogenesis

Retroperitoneal Anatomy: Spaces

Great Vessels

Transversalis Fascia

Posterior Fat Pads

Perirenal Space

Anterior Pararenal Space

Retroperitoneal Anatomy: Planes

Retromesenteric and Lateroconal Planes

Retrolenal Plane

Pelvic Extraperitoneal Spaces and Planes

Subperitoneal Spaces: Ligaments and Mesenteries

Upper Abdominal Ligaments

Lower Abdominal Ligaments

Peritoneal Spaces: Upper Abdomen

Left-Sided Peritoneal Spaces

Right-Sided Peritoneal Spaces

Peritoneal Spaces: Lower Abdomen and Pelvis

Inframesocolic Space

Pelvic Peritoneal Spaces

The peritoneum, subperitoneal space, and retroperitoneum are anatomic compartments frequently involved in pathologic processes that originate in the gastrointestinal tract. Because they represent the result of complex embryologic processes of organogenesis, rotation, folding, and fusion, the distribution of fluid collections resulting from such processes is often confusing. A working knowledge of the anatomic compartmentalization of disease spread in the abdomen is essential to the understanding of imaging findings in a variety of pathologic conditions.

This chapter focuses on the anatomy of the peritoneum, retroperitoneum, and subperitoneum as depicted by cross-sectional imaging methods. In normal individuals, the boundaries of these anatomic regions are defined poorly or not at all. When pathologic processes produce intra-abdominal fluid collections, the patterns of fluid distribution are directly determined by their relationships. The patterns of disease spread within the abdomen can be logically predicted from an understanding of the folds of mesenchymal tissue that envelop the

gut and the gut-derived solid viscera: the mesenteries. Most illustrations in this chapter feature the axial sections familiar to all practitioners of computed tomography (CT) and magnetic resonance imaging (MRI). In selected examples, however, the anatomic relationships are better displayed by coronal, sagittal, or volume rendered images.

Embryology

Embryology is the key to understanding all of the concepts presented in this chapter. This section provides an overview of the embryogenesis of the retroperitoneum and the mesenteries that form ligamentous attachments in the adult.¹ Some details are addressed in the sections on retroperitoneum and subperitoneum that follow.

UPPER ABDOMINAL EMBRYOGENESIS

The Gut and Its Derivatives

At about 3 weeks of fetal life, the lateral body plates (the mesodermal tissue forming the external fetal surface) of the fetus curl up to enclose a small portion of the celomic cavity to form an intraembryonic celomic cavity (Fig. 108-1A). Near the umbilicus, a portion of the yolk sac, which gives rise to the endodermal structures (the gut and all gut-derived solid organs), is enclosed and lined on all sides by fetal mesoderm. At this stage, there are well-demarcated right and left peritoneal spaces, divided by the mesenchyme suspending the gut from the ventral body wall (i.e., ventral mesentery), the gut and its surrounding mesenchyme, and the mesenchyme suspending the gut from the dorsal body wall (i.e., dorsal mesentery). Maternal blood from the umbilical vein courses through the ventral mesentery to supply the fetus, and blood from the now paired dorsal aortae establish vascular channels to the gut and developing viscera through the dorsal mesentery.

At about 4 weeks of fetal development, this symmetric arrangement is distorted. The liver begins to develop in the middle of the ventral mesentery, and it grows rapidly in all directions, bulging the contour of the right and left ventral peritoneal space and extending superiorly inside the ventral mesentery until it encounters the septum transversum (i.e., fetal diaphragm), which is growing from the ventral to the dorsal wall of the fetus to separate the thoracic from the abdominal cavity. The broad, roughly oval line of contact between the ventral mesentery and the septum transversum is not lined by mesothelium, and it becomes the bare area of the liver in the adult (Fig. 108-1B, C).

At the same time, the spleen and pancreas are beginning to grow within the leaves of the dorsal mesogastrium (Fig. 108-1D). The spleen generates just dorsal to the stomach, whereas

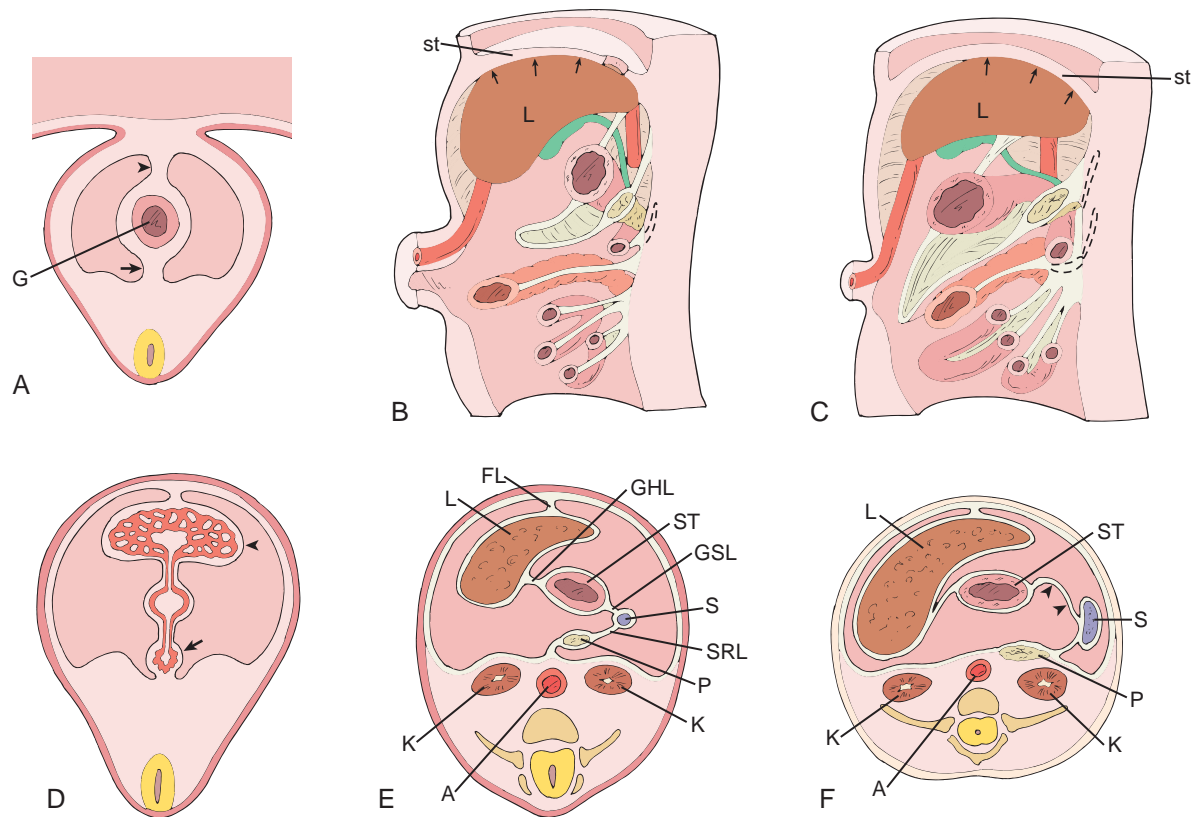


Figure 108-1 Embryogenesis of peritoneal spaces and ligaments. **A.** By the end of the third week of fetal development, the ventral body wall has fused, forming an enclosed abdominal cavity with the pinched-off primitive gut (G) in the center. The primitive gut is suspended within the abdomen by the dorsal (arrow) and ventral (arrowhead) mesenteries, which divide the cavity into symmetric right and left halves. **B.** Formation of the bare area of the liver. The line drawing of a sagittal view of an embryo from the left side shows the liver (L) within the ventral mesentery that is growing cephalad to encounter the mesoderm within the septum transversum (st). The surface of the liver in contact with the septum transversum (arrows) is not peritonealized and is known as the bare area. **C.** The line drawing depicts the rotation of the bare area into its adult position. As the septum transversum grows dorsally to separate the thorax from the abdomen, the bare area (arrows) shifts to a posterior position within the abdominal cavity. **D.** During the fourth week of fetal life, cords of tissue from the dorsal and ventral mesenteries grow rapidly, forming the liver, the spleen, and the tail off the pancreas. The liver (arrowhead) arises within the ventral mesentery. The spleen and the body and tail of the pancreas (arrow) grow from the dorsal mesentery. **E.** During the fifth week, the liver begins to grow rapidly and begins to occupy a large portion of the peritoneal space. Concurrently, the right peritoneal space expands toward the left, extending posterior to the stomach. **F.** The leftward expansion of the right peritoneal space causes the gastrosplenic ligament to billow laterally (arrowheads). The tail of the pancreas (P) fuses with the dorsal mesenchymal tissue. A, Aorta; FL, falciform ligament; GHL, gastrohepatic ligament; GSL, gastrosplenic ligament; K, kidney; L, liver; S, spleen; SRL, splenorenal ligament; ST, stomach.

the dorsal pancreas arises behind the duodenum. Part of the pancreas (i.e., the head and uncinate process in the adult) arises from a nest of cells within the ventral mesentery that ultimately rotates to join the dorsal pancreas later in fetal life. The all-enveloping mesenchyme continues to connect all of these developing organs with the body wall and the gut, and it persists into adult life as the abdominal ligaments (Fig. 108-1E). The ventral part of the ventral mesentery, connecting the liver to the anterior body wall, becomes the falciform ligament, through which courses the umbilical vein (and its fibrous remnant, the ligamentum teres, in the adult). The dorsal part of the ventral mesentery becomes the gastrohepatic and hepatoduodenal ligaments, which together compose the lesser omentum. The gastrohepatic ligament stretches between the lesser curvature of the stomach and the fissure for the ligamentum venosum. It contains the left gastric artery and vein and the lymph node group that drains the lesser curvature. The hepatoduodenal ligament, the caudal extension of the lesser omentum, contains

the portal vein, hepatic artery, common bile duct, and hepatic lymph node chain. The most inferior edge of the lesser omentum forms the roof of the foramen of Winslow.

The ventral part of the dorsal mesentery, connecting the stomach to the spleen, becomes the gastrosplenic ligament, identified by the short gastric arteries and veins that course within it (Fig. 108-1F). In the adult, the gastrosplenic ligament also forms the entirety of the greater omentum (i.e., gastrocolic ligament) and the cephalad portion of the transverse mesocolon (discussed later). These fat-filled structures are readily identified by their contained vessels, the gastroepiploic in the greater omentum and the middle colic in the transverse mesocolon. The dorsal part of the dorsal mesentery becomes the splenorenal (lienorenal) ligament, which contains the splenic vessels and connects the spleen with the tail of the pancreas. This latter mesenchyme fuses almost completely with the anterior renal fascia to become part of the retroperitoneum.

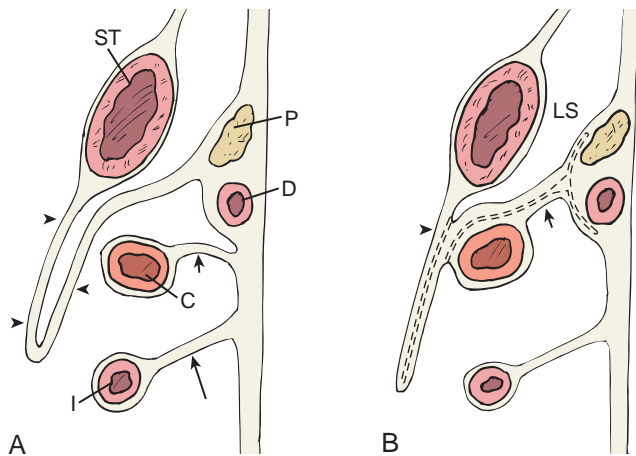


Figure 108-2 Formation of the gastrocolic ligament and transverse mesocolon. **A.** The leftward expansion of the right peritoneal cavity has elongated the gastrosplenic ligament caudally, forming an inferior recess of the developing lesser sac (arrowheads). Long arrow, small bowel mesentery; short arrow, transverse mesocolon. **B.** The posterior layer of the gastrosplenic ligament eventually fuses with the colonic mesentery to form the transverse mesocolon (arrow). The anterior and posterior layers of the gastrosplenic ligament also fuse to obliterate a portion of the right peritoneal space and in so doing form the gastrocolic ligament (arrowhead). What remains of the expanded retrogastric portion of the right peritoneal space eventually becomes the lesser sac (LS). C, transverse colon; D, duodenum; I, small intestine; P, pancreas; ST, stomach; arrows, mesenteries of the colon and small intestine.

During the fifth and sixth weeks of fetal life, the liver continues to grow rapidly and rotates into the right peritoneal space. Concurrently, the stomach undergoes a 90-degree clockwise rotation, such that its left side becomes ventral and its right side dorsal. This rotation pulls the dorsal mesogastrium to the left, allowing room for the right peritoneal space to expand behind the stomach and in front of the pancreas.

This part of the right peritoneal space becomes the lesser sac (i.e., omental bursa). The inferior margin of the gastrosplenic ligament elongates in a caudal direction to form a long inferior sinus. Later in fetal life, the redundant apposed layers of this part of the gastrosplenic ligament fuse to form the greater omentum (Fig. 108-2). During this period (roughly week 6 of fetal development), the midgut has lengthened to the extent that its midportion projects into the umbilical cord (i.e., physiologic herniation). During the 10th week, it returns to the abdomen. The cecum ultimately undergoes a 180-degree rotation (as viewed from above) to arrive at its normal location in the right lower quadrant. The ascending and descending colonic segments undergo further rotation such that their mesenteries fuse to the anterior renal fascia on each side (Fig. 108-3). On the right, the ascending colon rotates 90 degrees counterclockwise (as viewed from below) and normally becomes a fixed part of the retroperitoneum. On the left, the descending colon rotates 90 degrees clockwise (as viewed from below) to become a portion of the retroperitoneum. The transverse colon and its mesentery span the fetus from right to left, with a mesenteric surface facing ventrally. The posterior part of the gastrosplenic ligament then fuses with this surface to form the adult transverse mesocolon.

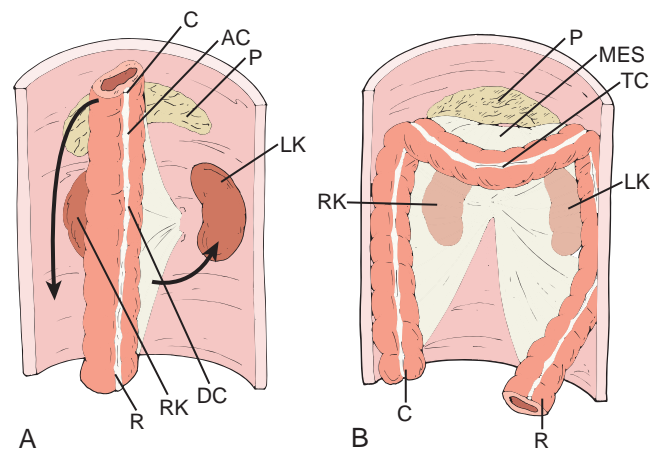


Figure 108-3 Rotation and fusion of colon mesentery. **A.** The line drawing of an embryo early in fetal development shows the distal midgut and hindgut segments that become the adult colon. The most caudal portion, the rectum (R), retains its position in the pelvis. The descending colon (DC) and its attached dorsal mesentery rotate (curved arrow) to cover the surface of the left kidney (LK). The more proximal portions, including the cecum (C) and ascending colon (AC), elongate and join the remainder of the midgut within the physiologic herniation through the umbilicus that occurs in about the sixth fetal week. When these segments return to the abdomen, they undergo a hairpin turn (arrow) so that the cecum is positioned in the right lower quadrant. **B.** After its relocation, the right colon and its attached mesentery rotate to cover the anterior surface of the right kidney (RK). The transverse colon (TC) and its mesentery (MES) face anteriorly at roughly the same level as the pancreas (P).

LOWER ABDOMINAL AND PELVIC EMBRYOGENESIS

Rectum, Urogenital Sinus, and Kidneys

The rectum and urogenital sinus initially develop as part of one structure, the cloaca, the distal part of the hindgut.² As the fetus develops, the urorectal fold, a peritoneal sinus, divides the anterior urinary system from the posterior gut (Fig. 108-4A). In the adult, the caudal part of the urorectal fold fuses to become Denonvilliers' fascia, but a sulcus of peritoneum persists in males and females, becoming the rectovesical pouch (i.e., pouch of Douglas). The rectum and perirectal fat are enveloped by an important fascial plane, the mesorectal fascia.

The anterior (urinary tract) system has several connections that determine adult anatomic landmarks. Superiorly, the urogenital sinus is connected to the umbilical stalk through the allantois, which undergoes fibrous degeneration to become the urachus in both sexes. Posteriorly, the midportion of the urogenital sinus (which becomes the urinary bladder) receives the metanephric duct, or ureter. The inferior part of the urogenital sinus receives the paramesonephric duct and the mesonephric duct; further development of the sinus and the two ducts it receives depends on gender differentiation. In the female embryo, the inferior parts of the paramesonephric ducts fuse to become the uterus and upper vagina, and the part closest to the gonad becomes the fallopian tube. The mesonephric duct almost completely degenerates. The inferior aspect of the urogenital sinus becomes the urethra, lower vagina, and vestibule, with associated Bartholin's glands (Fig. 108-4B).

In the male embryo, the paramesonephric ducts degenerate. The portion of the mesonephric duct closest to the gonads becomes the ductus deferens, and the part closest to the

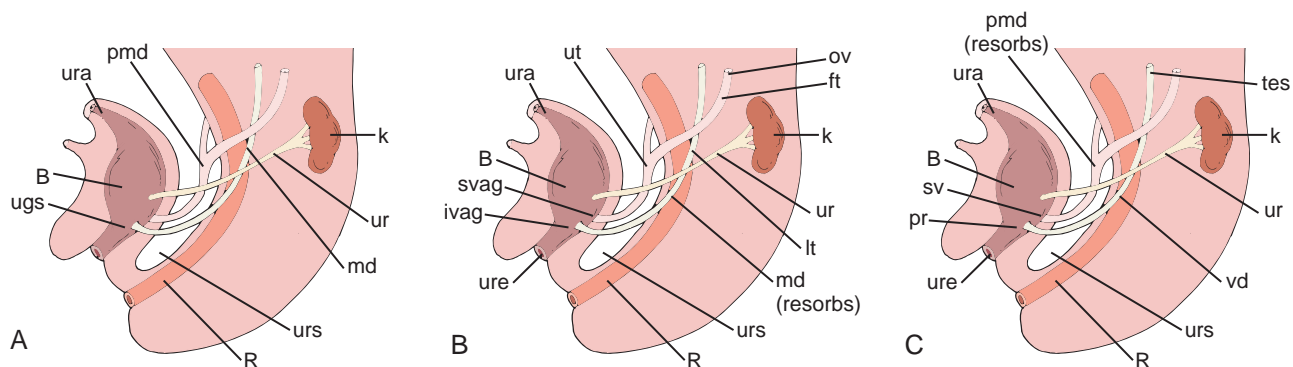


Figure 108-4 Embryology of the pelvis. **A.** Sagittally oriented line drawing of the pelvis in a developing fetus before gender differentiation shows the urorectal sinus (urs), a fold of peritoneum that divides the cloaca into a posterior alimentary tract component, including the rectum (R), and an anterior urogenital component (ugs). The central portion of the urinary component is the bladder (B), which drains superiorly into the allantoic stalk, which becomes the urachus (ura). Inferiorly, the bladder is attached to the urogenital sinus (urs), which differentiates further according to gender. The bladder receives the ureter (ur), and the urogenital sinus receives the paramesonephric duct (pmd) and the mesonephric duct (md), both of which contribute to genital formation. **B.** In the female, the mesonephric duct is almost completely resorbed; its superior portion becomes the ligamentum teres (lt). The central fused portion of the paramesonephric ducts becomes the uterus (ut), and the more superior paired portions close to the ovaries (ov) become the fallopian tubes (ft). The inferior paramesonephric duct becomes the superior vagina (svag). The urogenital sinus in females differentiates into the inferior portion of the vagina (ivag) and urethra (ure). **C.** In males, the paramesonephric duct (pmd) is resorbed. The portion closest to the testis (tes) becomes the vas deferens, and the part near the urogenital sinus differentiates into the seminal vesicles (sv). The urogenital sinus becomes the prostate (pr) and penile urethra (ure). k, Kidney; vd, vas deferens.

urogenital sinus develops into the seminal vesicles and ejaculatory duct. Meanwhile, the urogenital sinus becomes the prostate, urethra, and associated glands (Fig. 108-4C). The remnant of this embryologic derivation is a fascial plane (i.e., umbilicovesical fascia) that envelops the extraperitoneal portion of the bladder and is continuous with the structures that were embryologically in communication with the bladder surface. These structures include the urachus (i.e., median umbilical ligament), the obliterated umbilical arteries (i.e., medial umbilical ligaments), and, in males, the ductus deferens, seminal vesicles, and prostate. This fascia also covers the medial aspect of the ureters as they insert into the bladder base (see Fig. 108-15).

Retroperitoneal Anatomy: Spaces

The embryology previously discussed provides a rationale for the laminar nature of the retroperitoneum (Fig. 108-5). We consider four layers, proceeding from the outermost portion of the extraperitoneum (i.e., body wall and great vessels) to the innermost (i.e., anterior pararenal space). The basic concept to be stressed is that pathologic fluid collections rapidly fill their space of origin and then extend into some nearby expandable plane. If the origin of the fluid collection is within what was embryologically a mesentery (e.g., pancreatitis within the dorsal mesentery), a common mode of extension is within the ligament to which it is attached (e.g., the gastrosplenic ligament). This method of extension is known as subperitoneal spread, as shown in Figure 108-5A. Alternatively, fluid collections may progress between the layers that make up the retroperitoneal lamina (e.g., between the anterior pararenal space and the perirenal space). This is known as interfascial spread,³⁻⁹ and it provides potential communication between the upper abdomen and the pelvis (Fig. 108-5B, C). The remainder of this section provides clinical images of each form of spread, including examples of fluid and aggressive cellular collections.

GREAT VESSELS

The aorta and inferior vena cava course through an incompletely margined space in front of the vertebrae and anterior psoas fascia and posterior to the root of the small intestinal mesentery. An incomplete lateral boundary is formed by the medial aspect of the anterior and posterior renal fasciae, but this is pierced by the renal artery and vein. Superiorly, the great vessel space is continuous with the middle mediastinum; inferiorly, it extends between the abdominal portions of the ureters. Processes that begin in this space can extend easily into the perirenal fat or into the planes anterior and posterior to the perirenal space (Fig. 108-6).¹⁰⁻¹³ Hemorrhage from ruptured aortic aneurysms is particularly likely to enter the posterior interfascial plane. Other processes, such as retroperitoneal fibrosis, tend to be restricted to the great vessel space, encompassing the aorta and inferior vena cava and extending to involve both ureters in their abdominal course.

TRANSVERSALIS FASCIA

The transversalis fascia is the expandable plane that lines the inner surface of the entire abdominal wall. It forms the outermost layer of the retroperitoneum. It is continuous with the diaphragmatic fascia superiorly and with the deep pelvic fascia inferiorly, so that it provides a natural pathway for fluid collections to spread throughout the abdominal cavity.

POSTERIOR FAT PADS

There are two fat pads that provide a cushion for the kidneys; they are positioned in the posterolateral portion of the abdomen and extend into the upper portion of the pelvis. The larger of the two is a crescentic fat collection, the anterior part of which lies lateral to the ascending and descending colon; the posterior part lies on the posterior surface of the perirenal

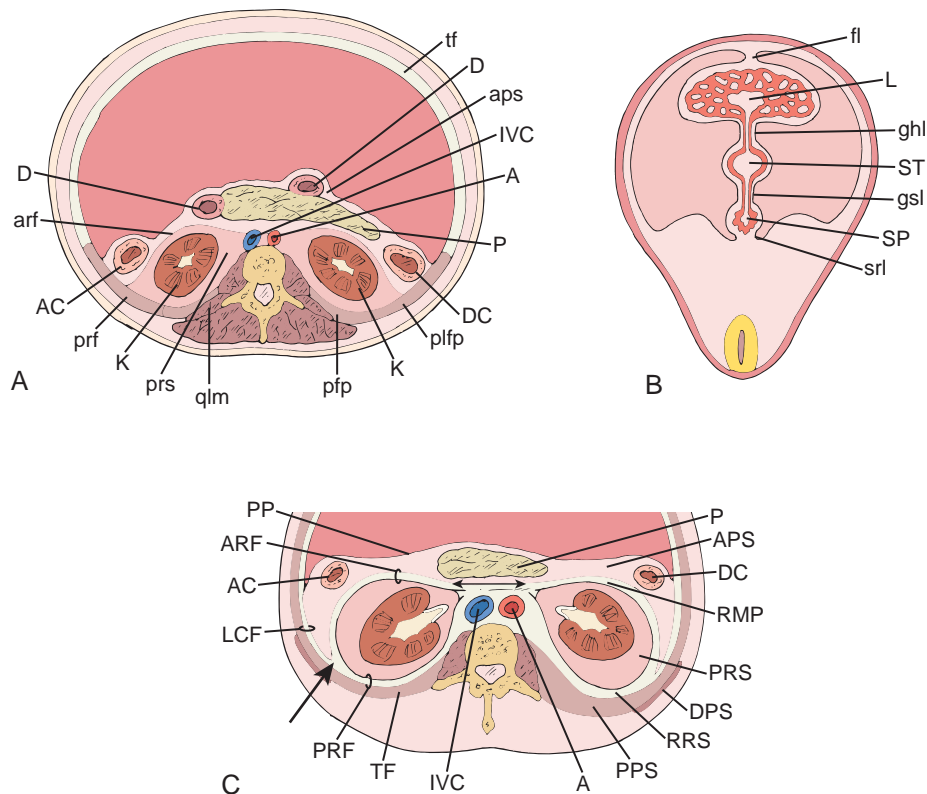


Figure 108-5 The layers of the retroperitoneum and concepts of fluid distribution. **A.** The line drawing depicts the four major retroperitoneal layers. The outermost is the transversalis fascia (tf), which extends from the inferior diaphragmatic fascia to the deep pelvic fascia and surrounds all abdominal organs. Just deep to the transversalis fascia, there are two organless fat pads. The posterior fat pad (pfp) is located just anterior to the quadratus lumborum muscle (qlm). The larger posterolateral fat pad (plfp) cushions the kidney (K) and perirenal fat and the mesentery surrounding the descending colon (DC). Between the two is a cleft, which is a part of the inferior lumbar triangle; the cleft is an important passageway between the deep retroperitoneum and the transversalis fascia. Just internal to the fat pads are the perirenal spaces (prs), which contain the kidneys, adrenal glands, and abundant fat. They are bounded by expandable fascial planes anteriorly (arf) and posteriorly (prf). They are loosely attached medially to the great vessel space around the inferior vena cava (IVC) and aorta (A). In adults, the two perirenal spaces do not communicate directly. The innermost space, which is the anterior pararenal space (aps), is composed of the dorsal mesenteries that contain the ascending (AC) and descending colon (DC) laterally and the duodenum (D) and pancreas (P) medially. **B.** The concept of subperitoneal disease spread is delineated. The line drawing of an early embryo emphasizes that the mesenteries surround every structure in the abdomen, providing a potential means of communication by way of the abdominal ligaments (derivatives of the mesenteries); the falciform ligament (fl) connects the liver (L) with the anterior abdominal wall. The stomach (ST) and duodenum are connected to the liver by the gastrohepatic ligament (ghl) or lesser omentum. The dorsal mesentery, containing the spleen (SP) and pancreas, communicates ventrally through the gastrosplenic ligament (gsl) and dorsally by way of the splenorenal ligament (srl). **C.** The diagram shows the retroperitoneal compartments and interfascial planes and spaces. The anterior pararenal space (APS) contains the duodenum (not shown), the ascending and descending colon, and the pancreas. The perirenal space contains the adrenal glands (not shown) and the kidneys. The perirenal spaces are closed medially. The posterior pararenal space (PPS) contains fat and lymph nodes. The renal fascia and lateroconal fascia are laminated planes composed of apposed layers of embryonic mesentery. By dissection of these layers, rapidly accumulating fluid collections or infiltrating disease may spread within retroperitoneal fascial planes. The thickness of the interfascial planes is exaggerated to illustrate their potentially expansile nature; all three interfascial planes are potential spaces. The retromesenteric plane (RMP) is continuous across the midline (bidirectional arrows). The retromesenteric plane, retrorenal plane (RRS), and lateroconal plane (LCF) communicate at the fascial trifurcation (arrow). The dorsal pleural sinus (DPS) may extend inferiorly to lie posterolateral to the PPS and the transversalis fascia (TF). ARF, Anterior renal fascia; PP, parietal peritoneum; PRF, posterior renal fascia. (C from Aizenstein RI, Wilbur AC, O'Neil HK: Interfascial and perinephric pathways in the spread of retroperitoneal disease: Refined concepts based on CT observations. *AJR Am J Roentgenol* 168:639-643, 1997.)

fat. This fat has been called the posterior pararenal space. Cutaneous nerves pass through this fat, but it contains no organs and is rarely the primary site of pathologic processes. The smaller fat pad lies just anterior to the transversalis fascia near the quadratus lumborum muscle. Between the two fat pads is a cleft, through which fluid may pass from the deep retroperitoneum outward to the transversalis fascia. Hernias containing fat or bowel can pass through this same cleft, which is a part of the inferior lumbar triangle (i.e., Petit's triangle). It is common for severe pancreatitis to spread by this route, producing inflammation or hemorrhage, or both, in the ipsilateral

flank; this is the rationale for the Grey Turner sign of hemorrhagic pancreatitis (Fig. 108-7).¹⁴

PERIRENAL SPACE

There has been considerable interest in delineating the precise anatomy of the perirenal space and its enveloping fascia,¹⁵⁻²⁰ and there is no universal agreement about its exact boundaries—whether its inferior part is open or closed to the pelvis²¹⁻²⁸ and whether the spaces communicate across the midline.²⁹ In our view, rapidly expanding retroperitoneal fluid collections extend

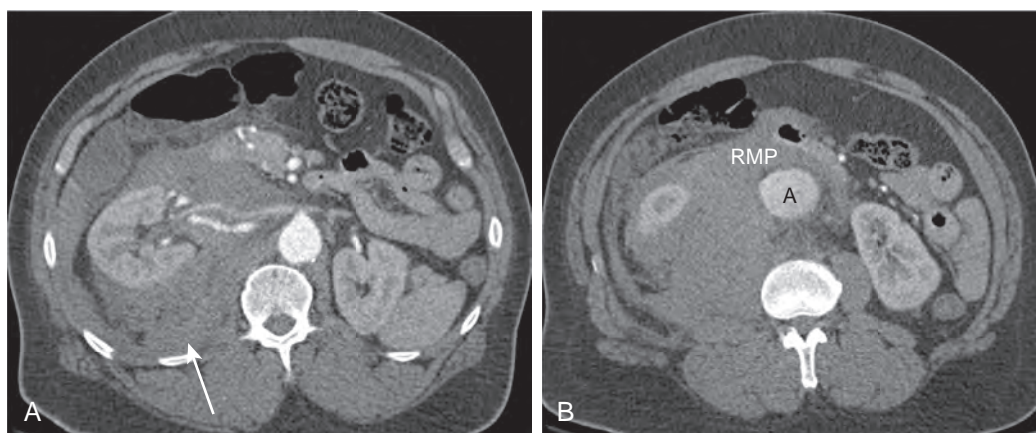


Figure 108-6 Ruptured abdominal aortic aneurysm. Scans obtained at two different levels (**A** and **B**) show hemorrhage in the retromesenteric plane (RMP) and the retrorenal plane (arrow). A, aortic aneurysm.

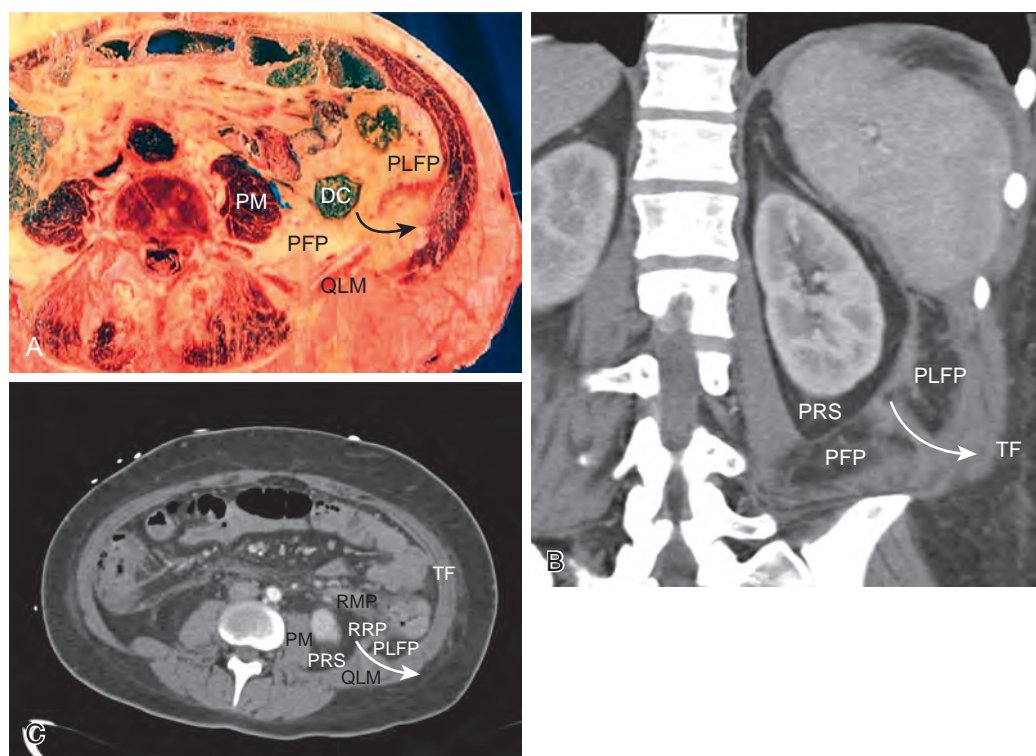


Figure 108-7 Inferior lumbar triangle pathway. **A.** Section from a cadaver shows the posterior fat pad (pfp) just lateral to the psoas muscle (PM) and anterior to the quadratus lumborum muscle (qlm). The posterolateral fat pad (plfp), also called the posterior pararenal space, has been displaced in this subject by a hernia (curved arrow) containing fat adjacent to the descending colon (DC). This inferior lumbar hernia occurs through the cleft between the two fat pads. **B.** Coronal CT section in a patient with severe pancreatitis shows pancreatic effusion from the deep retroperitoneal planes extending (curved arrow) through the inferior lumbar triangle pathway between the posterior fat pad (PFP) and the posterolateral fat pad (PLFP) to reach the transversalis fascia (TF). On the axial image (**C**), notice the preserved fat in the perirenal space (PRS), which divides the anterolateral retromesenteric plane (RMP) from the posterolateral retrorenal plane (RRP).

into the interfascial planes, where they can freely spread into the pelvic extraperitoneum and across the midline (examples are discussed later).

The embryology of the kidneys provides the explanation for the unusual appearance of the perirenal space. As the kidneys ascend from their pelvic origins, they are sheathed by a long, tapered cone of fat within the anterior and posterior renal fascia.³⁰ This space is thin at the diaphragm, typically most voluminous posterior to the lower renal pole, and thin again as

it extends inferiorly toward the pelvis. Fluid collections, such as urinomas or localized hematomas,³¹⁻³⁶ often gravitate toward the posteroinferior portion of the perirenal fat, which typically has the greatest volume. The lateral boundary of the perirenal space abuts the posterolateral fat pad, and its fusion with that space creates an expandable plane that extends behind and lateral to the kidney, the retrorenal plane. The laminar nature of this fusion plane was described by Raptopoulos and colleagues³⁷ and conforms to clinical observations. The anterior

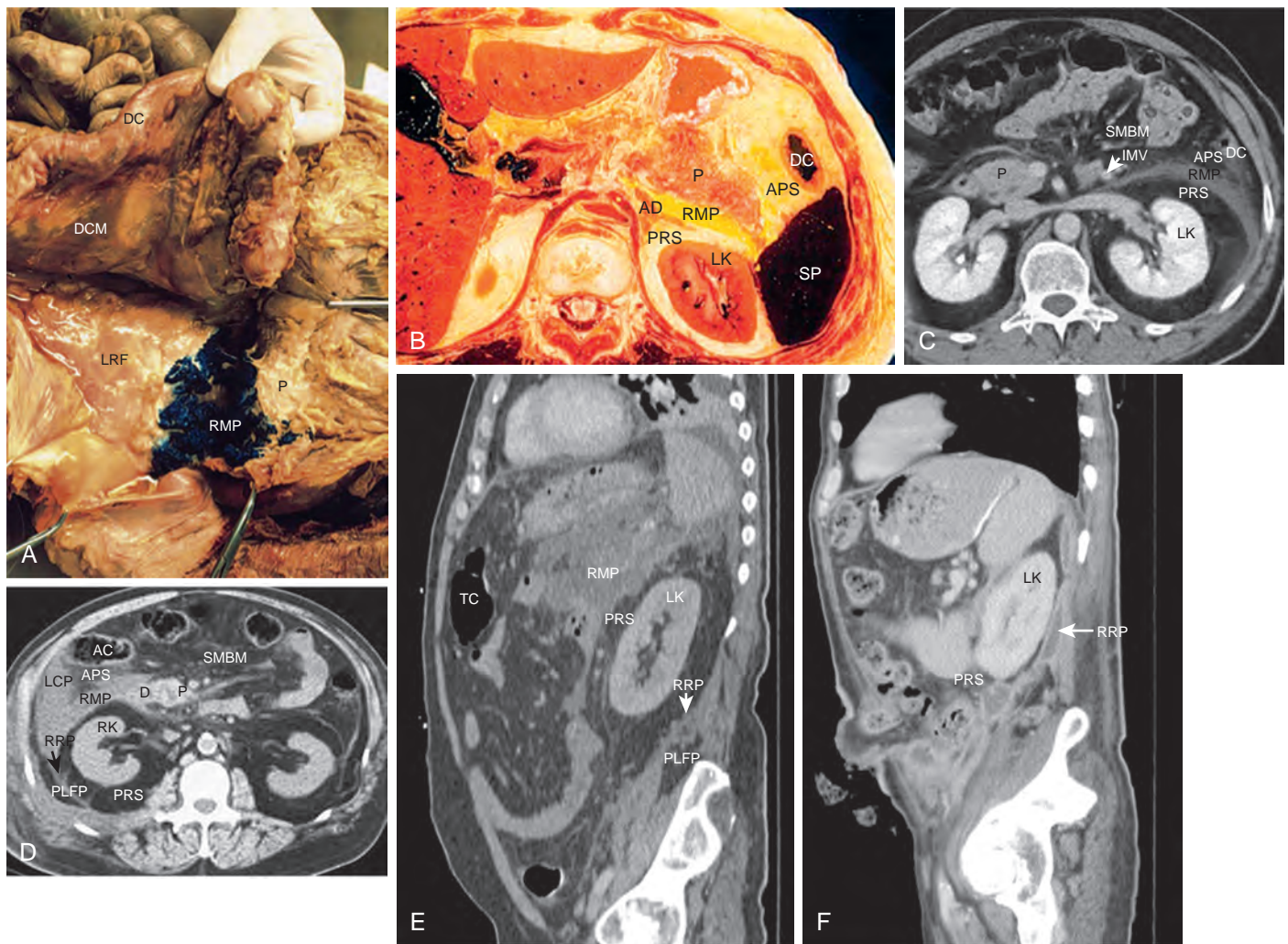


Figure 108-8 Retromesenteric and retrorenal escape planes. **A.** Photograph of a cadaver dissection prepared by injection of blue latex into the pancreatic parenchyma to simulate pancreatitis. The dissector retracts the descending colon (DC) and its mesentery (DCM) to expose the latex in the retromesenteric plane (RMP). This plane lies anterior to the left renal fascia (LRF) and just posterior to the pancreatic (P) tail. **B.** Cross section of a cadaver prepared as in **A** shows yellow latex filling the retromesenteric plane (rmp) anterior to the perirenal space (PRS), which contains the left kidney (LK) and adrenal (ad). Anterior to the latex collection lie the pancreas (P) and descending colon (DC) within the anterior pararenal space (APS), located above the spleen (SP). **C.** CT demonstrates retroperitoneal anatomy in a patient with pancreatitis. The effusion lies in the retromesenteric plane (RMP) anterior to the perirenal space (PRS) around the left kidney (LK). Anterior to the effusion is the anterior pararenal space (aps, identified by its contents), the descending colon (DC), and its mesentery, which is marked by the inferior mesenteric vein (IMV) that is near the pancreas (P). The small intestinal mesentery (SMBM) lies anterior to the anterior pararenal space. **D.** The CT section shows the symmetric arrangement of the intrafascial planes on the right in a patient with inflammation of the duodenum (D). The retromesenteric plane (RMP) lies anterior to the right kidney (RK) and surrounding fat in the perirenal space (PRS) and lies posterior to the ascending colon (AC) and its fat-filled mesentery in the anterior pararenal space (APS). In this example, fluid extends posteriorly between the posterolateral fat pad (PLFP) and the anterior pararenal space within the lateroconal plane (LCP) as well as posteriorly between the perirenal fat and the posterolateral fat pad in the retrorenal plane (RRP). The pancreas (P) and small intestinal mesentery (SMBM) are identified. **E.** Sagittal reformatted CT image of the fascial planes in a patient with severe necrotizing pancreatitis shows fluid expanding the retromesenteric plane (RMP). The plane lies anterior to the right kidney (RK) within the perirenal space (PRS). There is a smaller amount of fluid in the retrorenal plane (RRP) lying posterior to the perirenal space and anterior to the posterolateral fat pad (PLFP). Notice the long inferior continuation of perirenal fat and the transverse colon (TC). **F.** Sagittal reformatted CT image shows the retrorenal plane (RRP) lying behind the perirenal space (PRS) in another patient with pancreatitis. In this case, the fluid extends from the inferior diaphragmatic fascia beyond the level of the lower pole of the left kidney (LK).

boundary of the perirenal space abuts the anterior pararenal space and produces a similar laminar plane (i.e., retromesenteric plane) that also collects and distributes retroperitoneal effusions (Fig. 108-8).

Each perirenal space contains the kidney, adrenal gland, proximal ureter, renal artery, and renal vein. The fascial lining of the perirenal space is incomplete where the renal vessels pass through it, and the entire medial boundary of the space is poorly defined.³⁸ The study by Kunin³⁹ established that there

are well-structured pores within the perirenal fat, some of which course between one surface of the kidney and another (i.e., renorenal septa) and some of which communicate between the renal surface and the perirenal fascia (i.e., renofascial septa). The latter are responsible for the rapid egress of effusions (often urinomas⁴⁰) in the perirenal space into the retromesenteric or retrorenal plane (Fig. 108-9) and for involvement of the renal surface with effusions of extrarenal origin, such as pancreatitis.⁴¹⁻⁴³

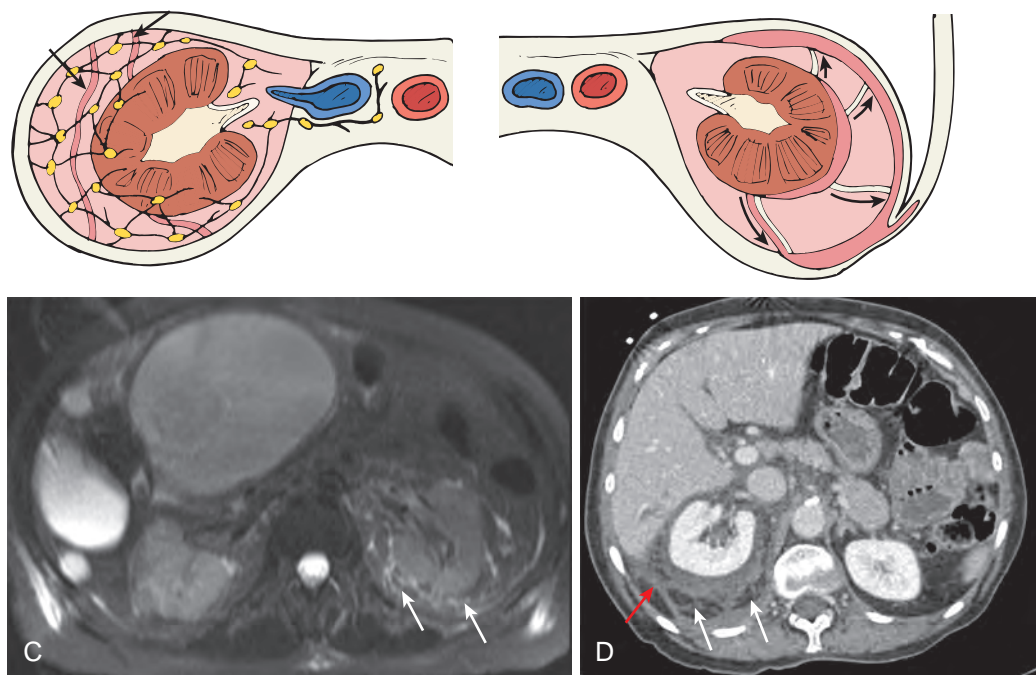


Figure 108-9 Perinephric space. **A.** Diagram depicting the perinephric space at the level of the midpole of the right kidney shows a rich network of bridging septa (arrows), arteries, veins, and lymphatics. The perirenal lymphatics communicate with the lymph nodes of the renal hilum, and these connect with the periaortic and pericaval lymph nodes. **B.** Renal pericapsular hematoma can spread along the perinephric bridging septa (arrows) toward the interfascial planes. Tense fluid collections, such as large urinomas and hematomas, that would otherwise be constricted by an intact renal capsule or by perinephric septa may decompress along perinephric channels and retroperitoneal interfascial planes. **C.** Fat-suppressed magnetic resonance image demonstrates bridging septa of Kunin (arrows) in a patient with recent forniceal rupture. **D.** Subcapsular hematoma of the right kidney is decompressing through the bridging septa (white arrows) into the posterior retrorenal plane (red arrow). (**A** and **B** from Aizenstein RI, Wilbur AC, O'Neil HK: *Interfascial and perinephric pathways in the spread of retroperitoneal disease: Refined concepts based on CT observations.* *AJR Am J Roentgenol* 168:639-643, 1997.)

ANTERIOR PARARENAL SPACE

The anterior pararenal space is entirely composed of visceral structures and their mesenteries of origin. Medially, the components consist of the pancreas (with remnants of the ventral mesentery surrounding the head and uncinate process and the dorsal mesentery supporting the neck, body, and tail) and the duodenum. These structures fuse posteriorly with the perirenal space, typically at the level of the renal hila. In the midline, the fusion plane passes between the great vessel space and the root of the intestinal mesentery. This part of the retromesenteric plane provides communication between the left and right retroperitoneum, and it is the only anatomic site where a passage exists across the midline (see Fig. 108-12C).

The lateral aspect of the pararenal space is formed by the ascending and descending colon and their attached dorsal mesenteries. These mesenteries fuse to the anterior aspect of the perirenal fat just lateral to the fusion of the duodenum, and they create a single retromesenteric plane on each side. Laterally, they fuse to the posterolateral fat pads to form the lateroconal plane (Fig. 108-10).

Retroperitoneal Anatomy: Planes

RETROMESENTERIC AND LATEROCONAL PLANES

The lateroconal planes are relatively small. They extend down the length of the ascending and descending colon just lateral to

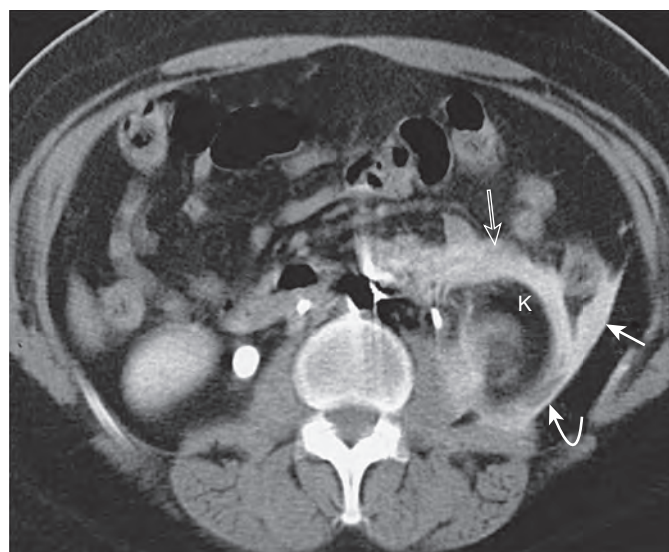


Figure 108-10 Ruptured renal pelvis. The retromesenteric plane (open arrow), lateroconal plane (solid arrow), and retrorenal plane (curved arrow) contain extraluminal contrast material because of the rupture of the left renal pelvis due to blunt trauma. K, Perinephric space.

the colonic lumen. The retromesenteric planes are major routes by which effusions are distributed in the extraperitoneal abdomen. They are especially important because they are the route of escape for common pathologic entities, such as pancreatitis and colitis. On the left, the retromesenteric plane

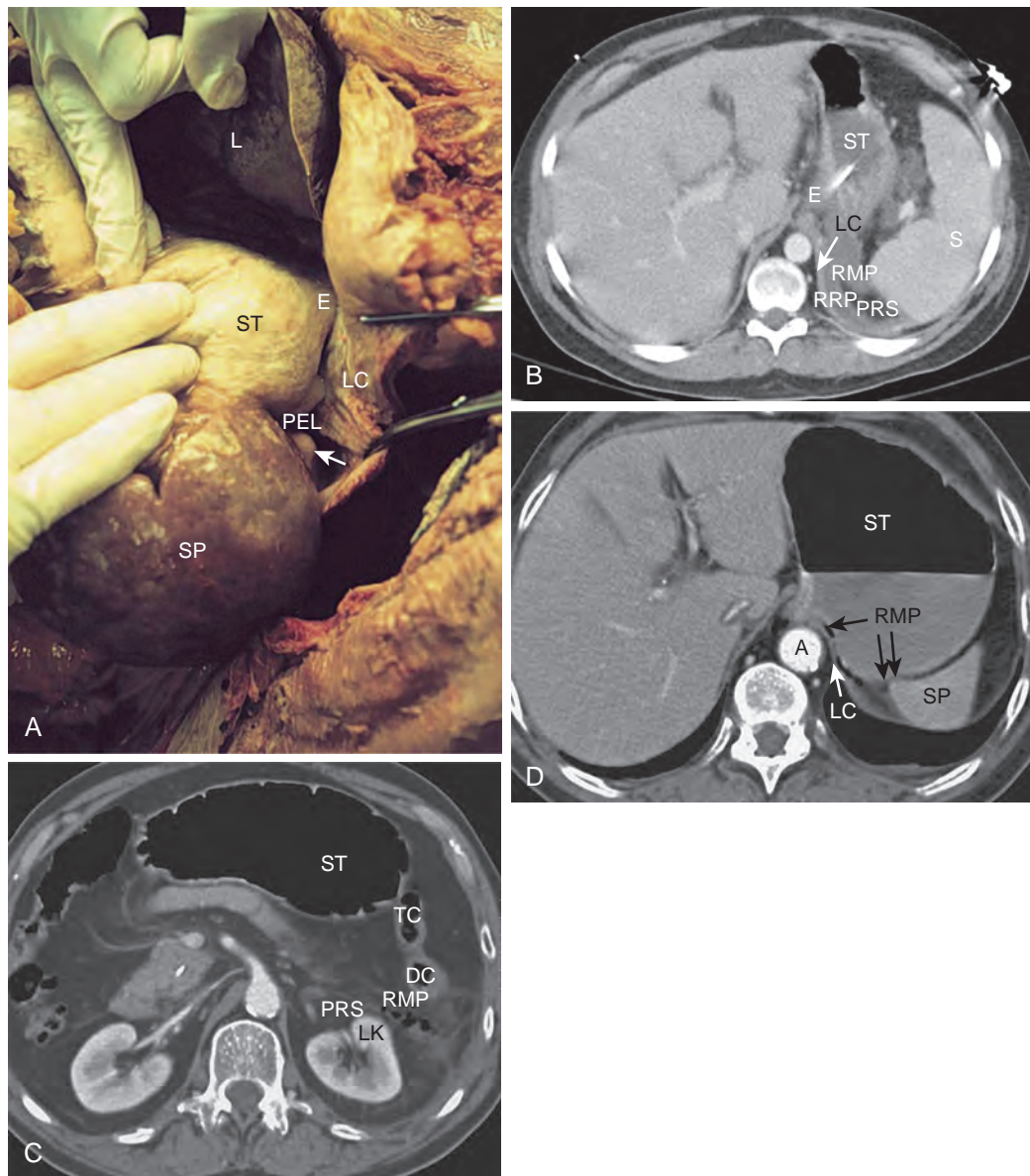


Figure 108-11 Superior extent of the interfascial planes: left side. **A.** Blunt dissection of a cadaver prepared as shown in [Figure 108-8A](#). The dissector's hand passes posterior to the pancreas (not shown) and hilum of the spleen (SP) to lie immediately posterior to the stomach (ST) just below its junction with the esophagus (E). The dissector's gloved fingertip (*arrow*) lies on the left crus of the diaphragm (LC) and is covered by the nearly transparent phrenicoesophageal ligament (PEL). **B.** CT shows a section from a clinical case illustrating the superior extent of the interfascial planes. In this patient with pancreatitis, fluid fills the retrorenal plane (RRP) and retromesenteric plane (RMP) surrounding the superior part of the perirenal space (PRS). The collection converges to its most superior location, just lateral to the left crus (LC), posterior and to the left of the esophagus (E), and posterior and to the right of the stomach (ST). This fluid defines the bare area of the stomach. **C.** The CT section was obtained in a patient who had a localized perforation of the tail of the pancreas during an interventional endoscopic procedure. Fluid and gas outline a portion of the retromesenteric plane (RMP) anterior to the perirenal space (PRS) containing the left kidney (LK). The anterior pararenal space is identified by the presence of the proximal descending colon (DC) and its mesenteric fat. TC, Transverse colon; ST, stomach. **D.** The CT section obtained 4 cm superior to that in **C** shows gas in the retromesenteric plane (RMP) adjacent to the left diaphragmatic crus (LC), outlining the bare area of the stomach (*single arrow*) and the bare area (*double arrow*) of the spleen (SP). A, Aorta; ST, stomach.

extends superiorly to abut the left crus of the diaphragm just posterior to the gastroesophageal junction ([Fig. 108-11](#)). On the right, the superior extent is less well understood; clinical observations suggest that the retromesenteric plane on the right (or possibly the superior part of the perirenal space^{44,45}) is directly continuous with the bare area of the liver ([Fig. 108-12](#)).

Inferiorly, the retromesenteric plane is limited and extends over the surface of the kidneys medially as far as the dorsal mesentery. Proceeding inferiorly, this plane becomes

progressively smaller as the perirenal space becomes thinner. Ultimately, it merges with the retrorenal plane below the cone of renal fascia to form the combined plane ([Fig. 108-13](#)).

RETRORENAL PLANE

Superiorly, the retrorenal plane extends to the inferior diaphragmatic fascia. At the level of the kidneys and below, the retrorenal plane typically extends as far medially as the psoas

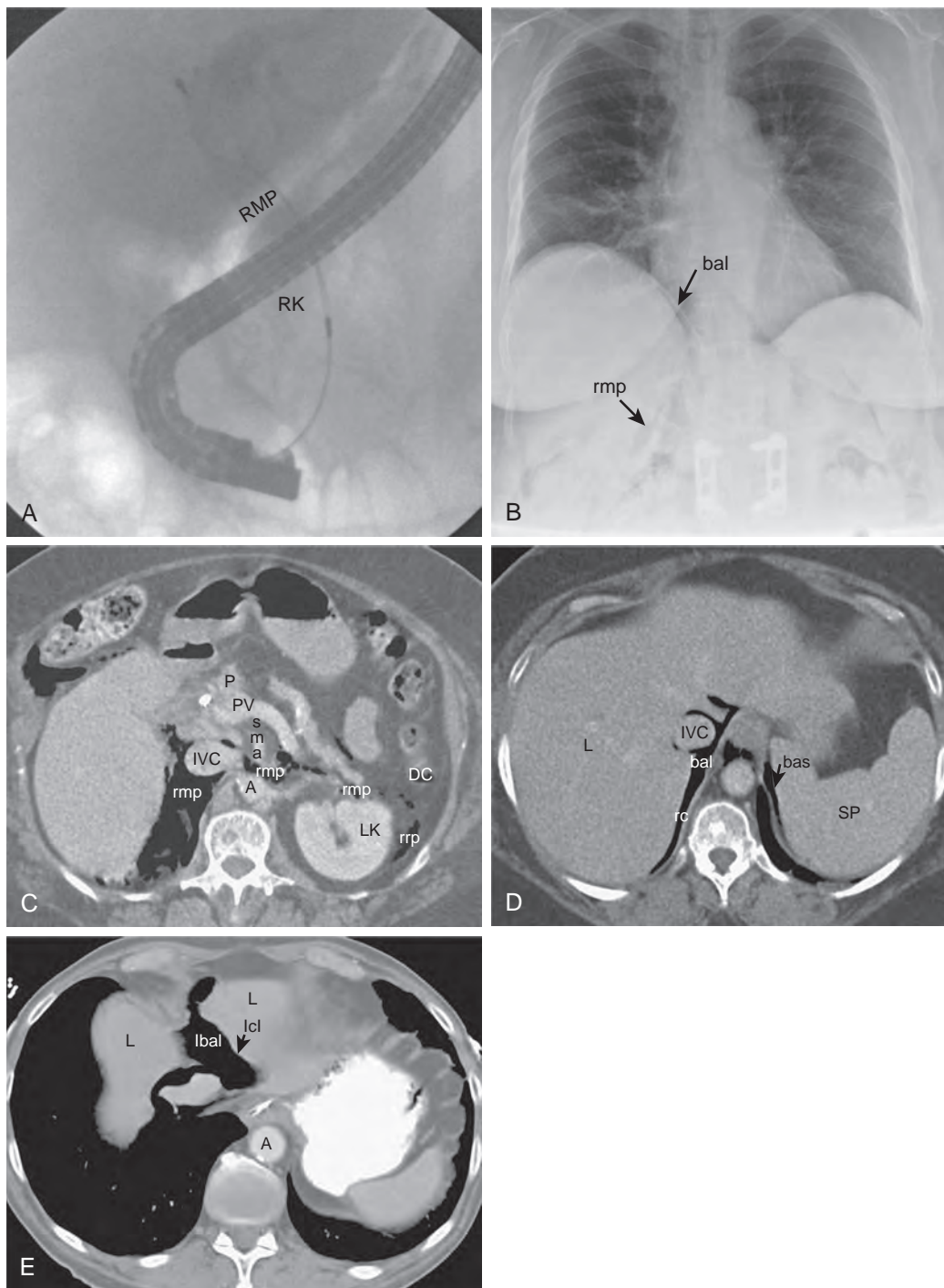


Figure 108-12 Superior extent of the intrafascial planes: right side. **A.** An oblique fluoroscopic image obtained during an interventional endoscopic procedure shows gas from a duodenal perforation outlining the retromesenteric plane (RMP) anterior to the right kidney (RK). **B.** The chest radiograph obtained immediately after the procedure shows a crescentic gas collection on the medial aspect of the right hemidiaphragm in the location of the bare area of the liver (bal). Gas in the retromesenteric plane (rmp) is discernible superior to the duodenal gas. **C.** CT section obtained in the same patient shows extensive gas filling the superior aspect of the retromesenteric plane (rmp). This gas continues anterior to the inferior vena cava (IVC) and extends to the left between the aorta (A) and superior mesenteric artery (sma) in the part of the retromesenteric plane created by fusion of the mesentery of the duodenum with the great vessels. This allows access of the right-sided plane to its counterpart on the left, anterior to the left kidney (LK) and behind the descending colon (DC). Some of the gas has dissected into the left retrorenal plane (rrp). P, Pancreas; PV, portal vein. **D.** The CT section obtained 4 cm superior to that in **C** shows gas outlining the bare area (bal) of the liver (L). The gas courses around the inferior vena cava (IVC) along the right diaphragmatic crus (rc). Some of the left-sided gas has ascended to the bare area (bas) of the spleen (SP). **E.** The CT section obtained 3 cm superior to that in **D** shows gas outlining the left portion of the bare area (lbal). This gas outlines the left coronary ligament (lcl), the edge of the peritoneal reflection of the left perihepatic spaces. L, Liver; A, aorta.

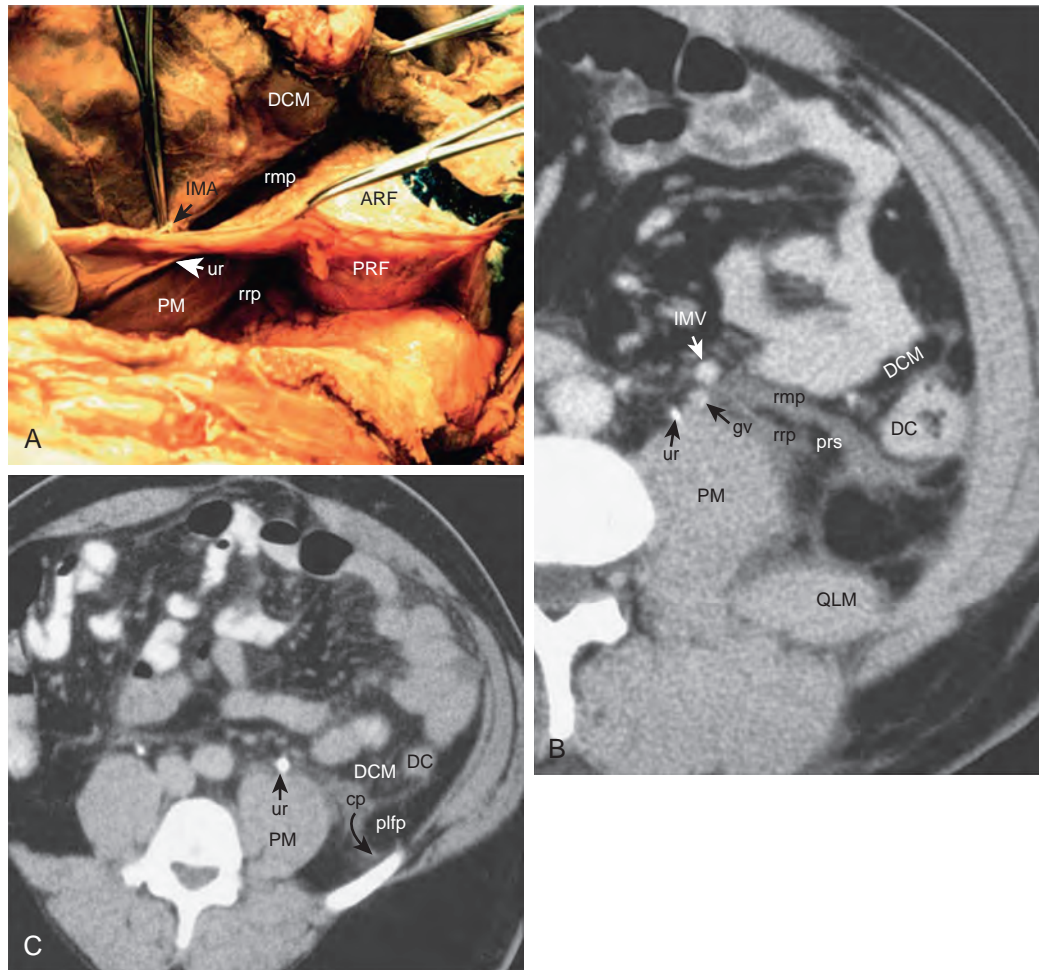


Figure 108-13 Communication of the intrafascial planes with the pelvis. **A.** Blunt dissection of a cadaver prepared as shown in [Figure 108-8A](#). The descending colon (not shown) is being retracted on its mesentery (DCM), identified by its major vessel, the inferior mesenteric artery (IMA). Just anterior to the anterior renal fascia (ARF) lies the retromesenteric plane (rmp), which extends laterally as far as the colonic mesentery. The perirenal fat (held by the dissector) becomes progressively smaller inferiorly. Posterior to the posterior renal fascia (PRF) is the retrorenal plane (rrp). This plane extends medially as far as the psoas muscle (PM) and ureter (ur). Fluid collections tend to occupy the larger retrorenal plane and extend into the pelvis along the margin of the psoas muscle (PM). **B.** CT shows a section of the inferior aspect of the perirenal space (prs) in a patient with pancreatitis. Fluid in the retromesenteric plane occupies the space immediately behind the descending colon (DC) and its mesentery (DCM), identified here by the inferior mesenteric vein (IMV). Just posterior to the perirenal space and anterior to the psoas muscle (PM) is the retrorenal plane (rrp). It extends medially almost as far as the ureter (ur). Between the ureter and inferior mesenteric vein is the right gonadal vein (gv). The quadratus lumborum muscle (QLM) is identified. **C.** The CT section 15 mm inferior to that in **B** shows no perceptible perirenal fat. The retrorenal and retromesenteric planes have merged to form a combined plane (cp), which occupies the anterolateral surface of the psoas muscle (PM) lateral to the ureter (ur). Notice the extension of the fluid into the lumbar triangle cleft (curved arrow) medial to the posterolateral fat plane (plfp).

muscle (see Fig. 108-13A). In general, retrorenal collections do not extend medial to the ipsilateral ureter. As the retrorenal plane extends inferior to the cone of renal fascia, it joins the retromesenteric plane to become a combined plane that is situated on the anterolateral surface of the psoas muscle, lateral to the ureter and medial to the iliac vessels. It continues into the pelvic extraperitoneum.

PELVIC EXTRAPERITONEAL SPACES AND PLANES

The urinary bladder, along with its embryologically derived attachments, is the central structure in the formation of the pelvic extraperitoneum. The bladder, urachus, obliterated umbilical vessels, and urogenital sinus derivatives are covered by umbilicovesical fascia.⁴⁶ This divides the pelvic extraperitoneum into a small-volume perivesical space and a prevesical space that lies between the perivesical space and the transversalis fascia. In a way analogous to the structure of the perirenal space and fascia, the fascial lining of the prevesical space forms an expandable plane surrounding the bladder. As shown in Figure 108-14, the obliterated umbilical artery (i.e., medial umbilical ligament) contains a variable amount of periligamentous fat and is covered anteriorly and posteriorly by fascia. The anterior fascia forms the umbilicoprevesical plane and passes just posterior to the inferior epigastric artery; laterally, it fuses with the transversalis fascia near the inguinal ring. The posterior fascia forms the umbilicovesical plane and fuses laterally to the combined plane, typically positioned just medial to the obturator fossa. Large collections occupying both of these

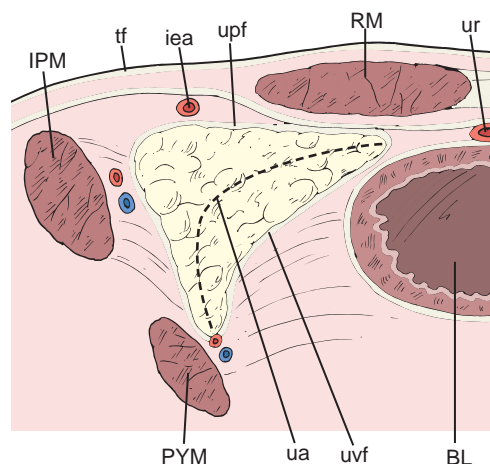


Figure 108-14 Fascial planes of the extraperitoneal pelvis. The bladder (BL) occupies the anterior midline and is surrounded by perivesical fascia. Fascia surrounds the triangular fat around the medial umbilical ligaments, containing the obliterated umbilical artery (ua). Posterior to the periligamentous fat is the umbilicovesical fascia (uvf), which blends with the fascial plane around the bladder. Anterior to the fat in the root of the medial umbilical ligament is the umbilicoprevesical fascia (upf), which extends posterior to the inferior epigastric artery (iea). Laterally, this fascia blends with the combined fascial plane medial to the iliopsoas muscle (IPM) and can potentially extend posteromedially, medial to the internal iliac vessels near the piriformis muscle (PYM). Just anterior to the bladder is the obliterated allantois, the urachus (ur), which is surrounded by a variable quantity of fat. The umbilicoprevesical fascia divides in the midline to surround this structure. RM, Rectus muscle; tf, transversalis fascia.

posterior planes straddle the urinary bladder and resemble a molar tooth.

Most fluid collections continue to extend through the prevesical space to involve the transversalis fascia. These can gain access to the combined plane lateral to the colon; from here, they extend posteriorly just medial to the obturator canal to involve the presacral fascia. Moreover, they can gain access to the inguinal canal to extend to the scrotum and to the femoral canal to progress to the lower extremity (Fig. 108-15).

In summary, there exists a complex and voluminous network of fascia capable of transmitting pathologic fluid collections that arise anywhere in the abdomen to locations remote from the original site of the process. This network explains how, for example, pancreatitis can mimic appendicitis or diverticulitis can clinically and radiographically resemble ureteral obstruction. Although fluid from pancreatitis remains the most common pathologic process to involve these planes, cellular spread of aggressive tumors can extend in an identical fashion. A diagrammatic summary of the spaces and planes in the retroperitoneum is shown in Figure 108-16.

Subperitoneal Spaces: Ligaments and Mesenteries

Pathologic fluid collections rapidly seek escape from their space of origin. The interfascial planes are major routes for such escape, but fluid also can extend within the mesentery that originally enfolded the diseased organ. This means of intramesenteric spread is referred to as subperitoneal spread, and it represents extension within the abdominal ligaments.⁴⁷

UPPER ABDOMINAL LIGAMENTS

Most of the mesenteries that persist into adult life as ligaments are present in the upper portion of the abdominal cavity, in part because the ventral mesentery distal to the foregut is resorbed. Described in the following sections are the remnants of the ventral and dorsal mesenteries that supported the gut and the intramesenteric growth of the gut-derived solid viscera: liver, spleen, and pancreas.

Falciform Ligament

The falciform ligament is the remnant of the ventral part of the ventral mesentery. It contains the obliterated umbilical vein, and it is the structure in which large collateral veins are recruited in patients with advanced portal hypertension. It subdivides the peritoneal spaces over the surface of the liver, and it is occasionally a conduit for spread of intrahepatic neoplasms, such as aggressive hepatomas (Fig. 108-17).

Gastrohepatic and Hepatoduodenal Ligaments

The gastrohepatic and hepatoduodenal ligaments are remnants of the dorsal part of the ventral mesentery, between the gut and the liver, and they are known collectively as the lesser omentum. The gastrohepatic ligament extends between the lesser curve of the stomach and the fissure for the ligamentum venosum; it contains the left gastric artery, coronary vein, and part of the hepatic chain of lymph nodes.⁴⁸ It is an important means of spread of gastric cancer into the hilum of the liver, and gastric perforations occasionally extend between its leaves (Fig. 108-18).

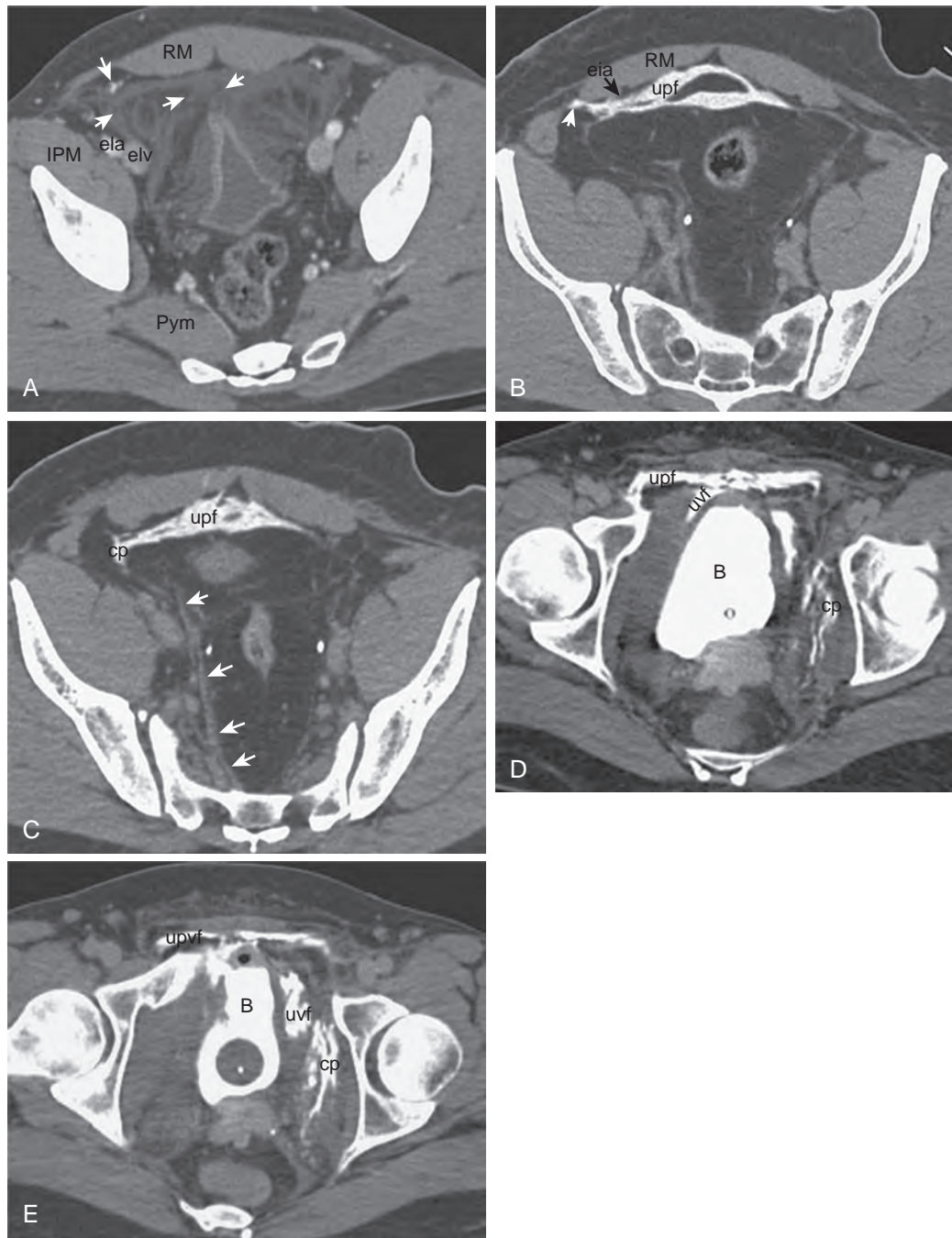


Figure 108-15 Retroperitoneal fascial planes. **A.** CT section of a patient with traumatic bladder perforation shows a small amount of urine in the perivesical space (pvs) surrounding the bladder (B). In this patient, there is a larger fat plane than usual around the medial umbilical ligament (mul). There is fluid within the umbilicoprevesical fascia (upvf) anteriorly and the umbilicovesical plane (uvp) posteriorly. On the right, the collection extends posteriorly toward the internal iliac vessels lying on the piriformis muscle (Pym). Anteriorly, the lateral part of the fascia extends posterior to the internal epigastric artery (iea) to blend with the combined plane (cp) near the external iliac vessels (eia and eiv). The iliopsoas muscle (IPM), rectus abdominis muscle (RM), and urachus (ura) are indicated. **B.** CT section in a different patient with a pelvic fracture producing extraperitoneal bladder perforation shows another pattern of fluid distribution in the pelvic extraperitoneum. Contrast material from the bladder has extended into the umbilicoprevesical fascia (upf), which divides in the midline to surround the fat surrounding the median umbilical ligament or urachus (ur). The umbilicoprevesical fascia extends laterally behind the external iliac artery (eia) and enters the transversalis fascia (tf) lateral to the boundary of the rectus abdominis muscle (RM). **C.** CT section obtained 15 mm inferior to that in **B** shows contrast material in the umbilicoprevesical fascia (upf) extending into the combined plane (cp) on the anterior surface of the fat around the medial umbilical ligament (mul). On the right, fluid, but not contrast material, extends posteriorly (arrows) just medial to the iliac vessels and lateral to the perirectal fat as far as the presacral space (PS). **D.** The CT section in another patient with extraperitoneal bladder rupture due to blunt trauma with multiple pelvic fractures shows contrast material from the perforated bladder (B) extending into the umbilicovesical fascia (uvf) and the umbilicoprevesical fascia (upf). On the left, some of this contrast material has entered the combined plane (cp), tracking posteriorly. **E.** A CT section 15 mm inferior to that in **D** shows further accumulation of contrast material in the combined plane (cp).

The hepatoduodenal ligament contains the portal vein, hepatic artery, common hepatic and central cystic ducts, and nodes of the porta hepatis.⁴⁹ At one time, this part of the ventral mesentery contained the ventral pancreas, which later in embryologic development rotated into the retroperitoneum. Pancreatitis recalls that embryologic connection and often extends into the liver through the porta hepatis. Because of this, intrahepatic portal vein thrombosis is a moderately common complication of acute pancreatitis (Fig. 108-19).

Gastrosplenic Ligament, Greater Omentum, and Transverse Mesocolon

The ventral part of the dorsal mesentery extends in the embryo between the greater curvature of the stomach and the spleen. When the right peritoneal cavity extends behind the stomach, this part of the dorsal mesentery is elongated so that a long, redundant surface extends inferiorly. The part of the dorsal mesentery closest to the spleen becomes the adult gastrosplenic ligament, and it can be recognized by the short gastric vessels that course through it. In cases of splenic vein thrombosis, the short gastric veins are routinely recruited as collaterals. A major route of escape for pancreatitis arising in the peripheral body and tail is into the gastrosplenic ligament.⁵⁰ Large intraligamentous collections are frequently mistaken for lesser sac effusions but do not communicate with the peritoneal cavity (Fig. 108-20).

The redundant portion of the gastrosplenic ligament forms two other ligamentous structures in the adult. The inferior portion fuses to form the gastrocolic ligament, or greater omentum. This structure is easily recognized by its contained gastroepiploic vessels, the veins of which dilate in the presence of splenic vein occlusion. The omentum also is the major site of implantation of processes involving the peritoneal cavity. Omental caking from ovarian, endometrial, or gastric primary cancers is commonly recognized (Fig. 108-21).

The posterior and superior part of the redundant gastrosplenic ligament fuses to the anterior leaf of the dorsal mesentery of the transverse colon to form the transverse mesocolon. The middle colic vessels mark the location of this structure; it provides a pathway for escape of pancreatitis that involves the midportion of the pancreas. Greater curvature gastric ulcers, benign or malignant, course down the transverse mesocolon to create gastrocolic fistulas (Fig. 108-22). The transverse mesocolon is also an important pathway of direct spread from tumors arising from the nearby pancreas.^{51,52}

Splenorenal Ligament

The tail of the pancreas arises in the splenorenal ligament. When the right peritoneal cavity creates the lesser sac, it also rotates the pancreas and the ligament clockwise, and they become part of the retroperitoneum. Effusions in the splenorenal ligament are difficult to distinguish from fluid in the anterior pararenal compartment.

Root of the Intestinal Mesentery

The small bowel mesentery is a broad fold of peritoneum connecting the intestine to the posterior abdominal wall just anterior to the great vessel space.^{53,54} It is recognized by the superior mesenteric artery and its branches and by the superior mesenteric vein and its tributaries. Mesenteric lymph nodes are readily observed on cross-sectional imaging. Pancreatitis occasionally extends into the root of the mesentery, but the mesentery is most commonly seen in patients with ascites, which outlines the mesenteric pleats.

LOWER ABDOMINAL LIGAMENTS

The sigmoid mesocolon contains the sigmoid and hemorrhoidal branches of the inferior mesenteric artery and the large inferior mesenteric vein, which can be traced to its junction

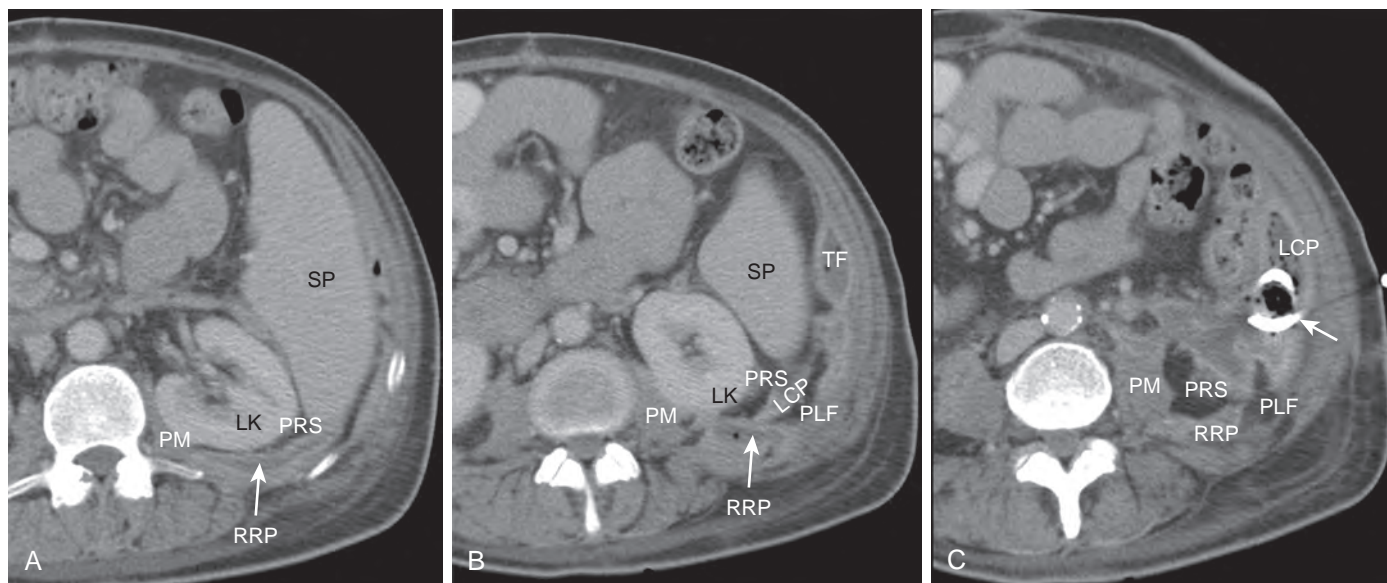


Figure 108-16 Collection in the retrorenal plane extending from the pelvis to the diaphragm. **A.** CT section at the level of the inferior left hemidiaphragm shows a collection in the retrorenal plane (RRP) extending lateral to the psoas muscle (PM) behind the fat in the perirenal space (PRS) and left kidney (LK), to the left of the spleen (SP). **B.** A CT section inferior to that in **A** shows the collection in the retrorenal plane (RRP), which has expanded into the posterolateral fat pad (PLF). There is extension of the collection into the superior extent of the lateroconal plane (LCP). Also note the collection along the transversalis fascia (TF). **C.** Inferior to section **B**, collections in the lateroconal plane and along the transversalis fascia have merged into one collection containing a drainage catheter (arrow).

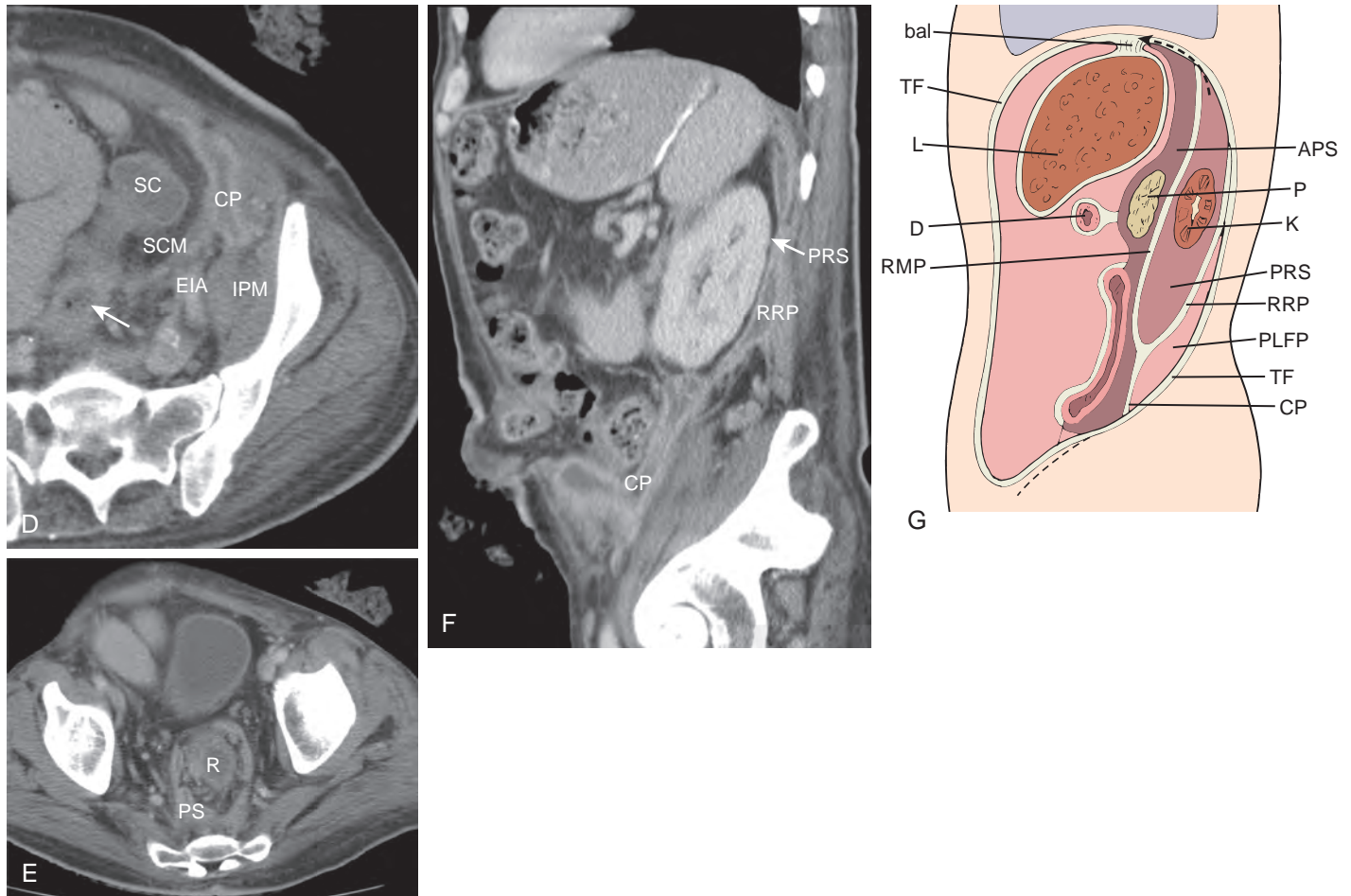


Figure 108-16, cont'd **D.** The CT section at the level of the true pelvic inlet shows the collection in the combined plane (CP), anterior to the iliopsoas muscle (IPM), extending between the sigmoid colon (SC) and its mesentery (SCM) and the iliac vessels (EIA), communicating with an extraperitoneal collection surrounding the rectum, the cranial portion of which is noted on this section (arrow). (Case courtesy Doug Kitchin, MD.) **E.** CT section from the same patient at the level of the acetabula shows collections extending medially into the extraperitoneal perirectal space (PS) surrounding the rectum (R). **F.** A sagittal reformatted image in the same patient shows the continuity of the retrorenal plane (RRP) extending from the left hemidiaphragm behind the perirenal space (prs) through the combined plane (cp) into the pelvic extraperitoneum. **G.** The line drawing depicts a sagittal view summarizing the retroperitoneal spaces and planes. Encircling the abdomen, the transversalis fascia (TF) provides an expandable plane available to fluid collections from any source. Internal to the transversalis fascia are the posterolateral fat pads (PLFP), or posterior pararenal spaces, which contain no viscera and rarely participate in pathologic processes. Internal to the posterior pararenal spaces are the perirenal spaces (PRS) surrounding the kidney (K) and adrenal glands. On the right, the perirenal space appears to be open to the bare area of the liver (dashed arrow). The boundary between the posterior pararenal and perirenal spaces creates an expandable plane, the retrorenal plane (RRP). Anterior to the perirenal spaces are the organs and mesenteries that compose the anterior pararenal space (APS). The boundary between these two spaces creates the retromesenteric plane (RMP). Below the cone of renal fascia, the retrorenal and retromesenteric spaces join to form the combined plane (CP) that extends to the pelvic extraperitoneum. BAL, bare area of the liver; D, duodenum; L, liver; P, pancreas.

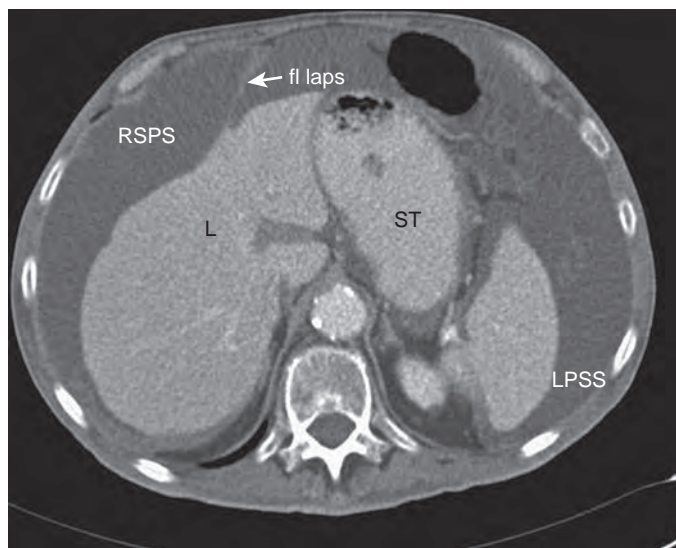


Figure 108-17 Falciform ligament. The falciform ligament (fl) is outlined by ascites in this patient with hepatic failure. There is fluid in the left anterior perihepatic space (laps) and in the right subphrenic space (RSPS), which are separated by a remnant of the ventral mesentery, the falciform ligament. L, Liver; LPSS, left posterior subphrenic space; ST, stomach.

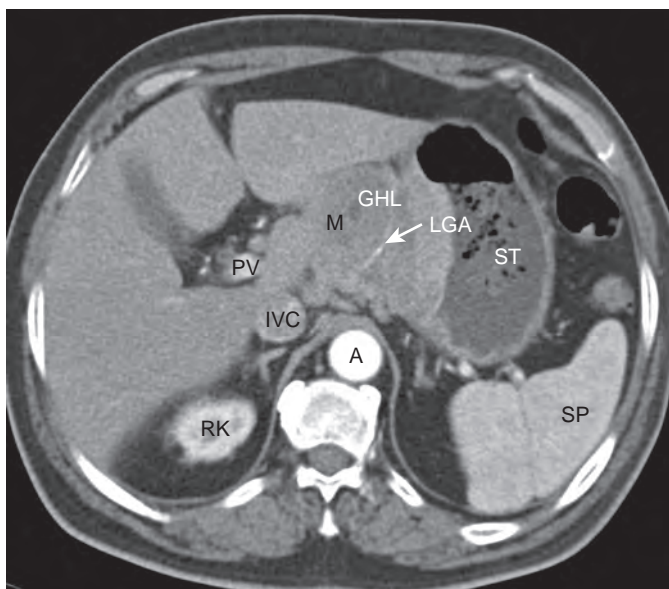


Figure 108-18 The gastrohepatic ligament. Gastric cancer has produced an extensive lobular mass (M) that extends from the stomach (ST) to the gastrohepatic ligament (GHL), which is identified by the left gastric artery (LGA). A, Aorta; IVC, inferior vena cava; RK, right kidney; PV, portal vein; SP, spleen.

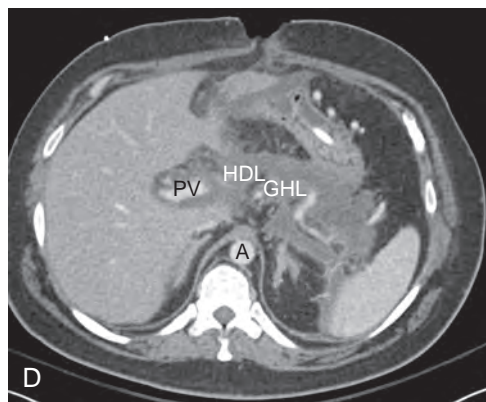
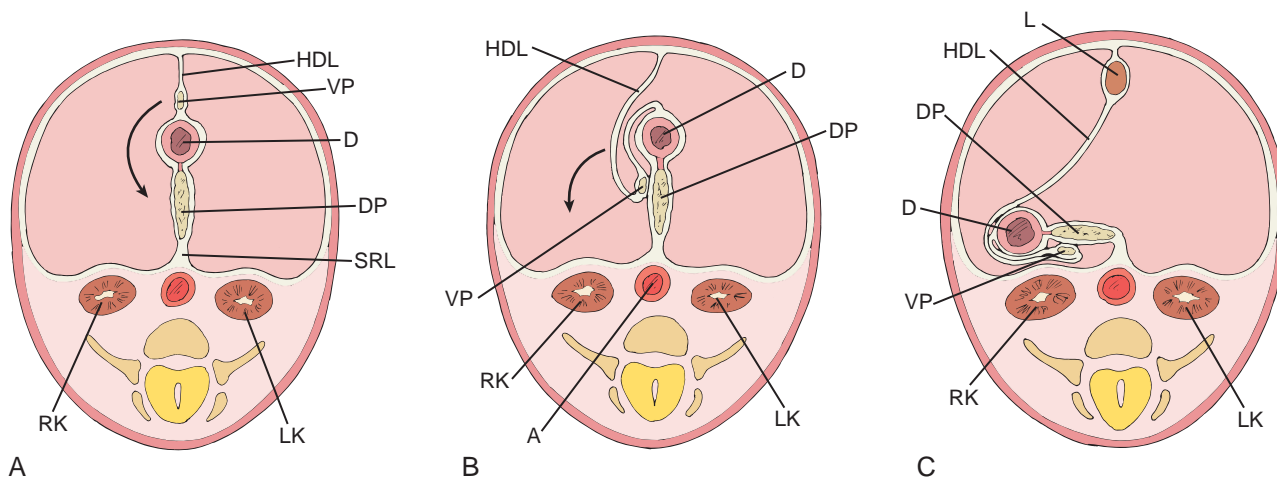


Figure 108-19 Embryologic explanation of subperitoneal spread from the pancreas to the liver hilum. **A.** Line drawing of an embryo during early development shows the intramesenteric development of the ventral pancreas (VP) in the ventral portion of the mesentery, which contains the developing liver (cephalic to this image). This mesentery ultimately becomes the hepatoduodenal ligament (HDL) in the adult. As the fetus develops, the ventral pancreas rotates in the direction of the arrow, along with the duodenum (D), to fuse with the dorsal pancreas (DP). LK, Left kidney; RK, right kidney; SRL, splenohepatic ligament. **B.** Somewhat later, the ventral pancreas (VP) is still attached to its mesentery (HDL) and is fused to the right side of the dorsal pancreas (DP). As the fetus develops further, both parts of the pancreas and the duodenum rotate in the direction of the arrow to fuse with the posterior surface of the retroperitoneum just anterior to the right kidney (RK). A, Aorta. **C.** After all rotations, a line drawing shows that the ventral pancreas (VP), now a part of the anterior pararenal space, retains its connection to the liver (L) through the HDL. **D.** Clinical case of pancreatitis shows extension of pancreatic fluid along the HDL into the hilum of the liver anterior to the portal vein (PV) as well as into the more superior gastrohepatic ligament (GHL). IVC, inferior vena cava.

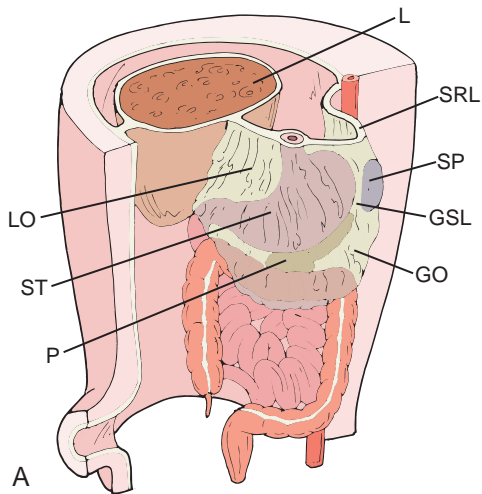


Figure 108-20 Subperitoneal spread into the gastrosplenic ligament. **A.** Line drawing of the ligaments in the upper abdomen shows the stomach (ST) attached through the ventral mesentery to the liver (L); this becomes the lesser omentum (LO) in the adult. The ventral part of the dorsal mesentery is called the gastrosplenic ligament (GSL), and it connects the greater curvature of the stomach to the spleen (SP). Its redundant inferior folds become the greater omentum (GO). The pancreas (P) lies in the dorsal part of the dorsal mesentery, most of which fuses to the dorsal body wall to become the splenorenal ligament (SRL). Effusions arising in the pancreatic tail can extend to any part of the dorsal mesentery. **B.** CT section in a patient with pancreatitis shows extension of the fluid collection into the gastrosplenic ligament (GSL), identified by the short gastric arteries (arrows) above the spleen (SP). A portion of this collection extends along the greater curvature of the stomach (ST). **C.** CT section in another patient with pancreatitis shows a large fluid collection within the gastrosplenic ligament (GSL) distorting the greater curvature of the stomach (ST). This collection is frequently misidentified as being in the lesser peritoneal sac. The spleen (SP) is identified on the right.

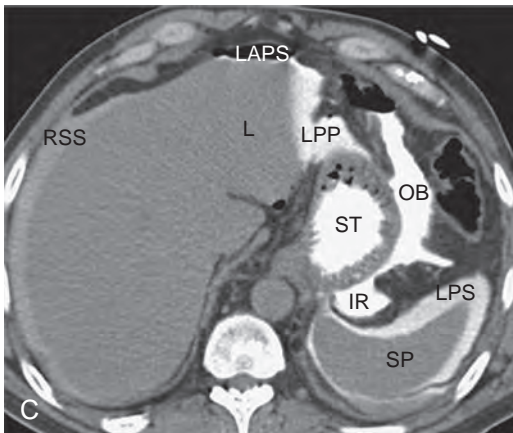
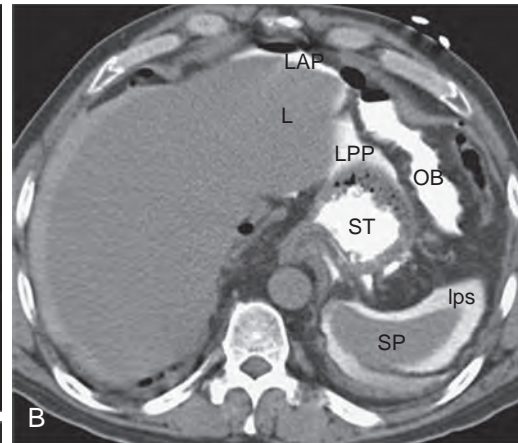
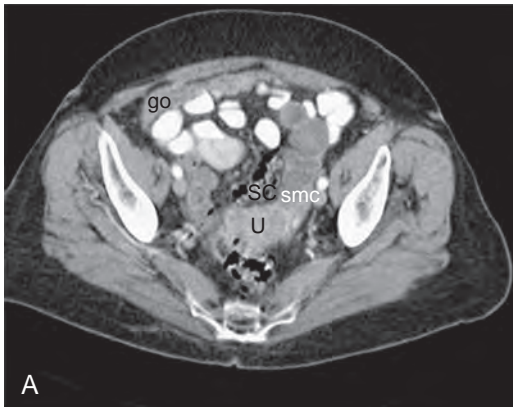
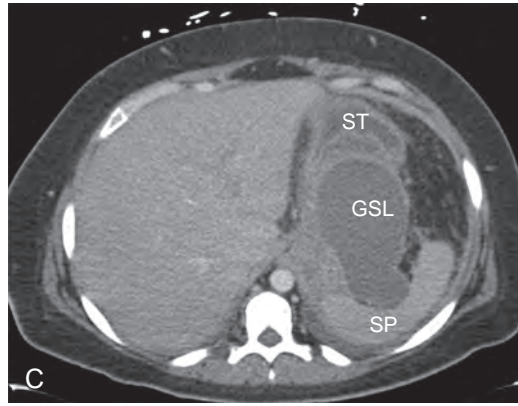


Figure 108-21 The greater omentum. **A.** CT section through the upper part of the pelvis in a patient with widespread peritoneal metastases from an ovarian primary shows extensive soft tissue deposits in the greater omentum (go) in its characteristic location in the anterior abdomen. There are also deposits in the sigmoid mesocolon (smc) adjacent to the sigmoid colon (SC) just anterolateral to the uterus (U). **B.** CT section through the upper abdomen in a patient with gastric perforation into the greater and lesser peritoneal sacs shows contrast material within the lumen of the stomach (ST) that has leaked into the left peritoneal spaces to occupy the left anterior perihepatic space (LAP) and left posterior perihepatic space (LPP) on the surface of the left lobe of the liver (L). There is also contrast material in the left posterior subphrenic (or perisplenic) space (lps) above the spleen (SP). Some dense contrast material has leaked into a space between the leaves of the greater omentum, filling the omental bursa (OB), part of the inferior recess of the lesser sac. **C.** CT section 15 mm inferior to that in B shows the communication between the inferior recess of the lesser sac (IR) and the contrast material collection within the greater omentum (OB). The right subphrenic space (RSS) is identified on the left. LAPS, Left anterior perihepatic space.

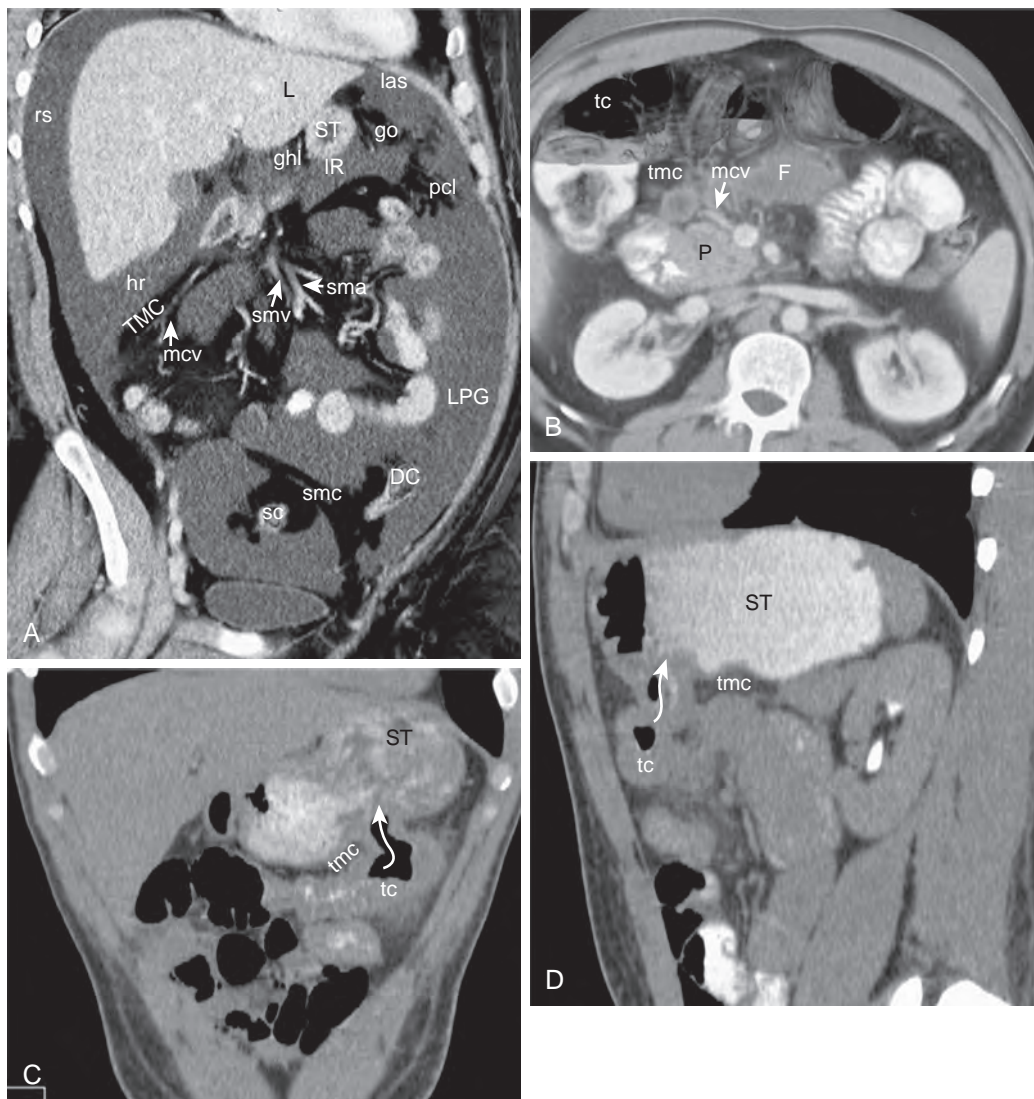


Figure 108-22 The transverse mesocolon. **A.** Coronal reformat image in a patient with voluminous ascites shows the transverse mesocolon (TMC), identified by the middle colic vein (mcv), which subdivides the peritoneal spaces into supramesocolic and inframesocolic compartments. A zone of continuity is located centrally between the transverse mesocolon and the root of the small bowel mesentery (marked by the superior mesenteric vessels [sma and smv]). There is ascitic fluid in the right subphrenic (rs) and hepatorenal (hr) spaces in the right supramesocolic peritoneum; some fluid is also seen within the inferior recess of the lesser sac (lr). Fluid in the left anterior subphrenic space (las) outlines the greater omentum (go) and the phrenicocolic ligament (pcl) and communicates with the left paracolic gutter (LPG) in the inframesocolic peritoneum. Fluid in the pelvic portion of the inframesocolic space outlines segments of the descending colon (DC) and sigmoid colon (SC) and the fat-rich sigmoid mesocolon (smc). L, Liver. **B.** CT section illustrates extension of pancreatitis to the transverse mesocolon (tmc). The fluid collection (F) extends along the middle colic vein (mcv) to lie within the leaves of the transverse mesocolon. The transverse colon (tc) and pancreatic head (P) are identified. **C.** Coronal reformat image in a patient with colon cancer shows extension of the primary tumor in the transverse colon (tc) through the transverse mesocolon (tmc) into the stomach (ST). **D.** Sagittal view of the same patient as in **C** shows the fistula (arrow) between the transverse colon (tc) and the stomach (ST) by means of the transverse mesocolon (tmc).

with the splenic vein. Processes that begin in the sigmoid colon, such as diverticulitis, seep through the porous mesentery to distend the combined interfascial plane. The sigmoid mesentery is also one of the common locations for peritoneal seeding in gynecologic primary carcinomas.

Peritoneal Spaces: Upper Abdomen

The peritoneal cavity consists of a series of communicating but compartmentalized potential spaces that are not depicted on conventional radiologic studies or by cross-sectional imaging

unless they are distended by fluid or air. The lining of the peritoneal cavity and of the abdominal and pelvic organs contained therein is a mesothelial surface known as peritoneum. Peritoneal spaces are bounded by extensions of the ventral and dorsal mesentery, the ligaments (Fig. 108-23). The abdominal cavity is subdivided to some extent by the largest of these ligaments, the transverse mesocolon, which forms an upper (supramesocolic) and a lower (inframesocolic) compartment.⁵⁵ In the supramesocolic compartment, the gut and its mesenteries effectively prevent communication between the right side of the peritoneal space and the left.

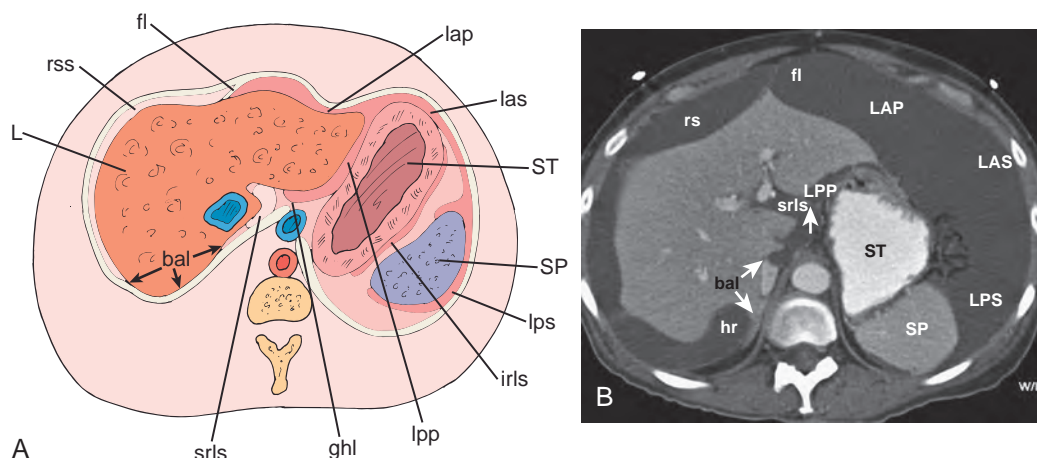


Figure 108-23 Supramesocolic peritoneal spaces. **A.** Line drawing of the supramesocolic peritoneal spaces shows the falciform ligament (fl) delimiting the right side of the left anterior perihepatic space (lap), formed when the lateral segment of the liver (L) grew to the left and distorted the peritoneum around it. The left posterior perihepatic space (lpp) is always parallel to the lesser curvature of the stomach (ST), and it is limited posteriorly and on the right by the gastrohepatic ligament (ghl). Between the stomach and the diaphragm lies the left anterior subphrenic space (las), which extends posteriorly to surround the spleen (SP) in the left posterior subphrenic space (lps). On the right, the right subphrenic space courses between the liver and right hemidiaphragm between the falciform ligament and the bare area of the liver (bal). The caudate lobe grows into the superior recess of the lesser sac (srls), deforming it into its characteristic boomerang shape. Posterior to the stomach lies the inferior recess of the lesser sac (irls). rsls, Right subphrenic space. **B.** CT section similar in location to that in **A** in a patient with voluminous ascites shows the falciform ligament (fl) outlined by a large collection in the left anterior perihepatic space (LAP). There is only a tiny fluid collection in the left posterior perihepatic space (LPP), but ascites fills the left anterior subphrenic (LAS) and left posterior subphrenic (LPS) spaces. On the right, the liver surface is distorted by the tense collection in the right subphrenic space (rs), and there is a large volume of fluid in the hepatorenal (hr) space. A small volume of fluid is present in the superior recess of the lesser sac (srls). Notice the thin gastrohepatic ligament (arrow) separating the left posterior perihepatic space from the superior recess. SP, Spleen; ST, stomach.

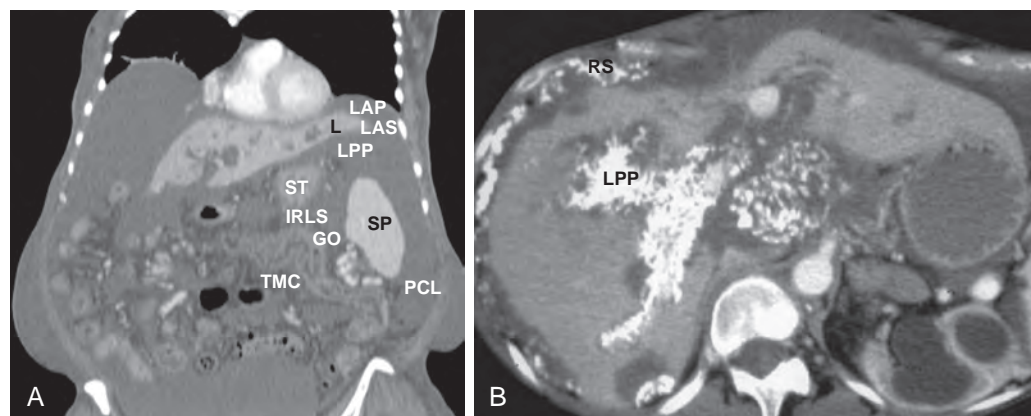


Figure 108-24 Left perihepatic spaces. **A.** Coronal reformatted image in a patient with ascites shows fluid surrounding the lateral segment of the liver (L) in the left anterior (LAP) and posterior (LPP) perihepatic spaces. Fluid in the left anterior subphrenic space (LAS) outlines the gastrocolic ligament, or greater omentum (GO). The left-most extension of the transverse mesocolon attaches to the left hemidiaphragm to form the phrenicocolic ligament (PCL), which forms an incomplete barrier between the supramesocolic and inframesocolic portions of the peritoneum. The stomach (ST) and inferior recess of the lesser sac (IRLS) are identified, as is the spleen (SP). **B.** CT section in a patient with widespread calcified mucinous tumor implants throughout the peritoneum shows the intrahepatic extent of the left posterior perihepatic space (LPP). Metastases occur over the diaphragmatic surface of the right lobe in the right subphrenic space (RS). Also noted is the transverse mesocolon.

LEFT-SIDED PERITONEAL SPACES

In the following discussion, the peritoneal spaces are arbitrarily divided into a number of subspaces. Although left-sided spaces can communicate freely, clinically observed pathologic fluid collections frequently occupy one or more of the subcompartments, separated by fibrous adhesions.

Perihepatic Space

Two left perihepatic spaces are formed as the left lateral segment of the liver grows into and distorts the left peritoneal cavity.

The anterior left perihepatic space extends over the surface of the liver, limited on the right by the falciform ligament. The posterior left perihepatic space (or gastrohepatic recess⁵⁶) extends between the lesser curvature of the stomach anterior to the gastrohepatic ligament and posterior to the left lobe of the liver. It can extend deeply into the liver parenchyma along Glisson's capsule, and peritoneal processes can mimic primary intrahepatic disease. Fluid in the gastrohepatic recess is immediately anterior to fluid in the superior recess of the lesser sac (Fig. 108-24).

Subphrenic Space

Immediately to the left of the perihepatic space is the anterior subphrenic space,⁵⁷ which is bounded by the diaphragm anteriorly and laterally and by the stomach posteriorly. Lateral to the stomach, the anterior subphrenic space communicates with the posterior subphrenic (or perisplenic) space. The perisplenic space almost completely surrounds the spleen,⁵⁸ except for a variable portion of splenic tissue lying within the splenorenal ligament. This bare area of the spleen prevents fluid from tracking medially at the level of the splenic hilum.⁵⁹ Inferior to the tip of the spleen, the attachment of the left side of the transverse mesocolon to the left hemidiaphragm creates the phrenocolic ligament, which almost completely effaces the posterior subphrenic compartment. It forms a relative barrier to fluid extension up the left paracolic gutter into the supramesocolic compartments.⁶⁰

RIGHT-SIDED PERITONEAL SPACES

Supramesocolic spaces on the right side of the abdomen are most influenced by the liver. A portion of the right peritoneal cavity, however, crosses behind the stomach through the epiploic foramen (or foramen of Winslow) and comes to lie to the left of the midline.

Subdiaphragmatic Space

The right subdiaphragmatic space is limited anteriorly by the falciform ligament and posteriorly by the hepatic bare area, which is broadest just below the junction of the inferior vena cava with the right atrium.⁶¹ Collections in this space frequently deform the surface of the liver (Fig. 108-25). Of note, subhepatic and subphrenic abscesses on the right side of the abdomen occur with a greater frequency than those on the left side owing to a shallower left paracolic gutter compared with its right-sided counterpart as well as flow limited by the phrenocolic ligament.⁶²

Hepatorenal Space

Just beneath the bare area, the right peritoneal space courses between the posterior surface of segment VI and the anterior renal fascia on its way to the epiploic foramen. This relatively small potential space is referred to as the hepatorenal fossa or, more commonly, Morison's pouch. Collections frequently form here in patients recovering from upper abdominal surgery (often cholecystectomy) because it is the most dependent portion of the right supramesocolic spaces.

Lesser Sac

There are two components to the lesser sac (i.e., omental bursa), the name applied to the portion of the right peritoneal space that passes posterior to the gastrohepatic omentum and stomach.⁶³⁻⁶⁵ The caudate lobe of the liver distorts the right side of the peritoneum to form a boomerang-shaped superior recess (Fig. 108-26). The larger inferior recess is bounded anteriorly by the stomach, posteriorly by the anterior pararenal space, and inferiorly and to the left by the transverse mesocolon. The inferior recess communicates with a potential space lying inside the leaves of the greater omentum (Fig. 108-27). Although fluid in the lesser sac is most commonly caused by generalized peritoneal fluid entering through the epiploic foramen, inflammation from pancreatitis, cholecystitis, or gastric perforation may cause ascites localized to the lesser sac.⁶⁶

Peritoneal Spaces: Lower Abdomen and Pelvis

INFRAMESOCOLIC SPACE

The inframesocolic compartment is divided into two unequal spaces by the small intestinal mesentery. The smaller right inframesocolic space is restricted inferiorly by the junction of the distal small bowel mesentery with the cecum, whereas the larger left inframesocolic space opens into the pelvis,

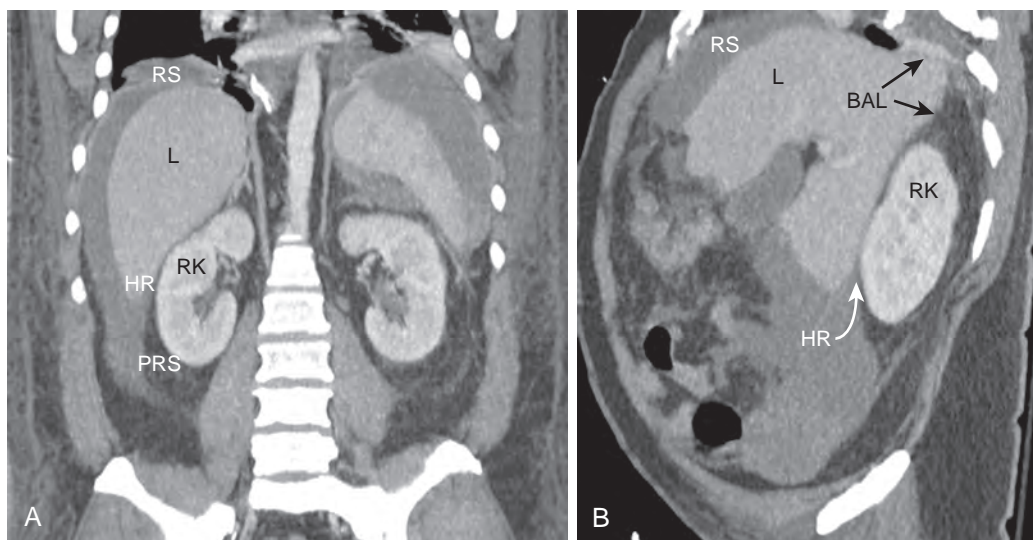


Figure 108-25 Right perihepatic spaces. A. Coronal reformatted image in a patient with ascites shows fluid between the right hemidiaphragm and the liver (L) in the right subphrenic space (RS). This is continuous with fluid in the hepatorenal recess (HR) on the inferior surface of the liver, superior to the right kidney (RK) and fat in the perirenal space (PRS). The hepatorenal space is also called Morison's pouch. **B.** Sagittal reformatted image in another patient shows the continuity between the right subphrenic space (rs) and Morison's pouch (HR), which extends between the liver (L) and the right kidney (RK). Notice the posterior location of the bare area of the liver (BAL), in which no ascites is present.

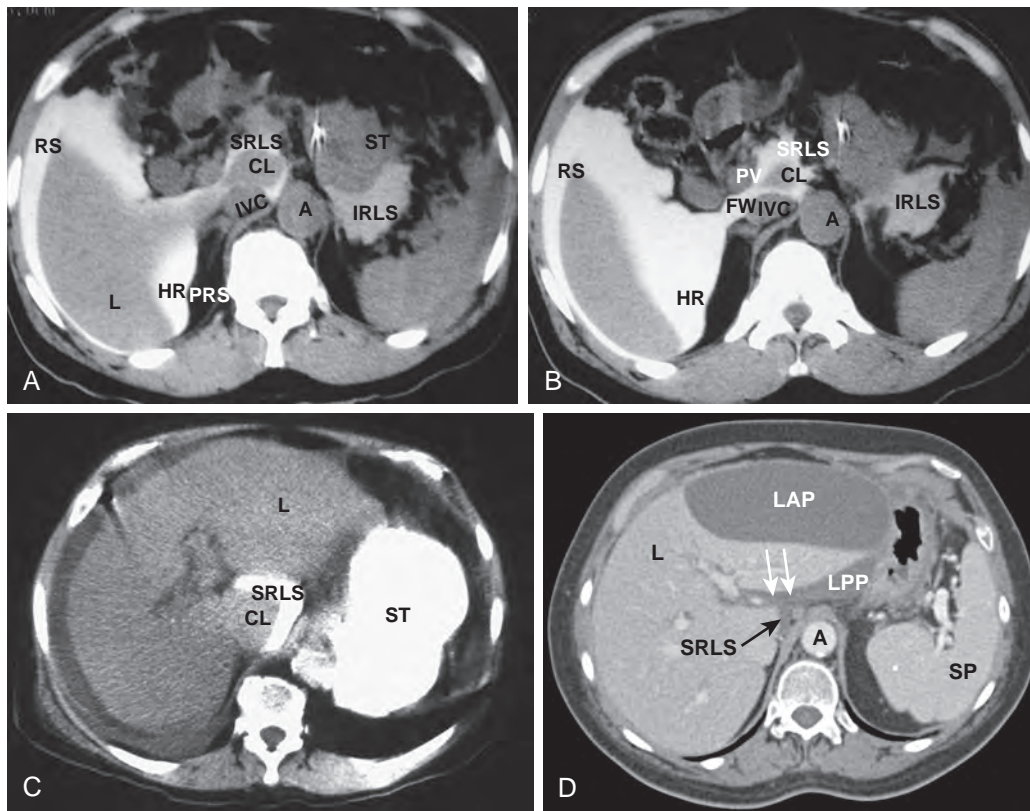


Figure 108-26 The foramen of Winslow. **A.** In a patient with peritoneal bladder perforation from trauma, CT shows contrast material from CT cystography filling the right subphrenic space (RS) around the liver (L) and flowing into the hepatorenal recess (HR) between the liver and the perirenal space (PRS). Some of this contrast material has extended into the two compartments of the lesser sac. The denser collection lies within the superior recess of the lesser sac (SRLS), surrounding the caudate lobe (CL), and the more dilute collection is in the inferior recess of the lesser sac (IRLS), posterior to the stomach (ST). **B.** CT section 15 mm inferior to that in **A** shows hepatorenal recess fluid (HR) funneling into the superior recess of the lesser sac (SRLS) through the narrow foramen of Winslow (FW), which lies between the inferior vena cava (IVC) and the portal vein (PV). The aorta (A), caudate lobe (CL), and inferior recess of the lesser sac (IRLS) are identified. **C.** CT section in another patient who proved to have a perforated gastric ulcer shows dense contrast material leaking from the lumen of the stomach (ST) into the superior recess of the lesser sac (SRLS), defining its characteristic boomerang shape on the medial surface of the caudate lobe (CL). The liver (L) is identified. **D.** CT section in a patient with ascites shows the relationship between the collection in the left posterior perihepatic space (LPP) and the smaller collection in the superior recess of the lesser sac (SRLS). Between the two collections lies the gastrohepatic ligament (arrows). The aorta (A), liver (L), stomach (ST), and spleen (SP) as well as a tense collection in the left anterior perihepatic space (LAP) also are identified.

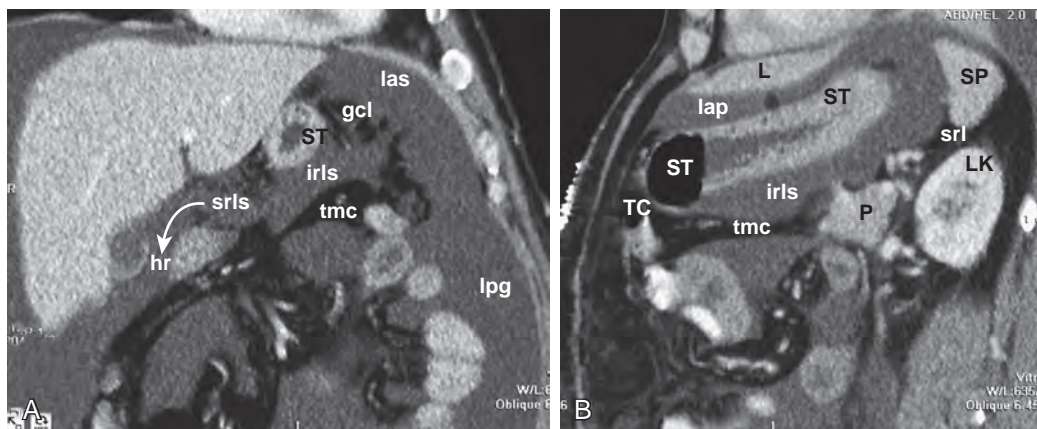


Figure 108-27 Boundaries of the inferior recess of the lesser sac. **A.** Oblique coronal reformatted image in a patient with ascites shows the inferior recess of the lesser sac (irls) bounded by the stomach (ST) superiorly, the gastrocolic ligament (gcl) on the left, and the transverse mesocolon (tmc) inferiorly. On the right, it is open to the superior recess of the lesser sac (srls), which empties into the hepatorenal recess (hr). The left anterior subphrenic space (las) and left paracolic gutter (lpg) also are identified. **B.** Sagittal reformatted image in the same patient shows the inferior recess of the lesser sac (irls) bounded superiorly by the stomach (ST), posteriorly by the splenorenal ligament (srl), and inferiorly by the transverse mesocolon (tmc). L, Liver; lap, left anterior perihepatic space; LK, left kidney; P, pancreas; SP, spleen; TC, transverse colon.

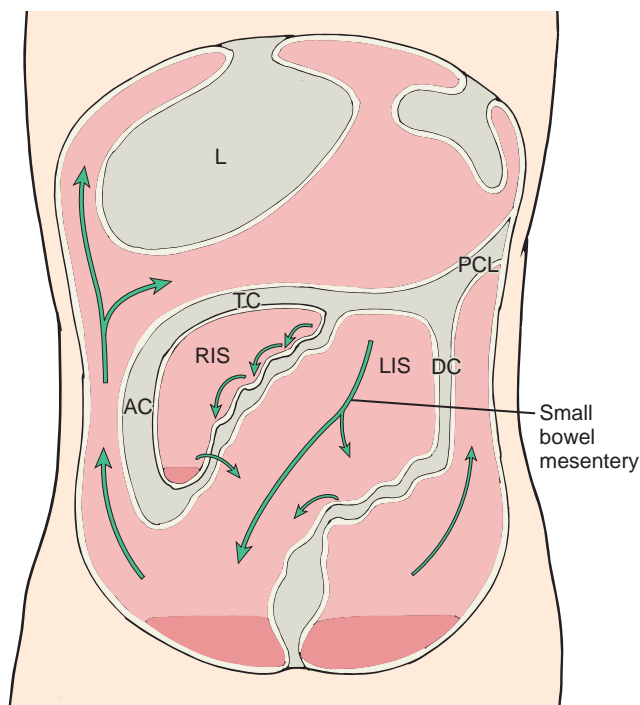


Figure 108-28 Intraperitoneal flow of ascites. The inframesocolic compartment is divided by the small bowel mesentery. The smaller right infracolic space (RIS) is restricted inferiorly by the junction of the distal small bowel mesentery with the cecum. Except where it is bounded by the sigmoid mesocolon, the larger left infracolic space (LIS) opens into the pelvis. The paracolic gutters are located lateral to the peritoneal reflections of the ascending colon (AC) and descending colon (DC). The right paracolic gutter freely communicates with the right supramesocolic spaces. The phrenicocolic ligament (PCL) forms a partial barrier between the left paracolic gutter and the left subphrenic space. L, Liver; TC, transverse colon.

except where it is bounded by the sigmoid mesocolon (Fig. 108-28). The paracolic gutters are located lateral to the peritoneal reflections of the ascending and descending colon. The right paracolic gutter freely communicates with the right supramesocolic spaces, and the phrenicocolic ligament forms a partial barrier between the left paracolic gutter and the left subphrenic space.

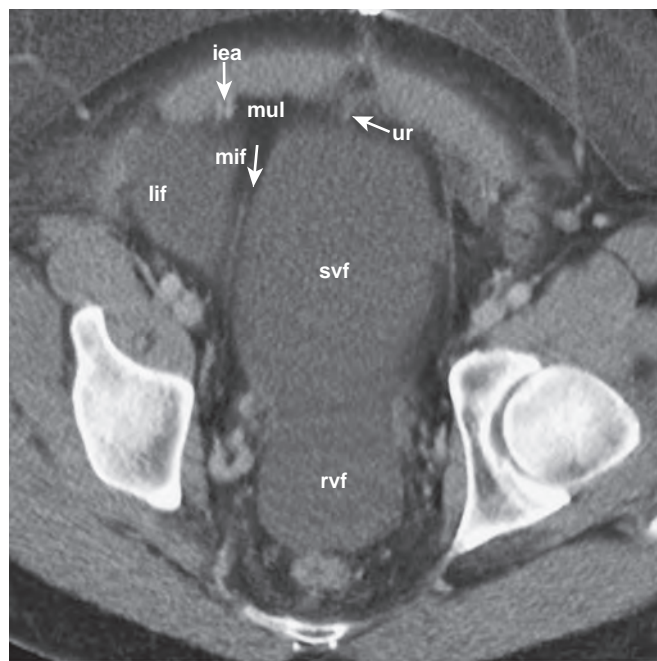


Figure 108-29 The pelvic peritoneum. The pelvic peritoneal spaces are depicted in a male patient with ascites. The large, medially positioned supravesical fossa (svf) is crossed on both sides by the medial umbilical ligaments (mul), which separate it from the inguinal spaces. The inguinal spaces are divided by the lateral umbilical fold, which contains the inferior epigastric artery (iea), into medial (mif) and lateral (lif) compartments. In women, the uterus separates the posteriorly located rectovesical pouch (rvf), also known as the pouch of Douglas, from the supravesical fossa. The urachus (ur) is identified.

PELVIC PERITONEAL SPACES

The most dependent portion of the peritoneal space in supine and erect positions is in the pelvis, and this anatomic feature explains the frequency of abscesses and peritoneal implantation of tumor in this region. In males, this cul-de-sac lies between the anterior mesorectal fascia and the posterior wall of the bladder. In females, the equivalent space lies between the uterine wall and the anterior mesorectal fascia.⁶⁷ Anteriorly, the pelvic peritoneum is indented by two folds. The medial umbilical folds, which contain the obliterated umbilical arteries, divide the peritoneum into medial and lateral compartments, and the inferior epigastric arteries divide the lateral compartment into medial and lateral inguinal fossae (Fig. 108-29).

REFERENCES

- Moore KL, Persaud TVN, Torchia MG: The Developing Human: Clinically Oriented Embryology, ed 9, Philadelphia, 2013, Saunders/Elsevier.
- Cochard LR, Netter FH: Netter's Atlas of Human Embryology, Teterboro, NJ, 2002, Icon Learning Systems.
- Hureau J, Agossou-Voyame AK, Germain M, Pradel J: [The posterior interparietoperitoneal spaces or retroperitoneal spaces. 1: Normal topographic anatomy]. J Radiol 72:101–116, 1991.
- Hureau J, Pradel J, Agossou-Voyame AK, Germain M: [The posterior interparietoperitoneal or retroperitoneal spaces. 2: Pathological x-ray computed tomographic image]. J Radiol 72:205–227, 1991.
- Molmenti EP, Balfe DM, Kanterman RY, et al: Anatomy of the retroperitoneum: Observations of the distribution of pathologic fluid collections. Radiology 200:95–103, 1996.
- Aizenstein RI, Owens C, Sabniss S, et al: The perinephric space and renal fascia: Review of normal anatomy, pathology, and pathways of disease spread. Crit Rev Diagn Imaging 38:325–367, 1997.
- Scialpi M, Scaglione M, Angelelli G, et al: Emergencies in the retroperitoneum: Assessment of spread of disease by helical CT. Eur J Radiol 50:74–83, 2004.
- Aizenstein RI, Wilbur AC, O'Neal HK: Interfascial and perinephric pathways in the spread of retroperitoneal disease: Refined concepts based on CT observations. AJR Am J Roentgenol 168: 639–643, 1997.
- Ishikawa K, Tohira H, Mizushima Y, et al: Traumatic retroperitoneal hematoma spreads through the interfascial planes. J Trauma 59: 595–607, discussion 607–608, 2005.
- Rosen A, Korobkin M, Silverman P, et al: CT diagnosis of ruptured abdominal aortic aneurysm. AJR Am J Roentgenol 143:265–268, 1984.
- Parke CE, Stanley RJ, Berlin AJ: Infrarenal vena caval injury following blunt trauma: CT findings. J Comput Assist Tomogr 17:154–157, 1993.
- Hashmonai M, Stahl S, Schramek A: Rupture of an aortic abdominal aneurysm presenting as

- painful obstructive jaundice. *J Cardiovasc Surg (Torino)* 22:187–189, 1981.
13. Politoske EJ: Ruptured abdominal aortic aneurysm presenting as an obstruction of the left colon. *Am J Gastroenterol* 85(6):745–747, 1990.
 14. Meyers MA, Feldberg MA, Oliphant M: Grey Turner's sign and Cullen's sign in acute pancreatitis. *Gastrointest Radiol* 14:31–37, 1989.
 15. Meyers MA, Whalen JP, Peelle K, Berne AS: Radiologic features of extraperitoneal effusions. An anatomic approach. *Radiology* 104:249–257, 1972.
 16. Meyers MA, Whalen JP, Peelle K, et al: Radiological features of the spread and localization of extraperitoneal gas and their relationship to its source. An anatomical approach. *Radiology* 111: 17–26, 1974.
 17. Parienty RA, Pradel J, Picard JD, et al: Visibility and thickening of the renal fascia on computed tomograms. *Radiology* 139:119–124, 1981.
 18. Nicholson RL: Abnormalities of the perinephric fascia and fat in pancreatitis. *Radiology* 139: 125–127, 1981.
 19. Korobkin M, Silverman PM, Quint LE, et al: CT of the extraperitoneal space: Normal anatomy and fluid collections. *AJR Am J Roentgenol* 159: 933–942, 1992.
 20. Bechtold RE, Dyer RB, Zagoria RJ, Chen MY: The perirenal space: Relationship of pathologic processes to normal retroperitoneal anatomy. *Radiographics* 16:841–854, 1996.
 21. Lei QF, Marks SC, Jr, Touloupoulos P, et al: Fascial planes and compartments of the posterior abdomen: The perirenal and pararenal pathways. *Clin Anat* 3:1–15, 1990.
 22. Mastromatteo JF, Mindell HJ, Mastromatteo MF, et al: Communications of the pelvic extraperitoneal spaces and their relation to the abdominal extraperitoneal spaces: Helical CT cadaver study with pelvic extraperitoneal injections. *Radiology* 202:523–530, 1997.
 23. Mindell HJ, Mastromatteo JF, Dickey KW, et al: Anatomic communications between the three retroperitoneal spaces: Determination by CT-guided injections of contrast material in cadavers. *AJR Am J Roentgenol* 164:1173–1178, 1995.
 24. Beaulieu CF, Mindelzun RE, Dolph J, et al: The infraconal compartment: A multidirectional pathway for spread of disease between the extraperitoneal abdomen and pelvis. *J Comput Assist Tomogr* 21:223–228, 1997.
 25. Thornton FJ, Kandiah SS, Monkhouse WS, Lee MJ: Helical CT evaluation of the perirenal space and its boundaries: A cadaveric study. *Radiology* 218:659–663, 2001.
 26. Aikawa H, Tanoue S, Okino Y, et al: Pelvic extension of retroperitoneal fluid: Analysis in vivo. *AJR Am J Roentgenol* 171:671–677, 1998.
 27. Wolfram-Gabel R, Kahn J, Rapp E: Is the renal space closed? *Clin Anat* 13:168–176, 2000.
 28. Raptopoulos V, Lei QF, Touloupoulos P, et al: Why perirenal disease does not extend into the pelvis: The importance of closure of the cone of the renal fasciae. *AJR Am J Roentgenol* 164: 1179–1184, 1995.
 29. Kneeland JB, Auh YH, Rubenstein WA, et al: Perirenal spaces: CT evidence for communication across the midline. *Radiology* 164:657–664, 1987.
 30. Chesbrough RM, Burkhard TK, Martinez AJ, et al: Gerota versus Zuckerkindl: The renal fascia revisited. *Radiology* 173:845–846, 1989.
 31. Bosniak MA: Spontaneous subcapsular and perirenal hematomas. *Radiology* 172:601–602, 1989.
 32. Belville JS, Morgentaler A, Loughlin KR, et al: Spontaneous perinephric and subcapsular renal hemorrhage: Evaluation with CT, US, and angiography. *Radiology* 172:733–738, 1989.
 33. Yip KTL, Peh WLG, Tam PC: Spontaneous rupture of renal tumours: The role of imaging in diagnosis and management. *Br J Radiol* 71: 146–154, 1998.
 34. Cass AS, Lee JY, Smith CS: Perirenal extravasation with blunt trauma from rupture of a calyceal fornix. *J Trauma* 35:20–22, 1993.
 35. Siegel JH, Balfe DM: Blunt renal and ureteral trauma in childhood: CT patterns of fluid collections. *AJR Am J Roentgenol* 152:1043–1047, 1989.
 36. Kawashima A, Sandler CM, Corriere JN, Jr, et al: Ureteropelvic junction injuries secondary to blunt abdominal trauma. *Radiology* 205:487–492, 1997.
 37. Raptopoulos V, Kleinman PK, Marks S, Jr, et al: Renal fascial pathway: Posterior extension of pancreatic effusions within the anterior pararenal space. *Radiology* 158:367–374, 1986.
 38. Raptopoulos V, Touloupoulos P, Lei QF, et al: Medial border of the perirenal space: CT and anatomic correlation. *Radiology* 205:777–784, 1997.
 39. Kunin M: Bridging septa of the perinephric space: Anatomic, pathologic, and diagnostic considerations. *Radiology* 158:361–365, 1986.
 40. Titton RL, Gervais DA, Hahn PF, et al: Urine leaks and urinomas: Diagnosis and imaging-guided intervention. *Radiographics* 23:1133–1147, 2003.
 41. Munkelwitz R, Krasnokutsky S, Mohan E, et al: Unusual presentation of a pancreatic pseudocyst. A case report and review of literature. *Int J Pancreatol* 21:91–94, 1997.
 42. Farman J, Morehouse H, Amis ES, Jr, Newhouse JH: CT of pancreatitis with renal and juxtarenal manifestations. *Clin Imaging* 21:183–188, 1997.
 43. Moertele KJ, Mergo PJ, Taylor HM, et al: Renal and perirenal space involvement in acute pancreatitis: Spiral CT findings. *Abdom Imaging* 25:272–278, 2000.
 44. Moertele KJ, Mergo PJ, Taylor HM, et al: Continuation of gas from the right perirenal space into the bare area of the liver. *J Comput Assist Tomogr* 21:667–670, 1997.
 45. Lim JH, Kim B, Auh YH: Anatomical communications of the perirenal space. *Br J Radiol* 71:450–456, 1998.
 46. Auh YH, Rubenstein WA, Schneider M, et al: Extraperitoneal paravesical spaces: CT delineation with US correlation. *Radiology* 159:319–328, 1986.
 47. Meyers MA, Oliphant M, Berne AS, et al: The peritoneal ligaments and mesenteries: Pathways of intraabdominal spread of disease. *Radiology* 163:593–604, 1987.
 48. Balfe DM, Mauro MA, Koehler RE, et al: Gastrohepatic ligament: Normal and pathologic CT anatomy. *Radiology* 150:485–490, 1984.
 49. Weinstein JB, Heiken JP, Lee JKT, et al: High resolution CT of the porta hepatis and hepatoduodenal ligament. *Radiographics* 6:55–74, 1986.
 50. Jeffrey RB, Federle MP, Laing FC: Computed tomography of mesenteric involvement in fulminant pancreatitis. *Radiology* 147:185–188, 1983.
 51. Vikram R, Balachandran A, Bhosale PR, et al: Pancreas: Peritoneal reflections, ligamentous connections, and pathways of disease spread. *Radiographics* 29:e34, 2009.
 52. Tirkes T, Sandrasegaran K, Patel AA, et al: Peritoneal and retroperitoneal anatomy and its relevance for cross-sectional imaging. *Radiographics* 32:437–451, 2012.
 53. Silverman PM, Kelvin FM, Korobkin M, et al: Computed tomography of the normal mesentery. *AJR Am J Roentgenol* 143:953–957, 1984.
 54. Silverman PM, Baker ME, Cooper C, et al: CT appearance of diffuse mesenteric edema. *J Comput Assist Tomogr* 10:67–70, 1986.
 55. Meyers MA: Distribution of intra-abdominal malignant seeding: Dependency on dynamics of flow of ascitic fluid. *Am J Roentgenol Radium Ther Nucl Med* 119:198–206, 1973.
 56. Vincent LM, Mauro MA, Mittelstaedt CA: The lesser sac and gastrohepatic recess: Sonographic appearance and differentiation of fluid collections. *Radiology* 150:515–519, 1984.
 57. Halvorsen RA, Jones MA, Rice RP, et al: Anterior left subphrenic abscess: Characteristic plain film and CT appearance. *AJR Am J Roentgenol* 139: 283–289, 1982.
 58. Rubenstein WA, Auh YH, Zirinsky K, et al: Posterior peritoneal recesses: Assessment using CT. *Radiology* 156:461–468, 1985.
 59. Vibhakar SD, Bellon EM: The bare area of the spleen: A constant CT feature of the ascitic abdomen. *AJR Am J Roentgenol* 142:953–955, 1984.
 60. Meyers MA: Roentgen significance of the phrenicocolic ligament. *Radiology* 95:539–545, 1970.
 61. Rubenstein WA, Auh YH, Whalen JP, et al: The perihepatic spaces: Computed tomographic and ultrasound imaging. *Radiology* 149:231–239, 1983.
 62. Kim S, Kim TU, Lee JW, et al: The perihepatic space: Comprehensive anatomy and CT features of pathologic conditions. *Radiographics* 27: 129–143, 2007.
 63. Jeffrey RB, Federle MP, Goodman PC: Computed tomography of the lesser peritoneal sac. *Radiology* 141:117–122, 1981.
 64. Dodds WJ, Foley WD, Lawson TL, et al: Anatomy and imaging of the lesser peritoneal sac. *AJR Am J Roentgenol* 144:567–575, 1985.
 65. Meyers MA: The spread and localization of acute intraperitoneal effusions. *Radiology* 95: 547–554, 1970.
 66. Yoo E, Kim JH, Kim MJ, et al: Greater and lesser omenta et al: Greater and lesser omenta: Normal anatomy and pathologic processes. *Radiographics* 27:707–720, 2007.
 67. Auh YH, Rubenstein WA, Markisz JA, et al: Intraperitoneal paravesical spaces: CT delineation with US correlation. *Radiology* 159:311–317, 1986.

Pathways of Abdominal and Pelvic Disease Spread

RICHARD M. GORE | MORTON A. MEYERS | DAVID N. RABIN

CHAPTER OUTLINE

Hematogenous Spread

Malignant Disease
Infection

Lymphatic Spread

Biliary Spread

Infection
Malignant Disease

Peritoneal Spread

Intraperitoneal Flow of Fluid
Pouch of Douglas
Perihepatic Spaces
Left Subphrenic Space
Lower Small Bowel Mesentery
Sigmoid Mesocolon

Retroperitoneal Spread

Anterior Pararenal Space
Perirenal Space
Posterior Pararenal Space

Subperitoneal Spread

Transverse Mesocolon
Gastrocolic Ligament and Greater Omentum
Gastrohepatic Ligament
Hepatoduodenal Ligament
Duodenocolic Ligament
Gastrosplenic Ligament
Splenorenal Ligament
Phrenicocolic Ligament
Small Bowel Mesentery
Sigmoid Mesocolon
Broad Ligament
Falciform Ligament and Ligamentum Teres
Coronary Ligament and Bare Area

Extraperitoneal Spread

Iliopsoas Muscle Route
Sacrosclatic Notch Route
Obturator Foramen Route
Abdominal Wall Route

Conclusions

Traditionally, the abdominal cavity has been divided into a number of peritoneal, retroperitoneal, and extraperitoneal spaces.¹ Although it is useful for learning abdominal anatomy and appreciating the confinement of disease in a particular space, this classic approach affords limited understanding of

the intra-abdominal spread of disease. Dissemination of disease between the retroperitoneum and the peritoneal cavity, between the subdivisions of the retroperitoneum, and within the subperitoneal spaces is difficult to conceptualize if the various spaces and compartments of the abdomen and pelvis are considered fixed, immutable, and isolated delineators of anatomy. Meyers and colleagues perceived that the abdominal cavity should be viewed rather as a continuous space that is punctuated by the abdominal mesenteries, ligaments, and fascia, which may confine disease or provide an avenue for its spread.²⁻⁷ Blood vessels, lymphatics, and the biliary system also contribute to the spread of a number of benign and malignant processes. This holistic schema provides a rationale for understanding the dissemination of intra-abdominal disease focally and to areas distant from the site of origin.

Hematogenous Spread

MALIGNANT DISEASE

Malignant neoplasms shed as many as 4 million cells per gram of tumor tissue into the bloodstream every day. Of these cells, more than 90% are cleared rapidly from the circulation.^{8,9} Despite this metastatic inefficiency, the abdominal organs and gut (Fig. 109-1) are common sites of hematogenous metastases from intra-abdominal and extra-abdominal primary sites.^{8,9}

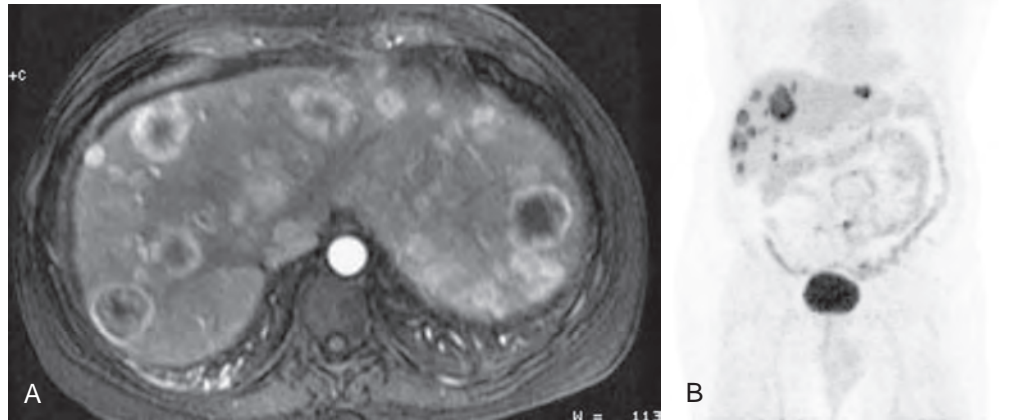
Liver Metastases

Because of its dual blood supply, the liver is a common site of metastatic disease.¹⁰ The portal system conveys cancer cells from tumors of the colon, pancreas, stomach, and small bowel, whereas the systemic arterial system carries metastases from any site but most often from the lung and breast. The liver is particularly vulnerable to the deposition of metastases because of its architecture. Kupffer cells extend into the hepatic sinusoids and impede the passage of tumor cells. These cells then subendothelially extravasate, indent the hepatocytes, and, because of their position adjacent to the sinusoids, receive a rich mixture of arterial and portal blood.¹¹⁻¹³ In this favorable milieu, it is not surprising that metastases in the liver grow four to six times faster than those at other sites, that the liver is the second most common site of metastases (after lymph nodes), and that 25% of all patients who die of cancer have liver metastases.¹²

The radiographic appearance of liver metastases depends on the tumor type, its vascularity, and the degree to which neovascularization occurs. Well-established metastases derive most of their blood supply from the hepatic artery, and this fact is important for planning local hepatic chemotherapy or embolization therapy.¹⁰

Figure 109-1 Hematogenous metastases: imaging spectrum.

A. Contrast-enhanced MR scan shows multiple hepatic metastases from a small bowel neuroendocrine tumor. **B.** PET scan in a different patient shows multiple hepatic metastases from a small bowel adenocarcinoma.



Gut Metastases

The hollow viscera are important but less frequent sites of hematogenous metastases. Carcinoma of the breast or lung and melanoma are the most common primary tumors. On occasion, symptoms of bowel metastases, such as obstruction or hemorrhage, may be the initial clinical manifestations of an occult primary neoplasm.¹⁴

The radiographic appearance of gut metastases depends on the primary tumor type, the degree of vascularity and rate of growth, and the tumor's ability to induce desmoplasia. Hematogenous metastases have a distinct predilection for the antimesenteric border of the bowel¹⁴ because tumor cells are trapped in the smallest capillaries, which are located on the antimesenteric side of the gut.¹⁵ The mesenteric vessels are larger at their entrance on the mesenteric border.¹⁶ A mass, ulcer, ulcerated mass, or area of stenosis may be seen radiographically.

INFECTION

Portal Vein

In the preantibiotic era, pyogenic liver abscesses were usually caused by portal vein pyemia resulting from appendicitis, diverticulitis, or pelvic inflammatory disease.¹⁷ In Western countries, portal vein pylephlebitis is now rare, and ascending biliary infections are the most common cause of pyogenic hepatic abscesses.¹⁸⁻²⁰

Approximately 10% of the world's population are infected by *Entamoeba histolytica*, and 10% of these infections cause clinical disease. The portal vein remains the principal conduit for invasive amebiasis of the colon. The protozoa gain access to the portal venous system by invading the colonic mucosa, and they are then carried to the liver, where they obstruct small portal and arterial radicles, producing parenchymal infarction and proteolysis with subsequent abscess formation.²¹

The portal vein also transmits the eggs of *Echinococcus granulosus* to the liver. The eggs are dissolved by the digestive juices, and the released oncospheres pass through the duodenal mucosa into the portal circulation. In the liver, the eggs disintegrate or grow into a hydatid cyst (see Chapter 88).^{21,22}

Schistosoma mansoni organisms are also carried to the liver through the portal vein. When the worm burden is sufficient, portal vein obstruction may occur, leading to portal hypertension. Schistosomiasis is the most common cause of portal hypertension in the world.^{21,22}

Systemic Arteries

Before the 1980s, hematogenous dissemination of bacterial infections to the abdomen was becoming less frequent and less lethal. This pathway, however, is making a grim comeback in injection drug users, patients with acquired immunodeficiency syndrome (AIDS), and other immunocompromised persons.²³ Pyogenic and nonpyogenic abscesses (as found in candidiasis, tuberculosis, and *Pneumocystis jiroveci* and *Cryptococcus neoformans* infections) occur with greater frequency in these patients.²⁴⁻²⁸

Lymphatic Spread

Neoplasms of the bile ducts, pancreas, stomach, small bowel, and colon (Fig. 109-2) commonly invade adjacent lymphatics. Although a specific discussion of each malignant neoplasm is beyond the scope of this chapter, several fundamental principles apply. Lymphatic tumor emboli from primary bowel neoplasms are not always arrested in the nearest draining lymph node. Lymphatic obstruction of a more remote node may occur because of cellular impaction. This can cause retrograde tumor spread to an adjacent segment of gut or a more distant portion of the alimentary tract. This may explain the phenomenon of anastomotic recurrence of colon cancer, even though a no-touch technique and wide surgical margins are used during resection.²⁹

Tumor-induced derangements of lymph flow produce a number of radiographic findings. In the colon, there may be edema of the bowel wall with mucosal thickening, loss of colonic haustra, and narrowing of the lumen. On computed tomography (CT) scans, increased attenuation of the pericolic fat may be seen.³⁰ With disease progression, nodular tumor deposits accompany the edema, leading to thumbprinting in the

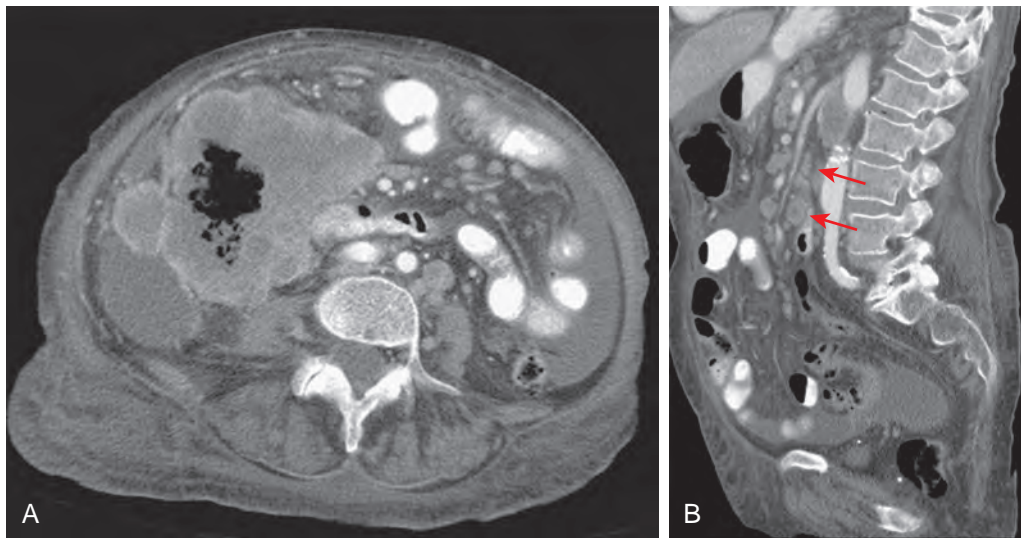


Figure 109-2 Lymphatic metastases: CT findings. **A.** Large necrotic carcinoma of the ascending colon with malignant ascites and retroperitoneal adenopathy. **B.** Sagittal reformatted image shows metastatic lymphadenopathy (arrows) within the small bowel mesentery.

colon and cobblestoning of the small bowel. These radiographic findings, which may simulate ischemic colitis and Crohn's disease, respectively, indicate extensive lymphatic permeation and suggest that resection will probably not be curative.⁶ Lymphatic obstruction by tumor at the root of the small bowel mesentery may cause focal or diffuse thickening of the valvulae conniventes from lymphedema or tumor infiltration. When the lymphatics of the liver are obstructed, periportal lymphedema develops, which may cause zones of periportal lucency on CT scans and periportal hyperintensity on T2-weighted magnetic resonance (MR) images of the liver.³¹

Infection and inflammatory disease can also be spread through lymphatics. Patients with viral hepatitis often show spread of the hepatic inflammatory process to regional lymph nodes (see Chapter 89).³²⁻³⁴

Biliary Spread

INFECTION

The biliary system is a major conduit for infectious disease.³⁵ Asian cholangiohepatitis is the most common biliary tract disease in parts of China, Japan, and other countries of the Far East. Most affected persons harbor parasites of *Clonorchis sinensis* or *Fasciola hepatica*, which may obstruct the bile ducts or act as a nidus for stone formation and chronic inflammation. These liver flukes migrate from the duodenum, through the ampulla of Vater, and on to any part of the biliary tract.³⁶⁻³⁸

Ascaris lumbricoides affects one fourth of the world's population. Adult worms often migrate from the duodenum through the ampulla of Vater to lodge in the gallbladder, the biliary tract, or less commonly the pancreatic duct. Patients may present with acute cholecystitis or biliary obstruction.³⁸⁻⁴² Established liver infections, such as hydatid cysts, may erode through and rupture into the biliary system, and the expelled contents may cause obstructive jaundice (see Chapter 88).⁴³

Ascending cholangitis is a pyogenic infection of the biliary tract and the most common cause of liver abscess in the Western world. It occurs in the clinical setting of obstruction

and biliary stasis proximal to an obstructing stone, stricture, or neoplasm.²⁰

Patients with AIDS are subject to a number of biliary and pancreatic duct abnormalities because of direct involvement by organisms such as *Cryptococcus* and *Cryptosporidium*, which also migrate from the duodenum through the ampulla. On radiographic evaluation, infection may produce an appearance similar to that of sclerosing cholangitis, papillary stenosis, or acute cholecystitis (see Chapter 80).⁴³⁻⁴⁹

MALIGNANT DISEASE

Hepatocellular carcinoma and cholangiocarcinoma uncommonly seed the biliary tract.^{42,50}

Peritoneal Spread

INTRAPERITONEAL FLOW OF FLUID

The peritoneal cavity contains a number of compartmentalized but communicating spaces (see Chapter 108). The peritoneal cavity can be divided into supramesocolic and inframesocolic spaces by the transverse mesocolon. Four intraperitoneal spaces are present in the supramesocolic portion of the abdomen: the suprahepatic and subhepatic spaces on the right and the subphrenic space and lesser sac on the left. The inframesocolic portion of the peritoneal cavity is divided into the right and left inframesocolic spaces by the small bowel mesentery. The large left inframesocolic space is open to the pelvis, except where it is bounded by the sigmoid mesocolon. The right inframesocolic space is smaller and caudally restricted by the junction of the distal small bowel mesentery with the cecum. The most dependent portions of the peritoneal cavity are the lateral paravesical spaces and the pouch of Douglas (i.e., cul-de-sac in women and rectovesical space in men). The pelvis communicates with the supramesocolic space through the paracolic gutters, which lie lateral to the attachments of the peritoneal reflections of the ascending and descending colon. The right paracolic gutter is continuous with the right subhepatic and suprahepatic space

and diaphragm. On the left, the phrenicocolic ligament forms a partial barrier between the left paracolic gutter and the left subphrenic space.⁵¹⁻⁵⁴

The natural flow of intraperitoneal fluid occurs along pathways determined by the anatomic compartmentalization of the peritoneal cavity, intraperitoneal pressure, position of the patient, site of fluid origin, nature of fluid, speed of fluid accumulation, presence of adhesions or previous surgery, degree of bladder distention, and density of fluid (Fig. 109-3).^{5,6,54-58} Abscesses form and malignant cells grow where natural flow allows the affected ascitic fluid to pool. Fluid in the inframesocolic space seeks the pelvis but may first seed the superior aspect of the sigmoid colon on the left and the medial aspect of the cecum on the right. In the pelvis, infected and malignant fluid fills the pouch of Douglas and then the lateral paravesical recesses. Pelvic fluid then ascends both paracolic gutters, driven by negative intra-abdominal pressure associated with respiration, volume considerations, and topographic anatomy of peritoneal recesses.^{5,54} The flow in the left paracolic gutter is modest and limited by the phrenicocolic ligament. Most flow occurs in the right paracolic space. Fluid in this gutter has access to Morison's pouch (the hepatorenal recess of the subhepatic space), the right subphrenic space, and potentially the lesser sac through the anterior subhepatic space and foramen of Winslow. The falciform ligament usually prevents fluid spread across the midline from the right to the left subphrenic spaces.⁵¹⁻⁵⁸

The most common sites of intraperitoneal abscess are the pelvis, the right subhepatic space, and the right subphrenic space. Similarly, the pouch of Douglas, the lower small bowel mesentery near the ileocecal junction, the sigmoid mesocolon, the right paracolic gutter, and the right subhepatic and subphrenic spaces are the most common sites for the growth of seeded peritoneal metastases.^{6,15,50-58}

POUCH OF DOUGLAS

Malignant Disease

The pouch of Douglas projects at the level of the lower second to fourth sacral segment in most people (Fig. 109-4). On barium studies, drop metastases to this pouch produce a nodular, serosal indentation or fixed parallel folds along the anterior aspect of the rectosigmoid junction. These changes, which clinically correlate with the classic Blumer shelf, reflect the coalescence of tumor deposits with a dense fibrous reaction. This radiographic appearance can be simulated by endometriosis, inflammation of the seminal vesicles, prostate neoplasm or infection, scirrhous colon cancer, or radiation-induced changes.^{5,6}

Infection

Infected fluid naturally pools in the pouch of Douglas, often leading to abscess formation (Fig. 109-5). On plain radiographs, this fluid may be seen as a soft tissue density superior to the urinary bladder. Abscesses may also cause extrinsic distortion of the bladder dome, compress the rectosigmoid junction, or posteriorly and superiorly displace the sigmoid colon.⁵⁻⁷

PERIHEPATIC SPACES

Malignant Disease

Perihepatic dissemination of ovarian carcinoma is commonly seen on CT scans and is manifested as nodular, plaque-like, or

sheetlike masses that may be calcified (Fig. 109-6). Free-floating ovarian carcinoma cells are removed from the peritoneum by lymphatic channels in the diaphragm, particularly on the right. The submesothelial lymphatic capillaries of the diaphragm penetrate the muscle to communicate with a similar plexus arising on the pleural surface. From these diaphragmatic lymphatics, lymph drains to the cardiophrenic and mediastinal lymph nodes. Accordingly, a pelvic malignant neoplasm such as ovarian carcinoma can cause adenopathy at the cardiophrenic angle. Malignant ascites and peritoneal implants occur when these lymphatics are obstructed by tumor.^{6,59}

Infection

Right subphrenic and subhepatic abscesses occur two to three times more frequently than left subphrenic and perisplenic abscesses because of the fact that more right-sided surgical procedures, such as cholecystectomy and appendectomy, are performed and because Morison's pouch acts as a sewer for the right paracolic gutter. Infected fluid on the right side does not extend to the left subphrenic space because it is blocked by the falciform ligament.^{5,60-62}

LEFT SUBPHRENIC SPACE

Left subphrenic space (Fig. 109-7) abscesses most commonly result from perforated anterior gastric or duodenal bulb ulcers or are a sequela of gastric, colonic, or splenic surgery. The negative intra-abdominal pressure beneath the diaphragm preferentially draws infected material toward the diaphragm. The phrenicocolic ligament and falciform ligament prevent transcoelomic spread of generalized peritonitis and tumor.^{5,6,61}

LOWER SMALL BOWEL MESENTERY

A series of peritoneal recesses is formed along the right side of the small bowel mesentery as the mesenteric ruffles extend from the root of the mesentery to support the small bowel loops. Disease-bearing fluid and cells cascade from recess to recess toward the right lower quadrant and pool at the level of the distal ileum and cecum before overflowing into the pelvis.^{15,63}

Malignant seeding down the small bowel mesentery (Fig. 109-8) may be manifested as a mesenteric mass, stricture, spiculation, ulceration, or tethering of small bowel loops. If multiple adjacent recesses are affected, palisading of small bowel loops, in which narrowed loops are aligned in parallel configuration, may be seen on barium studies.^{5,6,15,63}

SIGMOID MESOCOLON

Infected and malignant fluid from the left inframesocolic space collects on the superior aspect of the sigmoid mesocolon (Fig. 109-9). This may cause a serosal mass effect on the superior aspect of the sigmoid colon on barium enema studies.^{5,6}

Retroperitoneal Spread

The retroperitoneum extends from the pelvic brim inferiorly to the diaphragm superiorly. It is bounded ventrally by the posterior parietal peritoneum and dorsally by the transversalis fascia. The anterior (Gerota) and posterior (Zuckerkandl) limbs of renal fascia divide the retroperitoneum into three major

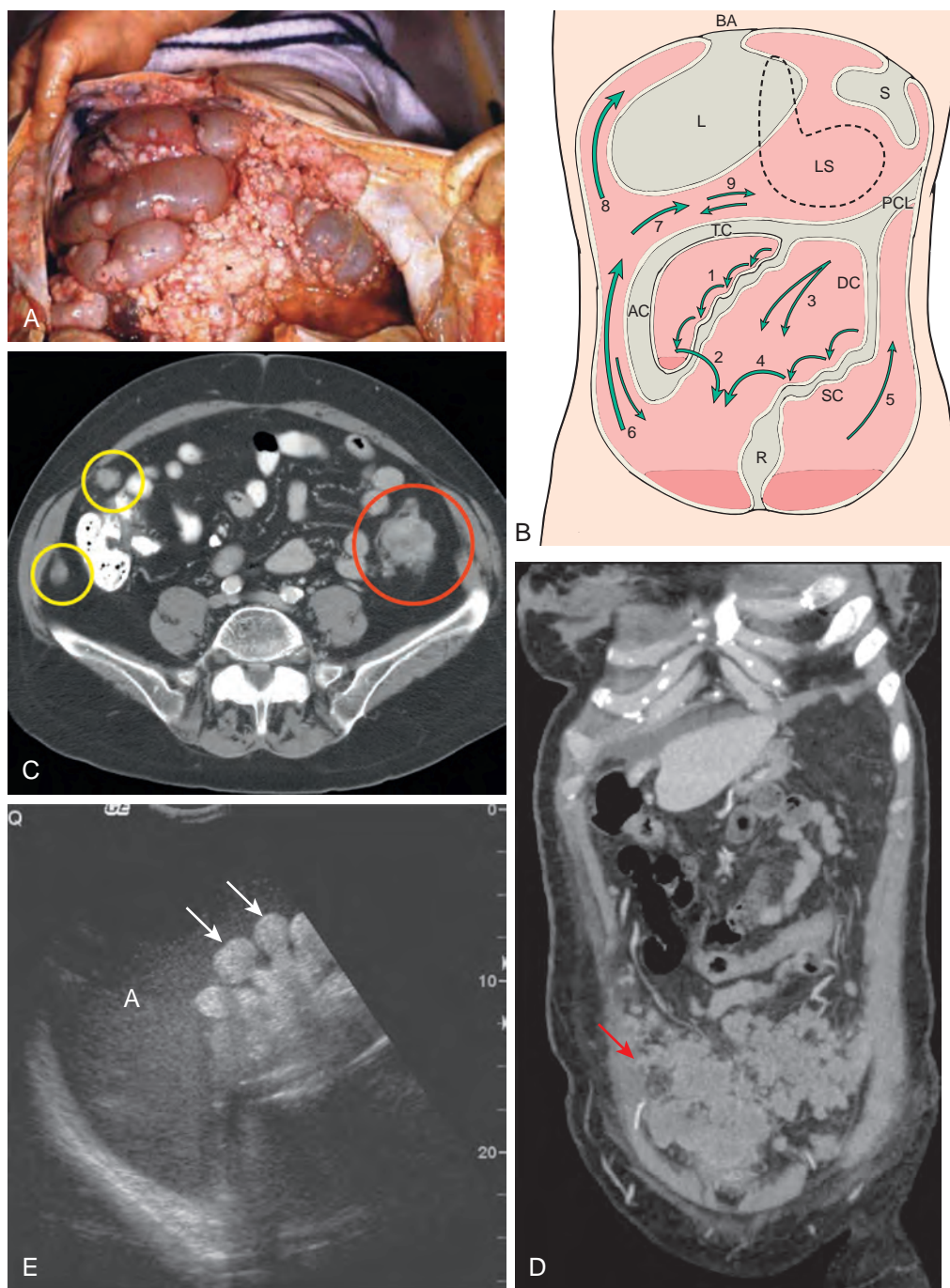


Figure 109-3 Intraperitoneal spread of tumor: spectrum of imaging findings. **A.** Gross peritoneal tumor implants are present in a patient with ovarian carcinomatosis. **B.** Fluid in the right inframesocolic space (1) cascades down the leaves of the small bowel mesentery, pools at the medial aspect of the cecum, and then overflows into the pelvis (2). Fluid in the left inframesocolic space (3) seeks the pelvis directly or is deposited on the superior aspect of the sigmoid mesocolon and then flows into the pelvis (4). Fluid in the pelvis may ascend the left paracolic gutter (5) but is stopped by the phrenicocolic ligament (PCL). Fluid in the right paracolic gutter (6) ascends to Morison's pouch (7) and then to the subphrenic space (8), where it is stopped by the bare area (BA) of the liver (L). There is potential communication with the lesser sac (LS) through the foramen of Winslow (9). AC, Ascending colon; DC, descending colon; R, rectum; S, stomach; SC, sigmoid colon; TC, transverse colon. **C.** Axial CT scan of a patient with carcinoma of the descending colon (red circle) and tumor implants in the greater omentum (yellow circles) adjacent to the right colon. **D.** Coronal reformatted CT shows an omental cake resulting from metastases from an ovarian carcinoma. **E.** Sonogram showing malignant ascites (A) contains fine, low-level echoes with matting of the bowel loops (arrows) centrally and posteriorly. (B modified from Meyers MA: The spread and localization of acute intraperitoneal effusions. *Radiology* 95:547-554, 1970; and from Meyers MA: Metastatic seeding along small bowel mesentery: Roentgen features. *Am J Roentgenol Radium Ther Nucl Med* 123:67-73, 1975.)

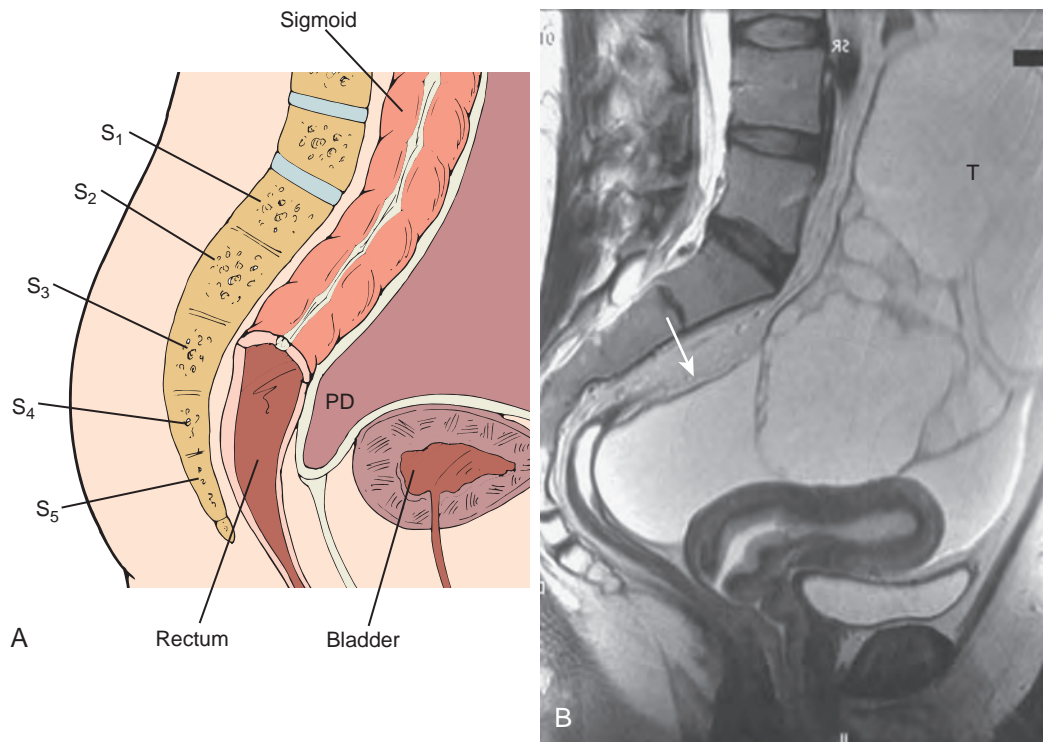


Figure 109-4 Pouch of Douglas **A.** The pouch of Douglas (PD) is the most dependent portion of the peritoneal cavity and a common site for abscess formation and drop metastases. This sagittal diagram shows the anatomic relationships of this space and indicates the positions of the sacral segments of the spine (S1 through S5). **B.** Sagittal T2-weighted MR image shows malignant fluid (arrow) resulting from a large ovarian neoplasm (T) distending the pouch of Douglas. (**A** from Meyers MA: *Distribution of intra-abdominal malignant fluid*. *Am J Roentgenol Radium Ther Nucl Med* 119:198–206, 1973. **B** courtesy of Rodney H. Reznek, MD, London, England.)

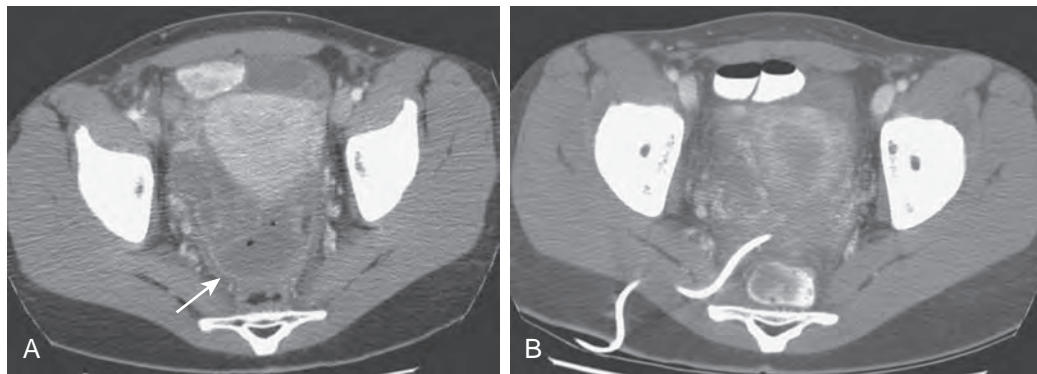
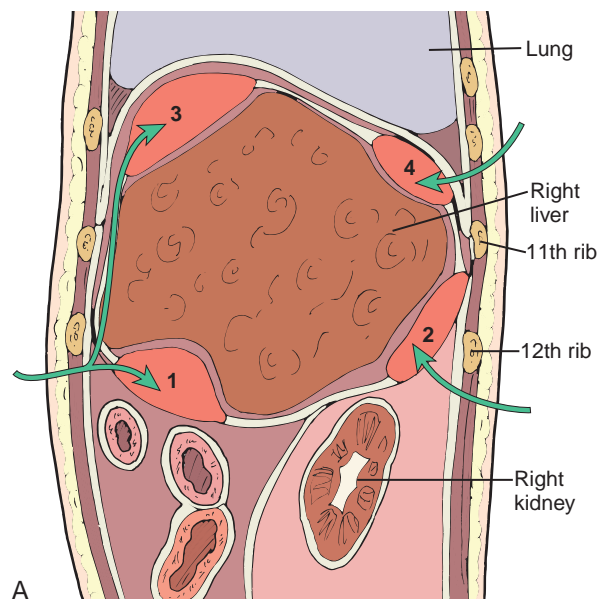


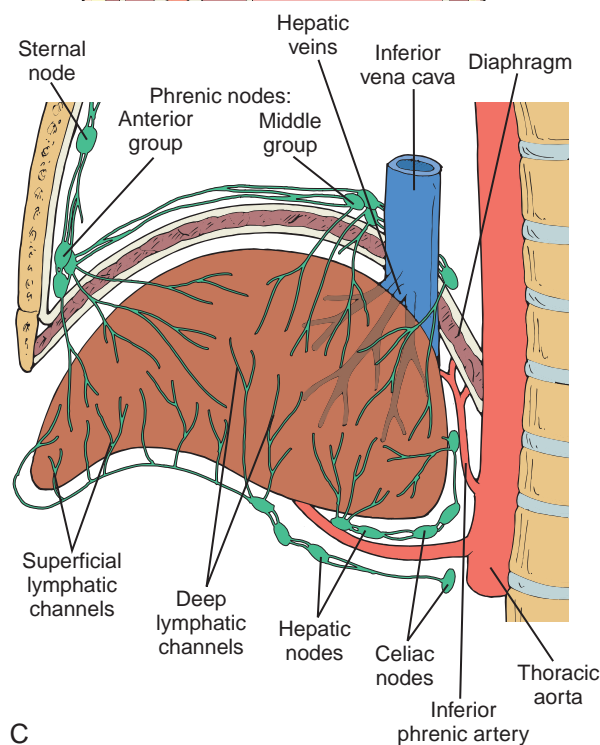
Figure 109-5 Pouch of Douglas abscess. **A.** A gas-containing pouch of Douglas abscess (arrow) is demonstrated on this CT scan of a patient 10 days after an appendectomy. **B.** The abscess has been successfully treated with a percutaneous drain introduced by a transgluteal approach.



A



B



C

Figure 109-6 Perihepatic spaces. **A.** Parasagittal diagram through the right lobe of the liver demonstrates the perihepatic spaces, the most common sites of abscess formation and peritoneal tumor localization in the right upper quadrant: 1, anterior subhepatic; 2, posterior subhepatic (Morison's pouch); 3, anterior subphrenic; 4, posterior subphrenic; arrows indicate surgical approaches to abscesses in the perihepatic spaces. **B.** The right subphrenic space (black arrow), the left subphrenic space (white arrow), and the anterior subhepatic space (dashed arrow) are depicted on this coronal T1-weighted MR image in a patient with ascites. **C.** The lymphatic drainage of the liver and perihepatic spaces is demonstrated on this sagittal diagram. Notice the presence of many lymphatics that traverse the diaphragm. (**A** from Meyers MA: *Dynamic Radiology of the Abdomen: Normal and Pathologic Anatomy*, 5th ed. New York, Springer-Verlag, 2000, pp 57–130. **C** from Woodburne RT, Burkell WE: *Essentials of Human Anatomy*. New York, Oxford University Press, 1988, pp 407–508.)

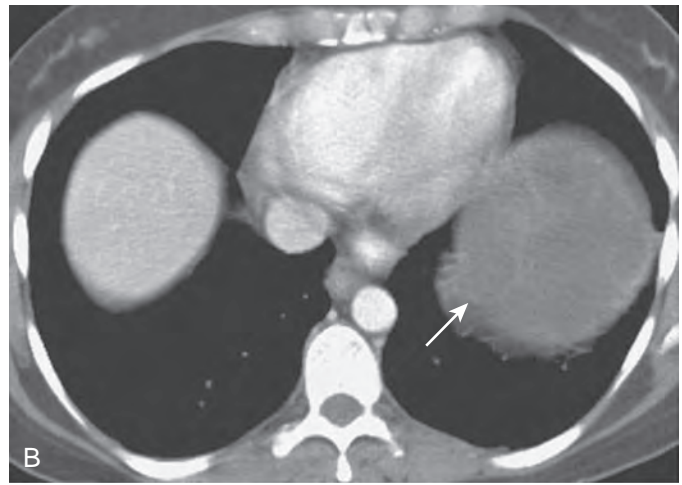
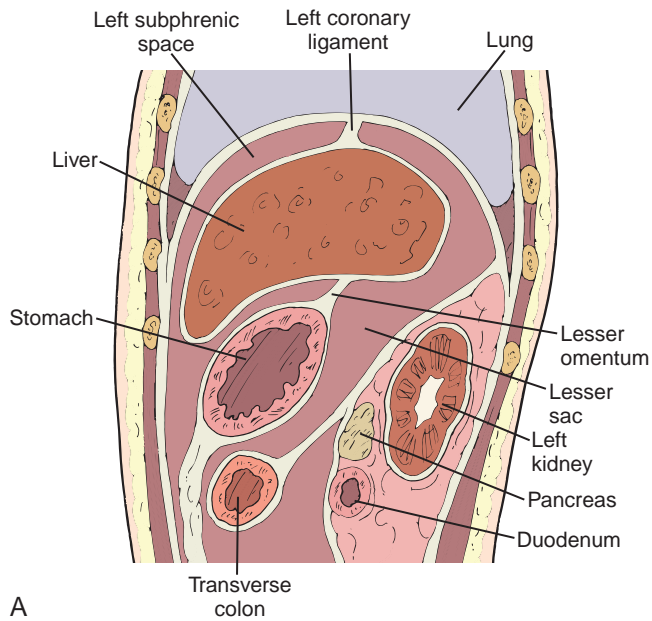


Figure 109-7 Left subphrenic space: anatomy and pathology. **A.** Sagittal diagram through the left lobe of the liver demonstrates the boundaries of the left subphrenic space, lesser sac, left coronary ligament, and lesser omentum. **B.** Cystic metastasis to the left subphrenic space (arrow) has resulted from carcinoma of the ovary. (**A** from Meyers MA: *Dynamic Radiology of the Abdomen: Normal and Pathologic Anatomy*, 3rd ed. New York, Springer-Verlag, 1988, pp 49–90.)

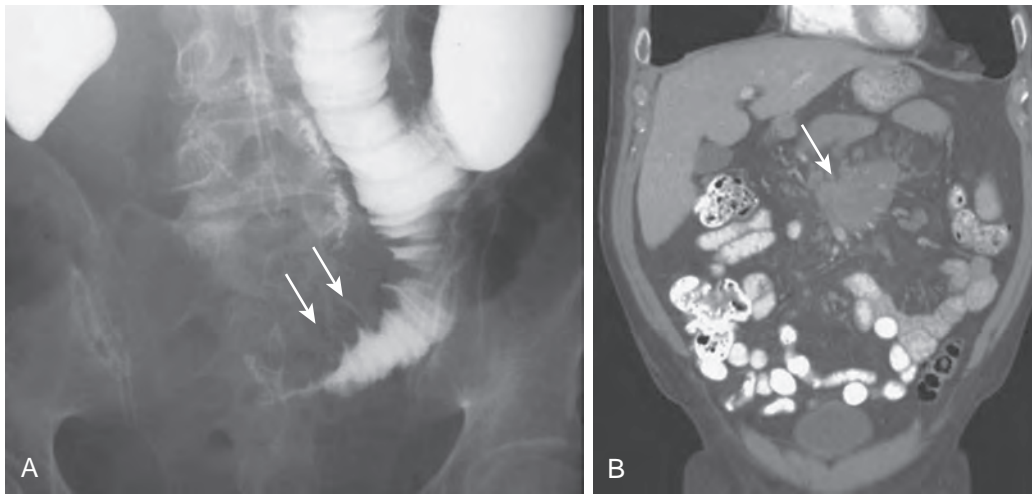


Figure 109-8 Mesenteric seeding of tumor. **A.** Malignant seeding down the small bowel mesentery from a gastric carcinoma is causing obstruction and spiculation of the valvulae conniventes (arrows) on the mesenteric side of the jejunum. **B.** Coronal reformatted CT image shows a carcinoid tumor infiltrating the root of the small bowel mesentery (arrow).

compartments: the anterior pararenal space, the perirenal space, and the posterior pararenal space (Fig. 109-10).⁶⁴⁻⁶⁶

ANTERIOR PARARENAL SPACE

The anterior pararenal space contains the retroperitoneal portions of the alimentary tract: the pancreas; the ascending and descending colon; and the second, third, and fourth portions of the duodenum. Consequently, it is the site of a large number of infectious, neoplastic, and inflammatory disorders, including appendicitis, diverticulitis, pancreatitis, and carcinoma. Fluid collections and gas in the anterior pararenal space tend to

remain on the right or left side, but they may involve both sides if they originate from the pancreas because that organ straddles the space across the midline. Concurrent disease in both anterior pararenal spaces most commonly occurs in patients with pancreatitis.^{64,65,67,68}

The anterior pararenal space is anatomically continuous with the bare area of the liver (Fig. 109-11), the root of the small bowel mesentery, and the transverse mesocolon, and it provides a pathway for widespread dissemination of gastrointestinal disease. Fluid in the anterior pararenal space can flow inferiorly around the caudal border of the renal fascia and then extend posteriorly to involve the posterior pararenal space. At this level,

the lateroconal fascia may disappear as a distinct boundary, permitting direct communication with the properitoneal fat stripe. The inflammatory process may track to the lateral abdominal wall, which accounts for Grey Turner's sign of pancreatitis.^{64,69}

PERIRENAL SPACE

The perirenal space lies within the anterior (Gerota) and posterior (Zuckerkandl) renal fasciae and contains the kidney, adrenal gland, and fat. The left kidney is intimately related to the distal transverse and proximal descending colon.^{70,71}

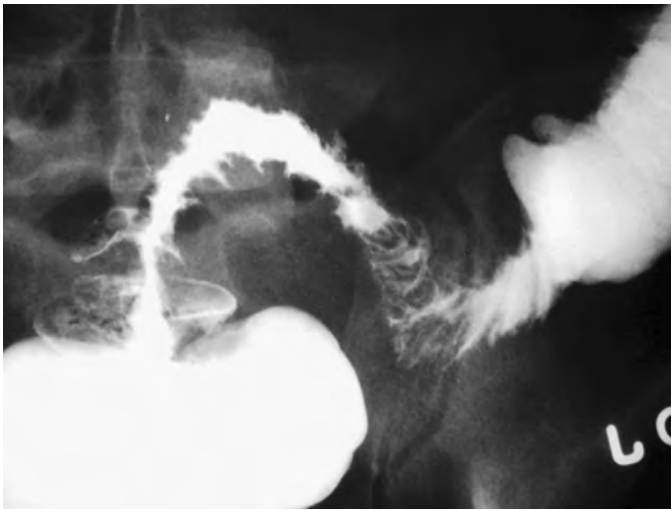


Figure 109-9 Drop metastases: carcinoma of the stomach metastatic to the sigmoid mesocolon. A barium enema study shows narrowing and spiculation of the mucosa of the sigmoid colon.

The lienorenal ligament, phrenicocolic ligament, transverse mesocolon, and peritoneal reflections of the descending colon merge near the anterior aspect of the left kidney. The right kidney lies adjacent to the descending duodenum and hepatic flexure of the colon. The root of the transverse mesocolon and peritoneal reflections of the ascending colon also lie in this area. Advanced renal infections and neoplasms may break through fascial boundaries and invade the adjacent bowel. Similarly, large neoplasms of the colon may invade the kidneys.^{70,71}

There is evidence of potential communication across the midline between the two perirenal spaces anterior to the lower aorta and inferior vena cava at the level of L3 to L5. This accounts for certain patterns of distribution of hemorrhage after abdominal aortic aneurysm rupture. When the disease process originates in the kidney, however, contralateral extension of fluid is impeded by fibrous septa and by the narrowness of the potentially communicating channel.⁷²

POSTERIOR PARARENAL SPACE

The posterior pararenal space contains primarily fat. Accordingly, it is usually involved secondarily by disease processes rather than being a primary site of disease. Perforations of the sigmoid colon and rectum may gain access to the posterior pararenal space.⁷³ In pancreatitis, fluid may extend directly into this space from the anterior pararenal space inferiorly.⁶⁴ However, most fluid collections seen posterior to the kidney in pancreatitis are caused by separation of the two laminae of the posterior limb of renal fascia.

Collections in the posterior pararenal space usually result from spontaneous retroperitoneal hemorrhage or from disease in contiguous musculoskeletal structures. The posterior pararenal space continues anteriorly as the properitoneal fat line, and disease in this space may obliterate the line.^{64,65}

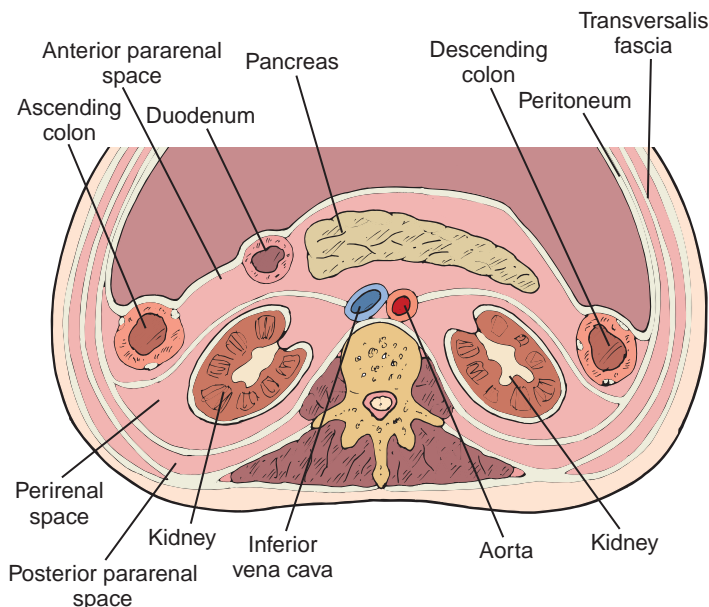


Figure 109-10 Retroperitoneal anatomy. Axial diagram of the abdomen at the level of the kidneys demonstrates the anatomy of the retroperitoneum. The anterior pararenal space contains the retroperitoneal portions of the alimentary tract: ascending colon, descending colon, duodenum, and pancreas. The perirenal space contains the kidneys and lies between the Gerota fascia and the fascia of Zuckerkandl. The posterior pararenal space contains fat. (Modified from Meyers MA: Acute extraperitoneal infection. *Semin Roentgenol* 8:445-464, 1973.)

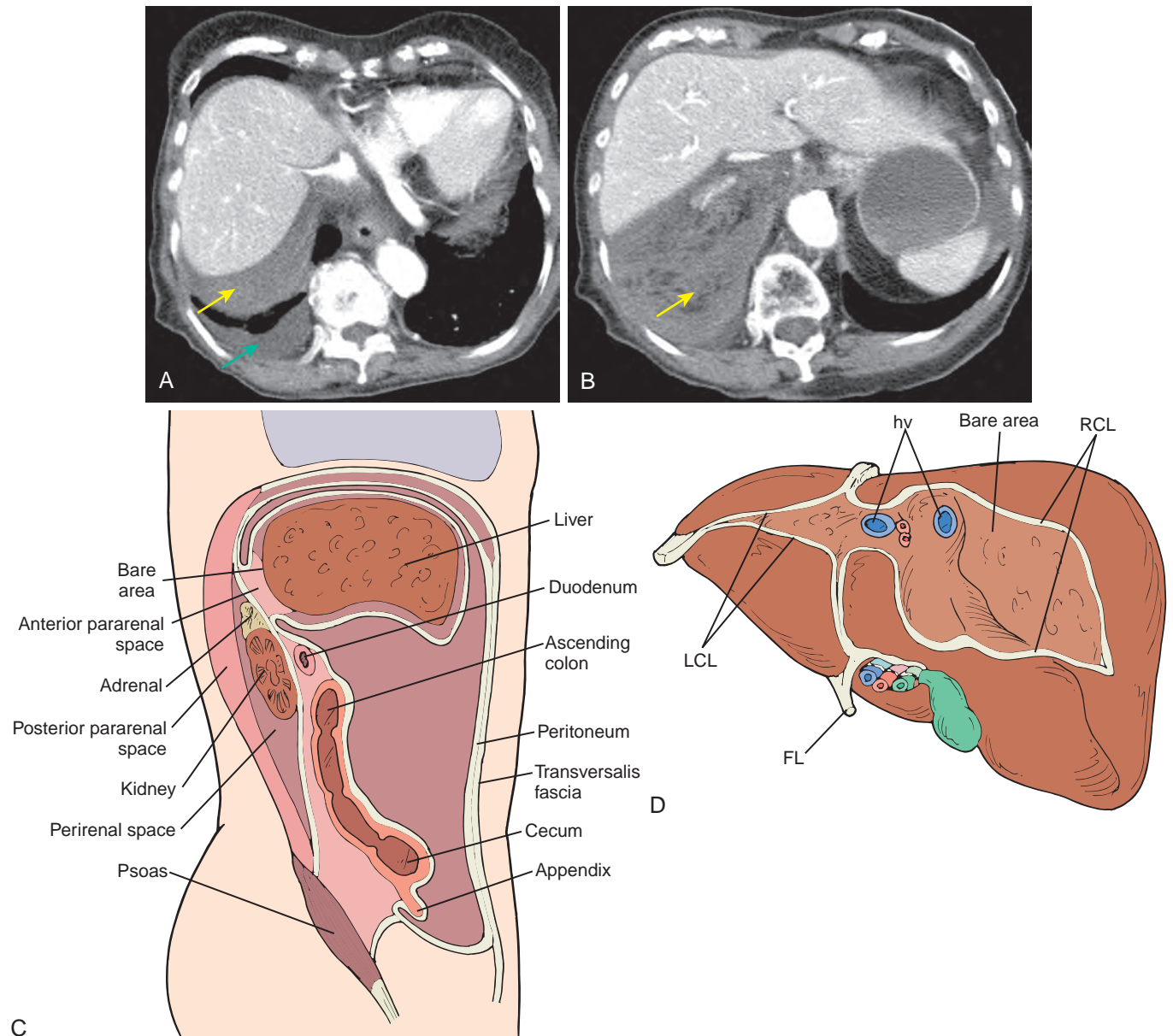


Figure 109-11 Hepatic bare area and anterior pararenal space: spread of hemorrhage. Communication between the bare area of the liver and the anterior pararenal space is illustrated in this patient who developed a spontaneous right renal bleed while being treated with anticoagulant drugs. **A.** Hemorrhage from a fractured right kidney is present in the bare area of the liver (yellow arrow). Blue arrow, Pleural effusion. **B.** The renal fracture is identified (arrow), and there is blood in the perinephric space and anterior pararenal space. Note the slitlike inferior vena cava. **C.** The anterior pararenal space is continuous with the bare area of the liver, explaining the findings in **B.** This sagittal drawing depicting the right retroperitoneal spaces also shows the perirenal space, containing the right kidney and adrenal gland, and the posterior pararenal space, which communicates with the inferior aspect of the anterior pararenal space. **D.** The diagram shows the posterior view of the bare area of the liver. LCL, Left coronary ligament; FL, falciform ligament; hv, hepatic veins; RCL, right coronary ligament. (**C** from Meyers MA: *Acute extraperitoneal infection*. *Semin Roentgenol* 8:445–464, 1973. **D** from Arenas AP, Sanchez LV, Albillos JM, et al: *Direct dissemination of pathologic abdominal processes through perihepatic ligaments: Identification with CT*. *RadioGraphics* 14:515–537, 1994.)

Subperitoneal Spread

The subperitoneal space is a large, unifying, anatomically continuous potential space that connects the peritoneal cavity with the retroperitoneum (Fig. 109-12). This space is formed by the subserosal areolar tissue that lines the inner surfaces of the peritoneum and the musculature of the abdomen and pelvis. It contains the branches of the vascular, lymphatic, and nervous systems that supply the viscera. The subperitoneal

space extends into the peritoneal cavity and is invested between the layers of the mesenteries and ligaments that support and interconnect the abdominal and pelvic organs. As such, it provides one large continuous space in which infectious, neoplastic, inflammatory, and hemorrhagic disease may spread in many directions.*

*References 2-4, 6, 7, 65-68, 74, 75.

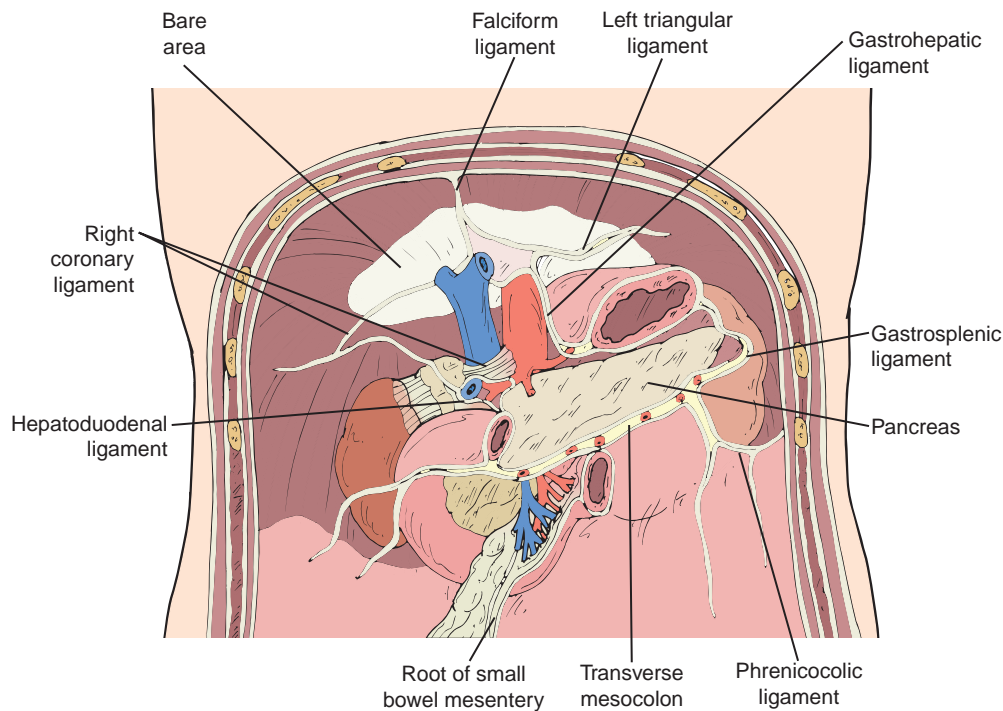


Figure 109-12 Subperitoneal spaces. Frontal diagram of the posterior parietal wall of the upper abdomen shows the planes of peritoneal reflections that constitute the major ligaments and mesenteries of the subperitoneal space. Anatomic continuity between intraperitoneal structures and between extraperitoneal and intraperitoneal sites is established along the bare areas at the roots of origin of the supporting ligaments and mesenteries. (From Meyers MA, Oliphant M, Berne AS, et al: *The peritoneal ligaments and mesenteries: Pathways of intraabdominal spread of disease*. Radiology 163:593–604, 1987.)

TRANSVERSE MESOCOLON

The transverse mesocolon is the linchpin that unites the various subperitoneal spaces and is a major conduit for focal and distant spread of disease. On the right, the transverse mesocolon is continuous with the duodenocolic ligament; on the left, it is continuous with the phrenicocolic ligament; and centrally, it communicates with the small bowel mesentery (Fig. 109-13).^{2-4,7}

The dissemination of fluid and enzymes in pancreatitis typifies the role of this space in disease spread. The inflammatory changes of pancreatitis can spread to the transverse colon and stomach (both intraperitoneal organs) by the gastrosplenic ligament, lesser sac, and gastrocolic ligament; to the left kidney (a retroperitoneal organ) by the splenorenal ligament; to the liver and gallbladder (intraperitoneal organs) by the hepatoduodenal ligament; and to the right lower quadrant by the root of the small bowel mesentery.^{2-4,67,68,75}

Because the transverse mesocolon inserts on the taenia mesocolica, pancreatic processes carried by this ligament preferentially affect the inferior border of the transverse colon.^{74,75} Fixation of the inferior margin and pseudosacculation of the superior (uninvolved) margin of the transverse colon may be seen on barium enema studies in patients with pancreatic disease. Colon neoplasms and diverticulitis can invade the transverse mesocolon and subsequently spread to the pancreas.²⁻⁴

GASTROCOLIC LIGAMENT AND GREATER OMENTUM

The gastrocolic ligament connects the greater curvature of the stomach to the transverse colon (Fig. 109-14). It is formed by

fusion of the four layers of peritoneum that invest the stomach. These layers descend a variable distance to form the greater omentum and then fuse at the level of the colon.

The potential space between the middle layers of the greater omentum forms the inferior recess of the lesser sac. In most adults, partial fusion of the middle layers prevents the lesser sac from extending below the transverse colon. The greater omentum consists of a trabecular framework of vessels with various amounts of adipose tissue, lymphatics, or macrophages. It has been called the abdominal policeman and is frequently involved by infectious and neoplastic processes.⁷⁶⁻⁷⁹

On the left, the gastrocolic ligament is continuous with the gastrosplenic ligament. On the right, it ends at the gastroduodenal junction, near the hepatoduodenal ligament. Carcinoma of the transverse colon can invade to the greater curvature of the stomach, and gastric neoplasms can spread to the superior aspect of the transverse colon by the gastrocolic ligament.^{74,75,79}

GASTROHEPATIC LIGAMENT

The gastrohepatic ligament is part of the lesser omentum. It joins the gastroesophageal junction and lesser curvature of the stomach to the liver at the fissure of the ligamentum venosum superiorly and the porta hepatis inferiorly. Beneath the diaphragm, the esophagus is invested by the gastrohepatic ligament on the right and the gastrophrenic ligament on the left. The gastrohepatic ligament contains the left gastric artery, coronary vein, and left gastric lymph node chain. The subperitoneal fat of the gastrohepatic ligament continues into the liver as Glisson's capsule. Lymph nodes and blood vessels seen in the gastrohepatic ligament by CT should be smaller than 8 mm in

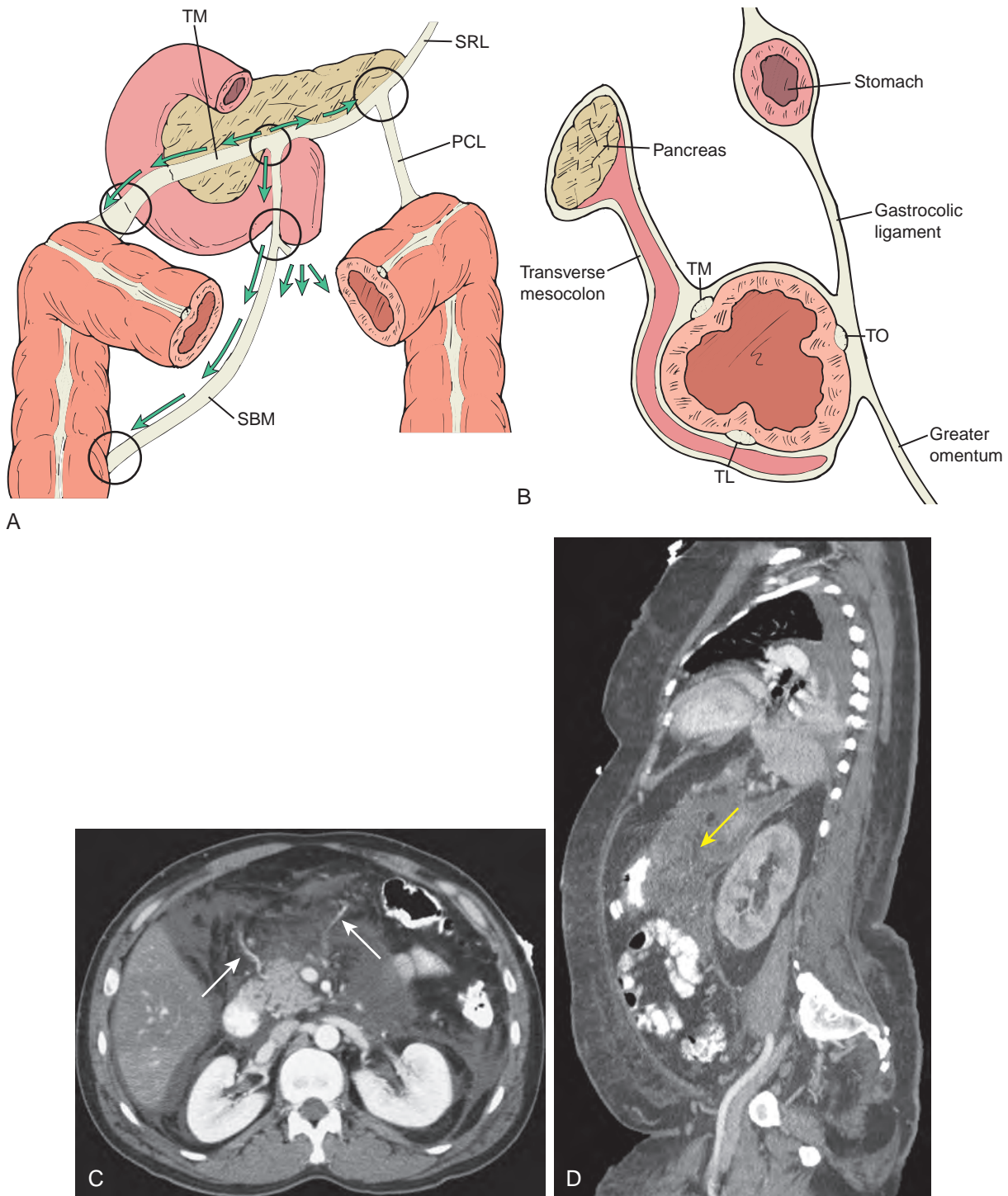


Figure 109-13 Transverse mesocolon: anatomic relationships and planes of disease spread. **A.** Frontal diagram shows the relationships of the transverse mesocolon (TM). The transverse mesocolon is continuous with the root of the small bowel mesentery (SBM), the splenorenal ligament (SRL), and the phrenicocolic ligament (PCL). **B.** Sagittal diagram through the transverse colon demonstrates preferential spread of pancreatic disease through the transverse mesocolon (TM) inferiorly along the taenia mesocolica–taenia libera (TL) haustra toward the taenia libera–taenia omentalis (TO) row. This constitutes the inferior border of the transverse mesocolon. **C.** Fluid surrounds the middle colic vessels (arrows) of the transverse mesocolon in this patient with pancreatitis. **D.** Sagittal reformatted image shows inflammatory pancreatic fluid traversing the transverse mesocolon to spread (arrow) to the transverse colon. (A from Okino Y, Kiyosue H, Mori H, et al: Root of the small-bowel mesentery: Correlative anatomy and CT features of pathologic conditions. *RadioGraphics* 21:1475–1490, 2001; modified from Meyers MA: *Dynamic Radiology of the Abdomen: Normal and Pathologic Anatomy*, 5th ed. New York, Springer-Verlag, 2000, pp 131–264. B from Meyers MA, Volberg F, Katzen B, et al: *Haustral anatomy and pathology: A new look. II. Roentgen interpretation of pathologic alterations. Radiology* 108:505–512, 1973.)

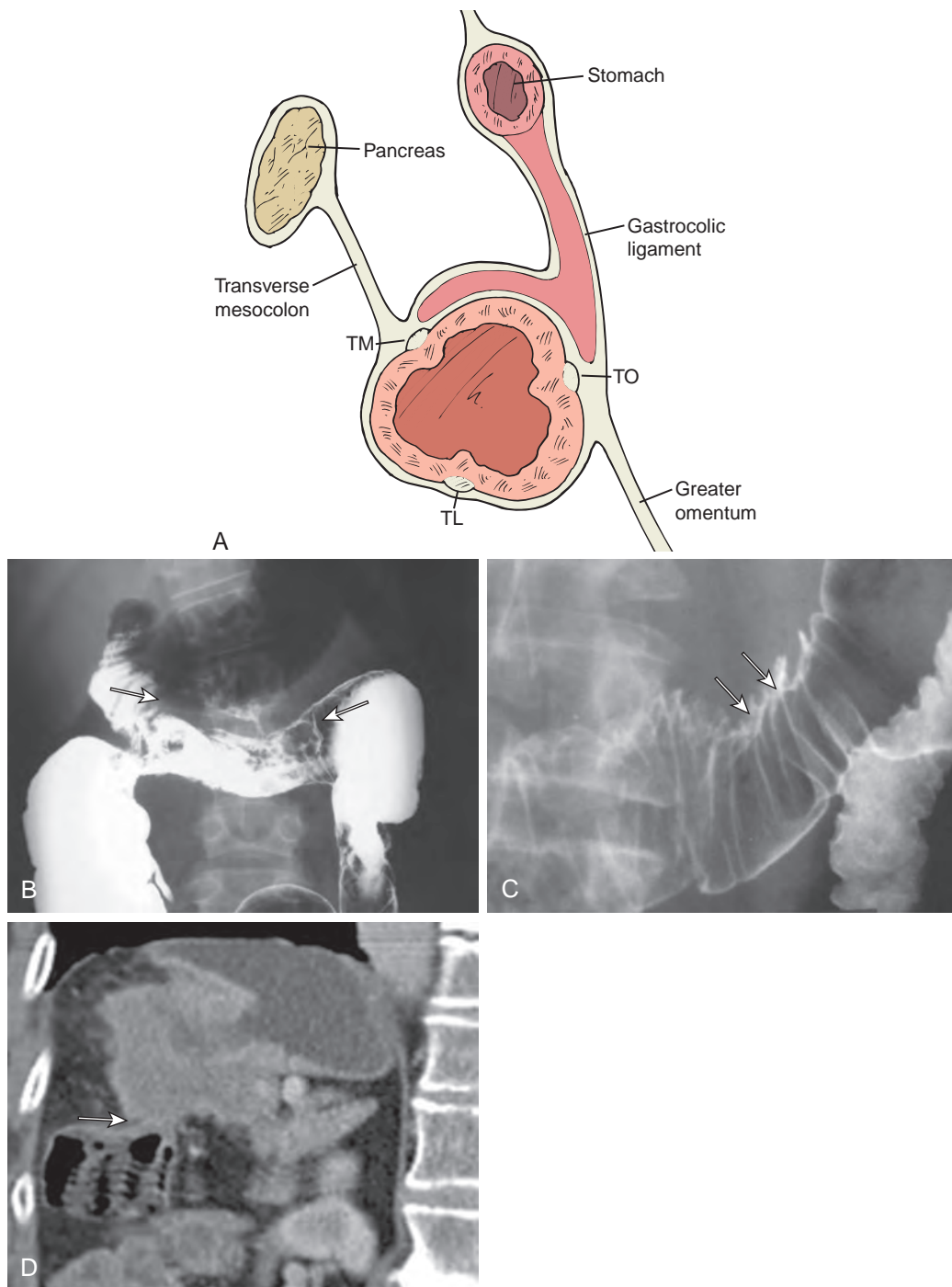


Figure 109-14 Gastrocolic ligament: normal anatomy and pathology. **A.** Sagittal diagram through the transverse colon demonstrates preferential spread of disease from the stomach, through the gastrocolic ligament, and along the taenia omentalis (TO)–taenia mesocolica (TM) haustral row. This constitutes the superior border of the transverse colon. The taenia libera (TL) is indicated. **B.** Barium enema in a patient with Crohn's disease demonstrates a fistula (arrows) from the transverse colon to the greater curvature aspect of the stomach by way of the gastrocolic ligament. **C.** Direct invasion (arrows) of the superior aspect of the transverse colon along the gastrocolic ligament occurs from a scirrhous carcinoma of the stomach. **D.** Sagittal reformatted image shows gastric cancer invading through the gastrocolic ligament into the superior aspect of the transverse colon (arrow). (A from Meyers MA, Volberg F, Katzen B, et al: *Haustral anatomy and pathology: A new look. II. Roentgen interpretation of pathologic alterations. Radiology* 108:505–512, 1973.)

diameter. Nonenhancing structures larger than 8 mm suggest adenopathy; if they enhance, varices should be considered.⁸⁰

Gastric cancers often spread first to the lymph nodes in the gastrohepatic ligament (Fig. 109-15). The left gastric nodes also receive direct lymphatic drainage from the distal esophagus,

and neoplasms in this region may produce gastrohepatic ligament adenopathy. Because the gastrohepatic ligament is contiguous with the hepatoduodenal ligament, adenopathy may occur in the porta hepatis and the peripancreatic area from spread of a gastric neoplasm. Direct spread of fundal gastric

malignant neoplasms into the left hepatic lobe occurs by means of this ligament and Glisson's capsule.⁴ Infectious, inflammatory, and autoimmune disorders of the liver often cause adenopathy in the gastrohepatic and gastroduodenal ligaments. Lymphoma and carcinoma of the breast, lung, and esophagus may spread to the same ligament.

HEPATODUODENAL LIGAMENT

The hepatoduodenal ligament is formed at the free edge of the gastrohepatic ligament and connects this portion of the peritoneal cavity with the right anterior pararenal space. It extends from the junction of the first and second portions of the duodenum to the porta hepatis and contains the blood vessels and

lymphatics that supply the liver, gallbladder, and biliary tree as well as the common bile duct to its insertion into the ampulla of Vater. Any hepatic or biliary process adjacent to the liver hilum, including the anterior portion of the caudate lobe, can spread by the hepatoduodenal ligament and subsequently extend to the gastrohepatic ligament, gastrocolic ligament, duodenocolic ligament, transverse mesocolon, and falciform ligament. Pancreatic neoplasms invade the porta hepatis by this ligament.⁸¹⁻⁸⁶

DUODENOCOLIC LIGAMENT

The duodenocolic ligament is the right margin of the transverse mesocolon. It provides a pathway for disease spread between the descending duodenum and the junction of the ascending and transverse colon.^{81,87}

GASTROSPLENIC LIGAMENT

The gastrosplenic ligament is formed by the left lateral extension of the peritoneal layers of the greater omentum and connects the greater curvature of the stomach with the splenic hilum. It contains the left gastroepiploic and short gastric vessels. The gastrosplenic ligament provides a pathway for spread of disease between the pancreatic tail, the spleen, and the stomach. Carcinoma of the stomach may spread to the splenic hilum along this ligament. Similarly, carcinoma of the pancreatic tail can spread to the stomach by invading first the splenic hilum and then the stomach by the gastrosplenic ligament. Because the pancreatic tail borders this ligament, this is a fairly common site of pseudocyst formation (Fig. 109-16). Benign gastric ulcers may penetrate into the spleen by this ligament.^{2-4,6,88}

SPLENORENAL LIGAMENT

The splenorenal ligament invests the pancreatic tail and affords communication between the anterior pararenal space, which contains the pancreas, and the perirenal space, which contains the kidney. Although pancreatitis (Fig. 109-17) and carcinoma

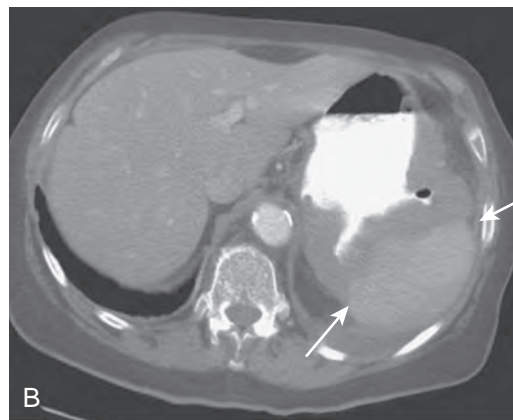


Figure 109-15 Spread of gastric cancer into the gastrohepatic ligament. Coronal reformatted CT image shows tumor invasion of the gastrohepatic ligament (black arrow). Peritoneal tumor implants (white arrows) are identified.



Figure 109-16 Gastric cancer spread to the spleen by means of the gastrosplenic ligament.

Coronal (A) and axial (B) images. The subperitoneal space of the gastrosplenic ligament (arrows) is serving as a conduit of tumor spread in this patient with adenocarcinoma of the greater curvature of the stomach.



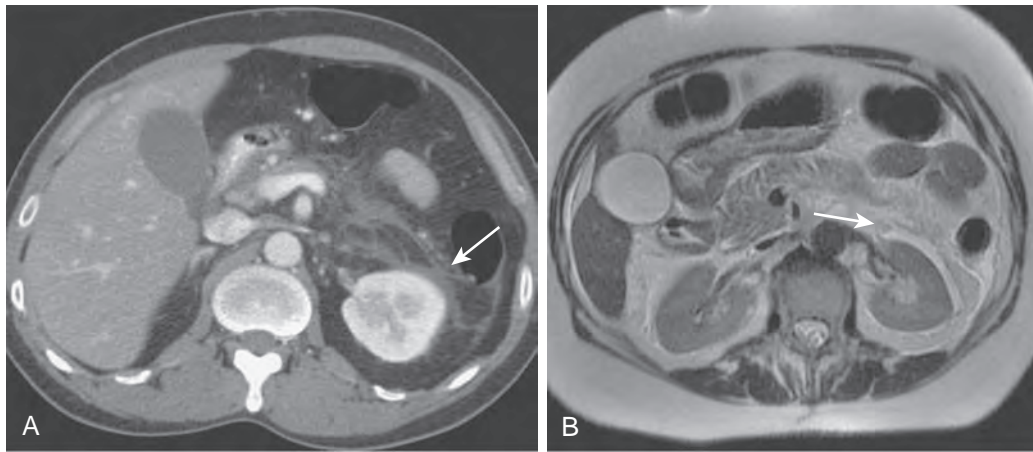


Figure 109-17 Inflammation of pancreatitis spreading from the pancreas to the left kidney by means of the splenorenal ligament: MRI and CT findings in the same patient. **A.** CT shows fluid inferior to the pancreatic tail that extends into the left perirenal space (arrow). **B.** Fat-suppressed, axial, T2-weighted MR image shows high signal intensity fluid (arrow) lateral to the left kidney in the perirenal space.

of the pancreas can commonly spread through this ligament, renal disease seldom involves the pancreatic tail.^{2-4,6}

PHRENICOCOLIC LIGAMENT

The phrenicocolic ligament is the left lateral extension of the transverse mesocolon. It acts as the suspensory ligament of the spleen, reflects the anatomic splenic flexure of the colon, and is directly continuous with the splenorenal ligament and transverse mesocolon. It can transmit neoplastic and inflammatory disease between the pancreas and the colon, the left kidney, and the spleen.^{2-6,67,68}

SMALL BOWEL MESENTERY

The small bowel mesentery occupies a major portion of the peritoneal cavity as it suspends the small bowel, and it represents an enormous potential space for disease spread.^{2-4,63,67,68} Seeded neoplastic or infectious material associated with free intraperitoneal fluid cascades along the mesenteric leaves in the inframesocolic space and is deposited on the medial aspect of the cecum on the right, on the superior border of the terminal ileum, and on the superior aspect of the sigmoid mesocolon on the left.^{5,6}

The subperitoneal space of the small bowel mesentery is continuous with the bare area of the ascending colon and the transverse mesocolon (Fig. 109-18). The leaves of the small bowel mesentery continue as the posterior peritoneum, overlying the posterior abdominal wall. The connective tissue in the small bowel mesentery merges with the subperitoneal tissue of the retroperitoneum. The subperitoneal tissue continues without interruption inferiorly, from the right lower abdomen over the pelvic musculature and along the lateral pelvic sidewalls. Because this space potentially communicates with the broad ligament, it provides a pathway for bidirectional disease spread between the abdomen and the pelvis.^{2-4,17}

SIGMOID MESOCOLON

The mesocolon or mesentery of the sigmoid colon provides a major avenue for spread of disease between the abdominal cavity and the pelvis. It is directly continuous with the posterior bare area of the colon, the bare area of the rectum, and, in

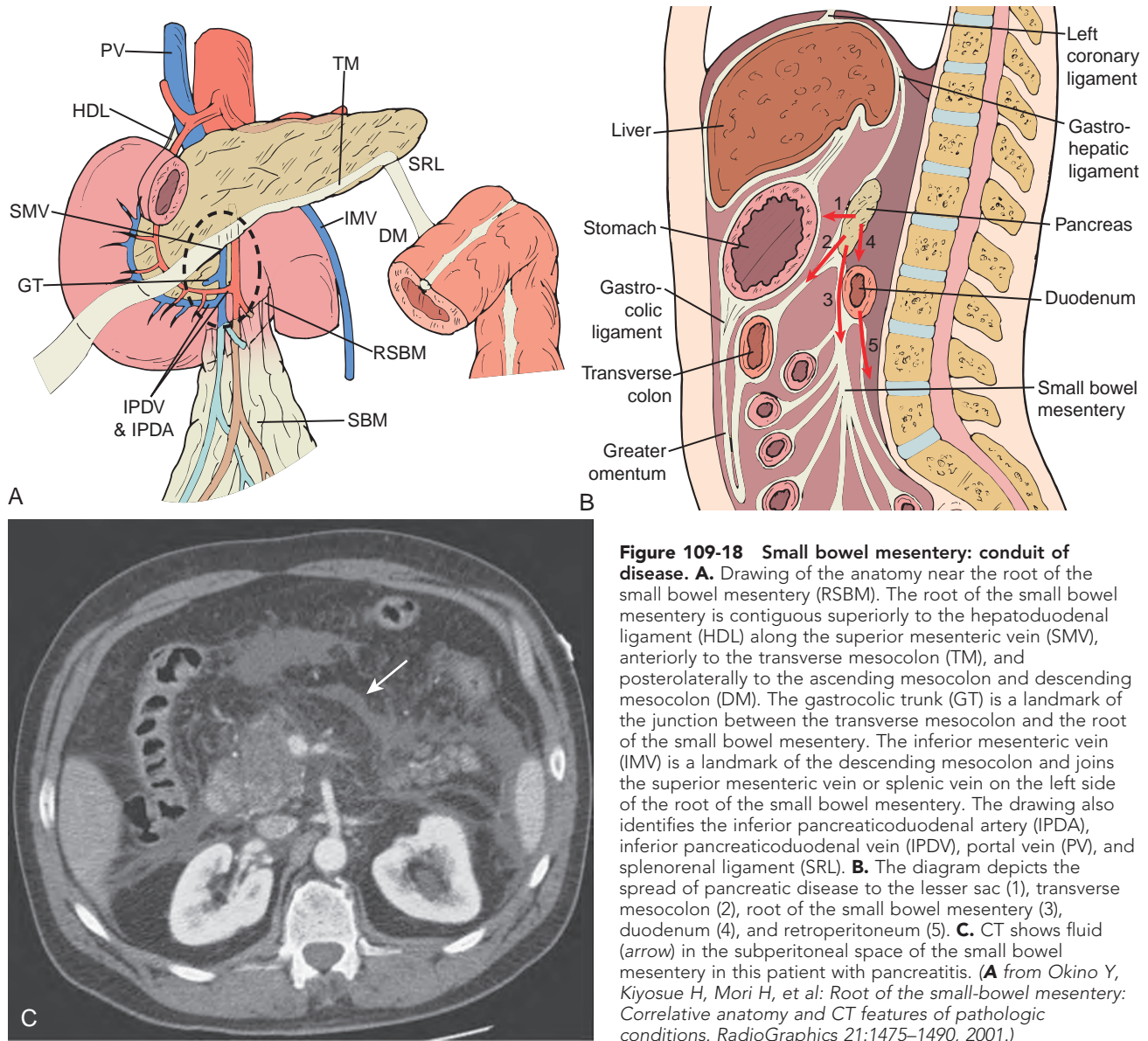
females, the broad ligament. Diverticulitis usually spreads into and is confined by the sigmoid mesocolon. Carcinoma of the sigmoid colon may spread to the ovary hematogenously or through the mesocolon and then along the broad ligament.^{2-4,7} Similarly, ovarian neoplasms or tubo-ovarian abscesses may directly spread by the broad ligament to the sigmoid mesocolon and subsequently involve the sigmoid colon.^{2-4,7}

BROAD LIGAMENT

The broad ligaments pass from the margins of the uterus to the lateral walls of the pelvis and together with the uterus form a septum across the lesser pelvis, dividing it into two parts. The anterior part contains the bladder and uterocystic recess; the posterior part includes the rectum, cul-de-sac, terminal ileum, and part of the sigmoid colon. These ligaments enclose the subperitoneal space, which includes the uterus, ovaries, fallopian tubes, arteries, nerves, lymphatics, and distal ureters as they enter the bladder. On the right side, communication with the base of the cecum and right inferolateral termination of the small bowel mesentery provides subperitoneal continuity for bidirectional spread of disease between the female pelvic organs and the retroperitoneal and peritoneal organs of the abdomen. On the left, the broad ligament communicates with the sigmoid mesocolon. Tumors of the cecum, appendicitis, Crohn's disease abscesses, and drop metastases can spread to the right ovary by this pathway. Similarly, an ovarian neoplasm or tubo-ovarian abscess may spread to the cecum and terminal ileum.⁷

FALCIFORM LIGAMENT AND LIGAMENTUM TERES

The ligamentum teres is located in the free edge of the falciform ligament and anchors the liver anterosuperiorly to the abdominal wall. Infections and malignant neoplasms in the porta hepatis can penetrate the falciform ligament when they extend along the fissure of the ligamentum teres. The superficial lymphatics of the liver also traverse the falciform ligament, providing additional pathways of disease spread. The ligamentum teres, gastrohepatic ligament, and hepatoduodenal ligament are continuous, deep to the porta hepatis near the left portal vein.^{2-4,89}



CORONARY LIGAMENT AND BARE AREA

The right coronary ligament suspends the right lobe of the liver from behind and together with the left coronary ligament defines the margins of the bare area of the liver. The bare area of the liver is continuous with the anterior pararenal space.^{4,64,65} The inferior vena cava lies within the bare area of the liver, and fluid in the anterior pararenal space can extend ventrally to the inferior vena cava (see Fig. 109-11), close to the epiploic foramen.^{2-4,89}

Extraperitoneal Spread

ILIOPSOAS MUSCLE ROUTE

Intraperitoneal and retroperitoneal disease can penetrate fascial boundaries and spread into the extraperitoneal space and its major muscles, the psoas and iliacus. These muscles are quite long and provide a pathway for disease spread from the level of

the pancreas to the level of the thigh and lesser trochanter. Carcinoma of the colon, pancreatitis, appendicitis, Crohn's disease with fistula formation, diverticulitis, ischiorectal abscess, periureteral abscess, renal abscess, traumatic perforation of the rectum, and foreign body perforation of the gut can potentially involve the psoas muscle and extend into the extraperitoneal space.⁹⁰⁻⁹⁴

SACROSCIATIC NOTCH ROUTE

Pelvic neoplasms arising from the rectosigmoid, prostate, uterus, and cervix can involve the extraperitoneal pelvic compartment and gluteal regions by intrinsic involvement of the piriformis and the obturator internus muscles or their surrounding fascial planes. Direct compression of the sciatic or sacral nerve may cause pain, simulating a cauda equina lesion. Similarly, hematoma or abscess fluid may spread from the pelvis to the gluteal region and vice versa.^{90,92}

The piriformis muscle can spread disease through the greater sciatic foramen onto the greater trochanter. The obturator internus muscle can be a disease conduit as it courses through the lesser sciatic foramen to insert on the greater trochanter.^{91,95}

OBTURATOR FORAMEN ROUTE

Infections and hernias may spread through the obturator foramen into the groin and legs and onto the lesser trochanter.

ABDOMINAL WALL ROUTE

The spread of infection in the abdominal wall is facilitated by copious fat and long muscle groups that contain few impeding fasciae. Abdominal wall disease may result from direct spread

of disease (e.g., Crohn's disease, perforated neoplasm) or from indirect spread from the peritoneal cavity by the falciform ligament. Contiguous spread of tumor to the abdominal wall is most frequently seen in tumors that arise in superficial organs, such as the omentum, transverse colon, gallbladder, and bladder.⁹⁶⁻⁹⁸

Conclusions

The abdominal and pelvic organs and their supporting ligaments, peritoneal reflections, and mesenteries form a complex interconnecting network. This unifying concept explains the presence of abdominal disease at sites distant from its origin. Knowledge of the various pathways of spread provides a clearer understanding of many disease processes and can help tailor the imaging approach to abdominal and pelvic disease.

REFERENCES

- Warwick R, Williams PL, editors: Peritoneum. In Gray's Anatomy, 35th British ed, Philadelphia, 1973, WB Saunders, pp 1257-1269.
- Oliphant M, Berne AS, Meyers MA: Subperitoneal spread of intra-abdominal disease. In Meyers MA, editor: Computed Tomography of the Gastrointestinal Tract, New York, 1986, Springer-Verlag, pp 95-138.
- Oliphant M, Berne AS: Computed tomography of the subperitoneal space: Demonstration of direct spread of intraabdominal disease. J Comput Assist Tomogr 6:1127-1137, 1982.
- Meyers MA, Oliphant M, Berne AS, et al: The peritoneal ligaments and mesenteries: Pathways of intraabdominal spread of disease. Radiology 163:593-604, 1987.
- Meyers MA: Dynamic Radiology of the Abdomen: Normal and Pathologic Anatomy, ed 5, New York, 2000, Springer-Verlag, pp 57-130.
- Meyers MA, Charnsangavej C, Oliphant M: Dynamic Radiology of the Abdomen: Clinical Anatomy of the Abdomen, ed 6, New York, 2011, Springer-Verlag, pp 23-408.
- Oliphant M, Berne AS, Meyers MA: Imaging the direct bidirectional spread of disease between the abdomen and the female pelvis via the subperitoneal space. Gastrointest Radiol 13:285-298, 1988.
- Coman DR, DeLong KP, McCutcheon M: Studies on the mechanism of metastasis: The distribution of tumors in various organs in relation to the distribution of arterial emboli. Cancer Res 11:648-651, 1981.
- Weiss L: Cancer cell traffic from lungs to liver: An example of metastatic inefficiency. Int J Cancer 25:385-392, 1980.
- Baker ME, Paulson EK: Hepatic metastatic disease. In Meyers MA, editor: Neoplasms of the Digestive Tract: Imaging, Staging, and Management, Philadelphia, 1998, Philadelphia, Lippincott-Raven, pp 361-395.
- Adson MA: Cannon lecture: Hepatic metastases in perspective. AJR Am J Roentgenol 140:695-700, 1983.
- Silverman PM: Liver metastases: Imaging considerations for protocol development with multislice CT (MSCT). Cancer Imaging 6:175-181, 2006.
- Arnold MM, Kreel L, Lo YF, et al: Are the hepatic arteries "end arteries"? Invest Radiol 26:337-342, 1991.
- Meyers MA, McSweeney J: Secondary neoplasms of the bowel. Radiology 105:1-11, 1972.
- Meyers MA: Metastatic seeding along small bowel mesentery: Roentgen features. Am J Roentgenol Radium Ther Nucl Med 123:67-73, 1975.
- Meyers MA: Clinical involvement of mesenteric and antimesenteric borders of small bowel loops. II. Radiologic interpretation of pathologic alterations. Gastrointest Radiol 1:49-58, 1976.
- Knockaert DC, Robaey GK, Cox EJ: Suppurative pyelothrombosis: A changing clinical picture. Gastroenterology 97:1028-1030, 1987.
- Frey CF, Zhu Y, Suzuki M, et al: Liver abscesses. Surg Clin North Am 69:259-271, 1989.
- Kurland JE, Brann OS: Pyogenic and amebic liver abscesses. Curr Gastroenterol Rep 6:273-279, 2004.
- Mohan S, Talwar N, Chaudhary A, et al: Liver abscess: A clinicopathological analysis of 82 cases. Int Surg 91:228-233, 2006.
- Yu SC, Ho SS, Lau WY, et al: Treatment of pyogenic liver abscess: Prospective randomized comparison of catheter drainage and needle aspiration. Hepatology 39:932-938, 2004.
- Giorgio A, de Stefano G, Di Sarno A, et al: Percutaneous needle aspiration of multiple pyogenic abscesses of the liver: 13-year single-center experience. AJR Am J Roentgenol 187:1585-1590, 2006.
- Chung RT, Friedman LS: Liver abscess and bacterial, parasitic, fungal, and granulomatous liver disease. In Feldman M, Scharschmidt BF, Sleisenger MH, editors: Gastrointestinal and Liver Disease, ed 6, Philadelphia, 1998, WB Saunders, pp 1170-1187.
- Radin DR, Baker EL, Klatt EC, et al: Visceral and nodal calcification in patients with AIDS-related *Pneumocystis carinii* infection. AJR Am J Roentgenol 154:27-31, 1990.
- Gore RM, Miller FH, Yaghamai V: Acquired immunodeficiency syndrome (AIDS) of the abdominal organs: Imaging features. Semin Ultrasound CT MR 19:175-189, 1998.
- Bartelsman JFWM: Diagnosis and treatment of gastrointestinal disease in patients with HIV infection. In Reenders JWA, Mathieson JR, editors: AIDS Imaging: A Practical Approach, Philadelphia, 1998, WB Saunders, pp 168-188.
- Wall SD, Yee J: Infections of the alimentary tract in AIDS. In Margulis AR, editor: Modern Imaging of the Alimentary Tube, Berlin, 1998, Springer-Verlag, pp 246-247.
- Ralls PW: Focal inflammatory disease of the liver. Radiol Clin North Am 36:377-390, 1998.
- Cohn I, Nance FC: Intermediate or precancerous lesions and malignant lesions. In Sabiston DC, editor: Textbook of Surgery, ed 13, Philadelphia, 1986, WB Saunders, pp 1003-1011.
- Merine D, Fishman EK, Jones B: CT of the small bowel and mesentery. Radiol Clin North Am 27:707-716, 1989.
- Karacaltincaba M, Haliloglu M, Akpınar E, et al: Multidetector CT and MRI findings in periportal space pathologies. Eur J Radiol 61:3-10, 2007.
- Forsberg L, Floren CH, Hederstrom E, et al: Ultrasound examination in diffuse liver disease. Clinical significance of enlarged lymph nodes in the hepato-duodenal ligament. Acta Radiol Diagn 28:281-290, 1987.
- Lyttkens K, Forsberg L, Hederstrom E: Ultrasound examination of lymph nodes in the hepato-duodenal ligament. Br J Radiol 63:26-30, 1990.
- Gore RM, Vogelzang RL, Nemcek AA: Lymphadenopathy in chronic active hepatitis: CT observations. AJR Am J Roentgenol 151:75-78, 1988.
- Bass NM: Sclerosing cholangitis and recurrent pyogenic cholangitis. In Feldman M, Scharschmidt BF, Sleisenger MH, editors: Gastrointestinal and Liver Disease, ed 6, Philadelphia, 1998, WB Saunders, pp 1275-1283.
- Liao WC, Wang HP, Chiu HM, et al: Multiple hepatic nodules: Rare manifestation of clonorchiasis. J Gastroenterol Hepatol 21:1497-1500, 2006.
- Fullerton JK, Vitale M, Vitale GC: Therapeutic endoscopic retrograde cholangiopancreatography for the treatment of *Fasciola hepatica* presenting as biliary obstruction. Surg Innov 13:179-182, 2006.
- Federle MP, Cello JP, Laing FC, et al: Recurrent pyogenic cholangitis in Asian immigrants. Use of ultrasonography, computed tomography and cholangiography. Radiology 143:151-156, 1982.
- Schulman A: Non-western patterns of biliary stones and the role of ascariasis. Radiology 162:425-430, 1987.

40. Shah OJ, Zargar SA, Robbani I: Biliary ascariasis: A review. *World J Surg* 30:1500–1506, 2006.
41. Macris GJ, Galanis NN: Rupture of *Echinococcus* cyst of the liver into the biliary ducts. *Am Surg* 32:36–39, 1966.
42. Zeman RK, Burrell MI: Gallbladder and Bile Duct Imaging, New York, 1987, Churchill Livingstone, pp 471–592.
43. Bonacini M, Nussbaum J, Ahluwalia C: Gastrointestinal, hepatic, and pancreatic involvement with *Cryptococcus neoformans* in AIDS. *J Clin Gastroenterol* 12:295–297, 1990.
44. Pol S, Romana CA, Richard S, et al: *Microsporidia* infection in patients with human immunodeficiency virus and unexplained cholangitis. *N Engl J Med* 328:95–99, 1993.
45. Grumbach K, Coleman BG, Gal AA, et al: Hepatic and biliary tract abnormalities in patients with AIDS. *J Ultrasound Med* 8:247–254, 1989.
46. McCarthy RA, Choudhri AH, Helbert M, et al: Radiological features of AIDS related cholangitis. *Clin Radiol* 40:582–585, 1989.
47. Wright TL: Cytomegalovirus infection and vanishing bile duct syndrome: Culprit or innocent bystander? *Hepatology* 16:494–496, 1992.
48. Kuhlman JE, Fishman EK: Acute abdomen in AIDS: CT diagnosis and triage. *Radiographics* 10:621–634, 1990.
49. Yana C, Frija J, Cyna-Gorse F, et al: Radiological appearance of non-calculous gallbladder and bile inflammation in AIDS. *J Radiol* 70:411–414, 1989.
50. Kokubo T, Itai Y, Ohtoma K, et al: Mucin-secreting intrahepatic biliary neoplasms. *Radiology* 168:609–614, 1988.
51. Meyers MA: Anatomy of the peritoneal cavity. In Taveras J, Ferrucci JT, editors: *Radiology*, vol 4, Philadelphia, 1990, JB Lippincott, pp 1–23.
52. DeMeo JH, Fulcher AS, Austin RF: Anatomic CT demonstration of the peritoneal spaces, ligaments, and mesenteries: Normal and pathologic processes. *Radiographics* 15:755–778, 1995.
53. Perry J, Pickhardt PJ, Bhalla: Unusual non-neoplastic peritoneal and subperitoneal conditions: CT findings. *Radiographics* 25:719–730, 2005.
54. Meyers MA: The spread and localization of acute intraperitoneal effusions. *Radiology* 95: 547–554, 1970.
55. Rosenshein N, Blake D, McIntyre PA, et al: The effect of volume on the distribution of substances instilled into the peritoneal cavity. *Gynecol Oncol* 6:106–110, 1978.
56. Proto AV, Lane EJ, Marangola JP: A new concept of ascitic fluid distribution. *AJR Am J Roentgenol* 126:974–980, 1976.
57. Churchill RJ: CT of intra-abdominal fluid collections. *Radiol Clin North Am* 27:653–666, 1989.
58. Churchill R, Meyers MA: Intraperitoneal fluid collections. In Meyers MA, editor: *Computed Tomography of the Gastrointestinal Tract*, New York, 1986, Springer-Verlag, pp 183–220.
59. Rubenstein WA, Auh YH, Whalen JP, et al: The perihepatic spaces: Computed tomographic and ultrasound imaging. *Radiology* 149:231–239, 1983.
60. Whalen JP: Anatomy and radiologic diagnosis of perihepatic abscesses. *Radiol Clin North Am* 14:406–428, 1976.
61. DeCrosse JJ, Paulin TL, Fox PS, et al: Subphrenic abscess. *Surg Gynecol Obstet* 138:841–846, 1974.
62. Halasz NA: Subphrenic abscess: Myths and facts. *JAMA* 214:724–726, 1970.
63. Meyers MA: *Dynamic Radiology of the Abdomen: Normal and Pathologic Anatomy*, ed 5, New York, 2000, Springer-Verlag, pp 493–538.
64. Meyers MA, Whalen JP, Peelle K, et al: Radiologic features of extraperitoneal effusions: An anatomic approach. *Radiology* 104:249–257, 1972.
65. Meyers MA: *Dynamic Radiology of the Abdomen: Normal and Pathologic Anatomy*, ed 3, New York, 1988, Springer-Verlag, pp 219–342.
66. Meyers MA, Mindelzun RE: Peritoneal reflections, ligaments, recesses, and mesenteries. In Margulis AR, editor: *Modern Imaging of the Alimentary Tube*, Berlin, 1998, Springer-Verlag, pp 159–184.
67. Meyers MA, Evans JA: Effects of pancreatitis on the small bowel and colon: Spread along mesenteric planes. *Am J Roentgenol Radium Ther Nucl Med* 119:151–165, 1973.
68. Meyers MA: *Dynamic Radiology of the Abdomen: Normal and Pathologic Anatomy*, ed 4, New York, 1993, Springer-Verlag, pp 405–430.
69. Meyers MA, Feldberg MAM, Oliphant M: Grey Turner's sign and Cullen's sign in acute pancreatitis. *Gastrointest Radiol* 14:31–37, 1989.
70. Meyers MA: The reno-alimentary relationships: Anatomic-roentgen study of their clinical significance. *Am J Roentgenol Radium Ther Nucl Med* 123:386–400, 1975.
71. Meyers MA: *Dynamic Radiology of the Abdomen: Normal and Pathologic Anatomy*, ed 3, New York, 1988, Springer-Verlag, pp 279–318.
72. Kneeland JB, Auh YH, Rubenstein WA, et al: Perirenal spaces: CT evidence for communication along the midline. *Radiology* 104:657–664, 1987.
73. Meyers MA: Radiologic features of the spread and localization of extraperitoneal gas and their relationship to its source: An anatomical approach. *Radiology* 111:17–26, 1974.
74. Meyers MA, Volberg F, Katzen B, et al: Hausrat identification of normal patterns and relationships. *Radiology* 108:497–504, 1973.
75. Meyers MA, Volberg F, Katzen B, et al: Hausrat anatomy and pathology: A new look. II. Roentgen interpretation of pathologic alterations. *Radiology* 108:505–512, 1973.
76. Okino Y, Kiyosue H, Mori H, et al: Root of the small-bowel mesentery: Correlative anatomy and CT features of pathologic conditions. *Radiographics* 21:1475–1490, 2001.
77. Sompayrac SW, Mindelzun RE, Silverman PM, et al: Greater omentum. *AJR Am J Roentgenol* 168:683–688, 1997.
78. Sheth S, Horton KM, Garland MR, et al: Mesenteric neoplasms: CT appearances of primary and secondary tumors and differential diagnosis. *Radiographics* 23:457–473, 2003.
79. Rubenstein SE, Levine MS, Glick SN: Gastric involvement by omental cakes. *Radiographic findings. Gastrointest Radiol* 11:223–228, 1986.
80. Balfe DM, Mauro MA, Koehler RE, et al: Gastrohepatic ligament: Normal and pathologic CT anatomy. *Radiology* 150:485–499, 1984.
81. Meyers MA: *Dynamic Radiology of the Abdomen: Normal and Pathologic Anatomy*, ed 4, New York, 1993, Springer-Verlag, pp 319–340.
82. Engels JT, Balfe DM, Lee JKT: Biliary carcinoma: CT evaluation of extrahepatic spread. *Radiology* 172:35–40, 1989.
83. Mori H, Aikawa H, Hirao K, et al: Exophytic spread of hepatobiliary disease via perihepatic ligaments: Demonstration with CT and US. *Radiology* 172:41–46, 1989.
84. Baker ME, Silverman PM, Halvorsen RA, et al: Computed tomography of masses in periportal hepatoduodenal ligament. *J Comput Assist Tomogr* 11:258–263, 1987.
85. Weil FS, Costa R, Racle A, et al: Ultrasound study of adenopathies within the hepatoduodenal ligament: The “rose-bud” pattern. *Gastrointest Radiol* 11:140–142, 1986.
86. Zeman RK, Schiebler M, Clark LR, et al: The clinical and imaging spectrum of pancreaticoduodenal lymph node enlargement. *AJR Am J Roentgenol* 144:1223–1228, 1985.
87. Meyers MA, Whalen JP: Roentgen significance of the duodenocolic relationships: An anatomic approach. *Am J Roentgenol Radium Ther Nucl Med* 117:263–274, 1973.
88. Glick SN, Levine MS, Teplick SJ, et al: Splenic penetration by benign gastric ulcer: Preoperative recognition with CT. *Radiology* 163:637–639, 1987.
89. Pannu HK, Bristow RE, Montz FJ, et al: Multi-detector CT of peritoneal carcinomatosis from ovarian cancer. *Radiographics* 23:687–701, 2003.
90. Raval B, Lakmi N: CT demonstration of preferential routes of the spread of pelvic disease. *Crit Rev Diagn Imaging* 27:17–48, 1987.
91. Meyers MA, Goodman KJ: Pathways of extrapelvic spread of disease: Anatomic-radiologic correlation. *Am J Roentgenol Radium Ther Nucl Med* 125:900–909, 1975.
92. Meyers MA, Charnsangavej C, Oliphant M: *Dynamic Radiology of the Abdomen: Clinical Anatomy of the Abdomen*, ed 6, New York, 2011, Springer-Verlag, pp 363–380.
93. Steinbach L, Schneider R, Goldman A, et al: Bursae and abscess cavities communicating with the hip. Diagnosis during arthrography and CT. *Radiology* 156:303–307, 1986.
94. Fox TA, Gomez J, Brave J: Subcutaneous emphysema of the lower extremity of gastrointestinal origin. *Dis Colon Rectum* 21:357–360, 1978.
95. Jager GJ, Rijssen HV, Lamers JHH: Subcutaneous emphysema of the lower extremity of abdominal origin. *Gastrointest Radiol* 15:253–258, 1990.
96. Goodman P, Balachandran S: CT evaluation of the abdominal wall. *Crit Rev Diagn Imaging* 33:461–493, 1992.
97. Martín J, Mellado JM, Solanas S, et al: MDCT of abdominal wall lumbar hernias: anatomical review, pathologic findings and differential diagnosis. *Surg Radiol Anat* 34:455–463, 2012.
98. Trainer V, Leung C, Owen RE, et al: External anterior abdominal wall and pelvic hernias with emphasis on the key diagnostic features on MDCT. *Clin Radiol* 68:388–396, 2013.

Ascites and Peritoneal Fluid Collections

RICHARD M. GORE | ROBERT I. SILVERS |
GERALDINE MOGAVERO NEWMARK | MARGARET D. GORE

CHAPTER OUTLINE

Pathophysiology

Clinical Findings

Diagnostic Paracentesis

Types of Peritoneal Fluid Collections

Transudates

Exudates

Hemorrhagic Ascites

Pus

Chylous Ascites

Neonatal Ascites

Pseudomyxoma Peritonei

Bile Ascites

Pancreatic Ascites

Urine Ascites

Cerebrospinal Fluid Ascites

Pathways of Fluid Distribution

Radiologic Findings

Chest Radiography

Plain Abdominal Radiography

Barium Studies

Ultrasonography

Computed Tomography

Magnetic Resonance Imaging

Differentiation of Ascites

Differentiation of Ascites from Pleural Fluid

Differentiation of Ascites from Subcapsular Fluid

Treatment

Diuretics

Therapeutic Paracentesis

Transjugular Intrahepatic Portosystemic Shunt

Surgical Shunting

Ascites is the pathologic accumulation of fluid in the peritoneal cavity. It is a common clinical finding that can be associated with a large number of diseases. In some disorders, peritoneal fluid represents a complication or late manifestation of disease, whereas in others, it is the first clinical expression of the disease process. For this reason, early detection and characterization of ascites and other peritoneal fluid collections are important.

Pathophysiology

The causes of ascites are protean and are listed in [Box 110-1](#). The imaging features that can help differentiate the various causes are listed in [Table 110-1](#). Although ascites may merely reflect generalized third-space fluid loss in conditions such as congestive heart failure, chronic renal disease, and massive fluid overload, it is more commonly related to intra-abdominal factors that produce peritoneal fluid more rapidly than it can be absorbed.¹⁻⁴ Cirrhosis and neoplasm are the two most common causes of ascites in the Western world. Tuberculosis and cirrhosis are the predominant causes worldwide.^{4,5}

Clinical Findings

A small amount of ascites is often asymptomatic, but as the amount of fluid increases, the patient develops a sense of fullness, discomfort, and abdominal distention. With tense ascites, the patient may experience respiratory distress, nausea, vomiting, anorexia, fever, or pain. Weight gain usually accompanies the fluid accumulation, unless it is associated with alcoholism, neoplasm, or poor nutrition, in which case the patient's weight may remain stable or drop.⁴

The physical diagnosis of ascites is difficult, unless there is at least 1.5 to 2 L of fluid in the peritoneal cavity.⁶ Physical examination reveals abdominal distention, with bulging flanks that are dull to percussion or a fluid wave. As little as 300 to 400 mL of fluid can be demonstrated by placing the patient on hands and knees and producing a dull sound by percussion over the dependent abdomen (i.e., the puddle sign).⁷ Umbilical hernias, penile or scrotal edema, and pleural effusion are indirect signs of ascites. Flank dullness is the most sensitive sign, and a fluid wave is the most specific sign of ascites on physical examination.²

Diagnostic Paracentesis

Diagnostic paracentesis is indicated for any patient who develops ascites for the first time and for patients with chronic ascites who develop fever, encephalopathy, or abdominal pain.⁸ Paracentesis for small volumes should be performed under sonographic guidance with an 18- or 20-gauge, plastic-sheathed catheter to avoid injury to the liver, spleen, or gut. With massive ascites, a blind tap can be performed 2 to 3 cm beneath the umbilicus in the midline to reduce the chance of bleeding along the linea alba or at a left-sided McBurney point to avoid injuring an enlarged liver or spleen.^{2,4} Fluid should be analyzed for protein, lactate dehydrogenase, amylase, blood cell count with differential, bacteriologic and cytologic tests, pH, and triglycerides.^{2,4,8}

Types of Peritoneal Fluid Collections

TRANSUDATES

Transudates are clear and colorless fluid collections with a protein content less than 2.5 g/dL and specific gravity less than 1.016. They are most commonly seen in patients with cirrhosis, long-standing heart failure, constrictive pericarditis, chronic

BOX 110-1 CAUSES OF ASCITES

PORTAL HYPERTENSION RELATED

- Cirrhosis
- Alcoholic hepatitis
- Fulminant hepatic failure
- Heart failure
- Constrictive pericardial disease
- Budd-Chiari syndrome
- Hepatic veno-occlusive disease
- Liver metastases

PERITONEAL DISEASES

- Carcinomatosis from ovarian, colon, gastric, pancreatic, hepatic, and other neoplasms
- Mesothelioma
- Tuberculosis
- Fungal infections
- Pyogenic infections
- Peritonitis
- Sarcoidosis
- Vasculitis
- Eosinophilic gastroenteritis
- Whipple's disease

MISCELLANEOUS CAUSES

- Myxedema
- Pancreatic ascites
- Chylous ascites
- Hemoperitoneum due to trauma or tumor hemorrhage
- Ruptured ovarian cyst
- Nephrotic syndrome
- Malnutrition
- Protein-losing enteropathy
- Hypoalbuminemia
- Meigs' syndrome
- Ovarian hyperstimulation syndrome

renal failure, hypoproteinemia, anasarca, and Budd-Chiari syndrome.^{2,4,8-10}

EXUDATES

Exudates are fluid collections with a density greater than 1.016 and a protein content greater than 2.5 g/dL. They are often yellowish but may be hemorrhagic in patients with metastatic peritoneal infiltration, infection, tuberculosis, or pancreatitis. An ascitic fluid-to-serum lactate dehydrogenase ratio greater than 0.6 suggests malignant disease. A polymorphonuclear leukocyte count greater than 500/mm³ suggests infection or pancreatic ascites, and a mononuclear cell count larger than 500/mm³ is commonly seen with tuberculosis.¹¹ A pH less than 7.35 also indicates tumor, infection, or pancreatitis. A fluid amylase value greater than 1000 U/L and a protein value greater than 3 g/dL are usually associated with pancreatic ascites.¹²

HEMORRHAGIC ASCITES

Hemorrhagic ascites usually occurs in the setting of hepatic or splenic trauma resulting from an accident (Fig. 110-1A), surgery, or biopsy. Sanguineous ascites is usually caused by malignant disease but may occur in patients with tuberculosis or chronic pancreatitis.

PUS

Pus is often present in the peritoneal cavity in patients with acute peritonitis. It is most often seen in young patients with pneumococcal or hemolytic streptococcal peritonitis. When peritonitis is caused by a perforated viscus (Fig. 110-1B), appendicitis, diverticulitis, or tubo-ovarian abscess, signs and symptoms are typically impressive, but the amount of intraperitoneal fluid is relatively small. The presence of more than 500 leukocytes/mm³ is indicative of infected ascites.^{9,13}

CHYLOUS ASCITES

Chylous ascites is a collection of yellowish white, milky fluid that results from obstruction or disruption of lymph flow

TABLE 110-1 Imaging Features of Benign and Complicated Ascites

Imaging Modality	Features Suggesting Benign Transudate	Features Suggesting Complicated Ascites
Ultrasonography	Anechoic collection Compressible collection Follows contours of gut and solid organs Bowel loops freely float in fluid to center of abdomen	Internal echoes (may represent blood, crystals, infection, tumor) Fluid does not conform to available spaces but displaces gut and solid organs Loculation (may represent tumor, infection, adhesion, inflammation)
Computed tomography	Seen first in cul-de-sac and Morison's pouch Uniform low attenuation (0-20 HU) Bowel loops freely float in fluid to center of abdomen	Loculation (may represent tumor, infection, adhesion, inflammation) High fluid attenuation (>30 HU suggests blood but may have hemoperitoneum with fairly normal attenuation) Delayed contrast enhancement (may indicate tumor or infection)
Magnetic resonance imaging	Low signal intensity on T1-weighted image Very high signal intensity on T2-weighted image Bowel loops freely float in fluid to center of abdomen	T1 relaxation shorter with exudates due to protein, tumor, or blood Acute blood (<48 hr) has low signal intensity on T1- and T2-weighted images due to deoxyhemoglobin Intermediate-age blood (2-7 days) has high signal intensity on T1-weighted image and low signal intensity on T2-weighted image due to methemoglobin Delayed contrast enhancement (may indicate tumor or infection) Loculation (may represent tumor, infection, adhesion, inflammation)

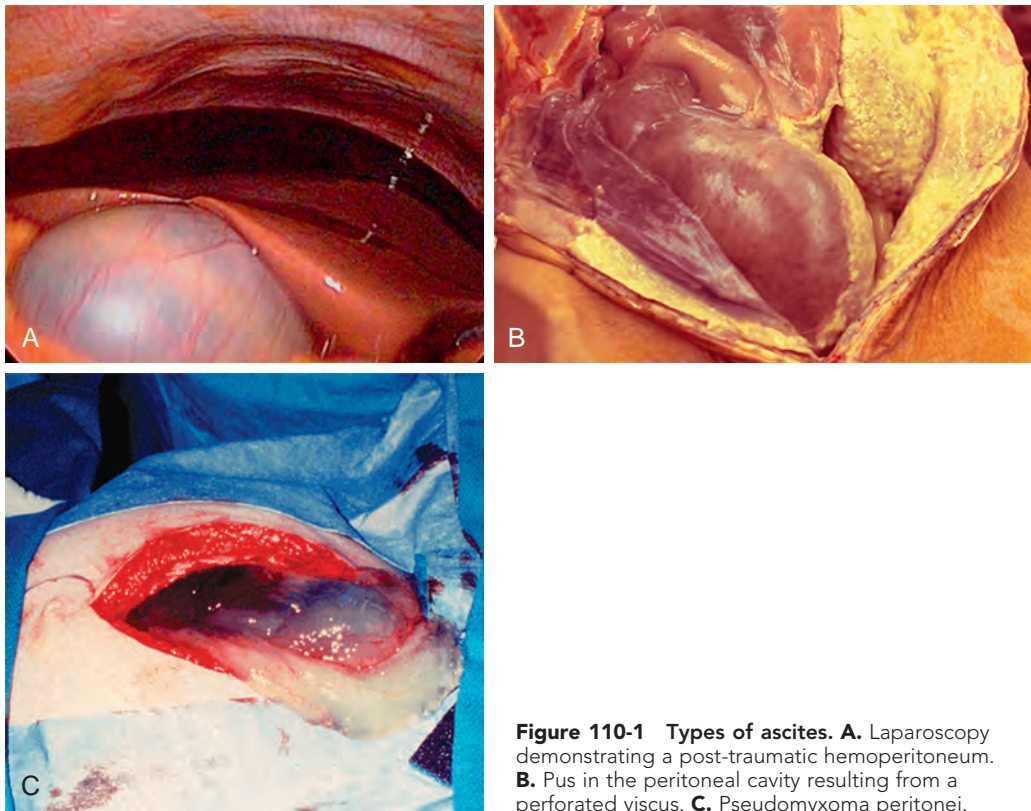


Figure 110-1 Types of ascites. **A.** Laparoscopy demonstrating a post-traumatic hemoperitoneum. **B.** Pus in the peritoneal cavity resulting from a perforated viscus. **C.** Pseudomyxoma peritonei.

through the cisterna chyli and thoracic duct.^{4,9} The milky appearance results from the presence of fat (mainly triglycerides in amounts greater than 400 mg/dL) and small amounts of cholesterol and phospholipid. Triglyceride levels may treble after a fatty meal. The causes of chylous ascites include blunt, penetrating, and surgical trauma; malignant infiltration of the cisterna chyli by lymphoma or carcinoma of the pancreas, stomach, colon, or ovary; left subclavian vein thrombosis; and tuberculous lymphadenitis. Cirrhosis, nephrotic syndrome, protein-losing enteropathy, congenital lymphatic disorders, chronic lymphocytic leukemia, sarcoidosis, and extremely high right-sided heart pressure that alters lymph flow are less common causes of chylous ascites.^{3,14-16} The discovery of milky ascites in an adult mandates a careful search for malignant disease, particularly lymphoma.¹⁷

NEONATAL ASCITES

Neonatal ascites may result from posterior urethral valves, perforated bladder, or urethral atresia that produces urine ascites. Ileal atresia, ileal perforation, ileal volvulus, ischemia, cardiac failure, and infections can also result in neonatal ascites.¹⁸

PSEUDOMYXOMA PERITONEI

Pseudomyxoma peritonei is characterized by the massive accumulation of gelatinous, mucinous material in the peritoneal cavity (Fig. 110-1C), mesentery, and omentum.¹⁹ It is produced by metastatic parietal and visceral peritoneal implants that are seeded after rupture of benign or malignant mucin-secreting tumors of the appendix or ovary. Less commonly, mucinous

tumors of the pancreas, stomach, colon, uterus, bile duct, urachus, omphalomesenteric duct, or pancreas cause pseudomyxoma peritonei.³

BILE ASCITES

Bile ascites can develop after trauma, cholecystectomy, biliary tract surgery, hepatic surgery, liver biopsy, and percutaneous biliary drainage. These collections typically occur in the right or the left supramesocolic spaces.

PANCREATIC ASCITES

Virtually all patients with clinically significant pancreatitis have peripancreatic fluid collections, most of which resolve within 6 weeks (see Chapter 96). These collections most often occur in the lesser sac and anterior pararenal space. Fluid accumulation in the greater peritoneal sac usually occurs in the setting of severe pancreatitis “burning” the peritoneum, in trauma, or after surgical resection.^{20,21} The cause of pancreatic ascites in all cases is disruption of the pancreatic duct. Endoscopic retrograde pancreatography is diagnostic in these cases.^{21,22} Pancreatic ascites should be part of the differential diagnosis of every patient with chronic ascites who has a history of pancreatitis, alcoholism, or abdominal trauma.

URINE ASCITES

Urine ascites usually follows a bladder tear or injury to another portion of the collecting system after direct trauma, seat belt-caused injury, or use of instrumentation. Most urinomas

accumulate in the retroperitoneum rather than in the peritoneal cavity.³

CEREBROSPINAL FLUID ASCITES

Cerebrospinal fluid ascites and pseudocyst formation account for 4.5% of all ventriculoperitoneal shunt complications. This type of ascites occurs when the peritoneal cavity fails to absorb the fluid or when lymphatic disruption diminishes return of fluid to the bloodstream. If the collection elicits an infectious or inflammatory response, adhesions may develop and cause encystation of the cerebrospinal fluid.³

Pathways of Fluid Distribution

A number of factors determine the distribution of fluid in the peritoneal cavity: volume; peritoneal pressures; position of the patient; region of origin; rate of fluid accumulation; presence of adhesions; density of the fluid; and peritoneal, mesenteric, and omental ligaments and reflections.²³⁻³⁵ The pathways of intraperitoneal fluid distribution are summarized in Figure 110-2. Briefly, fluid in the inframesocolic space seeks the pelvis: on the right, through the leaves of the small bowel mesentery, and on the left, through the medial side of the rectosigmoid.

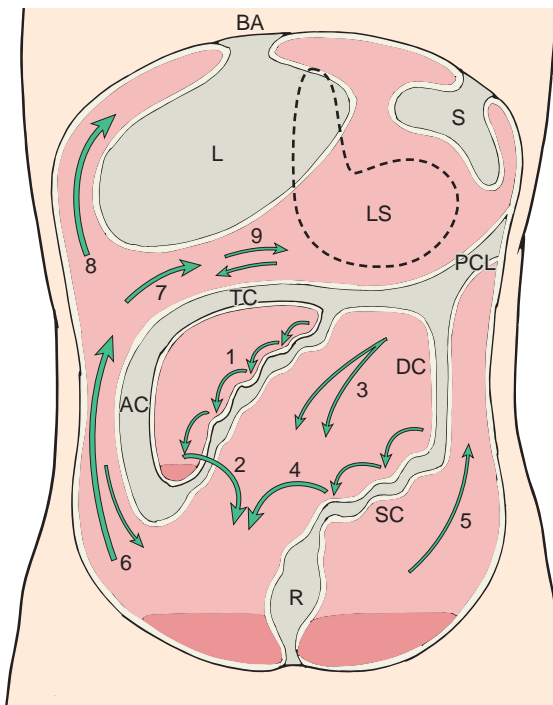


Figure 110-2 Common pathways of intraperitoneal fluid spread. Fluid in the right inframesocolic space (1) cascades down the leaves of the small bowel mesentery, pools at the medial aspect of the cecum, and then overflows into the pelvis (2). Fluid in the left inframesocolic space (3) seeks the pelvis directly or is deposited on the superior aspect of the sigmoid mesocolon and then flows into the pelvis (4). Fluid in the pelvis may ascend the left paracolic gutter (5) but is stopped by the phrenicocolic ligament (PCL). Fluid in the right paracolic gutter (6) ascends to Morison's pouch (7) and then to the subphrenic space (8), where it is stopped at the bare area (BA) of the liver (L). There is potential communication with the lesser sac (LS) through the foramen of Winslow (9). AC, ascending colon; DC, descending colon; R, rectum; S, spleen; SC, sigmoid colon; TC, transverse colon.

After fluid fills the pouch of Douglas, which is the most dependent portion of the peritoneal cavity, it fills the lateral paravesical recesses and then ascends the paracolic gutters. On the left, its cephalad extent is limited by the phrenicocolic ligament. Fluid in the right paracolic gutter, which structure represents the main communication between the upper and lower abdominal compartments, reaches Morison's pouch and subsequently the right subphrenic space.^{34,35} This is discussed more fully in Chapter 108.

Radiologic Findings

CHEST RADIOGRAPHY

Elevation of the diaphragm, with or without sympathetic pleural effusions (i.e., hepatic hydrothorax), is seen in patients with massive ascites. The cause of the ascites can sometimes be suggested by the chest radiograph. With chylous effusions, a superior mediastinal mass with tracheal deviation may be seen; pericardial calcification or effusion and mediastinal adenopathy are also helpful signs.^{3,36,37}

In patients with hiatal hernia, massive ascites can cause a mediastinal pseudotumor as fluid passes through the esophageal hiatus into the posterior mediastinum.^{38,39} This pseudotumor is caused by the fact that the stomach remains covered by peritoneum to the level of the gastroesophageal junction, regardless of where this point lies. Sometimes, the ascites may enlarge the hernial sac out of proportion to the size of the gastric pouch and cause dysphagia and produce a retrocardiac mass visible on barium studies. Cyclic negative intrathoracic pressure created during respiration may provide an alternative route for clearance of peritoneal fluid through defects in the tendinous diaphragm.^{37,40}

PLAIN ABDOMINAL RADIOGRAPHY

Plain radiographs are insensitive for the diagnosis of ascites and have been replaced by cross-sectional imaging. More than 500 mL of fluid is usually required for ascites to be diagnosed on plain radiographs.^{3,41,42}

Indirect signs of ascites on plain radiographs are often nonspecific or helpful only in the presence of massive peritoneal fluid: diffuse abdominal haziness, bulging of the flanks, indistinct psoas margins, poor definition of the intra-abdominal organs, erect-position density increase, separation of small bowel loops, and centralization of floating gas containing small bowel.^{3,4,42} The direct signs of ascites are more reliable and specific. In 80% of patients with ascites, the lateral liver edge is medially displaced from the adjacent thoracoabdominal wall (i.e., the Hellmer sign). Obliteration of the hepatic angle (visible in 80% of normal patients) is a close corollary to the Hellmer sign and is related to the fact that fluid in the superior mesocolic space accumulates around the margins of the liver (e.g., Morison's pouch).^{3,41-44} In the pelvis, fluid accumulates in the rectovesical pouch, then spills into the paravesical fossae. This fluid produces symmetric densities on both sides of the bladder, producing a dog's ear or a Mickey Mouse appearance, which is another good sign of ascites.⁴¹⁻⁴⁴ Another direct sign of ascites is medial displacement of the cecum and ascending colon and lateral displacement of the properitoneal fat line. This sign is present in more than 90% of patients with significant ascites.

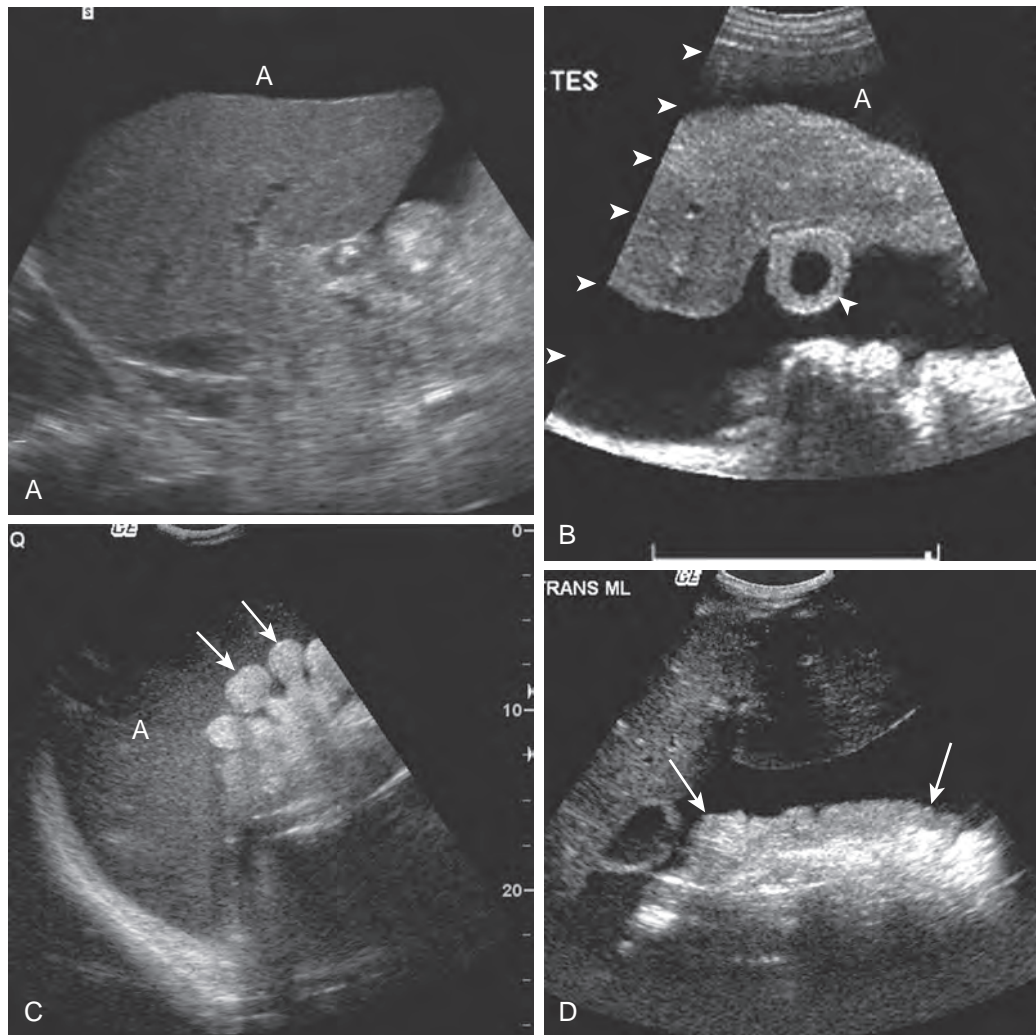


Figure 110-3 Ascites: sonographic findings. **A.** The sonogram of transudative ascites (A) in a patient with cirrhosis of the liver shows anechoic fluid and an echogenic liver. **B.** Mural thickening of the gallbladder (arrowhead) is seen in this patient with cirrhosis and ascites (A). Gallbladder wall thickening in the presence of ascites suggests benign disease. Normal mural thickness in the presence of ascites suggests malignant disease. **C.** The sonogram shows malignant ascites in a patient with carcinomatosis due to gastric cancer. Notice the echogenic fluid (A) and bowel loops (arrows) that are tethered posteriorly. Normally, these loops should be freely flowing. **D.** Peritoneal implants (arrows) are present in this patient with carcinomatosis.

BARIUM STUDIES

When the peritoneal fluid is malignant, barium studies may reveal metastatic serosal implants, mechanical small bowel obstruction, or the fixed colon sign, in which no change in colon position or course is observed on pre-evacuation and postevacuation radiographs. Large fluid collections in the lesser sac may simulate a large retrogastric mass on an upper gastrointestinal examination.

ULTRASONOGRAPHY

Real-time sonography is the easiest and most sensitive technique for detection of ascitic fluid.⁴⁵⁻⁴⁹ Volumes as small as 5 to 10 mL can be routinely visualized. Small amounts of fluid are commonly seen in the cul-de-sac of normal women during all phases of the menstrual cycle.⁵⁰

On sonographic examination, uncomplicated ascites appears as a homogeneous, freely mobile, anechoic collection in the

peritoneal cavity that demonstrates deep acoustic enhancement (Fig. 110-3A, B). Free ascites does not displace organs but typically insinuates itself between them, contouring to organ margins and demonstrating acute angles where the fluid borders the organ. The fluid compresses with increased transducer pressure and shifts with a change in the patient's position.⁵¹⁻⁵⁶

Benign ascites can occasionally cause perplexing sonographic artifacts. Perihepatic ascites may cause apparent discontinuity in the diaphragm as a result of reflection of the sound beam at the liver-fluid interface.⁵⁷ Echogenic hepatic pseudotumors can be seen in patients with a nodular liver surface. In this artifact, a focal concavity of the liver surface can act as an acoustic lens and transmit sound in a fashion analogous to the way in which a posterior wall of a cyst does.^{53,58} Other sources of confusion are the appendices epiploica of the colon, which can be mistaken for mesenteric or peritoneal metastatic implants.⁵⁹

The smallest amounts of fluid tend to collect in Morison's pouch and around the liver as a sonolucent band. Fluid may collect anteriorly, as a result of the capillary effect of the narrow

space between bowel loops and viscera.^{34,35,54} In a study of patients with ascites from liver disease, 92% had ascites around the liver, 77% in the pelvis, 69% in the paracolic gutters, and 63% in Morison's pouch.⁵² Although the pouch of Douglas is the most common location for the fluid accumulation of ascites, an overdistended bladder may obscure and displace the fluid to the peritoneal reflection adjacent to the uterine fundus—the so-called triangular fluid cap.^{50,54} In doubtful cases, changes in position produce significant alterations in the location, shape, and size of the fluid. Small amounts of intraperitoneal fluid are readily identified in the cul-de-sac, pouch of Douglas, and Morison's pouch. With more fluid, ascites can be identified in the paracolic gutters.^{45,52,54}

With massive ascites, the small bowel loops have a characteristic polycyclic, "lollipop," or arcuate appearance as they are arrayed on either side of the vertically floating mesentery. The intraluminal gas content and amount of mesenteric fat determine whether the small bowel loops float. In emaciated patients, the entire small bowel mesentery and gut may sink because of the paucity of mesenteric fat.^{45,52,54} The transverse colon and sigmoid colon usually float on top of the fluid because of the nondependent position of their gas content when the patient is supine. The ascending colon and descending colon do not float because they are fixed in the retroperitoneum.^{54,56} In some patients with massive ascites, the right kidney may also be displaced anteriorly and laterally because fluid in the right paracolic gutter exploits the lack of peritoneal attachment between the right renal fascia and liver or diaphragm.⁵⁹

Certain sonographic patterns suggest that the ascites may be an infected, inflammatory, or malignant exudate (Fig. 110-3C, D): coarse internal echoes (i.e., blood), fine internal echoes (i.e., chyle), multiple septa (i.e., tuberculous peritonitis or pseudomyxoma peritonei), loculation or atypical fluid distribution, matting or clumping of bowel loops, and thickening of interfaces between the fluid and adjacent structures.^{54,55,59-63} Absence of these findings does not entirely exclude an exudate because these complicated fluid collections may fulfill the sonographic criteria for transudates in one fourth of cases.^{54,55,60,61}

In malignant ascites, the bowel loops do not float freely but may be tethered along the posterior abdominal wall or plastered to the liver or other organs, or they may be surrounded by loculated fluid collections. Bowel loops are considered matted or infiltrated if they cannot be moved apart with compression by the transducer or if they fail to separate with fluid despite changes in the patient's position.^{51,60}

Loculated ascites usually indicates a malignant process or one associated with adhesions and bowel strictures.^{51,60} Loculated ascites usually has rounded or bulging contours, is not compressible with increased probe pressure, does not conform to the margins of organs, and shows no movement with changes in the patient's position.⁵¹

Another sign of malignant ascites is the presence of concordant fluid collections in the greater and lesser peritoneal sacs.⁶⁴ The significance of this finding is discussed in the section on computed tomography (CT). On sonographic evaluation, these fluid collections produce a butterfly- or wing-shaped lucency separated by the lesser omentum or gastrocolic ligament.⁶⁵

The presence or absence of gallbladder wall thickening is another predictor of benign or malignant ascites (see Fig.

110-3B). Most patients (95%) with carcinomatous peritonitis have a gallbladder wall less than 3 mm thick.^{64,66,67} Mural thickening of the gallbladder (>3 mm) is associated with benign ascites in 82% of cases.^{64,66,67} This thickening of the gallbladder is primarily a reflection of cirrhosis and portal hypertension. Benign, transudative ascites frequently accompanies these disorders.⁶⁸

The sonographic appearances of pseudomyxoma peritonei vary: an exudate with numerous echoes; highly echogenic masses containing numerous scattered cystic spaces; large intraperitoneal, septate, cystic-appearing masses; numerous thick-walled, multiseptate, fluid-filled masses; scalloping of the liver edge; and multiple rounded, echodense masses, which may cast a shadow resulting from calcification.^{54,69,70}

The sonographic appearance of bilomas is nonspecific, and needle aspiration is essential to confirm the diagnosis. Bilomas are usually anechoic collections that are located adjacent to hepatic or biliary structures, demonstrate acoustic enhancement, and have sharp margins.^{3,54}

The appearance of cerebrospinal fluid ascites is also nonspecific. A small amount of free intraperitoneal fluid is a normal finding in patients with a ventriculoperitoneal shunt and suggests normal shunt function. Its absence does not indicate malfunction. However, a localized fluid collection in association with the tip of the shunt tube is pathologic and implies malfunction.^{3,54,71}

The sonographic appearance of hemorrhage is highly variable and depends on the frequency of the transducer. Fresh hemorrhage imaged with 2.25- and 3.0-MHz transducers is typically anechoic with increased sound transmission.⁷² At 5.0, 7.5, and 10.0 MHz, the clot is intensely echogenic. This echogenicity is transient and usually disappears within 96 hours, as the clot undergoes hemolysis. As the clot organizes, internal echoes are generated that disperse evenly throughout the fluid or layer dependently. Chronic hematomas often have coarse clumps of highly echogenic material. With time, the clots may become completely anechoic seromas.^{3,54}

Although the sonographic findings of hematomas are nonspecific, in the appropriate clinical setting of trauma, acute anemia, blood loss, or pelvic pain, certain findings can be most instructive. For example, the presence of highly echogenic material in the cul-de-sac may be helpful in diagnosis of pelvic hemoperitoneum because most other pelvic fluid collections are predominantly anechoic, with low-level echoes.^{59,72}

COMPUTED TOMOGRAPHY

Ascites is well demonstrated by CT. Small amounts of ascitic fluid localize in the right perihepatic space, the posterior subhepatic space (i.e., Morison's pouch), and the pouch of Douglas.⁶⁴ When larger amounts of ascites are present, the fluid accumulates in the paracolic gutters, causing progressive centralization of bowel loops.⁴⁵ The fluid may accumulate in a triangular configuration within the leaves of the small bowel mesentery or adjacent to bowel loops.⁷³ A massive amount of fluid distends the peritoneal spaces.

It is usually difficult to characterize the nature of a peritoneal fluid collection on the basis of CT density,⁷⁴ but several general rules are helpful.⁷⁵ Simple ascites appears as a low-density collection of fluid (Fig. 110-4A) with an attenuation value ranging from 0 to 30 Hounsfield units (HU). The density of the ascitic fluid increases with increasing protein content

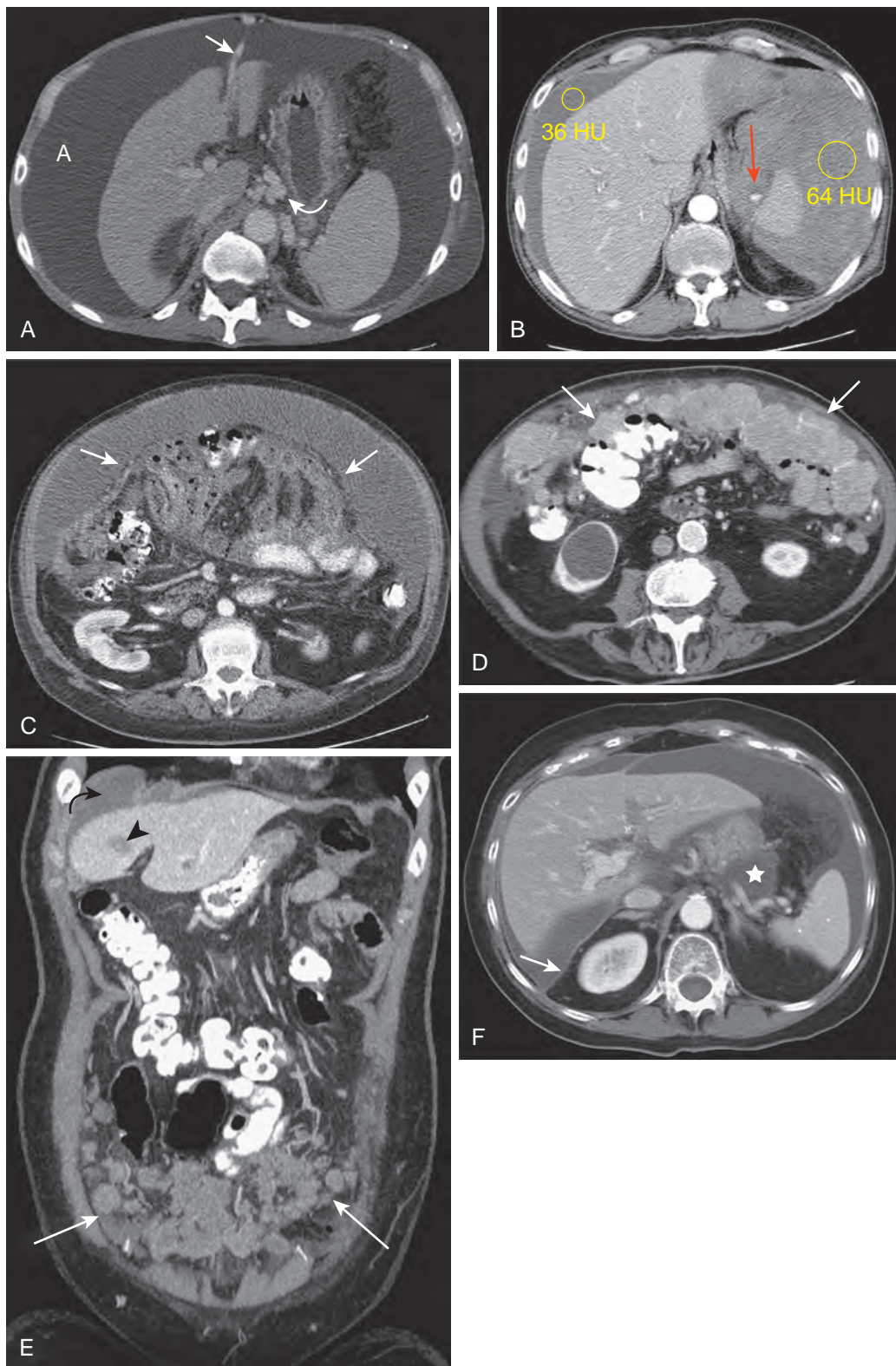


Figure 110-4 Ascites: CT features. **A.** Benign, transudative ascites (A) in a patient with cirrhosis and portal hypertension. A recanalized umbilical vein (*straight arrow*) and varices in the gastrohepatic ligament (*curved arrow*) can be seen. **B.** Hemoperitoneum and the sentinel clot sign are demonstrated in a patient with splenic trauma and active extravasation of contrast material (*arrow*). Note the higher density peritoneal fluid adjacent to the spleen (64 HU) and lower density fluid (36 HU) adjacent to the liver. **C.** Complicated ascites from an infection or tumor can cause retraction and a stellate appearance (*arrows*) of the mesentery. This patient had carcinomatosis from colon cancer. **D.** CT of a patient with ovarian cancer shows fluid associated with an omental cake (*arrows*), indicating carcinomatosis. The omental cake is caused by complete replacement of the omental fat by tumor. **E.** Coronal multiplanar reconstruction image shows omental cake (*straight arrows*), liver metastases (*arrowhead*), and ascites (*curved arrow*) in a patient with metastatic colon cancer. **F.** Fluid is identified in the lesser sac (*star*) and the greater peritoneal cavity. This finding and the abnormal enhancement and thickening of the peritoneum (*arrow*) suggest carcinomatosis in this patient with ovarian cancer.

and with exudates.^{3,32} Similarly, acute intraperitoneal hemorrhage can often be distinguished from other fluid collections because it has an attenuation value greater than 30 HU⁷⁴ (Fig. 110-4B). The CT characteristics of blood within the peritoneal cavity change in a matter of hours or days, in contrast with intracerebral bleeds, in which lysis of blood and consequently CT density evolve during days or weeks. These temporally dramatic changes are related to the impressive fibrinolytic activity of the peritoneum. High-density blood implies that the bleeding is recent or rapid and mandates careful observation of the patient.^{75,76} Several caveats are warranted in interpreting high-attenuation fluid. Delayed enhancement of ascites may follow infusion of a large dose of contrast medium for delayed hepatic CT scanning.^{77,78}

Chylous ascites attributable to traumatic or neoplastic disruption of the cisterna chyli has an attenuation value less than 0 HU.¹⁷ The presence of intraperitoneal and extraperitoneal water-density fluid (i.e., chyle) suggests chylous ascites in a trauma patient because most water-density abdominal fluid collections are confined to one peritoneal compartment.^{76,79,80} However, it is usually difficult to characterize the underlying cause of ascites on the basis of CT density.^{74,75}

After the CT diagnosis of ascites has been established, it is important to determine the cause. A number of CT features suggest neoplasia. Hepatic, adrenal, splenic, or lymph node lesions associated with masses arising from the ovary, gut, or pancreas are suggestive of malignant ascites.⁸⁰ However, these tumors are often advanced and clinically evident before the onset of ascites. Peritoneal seeding from ovarian, gastric, pancreatic, or colon metastases may produce nodular soft tissue masses along the peritoneal surface or along the liver capsule.^{81,82} Sometimes, the peritoneum shows thickening or abnormal enhancement, but these later findings are nonspecific (Fig. 110-4C, D). Omental and mesenteric masses are also commonly seen in carcinomatosis (Fig. 110-4E, F).

Patients with malignant ascites tend to have proportional fluid collections in the greater and lesser sacs, whereas in patients with benign transudates, the fluid is seen primarily in the greater sac and not in the lesser omental bursae.^{62,64} Similarly, benign fluid collections resulting from disease in structures that border the lesser sac (e.g., pancreatitis, posterior penetrating gastric ulcer) tend to remain confined to the lesser sac.⁸³ The foramen of Winslow is more a potential than a widely patent avenue of communication between these peritoneal bursae.^{62,83,84}

In malignant ascites, the small bowel may be tethered along the posterior abdominal wall (see Fig. 110-5C) or have a stellate appearance. Normally, gas-filled or contrast-filled gut should be able to reach the anterior abdominal wall and float freely and centrally in benign ascitic fluid.^{67,85-87} As observed sonographically, gallbladder wall thickening is another useful sign of benign ascites.

On CT scans, pseudomyxoma peritonei may be manifested as scalloping of the liver edge, as large low-attenuation fluid collections that appear to have multiple cysts, or as low-density masses with calcification. A sterile, nonhemorrhagic biloma has a nonspecific appearance and an attenuation value less than 20 HU. These bilious collections cannot be specifically distinguished from cysts, pseudocysts, loculated ascites, or abscess. Urine ascites also has a nonspecific CT appearance on unenhanced scans. Intravenously administered contrast medium often accumulates in these collections. Cerebrospinal

fluid ascites also has a nonspecific appearance, and infection usually cannot be excluded on the basis of CT appearance alone.³³

MAGNETIC RESONANCE IMAGING

Transudates have long T1 and T2 relaxation times (Fig. 110-5A, B). Exudates demonstrate intermediate to short T1 values and long T2 values. The T1 relaxation time of fluid decreases with increasing protein content.⁸⁸⁻⁹⁰ Although magnetic resonance imaging (MRI) offers potential for differentiating various types of abdominal fluid collections, it is not sufficiently specific to obviate paracentesis.³²

MRI is another method for detecting peritoneal fluid and in several studies was shown to be superior to CT in detecting peritoneal tumors and carcinomatosis (Fig. 110-5C, D). MRI sequences used included T1-weighted, fast spin-echo T2-weighted, immediate and delayed gadolinium-enhanced, breath-hold, and fast multiplanar sequences with fat saturation. A 2% barium solution is given orally to provide an effective source of stabilized water and bowel distention that facilitates depiction of serosal and adjacent peritoneal tumors.⁹¹⁻⁹³

Differentiation of Ascites

DIFFERENTIATION OF ASCITES FROM PLEURAL FLUID

In patients with small pleural effusions or ascites, it may be difficult to determine whether the fluid is supradiaphragmatic or subdiaphragmatic. Four useful signs have been described on CT and ultrasound studies.^{40,94-100}

Bare Area Sign

The right lobe of the liver is directly attached to the posterior abdominal wall and diaphragm by the coronary ligament, without intervening peritoneum. Intraperitoneal fluid cannot accumulate posterior to the liver (Fig. 110-6). If fluid is identified dorsal to the liver and medial to the attachment of the right superior coronary ligament, it must lie in the posterior sulcus of the pleural space. The spleen also demonstrates a bare area that maintains a constant relation to the superior ventral aspect of the left kidney, specifically Gerota's fascia. This bare area is about 2 cm long and is usually seen on two adjacent CT sections. It is postulated that the point of reflection of the splenorenal ligament at the bare area is correlated anatomically with the intermediate ridge of the spleen.¹⁰⁰

Diaphragm Sign

Fluid "inside" the diaphragm is ascites, whereas fluid "outside" the diaphragm is pleural effusion.⁹⁹

Displaced Crus Sign

The diaphragmatic crura represent focal muscle thickenings near the midline. If the crus is displaced away from the spine by an abnormal fluid collection, the fluid is pleural in origin. Ascites lies lateral and anterior to the crus.⁹⁷

Interface Sign

The location of a fluid collection can also be suggested by its interface with the liver. The apparent interface between ascites

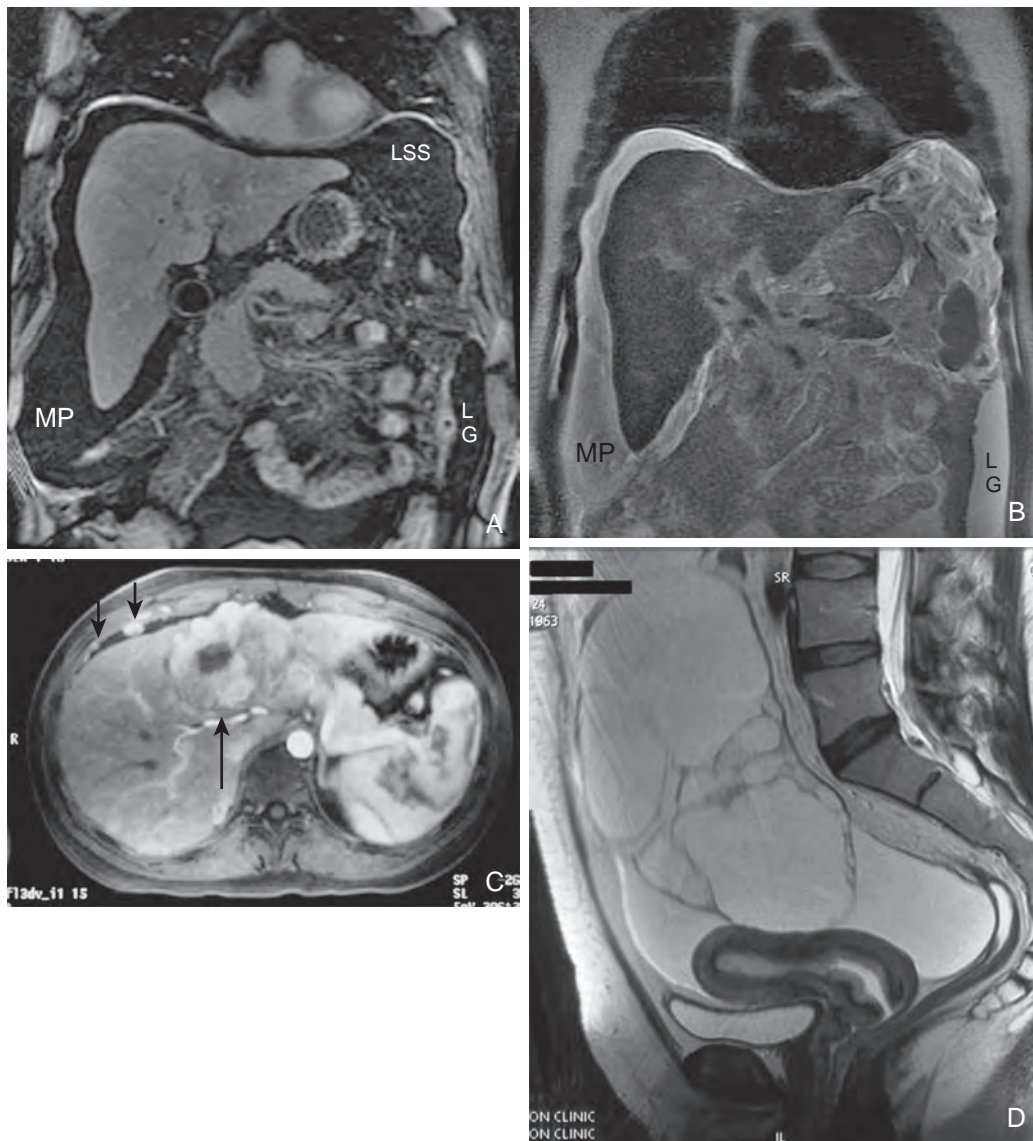


Figure 110-5 Ascites: MR features. Coronal T1-weighted (A) and T2-weighted (B) scans of the upper abdomen show benign fluid in Morison's pouch (MP), left paracolic gutter (LG), and left subphrenic space (LSS). C. Image of a patient with fibrolamellar hepatoma of the left lobe shows ascites and enhancing Glisson's capsule implants (arrows), indicating peritoneal spread of disease. D. Coronal T2-weighted image shows pseudomyxoma peritonei displacing the gut superiorly. (D courtesy Dr. Rodney H. Reznek, London, England.)

and the liver is sharp and well defined. The interface between pleural fluid and the liver is ill defined. This unsharpness in part reflects volume averaging at curved surfaces (e.g., the diaphragm) and is influenced by slice thickness.⁹⁸

DIFFERENTIATION OF ASCITES FROM SUBCAPSULAR FLUID

Subcapsular hepatic and splenic collections typically conform to the shape of the organ capsule. Subcapsular hepatic collections are confined by the falciform ligament and may extend medially to the attachment of the superior coronary ligament. Medial extension of intraperitoneal fluid collections is stopped by the coronary ligament. On real-time ultrasound studies, subcapsular collections move with the involved organ during respiration, whereas the organs "glide" within intraperitoneal fluid.⁵⁵

Treatment

The rationale for treatment of cirrhotic ascites is to reduce the risk for development of complications, such as spontaneous bacterial peritonitis, and to improve the patient's overall appearance, energy expenditure, and sense of well-being.^{4,101} Respiratory compromise resulting from compression of the diaphragm, anorexia caused by gastric distention, and abdominal discomfort from distention can be improved with therapy.^{3,4} Because these complications occur almost exclusively in patients with moderate to marked ascites, patients with small amounts of fluid usually require no specific treatment. Depending on the method and aggressiveness of therapy, the treatment of ascites is associated with several potentially serious side effects: acid-base and electrolyte abnormalities, hepatic encephalopathy, renal insufficiency, hypovolemia, and a variety of complications associated with the LeVeen peritoneovenous shunt.⁴

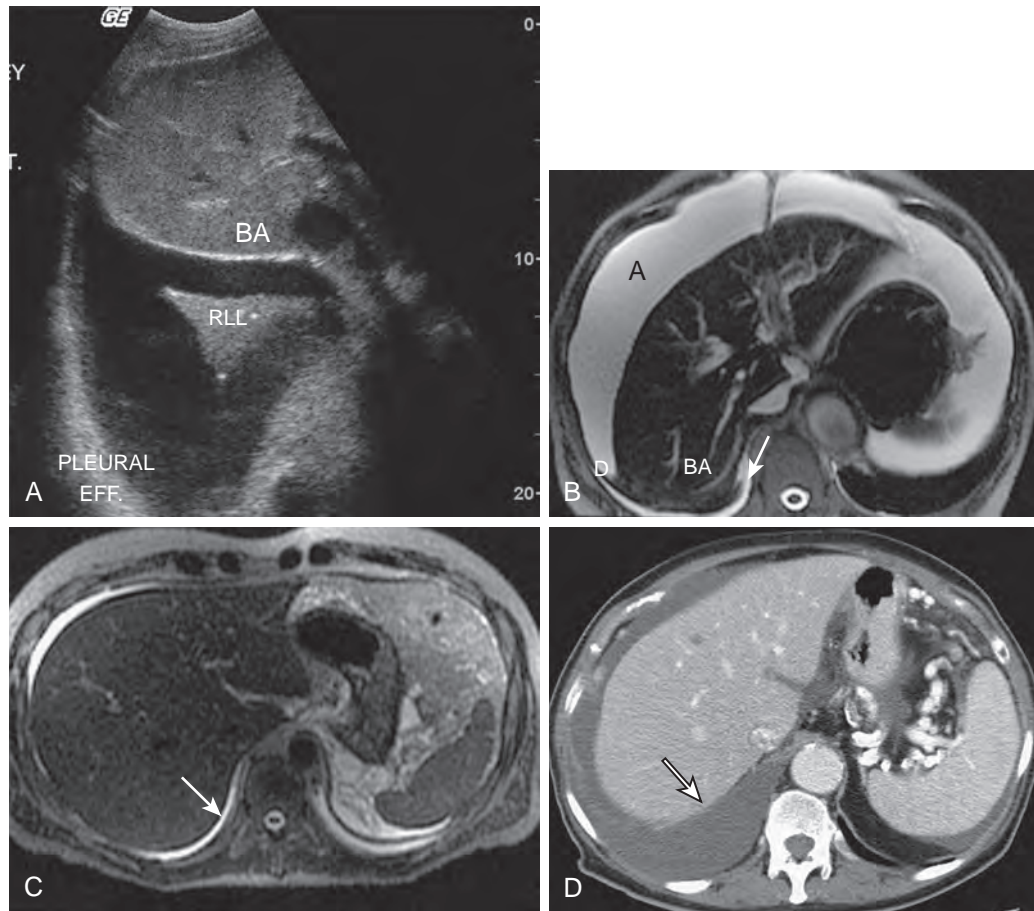


Figure 110-6 Differentiating ascites from pleural fluid. **A.** The bare area (BA) sign is demonstrated on this transverse sonogram, which shows pleural fluid posterior to the bare area of the liver. Ascites would not be present in this area because it is excluded from the peritoneum. *RLL*, Right lower lobe of lung. **B.** Diaphragm sign. An axial MR scan shows high signal intensity pleural fluid (arrow) outside the diaphragm (D) posterior to the bare area (BA) of the liver. *A*, Intraperitoneal fluid. **C.** Displaced crus sign. An axial MR image shows a sliver of high signal intensity fluid (arrow) separating the spine from the left hemidiaphragm. **D.** Interface sign. The interface between pleural fluid and liver (arrow) is less distinct than that between ascites and liver.

DIURETICS

Sodium restriction (20 to 30 mEq/day), water restriction (in the presence of hyponatremia), diuretics, and spironolactone constitute the standard medical management for ascites and are effective in 95% of patients.⁴ Therapeutic paracentesis should be reserved for patients who need rapid symptomatic relief of tense ascites.^{101,102}

THERAPEUTIC PARACENTESIS

Early reports stressed the dangers of large-volume paracentesis: hepatic encephalopathy, renal insufficiency, decreased cardiac output, hypovolemia, and hyponatremia. Later studies suggested that large-volume paracentesis of up to 5 L is tolerated well by most cirrhosis patients.¹⁰²⁻¹⁰⁶

TRANSJUGULAR INTRAHEPATIC PORTOSYSTEMIC SHUNT

The transjugular intrahepatic portosystemic shunt (TIPS) procedure has become increasingly popular in the short-term and long-term treatment of patients with refractory ascites (Fig. 110-7).¹⁰⁷⁻¹¹⁰ This procedure is described in Chapter 82.

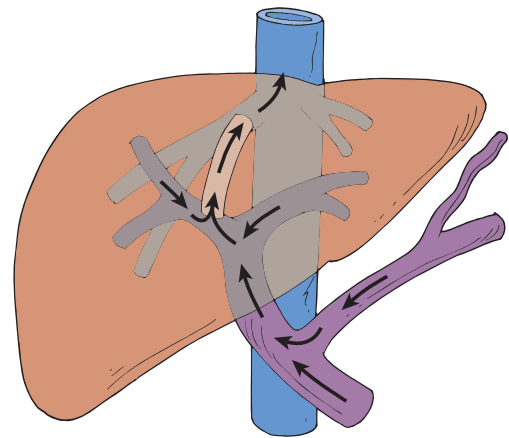


Figure 110-7 Ascites: therapy. Transjugular intrahepatic portosystemic shunt (TIPS) has become the first-line treatment for refractory massive ascites that fails medical management.

SURGICAL SHUNTING

The peritoneovenous shunt is the best surgical alternative for the less than 5% of patients with medically intractable ascites. First introduced by LeVeen, the shunt functions as a megalympathic that returns the ascitic fluid to the central venous

system. One end of the shunt lies in the peritoneal cavity; the efferent limb lies in the superior vena cava near the entrance of the right atrium. Later shunts (e.g., Denver, Cordis-Hakim) include a pumping mechanism to increase flow or to clear partially occluded shunts. Beneficial effects of these shunts include increased cardiac output, renal blood flow, glomerular filtration rate, urinary volume, and sodium excretion and decreased plasma renin activity and plasma aldosterone concentration.^{111,112}

Despite these apparent benefits, there is no indication that the peritoneovenous shunt improves survival of patients. These shunts are associated with a complication rate of 74% and a mortality rate of 24%.¹¹³ Sepsis, shunt malfunction, and disseminated intravascular coagulation are the major complications. This procedure should be reserved for patients who are truly refractory to medical management and the TIPS procedure.¹¹⁴

REFERENCES

- Nusrat S, Khan MS, Fazili J, et al: Cirrhosis and its complications. *World J Gastroenterol* 20: 5442–5460, 2014.
- Jafri SM, Gordon SC: Care of the cirrhotic patient. *Infect Dis Clin North Am* 26:979–994, 2012.
- Runyon BA: Approach to the patient with ascites. In Yamada T, editor: *Textbook of Gastroenterology*, ed 4, Philadelphia, 2003, Lippincott Williams & Wilkins, pp 1109–1127.
- Boyer TD: Diagnosis and management of cirrhotic ascites. In Zakim D, Boyer TD, editors: *Hepatology: A Textbook of Liver Disease*, ed 4, Philadelphia, 2003, WB Saunders, pp 631–658.
- Cardenas A, Arroyo V: Refractory ascites. *Dig Dis* 23:30–38, 2005.
- Cattau EL, Benjamin SB, Knuff TE, et al: The accuracy of the physical examination in the diagnosis of suspected ascites. *JAMA* 247:1164–1166, 1966.
- Lawson JD, Weissbein AS: The puddle sign—an aid in the diagnosis of minimal ascites. *N Engl J Med* 260:652–654, 1959.
- Thoeni RF: The role of imaging in patients with ascites. *AJR Am J Roentgenol* 165:16–18, 1995.
- Lipsky MS, Sternbach MR: Evaluation and initial management of patients with ascites. *Am Fam Physician* 54:1327–1333, 1996.
- Trey C, Trey G: Complications of cirrhosis: Ascites and hepatic encephalopathy. *Curr Opin Gastroenterol* 6:365–369, 1990.
- Montano-Loza AJ: Clinical relevance of sarcopenia in patients with cirrhosis. *World J Gastroenterol* 20:8061–8071, 2014.
- Attali P, Turner K, Pelletier G, et al: pH of ascitic fluid: Diagnostic and prognostic value in cirrhotic and noncirrhotic patients. *Gastroenterology* 90:1255–1260, 1986.
- Woolf GM, Runyon BA: Spontaneous salmonella infection of high protein noncirrhotic ascites. *J Clin Gastroenterol* 12:430–432, 1990.
- Hibbeln JE, Wehmuller MD, Wilbur AC: Chylous ascites: CT and ultrasound appearance. *Abdom Imaging* 20:138–141, 1995.
- Anbarasu A, Upadhyay A, Merchant SA, et al: Tuberculous chylous ascites: Pathognomonic CT findings. *Abdom Imaging* 22:50–53, 1997.
- Kuboki S, Shimizu H, Yoshidome H, et al: Chylous ascites after hepatopancreatobiliary surgery. *Br J Surg* 100:522–527, 2013.
- Steinemann DC, Dindo D, Clavien PA, et al: Atraumatic chylous ascites: Systematic review on symptoms and causes. *J Am Coll Surg* 212:899–905, 2011.
- Oei J, Garvey PA, Rosenberg AR: The diagnosis and management of neonatal urinary ascites. *J Paediatr Child Health* 37:513–515, 2001.
- Randle RW, Swett KR, Swords DS, et al: Efficacy of cytoreductive surgery with hyperthermic intraperitoneal chemotherapy in the management of malignant ascites. *Ann Surg Oncol* 2013. [Epub ahead of print].
- Krauetz GW, Cho KC, Baker SR: Radiologic evaluation of pancreatic ascites. *Gastrointest Radiol* 13:163–166, 1988.
- Sankaran S, Sugawa C, Walt AJ: Value of endoscopic retrograde pancreatography in ascites. *Surg Gynecol Obstet* 148:185–192, 1979.
- Weaver DW, Walt AJ, Sugawa C, et al: A continuing appraisal of pancreatic ascites. *Surg Gynecol Obstet* 154:845–848, 1982.
- Proto AV, Lane EJ, Marangola JP: A new concept of ascitic fluid distribution. *AJR Am J Roentgenol* 126:974–980, 1976.
- Raval B, Lakmi N: CT demonstration of preferential routes of the spread of pelvic disease. *Crit Rev Diagn Imaging* 26:17–48, 1987.
- Dunnick NR, Jones RB, Doppman JL, et al: Intraperitoneal contrast infusion for assessment of intraperitoneal fluid dynamics. *AJR Am J Roentgenol* 133:221–223, 1979.
- Rosenshein N, Blake D, McIntyre PA, et al: The effect of volume on the distribution of substances instilled into the peritoneal cavity. *Gynecol Oncol* 6:106–110, 1978.
- Wahl RL, Gyves J, Gross BH, et al: SPECT of the peritoneal cavity: Method of delineating intraperitoneal fluid distribution. *AJR Am J Roentgenol* 152:1205–1210, 1989.
- Fiske CE, Callen PW: Fluid collections ultrasonically simulating urinary bladder. *J Can Assoc Radiol* 31:254–255, 1980.
- Moss AA: Ascites. In Margulis AR, Burhenne HJ, editors: *Alimentary Tract Radiology*, vol 3, St. Louis, 1979, CV Mosby, pp 524–529.
- Wojtowicz L, Rzymiski K, Czarneck R: A CT evaluation of intraperitoneal fluid distribution. *Rofo* 137:95–99, 1982.
- Irving HC, Robinson PJ: The diagnosis and management of abdominal abscesses and other fluid collections. In Simpkins KC, editor: *A Textbook of Radiological Diagnosis*, vol 4, London, 1988, HK Lewis, pp 659–677.
- Heiken JP: Abdominal wall and peritoneal cavity. In Lee JKT, Sagel SS, Stanley RJ, editors: *Computed Body Tomography with MRI Correlation*, ed 3, Philadelphia, 1998, Lippincott-Raven, pp 961–1022.
- Churchill RA, Meyers MA: Intraperitoneal fluid collections. In Meyers MA, editor: *Computed Tomography of the Gastrointestinal Tract*, New York, 1986, Springer-Verlag, pp 183–220.
- Meyers MA: Dynamic Radiology of the Abdomen, ed 4, New York, 1994, Springer-Verlag, pp 55–114.
- Meyers MA: Dynamic Radiology of the Abdomen, ed 4, New York, 1994, Springer-Verlag, pp 115–218.
- Baker SR, Cho KC: The Abdominal Plain Film with Correlative Imaging, East Norwalk, CT, 1998, Appleton & Lange.
- Singh A, Bajwa A, Shujaat A: Evidence-based review of the management of hepatic hydrothorax. *Respiration* 86:155–173, 2013.
- Pandolfo I, Goeta M, Scribano E, et al: Mediastinal pseudotumor due to passage of ascites through the esophageal hiatus. *Gastrointest Radiol* 14:209–211, 1989.
- Baer JW: Extraperitoneal mass effect by ascites under tension. *Gastrointest Radiol* 15:3–8, 1990.
- Arenas AP, Sanchez LV, Albillos SM, et al: Direct dissemination of pathologic abdominal processes through perihepatic ligaments: Identification with CT. *Radiographics* 14:515–527, 1994.
- Gooding GAW, Cummings SR: Sonographic detection of ascites in liver disease. *J Ultrasound Med* 3:169–172, 1984.
- Bisset RAL, Khan AN: Differential Diagnosis in Abdominal Ultrasound, London, 1990, Baillière Tindall, pp 296–362.
- Budin E, Jacobson G: Roentgenographic diagnosis of small amounts of intraperitoneal fluid. *Radiology* 99:62–70, 1967.
- Love L, Demos TC, Reynes CJ, et al: Visualization of the lateral edge of the liver in ascites. *Radiology* 122:619–622, 1977.
- Gore RM: Ultrasound and CT scanning in the evaluation of ascites. *Med Times* 112:65–72, 1984.
- Bundrick TJ, Cho SR, Brewer WH, et al: Ascites: Comparison of plain film radiographs with ultrasonograms. *Radiology* 152:503–506, 1984.
- Goldberg BB, Goodman GA, Clearfield HR: Evaluation of ascites by ultrasound. *Radiology* 96:15–22, 1970.
- Hunig R, Kinser J: The diagnosis of ascites by ultrasonic tomography (B-scan). *Br J Radiol* 46:325–328, 1973.
- Goldberg BB, Clearfield HR, Goodman GA, et al: Ultrasonic determination of ascites. *Arch Intern Med* 131:216–220, 1973.
- Nyberg DA, Laing FC, Jeffrey RB: Sonographic detection of subtle pelvic fluid collections. *AJR Am J Roentgenol* 143:261–265, 1984.
- Shkolnik ML: Guide to the Ultrasound Examination of the Abdomen, New York, 1986, Springer-Verlag, pp 11–16.
- Sickler GK, Chen PC, Dubinsky TJ, et al: Free echogenic pelvic fluid: Correlation with hemo-peritoneum. *J Ultrasound Med* 17:431–435, 1998.

53. Gooding GAW, Cummings SR: Sonographic detection of ascites in liver disease. *J Ultrasound Med* 3:169–173, 1984.
54. Nguyen KT, Sauerbrei E, Nolan RL: The peritoneum and the diaphragm. In Rumack CM, Wilson SR, Charboneau JW, editors: *Diagnostic Ultrasound*, ed 2, St. Louis, 1998, CV Mosby, pp 501–518.
55. Vincent LM, Mauro MA, Mittlestaedt CA: The lesser sac and gastrohepatic recess: Sonographic appearance and differentiation of fluid collections. *Radiology* 150:515–519, 1984.
56. Yeh HS, Wolf BS: Ultrasonography in ascites. *Radiology* 124:783–790, 1977.
57. Jeffrey RB, McGahan JP: Gastrointestinal tract and peritoneal cavity. In McGahan JP, Goldberg BB, editors: *Diagnostic Ultrasound—A Logical Approach*, Philadelphia, 1998, Lippincott-Raven, pp 511–560.
58. Shwarok DJ, Goiney RC, Cooperberg PL: Hepatic pseudotumors in patients with ascites. *J Ultrasound Med* 5:5–8, 1986.
59. Derchi LE, Reggiani L, Rebaudi F, et al: Appendices epiploicae of the large bowel: Sonographic appearance and differentiation from peritoneal seeding. *J Ultrasound Med* 7:11–14, 1988.
60. Edell SL, Gefter WB: Ultrasonic differentiation of types of ascitic fluid. *AJR Am J Roentgenol* 133:111–114, 1979.
61. Franklin JT, Azose AA: Sonographic appearance of chylous ascites. *J Clin Ultrasound* 12:239–242, 1984.
62. Suresh S, Indrani S, Vijayalakshmi S: Ultrasonography in tropical diseases. *Ultrasound Q* 8:43–72, 1990.
63. Suslavich FJ, Turner NA, King PS, et al: Intraabdominal adhesions: intraoperative US. *Radiology* 172:387–388, 1989.
64. Gore RM, Callen PW, Filly RA: Lesser sac fluid in predicting the etiology of ascites. *AJR Am J Roentgenol* 142:701–705, 1982.
65. Weill FS, Rohmer P, Beloir A, et al: The butterfly sign: An indicator of fluid within both the greater peritoneal cavity and lesser omental bursa. *J Ultrasound Med* 2:161–164, 1983.
66. Tsujimoto F, Miyamoto Y, Tada S: Differentiation of benign from malignant ascites by sonographic evaluation of gallbladder wall. *Radiology* 157:503–504, 1985.
67. Seltzer SE: Analysis of the tethered-bowel sign on abdominal CT as a predictor of malignant ascites. *Gastrointest Radiol* 12:245–249, 1987.
68. Marti-Bonmati L, Andres JC, Aguado C: Sonographic relationship between gallbladder wall thickness and the etiology of ascites. *J Clin Ultrasound* 17:497–501, 1989.
69. Yeh HC, Shafir MK, Slater G, et al: Ultrasonography and computed tomography in pseudomyxoma peritonei. *Radiology* 153:507–510, 1984.
70. Seshol MB, Coulam CM: Pseudomyxoma peritonei: Computed tomography and sonography. *AJR Am J Roentgenol* 136:803–806, 1981.
71. Agha FP, Amendola MA, Shirazik R, et al: Unusual complications of ventriculoperitoneal shunts. *Radiology* 146:323–326, 1985.
72. Jeffrey RB, Laing FC: Echogenic clot: A useful sign of pelvic hemoperitoneum. *Radiology* 145:139–142, 1982.
73. Rust RJ, Kopecky KK, Holden RW: The triangle sign: A CT sign of intraperitoneal fluid. *Gastrointest Radiol* 9:107–113, 1984.
74. Bydder GM, Krel L: Attenuation values of fluid collections within the abdomen. *J Comput Assist Tomogr* 4:145–150, 1980.
75. Akriviadis EA: Hemoperitoneum in patients with ascites. *Am J Gastroenterol* 92:567–575, 1997.
76. Federle MP, Jeffrey RB: Hemoperitoneum studied by computed tomography. *Radiology* 148:187–192, 1983.
77. Minutoli A, Volta S, Gaeta M: Delayed enhancement of ascites following high dose contrast CT for liver metastases. *J Comput Assist Tomogr* 13:916–917, 1990.
78. Hammerman AM, Oberle PA, Susman N: Opacification of ascitic fluid on delayed contrast computed tomography scans. *Clin Imaging* 14:222–224, 1990.
79. Watanabe AT, Jeffrey RB: CT diagnosis of traumatic rupture of the cisterna chyli. *J Comput Assist Tomogr* 11:175–176, 1987.
80. Jolles H, Coulam CM: CT of ascites: Differential diagnosis. *AJR Am J Roentgenol* 135:315–322, 1980.
81. Callen PW, Marks WM, Filly RA: Computed tomography and ultrasonography in the evaluation of the retroperitoneum in patients with malignant ascites. *J Comput Assist Tomogr* 3:581–584, 1979.
82. Jeffrey RB: CT demonstration of peritoneal implants. *AJR Am J Roentgenol* 135:323–326, 1980.
83. Jeffrey RB, Federle MP, Goodman PC: Computed tomography of the lesser peritoneal sac. *Radiology* 141:117–122, 1981.
84. Raval B, Hall JT, Jackson H: CT diagnosis of fluid on lesser sac mimicking thrombosis of inferior vena cava. *J Comput Assist Tomogr* 9:956–958, 1985.
85. Demas BE: Imaging of peritoneal pathology. *Curr Opin Radiol* 2:472–476, 1990.
86. Hoffer FA, Kozakewich H, Colodny A, et al: Peritoneal inclusion cysts: Ovarian fluid in peritoneal adhesions. *Radiology* 169:189–191, 1988.
87. Wise SW, DeMeo JH, Austin RF, et al: Enhancing ascites: Aid to CT diagnosis. *Abdom Imaging* 21:67–69, 1996.
88. Low RN, Sigeti JS: MR imaging of peritoneal disease. *AJR Am J Roentgenol* 163:1131–1140, 1994.
89. Wallner B, Edelman RR, Finn JP, et al: Bright pleural effusion and ascites on gradient-echo MR images: A potential source of confusion in vascular MR studies. *AJR Am J Roentgenol* 155:1237–1240, 1990.
90. Cohen JM, Weinreb JC, Maravilla KR: Fluid collections in the intraperitoneal and extraperitoneal spaces: Comparison of MR and CT. *Radiology* 155:705–708, 1985.
91. Low RN, Barone RM, Lacey C, et al: Peritoneal tumor: MR imaging with dilute oral barium and intravenous gadolinium-containing contrast agents compared with unenhanced MR imaging and CT. *Radiology* 204:513–520, 1997.
92. Low RN, Carter WD, Saleh F, et al: Ovarian cancer: Comparison of findings with perfluorocarbon-enhanced MR imaging, In-III-CYT-103 immunoscintigraphy, and CT. *Radiology* 195:391–400, 1995.
93. Low RN, Francis IR: Imaging of the gastrointestinal tract with IV gadolinium and diluted barium oral contrast media compared with unenhanced MR imaging and CT. *AJR Am J Roentgenol* 169:1051–1059, 1997.
94. Halvorsen RA, Fedyskin PJ, Korobkin M, et al: Ascites or pleural effusion? CT differentiation: Four useful criteria. *Radiographics* 6:135–149, 1986.
95. Griffin DH, Gross BH, McCracken S, et al: Observation on CT differentiation of pleural and peritoneal fluid. *J Comput Assist Tomogr* 8:24–28, 1984.
96. Alexander ES, Proto AV, Clark RA: CT differentiation of subphrenic abscess and pleural effusion. *AJR Am J Roentgenol* 140:47–51, 1983.
97. Dwyer A: The displaced crus: A sign for distinguishing between pleural fluid and ascites on computed tomography. *J Comput Assist Tomogr* 2:598–599, 1978.
98. Teplick JG, Teplick SK, Goodman L, et al: The interface sign: A computed tomographic sign for distinguishing pleural and intraabdominal fluid. *Radiology* 144:359–362, 1982.
99. Nadich DP, Megibow AJ, Ross CR, et al: Computed tomography of the diaphragm: Peridiaphragmatic fluid localization. *J Comput Assist Tomogr* 7:633–640, 1983.
100. Vibhakor SD, Bellon EM: The bare area of the spleen: A constant CT feature of the ascitic abdomen. *AJR Am J Roentgenol* 141:953–955, 1984.
101. Dolz C, Ravrich JM, Ibanez J, et al: Ascites increases the resting energy expenditure in liver cirrhosis. *Gastroenterology* 100:738–744, 1991.
102. Hsu SJ, Huang HC: Management of ascites in patients with liver cirrhosis: Recent evidence and controversies. *J Chin Med Assoc* 76:123–130, 2013.
103. Liou IW: Management of end-stage liver disease. *Med Clin North Am* 98:119–152, 2014.
104. Choudhury J, Sanyal AJ: Treatment of ascites. *Curr Treat Options Gastroenterol* 6:481–491, 2003.
105. Ross GJ, Kessler HB, Clair MR, et al: Sonographically guided paracentesis for palliation of symptomatic malignant ascites. *AJR Am J Roentgenol* 153:1309–1311, 1989.
106. Zervos EE, Rosemurgy AS: Management of medically refractory ascites. *Am J Surg* 181:256–264, 2001.
107. Saad WE, Darwish WM, Davies MG, et al: Transjugular intrahepatic portosystemic shunts in liver transplant recipients for management of refractory ascites: Clinical outcome. *J Vasc Interv Radiol* 21:218–223, 2010.
108. Parvianian A, Bui JT, Knutinen MG, et al: Transjugular intrahepatic portosystemic shunt for the treatment of medically refractory ascites. *Diagn Interv Radiol* 20:58–64, 2014.
109. D'Amico G, Luca A, Morabito A, et al: Uncovered transjugular intrahepatic portosystemic shunt for refractory ascites: A meta-analysis. *Gastroenterology* 129:1282–1293, 2005.
110. Fidelman N, Kwan SW, LaBerge JM, et al: The transjugular intrahepatic portosystemic shunt: An update. *AJR Am J Roentgenol* 199:746–755, 2012.
111. Wong F: Management of ascites in cirrhosis. *J Gastroenterol Hepatol* 27:11–20, 2012.
112. Rosemurgy AS, Zervos EE, Clark WC, et al: TIPS versus peritoneovenous shunt in the treatment of medically intractable ascites: A prospective randomized trial. *Ann Surg* 239:883–889, 2004.
113. Gur I, Diggs BS, Orloff SL: Surgical portosystemic shunts in the era of TIPS and liver transplantation are still relevant. *HPB (Oxford)* 16:481–493, 2014.
114. Taki Y, Kanazawa H, Narahara Y, et al: Predictive factors for improvement of ascites after transjugular intrahepatic portosystemic shunt in patients with refractory ascites. *Hepatol Res* 44:871–877, 2014.

Mesenteric and Omental Lesions

APARNA BALACHANDRAN | TARA SAGEBIEL | PAUL M. SILVERMAN

CHAPTER OUTLINE

Anatomy

Primary Neoplasms

Desmoid Tumors
Malignant Peritoneal Mesothelioma
Primary Peritoneal Serous Carcinoma
Well-Differentiated Papillary Mesothelioma
Multicystic Peritoneal Mesothelioma
Desmoplastic Small Round Cell Tumor
Adenomatoid Tumor
Other Primary Mesenchymal Tumors

Secondary Tumors

Peritoneal Carcinomatosis
Carcinoid Tumor
Lymphoma

Inflammatory and Infiltrative Diseases

Pancreatitis
Diverticulitis
Crohn's Disease
Mesenteric Panniculitis or Sclerosing Mesenteritis
Tuberculosis
Whipple's Disease
Amyloidosis
Extramedullary Hematopoiesis
Trauma and Hemorrhage
Mesenteric Edema
Mesenteric Cysts

Omentum

Radiologic Features
Primary Neoplasms
Metastatic Disease and Lymphoma
Inflammatory Diseases
Miscellaneous Conditions

Anatomy

The mesentery is a part of the peritoneal lining that extends from the posterior peritoneum and suspends bowel loops. The mesentery is composed of two thin layers of fibrofatty tissue, which surrounds and contains the vascular and lymphatic structures supplying either the small bowel or colon. The purpose of the peritoneum and mesentery is to provide a smooth and frictionless surface between the solid organs.¹ The mesentery can be further divided according to whether it suspends small intestine or colon. The small bowel mesentery is obliquely placed in the peritoneal cavity and extends from the ligament of Treitz in the left upper quadrant to the terminal

ileum and ileocecal valve in the right lower quadrant. The transverse mesocolon extends from the pancreas and suspends the transverse mesocolon. The root of the transverse mesocolon passes across the second portion of the duodenum and the head, body, and tail of the pancreas. The plane of the transverse mesocolon can be identified by following the middle colic vessels.

The greater omentum is the continuation of the dorsal mesogastrium inferiorly from the greater curvature of the stomach. This extends inferiorly and doubles back anterior to the transverse colon and then continues posteriorly as the transverse mesocolon. The descending and ascending portions of the greater omentum usually fuse to form a four-layer vascular peritoneal fold (Fig. 111-1).

The peritoneal cavity is divided primarily by the transverse mesocolon into the supramesocolic and inframesocolic compartments. The peritoneal folds in the supramesocolic compartment consist of the falciform, coronary, gastrohepatic, hepatoduodenal, greater omentum, gastrosplenic, splenorenal, and phrenicocolic ligaments. The falciform ligament divides the subphrenic space into the right and left subphrenic spaces. The phrenicocolic ligament extends from the splenic flexure to the diaphragm and limits the cranial extent of the left paracolic gutter. The inframesocolic compartment is subdivided by the small bowel mesentery into the right and the larger left portion extending deep into the pelvis. The left inframesocolic space is limited in the lower left pelvis by the sigmoid mesocolon.

All the ligaments of the peritoneal cavity consist of fused peritoneal layers and form the subperitoneal space, which is a continuous potential space that connects the intraperitoneal compartment to the retroperitoneal compartment. The subperitoneal space also extends to the solid viscera. Thus, any disease process that involves the subperitoneal space can spread bidirectionally to involve either the peritoneal compartment or the retroperitoneum and may involve the abdominal organs.

In most patients, there is sufficient macroscopic fat on computed tomography (CT) to identify the small bowel mesentery, transverse mesocolon, and sigmoid mesocolon. Mesenteric fat has Hounsfield unit measurements of fat elsewhere and measures between -100 and -160 HU.²

Primary Neoplasms

Primary tumors arising from the peritoneum are rare and are usually of mesenchymal origin.

DESMOID TUMORS

These tumors are related to benign but locally aggressive fibroblast proliferation or fibromatosis.³ The morbidity associated with these tumors is related to their locally aggressive behavior with involvement of adjacent organs. They are uncommon,

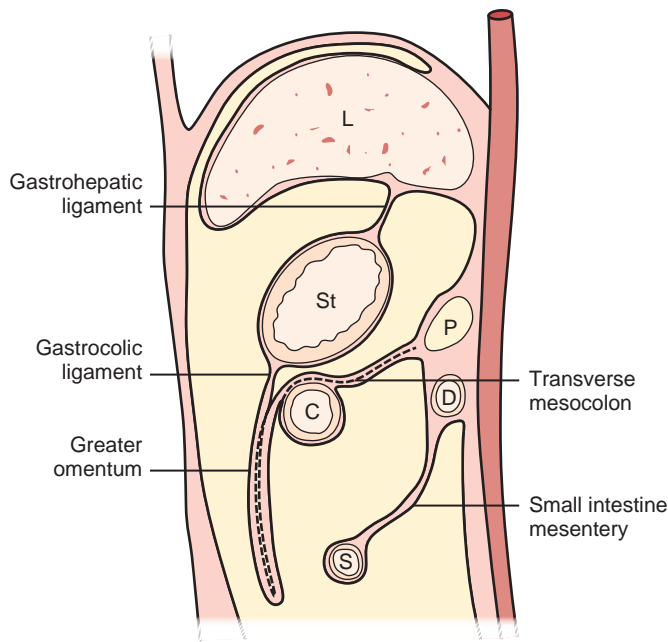


Figure 111-1 Schematic diagram of the anatomy of the greater omentum. L, Liver; St, stomach; C, colon; P, pancreas; D, duodenum; S, small intestine.

occurring in 2 to 4 per million people per year, and do not show the features of neoplasia. The cause is unknown, but there is an association with pregnancy and estrogen administration. They can occur either sporadically or in association with familial adenomatous polyposis. Familial adenomatous polyposis is an inherited syndrome characterized by innumerable polyps predominantly occurring in the colon. Gardner's syndrome is now considered to be a part of familial adenomatous polyposis, and both these conditions have a mutation of the APC gene.

Desmoid tumors can occur in 5% to 25% of patients with familial adenomatous polyposis.⁴ About half of the abdominal desmoids occur intra-abdominally, and the other half are found in the abdominal wall.⁴ Nearly one third of abdominal desmoids cause pain. Abdominal desmoids can involve the abdominal wall, mesentery, or retroperitoneum (Figs. 111-2 and 111-3). Many of these tumors are often associated with prior surgery, such as colectomy, and can recur at the surgical site. Surgery is thought to stimulate desmoid tumor growth.⁵ The most common site for mesenteric desmoids is at the base of the small bowel mesentery. Tumors can vary in size and range from a few centimeters to extremely large lesions. Desmoids are pseudoencapsulated lesions despite their relatively well defined gross appearance. On microscopic examination, they demonstrate infiltrative margins. Progressive growth may lead to bowel, ureteric, or vascular obstruction and occasionally fistulas.⁶ CT is an excellent imaging study to evaluate desmoid tumors and their relation to surrounding structures and in the follow-up of patients who undergo conservative medical therapy. Desmoid tumors are typically poorly enhancing solid lesions. They can usually be distinguished from postoperative fibrosis by the lack of mass effect of the fibrosis. On ultrasound, these appear as well-demarcated solid masses (Fig. 111-4) containing low to mid-level echoes.⁷ On magnetic resonance imaging (MRI), they

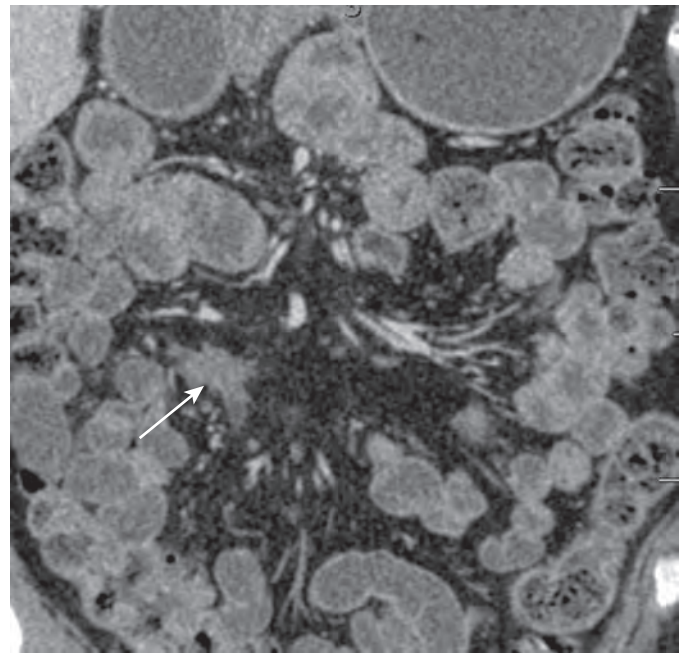


Figure 111-2 Desmoid tumor. Desmoid tumor (arrow) in the mesentery with radiating strands in the mesenteric fat.

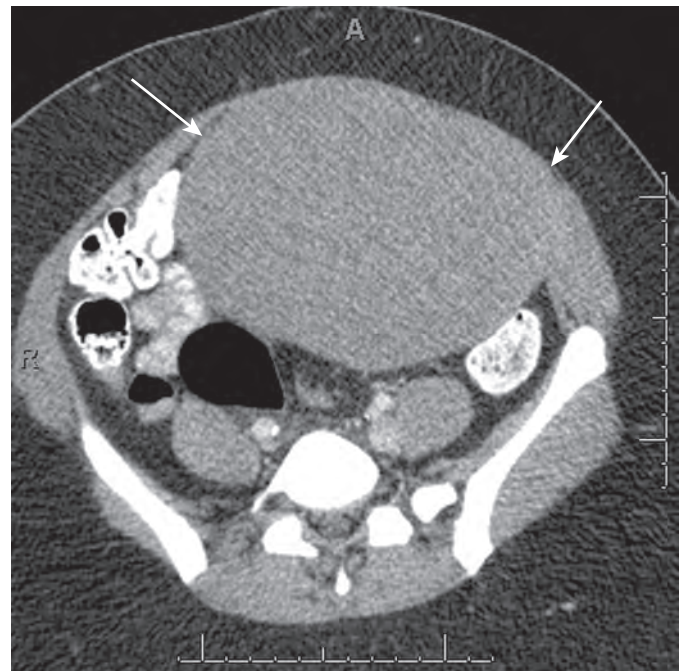


Figure 111-3 Desmoid tumor. Desmoid tumor (arrows) involving the abdominal wall.

are of low T1 and low T2 signal intensity (Fig. 111-5) with no or poor enhancement.⁸

MALIGNANT PERITONEAL MESOTHELIOMA

Malignant peritoneal mesothelioma (MPM) is a rare but aggressive tumor that arises from the serosa lining the pleura and the peritoneum.⁹ MPMs account for only 10% to 15% of all mesotheliomas.⁹ These may occur either alone or in conjunction

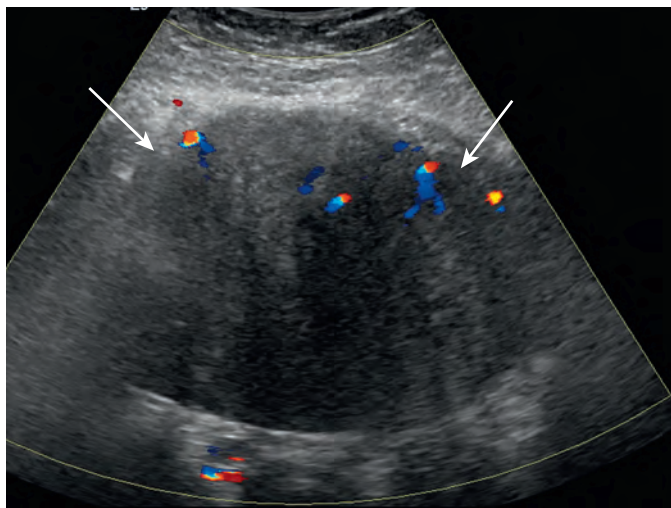


Figure 111-4 Desmoid tumor. Desmoid tumor (arrows) is a hypoechoic mass on ultrasound.

with pleural mesothelioma. Most patients have a history of exposure to asbestos.^{10,11} There is also a long latent period between exposure and appearance of peritoneal mesothelioma, typically 30 years after the exposure to asbestos. There is a slight male predominance, less than that of pleural mesotheliomas. It has been postulated that the patients with MPM have to have a higher cumulative exposure to asbestos than that of the patients with pleural mesothelioma.¹²

Peritoneal mesotheliomas can be classified into diffuse versus localized mesothelioma. The diffuse type is aggressive as opposed to the localized form, which has a better prognosis with surgery.

Peritoneal mesotheliomas can be classified into epithelial, sarcomatoid, and mixed types on the basis of histologic features. There is great variability in the histologic appearance, making the diagnosis difficult. Sarcomatoid histology is associated with a poor prognosis.¹³ Immunohistochemical staining has been proved to be of great benefit in differentiating MPMs from secondary tumors affecting the peritoneum.¹⁴ MPMs

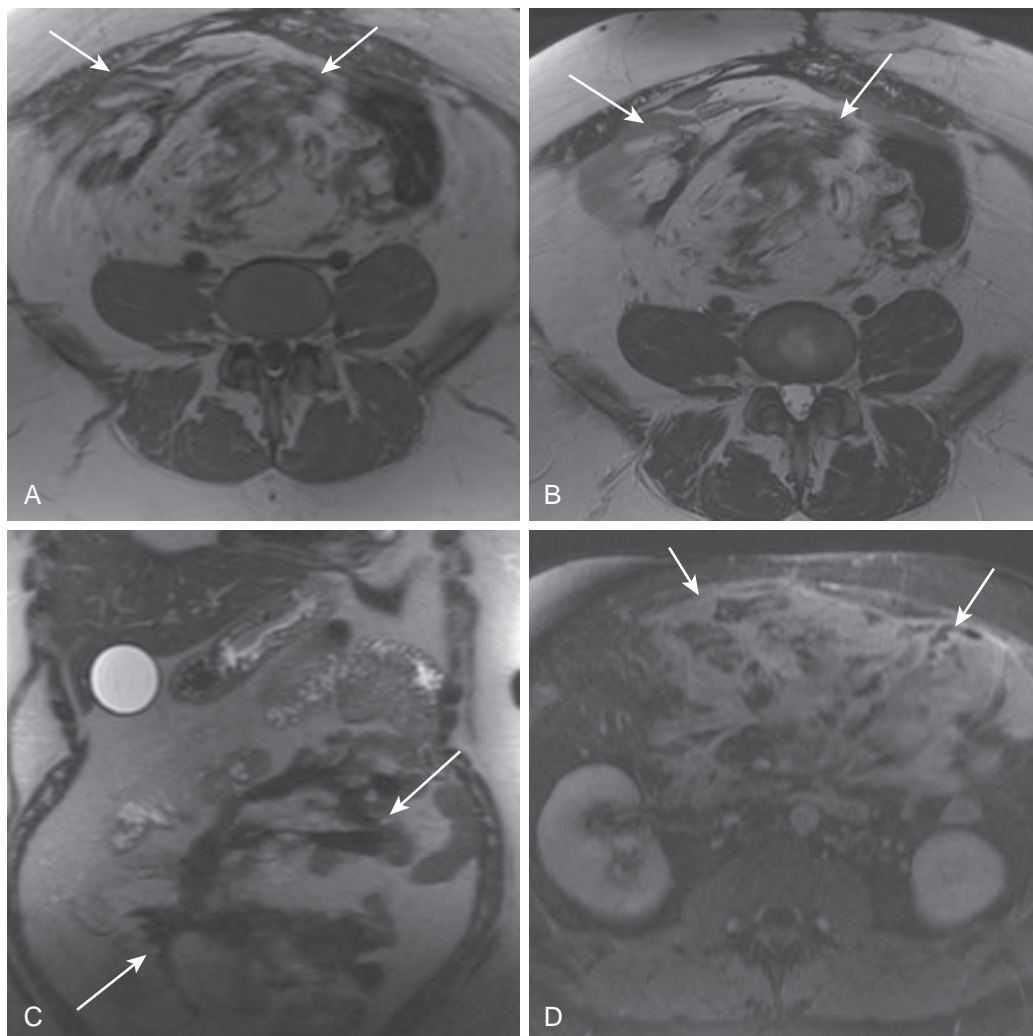


Figure 111-5 Desmoid tumor. Desmoid tumor (arrows) involving the mesenteric fat on axial T1 (A), axial T2 (B), coronal single-shot fast spin-echo (C), and postcontrast fat-saturated (D) sequences.

produce large amounts of hyaluronic acid and stain with colloidal iron. In contrast, MPMs do not stain positive for the presence of mucin. Symptoms are nonspecific and include abdominal distention, pain, and malaise. Fifty-five percent of patients fail to demonstrate evidence of asbestosis on chest radiographs.

CT is the most useful test in the initial evaluation of patients with increasing abdominal girth and pain. The nodules and masses in mesothelioma enhance with intravenous administration of contrast material. These can be manifested as sites of peritoneal thickening, infiltration, or nodularity (Fig. 111-6). A sheetlike pattern of growth with thickened appearance to the mesentery and bowel wall can also be seen. Bowel loops may be fixed from these infiltrative changes. Calcification is rare in MPMs. They can be associated with variable amounts of ascites. Scalloping or mass effect on adjacent organs is typically seen. On MRI, the nodules are of low T1 signal intensity and intermediate to high T2 signal intensity (Fig. 111-7).¹⁵ The peritoneal nodules can also be seen on dynamic or diffusion-weighted imaging.¹⁶ Positron emission tomography (PET) has a limited role in exact anatomic evaluation of MPMs.¹⁷ All the imaging modalities are limited in their detection of peritoneal nodules

less than 0.5 cm. Peritoneal mesothelioma is associated with poor survival; median survival time is 8 to 12 months after diagnosis.

CT is of help in evaluating for a primary tumor elsewhere in the gastrointestinal or genitourinary tracts, breast, and pancreas. The differential diagnosis includes metastatic disease, primary papillary serous carcinoma of the peritoneum, lymphoma, and granulomatous disease. The presence of marked and enlarged lymphadenopathy favors lymphoma or metastatic disease as the most likely diagnosis. Similarly, calcification of the peritoneal thickening makes MPMs less likely.

The mesenteric infiltration results in a characteristic stellate and fixed appearance.

PRIMARY PERITONEAL SEROUS CARCINOMA

Primary peritoneal serous carcinoma is a rare malignant neoplasm that typically occurs in postmenopausal women. This is a primary tumor of the peritoneum, but the cell origin is thought to be the extraovarian mesothelium with müllerian potential.¹⁸

According to the Gynecologic Oncology group, for a diagnosis of primary peritoneal serous carcinoma to be made, the

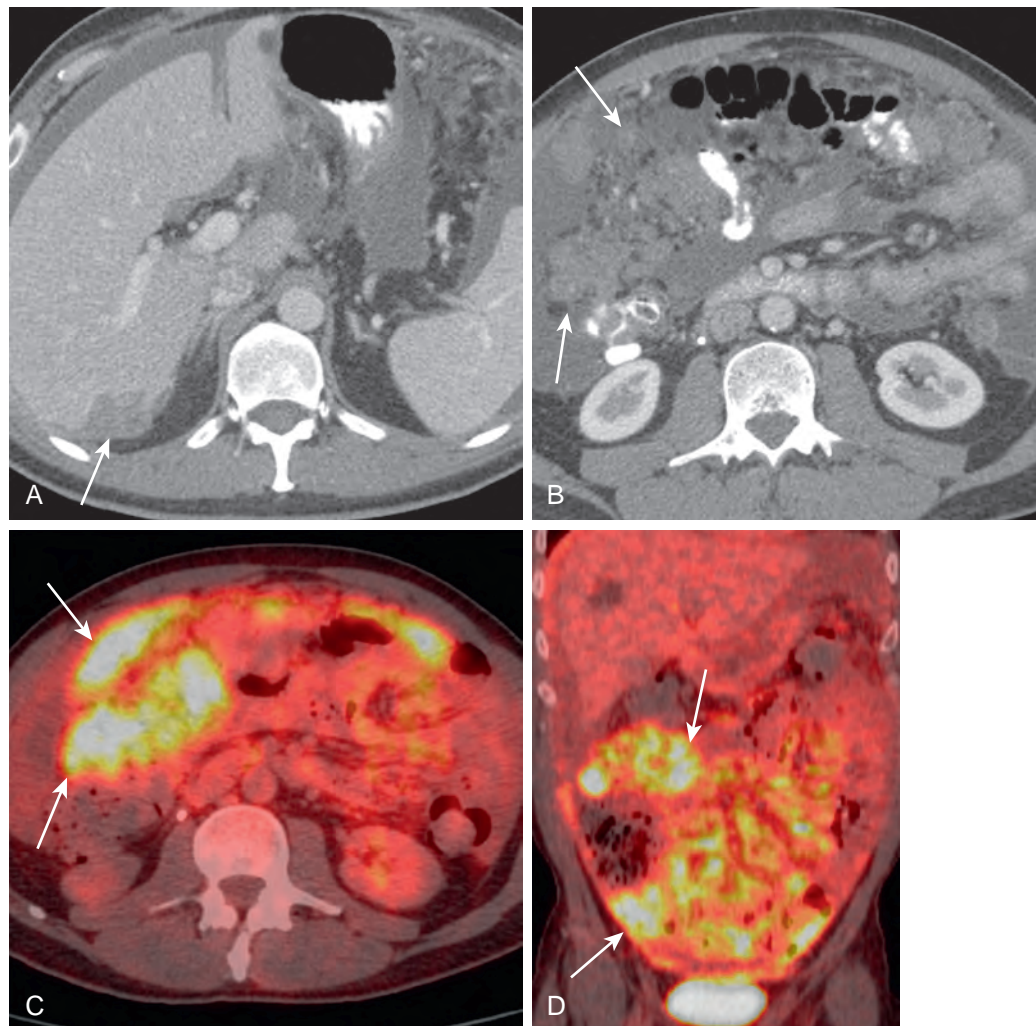


Figure 111-6 Mesothelioma. **A.** Patient with peritoneal mesothelioma demonstrating an implant (arrow) along the posterior liver. **B.** Infiltration with masses (arrows) along the mesentery. **C.** Axial PET/CT demonstrating FDG-avid masses (arrows) along the small bowel mesentery. **D.** Coronal PET/CT demonstrating diffuse peritoneal (arrows) involvement.

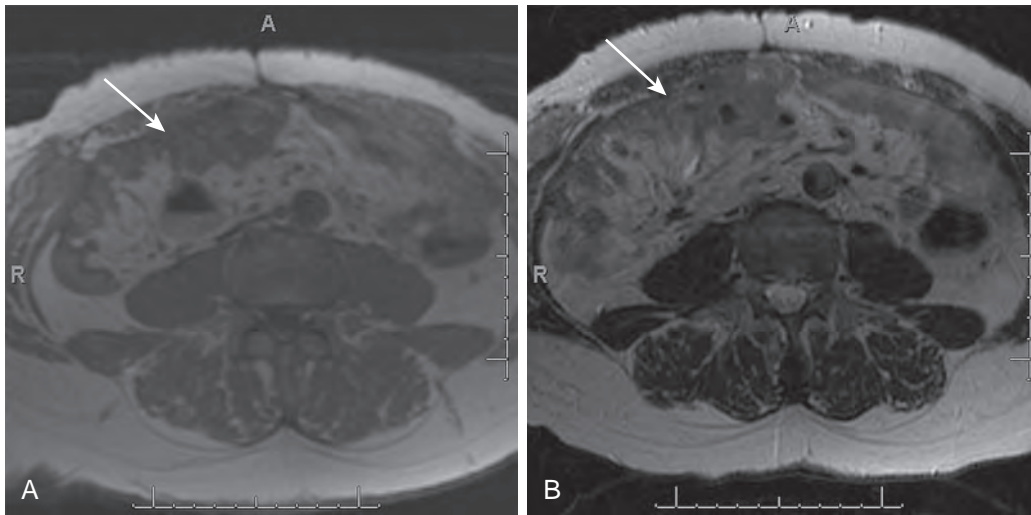


Figure 111-7 Peritoneal mesothelioma on MRI. Axial T1-weighted (A) and axial T2-weighted (B) images demonstrating infiltrative mass (arrow) involving the mesentery and omentum.

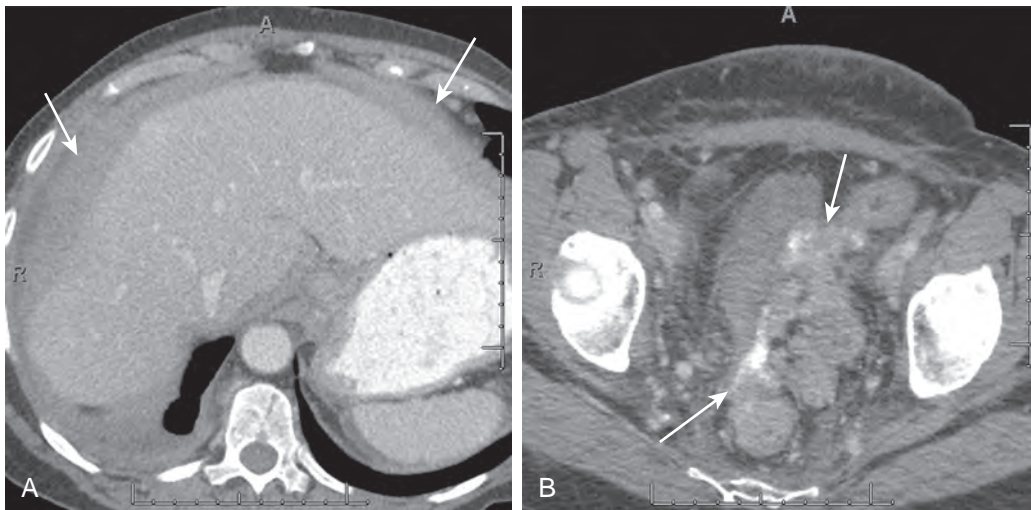


Figure 111-8 Primary peritoneal papillary serous carcinoma. A. Peritoneal involvement along the liver (arrows). B. Pelvic peritoneal involvement with calcifications (arrows).

ovaries should be normal in size or enlarged from a benign process, and the involvement of the extraovarian sites should be greater than ovarian involvement.¹⁹ The prognosis and treatment are similar to those of serous ovarian carcinoma. Calcification can be seen with this tumor and can help differentiate MPM from this tumor (Fig. 111-8). The CT and the pathologic appearance of primary peritoneal serous carcinoma is similar to that of carcinomatosis from serous ovarian cancer. Assessment for primary ovarian masses should be performed to exclude peritoneal carcinomatosis from ovarian cancer. Psammomatous calcifications can be seen in up to 30% of cases.²⁰

WELL-DIFFERENTIATED PAPILLARY MESOTHELIOMA

This is a rare subtype of mesothelioma that is clinically distinct from MPM. These tumors are seen typically in younger women and are not associated with asbestos exposure.²¹ They may be

detected and removed incidentally. These tumors tend to be small (Fig. 111-9). There is very little written about these tumors in the radiologic literature. These tumors can be manifested as calcifications of the peritoneal surface without associated mass but can also be multiple peritoneal nodules.^{22,23} The clinical course tends to be indolent after surgery. However, these tumors should be observed because of the small risk for development into MPMs.²⁴

MULTICYSTIC PERITONEAL MESOTHELIOMA

This is another rare subtype of peritoneal mesothelioma occurring predominantly in young and middle-aged women along the pelvic peritoneal surface. There is no association to asbestos exposure in these patients. A higher incidence of prior abdominal surgery or pelvic inflammatory disease is seen in these patients.²⁵ This tumor is composed of cysts that vary in size and are separated by septations or fibrous tissue.²⁶ It can appear as

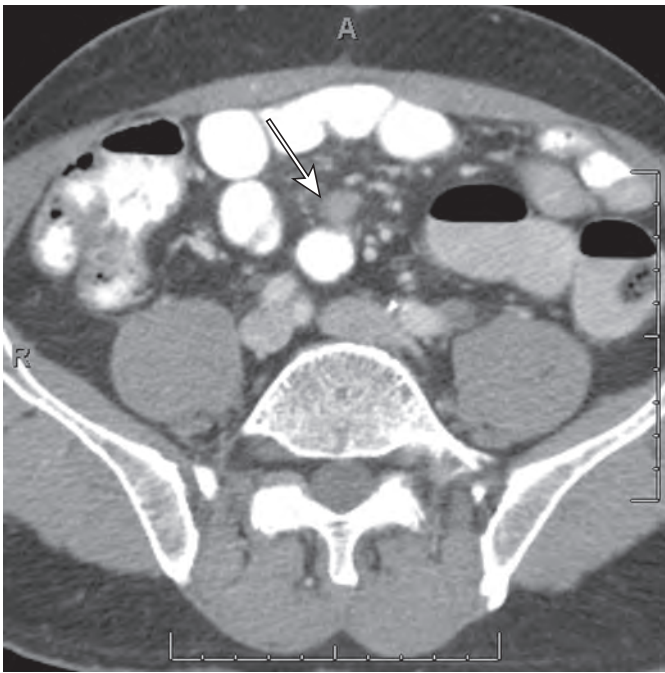


Figure 111-9 Papillary mesothelioma. Incidentally diagnosed small papillary mesothelioma (arrow) within the small bowel mesentery.

a multicystic mass, multiple unilocular cysts adjacent to each other, or a unilocular cystic mass.²³ On ultrasound, this tumor appears as a multiloculated lesion containing anechoic cystic spaces separated by echogenic septations. They can surround the ovaries, and the ovaries may appear entrapped within the cystic mass. On CT, this appears as a well-defined, noncalcified multiloculated cystic mass with enhancing internal septations. Fifty percent of these tumors tend to locally recur after surgical resection.²⁷

There is a slight risk for transformation into a malignant mesothelioma, and long-term follow-up should be performed in these patients.²⁸

DESMOPLASTIC SMALL ROUND CELL TUMOR

This is a rare but extremely aggressive tumor that typically occurs in adolescents and young adults and more commonly in men. The most common clinical complaint is abdominal distention. The prognosis is poor, and the 3-year survival is less than 30%.²⁹ CT shows multiple large solid intraperitoneal masses (Fig. 111-10) without an apparent primary site. The tumor predominantly involves the omentum and paravesical space. Areas of central low attenuation may correspond to hemorrhage or necrosis. Ascites and hepatic metastases are associated findings. There is both hematogenous and intraperitoneal

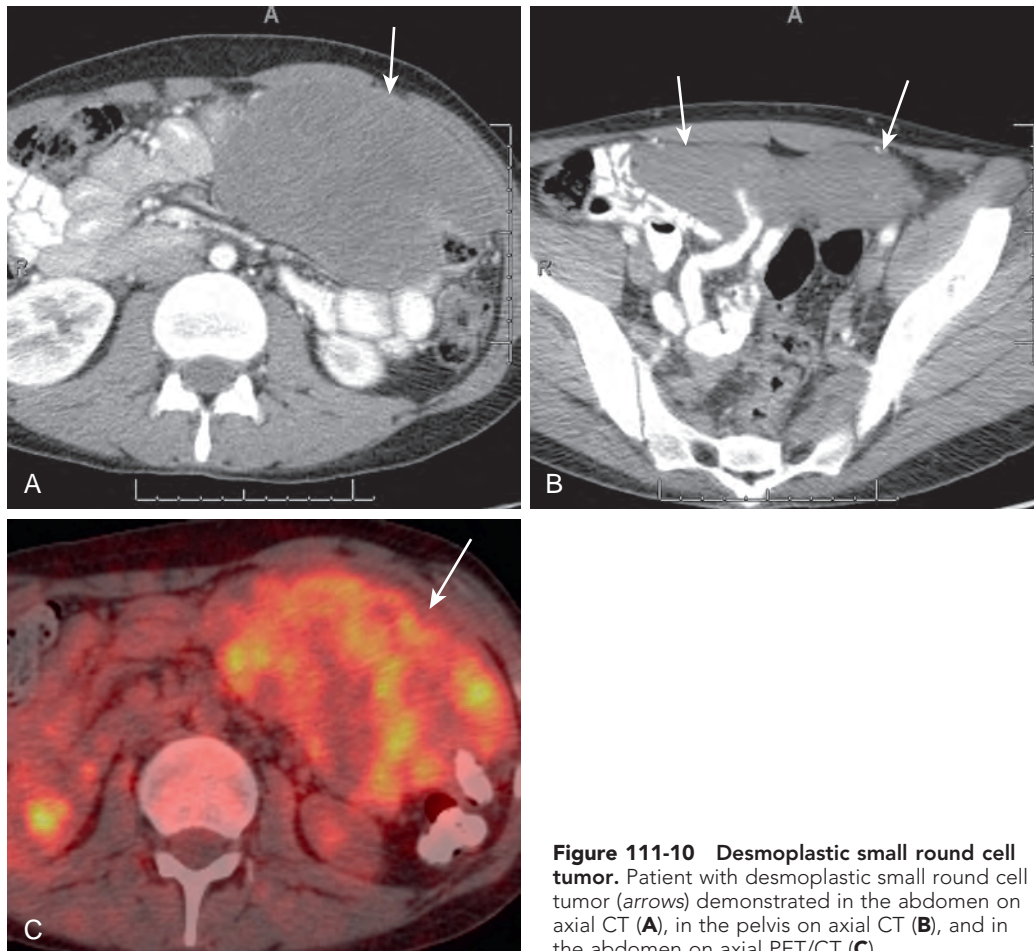


Figure 111-10 Desmoplastic small round cell tumor. Patient with desmoplastic small round cell tumor (arrows) demonstrated in the abdomen on axial CT (A), in the pelvis on axial CT (B), and in the abdomen on axial PET/CT (C).

spread that can be seen with this tumor. Retroperitoneal and paratesticular involvement has been reported with this tumor. Malignant ascites is frequently seen with these tumors. They tend to be of low T1 and high T2 signal intensity and demonstrate heterogeneous contrast enhancement.¹

ADENOMATOID TUMOR

This is a very rare tumor that is typically discovered incidentally. Adenomatoid tumor can occur in conjunction with the multicystic mesotheliomas.³⁰ It is typically small and characterized by epithelioid cells.¹

OTHER PRIMARY MESENCHYMAL TUMORS

Tumors may arise from the mesenchymal structures and may be of fatty, vascular, lymphatic, or neurogenic tissue origin.

Tumors of fatty origin can range from benign lipoma to the malignant liposarcoma. Benign lipoma is usually a well-defined homogeneous lesion containing tissue of fat attenuation on CT. Liposarcomas can be ill-defined heterogeneous lesions with a variable soft tissue component (Fig. 111-11). The diagnosis of liposarcoma³¹ can be made on CT if this mass contains fat interspersed with the soft tissue component or areas of enhancement.

Hemangiomas can occur in the mesentery. These are further divided into cavernous, capillary, and venous types. Cavernous hemangiomas containing large vascular sinusoids are the most common type of hemangioma to occur in the mesentery. They are typically of soft tissue attenuation and may contain phleboliths within them.^{32,33} Hemangiopericytomas can also occur in the mesentery and are typically large, vascular masses (Fig. 111-12).

Lymphangiomas are benign tumors of lymphatic origin. These can be either congenital tumors or benign tumors of

mesenchymal origin. They are typically multiloculated cystic masses with thin enhancing walls (Fig. 111-13). It can be difficult to differentiate them from cystic mesotheliomas.³⁴

Tumors of neurogenic origin are typically benign and are more common in the retroperitoneum than in the mesentery. On CT, these tumors are solid low-attenuation masses (Fig. 111-14) that show minimal contrast enhancement.³⁵ They are of low T1 signal intensity and intermediate to high T2 signal intensity and show minimal contrast enhancement. They may

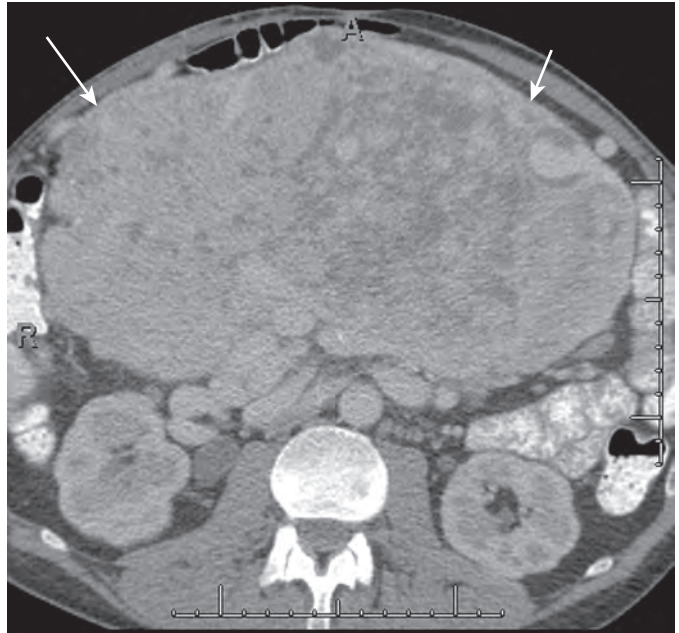


Figure 111-12 Hemangiopericytoma. Vascular hemangiopericytoma in the mesentery (arrows).

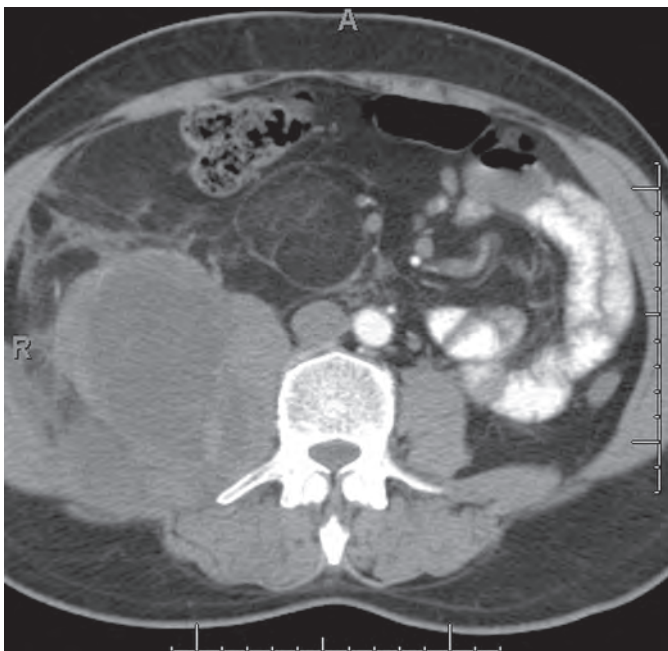


Figure 111-11 Liposarcoma. Liposarcoma with mixed appearance of solid nodules and fatty components.

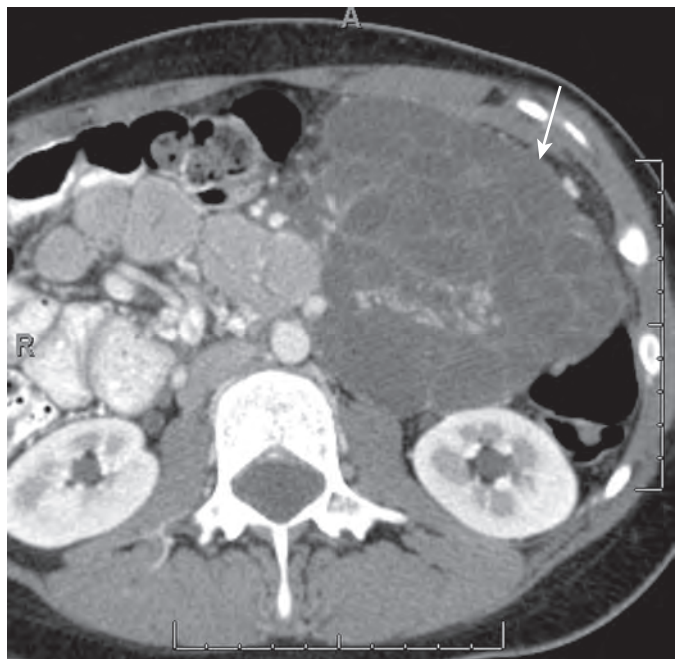


Figure 111-13 Mesenteric lymphangioma. Axial CT demonstrating a multicystic mass consistent with a mesenteric lymphangioma (arrow).

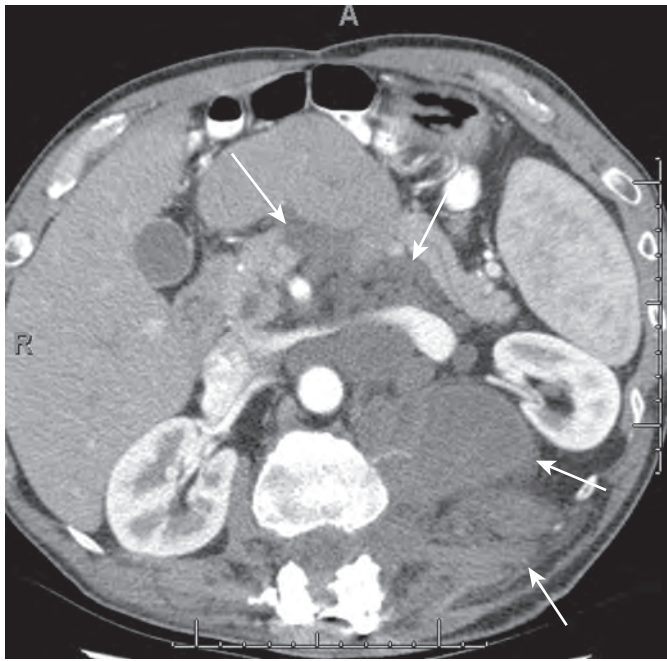


Figure 111-14 Neurofibroma. Axial CT demonstrating a low-attenuation, homogeneous mass involving the retroperitoneum and mesentery consistent with a neurofibroma (arrows).

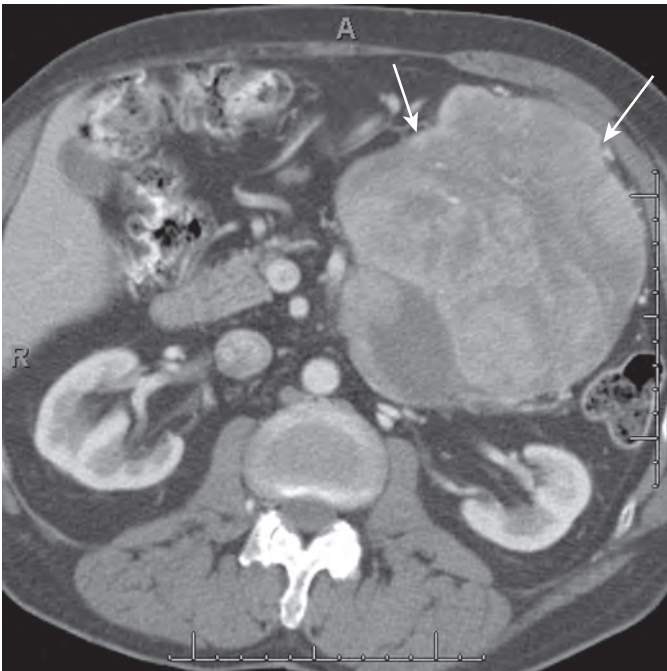


Figure 111-15 Fibrosarcoma. Axial CT demonstrating a heterogeneously enhancing fibrosarcoma in the mesentery (arrows).

show a tubular or elongated pattern. Uncommonly, they may show malignant degeneration.

Leiomyomatosis peritonealis disseminata is a rare entity characterized by multiple smooth muscle tumor nodules throughout the peritoneum. This is typically found in young women with uterine fibroids and detected incidentally.¹

Sarcomas are more common in the retroperitoneum compared with the mesentery. The tumors often arise in the retroperitoneum and extend into the peritoneum. They are typically large at the time of diagnosis (Fig. 111-15) and can show areas

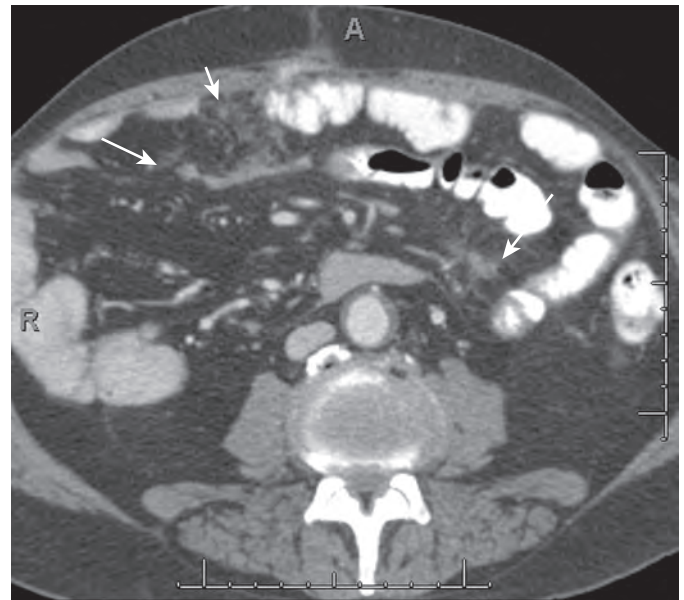


Figure 111-16 Peritoneal carcinomatosis. Patient with metastatic colon carcinoma who has small peritoneal nodules (arrows) from peritoneal metastases.

of central low attenuation related to necrosis or hemorrhage. Malignant fibrous histiocytoma is the most common peritoneal sarcoma.

Secondary Tumors

The intra-abdominal spread of metastatic disease can occur by (1) direct extension along the mesentery and ligaments, (2) intraperitoneal seeding, (3) lymphatic extension, and (4) hematogenous dissemination.³⁶

Direct extension occurs most commonly in gastrointestinal and pancreatic tumors and can involve the various ligaments surrounding the site of primary tumor. Intraperitoneal seeding is related to the movement of malignant cells within ascitic fluid, thereby being deposited in the peritoneal cavity. Lymphatic dissemination is most commonly seen with lymphoma. Hematogenous metastases typically occur on the antimesenteric border of the bowel loops by distal embolization. This is commonly seen in melanoma and breast and lung carcinoma.

PERITONEAL CARCINOMATOSIS

Peritoneal carcinomatosis is usually seen in tumors arising from the gastrointestinal tract, pancreas, melanoma, breast, lung, and ovary. Any of the four mechanisms listed before can seed the peritoneum, and this can cause peritoneal carcinomatosis. A variable amount of fluid exists in the peritoneal cavity. This circulates from the superior abdomen caudally to the pelvis and then back again to the superior abdomen. Both gravity and respiration play a role in the fluid circulation within the peritoneal cavity. Peritoneal carcinomatosis is manifested on CT as nodularity to the peritoneum (Fig. 111-16), which can progress to peritoneal masses. When the primary tumor is mucinous, such as in appendiceal or ovarian tumors, diffuse peritoneal involvement with cystic implants can be seen (Fig. 111-17). This is called pseudomyxoma peritonei. Detection of

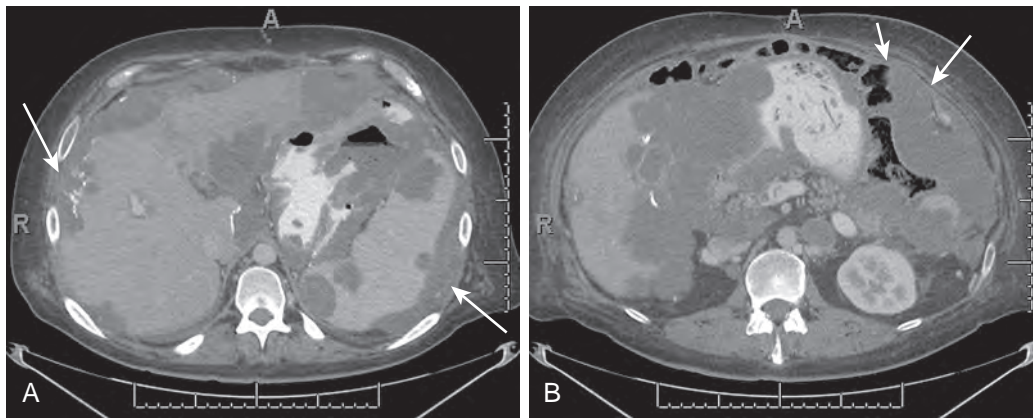


Figure 111-17 Metastatic mucinous appendiceal carcinoma. Axial CT demonstrating mucinous implants causing scalloping of the liver and spleen (arrows) with thin calcifications (A) and with mucinous implants causing mass effect (arrows) on bowel loops (B).

peritoneal carcinomatosis is difficult, especially when the nodules are subcentimeter in size. Peritoneal nodules can often mimic unopacified small bowel loops. Accurate assessment for peritoneal carcinomatosis requires adequate bowel opacification and the intravenous administration of contrast material. The nodules create mass effect on the organs adjacent to them. They can cause scalloping of the liver and spleen; they can cause mesenteric infiltration and thickening, leading to a stellate mesentery; and they can involve the surface of the bowel, causing bowel wall thickening and potentially bowel obstruction. Common sites of involvement include the right hemidiaphragm, right paracolic gutter, cul de sac, and omentum.³⁷

CARCINOID TUMOR

These are rare tumors and represent only 2% of all gastrointestinal tumors. However, carcinoid tumors are the second most common small bowel neoplasm and account for 25% of all small bowel masses.³⁸ They are derived from the enterochromaffin cells; 85% of all carcinoid tumors are found in the gastrointestinal tract. Carcinoid tumors of the gastrointestinal tract are most frequently found in the appendix (50%) and then in the small intestine, primarily the ileum. Metastatic adenopathy involving the mesenteric nodes is seen with small bowel carcinoids. There is intense desmoplastic reaction surrounding the mesenteric mass,³⁹ which can cause radiating strands from the mesenteric mass, rigidity and fixation of the small bowel loops, and sometimes kinking of small bowel loops (Fig. 111-18). The mesenteric fibrosis may also involve mesenteric vasculature and potentially cause mesenteric ischemia. Calcification within the mesenteric mass is seen in 70% of the cases. On MRI, the mesenteric mass is of low T1 signal intensity and intermediate T2 signal intensity and demonstrates evidence of contrast enhancement.

LYMPHOMA

Lymphoma can involve the mesentery, manifested as either enlarged adenopathy or less commonly peritoneal lymphomatosis. Mesenteric involvement by adenopathy is common in non-Hodgkin's lymphoma, occurring in nearly half of these patients (Fig. 111-19). The classic appearance on CT is that of confluent masses that surround the superior mesenteric artery

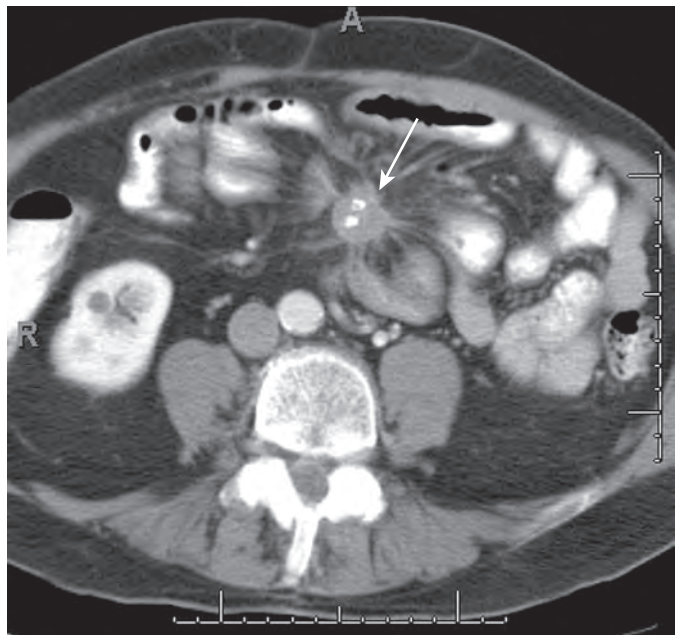


Figure 111-18 Carcinoid tumor. Axial CT in a patient with metastatic carcinoid tumor of the small bowel to the mesenteric nodes (arrow). This metastatic node causes a desmoplastic reaction with radiating strands into the mesentery.

and vein, producing the sandwich sign.⁴⁰ There is usually associated retroperitoneal adenopathy. Many other disease conditions can be manifested with enlarged mesenteric adenopathy, including metastatic disease and reactive adenopathy from granulomatous infections, acquired immunodeficiency syndrome (AIDS), Crohn's disease, and Whipple's disease.

Peritoneal lymphomatosis is much less common and can mimic peritoneal carcinomatosis (Fig. 111-20) and tuberculous peritonitis.⁴¹ Ascites is commonly seen. Bowel involvement by lymphoma is also often seen as bowel wall thickening or aneurysmal dilation of the bowel. Mesenteric and retroperitoneal enlarged adenopathy is also seen. Peritoneal lymphomatosis is typically seen in high-grade aggressive lymphomas, including small cell, large cell, and lymphoblastic lymphoma. This can mimic aggressive carcinomas.

Inflammatory and Infiltrative Diseases

PANCREATITIS

Acute pancreatitis is an acute and diffuse inflammation of the pancreas. This can range from mild acute pancreatitis to severe acute pancreatitis. Mild acute pancreatitis occurs in 75% to 80% of patients and is characterized by pancreatic interstitial edema and inflammation, which spontaneously resolves without complications. Severe acute pancreatitis is seen in a minority of patients and can be characterized by pancreatic or retroperitoneal fat necrosis and systemic distant organ failure. In the majority of cases, imaging is not necessary. In one third of

patients with pancreatitis, the pancreas may be normal on CT. In the other patients with mild acute pancreatitis, thickening and peripancreatic fat stranding and nodularity can be seen (Fig. 111-21). CT with intravenous administration of contrast material is of help in patients with severe acute pancreatitis and in patients with fevers and leukocytosis. The enhanced CT can help assess the extent of pancreatitis and the presence of peripancreatic fluid collections, hemorrhage, pancreatic or retroperitoneal necrosis, and pancreatic abscess formation. In these patients, the early use of CT has been shown to be beneficial to assess the severity and for follow-up. Peripancreatic fluid collections can dissect through the peritoneum and track along ligaments. They can be seen near the splenic hilum, in the gastrohepatic ligament, along the transverse mesocolon, and along the small bowel mesentery. The colon cutoff sign is seen when the fluid and inflammatory changes track to the transverse colon through the transverse mesocolon, causing an abrupt change in the caliber of the colon at the anatomic junction of the transverse and descending colon.

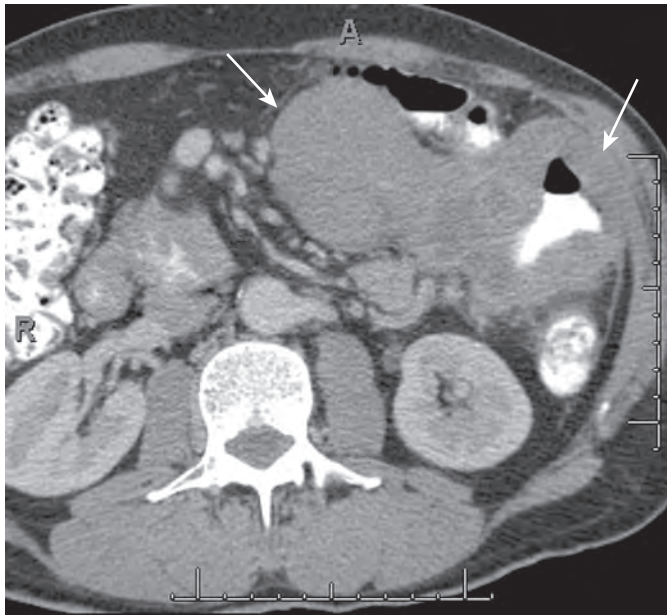


Figure 111-19 Lymphoma. Patient with lymphoma involving the jejunum with lymphadenopathy (arrows) extending into the small bowel mesentery.

DIVERTICULITIS

Diverticulosis of the colon is a common finding at CT. Diverticulitis of the colon develops in 15% to 30% of all patients with diverticulosis.⁴² This is characterized by thickening of the colonic wall with poor visualization of haustral folds and pericolonic fat stranding (Fig. 111-22). Diverticulitis can also cause colonic perforation, pericolonic abscess formation, fistula formation to adjacent structures, and colonic or ureteral obstruction due to the inflammatory changes.⁴³ These cases account for approximately one fifth of cases, and surgery may be required instead of conservative treatment. CT provides a noninvasive method to assess the extent of diverticulitis and presence of complications and has become the imaging test of choice in diverticulitis. CT also provides a road map for percutaneous drainage procedures for abscess collections. On occasion, perforated colonic neoplasms, pelvic inflammatory disease, endometriosis, and appendicitis can be confused with diverticulitis. Continued follow-up after resolution of acute symptoms is recommended to exclude a primary colonic malignant neoplasm.

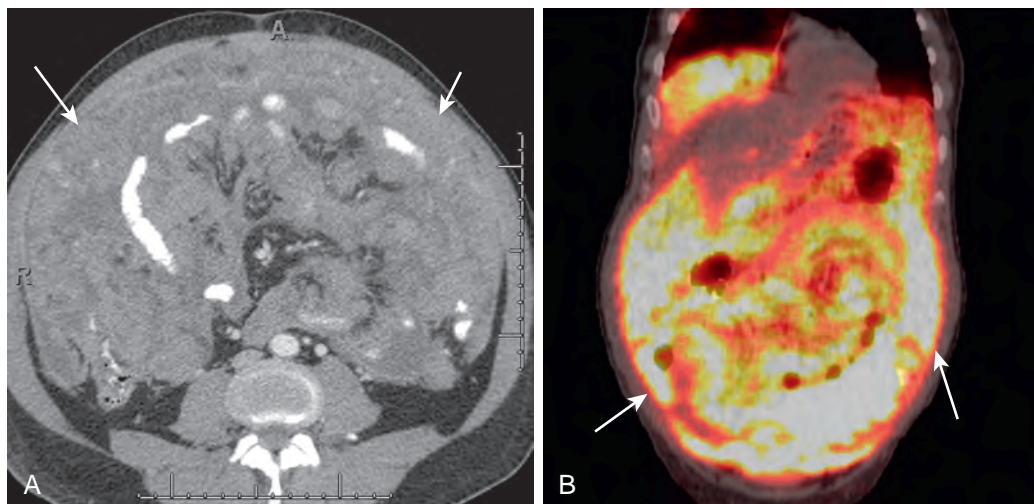


Figure 111-20 Peritoneal lymphomatosis. Axial CT (A) and coronal PET/CT (B) demonstrate peritoneal lymphomatosis (arrows). The imaging appearance is similar to that of peritoneal carcinomatosis.

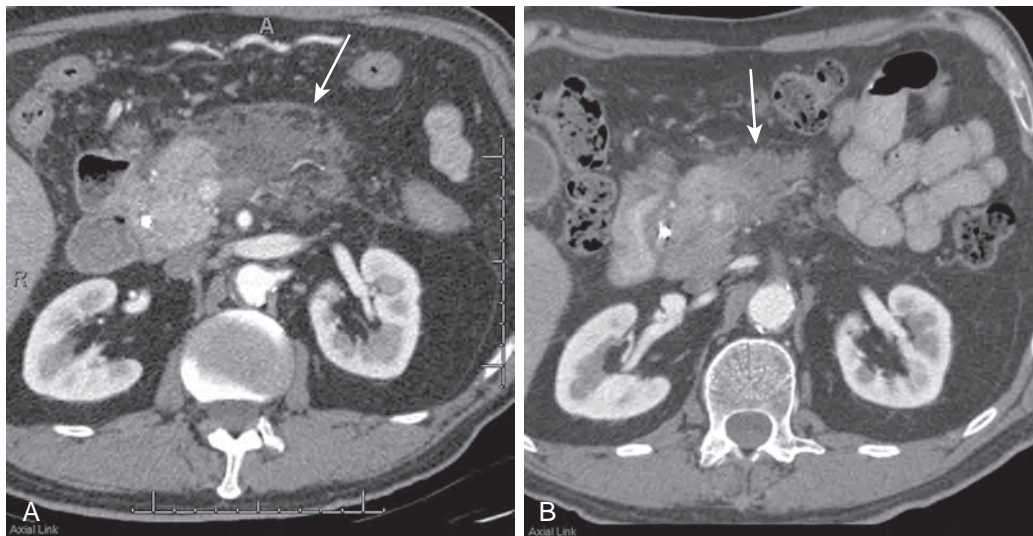


Figure 111-21 Pancreatitis. **A.** Axial CT at the time of acute pancreatitis demonstrates hazy soft tissue (arrow) surrounding the pancreas and extending into the root of the mesentery. **B.** Axial CT obtained 2 months later demonstrates evolution of the changes of pancreatitis with a more solid appearance (arrow).

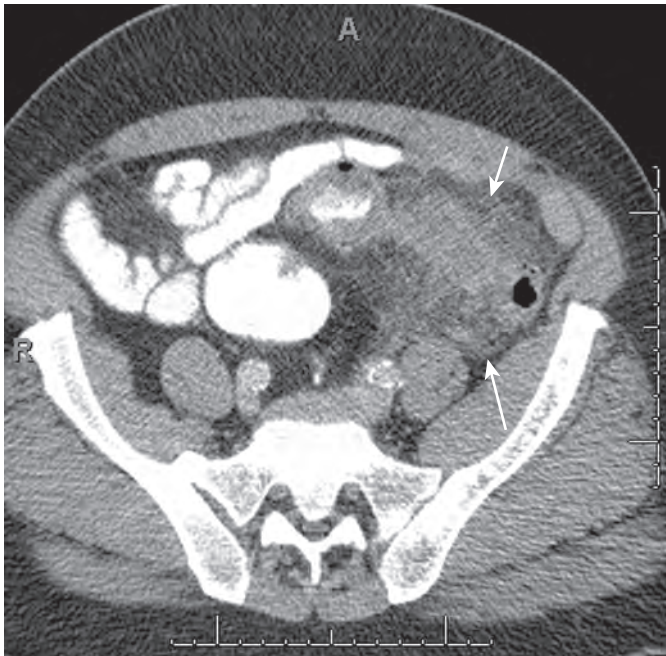


Figure 111-22 Diverticulitis. Axial CT in a patient with diverticulitis with stranding along the sigmoid colon (arrows).

CROHN'S DISEASE

Crohn's disease, a chronic granulomatous inflammatory disease of the gastrointestinal tract, can occur anywhere from the mouth to the anus. This is of unknown etiology and has a characteristic relapsing and remitting course involving discontinuous portions of the gastrointestinal tract. The small bowel and typically the distal ileum are the most commonly affected sites. CT findings include segmental bowel wall thickening, submucosal edema, and mucosal hyperenhancement in the acute phase.⁴⁴ CT can also show areas of bowel stenosis or narrowing with prestenotic dilation, fibrofatty proliferation surrounding the affected segment (Fig. 111-23), fistulization to adjacent structures, and abscess formation. The fibrofatty proliferation

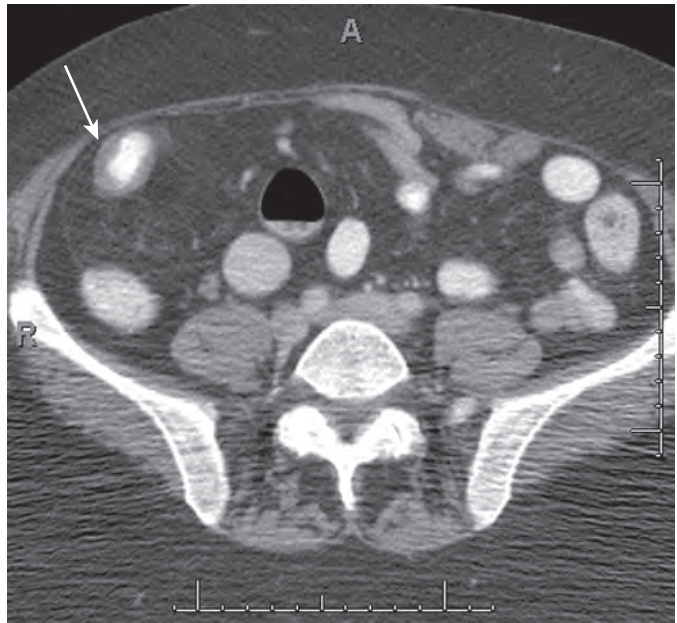


Figure 111-23 Crohn's disease. Axial CT in a patient with Crohn's disease. CT demonstrates a thickened small bowel loop (arrow) surrounded by normal-appearing small bowel loops.

can result in a marked increase in the amount of fat surrounding an affected bowel loop or in increased density of the fat due to inflammation. Fistulization can occur to adjacent bowel loops but occasionally can occur to the skin. Internal fistulization can occur in 15% to 40% of patients with active disease. Enlarged mesenteric adenopathy, especially involving the ileocolic nodes, can be seen in Crohn's disease. CT can be beneficial in assessing complications and monitoring therapy.

MR enterography is being increasingly used in young adults with Crohn's disease. The advantages of MRI include repeated imaging without unnecessary radiation; real-time imaging to assess fixed small bowel loops; and diffusion-weighted imaging, which can highlight areas of restricted diffusion thought to be arising from acute inflammation.^{45,46}

MESENTERIC PANNICULITIS OR SCLEROSING MESENTERITIS

This has various names, including retractile mesenteritis, mesenteric lipodystrophy, and xanthogranulomatous mesenteritis.⁴⁷ It is a rare condition of unknown etiology that is characterized by mesenteric inflammation, fibrosis, and variable amounts of fat necrosis. This is often associated with other inflammatory conditions, such as retroperitoneal fibrosis, sclerosing cholangitis, Riedel thyroiditis, orbital pseudotumor, and more recently along the spectrum of the immunoglobulin G4-elevated sclerosing disorders.⁴⁸ This has a wide age range with the peak incidence in the sixth and seventh decades and a male-to-female ratio of 1.8 to 1. Criteria for diagnosis require exclusion of pancreatitis, inflammatory bowel disease, and extra-abdominal fat necrosis, such as Weber-Christian disease. This typically involves the small bowel mesentery, especially at the root of the mesentery.

Common clinical symptoms include abdominal pain, weight loss, fever, nausea, vomiting, intestinal obstruction, and mesenteric ischemia. This condition may be manifested predominantly in one of three ways: mesenteric panniculitis, which is characterized by chronic inflammation and subtle increased density of the mesenteric fat; mesenteric lipodystrophy, which is characterized by fat necrosis; and retractile mesenteritis, which is characterized by fibrosis. Patients may present with all three manifestations.

On upper gastrointestinal and barium enema examinations, there is displacement of the bowel loops by a mesenteric mass, with the jejunal mesentery being most commonly involved. The bowel loops may be dilated, fixed, or narrowed, but complete obstruction is rare. On CT, the findings can vary from slightly increased density of the mesenteric fat to a spiculated soft tissue mass (Figs. 111-24 and 111-25). The soft tissue masses in this condition can cause intestinal obstruction and can infiltrate around mesenteric vessels to cause ischemia. There may be a small rim of fat preserved around the vessels called the fat ring

or halo sign, which may help in the diagnosis. On occasion, the area of mesenteritis can show areas of central calcification. Differential diagnosis includes carcinoid metastases to the mesentery and lymphoma. The finding of increased density of mesenteric fat on CT has a wide differential and is presented in Box 111-1.

TUBERCULOSIS

Tuberculous peritonitis occurs in less than 4% of patients with tuberculosis and has been described as the sixth most common site of extrapulmonary tuberculosis.⁴⁹ This is most commonly due to hematogenous dissemination, but ruptured involved bowel, nodes, or fallopian tubes may occasionally be the cause. As many as 80% of the cases of abdominal tuberculosis are now associated with underlying immunodeficiency.⁵⁰

This has been classified further into the wet, fixed and fibrotic, and dry plastic types. The wet type is the most common presentation (90%) and consists of large amounts of ascites (free flowing or loculated). The fixed fibrotic type is the next most common and is characterized by omental and mesenteric masses with fixed and matted bowel loops. The dry type is characterized by a fibrous thickening of the peritoneum and caseous lymph nodes.⁵⁰ There is often overlap between these three types.

The lymphadenopathy is typically found in the mesenteric and peripancreatic locations rather than retroperitoneally because of involvement of the small bowel and liver. The classic appearance is of rim-enhancing centrally necrotic nodes, likely related to caseous necrosis. The ascites is typically of high attenuation ranging between 20 and 45 HU due to the high cellular and protein content. Other findings that support the diagnosis include hepatosplenomegaly with focal hepatic and splenic lesions, peritoneal enhancement, and bowel involvement. Assessment of the bowel, especially in the ileocecal region, may

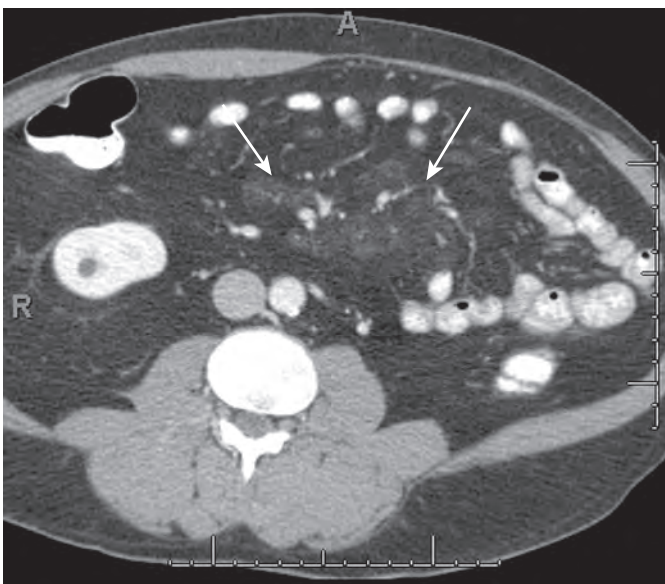


Figure 111-24 Sclerosing mesenteritis. Axial CT in a patient with a carcinoid tumor of the small bowel and incidental detection of haziness in the mesentery (arrows). This was proved to be sclerosing mesenteritis.

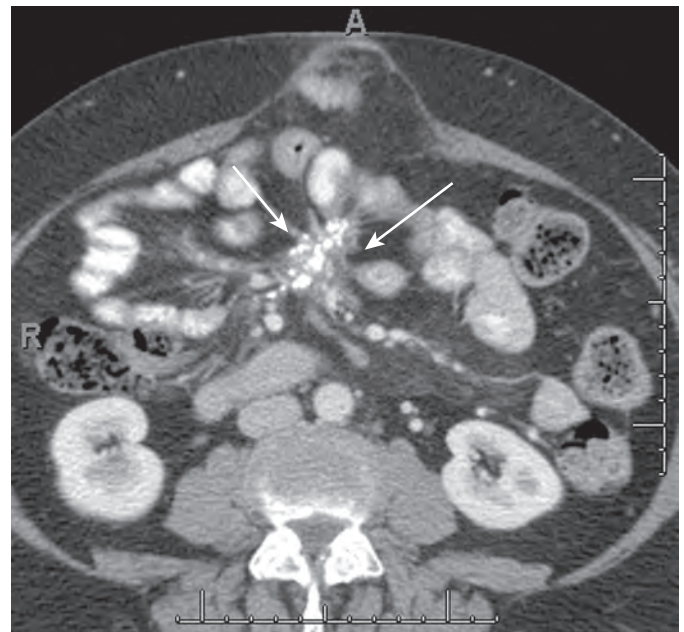


Figure 111-25 Sclerosing mesenteritis. Axial CT demonstrating sclerosing mesenteritis in another patient with mesenteric mass with multiple calcifications (arrows).

BOX 111-1 MISTY MESENTERY: DIFFERENTIAL DIAGNOSIS**MESENTERIC EDEMA**

Hypoalbuminemia
 Portal hypertension
 Cirrhosis
 Nephrotic syndrome
 Heart failure
 Constrictive pericarditis
 Portal vein thrombosis
 Superior mesenteric vein thrombosis
 Superior mesenteric artery thrombosis
 Budd-Chiari syndrome
 Vasculitis
 Trauma
 Neoplasm
 Surgery

LYMPHEDEMA

Inflammation
 Neoplasm
 Surgery
 Radiation therapy
 Congenital malformation

INFLAMMATION

Pancreatitis
 Appendicitis
 Diverticulitis
 Inflammatory bowel disease
 Tuberculosis
 Amyloidosis
 Mesenteric panniculitis

HEMORRHAGE

Trauma
 Bowel ischemia and infarction
 Anticoagulation

NEOPLASMS

Non-Hodgkin's lymphoma
 Mesothelioma
 Carcinoid tumor
 Pancreatic carcinoma
 Colon carcinoma
 Ovarian carcinoma
 Breast carcinoma
 Melanoma
 Gastrointestinal stromal tumor

further help with the diagnosis. Early diagnosis and treatment are crucial because of the high mortality rates.⁵⁰

WHIPPLE'S DISEASE

Whipple's disease is a rare multisystem infection caused by a gram-positive bacillus, *Tropheryma whipplei*. It affects multiple organs. There is abnormal accumulation of lipid-laden macrophages, which contain bacterial elements that stain with the periodic acid-Schiff method. These macrophages accumulate mainly in the submucosa of the small bowel. Clinical symptoms include weight loss, abdominal pain, arthralgias, and steatorrhea. Small bowel fold thickening is noted along with enlarged low-attenuation mesenteric nodes. The fold thickening is likely to be related to a combination of macrophage deposition and dilated lymphatics from nodal involvement. Enlarged low-attenuation mesenteric nodes, which can cause lymphatic stasis

and secondary bowel thickening, are typically seen. Enlarged nodes can be seen in the peripancreatic, retroperitoneal, and occasionally mediastinal locations.

The low attenuation of these nodes is characteristic for Whipple's disease.⁵¹ The differential diagnosis for low-attenuation nodes includes metastatic disease, such as treated testicular cancer, treated lymphoma, and tuberculosis.

AMYLOIDOSIS

Systemic amyloidosis is caused by the extracellular deposition of amyloid in an abnormal fibrillar form in multiple organs. This may occur as a primary process or secondary to a number of chronic diseases and can occur in multiple myeloma. Clinical symptoms and signs include bowel obstruction, pseudotumor, hepatomegaly, and macroglossia. The amyloid deposition can lead to bowel wall thickening and rarely to mesenteric and omental soft tissue infiltration. Discrete nodules and coarse dystrophic calcification within the involved peritoneum can be seen on CT. Mesenteric and retroperitoneal lymphadenopathy can also be seen.^{52,53}

EXTRAMEDULLARY HEMATOPOIESIS

Extramedullary hematopoiesis refers to conditions in which there is a compensatory response to decreased hematopoiesis (as in myelofibrosis) or in the presence of a hemoglobinopathy (such as thalassemia). The predominantly affected regions are the liver, spleen, and paraspinal soft tissues. Rarely, the mesentery and peritoneum may be involved. On CT, this is manifested as large soft tissue masses within the mesentery and peritoneum, with minimal mass effect on adjacent structures such as the bowel.⁵⁴ Differential diagnosis includes lymphoma.

TRAUMA AND HEMORRHAGE

Mesenteric hemorrhage is unusual but can be seen in blunt abdominal trauma, aneurysm rupture, anticoagulation, and thrombocytopenia. Acute hemorrhage can be dense (between 50 and 60 HU) on noncontrast CT,⁵⁵ which can decrease in attenuation during 2 weeks. Barium studies may demonstrate displacement of bowel loops and bowel wall thickening if there is bowel wall hemorrhage. On ultrasound, there can be a variety of appearances, depending on the age of the hemorrhage. Similarly, on MRI, there can be a variety of appearances on the basis of the age of the hemorrhage. Most acute hemorrhages have a high T1 signal intensity. Approximately 50% of the significant hemorrhages that occur with anticoagulation occur intra-abdominally and can involve bowel wall, retroperitoneum, and the abdominal wall.

MESENTERIC EDEMA

Mesenteric edema can be caused by conditions including systemic hypoalbuminemic states, such as cirrhosis or nephrotic syndrome, and lymphatic or venous obstruction. The typical finding on CT is diffuse increased hazy density of the fat of the mesentery and indistinctness of vessels within the mesentery. The term *misty mesentery*, used by Mindelzun and colleagues,² is often the sign of underlying mesenteric disease and is associated with an increase in the density of the fat in the mesentery. This is a nonspecific sign and can be seen in mesenteric edema,

hemorrhage, trauma, inflammation, and tumor involvement as shown in [Box 111-1](#). Careful assessment of the larger mesenteric veins for venous thrombus and venous obstruction related to a mass should be performed. In systemic conditions causing the mesenteric edema, subcutaneous and bowel wall edema can also be seen.

MESENTERIC CYSTS

Cystic lesions in the mesentery may be duplication cysts, enteric cysts, lymphangiomas, pseudocysts, teratomas, and mesothelial cysts.^{56,57} These are frequently congenital and benign lesions.

Lymphangiomas are multilocular cystic lesions with rim enhancement. The different locules may contain complex fluid. These can be adherent to adjacent bowel, necessitating bowel removal at the time of resection. Pseudocysts can be seen in patients with a prior history of pancreatitis ([Fig. 111-26](#)). They can be unilocular or multilocular and have a distinct wall. The wall typically shows contrast enhancement. They can demonstrate echogenic debris on ultrasound. Enteric duplication cysts also typically have thick walls ([Fig. 111-27](#)) compared with enteric cysts, which have a thin wall. Benign cystic mesotheliomas are also in the differential.

Omentum

The anatomy of the omentum is discussed earlier. The omentum also contains vessels and lymphatics along with areolar tissue, just like the other peritoneal folds. In addition to storing fat, the omentum plays an important role in walling off infections and scavenges inflammatory and neoplastic cells in the peritoneal cavity. The arterial supply is from branches of the celiac axis, and the venous drainage is through the splenic and superior mesenteric veins into the portal vein. Whereas the greater

omentum helps minimize the spread to transdiaphragmatic lymph channels, this may increase the spread to the portal circulation and liver.

RADIOLOGIC FEATURES

Plain abdominal radiographs rarely depict omental disease. In cases of large omental masses, secondary signs related to displacement of bowel loops may help make the diagnosis. Indirect evidence of omental infiltration on barium enema studies may be inferred by mass effect, tethering of folds, or luminal narrowing, especially along the superior border of the transverse colon.

Ultrasound may be of help in patients with large omental masses, but distinguishing smaller masses from bowel loops may be difficult. Ultrasound is also operator dependent, making reproducibility and assessment of response difficult.

The most commonly used imaging modality in assessment of omental and peritoneal disease is CT. With the advent of multidetector CT (MDCT), thinner slices and rapid speed of imaging have improved detection of small omental and peritoneal nodules. Optimal bowel contrast opacification is critical in imaging of patients with suspected omental and peritoneal disease. Lack of intra-abdominal fat may make the visualization of the omental disease difficult.

The normal greater omentum is routinely identified as a homogeneous fat-attenuating structure anterior to and lateral to the transverse colon. This should be distinguished from the more centrally located small bowel mesentery. The omentum is typically affected secondarily in disease processes such as peritoneal carcinomatosis and can be involved in inflammatory processes that affect the peritoneum and the adjacent organs. Primary omental disease is rare and may be seen with omental cysts, segmental infarction, torsion, and primary omental tumors.

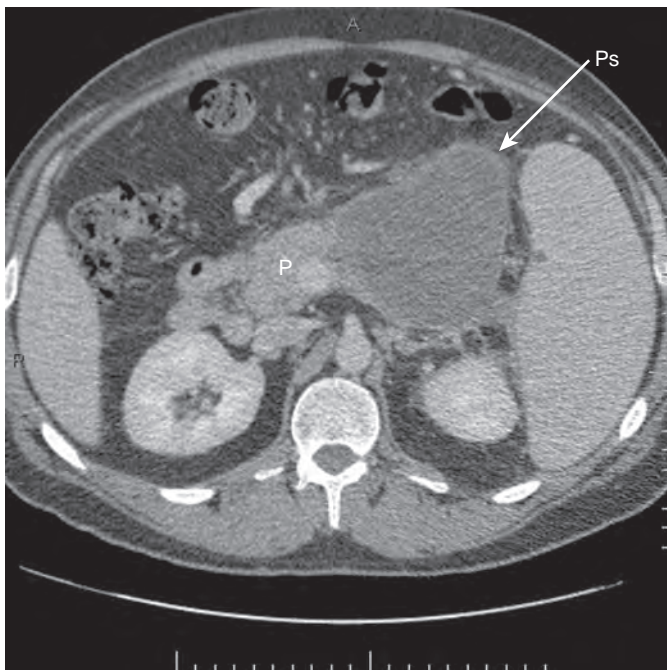


Figure 111-26 Pseudocyst. Axial CT demonstrating a pseudocyst (Ps, arrow) near the pancreas (P).

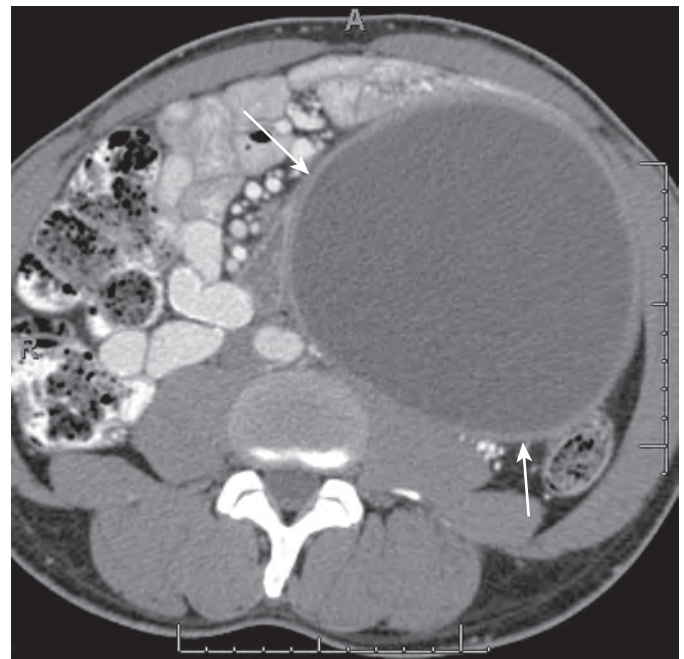


Figure 111-27 Enteric duplication cyst. Axial CT demonstrating a thick-walled enteric duplication cyst (arrows).

PRIMARY NEOPLASMS

Primary omental neoplasms are rare and can include tumors of mesenchymal origin, such as lipoma/liposarcoma, lipoblastoma, fibroma/fibrosarcoma, and leiomyoma/leiomyosarcoma.⁵⁸ Teratomas and hemangioblastomas of the omentum have also been described. Symptoms occur late in the course of disease and are nonspecific and may be related to abdominal bloating and pain. Approximately 33% of omental masses are malignant. The CT appearance for omental masses is often nonspecific. The presence of fat within the mass may further narrow the differential diagnosis to masses that contain fat, such as lipoma, lipoblastoma, and liposarcoma, and other non-neoplastic conditions, such as panniculitis, focal infarction, and torsion.

METASTATIC DISEASE AND LYMPHOMA

Metastatic disease is the most common cause of omental lesions. The metastatic cells can implant on the surface of the omentum and invade through the loosely bound basement membrane to proliferate in the omental fat. Omental infiltration favors a diagnosis of tumor involvement and usually indicates peritoneal involvement. The classic “omental cake” is from complete replacement of the omentum by tumor involvement ([Fig. 111-28](#)). On CT, a thick soft tissue mass is seen replacing the entire omentum and is located anterior to the transverse colon. This soft tissue mass can extend down into the pelvis also. The early manifestations of omental involvement on CT can begin as small areas of nodularity and fat stranding. Detection of small omental implants has improved with MDCT but still remains a challenge. Assessment for secondary signs of peritoneal involvement, such as ascites, may also be of help.

Ovarian cancer is the most frequent cause of metastatic disease to the omentum. Omental involvement is found at the time of initial laparotomy and is almost universally present at

autopsy. Although an abnormal-appearing omentum in a patient with ovarian cancer is strongly indicative of metastatic disease, a normal-appearing omentum on CT does not exclude involvement.⁵⁹ Tumors that commonly spread to the omentum include carcinomas of the colon, stomach, pancreas, breast, and endometrium and adenocarcinomas of unknown primary site.⁵⁸ Melanomas, sarcomas, and lymphomas can also involve the omentum. Calcified omental masses generally indicate tumors of mucinous origin, such as ovarian and colon tumors. Leiomyosarcomas typically tend to produce large, well-defined soft tissue masses in the omentum with areas of central necrosis.

INFLAMMATORY DISEASES

Pancreatitis

Inflammation from pancreatitis typically involves the peripancreatic fat, adjacent retroperitoneum, and lesser sac and can extend to involve the small bowel mesentery. In severe cases, the inflammation may extend to the colon and greater omentum. Omental changes, such as stranding and infiltration phlegmonous changes, pseudocyst and abscess formation, and occasionally ascites, can occur.

Tuberculosis

The CT appearance of tuberculous peritonitis can be indistinguishable from that of peritoneal carcinomatosis with omental nodularity, caking, and ascites. Centrally low attenuation, enlarged nodes may help narrow the differential diagnosis. Hepatosplenomegaly is an associated finding seen in tuberculosis. In patients with risk factors, tuberculous peritonitis should be considered because of the high mortality associated with this condition.

Panniculitis

Idiopathic panniculitis is inflammation of the fat in the omentum. The CT findings include increased density and stranding surrounding the omentum. The changes are identical to those observed in the small bowel mesentery, where they are more common.

MISCELLANEOUS CONDITIONS

A variety of other processes affect the omentum. These include traumatic hematoma, omental hernias, omental infarction, and torsion. Primary segmental infarction often involves the free edge of the right lateral omentum.⁶⁰⁻⁶³ Right lower quadrant pain mimicking appendicitis or cholecystitis can be the presenting symptom. This typically involves young adults (20 to 40 years old), and men are affected twice as commonly as women. The diagnosis on CT is suggested by the presence of focally infiltrated omental fat in the right lower quadrant with a normal-appearing appendix and gallbladder and associated complex intraperitoneal fluid. Omental torsion can be suggested in patients with acute abdominal pain if the CT findings show a fatty mass with fine concentric or swirling lines in the anterior abdomen.

In summary, peritoneal and omental disease may show a wide spectrum of findings on imaging studies. CT and MDCT are currently the most effective radiologic imaging modalities for detection and characterization of pathologic processes involving these areas. The specific feature and distribution of disease can often lead to a precise diagnosis.

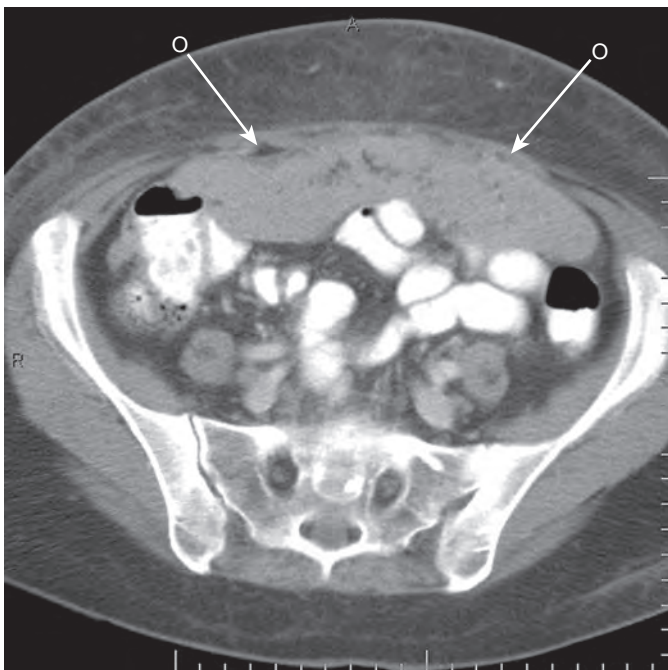


Figure 111-28 Omental cake. Axial CT demonstrating omental cake (arrows) in a patient with metastatic ovarian cancer.

REFERENCES

- Levy AD, Arnáiz J, Shaw JC, Sobin LH: From the archives of the AFIP: Primary peritoneal tumors: imaging features with pathologic correlation. *Radiographics* 28:583–607, 2008.
- Mindelzun RE, Jeffrey RB, Jr, Lane MJ, Silverman PM: The misty mesentery on CT: Differential diagnosis. *AJR Am J Roentgenol* 167:61–65, 1996.
- Dinauer PA, Brixey CJ, Moncur JT, et al: Pathologic and MR imaging features of benign fibrous soft-tissue tumors in adults. *Radiographics* 27:173–187, 2007.
- Clark SK, Neale KF, Landgrebe JC, Phillips RK: Desmoid tumours complicating familial adenomatous polyposis. *Br J Surg* 86:1185–1189, 1999.
- Soravia C, Berk T, McLeod RS, Cohen Z: Desmoid disease in patients with familial adenomatous polyposis. *Dis Colon Rectum* 43:363–369, 2000.
- Brooks AP, Reznick RH, Nugent K, et al: CT appearances of desmoid tumours in familial adenomatous polyposis: Further observations. *Clin Radiol* 49:601–607, 1994.
- Nance FC: Disease of the peritoneum, retroperitoneum, mesentery, and omentum. In Haubrich WS, Schaffner F, editors: *Bockus Gastroenterology*, ed 5, Philadelphia, 1995, WB Saunders, pp 3061–3096.
- Healy JC, Reznick RH, Clark SK, et al: MR appearances of desmoid tumors in familial adenomatous polyposis. *AJR Am J Roentgenol* 169:465–472, 1997.
- Teta MJ, Mink PJ, Lau E, et al: US mesothelioma patterns 1973–2002: Indicators of change and insights into background rates. *Eur J Cancer Prev* 17:525–534, 2008.
- Boffetta P: Epidemiology of peritoneal mesothelioma: A review. *Ann Oncol* 18:985–990, 2007.
- Rodriguez D, Cheung MC, Housri N, Koniari LG: Malignant abdominal mesothelioma: Defining the role of surgery. *J Surg Oncol* 99:51–57, 2009.
- Hodgson JT, Darnton A: The quantitative risks of mesothelioma and lung cancer in relation to asbestos exposure. *Ann Occup Hyg* 44:565–601, 2000.
- Sugarbaker PH, Welch LS, Mohamed F, Glehen O: A review of peritoneal mesothelioma at the Washington Cancer Institute. *Surg Oncol Clin N Am* 12:605–621, xi, 2003.
- Takeshima Y, Amatya V, Kushitani K, Inai K: A useful antibody panel for differential diagnosis between peritoneal mesothelioma and ovarian serous carcinoma in Japanese cases. *Am J Clin Pathol* 130:771–779, 2008.
- Szklaruk J, Tamm EP, Choi H, Varavithya V: MR imaging of common and uncommon large pelvic masses. *Radiographics* 23:403–424, 2003.
- Low RN, Barone RM: Combined diffusion-weighted and gadolinium-enhanced MRI can accurately predict the peritoneal cancer index preoperatively in patients being considered for cytoreductive surgical procedures. *Ann Surg Oncol* 19:1394–1401, 2012.
- Deraco M, Bartlett D, Kusumura S, Baratti D: Consensus statement on peritoneal mesothelioma. *J Surg Oncol* 98:268–272, 2008.
- Muto MG, Welch WR, Mok SC, et al: Evidence for a multifocal origin of papillary serous carcinoma of the peritoneum. *Cancer Res* 55:490–492, 1995.
- Pentheroudakis G, Pavlidis N: Serous papillary peritoneal carcinoma: Unknown primary tumour, ovarian cancer counterpart or a distinct entity? A systematic review. *Crit Rev Oncol Hematol* 75:27–42, 2010.
- Stafford-Johnson DB, Bree RL, Francis IR, Korobkin M: CT appearance of primary papillary serous carcinoma of the peritoneum. *AJR Am J Roentgenol* 171:687–689, 1998.
- Hoekman K, Tognon G, Risse EK, et al: Well-differentiated papillary mesothelioma of the peritoneum: A separate entity. *Eur J Cancer* 32A:255–258, 1996.
- Lovell FA, Cranston PE: Well-differentiated papillary mesothelioma of the peritoneum. *AJR Am J Roentgenol* 155:1245–1246, 1990.
- Park JY, Kim KW, Kwon HJ, et al: Peritoneal mesotheliomas: Clinicopathologic features, CT findings, and differential diagnosis. *AJR Am J Roentgenol* 191:814–825, 2008.
- Burris KE, Pfitzer P, Hort W: Well-differentiated papillary mesothelioma of the peritoneum: A borderline mesothelioma. Report of two cases and review of literature. *Virchows Arch A Pathol Anat Histopathol* 417:443–447, 1990.
- Weiss SW, Tavassoli FA: Multicystic mesothelioma. An analysis of pathologic findings and biologic behavior in 37 cases. *Am J Surg Pathol* 12:737–746, 1988.
- O'Neil JD, Ros PR, Storm BL, et al: Cystic mesothelioma of the peritoneum. *Radiology* 170:333–337, 1989.
- Katsube Y, Mukai K, Silverberg SG: Cystic mesothelioma of the peritoneum: A report of five cases and review of the literature. *Cancer* 50:1615–1622, 1982.
- Gonzalez-Moreno S, Yan H, Alcorn KW, Sugarbaker PH: Malignant transformation of “benign” cystic mesothelioma of the peritoneum. *J Surg Oncol* 79:243–251, 2002.
- Quaglia MP, Brennan MF: The clinical approach to desmoplastic small round cell tumor. *Surg Oncol* 9:77–81, 2000.
- Chan JK, Fong MH: Composite multicystic mesothelioma and adenomatoid tumour of the uterus: Different morphological manifestations of the same process? *Histopathology* 29:375–377, 1996.
- Waligore MP, Stephens DH, Soule EH, McLeod RA: Lipomatous tumors of the abdominal cavity: CT appearance and pathologic correlation. *AJR Am J Roentgenol* 137:539–545, 1981.
- Pickhardt PJ, Bhalla S: Primary neoplasms of peritoneal and sub-peritoneal origin: CT findings. *Radiographics* 25:983–995, 2005.
- Pickhardt PJ, Bhalla S: Unusual nonneoplastic peritoneal and subperitoneal conditions: CT findings. *Radiographics* 25:719–730, 2005.
- de Perrot M, Rostan O, Morel P, Le Coultre C: Abdominal lymphangioma in adults and children. *Br J Surg* 85:395–397, 1998.
- Matsuki K, Kakitsubata Y, Watanabe K, et al: Mesenteric plexiform neurofibroma associated with Recklinghausen's disease. *Pediatr Radiol* 27:255–256, 1997.
- Meyers MA, Oliphant M, Berne AS, Feldberg MA: The peritoneal ligaments and mesenteries: Pathways of intraabdominal spread of disease. *Radiology* 163:593–604, 1987.
- Pannu HK, Bristow RE, Montz FJ, Fishman EK: Multidetector CT of peritoneal carcinomatosis from ovarian cancer. *Radiographics* 23:687–701, 2003.
- Anzidei M, Napoli A, Zini C, et al: Malignant tumours of the small intestine: A review of histopathology, multidetector CT and MR aspects. *Br J Radiol* 84:677–690, 2011.
- Coulier B, Pringot J, Gielen I, et al: Carcinoid tumor of the small intestine: MDCT findings with pathologic correlation. *JBR-BTR* 90:507–515, 2007.
- Mueller PR, Ferrucci JT, Jr, Harbin WP, et al: Appearance of lymphomatous involvement of the mesentery by ultrasonography and body computed tomography: The “sandwich sign.” *Radiology* 134:467–473, 1980.
- Karaosmanoglu D, Karcaaltincaba M, Oguz B, et al: CT findings of lymphoma with peritoneal, omental and mesenteric involvement: Peritoneal lymphomatosis. *Eur J Radiol* 71:313–317, 2009.
- Rao PM, Rhea JT, Novelline RA, et al: Helical CT with only colonic contrast material for diagnosing diverticulitis: Prospective evaluation of 150 patients. *AJR Am J Roentgenol* 170:1445–1449, 1998.
- Gryspeerd S, Lefere P: Chronic diverticulitis vs. colorectal cancer: Findings on CT colonography. *Abdom Imaging* 37:1101–1109, 2012.
- McLaughlin PD, Maher MM: Nonneoplastic diseases of the small intestine: Differential diagnosis and Crohn disease. *AJR Am J Roentgenol* 201:W174–W182, 2013.
- Oto A, Kayhan A, Williams JT, et al: Active Crohn's disease in the small bowel: Evaluation by diffusion weighted imaging and quantitative dynamic contrast enhanced MR imaging. *J Magn Reson Imaging* 33:615–624, 2011.
- Makanyanga JC, Taylor SA: Current and future role of MR enterography in the management of Crohn disease. *AJR Am J Roentgenol* 201:56–64, 2013.
- Wat SY, Harish S, Winterbottom A, et al: The CT appearances of sclerosing mesenteritis and associated diseases. *Clin Radiol* 61:652–658, 2006.
- Kim JH, Byun JH, Lee SS, et al: Atypical manifestations of IgG4-related sclerosing disease in the abdomen: Imaging findings and pathologic correlations. *AJR Am J Roentgenol* 200:102–112, 2013.
- Vazquez Munoz E, Gómez-Cerezo J, Atienza Saura M, Vázquez Rodríguez JJ: Computed tomography findings of peritoneal tuberculosis: Systematic review of seven patients diagnosed in 6 years (1996–2001). *Clin Imaging* 28:340–343, 2004.
- Gore RM, Miller FH, Yaghai V: Acquired immunodeficiency syndrome (AIDS) of the abdominal organs: Imaging features. *Semin Ultrasound CT MR* 19:175–189, 1998.
- Gervaise A, Corberand D, Naulet P, et al: Whipple's disease with gastrointestinal involvement and multiple adenopathies. *Diagn Interv Imaging* 94:1145–1147, 2013.
- Horton KM, Corl FM, Fishman EK: CT of non-neoplastic diseases of the small bowel: Spectrum of disease. *J Comput Assist Tomogr* 23:417–428, 1999.
- Araoz PA, Batts KP, MacCarty RL: Amyloidosis of the alimentary canal: Radiologic-pathologic correlation of CT findings. *Abdom Imaging* 25:38–44, 2000.
- Holden C, Hennessy O, Lee WK: Diffuse mesenteric extramedullary hematopoiesis with ascites: Sonography, CT, and MRI findings. *AJR Am J Roentgenol* 186:507–509, 2006.

55. Brofman N, Atri M, Hanson JM, et al: Evaluation of bowel and mesenteric blunt trauma with multidetector CT. *Radiographics* 26:1119–1131, 2006.
56. Ros PR, Olmsted WW, Moser RP, Jr, et al: Mesenteric and omental cysts: Histologic classification with imaging correlation. *Radiology* 164:327–332, 1987.
57. Johnson PT, Horton KM, Fishman EK: Nonvascular mesenteric disease: Utility of multidetector CT with 3D volume rendering. *Radiographics* 29:721–740, 2009.
58. Hamrick-Turner JE, Chiechi MV, Abbitt PL, Ros PR: Neoplastic and inflammatory processes of the peritoneum, omentum, and mesentery: Diagnosis with CT. *Radiographics* 12:1051–1068, 1992.
59. Silverman PM, Osborne M, Dunnick NR, Bandy LC: CT prior to second-look operation in ovarian cancer. *AJR Am J Roentgenol* 150:829–832, 1988.
60. Singh AK, Gervais DA, Lee P, et al: Omental infarct: CT imaging features. *Abdom Imaging* 31:549–554, 2006.
61. Wang W, Wang ZJ, Webb EM, et al: Omental infarction preceded by anatomically upturned omentum. *Clin Imaging* 37:1125–1127, 2013.
62. Lubner MG, Simard ML, Peterson CM, et al: Emergent and nonemergent nonbowel torsion: Spectrum of imaging and clinical findings. *Radiographics* 33:155–173, 2013.
63. Wang W, Wang ZJ, Webb EM, et al: Omental infarction preceded by anatomically upturned omentum. *Clin Imaging* 37:1125–1127, 2013.

Hernias and Abdominal Wall Pathology

RICHARD M. GORE | GARY G. GHahremani |
CAROLYN K. DONALDSON | GAIL S. SMITH | LINDA C. SHERBAHN |
CHARLES S. MARN

CHAPTER OUTLINE

Hernia Classification

Hernias

Internal Abdominal Hernias

Abdominal Wall Hernias

Pelvic and Groin Hernias

Diaphragmatic Hernias

Anterior Abdominal Wall

Anatomy

Congenital Lesions

Fluid Collections

Neoplasms

Miscellaneous Conditions

Conclusions

Abdominal hernias are commonly encountered in clinical practice, and they account for approximately 750,000 operations per year in the United States.¹ Most herniations involving the anterior abdominal wall or groin can be easily diagnosed by inspection and palpation. In these cases, the radiologic examinations are useful for preoperative demonstration of the hernia's contents and associated complications, such as bowel obstruction or ischemia. Diagnostic radiology is the principal means of detecting the internal, diaphragmatic, and other nonpalpable or unsuspected hernias.²⁻⁷

Multidetector computed tomography (MDCT) can show several features of hernias that are critical to diagnosis and management: the precise anatomic site of the hernia sac; the shape of the sac and its connections; the contents of the sac; the hernia cuff and surrounding wall; and complications of the intestinal, vascular, omental, and mesenteric wall and cavity of the hernia sac. The multiplanar capabilities of MDCT offer exquisite detail of the anterior abdominal and pelvic wall. It can identify wall hernias and their contents, detect postoperative complications, and characterize hematomas, abscesses, and neoplasms.

This chapter describes the clinical and radiologic features of various abdominal herniations. In many instances, small and reducible hernias are discovered incidentally during gastrointestinal barium studies or CT of the abdomen performed to investigate unrelated conditions.²⁻⁷ Asymptomatic hernias do not warrant surgical repair, but their presence should always be brought to the attention of the patient and the referring physician. If intestinal obstruction attributable to an incarcerated

hernia develops at a future time, it can then be treated without undue delay while the underlying cause is sought.

Hernia Classification

Abdominal hernias can be classified as three major types. *Internal hernia* denotes protrusion of gut through a peritoneal or mesenteric aperture of omentum, mesentery, or peritoneal ligament, leading to its encapsulation within another compartment of the otherwise intact abdominal cavity. An *external hernia* (i.e., abdominal wall hernia) is caused by prolapse of an intestinal loop, omentum, or mesentery through a defect in the wall of the abdomen or pelvis. Diaphragmatic hernias, in which gut, omentum, or mesentery herniates into the chest, are usually considered a separate category.

The responsible hernia orifice is often a preexisting anatomic structure, such as the epiploic foramen of Winslow, inguinal canals, or esophageal hiatus. Pathologic defects of congenital, postsurgical, or traumatic origin are also potential sites of herniation.¹⁻⁷ Mobile segments of the small or large bowel are usually the content of abdominal hernias, but the greater omentum and various other viscera or pelvic organs are occasionally involved.

The nomenclature used for specific hernias indicates the anatomic location of their orifice rather than the nature of the protruding organ. The classification is therefore based on topographic distribution of the relatively common types of hernias (Box 112-1).

Hernias

INTERNAL ABDOMINAL HERNIAS

The autopsy incidence of internal hernias is in the range of 0.2% to 0.9%.^{2,4} They are becoming more common with increasing use of bariatric surgery and liver transplantation. Figure 112-1 shows their typical location.² Internal hernias may remain clinically silent if they are easily reducible, but the larger ones often cause vague epigastric discomfort, colicky periumbilical pain, and recurrent episodes of intestinal obstruction. Physical examination may reveal a palpable mass of herniated loops with localized tenderness. In these patients, the correct diagnosis can be made if barium study or CT of the abdomen is performed during the symptomatic periods. Otherwise, the hernia may not be recognized after it is reduced spontaneously or after bowel decompression with a nasogastric tube.

By far, the most common presentation of an incarcerated internal hernia is acute small bowel obstruction. In a large series of patients who underwent operation for bowel obstruction, the

BOX 112-1 CLASSIFICATION OF HERNIAS**INTERNAL ABDOMINAL HERNIAS**

Paraduodenal
Foramen of Winslow
Pericecal
Intersigmoid
Transmesenteric
Retroanastomotic

EXTERNAL ABDOMINAL OR PELVIC HERNIAS

Abdominal wall
Umbilical
Ventral
Spigelian
Lumbar
Incisional
Pelvic walls and groin
Inguinal
Femoral
Obturator
Sciatic
Perineal

DIAPHRAGMATIC HERNIAS

Esophageal hiatus
Foramen of Bochdalek
Foramen of Morgagni
Acquired defects

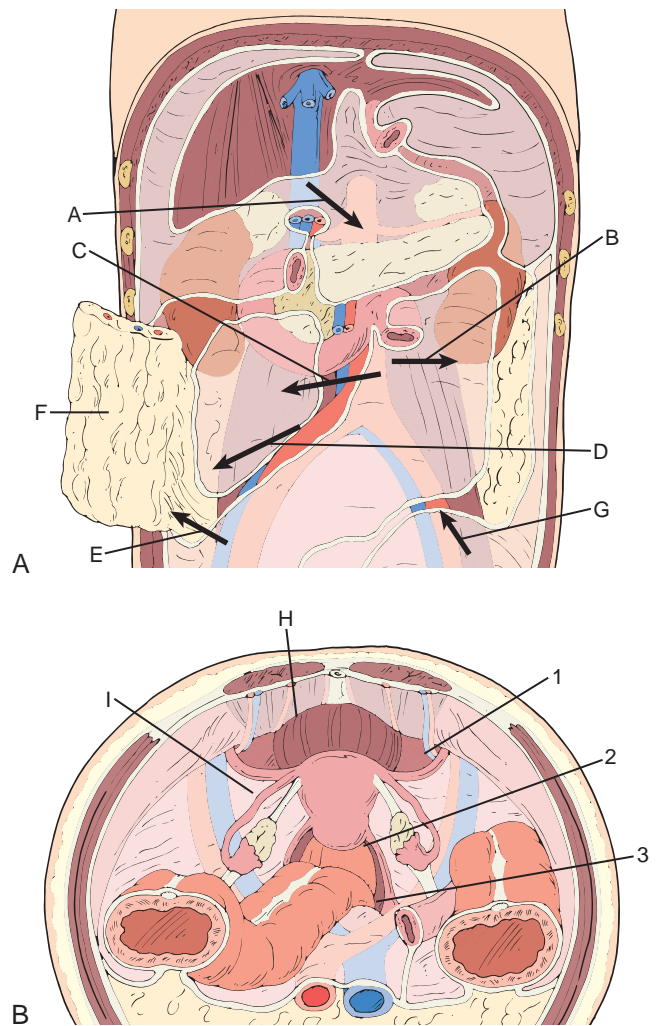


Figure 112-1 Abdominal and pelvic hernias. **A.** The drawing (coronal view) shows the locations and directions of internal hernias of the upper and lower abdominal peritoneal cavity: foramen of Winslow hernia (A), left paraduodenal hernia (B), right paraduodenal hernia (C), transmesenteric hernia (D), pericecal hernia (E), transomental hernia (F), and intersigmoid hernia (G). **B.** The drawing (superior view) shows the locations of internal hernias, pouches, and fossae of the pelvic cavity in a female patient: supravesical hernia (H), hernia through the broad ligament (I), vesicouterine pouch (1), Douglas (rectouterine) pouch (2), and perirectal fossa (3). (From Kudo M: *Operation for uterus*. In Takeda Y [ed]: *Anatomy for Obstetric and Gynecologic Surgery*, Tokyo, 1999, Medical View, pp 38–67; Asanuma Y: *Pancreas and spleen*. In Matsuno S, Hatakeyama K, Kanematsu T [eds]: *Comprehensive Anatomy for Gastroenterological Surgery: Small Intestine, Anorectal Disease, Colon, Liver, Gallbladder, Biliary Tract, Pancreas and Spleen*, Tokyo, 1999, Medical View, pp 108–144; Kuwahara M: *Anatomical precautions of adjacent organs*. In Yoshida O [ed]: *Anatomy for Urologic Surgery*, Tokyo, 1998, Medical View, pp 114–133.)

underlying causes proved to be internal hernia (4.1%), external hernia (17.5%), neoplasms (18%), or adhesions (32%).⁸

Each type of internal hernia has specific radiologic features (Table 112-1), which are described later in this chapter. As a general rule, barium studies and CT show certain diagnostic hallmarks shared by various internal hernias, including abnormal location of an intestinal segment in susceptible regions, such as the lesser sac; encapsulation and crowding together of several small bowel loops within the confines of the peritoneal cavity; stasis of contrast material in the lumen and dilation of more proximal bowel; and apparent fixation of the herniated loops, preventing their separation or dislodgment during fluoroscopic manipulations or by changing the position of the patient.^{2,4}

Preoperative radiologic diagnosis or a high index of suspicion for an internal hernia is important because at laparotomy, spontaneous reduction or inadvertent traction of the herniated loops may cause it to be overlooked. The usual abdominal exploration is inadequate for evaluating all peritoneal fossae and mesenteric defects that could serve as potential sites of herniations.^{2,4}

Paraduodenal Hernia

Paraduodenal hernias are the most common type of intra-abdominal herniation, and they account for 53% of the reported cases.^{2,9-13} They are more common in men than in women, with a ratio of about 3:1. Approximately 75% occur on the left and involve the paraduodenal fossa of Landzert. This peritoneal pocket is observed at 2% of autopsies. It is located just lateral to the ascending, or fourth, segment of the duodenum, beneath a peritoneal fold elevated by the inferior mesenteric vein and ascending left colic artery. Small bowel loops enter the sac from behind, where the duodenum emerges from its fixed retroperitoneal position. They protrude farther posteriorly and to the left, essentially herniating into the descending mesocolon and distal portion of the transverse mesocolon.^{2,4}

Twenty-five percent of paraduodenal hernias develop on the right side of the abdomen and typically involve the mesentericoparietal fossa of Waldeyer. This abnormal pocket in the jejunal mesentery is found at 1% of autopsies. Its orifice is located immediately behind the superior mesenteric artery and inferior to the transverse segment of the duodenum; however, the peritoneal pocket itself extends to the right and downward, directly in front of the posterior parietal peritoneum. Accordingly, the right paraduodenal hernia can be viewed as small bowel herniation into the ascending mesocolon.^{2,4,9}

The clinical manifestations of paraduodenal hernias range from intermittent and mild digestive complaints to acute

TABLE
112-1

Clinical and Imaging Findings for Internal Hernias

Hernia Type	Subtype	Incidence*	Characteristic Clinical Findings	Radiography and Barium Studies	CT Findings	Key Vessel
Left paraduodenal	Congenital, normal aperture	40% of all hernias, 75% of paraduodenal hernias	Postprandial pain, may date back to childhood	Encapsulated cluster of the jejunum in LUQ, lateral to the ascending duodenum; may have mass effect, indenting the posterior wall of stomach or displacing the transverse colon inferiorly	Clustered dilated small bowel loops between the stomach and pancreas, behind the pancreas itself, or between transverse colon and left adrenal gland	IMV in the neck of the hernia sac with anterior upward displacement of the IMV
Right paraduodenal	Congenital, normal aperture	13% of all hernias, 25% of paraduodenal hernias	Postprandial pain, may date back to childhood	Encapsulated loops lateral and inferior to the descending duodenum; associated with small bowel nonrotation	Encapsulated loops lateral and inferior to the descending duodenum; associated with small bowel nonrotation	SMA displaced anteriorly
Pericecal	Congenital or acquired, abnormal aperture	13%	RLQ pain, differential diagnosis of appendicitis; high incidence of occlusive symptoms	Clustered small bowel loops (usually distal) posterior and lateral to the cecum in the right paracolic gutter	Clustered small bowel loops (usually distal) posterior and lateral to the cecum in the right paracolic gutter	None
Foramen of Winslow	Congenital, normal aperture	8%	Symptoms of proximal obstruction because of mass effect on stomach; symptom onset often preceded by changes in intra-abdominal pressure (i.e., parturition, straining); relief of symptoms with forward bending	Circumscribed loops medial and posterior to the stomach; differential diagnosis of cecal volvulus	Loops in the lesser sac between the liver hilum and IVC	None; vessels stretched through the foramen of Winslow
Intersigmoid	Type 1: congenital, normal aperture Types 2 and 3: acquired, abnormal aperture	6%	None	U- or C-shaped cluster of small bowel posterior and lateral to the sigmoid colon	U- or C-shaped cluster of small bowel posterior and lateral to the sigmoid colon	None
Transmesenteric [†]	In children: congenital, abnormal aperture In adults: usually acquired, abnormal aperture	8%	Two typical patient populations: children and postsurgical adults In adults, less vomiting because fewer secretions in proximal gastric pouch, onset more acute	Variable, air within gastric remnant; may simulate a left paraduodenal hernia	Small bowel lateral to the colon; displaced omental fat with small bowel directly abutting the abdominal wall	None
Retroanastomotic [†]	Acquired, abnormal aperture	5%	Usually within the first postoperative month; less vomiting because fewer secretions in the proximal gastric pouch	Variable	Variable	None

*Incidences for the first six types are from Meyers¹¹²; they are historic data but are the only major source available. Incidences for these first six types of internal hernias total only 93% because the perivesical hernias reported¹¹² are not true internal hernias, so they were not included in this review.

[†]Probably more transmesenteric and retroanastomotic internal hernias currently because of the number of liver transplantations and gastric bypass operations being performed throughout the United States during the past decade. The 5% refers to the incidence after Roux loops were used during surgery for reasons other than liver transplantation or gastric bypass.

IMV, inferior mesenteric vein; IVC, inferior vena cava; LUQ, left upper quadrant; RLQ, right lower quadrant; SMA, superior mesenteric artery.

intestinal obstruction. Recurrent periumbilical cramps or postprandial epigastric pain and distention are frequently experienced before the onset of incarceration.^{2,9} Contrast examinations of the gastrointestinal tract are most likely to provide the correct diagnosis during symptomatic periods. After the hernia is reduced spontaneously, however, results of barium studies tend to be negative, and the patient may be mislabeled as psychoneurotic.

The characteristic radiographic features of left paraduodenal hernias have been described by several investigators.^{2,4,5,9-12} A circumscribed, ovoid mass of multiple jejunal loops occupies the left upper quadrant immediately lateral to the ascending duodenum (Fig. 112-2). The hernia indents the posterior gastric wall and depresses the distal transverse colon. Fluoroscopy and serial radiographs reveal a separation of encapsulated loops from the remaining small intestine. Dilatation of the involved segments and stasis of barium may also be evident. Because the duodenum is retroperitoneal and the herniated proximal jejunal

loops enter the fossa of Landert posteromedially, only one loop of distal small intestine exits through the hernia orifice. The inferior mesenteric vein and ascending left colic artery lie in the anteromedial border of the left paraduodenal hernia.^{2,4,9} These findings are best appreciated during laparotomy, but CT scans of the upper abdomen may help demonstrate them before operation.

Right paraduodenal hernias are manifested as a similar ovoid grouping of several small bowel loops just lateral and inferior to the descending duodenum (Fig. 112-3). They are usually more massive and fixed than those on the left side. Afferent and

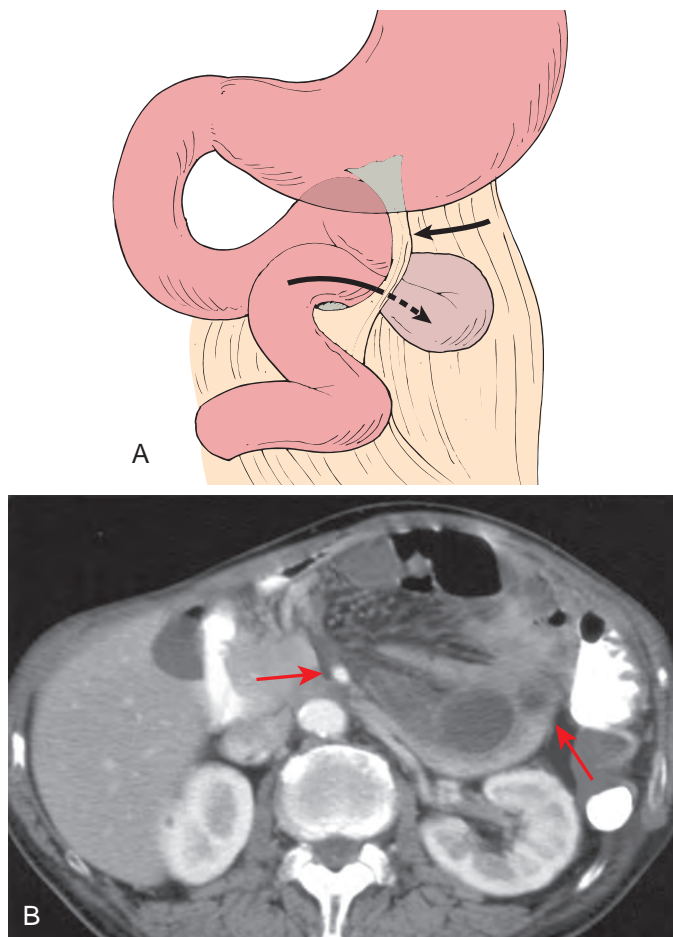


Figure 112-2 Left paraduodenal hernia. **A.** Graphic illustration of a left paraduodenal hernia depicts loop of small bowel prolapsing (curved arrow) through Landert's fossa, located behind inferior mesenteric vein and ascending left colic artery (straight arrow). Herniated bowel loops are therefore located lateral to the fourth portion of the duodenum. **B.** Axial CT scan shows a closed loop obstruction of a short segment of proximal jejunum (arrows). The mural thickening and mesenteric edema suggest superimposed ischemia. (A from Martin LC, Merkle EM, Thompson WM: Review of internal hernias: Radiographic and clinical findings. *AJR Am J Roentgenol* 186:703-717, 2006. Reprinted with permission from the American Journal of Roentgenology.)

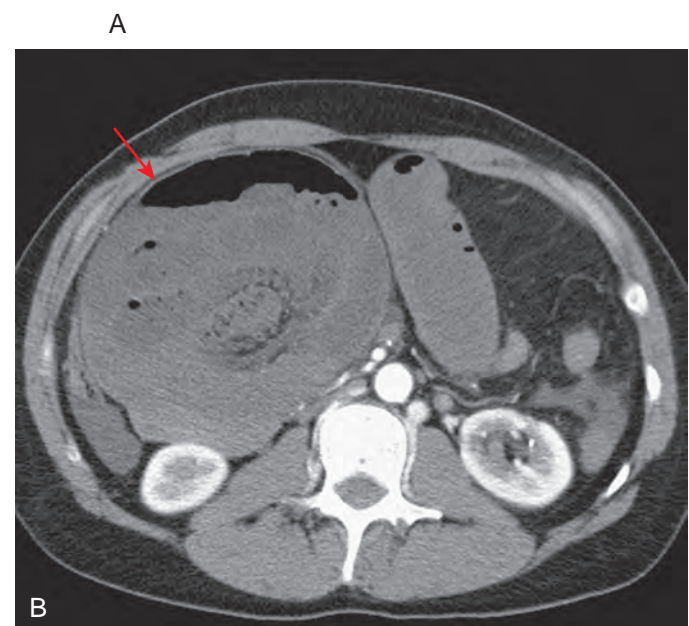
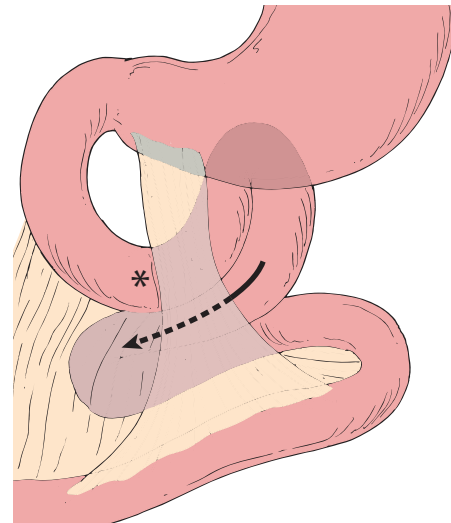


Figure 112-3 Right paraduodenal hernia. **A.** Graphic illustration of right paraduodenal hernia shows loop of small bowel prolapsing (arrow) through Waldeyer's fossa, behind superior mesenteric artery and inferior to third portion of duodenum (asterisk). **B.** Axial CT scan shows a cluster of jejunal loops (arrow) in a closed loop obstruction. Note the poor mural enhancement and edema in the adjacent mesentery, indicating ischemia. (A from Martin LC, Merkle EM, Thompson WM: Review of internal hernias: Radiographic and clinical findings. *AJR Am J Roentgenol* 186:703-717, 2006. Reprinted with permission from the American Journal of Roentgenology.)

effluent intestinal loops pass through the hernia orifice, where they are closely apposed and narrowed.^{2,4,5,7,13} Lateral radiographs are particularly useful for demonstrating the retroperitoneal displacement of the hernia contents. Barium enema examination shows that the ascending colon lies lateral to a right paraduodenal hernia, and the cecum retains its normal position.

The superior mesenteric artery and its ileocolic branches are situated in the anterior wall of the right paraduodenal hernia sac. The passage of herniated loops behind these vessels causes arteriographically detectable changes.² The jejunal arteries, which normally arise from the left side of the superior mesenteric artery, abruptly reverse direction to the right and course behind the parent vessel to supply the herniated loops in the fossa of Waldeyer.

Operative techniques for the correction of paraduodenal hernias are described elsewhere.⁹ Preoperative diagnosis and demonstration of their radiographic anatomy assist the surgeon to better understand the extremely confusing laparotomy findings. Blind division of the hernia sac should be avoided because it carries the risk of injury to the vital mesenteric vessels contained within its wall. It may create a mesenteric defect that could later serve as a potential site for an iatrogenic internal hernia.^{2,4}

Foramen of Winslow Hernia

The lesser sac communicates with the greater peritoneal cavity through the epiploic foramen of Winslow. This small opening can serve as a pathway for protrusion of viscera into the lesser sac, where 8% of all internal hernias occur.^{2,4-7,14} The small intestine is the herniated segment in 60% to 70% of cases. The terminal ileum, cecum, and ascending colon are involved in about 25% to 30%. The transverse colon, gallbladder, and omentum account for the remainder. Predisposing factors include an enlarged foramen of Winslow and excessively mobile intestinal loops because of a long mesentery or persistence of the ascending mesocolon. Herniation into the lesser sac may be provoked by a sudden increase in intra-abdominal pressure, like that experienced while lifting heavy weights or during parturition. An elongated right lobe of the liver can also be a contributing factor by directing the mobile intestinal loops toward the foramen of Winslow.

This type of internal hernia usually affects middle-aged patients and is manifested as progressive upper abdominal pain and acute onset of small bowel obstruction. Physical examination usually reveals localized tenderness and distention in the epigastric regions. A helpful sign is the relief of pain with forward bending or in the knee-chest position.

Several radiologic features of hernias through the foramen of Winslow are characteristic:

1. Plain radiographs of the abdomen show bowel loops containing gas within the lesser sac medial and posterior to the stomach, usually in conjunction with markedly dilated proximal small intestine. The right iliac fossa may appear empty if the cecum and ascending colon are the herniated segments.^{2,4,5}
2. Upper gastrointestinal examination demonstrates displacement of the stomach to the left and anteriorly because of extrinsic compression by the mass of herniated loops in the lesser sac. The first and second portions of the duodenum may be compressed and deviated to the left side.

3. Small bowel series show dilation and hyperperistalsis of the intestinal loops that indicate distal mechanical obstruction. Serial radiographs and fluoroscopy can localize the site of obstruction to the right upper abdomen, corresponding to the anatomic location of the foramen of Winslow between the duodenal bulb and the hilum of the liver.
4. If the herniation involves the cecum and ascending colon, barium enema examination may reveal a tapered narrowing or obstruction near the hepatic flexure.^{2,4}
5. CT scans of the abdomen show an aberrant position of the bowel loops between the liver, the stomach, and the pancreas (Fig. 112-4). CT is the optimal imaging technique to demonstrate the presence and content of herniations involving the lesser sac.^{5-7,14}
6. Gallbladder herniation into the lesser sac can be diagnosed when the opacified gallbladder appears elongated and its fundus is malpositioned on the left, indenting the gastric antrum or body of the pancreas. Manual compression of the epigastrium can reduce the hernia if the foramen of Winslow is widely patent. Gallbladder strangulation and perforation in the lesser sac may occur if the condition is not diagnosed and treated promptly.¹⁵

Besides the foramen of Winslow, there may be other openings for herniation into the lesser sac. For instance, a defect in the gastrohepatic ligament forming the anterior wall of the lesser sac may follow partial gastrectomy. A congenital or acquired defect may also be present in the transverse mesocolon or gastrocolic ligament, which constitutes the floor of the lesser sac. The intestinal loops can prolapse through these openings to occupy the lesser sac or reenter the greater peritoneal cavity by the foramen of Winslow.^{2,4,16,17}

Pericecal Hernia

Four peritoneal fossae located in the ileocecal region as well as congenital and acquired defects in the mesentery of the cecum or appendix may lead to development of a pericecal hernia.^{2,4,5} The various other terms used to classify these hernias (e.g., ileocolic, retrocecal, ileocecal, paracecal) appear to have limited practical value for radiologic differential diagnosis and surgical management.

In a collective review of 467 cases of internal hernia, 13% involved the ileocecal region.² The clinical manifestations are usually intermittent episodes of colicky right lower abdominal pain associated with small bowel distention, nausea, and vomiting. Chronic incarceration may produce symptoms compatible with periappendiceal abscess, regional enteritis, or intestinal obstruction caused by adhesions.

In most cases, an ileal segment herniates through a defect in the mesentery of the cecum and occupies the right paracolic gutter. The correct diagnosis may be suggested on plain radiographs of the abdomen (Fig. 112-5), provided the unusual relationship of the ileum to the cecum is recognized in association with small bowel obstruction. More useful are delayed radiographs of a small bowel series or a barium enema examination with retrograde opacification of the terminal ileum. Careful fluoroscopic evaluation and filming in lateral and oblique projections are particularly valuable for the demonstration of the fixed position of the herniated ileal loop posterolateral to the cecum.

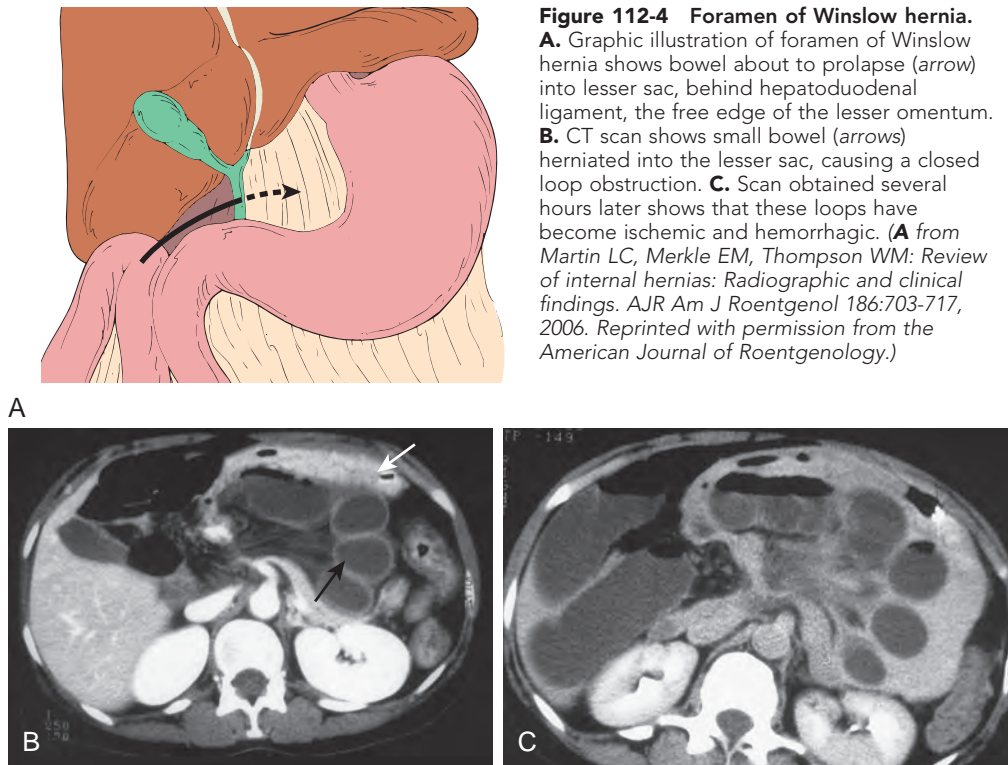


Figure 112-4 Foramen of Winslow hernia.
A. Graphic illustration of foramen of Winslow hernia shows bowel about to prolapse (arrow) into lesser sac, behind hepatoduodenal ligament, the free edge of the lesser omentum.
B. CT scan shows small bowel (arrows) herniated into the lesser sac, causing a closed loop obstruction.
C. Scan obtained several hours later shows that these loops have become ischemic and hemorrhagic. (**A** from Martin LC, Merkle EM, Thompson WM: Review of internal hernias: Radiographic and clinical findings. *AJR Am J Roentgenol* 186:703-717, 2006. Reprinted with permission from the American Journal of Roentgenology.)

Intersigmoid Hernia

Intersigmoid hernias involve the intersigmoid fossa, a peritoneal pouch located between the two loops of the sigmoid colon and its mesentery. This pocket is found at 65% of autopsies.^{2,4,5,18}

Intersigmoid hernias are usually reducible and are an incidental finding during laparotomy. Radiologic diagnosis is best made on barium enema studies in which retrograde filling of the small bowel has been achieved. The examination typically shows a portion of jejunum or ileum to be encapsulated between the sigmoid loops (Fig. 112-6).

In this context, two similar entities deserve a brief mention:

1. In *transmesosigmoid hernias*, a defect involving both layers of the sigmoid mesentery allows herniation of the small bowel loops toward the left lower abdomen, posterolateral to the sigmoid colon. The hernia ring is usually a long slit whose fibrous edge is bound by branches of the inferior mesenteric vessels.^{2,19}
2. In *intramesosigmoid hernia*, a congenital defect may be present in only one of the constituent leaves of the sigmoid mesentery. The small bowel loops passing through this orifice are incarcerated in a hernia sac, which is formed by separation of medial and lateral leaves of the mesosigmoid.^{4,18}

Radiologic differentiation of these three types of hernias involving the mesosigmoid is often difficult, and in terms of their ultimate surgical management, it is irrelevant.

Transmesenteric Hernia

Approximately 5% to 10% of all internal hernias occur through defects in the mesentery of the small bowel. They have no limiting sac, but their functional significance is similar to that of true internal hernias.^{4,19-23}

Almost 35% of transmesenteric hernias affect the pediatric age group, in which they constitute the most common type of internal herniation. The underlying mesenteric defects are usually 2 to 5 cm in diameter and located close to the ligament of Treitz or the ileocecal valve.^{2,4} A causal relationship to prenatal intestinal ischemic accidents seems likely because such mesenteric apertures and associated hernias are frequently found in infants with atretic bowel segments. In adults, however, most mesenteric defects are probably the result of previous gastrointestinal operations, abdominal trauma, or intraperitoneal inflammation.^{2,4,24}

In the absence of a limiting hernia sac, a considerable length of small intestine may protrude through the mesenteric aperture. Volvulus may further complicate the process and cause rapid strangulation and intestinal gangrene.²⁰⁻²⁴ Patients present with severe periumbilical cramps accompanied by hyperactive bowel sounds and progressive distention. A tender abdominal mass, representing the Gordian knot of herniated intestine, may be palpable. Plain radiographs of the abdomen demonstrate a mechanical small bowel obstruction and occasionally show a single, distended closed loop (Fig. 112-7). Small bowel examination may disclose a constriction around the closely approximated afferent and efferent limbs of the herniated intestine. The superior mesenteric arteriogram shows abrupt angulation and displacement of the visceral branches as they pass through the mesenteric defect to supply the herniated loops.²² These findings signal a surgical emergency, although clinical and radiologic differentiation of the mesenteric hernia from other closed loop obstructions (e.g., small bowel volvulus or entrapment beneath peritoneal adhesions) may be impossible.²³⁻²⁵

Defects in the mesenteric attachments of the colon are also the potential sites of internal herniation. For example, a congenital or postsurgical opening in the transverse mesocolon

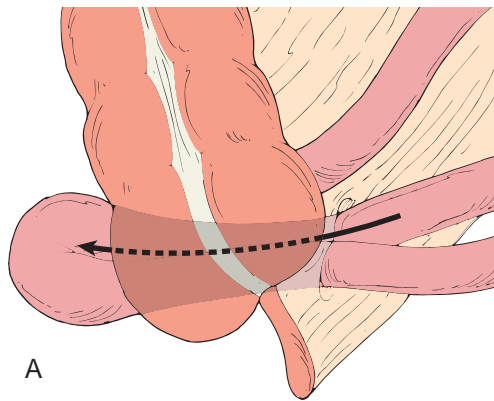


Figure 112-5 Pericecal hernia. **A.** Diagram of a pericecal hernia shows a loop of ileum prolapsing (arrow) through cecal mesenteric defect, behind and lateral to the cecum, into right paracolic gutter. **B.** CT scan shows small bowel loops (arrows) lateral to the proximal ascending colon. (A from Martin LC, Merkle EM, Thompson WM: Review of internal hernias: Radiographic and clinical findings. *AJR Am J Roentgenol* 186:703-717, 2006. Reprinted with permission from the American Journal of Roentgenology.)

permits small bowel loops to herniate into the lesser sac.^{2,4} A somewhat similar situation can be present in cases of congenital persistence of descending mesocolon. A defect in this structure may allow small bowel herniation into the left paracolic gutter, causing medial displacement of the descending colon.

Transomental Hernia

Approximately 1% to 4% of internal hernias occur through defects in the greater omentum.^{2,4,8} Fewer than 100 cases have been reported from observations made at surgery or autopsy. The hernia orifice is usually a slitlike opening up to 10 cm long, located in the periphery of the greater omentum. Most have a congenital origin, but trauma and inflammation may also produce omental perforations or weak areas. These defects can subsequently serve as potential sites for transomental herniation of the small intestine (Fig. 112-8) and other mobile segments, such as the cecum or sigmoid colon. The clinical and radiologic findings are almost identical to those of transmesenteric hernias.¹⁸⁻²³

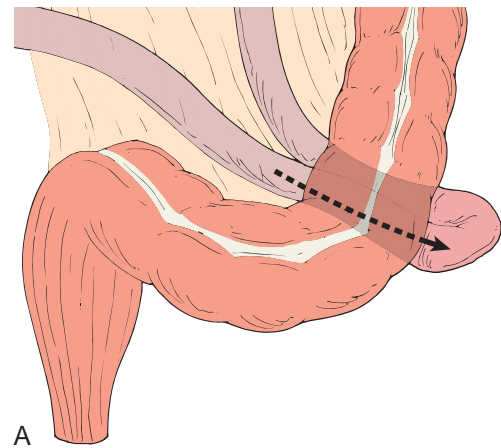


Figure 112-6 Intersigmoid hernia. **A.** Illustration of an intersigmoid hernia shows bowel protruding (arrow) through defect in sigmoid mesocolon to lie posterolateral to sigmoid colon itself. **B.** A small knuckle of ileum has herniated into the intersigmoid fossa, leading to small bowel obstruction. Notice the small bowel feces sign of the obstructed loop (arrows). (A from Martin LC, Merkle EM, Thompson WM: Review of internal hernias: Radiographic and clinical findings. *AJR Am J Roentgenol* 186:703-717, 2006. Reprinted with permission from the American Journal of Roentgenology.)

Retroanastomotic Hernia

Retroanastomotic hernias are a well-recognized and preventable complication of gastrointestinal surgery. They usually develop after partial gastrectomy and gastrojejunostomy. About 75% of cases involve incarceration of the efferent jejunal segment in the retroanastomotic space, which is created during antecolic or retrocolic anastomosis.^{2,4,26} The herniation is usually from right to left, so that the efferent jejunal loop or an excessively long afferent segment occupies the left upper quadrant of the abdomen. Less commonly, the ileum, the cecum, or the omentum is also involved.²⁷

Approximately half of these hernias occur in the first postoperative month, and the others occur within 1 year or several

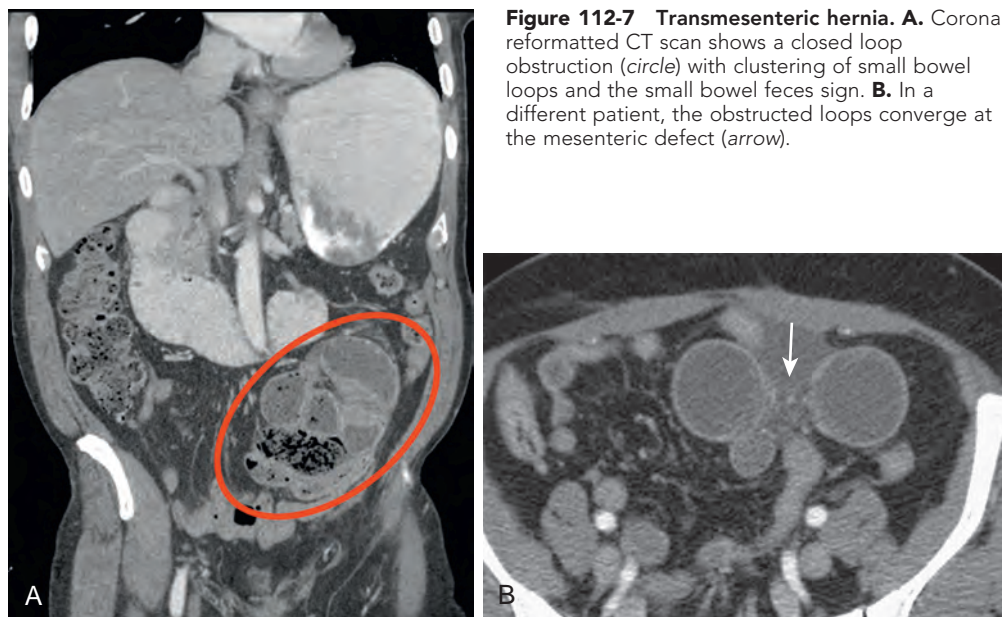


Figure 112-7 Transmesenteric hernia. **A.** Coronal, reformatted CT scan shows a closed loop obstruction (circle) with clustering of small bowel loops and the small bowel feces sign. **B.** In a different patient, the obstructed loops converge at the mesenteric defect (arrow).

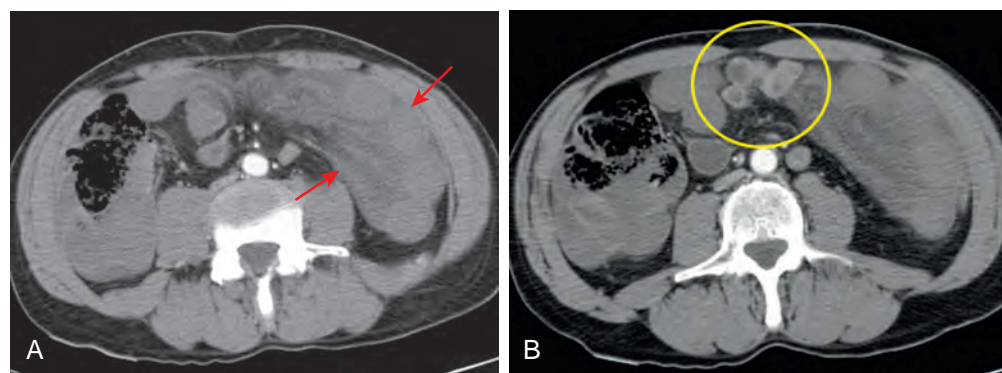


Figure 112-8 Transomental hernia. **A.** A group of ischemic small bowel loops (arrows) shows poor enhancement and mesenteric edema due to a strangulating transomental hernia. **B.** Note the clustering of small bowel loops (circle) at the origin of the hernia.

years after surgery.⁴ The presenting symptom is cramping abdominal pain, and the signs are those of high small bowel obstruction. The herniated loops are occasionally palpable as a tender mass in the left upper abdomen. These nonspecific findings may be mistaken for gastric outlet obstruction caused by stomal edema, dumping syndrome, or postoperative pancreatitis. Delay in establishing the correct diagnosis may lead to strangulation of the herniated loops; the associated mortality rate is up to 30% for surgically treated cases and almost 100% if the problem is not corrected.^{2,4,26}

Radiologic diagnosis of a retroanastomotic hernia requires careful fluoroscopic evaluation of the gastrointestinal tract after administration of barium or water-soluble contrast medium. The examination reveals that the site of obstruction is not the gastric stoma but is more distal in either of the anastomotic limbs. Gradual opacification of the partially obstructed efferent loop discloses its abnormal position lateral and posterior to the gastrojejunostomy (Fig. 112-9). The herniated segments of jejunum appear clumped or fixed in the left upper abdomen, usually associated with some degree of dilation and stasis.^{2,4,27}

The diagnosis of afferent loop hernia, which occurs primarily after an antecolic anastomosis, is more difficult. The clinical findings include persistent epigastric pain and tenderness, non-bilious vomiting, and elevated serum amylase level. Contrast studies of the upper gastrointestinal tract show patency of the anastomosis and the efferent loop; however, opacification of the herniated afferent limb may not occur or may be delayed. CT scans or sonograms of the upper abdomen usually disclose the obstructed afferent loop as a fluid-filled and markedly distended tubular structure.^{28,29} Scintigraphy is another diagnostic method for this entity. Radionuclide agents excreted by the biliary tract into the duodenum permit visualization of the dilated afferent loop and the site of obstruction.³⁰

Like any other symptomatic internal hernia, hernias involving the retroanastomotic space also require surgical correction. However, this iatrogenic hernia should be prevented during initial gastric operation by the use of a short afferent loop and the closure of the retroanastomotic space with sutures placed between the jejunal mesentery and the transverse mesocolon.^{2,4,26,27}

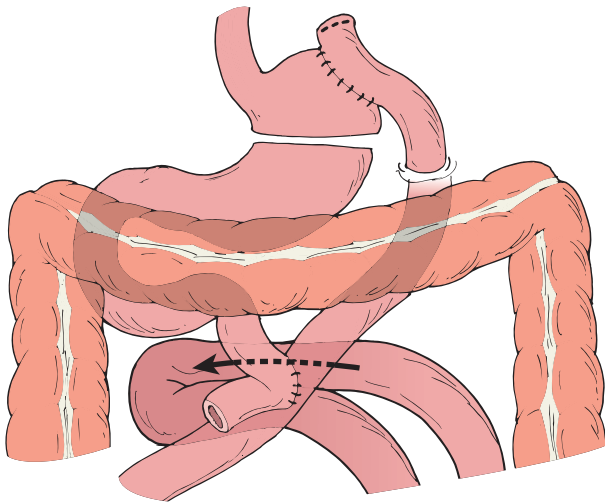


Figure 112-9 Retroanastomotic hernia. The diagram shows a retrocolic Roux-en-Y gastric bypass procedure. The arrow indicates a loop of small bowel protruding posterior to the enteroenterostomy, in keeping with a retroanastomotic internal hernia. (From Martin LC, Merkle EM, Thompson WM: *Review of internal hernias: Radiographic and clinical findings*. *AJR Am J Roentgenol* 186:703-717, 2006. Reprinted with permission from the American Journal of Roentgenology.)

ABDOMINAL WALL HERNIAS

Herniations through the walls of the abdominal cavity develop in approximately 1.5% of the population and usually involve specific sites of congenital weakness or previous surgical incision.¹⁻³ An outpouching of the peritoneum forms a hernia sac, which surrounds the protruding parts of the greater omentum, intestine, or other abdominal organs. The presenting symptoms are variable and depend on the size, location, and content of the hernia.

Umbilical Hernia

In infants and children, a patent umbilical ring is a common site of herniation. It often is manifested as a soft, asymptomatic bulge that tends to disappear spontaneously. In some instances, however, the development of umbilical tenderness and obstructive symptoms caused by incarceration necessitate surgical repair. The congenital entity known as an omphalocele is not a true umbilical hernia because the bowel loops never return to the peritoneal cavity during gestation in this disorder.

In adults, umbilical hernias occur predominantly in women with a history of multiple pregnancies and in patients with obesity or with increased abdominal pressure resulting from ascites and chronic bowel distention (Fig. 112-10). The hernia contents are usually the greater omentum and various segments of the small or large intestine. Adhesions often develop between the protruding viscera and the peritoneal sac and cause digestive symptoms and other complications.^{7,8}

The clinical diagnosis of an incarcerated umbilical hernia should be suspected when a patient presents with intestinal obstruction and umbilical tenderness, even if there is no obvious bulge on the surface. Radiographs of the abdomen usually show the distended bowel loops and a tumor-like density, the umbilical hernia. A coned-down lateral or cross-table view of the anterior abdominal wall using low peak kilovoltage can be

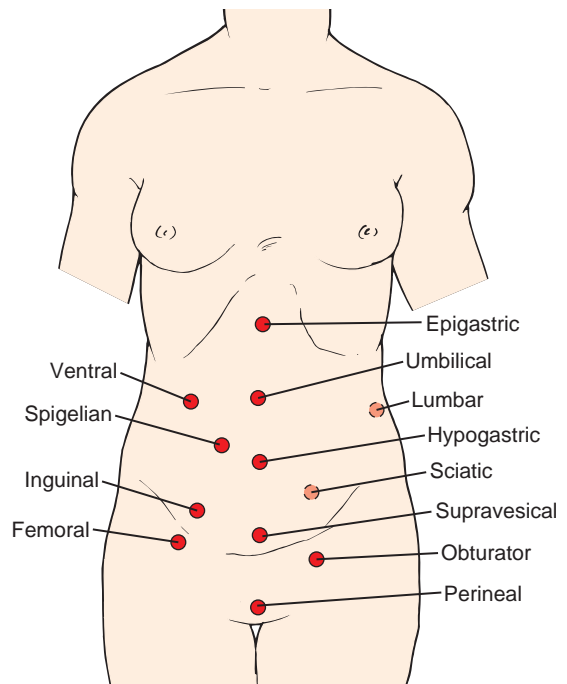


Figure 112-10 Types and locations of hernias. Herniations through the walls of the abdominal cavity usually involve specific sites of congenital weakness or previous surgical incision.

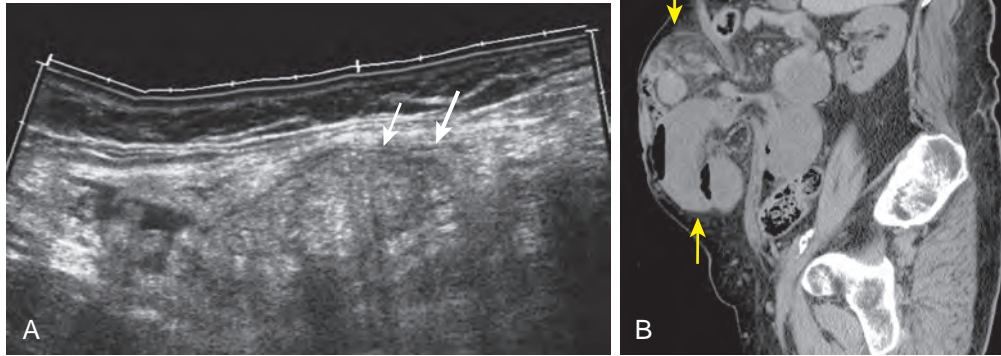
helpful in detecting the presence of omental fat or bowel loops in the umbilical hernia. Barium studies of the small or large intestine can show obstruction or protrusion of gut in the umbilical region. Ultrasound and CT studies of the abdomen establish the diagnosis when they demonstrate a “knuckle” of bowel protruding through an umbilical defect.³¹⁻³³

Ventral Hernia

The term *ventral hernia* encompasses several types of herniations through the anterior and lateral aspects of the abdominal wall (Fig. 112-11). Most occur in the midline and emerge through the aponeurosis forming the linea alba. They are referred to as epigastric or hypogastric hernias, depending on their location above or below the umbilicus, respectively. The hernia aperture is often a small, firm defect that allows portions of the greater omentum, properitoneal fat, or a bowel loop to protrude anteriorly.^{1,5-7,33} Incarceration and strangulation of the contents may occur frequently and produce symptoms out of proportion to the objective findings. The severity of abdominal pain may simulate a perforating peptic ulcer. The pain of a ventral hernia, however, is aggravated by exertion and associated with focal tenderness of the abdominal wall.

Lateral ventral hernias often occur spontaneously, but they frequently involve a site of previous abdominal surgery, laparoscopy, peritoneal dialysis, or stab wound. They are discussed later in conjunction with other incisional hernias. As a general rule, the radiologic features of various ventral hernias are similar to those of umbilical hernias. Barium studies demonstrate distended bowel loops proximal to a narrowing or obstruction in close relationship to a locally tender part of the abdominal wall. CT, magnetic resonance imaging (MRI), or sonography can reveal the defect and associated herniation in the ventral wall of the abdomen.^{5-7,31-34}

Figure 112-11 Ventral hernia. **A.** The longitudinal sonogram shows a ventral herniation of omental fat (arrows). **B.** Sagittal, reformatted image in a different patient shows herniated small bowel and mesentery (arrows).



Spigelian Hernia

Spigelian hernias are uncommon. They occur in the anterolateral aspect of the lower abdomen, along the semilunar line formed by fibrous union of the rectus sheath with the aponeuroses of the transversus abdominis and oblique abdominal muscles. The underlying cause is a congenital weakness in the posterior layer of transversalis fascia, through which the viscera prolapse between the lateral abdominal wall muscles as an interparietal or interstitial herniation.^{1,35-37}

Spigelian hernias are notoriously difficult to diagnose clinically because of their deep anatomic location and insidious development. Patients usually present with a prolonged history of intermittent lower abdominal pain and intestinal obstruction associated with a slight swelling or a vanishing anterolateral mass located midway between the umbilicus and the symphysis pubis. These hernias occur with almost equal frequency in males and females; they can be bilateral and associated with other ventral or inguinal hernias.

The usual contents of a spigelian hernia include the omentum and short segments of the small or large intestine. Barium enema or small bowel examination can be useful in establishing the diagnosis.³⁶ However, CT is the best imaging technique for visualizing the hernia defect involving the lateral border of the rectus sheath as well as interstitial protrusion of the omentum or intestinal loops (Fig. 112-12).^{5-7,37-39} Sonographic diagnosis can be made when there is a complex mass in the anterolateral wall of the lower abdomen, showing an echogenic component resulting from omental herniation or acoustic shadowing by the air-containing loops of incarcerated bowel.³⁷

Lumbar Hernia

Two areas of relative weakness in the flank can be sites of herniation. The superior lumbar space of Grynfeltt-Lesshaft is an inverted triangle bound by the 12th rib superiorly, the internal oblique muscle anteriorly, and the erector spinae muscle posteriorly.^{1,40,41} The inferior lumbar triangle (i.e., Petit's triangle) is bordered inferiorly by the iliac crest, anteriorly by the external oblique muscle, and posteriorly by the latissimus dorsi muscle.^{42,43}

Approximately 300 cases of lumbar hernia have been reported in the literature, and most involve the larger superior lumbar space. The contents usually include a bowel loop,

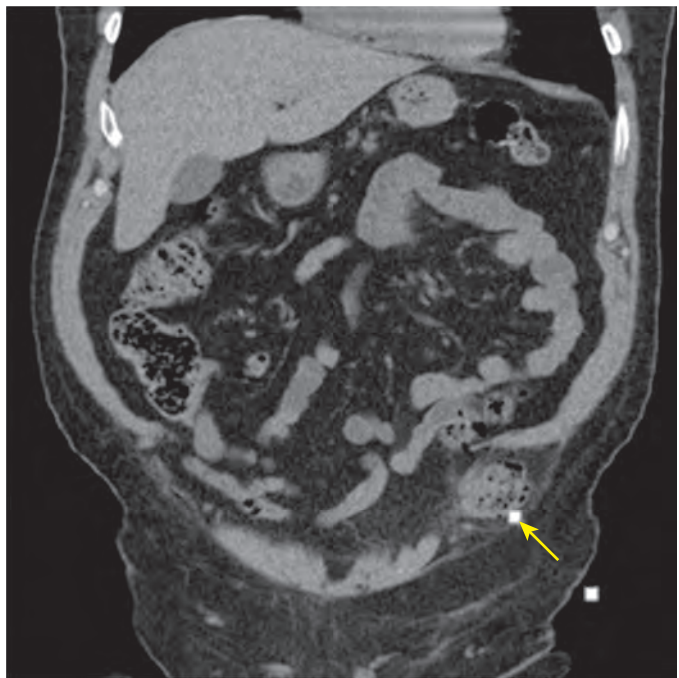


Figure 112-12 Spigelian hernia. CT shows herniated small bowel through a peritoneal defect at the lateral border of the left rectus muscle (arrow), which was a prior laparoscopic port site.

retroperitoneal fat, kidney, or, less frequently, other viscera. These hernias tend to enlarge gradually and cause symptoms ranging from chronic low back pain to intestinal obstruction. Bowel incarceration occurs in approximately 25% of these hernias and may lead to strangulation in about 10% of cases. The spontaneous and the post-traumatic types of lumbar hernias occur more frequently on the left side and in middle-aged men. The clinical manifestation as a soft, bulging mass in the flank may be mistaken for a lipoma or hematoma. Plain radiographs of the abdomen are often noncontributory, but barium studies can be useful when the bowel loops are contained within the hernia (Fig. 112-13). Certain articles indicate that CT can best delineate the precise location and content of lumbar hernias.^{5-7,40-43}

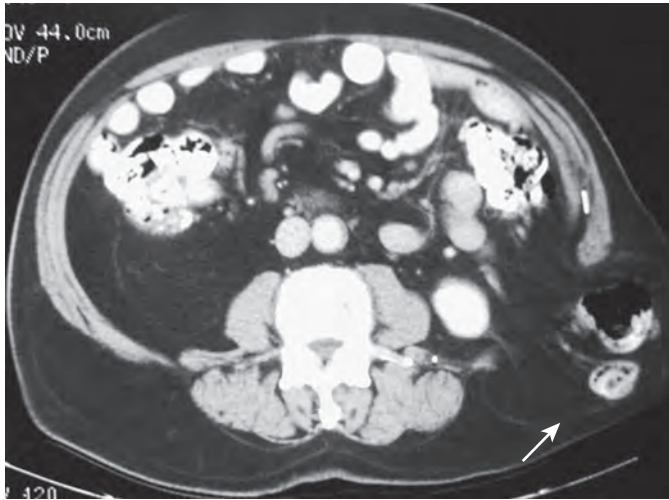


Figure 112-13 Lumbar hernia. CT shows the descending colon and mesentery herniating (arrow) posterolaterally through the left inferior lumbar space or Petit's triangle.

Incisional Hernia

Incisional hernias develop in approximately 5% of patients and represent a significant iatrogenic problem, given the fact that almost 3 million abdominal operations are performed annually in the United States. These hernias tend to occur during the first 4 months after surgery, a critical period for the healing of transected muscular and fascial layers of the abdominal wall. Their progressive enlargement is usually manifested within the first postoperative year, but 5% to 10% remain clinically silent for several years before they are detected.^{1,3,5}

The most common sites of involvement are along midline and paramedian incisions, although any surgical scar carries the potential risk of this complication. The clinical symptoms and physical findings of an incisional hernia depend on the size and rigidity of the underlying defect and on the extent of visceral protrusion. The properitoneal fat or the edge of the greater omentum is often the initial contents of a small incisional hernia, producing vague abdominal discomfort and localized tenderness of the healed scar. At a more advanced stage, a persistent bulging mass resulting from incarcerated bowel loops may be seen.

Approximately 10% of incisional hernias cannot be detected on physical examination. In obese patients, for example, the abundant subcutaneous fat can prevent palpation of a deeply seated peritoneal defect and the protruding viscera. The clinical diagnosis may also be difficult in patients with severe abdominal pain and distention or in the presence of a keloid or thick panniculus. The herniated segments occasionally dissect and are hidden between the muscular and the fascial layers of the abdominal wall. These interparietal or interstitial hernias often are manifested as localized swelling and tenderness adjacent to the surgical scar, but their actual content and internal orifice are seldom palpable. Under these circumstances, radiologic studies play a crucial role in establishing the correct diagnosis.^{3,5,34,44-47}

In patients with nonspecific abdominal pain and intermittent obstructive symptoms, a careful fluoroscopic evaluation of the gastrointestinal tract with barium may reveal a clinically occult or unsuspected incisional hernia. It is crucial that areas

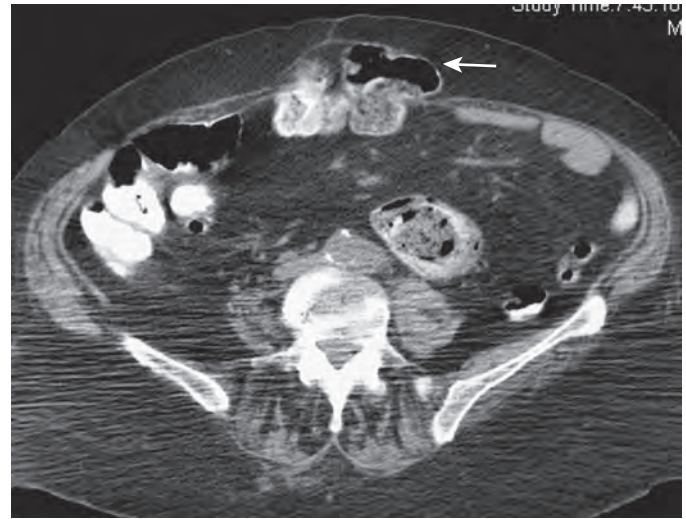


Figure 112-14 Incisional hernia. The CT scan performed 1 year after laparotomy shows a knuckle of transverse colon (arrow) protruding beneath a healed midline incision.

with old surgical scars be viewed in profile while the patient strains. This maneuver assists in detection of reducible hernias that may otherwise be overlooked.⁴⁶ CT can best show small defects in peritoneal and fascial layers of abdominal wall through which the omentum or a knuckle of intestine protrudes into the subcutaneous fat.^{3,31-34} It can also disclose ischemic changes caused by strangulated bowel loops, a sign of a surgical emergency (Fig. 112-14). Sonographic detection of an incisional hernia is also possible by visualization of a bowel loop causing acoustic shadowing within the disrupted abdominal wall layers beneath a healed scar.

Most incisional hernias are ventral, but other potential sites should be considered in patients who previously had abdominal surgery. For example, an acquired lumbar hernia may be present in the area of flank incision for nephrectomy.⁴¹ A parastomal herniation of the omentum or intestine may also occur where the distal bowel loop has tunneled through the abdominal wall (Fig. 112-15). In a similar manner, postcholecystectomy patients can develop intermittent bowel herniation beneath the right subcostal incision. These hernias may not be appreciated during physical examination but are easily detectable on barium studies or abdominal CT.^{3,5,7,44}

PELVIC AND GROIN HERNIAS

Almost 75% of all abdominal hernias occur in the groin and account for more than a half-million operations per year in the United States.^{1,34} Most are inguinal hernias that are easy to diagnose by inspection and palpation. Radiologic studies are performed primarily for preoperative delineation of the herniated viscera and associated complications or when the clinical findings are equivocal because of the deep location of a pelvic wall herniation.

Inguinal Hernia

In its most common type, known as indirect inguinal hernia, the peritoneal sac containing bowel loops protrudes through the inguinal canal and emerges at its external ring. This hernia occurs predominantly in males and can extend along the

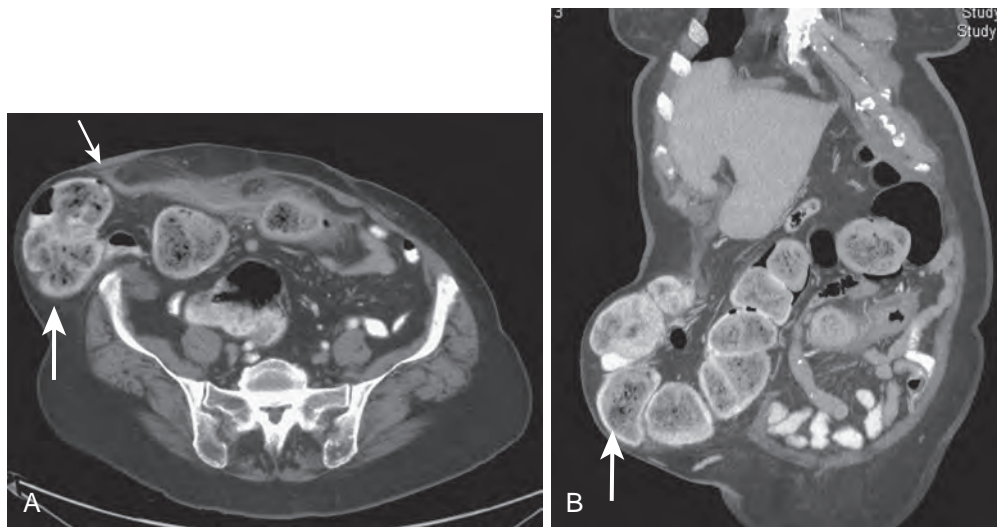


Figure 112-15 Peristomal hernia. **A.** Axial CT image demonstrates portions of the ascending colon (large arrow) along the posterolateral aspect of the patient's colostomy (small arrow) in a peristomal hernia. **B.** Coronal, reformatted CT image shows portions of the hepatic flexure of the colon (arrow) in the hernia.

spermatic cord into the scrotum (Fig. 112-16). In females, the hernia follows the course of the round ligament of the uterus into the labium majus.^{1,34}

The development of indirect inguinal hernia has a congenital basis. During embryologic migration of the testis, a peritoneal sac called the processus vaginalis accompanies testicular descent into the scrotum; in females, it follows the round ligament. In both sexes, this peritoneal communication is normally obliterated before birth; however, about one third of infants and 15% of adults have a patent processus vaginalis on one or both sides. This allows the subsequent development of an inguinal hernia when abdominal viscera are pushed into the open sac.^{34,37}

The contents of indirect inguinal hernias usually include small bowel loops or mobile colon segments such as the sigmoid colon, cecum, and appendix. The other viscera and pelvic adnexa are less frequently involved. The term *sliding inguinal hernia* is used when partially retroperitoneal organs, such as the urinary bladder, distal ureters, or ascending or descending colon, are included in the herniation. Their preoperative demonstration is important because retroperitoneal structures constitute the wall of the hernia sac and may be injured during its surgical repair. The blood vessels supplying the herniated segments of ascending or descending colon course in the posterior wall of sliding hernias and are subject to inadvertent trauma if an incorrect surgical approach is used.

Indirect inguinal hernias account for 15% of intestinal obstructions; only neoplasms (32%) and adhesions (18%) are more common causes.⁸ The symptoms of an incarcerated or strangulated hernia include bowel distention associated with painful and often tense swelling in a groin or the scrotum. Radiographs of the abdomen obtained with the patient supine can indicate the correct diagnosis by showing the convergence of distended intestinal loops toward the inguinal region and a soft tissue density or gas-containing mass overlying the obturator foramen on the affected side. Barium examination of the small or large bowel typically shows a tapered narrowing or obstruction of the intestinal segment as it enters the hernia orifice. Every attempt should be made to reduce the hernia

manually under fluoroscopy and to clearly visualize the afferent and efferent loops of protruding intestine. It is important to recognize that diverticulitis, appendicitis, and primary or metastatic tumors may occur within the hernia sac.⁴⁷⁻⁵⁰ CT and ultrasound examinations of the groin can also provide useful diagnostic information on the hernia contents and on its differentiation from other masses involving the groin or scrotum (see Fig. 112-16).^{32,34}

The *direct inguinal hernia* is a less common type of groin hernia that occurs mostly in men and seldom in women or children. It represents visceral protrusion directly through the lower abdominal wall in a weak area medial to the inferior epigastric vessels. This hernia appears as a small bulge in the groin. It rarely becomes incarcerated because of its short and blunt aperture.^{1,34} It can be differentiated from indirect hernias, which have an elongated, oblique course through the inguinal canal and frequently extend into the scrotum.

Simultaneous occurrence of direct and indirect inguinal hernias in the same groin is unusual. In these cases, the separation of the two adjacent hernia sacs by the inferior epigastric vessels creates a bilocular appearance. This entity is therefore referred to as a saddlebag, a pantaloons, or *combined inguinal hernia*.^{1,34,51}

Two other varieties of abdominal herniations occur:

1. In *Littre's hernia*, a Meckel diverticulum protrudes into the hernia sac. This usually occurs in the right inguinal region but may also be associated with other ventral or pelvic hernias.^{1,52}
2. *Richter's hernia* contains only a part of the bowel wall circumference as a localized outpouching (Fig. 112-17). The intestinal lumen remains patent, and no obstructive symptoms are produced despite intense pain and tenderness caused by incarceration of the bulging bowel wall into a postoperative or postlaparoscopic defect.^{3,53-55}

Femoral Hernia

Herniation into the femoral canal occurs predominantly in women and accounts for about one third of groin hernias in

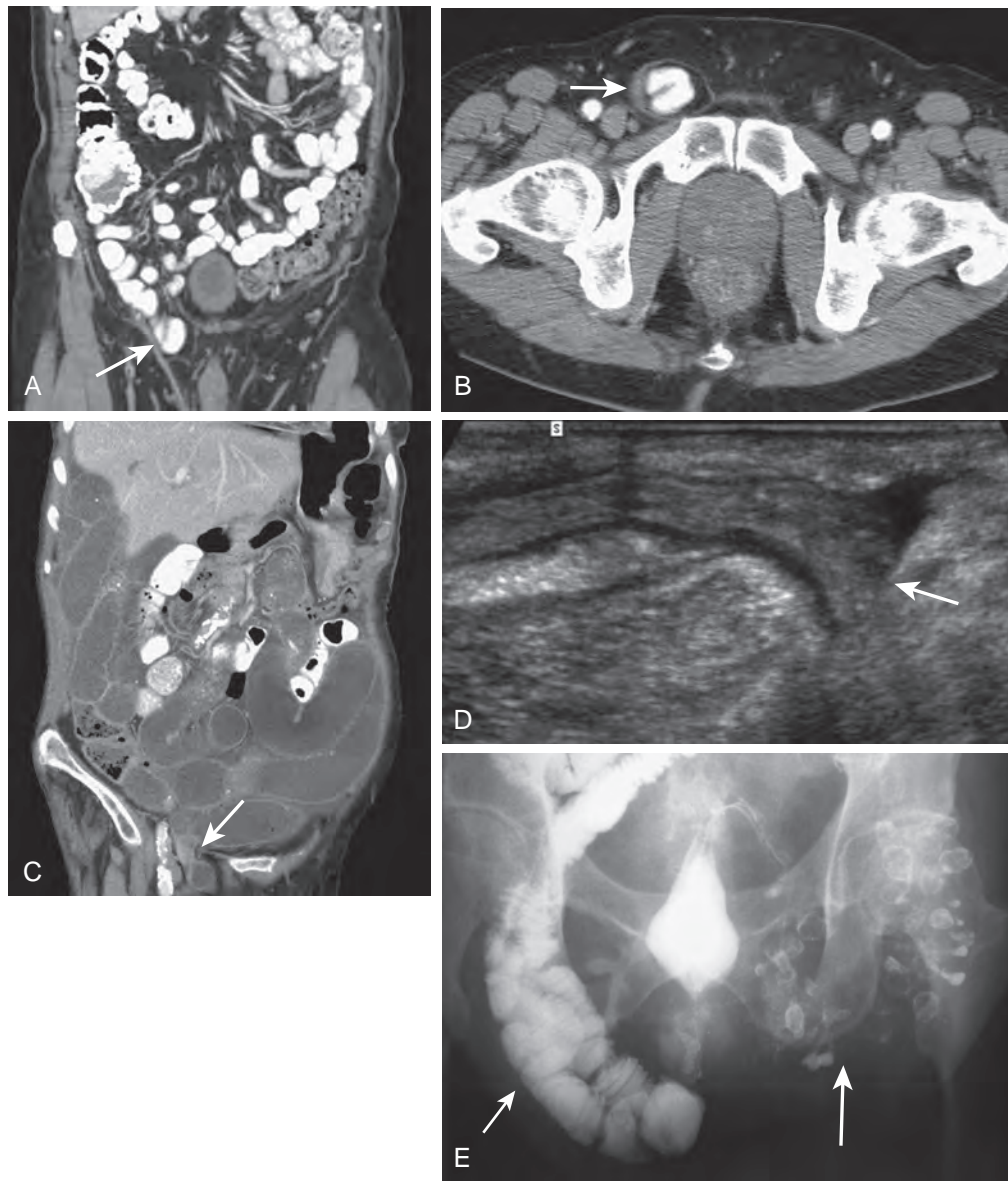


Figure 112-16 Inguinal hernia. **A.** Coronal, reformatted CT image shows a nonobstructing, right inguinal hernia containing small bowel (arrow). **B.** An axial image shows the herniated segment of ileum (arrow). **C.** Coronal, reformatted CT image reveals an obstructing, right inguinal hernia containing a small segment of ileum (arrow). **D.** Sagittal sonogram in a different patient demonstrates an inguinal hernia containing fat, fluid, and gut (arrow). **E.** Barium enema examination demonstrates herniation of the distal ileum into the right scrotum (small arrow). There is herniation of the sigmoid colon into a left inguinal hernia (large arrow).

women. The incidence in men is three to four times lower, and children are rarely affected.^{56,57} The hernia contents are usually properitoneal fat, edge of the omentum, or loop of small bowel (Fig. 112-18). They can displace or narrow the femoral vein and descend along the saphenous vein. However, the neck of a femoral hernia always remains below the inguinal ligament and lateral to the pubic tubercle.

Femoral hernias are often difficult to diagnose clinically because of the deep location of the femoral canal and the abundance of overlying adipose tissue. Nevertheless, they are 8 to 12 times more prone to incarceration and strangulation than are inguinal hernias because of the firm and unyielding margins of the femoral ring. The correct radiologic diagnosis can therefore be important.^{7,58-60}

Obturator Hernia

The site of this uncommon herniation is the obturator canal (Fig. 112-19) in the superolateral aspect of the obturator foramen. It is an obliquely oriented, fibro-osseous tunnel measuring about 2 to 3 cm long and 1 cm in diameter, through which the obturator nerve and vessels course.

Approximately 80% to 90% of obturator hernias occur in elderly women, probably because of enlargement of the obturator canal after pregnancies and aging. They are more common on the right and usually contain an ileal loop, but other viscera or pelvic adnexa may also be involved.^{1,34,60} The protruding structures are often incarcerated in the canal or in the space between the pectineus and the obturator muscles. Most patients

Figure 112-17 Incarcerated Richter's hernia. **A.** Double-contrast colon examination shows a funnel-shaped traction deformity involving the inferior border of the sigmoid loop (arrows). **B.** CT of the lower pelvis reveals a small left inguinal hernia containing the air-filled outpouching of sigmoid wall (arrow). **C.** Another section 2 cm caudad shows a fatty mass within the hernia sac (arrow), representing an incarcerated epiploic appendage that pulled the adjacent sigmoid wall.

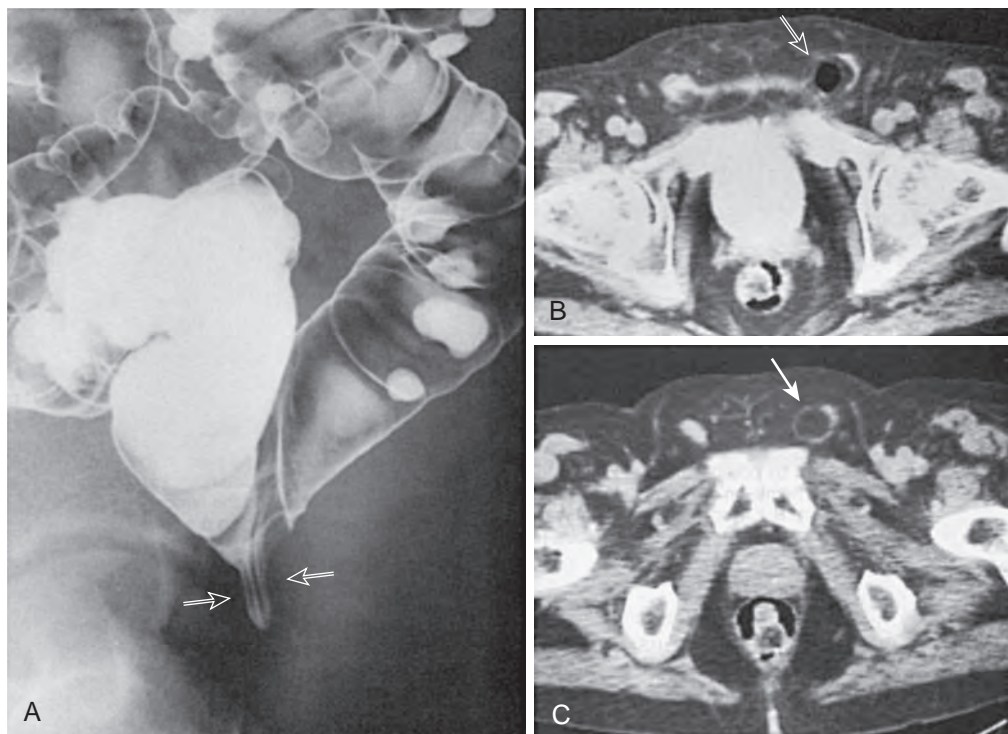
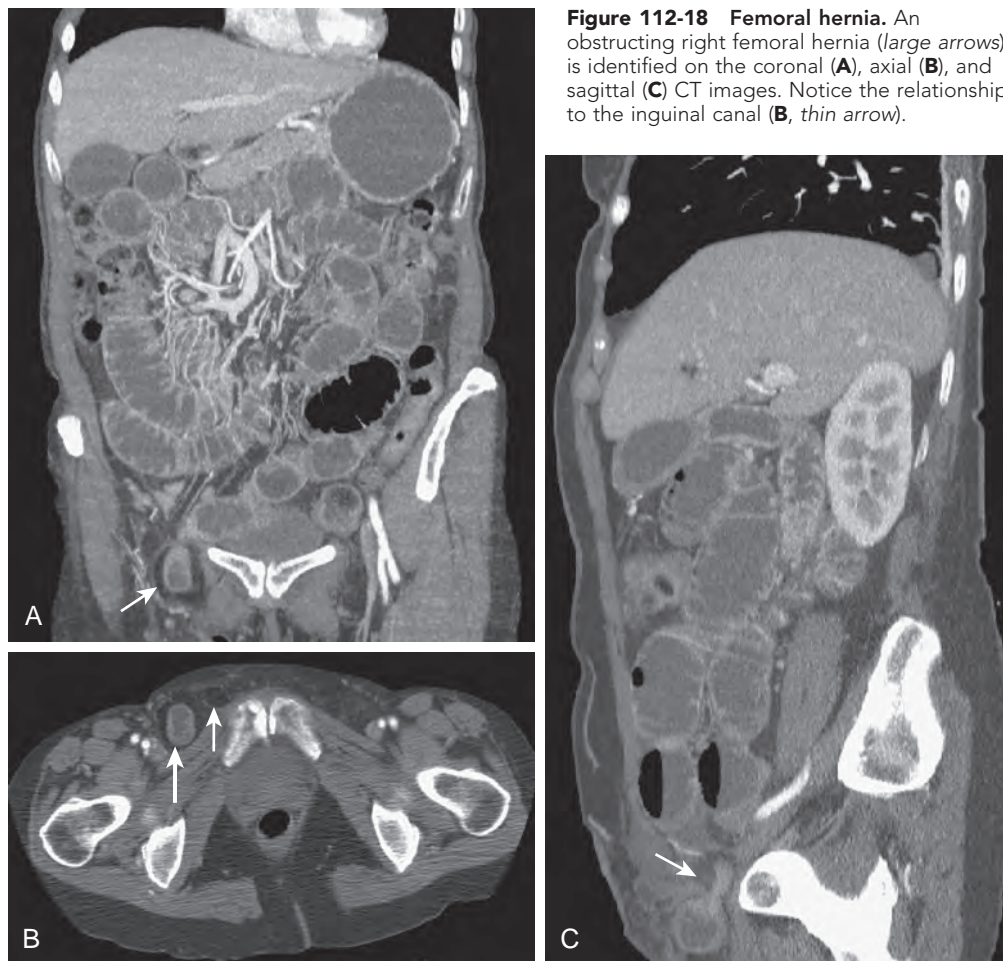


Figure 112-18 Femoral hernia. An obstructing right femoral hernia (large arrows) is identified on the coronal (**A**), axial (**B**), and sagittal (**C**) CT images. Notice the relationship to the inguinal canal (**B**, thin arrow).



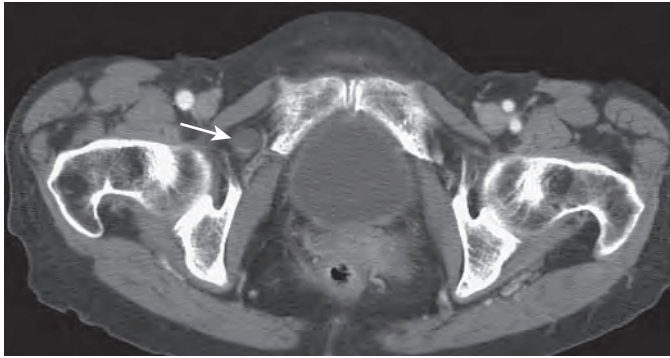


Figure 112-19 Obturator hernia. Pelvic CT reveals a small knuckle of ileum in a hernia (arrow) deep to the right pectineus and anterior to the right obturator internus muscles.

present with acute or recurrent bowel obstruction and a tender mass in the obturator region detected on rectal or vaginal examination. About half the patients experience pain radiating along the medial aspect of the thigh when the leg is extended or abducted (i.e., Howship-Romberg sign) because of obturator nerve compression by the hernia.

The radiologic diagnosis of obturator hernia should be considered whenever abdominal radiographs or barium studies show bowel obstruction together with a fixed loop containing some gas or contrast medium in the obturator region. CT of the pelvis is most valuable in revealing the hernia as a soft tissue mass or opacified loop that protrudes through the obturator foramen and extends between the pectineus and the obturator muscles.⁶¹⁻⁶³

Sciatic Hernia

The greater sciatic notch is bordered by the lateral margin of the sacrum and the inferior border of iliac bone. The sacrotuberous ligament converts this semicircular structure into the greater sciatic foramen. This opening is the pathway for the sciatic nerve, the gluteal vessels and nerves, and the piriformis muscle. It also represents a potential site of herniation of the pelvic or abdominal viscera into the subgluteal region.^{5,64-66} The lesser sciatic foramen, a small slit located farther caudally, is less prone to this complication.

About 50 cases of sciatic hernia have been reported, with most involving the distal ureter or a loop of the small bowel.^{64,66} Clinical manifestations are usually lower abdominal cramps, urinary symptoms, pain radiating to the dorsal aspect of the thigh or leg, and a palpable, tender mass in the gluteal region. Plain radiographs of the abdomen are seldom helpful, but excretory urography can disclose the characteristic curlicue appearance of herniated distal ureter. Barium studies of the small bowel or colon and CT scans may be used to show a bowel loop that has herniated through the sciatic foramen and extends laterally into the subgluteal region (Fig. 112-20).

Perineal Hernia

Herniations involving the pelvic floor are uncommon and occur mainly through the urogenital diaphragm. Defects in the levator ani or coccygeus muscle can lead to more posterior perineal hernias.^{60,67}

Most patients with perineal hernias are women older than 50 years. Causal factors include acquired weakness of the pelvic



Figure 112-20 Sciatic hernia. A small knuckle of ileum (arrow) is identified behind the right acetabulum. There is no associated obstruction.

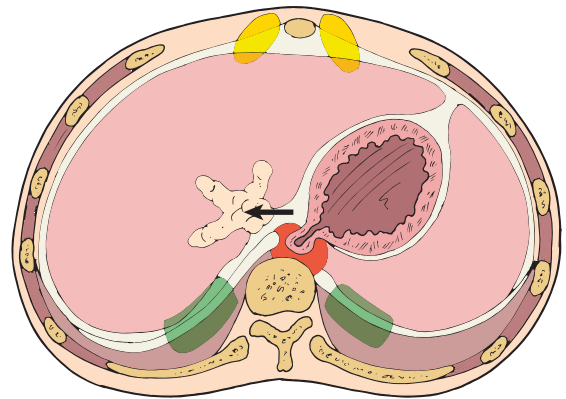


Figure 112-21 Diaphragmatic hernias. Cross-sectional drawing depicts the common locations of Morgagni, Bochdalek, and hiatal hernias. Several elements are indicated: juxtacaval fat (arrow), foramen of Bochdalek (green), esophageal hiatus (pink), and foramen of Morgagni (yellow). (From Gaerte SC, Meyer CA, Winer-Muram HT, et al: Fat-containing lesions of the chest. *RadioGraphics* 22:S61-S78, 2002.)

floor caused by increased abdominal pressure from pregnancy, obesity, or ascites; local inflammatory processes; and postsurgical defects after abdominoperineal resection or transperineal prostatectomy. Clinical findings usually consist of a perineal or gluteal mass, which may cause discomfort when sitting. Barium enema or small bowel examination can be used to demonstrate the protruding loop adjacent to the anus or in one of the buttocks.^{60,67} CT scans can also depict the hernia sac and its contents in the ischiorectal fossa.⁶⁸

DIAPHRAGMATIC HERNIAS

Diaphragmatic hernias (Fig. 112-21) are classified as four types: esophageal hiatus, Morgagni, Bochdalek, and traumatic. Esophageal hiatal hernias are discussed in Chapter 28.

Foramen of Morgagni Hernia

Foramen of Morgagni hernias usually contain the omentum and transverse colon (Fig. 112-22) and occasionally contain the stomach and small bowel, surrounded by their peritoneal sac. They protrude through the retrosternal foramen of Morgagni, which is wider than normal because of a natural weakness of the sternocostal muscle bundles. About 90% of cases occur on the right side. In adults, these hernias are usually asymptomatic.⁶⁸⁻⁷¹

Foramen of Bochdalek Hernia

Foramen of Bochdalek hernias occur through the lumbocostal trigone of Bochdalek. In these cases, there is defective closure of the pleuropulmonary hiatus (Fig. 112-23). In neonates, these hernias are conspicuous in size and often need surgical repair. In adults, these hernias are small and usually result from hypoplasia of the lumbocostal muscle bundles surrounding Bochdalek's foramen. They are usually found incidentally in

asymptomatic patients. MDCT is useful in determining the extent of the diaphragmatic defect and the contents of the hernia sac. This canal is a communication between the thoracic cavity and the retroperitoneal space. These hernias are more common on the left than on the right.⁶⁸⁻⁷¹

Traumatic Hernias

Diaphragmatic disruption can develop from blunt trauma (e.g., auto accidents, falls, crush injuries, bout of hyperemesis) or penetrating trauma (e.g., bullet and knife wounds, repair of hiatal hernia). Rupture occurs in 0.8% to 1.6% of all blunt trauma and represents 5% of all diaphragmatic hernias but 90% of all strangulated diaphragmatic hernias.⁶⁸⁻⁷¹

The left hemidiaphragm is injured three times more commonly than the right in traumatic diaphragmatic hernias. Organ herniation occurs in 32% to 58% of cases and most often involves, in descending order, the stomach, colon, small bowel, omentum, spleen, kidney, and pancreas.⁶⁸⁻⁷¹ The most frequent injuries associated with diaphragm rupture in auto accidents include laceration of the liver and spleen, rib and pelvic fractures, and pulmonary contusion. Bergqvist's triad includes rib fractures, spine or pelvic fractures, and diaphragmatic rupture.

The reported accuracy of CT in the detection of these hernias is variable, with a sensitivity ranging between 61% and 100% and specificity between 77% and 100%.⁶⁸⁻⁷¹ Coronal and sagittal reformatting of the volumetric MDCT data may be helpful in establishing the diagnosis but is not always definitive and can be misleading.

Several signs are helpful in identifying traumatic rupture: diaphragm discontinuity, segmental nonrecognition of diaphragm, intrathoracic herniation of abdominal contents, collar sign, elevated abdominal organs, thickened diaphragm, thoracic fluid abutting intra-abdominal organs, dependent viscera sign, hemothorax and hemoperitoneum, and extravasation of contrast material at level of diaphragm. The dependent viscera sign (Fig. 112-24) is contact of the upper third of the liver on the right or the stomach or bowel on the left with the posterior ribs. The collar or hourglass sign is focal constriction of the stomach or liver at the site of herniation through the diaphragm. Abrupt discontinuity of the diaphragm may be visible with or without herniation of viscera. The absent diaphragm sign is lack of visualization of the diaphragm in an area where it does not

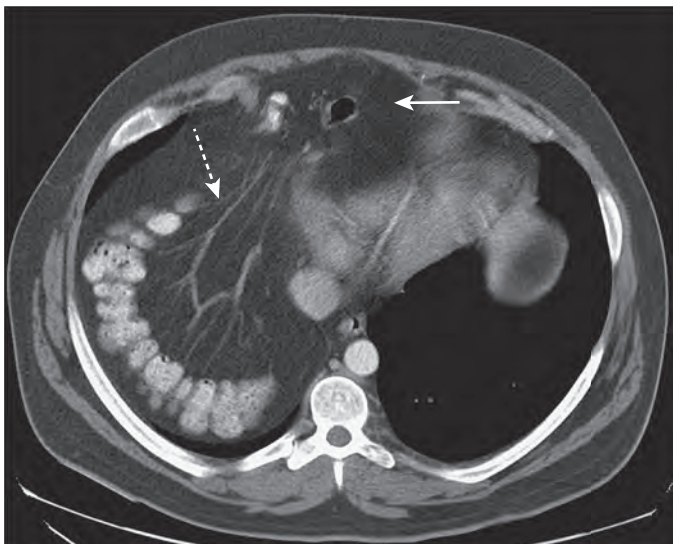


Figure 112-22 Foramen of Morgagni hernia. CT scan shows a retrosternal hernia that includes the omentum and colon (arrow). Notice the fanlike disposition of the mesenteric vessels (dashed arrow).

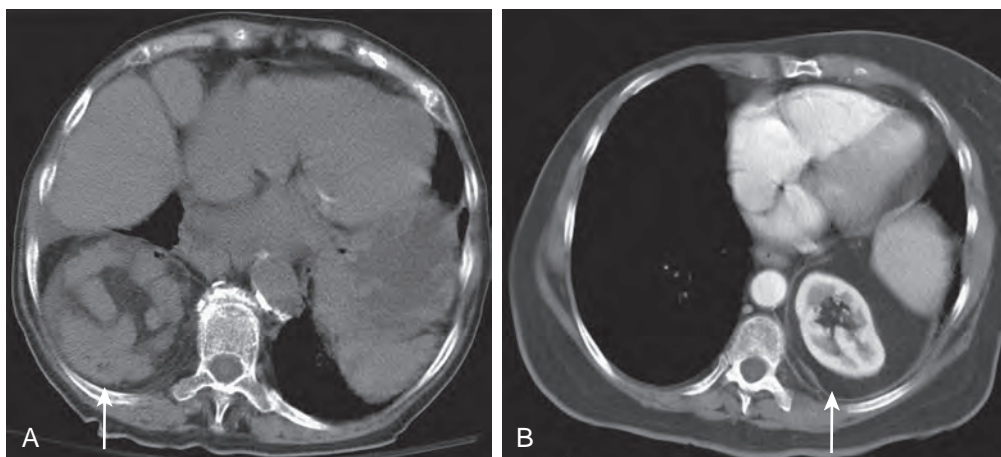


Figure 112-23 Foramen of Bochdalek hernias. **A.** Small bowel (arrow) is seen herniated in this right foramen of Bochdalek hernia. **B.** The left kidney and perinephric fat are contained in this left foramen of Bochdalek hernia (arrow).

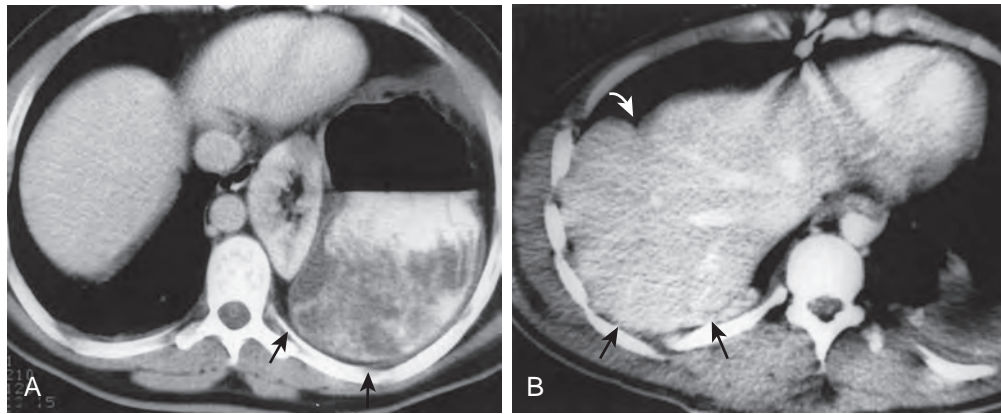


Figure 112-24 Traumatic diaphragmatic hernias: the dependent viscera sign. **A.** In a 32-year-old man with left-sided diaphragmatic rupture, an axial CT scan shows discontinuity of left hemidiaphragm (arrows indicate extent of diaphragmatic tear) with gastric and left renal herniation. The stomach lies dependent on left posterior ribs, which is a positive dependent viscera sign. **B.** In a 32-year-old woman with ruptured right hemidiaphragm, an axial CT scan shows the right lobe of the liver dependent on right posterior ribs (black arrows), which is the dependent viscera sign. A partial, waistlike constriction (white arrow)—the collar sign—is visible along anterior surface of right lobe of liver and is attributable to partial hepatic intrathoracic herniation. (**A** and **B** from Bergin D, Ennis R, Keogh C, et al: *The “dependent viscera” sign in CT diagnosis of blunt traumatic diaphragmatic rupture*. *AJR Am J Roentgenol* 177:1137-1140, 2001. Reprinted with permission from the American Journal of Roentgenology.)

contact and is normally seen. Active extravasation of contrast material at the level of the diaphragm and asymmetric thickening of the diaphragm also suggest injury. Elevation of the hemidiaphragm alone is not specific to diaphragmatic rupture because it can be the result of eventration, phrenic nerve injury, or preexisting paralysis.⁶⁸⁻⁷¹

This diagnosis is often difficult, and traumatic hernias often go undetected for days or even years because of subtle changes on chest radiographs, nonsurgical management of thoracic or abdominal injuries, and diversion of attention to more immediate life-threatening injuries. Other diagnostic difficulties arise because left-sided defects may be covered by omentum; right-sided defects may be sealed by the liver; positive pressure ventilation may prevent herniation of abdominal contents into the thorax until mechanical ventilation is discontinued; and atelectasis, pleural effusion, lung contusion, or phrenic nerve paralysis may mask the tear. Onset of symptoms may be so long delayed that the traumatic event is forgotten.⁶⁸⁻⁷¹

Anterior Abdominal Wall

The muscles and fascial layers of the anterior abdominal wall provide containment, support, and protection for the intraperitoneal contents and are involved in movement and breathing. These structures usually receive little attention in cross-sectional imaging, but they can be involved in a wide variety of congenital, inflammatory, neoplastic, and iatrogenic processes. In CT and MRI, routine imaging protocols are usually adequate to evaluate abdominal wall lesions; ultrasound examinations must be tailored to the evaluation of the anterior abdominal wall through the use of high-frequency (5-7.5 MHz) transducers with short focus. All of these techniques provide excellent anatomic detail for the evaluation of anterior abdominal wall disease.

ANATOMY

The anatomy of the anterior abdominal wall can be discussed in two regions. The anterior wall of the abdomen and upper

pelvis is a relatively simple, multilayered structure, whereas the fascial planes, spaces, and structures of the lower pelvis are more complex. These anatomic relationships dictate the origin and spread of disease processes.

In general, superficial to deep dissection of the anterior abdominal wall exposes skin, subcutaneous fat, superficial muscle fascia, one or more muscles, deep muscle fascia, properitoneal fat, and the peritoneum.^{72,73} The rectus muscle is present on either side of the midline linea alba, which runs from the xiphoid process to the symphysis pubis (Fig. 112-25). Along its superior aspect, the rectus abdominis muscle is surrounded by the aponeurosis of the three flank muscles. Approximately halfway between the umbilicus and the symphysis pubis, the aponeurosis of the internal oblique muscle and the transversus abdominis muscle no longer contribute to the posterior aspect of the rectus sheath. This transition, marked by the arcuate line, leaves the rectus invested posteriorly only by the thin transversalis fascia from the arcuate line to the pubic symphysis. The lateral abdominal muscles (from superficial to deep) include the external oblique, internal oblique, and transversus abdominis muscles, and they are separated from the rectus by the linea semilunaris. Asymmetry of abdominal wall muscles is common and often results from congenital variation or postoperative atrophy. The properitoneal fat stripe is frequently evident on plain radiographs. Ascites causes a shift of this lucency away from the adjacent colon, whereas inflammatory lesions of the peritoneal cavity or abdominal wall can obliterate it.

An anatomic model analogous to the retroperitoneal spaces around the kidneys has been advanced to simplify the understanding of the extraperitoneal spaces surrounding the bladder.⁷⁴ The umbilicovesical fascia originates at the umbilicus and spreads as a fan-shaped structure around the urachus, obliterated umbilical arteries, and bladder to terminate in the fascial layers of the deep pelvis. In this way, the umbilicovesical fascia is analogous to Gerota's fascia, creating a prevesical space anterior to the umbilicovesical fascia (like the anterior pararenal space) with a perivesical space between this fascia and the bladder (like the perirenal space). The analogy to the perirenal spaces is completed by noticing that the bladder, urachus, and

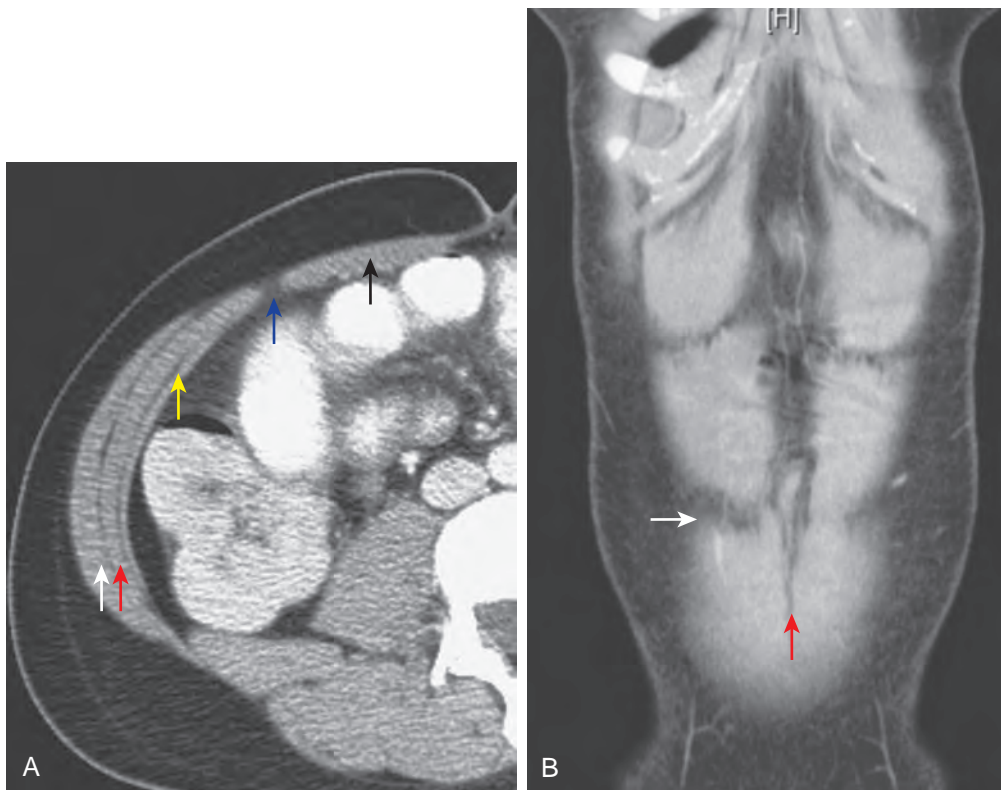


Figure 112-25 Anterior abdominal wall anatomy. **A.** Axial CT image of the normal anatomy of the abdominal wall: external oblique muscle (white arrow), internal oblique muscle (red arrow), transversus abdominis muscle (yellow arrow), linea semilunaris muscle (blue arrow), and rectus abdominis muscle (black arrow). **B.** Coronal CT image of the normal anatomy of the abdominal wall: aponeurosis (white arrow) and linea alba (red arrow).

obliterated umbilical arteries lie in the perivesical space, parallel to the kidneys, ureters, and adrenal glands in the perirenal space. The prevesical space represents a large potential space. Fluid collections in this space can be confined to the low pelvis, where this compartment is also known as the retropubic space or the space of Retzius. Larger collections, however, quickly track upward and laterally into the properitoneal space. Fluid in the prevesical space can also enter the rectus sheath below the level of the arcuate line, probably at perforations in the transversalis fascia of the inferior epigastric vessels. The perivesical space, however, is confined closely around the bladder.⁷⁴

CONGENITAL LESIONS

Urachal Abnormalities

The urachus is an extraperitoneal tubular structure that courses from the umbilicus to the bladder dome. It is the obliterated remnant of the allantois and perhaps of a portion of the cloaca. This three-layered cord is lined with transitional epithelium supported by a layer of blood vessels and lymphatics enclosed by a muscle layer.⁷⁵ Dissections of fetuses have shown that at or before birth, the urachus has involuted into a fibrous cord or is patent as a 1-mm tube extending from the bladder dome. This lumen is usually quickly obliterated.⁷⁶

Four congenital lesions of the urachus are known: patent urachus, urachal cyst, urachal sinus, and vesicourachal diverticulum.^{75,77} Patent urachus is evident in the first moments or days of life. The umbilical cord may be thickened and tense

from urine reflux, and an umbilical hernia may be present. Urine leaks from the umbilicus when it is ligated. Numerous series have reported an association between patent urachus and lower urinary tract obstruction (14%-50% of cases), but it is not clear whether urethral obstruction is the direct cause of patent urachus.⁷⁵ The diagnosis is confirmed by analyzing the expressed fluid for urea and creatinine, by observing a color change at the umbilicus when dye is injected into the bladder, or with fistulography performed by cannulating the opening at the umbilicus.⁷⁵ Voiding cystourethrography may demonstrate the communication, and it offers the additional benefit of excluding a lower obstruction.

If only a portion of the urachus remains unobliterated, a urachal cyst occurs. It frequently becomes apparent in adults as an enlarging mass, a sensation of fullness, or infection. These lesions require cross-sectional imaging for detection because there is no communication with the bladder or umbilicus.⁷⁸ CT or ultrasound offers the immediate advantage of cyst puncture and drainage for diagnostic purposes. A course of percutaneous drainage and antibiotic therapy is beneficial preoperatively to reduce infectious complications at surgery.⁷⁹ Untreated infected cysts usually drain to the anterior abdominal wall, but they may spontaneously rupture into the peritoneal cavity.⁷⁵ Definitive therapy requires complete excision with resection of a cuff of bladder dome.^{80,81}

A urachal sinus is likely the result of an infected urachal cyst that dissects and drains to the umbilicus or, less commonly, to the bladder. These lesions are manifested with umbilical

drainage or urinary tract infection. Other communicating tracts may exist if a remnant of the omphalomesenteric duct allows a connection to the bowel lumen, mesentery, or peritoneal space. Fistulography is useful for delineating the course of the tracts, and complete excision is required.

Omphalomesenteric Duct Abnormalities

Rarely, anomalies of the omphalomesenteric duct are manifested as periumbilical processes.^{75,77} This tubular structure connects the umbilicus to the gut in early embryonic development and is usually obliterated by the 10th week of gestation. A variety of malformations can arise if part or all of this communication from the gut to the umbilicus remains open.⁷⁷ Incomplete closure of the deep end of this structure leads to the development of Meckel's diverticulum, which is the most common omphalomesenteric abnormality. Rarely, a patent duct allows free communication from the ileum to the umbilicus. This lesion can be easily differentiated from patent urachus by noticing the nature of the discharge and by performing fistulography. If only the superficial end of the duct is patent, an omphalomesenteric sinus is present, which is manifested with mucoid discharge. A polypoid mass of small bowel mucosa may be present.⁸² If both ends of the duct close but the midportion is not obliterated, an omphalomesenteric (vitelline) cyst forms and mucoid secretions from the intestinal lining accumulate.⁷⁵

Prune-Belly Syndrome

Prune-belly syndrome, also known as Eagle-Barrett syndrome, is a constellation of absence of the anterior abdominal wall muscles, cryptorchidism, and dilation of ureters and bladder; it has no known cause.^{83,84} The manifestations vary; the most profoundly affected infants die at or shortly after birth of pulmonary hypoplasia resulting from oligohydramnios (i.e., Potter's syndrome). Milder cases are treated by repair of undescended testes or vesicoureteral reflux. Milder cases may have only slight wrinkling of the anterior abdominal wall or diastasis of the rectus musculature.⁸³ CT easily demonstrates the defects in the anterior abdominal wall and the genitourinary abnormalities.

FLUID COLLECTIONS

Hematoma

Hematomas of the anterior abdominal wall frequently involve the rectus sheath, although lateral collections do occur (Fig. 112-26).⁷³ These hematomas originate from tears in muscle fibers or blood vessels and may be spontaneous or related to trauma, surgery, anticoagulation, straining, coughing, or iatrogenic causes such as needle biopsy or aspiration.^{85,86} Pain, blood loss, ecchymosis, and abdominal mass may suggest the correct diagnosis, but clinical signs are often absent or nonspecific. Pain or fever may suggest the presence of abscess or other acute intra-abdominal process, and an accurate diagnosis is required to avoid unnecessary intervention.⁸⁶

Rectus sheath hematomas above the arcuate line are simple to diagnose because of their location and configuration. Transverse images demonstrate ovoid expansion of the rectus sheath. Longitudinal images show a spindle-shaped lesion.⁸⁶ Below the arcuate line, these collections extend into the prevesical space to displace and to compress the pelvic viscera.⁸⁷ Other diagnoses, such as urinoma, abscess, or lymphocele, must be considered for pelvic fluid collections. Conversely, urinomas, abscesses, or lymphoceles starting in the prevesical space can mimic a

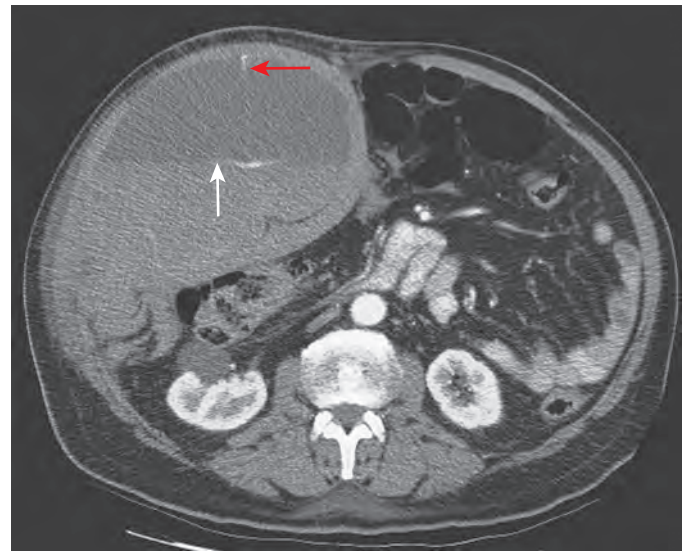


Figure 112-26 Lateral abdominal wall hematoma. A hematocrit effect (white arrow) is identified. Notice that active extravasation of contrast material (red arrow) is present.

rectus sheath hematoma if they track cranially. The subfascial hematoma from cesarean section is also a prevesical hematoma, located between the uterus and the anterior abdominal wall. Because the surgical approach is different, this lesion must be differentiated from a bladder flap hematoma, which arises between the lower uterine segment and the bladder.⁸⁸

Arterial puncture in the femoral sheath with subsequent hematoma formation has the potential to involve the anterior abdominal wall. The femoral sheath is contiguous superiorly with the transversalis fascia, and hematomas formed in the femoral sheath can expand rapidly to fill the prevesical space. These hematomas can extend into the rectus muscles or lateral abdominal wall muscles.¹⁸ Blood can also track directly from the groin into the lateral abdominal wall, primarily along the transversalis fascia and transversus abdominis muscle.^{89,90} In any case of retroperitoneal, extraperitoneal, or abdominal wall hematoma, clinical signs and symptoms are poorly localized and underrepresent the hematoma. CT is useful for documenting the full extent of the lesion, and changes over time are readily apparent. Continued bleeding requires surgical intervention.⁹¹

The CT, ultrasound, and MRI appearances of blood vary with the age of the clot, the hematocrit of the patient, and, in the case of CT or MRI, the use of contrast material, which alters the appearance of surrounding muscle.⁸⁵ On CT scans, blood is commonly hyperdense and heterogeneous. The hyperdensity is within areas of clot and is surrounded by lower attenuation collections of serum. Dependent layering of cellular elements in a hematoma can be demonstrated by CT or ultrasound (see Fig. 112-26).⁸⁵ The MRI appearance of blood is highly variable and can frequently be indistinguishable from tumor or abscess.⁹²

Urinoma

Bladder rupture usually occurs in the setting of blunt abdominal trauma, often with pelvic fracture. Penetrating and iatrogenic injuries to the bladder are occasionally encountered. The distended urinary bladder can rupture into the intraperitoneal space because of tears along the dome of the bladder.

Extraperitoneal bladder rupture can be confined solely to the perivesical space or can extend into the prevesical space of Retzius or into the scrotum, thigh, penis, or retroperitoneum.⁹³ Urinomas from bladder rupture are part of the differential diagnosis of anterior abdominal wall fluid collections. CT can frequently demonstrate these collections, but cystography is superior for urethral injury and remains required whenever bladder rupture or urethral injury is suspected.^{93,94}

Abscess and Cellulitis

Focal inflammatory lesions of the anterior abdominal wall can be postoperative, post-traumatic, or spontaneous (i.e., associated with diabetes mellitus or immunosuppression). They can also represent extension of an intra-abdominal process, such as abscess or Crohn's disease.^{73,95,96} Often, these lesions occur in postoperative or critically ill patients, with concomitant sepsis. Like hematomas, abdominal wall abscesses are difficult to fully delineate by clinical means. CT, MRI, and ultrasound have been advocated as methods for evaluation of abdominal wall infections.^{73,95,96} The goals of any cross-sectional examination for this indication are fourfold. First, the inflammatory lesion must be carefully localized. Whereas a subcutaneous abscess may respond to simple incision and drainage, deeper lesions may require more aggressive therapy. Second, evidence for underlying causative factors, such as Crohn's disease, infected or perforated tumor, or intra-abdominal abscess, should be sought. In this regard, ultrasound has a significant limitation because of the difficulty of recognizing bowel or mesenteric lesions.⁹⁶ Third, cellulitis or phlegmon without a well-defined fluid collection must be differentiated from frank abscess because antibiotic therapy alone is inadequate to cure an abscess. Fourth, percutaneous drainage should be offered in appropriately selected cases. CT remains the imaging procedure of choice for inflammatory lesions of the abdominal wall because it accurately delineates intraperitoneal and retroperitoneal associated processes and offers appropriate planning information and guidance for drainage.⁹⁵

Smaller abdominal wall abscesses are usually ovoid or spindle shaped. As they enlarge, they become progressively more mass-like. They may displace structures such as liver, spleen, or bladder and can be mistaken for intraperitoneal or retroperitoneal collections.⁹⁵ CT or ultrasound usually resolves the fluid components necessary to differentiate abscess from cellulitis (Fig. 112-27). In general, cellulitis and phlegmon have ill-defined margins, with the exception of any margin sharply defined by a fascial plane.⁹⁵

Necrotizing fasciitis is a rare form of aggressive soft tissue infection usually seen in diabetics or alcoholics. This entity is usually caused by an underlying infection of the lower genitourinary tract or soft tissues of the perianal region, and most infections are centered in the pelvis,⁹⁷ although necrotizing fasciitis has also been reported in other locations. It can arise spontaneously or from blunt or penetrating trauma, surgery, venous stasis, or decubitus ulcers.⁹⁸ Thrombosis of small subcutaneous arteries is seen on pathologic examination, and the resultant ischemia likely allows the aggressive infection to occur.⁹⁷ Soft tissue gas has been emphasized as the radiologic hallmark of this disorder,⁹⁸ but gas alone is not sufficient for the diagnosis to be made because soft tissue gas may result from fistulas, drains, penetrating injury, or molecular oxygen from hydrogen peroxide wound irrigation.⁹⁹ Most patients with necrotizing fasciitis are toxic at the time



Figure 112-27 Abdominal wall abscess. An abscess (arrow) involves the rectus abdominis muscles in this postoperative patient. Notice the inflammatory changes in the subcutaneous fat.

of presentation and require aggressive antibiotic therapy and surgical débridement. Mortality rates of 20% to 50% have been reported.⁹⁸ Another unusual form of abdominal wall infection is actinomycosis. This infection usually involves the abdominal wall by direct inoculation at trauma, extension from an infected intra-abdominal source, or blood-borne infection. Although these lesions are responsive to penicillin, they mimic neoplasm. The correct diagnosis is often not made until surgical biopsy.¹⁰⁰

NEOPLASMS

Primary Malignant Neoplasms

Primary malignant neoplasms of the anterior abdominal wall are uncommon. They include sarcomas, desmoid tumors (i.e., tumors of mesenchymal origin), and urachal carcinoma. Sarcomas are further subtyped histologically as rhabdomyosarcomas, fibrosarcomas, leiomyosarcomas, liposarcomas, synovial sarcomas, malignant schwannomas, malignant fibrous histiocytomas, and poorly differentiated sarcomas.^{101,102} Desmoid tumors represent a low-grade, nonmetastasizing variant of fibrosarcoma, and they have a unique tendency to arise in musculoaponeurotic planes. They are locally aggressive tumors and may involve bowel loops or bladder deep to the tumor or adjacent ribs or pelvic bones.^{101,102} Their histologic appearance, local invasiveness, and predilection for recurrence have inspired their other name of *aggressive fibromatosis*. Desmoid tumors most often occur in women of childbearing age and sometimes arise in a preexisting surgical scar.¹⁰¹⁻¹⁰³ Desmoid tumors arise frequently in the colectomy scar of patients with Gardner's syndrome and may be accompanied by desmoid tumors of the mesentery or paraspinous musculature.¹⁰⁴

Differentiation of desmoid tumors from the various sarcomas is often not possible unless distant metastatic disease is present.⁷³ Desmoids are frequently well defined.¹⁰⁵ Fibrous tumors are often hypoechoic sonographically and hyperdense compared with muscle on CT studies, particularly on postcontrast scans.¹⁰⁵⁻¹⁰⁷ MR scans show the expected low signal intensity of fibrous tissue on T1- and T2-weighted images, and the multiple imaging planes available with MR scanning may have

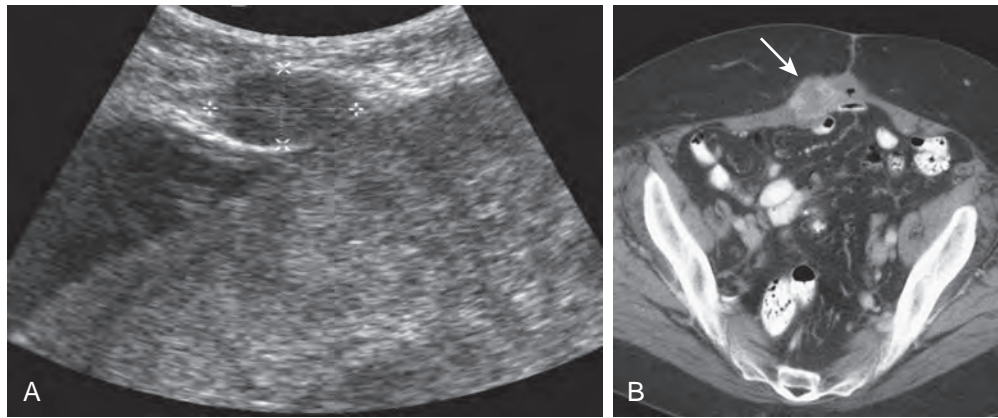


Figure 112-28 Abdominal wall metastatic malignant neoplasm. **A.** Longitudinal sonogram demonstrates a hypoechoic metastasis (cursors) within the subcutaneous fat of the anterior abdominal wall from a gastric carcinoma. **B.** Enhancing abdominal wall metastasis (arrow) from colon cancer.

some advantage in showing the origin and extent of these lesions.³⁷ These lesions require wide excision, and preoperative evaluation of the extent of the lesion is invaluable for surgical planning.¹⁰⁷

Urachal carcinoma is a rare lesion, usually arising in the juxtavesical segment of the urachus. Classic clinical features include the passage of blood or mucus in the urine. These lesions are most commonly adenocarcinoma (94%), and they usually occur in males (75%).¹⁰⁸ The lesion is frequently calcified; it deforms the bladder apex and may shift the ureters laterally.¹⁰⁸

Metastatic Disease

Although subcutaneous metastatic deposits are usually clinically evident, they may be overlooked, particularly in the obese patient. These soft tissue lesions are usually well visualized because of the naturally homogeneous background provided by subcutaneous fat. CT, ultrasound, or MRI can demonstrate these lesions, and changes in these metastases over time can be used as one marker of response to chemotherapy (Fig. 112-28).¹⁰⁹ Typical primary lesions that cause subcutaneous metastases include melanoma and lung, renal, and ovarian cancer.⁷³ Direct spread of a variety of intra-abdominal malignant neoplasms to the abdominal wall is also common. A unique, iatrogenic form of spread to the abdominal wall is occasionally seen in patients with indwelling drains placed to manage malignant obstruction of the biliary tract.¹¹⁰ Rarely, percutaneous biopsy can seed subcutaneous metastasis.¹¹¹ Gastric cancer has a peculiar predilection to produce an isolated metastasis near the umbilicus. This probably represents a form of peritoneal metastasis rather than nodal spread.¹¹²

Benign Lesions

A variety of benign tumors of the abdominal wall can be manifested as soft tissue masses. These lesions, discovered incidentally, include lipomas, neurofibromas, and other mesenchymal tumors.⁷³ On occasion, endometriomas can occur in the anterior abdominal wall, incorporated in a surgical scar, typically in the setting of prior cesarean section. These hormonally responsive lesions can be painful at the time of menses and can be easily missed with pelvic ultrasound if the near field is not carefully examined.¹¹³

MISCELLANEOUS CONDITIONS

Vascular Lesions

Small, subcutaneous blood vessels are frequently evident on abdominal CT scans; however, an increase in the size or number of these vessels (usually veins) should raise suspicion of an intra-abdominal venous abnormality. Veins are recognized by their intense enhancement and tubular or serpiginous configuration on multiple, contiguous images. Abdominal wall venous collateral vessels may occur in the setting of systemic venous occlusion or portal hypertension, and the appearance of the collateral vessels alone often does not lead to a definitive diagnosis. Patients with portal hypertension usually have a large number of associated findings that lead to the correct diagnosis, including retroperitoneal, mesenteric, perisplenic, or paraesophageal varices and cirrhotic hepatic changes.¹¹³⁻¹¹⁵ One specific collateral vessel, the recanalized umbilical or paraumbilical vein, is highly specific for portal hypertension.¹¹³⁻¹¹⁵ This vessel drains the portal venous system from the left portal vein along the falciform ligament into the anterior abdominal wall, terminating in many paraumbilical systemic veins, causing caput medusae.

Vascular Grafts

Surgically placed arterial grafts are easily identified in the subcutaneous tissues by CT, ultrasound, or MRI.⁷³ Axillary-femoral bypass grafts are oriented parallel to the long axis of the body along the lateral abdominal wall, whereas femoral-femoral grafts cross the lower abdomen just above the symphysis pubis. Patency of these grafts is usually apparent by palpation but can be confirmed by Doppler ultrasound.⁷³

Other Implanted Devices

Chronic ambulatory peritoneal dialysis is performed on patients in renal failure by sequentially infusing fluid into the peritoneal cavity and removing it to allow removal of toxins and regulation of electrolytes. This technique requires the placement of a catheter that crosses the anterior abdominal wall. Leaks, hernias, or fluid collections at the catheter entry site are optimally demonstrated by CT (Fig. 112-29). It is beneficial to infuse dialysate mixed with an iodinated contrast agent to enhance visualization of the configuration of the peritoneal lining at the catheter site.¹¹⁵



Figure 112-29 CSFoma: CT features. There is a fluid collection (arrow) in the subcutaneous fat of the anterior pelvic wall due to malposition of ventriculoperitoneal shunt tube (red arrow).

Other devices, such as infusion ports, chemotherapy reservoirs, and cardiac pacemakers, are commonly seen with cross-sectional imaging. Unless the device was placed recently, the presence of gas or fluid around the implant should raise suspicion of infection.

Calcifications

Hypercalcemic states, dermatomyositis, idiopathic calcinosis, Ehlers-Danlos syndrome, injection granulomas, and epidermolysis bullosa can cause subcutaneous calcification.¹¹⁵ These can be precisely located by CT.

Subcutaneous Gas

Although most cases of subcutaneous gas are caused by trauma or surgery, infection and ruptured viscus must also be considered.⁷³ These collections are well localized on CT scans, and underlying pathologic conditions, including fistulas to bowel and abscesses, also can be evaluated.¹¹⁵⁻¹¹⁷

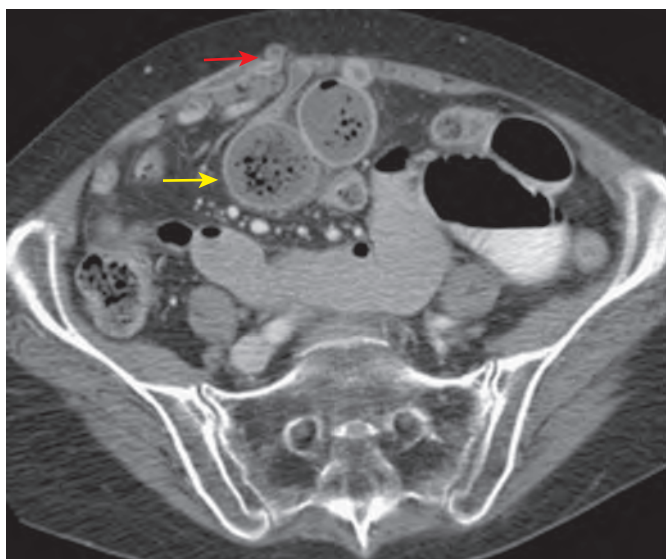


Figure 112-30 Trocar deformity. Anterior abdominal wall trocar-associated hernias (red arrow) are seen causing small bowel obstruction (yellow arrow) with the small bowel feces sign.

Laparoscopic Injuries

Laparoscopic surgery is being used for an increasing number of indications in the abdomen and pelvis. This surgery requires at least four holes in the abdominal wall created by a trocar. Each one of these holes can lead to the formation of a permanent defect (Fig. 112-30), which can serve as a pathway for future herniation.¹¹⁸⁻¹²⁰

Conclusions

Cross-sectional imaging provides an excellent, noninvasive means of evaluating pathologic processes of the anterior abdominal wall. Specific observations on the nature, location, extent, and underlying causes of these lesions can be made, therapy planned and instituted, and follow-up accomplished.

REFERENCES

1. Trainer V, Leung C, Owen RE, et al: External anterior abdominal wall and pelvic hernias with emphasis on the key diagnostic features on MDCT. *Clin Radiol* 68:388–396, 2013.
2. Aguirre DA, Santosa AC, Casola G, et al: Abdominal wall hernias: Imaging features, complications, and diagnostic pitfalls at multi-detector row CT. *Radiographics* 25:1501–1520, 2005.
3. Martin LC, Merkle EM, Thompson WM: Review of internal hernias: Radiographic and clinical findings. *AJR Am J Roentgenol* 186:703–717, 2006.
4. Mathieu D, Luciani A: Internal abdominal herniations. *AJR Am J Roentgenol* 183:397–404, 2004.
5. Murphy KP, O'Connor PJ, Maher MM: Adult abdominal hernias. *AJR* 202:W506–W511, 2014.
6. Blachar A, Federle MP, Brancatelli G, et al: Radiologist performance in the diagnosis of internal hernia by using specific CT findings with emphasis on transmesenteric hernia. *Radiology* 221:422–428, 2001.
7. Graf JL, Caty MG, Martin DJ, et al: Pediatric hernias. *Semin Ultrasound CT MR* 23:197–200, 2002.
8. Bower C, Roth JS: Economics of abdominal wall reconstruction. *Surg Clin North Am* 93:1241–1245, 2013.
9. Blachar A, Federle MP: Internal hernia: Clinical and imaging finding in 17 patients with emphasis on CT criteria. *Radiology* 218:68–74, 2001.
10. Suchato C, Pekkann P, Panjapiyakul C: CT findings in symptomatic left paraduodenal hernia. *Abdom Imaging* 21:148–149, 1996.
11. Osadchy A, Weisenberg N, Wiener Y, et al: Small bowel obstruction related to left-side paraduodenal hernia: CT findings. *Abdom Imaging* 30:53–55, 2005.
12. Oriuchi T, Kinouchi Y, Hiwatashi N, et al: Bilateral paraduodenal hernias: Computed tomography and magnetic resonance imaging appearance. *Abdom Imaging* 23:278–280, 1998.
13. Osadchy A, Weisenberg N, Wiener Y, et al: Small bowel obstruction related to left-side paraduodenal hernia: CT findings. *Abdom Imaging* 30:53–55, 2005.
14. Wojtasek DA, Codner MA, Nowak EJ: CT diagnosis of cecal herniation through the foramen of Winslow. *Gastrointest Radiol* 16:77–79, 1991.
15. Bach DB, Satin R, Palayew M, et al: Herniation and strangulation of the gallbladder through

- the foramen of Winslow. *AJR Am J Roentgenol* 142:541–542, 1984.
16. Tran TL, Regan F, Al-Kutobi MA: Computed tomography of lesser sac hernia through the gastrohepatic omentum. *Br J Radiol* 64:372–374, 1991.
 17. Inoue Y, Nakamura H, Mizumoto S, et al: Lesser sac hernia through the gastrocolic ligament: CT diagnosis. *Abdom Imaging* 21:145–147, 1996.
 18. Meissnitzer T, Meissnitzer MW, Forstner R, et al: Imaging of transmesocolic internal hernias following retrocolic Roux-Y reconstruction: Tips and tricks for radiologists. *Rofo* 185:419–427, 2013.
 19. Yip AWC, Tong KK, Cho TK: Mesenteric hernia through defects of the mesosigmoid. *Aust N Z J Surg* 60:396–399, 1990.
 20. Janin Y, Stone AM, Wise L: Mesenteric hernia. *Surg Gynecol Obstet* 150:747–754, 1980.
 21. Kessler RM, Lentz JC, Abdenour GE, et al: Mesenteric vascular gas secondary to ischemic bowel in transmesenteric hernia. *Radiology* 140:645–646, 1981.
 22. Cohen AM, Patel S: Arteriographic findings in congenital transmesenteric internal hernia. *AJR Am J Roentgenol* 133:541–543, 1979.
 23. Balthazar EJ, Birnbaum BA, Megibow AJ, et al: Closed loop and strangulating intestinal obstruction: CT signs. *Radiology* 185:769–775, 1992.
 24. Newson BD, Kukora JS: Congenital and acquired internal hernias: Unusual causes of small bowel obstruction. *Am J Surg* 152:279–285, 1986.
 25. Liakakos T, Liatas AC, Kakoulides D, et al: Multiple congenital internal hernias as a cause of acute abdominal symptoms in late adult life. *Eur J Surg* 158:561–562, 1992.
 26. Wang HH: Internal herniation of the efferent jejunal loop after gastroenterostomy. *Am J Surg* 124:587–590, 1972.
 27. Rutledge RH: Retroanastomotic hernias after gastrojejunal anastomoses. *Ann Surg* 177:547–553, 1973.
 28. Gale ME, Gerzof SG, Kiser LC, et al: CT appearance of afferent loop obstruction. *AJR Am J Roentgenol* 138:1085–1088, 1982.
 29. Lee DH, Lim JH, Ko YT: Afferent loop syndrome: Sonographic findings in seven cases. *AJR Am J Roentgenol* 157:41–43, 1991.
 30. Rao K, Gooneratne N, Asokan S, et al: Afferent loop obstruction documented with hepatobiliary imaging. *Gastrointest Radiol* 8:345–347, 1983.
 31. Wechsler RJ, Kurtz AB, Needleman L, et al: Cross-sectional imaging of abdominal wall hernias. *AJR Am J Roentgenol* 153:517–521, 1989.
 32. Zafar HM, Levine MS, Rubesin SE, et al: Anterior abdominal wall hernias: Findings in barium studies. *Radiographics* 26:691–699, 2006.
 33. Peters JC, Reinertson JS, Polansky SM, et al: CT demonstration of traumatic ventral hernia. *J Comput Assist Tomogr* 12:710–711, 1988.
 34. Harrison LA, Keesling CA, Martin NL, et al: Abdominal wall hernias: Review of herniography and correlation with cross-sectional imaging. *Radiographics* 15:315–332, 1995.
 35. Sucandy I, Miles M, Gallagher S, et al: Spigelian hernia, diagnosis, and minimally invasive repair: A case series of 11 patients. *Am Surg* 79:E284–E285, 2013.
 36. Holder LE, Schneider HJ: Spigelian hernias: Anatomy and roentgenographic manifestations. *Radiology* 112:309–313, 1974.
 37. Balthazar EJ, Subramanyam BR, Megibow A: Spigelian hernia: CT and ultrasonography diagnosis. *Gastrointest Radiol* 9:81–84, 1984.
 38. Luedke M, Scholz FJ, Larsen CR: Computed tomographic evaluation of spigelian hernia. *Comput Med Imaging* 12:123–129, 1988.
 39. Shenouda NF, Hyams BB, Rosenbloom MB: Evaluation of spigelian hernia by CT. *J Comput Assist Tomogr* 14:777–778, 1990.
 40. Baker ME, Weinerth JL, Andriani JL, et al: Lumbar hernia: Diagnosis by CT. *AJR Am J Roentgenol* 148:565–567, 1987.
 41. Faro SH, Racette CD, Lally JF, et al: Traumatic lumbar hernia: CT diagnosis. *AJR Am J Roentgenol* 154:757–759, 1990.
 42. Lawdahl RB, Moss CN, Van Dyke JA: Inferior lumbar (Petit's) hernia. *AJR Am J Roentgenol* 147:744–745, 1986.
 43. Siffring PA, Forrest TS, Frick MP: Hernias of the inferior lumbar space: Diagnosis with US. *Radiology* 170:190, 1989.
 44. Ghahremani GG, Gore RM: CT diagnosis of postoperative abdominal complications. *Radiol Clin North Am* 27:787–804, 1989.
 45. Hojer AM, Rygaard H, Jess P: CT in the diagnosis of abdominal wall hernias. *Eur Radiol* 7:1416–1418, 1997.
 46. Jaffe TA, O'Connell MJ, Harris JP, et al: MDCT of abdominal wall hernias: Is there a role for Valsalva's maneuver? *AJR Am J Roentgenol* 184:847–851, 2005.
 47. Bernardy MO, Umer MA, Flanagan RC: Computed tomography of hydrocele of the tunica vaginalis. *J Comput Assist Tomogr* 9:203–204, 1985.
 48. Salomonowitz E, Frick MP, Sommer G, et al: Symptomatic inguinal hernia: Association with intraabdominal mass lesions. *Gastrointest Radiol* 8:371–374, 1983.
 49. Van den Berg JC: Inguinal hernias: MRI and ultrasound. *Semin Ultrasound CT MRI* 23:143–156, 2002.
 50. Epner SL, Rozenblit A, Gentile R: Direct inguinal hernia containing bladder carcinoma: CT demonstration. *AJR Am J Roentgenol* 161:97–98, 1993.
 51. Kingsnorth AN: A clinical classification for patients with inguinal hernia. *Hernia* 8:242–246, 2004.
 52. Ghahremani GG: Radiology of Meckel's diverticulum. *Crit Rev Diagn Imaging* 26:1–43, 1986.
 53. Toms AP, Cash CC, Fernando B, et al: Abdominal wall hernias: A cross-sectional pictorial review. *Semin Ultrasound CT MR* 23:143–155, 2002.
 54. Middlebrook MR, Eftekhari F: Sonographic findings in Richter's hernia. *Gastrointest Radiol* 17:229–230, 1992.
 55. Boike G, Miller C, Spirtos N, et al: Bowel herniations after operative laparoscopy: A series of 19 cases and review of the literature. *Am J Obstet Gynecol* 172:1726–1733, 1995.
 56. Anderas P, Jona JZ, Glicklich M, et al: Femoral hernias in children: An infrequent problem. *Arch Surg* 122:950–951, 1987.
 57. Tam PKH, Lister J: Femoral hernia in children. *Arch Surg* 119:1161–1164, 1984.
 58. Markos V, Brown EF: CT herniography in the diagnosis of occult groin hernias. *Clin Radiol* 60:251–256, 2005.
 59. Lewin JR: Femoral hernia with upward extension into abdominal wall: CT diagnosis. *AJR Am J Roentgenol* 136:206–207, 1981.
 60. Ekberg O, Nordblom I, Fork FT, et al: Herniography of femoral, obturator and perineal hernias. *Rofo* 143:193–199, 1985.
 61. Nishina M, Chiiho F, Logino R, et al: Preoperative diagnosis of obturator hernia by computed tomography. *Semin Ultrasound CT MR* 23:193–196, 2002.
 62. Otsuka Y, Harihara Y, Nakajima K, et al: A case of bilateral obturator hernias; feasibility of combination study of computed tomography and ultrasonography to make diagnostic and therapeutic strategies. *Hepatogastroenterology* 50:1054–1056, 2003.
 63. Green BT: Strangulated obturator hernia: Still deadly. *South Med J* 94:81–83, 2001.
 64. Arat A, Haliloglu M, Cila A, et al: Demonstration of ureterosciatic hernia with spiral CT. *J Comput Assist Tomogr* 20:816–818, 1996.
 65. Ghahremani GG, Michael AS: Sciatic hernia with incarcerated ileum: CT and radiographic diagnosis. *Gastrointest Radiol* 16:120–122, 1991.
 66. Spring DB, Vandeman F, Watson RA: Computed tomographic demonstration of ureterosciatic hernia. *AJR Am J Roentgenol* 141:579–580, 1983.
 67. Silen W: Inguinal and incisional hernias. *Lancet* 363:83–84, 2004.
 68. Killeen KL, Shanmuganathan K, Mirvis SE: Imaging of traumatic diaphragmatic injuries. *Semin Ultrasound CT MRI* 23:184–192, 2002.
 69. Killeen KL, Mirvis SE, Shanmuganathan K, et al: Helical CT of traumatic diaphragmatic rupture secondary to blunt trauma. *AJR Am J Roentgenol* 173:1611–1616, 1999.
 70. Bergin D, Ennis R, Keogh C, et al: The “dependent viscera” sign in CT diagnosis of blunt traumatic diaphragmatic rupture. *AJR Am J Roentgenol* 177:1137–1140, 2001.
 71. Eren S, Ciris F: Diaphragmatic hernia: Diagnostic approaches with review of the literature. *Eur J Radiol* 54:448–459, 2005.
 72. Goodman P, Balachandran S: CT evaluation of the abdominal wall. *Crit Rev Diagn Imaging* 33:461–493, 1992.
 73. Wechsler RJ: *Cross-Sectional Analysis of the Chest and Abdominal Wall*, St. Louis, 1989, CV Mosby, pp 126–202.
 74. Balfe DM, Gratz B, Peterson C: Normal abdominal and pelvic anatomy. In Lee JKT, Sagel SS, Stanley RJ, et al, editors: *Computed Body Tomography with MRI Correlation*, ed 4, Philadelphia, 2006, Lippincott-Raven, pp 707–770.
 75. Bauer SB, Retik AB: Urachal anomalies and related umbilical disorders. *Urol Clin North Am* 5:195–211, 1978.
 76. Hammond G, Yglesias L, Davis JE: The urachus, its anatomy and associated fasciae. *Anat Rec* 80:271–287, 1941.
 77. DiSantis DJ, Siegel MJ, Katz ME: Simplified approach to umbilical remnant abnormalities. *Radiographics* 11:59–66, 1991.
 78. Sarno RC, Klauber G, Carter BL: Computer assisted tomography of urachal abnormalities. *J Comput Assist Tomogr* 7:674–676, 1983.
 79. Holten I, Lomas F, Mouratidis B, et al: Ultrasonic diagnosis of urachal abnormalities. *Australas Radiol* 40:2–8, 1996.
 80. Khati NJ, Enquist EG, Javitt MC: Imaging the umbilicus and periumbilical region. *Radiographics* 18:413–429, 1998.

81. Naiditch JA, Radhakrishnan J, Chin AC: Current diagnosis and management of urachal remnants. *J Pediatr Surg* 48:2148–2152, 2013.
82. Steck WD, Helwig EB: Umbilical granulomas, pilonidal disease, and the urachus. *Surg Gynecol Obstet* 120:1043–1057, 1965.
83. Berdon WE, Baker DH, Wigger HJ, et al: The radiologic and pathologic spectrum of the prune belly syndrome. *Radiol Clin North Am* 15:83–92, 1977.
84. Reinig JW, Curry NS, Schabel SI, et al: CT evaluation of the prune belly syndrome. *J Comput Tomogr* 5:548–549, 1981.
85. Davies RS, Goh GJM, Curtis JM, et al: Abdominal wall haematoma in anticoagulated patients: Role of imaging in diagnosis. *Australas Radiol* 40:109–113, 1996.
86. Fukuda T, Sakamoto I, Kohzaki S, et al: Spontaneous rectus sheath hematomas: Clinical and radiologic features. *Abdom Imaging* 21:58–61, 1996.
87. Berná JD, Garcia-Medina V, Guirao J, et al: Rectus sheath hematoma: Diagnostic classification by CT. *Abdom Imaging* 21:62–66, 1996.
88. Wiener MD, Bowie JD, Baker ME, et al: Sonography of subfascial hematoma after cesarean delivery. *AJR Am J Roentgenol* 148:907–910, 1987.
89. Trerotola SO, Kuhlman JE, Fishman EK: Bleeding complications of femoral catheterization: CT evaluation. *Radiology* 174:37–40, 1990.
90. Trerotola SO, Kuhlman JE, Fishman EK: CT and anatomic study of postcatheterization hematomas. *Radiographics* 11:247–258, 1991.
91. Illescas FF, Baker ME, McCann R, et al: CT evaluation of retroperitoneal hemorrhage associated with femoral arteriography. *AJR Am J Roentgenol* 146:1289–1292, 1986.
92. Anderson MW: Muscles. In Higgins CB, Hricak H, Helms CA, editors: *Magnetic Resonance Imaging of the Body*, ed 3, Philadelphia, 1997, Lippincott-Raven, pp 1321–1344.
93. Sandler CM, Hall JT, Rodriguez MB, et al: Bladder injury in blunt pelvic trauma. *Radiology* 158:633–638, 1986.
94. Kane NM, Francis IR, Ellis JH: The value of CT in the detection of bladder and posterior urethral injuries. *AJR Am J Roentgenol* 153:1243–1246, 1989.
95. Yeh H-C, Rabinowitz JG: Ultrasonography and computed tomography of inflammatory abdominal wall lesions. *Radiology* 144:859–863, 1982.
96. Sharif HS, Clark DC, Aabed MY, et al: MR imaging of thoracic and abdominal wall infections: Comparison with other imaging procedures. *AJR Am J Roentgenol* 154:989–995, 1990.
97. Clayton MD, Fowler JE, Jr, Sharifi R, et al: Causes, presentation and survival of fifty-seven patients with necrotizing fasciitis of the male genitalia. *Surg Gynecol Obstet* 170:49–55, 1990.
98. Fisher JR, Conway MJ, Takeshita RT, et al: Necrotizing fasciitis. Importance of roentgenographic studies for soft-tissue gas. *JAMA* 241:803–806, 1979.
99. Swayne LC, Ginsberg HN, Ginsburg A: Pneumoretroperitoneum secondary to hydrogen peroxide wound irrigations. *AJR Am J Roentgenol* 148:149–150, 1987.
100. Lau WY, Boey J, Fan T, et al: Primary actinomycosis of the abdominal wall. *Aust N Z J Surg* 56:873–875, 1986.
101. Shiu MH, Flancbaum L, Hajdu SI, et al: Malignant soft-tissue tumors of the anterior abdominal wall. *Arch Surg* 115:152–155, 1980.
102. Shiu MH, Weinstein L, Hajdu SI, et al: Malignant soft-tissue tumors of the anterior abdominal wall. *Am J Surg* 158:446–451, 1989.
103. Lou L, Teng J, Ban Y: Sonographic appearances of desmoid tumors. *J Ultrasound Med* 33:1519–1525, 2014.
104. Magid D, Fishman EK, Jones B, et al: Desmoid tumors in Gardner syndrome: Use of computed tomography. *AJR Am J Roentgenol* 142:1141–1145, 1984.
105. Einstein DM, Tagliabue JR, Desai RK: Abdominal desmoids: CT findings in 25 patients. *AJR Am J Roentgenol* 157:275–279, 1991.
106. Yeh HC, Rabinowitz JG, Rosenblum PJ: Complementary role of CT and ultrasonography in the diagnosis of desmoid tumor of abdominal wall. *Comput Radiol* 6:275–280, 1982.
107. Shinagare AB, Ramaiya NH, Jagannathan JP, et al: A to Z of desmoid tumors. *AJR Am J Roentgenol* 197:W1008–W1014, 2011.
108. Kwok-Liu JB, Zikman JM, Cockshott WP: Carcinoma of the urachus: The role of computed tomography. *Radiology* 137:731–734, 1980.
109. Dunnick NR, Schaner EG, Doppman JL: Detection of subcutaneous metastases by computed tomography. *J Comput Assist Tomogr* 2:275–279, 1978.
110. Williams KJ, Hayes AJ: A guide to oncological management of soft tissue tumours of the abdominal wall. *Hernia* 18:91–97, 2014.
111. Livraghi T, Damascelli B, Lombardi C, et al: Risk in fine-needle abdominal biopsy. *J Clin Ultrasound* 11:77–81, 1983.
112. Meyers MA: Gastric carcinoma: Imaging, staging, management. In Meyers MA, editor: *Neoplasms of the Digestive Tract*, Philadelphia, 1998, Lippincott-Raven, pp 93–110.
113. Amato MA, Levitt R: Abdominal wall endometrioma: CT findings. *J Comput Assist Tomogr* 8:1213–1214, 1984.
114. Yeh H-C, Stancato-Pasik A, Ramos R, et al: Paraumbilical venous collateral circulations: Color Doppler ultrasound features. *J Clin Ultrasound* 24:359–363, 1996.
115. Hollett MD, Marn CS, Ellis JH, et al: Complications of continuous ambulatory peritoneal dialysis: Evaluation with CT peritoneography. *AJR Am J Roentgenol* 159:983–989, 1992.
116. Lubat E, Gordon RB, Birnbaum BA, et al: CT diagnosis of posterior perineal hernia. *AJR Am J Roentgenol* 154:761–762, 1990.
117. Ianora AA, Midiri M, Vinci R, et al: Abdominal wall hernias: Imaging with spiral CT. *Eur Radiol* 10:914–919, 2000.
118. Meijer EJ, Timmermans L, Jeekel J, et al: The principles of abdominal wound closure. *Acta Chir Belg* 113:239–244, 2013.
119. Bower C, Roth JS: Economics of abdominal wall reconstruction. *Surg Clin North Am* 93:1241–1253, 2013.
120. Criss CN, Petro CC, Krpata DM, et al: Functional wall reconstruction improves core physiology and quality-of-life. *Surgery* 156:176–182, 2014.

SECTION
XIV

Pediatric Disease

Applied Embryology of the Gastrointestinal Tract

BRUCE R. JAVORS | ROI M. BITTANE

CHAPTER OUTLINE

Early Development

Division of the Intraembryonic Celom and Formation of the Diaphragm

Anomalies of Diaphragmatic Development

Diaphragmatic Hernia
Foramen of Morgagni Hernia
Eventration

Normal Liver Development

Abnormal Liver Development

Atypical Segmentation
Atypical Location

Normal Gallbladder and Bile Duct Development

Abnormal Gallbladder and Bile Duct Development

Phrygian Cap
Gallbladder Diverticulum
Positional Anomalies
Bifid Gallbladder or Duplication
Agenesis
Tracheobiliary Fistula
Biliary Atresia
Alagille's Syndrome
Cystic Disease
Caroli's Disease
Choledochal Cysts

Normal Development of the Esophagus

Abnormal Development of the Esophagus

Tracheoesophageal Fistula
Duplication
Stenosis
Esophageal Bronchus
Congenital Short Esophagus

Normal Development of the Stomach, Duodenum, and Lesser Omentum

Abnormal Development of the Stomach and Duodenum

Antral Web
Gastric Diverticula
Duplications
Duodenal Stenosis
Duodenal Web and Inverted Diverticulum

Normal Development of the Pancreas

Abnormal Development of the Pancreas

Annular Pancreas
Pancreas Divisum
Ectopic Pancreatic Tissue

Normal Development of the Lesser Sac and Greater Omentum

Abnormal Development of the Lesser Sac and Greater Omentum

Infracardiac Bursa
Omental Cyst

Normal Development of the Spleen

Abnormal Development of the Spleen

Accessory Spleen
Wandering Spleen
Asplenia
Polysplenia
Splenic-Gonadal Fusion

Normal Midgut Rotation and Fixation

Abnormal Midgut Rotation and Fixation

Duplication
Ileal Atresia
Mesenteric Cyst
Nonrotation
Reversed Rotation
Incomplete Rotation and Malrotation
Hyperrotation
Internal Herniations
Meckel's Diverticulum

The complex anatomy of the gastrointestinal tract and the peritoneal cavity arises from much simpler origins. The transition from the primitive straight tubular alimentary canal to the elongated and tortuous gut (and its accessory organs) suspended by mesenteries and encased by peritoneal reflections can readily be explained by a well-defined series of events. Although these processes are summarized individually, these multiple events often occur simultaneously with complex interactions.

Early Development

After fertilization, the zygote rapidly undergoes repeated mitotic divisions that result in an increased number of cells. This occurs without a corresponding increase in the cell mass.

Approximately 3 days after fertilization, a solid ball of cells (i.e., morula) develops. The next day, central cavities appear, which separate the cells into the trophoblast (from which part

of the placenta develops) and the embryoblast. Two days later, endometrial implantation begins.

During the second week of development, the spherical mass of cells flattens into a bilaminar disk. A primitive yolk sac also develops. During the third week, the embryonic disk rapidly develops into the embryo (i.e., gastrulation). The cells differentiate into the three classic germ cell layers: endoderm, mesoderm, and ectoderm.

The endoderm gives rise to the lining epithelium of the respiratory and gastrointestinal tracts as well as the glandular elements of the liver and pancreas. From the mesoderm arise the smooth muscle of the gastrointestinal tract, the connective tissues, and their associated blood vessels. Blood cells and their progenitors, striated muscle, bone, cartilage, and the reproductive and genitourinary tract are also mesodermal in origin. The ectoderm is the source of the epidermis and the nervous system.

Clefts appear within the lateral aspects of the developing intermediate mesodermal layer, forming the intraembryonic celom. These open laterally into the yolk sac. They lie between and separate the more dorsal somatic mesoderm from the ventral splanchnic mesoderm.¹ The somatic mesoderm, in association with the ectodermal layer, forms the embryonic body wall (i.e., somatopleure); the splanchnic mesoderm, along with the endoderm, forms the embryonic gut (i.e., splanchnopleure) (Fig. 113-1).

As the lateral margins of the embryonic disk move ventrally and medially, they begin to pinch off the yolk sac and the more laterally placed intraembryonic celom. Continued growth by the somatopleure and its eventual midline fusion complete the encompassment of the intraembryonic celom with formation of a cylindrical body cavity. The more centrally placed splanchnopleure also starts to close ventrally, partially separating the primary yolk sac into the gut and the secondary yolk sac, which is separated by the yolk stalk (Fig. 113-2).

A primitive alimentary tube is formed within the larger surrounding body cavity. The dorsal mesentery and its visceral peritoneum are derived from the splanchnopleure. Most of the ventral mesentery, also derived from the splanchnopleure, degenerates with time, leaving a large embryonic body cavity (i.e., celom).²

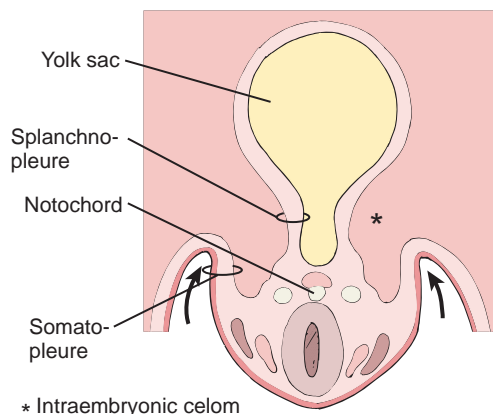


Figure 113-1 Embryologic development: early fourth week.

Cross section through the midportion of an embryo early in the fourth week shows infolding of the somatopleure as it begins to encase the intraembryonic celom. This eventually encompasses the body cavity. The splanchnopleure's contribution to the formation of the midgut is evident.

Division of the Intraembryonic Celom and Formation of the Diaphragm

During the fourth to sixth weeks of development, the large common intraembryonic celomic cavity is partitioned into pleural, pericardial, and peritoneal spaces. By the fourth week, a large pericardial cavity is connected to the peritoneal cavity by two smaller pericardioperitoneal canals. The pressure of the developing head causes the heart and pericardial cavity to be displaced caudally and ventrally. The pericardioperitoneal canals exit from the pericardium along its dorsal aspect to enter the peritoneum.

As the lung buds develop, they grow into the paired pericardioperitoneal canals. This produces two pairs of ridges. The cranial pair gives rise to the pleuropericardial membrane that eventually separates the primitive pericardial cavity into definitive pericardial and pleural spaces. The more caudal pair gives rise to the pleuroperitoneal membrane. This plays an important role in the development of the diaphragm. As the lung buds grow superiorly and the liver and peritoneal space expand inferiorly, these membranes become more prominent. They attach themselves to the abdominal wall along their dorsal and lateral margins. Their free edges project into the pericardioperitoneal canals.

During the sixth week, the free edges of the dorsolateral pleuroperitoneal membrane fuse with the midline dorsal mesentery of the esophagus, forming part of the primitive mediastinum at this point. The anterior half of the primitive diaphragm is formed by the septum transversum, which arises in the third week as a condensation of mesoderm. By the fourth week, it has thickened to form an incomplete division anteriorly between the pericardium and the peritoneal cavity (Fig. 113-3).

Between weeks 6 and 12, many changes take place in the relative contributions of these structures to the diaphragm that exists at birth. The large dorsolateral component formed by the pleuroperitoneal membranes decreases in size. Myoblasts from the abdominal wall migrate into the peripheral aspects of the membranes. These contribute to the growth of the diaphragm

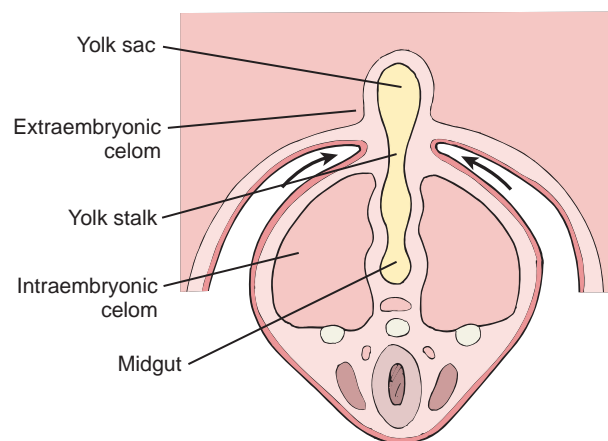


Figure 113-2 Embryologic development: late fourth week.

The cross section is similar to that in Figure 113-1, but it shows development at the end of the fourth week. The envelopment of the intraembryonic celom is almost complete. The yolk sac has separated into a more definitive yolk stalk and midgut.

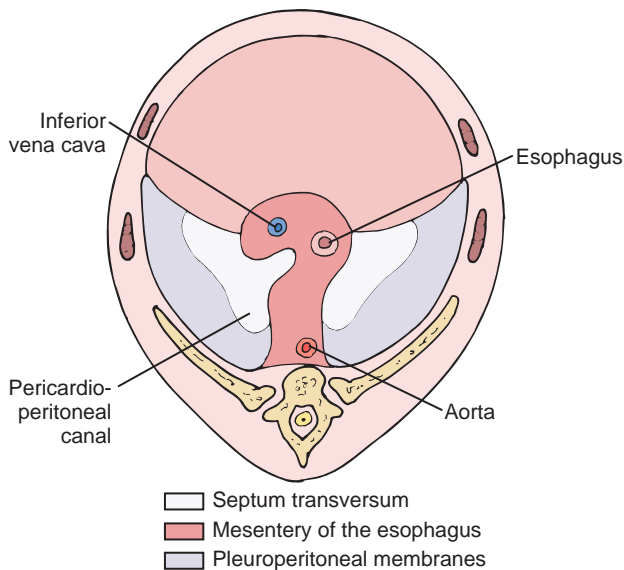


Figure 113-3 Embryologic development: fifth week. Diagram of a 5-week embryo as seen from below. The relative contributions of the septum transversum, esophageal mesentery, and pleuroperitoneal membranes change with further development.

and eventually give rise to the costophrenic sulci. Myoblasts also grow into the primitive dorsal esophageal mesentery, forming the diaphragmatic crura.

In addition to its complex formation, the diaphragm markedly shifts in position. In the fourth week, the septum transversum is at the level of the third to fifth cervical somites. The myoblasts and associated nerve innervation also arise from these levels. From the fourth to the sixth weeks, the dorsal part of the embryo grows rapidly, causing an apparent descent of the diaphragm. The mesenchyme of the septum transversum contributes its own myoblasts to the diaphragm, maintaining its original C3-C5 innervation. In its definitive state, the diaphragm lies at the level of the thoracolumbar junction while maintaining its phrenic nerve, midcervical innervation.

Anomalies of Diaphragmatic Development

DIAPHRAGMATIC HERNIA

If the pleuroperitoneal membrane fails to close entirely, a patent canal may persist between the pleural and the peritoneal cavities. If this dorsally and laterally placed canal is still present at the reduction of the physiologic herniation of the midgut at week 10 (discussed later), the returning bowel may herniate through this patent foramen of Bochdalek into the chest. This occurs most frequently on the left side.²

FORAMEN OF MORGAGNI HERNIA

A natural weakness in the anteromedial portion of the diaphragm (i.e., retrosternal) is caused by the passage of the superior epigastric vessels. Herniation of omentum or intestines may occur at this site, and it occurs most frequently on the right side.³

EVENTRATION

Defective muscle development of the dome of the diaphragm may lead to structural weakness and subsequent ballooning. Only a thin, aponeurotic sheet of tissue is then present. Abdominal contents may bulge into the thoracic cavity, simulating a difficult to differentiate eventration from a true herniation.

Normal Liver Development

During the fourth week of development, the caudal portion of the foregut develops a ventral bud called the primordial hepatic diverticulum. This endodermal liver bud enlarges and grows into and between the two layers of the ventral mesentery. More superiorly, it grows in contact with and into the mass of mesenchyme, the septum transversum. The ventral liver bud divides into cranial and caudal portions within the mesentery. The cranial portion gives rise to the liver and intrahepatic bile ducts; the caudal portion forms the gallbladder and cystic duct.⁴

The cranial liver bud further divides into right and left lobes, which are initially of equal size. The right lobe eventually becomes much larger than the left. The distal branches of the right and left lobe cords undergo canalization to become the definitive main right and left hepatic ducts. The intrahepatic biliary tree is thought to arise from the hepatic parenchyma. These cords of tissue extend along the randomly created pattern of portal vein tributaries (discussed later). Consequently, the pattern of intrahepatic bile ducts is variable.

The mature liver has two ligaments that represent remnants of embryologic vascular channels. These are the ligamentum teres (i.e., round ligament) within the falciform ligament and the ligamentum venosum. These develop from the vitelline and umbilical veins, respectively. The paired vitelline veins drain the yolk sac, pass through the developing liver and septum transversum, and empty into the right side of the primitive heart (i.e., sinus venosus). The vitelline veins within the liver create a meshlike network of vascular channels that become the hepatic sinusoids. Some of the lining cells of the sinusoids later differentiate into macrophages (i.e., Kupffer cells), the reticuloendothelial component of the liver.⁵ The segments of the vitelline veins proximal and distal to the sinusoids become, respectively, the hepatic veins and the hepatic portion of the portal vein.⁶

The paired umbilical veins drain the placenta and chorion. They pass through the septum transversum, contributing minimally to hepatic sinusoidal development, and then empty into the sinus venosus. The entire right umbilical vein and a segment of the left proximal (cephalad) to the liver atrophy. A large venous channel, the ductus venosus, arises from the hepatic sinusoidal network and carries blood from the distal (caudal) left umbilical vein into the sinus venosus, bypassing the liver. Eventually, the lumen of the ductus venosus is obliterated, and the structure becomes the ligamentum venosum. The distal portion of the left umbilical vein migrates medially to the liver edge, and its lumen closes. It then becomes the round ligament (i.e., ligamentum teres). This ligament, which connects the ligamentum venosum to the umbilicus, is encased within the most anterior portion of the ventral mesentery, the falciform ligament (Fig. 113-4).⁷

The mesenchymal septum transversum contributes to the ventral mesentery that surrounds the liver and gallbladder. The fibrous tissues of the liver, including Glisson's capsule,

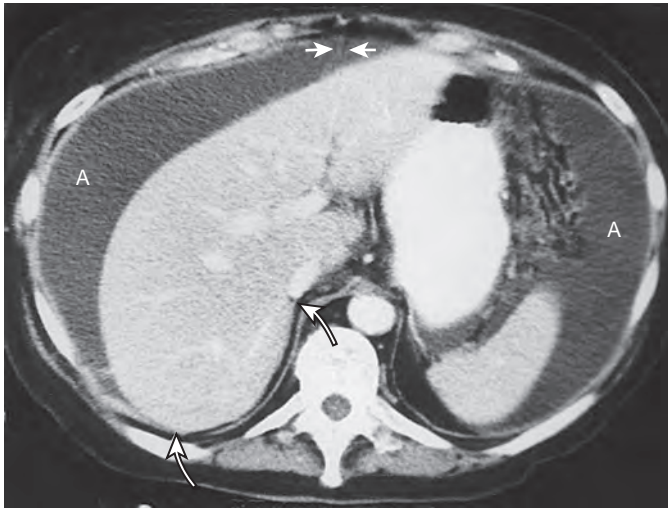


Figure 113-4 Falciform ligament and bare area of liver. CT of the upper abdomen shows a large amount of ascites (A) outlining the falciform ligament (*straight arrows*). Along the posterior aspect of the right lobe, there is a region not surrounded by the fluid: the bare area (*curved arrows*). This represents the portion of the liver that developed in contact with the septum transversum and that is not covered by the peritoneum.

embryonal hepatic hematopoietic tissues, and the Kupffer cells lining the sinusoids, are also derived from the septum transversum.⁷

The membranous ventral mesentery is a double-layered structure that encloses the liver and gallbladder to become their visceral peritoneum. The cephalic portion of the developing liver directly contacts the septum and therefore is not enveloped by the ventral mesentery. This region, devoid of peritoneum, is known as the bare area (see Fig. 113-4). The visceral peritoneum reflects off the liver onto the undersurface of the diaphragm as the coronary ligaments outlining this region.

Abnormal Liver Development

ATYPICAL SEGMENTATION

Variations of lobulation sometimes occur. A bipartite liver results from an exaggerated separation of the lobes, which may represent congenital absence of the medial segment of the left lobe.⁸

Absence of the right lobe may result from maldevelopment of the portal vein or the primordial hepatic diverticulum proper.^{9,10} A portal venous abnormality may account for an absent left lobe. Multilobar livers—as many as 16—may be seen.⁷ Hepatic anomalies are discussed further in Chapter 85.

ATYPICAL LOCATION

Hepatic lobes can develop in the thorax. They may undergo torsion when they have a separate mesentery.¹¹ Heterotopic liver tissue may also be found within structures that share a common embryologic development: gallbladder, pancreas, umbilical cord, and gastrohepatic ligament.¹²

Normal Gallbladder and Bile Duct Development

The fourth week of embryogenesis is marked by the appearance of the hepatic diverticulum. It then divides into cranial and caudal buds. The caudal bud forms the gallbladder, cystic duct, and extrahepatic bile ducts. Their development precedes that of the intrahepatic ducts by several weeks.

The common bile duct develops as a cord connecting the cystic and main hepatic ducts to the descending duodenum. The hollow gallbladder and common bile duct primordia become occluded with proliferating endoderm during the fifth week. They recanalize by vacuolization and cell degeneration by the end of that week. The recanalization of the common bile duct precedes that of the gallbladder and duodenum. As the duodenum rotates 90 degrees to the right, the common bile duct rotates an additional 180 degrees along with the ventral pancreatic anlage. The common duct is carried from its original ventral position to the right, then posteriorly, and finally to the medial aspect of the duodenal sweep.

The gallbladder and intrahepatic ducts also communicate through the cystohepatic ducts of Luschka during fetal life. These ducts usually atrophy in the adult but may remain patent in some patients. When they persist and are not recognized during cholecystectomy, a significant bile leak may result.¹³

Vacuoles in the wall of the duodenum coalesce to form two separate channels and then one single lumen for the adjacent common bile and main pancreatic ducts. Within the wall of the duodenum are primitive ampullary tissues that enlarge and displace the junction of the two ducts away from the duodenal lumen. This displacement is reversed by the growth of the duodenal wall smooth muscle. This accounts for the considerable variability seen in the junction of these two structures.^{14,15}

Abnormal Gallbladder and Bile Duct Development

PHRYGIAN CAP

The phrygian cap is an abnormal shape of the gallbladder. It represents a folding of the fundus on itself and is not truly pathologic.

GALLBLADDER DIVERTICULUM

The gallbladder diverticulum is the true diverticulum (containing all normal wall elements). It probably is the remnant of the cystohepatic duct. It can be a site of bile stasis and stone formation (see Chapter 76).¹⁶

POSITIONAL ANOMALIES

The most common anomaly of gallbladder position is that of a “wandering” or “floating” gallbladder. Elongation of the gallbladder mesenteric attachment to the undersurface of the liver results in excessive mobility. The gallbladder may herniate into the lesser sac, undergo torsion, or be located in other intra-abdominal locations (see Chapter 76).^{7,16-19}

BIFID GALLBLADDER OR DUPLICATION

A bifid gallbladder has two cavities but only one cystic duct. Each of the duplicate or triplicate gallbladders has its own cystic duct. These entities may result from a persistent outpouching of the extrahepatic duct or incomplete recanalization of the gallbladder.^{5,7,16,18} The latter may also give rise to a septate gallbladder (see Chapter 76).^{7,20}

AGENESIS

Agenesis, a rare entity, results from a lack of development of the caudal portion of the liver bud or improper recanalization of the gallbladder.^{6,7,18,21} It may be associated with a host of other anomalies affecting many other organ systems (see Chapter 76).

TRACHEOBILIARY FISTULA

Tracheobiliary fistula is characterized by the combination of bile-stained sputum and pneumobilia. It results when the biliary tree is connected to the carinal region.^{7,18,22}

BILIARY ATRESIA

In biliary atresia, the number of intrahepatic bile ducts is decreased. This may develop primarily or result from α_1 -antitrypsin deficiency, cystic fibrosis, or viral hepatitis (see Chapter 120).²³

ALAGILLE'S SYNDROME

Alagille's syndrome is an autosomal dominant syndrome of arteriohepatic dysplasia. It is characterized by a paucity of bile ducts, peripheral pulmonic stenosis, vertebral anomalies, and mental and physical retardation (see Chapter 119).²⁴

CYSTIC DISEASE

The spectrum of cystic diseases ranges from intrahepatic cysts or fibrosis to renal disease. Various patterns of inheritance also occur. Cysts may be attributable to defective development of the intrahepatic ducts. In other forms, bile duct hyperplasia and portal fibrosis may predominate (see Chapters 76 and 119).

CAROLI'S DISEASE

Caroli's disease is a nonfamilial entity characterized by segmental cystic dilation of the intrahepatic bile ducts. It may represent an intermediate form of disease between congenital hepatic fibrosis and choledochal cysts.¹⁸ A possible cause is perinatal hepatic artery occlusion.²⁵ Multiple episodes of cholangitis may result from bile stasis (see Chapter 76).

CHOLEDOCHAL CYSTS

Multiple theories have been proposed to explain choledochal cysts.²⁶⁻²⁸ These concepts include distal biliary ductal obstruction with subsequent weakening and ballooning of the wall, anomalous course of the bile duct through the duodenal wall, and deficient development of the bile duct wall. Additional theories include a high junction of the bile and pancreatic ducts proximal to the sphincter of Oddi, which

allows reflux of pancreatic enzymes up the common bile duct when the sphincter is contracted, resulting in cholangitis and dilation. Another theory suggests an excess quantity of epithelial cells in the primitive choledochus, followed by recanalization leading to cyst formation. Viral infection leading to infantile obstructive cholangiopathy is another widely favored theory. During the past decade, technologic advances in imaging have greatly enhanced the noninvasive evaluation of the biliary tract. For example, multidetector computed tomography (CT) and magnetic resonance cholangiopancreatography (MRCP) can accurately depict preoperative anatomy and enable delineation of an anomalous pancreaticobiliary junction.²⁹

Choledochal cysts are found more often in Asians and in females. Five classic radiographic types have been identified.³⁰ The most common type is aneurysmal dilation of the common duct, which often extends into the cystic duct and the main hepatic ducts. The rare second form is a diverticulum that projects off the distal common duct. The third form is that of a choledochoceles, which represents a dilation of the distal common bile duct that protrudes into the duodenum. This third form may also be a congenital duplication cyst of the duodenum through which the common duct courses (see Chapter 76).³¹

Two other types are included in the classification of choledochal cysts. One is multifocal segmental intrahepatic and extrahepatic ductal dilation. The other is Caroli's disease (discussed earlier).

Normal Development of the Esophagus

During the latter half of the fourth week, the respiratory system develops as a ventral bud of the foregut. The laryngotracheal groove forms at the caudal end of the primitive pharynx and becomes the laryngotracheal diverticulum. Longitudinal (tracheoesophageal) folds eventually separate the ventral respiratory apparatus from the dorsal esophagus.

Initially, the esophagus is relatively short. Growth of the heart and lungs contributes to the elongation of the esophagus. Its epithelium and epithelial glands proliferate and obliterate the hollow lumen. This cellular plug is resorbed by the eighth week, the end of the fetal period.

Abnormal Development of the Esophagus

TRACHEOESOPHAGEAL FISTULA

Partial fusion of the tracheoesophageal folds leads to incomplete separation of the respiratory and gastrointestinal tracts (i.e., tracheoesophageal fistula). This is usually accompanied by some narrowing of the associated lumens (i.e., esophageal atresia). This common anomaly is discussed further in Chapter 114.

DUPLICATION

Incomplete resorption of the endothelial plug may result in a duplication of the esophagus (see Chapter 114).³² Duplication cysts are manifested as submucosal masses and do not usually

communicate with the esophageal lumen. CT or endoscopic sonography can document its cystic nature.

STENOSIS

Weblike narrowing or long segmental strictures may occur in the distal esophagus. Stenosis results from incomplete recanalization (see Chapter 114).³³

ESOPHAGEAL BRONCHUS

An esophageal bronchus is evidence of the common origin of the respiratory and gastrointestinal tracts. In this entity, a branching bronchus arises from the esophagus, usually in association with a pulmonary sequestration.³⁴

CONGENITAL SHORT ESOPHAGUS

If the esophagus does not proportionally elongate as the body grows, a congenital short esophagus occurs.³³ Seen at birth in association with a hiatal hernia, it is distinct from the acquired form found in adults.

Normal Development of the Stomach, Duodenum, and Lesser Omentum

At the end of the fourth week, which is the midpoint of the fetal period, the primitive stomach is still a straight, hollow tube in the midsagittal plane. During the next 2 weeks, the future stomach dilates, first in a fusiform manner and then with preferential growth of its dorsal wall. This causes a dorsal bulge, which is the origin of the greater curvature.

During the sixth to eighth weeks of development, the stomach rotates along two different axes simultaneously. The first and major rotation about the longitudinal axis causes the dorsal bulge to form the lateral border of the stomach. The former ventral aspect forms the medial wall (i.e., lesser curvature).³³ This accounts for the left vagus nerve innervating the anterior wall of the stomach and the right vagus nerve innervating the posterior wall in the adult (Fig. 113-5).

The enlarging liver contributes to a second rotation about the anteroposterior axis. The stomach shifts from a

purely longitudinal orientation to one more transverse. The greater curvature convexity is directed inferiorly and laterally, whereas the lesser curvature is concave superiorly and medially.

The ventral mesentery of the distal foregut persists into adulthood. It continues to connect the lesser curvature of the stomach (i.e., former ventral wall) to the undersurface of the liver at the junction of the caudate lobe and the lateral segment of the left lobe as the gastrohepatic ligament (Fig. 113-6).³⁵ Within it lie the left gastric artery, coronary veins, and multiple lymph nodes. The more caudal portion of the lesser omentum forms the hepatoduodenal ligament. Within its free edge lie the hepatic artery, portal vein, common hepatic and bile ducts, and lymph nodes.³⁶ This free edge forms one of the borders of the foramen of Winslow, separating the lesser sac from the greater peritoneal cavity.

Unlike the dorsal bulge of the primitive stomach, the duodenum forms a ventral bulge. The proximal portion of the duodenum (i.e., from the pylorus to just past the papilla) is derived from the foregut, maintaining its blood supply from the celiac axis (i.e., major foregut artery). The remainder of the duodenum is derived from the midgut. Consequently, it is supplied by the superior mesenteric artery (i.e., major artery of the midgut), which passes through the persistent dorsal mesentery.

With gastric rotation, the duodenum also changes in position. The concave border formerly directed dorsally becomes open to the left (i.e., classic C loop). The dorsal mesentery is subsequently resorbed, leaving a covering of visceral peritoneum along its anterior surface. This loss of mesenteric attachment accounts for the final “retroperitoneal” location of the duodenum distal to the bulb.

Abnormal Development of the Stomach and Duodenum

ANTRAL WEB

An antral web is a thin, concentric narrowing of the antrum. It is composed of mucosa and submucosa (Fig. 113-7). It may be congenital in origin (i.e., a recanalization error) or may be associated with peptic ulcer disease.³⁷

GASTRIC DIVERTICULA

Gastric diverticula usually occur high on the posterior wall of the fundus, and they may be true diverticula or pseudodiverticula with an absent muscle wall.³⁷ The constancy of position suggests an underlying congenital basis.

DUPLICATIONS

Duplications usually are found along the greater curvature. These noncommunicating cystic masses vary greatly in size (see Chapter 116).^{37,38}

DUODENAL STENOSIS

Duodenal stenosis is manifested as a narrowing of variable length, usually in the third and fourth portions. It may result from faulty recanalization (see Chapter 116).³³

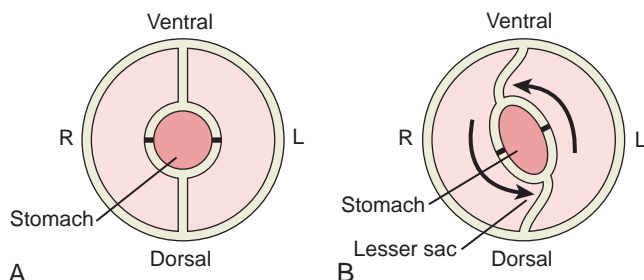


Figure 113-5 Gastric rotation and formation of the lesser sac. **A** and **B**. Schematic cross-sectional diagrams depict the rotation of the stomach about the body's longitudinal axis. The left vagus nerve is carried to the anterior wall of the stomach. The extension of the right peritoneal space posterior to the stomach starts the formation of the lesser sac.

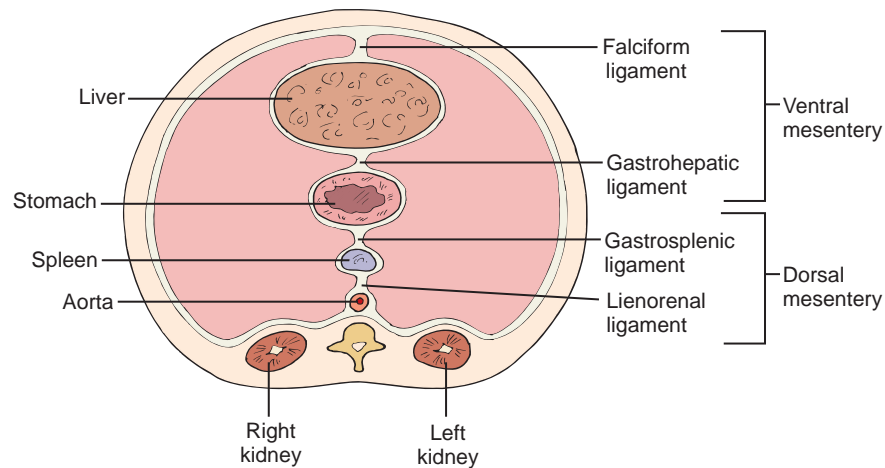


Figure 113-6 Embryologic origins of mesenteries and supporting ligaments. Cross section through a 5-week embryo at the level of the liver shows the paired superior peritoneum (right and left) separated by the ventral and dorsal mesenteries. Even at this stage of development, the origins of many of the suspensory ligaments of the adult are clearly demonstrated.



Figure 113-7 Antral web. There is a thin, linear, nonobstructive defect (arrows) in the gastric antrum.

DUODENAL WEB AND INVERTED DIVERTICULUM

A thin, narrow band of tissue may partially block the duodenum. With the continued pressure of peristalsis propelling intestinal contents, this web may stretch and balloon into a saclike structure within the normal duodenal lumen, the so-called inverted diverticulum or windsock deformity (see Chapter 116).³⁹

Normal Development of the Pancreas

The endoderm of the caudal foregut produces dorsal and ventral pancreatic buds during the fourth week of development.

The dorsal bud appears first and lies cephalad to the ventral anlage. The dorsal bud rapidly grows into the dorsal mesentery (i.e., mesoduodenum). It gives rise to the body and tail of the pancreas. The more caudal ventral pancreatic bud develops from the hepatic diverticulum. This bud is originally bifid, but the left side atrophies, and the right side persists to form the uncinete process and the head of the pancreas.^{40,41}

The dorsal bud has been reported to have a greater propensity for fatty infiltration than the ventral bud, which may be useful in distinguishing normal pancreatic parenchyma from diseased pancreas between the pancreatic buds on imaging studies.⁴² This propensity may stem from the different histologic composition of the pancreatic buds. Microscopic evaluation indicates that the parenchyma originating from the ventral bud contains densely packed pancreatic lobules, whereas the parenchyma originating from the dorsal bud is relatively loosely packed and contains more interposed adipose tissue.⁴³

CT evaluation of focal fatty infiltration, most often observed in the anterior aspect of the pancreatic head, demonstrates an isolated region of fat attenuation within the pancreatic parenchyma on non-contrast-enhanced or contrast-enhanced studies. However, contrast-enhanced CT studies may mask the presence of focal fatty infiltration as the normal parenchyma enhances and obscures the low-attenuation regions of fat. It is noteworthy that the delineation between the region of fatty infiltration and the remaining pancreatic parenchyma is often smooth and sharp, as would be expected in infiltration resulting from differing histologic composition.^{43,44}

On ultrasound, focal fatty infiltration is hyperechoic compared with the normal pancreatic parenchyma. As on CT, there is a discrete delineation between the segment of the pancreas with fatty infiltration and the remaining parenchyma.⁴⁴

Magnetic resonance imaging is an accurate modality for evaluating focal fatty infiltration (and differentiating it from a neoplastic lesion) because of its ability to clearly identify fatty tissues. Fatty tissue will show high signal intensity on T1- and T2-weighted images. In addition, with use of chemical shift imaging, it can be shown that fatty infiltration tissue shows a significant signal decrease on the out-of-phase T1 sequence compared with the in-phase T1 sequence.^{43,44}

There are several important imaging clues that help differentiate a mass from focal fatty infiltration of pancreatic parenchyma. Focal fatty infiltration is more often found in the anterior aspect of the pancreatic head, whereas the posterior aspect of the pancreatic head and the parenchyma adjacent to the pancreatic duct are spared. Compared with a malignant lesion, for example, fatty infiltration does not usually exert mass effect on the surrounding tissues or vessels and often maintains the normal contour of the pancreas. Finally, focal fatty infiltration tends to be stable on repeated studies.

As the duodenum rotates 90 degrees to the right, the dorsal pancreatic bud and its mesentery are carried along in the concavity of the primitive duodenal sweep (discussed earlier). They are ultimately situated along the left (medial) margin of the descending duodenum. The common bile duct and the right side of the ventral pancreatic anlage also complete this 90-degree rotation while undergoing an additional 180-degree rotation of their own. They come to lie along the concavity of the duodenal sweep after rotating through a total of 270 degrees (Fig. 113-8A, B).

Eventually, the duodenal dorsal mesentery fuses with the posterior peritoneal wall, resulting in the retroperitoneal location of the pancreas. However, a small portion of the tail of the pancreas maintains its intraperitoneal location near the hilum of the spleen in a portion of the mesogastrium that sometimes is not fully resorbed.⁴⁰

During the sixth week, the parenchyma of the ventral and dorsal buds and their ducts unite. The main pancreatic duct (Wirsung), which empties through the main papilla, is derived from the ventral anlage in the head and the dorsal anlage in the body and tail (Fig. 113-8C). The accessory duct (Santorini) is derived from the distal aspect of the dorsal anlage, and in 10% of patients, it empties through the minor papilla.⁴⁰ In the remaining cases, the main pancreatic duct is the predominant excretory pathway as the two ductal systems communicate.

The exocrine pancreatic tissue is derived from the pancreatic buds, which produce tubules. Vesicles form at the ends of these tubules, which give rise to acini. The endocrine islets of

Langerhans also derive from the endoderm.⁴⁰ The splanchnic mesenchyme adjacent to the pancreas provides its connective tissue stroma.³³

Abnormal Development of the Pancreas

ANNULAR PANCREAS

In 85% of cases of this anomaly, the descending duodenum is surrounded by a band of pancreatic tissue.^{40,41} An annular pancreas is most often found in male patients, and it may be associated with other congenital anomalies in up to 75% of cases (see Chapter 96).

According to one theory, the left bud of the originally bifid ventral pancreas persists and helps contribute to the ring of tissue around the duodenum.⁴⁵ Another theory proposes that the tip of the right bud abnormally adheres to the duodenum as it and the anlage rotate, thereby stretching and wrapping the pancreatic tissue around the duodenum.^{40,41}

PANCREAS DIVISUM

Pancreas divisum is caused by failure of the dorsal and ventral pancreatic buds to unite. This allows the uncinate process and a portion of the head to be drained by a short and narrow-caliber main pancreatic duct (Wirsung) through the major papilla. The remainder is drained by the accessory pancreatic duct (Santorini) through the minor papilla that lies cephalad and ventral to the major papilla. The narrow opening of the minor papilla may predispose these patients to pancreatitis (see Chapter 96).⁴⁶ Advances in MRCP have proved accurate in the diagnosis of pancreatic divisum. Multidetector CT using cine visualization or multiplanar reformatting may also improve the visualization of ductal anatomy in patients with pancreatic divisum.^{47,48} Endoscopic ultrasound with a linear array transducer can demonstrate atypical ductal anatomy. The cleavage plane between the ventral and dorsal

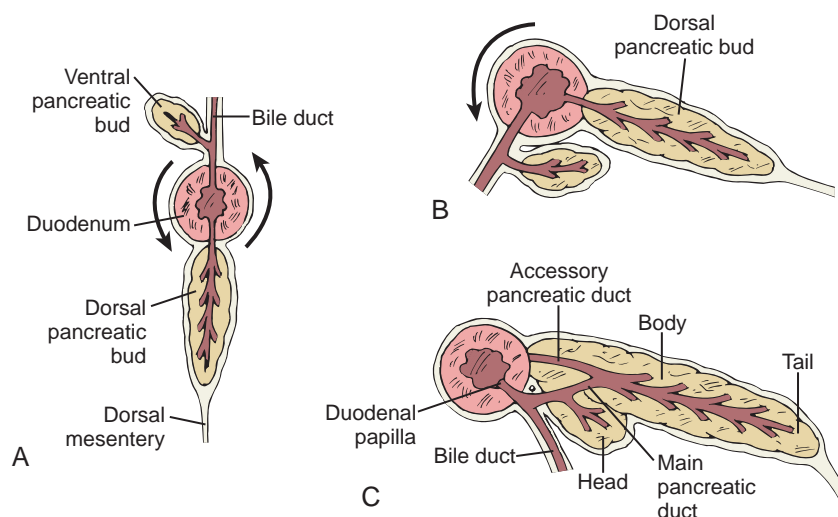


Figure 113-8 Stages of pancreatic development: superior perspective. **A.** Starting in the fourth week, the ventral pancreatic anlage rotates 180 degrees (first to the right and then posteriorly) as the duodenum rotates 90 degrees. This results in a total rotation of 270 degrees, with the original ventral anlage moving to the left of the duodenum. This rotation also carries the distal common bile duct posterior to the duodenum. **B.** The dorsal anlage is carried along by the duodenal rotation, such that it lies to the left of the duodenum. **C.** By the seventh to eighth week, the ducts of the two pancreatic buds fuse with the ventral pancreas, contributing the distal portion of the main pancreatic duct. Most of the proximal main duct arises from the dorsal anlage.

pancreatic anlagen may also be demonstrated by this technique.⁴⁹

ECTOPIC PANCREATIC TISSUE

Small islands of pancreatic tissue may grow along the greater curvature of the antrum or medial aspect of the duodenal sweep, with formation of submucosal nodules.^{37,39} Other sites of involvement, including the omentum, have also been reported (see Chapter 96). Fully developed ducts are rare.

Normal Development of the Lesser Sac and Greater Omentum

With the resorption of the ventral mesentery along the midgut and its persistence along the distal foregut, the abdomen is divided into paired (left and right) cephalic peritoneal spaces and a larger, common space caudally. As the primitive stomach develops, the dorsal mesentery (i.e., mesogastrium) with its accompanying vascular supply starts to elongate markedly. The elongated mesogastrium is carried along with the dorsal bulge of the stomach as it rotates (described earlier). This causes the right half of the paired cephalic peritoneal space to extend posterior to the stomach into the left upper quadrant, forming the lesser sac (see Fig. 113-5).

The most dorsal aspect of this elongated mesogastrium (containing the spleen) eventually fuses partially with the posterior abdominal wall, accounting for the retroperitoneal course of the splenic artery (Fig. 113-9).³⁶ The more ventral portion of the now redundant mesogastrium projects anteriorly and inferiorly. It hangs from the greater curvature of the stomach and overlies the transverse colon and mesenteric small bowel. It then loops back on itself to rejoin its already fused dorsal component at the posterior abdominal wall (Fig. 113-10A).

The two leaves of this redundant apron of mesentery fuse, obliterating the space between the two layers (i.e., inferior recess of the lesser sac). The greater omentum, composed of four layers of peritoneum, hangs like an apron over much of the peritoneal cavity. The greater omentum partially fuses with

the transverse colon and its suspending dorsal mesentery (Fig. 113-10B).^{33,36} Ventrally, this gives rise to the gastrocolic ligament as the greater omentum adheres to the superior aspect of the transverse colon. Dorsally, the mesogastrium and mesocolon fuse to form the definitive transverse mesocolon.^{33,36} This delineates the inferior border of the lesser sac. The transverse mesocolon takes rise over the pancreas and may act as a pathway for the spread of disease from the retroperitoneal pancreas to the intraperitoneal colon.⁵⁰ The retroperitoneum fascia is composed of multiple discrete layers that represent fused leaves of the apposed embryonic mesentery. These planes, which extend from the diaphragm to the pelvic floor, enable rapid accumulations of fluid to spread in the retroperitoneum (see Chapter 108).⁵¹

The foramen of Winslow is the entry point into the lesser sac. It is bordered by the free edge of the hepatoduodenal

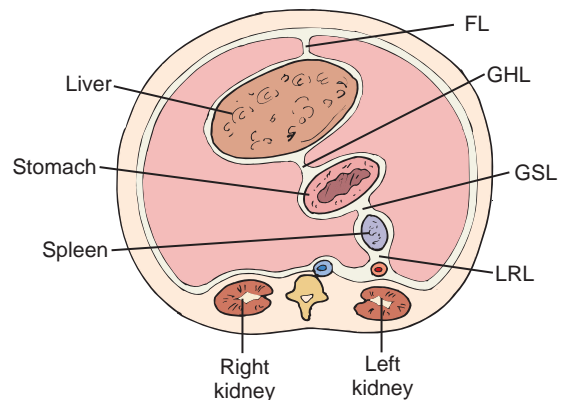


Figure 113-9 Rotation of the mesogastrium. Schematic cross-sectional diagram through the upper abdomen reveals continued rotation of the elongated mesogastrium containing the splenic bud. This rotation brings the dorsal mesentery to lie along the posterior abdominal wall. Eventual involution and fusion of the mesentery leaves the lienorenal ligament (LRL) as its remnant. The gastrosplenic ligament (GSL) forms one of the lateral borders of the lesser sac. The gastrohepatic ligament (GHL) persists as the lesser omentum. The falciform ligament (FL) continues to separate the right side of the peritoneum from the left, anteriorly and superiorly, in the subphrenic space.

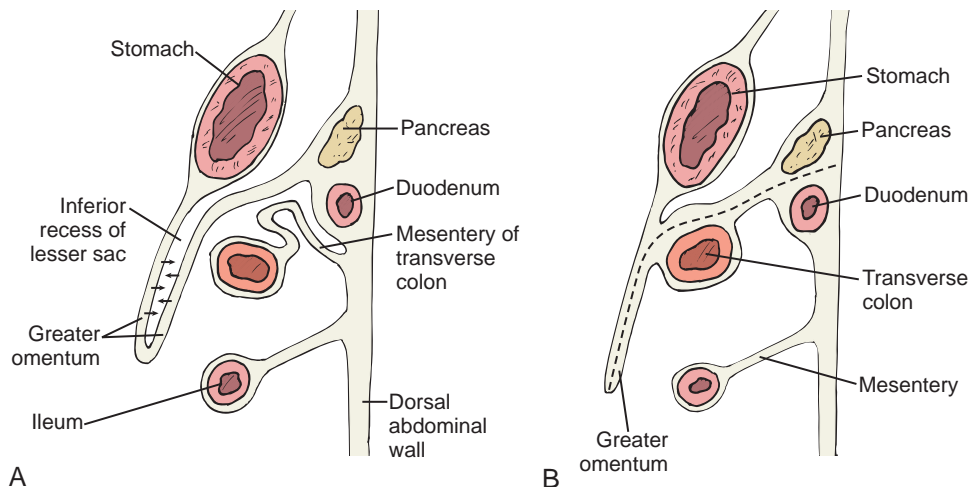


Figure 113-10 Formation of the greater omentum. **A.** Longitudinal schematic drawing shows the fusion of the two leaves of the greater omentum with obliteration of the inferior recess of the lesser sac. **B.** Fusion of the greater omentum with the transverse colon and its dorsal mesentery gives rise to the definitive gastrocolic ligament and the transverse mesocolon.

ligament ventrally, the caudate lobe of the liver superiorly, the inferior vena cava posteriorly, and a reflection of peritoneum from the pyloroduodenal region inferiorly.⁵²

The spleen develops within the stomach's elongated dorsal mesentery and divides it into two components that contribute to the lateral borders of the lesser sac. The lienorenal ligament represents the fusion of the dorsal portion of the mesogastrium to the retroperitoneum. The gastrosplenic ligament represents the more ventral remnant of the spleen's mesenteric origin between the stomach and the posterior abdominal wall (see Fig. 113-9).⁵²

The raised peritoneal ridge overlying the left gastric artery divides the lesser sac into two compartments. The smaller, medial compartment contains the submerged (subdiaphragmatic) portion of the esophagus. Inflammatory exudate in the medial lesser peritoneal sac may extend transdiaphragmatically through the esophageal hiatus into the mediastinum.

Abnormal Development of the Lesser Sac and Greater Omentum

INFRACARDIAC BURSA

Rarely, a persistent communication exists at the level of the diaphragm, with the medial lesser peritoneal sac extending into the mediastinum. This forms an infracardiac cystic space medial to the right lung.³³

OMENTAL CYST

A mesenchyme-lined omental cyst can develop within the leaves of the greater omentum, representing incomplete obliteration of the inferior recess of the greater omentum. Histologic differentiation of mesenteric, omental, duplication, and neurenteric cysts is based on their cell linings and other wall components.^{53,54}

Normal Development of the Spleen

The spleen develops from the mesenchyme within the mesogastrium during the fifth week of development. Initially, several distinct clusters of mesenchyme are formed. These coalesce and fuse to form the spleen, which develops its characteristic shape by the third month. Their fusion leads to the spleen's lobulated contour. Before birth, the splenic contour smooths; only a few notches remain along its anterosuperior border. The mesenchyme forms the reticular framework, trabeculae, and capsule of the spleen. The T and B lymphocytes arise in the bone marrow and migrate to the spleen. By the fourth month, the spleen is producing megakaryocytes and other blood cell precursors as part of its hematopoietic activity, a capacity that is retained in the adult spleen.

Abnormal Development of the Spleen

ACCESSORY SPLEEN

Accessory spleen refers to congenitally derived ectopic splenic tissue (see Chapter 104). This is separate and distinct from splenosis, which is ectopic splenic tissue resulting from trauma and subsequent implantation and growth of splenic fragments.

Accessory spleens may result from failure of the splenic clusters to fuse.⁵⁵ Alternatively, exaggerated lobulation may cause tissue to be pinched off and separated from the main spleen.⁵⁶ Up to 30% of the population has accessory splenic tissue.^{33,55} It is most commonly found in the splenic hilum, but it may be found elsewhere in the retroperitoneum.⁵⁷ Usually, only one accessory spleen is present. There is an association between having an accessory spleen and hematologic disorders.⁵⁸

WANDERING SPLEEN

The spleen may have an unusual degree of mobility and occupy an atypical location (see Chapter 104) in less than 0.2% of all patients.⁵⁵ It is most commonly found in multiparous women.^{59,60} Wandering spleen has been associated with incomplete fusion or even absence of the gastrosplenic and lienorenal ligaments.^{61,62} Its association with splenomegaly and increased frequency in postpartum women suggests an acquired cause.⁶³ The spleen's exaggerated mobility predisposes it to torsion and subsequent infarction.

ASPLENIA

Isolated absence of the spleen without accompanying abnormalities is usually an acquired condition.^{64,65} However, it occurs more frequently in boys and with a complex constellation of congenital abnormalities of multiple organ systems (see Chapter 122).⁶⁶ One theory suggests a link with maldevelopment of the body curvature in the embryo.⁶⁷ This accounts for the frequent situs abnormalities (especially dextroisomerism) in conjunction with asplenia.⁵⁵

POLYSPLENIA

Polysplenia is a component of a broader heterotaxy syndrome that is defined by a host of anatomic abnormalities. This heterotaxy syndrome is associated with levoisomerism, which suggests the presence of bilateral bilobed lungs and bilateral pulmonary atria. This syndrome is also associated with a central intra-abdominal liver, a randomly located stomach, and multiple spleens. Cardiac anomalies may also be present, but they are more common in asplenic rather than in polysplenia patients. The most common finding in heterotaxy syndrome with polysplenia is azygos (or hemiazygos) continuation of the inferior vena cava, which can be easily detected by cross-sectional imaging as well as on careful scrutiny of lateral plain films of the chest (Fig. 113-11). This constellation of findings in heterotaxy syndrome with polysplenia is not constant, and variations may be found from patient to patient.⁶⁸

As in the case of asplenia, the multiple organ system anomalies associated with polysplenia may be related to abnormal development of the embryo's body curvature.⁶⁷ Polysplenia is more common in females. Although polysplenic patients present with a wider spectrum of clinical manifestations compared with asplenic patients, reportedly more than 50% of those born with this condition die within the first year of life.^{55,69}

SPLENIC-GONADAL FUSION

Splenic-gonadal fusion is almost exclusively seen in boys and involves the left side.^{70,71} Continuous and discontinuous forms are seen with equal frequency. The continuous form involves a

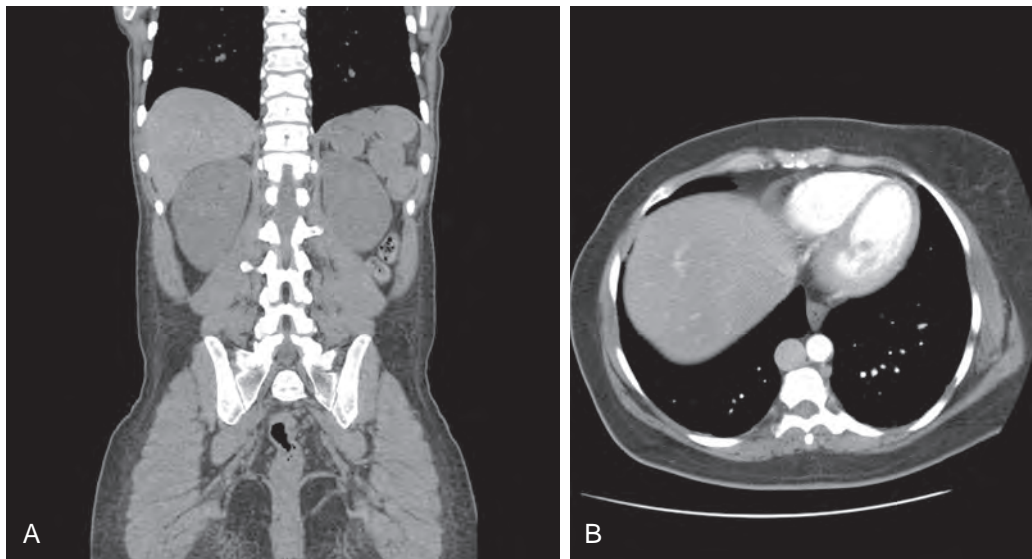


Figure 113-11 Polysplenia with azygos continuation of the inferior vena cava. **A.** Coronal CT scan demonstrating multiple spleens in the left upper quadrant. **B.** Axial CT scan demonstrates azygos continuation of the inferior vena cava in the same patient, a common finding in heterotaxy syndrome with polysplenia.

band of fibrous and splenic tissue connecting the left gonad to the spleen.⁷⁰ Approximately 25% of these patients have cryptorchidism. In the discontinuous form, ectopic splenic tissue is located in the gonad.

The developing gonad arises during the sixth week of embryogenesis from the mesonephros, which is adjacent to the splenic precursor in the dorsal mesentery.⁷² The gonadal tissue normally descends during the eighth week of development. Failure of these two anlagen to separate completely may account for this anomaly.

Normal Midgut Rotation and Fixation

Only anthropoid apes and humans have partial obliteration of the primitive dorsal mesentery. This most likely results from their upright posture.⁷³

During the third and fourth weeks of development, the embryo starts to grow much more rapidly than the yolk sac. By the fifth week, the intraembryonic and extraembryonic celomic cavities connect by a narrow stalk (i.e., omphalomesenteric or vitellointestinal duct or yolk stalk) (see Fig. 113-2).

Within the intraembryonic celom, the midgut starts to elongate and loop ventrally into the yolk sac. This midgut loop can be divided into two segments, originally of roughly equal length. The axis of this loop is the superior mesenteric artery, and its apex is marked by the omphalomesenteric duct. The prearterial segment starts at the foregut-midgut junction and ends at the apex of the loop. This gives rise to the duodenum distal to the papilla, the jejunum, and most of the ileum. The postarterial limb extends from the apex of the loop to the midgut-hindgut junction. From this segment arise the very distal and terminal ileum, cecum, appendix, ascending colon, and most of the transverse colon. The transition to the hindgut is usually in the distal third of the transverse colon, where the changeover from superior mesenteric artery (i.e., middle colic) to inferior mesenteric artery (i.e., left colic) distribution occurs (Fig. 113-12).

By the fifth week, a small swelling (i.e., cecal bud) in the proximal postarterial segment, just distal to the apex of the

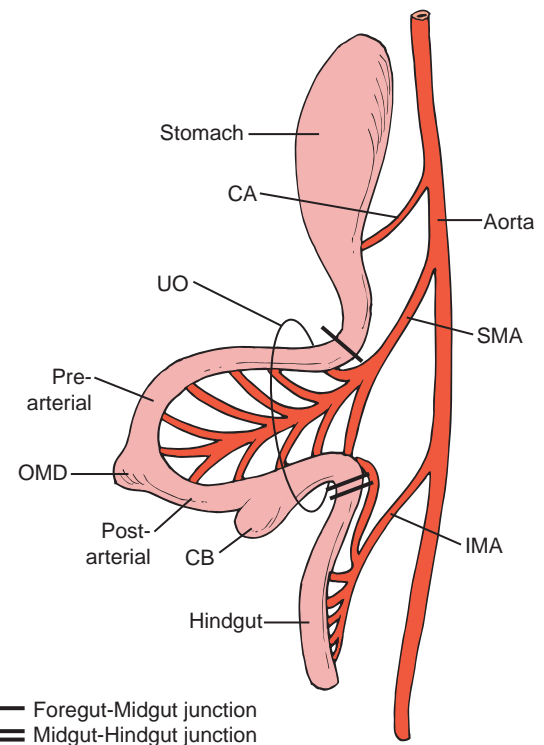


Figure 113-12 Intestinal tract development at 6 weeks.

Longitudinal view of the intestinal tract at 6 weeks of development shows that the superior mesenteric artery (SMA) acts as the axis for midgut rotation. The omphalomesenteric duct (OMD) divides the midgut into prearterial and postarterial limbs. Notice the physiologic herniation of the midgut through the umbilical orifice (UO). Heavy lines mark the foregut-midgut (/) and the midgut-hindgut (//) junctions. The celiac axis (CA) is the major artery of the foregut; the inferior mesenteric artery (IMA) supplies the hindgut. CB, Cecal bud.

umbilical loop, marks the beginning of the differentiation between small and large bowel.

The pioneering work of Snyder and Chaffin in the early 1950s prompted a major revision of the theory of how the midgut rotates.^{74,75} The herniation of the midgut takes place in

the sixth week of development. It is limited by dense condensations of the dorsal mesentery that bind the more proximal prearterial and more distal postarterial segments to the posterior peritoneum.⁷⁶ Within this hernia, the midgut markedly elongates. The growth predominantly involves the prearterial segment. Pressure from the enlarging right lobe of the liver, along with the rapid elongation, forces the prearterial segment down and to the right.^{33,76} The increase in length is accommodated by a series of convolutions and small loops. At this point, the postarterial segment occupies the left side of the umbilical hernia. Viewed from the front, this represents a 90-degree counterclockwise rotation.

By the 10th week, further growth in the peritoneal cavity and less rapid increase in the liver size allow sufficient room for the physiologic herniation of the midgut to reduce itself. First to return is the elongated, convoluted prearterial limb.^{33,74-76} These right-sided (originally cranial) loops enter the abdomen on the right side of the superior mesenteric artery but then pass behind that artery to occupy the left side of the abdomen. The now larger cecal bud may impede the return of the postarterial (originally caudal), now left-sided midgut until the prearterial return is complete (Fig. 113-13).³³

During the 11th week, the more slowly growing postarterial segment returns. As the herniation is reduced, the colon continues to rotate, first in front of and then to the right of the

superior mesenteric artery (Fig. 113-14). By the 12th week, the colon completes a 270-degree counterclockwise rotation. These 270 degrees comprise 90 degrees occurring during the umbilical herniation and an additional 180 degrees during its reduction. Flexion of the embryo carries the cecum to the level of the iliac crest. Its final, right lower quadrant position is a result of the continued growth of the ascending colon, not further midgut rotation.³³

The development of the appendix is a separate and distinct process.⁷⁷ Differential rates of growth between the base of the primitive cecum and its apex result in the rapid formation of a vermiform appendage, the appendix. Asymmetric growth of the lateral wall of the cecum after birth causes the appendix to migrate from the midline to the same side of the cecum as the ileocecal valve. The growth of the medial wall may be hindered by the presence of the ileum and its vascular pedicle.⁷⁷

From the 11th week to the end of the 5th month, a gradual, partial resorption of the dorsal mesentery occurs. The segments attaching the ascending and descending colon agglutinate with the parietal peritoneum of the posterior abdominal wall, leading to their final, so-called retroperitoneal location. In reality, they are usually covered by peritoneum on their anterior, medial, and lateral borders; only their posterior walls are truly retroperitoneal.

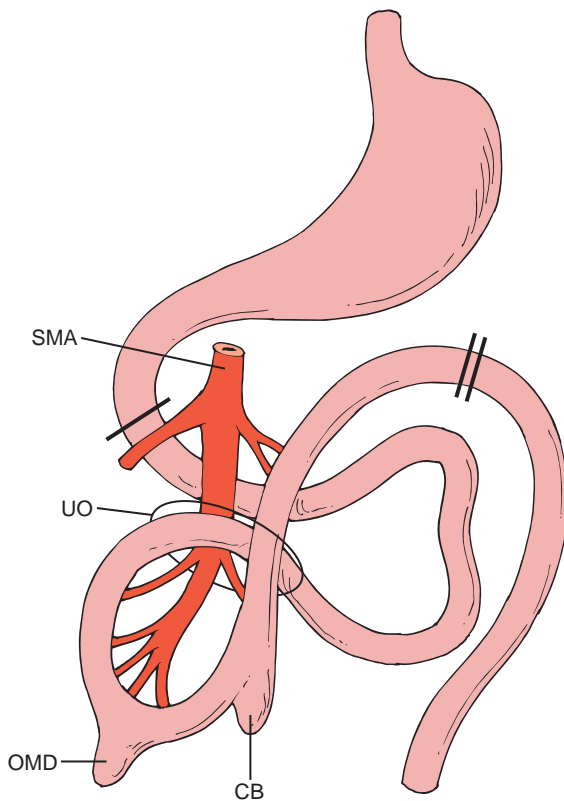


Figure 113-13 Intestinal tract development at 10 weeks. Frontal view of a 10-week fetus. The elongated, redundant prearterial limb has re-entered the abdomen and crossed to the left of and behind the superior mesenteric artery (SMA). This displaces the hindgut to the left. Heavy lines mark the foregut-midgut (/) and the midgut-hindgut (/) junctions. CB, Cecal bud; OMD, omphalomesenteric duct; UO, umbilical orifice.

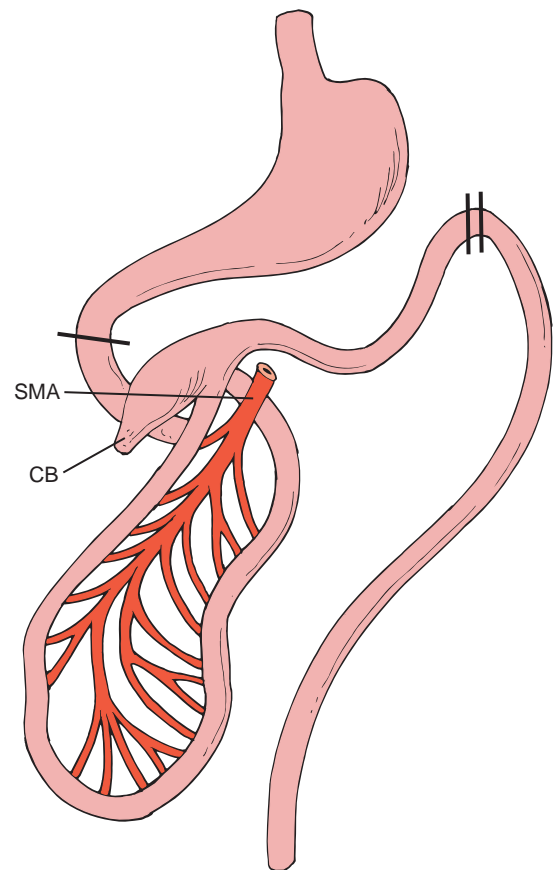


Figure 113-14 Intestinal tract development at 11 weeks. With development 1 week later than in Figure 113-13, reduction of the physiologic herniation is complete. The postarterial limb has partially completed its 180-degree rotation, and the cecum lies in the upper abdomen on its way to the right side. CB, Cecal bud; SMA, superior mesenteric artery.

The transverse colon mesentery (i.e., mesocolon) persists into adulthood. It partially fuses with the greater omentum, forming the gastrocolic ligament. The distal end of the transverse mesocolon (i.e., phrenicocolic ligament) serves as an anchor that fixes the splenic flexure in the left upper quadrant. It also seals the left paracolic gutter, preventing the spread of disease into the left upper quadrant from below.^{36,78}

In the small bowel, the thick proximal attachment of the prearterial segment lies to the left of the second lumbar vertebra, marking the duodenal-jejunal junction. This dorsal mesenteric remnant of the duodenum is also resorbed into the posterior abdominal wall, which results in “retroperitonealization” of the duodenum. The distal end of the small bowel mesentery is carried into the right lower quadrant, ending at the level of the fourth or fifth lumbar vertebra. The mesenteric small bowel is suspended from a short posterior attachment along the posterior abdominal wall.

The sigmoid colon maintains its dorsal mesenteric attachment as the sigmoid mesocolon. Its short length compared with the variable length of attached colon may contribute to the development of sigmoid volvulus.

Abnormal Midgut Rotation and Fixation

DUPLICATION

A second intestinal lumen may form parallel to the primary one because of errors in recanalization.^{33,54,79} The duplication does not usually communicate with the primary lumen, but they share a common muscle wall and blood supply. They are more often found in the ileum (see Chapter 117).^{33,53}

ILEAL ATRESIA

Atresias of all levels of the small bowel from duodenum to ileum have been attributed to in utero ischemic processes (see Chapter 117).^{80,81} Other authorities implicate intrauterine inflammatory disease in cases of multiple intestinal atresias.⁸²

MESENTERIC CYST

Cysts within the mesentery have various origins. Their differentiation depends on the histologic determination of their wall constituents and lining cells.^{53,54}

NONROTATION

Although commonly called malrotation, nonrotation represents an abnormal arrest of the midgut rotation after the first 90 degrees of rotation.^{33,54,83} At this point, the prearterial midgut lies to the right of the superior mesenteric artery, and the postarterial limb lies to the left. The postarterial limb is then first to return to the abdomen. Consequently, it lies in the left hemiabdomen. The returning prearterial segment is forced to remain on the right (Fig. 113-15). Both segments continue to share a common dorsal mesentery, which lies in the midline. This allows considerable mobility of the small and large bowels and predisposes to midgut volvulus.

REVERSED ROTATION

In the rare entity of reversed rotation, the order of the midgut return is reversed, with the postarterial limb preceding

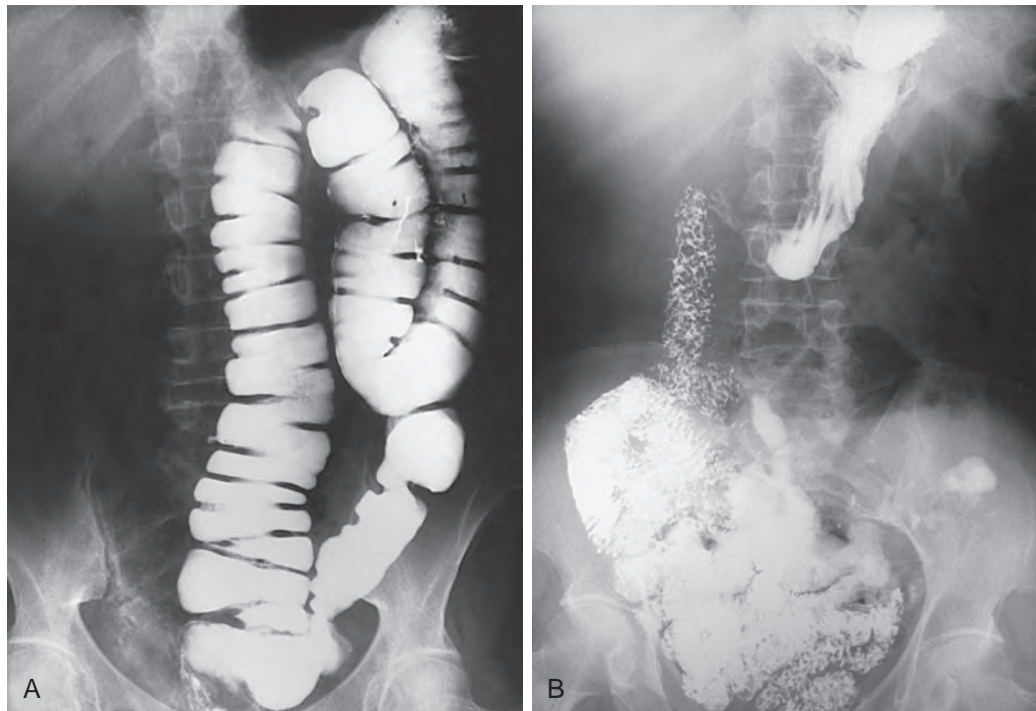


Figure 113-15 Nonrotation of the gut. A. Single-contrast barium enema shows that the entire colon lies in the left hemiabdomen. This reflects the premature return of the postarterial limb of the midgut after the first 90 degrees of rotation. **B.** An upper gastrointestinal series in the same patient demonstrates incomplete formation of the duodenal sweep. The jejunum and most of the small bowel lie in the right hemiabdomen. The prearterial limb of the midgut must remain on the right after the postarterial limb occupies the left.

the prearterial.^{33,54} This causes the colon to lie posterior to the superior mesenteric artery; the duodenum and small bowel cross anteriorly. Abnormal mesenteric bands may cause obstruction.

INCOMPLETE ROTATION AND MALFIXATION

Although rotation and fixation are two separate and distinct stages of development, abnormalities of rotation are frequently associated with malfixation.^{33,54,73,83} Most often, the colon fails to complete its final 180-degree rotation, ending in the right upper quadrant. There may be incomplete resorption of the dorsal mesentery that allows formation of elongated and mobile segments of colon. Many different variations and combinations of abnormal rotation and fixation may be encountered. The presence of an abnormally rotated proximal limb does not necessarily imply an abnormally rotated lower tract, but the presence of an abnormal lower tract is almost always associated with abnormal proximal rotation.

Multiple congenital anomalies of the gastrointestinal tract and other organ systems have been reported with abnormal intestinal rotation and fixation.⁸³ Duodenal atresia or web (11%) was the most common associated anomaly, followed by Meckel's diverticulum (11%), omphalocele (9%), other stenosis or atresia (5%), and Hirschsprung's disease (2%). Less common associated anomalies included cardiac and orthopedic anomalies, biliary atresia, pancreatic anomalies, microcolon, esophageal webs, and tracheoesophageal fistula.^{84,85}

HYPERROTATION

In hyperrotation, an elongated colon continues to rotate past its usual 270-degree stopping point.^{33,54} The cecum may cross the midline, sometimes reaching the left upper quadrant. Because the prearterial segment is normal in length and rotation, it lies in its normal position and is not affected in this entity.

INTERNAL HERNIATIONS

Abnormalities in the formation and resorption of the dorsal mesentery may allow fossae to develop into which loops of bowel may herniate (see Chapter 112). The most common of these fossae are those near the duodenum.^{33,54}

Left paraduodenal hernias are much more common than those on the right. The fossa of Landzert is formed by incomplete fusion of the descending colon mesentery.⁵⁴ Bowel loops may herniate under the colon and in front of the inferior mesenteric vein. A similar defect in the small bowel mesentery (i.e., fossa of Waldeyer or mesentericoparietal fossa) allows loops to herniate from the left upper quadrant beneath the superior mesenteric artery to the right.⁵⁴ This is a right paraduodenal hernia.

Similar but less common defects may exist in the periceal region, within the sigmoid mesocolon, and even in the transverse colon mesentery. Many different types and positions of internal herniations may be seen in these areas.

MECKEL'S DIVERTICULUM

If the omphalomesenteric duct fails to be completely obliterated, a persistent outpouching of the bowel may persist. Its

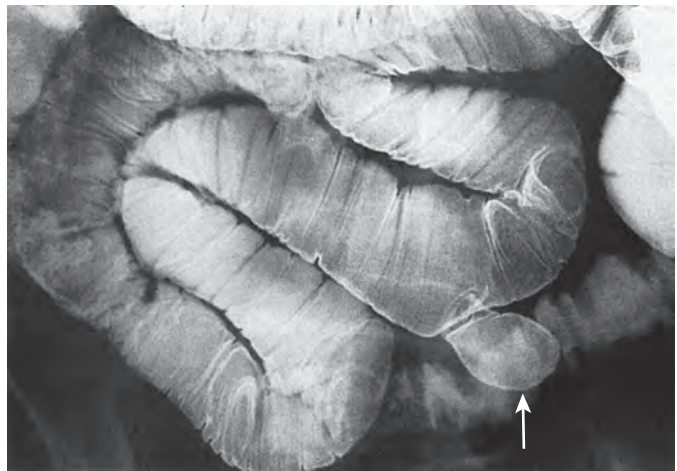


Figure 113-16 Meckel's diverticulum. Coned-down view from an enteroclysis shows Meckel's diverticulum (arrow) arising from the antimesenteric border of an ileal loop. This represents the remnant of the omphalomesenteric duct.

location at the apex of the physiologic herniation accounts for the location of Meckel's diverticula in the distal ileum (see Chapter 117).

Meckel's diverticulum has a wide spectrum of variation.⁵⁴ There may be cystic remnants between the small bowel and the umbilicus or fibrous bands. Communication with the bowel is the most common finding (Fig. 113-16), but draining umbilical sinuses also have been reported. The fibrous cord may act as an axis of rotation, allowing volvulus to develop.

These diverticula can contain ectopic gastric or pancreatic tissue. The presence of ectopic gastric tissue may lead to peptic ulceration and bleeding. Rare neoplasms have been reported within the mucosal lining. Stasis of intestinal contents within the diverticulum may give rise to enterolith formation. Rarely, the diverticulum may invert and act as the leading edge of an intussusception. In Littre's hernia, the diverticulum enters a hernia sac.⁵⁴ Some studies have demonstrated an increased incidence of Meckel's diverticulum in patients with known Crohn's disease. Meckel's diverticula were found in 17 (5.8%) of 294 patients with Crohn's disease, a rate that is about two to three times greater than in the general population.⁸⁶ In another study, however, only 10 (1.1%) of 877 patients with Crohn's disease had Meckel's diverticula.⁸⁷ Most patients with Crohn's disease and associated Meckel's diverticula were younger than 40 years and had ileal involvement with or without colonic involvement.⁸⁷ This study concluded that the overall presence of Meckel's diverticulum is not increased from that in the general population, and more important, the presence of Meckel's diverticula did not alter patient management.⁸⁷ In these studies, none of the patients with surgically proven Meckel's diverticula had heterotopic gastric mucosa. This finding implies that imaging with technetium in these patients would not yield positive results.^{86,87}

ACKNOWLEDGMENT

The authors wish to acknowledge the significant contributions of James H. Sloves, MD, and Joseph Patrick Mazzie, DO, in the preparation of this chapter.

REFERENCES

- Moore KL: The Developing Human, ed 4, Philadelphia, 1988, WB Saunders, pp 50–59.
- Moore KL: The Developing Human, ed 4, Philadelphia, 1988, WB Saunders, pp 159–169.
- Monie IW: Embryology. In Margulis AR, Burhenne HJ, editors: Alimentary Tract Roentgenology, ed 3, St. Louis, 1983, CV Mosby, pp 275–291.
- DuBois AM: The embryonic liver. In Roviller CH, editor: The Liver: Morphology, Biochemistry and Physiology, New York, 1963, Academic, pp 1–32.
- Kelly DE, Wood RL, Enders AC: Bailey's Textbook of Microscopic Anatomy, Baltimore, 1984, Williams & Wilkins, pp 590–593.
- Netter FH: Digestive System. Part III. Liver, Biliary Tract and Pancreas. The Ciba Collection of Medical Illustrations, vol 3, Summit, NJ, 1957, Ciba Pharmaceutical Products, pp 2–3.
- Giovannelli AS, Friedman A: Liver: Embryology, anatomy, histology and variations. In Friedman AC, editor: Radiology of the Liver, Biliary Tract, Pancreas, and Spleen, Baltimore, 1987, Williams & Wilkins, pp 3–36.
- Li YP, Morin ME, Tan A: Bipartite liver as a cause of 99m Tc liver scan defect. *Appl Radiol* 1:97–98, 1982.
- Radin DR, Colletti PM, Ralls PW, et al: Agenesis of the right lobe of the liver. *Radiology* 164:639–642, 1987.
- Champetier J, Yuer R, Letoublon C, et al: A general review of anomalies of hepatic morphology and their clinical implications. *Anat Clin* 7:285–299, 1985.
- Pujari BD, Deodhare SG: Symptomatic accessory lobe of the liver with review of the literature. *Postgrad Med J* 52:234–236, 1976.
- Rappaport AM: Physioanatomic considerations. In Schiff L, Schiff ER, editors: Diseases of the Liver, Philadelphia, 1987, JB Lippincott, pp 1–46.
- Hayes NA, Goldenberg IS, Bishop CC: The developmental basis for bile duct anomalies. *Surg Gynecol Obstet* 107:447–456, 1958.
- Snell RS: Clinical Anatomy for Medical Students, ed 2, Boston, 1981, Little, Brown, pp 202–205.
- Schwegler RA, Jr, Boyden EA: Development of pars intestinalis of common bile duct in human fetus with special reference to origin of ampulla of Vater and sphincter of Oddi. *Anat Rec* 67:441–467, 1937.
- Pontes JF, Pinotti WH: Anomalies of the gallbladder and biliary system. In Bockus HL, Berk JE, Haubrich WS, et al, editors: Gastroenterology, ed 3, Philadelphia, 1976, WB Saunders, pp 651–665.
- Berk RM: Oral cholecystography. In Berk RN, Ferrucci JT, Jr, Leopold GR, editors: Radiology of the Gallbladder and Bile Ducts, Diagnosis and Intervention, Philadelphia, 1983, WB Saunders, pp 121–142.
- Singleton E: Pediatric diseases of the gallbladder and bile ducts. In Berk RN, Ferrucci JT, Jr, Leopold GR, editors: Radiology of the Gallbladder and Bile Ducts, Diagnosis and Intervention, Philadelphia, 1983, WB Saunders, pp 513–546.
- Youndwith JD, Peters JC, Perry MC: The suprahepatic gallbladder. *Radiology* 149:57–58, 1983.
- Croce ES: The multiseptate gallbladder. *Arch Surg* 107:104–108, 1973.
- Hatfield PM, Wise RE: Anatomic variation in the gallbladder and bile ducts. *Semin Roentgenol* 11:157–164, 1976.
- Neuhauser EBD, Elkin M, Landing BH: Congenital direct communication between biliary system and respiratory tract. *Am J Dis Child* 83:654–658, 1952.
- Witzleben CL: Bile duct paucity (“intrahepatic atresia”). *Perspect Pediatr Pathol* 7:185–200, 1982.
- Alagille D: Intrahepatic biliary atresia (hepatic ductal hypoplasia). In Berenberg SR, editor: Liver Disease in Childhood, Baltimore, 1976, Williams & Wilkins, p 129.
- Doppman JL, Dunnick NR, Girton M, et al: Bile duct cysts secondary to liver infarcts: Report of a case and experimental production by small vessel hepatic artery occlusion. *Radiology* 130:1–5, 1979.
- Berger PE, Kuhn JP: Computed tomography of the hepatobiliary system in infancy and childhood. *Radiol Clin North Am* 19:431–441, 1981.
- Babbitt DP, Starshak RJ, Clemett A: Choledochal cyst: A concept of etiology. *AJR Am J Roentgenol* 119:57–62, 1973.
- Ghahremani GG, Lu CT, Woodlief RM, et al: Choledochal cyst in adults. A clinical and radiologic study in ten cases. *Gastrointest Radiol* 1:305–313, 1977.
- Levy AD, Rohrmann CA: Biliary cystic disease. *Curr Probl Diagn Radiol* 6:233–263, 2003.
- Todani T, Watanabe Y, Narusue M, et al: Congenital bile duct cysts. *Am J Surg* 134:263–268, 1977.
- Sherlock S: Diseases of the Liver and Biliary System, ed 6, Oxford, 1981, Blackwell Scientific, pp 406–412.
- Dodds WJ: Radiology (esophagus and esophagogastric region). In Margulis AR, Burhenne HJ, editors: Alimentary Tract Roentgenology, ed 3, St. Louis, 1983, CV Mosby, pp 529–603.
- Moore KL: The Developing Human, ed 4, Philadelphia, 1988, WB Saunders, pp 217–245.
- Franken EA, Jr, Smith WL: Pediatric esophagus. In Levine MS, editor: Radiology of the Esophagus, Philadelphia, 1989, WB Saunders, pp 337–362.
- Balfe DM, Mauro MA, Koehler RE, et al: Gastrohepatic ligament: Normal and pathologic CT anatomy. *Radiology* 150:485–490, 1984.
- Balfe DM, Peterson RR, van Dyke JA: Normal abdominal and pelvic anatomy. In Lee JKT, Sagel SS, Stanley RJ, editors: Computed Body Tomography with MRI Correlation, ed 2, New York, 1989, Raven Press, pp 415–475.
- Seaman WB: Nonneoplastic lesions (stomach and duodenum). In Margulis AR, Burhenne HJ, editors: Alimentary Tract Roentgenology, ed 3, St. Louis, 1983, CV Mosby, pp 529–603.
- Koehler RE, Balfe DM, Stanley RJ: Gastrointestinal tract. In Lee JKT, Sagel SS, Stanley RJ, editors: Computed Body Tomography with MRI Correlation, ed 2, New York, 1989, Raven Press, pp 477–520.
- Op den Orth JO: Duodenum. In Margulis AR, Burhenne HJ, editors: Alimentary Tract Roentgenology, ed 3, St. Louis, 1983, CV Mosby, pp 800–831.
- Friedman AC, Birns MT: Embryology, anatomy, histology and physiology (pancreas). In Friedman AC, editor: Radiology of the Liver, Biliary Tract, Pancreas and Spleen, Baltimore, 1987, Williams & Wilkins, pp 619–642.
- Ravitch MM: The pancreas in infants and children. *Surg Clin North Am* 55:377–385, 1975.
- Shirkhoda A, Gore R: The pancreas. In Shirkhoda A, editor: Variants and Pitfalls in Body Imaging, Philadelphia, 2000, Lippincott Williams & Wilkins, pp 293–294.
- Kawamoto S, Siegelman SS, Bluemke DA, et al: Focal fatty infiltration in the head of the pancreas: Evaluation with multidetector computed tomography with multiplanar reformation. *J Comput Assist Tomogr* 33:90–95, 2009.
- Low G, Panu A, Millo N, Leen E: Multimodality imaging of neoplastic and nonneoplastic solid lesions of the pancreas. *Radiographics* 31:993–1015, 2011.
- Glazer GM, Margulis AR: Annular pancreas: Etiology and diagnosis using ERCP. *Radiology* 133:303–306, 1979.
- Richter JM, Schapiro RM, Mulley AG, et al: Association of pancreas divisum and pancreatitis and its treatment by sphincteroplasty of the accessory ampulla. *Gastroenterology* 81:1104–1110, 1981.
- Itoh S, Takada A, Satake H, et al: Diagnostic value of multislice computed tomography for pancreas divisum: Assessment with oblique coronal reconstruction images. *J Comput Assist Tomogr* 29:452–460, 2005.
- Soto JA, Lucey BC, Stuhlfaut JW: Pancreas divisum: Depiction with multi-detector row CT. *Radiology* 235:503–508, 2005.
- Lai F, Freeman ML, Cass OW, Mallory S: Accurate diagnosis of pancreas divisum by linear-array endoscopic ultrasonography. *Endoscopy* 8:705–709, 2004.
- Morgan DE, Stanley RJ: Pancreas. In Lee JKT, Sagel SS, Stanley RJ, Heiken JP, editors: Computed Body Tomography with MRI Correlation, ed 4, Philadelphia, 2006, Lippincott Williams & Wilkins, pp 1007–1100.
- Gore RM, Balfe DM, Aizenstein RI, Silverman PM: The great escape: Interfascial decompression planes of the retroperitoneum. *AJR Am J Roentgenol* 175:363–370, 2000.
- Dodds WJ, Foley WD, Lawson TL, et al: Anatomy and imaging of the lesser peritoneal sac. *AJR Am J Roentgenol* 144:567–575, 1985.
- Ros PK, Olmsted WJ, Moser RP, Jr, et al: Mesenteric and omental cysts: Histologic classification with imaging correlation. *Radiology* 164:327–332, 1987.
- Maglinte DDT, Herlinger H: Congenital and developmental anomalies in adolescents and adults. In Herlinger H, Maglinte D, editors: Clinical Radiology of the Small Intestine, Philadelphia, 1989, WB Saunders, pp 249–273.
- Dachman AH: Anomalies and congenital disorders (spleen). In Friedman AC, editor: Radiology of the Liver, Biliary Tract, Pancreas, and Spleen, Baltimore, 1987, Williams & Wilkins, pp 913–930.
- Blaustein A: The Spleen, New York, 1963, McGraw-Hill, p 45.
- Halpert B, Gyorkey F: Lesions observed in accessory spleens of 311 patients. *Am J Clin Pathol* 32:165–168, 1959.
- Olsen WR, Beaudoin DE: Increased incidence of accessory spleens in hematologic disease. *Arch Surg* 98:762–763, 1969.
- Malins E: Rotation of the spleen; removal; recovery. *Lancet* 2:607, 1894.
- McClain GH, Leberz TB: Radiographic evidence of splenic torsion: Report of a case. *Obstet Gynecol* 29:475–478, 1967.
- Gordon DH, Burrell MI, Levin DC, et al: Wandering spleen: The radiological and clinical spectrum. *Radiology* 125:39–46, 1977.

62. Vermeylen C, Lebecque P, Claus D, et al: The wandering spleen. *Eur J Pediatr* 140:112–115, 1983.
63. Kelly KJ, Chusid MJ, Camitta BM: Splenic torsion in an infant associated with secondary disseminated *Hemophilus influenzae* infection. *Clin Pediatr* 21:365–366, 1982.
64. Monie IW: The asplenia syndrome: An explanation for absence of the spleen. *Teratology* 25: 212–219, 1982.
65. Tawfik AM, Batouty NM, Zaky MM, et al: Polysplenia syndrome: A review of the relationship with viscerotransposition and the spectrum of extra-cardiac anomalies. *Surg Radiol Anat* 35: 647–653, 2013.
66. Ivemark BI: Implications of agenesis of the spleen on the pathogenesis of conotruncus anomalies in childhood. An analysis of the heart malformations in the splenic agenesis syndrome with fourteen new cases. *Acta Paediatr* 44(Suppl 104):1–110, 1955.
67. Hutchins GM, Morre GW, Lipford EH, et al: Asplenia and polysplenia malformation complexes explained by abnormal embryonic body curvature. *Pathol Res Pract* 177:60–76, 1983.
68. Applegate KE, Goske MJ, Pierce G, Murphy D: Situs revisited: Imaging of the heterotaxy syndrome. *Radiographics* 19:837–852, 1999.
69. Rose V, Izukawa T, Moes CAF: Syndromes of asplenia and polysplenia: A review of cardiac and non-cardiac malformations in 60 cases with special reference to diagnosis and prognosis. *Br Heart J* 37:840–852, 1975.
70. Bearss RW: Splenic-gonadal fusion. *Urology* 16:277–279, 1980.
71. Ceccacci L, Tosi S: Splenic-gonadal fusion: Case report and review of the literature. *J Urol* 126: 387–389, 1981.
72. Putschar WGJ, Manion WC: Congenital absence of the spleen and associated anomalies. *Am J Clin Pathol* 26:429–445, 1956.
73. Balthazar EJ: Congenital positional anomalies of the colon: Radiographic diagnosis and clinical implications. II. Abnormalities of fixation. *Gastrointest Radiol* 2:49–56, 1977.
74. Snyder WH, Jr, Chaffin L: Intermediate stage in return of the intestines from the umbilical cord. *Anat Rec* 113:451–457, 1952.
75. Snyder WH, Jr, Chaffin L: Embryology and pathology of intestinal tract: Presentation of 40 cases of malrotation. *Ann Surg* 140:368–379, 1954.
76. Maglinte DDT, Herlinger H: Embryology of the small intestine. In Herlinger H, Maglinte D, editors: *Clinical Radiology of the Small Intestine*, Philadelphia, 1989, WB Saunders, pp 3–6.
77. Balthazar EJ, Gade M: The normal and abnormal development of the appendix. *Radiology* 121:599–604, 1976.
78. Heiken JP: Abdominal wall and peritoneal cavity. In Lee JKT, Sagel SS, Stanley RJ, editors: *Computed Body Tomography with MRI Correlation*, ed 2, New York, 1989, Raven Press, pp 661–705.
79. Kottra JJ, Dodds WJ: Duplication of the large bowel. *AJR Am J Roentgenol* 113:310–315, 1971.
80. Earlam RJ: A study of the aetiology of congenital stenosis of the gut. *Ann R Coll Surg Engl* 51:126–130, 1972.
81. de Sa DJ: Congenital stenosis and atresia of the jejunum and ileum. *J Clin Pathol* 25:1063–1070, 1972.
82. Puri P, Fujimoto T: New observations on the pathogenesis of multiple atresias. *J Pediatr Surg* 23:221–225, 1988.
83. Balthazar EJ: Congenital positional anomalies of the colon: Radiographic diagnosis and clinical implications. I. Abnormalities of rotation. *Gastrointest Radiol* 2:49–56, 1977.
84. Ford EG, Senac MO, Srikanth MS, Weitzman JJ: Malrotation of the intestine in children. *Ann Surg* 215:172–178, 1992.
85. Powell DM, Othersen HB, Smith CD: Malrotation of the intestines in children: The effect of age on presentation and therapy. *J Pediatr Surg* 24:777–780, 1989.
86. Andreyer HJ, Owen RA, Thompson I, Forbes A: Association between Meckel's diverticulum and Crohn's disease: A retrospective review. *Gut* 35:788–790, 1994.
87. Robustelli U, Manguso F, Armellino MF, et al: Acute symptomatic Meckel diverticulum management. *Ann Ital Chir* 85:129–135, 2014.

CHAPTER OUTLINE

Rotational Anomalies

Embryology
Clinical Findings
Radiologic Findings

Gastroschisis

General Considerations
Clinical Findings
Treatment
Radiologic Findings

Omphalocele

Clinical Findings
Radiologic Findings

Diaphragmatic Hernia

Foramen of Bochdalek Hernia
Foramen of Morgagni Hernia

Normal and Abnormal Neonatal Bowel Gas**Abdominal Masses**

Clinical Findings
Radiologic Findings

Necrotizing Enterocolitis

Clinical Findings
Radiologic Findings

Esophageal Atresia

General Considerations
Radiologic Findings

Laryngotracheal Cleft**Jejunal and Ileal Stenosis and Atresia**

Treatment
Radiologic Findings

Meconium Peritonitis

Clinical Findings
Radiologic Findings

Colonic Atresia

General Considerations
Radiologic Findings

Imperforate Anus

Clinical Findings
Treatment
Radiologic Findings

Imperforate Anus Variants

Cloacal Malformation
Treatment
Radiologic Findings

Caudal Regression**Currarino Triad****Other Low Obstructive Lesions**

Meconium Ileus
Meconium Plug Syndrome
Megacystis–Microcolon–Intestinal Hypoperistalsis Syndrome
Hirschsprung's Disease

This chapter discusses gastrointestinal malformations that are manifested during the neonatal period. Some are grossly apparent at birth (e.g., gastroschisis, omphalocele, diaphragmatic hernia); others usually are manifested within the first hours or days of life (e.g., esophageal, small bowel, or colonic atresia; meconium ileus; meconium plug; Hirschsprung's disease). Many of these diagnoses can be suggested by prenatal ultrasound.

Rotational Anomalies**EMBRYOLOGY**

During the sixth gestational week, rapid elongation of the midgut and hindgut results in their herniation into a sac in the midline of the anterior abdominal wall. Before returning to the peritoneal cavity during the ninth week of gestation, the midgut revolves 90 degrees around the superior mesenteric artery. Once it is within the abdominal cavity, the bowel rotates

an additional 180 degrees, which positions the duodenojejunal junction to the left of the spine at the level of the stomach, the jejunum in the left upper quadrant, and the ileum in the right hypochondrium or right lower quadrant.¹⁻³ The colon undergoes a separate counterclockwise rotation of 270 degrees, which brings the cecum into the right lower quadrant. This normal rotation is associated with a broad mesenteric base, extending from the left upper quadrant to the right lower quadrant. Attachments at two sites keep the bowel fixed in proper position: the ligament of Treitz at the duodenojejunal junction and an attachment at the cecal base.

Deviation from normal rotation and fixation occurs universally in children with omphalocele, gastroschisis, and diaphragmatic hernia. Variations of rotation may also be present in children with asplenia and polysplenia syndromes, duodenal stenosis or atresia, and Hirschsprung's disease. However, malrotation frequently exists as an isolated anomaly.

The spectrum of rotational abnormalities is broad (Figs. 114-1 to 114-3).³⁻¹⁰ In some children, the process of rotation

takes place, but fixation fails to occur. In others, there are only minor variations from the normal position. Complete nonrotation is said to be present when the jejunum is to the right of the spine and the ileum is in the pelvis or to the left of the spine. Most clinical problems arise in children with the greatest deviation from the normal rotational pattern. In classic malrotation,

the cecum lies in the midabdomen or left of the midline (see Fig. 114-2) and may be fixed in place by broad bands that emanate from the undersurface of the liver. These Ladd bands cross the duodenum and may cause extrinsic compression and obstruction of the gut at this level (see Fig. 114-3).

CLINICAL FINDINGS

Most children with malrotation present in the first few months of life. They have acute abdominal symptoms if there has been acute volvulus with twisting of the bowel on its shortened mesentery or chronic vomiting and failure to thrive because of the obstructing Ladd bands (see Fig. 114-3). Midgut volvulus may produce vascular compromise, which can lead to gangrene of the entire small bowel if it is not promptly diagnosed and treated (Fig. 114-4).⁴⁻¹⁰

In some children, malrotation is not detected until later, when studies are done for other purposes. Uncommonly, malrotation can be associated with chronic volvulus. This condition interferes with lymphatic and venous drainage, which produces malabsorption or failure to thrive.¹¹⁻¹⁴ Acute volvulus with infarction of bowel does occur, although rarely, in older children and adults. Motility abnormalities may persist after corrective surgery. Other duodenal abnormalities occur frequently in children with malrotation: duodenal atresia, annular pancreas, and preduodenal portal vein.

RADIOLOGIC FINDINGS

Abdomen radiographs are of little value in the child with an uncomplicated rotational abnormality because the positions of the duodenojejunal junction and cecum are rarely definable without positive contrast media. Sometimes, abnormal configuration of the gas in the right hypochondrium (i.e., duodenal triangle) may suggest the diagnosis of malrotation with volvulus.¹¹ Normal findings on radiographs do not exclude the diagnosis of malrotation with volvulus.^{4-6,10}



Figure 114-1 Rotational variation. The duodenal bulb overlies the spine, and multiple jejunal loops are seen throughout the right side of the abdomen.



Figure 114-2 Malrotation demonstrated on barium enema. **A.** The cecum (C) lies in the left lower quadrant. Contrast medium is visible in the appendix (arrows). **B.** In a different child, the cecum (C) is in the left upper quadrant.

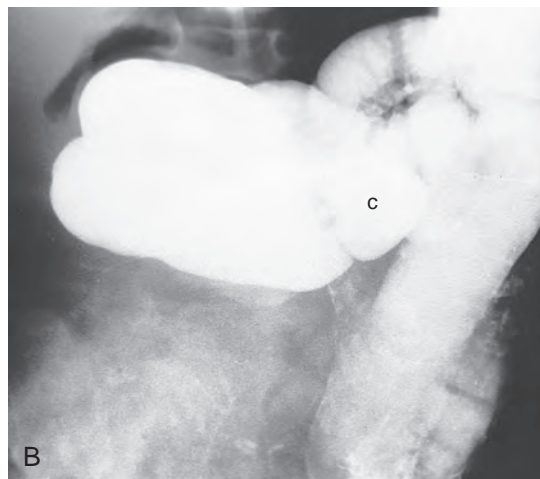




Figure 114-3 Malrotation with Ladd bands. This upper gastrointestinal series shows a partially obstructing, extrinsic defect (arrow) in the duodenum.

In the neonate or child with abdominal pain or vomiting, abdomen radiographs showing gaseous distention of the stomach and duodenal bulb suggest a high obstruction (see Fig. 114-4). This appearance (i.e., double bubble) can also be seen in duodenal atresia and annular pancreas. A contrast study may be necessary for differentiation between the relatively benign complication of Ladd bands (see Fig. 114-3) and the surgical emergency of volvulus (see Fig. 114-4).

In the child with midgut volvulus, the abdominal gas pattern may be normal or show high or low obstruction, or the abdomen may be gasless.⁵⁻⁷ Because abdomen radiographs are usually nondiagnostic and the consequences of delayed diagnosis are grim, contrast studies should be performed emergently when volvulus is suspected.

The first study performed to detect the malrotation and its complications should be an upper gastrointestinal series. The barium enema can show a malpositioned or malfixed cecum (see Fig. 114-2), but normal results of a barium enema do not exclude malrotation with volvulus. For this reason, an upper gastrointestinal series may need to be performed after the enema if a low obstructive lesion is not found and malrotation is still considered.

The diagnosis of malrotation can be made sonographically, although it is usually an incidental finding on studies performed for other reasons.^{14,15} Failure of the bowel to rotate normally produces an abnormal relationship between the superior mesenteric artery and vein. With volvulus, the superior mesenteric vein may wind around the superior mesenteric artery, inconsistently producing the whirlpool sign on ultrasound.¹⁵ Sonography may exclude malrotation by showing the third portion of the duodenum between the aorta and superior mesenteric artery.^{16,17} Computed tomography (CT) can also show these vascular changes and demonstrate malpositioned and twisted bowel.¹⁸

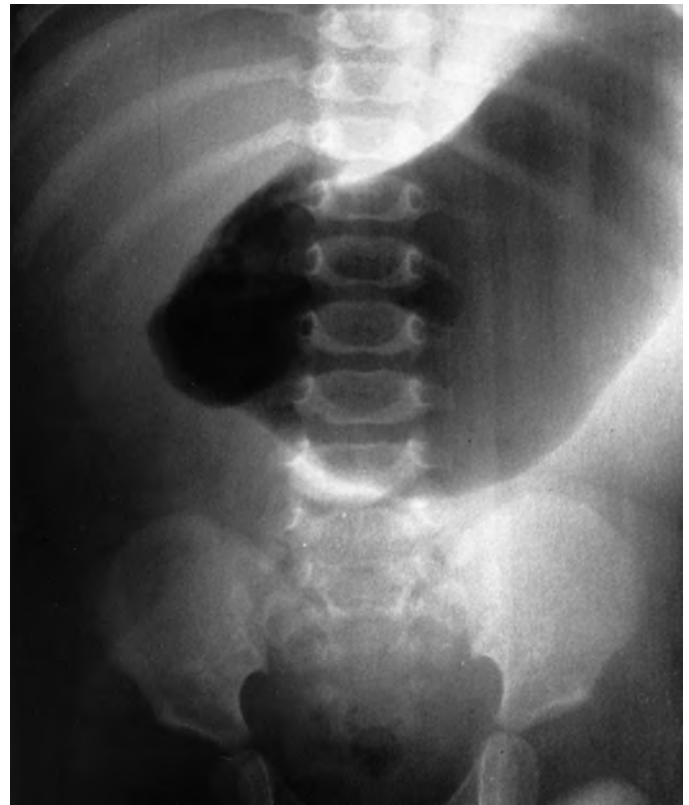


Figure 114-4 Midgut volvulus. Plain radiograph demonstrates air only in the stomach and duodenum in this acutely ill infant with midgut volvulus.

Gastroschisis

GENERAL CONSIDERATIONS

Development of the anterior abdominal wall is complex, with the orderly ingrowth of four separate folds (i.e., cranial, caudal, and two lateral) necessary for normal closure.^{19,20} Gastroschisis is a parasagittal defect, usually to the right of the normally positioned and normal-appearing umbilical cord, through which bowel herniates into the amniotic fluid.

CLINICAL FINDINGS

The herniated bowel has no covering membrane or sac and is therefore associated with a rise in the maternal serum α -fetoprotein level. Occurring in about 1 of 10,000 live births, gastroschisis can be diagnosed prenatally with sonography.²¹⁻²³ At birth, the defect and herniated bowel are apparent and not easily confused with other abdominal wall defects.

Malrotation or nonrotation of the bowel is the rule in gastroschisis, but it rarely leads to complications. Bowel atresia, present in 20% of cases, is usually the only anomaly, but it is an important factor contributing to postoperative morbidity.²⁴⁻²⁸

TREATMENT

Even though a small amount of bowel usually is herniated through a small defect, surgical repair is associated with a postoperative mortality rate of 5% to 25%, with major complications of sepsis and electrolyte problems.²²⁻²⁹ Antenatal exposure

to amniotic fluid produces bowel wall edema and inflammatory thickening of the serosa, which interferes with peristaltic function, even after repair.²⁸ In utero, the exposed bowel and mesentery may become shortened and coiled, which also affects postnatal function. Short gut syndrome may decrease intestinal absorption and cause diminished constitutional growth. Children with short gut or hypoperistalsis can be supported with parenteral hyperalimentation, but this also can create management problems: venous thrombosis, liver disease, and cholelithiasis. Cesarean section, once routine in an attempt to diminish the intrauterine bowel changes, has been shown to produce no difference in postnatal and postoperative bowel function.^{20,23,29}

The type of surgical correction, primary or delayed, depends on the size of the defect and the presence of other complications, such as atresia and short gut.²⁶⁻²⁹ In addition to covering the herniated bowel, with placement of an abdominal silo, it may be necessary to create a stoma to decompress the dilated bowel proximal to an atresia.

After surgery, motility changes are universal in children with gastroschisis.²⁷⁻³¹ The initial postoperative paralytic ileus is frequently followed by marked prolongation of intestinal transit. These children also have a high incidence of significant gastroesophageal reflux. Even though they are usually term infants, necrotizing enterocolitis (NEC) occurs in 23% of cases at 1 to 4 months after repair and may be manifested atypically; only 36% of affected children have blood-streaked stool.³⁰

RADIOLOGIC FINDINGS

The prenatal sonographic diagnosis of gastroschisis is based on the observation of normal umbilical cord insertion in a fetus with an anterior abdominal wall defect through which bowel has herniated.^{19,21,23} No membrane covers the bowel; if fetal ascites or a covering membrane is present or if the liver is detected in the herniated viscera, omphalocele is the more likely diagnosis.^{19,22,32} Thickening of the exteriorized bowel loops strongly suggests gastroschisis. Amniotic fluid volume is usually normal. A bowel caliber of more than 17 mm suggests that an atresia is present; similarly, bowel of a smaller diameter is usually associated with bowel continuity.

Abdomen radiographs show the normally positioned umbilical clamp separated from herniated bowel loops, which are outlined by air (Fig. 114-5). Postoperative radiographs should be scrutinized to detect changes of NEC: ileus, dilated bowel loops, and intramural air.^{27,30} Postsurgical barium studies are used to detect gastroesophageal reflux, bowel loop dilation, obstructive adhesions, amount of bowel present, and abnormalities of position, peristalsis, or transit time.³³

Omphalocele

CLINICAL FINDINGS

Omphalocele, present in about 1 of 5000 live births, is a midline defect of variable size through which bowel, liver, spleen, pancreas, and uterus may protrude.^{19,21,32} A membrane or sac usually covers the herniated organs, but the sac may be ruptured at birth. The umbilical cord inserts into the apex of the sac. The bowel is malrotated, and 8% to 20% of these children have Meckel's diverticulum.

The diagnosis of omphalocele can be made with prenatal ultrasound.^{19,21,22,32} Maternal α -fetoprotein levels may be

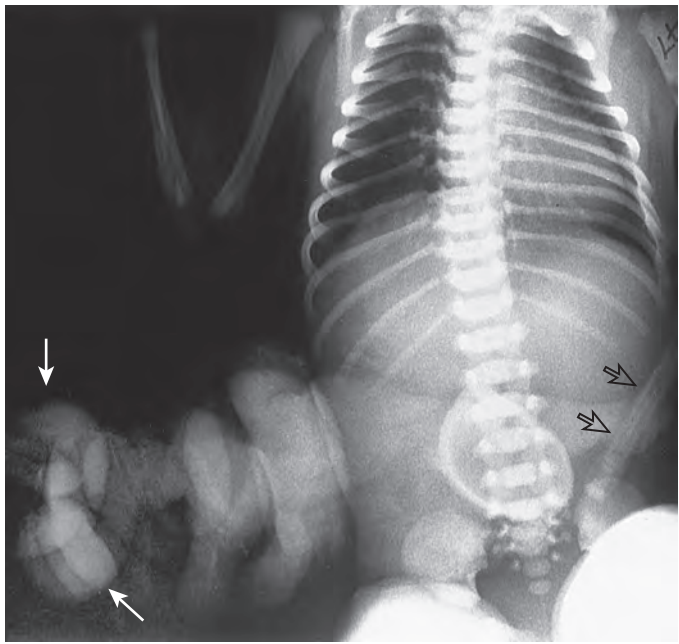


Figure 114-5 Gastroschisis. Exteriorized bowel loops (white arrows) extend lateral to the abdominal wall in this neonate with gastroschisis. Because the loops lack a covering membrane, each is clearly outlined by air. The normally inserted umbilical cord is in the midline, defined by the umbilical clamp to the left of midline (open arrows).

elevated, but because of the covering sac, they tend to be less than those found with gastroschisis. Associated anomalies are seen in about 50% to 80% of infants with omphalocele, including tetralogy of Fallot and atrial septal defect as well as other cardiac, central nervous system, and gastrointestinal anomalies. Detection of anomalies may influence the outcome or management of the pregnancy; certain anomalies are associated with fetal demise, and others may result in planned termination of pregnancy.³⁴⁻³⁶ Children with Beckwith-Wiedemann syndrome account for almost 12% of the population with omphalocele. These infants are large at birth and have a large tongue. A specific pancreatic abnormality, nesidioblastosis, predisposes the infants to hypoglycemia, even in the neonatal period. Down syndrome (i.e., trisomy 21), trisomy 13, and trisomy 18 are associated with an increased incidence of omphalocele.^{32,34-36}

Children with small anterior abdominal defects (e.g., gastroschisis, small omphalocele) tend to have a normally developed thorax. Those with giant omphaloceles (i.e., containing liver and bowel) have a small thorax and an increased incidence of pulmonary hypoplasia and respiratory insufficiency. They may require ventilatory support after surgery.^{36,37}

Surgical management may take many forms.³⁸ In most children, the defect is corrected by primary skin closure or closure with a silo. The surgical approach is determined by the size of the defect, and larger defects may require a staged reduction.

RADIOLOGIC FINDINGS

Prenatal sonographic diagnosis of omphalocele is based on visualization of the umbilical cord inserting into the membrane covering structures anterior to the abdominal wall of the fetus.^{19,21-23,32,35} Fetal ascites, abnormal amounts of amniotic fluid, and associated congenital defects are supportive ancillary

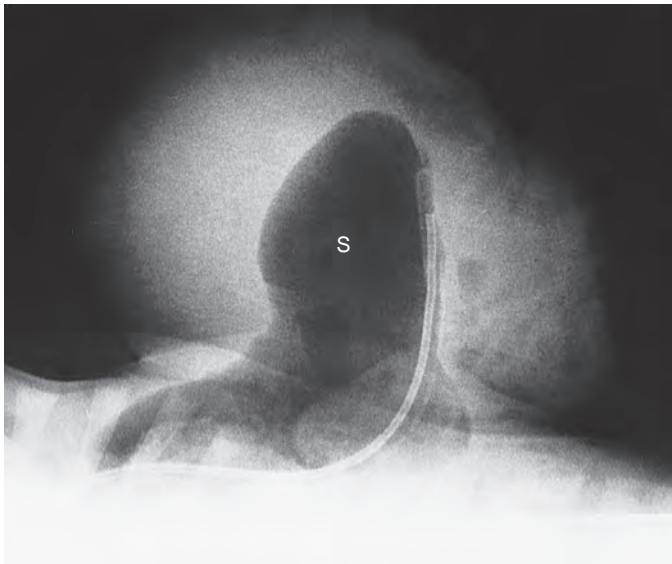


Figure 114-6 Omphalocele. Lateral abdomen radiograph reveals a membrane-covered omphalocele. The sac of the omphalocele is outlined by air and clearly seen, but individual bowel loops cannot be identified because they are not exposed to air, unlike the situation in gastroschisis. The air-filled stomach (S) protrudes into the omphalocele.

findings. Thickening of exteriorized bowel loops or absence of membrane or sac suggests the diagnosis of gastroschisis.

Postnatal abdominal radiographs (Fig. 114-6) depict the omphalocele as a soft tissue density whose margins are well defined by the adjacent air. Unlike gastroschisis (see Fig. 114-5), the bowel loops are not individually seen unless the omphalocele sac has ruptured. Malrotation of the bowel and malposition of other organs are identified on postoperative imaging studies.³⁹

Diaphragmatic Hernia

FORAMEN OF BOCHDALEK HERNIA

Embryology

In early fetal life, the peritoneal cavity and the pleural space are in continuity. At week 8, just before anteriorly herniated bowel returns to the abdominal cavity, the communication between these two spaces is closed by the development of the diaphragm.⁴⁰ If the bowel returns to the abdomen prematurely or if the diaphragm develops late or incompletely, a diaphragmatic hernia develops. Affected children have malrotation of the bowel because the normal rotation that occurs as the bowel returns to the abdomen is interrupted. A membrane covers the herniated gut in only 10% of Bochdalek hernias.

Clinical Findings

The posterolateral or Bochdalek hernia occurs in approximately 1 of 3000 live births.⁴⁰ Some diaphragmatic hernias may be acquired after trauma or infection. In the neonatal period, diaphragmatic hernias can develop in association with group B streptococcal infection.⁴¹ Late presentation or detection of an asymptomatic diaphragmatic hernia has also been described.^{41,42}

Congenital diaphragmatic hernia occurs six to nine times more often on the left, presumably because the pleuroperitoneal

canal closes earlier on the right; about 3% of children have bilateral diaphragmatic hernia. Left-sided hernias usually contain portions of the gastrointestinal tract. The liver may extend into the thorax with left or right diaphragmatic hernias. Regardless of the side on which the hernia occurs, the ipsilateral and contralateral lungs are compressed, and the most critical factor in determining the neonate's outcome is the degree of pulmonary hypoplasia.⁴³⁻⁴⁸

Diaphragmatic hernia should be suspected clinically when a neonate with severe respiratory distress has a scaphoid abdomen. Because bowel contents are in the thorax, the abdomen lacks its normal protuberant appearance. Most newborns with diaphragmatic hernia are rapidly intubated and resuscitated; when they are stable, they undergo surgical repair. All children are carefully inspected for midline defects (i.e., cleft lip and palate, spina bifida, and omphalocele) and cardiac lesions (i.e., ventricular septal defect and tetralogy of Fallot) because associated anomalies also determine outcome.^{42,43}

Despite ventilatory support and pharmacologic manipulation including inhaled nitric oxide to correct pulmonary hypertension, a common complication of diaphragmatic hernias, early presurgical mortality rates range from 20% to 80%.⁴³ To improve survival, extracorporeal membrane oxygenation (ECMO) is used in infants who experience significant respiratory insufficiency resulting from pulmonary hypoplasia.^{48,49} ECMO may be performed before, during, or after surgery. This lung bypass system entails placement of large-bore cannulas into the aortic arch through the right common carotid artery and the right atrium (venoarterial approach) or a single double-lumen catheter into the right atrium (venovenous approach) through the right internal jugular vein.⁵⁰ Heparinization is routine. The lungs are minimally ventilated and given the chance to mature and grow. ECMO has increased postsurgical survival to more than 80%, but it is not without complications: bleeding at the neck wounds, intracerebral and pleural hemorrhage, and difficulty with later central line placement. Children who require ECMO have a poorer neurologic outcome than those who do not. Because these children are sicker from the moment of birth, the neurologic deficits have a multifactorial cause, including ECMO.⁵¹

The fact that many infants with diaphragmatic hernias still died before undergoing repair drove the research in prenatal surgical intervention throughout the 1990s. The observed-to-expected fetal lung volume measured by magnetic resonance imaging (MRI) is reported to be a predictor of survival.⁴⁴ In fetuses with a very low observed-to-expected fetal lung volume, one fetal surgical technique employed involves fetal tracheal occlusion; this causes fluid to fill the lungs and encourages their expansion despite the extrinsic pressure produced by herniated abdominal contents.⁵² The clip or balloon occluding the trachea is removed at the time of birth, allowing normal respiration. Results with this technique, used only in those whose prenatal ultrasound indicates severely compromised lung parenchyma, have been promising.⁵²

Radiologic Findings

The prenatal sonographic diagnosis of diaphragmatic hernia is made when the heart and other mediastinal contents are shifted from the midline and a "mass" (i.e., liver or gut) is present in the thorax.^{40,43-45} A fetal abdominal circumference below the fifth percentile correlates with a poor prenatal and postnatal course in some studies.⁵³ Fetal ascites, pleural effusion, and

polyhydramnios have been associated with diaphragmatic hernia.

Prenatal ultrasound and MRI have documented the presence of a portion or all of the liver in many diaphragmatic hernias.^{44,47} When it is not diagnosed prenatally, the affected infant presents with respiratory distress shortly after birth. Abdomen radiographs can determine the amount of bowel present in the abdomen. Chest radiographs can exclude other causes of neonatal respiratory distress: pulmonary immaturity, congenital pulmonary airway malformation, and pneumonia. Complications of resuscitation and other congenital abnormalities that may affect management should be sought. Pneumothorax is common and requires prompt treatment.

On early radiographs, the herniated bowel loops may appear as a soft tissue mass. With time and air swallowing, the chest radiographs have a more typical bubbly appearance (Fig. 114-7). Diaphragmatic hernias that contain liver may appear more solid and may be accompanied by a pleural collection. On occasion, mild diaphragmatic hernias are not diagnosed until later in childhood.⁴⁰

If the nature of the thoracic contents is uncertain, a nasogastric tube should be inserted to define the stomach and to introduce air into the bowel. Contrast studies are rarely needed to visualize the upper or lower gastrointestinal tract before surgery (Fig. 114-8).

The mediastinum remains shifted to the side opposite the hernia on immediate postoperative chest radiographs. The ipsilateral lung appears as a soft tissue density outlined with air close to the mediastinum. The ipsilateral pneumothorax is expected and may simulate tension pneumothorax because of the long-standing mediastinal shift. Attempts to evacuate this pneumothorax may result in overexpansion of the hypoplastic

contralateral lung and cause contralateral pneumothorax. During the first few postoperative days, as the ipsilateral lung expands, fluid may occupy a portion of the pleural space and produce haziness on that side of the thorax.

Before a child is placed on ECMO, cardiac, cranial, and abdominal ultrasound is performed to identify those who can safely receive this treatment. Neonates with intracranial hemorrhage or with a lethal anomaly are excluded from ECMO.

Neonates treated with ECMO receive a daily chest radiograph. Evaluation of line placement is necessary; kinking and dislodgment of support lines may occur and compromise treatment. Lung opacity is often diffusely increased because of the planned underventilation, increased fluid in the lungs, and, uncommonly, bleeding.^{54,55} Pleural hemorrhage develops in about 30% of children on ECMO and may be manifested as a typical pleural collection or, when it is associated with pneumothorax, an unexpected mediastinal shift.⁵⁵ The esophagus may appear as a mediastinal air or fluid mass in the midline because it frequently dilates from gastroesophageal reflux.⁵⁶ Although the replacement of the bowel loops into the abdomen usually is well tolerated, about 20% of long-term survivors experience intestinal obstruction, and about 13% require surgery for relief of the obstruction.⁵⁷

The most striking finding on the chest radiographs of many long-term survivors is the degree to which the hypoplastic lungs may grow and develop. In many children, a chest radiograph at age 2 or 3 years has a nearly normal appearance.⁵⁸

FORAMEN OF MORGAGNI HERNIA

Herniation of colon or other abdominal structures into the retrosternal space is rare and occurs when the anteromedial aspect of the diaphragm develops abnormally. The so-called foramen of Morgagni hernia accounts for about 2% to 4% of all diaphragmatic hernias.^{40,43,59}

Respiratory and gastrointestinal complaints are common but not necessarily related to the hernia.^{59,60} The child may be asymptomatic, and the abnormality may be detected on a chest radiograph obtained for a nonrelated purpose. Only 50% are detected by age 5 years.⁶¹

Although the amount of bowel herniated into the chest in Morgagni hernias is usually much less than in Bochdalek hernias, malrotation or malfixation is common. In contrast to Bochdalek hernias, Morgagni hernias usually are right sided and have a covering or sac.^{62,63}

The differential diagnosis of air-containing Morgagni hernias includes pneumonia, atelectasis, pneumatocele, abscess, and congenital pulmonary airway malformation. If the liver is herniated, the solid appearance may simulate a tumor of the diaphragm, a pericardial mass, or an anterior mediastinal mass. Morgagni hernias are corrected even in asymptomatic children because of the potential for incarceration and strangulation.

Radiologic Findings

Anteroposterior chest radiographs may show a soft tissue opacity or air along the heart border (Fig. 114-9). On the lateral projection, the anterior location of the hernia and visualization of bowel establish the diagnosis. In some cases, additional imaging may be needed to identify the nature and extent of the hernia (see Fig. 114-9).⁶³

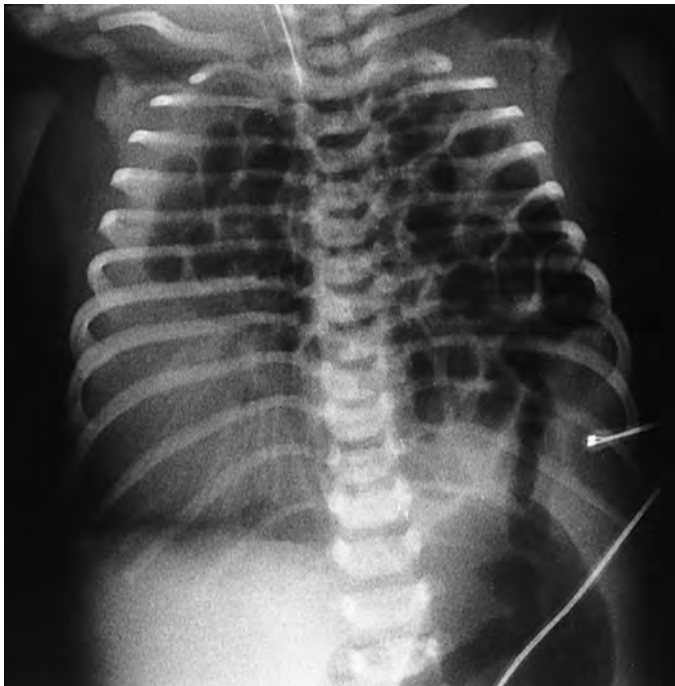


Figure 114-7 Left Bochdalek hernia. Multiple, air-filled bowel loops fill the left thorax and right apex. The mediastinum is shifted to the right, and the soft tissues of the heart and the hypoplastic right lung merge.

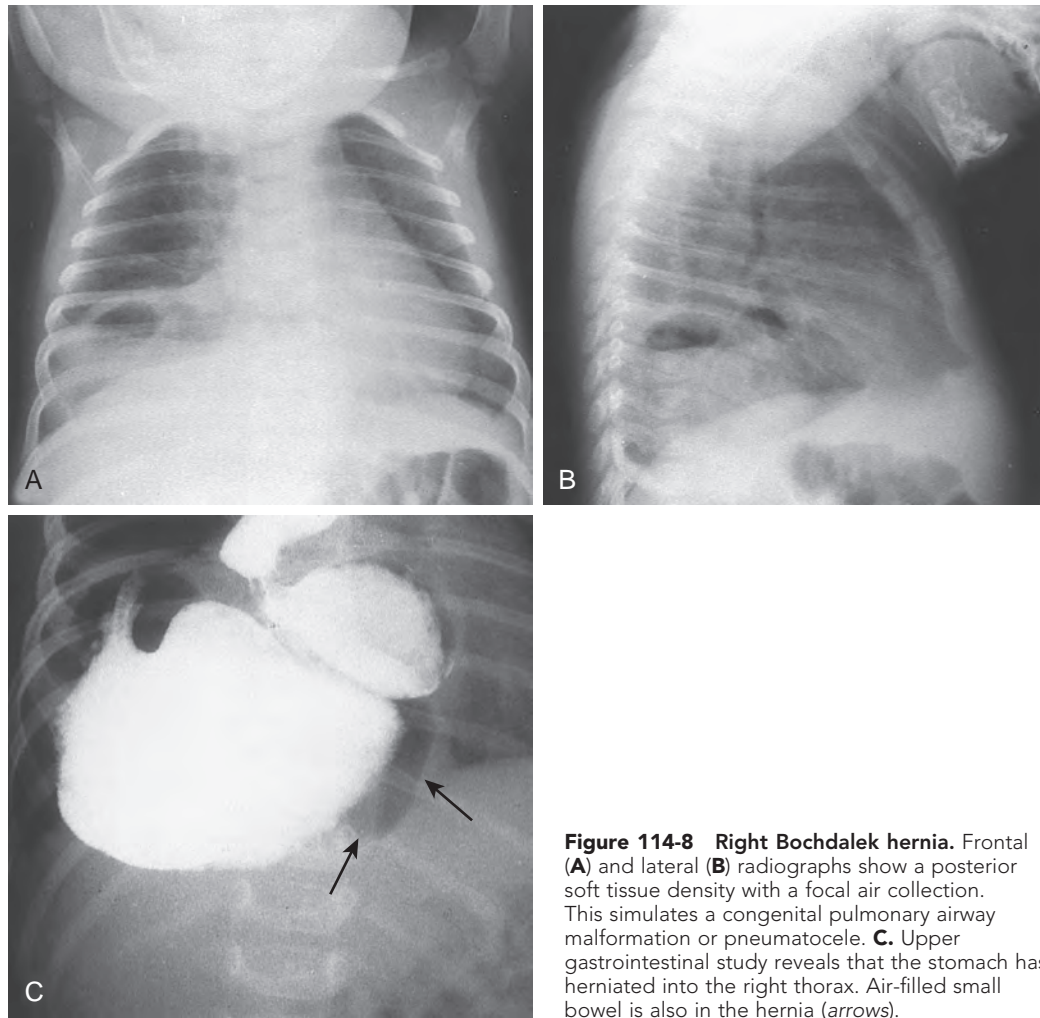


Figure 114-8 Right Bochdalek hernia. Frontal (A) and lateral (B) radiographs show a posterior soft tissue density with a focal air collection. This simulates a congenital pulmonary airway malformation or pneumatocele. C. Upper gastrointestinal study reveals that the stomach has herniated into the right thorax. Air-filled small bowel is also in the hernia (arrows).

Normal and Abnormal Neonatal Bowel Gas

With the first breath, the neonate begins to aerate the respiratory and gastrointestinal tracts. Unless there is obstruction, these processes tend to parallel each other. Several problems delay the passage of air into the gastrointestinal tract. The most obvious is a mechanical obstruction in the oral cavity or esophagus, most often esophageal atresia. Drugs given during labor and delivery can depress the swallowing mechanism, diminish the amount of air swallowed, and delay passage of air distally into the small bowel and colon.

Abdomen radiographs that are initially normal but then become gasless raise the possibility that the neonate has sepsis, has developed electrolyte imbalance, is receiving gastric suction, or is being paralyzed while being ventilated. These processes decrease the amount of air swallowed and the amount available for passage into distal bowel.

The bowel gas pattern should be carefully scrutinized in any neonate with respiratory or gastrointestinal symptoms. Gas should be symmetrically distributed throughout the abdomen in a mosaic pattern. Paucity or malposition of the gas may confirm a suspected diaphragmatic hernia. An abdominal mass may displace bowel loops and, through pressure on the

diaphragm, cause respiratory distress. With a high bowel obstruction, a few loops of bowel in the upper abdomen are distended with air and fluid (Fig. 114-10). With distal obstruction, dilated bowel loops fill the abdomen (Fig. 114-11).

In the neonate, it may be difficult to differentiate small from large bowel because haustra are poorly developed. Although location may allow differentiation of small from large bowel, distended small bowel may fill the space usually occupied by the colon or even simulate a distended stomach.

It is important to determine the most distal extent of air because the differential diagnosis depends on the level of the obstruction. Additional views may be necessary to detect air within the colon. Prone lateral rectal views may be useful if an extremely distal lesion is suspected. A contrast study of the colon may be performed to determine if there is an obstruction or to identify the level and nature of the obstruction.

Abdominal Masses

CLINICAL FINDINGS

The differential diagnosis of abdominal mass in the newborn is extensive: ovarian cyst or tumor, alimentary tract duplication, mesenteric or omental lymphangioma, cyst or tumor of the

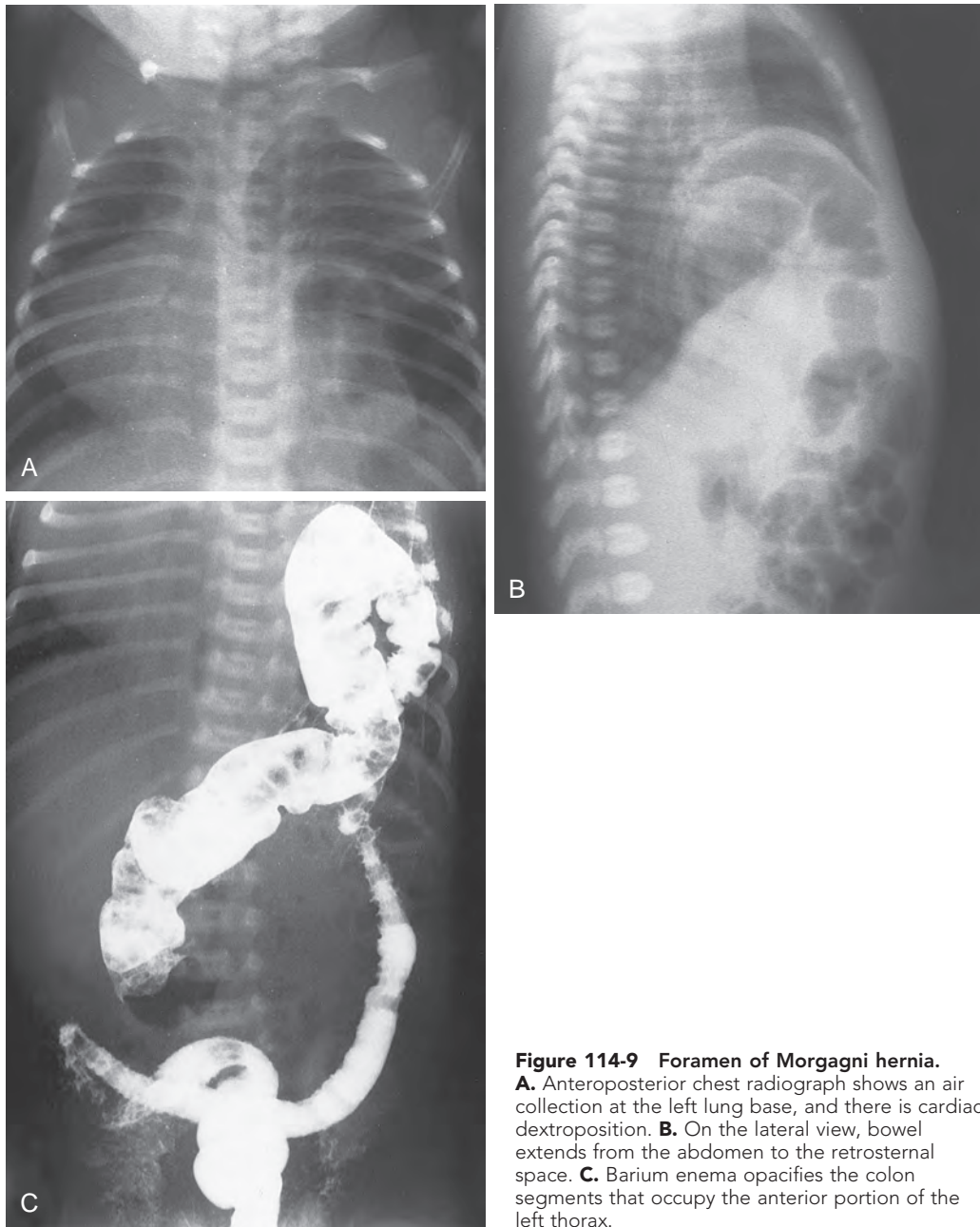


Figure 114-9 Foramen of Morgagni hernia.

A. Anteroposterior chest radiograph shows an air collection at the left lung base, and there is cardiac dextroposition. **B.** On the lateral view, bowel extends from the abdomen to the retrosternal space. **C.** Barium enema opacifies the colon segments that occupy the anterior portion of the left thorax.

spleen or liver, choledochal cyst, cystic meconium peritonitis, hydrometrocolpos, and retroperitoneal masses.^{60,64-67} Most neonatal abdominal masses originate in the kidneys; ureteropelvic junction obstruction and multicystic dysplastic kidneys are the most common causes. Gastrointestinal lesions account for 8% to 15% of neonatal abdominal masses.

The mass may be detected by prenatal sonography or by abdominal palpation after birth. In some neonates, the mass is sufficiently large to distend or distort the abdominal wall and cause respiratory distress. Ascites may be present or simulated. Pain or obstruction results if the mass is producing pressure on an adjacent structure or if there is torsion of the mass.

A bruit over the liver in an infant with congestive heart failure suggests a hepatic hemangioma. If a mass is present over

the buttocks, the abdominal mass may represent internal extension of a sacrococcygeal teratoma.⁶⁶

RADIOLOGIC FINDINGS

Abdomen radiographs may show obstruction or displacement of bowel, relatively nonspecific findings. Calcifications suggest meconium peritonitis, teratoma, and hepatoblastoma; spinal anomalies suggest anterior sacral meningocele, obstructed cloacal deformity, and sacrococcygeal teratoma with an internal component.

Ultrasound is the premier imaging technique for abdominal and pelvic masses in neonates (Fig. 114-12).^{60,65,66} The following questions should be addressed:

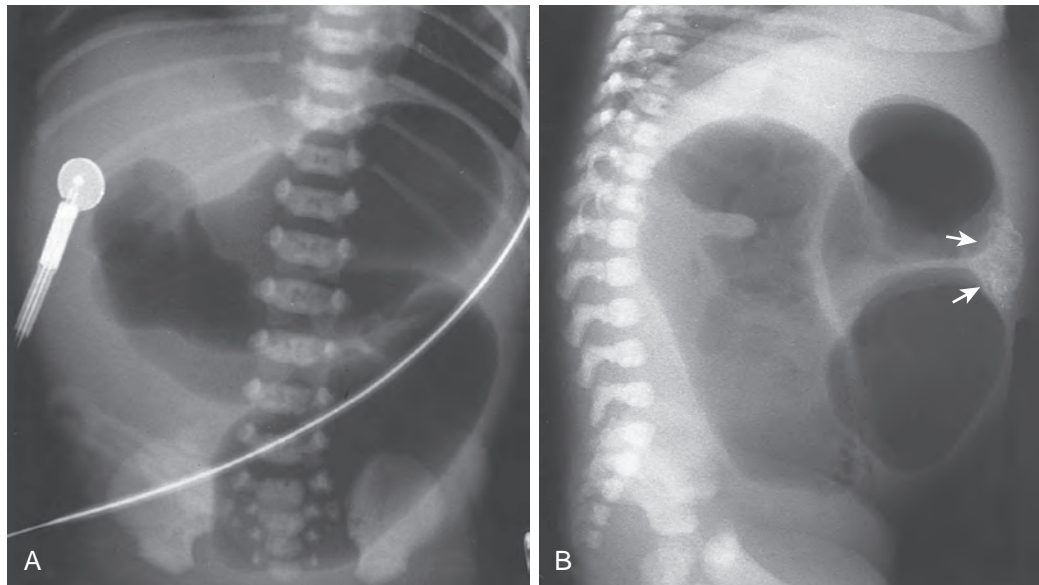


Figure 114-10 High obstruction. Anteroposterior (A) and lateral (B) abdomen radiographs in a child with jejunal atresia show several markedly distended bowel loops that fill the abdomen. The calcification along the anterior abdominal wall (arrows) indicates prior bowel perforation and meconium peritonitis.



Figure 114-11 Low obstruction. Colonic obstruction from Hirschsprung's disease has produced dilation of multiple bowel loops throughout the abdomen. Because discrete haustral markings cannot be identified, it is difficult to appreciate that the colon is dilated in addition to the entire small bowel.

From what compartment or organ does the mass originate?

Is the mass solid, cystic, or septate?

Is there a wall, membrane, or capsule around it?

Do the structures surrounding the mass look normal?

Is there ascites?

Are there any sites of spread or extension within the abdomen or retroperitoneum?

On the basis of the information obtained, the child may proceed to surgery, undergo further radiologic evaluation, or be observed and restudied after a period of observation.

Necrotizing Enterocolitis

CLINICAL FINDINGS

NEC is a life-threatening process that primarily affects the gastrointestinal tracts of premature infants. Signs and symptoms of NEC usually develop in the first 2 weeks of life: rising gastric residual volume, abdominal distention, bloody stools, lethargy, and even changing respiratory status.^{68,69}

Associations other than prematurity have been noted: bowel ischemia of any cause; abnormal gut hormones, immunoglobulins, or peristalsis; enteral feedings, especially high volumes of formula with high calorie concentration; and maternal cocaine use.^{70,71} The occasional epidemic nature of NEC indicates that a viral or bacterial agent may play a role in some cases.

Pathologic examination reveals ulceration that begins in the mucosa and extends to the submucosa; inflammatory cells may be present in multiple bowel layers.⁷² Pneumatosis intestinalis is seen in the submucosa and subserosa. In 50% of cases, normal areas of bowel are interposed between diseased segments. Inflammatory pseudomembranes occur in less than 10%. Many specimens concurrently show acute changes and reparative changes in the same bowel segment. Complications of these processes include gangrene, perforation with peritonitis or enterocyst formation or stricture formation, enteric fistulas, and sepsis.⁷²⁻⁷⁴

Timing of surgery is crucial; ideally, surgery should take place when necrosis is present but before bowel perforation. Erythema of the abdominal wall or positive result of paracentesis suggests bowel perforation and mandates surgical treatment.⁷⁵⁻⁷⁷ Pneumoperitoneum is an indication for surgery. These clinical and radiologic signs clearly indicate that perforation has occurred.

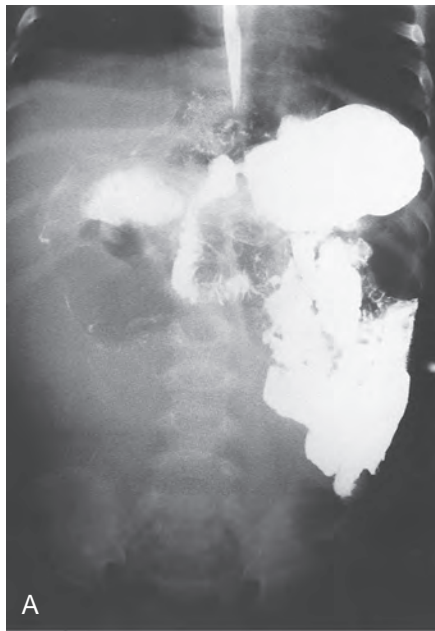
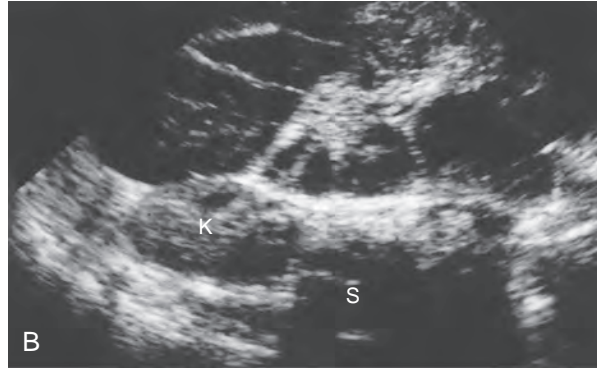


Figure 114-12 Neonatal abdominal mass: mesenteric lymphangioma. **A.** Barium is present in the stomach, duodenum, and small bowel. Gastroesophageal reflux is filling the distal esophagus. The duodenal sweep is displaced to the left. Upwardly displaced, compressed, and opacified bowel loops are seen in the right upper quadrant. **B.** Transverse abdomen sonogram to the right of the midline demonstrates multiple, fluid-filled structures. None of these structures had visible peristalsis because they were portions of the lymphangioma. K, Kidney; S, spine.



Strictures are late findings that develop in about 9% to 35% of children with NEC. About 75% occur in the colon, usually in the region of the splenic flexure; 15% are multiple; and the terminal ileum is involved in 15% of affected infants. They can be manifested after a delay of 20 months, but when they are seen on early studies, they may resolve spontaneously.^{73,78} Children whose NEC-induced bowel perforations are treated with bowel diversion or percutaneous peritoneal drainage have a lower rate of stricture formation than do those who received only medical management. To exclude a stricture, children with NEC may undergo an antegrade contrast study of the entire gastrointestinal tract before feeding is resumed. In infants with diversions, the bypassed bowel should be studied to exclude a stricture before bowel continuity is reestablished.^{73,78} Medical management of infants with suspected NEC includes parenteral nutrition and antibiotic therapy.⁷¹

Most children with NEC, treated medically and surgically, survive. The greatest mortality rate is seen for small premature infants who, too frail to undergo standard laparotomy, are treated with percutaneous peritoneal drainage. Late complications include short gut syndrome, sepsis, abdominal abscess, recurrent NEC, and stricture formation as well as some extra-gastrointestinal problems. NEC survivors constitute the largest group of children with short gut syndrome.

RADIOLOGIC FINDINGS

Abdomen radiograph findings include gastric dilation, a persistently dilated bowel loop, or an unchanging bowel gas pattern.⁷⁹ Pneumatosis intestinalis (Figs. 114-13 and 114-14) is manifested later, and large collections of intramural gas create a linear streaky pattern that parallels the bowel wall or, when seen en face, is manifested as circular lucency around the bowel lumen. Although the bubbly appearance of pneumatosis intestinalis may suggest feces, the premature infant rarely has formed stool within the colon in the first 2 weeks of life.

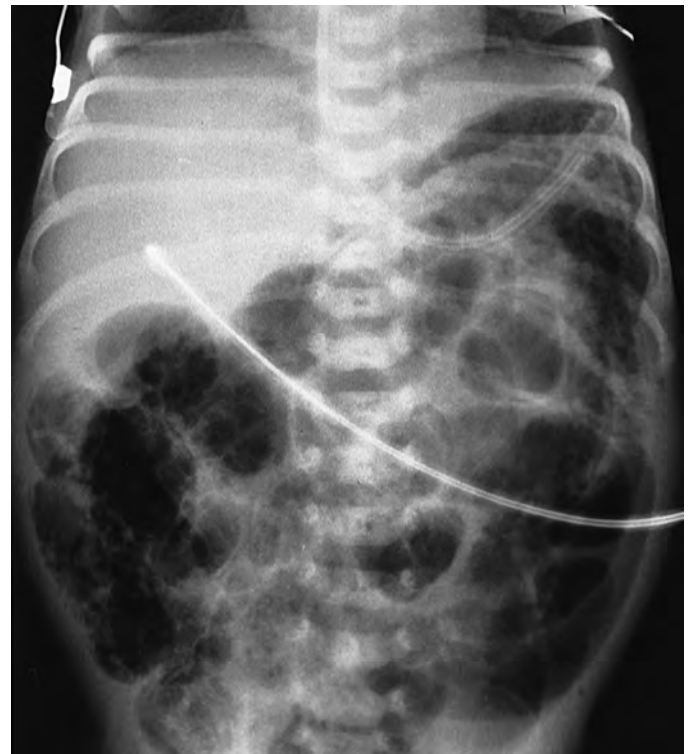


Figure 114-13 Necrotizing enterocolitis with pneumatosis intestinalis. The bubbly appearance of the abdomen is caused by air within the bowel wall. In some segments, the intramural air clearly parallels the lumen; in other segments, it is seen as a circular pattern surrounding the lumen.

Gas enters the mesenteric veins and subsequently the portal vein and its branches, producing streaky lucencies radiating to the periphery of the liver (see Fig. 114-14). This is an evanescent sign in most children, but to many physicians, it indicates the need for surgery.⁷⁷

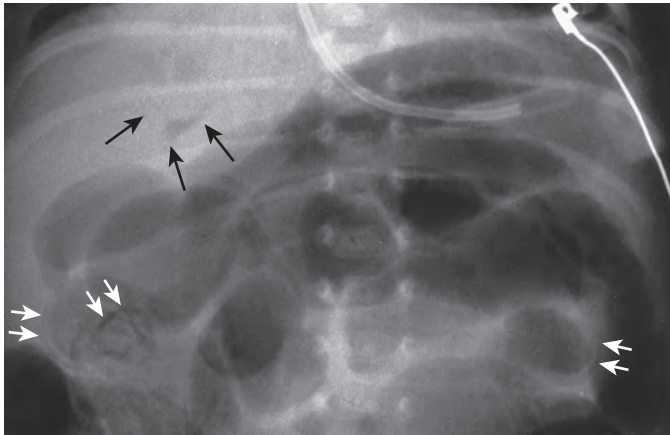


Figure 114-14 Necrotizing enterocolitis with portal venous air. Branching lucencies throughout the liver represent gas within the portal venous system (black arrows). Intramural air is also present (white arrows).

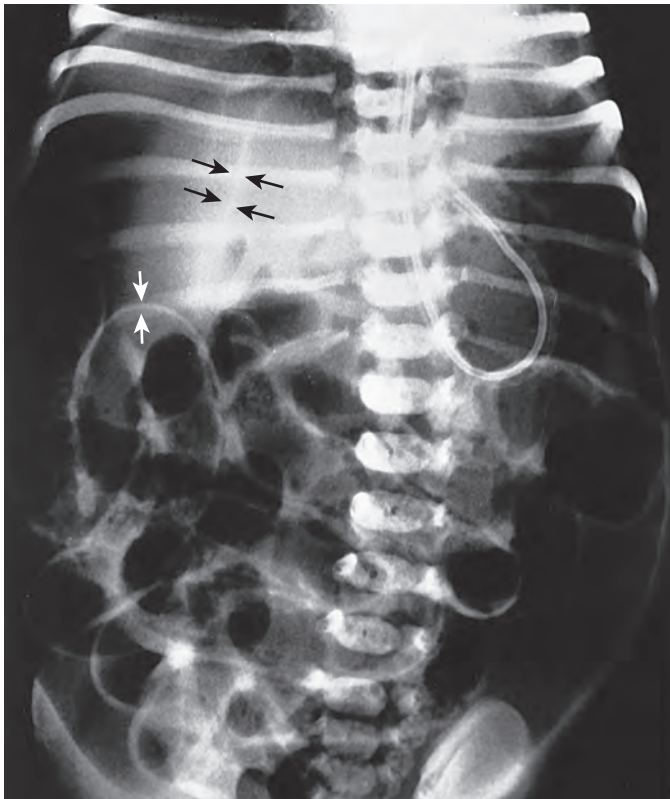


Figure 114-15 Necrotizing enterocolitis with perforation: the football sign. A large amount of free peritoneal air outlines the falciform ligament (black arrows). The air has also given the entire right upper quadrant an unusual lucent appearance. The inner and outer walls (white arrows) of multiple bowel loops are visible, another sign of free peritoneal air.

Bowel perforation, the most serious complication of NEC, is manifested by free intraperitoneal air. When the amount of air is large, a diffuse lucency appears over the liver or midabdomen. Air may outline the falciform ligament (Fig. 114-15). The inner and outer surfaces of the bowel wall may be clearly seen. In a few children, air surrounds the umbilical arteries and produces an inverted V sign in the pelvis. Air in Morison's pouch produces a triangular lucency.⁸⁰



Figure 114-16 Colonic stricture from necrotizing enterocolitis. Water-soluble enema depicts an area of minor narrowing in the midtransverse colon (straight arrow) and a more severely narrowed segment at the hepatic flexure (curved arrows).

When free air is suspected, supine abdomen radiographs are supplemented by cross-table lateral radiographs, which are more easily obtained than decubitus or upright radiographs. Free air is visible as lucency anterior to the liver and stomach or as small, triangular lucencies projecting downward from the abdominal wall between the bowel loops.⁸¹

Although ultrasound is not the primary imaging technique for NEC, it can show mural thickening of affected loops and portal venous gas before their detection on radiographs.^{82,83} Intrahepatic portal venous gas is seen as bright reflectors bubbling through the liver. The hepatic parenchyma develops unusually bright echoes in a patchy distribution. Severely affected (gangrenous) bowel loops may demonstrate diminished or absent blood flow when color Doppler imaging is used.⁸³ Focal fluid collections, echogenic free fluid, increased bowel wall echogenicity, and increased bowel wall thickness are also ultrasonographic signs predicting poor outcome.⁸⁴ Early diagnosis of NEC prompts therapy that in most cases aborts the process. When NEC is suspected clinically, the infant is treated accordingly, even in the absence of radiographic findings. If confirmation is required, the neonate can undergo upper gastrointestinal imaging with low-osmolality contrast agents or even contrast enema. A novel approach to confirming NEC employs CT. Urine specimens collected from neonates with NEC who have ingested diluted low-osmolality contrast material have a significantly higher mean CT attenuation value than the urine of normal infants.⁸⁵

Strictures that can develop in the natural history of NEC can cause clinical and radiographic signs of bowel obstruction. Contrast enema (Fig. 114-16) should be used to evaluate the

entire colon and terminal ileum. Although some of the strictures may spontaneously regress, most are resected surgically or dilated with balloon catheters.^{78,86}

Esophageal Atresia

GENERAL CONSIDERATIONS

Esophageal atresia (EA) occurs in about 1 in 5000 live births; boys and girls are equally affected. In more than 80%, the trachea is connected to the distal esophagus by a congenital tracheoesophageal fistula (TEF), but in about 10%, the EA is complete (Fig. 114-17). About 3% to 4% have a proximal fistula (with or without the distal fistula), and about 5% have no atresia but have an aberrant connection between the trachea and esophagus (i.e., H-type fistula).

EA can be diagnosed prenatally but is more often diagnosed at birth, when the infant has difficulty handling secretions, or with the first feeding, when the infant has respiratory distress.⁸⁷ Attempts to pass a nasogastric tube are usually unsuccessful; rarely, the tube may enter the trachea and pass into the TEF and distal esophagus. Prompt diagnosis of EA is necessary to protect the lungs.

The neonate with EA or with EA and TEF must be evaluated for exclusion of other anomalies, including trisomy 21 and the VATER association. The acronym VATER or VACTERL emphasizes that vertebral, anorectal, cardiac, tracheoesophageal, renal, and limb anomalies may occur together.⁸⁸⁻⁹¹ Physical

examination and imaging studies are performed before surgery to find other anomalies that need emergent correction (e.g., duodenal atresia), influence the standard surgical correction of TEF (e.g., right aortic arch), or affect mortality (e.g., renal agenesis, duct-dependent cardiac lesions). In about 50% of infants, EA is an isolated anomaly.

The presence of a distal fistula can be diagnosed clinically (see Fig. 114-17) because the affected neonate has a rounded abdomen and bowel sounds. The infant with EA and no distal fistula has a scaphoid abdomen and absent bowel sounds.

The stable neonate with EA and TEF undergoes surgical correction in the first few days of life. Surgical options include end-to-end or end-to-side anastomosis.^{90,91} Surgery can be performed through traditional thoracotomy or video-assisted thoracotomy.^{92,93} Parenteral nutrition is provided for a few days until postoperative studies confirm that the anastomosis is intact and oral feedings can be given safely.

When there is a large gap between the proximal and distal segments, a common problem in the child with EA and no TEF, primary correction is usually not attempted in the neonatal period. Nutritional needs are met by a gastrostomy tube placed under surgical or radiologic guidance.⁹⁴ The upper pouch is diverted so that secretions within it will not be aspirated. A neoesophagus is later created by interposing a segment of bowel or pulling the stomach into the esophagus, creating an anastomosis between the proximal esophagus and the stomach.⁹⁵⁻⁹⁷ This surgery is often delayed until the child is 1 year old. Nonsurgical anastomosis in EA may be created by magnetic lengthening of the esophageal segments with placement of a magnet in both ends of the upper and lower pouches, using the mouth and gastrostomy for catheter insertion.⁹⁸ Postoperative complications are numerous, regardless of the type of repair performed. An anastomotic leak is seen in 10% to 20% of children who undergo primary repair in the neonatal period (Fig. 114-18). Anastomotic narrowing or stricture formation (Figs. 114-19 and 114-20) occurs in 15% to 30% of cases because of anastomotic leaks with scarring, ischemic change from tension on the anastomosis, or gastroesophageal reflux.⁹⁹⁻¹⁰² A change in caliber at the anastomosis does not always indicate stricture but may instead result from residual dilation of the previously obstructed upper esophageal segment. Distal esophageal narrowing may be caused by congenital esophageal stenosis or gastroesophageal reflux (Fig. 114-21).¹⁰⁰ Bougienage and balloon dilation are used to treat these strictures.¹⁰³

Development of a fistula at the surgical site (Fig. 114-22) or late detection of a proximal pouch fistula (Fig. 114-23) may cause postoperative feeding difficulty simulating aspiration. Children with an H-type fistula (Fig. 114-24) may have only intermittent feeding problems because the fistula may not be patent at all times. The muscle wall of the fistula may contract, or the fistula may be blocked with mucus or food. The H-type fistula can remain undetected for years, until esophagography is performed to evaluate the cause of multiple pneumonias.

Symptomatic gastroesophageal reflux and pulmonary disease are common throughout the lives of children with EA and TEF. Gastroesophageal reflux results from a primary abnormality of the distal esophagus, postsurgical changes in the anatomy of the gastroesophageal junction, poor antegrade peristalsis, or delayed gastric emptying.^{100,101,104} Virtually all children with EA have disordered esophageal motility. If a fundoplication is needed to

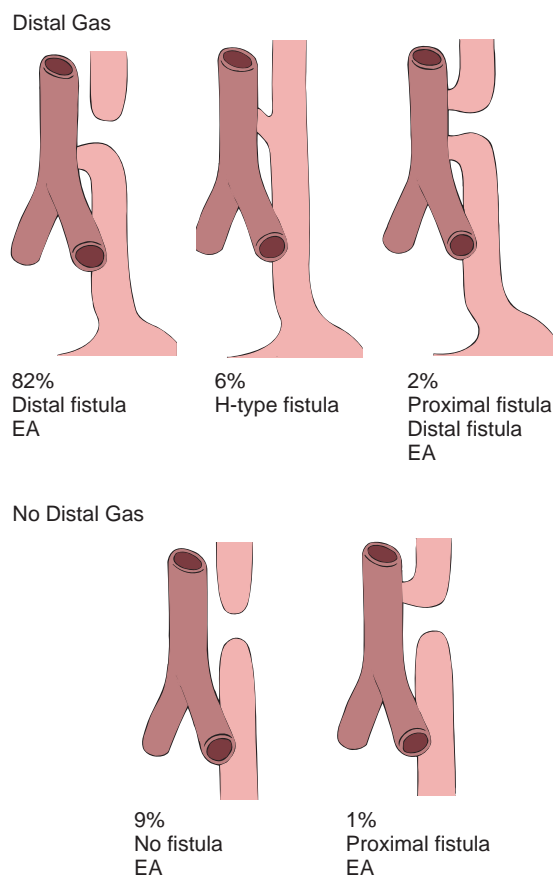


Figure 114-17 Types of esophageal atresia. Common forms of esophageal atresia (EA) are depicted.

treat the gastroesophageal reflux, it must be modified so that it does not obstruct the poorly peristaltic esophagus.¹⁰⁵

CT studies done years after repair have documented structural and functional abnormalities of the trachea and puddling of fluid in the dilated upper esophagus.¹⁰⁶ Tracheal

abnormalities may be caused by maldevelopment of the foregut or surgical changes.¹ Respiratory tract symptoms may persist throughout life.^{99,101}

RADIOLOGIC FINDINGS

The prenatal diagnosis of EA without TEF is suggested by the presence of polyhydramnios with absence of fluid in the

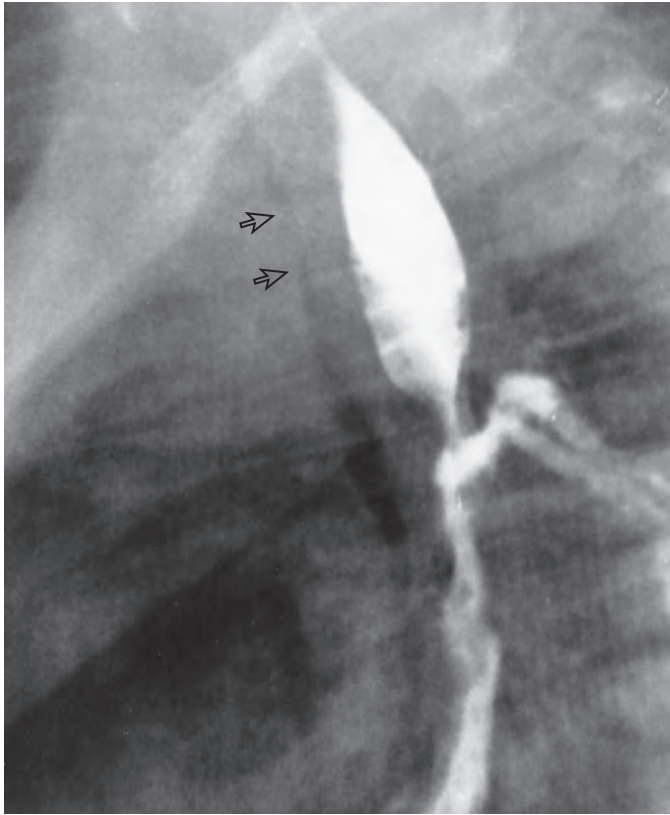


Figure 114-18 Anastomotic leak after esophageal atresia and tracheoesophageal fistula repair. As contrast material reaches the anastomosis, it passes into the distal esophagus and into the posteriorly directed leak. Notice the narrowing of the proximal trachea (arrows).

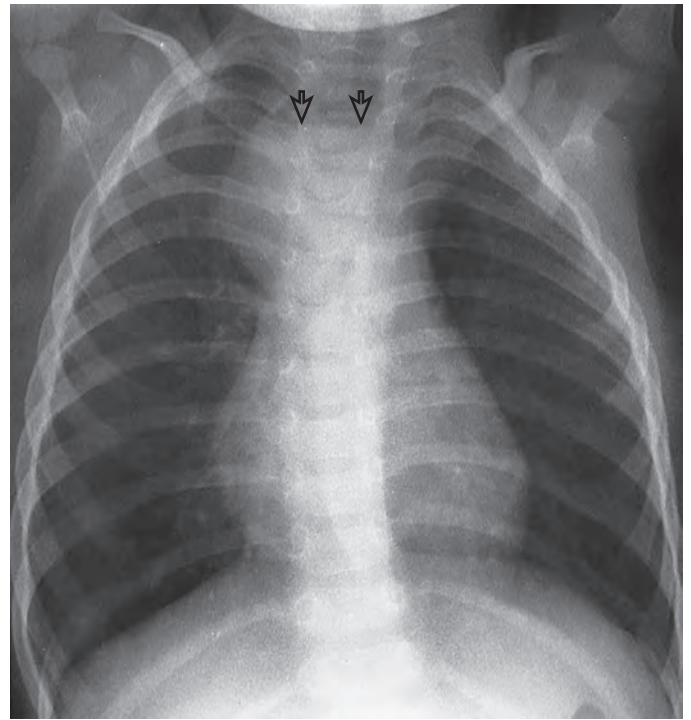


Figure 114-20 Anastomotic stricture after tracheoesophageal fistula repair. A soft tissue density with air-fluid level (arrows) displaces the trachea to the left. This is the dilated upper pouch above a narrowed anastomosis. The child is acutely symptomatic because food is impacted at the anastomosis.

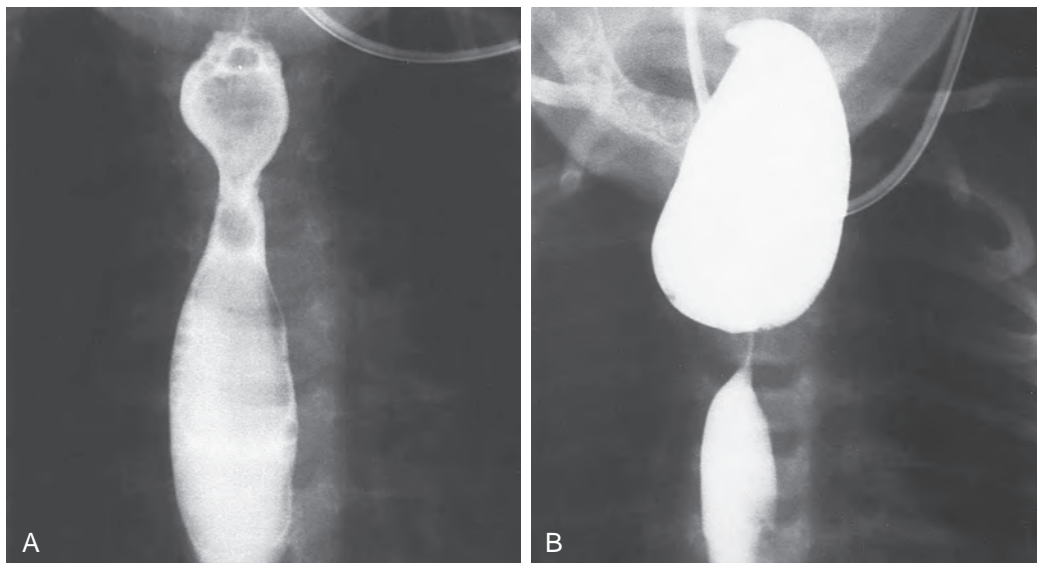


Figure 114-19 Stricture formation after esophageal atresia and tracheoesophageal fistula repair. **A.** A study performed in the early postoperative period demonstrates mild narrowing at the anastomotic site. This can be normal. **B.** Several months later, a study shows a severe stricture causing increased dilation of the proximal esophagus.

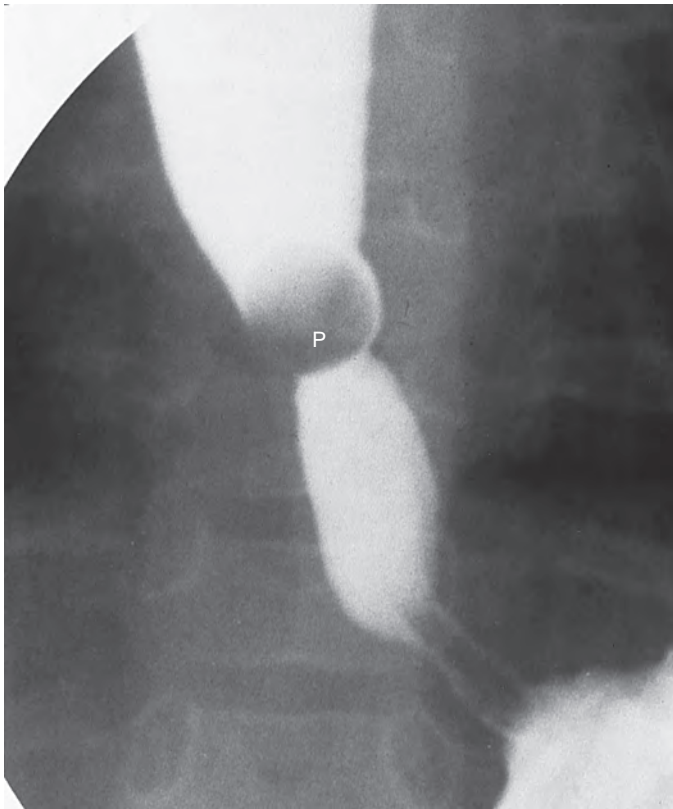


Figure 114-21 Gastroesophageal reflux after tracheoesophageal fistula repair. Reflux has produced such severe narrowing of the distal esophagus that a pea (P), swallowed whole, could not pass into the stomach.

stomach.^{87,107} The fluid-filled upper pouch may be detected with ultrasound, with MRI occasionally used for confirmation.

Radiographs

Chest and abdomen radiographs should be scrutinized for vertebral segmentation and limb anomalies as part of the VACTERL association (Fig. 114-25); tetralogy of Fallot and right-sided aortic arch, for avoidance of injury during thoracotomy, which is usually performed on the right; and bowel gas, to differentiate pure EA from EA with TEF and to detect other gut atresias.

Preoperative Contrast Studies

Preoperative identification of a proximal fistula is desired at some institutions and not at others. Evaluation for possible fistula is performed with lateral fluoroscopy of the upper esophagus with the child supported in a semiupright position. A slow, manual injection of a few milliliters of low-osmolality contrast agent through a feeding tube placed in the upper pouch defines the pouch (Fig. 114-26; see also Fig. 114-23). As soon as a fistula is identified, the injection is stopped. When there is no fistula, contrast material is removed through the feeding tube.

In the child with EA and no TEF, barium studies are done through the gastrostomy tube to define the length of the lower esophageal segment before surgery. The lowest extent of the upper pouch is defined by a large-bore catheter. The lower segment may be seen with refluxed contrast material or by means of a tube passed cephalad through the gastrostomy. The

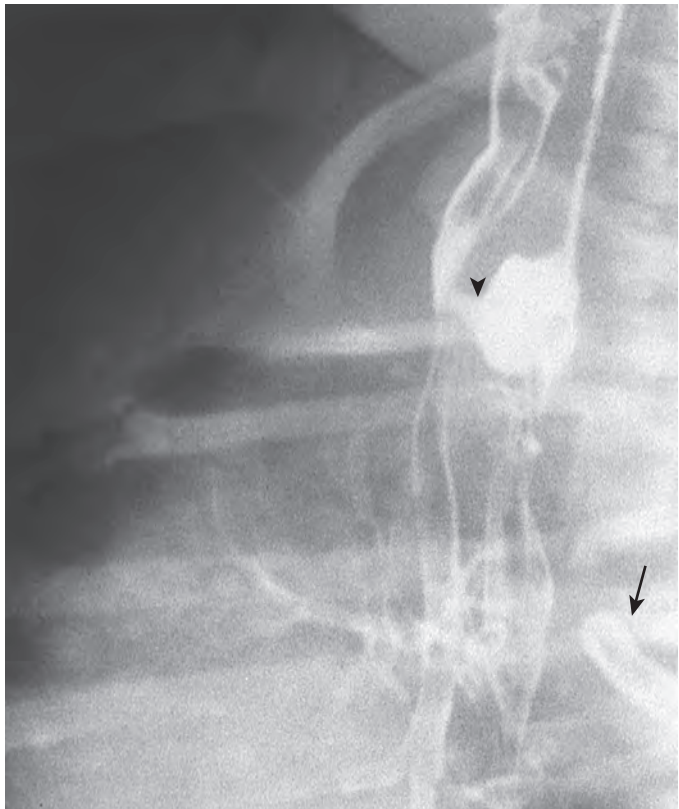


Figure 114-22 Postsurgical esophageal atresia and tracheoesophageal fistula. This fistula is demonstrated several days after surgery. Contrast material instilled into the upper esophagus passes through a fistula (arrowhead) into the trachea. A pleural drain (arrow) is identified.

distal segment tends to extend above the diaphragm for only a small distance (Fig. 114-27).

Because the H-type TEF is not always patent, it may be difficult to demonstrate. The esophagus must be distended, and in some children, a second or third study may be necessary to see the fistula. Repeated barium esophagography may be performed by placing a feeding tube in the upper esophagus and giving a bolus injection of contrast medium manually. The fistula has an N rather than an H shape as it passes superiorly and anteriorly from esophagus to trachea (see Fig. 114-24). Although CT performed in the sagittal plane can demonstrate EA, a distal TEF, and the length of the gap between the upper and lower segments, there has been little application of this technique.

Ultrasound Studies

Sonography is performed to search for kidney malformations included in the VACTERL association: agenesis, ectopia, and fusion anomalies. Associated urethral anomalies are usually detected by clinical inspection.

Postoperative Contrast Studies

About 5 days after surgery, esophagography is performed to detect anastomotic leakage (Fig. 114-28; see also Fig. 114-18). Low-osmolality contrast agent may be used initially, and if the esophagus is intact, the remainder of the study can be performed with barium.

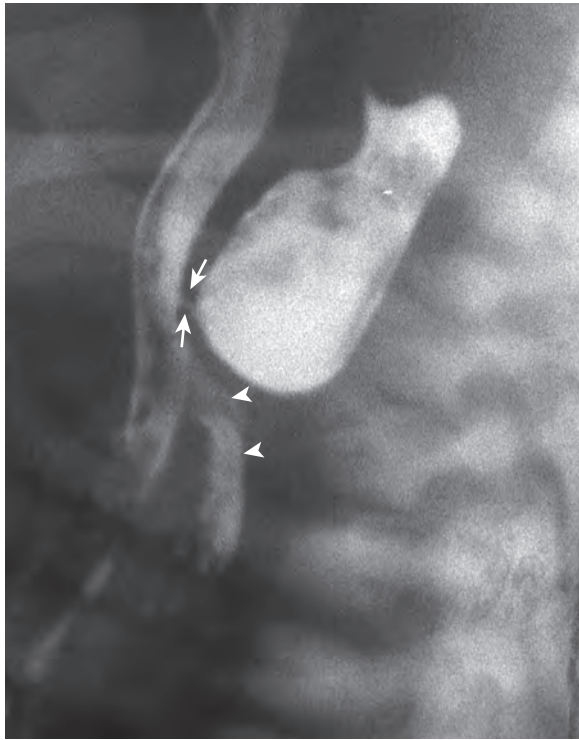


Figure 114-23 Poorly performed preoperative study of the upper pouch: esophageal atresia with proximal and distal fistulas. The upper pouch is overfilled with contrast medium. The trachea is being filled through a tiny fistula (arrows). Contrast material from the trachea is outlining the distal tracheoesophageal fistula and the upper portion of the distal esophageal segment (arrowheads). The upper and lower esophageal segments are closely apposed.

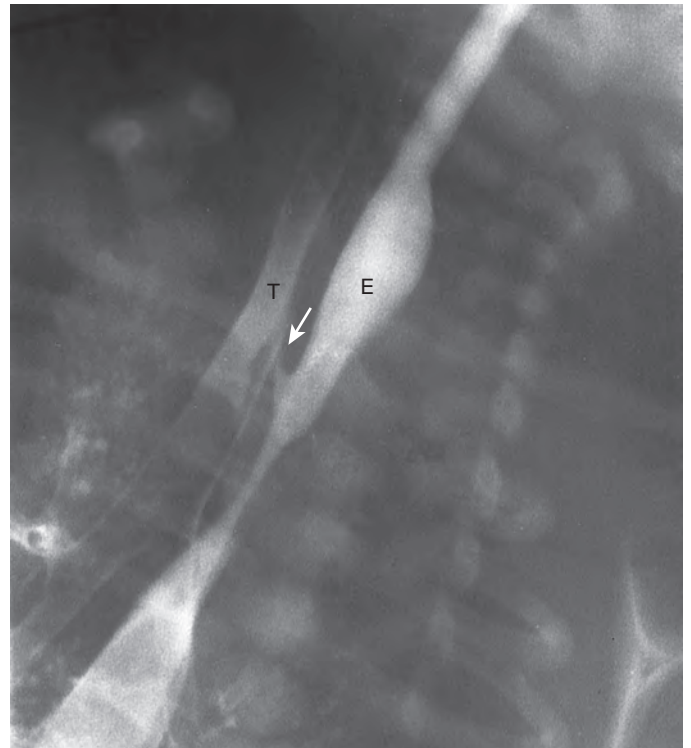


Figure 114-24 H-type tracheoesophageal fistula. The contrast agent injected into the upper esophagus fills the esophagus (E), the fistula (arrow), and the trachea (T).

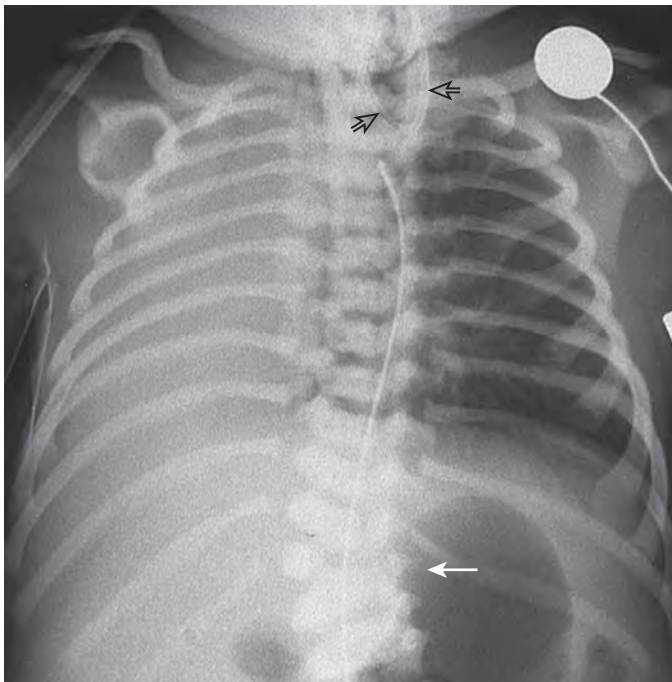


Figure 114-25 VATER association. A feeding tube is coiled in the upper esophageal pouch (open arrows). Eleven ribs are present on the left and 12 on the right. Segmentation anomalies, including a hemivertebra, are seen at the thoracolumbar level (solid arrow). The right hemithorax is opacified, and the mediastinal contents are shifted to the right because the right lung is agenetic. This child also had unilateral renal agenesis.

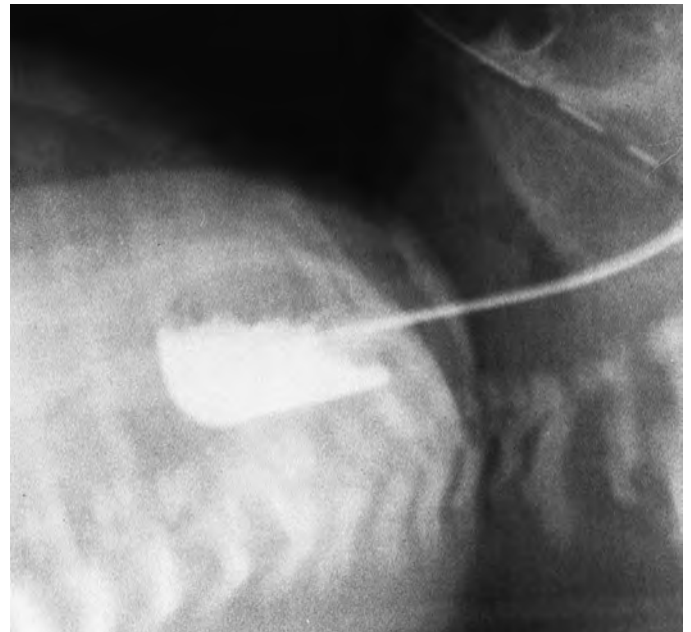


Figure 114-26 Esophageal atresia without tracheoesophageal fistula. The upper pouch is filled with a small amount of contrast material. No fistula is identified. This study was performed with the patient in the supine rather than in the preferred upright position.

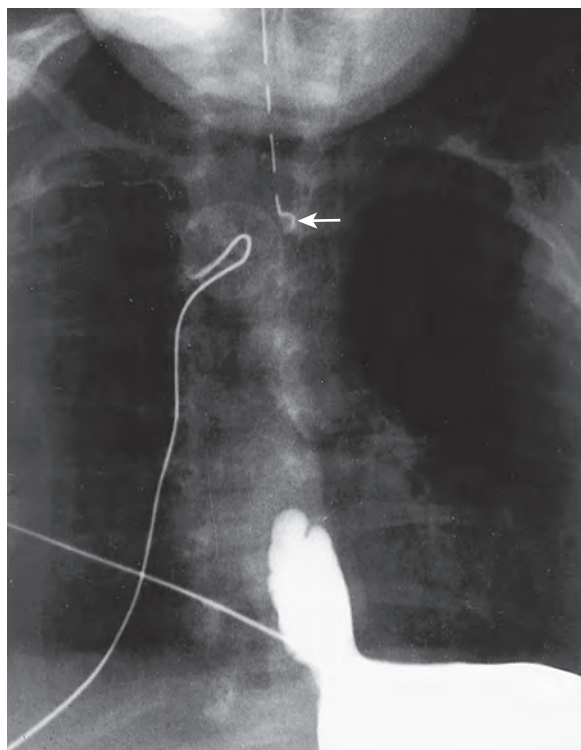


Figure 114-27 Gastrostomy injection of an esophageal atresia without a tracheoesophageal fistula. A feeding tube is in the upper esophageal pouch (arrow). Contrast material injected into the stomach through a gastrostomy has refluxed into the short distal esophageal segment. The distance between the distal aspect of the upper pouch and the proximal aspect of the distal esophagus is approximately the height of five vertebral bodies.

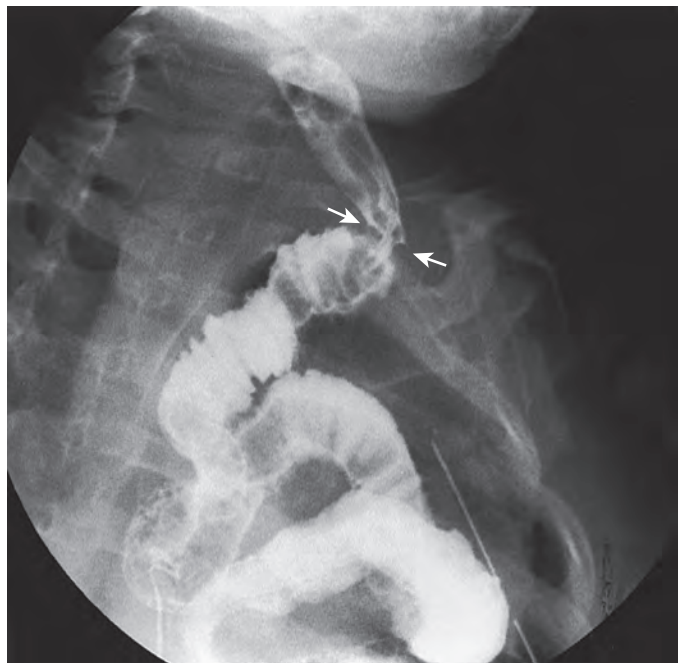


Figure 114-28 Postoperative study in a child with esophageal atresia and no tracheoesophageal fistula. Contrast material passes through the anastomosis (arrows) between the previously diverted upper esophageal segment and the redundant neoesophagus created from multiple small bowel loops.

When a child's eating pattern deteriorates, barium esophagography should be performed to exclude narrowing at the anastomosis or distal esophagus. Refusal of solid food may be the first sign of narrowing. During this examination, the anastomosis must be challenged with large amounts of contrast material. Small sips poorly distend the esophagus, allowing an abnormal segment to be overlooked. A child who presents with drooling or complete refusal to eat may need a contrast study to detect a foreign body or food impacted above the anastomosis or distal esophagus (see Figs. 114-20 and 114-21).¹⁰⁸

Laryngotracheal Cleft

Laryngotracheal or laryngotracheoesophageal cleft is a rare, severe failure of foregut division that has a slight male predominance. The cleft is of variable length and is frequently associated with EA and TEF.¹⁰⁹ The EA and TEF may mask the laryngotracheal cleft because the symptoms are similar: coughing, inability to handle secretions, and recurrent pneumonias. This anomaly, which causes a toneless cry, is also associated with the anomalies that compose the VACTERL association and with coarctation of the aorta and transposition of the great vessels.¹⁰⁹⁻¹¹¹ Death in the neonatal period is common because of the multiple anomalies.

The diagnosis of laryngotracheal cleft is confirmed with endoscopy. Postoperative radiologic studies should be performed with small amounts of contrast agent given slowly so that any residual cleft can be differentiated from aspiration. Surgery is necessary to divide the trachea from the esophagus. The extent of the cleft and the associated tracheomalacia make reconstruction difficult in many children.

Jejunal and Ileal Stenosis and Atresia

Duodenal atresia is discussed in Chapter 116. Jejunal and ileal atresia occur in about 1 of 5000 births.¹¹² Prenatal ultrasound shows polyhydramnios in about 50% of cases. Atresia may be diagnosed after birth when vomiting and abdominal distention develop.

Jejunal and ileal atresia are thought to result from a vascular insult to the bowel by focal pressure, by compromise of the mesenteric root, by intravascular thrombosis, or by failure of complete recanalization of the bowel.¹¹²⁻¹¹⁷ Multiple levels of atresia are seen in 30% of affected neonates.¹¹²⁻¹¹⁷ Most cases occur sporadically, although hereditary syndromes of multiple gastrointestinal atresias have been described.^{118,119}

Atresias are classified by differences in the discontinuity of the bowel and the mesentery (Fig. 114-29).¹¹⁵ Atresia is about six times more frequent than congenital stenosis.¹¹⁴ About one third of children with jejunoileal atresia have malrotation of the bowel.³

TREATMENT

Improvements in operative technique and postoperative care have significantly enhanced the outcome of patients with small bowel atresia. The choice of operation depends on the site, extent, and type of atresia and the extent of proximal bowel dilation.¹¹²⁻¹¹⁷ Short gut, defined as a residual bowel with less than half of its normal length of 200 cm, has been a consistent

cause of morbidity and mortality. Short gut may initially be compensated for by total parenteral nutrition, but the most severely affected children are candidates for liver transplantation because of complications from total parenteral nutrition hepatitis.

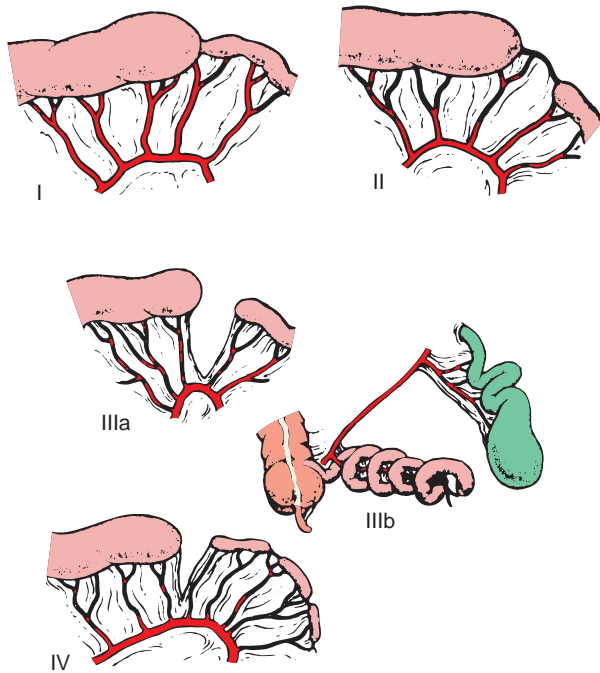


Figure 114-29 Classification of bowel atresia. In type I, there is a web or diaphragm between adjacent bowel loops. In type II, there is a discontinuity of bowel, usually with dilation of the proximal segment. The mesentery is intact. In type IIIa, there is a gap in the mesentery and a discontinuity between the bowel loops. In type IIIb, there is a long segment of atretic small bowel. The remaining small bowel has a corkscrew or apple peel appearance. In type IV, there are multiple areas of intestinal atresia. (From Grosfeld JL, Ballantine TVN, Shoemaker R: *Operative management of intestinal atresia and stenosis based on pathologic findings*. *J Pediatr Surg* 3:368–375, 1979.)

RADIOLOGIC FINDINGS

When prenatal sonography demonstrates polyhydramnios in conjunction with dilated bowel, small bowel atresia should be considered.^{120,121} Prenatal sonography is more successful at detecting duodenal atresia than other intestinal atresias.¹²⁰ MRI can also demonstrate fetal bowel atresia. Postnatal abdomen radiographs demonstrate dilated, air-filled bowel loops proximal to the atretic or stenotic segment. The proximal loop nearest to the obstruction may be dilated out of proportion to the other segments and have a round edge (see Fig. 114-10). No distal bowel gas is observed in atresia, whereas a paucity of distal air is found in stenosis. Peritoneal calcifications indicate that the atresia is complicated by meconium peritonitis (Fig. 114-30; see also Fig. 114-10). However, meconium peritonitis can be present even when no calcifications are seen radiographically or at surgery (Fig. 114-31). Intramural calcifications have been reported in children with intestinal atresia but may also occur without atresia.

Air usually provides adequate contrast for determining the level of obstruction. With jejunal atresia, few loops are filled with air or have air-fluid levels (see Fig. 114-10). When multiple dilated loops are present, the obstruction is more likely to be in the ileum (Fig. 114-32). When there is an extremely low ileal obstruction, the dilated loops may fill the entire abdomen and make differentiation from colonic obstruction impossible.

To exclude a second distal obstruction in the child with suspected jejunal atresia, a contrast enema may be performed. Because of the risk of perforation, low-osmolality contrast agents are preferred for these studies. A normal-caliber colon is present when the obstruction is high because the secretions of the bowel distal to the obstruction are passed into the colon, which preserves its reservoir function. A small-caliber colon implies that there is an obstruction in the distal small bowel and that small bowel contents cannot enter the colon (see Fig. 114-30). Rarely, extrinsic compression can so completely obstruct patent bowel that microcolon can develop.¹²² Ultrasound may be useful when secondary intraperitoneal processes, including

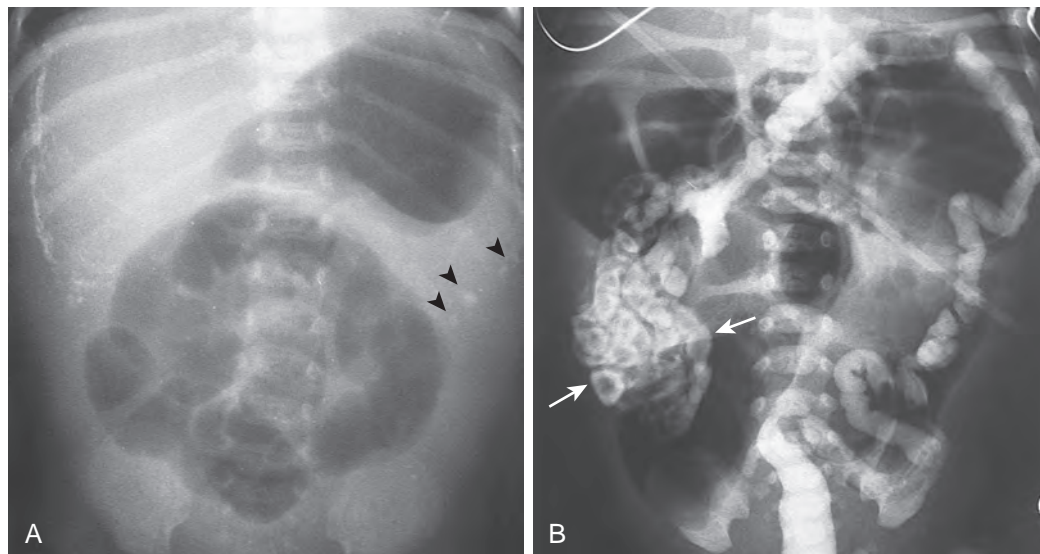


Figure 114-30 Ileal atresia. **A.** Dense calcifications (arrowheads) rim the lateral aspect of the upper abdomen. Notice the dilated bowel loops proximal to a surgically proven high ileal atresia. **B.** Contrast enema in a different patient with ileal atresia shows a small-caliber colon and reflux of contrast material into a meconium-filled terminal ileum (arrows).

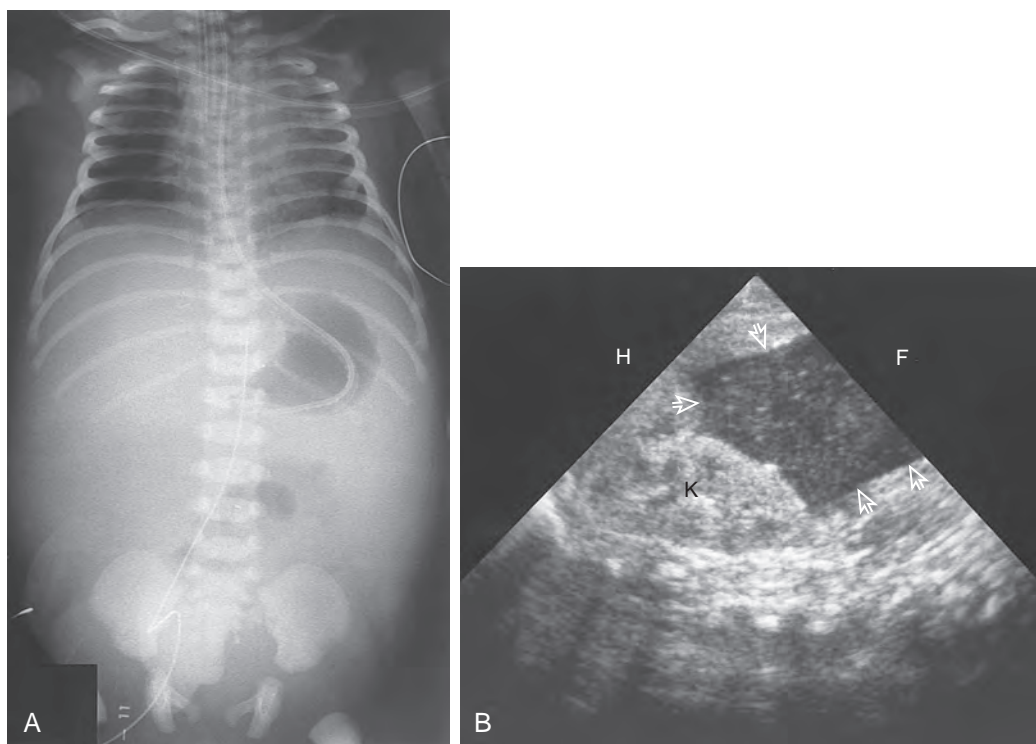


Figure 114-31 Meconium peritonitis. **A.** On the chest and abdomen radiograph, there is a paucity of abdominal gas, perhaps because of suction and ventilation through the endotracheal tube. Meconium peritonitis causes generalized abdominal haziness, bulging flanks, and centralization of bowel loops. **B.** The longitudinal sonogram reveals a peritoneal collection of meconium (arrows) anterior to the echogenic neonatal kidney (K). The meconium is less echogenic than the solid structures, but it contains more echoes than simple transudative ascites. H, Cephalic; F, caudal.



Figure 114-32 Colonic atresia. Multiple dilated bowel loops are present. Water-soluble contrast material fills a small-caliber colon. The contrast material did not pass proximal to the hepatic flexure, the site of the atresia.

meconium peritonitis, are suspected. Free fluid, free meconium, or enterocysts may be detected (see Fig. 114-31). Meconium is echogenic because it is a complex substance composed of secretions, desquamated cells, and lanugo hairs.¹²³

If a large amount of bowel is atretic or resected, postoperative barium studies of the small bowel may show many changes that represent the bowel's attempts to compensate for its loss of length.¹²⁴ The small bowel becomes dilated, the folds become thicker than usual, and transit time may be increased.

Meconium Peritonitis

When bowel perforation occurs in utero, sterile meconium leaks into the peritoneal cavity and creates a chemical peritonitis: meconium peritonitis. The perforation is caused by any process that may produce bowel ischemia: volvulus, internal hernia, intussusception, or meconium ileus with or without cystic fibrosis.¹²⁵⁻¹²⁹ The peritonitis is associated with atresia, adhesions, intra-abdominal cystic masses, ascites, scrotal masses, and, in many cases, intraperitoneal or scrotal calcifications (see Figs. 114-10 and 114-30).¹²⁵⁻¹³¹ Meconium peritonitis occurs in 1 of 35,000 live births.

Meconium peritonitis sometimes has been categorized as several distinct forms: fibroadhesive, cystic, and generalized. Fibroadhesive meconium peritonitis is defined by dense bands and membranes that form around and across bowel loops in response to the peritoneal process. Cystic meconium peritonitis develops when the perforation is contained by inflammatory tissue and adjacent loops of bowel that are matted together. After birth, the "cyst" may be filled with fluid if the perforation

has sealed or with air and bowel contents if the cavity remains in continuity with the bowel lumen. In the generalized form of meconium peritonitis, loosely adherent or free-floating plaques of calcium are scattered throughout the peritoneal cavity. The calcifications may not be visible on abdominal radiographs.

CLINICAL FINDINGS

Many children with meconium peritonitis are diagnosed prenatally.¹²⁸⁻¹³⁰ Most of those diagnosed postnatally present within the first 24 hours of life with abdominal distention and bilious vomiting resulting from adhesive bands, small bowel atresia, or meconium ascites (see Figs. 114-10, 114-30, and 114-31). Asymptomatic children may not be diagnosed until abdomen radiographs obtained for other reasons demonstrate peritoneal calcification.

Meconium peritonitis and cystic fibrosis may occur independently, and calcification of meconium most often occurs in the absence of cystic fibrosis.¹³¹ The differential diagnosis of abdominal calcifications in a neonate is limited: tumors (e.g., neuroblastoma, hepatoblastoma, teratoma), calcification in the walls or lumen of a bowel loop, and retroperitoneal calcifications from prenatal adrenal hemorrhage or renal vein thrombosis. Although all children with meconium peritonitis should undergo a sweat chloride and stool trypsin and chymotrypsin tests to exclude cystic fibrosis, less than 10% of patients have the disease.¹³⁰ The prognosis for those with meconium peritonitis is good, with a survival rate of about 90%.¹²⁸⁻¹³⁰

RADIOLOGIC FINDINGS

The sonographic criteria for meconium peritonitis include fetal ascites that may have echogenic debris, echogenicity along the peritoneal surfaces, abnormal cystic abdominal masses, and bowel dilation.^{129,130} Ascites alone may be a sign of meconium peritonitis; in utero, this may simulate fetal hydrops. Abdominal radiographs may show peritoneal calcifications (see Figs. 114-10 and 114-30), intestinal obstruction, mass effect, and, uncommonly, pneumoperitoneum.

Sonography should be used if there is ascites or a palpable mass in the pelvis or abdomen because it can define the size of the mass and exclude other masses or obstructive lesions. Sonography can differentiate the usual ascites from meconium peritonitis with “dirty” ascites (see Fig. 114-31). Radiographs of the skeleton may show metaphyseal dense bands, which are thought to develop at the time of the perforation.¹³²

Colonic Atresia

GENERAL CONSIDERATIONS

The incidence of atresia is lower in the colon than elsewhere in the gut; it occurs in about 1 of 40,000 live births.¹¹⁵ The transverse colon is more frequently involved than other sites, and there is a slight female predominance.¹³³ In contrast to the increased rate of prematurity found with other intestinal atresias, children with colonic atresia are more likely to be born at term. The neonate with colonic atresia presents with vomiting and abdominal distention. Meconium might have passed normally.

The differential diagnosis of colonic atresia includes other causes of low obstruction: Hirschsprung’s disease, duplication,

meconium plug, intussusception, and distal ileal processes. A contrast enema should be performed to narrow the diagnostic possibilities and to direct additional testing and therapy.

RADIOLOGIC FINDINGS

As with other intestinal atresias, prenatal sonography of colon atresia frequently demonstrates polyhydramnios and dilated, fluid-filled bowel loop. Postnatal abdomen radiographs indicate a low obstruction, and the dilated bowel loops may have air-fluid levels or a bubbly appearance because of intraluminal meconium. The radiographic diagnosis of colonic atresia is difficult, particularly in the first few hours of life because air may not have reached the most distal bowel segment.

Sonography is useful for excluding the presence of ascites or mass lesion. A contrast enema with a low-osmolality contrast agent is the diagnostic study of choice. The examination should be performed with great caution because of an increased incidence of colonic rupture in patients with atresia. The contrast column ends abruptly and may taper or have a round, “cobra head” or club deformity if a membrane is present (Fig. 114-32).¹³⁴ The colon may be normal or small in caliber, depending on when luminal occlusion occurred. If a transition zone is observed, Hirschsprung’s disease also may be present.¹³⁵

Imperforate Anus

CLINICAL FINDINGS

Imperforate anus is a complex anomaly that occurs in about 1 of 5000 live births, with a slight male predominance.¹³⁶⁻¹⁴⁰ The spectrum of anorectal malformations is broad and varies with the patient’s sex (Fig. 114-33). Numerous classifications of the variants of imperforate anus have been made; one widely used system is the Wingspread classification.¹³⁶ Others with a strong basis on clinical inspection performed at age 1 day have been developed.^{137,138} Boys are more likely than girls to have enterourinary fistulas because they lack interposed genital structures (Fig. 114-34). Girls have a high incidence of enterovaginal fistulas and cloacal anomalies.

The distal extent of the rectum must be delineated because it determines whether the infant needs neonatal colostomy and the probability that other malformations are present.¹³⁷⁻¹⁴² The position of the distal rectal pouch in relation to the levator ani muscles is used to categorize grossly the different types of imperforate anus. When the rectum ends above the levator ani muscles, the infant has a high or supralevator imperforate anus. When the rectum ends below these muscles, the infant has a low or infralevator imperforate anus. Radiologic and clinical data are used to differentiate high from low lesions. Abdomen radiographs, ultrasound, CT, and MRI may have roles in this process.

A low lesion is suggested when there is a fistula, perineal pearls, corrugated appearance of the extrinsic sphincter, or normal-appearing female urethra and vagina. The presence of meconium on the perineum or in the urine suggests a low lesion.^{137,139} Infants with low lesions undergo anoplasty or temporary enlargement of the fistula. High lesions should be suspected when there is no fistula, when there is a smooth perineum, or when a girl has a single perineal orifice (i.e., cloacal anomaly). Neonates with high lesions undergo a colostomy. A corrective pull-through procedure is performed when the child is about 1 year old.

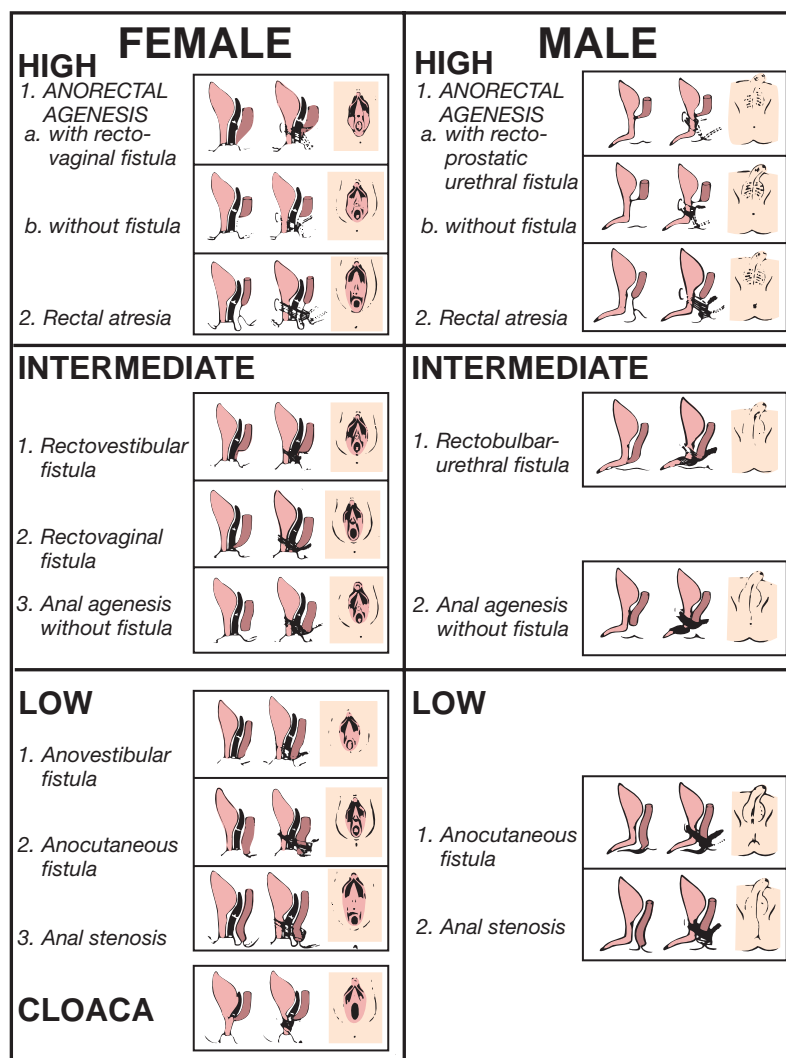


Figure 114-33 Classification of imperforate anus. This diagram shows many of the possible relationships of the imperforate anus to the internal organs in children of both sexes. (Modified from Grosfeld JL, Ballantine TVN, Shoemaker R: *Operative management of intestinal atresia and stenosis based on pathologic findings*. *J Pediatr Surg* 3:368–375, 1979.)

Genitourinary abnormalities are common in infants with imperforate anus.¹⁴⁰⁻¹⁴² Renal anomalies (e.g., absence, agenesis, ectopia, horseshoe kidney) are more common and more severe in children with high imperforate anus. A fistulous connection to the urinary tract, usually to the urethra or the bladder, is present in about 23% of children with supralelevator imperforate anus. The fistula may be diagnosed at birth when there is air in the bladder on early postnatal plain abdomen radiographs or meconium in the urine. Otherwise, the fistula is sought with voiding cystourethrography in the neonatal period or pressure antegrade colography before colostomy closure.¹⁴³ In children with the VACTERL association, there is an increased incidence of congenital urethral lesions: duplications, stricture, and megalourethra.¹⁴⁰

The incidence of cardiovascular malformations, especially tetralogy of Fallot and ventricular septal defect, is increased in children with otherwise isolated imperforate anus. The cardiac anomalies contribute significantly to the mortality rate of children with imperforate anus. Tethered spinal cord may occur

with or without vertebral anomalies in up to 20% of children with imperforate anus.¹⁴⁴

TREATMENT

The corrective procedure depends on the anatomy of the congenital lesion and surgical preference. Most procedures for high imperforate anus are variants of the posterior sagittal anorectoplasty.^{145,146} The goal of surgery is to preserve and, if necessary, to enhance the mechanisms of continence. Urinary tract anomalies that need correction are repaired at the time of imperforate anus surgery.

The incidence of spinal deformity and intraspinal lesions is lower in children with low imperforate anus than in those with high imperforate anus. These children also tend to have better development of the levator sling, a more intact neural arc, and more normal evacuation patterns after surgery than children with high imperforate anus. After the corrective surgery, girls have greater success at achieving continence than boys do.^{140,145}



Figure 114-34 Rectourethral fistula. A catheter placed in the urethra for voiding cystourethrography passed into the rectourethral fistula. Contrast material outlines the distal rectal segment.

This difference probably reflects the fact that more than 90% of boys but only 69% of affected girls have supralelevator imperforate anus.

RADIOLOGIC FINDINGS

Prenatal Ultrasound

Prenatal ultrasound may suggest bowel obstruction in patients with imperforate anus; however, dilated bowel is seen only in the later stages of gestation. Intraluminal enteroliths may be seen in fetuses with imperforate anus. Because infants with jejunal and ileal atresia have few extragastrointestinal abnormalities, detection of any of the stigmata of the VACTERL association in a fetus with multiple dilated bowel loops suggests imperforate anus.

Radiographs

A number of associated anomalies of imperforate anus can be visualized on radiographs of the chest and abdomen: spinal deformity with absent, additional, or fused segments; scimitar sacrum; tetralogy of Fallot; and ventricular septal defect. The bowel gas pattern may show little except changes of distal obstruction. The intraluminal calcification reported in a small number of infants with imperforate anus may be caused by prenatal mixture of urine and colon contents, although it can occur in the absence of obstruction or fistulous communication between the gut and the genitourinary tract (Fig. 114-35; see also Fig. 114-34).

When the physical examination does not provide enough information about the level of the distal pouch, it must be defined radiographically. A lateral radiograph of the rectum obtained with the infant inverted (i.e., invertogram) was once the standard way to assess rectal position.¹⁴⁶ The level of the



Figure 114-35 Imperforate anus with rectourethral fistula. A rectourethral fistula is demonstrated on this voiding cystourethrogram. As the child voids and fills the urethra, contrast material passes through the fistula (arrow) into the blind-ending rectum. The fistula is demonstrated best on lateral radiographs.

levator sling was considered to be the same as the pubococcygeal line: a line drawn from the junction of the superior third of the pubis with the middle third to the inferior aspect of the fifth sacral vertebra. If the rectal air stopped proximal to this line, the imperforate anus was considered to be high, but if it stopped below, it was considered to be low. The invertogram is now not used, and a prone cross-table lateral radiograph of the rectum is obtained with the infant's knees tucked beneath (Fig. 114-36).^{147,148} The prone or knee-chest position is physiologically better for the infant than the invertogram; it also encourages colonic gas to pass to the rectum and tends to prevent distal air from escaping through a fistula. The landmarks used are the same as on the standard invertogram. The radiograph is more accurate when it is obtained after the first 24 hours of life because the delay allows gas to be driven to the most distal portion of bowel.^{147,148}

The CT invertogram (obtained with the child prone or in the knee-chest position) provides better delineation of the anatomy than do abdomen radiographs, but it is not commonly used.¹⁴⁹ On sagittal reconstruction, the distal colon can be seen in relation to the midline bone structures even if it has not yet been filled with air. Percutaneous injection of contrast material through the rectal dimple in an attempt to find a poorly seen distal pouch is rarely performed.

Ultrasound Studies

Sonography can identify the distal rectal pouch because it contains echogenic meconium and can therefore define the anomaly

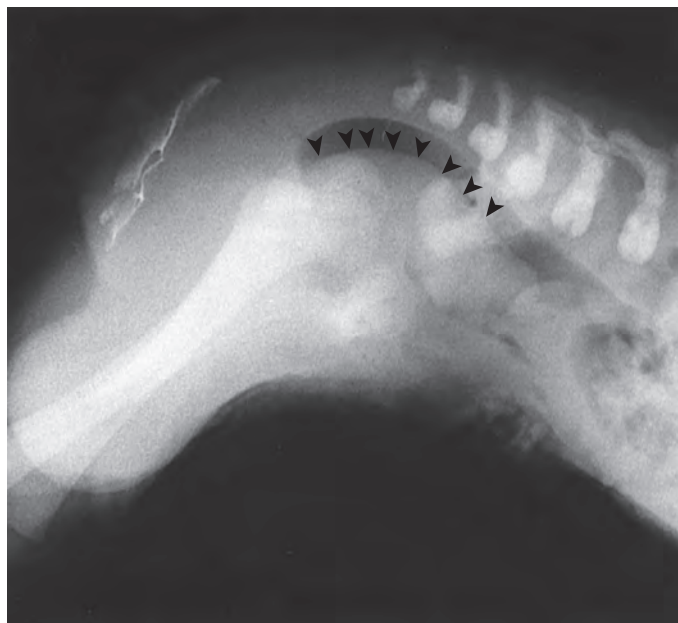


Figure 114-36 Jackknife position invertogram demonstrating an imperforate anus. The child is positioned prone with the hips elevated on a cloth roll. Barium paste marks the anus. Meconium (arrowheads) in the rectal pouch is outlined by air.

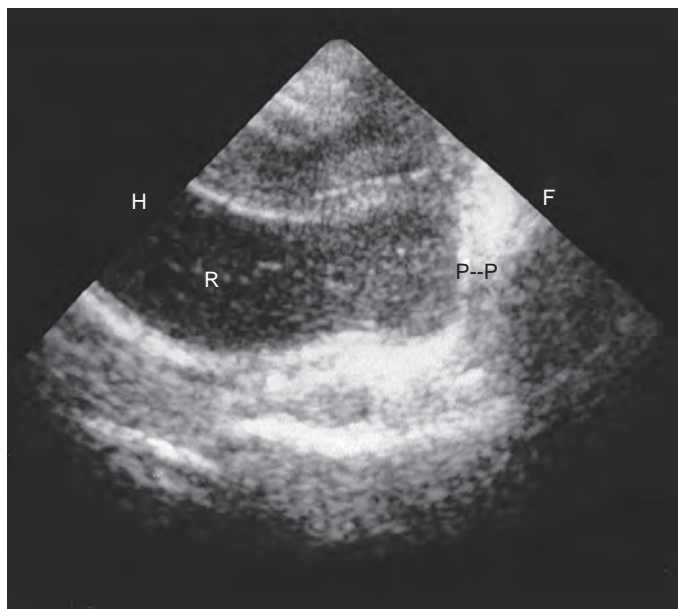


Figure 114-37 Imperforate anus. On a longitudinal sonogram of the rectal pouch in an infant with imperforate anus, the echogenic meconium distends and defines the distal rectal (R) pouch. The pouch-to-perineum distance (P-P) is only a few millimeters. F, inferior; H, superior.

as a high or low lesion (Fig. 114-37).¹⁵⁰ When the pouch cannot be easily classified, it is usually a high imperforate anus. Transperineal sonography has also been used to assess the distal pouch and the puborectalis muscle around it.¹⁵¹ Renal sonography should be routine, and spinal ultrasound is performed even when abdomen radiographs do not demonstrate a spinal anomaly.

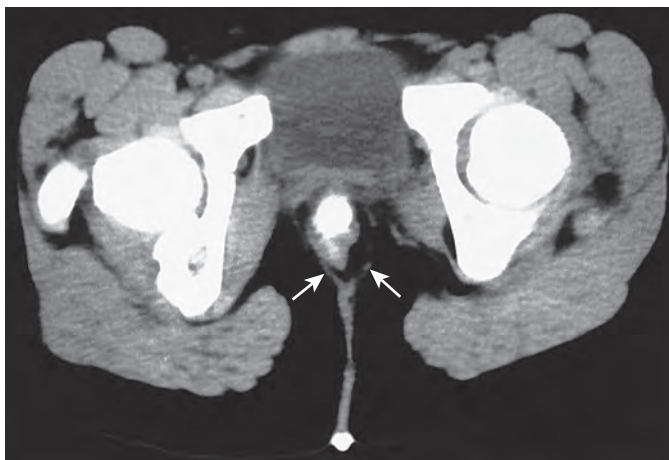


Figure 114-38 Imperforate anus: postoperative CT. For the postoperative evaluation of the sphincter muscle in an infant with imperforate anus, pelvic CT shows that the sphincter muscles (arrows) are extremely thin and underdeveloped.

Gastrointestinal and Genitourinary Contrast Studies

Voiding cystourethrography is routinely performed to exclude vesicoureteral reflux, which occurs in almost 50% of children with high imperforate anus and in 35% of children with low imperforate anus. In boys, voiding cystourethrography is also necessary to exclude rectourinary fistula, which requires ligation at the time of pull-through surgery.

Because the fistula may not always fill on the initial examination, pressure-augmented antegrade colography or repeated voiding cystourethrography precedes corrective surgery if the result of the neonatal study was normal.¹⁴³ Water-soluble contrast agents, rather than barium, should be used to fill this unused segment to avoid barium in the urinary tract. The fistula is best seen when the distal colon segment is distended and the infant is in the lateral position (see Fig. 114-35).

Computed Tomography and Magnetic Resonance Imaging

Preoperative evaluation of the levator sling can be performed with CT or MRI, but it is not routine.^{149,150} MRI displays the sphincteric muscle complex better than CT, which is limited by the small amount of fat present in the neonate. MRI also can better demonstrate the muscles best imaged in the coronal or sagittal planes. When there is insufficient intrinsic muscle to produce continence, surgical results may be disappointing unless special procedures to buttress the muscles are also performed.¹⁵²

MRI is useful in evaluating the spinal cord when an abnormality is detected on ultrasonography.¹⁵³⁻¹⁵⁵ In the neonatal period, MRI also displays the distal portion of the colon well; the impacted meconium produces an intense signal.

Postoperative Studies

Postoperative studies are performed when there is clinical suspicion of an anastomotic leak. Later contrast studies are performed if there is fecal soiling or severe constipation. CT and MRI are occasionally used to assess the position of the colon pull-through in relation to the sphincteric muscle complex (Figs. 114-38 and 114-39).¹⁵⁶ The rectum should be centrally

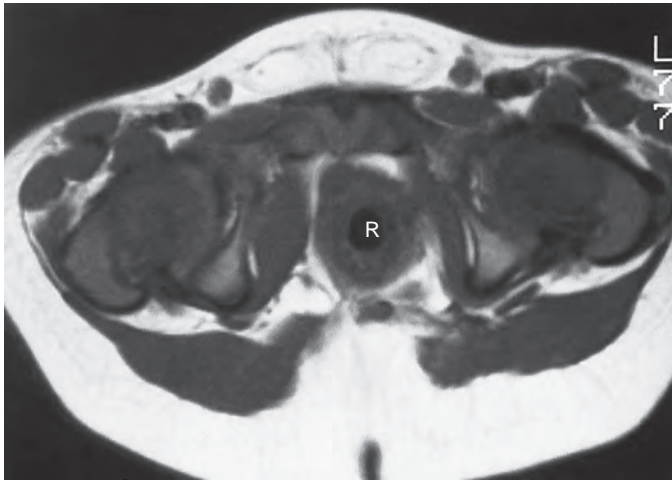


Figure 114-39 Imperforate anus: MRI of pull-through. Axial MRI shows the anal pull-through in a good position. The rectum (R) is centrally placed within a well-developed sphincteric muscle complex.

positioned within the sphincteric muscle complex to ensure proper function. Poor centralization of the neorectum is more common in children with a poorly developed sphincteric muscle complex than in those with normally developed muscles (Fig. 114-38). A child who evacuates well initially but later develops incontinence should be evaluated for a spinal cord lesion that produces tethering.¹⁵³⁻¹⁵⁵ A child who has difficulty beginning at the time of surgery should be evaluated for Hirschsprung's disease, a disorder that occurs with increased frequency in patients with imperforate anus. In some children, especially those prone to constipation, fecal continence is achieved by percutaneous cecostomy and antegrade enema.¹⁵⁷

Imperforate Anus Variants

CLOACAL MALFORMATION

In girls, a variant of imperforate anus associated with more profound renal, vaginal, and uterine abnormalities is the cloacal malformation.^{136,158-160} It occurs in 1 of 40,000 to 50,000 births. This anomaly can be diagnosed at birth when a "bland" or "featureless" perineum with only one opening is detected. This opening is usually beneath an enlarged clitoris. The external anatomy indicates that at some level, the bladder, urethra, vagina, and rectum merge into a common distal channel of variable length. The numerous possible configurations depend on which distal channel is dominant.

In one third of neonates with cloaca, the vaginal opening of the confluent channel is stenotic, which causes hydrocolpos with resultant abdominal mass.¹⁶⁰⁻¹⁶² Urinary sepsis may develop if the bladder cannot drain freely or if there is associated reflux. Management in the neonatal period requires that urinary tract abnormalities be corrected and that the fecal stream be diverted.

Genitourinary tract anomalies, such as solitary kidney, renal ectopia, ureteral obstruction, vesicoureteral reflux, and bladder diverticula, are common. Failure of the fusion of müllerian structures is frequent and results in duplication of the vagina, a vaginal septum, and uterine duplication. Cardiac, skeletal, and other gastrointestinal anomalies are also seen with increased frequency.

TREATMENT

Corrective surgery is frequently delayed until after 1 year of age.^{159,160} Although in some girls the anatomy lends itself to a one-stage correction, those with a long common channel need a staged repair for creation of a urethra, a separate vagina, and a functioning anus. The goal of surgery is to achieve fecal and urinary continence and normal sexual function.

RADIOLOGIC FINDINGS

To prevent injury or deterioration of the urinary tract, the internal anatomy must be accurately delineated in the neonatal period. An abdomen radiograph can document the presence or absence of vertebral deformity, abdominal calcifications, or a large pelvic mass (i.e., dilated vagina).

Water-soluble contrast studies are needed to visualize the length of the common channel and the relationships of each of the systems above it. These studies are performed with catheters introduced through and occluding the perineal opening while the contrast agent is being injected; the catheter is introduced from above if colostomy, vesicostomy, or vaginostomy is present.^{161,162} Any accessory openings should also be injected with contrast material.

Ultrasound is useful for detecting renal, uterine, or vaginal abnormalities. However, the common channel is difficult to visualize with ultrasound or CT.^{161,162} Three-dimensional magnetic resonance genitography with instillation of gadolinium solution into the common channel, vesicostomy, and distal colon by augmented pressure delineates the complex anatomy.¹⁶³ MRI is helpful in evaluating the spinal cord; tethering of the cord is common, and this affects later bowel and bladder function.

Caudal Regression

Caudal regression is a rare association of severe malformations of the lower spine, lower limbs, genitourinary tract, and anorectum that occurs in about 1% of the offspring of diabetic mothers.^{164,165} The infant with fusion of the lower limbs into a single structure is said to have a specific form of caudal regression: sirenomelia, or mermaid deformity.¹⁶⁶ This is usually a lethal variant associated with complete renal agenesis. Other children with milder changes of caudal regression present with many of the classic stigmata of the VACTERL association. The lower limbs may be atrophied, malrotated, or contracted. The genitourinary anomalies are the same as those seen in imperforate anus, and the degree of bladder dysfunction reflects but does not parallel the spinal deformity.

Many of the changes can be diagnosed prenatally.¹⁶⁷ The spinal and limb changes are usually apparent earlier than the anorectal anomaly. Spinal anomalies are usually evaluated by MRI.¹⁶⁸

Currarino Triad

Another variant of anorectal malformations is the Currarino triad, which additionally includes a sacral deformity and presacral mass.¹⁶⁹⁻¹⁷¹ The anorectal lesion has been described as being anal stenosis, anal ectopia, imperforate anus, or Hirschsprung's disease.¹⁷² Sacral lesions are not uncommon in children with anorectal malformations, but presacral masses (e.g., anterior

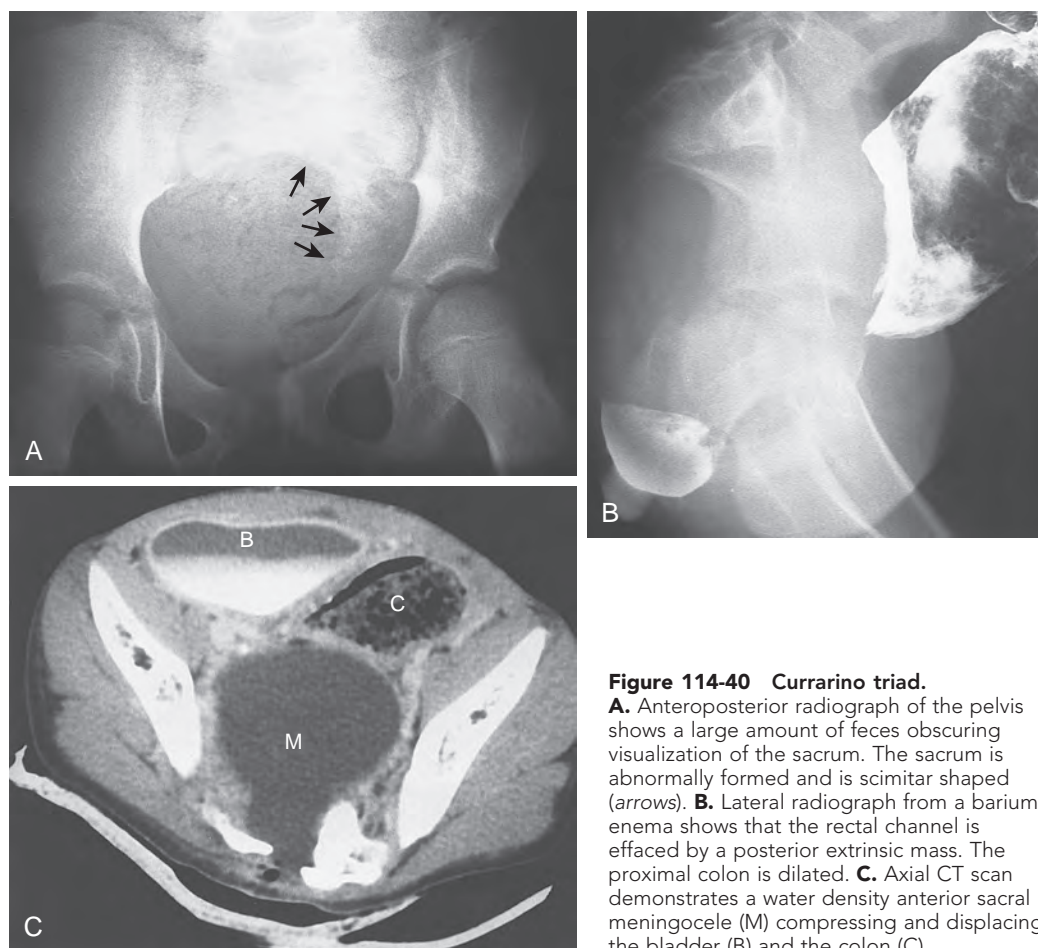


Figure 114-40 Currarino triad.

A. Anteroposterior radiograph of the pelvis shows a large amount of feces obscuring visualization of the sacrum. The sacrum is abnormally formed and is scimitar shaped (arrows). **B.** Lateral radiograph from a barium enema shows that the rectal channel is effaced by a posterior extrinsic mass. The proximal colon is dilated. **C.** Axial CT scan demonstrates a water density anterior sacral meningocele (M) compressing and displacing the bladder (B) and the colon (C).

meningocele, duplication, teratoma) are. In some children, the presacral mass is detected years after the anal lesion has been repaired (Fig. 114-40).

In about 50% of cases, the triad is inherited in an autosomal dominant manner.^{168,170} As in other variants of imperforate anus, ultrasound evaluation of the spinal cord followed by MRI when the ultrasound finding is abnormal is an important part of patient evaluation because tethering of the cord is common in this entity.¹⁷³

Other Low Obstructive Lesions

Many low obstructive lesions are functional rather than mechanical. When a contrast enema is performed in a child with signs of Hirschsprung's disease, the diseases described in the following sections should be considered. Any process that causes ileus may simulate obstruction and should be excluded clinically.

MECONIUM ILEUS

Clinical Findings

Meconium ileus indicates cystic fibrosis in more than 80% of patients.¹²⁵ The narrowed lumen of the distal ileum is impacted with meconium pellets, and the dilated segment above contains thick meconium. The neonate does not pass meconium or stool.¹²⁵ The first-year mortality rate for affected infants has

diminished markedly but remains about 10%. Further discussion of meconium ileus is included in Chapter 118.

Therapy

Cleansing enemas of hypertonic, water-soluble contrast agents have long been used to diagnose and to treat this disorder.¹⁷⁴ Because fluid drawn into the bowel lumen from the intravascular space may produce dehydration, the neonate should have an intravenous line in place. The necessity of refluxing contrast material into the obstructed terminal ileum may result in perforation of the unused microcolon; most children with perforation do well, despite the need for immediate surgery.¹⁷⁵

Radiologic Findings

Abdomen radiographs show multiple, dilated small bowel loops (Fig. 114-41). A granular appearance of the right lower quadrant and the absence of air-fluid levels in this region result from the abnormally thick intraluminal meconium, which does not change position with gravity.

Contrast enema demonstrates a small-caliber colon that is malrotated in 33% to 50% of patients.¹²⁵⁻¹²⁷ Contrast material refluxed into the terminal ileum outlines the impacted meconium (see Fig. 114-41). To avoid perforation, the physician should not attempt to fill the entire obstructed segment with the first contrast enema. When some of the terminal ileum is filled, the study is concluded. The infant is returned to the nursery and observed clinically. If there is continued

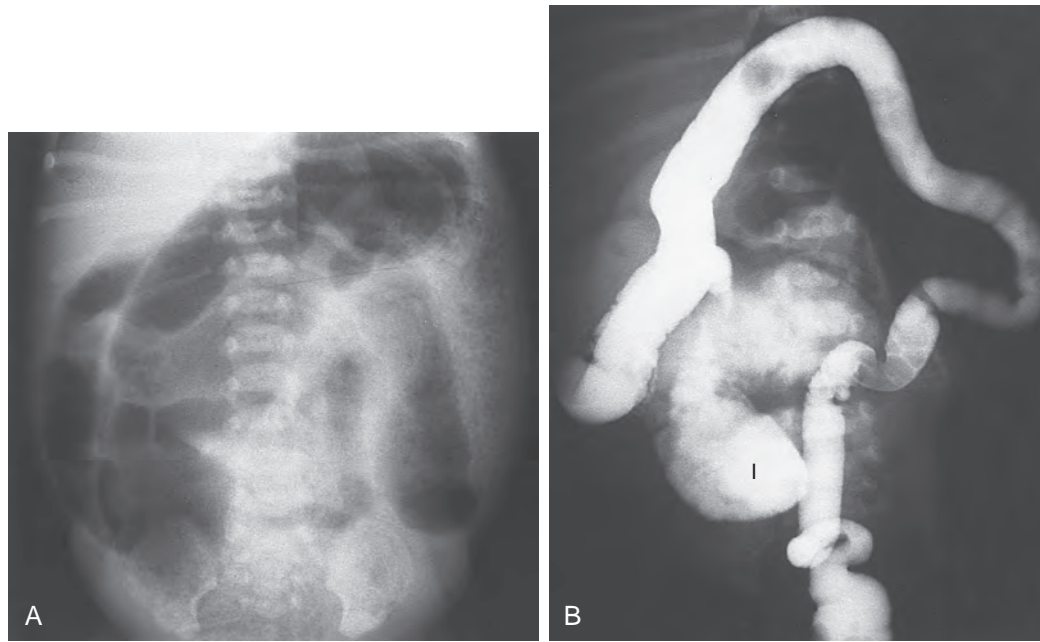


Figure 114-41 Meconium ileus. **A.** Air-filled, dilated bowel loops are present throughout the abdomen. Multiple loops of meconium-filled gut are seen above the distal meconium impaction. **B.** The caliber of the colon is slightly diminished on contrast enema. As contrast material refluxes into the dilated and obstructed terminal ileum (I), it is diluted by the intraluminal meconium.

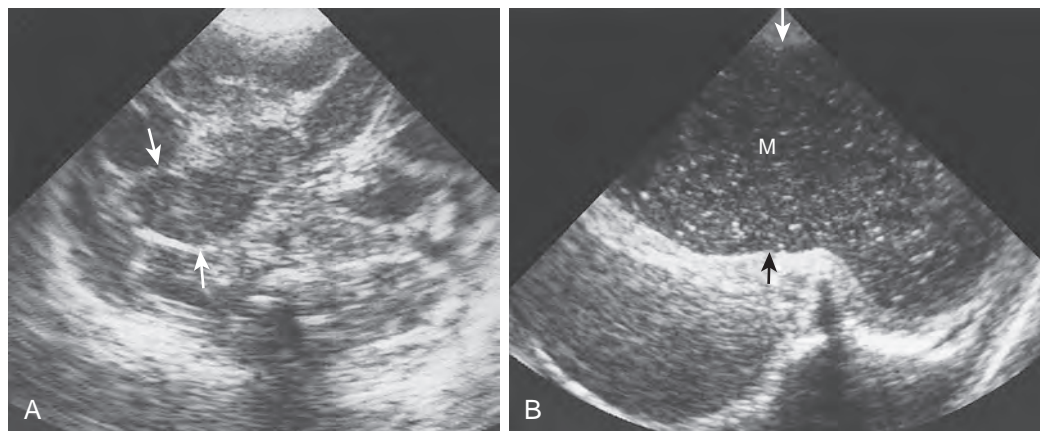


Figure 114-42 Ultrasound appearance of meconium ileus. **A.** Round loops of bowel (arrows) full of echogenic meconium are visualized on this transverse scan. **B.** Echogenic meconium (M) fills the dilated bowel loop (arrow).

obstruction, additional enemas are given, usually 1 day apart. Each time, it is necessary to observe that the retrograde flow reaches the impacted meconium and ultimately enters the dilated bowel loops above.

Prenatal or postnatal sonography can show the inspissated meconium or meconium in the dilated proximal bowel loops (Fig. 114-42).^{120,121} Prenatal diagnosis of meconium ileus is increasingly common.

MECONIUM PLUG SYNDROME

Delayed passage of meconium and abdominal distention are the presenting findings in neonates with meconium plug syndrome, also called small left colon syndrome or functional immaturity of the colon, which occurs in about 1 of 500 to 1000 neonates. Of these, up to 25% have cystic fibrosis, and another 5% to 13%

have Hirschsprung's disease.¹⁷⁶⁻¹⁸² Other factors associated with meconium plug include prematurity, maternal diabetes, and maternal treatment with magnesium sulfate.^{179,181,182} In most children, meconium plug is an isolated process without a specific cause.

Most children are promptly and completely relieved by contrast enema, which stimulates passage of the plug. If the obstruction recurs, it is necessary to exclude Hirschsprung's disease by rectal biopsy and to evaluate the patient for cystic fibrosis. When obstructive symptoms develop after an uneventful perinatal period, a contrast enema may be done to exclude Hirschsprung's disease. If it shows filling defects in the terminal ileum, milk curd syndrome should be considered. This also can be treated with a hypertonic contrast enema.¹⁸³ Boys are affected with milk curd syndrome about five times more often than girls are.

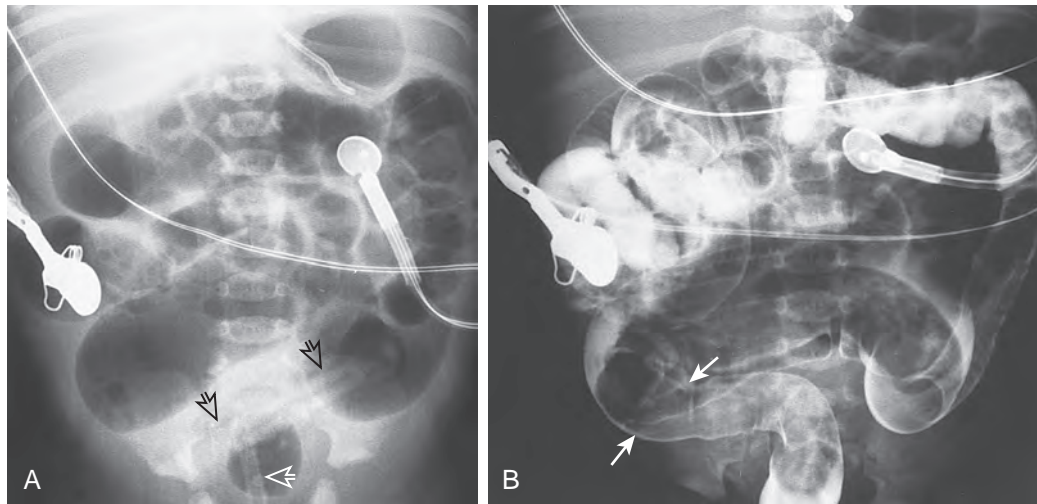


Figure 114-43 Meconium plug in Hirschsprung's disease. **A.** Multiple dilated bowel loops fill the abdomen. None can be specifically identified as the colon. The umbilical clamp projects (black arrows) over the lower abdomen. An enema tip is in place (white arrow). **B.** An intraluminal tubular defect (arrows) extends from the descending colon to the rectum. There is a subtle change in the caliber of the colon, with the sigmoid colon being larger than the rectum.

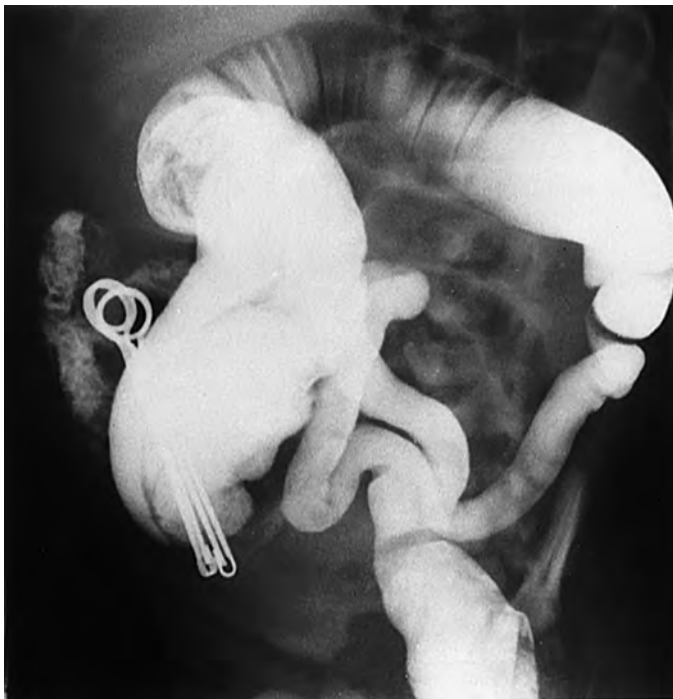


Figure 114-44 Small left colon syndrome. The rectum is large, but the descending colon and sigmoid colon are much smaller than normal. There is an abrupt change in caliber at the level of the splenic flexure, a classic finding.

Radiologic Findings

In children with the meconium plug syndrome, abdomen radiographs demonstrate multiple, dilated bowel loops (Fig. 114-43A).^{177,180} Contrast enema, performed with a water-soluble agent, outlines the adherent plug, which fills the lumen (Fig. 114-43B). The colon may be normal in caliber or have a diminished caliber up to the splenic flexure (Fig. 114-44), as seen in neonates with small left colon syndrome.¹⁸¹

MEGACYSTIS–MICROCOLON–INTESTINAL HYPOPERISTALSIS SYNDROME

The pathophysiologic mechanism of megacystis–microcolon–intestinal hypoperistalsis (MMIH) syndrome has been investigated by many but remains poorly understood.¹⁸³⁻¹⁸⁶ Abnormalities of autonomic inhibitory input to the smooth muscle cells of the small intestine, imbalance of gut peptides, and fibrosis after inflammation have been postulated.

Clinical Findings

MMIH syndrome is a rare condition that occurs almost exclusively in girls.¹⁸⁶ Most cases are sporadic, but in some, there has been a pattern of autosomal recessive inheritance. The clinical presentation may overlap with the chronic intestinal pseudo-obstruction syndrome, which has similar problems of the gastrointestinal tract but variable urinary tract involvement.¹⁸⁷

The affected infant presents shortly after birth with abdominal distention and vomiting. The wrinkled appearance of the abdomen, similar to that of the prune-belly syndrome, may not be appreciated until the huge bladder is catheterized and drained.

Virtually all children with MMIH syndrome die in infancy. Neither pharmacologic stimulation nor ileostomy or colostomy improves gastrointestinal tract function. Hyperalimentation improves nutritional status, but it is a temporizing measure because bowel function is never corrected.

The main alternative diagnosis to MMIH syndrome is Hirschsprung's disease, which is not usually associated with microcolon or a large bladder. In some children, biopsy of the colon may be necessary to exclude the diagnosis.

Radiologic Findings

The MMIH syndrome can be suggested in utero by finding a markedly dilated bladder and upper urinary tract in a female infant.^{188,189} It can be differentiated from other syndromes with bladder distention and upper urinary tract changes because it is not associated with a decreased amount of amniotic fluid.

Male infants with a distended bladder and upper tract abnormalities are more likely to have posterior urethral valves or prune-belly syndrome.

Postnatal radiologic studies may show the dilated upper urinary tract but fail to disclose any site of mechanical obstruction. A contrast enema easily fills the microcolon, which in infants with MMIH syndrome has a tendency to be abnormally rotated or fixed. Contrast studies of the genitourinary tract are

routinely performed to exclude vesicoureteral reflux, a common neonatal cause of dilation. Sonography can show the dilated bladder mass.¹⁹⁰

HIRSCHSPRUNG'S DISEASE

Hirschsprung's disease typically is manifested in the neonatal period. This disorder is discussed in Chapter 118.

REFERENCES

- Cyr DR, Mack LA, Schoenecker SA, et al: Bowel migration in the normal fetus: US detection. *Radiology* 161:119–121, 1986.
- Parulekar SG: Sonography of normal fetal bowel. *J Ultrasound Med* 10:211–220, 1991.
- Strouse PJ: Disorders of intestinal rotation and fixation ("malrotation"). *Pediatr Radiol* 34: 837–851, 2004.
- Long FR, Kramer SS, Markowitz RI, et al: Radiographic patterns of intestinal malrotation in children. *Radiographics* 16:547–556, 1996.
- Torres AM, Ziegler MM: Malrotation of the intestine. *World J Surg* 17:211–220, 1993.
- Ilce Z, Celayir S, Akova F, et al: Intestinal rotation anomalies in childhood: Review of 22 years' experience. *Surg Today* 33:893–895, 2003.
- Whinney J, Paul SP, Candy DC: Clinical update: Vomiting in infants. *Community Pract* 86:44–47, 2013.
- Berdon WE: The diagnosis of malrotation and volvulus in the older child and adult: A trap for radiologists. *Pediatr Radiol* 25:101–103, 1995.
- Mori H, Hayashi K, Futagawa S, et al: Vascular compromise in chronic volvulus with midgut malrotation. *Pediatr Radiol* 17:277–281, 1987.
- Verma TR, Bankole MA: Lymphovenous obstruction in anomalous midgut rotation. *Arch Dis Child* 48:154–156, 1973.
- Potts SR, Thomas PS, Garstin WI, et al: The duodenal triangle: A plain film sign of midgut malrotation and volvulus in the neonate. *Clin Radiol* 36:47–49, 1985.
- Patino MO, Munden MM: Utility of the sonographic whirlpool sign in diagnosing midgut volvulus in patients with atypical clinical presentations. *J Ultrasound Med* 23:397–401, 2004.
- Weinberger E, Winters W, Liddell R, et al: Sonographic diagnosis of intestinal malrotation in infants. *AJR Am J Roentgenol* 159:825–828, 1992.
- Pracos JP, Sann L, Genin G, et al: Ultrasound diagnosis of midgut volvulus: The "whirlpool" sign. *Pediatr Radiol* 22:18–20, 1992.
- Shimanuki Y, Aihara T, Takano H, et al: Clockwise whirlpool sign at color Doppler US: An objective and definite sign of midgut volvulus. *Radiology* 199:261–264, 1996.
- Yousefzadeh DK, Kang L, Tessini L: Assessment of retromesenteric position of the third portion of the duodenum: an US feasibility study in 33 newborns. *Pediatr Radiol* 40:1476–1484, 2010.
- Menten R, Reding R, Godding V, et al: Sonographic assessment of the retroperitoneal position of the third portion of the duodenum: An indicator of normal intestinal rotation. *Pediatr Radiol* 42:941–945, 2012.
- Aidlen J, Anupindi SA, Jaramillo D, et al: Malrotation with midgut volvulus: CT findings of bowel infarction. *Pediatr Radiol* 35:529–531, 2005.
- Emanuel PG, Garcia GI, Angtuaco TL: Prenatal detection of anterior abdominal wall defects with US. *Radiographics* 15:517–530, 1995.
- Ergun O, Barksdale E, Ergun FS, et al: The timing of delivery of infants with gastroschisis influences outcome. *J Pediatr Surg* 40:424–428, 2005.
- Barisic I, Clementi M, Hausler M, et al: Evaluation of prenatal ultrasound diagnosis of fetal abdominal wall defects by 19 European registries. *Ultrasound Obstet Gynecol* 18:309–316, 2001.
- Hwang PJ, Kouseff BG: Omphalocele and gastroschisis: An 18-year review study. *Genet Med* 6:232–236, 2004.
- Saada J, Oury JE, Vuillard E, et al: Gastroschisis. *Clin Obstet Gynecol* 48:964–972, 2005.
- Durfee SM, Downard CD, Benson CB, et al: Postnatal outcome of fetuses with the prenatal diagnosis of gastroschisis. *J Ultrasound Med* 21:269–274, 2002.
- Molik KA, Gingalewski CA, West KW, et al: Gastroschisis: A plea for risk categorization. *J Pediatr Surg* 36:51–55, 2001.
- Baerg J, Kaban G, Tonita J, et al: Gastroschisis: A sixteen-year review. *J Pediatr Surg* 38:771–774, 2003.
- Ramsden WH, Arthur RJ, Martinez D: Gastroschisis: A radiological and clinical review. *Pediatr Radiol* 27:166–169, 1997.
- Vegunta RK, Wallace LJ, Leonardi MR, et al: Perinatal management of gastroschisis: Analysis of a newly established clinical pathway. *J Pediatr Surg* 40:528–534, 2005.
- Bucher BT, Mazotas IG, Warner BW, et al: Effect of time to surgical evaluation on outcomes of infants with gastroschisis. *J Pediatr Surg* 47:1105–1110, 2012.
- Kelly KB, Ponsky TA: Pediatric abdominal wall defects. *Surg Clin North Am* 93:1255–1267, 2014.
- Japaraj RP, Hockey R, Chan FY: Gastroschisis: Can prenatal sonography predict neonatal outcome? *Ultrasound Obstet Gynecol* 21:329–333, 2003.
- Blazer S, Zimmer EZ, Gover A, et al: Fetal omphalocele detected early in pregnancy: Associated anomalies and outcomes. *Radiology* 232:191–195, 2004.
- Soboleski D, Daneman A, Manson D, et al: Tailoring the small bowel follow-through examination postoperatively in gastroschisis patients. *Pediatr Radiol* 25:267–268, 1995.
- Getachew MM, Goldstein RB, Edge V, et al: Correlation between omphalocele contents and karyotypic abnormalities: Sonographic study in 37 cases. *AJR Am J Roentgenol* 158: 133–136, 1992.
- Brantberg A, Blaas HGK, Haugens SE, et al: Characteristics and outcome of 90 cases of fetal omphalocele. *Ultrasound Obstet Gynecol* 26:527–537, 2005.
- Stoll C, Alembik Y, Dott B, et al: Risk factors in congenital abdominal wall defects (omphalocele and gastroschisis): A study in a series of 265,858 consecutive births. *Am Genet* 44:201–208, 2001.
- Tsakayannis DE, Zurakowski D, Lillehei CW: Respiratory insufficiency at birth: A predictor of mortality for infants with omphalocele. *J Pediatr Surg* 31:1088–1090, 1996.
- Islam S: Advances in surgery for abdominal wall defects: Gastroschisis and omphalocele. *Clin Perinatol* 39:376–386, 2012.
- Zaccara A, Iacobelli BD, La Sala E, et al: Sonographic biometry of liver and spleen size long after closure of abdominal wall defects. *Eur J Pediatr* 162:490–492, 2003.
- Hollinger LE, Lally PA, Tsao K, et al: A risk-stratified analysis of delayed congenital diaphragmatic hernia repair: Does timing of operation matter? *Surgery* 156:475–482, 2014.
- Baglaj M, Dorobisz U: Late-presenting congenital diaphragmatic hernia in children: A literature review. *Pediatr Radiol* 35:478–488, 2005.
- Colvin J, Bower C, Dickinson JE, et al: Outcomes of congenital diaphragmatic hernia: A population-based study in Western Australia. *Pediatrics* 116:356–363, 2005.
- Fauza DO, Wilson JM: Congenital diaphragmatic hernia and associated anomalies: Their incidence, identification, and impact on prognosis. *J Pediatr Surg* 29:1113–1117, 1994.
- Busing KA, Kilian AK, Schaible T, et al: MR relative fetal lung volume in congenital diaphragmatic hernia: Survival and need for extracorporeal membrane oxygenation. *Radiology* 248:240–246, 2008.
- Gorincour G, Bouvenot J, Mourot MG, et al: Prenatal prognosis of congenital diaphragmatic hernia using magnetic resonance imaging of fetal lung volume. *Ultrasound Obstet Gynecol* 26:738–744, 2005.
- Kitano Y, Nakagawa S, Kuroda T, et al: Liver position in fetal congenital diaphragmatic hernia retains a prognostic value in the era of lung protective strategy. *J Pediatr Surg* 40:27–32, 2005.
- Hubbard AM, Adzick NS, Crombleholme TM, et al: Congenital chest lesions: Diagnosis and characterization with prenatal MR imaging. *Radiology* 212:43–48, 1999.
- Metkus AP, Filly RA, Stringer MD, et al: Sonographic predictors of survival in fetal diaphragmatic hernia. *J Pediatr Surg* 31:148–151, 1996.
- Reickert CA, Hirschl RB, Atkinson JB, et al: Congenital diaphragmatic hernia survival and use of extracorporeal life support at selected level III nurseries with multimodality support. *Surgery* 123:305–310, 1998.

50. Dimmitt RA, Moss L, Rhine WD, et al: Veno-arterial versus venovenous extracorporeal membrane oxygenation in congenital diaphragmatic hernia: The Extracorporeal Life Support Organization Registry, 1990-1999. *J Pediatr Surg* 36:1199-1204, 2001.
51. Leeuwen L, Walker K, Halliday R, et al: Neurodevelopmental outcome in Congenital Diaphragmatic Hernia survivors during the first three years. *Early Hum Dev* 90:413-415, 2014.
52. Done E, Gratacos E, Nicolaides KH, et al: Predictors of neonatal morbidity in fetuses with severe isolated congenital diaphragmatic hernia undergoing fetoscopic tracheal occlusion. *Ultrasound Obstet Gynecol* 42:77-83, 2013.
53. Teixeira J, Sepulveda W, Hassan J, et al: Abdominal circumference in fetuses with congenital diaphragmatic hernia: Correlation with hernia content and pregnancy outcome. *J Ultrasound Med* 16:407-410, 1997.
54. Taylor GA, Lotze A, Kapur S, et al: Diffuse pulmonary opacification in infants undergoing extracorporeal membrane oxygenation: Clinical and pathologic correlation. *Radiology* 161:347-350, 1986.
55. Gross GW, Dougherty CH: Pleural hemorrhage in neonates on extracorporeal membrane oxygenation after repair of congenital diaphragmatic hernia: Imaging findings. *AJR Am J Roentgenol* 164:951-955, 1995.
56. Kieffer J, Sapin E, Berg A: Gastroesophageal reflux after repair of congenital diaphragmatic hernia. *J Pediatr Surg* 30:1330-1333, 1995.
57. Vanamo K, Rintala RJ, Lindahl H, et al: Long-term gastrointestinal morbidity in patients with congenital diaphragmatic hernia. *J Pediatr Surg* 31:551-554, 1996.
58. Traschel D, Selvadurai H, Bohn D, et al: Long-term pulmonary morbidity in survivors of congenital diaphragmatic hernia. *Pediatr Pulmonol* 39:433-439, 2005.
59. Guibaud L, Filiatrault D, Garel L, et al: Fetal congenital diaphragmatic hernia: Accuracy of sonography in the diagnosis and prediction of the outcome after birth. *AJR Am J Roentgenol* 166:1195-1202, 1996.
60. Loong TPF, Kocher HM: Clinical presentation and operative repair of hernia of Morgagni. *Postgrad Med J* 81:41-44, 2005.
61. Groff DB: Diagnosis of a Morgagni hernia complicated by a previous normal chest x-ray. *J Pediatr Surg* 25:556-557, 1990.
62. Sarihan H, Imamoglu M, Abes M, et al: Pediatric Morgagni hernia: Report of two cases. *J Cardiovasc Surg* 37:195-197, 1996.
63. Newman B, Davis PL: Sonographic and magnetic resonance imaging of an anterior diaphragmatic hernia. *Pediatr Radiol* 20:110-112, 1989.
64. Sbargia L, Paek BW, Feldstein VA, et al: Outcome of prenatally diagnosed solid fetal tumors. *J Pediatr Surg* 36:1244-1247, 2001.
65. Heling KS, Chaoui R, Kirchmair F, et al: Fetal ovarian cysts: Prenatal diagnosis, management, and postnatal outcome. *Ultrasound Obstet Gynecol* 20:47-50, 2002.
66. Kirkinen P, Partanen K, Merikanto J, et al: Ultrasonic and magnetic resonance imaging of fetal sacrococcygeal teratoma. *Acta Obstet Gynecol Scand* 76:917-922, 1997.
67. Siegel MJ: MR imaging of pediatric abdomen. *Magn Reson Imaging Clin North Am* 3:161-182, 1995.
68. Neu J: Neonatal necrotizing enterocolitis: An update. *Acta Pediatr Suppl* 94:100-105, 2005.
69. Engum SA, Grosfeld JL: Necrotizing enterocolitis. *Curr Opin Pediatr* 10:123-130, 1998.
70. Martinez-Tallo E, Claire N, Bancalari E: Necrotizing enterocolitis in full-term or near-term infants: Risk factors. *Biol Neonate* 71:292-298, 1997.
71. Hsueh W, Caplan MS, Qu XW, et al: Neonatal necrotizing enterocolitis: Clinical considerations and pathogenetic concepts. *Pediatr Dev Pathol* 6:6-23, 2003.
72. Stringer MD, Cave E, Puntis JW, et al: Enteric fistulas and necrotizing enterocolitis. *J Pediatr Surg* 31:1268-1271, 1996.
73. Hartman GE, Drugas GT, Sochat SJ: Post-necrotizing enterocolitis strictures presenting with sepsis or perforation: Risk of clinical observation. *J Pediatr Surg* 23:562-566, 1988.
74. Horwitz JR, Lally KP, Cheu HW, et al: Complications after surgical intervention for necrotizing enterocolitis: A multicenter review. *J Pediatr Surg* 30:994-999, 1995.
75. Rescorla FJ: Surgical management of pediatric necrotizing enterocolitis. *Curr Opin Pediatr* 7:335-341, 1995.
76. Sharma R, Tepas JJ, Hudak ML, et al: Portal venous gas and surgical outcome of neonatal necrotizing enterocolitis. *J Pediatr Surg* 40:371-376, 2005.
77. Kosloske AM: Indications for operation in necrotizing enterocolitis revisited. *J Pediatr Surg* 5:663-666, 1994.
78. Tonkin IL, Bjelland JC, Hunter TB, et al: Spontaneous resolution of colonic strictures caused by necrotizing enterocolitis: Therapeutic implications. *AJR Am J Roentgenol* 130:1077-1081, 1978.
79. Morrison SC, Jacobson JM: The radiology of necrotizing enterocolitis. *Clin Perinatol* 21:347-363, 1994.
80. Brill PW, Olson SR, Winchester P: Neonatal necrotizing enterocolitis: Air in Morison pouch. *Radiology* 174:469-471, 1990.
81. Seibert JJ, Parvey LS: The telltale triangle: Use of the supine cross table lateral radiograph of the abdomen in early detection of pneumoperitoneum. *Pediatr Radiol* 5:209-210, 1977.
82. Merritt CRB, Goldsmith JP, Sharp MJ: Sonographic detection of portal venous gas in infants with necrotizing enterocolitis. *AJR Am J Roentgenol* 143:1059-1062, 1984.
83. Faingold R, Daneman A, Tomlinson G, et al: Necrotizing enterocolitis: Assessment of bowel viability with color Doppler US. *Radiology* 235:587-594, 2005.
84. Muchantef K, Epelman M, Darge K, et al: Sonographic and radiographic imaging features of the neonate with necrotizing enterocolitis: Correlating findings with outcomes. *Pediatr Radiol* 43:1444-1452, 2013.
85. Rencken IO, Sola A, Al-Ali F, et al: Necrotizing enterocolitis: Diagnosis with CT examination of urine after internal administration of iodinated water-soluble contrast material. *Radiology* 205:87-90, 1997.
86. Ball WS, Seigel RS, Goldthorn JF, et al: Colonic strictures in infants following intestinal ischemia: Treatment by balloon catheter dilatation. *Radiology* 149:469-472, 1983.
87. Stringer MD, McKenna KM, Goldstein RB, et al: Prenatal diagnosis of esophageal atresia. *J Pediatr Surg* 30:1258-1263, 1995.
88. Quan L, Smith DW: The VATER association, vertebral defects, anal atresia, T-E fistula with esophageal atresia, radial and renal dysplasia: A spectrum of associated defects. *J Pediatr* 82:104-107, 1973.
89. Usui N, Kamata S, Ishikawa S, et al: Anomalies of the tracheobronchial tree in patients with esophageal atresia. *J Pediatr Surg* 31:258-262, 1996.
90. Botto LD, Khoury MJ, Mastroiacovo P, et al: The spectrum of congenital anomalies of the VATER association: An international study. *Am J Med Genet* 71:8-15, 1997.
91. Shaw-Smith C: Oesophageal atresia, tracheo-oesophageal fistula and the VACTERL association: Review of genetics and epidemiology. *J Med Genet* 43:545-554, 2006.
92. Touloukian RJ, Seashore JH: Thirty-five year institutional experience with end-to side repair for esophageal atresia. *Arch Surg* 139:371-374, 2004.
93. Holcomb GW, Rothenberg SS, Bax KM, et al: Thoracoscopic repair of esophageal atresia and tracheoesophageal fistula. *Ann Surg* 242:422-428, 2005.
94. Aziz D, Chait P, Kreichman F, et al: Image-guided percutaneous gastrostomy in neonates with esophageal atresia. *J Pediatr Surg* 39:1648-1650, 2004.
95. Spitz L, Kiely E, Pierro A: Gastric transposition in children—a 21-year experience. *J Pediatr Surg* 39:276-281, 2004.
96. Pedersen JC, Klein RL, Andrews DA: Gastric tube as the primary procedure for pure esophageal atresia. *J Pediatr Surg* 31:1233-1235, 1996.
97. Raffensperger JG, Luck SR, Reynolds M, et al: Intestinal bypass of the esophagus. *J Pediatr Surg* 31:38-46, 1996.
98. Zartizky M, Ben R, Zylberg GI, et al: Magnetic compression anastomosis as a nonsurgical treatment for esophageal atresia. *Pediatr Radiol* 39:945-949, 2009.
99. Kovesi T, Rubin S: Long-term complications of congenital esophageal atresia and/or tracheoesophageal fistula. *Chest* 126:915-925, 2004.
100. Rintala RJ, Pakarinen MP: Long-term outcome of esophageal anastomosis. *Eur J Pediatr Surg* 23:219-225, 2013.
101. Little DC, Rescorla FJ, Grosfeld JL, et al: Long-term analysis of children with esophageal atresia and tracheoesophageal fistula. *J Pediatr Surg* 38:852-856, 2003.
102. Newman B, Bender TM: Esophageal atresia/tracheoesophageal fistula and associated congenital esophageal stenosis. *Pediatr Radiol* 27:530-534, 1997.
103. Yeming W, Somme S, Chenren S, et al: Balloon catheter dilatation in children with congenital and acquired esophageal anomalies. *J Pediatr Surg* 37:398-402, 2002.
104. Romeo C, Bonanno N, Baldari S, et al: Gastric motility disorders in patients operated on for esophageal atresia and tracheoesophageal fistula: Long-term evaluation. *J Pediatr Surg* 35:740-744, 2000.
105. Snyder CL, Ramachandran V, Kennedy AP, et al: Efficacy of partial wrap fundoplication for gastroesophageal reflux after repair of esophageal atresia. *J Pediatr Surg* 32:1089-1091, 1997.
106. Griscom NT, Martin TR: The trachea and esophagus after repair of esophageal atresia and distal fistula: Computed tomographic observations. *Pediatr Radiol* 20:447-450, 1990.
107. Langer JC, Hussain H, Khan A, et al: Prenatal diagnosis of esophageal atresia using sonography and magnetic resonance imaging. *J Pediatr Surg* 36:804-807, 2001.

108. Zigman A, Yazbeck S: Esophageal foreign body obstruction after esophageal atresia repair. *J Pediatr Surg* 37:776–778, 2002.
109. Carr MM, Clarke KD, Webber E, et al: Congenital laryngotracheal cleft. *J Otolaryngol* 28:112–117, 1999.
110. Kubbe H, Gibson D, Bailey M, et al: Techniques and outcomes of laryngeal cleft repair: An update on the Great Ormond Street Hospital series. *Ann Otol Rhinol Laryngol* 114: 309–313, 2005.
111. Garabedian EN, Ducroz V, Roger G, et al: Posterior laryngeal clefts: Preliminary report of a new surgical procedure using tibial periosteum as an interposition graft. *Laryngoscope* 108: 899–902, 1998.
112. Cragan JD, Martin ML, Moore CA, et al: Descriptive epidemiology of small intestinal atresia, Atlanta, Georgia. *Teratology* 48:441–450, 1993.
113. Heij HA, Moorman-Voestermans CG, Vos A: Atresia of jejunum and ileum: Is it the same disease? *J Pediatr Surg* 25:635–637, 1990.
114. Komuro H, Hori T, Amagai T, et al: The etiologic role of intrauterine volvulus and intussusception in jejunoileal atresia. *J Pediatr Surg* 39:1812–1814, 2004.
115. Dalla Vecchia LK, Grosfeld JL, West KW, et al: Intestinal atresia and stenosis: A 45-year experience with 277 cases. *Arch Surg* 133:490–496, 1998.
116. Touloulou AJ: Diagnosis and treatment of jejunoileal atresia. *World J Surg* 17:310–317, 1993.
117. Sweeney B, Surana R, Puri P: Jejunoileal atresia and associated malformations: Correlation with the timing of in utero insult? *J Pediatr Surg* 36:774–777, 2001.
118. Waldhausen JH, Sawin RS: Improved long-term outcome for patients with jejunoileal apple peel atresia. *J Pediatr Surg* 32:1307–1309, 1997.
119. Bilodeau A, Prasil P, Cloutier R, et al: Hereditary multiple intestinal atresia: Thirty years later. *J Pediatr Surg* 39:726–730, 2004.
120. Haeusler MC, Berghold A, Stoll C, et al: Prenatal ultrasonographic detection of gastrointestinal obstruction: Results from 18 European congenital anomaly registries. *Prenat Diagn* 22:616–623, 2002.
121. Iacobelli BD, Zaccara A, Spiryakis I, et al: Prenatal counseling of small bowel atresia: Watch the fluid! *Prenat Diagn* 26:214–217, 2006.
122. Leonidas JC: Microcolon in the absence of small bowel obstruction in the newborn. *J Pediatr Surg* 24:180–182, 1989.
123. Neal MR, Seibert JJ, Vanderzalm T, et al: Neonatal ultrasonography to distinguish between meconium ileus and ileal atresia. *J Ultrasound Med* 16:263–266, 1997.
124. Kalifa G, Devred PH, Riccour C, et al: Radiological aspects of the small bowel after extensive resection in children. *Pediatr Radiol* 8: 70–75, 1979.
125. Agrons GA, Corse WR, Markowitz RI, et al: Gastrointestinal manifestations of cystic fibrosis: Radiologic-pathologic correlation. *Radiographics* 16:871–893, 1996.
126. Chaudry G, Navarro OM, Levine DS, et al: Abdominal manifestations of cystic fibrosis in children. *Pediatr Radiol* 36:233–240, 2006.
127. Navarro OM, Daneman A, Miller SF: Contrast enema depiction of small bowel volvulus in complicated neonatal bowel obstruction. *Pediatr Radiol* 34:1020–1023, 2004.
128. Eckoldt F, Heling KS, Woderich R, et al: Meconium peritonitis and pseudocyst formation: Prenatal diagnosis and postnatal course. *Prenat Diagn* 23:904–908, 2003.
129. Chan KL, Tang MH, Tse HY, et al: Meconium peritonitis: Prenatal diagnosis, postnatal management and outcome. *Prenat Diagn* 25:676–682, 2005.
130. Dirkes K, Crombleholme TM, Craigo SD, et al: The natural history of meconium peritonitis diagnosed in utero. *J Pediatr Surg* 30:979–982, 1995.
131. Pan EY, Chen LY, Zang JZ, et al: Radiographic diagnosis of meconium peritonitis. *Pediatr Radiol* 13:199–205, 1983.
132. Wolfson JJ, Engel RR: Anticipating meconium peritonitis from metaphyseal bands. *Radiology* 92:1055–1060, 1969.
133. Cox SG, Numanoglu A, Millar AJ, et al: Colonic atresia: Spectrum of presentation and pitfalls in management. A review of 14 cases. *Pediatr Surg Int* 21:813–818, 2005.
134. Landes A, Shuckett B, Skarsgard E: Non-fixation of the colon in colonic atresia: A new finding. *Pediatr Radiol* 24:167–169, 1994.
135. Kim PC, Superina RA, Ein S: Colonic atresia combined with Hirschsprung's disease: A diagnostic and therapeutic challenge. *J Pediatr Surg* 30:1216–1217, 1995.
136. Stephens FD: Wingspread anomalies, rarities, and super rarities of the anorectum and cloaca. *Birth Defects* 24:581–585, 1988.
137. Siebert JJ, Golladay ES: Clinical evaluation of imperforate anus: Clue to type of anal-rectal anomaly. *AJR Am J Roentgenol* 133:289–292, 1979.
138. Levitt MA, Pena A: Outcomes from the correction of anorectal malformations. *Curr Opin Pediatr* 17:394–401, 2005.
139. Shaul DB, Harrison EA: Classification of anorectal malformations—initial approach, diagnostic test, and colostomy. *Semin Pediatr Surg* 6:187–195, 1997.
140. Bischoff A, Levitt MA, Peña A: Update on the management of anorectal malformations. *Pediatr Surg Int* 29:899–904, 2013.
141. Metts JC, 3rd, Kotkin L, Kasper S, et al: Genital malformations and coexistent urinary tract or spinal anomalies in patients with imperforate anus. *J Urol* 158:1298–1300, 1997.
142. Fernbach SK: Urethral anomalies in male neonates with VATER association. *AJR Am J Roentgenol* 156:137–140, 1991.
143. Gross GW, Wolfson PJ, Peña A: Augmented-pressure colostogram in imperforate anus with fistula. *Pediatr Radiol* 21:560–562, 1991.
144. Nah SA, Ong CCP, Lakshmi NK, et al: Anomalies associated with anorectal malformations according to the Krikenbeck anatomic classification. *J Pediatr Surg* 47:2273–2278, 2012.
145. Javid PJ, Barnhart DC, Hirschl RB, et al: Immediate and long-term results of surgical management of low imperforate anus in girls. *J Pediatr Surg* 33:198–203, 1998.
146. Wagensteen OH, Rice CO: Imperforate anus: Method of determining surgical approach. *Arch Surg* 92:77–91, 1930.
147. Narasimharao KL, Prasad GR, Katariya S, et al: Prone cross-table lateral view: An alternative to the invertogram in imperforate anus. *AJR Am J Roentgenol* 140:227–229, 1983.
148. Berdon WE, Baker DH: The inherent errors in measurements of inverted films in patients with imperforate anus. *Ann Radiol* 10:235–240, 1967.
149. Leighton DM, de Campo M: CT invertograms. *Pediatr Radiol* 19:176–178, 1989.
150. Donaldson JS, Black CT, Reynolds M, et al: Ultrasound of the distal pouch in infants with imperforate anus. *J Pediatr Surg* 24:465–468, 1989.
151. Han TI, Kim IO, Kim WS: Imperforate anus: US determination of the type with infracoccygeal approach. *Radiology* 228:226–229, 2003.
152. Meehan JJ, Hardin WD, Jr, Georgeson KE: Gluteus maximus augmentation for the treatment of fecal incontinence. *J Pediatr Surg* 32:1045–1047, 1997.
153. Golonka NR, Haga LJ, Keating RP, et al: Routine MRI evaluation of low imperforate anus reveals unexpected high incidence of tethered spinal cord. *J Pediatr Surg* 37:966–969, 2002.
154. Appignani BA, Jaramillo D, Barnes PD, et al: Dysraphic myelodysplasia associated with urogenital and anorectal anomalies: Prevalence and types seen with MR imaging. *AJR Am J Roentgenol* 163:1199–1203, 1994.
155. Long FR, Hunter JV, Mahboubi S, et al: Tethered cord and associated vertebral anomalies in children with imperforate anus: Evaluation with MR imaging and plain films. *Radiology* 200:377–382, 1996.
156. Vade A, Reyes H, Wilbur A, et al: The anorectal sphincter after rectal pull-through surgery for anorectal anomalies: MRI evaluation. *Pediatr Radiol* 19:179–183, 1989.
157. Chait PG, Shlomovitz E, Connolly BL, et al: Percutaneous cecostomy: Updates in techniques and patient care. *Radiology* 227:246–250, 2003.
158. Stephens FD: Embryology of the cloaca and embryogenesis of anorectal malformations. *Birth Defects* 24:177–209, 1988.
159. Lund DP, Hendren WH: Cloacal exstrophy: Experience with 20 cases. *J Pediatr Surg* 28: 1360–1368, 1993.
160. Pena A, Levitt MA, Hong AR, et al: Surgical management of cloacal malformations: A review of 339 patients. *J Pediatr Surg* 39:470–479, 2004.
161. Jaramillo D, Lebowitz RL, Hendren WH: Cloacal malformations: Radiologic findings. *Radiology* 177:441–448, 1990.
162. Wood BP: Cloacal malformations and exstrophy syndromes. *Radiology* 177:326–327, 1990.
163. Baughman SM, Richardson RR, Podberesky DJ, et al: 3-Dimensional magnetic resonance genitography: A different look at cloacal malformations. *J Urol* 178:1675–1679, 2007.
164. Goto MP, Goldman AS: Diabetic embryopathy. *Curr Opin Pediatr* 6:486–491, 1994.
165. Cama A, Palmieri A, Capra V, et al: Multidisciplinary management of caudal regression syndrome. *Eur J Pediatr Surg* 1:44–45, 1996.
166. Guidera KJ, Raney E, Ogden JA, et al: Caudal regression: A review of seven cases, including the mermaid syndrome. *J Pediatr Orthop* 11: 743–747, 1991.
167. Adra A, Cordero D, Mejides A, et al: Caudal regression syndrome: Etiopathogenesis, prenatal diagnosis, and perinatal management. *Obstet Gynecol Surv* 49:508–516, 1994.
168. Nievelstein RA, Valk JM, Smit LM, et al: MR of the caudal regression syndrome: Embryologic implications. *AJNR Am J Neuroradiol* 15: 1021–1029, 1994.
169. Currarino G, Coln D, Votteler T: Triad of anorectal, sacral, and presacral anomalies. *AJR Am J Roentgenol* 137:395–398, 1981.

170. Kole MJ, Fridley JS, Jea A, et al: Currarino syndrome and spinal dysraphism. *J Neurosurg Pediatr* 13:685–689, 2014.
171. Pfluger T, Czekalla R, Koletzko S, et al: MRI and radiographic findings in Currarino's triad. *Pediatr Radiol* 26:524–527, 1996.
172. Baltogiannis N, Mavridis G, Soutis M, et al: Currarino triad associated with Hirschsprung's disease. *J Pediatr Surg* 38:1086–1089, 2003.
173. Martucciello G, Torre M, Belloni E, et al: Currarino syndrome: Proposal of a diagnostic and therapeutic protocol. *J Pediatr Surg* 39:1305–1311, 2004.
174. Kao SC, Franken EA, Jr: Nonoperative treatment of simple meconium ileus: A survey of the Society for Pediatric Radiology. *Pediatr Radiol* 25:97–100, 1995.
175. Ein SH, Shandling B, Reilly BJ, et al: Bowel perforation with nonoperative treatment of meconium ileus. *J Pediatr Surg* 22:146–147, 1987.
176. Rosenstein BJ: Cystic fibrosis presenting with the meconium plug syndrome. *Am J Dis Child* 132:167–169, 1978.
177. Berdon WE, Slovis TL, Campbell JB, et al: Neonatal left colon syndrome: Its relationship to aganglionosis and meconium plug syndrome. *Radiology* 125:457–462, 1977.
178. Amodio J, Berdon W, Abramson S, et al: Microcolon of prematurity: A form of functional obstruction. *AJR Am J Roentgenol* 146: 239–244, 1986.
179. Burge D, Drewett M: Meconium plug obstruction. *Pediatr Surg Int* 20:108–110, 2004.
180. De Backer AI, De Schepper AM, Deprettere A, et al: Radiographic manifestations of intestinal obstruction in the newborn. *JBR-BTR* 82:159–166, 1999.
181. Davis WS, Allen RP, Favara BE, et al: Neonatal small left colon syndrome. *AJR Am J Roentgenol* 120:322–329, 1974.
182. Keckler SJ, St. Peter SD, Spilde TL, et al: Current significance of meconium plug syndrome. *J Pediatr Surg* 43:896–898, 2008.
183. Konvolinka CW, Frederick J: Milk curd syndrome in neonates. *J Pediatr Surg* 24:497–498, 1990.
184. Kubota M, Ikeda K, Shono T, et al: Autonomic innervation of the intestine from a baby with megacystis microcolon intestinal hypoperistalsis syndrome. I. Immunohistochemical study. *J Pediatr Surg* 24:1264–1266, 1989.
185. Kubota M, Ikeda K, Ito Y: Autonomic innervation of the intestine from a baby with megacystis microcolon intestinal hypoperistalsis syndrome. II. Electrophysiological study. *J Pediatr Surg* 24:1267–1270, 1989.
186. Young LW, Yunis EJ, Girdany BR, et al: Megacystis-microcolon-intestinal hypoperistalsis syndrome: Additional clinical, radiological, surgical, and histopathologic aspects. *AJR Am J Roentgenol* 137:749–755, 1981.
187. Goulet O, Jobeer-Giraud A, Michel JL, et al: Chronic intestinal pseudo-obstruction syndrome in pediatric patients. *Eur J Pediatr Surg* 9:83–89, 1999.
188. Manco LG, Osterdahl P: The antenatal diagnosis of megacystis-microcolon-intestinal hypoperistalsis syndrome. *J Clin Ultrasound* 12: 595–598, 1984.
189. Carlsson SA, Hokegard KH, Mattsson LA: Megacystis-microcolon-intestinal hypoperistalsis syndrome: Antenatal appearance in two cases. *Acta Obstet Gynecol Scand* 71:645–648, 1992.
190. Tuzovic L, Anyane-Yeboah K, Mills A, et al: Megacystis-microcolon-intestinal hypoperistalsis syndrome. *Fetal Diagn Ther* 36:74–80, 2014.

CHAPTER OUTLINE

Congenital Anomalies of the Esophagus

Overview

Swallowing Disorders

Vascular Rings

Acquired Abnormalities of the Esophagus

Gastroesophageal Reflux Disease

Eosinophilic Esophagitis

Achalasia

Esophageal Varices

Foreign Body and Caustic Ingestion

Other Esophageal Injuries

Congenital Anomalies of the Esophagus**OVERVIEW**

Many congenital lesions affect esophageal morphology and function. Duplications may be asymptomatic or may be manifested with respiratory or swallowing problems. Esophageal atresia is a complex anomaly, frequently accompanied by anomalies of other organ systems. These disorders are described in Chapter 113.

Some congenital bronchopulmonary foregut malformations, such as agenesis and congenital stenosis of the trachea, are rare and may be associated with esophageal atresia (Fig. 115-1).¹⁻⁷ Also included in the spectrum of bronchopulmonary foregut malformations is esophageal bronchus, characterized by communication between an isolated portion of lung and the esophagus (Fig. 115-2).⁸

Webs and diverticula are also uncommon and may be manifested in childhood with mucosal inflammation and dysphagia (Fig. 115-3).^{6,7} Esophageal diverticulum may be an isolated finding or a manifestation of Ehlers-Danlos syndrome.⁹ In neonates, a posteriorly directed diverticulum should be differentiated from a cavity produced by traumatic passage of a nasogastric or endotracheal tube.¹⁰

Ectopic gastric or respiratory epithelium and tracheal cartilage in the esophagus are associated with focal narrowing and dysphagia.^{2,5,11} Although the incidence of ectopic gastric mucosa in the upper esophagus approaches 21% in pediatric autopsy series, these cases are rare clinically.¹¹

Intramural leiomyomas in children may be familial, syndromic, or isolated.¹²⁻¹⁵ They may produce luminal esophageal narrowing and may be difficult to differentiate from other masses of the middle mediastinum by imaging (Fig. 115-4). Leiomyoblastomas may arise in the esophageal wall in association with other pathologic anomalies, such as pulmonary chondromas.¹³

SWALLOWING DISORDERS

Derangement of the oral portion of swallowing may be due to congenital anomalies, such as absence of the tongue, macroglossia, cleft palate, and micrognathia.^{16,17} Acquired swallowing problems often result from neurologic disorders, such as cerebral palsy, cranial trauma, meningomyelocele, or central nervous system tumors.¹⁶⁻¹⁹

All stages of the swallowing process (oral, pharyngeal, and esophageal) should be observed as part of a real-time, video-fluoroscopic swallowing examination, which is an excellent method for assessing oropharyngeal swallow biomechanics and can be performed with minimal radiation dose.^{16,20,21} Older children are given age-appropriate foods to assess completeness of mastication and the ability to centralize the food within the oral cavity. Some children swallow liquids and puréed foods well but have difficulty swallowing solids. The modified barium swallow is performed with the child in a supported semiupright position, simulating the way the child usually eats. Maneuvers to augment swallowing (e.g., stroking the cheek, additional chin and head support) are more easily performed in this position as well.

Neuromuscular disorders can affect multiple anatomic locations that disrupt the normal swallowing process. Organs that may be impaired include the tongue, which causes poor bolus formation; the palate, which causes nasopharyngeal reflux (Fig. 115-5A); the epiglottis, which causes tracheal penetration or aspiration; the pharynx, which causes poor emptying and premature laryngeal “spillage”; and the cricopharyngeal muscle, which causes obstruction of the passage of the bolus. Failure of cricopharyngeal muscle relaxation is called cricopharyngeal spasm or cricopharyngeal bar and occurs transiently in some normal children (Fig. 115-5B).

Swallowing studies should be performed in conjunction with a speech or occupational therapist who can determine the optimal food volume and feeding implements and may perform compensatory maneuvers that assist swallowing. The examination should be recorded on videotape or digital medium to allow subsequent review.

VASCULAR RINGS*Clinical Findings*

Vascular rings occur when the esophagus and trachea are encircled, displaced, or compressed by the aorta, its branches, or remnants of the fetal circulation.²²⁻²⁴ Some rings are incomplete, but others, such as the double aortic arch, completely surround and frequently compress the esophagus and trachea (Fig. 115-6).

Asymptomatic rings are often incidentally discovered on chest radiographs. In childhood, vascular rings commonly are manifested with stridor during feeding because transient esophageal dilation produces additional tracheal compression;

adults instead tend to have dysphagia as a presenting symptom. Reflex apnea is another presentation and may prompt urgent surgery. Twenty percent of these children also have congenital heart disease.²⁵

The double aortic arch, the most common vascular ring, is usually formed by the larger and more cephalad right aortic arch and the smaller and more caudad left aortic arch. The second most common ring occurs if an aberrant right subclavian artery arises as the last rather than the first branch of a left aortic arch. To reach its normal position, this vessel must pass

from left to right in an oblique, cephalad direction, indenting the posterior aspect of the esophagus. If the left subclavian artery arises as the last branch of a right aortic arch, it produces more tracheal and esophageal impingement because the subclavian originates from the usually small but space-occupying diverticulum of Kommerell, and the normal left-sided ligamentum arteriosum persists.

The right innominate artery, the first vessel to arise from the aorta, originates completely or partially to the left of midline in most children.²⁶ As it crosses from left to right, it may indent the anterior aspect of the trachea. Because many children with this finding are asymptomatic and many symptomatic children outgrow the symptoms, the aberrant right innominate artery is often considered to be a normal variant.²⁶ Severely symptomatic children may respond to innominopecty, a surgical procedure that elevates and fixes the artery away from the trachea.

A vascular sling is an anomaly of the pulmonary artery in which the left pulmonary artery arises in an aberrant fashion from the right pulmonary artery, rather than normally from the main pulmonary artery. The anomalous left pulmonary artery courses from the right to the left in the space between the trachea and esophagus. Children with pulmonary sling have an increased incidence of intracardiac and bronchial anomalies, including ventricular septal defects and variations in the normal branching pattern.

Imaging Findings

Plain radiographs can often suggest the diagnosis of a vascular ring. On the frontal view of the airway or chest, the position of the aortic arch and trachea should always be carefully evaluated (Figs. 115-7 and 115-8). The presence of a right aortic arch in a child with respiratory symptoms suggests that there may be a double aortic arch or right aortic arch with an aberrant left subclavian artery.²² A lateral chest radiograph showing anterior displacement of the trachea suggests the presence of a vascular ring.

Although it is less frequently performed than in the past, barium esophagography often remains the initial imaging study

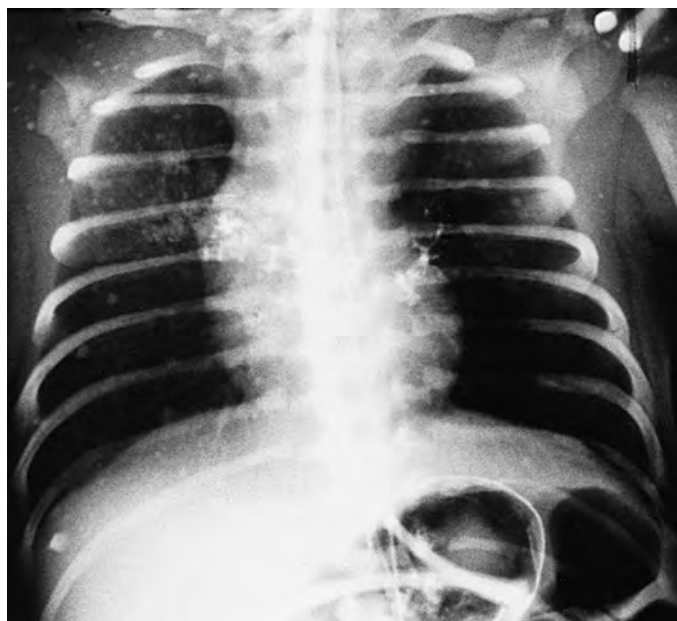


Figure 115-1 Tracheal agenesis. Despite apparent aeration and development of both lungs, this child had marked respiratory distress. Endoscopy performed after several unsuccessful attempts at intubation revealed tracheal agenesis. The intraoperative study shows that both main bronchi contain barium because they arise from the esophagus.

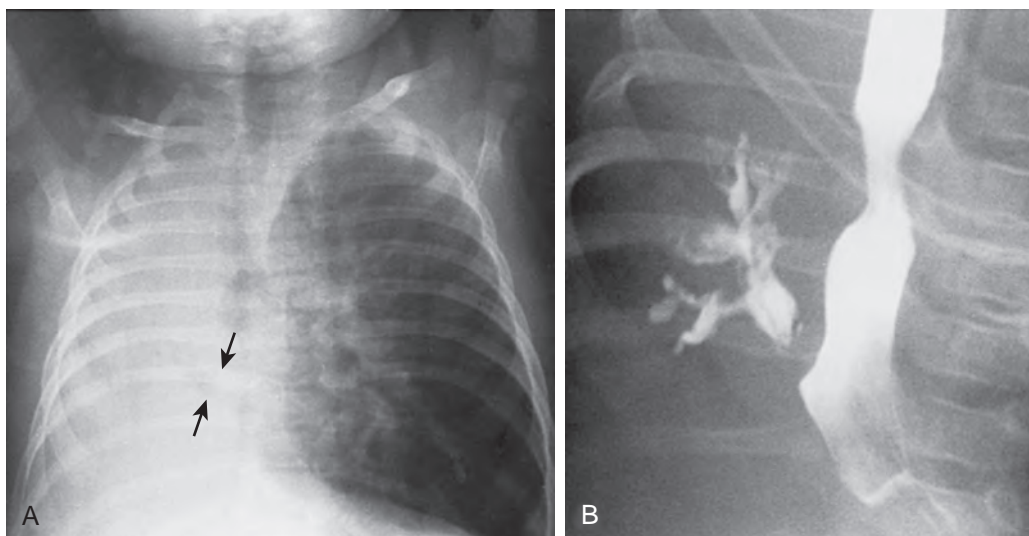


Figure 115-2 Esophageal origin of right main stem bronchus. **A.** The mediastinum is shifted to the opacified right hemithorax. An air collection in the midline over the lower third of the thorax (arrows) corresponds to the right main bronchus. **B.** The bronchus to the right lung originates and fills with contrast material from the esophagus.

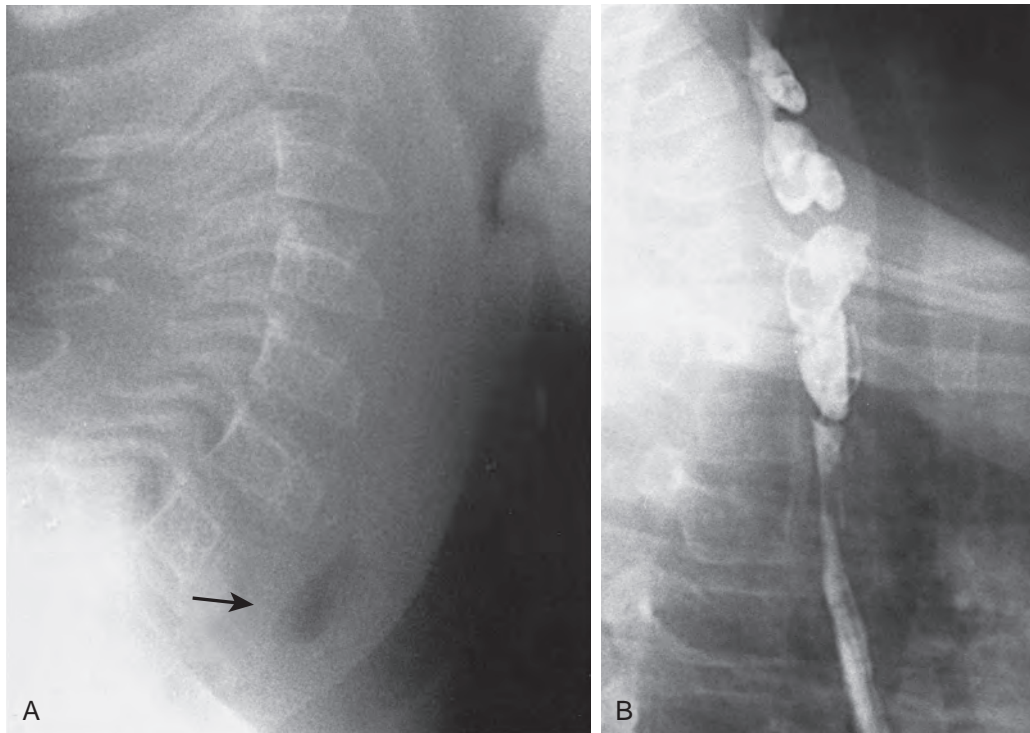


Figure 115-3 Esophageal webs. **A.** On the lateral projection, a small air collection in the prevertebral space (arrow) represents dilated esophagus. **B.** Esophagram shows discrete and partially obstructed esophageal segments separated by multiple webs.

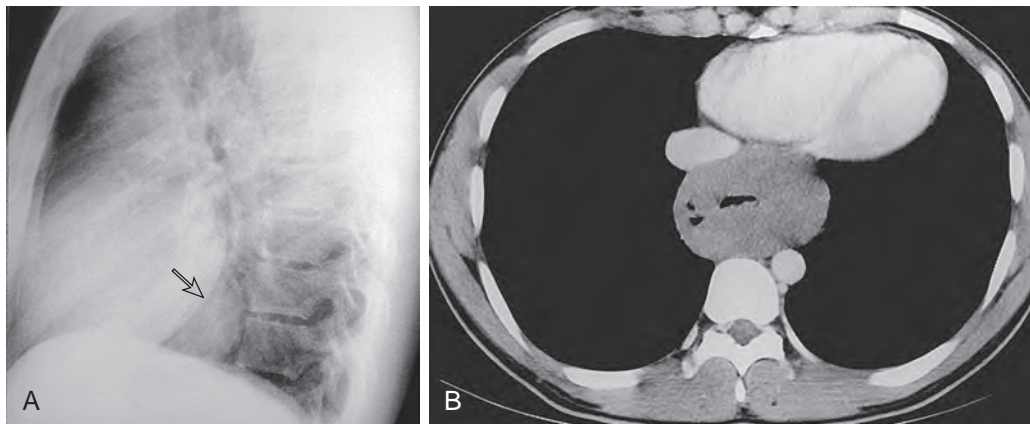


Figure 115-4 Esophageal leiomyoma. **A.** Lateral chest radiograph demonstrates a soft tissue mass (arrow) between the heart and the spine. **B.** CT scan shows the homogeneous mass encircling the distal esophagus. Tiny air collections in the mass resulted from prior biopsy.

in patients with symptomatic vascular rings. Therefore, radiologists must be able to recognize the characteristic impression that each type of ring produces on the upper esophagus, especially on the lateral view (Figs. 115-9 and 115-10).²²

Even after a vascular ring has been detected by plain radiography or esophagography, advanced cross-sectional imaging is recommended for more detailed evaluation. Magnetic resonance (MR) angiography with and without intravenous administration of contrast material and contrast-enhanced multidetector computed tomography (CT) angiography allow production of high-resolution multiplanar reformatted images and three-dimensional reconstructions that assist in detailing

the complex anatomic relationships between aortic arch structures, trachea, and esophagus (Figs. 115-11 and 115-12). CT and MR angiography are particularly useful for presurgical planning and postoperative and postendovascular evaluation and have largely supplanted conventional catheter angiography for direct visualization of vascular anatomy.^{23,24,27,28} State-of-the-art MR angiography is usually preferred to CT angiography in pediatric patients because it does not require radiation or iodinated contrast material and can provide hemodynamic information. Multidetector CT angiography can be performed when MR angiography is not available, is contraindicated, or is likely to be nondiagnostic.²⁷

Figure 115-5 Abnormal swallowing.

A. Nasopharyngeal reflux. As barium passes over the tongue (T), the palate (P) does not close off the nasopharynx, which fills with barium. **B.** Cricopharyngeal spasm. There is narrowing of the esophagus at the C5 level at the upper esophageal sphincter, which is the cricopharyngeal muscle (arrows).

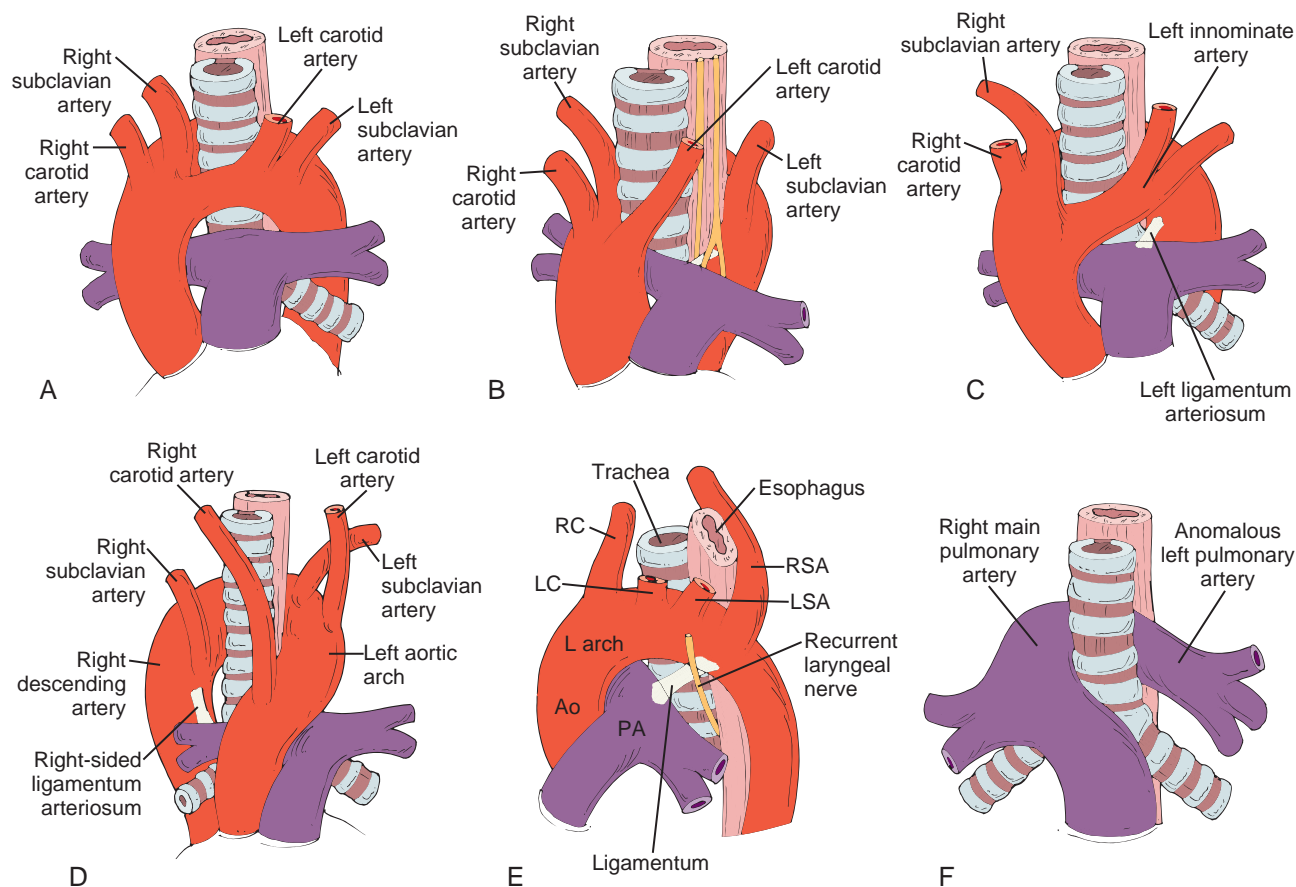
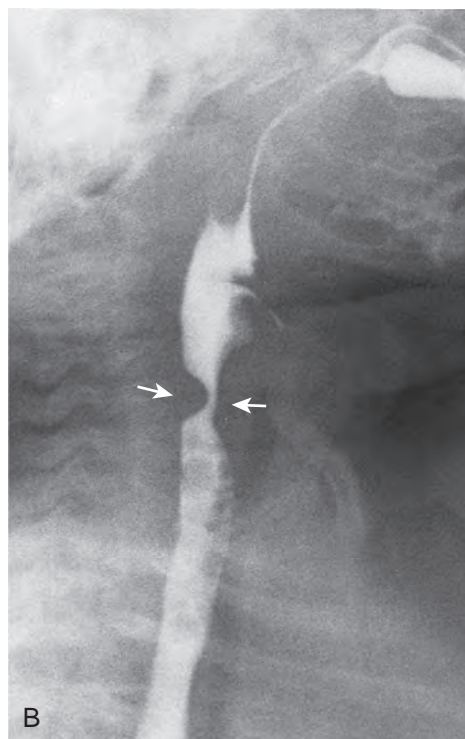
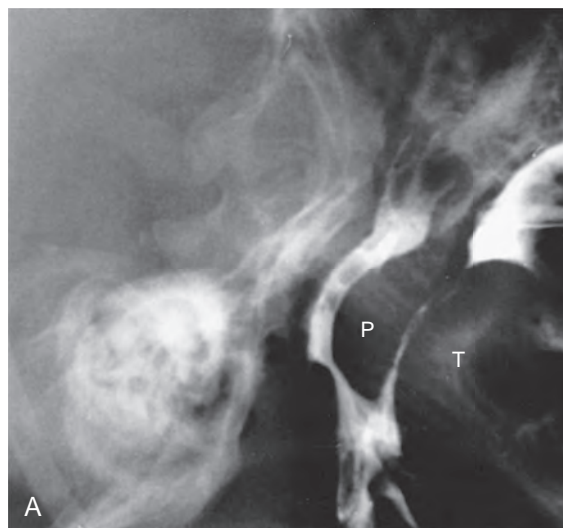


Figure 115-6 Vascular rings and slings. **A.** Double aortic arch. **B.** Right aortic arch with aberrant left subclavian artery and left ligamentum arteriosum. **C.** Right aortic arch with mirror-image branching and retroesophageal ligamentum arteriosum. **D.** Left aortic arch with right descending aorta and right ligamentum arteriosum. **E.** Left aortic arch, aberrant retroesophageal right subclavian artery, and left ligamentum arteriosum. **F.** Aberrant left pulmonary artery or pulmonary artery sling. (Courtesy Jane M. Eggerstedt, MD, Shreveport, LA.)

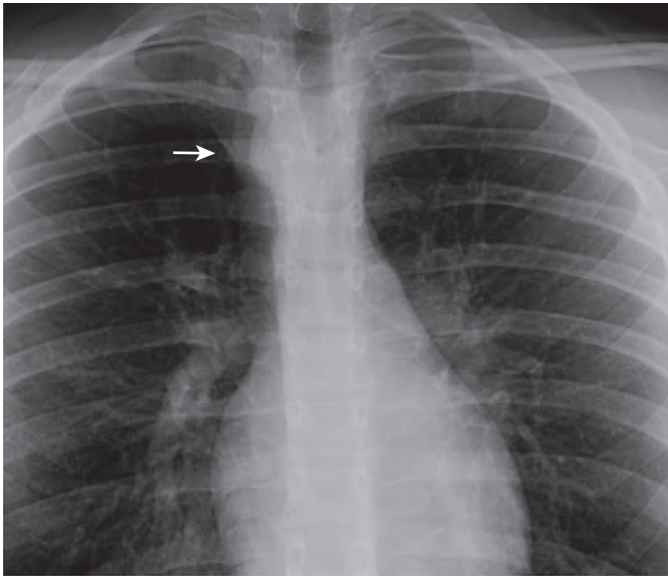


Figure 115-7 Right aortic arch. The right aortic arch (arrow) indents and displaces the trachea to the left. Normal left-sided aortic knob is absent.

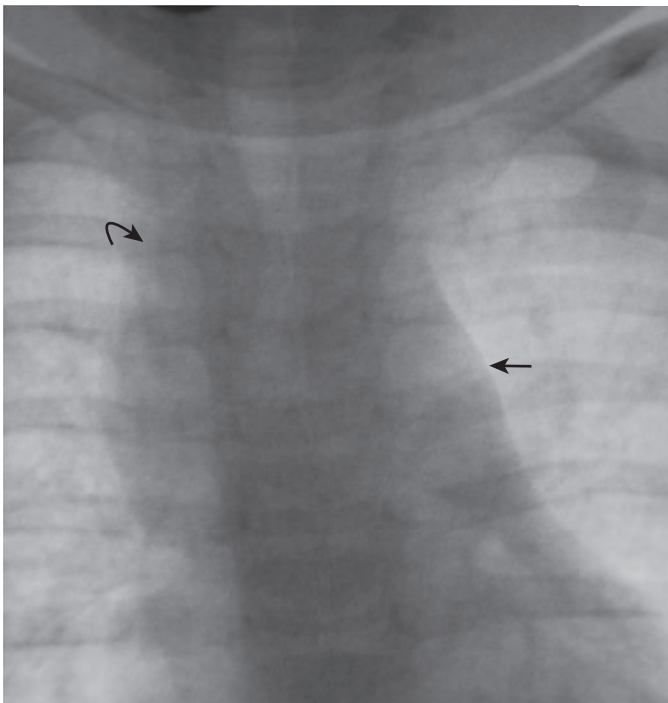


Figure 115-8 Double aortic arch. The larger and higher right arch (curved arrow) indents and displaces the trachea toward the left. Impression from the smaller and lower left aortic arch (straight arrow) is seen along the left margin of the trachea.

Acquired Abnormalities of the Esophagus

GASTROESOPHAGEAL REFLUX DISEASE

Clinical Findings

Gastroesophageal reflux (GER) is a common, almost physiologic process in infants and children.²⁹⁻³² It usually results from

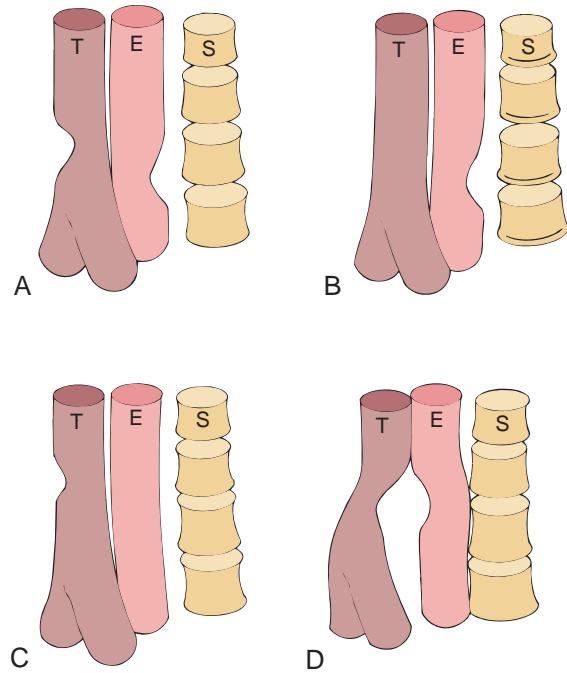


Figure 115-9 Vascular impressions on trachea and esophagus on lateral view. **A.** Double aortic arch. The trachea is indented by the anterior portion of the arch and the esophagus by the posterior portion. **B.** Aberrant right or left subclavian artery. The trachea has a normal appearance. The esophagus is indented posteriorly by the anomalous vessel. **C.** Anomalous innominate artery. The trachea is flattened anteriorly by the innominate artery. The esophagus has a normal appearance. **D.** Pulmonary sling. The trachea is displaced anteriorly and the esophagus posteriorly by the left pulmonary artery, which is passing between them. E, Esophagus; S, spine; T, trachea. (Modified from Berdon WE, Baker DH: Vascular anomalies and the infant lung: Rings, slings, and other things. *Semin Roentgenol* 7:39-64, 1972.)

the failure of the lower esophageal sphincter to maintain an adequate resting pressure, but approximately 35% of children with GER may have additional disorders of esophageal motility.³⁰ GER is pathologic when it is associated with hematemesis, failure to thrive, esophageal stricture formation, apnea, and bradycardia.³¹ Additional extraesophageal or supraesophageal symptoms of GER, such as otitis media, asthma, recurrent upper respiratory tract infections, and sleep disturbances, are becoming increasingly recognized.^{29,31-34} GER is also responsible for the development of Barrett's mucosa in the esophagus.³⁵

GER can be an isolated problem, but it occurs with increased frequency in children with neuromuscular disorders; repair of tracheoesophageal fistula, diaphragmatic hernia, or gastroschisis; cystic fibrosis; and collagen-vascular diseases. Medications given to decrease bronchial spasm and to enhance aeration in children with bronchopulmonary dysplasia and asthma may reduce lower esophageal pressure, cause or worsen GER, and conversely exacerbate respiratory symptoms. Secondary GER occurs in infants and children with gastric outlet obstruction and may disappear after the obstruction is corrected. Delayed gastric emptying coexists in 50% of children with primary GER.³⁶

Although GER can be suspected on clinical grounds (i.e., infant who vomits after every feeding), some pediatricians prefer to document and quantify the reflux before beginning

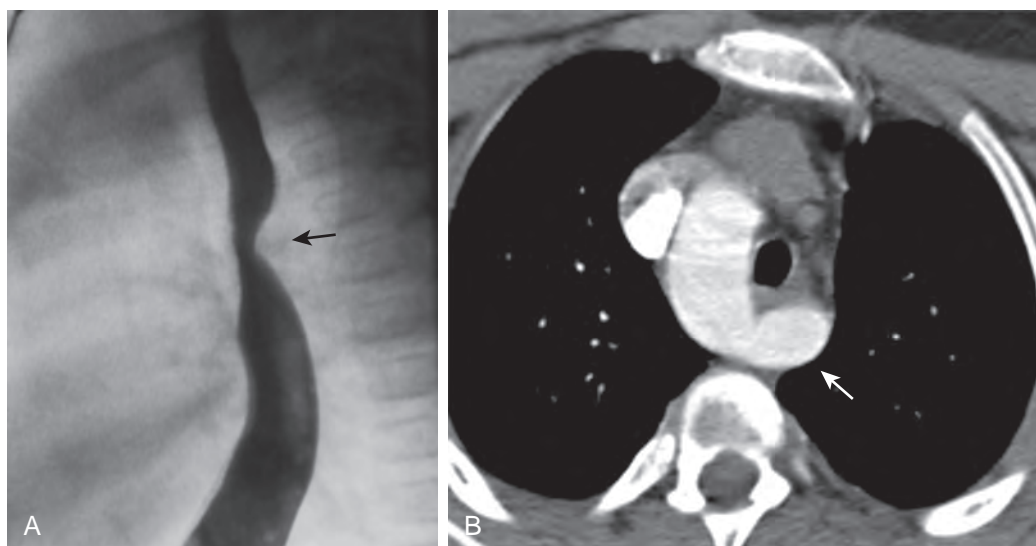


Figure 115-10 Right aortic arch with aberrant left subclavian artery. **A.** Lateral view of esophagus shows pronounced posterior impression on the esophagus by the aberrant vessel (arrow). **B.** Contrast-enhanced CT shows the aberrant left subclavian artery (arrow) arising from the right aortic arch and coursing posterior to the collapsed esophagus.

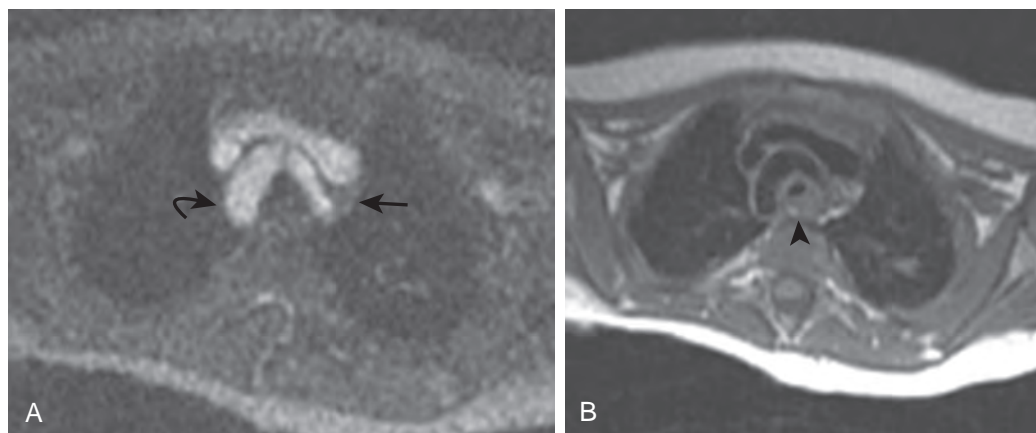


Figure 115-11 Double aortic arch: MR findings. **A.** White blood, steady-state free precession image demonstrates larger right (curved arrow) and smaller left (straight arrow) aortic arches. **B.** Corresponding black blood T1-weighted image shows the double aortic arches encircling the trachea and the collapsed esophagus (arrowhead).

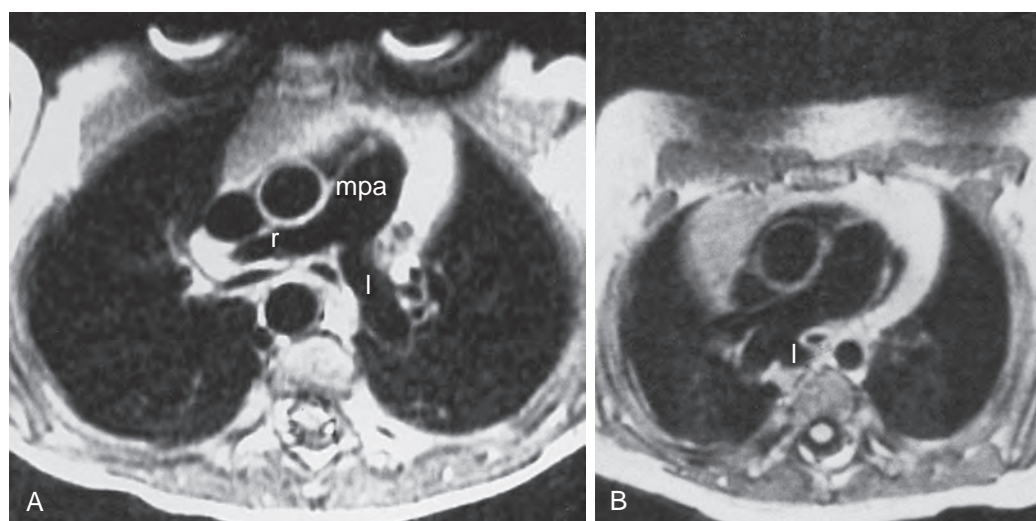


Figure 115-12 Pulmonary sling: MR findings. **A.** Normal anatomy. The main pulmonary artery (mpa) divides into the right (r) and left (l) pulmonary arteries. **B.** In pulmonary sling, the anomalous left pulmonary artery (l) arises from the right pulmonary artery.

therapy. Barium esophagography, the most commonly used test, is inexpensive and readily available. The greatest value of barium esophagography may be not in its ability to diagnose GER but in its ability to detect other causes of the child's symptoms and to exclude gastric or duodenal obstruction. Radionuclide scintigraphy is much less used to diagnose GER than in the past. Esophageal manometry and pH probe monitoring of the esophagus provide additional information about the frequency and duration of reflux.^{37,38} Endoscopy can document the presence and severity of GER-induced esophagitis.

Most children with isolated GER outgrow the process, but those with underlying abnormalities are less likely to do so.^{30,31,39} Symptomatic GER can be treated by thickening the infant's formula, giving smaller amounts at each meal, and positioning the infant appropriately after eating. Proton pump inhibitors and antacids are commonly given. Prokinetic agents have debatable success in treatment.³² Discontinuation of potentially provocative medications or correction of a gastric or duodenal obstruction may also eliminate GER.

Those failing to respond to medical regimens may undergo a fundoplication, which is a surgical augmentation of the lower esophageal sphincter with a gastric wrap around the lower esophagus.^{40,41} In the most common variant of the procedure, the Nissen fundoplication, the gastric fundus is wrapped 360 degrees around the esophagus; however, partial rather than complete wraps may also be performed, especially in children with poor esophageal motility.³⁹⁻⁴² Antireflux surgery produces less morbidity and is more successful in children with isolated GER than in those with a complex medical or surgical history.^{40,41} Before fundoplication is performed, it is important to exclude a lesion that interferes with gastric emptying. If one is found, the antireflux surgery may be complemented by pyloroplasty or pyloromyotomy. For certain patient populations, laparoscopic fundoplication is favored to an open procedure in many centers. The success rate of laparoscopic fundoplication is equal to that of conventional fundoplication, and benefits include shorter hospital stays, decreased need for pain medication, better cosmetic result, and earlier institution of feeding.^{39,41-43}

In some children, GER is associated with torticollis and abnormal movements of the trunk, head, and neck simulating a neurologic abnormality. This is called Sandifer's syndrome.⁴⁴ The abnormal movements cease after the GER is corrected and may be the result of the pain caused by the GER or may represent attempts to minimize reflux.

Imaging Findings

Barium Studies. To optimize detection of GER during barium esophagography, the esophagogastric junction should be challenged by an adequate amount of liquid in the stomach, and intermittent observation should be performed during several minutes. If the child refuses to drink the necessary volume of barium or has neurologic impairment of swallowing, it can be instilled into the stomach through a nasogastric tube. If the child has ingested almost as much barium as necessary then refuses to drink more, formula or juice may be given to supplement the volume. The dilution of barium does not change the ability to detect GER.

Fluoroscopy is used to define the frequency, volume, and cephalad extent of the GER (Fig. 115-13). Aspiration rarely occurs as a result of GER but may be demonstrated during the swallowing portion of esophagography. The rate at which the

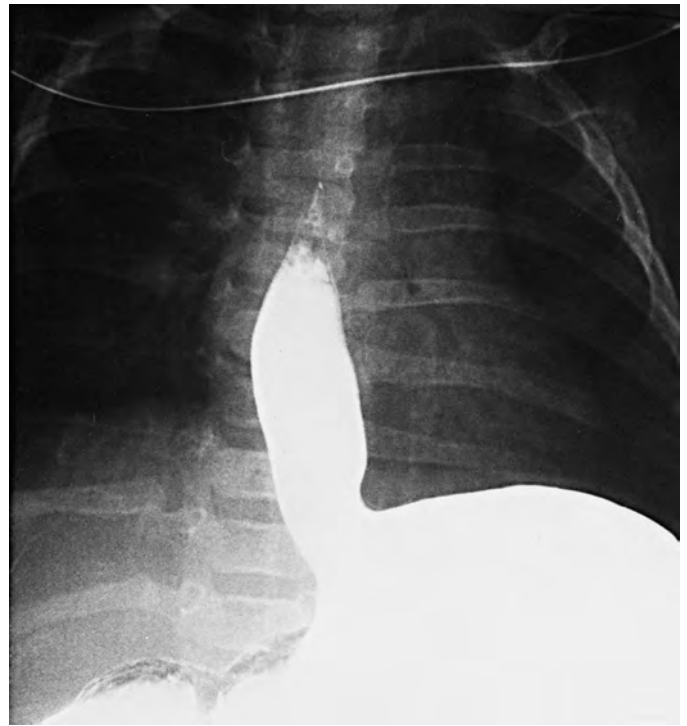


Figure 115-13 Gastroesophageal reflux. A large volume of contrast material refluxes to the level of the carina. The gastroesophageal junction is patulous.

refluxed barium clears from the esophagus should be evaluated; children with rapid clearing are less likely to aspirate or to develop esophagitis.³⁰ GER-induced esophagitis is rarely seen on standard contrast studies. After the question of GER has been addressed, the stomach and duodenum should be observed to exclude delayed gastric emptying, gastric outlet obstruction, duodenal obstruction, or malrotation.

Nuclear Scintigraphy. The radionuclide scan is extremely sensitive in the diagnosis of GER. The child is given formula or juice containing technetium Tc 99m sulfur colloid (or other technetium chelate) and is continuously scanned for 60 minutes, allowing documentation of the number of reflux episodes during this prolonged time.³⁸ This is a major advantage over fluoroscopy, which must be intermittent to minimize radiation exposure to the child. The radionuclide study compares favorably with the "gold standard" of 24-hour pH probe study for gastroesophageal reflux disease and provides additional information about gastric emptying, aspiration into the lung, and abnormal esophageal contraction.^{36,38}

Ultrasound. Ultrasound can accurately demonstrate episodes of GER and correlates well with the results of barium studies and esophageal pH monitoring, but it has failed to replace other tests in the primary diagnosis of GER.⁴⁵⁻⁴⁷ The anatomy of the gastroesophageal junction is well visualized with ultrasound, which can be used in conjunction with other studies to evaluate reflux.⁴⁸ After feeding, GER is seen as retrograde passage of highly echogenic material toward the esophagus. Sonography has also been used to evaluate the length of the intra-abdominal portion of the esophagus, a factor that correlates with the likelihood of GER.⁴⁷

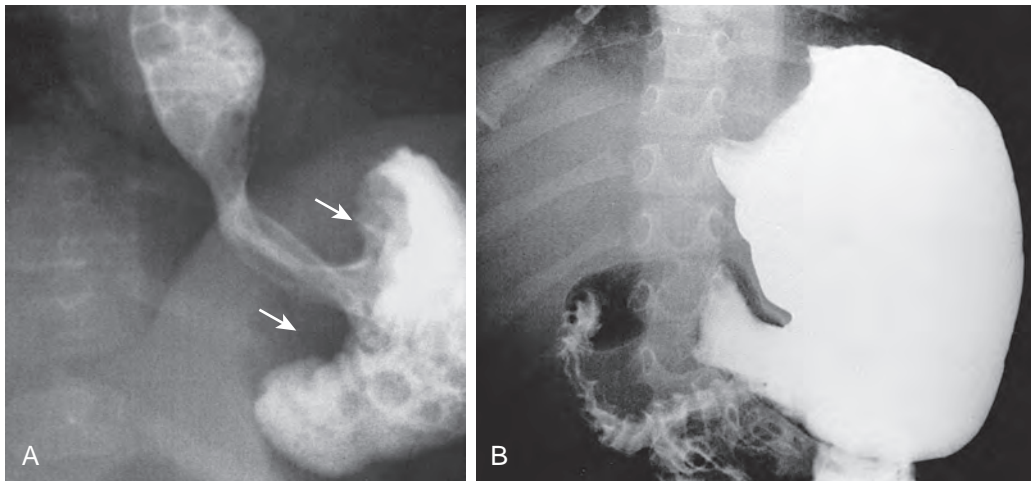


Figure 115-14 Barium esophagogram after fundoplication. A. The gastric wrap has produced narrowing of the distal esophagus and a mass effect on the gastric fundus (arrows). **B.** The concavity of the fundus is at the site of fundoplication.

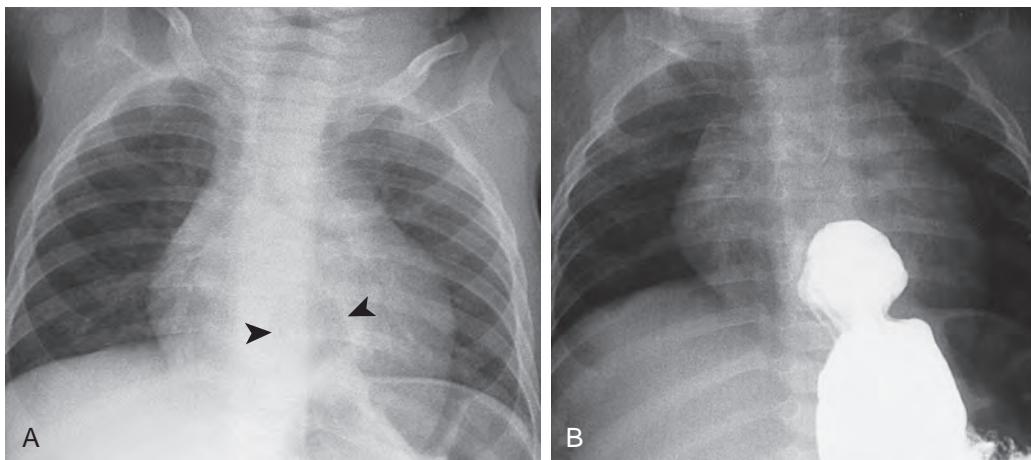


Figure 115-15 Failed Nissen fundoplication. A. A rounded retrocardiac air collection (arrowheads) on the chest radiograph represents the herniated stomach. **B.** The abnormally located gastric fundus is filled with barium. The indentation indicates the remnants of the gastric wrap.

Postsurgical Studies. Indications for postsurgical studies include dysphagia, which may indicate that the fundoplication is too tight, and continued GER symptoms, which suggest that the gastric wrap is too loose or has become undone.⁴⁹ On radiographic examination, the intact wrap produces a mass effect at the gastroesophageal junction (Fig. 115-14). Breakdown of the wrap may be associated with paraesophageal hernia or GER (Fig. 115-15).

EOSINOPHILIC ESOPHAGITIS

Clinical Findings

During the last several decades, eosinophilic esophagitis has become increasingly recognized as a distinct form of esophagitis in children and less commonly in adults. Although this disease is manifested with symptoms that share significant overlap with those of GER, it possesses characteristic clinicopathologic features that distinguish it from GER. Clinical manifestations of eosinophilic esophagitis in children are related to esophageal dysfunction and vary by age.

Infants and toddlers often present with feeding difficulties, whereas school-aged children and adolescents are more likely to present with vomiting, pain, and dysphagia. Food impaction, which is a characteristic presentation of the disease in adults, is less commonly seen in children.⁵⁰ Eosinophilic esophagitis, which has a reported incidence in children of at least 1 in 10,000 and a high male predominance, should be suspected in children with GER symptoms who are unresponsive to conventional treatment with proton pump inhibitors.⁵¹⁻⁵³

Eosinophilic esophagitis is a chronic, immune- and antigen-mediated disease isolated to the esophagus and characterized histologically by eosinophilic inflammation.^{50,54} Endoscopy with biopsy is currently the only reliable diagnostic test for eosinophilic esophagitis, with at least 15 eosinophils per high-power field required for diagnosis.⁵⁵ In children, eosinophilic esophagitis is most often present in association with other manifestations of atopy, such as food allergy, asthma, and eczema, and is responsive to elimination of specific dietary antigens, topical steroids, or both.^{54,55}

Imaging Findings

Because the symptoms of eosinophilic esophagitis are nonspecific and often mistaken for GER, a diagnostic work-up including upper gastrointestinal examination or esophagography is frequently performed.⁵² Characteristic findings on esophagography reported in adults include long-segment, smooth mid or distal esophageal stricture and esophageal dysmotility (Fig. 115-16).^{52,53} Diffuse esophageal narrowing producing a small-caliber esophagus measuring less than 20 mm in diameter and distinctive multiple concentric indentations producing a ringed esophagus have been described in adults with eosinophilic esophagitis and can also be seen in pediatric patients.^{56,57} Schatzki rings of the distal esophagus are rare in children but, when seen, are often associated with underlying eosinophilic esophagitis.⁵⁸ Despite the plethora of radiologic abnormalities described in conjunction with eosinophilic esophagitis, the fact remains that in more than half of affected children, including those with severe symptoms and documented food impaction, the esophagram is normal, indicating that esophagography is not a reliable technique to detect this entity.⁵³

ACHALASIA

Clinical Findings

Children account for only 3% of patients with achalasia.⁵⁹ Achalasia is usually an isolated finding but may rarely be associated with syndromes. A specific association, the triple A syndrome

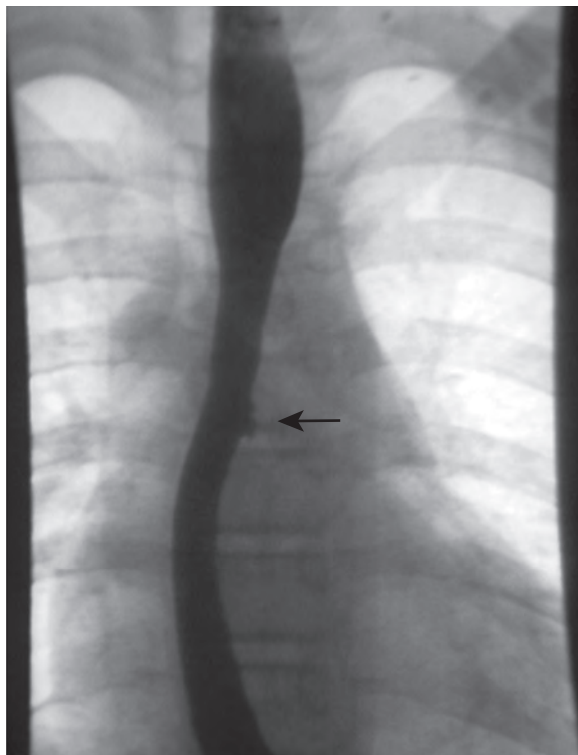


Figure 115-16 Eosinophilic esophagitis. Abnormally narrowed caliber of the mid and distal esophagus secondary to long-segment, smoothly marginated stricture is seen in this teenager with dysphagia. A small outpouching of contrast material (arrow) represents a localized perforation of the esophagus complicating an endoscopic biopsy.

(i.e., achalasia, alacrima, and corticotropin [ACTH] insensitivity), is also known as Allgrove's syndrome.⁶⁰

Affected children typically present with dysphagia or regurgitation of undigested food. Recurrent pneumonia may result from aspiration of esophageal contents at night by the recumbent, sleeping child. The enlarged esophagus may compress the trachea, producing airway symptoms, and weight loss or failure to thrive may develop.^{61,62}

Pneumatic dilation of the esophagus is used in some patients,⁶³ and injection of the affected esophageal segment with botulinum toxin has produced transient improvement.^{64,65} Such an injection can be repeated as necessary. In those whose achalasia is refractory to botulinum toxin injection or dilation, surgery (i.e., modified esophagomyotomy) is performed, often with laparoscopic technique.⁶⁶⁻⁶⁸ To control the frequently associated postoperative GER, fundoplication may be performed at the time of myotomy.⁶⁸

Imaging Findings

The radiologic findings of achalasia in children are similar to those of adults. Chest radiographs may show a dilated, fluid-filled esophagus that compresses or displaces the trachea, evidence of chronic aspiration, and absence of the gastric air bubble. Barium studies reveal a dilated, fluid-filled, atonic or poorly contractile esophagus that ends in a tapered, narrowed segment with beaking.

ESOPHAGEAL VARICES

Esophageal varices are rare in children, usually occurring as a consequence of extrahepatic obstruction (i.e., cavernous transformation) of the portal vein rather than parenchymal liver disease.⁶⁹ The cause of the portal venous thrombosis is unknown in most children, but there are several predisposing risk factors: dehydration, intra-abdominal infection, and umbilical venous catheterization.⁶⁹⁻⁷¹ Intrahepatic portal venous obstruction is caused by congenital or acquired diseases that produce hepatic fibrosis: biliary atresia, α_1 -antitrypsin deficiency, polycystic kidney disease, and cystic fibrosis.^{69,70}

Most commonly, the dilated venous collaterals are diagnosed at endoscopy. However, they can also be directly visualized by CT or sonography or even occasionally indirectly visualized on esophagography as tortuous, linear filling defects extending cephalad into the esophagus from the gastric fundus (Fig. 115-17).^{71,72}

FOREIGN BODY AND CAUSTIC INGESTION

Clinical Findings

Young children instinctively place objects in their mouths, and it is not surprising that most caustic and foreign body ingestions occur in children younger than 5 years. Few ingestions occur in infants younger than 6 or 7 months because infants lack the ability to place grasped objects in their mouths.

With regard to caustic ingestion, the type and location of mucosal injury depend on the pH of the ingested material.⁷³⁻⁷⁵ Caustic agents, such as lye and laundry detergents, have a high pH and cause most damage in the mouth and upper esophagus. Although most children recover without sequelae, perforation or stricture formation occurs in about 3% of patients.⁷⁴ Acids and other low-pH corrosive agents (e.g., toilet bowl cleaners) primarily injure the gastric antrum but can produce burns and

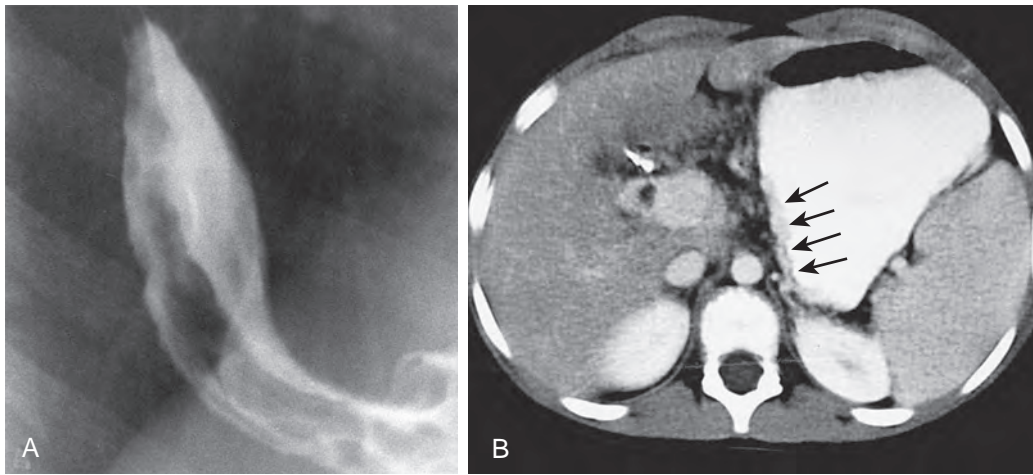


Figure 115-17 Esophageal varices. **A.** Barium esophagogram. A spot film of the esophagogastric junction demonstrates a large, linear varix. **B.** CT scan shows varices (arrows) along the posterior and medial aspects of the fluid-filled stomach.

scars in the esophagus. Contact between acid and the upper airway can produce life-threatening epiglottitis in some children. Bleaches have a neutral pH of 7 and generally cause only transient irritation of the esophagus without long-term complications. Bleach ingestion has been reported occasionally to produce deeper lesions.

In the setting of caustic ingestion, endoscopy is performed nonemergently, about 2 or 3 days after the ingestion, to assess the degree and extent of damage; this information aids in treatment and prognosis. Approximately one third of children with a history of ingestion have esophageal changes discovered by endoscopy.⁷⁵ Clinical findings (e.g., oral burns, stridor, drooling, vomiting) do not correlate with the extent of injury found endoscopically, but the number of clinical findings does correlate with the degree of mucosal damage.⁷⁶ Children with dysphagia or prolonged drooling are likely to have developed esophageal strictures or scars.

Foreign body ingestion, most commonly with coins, may be manifested with a wide range of symptoms. Children with a foreign object impacted in the esophagus may present with gastrointestinal complaints, including dysphagia, choking, and drooling. However, these children may also present with respiratory complaints, such as wheezing, respiratory distress, and cough, particularly with impaction of prolonged duration. Therefore, a high index of suspicion for esophageal foreign body should be adopted even when the ingestion is not witnessed.⁷⁷ Not infrequently, unexpected esophageal foreign bodies are discovered when a radiograph is performed for work-up of respiratory complaints. Up to 14% of children with esophageal foreign body impaction have an underlying structural abnormality, such as stricture or ring.⁷⁷ Food bolus impaction in particular has a high association with underlying esophageal disease, such as eosinophilic esophagitis.⁷⁷

Complications associated with esophageal foreign body impaction include mucosal ulceration, perforation, and fistula. These types of esophageal injury are most likely to occur when the foreign body has been present for a prolonged period exceeding 24 hours.⁷⁷ In addition, the type of foreign body may affect the likelihood of complication. Button or disc batteries, which are an increasingly common household item, are well

known to cause tissue injury when they are impacted in the esophagus. The battery can cause severe focal damage to the esophagus, sometimes within a few hours, and therefore prompt removal is imperative. Mechanisms of injury include pressure necrosis, chemical injury from fluid leaked from the battery, and low-voltage electrical injury.⁷⁸⁻⁸⁰ The 20-mm button batteries composed of lithium generate especially intense electric current that may result in particularly high rates of complications when they are ingested.⁸¹ Disc batteries smaller than 15 mm usually pass without difficulty and are less likely to cause injury.⁸⁰

Not all foreign bodies require removal. In asymptomatic children, a recently swallowed coin lodged in the esophagus below the thoracic inlet may be allowed to pass without intervention. Coin removal is necessary only when symptoms develop or serial radiographs show that the position of the coin has not changed.⁷⁶ When removal is necessary, endoscopy with rigid esophagoscopy is the preferred method.⁷⁸ Despite the need for general anesthesia, the procedure has proved to be safe and effective and can provide information about the esophagus at the site of impaction.⁸² A less frequently performed alternative is fluoroscopically guided balloon extraction, which can be a cost-effective method of foreign body removal, with reported success rates of more than 80%.^{81,83-85} When the impacted foreign body is a button battery, however, endoscopic removal is preferred because this allows determination of extent of injuries and evaluation of possible complications.⁸¹

Imaging Findings

After caustic ingestion, airway and chest radiographs should be obtained. Any swelling of the epiglottis or edema of the airway should prompt measures to ensure airway patency. Lung damage, although rare, may occur. Mediastinal air, indicating perforation of the esophagus, may not develop acutely but should be sought on early and later radiographs.

Barium studies are not useful in diagnosis or management immediately after caustic ingestion. Endoscopic evaluation of the esophagus is more precise during this period.⁷⁵ In the early recuperative period, contrast studies may show abnormalities

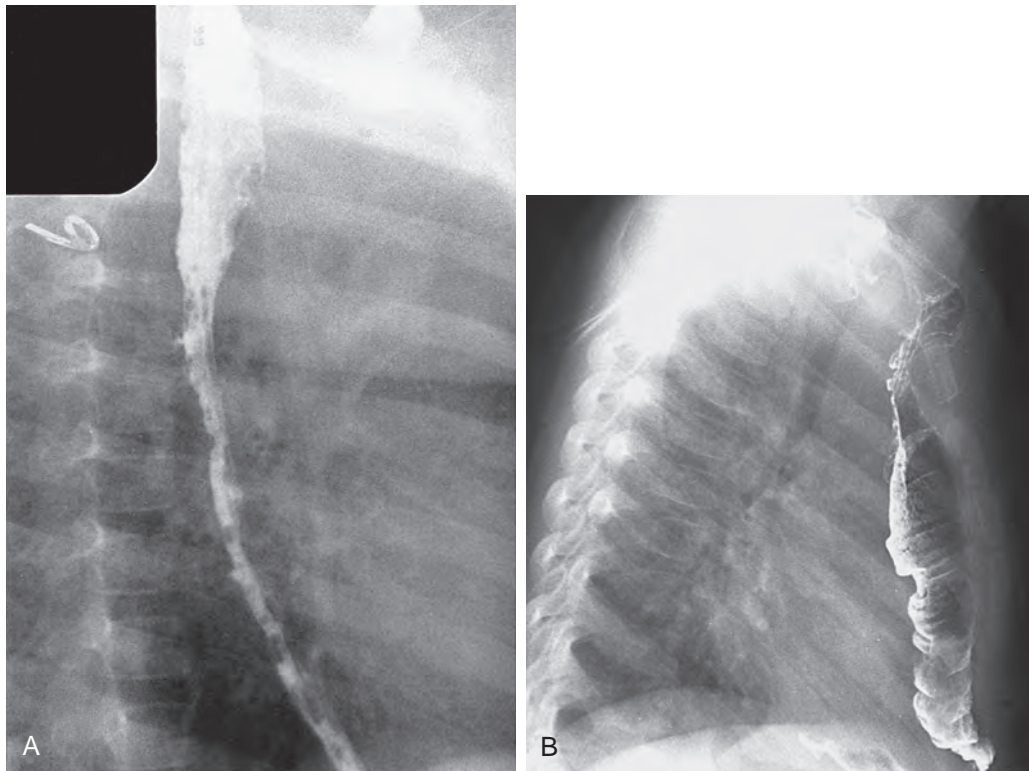


Figure 115-18 Lye ingestion and surgical correction. **A.** Irregularity of the distal esophagus and lack of distensibility indicate the degree of damage done by the ingestion of lye. **B.** The stricture was treated surgically by esophagectomy and colonic interposition graft. The interposed colon, coated with contrast material, is seen in the retrosternal space.

of predictive value. Retention of contrast material within the wall of the esophagus and persistent gaseous dilation of the esophagus usually signify severe injury and may precede perforation. Caustic-induced dysmotility may be associated with the appearance of transverse folds in the esophagus, and strictures can develop at these sites.^{86,87} Barium studies are of value in detecting late changes of the esophagus, such as stricture, or abnormalities in sites not visualized during endoscopy.⁸⁸ Esophagectomy with colonic interposition may be necessary to treat a long stricture or one that is resistant to dilation (Fig. 115-18).⁸⁹

Foreign bodies are easy to detect if they contain radiodense metal. Coins are the most frequently seen foreign bodies on chest radiographs.^{75,90,91} Aluminum-containing foreign bodies, especially the ring from pop-top soda cans, may be difficult to see, as are some foreign coins made from metals that are only slightly radiodense.^{92,93} Visualization of glass depends on the size of the piece ingested and on the presence of overlying structures.⁹¹ However, most swallowed foreign objects, such as food and small plastic toys, are not radiopaque and can be detected only with esophagography or endoscopy (Fig. 115-19).

Imaging work-up for suspected coin or battery ingestion should begin with anteroposterior and lateral chest radiographs for identification of type and number of the foreign body.⁷⁸ Radiographs can also aid in localization of the foreign body and of complications such as perforation. Ingested foreign bodies typically become lodged in the esophagus at several physiologic sites of narrowing, namely, the thoracic inlet, the level of the

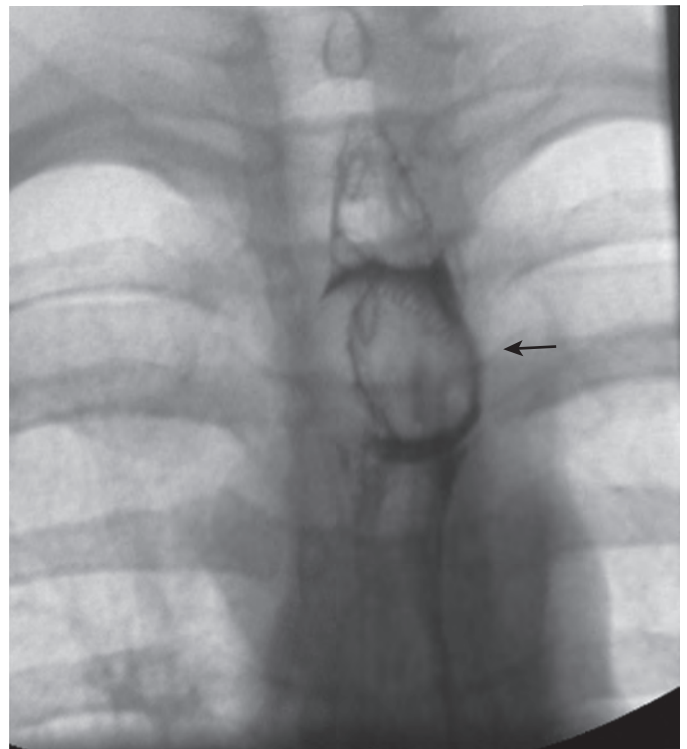


Figure 115-19 Esophageal foreign body. Round, radiolucent filling defect in esophagus (arrow) is outlined by contrast material and represents an ingested plastic bottle cap impacted at the level of the aortic arch.

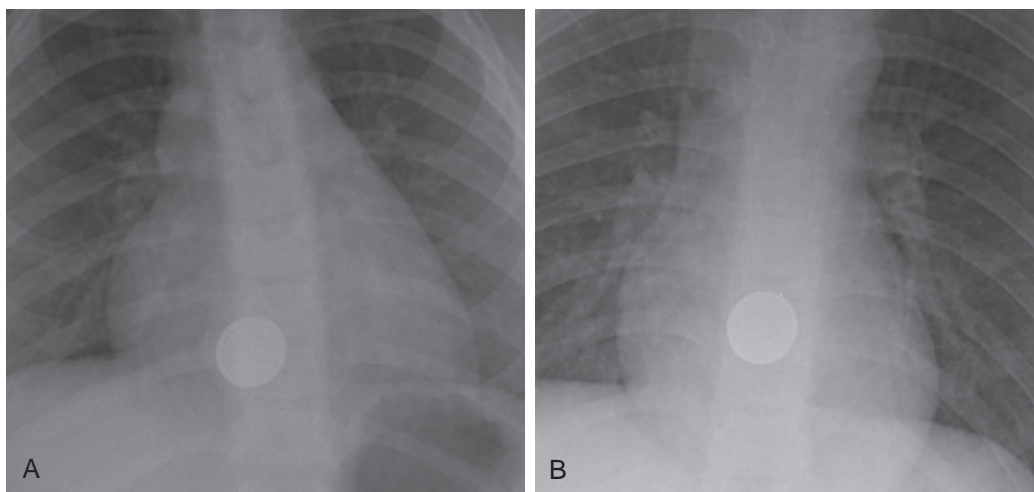


Figure 115-20 Distinguishing ingested disc battery from coin. **A.** A disc battery lodged in the distal esophagus demonstrates a distinctive appearance of two concentric densities separated by a circumferential lucent ring. **B.** In contrast, an impacted coin is homogeneous in density and lacks the characteristic features of the battery.

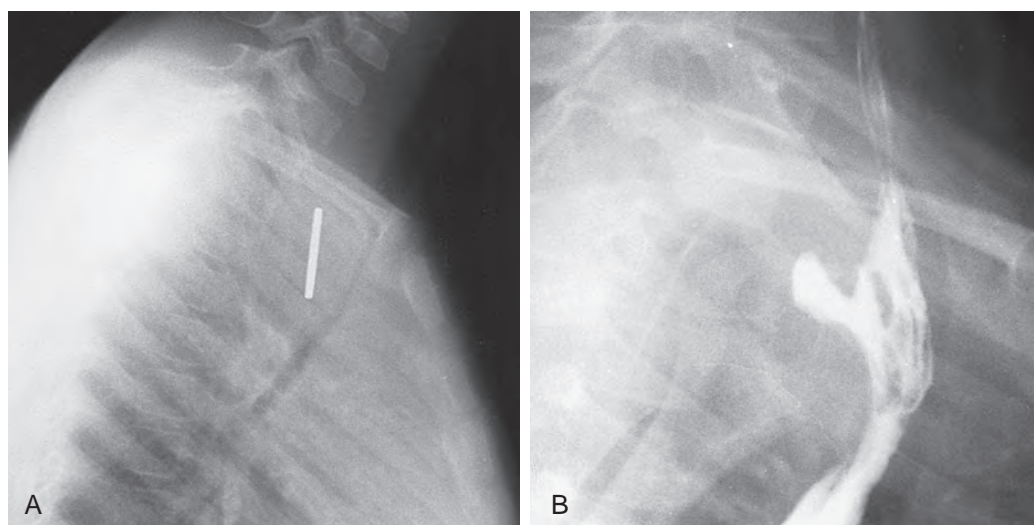


Figure 115-21 Esophageal perforation complicating coin ingestion. **A.** The coin is seen in the upper esophagus. The trachea is bowed anteriorly and is narrowed. **B.** After removal of the coin, the contrast study demonstrates that the coin had perforated the esophagus posteriorly and that the esophagus was pushed anteriorly by the inflammatory process surrounding the site of perforation.

aortic knob, and the gastroesophageal junction. Foreign body impaction at any other level should raise the suspicion of underlying stricture or vascular ring.

The urgency for removal of batteries from the esophagus is much higher than for coins, but coins may occasionally mimic the shape, size, and contour of round, button batteries, confounding the correct diagnosis and resulting in delayed treatment.^{78,79} Careful inspection of the radiographic features of the foreign body should be performed to discern the characteristic double density or concentric halo seen with disc batteries that distinguishes them from coins (Fig. 115-20).^{79,82}

Findings on plain radiographs of the airway or chest may be entirely normal when the esophageal foreign body is radiolucent. The mediastinum should be carefully analyzed on the lateral projection; thickening of the soft tissues between the esophagus and the trachea may be a sign of esophageal edema,

which decreases the likelihood of successful retrieval of the foreign body by catheter. Thickening or anterior bowing of the esophagus may result from mediastinitis, which develops after esophageal perforation (Fig. 115-21).

If an otherwise healthy-appearing child presents with recent onset of drooling or dysphagia, a barium study is recommended to exclude a nonopaque foreign body, a congenital lesion that has become symptomatic, or an acquired inflammatory lesion. The swallowing mechanism and common locations of physiologic narrowing should be scrutinized because these sites are where foreign bodies are most likely to lodge. After an esophageal foreign body has been removed, a contrast study may be used to exclude intrinsic esophageal disease and to detect complications, including post-traumatic esophageal diverticulum, tracheoesophageal fistula, and esophageal-aortic fistula (Fig. 115-22).^{79,94,95}

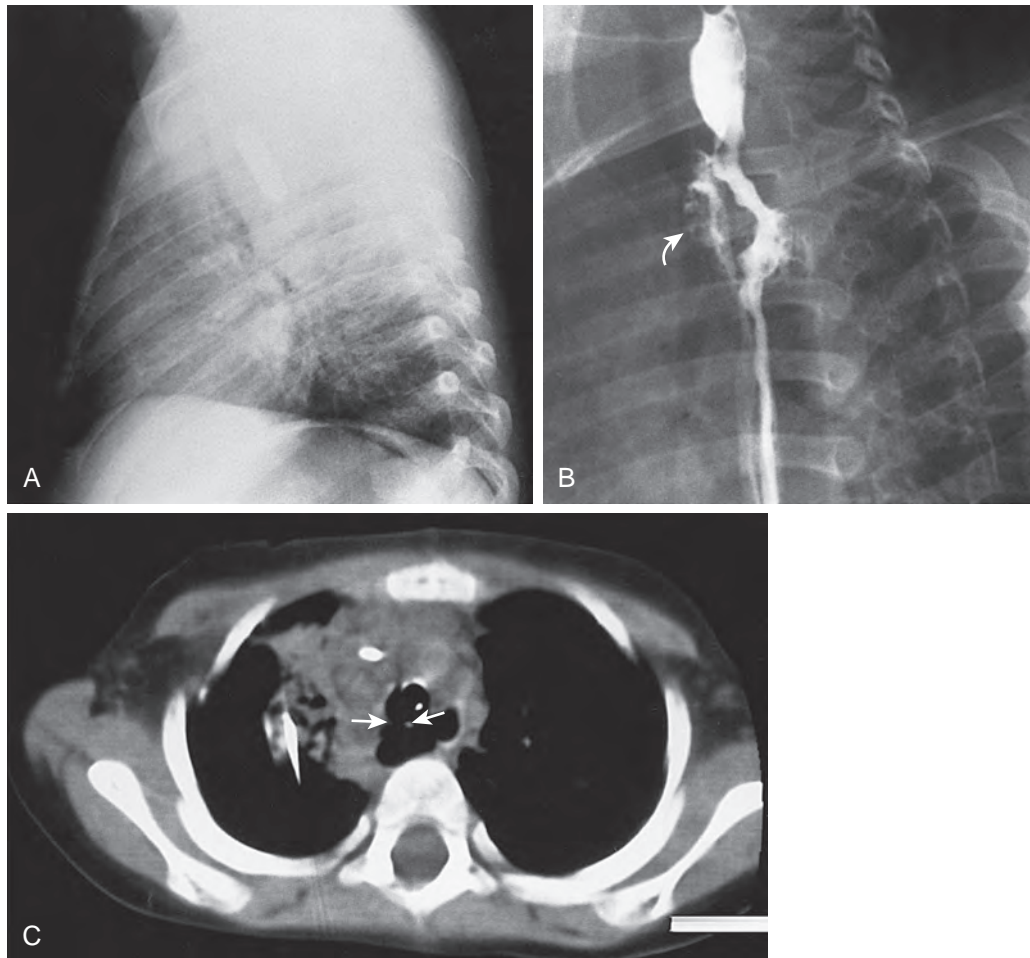


Figure 115-22 Battery-induced tracheoesophageal fistula. **A.** Lateral chest radiograph. The lodged radiopaque battery is associated with thickening of the soft tissue between the trachea and esophagus and anterior bowing of the trachea. **B.** Esophagogram. Water-soluble contrast material passes from the normal cervical esophagus into the irregular-appearing region where the battery was previously seen. The anterior collection (arrow) of contrast material indicates that perforation occurred. **C.** CT scan. After several days of antibiotics and feeding through a gastrostomy tube, the child developed a fever. A fistula (arrows) was identified between the trachea and traumatically widened esophagus.

OTHER ESOPHAGEAL INJURIES

Radiation therapy, particularly if it is combined with certain chemotherapeutic agents, can produce esophagitis, stricture, and fistula formation (Fig. 115-23).^{96,97} Motility and mucosal abnormalities are also seen acutely in children receiving chemotherapy alone. Because of immunosuppression, esophageal infections by opportunistic organisms, such as herpesvirus, *Candida albicans*, and cytomegalovirus, are common.⁹⁸ Many oral medications can produce focal esophageal injury, presumably caused by direct mucosal contact with the tablet.

Esophageal narrowing requiring dilation has been described as part of the Stevens-Johnson syndrome.⁹⁹ Esophageal involvement in epidermolysis bullosa usually takes the form of short or long, multiple or single strictures. Webs, pseudodiverticula, and overall esophageal shortening may occur in this cutaneous disorder. An increased incidence of pyloric atresia is observed among children with epidermolysis bullosa, and it appears to be localized within a genetic subgroup of those with epidermolysis bullosa.¹⁰⁰⁻¹⁰³



Figure 115-23 Radiation-associated and chemotherapy-associated esophagitis. This teenage girl received chemotherapy and radiotherapy for a lower thoracic primitive neuroectodermal tumor. The esophagogram performed because of dysphagia demonstrates a long, narrowed segment.

REFERENCES

1. Sulkowski JP, Cooper JN, Lopez JJ, et al: Morbidity and motility in patients with esophageal atresia. *Surgery* 156:483–491, 2014.
2. Achildi O, Grewal H: Congenital anomalies of the esophagus. *Otolaryngol Clin North Am* 40:219–244, 2007.
3. Sumner TE, Auringer ST, Cox TD: A complex communicating bronchopulmonary foregut malformation: Diagnostic imaging and pathogenesis. *Pediatr Radiol* 27:799–801, 1997.
4. Grabowski ST, Andrews DA: Upper esophageal stenosis: Two case reports. *J Pediatr Surg* 32:936–937, 1997.
5. Berrocal T, Madrid C, Novo S, et al: Congenital anomalies of the tracheobronchial tree, lung and mediastinum: Embryology, radiology, and pathology. *Radiographics* 24:e17, 2004.
6. Maclean AD, Houghton-Allen BW: Upper oesophageal web in childhood. *Pediatr Radiol* 3:240–241, 1975.
7. Fordham LA: Imaging of the esophagus in children. *Radiol Clin North Am* 43:283–302, 2005.
8. Katz R, Pitt R, Kim D, Wingrove B: Thoracoscopic pneumonectomy for communicating bronchopulmonary foregut malformation in a 4-month-old child. *J Pediatr Surg* 45:427–429, 2010.
9. Toyohara T, Kaneko T, Araki H, et al: Giant epiphrenic diverticulum in a boy with Ehlers-Danlos syndrome. *Pediatr Radiol* 19:437, 1989.
10. Flanary VA, Flanary CJ: Conservative management of traumatic pseudodiverticulum in the neonate. *Ear Nose Throat J* 77:186–189, 1998.
11. Variend S, Howat AJ: Upper oesophageal heterotopia: A prospective necropsy study in children. *J Clin Pathol* 4:742–745, 1988.
12. Anker MC, Arnemann J, Neumann K, et al: Alport syndrome with diffuse leiomyomatosis. *Am J Med Genet A* 119A:381–385, 2003.
13. Levine MS, Buck JL, Pantongrag-Brown L: Esophageal leiomyomatosis. *Radiology* 199:533–536, 1996.
14. Mazas-Artasona L, Romeo M, Felices R, et al: Gastro-oesophageal leiomyoblastomas and multiple pulmonary chondromas: An incomplete variant of Carney's triad. *Br J Radiol* 61:1181–1184, 1988.
15. Jolley SG, McClelland KK, Mosesso-Rousseau M: Pharyngeal and swallowing disorders in infants. *Semin Pediatr Surg* 4:157–165, 1995.
16. Miller CK, Willging JP: Advancement in the evaluation and management of pediatric dysphagia. *Curr Opin Otolaryngol Head Neck Surg* 11:442–446, 2003.
17. Arvedson JC: Dysphagia in pediatric patients with neurologic damage. *Semin Neurol* 16:371–386, 1996.
18. Taniguchi MH, Moyer RS: Assessment of risk factors for pneumonia in dysphagic children: Significance of videofluoroscopic swallowing evaluation. *Dev Med Child Neurol* 36:495–502, 1994.
19. Aloysius A, Born P, Kinali M, et al: Swallowing difficulties in Duchenne muscular dystrophy: Indications for feeding assessment and outcome of videofluoroscopic swallow studies. *Eur J Paediatr Neurol* 12:239–245, 2008.
20. Zerilli KS, Stefans VA, DiPietro MA: Protocol for the use of videofluoroscopy in pediatric swallowing dysfunction. *Am J Occup Ther* 44:441–446, 1990.
21. Zammit-Maempel I, Chapple CL, Leslie P: Radiation dose in videofluoroscopic swallow studies. *Dysphagia* 22:13–15, 2007.
22. Etesami M, Ashwath R, Kanne J, et al: Computed tomography in the evaluation of vascular rings and slings. *Insights Imaging* 5:507–521, 2014.
23. Hernanz-Schulman M: Vascular rings: A practical approach to imaging diagnosis. *Pediatr Radiol* 35:961–979, 2005.
24. Backer CL, Mavroudis C, Rigsby CK, et al: Trends in vascular surgery. *J Thorac Cardiovasc Surg* 129:1339–1347, 2005.
25. van Son JA, Julsrud PR, Hagler DJ, et al: Surgical treatment of vascular rings: The Mayo Clinic experience. *Mayo Clin Proc* 68:1056–1063, 1993.
26. Strife JL, Baumel AS, Dunbar JS: Tracheal compression by the innominate artery in infancy and childhood. *Radiology* 139:73–75, 1981.
27. Hellinger JC, Daubert M, Lee EY, Epelman M: Congenital thoracic vascular anomalies: Evaluation with state-of-the-art MR imaging and MDCT. *Radiol Clin North Am* 49:969–996, 2011.
28. Ramos-Duran L, Nance JW, Jr, Schoepf UJ, et al: Developmental aortic arch anomalies in infants and children assessed with CT angiography. *AJR Am J Roentgenol* 198:W466–W474, 2012.

29. Sload RL, Brigger MT: Surgery for reflux induced airway disease: A systematic review. *Int J Pediatr Otorhinolaryngol* 78:1211–1215, 2014.
30. Glassman M, George D, Grill B: Gastroesophageal reflux in children. *Gastroenterol Clin North Am* 24:71–98, 1995.
31. Hassall E: Decision in diagnosing and managing chronic gastroesophageal reflux disease in children. *J Pediatr* 146:S3–S12, 2005.
32. Gottrand F: Gastroesophageal reflux in infants, children, and adults. *Rev Prat* 15:95–98, 2007.
33. Craig WR, Hanlon-Dearman A, Sinclair C, et al: Metoclopramide, thickened feedings, and positioning for gastroesophageal reflux in children under two years. *Cochrane Database Syst Rev* (18):CD003502, 2004.
34. Freed GE, Steinschneider A, Glassman M, et al: Sudden infant death syndrome prevention and an understanding of selected clinical issues. *Pediatr Clin North Am* 41:967–990, 1994.
35. Snyder JD, Goldman H: Barrett's esophagus in children and young children: Frequent association with mental retardation. *Dig Dis Sci* 35:1185–1189, 1990.
36. Heyman S: Gastric emptying in children. *J Nucl Med* 39:865–869, 1998.
37. Orenstein SR, Klein HA, Rosenthal MS: Scintigraphy versus pH probe for quantification of pediatric gastroesophageal reflux: A study using concurrent multiplexed data and acid feedings. *J Nucl Med* 34:1228–1234, 1993.
38. Warrington JC, Charron M: Pediatric gastrointestinal nuclear medicine. *Semin Nucl Med* 37:269–285, 2007.
39. Mauritz FA, van Herwaarden-Lindeboom MY, Stomp W, et al: The effects and efficacy of anti-reflux surgery in children with gastroesophageal reflux disease: A systematic review. *J Gastrointest Surg* 15:1872–1878, 2011.
40. Fonkalsrud EW, Burstoff-Silva J, Perez CA, et al: Antireflux surgery in children under 3 years of age. *J Pediatr* 34:527–531, 1999.
41. Diaz DM, Gibbons TE, Heiss K, et al: Antireflux surgery outcomes in pediatric gastroesophageal reflux disease. *Am J Gastroenterol* 100:1844–1852, 2005.
42. Kane TD, Brown MF, Chen MK: Members of the APSA New Technology Committee: Position paper on laparoscopic antireflux operations in infants and children for gastroesophageal reflux disease. *American Pediatric Surgery Association. J Pediatr Surg* 44:1034–1040, 2009.
43. Rothenberg SS: The first decade's experience with laparoscopic fundoplication in infants and children. *J Pediatr Surg* 40:142–147, 2005.
44. Gorroategi P, Reguilon MJ, Arana J, et al: Gastroesophageal reflux in association with the Sandifer syndrome. *Eur J Pediatr Surg* 5:203–205, 1995.
45. Westra SJ, Wolf BHM, Staalman CR: Ultrasound diagnosis of gastroesophageal reflux and hiatal hernia in infants and young children. *J Clin Ultrasound* 18:477–485, 1990.
46. Naik DR, Bolia A, Moore DJ: Comparison of barium swallow and ultrasound in diagnosis of gastro-oesophageal reflux in children. *BMJ* 290:1943–1945, 1985.
47. Koumanidou C, Vakaki M, Pitsoulakis G, et al: Sonographic measurement of the abdominal esophagus length in infancy: A diagnostic tool for gastroesophageal reflux. *AJR Am J Roentgenol* 183:801–807, 2004.
48. Savino A, Cecamore C, Matronola MF, et al: US in the diagnosis of gastroesophageal reflux in children. *Pediatr Radiol* 42:515–524, 2012.
49. Trinh TD, Benson JE: Fluoroscopic diagnosis of complications after Nissen antireflux fundoplication in children. *AJR Am J Roentgenol* 169:1023–1028, 1997.
50. Furuta GT: Eosinophilic esophagitis in children and adults. *Gastroenterol Hepatol* 4:775–777, 2008.
51. Liacouras CA: Clinical presentation and treatment of pediatric patients with eosinophilic esophagitis. *Gastroenterol Hepatol* 7:264–267, 2011.
52. Diniz LO, Putnum PE, Towbin AJ: Fluoroscopic findings in pediatric eosinophilic esophagitis. *Pediatr Radiol* 42:721–727, 2012.
53. Binkovitz LA, Lorenz EA, Di Lorenzo C, Kahwash S: Pediatric eosinophilic esophagitis: Radiologic findings with pathologic correlation. *Pediatr Radiol* 40:714–719, 2010.
54. Rea F, Caldarò T, Tambucci R, et al: Eosinophilic esophagitis: Is it also a surgical disease? *J Pediatr Surg* 48:304–308, 2013.
55. Liacouras CA, Furuta GT, Hirano I, et al: Eosinophilic esophagitis: Updated consensus recommendations for children and adults. *J Allergy Clin Immunol* 128:3–20.e6, quiz 21–22, 2011.
56. Zimmerman SL, Levine MS, Rubesin SE, et al: Idiopathic eosinophilic esophagitis in adults: The ringed esophagus. *Radiology* 236:159–165, 2005.
57. White SB, Levine MS, Rubesin SE, et al: The small-caliber esophagus: Radiographic sign of idiopathic eosinophilic esophagitis. *Radiology* 256:127–134, 2010.
58. Towbin AJ, Diniz LO: Schatzki ring in pediatric and young adult patients. *Pediatr Radiol* 42:1437–1440, 2012.
59. Hussain SZ, Thomas R, Tolia V: A review of achalasia in 33 children. *Dig Dis Sci* 47:2538–2543, 2002.
60. Khelif K, De Laet MH, Chaouachi B, et al: Achalasia of the cardia in Allgrove's (triple A) syndrome: Histopathologic study of ten cases. *Am J Surg Pathol* 27:667–672, 2003.
61. Roskies M, Zielinski D, Levesque D, Daniel SJ: Atypical presentations of achalasia in the pediatric population. *J Otolaryngol Head Neck Surg* 41:E44–E46, 2012.
62. Hallal C, Kielling CO, Nunes DL, et al: Diagnosis, misdiagnosis, and associated diseases of achalasia in children and adolescents: A twelve-year single center experience. *Pediatr Surg Int* 28:1211–1217, 2012.
63. Perisic V, Scepanovic D, Radlovic N: Nonoperative treatment of achalasia. *J Pediatr Gastroenterol Nutr* 22:45–46, 1996.
64. Hurwitz M, Bahar RJ, Ament ME, et al: Evaluation of the use of botulinum toxin in children with achalasia. *J Pediatr Gastroenterol Nutr* 30:509–514, 2000.
65. Franklin AL, Petrosyan M, Kane TD: Childhood achalasia: A comprehensive review of disease diagnosis and therapeutic management. *World J Gastrointest Endosc* 16:105–111, 2014.
66. Esposito C, Mendoza-Sagaon M, Roblot M, et al: Complications of laparoscopic treatment of esophageal achalasia in children. *J Pediatr Surg* 35:680–683, 2000.
67. Mattioli G, Esposito C, Prato AP: Results of the laparoscopic Heller-Dor procedure for pediatric esophageal achalasia. *Surg Endosc* 17:1650–1652, 2003.
68. Garzi A, Valla JS, Molinaro F, et al: Minimally invasive surgery for achalasia. *J Pediatr Gastroenterol Nutr* 44:587–591, 2007.
69. Fonkalsrud EW: Treatment of variceal hemorrhage in children. *Surg Clin North Am* 70:475–487, 1990.
70. Agrons GA, Corse WR, Markowitz RI, et al: Gastrointestinal manifestations of cystic fibrosis: Radiologic-pathologic correlation. *Radiographics* 16:871–893, 1996.
71. Cho KC, Patel YD, Wachsberg RH, et al: Varices in portal hypertension: Evaluation with CT. *Radiographics* 15:609–622, 1995.
72. Coley BD: Pediatric application of abdominal vascular Doppler imaging. Part I. *Pediatr Radiol* 34:757–771, 2004.
73. Nuutinen M, Uhari M, Karvali T, et al: Consequences of caustic ingestions in children. *Acta Paediatr* 83:1200–1205, 1994.
74. Gundogdu HZ, Tanyel FC, Bukyupamku N, et al: Conservative treatment of caustic esophageal strictures in children. *J Pediatr Surg* 27:767–770, 1992.
75. Duncan M, Wong RKH: Esophageal emergencies: Things that will wake you from a sound sleep. *Gastroenterol Clin North Am* 32:1035–1052, 2003.
76. Shariief GQ, Brousseau TJ, Bradshaw JA, et al: Acute esophageal coin ingestions: Is immediate removal necessary? *Pediatr Radiol* 33:359–363, 2003.
77. Denney W, Ahmad N, Dillard B, Nowicki MJ: Children will eat the strangest things: A 10-year retrospective analysis of foreign body and caustic ingestions from a single academic center. *Pediatr Emerg Care* 28:731–734, 2012.
78. Marom T, Goldfarb A, Russo E, Roth Y: Battery ingestion in children. *Int J Pediatr Otorhinolaryngol* 74:849–854, 2010.
79. Kimball SJ, Park AH, Rollins MD, 2nd, et al: A review of esophageal disc battery ingestions and a protocol for management. *Arch Otolaryngol Head Neck Surg* 136:866–871, 2010.
80. Yardeni D, Yardeni H, Coran AG, et al: Severe esophageal damage due to button battery ingestion: Can it be prevented? *Pediatr Surg Int* 20:496–501, 2004.
81. Litovitz T, Whitaker N, Clark L, et al: Emerging battery-ingestion hazard: Clinical implications. *Pediatrics* 125:1168–1177, 2010.
82. Myer CM, III: Potential hazards of esophageal foreign body extraction. *Pediatr Radiol* 20:97–98, 1991.
83. Campbell JB, Condon VR: Catheter removal of blunt foreign bodies in children: Survey of the Society for Pediatric Radiology. *Pediatr Radiol* 19:361–365, 1989.
84. Harned RK, Strain JD, Hay TC, et al: Esophageal foreign bodies: Safety and efficacy of Foley catheter extraction of coins. *AJR Am J Roentgenol* 168:443–446, 1997.
85. Little DC, Shah SR, St Peter SD, et al: Esophageal foreign bodies in the pediatric population: Our first 500 cases. *J Pediatr Surg* 41:914–918, 2006.
86. Cadranet S, Di Lorenzo C, Rodesch P, et al: Caustic ingestion and esophageal function. *J Pediatr Gastroenterol Nutr* 10:164–168, 1990.
87. Reeder JD, Kramer SS, Dudgeon DL: Transverse esophageal folds: Association with corrosive injury. *Radiology* 155:303–304, 1985.
88. Subbarao KS, Kakar AK, Chandrasekhar V, et al: Cicatricial gastric stenosis caused by corrosive ingestion. *Aust N Z J Surg* 58:143–146, 1988.

89. Gundogdu HZ, Tanyel FC, Buyukpamukcu N, et al: Colonic replacement for the treatment of caustic esophageal strictures in children. *J Pediatr Surg* 27:771–774, 1992.
90. Wright CC, Closson FT: Updates in pediatric gastrointestinal foreign bodies. *Pediatr Clin North Am* 60:1221–1239, 2013.
91. Sahn B, Mamula P, Ford CA: Review of foreign body ingestion and esophageal food impaction management in adolescents. *J Adolesc Health* 55:260–266, 2014.
92. Egli KD, Potter BM, Garcia V, et al: Delayed diagnosis of esophageal perforation by aluminum foreign bodies. *Pediatr Radiol* 16:511–516, 1986.
93. Valente JH, Lemke T, Ridlen M, et al: Aluminum foreign bodies: Do they show up on x-ray? *Emerg Radiol* 12:30–33, 2005.
94. Glover P, Westmoreland T, Roy R, et al: Esophageal diverticulum arising from a prolonged retained esophageal foreign body. *J Pediatr Surg* 48:e9–e12, 2013.
95. Grisel JJ, Richter GT, Casper KA, Thompson DM: Acquired tracheoesophageal fistula following disc-battery ingestion: Can we watch and wait? *Int J Pediatr Otorhinolaryngol* 72:699–706, 2008.
96. Mahboubi S, Silber JH: Radiation-induced esophageal strictures in children with cancer. *Eur Radiol* 7:119–122, 1997.
97. Lal DR, Foroutan HR, Su WT, et al: The management of treatment-related esophageal complications in children and adolescents with cancer. *J Pediatr Surg* 41:495–499, 2006.
98. Haller JO, Cohen HL: Gastrointestinal manifestations of AIDS in children. *AJR Am J Roentgenol* 162:387–393, 1994.
99. Lamireau T, Leauté-Labrèze C, Le Bail B, Taieb A: Esophageal involvement in Stevens-Johnson syndrome. *Endoscopy* 33:550–553, 2001.
100. Mauro MA, Parker LA, Hartley WS, et al: Epidermolysis bullosa: Radiographic findings in 16 cases. *AJR Am J Roentgenol* 149:925–927, 1987.
101. Lin AN: Pyloric atresia and epidermolysis bullosa. *Pediatr Dermatol* 14:406–408, 1997.
102. Featherstone C: Epidermolysis bullosa. *J Invest Dermatol* 127:256–259, 2007.
103. Fine JD, Bruckner-Tuderman L, Eady RA, et al: Inherited epidermolysis bullosa: Updated recommendations on diagnosis and classification. *J Am Acad Dermatol* 70:1103–1126, 2014.

Diseases of the Pediatric Stomach and Duodenum

JENNIFER E. LIM-DUNHAM | RICHARD M. GORE

CHAPTER OUTLINE

Congenital Anomalies

Pyloric and Antral Atresias
Antral Mucosal Diaphragm
Microgastria
Duodenal Atresia and Stenosis
Duplication Cyst
Malrotation

Acquired Diseases

Gastric Perforation
Pyloric Stenosis
Gastric and Duodenal Hematomas
Gastric and Duodenal Foreign Bodies
Neoplasms
Peptic Ulcer Disease
Inflammatory Disorders Other Than Peptic Disease
Gastric or Duodenal Distention

Congenital Anomalies

Most anomalies that affect the stomach and duodenum are evident on plain radiographs of the abdomen. Complete atresia of the pylorus results in a single bubble of air, atresia of the duodenum is manifested as the well-known radiographic double bubble, and duplication cysts can displace or obstruct bowel. Microgastria results in absence of the normal gastric bubble and is associated with cardiovascular and splenic anomalies. When an anomaly of stomach or duodenum is encountered, careful search for other anomalies is mandatory.

PYLORIC AND ANTRAL ATRESIAS

Pyloric and antral atresias are rare anomalies in which the neonate is unable to feed without vomiting. The abdomen is gasless except for the stomach bubble. Sonograms performed on infants with pyloric atresia show neither a normal canal nor muscle of the pylorus.¹ A pyloric channel should be apparent in babies who have a complete pyloric membrane.^{2,3} The rare neonate who has pyloric stenosis has incomplete obstruction and typical features of pyloric stenosis. Differentiation between atresia and membrane usually rests with the surgeon because plain radiographs showing complete obstruction in the first day of life mandate an operation. There is an association between pyloric atresia and epidermolysis bullosa.⁴ In affected patients, minimal trauma to the skin results in blisters and erosions. Pyloric obstruction in these patients may begin in utero or develop postnatally.

ANTRAL MUCOSAL DIAPHRAGM

Complete mucosal diaphragm or web of the antrum is an uncommon anomaly that may cause vomiting or failure to thrive in infants.⁵ Older children may present because of gastric retention of a coin or other foreign body.⁶ On upper gastrointestinal studies, the thin membrane is manifested as a linear filling defect at the level of the antrum (Fig. 116-1). In symptomatic infants, the aperture of the diaphragm is often 5 mm in diameter or less, although the size of the aperture cannot be judged accurately on fluoroscopic examination.⁷ Asymptomatic, incidentally discovered webs probably do not require intervention, although some physicians advocate a more aggressive approach.^{7,8}

MICROGASTRIA

Microgastria is often associated with absence of the spleen and mesenteric abnormalities.^{9,10} An association with laryngo-tracheoesophageal clefts, tracheoesophageal fistula, and the VACTERL (vertebral, anorectal, cardiac, tracheoesophageal, renal, and limb) spectrum of anomalies has been documented.^{11,12} In those patients with isolated microgastria, plain radiographs show no normal gastric air bubble and the esophagus is often dilated because it functions as an accessory stomach through reflux.¹³ The miniature stomach empties into a duodenum of normal caliber, which may be in an abnormal position (Fig. 116-2). Treatment is directed toward increasing gastric capacity by creating and attaching a jejunal pouch.¹⁴

DUODENAL ATRESIA AND STENOSIS

Clinical Findings

Atresia and stenosis are related congenital obstructive anomalies of the proximal duodenum attributable to failed canalization of the duodenum during the 8th to 10th weeks in utero. Atresia is characterized by complete luminal occlusion; stenosis is characterized by incomplete occlusion. Stenosis can take several forms, including segmental narrowing and a diaphragm or web with one or more openings partially occluding the duodenal lumen.¹⁵

Duodenal atresia has an incidence of 1 in 10,000 live births and is much more common than stenosis.¹⁶ The newborn usually has bilious vomiting because the atresia is located distal to the ampulla of Vater in 75% of patients.¹⁵ Duodenal stenosis or web, on the other hand, may not become clinically evident until later in life. The small lumen may become plugged with food only after the infant graduates from a liquid to a solid diet.¹⁷

Duodenal atresia and stenosis are associated with other anomalies, including trisomy 21, which is found in approximately one third of infants who have atresia or stenosis.¹⁵ Other



Figure 116-1 Antral web. Single-contrast view of the stomach in the prone, right anterior oblique position demonstrates a thin, linear filling defect across the barium-filled antrum (arrows). The infant presented a few hours after birth with postprandial projectile vomiting.

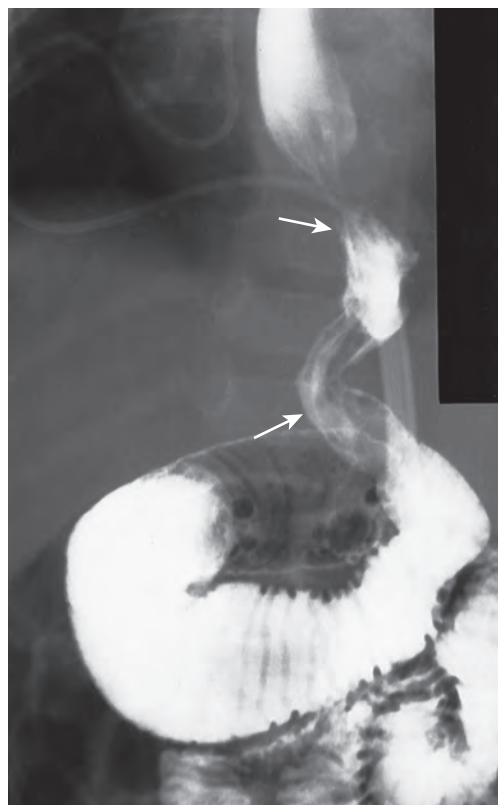


Figure 116-2 Microgastria. Supine, frontal view shows a miniature stomach (arrows). The moderately dilated duodenum is in the normal position. The infant had marked gastroesophageal reflux during the examination. This upper gastrointestinal series was obtained as part of an evaluation of the failure to thrive of an 8-month-old infant. The overlying catheter is a central venous line.

associations include the VACTERL spectrum of abnormalities, cardiac anomalies, and malrotation.^{16,18,19}

Annular pancreas may be found in up to 20% of patients with duodenal atresia or stenosis but is rarely the primary cause of the duodenal obstruction.¹⁵ Because the surgical approach to duodenal stenosis does not differ significantly when annular pancreas is present, an extensive preoperative evaluation is unnecessary.

Imaging Findings

Duodenal atresia and other congenital obstruction of the duodenum are reliably diagnosed with prenatal ultrasonography at or before 20 weeks of gestation.^{16,20,21} Typically, the sonogram shows a double bubble sign of fluid-filled, dilated fetal stomach and duodenum, although this observation has also been reported as a transient finding in otherwise normal fetuses (Fig. 116-3).¹⁶

After birth, the abdominal plain radiograph is usually diagnostic and shows the double bubble, with gas filling a distended stomach and proximal duodenum with no distal gas (Fig. 116-4). The radiograph may be nondiagnostic if the stomach and duodenum are decompressed by vomiting or a nasogastric tube. If plain radiographs are not diagnostic, air or barium can be injected through the nasogastric tube. In incomplete duodenal obstructions, a double bubble is accompanied by gas in distal bowel.^{16,22} An important condition that may mimic duodenal atresia or stenosis on plain radiographs is malrotation with midgut volvulus.

Infants with clinical and plain radiographic evidence of complete or partial high-grade duodenal stenosis will rarely require additional imaging with contrast upper gastrointestinal examination because surgical intervention is required to relieve the obstruction. Surgery can be delayed if necessary for duodenal atresia or stenosis but not for malrotation and midgut volvulus. If a delay in surgery is contemplated, upper gastrointestinal



Figure 116-3 Duodenal atresia prenatal ultrasound. Abnormally dilated and fluid-filled stomach (arrowhead) and duodenal bulb (arrow) suggest duodenal atresia in this fetal ultrasound obtained at 29 weeks of gestation.

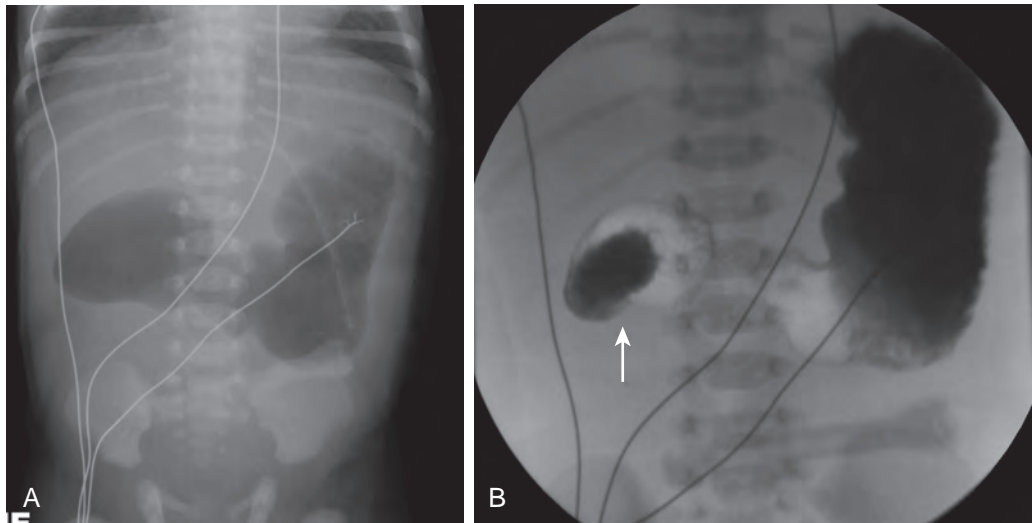


Figure 116-4 Duodenal atresia. **A.** Abdominal radiograph of a newborn infant shows the classic double bubble with dilated, air-filled stomach and duodenum. **B.** Upper gastrointestinal examination shows the duodenum dilated out of proportion to the stomach, a characteristic appearance for duodenal atresia, and complete obstruction of passage of contrast material beyond the level of the atretic segment (arrow).

examination or ultrasound should be performed to confirm absence of malrotation.²²

Complete obstruction of the duodenum with failure of contrast material to pass beyond the atretic segment and duodenal bulb dilation out of proportion to the stomach are typical findings on upper gastrointestinal examination in atresia. In duodenal stenosis, narrowing of the second portion of the duodenum is seen, but the corkscrew appearance of the duodenum and displacement of the duodenojejunal junction (DJJ) seen in malrotation and volvulus are absent.²² Duodenal diaphragm or web, which may also be called intraluminal diverticulum, appears as a fine linear filling defect within the barium-filled duodenum (Fig. 116-5).²³ In older children, the diaphragm that has been stretched for years may take on the appearance of a windsock on both barium and ultrasonographic studies.²⁴

DUPLICATION CYST

Clinical Findings

Duplication cysts are rare in the stomach and duodenum.²⁵⁻²⁷ Duplications that arise from the gastroesophageal junction may contain respiratory and enteric tissue, and they probably represent a bronchopulmonary foregut malformation.^{25,28} If a cystic mass is discovered at the gastroesophageal junction, chest radiographs should be scrutinized for a mediastinal or pulmonary component to the cyst. Duplication cysts of the distal stomach and duodenum may be enteric or neurenteric in origin.²⁶ In early intrauterine life, a neurenteric canal connects ectoderm to endoderm and passes through dorsal neural folds. Persistence of this or an accessory canal (i.e., split notochord syndrome) gives rise to a series of anomalies, including diastematomyelia, hemivertebrae, and enteric cysts.²⁹ Most gastric and duodenal cysts are considered the result of abnormal canalization of the intestinal tract.³⁰ Duplication cysts are often diagnosed prenatally.^{31,32}

The common features of gastric or duodenal duplication cysts include obstruction, palpable upper abdominal mass, gastrointestinal bleeding, and respiratory distress. Most duplication cysts are diagnosed during the first year of life.^{32,33-35}

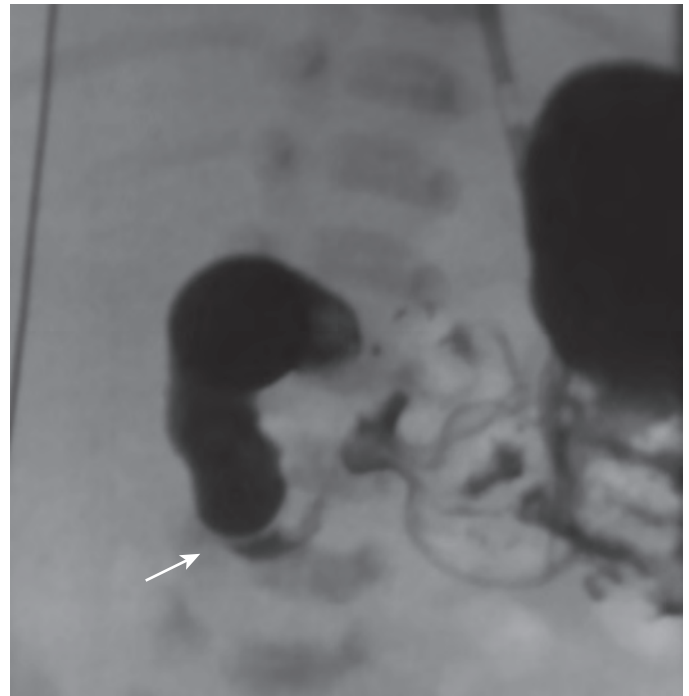


Figure 116-5 Duodenal diaphragm or web. The partially obstructing duodenal web is seen as a thin linear filling defect in the second portion of the duodenum (arrow).

Imaging Findings

Gastric duplication cysts can be evaluated by upper gastrointestinal examination, ultrasonography, or both (Fig. 116-6). At fluoroscopy, a “beak” results when contrast material in the gastrointestinal tract lumen surrounds the proximal portion of an obstructive duplication cyst.^{36,37} On ultrasound, enteric duplication cysts can usually be recognized by a characteristic pattern of echoes in the bowel wall, which mirrors that seen in the native bowel. This pattern has been termed the gut signature and consists of an inner hyperechoic ring representing mucosa

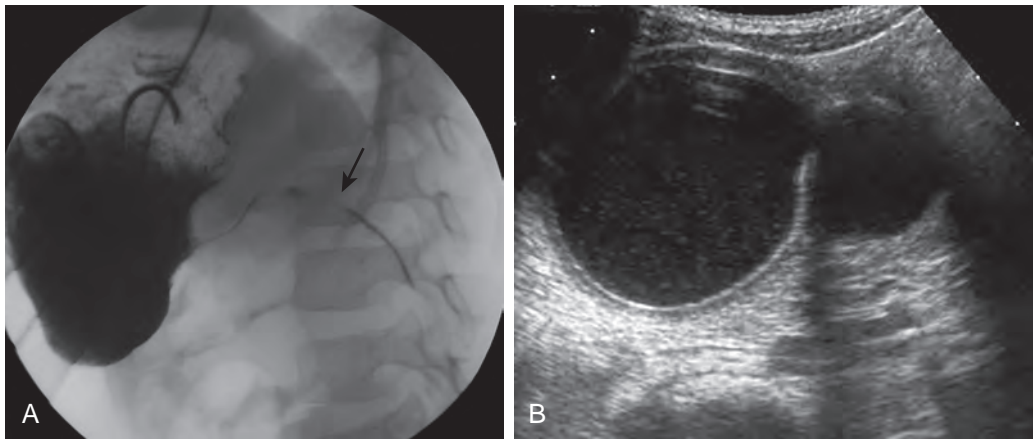


Figure 116-6 Gastric duplication cyst. **A.** Upper gastrointestinal examination in this 7-week-old infant with persistent vomiting shows extrinsic compression and mass effect on the gastric antrum and severe luminal narrowing of the proximal duodenum (arrow) with nearly complete obstruction. **B.** Corresponding sonogram confirms that the mass effect is caused by a large, bilobed cyst containing low-level internal echoes. The cyst wall exhibits the characteristic alternating hypoechoic and hyperechoic layers of bowel wall.

and submucosa and an outer hypoechoic ring representing muscularis propria.^{33,34,38}

MALROTATION

Clinical Findings

The developing gastrointestinal tract normally has two zones, the duodenojejunal and the cecocolic, that seem to be able to pull adjacent bowel along with them. Before the 8th week of intrauterine life, the duodenojejunal segment returns to the peritoneal cavity from the omphalus, having coursed counterclockwise to the left of the midline, under the superior mesenteric artery (SMA). Later, after the 10th week of life, the cecocolic segment undergoes a counterclockwise rotation toward the right lower quadrant.³⁹⁻⁴¹ Intestinal malrotation refers to improper completion of the normal rotational process, resulting in formation of abnormal mesenteric attachments (i.e., Ladd's bands) and shortening of the mesenteric base. Arrest of rotation may occur at any phase of development or involve only a part of the midgut, resulting in a wide spectrum of rotational anomalies ranging from nonrotation (in which the small bowel lies to the right of the mesenteric vessels and the colon to the left) to minor degrees of cecal elevation.⁴¹⁻⁴³

Particular attention should be paid to two critical anatomic landmarks in malrotation. First is the ligament of Treitz, which is a suspensory ligament of connective tissue and smooth muscle that runs from the root of the SMA to the junction of the fourth portion of the duodenum with the jejunum.^{41,44} Its presence is inferred on an upper gastrointestinal examination by normal position of the duodenal-jejunal junction (DJJ) in relation to the stomach, proximal duodenum, and spine. The DJJ and ligament of Treitz are located in the left upper quadrant of the abdomen in normal individuals but are displaced medially and inferiorly in those with malrotation.⁴⁵ Second is the third and fourth portions of the duodenum, which are fixed in the retroperitoneum under the SMA in normal individuals but freely movable in the peritoneal cavity in those with malrotation.⁴⁶

It is not the malrotation that causes symptoms but rather complications arising from the malrotated, abnormally

positioned intestine. The most grave is a midgut volvulus that results from twisting of the mesentery around the abnormally narrowed and shortened vascular pedicle. Volvulus may be fixed or intermittent and is a life-threatening emergency because of potential for bowel ischemia and necrosis.⁴⁷ Obstruction may also result from Ladd's bands across the duodenum. Affected individuals are usually symptomatic in the first year of life, but malrotation can be manifested at any age.⁴⁵ Bilious emesis is the classic symptom, and a high index of suspicion for malrotation and volvulus should be maintained for those infants presenting in this manner.^{43,45} On occasion, a child may tolerate obstruction from intermittent volvulus and come to medical attention because of episodic pain or symptoms of malabsorption.^{48,49} Chronic, intermittent volvulus is a cause of secondary lymphangiectasia and chylous ascites.

Urgent surgical treatment of malrotation is indicated to avoid the potentially catastrophic complications of bowel necrosis associated with volvulus. The definitive treatment is Ladd's procedure, in which the midgut volvulus is untwisted, Ladd's bands are divided, cecum is mobilized, appendix is removed, and mesentery is widened, with placement of small bowel in the right hemiabdomen and colon in the left hemiabdomen.⁵⁰

Imaging Findings

Plain radiographs of patients with malrotation or volvulus show a variety of appearances ranging from paucity of distal bowel gas to unusual position of the air-filled stomach or intestinal loops, gaseous dilation of the stomach or duodenal bulb due to obstruction, and grossly distended air-filled loops with mural thickening if there is a closed-loop distal bowel obstruction and ischemia from volvulus. Most often, however, the findings on plain radiography are normal.^{44,45}

There is considerable debate in the literature concerning the best diagnostic approach to document position of bowel and presence of obstruction in suspected midgut volvulus.⁵¹⁻⁵⁴ The methods described in the following paragraphs are not foolproof, and ultimately, because the stakes of missing a malrotation are so high, in inconclusive cases, the radiologist should

not hesitate to repeat a study or to use a different, complementary modality to reach the correct diagnosis.^{44,45,55}

A carefully controlled upper gastrointestinal series, with delivery of barium or water-soluble contrast material orally or through a nasogastric tube placed in the stomach or, better yet, in the proximal duodenum, is generally considered the “gold standard.”^{45,55} The critical anatomy to document is the DJJ in a well-positioned straight frontal view of the first passage of contrast material through the duodenum.^{55,56} The DJJ, and by inference the ligament of Treitz, is considered normal when it is at or above the level of the superior end plate of the L2 vertebral body or the duodenal bulb and to the left of the left pedicle of this vertebral body.^{41,57} On lateral views, the second and third portions of the duodenum are posterior because they are retroperitoneal.^{45,55,56}

Displacement of the DJJ inferiorly or medially on the anteroposterior view and anteriorly on the lateral view is a sign of malrotation (Fig. 116-7). Ladd’s bands typically cause a complete or partial obstruction of the duodenum; midgut volvulus causes a corkscrew, Z, or ribbon-like appearance of the duodenum and jejunum, sometimes with proximal dilation and partial obstruction of the duodenum (Fig. 116-8).^{39,40,41,54}

On occasion, normal anatomic variations of the duodenum may be difficult to distinguish from genuine malrotation, or the DJJ may not be visualized because of technical factors. Normal variations that may mimic malrotation include inferior displacement of the DJJ by dilated stomach or bowel in infants with gastric overdistention or distal bowel obstruction; mobility of the DJJ in children younger than 4 years; and redundancy of

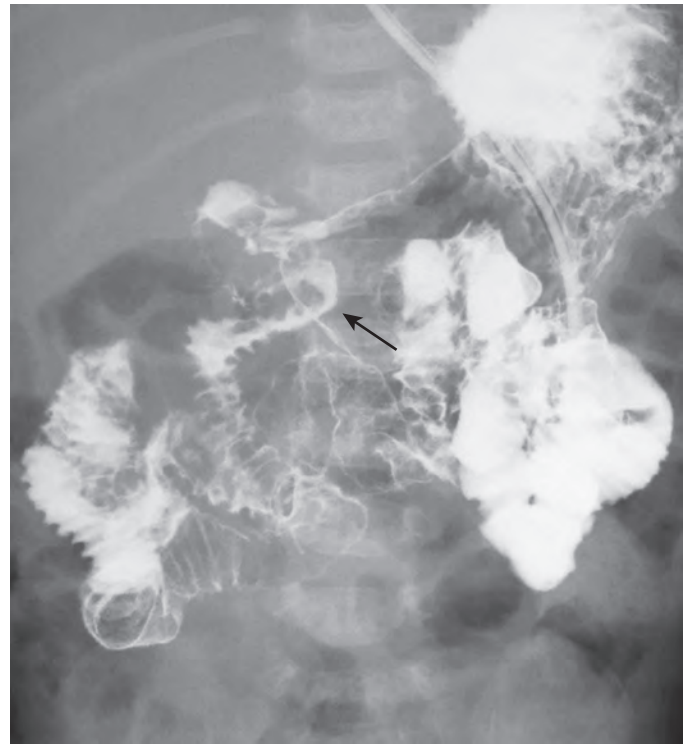


Figure 116-7 Malrotation. Upper gastrointestinal examination shows abnormally positioned duodenojejunal junction (arrow) to the right of the left pedicle and below the level of the L2 vertebral body superior end plate.

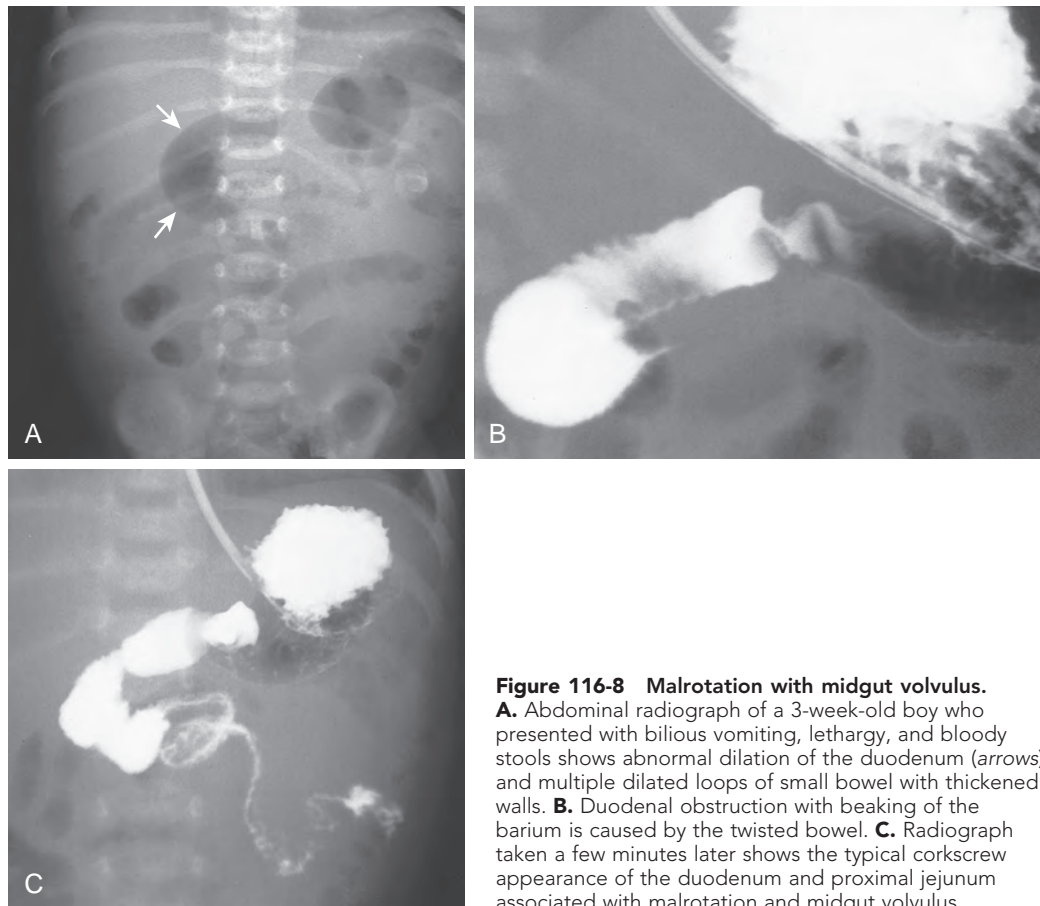


Figure 116-8 Malrotation with midgut volvulus.

A. Abdominal radiograph of a 3-week-old boy who presented with bilious vomiting, lethargy, and bloody stools shows abnormal dilation of the duodenum (arrows) and multiple dilated loops of small bowel with thickened walls. **B.** Duodenal obstruction with beaking of the barium is caused by the twisted bowel. **C.** Radiograph taken a few minutes later shows the typical corkscrew appearance of the duodenum and proximal jejunum associated with malrotation and midgut volvulus.

the second portion of the duodenum, also known as mobile duodenum or water-trap duodenum.^{48,57-60} In cases in which the position of the DJJ is equivocal, the position of the cecum can be evaluated by either following the contrast material into the colon or performing a contrast enema.^{44,59} However, the cecum, although usually located in the right lower quadrant, may have a wide range of normal in infants and may be in a normal position even with malrotation.^{39,40,44} Of children with surgically proved malrotation, only 87% had an abnormally positioned cecum compared with 97% with an abnormally positioned DJJ.⁴⁵

Several sonographic features of malrotation have been described. Inversion of locations of the SMA and superior mesenteric vein (SMV) is one finding that has been described in malrotation. The SMV usually lies to the right of the SMA on a transverse image at the level of the junction with the portal vein. If the SMV is to left of the SMA, the diagnosis of malrotation should be entertained. However, this is an inconstant finding, with sensitivity of 67% to 100% and specificity of 75% to 83%, and normal relationships are present in malrotation and inverted relationships are present without malrotation.^{44,45,56} The whirlpool sign, indicating a midgut volvulus, can be seen on ultrasound when the bowel, SMV, and SMA are twisted and wrapped around the vascular mesentery (Fig. 116-9). Finally, sonographic demonstration of the third portion of the duodenum in a retroperitoneal position between the SMA and the aorta is a reliable but not infallible sign of normal intestinal rotation.^{43,46,56} Likewise, absence of a retroperitoneal duodenum is a strong indicator of malrotation.⁴⁶

After Ladd's procedure for malrotation and volvulus, upper gastrointestinal examination shows the expected postoperative appearance of persistently displaced DJJ, small bowel in the right hemiabdomen, and colon in the left hemiabdomen (Fig. 116-10).⁵⁰ Other possible complications include adhesions and small bowel obstruction, reported in up to 24% of patients, and recurrent volvulus, reported in up to 7% of patients.⁵⁰

Acquired Diseases

GASTRIC PERFORATION

The incidence of acute spontaneous gastric perforation in neonates is declining.^{61,62} Predisposing factors include acute distention of the stomach, ischemic necrosis associated with perinatal asphyxia, and distal obstruction such as annular pancreas or

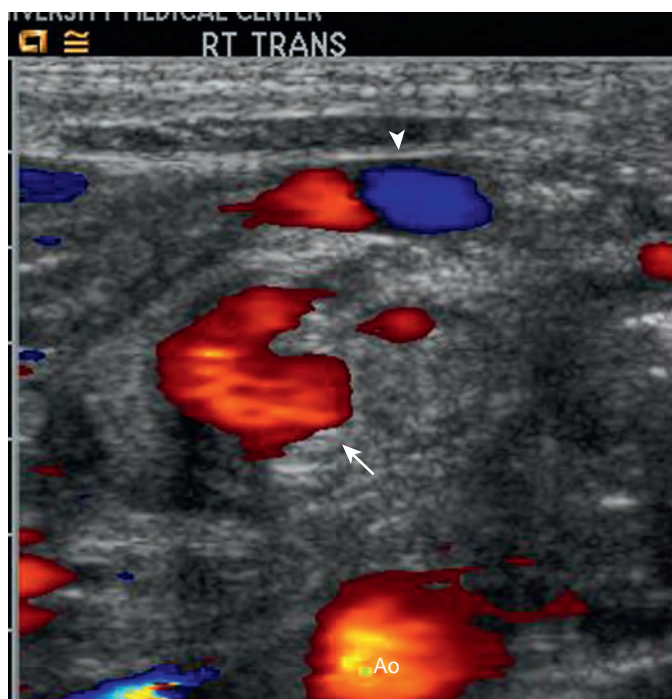


Figure 116-9 Malrotation with midgut volvulus. Transverse color Doppler sonogram of an epigastric mass shows the whirlpool sign consisting of the SMA (arrow) and SMV (arrowhead) twisted and draped clockwise around the mesentery, indicating midgut volvulus.

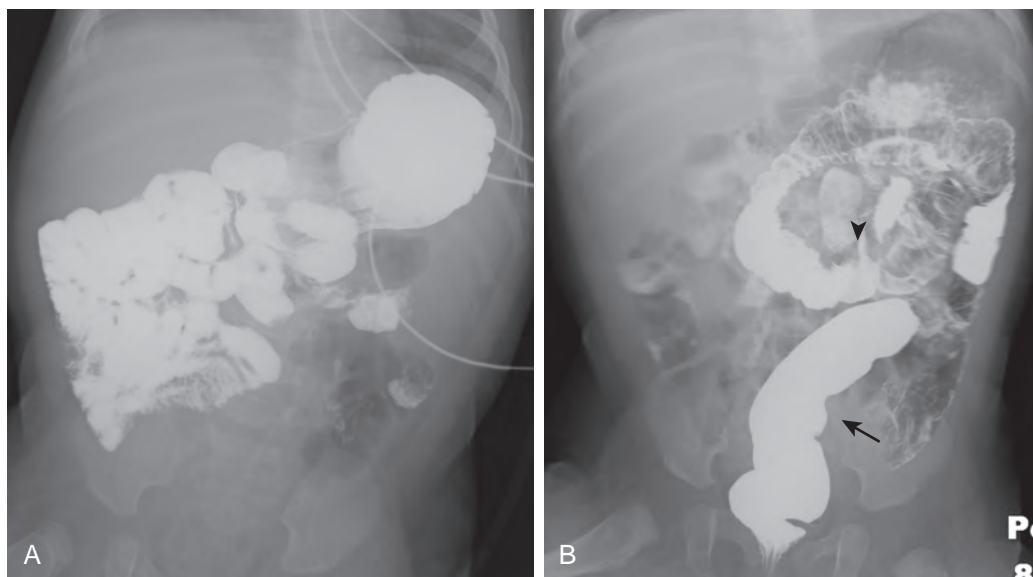


Figure 116-10 Ladd's procedure for malrotation. **A.** Small bowel examination shows the expected postoperative appearance after Ladd's procedure with jejunum and ileum located in the right upper quadrant. **B.** The entire colon, including the rectosigmoid (arrow) and the cecum (arrowhead), is located in the left hemiabdomen.

duodenal stenosis.⁶¹⁻⁶⁵ Plain radiographs show pneumoperitoneum and absence of a gastric air-fluid level on upright views.⁶⁶ Neonatal duodenal perforation is rare.⁶⁷

Gastric perforation in older children occurs in the following clinical settings: perforated peptic ulcer, dermatomyositis (although duodenal perforation is more common), migration of tubes and catheters through the gastric wall, and prior ingestion of caustic substances.⁶⁸⁻⁷² Complications of the Nissen and other funduplications include gastric bloat and gastric rupture or infarction when patients also have distal small bowel obstruction.⁷³⁻⁷⁵ Blunt trauma to the upper abdomen, when the stomach is distended, occasionally results in gastric rupture.

PYLORIC STENOSIS

Clinical Findings

Hypertrophic pyloric stenosis, which occurs in approximately 3 of 1000 infants, is one of the most common indications for surgery in infants. This disorder with familial predisposition is of unknown etiology but probably results from a complex interaction of genetic and environmental factors.^{76,77} Males, especially first-born males, are affected more frequently.^{78,79}

Classically, pyloric stenosis is manifested in a previously healthy infant between the age of 2 and 12 weeks with repeated nonbilious emesis that is sometimes forceful or projectile. The gradual onset of the symptoms may be mistaken for new or worsening gastroesophageal reflux. Presentation outside of this age range or emesis that is bilious should prompt evaluation for alternative diagnoses, such as malrotation. Pyloromyotomy, which can be performed nonemergently, is the treatment of choice for pyloric stenosis.⁷⁶ Because of better cosmetic result, shorter hospital stays, and lower wound infection rates, laparoscopic surgery is increasingly favored over an open procedure.^{76,78}

Imaging Findings

Ultrasonography is the established imaging examination for the diagnosis of pyloric stenosis and has been found to be highly sensitive and specific.⁷⁶⁻⁷⁸ In contemporary medical practice, the reliance on imaging has progressed to the point that ultrasound is now considered an intrinsic part of evaluation for pyloric stenosis, whereas the classically described palpable "olive" is found on physical examination with decreasing frequency.^{76,80,81} Features easily depicted by sonography include a thickened, hypoechoic pyloric muscle (doughnut or cervix sign) and a double layer of redundant echogenic mucosa (sonographic double-track sign) (Fig. 116-11).^{77,82-84} A muscle thickness of more than 3.0 to 3.5 mm measured in the long axis of the pylorus is a reliable indicator of pyloric stenosis, regardless of the patient's age or weight.^{52,76,79,85-87} A pyloric channel length of more than 15 to 18 mm is also considered abnormal.⁸² As important as the quantitative measurements in diagnosis of pyloric stenosis is the morphologic appearance of the pylorus and the real-time observation of little or no passage of gastric contents through the pylorus.

In pyloric stenosis, the thickened muscle is a fixed abnormality that does not change with time. Pylorospasm, which is a condition in which the muscle enlargement is transient rather than fixed and which is treated nonoperatively, may mimic pyloric stenosis on sonography. The muscle may be thickened, but the degree of thickening is often less pronounced than in pyloric stenosis, usually less than 3.0 mm. In addition, whereas

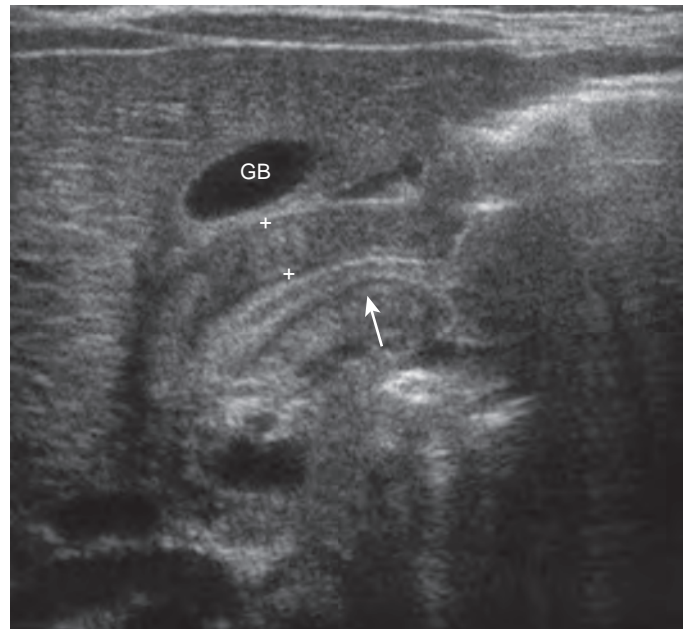


Figure 116-11 Pyloric stenosis: ultrasonography. In this image obtained along the long axis of the pylorus, the hypoechoic pyloric muscle (between calipers) is abnormally hypertrophied and thickened, measuring more than 3.5 mm, and can be seen on either side of the parallel, linear echoes (arrow) that represent the redundant mucosa of the narrowed pyloric channel. The gallbladder (GB) is a useful anatomic landmark for locating the pylorus.

muscle thickening is persistent in pyloric stenosis, it is intermittent in pylorospasm, with occasional relaxation of the pyloric muscle allowing passage of gastric contents. Thus, extending the length of time of observation of the pylorus to at least 5 to 10 minutes is an essential part of the sonographic study that can prevent false-positive diagnosis of pyloric stenosis.⁸⁴ In equivocal cases, repeated sonography in 1 to 3 days can be performed to detect early or evolving pyloric stenosis.⁷⁶⁻⁷⁸

Sonography should be performed with a high-frequency linear array transducer placed with the liver as an acoustic window.⁷⁷ To allow adequate filling of the antrum with fluid and assessment of patency of the pyloric channel, the infant can be turned to the right posterior oblique position and fluid can be given orally (Fig. 116-12). These maneuvers can help demarcate the landmarks denoting the beginning and end of the pyloric channel, namely, the prepyloric antrum and the duodenal bulb.⁷⁷ Fluid should not be given if the stomach is already distended as an overdistended stomach displaces the pylorus behind the stomach, making visualization difficult and possibly leading to false-negative results.⁷⁷

Contrast upper gastrointestinal examination is rarely performed if pyloric stenosis is the primary diagnostic consideration, but radiologists should still recognize findings because unexpected pyloric stenosis is occasionally found in infants undergoing upper gastrointestinal examination for suspected reflux. Upper gastrointestinal examination is also an alternative examination in the event that sonographic expertise is not available.⁷⁶ The classic features of pyloric stenosis on barium radiography include partial or complete gastric outlet obstruction, hyperperistalsis of the stomach, elongation of the pyloric channel, single (i.e., string sign) or double (i.e., train track sign) streaks of barium within the compressed lumen of the

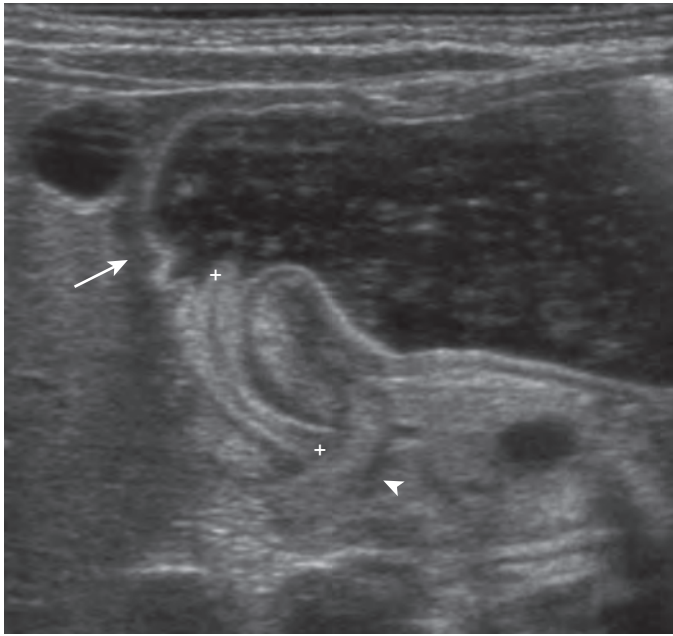


Figure 116-12 Pyloric stenosis: ultrasonography. Gastric outlet obstruction secondary to hypertrophied pyloric muscle. The stomach is distended with fluid given orally. The pyloric channel (between calipers) is abnormally elongated to more than 17 mm and does not open to allow passage of fluid. Reliable sonographic landmarks demarcating the beginning and end of the pylorus are the fluid-filled gastric antrum (arrow) and the echogenic, triangular duodenal bulb (arrowhead), respectively.

channel, and the shoulder sign of a pyloric mass indenting the barium-filled stomach and the base of the duodenal bulb (Fig. 116-13).^{76,82}

The radiographic appearance in the immediate postoperative period after pyloromyotomy is difficult to interpret because it is similar to that of preoperative studies, with a string sign and antropylorospasm (Fig. 116-14).⁷⁶ By 6 weeks, however, the sonographic and radiographic appearance should be normal for most patients. Until then, there is often asymmetry of the channel as the mucosa eventrates through the defect of the “cracked” muscle. Incomplete pyloromyotomy results in persistence of an elongated, narrowed channel with poor gastric emptying.⁸⁸ Patients who have had a past history of successful pyloromyotomy may be left with some antropyloric dysfunction, which has led to retention of foreign bodies (e.g., coins) in some patients.^{76,89}

GASTRIC AND DUODENAL HEMATOMAS

Clinical Findings

Gastric hematoma from blunt abdominal trauma is unusual. Duodenal hematoma is more common because the duodenum is sandwiched between the spine and the anterior abdominal wall of the epigastrium. A typical history in such cases is a child falling onto the handlebars of a bicycle or being struck in the abdomen during play or an athletic event.^{90,91} Duodenal hematomas are associated with pancreatic injury because the pancreas is also located in the retroperitoneum in a position vulnerable to blunt epigastric trauma.⁹²

Child abuse should be considered when any child has a suspicious history.^{93,94} Other risk factors for duodenal hematoma

include Henoch-Schönlein purpura, bleeding associated with leukemia, coagulopathies, idiopathic thrombocytopenia purpura, endoscopic biopsy, and anticoagulant therapy.⁹⁵ Surgery is mandatory when perforation is present, but otherwise most uncomplicated duodenal hematomas are managed conservatively.^{90,94,96}

Imaging Findings

The diagnosis of duodenal hematoma can be suggested by plain radiographs that demonstrate gastric distention, soft tissue mass in the right hemiabdomen, and sparse distal gas. Retroperitoneal air can be seen on the plain radiograph or computed tomography (CT) scan as a sign of transmural leakage.⁹⁶⁻⁹⁸ Upper gastrointestinal study with contrast material shows the intramural mass effect of the hematoma but may not demonstrate the perforation if the hematoma is plugging the mural rent (Fig. 116-15A).

Ultrasonography can demonstrate and monitor the hematoma and adjacent pancreatic injury that is commonly present, but it cannot reliably demonstrate perforation (Fig. 116-15B).^{92,99} CT is the preferred method of imaging if there has been severe upper abdominal trauma, especially crush injury, because it can image all organs well (Fig. 116-16).⁹⁶ However, CT can miss subtle cases of duodenal rupture.¹⁰⁰ As the hematoma resolves, perforation and duodenal diastasis may become apparent, and every child with a duodenal hematoma must be carefully watched during the first 7 to 10 days after trauma.⁹⁹

GASTRIC AND DUODENAL FOREIGN BODIES

Clinical Findings

A gastric mass in a child can be an ingested foreign body or a bezoar. The most common bezoar in childhood is a trichobezoar, or hairball, but other indigestible materials, such as vegetable or fruit (phytobezoar), may also form a mass that may cause obstruction.¹⁰¹ Trichobezoar in adolescence is usually associated with psychiatric problems and pica, which is ingestion of non-nutritive substances. The trichobezoar is usually confined to the stomach, but a tail may extend into the duodenum and, rarely, throughout the small bowel.¹⁰² Lactobezoars have been described in premature infants, and they probably form as a result of immature mechanisms of gastric emptying.¹⁰³ The symptoms of bezoars are usually those of insidious obstruction, such as nausea, vomiting, abdominal pain, early satiety, and decreased appetite.^{101,102}

Ingestion of foreign bodies is extremely common in young children, particularly in those between the ages of 6 months and 3 years. Because most objects pass without complication, even in small children, a conservative approach is taken by surgeons and pediatricians. Of foreign bodies that reach the stomach, 90% to 95% pass spontaneously in the absence of underlying stomach and duodenum structural abnormality.¹⁰⁴⁻¹⁰⁶

Because of unfavorable size, shape, or composition, several types of ingested foreign bodies are more likely to cause complications and should be approached with more caution than for other types of foreign bodies. These include sharp pointed objects, objects longer than 6 cm, disc batteries, and magnets.¹⁰⁶

Ingested disc or button batteries can potentially cause injury because prolonged contact of the battery with tissue is known to cause focal injury and possible perforation due to pressure necrosis or low-voltage electrical injury.¹⁰⁶ Although batteries

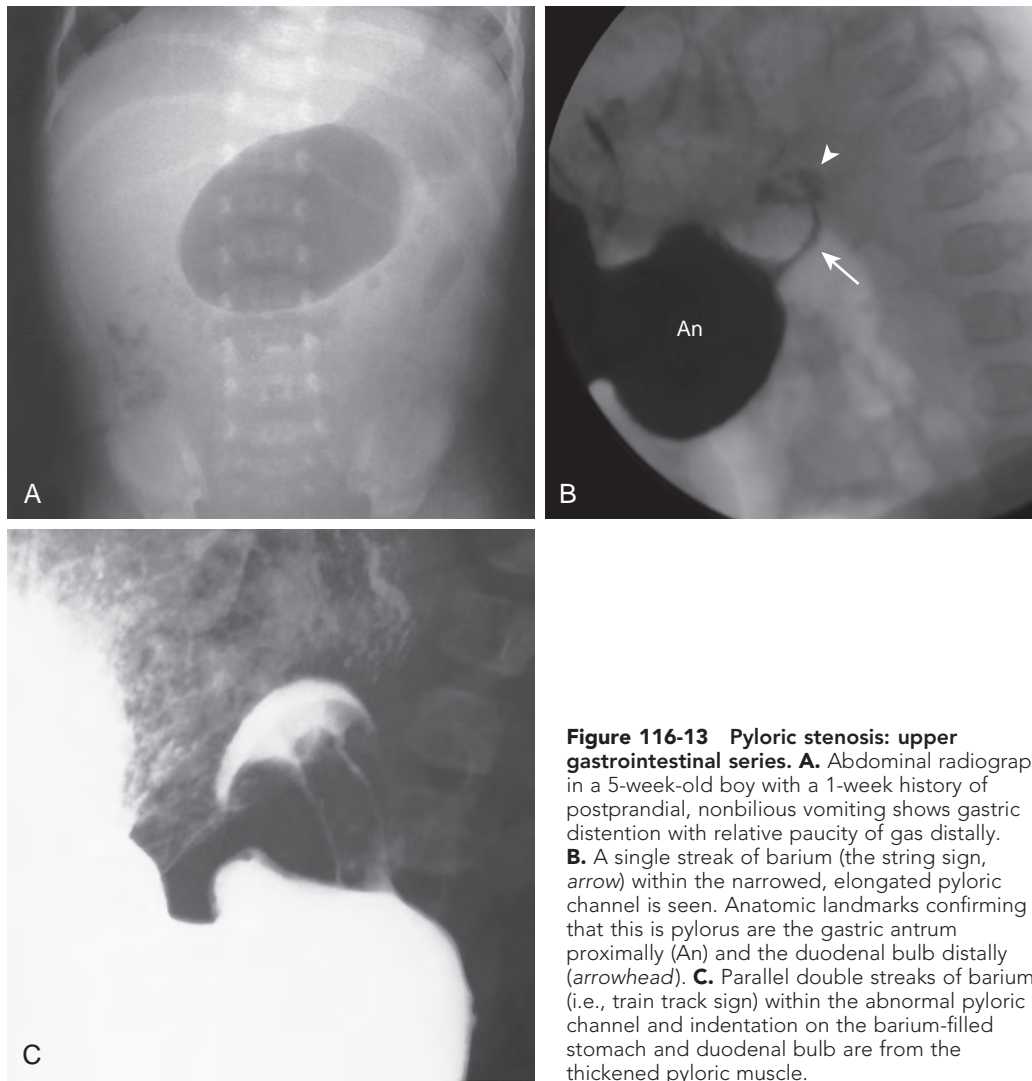


Figure 116-13 Pyloric stenosis: upper gastrointestinal series. **A.** Abdominal radiograph in a 5-week-old boy with a 1-week history of postprandial, nonbilious vomiting shows gastric distention with relative paucity of gas distally. **B.** A single streak of barium (the string sign, arrow) within the narrowed, elongated pyloric channel is seen. Anatomic landmarks confirming that this is pylorus are the gastric antrum proximally (An) and the duodenal bulb distally (arrowhead). **C.** Parallel double streaks of barium (i.e., train track sign) within the abnormal pyloric channel and indentation on the barium-filled stomach and duodenal bulb are from the thickened pyloric muscle.

are more likely to lodge in the esophagus than in the stomach, if a battery fails to pass beyond the stomach after several days, removal is recommended.¹⁰⁶ Management of disc batteries impacted in the esophagus is discussed in Chapter 115.

Ingested rare earth magnets that are small but powerful have become increasingly recognized as a potential cause of gastrointestinal injury that requires active management. Two or more magnets or a magnet coupled with a metallic foreign body may lodge in two adjacent but separate segments of the gastrointestinal tract and adhere to each other because of magnetic attraction, resulting in entrapment, necrosis, and perforation of the interposed bowel wall.¹⁰⁶⁻¹⁰⁸ Although most commonly this occurs in the small bowel, any segment of intestinal tract from esophagus to colon can be affected. In the setting of abdominal pain or other clinical signs of obstruction or perforation, the threshold is low for endoscopic removal of the magnets within endoscopic reach and possible surgical removal for those beyond endoscopic reach.¹⁰⁶

Imaging Findings

Large trichobezoars in the stomach can often be visualized on plain radiographs and confirmed with barium upper gastroin-

testinal examination (Fig. 116-17). They may also be incidentally discovered on cross-sectional imaging.

In cases of suspected foreign body ingestion, witnessed ingestion and reliable history are often absent, making plain radiographs an important part of management. Anteroposterior and lateral radiographs of the chest and abdomen are recommended to confirm the presence, type, and location of the foreign body and evidence of perforation, such as free intraperitoneal air. Care should be taken not to mistake a round disc battery, which has a characteristic beveled, double density rim or edge on plain radiographs, with a coin. Sequential radiographs should be obtained several hours apart to document movement of the foreign body through the gastrointestinal tract. In the case of multiple magnets or a combination of magnet and metallic foreign body, failure of movement of the foreign body or presence of a gap between two magnets should raise suspicion of bowel wall entrapment between the objects and need for intervention (Fig. 116-18). Pitfalls in plain film interpretation include stacked magnets simulating a single object and assuming that adhered magnets are located in a single segment of bowel without intervening bowel wall.¹⁰⁶

NEOPLASMS

Gastric and duodenal neoplasms are rare in children. There are a wide variety of masses arising from the stomach that overlap significantly in imaging characteristics and are difficult to distinguish from each other radiographically.¹⁰⁹ Masses arising external to the stomach, such as large pancreatic pseudocysts or hepatic masses, can also indent the stomach, causing mass effect, and mimic a gastric mass.

Gastric teratomas occur in infancy, most commonly in boys.¹¹⁰ Virtually all of these patients present with upper abdominal masses during the first year of life.¹¹¹⁻¹¹⁴



Figure 116-14 Postoperative pyloromyotomy. There is residual deformity of the pylorus but normal gastric emptying after surgery for pyloric stenosis. The follow-up examination was performed for persistent "spitting" postoperatively. The patient responded to conservative medical therapy.

Plain radiographs typically show calcification within a mass that displaces the gastric air bubble.¹¹³ Without cross-sectional imaging, differentiation from retroperitoneal neuroblastoma may be difficult in some patients. Leiomyomas and leiomyosarcomas are lobulated or polypoid masses arising from the gastric wall that can be differentiated only by histologic examination.^{115,116} Leiomyoblastoma is an uncommon tumor of the gastric wall that tends to grow in an intraluminal fashion, causing ulceration of the overlying mucosa. Its biologic behavior is generally benign, but metastases have been reported, with the liver being the most frequent site.¹¹⁷

Other rare tumors of the stomach include lymphoma, which may be a primary lesion or, rarely, part of generalized involvement with Burkitt's lymphoma.^{118,119} In either case, the appearance is similar: diffuse infiltration of the gastric wall, mucosal thickening, ulcerations, and a discrete gastric mass. Gastric adenocarcinomas, which appear similar to lymphoma and leiomyosarcoma on barium studies, are unusual in children and are associated with ataxia-telangiectasia and



Figure 116-16 Duodenal hematoma. CT scan shows the duodenal hematoma (arrow) in the wall of the second portion of the duodenum, which causes eccentric compression of the contrast-filled lumen.

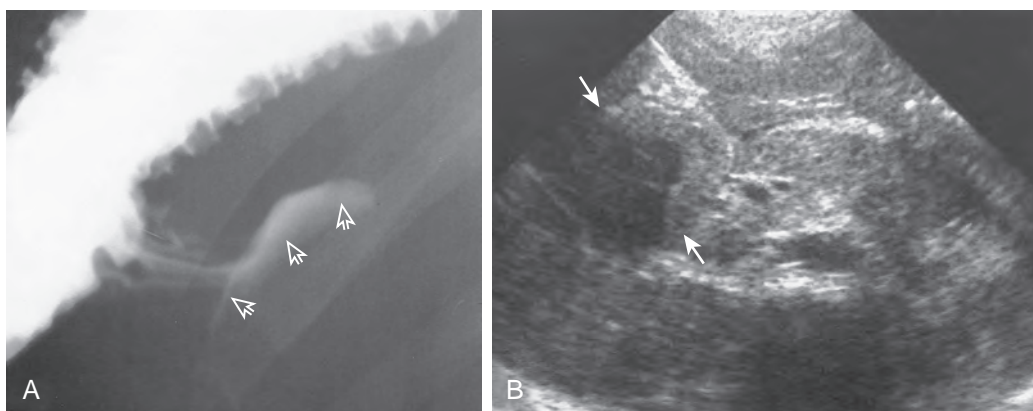


Figure 116-15 Duodenal hematoma. A. Prone, oblique view from an upper gastrointestinal series shows duodenal obstruction with barium (arrows) outlining a duodenal mass. **B.** Transverse sonogram of the upper abdomen demonstrates the mass to be a duodenal hematoma (arrows) in this 10-year-old child who sustained a bicycle handlebar injury to the upper abdomen. The complete sonographic study also demonstrated pancreatic swelling and peripancreatic fluid from the injury (not shown).

immunodeficiency.^{120,121} Gastrointestinal stromal tumor, a mesenchymal malignant tumor of the gastrointestinal tract, involves the stomach in more than 50% of cases (Fig. 116-19).^{109,122}

Gastric inflammatory pseudotumor can simulate a malignant tumor on radiographic studies and should be considered when a gastric mass contains an ulcer or confined perforation; if the child has another unusual associated problem, such as retroperitoneal fibrosis or sclerosing cholangitis; or if the child has Castleman's syndrome.¹²³

Polyps of the stomach and duodenum are most commonly hamartomatous and part of the Peutz-Jeghers syndrome (Fig. 116-20). Fundic gland polyposis has been described in children

and adults who have familial adenomatosis coli and Gardner's syndrome.¹²⁴ Other gastric polyps in children include inflammatory fibroid polyp, solitary hyperplastic polyp, and polypoid focal foveolar hyperplasia.¹²⁵⁻¹²⁸

Neurofibromas can develop in the gastric or duodenal wall. Although these lesions usually are benign, they can cause vomiting, jaundice, and hematemesis.¹²⁹ Neurofibromas usually occur with other stigmata of von Recklinghausen's



Figure 116-17 Trichobezoar. There is a large filling defect within the barium-filled stomach of this 12-year-old girl with a 2-year history of trichophagia, which left bald patches on her head. At surgery, a 500-g mass of matted, brunette hair was removed from the stomach.



Figure 116-18 Ingested magnets in the stomach. Ten magnetic balls arranged in a linear mass in the expected region of the gastroesophageal junction and proximal stomach are seen in this patient with several days of acute abdominal pain. At endoscopy, the separate magnets had adhered together, with the most proximal magnet in the distal esophagus and the others in the gastric cardia, entrapping esophageal and stomach wall between them. There was no bowel wall erosion or perforation.

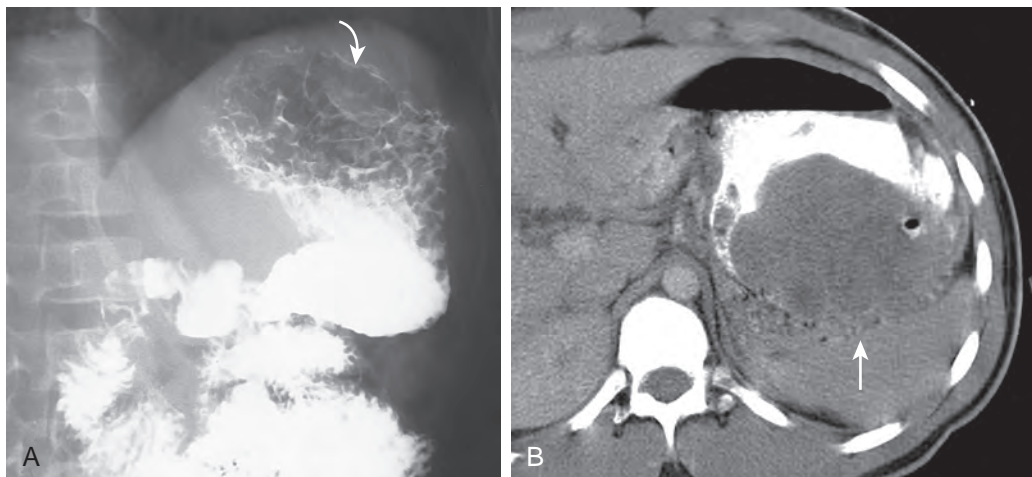


Figure 116-19 Gastrointestinal stromal tumor of stomach. **A.** The upper gastrointestinal series demonstrates a large filling defect (arrow) in the gastric fundus. **B.** CT scan shows the fundal, intraluminal soft tissue mass (arrow represents the tumor outlined by contrast material in the stomach).



Figure 116-20 Peutz-Jeghers syndrome. Barium and air administered through a gastrostomy tube in this patient with known Peutz-Jeghers syndrome outline multiple filling defects representing hamartomatous polyps.

disease. Pancreatic rests, manifested as masses along the greater curvature of the stomach or inner margin of the duodenum, are congenital abnormalities that are rarely diagnosed in infancy.¹³⁰ Choledochoceles may be manifested as a smooth, well-defined mass at the ampulla of Vater. Intussusception of the duodenum or stomach can occur when a large hamartomatous polyp, gastrostomy tube, or Foley catheter acts as a lead point.¹³¹

PEPTIC ULCER DISEASE

Helicobacter pylori, a gram-negative, motile bacterium, is a common human pathogen associated with peptic ulcer disease and gastritis, with reported incidence of up to 50% in lower socioeconomic classes in the United States.¹³²⁻¹³⁶ Whereas most infections are acquired during childhood, symptoms typically are not manifested for decades, and consequently peptic ulcer disease in children is remarkably uncommon.¹³⁶⁻¹³⁸ Perforated peptic ulcer disease is even more uncommon, with one series spanning 20 years reporting only 52 cases and describing characteristic acute rather than chronic presentation and association with an older, adolescent-age group and male gender.¹³⁹

Peptic ulcer disease may also occur secondary to stress in infancy and early childhood. Shock, respiratory failure, sepsis, hypoglycemia, severe burns (i.e., Curling's ulcer), intracranial lesions (i.e., Cushing's ulcer), and chronic systemic disease have been implicated in addition to aspirin, other nonsteroidal anti-inflammatory drugs, corticosteroids, and tolazoline.^{68,138}

Zollinger-Ellison syndrome, which is due to excessive gastrin production by gastrinoma and resultant gastric acid hypersecretion, is a rare cause of peptic ulcer disease in children; the registry tabulating this disease recorded only 28 children in 21

years.^{68,136} Peptic ulceration, gastric acid hypersecretion, and hypergastrinemia have occasionally occurred in children with antral G-cell hyperplasia.⁶⁸

INFLAMMATORY DISORDERS OTHER THAN PEPTIC DISEASE

Ménétrier's disease is a rare inflammatory disorder characterized by enlarged gastric folds, predominantly in the body and fundus, and proliferation of gastric glands.¹⁴⁰⁻¹⁴² This disease has a bimodal distribution, occurring in children younger than 10 years and also in adulthood. In contrast to the progressive clinical course of the disease in adults, the childhood form of the disease is linked to cytomegalovirus infection and has an acute onset with spontaneous resolution in weeks or months.¹⁴¹ Affected children present with upper abdominal pain, nausea, and vomiting that is occasionally complicated by hematemesis, anemia, and marked hypoproteinemia. Abnormally thickened gastric folds and gastric wall thickening can be seen with barium studies, CT, or sonography.¹⁴⁰⁻¹⁴⁴

Eosinophilic gastritis and eosinophilic gastroenteritis are classified within the larger group of primary eosinophilic gastrointestinal disorders in children characterized by eosinophil-rich inflammation of the gastrointestinal tract without known cause.^{145,146} Eosinophilic esophagitis, which is also subsumed in this classification, is discussed in more detail in Chapter 115. An allergic mechanism, including generalized atopy and food allergy, is proposed in at least a large subset of children with eosinophilic gastritis and eosinophilic gastroenteritis who may have a history of asthma, eczema, or allergic rhinitis in addition to exhibiting a variety of nonspecific symptoms including abdominal pain, vomiting, failure to thrive, anemia, and protein-losing enteropathy.^{145,146} Imaging has low sensitivity and specificity, but findings in the stomach include mucosal irregularity and lacy pattern, gastric fold and wall thickening, and luminal narrowing, usually confined to the gastric antrum.^{145,147,148}

Chronic granulomatous disease is a hematologic disorder, usually occurring in boys, in which there is a defect in the mechanism for producing superoxide. This results in ineffective lysis of certain bacteria by polymorphonuclear leukocytes and mobilization of macrophages and other granulomatous responses. In addition to the well-known infectious complications of the disease, involvement of any portion of the gastrointestinal tract has been reported in a large number of patients.^{149,150} The most characteristic gastrointestinal tract finding, fold and wall thickening of the gastric antrum that may lead to luminal narrowing and gastric outlet obstruction, is found in only 16% of cases (Fig. 116-21).¹⁵⁰⁻¹⁵²

Crohn's disease affecting the stomach and duodenum is unusual in children and, if present, usually is found in patients with well-established small bowel and colonic disease.¹⁵³⁻¹⁵⁵ Mucosal nodularity and ulceration, fistula and sinus tracks, and irregular narrowing and pseudodiverticula formation are the major radiographic findings in gastroduodenal Crohn's disease (Fig. 116-22).¹⁵⁵

The most common sites of gastrointestinal involvement of Henoch-Schönlein purpura are the duodenum and small bowel, which is discussed further in Chapter 117. Thickening of the wall of the duodenum, usually the second portion of the duodenum, is seen and may rarely be accompanied by ulceration.¹⁵⁶⁻¹⁵⁸ The characteristic rash may appear after abdominal symptoms of pain and vomiting.

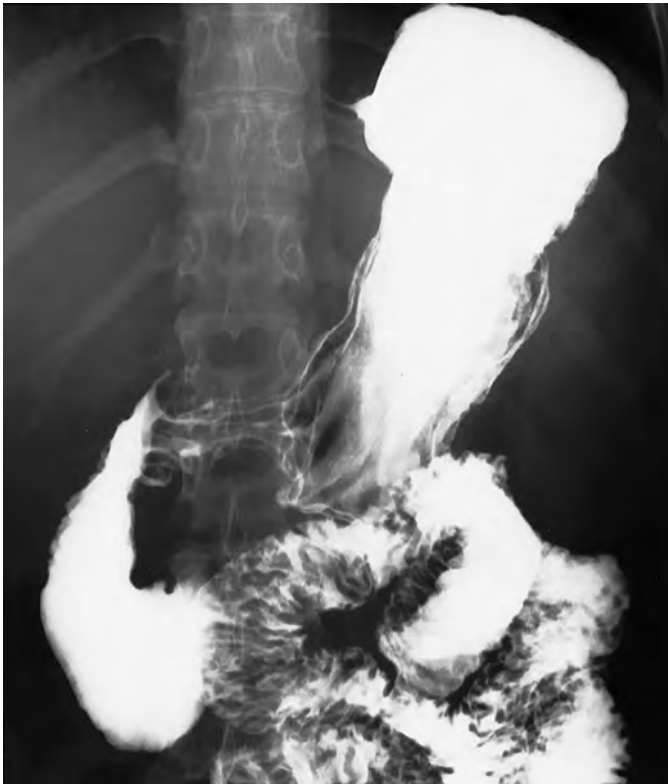


Figure 116-21 Chronic granulomatous disease. Thickened gastric folds with marked antral narrowing are seen in this patient with a long-standing history of chronic granulomatous disease. This study was prompted by symptoms of epigastric discomfort and vomiting.



Figure 116-22 Gastritis in Crohn's disease. A 12-year-old boy presented with upper abdominal pain and weight loss. Mucosal nodularity is apparent on this radiograph from an upper gastrointestinal series.

Twenty-five percent of the world's population harbor *Ascaris lumbricoides*, and most infected people are children.¹⁵⁹ This is the only parasite that ingests barium.¹⁵⁹ When the worm burden is sufficiently large, obstruction can result, and radiologists working in endemic areas become skilled at differentiating clumps of intraluminal worms from stool and other masses (Fig. 116-23). Gastric mucosal penetration by the larvae of *Anisakis*, ingested with a meal of infected raw fish, causes acute, severe abdominal pain. Double-contrast barium studies can be diagnostic; threadlike filling defects are associated with a mound of mucosal edema at the site of larval penetrations of gastric wall.¹⁶⁰ Endoscopic removal of the larvae results in resolution of abdominal pain.

Although giardiasis may occur in the setting of dysgammaglobulinemia, immunocompetent children can be infected if the water source is contaminated. Duodenal spasm, thickening of the mucosa, and increased intraluminal fluid are characteristic but nonspecific radiologic features of infection.¹⁶¹ *Strongyloides* also affects duodenal mucosa and provokes an inflammatory response. Chronic disease results in a fixed, narrowed, and featureless duodenum.¹⁶²

The location and type of injury that occurs secondary to ingestion of caustic substances are largely dependent on the pH of the ingested agent. High-pH, alkaline agents are more viscous, leading to relatively prolonged contact time with the esophagus (see Chapter 115). On the other hand, low-pH, acidic agents are less viscous, resulting in rapid transit through the esophagus into the stomach, with predilection for pooling in the antrum

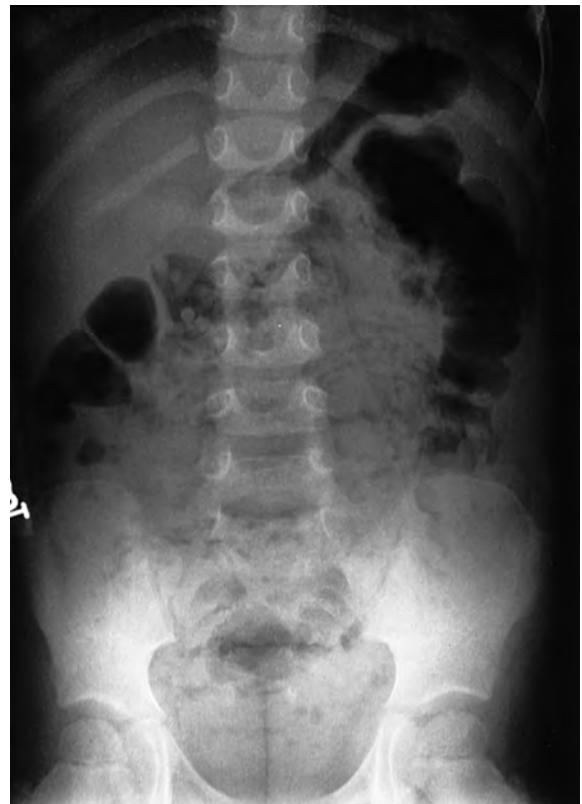


Figure 116-23 Ascariasis. A 5-year-old girl from Puerto Rico had a 2-month history of abdominal pain. Diarrhea was accompanied by vomiting, and the vomitus contained worms. Notice the unusual gas pattern in the middle duodenum and jejunum.

and pylorus.¹⁶³ Because the type of necrosis induced by acids is characterized by coagulation rather than by liquefaction, the wall penetration and subsequent perforation that are seen with alkali agents in the esophagus are less frequently encountered with acid injury in the stomach.¹⁶³ More often, mucosa of the stomach, and sometimes the duodenum, becomes thickened or ulcerated, resulting in gastric outlet obstruction, which is the most commonly reported complication of acid ingestion (Fig. 116-24).¹⁶³⁻¹⁶⁵ Radiology is useful in the follow-up of prior caustic injury because scarring takes weeks to months to evolve.

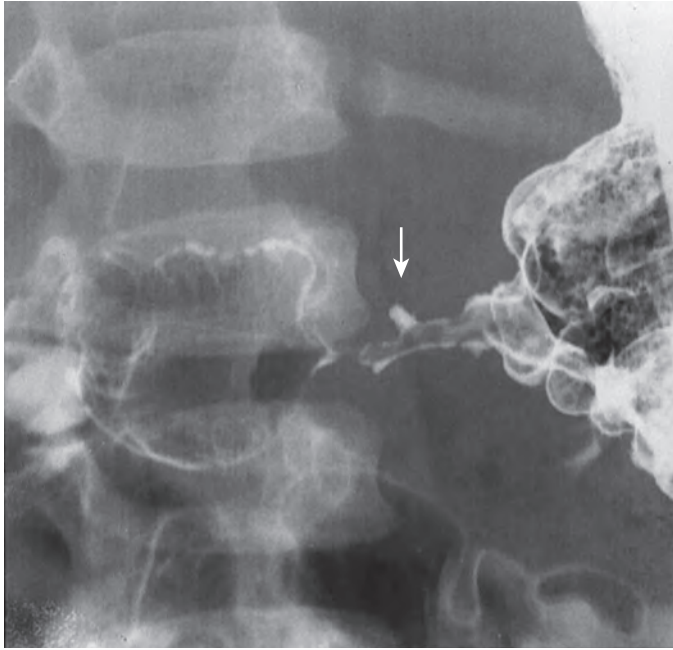


Figure 116-24 Gastritis from caustic ingestion. Marked antral narrowing with fold thickening and ulceration (arrow) are seen in this 7-year-old boy, who accidentally swallowed sulfuric acid.

Stenosis and contraction of the stomach and rigidity of the duodenal loop are characteristic of prior caustic ingestion.¹⁶⁶

GASTRIC OR DUODENAL DISTENTION

Gaseous distention of the stomach is seen in several disorders peculiar to the pediatric population. Many children swallow air when crying or nervous. There is overt aerophagia in some groups of youngsters with neuromuscular impairment and developmental delay.^{167,168} Gastric distention with air occurs with tracheoesophageal fistula, with or without esophageal atresia, or after an endotracheal tube is inadvertently placed in the esophagus. Diabetes mellitus and prior starvation are causes of gastric dilation that probably results from atony.

Distention of the stomach predisposes it to volvulus. Volvulus is also associated with deficient mesenteric and ligamentous attachments and diaphragmatic defects.^{167,168} Mesenteroaxial volvulus is a twist along an axis joining the lesser and greater curvature of the stomach. It has a characteristic appearance on plain radiographs.¹⁴⁷ Organoaxial volvulus is a twist along the gastric axis.¹⁶⁹ Intrathoracic gastric volvulus may accompany a large congenital hiatal or diaphragmatic hernia (Fig. 116-25).^{170,171}

SMA syndrome is obstructive compression of the third and fourth parts of the duodenum by the SMA and the root of the mesentery.¹⁷²⁻¹⁷⁵ It may follow surgery and casting for correction of scoliosis (i.e., cast syndrome) or may occur after severe weight loss. Plain radiographs and upper gastrointestinal series show distention of the stomach and proximal duodenum and a sharp cutoff in the midtransverse portion of the duodenum. Feeding in the prone position, hyperalimentation, or nasojejunal feeding alleviates the symptoms in most patients, and operative treatment is rarely necessary.¹⁷²⁻¹⁷⁵

Idiopathic megaduodenum is part of the spectrum of chronic intestinal pseudo-obstruction, and it may occur sporadically or in families.^{176,177} The condition is caused by disease of the smooth muscle, abnormal extrinsic or intrinsic nerves, or alteration of the neuroendocrine environment. Dilation of sections

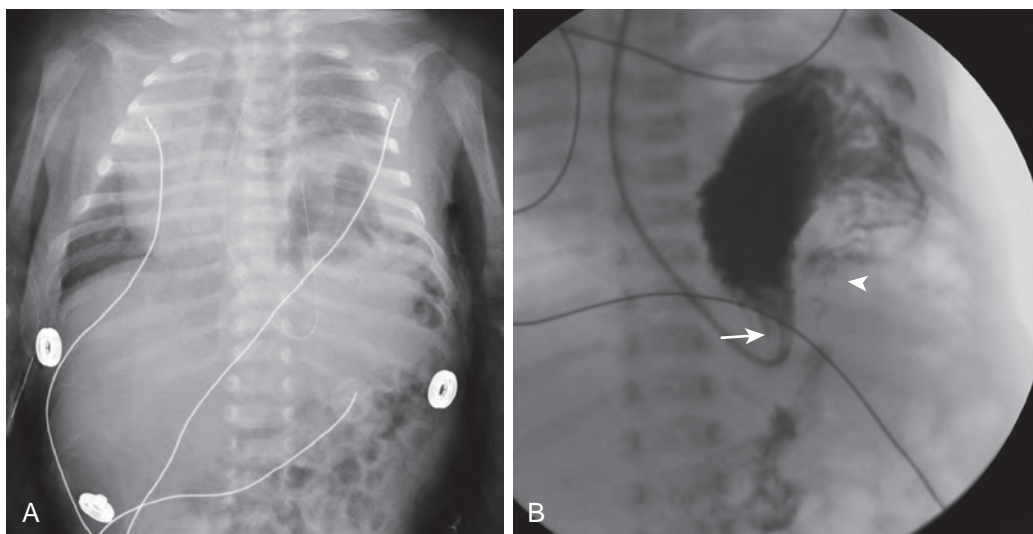


Figure 116-25 Gastric volvulus. **A.** Abdominal radiograph shows congenital left diaphragmatic hernia. **B.** Upper gastrointestinal examination shows gastric volvulus associated with the herniated stomach. Arrow identifies the gastroesophageal junction. There are both organoaxial, with greater curvature superior to lesser curvature, and mesenteroaxial, with duodenum (arrowhead) to the left of the stomach, components to the volvulus.

of the gastrointestinal tract without anatomic obstruction is characteristic. Bacterial overgrowth and diarrhea are common problems. Secondary megaduodenum from diabetes, scleroderma, and amyloidosis are always mentioned in differential diagnoses, but these disorders are rare in pediatric patients.

Radiographically demonstrable abnormalities of the duodenum are common in cystic fibrosis and most prevalent in the second portion of the duodenum.^{178,179} Thickened mucosal

folds, nodular mucosa, and increased intraluminal fluid are typical features. These findings have been attributed to hyperplasia of the Brunner glands, tenacious mucus, mucosal edema, or inappropriate contraction of the muscularis mucosae.¹⁸⁰ Because an ulcer is difficult to detect on this background of abnormal mucosa radiographically, endoscopy is recommended in patients with cystic fibrosis who have symptoms of peptic ulcer disease.¹⁸⁰

REFERENCES

- Naik-Mathuria B, Olutoye OO: Foregut abnormalities. *Surg Clin North Am* 86:261–284, 2006.
- Gerber BC, Aberdeen SD: Prepyloric diaphragm: An unusual abnormality. *Arch Surg* 90:472–480, 1965.
- Gupta AK, Guglani B: Imaging of congenital anomalies of the gastrointestinal tract. *Indian J Pediatr* 72:403–414, 2005.
- Lin AN: Pyloric atresia and epidermolysis bullosa. *Pediatr Dermatol* 14:406–408, 1997.
- Pratap A, Tiwari A, Agrawal CS, et al: Antral mucosal valve: A rare cause of gastric outlet obstruction in newborn. *J Pediatr Surg* 41:856–858, 2006.
- Oak S, Bhatnagar M, Kulkarni B, et al: Prepyloric membrane detected following foreign body ingestion. *Indian J Gastroenterol* 15:109–110, 1996.
- Blazek FD, Boeckman CR: Prepyloric antral diaphragm: Delays in treatment. *J Pediatr Surg* 22:948–949, 1987.
- Tunnell WP, Smith EI: Antral web in infancy. *J Pediatr Surg* 15:152–155, 1980.
- Mandell GA, Heyman S, Alavi A, et al: A case of microgastria in association with splenic-gonadal fusion. *Pediatr Radiol* 13:95–98, 1983.
- Kroes EJ, Festen C: Congenital microgastria: A case report and review of literature. *Pediatr Surg Int* 13:416–418, 1998.
- Samuel M, Burge DM, Griffiths DM: Prenatal diagnosis of laryngotracheoesophageal clefts. *Fetal Diagn Ther* 12:260–265, 1997.
- Hasegawa S, Kohno S, Tamura K, et al: Congenital microgastria in an infant with the VACTERL association. *J Pediatr Surg* 28:782–784, 1993.
- Sharma SC, Menon P: Congenital microgastria with esophageal stenosis and diaphragmatic hernia. *Pediatr Surg Int* 21:292–294, 2005.
- Ramos CT, Moss RL, Musmeche CA: Microgastria as an isolated anomaly. *J Pediatr Surg* 31:1445–1447, 1996.
- Fonkalsrud EW, deLorimier AA, Hays DM: Congenital atresia and stenosis of the duodenum: A review compiled from the members of the Surgical Section of the American Academy of Pediatrics. *Pediatrics* 43:79–83, 1969.
- Choudhry MS, Rahman N, Boyd P, Lakhoo K: Duodenal atresia: Associated anomalies, prenatal diagnosis and outcome. *Pediatr Surg Int* 25:727–730, 2009.
- Smith GV, Teele RL: Delayed diagnosis of duodenal obstruction in Down syndrome. *AJR Am J Roentgenol* 120:315–321, 1980.
- Grosfeld JL, Rescoria FJ: Duodenal atresia and stenosis: Reassessment of treatment and outcome based on antenatal diagnosis, pathologic variance, and long-term follow-up. *World J Surg* 17:301–309, 1993.
- Samuel M, Wheeler RA, Mami AG: Does duodenal atresia and stenosis prevent midgut volvulus in malrotation? *Eur J Pediatr Surg* 7:11–12, 1997.
- Latzman JM, Levin TL, Nafday SM: Duodenal atresia: Not always a double bubble. *Pediatr Radiol* 44:1031–1034, 2014.
- Miro J, Bard H: Congenital atresia and stenosis of the duodenum: The impact of a prenatal diagnosis. *Am J Obstet Gynecol* 158:555–559, 1988.
- Gilbertson-Dahdal DL, Dutta S, Varich LJ, Barth RA: Neonatal malrotation with midgut volvulus mimicking duodenal atresia. *AJR Am J Roentgenol* 192:1269–1271, 2009.
- Karoll MP, Ghahremani GG, Port RB, et al: Diagnosis and management of intraluminal duodenal diverticulum. *Dig Dis Sci* 28:411–416, 1983.
- Cremin BJ, Solomon DJ: Ultrasonic diagnosis of duodenal diaphragm. *Pediatr Radiol* 17:489–490, 1987.
- Heithoff KB, Sane SM, Williams JH, et al: Bronchopulmonary foregut malformations: A unifying etiological concept. *AJR Am J Roentgenol* 126:46–55, 1976.
- Murty TVM, Bhargava RK, Rakas FS: Gastro-duodenal duplication. *J Pediatr Surg* 27:515–517, 1992.
- Bower RJ, Sieber WK, Kiesewetter WB: Alimentary tract duplications in children. *Ann Surg* 188:669–674, 1978.
- Achildi O, Grewal H: Congenital anomalies of the esophagus. *Otolaryngol Clin North Am* 40:219–244, 2007.
- Neuhauser EBD, Harris GBC, Berret A: Roentgenographic features of neurenteric cysts. *AJR Am J Roentgenol* 79:235–240, 1958.
- Merrot T, Anastasescu R, Pankevych T, et al: Duodenal duplications. Clinical characteristics, embryological hypotheses, histological findings, treatment. *Eur J Pediatr Surg* 16:18–23, 2006.
- Richards DS, Langham MR, Anderson CD: The prenatal sonographic appearance of enteric duplication cysts. *Ultrasound Obstet Gynecol* 7:17–20, 1996.
- Ozman MN, Onderoglu L, Ciftci AO, et al: Prenatal diagnosis of gastric duplication cyst. *J Ultrasound Med* 16:219–222, 1997.
- Teel RL, Henschke CI, Tapper D: The radiographic and ultrasonographic evaluation of enteric duplication cysts. *Pediatr Radiol* 10:9–14, 1980.
- Lamont AC, Starinsky R, Cremin BJ: Ultrasonic diagnosis of duplication cysts in children. *Br J Radiol* 57:463–467, 1984.
- Gupta AK, Berry M, Mitra DK: Gastric duplication cyst in children: Report of two cases. *Pediatr Radiol* 24:346–347, 1994.
- Blake NS: Beak sign in duodenal duplication cyst. *Pediatr Radiol* 14:232–233, 1984.
- Hamada Y, Inoue K, Hioki K: Pyloroduodenal duplication cyst: Case report. *Pediatr Surg Int* 12:194–195, 1997.
- Cheng G, Soboleski D, Daneman A, et al: Sonographic pitfalls in the diagnosis of enteric duplication cysts. *AJR Am J Roentgenol* 184:521–525, 2005.
- Ortiz-Neira CL: The corkscrew sign of midgut volvulus. *Radiology* 242:315–316, 2007.
- Berdon WE, Baker DH, Bull S, et al: Midgut malrotation and volvulus. Which films are most helpful? *Radiology* 96:375–383, 1970.
- Long FR, Kramer SS, Markowitz RI, et al: Radiographic patterns of intestinal malrotation in children. *Radiographics* 16:547–556, 1996.
- Taylor GA: CT appearance of the duodenum and mesenteric vessels in children with normal and abnormal bowel rotation. *Pediatr Radiol* 41:1378–1383, 2011.
- Daneman A: Malrotation: The balance of evidence. *Pediatr Radiol* 39(Suppl 2):S164–S166, 2009.
- Jit I: The development and the structure of the suspensory muscle of the duodenum. *Anat Rec* 113:395–407, 1952.
- Applegate KE: Evidence-based diagnosis of malrotation and volvulus. *Pediatr Radiol* 39(Suppl 2):S161–S163, 2009.
- Yousefzadeh DK: The position of the duodenojejunal junction: The wrong horse to bet on in diagnosing or excluding malrotation. *Pediatr Radiol* 39(Suppl 2):S172–S177, 2009.
- Rescoria FJ, Shedd FJ, Grosfeld JL, et al: Anomalies of intestinal rotation in childhood: Analysis of 447 cases. *Surgery* 108:710–715, 1990.
- Palmas G, Maxia L, Fanos V: Volvulus and intestinal malrotation in the newborn. *Pediatr Med Chir* 27:62–66, 2005.
- Epelman M: The whirlpool sign. *Radiology* 240:910–911, 2006.
- El-Gohary Y, Alagtal M, Gillick J: Long-term complications following operative intervention for intestinal malrotation: A 10-year review. *Pediatr Surg Int* 26:203–206, 2010.
- Blumhagen JD: The role of ultrasonography in the evaluation of vomiting in infants. *Pediatr Radiol* 16:324–327, 1986.
- Bowen AD: The vomiting infant: Recent advances and unsettled issues in imaging. *Radiol Clin North Am* 26:377–392, 1988.
- Cohen HL, Haller JO, Mestel AL, et al: Neonatal duodenum: Fluid-aided US examination. *Radiology* 164:805–809, 1987.
- Applegate KE, Anderson JM, Klatte EC: Intestinal malrotation in children: A problem-solving approach to the upper gastrointestinal series. *Radiographics* 26:1485–1500, 2006.

55. Tang V, Daneman A, Navarro OM, Gerstle JT: Disorders of midgut rotation: Making the correct diagnosis on UGI series in difficult cases. *Pediatr Radiol* 43:1093–1102, 2013.
56. Menten R, Reding R, Godding V, et al: Sonographic assessment of the retroperitoneal position of the third portion of the duodenum: An indicator of normal intestinal rotation. *Pediatr Radiol* 42:941–945, 2012.
57. Katz ME, Siegel MJ, Shackelford GD, et al: The position and mobility of the duodenum in children. *AJR Am J Roentgenol* 148:947–951, 1987.
58. Taylor GA, Teele RL: Chronic intestinal obstruction mimicking malrotation in children. *Pediatr Radiol* 15:392–394, 1985.
59. Long FR, Kramer SS, Markowitz RI, et al: Intestinal malrotation in children: Tutorial on radiographic diagnosis in difficult cases. *Radiology* 198:775–780, 1996.
60. Lim-Dunham JE, Ben-Ami T, Yousefzadeh DK: Manual epigastric compression during upper gastrointestinal examination of neonates: Value in diagnosis of intestinal malrotation and volvulus. *AJR Am J Roentgenol* 173:979–983, 1999.
61. Shaw A, Blanc WA, Santulli TV, et al: Spontaneous rupture of the stomach in the newborn: A clinical and experimental study. *Surgery* 58:561–571, 1965.
62. Young AE, Sury MR: Spontaneous neonatal gastric perforation. *Pediatr Anaesth* 6:143–145, 1996.
63. Lloyd JR: The etiology of gastrointestinal perforation in the newborn. *J Pediatr Surg* 4:77–84, 1969.
64. Odita JC, Omene JA, Okolo AA: Gastric distension in neonatal necrotizing enterocolitis. *Pediatr Radiol* 17:202–205, 1987.
65. Ibach JR, Inouye WY: Neonatal gastric perforation secondary to annular pancreas. *Am J Surg* 110:985–987, 1965.
66. Pochaczewsky R, Bryk DK: New roentgenographic signs of neonatal gastric perforation. *Radiology* 102:145–147, 1972.
67. Miller BM, Kumar A: Neonatal duodenal perforation. *J Pediatr Gastroenterol Nutr* 11:407–410, 1990.
68. Nord KS: Peptic ulcer disease in the pediatric population. *Pediatr Clin North Am* 35:117–140, 1988.
69. Magill HL, Hixson SD, Whittington G, et al: Duodenal perforation in childhood dermatomyositis. *Pediatr Radiol* 14:28–30, 1984.
70. Schullinger JN, Jacobs JC, Berdon WE: Diagnosis and management of gastrointestinal perforations in childhood dermatomyositis with particular reference to perforations of the duodenum. *J Pediatr Surg* 20:521–524, 1985.
71. Oi SZ, Shose Y, Asano N, et al: Intragastric migration of a ventriculoperitoneal shunt catheter. *Neurosurgery* 21:255–257, 1987.
72. Estrera A, Taylor W, Mills LF, et al: Corrosive burns of the esophagus and stomach: A recommendation for an aggressive surgical approach. *Ann Thorac Surg* 41:276–283, 1986.
73. Glick PL, Harrison MR, Adzick NS, et al: Gastric infarction secondary to small bowel obstruction: A preventable complication after Nissen fundoplication. *J Pediatr Surg* 22:941–943, 1987.
74. Richter JE: Gastroesophageal reflux disease treatment: Side effects and complications of fundoplication. *Clin Gastroenterol Hepatol* 11:465–471, quiz e39, 2013.
75. Rohof WO, Bisschops R, Tack J, Boeckxstaens GE: Postoperative problems 2011: Fundoplication and obesity surgery. *Gastroenterol Clin North Am* 40:809–821, 2011.
76. Pandya S, Heiss K: Pyloric stenosis in pediatric surgery: An evidence-based review. *Surg Clin North Am* 92:527–539, vii–viii, 2012.
77. Cogley JR, O'Connor SC, Houshyar R, Al Dulaimy K: Emergent pediatric US: What every radiologist should know. *Radiographics* 32:651–665, 2012.
78. Ranells JD, Carver JD, Kirby RS: Infantile hypertrophic pyloric stenosis: Epidemiology, genetics, and clinical update. *Adv Pediatr* 58: 195–206, 2011.
79. Haller JO, Cohen HL: Hypertrophic pyloric stenosis: Diagnosis using ultrasound. *Radiology* 161:335–339, 1986.
80. Aspelund G, Langer JC: Current management of hypertrophic pyloric stenosis. *Semin Pediatr Radiol* 16:27–33, 2007.
81. Mandell GA, Wolfson PJ, Adkins ES, et al: Cost-effective imaging approach to nonbilious vomiting infant. *Pediatrics* 103:1198–1202, 1999.
82. Hernanz-Schulman M: Infantile hypertrophic pyloric stenosis. *Radiology* 227:319–331, 2003.
83. Hernanz-Schulman M, Lowe LH, Johnson J, et al: In vivo visualization of pyloric mucosal hypertrophy in infants with hypertrophic pyloric stenosis: Is there an etiologic role? *AJR Am J Roentgenol* 177:843–848, 2001.
84. Cohen HL, Blumer SL, Zucconi WB: The sonographic double-track sign: Not pathognomonic for hypertrophic pyloric stenosis; can be seen in pylorospasm. *J Ultrasound Med* 23:641–646, 2004.
85. Blumhagen JD, Maclin L, Krauter D, et al: Sonographic diagnosis of hypertrophic pyloric stenosis. *AJR Am J Roentgenol* 150:1367–1370, 1988.
86. Finkelstein MS, Mandell GA, Tarbell KV: Hypertrophic pyloric stenosis: Volumetric measurement of nasogastric aspirate to determine the imaging modality. *Radiology* 177: 759–761, 1990.
87. Iqbal CW, Rivard DC, Mortellaro VE, et al: Evaluation of ultrasonographic parameters in the diagnosis of pyloric stenosis relative to patient age and size. *J Pediatr Surg* 47:1542–1547, 2012.
88. Jamroz GA, Blocker SH, McAlister WH: Radiographic findings after incomplete pyloromyotomy. *Gastrointest Radiol* 11:139–141, 1986.
89. Cass DT: Gastric retention of a swallowed coin after surgical treatment of pyloric stenosis. *Aust Paediatr J* 25:299–301, 1989.
90. Jewett TC, Jr, Caldarola V, Karp MP, et al: Intramural hematoma of the duodenum. *Arch Surg* 123:54–58, 1988.
91. Hernanz-Schulman M, Genieser NB, Ambrosino M: Sonographic diagnosis of intramural duodenal hematoma. *J Ultrasound Med* 8:273–276, 1989.
92. Foley C, Teele RL: Ultrasound of epigastric injuries after blunt abdominal trauma. *AJR Am J Roentgenol* 132:593–598, 1979.
93. Iuchtman M, Steiner T, Faierman T, et al: Post-traumatic intramural duodenal hematoma in children. *Isr Med Assoc J* 8:95–97, 2006.
94. Clendenon JN, Meyers RL, Nance ML, Scaife ER: Management of duodenal injuries in children. *J Pediatr Surg* 39:964–968, 2004.
95. Bechtel K, Moss RL, Leventhal JM, et al: Duodenal hematoma after upper endoscopy and biopsy in a 4-year-old girl. *Pediatr Emerg Care* 22:653–654, 2006.
96. Megremis S, Segkos N, Andrianaki A, et al: Sonographic diagnosis and monitoring of an obstructing duodenal hematoma after blunt trauma: Correlation with computed tomographic and surgical findings. *J Ultrasound Med* 23:1679–1683, 2004.
97. Tu RK, Starshak RJ, Brown B: CT diagnosis of gastric rupture following blunt abdominal trauma in a child. *Pediatr Radiol* 22:146–147, 1992.
98. Sidhu MK, Weinberger E, Healey P: Intramural duodenal hematoma after blunt abdominal trauma. *AJR Am J Roentgenol* 170:38, 1998.
99. Touloukian RJ: Protocol for the nonoperative treatment of obstructing intramural duodenal hematoma during childhood. *Am J Surg* 145: 330–334, 1983.
100. Cook DE, Walsh JW, Vick CW, et al: Upper abdominal trauma: Pitfalls in CT diagnosis. *Radiology* 159:65–69, 1986.
101. Saito JM: Beyond appendicitis: Evaluation and surgical treatment of pediatric acute abdominal pain. *Curr Opin Pediatr* 24:357–364, 2012.
102. Wolfson PJ, Fabius RJ, Leibowitz AN: The Rapunzel syndrome: An unusual trichobezoar. *Am J Gastroenterol* 82:365–367, 1987.
103. Yoss BS: Human milk lactobezoars. *J Pediatr* 105:819–822, 1984.
104. Ament ME, Berquist WE, Vargas J, et al: Fiberoptic upper intestinal endoscopy in infants and children. *Pediatr Clin North Am* 35:141–155, 1988.
105. Litovitz T, Whitaker N, Clark L, et al: Emerging battery-ingestion hazard: Clinical implications. *Pediatrics* 125:1168–1177, 2010.
106. Otjen JP, Rohrmann CA, Jr, Iyer RS: Imaging pediatric magnet ingestion with surgical-pathological correlation. *Pediatr Radiol* 43: 851–859, 2013.
107. Kircher MF, Milla S, Callahan MJ: Ingestion of magnetic foreign bodies causing multiple bowel perforations. *Pediatr Radiol* 37:933–936, 2007.
108. Tavaréz MM, Saladino RA, Gaines BA, Manole MD: Prevalence, clinical features and management of pediatric magnetic foreign body ingestions. *J Emerg Med* 44:261–268, 2013.
109. Hueman MT, Schlick RD: Management of gastrointestinal stromal tumors. *Surg Clin North Am* 88:599–614, vii, 2008.
110. Gengler JS, Ashcroft KW, Slattery P: Gastric teratoma: The sixth reported case in a female infant. *J Pediatr Surg* 30:889–890, 1995.
111. Niedzwiecki G, Wood BP: Radiological cases of the month. Gastric teratoma. *Am J Dis Child* 144:1147–1148, 1990.
112. Dunlap JP, James DA, Maxson RT, et al: Gastric teratoma with intramural extension. *Pediatr Radiol* 25:383–384, 1995.
113. Atwell JD, Claireaux AE, Nixon HH: Teratoma of the stomach in the newborn. *J Pediatr Surg* 2:197–204, 1967.
114. Nelson RS, Word R, McGill C: Clinical quiz: Gastric teratoma. *J Pediatr Gastroenterol Nutr* 42:249–250, 2006.
115. Ablin DS, Brant WE: Cystic leiomyosarcoma of the stomach in a child. *J Clin Ultrasound* 20: 72–76, 1992.
116. Wurliizer FP, Mares AJ, Isaacs H, Jr, et al: Smooth muscle tumors of the stomach in childhood and adolescence. *J Pediatr Surg* 8: 421–427, 1973.
117. Van Steenberg W, Kojima T, Geboes K, et al: Gastric leiomyoblastoma with metastases to

- the liver: A 36-year follow-up study. *Gastroenterology* 89:875–881, 1985.
118. Krudy AG, Long JL, Magrath IT, et al: Gastric manifestations of North American Burkitt's lymphoma. *Br J Radiol* 56:697–702, 1983.
 119. Choe BK, Kim JY, Hwang JB, et al: A case of primary gastric lymphoma in a child. *J Pediatr Hematol Oncol* 28:296–299, 2006.
 120. Ladd AP, Grosfeld JL: Gastrointestinal tumors in children and adolescents. *Semin Pediatr Surg* 15:37–47, 2006.
 121. Haerer AF, Jackson JF, Evers CG: Ataxia-telangiectasia with gastric adenocarcinoma. *JAMA* 210:1884–1887, 1969.
 122. Benesch M, Wardelmann E, Ferrari A, et al: Gastrointestinal stromal tumors (GIST) in children and adolescents: A comprehensive review of the current literature. *Pediatr Blood Cancer* 53:1171–1179, 2009.
 123. Maves CK, Johnson JF, Bove D, et al: Gastric inflammatory pseudotumor in children. *Radiology* 173:381–383, 1989.
 124. Iida M, Yao T, Itoh H, et al: Natural history of fundic gland polyposis in patients with familial adenomatous coli/Gardner's syndrome. *Gastroenterology* 89:1021–1025, 1985.
 125. Schroeder BA, Wells RG, Sty JR: Inflammatory fibroid polyp of the stomach in a child. *Pediatr Radiol* 17:71–72, 1987.
 126. Buts J-P, Gosseye S, Claus D, et al: Solitary hyperplastic polyp of the stomach. *Am J Dis Child* 135:846–847, 1981.
 127. Katz ME, Blocker SH, McAlister WH: Focal foveolar hyperplasia presenting as an antral-pyloric mass in a young infant. *Pediatr Radiol* 15:136–137, 1985.
 128. McAlister WH, Katz ME, Perlman JM, et al: Sonography of focal foveolar hyperplasia causing gastric obstruction in an infant. *Pediatr Radiol* 18:79–81, 1988.
 129. Tishler JM, Han SY, Colcher H, et al: Neurogenic tumors of the duodenum in patients with neurofibromatosis. *Radiology* 149:51–53, 1983.
 130. Kilman WJ, Berk RN: The spectrum of radiographic features of aberrant pancreatic rests involving the stomach. *Radiology* 123:291–296, 1977.
 131. Lamont AC, Rode H: Retrograde jejuno-duodeno-gastric intussusception. *Br J Radiol* 58:559–561, 1985.
 132. Levine MS, Rubesin SE: The *Helicobacter pylori* revolution: Radiologic perspective. *Radiology* 195:593–596, 1995.
 133. Costa Lopes AI, Palha A, Monteiro L, et al: *Helicobacter pylori* genotypes in children from a population at high gastric cancer risk: No association with gastroduodenal histopathology. *Am J Gastroenterol* 101:2113–2122, 2006.
 134. Blecker U: *Helicobacter pylori* disease in childhood. *Clin Pediatr* 35:175–183, 1996.
 135. Mitchell JD, Mitchell HM, Tobias V: Acute *Helicobacter pylori* in recurrent, functional abdominal pain in children. *Am J Gastroenterol* 87:347–349, 1992.
 136. Czinn SJ: *Helicobacter pylori* infection: Detection, investigation, and management. *J Pediatr* 146(Suppl):S21–S26, 2005.
 137. Sykora J, Rowland M: *Helicobacter pylori* in pediatrics. *Helicobacter* 16(Suppl 1):59–64, 2011.
 138. Schwartz S, Edden Y, Orkin B, Erlichman M: Perforated peptic ulcer in an adolescent girl. *Pediatr Emerg Care* 28:709–711, 2012.
 139. Hua MC, Kong MS, Lai MW, Luo CC: Perforated peptic ulcer in children: A 20-year experience. *J Pediatr Gastroenterol Nutr* 45:71–74, 2007.
 140. Marks MP, Lanza MV, Kahlstrom EJ, et al: Pediatric hypertrophic gastropathy. *AJR Am J Roentgenol* 147:1031–1034, 1986.
 141. Trout AT, Dillman JR, Neef HC, et al: Case 189: Pediatric Ménétrier disease. *Radiology* 266:357–361, 2013.
 142. Friedman J, Platnick J, Farruggia S, et al: Ménétrier disease. *Radiographics* 29:297–301, 2009.
 143. Cardenas A, Kelly C: Ménétrier disease. *Gut* 53(330):338, 2004.
 144. Gassner I, Strasser K, Bart G, et al: Sonographic appearance of Ménétrier's disease in a child. *J Ultrasound Med* 9:537–539, 1990.
 145. Fleischer DM, Atkins D: Evaluation of the patient with suspected eosinophilic gastrointestinal disease. *Immunol Allergy Clin North Am* 29:53–63, ix, 2009.
 146. Rothenberg ME: Eosinophilic gastrointestinal disorders (EGID). *J Allergy Clin Immunol* 113:11–28, quiz 29, 2004.
 147. Vitellas KM, Bennett WF, Bova JG, et al: Radiographic manifestations of eosinophilic gastroenteritis. *Abdom Imaging* 20:406–413, 1995.
 148. Teele RL, Katz AJ, Goldman H, et al: The radiographic features of eosinophilic gastroenteritis (allergic gastroenteropathy) of childhood. *AJR Am J Roentgenol* 132:575–580, 1979.
 149. Marciano BE, Rosenzweig SD, Kleiner DE, et al: Gastrointestinal involvement in chronic granulomatous disease. *Pediatrics* 114:462–468, 2004.
 150. Towbin AJ, Chaves I: Chronic granulomatous disease. *Pediatr Radiol* 40:657–668, quiz 792–793, 2010.
 151. Griscom NTG, Kirkpatrick JA, Jr, Girdany BR, et al: Gastric antral narrowing in chronic granulomatous disease of childhood. *Pediatrics* 54:456–460, 1974.
 152. Kopen PA, McAlister WH: Upper gastrointestinal and ultrasound examinations of gastric antral involvement in chronic granulomatous disease. *Pediatr Radiol* 14:91–93, 1984.
 153. Kirschner BS: Inflammatory bowel disease in children. *Pediatr Clin North Am* 35:189–208, 1988.
 154. Manson DE, Stringer DA, Durie PR, et al: The radiologic and endoscopic investigation and etiologic classification of gastritis in children. *Can Assoc Radiol J* 41:201–206, 1990.
 155. Shimoyama Y, Kusano M, Hirano Y, et al: Onset of gastric Crohn's disease observed endoscopically. *Gastrointest Endosc* 72:1060–1061, 2010.
 156. Kagimoto S: Duodenal findings on ultrasound in children with Schönlein-Henoch purpura and gastrointestinal symptoms. *J Pediatr Gastroenterol Nutr* 16:178–182, 1993.
 157. Ozdemir H, Isik S, Buyan N, et al: Sonographic demonstration of intestinal involvement in Henoch-Schönlein syndrome. *Eur J Radiol* 20:32–34, 1995.
 158. Rathore M, Shrivastava R, Goyal R, et al: Henoch Schönlein purpura presenting as duodenal ulcer and gastric outlet obstruction. *Indian J Pediatr* 81:189–190, 2014.
 159. Palmer PES: Diagnostic imaging in parasitic infections. *Pediatr Clin North Am* 32:1019–1040, 1985.
 160. Sugimachi K, Inokuchi K, Ooiwa T, et al: Acute gastric anisakiasis. Analysis of 178 cases. *JAMA* 253:1012–1013, 1985.
 161. Marshak RH, Ruoff M, Lindner AE: Roentgen manifestations of giardiasis. *AJR Am J Roentgenol* 104:557–560, 1968.
 162. Berkmen YM, Rabinowitz J: Gastrointestinal manifestations of the strongyloidiasis. *AJR Am J Roentgenol* 115:306–311, 1972.
 163. Kay M, Wyllie R: Caustic ingestions in children. *Curr Opin Pediatr* 21:651–654, 2009.
 164. Ceylan H, Ozokutan BH, Gunduz F, Gozen A: Gastric perforation after corrosive ingestion. *Pediatr Surg Int* 27:649–653, 2011.
 165. Martel WM: Radiologic features of esophagogastritis secondary to extremely caustic agents. *Radiology* 103:31–36, 1972.
 166. Goldman LP, Weigert JM: Corrosive substance ingestion: A review. *Am J Gastroenterol* 79:85–90, 1984.
 167. Ziprkowski MN, Teele RL: Gastric volvulus in childhood. *AJR Am J Roentgenol* 132:921–925, 1979.
 168. Elhalaby EA, Mashaly EM: Infants with radiologic diagnosis of gastric volvulus: Are they over-treated? *Pediatr Surg Int* 17:596–600, 2001.
 169. Chang SW, Lee HC, Yeung CY, et al: Gastric volvulus in children. *Acta Paediatr Taiwan* 47:18–24, 2006.
 170. Bonadio WA, Wood BP: Radiological case of the month. Intrathoracic stomach with volvulus. *Am J Dis Child* 143:503–504, 1989.
 171. Reddy ER, Onyett H, Fitzgerald GW: Gastric torsion. *Can Assoc Radiol J* 40:47–48, 1989.
 172. Moskovich R, Cheong-Leen P: Vascular compression of the duodenum. *J R Soc Med* 79:465–467, 1986.
 173. McClenahan JH, Wood BP: Radiological case of the month. Hyperthyroidism as a cause of superior mesenteric artery syndrome. *Am J Dis Child* 142:685–686, 1988.
 174. Ortiz C, Cleveland RH, Blickman JG, et al: Familial superior mesenteric artery syndrome. *Pediatr Radiol* 20:588–589, 1990.
 175. Marchant EA, Alvear DT, Fagelman KM: True clinical entity of vascular compression of the duodenum in adolescence. *Surg Gynecol Obstet* 168:381–386, 1989.
 176. Eaves ER, Schmidt GT: Chronic idiopathic megaduodenum in a family. *Aust N Z J Med* 15:1–6, 1985.
 177. Milla PJ: Gastrointestinal motility disorders in children. *Pediatr Clin North Am* 35:311–330, 1988.
 178. Phelan MS, Fine DR, Zentler-Munro PL, et al: Radiographic abnormalities of the duodenum in cystic fibrosis. *Clin Radiol* 34:573–577, 1983.
 179. Carty H: Abdominal radiology in cystic fibrosis. *J R Soc Med* 88(Suppl 25):18–23, 1995.
 180. Selimoglu MA, Karabiber H, Otlu B, et al: Correlation of clinical, endoscopic, and histologic findings with virulence factors in children with *Helicobacter pylori* gastritis. *Eur J Gastroenterol Hepatol* 26:602–606, 2014.

CHAPTER OUTLINE

Meckel's Diverticulum

Clinical Findings

Imaging Findings

Intestinal Lymphangiectasia

Clinical Findings

Imaging Findings

Henoch-Schönlein Purpura

Clinical Findings

Imaging Findings

Meckel's Diverticulum**CLINICAL FINDINGS**

Meckel's diverticulum is a common congenital abnormality of the gastrointestinal tract that can produce varied complications and therefore diverse clinical manifestations. It is the most frequent in a spectrum of abnormalities that occur in the small bowel secondary to failed regression in early fetal life of the omphalomesenteric (vitelline) duct, the tract through which the primitive midgut communicates with the yolk sac. Incomplete resorption of the duct can produce abnormalities anywhere along its course between the ileum and the umbilicus, which in addition to Meckel's diverticulum include omphalomesenteric or mesodiverticular bands, vitelline fistula, omphalomesenteric cyst, and umbilical polyps (Fig. 117-1).¹⁻⁹

Meckel's diverticulum is a result of the patency of the ileal end and closure of the umbilical end of the omphalomesenteric duct and is a true diverticulum, composed of all bowel layers. Unlike alimentary duplications and most other bowel diverticula, Meckel's diverticulum arises from the antimesenteric border of the bowel and has a separate blood supply, the vitelointestinal artery.^{5,8} According to the "rule of 2's," Meckel's diverticulum has an incidence of approximately 2%, arises in the ileum within 2 feet of the ileocecal valve, and becomes clinically symptomatic by the age of 2 years.^{8,10}

Clinical symptoms secondary to complications of Meckel's diverticulum are varied and occur in approximately 4% of patients with Meckel's diverticulum. The most common complications are rectal hemorrhage and intussusception.^{1-5,8}

Painless lower gastrointestinal bleeding is a major complication of the approximately 20% to 55% of Meckel's diverticula that contain acid-secreting ectopic gastric mucosa and is more frequent in children than in adults.^{1,3} The small bowel adjacent to the ectopic gastric mucosa becomes ulcerated from exposure to the acid, resulting in hemorrhage. Ileoileal and ileocolic intussusceptions result when Meckel's diverticulum serves as a lead point, and an irreducible intussusception should raise suspicion for Meckel's diverticulum.^{1,2,4-6,8,10} Other

less common complications of Meckel's diverticulum include small bowel obstruction from volvulus or hernia around an associated omphalomesenteric band; bowel perforation; diverticulitis or inflammation of the diverticulum itself; and Littre hernia, which is an inguinal hernia containing Meckel's diverticulum.^{1-2,8-10}

A specific form of Meckel's diverticulum is giant Meckel's diverticulum, which tends to be larger than the average size of 2×3 cm and is long with a narrow neck.¹¹ It can serve as a lead point for focal volvulus or may undergo torsion at its base.^{11,12} Stasis in enormous Meckel's diverticula may lead to bacterial overgrowth, resulting in malabsorption.

IMAGING FINDINGS

Plain abdominal radiographs usually have normal findings but may show obstruction if the diverticulum is complicated by intussusception. Meckel's diverticulum rarely fills on routine barium studies, possibly because of small size or blockage of the lumen with ingested debris, but it may opacify with the higher pressures of enteroclysis.^{8,13} Difficulty in detection is compounded by overlying bowel loops that may obscure the diverticulum unless they are displaced with compression. A mucosal triangular plateau or a triradiate fold pattern in the right lower quadrant has been described in small bowel examinations in patients with Meckel's diverticulum.¹³ Air-filled giant Meckel's diverticula may fill with contrast medium on delayed studies (Fig. 117-2).¹² Children with small bowel hernia or volvulus around an omphalomesenteric band often show nonspecific findings of lower small bowel obstruction (Fig. 117-3).

Advanced imaging including computed tomography (CT) and ultrasound is routinely used to study children who present with symptoms of an acute abdomen, especially right lower quadrant pain. Meckel's diverticulum itself as well as secondary complications such as intussusceptions can be detected (Fig. 117-4). On sonography, inflamed Meckel's diverticulum can appear as a cystic or tubular structure with thickened walls, sometimes displaying the characteristic alternating hyperechoic and hypoechoic bands of intestinal wall.⁴⁻⁷ Doppler and color Doppler sonography may demonstrate the inflammatory changes more clearly.⁴⁻⁷ By CT or magnetic resonance (MR) enterography, the inflamed diverticulum may appear as an air-, fluid- or contrast-filled blind-ending pouch with thickened walls in the right lower quadrant with inflammatory changes in the adjacent mesentery.^{3-6,14} Inverted Meckel's diverticulum, often the lead point of an intussusception, may also be seen as a filling defect in the opacified lumen.^{15,16}

Dilated and inflamed Meckel's diverticulum can resemble the dilated and inflamed appendix in appendicitis by sonography and CT. Clinical symptoms of right lower quadrant pain and fever also overlap in the two entities, and identification of the normal appendix in cases of suspected Meckel's diverticulum is recommended to aid in differentiation between the

two.^{8,10,14} An ileal duplication cyst may mimic Meckel's diverticulum; Meckel's diverticulum is distinguishable from an ileal duplication cyst by its thicker, more irregular wall and the presence of peristalsis.^{8,14}

Technetium Tc 99m pertechnetate nuclear scintigraphy is the most widely used method for diagnosis of bleeding Meckel's diverticula, and it has a sensitivity of 85%.^{4,5,8,17,18} The intravenously injected isotope localizes in the right lower quadrant of the abdomen within the ectopic gastric mucosa, with rate and pattern of activity mirroring that of gastric mucosa in the stomach (Fig. 117-5). Administration of pentagastrin before scintigraphy may be used to stimulate diverticular gastric mucosal uptake and thereby enhance sensitivity of detection if the result of a prior study has been negative or equivocal and Meckel's diverticulum is still strongly suspected.¹⁸

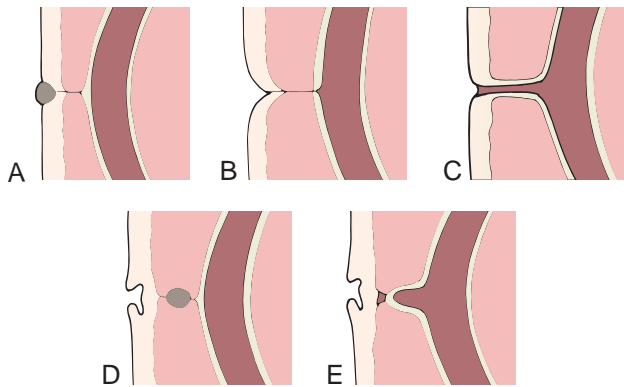


Figure 117-1 Abnormalities of regression of the omphalomesenteric duct. **A.** Umbilical polyp. **B.** Mesodiverticular or omphalomesenteric band. **C.** Patent omphalomesenteric duct or vitelline fistula. **D.** Vitelline cyst. **E.** Meckel's diverticulum.

False-negative study results can occur when residual gastrointestinal barium absorbs the emitted gamma rays, when profound ulceration or infarction has destroyed the gastric mucosa within the diverticulum, or when the isotope is incorrectly interpreted as being within the genitourinary tract. Lateral



Figure 117-2 Giant Meckel's diverticulum. The radiograph obtained after barium enema demonstrates residual contrast material within the colon and several small bowel loops. The large, rounded gas collection in the midabdomen, causing proximal small bowel obstruction, is a giant Meckel diverticulum.

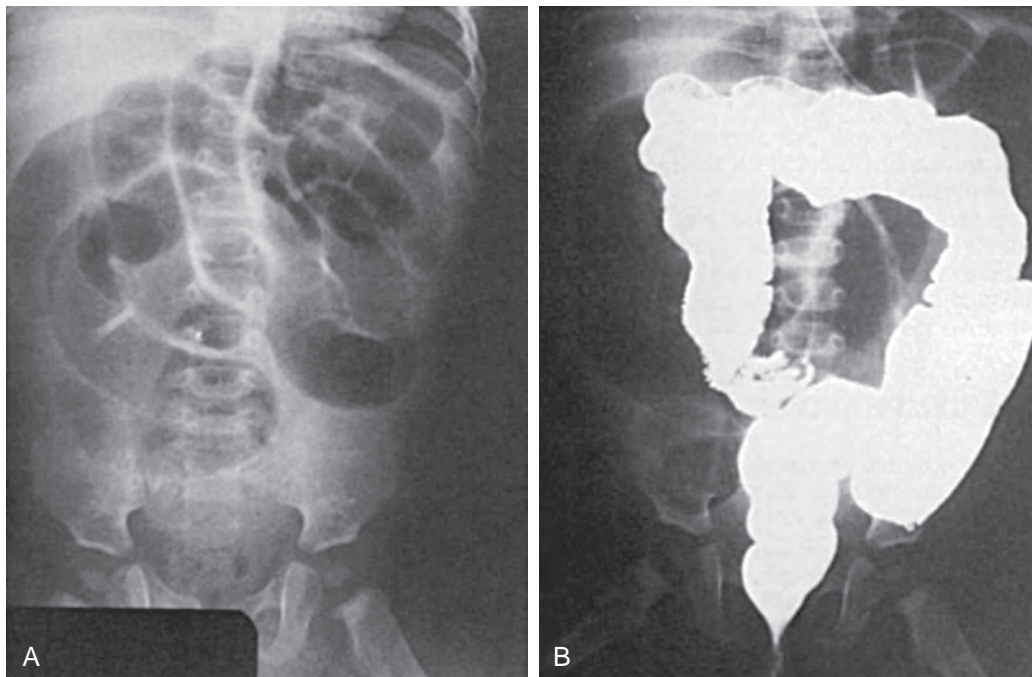


Figure 117-3 Omphalomesenteric band. **A.** Multiple, dilated small bowel loops suggest a low obstruction on the plain abdominal radiograph of an infant. **B.** The colon was normal, except that the right colon was displaced from the lateral abdominal wall, and it was impossible to distend the cecum. At surgery, small bowel that had herniated beneath the omphalomesenteric duct was found to be entrapped.

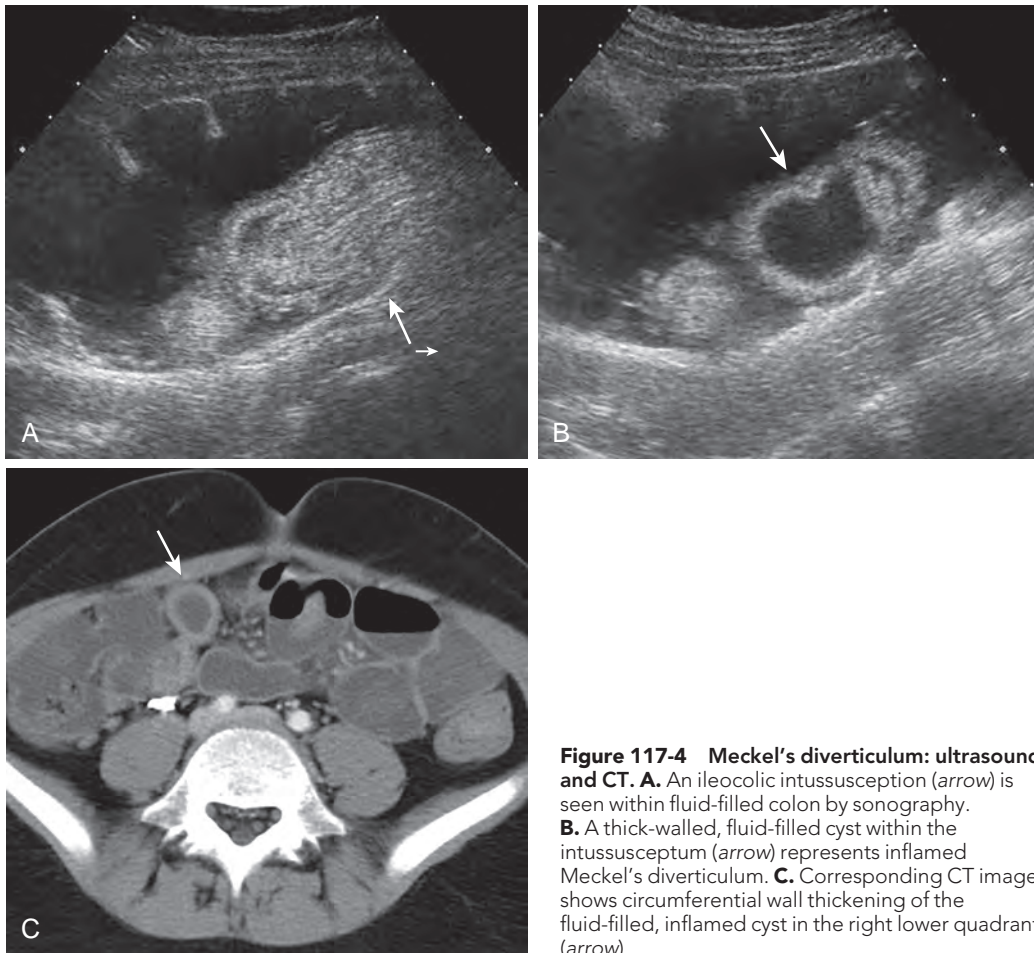


Figure 117-4 Meckel's diverticulum: ultrasound and CT. **A.** An ileocolic intussusception (arrow) is seen within fluid-filled colon by sonography. **B.** A thick-walled, fluid-filled cyst within the intussusceptum (arrow) represents inflamed Meckel's diverticulum. **C.** Corresponding CT image shows circumferential wall thickening of the fluid-filled, inflamed cyst in the right lower quadrant (arrow).

scans of the abdomen are performed routinely to minimize the last error.⁸ False-positive study results can also occur, but they are easier to recognize. Ectopic gastric mucosa in alimentary cysts is responsible for most of the false-positive results. Inflammatory processes may rarely localize the isotope, despite the absence of gastric mucosa.

Intestinal Lymphangiectasia

CLINICAL FINDINGS

Congenital and acquired disorders of the small bowel lymphatics can produce protein loss, diarrhea, and decreased immunoglobulin levels.¹⁹ Histologic changes include diffuse or focal dilation of lymphatics in all bowel layers that may be accompanied by villous changes and infiltration of the mucosa by inflammatory cells.¹⁹⁻²² Leakage of protein-rich lymphatic fluid from the dilated lymphatic channels into the gastrointestinal tract results in protein-losing enteropathy. Congenital lymphatic structural malformation is termed primary intestinal lymphangiectasia (Waldmann's disease) and typically is manifested before 3 years of age. Common symptoms include bilateral lower extremity edema and gastrointestinal complaints such as diarrhea, abdominal pain, nausea, and vomiting.²²

Because of the protein loss through the small bowel, the child may fail to thrive. Similar loss of lymph cells may produce lymphopenia. Definitive diagnosis of primary lymphangiectasia is made by endoscopy and intestinal biopsy.²³ Elevated levels of α_1 -antitrypsin in a 24-hour stool sample are indicative of protein-losing enteropathy and support the diagnosis.^{22,23}

When dilation of lymphatic channels is secondary to venous obstruction or elevated venous pressure, the disorder is termed secondary lymphangiectasia. Conditions known to cause secondary lymphangiectasia include inflammatory bowel disease, sarcoidosis, lymphoma, congestive heart failure, and constrictive pericarditis.²² Secondary lymphangiectasia is an uncommon but well-recognized complication in children who have undergone a Fontan procedure for complex congenital heart disease. Intestinal lymphangiectasia has long been recognized as part of the Noonan, Turner, Klippel-Trénaunay, and von Recklinghausen syndromes.²² Hennekam syndrome, an autosomal recessive disorder with mild to moderate mental retardation, peculiar facies, and ear defects, is also associated with lymphangiectasia.²⁴⁻²⁶

IMAGING FINDINGS

Small bowel series show thickening of the valvulae conniventes, nodularity of the mucosa, and excess secretions if

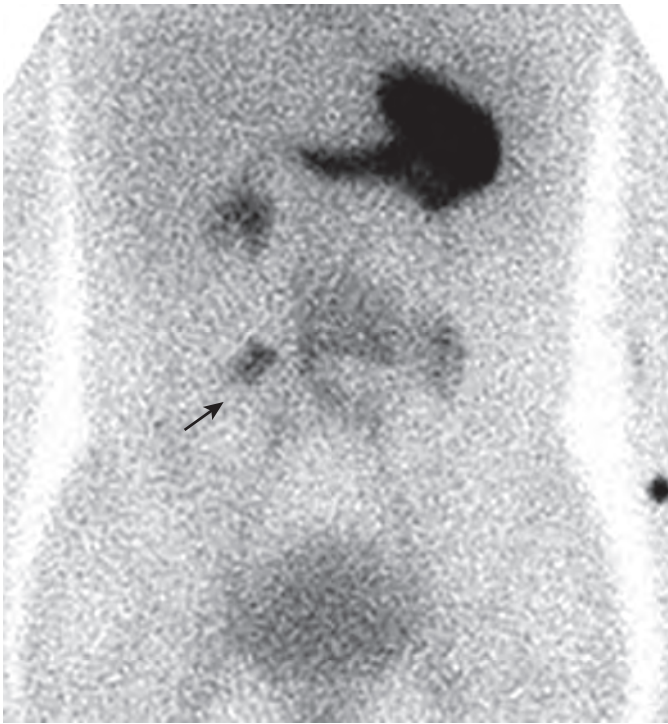


Figure 117-5 Meckel's diverticulum: nuclear scintigraphy. Technetium pertechnetate has passed from the stomach into the proximal small bowel. A small region of abnormal and persistent activity in the right lower quadrant (arrow) represents isotope localizing within ectopic gastric mucosa within Meckel's diverticulum.

there is malabsorption.¹⁹ The caliber of the gut is normal. Barium enema examination may show thickening of affected colonic folds.

Sonography and CT can also demonstrate the nonspecific findings of ascites, dilated lymphatics, and thickened bowel walls and mesentery.^{23,27-29} The last changes may be primary or result from the hypoproteinemia caused by this protein-losing enteropathy.

Functional imaging with human serum albumin nuclear medicine scintigraphy plays an important role in the work-up of suspected intestinal lymphangiectasia and has the advantage over α_1 -antitrypsin stool sampling of the ability not only to confirm the presence of the protein loss from the gastrointestinal tract but also to localize the anatomic site of protein leakage. In this diagnostic procedure, ^{99m}Tc -labeled human serum albumin is injected intravenously, and periodic images of the abdomen are obtained during a 24-hour period in search of abnormal radiotracer activity seeping in the bowel. Other radiopharmaceuticals used for this purpose include ^{99m}Tc -methylene diphosphonate and ^{99m}Tc -dextran.^{22,23,28}

Henoch-Schönlein Purpura

CLINICAL FINDINGS

Henoch-Schönlein purpura is the most common systemic vasculitis of childhood, typically involving the small bowel and kidney, and is associated with a distinctive rash.^{30,31} Henoch-Schönlein purpura spares the very young and is most common

in children between the ages of 3 and 10 years, occurring with a slight male predominance. As many as 30% of affected patients may be older than 20 years.^{30,31} It occurs more often in the winter than in other seasons.

Small bowel involvement in Henoch-Schönlein purpura is characterized by ischemia or hemorrhage into the bowel wall. The subsequent abdominal pain may be intense, simulating that of a surgical abdomen.³²⁻³⁶ Surgery may be needed in the 3% to 5% of children with Henoch-Schönlein purpura who develop complications, including bowel perforation and irreducible intussusception.³²⁻³⁴ Ileoileal intussusception occurs as often as the more common ileocolic intussusception. When the intussusception involves the small bowel alone, it frequently reduces spontaneously despite the underlying disease process. Gastrointestinal bleeding, which is less common in older patients, occurs in about half of the pediatric patients but is unlikely to require transfusion. Most children recover completely without residua of the acute process.

Renal disease usually is manifested as hematuria, whereas a significant decline in renal function is uncommon. Renal biopsy may document glomerulonephritis or changes of immunoglobulin A nephritis. The associated rash may evolve from a urticarial to a maculopapular rash to become the classically described palpable purpuric lesions. The skin lesions are most prominent over the buttocks and lower extremities. Biopsy of the skin lesions shows granulocytes around arterioles and venules.³¹ Brain involvement is less common but may take many forms, including seizures, blindness, and headache.³⁷ Genitourinary involvement is uncommon but may produce testicular or epididymal pain and simulate testicular torsion or epididymo-orchitis.³⁸ Arthralgias typically occur in a few large joints and can precede the skin lesions.

IMAGING FINDINGS

Plain radiographs of the abdomen usually have normal findings unless there has been perforation, intussusception with small bowel obstruction, or sufficient bowel wall thickening to produce thumbprinting of segments distended with air.³⁴ Studies of the upper gastrointestinal tract with contrast material show mucosal thickening and submucosal edema that tend to be localized (Fig. 117-6).³⁴ Obstruction or intussusception may be detected. Contrast enemas performed to reduce an ileocolic intussusception are well tolerated but usually are unsuccessful.³⁹

Sonography demonstrates mural thickening and sometimes fluid distention of affected bowel segments, usually jejunum or ileum (Fig. 117-7), which is often distended with fluid.^{34,39,40} Sonography is also useful in excluding associated abdominal processes such as intussusception. Sonography or scintigraphy has been used to evaluate those who develop acute scrotal pain or tenderness.^{38,41,42}

Diagnostic features of Henoch-Schönlein purpura, including bowel wall thickening and wall enhancement, are well demonstrated by advanced dedicated bowel imaging techniques such as CT and MR enterography performed with intravenous administration of contrast material as well as an oral contrast agent to achieve bowel distention (Fig. 117-8).^{35,43-45} Similar bowel abnormalities can be seen in a variety of other disorders, including graft-versus-host disease, ischemic or infectious enteritis, and inflammatory bowel disease.^{35,43,46,47}



Figure 117-6 Henoch-Schönlein purpura: small bowel examination. The valvulae are thickened in the jejunum. Contrast medium is diluted as it passes into more distal, fluid-filled loops.

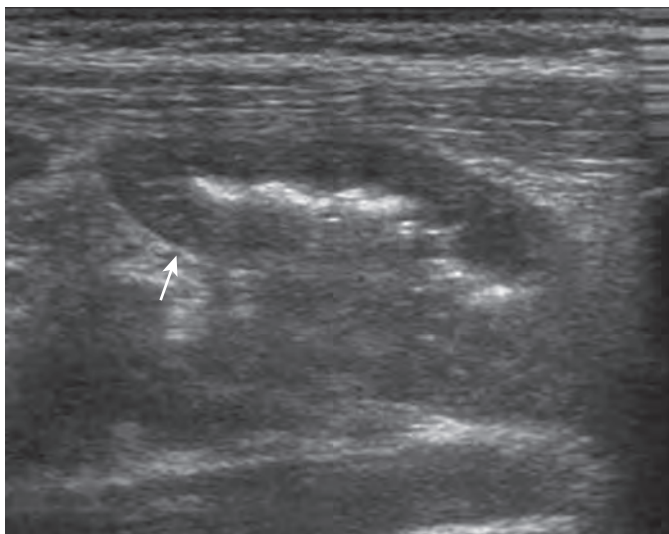


Figure 117-7 Henoch-Schönlein purpura: ultrasonography. Abnormal loop of small bowel showing marked thickening of the wall (arrow).

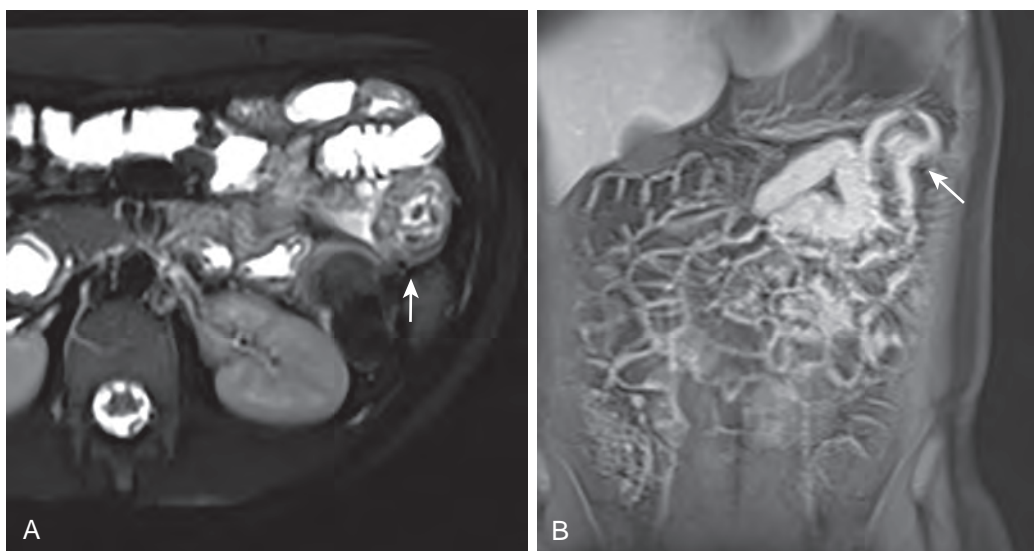


Figure 117-8 Henoch-Schönlein purpura: MR enterography. A. Axial T2-weighted half-Fourier acquisition single-shot turbo spin-echo (HASTE) fat-saturated image shows focal, circumferential wall thickening of a loop of jejunum in the left upper quadrant (arrow). **B.** Coronal T1-weighted fat-saturated three-dimensional volume-interpolated breath-hold examination (VIBE) delayed image after intravenous administration of gadolinium demonstrates abnormal wall enhancement of the same loop of bowel (arrow).

REFERENCES

- Alemayehu H, Hall M, Desai AA, et al: Demographic disparities of children presenting with symptomatic Meckel's diverticulum in children's hospitals. *Pediatr Surg Int* 30:649–653, 2014.
- St-Vil D, Brandt ML, Panic S, et al: Meckel's diverticulum in children: A 20-year review. *J Pediatr Surg* 26:1289–1292, 1991.
- Bennett GL, Birnbaum BA, Balthazar EJ: CT of Meckel's diverticulitis in 11 patients. *AJR Am J Roentgenol* 182:625–629, 2004.
- Rossi P, Gourtsoyannis N, Bezzi M, et al: Meckel's diverticulum: Imaging diagnosis. *AJR Am J Roentgenol* 166:567–573, 1996.
- Levy AD, Hobbs CM: From the archives of the AFIP. Meckel diverticulum: Radiologic features with pathologic correlation. *Radiographics* 24: 565–587, 2004.
- Daneman A, Lobo E, Alton DJ, et al: The value of sonography, CT, and air enema for detection of complicated Meckel diverticulum in children with nonspecific clinical presentation. *Pediatr Radiol* 28:928–932, 1998.
- Baldisserotto M, Maffazzoni DR, Dora MD: Sonographic findings of Meckel's diverticulitis in children. *AJR Am J Roentgenol* 180:425–428, 2003.
- Kotecha M, Bellah R, Pena AH, et al: Multimodality imaging manifestations of the Meckel diverticulum in children. *Pediatr Radiol* 42:95–103, 2012.
- Sun C, Hu X, Huang L: Intestinal obstruction due to congenital bands from vitelline remnants: Sonographic features and review of the literature. *J Ultrasound Med* 31:2035–2038, 2012.
- Pepper VK, Stanfill AB, Pearl RH: Diagnosis and management of pediatric appendicitis, intussusception, and Meckel diverticulum. *Surg Clin North Am* 92:505–526, vii, 2012.
- Limas C, Seretis K, Soultanidis C, Anagnostoulis S: Axial torsion and gangrene of a giant Meckel's diverticulum. *J Gastrointest Liver Dis* 15:67–68, 2006.
- Galifer RB, Noblet D, Ferran JL: "Giant Meckel's diverticulum": Report of an unusual case in a child with preoperative x-ray diagnosis. *Pediatr Radiol* 11:217–218, 1981.
- Maglinte DDT, Elmore MF, Isenberg M, et al: Meckel diverticulum: Radiologic demonstration by enteroclysis. *AJR Am J Roentgenol* 134:925–932, 1980.
- Hegde S, Dillman JR, Gadepalli S, et al: MR enterography of perforated acute Meckel diverticulitis. *Pediatr Radiol* 42:257–262, 2012.
- Pantongrag-Brown L, Levine MS, Elsayed AM, et al: Inverted Meckel diverticulum: Clinical, radiologic, and pathologic findings. *Radiology* 199:693–696, 1996.
- Kim G, Daneman A, Alton DJ, et al: The appearance of inverted Meckel diverticulum with intussusception on air enema. *Pediatr Radiol* 27: 647–650, 1997.
- Society of Nuclear Medicine: Procedure guideline for gastrointestinal bleeding and Meckel's diverticulum scintigraphy. *J Nucl Med* 40:1226–1232, 1999.
- Emamian SA, Shalaby-Rana E, Majd M: The spectrum of heterotopic gastric mucosa in children detected by Tc-99m pertechnetate scintigraphy. *Clin Nucl Med* 26:529–535, 2001.
- Olmsted WW, Madewell JE: Lymphangiectasia of the small intestine: Description and pathophysiology of roentgenographic signs. *Gastrointest Radiol* 1:241–243, 1976.
- Abramowsky C, Hupertz V, Kilbridge P, et al: Intestinal lymphangiectasia in children: A study of upper gastrointestinal endoscopic biopsies. *Pediatr Pathol* 9:289–297, 1989.
- Yang DM, Jung DH: Localized intestinal lymphangiectasia: CT findings. *AJR Am J Roentgenol* 180:213–214, 2003.
- Braamskamp MJ, Dolman KM, Tabbers MM: Clinical practice. Protein-losing enteropathy in children. *Eur J Pediatr* 169:1179–1185, 2010.
- Vignes S, Bellanger J: Primary intestinal lymphangiectasia (Waldmann's disease). *Orphanet J Rare Dis* 3:5, 2008.
- Bloomfield FH, Hadden W, Gunn TR: Lymphatic dysplasia in a neonate with Noonan's syndrome. *Pediatr Radiol* 27:321–323, 1997.
- Hennekam RC, Geerdink RA, Hamel BC, et al: Autosomal recessive intestinal lymphangiectasia and lymphedema, with facial anomalies and mental retardation. *Am J Med Genet* 34:593–600, 1989.
- Forzano F, Faravelli F, Loy A, et al: Severe lymphedema, intestinal lymphangiectasia, seizures and mild mental retardation: Further case of Hennekam syndrome with a severe phenotype. *Am J Med Genet* 111:68–70, 2002.
- Dorne HL, Jequier S: Sonography of intestinal lymphangiectasia. *J Ultrasound Med* 5:13–16, 1986.
- Puri AS, Aggarwal R, Gupta RK, et al: Intestinal lymphangiectasia: Evaluation by CT and scintigraphy. *Gastrointest Radiol* 17:119–121, 1991.
- Mazzie JP, Maslin PI, Moy L, et al: Congenital intestinal lymphangiectasia: CT demonstration in a young child. *Clin Imaging* 27:330–332, 2003.
- Saulsbury FT: Henoch-Schönlein purpura. *Curr Opin Rheumatol* 13:35–40, 2001.
- Dillon MJ: Henoch-Schönlein purpura: Recent advances. *Clin Exp Rheumatol* 25:S66–S68, 2007.
- Sonmez K, Turkyilmaz Z, Demirogullari B, et al: Conservative treatment for small intestinal intussusception associated with Henoch-Schönlein purpura. *Surg Today* 32:1031–1034, 2002.
- Yang YH, Yu HH, Chiang BL: The diagnosis and management of Henoch-Schönlein purpura. *Autoimmun Rev* 13:355–358, 2014.
- Chang WL, Yang YH, Lin YT, et al: Gastrointestinal manifestations in Henoch-Schönlein purpura: A review of 261 patients. *Acta Paediatr* 93:1427–1431, 2004.
- Hammer MR, Podberesky DJ, Dillman JR: Multidetector computed tomographic and magnetic resonance enterography in children: State of the art. *Radiol Clin North Am* 51:615–636, 2013.
- Ebert EC: Gastrointestinal manifestations of Henoch-Schönlein purpura. *Dig Dis Sci* 53: 2011–2019, 2008.
- Woolfenden AR, Hukin J, Poskitt KJ, et al: Encephalopathy complicating Henoch-Schönlein purpura: Reversible MRI changes. *Pediatr Neurol* 19:74–77, 1998.
- Soreide K: Surgical management of nonrenal genitourinary manifestations in children with Henoch-Schönlein purpura. *J Pediatr Surg* 40: 1243–1247, 2005.
- Schwab J, Benya E, Lin R, et al: Contrast enema in children with Henoch-Schönlein purpura. *J Pediatr Surg* 40:1221–1223, 2005.
- Connolly B, O'Halpin D: Sonographic evaluation of the abdomen in Henoch-Schönlein purpura. *Clin Radiol* 49:320–323, 1994.
- Sudakoff GS, Burke M, Rifkin MD: Ultrasonographic and color Doppler imaging of hemorrhagic epididymitis in Henoch-Schönlein purpura. *J Ultrasound Med* 11:619–623, 1993.
- Saulsbury FT: Clinical update: Henoch-Schönlein purpura. *Lancet* 369:976–978, 2007.
- Amzallag-Bellenger E, Oudjit A, Ruiz A, et al: Effectiveness of MR enterography for the assessment of small-bowel diseases beyond Crohn disease. *Radiographics* 32:1423–1444, 2012.
- Applegate KE, Maglinte DD: Imaging of the bowel in children: New imaging techniques. *Pediatr Radiol* 38(Suppl 2):S272–S274, 2008.
- Darge K, Anupindi SA, Jaramillo D: MR imaging of the abdomen and pelvis in infants, children, and adolescents. *Radiology* 261:12–29, 2011.
- Smith EA: Advanced techniques in pediatric abdominopelvic oncologic magnetic resonance imaging. *Magn Reson Imaging Clin N Am* 21:829–841, 2013.
- Sada DM, Vellody R, Liu PS: Magnetic resonance angiography of the pediatric abdomen and pelvis: Techniques and imaging findings. *Magn Reson Imaging Clin N Am* 21:843–860, 2013.

CHAPTER OUTLINE

Lymphoid Follicular Pattern and Lymphoid Hyperplasia**Anterior Anus**

Radiologic Findings

Hirschsprung's Disease

Pathologic Findings

Clinical Findings

Therapy

Radiologic Findings

Inflammatory Bowel Disease**Other Colitides and Causes of Diarrhea****Hemolytic Uremic Syndrome**

Clinical Findings

Radiologic Findings

Appendicitis

Clinical Findings

Radiologic Findings

Typhlitis

Clinical Findings

Radiologic Findings

Intussusception

Clinical Findings

Therapeutic Considerations

Radiologic Findings

Volvulus of the Colon

Clinical Findings

Radiologic Findings

Juvenile Polyps

Clinical Findings

Radiologic Findings

Colon Carcinoma

Clinical Findings

Radiologic Findings

Fibrosing Colonopathy

Clinical Findings

Radiologic Findings

contrast barium enema studies and may be seen in 50% to 70% of such examinations in children (Fig. 118-1).^{1,2} Normal follicles are 2 mm in diameter, are uniform in size, and often have central umbilications. They can simulate familial polyposis in the way they carpet the colon. Follicles larger than 2 to 3 mm are associated with nodular lymphoid hyperplasia, which occurs in response to a number of immunologic, infectious, inflammatory, or allergic stimuli.^{3,4}

Anterior Anus

The anterior anus, an organic cause of constipation, is seen in some children who were previously said to have psychogenic constipation or suspected of having Hirschsprung's disease (HD).^{5,6} The anterior anus may be a mild variant of imperforate anus with perineal fistula.^{5,6}

The amount of anal displacement may be minimal and difficult to appreciate by physical examination. The external changes may be more difficult to discern in boys than in girls. The position of the anus does not by itself determine the degree of dysfunction.⁷ Affected children may have an abnormal evacuation history from birth or may evacuate normally for several months. A long interval between bowel movements, straining with defecation, and fecal soiling are also common complaints.^{5,6}

Treatment is surgical. The anorectal canal and internal anal sphincter are mobilized, and a neorectum is created in a normal location. The surgery has a low complication rate and allows development of nearly normal evacuation patterns.^{5,7-9}

The differential diagnosis of anterior anus includes HD, neurologic constipation, and psychogenic constipation. These disorders can usually be excluded on the basis of physical examination, spine radiographs, rectal manometry, and rectal biopsy.

RADIOLOGIC FINDINGS

Conventional radiographs are used to evaluate the amount of stool present and to detect spinal anomalies. If a large amount of stool obscures the sacrum, a lateral spine radiograph may be necessary to exclude sacral deformities that may be associated with neurogenic rectal dysfunction.

On barium enema examination, the lateral rectal view is key in diagnosis. In children with anterior anus, there is a deep posterior recess or shelf behind the rectal catheter (Fig. 118-2). The rectum descends below the last turn of the colon as it passes anteriorly to become the anus. Postevacuation radiographs, with the rectal tube removed, show that the anus is more anterior than usual and lies at an angle to the posterior rectal shelf, which is in a normal position a few millimeters anterior to the sacrum.

Lymphoid Follicular Pattern and Lymphoid Hyperplasia

Lymphoid follicles are a normal feature of the gastrointestinal tract and are much more prominent in children than in adults. The lymphoid follicular pattern is best appreciated on double-



Figure 118-1 Lymphoid follicular pattern. Fine nodules of similar size are seen throughout the colon on this double-contrast barium enema study.

Hirschsprung's Disease

PATHOLOGIC FINDINGS

HD is characterized by absence of ganglion cells in Auerbach's and Meissner's plexus in the affected bowel.¹⁰ The process is probably caused by arrest of the usual craniocaudal migration of primitive neuroblasts, which in some children is associated with other abnormalities of the neural crest. Research indicates that children with central hypoventilation syndrome have an increased incidence of HD.¹¹

The involved segment is of variable length and is always distal. Approximately 85% of cases are limited to the descending colon and distal segments; 55% of all cases involve the rectosigmoid colon and distal segments.^{10,12} Total colonic aganglionosis, with or without small bowel involvement, is seen in 8% of affected children.^{10,12-14} Extensive aganglionosis is a rare, usually lethal variant in which the entire small bowel and even the stomach lack normal ganglion cells.¹⁴ Zonal aganglionosis is rare and may be an acquired lesion or have a different embryologic basis.

CLINICAL FINDINGS

Two thirds to three fourths of children with classic HD are male. Boys and girls are equally affected with total colonic aganglionosis. HD is the most common cause of neonatal obstruction of the colon, and more than 70% of cases are diagnosed in this period.^{10,12} Neonates present with delayed passage of meconium, abdominal distention, or vomiting. Delay in diagnosis

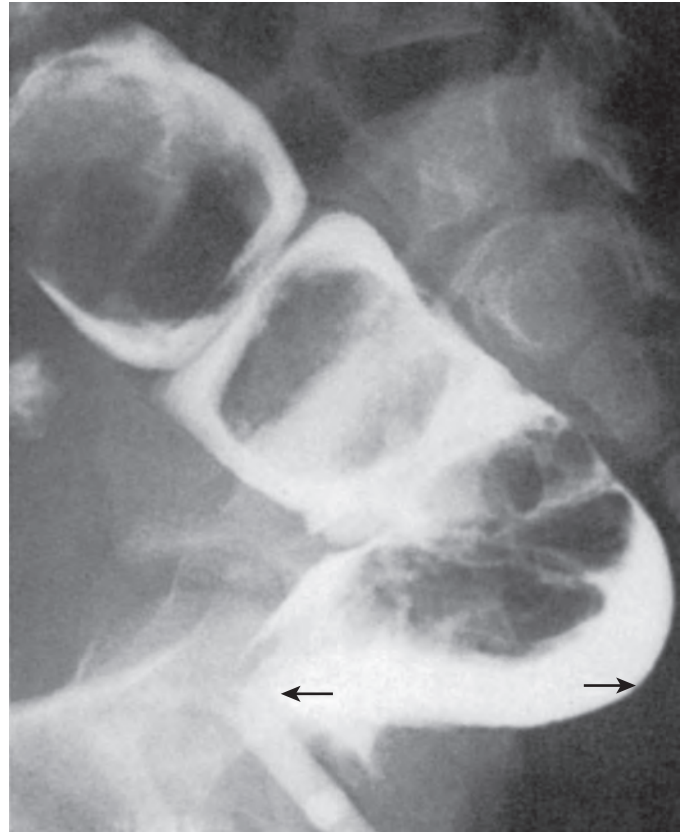


Figure 118-2 Anterior anus. Barium enema study shows that the rectum is capacious and contains much fecal debris. A deep posterior segment of the rectum (arrows) far behind the anus is identified by the catheter tip.

can lead to bowel perforation or potentially fatal enterocolitis.¹⁵⁻¹⁷ About 5% of children with HD die of enterocolitis, usually within the first 3 months of life, and about 10% of children with HD develop enterocolitis before surgery. Pseudomembranous colitis may also occur in these children, even without recent exposure to antibiotics, and it can lead to perforation of the appendix and proximal colon in 5% of cases.¹⁸ Because pseudomembranous colitis is treatable, it may be useful to obtain stool cultures in children with HD and "typical" colitis.¹⁷

Older children with undiagnosed HD usually have an abnormal neonatal stooling history and unremitting constipation.^{19,20} On occasion, the diagnosis is delayed until the second and third decades of life, leading to chronic constipation, chronic laxative abuse, and colonic distention, which predispose the colon to volvulus.

The clinical history and physical examination findings usually are specific. In contrast to children with psychogenic constipation, whose symptoms begin at the time of toilet training, children with HD have an abnormal stooling history as neonates and rarely have fecal soiling. On physical examination, the rectal ampulla is full in children with psychogenic constipation and empty in those with HD.

Distention of the rectum fails to produce normal reflex relaxation of the internal sphincter in children with HD.²¹ Rectal manometry may be performed if the diagnosis remains uncertain, particularly in children with a normal barium enema result who do not respond to medical therapy for

constipation.²¹ Rectal manometry may give equivocal or incorrect results in approximately 18% of those younger than 1 month and in 10% older than this.²¹

Suction biopsy of the rectal mucosa excludes the diagnosis of HD by histologic demonstration of ganglion cells. Full-thickness biopsy of the rectum is reserved for problem situations, such as when the radiologic pattern is atypical or when the mucosal biopsy is inconclusive.²²

In most children, HD is an isolated finding, but there is an increased incidence of this disorder among children with trisomy 21, Waardenburg's syndrome, Smith-Lemli-Opitz syndrome, and several other syndromes. In some families, HD appears to be genetically transmitted.²³⁻²⁵ Genetic factors may be present in up to 20% of patients, and a dominant inheritance pattern has been identified in several families. Multiple genes have been implicated in HD, and many mutations have been observed with neurodevelopmental genes.²⁶

There is an increased incidence of malrotation in children with HD.²⁷ In utero, this malrotation may lead to volvulus and ischemia and contribute to the increased incidence of intestinal atresia in children with HD.^{27,28} The association of HD with intestinal atresia also suggests that the ischemic event that produced the atresia might have interfered with the craniocaudal migration of neuroblasts.

THERAPY

Initial treatment of HD is directed toward decompressing the colon to prevent enterocolitis. Although this can be achieved with saline solution enemas, a one-stage neonatal repair may be done. This consists of a transanal endorectal pull-through without or with laparoscopic assistance by intraoperative pathologic guidance to define the true transition zone. In children with markedly dilated colon or those weighing less than 2 kg, a colostomy is performed. Definitive or corrective surgery is usually delayed several months. All operations (i.e., Swenson, Soave, and Duhamel procedures) attempt to restore normal function by removing or bypassing the aganglionic segment.^{10,12} Postoperative complications include leakage at the anastomosis, continued obstruction, and, rarely, development of secondary aganglionosis in a previously normal segment.

When HD is diagnosed in an older child, a colostomy is performed before corrective surgery to enable the enlarged colon to normalize in caliber. This makes later surgery easier. Children with total colonic aganglionosis undergo ileostomy under histologic intraoperative guidance to enable placement of the ileostomy in a segment that contains ganglion cells. Later, these children undergo total colectomy and ileoanal endorectal pull-through.¹⁹

RADIOLOGIC FINDINGS

Early diagnosis of HD can be lifesaving. Unfortunately, radiologic diagnosis is more difficult in the neonatal period than in later life. Conventional radiographs show changes of distal bowel obstruction. Rarely, calcifications may be present in bowel lumen.²⁹

Contrast enema examination is performed for diagnosis and to exclude other causes of distal obstruction, such as meconium plug, small left colon syndrome, and ileal atresia. When HD is suspected, a small-caliber enema tip may be used to avoid dilating the rectum.

The enema is begun with the infant or child in the left lateral decubitus position to improve visualization of the segments most likely to be abnormal: the rectum and the rectosigmoid (Fig. 118-3). In infants, a funnel- or cone-shaped appearance suggests HD (Fig. 118-4). Despite reports that delayed abdomen radiographs demonstrating retained barium are valuable in confirming the diagnosis, filling of the colon proximal to an abnormal configuration is not recommended in case the barium becomes impacted. A lateral radiograph of the rectum obtained after the enema tip has been removed may be key to appreciating the abnormally small rectal vault and demonstrating the abnormal rectosigmoid index.^{30,31} A crinkled appearance of the distal colon, the corrugated rectum, is another finding of

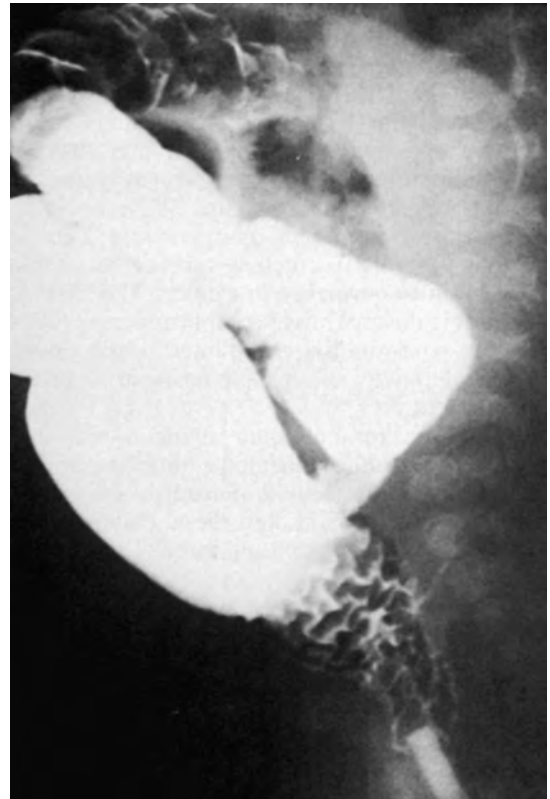


Figure 118-3 Hirschsprung's disease. On this lateral view from a barium enema study, the rectum is smaller than the sigmoid colon. The corrugated appearance of the rectum has also been described in Hirschsprung's disease.

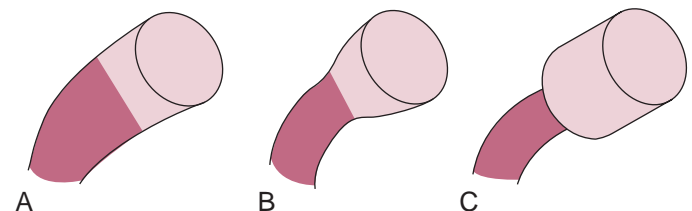


Figure 118-4 Hirschsprung's disease. The diagram (lateral view) depicts the varied appearance of the transition zone in the rectum in Hirschsprung's disease. **A.** In the very young, the transition zone may be cone shaped, with the caliber imperceptibly decreasing as it goes from the sigmoid colon to the rectum. **B** and **C.** A discrete change in caliber is more typical, with the radiologic transition zone more clearly defined in **C.**

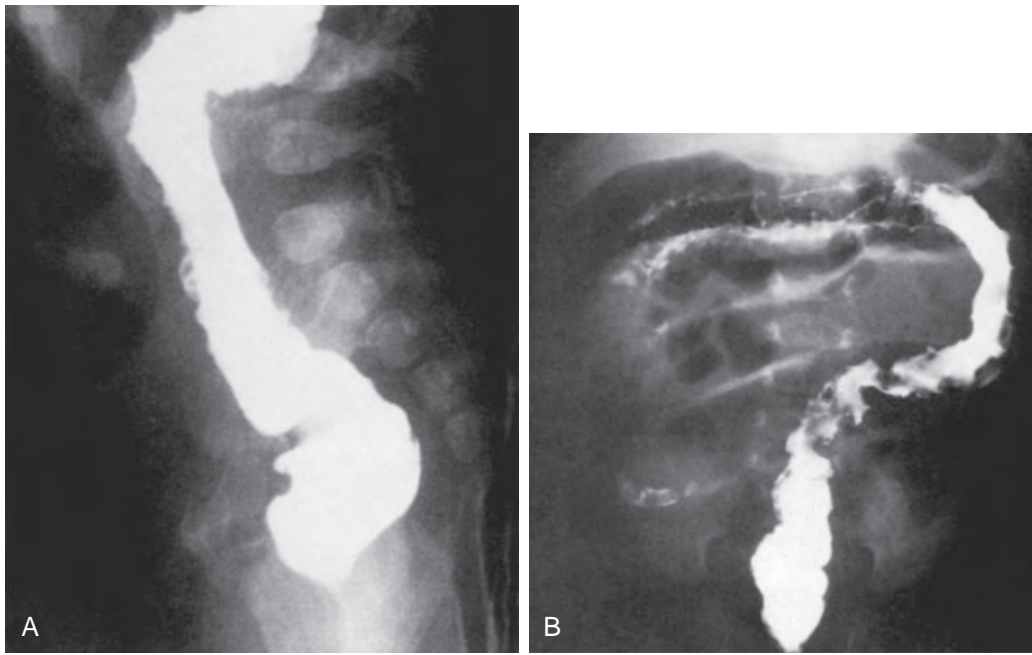


Figure 118-5 Total colonic Hirschsprung's disease. Frontal (A) and lateral (B) views from a barium enema study show that the rectum is larger than the more proximal colon. Intense spasm from colitis prevents colonic distention. Spiculation and mucosal ulcerations are present throughout, except in the rectum.

aganglionosis and may become more apparent after the catheter tip is removed.

In the neonate with total colonic aganglionosis, the colon may fill easily with rapid reflux into the small bowel, with a transition zone demonstrated between normal and dilated bowel in the ileum and with loss of the normal colonic redundancy. The abnormal colon may instead appear normal, have a meconium plug, or be a microcolon.^{32,33}

HD-induced colitis produces a spastic, difficult to distend colon with a spiculated or saw-toothed mucosa (Fig. 118-5). Active colitis produces rapid expulsion of barium, which accounts for false-negative, delayed postevacuation radiographs in children with HD.

In the older child with a history of constipation, the contrast enema is performed in an unprepared colon because decompression of the dilated colon and dilation of the rectum may decrease the abrupt changes that produce the classic transition zone. *Transition zone* is the term applied to the region in which there is a perceptible change in caliber, with the dilated normal colon above and the narrowed aganglionic colon below. The dilated segment may contain aganglionic bowel because the innervated enlarged colon pushes its contents distally and dilates the abnormal segment.^{34,35} Pathologic confirmation of the true transition zone is always obtained before palliative or corrective surgery is performed.

When barium enema examination shows a dilated rectum and sigmoid colon, classic HD has been excluded; the colon above is filled to see the extent of colonic distention and to evaluate bowel rotation. Parents should be instructed in ways to enhance the passage of barium afterward. When the child undergoes a bypass procedure as the initial surgical therapy, the distal segment is usually studied with contrast enema before gastrointestinal continuity is reestablished. It may appear poorly distensible and rigid with mucosal thickening, nodularity, and

polypoid lymphoid hyperplasia.³⁶ Redundancy, if present, is a result of prior dilation of the ganglionic portion of this segment.

After definitive corrective surgery, there is no routine time or indication for radiologic study. If the child is septic in the immediate postoperative period, gentle instillation of water-soluble contrast material into the rectum through a small catheter can demonstrate an anastomotic leak. Alternatively, contrast-enhanced computed tomography (CT) of the pelvis may demonstrate the suspected collection or abscess and better define its extent and secondary complications.

Inflammatory Bowel Disease

The pathology, epidemiology, and radiographic findings in ulcerative and Crohn's colitis are discussed in Chapter 57. This short discussion focuses on a few aspects of ulcerative colitis in the child. Pediatric Crohn's disease is presented in Chapter 116.

Ulcerative colitis is rare during the first and uncommon in the second decade of life. The symptoms of diarrhea with blood or mucus, abdominal pain, and fever suggest a juvenile polyp, Meckel's diverticulum, or infectious or allergic colitis. Anemia and weight loss may also develop.³⁷⁻⁴⁰

The radiographic findings in children with ulcerative colitis are identical to those in adults. Toxic megacolon, however, occurs much less commonly in children.

Other Colitides and Causes of Diarrhea

Persistent bloody or watery diarrhea is unusual in children and is a cause for concern because it may lead to electrolyte abnormalities, protein and weight loss, and irritation of the buttocks. Viral, bacterial, or parasitic processes are frequently the source

of the problem.⁴¹⁻⁴³ In up to 28% of children, the cause of the diarrhea may elude diagnosis despite numerous diagnostic tests. Celiac disease, usually considered to be a small bowel disorder, may be the most common noninfectious cause of diarrhea. Diagnosis is based on response to a gluten-free diet and results of a small bowel biopsy.⁴⁴

Milk allergy and lactose intolerance can cause diarrhea in children.^{45,46} The inability to digest lactose can cause diarrhea in the first year of life. Removal of the offending disaccharide results in remission of symptoms. The proteins in cow's milk and soy-based milk can damage the gastrointestinal mucosa in some children with allergy to these foods. Rectal biopsy may show diagnostic histologic changes. Barium enema examination may show nonspecific changes of colitis: narrowing, thumbprinting, and spasm. Although these changes usually involve the entire colon, segmental changes have been described. The small bowel may also be affected, producing thickening of the valvulae conniventes or narrowing of involved segments.

A rare cause of diarrhea in children is collagenous colitis.⁴⁷⁻⁴⁹ This colitis is associated with watery diarrhea and colicky pain. Microscopic analysis of biopsy specimens of mucosa is necessary for diagnosis. Widening of the collagen band of the basement membrane, few inflammatory cells, and edema of the lamina propria are observed. Symptoms usually respond to corticosteroids or sulfasalazine but may recur after the medications have been withdrawn.

Tumor is a rare cause of watery diarrhea. A few ganglioneuromas and ganglioneuromas secrete vasoactive intestinal polypeptide, which, as its name suggests, produces increased intestinal motility.⁵⁰ This disorder is often unsuspected, but the diagnosis is made when the conventional radiograph preceding barium enema reveals paravertebral mass or calcifications. Plasma levels of vasoactive intestinal polypeptide can be measured to confirm the diagnosis, and CT or sonography may be useful in delineating tumor size and tissue of origin. Removal of the tumor is followed by cessation of the diarrhea.

Kawasaki's disease may cause a variety of physical and physiologic changes: abdominal pain, serum abnormalities indicative of liver disease, frank organ necrosis, and atypical colitis simulating ischemic colitis.⁵¹

Hemolytic Uremic Syndrome

CLINICAL FINDINGS

Hemolytic uremic syndrome (HUS) is a pathologic entity with two different groups of affected patients.⁵²⁻⁵⁴ In some, an infection with a specific *Escherichia coli* is associated with the development of HUS. In others, especially those with relapses of the disease, there may be a genetic component. Both groups suffer an acute microangiopathic hemolytic anemia, oliguric renal failure, and thrombocytopenia.⁵²⁻⁵⁴ HUS usually occurs in toddlers and children between 2 and 10 years old, who present with an influenza-like illness, gastroenteritis, and bloody diarrhea that precede the more striking renal and hematologic manifestations by several days or weeks. The gastrointestinal manifestations of the prodromal period are protean, requiring differentiation from ulcerative colitis, pseudomembranous colitis, granulomatous colitis, shigellosis, salmonellosis, intussusception, and causes of an acute surgical abdomen.⁵²⁻⁵⁶ Diagnosis is often delayed until anemia, thrombocytopenia, or renal failure appears. Urinalysis provides vital information because

most patients have proteinuria, hemoglobinuria, or hematuria (microscopic or gross) early in the course of the disease. Those who present without diarrhea have a worse prognosis for renal disease than those who have diarrhea at presentation.⁵⁷ The peripheral blood smear is also suggestive when schistocytes and burr cells are present. Patients may experience central nervous system symptoms, sometimes associated with abnormal findings on CT and magnetic resonance (MR) examinations.⁵⁸

The vigorous fluid therapy given to children with active peritoneal signs typical of HUS may result in overhydration and cause peripheral and pulmonary edema when acute renal failure develops. Prompt diagnosis may avert an unwarranted laparotomy and contribute to the proper management of fluid needs. Dialysis is necessary until renal function resumes.

Most patients recover without sequelae. Death, more frequent in children with anuria, is attributable to the manner in which the thrombotic process affects organs other than the kidneys.

RADIOLOGIC FINDINGS

Conventional radiographs often have abnormal findings but are nondiagnostic. A disordered bowel gas pattern and thickening or thumbprinting of affected bowel loops may be observed.⁵⁹

The colon may demonstrate spasm, thumbprinting, ulceration, straightening, and narrowing of edematous segments (Fig. 118-6) on barium enema examination. Later, strictures may form.

Sonography is useful in excluding causes of a surgical abdomen and in showing changes that suggest the diagnosis:



Figure 118-6 Hemolytic uremic syndrome. Spasm and ulceration are present in the descending colon, and mild thumbprinting deforms the transverse colon on this barium enema study.

peritoneal fluid, bowel wall thickening, and increased echogenicity of the renal parenchyma.⁶⁰ During periods of oliguria or anuria, there are profound abnormalities of systolic and diastolic blood flow on Doppler studies. A return of normal blood flow heralds impending diuresis, useful information in children undergoing dialysis.⁶⁰

Appendicitis

CLINICAL FINDINGS

The most common indication for emergency laparotomy in children is an inflamed or ruptured appendix. The diagnosis is based on symptoms (e.g., abdominal pain, vomiting, low-grade fever), signs (e.g., pain on palpation of the right lower quadrant, rebound tenderness), and laboratory data (e.g., low-grade leukocytosis, absence of urinary tract infection). When the presentation is classic, surgery is usually performed without radiologic studies. Imaging is performed in those whose atypical presentation suggests the possibility of other, even nonsurgical, diagnoses. Sonography has demonstrated that alternative diagnoses may be established in up to 25% of the patients with suspected appendicitis.⁶¹

Infectious enteritis, Crohn's disease, mesenteric lymphadenitis, intussusception, acute pyelonephritis, omental infarction, and Meckel's diverticulitis are other possibilities that can be suggested with sonography or CT in the setting of suspected appendicitis. In teenage girls, gynecologic conditions, including pelvic inflammatory disease, ovarian cyst, hematometrocolpos, ovarian torsion, and pregnancy, may be diagnosed.⁶¹

Rupture or perforation occurs more commonly in children than in adults.⁶²⁻⁶⁵ In pediatric patients who have had preoperative imaging studies, the perforation rate at surgery is as high as 50%.⁶⁶ After rupture, the abdominal symptoms may temporarily diminish, which obscures the diagnosis.

If rupture has occurred, the inflammation of the local soft tissues (e.g., bowel, omentum) is called a phlegmon. Phlegmon or periappendiceal abscess is reported in as many as 37% of children with acute appendicitis and is more common in those whose symptoms are of longer duration.⁶⁴ Phlegmon or periappendiceal abscess may be palpated as a right lower quadrant mass. A complete discussion of the diagnosis, treatment, and prognosis of appendiceal abscess is presented in Chapter 56.

RADIOLOGIC FINDINGS

The radiologic findings in children with appendicitis are identical to those in adults and are discussed in Chapter 56. Certain features of pediatric appendicitis should be considered. Appendicoliths are more common in children than in adults with appendicitis and, when present, are more likely to be associated with appendiceal rupture (Figs. 118-7 and 118-8).

The choice of imaging modality (and even whether to image) can be confusing. In some series, the use of preoperative imaging has increased the number of alternative, nonsurgical diagnoses and decreased the number of negative appendectomies, but others have opposite results and see a negative value in waiting for the study to be done. When cross-sectional imaging is indicated, sonography (Fig. 118-9) and CT (Figs. 118-10 and 118-11) have a specificity and sensitivity of more than 90%.⁶¹⁻⁶⁸ A normal appendix may be identified on sonography in up to 81% of children who do not have appendicitis (Fig. 118-12).⁶⁹



Figure 118-7 Appendicolith. A large, calcified appendicolith is seen below the right sacroiliac joint (arrow).



Figure 118-8 Appendiceal abscess. The terminal ileum is extrinsically compressed by and displaced around an appendiceal abscess on this small bowel series.

In thin children, ultrasound is a reasonable first-line choice. In heavier children or when ultrasound is not readily available, CT has been equally successful in diagnosing or excluding appendicitis or detecting alternative disease processes. MR imaging may be useful in the diagnosis of appendicitis when

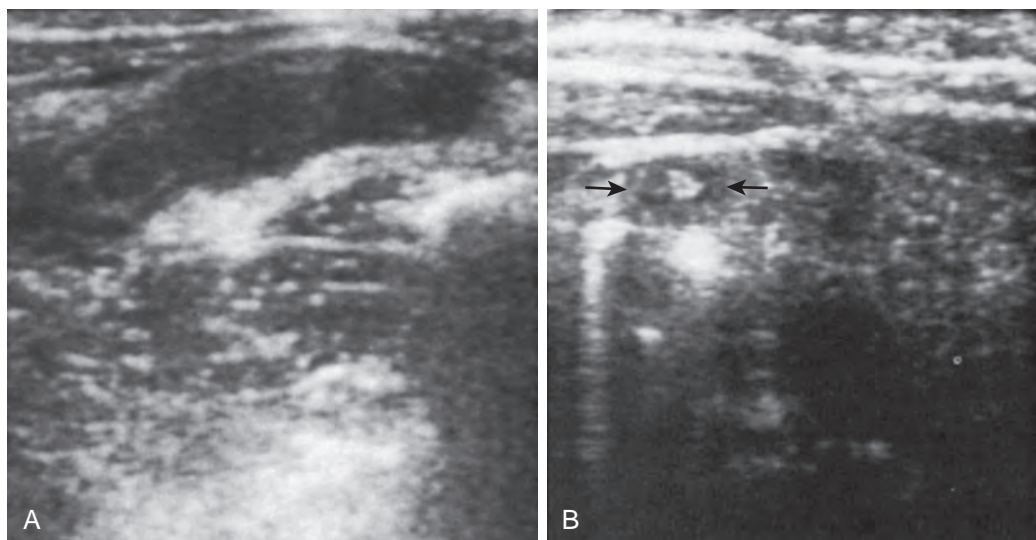


Figure 118-9 Sonography of appendicitis. **A.** A dilated, incompressible appendix lies beneath the abdominal musculature on this longitudinal scan. **B.** Transverse scan of the right lower quadrant in a different child shows a widened appendix (arrows), suggesting appendicitis. The echogenic focus in the center causing distal shadowing is an appendicolith.

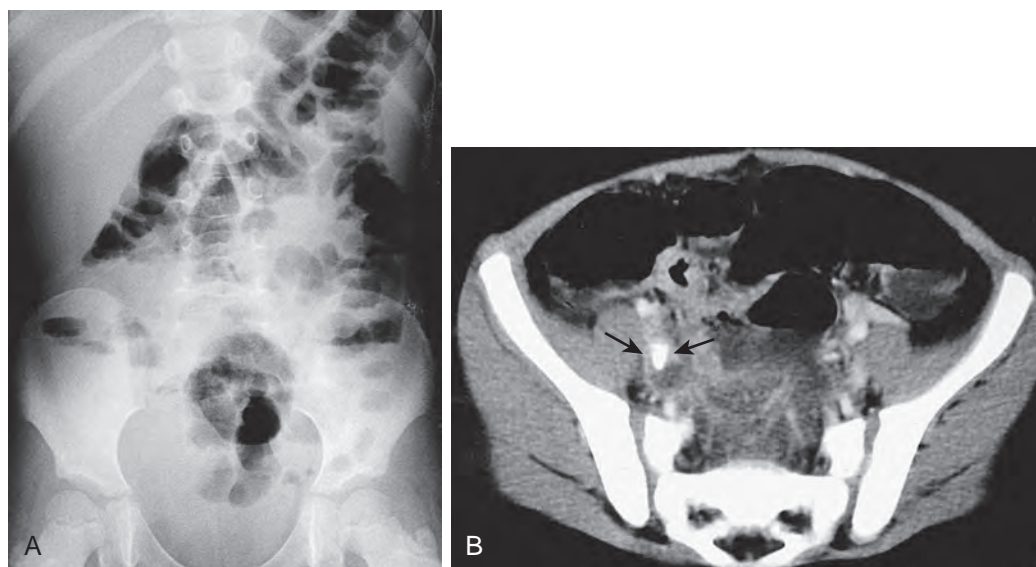


Figure 118-10 Appendicitis: abdomen radiograph and CT. **A.** Abdomen radiograph demonstrates a mild left lumbar scoliosis due to right psoas spasm. Several air-fluid levels are present in the lower quadrant bowel loops, a sign of focal ileus. **B.** CT demonstrates an appendicolith (arrows) in the dilated appendix.

ultrasonography is equivocal.⁷⁰ Controversy about how the CT study should be done (i.e., full abdomen and pelvis or focused to the abdomen and pelvis below the lower pole of the right kidney) and what is the proper preparation (i.e., rectal, oral, intravenous, or some combination of these) indicates that many techniques produce excellent diagnostic results.^{71,72}

An acutely ruptured appendix may be challenging to diagnose with sonography for a number of reasons. The decompressed appendix may have a diameter of less than 6 mm, an appendix may not be identified because of overlying bowel gas, and only questionable appendiceal remnants may be present after the inflammatory response develops in the surrounding tissues. Sonography and CT are helpful in differentiating

Yersinia enterocolitis (frequently associated with right lower quadrant pain) from appendicitis (Fig. 118-13). In addition to imaging of appendicitis, radiologists can percutaneously drain the appendiceal abscesses.⁷³

Typhlitis

Typhlitis, also known as neutropenic colitis because it may affect any segment of the colon, is acute inflammation of the cecum that occurs in immunosuppressed patients. It was originally described in children with immunosuppression due to treatment of acute myelogenous leukemia.⁷⁴ Typhlitis is seen in children and affects adults with many forms of immunosuppression; chemotherapy for treatment of malignant disease,



Figure 118-11 CT of appendiceal abscess. **A.** Moderate dilation of the right pelvicalyceal system and proximal ureter due to the mass effect of the right lower quadrant process is demonstrated on this retrograde pyelogram. **B.** CT reveals a complex mass (arrows), which compresses the right ureter.

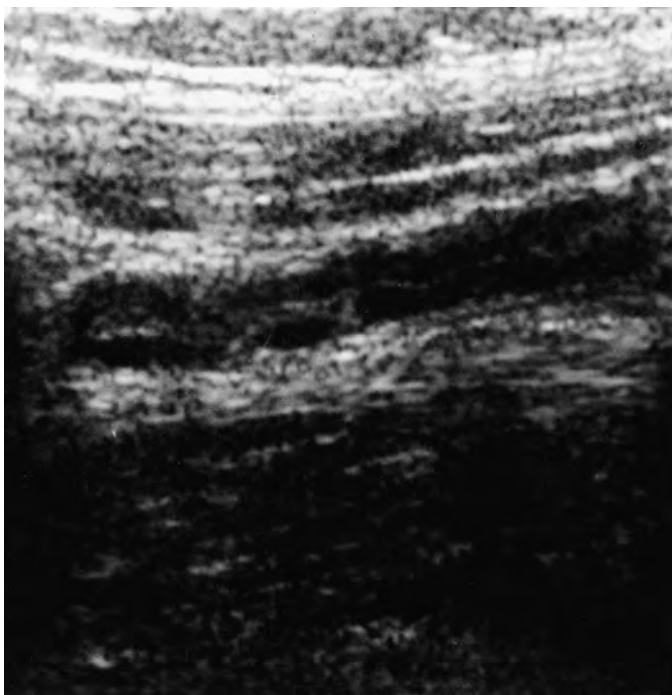
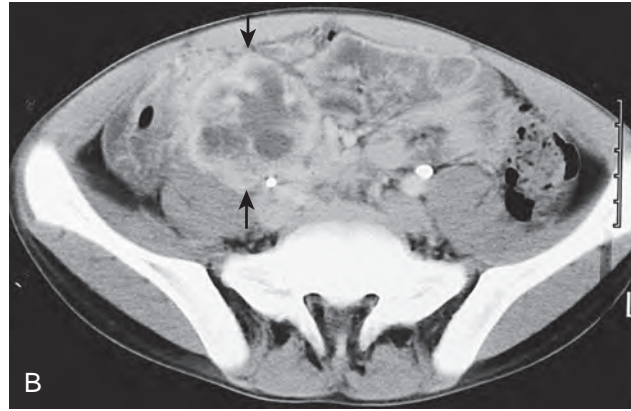


Figure 118-12 Normal appendix. The blunt distal tip of the nontender, compressible appendix is superior to its proximal portion on this longitudinal scan.

organ and bone marrow transplantation, and AIDS are other significant risk factors.⁷⁴⁻⁷⁸

CLINICAL FINDINGS

Children with typhlitis present with right lower quadrant pain, neutropenia, fever, and peritoneal signs; they occasionally

present with an inflammatory mass and uncommonly with lower gastrointestinal hemorrhage. Perforation of the cecum may occur but is not necessarily lethal when it is treated immediately. Granulocyte transfusions, antibiotics, and surgical resection of affected bowel may stop the progress of the inflammation.^{77,78} Diagnostic delay may lead to perforation, sepsis, and death.

The differential diagnosis of typhlitis includes appendicitis clinically and pneumatosis intestinalis radiologically. A study of more than 450 children treated for hematologic malignant disease found that appendicitis and typhlitis occurred with almost equal frequency and demonstrated that CT studies were key in differentiating these diagnoses.⁷⁹

RADIOLOGIC FINDINGS

Conventional radiographs of patients with typhlitis may show an abnormal amount of bowel gas or a soft tissue mass in the right lower quadrant, ascites, or pneumatosis intestinalis. The pneumatosis may have a benign course. Free intraperitoneal air is a more ominous sign and indicates the need for surgery unless another source of the air is apparent.

Contrast enema has been reported to show changes in the appearance of the inflammatory process in the cecum but may lead to perforation. It is not recommended in patients with suspected typhlitis.

Angiography, rarely used for diagnosis, may demonstrate hyperemic changes of the mucosa, staining at sites of ulceration, and arteriovenous shunting.⁷⁵ Embolotherapy may be performed if bleeding is massive.

Sonography shows mural thickening of the cecum, ascending colon, and ileum.^{80,81} Color Doppler demonstrates increased transmural blood flow, in contrast to other processes, which may primarily affect the mucosa or instead be associated with diminished blood flow and ischemic change. Sonography is also useful in identifying abscesses and in excluding appendiceal inflammation. The success of CT in differentiating typhlitis

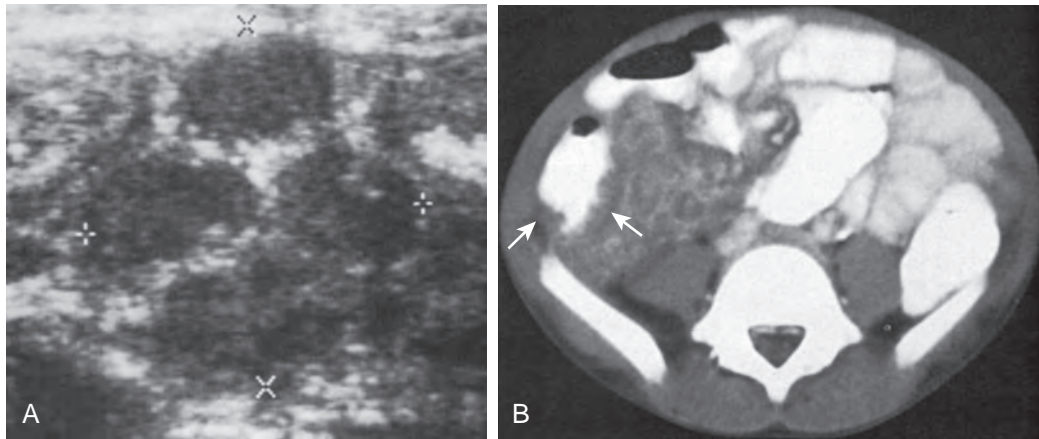


Figure 118-13 *Yersinia enterocolitis*. **A.** Several enlarged lymph nodes (cursors) are seen on this sagittal sonogram of a child whose appendix appeared normal. **B.** The enlarged lymph nodes produce an inhomogeneous mass in the right iliac fossa. The wall of the cecum (arrows) is thickened on the CT scan.

from other processes in this fragile population has fostered its increased use for this purpose.^{82,83}

Intussusception

Intussusception occurs when a proximal segment of bowel passes into the lumen of a more distal segment, and through peristalsis, it is propelled distally. The proximal segment is referred to as the intussusceptum, and the distal segment is called the intussusciens. Intussusceptions are named by the segments involved. The most common form (70%-90%) is ileocolic, in which the ileum is prolapsed into the colon for a variable distance. Less common types of intussusceptions are ileoileocolic, ileoileal, and jejunoileal.

Despite a seasonal variation in the incidence, which suggests a predisposing viral agent, most children with intussusception have no prodrome or discernible cause. Only 3% to 10% of children have an intrinsic bowel abnormality that serves as the lead point for the intussusception: duplication, hemangioma, polyp, Meckel's diverticulum, or lymphoma.⁸⁴⁻⁸⁶ Intussusception is a known but rare complication of surgery.⁸⁷ Most intussusceptions occur in children between 3 months and 3 years old, with a 2:1 male predominance. Almost one third of children who develop an intussusception outside this age range have a pathologic lead point.⁸⁴⁻⁸⁶ Nevertheless, radiologic reduction of the intussusception should be attempted in older children because most do not have a lead point and can therefore avoid surgery.

CLINICAL FINDINGS

Children with intussusception present with colicky abdominal pain. The stools may test positive for occult blood or have the classic but infrequent currant jelly appearance. Vomiting, diarrhea, and other gastrointestinal symptoms occur in more than 90% of cases. An abdominal mass may be palpated in slightly more than half of the affected children. A few children are lethargic or dehydrated. In neonates, vomiting is usually the most striking clinical finding. Rectal bleeding is also more common in the neonate with intussusception than in the older child and may suggest necrotizing enterocolitis rather than the correct diagnosis.

THERAPEUTIC CONSIDERATIONS

Barium enema or air enema may be used to diagnose and to treat ileocolic intussusception. The hydrostatic or pneumatic pressure of the enema is used to drive the infolded segment of bowel in a retrograde direction to its normal position. Surgery is required to reduce intussusceptions that do not respond to this pressure and to treat children whose clinical status precludes radiologic intervention. Children with fever, elevated white blood cell count, peritoneal signs, or marked systemic toxicity should have immediate surgery because these findings suggest perforated bowel or gangrenous gut. Spontaneous reduction may occur, often as a result of general anesthesia, and about 14% of children with documented intussusception may have none of these findings at surgery.^{83,84}

When there is evidence of small bowel obstruction or the presence of symptoms for more than 24 hours, the success rate for reduction is decreased.⁸⁷⁻⁸⁹ Whereas the success rate may be greater than 75% in children seen acutely, it is half of that rate in those who have symptoms for more than 48 hours. Because the only alternative to hydrostatic or pneumatic reduction is surgery, with its increased morbidity and cost, reduction should be attempted in all children who do not have the medical problems described previously.

Recurrent intussusception develops in 7% to 10% of the children who have had successful reductions. Second and even third episodes of intussusception do not necessarily indicate that there is a lead point. In a large series, only 10% to 20% of children with recurrence had lead points found at surgery.⁹⁰ For this reason, hydrostatic or air reduction should be attempted despite recurrence.

Children with Henoch-Schönlein purpura, recent abdominal surgery, or cystic fibrosis have an increased incidence of intussusception. Standard reduction methods may work in these populations, but they are usually less successful in children with Henoch-Schönlein purpura.⁹¹

RADIOLOGIC FINDINGS

The diagnosis of intussusception is often suggested on conventional radiographs when the amount of intestinal gas is subnormal; bowel loops are displaced from the right hypochondrium;

the appendix, if air filled, is in an abnormal location; or the intussusceptum can be identified as a soft tissue mass.⁹²⁻⁹⁴ When there is a suspicion of intussusception, the child may go directly to a contrast enema with barium, air, or water-soluble agents performed for diagnosis and treatment.

In many institutions, a diagnostic sonogram is performed. Sensitivity for diagnosis approaches 100% and specificity is more than 90%.⁹⁵⁻⁹⁷ Pitfalls of sonographic diagnosis include false-positive results produced when the bowel is thickened for other reasons, such as lymphoma or Crohn's disease, and false-negative results when the amount of bowel gas present precludes a complete abdominal examination. Detection of false lead points has also been reported.⁹⁴

The therapeutic enema examination is performed only in the medically stable child. Surgical consultation should be obtained before the study in case reduction is unsuccessful or a complication occurs. The lethargic or dehydrated child should be resuscitated before the examination is started. A large-bore catheter (with or without inflatable balloon) is placed securely in the rectum, and the buttocks are firmly taped shut. First the barium enema and then the air enema are described.

The bag of barium or water-soluble contrast agent is suspended 36 to 39 inches above the fluoroscopy table. Flow of contrast material is continued until the colon is filled and there is free reflux into the small bowel or until the intussusceptum is encountered (Fig. 118-14). The contrast medium bag remains open to the patient throughout the study to maintain a constant pressure in an attempt to push the gut to its original position.

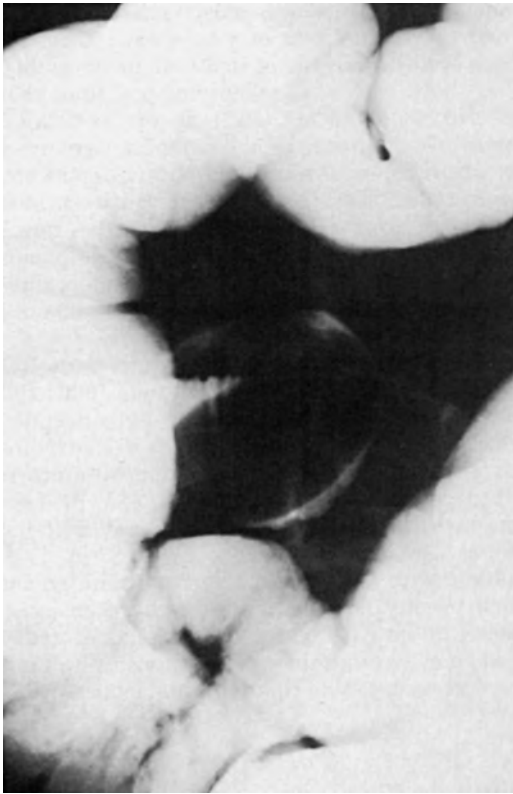


Figure 118-14 Intussusception. A persistent filling defect is seen on barium enema examination in the ileum in this child who had a normal-appearing colon. Because the sonogram that preceded this study showed the intussusception, it was necessary to reflux into more ileal loops than usual to confirm and treat the problem.

Manual pressure on the abdomen should be avoided because it may increase the risk of perforation. The flow of contrast material continues as long as there is retrograde motion of the intussusceptum. When there is a standstill, the bag should remain open to the patient for another 3 to 5 minutes. If there is no movement during this period, the contrast material is drained from the colon, and the child is allowed to rest for a few minutes. Enema reduction is attempted again, and this sequence is followed up to three times. If incomplete or no reduction has occurred, surgery is indicated. Successful reduction with this technique occurs in almost 90% of children. Recent literature suggests that in some children, delayed repeated attempts at intussusception reduction are successful and may avert surgery.^{90,98,99} Analgesia and sedation may be given if the first reduction attempt is unsuccessful.¹⁰⁰ This tends to make the child more comfortable and may aid in spontaneous reduction. Children with suspected intussusception are not routinely sedated before beginning of a contrast enema because the medication may obscure the nature of the abdominal process in children who do not have an intussusception. Glucagon, an effective smooth muscle relaxant, has not proved helpful in intussusception reduction in children.¹⁰¹

Barium dissecting between the intussusceptum and the intussusciptens has been reported as a sign of nonreduction and is associated with an increased incidence of necrotic bowel (Fig. 118-15). However, reduction is possible in as many as 40% of these children, and a nonvigorous attempt, perhaps with water-soluble contrast medium, may avoid surgery.

Reduction exists only when there is free reflux of contrast material into small bowel loops. They should be carefully



Figure 118-15 Dissection sign of intussusception on barium enema study. Contrast medium is seen along the sides of the intussusception, which has a coil-spring appearance. When this sign is observed, the likelihood of successful reduction is diminished, although reduction is still possible.

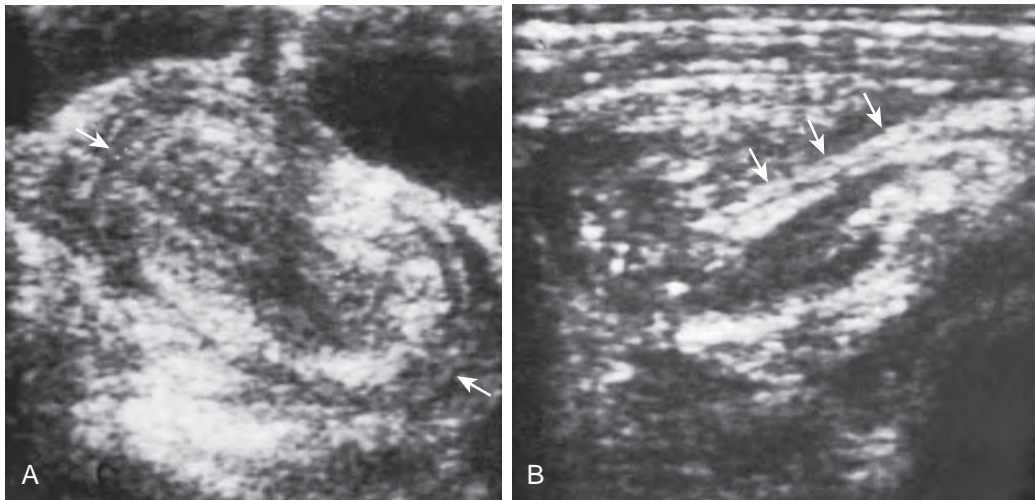


Figure 118-16 Sonography of intussusception. **A.** The target (arrows) appearance of intussusception is demonstrated on this longitudinal sonogram. The hypoechoic structures anteriorly are dilated bowel loops. **B.** Transverse scan of a different patient shows the parallel echogenic mucosa (arrows) of the intussusciens and intussusceptum.

evaluated by fluoroscopy and on filled and postevacuation radiographs in an attempt to find a lead point.

After reduction, the ileocecal valve may be edematous and may simulate a persistent intussusception or lead point.¹⁰² In older children, a delayed abdominal radiograph is helpful in identifying a residual cecal mass that may represent lymphoma or another lead point.

Perforation can occur during the reduction procedure at the site of the intussusception, the distal colon, or the rectum if the balloon is overinflated.^{103,104} Perforation is rare, occurring in less than 1% of reductions.

Water-soluble contrast medium or air should be used when there is concern about the viability of the underlying bowel, if symptoms have been present for more than 48 hours, and in neonates and infants. Water-soluble contrast medium exerts less hydrostatic pressure than barium, allowing the enema bag to be raised slightly higher than the standard 3 feet.¹⁰⁵

Intussusception reduction by enema with room air is widely used.¹⁰⁶⁻¹¹⁰ This technique has an impressive success rate, few complications, and many advantages. No foreign agent is introduced if there is perforation into the peritoneal cavity, and reduction attempts are less messy. Original reports indicated that radiation exposure was reduced because fluoroscopy time was often shorter and lower fluoroscopic techniques can be used, but a later article confirmed that fluoroscopy times were widely varied and depended on the radiologist and the ease of reduction.¹⁰⁷ For the novice, it may be difficult to determine when reduction has occurred because air may pass into and distend the small bowel before complete reduction has occurred.^{109,110}

Air reduction has many of the same requirements as hydrostatic reduction: placement of a rectal tube, a good seal of the rectum, and fluoroscopy. Air can be delivered by intermittent manual insufflation or through a continuous delivery system. Pressure is controlled by manometry so that the desired pressures are reached but not exceeded. Low pressure (60 mm Hg) and a low flow rate (1 L/min) may aid visualization of the intussusceptum at the beginning of the study, but pressures between 80 and 120 mm Hg are used routinely during most of the study.¹⁰⁶ Tension pneumoperitoneum secondary to perforation during air reduction may be life-threatening.¹⁰⁴ An 18-gauge

needle is standard equipment to immediately perform a paracentesis.

The sonographic findings of intussusception are well described.^{94-97,110-114} The mass of infolded bowel and the layering of the bowel walls produce a target or doughnut appearance on transverse scans (Fig. 118-16A) and a pseudokidney or sand-wich sign on longitudinal scans (Fig. 118-16B). Sonography may be diagnostic and therapeutic. At some institutions, Ringer, Hartmann, or saline solution enemas or air enemas are used to reduce the intussusception under sonographic guidance.¹¹⁵⁻¹¹⁸ The CT appearance of intussusception has been described in adults (see Chapter 62) and children.¹¹⁹ CT is not a useful screening technique because of radiation dose considerations and expense. CT or sonography may be of use in the child with no visible intussusceptum on enema but a competent ileocecal valve. In this setting, it is important to differentiate the child with a reduced intussusception from the child with residual ileoileal or other intussusception variant.

Volvulus of the Colon

CLINICAL FINDINGS

Volvulus of the colon is rare in children and occurs most commonly in the setting of malrotation and other anomalies of mesenteric attachment; constipation associated with mental retardation, HD, or cystic fibrosis; or aerophagia.¹²⁰⁻¹²³ Cecal volvulus may include twisting of the adjacent small bowel; it has been reported in children who have achieved continence by cecostomy button or tube and antegrade enema.¹²⁴

The very young are spared, and the presentation of childhood volvulus is usually between 7 and 10 years. Colonic volvulus generally and sigmoid volvulus specifically occur four to five times more frequently in boys than in girls. At presentation, the child has abdominal pain and, less frequently, vomiting accompanying the physical findings of abdominal distention and tenderness. This presentation may simulate intussusception, although this diagnosis would be unlikely in an older child.

Treatment consists of a diagnostic enema and proctoscopy or colonoscopy with or without insertion of a large-bore

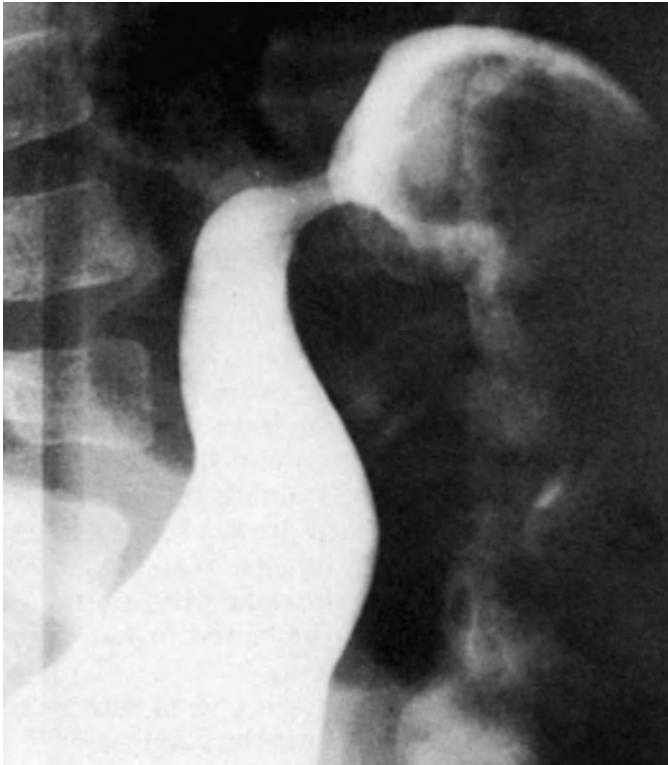


Figure 118-17 Sigmoid volvulus. Twisting of the colon produces narrowing just above the rectum. The segment above the volvulus is dilated and full of feces.

catheter for decompression. Operative treatment is needed if decompression is not achieved or if the volvulus recurs, which it does in one third of cases. If there are signs of peritonitis, surgery is indicated because gangrenous bowel can result from vascular compromise of the involved gut.

RADIOLOGIC FINDINGS

In patients with volvulus, conventional radiographs may be interpreted as normal, show nonspecific changes of colonic or small bowel obstruction, or less commonly demonstrate the bean-shaped, abnormally twisted loop. The value of the northern exposure sign (i.e., the dilated, volvulated sigmoid colon projects above the transverse colon) has not been determined in children.¹²⁵ Cecal volvulus may be manifested as an air-filled structure in the left midabdomen or left upper quadrant. Conventional radiographs are most useful for excluding other causes of abdominal pain and free air.

The contrast enema study characteristically demonstrates the narrowing, twisting, or bird-beak deformity of the volvulus (Fig. 118-17). The pressure of the enema may untwist the affected segment. Further discussion of volvulus can be found in Chapter 62.

Juvenile Polyps

CLINICAL FINDINGS

Juvenile polyps are benign, “inflammatory” polyps that are not hereditary or associated with inflammatory bowel disease. They are slightly more common in males than in females.¹²⁶⁻¹²⁹ These

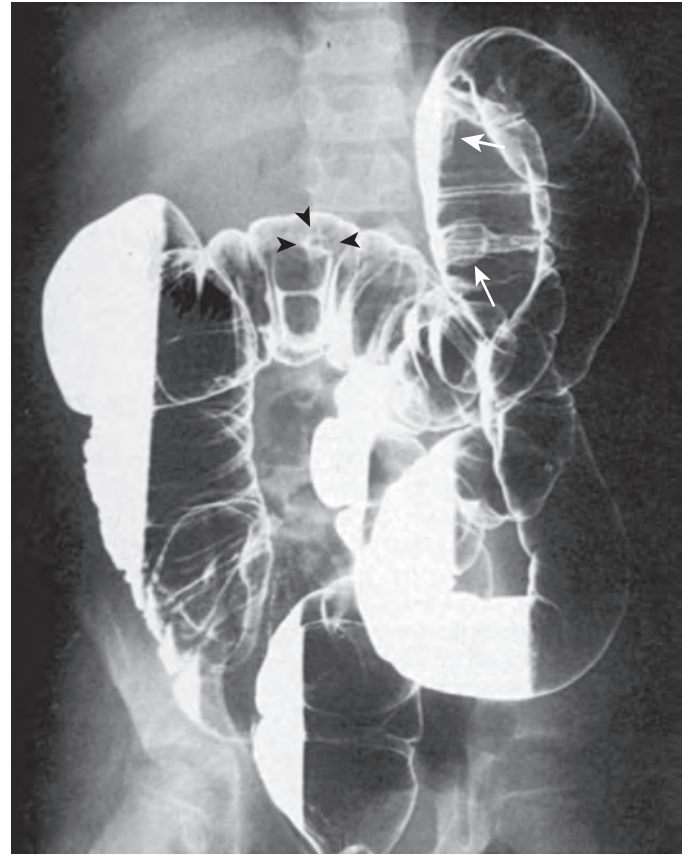


Figure 118-18 Juvenile polyps. Double-contrast barium enema examination demonstrates three polyps, two on stalks in the region of the splenic flexure (arrows) and the third en face (arrowheads) in the transverse colon.

polyps are rare in the neonate and are manifested in the middle and latter part of the first decade of life with blood in the stools. The bleeding is not accompanied by diarrhea or extragastrointestinal symptoms to suggest infectious or inflammatory bowel disease. Inspection of the anus can exclude fissure or tear as a cause of blood. On occasion, the polyp may be manifested as a prolapsing rectal mass. These polyps should be differentiated from those seen in juvenile polyposis, an autosomal dominant form of polyposis with few distinguishing extracolonic manifestations, and from polyps that occur in syndromes such as Peutz-Jeghers syndrome and familial adenomatous polyposis.¹²⁹⁻¹³² Because up to one third of these polyps are proximal to the splenic flexure, colonoscopy is recommended. Treatment consists of polypectomy at the time of colonoscopy.

RADIOLOGIC FINDINGS

Juvenile polyps are best demonstrated on double-contrast barium enema studies. Although most juvenile polyps are left sided, the entire colon must be carefully assessed. Demonstration of one polyp should not detract from the search for an additional one because approximately 20% to 30% of children have more than one juvenile polyp. Most polyps appear smooth and pedunculated (Fig. 118-18). The radiologic criteria for differentiating benign from malignant polyps in adults are of little value in children because virtually all juvenile polyps are benign, regardless of their appearance.

Imaging of polyps by sonography with compression of the colon and CT colonography are emerging areas of interest.¹³³⁻¹³⁵ However, colonoscopy is the first line of evaluation in most settings.

Colon Carcinoma

Primary colon cancer is rare in children, and on pathologic examination, these cancers are more often mucinous or colloid variants.¹³⁶⁻¹⁴² Most occur in the rectum and sigmoid colon. These cancers may arise spontaneously or may result from ulcerative colitis or familial adenomatous polyposis.

CLINICAL FINDINGS

A mass is palpable in about 10% of patients. The symptoms of colon cancer (e.g., vomiting, pain, constipation, bleeding) warrant early and complete evaluation, although the rarity of this neoplasm in children tends to delay a thorough diagnostic work-up. Consequently, the disease is often advanced at the time of diagnosis. Patients do poorly despite surgery and chemotherapy.

The differential diagnosis of colon cancer is limited. Non-neoplastic lesions such as intussusception, appendicitis, gastroenteritis, and parasitic infestations should be considered and excluded with appropriate tests. Obstruction, mass, and rectal bleeding can also be the presenting signs of a number of other neoplasms, including hemangioma, lymphoma, leiomyomas, and other spindle cell tumors.¹⁴¹

RADIOLOGIC FINDINGS

Single- and double-contrast barium enema characteristics of colon cancer in children are identical to those found

in adults (see Chapter 59). Mucosal irregularity or narrowing of the caliber of the colon with a typical apple-core deformity may be present. As in adults, sonography or CT is useful in looking for local, metastatic, or recurrent disease.

Fibrosing Colonopathy

CLINICAL FINDINGS

Fibrosing colonopathy (FC) has been recognized in children and adults with cystic fibrosis.¹⁴³⁻¹⁴⁸ It is a complication of enzyme replacement therapy, and it is usually seen in children in the first decade of life. It is unclear whether FC is related to high-dose preparations or to the total dose of enzyme that has been received. FC results in luminal narrowing of the colon and is distinct from Crohn's disease. Although patients with FC have diarrhea and abdominal pain, FC may not be immediately diagnosed because enzyme-refractory diarrhea and abdominal pain are fairly common in children with cystic fibrosis. In patients with FC and obstruction, distal intestinal obstruction syndrome or intussusception may be simulated. A contrast enema can differentiate these complications.

Treatment consists of decreasing the enzyme dose and amount of fat in the diet. Severe obstruction is common and may require surgery.¹⁴⁹

RADIOLOGIC FINDINGS

Barium enema examination reveals colonic stricture of varying severity extending distally from the cecum.¹⁴⁵ The rectum is usually spared. The colon is foreshortened, and the haustra are obliterated in the affected segments.^{150,151}

REFERENCES

- Laufer I, de Sa D: Lymphoid follicular pattern: A normal feature of the pediatric colon. *AJR Am J Roentgenol* 130:51-55, 1978.
- Glick S, Teplick SK, Ross WM: Colonic lymphoid follicles associated with colonic neoplasms. *Radiology* 168:603-607, 1988.
- Crooks DJM, Brown WR: The distribution of intestinal nodular lymphoid hyperplasia in immunoglobulin deficiency. *Clin Radiol* 31:701-706, 1980.
- Iacono G, Ravelli A, di Prima L, et al: Colonic lymphoid hyperplasia in children: Relationship to food hypersensitivity. *Clin Gastroenterol Hepatol* 5:361-366, 2007.
- Hendren WH: Constipation caused by anterior location of the anus and its surgical correction. *J Pediatr Surg* 13:505-512, 1978.
- Leape LL, Ramenofsky ML: Anterior ectopic anus: A common cause of constipation in children. *J Pediatr Surg* 13:627-630, 1978.
- Gene A, Tanelli C, Tansug N, et al: Evaluation of the location of the anus by a modified technique in the neonate. *J Pediatr Surg* 37:80-82, 2002.
- Hofman AD, Puri P: Association of Hirschsprung's disease and anorectal malformation: A systematic review. *Pediatr Surg Int* 29:913-917, 2013.
- Wakhlu A, Kureel SN, Tandon RK, Wakhlu AK: Long-term results of anterior sagittal anorectoplasty for the treatment of vestibular fistula. *J Pediatr Surg* 44:1913-1919, 2009.
- Swenson O, Sherman JO, Fisher JH: Diagnosis of congenital megacolon: An analysis of 501 patients. *J Pediatr Surg* 8:587-594, 1983.
- Gaultier C, Trang H, Duager S, et al: Pediatric disorders with autonomic dysfunction: What role for *PHOX2B*? *Pediatr Res* 58:1-6, 2005.
- Foster P, Cowan G, Wrenn EL, Jr: Twenty-five years' experience with Hirschsprung's disease. *J Pediatr Surg* 25:531-534, 1990.
- Suita S, Taguchi T, Kamimura T, et al: Total colonic aganglionosis with or without small bowel involvement: A changing profile. *J Pediatr Surg* 32:1537-1541, 1997.
- Jasonni V, Martucciello G: Total colonic aganglionosis. *Semin Pediatr Surg* 7:174-180, 1998.
- Teitelbaum DH, Coran AG: Enterocolitis. *Semin Pediatr Surg* 7:162-169, 1998.
- Newman B, Nussbaum A, Kirkpatrick JA, Jr: Bowel perforation in Hirschsprung's disease. *AJR Am J Roentgenol* 148:1195-1197, 1987.
- Arliss J, Holgerson LO: Neonatal perforation and Hirschsprung's disease. *J Pediatr Surg* 25:694-695, 1990.
- Brook I: Pseudomembranous colitis in children. *J Gastroenterol Hepatol* 20:182-186, 2005.
- Nurko S, Zimmerman LA: Evaluation and treatment of constipation in children and adolescents. *Am Fam Physician* 90:82-90, 2014.
- Ghosh A, Griffiths DM: Rectal biopsy in the investigation of constipation. *Arch Dis Child* 79:266-268, 1998.
- Penninckx F, Lestar B, Kerremans R: Pitfalls and limitations of testing the rectoanal inhibitory reflex in screening for Hirschsprung's disease. *Pediatr Surg Int* 5:260-265, 1990.
- Diamond IR, Casadiego G, Traubici J, et al: The contrast enema for Hirschsprung disease: Predictors of a false positive result. *J Pediatr Surg* 42:792-795, 2007.
- Amiel J, Lyonnet S: Hirschsprung disease, associated syndromes, and genetics: A review. *J Med Genet* 38:729-739, 2001.
- Shahar E, Shinawi M: Neurocristopathies presenting with neurologic abnormalities associated with Hirschsprung's disease. *Pediatr Neurol* 28:385-391, 2003.
- Seri M, Yin L, Barone V, et al: Frequency of RET mutations in long- and short-segment Hirschsprung disease. *Hum Mutat* 9:243-249, 1997.

26. Moore SW: Chromosomal and related Mendelian syndromes associated with Hirschsprung's disease. *Pediatr Surg Int* 28:1045–1058, 2012.
27. Filston HC, Kirks DR: The association of malrotation and Hirschsprung's disease. *Pediatr Radiol* 12:6–10, 1982.
28. Moore SW, Rode H, Millar AJW, et al: Intestinal atresia and Hirschsprung's disease. *Pediatr Surg Int* 5:182–184, 1990.
29. Fletcher BD, Yulish BS: Intraluminal calcifications in the small bowel of newborn infants with total colonic aganglionosis. *Radiology* 126:451–455, 1978.
30. Pochaczewsky R, Leonidas JC: The "rectosigmoid index." A measurement for the early diagnosis of Hirschsprung's disease. *AJR Am J Roentgenol* 123:770–777, 1975.
31. Siegel MJ, Shackelford GD, McAlister WH: The rectosigmoid index. *Radiology* 139:497–499, 1981.
32. DeCampo JF, Mayne V, Boldt DW, et al: Radiological findings in total aganglionosis coli. *Pediatr Radiol* 14:205–209, 1984.
33. Berdon WE, Koontz P, Baker DH: The diagnosis of colonic and terminal ileal aganglionosis. *AJR Am J Roentgenol* 91:680–689, 1984.
34. Jamieson DH, Dundas SE, Belushi SA, et al: Does the transition zone reliably delineate aganglionic bowel in Hirschsprung's disease? *Pediatr Radiol* 34:811–815, 2004.
35. Proctor ML, Traubici J, Langer JC, et al: Correlation between radiographic transition zone and level of aganglionosis in Hirschsprung's disease: Implications for surgical approach. *J Pediatr Surg* 38:775–778, 2003.
36. Leonidas JC, Krasna IH, Strauss L, et al: Roentgen appearance of the excluded colon after colostomy for infantile Hirschsprung's disease. *AJR Am J Roentgenol* 112:116–122, 1971.
37. Heyman MB, Kirschner BS, Gold BD, et al: Children with early-onset inflammatory bowel disease (IBD): Analysis of a pediatric IBD consortium registry. *J Pediatr* 146:35–40, 2005.
38. Mack DR: Ongoing advances in inflammatory bowel disease, including maintenance therapies, biologic agents, and biology of disease. *Curr Opin Pediatr* 10:499–506, 1998.
39. Aideyan UO, Smith WL: Inflammatory bowel disease in children. *Radiol Clin North Am* 34:885–902, 1996.
40. Wyllie R, Sarigol S: The treatment of inflammatory bowel disease in children. *Clin Pediatr* 37:421–425, 1998.
41. Denno DM, Stapp JR, Boster DR, et al: Etiology of diarrhea in pediatric outpatient settings. *Pediatr Infect Dis J* 24:142–148, 2005.
42. Dennehy PH: Acute diarrheal disease in children: Epidemiology, prevention, and treatment. *Infect Dis Clin North Am* 19:585–602, 2005.
43. Cohen MB, Nataro JP, Bernstein DI, et al: Prevalence of diarrheogenic *Escherichia coli* in acute childhood enteritis: A prospective controlled study. *J Pediatr* 146:54–61, 2005.
44. Guandalini S, Assiri A: Celiac disease: A review. *JAMA Pediatr* 168:272–278, 2014.
45. Moon A, Kleinman RE: Allergic gastroenteropathy in children. *Ann Allergy Asthma Immunol* 74:5–12, 1995.
46. Garci-Carceaga M, Jr, Kerner JA, Jr: Gastrointestinal manifestations of food allergies in pediatric patients. *Nutr Clin Pract* 20:526–535, 2005.
47. Camarero C, Leon F, Colino E, et al: Collagenous colitis in children: Clinicopathologic, microbiologic, and immunologic features. *J Pediatr Gastroenterol Nutr* 37:508–513, 2003.
48. Gremse DA, Boudreaux CW, Mancini EA: Collagenous colitis in children. *Gastroenterology* 104:906–909, 1993.
49. Yardley JH, Lazenby AJ, Kornacki S: Collagenous colitis in children. *Gastroenterology* 105:647–648, 1993.
50. Nikou GC, Toubanakis C, Nikolaou P, et al: VIPomas: An update in diagnosis and management in a series of 11 patients. *Hepatogastroenterology* 52:1259–1269, 2005.
51. Chung CJ, Rayder S, Meyers W, et al: Kawasaki disease presenting as focal colitis. *Pediatr Radiol* 26:455–457, 1996.
52. Petermann A, Offermann G, Distler A, et al: Familial hemolytic-uremic syndrome in three generations. *Am J Kidney Dis* 32:1063–1067, 1998.
53. Siegler R, Oakes R: Hemolytic uremic syndrome: Pathogenesis, treatment, and outcome. *Curr Opin Pediatr* 17:200–204, 2005.
54. Siegler RL: The hemolytic uremic syndrome. *Pediatr Clin North Am* 42:1505–1529, 1995.
55. Seror D, Szold A, Udassin R, et al: Surgical complications in hemolytic-uremic syndrome: Gangrenous appendicitis. *Pediatr Surg Int* 5:214–215, 1990.
56. Brandt ML, O'Reagan S, Rousseau E, et al: Surgical complications of the hemolytic-uremic syndrome. *J Pediatr Surg* 25:1109–1112, 1990.
57. Gianviti A, Tozzi AE, De Petris L, et al: Risk factors for poor renal prognosis in children with hemolytic uremic syndrome. *J Pediatr Nephrol* 18:1229–1235, 2003.
58. Steinborn M, Leiz S, Rudisser K, et al: CT and MRI in haemolytic uraemic syndrome with central nervous system involvement: Distribution of lesions and prognostic value of imaging findings. *Pediatr Radiol* 34:805–810, 2004.
59. Rahman RC, Cobenas CJ, Drut R, et al: Hemorrhagic colitis in postdiarrheal hemolytic uremic syndrome: Retrospective analysis of 54 children. *Pediatr Nephrol* 27:229–233, 2012.
60. Patriquin HB, O'Reagan S, Robitaille P, et al: Hemolytic-uremic syndrome: Intrarenal arterial Doppler patterns as a useful guide to therapy. *Radiology* 172:625–628, 1989.
61. Carrico CW, Fenton LZ, Taylor GA, et al: Impact of sonography on the diagnosis and treatment of acute lower abdominal pain in children and young adults. *AJR Am J Roentgenol* 172:513–516, 1999.
62. Patriquin HB, Garcier J-M, Lafortune M, et al: Appendicitis in children and young adults: Value of sonography in detecting perforation. *AJR Am J Roentgenol* 166:629–633, 1996.
63. Chang YJ, Kong MS, Hsia SH, et al: Usefulness of ultrasonography in acute appendicitis in early childhood. *J Pediatr Gastroenterol Nutr* 44:592–595, 2007.
64. Emil S, Mikhail P, Laberge JM, et al: Clinical versus sonographic evaluation of acute appendicitis in children: A comparison of patient characteristics and outcomes. *J Pediatr Surg* 36:780–783, 2001.
65. Ramachandran P, Sivit CJ, Newman KD, et al: Ultrasonography as an adjunct in the diagnosis of acute appendicitis: A 4-year experience. *J Pediatr Surg* 31:164–169, 1996.
66. Friedland JA, Siegel MJ: CT appearance of acute appendicitis in childhood. *AJR Am J Roentgenol* 168:439–442, 1997.
67. van Heurn LW, Pakarinen MP, Wester T: Contemporary management of abdominal surgical emergencies in infants and children. *Br J Surg* 101:e24–e33, 2014.
68. Kaiser S, Frenckner B, Jorulf HK: Suspected appendicitis in children: US and CT—a prospective randomized study. *Radiology* 223:633–668, 2002.
69. Wiersma F, Sramek A, Holscher HC: US features of the normal appendix and surrounding area in children. *Radiology* 235:1018–1022, 2005.
70. Herliczek TW, Swenson DW, Mayo-Smith WW: Utility of MRI after inconclusive ultrasound in pediatric patients with suspected appendicitis: Retrospective review of 60 consecutive patients. *AJR Am J Roentgenol* 200:969–973, 2013.
71. Fefferman NR, Roche KJ, Pinkney LP, et al: Suspected appendicitis in children: Focused CT technique for evaluation. *Radiology* 220:691–695, 2001.
72. Mittal VK, Goliath J, Sabir M, et al: Advantages of focused helical computed tomographic scanning with rectal contrast only vs triple contrast in the diagnosis of clinically uncertain acute appendicitis: A prospective randomized study. *Arch Surg* 139:495–499, 2004.
73. Jamieson DH, Chait PG, Filler R: Interventional drainage of appendiceal abscesses in children. *AJR Am J Roentgenol* 169:1619–1622, 1997.
74. Abramson SJ, Berdon WE, Baker DH: Childhood typhlitis: Its increasing association with acute myelogenous leukemia. *Radiology* 146:61–64, 1983.
75. Meyerovitz MF, Fellows KE: Typhlitis: A cause of gastrointestinal hemorrhage in children. *AJR Am J Roentgenol* 143:833–835, 1984.
76. Merine DS, Fishman EK, Jones B, et al: Right lower quadrant pain in the immunocompromised patient: CT findings in 10 cases. *AJR Am J Roentgenol* 149:1177–1179, 1987.
77. Sloas MM, Flynn PM, Kaste SC, et al: Typhlitis in children with cancer: A 30-year experience. *Clin Infect Dis* 17:484–490, 1993.
78. McCarville MB, Adelman CS, Li C, et al: Typhlitis in childhood cancer. *Cancer* 104:380–387, 2005.
79. Hobson MJ, Carney DE, Molik KA, et al: Appendicitis in childhood hematologic malignancies: Analysis and comparison with typhlitis. *J Pediatr Surg* 40:214–219, 2005.
80. McCarville MB, Thompson J, Li C, et al: Significance of appendiceal thickening in association with typhlitis in pediatric oncology patients. *Pediatr Radiol* 34:245–249, 2004.
81. Teefey SA, Montana MA, Goldfogel GA, et al: Sonographic diagnosis of neutropenic typhlitis. *AJR Am J Roentgenol* 149:731–733, 1987.
82. Schlatter M, Snyder K, Freyer D: Successful nonoperative management of typhlitis in pediatric oncology patients. *J Pediatr Surg* 37:1151–1155, 2002.
83. Agrawal AK, Saini N, Gildenogorin G, Feusner JH: Is routine computed tomographic scanning justified in the first week of persistent febrile neutropenia in children with malignancies? *Pediatr Blood Cancer* 57:620–624, 2011.
84. Schuh S, Wesson DE: Intussusception in children 2 years of age or older. *CMAJ* 136:269–272, 1987.
85. Gray MP, Li Sh, Hoffman RG, et al: Recurrence rates after intussusception enema reduction: A meta-analysis. *Pediatrics* 134:110–119, 2014.

86. Ong NT, Beasley SW: The lead point in intussusception. *J Pediatr Surg* 25:640–643, 1990.
87. Klein JD, Turner CG, Kamran SC, et al: Pediatric postoperative intussusception in the minimally invasive surgery era: A 13-year, single center experience. *J Am Coll Surg* 16: 1089–1093, 2013.
88. Stephenson CA, Seibert JJ, Strain JD, et al: Intussusception: Clinical and radiographic factors influencing reducibility. *Pediatr Radiol* 20:57–60, 1989.
89. Fike FB, Mortellaro VE, Holcomb GW, 3rd, St Peter SD: Predictors of failed enema reduction in childhood intussusception. *J Pediatr Surg* 47:925–927, 2012.
90. Navarro O, Daneman A, Chae A: Intussusception: The use of delayed, repeated attempt and the management of intussusceptions due to pathologic lead points in pediatric patients. *AJR Am J Roentgenol* 182:1169–1176, 2004.
91. Schwab J, Benya E, Lin R, et al: Contrast enema in children with Henoch-Schönlein purpura. *J Pediatr Surg* 40:1221–1223, 2005.
92. Hernandez JA, Swischuk LE, Angel CA: Validity of plain films in intussusception. *Emerg Radiol* 10:323–326, 2004.
93. Ratcliffe JE, Fong S, Cheong I, et al: Plain film diagnosis of intussusception: Prevalence of the target sign. *AJR Am J Roentgenol* 158:619–621, 1992.
94. Daneman A, Navarro O: Intussusception. Part 1. A review of diagnostic approaches. *Pediatr Radiol* 33:79–85, 2003.
95. Hryhorczuk AL, Strouse PJ: Validation of US as a first-line diagnostic test for assessment of pediatric ileocolic intussusception. *Pediatr Radiol* 39:1075–1079, 2009.
96. Bhisitkul DM, Listerick R, Shkolnik A, et al: Clinical application of ultrasonography in the diagnosis of intussusception. *J Pediatr* 121: 182–186, 1992.
97. Verschelden P, Filiatrault D, Garel L, et al: Intussusception in children: Reliability of US in diagnosis—a prospective study. *Radiology* 184:741–744, 1992.
98. Collins DL, Pickney LE, Miller KE, et al: Hydrostatic reduction of ileocolic intussusception: A second attempt in the operating room with general anesthesia. *J Pediatr* 115:204–207, 1989.
99. Naiditch JA, Rigsby C, Chin A: Delayed repeated enema and operative findings after unsuccessful primary enema for intussusception. *Eur J Pediatr Surg* 22:404–408, 2012.
100. Touloukian RJ, O'Connell JB, Markowitz RI, et al: Analgesic premedication in the management of ileocolic intussusception. *Pediatrics* 79:432–434, 1987.
101. Franken EA, Smith WL, Chernish SM, et al: The use of glucagon in hydrostatic reduction of intussusception: A double blind study of 30 patients. *Radiology* 146:687–689, 1983.
102. Devred PH, Faure F, Padovani J: Pseudotumoral cecum after hydrostatic reduction of intussusception. *Pediatr Radiol* 14:295–298, 1984.
103. Bramson RT, Blickman JG: Perforation during hydrostatic reduction of intussusception: Proposed mechanism and review of the literature. *J Pediatr Surg* 27:589–591, 1992.
104. Daneman A, Alton DJ, Ein S, et al: Perforation during attempted intussusception reduction in children—a comparison of perforation with barium and air. *Pediatr Radiol* 25:81–86, 1995.
105. Kuta AJ, Benator RM: Intussusception: Hydrostatic pressure equivalents for barium and meglumine sodium diatrizoate. *Radiology* 175: 125–126, 1990.
106. Schmit P, Rohrschneider WK, Christmann D: Intestinal intussusception survey about diagnostic and nonsurgical therapeutic procedures. *Pediatr Radiol* 29:752–761, 1999.
107. Heenan SD, Kyriou J, Fitzgerald M, et al: Effective dose at pneumatic reduction of paediatric intussusception. *Clin Radiol* 55:811–816, 2000.
108. Guo J, Ma X, Zhou Q: Results of air pressure enema reduction of intussusception: 6,396 cases in 13 years. *J Pediatr Surg* 21:1201–1203, 1986.
109. Hedlund GL, Johnson JF, Strife JL: Ileocolic intussusception: Extensive reflux of air preceding pneumatic reduction. *Radiology* 174:187–189, 1990.
110. Daneman A, Navarro O: Intussusception. Part 2. An update on the evolution of management. *Pediatr Radiol* 34:97–108, 2004.
111. Britton I, Wilkinson AG: Ultrasound features of intussusception predicting outcome of air enema. *Pediatr Radiol* 29:705–710, 1999.
112. Swischuk LE, Hayden CK, Boulden T: Intussusception: Indications for ultrasonography and an explanation of the doughnut and pseudokidney signs. *Pediatr Radiol* 15:388–391, 1985.
113. Alessi V, Salerno G: The “hay-fork” sign in the ultrasonographic diagnosis of intussusception. *Pediatr Radiol* 10:177–179, 1985.
114. Pracros JP, Tran-Minh VA, Morin de Finfe CH, et al: Acute intestinal intussusception in children: Contribution of ultrasonography (145 cases). *Ann Radiol* 30:525–530, 1987.
115. Gu L, Zhu H, Wang S, et al: Sonographic guidance of air enema for intussusception reduction in children. *Pediatr Radiol* 30:339–340, 2000.
116. Crystal P, Hertzmann Y, Farber B, et al: Sonographically guided hydrostatic reduction of intussusception in children. *J Clin Ultrasound* 30:343–348, 2002.
117. Khong PL, Peh WC, Lam CH, et al: Ultrasound-guided hydrostatic reduction of childhood intussusception: Technique and demonstration. *Radiographics* 20:E1, 2000.
118. del-Pozo G, Albillos JC, Tejedor D, et al: Intussusception in children: Current concepts in diagnosis and enema reduction. *Radiographics* 19:299–319, 1999.
119. Cox TD, Winters WD, Weinberger E: CT of intussusception in the pediatric patient: Diagnosis and pitfalls. *Pediatr Radiol* 26:26–32, 1996.
120. Puneet P, Khanna R, Gangopadhyay AN, et al: Sigmoid volvulus in childhood: Report of six cases. *Pediatr Surg Int* 16:132–133, 2000.
121. Zeng M, Amodio J, Schwarz S, et al: Hirschsprung disease presenting as sigmoid volvulus: A case report and review of the literature. *J Pediatr Surg* 48:243–246, 2013.
122. Atamanalp SS, Yildiran MI, Basoglu M, et al: Sigmoid colon volvulus in children: A review of 19 cases. *Pediatr Surg Int* 20:492–495, 2004.
123. Folaranmi SE, Cho A, Tareen F, et al: Proximal large bowel volvulus in children: 6 new cases and review of the literature. *J Pediatr Surg* 47: 1572–1575, 2012.
124. Kokoska ER, Herndon CD, Carney DE, et al: Cecal volvulus: A report of two cases occurring after the antegrade colonic enema procedure. *J Pediatr Surg* 39:916–919, 2004.
125. Javors BR, Baker SR, Miller JA: The northern exposure sign: A newly described finding in sigmoid volvulus. *AJR Am J Roentgenol* 173: 571–574, 1999.
126. Latt TT, Nichol R, Domizio P, et al: Rectal bleeding and polyps. *Arch Dis Child* 69:144–147, 1993.
127. Pillai RB, Tolia V: Colonic polyps in children: Frequently multiple and recurrent. *Clin Pediatr* 37:253–257, 1998.
128. Cohen S, Gorodnichenko A, Weiss B, et al: Polyposis syndromes in children and adolescents. *Eur J Gastroenterol Hepatol* 26:972–977, 2014.
129. Guota SK, Fitzgerald JF, Croffie JM, et al: Experience with juvenile polyps in North American children: The need for pancolonoscopy. *Am J Gastroenterol* 96:1695–1697, 2001.
130. Erdman SH, Barnard JA: Gastrointestinal polyps and polyposis syndromes in children. *Curr Opin Pediatr* 14:576–582, 2002.
131. Hyer W, Beveridge I, Domizio P, et al: Clinical management and genetics of gastrointestinal polyps in children. *J Pediatr Gastroenterol Nutr* 31:469–479, 2000.
132. Thakkar K, Fishman DS, Gilger MA: Colorectal polyps in childhood. *Curr Opin Pediatr* 24:632–637, 2012.
133. Baldisserotto M, Spolidoro JV, Bahu Mda G: Graded compression of the colon in the diagnosis of polyps in pediatric patients. *AJR Am J Roentgenol* 79:201–205, 2002.
134. Wei C, Dayong W, Liquin J, et al: Colorectal polyps in children: A retrospective study of clinical features and the value of ultrasonography in their diagnosis. *J Pediatr Surg* 47:1853–1858, 2012.
135. Anupindi S, Jaramillo D, Zalis ME, et al: Low-dose CT colonography in children: Initial experience, technical feasibility, and utility. *Pediatr Radiol* 35:518–524, 2005.
136. Steinberg JB, Tuggle DW, Postier RG: Adenocarcinoma of the colon in adolescents. *Am J Surg* 156:460–462, 1988.
137. Jerkic S, Rosewich H, Scharf JG, et al: Colorectal cancer in two pre-teenage siblings with familial adenomatous polyposis. *Eur J Pediatr* 164:306–310, 2005.
138. Lamego CMB, Torloni H: Colorectal adenocarcinoma in childhood and adolescence. Report of 11 cases and review of the literature. *Pediatr Radiol* 19:504–508, 1989.
139. Al Sasi O, Sathiapalan R, Rafai A, et al: Colonic neuroendocrine carcinoma in a child. *Pediatr Radiol* 35:339–343, 2005.
140. McCarville MB, Hill DA, Miller BE, et al: Secondary ovarian neoplasms in children: Imaging features with histopathologic correlation. *Pediatr Radiol* 31:358–364, 2001.
141. Terada R, Ito S, Akama F, et al: Clinical and histopathological features of colonic stromal tumor in a child. *J Gastroenterol* 35:456–459, 2000.
142. Kim G, Baik SH, Lee KY, et al: Colon carcinoma in childhood: Review of the literature with four case reports. *Int J Colorectal Dis* 28:157–164, 2013.
143. Schwartzberg SJ, Wielnski CL, Shamieh I, et al: Cystic fibrosis-associated colitis and fibrosing colonopathy. *J Pediatr* 127:565–570, 1995.
144. Borowitz D, Gelfond D: Intestinal complications of cystic fibrosis. *Curr Opin Pulm Med* 19:676–680, 2013.

145. Zerin JM, Kuhn-Fulton J, White SJ, et al: Colonic strictures in children with cystic fibrosis. *Radiology* 194:223–226, 1995.
146. Ramsden WH, Moya EF, Littlewood JM: Colonic wall thickness, pancreatic enzyme dose and type of preparation in cystic fibrosis. *Arch Dis Child* 79:339–343, 1998.
147. FitzSimmons SC, Burkhart GA, Borowitz D, et al: High-dose pancreatic-enzyme supplements and fibrosing colonopathy in children with cystic fibrosis. *N Engl J Med* 336:1283–1289, 1997.
148. Lloyd-Still JD, Beno DW, Kimura RM: Cystic fibrosis colonopathy. *Curr Gastroenterol Rep* 1:231–237, 1999.
149. Escobar MA, Grosfeld JL, Burdick JJ, et al: Surgical considerations in cystic fibrosis: A 32-year evaluation of outcomes. *Surgery* 138:560–571, 2005.
150. Fields TM, Michel SJ, Buttler CL, et al: Abdominal manifestations of cystic fibrosis in older children and adults. *AJR Am J Roentgenol* 187: 1199–2003, 2006.
151. Kuo W, Ciet P, Tiddens HA, et al: Monitoring cystic fibrosis lung disease by computed tomography. Radiation risk in perspective. *Am J Respir Crit Care Med* 189:1328–1336, 2014.

Diseases of the Pediatric Gallbladder and Biliary Tract

JENNIFER L. NICHOLAS

CHAPTER OUTLINE

Imaging Modalities

Normal Gallbladder

Normal Bile Ducts

Evaluation of Infants and Children with Cholestasis

Neonatal Jaundice

Biliary Atresia

Alagille's Syndrome

Progressive Familial Intrahepatic Cholestasis

Choledochal Malformations

Caroli's Disease

Bile Plug Syndrome or Inspissated Bile Syndrome

Gallbladder Disease

Cholelithiasis

Acalculous Cholecystitis

Gallbladder Dyskinesia

Gallbladder Hydrops

Bile Duct Disease

Choledocholithiasis

Biliary Changes with Cystic Fibrosis

Primary Sclerosing Cholangitis

Neoplasms

Imaging Modalities

Ultrasound is typically the first imaging modality used in the evaluation of children with suspected biliary disease because it is noninvasive and relatively inexpensive and does not involve contrast agents, sedation, or radiation exposure. Ultrasound is particularly useful in differentiating obstructive from nonobstructive causes of jaundice.¹ In general, the only preparation needed for an ultrasound study in the work-up of suspected biliary disease is for the child to have nothing by mouth for as close to 4 to 6 hours as possible to ensure optimal distention of the biliary system.

Computed tomography (CT) and magnetic resonance imaging (MRI) can also be useful in the evaluation of the biliary system in children, but CT exposes the child to radiation and both imaging modalities may require sedation. Specific protocols for evaluating the biliary system have been developed for CT and MRI. CT cholangiography, performed after the intravenous administration of a contrast agent that is excreted by the liver into the biliary system (meglumine iodoxamic acid), is not typically used in the pediatric population.² Magnetic resonance cholangiopancreatography (MRCP) is a noninvasive

means of evaluating the biliary system, the surrounding liver parenchyma, and other abdominal viscera that can usually be performed without administration of a contrast agent and does not expose the child to radiation.² MRCP is limited in neonates and infants, however, as biliary ducts less than 1 mm in diameter are difficult to visualize on MRCP.³ In preparation for MRCP, it is essential that the child be given nothing by mouth for as close to 4 to 6 hours as possible so that the biliary system is optimally distended and the stomach is empty.³ During acquisition of the images for MRCP, breath-hold techniques can be used in children who are able to cooperate, and non-breath-hold techniques with respiratory gating can be used in children who are not able to cooperate.^{3,4}

Percutaneous transhepatic cholangiography, percutaneous cholecystocholangiography, intraoperative cholangiography, and endoscopic retrograde cholangiopancreatography (ERCP) are also used in evaluation of the pediatric biliary system, but they are invasive examinations, expose the child to radiation and sedation, and can be technically challenging. ERCP, for example, has a complication rate in pediatric patients of one in three (33%), which is higher than the complication rate for adults.⁵

Nuclear medicine hepatobiliary scintigraphy, which is performed with either ^{99m}Tc-disofenin ([2,6-diisopropylacetanilido]-iminodiacetic acid) or ^{99m}Tc-mebrofenin (bromo-2,4,6-trimethylacetanilidoiminodiacetic acid), provides more physiologic information than anatomic information, particularly regarding the patency of the biliary system.

Normal Gallbladder

Ultrasound is an ideal imaging modality for evaluating the gallbladder in children because it allows real-time evaluation of the gallbladder in multiple planes and with the patient in various positions. The normal pediatric gallbladder is approximately 1.3 cm in length in neonates and 3.4 cm in length in infants and less than 1 cm in width.⁶ The average length of the gallbladder in a 16-year-old is 8 cm, with an average width of less than 3.5 cm.⁷

The normal sonographic appearance of the gallbladder wall is well defined, hyperechoic, and less than 3 mm in thickness when the child is fasting.^{6,7} Duplication of the gallbladder is rare⁸ and is often asymptomatic, but when it is encountered, it may be mistaken for a pathologic process such as choledochal malformation, dilated bile ducts, or gallbladder diverticulum (Fig. 119-1). Other congenital anomalies of the gallbladder include ectopia (most commonly retrohepatic, intrahepatic, or suprahepatic), septations, and agenesis.⁶ The normal pediatric gallbladder may have folds or kinks, which can mimic pathologic processes such as stones and dilated bile ducts. Imaging in more than one plane or with the patient in different positions

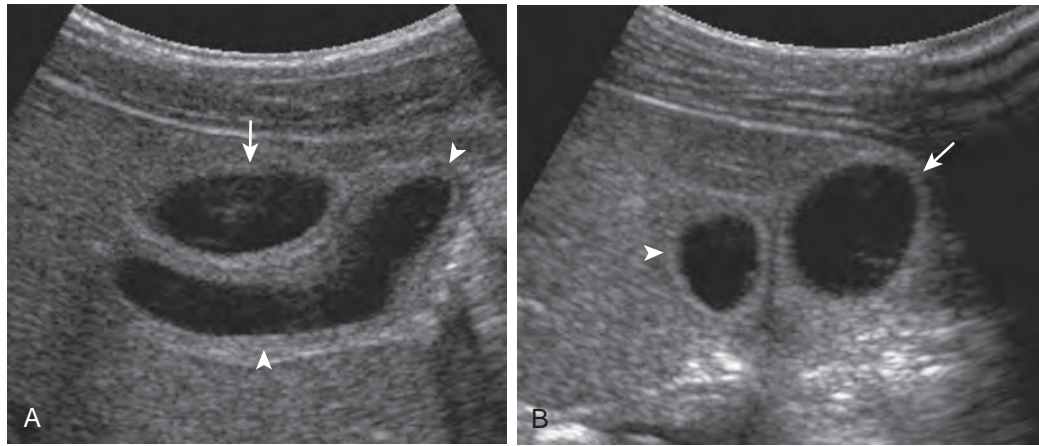


Figure 119-1 Duplication of the gallbladder. **A** and **B.** Sonograms in two planes demonstrate two gallbladders (arrows and arrowheads) in a 10-year-old child with biliary colic.

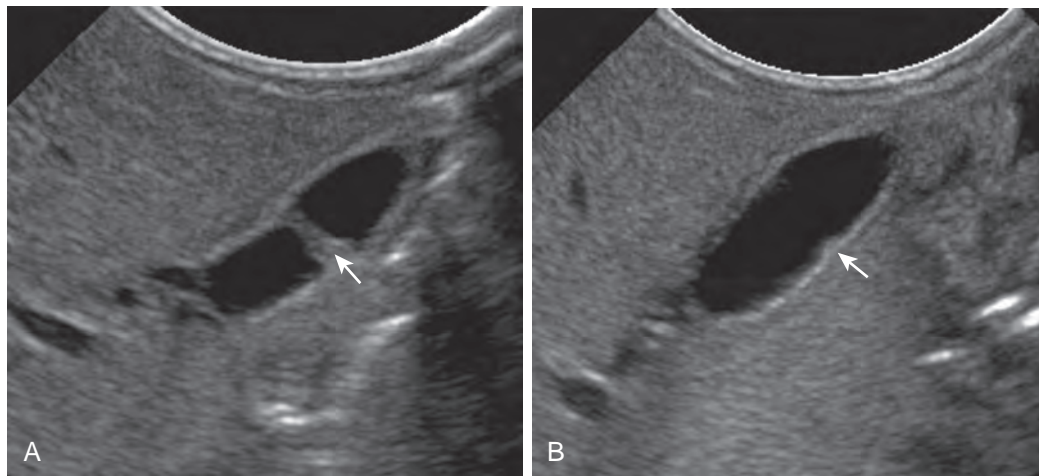


Figure 119-2 Normal gallbladder with a fold. **A.** Male infant at 21 days old. The sonographic image demonstrates a fold (arrow) that mimics a septum traversing the gallbladder lumen. **B.** Imaging in another plane demonstrates that the gallbladder lumen is not compartmentalized. The fold simulates focal thickening of the gallbladder wall (arrow).

can help differentiate normal folds from abnormal pathologic processes (Fig. 119-2).⁶

Gallbladder wall thickening in children, which is defined as more than 3 mm in thickness, can be seen in the setting of acute or chronic cholecystitis,⁶ hypoalbuminemia, ascites, systemic venous hypertension,⁹ and acute hepatitis.¹⁰ Children with ascites and hypoalbuminemia can have normal gallbladder wall thickness, however.⁹ Cholecystitis can occur in children without gallbladder wall thickening as well.⁹ The gallbladder wall may appear falsely thickened if fluid is trapped in the mesentery between the gallbladder and liver, creating a halo effect, or if fluid is otherwise surrounding the intraperitoneal gallbladder.⁹ Technical factors, such as the angle of the transducer, can also affect the appearance of the gallbladder wall. If the gallbladder is not optimally distended because of a contraction from a recent meal, the gallbladder wall may appear falsely thickened, and repeated imaging after the patient has been fasting for 4 to 6 hours is recommended for more accurate evaluation.

Normal Bile Ducts

Bile excreted by hepatocytes of the liver is collected by bile canaliculi that merge into the canals of Hering. Bile then flows into interlobular bile ducts, more peripheral intrahepatic bile ducts, and then into the left and right hepatic ducts. The left and right hepatic ducts merge into the common hepatic duct, which exits the liver and joins the cystic duct (from the gallbladder), which then forms the common bile duct. The common bile duct then joins the pancreatic duct, forming the ampulla of Vater, which delivers the bile to the second portion of the duodenum.

Peripheral intrahepatic ducts are not typically visualized on ultrasound, CT, or MRI (even MRCP) unless they are dilated. The normal left and right hepatic ducts may be seen on ultrasound, MRI, and CT in older children. The common hepatic duct, cystic duct, and common bile duct may be visualized more readily, but their small size can make visualization challenging. As measured on ultrasound from inner wall to inner wall, the

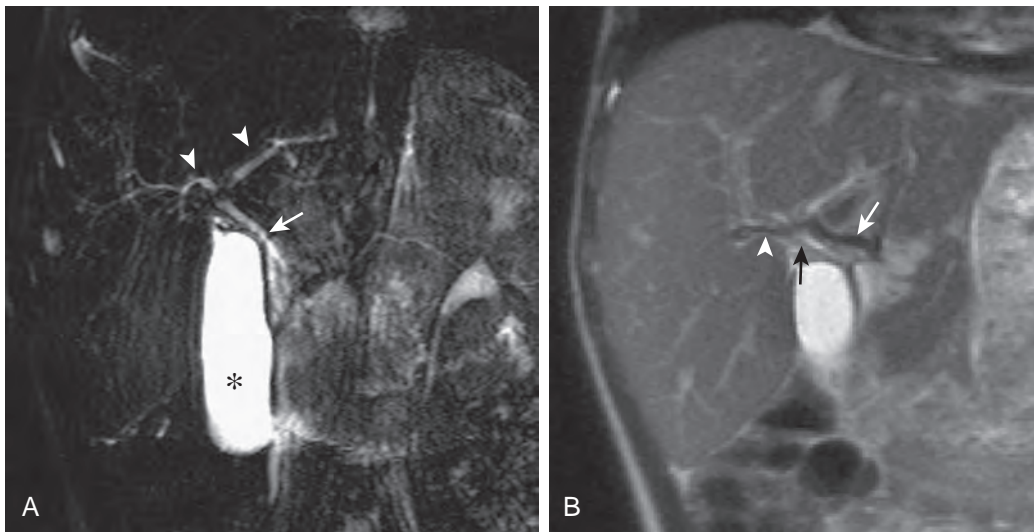


Figure 119-3 Normal findings on MRCP. MRCP was obtained to evaluate the biliary tract in a child with sickle cell disease. **A.** The coronal, thick-slab, T2-weighted image demonstrates patency of the common bile duct (arrow), the common hepatic duct, and the right and left hepatic ducts (arrowheads). There is loss of signal where the hepatic artery crosses at the confluence of the right and left hepatic ducts. Individual source images (not shown) demonstrate duct patency. The gallbladder is distended with bile (asterisk). **B.** Coronal half-Fourier acquisition single-shot turbo spin-echo (HASTE) image demonstrates the flow void in the main hepatic artery (white arrow) and right branch of the hepatic artery (arrowhead). The black arrow marks the origin of the common hepatic duct.

diameter of the common bile duct should be less than 1.6 mm in children younger than 1 year and less than 3.3 mm during childhood and early adolescence.¹¹ The cystic duct is usually seen only if it is dilated, and even then, only the distal portion of the cystic duct is typically visualized.⁶

On MRCP, the pediatric biliary tree is considered normal if the right hepatic, left hepatic, common hepatic, and common bile ducts are visualized, are of normal caliber, and have confluent, uniform branching (Fig. 119-3).¹²⁻¹⁴ In neonates, however, the extrahepatic biliary ducts may be the only ducts visible.

Evaluation of Infants and Children with Cholestasis

NEONATAL JAUNDICE

Normal transient physiologic jaundice (unconjugated hyperbilirubinemia) can occur in term and preterm infants in the first 2 weeks of life.¹⁵ The Cholestasis Guideline Committee recommends evaluation for cholestasis (abnormal accumulation of conjugated bilirubin), however, in jaundiced, non-breast-fed infants who are more than 2 weeks old.¹⁵ Breast-fed infants may have elevated bilirubin during the first 3 weeks of life, but hyperbilirubinemia in these babies should be considered abnormal if the urine is dark or the stools are light.¹⁵ Cholestasis is diagnosed when the serum conjugated bilirubin concentration is more than 1.0 mg/dL if the total serum bilirubin concentration is less than 5.0 mg/dL or when it is more than 20% of the total serum bilirubin concentration if the total serum bilirubin concentration is less than 5.0 mg/dL.

Transient neonatal jaundice can be due to hemolysis, hepatic infection, sepsis, metabolic diseases, bile plug syndrome, or adrenal hemorrhage. Some medications and total parenteral nutrition can also cause transient jaundice. Neonatal hepatitis, biliary atresia, and choledochal malformation are the most common causes of persistent neonatal jaundice,¹ with hepatitis

and biliary atresia accounting for 70% to 80% of cases.¹⁶ Alagille's syndrome and spontaneous bile duct perforation are less common causes of persistent neonatal jaundice.¹⁶ Caroli's disease is a congenital abnormality of the intrahepatic bile ducts that can also cause persistent jaundice, but clinical presentation more commonly occurs in childhood or adolescence.¹⁷

Biliary atresia is the most common cause of persistent neonatal jaundice that requires surgical intervention. Other less common surgically amenable causes of persistent neonatal jaundice include inspissated bile syndrome, choledochal malformation, and spontaneous perforation of the bile ducts.¹⁸ The initial imaging study in a child with neonatal jaundice is usually an ultrasound examination of the abdomen and pelvis. The liver size, vasculature, parenchymal echogenicity and echotexture, and intrahepatic and extrahepatic biliary ducts are evaluated with gray-scale and Doppler imaging. If a gallbladder is present, it is evaluated for size, wall thickness, presence of stones or sludge, and pericholecystic fluid. The spleen and pancreas are also evaluated. Ultrasound of the abdomen and pelvis provides good anatomic evaluation for potential sources of cholestasis; hepatocyte function and biliary drainage can be evaluated with nuclear medicine hepatobiliary scintigraphy, preferably performed with ^{99m}Tc-mebrofenin.

BILIARY ATRESIA

Background

Biliary atresia is a progressive, fibrosing, obliterative disease that affects the biliary tree. Biliary atresia typically begins in the neonatal period but may begin before birth.^{19,20} Biliary atresia results in cholestasis, which then leads to hepatic fibrosis and cirrhosis.²⁰ Children with biliary atresia typically present with persistent neonatal jaundice and often also have icterus or clay-colored (acholic) stool.²¹ Biliary atresia occurs in 1 of 8000 to 16,700 live births, with a higher incidence in Asian populations.²²⁻²⁴

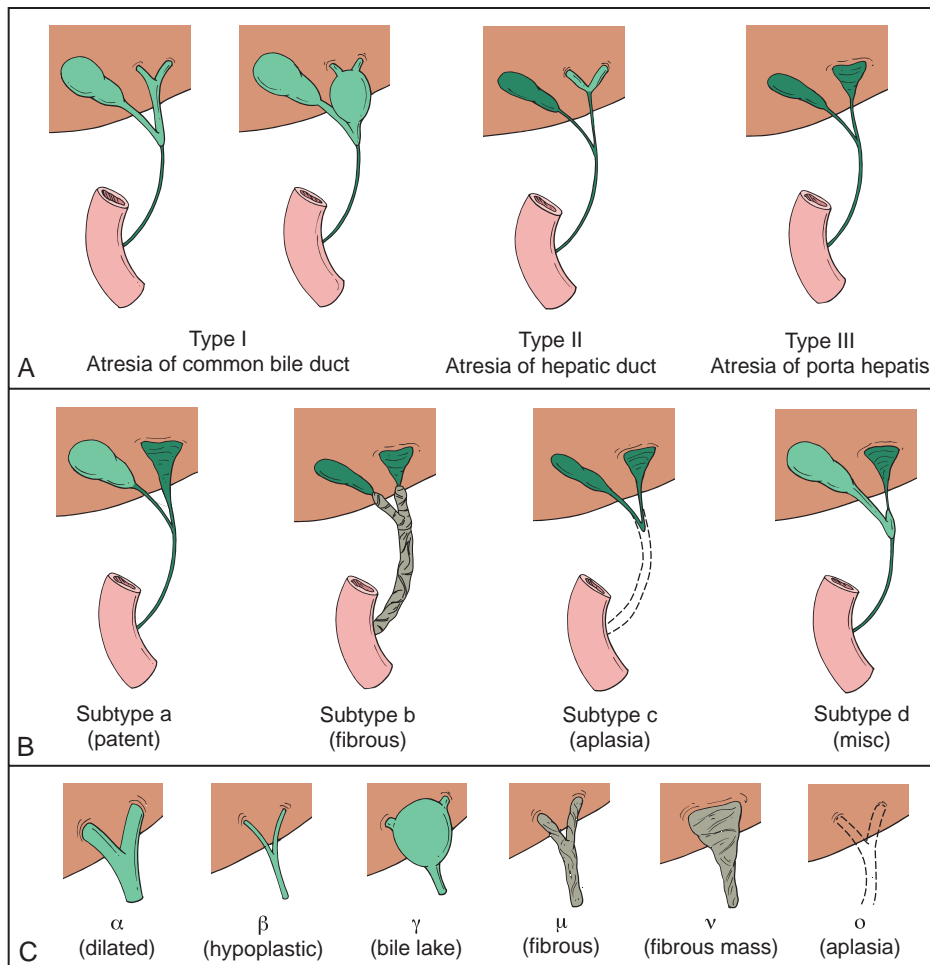


Figure 119-4 Schematic of Ohi used in the classification of biliary atresia. **A.** The three main types of biliary atresia (type I is considered surgically “correctable”). **B.** The subtypes for biliary atresia of the distal biliary ducts. **C.** The subtypes for biliary atresia of the proximal biliary ducts. (From Superina R, Magee JC, Brandt ML, et al: *The anatomic pattern of biliary atresia identified at time of Kasai hepatopuertoenterostomy and early postoperative clearance of jaundice are significant predictors of transplant-free survival.* *Ann Surg* 254:577–585, 2011.)

Several classification systems for biliary atresia have been developed, generally based on which part of the biliary tree is involved and to what degree.¹ The classification system for biliary atresia initially proposed and Ohi^{25,26} is one of the more widely used. In the system developed by Ohi, type I is atresia of the common bile duct, with patency of the proximal biliary ducts (right hepatic, left hepatic, and common hepatic), and it is considered to be the surgically “correctable” type of biliary atresia. Type II is atresia of the hepatic duct. Type III is involvement of the extrahepatic biliary tree and intrahepatic ducts of the porta hepatis.²⁵ Varying degrees of atresia may occur in the distal ducts, ranging from hypoplasia to fibrosis, aplasia, or a miscellaneous combination of these degrees of atresia (subtypes a to d, respectively). Involvement of the proximal ducts is further divided into subtypes that are assigned lowercase Greek letters: alpha (α) is dilation of the proximal ducts, beta (β) is hypoplasia of the proximal ducts, gamma (γ) involves a bile lake at the porta hepatis, mu (μ) is fibrosis of the proximal ducts, nu (ν) is a fibrous mass at the porta hepatis, and omicron (\omicron) is aplasia of the proximal ducts (Figs. 119-4 and 119-5).

Associated Anomalies and Malformations

Approximately 70% to 85% of infants with biliary atresia will not have any other anomalies or malformations, which has been referred to as perinatal biliary atresia.^{27–29} Typically, these children are born without jaundice, but jaundice develops and

stools become progressively acholic within the first 2 months of life.

Approximately 10% to 15% of infants with biliary atresia have associated laterality malformations, which is known as biliary atresia splenic malformation³⁰ or embryonal biliary atresia. Abnormalities associated with biliary atresia include situs inversus, symmetric bilobed liver, asplenia or polysplenia, intestinal malrotation, interrupted or absent inferior vena cava, preduodenal portal vein, aberrant hepatic artery, and cardiac anomalies.^{30,31} If polysplenia or situs inversus is encountered in a jaundiced infant, biliary atresia is almost invariably present.¹⁸ The association is important because the complex anatomy in patients with laterality malformations complicates the surgical treatment of biliary atresia.²³

The remaining 5% to 10% of biliary atresia cases are associated with other congenital malformations, including intestinal atresia, imperforate anus, kidney anomalies, and cardiac anomalies.^{28,32,33}

Treatment

If it is untreated, biliary atresia is fatal, with an average survival of 18 months.³⁴ In patients with biliary atresia, the goal is to achieve adequate biliary drainage with the Kasai procedure (also known as the Kasai portoenterostomy, hepatic portoenterostomy, and hepatopuertoenterostomy). The Kasai procedure involves excision of the obliterated biliary remnant with

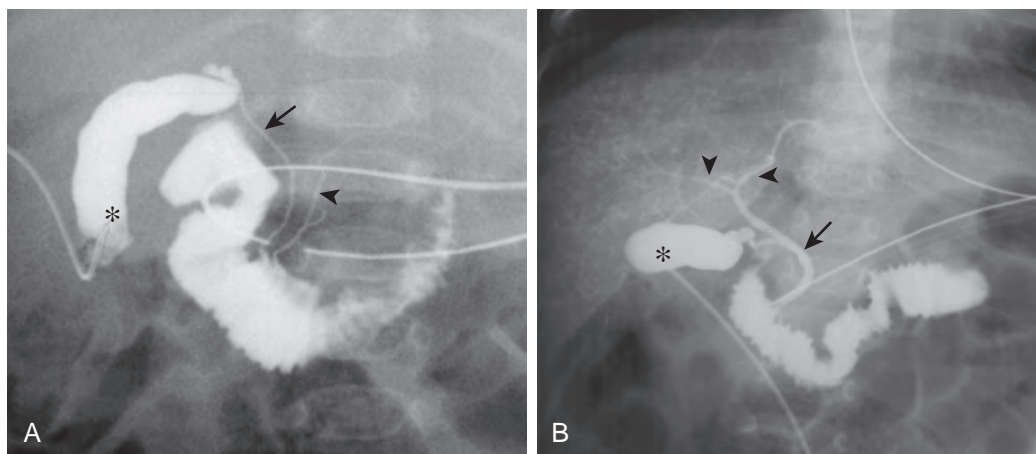


Figure 119-5 Biliary atresia: cholangiographic features. **A.** Intraoperative cholangiography is performed by catheterization of the gallbladder (asterisk) and injection of contrast material. This infant has an extremely hypoplastic but patent common bile duct (arrow). There is no filling of the common hepatic duct or intrahepatic ducts. The pancreatic duct (arrowhead) is opacified. **B.** Normal findings on intraoperative cholangiography in an infant. The gallbladder (asterisk) is cannulated. The union of the cystic duct and common hepatic duct forms the common bile duct (arrow). The right and left hepatic ducts are opacified (arrowheads), and intrahepatic duct branching is evident.

anastomosis of the portal plate to the small bowel with a Roux-en-Y hepatojejunostomy. For the biliary atresia to be considered surgically correctable, a portion of the proximal common hepatic duct must be patent, which can be directly anastomosed to the jejunum after the resection of the fibrotic bile duct remnant, ideally preventing the long-term sequelae of biliary atresia and the need for liver transplantation. Unfortunately, the truly correctable type of biliary atresia is uncommon, accounting for only approximately 10% to 15% of cases. Even though the remaining forms of biliary atresia are not considered correctable surgically, the Kasai procedure is used palliatively until a liver transplant is needed, with a survival rate of more than 95%.¹⁸ Adequate biliary drainage after a Kasai procedure has been defined as a total bilirubin concentration of less than 2.0 mg/dL anytime within the first 3 months after surgery.²⁶

It was initially accepted that the Kasai procedure should be performed before an infant diagnosed with biliary atresia reaches 2 months of age.³⁵ Subsequently, however, this was not the conclusion of a more comprehensive analysis from the Japanese registry,³⁶ nor was it the conclusion of Davenport, who reported a 5-year 45% transplant-free survival in a smaller cohort of children who underwent the Kasai procedure at more than 100 days of age.³⁷ A collaborative North American study, which prospectively evaluated 530 patients with biliary atresia from 2004 to 2010, found that infants younger than 75 days undergoing the Kasai procedure were no more likely than infants older than 75 days to achieve adequate biliary drainage (total bilirubin concentration of less than 2.0 mg/dL within the first 3 months).²⁶ In the same study, however, Suprina and colleagues²⁶ did show that having the Kasai procedure done before 75 days of age was associated with improved transplant-free survival, suggesting that efforts to identify and to treat infants with biliary atresia as early as possible are worthwhile.

Cholangitis is a serious potential complication of the Kasai procedure that can lead to sudden cessation of bile drainage. The greatest risk factor for development of cholangitis after a Kasai procedure is inadequate biliary drainage. Cholangitis

should be suspected when the child has fever and acholic stools or fever and jaundice with an elevated direct bilirubin level and positive C-reactive protein result.^{38,39} Some investigators expand the diagnosis of cholangitis to include any unexplained fever in a patient who has had a Kasai procedure. Most patients who have undergone the Kasai procedure have at least one episode of cholangitis, and 90% occur in children younger than 2 years.³⁹ Episodes of cholangitis in this population have been shown to adversely affect survival rates.³⁹

Imaging

Ultrasound, nuclear medicine hepatobiliary scintigraphy, CT, and MRI are the primary imaging modalities used in the work-up for biliary atresia. When necessary, transhepatic cholangiography, intraoperative cholangiography, and traditional angiography may be used. Preoperative definition of the patient's anatomy with Doppler ultrasound, CT, MRI, and angiography is used in technical planning of the surgical procedure. Traditional angiography may be necessary to demonstrate the location and size of the portal trunk in cases in which it is not seen by CT or MRI.⁴⁰

Ultrasound should be the initial imaging modality for infants with cholestatic jaundice and suspected biliary atresia.²² The infant is kept fasted for as close to 4 hours as possible before the ultrasound examination in an attempt to maximize distention of the biliary tree and gallbladder, if one is present. A high-frequency linear transducer or microconvex transducer is used for optimal visualization of the biliary system.^{20,22}

Sonographic findings in children with biliary atresia are variable. The liver parenchyma may be normal in echogenicity and echotexture,⁴ or there may be absence of identifiable bile ducts resulting in a homogeneous appearance of the liver parenchyma (Fig. 119-6).¹⁸ If the patient presents later in the course of the disease, findings of cirrhosis and portal hypertension may be present (Fig. 119-7). The common bile duct may not be seen. If the liver is not interrogated by color Doppler imaging, the hepatic artery can be mistaken for the common bile duct, resulting in a false-negative study. False-negative examination results can also occur when there is a patent portion of the

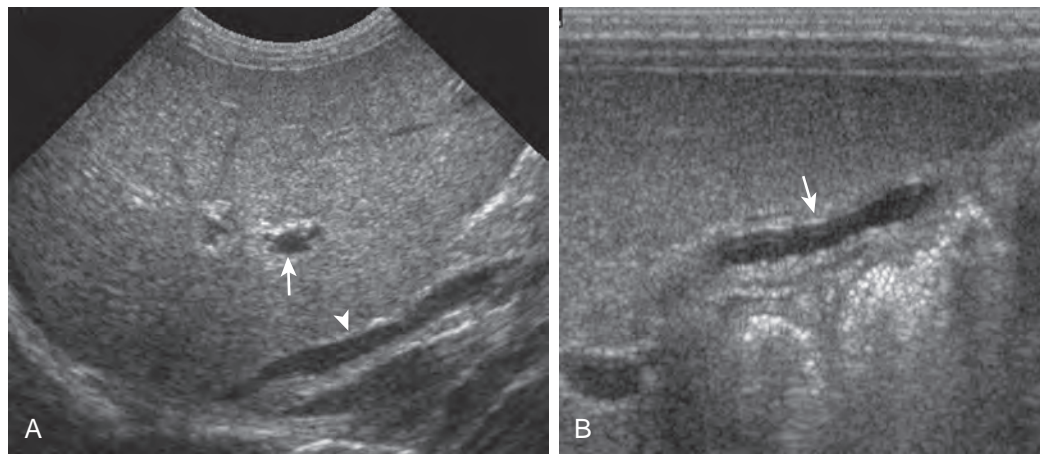


Figure 119-6 Biliary atresia: sonographic features. **A.** Longitudinal sonogram of a 22-day-old girl with cholestatic jaundice. The liver has a normal, uniform echotexture. The intrahepatic inferior vena cava (arrowhead), hepatic veins, and portal veins (arrow) are seen, but bile ducts are not identified. **B.** A small gallbladder (arrow) with an irregular wall is identified. There is no bile duct dilation. Biliary atresia was confirmed with nuclear scintigraphy, liver biopsy, and intraoperative cholangiography before treatment with a Kasai procedure.

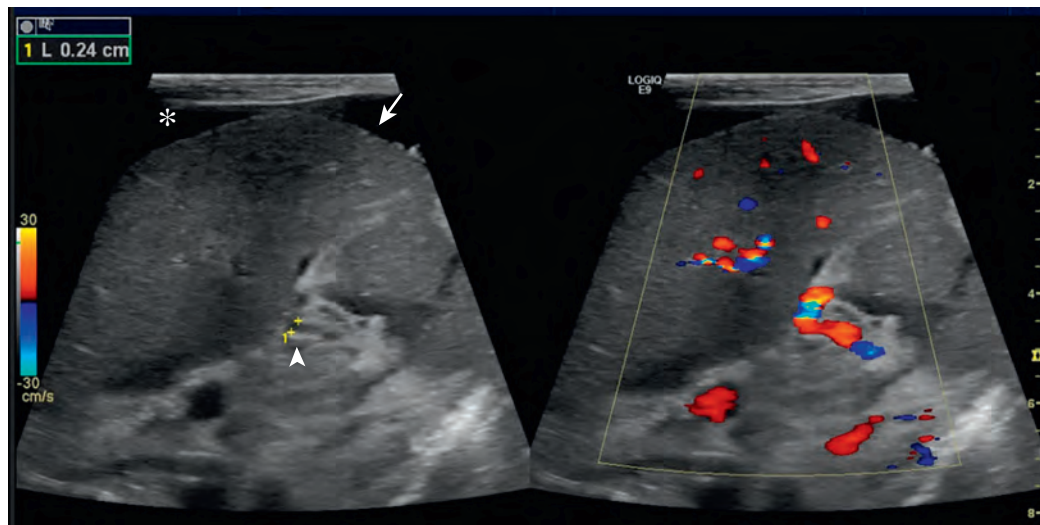


Figure 119-7 Biliary atresia: progression to cirrhosis with portal hypertension and ascites. Gray-scale and color Doppler images of the liver with a high-frequency linear transducer in a 3-month-old boy with biliary atresia show nodular contour of the liver surface (arrow), ascites (asterisk), and an enlarged hepatic artery (arrowhead). This patient was not a candidate for the Kasai procedure because he presented after he had ascites and cirrhosis. He received a liver transplant approximately 1 month later.

common bile duct²¹ or if there is cystic dilation of the extrahepatic duct.¹⁸

When the hepatic artery is correctly identified, its size may be helpful in making the diagnosis of biliary atresia. It has been shown that the diameter of the right hepatic artery in patients with biliary atresia (1.9 ± 0.4 mm) is significantly larger than the diameter of the hepatic artery in infants with hepatitis (1.4 ± 0.3 mm) and infants in the control group (1.2 ± 0.2 mm).⁴¹ In the same study, the hepatic artery diameter-to-portal vein diameter ratio in the biliary atresia group (0.52 ± 0.12) was larger than that in hepatitis (0.40 ± 0.07) and control (0.40 ± 0.10) groups ($P < .001$).⁴¹ On the basis of these findings, cutoff values for diagnosis of biliary atresia were 1.5 mm (sensitivity, 92%; specificity, 87%; accuracy, 89%) for hepatic artery diameter and 0.45 for hepatic artery diameter-to-portal vein diameter ratio (sensitivity, 76%; specificity, 79%; accuracy, 78%).⁴¹

Another ultrasound finding that can be helpful in the diagnosis of biliary atresia is a focal triangular or tubular hyperechoic structure just anterior and slightly superior to the main portal vein bifurcation (Fig. 119-8), known as the triangular cord sign. This echogenic structure represents the fibrotic remnant of the obliterated common bile duct.^{4,20,22,42,43} Flow is not seen within the triangular cord on Doppler evaluation. The triangular cord may not be obvious in the early stages of the disease, or it may be obscured by a large right hepatic artery.⁴² The triangular cord can also be masked by diffuse periportal hyperechogenicity due to inflammation or cirrhosis, or it may be difficult to appreciate if the fibrotic cord is small.²⁰ Short-term follow-up ultrasound is warranted if the infant has findings on initial ultrasound that appear normal or that suggest neonatal hepatitis but the cholestatic jaundice is not improving or is worsening.⁴⁴

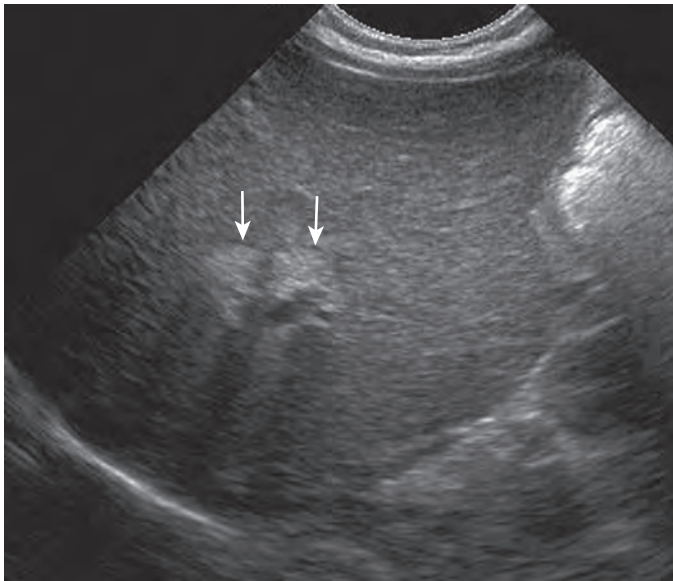


Figure 119-8 Biliary atresia: triangular cord sign on ultrasound. The triangular cord sign describes the fibrotic, obliterated common bile duct in infants with biliary atresia. It is seen as a focal hyperechoic area just cephalad to the main portal vein bifurcation, or it can be measured as the echogenic anterior wall of the right portal vein (arrows). The hypoechoic area within this is a branch of the right hepatic artery. (Courtesy Myung-Joon Kim, MD, Yonsei University College of Medicine, Severance Hospital, Seoul, Korea.)

A triangular cord larger than 4 mm in a neonate with cholestatic jaundice has been shown to be 80% sensitive and 98% specific and to have positive and negative predictive values of 94% for the diagnosis of biliary atresia.⁴⁵ Round, linear, or tubular hypoechoic or cystic lesions within the triangular cord have been described that are cleftlike cystic lesions within the fibrotic mass histopathologically.⁴ These cystic clefts can also be seen as triangular areas of increased signal intensity on T2-weighted MRCP images.⁴

The gallbladder is usually small or absent in patients with biliary atresia,^{4,14,20-22} but visualization of a normal gallbladder does not exclude the diagnosis of biliary atresia.⁴² Jaundiced, preterm infants receiving total parenteral nutrition without biliary atresia can also have small gallbladders.²⁰ The gallbladder ghost triad has been described in association with biliary atresia: an atretic gallbladder (<1.9 cm long); thinned mucosa or lack of a smooth, complete echogenic gallbladder mucosal lining with indistinct walls; and a knobby, irregular or lobular gallbladder contour (Fig. 119-9).²⁰ These findings are presumed to be caused by the atretic state, immaturity, and lack of function of the gallbladder in infants with biliary atresia. Gallbladder wall thickening is not a feature of biliary atresia, but it has been described in 25% of jaundiced infants without biliary atresia and may be useful in directing the work-up away from the diagnosis of biliary atresia.²⁰

When ultrasound is not diagnostic of biliary atresia, the next diagnostic test is usually a nuclear medicine hepatobiliary scintigraphy study.⁴² This study is performed with ^{99m}Tc and an iminodiacetic acid derivative, preferably mebrofenin,⁴⁶ because of its higher hepatic excretion.⁴⁷ Ideally, a 3- to 7-day course of oral phenobarbital (5 mg/kg/day in two divided doses)^{46,47} is given to the child in preparation for the examination because it is thought that phenobarbital enhances bile excretion and flow,

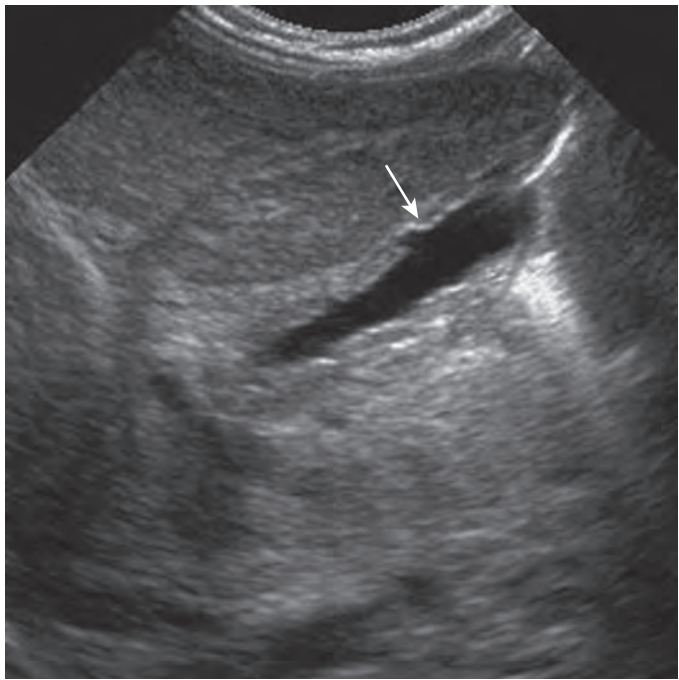


Figure 119-9 Biliary atresia: gallbladder ghost triad on ultrasound. The combination of an atretic gallbladder with irregular mucosa and wall contour (arrow) has been called the gallbladder ghost triad. It is associated with biliary atresia. (Courtesy Myung-Joon Kim, MD, Yonsei University College of Medicine, Severance Hospital, Seoul, Korea.)

which can help differentiate biliary atresia from neonatal hepatitis. If the infant is approaching the age before which a Kasai procedure is ideally performed (60-75 days), the hepatobiliary study may be attempted without the phenobarbital preparation or with a shorter 2- to 3-day pretreatment with ursodeoxycholic acid (20 mg/kg/day in two divided doses, continued until the test is finished)^{47,48} in an effort to save time and to prevent a delay in the diagnosis.

According to the practice guidelines of the Society of Nuclear Medicine, an infant who is having a hepatobiliary scan should be kept fasted for at least 2 hours before the intravenous administration of 1 mCi of ^{99m}Tc-mebrofenin.⁴⁷ Anterior images are then acquired dynamically, starting at the time of injection and continuing for 60 minutes, at 1 minute per frame.⁴⁷ Delayed images in the anterior and right lateral projections are obtained after a diaper change, including 5-minute images at 4 to 6 hours and 10-minute images at 24 hours if no radiopharmaceutical has been visualized in the small bowel.

The findings on the hepatobiliary scintigraphy study are considered normal if the hepatic parenchyma is visualized almost immediately after intravenous administration of the isotope, followed sequentially by activity in the intrahepatic biliary ducts, the extrahepatic biliary ducts, the gallbladder, and the small bowel, ideally within 1 hour after administration of the isotope. Neonatal hepatitis is presumed when there is delayed hepatocyte clearance of the radiopharmaceutical but activity is seen in the small bowel by 24 hours. If the radiopharmaceutical is excreted into the bowel by 24 hours, the diagnosis of biliary atresia is essentially excluded.^{34,42,49} When no radiopharmaceutical is seen in the bowel on the 24-hour delayed images, biliary atresia should be strongly considered (Fig. 119-10). However, nonvisualization of the

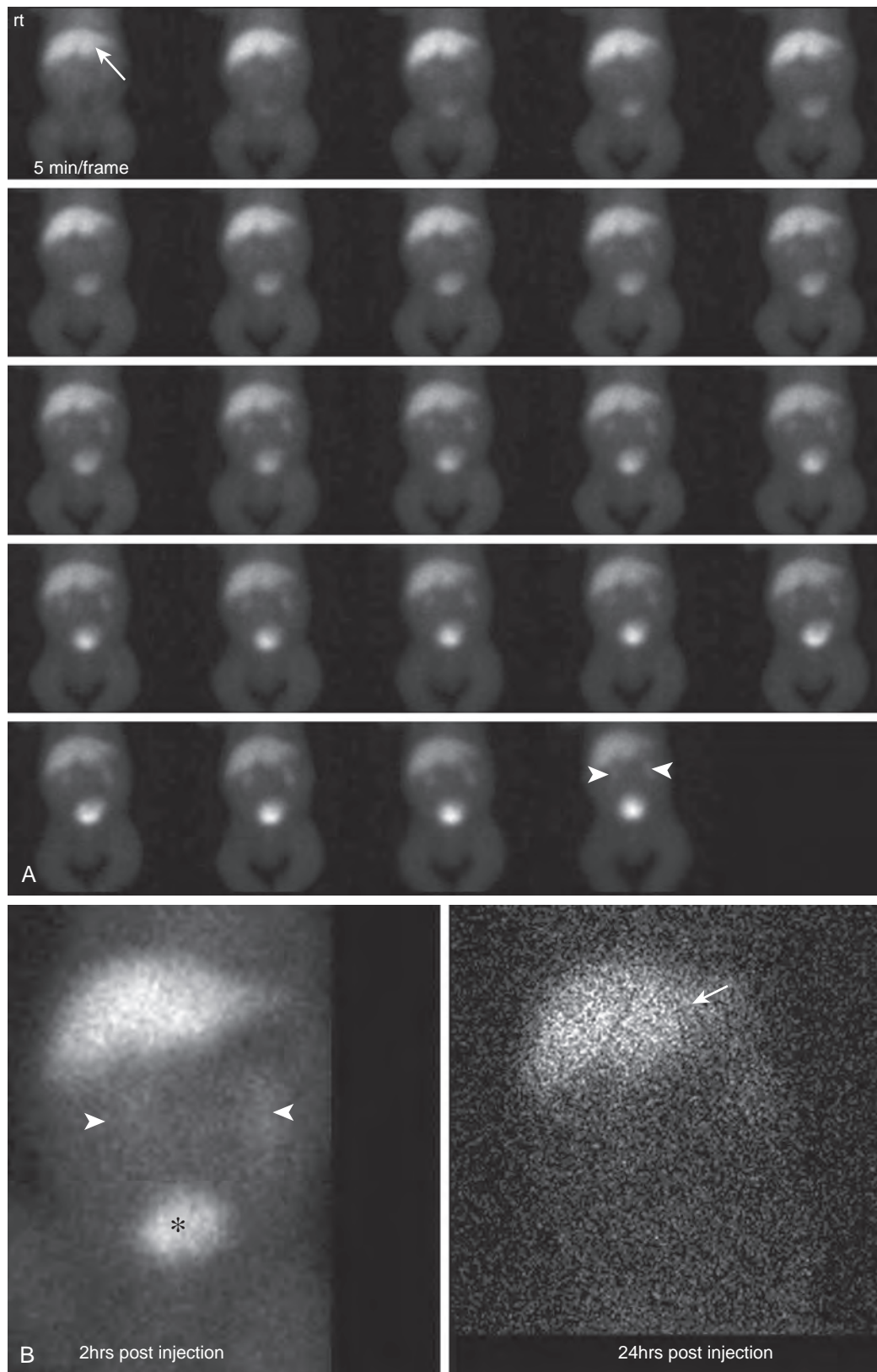


Figure 119-10 Biliary atresia: hepatobiliary nuclear scintigram. A. Anterior images of the abdomen and pelvis filmed at 5 minutes/frame demonstrate good uptake of ^{99m}Tc -disofenin by the hepatocytes in the liver (arrow). There is no evidence of activity in the gallbladder, common bile duct, or intestines. Renal uptake (arrowheads) and excretion into the urinary bladder are evident. **B.** Anterior delayed images. After a 2-hour delay, there is persistent activity within the liver and continued clearance by the kidneys (arrowheads) with excreted radiopharmaceutical detected within the urinary bladder (asterisk). The 24-hour image also demonstrates some activity in the liver (arrow) but no evidence of biliary excretion into the small intestine.

radiopharmaceutical in the bowel at 24 hours is not highly specific for biliary atresia because hepatocellular dysfunction in infants with neonatal hepatitis can sometimes be pronounced enough that the radiopharmaceutical is not excreted within the first 24 hours.⁵⁰ The reported diagnostic accuracy of hepatobiliary scintigraphy in the diagnosis of biliary atresia is 56% to 81.6%, with a sensitivity of 91.7% to 100% and a specificity of 35% to 76.9%.^{14,20,42}

For biliary atresia to be excluded, the patency of the common hepatic duct and common duct should be demonstrated,⁴⁹ but this is not always achieved with ultrasound and hepatobiliary scintigraphy. MRCP may eliminate the need in children for more invasive imaging, such as percutaneous transhepatic or intraoperative cholangiography, biopsy, or exploratory surgery, if normal biliary tract anatomy can be demonstrated.¹³ The diagnosis of biliary atresia is made on MRCP when the common bile duct or the common hepatic duct is not visualized.⁴⁹ In infants with cholestatic jaundice, Han and colleagues⁵¹ demonstrated that MRCP had an accuracy of 98%, sensitivity of 100%, and specificity of 96% for the diagnosis of biliary atresia. As on ultrasound, MRCP findings of biliary atresia include nonvisualization of the extrahepatic bile ducts, a small or absent gallbladder, and periportal fibrosis (the triangular cord sign on ultrasound). Periportal fibrosis is often seen as a triangular area of high signal intensity ventral to the porta hepatis on the T2-weighted images^{3,4,49} and as a hypointense signal paralleling the portal vein branches on T1-weighted sequences that becomes isointense with liver after administration of gadolinium.⁵² Gadolinium administration distinguishes the enhancing periportal fibrosis from the nonenhancing, dilated periportal ducts seen in other disease processes.⁵² On T2-weighted images, a focal region of hyperintense signal thought to be fluid has been described within the high signal intensity periportal fibrosis in some children with biliary atresia (Fig. 119-11).⁴

False-positive MRCP results for biliary atresia have been reported; these are in part due to the fact that MRCP relies on the production and excretion of bile into the bile ducts to visualize the biliary tract.¹³ Children with disease states that result in decreased hepatobiliary function and subsequent decreased bile production, such as sclerosing cholangitis, may have false-positive examination findings because the biliary tree is not visualized on MRCP owing to a relative lack of bile within the ducts.^{12,13}

Liver biopsy can help confirm the diagnosis of biliary atresia. An 18-gauge needle biopsy of the liver has been shown to be 90% sensitive, 96% specific,⁴² and 85%¹⁸ to 93%⁴² accurate for the diagnosis of biliary atresia in cholestatic children.⁴² Neonatal hepatitis and early biliary atresia may have identical ultrastructural and light microscopic features.⁵³ If the biopsy is performed early in a particular patient's disease process, the typical ultrastructural features of biliary atresia (i.e., proliferation of the intralobular bile ductules with loss of ductular microvilli, periductal inflammatory fibrosis, and bile plugging) may not yet be present, and a false-negative result may occur.⁵³ If the clinical course and liver biopsy results are not concordant, repeated biopsy may be warranted.

In some children, ultrasound, nuclear scintigraphy, MRCP, and liver biopsy results may all be inconclusive. In these children, visualization of the bile ducts by cholangiography

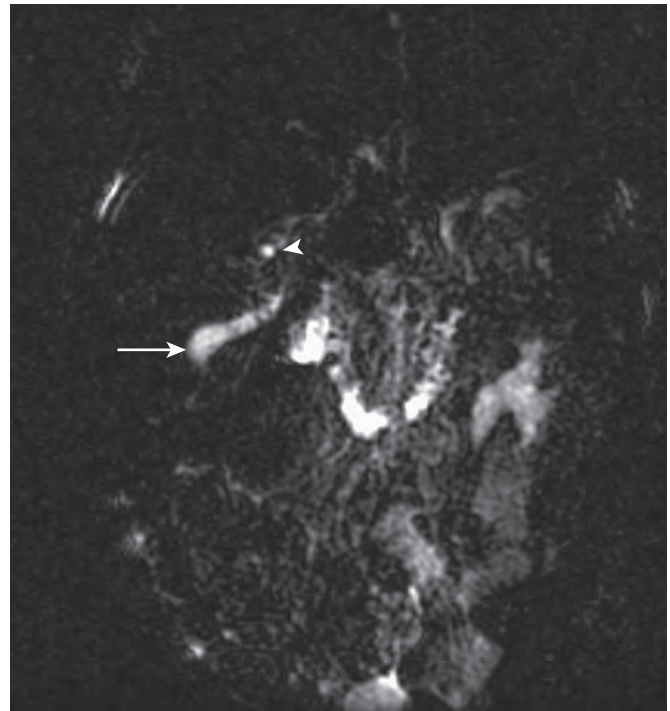


Figure 119-11 Biliary atresia: MRCP findings. Coronal, thick-slab, T2-weighted image of a 19-day-old infant with cholestasis shows a small focus of increased signal intensity (arrowhead) in the porta hepatis that represents a cystic lesion within the porta hepatis. A gallbladder is identified (arrow), but no linear or branching structures suggesting bile ducts are identified. Lack of identification of the right, left, and main hepatic ducts and common bile duct is consistent with biliary atresia. (Courtesy Myung-Joon Kim, MD, Yonsei University College of Medicine, Severance Hospital, Seoul, Korea.)

intraoperatively, percutaneously through the liver or gallbladder, or by endoscopy may be necessary.

In children with biliary atresia who have undergone the Kasai procedure, it is important to monitor for changes of fibrosis, cirrhosis, and portal hypertension on postoperative imaging. It is also important to know the patient's baseline anatomy and to remember that the loop of jejunum that is anastomosed to the porta hepatis can be seen as a fluid-filled structure, which can be mistaken for a postoperative fluid collection. If necessary, patency of the anastomosis can be confirmed by nuclear scintigraphy.

ALAGILLE'S SYNDROME

Background

Alagille's syndrome, also known as arteriohepatic dysplasia, is a rare autosomal dominant disease characterized by chronic cholestasis due to a paucity of interlobular bile ducts relative to the number of portal areas within the liver.^{54,55} Children with Alagille's syndrome usually present as neonates but may present later.⁵⁶ For diagnosis, at least three of the five typical features of the disease are exhibited: chronic cholestasis from interlobular bile duct paucity, congenital heart disease typically involving hypoplasia or stenosis of the peripheral pulmonary arteries, "butterfly" vertebrae, posterior embryotoxon (an ocular abnormality), and peculiar facies.^{56,57}

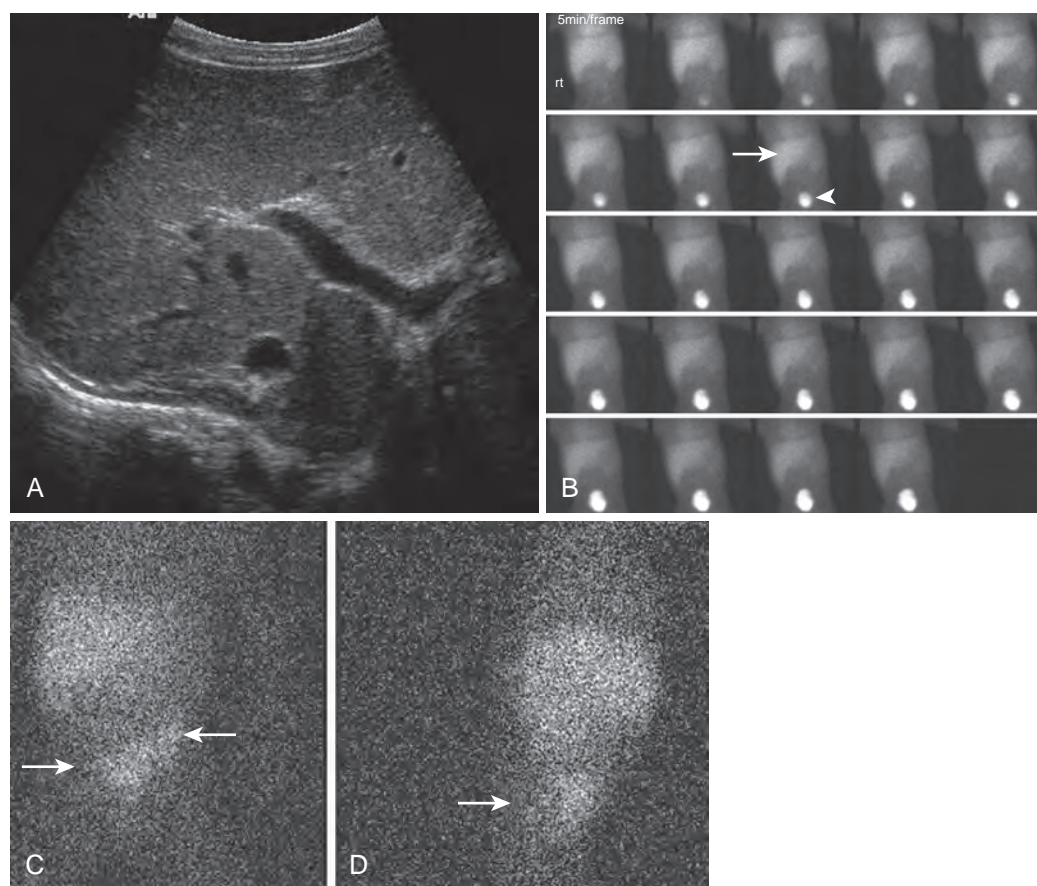


Figure 119-12 Nonsyndromic intrahepatic bile duct paucity: ultrasound and hepatobiliary scintigram. **A.** The cholestatic infant has a lack of sonographically identifiable gallbladder or intrahepatic bile ducts. **B.** Nuclear scintigraphy demonstrates poor hepatic extraction (arrows) of the radiopharmaceutical. Some radiopharmaceutical is seen in the urinary bladder (arrowhead). **C** and **D.** There is minimal small bowel activity at 24 hours (arrow). These findings can be seen in the setting of neonatal hepatitis or paucity of intrahepatic bile ducts with cholestasis. Liver biopsy confirmed a paucity of intrahepatic ducts (arrows). This child lacked other clinical abnormalities that are associated with Alagille's syndrome.

Pulmonary artery stenosis at various levels is one of the most common manifestations of Alagille's syndrome. Other associated vascular anomalies include basilar or middle cerebral artery aneurysms, internal carotid artery anomalies, aortic coarctation or aneurysm, and moyamoya syndrome. The intracranial vascular anomalies account for up to 34% of the mortality in these patients.⁵⁷ Renal artery involvement may result in hypertension.⁵⁷

Imaging

The sonographic findings of Alagille's syndrome are similar to those of neonatal hepatitis. In neonatal hepatitis, the liver size and echogenicity may be normal or increased, and the intrahepatic bile ducts are typically not visualized.⁶ Nuclear hepatobiliary scintigraphy may initially resemble biliary atresia⁴⁶ and typically fails to show normal excretion of the radiopharmaceutical into the bowel (Fig. 119-12).⁵⁰ Cholangiography or MRCP should demonstrate patency of the extrahepatic bile ducts, excluding the diagnosis of biliary atresia, but because Alagille's syndrome is rare, this diagnostic step is occasionally foregone, leading to treatment with the Kasai procedure before the pathologic diagnosis of Alagille's syndrome is made.⁵⁶

Biliary cirrhosis occurs in 12% of children with Alagille's syndrome resulting from chronic cholestasis.⁵⁸ Children presenting with Alagille's syndrome at an older age may have findings of cirrhosis. Benign lesions such as nodular hyperplasia have also been described in children with Alagille's syndrome and cirrhosis.⁵⁹ Liver transplantation may ultimately be required.

PROGRESSIVE FAMILIAL INTRAHEPATIC CHOLESTASIS

Background

Progressive familial intrahepatic cholestasis (PFIC) is a group of three slightly distinct autosomal recessive intrahepatic cholestatic disease processes that begin in infancy and progress to cirrhosis, typically within the first decade of life. Children with PFIC present with cholestasis, jaundice, failure to thrive, steatorrhea, pruritus, or rickets.⁶⁰ The average age at onset is 3 months, but some patients may not present until later, even into adolescence. Without treatment, few patients have survived into the third decade of life.⁶¹

The first subtype of what is now known as PFIC was initially identified in Amish descendants of Jacob Byler and was named

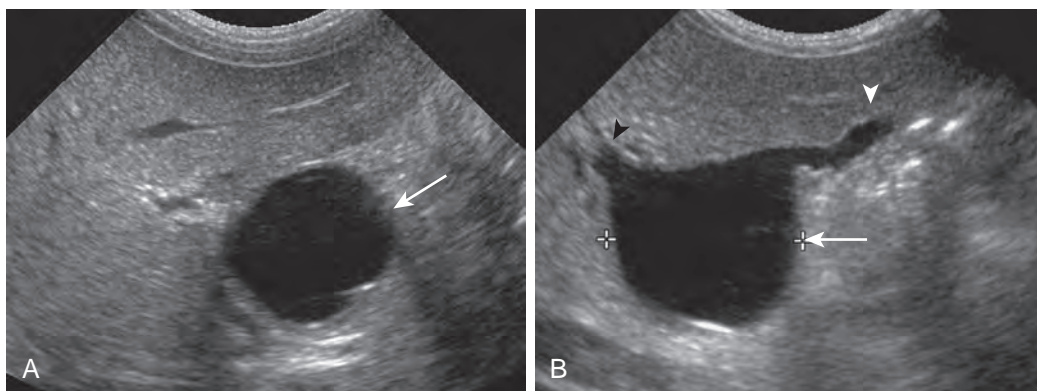


Figure 119-13 Choledochal malformation: cystic type. **A** and **B.** Ultrasound images obtained on the third day of life show the small gallbladder (white arrowhead) that empties into the choledochal cyst (arrow). At surgery, the cyst was amputated proximally at the common hepatic duct (black arrowhead).

Byler's disease.⁶² A similar disease was identified in Greenland Eskimo children and was named cholestasis familiaris groenlandica.⁶³ Subsequently, several non-Amish but phenotypically similar patients were reported to have a similar condition, and the broader term Byler's syndrome was adopted.

What were formerly known as Byler's disease and cholestasis familiaris groenlandica have been found to be the same disease and are now grouped into a subtype known as PFIC-1. PFIC-2 is clinically similar to PFIC-1 but primarily occurs in families in the Middle East and Europe. Although both PFIC-1 and PFIC-2 involve life-threatening cholestasis, patients with these diseases have low γ -glutamyl transpeptidase levels. Important clinical features of PFIC-1 include diarrhea, pancreatitis, and hearing loss; PFIC-2 is associated with increased risk of hepatobiliary malignant neoplasms.⁶⁴ Both PFIC-1 and PFIC-2 are caused by the absence of gene products required for canalicular export and bile formation.⁶⁵

Despite a similar clinical presentation, patients with PFIC-3 have elevated levels of serum γ -glutamyl transpeptidase. Rather than defective bile acid export as seen in PFIC-1 and PFIC-2, patients with PFIC-3 have deficient hepatocellular phospholipid export, which leads to unstable micelles that have a toxic effect on the bile ducts, leading to biliary obstruction.⁶⁶

Imaging

Ultrasound findings in patients with PFIC may be normal in the early stages of the disease but will eventually show cirrhosis, including coarsened echotexture, nodular contour, and features of portal hypertension. Nuclear medicine hepatobiliary scintigraphy does not typically have a role in the initial diagnosis of PFIC but is sometimes used after the palliative biliary diversion procedure⁶⁷ to assess for patency.

CHOLEDOCHAL MALFORMATIONS

Background

Choledochal malformations are dilated bile ducts that may be extrahepatic, intrahepatic, or both.³ Choledochal malformations are uncommon, with an estimated incidence of 1 case in 750,000 live births.¹⁸ Choledochal malformations are four to six times more common in girls than in boys.^{68,69}

Infants with choledochal malformations typically present with a palpable abdominal mass that corresponds to an underlying cystic mass (Fig. 119-13), jaundice, and acholic stool.

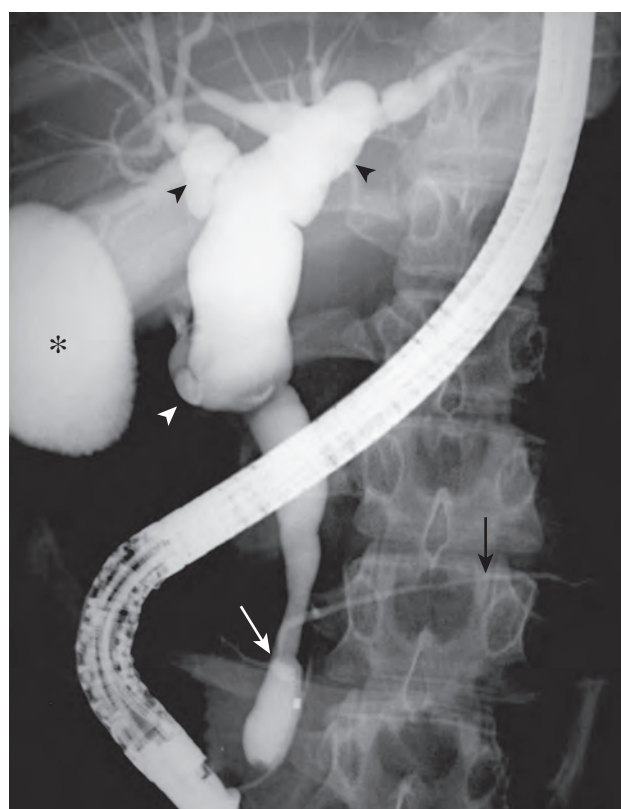


Figure 119-14 Choledochal malformation: fusiform type on ERCP. There is fusiform dilation of the right and left hepatic ducts (black arrowheads) and their primary intrahepatic branches. The cystic duct (white arrowhead) joins the dilated common hepatic duct to form the common bile duct, and there is an anomalous union of the common bile duct (white arrow) and the pancreatic duct (black arrow). The gallbladder is distended with contrast material (asterisk). No stones are identified.

These children less often have symptoms of vomiting, pain or discomfort, and fever. Children who present with choledochal malformations after 1 year of age have more variable symptoms.

Choledochal malformations are classified morphologically as cylindrical, fusiform (Fig. 119-14), or spindle shaped.⁶⁹ Todani and colleagues⁷⁰ proposed a classification system that

considers the location of the malformation within the biliary tree:

- Type I (most common)
 - A. Dilation of the common bile duct above the level of insertion of the cystic duct
 - B. Dilation of the common bile duct below the level of insertion of the cystic duct
 - C. Diffuse or cylindrical dilation
- Type II. One or more diverticula of the common bile duct
- Type III. Choledochoceles (dilation of the intraduodenal portion of the duct, with both the common bile duct and pancreatic duct emptying into it)
- Type IV. Multiple cysts
 - A. Multiple intrahepatic and extrahepatic ductal cysts
 - B. Multiple extrahepatic ductal cysts only
- Type V (Caroli's disease). Intrahepatic bile duct cyst (single or multiple)

A subtype of Todani type I choledochal malformation (Todani ID) was recently proposed.⁷¹ In addition to dilation of the common hepatic and the common bile duct, this type of choledochal malformation also has dilation of the central portion of the cystic duct, resulting in a bicornal configuration to the malformation.⁷¹

One of the leading theories concerning the cause of choledochal malformations is anomalous union of the pancreatic duct and common bile duct proximal to the ampulla, with subsequent reflux of pancreatic enzymes into the bile ducts.⁷² The pancreatic duct has higher pressure than the common bile duct, and pancreatic fluid may directly reflux into the common bile duct, which is not protected by the choledochal sphincter because the pancreatobiliary malunion occurs outside of the duodenal wall.⁷² This may account for the high level of pancreatic enzymes in the bile within some choledochal malformations.⁶⁹ Choledochal malformations are associated with the following findings: intraductal calculi, intrahepatic biliary dilation, anomalous hepatic biliary ducts, recurrent pancreatitis, and extrahepatic bile duct perforation.^{3,72}

Imaging

Ultrasound is useful in the evaluation for choledochal malformations (see Fig. 119-13).^{2,3,69} Choledochal malformations may be seen on routine prenatal ultrasound (Fig. 119-15).^{12,68} On ultrasound, a choledochal malformation may be seen as a large, lobular, right upper quadrant cystic structure that is distinct

from the gallbladder, extends to the porta hepatis,⁵⁶ and communicates with the biliary ductal system (Fig. 119-16).¹ The intrahepatic ducts are usually normal in caliber and appearance but may be dilated to varying degrees.⁷³

Nuclear hepatobiliary scintigraphy typically confirms the biliary origin of the cystic structure, and the structure can often be distinguished from the gallbladder.⁷⁴ In some patients, the choledochal malformation does not fill with radiopharmaceutical and may cause a photopenic defect in the liver that correlates with sonographic findings.⁷⁴ Additional cross-sectional imaging with MRCP may be a useful adjunct to sonography for preoperative planning.² The need for preoperative ERCP or intraoperative cholangiography, which lengthens operating room time, may be eliminated in the subset of patients in whom MRCP demonstrates the pancreatic duct and the common channel.⁷¹ MRCP can also depict stenosis of intrahepatic ducts or the presence of anomalous hepatic biliary ducts.

The treatment of choledochal malformations in children with persistent or intermittent jaundice is excision of the malformation followed by Roux-en-Y hepaticojejunostomy.¹⁸ In the newborn period, choledochal malformations may be drained externally, followed by excision and biliary reconstruction when the child is older (typically around 5 months old).⁶⁹

There is an approximate 4% risk of malignant transformation in the malformation or the nearby bile or pancreatic duct.⁷⁵ This risk of cancer is approximately 80 times greater than in the general population.⁷⁵ Types of cancer reported include adenocarcinoma, squamous cell carcinoma, and adenoacanthoma.⁷⁰

The differential diagnosis of choledochal malformation includes mesenchymal hamartoma, hepatic cyst, enteric duplication cyst, pancreatic pseudocyst, hepatic artery aneurysm, spontaneous perforation of the common bile duct,¹ and biliary cystadenoma.

CAROLI'S DISEASE

Background

Caroli's disease is also known as Todani type V choledochal malformation^{3,70} and as communicating cavernous ectasia of intrahepatic bile ducts.⁷⁶ Caroli's disease is a rare, congenital disease in which there is segmental nonobstructive dilation of the intrahepatic biliary ducts.⁷⁷ Caroli's disease may affect one or both lobes of the liver, but more commonly the left lobe of the liver is involved.¹⁷ When ectasia is limited to the intrahepatic biliary tree, without other hepatic abnormalities, Caroli's disease

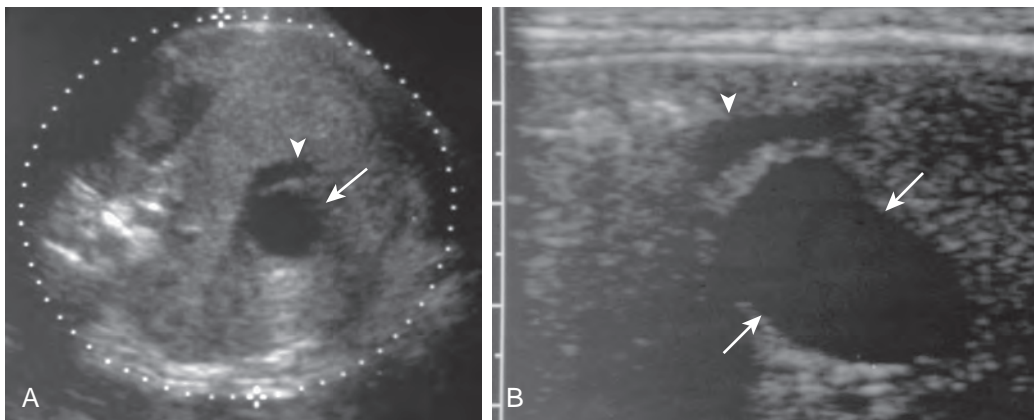


Figure 119-15 Prenatal diagnosis of choledochal malformation. **A.** Prenatal sonogram demonstrates a cystic structure in the periportal region (arrow). The gallbladder (arrowhead) is also identified. **B.** Postnatal sonogram of the same infant on the day of birth confirms the presence of a choledochal cyst (arrows) involving the extrahepatic bile duct. The gallbladder (arrowhead) is identified as a separate structure.

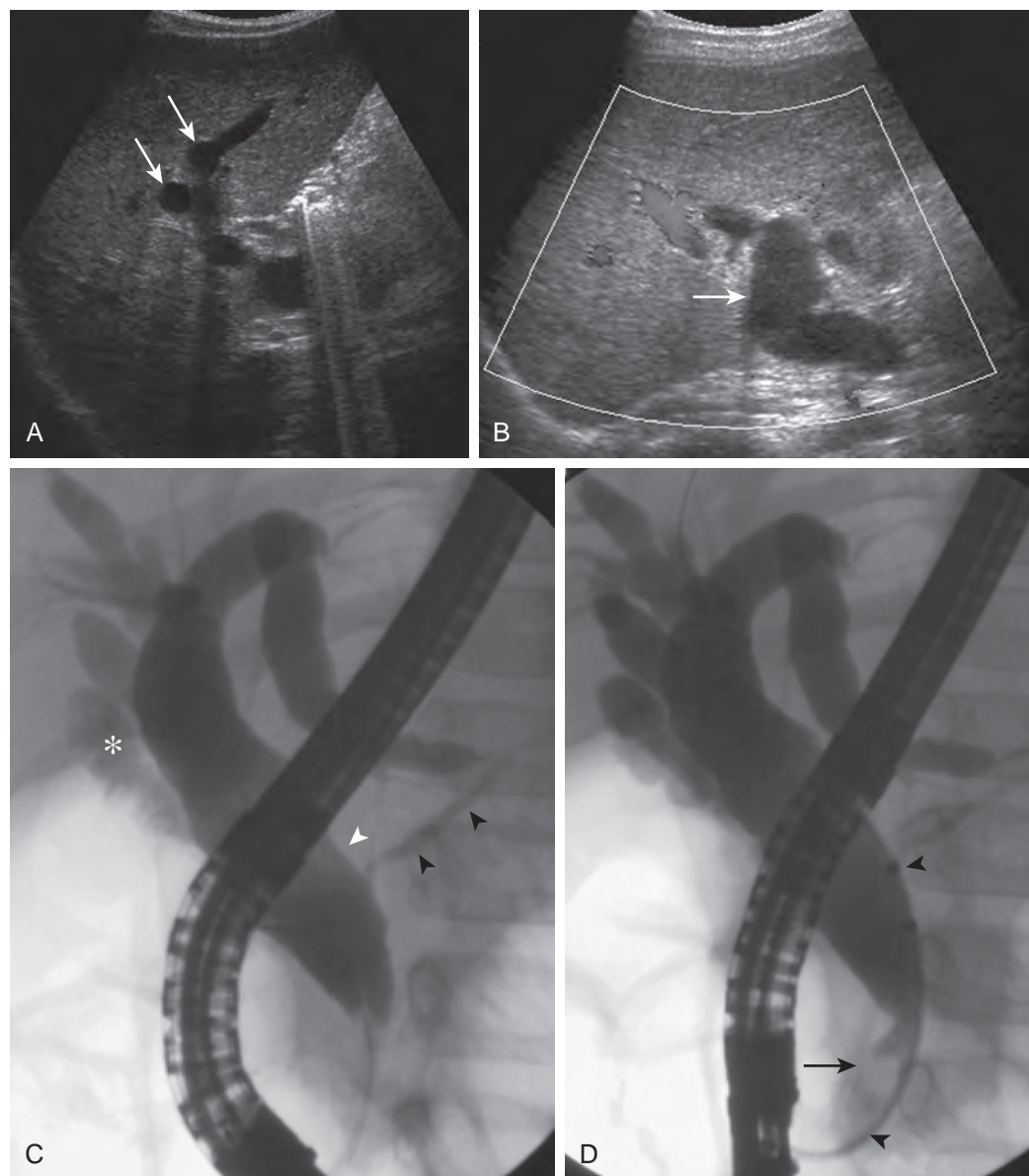


Figure 119-16 Fusiform choledochal malformation.

A and **B**. Sonogram of a 4-year-old child with recurrent pancreatitis. The images demonstrate fusiform dilation of the intrahepatic (**A**, arrows) and extrahepatic (**B**, arrow) bile ducts. **C**. ERCP shows fusiform dilation of the common bile duct (white arrowhead) and the common hepatic duct and its primary branches. The gallbladder (asterisk) is identified. There is an irregularity of the pancreatic duct (black arrowheads) that has an anomalous insertion into the common bile duct. **D**. The common pancreaticobiliary channel (arrowheads) contains a 5-mm stone (arrow).

is the term used. Caroli's syndrome, which is more common than Caroli's disease, involves ectasia of small and large bile ducts and is associated with congenital hepatic fibrosis. Periportal fibrosis can lead to cirrhosis and portal hypertension in patients with Caroli's syndrome.^{77,78}

Both Caroli's disease and Caroli's syndrome are transmitted in an autosomal recessive manner. There is an association between Caroli's disease and Caroli's syndrome and renal cystic diseases, including autosomal recessive polycystic kidney disease (Fig. 119-17), renal tubular ectasia, medullary sponge kidney, and nephronophthisis with cysts in the renal medulla and corticomedullary junction.^{3,73}

One of the most accepted theories regarding the pathogenesis of Caroli's disease is that it results from arrest during remodeling of the embryonic ductal plate. The ductal plate is a sleeve-like layer of hepatic precursor cells (hepatoblasts) that surrounds the portal venous branches. The ductal plate cells duplicate and separate, creating a slitlike lumen between the two

epithelial layers. The ductal plate remodels throughout fetal life to form the intrahepatic bile ducts. Incomplete remodeling is thought to result in a ductal plate malformation and eventually Caroli's disease.⁷⁸

Most patients with Caroli's disease or Caroli's syndrome present during childhood or as young adults with fever, recurrent or crampy abdominal pain, and transient jaundice.^{1,79} These presenting symptoms result from bile stasis and stone formation.⁷⁹ Young children may present with recurrent abdominal pain, pruritus, acholic stools, and intermittent jaundice. The liver may be enlarged.⁷⁹

Cholangiocarcinoma has been reported in up to 7% of people with congenital cystic dilation of the intrahepatic bile ducts,⁷⁷ which is more than 100 times greater than in the general population.⁶⁷ The cause of the malignant transformation is unknown. Early diagnosis of malignant transformation is difficult because the symptoms may mimic cholangitis.⁷⁷

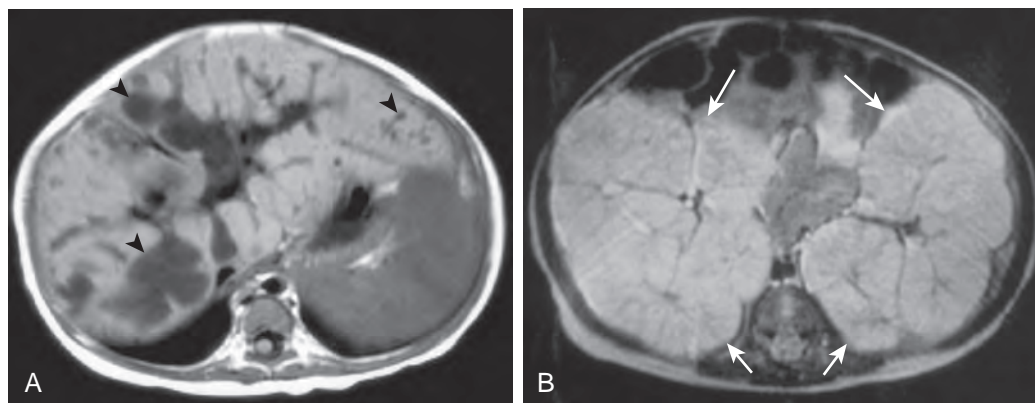


Figure 119-17 Caroli's disease: MR features. **A.** Axial view, T1-weighted MR image demonstrates diffuse intrahepatic bile duct dilation with scattered areas of saccular dilation (arrowheads). **B.** Axial view, T2-weighted MR image of the kidneys. The kidneys (arrows) are diffusely enlarged without hydronephrosis. The constellation of findings is consistent with Caroli's disease with associated autosomal recessive polycystic kidney disease.

Imaging

Sonographic findings in Caroli's disease include ectatic intrahepatic bile ducts with echogenic septa that completely or incompletely traverse the dilated duct lumen and small portal venous branches that are partly or completely surrounded by the dilated bile ducts.⁸⁰ On CT, the centrally enhancing portal radicle surrounded by the low-attenuation, dilated bile ducts is called the central dot sign.⁴³

BILE PLUG SYNDROME OR INSPISSATED BILE SYNDROME

Inspissated bile is the second most common cause of surgically treatable neonatal jaundice after biliary atresia. It is slightly more common than choledochal malformation.¹⁸ Ultrasound may show a dilated common bile duct with a normal-appearing gallbladder. The occluding bile plug is evident sonographically in 30% of children.¹⁸ Inspissated bile is slightly hyperechoic and does not cause acoustic shadowing. A fluid-debris level may be seen in the dilated obstructed bile duct.¹ Sludge can be isoechoic with the liver, and if it fills the gallbladder lumen, it may make the gallbladder difficult to visualize.⁶ The hepatic echotexture may be increased because of cholestasis.¹

The diagnosis can be confirmed by percutaneous transhepatic cholangiography and treated during the procedure with therapeutic saline lavage of the biliary tree. Postprocedural follow-up ultrasounds shows return of the bile ducts to normal caliber.¹⁸

Gallbladder Disease

CHOLELITHIASIS

Gallstones can be seen in children of any age (Fig. 119-18).⁸¹ The classic risk factors for cholelithiasis in children include hemolysis, prior gastrointestinal surgery, and total parenteral nutrition.⁸²⁻⁸⁴ In neonates and infants, additional proposed risk factors include prematurity, prolonged fasting,⁸⁴ and furose-mide treatment.^{82,85} Stones have also been found in newborns and infants with a history of septicemia, hyperbilirubinemia requiring phototherapy, and intestinal malabsorption.⁸⁶ In

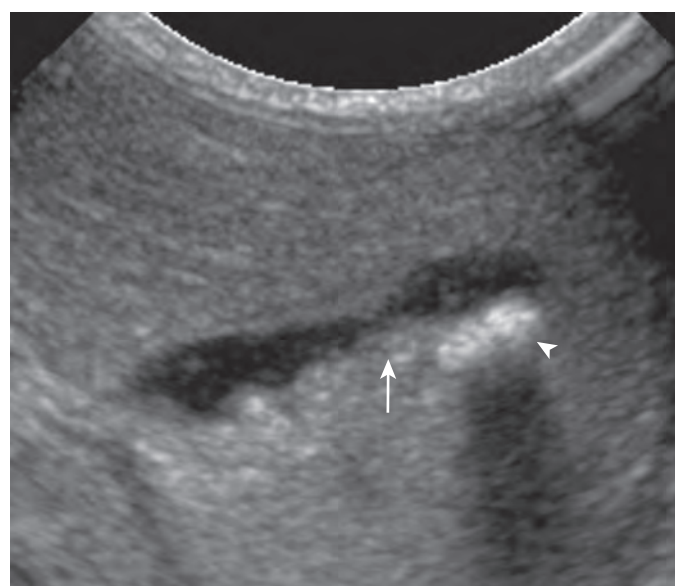


Figure 119-18 Neonatal gallstone. Ultrasound image of a 1-day-old infant (gestational age of 37 weeks) demonstrates a gallstone (arrowhead) and sludge (arrow) within the gallbladder.

older children, the causes of biliary stones are numerous and include sickle cell disease,⁸⁷ total parenteral nutrition, ileal resection, hemolytic anemia, and cystic fibrosis.^{88,89} The rate of cholelithiasis in children with sickle cell disease increases with advancing age, up to 42% in the 15- to 18-year-old age group.⁸⁷ In the adolescent population, cholelithiasis is associated with pregnancy,^{84,89} use of birth control pills, and obesity.⁸⁴ The imaging features of gallstones are described in Chapter 77.

ACALCULOUS CHOLECYSTITIS

Acalculous cholecystitis is inflammation of the gallbladder without gallstones. Acalculous cholecystitis is considered acute if the symptoms are present for less than 1 month or chronic if the symptoms persist for longer than 3 months.⁹⁰

The symptoms of acalculous cholecystitis include fever, jaundice, abdominal pain, right upper quadrant pain, and

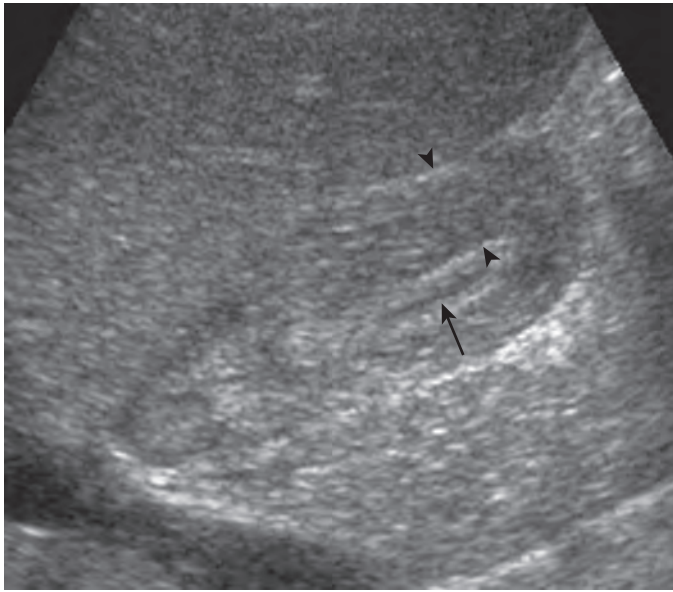


Figure 119-19 Acute acalculous cholecystitis: sonographic findings. The gallbladder wall is diffusely thickened (arrowheads). The tiny, hypoechoic lumen is free of stones (arrow).

vomiting.^{84,90} Most children with acute acalculous cholecystitis also have leukocytosis and abnormal liver function test results. Acute acalculous cholecystitis is most often seen in the immediate postoperative period or in association with a systemic medical illness, severe trauma, burns, metabolic illness, multiple transfusions, intravenous narcotic use, or hyperalimentation.⁹⁰ *Salmonella* sepsis should also be considered an infectious cause in children.⁸² Acute acalculous cholecystitis can be treated medically or with cholecystectomy.⁹¹

On ultrasound, the gallbladder is free of stones, although it may contain sludge, may be distended, and may have a thick wall (Fig. 119-19).^{73,81} This wall thickening may be caused by edema or focal hemorrhage.⁸¹ Chronic cholecystitis in children is more often associated with cholelithiasis.⁷³

GALLBLADDER DYSKINESIA

Gallbladder dyskinesia is characterized by poor gallbladder contractility. Children and adolescents with this disorder have chronic abdominal pain. A ^{99m}Tc hepatobiliary scan, followed with cholecystokinin injection to induce gallbladder contraction, may be diagnostic. An ejection fraction of less than 35% is considered abnormal.⁸⁴

Rescorla⁷³ reported that 20% of children undergoing laparoscopic cholecystectomy had a preoperative diagnosis of biliary dyskinesia. In that series, pathologic evaluation revealed changes of chronic cholecystitis in 71%, but 93% were relieved of their pain after cholecystectomy.

GALLBLADDER HYDROPS

Hydrops of the gallbladder is abnormal distention of the gallbladder without gallbladder wall thickening or inflammation.⁹² The bile within the gallbladder may be abnormally thick and transiently obstruct the cystic duct,⁹³ or the obstruction may be extrinsic,⁶ possibly caused by enlarged periportal lymph nodes.⁹³

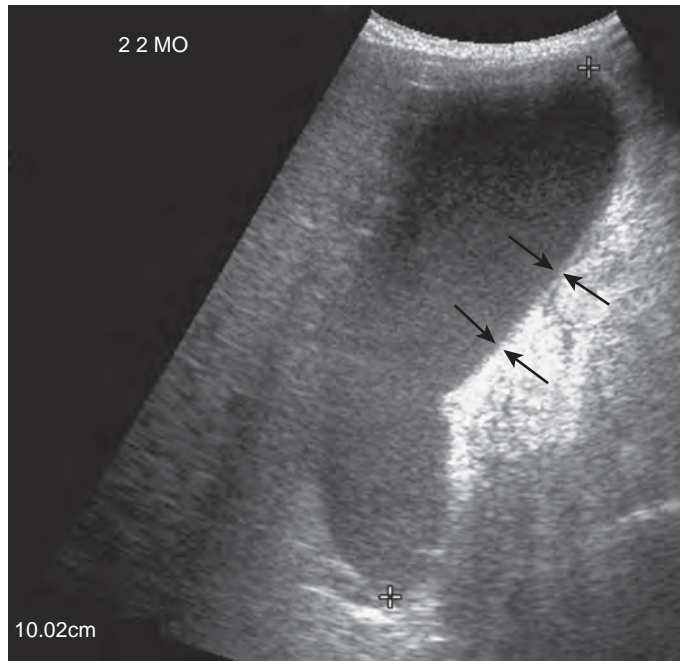


Figure 119-20 Gallbladder hydrops. The gallbladder is abnormally distended, measuring more than 10 cm long in this 22-month-old child after bone marrow transplantation. The gallbladder wall is thin (arrows), and there is echogenic sludge within the lumen. The gallbladder was later drained with a cholecystostomy tube.

Vasculitis can also be a causative factor in gallbladder hydrops.⁶ After the initial obstruction, the gallbladder is further distended by serous fluid secreted by the gallbladder mucosa.⁶ Bowen argues that the transient, acute distention of the gallbladder occurring in infants who are not fed or in those with acute obstruction of the cystic duct is “transient gallbladder dilation” and that the term *hydrops* may best be reserved for cases in which the cystic duct is obstructed so long that bile within the gallbladder is replaced by clear, thin, colorless liquid.⁹³

Hydrops of the gallbladder is typically caused by bile stasis resulting from dehydration or prolonged fasting.⁶ Neonatal hydrops can be seen in the setting of infection or hyperalimentation.^{92,93} In older children, there is a reported association with mucocutaneous lymph node syndrome (Kawasaki’s syndrome) and a variety of infections.⁹³ Presentation may include jaundice, abdominal distention, and a palpable right upper quadrant mass,^{92,93} but it may be asymptomatic.⁶

In acute hydrops, the ultrasound measurement of the gallbladder length is more than 3 cm in infants and more than 7 cm in older children.⁶ The wall is not thickened, and there may or may not be sludge (Fig. 119-20); the biliary tract is otherwise not abnormally dilated.⁶

Bile Duct Disease

CHOLEDOCHOLITHIASIS

Gallbladder stones and choledocholithiasis coexist in up to 13% of children with cholelithiasis requiring cholecystectomy.^{84,94} The common duct stones are spontaneously passed without the need for routine preoperative or postoperative ERCP in most children.⁹⁴ However, complete obstruction of

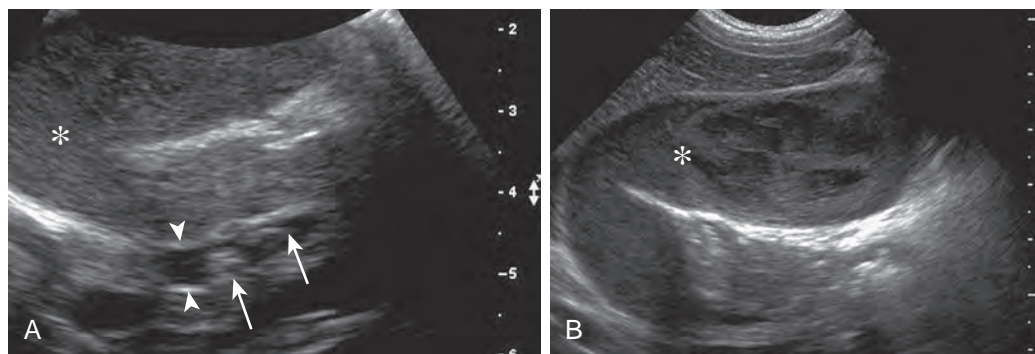


Figure 119-21 Common bile duct stone or sludge: sonographic features. **A.** The common bile duct (arrowheads) is abnormally dilated and contains hyperechoic stones, sludge, or both (arrows). **B.** The gallbladder is grossly distended with sludge (asterisk) in this 8-year-old child with sickle cell disease.

the biliary tract or pancreatitis can occur.^{84,94} In a series by Vrochides and colleagues,⁹⁴ 11 of 12 children undergoing cholecystectomy who had an intraoperative cholangiographic diagnosis of choledocholithiasis were asymptomatic postoperatively, even without surgical removal of the intraductal stones. One-week follow-up sonography demonstrated no stones or evidence of obstruction. In children, postoperative ERCP with sphincterotomy and stone removal are warranted in the unusual circumstance of symptomatic postoperative retention of common bile duct stones.⁹⁴

Ultrasound is accurate in the detection of calculi within the gallbladder but less so in the intrahepatic and extrahepatic ducts.³ Choledocholithiasis appears sonographically as a brightly echogenic, shadowing structure within the biliary ducts, often with proximal ductal dilation (Fig. 119-21).¹

MRCP in adults has been reported to have 95% sensitivity, 100% specificity, 100% positive predictive value, and 98% negative predictive value for diagnosis of choledocholithiasis.⁹⁵ MRCP evaluation of choledocholithiasis has not been extensively studied in children.³

BILIARY CHANGES WITH CYSTIC FIBROSIS

In addition to the hepatic fibrosis and cirrhosis, patients with cystic fibrosis may develop biliary disease, including cholelithiasis and bile sludge formation.^{88,89} Gallstones (usually cholesterol) occur in approximately 10% of patients with cystic fibrosis.⁹⁶ Neonates with cystic fibrosis may have prolonged jaundice related to inspissated bile.⁹⁶

Ultrasound and MRCP are used as noninvasive tools to assess for these changes.⁹⁷ On sonography, a thick-walled, tiny gallbladder can be seen in children with cystic fibrosis.⁹ Although approximately one in three patients with cystic fibrosis has a small gallbladder, gallbladder function is usually normal.⁹⁶ Some children have painful focal bile ductule stenosis, which is manifested as delayed excretion of radiopharmaceutical on hepatobiliary scintigraphy.⁹⁶ MRCP can be used to assess the biliary tract in addition to evaluating patients for the typical pancreatic, hepatic, and splenic abnormalities associated with cystic fibrosis.⁹⁷ These findings include a tiny gallbladder with or without stones; intraductal cholelithiasis; intrahepatic and extrahepatic bile duct strictures; duct wall irregularity; and areas of duct dilation, which in some cases result in a beaded appearance.⁹⁷

Historically, 23% of cystic fibrosis patients at autopsy have gallbladders of abnormal size or with abnormal contents, without inflammatory changes.⁹⁸ The gallbladder may be hypoplastic, atrophied, or dilated, and there may be numerous, epithelial cell-lined, multiloculated, mucoid-containing “cysts” in and just below the mucosa. The gallbladder lumen may contain clear or gray mucus rather than bile.⁹⁸

PRIMARY SCLEROSING CHOLANGITIS

Primary sclerosing cholangitis (PSC) is a chronic progressive disorder that involves inflammation, fibrosis, and subsequent stricturing of medium and large intrahepatic and extrahepatic biliary ducts. Most children have intrahepatic and extrahepatic involvement, although the disease may be limited to either site.⁹⁹ PSC may affect only isolated areas of the intrahepatic bile ducts, unlike Caroli's disease, in which the large central intrahepatic ducts are typically affected.⁷⁶

Most children with PSC are symptomatic at the time of diagnosis and present with abnormal liver function test results and one or more of the following signs or symptoms: abdominal pain, fatigue, jaundice, splenomegaly with or without hepatomegaly, ascites, fever, and weight loss.^{99,100} As many as 81% of the children have associated inflammatory bowel disease, typically ulcerative colitis.⁹⁹ Other children have comorbid extrabiliary disease, such as Langerhans cell histiocytosis, immunodeficiency,¹⁰⁰ systemic lupus erythematosus, insulin-dependent diabetes mellitus, or autoimmune thyroiditis.⁹⁹ Thirty-five percent of the children with PSC also have histologic features consistent with autoimmune hepatitis.⁹⁹ Many children with PSC progress to end-stage liver disease and require liver transplantation. PSC may recur in the allograft.⁹⁹

Sonographic findings of sclerosing cholangitis include dilated intrahepatic and, less often, extrahepatic bile ducts,¹⁰⁰ bile duct wall thickening, intrahepatic and extrahepatic duct stones, gallstones, and segmental ductal narrowing due to strictures. The strictures may be difficult to detect unless there is also duct dilation.⁶ There may be signs of cirrhosis or portal hypertension.¹⁰⁰ MRCP or conventional cholangiography may show intrahepatic or extrahepatic bile duct wall irregularity, long- or short-segment strictures, filling defects, and abnormal dilations with or without interpositional annular strictures (Fig. 119-22).¹⁰⁰ The imaging features of PSC are discussed further in Chapter 80.

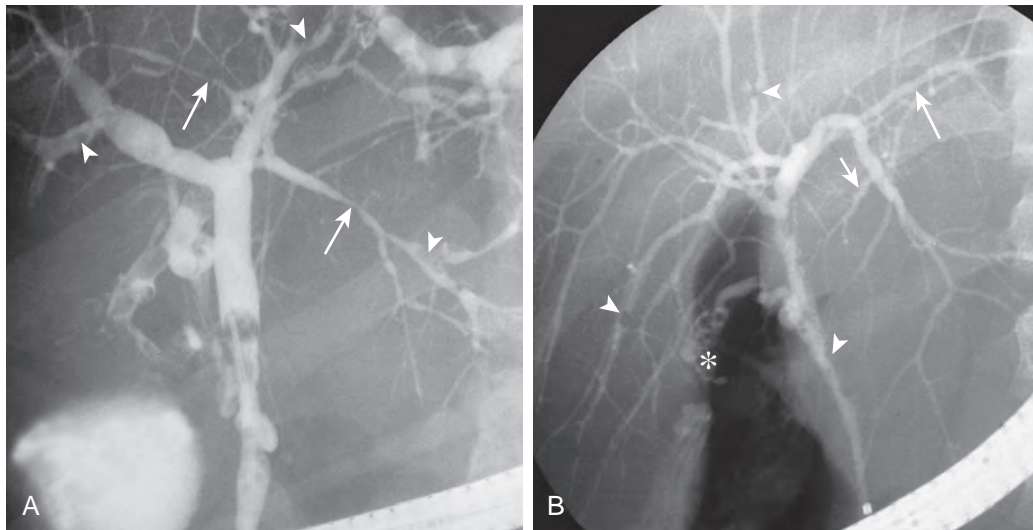


Figure 119-22 Sclerosing cholangitis: ERCP findings. **A.** ERCP image of a teen with Crohn's disease and sclerosing cholangitis. There are filling defects within the ducts that may represent stones (arrowheads). Segmental narrowing or strictures (arrows) are present throughout the intrahepatic bile ducts. (Courtesy Lisa Lowe, MD, Children's Mercy Hospital and Clinics, University of Missouri, Kansas City, MO.) **B.** ERCP image of a 9-year-old child with ulcerative colitis and sclerosing cholangitis. Arrowheads mark the intraluminal filling defects, which are probably calculi. There are multiple filling defects within the gallbladder (asterisk), and there is mild duct wall irregularity (arrows) without significant stricture formation. (Courtesy Laura Z. Fenton, MD, The Children's Hospital and University of Colorado Health Sciences, Denver, CO.)

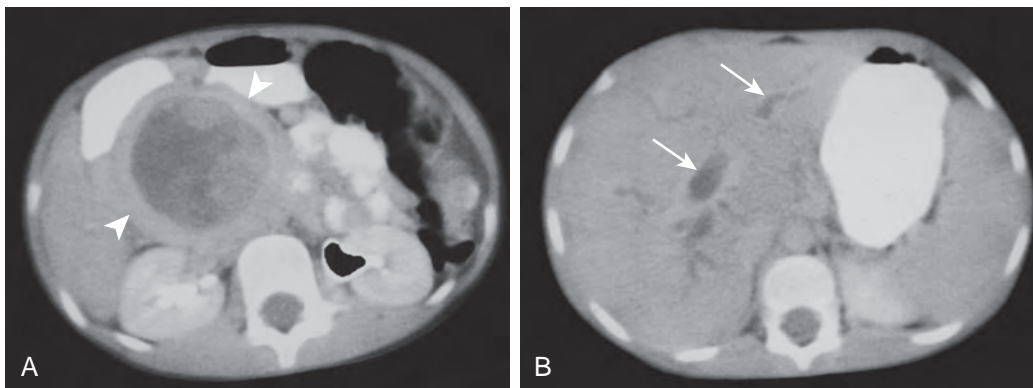


Figure 119-23 Biliary obstruction by a pancreatic head neoplasm. **A.** The large, mixed density mass with a thick wall (arrowheads) originating in the pancreatic head is a solid and papillary epithelial neoplasm of the pancreas in this 2-year-old child. **B.** The mass is obstructing the common bile duct, and there is subsequent intrahepatic bile duct dilation (arrows). (Courtesy Laura Z. Fenton, MD, The Children's Hospital and University of Colorado Health Sciences, Denver, CO.)

Neoplasms

Extrahepatic neoplasms, such as pancreaticobiliary lymphoma, can create mass effect on the bile ducts. Intraductal neoplasms, such as rhabdomyosarcoma, also result in biliary obstruction. Presenting symptoms include anorexia, jaundice, itching, fever, abdominal distention (with or without pain), vomiting, and a palpable abdominal mass.¹⁰¹⁻¹⁰³ Mass effect from tumors such as biliary rhabdomyosarcoma,¹⁰¹ lymphoma,¹⁰² pancreatic head neoplasm such as hemangioendothelioma,¹⁰⁴ and pancreatic adenocarcinoma with extension to the common bile duct¹⁰⁵ has been reported to cause obstructive jaundice (Fig. 119-23).¹⁰²

Rhabdomyosarcoma is the only primary neoplasm to arise within the pediatric biliary tree.¹⁰⁶ It is typically the embryonal variety (i.e., sarcoma botryoides).^{103,107} Rhabdomyosarcoma may arise from the ampulla,¹⁰¹ common bile duct,¹⁰³ or hepatic

ducts.¹⁰⁷ Most children present with intermittent jaundice, fever, and anorexia with or without abdominal distention.¹⁰³ Ultrasound may demonstrate a mass in the porta hepatis.¹⁰³ On CT, the soft tissue mass is seen distending the affected bile ducts (Figs. 119-24 and 119-25).¹⁰⁶ There may be secondary intrahepatic duct dilation. CT may also show retroperitoneal and mesenteric lymphadenopathy.¹⁰⁶ The tumor may extend into the liver. Metastases to regional nodes, peritoneum, and omentum occur in 30% of the children.¹⁰³ Pediatric ampullary rhabdomyosarcoma has been successfully treated by pancreaticoduodenectomy with adjuvant chemotherapy, irradiation, or both.¹⁰¹

Pancreaticobiliary lymphoma can involve the porta hepatis and the gallbladder without causing obstruction.¹⁰² The lymphomatous masses that do obstruct the biliary tree often respond quickly to chemotherapy and may not require a biliary drainage procedure.^{102,108,109}

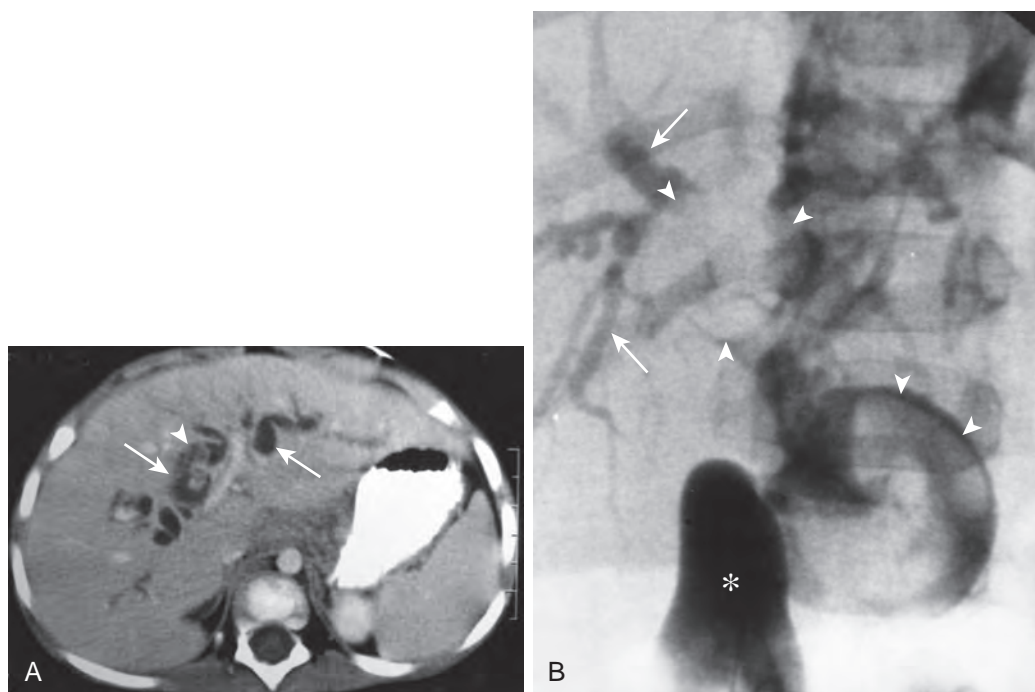


Figure 119-24 Biliary rhabdomyosarcoma. **A.** Contrast-enhanced CT of a 2-year-old child with fever, malaise, and jaundice. The arrows indicate the dilated intrahepatic bile ducts. In one area, there is a higher attenuation substance that may represent intraluminal sludge or an intraductal mass (arrowhead). **B.** Intraoperative cholangiogram obtained by injection of contrast material into the gallbladder (asterisk) demonstrates multiple filling defects (arrowheads) within the dilated bile ducts, including the common bile duct. The bile ducts proximal to the intraductal masses are also dilated (arrows). Surgical biopsy confirmed the diagnosis of embryonal rhabdomyosarcoma. (From Donnelly LF, Bisset GS III, Frush DP: Case 2: Embryonal rhabdomyosarcoma of the biliary tree. *Radiology* 208:621–623, 1998.)



Figure 119-25 Biliary rhabdomyosarcoma. **A.** Ultrasound image of the liver in a 3-year-old child with malaise and jaundice shows dilated intrabiliary ducts (arrows). **B.** Coronal T2-weighted MRCP image from the same patient. The arrows indicate the dilated intrahepatic bile ducts and common hepatic duct. Extensive tumor involvement is seen in the common bile duct (asterisk).

REFERENCES

- Gubernick JA, Rosenberg HK, Ilaslan H, Kessler A: US approach to jaundice in infants and children. *Radiographics* 20:173–195, 2000.
- Lam WW, Lam TP, Saing H, et al: MR cholangiography and CT cholangiography of pediatric patients with choledochal cysts. *AJR Am J Roentgenol* 173:401–405, 1999.
- Egbert ND, Bloom DA, Dillman JR: Magnetic resonance imaging of the pediatric pancreaticobiliary system. *Magn Reson Imaging Clin N Am* 21:681–696, 2013.
- Kim MJ, Park YN, Han SJ, et al: Biliary atresia in neonates and infants: Triangular area of high signal intensity in the porta hepatis at T2-weighted MR cholangiography with US and histopathologic correlation. *Radiology* 215:395–401, 2000.

5. Saito T, Terui K, Mitsunaga T, et al: Role of pediatric endoscopic retrograde cholangiopancreatography in an era stressing less-invasive modalities. *J Pediatr Gastroenterol Nutr* 59:204–209, 2014.
6. Siegel MJ: *Pediatric Sonography*, ed 4, Philadelphia, 2011, Wolters Kluwer/Lippincott Williams & Wilkins.
7. McGahan JP, Phillips HE, Cox KL: Sonography of the normal pediatric gallbladder and biliary tract. *Radiology* 144:873–875, 1982.
8. Kinoshita LL, Callen PW, Filly RA, Hill LM: Sonographic detection of gallbladder duplication: Two cases discovered in utero. *J Ultrasound Med* 21:1417–1421, 2002.
9. Patriquin HB, DiPietro M, Barber FE, Teele RL: Sonography of thickened gallbladder wall: Causes in children. *AJR Am J Roentgenol* 141: 57–60, 1983.
10. Toppet V, Souayah H, Delplace O, et al: Lymph node enlargement as a sign of acute hepatitis A in children. *Pediatr Radiol* 20:249–252, 1990.
11. Hernanz-Schulman M, Ambrosino MM, Freeman PC, Quinn CB: Common bile duct in children: Sonographic dimensions. *Radiology* 195:193–195, 1995.
12. Guibaud L, Lachaud A, Touraine R, et al: MR cholangiography in neonates and infants: Feasibility and preliminary applications. *AJR Am J Roentgenol* 170:27–31, 1998.
13. Norton KI, Glass RB, Kogan D, et al: MR cholangiography in the evaluation of neonatal cholestasis: Initial results. *Radiology* 222:687–691, 2002.
14. Jaw TS, Kuo YT, Liu GC, et al: MR cholangiography in the evaluation of neonatal cholestasis. *Radiology* 212:249–256, 1999.
15. Moyer V, Freese DK, Whittington PE, et al: Guideline for the evaluation of cholestatic jaundice in infants: Recommendations of the North American Society for Pediatric Gastroenterology, Hepatology and Nutrition. *J Pediatr Gastroenterol Nutr* 39:115–128, 2004.
16. Balistreri WF: Neonatal cholestasis. *J Pediatr* 106:171–184, 1985.
17. Watts DR, Lorenzo GA, Beal JM: Proceedings: Congenital dilatation of the intrahepatic biliary ducts. *Arch Surg* 108:592–598, 1974.
18. Davenport M, Betalli P, D'Antiga L, et al: The spectrum of surgical jaundice in infancy. *J Pediatr Surg* 38:1471–1479, 2003.
19. Ikeda S, Sera Y, Ohshiro H, et al: Gallbladder contraction in biliary atresia: A pitfall of ultrasound diagnosis. *Pediatr Radiol* 28:451–453, 1998.
20. Tan Kendrick AP, Phua KB, Ooi BC, et al: Making the diagnosis of biliary atresia using the triangular cord sign and gallbladder length. *Pediatr Radiol* 30:69–73, 2000.
21. Jiang LP, Chen YC, Ding L, et al: The diagnostic value of high-frequency ultrasonography in biliary atresia. *Hepatobiliary Pancreat Dis Int* 12:415–422, 2013.
22. Tan Kendrick AP, Phua KB, Ooi BC, Tan CE: Biliary atresia: Making the diagnosis by the gallbladder ghost triad. *Pediatr Radiol* 33:311–315, 2003.
23. McIlhenny J, Campbell SE, Raible RJ, Antaki GM: Pediatric case of the day. Biliary atresia and polysplenia syndrome. *AJR Am J Roentgenol* 167:269, 271–273, 1996.
24. Baumann U, Ure B: Biliary atresia. *Clin Res Hepatol Gastroenterol* 36:257–259, 2012.
25. Ohi R, Kasai M, Takahashi T: Intrahepatic biliary obstruction in congenital bile duct atresia. *Tohoku J Exp Med* 99:129–149, 1969.
26. Superina R, Magee JC, Brandt ML, et al: The anatomic pattern of biliary atresia identified at time of Kasai hepatoporeostomy and early postoperative clearance of jaundice are significant predictors of transplant-free survival. *Ann Surg* 254:577–585, 2011.
27. Haber BA, Russo P: Biliary atresia. *Gastroenterol Clin North Am* 32:891–911, 2003.
28. Schwarz KB, Haber BH, Rosenthal P, et al: Extrahepatic anomalies in infants with biliary atresia: Results of a large prospective North American multicenter study. *Hepatology* 58: 1724–1731, 2013.
29. Shneider BL, Brown MB, Haber B, et al: A multicenter study of the outcome of biliary atresia in the United States, 1997 to 2000. *J Pediatr* 148:467–474, 2006.
30. Davenport M, Savage M, Mowat AP, Howard ER: Biliary atresia splenic malformation syndrome: An etiologic and prognostic subgroup. *Surgery* 113:662–668, 1993.
31. Mirza B, Iqbal S, Sheikh A: Biliary atresia associated with polysplenia syndrome, situs inversus abdominus, and reverse rotation of intestine. *APSP J Case Rep* 3:14, 2012.
32. De Matos V, Erlichman J, Russo PA, Haber BA: Does “cystic” biliary atresia represent a distinct clinical and etiological subgroup? A series of three cases. *Pediatr Dev Pathol* 8:725–731, 2005.
33. Muise AM, Turner D, Wine E, et al: Biliary atresia with choledochal cyst: Implications for classification. *Clin Gastroenterol Hepatol* 4:1411–1414, 2006.
34. Dolgin SE: Answered and unanswered controversies in the surgical management of extrahepatic biliary atresia. *Pediatr Transplant* 8: 628–631, 2004.
35. Kasai M, Ohi R: Long-term follow-up results of patients with biliary atresia. *Indian J Pediatr* 50:209–217, 1983.
36. Ibrahim M, Miyano T, Ohi R, et al: Japanese Biliary Atresia Registry, 1989 to 1994. *Tohoku J Exp Med* 181:85–95, 1997.
37. Davenport M, De Ville de Goyet J, Stringer MD, et al: Seamless management of biliary atresia in England and Wales (1999–2002). *Lancet* 363:1354–1357, 2004.
38. Nio M, Sano N, Ishii T, et al: Cholangitis as a late complication in long-term survivors after surgery for biliary atresia. *J Pediatr Surg* 39: 1797–1799, 2004.
39. Wu ET, Chen HL, Ni YH, et al: Bacterial cholangitis in patients with biliary atresia: Impact on short-term outcome. *Pediatr Surg Int* 17: 390–395, 2001.
40. Hasegawa T, Kimura T, Sasaki T, Okada A: Living-related liver transplantation for biliary atresia associated with polysplenia syndrome. *Pediatr Transplant* 6:78–81, 2002.
41. Kim WS, Cheon JE, Youn BJ, et al: Hepatic arterial diameter measured with US: Adjunct for US diagnosis of biliary atresia. *Radiology* 245:549–555, 2007.
42. Park WH, Choi SO, Lee HJ, et al: A new diagnostic approach to biliary atresia with emphasis on the ultrasonographic triangular cord sign: Comparison of ultrasonography, hepatobiliary scintigraphy, and liver needle biopsy in the evaluation of infantile cholestasis. *J Pediatr Surg* 32:1555–1559, 1997.
43. Choi BI, Yeon KM, Kim SH, Han MC: Caroli disease: Central dot sign in CT. *Radiology* 174: 161–163, 1990.
44. Jiang LP, Chen YC, Ding L, et al: The diagnostic value of high-frequency ultrasonography in biliary atresia. *Hepatobiliary Pancreat Dis Int* 12:415–422, 2013.
45. Lee HJ, Lee SM, Park WH, Choi SO: Objective criteria of triangular cord sign in biliary atresia on US scans. *Radiology* 229:395–400, 2003.
46. Treves ST: *Pediatric Nuclear Medicine/PET*, ed 3, New York, 2007, Springer.
47. Tulchinsky M: The SNM practice guideline on hepatobiliary scintigraphy. *J Nucl Med* 51:1825, 2010.
48. Poddar U, Bhattacharya A, Thapa BR, et al: Ursodeoxycholic acid-augmented hepatobiliary scintigraphy in the evaluation of neonatal jaundice. *J Nucl Med* 45:1488–1492, 2004.
49. Fitoz S, Erden A, Boruban S: Magnetic resonance cholangiopancreatography of biliary system abnormalities in children. *Clin Imaging* 31:93–101, 2007.
50. Kuhn JP, Slovis TL, Haller JO, editors: *Caffey's Pediatric Diagnostic Imaging*, ed 10, Philadelphia, 2004, Mosby.
51. Han SJ, Kim MJ, Han A, et al: Magnetic resonance cholangiography for the diagnosis of biliary atresia. *J Pediatr Surg* 37:599–604, 2002.
52. Avni FE, Segers V, De Maertelaer V, et al: The evaluation by magnetic resonance imaging of hepatic periportal fibrosis in infants with neonatal cholestasis: Preliminary report. *J Pediatr Surg* 37:1128–1133, 2002.
53. Petersen C, Davenport M: Aetiology of biliary atresia: What is actually known? *Orphanet J Rare Dis* 8:128, 2013.
54. Alagille D, Estrada A, Hadchouel M, et al: Syndromic paucity of interlobular bile ducts (Alagille syndrome or arteriohepatic dysplasia): Review of 80 cases. *J Pediatr* 110:195–200, 1987.
55. Alagille D, Odievre M, Gautier M, Dommergues JP: Hepatic ductular hypoplasia associated with characteristic facies, vertebral malformations, retarded physical, mental, and sexual development, and cardiac murmur. *J Pediatr* 86:63–71, 1975.
56. Lykavieris P, Hadchouel M, Chardot C, Bernard O: Outcome of liver disease in children with Alagille syndrome: A study of 163 patients. *Gut* 49:431–435, 2001.
57. Kamath BM, Spinner NB, Emerick KM, et al: Vascular anomalies in Alagille syndrome: A significant cause of morbidity and mortality. *Circulation* 109:1354–1358, 2004.
58. Perrault J: Paucity of interlobular bile ducts: Getting to know it better. *Dig Dis Sci* 26:481–484, 1981.
59. Tajima T, Honda H, Yanaga K, et al: Hepatic nodular hyperplasia in a boy with Alagille syndrome: CT and MR appearances. *Pediatr Radiol* 31:584–588, 2001.
60. Kliegman R, Nelson WE: *Nelson Textbook of Pediatrics*, ed 19, Philadelphia, 2011, Elsevier/Saunders.
61. Davit-Spraul A, Gonzales E, Baussan C, Jacquemin E: Progressive familial intrahepatic cholestasis. *Orphanet J Rare Dis* 4:1, 2009.
62. Arun BR, Padma S, Mallick A, et al: Unsuspected right lobe liver infarction in Byler's disease—identified by hepatobiliary scintigraphy. *Indian J Pediatr* 81:512–513, 2014.
63. Nielsen IM, Eiberg H: Cholestasis familiaris groenlandica: an epidemiological, clinical and genetic study. *Int J Circumpolar Health* 63 (Suppl 2):192–194, 2004.

64. Knisely AS, Strautnieks SS, Meier Y, et al: Hepatocellular carcinoma in ten children under five years of age with bile salt export pump deficiency. *Hepatology* 44:478–486, 2006.
65. Eppens EF, van Mil SW, de Vree JM, et al: FIC1, the protein affected in two forms of hereditary cholestasis, is localized in the cholangiocyte and the canalicular membrane of the hepatocyte. *J Hepatol* 35:436–443, 2001.
66. de Vree JM, Jacquemin E, Sturm E, et al: Mutations in the MDR3 gene cause progressive familial intrahepatic cholestasis. *Proc Natl Acad Sci U S A* 95:282–287, 1998.
67. Halaweish I, Chwals WJ: Long-term outcome after partial external biliary diversion for progressive familial intrahepatic cholestasis. *J Pediatr Surg* 45:934–937, 2010.
68. Davenport M, Basu R: Under pressure: Choledochal malformation manometry. *J Pediatr Surg* 40:331–335, 2005.
69. Todani T, Urushihara N, Morotomi Y, et al: Characteristics of choledochal cysts in neonates and early infants. *Eur J Pediatr Surg* 5: 143–145, 1995.
70. Todani T, Watanabe Y, Narusue M, et al: Congenital bile duct cysts: Classification, operative procedures, and review of thirty-seven cases including cancer arising from choledochal cyst. *Am J Surg* 134:263–269, 1977.
71. Michaelides M, Dimarellos V, Kostantinou D, et al: A new variant of Todani type I choledochal cyst. Imaging evaluation. *Hippokratia* 15:174–177, 2011.
72. Todani T, Watanabe Y, Fujii T, Uemura S: Anomalous arrangement of the pancreatobiliary ductal system in patients with a choledochal cyst. *Am J Surg* 147:672–676, 1984.
73. Rescorla FJ: Cholelithiasis, cholecystitis, and common bile duct stones. *Curr Opin Pediatr* 9:276–282, 1997.
74. Johnson K, Alton HM, Chapman S: Evaluation of mebrofenin hepatoscintigraphy in neonatal-onset jaundice. *Pediatr Radiol* 28:937–941, 1998.
75. Bloustein PA: Association of carcinoma with congenital cystic conditions of the liver and bile ducts. *Am J Gastroenterol* 67:40–46, 1977.
76. Fulcher AS, Turner MA, Sanyal AJ: Case 38: Caroli disease and renal tubular ectasia. *Radiology* 220:720–723, 2001.
77. Dayton MT, Longmire WP, Jr, Tompkins RK: Caroli's Disease: A premalignant condition? *Am J Surg* 145:41–48, 1983.
78. Desmet VJ: Ludwig symposium on biliary disorders—part I. Pathogenesis of ductal plate abnormalities. *Mayo Clin Proc* 73:80–89, 1998.
79. Zhang DY, Ji ZF, Shen XZ, et al: Caroli's disease: A report of 14 patients and review of the literature. *J Dig Dis* 13:491–495, 2012.
80. Marchal GJ, Desmet VJ, Proesmans WC, et al: Caroli disease: High-frequency US and pathologic findings. *Radiology* 158:507–511, 1986.
81. Stringer MD, Lim P, Cave M, et al: Fetal gallstones. *J Pediatr Surg* 31:1589–1591, 1996.
82. Brill PW, Winchester P, Rosen MS: Neonatal cholelithiasis. *Pediatr Radiol* 12:285–288, 1982.
83. Matos C, Avni EF, Van Gansbeke D, et al: Total parenteral nutrition (TPN) and gallbladder diseases in neonates. Sonographic assessment. *J Ultrasound Med* 6:243–248, 1987.
84. Svensson J, Makin E: Gallstone disease in children. *Semin Pediatr Surg* 21:255–265, 2012.
85. Blickman JG, Herrin JT, Cleveland RH, Jaramillo D: Coexisting nephrolithiasis and cholelithiasis in premature infants. *Pediatr Radiol* 21:363–364, 1991.
86. St-Vil D, Yazbeck S, Luks FI, et al: Cholelithiasis in newborns and infants. *J Pediatr Surg* 27:1305–1307, 1992.
87. Sarnaik S, Slovis TL, Corbett DP, et al: Incidence of cholelithiasis in sickle cell anemia using the ultrasonic gray-scale technique. *J Pediatr* 96:1005–1008, 1980.
88. Henschke CI, Teele RL: Cholelithiasis in children: Recent observations. *J Ultrasound Med* 2:481–484, 1983.
89. Reif S, Sloven DG, Lebenthal E: Gallstones in children. Characterization by age, etiology, and outcome. *Am J Dis Child* 145:105–108, 1991.
90. Tsakayannis DE, Kozakewich HP, Lillehei CW: Acalculous cholecystitis in children. *J Pediatr Surg* 31:127–130, discussion 130–131, 1996.
91. Garel L, Lucaya J, Piqueras J: Acute acalculous cholecystitis owing to salmonella sepsis. *Pediatr Radiol* 33:905–906, 2003.
92. Appleby GA, Forestier E, Starck CJ: Hydrops of the gallbladder in the neonatal period. *Acta Paediatr Scand* 70:117–120, 1981.
93. Bowen A: Acute gallbladder dilatation in a neonate: Emphasis on ultrasonography. *J Pediatr Gastroenterol Nutr* 3:304–308, 1984.
94. Vrochides DV, Sorrells DL, Jr, Kurkchubasche AG, et al: Is there a role for routine preoperative endoscopic retrograde cholangiopancreatography for suspected choledocholithiasis in children? *Arch Surg* 140:359–361, 2005.
95. Topal B, Van de Moortel M, Fieus S, et al: The value of magnetic resonance cholangiopancreatography in predicting common bile duct stones in patients with gallstone disease. *Br J Surg* 90:42–47, 2003.
96. Ruzal-Shapiro C: Cystic fibrosis. An overview. *Radiol Clin North Am* 36:143–161, 1998.
97. King LJ, Scurr ED, Murugan N, et al: Hepatobiliary and pancreatic manifestations of cystic fibrosis: MR imaging appearances. *Radiographics* 20:767–777, 2000.
98. Akata D, Akhan O: Liver manifestations of cystic fibrosis. *Eur J Radiol* 61:11–17, 2007.
99. Feldstein AE, Perrault J, El-Youssif M, et al: Primary sclerosing cholangitis in children: A long-term follow-up study. *Hepatology* 38: 210–217, 2003.
100. Mieli-Vergani G, Vergani D: Paediatric autoimmune liver disease. *Arch Dis Child* 98:1012–1017, 2013.
101. Caty MG, Oldham KT, Prochownik EV: Embryonal rhabdomyosarcoma of the ampulla of Vater with long-term survival following pancreaticoduodenectomy. *J Pediatr Surg* 25: 1256–1258, 1990.
102. Pietsch JB, Shankar S, Ford C, Johnson JE: Obstructive jaundice secondary to lymphoma in childhood. *J Pediatr Surg* 36:1792–1795, 2001.
103. Ruymann FB, Raney RB, Jr, Crist WM, et al: Rhabdomyosarcoma of the biliary tree in childhood. A report from the Intergroup Rhabdomyosarcoma Study. *Cancer* 56:575–581, 1985.
104. Sauer L, Harrison MR, Bond SJ, et al: Long-term percutaneous biliary drainage in an infant with hemangioendothelioma. *J Pediatr Surg* 22:606–608, 1987.
105. Nijs E, Callahan MJ, Taylor GA: Disorders of the pediatric pancreas: Imaging features. *Pediatr Radiol* 35:358–373, 2005.
106. Donnelly LF, Bisset GS, 3rd, Frush DP: Diagnosis please. Case 2: Embryonal rhabdomyosarcoma of the biliary tree. *Radiology* 208: 621–623, 1998.
107. Brugières L, Branchereau S, Laithier V: Paediatric malignant liver tumours. *Bull Cancer* 99:219–228, 2012.
108. Arenas Garcia BR: Primary pancreatic lymphoma in pediatric patients. *Radiologia* 49: 125–127, 2007.
109. Arellano CM, Kritsaneeapiboon S, Lee EY: CT Imaging findings of malignant neoplasms arising in the epigastric region in children. *Clin Imaging* 35:10–20, 2011.

CHAPTER OUTLINE

Imaging Approach for a Suspected Hepatic Mass**Congenital Anomalies**

Malformations and Hernias

Fibropolycystic Diseases of the Liver

Hepatic Cysts

Malignant Hepatic Neoplasms

Primary Malignant Neoplasms

Secondary Malignant Neoplasms

Benign Hepatic Neoplasms and Neoplasm-Like Abnormalities

Pediatric Hepatic Vascular Lesions

Mesenchymal Hamartoma

Hepatic Adenoma

Focal Nodular Hyperplasia

Lymphoproliferative Disorders

Focal Inflammatory-Infectious Lesions of the Liver**Neonatal Jaundice****Cirrhosis and Diffuse Disorders of the Liver** α_1 -Antitrypsin Deficiency

Cystic Fibrosis

Glycogen Storage Diseases

Gaucher's Disease

Liver disease is less common in the pediatric population than it is in the adult population, but the sequelae can be equally devastating and may lead to the need for liver transplantation. This chapter addresses the more common congenital, neoplastic, infectious, vascular, and metabolic disorders of the pediatric liver.

At birth, the liver occupies approximately 40% of the abdominal cavity and represents 5% of the infant's total body weight. The relative size of the liver to the abdominal cavity decreases as a child grows. During infancy, the inferior hepatic margin is normally several centimeters below the costal margin, but it becomes less prominent throughout childhood.

Imaging of the pediatric liver may be prompted by hepatomegaly, abnormal liver function test results, jaundice, a palpable mass, or an abnormality detected on prenatal ultrasound. Imaging also plays an important role in evaluation of the liver before and after liver transplantation. This chapter focuses on liver masses and diseases that are unique to the pediatric population, particularly when the imaging approach diverges from that used in the adult population.

Imaging Approach for a Suspected Hepatic Mass

A palpable abdominal mass is the most common clinical presentation in a child with a liver mass. Other frequently encountered presenting signs and symptoms include hepatomegaly, abdominal pain, weight loss, anorexia, jaundice, and paraneoplastic syndromes. In addition, large vascular malformations may be manifested as congestive heart failure or consumptive coagulopathy (Kasabach-Merritt syndrome). Ultrasound is a useful imaging modality in the work-up of a suspected liver mass in a child because it allows evaluation of the abdominal viscera and vasculature. Ultrasound is relatively inexpensive, does not expose the child to ionizing radiation, and usually does not require that the patient be sedated. When an abdominal mass is identified, ultrasound can help determine the organ of origin, whether the mass is cystic or solid, if there is vascular flow to the mass, whether the mass contains calcifications, and involvement of other abdominal organs.

After the presence of a liver mass is confirmed by ultrasound, additional imaging with computed tomography (CT) or magnetic resonance imaging (MRI) is usually performed. Because surgical resection is the first line of treatment for many pediatric liver masses, precise anatomic delineation of the mass is important. The decision to pursue CT or MRI as the subsequent imaging modality is often driven by institutional and individual preferences because each modality has its own strengths and limitations. MRI is often preferred because it provides detailed multiplanar anatomic information, does not rely on proper timing of bolus contrast material administration for delineation of the vasculature, and imparts no ionizing radiation. CT is often more readily available than MRI and less commonly requires sedation.

When focal nodular hyperplasia is a consideration, technetium Tc 99m sulfur colloid scintigraphy may be a helpful adjunct study. Focal nodular hyperplasia demonstrates normal to increased uptake of the radiopharmaceutical, whereas other hepatic masses create photopenic areas. Tagged red blood cell studies can also be helpful in differentiating hemangiomas from other masses in the liver; hemangiomas demonstrate increased radiopharmaceutical activity, whereas other hepatic masses do not.

Congenital Anomalies**MALFORMATIONS AND HERNIAS**

The major congenital malformations of the liver include anomalous lobar development, lobar hypoplasia, and complete lobar agenesis. Agenesis and hypoplasia of the liver most commonly involve segment IV in the left lobe and segments V and VIII in the right lobe.¹ The best diagnostic clue, besides obvious absence of liver parenchyma, is absence of the respective hepatic and

portal veins and intrahepatic biliary ducts.¹ With congenital agenesis or hypoplasia of a lobe of the liver, compensatory enlargement of the remaining hepatic parenchyma usually occurs. Hepatic agenesis is associated with biliary tract disease, portal hypertension, and other congenital anomalies.² Herniation of the liver parenchyma through a diaphragmatic hernia is typically present at birth but may be delayed. For example, group B streptococcal pneumonia has been associated with late-onset, right-sided diaphragmatic hernia.³

FIBROPOLYCYSTIC DISEASES OF THE LIVER

Fibropolycystic diseases of the liver are thought to be the sequelae of ductal plate malformations, which involve partial or total arrest of remodeling of the ductal plate and result in persistence of embryonic biliary structures.⁴ Ductal plate malformations may involve segmental bile ducts (large), interlobular bile ducts (medium sized), or the smallest bile duct ramifications, resulting in distinct disease entities. Choledochal malformations (extrahepatic) and Caroli's disease (intrahepatic) involve malformations of large embryologic hepatobiliary ducts. Autosomal dominant polycystic liver disease (ADPLD) involves malformations of medium-sized embryologic hepatobiliary ducts. Fibropolycystic liver diseases involving malformations of small embryologic hepatobiliary ducts include congenital hepatic fibrosis and biliary hamartomas (von Meyenburg complexes).⁵ Caroli's syndrome (Caroli's disease with congenital hepatic fibrosis) involves large and small biliary ducts.⁶

Choledochal malformations (also known as choledochal cysts) and Caroli's disease (also known as type V choledochal cyst) are characterized by dilated extrahepatic and intrahepatic bile ducts, respectively, and are thought to happen during early bile duct embryogenesis. A second widely accepted theory of development of choledochal malformations is abnormal proximal insertion of the pancreatic duct into the common bile duct, which causes reflux of pancreatic enzymes into the common bile duct that weaken the duct wall and results in abnormal dilation.^{7,8} Caroli's disease and choledochal malformations, their diagnostic work-up, and imaging findings are discussed in Chapter 119.

ADPLD involves malformations of medium-sized bile ducts and is associated with autosomal dominant polycystic kidney disease (ADPKD) (Fig. 120-1). ADPLD is very rarely seen

without ADPKD. The development of liver cysts usually occurs after the development of renal cysts, and because renal cysts in ADPKD typically are not manifested until the second or third decade of life, ADPLD rarely is manifested in childhood. ADPLD is manifested in 29% to 48% of people with ADPKD.⁹ Hepatomegaly is usually the first indication that there may be underlying polycystic liver disease. Ultrasound, CT, MRI, and magnetic resonance cholangiopancreatography (MRCP) are useful in the detection of cysts in the liver. Ultrasound demonstrates multiple anechoic, thin-walled lesions, with posterior acoustic enhancement. On CT, the hepatic cysts are fluid attenuation; on MRI and MRCP, the cysts are hypointense on T1-weighted sequences and hyperintense on T2-weighted sequences. If there has been hemorrhage into the cysts, prior infection, or other reasons that the fluid may be more complex, the echogenicity, attenuation, and signal will change accordingly.^{5,10}

Congenital hepatic fibrosis involves defective remodeling of the smaller interlobular bile ducts and is characterized by abnormal branching of the intrahepatic portal veins and progressive fibrosis of the portal tracts.¹¹ Congenital hepatic fibrosis may occur with or without macroscopically visible cystic dilations of the intrahepatic biliary ducts. Congenital hepatic fibrosis with macroscopic liver cysts that communicate with the biliary ducts (also known as Caroli's disease) is referred to as Caroli's syndrome. Caroli's disease is much rarer than Caroli's syndrome. Caroli's disease and Caroli's syndrome can occur in different members of the same family, suggesting that these two disease entities may be on the same continuum. Congenital hepatic fibrosis sometimes is manifested in early childhood but may not be manifested until later in life.

Congenital hepatic fibrosis and Caroli's syndrome are associated with fibrocystic renal disease, including autosomal recessive polycystic kidney disease (ARPKD) and ADPKD; glomerulocystic kidney disease; diffuse cystic dysplastic kidneys; tubulointerstitial disorders, such as nephronophthisis, chronic tubulointerstitial disease, and urine-concentrating defect; and medullary sponge kidney (a radiologic term for microcystic dilations of renal collecting ducts on contrast-enhanced imaging that may be seen with or without nephrocalcinosis). All patients with ARPKD who survive the neonatal period develop clinical findings of congenital hepatic fibrosis.¹² Nonobstructive dilation of the intrahepatic bile ducts in the liver (Caroli's disease) is seen at the histologic level in a subset of patients as well.¹²

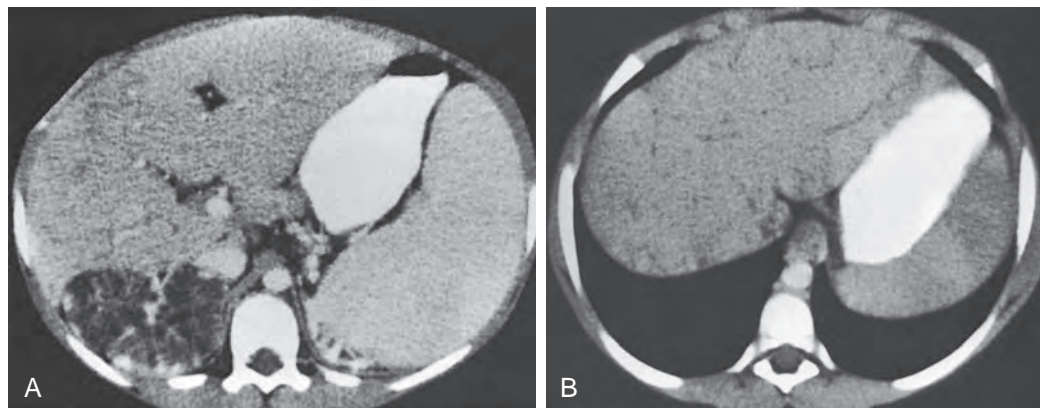


Figure 120-1 Autosomal dominant polycystic kidney disease. A. CT scan through the upper abdomen reveals multiple, small renal cysts. B. Numerous, small liver cysts are seen better on a higher section.

On ultrasound, patients with congenital hepatic fibrosis may have normal or increased parenchymal echogenicity, normal or coarsened parenchymal echotexture, hyperechoic portal triads, or poorly defined portal vessels. Cysts may be seen in the parenchyma, and the left lobe of the liver may be enlarged; there may be signs of portal hypertension, including reversal of flow in the portal vein, splenomegaly, and varices.¹³ Because of the association with fibrocystic kidney disease, the kidneys may be abnormal as well, and evaluation with a high-frequency transducer may be useful for detailed evaluation of the renal parenchyma. On CT, the liver is heterogeneous in attenuation, the left lobe of the liver is enlarged, and the associated findings of portal hypertension and fibrocystic renal disease may be evident. Findings of congenital hepatic fibrosis on MRI include hypointense signal in the liver parenchyma on T1- and T2-weighted sequences with hyperintense signal within the portal vessels on T2-weighted imaging (which reflects the periportal fibrosis), enlarged spleen, and accompanying fibrocystic changes in the kidneys.¹³ When associated Caroli's disease is present, MRCP may reveal cystic or fusiform dilations and irregularities of the intrahepatic bile ducts.¹⁴ Complications of congenital hepatic fibrosis include ascending cholangitis, sequelae of portal hypertension including cirrhosis and variceal bleeding, and increased risk of hepatocellular carcinoma.¹⁴

Biliary hamartomas (also known as biliary microhamartomas or von Meyenburg complexes) are also thought to be due to small interlobular ductal plate malformations. Biliary hamartomas can be confused with metastatic disease, and therefore definite diagnosis requires a tissue sample. On ultrasound, biliary hamartomas may be hypoechoic or hyperechoic. On CT, biliary hamartomas typically are uniform in size and do not enhance.¹⁴ On MRI, biliary hamartomas are typically hypointense on T1-weighted sequences and hyperintense on T2-weighted sequences.¹⁴

HEPATIC CYSTS

Hepatic cysts are thought to represent growth arrest and dilation of the biliary tract, although there is some support for a theory of vascular insult leading to necrosis and cyst formation (Fig. 120-2). They may be detected prenatally, but a definitive

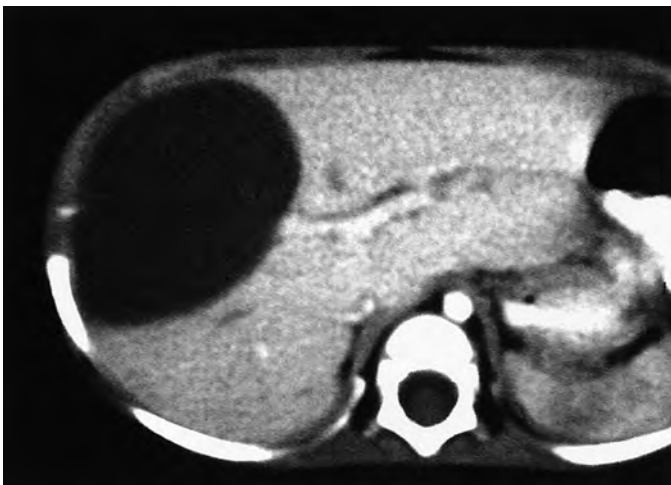


Figure 120-2 Hepatic cyst. A simple liver cyst in a 6-month-old infant was initially detected on prenatal ultrasound. Continued enlargement led to additional imaging and surgical resection.

diagnosis may not be possible until after birth. Differential diagnosis for peripheral lesions includes cystic hepatoblastoma, mesenchymal hamartoma, and vascular malformation. When the cyst has a subhepatic location, choledochal cyst, pancreatic pseudocyst, alimentary duplication, mesenteric cyst, and urachal cyst are additional considerations.¹⁵

Malignant Hepatic Neoplasms

In children, hepatic masses are relatively uncommon, accounting for 5% to 6% of all abdominal masses in the pediatric population.¹⁶ Primary neoplasms of the liver represent only 0.5% to 2% of all childhood malignant neoplasms, but they are by far the most common primary malignant neoplasms of the pediatric gastrointestinal tract. Primary hepatic neoplasms are the third most common abdominal malignant neoplasm in childhood, after Wilms' tumor and neuroblastoma.¹⁷

PRIMARY MALIGNANT NEOPLASMS

No hepatic malignant neoplasm has imaging features so pathognomonic as to obviate tissue diagnosis.^{17,18} The primary purpose of imaging is to characterize the lesion and to define the extent of disease relative to segmental anatomy, vascular structures, and the biliary system for potential chemotherapeutic intervention and preoperative planning.^{19,20} Follow-up imaging is necessary for assessment of tumor response to treatment protocols and determination of the potential for resection. Most malignant pediatric liver tumors require complete resection or transplantation as a prerequisite for cure.²¹

Hepatoblastoma, hepatocellular carcinoma, and the less frequently encountered embryonal sarcoma account for approximately two thirds of primary malignant hepatic tumors in children. The remaining primary tumors of the liver are uncommon in children and include fibrolamellar hepatocellular carcinoma, angiosarcoma, epithelioid hemangioendothelioma (a very rare tumor that is on the continuum between angiosarcoma and hemangioma), rhabdoid tumor, endodermal sinus tumor, and lymphosarcoma. Embryonal rhabdomyosarcoma is the most common malignant neoplasm to arise from the biliary tract in children and is discussed in Chapter 119.²²

Hepatoblastoma

Hepatoblastoma is the most common pediatric hepatic malignant neoplasm, accounting for 1% of all pediatric malignant neoplasms.²³ Hepatoblastomas are embryonal tumors derived from pluripotent stem cells with the capability of differentiating into hepatocytes and biliary epithelial cells. On histologic examination, these tumors are classified as epithelial, mixed (i.e., epithelial and mesenchymal), or anaplastic type. The epithelial type is the most common, accounting for approximately 60% of all hepatoblastomas.²⁴⁻²⁶ The epithelial type is further subdivided into fetal and embryonal forms. Pure fetal histology carries a better prognosis, and anaplastic or undifferentiated histology carries a poorer prognosis. With the mixed-type tumors, the presence of mesenchymal components carries a more favorable prognosis. The most commonly found mesenchymal components are cartilage and osteoid.^{24,25}

Hepatoblastoma usually occurs in infants and children younger than 3 years, with a median age of occurrence of approximately 1 year. This tumor is slightly more common in boys than in girls, with a male-to-female ratio of approximately

3:2.²⁷ No environmental risk factors have been definitively linked to hepatoblastoma, but an increased incidence of hepatoblastoma has been reported in infants with prematurity or low birth weight.^{28,29} Hepatoblastomas occurring within families have also been reported, with increased risk in children with Beckwith-Wiedemann syndrome and familial adenomatous polyposis. The association between hepatoblastoma and these two syndromes suggests that aberrations of chromosomes 11 and 5 play a role in pathogenesis.^{30,31} Several other conditions that demonstrate an increased incidence of hepatoblastoma are hemihypertrophy, Wilms' tumor, and biliary atresia.

Hepatoblastoma usually is manifested as a painless abdominal mass, but weight loss, anorexia, abdominal pain, jaundice, and rarely precocious puberty may be present. Most patients have no underlying liver disease. On occasion, levels of human β -chorionic gonadotropin are elevated, producing virilization and moderate thrombocytosis. Serum α -fetoprotein levels are elevated in more than 90% of children with hepatoblastoma. In a child younger than 3 years with a liver mass and an elevated α -fetoprotein level, hepatoblastoma should be the primary consideration.

The most common site of involvement of hepatoblastoma is the right lobe of the liver, although bilateral disease is seen in approximately 35% of cases (Figs. 120-3 and 120-4).³¹ Distant metastases are present in 20% of patients at the time of diagnosis, most commonly within the lungs.²⁹ On pathologic examination, hepatoblastomas have a tendency to be pseudo-encapsulated, well defined, and large at the time of presentation. On average, these liver masses are 10 to 20 cm in diameter at presentation.^{25,32} Hepatoblastoma commonly appears sonographically as a well-circumscribed, predominantly echogenic, solid mass.³³ Calcifications are apparent by ultrasound in up to one third of patients and are manifested as punctuate heterogeneous hyperechoic areas with posterior shadowing. Rarely, hepatoblastomas are cystic.³⁴

CT usually demonstrates a large, hypoattenuating, well-defined mass with homogeneous enhancement after the intravenous administration of contrast material (Fig. 120-5). CT better defines calcifications than ultrasound or MRI.

Calcifications tend to be punctate and delicate in epithelial-type tumors, but they are more often extensive and coarse in the mixed-type tumors.³⁵ MRI most commonly depicts a well-defined hepatic mass that is hypointense on T1-weighted sequences and hyperintense on T2-weighted sequences.^{25,35} When necrosis or hemorrhage exists within the tumor, there may be regions of hyperintense T1-weighted signal within the mass. Contrast-enhanced CT and MRI readily depict invasion, encasement, or thrombosis of the main portal vein or the hepatic artery. The presence or absence of these findings strongly affects tumor resectability.³⁶ The advent of combined adjuvant and neoadjuvant chemotherapy, hepatic resection, and, in some cases, liver transplantation has led to a dramatic improvement in survival. The 5-year survival rate for children with hepatoblastoma is 75%.³⁷



Figure 120-4 Multifocal hepatoblastoma. Contrast-enhanced CT demonstrates multiple, low-attenuation hepatic masses and thrombosis of the portal vein in a 1-year-old child.

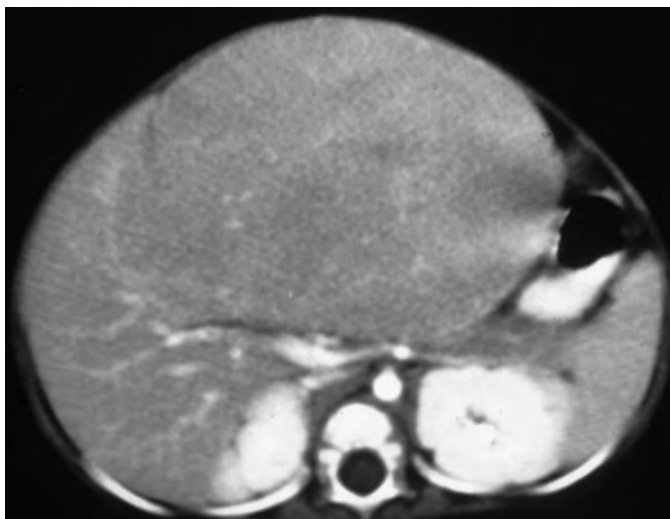


Figure 120-3 Hepatoblastoma. Contrast-enhanced CT through the upper abdomen in a 6-month-old child reveals a large isoattenuating mass arising from the medial segment of the left hepatic lobe.



Figure 120-5 Hepatoblastoma. A 3-year-old boy presented with an abdominal mass. Contrast-enhanced CT demonstrates a low-density, well-margined mass in the right lobe of the liver.

Hepatocellular Carcinoma

Hepatocellular carcinoma is rare in childhood, accounting for approximately 0.5% of all pediatric malignant neoplasms. After hepatoblastoma, hepatocellular carcinoma is the second most common primary hepatic tumor of childhood and the most common primary liver tumor in children older than 4 years.^{37,38} Histologic features of hepatic cellular carcinoma in children are similar to those in adults, with tumor cells that closely resemble hepatocytes. Tumor growth varies, but these lesions often are manifested as multicentric, diffuse, or infiltrative masses.³⁹ If necrosis is present, portions of the tumor may appear cystic. Hepatocellular carcinoma occurs more commonly in boys and older children. It has a bimodal age distribution. The first peak occurs at age 4 to 5 years, and the second peak occurs at age 12 to 14 years. The mean age at diagnosis is 12 years.⁴⁰

Although histologic and gross specimen characteristics follow the patterns seen in adults, the underlying causes in children are for the most part unique: biliary atresia, Fanconi anemia, hepatitis B viral infection, familial cholestasis, hereditary tyrosinemia, and glycogen storage disease type 1A. Glycogen storage disease type 1A results from a deficiency of glucose-6-phosphatase and leads to the development of hepatic adenomas in approximately 50% of patients. These patients are also at risk for hepatocellular carcinoma from malignant transformation of existing adenomas or from development of new tumors.^{41,42} Hyperalimentation, treatment with androgenic steroids or methotrexate, and use of oral contraceptives are also associated with an increased risk for hepatocellular carcinoma.⁴³ More than 50% of children with hepatocellular carcinoma have no preexisting liver disease or other risk factors, however.^{39,44} Many pediatric hepatocellular carcinomas are *de novo* cases that usually are not related to hepatic cirrhosis or other preexisting liver disease. This is in contrast to hepatocellular carcinoma in adults, in whom 70% to 90% of cases are related to cirrhosis.⁴³⁻⁴⁶

Despite differences in etiology, the macroscopic and microscopic features of hepatocellular carcinoma in children and adults are similar.⁴⁷ The classic trabecular pattern and fibrolamellar variants are the two most common types of hepatocellular carcinoma in children. It has been observed that there are improved outcomes associated with the fibrolamellar subtype in adults, but this has not been reported in the pediatric population.^{24,48-50}

Hepatocellular carcinoma frequently is manifested with abdominal fullness associated with pain or discomfort. Other common signs and symptoms include weight loss and fatigue. The most common clinical finding on physical examination is hepatomegaly. At presentation, between 60% and 80% of children with hepatocellular carcinoma have elevated serum α -fetoprotein levels. Metastatic disease at the time of presentation is common, and typical sites of metastasis include regional lymph nodes, lungs, and bone. Therapeutic results are uniformly poor, with an overall survival rate of about 20%.^{47,51-54} Complete tumor excision remains the only chance for long-term survival. Because of a high rate of metastatic disease at presentation (up to 50% of children) and because hepatocellular carcinoma in children is often multifocal, complete tumor excision is possible in only a minority of cases.^{26,39,51} The question of optimal therapy for pediatric hepatocellular carcinoma remains controversial, and the role of liver transplantation remains a matter for debate.

The imaging findings for hepatocellular carcinoma in children do not differ significantly from those seen in adults and are nonspecific, with variable appearance of the tumors on ultrasound, CT, and MRI. On ultrasound, hepatocellular carcinoma is typically hypoechoic to isoechoic compared with normal hepatic parenchyma. When the tumor is infiltrative, there may be subtle disruption of the normal liver echotexture.⁵⁵ CT can demonstrate a solitary mass, infiltrative tumor, or multiple, confluent masses that are low attenuating to isoattenuating relative to normal hepatic parenchyma on noncontrast or portal venous phase studies. With contrast-enhanced CT, these tumors may be hyperattenuating (Fig. 120-6). Calcifications are uncommon, but hemorrhage and necrosis are frequently seen. With T1-weighted MRI, hepatocellular carcinoma is frequently hypointense to normal hepatic parenchyma, but tumors may also appear isointense to hyperintense. Lesions of mixed signal intensity are seen in the setting of hemorrhage, necrosis, or fatty metaplasia. On T2-weighted images, most lesions demonstrate moderately increased signal intensity.

Undifferentiated Embryonal Sarcoma

Undifferentiated embryonal sarcoma is a rare, highly malignant hepatic neoplasm of mesenchymal origin that occurs almost exclusively in the pediatric population. It is the third most common primary hepatic malignant neoplasm of childhood. The age distribution for undifferentiated embryonal sarcoma

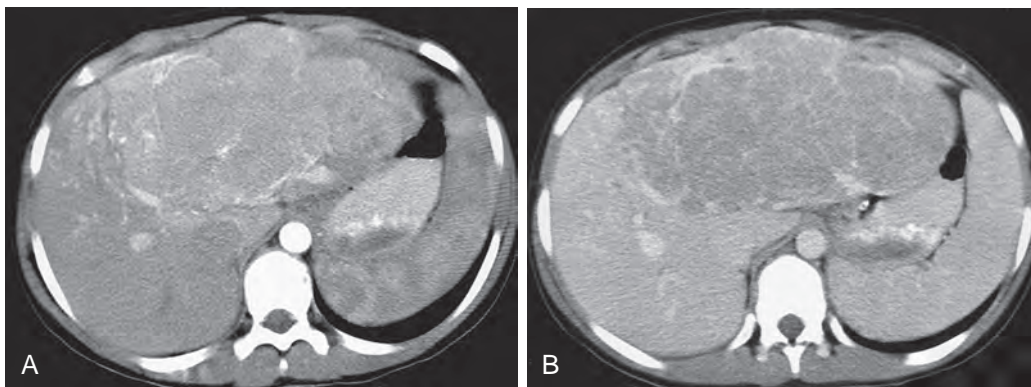


Figure 120-6 Hepatocellular carcinoma. Arterial phase (A) and portal venous phase (B) dynamic CT through the upper abdomen in a 12-year-old girl who presented with an abdominal mass demonstrates a large, heterogeneous mass with early enhancement on the arterial phase CT scan. The child had no underlying liver disease.

falls between the peak ages of the incidence for hepatoblastoma and hepatocellular carcinoma, in children between the ages of 6 and 10 years, with no gender predilection.¹⁷ On histologic examination, this tumor consists of undifferentiated spindle cells that resemble embryonal cells with a myxoid stroma. The tumor typically is well demarcated by a fibrous pseudocapsule.⁵⁶

Undifferentiated embryonal sarcoma usually is manifested as a large abdominal mass, although pain, fever, jaundice, and weight loss have been reported.²⁵ On occasion, children with this tumor present with an acute abdomen after the tumor ruptures. There are no reliable serum markers for this tumor, although leukocytosis and anemia may be present. Serum α -fetoprotein levels are normal.⁵⁷

Undifferentiated embryonal sarcoma varies in sonographic appearance from a septate, cystic mass to a heterogeneous, predominantly solid lesion. The solid lesions may demonstrate high-level echoes with acoustic shadowing from calcifications. On noncontrast CT, undifferentiated embryonal sarcoma is frequently hypoattenuating. There may be enhancement of the internal septa and fibrous capsule after administration of contrast material.⁵⁸ On MRI, undifferentiated embryonal sarcomas typically appear heterogeneous; these tumors usually are hypointense on T1-weighted sequences and hyperintense on T2-weighted sequences, corresponding to the cystic components of the mass. The fibrous pseudocapsule and internal septations appear hypointense on T1-weighted and T2-weighted sequences (Fig. 120-7).⁵⁹

Hepatic Angiosarcoma

Hepatic angiosarcoma is a rare, high-grade malignant neoplasm of endothelial cells.⁶⁰⁻⁶⁴ Unlike hepatic angiosarcoma in the adult population, pediatric hepatic angiosarcoma affects girls more than boys, with a female-to-male ratio of approximately 2:1. There is a lack of clear association with environmental carcinogens such as arsenic and polyvinyl chloride.⁶⁵ The mean age at presentation is 40 months. Pediatric hepatic angiosarcoma usually is manifested as an abdominal mass that may be associated with jaundice, abdominal pain, vomiting, fever, tachypnea, dyspnea, or anemia (Fig. 120-8). Consumption coagulopathy, which frequently occurs in adults with hepatic angiosarcoma, has not been described in children.

Pediatric hepatic angiosarcoma differs histologically from adult hepatic angiosarcoma. Pediatric hepatic angiosarcoma

can have hypercellular whorls of sarcomatous cells or kaposiform spindle cells similar to kaposiform hemangioendothelioma of soft tissue in addition to the features of adult angiosarcoma.⁶⁶ This tumor typically is manifested as a rapidly enlarging abdominal mass, and it usually is unresectable at presentation. Metastatic disease, particularly to the lungs, is a common early occurrence.^{61,62,67} Pediatric hepatic angiosarcoma has been described in the background of infantile hemangioendothelioma, and it therefore may be missed on the initial biopsy specimen.^{61,62,67,68} Because of the possibility of an association between infantile hemangioendothelioma and pediatric hepatic angiosarcoma, a presumptive diagnosis of infantile hemangioendothelioma in a child older than 1 year should probably be followed by a biopsy. There are no clear radiographic features to distinguish the two tumors.⁶⁷

Epithelioid Hemangioendothelioma

Epithelioid hemangioendothelioma is a very rare malignant neoplasm of vascular origin arising in soft tissues, lung, and liver that has malignant potential intermediate between infantile hemangioendothelioma and hepatic angiosarcoma.^{69,70} On histopathologic examination, the tumor consists of epithelioid and dendritic cells. The center of the tumor is predominantly

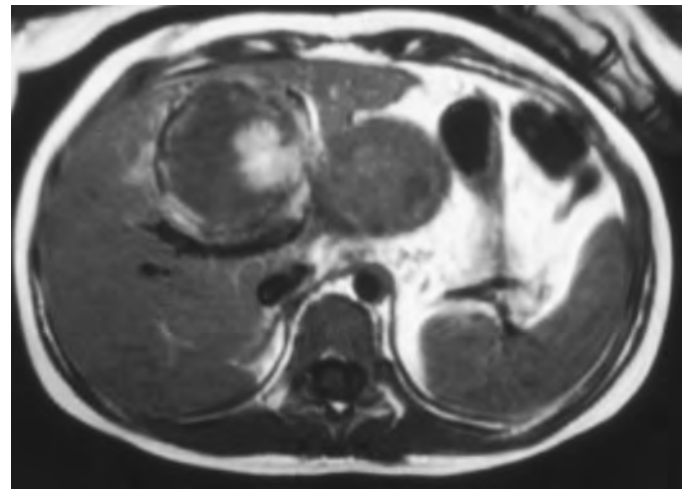


Figure 120-7 Undifferentiated embryonal sarcoma. Axial T1-weighted MRI through the upper abdomen in an 8-year-old girl demonstrates a bilobed mass arising from the left hepatic lobe.

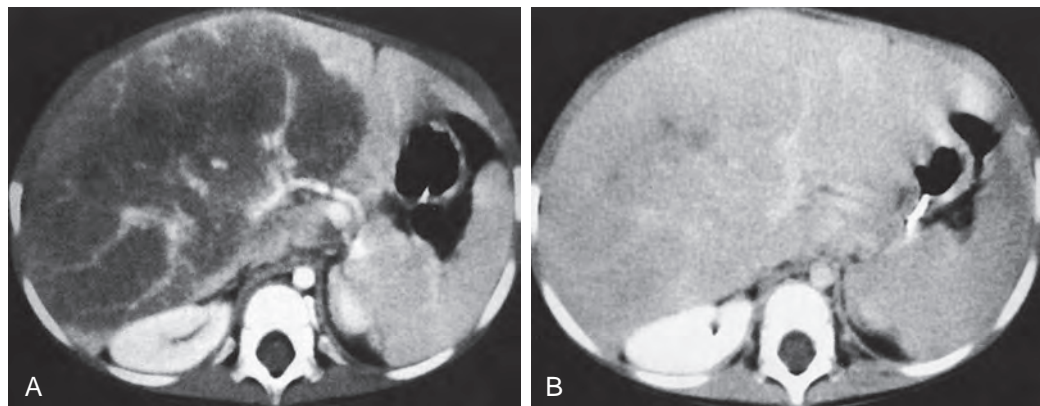


Figure 120-8 Hepatosarcoma. Dynamic, contrast-enhanced CT image reveals a large, low-density liver mass arising in the right lobe and extending into the medial segment of the left lobe. **A.** Arterial phase. **B.** Delayed scan.

fibrous stroma. This tumor may infiltrate the hepatic sinusoids and portal branches and, in doing so, obliterate them. These features may be misinterpreted as veno-occlusive disease.⁷¹ Splenomegaly, ascites, and portal hypertension may be present. Epithelioid hemangioendothelioma typically occurs after the second decade of life and is manifested with various clinical symptoms.

Epithelioid hemangioendotheliomas tend to be multifocal or multicentric at presentation. Metastatic disease is seen at presentation in approximately 27% to 45% of patients.^{71,72} Ultrasound characteristics of this tumor vary and are nonspecific. Tumors have been described as hypoechoic, isoechoic, and hyperechoic.⁷² Internal calcifications may be present. The lesions are hypoattenuating relative to normal hepatic parenchyma on unenhanced CT. After intravenous administration of contrast material, there is typically peripheral enhancement followed by relatively uniform enhancement that is isoattenuating compared with hepatic parenchyma. MRI may depict tumor characteristics better than CT.⁷³ On T1-weighted sequences, the tumor typically demonstrates decreased signal relative to normal hepatic parenchyma and demonstrates peripheral enhancement after intravenous administration of gadolinium. The lesions may be relatively heterogeneous on T2-weighted sequences.⁷³

Epithelioid hemangioendothelioma tumors are notable for resistance to chemotherapy and radiation therapy. The primary treatment of choice is radical hepatic resection or liver transplantation.

SECONDARY MALIGNANT NEOPLASMS

The most commonly encountered secondary or metastatic hepatic malignant neoplasms in children include neuroblastoma, Wilms' tumor, lymphoma, and leukemia. Metastatic disease typically appears as solitary or multiple discrete masses within the hepatic parenchyma, although leukemia may be manifested with a diffuse infiltrative pattern.^{16,17} Stage IVS neuroblastoma, in which infants have metastases confined to the liver, skin, or bone marrow, usually is manifested as diffuse infiltration of the hepatic parenchyma. Hepatic metastases usually appear hypoechoic on ultrasound, but diffuse involvement of the liver may be difficult to detect. On CT, metastatic disease typically appears as hypoattenuating lesions, although care should be taken during portal venous phase scanning

because some metastases become isoattenuating during this phase (Figs. 120-9 and 120-10). Metastatic disease in the liver typically has low signal intensity on T1-weighted MR sequences and high signal intensity on T2-weighted sequences.

Benign Hepatic Neoplasms and Neoplasm-Like Abnormalities

PEDIATRIC HEPATIC VASCULAR LESIONS

Vascular lesions of the pediatric liver can be divided into two main categories by their biologic characteristics.⁷⁴ Hepatic vasoproliferative tumors include infantile hemangioendothelioma, angiosarcoma, and epithelioid hemangioendothelioma. Vascular malformations include arteriovenous malformations, arterioportal fistula, and portosystemic shunts.

Infantile Hemangioendothelioma

Infantile hemangioendothelioma is a benign but frequently symptomatic vascular neoplasm. These lesions are the most

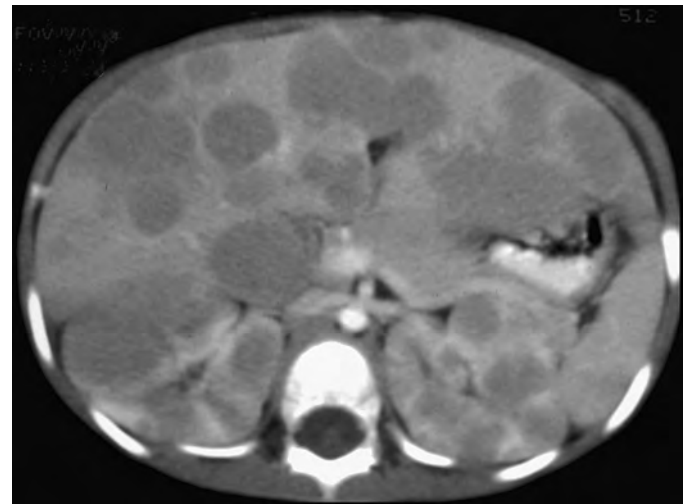


Figure 120-9 Burkitt's lymphoma. Contrast-enhanced CT of the upper abdomen reveals multiple, low-attenuation liver masses from metastatic Burkitt's lymphoma in a 6-year-old boy. Notice the multiple, low-attenuation renal lesions, which also result from metastatic Burkitt's lymphoma.

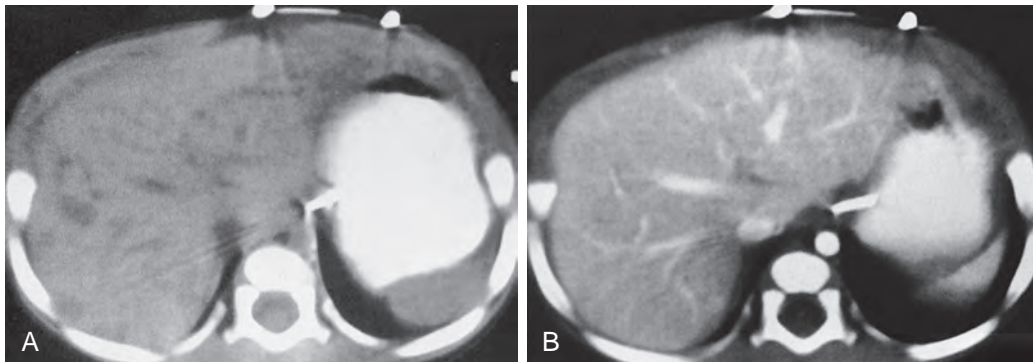


Figure 120-10 Liver metastases from neuroblastoma. A 12-month-old child with a primary pelvic neuroblastoma was found to have multiple liver metastases. The focal lesions are best seen on precontrast scans (A), and they become almost isodense after administration of contrast material (B).

common hepatic masses in infancy, and most are manifested within the first 2 to 6 months of life.^{75,76} Only 5% of infantile hemangioendotheliomas are detected in children older than 1 year. Girls are more frequently affected than boys, with a ratio of between 1.3 and 2 girls to 1 boy. Infantile hepatic hemangioendothelioma is a proliferative, predominantly endothelial cell hepatic neoplasm, with characteristic periods of rapid growth due to cellular proliferation followed by spontaneous involution. It is important to differentiate infantile hemangioendothelioma from epithelioid hemangioendothelioma and adult hepatic hemangioma. Epithelioid hemangioendothelioma is a proliferative neoplasm with malignant potential that does not involute over time, and adult hepatic hemangioma represents a vascular malformation that does not spontaneously regress.

Infantile hemangioendotheliomas typically are manifested in young infants as hepatomegaly. In 10%, there is associated high-output congestive heart failure due to vascular shunting. Failure to thrive, anemia, thrombocytopenia, and respiratory distress are other commonly associated symptoms. Anemia and thrombocytopenia may be related to consumptive coagulopathy (Kasabach-Merritt syndrome). Tumor rupture with intraperitoneal hemorrhage has also been described.^{77,78} Cutaneous hemangiomas and hemangiomas of other organs are seen in approximately 50% of children with these tumors.

Ultrasound, CT, and MRI are able to define the classic secondary features of these high-flow lesions, including tapering of the abdominal aorta below the level of the superior mesenteric artery and prominent feeding vessels. Typically, these lesions are well-circumscribed, hypoechoic lesions on ultrasound, although the solitary or focal lesions may be more heterogeneous (Fig. 120-11).⁵⁵ On noncontrast CT, most hemangioendotheliomas appear hypoattenuating compared with normal hepatic parenchyma. Finely stippled calcifications may be observed. After injection of contrast material, there is centripetal enhancement of the lesion, with the periphery of a lesion enhancing first (Fig. 120-12). Delayed scans generally demonstrate uniformly hyperattenuating masses or mass. Large focal lesions may appear heterogeneous with varying enhancement patterns, including lack of enhancement in the central portion because of fibrosis (Fig. 120-13).⁷⁹ The MR appearance of hemangioendotheliomas depends on the degree of tumoral necrosis or hemorrhage. Classically, infantile

hemangioendothelioma appears as a well-defined, spherical lesion with signal characteristics that are hypointense relative to liver on T1-weighted sequences and vividly hyperintense on T2-weighted sequences. Intratumoral flow voids related to increased vascular shunting may be present.

Initial management of an infant with a hepatic hemangioendothelioma should be conservative because most lesions spontaneously involute without therapy during several months to years.¹⁶ These lesions are often observed with sequential ultrasound examinations until they involute. Therapeutic

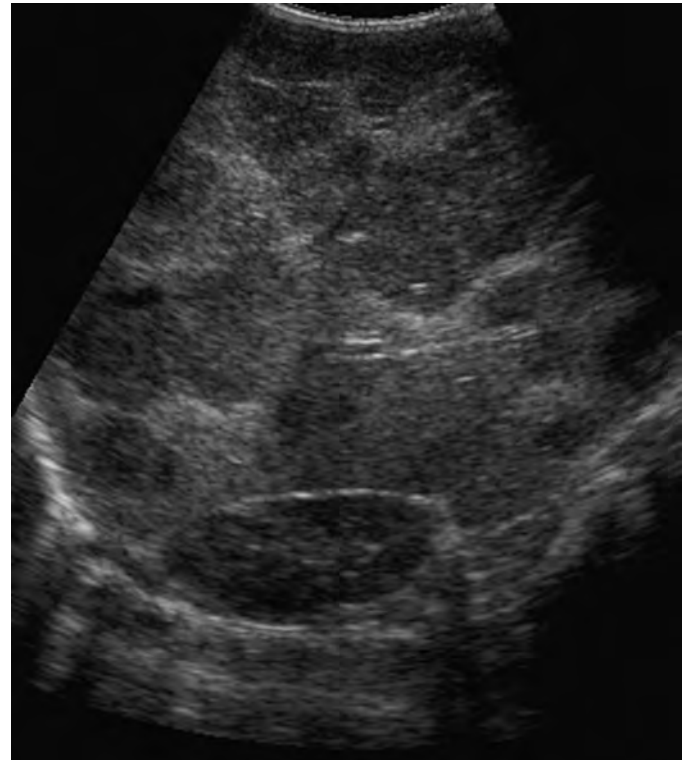


Figure 120-11 Hemangioendothelioma. Ultrasound of the liver in the sagittal plane in a 1-month-old girl with hepatomegaly demonstrates multiple, hypoechoic masses throughout the hepatic parenchyma due to multicentric hemangioendothelioma.

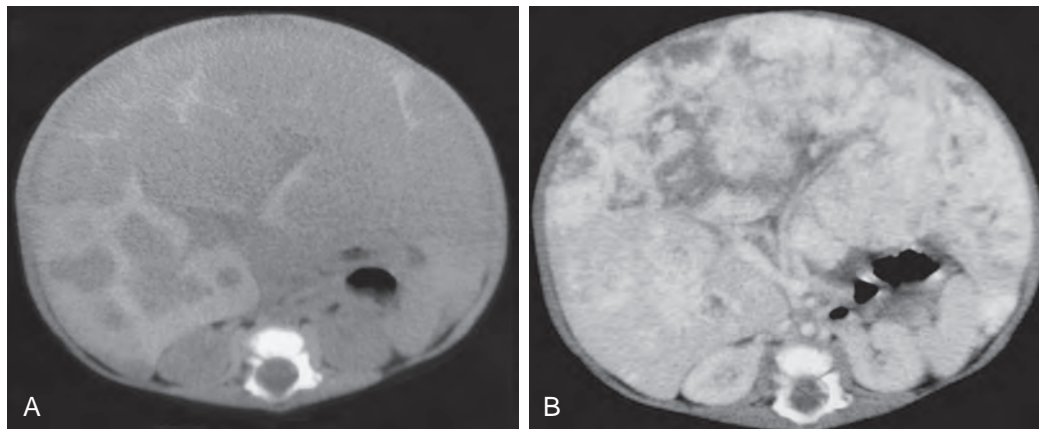


Figure 120-12 Multifocal hemangioendothelioma of the liver in a 2-week-old girl who presented with hepatomegaly. **A.** Noncontrast CT of the abdomen demonstrates multiple, low-attenuation lesions within both lobes of the liver. **B.** After the intravenous administration of contrast material, there is dense peripheral enhancement of these lesions.

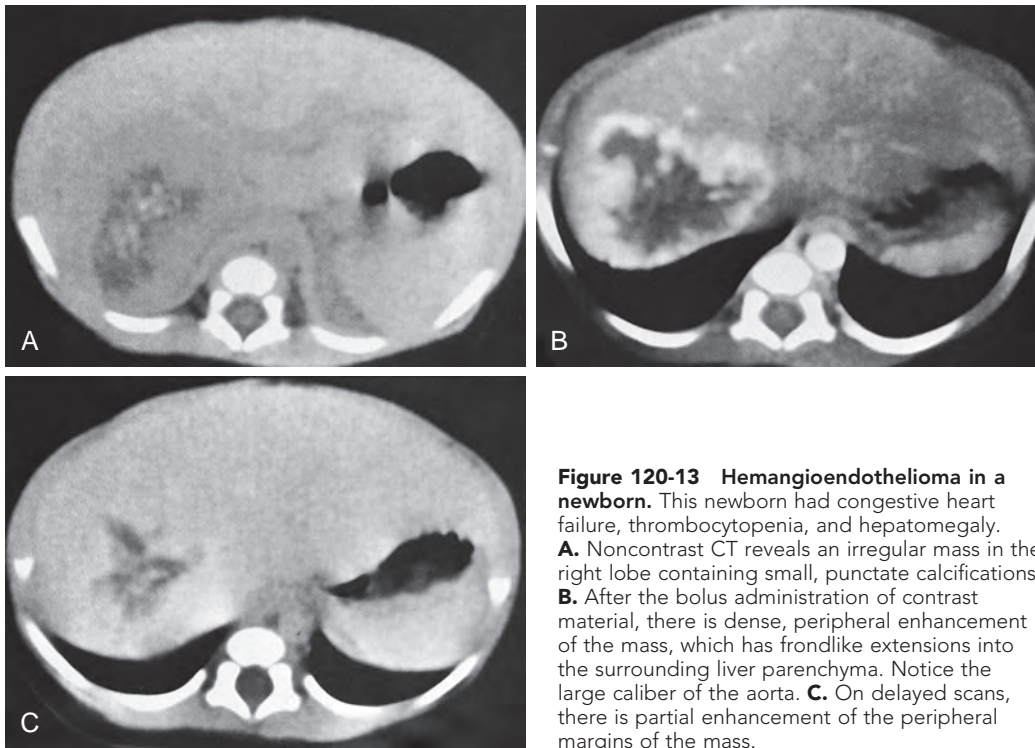


Figure 120-13 Hemangioendothelioma in a newborn. This newborn had congestive heart failure, thrombocytopenia, and hepatomegaly. **A.** Noncontrast CT reveals an irregular mass in the right lobe containing small, punctate calcifications. **B.** After the bolus administration of contrast material, there is dense, peripheral enhancement of the mass, which has frondlike extensions into the surrounding liver parenchyma. Notice the large caliber of the aorta. **C.** On delayed scans, there is partial enhancement of the peripheral margins of the mass.

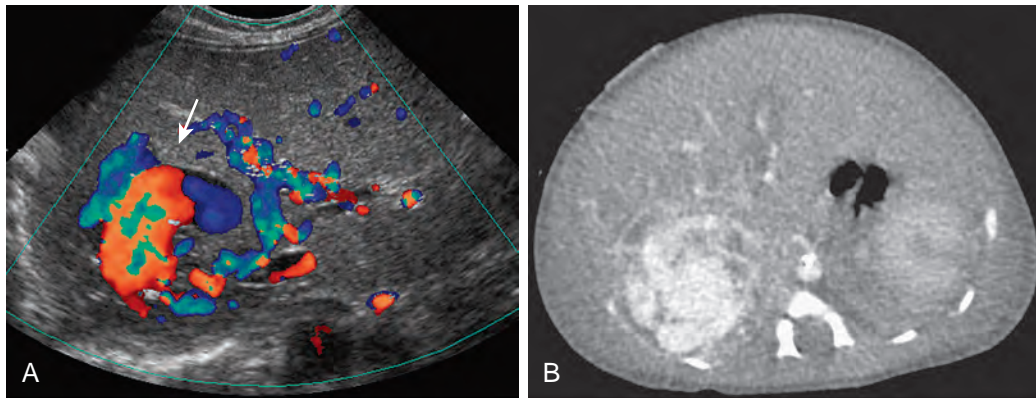


Figure 120-14 Hepatic arteriovenous malformation. **A.** Ultrasound of the posterior right hepatic lobe in an infant reveals a large arteriovenous malformation with direct communication between the right hepatic vein and the hepatic artery (arrow). **B.** On the axial contrast-enhanced CT scan of the liver in the same infant with a large arteriovenous malformation involving the posterior right hepatic lobe, notice the lack of hepatic parenchyma between the abnormal vessels.

options include steroids, interferon alfa-2a, embolization, and, less frequently, chemotherapy, radiotherapy, surgery, or liver transplantation in refractory cases.

Arteriovenous Malformations

Hepatic arteriovenous malformations (AVMs) are congenital abnormalities of blood vessels that result in shunting of blood through direct communications between the arterial and venous systems. These anomalies contain no abnormal tissue between the anomalous vessels and lack potential for growth or regeneration. In the neonatal period, hepatic AVMs are manifested with congestive heart failure, anemia, hepatomegaly, and portal hypertension. In infants, AVMs are usually solitary, and imaging findings may show considerable overlap with those seen in the

setting of a solitary hepatic hemangioma (see Fig. 120-15). Patients with hereditary hemorrhagic telangiectasia may present in late childhood with symptoms of congestive heart failure, hepatic ischemia, and portal hypertension. Unlike with the AVMs typically encountered during infancy, children with hereditary hemorrhagic telangiectasia typically have diffuse disease.

Hepatic AVMs may appear sonographically as a cluster of enlarged, tortuous vessels confined to one lobe of the liver, with increased venous pulsatility and decreased arterial resistive indices (Fig. 120-14). These lesions demonstrate intense homogeneous enhancement on CT with the intravenous administration of contrast material during the arterial or early portal venous phase, followed by rapid clearing of the contrast

material. MRI is particularly useful for differentiating hepatic AVMs from hepatic hemangiomas.⁸⁰ On contrast-enhanced MRI, AVMs lack the delayed contrast enhancement around the tortuous vessels that is commonly seen with hemangiomas.⁸¹

Arterioportal Fistula

Most hepatic arterioportal fistulas are isolated congenital anomalies, although these vascular lesions may be acquired and can be seen in the setting of hereditary hemorrhagic telangiectasia or Ehlers-Danlos syndrome.⁸² In infants and young children, a hepatic arterioportal fistula most commonly is manifested as portal hypertension with ascites, malabsorption, and gastrointestinal bleeding, although high-output cardiac failure has also been described.⁸² The lesion has a variable appearance, but it typically contains a large intrahepatic varix with a single arteriovenous connection that distinguishes it from an AVM, which contains multiple feeding vessels.⁸³ This lesion may be differentiated from focal hemangioma in infants by the lack of enhancing tissue around the varix. Treatment may consist of lobectomy if embolization is unsuccessful.⁸⁴

Portosystemic Shunts

Congenital portosystemic shunts, although rare, are a recognized cause of hyperammonemia and galactosemia in infants and children.⁸⁵⁻⁸⁷ Intrahepatic and extrahepatic portosystemic shunts have been described.^{80,85-89} Prognostic factors are related to the type of shunt, shunt ratio, and age of the patient. Most intrahepatic portosystemic shunts spontaneously close within the first 2 years of life, and asymptomatic children with this anomaly may be observed with serial ultrasound examinations.^{80,85}

Congenital intrahepatic portosystemic shunts are anomalous communications between branches of the portal vein and hepatic veins that are thought to be the sequelae of absent venous sinusoids.⁸⁸ Ultrasound of the liver typically shows communication of the hepatic and portal vein branches through tubular, anechoic structures. Doppler evaluation may be useful for documentation of the vascular communication and evaluation of the shunt ratio. The presence of a portosystemic shunt should be suspected when a pulsatile biphasic or triphasic spectral pattern is encountered in the portal vein or its branches.

Extrahepatic portosystemic shunts include congenital absence of the portal vein and a side-to-side communication

between the portal vein and the inferior vena cava. These anomalies have a high association with other congenital malformations, such as complex congenital heart disease, heterotaxy syndromes, Goldenhar's syndrome, and biliary atresia, but they have also been described in asymptomatic children undergoing imaging for other reasons.⁸⁰ Absence of the portal vein may be detected with ultrasound by the presence of only the hepatic artery and common bile duct at the hepatic hilum. Cross-sectional imaging with CT or MRI provides better delineation of the course of the extrahepatic portosystemic shunt, particularly when postprocessing volume-rendering techniques are used.

MESENCHYMAL HAMARTOMA

Mesenchymal hamartoma of the liver is a rare, benign, predominantly cystic mass of infancy and young childhood; most patients present before the age of 2 years. This lesion is considered to be a developmental anomaly rather than a true neoplasm of the liver, and it is composed of bile ducts, hepatocytes, mesenchymal tissue, and vessels. The tumor is commonly predominantly cystic, but tumors with a large solid component occasionally occur.⁹⁰ The tumor is often large at presentation, frequently weighing more than 1000 g, and it commonly occupies the right hepatic lobe, although both lobes may be involved. Patients typically present with a large, asymptomatic abdominal mass and have normal serum α -fetoprotein levels.

Ultrasound can characterize these lesions well by delineating the cystic and septate nature of the mass and any solid components, but contrast-enhanced CT better delineates the relationship of the mass to adjacent structures. There should be little enhancement of the septa after intravenous administration of contrast material, but when a soft tissue component is present, enhancement may be inhomogeneous (Fig. 120-15). On MRI, the cystic component demonstrates inconsistent signal patterns that correspond to the variable content of proteinaceous fluid.⁹¹

Although mesenchymal hamartoma is a benign lesion and can often be differentiated from other liver tumors radiographically with a high degree of confidence, surgical resection remains the mainstay of treatment. Resection is generally curative, although enucleation followed by incision and drainage

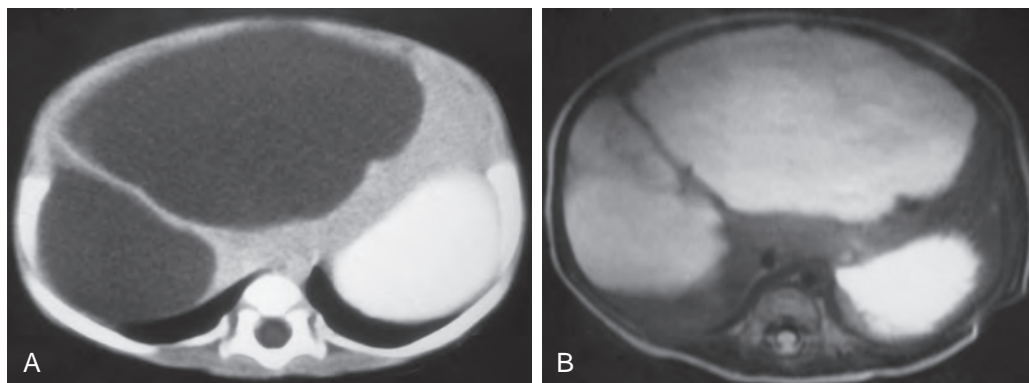


Figure 120-15 Mesenchymal hamartoma. **A.** Contrast-enhanced axial CT through the upper abdomen in an infant demonstrates a large cystic liver mass occupying both lobes. Notice the enhancement of the single septation. **B.** Axial T1-weighted MRI demonstrates the same lesion, which is almost entirely cystic.

of the cystic components and nonoperative management with serial imaging have been reported.^{92,93} Transplantation remains an option in children for whom surgical resection is not possible.⁹⁴

HEPATIC ADENOMA

Hepatic adenomas are unusual tumors in the general pediatric population, but they may be encountered more frequently in children with predisposing systemic diseases or in teenage girls, particularly those taking oral contraceptive pills. Children with Fanconi anemia who are treated with exogenous steroids and patients with type 1 glycogen storage disease are at increased risk for adenomas and other hepatic neoplasms.⁹⁵⁻⁹⁷ In children with type 1 glycogen storage disease, hepatic adenomas are more likely to be multiple (Fig. 120-16).⁹⁸

Adenomas are typically solitary lesions associated with normal serum α -fetoprotein levels. They may be found incidentally, but they are prone to acute hemorrhage, causing sudden

onset of abdominal pain (Fig. 120-17). Because of the complications related to sudden hemorrhage, these lesions are treated with surgical resection.

FOCAL NODULAR HYPERPLASIA

Focal nodular hyperplasia is the second most common benign, solid hepatic neoplasm in adults after hemangioma, but it is rare in the pediatric population (Fig. 120-18). Historically, focal nodular hyperplasia was considered a hamartoma or neoplasm related to ischemic changes, but this benign tumor is now considered to be a non-neoplastic, hyperplastic response to a congenital or acquired vascular malformation.³ It is postulated that focal circulatory disturbances cause arterial and portal venous thrombosis. Vascular recanalization and reperfusion of hepatic tissue may lead to hepatocyte proliferation and the development of focal nodular hyperplasia^{3,99} and other non-neoplastic lesions, such as regenerative nodules.¹⁰⁰

LYMPHOPROLIFERATIVE DISORDERS

Lymphoproliferative disorder is becoming more common in the pediatric population as the number of immunocompromised children grows. Solid organ and stem cell transplantation are being used more widely in children, and there is increased survival of children with immunologic disorders. Lymphoproliferative disorder results from T-cell dysfunction and abnormal proliferation of B cells infected with Epstein-Barr virus. This disorder encompasses a wide spectrum of disease, from polyclonal B-cell hyperplasia to monoclonal B-cell lymphoma.^{101,102} Lymphoproliferative disorder is most commonly seen after solid organ transplantation, but it also occurs in children after stem cell transplantation.

After solid organ transplantation, lymphoproliferative disorder commonly occurs in the region of the allograft, with hepatic involvement most frequently occurring after liver transplantation.¹⁰² Hepatic disease may be manifested as regions of periportal low attenuation or discrete masses.^{102,103} Hepatic masses related to lymphoproliferative disorder may be distinguished from other causes of liver masses by their tendency to invade and encase the portal veins rather than displace them.¹⁸



Figure 120-16 Adenoma. Contrast-enhanced CT through the liver of a child with Gaucher's disease reveals an enhancing, well-circumscribed mass arising from the lateral aspect of the left hepatic lobe. At surgical resection, this lesion proved to be an adenoma. Notice the hepatomegaly and decreased attenuation of the liver due to Gaucher's disease.

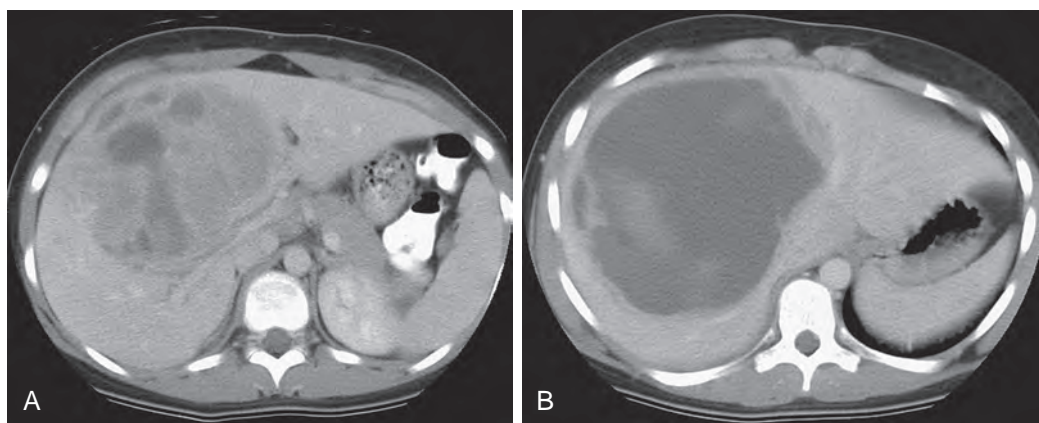


Figure 120-17 Adenoma with hemorrhage. A and B. Axial CT images after intravenous contrast enhancement in an 11-year-old girl who experienced acute onset of abdominal pain after karate class. The large, hemorrhagic tumor occupying the right hepatic lobe was found to be an adenoma at resection.

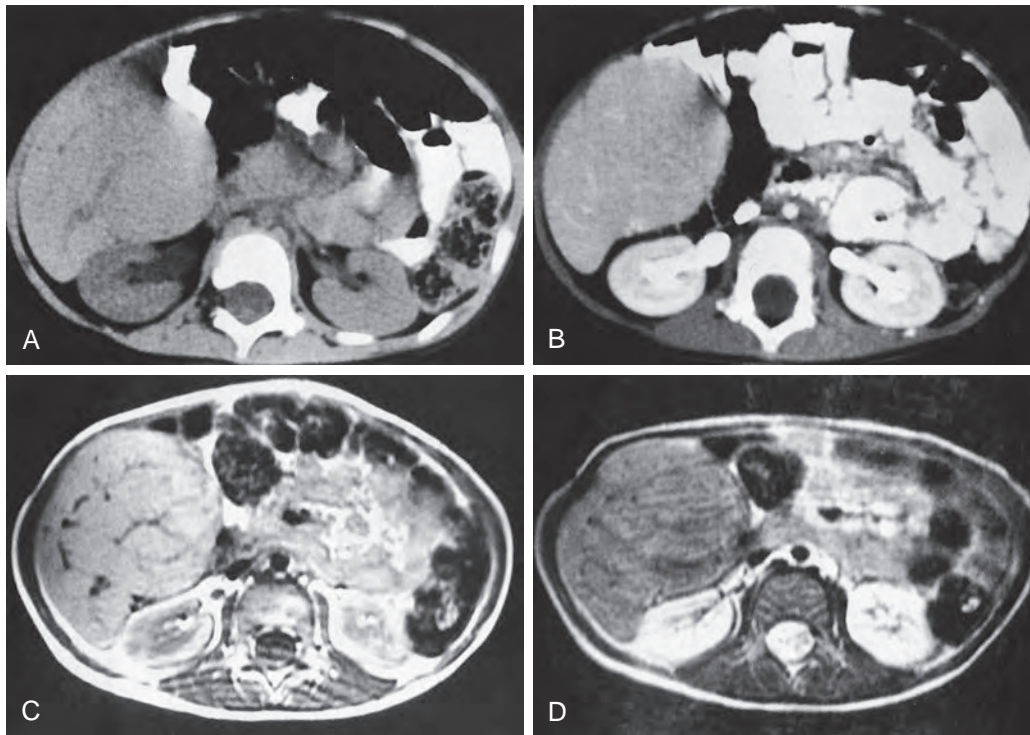


Figure 120-18 Focal nodular hyperplasia. The newborn was found to have an enlarged liver on physical examination. CT images reveal a round mass in the inferior aspect of the right lobe that has the same density as surrounding parenchyma before (A) and after (B) contrast enhancement. MRI reveals a signal intensity equal to that of surrounding parenchyma on T1-weighted (600/30) (C) and T2-weighted (2000/80) (D) sequences.

Focal Inflammatory-Infectious Lesions of the Liver

Focal hepatic infections are described in detail in Chapter 88. This section focuses on the aspects of hepatic inflammatory lesions specific to children. Hepatic abscesses are often caused by bacterial, fungal, or granulomatous infections. Amebic abscesses and hydatid cysts are common worldwide but occur infrequently in the general pediatric population in developed countries.

Pyogenic bacterial hepatic abscesses require prompt diagnosis and treatment because they may be life-threatening. In infants, hepatic abscesses are associated with generalized sepsis or may be a sequela of umbilical line placement. In older children, sepsis is a common cause, although pyogenic liver abscesses may also be seen after trauma or in immunocompromised patients such as children with sickle cell anemia or an immunologic deficiency (Fig. 120-19). On occasion, pyogenic hepatic abscesses can result from perforated appendicitis (Fig. 120-20). In children who have undergone stem cell transplantation or who are immunocompromised as the result of chemotherapy, hepatic and splenic abscesses related to disseminated fungal infection are more common.¹⁸ The most frequent causative organisms in these patients are *Candida albicans* and *Aspergillus* species. Cat-scratch disease is a benign, self-limited systemic infection associated with regional lymphadenopathy that commonly affects the liver. Hepatic involvement typically is manifested as multiple, small, nodular lesions. This infection, caused by *Bartonella henselae*, typically follows a cat scratch or multiple skin abrasions.

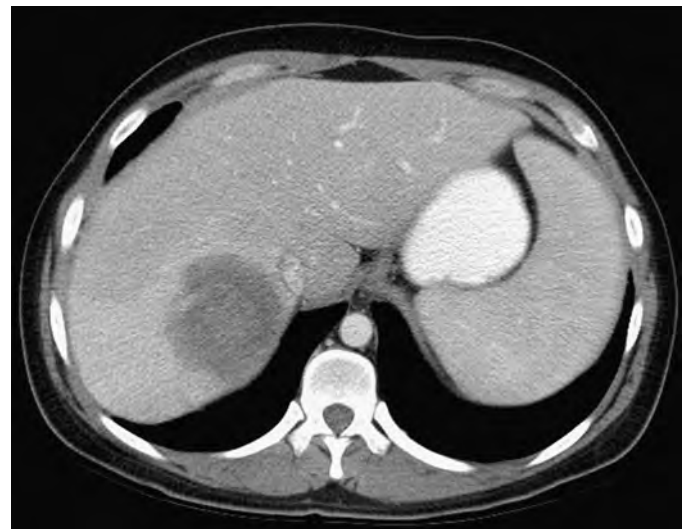


Figure 120-19 Chronic granulomatous disease. A low-attenuation hepatic abscess is seen in the dome of the right hepatic lobe in a teenage boy. Percutaneous drainage is unrewarding because there is little purulent material and mostly granuloma.

Chronic granulomatous disease is an inherited immune deficiency that results in an abnormality of leukocytes. This disorder is most commonly inherited in an X-linked fashion and therefore occurs most commonly in boys. Chronic granulomatous disease is characterized by a combination of several molecular defects that result in defective NADPH oxidase activity in

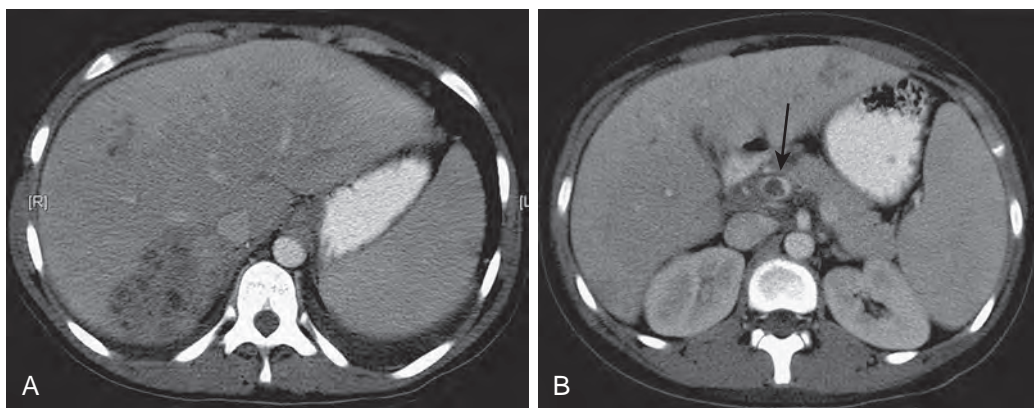


Figure 120-20 Pyogenic liver abscess. **A.** Multiple, mixed-attenuation lesions are seen in the liver of this 15-year-old girl with perforated appendicitis. **B.** Notice the thrombus in the superior mesenteric vein (arrow) in the same child.

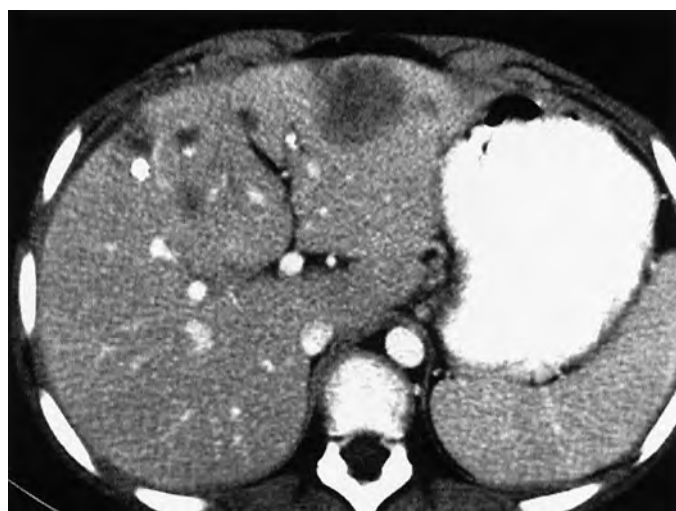


Figure 120-21 Chronic granulomatous disease. Multiple hepatic lesions are found on the CT scan of a 9-year-old boy. CT demonstrates calcifications from prior infections and low-attenuation masses from an active infection.

leukocytes.¹⁰⁴ Children with chronic granulomatous disease develop recurrent infections, commonly with catalase-positive bacteria such as *Staphylococcus aureus* or fungi, including *Aspergillus*, because of defective intracellular killing by neutrophils (Fig. 120-21).¹⁰⁵ This disease usually is manifested in children younger than 1 year with pulmonary infections. Other sites of involvement include the lymph nodes, skin, liver, gastrointestinal tract, and bones.¹⁰⁶

Neonatal Jaundice

Unconjugated hyperbilirubinemia is a common physiologic event in normal newborns, occurring in approximately 60% of term infants and 80% of preterm infants. Hyperbilirubinemia generally peaks in days 5 to 7 of life, with bilirubin levels typically below 12 to 14 mg/dL.¹⁰⁷ Infants who are breast-fed may have prolonged elevation of bilirubin through the second week of life. Onset of neonatal jaundice within the first 24 hours of life, rapid rise of serum bilirubin levels (>5 mg/dL in 24 hours), persistent jaundice, new onset of jaundice after 2 weeks of life, or a direct bilirubin level above 1 mg/dL should increase

suspicion that the neonatal jaundice may be pathologic.^{108,109} In these children, further evaluation is needed for infectious, metabolic, or surgical causes of jaundice. During the neonatal period, neonatal hepatitis, biliary atresia, and choledochal malformation/cyst are the three most common causes of jaundice.¹¹⁰ Biliary atresia and choledochal cysts are discussed in detail in Chapter 119.

Neonatal hepatitis is more common in male infants than in female infants and typically occurs during the first month of life. The spectrum of diseases associated with neonatal hepatitis includes hepatitis A, hepatitis B, hepatitis C, protozoan infections, toxoplasmosis, syphilis, rubella, cytomegalovirus infection, herpesvirus infection, inborn errors of metabolism, familial cholestasis, and idiopathic causes.¹⁰⁸⁻¹¹⁰

Ultrasound is the initial imaging tool in neonates with jaundice and is particularly useful in the differentiation of a choledochal cyst or dilation of the bile ducts from other causes of obstruction. In infants with neonatal hepatitis, the sonographic appearance of the liver may be normal to enlarged, with variable increased or decreased echogenicity. The biliary ducts and gallbladder are typically normal, except in cases with severe hepatocellular dysfunction. In these infants, decreased bile production may cause the gallbladder to appear small.¹¹⁰ In neonates with poor bile excretion due to hepatic dysfunction, sonographic differentiation of neonatal hepatitis from biliary atresia can be challenging. In these children, nuclear medicine hepatobiliary scintigraphy should be performed to assess for excretion of bile into the small intestine.

Cirrhosis and Diffuse Disorders of the Liver

Cirrhosis is a diffuse disease of the liver that results from destruction of normal hepatic parenchyma and the development of fibrosis. Regeneration of liver parenchyma occurs in a focal nodular pattern that may be micronodular or macronodular. Portal hypertension is commonly seen in the setting of cirrhosis. Cirrhosis in children usually occurs as the sequela of congenital or acquired disease of the liver, including biliary atresia, hepatitis, congenital hepatic fibrosis, cystic fibrosis, Budd-Chiari syndrome, and chronic biliary obstruction. Cirrhosis is also a secondary phenomenon in a variety of metabolic disorders, including α_1 -antitrypsin deficiency, Wilson's



Figure 120-22 Tyrosinemia. The liver has irregular contours, multiple low-attenuation lesions within the parenchyma, and patchy enhancement in a patient with tyrosinemia. The child underwent transplantation.

disease, glycogen storage disease, tyrosinemia, and galactosemia (Fig. 120-22).

α_1 -ANTITRYPSIN DEFICIENCY

The most common genetic cause of severe liver disease in children is α_1 -antitrypsin deficiency. A relative deficiency of an antiproteolytic enzyme results in accumulation of hepatic toxins, which leads to the destruction of hepatic architecture and cirrhosis, with the associated imaging findings. Individuals are also at risk for clinical manifestations such as emphysema, panniculitis, and perhaps even granulomatosis with polyangiitis (formerly Wegener's granulomatosis).¹¹¹⁻¹¹³

CYSTIC FIBROSIS

The frequency and severity of hepatobiliary complications in children with cystic fibrosis have increased with the improved life expectancy of those with this disorder.¹¹⁴ Cystic fibrosis-related hepatobiliary disease includes chronic cholangitis, fibrosis, fatty changes, and focal biliary cirrhosis that may progress to profound hepatic cirrhosis with portal hypertension, abnormalities of the bile ducts, and gallbladder abnormalities, including cholelithiasis.¹¹⁵

GLYCOGEN STORAGE DISEASES

The glycogen storage diseases are a group of inherited metabolic disorders, most of which have an abnormality in the breakdown of glycogen to glucose, which is manifested as



Figure 120-23 Gaucher's disease. CT scan through the liver of a 9-year-old boy reveals a distorted hepatic contour, peripheral parenchymal enhancement, and central region of relatively low density surrounding the portal branches. The patient died within a few days of this CT study. At autopsy, the central portion of the liver was replaced with fibrosis.

abnormal structure or concentration of glycogen. The six types are classified by differences in a specific enzyme defect. Type 1 (von Gierke's disease) is distinguished by a defect in the breakdown of glycogen to glucose, resulting in excess accumulation of glycogen within hepatocytes and the proximal convoluted tubules of the kidneys. Children with type 1 glycogen storage disease have an increased incidence of hepatic adenomas and hepatocellular carcinomas. Hepatomegaly, splenomegaly, and cirrhosis are characteristic in several different types of glycogen storage disease.

GAUCHER'S DISEASE

Gaucher's disease is a rare genetic disorder of glycolipid metabolism that leads to abnormal accumulation of glucocerebroside in cells of the reticuloendothelial system. Hepatomegaly may be the only imaging abnormality seen in the liver, but some children exhibit focal areas of low-intensity T1-weighted and high-intensity T2-weighted signal on MRI, patterns that are presumably related to deposition of Gaucher cells and fibrosis. Portal hypertension in these children is uncommon. Liver and spleen volumes determined by ultrasound, CT, or MRI are useful as an indicator of disease progression and may correlate with changes in the bone marrow and the development of avascular necrosis (Fig. 120-23).¹¹⁶⁻¹¹⁹

REFERENCES

- Caseiro-Alves F, Seco M, Bernardes A: Liver anatomy, congenital anomalies, and normal variants. In Hamm B, Ros P, editors: *Abdominal Imaging*. New York, 2013, Springer, pp 983–1000.
- Makanjuola D, Al-Smayer S, Al-Orainy I, et al: Radiographic features of lobar agenesis of the liver. *Acta Radiol* 37(Pt 1):255–258, 1996.
- Dimitroulis D, Charalampoudis P, Lainas P, et al: Focal nodular hyperplasia and hepatocellular adenoma: Current views. *Acta Chir Bleg* 113:162–169, 2013.
- Desmet VJ: [Cystic diseases of the liver. From embryology to malformations]. *Gastroenterol Clin Biol* 29:858–860, 2005.

5. Veigel MC, Prescott-Focht J, Rodriguez MG, et al: Fibropolycystic liver disease in children. *Pediatr Radiol* 39:317–327, 2009.
6. Desmet VJ: [Cystic diseases of the liver. From embryology to malformations]. *Gastroenterol Clin Biol* 29:858–860, 2005.
7. Wiedmeyer DA, Stewart ET, Dodds WJ, et al: Choledochal cyst: Findings on cholangiopancreatography with emphasis on ectasia of the common channel. *AJR Am J Roentgenol* 153:969–972, 1989.
8. Kim OH, Chung HJ, Choi BG: Imaging of the choledochal cyst. *Radiographics* 15:69–88, 1995.
9. Bistriz L, Tamboli C, Bigam D, Bain VG: Polycystic liver disease: Experience at a teaching hospital. *Am J Gastroenterol* 100:2212–2217, 2005.
10. Morgan DE, Lockhart ME, Canon CL, et al: Polycystic liver disease: Multimodality imaging for complications and transplant evaluation. *Radiographics* 26:1655–1668, quiz 1655, 2006.
11. Desmet VJ: Ludwig symposium on biliary disorders—part I. Pathogenesis of ductal plate abnormalities. *Mayo Clin Proc* 73:80–89, 1998.
12. Büscher R, Büscher AK, Weber S, et al: Clinical manifestations of autosomal recessive polycystic kidney disease (ARPKD): Kidney-related and non-kidney-related phenotypes. *Pediatr Nephrol* 2013 Oct 10. [Epub ahead of print].
13. Akhan O, Karaosmanoglu AD, Ergen B: Imaging findings in congenital hepatic fibrosis. *Eur J Radiol* 61:18–24, 2007.
14. Brancatelli G, Federle MP, Vilgrain V, et al: Fibropolycystic liver disease: CT and MR imaging findings. *Radiographics* 25:659–670, 2005.
15. Avni EF, Rypens F, Donner D, et al: Hepatic cysts and hyperechogenicities: Perinatal assessment and unifying theory on their origin. *Pediatr Radiol* 24:569–572, 1994.
16. Pobel RS, Bisset GS, 3rd: Pictorial essay: Imaging of liver tumors in the infant and child. *Pediatr Radiol* 25:495–506, 1995.
17. Davey MS, Cohen MD: Imaging of gastrointestinal malignancy in childhood. *Radiol Clin North Am* 34:717–742, 1996.
18. Donnelly LF, Bisset GS, III: Pediatric hepatic imaging. *Radiol Clin North Am* 36:413–427, 1998.
19. Finn JP, Hall-Craggs MA, Dicks-Mireaux C, et al: Primary malignant liver tumors in childhood: Assessment of resectability with high-field MR and comparison with CT. *Pediatr Radiol* 21:34–38, 1990.
20. Tiao GM, Bobey N, Allen S, et al: The current management of hepatoblastoma: A combination of chemotherapy, conventional resection, and liver transplantation. *J Pediatr* 146:204–211, 2005.
21. Czauderna P, Otte JB, Aronson DC, et al: Childhood Liver Tumour Strategy Group of the International Society of Paediatric Oncology (SIOPEL): Guidelines for surgical treatment of hepatoblastoma in the modern era—recommendations from the Childhood Liver Tumour Strategy Group of the International Society of Paediatric Oncology (SIOPEL). *Eur J Cancer* 41:1031–1036, 2005.
22. Sanz N, de Mingo L, Florez F, Rollan V: Rhabdomyosarcoma of the biliary tree. *Pediatr Surg Int* 12:200–201, 1997.
23. Mann JR, Kasthuri N, Raafat F, et al: Malignant hepatic tumours in children: Incidence, clinical features and aetiology. *Paediatr Perinat Epidemiol* 4:276–289, 1990.
24. Hass JE, Mcynski KA, Krailo M, et al: Histopathology and prognosis in childhood hepatoblastoma and hepatocarcinoma. *Cancer* 64:1082–1095, 1989.
25. Helmberger TK, Ros PR, Mergo PJ, et al: Pediatric liver neoplasms: A radiologic-pathologic correlation. *Eur Radiol* 9:1339–1347, 1999.
26. Emre S, McKenna GJ: Liver tumors in children. *Pediatr Transplant* 8:632–638, 2004.
27. Bulterys M, Goodman MD, Smith MA, et al: Cancer Incidence and Survival Among Children and Adolescents: United States SEER Program 1975–1995. National Cancer Institute SEER Program, NIH publication no. 99-4649, Bethesda, MD, 1999, National Cancer Institute, pp 91–97.
28. Fernandez-Pineda I, Cabello-Laureano R: Differential diagnosis and management of liver tumors in infants. *World J Hepatol* 6:486–495, 2014.
29. Feusner J, Plaschkes J: Hepatoblastoma and low birth weight: A trend or chance observation? *Med Pediatr Oncol* 39:508–509, 2002.
30. Haas OA, Zoubek A, Grumayer ER, Gardner H: Constitutional interstitial deletion of 11p11 and pericentric inversion of chromosome 9 in a patient with Wiedemann-Beckwith syndrome and hepatoblastoma. *Cancer Genet Cytogenet* 23:95–104, 1986.
31. Steenman M, Westerveld A, Mannens M: Genetics of Beckwith-Wiedemann syndrome—associated tumors: Common genetic pathways. *Genes Chromosomes Cancer* 28:1–13, 2000.
32. Hartley AL, Birch JM, Kelsey AM, et al: Epidemiological and familial aspects of hepatoblastoma. *Med Pediatr Oncol* 18:103–109, 1990.
33. de Campo M, de Campo JF: Ultrasound of primary hepatic tumours in childhood. *Pediatr Radiol* 19:19–24, 1988.
34. Miller JH: The ultrasonographic appearance of cystic hepatoblastoma. *Radiology* 138:141–143, 1981.
35. Boechat MI, Kangaroo H, Ortega J, et al: Primary liver tumors in children: Comparison of CT and MR imaging. *Radiology* 169:727–732, 1988.
36. Herzog CE, Andrassy RJ, Eftekhari F: Childhood cancers: Hepatoblastoma. *Oncologist* 5:445–453, 2000.
37. Schnater JM, Kohler SE, Lamers WH, et al: Where do we stand with hepatoblastoma? A review. *Cancer* 98:668–678, 2003.
38. Czauderna P, Mackinlay G, Perilongo G, et al: Hepatocellular carcinoma in children: Results of the first prospective study of the International Society of Pediatric Oncology group. *J Clin Oncol* 20:2798–2804, 2002.
39. Ni YH, Chang MH, Hsu HY, et al: Hepatocellular carcinoma in childhood. Clinical manifestations and prognosis. *Cancer* 68:1737–1741, 1991.
40. Bellani FF, Massimino M: Liver tumors in childhood: Epidemiology and clinics. *J Surg Oncol Suppl* 3:119–121, 1993.
41. Howell RR, Stevenson RE, Ben-Menachem Y, et al: Hepatic adenomata with type I glycogen storage disease. *JAMA* 236:1481–1484, 1976.
42. Franco LM, Krishnamurthy V, Bali D, et al: Hepatocellular carcinoma in glycogen storage disease type Ia: A case series. *J Inher Metab Dis* 28:153–162, 2005.
43. Weinberg AG, Finegold MJ: Primary hepatic tumor of childhood. *Human Pathol* 14:512–537, 1983.
44. Czauderna P: Adult type vs. childhood hepatocellular carcinoma—are they the same or different lesions? Biology, natural history, prognosis, and treatment. *Med Pediatr Oncol* 39:519–523, 2002.
45. Ducreux M, Elias D, Rougier P, et al: [Treatment of hepatocellular carcinoma in the presence of liver cirrhosis]. *J Chir (Paris)* 132:279–286, 1995.
46. Kew MC: Hepatocellular carcinoma with and without cirrhosis. A comparison in southern African blacks. *Gastroenterology* 97:136–139, 1989.
47. Moore SW, Hesselning PB, Wessels G, et al: Hepatocellular carcinoma in children. *Pediatr Surg Int* 12:266–270, 1997.
48. Farhi DC, Shikes RH, Murari PJ, et al: Hepatocellular carcinoma in young people. *Cancer* 52:1516–1525, 1983.
49. Hegde SV, Dillman JR, Lopez MJ, Strouse PJ: Imaging of multifocal liver lesions in children and adolescents. *Cancer Imaging* 12:516–529, 2013.
50. Katzenstein HM, Krailo MD, Malogolowkin MH, et al: Fibrolamellar hepatocellular carcinoma in children and adolescents. *Cancer* 97:2006–2012, 2003.
51. Chen JC, Chen CC, Chen WJ, et al: Hepatocellular carcinoma in children: Clinical review and comparison with adult cases. *J Pediatr Surg* 33:1350–1354, 1998.
52. von Schweinitz D, Fuchs J, Mildnerberger H: [Surgical strategy in pediatric liver malignancies]. *Langenbecks Arch Chir Suppl Kongressbd* 113:1091–1094, 1996.
53. King DR, Ortega J, Campbell J, et al: The surgical management of children with incompletely resected hepatic cancer is facilitated by intensive chemotherapy. *J Pediatr Surg* 26:1074–1080, discussion 1080–1081, 1991.
54. Gauthier F, Valayer J, Thai BL, et al: Hepatoblastoma and hepatocarcinoma in children: Analysis of a series of 29 cases. *J Pediatr Surg* 21:424–429, 1986.
55. Das CJ, Dhillon S, Gupta AK, et al: Imaging of paediatric liver tumours with pathological correlation. *Clin Radiol* 64:1015–1025, 2009.
56. Bisogno G, Pilz T, Perilongo G, et al: Undifferentiated sarcoma of the liver in childhood: A curable disease. *Cancer* 94:252–257, 2002.
57. Horowitz ME, Etcubanas E, Webber BL, et al: Hepatic undifferentiated (embryonal) sarcoma and rhabdomyosarcoma in children. Results of therapy. *Cancer* 59:396–402, 1987.
58. Moon WK, Kim WS, Choi BI, et al: Undifferentiated embryonal sarcoma of the liver treated with chemotherapy: CT imaging in four patients. *Abdom Imaging* 20:133–137, 1995.
59. Psatha EA, Semelka RC, Fordham L, et al: Undifferentiated (embryonal) sarcoma of the liver (USL): MRI findings including dynamic gadolinium enhancement. *Magn Reson Imaging* 22:897–900, 2004.
60. Kirchner SG, Heller RM, Kasselberg AG, Greene HL: Infantile hepatic hemangioendothelioma with subsequent malignant degeneration. *Pediatr Radiol* 11:42–45, 1981.
61. Selby DM, Stocker JT, Ishak KG: Angiosarcoma of the liver in childhood: A clinicopathologic and follow-up study of 10 cases. *Pediatr Pathol* 12:485–498, 1992.
62. Falk H, Herbert JT, Edmonds L, et al: Review of four cases of childhood hepatic angiosarcoma—elevated environmental arsenic exposure in one case. *Cancer* 47:382–391, 1981.
63. Noronha R, Gonzalez-Crussi F: Hepatic angiosarcoma in childhood. A case report and

- review of the literature. *Am J Surg Pathol* 8: 863–871, 1984.
64. Strate SM, Rutledge JC, Weinberg AG: Delayed development of angiosarcoma in multinodular infantile hepatic hemangioendothelioma. *Arch Pathol Lab Med* 108:943–944, 1984.
 65. Dimashkieh HH, Mo JQ, Wyatt-Ashmead J, Collins MH: Pediatric hepatic angiosarcoma: Case report and review of the literature. *Pediatr Dev Pathol* 7:527–532, 2004.
 66. Bruegel M, Muenzel D, Waldt S, et al: Hepatic angiosarcoma: Cross-sectional imaging findings in seven patients with emphasis on dynamic contrast-enhanced and diffusion-weighted MRI. *Abdom Imaging* 38:745–754, 2013.
 67. Awan S, Davenport M, Portmann B, Howard ER: Angiosarcoma of the liver in children. *J Pediatr Surg* 31:1729–1732, 1996.
 68. Dehner LP, Ishak KG: Vascular tumors of the liver in infants and children. A study of 30 cases and review of the literature. *Arch Pathol* 92:101–111, 1971.
 69. Furui S, Itai Y, Ohtomo K, et al: Hepatic epithelioid hemangioendothelioma: Report of five cases. *Radiology* 171:63–68, 1989.
 70. Weiss SW, Enzinger FM: Epithelioid hemangioendothelioma: A vascular tumor often mistaken for a carcinoma. *Cancer* 50:970–981, 1982.
 71. Makhlouf HR, Ishak KG, Goodman ZD: Epithelioid hemangioendothelioma of the liver: A clinicopathologic study of 137 cases. *Cancer* 85:562–582, 1999.
 72. Stringer MD: The role of liver transplantation in the management of paediatric liver tumours. *Ann R Coll Surg Engl* 89:12–21, 2007.
 73. Van Beers B, Roche A, Mathieu D, et al: Epithelioid hemangioendothelioma of the liver: MR and CT findings. *J Comput Assist Tomogr* 16:420–424, 1992.
 74. Mulliken JB, Glowacki J: Hemangiomas and vascular malformations in infants and children: A classification based on endothelial characteristics. *Plast Reconstr Surg* 69:412–422, 1982.
 75. Fan F, Yang X, Zhu B, et al: Clinical and radiological characteristics of Chinese patients with hepatic epithelioid hemangioendothelioma. *Ann Saudi Med* 33:334–338, 2013.
 76. Boon LM, Burrows PE, Patel HJ, et al: Hepatic vascular anomalies in infancy: A twenty-seven-year experience. *J Pediatr* 129:346–354, 1996.
 77. von Schweinitz D, Gluer S, Mildenberger H: Liver tumors in neonates and very young infants: Diagnostic pitfalls and therapeutic problems. *Eur J Pediatr Surg* 5:72–76, 1995.
 78. Dachman AH, Lichtenstein JE, Friedman AC, Hartman DS: Infantile hemangioendothelioma of the liver: A radiologic-pathologic-clinical correlation. *AJR Am J Roentgenol* 140: 1091–1096, 1983.
 79. Yoshikawa J, Matsui O, Kadoya M, et al: Delayed enhancement of fibrotic areas in hepatic masses: CT-pathologic correlation. *J Comput Assist Tomogr* 16:206–211, 1992.
 80. Gallego C, Miralles M, Marin C, et al: Congenital hepatic shunts. *Radiographics* 24:755–772, 2004.
 81. Singh S, Swanson KL, Hatchcock MA, et al: Identifying the presence of clinically significant hepatic involvement in hereditary haemorrhagic telangiectasia using a simple clinical scoring index. *J Hepatol* 61:124–131, 2014.
 82. Burrows PE, Dubois J, Kassarian A: Pediatric hepatic vascular anomalies. *Pediatr Radiol* 31:533–545, 2001.
 83. Marchand V, Uflacker R, Baker SS, et al: Congenital hepatic arterioportal fistula in a 3-year-old child. *J Pediatr Gastroenterol Nutr* 28: 435–441, 1999.
 84. Tasar M, Gulec B, Bozlar U, et al: Intrahepatic arterioportal fistula and its treatment with detachable balloon and transcatheter embolization with coils and microspheres. *Clin Imaging* 29:325–330, 2005.
 85. Akahoshi T, Nishizaki T, Wakasugi K, et al: Portal-systemic encephalopathy due to a congenital extrahepatic portosystemic shunt: Three cases and literature review. *Hepatogastroenterology* 47:1113–1116, 2000.
 86. Florio F, Nardella M, Balzano S, et al: Congenital intrahepatic portosystemic shunt. *Cardiovasc Intervent Radiol* 21:421–424, 1998.
 87. Kim SZ, Marz PL, Laor T, et al: Elevated galactose in newborn screening due to congenital absence of the portal vein. *Eur J Pediatr* 157: 608–609, 1998.
 88. Park JH, Cha SH, Han JK, Han MC: Intrahepatic portosystemic venous shunt. *AJR Am J Roentgenol* 155:527–528, 1990.
 89. Lane MJ, Jeffrey RB, Jr, Katz DS: Spontaneous intrahepatic vascular shunts. *AJR Am J Roentgenol* 174:125–131, 2000.
 90. Craig JR: Mesenchymal tumors of the liver. Diagnostic problems for the surgical pathologist. *Pathology (Phila)* 3:141–160, 1994.
 91. Ros PR, Goodman ZD, Ishak KG, et al: Mesenchymal hamartoma of the liver: Radiologic-pathologic correlation. *Radiology* 158:619–624, 1986.
 92. Qian LJ, Zhu J, Zhuang ZG, et al: Spectrum of multilocular cystic hepatic lesions: CT and MR imaging findings with pathologic correlation. *Radiographics* 33:1419–1433, 2013.
 93. Patel SR, Misra V, Verma K, et al: Benign Hepatic Mesenchymal Hamartoma (HMH)—A case report. *J Clin Diagn Res* 8:119–120, 2014.
 94. Tepetes K, Selby R, Webb M, et al: Orthotopic liver transplantation for benign hepatic neoplasms. *Arch Surg* 130:153–156, 1995.
 95. Hung CH, Changchien CS, Lu SN, et al: Sonographic features of hepatic adenomas with pathologic correlation. *Abdom Imaging* 26: 500–506, 2001.
 96. Fulcher AS, Sterling RK: Hepatic neoplasms: Computed tomography and magnetic resonance features. *J Clin Gastroenterol* 34:463–471, 2002.
 97. Brancatelli G, Federle MP, Vullierme MP, et al: CT and MR imaging evaluation of hepatic adenoma. *J Comput Assist Tomogr* 30:745–750, 2006.
 98. Lee PJ: Glycogen storage disease type I: Pathophysiology of liver adenomas. *Eur J Pediatr* 161(Suppl 1):S46–S49, 2002.
 99. Bouyn CI, Leclerc J, Raimondo G, et al: Hepatic focal nodular hyperplasia in children previously treated for a solid tumor. Incidence, risk factors, and outcome. *Cancer* 97:3107–3113, 2003.
 100. Brancatelli G, Federle MP, Grazioli L, et al: Large regenerative nodules in Budd-Chiari syndrome and other vascular disorders of the liver: CT and MR imaging findings with clinicopathologic correlation. *AJR Am J Roentgenol* 178:877–883, 2002.
 101. Day DL, Shapiro RS, Yueh N, et al: B-cell lymphoproliferative disorders in children after bone marrow transplantation: Radiologic manifestations. *Radiology* 162:807–810, 1987.
 102. Donnelly LF: CT imaging of immunocompromised children with acute abdominal symptoms. *AJR Am J Roentgenol* 167:909–913, 1996.
 103. Donnelly LF, Frush DP, Marshall KW, White KS: Lymphoproliferative disorders: CT findings in immunocompromised children. *AJR Am J Roentgenol* 171:725–731, 1998.
 104. Kishimoto TK, Springer TA: Human leukocyte adhesion deficiency: Molecular basis for a defective immune response to infections of the skin. *Curr Probl Dermatol* 18:106–115, 1989.
 105. Dinanuer MC: Disorders of neutrophil function: An overview. *Methods Mol Biol* 1124: 501–515, 2014.
 106. Pennington DJ, Lonergan GJ, Benya EC: Pulmonary disease in the immunocompromised child. *J Thorac Imaging* 14:37–50, 1999.
 107. Behrman RE, editor: *Nelson Textbook of Pediatrics*, ed 14, Philadelphia, 1992, WB Saunders, p 478.
 108. Kessler A, Rosenberg HK: Sonographic approach to infants and children with jaundice. In Lombay B, editor: *1993 Yearbook of Pediatric Radiology*, vol 5, Miskolc, Hungary, 1993, Central Medical Library of County Hospital, pp 3–22.
 109. Smith WL: The liver. In Franken EA, Jr, Smith WL, editors: *Gastrointestinal Imaging in Pediatrics*, ed 2, New York, 1982, Harper & Row, pp 425–458.
 110. Gubernick JA, Rosenberg HK, Ilaslan H, Kessler A: US approach to jaundice in infants and children. *Radiographics* 20:173–195, 2000.
 111. Fink S, Schilsky ML: Inherited metabolic disease of the liver. *Curr Opin Gastroenterol* 23:237–243, 2007.
 112. Barnett VT, Sekosan M, Khurshid A: Wegener's granulomatosis and alpha₁-antitrypsin-deficiency emphysema: Proteinase-related diseases. *Chest* 116:253–255, 1999.
 113. Mahr AD, Edberg JC, Stone JH, et al: Alpha₁-antitrypsin deficiency-related alleles Z and S and the risk of Wegener's granulomatosis. *Arthritis Rheum* 62:3760–3767, 2010.
 114. King LJ, Scurr ED, Murugan N, et al: Hepatobiliary and pancreatic manifestations of cystic fibrosis: MR imaging appearances. *Radiographics* 20:767–777, 2000.
 115. Willi UV, Reddish JM, Teele RL: Cystic fibrosis: Its characteristic appearance on abdominal sonography. *AJR Am J Roentgenol* 134:1005–1010, 1980.
 116. Hill SC, Damaska BM, Ling A, et al: Gaucher disease: Abdominal MR imaging findings in 46 patients. *Radiology* 184:561–566, 1992.
 117. Terk MR, Esplin J, Lee K, et al: MR imaging of patients with type 1 Gaucher's disease: Relationship between bone and visceral changes. *AJR Am J Roentgenol* 165:599–604, 1995.
 118. States LJ: Imaging of metabolic bone disease and marrow disorders in children. *Radiol Clin North Am* 39:749–772, 2001.
 119. Razeq AA, Abdalla A, Fathy A, et al: Apparent diffusion coefficient of the vertebral bone marrow in children with Gaucher's disease type I and III. *Skeletal Radiol* 42:283–287, 2013.

Diseases of the Pediatric Pancreas

MARIAM M. KAPPIL | DARSHIT J. THAKRAR

CHAPTER OUTLINE

Imaging of the Pediatric Pancreas

Trauma

Pancreatitis

Acute Pancreatitis

Chronic Pancreatitis

Cystic Fibrosis

Shwachman-Diamond Syndrome

Nesidioblastosis

Pancreatic Masses

Congenital Cysts

Neoplasms

Metastatic Disease

Miscellaneous Processes

von Hippel–Lindau Disease

Beckwith–Wiedemann Syndrome

Autosomal Dominant Polycystic Kidney Disease

Imaging of the Pediatric Pancreas

Ultrasound is the initial imaging modality of choice for evaluation of the pediatric pancreas. The relatively large left hepatic lobe serves as an acoustic window and children have a thin body habitus, which makes this possible.¹ Ultrasound is also ideal for imaging of children because it is noninvasive and does not require sedation, along with the lack of ionizing radiation.² On sonography, the normal pancreas has a homogeneous echotexture (Fig. 121-1).³ The pancreas in preterm infants and neonates usually is more echogenic than the liver.⁴ As children grow, it usually becomes nearly isoechoic to the liver. The normal pancreatic duct is commonly seen in the body of the gland as an echogenic line or an anechoic lumen with echogenic borders (Fig. 121-2).^{1,3} Relative to body size, the pancreas is larger in children than in adults, although it tends to shrink relatively with age.^{2,5} The head and tail of the pancreas typically are thicker than the body and neck. The usual prominence of the head can sometimes be mistaken for abnormality. The pancreatic duct normally is less than 2 mm in diameter.⁶

Given the ionizing radiation, the need for intravenous and oral administration of contrast material, and the possible need for sedation of young patients, computed tomography (CT) is usually reserved for when the ultrasound study is nondiagnostic. It is also used to more clearly define anatomic detail (such as pancreatic mass, severe pancreatitis, or the complete extent of disease), to evaluate blunt abdominal trauma,¹ and to assess the distant complications of pancreatic disease. On CT, the normal pediatric pancreas has a generally smooth or slightly

lobulated surface and a homogeneous soft tissue attenuation² that is usually similar to that of the liver (Fig. 121-3).⁵

Magnetic resonance imaging (MRI), when it is coupled with magnetic resonance cholangiopancreatography (MRCP), is a powerful, noninvasive tool for imaging of the pancreatic and biliary ductal systems.² On fat-saturated T1-weighted images, the pancreas demonstrates intrinsic T1 hyperintensity and is of bright signal compared with other organs. On T2-weighted images, the pancreas should be isointense to the liver.⁷ MRCP is useful to evaluate the ductal anatomy in children with acute or recurrent pancreatitis for congenital abnormalities, such as pancreas divisum or an abnormal pancreatobiliary junction.⁸ The disadvantages of MRI include its expense, technical difficulty (particularly in younger children, who are unable to cooperate), and poor spatial resolution with regard to peripheral pancreatic and biliary anatomy.⁸

Whereas endoscopic retrograde cholangiopancreatography (ERCP) has been the “gold standard” for evaluating the pancreatic and biliary ductal systems, its utility has decreased with the advent of MRCP. This technique has the disadvantages of being invasive, requiring general anesthesia in children, and having the potential complication of pancreatitis, which occurs in at least 3% of children.¹ Thus, ERCP is now usually reserved for cases that require intervention or for manometry of biliary and pancreatic sphincters.⁹

Trauma

Blunt abdominal trauma accounts for most abdominal injuries in children.¹⁰ Children are more prone to trauma-induced pancreatic injury than adults are because of underdeveloped abdominal musculature.² The mechanism of injury most commonly involves compression of the pancreas against the spine, as seen in motor vehicle collisions or nonaccidental trauma, or discrete focal trauma,¹⁰ commonly seen in bicycle handlebar injuries.⁵ There is overall approximately 3% to 12% incidence of pancreatic injury in children,¹⁰ with 90% of these patients also concurrently having injuries to other structures, including the liver, spleen, bowel, and adjacent vasculature.¹¹ The bicycle handlebar type is the most likely to cause isolated injury to the pancreas (Fig. 121-4).¹²

The signs and symptoms of pancreatic injury may be delayed for hours or days after the trauma, particularly if the injury is isolated to the pancreas.¹⁰ Symptoms are often atypical and nonspecific, including abdominal pain, nausea, vomiting, and fever.² The initial serum amylase level has a low sensitivity and specificity for detecting pancreatic injury, and it may be normal, even in the setting of significant pancreatic injury.¹²

The utility of ultrasound is limited in the setting of blunt abdominal trauma, with a sensitivity of only 67% for detecting pancreatic injury seen by CT.¹² Contrast-enhanced CT is superior to ultrasound for evaluating pancreatic trauma, with a sensitivity for detecting all pancreatic injuries of 85% within 24

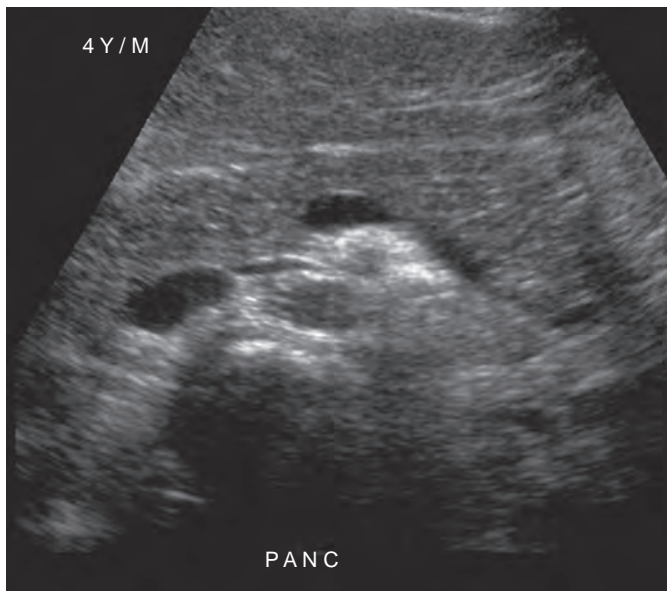


Figure 121-1 Normal pancreas. The transverse ultrasound image of the pancreas demonstrates pancreatic echogenicity similar to that of the adjacent liver.

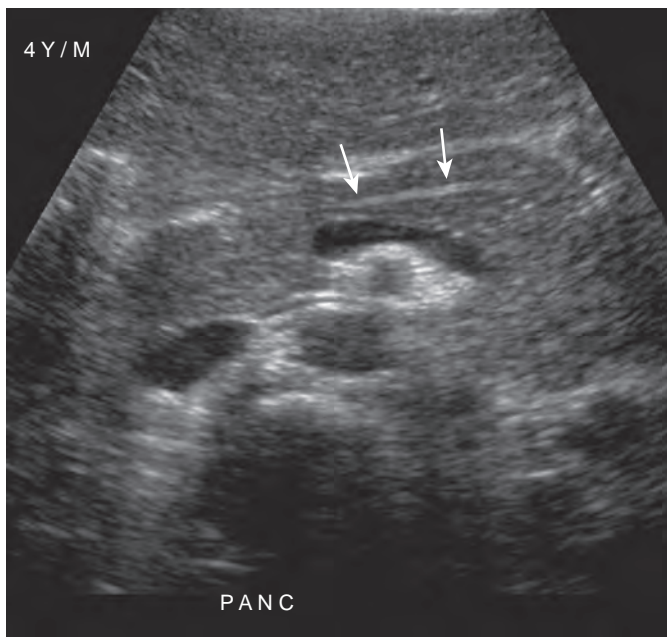


Figure 121-2 Normal pancreatic duct. The transverse sonographic image of the pancreas demonstrates parallel echogenic lines in the body of the pancreas consistent with a normal pancreatic duct (arrows).

hours of admission.¹² Admission CT findings may be normal in patients later proved to have pancreatic injury by repeated imaging or laparotomy.¹⁰ Early findings of pancreatic injury can be subtle, especially immediately after trauma.² Unlike other traumatized abdominal solid organs, the pancreas can have little change in attenuation with lacerations and fractures, making diagnosis difficult, particularly if there is no separation of the parenchymal fragments (Fig. 121-5).^{2,13}

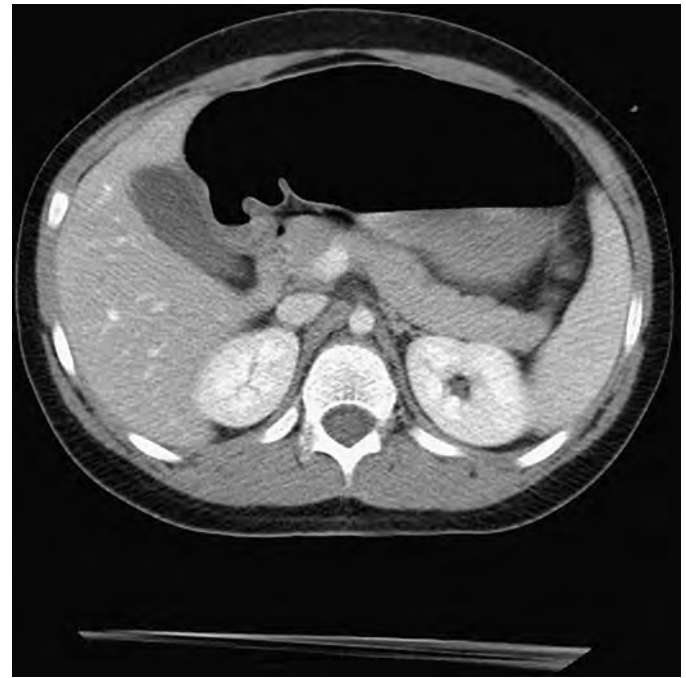


Figure 121-3 Normal pancreas. The contrast-enhanced CT scan demonstrates a normal pancreas with a gently lobulated surface in a 7-year-old girl. The attenuation of the pancreas is similar to that of the adjacent liver.

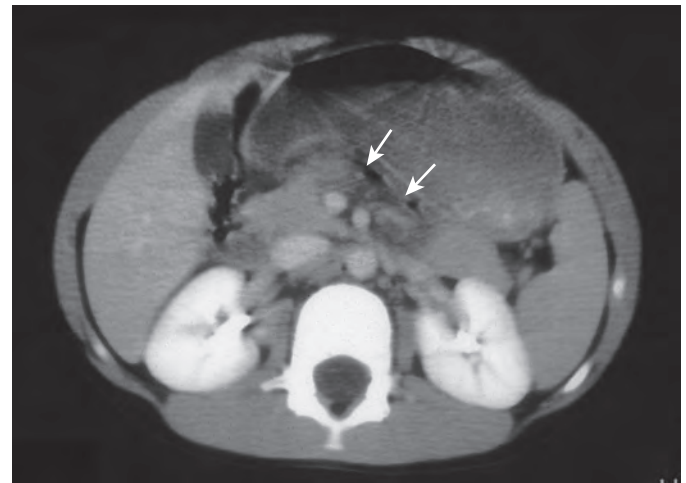


Figure 121-4 Pancreatic contusion. The CT scan through the pancreas reveals focal low attenuation in the body of the pancreas caused by contusion (arrows) in a young boy after abdominal trauma from a bicycle handlebar.

Pancreatic contusions or lacerations tend to occur at the junction of the body and tail of the pancreas.¹⁴ They are manifested as linear areas of low attenuation perpendicular to the long axis of the pancreas (Fig. 121-6),^{1,2,5} and there may be associated pancreatic edema and enlargement, pancreatic or duodenal hematoma, and pancreatic duct dilation.^{2,12} Peripancreatic fluid or fluid in the lesser sac is a useful marker for pancreatic injury, particularly in the absence of injury to other organs.¹ The failure to visualize a portion of the gland should suggest the diagnosis of pancreatic

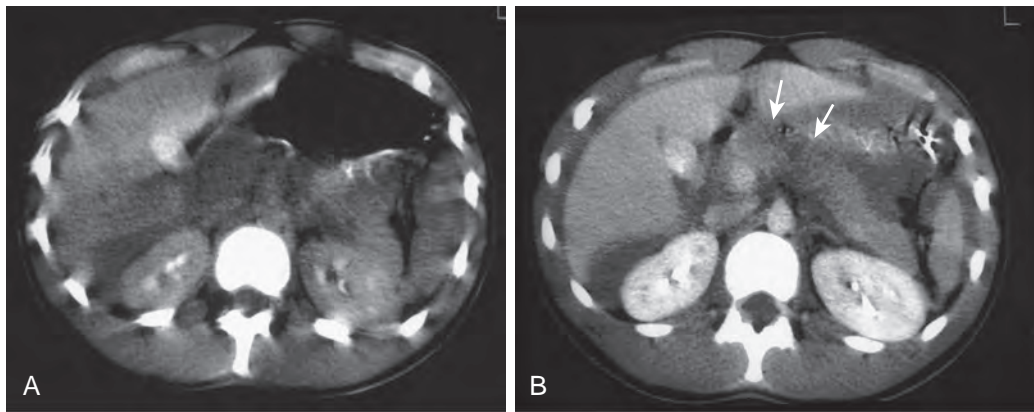


Figure 121-5 Pancreatic contusion. **A.** The CT scan through the upper abdomen of a young girl involved in a motor vehicle accident is limited by significant motion artifact. **B.** The repeated scan through the upper abdomen shows heterogeneous low attenuation in an enlarged pancreas that represents pancreatic contusion and edema (arrows). The patient also has moderate free intraperitoneal fluid.

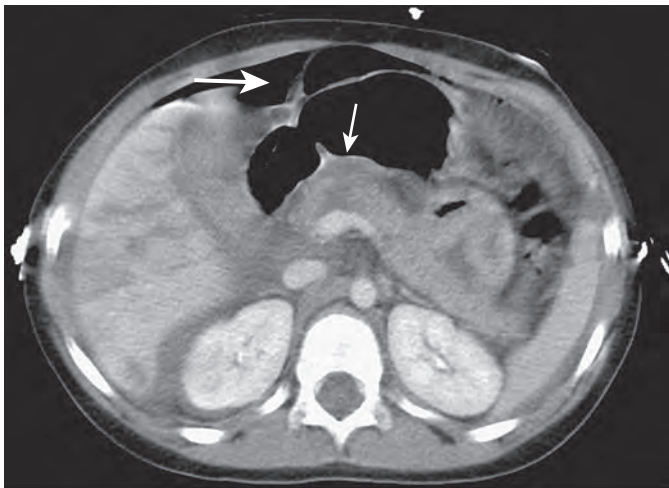


Figure 121-6 Pancreatic contusion. The CT scan through the upper abdomen of a 3-year-old boy after a motor vehicle accident shows focal low attenuation in the pancreatic head in the typical distribution anterior to the spine (small arrow). The patient also has free intraperitoneal air from a duodenal laceration (large arrow).

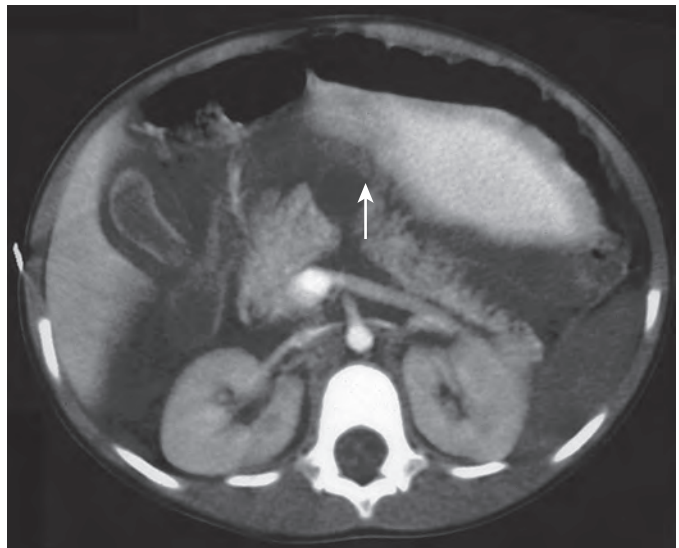


Figure 121-7 Pancreatic transection. The CT scan through the pancreas in a young child after nonaccidental trauma demonstrates complete pancreatic transection (arrow).

laceration.¹⁴ Complete pancreatic transection is rare (Fig. 121-7).¹⁴ Blunt trauma is the most common cause of acute pancreatitis in children.⁵ In the setting of post-traumatic acute pancreatitis in children, CT imaging can demonstrate the typical findings of acute pancreatitis. Pancreatic pseudocysts develop in approximately 40% of children with traumatic pancreatic injury, and approximately half of these resolve spontaneously.^{1,10}

ERCP, where it is available, can be used to assess for ductal injury if CT findings are equivocal. ERCP has the added benefit of potential intervention as well, with placement of a stent to treat pancreatic duct injury.¹⁵ The routine use of ERCP can also lead to more cases of pancreatic injury being treated nonoperatively.¹⁶

Once pancreatic injury is diagnosed, management depends on the severity and location of the injury and on the presence of associated intra-abdominal injuries.¹⁰ Most patients are treated nonoperatively with bowel rest and total parenteral

nutrition.¹⁷ The decision to intervene surgically is based on hemodynamic instability and the degree of spill of pancreatic fluid into the intraperitoneal or retroperitoneal space.¹⁸ Injury to the proximal pancreatic duct usually is treated conservatively with bowel rest, nasogastric decompression, and hyperalimentation. Transection of the distal pancreatic duct, however, may be treated with distal pancreatectomy with preservation of the spleen.^{10,19}

Abnormal pancreatic enhancement can be seen in the setting of hypoperfusion complex, a rare process seen in young children with hypovolemic shock. This complex tends to occur in those who suffer severe central nervous system or abdominal injury⁵ and have evidence of profound acidemia.²⁰ Imaging findings of hypoperfusion complex include “shock bowel,” with diffusely dilated, fluid-filled bowel with abnormal mural enhancement²; intense enhancement of the pancreas, kidneys, adrenal glands,⁵ and mesentery²; moderate to large intraperitoneal hematomas; and diminished caliber



Figure 121-8 Hypoperfusion complex. The CT scan through the pancreas in a teenager after a motor vehicle accident demonstrates findings of hypoperfusion complex, including intense enhancement of the pancreas and diminished calibers of the aorta and inferior vena cava.

of the abdominal aorta²⁰ and a slitlike inferior vena cava (Fig. 121-8).

Pancreatitis

ACUTE PANCREATITIS

Pancreatitis is an uncommon cause of abdominal pain in children. The clinical diagnosis of acute pancreatitis is based on the presence of upper abdominal pain and tenderness and evaluation of pancreatic enzymes. With a mortality rate⁵ for acute pancreatitis in children as high as 21% and protean clinical presentations, a high level of clinical suspicion is essential for prompt diagnosis.

The causes of acute pancreatitis in children differ significantly from those in adults. In adults, pancreatitis is associated with alcoholism and biliary tract disease in 80% of cases.²¹ The most common cause of acute pancreatitis in children is blunt abdominal trauma,²² followed by infection and drug use.²¹ Numerous drugs and toxins have been implicated in causing acute pancreatitis. The most commonly associated medication in children is the antiseizure drug valproic acid.²³ Infections causing acute pancreatitis in the pediatric population tend to be viral and include the mumps virus,¹⁴ coxsackievirus B, and varicella-zoster virus.²³ Fifteen percent of cases of acute pancreatitis in children are caused by structural anomalies.²⁴ These include congenital anomalies (e.g., pancreas divisum), Crohn's disease, and duodenal ulcers that involve the periampullary region.²⁵ Multisystemic disease, including vasculitis, lupus, sepsis, sickle cell disease, and hemolytic uremic syndrome, accounts for approximately 14% of cases of acute pancreatitis.²⁴ In cases of unexplained pancreatitis, diagnostic considerations, particularly in a young child, should include nonaccidental trauma, inborn errors of organic acid metabolism, hereditary pancreatitis, hemolytic uremic syndrome, and biliary tract disease.⁵ Other causes of pediatric pancreatitis are listed in Table 121-1. In up to 25% of cases, no cause is found.

Plain radiographs are not sensitive for detection of acute pancreatitis, but some reactive findings can be seen (Fig. 121-9). These include atelectasis, elevation of the hemidiaphragms,

TABLE
121-1

Causes of Pediatric Pancreatitis

Trauma

- Motor vehicle collision
- Nonaccidental trauma
- Bicycle handlebar injury

Drugs or toxins

- Antiseizure medications, particularly valproic acid
- Chemotherapeutic agents
- Steroids
- L-Asparaginase
- Acetaminophen
- Sulfasalazine
- Thiazides
- Furosemide

Infections

- Mumps
- Coxsackievirus B
- Varicella-zoster virus
- Ascariasis
- Escherichia coli*
- Fungal infection (immunosuppression)

Structural anomalies

- Pancreas divisum
- Choledochal cysts
- Intestinal duplication cysts
- Periampullary lesions, including Crohn's disease and duodenal ulcers

Metabolic disorders

- Cystic fibrosis
- Hypercalcemia
- Hyperlipidemia

Collagen-vascular diseases

- Lupus
- Vasculitis
- Hemolytic uremic syndrome

Sepsis

Shock

Sickle cell disease

Thalassemia

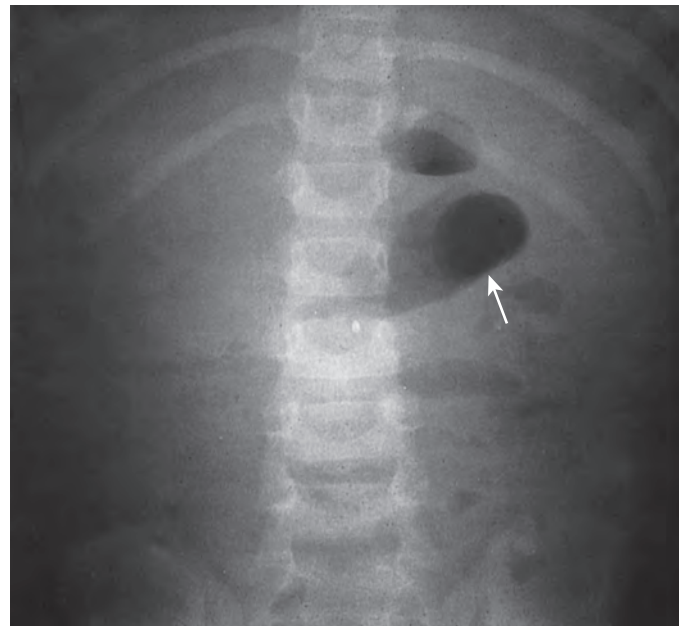


Figure 121-9 Sentinel loop. The anteroposterior radiograph shows focal dilation of a small bowel loop in the left upper abdomen (arrow), representing a localized ileus caused by peripancreatic inflammation in a 2-year-old boy with abusive traumatic pancreatitis.

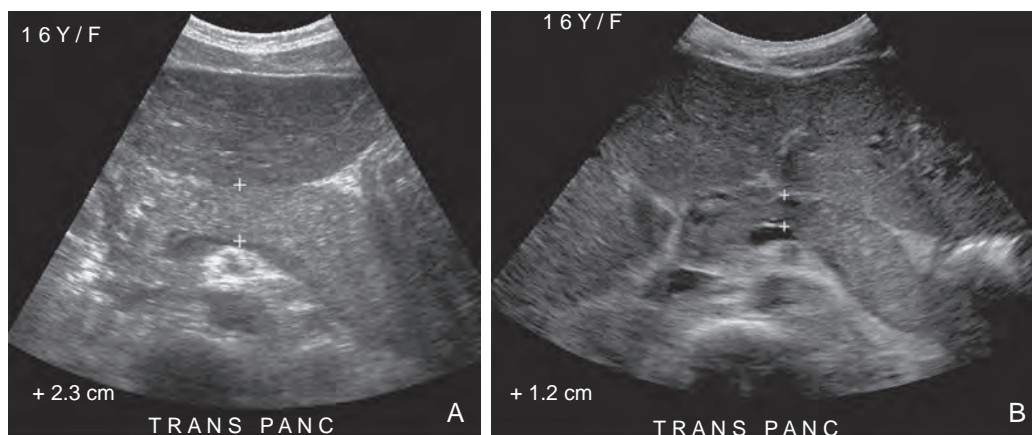


Figure 121-10 Acute pancreatitis. **A.** The transverse sonographic image through the pancreas shows a diffusely enlarged pancreas that is echogenic compared with the liver in a 17-year-old girl with a history of thrombotic thrombocytopenic purpura. **B.** Follow-up ultrasound of the same patient 2 weeks later demonstrates interval decrease in the size of the pancreas, with decreased echogenicity compared with the liver.

left pleural effusion, pericardial effusion, and pulmonary edema on chest radiographs.²¹ A sentinel loop in the left upper quadrant or diffuse small bowel ileus (see Fig. 121-9), a dilated transverse colon, or paucity of gas within the descending colon can be seen on abdominal radiographs. Additional findings may include mass effect from a pancreatic pseudocyst and peripancreatic extraluminal gas (if it is associated with an abscess).²¹

Ultrasound is usually the first imaging study performed for the evaluation of suspected pediatric pancreatitis.¹ Enlargement of the pancreas can be seen, either diffuse or focal, usually involving the head¹ (Fig. 121-10). However, there is a wide variation in pancreatic size in children, and there can be overlap between healthy patients and those with pancreatitis.³ The pancreatic echotexture can also become hypoechoic with acute pancreatitis,²¹ but increased echogenicity has also been described.² The most reliable finding in children appears to be dilation of the pancreatic duct.⁹ A dilated duct with poorly defined borders²⁶ can be seen in acute and chronic pancreatitis, with the duct diameter tending to be greater in patients with chronic pancreatitis. The duct diameter associated with pancreatitis is greater than 1.5 mm in children 1 to 6 years of age, greater than 1.9 mm in children 7 to 12 years of age, and greater than 2.2 mm at 13 to 18 years of age.⁶ In mild cases of pancreatitis, the pancreas can appear normal.² Other findings that can be seen on ultrasound include gallstones, biliary sludge, and intrahepatic or extrahepatic biliary ductal dilation.²⁵ Ascites and extrapancreatic fluid collections¹ are frequently observed. Ultrasound is also the modality of choice for follow-up of pancreatitis fluid collections.¹

CT is more sensitive than ultrasound to detect early findings of pancreatitis² and is best for evaluating the severity of pancreatitis and the potential for complications.²¹ CT evaluation of acute pancreatitis in pediatric patients demonstrates a spectrum of findings. These include diffuse gland enlargement with heterogeneous attenuation and enhancement; poorly defined pancreatic margins, peripancreatic fluid, and edema; and fat and soft tissue inflammation (Fig. 121-11).^{5,27} Areas of decreased attenuation and poor contrast enhancement indicate pancreatic necrosis and increased severity of pancreatitis.² A normal pancreas on initial imaging can be seen in up to one third of patients with acute pancreatitis.⁵



Figure 121-11 CT findings of acute pancreatitis. The CT scan shows diffuse enlargement of the pancreas with inflammation of the peripancreatic fat (arrows) in a 7-year-old boy who developed acute pancreatitis after therapy with asparaginase for acute lymphocytic leukemia.

Studies suggest an increasing role for MRI with MRCP in the evaluation of acute pancreatitis, especially given its lack of radiation and excellent soft tissue contrast. MRI may also be more sensitive for detection of acute pancreatitis compared with CT.⁷ MRI demonstrates an enlarged gland with abnormal signal intensity with surrounding inflammation and edema in acute pancreatitis. Specifically, there is loss of the normal intrinsic T1 hyperintensity of the gland and increased T2 signal due to the edema.⁷ MRCP can show congenital anomalies, such as pancreas divisum and abnormal junction of the pancreatobiliary junction, or biliary stones as the etiology of the acute pancreatitis.^{8,25}

ERCP is reserved for children with unexplained recurrent bouts of pancreatitis and patients with a prolonged course to exclude possible structural abnormalities or duct disruption.

ERCP may also be diagnostic and therapeutic in patients with gallstone pancreatitis.²⁵

Approximately half of pediatric patients with acute pancreatitis develop fluid collections outside the pancreas: acute pancreatic fluid, pseudocysts, and abscesses. Of all these, pseudocyst formation is the most common complication of pancreatitis.^{24,26} The most common locations for pseudocyst formation in children are the anterior pararenal space (71%), lesser sac (57%), lesser omentum (50%), and transverse mesocolon.²⁷ Less than 10% of pseudocysts occur within the pancreatic parenchyma in children.²⁸ Pseudocysts with a diameter of less than 10 cm tend to resolve spontaneously. Drainage has been suggested for pseudocysts with a diameter greater than 10 cm or for those less than 10 cm in diameter that do not resolve after 6 weeks.¹⁸ A persistent fluid collection should raise the suspicion of an underlying structural abnormality,²⁷ and further evaluation of the pancreatic duct may be necessary.⁵ Pseudocysts typically are homogeneous in appearance, with an attenuation approaching that of water (Fig. 121-12), unless they are complicated by hemorrhage or infection.¹⁴ Abscesses usually occur more than 4 weeks after the onset of pancreatitis⁵ and can develop from acute pancreatic fluid collections and pseudocysts.

CHRONIC PANCREATITIS

Chronic pancreatitis consists of progressive, irreversible pancreatic destruction due to recurrent pancreatic inflammation that produces fibrosis, fatty degeneration, or calcium deposits.²⁶ It is thought that susceptibility to chronic pancreatitis is influenced by genetic and environmental factors.²⁵ The most common cause worldwide is juvenile tropical pancreatitis, which is associated with pure protein malnutrition and occurs in equatorial, Third World countries.⁵ In the United States, the most common causes are hereditary pancreatitis and cystic fibrosis.²⁵ Hereditary pancreatitis is defined by recurrent attacks of pancreatitis¹⁴ that occur in families during two or more generations without other known predisposing factors.²¹ Most commonly seen in

white children, it is inherited in an autosomal dominant fashion with variable penetrance (40%-80%).¹⁴ The median age at presentation is 10 years.²⁵ Approximately half of the patients develop chronic pancreatitis 10 years after the first bout of acute pancreatitis.²⁵ Complications occur more frequently in patients with hereditary pancreatitis than in those with nonhereditary chronic pancreatitis.²¹ Less common causes include steroid therapy, hyperparathyroidism, pancreas divisum,¹⁴ hypercalcemia,²³ and malnutrition.²⁶

Patients with chronic pancreatitis have chronic, midepigastri abdominal pain.⁵ Pancreatic insufficiency with diabetes is a late-stage complication, occurring when there is less than 10% of residual pancreatic function.^{5,23} Chronic pancreatitis demonstrates increased pancreatic echogenicity sonographically. Irregular contours, with intraparenchymal calcifications and pancreatic duct dilation (Fig. 121-13), are commonly seen.²⁶ CT better characterizes the parenchymal atrophy, duct dilation, and calcifications (Fig. 121-14).⁵ Complications of chronic pancreatitis include recurrent bouts of acute pancreatitis, pseudocyst formation, and increased risk for pancreatic adenocarcinoma.¹⁴ Other major complications include diabetes mellitus, ascites, pleural effusions, portal hypertension, thrombosis of the portal and splenic veins, and exocrine pancreatic insufficiency.²¹

Cystic Fibrosis

Cystic fibrosis is the most common lethal recessive genetic trait in white individuals,² with an incidence of 1 case in 2500 live births.²⁹ Inherited in an autosomal recessive fashion,⁵ cystic fibrosis is a multisystemic disease caused by a variety of mutations in the cystic fibrosis transmembrane conductance regulator (CFTR) gene.³⁰ The defective gene causes abnormal chloride transport across the membrane of epithelial cells that express CFTR, resulting in abnormally thick exocrine gland secretions that typically affect the lungs, pancreas, and liver²⁶ and also the paranasal sinuses and reproductive tract.²⁹ Although lung

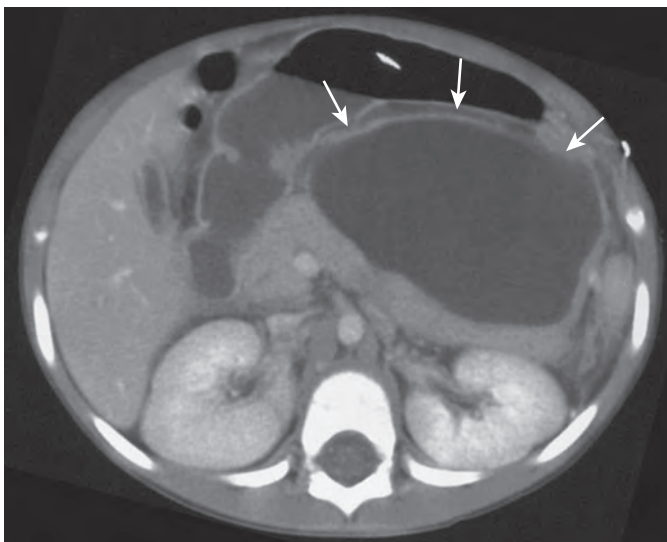


Figure 121-12 Pancreatic pseudocyst. The CT scan through the pancreas shows a large cystic fluid collection in the midabdomen with a mass effect on the stomach that represents a pseudocyst (arrows) in a young patient with a history of pancreatitis.

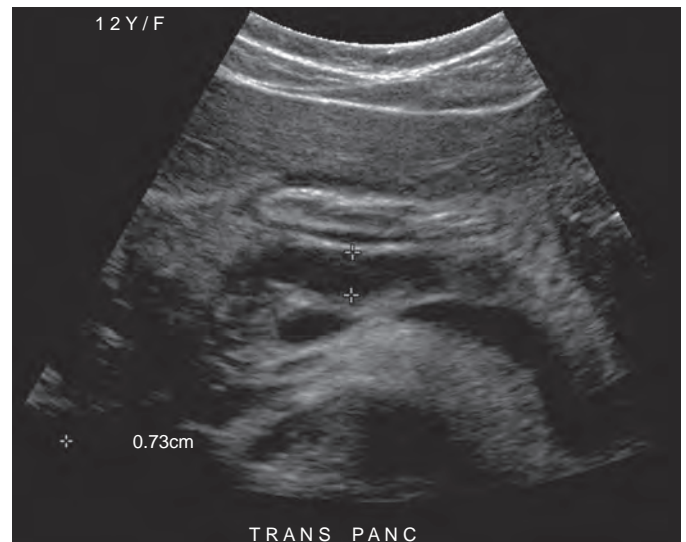


Figure 121-13 Chronic pancreatitis. The transverse sonographic image of the pancreas reveals dilation of the main pancreatic duct in a 12-year-old girl with chronic pancreatitis.

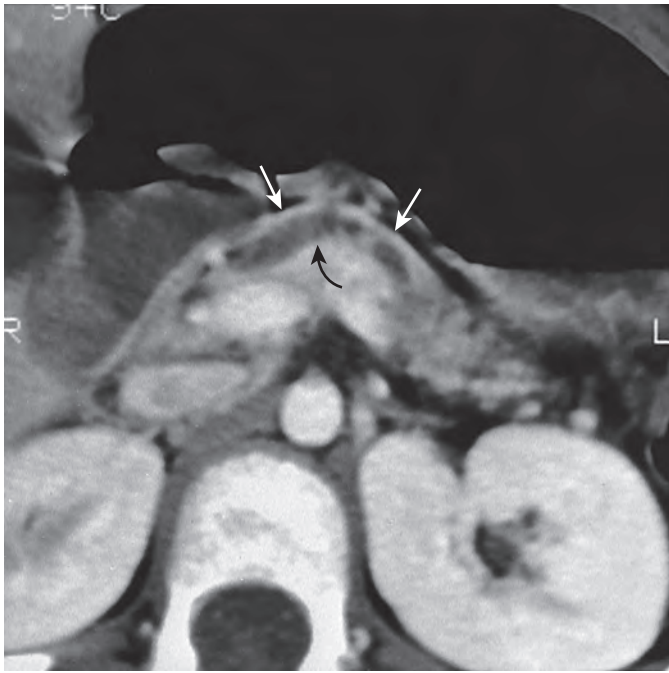


Figure 121-14 CT findings of chronic pancreatitis. CT demonstrates thinning of the pancreatic parenchyma (straight arrows) with dilation of the pancreatic duct (curved arrow) in a 5-year-old girl with chronic pancreatitis.

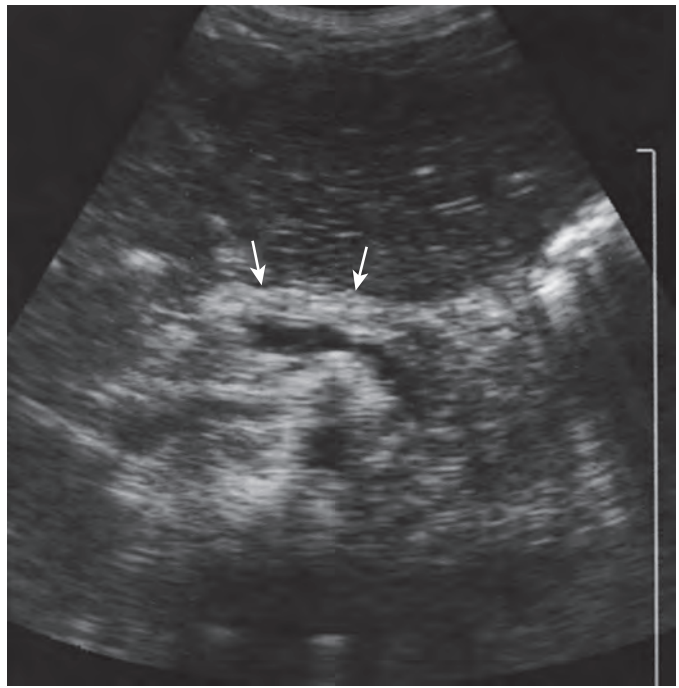


Figure 121-15 Ultrasound findings of the pancreas in cystic fibrosis. Transverse ultrasound shows the pancreas to be thin and markedly echogenic as a result of atrophy and fat infiltration (arrows) in a 7-year-old boy with cystic fibrosis.

disease is the leading cause of morbidity and mortality in persons with cystic fibrosis,³¹ improved treatment of lung disease has resulted in longer survival and increased morbidity from involvement of other organs,²⁹ including the pancreas.

The tenacious pancreatic secretions of cystic fibrosis cause obstruction of pancreatic ducts with upstream acinar and ductal distention and end-stage atrophy of acinar tissue.⁵ If it is severe enough, the degeneration eventually results in replacement of pancreatic parenchyma with fibrosis and fat.^{5,26} Cystic fibrosis is responsible for 85% to 90% of exocrine pancreatic insufficiency in children.² It occurs at or soon after birth as a result of chronic obstruction.³⁰ Only 10% to 15% of patients maintain enough pancreatic function to avoid steatorrhea. Endocrine dysfunction in cystic fibrosis is less common, with 30% to 50% of cystic fibrosis patients demonstrating glucose intolerance and 13% of adult patients having diabetes.³¹

Several patterns of pancreatic changes have been described in cystic fibrosis: complete replacement of the pancreas by fibrofatty tissue with enlargement of the pancreas, partial replacement of the pancreas by fibrofatty tissue, complete pancreatic atrophy without fatty replacement, diffuse pancreatic fibrosis, and cystic transformation of the pancreas.²⁹ Pancreatic calcifications and small pancreatic cysts that do not exceed several millimeters in diameter are not uncommon imaging features in cystic fibrosis.²⁹ Pancreatic cystosis is a usual complication of cystic fibrosis, with larger cysts distributed throughout the gland.²⁹ These true cysts are caused by obstruction of pancreatic ducts by tenacious secretions, resulting in upstream dilation.²⁹ Pancreatic calcifications are typically seen in dilated pancreatic ducts after ductal and ductular obstruction by calcium-rich inspissated material.³² Although cystic fibrosis is one of the most common causes of chronic pancreatitis, acute

pancreatitis is not a common manifestation because there is generally not enough functioning residual pancreatic tissue to mount the inflammatory reaction.^{5,25} Acute pancreatitis should be suspected, however, if there is enlargement of the pancreatic head.¹

The sonographic findings of cystic fibrosis include increased pancreatic echogenicity due to fatty replacement and decreased pancreatic size due to pancreatic atrophy (Fig. 121-15).²⁹ Other findings can include calcifications and single or multiple cysts.² In the setting of pancreatic cystosis, multiple anechoic lesions are seen with smooth, thin walls without nodules and enhanced through-transmission.

CT evaluation of the pancreas in patients with cystic fibrosis demonstrates diffuse, low attenuation throughout an enlarged pancreas, consistent with fatty replacement (Fig. 121-16). When complete atrophy is present, it is seen as a small pancreas with soft tissue attenuation and with no enhancement after administration of contrast material.²⁹ Other findings may include parenchymal calcifications and the cysts of pancreatic cystosis.²

MRI demonstrates complete fatty replacement of the pancreas, which is manifested as an enlarged pancreas with high signal intensity on T1-weighted images. Fibrosis of the pancreas is seen as low signal intensity on T1- and T2-weighted images, without the high signal intensity of fat on T1-weighted images.^{29,32} A disadvantage of pancreatic MRI is the inability to reliably demonstrate small calcifications.²⁸ On MRCP, the main pancreatic duct usually is not well delineated in cystic fibrosis because of pancreatic duct narrowing.³² When cysts are present, they have low signal intensity on T1-weighted images and high signal intensity on T2-weighted images with thin, smooth walls that have low signal intensity.²⁹

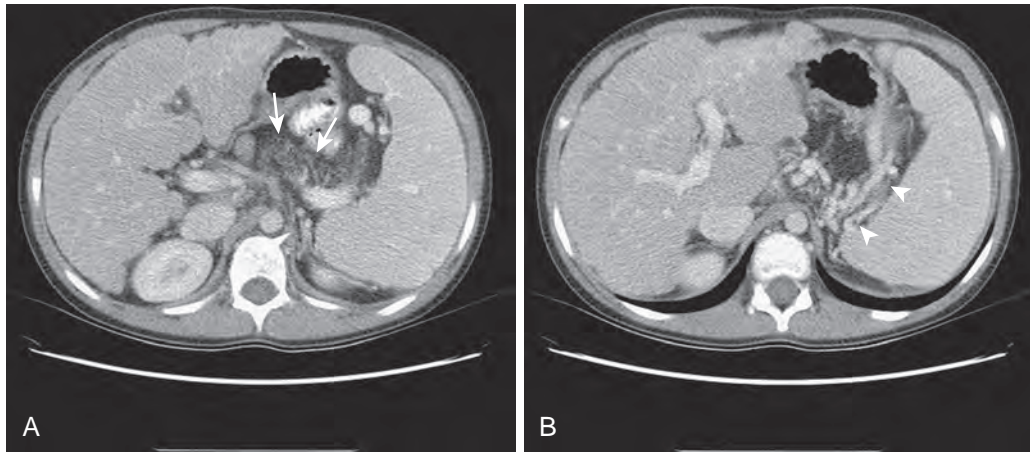


Figure 121-16 CT findings of the pancreas in cystic fibrosis. **A** and **B**. CT demonstrates fatty replacement of the pancreas (arrows) in a teenaged girl. The patient also has a nodular liver from hepatic fibrosis and has splenic varices (arrowheads) and splenomegaly from portal hypertension.

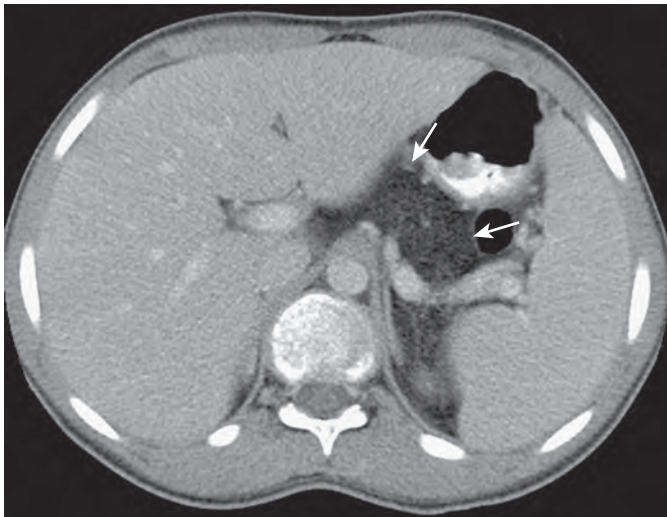


Figure 121-17 Shwachman-Diamond syndrome. CT shows the loss of pancreatic parenchyma from atrophy and infiltration of the pancreas by fat (arrows) in a young boy with Shwachman-Diamond syndrome.

Shwachman-Diamond Syndrome

Shwachman-Diamond syndrome is the second most common cause of exocrine pancreatic insufficiency in childhood after cystic fibrosis, with a clinical spectrum from mild to nearly complete absence of exocrine function.³³ It is inherited in an autosomal recessive fashion, and other associated manifestations include skeletal and bone marrow abnormalities. These patients have exocrine pancreatic insufficiency with a normal sweat test result,³⁴ allowing the syndrome to be distinguished from cystic fibrosis.⁵ Clinically, patients with Shwachman-Diamond syndrome present with steatorrhea during infancy.²¹ Unlike with cystic fibrosis, the clinical condition of patients with Shwachman-Diamond syndrome tends to improve with age.⁵ On pathologic examination, there is fatty infiltration of the pancreas with reduction of the acini, but the islets and ducts are preserved^{1,21,34} (Fig. 121-17).³³ Initially, the pancreas may be enlarged, but the size later becomes normal or slightly small.¹⁴

Patients may demonstrate hepatomegaly or splenomegaly, which may be caused by infection or malnutrition.³³ Pancreatic calcifications and cysts are not associated with Shwachman-Diamond syndrome, which distinguishes this disease from cystic fibrosis.⁵

Nesidioblastosis

Nesidioblastosis, also known as persistent hyperinsulinemic hypoglycemia of neonates and infants and as diffuse adenomatosis, is a congenital anomaly characterized by persistence of the fetal state of the pancreas. On pathologic examination, there is proliferation and persistence of nesidioblasts, cells that differentiate from ductal epithelium.²⁶ These nesidioblasts produce insulin, and patients present with symptoms of hypoglycemia, usually detected in the newborn and infant stage.^{1,26} Diagnosis of nesidioblastosis is made by the persistence of symptomatic hypoglycemia with inappropriately high levels of insulin and with the inappropriate response to intravenous glucagon.³⁵ The diagnosis can also be made by selective venous sampling in pancreatic veins, evaluating for elevated insulin levels.³⁶ Two forms have been identified, one with focal adenomatous hyperplasia and the second with diffuse B-cell abnormalities.³⁶ Ultrasound of the pancreas sometimes demonstrates diffuse increased echogenicity and increased size of the pancreatic head, body, and tail in the diffuse form. The lesions in the focal form are not well visualized radiologically.³⁶ Nearly total pancreatectomy is necessary in the setting of persistent hypoglycemia with the diffuse form; with the focal form, only that particular lesion needs to be resected.³⁷

Pancreatic Masses

CONGENITAL CYSTS

True congenital cysts of the pancreas are rare and are the result of anomalous development of the pancreatic ducts.^{26,38} During prenatal ultrasound scanning, the cysts may be manifested incidentally or may be associated with polyhydramnios. Postnatally, the cysts can be diagnosed at any age.¹ Patients are usually asymptomatic, and the cysts are found incidentally.³⁸ There is a

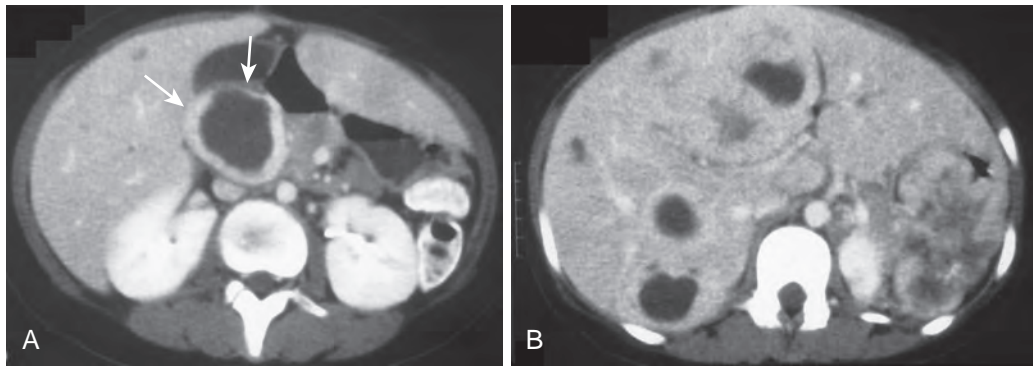


Figure 121-18 Pancreatoblastoma. **A.** CT demonstrates a large, well-defined mass in the head of the pancreas (arrows) of a young boy with pancreatoblastoma. **B.** CT scan through the liver demonstrates multiple, heterogeneous masses within the hepatic parenchyma consistent with metastatic disease.

female predominance.³⁸ Congenital pancreatic cysts have an epithelial lining, are usually singular and unilocular, and are typically located in the body or tail of the pancreas.^{5,38} Communication with the pancreatic duct is rare.³⁸ On sonography, congenital pancreatic cysts usually are anechoic and may range in size from microscopic up to 5 cm in diameter. On CT, the cysts generally have low attenuation and demonstrate no mural enhancement.³⁸ When they are multiple, congenital cysts may be seen in association with a variety of syndromes, including Beckwith-Wiedemann syndrome, autosomal dominant polycystic kidney disease (ADPKD), and von Hippel–Lindau disease (VHL).²⁶

NEOPLASMS

Tumors of the pediatric pancreas are extremely rare. They are classified as epithelial or nonepithelial in origin; the epithelial tumors are further subdivided into exocrine and endocrine tumors.³⁷ In the pediatric population, the most common exocrine tumors are pancreatoblastoma and adenocarcinoma. Endocrine tumors can be hormonally functioning or nonfunctioning. Mesenchymal tumors of the pediatric pancreas are even rarer.

Exocrine Tumors of the Pancreas

Pancreatoblastoma. Pancreatoblastoma, also known as infantile carcinoma of the pancreas, is the most common pancreatic neoplasm of childhood.²⁸ This rare epithelial tumor,¹⁴ which is often misdiagnosed as neuroblastoma or hepatoblastoma,⁵ has a 2:1 male-to-female ratio.^{2,28} The mean age at diagnosis is 4 years, but it can be manifested at any time from the newborn period to adulthood.² It is associated with Beckwith-Wiedemann syndrome^{2,28} and has an increased incidence in East Asia.² Patients usually present with abdominal distention or with a large, palpable abdominal mass. The mass may be associated with nonspecific symptoms, including failure to thrive, epigastric pain, anorexia, vomiting, diarrhea, and weight loss.²⁸ Obstructive jaundice may also be present. The serum α -fetoprotein level is elevated in 25% to 55% of patients, and the tumor may secrete adrenocorticotrophic hormone.^{2,39}

Pancreatoblastoma can be located anywhere in the pancreas; it may be exophytic or may entirely replace the pancreas.²⁸ The mass tends to be large at the time of presentation, with a diameter of 7 to 18 cm. It is usually solitary, well defined, and surrounded by a fibrous capsule.^{14,28} Metastases are most

commonly seen in the liver but may also occur in regional lymph nodes, lungs, and, rarely, bone.³⁹ Local invasion of the bowel and peritoneal cavity as well as of adjacent structures like the spleen, kidney, and adrenal gland can also occur.^{28,39} When metastatic disease is present, the prognosis is typically poor.²

In general, imaging demonstrates a solid mass with an appearance suggestive of but not specific for pancreatoblastoma.¹ The pancreatoblastoma usually is large and well defined, and it may be lobulated.⁵ Sonography demonstrates a well-demarcated, heterogeneous mass with both solid and cystic components.³⁷ A predominantly hypoechoic solid mass may also be seen.³⁹ CT usually demonstrates a mass with heterogeneous contrast enhancement and areas of low attenuation, suggestive of cystic necrosis (Fig. 121-18).³⁹ Metastases to the liver tend to be hypodense and may also contain areas of central necrosis.³⁹ On MRI, pancreatoblastoma is low to intermediate signal intensity on T1-weighted images and high signal intensity on T2-weighted images.³⁷ Vascular encasement of the mesenteric vessels and the inferior vena cava may develop, and calcifications can be present, which may make differentiation from neuroblastoma difficult.³⁹

Given the nonspecific imaging findings of pancreatoblastoma, the diagnosis is generally established by percutaneous biopsy.¹ Treatment consists of surgical excision, with chemotherapy administered for metastatic disease.²⁸ Radiation therapy is used for local recurrence or incomplete resection.^{1,40} Although some patients are cured with excision alone, recurrence has been described in up to 60% of patients.⁴⁰

Adenocarcinoma. Adenocarcinomas, both the ductal and acinar types, are extremely rare in children. Of these, the acinar type is more frequently seen in children and is pathologically related to pancreatoblastoma.³⁷ The mass can occur anywhere in the pancreas and tends to be manifested with symptoms related to local tumor expansion or metastases.² Metastases are commonly present at the time of diagnosis.²⁶ Imaging demonstrates a well-circumscribed, nodular mass with areas of necrosis.² On sonography, the mass is usually cystic or has mixed solid and cystic components.²⁶ CT imaging demonstrates hemorrhagic and cystic areas with heterogeneous enhancement.⁵ Calcification can also be seen.

The ductal type typically occurs in adults but has been reported in teenaged patients.²⁸ It is most commonly located in the head of the pancreas. Patients present with pain and weight loss, and more than half have obstructive jaundice. Imaging

demonstrates a small hypovascular mass, often with dilation of the main pancreatic duct and common bile duct proximal to the mass.²

Endocrine Tumors of the Pancreas

Islet Cell Tumors. Islet cell tumors can be classified as functioning or nonfunctioning endocrine tumors.² If they are functioning, islet cell tumors are associated with hypoglycemia (insulinoma) or Zollinger-Ellison syndrome (gastrinoma); ACTHomas and VIPomas are less common in children.³⁷ Nonfunctioning islet cell carcinoma is much more common in the pediatric population than in adults and usually is manifested as an abdominal mass. Metastases are common at presentation because of the delay in diagnosis of this nonfunctioning tumor.²⁸

METASTATIC DISEASE

Metastatic disease to the pancreas is more common than primary pancreatic neoplasms in the pediatric population. Burkitt's lymphoma is the most common cause of metastases (Fig. 121-19). The mean age at the time of presentation is 11 years, and the clinical picture is nonspecific.²⁶ Sonographic evaluation may demonstrate a solitary lesion, diffuse infiltration of the pancreas, or multiple lesions, which usually are solid, well defined, and hypoechoic.²⁶ Metastases can also be seen from other malignant neoplasms, including primitive neuroectodermal tumor, Kaposi's sarcoma, and neuroblastoma. Neuroblastoma usually involves the pancreas through lymphatic spread or by direct invasion.⁵

Miscellaneous Processes

VON HIPPEL-LINDAU DISEASE

VHLD is an autosomal dominant disorder with variable penetrance (80%-100%)^{41,42} and variable delayed expressivity; it

usually becomes clinically apparent in the second or third decade.⁵ The clinical manifestations of VHLD are broad and include both benign and malignant lesions in multiple organ systems; the most common manifestations are pancreatic cysts and tumors, renal cysts and clear cell carcinomas, retinal and cerebellar hemangioblastomas, and pheochromocytomas.⁴³ Renal cysts are the most common abdominal lesions of VHLD, seen in approximately 76% of patients.⁴⁴ These cysts can range from single to innumerable, simulating polycystic kidney disease.⁴¹

Cysts, which range from the typical simple pancreatic cyst⁴⁴ to cystic replacement of the pancreas, are the most common pancreatic lesion of VHLD.⁴¹ Cysts have been described in 30% to 50% of VHLD patients on imaging in some series,^{5,44} and an autopsy series described these cysts in approximately 72% of patients with known VHLD.⁴⁴ The cysts tend to occur in the body and tail of the pancreas⁵ (Figs. 121-20 and 121-21) and typically are small. Diabetes has been described in patients with extensive cystic replacement of the pancreas,⁴⁴ and large cysts may cause obstruction of the common bile duct.¹⁴ Other lesions involving the pancreas in VHLD include nonfunctioning islet cell tumors,⁴⁴ hemangioblastomas,⁴¹ serous cystadenoma (i.e., microcystic adenoma), and adenocarcinoma of the ampulla of Vater.^{2,42} Pancreatic carcinoma has been described in families with VHLD and may be a source of mortality in some families.⁴⁴

BECKWITH-WIEDEMANN SYNDROME

Beckwith-Wiedemann syndrome is a rare disorder characterized by the classic triad of omphalocele, macroglossia, and gigantism. Although it can be familial, with autosomal dominant inheritance, variable expressivity, and reduced penetrance, most cases are sporadic.⁴⁵ Patients may demonstrate hemihypertrophy and various degrees of visceromegaly of the kidneys, liver, pancreas, and adrenal glands (Fig. 121-22).² Cysts have also been reported in the kidneys and rarely in the adrenals.⁴⁵ Patients are also at increased risk for development of malignant neoplasms.⁴⁵

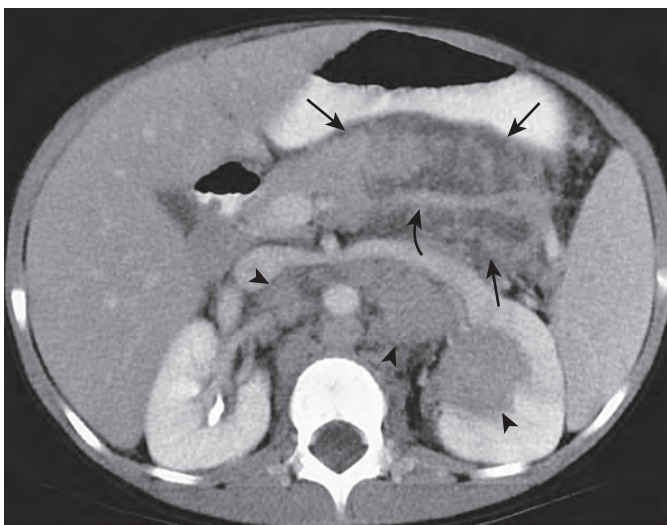


Figure 121-19 Lymphoma infiltrating the pancreas. The CT scan shows enlargement of the pancreas with infiltration by nodular soft tissue representing nodal enlargement (straight arrows) in a 7-year-old boy with Hodgkin's lymphoma. Notice the blood vessel (curved arrow) coursing through this region and the retroperitoneal adenopathy extending into the left renal hilum (arrowheads).

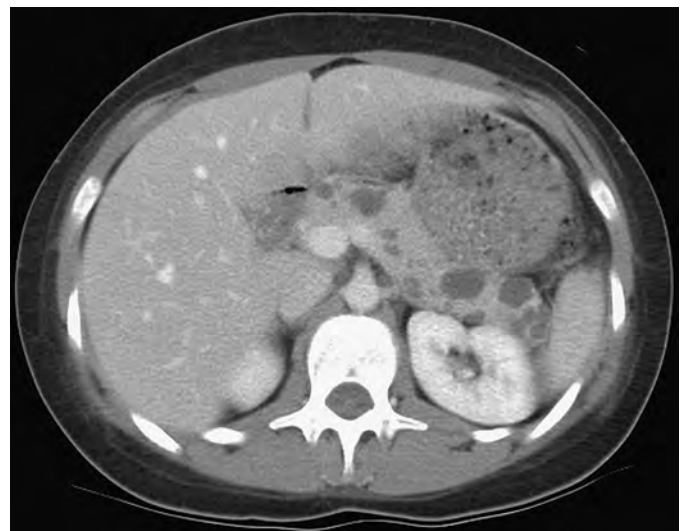


Figure 121-20 Pancreatic cysts in von Hippel-Lindau disease. The CT scan demonstrates numerous, small cysts within the pancreas in a young woman with von Hippel-Lindau disease.

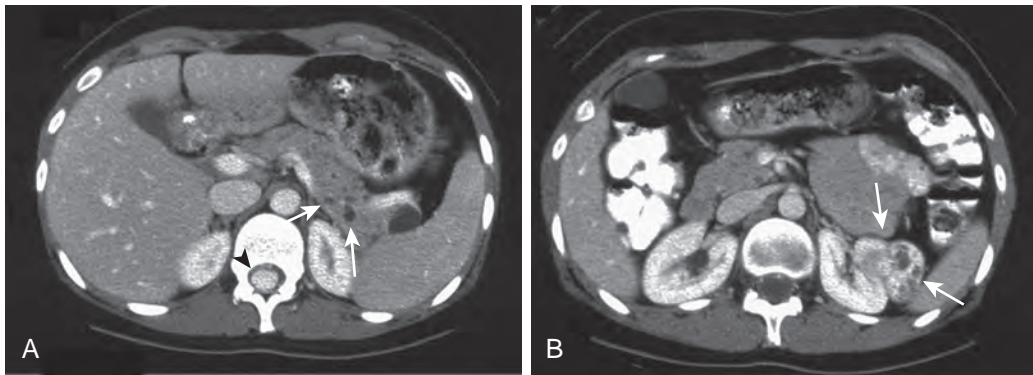


Figure 121-21 von Hippel–Lindau disease. **A.** CT scan through the pancreas demonstrates small cysts within the tail of the pancreas (arrows) in a young woman with von Hippel–Lindau disease. A hyperenhancing mass within the spinal canal is consistent with a hemangioblastoma (arrowhead). **B.** CT scan through the level of the kidneys demonstrates a heterogeneous mass within the left kidney consistent with a renal cell carcinoma (arrows).

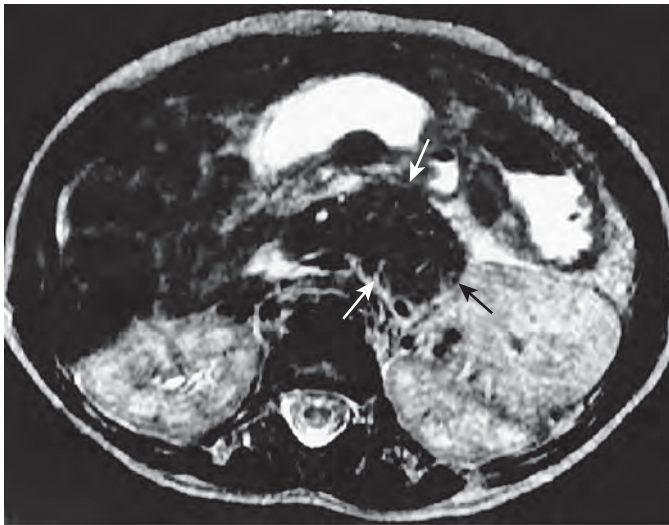


Figure 121-22 Pancreatic enlargement in Beckwith-Wiedemann syndrome. Axial-view, turbo T2-weighted MRI shows diffuse enlargement of the pancreas (arrows), which has normal signal intensity, in a 19-month-old girl with Beckwith-Wiedemann syndrome being observed for hepatoblastoma.

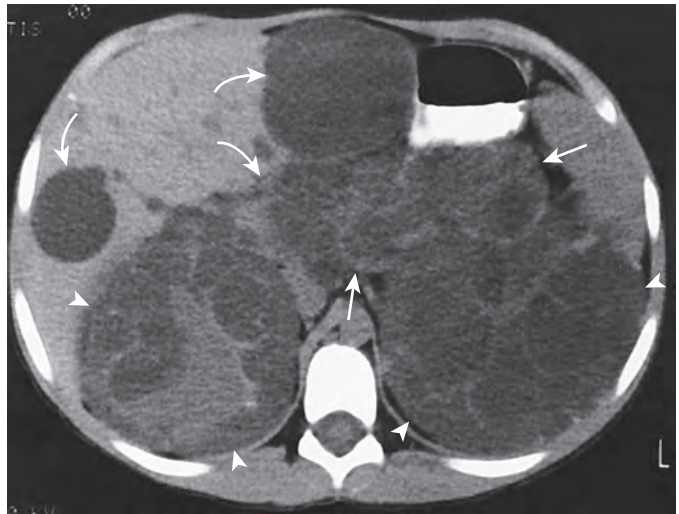


Figure 121-23 Pancreatic cysts in autosomal dominant polycystic kidney disease. The CT scan shows a pancreas (straight arrows) that is nearly replaced by large cysts in a 12-year-old boy with autosomal dominant polycystic kidney disease. The cysts also are demonstrated in the liver (curved arrows), and both kidneys are enlarged and contain many cysts (arrowheads).

Beckwith-Wiedemann syndrome is associated with a high risk of neonatal hypoglycemia.⁴⁵ Hypoglycemia often occurs in the first few days of life, and if it is severe enough, it may cause mental retardation.⁴⁵ Long-term prognosis depends on the occurrence of neoplasms, which are usually intra-abdominal.⁴⁶ Associated malignant neoplasms include Wilms' tumor⁴⁵ and pancreatoblastoma.²

Findings suggestive of Beckwith-Wiedemann syndrome on prenatal ultrasound include fetal macrosomia and anterior abdominal wall defects, most commonly omphalocele, hepatomegaly, nephromegaly, and macroglossia.⁴⁵ Because of the increased risk of intra-abdominal malignant neoplasms, routine abdominal ultrasounds are recommended at least every 4 months until the age of 7 or 8 years.⁴⁷

AUTOSOMAL DOMINANT POLYCYSTIC KIDNEY DISEASE

ADPKD is an autosomal dominant disorder with nearly 100% penetrance. Although renal cysts are the dominant feature, cysts can be seen in additional abdominal organs, including the pancreas, liver, spleen, and adrenal glands.² Pancreatic cysts occur in approximately 10% of patients with ADPKD,² and when pancreatic cysts are present, renal cysts usually are present.⁵ Sonography and CT usually demonstrate simple cysts, which can be multiple, are usually small, and may be present anywhere in the gland.⁴⁸ The cystic changes are typically not as severe as those involving the kidneys or liver, but cystic transformation of the pancreas has been described (Fig. 121-23).^{26,49}

REFERENCES

- Enriquez G, Vazquez E, Aso C, et al: Pediatric pancreas: An overview. *Eur Radiol* 8:1236–1244, 1998.
- Nijs E, Callahan MJ, Taylor GA: Disorders of the pediatric pancreas: Imaging features. *Pediatr Radiol* 35:358–373, 2005.
- Siegel MJ, Martin KW, Worthington JL: Normal and abnormal pancreas in children: US studies. *Radiology* 165:15–18, 1987.
- Walsh E, Cramer B, Pushpanathan C: Pancreatic echogenicity in premature and newborn infants. *Pediatr Radiol* 20:323–325, 1990.
- Vaughn DD, Jabra AA, Fishman EK: Pancreatic disease in children and young adults: Evaluation with CT. *Radiographics* 18:1171–1187, 1998.
- Chao HC, Lin SJ, Kong MS, Luo CC: Sonographic evaluation of the pancreatic duct in normal children and children with pancreatitis. *J Ultrasound Med* 19:757–763, 2000.
- Thai TC, Riherd DM, Rust KR: MRI manifestations of pancreatic disease, especially pancreatitis, in the pediatric population. *AJR Am J Roentgenol* 201:W877–W892, 2013.
- Egbert ND, Bloom DA, Dillman JR: Magnetic resonance imaging of the pediatric pancreaticobiliary system. *Magn Reson Imaging Clin N Am* 21:681–696, 2013.
- Darge K, Anupindi S: Pancreatitis and the role of US, MRCP and ERCP. *Pediatr Radiol* 39(Suppl 2):S153–S157, 2009.
- Maeda K, Ono S, Baba K, et al: Management of blunt pancreatic trauma in children. *Pediatr Surg Int* 29:1019–1022, 2013.
- Houben CH, Ade-Ajayi N, Patel S, et al: Traumatic pancreatic duct injury in children: Minimally invasive approach to management. *J Pediatr Surg* 42:629–635, 2007.
- Arkovitz MS, Johnson N, Garcia VF: Pancreatic trauma in children: Mechanisms of injury. *J Trauma* 42:49–53, 1997.
- Sheybani EF, Gonzalez-Araiza G, Kousari YM, et al: Pediatric nonaccidental abdominal trauma: What the radiologist should know. *Radiographics* 34:139–153, 2014.
- Herman TE, Siegel MJ: CT of the pancreas in children. *AJR Am J Roentgenol* 157:375–379, 1991.
- Wood JH, Partrick DA, Bruny JL, et al: Operative vs nonoperative management of blunt pancreatic trauma in children. *J Pediatr Surg* 45:401–406, 2010.
- Maeda K, Ono S, Baba K, Kawahara I: Management of blunt pancreatic trauma in children. *Pediatr Surg Int* 29:1019–1022, 2013.
- Mattix KD, Tataria M, Holmes J, et al: Pediatric pancreatic trauma: Predictors of nonoperative management failure and associated outcomes. *J Pediatr Surg* 42:340–344, 2007.
- Kouchi K, Tanabe M, Yoshida H, et al: Nonoperative management of blunt pancreatic injury in childhood. *J Pediatr Surg* 34:1736–1739, 1999.
- Reynolds EM, Curnow AJ: Laparoscopic distal pancreatectomy for traumatic pancreatic transection. *J Pediatr Surg* 38:E7–E9, 2003.
- Taylor GA, Fallat ME, Eichelberger MR: Hypovolemic shock in children: Abdominal CT manifestations. *Radiology* 164:479–481, 1987.
- Lerner A, Branski D, Lebenthal E: Pancreatic diseases in children. *Pediatr Clin North Am* 43:125–156, 1996.
- Coffey MJ, Nightingale, Ooi CY: Diagnosing acute pancreatitis in children. *Pancreatol* 14:251–256, 2014.
- Brown A: Pediatric acute pancreatitis—deciphering the black box. *J Clin Gastroenterol* 37:100–102, 2003.
- Gómez Beltrán O, Roldán Molleja L, Garrido Pérez JJ, et al: Acute pancreatitis in children. *Cir Pediatr* 26:21–24, 2013.
- Mekitarian Filho E, Carvalho WB, Silva FD: Acute pancreatitis in pediatrics: A systematic review of the literature. *J Pediatr (Rio J)* 88:101–114, 2012.
- Berrocal T, Prieto C, Pastor I, et al: Sonography of pancreatic disease in infants and children. *Radiographics* 15:301–313, 1995.
- King LR, Siegel MJ, Balfe DM: Acute pancreatitis in children: CT findings of intra- and extrapancreatic fluid collections. *Radiology* 195:196–200, 1995.
- Johnson PR, Spitz L: Cysts and tumors of the pancreas. *Semin Pediatr Surg* 9:209–215, 2000.
- Berrocal T, Pajares MP, Zubillaga AF: Pancreatic cystosis in children and young adults with cystic fibrosis: Sonographic, CT, and MRI findings. *AJR Am J Roentgenol* 184:1305–1309, 2005.
- Ferrozzi F, Bova D, Campodonico F, et al: Cystic fibrosis: MR assessment of pancreatic damage. *Radiology* 198:875–879, 1996.
- Soyer P, Spelle L, Pelage JP, et al: Cystic fibrosis in adolescents and adults: Fatty replacement of the pancreas—CT evaluation and functional correlation. *Radiology* 210:611–615, 1999.
- King LJ, Scurr ED, Murugan N, et al: Hepatobiliary and pancreatic manifestations of cystic fibrosis: MR imaging appearances. *Radiographics* 20:767–777, 2000.
- Bom EP, van der Sande FM, Tjon RT, et al: Shwachman syndrome: CT and MR diagnosis. *J Comput Assist Tomogr* 17:474–476, 1993.
- Myers KC, Bolyard AA, Otto B, et al: Variable clinical presentation of Shwachman-Diamond syndrome. *J Pediatr* 164:866–870, 2014.
- Krampitz GW, Norton JA: L Pancreatic neuroendocrine tumors. *Curr Probl Surg* 50:509–545, 2013.
- Sempoux C, Guiot Y, Lefevre A, et al: Neonatal hyperinsulinemic hypoglycemia: Heterogeneity of the syndrome and keys for differential diagnosis. *J Clin Endocrinol Metab* 83:1455–1461, 1998.
- Chung EM, Travis MD, Conran RM: Pancreatic tumors in children: Radiologic-pathologic correlation. *Radiographics* 26:1211–1238, 2006.
- Shet NS, Cole BL, Iyer RS: Imaging of pediatric pancreatic neoplasms with radiologic-histopathologic correlation. *AJR* 202:1337–1348, 2014.
- Roebuck DJ, Yuen MK, Wong YC, et al: Imaging features of pancreatoblastoma. *Pediatr Radiol* 31:501–506, 2001.
- Glick RD, Pashankar FD, Pappo A, et al: Management of pancreatoblastoma in children and young adults. *J Pediatr Hematol Oncol* 34(Suppl 2):S47–S50, 2012.
- Fill WL, Lamiell JM, Polk NO: The radiographic manifestations of von Hippel–Lindau disease. *Radiology* 133:289–295, 1979.
- Hough DM, Stephens DH, Johnson CD, Binkovitz LA: Pancreatic lesions in von Hippel–Lindau disease: Prevalence, clinical significance, and CT findings. *AJR Am J Roentgenol* 162:1091–1094, 1994.
- Leung RS, Biswas SV, Duncan M, Rankin S: Imaging features of von Hippel–Lindau disease. *Radiographics* 28:65–79, 2008.
- Haas NB, Nathanson KL: Hereditary kidney cancer syndromes. *Adv Chronic Kidney Dis* 21:81–90, 2014.
- Fremont B, Poulain P, Odent S, et al: Prenatal detection of a congenital pancreatic cyst and Beckwith–Wiedemann syndrome. *Prenat Diagn* 17:276–280, 1997.
- Sirinelli D, Silberman B, Baudon JJ, et al: Beckwith–Wiedemann syndrome and neural crest tumors. A report of two cases. *Pediatr Radiol* 19:242–245, 1989.
- Choyke PL, Siegel MJ, Craft AW, et al: Screening for Wilms tumor in children with Beckwith–Wiedemann syndrome or idiopathic hemihypertrophy. *Med Pediatr Oncol* 32:196–200, 1999.
- Ros PR, Hamrick–Turner JE, Chiechi MV, et al: Cystic masses of the pancreas. *Radiographics* 12:673–686, 1992.
- Chung EM, Conran RM, Schroeder JW, et al: From the radiologic pathology archives: Pediatric polycystic kidney disease and other ciliopathies: Radiologic-pathologic correlation. *Radiographics* 34:155–178, 2014.

Diseases of the Pediatric Spleen

JARED R. GREEN | MARTHA COTSEN SAKER

CHAPTER OUTLINE

Splenic Histology and Function

Spleen Size

Congenital Abnormalities

Splenules
Polysplenia and Asplenia
Wandering Spleen
Splenogonadal Fusion

Cystic Lesions

True Cysts and Pseudocysts
Lymphatic Malformations

Benign Lesions

Hemangiomas
Vascular Malformations
Hamartoma

Malignant Lesions

Lymphoma
Leukemia
Metastatic Disease

Trauma

Blunt Trauma
Splenosis

Infections

Candidiasis
Cat-Scratch Disease
Infectious Mononucleosis

Infarction

Sickle Cell Disease

Sequestration
Normal Islands of Splenic Tissue
Functional Asplenia

Peliosis

Gaucher's Disease

Histiocytic Syndromes

Splenic Histology and Function

Splenic tissue is composed of red pulp and white pulp. The red pulp is composed of vascular sinusoids, and the white pulp is composed of lymphoid follicles with white blood cells.¹ The proportion of white pulp relative to red pulp increases with age and antigenic stimulation.^{1,2} Mononuclear phagocytic cells of the red pulp remove abnormal or senescent red blood cells from circulation.^{3,4}

The radiographic appearance of the spleen depends on the imaging modality, age of the patient, splenic composition and

size,¹ and timing of intravenous administration of contrast agents.⁵ The spleen has the shape of a curved wedge and may have normal clefts, notches, or lobules.^{3,6}

On ultrasound, the normal spleen has a homogeneous echotexture that is hyperechoic to the pediatric kidney and isoechoic or hyperechoic to the liver on gray-scale images (Figs. 122-1 and 122-2). The parenchyma is exceptionally vascular on color flow Doppler imaging.³

Precontrast computed tomography (CT) examination of the normal spleen demonstrates uniform parenchymal attenuation that is slightly less than that of the normal liver.² On contrast-enhanced examinations, the spleen's appearance depends on the timing of the intravenous administration of the contrast bolus and image acquisition. Transient heterogeneous enhancement of the spleen is presumed to result from differences in relative flow rates through the red and white pulp. The mean time of initial visualization of the heterogeneity after infusion of the contrast agent is 19.2 seconds (range, 9-44 seconds). Normal transient heterogeneity persists 70 seconds after administration of the contrast agent in only 6% of children.⁵ The patterns as seen on contrast-enhanced CT and magnetic resonance imaging (MRI) examinations are varied and include arcs, stripes (Fig. 122-3), and focal areas of relatively delayed perfusion. Heterogeneous areas in the spleen on images acquired more than 70 seconds after the administration of contrast material may indicate an abnormality.⁵

The tissue characteristics related to the ratio of red and white pulp probably dictate the signal intensity on MRI. In the neonate, the lymphoid tissue of the white pulp is not well developed, and the spleen is composed primarily of the vascular sinusoids of the red pulp. In the first week of life, the spleen usually is isointense or hypointense relative to the liver on T1- and T2-weighted, spin-echo images (Fig. 122-4A, B).¹ With the maturation of high cellular water content lymphoid tissue, the spleen becomes minimally hyperintense relative to the liver on T2-weighted images at approximately the second week of life.⁶ When the child is 1 month old, the spleen is moderately hypointense relative to the liver.¹ There is a relative increase in the size and number of lymphoid follicles and a relative decrease in the extent of red pulp up to the age of 7 months (Fig. 122-4C, D). After the child is 8 months old, the signal characteristics of the pediatric spleen are the same as in the adult.¹ As on contrast-enhanced CT, the spleen often shows heterogeneous enhancement during the arterial phase of dynamic contrast-enhanced MRI.^{7,8} It has been theorized that the decreased signal intensity of the spleen relative to the liver in patients after chemotherapy, with or without associated blood transfusions, may result from reduction or elimination of the white pulp's high water content and lymphoid tissue.⁹

Nuclear medicine studies to evaluate the spleen include technetium ^{99m}Tc sulfur colloid scintigraphy and ^{99m}Tc-denatured (heat-damaged) red cell scintigraphy. Sulfur colloid is phagocytosed by the reticuloendothelial cells of the spleen

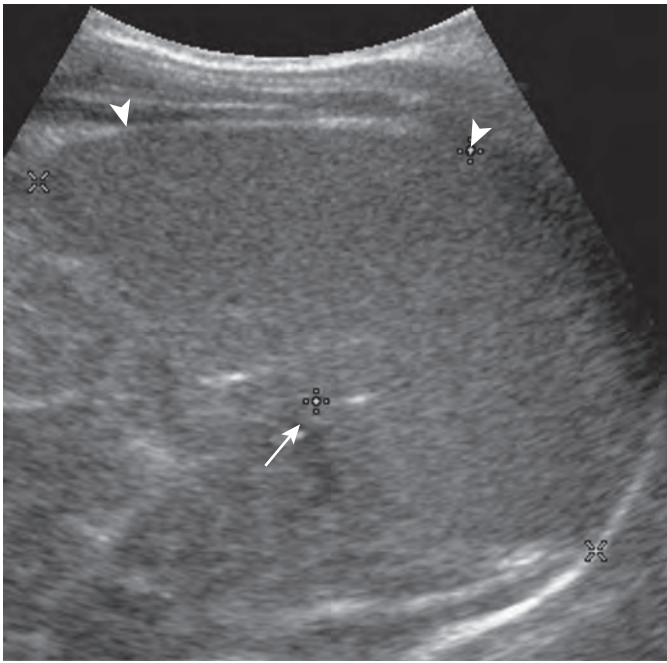


Figure 122-1 Normal spleen on ultrasound. Sonogram of a normal pediatric spleen demonstrates a uniform parenchymal echotexture, smooth outer capsular surface (arrowheads), and concave hilum (arrow).

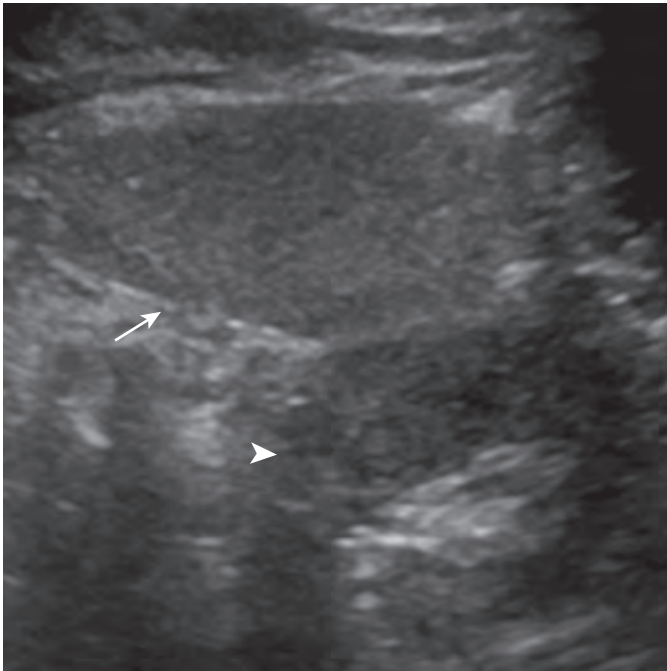


Figure 122-2 Normal spleen on ultrasound. Sonogram of a normal pediatric spleen demonstrates the normal uniform echotexture of the spleen (arrow) that is hyperechoic to the normal kidney (arrowhead).

and liver, and denatured red cells are sequestered in the spleen. Indications for splenic scintigraphy include evaluation of abdominal trauma, splenomegaly, and left upper quadrant mass; search for accessory spleens or splenosis; and assessment of infarction, functional asplenia, polysplenia, and the heterotaxy syndrome.¹⁰

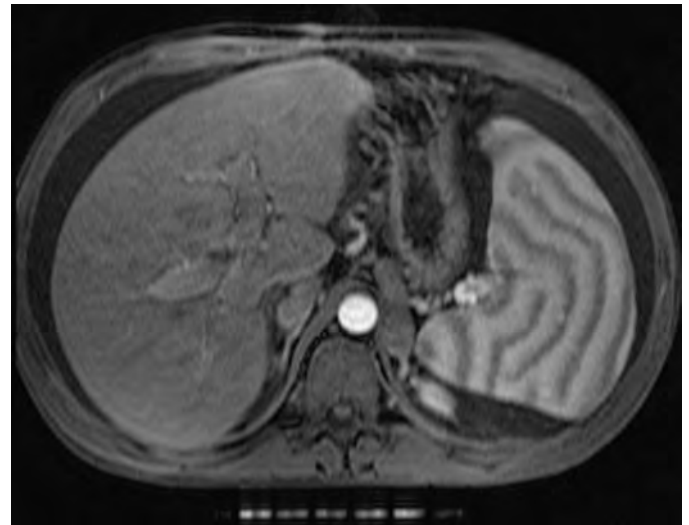


Figure 122-3 Splenic MR perfusion artifact. Axial view, volumetric interpolated breath-hold examination (VIBE) MR image obtained during administration of contrast material demonstrates transient splenic parenchymal perfusion patterns, including arcs and stripes.

Spleen Size

The spleen increases in length and volume as the child grows. Splenic length is typically measured sonographically in the coronal plane through the hilum, from the dome of the spleen to the inferior tip.¹¹ Upper limits of normal for age are 6 cm at 3 months, 6.5 cm at 6 months, 7 cm at 12 months, 8 cm at 2 years, 9 cm at 4 years, 9.5 cm at 6 years, 10 cm at 8 years, 11 cm at 10 years, 11.5 cm at 12 years, and 12 cm at and beyond 15 years for girls and 13 cm for boys 15 years and older.¹¹ Secondary imaging signs of splenomegaly include extension of the spleen below the inferior margin of the left kidney or the right hepatic lobe, medial extension to the aorta, and loss of the concavity of the hilum (Fig. 122-5).³

Congenital Abnormalities

SPLENULES

Splenules are congenital rests of normal splenic tissue that form when mesenchymal cells fail to fuse with the rest of the splenic mesenchyme.^{12,13} A splenule is also known as an accessory spleen, supernumerary spleen, or splenunculus. Splenules are typically located near the main splenic hilum anteriorly or posteriorly but are rarely lateral to the main spleen and have not been documented superior to the main spleen.¹⁴

Splenules are circumscribed, round, oval,¹³ or triangular, and they are homogeneous with and without enhancement (Fig. 122-6).¹⁴ Splenules vary in size from millimeters to centimeters, usually less than 3.2 cm in diameter, and are capable of significant hypertrophy.^{4,13,15}

Splenic artery supply to a splenule may be visible on CT. On CT, 16% of people have one to three accessory spleens,¹⁴ and the presence of 10 splenules has been described.¹⁶ Splenules are seen in 10% to 30% of people at surgery or autopsy.¹⁵ Subcentimeter splenules may have lower attenuation than the main spleen because of volume averaging with surrounding fat and the CT collimation used.¹⁴

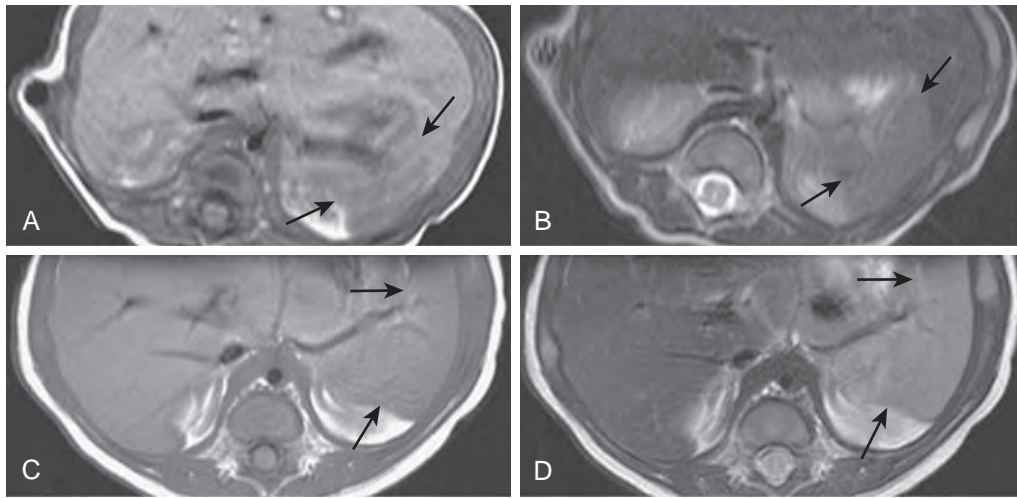


Figure 122-4 Normal spleen: MR findings. MRI demonstrates the normal change in signal intensity of the spleen (arrows) relative to the liver in a 9-day-old neonate (**A** and **B**) and in the same child at 12 weeks (**C** and **D**). In the T1-weighted image (**A**) and fast spin-echo T2-weighted image (**B**) of the 9-day-old infant, the neonatal spleen has relatively lower signal intensity, particularly on T2-weighted sequences, because of the higher ratio of vascular red pulp to white pulp. The T1-weighted image (**C**) demonstrates MR findings for the same child at age 12 weeks. As the lymphoid tissue of the white pulp matures, the spleen (arrows) becomes moderately hyperintense to the liver on fast spin-echo T2-weighted images (**D**).

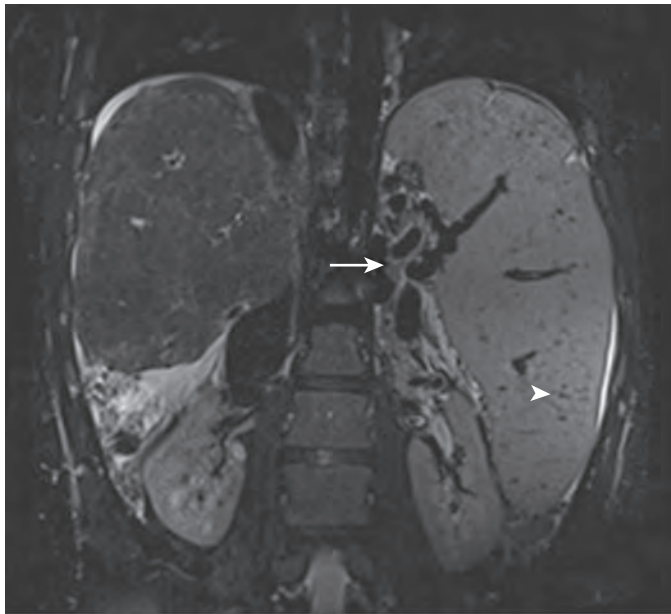


Figure 122-5 Splenomegaly: MR findings. The spleen is grossly enlarged, extending inferior to the cirrhotic right hepatic lobe. Note the splenic hilar varices (arrow) and punctate hypointense splenic siderotic nodules (arrowhead) on this T2-weighted coronal image.

Splenules need to be removed if the patient is undergoing therapeutic splenectomy for a hematologic disease because the residual splenic tissue can be responsible for recurrent disease.¹⁶⁻¹⁸ Accessory spleens may resemble lymphadenopathy or neoplasm if they are situated near the greater curve of the stomach,¹⁵ in the left adrenal,¹⁹ or within the pancreatic tail.^{15,20} Splenules may become symptomatic if they twist.²¹

POLYSPLENIA AND ASPLENIA

Multiple spleens (i.e., polysplenia) or absence of the spleen (i.e., asplenia) at birth can be associated with multiple congenital



Figure 122-6 Normal splenules. In the contrast-enhanced CT scan of an 18-year-old girl with abdominal pain, two splenules are seen at the hilar surface (arrows). They are 2.0 × 2.3 cm in the greatest dimension. The splenules have the same attenuation as the normal spleen on this 5-mm, axial view, contrast-enhanced CT image.

anomalies under the heading of heterotaxy or situs ambiguus.²² In polysplenia, multiple small spleens are always seen on the same side as the stomach²² because of the origin of splenic tissue from the dorsal mesogastrium (Fig. 122-7).¹² Polysplenia is often associated with an interrupted inferior vena cava with azygos continuation, bilateral left-sidedness, and congenital heart disease.²² There may also be associated absence of the gallbladder, biliary atresia, preduodenal portal vein,²² and malrotation of the bowel.²²⁻²⁴

Asplenia is the absence of splenic tissue and is associated with bilateral right-sidedness and complex cyanotic heart disease.^{6,25} There is an association with gallbladder duplication,^{6,8} midgut malfixation or malrotation, and microgastria.²⁶

Nuclear scintigraphy with ^{99m}Tc-sulfur colloid or heat-damaged ^{99m}Tc-labeled erythrocytes can evaluate for the presence or absence of splenic tissue.²⁵



Figure 122-7 Polysplenia. Axial view, contrast-enhanced CT shows multiple spleens of various sizes in the retrogastric area of the left upper quadrant (arrows). The azygos vein is enlarged (arrowhead), and the intrahepatic inferior vena cava is absent.

WANDERING SPLEEN

The spleen is primarily supported by the gastrosplenic and splenorenal ligaments.^{3,12,27,28} If the support ligaments are absent or lax, the spleen may be ectopic from its normal position and is referred to as a wandering spleen. It is rare in children.²⁷⁻²⁹ The degree of ectopia is limited by the length of the vascular pedicle.³⁰ The absence of the spleen in its usual position and presence of a soft tissue mass elsewhere with the imaging characteristics of the spleen characterize this entity (Fig. 122-8). There may be a history of intermittent abdominal pain^{27,31} or an intermittently palpable abdominal mass.⁶ The child with torsion of a wandering spleen usually presents with an acute surgical abdomen.^{27-29,32}

Ultrasound evaluation of torsion of the wandering spleen may demonstrate areas of hyperechoic hemorrhage and hypoechoic infarction and congestion. Early, the gray-scale echotexture may be preserved with or without splenomegaly,³³ and color Doppler examination may demonstrate splenic vein occlusion or stasis with preserved arterial flow and intraparenchymal flow. As the torsion persists, arterial inflow eventually decreases or ceases to be detectable.^{33,34}

On CT, the spleen with torsion may be heterogeneously enhancing and have decreased attenuation, depending on the extent of perfusion. The enhancing hilar vessels twist with the interpositional hilar fat and yield a whorled or banded appearance (Fig. 122-9).²⁷ On ultrasound examination, twisted hilar vessels appear as a splenic hilar mass, which may be an important finding for cases in which the diagnosis is not yet made and the twisted spleen is not ectopic.³³ The wandering spleen is associated with deficiency of anterior abdominal wall musculature³⁴ and is rarely reported with prune-belly syndrome.³⁵

After diagnosis of torsion of a wandering spleen, if the spleen is not infarcted, splenopexy may be performed in an effort to preserve splenic function by preventing future torsion.^{28,29,31,33}

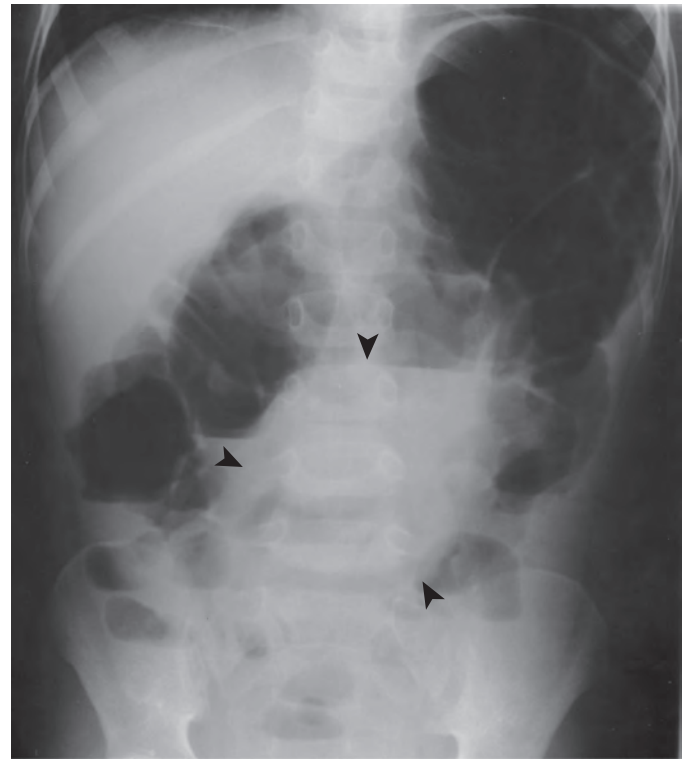


Figure 122-8 Ectopic wandering spleen. A plain radiograph demonstrates gaseous distention of the colon in the left upper quadrant, with no mass effect in the expected location of the spleen. In the midabdomen, the ectopic spleen (arrowheads) displaces the bowel, as confirmed on cross-sectional imaging. Air-fluid levels are seen in the small bowel.

SPLENOGONADAL FUSION

The splenic anlage and ipsilateral gonadal anlage have a close developmental relationship and may fuse, forming a long, *continuous* cord from the gonad cephalad to the main spleen.⁴ The connection to the main spleen may be totally or partially fibrous³⁶ and is associated with cryptorchidism.⁴ Alternatively, a portion of the splenic tissue may separate from the main spleen (*discontinuous*) and descend with the gonad,⁴ known as splenogonadal fusion.

Male children with splenogonadal fusion typically present with a painless testicular mass.³⁶ Splenogonadal fusion should be considered preoperatively in evaluation of a scrotal mass because failure to do so may result in unnecessary orchiectomy. The ectopic splenic tissue attached to the testicle mimics testicular duplication on ultrasound and has been described as an encapsulated, homogeneous extratesticular mass that is isoechoic with the normal testis and shows no hyperemia on color Doppler ultrasound. The presence of ectopic splenic tissue can be confirmed with nuclear ^{99m}Tc-sulfur colloid scintigraphy.⁴

Cystic Lesions

TRUE CYSTS AND PSEUDOCYSTS

True cysts, such as congenital or epithelial cysts and echinococcal cysts, have an epithelial cell lining, but pseudocysts do not.^{6,7}

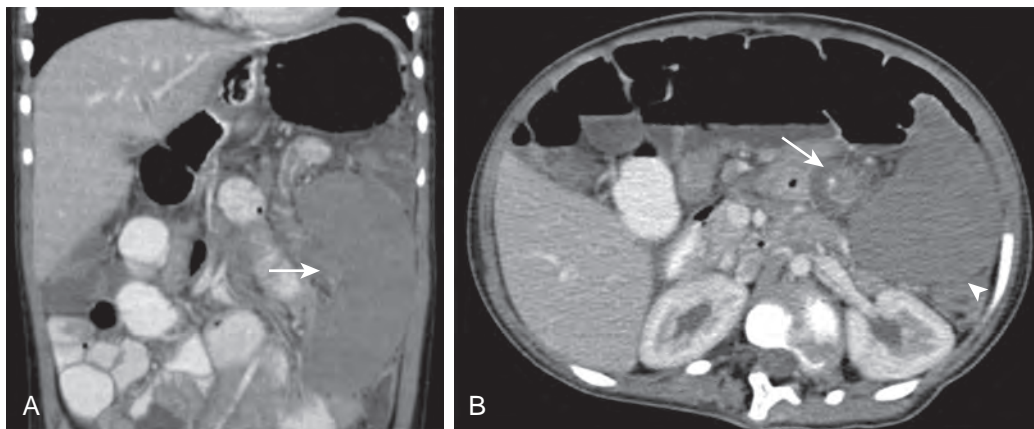


Figure 122-9 Splenic torsion. **A.** Torsion of the wandering spleen demonstrates absence of enhancement (arrow) on this contrast-enhanced CT coronal reformation. **B.** Note the whorled appearance of the splenic hilar vessels (arrow) and the lack of enhancement of the spleen parenchyma.

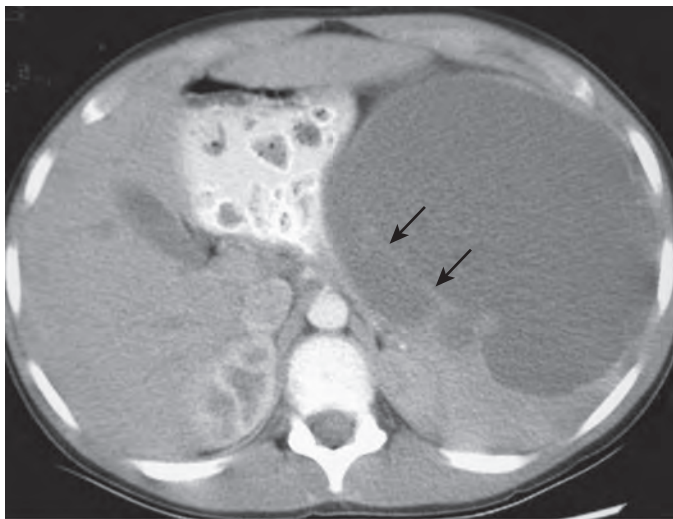


Figure 122-10 Epidermoid cyst. Contrast-enhanced CT demonstrates a large, intrasplenic cystic mass with a relatively thin wall. Notice the septa or trabeculae (arrows).

It is not possible to reliably differentiate between true cysts and pseudocysts by imaging.³⁷

Epithelial cysts can be further categorized as mesothelial, epidermoid, or dermoid. Epidermoid cysts are lined by stratified squamous epithelium, which macroscopically appears coarsely trabeculated.^{37,38} Epidermoid cysts may be familial, are often several centimeters in diameter, and have a tendency to rupture.³⁸

Epidermoid cysts on ultrasound appear as relatively thin walled, anechoic lesions that do not change over time. Mural calcification is seen in 10% of cases, although it is seen more often in acquired pseudocysts.³⁷ There may be septations and wall trabeculation, which are seen more often in true cysts.³⁷ The fluid may have some internal echoes caused by cholesterol crystals, inflammatory debris, or blood products from prior hemorrhage.³⁷ On CT and MRI, cysts follow fluid attenuation and signal character, with or without septations and calcification (Fig. 122-10).^{6,39,40} These cysts show no central or rim enhancement.⁷

Echinococcal cysts are true cysts. They can have peripheral calcification and often appear to have multiple septa.^{7,41} In echinococcal cysts, there may be internal areas of increased attenuation on CT due to dense debris, also known as hydatid sand. Peripherally located small daughter cysts may be present.⁴¹

Acquired pseudocysts, most often post-traumatic, are more common than true cysts.^{41,42} They are indistinguishable on imaging from true cysts and may have mural calcification,^{41,42} but septa are uncommon.⁴¹

LYMPHATIC MALFORMATIONS

Lymphatic malformations of the spleen, also known as lymphangiomas, are congenital and are composed of dilated lymphatic channels.^{43,44} Despite their rarity in the spleen,⁴⁵ lymphatic malformations are the second most common benign splenic lesion.⁸ They are not neoplastic, and their growth is commensurate with that of the child.^{46,47} An abrupt change in lymphatic pressure or flow, infection, or hemorrhage into the lesion can cause an abrupt increase in size.⁴⁶⁻⁴⁸ They are frequently asymptomatic and are found incidentally (Fig. 122-11).³⁹

The lymphatic channels and compartments are lined by a single layer of flattened endothelial cells and contain lymphatic fluid.⁴⁵ They can be solitary, or they may be associated with other lymphatic malformations of the viscera, bone, or soft tissues.^{45,49}

On imaging, lymphatic malformations of the spleen appear similar to lymphatic malformations elsewhere in the body, with a multiloculated, cystic configuration.⁴⁵ On ultrasound, there are well-defined, hypoechoic or anechoic spaces of various sizes, typically with septations and proteinaceous debris that may produce internal echoes.^{43,45,49} Radionuclide ^{99m}Tc-sulfur colloid scans show a focal area of decreased uptake.⁴⁵

On CT, lymphatic malformations are hypodense with non-enhancing discrete areas⁴⁹ that are often subcapsular, but they can be diffuse.^{43,50} The walls and septa may faintly enhance after administration of contrast material.^{44,50}

On MRI, the cystic areas are usually hypointense on T1-weighted images and hyperintense on T2-weighted images.^{7,44,49} They may appear hyperintense on T1-weighted images because of proteinaceous contents or prior hemorrhage, with or without fluid-fluid levels on T2-weighted sequences.^{8,44}

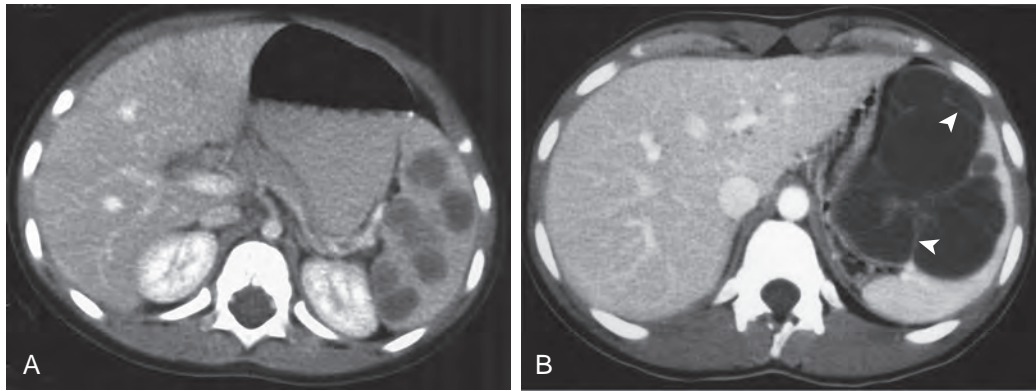


Figure 122-11 Lymphatic malformation. **A.** Multiple, nonenhancing, well-defined, low-attenuation, intrasplenic cystic lesions were incidentally found in a 3-year-old child. Lesions were stable during 1 month. Subsequent PET/CT examination showed no evidence of hypermetabolic features. Multiple lymphatic malformations were diagnosed at splenectomy. **B.** Contrast-enhanced CT in a different child demonstrates multiple septations (arrowheads) within this single, large lymphatic malformation that originates within the spleen. Although the septations may enhance, the cystic spaces of lymphatic malformations do not.

The cystic areas do not enhance, but the septa may enhance on the delayed phase images.⁷

Benign Lesions

HEMANGIOMAS

Before the classification by Mulliken and Glowacki,⁵¹ hemangiomas and vascular malformations had variable nomenclature in the literature, leading to classification confusion. The International Society for the Study of Vascular Anomalies (ISSVA) has subsequently established guidelines based on the histopathology, clinical course, and treatment of these lesions.⁵² Despite the criteria outlined in the ISSVA guidelines, lesions referred to as hemangiomas are the most common benign lesions of the spleen.^{13,50,53,54}

The imaging appearance of pediatric splenic hemangiomas on ultrasound, CT, and MRI is variable, as reported in the literature.^{13,41,50,53-56} This probably reflects the widespread use of inaccurate terminology in the medical literature, as some authors were likely describing vascular neoplasms, whereas others were describing vascular malformations.^{52,57}

Hemangiomas are benign and usually asymptomatic solid neoplasms composed predominantly of a mass of endothelial cells.^{44,52} Proliferating hemangiomas may cause clinical complications by location, mass effect, or platelet sequestration. They have an initial proliferative phase during the first year of life, followed by an involution phase.^{44,58} In the proliferative phase, a hemangioma is seen on MRI as a solid, lobulated, soft tissue mass that is isointense or hypointense to muscle on T1-weighted images and hyperintense on T2-weighted images, with uniform contrast enhancement. Feeding arteries and draining veins may be seen and can demonstrate prominent flow voids.^{44,58} During involution, there is fatty replacement of the neoplasm. There is a variable increase in signal on T1-weighted images and decreased signal on T2-weighted images.⁴⁴

VASCULAR MALFORMATIONS

Vascular malformations are congenital lesions composed of some combination of arterial, capillary, venous, and lymphatic

channels. They are described by their flow characteristics (i.e., high or low flow).^{44,52,58} Venous malformations are low-flow vascular malformations that were formerly known as cavernous hemangiomas, varicose hemangiomas, or lymphangiohemangiomas.⁴⁴ Vascular malformations are distinguished from vascular neoplasms, such as hemangiomas, by the lack of increased endothelial cell turnover.⁵² They are composed of endothelial cell-lined channels, with interconnecting venous spaces and various connections to normal or dysplastic draining veins. The spaces are filled with blood, and there is no true solid mass. They may contain phleboliths. They have low signal intensity on T1-weighted images and high signal intensity on T2-weighted images. The walls of the vascular spaces may appear as septations that do not enhance, whereas the vascular spaces do enhance if they are not thrombosed. Fluid-fluid levels may be seen. Phleboliths appear as signal voids on MRI.⁴⁴

HAMARTOMA

Hamartomas are rare, non-neoplastic, disorganized mixtures of normal splenic components.^{6,55,59} They usually are not encapsulated⁶⁰ but are well-circumscribed,^{59,60} solid, nodular lesions.⁵⁰ They often appear hyperechoic and may have cystic areas within them.^{8,40} Some are heterogeneous and may contain minute, speckled calcifications⁵⁰ or a central, stellate scar. Hamartomas range in size from a few millimeters to centimeters, with a median size of 5 cm.^{55,61}

Almost half of children with splenic hamartomas are symptomatic at presentation.⁵⁹ Children may present with splenomegaly, recurrent infections, periodic low-grade fever with night sweats, growth retardation, or hematologic abnormalities.^{59,60,62}

Nuclear scintigraphy may demonstrate splenomegaly without a shift in radionuclide uptake. The cross-sectional imaging appearance and degree of contrast enhancement vary.⁵⁰ CT may demonstrate splenomegaly⁶² with or without a contour abnormality.⁵⁵ On MRI, splenic hamartomas are often isointense with normal spleen on T1-weighted images and have variable signal intensity on T2-weighted images.^{8,62} There is diffuse heterogeneous early enhancement after administration of contrast material⁵⁵ and more uniform, prolonged enhancement on

delayed images, except in cystic areas or central scar.⁸ MR characteristics of the mass, combined with uptake of ^{99m}Tc-sulfur colloid, are most suggestive of a benign hamartoma.⁶² Splenic hamartomas have been reported in association with tuberosus sclerosis.^{40,63}

Malignant Lesions

LYMPHOMA

Lymphoma is the most common pediatric splenic solid malignant neoplasm.⁴⁰ Metastatic disease, even in the case of lymphoma, is more common than primary splenic malignant disease.⁸ Approximately one third of patients with lymphoma have splenic involvement.⁴² Splenic involvement in lymphoma can be focal or diffuse. Focal lesions may be miliary, small or large, and single or multiple.^{7,8,42} Diffuse involvement may mimic idiopathic splenomegaly without a discrete lesion. Approximately one third of lymphoma patients have splenomegaly; however, splenomegaly in the absence of splenic lymphoma can occur in children with lymphoma.³

Focal lesions on ultrasound are typically hypoechoic relative to the normal spleen^{40,41,64} and in some cases may resemble cysts.⁵⁶ Focal lymphomatous lesions are typically low density and nonenhancing on CT examination (Fig. 122-12).⁴¹ Central areas of old hemorrhage, necrosis, or abscess may be present.⁴¹

Lesions are often isointense to hypointense to muscle on T1-weighted images and isointense to hyperintense on T2-weighted images. With dynamic contrast enhancement, certain occult lesions may stand out as hypointense areas in contrast to the enhancing normal spleen.^{7,53} Diffuse infiltration of the spleen with lymphoma may not be detectable on T1- or T2-weighted images,⁴¹ and imaging with ¹⁸F-fluorodeoxyglucose

positron emission tomography (¹⁸F-FDG PET) may help identify diffuse splenic involvement.⁴⁰

In a review of 154 children with Hodgkin's lymphoma who underwent splenectomy for staging laparotomy, the two most important clinical predictors of splenic involvement at the time of surgery were fine to coarse surface nodulation of the spleen and lymph node involvement at the splenic hilum and pancreatic tail.⁶⁵ Seventy-one percent of children with enlarged lymph nodes at the splenic hilum or pancreatic tail had pathologically proven splenic involvement.⁶⁵

LEUKEMIA

The spleen often harbors leukemic cells in children. Sonographic findings at diagnosis usually include splenomegaly with hypoechoic echotexture. Unlike in lymphoma, focal masses are not typical. Hilar or retroperitoneal lymphadenopathy may also be present. After successful chemotherapy, the spleen decreases in size, and echotexture normalizes.³ Despite marked splenomegaly due to leukemic infiltration, the spleen usually maintains a normal, homogeneous attenuation value on CT examination.¹³

METASTATIC DISEASE

Metastatic disease to the spleen is uncommon⁵³ but is the most common splenic malignant disease. Splenic metastases are often microscopic and may not be evident by imaging or gross inspection.¹³ Metastatic lesions can have cystic-appearing areas of hemorrhage or necrosis and can become secondarily infected.⁴¹

Trauma

BLUNT TRAUMA

The spleen is the most commonly injured abdominal organ in children by blunt abdominal trauma, and most of these lesions are managed nonoperatively.⁶⁶⁻⁶⁹ In a meta-analysis of 26 cohort studies, evaluating 1083 children with blunt splenic injury and nonoperative management, 85% of the children had follow-up imaging and 15% did not. None of the children had delayed (after discharge from the hospital) splenic rupture, and there were no deaths.⁷⁰ Injuries are graded by the organ injury scale of the American Association for the Surgery of Trauma for CT imaging.⁷¹ The hemodynamic state and clinical status of the child are the major determinants of whether surgical treatment is necessary.^{2,66,67,72}

Ultrasound is less sensitive than CT in the diagnosis of splenic injuries. Ultrasound often underestimates the size of the splenic injury,⁷³ possibly because the hemorrhage and injury may acutely be isoechoic to normal spleen tissue.

Active extravasation of intravenous contrast material is manifested as a jet or blush of contrast material swirling into an expanding hematoma or blood pool at the site of splenic injury (Fig. 122-13A).⁷⁴ This finding indicates rapid, active bleeding and may necessitate surgical intervention, particularly in adults.^{66,75} Contrast blush in children with splenic injury is associated with higher grades of splenic injury, but only one of six children with this sign required operative management that included splenectomy and left nephrectomy.⁶⁶ Surgery or embolization (Fig. 122-13B, C) may reduce or eliminate the need for transfusion.⁶⁸

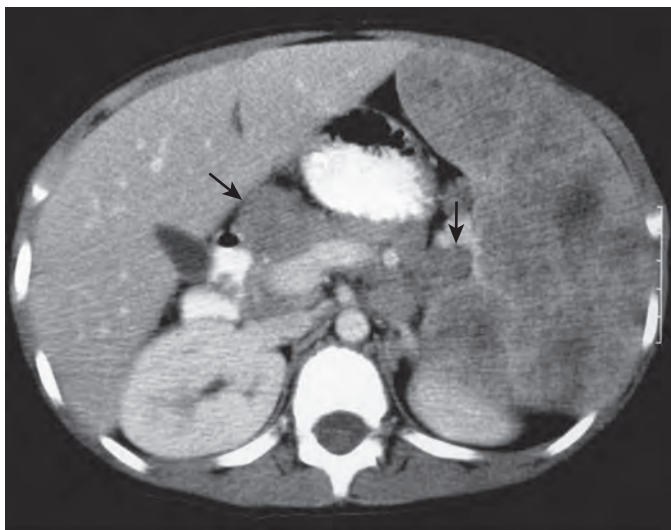


Figure 122-12 Lymphoma. The splenomegaly is associated with multiple low-attenuation lesions that do not significantly enhance. Lymphadenopathy is present in the region of the splenic hilum near the pancreatic tail and anterior to the portal vein (arrows). (Courtesy Lisa Lowe, MD, Children's Mercy Hospital and Clinics, University of Missouri, Kansas City, MO.)

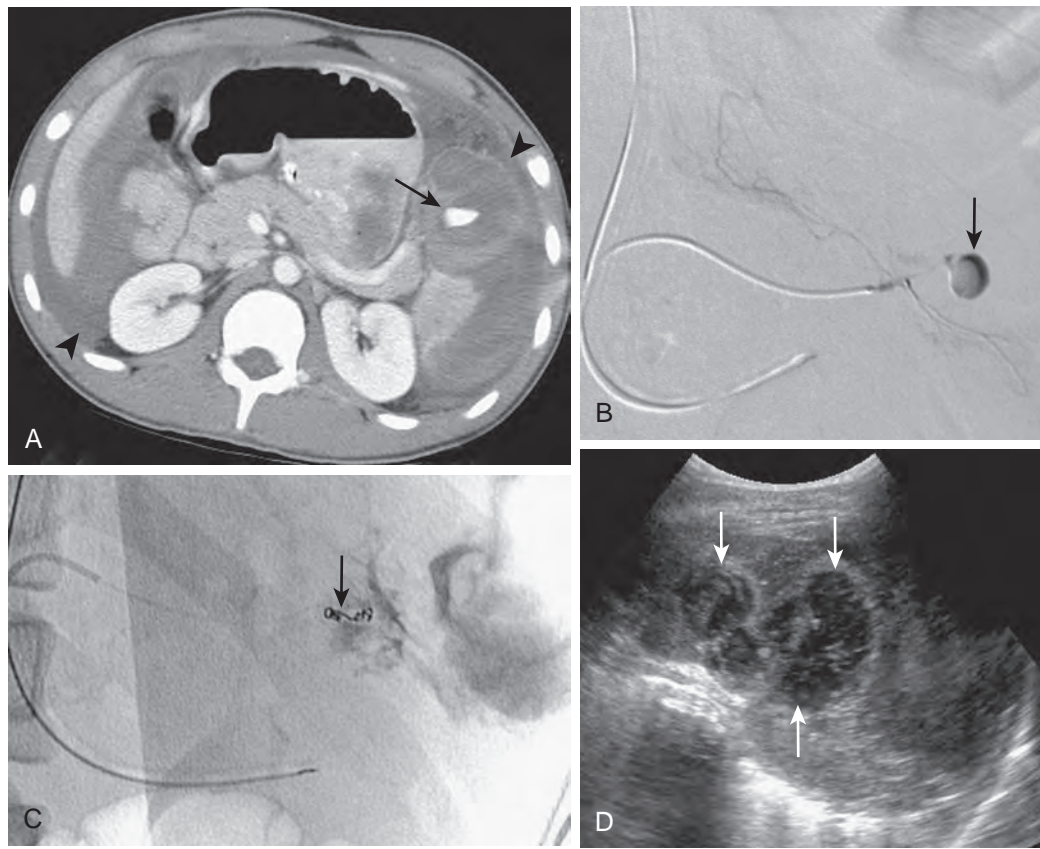


Figure 122-13 Splenic trauma. **A.** Contrast-enhanced CT of 14-year-old boy with a splenic injury after a motor vehicle collision. One month later, the boy had a syncopal episode and was hypotensive. The healing fractured spleen had spontaneously ruptured. Intraperitoneal blood surrounds the liver and the fractured spleen (arrowheads). There is a mixed-attenuation hematoma with a focal concentrated collection of extravasated intravenous contrast material (arrow), indicating active bleeding in the anterior aspect of the spleen. **B.** Selective arteriogram of a splenic end artery demonstrates focal extravasation (arrow). **C.** Coil (arrow) embolization was performed to stop hemorrhage. **D.** Healing spleen has a heterogeneous echotexture. Relatively hypoechoic areas (arrows) are likely to represent an evolving hematoma and necrotic splenic tissue.

If the patient with an isolated splenic or hepatic injury remains hemodynamically stable, repeated imaging is usually not indicated.^{70,72,76} Cyst formation in the area of prior injury is likely to represent resolving hematoma (Fig. 122-13D).⁷⁶ The time for healing, as determined by ultrasound imaging, increases with the severity of the splenic injury.⁷⁶

SPLENOSIS

Splenosis occurs when the splenic capsule is disrupted, by trauma or surgery, allowing intraperitoneal spread of splenic pulp.^{4,77,78} Unlike congenital splenules, the splenic tissue in splenosis may be located anywhere in the peritoneum or may be intrathoracic if the diaphragm is not intact, has a blood supply donated by local tissue, and lacks a capsule.⁷⁸

Splenosis is frequently asymptomatic. However, complications have been reported, including abdominal or pelvic pain, bowel obstruction, splenic implant torsion, relapse of hemolytic disease after splenectomy, and traumatic rupture.^{4,79}

Imaging may demonstrate multiple 1-mm to 5-cm soft tissue masses with an imaging appearance of normal splenic tissue.⁷⁹ They can be located anywhere in the abdominal cavity, most frequently on the small bowel serosa. Splenosis may be mistaken for a disease process such as lymphoma, peritoneal

carcinomatosis, or endometriosis.⁷⁷ Nuclear scintigraphy with ^{99m}Tc-sulfur colloid or denatured red blood cells may confirm the diagnosis of splenosis.^{10,80}

Infections

CANDIDIASIS

Multiple splenic abscesses are usually seen with nonbacterial organisms, most frequently *Candida* infections. Fungal microabscesses are typically seen in children with immunosuppression related to hematologic malignant neoplasms.⁸ These microabscesses may be too small to resolve on imaging.⁸ On ultrasound examination, there are several patterns of hepato-splenic candidiasis. Most commonly, there is a nonspecific pattern of uniformly hypoechoic lesions, although punctate echogenic foci less than 5 mm with variable posterior acoustic shadowing are seen late in the disease and are related to fibrosis with or without calcification (Fig. 122-14).⁸¹ On CT examination, acute microabscesses are typically hypodense to normal spleen and rarely have a central high-density focus, although over time they may become hyperattenuating and may calcify.⁸¹ On MR examination, microabscesses are seen as multiple intermediate signal intensity T1-weighted and hyperintense

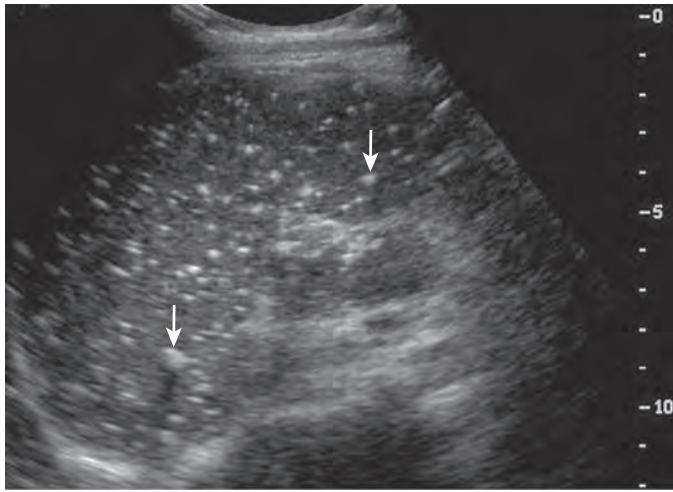


Figure 122-14 Candidiasis. For a leukemia patient with a history of *Candida* infection, sonography demonstrates innumerable, punctate, hyperechoic foci (arrows) throughout the spleen, consistent with healed granulomas.

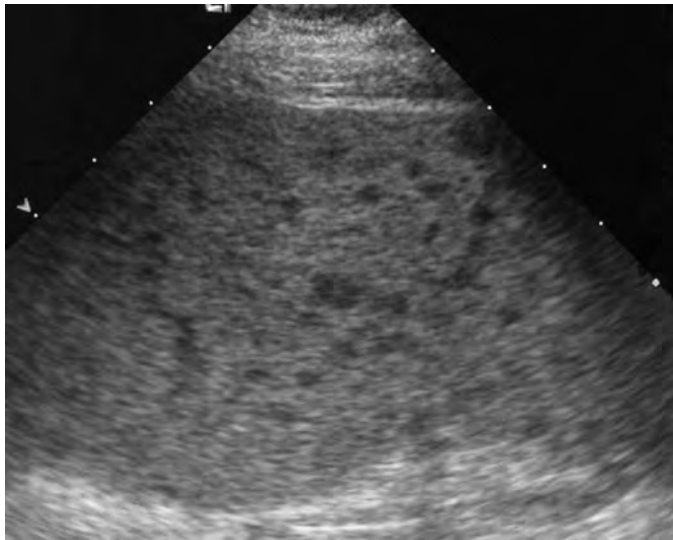


Figure 122-15 Cat-scratch disease. The enlarged spleen has innumerable hypoechoic foci that are consistent with microabscesses. This appearance is not specific for a given organism, and in this 10-year-old girl, it represented infection with *Bartonella henselae*. The lesions may calcify as they heal. (Courtesy Lisa Lowe, MD, Children's Mercy Hospital and Clinics, University of Missouri, Kansas City, MO.)

T2-weighted lesions. They may have peripheral ring enhancement or a target enhancement pattern after administration of gadolinium.⁸

CAT-SCRATCH DISEASE

Cat-scratch disease is caused by the gram-negative bacillus *Bartonella henselae*.⁸² Patients present with unilateral, regional lymphadenitis proximal to the inoculation site as well as constitutional symptoms.^{83,84} In a minority of patients, reticuloendothelial system involvement results in granulomatous or suppurative lesions of the liver and spleen.⁸³ Patients may develop splenomegaly with microabscesses and necrotizing granulomas, which may calcify with healing.⁸³ Multiple hypoechoic splenic lesions are seen on ultrasound (Fig. 122-15).

On CT examination, there are multiple, well-defined, low-attenuation splenic lesions that are better defined after intravenous administration of contrast material.⁸³

The differential diagnosis of the imaging findings includes other granulomatous diseases, such as tuberculosis, histoplasmosis, sarcoidosis, and *Candida* infections, and neoplasms such as lymphoma or other metastatic disease.^{8,83}

INFECTIOUS MONONUCLEOSIS

Infectious mononucleosis is caused by the Epstein-Barr virus. At least 50% of people with infectious mononucleosis acutely develop splenomegaly⁸⁵ from congestion with numerous, activated T lymphocytes.⁸⁶ The spleen may become markedly enlarged^{87,88} and rarely is complicated by spontaneous splenic rupture.^{87,89} Symptoms of spontaneous rupture include acute left upper quadrant pain and referred left shoulder pain (i.e., Kehr's sign).⁸⁷⁻⁹⁰

Ultrasound examination of spontaneous splenic rupture may demonstrate hypoechoic areas within the spleen, perisplenic and subcapsular fluid collections, and intraperitoneal fluid.

Infarction

Splenic artery branches are end arteries, and splenic vascular occlusion may therefore lead to infarction.^{2,8} Sickle cell hemoglobinopathy is the most common cause of splenic infarcts in pediatric patients. Splenic infiltration by leukemia or lymphoma can also cause infarcts.² Causes of splenic vascular occlusion include embolization, torsion, portal hypertension, collagen-vascular disease, and infiltrative disorders such as Gaucher's disease.² Possible complications of infarctions include fever, abscess or pseudocyst formation, splenic rupture, and hemorrhage.^{2,91}

Splenic infarcts are most commonly peripheral and wedge shaped, although on ultrasound they may appear as one or multiple poorly margined, hypoechoic regions, mimicking abscess or neoplasm.² With time, infarcts become more rounded and better delineated.⁴¹ Eventually, areas of infarction may completely resolve or may leave areas of calcification or small peripheral defects.^{2,91} If the entire spleen is recently infarcted, a hypodense spleen with only capsular enhancement may be seen on contrast-enhanced CT (Fig. 122-16).⁴²

Sickle Cell Disease

The spectrum of hemoglobinopathies in sickle cell disease includes homozygous sickle cell disease (SS), heterozygous sickle cell trait (SC), sickle cell-B⁰ thalassemia, and sickle cell-B⁺ thalassemia.⁹²

SEQUESTRATION

Children with SS disease may develop splenomegaly from sequestration of abnormal cells.² Acute splenic sequestration crisis is an emergent cause of potentially painful splenomegaly in children with SS disease. With sequestration, the splenic outflow is obstructed by sickled red blood cells,⁹³ leading to rapidly increasing spleen size. Hypovolemic shock and death may occur as the spleen traps large volumes of blood.^{94,95}

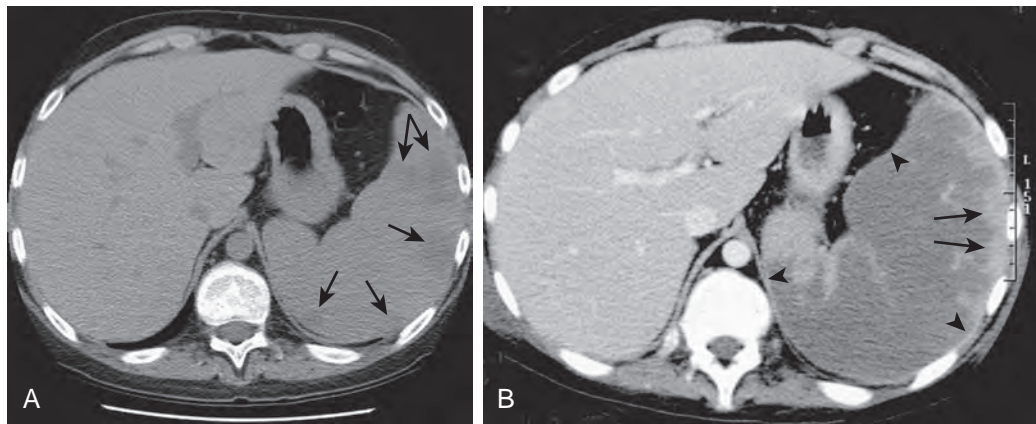


Figure 122-16 Leukemia and infarction. **A.** Noncontrast CT performed to assess pulmonary infection demonstrates splenomegaly in a teenager with leukemia. Peripherally located, hypoattenuating areas (arrows) may represent areas of infarction, infection, or tumor infiltration. **B.** Contrast-enhanced CT obtained 13 days later to evaluate the acute onset of left upper quadrant pain demonstrates an interval increase in spleen size. The spleen has a large area of decreased attenuation and relative lack of enhancement. The capsule (arrowheads) and some peripheral parenchyma (arrows) have normal attenuation and enhancement. Splenectomy confirmed splenic infarction.

Affected children are typically younger than 2 years,² although episodic sequestration in the spleen may occur up to the age of 5 years with SS disease^{93,94} and in older children and adolescents with SC disease.⁹³

Sonography reveals an enlarged and heterogeneous spleen with hypoechoic areas internally. Doppler examination shows patency of the main splenic vein and intrasplenic veins.⁹⁶

Contrast-enhanced CT may demonstrate multiple peripheral, nonenhancing, low-attenuation areas or large, diffuse nonenhancing low-attenuation areas. The spleen may return to a normal, homogeneous appearance, although splenomegaly may persist.⁹³

NORMAL ISLANDS OF SPLENIC TISSUE

Over time, the spleen of children with sickle cell disease becomes increasingly heterogeneous. On ultrasound examination, hyperechoic areas are thought to represent areas of prior infarction, and hypoechoic areas are thought to represent areas of normal splenic tissue.

On MR, islands of normal splenic tissue retain normal signal, whereas areas of decreased signal intensity on T1- and T2-weighted images are seen with hemosiderin deposition^{53,97} (Fig. 122-17) and calcification.^{97,98} T1-weighted, gradient-echo recalled in-phase and opposed-phase sequences can further accentuate the presence of iron because of the T2* effects.⁹⁹ Normal islands of splenic tissue do not significantly change in signal intensity between in-phase and opposed-phase sequences (Fig. 122-18). However, because of the continued decay of the transverse magnetization imposed by the iron's paramagnetic effects, there is appreciable signal loss on the second phase of the double gradient-echo technique in tissue with abnormal iron deposition.⁹⁹

The spleen may eventually develop dense calcifications, which may accumulate radiotracer during bone scintigraphy. Photopenic areas may correlate with the normal residual islands of functioning splenic tissue.¹⁰⁰ These normal islands accumulate ^{99m}Tc-sulfur colloid, indicating functioning splenic tissue, and have normal signal intensity on T1- and T2-weighted images, which can help differentiate these normal

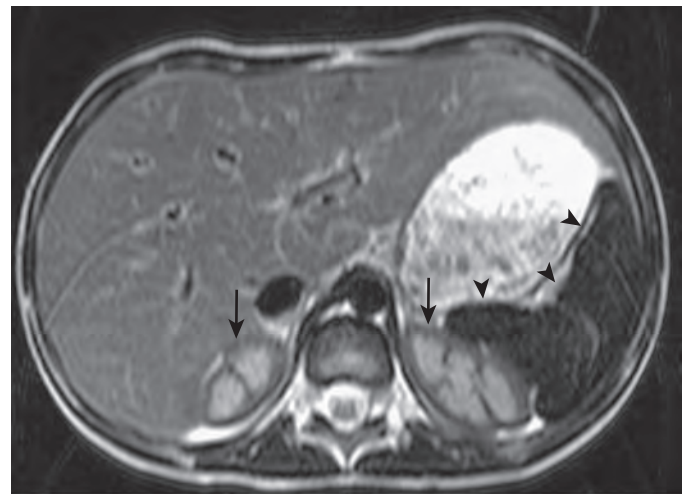


Figure 122-17 Sickle cell disease. The half-Fourier acquisition single-shot turbo spin-echo (HASTE) image shows low signal intensity of the renal cortex (arrows) and the spleen (arrowheads), indicating iron deposition.

islands from pathologic processes such as abscess, infarct, or neoplasm.^{98,100}

FUNCTIONAL ASPLENIA

Recurrent vaso-occlusive events may lead to a complete functional loss of the spleen's reticuloendothelial cells by the age of 7 years.¹⁰¹ Autosplenectomy and splenic atrophy are seen most often in the hemoglobin SS patients. Nevertheless, the spleen is sonographically visible in 64% of children 9 to 17 years old with SS disease, compared with 96% to 100% sonographic visibility of the spleen in other sickle cell subtypes.⁹²

It has been reported that splenic function has returned after bone marrow transplantation in children with sickle cell disease and functional asplenia, with return of splenic uptake documented on nuclear scintigraphy.¹⁰¹

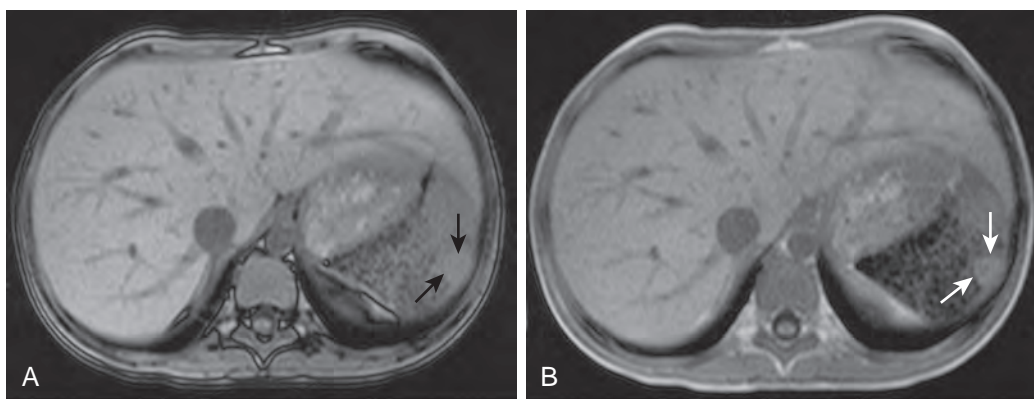


Figure 122-18 Normal island of splenic tissue (arrows) among siderotic nodules. **A.** Opposed-phase image (TE = 2.4 ms) of a double gradient-echo technique is characterized by the fat-water cancellation (i.e., chemical shift) artifact. **B.** The in-phase image (TE = 5.0 ms) is acquired last. The siderotic nodules have a pronounced decrease in signal intensity relative to their signal on the opposed-phase image. The liver and the normal splenic tissues (arrows) do not contain abnormal amounts of iron and do not demonstrate a significant change in signal intensity between phases.

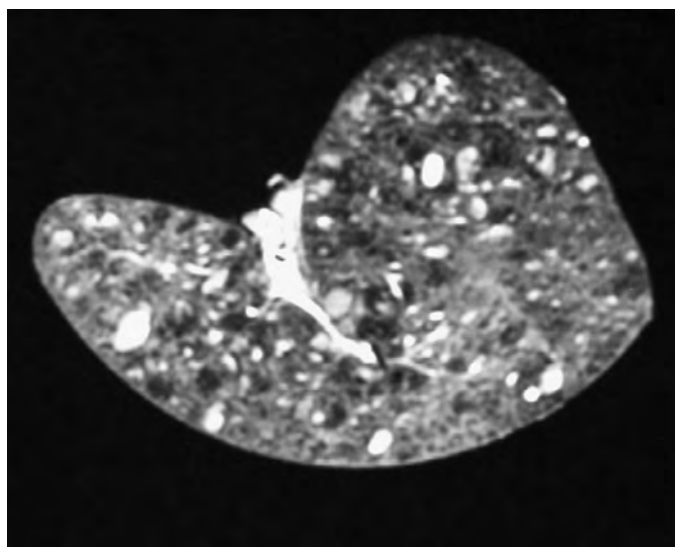


Figure 122-19 Peliosis hepatis. In the T2-weighted MR image of a surgically resected spleen with peliosis, the signal intensity of the innumerable, subcentimeter, blood-filled spaces is extremely variable.

Peliosis

Peliosis hepatis is characterized by multiple irregular cystic blood-filled spaces located within the liver and occasionally in the spleen or bone marrow. The pathogenesis of peliosis is uncertain,^{102,103} although it has been described in patients with tuberculosis, anabolic steroid use, oral contraceptive use, and human immunodeficiency virus infection.^{8,104,105}

On CT examination, peliosis is often characterized by subcentimeter lesions with variable attenuation; these lesions may resemble microabscesses.¹⁰⁵ The MR signal intensity tends to follow that of blood products, and the T1- and T2-weighted MR signal intensities are variable (Fig. 122-19).¹⁰⁵

Gaucher's Disease

Gaucher's disease is a lysosomal storage disorder caused by deficiency of the enzyme glucocerebrosidase.¹⁰⁶ Glucocerebroside accumulation within the reticuloendothelial system results in hepatosplenomegaly and bone marrow

infiltration.^{6,107,108} Splenomegaly can be marked, with symptoms due to mass effect on adjacent organs.^{107,108} Approximately 30% of patients with Gaucher's disease have numerous splenic nodules,¹⁰⁸ secondary to focal collections of the Gaucher cells and dilated, blood-filled sinusoids. The nodules typically are less than 2.5 cm in diameter.¹⁰⁸

On sonography, the multiple Gaucher nodules can be hypoechoic or hyperechoic within the same patient.¹⁰⁷ On CT, the nodules are hypodense and nonenhancing. On MRI, the nodules are slightly hypointense,¹⁰⁷ isointense, or, least often, hyperintense¹⁰⁸ on T1-weighted images and predominantly hypointense on T2-weighted images.¹⁰⁷ Gaucher nodules have also been described as being hyperintense, target-like (with central hyperintensity), or heterogeneous on T2-weighted images.¹⁰⁷ There may be associated areas of splenic infarction in 33% of patients, particularly in those individuals with larger spleens.¹⁰⁸

Histiocytic Syndromes

Histiocytic syndromes in children are divided into three categories: Langerhans cell histiocytosis; histiocytosis of mononuclear phagocytes other than Langerhans cells, including hemophagocytic lymphohistiocytosis (HLH); and malignant forms, including acute monocytic leukemia and malignant histiocytosis.¹⁰⁹

Langerhans cell histiocytosis is a proliferation of bone marrow-derived histiocytes in aggregates with mature eosinophils.¹¹⁰ Disease may be local or systemic. Splenomegaly with multiple, round, hypoechoic lesions of various sizes that resolve with systemic therapy has been described.¹¹¹

HLH is characterized by uncontrolled activation of the cellular immune system. Clinical criteria include fever, splenomegaly, pancytopenia, hypertriglyceridemia, and hypofibrinogenemia. The three primary sonographic findings in children with HLH are nonspecific and include dramatically striated gallbladder wall thickening of 5 to 7.5 mm; hyperechogenicity of the periportal region, thickened to 6 to 9 mm anterior to the portal vein; and porta hepatis lymphadenopathy.¹⁰⁹ Nodes are less often seen in the splenic hilum, and there is no biliary dilation. Splenomegaly occurs with or without portal hypertension. Half of children have anechoic peritoneal fluid. Because the findings are nonspecific and are seen in children with hepatitis, HLH can be considered if serologic test results for hepatitis are negative.¹⁰⁹

REFERENCES

- Donnelly LF, Emery KH, Bove KE, Bissett GS 3rd: Normal changes in the MR appearance of the spleen during early childhood. *AJR Am J Roentgenol* 166:635–639, 1996.
- Tonolini M, Bianco R: Nontumorous splenic emergencies: Cross-sectional imaging findings and triage. *Emerg Radiol* 20:323–332, 2013.
- Siegel MJ: *Pediatric Sonography*, ed 3, Philadelphia, 2002, Lippincott Williams & Wilkins.
- Sty JR, Conway JJ: The spleen: Development and functional evaluation. *Semin Nucl Med* 15:276–298, 1985.
- Donnelly LF, Foss JN, Frush DP, Bissett GS, 3rd: Heterogeneous splenic enhancement patterns on spiral CT images in children: Minimizing misinterpretation. *Radiology* 210:493–497, 1999.
- Paterson A, Frush DP, Donnelly LF, et al: A pattern-oriented approach to splenic imaging in infants and children. *Radiographics* 19:1465–1485, 1999.
- Ito K, Mitchell DG, Honjo K, et al: MR imaging of acquired abnormalities of the spleen. *AJR Am J Roentgenol* 168:697–702, 1997.
- Hilmes MA, Strouse PJ: The pediatric spleen. *Semin Ultrasound CT MR* 28:3–11, 2007.
- Donnelly LF, Bissett GS, 3rd: Dark spleens and livers on MRI after chemotherapy: Is it really iron overload? *Pediatr Radiol* 28:486, 1998.
- Treves ST: *Pediatric Nuclear Medicine*, ed 2, New York, 1995, Springer-Verlag.
- Rosenberg HK, Markowitz RI, Kolberg H, et al: Normal splenic size in infants and children: Sonographic measurements. *AJR Am J Roentgenol* 157:119–121, 1991.
- Larsen WJ: *Human Embryology*, New York, 2001, Churchill Livingstone.
- Freeman JL, Jafri SZ, Roberts JL, et al: CT of congenital and acquired abnormalities of the spleen. *Radiographics* 13:597–610, 1993.
- Mortele KJ, Mortele B, Silverman SG: CT features of the accessory spleen. *AJR Am J Roentgenol* 183:1653–1657, 2004.
- Thipphavong S, Duignan S, Schindera ST: Nonneoplastic, benign, and malignant splenic diseases. *AJR* 203:315–322, 2014.
- Curtis GM, Movitz D: The surgical significance of the accessory spleen. *Ann Surg* 123:276–298, 1946.
- Jacir NN, Robertson FM, Crombleholme TM, Harris BH: Recurrence of immune thrombocytopenic purpura after splenectomy. *J Pediatr Surg* 31:115–116, 1996.
- Facon T, Caulier MT, Fenaux P, et al: Accessory spleen in recurrent chronic immune thrombocytopenic purpura. *Am J Hematol* 41:184–189, 1992.
- Stiris MG: Accessory spleen versus left adrenal tumor: Computed tomographic and abdominal angiographic evaluation. *J Comput Assist Tomogr* 4:543–544, 1980.
- Jang KM, Kim SH, Lee SJ, et al: Differentiation of an intrapancreatic accessory spleen from a small (<3-cm) solid pancreatic tumor: Value of diffusion-weighted MR imaging. *Radiology* 266:159–167, 2013.
- Gok M, Karakas SP: Torsion of a splenule. *Pediatr Radiol* 40:S88, 2010.
- Applegate KE, Goske MJ, Pierce G, Murphy D: Situs revisited: Imaging of the heterotaxy syndrome. *Radiographics* 19:837–852, 1999.
- Vanderdood K, Op de Beeck B, Desprechins B, Osteaux M: Biliary atresia and cerebellar hypoplasia in polysplenia syndrome. *Pediatr Radiol* 33:652–654, 2003.
- Hasegawa T, Kimura T, Sasaki T, Okada A: Living-related liver transplantation for biliary atresia associated with polysplenia syndrome. *Pediatr Transplant* 6:78–81, 2002.
- Strouse PJ, Haller JO, Berdon WE, et al: Horseshoe adrenal gland in association with asplenia: Presentation of six new cases and review of the literature. *Pediatr Radiol* 32:778–782, 2002.
- Bakir M, Bilgic A, Ozmen M, Caglar M: The value of radionuclide splenic scanning in the evaluation of asplenia in patients with heterotaxy. *Pediatr Radiol* 24:25–28, 1994.
- Swischuk LE, Williams JB, John SD: Torsion of wandering spleen: The whorled appearance of the splenic pedicle on CT. *Pediatr Radiol* 23:476–477, 1993.
- Herman TE, Siegel MJ: CT of acute splenic torsion in children with wandering spleen. *AJR Am J Roentgenol* 156:151–153, 1991.
- Allen KB, Andrews G: Pediatric wandering spleen—the case for splenopexy: Review of 35 reported cases in the literature. *J Pediatr Surg* 24:432–435, 1989.
- Gunning KA, Rosenberg IL: Symptomatic wandering spleen. *Br J Surg* 80:93, 1993.
- Steinberg R, Karmazyn B, Dlugy E, et al: Clinical presentation of wandering spleen. *J Pediatr Surg* 37:E30, 2002.
- Crosta ID, Inserra A, Gil CP, et al: Abdominal pain and wandering spleen in young children: The importance of an early diagnosis. *J Pediatr Surg* 44:1446–1449, 2009.
- Kessler A, Miller E, Keidar S, et al: Mass at the splenic hilum: A clue to torsion of a wandering spleen located in a normal left upper quadrant position. *J Ultrasound Med* 22:527–530, 2003.
- Nemcek AA, Jr, Miller FH, Fitzgerald SW: Acute torsion of a wandering spleen: Diagnosis by CT and duplex Doppler and color flow sonography. *AJR Am J Roentgenol* 157:307–309, 1991.
- Teramoto R, Opas LM, Andrassy R: Splenic torsion with prune belly syndrome. *J Pediatr* 98:91–92, 1981.
- Cirillo RL, Jr, Coley BD, Binkovitz LA, Jayanthi RV: Sonographic findings in splenogonadal fusion. *Pediatr Radiol* 29:73–75, 1999.
- Dachman AH, Ros PR, Murari PJ, et al: Non-parasitic splenic cysts: A report of 52 cases with radiologic-pathologic correlation. *AJR Am J Roentgenol* 147:537–542, 1986.
- Spencer NJ, Arthur RJ, Stringer MD: Ruptured splenic epidermoid cyst: Case report and imaging appearances. *Pediatr Radiol* 26:871–873, 1996.
- Malhotra A, Jones LT: Epidermoid cyst of the spleen. *Pediatr Radiol* 38:714, 2008.
- Ladino-Torres ME, Strouse PJ: Gastrointestinal tumors in children. *Radiol Clin North Am* 49:665–677, 2011.
- Urrutia M, Mergo PJ, Ros LH, et al: Cystic masses of the spleen: Radiologic-pathologic correlation. *Radiographics* 16:107–129, 1996.
- Taylor AJ, Dodds WJ, Erickson SJ, Stewart ET: CT of acquired abnormalities of the spleen. *AJR Am J Roentgenol* 157:1213–1219, 1991.
- Pistola F, Markowitz SK: Splenic lymphangiomatosis: CT diagnosis. *AJR Am J Roentgenol* 150:121–122, 1988.
- Robertson RL, Robson CD, Barnes PD, Burrows PE: Head and neck vascular anomalies of childhood. *Neuroimaging Clin N Am* 9:115–132, 1999.
- Rao BK, AuBuchon J, Lieberman LM, Polcyn RE: Cystic lymphangiomatosis of the spleen: A radiologic-pathologic correlation. *Radiology* 141:781–782, 1981.
- Cope C: *Current Techniques in Interventional Radiology*, ed 2, New York, 1996, McGraw-Hill.
- Mulliken JB, Young A: *Vascular Birthmarks: Hemangiomas and Malformations*, Philadelphia, 1988, WB Saunders.
- Greene AK, Burrows PE, Smith L, Mulliken JB: Periorbital lymphatic malformation: Clinical course and management in 42 patients. *Plast Reconstr Surg* 115:22–30, 2005.
- Wadsworth DT, Newman B, Abramson SJ, et al: Splenic lymphangiomatosis in children. *Radiology* 202:173–176, 1997.
- Ferrozzi F, Bova D, Draghi F, Garlaschi G: CT findings in primary vascular tumors of the spleen. *AJR Am J Roentgenol* 166:1097–1101, 1996.
- Mulliken JB, Glowacki J: Hemangiomas and vascular malformations in infants and children: A classification based on endothelial characteristics. *Plast Reconstr Surg* 69:412–422, 1982.
- Lowe LH, Marchant TC, Rivard DC, Scherbel AJ: Vascular malformations: Classification and terminology the radiologist needs to know. *Semin Roentgenol* 47:106–117, 2012.
- Elsayes KM, Narra VR, Mukundan G, et al: MR imaging of the spleen: Spectrum of abnormalities. *Radiographics* 25:967–982, 2005.
- Abbott RM, Levy AD, Aguilera NS, et al: From the archives of the AFIP: Primary vascular neoplasms of the spleen: Radiologic-pathologic correlation. *Radiographics* 24:1137–1163, 2004.
- Ramani M, Reinhold C, Semelka RC, et al: Splenic hemangiomas and hamartomas: MR imaging characteristics of 28 lesions. *Radiology* 202:166–172, 1997.
- Solbiati L, Bossi MC, Bellotti E, et al: Focal lesions in the spleen: Sonographic patterns and guided biopsy. *AJR Am J Roentgenol* 140:59–65, 1983.
- Ros PR, Moser RP, Jr, Dachman AH, et al: Hemangioma of the spleen: Radiologic-pathologic correlation in ten cases. *Radiology* 162:73–77, 1987.
- Burrows PE, Robertson RL, Barnes PD: Angiography and the evaluation of cerebrovascular disease in childhood. *Neuroimaging Clin N Am* 6:561–588, 1996.
- Zhang LF, Tou JF, Wang X, et al: Splenic hamartomas in two children. *World J Surg Oncol* 12:180–185, 2014.
- Gaetke-Udager K, Wasnik AP, Kaza RK, et al: Multimodality imaging of splenic lesions and the role of non-vascular, image-guided intervention. *Abdom Imaging* 39:570–587, 2014.
- Lee H, Maeda K: Hamartoma of the spleen. *Arch Pathol Lab Med* 133:147–151, 2009.
- Thompson SE, Walsh EA, Cramer BC, et al: Radiological features of a symptomatic splenic hamartoma. *Pediatr Radiol* 26:657–660, 1996.
- Darden JW, Teeslink R, Parrish A: Hamartoma of the spleen: A manifestation of tuberous sclerosis. *Am Surg* 41:564–566, 1975.
- Goerg C, Schwerk WB, Goerg K: Sonography of focal lesions of the spleen. *AJR Am J Roentgenol* 156:949–953, 1991.

65. Schellong G, Waubke-Landwehr AK, Langermann HJ, et al: Prediction of splenic involvement in children with Hodgkin's disease. Significance of clinical and intraoperative findings. A retrospective statistical analysis of 154 patients in the German therapy study DAL-HD-78. *Cancer* 57:2049-2056, 1986.
66. Lutz N, Mahboubi S, Nance ML, Stafford PW: The significance of contrast blush on computed tomography in children with splenic injuries. *J Pediatr Surg* 39:491-494, 2004.
67. Lynn KN, Werder GM, Callaghan RM, et al: Pediatric blunt splenic trauma: A comprehensive review. *Pediatr Radiol* 39:904-916, 2009.
68. Cox CS, Jr, Geiger JD, Liu DC, Garver K: Pediatric blunt abdominal trauma: Role of computed tomography vascular blush. *J Pediatr Surg* 32:1196-1200, 1997.
69. Church NG, May G, Sigalet DL: A minimally invasive approach to bile duct injury after blunt liver trauma in pediatric patients. *J Pediatr Surg* 37:773-775, 2002.
70. Huebner S, Reed MH: Analysis of the value of imaging as part of the follow-up of splenic injury in children. *Pediatr Radiol* 31:852-855, 2001.
71. Tinkoff G, Esposito TJ, Reed J, et al: American Association for the Surgery of Trauma organ injury scale I: Spleen, liver and kidney, validation based on the National Trauma Data Bank. *J Am Coll Surg* 207:646-655, 2008.
72. Mehall JR, Ennis JS, Saltzman DA, et al: Prospective results of a standardized algorithm based on hemodynamic status for managing pediatric solid organ injury. *J Am Coll Surg* 193:347-353, 2001.
73. Krupnick AS, Teitelbaum DH, Geiger JD, et al: Use of abdominal ultrasonography to assess pediatric splenic trauma. Potential pitfalls in the diagnosis. *Ann Surg* 225:408-414, 1997.
74. van Schuppen J, Olthof DC, Wilde JC, et al: Diagnostic accuracy of a step-up imaging strategy in pediatric patients with blunt abdominal trauma. *Eur J Radiol* 83:206-211, 2014.
75. Leinwand MJ, Atkinson CC, Mooney DP: Application of the APSA evidence-based guidelines for isolated liver or spleen injuries: A single institution experience. *J Pediatr Surg* 39:487-490, discussion 487-490, 2004.
76. Emery KH, Babcock DS, Borgman AS, Garcia VF: Splenic injury diagnosed with CT: US follow-up and healing rate in children and adolescents. *Radiology* 212:515-518, 1999.
77. Mathurin J, Lallemand D: Splenosis simulating an abdominal lymphoma. *Pediatr Radiol* 21: 69-70, 1990.
78. Brancatelli G, Vilgrain V, Zappa M, Lagalla R: Case 80: Splenosis. *Radiology* 234:728-732, 2005.
79. Levy AD, Shaw JC, Sobin LH: Secondary tumors and tumorlike lesions of the peritoneal cavity: Imaging features with pathologic correlation. *Radiographics* 29:347-373, 2009.
80. Gunes I, Yilmazlar T, Sarikaya I, et al: Scintigraphic detection of splenosis: Superiority of tomographic selective spleen scintigraphy. *Clin Radiol* 49:115-117, 1994.
81. Pastakia B, Shawker TH, Thaler M, et al: Hepatosplenic candidiasis: Wheels within wheels. *Radiology* 166:417-421, 1988.
82. Sander A, Posselt M, Oberle K, Bredt W: Sero-prevalence of antibodies to *Bartonella henselae* in patients with cat scratch disease and in healthy controls: Evaluation and comparison of two commercial serological tests. *Clin Diagn Lab Immunol* 5:486-490, 1998.
83. Rappaport DC, Cumming WA, Ros PR: Disseminated hepatic and splenic lesions in cat-scratch disease: Imaging features. *AJR Am J Roentgenol* 156:1227-1228, 1991.
84. Moriarty RA, Margileth AM: Cat scratch disease. *Infect Dis Clin North Am* 1:575-590, 1987.
85. Sakulsky SB, Wallace RB, Silverstein MN, Dockerty MB: Ruptured spleen in infectious mononucleosis. *Arch Surg* 94:349-352, 1967.
86. Kumar V, Fausto N, Abbas A: Robbins and Cotran's Pathologic Basis of Disease, ed 7, Philadelphia, 2005, Elsevier.
87. Safran D, Bloom GP: Spontaneous splenic rupture following infectious mononucleosis. *Am Surg* 56:601-605, 1990.
88. Vezina WC, Nicholson RL, Cohen P, Chamberlain MJ: Radionuclide diagnosis of splenic rupture in infectious mononucleosis. *Clin Nucl Med* 9:341-344, 1984.
89. Farley DR, Zietlow SP, Bannon MP, Farnell MB: Spontaneous rupture of the spleen due to infectious mononucleosis. *Mayo Clin Proc* 67:846-853, 1992.
90. Johnson MA, Cooperberg PL, Boisvert J, et al: Spontaneous splenic rupture in infectious mononucleosis: Sonographic diagnosis and follow-up. *AJR Am J Roentgenol* 136:111-114, 1981.
91. Rabushka LS, Kawashima A, Fishman EK: Imaging of the spleen: CT with supplemental MR examination. *Radiographics* 14:307-332, 1994.
92. Walker TM, Serjeant GR: Focal echogenic lesions in the spleen in sickle cell disease. *Clin Radiol* 47:114-116, 1993.
93. Sheth S, Ruzal-Shapiro C, Piomelli S, Berdon WE: CT imaging of splenic sequestration in sickle cell disease. *Pediatr Radiol* 30:830-833, 2000.
94. Magid D, Fishman EK, Siegelman SS: Computed tomography of the spleen and liver in sickle cell disease. *AJR Am J Roentgenol* 143:245-249, 1984.
95. Brousse V, Buffet P, Rees D: The spleen and sickle cell disease. *Br J Haematol* 166:165-176, 2014.
96. Roshkow JE, Sanders LM: Acute splenic sequestration crisis in two adults with sickle cell disease: US, CT, and MR imaging findings. *Radiology* 177:723-725, 1990.
97. Adler DD, Glazer GM, Aisen AM: MRI of the spleen: Normal appearance and findings in sickle-cell anemia. *AJR Am J Roentgenol* 147: 843-845, 1986.
98. Levin TL, Berdon WE, Haller JO, et al: Intrasplicenic masses of "preserved" functioning splenic tissue in sickle cell disease: Correlation of imaging findings (CT, ultrasound, MRI, and nuclear scintigraphy). *Pediatr Radiol* 26:646-649, 1996.
99. Merkle EM, Nelson RC: Dual gradient-echo in-phase and opposed-phase hepatic MR imaging: A useful tool for evaluating more than fatty infiltration or fatty sparing. *Radiographics* 26:1409-1418, 2006.
100. Heck LL, Brittin GM: Splenic uptake of both technetium-99m diphosphonate and technetium-99m sulfur colloid in sickle cell β^0 thalassemia. *Clin Nucl Med* 14:557-563, 1989.
101. Ferster A, Bujan W, Corazza F, et al: Bone marrow transplantation corrects the splenic reticuloendothelial dysfunction in sickle cell anemia. *Blood* 81:1102-1105, 1993.
102. Yanoff M, Rawson AJ: Peliosis hepatis: An anatomic study with demonstration of two varieties. *Arch Pathol* 77:159-165, 1932.
103. Davidson J, Tung K: Splenic peliosis: An unusual entity. *Br J Radiol* 83:e126-e128, 2010.
104. Zak FG: Peliosis hepatis. *Am J Pathol* 26:1-15, 1950.
105. Maves CK, Caron KH, Bisset GS, 3rd, Agarwal R: Splenic and hepatic peliosis: MR findings. *AJR Am J Roentgenol* 158:75-76, 1992.
106. Brady RO, Kanfer JN, Bradley RM, Shapiro D: Demonstration of a deficiency of glucocerebrosidase-cleaving enzyme in Gaucher's disease. *J Clin Invest* 45:1112-1115, 1966.
107. Poll LW, Koch JA, vom Dahl S, et al: Gaucher disease of the spleen: CT and MR findings. *Abdom Imaging* 25:286-289, 2000.
108. Hill SC, Damaska BM, Ling A, et al: Gaucher disease: Abdominal MR imaging findings in 46 patients. *Radiology* 184:561-566, 1992.
109. Chateil J, Brun M, Perel Y, et al: Abdominal ultrasound findings in children with hemophagocytic lymphohistiocytosis. *Eur Radiol* 9:474-477, 1999.
110. Mampaey S, Warson F, Van Hedent E, De Schepper AM: Imaging findings in Langerhans' cell histiocytosis of the liver and the spleen in an adult. *Eur Radiol* 9:96-98, 1999.
111. Muwakkit S, Gharagzloo A, Souid AK, Spirt BA: The sonographic appearance of lesions of the spleen and pancreas in an infant with Langerhans' cell histiocytosis. *Pediatr Radiol* 24:222-223, 1994.

Diseases of the Pediatric Abdominal Wall, Peritoneum, and Mesentery

KEVIN P. BOYD | ARTHUR B. MEYERS | ANA MARIA GACA |
GEORGE S. BISSETT III

CHAPTER OUTLINE

Embryology

Defects of the Anterior Abdominal Wall

Pentalogy of Cantrell

Omphalocele

Gastroschisis

Exstrophy of the Bladder

Prune-Belly Syndrome

Peritoneum

Peritonitis

Mesenteric and Omental Cysts

Lymphadenopathy and Neoplasms of the Mesentery and Peritoneum

Embryology

At the end of the third week of gestation, the embryo, a relatively flat disk, begins to form a tube by means of four folds. These include one cephalic, one caudal, and two lateral folds, which combine to form the anterior abdominal wall at the region of the umbilicus. Failure of these folds to completely unite may result in defects of the anterior abdominal wall. The type of defect created depends on which of the folds has failed to fuse.

In the developing embryo, the midgut, the portion of bowel from the insertion of the bile duct to the splenic flexure of the colon, rapidly elongates at approximately the fifth to sixth week of gestation, and the abdominal cavity transiently becomes too small to accommodate this bowel. This results in physiologic herniation of bowel into the extraembryonic celom in the umbilical cord. These herniated loops of bowel return to the abdomen at approximately the 10th week of gestation. During this time, the bowel undergoes a 270-degree counterclockwise rotation. The failure of the bowel to return to the abdominal cavity results in an omphalocele. Gastroschisis occurs when herniation of abdominal viscera occurs through a defect in the anterior abdominal wall, usually to the right of the umbilicus.¹

The increasing use of prenatal ultrasound and routine screening with maternal serum α -fetoprotein has enabled earlier diagnosis of defects of the anterior abdominal wall, including pentalogy of Cantrell, omphalocele, gastroschisis, and bladder exstrophy. Although effort has been made to find a common cause for these abdominal wall defects, they seem to be disparate entities.² Overall, the prognosis for these conditions tends to depend on associated congenital anomalies.

Defects of the Anterior Abdominal Wall

PENTALOGY OF CANTRELL

Pentalogy of Cantrell is composed of two major abnormalities—ectopia cordis and a midline thoracoabdominal wall defect—associated with abnormalities of the tissues between these two areas and with defects of the lower sternum, diaphragmatic pericardium, and anterior diaphragm. Less severe cases have been described, which are considered to be incomplete forms. The cause is unclear, but there may be a genetic component. Numerous other abnormalities are associated with pentalogy of Cantrell, including cleft lip and palate³ and limb anomalies.⁴

Clinically, patients generally present with dyspnea and cyanosis. These newborns have an anterior abdominal wall defect, usually an omphalocele, and a structural heart defect, such as atrial septal defect, ventricular septal defect, or tetralogy of Fallot. The anterior abdominal wall defect, paired with the short or cleft sternum, gives the appearance of a high epigastrium filled by the heart.⁴

Diagnosis of pentalogy of Cantrell is usually made by prenatal ultrasound, when findings of omphalocele, ectopia cordis, and congenital heart disease are confirmed. Postnatally, chest radiographs demonstrate abnormal positioning of the heart, usually with dextrorotation. Thoracic abnormalities may also be evident, including pulmonary hypoplasia and rib anomalies.⁴ Computed tomography (CT) can be useful in preoperative evaluation of the thoracic cavity before repair of ectopia cordis.³ CT angiography and magnetic resonance imaging (MRI) can define cardiovascular anatomy, the degree of diaphragmatic deficiency, and the degree of transdiaphragmatic herniation of the bowel or liver.⁵

Treatment of pentalogy of Cantrell involves closure of the thoracoabdominal wall defect, but success with corrective surgery has been limited. Postoperative complications include increased intrathoracic and intra-abdominal pressures, which can result in respiratory and cardiovascular compromise.⁴ The prognosis depends on the severity of the cardiac anomalies and on the severity of any other associated abnormalities.³

OMPHALOCELE

An omphalocele is herniation of abdominal viscera into the intact umbilical cord, with a membranous covering over the eviscerated organs unless there has been membrane rupture (Fig. 123-1). The spectrum of severity ranges from a small umbilical hernia to a large defect, resulting in evisceration of all abdominal organs.⁶ The incidence of omphalocele is 1 case in 4000 to 7000 live births.² Although an omphalocele can be an

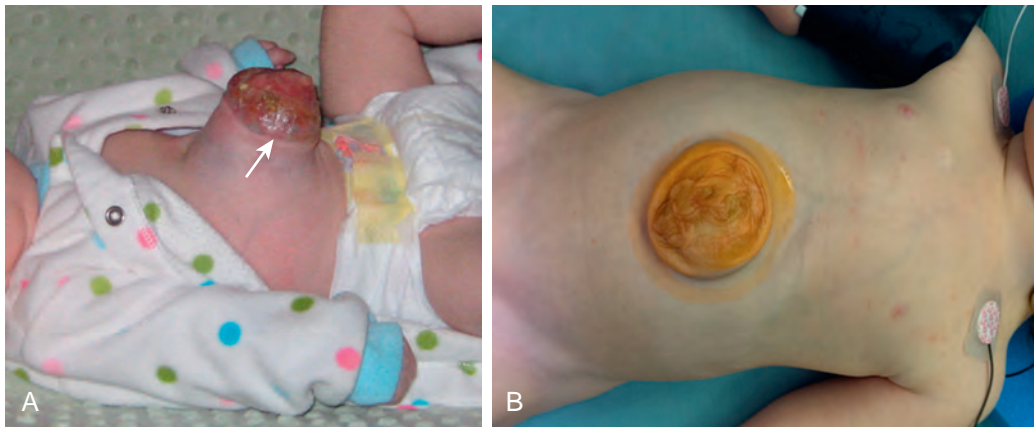


Figure 123-1 Giant omphalocele. Giant omphalocele with staged closure at 1 year of age. **A.** Paint and wait technique with progression of keratinization at the base (arrow). **B.** Preoperative image demonstrates a smaller, completely keratinized sac. (Courtesy J. Densmore, MD, Children's Hospital of Wisconsin, Milwaukee, WI.)

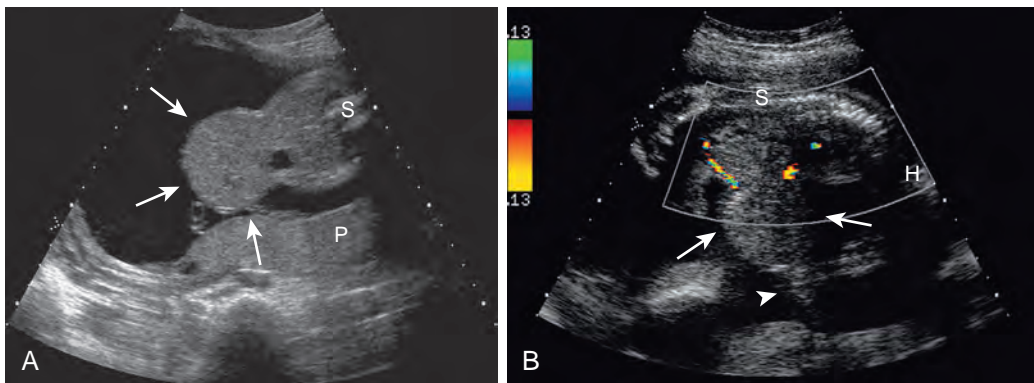


Figure 123-2 Omphalocele. **A.** Transverse prenatal ultrasound image demonstrates the liver herniating through an anterior abdominal wall defect (arrows) in a fetus with an omphalocele. **B.** Sagittal image also demonstrates the eviscerated liver (arrows), with the umbilical cord inserting into the membrane containing the liver (arrowhead). H, Head; P, placenta; S, spine.

isolated abnormality, associated anomalies are more common with an omphalocele than with gastroschisis.⁷ Associated genetic abnormalities are seen in up to 54% of patients; trisomy 18 is most common, but trisomy 13, Beckwith-Wiedemann syndrome, and rarely uniparental disomy (i.e., inheritance of both copies of a chromosome pair from one parent and none from the other) also occur. Studies suggest that associated chromosomal abnormalities are more likely in patients with a small omphalocele that does not include herniated liver.^{2,7} Visceral abnormalities are seen in up to 70%, including neural tube defects and cardiac, renal, facial, and skeletal abnormalities and pentalogy of Cantrell.^{2,7} Gastrointestinal anomalies can include imperforate anus, colonic atresia, and Hirschsprung's disease.

Physiologic herniation of bowel is normally seen between the 8th and 12th weeks of gestation; omphalocele cannot be reliably diagnosed until after this period. Omphalocele usually is diagnosed on prenatal ultrasound; patients with omphalocele demonstrate abdominal viscera within a mass at the umbilical cord insertion site⁶ with a covering membrane (Fig. 123-2). The abdominal wall defect of an omphalocele tends to be large.⁷ The herniated viscera usually include liver with various amounts of bowel.⁶ When the omphalocele contains herniated liver and biliary structures, it is referred to as a giant omphalocele (Fig. 123-3).² Ascites can be seen within the abdomen

or omphalocele, and polyhydramnios may be present.⁶ Prenatal diagnosis should also include a thorough search for associated anomalies.⁷ Fetal MRI is increasingly performed in patients with omphalocele to characterize the size and location of the anterior wall defect, to characterize the sac and its contents, and to identify associated anomalies (see Fig. 123-3).⁸ In addition, fetal MRI can be used to calculate lung volumes in patients with giant omphalocele to predict the degree of pulmonary hypoplasia, which is predictive of postnatal morbidity.⁹ Postnatal imaging of infants with omphalocele is generally reserved for identification of associated anomalies and should include echocardiography and renal ultrasound.

Studies of the route of delivery for infants with omphalocele have demonstrated no significant improvement in outcome with cesarean delivery compared with vaginal delivery. Cesarean delivery usually is reserved for patients with obstetric indications. Exceptions are patients who have a giant omphalocele, who are at increased risk of fatal hemorrhage from liver injury.²

Unlike in gastroschisis, the herniated bowel and liver in an omphalocele are morphologically and functionally normal.⁷ The membrane that covers the herniated viscera in an omphalocele decreases fluid loss and protects against the metabolic abnormalities commonly seen in patients with gastroschisis.²



Figure 123-3 Omphalocele. Sagittal balanced gradient-echo MR sequence in a 24-week-gestational-age fetus with a giant omphalocele. There is a large anterior abdominal wall defect (white solid arrows) with herniation of a large portion of the liver (arrowheads) and loops of small bowel (dashed arrow). The covering membrane of the omphalocele is clearly seen (open arrows), and a portion of the umbilical cord is seen attaching to the apex of the sac (black arrow).

The treatment of omphalocele is dictated by the presence of comorbidities (cardiovascular compromise, pulmonary insufficiency), the coexisting congenital syndromes or anomalies, and the size of the defect. Surgical options include primary closure for smaller defects and delayed closure, by the “paint and wait” technique, allowing time for the patient to grow enough to accommodate larger omphaloceles (see Fig. 123-1).¹⁰ Functionally, patients with omphalocele are typically spared the problems of bowel motility associated with gastroschisis. The protective covering membrane over the omphalocele affords a protective barrier to amniotic fluid exposure. The prognosis of patients with omphalocele predominantly depends on associated chromosomal or structural anomalies.^{2,7} Infants with an omphalocele and a cardiac anomaly have a mortality rate approaching 80%.² Prognosis is poorer when the covering membrane has ruptured because these patients tend to have significantly smaller birth weight than those with an intact membrane, regardless of omphalocele size. Patients with giant omphaloceles also tend to have pulmonary hypoplasia, which can complicate primary repair.^{6,11}

GASTROSCHISIS

Gastroschisis refers to herniation of abdominal viscera, usually the small and large bowel, through a defect in the anterior abdominal wall, typically to the right of the umbilicus. The umbilical cord insertion is intact, and there is no membrane covering the eviscerated organs (Fig. 123-4).² These bowel loops are subsequently exposed to amniotic fluid in utero.¹²

The incidence of gastroschisis is 1 case in 10,000 live births,² but epidemiologic studies from the United States, Europe, and Japan have found increasing rates of gastroschisis, by as much as 10-fold, during the past decade. This is not thought to represent improved detection or reporting because the incidence of omphalocele has remained stable during the same period,

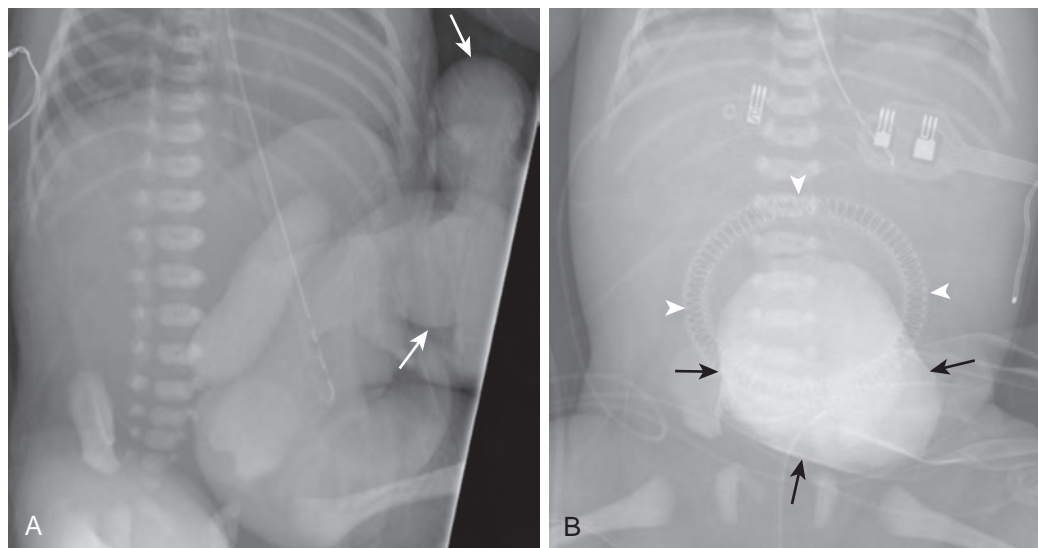


Figure 123-4 Gastroschisis. **A.** Frontal radiograph of the abdomen in a newborn with gastroschisis on the first day of life. There are multiple fluid-filled loops of bowel outside of the abdomen (arrows) that do not contain a covering. **B.** Frontal radiograph of the abdomen in the same patient after silo placement. The bowel loops (arrows) are now contained within the silo covering. The spring within the base of the silo is indicated by arrowheads.

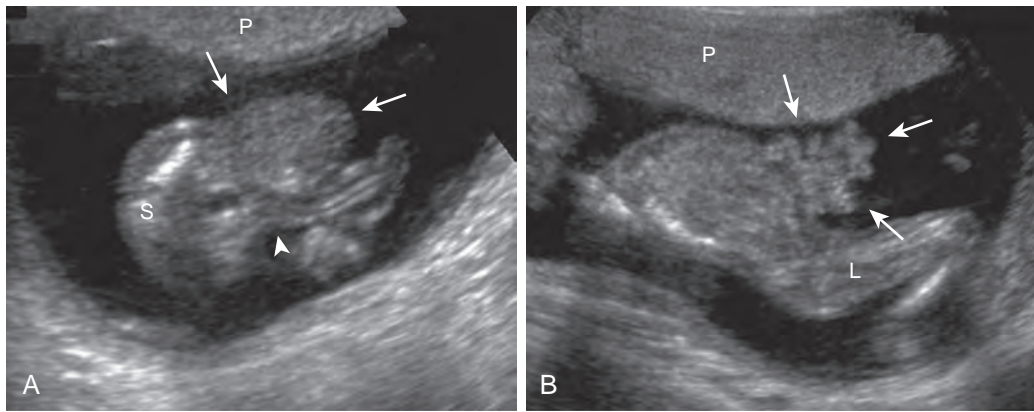


Figure 123-5 Gastroschisis. **A.** The prenatal transverse ultrasound image demonstrates the bowel (arrows) herniating through an anterior abdominal wall defect to the right of the umbilical cord insertion (arrowhead). **B.** The sagittal image demonstrates eviscerated bowel floating loosely in amniotic fluid without a membranous covering (arrows). L, Lower extremity; P, placenta; S, spine.

and the rate at which the incidence has increased suggests environmental risk factors rather than genetic ones.¹³⁻¹⁵ Although reports of familial gastroschisis suggest an inherited propensity, numerous studies have suggested that teratogens play a role. Gastroschisis is more likely to occur in young mothers who are heavy smokers, use alcohol during pregnancy, have poor nutrition during pregnancy, or use over-the-counter medications with vasoactive properties (e.g., acetaminophen, aspirin, pseudoephedrine, phenylpropanolamine, ephedrine, methylenedioxymethamphetamine [ecstasy]) early in pregnancy. Clusters of infants with this defect have also been described near toxic waste sites.^{2,15}

Unlike omphalocele, gastroschisis tends not to be associated with chromosomal abnormalities. Up to 31% of male patients with gastroschisis have cryptorchidism, and the testicles may be part of the herniated viscera.² Up to 25% of patients with gastroschisis have intestinal atresia or stenosis or other bowel complications. Other than bowel atresias and cryptorchidism, associated anomalies are rare.¹⁵

The cause of intestinal atresia with gastroschisis is unclear, with theories suggesting a common vascular insult causing the gastroschisis and atresia rather than bowel ischemia from constriction by the defect in the anterior abdominal wall.^{2,7} In addition to atresia, the herniated bowel in patients with gastroschisis is usually damaged, with bowel shortening, thickening, and development of a fibrous covering. Most patients have problems with poor bowel motility and absorptive function long after surgical correction of the defect.⁷ Studies have suggested that the causes include exposure to amniotic fluid, constriction-induced injury at the defect, and altered gene expression within enterocytes.^{6,12} The bowel injury that occurs in utero seems to occur late in pregnancy, with findings of progressive bowel dilation and thickening.⁷ Asymmetric bowel wall dilation, with or without meconium peritonitis, suggests bowel atresia.^{6,12} Not all bowel injury occurs in utero; improved prognosis has been described for early repair or silo application, suggesting that some damage may occur postnatally.⁷

The diagnosis of gastroschisis is typically made on prenatal ultrasound, and maternal screening demonstrates elevated serum levels of α -fetoprotein.^{7,12} The diagnosis of gastroschisis can be made as early as 12 weeks of gestation⁷ by ultrasonographic identification of herniated viscera without a covering membrane in the presence of a normal umbilical cord insertion

(Fig. 123-5). The abdominal wall defect is usually small, most often less than 4 cm in diameter. In addition to bowel, organs that can herniate include liver, stomach, testes, and fallopian tubes.⁶

Prenatal diagnosis enables early diagnosis of other abnormalities and allows decisions to be made about the location and timing of delivery, optimizing postnatal care. As with omphalocele, studies have failed to show improved survival or better outcomes for infants with gastroschisis delivered by cesarean section compared with vaginal delivery, with the exception of cases with eviscerated liver.¹² Infants delivered at medical centers with postnatal and surgical experience in the care of gastroschisis have improved outcome compared with patients delivered elsewhere.⁶

Treatment of gastroschisis involves the return of the herniated organs to the abdominal cavity with primary closure, if possible. This tends to be more urgent with gastroschisis than with omphalocele because the lack of a covering membrane results in increased fluid loss. If the abdominal cavity is too small to tolerate a primary repair because of size, a silo repair may be necessary, with the gradual return of the eviscerated organs to the abdominal cavity during several days (see Fig. 123-4). One risk of closure includes increased intra-abdominal pressures that can cause vascular and respiratory compromise,² urethral obstruction, and bowel ischemia.⁶ In cases of cryptorchidism, the testicles are usually returned to the abdominal cavity at the time of repair of the abdominal wall defect, and most eventually descend to the normal scrotal position.²

The prognosis for patients with gastroschisis depends on the presence of small bowel atresia or stenosis and on the condition of the herniated bowel.^{7,12} Postnatal imaging may be requested to detect small bowel strictures or areas of perforation, both of which are seen in complex gastroschisis and may not be predicted by prenatal imaging (Fig. 123-6).¹⁶ Although the cause of bowel injury is unclear, it affects outcome by leading to intrauterine growth retardation, amniotic fluid abnormalities, and preterm labor.⁷ Postnatally, the bowel injury results in poor weight gain, decreased bowel motility, and feeding intolerance.² Return of bowel motility is slow, regardless of the presence or absence of bowel atresia or stenosis.¹²

Mortality of patients with gastroschisis is commonly related to short gut, which can be congenital or can result from volvulus

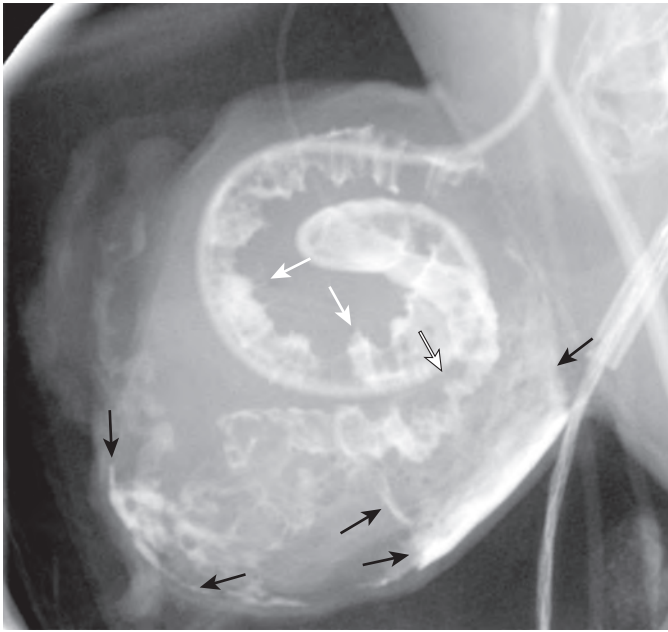


Figure 123-6 Complicated gastroschisis. Fluoroscopic image after injection of water-soluble contrast material through a jejunostomy tube. There is irregularity of jejunal loops (white arrows) and extraluminal extravasation of contrast material and pooling of contrast material in the silo in at least two separate areas (black arrows).

or necrotizing enterocolitis.¹⁷ Mortality can also be tied to liver disease from prolonged parenteral nutrition, particularly in patients with bowel atresia.²

EXSTROPHY OF THE BLADDER

With an incidence of approximately 2 cases per 100,000 live births, bladder exstrophy is a rare congenital anomaly. Epidemiologic studies suggest an equal male-to-female ratio and a higher incidence among white patients compared with non-white patients (e.g., blacks, Hispanics, Asians).¹⁸

Bladder exstrophy results from a failure of closure of the anterior abdominal wall at the ventral end of the cloacal membrane.⁷ This defect produces anterior herniation of the bladder, bladder neck, and urethra.¹⁹ There is also malformation of the external genitalia, including epispadias and a small phallus in male patients and an open urethral plate and labial separation in female patients.²⁰ Other associated anomalies can include cleft palate, neural tube defects, cardiovascular and musculoskeletal abnormalities, and preterm birth.¹⁸

Because the findings of bladder exstrophy can be subtle, the diagnosis is often not made on the basis of routine screening prenatal ultrasound.²¹ Persistent nonvisualization of the bladder in combination with normal-appearing kidneys and a normal volume of amniotic fluid should raise the suspicion of bladder exstrophy. Care must be taken to avoid mistaking a completely empty bladder for an absent one because the fetal bladder normally fills and empties every 50 to 155 minutes. A soft tissue mass that can be seen in the lower abdominal wall represents the exstrophied bladder. Additional findings of bladder exstrophy include a low insertion of the umbilical cord, a small phallus and epispadias in male patients, and splaying of the iliac crests.^{20,22}



Figure 123-7 Prune-belly syndrome. Photograph of newborn infant with prune-belly syndrome shows the typical appearance, with redundant, wrinkled skin covering a protuberant abdomen that lacks normal musculature.

Bladder exstrophy repair usually is staged. The initial stage includes closure of the bladder, posterior urethra, and anterior abdominal wall, possibly with pelvic osteotomy, depending on the amount of pubic diastasis present at birth. Subsequent stages include epispadias repair and bladder neck reconstruction.²³ Findings suggest greater success when bladder closure is performed early.²⁴

As with other defects of the anterior abdominal wall, there has been no evidence to suggest that cesarean section improves outcome, but delivery at a hospital with experience in surgical care of bladder exstrophy is recommended because of resultant improved outcomes.^{7,23} There is no significant perinatal mortality associated with bladder exstrophy; however, there can be significant long-term morbidity, particularly urinary, with approximately 70% of patients requiring major reconstruction to achieve continence. Male and female patients experience decreased fertility.²¹

Prune-Belly Syndrome

Prune-belly syndrome, also known as Eagle-Barrett syndrome or triad syndrome,²⁵ is composed of abdominal wall muscle laxity, bilateral undescended testes, and urologic abnormalities.^{26,27} *Pseudo-prune-belly syndrome* refers to patients in whom not all of the classic triad is present.²⁸ The term *prune belly* is derived from the wrinkled appearance of the skin overlying the anterior abdominal wall due to the muscle laxity (Fig. 123-7).²⁵

The cause of prune-belly syndrome is unknown. Theories include a fetal insult resulting in poor abdominal muscle development and muscle atrophy from chronic intrauterine abdominal distention (i.e., chronic bladder distention from posterior urethral valves).^{25,28} There also seems to be a familial form of the disease with an unclear mode of transmission.²⁷ Prune-belly syndrome occurs almost exclusively in boys,²⁵ although in the familial form it is slightly more common in girls (28% of patients, compared with 5% in the nonfamilial form).²⁷

Structural abnormalities of the genitourinary tract include various degrees of renal dysplasia. The ureters are dilated and tortuous bilaterally. The bladder is capacious, often with a urachal remnant, including a urachal diverticulum or fistula. The patient may have urethral abnormalities, including urethral hypoplasia or atresia.^{26,28}

Other anomalies associated with prune-belly syndrome involve the musculoskeletal, cardiovascular, and gastrointestinal systems.²⁵ Gastrointestinal anomalies include malrotation, imperforate anus, and Hirschsprung's disease.²⁸ These patients are prone to pulmonary infections and tend to develop scoliosis due to abdominal muscle weakness.²⁶

On sonographic evaluation, patients with prune-belly syndrome demonstrate dilated, tortuous ureters and bilateral hydronephrosis. The kidneys may be dysmorphic or demonstrate cystic changes.²⁵ The bladder tends to be enlarged but does not appear trabeculated.²⁵ On voiding cystourethrography, patients are found to have a large, elongated bladder, often with a urachal diverticulum or fistula. Eighty-five percent of these patients have vesicoureteral reflux, which often is bilateral, into dilated tortuous ureters (Fig. 123-8). On voiding, the prostatic urethra is generally dilated, with tapering into the membranous urethra. Contrast material can also reflux into the prostatic utricle.²⁵ Patients tend to have large postvoid residual volumes of the bladder.

With regard to prognosis, there seems to be two groups of patients. The first group includes patients with significant genitourinary abnormalities, particularly chronic urethral obstruction, and pulmonary hypoplasia. They tend to be stillborn or die shortly after birth.²⁶ The second group tends to have adequate renal function, although anatomic and functional abnormalities may be present, including dilation of the urinary tract and vesicoureteral reflux. The prognosis for the second group depends on the occurrence of obstruction, sepsis, and chronic renal failure from recurrent urinary tract infections. Many die within the first 2 years of life.^{25,26} Dilation of the urinary tract does not correlate with renal function.²⁹

Peritoneum

PERITONITIS

Bacterial peritonitis in the pediatric population is commonly a result of bowel perforation in association with appendicitis, although other causes include infection from peritoneal dialysis catheters and ventriculoperitoneal shunts (Fig. 123-9).³⁰ Primary bacterial peritonitis, an inflammatory condition of the abdomen of unknown origin, is a rare entity in the pediatric population. Clinical presentation may be similar to acute appendicitis with diffuse abdominal pain, fever, and leukocytosis. Primary bacterial peritonitis is most commonly seen in patients with an underlying chronic illness, such as chronic renal disease, disseminated lupus, liver disease, or

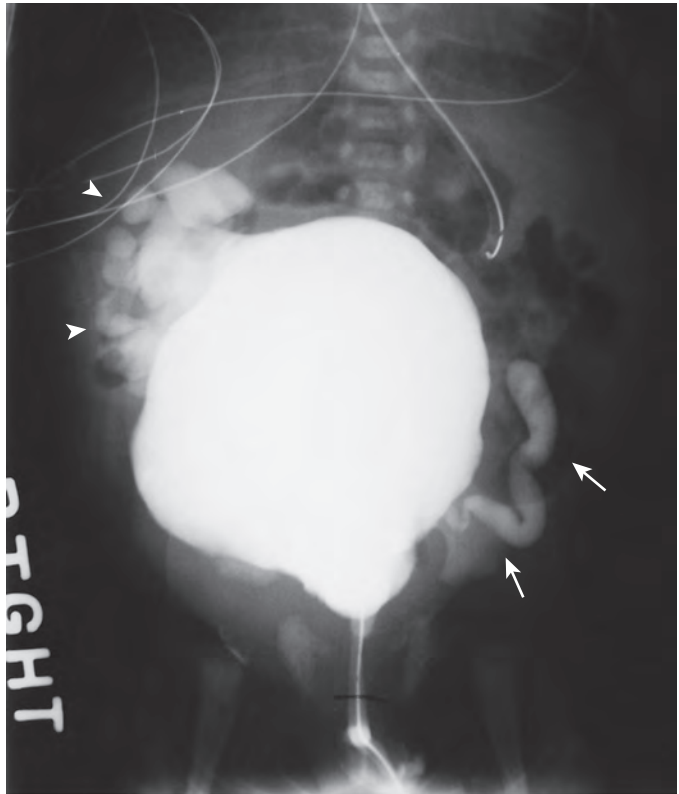


Figure 123-8 Prune-belly syndrome. Anteroposterior view of the abdomen during voiding cystourethrography demonstrates an enlarged, capacious bladder with reflux into the left ureter (arrows) and into the right renal collecting system, with right pelvocaliectasis (arrowheads).

immunosuppression.^{31,32} Peritoneal cultures typically grow a single strain of bacteria, typically gram-positive cocci, thought to reach the peritoneum by hematogenous, lymphatic, or transmural spread.

Imaging findings of primary bacterial peritonitis include complex ascites (fluid with septations and enhancement of the peritoneum) and omental inflammation, both of which may be out of proportion to any inflammatory changes in bowel. The diagnosis is confirmed with paracentesis and a fluid culture that demonstrates growth of a single bacterial species. Growth of multiple species is more consistent with perforated bowel than with primary bacterial peritonitis.³¹

Mesenteric and Omental Cysts

Omental and mesenteric cystic lesions are most often lymphatic malformations.³³ Lymphatic malformation is the preferred term of lesions that were formerly referred to as lymphangiomas or cystic hygromas.³⁴ These rare intra-abdominal cystic masses have an origin in abnormal lymphatics that lack a normal connection to the central lymphatic system.³⁵ The lesions tend to be multiseptate, mobile, and thin walled.³⁵

Mesenteric lymphatic malformations are most commonly found within the mesentery of the small bowel, but they can occur anywhere along the gastrointestinal tract from the duodenum to the rectum³⁶ or can be attached to the peritoneal lining of the abdominal cavity.³⁷ Within the mesentery, these lesions can extend from the base of the mesentery into the

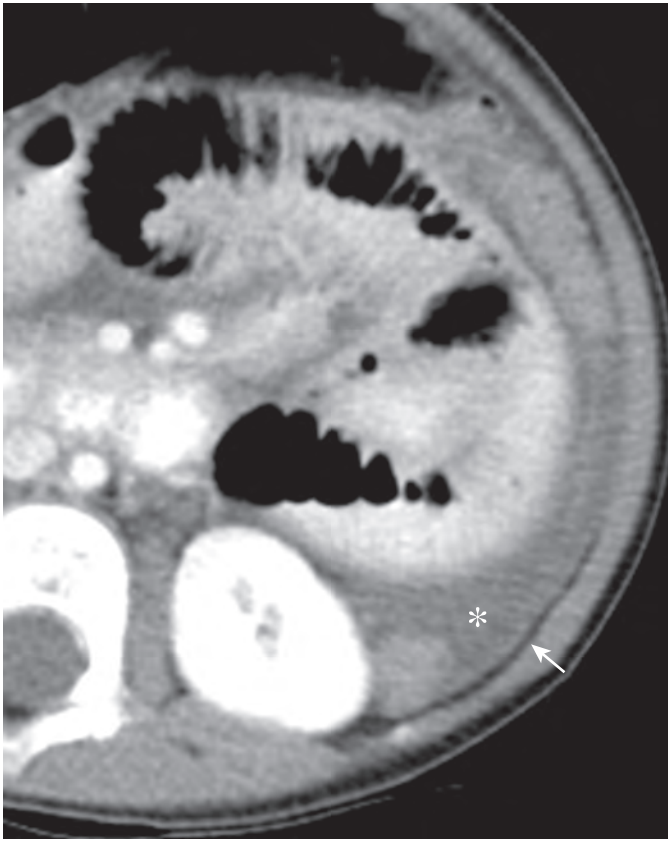


Figure 123-9 Peritonitis. A 3-year-old boy presenting with diffuse abdominal pain and physical examination findings consistent with peritonitis. Axial contrast-enhanced CT of the abdomen and pelvis revealed peritoneal thickening and enhancement (arrow) with complex ascites (asterisk). Surgery confirmed perforated appendicitis (not shown).

retroperitoneum. Approximately 75% of mesenteric cystic lesions are found in young adults or children older than 10 years.³⁵ Omental cystic lesions are contained within the greater or lesser omentum,³⁶ and they are usually seen in children, with 68% occurring in patients younger than 10 years.³⁸

Although patients with both types of lesions can be asymptomatic at the time of diagnosis, some may present with findings of abdominal distention or a “pulling sensation” in the abdomen.³⁵ Patients may also present with findings of an acute abdomen related to bowel obstruction from volvulus or mass effect, from infection or hemorrhage into the lesion,³⁵ or from the lesion’s undergoing torsion or rupture.³⁸ Rarely, patients may develop respiratory, hepatic, or renal compromise from the mass effect.³⁸ Although the diagnosis of a mesenteric or omental lymphatic malformation usually is made with ultrasound, CT, or MRI, radiographs of the abdomen classically demonstrate a homogeneous, water density mass that displaces bowel loops. These findings are nonspecific, however, and radiographs and fluoroscopic studies can be nondiagnostic.³⁹

Because of its lack of ionizing radiation and ready availability, ultrasound is the initial imaging modality of choice. Ultrasound imaging demonstrates an intra-abdominal cystic mass, usually with thin septations. Internal debris may be seen, consistent with hemorrhage or infection (Fig. 123-10).³⁶ CT imaging demonstrates a large, low-attenuation mass with a very thin or



Figure 123-10 Mesenteric cyst. Transverse ultrasound image of an 8-year-old boy with gradually worsening abdominal pain demonstrates a multiloculated cystic mass in the epigastric region with internal debris. The pancreas could not be visualized on this examination.

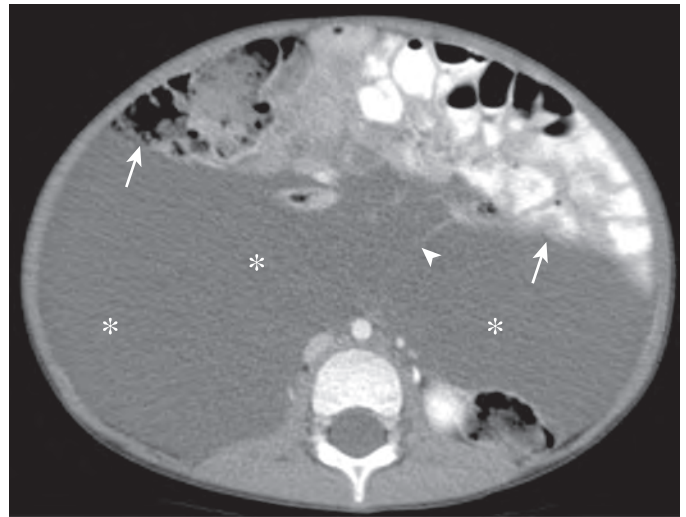


Figure 123-11 Mesenteric lymphatic malformation. A 3-year-old boy with a mesenteric lymphatic malformation. Axial postcontrast CT images of the abdomen show a large hypoattenuating mass in the abdomen and pelvis (asterisks) with a few thin septations (arrowhead), which causes anterior displacement of bowel (arrows).

indiscernible wall (Fig. 123-11).⁴⁰ The lesion may be multiseptate and have fine mural calcifications (Fig. 123-11).³⁶ MRI shows signal characteristics similar to lymphatic malformations in other locations, with a mass that is predominantly increased signal intensity on T2-weighted images with low signal intensity septations, decreased signal intensity on precontrast T1 images, and peripheral and septal enhancement after administration of

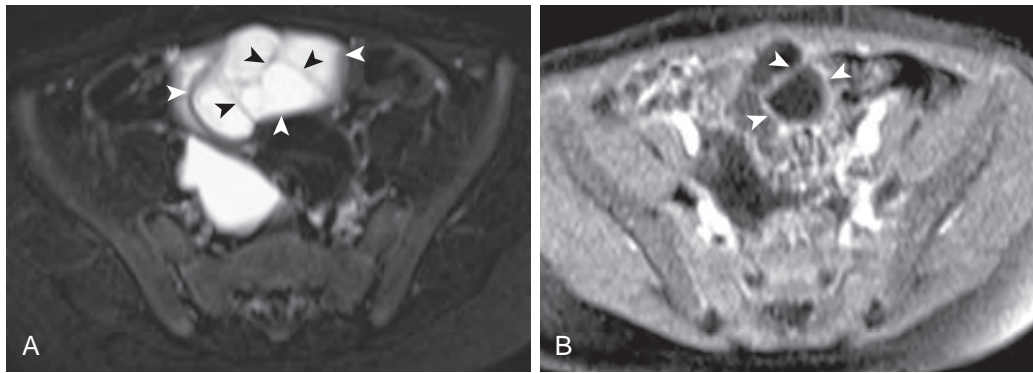


Figure 123-12 Mesenteric lymphatic malformation. A 4-year-old boy with a mesenteric lymphatic malformation. **A.** Axial T2-weighted fat-suppressed MR image of the pelvis shows a mesenteric mass with increased signal intensity (white arrowheads) and multiple low signal intensity thin septations (black arrowheads). **B.** Axial T1-weighted fat-suppressed MR image of the pelvis shows only thin peripheral and septal enhancement (arrowheads).



Figure 123-13 Mesenteric cyst. Gross image of a mesenteric cyst (arrows) centered in the mesentery of the distal small bowel.

contrast material (Fig. 123-12).⁴¹ CT and MRI can be helpful in demonstrating that this mass does not arise from the kidneys, ovaries, or pancreas.³⁷ Whereas a mesenteric cyst tends to be surrounded by bowel loops or to compress the bowel anteriorly if it arises at the base of the mesentery, an omental cyst tends to compress bowel posteriorly.³⁶

The treatment of mesenteric and omental cysts involves surgical resection to prevent torsion, bleeding, or infection³⁸ and usually results in resolution of symptoms.³⁷ Complete excision is recommended to prevent recurrence (Fig. 123-13).³⁵ More recently, percutaneous image-guided sclerotherapy of abdominal lymphatic malformations with doxycycline has been shown to be a safe and effective primary treatment.⁴²

Lymphadenopathy and Neoplasms of the Mesentery and Peritoneum

In the pediatric population, focal solid masses within the abdominal mesentery may be lymphomas, desmoids, teratomas, and lipomas. When the masses are multiple, they usually represent lymphadenopathy, which in the pediatric population

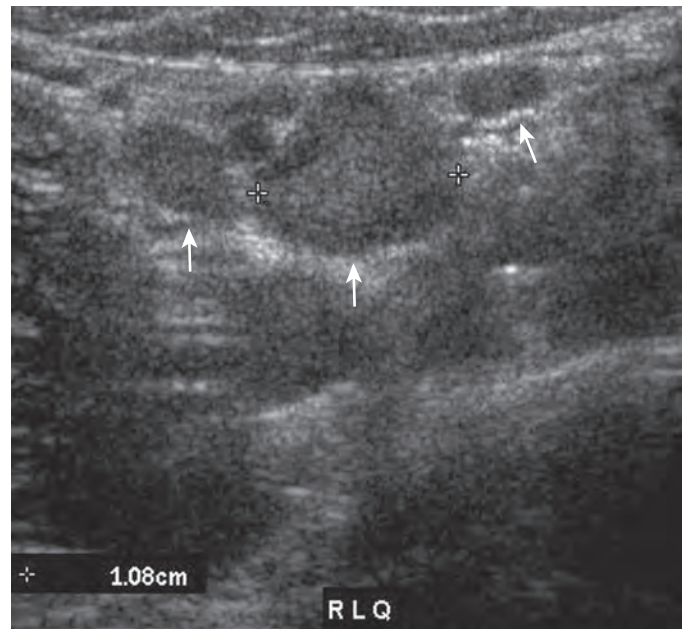


Figure 123-14 Mesenteric adenitis: ultrasound features.

Sonographic evaluation of a 12-year-old boy with abdominal pain demonstrates lymphadenopathy (arrows) in the right lower quadrant (cursors). The appendix was normal (not shown).

is more likely to be inflammatory or infectious than neoplastic. In the pediatric population, malignant lymphadenopathy is commonly caused by lymphoma, lymphoproliferative disorders, and metastatic disease.⁴⁰

On sonographic evaluation, the standard for mesenteric lymphadenopathy in children has been defined⁴³ as a short-axis diameter greater than 4 mm⁴⁴ and a long-axis diameter greater than 10 mm determined by graded compression sonography (Fig. 123-14). Abdominal lymphadenopathy, however, can be underestimated by ultrasound because of obscuration by bowel gas, a limited field of view, and operator dependence.⁴⁵ CT is a more sensitive imaging modality for the evaluation of abdominal lymph nodes. The pediatric standard for mesenteric lymphadenopathy determined by CT is a short axis greater than 8 mm; studies have shown that this standard would result in a false-positive rate for 5% of children.⁴⁵ The echogenicity of a

node is not sensitive for distinguishing normal nodes from lymphadenopathy.⁴⁶

A common cause of mesenteric lymphadenopathy in the pediatric population is mesenteric adenitis. Mesenteric adenitis is characterized by benign inflammation of mesenteric lymph nodes and is sometimes associated with enteritis.⁴⁰ Patients tend to present with acute, chronic, or recurrent abdominal pain with no evidence of other disease,⁴⁵ and they can have additional findings of nausea, vomiting, diarrhea, right lower quadrant pain and tenderness, fever, and leukocytosis. Mesenteric adenitis can be difficult to differentiate from acute appendicitis because of the similarities in clinical presentation.⁴⁰ Confounding this issue is the fact that enlarged lymph nodes have been described in normal, asymptomatic children in the ileocecal and para-aortic regions.⁴⁶

CT findings of mesenteric adenitis include lymphadenopathy anterior to the right psoas muscle and in the small bowel mesentery. This adenopathy tends to be more widespread than that seen with appendicitis, which tends to be isolated just anterior to the right psoas. Inflammatory changes of the mesentery have also been described.⁴⁰

Infectious or inflammatory lymphadenopathy in the pediatric population may result from tuberculosis, cat-scratch disease, fungal infection, or sarcoidosis.⁴⁰ Although most lymphadenopathy on CT is homogeneous, with attenuation similar to that of muscle, nodes that demonstrate central low attenuation with peripheral enhancement are more consistent with an infectious or inflammatory process than a neoplastic one.⁴⁰ This pattern of enhancement has been described as characteristic of tuberculosis (seen in approximately 60% of cases), but it can be seen in any process associated with central node necrosis. Tuberculosis has also been described as having more marked mesenteric than retroperitoneal lymphadenopathy.⁴⁰

Mesenteric lymphadenopathy is commonly seen in patients with Crohn's disease. Affected lymph nodes can be seen throughout the mesentery, from the root to the periphery, or they can be more focal and found in the right lower quadrant. Associated inflammatory bowel changes are not necessary for adenopathy to be present (Fig. 123-15).⁴⁷ Mesenteric adenopathy can also be seen with sarcoidosis and connective tissue disorders, but it is usually not the only imaging abnormality.⁴⁷

In the pediatric population, malignant lymphadenopathy commonly results from lymphoma, lymphoproliferative disorders, and metastatic disease. In lymphoma, nodes tend to start as small and discrete but can coalesce, forming a soft tissue mass (Fig. 123-16). This nodal mass has a characteristic appearance, growing around and displacing normal vessels and bowel.⁴⁷ On CT, the nodes usually demonstrate soft tissue attenuation with homogeneous enhancement, although peripheral enhancement has been described. Calcified lymph nodes are rare in untreated lymphoma, with a prevalence of less than 1%, but nodes commonly calcify after treatment.⁴⁷

Lymphoma that is manifested with abdominal lymphadenopathy is usually non-Hodgkin's lymphoma, and the adenopathy usually involves the mesentery and the retroperitoneum.⁴⁰ The lymphoproliferative disorders induced by Epstein-Barr virus tend to have extranodal parenchymal involvement rather than lymphadenopathy.^{48,49}

Solid masses of the mesentery are rare in the pediatric population. Desmoid tumors can be seen in patients with a history of Gardner's syndrome or with a history of prior

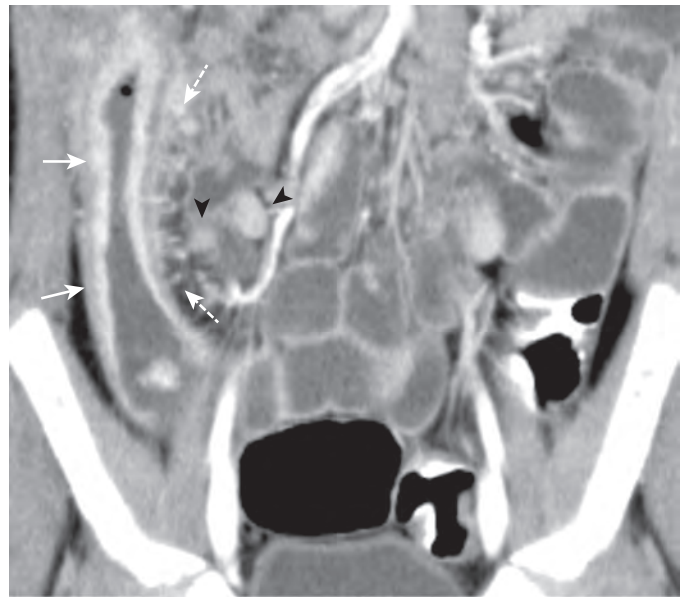


Figure 123-15 Lymphadenopathy. An 8-year-old girl with Crohn's disease. Coronal reformat image from a contrast-enhanced CT scan of the abdomen and pelvis. There is bowel wall thickening and hyperenhancement of the terminal ileum (solid arrows). Multiple enlarged mesenteric lymph nodes are present in the right lower quadrant (arrowheads). Engorgement of the vasa recta is also noted (dashed arrows).

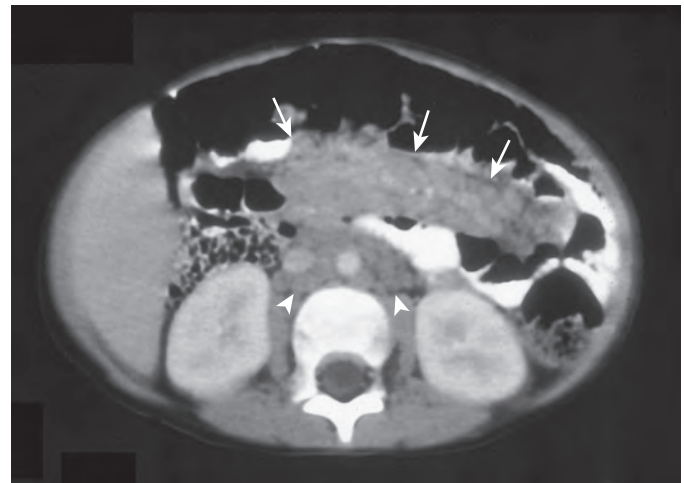


Figure 123-16 Lymphoma. Transverse CT image of 3-year-old child with lymphoma demonstrates a soft tissue nodal mass along the mesentery (arrows) and para-aortic and aortocaval retroperitoneal lymphadenopathy (arrowheads).

surgery or trauma.⁴⁰ Additional differential considerations for mesenteric masses include a solitary inflammatory or neoplastic lymph node and inflammatory pseudotumor.⁴⁰ Desmoplastic small round cell tumor is a rare malignant tumor that usually is manifested as a dominant mass in the pelvis with multiple peritoneal metastases as well as other metastatic disease at diagnosis (Fig. 123-17).^{50,51} Peritoneal metastases are rare in children but can also be seen with malignant ovarian tumors.

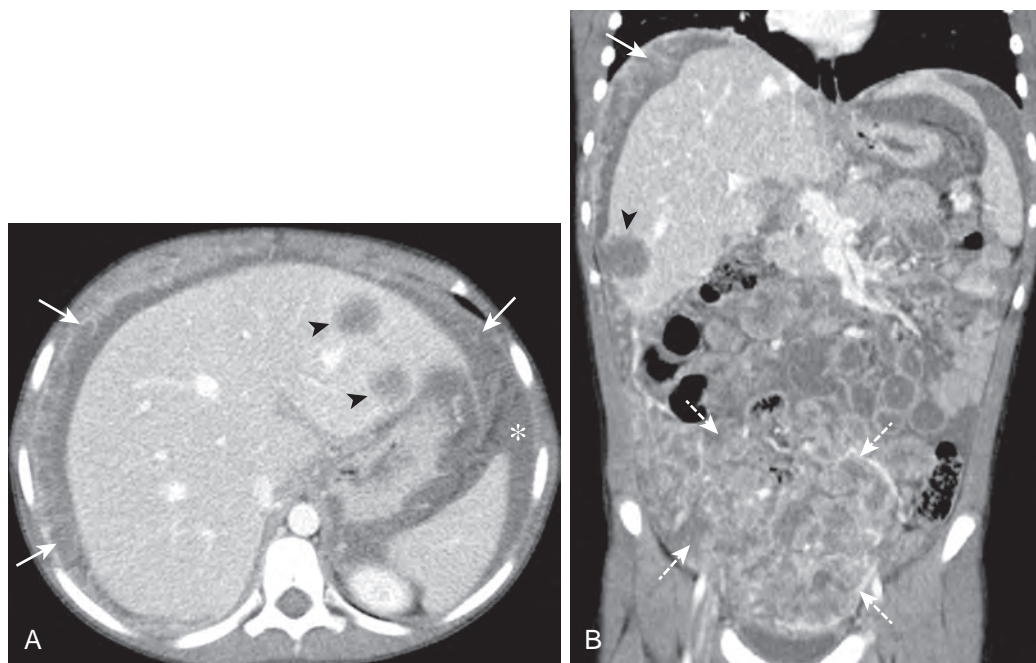


Figure 123-17 Desmoplastic small round cell tumor. An 8-year-old girl with desmoplastic small round cell tumor of the abdomen. Contrast-enhanced CT of the abdomen and pelvis. **A.** Axial image shows multiple peritoneal implants (arrows), complex ascites (asterisk), and hepatic metastases (arrowheads). **B.** Coronal image shows a large mesenteric mass (dashed arrows) in addition to the peritoneal implants (solid arrow) and hepatic metastasis (arrowhead).

REFERENCES

- Sadler TW: Langman's Medical Embryology, ed 7, Baltimore, 1995, Williams & Wilkins.
- Prefumo F, Izzi C: Fetal abdominal wall defects. Best Pract Res Clin Obstet Gynaecol 28:391–402, 2014.
- Correa-Rivas MS, Matos-Llovet I, Garcia-Fragoso L: Pentology of Cantrell: A case report with pathologic findings. Pediatr Dev Pathol 7:649–652, 2004.
- Liu H, Juan H, Liang C, et al: Multidetector computed tomography angiography imaging pentology of Cantrell. Circulation 129:1618–1620, 2014.
- Oka T, Shiraishi I, Iwasaki N, et al: Usefulness of helical CT angiography and MRI in the diagnosis and treatment of pentology of Cantrell. J Pediatr 142:84, 2003.
- Wilson RD, Johnson MP: Congenital abdominal wall defects: An update. Fetal Diagn Ther 19: 385–398, 2004.
- Langer JC: Abdominal wall defects. World J Surg 27:117–124, 2003.
- Nakagawa M, Hara M, Shibamoto Y: MRI findings in fetuses with an abdominal wall defect: Gastroschisis, omphalocele, and cloacal exstrophy. Jpn J Radiol 31:153–159, 2013.
- Danzer E, Victoria T, Bebbington MW: Fetal MRI-calculated total lung volumes in the prediction of short-term outcome in giant omphalocele: Preliminary findings. Fetal Diagn Ther 31:248–253, 2012.
- Ein SH, Langer JC: Delayed management of giant omphalocele using silver sulfadiazine cream: An 18-year experience. J Pediatr Surg 47: 494–500, 2012.
- Kamata S, Ishikawa S, Usui N, et al: Prenatal diagnosis of abdominal wall defects and their prognosis. J Pediatr Surg 31:267–271, 1996.
- Saxena AK, Hulskamp G, Schleef J, et al: Gastroschisis: A 15-year, single-center experience. Pediatr Surg Int 18:420–424, 2002.
- Mastroiacovo P, Lisi A, Castilla EE, et al: Gastroschisis and associated defects: An international study. Am J Med Genet A 143:660–671, 2007.
- Di Tanna GL, Rosano A, Mastroiacovo P: Prevalence of gastroschisis at birth: Retrospective study. BMJ 325:1389–1390, 2002.
- Weir E: Congenital abdominal wall defects. CMAJ 169:809–810, 2003.
- Emil S, Canvasser N, Chen T, et al: Contemporary 2-year outcomes of complex gastroschisis. J Pediatr Surg 47:1521–1528, 2012.
- Singh SJ, Fraser A, Leditschke JF, et al: Gastroschisis: Determinants of neonatal outcome. Pediatr Surg Int 19:260–265, 2003.
- Nelson CP, Dunn RL, Wei JT: Contemporary epidemiology of bladder exstrophy in the United States. J Urol 173:1728–1731, 2005.
- Mitchell ME: Bladder exstrophy repair: Complete primary repair of exstrophy. Urology 65: 5–8, 2005.
- Gearhart JP, Ben-Chaim J, Jeffs RD, Sanders RC: Criteria for the prenatal diagnosis of classic bladder exstrophy. Obstet Gynecol 85:961–964, 1995.
- Wilcox DT, Chitty LS: Non-visualisations of the fetal bladder: Aetiology and management. Prenat Diagn 21:977–983, 2001.
- Lee EH, Shim JY: New sonographic finding for the prenatal diagnosis of bladder exstrophy: A case report. Ultrasound Obstet Gynecol 21:498–500, 2003.
- Gearhart JP: Complete repair of bladder exstrophy in the newborn: Complications and management. J Urol 165(Pt 2):2431–2433, 2001.
- Nelson CP, Bloom DA, Dunn RL, Wei JT: Bladder exstrophy in the newborn: A snapshot of contemporary practice patterns. Urology 66:411–415, 2005.
- Berrocal T, Lopez-Pereira P, Arjonilla A, Gutierrez J: Anomalies of the distal ureter, bladder, and urethra in children: Embryologic, radiologic, and pathologic features. Radiographics 22: 1139–1164, 2002.
- Denes FT, Arap MA, Giron AM, et al: Comprehensive surgical treatment of prune belly syndrome: 17 years' experience with 32 patients. Urology 64:789–793, discussion 793–794, 2004.
- Ramasamy R, Haviland M, Woodard JR, Barone JG: Patterns of inheritance in familial prune belly syndrome. Urology 65:1227, 2005.
- Levin TL, Soghier L, Blitman NM, et al: Megacystis–microcolon–intestinal hypoperistalsis and prune belly: Overlapping syndromes. Pediatr Radiol 34:995–998, 2004.
- Ekwunife OH, Ugwu JO, Modekwe V: Prune belly syndrome. Niger J Clin Pract 17:425–430, 2014.
- Haecker FM, Berger D, Schumacher U, et al: Peritonitis in childhood: Aspects of pathogenesis and therapy. Pediatr Surg Int 16:182–188, 2000.
- Dann PH, Amodio JB, Rivera R, Fefferman NR: Primary bacterial peritonitis in otherwise healthy children: Imaging findings. Pediatr Radiol 35:198–201, 2005.
- Navia MJ, Caroli PL: Primary peritonitis in previously healthy children [Spanish]. An Pediatr (Barc) 61:554–557, 2004.
- Hebra A, Brown MF, McGeehin KM, Ross AJ: Mesenteric, omental, and retroperitoneal cysts

- in children: A clinical study of 22 cases. *South Med J* 86:173–176, 1993.
34. Mulliken JB, Fishman SJ, Burrows PE: Vascular anomalies. *Curr Probl Surg* 37:517–584, 2000.
 35. Mahaffey SM, Ryckman FC, Martin LW: Clinical aspects of abdominal masses in children. *Semin Roentgenol* 23:161–174, 1988.
 36. Egozi EI, Ricketts RR: Mesenteric and omental cysts in children. *Am Surg* 63:287–290, 1997.
 37. Cain WC, Kennedy S, Evans N, et al: Renal failure as a result of mesenteric cyst. *J Pediatr Surg* 39:1440–1443, 2004.
 38. Uramatsu M, Saida Y, Nagao J, et al: Omental cyst: Report of a case. *Surg Today* 31:1104–1106, 2001.
 39. Ranganath SH, Lee EY, Eisenberg RL: Focal cystic abdominal masses in pediatric patients. *AJR* 199:W1–W16, 2012.
 40. Zarewycz ZM, Donnelly LF, Frush DP, Bisset GS, 3rd: Imaging of pediatric mesenteric abnormalities. *Pediatr Radiol* 29:711–719, 1999.
 41. Navarro OM: Imaging of bone and soft tissue tumors soft tissue masses in children. *Radiol Clin North Am* 49:1235–1259, 2011.
 42. Shergill A, John P, Amaral JG: Doxycycline sclerotherapy in children with lymphatic malformations: Outcomes, complications and clinical efficacy. *Pediatr Radiol* 42:1080–1088, 2012.
 43. Grossman M, Shiramizu B: Evaluation of lymphadenopathy in children. *Curr Opin Pediatr* 6:68–76, 1994.
 44. Sivrit CJ, Newman KD, Chandra RS: Visualization of enlarged mesenteric lymph nodes at US examination: Clinical significance. *Pediatr Radiol* 23:471–475, 1993.
 45. Karmazyn B, Werner EA, Rejaie B, Applegate KE: Mesenteric lymph nodes in children: What is normal? *Pediatr Radiol* 35:774–777, 2005.
 46. Watanabe M, Ishii E, Hirowatari Y, et al: Evaluation of abdominal lymphadenopathy in children by ultrasonography. *Pediatr Radiol* 27:860–864, 1997.
 47. Lucey BC, Stuhlfaut JW, Soto JA: Mesenteric lymph nodes seen at imaging: Causes and significance. *Radiographics* 25:351–365, 2005.
 48. Rathaus V, Shapiro M, Grunebaum M, et al: Enlarged mesenteric lymph nodes in asymptomatic children: The value of the finding in various imaging modalities. *Br J Radiol* 78:30–33, 2005.
 49. Simanovsky N, Hiller N: Importance of sonographic detection of enlarged lymph nodes in children. *J Ultrasound Med* 26:581–584, 2007.
 50. Arora VC, Price AP, Fleming S, et al: Characteristic imaging features of desmoplastic small round cell tumour. *Pediatr Radiol* 43:93–102, 2013.
 51. Hayes-Jordan A, Green HL, Lin H, et al: Complete cytoreduction and HIPEC improves survival in desmoplastic small round cell tumor. *Ann Surg Oncol* 21:220–224, 2014.

SECTION

XV

Common Clinical Problems

The Acute Abdomen

RICHARD M. GORE | KIRAN H. THAKRAR | DANIEL R. WENZKE |
ROBERT I. SILVERS | UDAY K. MEHTA |
GERALDINE MOGAVERO NEWMARK | JONATHAN W. BERLIN

CHAPTER OUTLINE

Technical Considerations

Appendicitis

Diverticulitis

Bowel Obstruction

Acute Cholecystitis

Choledocholithiasis

Peptic Ulcer Disease

Pancreatitis

Perforation

Intestinal Ischemia

Abdominal Sepsis

Epiploic Appendagitis

Omental Torsion and Infarction

Mesenteric Adenitis

Infectious Enterocolitides

Inflammatory Bowel Disease

Small Bowel Diverticulitis

Abdominal Aortic Disease

Hemorrhage

Hepatosplenic Vascular Disease

Renal Colic

Conclusions

The term *acute abdomen* defines a clinical syndrome characterized by the sudden onset of severe abdominal pain requiring emergency medical or surgical treatment. A prompt and accurate diagnosis is essential to minimize morbidity and mortality. The differential diagnosis includes an enormous spectrum of infectious, inflammatory, obstructive, and neoplastic disorders ranging from benign self-limited diseases to conditions that require emergency surgery (Fig. 124-1). In a review of approximately 30,000 patients with acute abdomen, Shah observed that 28% of patients had appendicitis, 9.7% had acute cholecystitis, 4.1% had obstruction of the small bowel, 4% had acute gynecologic disease, 2.9% had acute pancreatitis, 2.9% had acute renal colic, 2.5% had perforated peptic ulcer, and 1.5% had diverticulitis. For one third of patients, no cause could be determined.¹

The clinical diagnosis of acute abdomen can be challenging because results of physical examination, clinical presentation, and laboratory examination are often nonspecific and nondiagnostic.²⁻⁵ Sonography has developed a niche in evaluating the gallbladder in all patients and the appendix in children and pregnant women. Magnetic resonance (MR) is being used with increasing frequency in pregnant women. Multidetector computed tomography (MDCT), however, has become the premier technique for triage of most patients with acute abdomen. MDCT has earned this role because it can provide a global perspective of the gut, mesenteries, omenta, peritoneum, retroperitoneum, subperitoneum, and extraperitoneum uninhibited by the presence of bowel gas and fat. MDCT scanning allows thinner contiguous images to be obtained without increasing radiation exposure and without respiratory misregistration. Multiplanar reformatted images can be obtained with virtually isotropic data sets. The rapidity of scanning allows several acquisitions to be obtained during different phases of a single intravenous bolus of contrast material.⁶ The cross-sectional imaging features of the most common abdominal disorders causing the acute abdomen are discussed in this chapter.

Technical Considerations

A variety of MDCT protocols for preparation of the patient and scanning have been created to study the diversity of diseases that can cause acute abdomen. The selection of an imaging technique depends on the most likely diagnosis, clinical setting, and local expertise. The examination should be tailored to each patient. See Chapter 5 for a more complete discussion of abdominal CT protocols.

It is best to obtain a general survey examination that includes the entire abdomen and pelvis. Diagnostic errors will occur if the anatomic coverage is dictated solely by the vagaries of clinical diagnosis. Scans are obtained from the diaphragm to beneath the symphysis pubis. Coronal and sagittal reformatted images are helpful in establishing a diagnosis.³

Intravenous administration of contrast material is helpful in the diagnosis of splanchnic venous thrombosis, bowel ischemia, aneurysms, and active arterial extravasation as well as solid parenchymal organ abnormalities. Inflammatory mural changes in appendicitis, cholecystitis, diverticulitis, Crohn's disease, and infectious enterocolitis are also better depicted with vascular enhancement. Neoplasms, abscesses, and infarcts in the liver, spleen, and kidneys are well portrayed on contrast-enhanced scans. Intravenously administered iodinated contrast material carries the risk of nephrotoxicity and potential reaction to the agent, and it may obscure renal and ureteral stones. However, in most patients, the information provided justifies the risk and extra expense. Between 125 and 150 mL of 60% iodinated

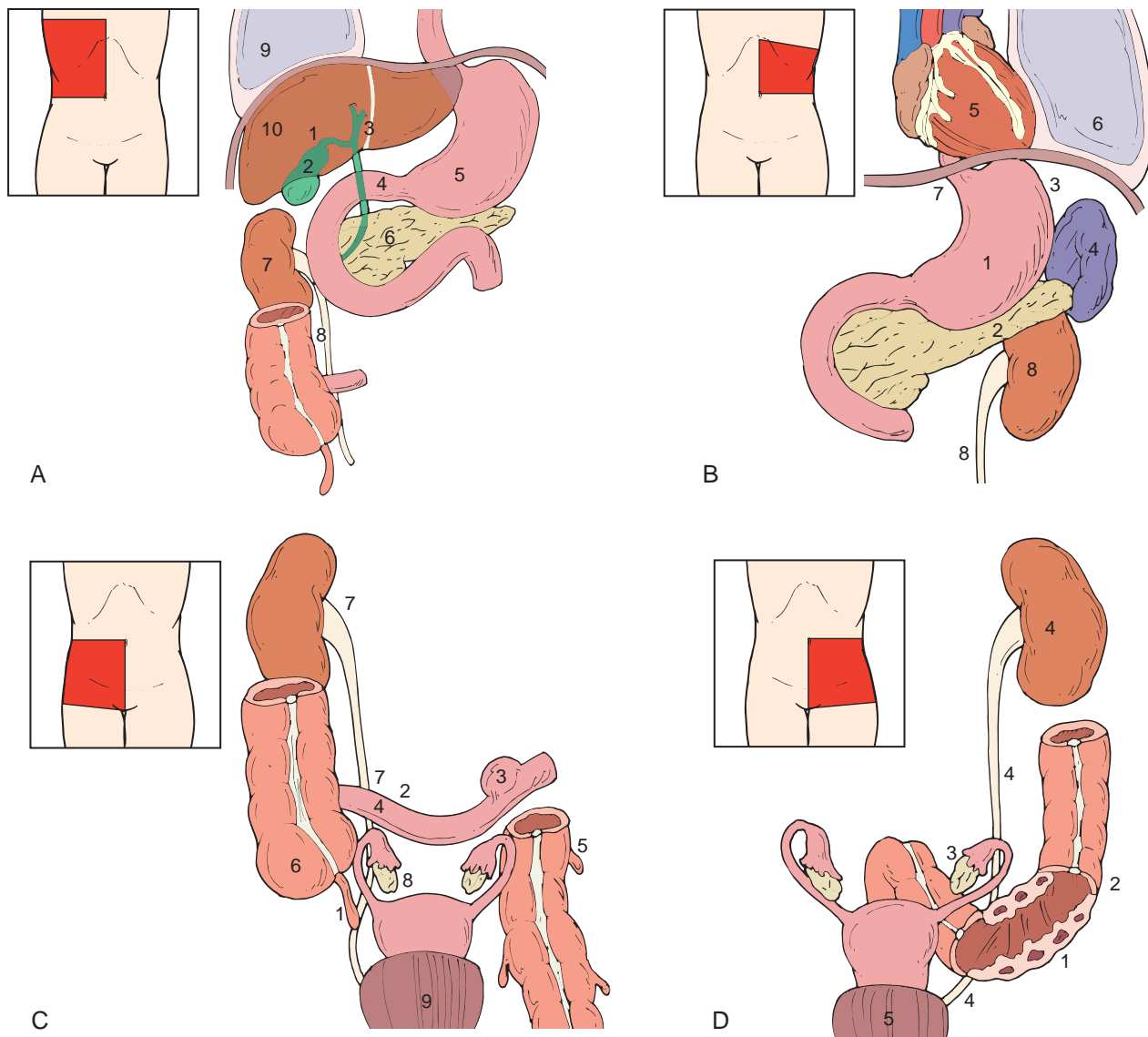


Figure 124-1 Leading causes of acute abdominal pain by quadrants. **A.** Causes of right upper quadrant pain: 1, cystic duct obstruction; 2, cholecystitis; 3, cholangitis, biliary obstruction; 4, duodenitis, duodenal ulcer; 5, gastritis, gastric ulcer; 6, pancreatitis, pancreatic cancer; 7, pyelonephritis, renal infarction, renal or ureteric stone, hydronephrosis; 8, subhepatic appendicitis; 9, pneumonia, pleural effusion, pulmonary embolism; 10, hepatitis, liver abscess, hemorrhage in liver tumor, acute hepatic congestion (right-sided heart failure), Budd-Chiari syndrome, portal vein thrombosis. **B.** Causes of left upper quadrant pain: 1, gastritis, gastric ulcer; 2, pancreatitis, pancreatic cancer; 3, subphrenic abscess; 4, splenic infarction and infection; 5, cardiac causes, including pericarditis, pericardial effusion, myocardial infarction; 6, left lower lobe pneumonia, effusion, pulmonary embolism; 7, hiatal hernia, gastroesophageal reflux disease; 8, pyelonephritis, renal infarction, ureteric stone. **C.** Causes of right lower quadrant pain: 1, appendicitis; 2, mesenteric adenitis, torsion of the greater omentum; 3, Meckel's diverticulum, ileal diverticulitis; 4, Crohn's disease, infectious or ischemic ileitis; 5, diverticulitis of a redundant sigmoid colon; 6, infectious, ischemic, or inflammatory colitis, epiploic appendagitis; 7, renal infection or infarction, ureteric stone; 8, ovarian disease, including cyst rupture, torsion, pelvic inflammatory disease, ectopic pregnancy; 9, infectious and inflammatory cystitis. **D.** Causes of left lower quadrant pain: 1, diverticulitis, epiploic appendagitis; 2, infectious, inflammatory, or ischemic colitis; 3, ovarian disease, including cyst rupture, torsion, pelvic inflammatory disease, ectopic pregnancy; 4, pyelonephritis, renal or ureteric stone; 5, infectious and inflammatory cystitis. (From Dieter B, Modder U: *Diagnostic Imaging of the Acute Abdomen*. Berlin, Springer-Verlag, 1988, p 5.)

contrast material should be injected intravenously at a rate of at least 3 mL/s. Scans are obtained during the portal venous phase with a 60- to 70-second delay. Arterial phase imaging (40-second delay) is useful in patients with suspected hemorrhage, bowel ischemia, and arterial thrombosis. Delayed scans through the kidneys and pelvis can reveal pyelonephritis, renal masses, and bladder disease that might have been overlooked during earlier phases.⁴⁻⁶

When bowel obstruction, intestinal ischemia or infarction, ileus, intestinal infection, or inflammation is suspected, the intrinsic fluid in the gut often serves as an excellent gastrointestinal luminal contrast agent. Positive contrast agents may lead to algorithm undershoot or overshoot and may interfere with assessment of bowel enhancement and viability. No oral contrast agent, water, or a low-contrast agent such as VoLumen may be given in these cases. For suspected kidney or ureteric

stones and ruptured abdominal aortic aneurysms, scans without oral or intravenous administration of contrast material should first be obtained.

For patients with nonspecific symptoms and signs, we prefer to give 800 to 1000 mL of a 2% solution of oral, diluted, water-soluble contrast material at least 1 hour before scanning. Oral contrast material is administered primarily to differentiate bowel loops from abdominal and pelvic masses and abscesses. Oral contrast material may obscure the diagnosis of bowel hemorrhage or ischemia and limit the detection of ureteral stones, appendicoliths, and bile duct stones. Practical difficulties of using oral contrast material include the time it takes to opacify the gut, the randomness of contrast opacification, and the inability of sick patients to consume and to retain sufficient quantities of the agent.

The use of rectal contrast material is advocated by some investigators to optimize the detection of appendicitis, diverticulitis, and epiploic appendagitis. With the patient in the left decubitus position, 400 to 600 mL of a 3% solution of water-soluble contrast agent is administered by gravity through a soft rubber rectal catheter without use of a balloon. The patient is then turned to the supine position for scanning.

An alternative approach to the patient with acute abdomen is to perform CT without oral, intravenous, or rectal administration of contrast media. This technique is fast, is virtually risk free, and causes no patient discomfort. However, these scans are the most difficult to interpret, particularly in patients with little abdominal or pelvic fat.

Appendicitis

Acute appendicitis (Fig. 124-2) is the most common abdominal surgical emergency, affecting approximately 250,000 people annually in the United States.⁷ Although the correct diagnosis can be made in most patients on the basis of the history, physical examination findings, and laboratory test results, the diagnosis is uncertain in 20% to 33% of patients who present with atypical symptoms. The diagnosis is most difficult for infants, young children, elderly patients, and women of reproductive age. In the past, an average negative laparotomy rate



Figure 124-2 Appendicitis. This intraoperative image shows an enlarged and diffusely inflamed appendix.

of 20% was acceptable.⁷ The widespread use of MDCT for patients with suspected appendicitis positively affects patient outcomes and increases the number of laparotomies with positive results. The surgical misdiagnosis rate has been reduced from 20% to 40% without imaging to a current rate of approximately 5% to 10%.^{8,9}

The MDCT, ultrasound, and MR findings of acute appendicitis reflect the extent and severity of inflammation (Fig. 124-3). In mild disease, the appendix appears as a slightly distended (6-15 mm in diameter), fluid-filled structure that shows circumferential symmetric mural thickening (Fig. 124-4). Sometimes, only the tip is inflamed (so-called tip appendicitis). On sonographic examination, periappendiceal inflammation may be encountered, and pain over the appendix may be elicited. The inflamed appendix is often hypervascular on color Doppler ultrasound.^{10,11}

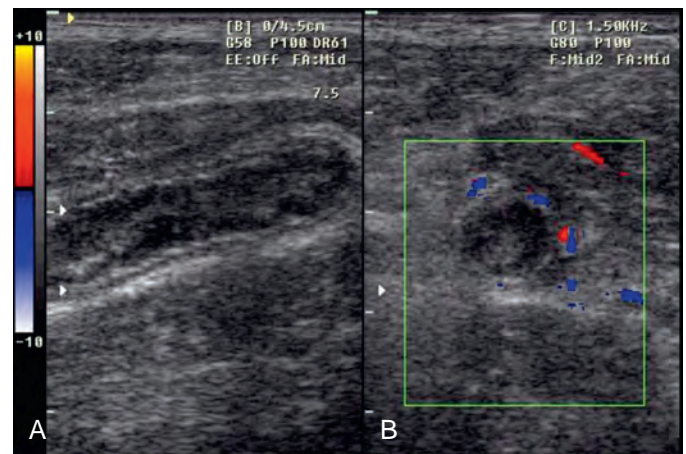


Figure 124-3 Appendicitis: sonographic features. **A.** A dilated, inflamed appendix is visualized along its long axis on this sonogram of the right lower quadrant. **B.** The inflamed appendix, imaged along its transverse axis, shows mural thickening and increased color Doppler flow to the appendiceal wall, attesting to the hyperemia accompanying the inflammation.

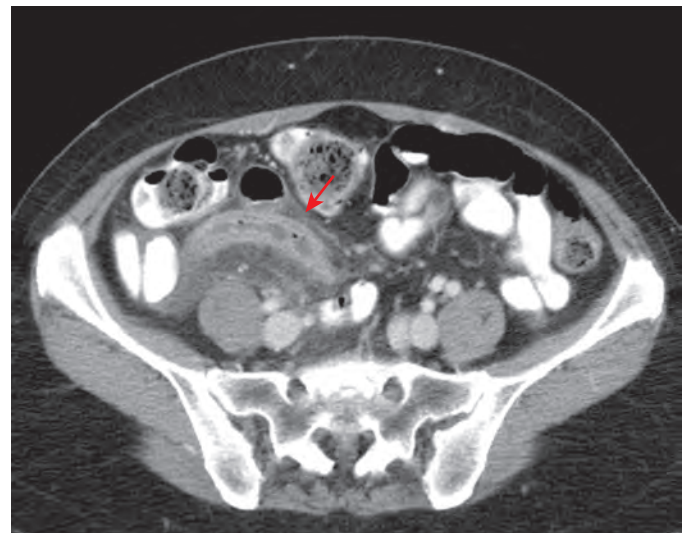


Figure 124-4 Appendicitis: CT features. Axial image shows a dilated, fluid- and gas-filled appendix (arrow), with mural thickening and periappendiceal inflammatory changes.

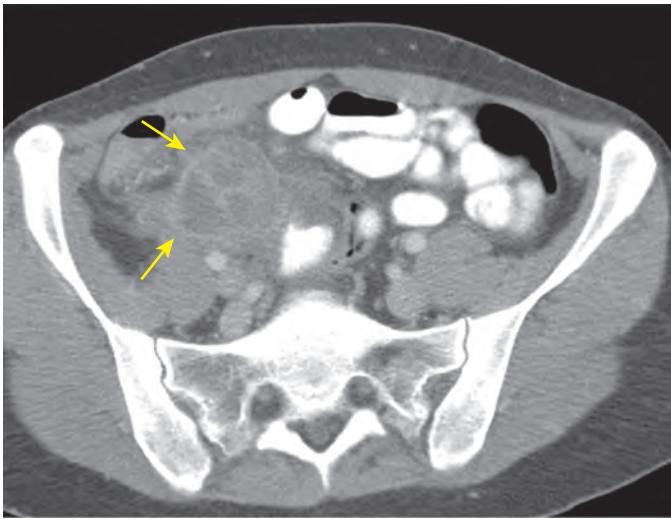


Figure 124-5 Appendiceal abscess. A right lower quadrant abscess (arrows) is identified along the medial aspect of the cecum.

Homogeneous, dense contrast enhancement of the wall is typical on MDCT, but a target sign may be seen on axial images (see Fig. 124-4). Periappendiceal inflammation is manifested as slight haziness of the mesoappendix fat. A calcified appendicolith is more reliably revealed on CT than on plain radiography.¹²⁻²⁰ When it is present, the appendicolith is less well visualized than on CT or ultrasound. With disease progression and perforation, the appendix becomes fragmented, destroyed, and replaced by a phlegmon or abscess (Fig. 124-5). Associated mural thickening of the adjacent distal ileum and cecum may also occur. In patients with these symptoms, the specific diagnosis of appendicitis can be made if an appendicolith is seen in the abscess or phlegmon. If not, the diagnosis of appendicitis can only be suggested within a differential diagnosis that includes cecal diverticulitis, ileal diverticulitis, Meckel's diverticulitis, perforated neoplasm (cecal, appendiceal, or ileal), and Crohn's disease with abscess formation.²⁰⁻³⁰

MR (Fig. 124-6) is becoming increasingly used in pregnant patients with high clinical suspicion of appendicitis. The MR features are similar to those seen on CT. The appendix is distended to a caliber greater than 6 to 7 mm in diameter with surrounding inflammatory change in the mesoappendix. See Chapter 56 for a more complete discussion of appendicitis.

Diverticulitis

Diverticulitis occurs in 10% to 25% of patients with known diverticulosis. It results from a microperforation or, much less commonly, a macroperforation of a diverticulum into the rich pericolic fat in the subperitoneal spaces surrounding the colon. These patients typically present with left lower quadrant pain, fever, and leukocytosis. Clinical misdiagnosis rates range from 34% to 67%.^{31,32} The role of CT for these patients is to confirm the diagnosis, to establish the presence of complications (e.g., abscess), to provide a road map for percutaneous or surgical therapy, and to suggest alternative diagnoses for patients in whom diverticulitis has been excluded.^{33,34}

The CT hallmark of diverticulitis is inflammatory change in the pericolic fat, which is observed in 98% of patients (Fig. 124-7). Minimal haziness of adjacent fat occurs in mild cases. Small

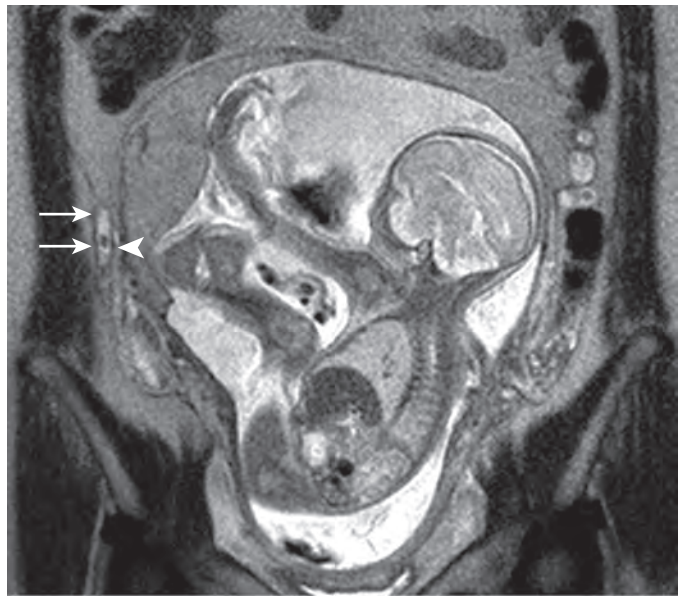


Figure 124-6 Appendicitis: MR features. An inflamed appendix (arrows and arrowhead) characterized by mural thickening, intraluminal fluid, and periappendiceal inflammation is depicted along the lateral aspect of the placenta on this T2-weighted coronal image obtained in a pregnant woman in the third trimester.

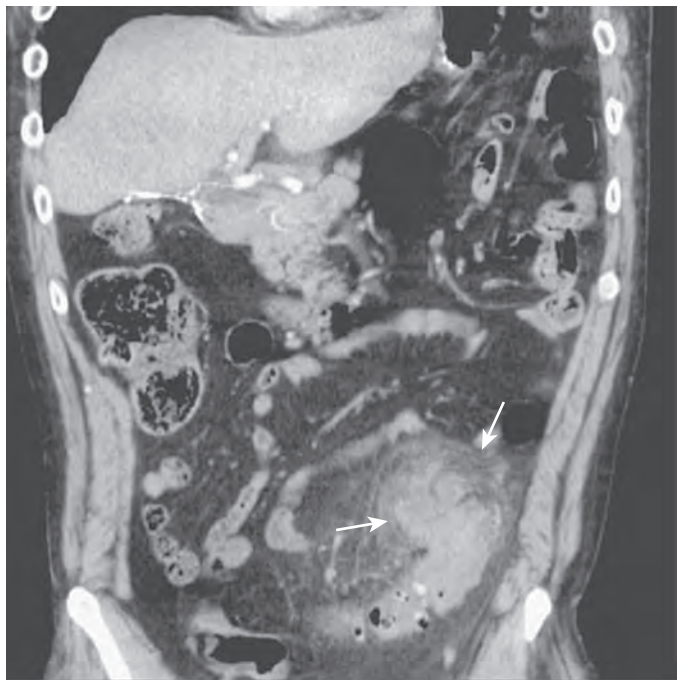


Figure 124-7 Diverticulitis of the sigmoid colon: CT findings. Coronal reformatted image shows mural thickening of the junction of the sigmoid and descending colon and a phlegmon (arrows) in the sigmoid mesocolon.

fluid collections, fine linear strands, and extraluminal gas bubbles may also occur. In more severe cases, phlegmon or frank abscess formation can occur. Diverticula are evident in more than 80% of patients, and symmetric mural thickening of more than 4 mm is seen in about 70% of patients. Other typical features include engorgement of the vasa recta and the presence

of fluid in the inferior portion of the combined interfascial plane.³¹⁻³⁴

In some patients, contrast material collects in an arrowhead shape adjacent to the inflamed colonic diverticulum (i.e., arrowhead sign of diverticulitis). The offending inflamed diverticulum may appear as a rounded paracolic outpouching centered in the paracolic inflammation with soft tissue calcium, barium, or air attenuation.³¹⁻³⁴

A perforated carcinoma is the major differential diagnostic consideration for patients with sigmoid diverticulitis. Although the colon wall is usually less than 1 cm thick in acute diverticulitis, in patients with severe muscle hypertrophy, the wall may be 2 to 3 cm thick, simulating carcinoma. CT findings favoring the diagnosis of acute diverticulitis include a tethered or saw-toothed luminal configuration, the presence of fluid in the combined interfascial plane, and engorged vasa recta. An abrupt zone of transition with normal bowel, enlarged local lymph nodes, and mural thickness greater than 1.5 cm favors carcinoma.³¹⁻³⁴

Complications of acute diverticulitis include abscess formation (Fig. 124-8), obstruction of the large and small bowel, secondary inflammation of the appendix, fistula, sinus tracks, and frank intraperitoneal perforation. Right-sided diverticulitis is usually difficult to diagnose clinically. Compared with patients with appendicitis, individuals with right-sided diverticulitis have a more protracted history, milder pain, and a higher point of maximum tenderness, which may clinically simulate acute cholecystitis. A palpable mass is present in up to one third of patients and can mimic an appendiceal or cecal tumor.

The MDCT findings of right-sided diverticulitis consist of focal pericolic inflammatory change, slight mural thickening, and visualization of diverticulum as an outpouching of the right colon at the level of maximum wall thickness. The offending diverticulum contains gas, fluid, contrast material, or calcified material. The normal appendix should be seen. If the



Figure 124-8 Abscess due to sigmoid diverticulitis. A large abscess (A) with an air-fluid level is identified in the sigmoid mesocolon.

appendix is not visualized, appendicitis, epiploic appendagitis, typhlitis, or perforated cecal carcinoma must be considered in the differential diagnosis.³¹⁻³⁴ See Chapter 55 for a more complete discussion of diverticulitis.

Bowel Obstruction

Obstruction of the small intestine and colon accounts for approximately 20% of acute abdominal surgical conditions.³⁵ MDCT has replaced conventional contrast studies because it can more reliably answer several questions. Is obstruction present? What is the level of obstruction? What is the cause of obstruction? What is the severity of obstruction? Is the obstruction simple or a closed loop? Is strangulation or ischemia present?

It is important to differentiate between simple and closed-loop obstruction (Fig. 124-9) because the simple obstruction can be treated conservatively, whereas closed-loop obstruction requires prompt surgical intervention. For patients with bowel obstruction, scans are best obtained without oral contrast material because intraluminal fluid and gas serve as natural contrast agents. Intravenous contrast material is important in assessing intestinal perfusion and ischemia and in delineating the size, configuration, and patency of the mesenteric vessels.³⁶ If oral contrast material is given, a delayed plain abdominal radiograph obtained several hours later can determine if the contrast material has passed into the colon.

The CT hallmark of bowel obstruction is the delineation of a transition zone between dilated and decompressed bowel. Careful inspection of the transition zone and luminal contents often reveals the underlying causes of obstruction. CT is most helpful in patients with internal and external hernias, neoplasms, gallstone ileus, various forms of enteroenteric intussusception, and afferent loop obstruction after a Billroth II operation. If no mass, hernia, intussusception, abscess, or inflammatory thickening is present, adhesion is the most likely diagnosis. The typical adhesion has a beaklike narrowing, and the affected gut may be difficult to view, depending on the orientation of the loop relative to the axial plane. Use of the scroll or leaf function and multiplanar reformations in the coronal and sagittal planes can help establish the correct diagnosis.³⁷⁻⁴⁷



Figure 124-9 Strangulated small bowel obstruction. The intraoperative photograph shows a hemorrhagic-necrotic small bowel due to strangulation caused by a volvulus surrounding an adhesion.



Figure 124-10 Closed-loop small bowel obstruction: CT features. Axial image shows the obstructed ileal loops converging to a central point in this patient with a transmesenteric internal hernia. There is mural thickening of the obstructed loops, hypoenhancement of several of the loops (arrows), and edema of the adjacent small bowel mesentery. Ischemic bowel was found at the time of surgery.

The anterior abdominal wall should be carefully inspected to search for prior surgical scars. The small bowel feces sign is often seen just proximal to the obstruction. If positive oral contrast material is present, it becomes progressively more dilute as it approaches the level of obstruction. Also the degree of small bowel dilation is largest closest to the level of obstruction.

An incarcerated or closed-loop obstruction is manifested as a loop-shaped, fluid-filled structure causing proximal segments to dilate with gas and fluid. The mesenteric vessels have a radial distribution (Fig. 124-10) because they become stretched and converge toward the U- or C-shaped loop. Two adjacent and collapsed round, oval, or triangular segments typically represent the afferent and efferent entry points of the torsion site. The mesenteric vasculature may have an unusual course. When ischemia develops, the bowel wall may thicken and have a target appearance caused by submucosal edema. Enhancement of the involved bowel wall may be poor or delayed. Fluid and hemorrhage may collect in the mesentery, bowel wall, and lumen of the involved segment. The mesentery becomes hazy in appearance, and ascites may develop.³⁷⁻⁴⁷

In patients with high-grade obstruction of the small bowel, CT has a reported sensitivity of 90% to 99%. CT is less accurate in patients with low-grade obstruction. Obstruction of the large bowel (Fig. 124-11) can also be demonstrated by MDCT. See Chapters 46 and 62 for a more complete discussion of bowel obstruction.

Acute Cholecystitis

Acute cholecystitis results from obstruction of the gallbladder and its attendant mural inflammation associated with infection and sometimes necrosis. Most cases are caused by obstructing gallstones in the gallbladder neck or cystic duct. Because acute cholecystitis develops in only 20% of patients with gallstones, many patients with gallstones with right upper quadrant pain have other pathologic conditions responsible for their symptoms.⁴⁸

Only 20% to 30% of patients with right upper quadrant pain have acute cholecystitis. The primary sonographic diagnostic



Figure 124-11 Carcinoma of the sigmoid colon causing large bowel obstruction. The coronal reformatted image shows the obstructing sigmoid mass (curved arrows). The cecum is dilated (double-headed arrow), and there are liver metastases.

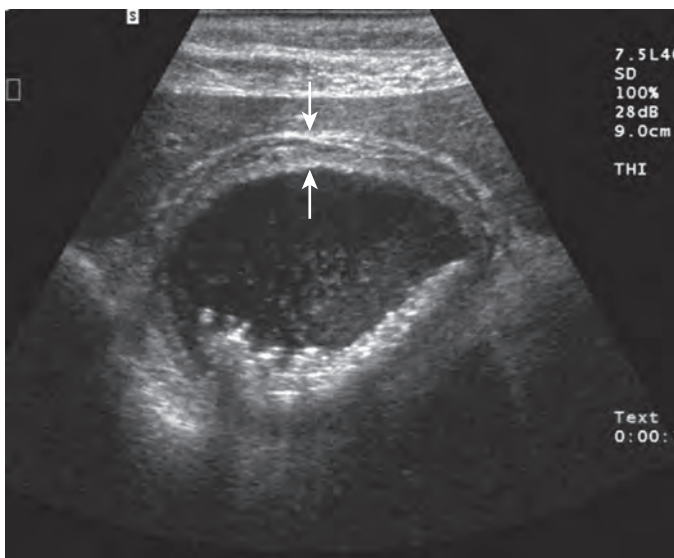


Figure 124-12 Acute cholecystitis: sonographic features.

Transverse sonogram of the right upper quadrant shows sludge and shadowing stones within the gallbladder. Mural thickening (arrows) is associated with edema, producing wall stratification. The patient also had a sonographic Murphy sign.

criterion is the sonographic Murphy sign associated with gallstones. Secondary signs of acute cholecystitis include mural thickening (>3 mm) and stratification, a distended or hydropic gallbladder with loss of the normal tapered neck and development of an elliptical or rounded shape, and pericholecystic fluid (Fig. 124-12).^{48,49}

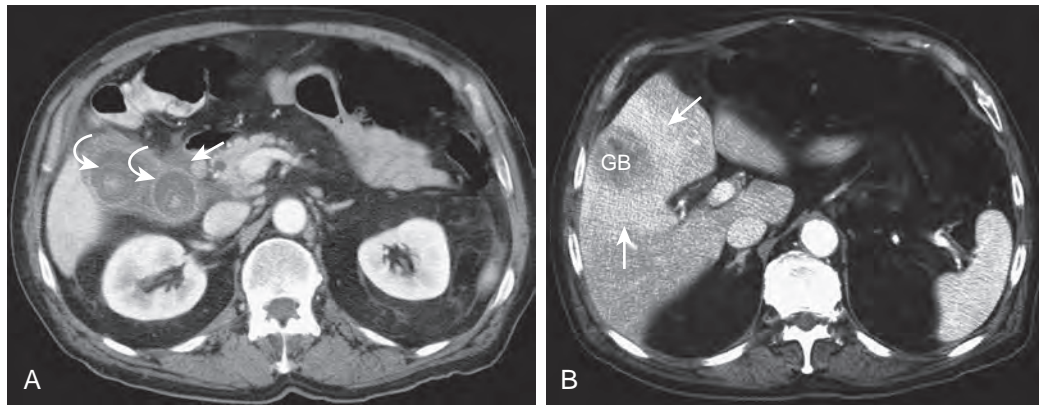


Figure 124-13 Acute cholecystitis: CT features. **A.** Two large stones (curved arrows) are identified within a thick-walled gallbladder. Notice the pericholecystic fluid (straight arrow). **B.** The more cephalad scan, displayed with a narrow window, shows a region of transient hepatic attenuation difference (arrows) surrounding the inflamed gallbladder (GB).

Although sonography is the preferred method for diagnosis of acute cholecystitis, CT is frequently the initial examination because the diagnosis is unclear. The most sensitive CT findings of acute cholecystitis are mural thickening greater than 3 mm (in the setting of a distended gallbladder) and enhancement of the inflamed wall (Fig. 124-13A). Transient, focally increased attenuation of the liver may develop adjacent to the inflamed gallbladder, resulting from hepatic artery hyperemia and early venous drainage (Fig. 124-13B). Less specific signs include pericholecystic fluid, haziness of the pericholecystic fat, and increased attenuation of the gallbladder bile. CT can also depict complications of acute cholecystitis, including perforation and gangrene. Intramural or intraluminal gas is present in emphysematous cholecystitis.^{49,50} See Chapter 77 for a complete discussion of acute cholecystitis.

Choledocholithiasis

Patients with choledocholithiasis typically present with acute right upper quadrant pain, fever, jaundice, and pancreatitis. Thin-collimation scans are needed to optimize the detection of stones on MDCT. A high-density nidus may be visualized in the duct, or alternating low- and high-density rings of mixed cholesterol-calcium stones may be seen. Biliary dilation may be evident proximally. MDCT has a sensitivity of 88%, specificity of 97%, and accuracy of 94% in the detection of choledocholithiasis; however, positive intraluminal and intravascular contrast agents can obscure the detection of peripherally calcified stones.^{49,51,52} MR and MR cholangiopancreatography are the premier means of establishing the diagnosis of choledocholithiasis.

Peptic Ulcer Disease

Patients with peptic ulcer disease often present with nonlocalizing signs and symptoms indistinguishable from those of acute pancreatitis or cholecystitis, and MDCT is normally the first examination ordered. The most common MDCT result is focal mural thickening, which is a nonspecific finding. On occasion, an active ulcer or perforation (Fig. 124-14) is identified, accompanied by inflammatory change of the adjacent fat, mesenteries, and omenta.⁵³

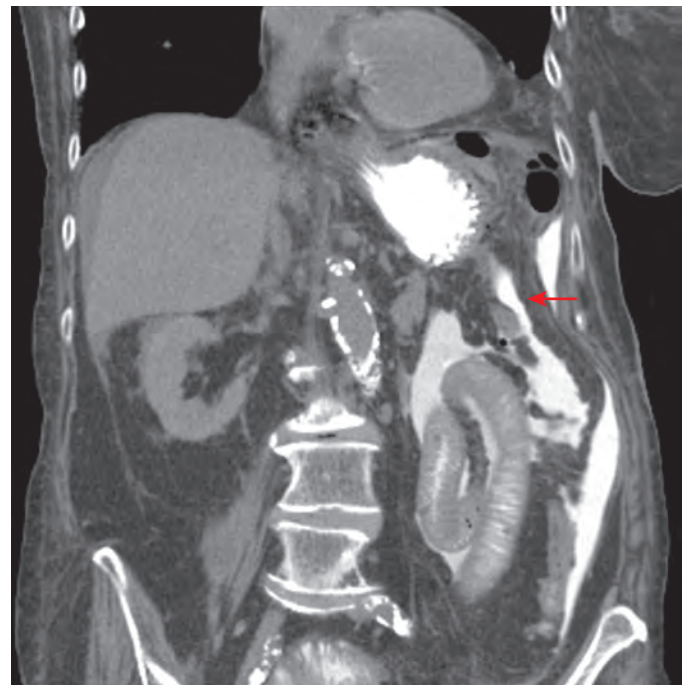


Figure 124-14 Perforated gastric ulcer: CT findings. Extravasated contrast material (arrow) is present in peritoneal spaces of the left upper quadrant.

Pancreatitis

MDCT plays a vital role in the clinical diagnosis (Fig. 124-15), treatment, and staging of patients with acute pancreatitis. MDCT can reveal hemorrhage or necrosis in the pancreas and identify the extension of inflammation in adjacent organs. MDCT findings of acute pancreatitis reflect edema of the gland and surrounding fat and may be normal in up to 28% of mild cases.⁵⁴ The entire gland may become diffusely enlarged and have a shaggy, irregular contour. In mild cases, the peripancreatic fat contains wisps of high attenuation, the vascular margins are cuffed, and the fascial planes are thickened. Mild peripancreatic inflammation may be present around an otherwise normal-appearing gland. Segmental pancreatitis occurs in 10%

to 18% of patients and is usually associated with stone disease. Typically, the gland shows uniform enhancement.⁵⁵

In more advanced cases, intraglandular intravasation of pancreatic fluid leads to the formation of many small, intrapancreatic fluid collections. In necrotizing pancreatitis, the gland becomes enlarged and is often enveloped by high-attenuation exudates. Necrotic parenchyma shows decreased or no enhancement that is sharply demarcated from normally enhancing viable tissue. The body and tail are usually involved; the head is spared because of its rich collateral vascular network. Enhancing islands of viable tissue may be scattered throughout the gland. The poorly defined peripancreatic exudates obliterate the peripancreatic fat, dissect fascial planes, and penetrate through fascial and peritoneal boundaries and ligaments. These collections typically accumulate in the lesser sac, anterior pararenal space, and anterior interfascial space. MDCT is also useful in revealing vascular complications, such as pseudoaneurysms and splenic and portal vein thrombosis.

MDCT can help predict patient outcomes by delineating necrosis. In one study, patients with no evidence of necrosis on

MDCT had 0% mortality and only 6% morbidity rates, whereas patients with large areas of necrosis (50%) had a 75% to 100% morbidity rate and an 11% to 25% mortality rate.⁵⁵ See Chapter 97 for a complete discussion of pancreatitis.

Perforation

Gastrointestinal perforation usually indicates a catastrophic complication of peptic ulcer disease, diverticulitis, severe intestinal inflammation, infarction, trauma, neoplasm, or closed-loop obstruction. MDCT is ideal for evaluating patients with signs of peritonitis, which is often misdiagnosed as another acute lesion. MDCT can detect pneumoperitoneum that may be overlooked on chest or abdominal radiography.⁵⁶⁻⁵⁹ The visualization of extraluminal gas is facilitated by scrolling through the images with lung windows.

Detection of the site of perforation is often difficult but can be assisted by the oral and intravenous administration of contrast material. Loculated fluid and gas (Fig. 124-16), focal mesenteric or omental infiltration, and focal enhancement of the parietal peritoneum can help pinpoint the site of perforation.⁵⁶⁻⁵⁹

Intestinal Ischemia

Vascular insufficiency of the gut is a differential diagnosis for elderly patients with acute abdominal pain or for any patient with a history of coronary artery disease, peripheral vascular disease, arteritis, hypotension, dehydration, or cardiac decompensation. Patients with intestinal ischemia have a broad range of symptoms that make a clinical diagnosis difficult. The major causes of intestinal ischemia include hypoperfusion and arterial or venous occlusion or thrombosis. Typically, the predominance of one factor determines the outcome. CT plays an important role in identifying the early changes of ischemia. Rapid intravenous administration of contrast material (>3 mL/s) is required to optimize vascular opacification and to assess the patency of the superior mesenteric artery and vein.⁶⁰⁻⁶³

The CT features of intestinal ischemia depend on its cause, chronicity, and severity. Mural thickening of the gut is the most common finding, and the wall may have a target or halo appearance caused by submucosal edema. Thickened edematous wall is best appreciated in bowel distended by fluid, air, or contrast

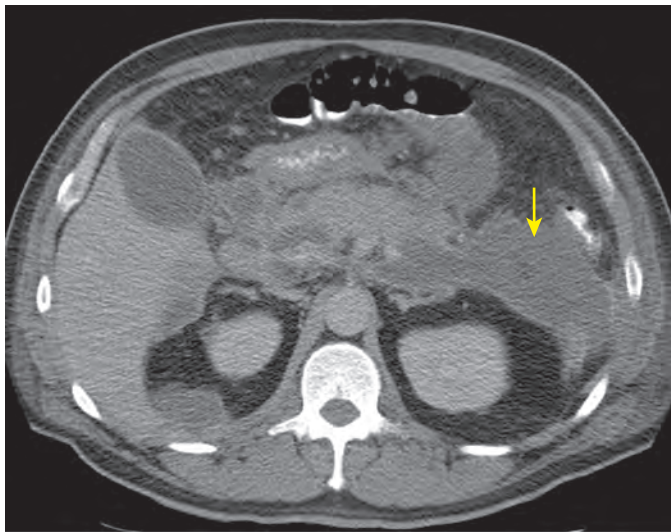


Figure 124-15 Pancreatitis: CT features. An inflammatory fluid collection (arrow) is identified in the left anterior interfascial plane on this axial image.

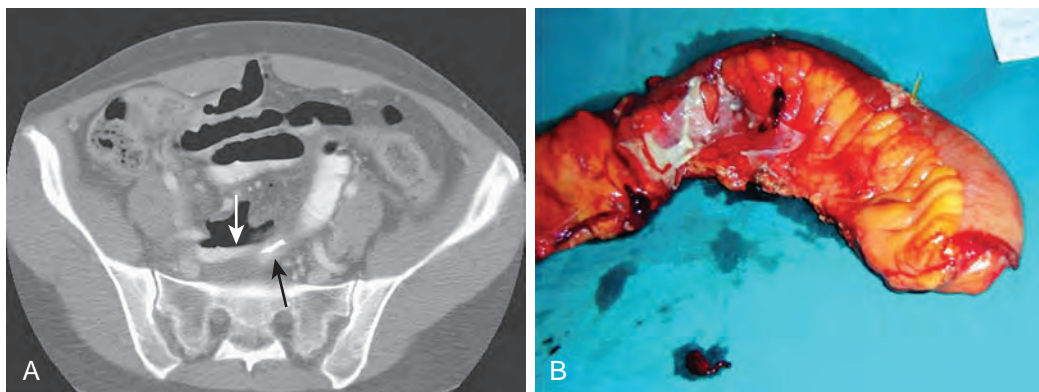


Figure 124-16 Small bowel perforation due to a chicken bone: CT and gross pathologic findings. **A.** CT shows an air-contrast material level (white arrow) in the small bowel mesentery due to perforation by a chicken bone (black arrow). **B.** Surgical specimen shows the site of the perforation.

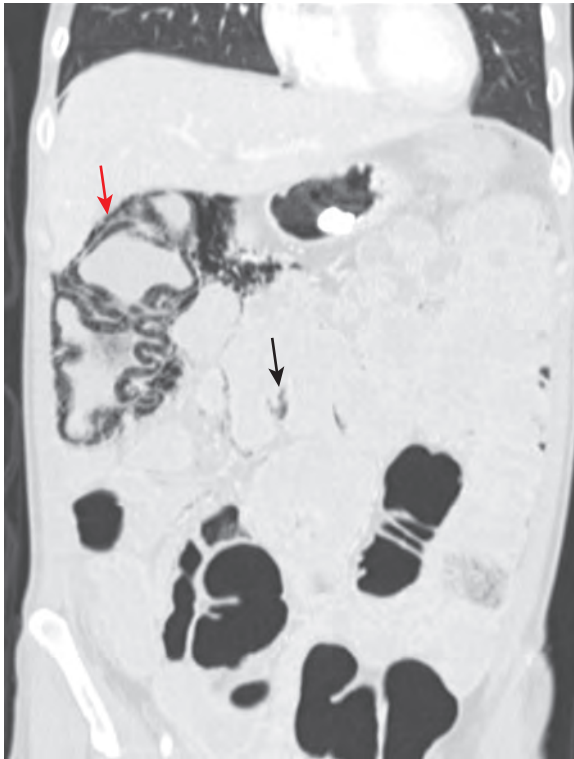


Figure 124-17 Colonic infarction with pneumatosis intestinalis and mesenteric venous gas: CT features. Coronal CT image shows pneumatosis (red arrow) in the region of the hepatic flexure of the colon and gas in the superior mesenteric vein (black arrow).

material. This appearance is nonspecific and can be seen in infectious and inflammatory bowel disease. Mesenteric haziness reflects edema and hemorrhage. The presence of focal pneumatosis or thrombus in the celiac, superior mesenteric, and inferior mesenteric arteries and veins permits a specific diagnosis to be made. Air in the bowel wall, mesentery, and portal venous system has grave prognostic implications for patients with ischemic bowel (Fig. 124-17). CT is far more sensitive than radiography in detecting pneumatosis and portal venous gas.⁶⁴⁻⁶⁸

Colonic ischemia usually results from hypoperfusion or hypotension, and mesenteric thrombus is rare. MDCT reveals segmental thickening of the colon with scalloped, irregular margins caused by submucosal edema.⁶⁵ Bowel ischemia is discussed more fully in Chapters 47 and 62.

Abdominal Sepsis

Patients with an abdominal abscess or peritonitis can present with an acute abdomen. Abdominal infections most commonly result from the contiguous spread of bacteria from the gut, biliary tract, or genitourinary system. These infections are typically polymicrobial in nature and include both aerobic and anaerobic organisms. MDCT is the most accurate imaging examination for the diagnosis of intra-abdominal abscesses. Initially, abscesses appear as a mass of soft tissue attenuation caused by the influx of inflammatory cells. With maturation, the abscess undergoes central liquefaction necrosis, and highly vascularized peripheral connective tissue develops. As a result, this lesion has a low-attenuation center with an enhancing rim. Small gas bubbles or air-fluid levels are present in 40% to 50%

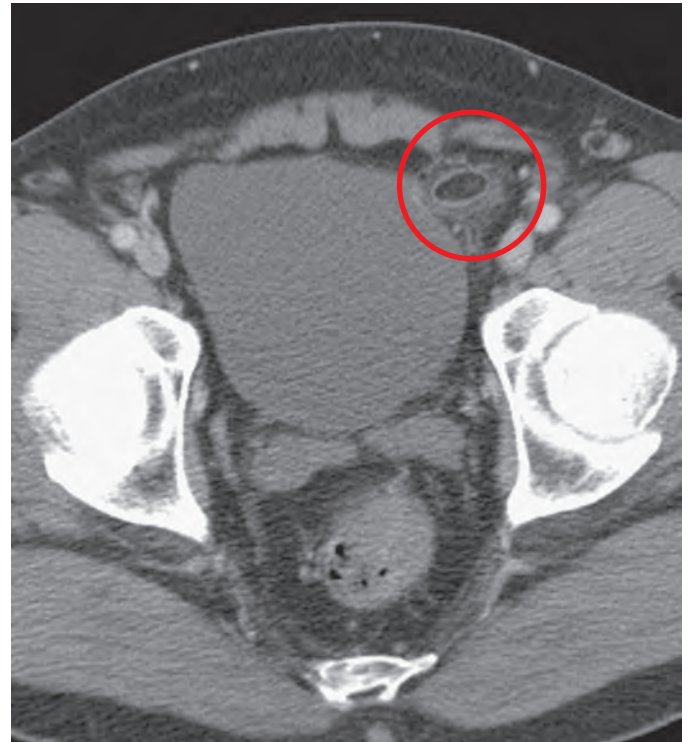


Figure 124-18 Epiploic appendagitis. CT shows an elliptical fat density structure (circle), the epiploic appendage, surrounded by increased attenuation in the pericolic fat.

of patients, and they suggest intra-abdominal sepsis. Abscesses tend to be round or oval unless they are adjacent to a solid organ. In these patients, abscesses may develop a lentiform or crescentic configuration. Abscesses also displace surrounding structures, obliterate or thicken adjacent fascial planes, and cause inflammation of the contiguous mesenteric or omental fat.³⁻⁵ See Chapter 72 for a more complete discussion of abdominal abscesses.

Epiploic Appendagitis

This unusual condition occurs when an epiploic appendage of the colon develops inflammation, torsion, or ischemia. Epiploic appendagitis can simulate appendicitis and right- and left-sided diverticulitis clinically and on MDCT scans. The inflamed appendage is manifested as a small, fat-attenuation mass with a hyperattenuating rim that abuts the serosal surface of the colon. At the center of the lesion, a small, round or linear, hyperdense focus may be seen, probably representing vascular thrombosis. Epiploic appendagitis also produces a mass effect, focal thickening of the adjacent bowel, infiltration of the mesenteric fat, and focal thickening of the surrounding peritoneum (Fig. 124-18).⁶⁹⁻⁷¹

MDCT is usually diagnostic. Surgery can be avoided in many cases because epiploic appendagitis is a self-limited disorder. See Chapter 62 for a more complete discussion of epiploic appendagitis.

Omental Torsion and Infarction

Omental torsion or infarction is an uncommon disorder. Portions of the greater omentum undergo torsion or spontaneous

Figure 124-19 Focal torsion-infarction of the greater omentum: CT findings. Axial (A) and coronal (B) images show focal increased attenuation (arrows) of a small portion of omental fat.

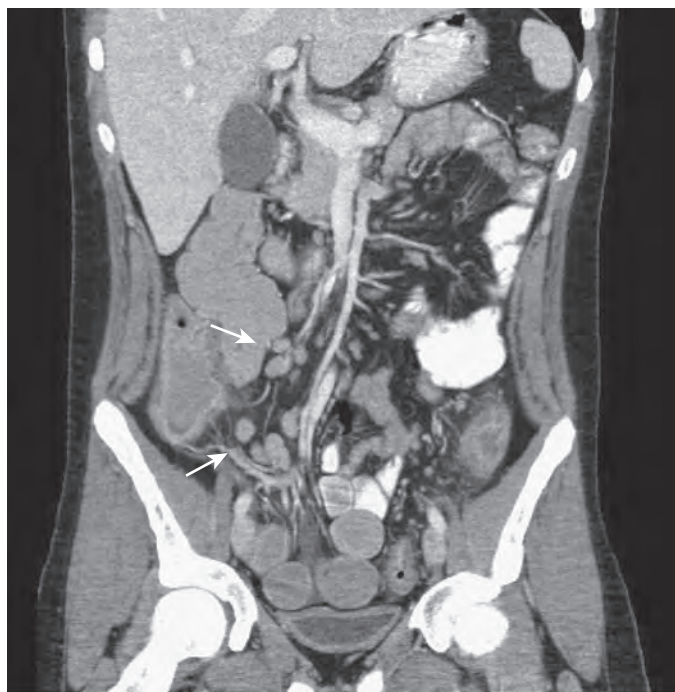
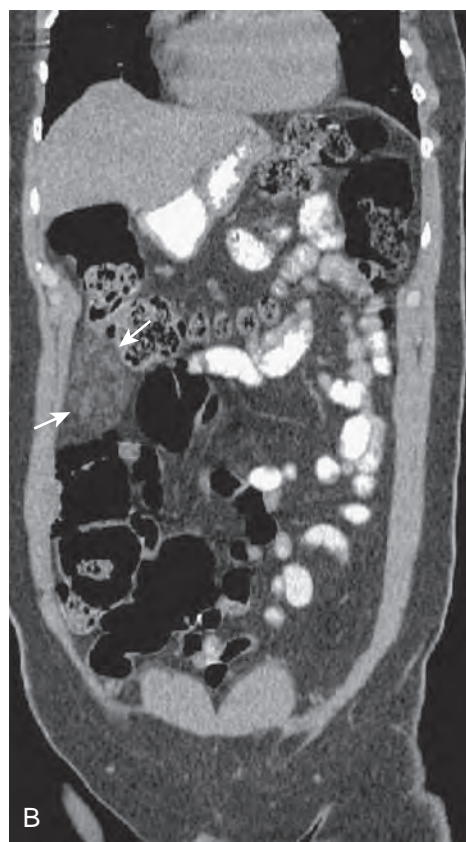


Figure 124-20 Mesenteric adenitis: CT features. Coronal reformatted image shows multiple, borderline, enlarged lymph nodes (arrows) in the ileocolic mesentery.

venous thrombosis, or both, which leads to severe abdominal pain associated with exquisite point tenderness. This usually occurs in the right lower quadrant, in which case it clinically simulates acute appendicitis, or in the right upper quadrant, in which case acute cholecystitis is simulated. This right-sided predilection may reflect variant vascular development, which predisposes to right-sided venous thrombosis.⁷²

CT demonstrates a region of increased attenuation within the greater omentum in the involved segment (Fig. 124-19). This region must be differentiated from an omental primary or secondary malignant neoplasm (e.g., carcinomatosis), omental infection (e.g., tuberculosis), and epiploic appendagitis. The size of the omental abnormality typically is larger in omental infarction and torsion than in epiploic appendagitis.⁷³ See Chapter 62 for a more complete discussion of omental torsion and infarction.

Mesenteric Adenitis

Benign inflammation of the ileocolic lymph nodes can cause mesenteric adenitis, which often simulates appendicitis clinically. *Yersinia enterocolitica*, *Yersinia pseudotuberculosis*, and *Helicobacter jejuni* are the most commonly implicated organisms. The appendix is normal, and there may be thickening of the adjacent ileum and cecum. On MDCT, the mesenteric lymph nodes are enlarged (>5 mm), and there may be inflammatory change in the surrounding mesentery (Fig. 124-20).⁷⁴

Infectious Enterocolitides

Gastroenteritis and the infectious enterocolitides are responsible for almost 70% of emergency department visits prompted by abdominal pain. Most cases are self-limited and do not require imaging. In atypical cases, colicky abdominal pain rather than diarrhea may be the predominant symptom. MDCT scans may show normal findings or may show nonspecific mural thickening in more severe cases of infection with invasive *Escherichia coli*, *Shigella*, *Salmonella*, *Yersinia*, and *Entamoeba* organisms.⁷⁵

In pseudomembranous colitis, potent antibiotics disrupt the normal bacterial flora of the colon, resulting in the overgrowth of *Clostridium difficile*. The release of its enterotoxins causes mucosal inflammation and the development of pseudomembranes, consisting of mucus and inflammatory debris. On MDCT, mural thickening averages 15 to 20 mm, with a target or halo pattern caused by submucosal edema.⁷⁵ Contrast material caught between thick haustra may simulate deep ulceration and produce an accordion-like appearance (Fig. 124-21). The lumen may be completely effaced. Ascites and pericolic inflammatory changes accompany these features.⁷⁵ MDCT is most useful in differentiating the panoply of inflammatory, infectious, and neoplastic disorders that can cause acute abdomen in AIDS patients. Infections such as cryptosporidiosis and cytomegalovirus infection produce thickening of the gut wall, edema of the submucosa, and increased enhancement of the mucosa.⁷⁵

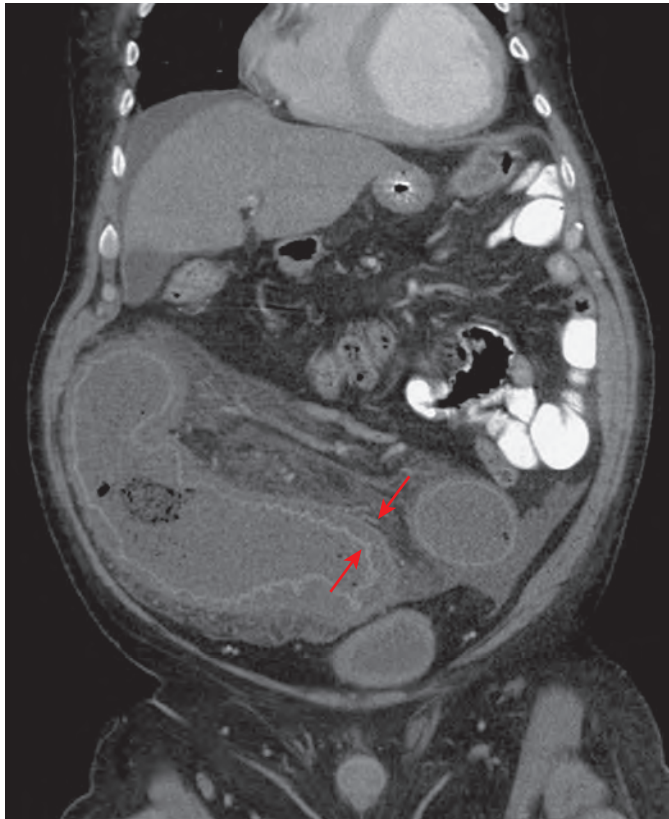


Figure 124-21 Pseudomembranous colitis: CT findings. Coronal reformatted CT image shows marked mural thickening with submucosal edema (arrows) of a redundant sigmoid colon. Note the ascites and inflammatory change in the adjacent sigmoid mesocolon.

Neutropenic enterocolitis (i.e., typhlitis) is an acute inflammatory and necrotizing process that affects the cecum or terminal ileum and appendix of immunocompromised patients with profound neutropenia. In this disorder, ulceration of the mucosa is followed by bacterial and fungal invasion. CT features are nonspecific and include segmental mural thickening of the cecum, intramural regions of edema or necrosis, pericolic fluid, and perienteric stranding (Fig. 124-22). In advanced cases, pneumatosis intestinalis and frank perforation may develop.⁷⁵ See Chapter 58 for a discussion of the infectious enterocolitides.

Inflammatory Bowel Disease

Most patients with inflammatory bowel disease experience chronic symptoms punctuated by periodic exacerbations. Fortunately, true emergencies are uncommon, but emergencies are associated with high rates of morbidity and mortality. Bowel obstruction and abscess formation are the most common emergencies for patients with Crohn's disease, whereas fulminant colitis, toxic megacolon, and perforation develop in patients with ulcerative colitis.⁷⁵⁻⁷⁸

Abscesses develop in almost 25% of patients with Crohn's disease, and MDCT is the preferred means of establishing a diagnosis and guiding percutaneous drainage. In patients with obstruction, the status of the diseased bowel, as depicted on MDCT, can significantly influence treatment of the patient. MDCT scans that reveal mural stratification (i.e., the ability to visualize distinct mucosal, submucosal, and muscularis propria layers) indicate the presence of submucosal edema. This edema may improve with steroids, biologic agents, and other immunosuppressive therapy. The reduced edema can lead to widening of the lumen caliber, with subsequent amelioration of the obstruction. If mural stratification is lost, transmural fibrosis is probably present, and the obstruction may require surgery or strictureplasty. MDCT may also reveal other, nonemergent complications of Crohn's disease, including fibrofatty proliferation of the mesentery, fistulas, and reactive adenopathy. In patients with fulminant ulcerative colitis, MDCT is the preferred noninvasive means of assessing the status of the bowel wall and detecting early perforation in toxic megacolon.⁷⁵⁻⁷⁸ See

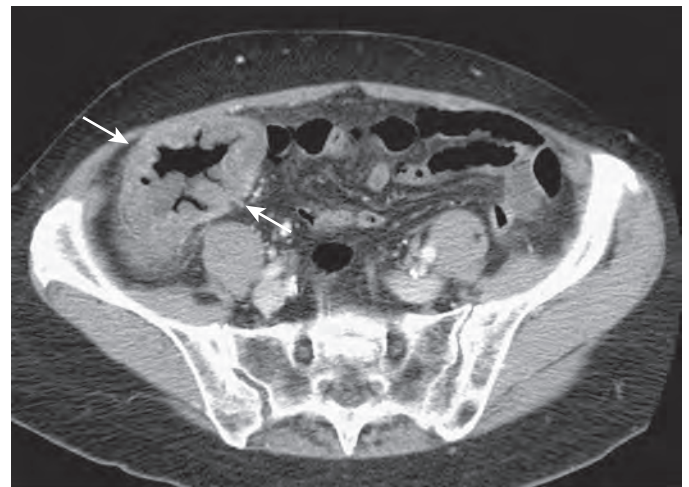


Figure 124-22 Typhlitis: CT features. Axial scan shows marked mural thickening of the cecum (arrows) in this patient with acute lymphocytic leukemia.

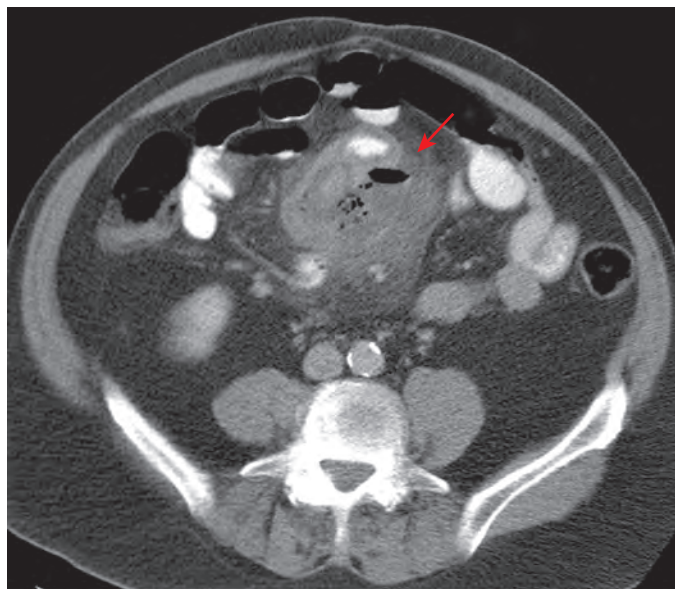


Figure 124-23 Meckel's diverticulitis: CT features. Axial CT image shows a gas-containing abscess (arrow) and inflammatory change in the ileocolic mesentery.

Chapters 41 and 57 for a more complete discussion of inflammatory bowel disease.

Small Bowel Diverticulitis

Small bowel diverticulitis is an unusual condition caused by the inflammation of a jejunal or ileal pseudodiverticulum or Meckel's diverticulum. CT findings are nonspecific and include perienteric inflammation (Fig. 124-23). On occasion, an air-filled or enterolith-filled diverticulum can be identified in the inflammatory process.⁷⁹

Abdominal Aortic Disease

MDCT is superb in depicting thoracoabdominal aortic dissections. Multiplanar reconstructions performed in the sagittal (Fig. 124-24) and coronal planes often help establish the diagnosis.⁸⁰

The clinical triad of symptoms of a ruptured aortic aneurysm includes abdominal pain, a pulsatile mass, and hypotension. Almost one third of patients do not have this classic presentation and are misdiagnosed as having renal colic and diverticulitis. The diagnosis of ruptured aneurysm should be considered for elderly men who are smokers because they run a higher risk of rupture. MDCT is the imaging procedure of choice for patients with suspected aneurysm dissection and rupture. Positive contrast agents should not be administered. Unenhanced images are initially obtained to search for hyperdense blood associated with one of the following signs of impending rupture: the draped aorta sign, in which the posterior wall of the aorta cannot be identified and is closely applied to the spine; the high-attenuation crescent sign (Fig. 124-25), attributed to hemorrhage in mural thrombus or in the wall of the aneurysm, which may be the first sign of aneurysm rupture; and focal discontinuity of intimal calcification.^{81,82}

Rapid infusion of contrast material (>3 mL/s) and thin collimation are required for optimal vascular resolution, depiction



Figure 124-24 Dissection of the infrarenal abdominal aorta. The sagittal reformatted image shows the intimal flap (arrows) in this normal-caliber aorta.

of intimal flaps, and multiplanar, three-dimensional vascular image creation. Although the atherosclerotic walls of aneurysms enhance and are perfused by the vasa vasorum, necrotic areas of the aortic wall reveal nonenhancing focal areas of low density. On MDCT, direct signs of rupture include a retroperitoneal hematoma and frank extravasation of intravenous contrast material (Fig. 124-26).^{81,82}

Hemorrhage

Acute hemorrhage in the gut, mesenteries, omenta, retroperitoneum, or abdominal musculature can cause acute abdomen. Patients with significant bleeding have a declining hematocrit and hypotension. Unenhanced scans should be obtained to detect a hyperdense hematoma. Intravenous contrast material delivered at a high rate (4-5 mL/s) may identify an active site of hemorrhage and provide a useful guide for subsequent angiographic embolization. Bleeding may occur into the rectus sheath or the psoas muscle. Most spontaneous hemorrhages are caused by anticoagulation (Fig. 124-27); however, they may result from tumor hemorrhage, most commonly in cases of renal cell carcinoma and hepatocellular carcinoma.⁸³

Hepatosplenic Vascular Disease

Acute right-sided heart decompensation can lead to dilation of the inferior vena cava and hepatic veins. This can cause hepatic engorgement and distention of Glisson's capsule, an underappreciated cause of right upper quadrant pain. MDCT findings

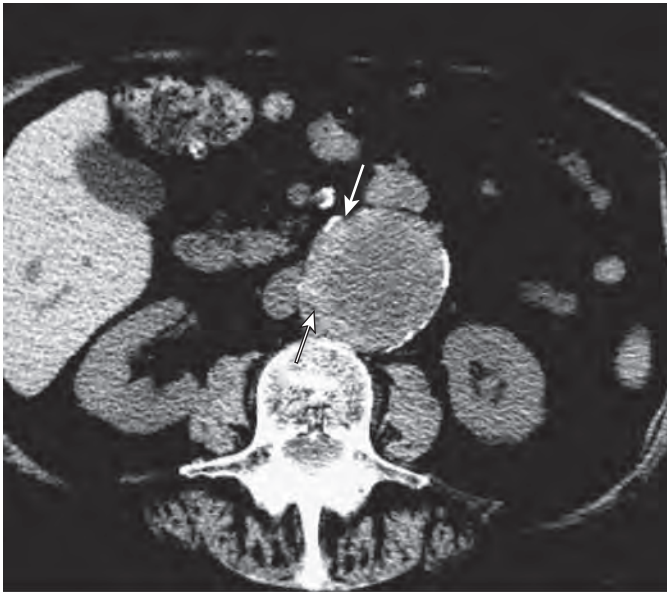


Figure 124-25 The crescent sign of impending aortic rupture. An aneurysmal infrarenal aorta, photographed at narrow window width, shows a hyperdense thrombus (arrows), which is associated with an increased incidence of rupture.



Figure 124-26 Active rupture of an abdominal aortic aneurysm: CT findings. Contrast material (arrow) is actively extravasating from the left lateral aspect of the aorta. Notice the hemorrhage into the surrounding intraperitoneal, retroperitoneal, subperitoneal, and extraperitoneal spaces.

show the venous dilation and reflux of contrast material into the dilated inferior vena cava and hepatic veins.⁸⁴

Patients with hepatic venous (i.e., Budd-Chiari syndrome), portal venous, and hepatic arterial thrombosis can present with acute right upper quadrant pain. The severity of symptoms depends on the extent and speed of onset of the occlusion.⁸⁵

Budd-Chiari syndrome has many causes, including coagulopathy, polycythemia vera, myeloproliferative disorders, and neoplasms. Thrombus may occur in the hepatic veins and the inferior vena cava. On early scans, the liver shows patchy enhancement, with the central portions having increased enhancement and the periphery having decreased enhancement. Delayed images show a reversal of this pattern.⁸⁵

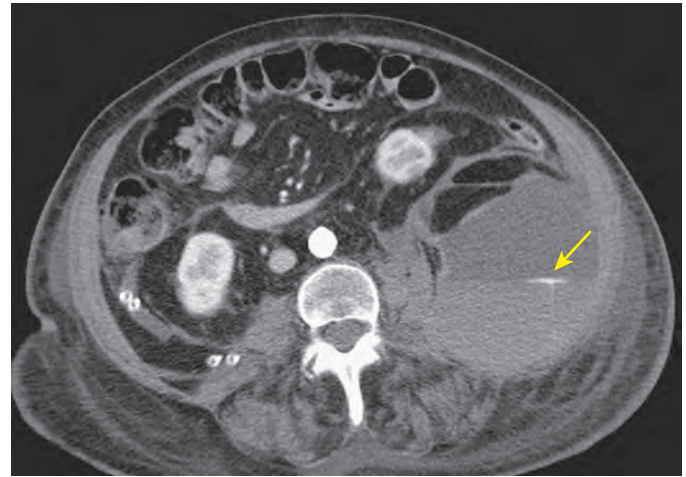


Figure 124-27 Spontaneous retroperitoneal bleed: CT features. Active extravasation of contrast material (arrow) is identified in the left flank of this patient who was overly anticoagulated. Blood is identified in multiple spaces: retroperitoneal, extraperitoneal, and interfascial.

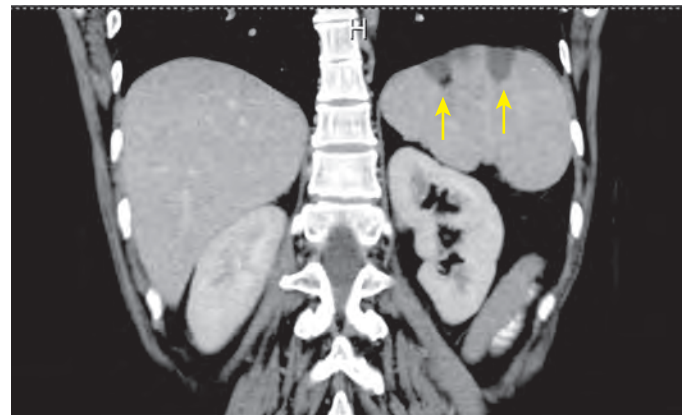


Figure 124-28 Splenic infarcts: CT findings. Coronal reformatted CT image shows two low-density regions (arrows) within the superior aspect of the spleen in this patient with atrial fibrillation.

Portal vein thrombosis develops in patients with cirrhosis, hepatic neoplasms, pancreatitis, and mesenteric pyelphlebitis. Portal vein thrombosis appears as a low-density central zone surrounded by an enhanced periphery on contrast-enhanced scans. Transient inhomogeneous enhancement of the affected liver segment also occurs. Tumor thrombus may dilate the vein and produce arterial phase enhancement.⁸⁵

Hepatic infarction is rare because the liver has a dual blood supply. Hepatic infarction usually results from thrombosis of the hepatic artery, which can be seen in patients with sepsis, shock, oral contraceptive use, transplanted liver, sickle cell disease, eclampsia, bacterial endocarditis, trauma, and polyarteritis nodosa. MDCT reveals wedge-shaped peripheral areas of low attenuation without contrast enhancement. Splenic and renal infarcts may also be present.⁸⁴

Splenic infarction is manifested as acute left upper quadrant pain but may be clinically silent. Bacterial endocarditis, pancreatitis, portal hypertension, sickle cell disease, and splenomegaly are responsible for most infarcts. On MDCT, focal infarcts are manifested as wedge-shaped zones of decreased attenuation that extend to the splenic capsule (Fig. 124-28). Although some

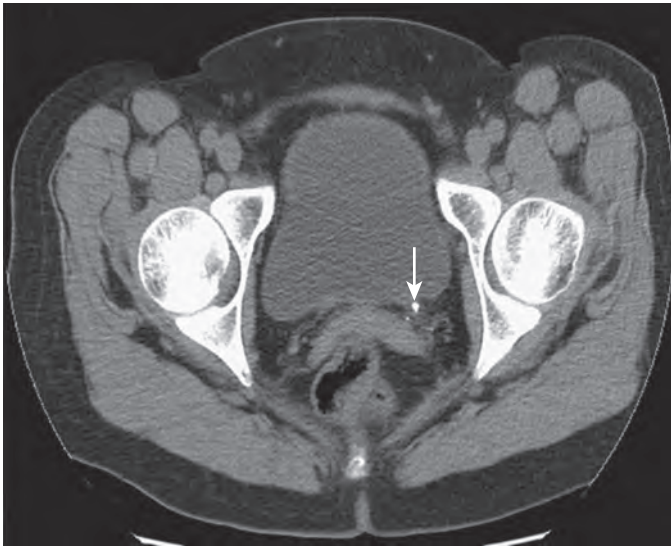


Figure 124-29 Ureterolithiasis: CT features. A 2-mm stone (arrow) is lodged at the left ureteropelvic junction.

peripheral enhancement may be caused by perfusion of capsular vessels, global infarction can cause diffuse splenic hypodensity.⁸⁶ See Chapter 90 for a more complete discussion of hepatosplenic vascular disorders.

Renal Colic

MDCT has transformed the evaluation of patients with acute flank pain suspected of having acute ureteral obstruction from an impacted stone. MDCT has positive and negative predictive values of more than 95% for the diagnosis of obstructing urinary calculi. MDCT can accurately determine the site and size of ureteral calculi and reveal the cause of flank pain in the 25% of patients without ureterolithiasis (e.g., appendicitis, diverticulitis, pancreatitis, cholecystitis, bowel obstruction, abdominal aortic aneurysms, ovarian disease).⁸⁷⁻⁹⁰

Most calculi are visible on MDCT. They appear as calcifications within the expected course of the ureter (Fig. 124-29). There is typically a thin rim of surrounding soft tissue that represents the edema within the ureteral wall, which strongly favors calcification as a calculus rather than a phlebolith. Secondary signs include hydronephrosis, hydroureter, perinephric stranding, and periureteric stranding. The affected kidney may have an attenuation value lower than that of the unobstructed kidney. A density difference of more than 5 HU is considered significant. Many of these patients are dehydrated, leading to minimal increased medullary attenuation on the normal side and lower attenuation on the obstructed side.⁸⁷⁻⁹⁰

Diagnostic pitfalls include misdiagnosing phleboliths as stones; attributing ureteral dilation to stones when it results from urinary tract infection or inflammation, reflux, or other benign and malignant causes of obstruction; and not detecting calculi that form in patients with human immunodeficiency virus infection undergoing indinavir therapy. The lack of intravenous contrast limits the ability of MDCT to diagnose other acute renal disease, such as pyelonephritis, renal vein thrombosis, and renal infarction. If the initial scan result is normal or inconclusive for the detection of obstructing calculi, a



Figure 124-30 Pyelonephritis: CT features. The infected right kidney is enlarged and edematous, and it produces a diminished, striated nephrogram on this coronal reformatted image.

contrast-enhanced scan can be obtained to search for other causes of the patient's pain (Fig. 124-30). A presumptive diagnosis of recent stone passage can be made when hydroureteronephrosis and perinephric and periureteric stranding are present without a calculus in a patient with clinical improvement and the absence of other findings.⁸⁷⁻⁹²

Conclusions

The subjective nature of pain, its complex neuroanatomic pathways, and the fact that a common symptom can arise from a broad spectrum of diseases make the acute abdomen difficult to diagnose. Nevertheless, two important decisions must be made. Does the patient need surgery, and if so, how soon? Immediate surgery is required for patients with massive hemorrhage (e.g., abdominal aortic aneurysm rupture); other conditions (e.g., perforation, intestinal ischemia) require surgical intervention in a few hours because additional delay increases morbidity. A delay of more than 6 hours is detrimental for patients with disorders such as appendicitis, mesenteric venous thrombosis, and strangulated small bowel obstruction.

MDCT has become the most important noninvasive imaging tool for diagnosing acute abdomen and for answering the questions previously posed. MDCT has the potential to positively affect the outcome, length of stay, and overall health care expenditures of patients with an acute abdomen.

REFERENCES

- Shah S: An update on common gastrointestinal emergencies. *Emerg Med Clin North Am* 31: 775–793, 2013.
- Crownover BK, Bepko JL: Appropriate and safe use of diagnostic imaging. *Am Fam Physician* 87:494–501, 2013.
- Gore RM, Miller FH, Pereles FS, et al: Helical CT in the evaluation of the acute abdomen. *AJR Am J Roentgenol* 174:901–913, 2000.
- Balachandran B, Singhi S, Lal S: Emergency management of acute abdomen in children. *Indian J Pediatr* 80:226–234, 2013.
- Khandelwal A, Fasih N, Kielar A: Imaging of acute abdomen in pregnancy. *Radiol Clin North Am* 51:1005–1022, 2013.
- Dewhurst C, Beddy P, Pedrosa I: MRI evaluation of acute appendicitis in pregnancy. *J Magn Reson Imaging* 37:566–575, 2013.
- Drake FT, Flum DR: Improvement in the diagnosis of appendicitis. *Adv Surg* 47:299–328, 2013.
- Teixeira PG, Demetriades D: Appendicitis: Changing perspectives. *Adv Surg* 47:119–140, 2013.
- McGory ML, Zingmond DS, Nanayakkara D, et al: Negative appendectomy rate: Influence of CT scans. *Am Surg* 71:803–808, 2005.
- Keyzer C, Zalcman M, De Maertelaer V, et al: Comparison of US and unenhanced multidetector row CT in patients suspected of having acute appendicitis. *Radiology* 236:527–534, 2005.
- Rosen MP, Ding A, Blake MA, et al: ACR Appropriateness Criteria right lower quadrant pain—suspected appendicitis. *J Am Coll Radiol* 8: 749–755, 2011.
- Johansson EP, Rydh A, Riklund KA: Ultrasound, computed tomography, and laboratory findings in the diagnosis of appendicitis. *Acta Radiol* 48:267–273, 2007.
- Leite NP, Pereira JM, Cunha R, et al: CT evaluation of appendicitis and its complications: Imaging techniques and key diagnostic findings. *AJR Am J Roentgenol* 185:406–417, 2005.
- Parker L, Nazarian LN, Gingold EL, et al: Cost and radiation savings of partial substitution of ultrasound for CT in appendicitis evaluation: A national projection. *AJR Am J Roentgenol* 202: 124–135, 2014.
- Levine CD, Aizenstein O, Levari O, et al: Why we miss the diagnosis of appendicitis on abdominal CT: Evaluation of imaging features of appendicitis incorrectly diagnosed on CT. *AJR Am J Roentgenol* 184:855–859, 2005.
- Leeuwenburgh MM, Wiezer MJ, Wiarda BM, et al: Accuracy of MRI compared with ultrasound imaging and selective use of CT to discriminate simple from perforated appendicitis. *Br J Surg* 101:e147–e155, 2014.
- Ganguli S, Raptopoulos V, Komlos F, et al: Right lower quadrant pain: Value of the nonvisualized appendix in patients at multidetector CT. *Radiology* 241:175–180, 2006.
- Paulson EK, Harris JP, Jaffe TA, et al: Acute appendicitis: Added diagnostic value of coronal reformations from isotropic voxels at multidetector row CT. *Radiology* 235:879–885, 2005.
- Lee SY, Coughlin B, Wolfe JM, et al: Prospective comparison of helical CT of the abdomen and pelvis without and with oral contrast in assessing acute abdominal pain in adult emergency department patients. *Emerg Radiol* 12:150–157, 2006.
- Le J, Kurian J, Cohen HW, et al: Do clinical outcomes suffer during transition to an ultrasound-first paradigm for the evaluation of acute appendicitis in children? *AJR Am J Roentgenol* 201:1348–1352, 2013.
- Bachar I, Perry ZH, Dukhno L, et al: Diagnostic value of laparoscopy, abdominal computed tomography, and ultrasonography in acute appendicitis. *J Laparoendosc Adv Surg Tech A* 23:982–989, 2013.
- Horrow MM, White DS, Horrow JC: Differentiation of perforated from nonperforated appendicitis at CT. *Radiology* 227:46–51, 2003.
- Chu LL, Webb EM, Stengel JW, et al: CT of acute appendicitis: Can diagnostic accuracy serve as a practical performance metric for readers specialized in abdominal imaging? *Clin Imaging* 38:56–59, 2014.
- Rodgers PM, Verma R: Transabdominal ultrasound for bowel evaluation. *Radiol Clin North Am* 51:133–148, 2013.
- Shademan A, Tappouni RF: Pitfalls in CT diagnosis of appendicitis: Pictorial essay. *J Med Imaging Radiat Oncol* 57:329–336, 2013.
- Yu J, Fulcher AS, Turnern MA, et al: Helical CT evaluation of acute right lower quadrant pain. Part I. Common mimics of appendicitis. *AJR Am J Roentgenol* 184:1136–1142, 2005.
- Daly CD, Cohan RH, Francis IR, et al: Incidence of acute appendicitis in patients with equivocal CT findings. *AJR Am J Roentgenol* 184:1813–1820, 2005.
- Sung T, Callahan MJ, Taylor GA, et al: Clinical and imaging mimickers of acute appendicitis in the pediatric population. *AJR Am J Roentgenol* 186:67–74, 2006.
- Yu J, Fulcher AS, Turner MA, et al: Helical CT evaluation of acute right lower quadrant pain. Part II. Uncommon mimics of appendicitis. *AJR Am J Roentgenol* 184:1143–1149, 2005.
- Macari M, Balthazar EJ: The acute right lower quadrant: CT evaluation. *Radiol Clin North Am* 41:1117–1136, 2003.
- Lohrmann C, Ghanem N, Pache G, et al: CT in acute perforated sigmoid diverticulitis. *Eur J Radiol* 56:78–83, 2005.
- Kaiser AM, Jiang JK, Lake JP, et al: The management of complicated diverticulitis and the role of computed tomography. *Am J Gastroenterol* 100:910–917, 2005.
- Siewert B, Tye G, Kruskal J, et al: Impact of CT-guided drainage in the treatment of diverticular abscesses: Size matters. *AJR Am J Roentgenol* 186:680–686, 2006.
- Castronovo G, Ciulla A, Tomasello G, et al: Diverticular disease of right colon: Clinical variants and personal experience. *Chir Ital* 58:213–217, 2006.
- Mak SY, Roach SC, Sukumar SA: Small bowel obstruction: Computed tomography features and pitfalls. *Curr Probl Diagn Radiol* 35:65–74, 2006.
- Jaffe TA, Martin LC, Thomas J, et al: Small-bowel obstruction: Coronal reformations from isotropic voxels at 16-section multi-detector row CT. *Radiology* 238:135–142, 2006.
- Zalcman M, Sy M, Donckier D, et al: Helical CT signs in the diagnosis of intestinal ischemia in small-bowel obstruction. *AJR Am J Roentgenol* 175:1601–1607, 2000.
- Nicolaou S, Kai B, Ho S, et al: Imaging of acute small-bowel obstruction. *AJR Am J Roentgenol* 185:1036–1044, 2005.
- Hayanga AJ, Bass-Wilkins K, Bulkley GB: Current management of small-bowel obstruction. *Adv Surg* 39:1–33, 2005.
- Yaghmai V, Nikolaidis P, Hammond NA, et al: Multidetector-row computed tomography diagnosis of small bowel obstruction: Can coronal reformations replace axial images? *Emerg Radiol* 13:69–72, 2006.
- Petrovic B, Nikolaidis P, Hammond NA, et al: Identification of adhesions on CT in small-bowel obstruction. *Emerg Radiol* 12:88–93, 2006.
- Aufort S, Charra L, Lesnik A, et al: Multidetector CT of bowel obstruction: Value of post-processing. *Eur Radiol* 15:2323–2329, 2005.
- Taylor MR, Lalani N: Adult small bowel obstruction. *Acad Emerg Med* 20:528–544, 2013.
- Nicolaou S, Kai B, Ho S, et al: Imaging of acute small-bowel obstruction. *AJR Am J Roentgenol* 185:1036–1044, 2005.
- Santillan CS: Computed tomography of small bowel obstruction. *Radiol Clin North Am* 51: 17–27, 2013.
- Huang BY, Warshauer DM: Adult intussusception: Diagnosis and clinical relevance. *Radiol Clin North Am* 41:1137–1152, 2003.
- Mathieu D, Luciani A: Internal abdominal herniations. *AJR Am J Roentgenol* 183:397–404, 2004.
- Bennett GL, Balthazar EJ: Ultrasound and CT evaluation of emergent gallbladder pathology. *Radiol Clin North Am* 41:1203–1216, 2003.
- Kogut MJ, Bastawrous S, Padia S, et al: Hepatobiliary oncologic emergencies: Imaging appearances and therapeutic options. *Curr Probl Diagn Radiol* 42:113–126, 2013.
- Singh AK, Sagar P: Gangrenous cholecystitis: Prediction with CT imaging. *Abdom Imaging* 30:218–221, 2005.
- Tonolini M, Ravelli A, Villa C, et al: Urgent MRI with MR cholangiopancreatography (MRCP) of acute cholecystitis and related complications: Diagnostic role and spectrum of imaging findings. *Emerg Radiol* 19:341–348, 2012.
- Hou LA, Van Dam J: Pre-ERCP imaging of the bile duct and gallbladder. *Gastrointest Endosc Clin N Am* 23:185–197, 2013.
- Pun E, Firkin A: Computed tomography and complicated peptic ulcer disease. *Australas Radiol* 48:516–519, 2004.
- Otsuki M, Takeda K, Matsuno S, et al: Criteria for the diagnosis and severity stratification of acute pancreatitis. *World J Gastroenterol* 19: 5798–5805, 2013.
- Banks PA, Bollen TL, Dervenis C, et al: A classification of acute pancreatitis—2012: Revision of the Atlanta classification and definitions by international consensus. *Gut* 62:102–111, 2013.
- Rubesin SE, Levine MS: Radiologic diagnosis of gastrointestinal perforation. *Radiol Clin North Am* 41:1095–1116, 2003.
- Hines J, Rosenblat J, Duncan DR, et al: Perforation of the mesenteric small bowel: Etiologies and CT findings. *Emerg Radiol* 20:155–161, 2013.
- Grassi R, Romano S, Pinto A, Romano L: Gastrointestinal perforations: Conventional plain film, US and CT findings in 166 consecutive patients. *Eur J Radiol* 50:30–36, 2004.
- Hainaux B, Agneessens E, Bertinotti R, et al: Accuracy of MDCT in predicting site of gastrointestinal tract perforation. *AJR Am J Roentgenol* 187:1179–1183, 2006.

60. Macari M, Balthazar EJ: CT of bowel wall thickening: Significance and pitfalls of interpretation. *AJR Am J Roentgenol* 176:1105–1116, 2001.
61. Segatto E, Morteale KJ, Ji H, et al: Acute small bowel ischemia: CT imaging findings. *Semin Ultrasound CT MR* 24:364–376, 2003.
62. Chou CK, Wu RH, Mak CW, et al: Clinical significance of poor CT enhancement of the thickened small-bowel wall in patients with acute abdominal pain. *AJR Am J Roentgenol* 186:491–498, 2006.
63. Chou CK, Mak CW, Tzeng WS, et al: CT of small bowel ischemia. *Abdom Imaging* 29:18–22, 2004.
64. Macari M, Chandarana H, Balthazar E, et al: Intestinal ischemia versus intramural hemorrhage: CT evaluation. *AJR Am J Roentgenol* 180:177–184, 2003.
65. Lee R, Tung HK, Tung PH, et al: CT in acute mesenteric ischaemia. *Clin Radiol* 58:279–287, 2003.
66. Rha SE, Ha HK, Lee SH, et al: CT and MR imaging findings of bowel ischemia from various primary causes. *Radiographics* 20:29–42, 2000.
67. Wiesner W, Khurana B, Ji H, et al: CT of acute bowel ischemia. *Radiology* 226:635–650, 2003.
68. Angelelli G, Scardapane A, Memeo M, et al: Acute bowel ischemia: CT findings. *Eur J Radiol* 50:37–47, 2004.
69. Hwang JA, Kim SM, Song HJ, et al: Differential diagnosis of left-sided abdominal pain: Primary epiploic appendagitis vs colonic diverticulitis. *World J Gastroenterol* 19:6842–6848, 2013.
70. Oztunali C, Kara T: Radiologic findings of epiploic appendagitis. *Med Ultrason* 15:71–72, 2013.
71. Pereira JM, Sirin CB, Pinto PS, et al: CT and MR imaging of extrahepatic fatty masses of the abdomen and pelvis: Techniques, diagnosis, differential diagnosis, and pitfalls. *Radiographics* 25:69–85, 2005.
72. Le Roux F, Gennuso F, Lipsker A, et al: Omental torsion, a rare cause of acute surgical abdomen. *J Visc Surg* 150:421–422, 2013.
73. Coulier B: Contribution of US and CT for diagnosis of intraperitoneal focal fat infarction (IFFI): A pictorial review. *JBR-BTR* 93:171–185, 2010.
74. Wertheimer J, Galloy MA, Régent D, et al: Radiological, clinical and histological correlations in a right segmental omental infarction due to primary torsion in a child. *Diagn Interv Imaging* 95:325–331, 2014.
75. Thoeni RF, Cello JP: CT imaging of colitis. *Radiology* 240:623–638, 2006.
76. Patak MA, Morteale KJ, Ros PR: Multidetector row CT of the small bowel. *Radiol Clin North Am* 43:1063–1077, 2005.
77. Huprich JE, Barlow JM, Hansel SL, et al: Multi-phase CT enterography evaluation of small-bowel vascular lesions. *AJR Am J Roentgenol* 201:65–72, 2013.
78. Hong SS, Kim AY, Byun JH, et al: MDCT of small bowel disease: Value of 3D imaging. *AJR Am J Roentgenol* 187:1212–1221, 2006.
79. Bennett GL, Birnbaum BA, Balthazar EJ: CT of Meckel's diverticulitis in 11 patients. *AJR Am J Roentgenol* 182:625–629, 2002.
80. Bhalla S, Menias CO, Heiken JP: CT of acute abdominal aortic disorders. *Radiol Clin North Am* 41:1153–1170, 2003.
81. Ahmed MZ, Ling L, Ettles DF: Common and uncommon CT findings in rupture and impending rupture of abdominal aortic aneurysms. *Clin Radiol* 68:962–971, 2013.
82. Desjardins B, Dill KE, Flamm SD, et al: ACR Appropriateness Criteria pulsatile abdominal mass, suspected abdominal aortic aneurysm. *Int J Cardiovasc Imaging* 29:177–183, 2013.
83. Morteale KJ, Cantisani V, Brown DL, et al: Spontaneous intraperitoneal hemorrhage: Imaging features. *Radiol Clin North Am* 41:1183–1202, 2003.
84. Giovine S, Pinto A, Crispano S, et al: Retrospective study of 23 cases of hepatic infarction: CT findings and pathological correlations. *Radiol Med* 111:11–21, 2006.
85. Brancatelli G, Vilgrain V, Federle MP, et al: Budd-Chiari syndrome: Spectrum of imaging findings. *AJR Am J Roentgenol* 188:168–176, 2007.
86. Warshauer DM, Hall HL: Solitary splenic lesions. *Semin Ultrasound CT MR* 27:370–388, 2006.
87. Langer JE: Computed tomography and ultrasonography of acute renal abnormalities. *Semin Roentgenol* 36:99–108, 2001.
88. Amilineni V, Lackner DF, Morse WS, et al: Contrast-enhanced CT for acute flank pain caused by acute renal artery occlusion. *AJR Am J Roentgenol* 174:105–106, 2000.
89. Moore CL, Daniels B, Singh D, et al: Prevalence and clinical importance of alternative causes of symptoms using a renal colic computed tomography protocol in patients with flank or back pain and absence of pyuria. *Acad Emerg Med* 20:470–478, 2013.
90. Zwank MD, Ho BM, Gresback D, et al: Does computed tomographic scan affect the diagnosis and management of patients with suspected renal colic? *Am J Emerg Med* 32:362–370, 2014.
91. Paick SH, Choo GY, Baek M, et al: Clinical value of acute pyelonephritis grade based on computed tomography in predicting severity and course of acute pyelonephritis. *J Comput Assist Tomogr* 37:440–442, 2013.
92. Barkin J, Rosenberg MT, Miner M: A guide to the management of urologic dilemmas for the primary care physician (PCP). *Can J Urol* 21:55–63, 2014.

Gastrointestinal Hemorrhage

JAMES E. HUPRICH | JEFFREY A. ALEXANDER | BRIAN P. MULLAN | ANTHONY W. STANSON

CHAPTER OUTLINE

Etiology

Clinical Presentation and Evaluation

Diagnostic and Therapeutic Procedures

Endoscopy

Capsule Endoscopy

Deep Enteroscopy

Multidetector Computed Tomography

Nuclear Scintigraphy

Angiography

Barium Studies

Upper Gastrointestinal Hemorrhage

Peptic Ulcers

Esophageal Varices

Gastritis

Mallory-Weiss Tear

Midgut Hemorrhage

Small Bowel Vascular Lesions

Small Bowel Ulcers

Small Bowel Neoplasms

Lower Gastrointestinal Hemorrhage

Diverticular Hemorrhage

Colon Neoplasms

Gastrointestinal hemorrhage is one of the most common and challenging clinical problems encountered by the gastroenterologist. Approximately 400,000 patients with signs and symptoms of gastrointestinal hemorrhage seek medical attention each year in the United States. Fortunately, in the majority of cases, gastrointestinal hemorrhage resolves spontaneously. However, in 25% of patients with recurrent or persistent bleeding, morbidity and mortality are significant.^{1,2} In these patients, rapid and accurate diagnosis and treatment of the bleeding source are necessary to prevent death and to limit morbidity. In many patients, bleeding may be chronic and intermittent, and patients may present with subtle signs of blood loss, such as anemia. Patients with chronic gastrointestinal blood loss have a lower mortality rate compared with patients with acute bleeding, but the toll on quality of life and the cost of care due to repeated hospitalizations and diagnostic procedures are substantial.

The classification of gastrointestinal hemorrhage is based on the severity of bleeding and the site of bleeding within the gastrointestinal tract. Patients experiencing gastrointestinal blood loss who exhibit signs of hemodynamic instability require rapid resuscitation and prompt identification and treatment of the bleeding site in an inpatient setting. On the other hand,

hemodynamically stable patients with signs of chronic blood loss may be managed as outpatients.

On the basis of endoscopic accessibility, gastrointestinal tract bleeding is also classified by the segment of the gastrointestinal tract in which the bleeding occurs. Upper gastrointestinal tract bleeding is defined as bleeding that originates from a lesion proximal to the ligament of Treitz, that is, the segment of bowel routinely accessible by upper endoscopy. Midgut bleeding occurs between the ampulla of Vater and the terminal ileum (accessible by deep endoscopy); and lower gastrointestinal tract bleeding occurs distal to the terminal ileum (accessible by colonoscopy). The approximate frequency of bleeding in each of these segments is 75% to 80%, 5% to 10%, and 20% to 25%, respectively.

The remainder of this chapter discusses an approach to the diagnosis and treatment of patients with gastrointestinal hemorrhage with emphasis on the imaging tools used to detect the nature and location of bleeding and the common methods used in the treatment of gastrointestinal hemorrhage.

Etiology

The list of gastrointestinal bleeding sources is extensive (Table 125-1). Most disorders are more common in specific segments of the gastrointestinal tract, and the more common conditions responsible for bleeding are discussed in the appropriate sections.

Past medical history often provides helpful clues to the source of gastrointestinal bleeding. Up to 60% of patients with a history of upper gastrointestinal hemorrhage bleed from the same lesion.³ Comorbid conditions may also suggest a potential cause of bleeding:

- Liver disease or alcohol abuse: varices
- Renal disease, aortic stenosis, or Osler-Weber-Rendu disease: angiodysplasia
- Abdominal aortic aneurysm or aortic graft: aortoenteric fistula
- *Helicobacter pylori* infection: peptic ulcer disease
- Smoking, alcohol abuse, *H. pylori* infection: malignant disease
- Gastroenteric anastomosis: marginal ulcers
- Chronic diarrhea and abdominal pain: inflammatory bowel disease

Clinical Presentation and Evaluation

Gastrointestinal hemorrhage has five clinical presentations: hematemesis, which is bloody vomitus that may be fresh and bright red or older with a coffee-ground appearance; melena, which is black, shiny, sticky, foul-smelling fecal matter that results from the degradation of blood in the gut; hematochezia, which is the passage of bright red or maroon blood, bloody

TABLE 125-1 Causes of Gastrointestinal Hemorrhage**Upper Tract Hemorrhage**

Duodenal ulcer
 Gastric ulcer
 Gastritis
 Marginal ulcer
 Esophagitis
 Esophageal and gastric varices
 Mallory-Weiss tear
 Barrett's ulcer
 Hematobilia
 Ménétrier's disease
 Hiatal and paraesophageal hernias

Upper and Lower Tract Hemorrhage

Neoplasms
 Carcinoma
 Leiomyosarcoma, leiomyoma
 Hemangioma
 Lymphoma
 Metastases
 Polyps
 Aortoenteric fistulas
 Vascular anomalies
 Osler-Weber-Rendu syndrome
 Blue rubber bleb nevus syndrome
 CRST syndrome (calcinosis cutis, Raynaud's phenomenon, sclerodactyly, and telangiectasia)
 Angiodysplasia
 Arteriovenous malformations
 Amyloidosis
 Elastic tissue disorders
 Pseudoxanthoma elasticum
 Ehlers-Danlos syndrome
 Hematologic disorders and diatheses
 Vasculitides

LOWER TRACT HEMORRHAGE

Hemorrhoids
 Anal fissures
 Diverticulosis of the small bowel and colon
 Ischemic bowel disease
 Inflammatory bowel disease
 Solitary colonic ulcer
 Intussusception

Modified from Rockey DC: Gastrointestinal bleeding. In Feldman M, Friedman LS, Brandt LJ (eds): *Gastrointestinal and Liver Disease*, 8th ed. Philadelphia, Saunders, 2010, pp 247–298.

diarrhea, or blood mixed with formed stool; occult blood, found only by testing of the stool with a chemical reagent; and symptoms of blood loss, such as dyspnea, dizziness, or shock (in massive bleeding) or iron deficiency anemia (in chronic bleeding).⁴⁻⁷

A major goal in the diagnosis of gastrointestinal hemorrhage is differentiation of upper from more distal gastrointestinal tract sources of bleeding. Proximal lesions tend to cause hematemesis or melena, whereas distal lesions more commonly produce hematochezia. Hematochezia stemming from an upper gastrointestinal source usually reflects a massive hemorrhage, which, if it is associated with a bloody nasogastric aspirate, has a mortality of nearly 30%. Hematemesis almost invariably localizes the source of hemorrhage proximal to the ligament of Treitz. However, up to 40% to 50% of patients with upper gastrointestinal bleeding do not experience hematemesis. About 20% of patients with bleeding ulcers present with melena, 30%

with hematemesis, 50% with both, and as many as 5% with hematochezia.⁸⁻¹¹ Melena can result when as little as 50 mL of blood is instilled into the upper gastrointestinal tract; the instillation of 1000 mL or more leads to hematochezia.

Aspiration of gastric contents with a nasogastric tube may reveal blood, which is diagnostic of an upper gastrointestinal bleeding source. The absence of blood, however, does not entirely exclude the possibility of an upper gastrointestinal hemorrhage because the bleeding might have ceased before passage of the tube or might have occurred distal to a competent pyloric sphincter. The presence of bile in the gastric aspirate indicates that the bowel distal to the pylorus has been sampled. Nasogastric lavage may help clear the stomach of blood clots and debris before endoscopy; however, there is little evidence to suggest that lavage helps stop bleeding.

Diagnostic and Therapeutic Procedures

ENDOSCOPY

Upper endoscopy and colonoscopy are the most important tools for evaluation of patients with gastrointestinal bleeding because they permit direct visualization of the bowel lumen and provide a method for rapid diagnosis and treatment of abnormalities within the upper gastrointestinal tract and within the colon and terminal ileum. Endoscopy can determine the cause of bleeding with a 90% to 95% accuracy while affording access for therapeutic procedures and providing valuable prognostic information.¹⁰

Whereas endoscopy remains the cornerstone of diagnosis and therapy for gastrointestinal bleeding originating in the upper gastrointestinal tract and colon, until recently the small bowel has been inaccessible. Recent advances in endoscopic techniques, including capsule endoscopy and deep enteroscopy, have extended the usefulness of endoscopy to the entire gastrointestinal tract, including the small bowel.

CAPSULE ENDOSCOPY

Capsule endoscopy (CE) was introduced in 2000 and enables visualization of the entire gastrointestinal tract, including the small bowel, which until then was virtually inaccessible with conventional endoscopic techniques. This technique involves the oral or endoscopic introduction of a small capsule equipped with a light source, lens, battery, radiofrequency transmitter, and antenna into the stomach or duodenum. The capsule acquires images of the gastrointestinal tract at two frames per second and transmits data to a data recorder worn on the patient's waist. The images are then downloaded and viewed on a computer. CE allows visualization of the entire small bowel in 79% to 90% of patients.¹²

CE does have several disadvantages. Trivial findings are commonly detected and occur in up to 23% of healthy patients undergoing CE.¹³ In addition, because the device is purely diagnostic, additional therapeutic procedures may be indicated if significant abnormalities are found. The most serious disadvantage of CE is capsule retention in patients with a stricture or bowel obstruction, sometimes requiring surgical removal. This is more common in patients with Crohn's disease and small bowel tumors. Patency capsules are useful for minimizing the

risk of retention by selecting those patients who may safely undergo CE.¹⁴

DEEP ENTEROSCOPY

These techniques, used primarily to evaluate the small bowel, include double-balloon enteroscopy (DBE), single-balloon enteroscopy, and spiral enteroscopy. These techniques offer an advantage over CE because they not only permit visualization of the entire small bowel but also allow therapeutic interventions. These advanced techniques require special technical skill and have associated complications, such as bleeding and bowel perforation; therefore, they are usually performed only after a positive finding on CE or other imaging studies suggesting a small bowel abnormality.

Double- and single-balloon enteroscopes consist of an enteroscope and an overtube with an inflatable balloon. Double-balloon enteroscopes also have a balloon attached to the end of the enteroscope. Advancement through the small bowel is achieved by a series of push-pull maneuvers in which the balloon is alternately inflated and deflated as the enteroscope and overtube are advanced as the small bowel is shortened like the bellows of an accordion. These procedures can be performed by an antegrade or retrograde approach. The antegrade approach is selected for suspected lesions in the proximal 75%; the retrograde approach is selected for distal lesions. The choice of approach is based on CE or other imaging findings. The success rate for examination of the entire small bowel ranges from 16% to 86%.¹⁵ The complication rate for diagnostic DBE is 0.8%; for therapeutic procedures, it is 4%.

Spiral enteroscopy is a new technique using a spiral overtube, which has a 21-cm raised helix at the distal end. The overtube is placed over the enteroscope, and the paired device is advanced by rotation in a clockwise fashion until the farthest extent of the small bowel is reached. The enteroscope is then advanced alone, followed by rotation of the spiral overtube. This device permits significantly shorter examination time and has a complication rate similar to that of DBE.

MULTIDETECTOR COMPUTED TOMOGRAPHY

The utility of multidetector computed tomography (MDCT) in the diagnosis of gastrointestinal hemorrhage has become increasingly accepted. In a meta-analysis of 22 studies involving 672 patients with acute episodes of gastrointestinal bleeding, CT angiography achieved a sensitivity of 85% and specificity of 92% in detecting active bleeding.¹⁶ MDCT techniques also appear useful in evaluating the source of bleeding in hemodynamically stable patients. In a prospective study of outpatients with obscure gastrointestinal bleeding, multiphase CT enterography (CTE) identified a bleeding source in 14 of 16 patients.¹⁷

In the majority of reports, the method used for evaluation of gastrointestinal bleeding is a modification of CTE technique¹⁸ (see Chapter 38). The patient drinks a large volume of low-concentration barium solution (e.g., VoLumen) to produce bowel distention. Water can be substituted, but it produces suboptimal bowel distention because of rapid intestinal absorption. Both agents are of neutral density to permit optimal bowel wall visualization. The presence of positive contrast material within the bowel, as is common with most CT scan studies, obscures the bowel wall and may mask subtle vascular lesions and prevent the identification of active bleeding.

A variety of scan techniques for evaluation of gastrointestinal bleeding have been reported. These usually involve two- or three-phase acquisitions (e.g., arterial, portal venous, delayed) after intravenous administration of contrast material, sometimes combined with a preliminary noncontrast scan. Obviously, the greater the number of acquisitions, the higher the patient's radiation dose. However, a greater number of acquisitions may improve detection of a bleeding source. The evolving appearance of active bleeding producing intraluminal accumulation of contrast material is best appreciated over time with multiple scan acquisitions (Fig. 125-1). Also, some lesions have characteristic enhancement patterns that may permit a specific diagnosis and therefore encourage timely management. In addition, vascular lesions may be visible only transiently, and abnormalities may go undetected if the acquisition is too early or too late.¹⁹ The choice of technique depends on the patient's age and clinical history. In our practice, we prefer to use three-phase acquisition for the evaluation of the majority of patients with obscure gastrointestinal bleeding.¹⁷

NUCLEAR SCINTIGRAPHY

Radionuclide imaging in the evaluation of gastrointestinal hemorrhage can be classified into direct and indirect methods. Direct nuclear scintigraphic methods use either technetium Tc 99m sulfur colloid or the preferred ^{99m}Tc-labeled red blood cell (RBC). Indirect evaluation of gastrointestinal blood loss relates to the use of ^{99m}Tc-pertechnetate scintigraphy in suspected Meckel's diverticulum, which is of particular value in younger patients.²⁰

^{99m}Tc-sulfur colloid studies can be useful in demonstrating rapid gastrointestinal blood loss, but with a short intravascular residence time (half-life of 2-3 minutes) and increasing uptake in the bone marrow, liver, and spleen, it has limited usefulness in gastrointestinal blood loss, as active bleeding is almost always intermittent. This allows a limited imaging window of approximately 15 minutes to demonstrate the bleeding site. It is also an "off-label" indication for this radionuclide tracer.

^{99m}Tc-labeled RBC scintigraphy is considered a sensitive noninvasive method for detection of gastrointestinal blood loss, with sensitivity ranging from 40% to 90%. In the animal model, it can detect blood loss rates on the order of 0.1 mL/min compared with 0.5 to 1.0 mL/min with contrast angiography.²¹⁻²⁶

The examination requires little preparation of the patient, has relatively low radiation exposure (0.3 rad/20 mCi), and can usually cover more than 12 hours of intermittent imaging. Sensitive imaging is predicated on high and durable RBC labeling efficiency, on the order of 95% by postlabeling quality control. The highest labeling efficiency is by the *in vitro* labeling methodology with use of a commercial kit such as UltraTag (Mallinckrodt, St. Louis, MO). The labeling procedure takes 20 to 30 minutes, and the labeled RBCs are reinjected, acquiring anterior abdominal dynamic images under a large field of view gamma camera. Typically, 60 to 90 minutes of initial imaging is standard, with subsequent delayed images if initial images are normal, as dictated by the patient's clinical status.²⁷

Image interpretation relies on viewing extravasation of the tracer into the bowel with subsequent peristaltic movement through the bowel (Fig. 125-2). The configuration, location, and movement of the tracer over time determine whether the gastrointestinal bleeding site is from the small or large bowel,

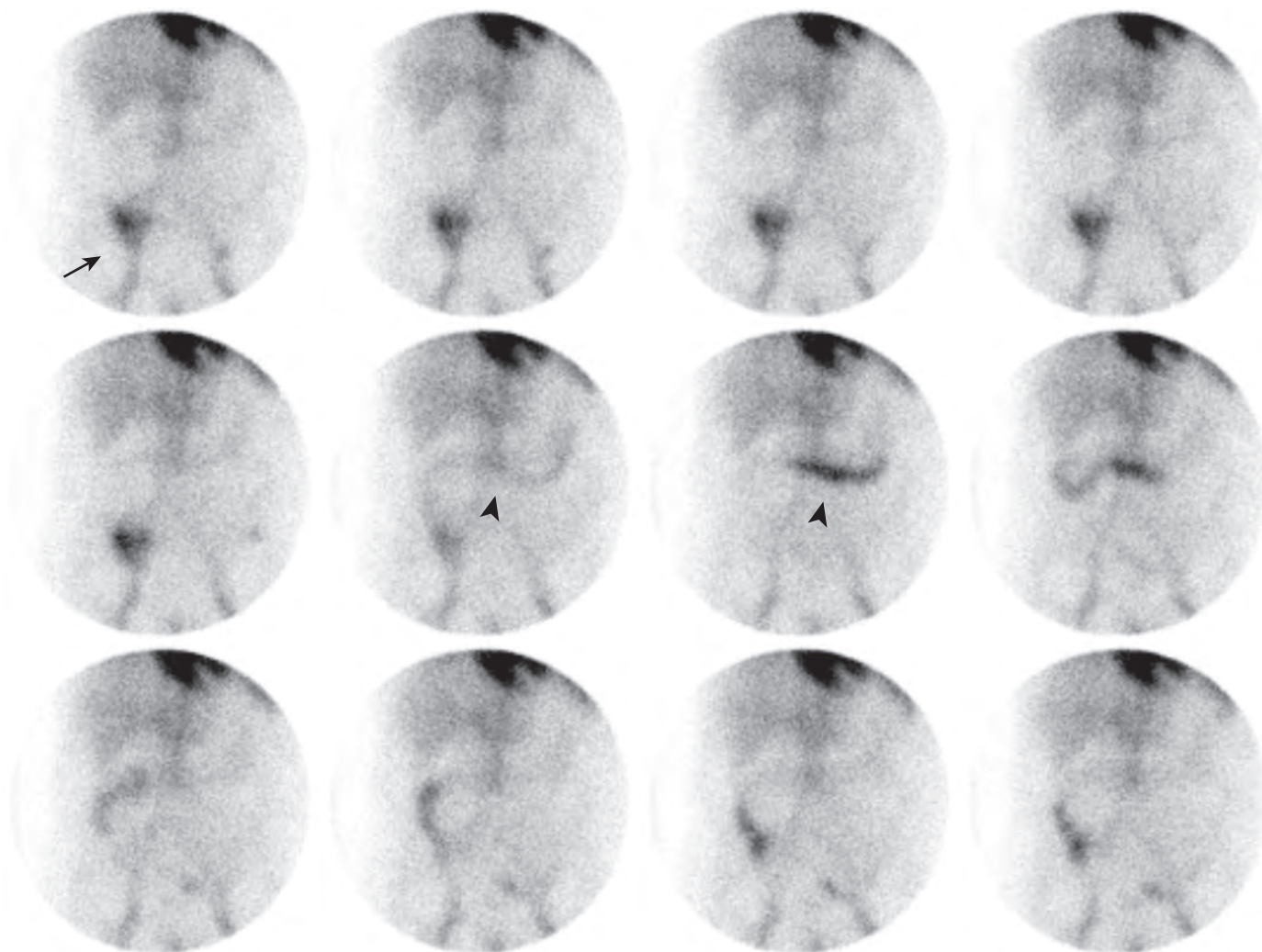


Figure 125-1 Active colonic bleeding. Sequential 5-minute dynamic composite anterior ^{99m}Tc -labeled RBC images in a patient with active gastrointestinal blood loss. Note the prompt appearance of abnormal tracer uptake in the right lower quadrant (arrow) with subsequent antegrade movement of tracer from the cecal region through the right colon to the transverse colon (arrowheads).



Figure 125-2 Active small bowel bleeding. An 82-year-old woman taking warfarin for aortic valve replacement experienced melena and anemia; findings on capsule endoscopy were normal. Axial arterial (A), enteric (B), and delayed (C) phase images from multiphase CTE demonstrate progressive accumulation of contrast material in the dependent portion of the bowel (arrow and arrowheads) due to active bleeding from an ileal ulcer. (From Huprich J, Fletcher J, Fidler J, et al: Prospective blinded comparison of wireless capsule endoscopy and multiphase CT enterography in obscure gastrointestinal bleeding. *Radiology* 260:744–751, 2011.)

noting that both antegrade and less commonly retrograde tracer movement can occur.

Imaging pitfalls can be due to free technetium within the stomach and renal system. This may be seen with a poor ^{99m}Tc -RBC label, unusual or prominent blood pool foci (such as abdominal aortic aneurysm), esophageal varices, penile activity, and vascular grafts as well as with miscellaneous items such as accessory splenic tissue and hemangiomas.

ANGIOGRAPHY

Persistent or recurrent bleeding occurs in 7% to 16% of patients with upper gastrointestinal bleeding²⁸ and in up to 25% of patients with lower gastrointestinal bleeding.²⁹ Such patients may require angiographic intervention to locate or to treat the source of bleeding.

In most cases, angiographic control of gastrointestinal bleeding requires that the site of bleeding first be identified. Angiographic detection of active bleeding requires a minimum bleeding rate of 0.5 mL/min. Because isotope-labeled RBC scans can detect lower bleeding rates (0.1 mm/min), a positive nuclear study may predict a positive angiographic examination.

Therapeutic angiographic intervention has a wide spectrum of applications, from embolization of arterial lesions, to direct infusion of vasopressin, to performing a transjugular intrahepatic portal systemic shunt (TIPS). Intra-arterial vasopressin causes generalized vasoconstriction by a direct action on vessel walls, thereby decreasing perfusion pressure to all stable clot formation. Unfortunately, rebleeding is common after cessation of the infusion. As a potent peripheral vasoconstrictor, vasopressin must be used with caution in patients with coronary artery disease, congestive cardiomyopathy, severe hypertension, and peripheral vascular disease.

Therapeutic embolization causes mechanical occlusion of the blood supply to the bleeding site. The embolic agents used can produce temporary (0-21 days) or permanent vessel occlusion. The embolic agent is delivered through an end-hole catheter into the target vessel. Complications occur in 5% to 9%, with ischemia and infarction being the most common. The use of superselective catheters has decreased complications related to ischemia. The use of angiography in specific cases of gastrointestinal bleeding is discussed in the following sections.

BARIUM STUDIES

Barium studies have no significant role to play in assessing the patient with massive gastrointestinal hemorrhage. Barium in the bowel lumen interferes with endoscopic studies, diagnostic MDCT, and diagnostic and therapeutic angiography.³⁰⁻³² In patients with anemia and occult gastrointestinal bleeding, barium studies have been replaced by upper gastrointestinal endoscopy, colonoscopy, CE, and MDCT.

Upper Gastrointestinal Hemorrhage

Upper gastrointestinal tract bleeding constitutes 75% to 80% of all cases of acute gastrointestinal tract bleeding. The incidence has decreased significantly in recent times; however, the mortality rate from acute nonvariceal upper gastrointestinal tract bleeding has decreased only minimally in the past 50 years, ranging from 2.5% to 10%.^{33,34} This lack of change in mortality rate likely is related to the increasing age of patients

who present with upper gastrointestinal bleeding and an increase in associated comorbid conditions.

Peptic ulcers are the most common source of upper gastrointestinal bleeding, accounting for 20% to 40% of cases. Other major causes are gastric erosions (15%-25% of cases), bleeding varices (5%-30%), and Mallory-Weiss tears (5%-15%). The use of aspirin or nonsteroidal anti-inflammatory drugs is prevalent in 45% to 60% of all cases of acute upper gastrointestinal bleeding. Moreover, the risk of upper gastrointestinal bleeding is increased in patients who take as few as one "baby aspirin" (81 mg) per day.

The initial evaluation of a patient with upper gastrointestinal bleeding should focus on assessment of hemodynamic status and comorbid conditions. Factors associated with severe upper gastrointestinal bleeding include red blood from nasogastric lavage, tachycardia, and hemoglobin level below 8 g/dL.

As in all cases of gastrointestinal bleeding, consideration must be given to comorbid illnesses that predispose patients to hypoxia (coronary artery disease, chronic obstructive pulmonary disease), volume overload (congestive heart failure, renal failure), bleeding (coagulopathies, thrombocytopenia, liver disease), and aspiration (dementia, hepatic encephalopathy) in choosing diagnostic and therapeutic procedures.

Expedited use of upper endoscopy is the diagnostic procedure of choice for acute upper gastrointestinal bleeding. Its reported sensitivity and specificity for the diagnosis of upper gastrointestinal bleeding are 92% to 98% and 30% to 100%, respectively.² In addition, once bleeding is identified, endoscopic treatment can achieve hemostasis and prevent recurrent bleeding in most patients.

Urgent endoscopy, however, cannot be advocated for all patients with acute upper gastrointestinal hemorrhage. Several prospective, randomized studies published in the early 1980s failed to demonstrate a decrease in morbidity or mortality rates associated with endoscopy in diagnosis of upper gastrointestinal hemorrhage.³⁵

Upper gastrointestinal endoscopy, however, should be performed as soon as possible in high-risk individuals: alcoholic patients who may be bleeding from a variety of sources; patients with suspected aortoenteric fistula; those with a quantitatively large volume of blood loss; those with suspected active hemorrhage; and those experiencing or unlikely to tolerate a recurrent hemorrhagic episode, including those who object to blood transfusions on religious grounds.³⁶ Patients with minor bleeding (i.e., without tachycardia, hypotension, or decreased hematocrit) can wait until the next day for elective endoscopy. Younger, otherwise healthy patients with trivial bleeding can be discharged without diagnostic testing with outpatient follow-up evaluation.³⁷

PEPTIC ULCERS

Bleeding from gastric or duodenal ulcers remains the most common cause of upper gastrointestinal tract hemorrhage. The most common risk factors for peptic ulcer disease are *Helicobacter pylori* infection, nonsteroidal anti-inflammatory drugs, physiologic stress, and excess gastric acid (e.g., Zollinger-Ellison syndrome).

The approach to a patient who has bled from peptic ulcer disease is determined at the time of endoscopy. There are many options for endoscopic therapy. Thermal-coaptive coagulation (an endoscopic technique used to ablate bleeding ulcers in

which two vessel walls are compressed and “fried”) involves the placement of the coagulating probe directly on the bleeding vessel. This is uniformly effective for vessels up to 2 mm in diameter with the heater probe. Injection therapy results in short-term tamponade and vasospasm and can be induced with the liberal use of epinephrine (1:10,000). Vasodestruction is long term and can be induced by sclerosants or alcohol (total injection volume not to exceed 2 mL). Endoscopic clipping has not been shown to be any more effective than thermal therapy³⁸; however, it may have appeal for use in patients with coagulation disorders or in cases in which further coaptive coagulation may not be desirable.

Endoscopic therapy is indicated for patients with active arterial bleeding and those with a nonbleeding visible vessel (pigmented protuberance). An adherent clot is a predictor of rebleeding and can be managed with endoscopic therapy or high-dose proton pump inhibitor therapy (or both).³⁹⁻⁴¹ All three endoscopic treatment options have been shown to have a relatively similar efficacy. However, epinephrine injection, followed by a more permanent form of treatment (coagulation, vasodestruction, or clipping), has been shown to be more effective than epinephrine therapy alone.⁴² Patients with a clean ulcer base (rebleeding rates, <5%) and a flat pigmented spot (rebleeding rates, 5%-10%) do not require endoscopic therapy and probably could be discharged soon after endoscopy. Deep ulcers may tend to expose larger vessels that may not be amenable to endoscopic coagulation. Deep ulcers in the stomach, particularly those in the upper body on the lesser curvature (left gastric artery), or posterior duodenal bulb (gastroduodenal artery) with nonbleeding visible vessels more than 2 to 3 mm in diameter should not be treated endoscopically. These patients may benefit from therapeutic embolization.

Rebleeding after endoscopic therapy occurs 20% to 30% of the time. Re-treatment for recurrent bleeding achieves long-term hemostasis in more than 70% of cases.⁴³ The endoscopic appearance of the ulcer may predict its likelihood of rebleeding. An endoscopically visualized, actively bleeding ulcer carries an 80% chance of persistent or recurrent bleeding.¹¹ A nonbleeding visible vessel is associated with a 50% chance of rebleeding.^{11,13}

If endoscopic therapy fails, angiographic embolization of the bleeding vessel is a preferable option to surgical intervention.³⁸ Vasopressin is effective at controlling gastric bleeding (70%). Bleeding duodenal ulcers are relatively unresponsive to vasopressin infusion because of the dual blood supply to the duodenum; the inflammatory reaction produced by the penetrating ulcer; and the large size of the vessels involved, which do not constrict in response to the vasopressin. However, rebleeding is common. Initial control of upper gastrointestinal bleeding with embolization can be achieved in 84%; however, rebleeding occurs in 27%.⁴⁴

ESOPHAGEAL VARICES

Portal hypertension develops from an increase in resistance to portal venous outflow from both mechanical and vascular factors and is maintained by a systemic hyperdynamic circulation and peripheral vasodilation. A hepatic venous pressure gradient of at least 10 mm Hg is required for the development of esophageal varices, and a gradient of at least 12 mm Hg is generally required for the development of variceal bleeding. Gastroesophageal varices are present in approximately half of

cirrhotic patients, and variceal hemorrhage occurs at a rate of 5% to 15% per year. Although survival has improved in recent years, variceal bleeding is associated with a mortality of at least 20% at 6 weeks.⁴⁵ Variceal size, endoscopic stigmata, and advanced liver disease are predictors of variceal bleeding.

Prophylactic treatment of patients with varices without bleeding is recommended with nonselective β -adrenergic blockers, which decreases portal venous pressure. These agents should be used in patients with small varices with a higher risk of bleeding, specifically those with red wale signs or those with advanced liver disease. Bleeding prophylaxis is similarly recommended for patients with large varices with either β blockade or variceal band ligation.

Therapy for acute esophageal variceal bleeding includes vasoactive drug treatment (octreotide in the United States) for 2 to 5 days, endoscopic variceal band ligation, and prophylactic antibiotics. A percutaneously placed TIPS is used for the 10% to 20% of patients who fail to respond to the standard therapy. In those with advanced liver disease, TIPS may potentially have a survival advantage over standard therapy.⁴⁵ Endoscopic variceal band ligation with or without β blockade is used for the prevention of rebleeding. Acute gastric variceal bleeding should be managed with pharmacologic therapy and antibiotics as well. Gastroesophageal and fundic varices can undergo banding acutely. Isolated gastric varices can be treated in the face of active bleeding with cyanoacrylate glue (not currently available in the United States). TIPS is used to prevent rebleeding from gastric varices. There are concerns with TIPS regarding shunt clotting, worsening hepatic encephalopathy, and deterioration of liver function.

GASTRITIS

Gastric mucosal bleeding attributable to stress, alcohol abuse, and use of nonsteroidal anti-inflammatory agents accounts for almost 30% of major gastrointestinal hemorrhage. The superficial erosions result from the breakdown of the mucosal barrier, allowing back diffusion of acid into the submucosa. Most patients with diffuse gastritis stop bleeding spontaneously. If they do not, transcatheter therapy should be attempted because surgery has a high mortality rate (21%) in this setting.⁴⁶

Diffuse hyperemia of the mucosa is seen angiographically in patients with hemorrhagic gastritis. If no extravasation of contrast medium is seen, intra-arterial injection of vasopressin should be performed. Embolization should be used in patients with active extravasation. These techniques are successful in approximately 80% of patients.

MALLORY-WEISS TEAR

Mallory Weiss syndrome is characterized by longitudinal mucosal lacerations in the distal esophagus and proximal stomach. Patients usually have a history of recent retching or vomiting and present with excruciating epigastric and left-sided chest pain radiating to the back. This condition accounts for approximately 5% of upper gastrointestinal tract bleeding. Diagnosis is made endoscopically.

Forty percent to 70% of patients with Mallory-Weiss syndrome require blood transfusion; however, 75% to 80% of patients are successfully treated with bed rest, sedation, and vigorous fluid and blood replacement.⁴⁷ Endoscopic treatment, with the injection of epinephrine or ethanol followed by thermal

coagulation, is successful in the majority of cases that fail conservative treatment. In rare cases in which endoscopy fails to staunch the hemorrhage, diagnostic and therapeutic angiography is indicated. After the bleeding vessel (usually a branch of the left gastric artery) is identified, a nonpermanent embolic agent such as Gelfoam pledgets should be used because this disorder is self-limited. Because the blood supply to the esophagus is complex, intra-arterial injection of vasopressin usually is not successful.

Midgut Hemorrhage

In approximately 5% of patients presenting with gastrointestinal bleeding, no bleeding source is identified at upper endoscopy and colonoscopy. This condition is defined by the American Gastroenterological Association as obscure gastrointestinal bleeding.⁴⁸ Repeated endoscopy may reveal a bleeding source missed at initial endoscopy in 15%, usually located in the upper gastrointestinal tract. Of the remaining patients, 75% will have a small bowel source for blood loss. Angiectasias (also called angiodysplasia) are the most common cause of bleeding in patients older than 65 years (54%), followed by small intestinal ulcers (13%) and tumors (12%). In patients younger than 41 to 64 years of age, angiectasias (35%) and small bowel tumors (31%) are most common. Before the age of 40 years, Crohn's disease is the most common cause of small bowel bleeding (34%), followed by small bowel tumors (23%) and nonspecific enteritis (11%).⁴⁹

In the majority of patients with a small bowel bleeding source, blood loss is slow and chronic. They may present with iron deficiency anemia with or without melena or hematochezia. In these patients, wireless CE is the preferred initial diagnostic procedure. The yield of CE in obscure gastrointestinal bleeding is up to 90% if it is performed within 1 to 2 weeks of the bleeding episode and drops to 60% to 70% if it is performed more than 2 weeks after the bleeding event.^{50,51} In patients with normal examination findings, repeated CE has been recommended and may reveal significant abnormalities in 55%.⁵²

Overall, CE outperforms CT enteroclysis in evaluation of patients with obscure gastrointestinal bleeding presenting with iron deficiency anemia, with sensitivities of 78% and 22%, respectively.⁵³ A pooled analysis of 24 CE trials reported an overall yield of 87% in obscure gastrointestinal bleeding.⁵⁴ Multiphase CTE may have a complementary role to CE in evaluating patients with suspected small bowel bleeding because of its ability to detect submucosal masses that may go undetected by CE. CE may fail to detect significant small bowel masses, particularly as some small bowel tumors, such as carcinoids and gastrointestinal stromal tumor, may not have a mucosal component.⁵⁵⁻⁵⁷ A total of 19 false-negative CE examinations were described in three reports, and 18 of 19 (95%) missed lesions were masses. Ross and coworkers⁵⁸ reported false-negative CE findings in 10 of 15 patients (67%) with small bowel tumors. In a retrospective study of 17 patients with small bowel tumors who underwent both CTE and CE, sensitivities were 94% and 35%, respectively.⁵⁹ In another prospective study comparing multiphase CTE with CE in obscure gastrointestinal bleeding, CTE detected 9 of 9 small bowel tumors compared with 3 of 9 for CE.¹⁷ Therefore, patients with normal findings on CE should be considered for multiphase CTE to exclude disease missed by CE, especially neoplasms.

Patients with signs of mild blood loss, such as iron deficiency anemia, in which a neoplasm has been excluded, may be considered for medical therapy. In patients in whom a small bowel neoplasm cannot be excluded or in whom bleeding is significant, requiring ongoing transfusions, additional more invasive procedures are warranted.

Deep enteroscopy can be performed by DBE, single-balloon enteroscopy, or spiral enteroscopy. The choice depends on the available expertise. DBE is the most widely used, and therefore most reports in the literature are based on this technique. The diagnostic yield of DBE in patients with obscure gastrointestinal bleeding ranges from 60% to 80%.

Angiography is used primarily to confirm the presence of a small bowel vascular lesion, especially arterial lesions. If such a lesion is detected on the angiogram in the clinical setting of acute gastrointestinal hemorrhage and no other lesion is found, catheter embolization is indicated even if acute hemorrhage is not detected at that time. However, if the lesion cannot be safely embolized, a microcatheter can be secured and the patient taken to surgery for methylene blue injection at the time of operative exposure to identify the short segment of bowel to be resected.⁶⁰

Intraoperative enteroscopy can be used in cases of failed enteroscopy. It allows the highest success rate in evaluating the entire small bowel. Rebleeding after therapeutic surgical intervention is low compared with deep enteroscopy. However, surgery is associated with higher morbidity than other therapies are.

SMALL BOWEL VASCULAR LESIONS

Vascular lesions of the small bowel include angiectasias, arterial lesions (arteriovenous malformations and Dieulafoy lesions), and venous lesions (venous angiomas and small bowel varices). Endoscopy and CTE appear to be complementary in detection of these lesions.¹⁹

Angiectasias are the most common vascular lesion associated with obscure gastrointestinal bleeding. Angiectasias can occur anywhere in the gastrointestinal tract. Much of what we know about angiectasias (also known as angiodysplasias) is based on findings at colonoscopy,⁶¹ although there is no evidence to suggest that small bowel angiectasias differ in any significant way from colonic lesions. Angiectasias consist of thin tortuous veins that lack an internal elastic layer. Peak incidence of these lesions is in the seventh and eighth decades of life. Reports indicate that angiectasias are multiple in 40% to 75% of patients with gastrointestinal bleeding. In addition, angiectasias are seen at colonoscopy in 2.6% to 6.2% of patients having the procedure performed for a variety of indications.⁶¹ Angiectasias appear as tiny focal areas of enhancement within the bowel wall (Fig. 125-3). On endoscopic examination, angiectasias consist of punctate or patchy areas of erythema, 2 to 10 mm in size. Angiectasias are treated endoscopically with ablation therapy. Unfortunately, recurrent bleeding is common.

Arterial lesions include arteriovenous malformations and fistulas and Dieulafoy lesions and are much less common than angiectasias. Dieulafoy lesions are most common in the stomach but can be seen throughout the gastrointestinal tract. They are a rare cause of obscure gastrointestinal bleeding. These lesions may be congenital and consist of a submucosally located artery with overlying ulceration. They are estimated to occur in 3.5% of patients with obscure gastrointestinal bleeding.⁶²

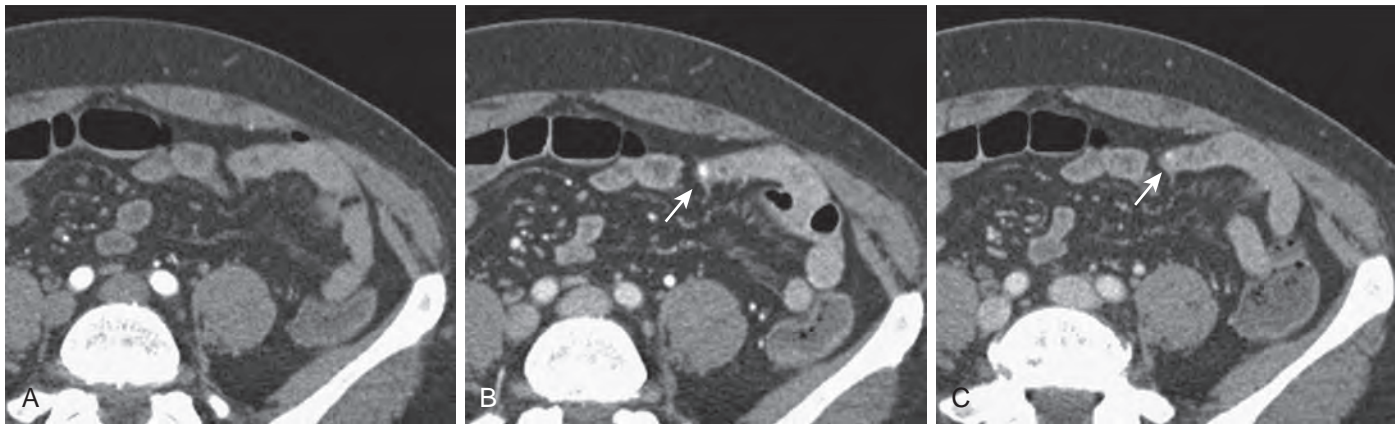


Figure 125-3 Angioectasia. A 65-year-old woman with multiple episodes of melena. Arterial (A), enteric (B), and delayed (C) phase axial images from a multiphase CTE study demonstrate a focal, less than 5 mm nodular area of enhancement in the distal jejunum (arrows), undetectable on the arterial phase and brightest on the enteric phase. Angioectasia was subsequently ablated during balloon-assisted endoscopy. (From Huprich J, Barlow J, Hansel S, et al: Multiphase CT enterography of small bowel vascular lesions. *AJR* 201:65–72, 2013.)

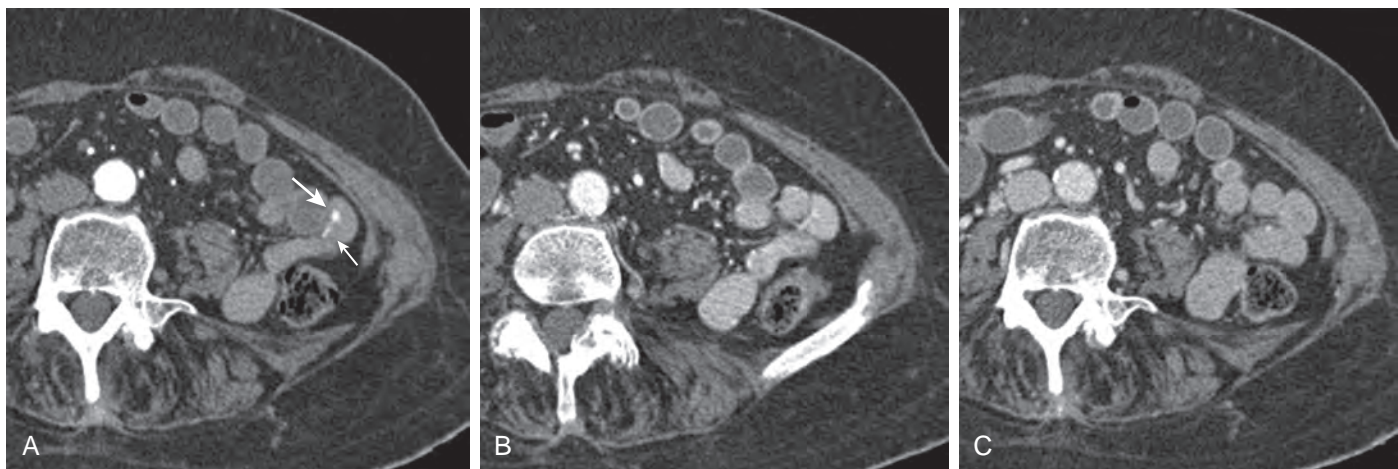


Figure 125-4 Dieulafoy lesion. A 58-year-old man with hematochezia. Arterial (A), enteric (B), and delayed (C) phase axial images from a multiphase CTE study demonstrate a small nodular area of enhancement in the distal jejunum visible only on the arterial phase (large arrow). Adjacent linear collection of contrast material (small arrow) may represent active bleeding. (From Huprich J, Barlow J, Hansel S, et al: Multiphase CT enterography of small bowel vascular lesions. *AJR* 201:65–72, 2013.)

Arterial lesions have characteristic findings on multiphase CTE, enhancing brightly on arterial phase images and fading or disappearing on subsequent phases (Fig. 125-4). Therefore, arterial lesions may go undetected if arterial phase images are omitted. Arteriovenous malformations and fistulas may be accompanied by an early draining vein, which distinguishes them from Dieulafoy lesions. Because arterial lesions are exposed to high arterial pressure, there is a significant potential for life-threatening bleeding. Treatment consists of endoscopic laser or mechanical ablation, embolization, or surgical resection.

Venous lesions consist of small bowel varices and venous angiomas. Small bowel varices form within adhesions in the setting of mesenteric venous hypertension because of either mesenteric venous obstruction or portal hypertension. Adhesions between adjacent bowel loops or between the bowel and peritoneum provide a pathway for the varices to form. Small

bowel varices should be suspected in patients who have had prior abdominal surgery and have evidence of mesenteric venous hypertension.⁶³ Venous angiomas are rare lesions of the small bowel that may occur in isolation or may be associated with Klippel-Trénaunay or blue rubber bleb nevus syndrome. The lesions are classified pathologically as hamartomas and consist of large blood-filled sinuses lined by endothelial cells. Venous lesions are usually treated by surgical resection.

SMALL BOWEL ULCERS

Ulcerations of the small bowel are a common cause of bleeding. Whereas there are many causes, nonsteroidal anti-inflammatory drugs are probably the most common cause of small bowel ulceration. Patients may present with small bowel obstruction due to associated strictures. Diagnosis of small bowel ulcerations is made by endoscopy. Radiology does not

play a significant role in diagnosis or management of ulcers. Enteroclysis techniques may be helpful in detecting those with associated strictures. Segmental resection of the affected small bowel may be necessary to avoid stricturing.

SMALL BOWEL NEOPLASMS

Small bowel neoplasms are the second most common lesions associated with obscure gastrointestinal bleeding. Most small bowel neoplasms are potentially malignant; therefore, their detection is important not only to treat the bleeding but also to minimize morbidity and mortality due to disease progression. Small bowel tumors are discussed elsewhere in the text.

Lower Gastrointestinal Hemorrhage

Lower gastrointestinal bleeding represents approximately 25% of all gastrointestinal bleeding and is associated with a significantly lower mortality (4%) compared with upper gastrointestinal bleeding. Bleeding will stop spontaneously in 80% to 85% of patients with lower gastrointestinal bleeding.⁶⁴ Compared with upper gastrointestinal bleeding, patients with lower gastrointestinal bleeding are older, which is probably explained by the increasing prevalence of colonic diverticulosis and angiodysplasia with age.

The majority of patients with hematochezia have a lower gastrointestinal bleeding source. As stated before, patients with hematochezia will usually undergo nasogastric lavage to exclude massive upper gastrointestinal bleeding. Blood originating from the left colon is usually bright red, whereas bleeding from the right colon is dark or maroon-colored owing to the more prolonged transit. However, rapid transit from massive right-sided bleeding may be bright red, and bleeding from the cecum can rarely appear as melena. Bacterial metabolism needs sufficient time for melena to be generated from fresh blood. If blood is limited to the toilet paper or surface of formed stool, a perianal source is likely. Tenesmus suggests a rectal origin (e.g., proctitis).

In a review of several large series, the most common causes of hematochezia were diverticulosis (42%), ischemic colitis (18%), anorectal disorders (hemorrhoids, fissure, rectal ulcers; 16%), neoplasms (11%), and angiodysplasias (3%).⁶⁵

After initial resuscitation and exclusion of an upper gastrointestinal bleeding source, colonoscopy is the procedure of choice for evaluation of hematochezia. A definite or potential bleeding source is seen at colonoscopy in 45% to 90% of patients with lower gastrointestinal bleeding.⁶⁵ The benefit of performing urgent colonoscopy is unclear. Some clinicians perform colonoscopy on an unprepared bowel; however, studies of colonoscopy for lower gastrointestinal bleeding without bowel cleansing report lower success rates. Most centers perform colonoscopy after adequate bowel preparation has been given. In patients in whom colonoscopy is incomplete or unsuccessful who continue to bleed, additional techniques should be used.

Radionuclide-labeled RBC scans may help localize bleeding sites. A major disadvantage of this test is that it requires active bleeding to detect the source and can localize the bleeding only to a general area of the abdomen. Accuracy rates vary substantially from 24% to 91%. Poor localization is the result of peristaltic and antiperistaltic action moving and dispersing

the radionuclide away from the bleeding site. In a study of 203 patients undergoing RBC scans for lower gastrointestinal bleeding, the scan was positive in 52 cases; however, it incorrectly localized the bleeding site in 13, causing unnecessary surgical procedures in 8 patients.⁶⁶

CT angiography may be useful in localization of active gastrointestinal bleeding.¹⁶ In a review of 124 patients with lower gastrointestinal bleeding, CT angiography demonstrated an accuracy of 100%.⁶⁷ This technique is appealing because of its expediency and wide availability. However, it subjects patients to radiation exposure and risks contrast-induced nephropathy, especially in those patients who require subsequent angiographic therapy.

Angiography is typically reserved for patients in whom endoscopy is not feasible because of severe bleeding with hemodynamic instability or those with persistent or recurrent bleeding and a nondiagnostic colonoscopy. Identification of active bleeding requires bleeding rates of 0.5 to 1 mL/min. Radionuclide-labeled RBC scans may be useful in confirming the presence of active bleeding and in localizing the bleeding site. In the absence of a positive RBC scan, angiography is carried out by first evaluating the superior mesenteric artery, which most often supplies the bleeding site. If the result is negative, the inferior mesenteric and celiac arteries are examined. The success rate of angiography for localizing the bleeding site varies widely from 25% to 70%.⁶⁸ Angiography also offers the ability to treat the bleeding site by delivery of vasoconstrictive agents and therapeutic embolization.

Rarely, patients with exsanguinating bleeding will need urgent surgery. The morbidity and mortality associated with colectomy in the absence of preoperative localization of the bleeding site are higher than in patients who have the bleeding site located preoperatively. Therefore, every effort should be made to locate the bleeding site before surgery.

DIVERTICULAR HEMORRHAGE

Patients with diverticular bleeding typically present with acute blood loss as manifested by maroon-colored stools or hematochezia. Minor or occult bleeding is not characteristic of diverticular bleeding or diverticulosis. Diverticular bleeding and diverticulitis are distinct conditions that rarely occur together. Diverticular bleeding is painless except for the cramping that may occur with the cathartic effect of blood within the colon.

Diverticular bleeding is thought to originate more commonly from the right colon, where ostia tend to be wider and the colon wall thinner. It is estimated that 3% to 5% of patients with diverticulosis will develop diverticular bleeding. Bleeding most commonly occurs during the sixth and seventh decades of life and stops spontaneously in more than 75% of patients. In general, rebleeding occurs in about 15% to 25% of patients.⁶⁹ After a second episode, the risk of rebleeding is approximately 25% to 50%.

Identification of the bleeding diverticulum by colonoscopy may be difficult because diverticula are numerous and bleeding may be intermittent. A definite colonic diverticular bleeding source may be identified in only 21%.⁷⁰ Endoscopic treatment options include submucosal injection of epinephrine, bipolar coagulation, and application of hemoclips and bands. In general, if the bleeding site can be identified endoscopically, treatment is effective with low rebleeding rates.

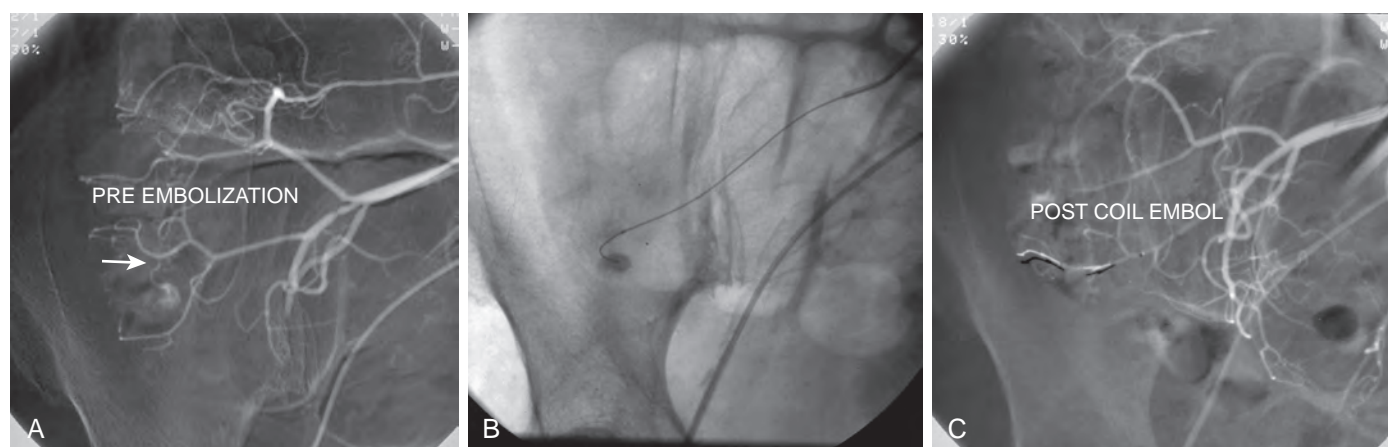


Figure 125-5 Bleeding colonic diverticulum. A 76-year-old man with acute bleeding from a diverticulum in the cecum. **A.** Angiogram of the ileocolic artery shows brisk bleeding into the cecum from a small terminal branch (arrow). **B.** Distal placement of a microcatheter into the terminal branch with the guidewire advanced 2 cm beyond the microcatheter tip. Note the round outline of the extravasated contrast material indicating hemorrhage into a diverticulum. **C.** Postembolization angiogram shows two metallic coils occluding the bleeding artery. (From McDonald M, Farrell M, Stanson A, et al: Preoperative highly selective catheter localization of occult small-intestinal hemorrhage with methylene blue dye. *Arch Surg* 130:106–108, 1995.)

For ongoing or recurrent bleeding after colonoscopy, angiography often is performed with the intention of identifying an actively bleeding vessel (Fig. 125-5). If the vessel is identified, transcatheter embolization can be attempted, although in some series colonic infarction has been as high as 20%. Transcatheter vasopressin can control bleeding in 90% of cases, but rebleeding rates are high.⁷¹

COLON NEOPLASMS

Colon cancer commonly causes occult lower gastrointestinal bleeding, frequently presenting with a positive result of the fecal occult blood test. It is an uncommon cause of hematochezia and is responsible for 10% of cases of rectal bleeding in patients older than 50 years. Colon neoplasms are discussed elsewhere in the text.

REFERENCES

- Ghassemi KA, Jensen DM: Lower GI bleeding: epidemiology and management. *Curr Gastroenterol Rep* 15:333, 2013.
- Lee E, Laberge J: Differential diagnosis of gastrointestinal bleeding. *Tech Vasc Interv Radiol* 7:112–122, 2004.
- Palmer E: The vigorous diagnostic approach to upper-gastrointestinal tract hemorrhage. A 23-year prospective study of 1400 patients. *JAMA* 207:1477, 1969.
- Di Fiore F, Lacleire S, Merle V, et al: Changes in characteristics and outcome of acute upper gastrointestinal hemorrhage: A comparison of epidemiology and practices between 1996 and 2000 in a multicentre French study. *Eur J Gastroenterol Hepatol* 17:641–647, 2005.
- Klebl F, Bregenzner N, Schofer L, et al: Risk factors for mortality in severe upper gastrointestinal bleeding. *Int J Colorectal Dis* 20:49–56, 2005.
- Kwan V, Norton I: Endoscopic management of non-variceal upper gastrointestinal hemorrhage. *ANZ J Surg* 77:222–230, 2007.
- Lee J: What is the value of early endoscopy in upper gastrointestinal bleeding? *Nat Clin Pract Gastroenterol Hepatol* 3:534–535, 2006.
- Geyer M, Stamenic I, Buhler H, et al: Epidemiology of gastrointestinal bleeding in the elderly. *Schweiz Rundsch Med Prax* 95:757–765, 2006.
- Gleeson E, Clarke E, Lennon J, et al: Outcome of accident and emergency room triaged patients with low risk of non-variceal upper gastrointestinal hemorrhage. *Ir Med J* 99:114–117, 2006.
- Gralnek I, Dulai G: Incremental value of upper endoscopy for triage of patients with acute non-variceal upper-GI hemorrhage. *Gastrointest Endosc* 60:9–14, 2004.
- Schemmer P, Decker F, Dei-Anane G, et al: The vital threat of an upper gastrointestinal bleeding: Risk factor analysis of 121 consecutive patients. *World J Gastroenterol* 12:3597–3601, 2006.
- Hale MF, Sidhu R, McAlindon ME: Capsule endoscopy: Current practice and future directions. *World J Gastroenterol* 24:7752–7759, 2014.
- Nadler M, Eliakim R: The role of capsule endoscopy in acute gastrointestinal bleeding. *Therapy Adv Gastroenterol* 7:87–92, 2014.
- Pasha S, Leighton J: Endoscopic techniques for small bowel imaging. *Radiol Clin North Am* 51:177–187, 2013.
- Leighton J: The role of endoscopic imaging of the small bowel in clinical practice. *Am J Gastroenterol* 106:27–36, 2011.
- Garcia-Blazquez V, Vicente-Bartulos A, Olavarria-Delgado A, et al: Accuracy of CT angiography in the diagnosis of acute gastrointestinal bleeding: A systematic review and meta-analysis. *Eur Radiol* 23:1181, 2013.
- Huprich J, Fletcher J, Fidler J, et al: Prospective blinded comparison of wireless capsule endoscopy and multiphase CT enterography in obscure gastrointestinal bleeding. *Radiology* 260:744–751, 2011.
- Huprich JE, Fletcher JG, Alexander JA, et al: Obscure gastrointestinal bleeding: Evaluation with 64-section multiphase CT enterography—initial experience. *Radiology* 246:562–571, 2008.
- Huprich J, Barlow J, Hansel S, et al: Multiphase CT enterography of small bowel vascular lesions. *AJR* 201:65–72, 2013.
- Sfakianakis G, Conway J: Detection of ectopic gastric mucosa in Meckel's diverticulum and in other aberrations by scintigraphy: 1. Pathophysiology and 10-year clinical experience. *J Nucl Med* 22:647–654, 1981.
- Bentley D, Richardson J: The role of tagged red blood cell imaging in the localization of gastrointestinal bleeding. *Arch Surg* 126:821–824, 1991.
- Emslie I, Zarnegar K, Siegel M, et al: Technetium-99m-labeled red blood cell scans in the investigation of gastrointestinal bleeding. *Dis Colon Rectum* 39:750–754, 1996.
- Gutierrez C, Mariano M, Vander Laan T, et al: The use of technetium-labeled erythrocyte scintigraphy in the evaluation and treatment of lower gastrointestinal hemorrhage. *Am Surg* 64:989–992, 1998.
- Howarth D: The role of nuclear medicine in the detection of acute gastrointestinal bleeding. *Semin Nucl Med* 36:133–146, 2006.
- Kotani K, Kawabe J, Higashiyama S, et al: Diagnostic ability of (99m)Tc-HSA-DTPA scintigraphy in combination with SPECT/CT for gastrointestinal bleeding. *Abdom Imaging* 39: 677–684, 2014.
- Suzman M, Talmor M, Jennis R, et al: Accurate localization and surgical management of active lower gastrointestinal hemorrhage with

- technetium-labeled erythrocyte scintigraphy. *Ann Surg* 224:29–36, 1996.
27. O'Connor M: The Mayo Clinic Manual of Nuclear Medicine, New York, 1996, Churchill Livingstone.
28. Wee E: Management of nonvariceal upper gastrointestinal bleeding. *J Postgrad Med* 57:161, 2011.
29. Edelman D, Sugawa C: Lower gastrointestinal bleeding: A review. *Surg Endosc* 21:514–520, 2007.
30. Antes G, Neher M, Hiemeyer V, et al: Gastrointestinal bleeding of obscure origin: Role of enteroclysis. *Eur Radiol* 6:851–854, 1996.
31. Malik A, Lukaszewski K, Caroline D, et al: A retrospective review of enteroclysis in patients with obscure gastrointestinal bleeding and chronic abdominal pain of undetermined etiology. *Dig Dis Sci* 50:649–655, 2005.
32. Thoeni R, Venbrux A: The value of colonoscopy and double-contrast barium enema examinations in the evaluation of patients with subacute and chronic lower intestinal bleeding. *Radiology* 146:603–607, 1993.
33. Laine L, Yang H, Chang S, Datto C: Trends for incidence of hospitalization and death due to GI complications in the United States from 2001 to 2009. *Am J Gastroenterol* 107:1190–1195, 2012.
34. Lanis A: Upper GI bleeding—associated mortality: Challenges to improving a resistant outcome [editorial]. *Am J Gastroenterol* 105:90–92, 2010.
35. Parente F, Anderloni A, Bargiggia S, et al: Outcome of non-variceal acute upper gastrointestinal bleeding in relation to the time of endoscopy and the experience of the endoscopist: A two year survey. *World J Gastroenterol* 11:7122–7130, 2005.
36. Targownik L, Gralnek I, Dulai G, et al: Management of acute non-variceal upper gastrointestinal hemorrhage: Comparison of an American and a Canadian medical centre. *Can J Gastroenterol* 17:489–495, 2003.
37. Oei T, Dalai G, Gralnek I, et al: Hospital care for low-risk patients with acute, non-variceal upper GI hemorrhage: A comparison of neighboring community and tertiary care centers. *Am J Gastroenterol* 97:2271–2278, 2002.
38. Sung J, Tsoi K, Lai L, et al: Endoscopic clipping versus injection and thermo-coagulation in the treatment of non-variceal upper gastrointestinal bleeding: A meta-analysis. *Gut* 56:1364–1373, 2007.
39. Barkun A, Bardou M, Kuipers E, et al: International consensus recommendations on the management of patients with nonvariceal upper gastrointestinal bleeding. *Ann Intern Med* 152:101–113, 2010.
40. Gralnek I, Barkun A, Bardou M: Management of acute bleeding from a peptic ulcer. *N Engl J Med* 359:928–937, 2008.
41. Laine L, Jensen D: Management of patients with ulcer bleeding. *Am J Gastroenterol* 107:345–360, 2012.
42. Vergara M, Calvet X, Gisbert J: Epinephrine injection versus epinephrine injection and a second endoscopic method in high risk bleeding ulcers. *Cochrane Database Syst Rev* (2): CD005584, 2007.
43. Lau J, Sung J, Lam Y, et al: Endoscopic retreatment compared with surgery in patients with recurrent bleeding after initial endoscopic control of bleeding ulcers. *N Engl J Med* 340:751–756, 1999.
44. Mirsadraee S, Tirukonda P, Nicholson A, et al: Embolization of non-variceal upper gastrointestinal tract haemorrhage: A systematic review. *Clin Radiol* 66:500–509, 2011.
45. Garcia-Tsao G, Bosch J: Management of varices and variceal hemorrhage in cirrhosis. *N Engl J Med* 362:823–832, 2010.
46. Gore R, Levine M, Ghahremani G: Drug-induced injury of the stomach. *Abdom Imaging* 24:17–24, 1999.
47. Feinman M, Haut ER: Upper gastrointestinal bleeding. *Surg Clin North Am* 94:43–53, 2014.
48. Raju GS, Gerson L, Das A, Lewis B: American Gastroenterological Association (AGA) Institute technical review on obscure gastrointestinal bleeding. *Gastroenterology* 133:1697–1717, 2007.
49. Zhang B, Chen C, Li Y: Capsule endoscopy examination identifies different leading causes of obscure gastrointestinal bleeding in patients of different ages. *Turk J Gastroenterol* 23:220–225, 2012.
50. Hartman D, Schmidt H, Bolz G: A prospective two-center study comparing wireless capsule endoscopy with intraoperative enteroscopy in patients with obscure GI bleeding. *Gastrointest Endosc* 61:826–832, 2005.
51. Pennazio M, Santucci R, Rondonotti E, et al: Outcome of patients with obscure gastrointestinal bleeding after capsule endoscopy: Report of 100 consecutive cases. *Gastroenterology* 126:643, 2004.
52. Svarta S, Segal B, Law J, et al: Diagnostic yield of repeat capsule endoscopy and the effect on subsequent patient management. *Can J Gastroenterol* 24:441, 2010.
53. Milano A, Balatsinou C, Filippone A, et al: A prospective evaluation of iron deficiency anemia in the GI endoscopy setting: Role of standard endoscopy, videocapsule endoscopy, and CT-enteroclysis. *Gastrointest Endosc* 73:1002–1008, 2011.
54. Lewis B, Eisen G, Friedman L: A pooled analysis to evaluate the results of capsule endoscopy trial. *Endoscopy* 37:960–965, 2005.
55. Baichi MM, Arifuddin RM, Mantry PS: Capsule endoscopy for obscure GI bleeding: Therapeutic yield of follow-up procedures. *Dig Dis Sci* 52:1370–1375, 2007.
56. Zhang Q, He Q, Liu J, et al: Combined use of capsule endoscopy and double-balloon enteroscopy in the diagnosis of obscure gastrointestinal bleeding: Meta-analysis and pooled analysis. *Hepatogastroenterology* 60:1885–1891, 2013.
57. Postgate A, Despott E, Burling D, et al: Significant small-bowel lesions detected by alternative diagnostic modalities after negative capsule endoscopy. *Gastrointest Endosc* 68:1209–1214, 2008.
58. Ross A, Mehdizadeh S, Tokar J, et al: Double balloon enteroscopy detects small bowel mass lesions missed by capsule endoscopy. *Dig Dis Sci* 53:2140–2143, 2008.
59. Hakim F, Alexander J, Huprich J, et al: CT-enterography may identify small bowel tumors not detected by capsule endoscopy: Eight years experience at Mayo Clinic Rochester. *Dig Dis Sci* 56:2914–2919, 2011.
60. McDonald M, Farnell M, Stanson A, et al: Pre-operative highly selective catheter localization of occult small-intestinal hemorrhage with methylene blue dye. *Arch Surg* 130:106–108, 1995.
61. Foucht P: Angiodysplasia of the gastrointestinal tract. *Am J Gastroenterol* 88:806–818, 1993.
62. Dulic-Lakovic E, Dulic M, Hubner D, et al: Bleeding Dieulafoy lesions of the small bowel: A systematic study on the epidemiology and efficacy of enteroscopic treatment. *Gastroenterol Endosc* 74:573–580, 2011.
63. Tang SJ, Jutabha R, Jensen DM: Push enteroscopy for recurrent gastrointestinal hemorrhage due to jejunal anastomotic varices: A case report and review of the literature. *Endoscopy* 34:735–737, 2002.
64. Farrell J, Friedman L: Review article: The management of lower gastrointestinal bleeding. *Aliment Pharmacol Ther* 21:1281, 2005.
65. Feinman M, Haut ER: Lower gastrointestinal bleeding. *Surg Clin North Am* 94:55–63, 2014.
66. Hunter J, Pezim M: Limited value of technetium 99m-labeled red cell scintigraphy in localization of lower gastrointestinal bleeding. *Am J Surg* 159:504–506, 1990.
67. Strate L, Naumann C: The role of colonoscopy and radiological procedures in the management of acute lower intestinal bleeding. *Clin Gastroenterol Hepatol* 8:333, 2010.
68. Cohn S, Moller B, Zieg P, et al: Angiography for preoperative evaluation in patients with lower gastrointestinal bleeding: Are the benefits worth the risks? *Arch Surg* 133:50, 1998.
69. Jensen DM: The ins and outs of diverticular bleeding. *Gastrointest Endosc* 75:388–391, 2012.
70. Jensen D, Machicado G, Jutabha R, et al: Urgent colonoscopy for the diagnosis and treatment of severe diverticular hemorrhage. *N Engl J Med* 342:78, 2000.
71. Heianna J, Miyauchi T, Yamano H, et al: Management of angiogram-negative acute colonic hemorrhage: Safety and efficacy of colonoscopy-guided superselective embolization. *Tech Coloproctol* 18:647–652, 2014.

CHAPTER OUTLINE

Mechanisms of Injury in Abdominal Trauma**Diagnostic Techniques in Patients with Abdominal Trauma****Computed Tomography Use in Abdominal Trauma****Computed Tomography Imaging Techniques and Interpretation**

Contrast Material
 Multiphasic Imaging
 Radiation Dose
 Image Processing

Approach to Computed Tomography Interpretation**Computed Tomography Findings in Abdominal Injury**

Liver and Spleen
 Pancreas
 Kidneys

Computed Tomography and Bowel Injury**Computed Tomography Findings in Bowel and Mesenteric Injury**

Bowel Wall Discontinuity
 Extravasation of Oral Contrast Material
 Extraluminal Air
 Focal Bowel Wall Thickening
 Abnormal Bowel Wall Enhancement
 Mesenteric Injury
 Free Intraperitoneal Fluid

Conclusions

Trauma is the leading cause of death in Americans younger than 45 years and the fifth leading overall cause in the United States.¹ Preliminary data approximate that more than 122,000 people died of traumatic injury in 2011.¹ Trauma has a significant economic burden on U.S. health care, with more than 45 million emergency department visits every year and approximately \$80 billion spent in direct medical costs.^{2,3} It is also the leading cause of disability and exceeds any other disease in productive years lost. In the year 2000, productivity losses due to trauma cost the United States \$326 billion.⁴

Appropriate prompt evaluation of trauma patients is essential to avoid serious morbidity and mortality. Although the physical examination is still vital in the initial assessment of these patients, some studies have shown sensitivity in the range of only 55% to 65% in the setting of blunt abdominal trauma.^{5,6} Furthermore, patients who show no obvious signs of trauma or physical examination findings (such as a seat belt sign, abdominal tenderness, or guarding) may still have significant internal organ injury. Therefore, imaging has come

to play a critically important role in trauma diagnosis and management.

In this chapter, we describe the mechanisms of injury in abdominal trauma as well as the role of imaging modalities—with a focus on computed tomography (CT)—in the evaluation of the trauma patient. We also review CT imaging techniques and the diagnostic criteria used for interpretation in abdominal trauma, with an emphasis on the role of abdominal CT in bowel injury.

Mechanisms of Injury in Abdominal Trauma

Abdominal injury can be divided into blunt and penetrating subtypes. Blunt trauma is the cause of more than 80% of abdominal injuries, whereas penetrating injuries account for approximately 20%.^{7,8} Penetrating injuries include stab and gunshot wounds, with stab wounds being encountered approximately three times more often than gunshot wounds.⁹ Penetrating trauma can have a more straightforward evaluation compared with blunt injury in that the point of wound entry is usually evident, and in the case of gunshot wounds, the exit wound can also be identified. However, the extent of injury with blunt trauma is less conspicuous on physical examination and is thus associated with higher morbidity and mortality.⁶

Most blunt injuries occur after a motor vehicle collision, followed by a pedestrian versus vehicle collision and direct blows to the abdomen by falls, assaults, or sports injuries.^{6,10} Three mechanisms are often used to describe blunt trauma. These are deceleration injuries, crush injuries, and external compression. Rapid deceleration creates significant shearing forces between fixed and mobile parts of organs that can result in lacerations at these areas or at points of attachment to the peritoneum. These forces can also lead to vascular tears or cause stretch injuries to arteries, resulting in infarction of susceptible organs.¹⁰ External objects such as the seat belt or steering wheel can lead to crush injury of the organs between the abdominal wall anteriorly and the thoracic ribs or vertebral column posteriorly.⁹ Finally, a sudden increase in intra-abdominal pressure by external compression can lead to perforation of hollow viscera.

Oftentimes, more than one mechanism occurs during the traumatic incident with simultaneous injury to multiple organs. For instance, an unrestrained driver in a motor vehicle accident who is ejected from the vehicle could initially strike the windshield, producing the first set of injuries, and then could strike the ground outside the vehicle, producing a second set of injuries. If the patient is still moving rapidly, a third or fourth set of injuries may occur until the patient eventually comes to a stop. Injuries may be clustered in one portion of the body, but multiple sites of injury may exist in the same patient. Thus, in

assessing patients with history of trauma, it is helpful to know details of the type of trauma as this can be useful in determining specific patterns of injured organs. In addition, the mechanism of injury has been found to be an independent predictor for mortality and long-term functional impairment.⁷

The spleen is the most commonly injured intra-abdominal organ and may be the only affected organ in up to 60% of cases.⁷ Following the spleen, in order of decreasing frequency, the other commonly injured organs are the liver, kidneys, small bowel or mesentery, bladder, colon or rectum, diaphragm, pancreas, and major vessels.¹⁰

Diagnostic Techniques in Patients with Abdominal Trauma

The diagnostic approach to trauma patients varies according to their hemodynamic status. Patients who remain hemodynamically unstable despite appropriate resuscitation efforts are usually taken to the operating room for emergent laparotomy because of high suspicion of ongoing hemorrhage. Diagnostic techniques for abdominal trauma include the focused assessment with sonography for trauma (FAST) and diagnostic peritoneal lavage. In short, FAST is used to evaluate for free intraperitoneal fluid and is usually performed before exploratory laparotomy. It is a rapid, noninvasive test that can be performed at the bedside and has been shown to have up to 90% specificity for blood products in the abdomen and pelvis.¹¹ However, it is an operator-dependent examination that does not focus on direct signs of organ trauma. It also has a low sensitivity (29%-35%) for organ injury in the absence of hemoperitoneum.¹¹ Because intra-abdominal injury cannot be ruled out with normal findings on FAST scan, further diagnostic testing, such as diagnostic peritoneal lavage or CT, is often necessary.

Diagnostic peritoneal lavage is used to evaluate for intra-abdominal hemorrhage and hollow organ injury. Its use has markedly decreased because of advances in imaging technology and increased nonoperative management after trauma. The principle of this technique is to infuse saline into the peritoneum to mix with possible blood and then to recover the fluid for analysis. Diagnostic peritoneal lavage has high sensitivity in the detection of peritoneal bleeding, and some trauma surgeons appreciate its capacity of providing them prompt and easy-to-interpret information in settings in which radiologists are not readily available to interpret films.¹² However, its disadvantages include lack of specificity for the source of bleeding and that it is an invasive procedure with associated risks and morbidity.^{13,14}

Computed Tomography Use in Abdominal Trauma

The speed and accuracy of CT as well as its widespread availability in emergency departments and trauma centers have led this imaging modality to play a principal role in the triage and diagnosis of trauma patients. Although the use of CT in abdominal trauma dates to the 1980s,¹⁵ the advent of helical scanning and multidetector helical computed tomography (MDCT) has allowed it to be more widely used with reduced scan times and improved image quality.

In the past, trauma patients were initially evaluated with conventional chest, cervical spine, and pelvic radiographs. CT scans were obtained only for hemodynamically stable patients with blunt abdominal trauma, in those with no evidence of penetrating injury, or in those who presented obtunded. Today, CT is more frequently used in patients with some degree of clinical instability, provided they respond to initial resuscitation and are stable enough to undergo CT. In fact, a study published in 2009 found that of patients who underwent whole-body CT, one of every five had been in shock at the scene of the trauma and one of six at the time of admission.¹⁶ CT is now also routinely used in patients with chest injuries or penetrating wounds.

When it comes to clinical decision making, CT scanning has proved to be superior to other methods in the diagnosis of injuries that require surgical intervention. In a study conducted by Deunk and coworkers,¹⁷ researchers found that MDCT findings after trauma often result in a change in treatment decisions. Moreover, increased CT use after trauma has led to a shift to nonoperative management and decreased morbidity and in-hospital mortality. A large number of injuries involving the liver, spleen, and kidneys are now managed conservatively if patients are hemodynamically stable.

Computed Tomography Imaging Techniques and Interpretation

Trauma CT protocols should attempt to optimize images to help radiologists detect injuries while minimizing risks to the patient. To achieve this goal, it is important to consider various aspects of image acquisition and analysis. These include the use of contrast material, different phases of acquisition with their varying degrees of contrast enhancement, radiation dose, and image processing.

CONTRAST MATERIAL

The intravenous use of contrast material improves the sensitivity and specificity of CT for detection of injury. The American College of Radiology developed the Appropriateness Criteria, which are evidence-based guidelines meant to aid in the selection of imaging and routes of administration of contrast material in different emergency scenarios. The guidelines state that the intravenous use of contrast material is critical to identify bowel, visceral, or vascular injury in the setting of blunt abdominal trauma.¹⁸ In addition, they recommend against the use of oral contrast material in the setting of blunt abdominal injury, probably because of lack of additional diagnostic value as well as potential delay in obtaining the CT images owing to wait time for enteric contrast material to progress.¹⁹

One of the more controversial issues surrounding the intravenous use of contrast material is the risk of acute kidney injury, especially in the elderly, those with established renal insufficiency, and patients with chronic diseases, such as diabetes mellitus, congestive heart failure, and hypertension. This is especially worrisome in the setting of trauma, when oftentimes one cannot obtain a thorough history and testing for renal function might delay possible treatment.

Some centers have recently been looking at point-of-care (POC) creatinine testing in patients presenting for imaging with nonspecific history that could be concerning for kidney disease.²⁰ A study by Lee-Lewandrowski and colleagues²¹ looked

at POC creatinine testing and its impact on clinical operations in the radiology department of a large academic medical center. This group found that 5.3% of patients (441 per month) who presented for scans did not have a recent creatinine level or estimated glomerular filtration rate; 26% of these were determined to be abnormal. They also found good agreement between POC and central laboratory plasma creatinine testing; however, the POC creatinine testing was approximately 47% more expensive than central laboratory plasma creatinine testing. However, because of the increased timeliness and improved quality of scans with intravenous contrast material, the authors suggested that POC creatinine testing improves clinical operations and is likely to be cost-effective.²¹ A study of POC creatinine testing in the emergency department also showed good correlation between POC and serum testing, leading the authors to conclude that because of its ease of use and rapid turnaround time, it could be of substantial benefit in the emergent setting.²²

MULTIPHASIC IMAGING

Because of increased image acquisition speed, it is possible to achieve multiphasic imaging with a single bolus of contrast material. However, there is no current consensus on the optimal number of phases needed for a trauma protocol as peak contrast enhancement varies between organs and there are advantages to each of the phases. Some researchers believe that the portal venous phase, which occurs 65 to 80 seconds after initiation of administration of the contrast material, is a good compromise in the diagnosis of parenchymal injury.¹⁰ In a study of the role of multiphasic imaging in pancreatic injury detection, for instance, researchers found that the portal venous phase was the most accurate to determine signs suggestive of ductal injuries.²³ Results of a study on splenic trauma by Boscak and associates²⁴ showed that the portal venous phase was more sensitive than the arterial phase in the diagnosis of parenchymal injury and active hemorrhage, yet the arterial phase was more sensitive for pseudoaneurysm detection. The authors suggested that dual phase imaging offers optimal overall performance.

Multiphasic imaging is also beneficial in trying to further characterize vascular injuries. Acquiring images at different points in time helps differentiate between contained injury and active vascular hemorrhage as well as distinguish arterial from venous sources.²⁵ By using delayed imaging, one can theoretically characterize the rate of bleed by looking for enlarged areas of extravasation of contrast material²⁶ as well as evaluate the collecting system of the kidneys.

RADIATION DOSE

With regard to radiation dose, as with all imaging, a risk-benefit analysis needs to be performed for each patient to determine if CT is appropriate. Specifically, the risks of radiation and intravenous administration of contrast material must be weighed against the benefits from diagnosis of traumatic injuries. In light of the fact that CT is superior to clinical evaluation and modalities such as diagnostic peritoneal lavage for diagnosis of clinically significant abdominal injuries,^{27,28} CT is a mainstay in the imaging of acute traumatic injury. It is critical to adhere to the concept of ALARA (as low as reasonably achievable) in performing CT; that is, image quality should be maximized but not at the expense of increased radiation dose to the patient.¹⁰

As such, there are multiple dose reduction tools available on current CT scanner platforms, including automatic tube current modulation, which allows the tube current to automatically change with the region of the body being imaged,²⁹ thereby lowering radiation dose.³⁰ In addition, whereas most CT is reconstructed with conventional filtered back projection, new research is focused on a host of new iterative reconstruction algorithms designed to reduce dose while maintaining image quality.³¹⁻³⁷ Willemink and associates³⁸ recently showed that although the mean time required for CT image reconstruction for whole-body trauma CT is statistically significantly higher with iterative reconstruction as opposed to filtered back projection, this difference is on the order of 45 seconds, likely making this a clinically insignificant delay in the trauma setting. This study was limited in that it was performed with one CT vendor's software only; additional studies with the other major vendor's iterative reconstruction products are likely needed to assess whether this holds true for other iterative reconstruction algorithms.

IMAGE PROCESSING

Current multidetector CT platforms have the ability to acquire data at submillimeter section thickness with isotropic data sets. Interpretation of these submillimeter-thick data sets can be cumbersome, and most centers will reconstruct these images at 2.5- or 5.0-mm section thickness to facilitate image interpretation.¹⁰

In addition, reconstruction of axial data sets in the coronal and sagittal planes can often be performed by the CT technologist at the console and sent to a picture and archiving communication system for interpretation by the radiologist in conjunction with the axial data sets. Coronal and sagittal reconstructions have the ability to help confirm diagnoses made on axial images as well as to aid in diagnosis of injuries of other structures, such as the bladder, diaphragm, and spine (Fig. 126-1).³⁹⁻⁴³

Approach to Computed Tomography Interpretation

The mechanisms of traumatic injuries are often complex and can lead to multiorgan injury. As such, a consistent and repeatable search pattern can help minimize missed injuries. The use of a rigorous routine in the interpretation of trauma patient CT studies significantly diminishes the number of missed traumatic lesions, especially in the setting of multiple injuries.^{44,45} As with any CT interpretation, the specific search pattern used is less important than simply having and following a comprehensive search pattern in each case.

Computed Tomography Findings in Abdominal Injury

LIVER AND SPLEEN

Currently, most splenic and liver injuries are managed conservatively in the hemodynamically stable patient. The major types of blunt hepatic and splenic trauma include subcapsular and intraparenchymal hematomas (Fig. 126-2), lacerations (Fig. 126-3), active hemorrhage, and other vascular injuries.^{46,47} Of

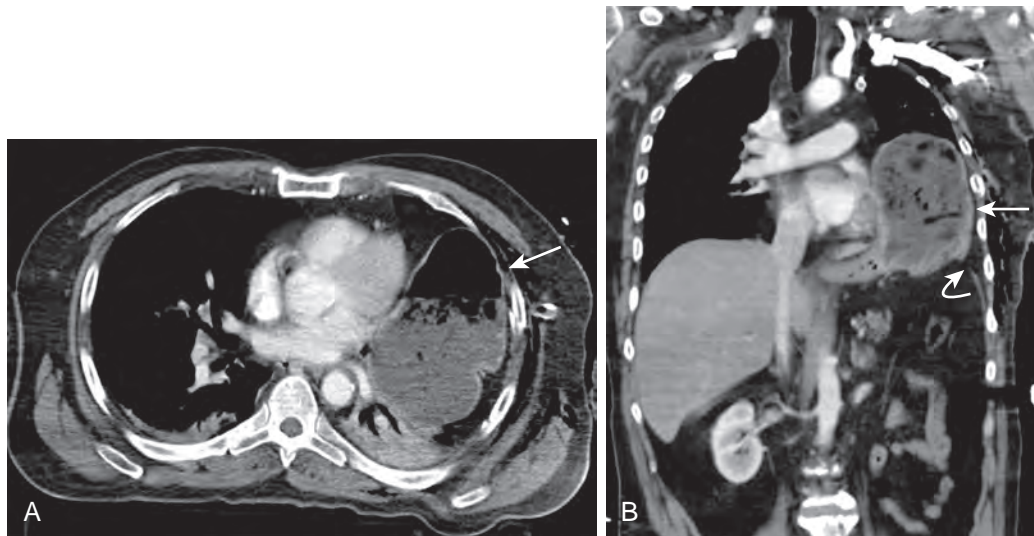


Figure 126-1 Left diaphragmatic rupture. A 55-year-old man who was driving a motorcycle and was struck by a motor vehicle. **A.** Axial image of a contrast-enhanced CT scan reveals the majority of the stomach in the thorax just lateral to the heart, indicating diaphragmatic rupture (arrow). **B.** Coronal reformatted image again shows the stomach herniating into the thorax and a ruptured diaphragm (curved arrow). The patient was taken to the operating room, where his 12-cm left diaphragmatic rupture was repaired. This case illustrates the value of coronal reformatted images in the acute traumatic setting.

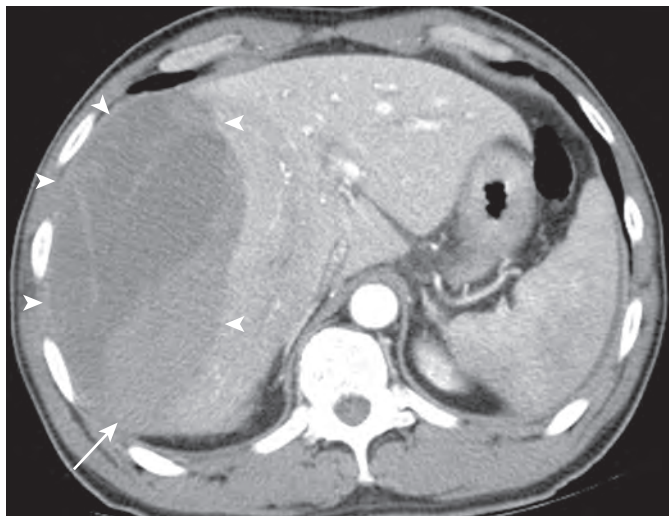


Figure 126-2 Subcapsular hematoma. A 55-year-old man was evaluated after blunt abdominal trauma. Contrast-enhanced CT scan of the abdomen reveals a subcapsular hematoma on the right hepatic lobe (arrowheads). Note the differing densities of the contents that indicate this is a hematoma, with more dense blood products along the gravity-dependent aspects of the hematoma (arrow).

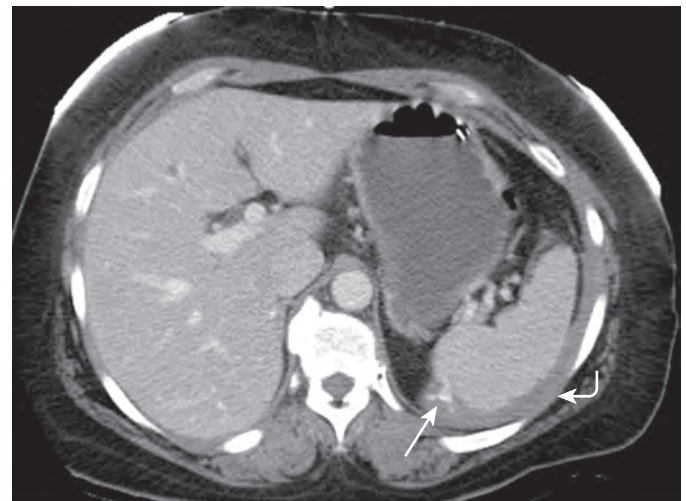


Figure 126-3 Splenic injury with active extravasation. A 45-year-old woman who was involved in a motor vehicle collision. Contrast-enhanced CT of the abdomen reveals a splenic injury with hemorrhage adjacent to the spleen (curved arrow) and an area of active extravasation (straight arrow). Splenic injury with active bleeding was confirmed at exploratory laparotomy with subsequent splenectomy.

note, vascular injury can be subtle, and its only sign may be end-organ damage. The American Association for the Surgery of Trauma (AAST) has devised injury grading scales for both liver and splenic injuries (Tables 126-1 and 126-2).

PANCREAS

In the pancreas, two thirds of injuries occur in the body of the organ; the rest occur equally in the head, neck, and tail (Fig. 126-4). In addition, pancreatic injuries are rarely isolated; it is estimated that 70% to 90% of injuries to the pancreas are

accompanied by injuries to other organs.⁴⁸ The AAST grading scale for pancreatic injury is based on the location of injury as well as on the degree of parenchymal and ductal destruction (Table 126-3).

Hepatic, pancreatic, and splenic injuries are further discussed in Chapters 91, 99, and 106, respectively.

KIDNEYS

CT is the imaging modality of choice to evaluate for renal injury after trauma because of its ability to accurately depict the renal

parenchyma, collecting system, and blood vessels.⁴⁹ Renal injury can be found in approximately 8% to 10% of abdominal traumas, although 80% to 90% of injuries result from blunt rather than from penetrating trauma.^{49,50} Trauma to the kidneys can result in contusion, laceration, hemorrhage, or avulsion of the renal pedicle (Fig. 126-5). Gross hematuria after trauma should prompt evaluation of the renal system, although the absence of this finding does not exclude injury.^{49,50}

Early and delayed imaging is necessary to fully evaluate the urinary system as delayed images are essential to determine the integrity of the collecting system.^{10,49,50} The AAST has devised an injury grading scale based on depth of injury as well as involvement of renal vasculature and the collecting system

(Table 126-4). Grade I injuries account for approximately 75% to 80% of traumatic injuries, whereas grade II injuries account for 10%.⁴⁹ Thus, as is the trend with other organs, most renal injuries are managed conservatively.

In addition to routine MDCT, CT cystography is recommended in patients who present with gross hematuria and a pelvic fracture to search for serious bladder injury. Most bladder ruptures (85%-100%) are manifested with pelvic fractures, yet only 6% to 8% of patients with pelvic fractures due to trauma present with a ruptured bladder (Fig. 126-6).⁵¹ The location of rupture is important for management decisions as most cases of extraperitoneal rupture can be managed conservatively with drainage (Fig. 126-7), whereas intraperitoneal ruptures

TABLE 126-1	American Association for the Surgery of Trauma Liver Injury Scale	
Grade*	Lesion	Injury Description
I	Hematoma	Subcapsular, <10% surface area
II	Laceration	Capsular tear, <1 cm parenchymal depth
	Hematoma	Subcapsular, 10% to 50% surface area
III	Laceration	Intraparenchymal, <10 cm in diameter
		Capsular tear, active bleeding
IV		1-3 cm parenchymal depth, <10 cm in length
		Subcapsular, >50% surface area or ruptured with active bleeding
V		Intraparenchymal hematoma >10 cm or expanding
	Laceration	>3 cm parenchymal depth
VI	Laceration	Parenchymal disruption involving 25% to 75% of hepatic lobe or 1-3 Couinaud segments within a single lobe
		Parenchymal disruption involving >75% of hepatic lobe or >3 Couinaud segments within a single lobe
V	Vascular	Juxtahepatic venous injuries (i.e., retrohepatic vena cava and/or central major hepatic veins)
	Vascular	Hepatic avulsion

From Moore EE, Cogbill TH, Jurkovich GJ, et al: Organ injury scaling: Spleen and liver (1994 revision). *J Trauma* 38:323-324, 1995.
*Advance one grade (up to grade III) for multiple injuries.

TABLE 126-2	American Association for the Surgery of Trauma Splenic Injury Scale	
Grade*	Lesion	Injury Description
I	Hematoma	Subcapsular, <10% surface area
II	Laceration	Capsular tear, <1 cm parenchymal depth
	Hematoma	Subcapsular, 10% to 50% surface area
III	Laceration	Intraparenchymal, <5 cm in diameter
		Capsular tear, active bleeding
IV		1-3 cm parenchymal depth, does not involve trabecular vessels
		Subcapsular, >50% surface area or expanding
V		Ruptured subcapsular or intraparenchymal hematoma
		Intraparenchymal hematoma >5 cm or expanding
V	Laceration	>3 cm parenchymal depth or involves trabecular vessels
	Laceration	Involves segmental or hilar vessels, producing major devascularization (>25% of spleen)
V	Vascular	Completely shattered spleen
	Vascular	Hilar vascular injury that devascularized the spleen

From Moore EE, Cogbill TH, Jurkovich GJ, et al: Organ injury scaling: Spleen and liver (1994 revision). *J Trauma* 38:323-324, 1995.
*Advance one grade (up to grade III) for multiple injuries.

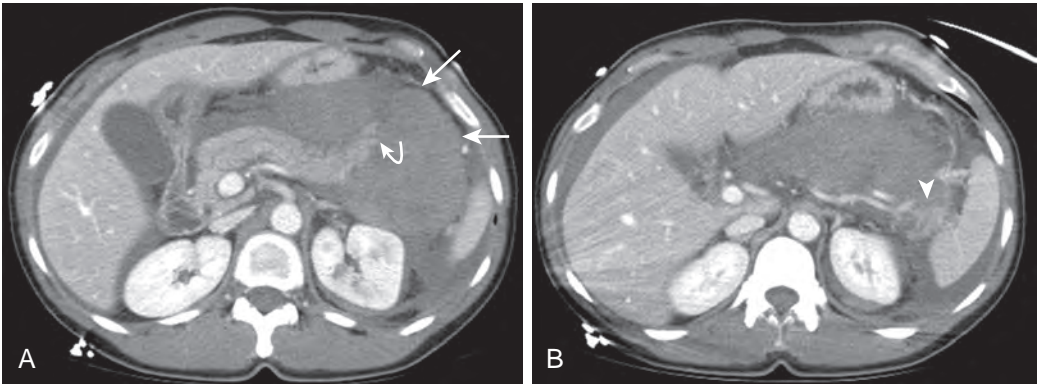


Figure 126-4 Pancreatic transection with retroperitoneal and intraperitoneal hemorrhage. A 42-year-old woman after a bicycle accident in which she suddenly braked and fell over the handlebars onto the pavement. **A.** Contrast-enhanced CT reveals a large amount of retroperitoneal and intraperitoneal hemorrhage (straight arrows). The pancreatic tail is deviated anteriorly by the hemorrhage (curved arrow). **B.** A portion of the transected pancreatic tail is seen in its expected location in the left upper quadrant (arrowhead). The diagnosis of pancreatic transection was confirmed at exploratory laparotomy, at which distal pancreatectomy and splenectomy were performed.

(Fig. 126-8) usually require surgical intervention for repair.⁵² Other findings of bladder trauma include contusions and interstitial injury, which are managed conservatively, and combined rupture, which usually requires repair.⁵³

Computed Tomography and Bowel Injury

Studies have historically shown that bowel injury occurs in approximately 1% to 5% of abdominal trauma patients. In a

more recent study of patients after blunt abdominal trauma, 9% were found to have hollow viscus injury. One third of these (approximately 3%) were in the stomach and the rest in the bowel.⁵⁴ The detection of a bowel injury in a blunt trauma patient can be difficult because clinical signs are often

TABLE 126-3 American Association for the Surgery of Trauma Pancreatic Injury Scale

Grade*	Lesion	Injury Description
I	Hematoma	Minor contusion without duct injury
	Laceration	Superficial laceration without duct injury
II	Hematoma	Major contusion without duct injury or tissue loss
	Laceration	Major laceration without duct injury or tissue loss
III	Laceration	Distal transection or parenchymal injury with duct injury
IV	Laceration	Proximal [†] transection or parenchymal injury involving ampulla
V	Laceration	Massive disruption of pancreatic head

From Moore EE, Cogbill TH, Malangoni MA, et al: Organ injury scaling, II: Pancreas, duodenum, small bowel, colon, and rectum. *J Trauma* 30:1427–1429, 1990.

*Advance one grade (up to grade III) for multiple injuries.

[†]Proximal pancreas is to the patient's right of the superior mesenteric vein.



Figure 126-5 Splenic laceration and renal injury secondary to gunshot wound. A 23-year-old pregnant woman after a gunshot wound to the left upper abdomen. Contrast-enhanced CT of the abdomen and pelvis reveals a splenic laceration (straight arrow). Note the extensive hemorrhage and gas inside the left renal fossa (arrowhead) and the left renal parenchymal injury (curved arrow). The patient underwent an exploratory laparotomy and splenectomy. Intraoperative evaluation of the left kidney revealed renal laceration and collecting system injury.

TABLE 126-4 American Association for the Surgery of Trauma Kidney Injury Scale

Grade*	Lesion	Injury Description
I	Contusion	Microscopic or gross hematuria, urologic studies normal
	Hematoma	Subcapsular, nonexpanding without parenchymal laceration
II	Hematoma	Nonexpanding perirenal hematoma confined to renal retroperitoneum
	Laceration	<1.0 cm parenchymal depth of renal cortex without urinary extravasation
III	Laceration	<1.0 cm parenchymal depth of renal cortex without collecting system rupture or urinary extravasation
IV	Laceration	Parenchymal laceration extending through renal cortex, medulla, and collecting system
	Vascular	Main renal artery or vein injury with contained hemorrhage
V	Laceration	Completely shattered kidney
	Vascular	Avulsion of renal hilum which devascularizes kidney

From Moore EE, Shackford SR, Pachter HL, et al: Organ injury scaling: Spleen, liver, and kidney. *J Trauma Acute Care Surg* 29:1664, 1989.

*Advance one grade (up to grade III) for multiple injuries.

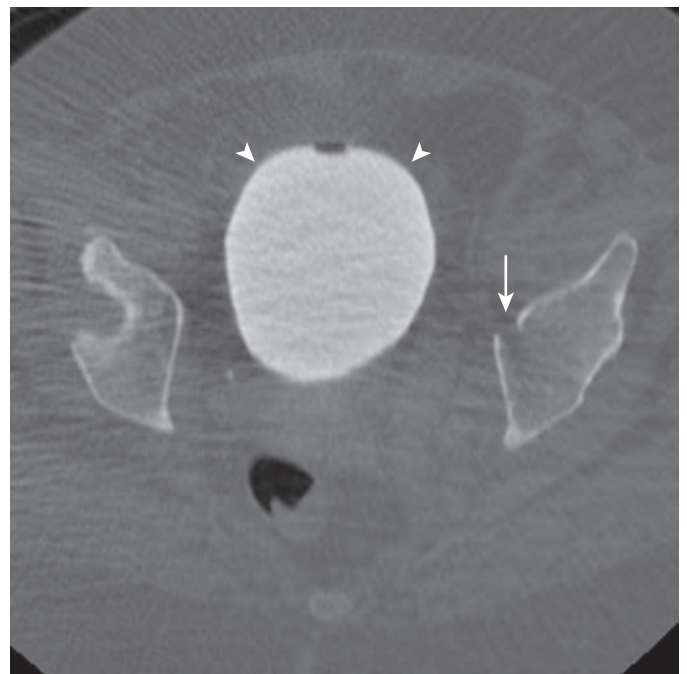


Figure 126-6 Pelvic trauma with normal findings on CT cystography. A 45-year-old man is evaluated after a motor vehicle collision. CT of the pelvis revealed multiple pelvic fractures and pelvic hemorrhage (left anterior acetabular fracture is denoted by the straight arrow). The patient underwent CT cystography, revealing smooth contour of the urinary bladder wall (arrowheads) and no evidence of bladder injury.

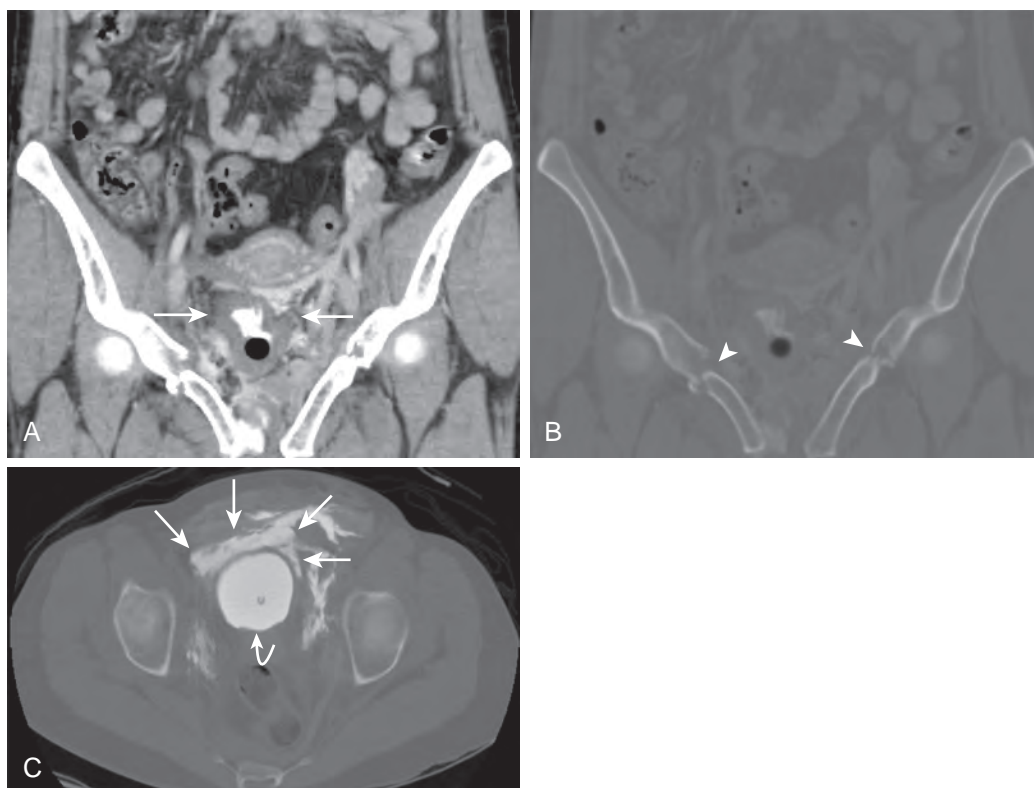


Figure 126-7 Extraperitoneal bladder rupture. A 51-year-old woman after a motorcycle accident. **A.** Coronal reformatted CT scan of the abdomen and pelvis revealed extensive pelvic fractures with pelvic hemorrhage. A decompressed urinary bladder with a Foley catheter contains contrast material from initial intravenous injection (*between straight arrows*). **B.** Coronal reformatted image of the abdomen and pelvis viewed on bone windows shows some of the representative pelvic fractures (*arrowheads*). **C.** Because of the extensive pelvic trauma, the patient underwent CT cystography, revealing an appropriately distended urinary bladder (*curved arrow*) as well as extravasated contrast material anterior and lateral to the bladder (*straight arrows*). These findings are compatible with an extraperitoneal bladder rupture.

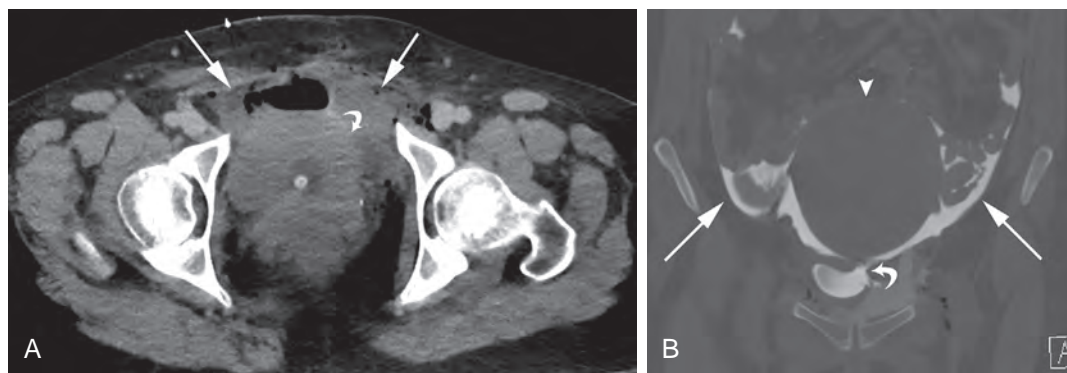


Figure 126-8 Intraperitoneal bladder rupture. A 33-year-old woman after penetrating pelvic injury. **A.** Contrast-enhanced CT scan reveals hematoma and air in the pelvis bilaterally (*straight white arrows*). A partially decompressed urinary bladder is seen containing a Foley catheter (*curved arrow*). **B.** Because of extensive hemorrhage in the pelvis, CT cystography was performed, and coronal reformatted images reveal extravasated contrast outlining bowel loops in the intraperitoneal space (*straight white arrows*). Note the approximate site of rupture at the left lateral bladder wall (*curved arrow*). Notice is made of an enlarged postpartum uterus in the central part of the image (*arrowhead*).

nonspecific or delayed in presentation. Moreover, in patients with polytrauma, subtle findings of a bowel injury can be overlooked in the presence of other organ injuries, especially if there is no evidence of extraluminal gas. The goal of diagnosis is to determine which patients require surgical intervention and which can be managed nonoperatively.

With the increasing number of patients who are managed conservatively, prompt accurate diagnosis is essential to minimize morbidity and mortality.¹⁰ Studies have shown that delay

in intervention because of delay in diagnosis leads to increased morbidity and mortality. One study showed that delays as short as 8 hours were more likely to result in sepsis, peritonitis, and death in patients who underwent laparotomies, whereas another demonstrated that delays longer than 24 hours could lead to acute respiratory distress syndrome and sepsis in patients with hollow viscus injury.^{55,56} A more recent study showed that morbidity increased threefold with a 5-hour delay between admission and laparotomies.⁵⁷

The sensitivity and specificity of CT in the evaluation of bowel injuries vary in the literature. Cited sensitivities range from 64% to 95%, and specificities are between 92% and 100%.^{10,58-61} Atri and colleagues⁶² also cited a high negative predictive value of CT with a less than 1% post-test probability of injury with normal findings on CT scan. Reasons for missed diagnosis include major injury to other organs causing readers to overlook minor bowel trauma, patient body habitus, support and monitoring devices that can cause artifact, and absence of extraluminal gas.⁴⁴ Thus, it is imperative that readers establish a specific search pattern while reading images to minimize false-negative readings.

Computed Tomography Findings in Bowel and Mesenteric Injury

Injury to the bowel and mesentery can have a range of appearances on CT from a small mesenteric hematoma with no direct evidence of bowel damage to a complete transmural rupture of bowel wall. More specifically, the mucosal surface of the bowel wall can be torn with an intact serosal surface, there can be bleeding into the bowel wall with intact mucosal and serosal layers, or there can be edema in the bowel wall representing bowel contusion. Alternatively, the serosal surface of the bowel may be injured, producing a hematoma adjacent to the bowel without frank perforation. The mesentery can also be injured by disruption of the arterial supply or venous drainage or by a hematoma from capillary injury. Alternatively, a segment of the mesentery can be avulsed, with its vessels and fat separated from the remainder of the mesentery.

Small bowel injuries occur twice as frequently as colonic injuries because the small bowel is more mobile. The proximal jejunum and distal ileum are particularly susceptible to blunt injury as shearing forces that result from this type of trauma

often affect the mobile loops associated with fixed points.⁶³ The transverse colon is the most vulnerable portion of the large bowel because of its exposed location, whereas the ascending and descending colon are relatively fixed in the retroperitoneum and are less susceptible. In terms of penetrating trauma, the small bowel⁶ and colon are two of the most commonly injured organs because of firearms. The liver, small bowel, and colon are the three most commonly injured organs from injuries inflicted by knives.⁶⁴

There are various CT findings that are helpful in the diagnosis of clinically important bowel and mesenteric injury. Unfortunately, these findings are not uniformly present in patients with bowel injury and therefore vary in sensitivity and specificity.¹⁰ It is important to look for these signs carefully as the presence of several findings might increase the likelihood of significant injury. The CT signs with highest specificity include bowel wall discontinuity, extraluminal contrast material, and free air. Other, less specific but more sensitive signs include focal wall thickening, abnormal bowel wall enhancement, mesenteric stranding, and free intraperitoneal fluid.⁶³

BOWEL WALL DISCONTINUITY

Focal wall discontinuity is 100% specific for bowel injury, and the most severe bowel injuries—frank perforations—usually are manifested with this sign (Fig. 126-9). Nonetheless, only 7% of injuries present with this finding, resulting in a low sensitivity.⁶⁵ The size of the perforation defect is usually small, which also contributes to the infrequency of the finding.⁶⁶

EXTRAVASATION OF ORAL CONTRAST MATERIAL

Many institutions do not administer oral contrast material on a routine basis for trauma CT because of potential delay in

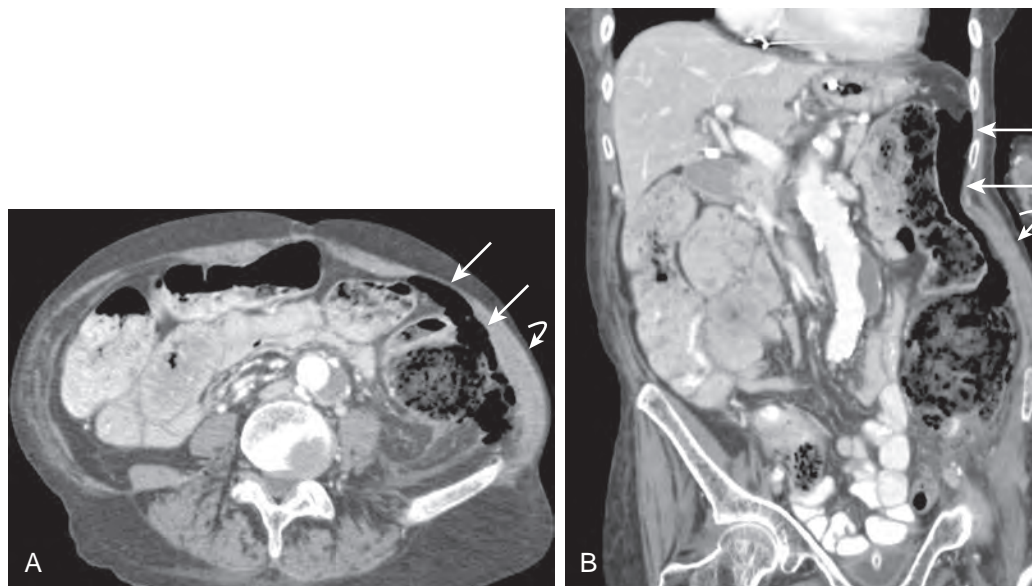


Figure 126-9 Colonic perforation from stab wound. A 65-year-old man presented with a stab wound to his left flank. **A.** Axial CT scan of the abdomen and pelvis reveals free intraperitoneal air (*straight arrows*) with discontinuity of the descending colonic wall, compatible with traumatic colonic perforation. Note is also made of a hematoma within the left flank musculature at the site of the stab wound (*curved arrow*). **B.** Coronal reconstruction of the CT image again reveals free intraperitoneal air (*straight arrows*) and left flank musculature hematoma (*curved arrow*). Incidental note is also made of an abdominal aortic aneurysm.

scanning from time required to get contrast material through the bowel. Thus, even though extravasation of oral contrast material is a specific sign⁶³ for bowel perforation, it is uncommonly seen.

EXTRALUMINAL AIR

Detection of extraluminal gas on CT after bowel injury has been reported over a wide range of 20% to 75% of cases.⁶³ Free air in the peritoneal or retroperitoneal cavity is relatively specific for injury, but the amount of free air may be low, thereby making detection more challenging. For instance, a loop of bowel may be fluid filled when it is ruptured with no initial release of gas into the peritoneum; the perforation can be self-contained by sealing spontaneously; or injury can lead to development of an ileus, which prevents air from being pushed down the intestine.⁶³ Lung and bone windows are often used to optimize detection of extraluminal air.

Pneumoperitoneum secondary to bowel rupture usually accumulates behind the anterior abdominal wall (see Fig. 126-9), below the diaphragm, or along the peritoneal surfaces of the liver and spleen. Air might also be seen in the porta hepatis, mesentery, mesenteric veins, or portal vein.⁶⁶ Detection of extraluminal gas is not 100% specific for bowel injury and can be caused by other factors. These include penetrating injuries (which introduce external air into the body), mechanical ventilation, bladder rupture with Foley catheter, barotrauma, pneumothorax, and peritoneal lavage before CT.^{63,66} Air contained between the inner layer of the abdominal wall and the parietal peritoneum, known as pseudopneumoperitoneum, can also lead to a false-positive bowel injury diagnosis.⁵⁹ Thus, free air can increase the probability of bowel injury when it is found in association with other signs; but if it is an isolated finding, other causes could be considered.

FOCAL BOWEL WALL THICKENING

With appropriate bowel distention, normal bowel wall thickness should not exceed 3 mm. Localized thickening of the bowel wall can be a clinically important sign and is found in approximately 45% to 75% of bowel injuries.^{44,62,66} In the absence of other findings, such as free fluid in the pelvis or stranding or fluid in the adjacent mesentery, focal bowel thickening is less likely to require surgical intervention.^{10,66} In other words, an isolated, focal finding of thickened bowel after trauma could be secondary to peristalsis or a focal bowel wall contusion that might not require operative management.⁵⁹

Compared with localized injuries as a direct result of trauma, generalized bowel wall thickening can be a sign of hypoperfusion or “shock bowel.”¹⁰ Other signs of decreased volume status, known as the hypoperfusion complex, include a flattened inferior vena cava, a narrowed aorta, and increased enhancement of the adrenal glands, kidneys, and bowel (Fig. 126-10).⁶⁷ Volume overload, usually secondary to overhydration with intravenous fluids, can also lead to diffuse wall thickening in the absence of all other findings of the hypoperfusion complex.⁵⁹

ABNORMAL BOWEL WALL ENHANCEMENT

Abnormal bowel wall enhancement can result from either hypoperfusion or local vascular injury, which can lead to increased vascular permeability and leakage of contrast material

into the interstitium.^{44,68} Several studies suggest that irregular increased enhancement after administration of contrast material is often a sign of full-thickness injury.^{63,69} On the other hand, decreased enhancement of the bowel wall can be a sign of ischemia.⁵⁹ Reference points often used to evaluate abnormal enhancement include nearby blood vessels and adjacent bowel loops.⁶⁸

MESENTERIC INJURY

Mesenteric injuries include mesenteric infiltration (also known as stranding), hematomas, and beading or abrupt termination of vessels.⁵⁹ Mesenteric stranding is often a sign of mesenteric injury and can be present with or without accompanying bowel injury (Fig. 126-11). This finding, when it is present with focal bowel thickening, likely represents a clinically important injury.^{44,59} However, it can also represent isolated mesenteric damage and thus has a low specificity for bowel injury.⁶³ For instance, a localized mesenteric hematoma without any other signs or findings indicative of bowel injury suggests an isolated injury of a mesenteric vessel.⁴⁴

Mesenteric hematomas are often triangular when small, but they may be rounded or oval when larger. In the presence of a larger hematoma, it is often important to look at delayed phase imaging to assess whether there is active bleeding that requires emergent surgery to prevent ischemic bowel. An irregular pattern, or beading, of mesenteric vessels and the abrupt termination of mesenteric arteries or veins are also signs of vascular injury that could require intervention (Fig. 126-12).⁵⁹

FREE INTRAPERITONEAL FLUID

Intraperitoneal fluid detection is a highly sensitive (90%-100%) but nonspecific (10%-15%) finding for bowel injury as peritoneal fluid may have a traumatic or nontraumatic origin.^{10,70} Sources of traumatic intraperitoneal fluid include blood from a solid organ, bowel, or mesenteric injury; bile from a ruptured gallbladder or bile duct; and urine from a ruptured bladder. Nontraumatic causes of fluid include ascites from a comorbid condition such as cirrhosis and physiologic fluid in the pelvis of women of childbearing age, among others.

The location of intraperitoneal fluid can often lead to the correct diagnosis.^{63,71} If fluid is seen only adjacent to bowel or caught between the leaves of the mesentery, it likely results from a bowel injury. If it is seen throughout the abdomen including upper and lower peritoneal compartments as well as the pelvis and a large amount of blood is present, the injury is more likely in a solid organ, such as a splenic or hepatic laceration. Upper abdominal solid organ injuries initially bleed into the major peritoneal space adjacent to the organ, and blood then migrates in an anatomic pathway down the paracolic gutters to the pelvis (Fig. 126-13).^{26,63} Thus, if a patient demonstrates blood caught between the leaves of the mesentery and does not have blood in the paracolic gutters or in the pelvis, the source of bleeding is likely bowel.

The density of intra-abdominal fluid in a trauma patient can also help identify the site of bleeding. Clotted blood is denser than serous blood, which is denser than urine or bile. The sentinel clot, which is usually found adjacent to the bleeding site, can be recognized on CT by its higher attenuation (45-70 HU), whereas unclotted blood found farther from the source has lower attenuation (30-45 HU).⁷² However, attenuation can be

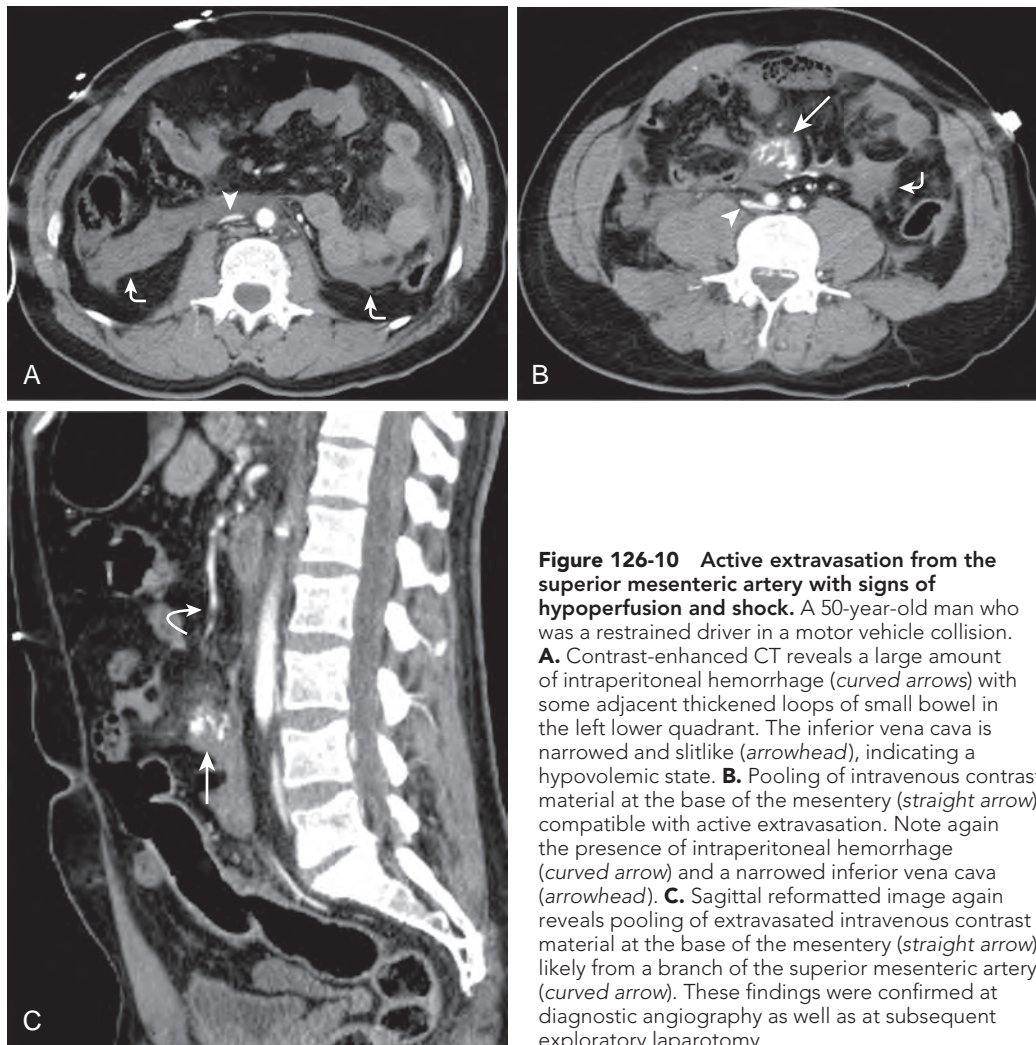


Figure 126-10 Active extravasation from the superior mesenteric artery with signs of hypoperfusion and shock. A 50-year-old man who was a restrained driver in a motor vehicle collision. **A.** Contrast-enhanced CT reveals a large amount of intraperitoneal hemorrhage (*curved arrows*) with some adjacent thickened loops of small bowel in the left lower quadrant. The inferior vena cava is narrowed and slitlike (*arrowhead*), indicating a hypovolemic state. **B.** Pooling of intravenous contrast material at the base of the mesentery (*straight arrow*), compatible with active extravasation. Note again the presence of intraperitoneal hemorrhage (*curved arrow*) and a narrowed inferior vena cava (*arrowhead*). **C.** Sagittal reformatted image again reveals pooling of extravasated intravenous contrast material at the base of the mesentery (*straight arrow*), likely from a branch of the superior mesenteric artery (*curved arrow*). These findings were confirmed at diagnostic angiography as well as at subsequent exploratory laparotomy.



Figure 126-11 Mesenteric hematoma. An 80-year-old man after a motor vehicle collision with a tree. Contrast-enhanced CT of the abdomen and pelvis revealed fat stranding and induration within the right lower quadrant mesentery (*arrows*) adjacent to the ascending colon. Findings were compatible with colonic contusion and mesenteric hematoma.

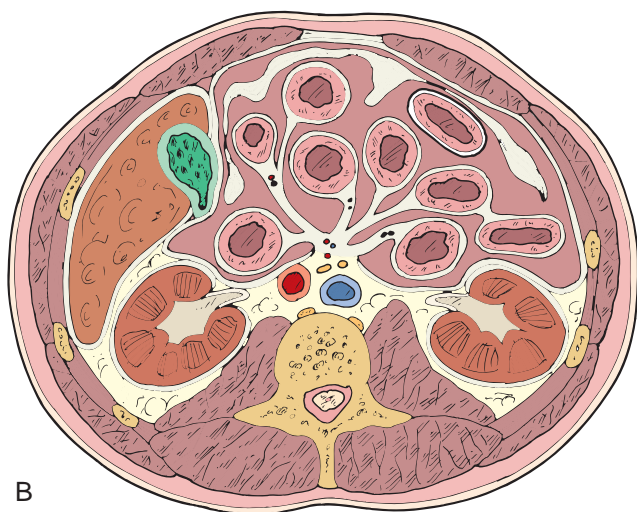
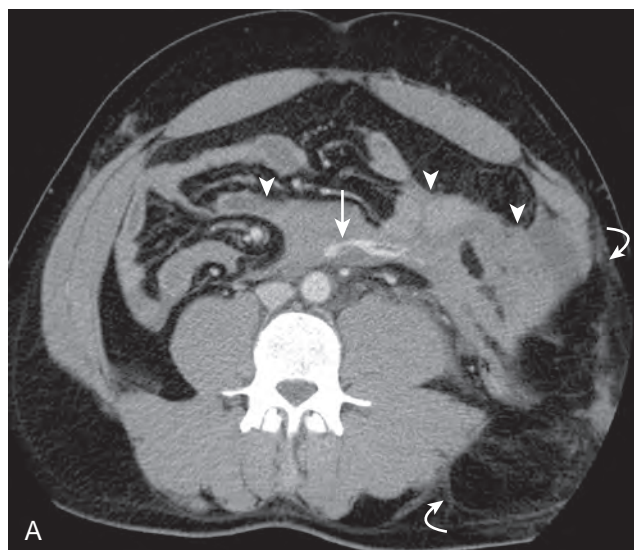


Figure 126-12 Traumatic abdominal hernia and active extravasation of intravenous contrast material. **A.** A 41-year-old man is evaluated after a motor vehicle collision. Contrast-enhanced CT of the abdomen and pelvis revealed traumatic left abdominal wall hernia (curved arrows) with hemoperitoneum (arrowheads) and active extravasation in the posterior mesentery in the region of a branch of the inferior mesenteric artery (straight arrow). **B.** Diagram of the midabdomen shows leaves of mesentery forming boundaries of the triangular interloop peritoneal spaces. This is similar to the findings seen in **A** with the mesenteric hemorrhage.

decreased in patients with hemorrhages that occurred more than 48 hours before the scan and in those patients with a low hematocrit.⁷² The density of bile and urine is closer to that of water, and thus their attenuation usually ranges from 0 to 15 HU.

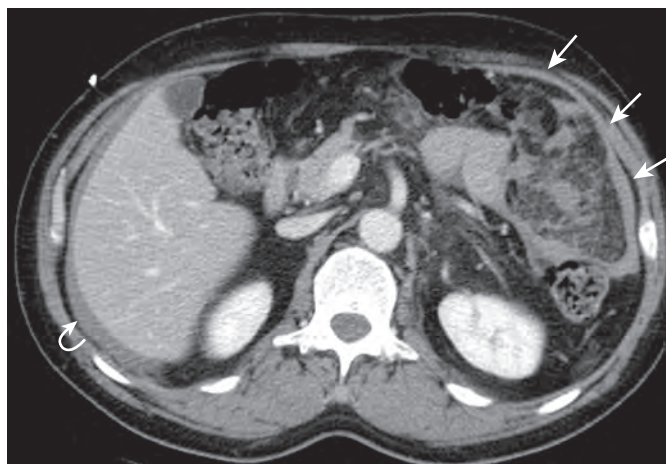


Figure 126-13 Omental laceration. A 56-year-old is evaluated after a motorcycle accident. Contrast-enhanced CT of the abdomen and pelvis revealed hemorrhage and thickening in the region of the omentum in the left upper quadrant (straight arrows). This hemorrhage extended to the splenic flexure of the colon. Additional hemorrhage was identified surrounding the liver (curved arrow). The patient was taken emergently to exploratory laparotomy, which revealed an omental laceration and a partial-thickness tear of the colon at the level of the splenic flexure.

Conclusions

Trauma is the leading cause of death in Americans younger than 45 years and the fifth leading overall cause in the United States. Appropriate prompt evaluation of trauma patients is essential to avoid serious morbidity and mortality. Because of the unreliability of the physical examination and risks from delayed diagnosis, imaging has come to play a critically important role in trauma diagnosis and management.

CT is the primary imaging modality used in the evaluation of patients in the acute traumatic setting because of its speed of acquisition, widespread availability, and high spatial resolution. It can be used after both blunt and penetrating abdominal injuries, and information obtained from CT often guides clinical decision making and treatment planning. Contrast-enhanced CT helps in the diagnosis of solid abdominal organ injury, and its use during the last three decades has led to a paradigm shift from surgical exploration to more conservative management in the hemodynamically stable patient.

Maintaining a consistent scan interpretation pattern is essential for radiologists to avoid “satisfaction of search” as traumatic injuries rarely occur in isolation. This is particularly important in the evaluation of bowel injury as its signs can range from pneumoperitoneum and extravasation of contrast material to more subtle presentations, such as focal bowel wall thickening and adjacent mesenteric hematomas. Radiologists are key members of the trauma team and make a substantial contribution to patient care.

REFERENCES

1. Hoyert DL, Xu J: Deaths: Preliminary data for 2011. *Natl Vital Stat Rep* 61:1–65, 2012.
2. Haegerich TM, Dahlberg LL, Simon TR, et al: Prevention of injury and violence in the USA. *Lancet* 384:64–74, 2014.
3. Web-based Injury Statistics Query and Reporting System (WISQARS), Atlanta, GA, 2010, US Department of Health and Human Services, Centers for Disease Control and Prevention, National Center for Injury Prevention and Control.
4. Finkelstein EA, Corso PS, Miller TR: *The Incidence and Economic Burden of Injuries in the United States*, New York, 2006, Oxford University Press.
5. Brown CK, Dunn KA, Wilson K: Diagnostic evaluation of patients with blunt abdominal

- trauma: A decision analysis. *Acad Emerg Med* 7:385–396, 2000.
6. Isenhour J, Marx J: Abdominal trauma. In Legome E, Shockley LW, editors: *Trauma: A Comprehensive Emergency Medicine Approach*, Cambridge, 2011, Cambridge University Press, p 213.
7. Haider AH, Chang DC, Haut ER, et al: Mechanism of injury predicts patient mortality and impairment after blunt trauma. *J Surg Res* 153:138–142, 2009.
8. Nishijima DK, Simel DL, Wisner DH, Holmes JF: Does this adult patient have a blunt intra-abdominal injury? *JAMA* 307:1517–1527, 2012.
9. Hughes TM, Elton C: The pathophysiology and management of bowel and mesenteric injuries due to blunt trauma. *Injury* 33:295–302, 2002.
10. Soto JA, Anderson SW: Multidetector CT of blunt abdominal trauma. *Radiology* 265:678–693, 2012.
11. Brooks A, Simpson JAD: Blunt and penetrating abdominal trauma. *Surgery* 27:266–271, 2009.
12. Pal JD, Victorino GP: Defining the role of computed tomography in blunt abdominal trauma: Use in the hemodynamically stable patient with a depressed level of consciousness. *Arch Surg* 137:1029–1032, discussion 1032–1033, 2002.
13. Melo EL, de Menezes MR, Cerri GG: Abdominal gunshot wounds: Multi-detector-row CT findings compared with laparotomy: A prospective study. *Emerg Radiol* 19:35–41, 2012.
14. Wang YC, Hsieh CH, Fu CY, et al: Hollow organ perforation in blunt abdominal trauma: The role of diagnostic peritoneal lavage. *Am J Emerg Med* 30:570–573, 2012.
15. Milia DJ, Brasel K: Current use of CT in the evaluation and management of injured patients. *Surg Clin North Am* 91:233–248, 2011.
16. Huber-Wagner S, Lefering R, Quick LM, et al: Effect of whole-body CT during trauma resuscitation on survival: A retrospective, multicentre study. *Lancet* 373:1455–1461, 2009.
17. Deunk J, Brink M, Dekker HM, et al: Routine versus selective computed tomography of the abdomen, pelvis, and lumbar spine in blunt trauma: A prospective evaluation. *J Trauma* 66:1108–1117, 2009.
18. Sudakoff G, Yucl E, Rosen M, et al: Expert panels on vascular imaging, gastrointestinal imaging, and urologic imaging. ACR Appropriateness Criteria blunt abdominal trauma [online publication], Reston, VA, 2008, American College of Radiology.
19. Broder JS, Hamedani AG, Liu SW, Emerman CL: Emergency department contrast practices for abdominal/pelvic computed tomography—a national survey and comparison with the American College of Radiology Appropriateness Criteria. *J Emerg Med* 44:423–433, 2013.
20. Haneder S, Gutfleisch A, Meier C, et al: Evaluation of a handheld creatinine measurement device for real-time determination of serum creatinine in radiology departments. *World J Radiol* 4:328–334, 2012.
21. Lee-Lewandrowski E, Chang C, Gregory K, Lewandrowski K: Evaluation of rapid point-of-care creatinine testing in the radiology service of a large academic medical center: Impact on clinical operations and patient disposition. *Clin Chim Acta* 413:88–92, 2012.
22. You JS, Chung YE, Park JW, et al: The usefulness of rapid point-of-care creatinine testing for the prevention of contrast-induced nephropathy in the emergency department. *Emerg Med J* 30:555–558, 2013.
23. Wong YC, Wang LJ, Fang JF, et al: Multidetector-row computed tomography (CT) of blunt pancreatic injuries: Can contrast-enhanced multiphasic CT detect pancreatic duct injuries? *J Trauma* 64:666–672, 2008.
24. Boscak AR, Shanmuganathan K, Mirvis SE, et al: Optimizing trauma multidetector CT protocol for blunt splenic injury: Need for arterial and portal venous phase scans. *Radiology* 268:79–88, 2013.
25. Vu M, Anderson SW, Shah N, et al: CT of blunt abdominal and pelvic vascular injury. *Emerg Radiol* 17:21–29, 2010.
26. Willmann JK, Roos JE, Platz A, et al: Multidetector CT: Detection of active hemorrhage in patients with blunt abdominal trauma. *AJR Am J Roentgenol* 179:437–444, 2002.
27. Catre M: Diagnostic peritoneal lavage versus abdominal computed tomography in blunt abdominal trauma: A review of prospective studies. *Can J Surg* 38:117, 1995.
28. Gonzalez RP, Ickler J, Gachassin P: Complementary roles of diagnostic peritoneal lavage and computed tomography in the evaluation of blunt abdominal trauma. *J Trauma Acute Care Surg* 51:1128–1136, 2001.
29. Huda W, Scalzetti EM, Levin G: Technique factors and image quality as functions of patient weight at abdominal CT. *Radiology* 217:430–435, 2000.
30. Hara AK, Wellnitz CV, Paden RG, et al: Reducing body CT radiation dose: Beyond just changing the numbers. *AJR Am J Roentgenol* 201:33–40, 2013.
31. Leipsic J, LaBounty TM, Heilbron B, et al: Estimated radiation dose reduction using adaptive statistical iterative reconstruction in coronary CT angiography: The ERASIR study. *AJR Am J Roentgenol* 195:655–660, 2010.
32. Moscariello A, Takx RA, Schoepf UJ, et al: Coronary CT angiography: Image quality, diagnostic accuracy, and potential for radiation dose reduction using a novel iterative image reconstruction technique—comparison with traditional filtered back projection. *Eur Radiol* 21:2130–2138, 2011.
33. Pontana F, Duhamel A, Pagniez J, et al: Chest computed tomography using iterative reconstruction vs filtered back projection (Part 2): Image quality of low-dose CT examinations in 80 patients. *Eur Radiol* 21:636–643, 2011.
34. Sato J, Akahane M, Inano S, et al: Effect of radiation dose and adaptive statistical iterative reconstruction on image quality of pulmonary computed tomography. *Jpn J Radiol* 30:146–153, 2012.
35. Singh S, Kalra MK, Gilman MD, et al: Adaptive statistical iterative reconstruction technique for radiation dose reduction in chest CT: A pilot study. *Radiology* 259:565–573, 2011.
36. Willemink MJ, de Jong PA, Leiner T, et al: Iterative reconstruction techniques for computed tomography part 1: Technical principles. *Eur Radiol* 23:1623–1631, 2013.
37. Willemink MJ, Leiner T, de Jong PA, et al: Iterative reconstruction techniques for computed tomography part 2: Initial results in dose reduction and image quality. *Eur Radiol* 23:1632–1642, 2013.
38. Willemink MJ, Schilham AM, Leiner T, et al: Iterative reconstruction does not substantially delay CT imaging in an emergency setting. *Insights Imaging* 4:391–397, 2013.
39. Bhullar IS, Block EF: CT with coronal reconstruction identifies previously missed smaller diaphragmatic injuries after blunt trauma. *Am Surg* 77:55–58, 2011.
40. Chan DP, Abujudeh HH, Cushing GL, Novelline RA: CT cystography with multiplanar reformation for suspected bladder rupture: Experience in 234 cases. *AJR Am J Roentgenol* 187:1296–1302, 2006.
41. Lucey BC, Stuhlfaut JW, Hochberg AR, et al: Evaluation of blunt abdominal trauma using PACS-based 2D and 3D MDCT reformations of the lumbar spine and pelvis. *AJR Am J Roentgenol* 185:1435–1440, 2005.
42. Rees O, Mirvis S, Shanmuganathan K: Multidetector-row CT of right hemidiaphragmatic rupture caused by blunt trauma: A review of 12 cases. *Clin Radiol* 60:1280–1289, 2005.
43. Roos JE, Hilfiker P, Platz A, et al: MDCT in emergency radiology: Is a standardized chest or abdominal protocol sufficient for evaluation of thoracic and lumbar spine trauma? *AJR Am J Roentgenol* 183:959–968, 2004.
44. Brody JM, Leighton DB, Murphy BL, et al: CT of Blunt trauma bowel and mesenteric injury: Typical findings and pitfalls in diagnosis. *Radiographics* 20:1525–1536, 2000.
45. Halvorsen RA, Jr, McCormick VD, Evans SJ: Computed tomography of abdominal trauma: A step-by-step approach. *Emerg Radiol* 1:283–291, 1994.
46. Clark TJ, Cardoza S, Kanth N: Splenic trauma: Pictorial review of contrast-enhanced CT findings. *Emerg Radiol* 18:227–234, 2011.
47. Yoon W, Jeong YY, Kim JK, et al: CT in blunt liver trauma. *Radiographics* 25:87–104, 2005.
48. Venkatesh SK, Wan JMC: CT of blunt pancreatic trauma—a pictorial essay. *Eur J Radiol* 67:311–320, 2008.
49. Park SJ, Kim JK, Kim KW, Cho K-S: MDCT findings of renal trauma. *AJR Am J Roentgenol* 187:541–547, 2006.
50. Kawashima A, Sandler CM, Corl FM, et al: Imaging of renal trauma: A comprehensive review. *Radiographics* 21:557–574, 2001.
51. Avey G, Blackmore CC, Wessells H, et al: Radiographic and clinical predictors of bladder rupture in blunt trauma patients with pelvic fracture. *Acad Radiol* 13:573–579, 2006.
52. Srinivasa R, Akbar S, Jafri S, Howells G: Genitourinary trauma: A pictorial essay. *Emerg Radiol* 16:21–33, 2009.
53. Vaccaro JP, Brody JM: CT cystography in the evaluation of major bladder trauma. *Radiographics* 20:1373–1381, 2000.
54. Joseph DAK, Kunac A, Kinler RL, et al: Diagnosing blunt hollow viscus injury: Is computed tomography the answer? *Am J Surg* 205:414–418, 2013.
55. Fakhry SM, Watts DD, Luchette FA: Current diagnostic approaches lack sensitivity in the diagnosis of perforated blunt small bowel injury: Analysis from 275,557 trauma admissions from the EAST multi-institutional HVI trial. *J Trauma Acute Care Surg* 54:295–306, 2003.
56. Niederee MJ, Byrnes MC, Helmer SD, Smith RS: Delay in diagnosis of hollow viscus injuries: Effect on outcome. *Am Surg* 69:293, 2003.
57. Malinoski DJ, Patel MS, Yakar DO, et al: A diagnostic delay of 5 hours increases the risk of death after blunt hollow viscus injury. *J Trauma Acute Care Surg* 69:84–87, 2010.
58. Allen TL, Mueller MT, Bonk RT, et al: Computed tomographic scanning without oral contrast solution for blunt bowel and mesenteric injuries in abdominal trauma. *J Trauma Acute Care Surg* 56:314–322, 2004.

59. Brofman N, Atri M, Hanson JM, et al: Evaluation of bowel and mesenteric blunt trauma with multidetector CT. *Radiographics* 26:1119–1131, 2006.
60. Khan I, Bew D, Elias DA, et al: Mechanism of injury and CT findings in bowel and mesenteric trauma. *Clin Radiol* 69:639–647, 2014.
61. Ekeh AP, Saxe J, Walusimbi M, et al: Diagnosis of blunt intestinal and mesenteric injury in the era of multidetector CT technology—are results better? *J Trauma Acute Care Surg* 65:354–359, 2008.
62. Atri M, Hanson JM, Grinblat L, et al: Surgically important bowel and/or mesenteric injury in blunt trauma: Accuracy of multidetector CT for evaluation. *Radiology* 249:524–533, 2008.
63. LeBedis CA, Anderson SW, Soto JA: CT imaging of blunt traumatic bowel and mesenteric injuries. *Radiol Clin North Am* 50:123–136, 2012.
64. Castrillon GA, Soto JA: Multidetector computed tomography of penetrating abdominal trauma. *Semin Roentgenol* 47:371–376, 2012.
65. Stuhlfaut JW, Soto JA, Lucey BC, et al: Blunt abdominal trauma: Performance of CT without oral contrast material. *Radiology* 233:689–694, 2004.
66. Yu J, Fulcher AS, Turner MA, et al: Blunt bowel and mesenteric injury: MDCT diagnosis. *Abdom Imaging* 36:50–61, 2011.
67. Prasad KR, Kumar A, Gamanagatti S, Chandrasekhara S: CT in post-traumatic hypoperfusion complex—a pictorial review. *Emerg Radiol* 18:139–143, 2011.
68. Romano S, Scaglione M, Tortora G, et al: MDCT in blunt intestinal trauma. *Eur J Radiol* 59:359–366, 2006.
69. Hawkins A, Mirvis S: Evaluation of bowel and mesenteric injury: Role of multidetector CT. *Abdom Imaging* 28:505–514, 2003.
70. Hassan R, Mohamed S: Computed tomography (CT) of bowel and mesenteric injury in blunt abdominal trauma: A pictorial essay. *Med J Malaysia* 67:445–451, 2012.
71. Tan K-K, Liu JZ, Go T-S, et al: Computed tomography has an important role in hollow viscus and mesenteric injuries after blunt abdominal trauma. *Injury* 41:475–478, 2010.
72. Lubner M, Menias C, Rucker C, et al: Blood in the belly: CT findings of hemoperitoneum. *Radiographics* 27:109–125, 2007.

Monitoring Gastrointestinal Tumor Response to Therapy

KUMAR SANDRASEGARAN

CHAPTER OUTLINE

World Health Organization and RECIST 1.0 Guidelines

Evolution of RECIST 1.1

Other Tumor Response Assessment Criteria

EASL and Modified RECIST Criteria

Choi Criteria

MASS Criteria

PERCIST

Functional Magnetic Resonance Imaging Techniques

Conclusion

Imaging plays a crucial role in the objective assessment of tumor response to various cancer therapies. Assessment of tumor response serves as an important clinical endpoint in phase II clinical trials and can reasonably predict the overall survival and other clinical events, such as time to progression.^{1,2} More than 70% of recent Food and Drug Administration approvals of oncologic drugs have been based on radiologic response.³ Several response assessment criteria have been used in oncology for assessment of response to gastrointestinal malignant neoplasms. Not only are these for use in research or drug trials, but they may also be incorporated into routine clinical practice. Early detection of therapy resistance may enable individualized treatment approaches tailored to the patient.

World Health Organization and RECIST 1.0 Guidelines

The World Health Organization (WHO) tumor response criteria, published in 1981, recommended the use of the cross product obtained by multiplying the longest diameter in the axial plane and the largest perpendicular diameter.⁴ Treatment response was categorized as complete response, indicating tumor disappearance; partial response, indicating more than 50% decrease in cross product; disease progression, indicating more than 25% increase in cross product; or stable disease, indicating changes that lay between partial response and disease progression. The WHO criteria suggested that in the presence of multiple lesions, the sum of the cross products of individual target lesions may be used to categorize the response. Since their inception, the WHO criteria were widely used for more than two decades.^{5,6} However, their deficiencies became obvious over time. No indication was given of the minimum number of lesions or the minimum size for a lesion to be categorized as a target lesion, and there were no guidelines on what type of

imaging modality may be used. The bidimensional measurements were cumbersome, with minor errors in measurement resulting in a large change to the cross product.⁷ To alleviate these difficulties, several modifications were attempted, but none of these methods was uniformly accepted.⁸

In the year 2000, the Response Evaluation Criteria in Solid Tumors (RECIST) guidelines were published by a task force that included members of the European Organization for Research and Treatment in Oncology, the National Cancer Institute of the United States, and the National Cancer Institute of Canada.⁹ This recommendation was based on a retrospective evaluation of more than 4000 patients in 14 different trials. These guidelines addressed most but not all of the deficiencies in the WHO criteria. RECIST guidelines recommended the use of one-dimensional tumor measurements (the longest diameter) rather than the cross product ([Fig. 127-1](#)). Lesions were categorized as measurable and nonmeasurable; those measuring more than 20 mm on conventional imaging techniques or more than 10 mm on helical computed tomography (CT) were considered measurable. The measurable lesions were categorized as target and nontarget lesions on the basis of the size and reproducibility of measurements. Only target lesions were used for response categorization. The RECIST guidelines recommended that up to 10 target lesions, in up to five organs, may be used in response assessment. The nontarget lesions were not measured unless there was an unequivocal progression of these lesions that indicated progressive disease. As in the WHO criteria, the tumor responses were complete response, indicating the disappearance of all target lesions; partial response, indicating a decrease of more than 30% in the sum of the greatest dimension of target lesions; progressive disease, indicating an increase of more than 20% in the sum of the greatest dimension of target lesions or the appearance of new lesions or unequivocal progression of nontarget lesions; and stable disease as tumors not classified in the other three classes. Major differences between the WHO and RECIST criteria are highlighted in [Table 127-1](#).

Despite the several improvements over WHO guidelines, RECIST 1.0 guidelines did not address many relevant issues, including the measurement of lymph nodes, the utility of newer functional imaging techniques such as positron emission tomography with ¹⁸F-fluorodeoxyglucose (¹⁸F-FDG PET) and perfusion magnetic resonance imaging (MRI), and the assessment in clinical trials using noncytotoxic drugs.^{10,11}

Evolution of RECIST 1.1

In an effort to address these limitations, the RECIST working group made several modifications to the existing criteria after evaluation of prospectively documented data from clinical trials with a total of more than 6500 patients who had more than

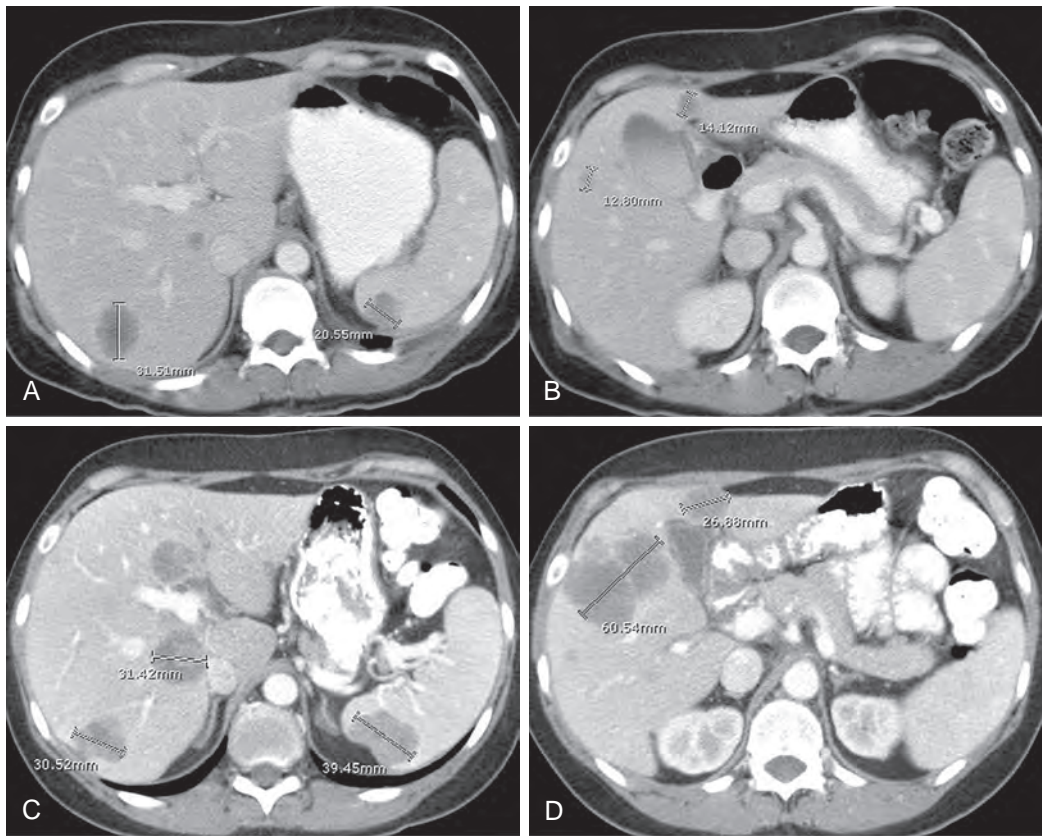


Figure 127-1 RECIST 1.0. A 39-year-old man with hepatic metastases from colon cancer. Sum of longest diameter of target lesions on initial scan was 77 mm (A and B). On follow-up CT (C and D), there was progressive disease per RECIST 1.1, with sum of longest diameter of target lesions of 238 mm.

TABLE 127-1 Comparison Between WHO Criteria and RECIST Guidelines		
	WHO	RECIST 1.0
Imaging modality	No particular mention of imaging modality	CT, MRI, and chest radiography are recommended modalities
Definition of measurable lesions	Should be measurable in two dimensions; no limitation on minimal size of the lesion	Should be accurately measurable in at least one dimension; longest diameter >20 mm for nonspiral CT and >10 mm for spiral CT
Method of measurement	Cross product of longest diameter and greatest perpendicular diameter	Longest diameter in axial plane
Number of lesions to be measured	No particular number of lesions specified	Up to total of 10 target lesions (5 per organ) measured
Response evaluation	Complete response: disappearance of all lesions Partial response: 30% decrease in sum of the longest diameters compared with baseline measurements Stable disease: neither partial response nor progressive disease Progressive disease: 20% increase in sum of longest diameters compared with smallest sum of longest diameters, appearance of new lesions, or unequivocal progression of nontarget lesions	Complete response: disappearance of all lesions Partial response: 50% decrease in target lesions, without 25% increase in any one target lesion Stable disease: neither partial response nor progressive disease Progressive disease: 25% increase in size of measurable lesions, appearance of new lesions, or unequivocal progression of nontarget lesions

18,000 target lesions.⁶ Major differences between RECIST 1.1 and RECIST 1.0 are highlighted in Table 127-2.⁶ Modifications in RECIST 1.1 include the following: reduced number of target lesions from a total of 10 per patient (and five per organ) to five per patient (and two per organ); classifying lymph nodes as target lesions and measuring their short axis (not the long axis; the long axis is used for other types of target

lesions); new definitions of how lesions previously determined to be nonmeasurable (e.g., bone lesions) may now be measured (Fig. 127-2); and modifications of guidelines on imaging modalities to be used.^{12,13} As in RECIST 1.0, the tumor lesions are categorized as measurable and nonmeasurable on the basis of their size. A measurable lesion is a lesion with longest axial diameter of more than

10 mm by CT scan (with slice thickness not more than 5 mm) and 20 mm by chest radiography. Lymph nodes greater than 15 mm in short axes are considered measurable (Fig. 127-3). Lesions smaller than 10 mm in longest diameter and lymph nodes with short-axis diameter between 11 and 15 mm are considered nonmeasurable. RECIST 1.1 designates several other lesions nonmeasurable. These include small tumors (nodules with a short-axis dimension <10 mm), leptomeningeal disease, lymphangitic spread, inflammatory breast disease, pericardial/pleural effusions, palpable abdominal masses/organomegaly not reproducible on imaging studies, lesions surrounded by

postradiation scar tissue, and bone metastases without soft tissue masses measuring more than 10 mm. The presence or absence of nonmeasurable lesions should be noted, as unequivocal progression of these lesions indicates progressive disease. As in RECIST 1.0, it is recommended to have baseline documentation of all target and nontarget lesions.

RECIST 1.1 relies on modalities that are reproducible and accurate. For instance, chest CT is preferred to chest radiography; however, if the lesion is clearly defined on a chest radiograph, it may be considered measurable. Overall, CT is considered the most reliable available method for lesion

TABLE
127-2

Comparison Between RECIST 1.0 and RECIST 1.1

	RECIST 1.0	RECIST 1.1
LESION MEASUREMENT		
Minimum size of measurable lesions	CT: 10 mm, spiral; 20 mm, nonspiral	CT: 10 mm; reference to spiral scan deleted
Lymph nodes	Not mentioned	Target lesions >15 mm; nontarget lesions 10-15 mm; nonpathologic <10 mm (short-axis measurements)
Number of lesions to be measured	10 lesions (5 per organ)	5 lesions (2 per organ)
Special considerations on lesion measurability	Cystic lesions; bone lesions considered nonmeasurable	Notes included on measurement of bone lesions, cystic lesions
RESPONSE CRITERIA		
Target lesions	Complete response: lymph node not mentioned Progressive disease: 20% increase over smallest sum on study or new lesions	Complete response: lymph nodes must be <10 mm in short axis Progressive disease: 20% increase over smallest sum on study (including baseline); at least 5-mm increase or new lesions
Nontarget disease	Unequivocal progression considered progressive disease	More detailed description of unequivocal progression; must be representative of overall disease status change, not a single-lesion increase
Overall response	Table with integrated target and nontarget lesions	Two tables, one integrating target and nontarget and the other of nontarget only
Confirmatory measure	For complete response and partial response: criteria must be met again 4 weeks after initial documentation	Retain this requirement <i>only</i> for nonrandomized trials with primary endpoint of response
Progression-free survival	General comments only	More specific comments on use of progression-free survival (or proportion progression free) as phase II endpoint Greater detail on progression-free survival assessment in phase III trials Divided into phase II and phase III Nine categories reduced to 5 In phase III, guidance given about reporting response
Reporting of response results	Nine categories suggested for reporting of phase II results	This section removed; no need to have different criteria for phase II and phase III
Response in phase III trials	More relaxed guidelines if protocol specified	

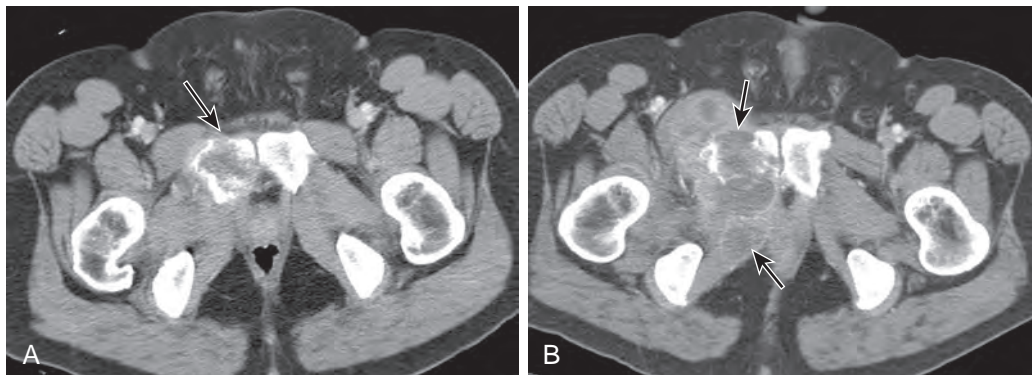


Figure 127-2 Measurement of bone lesions per RECIST 1.1. Initial (A) and follow-up (B) axial contrast-enhanced CT of the pelvis showed a lytic lesion in the right pubic bone (arrows) with significant interval increase in the soft tissue component on follow-up scan (B) consistent with progressive disease. RECIST1.1, unlike RECIST 1.0, has clear-cut guidelines on measurement of soft tissue components of bone metastases.

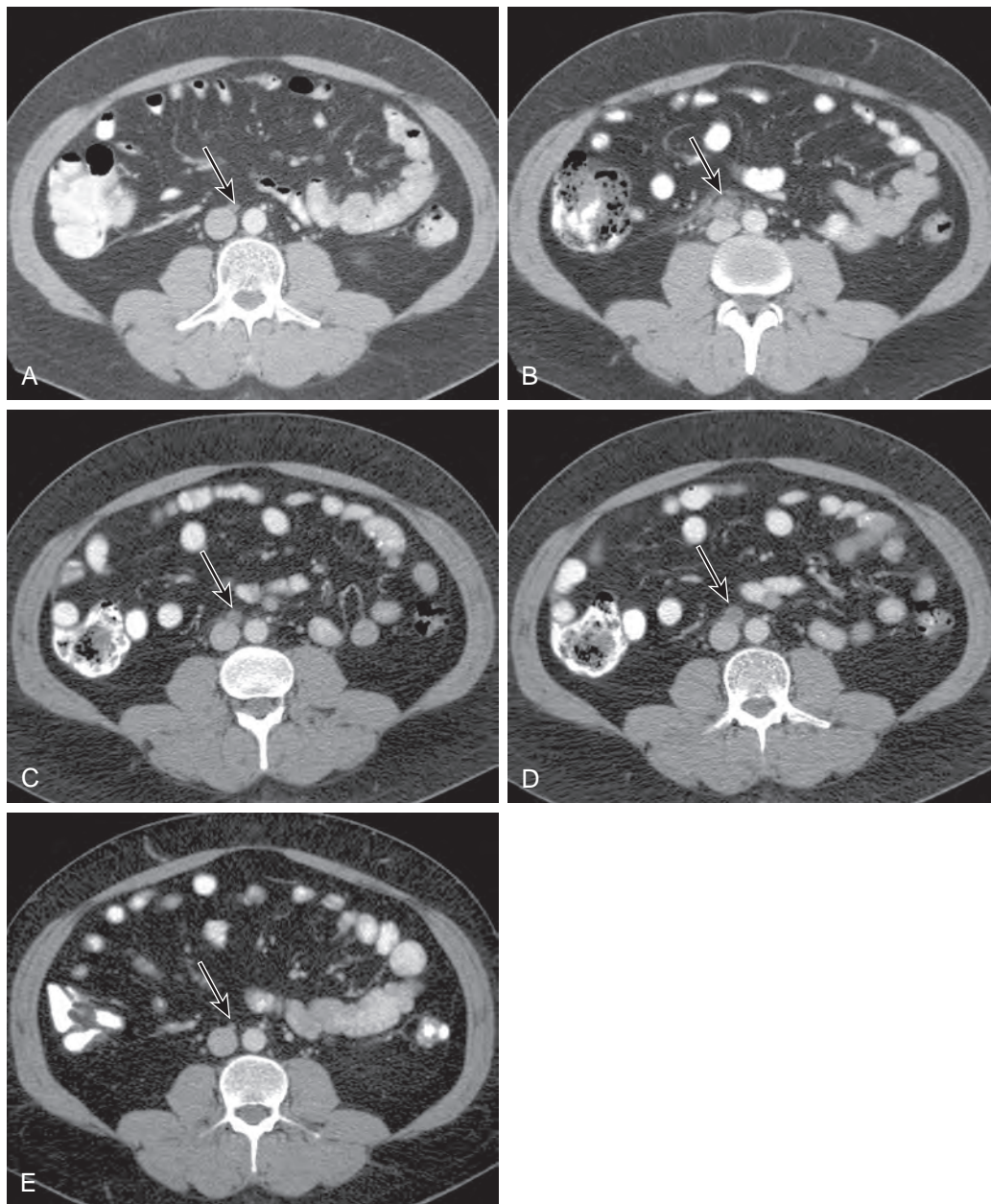


Figure 127-3 Measurement of lymph nodes per RECIST 1.1 (arrows). Short-axis measurements are used for lymph nodes in RECIST 1.1 and incorporated with the sum of the longest diameters of other metastatic lesions, if present. Serial axial contrast-enhanced CT images in a 35-year-old man with testicular cancer demonstrated an interaortocaval lymph node that had increased in size from 5 mm in May 2007 (**A**) to 18 mm in April 2008 (**B**), consistent with progressive disease. After chemotherapy, the node demonstrated interval decrease in size to 11 mm in July 2008 (**C**), which was consistent with partial response. In September 2008 (**D**), the node measured 14 mm. This was more than 20% increase in short-axis size but was not considered progressive disease because there also had to be 5 mm of absolute increase in size to qualify for progressive disease. Hence, this was considered stable disease. In December 2008 (**E**), the node measured 4 mm, which was considered a complete response (i.e., nodal size <10 mm).

measurement. Contrast-enhanced MRI may also be used to assess response. Ultrasound, endoscopy, laparoscopy, and tumor markers are considered to be reliably reproducible and not recommended for lesion measurement. PET scan may be helpful in some instances, such as confirming lack of metabolic activity in a site of radiation scar tissue, indicating complete response. New hypermetabolic sites are considered to indicate progressive disease as long as they are confirmed on subsequent CT.

Whereas RECIST 1.1 maintains the four major response categories as in RECIST 1.0, the definition of progressive

disease is modified. In addition to a 20% increase in the sum of diameters of target lesions, an absolute increase of at least 5 mm is required in small lesions. Appearance of new lesions is also considered progression. Inclusion of lymph nodes in RECIST 1.1 needs additional clarifications to avoid confusion. If all lymph nodes have a short axis of less than 10 mm, the result is categorized as complete response. This eliminates the major drawback with RECIST 1.0, whereby normal-sized lymph nodes could not be categorized as complete response.

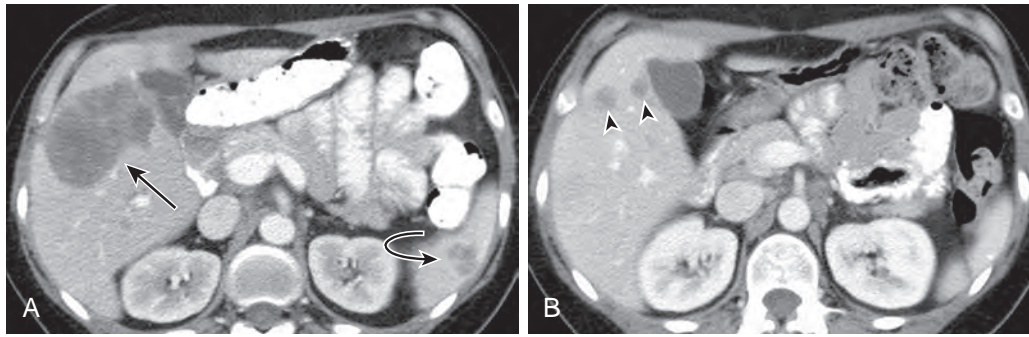


Figure 127-4 Handling of lesion splitting. Hepatic metastases in a 59-year-old woman with breast cancer. **A.** Initial axial contrast-enhanced CT demonstrated a large hepatic segment V lesion (*straight arrow*). Note splenic metastasis (*curved arrow*). **B.** Post-treatment axial contrast-enhanced CT image demonstrated splitting of the lesion into two smaller lesions (*arrowheads*). The sum of the longest diameter of each individual lesion is used on follow-up scan to assess for changes in tumor size.

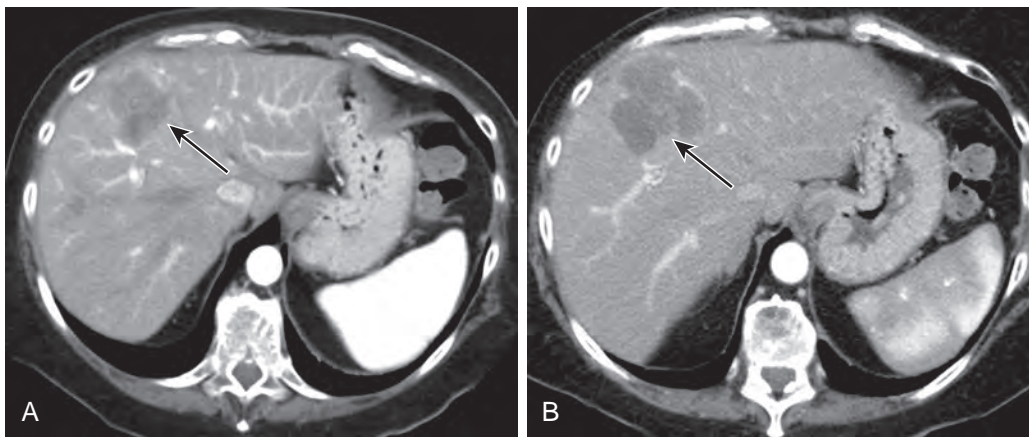


Figure 127-5 Pitfalls of RECIST 1.1. A 46-year-old man with poorly differentiated hepatocellular cancer. Axial contrast-enhanced CT images before (**A**) and 1-month after yttrium 90 (^{90}Y) radioembolization therapy (**B**) demonstrated increase in size of the mass (*arrows*), classified as progressive disease. Follow-up CT scans (not shown) revealed favorable response with decrease in tumor size and enhancement. Tumors treated with targeted therapy, including ablation and embolization, may show initial growth because of hemorrhage and edema.

RECIST 1.0 did not have a consensus on how to measure when a lesion splits or when multiple lesions coalesce. In RECIST 1.1, if the lesion splits, the sum of the longest diameters of individual lesions is used and reported as the target lesion sum (Fig. 127-4). If lesions become coalesced and inseparable from one another, the longest diameter of the coalesced lesion is recorded.

Other Tumor Response Assessment Criteria

RECIST 1.1 has limitations, some of which are specific to the tumor subtypes. The two major limitations of RECIST 1.1 are that it solely depends on the anatomic measurements and does not consider the tumor vascularity or parameters of functional imaging. Traditional cancer chemotherapy with cytotoxic agents often resulted in reduction in tumor size. In the last decade, there has been a paradigm shift in the understanding of cytogenetics and molecular biology of neoplasms, with advent of targeted tumor therapies. Several of these new agents are designed to interfere with or to inhibit one or more of the molecular mechanisms of tumor growth and are primarily

cytostatic rather than cytotoxic (Figs. 127-5 and 127-6). Examples of currently used cytostatic agents include antiangiogenic agents (bevacizumab for metastatic colorectal cancers), mammalian target of rapamycin (mTOR) inhibitors (temsirolimus for renal cell cancer), tyrosine kinase inhibitors (imatinib for gastrointestinal stromal tumors), and estrogen blockers (trastuzumab for breast cancer).¹⁴ Studies of several other cancer types, such as prostate cancer, malignant mesothelioma, soft tissue sarcoma, and neuroendocrine tumors, have also shown that RECIST 1.1 criteria are inaccurate in the assessment of response to therapy.

EASL AND MODIFIED RECIST CRITERIA

Forner and colleagues¹² found that RECIST criteria underestimated the tumor response in patients with hepatocellular carcinoma treated with transarterial chemoembolization or radiofrequency ablation. They recommended the use of European Association for the Study of the Liver (EASL) guidelines, which use tumor density measurements in addition to the tumor size for response assessment. These criteria have been successfully used in clinical trials dealing with assessment response to locoregional therapy for hepatocellular cancer.

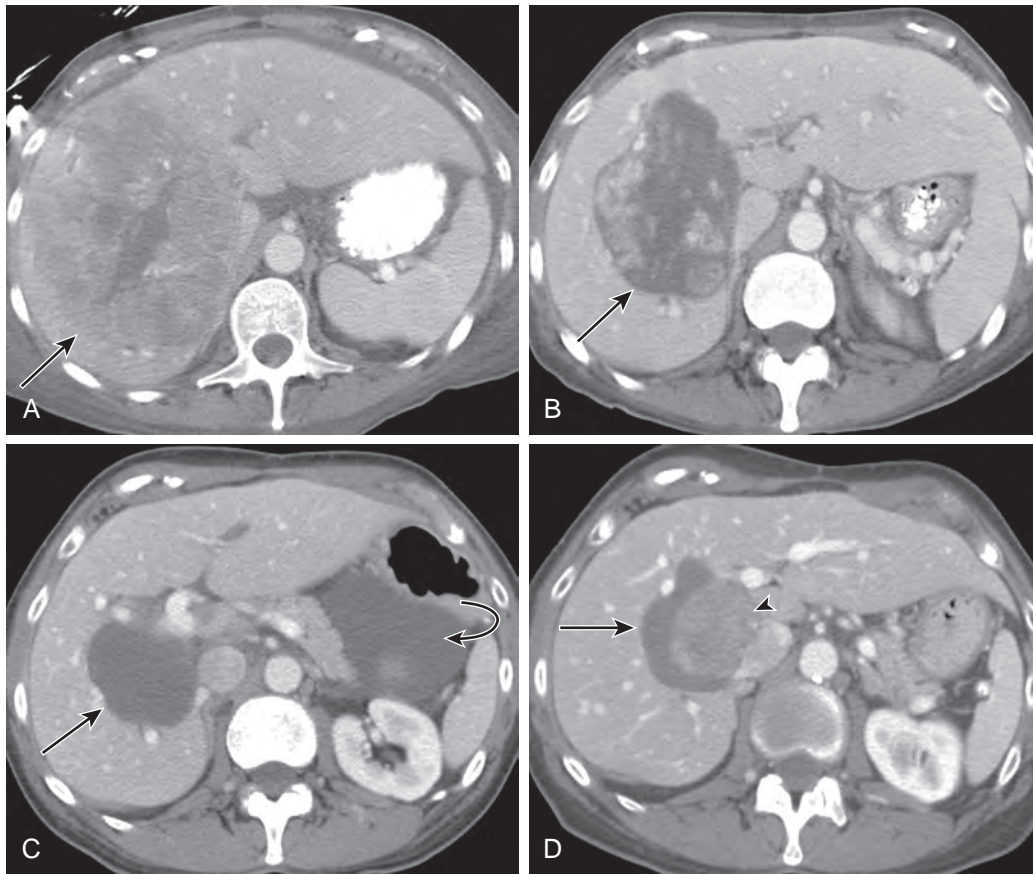


Figure 127-6 Response to biologic therapy. A 60-year-old woman with metastatic gastrointestinal stromal tumor treated by imatinib mesylate (Gleevec). **A.** Pretreatment (June 2006) contrast-enhanced axial CT showed a large lesion in the right lobe (arrow). **B.** Two months after starting of therapy (August 2006), the lesion (arrow) showed reduction in size but also substantial reduction in central density. **C.** In April 2007, the lesion was still present but completely cystic (straight arrow). This was considered partial response by RECIST 1.1 criteria but would have been considered complete response by Choi criteria. There was new-onset ascites (curved arrow), which was erroneously reported as metastatic tumor. Ascites is often seen because of hypoproteinemia induced by imatinib, and in the absence of solid peritoneal nodules, it should not be considered tumor recurrence. Radiologic error was recognized clinically and the dose of imatinib was reduced. **D.** In December 2009, a mural nodule (arrowhead) within the cystic mass (arrow) was seen, indicating tumor progression, even though total lesion size had not increased. New intratumoral nodules are considered progressive disease in the Choi criteria. This case illustrates many concepts. RECIST 1.1 is not satisfactory in assessing tumor response to biologic agents. Completely cystic hepatic or peritoneal masses after imatinib therapy should not be mistaken for benign cysts or nonviable tumors. Breakthrough clonal proliferation of gastrointestinal stromal tumor may occur after several months of good response to imatinib, especially if the dose is reduced. Ascites is not necessarily an indicator of metastatic peritoneal disease and is more likely secondary to drug effect.

Lencioni and Llovet¹³ proposed a set of modified RECIST (mRECIST) criteria for evaluation of response assessment in hepatocellular cancer. The mRECIST criteria are similar to RECIST criteria except that only the long dimension of the arterially enhancing component of the tumor is used (Fig. 127-7).

CHOI CRITERIA

Choi and associates¹⁵ formulated criteria for assessment of tumor response in gastrointestinal stromal tumors treated with imatinib, incorporating changes in tumor density and tumor size (Table 127-3). Imatinib is a tyrosine kinase inhibitor that primarily acts by inducing tumor apoptosis. On the basis of their study of 173 lesions in patients with advanced gastrointestinal stromal tumor, the authors recommended that a 15% reduction in tumor density or 10% reduction in tumor size should indicate a partial response (Fig. 127-8; see also Fig.

127-6). These criteria had a 97% correlation with ¹⁸F-FDG PET in determining good responders.

MASS CRITERIA

In 2010, Smith and colleagues¹⁶ proposed the morphology, attenuation, size, and structure (MASS) criteria for metastatic renal cell cancer (Table 127-4). Three categories of disease response were proposed: favorable response, intermediate response, and unfavorable response. In their study of 84 metastatic renal cell cancer patients treated with sunitinib or sorafenib, Smith and colleagues found that the accuracy for detection of progression-free survival was higher with MASS criteria (89%) compared with the RECIST criteria (36%) (Fig. 127-9). The authors concluded that time to progression and disease-specific survival differed significantly between the three categories of MASS criteria, indicating that these criteria were able to better differentiate aggressive from nonaggressive disease.

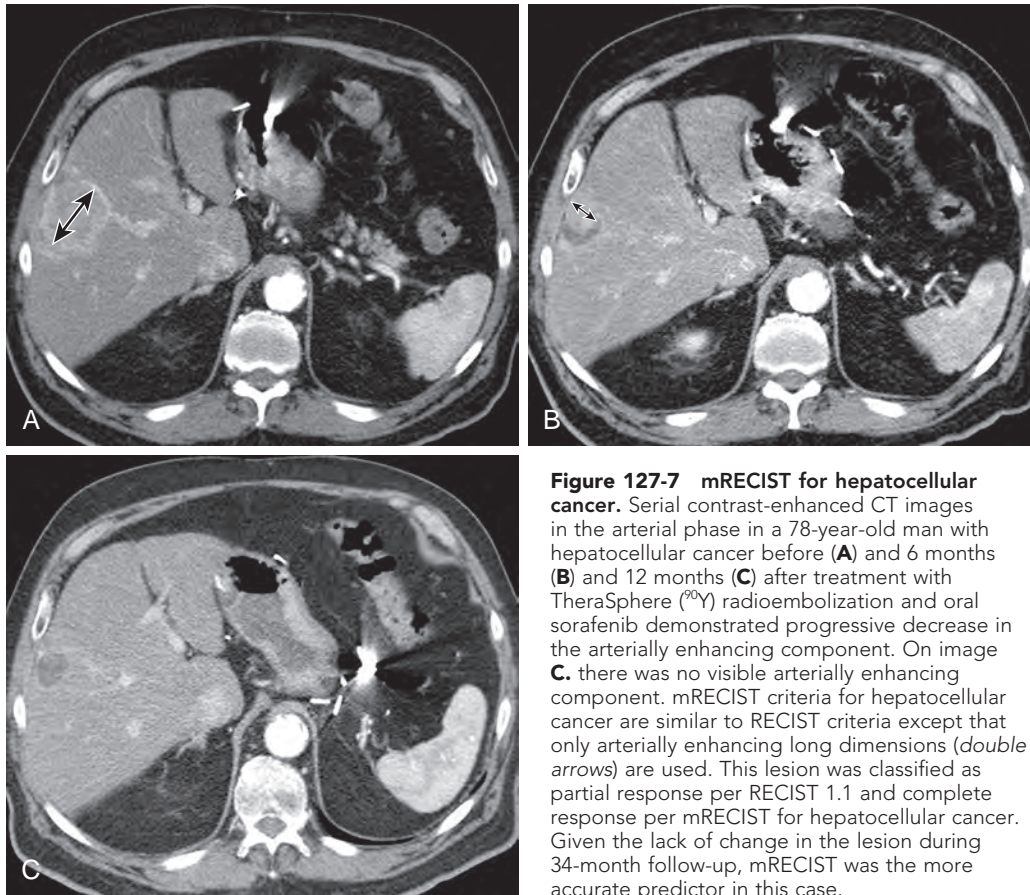


Figure 127-7 mRECIST for hepatocellular cancer. Serial contrast-enhanced CT images in the arterial phase in a 78-year-old man with hepatocellular cancer before (A) and 6 months (B) and 12 months (C) after treatment with TheraSphere (^{90}Y) radioembolization and oral sorafenib demonstrated progressive decrease in the arterially enhancing component. On image C, there was no visible arterially enhancing component. mRECIST criteria for hepatocellular cancer are similar to RECIST criteria except that only arterially enhancing long dimensions (double arrows) are used. This lesion was classified as partial response per RECIST 1.1 and complete response per mRECIST for hepatocellular cancer. Given the lack of change in the lesion during 34-month follow-up, mRECIST was the more accurate predictor in this case.

TABLE 127-3 Choi Response Criteria for Gastrointestinal Stromal Tumors

Complete response	Disappearance of lesions and No new lesions
Partial response	Decrease in size >10% (no new lesions) or Decrease in density >15% (no new lesions)
Progressive disease	New lesions or Increase in size by 10% (but no decrease in density by >15%) or New intratumoral nodules or increase in size of existing intratumoral nodules
Stable disease	None of the above

PERCIST

Two issues to consider in using PET for quantitative tumor assessment are the uniformity of measurement and the reproducibility of results. There have been several previous attempts to standardize PET, including those issued by the European Organization for Research and Treatment of Cancer¹⁷ and the National Cancer Institute.¹⁸ Positron Emission Tomography Response Criteria in Solid Tumors (PERCIST 1.0) represent the most recent effort to create standardized PET criteria.¹⁹ Tumor response is inherently continuous, and discrete categorization, for example, into complete or partial response, may result in the loss of useful data. PERCIST specifies that the percentage of

TABLE 127-4 MASS Criteria for Renal Cell Cancer

Response Type	Definition
Favorable response	No new lesion and any one of the following: Decrease in tumor size >20% One or more predominantly solid enhancing lesions with marked central necrosis or marked decreased attenuation (>40 HU)
Indeterminate response	Does not fit criteria for favorable response or unfavorable response
Unfavorable response	Any of the following: Increase in tumor size of >20% in absence of marked central necrosis or marked decreased attenuation New metastases, marked central fill-in or new enhancement of previously homogeneously hypoattenuating, nonenhancing mass

change in metabolic activity from baseline to post-treatment scans be recorded to provide a continuous plot of tumor activity.

The primary determinant of response with use of PET is the standardized uptake value (SUV), a semiquantitative measure of activity that is most commonly calculated by dividing the measured tumor activity by injected dose/body weight. Among the many variants of SUV, SUV corrected for lean body

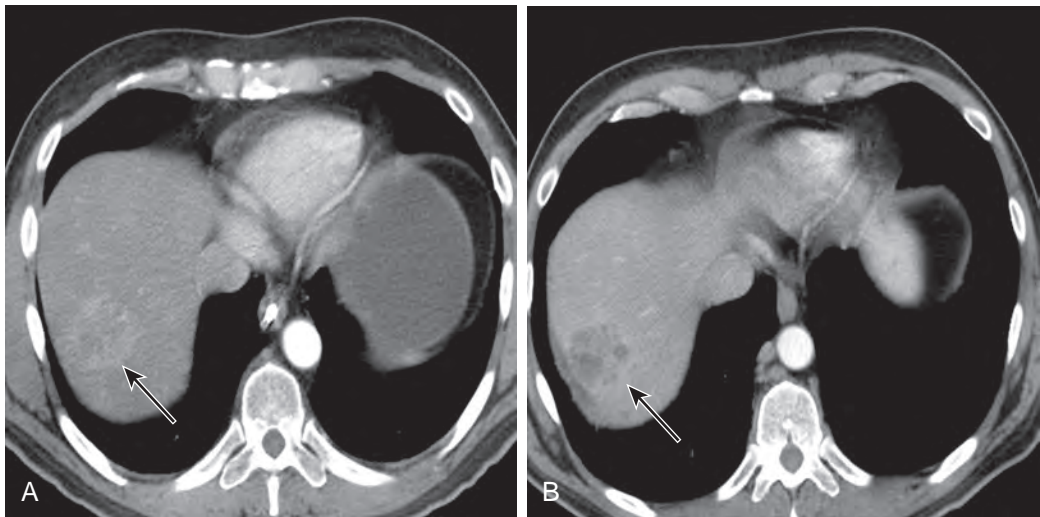


Figure 127-8 Choi criteria in gastrointestinal stromal tumor. Axial contrast-enhanced CT images in a patient with metastatic gastrointestinal stromal tumor before (A) and after (B) treatment with imatinib mesylate. Hepatic metastasis (arrows) measured 3.2 cm with attenuation of 145 HU on initial scan (A) and 3.0 cm with attenuation of 84 HU on follow-up scan (B). These findings were considered stable disease according to RECIST 1.1 and partial response according to Choi criteria.

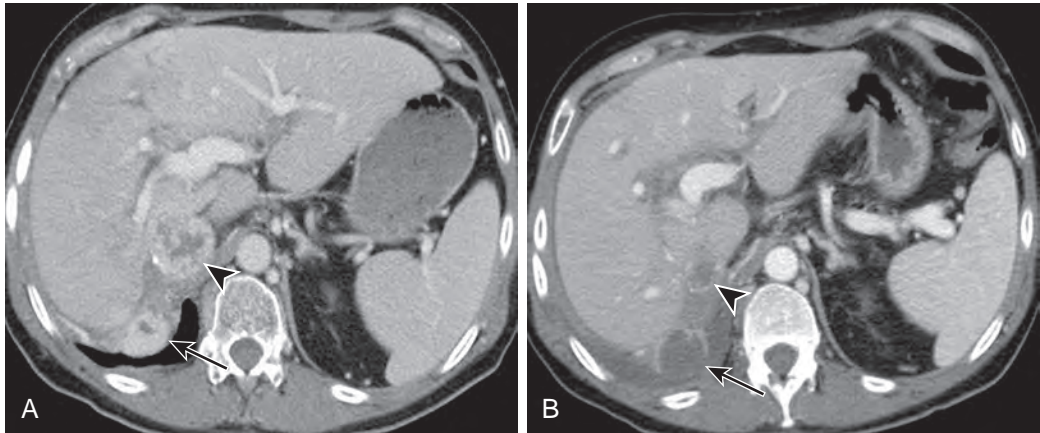


Figure 127-9 MASS criteria. A 52-year-old man with metastatic papillary renal cell cancer treated with sunitinib. Pretreatment (A) and post-treatment (B) images demonstrated mild increase in size of the posterior lesion (arrows) and significant decrease in attenuation/enhancement. Anterior lesion (arrowheads) showed reduction in size and density. This was consistent with favorable response per MASS criteria.

mass (SUL) was selected for use with PERCIST because this parameter has been shown to be less susceptible to variations in the patient’s body weight than the other SUV metrics.^{20,21} The SUL peak is obtained on the single most active lesion on each scan. This peak is defined as the average activity within a spherical region of interest measuring 1.2 cm in diameter (equivalent to a volume of 1 cm³) centered on the most metabolic portion of the tumor. The SUL peak may be located in a different lesion on a follow-up scan. By use of the same concept as RECIST, PERCIST recommends that the sum of the activity of up to five target lesions (up to two per organ) be used as a secondary determinant of response. As an additional metrics to SUL, PERCIST also suggests the measurement of total lesion glycolysis (TLG), so that the value of TLG may be evaluated. TLG is a measure of the FDG uptake of the entire tumor above a preset threshold and is calculated by multiplying the mean SUV by total tumor volume (in milliliters).²² PERCIST provides four response categories as shown in Table 127-5 (Figs. 127-10 and 127-11).

TABLE 127-5 PERCIST 1.0	
Response Type	Definition
Complete response	Disappearance of all FDG-avid lesions
Partial response	>30% reduction and at least 0.8 SUL mean unit reduction in most avid lesion
Progressive disease	>30% increase and at least 0.8 SUL mean unit increase in most avid lesion
Stable disease	New FDG-avid lesion None of the above

PET has also been incorporated in the revised International Working Group criteria for assessing treatment response of lymphoma. These are a complex set of criteria that use CT, PET, and bone marrow biopsy.²³⁻²⁵ Because this classification system does not deal with gastrointestinal cancers, they are not dealt with further in this chapter.

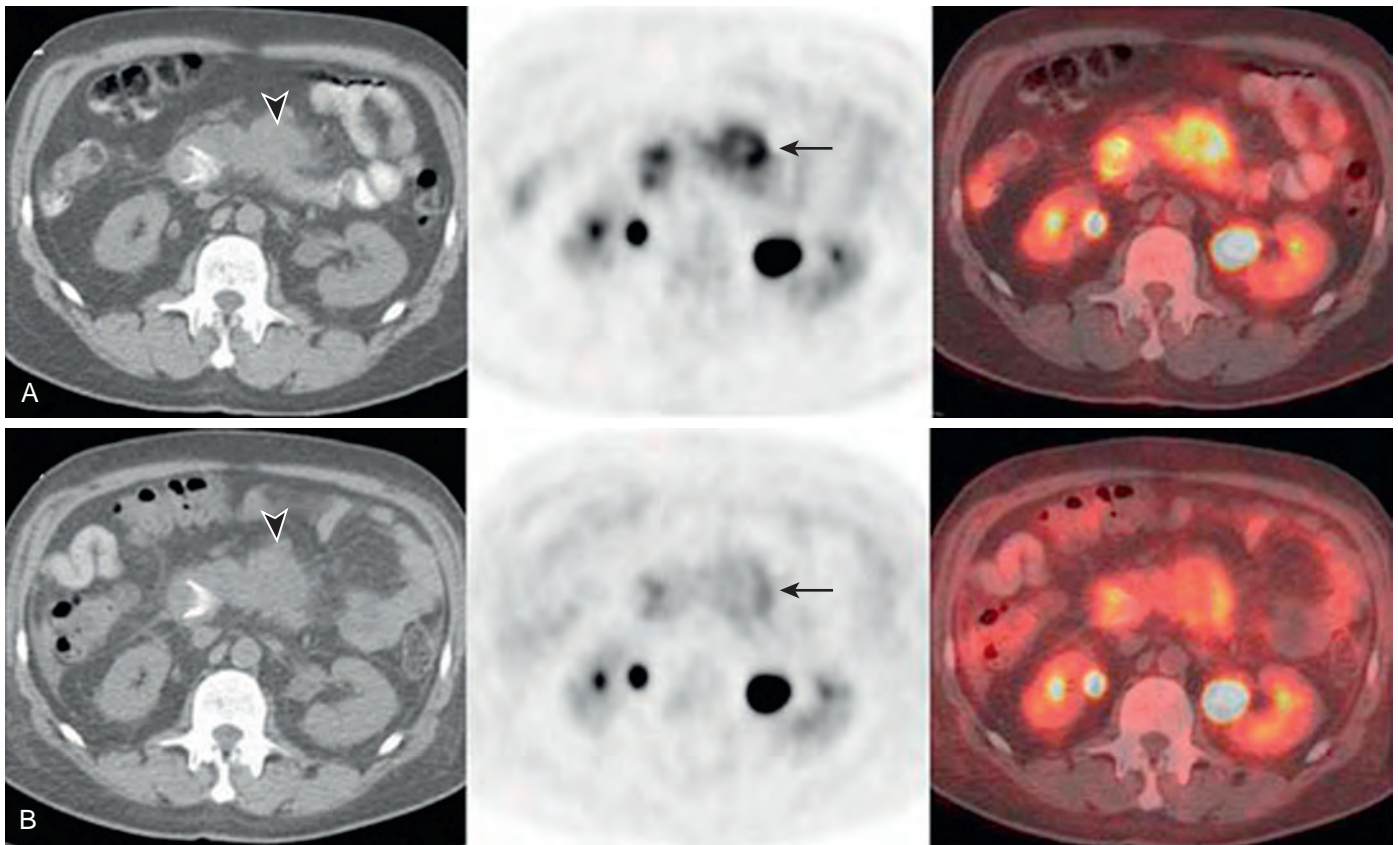


Figure 127-10 PERCIST criteria. Pretreatment (**A**) and post-treatment (**B**) PET/CT image sets in a 59-year-old man with pancreatic cancer demonstrated stable tumor sizes on CT (arrowheads). However, there was 41% decrease in SUL, indicating that tumor (arrows) has responded (partial response). PERCIST compares the metabolically most active lesion as measured with SUL peak.

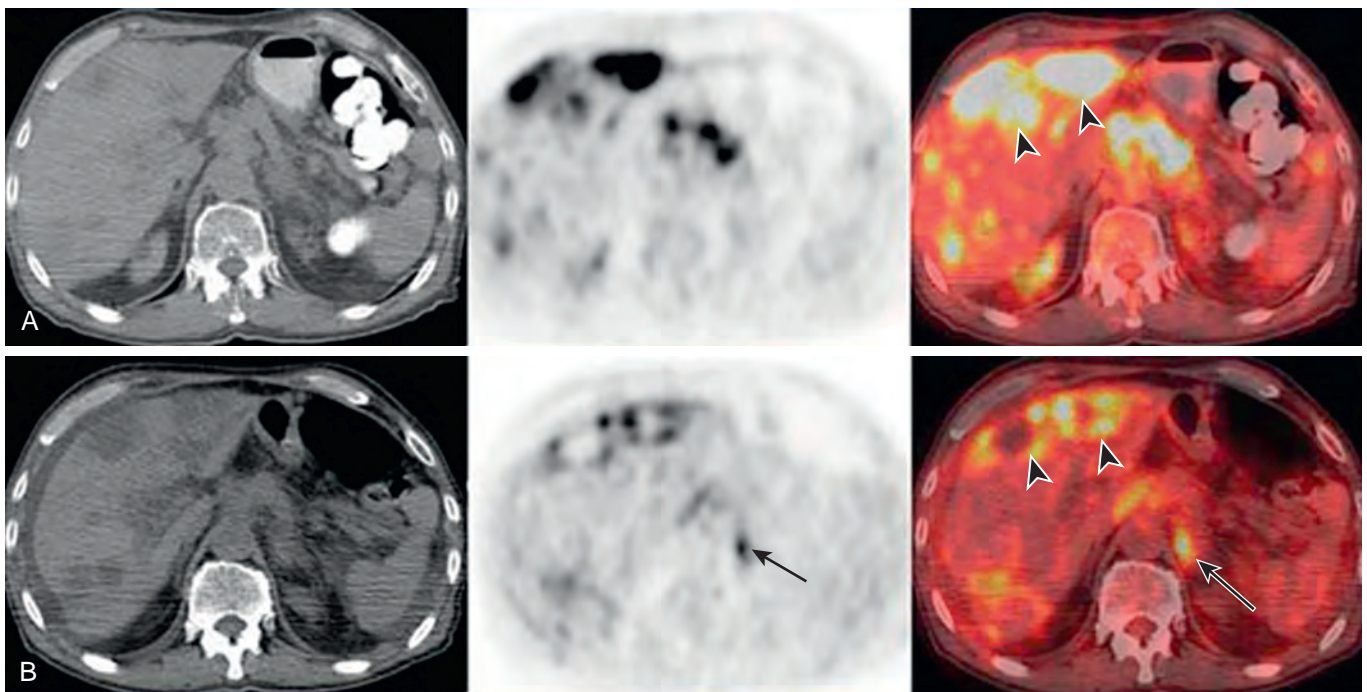


Figure 127-11 PERCIST criteria. A 53-year-old with colorectal cancer metastases undergoing combined chemotherapy with gemcitabine and irinotecan. Pretreatment (**A**) and post-treatment (**B**) PET/CT image sets showed 50% decrease in SUL in previously seen hepatic metastasis (arrowheads). However, a new hypermetabolic retroperitoneal lesion (arrows) was seen on image **B**, indicating progressive disease.

Functional Magnetic Resonance Imaging Techniques

Several MRI techniques, such as dynamic contrast-enhanced MRI (DCE-MRI), diffusion-weighted imaging, and MR spectroscopy, have been evaluated as a marker of tumor response. As of yet, there are no standardized protocols or clearly defined cutoffs for objective assessment of tumor response with these techniques. Most of the data regarding these techniques have come from single-center, predominantly retrospective studies and need to be validated in larger prospective randomized studies.

DCE-MRI involves acquisition of serial images before, during, and after intravenous administration of low-molecular weight gadolinium chelate. Typically, each image set is obtained with a temporal resolution of only a few seconds. DCE-MRI measures tissue vascularity when it is performed with T1-weighted contrast-enhanced techniques.²⁶ Other less widely used techniques of MR perfusion include dynamic susceptibility contrast-enhanced MRI, which assesses changes in T2* during the first-pass of gadolinium, and noncontrast arterial spin labeling. T1-weighted DCE-MRI may be performed semi-quantitatively, yielding parameters that may be obtained directly from the signal intensity–time plot, such as time to peak concentration and slope of enhancement curve. Such parameters are highly dependent on type of scanner and scan protocol used. In addition, the signal intensity is not proportional to the gadolinium concentration in tissue. In an effort to offer a greater degree of uniformity between different studies, quantitative techniques were developed. The details of the quantitative techniques, including the measurement of arterial input function and types of models used, are beyond the scope of this text and discussed elsewhere.^{26–30} A frequently used model (Toft's model) assumes that gadolinium infuses freely between the plasma and extravascular extracellular space and yields parameters such as the wash-in rate (K^{trans}), washout rate (K_{ep}), and fractional extracellular space volume (v_e).³⁰

Most studies on DCE-MRI have been performed in the pelvis (female gynecologic cancers, rectal or prostate cancers). Respiratory motion in the upper abdomen makes high temporal resolution DCE-MRI technically challenging. A few studies

have shown that high pretreatment K^{trans} indicates a better response of abdominal tumors to chemotherapy or antiangiogenic therapy.³¹ These results are concordant with studies on head and neck, brain, and breast cancers.^{26–28,32,33} A dramatic drop in K^{trans} after therapy is also suggestive of good response. Nevertheless, standardization of methodology and more widespread verification of results are required before DCE-MRI may be used clinically for tumor response assessment.

Diffusion-weighted MRI has been explored as a potential tool for response assessment in primary and metastatic liver disease, pancreas cancer, and rectal cancer.^{34,35} The results of these studies are somewhat discordant. Low pretreatment apparent diffusion coefficient (ADC) was shown to be a predictor of poor response in pancreas cancer, whereas high pretreatment ADC was shown to indicate therapy failure in liver metastasis and primary rectal cancer.^{36–38} An increase in ADC has been shown to correlate with good response in hepatocellular cancer treated with targeted therapy and in colorectal liver metastases treated with chemotherapy.^{39,40} However, the optimal timing of scans is unknown. ADC changes may reflect pathologic changes to the tumor tissue after treatment. A decrease of ADC value may be observed in the first 24 to 48 hours after treatment, probably because of cytotoxic edema and reduced extracellular space. In the first 2 weeks, tumor necrosis results in an increase of ADC values, which is often seen before tumor size change is measurable. A subsequent reduction in ADC values may be related to a cellular inflammatory exudate, tumor repopulation, fibrosis, or decreased perfusion.⁴¹ Further research is required before diffusion-weighted imaging is clinically used for assessment of tumor response.

Conclusion

Imaging plays a crucial role in the assessment of tumor response to various therapies. The advent of molecular targeted therapy has increased the need to determine tumor biology, which may not correlate with changes in tumor size. At present, RECIST 1.1 is the predominant method of formally assessing tumor response. In the future, techniques that involve PET or functional MRI may be used to overcome the limitations of anatomic measurements.

REFERENCES

- Hopper KD, Singapuri K, Finkel A: Body CT and oncologic imaging. *Radiology* 215:27–40, 2000.
- Saini S: Radiologic measurement of tumor size in clinical trials: Past, present, and future. *AJR Am J Roentgenol* 176:333–334, 2001.
- Millar AW, Lynch KP: Rethinking clinical trials for cytostatic drugs. *Nature Rev Cancer* 3:540–545, 2003.
- Miller AB, Hoogstraten B, Staquet M, et al: Reporting results of cancer treatment. *Cancer* 47:207–214, 1981.
- Padhani AR, Ollivier L: The RECIST (Response Evaluation Criteria in Solid Tumors) criteria: Implications for diagnostic radiologists. *Br J Radiol* 74:983–986, 2001.
- Schwartz LH, Bogaerts J, Ford R, et al: Evaluation of lymph nodes with RECIST 1.1. *Eur J Cancer* 45:261–267, 2009.
- Warr D, McKinney S, Tannock I: Influence of measurement error on assessment of response to anticancer chemotherapy: Proposal for new criteria of tumor response. *J Clin Oncol* 2:1040–1046, 1984.
- Green S, Weiss GR: Southwest Oncology Group standard response criteria, endpoint definitions and toxicity criteria. *Invest New Drugs* 10:239–253, 1992.
- Therasse P, Arbuck SG, Eisenhauer EA, et al: New guidelines to evaluate the response to treatment in solid tumors. European Organization for Research and Treatment of Cancer, National Cancer Institute of the United States, National Cancer Institute of Canada. *J Natl Cancer Inst* 92:205–216, 2000.
- Suzuki C, Jacobsson H, Hatschek T, et al: Radiologic measurements of tumor response to treatment: Practical approaches and limitations. *Radiographics* 28:329–344, 2008.
- Therasse P, Eisenhauer EA, Verweij J: RECIST revisited: A review of validation studies on tumour assessment. *Eur J Cancer* 42:1031–1039, 2006.
- Forner A, Ayuso C, Varela M, et al: Evaluation of tumor response after locoregional therapies in hepatocellular carcinoma: Are response evaluation criteria in solid tumors reliable? *Cancer* 115:616–623, 2009.
- Lencioni R, Llovet JM: Modified RECIST (mRECIST) assessment for hepatocellular carcinoma. *Semin Liver Disease* 30:52–60, 2010.
- Contractor KB, Aboagye EO: Monitoring predominantly cytostatic treatment response with ¹⁸F-FDG PET. *J Nucl Med* 50(Suppl 1):97S–105S, 2009.
- Choi H, Charnsangavej C, Faria SC, et al: Correlation of computed tomography and positron emission tomography in patients with metastatic gastrointestinal stromal tumor treated at

- a single institution with imatinib mesylate: Proposal of new computed tomography response criteria. *J Clin Oncol* 25:1753–1759, 2007.
16. Smith AD, Shah SN, Rini BI, et al: Morphology, attenuation, size, and structure (MASS) criteria: Assessing response and predicting clinical outcome in metastatic renal cell carcinoma on antiangiogenic targeted therapy. *AJR Am J Roentgenol* 194:1470–1478, 2010.
 17. Young H, Baum R, Cremerius U, et al: Measurement of clinical and subclinical tumour response using [^{18}F]-fluorodeoxyglucose and positron emission tomography: Review and 1999 EORTC recommendations. European Organization for Research and Treatment of Cancer (EORTC) PET Study Group. *Eur J Cancer* 35:1773–1782, 1999.
 18. Shankar LK, Hoffman JM, Bacharach S, et al: Consensus recommendations for the use of [^{18}F]-FDG PET as an indicator of therapeutic response in patients in National Cancer Institute Trials. *J Nucl Med* 47:1059–1066, 2006.
 19. Wahl RL, Jacene H, Kasamon Y, et al: From RECIST to PERCIST: Evolving considerations for PET response criteria in solid tumors. *J Nucl Med* 50(Suppl 1):122S–150S, 2009.
 20. Sugawara Y, Zasadny KR, Neuhoff AW, et al: Reevaluation of the standardized uptake value for FDG: Variations with body weight and methods for correction. *Radiology* 213:521–525, 1999.
 21. Zasadny KR, Wahl RL: Standardized uptake values of normal tissues at PET with 2-[fluorine- 18]-fluoro-2-deoxy-D-glucose: Variations with body weight and a method for correction. *Radiology* 189:847–850, 1993.
 22. Costelloe CM, Chuang HH, Madewell JE, et al: Cancer response criteria and bone metastases: RECIST 1.1, MDA and PERCIST. *J Cancer* 1:80–92, 2010.
 23. Cheson BD, Horning SJ, Coiffier B, et al: Report of an international workshop to standardize response criteria for non-Hodgkin's lymphomas. NCI Sponsored International Working Group. *J Clin Oncol* 17:1244, 1999.
 24. Cheson BD, Pfistner B, Juweid ME, et al: Revised response criteria for malignant lymphoma. *J Clin Oncol* 25:579–586, 2007.
 25. Tirkes T, Hollar MA, Tann M, et al: Response criteria in oncologic imaging: Review of traditional and new criteria. *Radiographics* 33:1323–1341, 2013.
 26. Li SP, Padhani AR: Tumor response assessments with diffusion and perfusion MRI. *J Magn Reson Imaging* 35:745–763, 2012.
 27. Zahra MA, Hollingsworth KG, Sala E, et al: Dynamic contrast-enhanced MRI as a predictor of tumour response to radiotherapy. *Lancet Oncol* 8:63–74, 2007.
 28. Hylton N: Dynamic contrast-enhanced magnetic resonance imaging as an imaging biomarker. *J Clin Oncol* 24:3293–3298, 2006.
 29. Barrett T, Brechbiel M, Bernardo M, et al: MRI of tumor angiogenesis. *J Magn Reson Imaging* 26:235–249, 2007.
 30. Tofts PS, Brix G, Buckley DL, et al: Estimating kinetic parameters from dynamic contrast-enhanced T1-weighted MRI of a diffusible tracer: Standardized quantities and symbols. *J Magn Reson Imaging* 10:223–232, 1999.
 31. Akisik MF, Sandrasegaran K, Bu G, et al: Pancreatic cancer: Utility of dynamic contrast-enhanced MR imaging in assessment of antiangiogenic therapy. *Radiology* 256:441–449, 2010.
 32. Provenzale JM, Mukundan S, Barboriak DP: Diffusion-weighted and perfusion MR imaging for brain tumor characterization and assessment of treatment response. *Radiology* 239:632–649, 2006.
 33. Punwani S: Contrast enhanced MR imaging of female pelvic cancers: Established methods and emerging applications. *Eur J Radiol* 78:2–11, 2011.
 34. Schmid-Tannwald C, Oto A, Reiser MF, et al: Diffusion-weighted MRI of the abdomen: Current value in clinical routine. *J Magn Reson Imaging* 37:35–47, 2013.
 35. Thoeny HC, Ross BD: Predicting and monitoring cancer treatment response with diffusion-weighted MRI. *J Magn Reson Imaging* 32:2–16, 2010.
 36. Koh DM, Scurr E, Collins D, et al: Predicting response of colorectal hepatic metastasis: Value of pretreatment apparent diffusion coefficients. *AJR Am J Roentgenol* 188:1001–1008, 2007.
 37. Dzik-Jurasz A, Domenig C, George M, et al: Diffusion MRI for prediction of response of rectal cancer to chemoradiation. *Lancet* 360:307–308, 2002.
 38. Niwa T, Ueno M, Ohkawa S, et al: Advanced pancreatic cancer: The use of the apparent diffusion coefficient to predict response to chemotherapy. *Br J Radiol* 82:28–34, 2009.
 39. Cui Y, Zhang XP, Sun YS, et al: Apparent diffusion coefficient: Potential imaging biomarker for prediction and early detection of response to chemotherapy in hepatic metastases. *Radiology* 248:894–900, 2008.
 40. Kamel IR, Liapi E, Reyes DK, et al: Unresectable hepatocellular carcinoma: Serial early vascular and cellular changes after transarterial chemoembolization as detected with MR imaging. *Radiology* 250:466–473, 2009.
 41. Lewis S, Dyvorne H, Cui Y, et al: Diffusion-weighted imaging of the liver: Techniques and applications. *Magn Reson Imaging Clin N Am* 22:373–395, 2014.

- A**
- Abdomen**
- acute, 2255-2270, 2256f
 - from abdominal aortic disease, 2263f, 2266f
 - from appendicitis, 2257-2258, 2257f-2258f
 - from bowel obstruction, 2259-2260, 2259f-2260f
 - causes of, by quadrant, 2256f
 - from cholecystitis, 2260-2261, 2260f-2261f
 - from choledocholithiasis, 2261
 - from diverticulitis, 2258-2259, 2258f-2259f
 - from epiploic appendagitis, 2263, 2263f
 - from hemorrhage, 2266
 - from hepatosplenic vascular disease, 2266-2268
 - from infectious enterocolitides, 2265, 2265f
 - from inflammatory bowel disease, 2265-2266
 - from intestinal ischemia, 2262-2263, 2263f
 - from mesenteric adenitis, 2264, 2264f
 - from omental torsion-infarction, 2263-2264, 2264f
 - from pancreatitis, 2261-2262, 2262f
 - from peptic ulcer disease, 2261, 2261f
 - from perforation, 2262, 2262f
 - from renal colic, 2268
 - from sepsis, 2263
 - from small bowel diverticulitis, 2266, 2266f
 - technical considerations on, 2255-2257
 - trauma to, 2282-2294
 - computed tomography on, 2283
 - bowel, 2287-2292
 - image interpretation in, 2284
 - imaging techniques and interpretation with, 2283-2284
 - kidneys, 2285-2287, 2287f, 2288f
 - liver and spleen, 2284-2285, 2285f, 2286f, 2287f
 - mesentery, 2290, 2291f-2292f
 - pancreas, 2283, 2286f, 2287f
- Abdominal heterotaxy, 1151f**
- Abdominal radiographs, 165-177**
- abnormal bowel gas patterns in, 179-184
 - abnormal soft tissue structures on, 192-194
 - of abscesses, 191, 191f
 - of the adrenal glands, 172, 172f-173f
 - of the anterior pararenal space, 173, 173f
 - of appendicitis, 184-185, 185f
 - of caustic esophagitis, 332, 332f
 - of the coccygeus muscle, 175
 - of the colon, 171
 - of colonic ischemia, 1114-1116, 1115f
 - of colonic obstruction, 169f
 - in colorectal transit studies, 1122, 1123f
 - of the diaphragmatic crura, 174
 - of the gallbladder, 169, 170f
 - of gastric carcinoma, 550, 550f
 - of gastric outlet obstruction, 179
 - on gastric varices, 604
 - of intestinal perforations, 167f
 - of the ischioanal fossa, 175, 175f
 - of the kidneys, 172, 173f
 - on large bowel obstruction, 1103, 1103f
 - left lateral decubitus, 166, 168f
- Abdominal radiographs (Continued)**
- of the liver, 168, 170f, 1529
 - major signs of free air on, 187
 - normal anatomy on, 168-176
 - normal bowel gas patterns in, 178, 179f
 - normal soft tissue structures on, 191, 192f
 - normal supine and upright, 166f
 - of the obturator internus muscle, 174-175
 - on pancreatitis, 1811-1812, 1812f
 - of the pelvic viscera, 175-176
 - of the pelvis, 174-176
 - peritoneal cavity, 168-172
 - of the piriformis muscle, 174, 175f
 - of pneumobilia, 188-189
 - of pneumoperitoneum, 166, 167f, 186-187
 - of pneumoretroperitoneum, 187-188
 - of the posterior pararenal space, 173, 173f
 - of potential intraperitoneal spaces, 171-172, 172f
 - of the psoas muscle, 173-174, 174f
 - of the quadratus lumborum muscle, 174
 - of the retroperitoneum and abdominal wall, 172-174, 173f
 - of the sacrospinous ligament, 175
 - of small bowel obstructions, 167f, 808, 808f-809f
 - of the small intestine, 171
 - of the spleen, 169, 170f
 - standard projections, 165, 166f
 - of the stomach, 170, 170f
 - supplemental projections, 165-168
 - techniques, 165-168
 - of toxic megacolon, 185-186, 186f
- Abdominal wall**
- anterior
 - anatomy of, 2070f
 - bladder exstrophy, 2245
 - calcifications, 2074
 - congenital lesions of, 2070-2071
 - prune-belly syndrome, 187
 - urachal abnormalities, 2070-2071
 - fluid collections in, 2071-2072
 - abscesses and cellulitis, 2072, 2072f
 - hematomas, 2071, 2071f
 - urinomas, 2071-2072
 - gastroschisis of, 2097-2098, 2242-2245, 2243f-2244f
 - implanted devices in, 2073-2074, 2074f
 - laparoscopic injuries to, 2074, 2074f
 - neoplasms of, 2072-2073
 - benign, 2073
 - metastatic, 2073, 2073f
 - primary malignant, 2072-2073
 - pediatric disorders of, 2241-2245
 - pentology of Cantrell, 2241
 - prune-belly syndrome, 1151f, 1912, 2071, 2245-2246, 2245f-2246f
 - subcutaneous gas in, 2074
 - vascular grafts of, 2073
 - vascular lesions of, 2073
 - embryology of, 2241
- Abdominopelvic survey examinations, 1162, 1162f**
- Abdominoperineal resection, 1138**
- Abetalipoproteinemia, 784, 784f, 786, 871f**
- Ablation techniques**
- chemical, 1506
 - combined with TACE, 1515
 - liver, 1506-1510
- Ablation techniques (Continued)**
- complications with, 1509-1510
 - contraindications to, 1508
 - follow-up after, 1510
 - of hepatocellular carcinomas before liver transplantation, 1740
 - indications for, 1508
 - technique for, 1508-1509
 - with metastatic disease, 1508-1509
 - radiofrequency, 1507-1508
 - with chemoembolization, 1726
 - for liver tumors, 1724, 1724f-1725f
 - spleen, 1908
 - alcohol, 1908, 1908f
 - radiofrequency, 1908
 - thermal, 1506-1508, 1509f, 1511f
- Abscesses. See also Percutaneous catheter drainage of abdominal abscesses**
- abdominal, 1254-1278
 - catheter management after drainage of, 1266-1272, 1270f
 - enteric, 1274-1275
 - with fistulous communication, 1272
 - fungal, 1271-1272
 - image-guided intervention with, 1258-1276
 - catheter fixation, 1263
 - combined modality approach in, 1264-1266, 1267f
 - diagnostic aspiration, 1259, 1259f
 - gantry angulation, 1264, 1265f
 - hydrodissection, 1266, 1268f
 - organ traversal, 1263-1264, 1265f
 - percutaneous drainage, advantages and disadvantages of, 1261
 - percutaneous drainage, clinical considerations in, 1259-1261
 - percutaneous drainage, technique in, 1261-1263, 1261f-1262f
 - Seldinger technique, 1263, 1263f
 - surgical drains and, 1264, 1266f
 - imaging techniques for, 1254-1258
 - advantages and disadvantages of, 1255
 - computed tomography, 1255-1257, 1257f-1258f
 - magnetic resonance imaging, 1257-1258, 1258f
 - plain radiography or fluoroscopy, 1254-1255
 - scintigraphy, 1258
 - ultrasound, 1255, 1256f
 - outcome after drainage of, 1269-1272, 1269f, 1269t
 - pathogenesis of, 1254
 - thrombolytic agents for drainage of, 1271, 1271f
 - abdominal radiographs of, 191, 191f
 - abdominal wall, 2072, 2072f
 - appendiceal, 960, 961f-962f, 1275
 - pediatric, 2169, 2169f, 2171f
 - biliary tract, after laparoscopic cholecystectomy, 1443-1447, 1449f, 1454f
 - bowel, after guided biopsy, 1251
 - colon
 - with anastomoses, 1138, 1138f
 - in cecal diverticulitis, 946, 947f
 - from colorectal cancer, 1036-1039
 - in diverticulitis, 941, 942f

Abscesses (Continued)

- in Crohn's disease, 63, 1004
- crypt, in ulcerative colitis, 988, 989f
- diverticular, 1274-1275, 1275f
- drainage of gastric, 128f, 129f
- gallbladder, 1336, 1337f
- intraabdominal, 1275-1276, 2009f
- liver, 1272-1273, 1273f
 - after trauma, 1716
 - amebic, 1611-1614
 - clinical findings on, 1612
 - complications with, 1612-1614
 - incidence of, 1611
 - pathogenesis of, 1612, 1613f
 - pathology of, 1612
 - radiologic findings on, 1612
 - treatment of, 1614
 - aspiration and drainage of, 1501-1502, 1502f
 - bacterial (pyogenic) abscesses, 1608-1611
 - clinical findings in, 1609
 - incidence of, 1608
 - pathogenesis of, 1608-1609, 1609f
 - pathology of, 1609, 1609f
 - radiologic findings on, 1609-1610, 1609f-1611f
 - treatment of, 1610-1611
 - on diffusion-weighted MRI, 1223
 - from diverticulitis, 939f, 949
 - epidemiology and symptoms of, 1501
 - hepatic resection for, 1720
 - with inflammatory bowel disease, 1010
 - pediatric, 2211
 - THADs and THIDs from, 1679f
- pancreatic
 - interventional radiologic management of, 1793-1794, 1794f
 - with pancreatitis, 1811
 - from trauma, 1860
- pelvic, 1274
- peripancreatic, 1273-1274, 1274f
- peritoneal spread of, 2009
- psaos, with inflammatory bowel disease, 1012
- pyogenic
 - hematogenous spread of, 2007
 - pediatric liver, 2211
 - spleen, 1939-1941, 1940f
- retroperitoneal, 1274
- small bowel
 - on computed tomography enterography, 688
 - peripouch, 858, 858f
- small bowel transplantation for, 858
- spleen
 - after splenectomy, 1973, 1973f
 - micro, 1936-1937
 - percutaneous catheter drainage of, 1907-1908, 1907f
 - pyogenic, 1939-1941, 1940f
 - with trauma, 1972
- splenic, 1273
- tubo-ovarian
 - colonic involvement of, 1113
- tumor, 1276

Absorbed dose, 1158

Acalculous cholecystitis, 1394

- acute, 1360-1362, 1361f-1362f
 - computed tomography, 1361f, 1362
 - ultrasound of, 1361-1362, 1361f-1362f
- cholescintigraphy on, 1362
- chronic, 1369
 - cholescintigraphy on, 1369
 - interventional radiology for, 1394
 - magnetic resonance imaging of, 1362, 1362f
 - pediatric, 2193-2194, 2194f

Acanthosis nigricans

- differential diagnosis of, 463t
- mucosal nodularity with, 301

Accessory fissures, liver, 1520, 1521f

Achalasia, 281-284

- advanced, 283f
 - Candida* esophagitis with, 317f
 - cardiomyotomy for, 460, 460f
 - differentiating primary and secondary, 398
 - fluoroscopic assessment of, 282f
 - idiopathic intestinal pseudo-obstruction and, 289
 - pathogenesis of, 397-398
 - pediatric, 2133
 - pneumatic dilation for, 459-460
 - primary, 400f
 - secondary, 284f, 396-399, 400f
 - caused by gastric carcinomas, 556-557, 557f
 - from metastatic disease, 396-399, 399f-401f
 - with sigmoid esophagus, 283f
 - squamous cell carcinoma associated with, 367, 373, 375f
 - surgical treatment of, 459-460
- Acid-base imbalances, chronic gastric dilation
 - caused by, 615, 616f
- Acoustic enhancement, 1173, 1173f
- Acquired retention cysts, 354
- Actinomyces israelii*, 1019
- Actinomycosis, 322, 323f
 - colon, 1019
 - small bowel, 769f
 - gastric, 512
 - pelvic infection with, 688
 - small bowel, 768
- Actinomyces israelii*, 322
- Acute cellular rejection, 1752
- Acute hepatic necrosis, liver transplantation for, 1738
- Acute mesenteric ischemia, 125f
 - arterial occlusive versus venous occlusive, 834-835, 836f
 - bowel dilation with, 833-835
 - bowel wall attenuation and abnormal enhancement in, 834
 - bowel wall thickening in, 833-834, 835f
 - pneumatosis and portomesenteric venous air in, 834
 - stranding and ascites in, 834
- Acute necrotizing collection (ANC), 1195
- Acute pancreatic fluid collection (APFC), 1195
- Adaptive statistical iterative reconstruction (ASIR), 1485
- Adenitis, mesenteric, 3248f, 2249
- acute abdomen from, 2264, 2264f
- Adenocarcinomas
 - cecal, 1050f
 - colon
 - hamartomas with, 1093
 - magnetic resonance imaging of, 1035-1037, 1044f, 1051f
 - perforation of, 1048f
 - of colon
 - computed tomography on, 1043f-1044f
 - colonic
 - magnetic resonance colonography on, 930, 930f
 - Crohn's associated, 752, 798-799
 - esophageal, 374-378
 - advanced, 378-380
 - clinical aspects of, 378
 - differential diagnosis of, 379-380, 463t
 - early, 378-379, 378f-379f
 - epidemiology and pathogenesis of, 374-377
 - pathology of, 377
 - radiographic findings and staging of, 378
 - routes of spread of, 377
 - gastric
 - mucinous, 558, 558f
 - gastroduodenal
 - pediatric, 2150-2151

Adenocarcinomas (Continued)

- gastrointestinal
 - in Peutz-Jeghers syndrome, 1093
 - metastatic, 1589
 - nonmucinous appendiceal, 977, 978f
 - pancreatic
 - cystic, 1849
 - differential diagnosis of, 1893t
 - differentiated from groove pancreatitis, 1830, 1831f
 - diffusion-weighted MRI of, 1223
 - ductal, 1838-1845
 - magnetic resonance imaging of, 1197
 - MRI in detection of, 1781
 - mucinous cystadenocarcinomas, 1846-1847
 - PET/CT of, 1020-1021, 1208-1209
 - ultrasound on, 1161
 - pancreatic ductal, 1793-1794
 - multiple, 1787
 - rectal, 1043f
 - small bowel, 798-799
 - with celiac disease, 763f
 - computed tomography enteroclysis on, 697-699
 - differential diagnosis of, 874f-875t
 - obstruction by, 817-818
 - obstruction from, 819f
 - PET/CT of, 102-103
 - site predilection of, 875t
- Adenoid cystic carcinoma
 - colonic, 1081
 - esophageal, 408
- Adenomas
 - adrenal
 - magnetic resonance imaging of, 1197-1198, 1197f
 - PET/CT of, 1211, 1213f
 - bile duct, 1556
 - biliary tract, 1424, 1424f
 - colon
 - with familial adenomatous polyposis syndrome, 1091
 - villous, 1032-1035, 1033f
 - esophageal
 - benign, 350, 352f
 - differential diagnosis of, 463t
 - gallbladder, 1410, 1411f
 - gastroduodenal
 - polyp progression to, 523, 527f-528f
 - liver
 - with glycogen storage disease, 1644-1645
 - hepatocellular carcinomas differentiated from, 1573
 - magnetic resonance imaging of, 1187-1189, 1189f
 - pediatric, 2210, 2210f
 - malignant, 1093
 - pancreatic
 - magnetic resonance cholangiopancreatography on, 1328
 - mucinous cystadenomas, 1846-1847
 - small bowel
 - benign, 790, 790f
 - thyroid, 1095
 - villous
- Adenomatoid tumors, 2042
- Adenomatosis, 1644
 - diffuse, 2223
- Adenomatous polyposis coli, 1074
- Adenomatous polyps
 - differential diagnosis of, 658t
 - in familial adenomatous polyposis syndrome, 1091
- gastroduodenal, 526-527, 527f

- Adenomyomatosis, 1381-1385, 1381f, 1385f, 1408
magnetic resonance cholangiopancreatography on, 1336, 1337f
pearl necklace sign in, 1337f
- Adenomyosis, 539
gallbladder, 1287
- Adenopathy
in mesenteric lymph nodes, 76-77, 76f
metastatic
duodenal, 575f
- Adenosquamous carcinomas
gastric, 598
- Adenovirus
in graft-versus-host disease, 764
- Adhesions
biliary tract
after laparoscopic cholecystectomy, 1453
colon obstruction from, 1109-1110
computed tomography enteroclysis on, 699, 699f
rectal varices associated with, 1118-1119
small bowel
differential diagnosis of, 875t
small bowel intussusceptions caused by, 822-824, 822f
small bowel obstructions from, 804, 811-812, 812f
- Adipose tissue
in fibrovascular polyps, 359
- Adrenal glands
calcified, 172f
duodenal displacement from, 616
image-guided biopsy of, 1244-1245, 1247, 1247f
incidentalomas, 1210
lymphomas, 1202-1203, 1211f
magnetic resonance imaging of, 1197-1198, 1197f
adrenal adenomas, 1197-1198, 1197f
myelolipomas, 1198
pheochromocytomas, 1198
metastases in
PET/CT on, 1210-1211, 1210f
normal anatomy of, 175f
in perirenal space, 1989
PET/CT of, 1210-1211, 1211f
pheochromocytomas, 1202-1204
- Adrenal rest tumors, 1556
- Adrenocortical carcinomas, 1210-1211
- Adverse reactions
to contrast, 12-13
nephropathy, 6
premedication against, 5
risk factors for, 4
treatment of, 5-6
types of, 4-5
to contrast agents, 4-6
- Adynamic ileus, 179-180
- Afferent loop hernias, 206f
- Afferent loop syndrome, 638
- AIDS (acquired immune deficiency syndrome)
actinomycosis with, 322, 769f
bacterial enteritis in, 721f
biliary spread of infections in, 2008
Candida esophagitis with, 301, 312-313
candidiasis infection with
liver, 1622
cholangiopathy with, 1356
cholangitis, 1436-1437, 1437f
cryptosporidiosis with, 513
cytomegalovirus infections with, 512
colitis from, 1019-1020, 1019f
small bowel, 765-766, 766f
esophageal lymphomas in, 400
gastrointestinal infections in, 765
hematogenous spread of infection in, 2007
- AIDS (acquired immune deficiency syndrome) (Continued)
ileal wall thickening in, 770f
Kaposi's sarcomas in
esophageal, 407
gastroduodenal, 591-593, 595f-596f
leiomyomas with, 1080
liver involvement in, 1651-1654
pathologic findings on, 1653
lymphadenopathy in, 782
lymphomas with, 770f, 1948-1949
small bowel, 801-802
spleen, 1950f
magnetic resonance enterography on, 721, 721f
non-Hodgkin's lymphomas in
esophageal, 403f
peliosis hepatis with, 1690
periportal fluid in, 1638
periportal low density in, 1710
P. jirovecii infection in, 1625, 1938
small bowel
luminal narrowing in, 873t
small bowel fold thickening in, 872t
small bowel intussusceptions in, 823-824
splenic pyogenic abscesses in, 1939
stromal tumors in, 1080
strongyloidiasis with, 513
tuberculosis with
gastroduodenal involvement in, 511
gastrointestinal involvement in, 1018-1019
intestinal, 760
tuberculous esophagitis in, 320, 322, 322f
typhlitis with, 1023, 1023f
- Alagille's syndrome, 2188-2189
- Alcohol ablation sclerotherapy, 1908, 1908f
- Alcoholic liver disease
liver transplantation for, 1757
- Alcoholism
acute alcohol-induced esophagitis in, 341-342, 342f
colorectal cancer and, 1028-1029
esophageal carcinoma and, 366
esophageal motility disorders with, 289
hepatic steatosis in, 1629-1630
hepatitis in, 1638-1639
malabsorption related to, 774
necrotizing fasciitis with, 2072
- Alcohol use
antral gastritis caused by, 499
cirrhosis from, 1190
erosive gastritis caused, 496
ulcers caused by, 468
- Alendronate
drug-induced esophagitis from, 327
- Alagille's syndrome, 1432
- Alkaline reflux esophagitis, 340-341, 341f
differential diagnosis of, 462t, 464t
- Alport's syndrome, 356
- Amebiasis
colonic, 1020
life cycle of, 1613f
liver abscesses in, 1273, 1611-1614
peritoneal, 1614
pleuropulmonary, 1612
toxic megacolon with, 1009
- American Association for the Surgery of Trauma
classifications, 1716, 1857b, 1971t
- Amiodarone toxicity, 1639-1640, 1640f
- Ampulla of Vater, 1773
congenital abnormalities in, 1806
embryology of, 1797
historical perspective on, 1771
liver fluke access through, 1440
neoplasms, 1419-1421, 1422f-1423f
- Ampullary carcinomas, 566, 567f
- Amyloidosis, 627, 627f
colonic involvement in, 1126
differential diagnosis in, 659t
fold enlargement in, 786
gastric narrowing from, 659t
liver involvement in, 1645-1646
malabsorption in, 776, 776b, 783, 783f
mesenteric, 2048
small bowel fold thickening in, 872t
- Anyotrophic lateral sclerosis
dysphagia and, 231
- Anal canal. *See also* Colon
cloacogenic carcinomas in, 1081-1082
hemorrhoids
internal, 1117-1118, 1118f
length of, 895-896
Anal incontinence, 890
- Anal manometry, 902
- Anastomosis
after esophagogastrectomy, 454
biliary-enteric, 1454-1456
background, indications, and technical considerations for, 1454-1455
complications after, 1455-1456
biliary leaks, 1455
strictures, 1455-1456
biliary tract strictures, 1312, 1313f
colocolic, 1133, 1134f
colon
leaks from, 1140, 1140f-1141f
esophageal, postoperative, 449, 450f
ileal-ascending colonic, 1136, 1136f
ileal pouch-anal, 1139-1142, 1139f-1140f, 1142f
ileoanal pouches with, 856-858, 857f, 997, 997f
ileocolic, 1133, 1134f
ileorectal, 997
I-pouch, 1137, 1137f-1138f
pancreas transplantation, leaks after, 154
pancreaticobiliary tract
magnetic resonance
cholangiopancreatography on, 1332-1334, 1333f
side-to-side enterocolic, 1133, 1134f
small bowel, 675-676, 852-855, 853f-854f
blind pouch and loop, 853-855, 854f
differential diagnosis of, 874t
- Anastomotic leaks
after esophagocystostomy, 640, 640f
after gastric resection, 635-636, 635f-636f
- Anabolic steroids
peliosis hepatis associated with, 1690
- Ancylostoma duodenale*, 757
- Ancylostomiasis, 757-758
- Anemia
after gastric and duodenal surgery, 640-641
after gastric resection, 635
in hemolytic uremic syndrome, 2168
pernicious
atrophic gastritis associated with, 504-506
in common variable immunodeficiency, 763
malabsorption related to, 775t
sickle cell (*See* Sickle cell disease)
- Anemia, pernicious
gastric carcinoma linked to, 547
gastric carcinomas and, 547
- Anesthesia
in enteroclysis, 671
- Aneurysmal dilation of bowel, 802, 803f
- Aneurysms
with acute pancreatitis, 1195
aortic, 139-141, 140f
pseudo-, 1710, 1712
after radioembolization, 1711t

- Aneurysms (Continued)**
 small bowel obstruction by, 817
 splanchnic artery, 845, 845f-846f
 embolization of, 1909-1910
 from trauma, 1968
 splanchnic vein, 1701, 1701f
 visceral artery, 159, 1699-1701, 1699f
- Angiodysplasia**
 acute small bowel bleeding in, 841
 colon, 1076-1077
- Angiodysplasia of the colon, 122, 122f**
- Angioectasias**
 GI bleeding from, 688-689
 hemorrhage from, 2277, 2278f, 2279
- Angioedema**
 segmental small bowel mural hyperenhancement in, 686, 687f
- Angioembolization, 1716**
- Angiography. See also Computed tomography**
 angiography (CTA)
 abdominal CT, 135-148
 of acute mesenteric ischemia, 123-126, 124f-125f
 arterial anatomy of gut sections and, 113-120
 in bowel mass biopsy, 127
 catheter
 on acute small bowel bleeding, 841-842
 catheter selection for, 112
 of the colon and rectum, 116-119
 equipment for, 113
 of the esophagus, 113
 on gastric varices, 604-606, 606f
 gastrointestinal catheter and needle placement in, 126-127
 on gastrointestinal hemorrhage, 692
 on hepatopulmonary syndrome, 433
 liver
 on angiosarcomas, 1586
 on Budd-Chiari syndrome, 1686, 1687f
 on cystadenomas and cystadenocarcinomas, 1584
 on fibrolamellar carcinoma, 1575
 on focal nodular hyperplasias, 1539
 on hepatoblastomas, 1579
 of hepatocellular adenomas, 1584
 on hepatocellular carcinomas, 1567
 on infantile hemangioidendothelioma, 1584
 on intrahepatic cholangiocarcinomas, 1580
 on lipomas, 1549-1550
 of mesenchymal hamartomas, 1555
 of metastases, 1599-1600
 of nodular regenerative hyperplasia, 1549
 on schistosomiasis, 1625
 on undifferentiated (embryonal) sarcomas, 1587
 of liver hemangiomas, 1533
 on lower gastrointestinal hemorrhage, 2270
 of major visceral vessels, 113
 pancreas
 on annular pancreas, 1805
 post-transplant, 1874, 1876f
 on pancreatitis, 1812
 patient preparation for, 112
 of primary vascular disease, 120-121
 of the small bowel, 115-116
 spleen, 1923-1924
 anatomy in, 1899-1900
 on angiosarcomas, 1947, 1949f
 on hamartomas, 1928
 on hemangiomas, 1928
 on infarctions, 1943
 on lymphangiomas, 1930
 on pyogenic abscesses, 1940-1941
 wandering, 1914
 of the stomach, 114-115
 vascular access in, 112
 of venous anatomy, 120
- Angiography, CT, 1164**
- Angiomyolipomas, 1198, 1198f**
 liver, 1549-1550, 1550f
- Angiosarcomas, 1584-1586**
 incidence and clinical presentation of, 1584-1585
 pathologic findings on, 1584, 1585f
 radiologic findings on, 1585-1586, 1586f
 spleen, 1947, 1948f
- Angiotensin-converting enzyme (ACE) inhibitors**
 in small bowel angioedema, 845-846
- Angulation, in double-contrast studies, 54f, 55**
- Anisakiasis, 758-759, 2153**
 colonic, 1020
- Anismus, 899-900, 900f**
- Ankylosing spondylitis, 1011**
- Ann Arbor staging system, 581**
- Annular carcinomas**
 gastric outlet obstruction caused by, 612, 612f
- Annular lesions, double-contrast studies of, 47, 49f**
- Annular pancreas, 1803-1805, 1803f-1805f, 2079**
- Anorectal angle, 895, 895f**
 during defecation, 893-895
 normal variations in, 902
 with paradoxical puborectalis contraction, 900
- Anorectal disease**
 with Crohn's disease, 1002, 1005f
- Anorectal dysfunction, 890-904**
- Anorectal junction, 896**
- Anorectal manometry, 1122**
- Anterior anus, 2164, 2165f**
- Anterior mucosal prolapse, 900, 901f**
- Anterior pararenal space, 1990, 1990f, 1992f**
 disease spread through, 2013-2014, 2015f
- Anterior wall prolapse, 898**
- Antiangiogenic therapy**
 perfusion MRI as biomarker for, 1236
- Antibiotics**
 in abdominal abscess drainage, 1260
 for *H. pylori* gastritis treatment, 501
- Anticholinergic agents, 19**
 for diffuse esophageal spasm, 285-286
- Anticoagulant agents**
 management of for image-guided biopsy, 1240-1241, 1241f
- Anti-epidermal growth factor receptor antibodies, 1206-1207**
- Antifungal agents**
 for candida esophagitis, 312
- Antilutetic therapy, 512**
- Antiperistaltic agents, 82**
 for magnetic resonance enterography, 712
- Antiplatelet agents**
 management of for image-guided biopsy, 1240-1241, 1241f
- Amisecretory agents**
 for GIST treatment, 474-475
 for *H. pylori* gastritis treatment, 501
 for hypertrophic gastritis treatment, 503
- Antispasmodic agents, 1121-1122**
- α_1 -antitrypsin deficiency**
 liver transplantation for, 1738
 pediatric, 2213
- Anti-tumor necrosis factor (TNF) agents**
 for Crohn's disease, 1007
 for ulcerative colitis, 996
- Anti-vascular endothelial growth factor antibodies, 1206-1207**
- Antral diaphragm, 610, 611f**
 gastric narrowing from, 659f
- Antral gastritis, 499-500, 500f**
 differential diagnosis of, 659f
- Antral-pyloric fold, hypertrophied, 499-500, 500f**
- Antral webs, 610, 611f, 2084, 2085f**
 gastric narrowing from, 659f
- Antrectomy**
 for peptic ulcer disease, 652
- Anus. See also Colon**
 anterior, 2164
 caudal regression in, 2117
 Currarino triad in, 2117-2118
 imperforate, 2113-2117
 squamous cell carcinomas of, 1081-1082
- Aorta**
 anatomy of, 1986
 in vascular rings, 2125-2127, 2128f-2129f
- Aortic aneurysm**
 acute abdomen from, 2266, 2266f
 crescent sign of impending rupture of, 2267f
 rupture of, 1988f
- Aortic aneurysms**
 aortoduodenal fistulas with, 625-626
 aorto-esophageal fistulas from, 421-422, 423f
 duodenal compression or displacement by, 580, 661f
 splanchnic, 845, 845f
- Aortic arch abnormalities, 2125-2127, 2129f-2130f**
- Aortic dissection**
 abdominal aorta, 138-139, 139f
- Aortoduodenal fistulas, 625-626, 626f**
 duodenal obstruction caused by, 614
- Aorto-esophageal fistulas, 421-422, 423f**
- APC gene, 1089**
- Aphthoid ulcers**
 in Crohn's disease, 728f
 in differential diagnosis, 768-769
 double-contrast studies of, 47-51, 51f
 in salmonellosis, 1017
 small bowel, 667-668, 669f
- Apparent diffusion coefficient (ADC), 1215, 1490-1491**
- Apparent diffusion coefficient (ADC) maps, 1183**
- Appendectomy, 1138, 1139f**
- Appendicitis**
 abscesses in, 1254, 2258f
 acute abdomen caused by, 2257-2258, 2257f-2258f
 liver abscesses from, 1608-1609
 pediatric, 2169-2170, 2169f-2171f
- Appendicoliths, 185, 960f**
 lamellated, 199, 199f
 pediatric, 2169, 2169f
- Appendix, 955-983**
 abscesses of, 960, 961f-962f, 1278
 appendicitis, 956-971
 acute suppurative, 60f
 barium enema findings on, 956f
 causes of, 957-958
 cecal diverticulitis differentiated from, 946
 clinical and radiologic assessment of, 958-959
 clinical findings on, 959-960
 differential diagnosis of, 969-971, 969f-971f
 distal, 964, 965f
 diverticulitis as left-sided, 938
 epidemiology of, 956-957
 imaging findings on, 960-969, 960f
 magnetic resonance imaging of, 88, 88f
 mimics of acute, 60, 61b
 pathophysiology of, 958, 958f-959f
 radiographic signs of, 184-185
 with small bowel obstruction, 185f
 sonographic criteria for, 60b
 transabdominal ultrasonography of, 59-60
 arrested development of, 955, 957f
 carcinoid tumors in, 1077
 Crohn's disease in, 971-972
 diverticulitis of, 973
 embryology of, 955-956, 956f
 endometriosis in, 972-973
 intussusception of, 973-974
 lesions of, differential diagnosis of, 1148f

- Appendix (Continued)
- metastases in, 979
 - neoplasms of, 974-979
 - carcinoid, 978-979, 979f
 - lymphoma, 979
 - mucinous cystadenoma and cystadenocarcinoma, 975-977, 978f
 - mucoceles, 976f-977f
 - nonmucinous adenocarcinoma, 977
 - normal, 2171f
 - ulcerative colitis in, 972
 - variations in position of, 955, 957f
 - Apple core lesions, 1037f, 1146f
 - Areae gastricae, 478
 - in atrophic gastritis, 506
 - enlarged in *H. pylori* gastritis, 501
 - with GISTs, 531
 - lymphoid hyperplasia differentiated from, 503
 - mucosal nodularity differentiated from, 586
 - A rings. *See* Muscular rings, esophageal
 - Arteriography
 - liver, differential diagnosis with, 1764
 - Arteriohepatic dysplasia, 1432
 - Arterioportal fistula, 2209
 - Arteriovenous malformations (AVMs), 690, 2208-2209, 2208f
 - hemorrhage from, 2277
 - Arthritis
 - with inflammatory bowel disease, 1011
 - rheumatoid
 - amyloidosis with, 783
 - septic
 - with inflammatory bowel disease, 1012
 - in Whipple's disease, 782
 - Arthropathy, 1011
 - in hemochromatosis, 1641
 - Artifacts
 - bowel motion, 1006
 - comet-tail or ring-down, 1174, 1175f
 - in computed tomography
 - tissue harmonic imaging, 1172
 - in diffusion-weighted MRI, 1220, 1220f
 - eddy current, 1218f
 - in esophagography, 300-301
 - in magnetic resonance
 - cholangiopancreatography, 1326-1327
 - in magnetic resonance colonography, 950f
 - in magnetic resonance enterography, 712
 - magnetic resonance imaging
 - minimization of, 1492
 - in magnetic resonance imaging, 1183-1184, 1184f
 - on Crohn's disease, 1006
 - diffusion-weighted, 1217-1220
 - susceptibility, 1184, 1185f
 - magnetic susceptibility, 1287
 - mirror image, 1174, 1174f
 - respiratory motion, 1006, 1183-1184, 1185f
 - in diffusion-weighted MRI, 1217-1218, 1220
 - reverberation, 1382-1384, 1384f
 - see-through, mimicking hyperplastic polyps, 526f
 - stalactites, 484
 - that mimic gallstones, 1462f
 - in ultrasonography, 1175-1176, 1174f
 - liver, 1478
 - Ascariasis, 757, 758f
 - biliary tract, 1437, 1438f
 - life cycle of, 1438f
 - pediatric, 2153, 2153f
 - Ascaris lumbricoides*, 757
 - biliary spread of, 2008
 - biliary tract infestations, 1437, 1438f
 - Ascites, 2024-2035
 - in acute mesenteric ischemia, 834
 - causes of, 2025b
 - with cirrhosis, 1655
 - clinical findings on, 2024
 - diagnostic paracentesis on, 2024
 - differentiation of, 2031-2032
 - diffusion-weighted MRI of, 1224
 - distribution pathways of, 2027, 2027f
 - gallbladder wall thickening in, 1356
 - with gastric carcinoma, 548
 - image-guided biopsy and, 1248
 - imaging features of, 2025f
 - intraoperative flow of, 2002-2004, 2004f
 - pancreatic
 - surgery for, 1861
 - treatment of, 1815-1816
 - pathophysiology of, 2024
 - perivesical fat demarcation with, 176f
 - radiologic findings on, 2027-2031
 - barium studies, 2028
 - chest radiography, 2027
 - computed tomography, 2029-2031, 2030f
 - magnetic resonance imaging, 2031, 2032f
 - plain abdominal, 2027
 - ultrasound, 2028-2029, 2028f
 - in root of the mesentery, 1996
 - signs on abdominal radiographs, 193-194, 193f
 - small bowel
 - differential diagnosis of, 875f
 - treatment of, 2032-2034
 - types of, 2025-2027, 2026f
 - bile, 2026
 - cerebrospinal fluid, 2027
 - chylous, 2025-2026
 - exudates, 2025
 - hemorrhagic, 2025
 - neonatal, 2026
 - pancreatic, 2026
 - pseudomyxoma peritonei, 2026
 - pus, 2025
 - transudates, 2025
 - urine, 2026-2027
- Asian cholangiohepatitis, 2008
- Aspergillus*, splenic infection with, 1936f
- Aspiration
 - after esophagogastricomy, 454
 - prevention of, 226-227
- Aspirin. *See* also Nonsteroidal anti-inflammatory drugs (NSAIDs)
 - erosive gastritis caused, 496
 - ulcers caused by, 468, 471
 - greater curvature, 472-473, 473f
- Asplenia, 1151f, 2088
 - functional, 2237
 - pediatric, 2230
- Asplenia syndrome, 1917-1918, 1917b, 1917f
- Astrovirus, in graft-versus-host disease, 764
- Atherosclerotic disease, chronic mesenteric ischemia caused by, 837
- Atresias
 - biliary
 - pediatric, 2182-2188
 - anomalies and malformations with, 2183
 - classification of, 2183f
 - imaging of, 2184-2188, 2184f-2188f
 - treatment of, 2183-2184
 - colon, 2112f, 2113
 - duodenal, 2141-2143, 2142f-2143f
 - esophageal, 2106-2110, 2106f
 - pediatric, 2125
 - ileal, 2091
 - intestinal, with gastroschisis, 2244, 2245f
- Atresias (Continued)
 - jejunal and ileal pediatric, 2110-2112, 2111f-2112f
 - classification of, 2111f
 - pyloric and antral, 2141
- Atrophic gastritis, 504-506, 506f
 - gastric carcinoma linked to, 547
 - gastric narrowing from, 659f
- Attenuated familial adenomatous polyposis syndrome (AFAPS), 1089
- Autoimmune conditions
 - pancreatitis, 1831-1833, 1831f-1832f
 - with primary biliary cirrhosis, 1649-1650
- Automatic modulation of tube current (ATCM), 1484
- Autosomal dominant polycystic kidney disease, 2201, 2201f
 - pancreatic cysts with, 2226, 2226f
- Autosomal dominant polycystic liver disease, 2201-2202
- Avascular lesions, liver, 1764f
- Avascular necrosis, 746-748, 1011
- Azathioprine
 - for Crohn's disease, 1007
 - hepatotoxicity of, 1639
- B**
- Backwash ileitis
 - segmental small bowel mural hyperenhancement in, 686, 687f
 - in ulcerative colitis, 990, 991f
 - Bacterial infections. *See* also *Escherichia coli*; Tuberculosis
 - after image-guided biopsy, 1250-1251
 - biliary tract
 - after laparoscopic cholecystectomy, 1453
 - in obstructive cholangitis, 1434-1435, 1436f
 - campylobacteriosis, 761-762, 873f, 1018
 - colon, 1017-1019
 - E. coli* colitis, 1018, 1019f
 - shigellosis, 1018
 - tuberculosis, 1018-1019
 - Yersinia enterocolitis*, 1018
 - hematogenous spread of, 2007
 - liver abscesses from, 1608-1611
 - salmonellosis, 761, 873f, 1017-1018
 - small bowel, 760-762
 - salmonellosis, 761
 - tuberculosis, 760-761, 760f
 - yersiniosis, 761, 761f
 - Yersinia enterocolitis*, 985, 2170, 2172f, 2264
 - Bacterial overgrowth, malabsorption due to, 775-778
 - Balloon dilation of strictures, 1007
 - Bannayan-Riley-Ruvalcaba syndrome (BRRS), 1093, 1097
 - Bannayan-Zonana syndrome. *See* Bannayan-Riley-Ruvalcaba syndrome (BRRS)
 - Barcelona Clinic Liver Cancer (BCLC) guidelines, 1508
 - Bare area, 199f, 1991, 2016f
 - embryology of, 1983, 1984f
 - Bare area sign, 2031
 - Bariatric surgery, 630, 641-654
 - biliopancreatic diversion with duodenal switch, 654, 654f
 - gastric banding, 646-651, 648f
 - imaging after, 647-651
 - malabsorptive procedures, 642
 - restrictive procedures, 642
 - Roux-en-Y gastric bypass, 642-646

Bariatric surgery (*Continued*)

- sleeve gastrectomy, 651-654, 652f
- imaging after, 652
- vertical banded gastroplasty, 642
- Barium. *See also* Contrast agents
- obturator obstruction from retained, 1110
- tagging agents, 907-908
- Barium enemas. *See* Enteroclysis
- Barium studies, 23-39. *See also* Enteroclysis
- anatomic considerations in, 271-273
- on ascites, 2028
- with barium suspensions, 269
- colon, 879-889
 - complications in, 886, 887f
 - double-contrast barium enema, 879-884, 888f
 - normal, 881f-883f, 883-884
 - single-contrast barium enema, 884
 - single- versus double-contrast, 879
 - technical problems in, 884-886, 885f
 - technique variations in, 886-887
- components for, 269
- on Crohn's disease, 727-733
- on diverticulosis, 935-937, 936f
- double-contrast, 30-36
 - artifacts in, 36, 38f
 - distention in, 31
 - interpretation of, 31-36
 - barium pool in, 35-36, 36f, 37f
 - of dependent and nondependent surfaces, 31-33, 33f
 - of depressed lesions, 33-35, 35f
 - of protrusions, 33, 33f
 - mucosal coating in, 30, 31f
 - performance of, 30-31
- of the duodenum, 273
- effervescent agents in, 269
- esophageal
 - for achalasia, 284
 - artifacts in, 300-301
 - of carcinoma, 389
 - with epidermolysis bullosa dystrophica, 338
 - of GERD, 288
 - of leiomyosarcomas, 405
 - of metastases, 394-396, 395f-396f
 - of motility, 279-283
 - of perforations, 415-416, 416f
 - of presbyesophagus, 286-287
 - of scleroderma, 288-289
 - of squamous cell carcinoma, 371
- flow technique for, 271, 271f
- gastric, 272-273, 274f
 - of carcinoma, 350-354
 - on dilation, 615
 - of varices, 604
- of gastroesophageal junction abnormalities, 438
- on gastroesophageal reflux disease, 2131, 2131f
- of GERD, 291
- high-density, 416-417, 416f
- hypotonic agents in, 269
- leiomyomas in, 354
- pancreatic, 1776
 - on annular pancreas, 1804-1805, 1804f, 1806f
 - in pancreatitis, 1832, 1833f
- of peptic ulcers, 477-478, 484
- proximal escape in, 280-281, 281f
- radiographic components in, 269
- reflux of barium in, 672
- Schatzki rings in, 441-443, 442f
- single-contrast, 23-30
 - barium enema, 28-30
 - barium suspensions for, 24
 - diagnostic principles in, 23
 - equipment for, 23-24
 - esophagography, 25
 - quality controls in, 24-25

Barium studies (*Continued*)

- small bowel, 26-27
 - upper gastrointestinal series, 25-26
- single- versus double-contrast, 879
- small bowel, 665-683
 - follow-through, 668-670
 - normal anatomy in, 665-666
 - of obstructions, 810-811, 810f-811f
 - principles for performing and interpreting, 667-668
- stalactites in, 484
- technique in upper gastrointestinal, 270-271, 271f
- upper gastrointestinal, 269-278
 - technique variations in, 273-275
- whiskering in, 530, 530f
- Barium sulfate contrast agents, 7
 - adverse reactions to, 12-13
 - in magnetic resonance colonography, 932
 - in magnetic resonance enterography, 711
 - in magnetic resonance imaging, 81-82
- Barium suspensions, 269
- Barrett's esophagus, 303-308
 - adenocarcinomas in, 368, 374-378, 378f-379f
 - adenomas in, 350, 352f
 - carcinoma of the gastric cardia and, 560
 - clinical findings in, 304
 - differential diagnosis of, 308, 463t-464t
 - distinguished from pemphigoid, 338
 - double-contrast esophagography on, 291
 - endoscopic and histologic findings of, 305
 - epithelial dysplasia in, 376-377
 - intramural pseudodiverticulosis with, 345
 - long-segment, 305-307, 306f
 - radiographic findings of, 305-308
 - relationship of with scleroderma, adenocarcinoma, and, 377
 - reticular mucosal patterns in, 306-308, 307f
 - short-segment, 307-308
 - surgery for, 450
 - surveillance and management of, 377
 - ulceration in, 305-306, 306f
- Bartonella infections, 2211
 - with AIDS, 1652
 - cat-scratch disease, 1938
- Basaloid carcinomas. *See* Cloacogenic carcinomas
- Beam hardening, 914f, 915
- Beckwith-Wiedemann syndrome, 1578, 2098, 2225-2226, 2226f
- Beger procedure, 1864, 1866f
- Behçet's disease, 343, 344f, 840-841, 841f
 - colonic involvement of, 1126
 - differential diagnosis of, 4621
- small bowel
 - luminal narrowing in, 873t
 - obstructions from, 819
- Belsey Mark IV repair, 450
- Benign lymphoid hyperplasia, 541, 541f
- Bevacizumab, hepatotoxicity of, 1639
- Bezoars, 622f
 - after gastric resection, 637, 637f
 - differential diagnosis of, 658t
 - obstruction by, 1110
 - pediatric, 2148-2149, 2151f
 - small bowel, 867
- Bile
 - ascites, 2026
 - leaks after liver surgery, 1728, 1728f
 - milk of calcium, 1385, 1386f
 - reflux, ulcers caused by, 468
 - reflux gastritis, 638-639, 639f
- Bile plug syndrome, 2193
- Bile salt insufficiency, 774
- Biliary atresia, 2182-2188
 - anomalies and malformations with, 2183
 - background on, 2182-2183

Biliary atresia (*Continued*)

- classification of, 2183, 2183f
- imaging of, 2183-2188, 2184f-2188f
- treatment of, 2183-2184
- Biliary calculi, 198, 198f, 1179-1180, 1179f. *See also* Cholelithiasis
- Biliary ducts, 1282-1283. *See also* Biliary tract
- Biliary-enteric anastomosis, 1454-1456
 - background, indications, and technical considerations for, 1454-1455
 - complications after, 1455-1456
 - biliary leaks, 1455
 - strictures, 1455-1456
- Biliary sludge, 1352, 1354f-1355f
- Biliary tract
 - abnormalities in, 1342-1345, 1343f
 - adenomas, 1556
 - AIDS involvement in, 1655
 - bile duct injuries, 1398-1399
 - Caroli's disease, 606f-607f, 607
 - choledochal cysts in, 1343-1345, 1343f-1345f
 - choledochoceles, 1344f, 1345
 - congenital anomalies
 - magnetic resonance cholangiopancreatography on, 1350-1352
 - contrast agents affecting, 20-21
 - diameter of, 1305
 - differential diagnosis of, 1460-1467
 - dilation, differential diagnosis of, 1464t
 - ductal diameter and obstructions in, 1290
 - duct system, 1773f
 - echinococcal disease, 1620
 - embryology of, 1340
 - endoscopic retrograde
 - cholangiopancreatography on, 1303-1324
 - technique for, 1303
 - examination techniques for, 1287-1300
 - cholecystokinin sonography, 1293
 - cholescintigraphy, 1286, 1287f
 - computed tomography, 1290-1292
 - computed tomography cholangiography, 1292, 1292f
 - direct cholangiography, 1295-1299
 - fatty meal before, 1290
 - magnetic resonance
 - cholangiopancreatography, 1292-1295, 1293f
 - magnetic resonance imaging, 1286-1287, 1287f
 - plain radiography, 1288
 - scintigraphy, 1299-1300, 1299f
 - ultrasound, 1288-1290
 - familial adenomatous polyposis syndrome in, 1091
 - filling defects, differential diagnosis of, 1465t
 - fistulas
 - differential diagnosis of, 1461t
 - gallbladder carcinoma metastases to, 1409, 1409f
 - gas in, differential diagnosis of, 1461t, 1759t
 - hamartomas, 1190, 1424, 1649, 1649f
 - pediatric, 2202
 - image-guided biopsy of, 1246f
 - infection and inflammation in, 1311-1320
 - inflammatory bowel disease complications in, 1009-1010, 1010b
 - inflammatory disorders of, 1427-1441
 - AIDS-related cholangitis, 1436-1437, 1437f
 - differential diagnosis of, 1464t-1465t
 - echinococcal cholangitis, 1440
 - floxuridine cholangitis, 1437
 - obstructive cholangitis, 1434-1435, 1436f
 - parasitic infestations, 1437-1440, 1438f
 - primary biliary cirrhosis, 1432-1434, 1433f, 1435f
 - pyogenic cholangitis
 - recurrent, 1376c, 1435-1436, 1436f

Biliary tract (*Continued*)

- interventional radiology
 - for bile duct injuries, 1398-1399, 1399f
 - for biopsy, 1399-1400
- common duct stone removal, 1398
- of percutaneous cholecystostomy, 1392-1394
- percutaneous transhepatic cholangiography and drainage, 1395-1396, 1395f
- for primary sclerosing cholangitis, 1399
- interventional radiology of, 1392-1401
- preprocedural management for, 1392
- liver abscesses from disease in, 1608-1609
- liver transplantation and
 - assessment of for living donor transplants, 1743
 - complications involving, 1749-1752
 - anastomotic strictures, 1750-1751, 1751f
 - leaks, 1752, 1752f
 - nonanastomotic strictures, 1751-1752, 1751f
 - obstruction, 1749-1750
 - normal findings after, 1749, 1750f
- liver trauma and complications in, 1717
- magnetic resonance cholangiopancreatography on, 1325-1339
 - on calculi, 1326-1328, 1327f-1328f
 - clinical applications of, 1326-1332
 - on congenital anomalies, 1330-1332
 - on neoplasms, 1328-1330
 - normal anatomy in, 1294-1295, 1326f
 - technique for, 1293-1294, 1294f, 1325-1326
- magnetic resonance imaging of, 1190, 1190f, 1192-1194, 1193f, 1195f
 - acute cholecystitis and, 1192-1193, 1193f
 - cholangiocarcinomas, 1194, 1195f
 - cholelithiasis and choledocholithiasis, 1192, 1193f
 - contrast agents in, 1186
 - lesions originating in, 1190
- metastatic disease in, 2008
- neoplasia, 1306-1311
- neoplasms, 1402
 - benign, 1424
 - cholangiocarcinomas, 1410-1419
 - extrahepatic, 1419, 1421f
 - cystadenomas and cystadenocarcinomas, 1421, 1423f
 - other malignant, 1422, 1424f
 - periampullary carcinomas, 1419-1421
 - normal anatomy
 - on endoscopic retrograde cholangiopancreatography, 1303-1306, 1304f
 - variations in, 1283, 1330-1332, 1332f, 1340-1347
 - normal anatomy of, 1281-1283, 1282f, 1476, 1477f
 - on cholangiography, 1297-1298
 - on computed tomography, 1291-1292
 - on magnetic resonance cholangiography, 1294-1295
 - on ultrasound, 1289
- obstructions in
 - differential diagnosis of, 1463f
- pediatric disorders of
 - Alagille's syndrome, 2188-2189
 - bile plug and inspissated bile syndromes, 2193
 - choledochal malformations, 2190-2191, 2190f-2192f
 - choledocholithiasis, 2194-2195, 2195f
 - cystic fibrosis, 2195
 - imaging modalities for, 2180
 - neonatal jaundice and, 2182
 - normal, 2181-2182, 2182f

Biliary tract (*Continued*)

- primary sclerosing cholangitis, 2195, 2196f
 - progressive familial intrahepatic cholestasis, 2189-2190
 - pericholecystic fluid, differential diagnosis of, 1461f
 - PET/CT of, 1202-1204
 - cholangiocarcinomas, 1202-1203, 1203f
 - from gallbladder carcinomas, 1203-1204
 - postcholecystectomy dilation of, 1290
 - postoperative
 - after biliary-enteric anastomosis, 1434-1436
 - after cholecystectomy, 1442-1453
 - after laparoscopic cholecystectomy, 1442-1453
 - abscesses, 1445-1447, 1449f, 1454f
 - bile duct injury and bile leakage, 1445-1448, 1445f-1448f
 - complications after, 1444-1453
 - imaging of, 1442-1443, 1444f, 1450-1452
 - retained biliary stones, 1448, 1450f
 - spilled biliary stones, 1452-1453, 1452f-1454f
 - strictures, 1449-1452, 1450f
 - technical considerations for, 1442, 1443f
 - magnetic resonance cholangiopancreatography on, 1332-1334, 1333f
 - post-traumatic lesions of, 1456-1457, 1456f-1457f
 - primary sclerosing cholangitis in, 1010, 1011f, 1427-1432
 - magnetic resonance pancreatography on, 1334-1335, 1334f-1335f
 - segmental lesions, differential diagnosis of, 1463f
 - in spread of infectious disease, 2008
 - strictures in, 1307b
 - benign, 1397-1398, 1397f
 - differential diagnosis of, 1463f
 - interventional radiology for, 1396-1398, 1397f
 - malignant, 1396-1397
 - ultrasonography on, 1178-1180, 1179f
 - gas in, 1175f
- Biliopancreatic diversion with duodenal switch (BPD-DS), 654, 654f
- Bilroth I procedure, 630, 633, 633f
 - bezoar formation after, 637f
 - for gastric masses, 640
 - leaks after, 635
 - stomal and anastomotic ulceration after, 637
- Bilroth II procedure, 630, 633, 634f
 - computed tomography enteroclysis on, 700-701
 - for gastric masses, 640
 - leaks after, 635-636, 635f-636f
 - stomal and anastomotic ulceration after, 637
 - stomal stenosis after, 636f
 - ulcer recurrence after, 638f
- Bilioenteric fistulas, 1193
- Bilomas, 1706, 1712, 1712f-1713f
 - liver, after transplantation, 1753
 - on ultrasound, 1714
- Biopsies. *See also* Percutaneous tissue acquisition techniques
- biliary tract, 1399-1400
- of bowel masses, 127
- liver
 - for biliary atresia, 2188
 - for fat quantification, 1635-1636
 - percutaneous, 1498-1501, 1499f-1500f
 - subcapsular hematoma from, 1706
 - transjugular, 1501
- pancreas, 1785-1789
 - background on, 1785
 - complications with, 1789
 - diagnostic effectiveness of, 1788-1789

Biopsies (*Continued*)

- indications for, 1785-1787, 1786f-1788f
- technical considerations in, 1787-1788
- ultrasound-guided, 153
- percutaneous, 1239-1253
 - pancreas, 1785-1789
 - preprocedure evaluation for, 1239-1241
- spleen
 - of angiosarcomas, 1947
 - image-guided, 1905-1907, 1906f-1907f
 - complications of, 1906f
 - transcatheter, 127
- Bismuth classification system, 1307, 1310f
- Bismuth-Corlette classification system, 1398-1399
- Bismuth-Couinaud classification system, 1473-1475, 1473f
- Black attenuation pattern, 73, 74f-75f
- Blastomycosis*, esophagitis caused by, 322
- Blind pouch and loop anastomoses, 853-855, 854f
- Blood vessels, engorgement of mesenteric, 75, 75f
- Blue rubber bleb nevus syndrome, 846-848, 1076
- Blumer shelf, 2009
- Blunt trauma. *See also* Trauma
 - abdominal
 - small bowel obstructions from, 820
 - liver, 1707, 1709f, 1712f
 - spleen, pediatric, 2234-2235, 2235f
- Body mass index, 641
- Boerhaave's syndrome, 414, 416f-417f, 417
- Bolus tracking systems, 1161, 1164, 1166
- Borrmann classification of gastric carcinoma, 558, 558f
- Botulinum toxin, achalasia treatment with, 284
- Bouveret's syndrome, 621, 1377, 1380f
- Bowel. *See also* Cecum; Colon; Large bowel; Rectum; Small bowel
 - abnormal gas patterns in, 179-184
 - adynamic ileus in, 179-180
 - altered blood flow in, 57
 - attenuation patterns in, 71f
 - biopsy of masses in, 127
 - decompression of, 129-130
 - delayed activity in, differential diagnosis of, 1463f
 - extramural and mesenteric changes in, 57-58
 - gastroschisis of, 2097-2098
 - image-guided biopsy of, 1250-1251
 - inadvertent catheterization of the, 126
 - infectious disease of, 86-88
 - infectious enterocolitis, 64-65
 - ischemia of, 64, 64f
 - loops
 - centrally located with bulging flanks, 194
 - separation of, 194
 - lumen of, 56
 - mural thickening in, 71f
 - normal gas patterns in, 178, 179f
 - neonatal, 2101, 2103f
 - obstructions
 - acute abdomen from, 2259-2260, 2260f
 - after biliopancreatic diversion with duodenal switch, 654
 - closed loop, 182
 - meconium ileus, 2118-2119, 2119f
 - meconium plug syndrome, 2119-2120, 2120f
 - with necrotizing enterocolitis, 2105-2106
 - in neonates and children, 2101, 2103f
 - pathologic changes in wall of, 70
 - plasticity, mobility, peristalsis in, 56-57
 - puncture of to confirm identity, 127
 - trauma to, 2287-2292
 - ultrasound features of abnormal, 56-58
 - ultrasound features of normal, 56

Bowel (Continued)

- volvulus, 182-184
- wall
 - computed tomography of normal, 69-70
 - layers of, 56
 - thickening of, 56, 61-62
- Bowler hat sign, 1032
- Branchial clefts, 238
- Branchial pouches, 238-239, 239f
- Breast cancer
 - chemotherapy hepatotoxicity in, 1659
 - with Cowden's disease, 1095
 - with Cowden's syndrome, 794
 - esophageal metastases in, 394, 398f-399f
 - hematogenous spread of, 2006
 - metastases from
 - to the colon, 1086
 - gallbladder, 1410
 - gastric, 548, 560, 574f
 - gastric narrowing from, 659f
 - linitis plastica appearance of, 572-573, 573f-574f, 579-580
 - liver, 1591t
 - omental, 577-578
 - small bowel obstruction from, 816
 - with Peutz-Jeghers syndrome, 1093-1095
- Bright liver, 1759f
- Broad ligaments, 2020
- Bronchopulmonary foregut malformations, 2125, 2126f
- Bronchus
 - esophageal, 2084
 - esophageal cancer invasion of, 381-382, 384f
- Brooke ileostomy, 996
- Brunner's gland
 - hyperplasias of, 539-541, 540f, 2155
 - differential diagnosis of, 661t
 - in Meckel's diverticulum, 861
- Brush border cells, 774
- Brush border disease, 775
- Bubbly bulb, 519, 519f
- Budd-Chiari syndrome, 413-414, 1504, 1680-1688
 - acute abdomen from, 2267
 - causes of, 1677f-1678f
 - clinical findings on, 1681
 - echinococcal disease with, 1620
 - etiology of, 1681-1682
 - hepatic steatosis with, 1639
 - imaging findings on, 1766f
 - nodular regenerative hyperplasia in, 1686, 1688f
 - pathologic findings on, 1682, 1683f
 - posthepatic obstruction in, 1656
 - radiologic findings on
 - angiography, 1686, 1687f
 - computed tomography, 1683-1684, 1685f
 - magnetic resonance imaging, 1684-1686, 1685f, 1687f
 - ultrasound, 1682-1683, 1684f-1685f
 - THADs and THIDs in, 1680
 - treatment of, 1686-1688
- Bull's-eye lesions, 499, 504
 - with ascariasis, 1457
 - double-contrast studies of, 47, 50f
 - ectopic pancreatic rests, 539
 - gastric, 587
 - gastric lymphomas, 583f
 - in hematogenous metastases, 571, 572f
 - intussusceptions, 1109
 - in Kaposi's sarcoma, 593, 595f
 - lipomas, 535-536
 - in liver metastases, 1593
 - in splenic fungal infections, 1936-1937, 1936f
- Burkitt's lymphoma, 1950f, 2206, 2206f, 2225, 2225f
- Byler's disease, 2189-2190

C

- Calcifications, 197-203
 - anterior abdominal wall, 2074
 - classification of, 198, 201-202
 - concretions, 198-199
 - conduit wall, 199-200, 199f
 - cystic, 200, 200f
 - in dermatomyositis, 2074
 - dystrophic, 197
 - in gastrointestinal stromal tumors, 531, 532f, 590f
 - liver
 - differential diagnosis of, 1758f
 - in metastatic disease, 1591, 1591f, 1596f
 - location of, 202
 - lymph node, 201, 201f
 - metastatic, 197
 - mobility of, 202, 203f
 - morphology of, 197-202
 - omental and mesenteric, 77, 77f
 - pancreatic, differential diagnosis of, 1889f
 - physiology of, 197
 - retroperitoneal teratomas, 198f
 - serous cystadenocarcinomas, 197, 198f
 - solid mass, 200-201, 201f
 - spleen
 - differential diagnosis of, 1979f
 - with lymphomas, 1952, 1954f
 - in sickle cell disease, 2237
 - sources of, 1924b
- Calcium channel blockers, for diffuse esophageal spasm, 285-286
- Campylobacter, 761-762, 1018
- Campylobacteriosis, 761-762, 753t, 1018
- Cancer. *See also specific cancers*
 - gastrocolic and duodenocolic fistulas, 624, 624f-625f
 - gastroduodenal
 - carcinoid tumors, 408
 - differential diagnosis of, 657f
 - GISts, 587-591
 - hematogenous spread of, 2006
 - Kaposi's sarcoma, 405
 - lymphomas, 580-587
 - metastases from
 - to gastrohepatic ligament, 2018-2019, 2019f
 - gastrosplenic ligament in spread of, 2019
 - liver, 1591t
 - peritoneal spread of, 2014f
 - metastatic, 571-580
 - appendiceal, 979
 - clinical findings in, 571
 - differential diagnosis of, 578-580
 - direct invasion of, 576-578
 - from gastric carcinoids, 596
 - hematogenous, 571-574
 - lymphatic spread of, 574-576
 - radiographic findings in, 571-578
 - PET/CT of, 100-102
 - surgical procedures for gastric masses, 632
 - villous tumors associated with, 528-530
- Candida albicans*
 - intra-abdominal abscesses from, 1271-1272
 - in liver abscesses, 2211
 - odynophagia caused by, 319
 - splenic infections, 1936-1937, 1936f
- Candida esophagitis*, 288-289, 293, 312-315
 - clinical findings with, 312
 - differential diagnosis of, 315, 462t-463t
 - differentiated from carcinoma, 381f
 - differentiated from glycogenic acanthosis, 353f
 - differentiated from herpes esophagitis, 317
 - endoscopic findings in, 312-313
 - with foamy esophagus, 317f
 - pathogenesis of, 312
 - plaquelike lesions in, 313, 313f-314f
 - radiographic findings in, 313-314
- Candida esophagitis* (Continued)
 - with scleroderma, 314, 316f
 - with shaggy esophagus, 313, 315f
 - strictures from, 314, 316f
- Candida glabrata*, intra-abdominal abscesses from, 1271-1272
- Candida pharyngitis*, 246f
- Candidiasis
 - gastric, 512
 - liver, 1622-1623, 1622f
 - splenic infection with, 1936-1937, 1936f
 - pediatric, 2235-2236
- Capsular retraction, 1729, 1758f
- Capsule endoscopy
 - on acute small bowel bleeding, 841
 - computed tomography enterography with, 684
 - on gastrointestinal hemorrhage, 2272-2273
 - integration of with computed tomography enterography, 692
 - small bowel neoplasms on, 689
 - video, 726-727, 728f
- Carbenoxolone, 469
- Carbohydrate digestion and absorption, 773
- Carbon dioxide insufflation
 - complications with, 922
 - computed tomography colonography, 909-910, 909f
 - for magnetic resonance colonography, 928
- Carcinoembryonic antigen (CEA), 1789
- Carcinoid syndrome, 799
- Carcinoid tumors
 - appendiceal, 978-979, 979f
 - colonic, 1077, 1078f
 - esophageal, 408
 - with familial adenomatous polyposis syndrome, 1092
 - gallbladder, 1408, 1410
 - gastroduodenal, 408
 - clinical findings on, 408
 - differential diagnosis of, 658t
 - pathology of, 408
 - ileal, 690f
 - mesenteric, 2044, 2044f
 - small bowel, 668f, 799, 799f
 - computed tomography enteroclysis on, 697-699
 - on computed tomography enterography, 689, 690f
 - differential diagnosis of, 874t
 - mesenteric ischemia caused by, 832f
 - obstruction by, 816-817, 817f-818f
 - site predilection of, 875t
- Carcinomas
 - adenosquamous, 598
 - adrenocortical, 1210-1211
 - annular, gastric outlet obstruction caused by, 612, 612f
 - appendiceal, 975-977, 978f
 - biliary tract, 566, 566f, 1307, 1310-1311, 1313f, 1319-1321
 - cecal, 971, 973f
 - cholangiocarcinoma
 - magnetic resonance imaging of, 1194, 1195f
 - PET/CT of, 1202-1204, 1203f
 - cloacogenic, 1119, 1120f-1121f
 - colonic
 - cloacogenic, 1081-1082, 1082f
 - computed tomography on, 1041f
 - differentiation of from diverticulitis, 943-944, 945f
 - diverticulitis and, 938
 - duodenal displacement from, 616
 - with familial adenomatous polyposis syndrome, 1090, 1090f-1091f
 - fistulas with, 1040f

Carcinomas (Continued)

- gastroduodenal metastases from, 576-577
- giant sigmoid diverticulum with, 952
- with inflammatory bowel disease, 1008-1009, 1008f, 1036
- obstructions from, 1039f, 1104-1105
- pediatric, 217b
- perforations from, 1040f
- recurrence of, 1060f
- in Turcot syndrome, 1092
- colorectal
 - computed tomography of, 1039-1050
 - with inflammatory bowel disease, 1008-1009, 1008f
 - primary, 1039-1047
 - recurrence of, 1067-1068
- downhill varices caused by, 432-433, 434f
- duodenal
 - ampullary, 566, 567f
 - annular, 510
 - periampullary, 566, 566f
- esophageal, 366-393
 - achalasia differentiated from, 283-284
 - adenocarcinoma, 336
 - from adenomas, 350
 - from caustic ingestion, 334f, 455
 - differential diagnosis of, 379-380
 - gastroduodenal metastases from, 576
 - infiltrating, 371, 372f-373f, 379, 380f
 - intramural pseudodiverticulosis with, 345
 - mucosal nodularity with, 301
 - palliative intubation for, 458-459, 459f
 - peptic strictures and, 300
 - plaques and nodules caused by, 315
 - polypoid, 371, 372f, 379, 380f
 - with pseudodiverticulosis, 345
 - small cell, 407-408, 408f
 - spindle cell, 402-403, 405f, 407, 463a
 - strictures from, 464t
 - surgical treatment of, 453-459
 - survival rates for, 453
 - tumor patterns, 371-372, 372f
 - ulcerative, 371-372, 372f, 379-380, 380f
 - varicoid, 302, 372, 372f, 380, 380f, 464t
- fibrolamellar, 1573-1577, 1574f
- fibrolamellar hepatocellular, 1187, 1188f
- gallbladder, 1203-1204
 - classification and staging of, 1402-1403, 1404f
 - clinical findings on, 1403
 - differential diagnosis of, 1408
 - epidemiology of, 1402
 - etiology of, 1402
 - fossa masses, 1406-1408, 1407f
 - gastroduodenal metastases from, 577, 579f
 - magnetic resonance
 - cholangiopancreatography on, 1156
 - magnetic resonance imaging of, 1193-1194, 1194f
 - pathologic findings in, 1402-1405
 - pathways of spread in, 1408-1409
 - PET/CT of, 1203-1204, 1204f
 - polypoid masses, 1406, 1407f
 - radiographic findings on, 1403-1409, 1404f-1405f
 - treatment and prognosis of, 1409-1410
 - wall thickening in, 1403-1406, 1405f
- gastric, 546-565
 - advanced, 550-554, 560
 - after partial gastrectomy, 547
 - atrophic gastritis and, 506, 547
 - of the cardia, 535-557, 556f
 - classification of, 548, 558
 - clinical findings in, 548-549

Carcinomas (Continued)

- with common variable immunodeficiency, 763
- Crohn's disease association with, 508
- CT findings on, 557-559, 557f-559f, 561-562, 562f
- dietary factors in, 546-547
- differential diagnosis of, 559-560, 658t-659t
- early, 549-550, 550f, 559
- endoscopic findings on, 549
- endoscopic ultrasonography of, 562-565, 563f-564f
- epidemiology of, 546
- esophageal metastases from, 394
- gastric outlet obstruction from, 660t
- gastric polyps in, 547
- hereditary factors in, 547
- H. pylori* in, 500-501, 546-547
- hyperplastic polyps and, 523
- infiltrating, 528f
- Ménétrier's disease and, 547
- metastatic, 560f-561f, 563f
 - differential diagnosis of, 578-580
- pathology of, 547-548
- pernicious anemia in, 547
- polypoid, 551, 551f-552f
 - differentiated from adenomatous polyps, 526, 527f
- prolapsed, 552f
- radiographic findings on, 549-555, 550f
- recurrence of after gastrectomy, 641
- routes of spread of, 548
- scirrhous, 529f, 550, 551f, 554-555, 555f-556f
- secondary achalasia caused by, 556-557, 557f
- staging, 560-565
- survival rates for, 580
- synchronous, 552f
- treatment and prognosis of, 565
- ulcerated, 527f-528f, 529, 551-553
- gastric cardia, 446, 446f
- hepatocellular, 1190-1192
 - diffusion-weighted MRI of, 1222
 - pediatric, 2204, 2204f
- kidneys
 - renal cell, 1198-1199, 1199f
 - transitional cell, 1199, 1199f
- oat cell, 1589-1590
- ovarian, 1111-1113
- pancreatic
 - gastroduodenal metastases from, 574-576, 577f-578f
 - magnetic resonance
 - cholangiopancreatography on, 1328, 1329f
 - PET/CT in staging, 1781
- periampullary, 566, 566f, 1307, 1310-1311, 1311f
- renal cell, 576, 1198-1199
- small bowel
 - computed tomography enteroclysis on, 697-699
 - obstruction from, 819f
 - superficial spreading
 - differential diagnosis of, 463t
- thyroid, 1095
- ulcerated, 477-479
- urachal, 2073
- varicoid, 431, 431f
- Carcinomatosis
 - peritoneal, 2043-2044, 2043f-2044f
 - small bowel, 816
- Cardiac disease
 - diffusion-weighted MRI on, 1218-1219
 - with imperforate anus, 2114
 - liver in, 1688-1689

- Cardiac rosette, 439, 439f, 555
- esophageal carcinoma and changes in, 576
- Cardiomyotomy, for achalasia, 460, 460f
- Carman-Kirklin meniscus complex, 553
- Caroli's disease, 606f-607f, 607, 2191-2193, 2193f, 2201-2202. *See also* Choledochal cysts
- hepatic resection for, 1720
- Caroli's syndrome, 2191-2192, 2201
- Carpet lesions
 - colon, 1032, 1034f
 - double-contrast studies of, 47, 49f
- Cartilaginous tumors
 - of the pharynx, 252
- β -catenin-mutated hepatocellular adenomas, 1189
- Cathartic agents
 - for computed tomography colonography, 905-907, 907f
- Cathartic colon, 1126, 1126f
- Catheter drainage. *See* Percutaneous catheter drainage of abdominal abscesses
- Cat-scratch disease, 1938, 2211, 2236, 2236f
- Caudal regression, 2117
- Caustic colitis, 1022-1023
- Caustic esophagitis
 - contrast agents with, 332
 - dysphagia from, 331
 - esophageal ulcers in, 332, 332f-333f
 - strictures from, 331-332, 333f-334f, 367, 373
- Caustic ingestion
 - antral narrowing from, 560
 - differential diagnosis of, 464t
 - duodenitis from, 519
 - esophagitis from, 330-333, 332f-333f
 - gastric and duodenal damage from
 - pediatric, 2153-2154, 2154f
 - gastric narrowing from, 659f
 - gastric outlet obstruction from, 613
 - gastroduodenal injuries from, 515-516, 516f-517f
 - midesophageal strictures caused by, 308, 308f
 - multiple duodenal ulcers from, 484
 - pediatric
 - esophageal damage from, 2153-2156, 2155f-2157f
 - squamous cell carcinoma associated with, 367, 373
 - strictures from, 464t
 - surgery for, 453
 - thickened gastric folds from
 - differential diagnosis of, 659t
- Cavernous hemangiomas, 1186-1187, 1187f
- differential diagnosis of, 1767f
- Cavernous transformation of the portal vein (CTPV), 1693, 1695f-1696f
- CD-117 expression, 531, 587
- Cecal bascule, 1109-1110
- Cecostomy, 1136, 1136f
- Cecum. *See also* Appendix
 - adenocarcinomas of, 1050f
 - adhesions in, 1109-1110
 - with appendicitis, 185
 - carcinomas
 - differentiated from appendicitis, 971, 973f
 - coned, differential diagnosis of, 1148t
 - diverticulitis in, 946, 947f
 - filling defects, differential diagnosis of, 1148t
 - mobile, 1151t
 - volvulus of, 183-184, 184f, 1105, 1107f
- Celiac artery
 - in pancreatic blood supply, 1773

- Celiac artery aneurysms, 1700
- Celiac disease
- with bubbly bulb, 319, 319f
 - complications with, 765-766
 - duodenal carcinoma with, 365
 - duodenal lymphoma with, 387
 - on enteroclysis, 681, 681f
 - fold enlargement in, 786
 - GI bleeding from, 688-689
 - lymphadenopathy in, 769, 782
 - magnetic resonance enterography on, 720-721
 - malabsorption in, 778-781
 - megaduodenum in, 661f
 - mesenteric adenitis in, 969
 - peliosis hepatis with, 1690
 - with primary biliary cirrhosis, 1649-1650
 - radiographic findings on, 758f, 765
 - small bowel
 - luminal narrowing in, 873f
 - site predilection of, 875f
 - small bowel fold thickening in, 872f
 - squamous cell carcinoma associated with, 367
 - thickened duodenal folds from, 661f
 - villous atrophy in, 758f, 762
- Celiac nerve blocks, 1776
- Celiac plexus, 1897
- Cellulitis, abdominal wall, 2072
- Central nervous system
- abnormalities with Cowden's disease, 1095
 - malignancies, in Turcot syndrome, 1092
- Centrilobular pattern, 1637
- Cerebrospinal fluid ascites, 2022
- Cerebrovascular accident
- dysphagia after, 231
- Ceruletide
- effects of on gallbladder, 21
 - gastrointestinal effects of, 20
- Cervical carcinoma
- colonic involvement of, 1113
- Cervical esophageal pouches, 241
- Cervical esophageal webs, 241-242, 243f
- Cesarean section, hematomas from, 2071
- Cestodes, 759
- Chagas' disease
- esophageal motility disorder from, 289
 - malabsorption in, 776b
 - nonobstructive megacolon in, 1123
 - secondary achalasia from, 396-397
 - small bowel infection in, 760
 - superior mesenteric root syndrome caused by, 614
- Chemical ablation, 1506
- Chemical shift imaging, 1633-1635
- Chemoembolization
- of hepatocellular carcinomas, 1740f
 - of liver tumors, 1725-1726, 1728-1729
 - radiofrequency ablation with, 1726
 - transarterial, 1505-1506, 1512, 1512f
- Chemoradiation therapy
- Chemotherapy
- biliary tract strictures from, 1435f
 - candidiasis infection with, 762f
 - esophagitis from, 2138, 2138f
 - fluorinated antipyrimidines in, 762-763, 763f
 - for gastric lymphomas, 584, 584f-585f
 - for GIST, 800, 802f
 - hepatic steatosis from, 1629-1630
 - for liver metastases, 1206-1207
 - liver toxicity from, 1639
 - sinusoidal obstruction syndrome in, 1680
 - for small bowel lymphomas
 - perforation risk with, 802-804, 803f
 - transarterial chemoembolization, 1505-1506, 1512f
- Chest pain
- in chronic graft-versus-host disease, 342
 - with diffuse esophageal spasm, 284-286
- Chest pain (Continued)
- with esophageal intramural pseudodiverticulum, 346
 - with presbyesophagus, 286-287
- Chest radiography
- on ascites, 2027
 - epiphrenic diverticulum on, 425
 - of esophageal squamous cell carcinoma, 371, 371f
 - on hepatopulmonary syndrome, 433
 - on pancreatitis, 1812
 - of postoperative esophagus, 449
- Chlamydia
- in pelvic inflammatory disease, 1113
 - in ulcerative colitis, 985
- Choi criteria of tumor response, 2300, 2301f, 2302f
- Cholangiocarcinomas, 1307, 1309f, 1410-1419
- bile leaks after resection of, 1455
 - with Caroli's disease, 2192
 - clinical findings on, 1411
 - clonorchiasis associated with, 1440
 - delayed iodine scanning on, 1483-1484
 - differential diagnosis of, 1408, 1431-1432
 - epidemiology of, 1410-1411
 - extrahepatic, 1419, 1421f
 - hilar, 1415-1417, 1416f-1418f
 - magnetic resonance
 - cholangiopancreatography on, 1329-1330, 1420f
 - surgical resectability of, 1418f
 - intraductal growing, 1411, 1413f
 - intrahepatic, 1413-1415, 1414f-1415f, 1579-1581
 - incidence and clinical presentation of, 1580
 - pathologic findings on, 1579-1580, 1580f, 1580t
 - radiologic findings on, 1580-1581, 1580t
 - liver transplantation for, 1737
 - magnetic resonance cholangiopancreatography
 - on, 1329-1330, 1330f
 - magnetic resonance imaging of, 1194, 1195f
 - mass forming, 1411, 1412f, 1413-1415, 1414f
 - metastatic
 - biliary spread of, 2008
 - mucin-secreting, 1414-1415, 1416f
 - papillary, 1307, 1309f-1310f
 - pathologic findings on, 1411
 - periductal infiltrating, 1411, 1412f
 - PET/CT of, 1202-1203, 1203f
 - radiographic findings on, 1411-1419, 1412f-1413f
 - with sclerosing cholangitis, 1421f, 1427
 - transarterial chemoembolization of, 1512
 - treatment of, 1419
- Cholangiography. *See also* Endoscopic retrograde cholangiopancreatography (ERCP); Magnetic resonance cholangiopancreatography (MRCP)
- contrast agents for, 13-14
 - direct, 1295-1299
 - of hilar cholangiocarcinomas, 1416-1417, 1419f
 - on liver abscesses, 1609
 - normal anatomy in, 1297-1298
 - operative and postoperative, 1298-1299, 1298f-1299f
 - percutaneous transhepatic, 1281, 1295-1297, 1296f
 - on primary sclerosing cholangitis, 1428
 - transcholecystic, 1297
- Cholangiopancreatography. *See* Endoscopic retrograde cholangiopancreatography (ERCP); Magnetic resonance cholangiopancreatography (MRCP)
- Cholangitis
- ascending, biliary spread of, 2006
 - with cholangiocarcinomas, 1411
 - echinococcal, 1440
 - from endoscopic retrograde cholangiopancreatography, 1322
 - eosinophilic, 1432
- Cholangitis (Continued)
- floxuridine, 1437
 - obstructive, 1434-1435, 1436f
 - primary sclerosing
 - differential diagnosis of, 1465f
 - interventional radiography for, 1399
 - with primary sclerosing cholangitis, 1427
 - pyogenic
 - recurrent, 1376f
- Cholecystectomy, 1178
- biliary complications after, 1311, 1315f
 - biliary duct dilation after, 1290
 - cholangiography in, 1298-1299, 1299f
 - laparoscopic, 1442-1453
 - biliary tract complications after, 1444-1453
 - abscesses, 1445-1447, 1449f, 1454f
 - bile duct injury and bile leakage, 1445-1448, 1445f-1448f
 - imaging of, 1450-1452
 - retained biliary stones, 1448, 1450f
 - spilled biliary stones, 1452-1453, 1452f-1454f
 - strictures, 1449-1452, 1450f
 - general complications after, 1441
 - normal imaging findings after, 1442-1443, 1444f
 - technical considerations for, 1442, 1443f
 - percutaneous, 1392-1394, 1394f
 - spilled gallstones after laparoscopic, 1375-1377, 1378f
- Cholecystitis
- acalculous
 - acute, 1360-1362, 1361f-1362f
 - chronic, 1369
 - interventional radiology for, 1394
 - pediatric, 2193-2194
 - acute, 1352-1360
 - acute abdomen from, 2260-2261, 2260f-2261f
 - complications of, 1362-1369
 - differential diagnosis of, 1464f
 - gallbladder perforation with, 1367-1369, 1368f-1369f
 - gallbladder wall thickening in, 1404
 - imaging of, 1355-1360, 1358f
 - cholescintigraphy, 1348, 1356
 - computed tomography, 1359-1360, 1359f-1360f
 - Doppler, 1356-1359, 1359f
 - magnetic resonance, 1360, 1361f
 - ultrasound, 1358f-1359f
 - pathogenesis and epidemiology of, 1352-1354
 - percutaneous gallbladder aspiration for, 1394
 - acute acalculous, 1361f
 - with AIDS, 1653
 - cholecystoduodenal fistulas caused by, 625, 625f
 - cholescintigraphy on, 1286
 - chronic, 1369-1370
 - differential diagnosis of, 1464f
 - with gallbladder carcinomas, 1404
 - imaging of, 1369, 1370f
 - pathogenesis and epidemiology of, 1369
 - xanthogranulomatous, 1369-1370, 1371f
 - emphysematous, 1365-1367, 1366f-1367f
 - with gallbladder duplication, 1341
 - gangrenous, 1193, 1356, 1362-1364, 1363f
 - gastric outlet obstruction from, 613
 - hemorrhagic, 1364-1365, 1365f
 - liver abscesses from, 1608-1609
 - magnetic resonance cholangiopancreatography
 - on, 1356, 1337f
 - xanthogranulomatous, 1408
- Cholecystoduodenal fistulas, 625, 625f
- Cholecystojejunostomy, 1868
- Cholecystokinin, 20
- Cholecystolithotomy, percutaneous, 1398
- Cholestyramine, 1342

- Cholecystoses, hyperplastic, 1379-1385
 adenomyomatosis, 1381-1385, 1383f-1385f
 cholesterosis, 1379-1380, 1382f
- Cholecystostomy
 percutaneous, 130f
- Choledochal cysts, 1343-1345, 1422, 2201
 cholangiocarcinomas with, 1419, 1422f
 classification of, 1343f-1345f
 magnetic resonance cholangiopancreatography on, 1330, 1332f
 widening of the duodenal sweep caused by, 618, 618f
- Choledochal malformations, 2182, 2190-2191, 2190f-2192f
- Choledochal sphincter, 1283
- Choledochoceles, 1344f, 1345
 pediatric, 2151-2152
- Choledochoduodenal fistulas, 491, 491f
- Choledochojunostomy, 1868
- Choledocholithiasis, 1193f, 1370-1374
 acute abdomen from, 226f
 imaging of, 1371-1374
 computed tomography, 1371-1372, 1372f-1373f
 endoscopic retrograde cholangiopancreatography, 137f
 magnetic resonance, 1372-1374, 1373f-1374f
 ultrasound, 1371, 1372f
 magnetic resonance cholangiopancreatography on, 1292, 1326-1328, 1327f-1328f
 magnetic resonance imaging of, 1192, 1193f
 pancreas ultrasound of, 1777-1778
 pathogenesis and epidemiology of, 1370-1371
 pediatric, 2194-2195, 2195f
- Cholelithiasis, 746-748, 1348-1351. *See also* Mirizzi syndrome
 abdominal radiography on, 1349, 1349f
 acute cholecystitis and, 1192-1193, 1193f, 1352-1354
 artifacts that mimic, 1462t
 common duct stone removal, 1398
 complications with
 gallstone ileus, 1348, 1377-1379, 1380f-1381f
 spilled gallstones after laparoscopic cholecystectomy, 1375-1377, 1377f-1378f
 computed tomography on, 1353f, 1377-1379
 with Crohn's disease, 1010
 with gallbladder duplication, 1341
 gallstone ileus from, 1348, 1377-1379
 intragastric and intraduodenal, 621
 magnetic resonance imaging of, 1192, 1193f
 magnetic resonance imaging on, 1351, 1354f
 pathogenesis and epidemiology of, 1348-1349
 pediatric, 2193-2194, 2193f
 retained biliary stones after laparoscopic cholecystectomy, 1448, 1450f
 small bowel obstructions by, 821, 822f
 spilled biliary stones after laparoscopic cholecystectomy, 1452-1453, 1452f-1454f
 ultrasound on, 1178-1179, 1179f, 1349-1350, 1350f
 wall-echo-shadow sign, 1350-1351
- Cholelithoptysis, 1453
- Cholescintigraphy, 1286
 acute cholecystitis imaging in, 1355-1356, 1357f
 acalculous, 1362
 chronic cholecystitis in
 acalculous, 1369
- Cholestasis, 2182
- Cholestasis familiaris groenlandica, 2189-2190
- Cholestasis Guideline Committee, 2182
- Cholesterol, 774
 in gallstones, 1348-1349
 polyps, 1406, 1408, 1410
- Cholesterosis, 1379-1380, 1382f
- Chondrosarcomas
 esophageal, 408
- Choriocarcinomas
 gastroduodenal, 598
- Chromophobe cell renal cell carcinomas, 1198-1199
- Chronic granulomatous disease, 1022, 2152, 2153f, 2211-2212
- Chronic mesenteric ischemia, 835-838, 837f
- Chronic mucocutaneous candidiasis, 314
- Chronic remnant gastritis, 638-639
- Churg-Strauss syndrome, 838-839
- Chylomicrons, nonformation of, 784, 784f
- Chylous ascites, 2025-2026
- Circumferential resection margin (CRM)
 for colorectal cancer, 92-93
- Cirrhosis, 1654-1670
 with AIDS, 1652
 ascites from, 2024, 2032-2034
 biopsies with, 1500-1501
 classification of, 1655f
 computed tomography on, 1164
 contrast agents with, 1452
 diagnosis of with diffusion-weighted MRI, 1223
 epidemiology of, 1654
 etiology of, 1655f
 fibrolamellar carcinomas with, 1573-1575
 glycogen storage disease and, 1644
 hepatocellular carcinomas differentiated from, 1567-1569
 hypersplenism in, 1909
 image-guided biopsy with, 1248
 imaging findings on, 1765t
 intestinal edema with, 867, 867f
 left hepatic lobe atrophy from, 1525
 liver surface nodularity in, 1178
 liver transplantation for, 1738
 preoperative imaging for, 1739
 magnetic resonance imaging of, 1190-1192
 nonalcoholic fatty liver disease-related, 1630
 pathophysiology of, 1654-1655, 1654f
 pediatric, 2212-2215, 2213f
 portal hypertension in, 1655-1656, 1655f
 classification of, 1655t
 computed tomography on, 1668-1670, 1669f
 magnetic resonance imaging on, 1670, 1670f
 transjugular intrahepatic portosystemic shunt for, 1670, 1671f
 ultrasound on, 1665-1668, 1665f-1667f
- primary biliary, 1432-1434, 1433f, 1435f, 1649-1650, 1649f
 differential diagnosis of, 1465t
 with primary sclerosing cholangitis, 1428f, 1431f
 radiologic findings on, 1656-1659
 extrahepatic, 1659-1662, 1665
 liver morphology, 1656-1665, 1657f, 1658f
 specific, 1658-1659, 1659f
 on ultrasound, 1659-1660
 vascular changes, 1661
 secondary biliary, 1650-1651, 1651f-1652f
 with double gallbladder, 1341
 from steatosis, 1630
 transjugular intrahepatic portosystemic shunts for, 1670, 1670f
 ultrasound on, 1170f
 varices with, 1656
 vascular changes in, 1660
 with viral hepatitis, 1637-1638
- Cisapride, 20
- C-kit. *See* CD-117 expression
- Clear cell renal cell carcinomas, 1198-1199
- Cloacal malformation, 2117
- Cloacogenic carcinomas, 1081-1082, 1082f, 1119, 1120f-1121f
- Clonorchiasis, 1413-1414, 1414f
 biliary tract, 1437-1440, 1438f
 life cycle of, 1439f
- Clonorchis sinensis*, 1410, 1411
 biliary spread of, 2008
- Closed loop obstruction, 182
- Clostridium difficile*
 in graft-versus-host disease, 764
 in pseudomembranous colitis, 64, 65f, 1024, 1024f, 2265
- Clostridium perfringens*
 in emphysematous gastritis, 514-515
- Cobblestoning
 Brunner gland hyperplasia associated with, 540-541, 540f
 in Crohn's disease, 62f, 507-508, 729-730, 729f, 988, 1001, 1002f
 in double-contrast studies, 42, 43f
 on small bowel follow-through, 678
- Coccygeus muscle, 175, 175f
- Coffee
 antral gastritis caused by, 499
 ulcers caused by, 468
- Coiled spring sign, 43, 44f, 822-823
 in appendiceal intussusception, 973-974
 of intussusceptions, 1109
- Colchicine, 1625
- Colectomy
 for familial adenomatous polyposis syndrome, 1089-1090
- Colitis, 984-1016
 after pancreas transplantation, 154
 caustic, 1022-1023
 collagenous, 1021, 2166
 cystica profunda, 1120, 1122f, 1127
 cytomegalovirus, 1019-1020, 1019f
E. coli in, 1018, 1019f
 eosinophilic, 1021
 granulomatous, 1013
 microscopic (collagenous), 1021
 neutropenic (*See* typhlitis)
 noninfectious, 1021-1022
 pediatric, 2167-2168
 pseudomembranous, 1024, 1024f
 radiation, 1116-1117, 1117f
 toxic megacolon with, 1009
 ulcerative (*See* Ulcerative colitis) pediatric, 2167
- Collagenous colitis, 1021, 2168
- Collagen vascular diseases
 colonic, 1124
 esophageal, 288-289, 288f-289f
- Collar button ulcers
 in double-contrast studies, 51, 52f
 in ulcerative colitis, 988, 989f
- Collecting duct renal cell carcinomas, 1198-1199
- Colloidal bismuth, 469
- Colon. *See also* Appendix; Colitis
 adenocarcinomas of
 computed tomography on, 1043f-1044f
 angiodysplasia, 1076-1077
 angiodysplasia of the, 122, 122f
 angiography of, 116-119, 119f
 anorectal and pelvic floor dysfunction and, 890-904
 with appendicitis, 185
 atresia of, 2112f, 2113
 barium studies of, 879-889
 cancer, 1027-1073
 adenocarcinomas, 1035-1057
 advanced, 1035-1036, 1037f

Colon (*Continued*)

- benign polyps versus, 1031-1035
- with carpet lesions, 1032, 1034f
- causative factors for, 1027
- clinical aspects of, 1029
- complications with, 1027-1029
- computed tomography of, 1039-1050, 1061-1062, 1061f, 1063f
- cross-sectional imaging on, 1057-1058, 1067-1068
- differential diagnosis of soft tissue stranding and, 1062b
- differential diagnosis of wall thickening and, 1058b
- early, 1035, 1035f-1036f
- endoluminal ultrasonography on, 1055-1056
- epidemiology, 1027
- evaluation of, 1028f
- factors in, 1027-1029
- hereditary factors in, 1028
- immunoscintigraphy on, 1066f
- immunoscintigraphy with monoclonal antibodies on, 1056, 1066, 1066f
- with juvenile polyposis, 1096, 1097f
- magnetic resonance imaging of, 1050-1054, 1050f-1051f, 1062-1065, 1063f-1065f
- recurrent, 1066f
- metastatic, 1045f-1046f, 1082-1086, 1084f, 1113-1114
- in the biliary tract, 1313j
- from cervix, 1113
- direct invasion from contiguous, 1082-1083, 1083f-1084f
- direct invasion from noncontiguous, 1083-1084, 1084f-1085f
- embolic, 1086
- gynecologic, 1111
- intrapertitoneal seeding of, 1084-1086, 1085f-1086f
- from the liver, 1591i
- from ovaries, 112f
- pathology of, 1590
- mosaic-submucosal edema pattern in, 1145f
- obstruction rates in, 1104
- pathogenesis of, 1029
- positron emission tomography on, 1066-1067, 1067f-1068f
- postoperative, 1058-1067
- radiology and diagnostic methods for, 1029-1031
- colonoscopy, 1030
- contrast enema, 1029-1030, 1030f
- cross-sectional imaging, 1030-1031
- recurrence of, 1043, 1060f, 1062f-1063f
- cross-sectional imaging on, 1067-1068
- staging, 1047-1050, 1048e-1049t
- with immunoscintigraphy with monoclonal antibodies, 1056
- with magnetic resonance imaging, 1052f-1053f, 1052t, 1053-1054
- with positron emission tomography, 1056-1057
- with scintigraphy, 1056
- synchronous tumors in, 1036, 1038f
- transrectal ultrasound on, 1054-1056, 1055f, 1065
- Turcot syndrome, 1092
- carcinomas of
- cloacogenic, 1081-1082, 1082f, 1119, 1120f-1121f
- computed tomography on, 1039-1050, 1041f-1042f
- gastrointestinal metastases from, 576-577, 579f
- obstructions from, 1104-1105
- ovarian metastases, 580f
- squamous cell, 1080-1081, 1081f

Colon (*Continued*)

- cathartic, 1126, 1126f
- computed tomography colonography of, 905-927
- diameter of, in ulcerative colitis, 987
- differential diagnosis of, 1144-1151
- annular "apple-core" lesions, 1146t
- anterior indentation on the rectosigmoid junction, 1151t
- appendiceal lesions, 1148t
- cecal filling defects, 1148t
- coned cecum, 1148t
- distention without obstruction, 1147t
- enlarged ileocecal valve, 1148t
- filling defects, multiple, 1145t
- filling defects, solitary, 1145t
- fistulas, 1149t
- gas in the colon wall, 1148t
- mosaic-submucosal edema patterns, 1145t
- obstruction in newborns, 1147t
- obstruction in postneonatal children, 1147t
- pneumatosis cystoides coli, 1148t
- segmental narrowing, 1146t
- toxic megacolon, 1148t
- distention of without obstruction, 1147t
- diversion colitis, 1125-1126
- diverticular disease of, 934-954
- carcinoma detection with, 1036, 1039f
- diverticular hemorrhage, 951, 951f-952f
- diverticulitis, 60-61, 61f, 937-949
- diverticulosis, 934-937
- giant sigmoid diverticulum, 952, 952f
- transverse, duodenal displacement from, 616
- duodenal impressions by, 661t
- embryology of, 1985, 1985f
- endocrine tumors in, 1077, 1078f
- eudometriosis in, 1111
- extracolonic diseases involving, 1110-1114
- fatty lesions of, 1077-1079, 1078f-1079f
- fluid absorption in, 774
- functional disorders of, 1120-1124
- hyperrotation of, 2092
- ileus of, 181
- inflammatory conditions of, 1017-1026 (*See also* Inflammatory bowel disease [IBD])
- bacterial infections, 1017-1019
- exogenous colitis, 1022-1024
- fungal infections, 1021
- neutrophil and macrophage dysfunction, 1022
- noninfectious colitis, 1021-1022
- parasitic infections, 1020-1021
- viral infections, 1019-1020, 1019f
- ischemia of, 1114-1116, 1114f-1115f
- lymphangiomas of, 1076
- lymphomas of, 1074-1075, 1075f
- magnetic resonance colonography, 928-933
- malignancies of
- magnetic resonance imaging of, 90-93
- metastatic, 93f
- megacystis-microcolon-intestinal hypoperistalsis syndrome in, 2120-2121, 2120f
- mesenteric attachments of, 578t
- metastatic cancer in, 105f
- normal anatomy of, 171, 173
- normal walls of, 70
- obstruction of, 1102-1110
- major types of, 1104-1110
- radiographs of, 169f
- obstructions of, 181-182, 182f
- pediatric disorders of, 2164-2179
- anterior anus, 2164, 2165f
- appendicitis, 2169-2170, 2169f
- carcinoma, 2176
- colitides and causes of diarrhea, 2165-2168
- fibrosing colonopathy, 2176

Colon (*Continued*)

- hemolytic uremic syndrome, 2168-2169, 2168f
- Hirschsprung's disease, 2165-2167, 2166f-2167f
- inflammatory bowel disease, 2167
- intussusception, 2172-2174, 2173f-2174f
- juvenile polyps, 2175-2176
- lymphoid follicular pattern and hyperplasia, 2164, 2165f
- typhilitis, 2170-2172
- volvulus, 2174-2175, 2175f
- PET/CT of, 103-107
- polyposis syndromes in, 1089-1101
- familial adenomatous, 1089-1093
- polyps
- adenocarcinomas, 1035-1057
- benign, 1031-1035
- detection of, 1032-1035, 1034f-1035f
- distribution of, 1031f
- endoscopic polypectomy of, 1032f
- incidence of, 1031, 1031f
- pathology of, 1031
- carpet lesions, 1032, 1034f
- postoperative, 1133-1143
- after abdominoperineal resection, 1138
- after appendectomy, 1138, 1139f
- after cecostomy, 1136, 1136f
- after colonoscopy, 1133-1136, 1135f-1136f
- after Hartmann procedures, 1138, 1138f
- after ileal pouch-anal anastomosis, 1139-1142, 1139f, 1142f
- leaks from, 1140f-1141f
- after low anterior resection, 1136-1137, 1137f
- after mucous fistula, 1138
- after proctectomy and coloanal anastomoses, 1137-1138, 1137f-1138f
- after segmental resection, 1133, 1134f
- after side-to-side enterocolic anastomosis, 1133, 1134f
- segmental resection, 1134f
- sexually transmitted diseases in, 1113
- stromal tumors, 1079-1080, 1081f
- toxic megacolon, 185-186, 186f
- transit studies, 902
- transverse
- carcinomas of
- omental metastases of, 578
- vascular lesions, 1075-1077
- anorectal, 1117-1120
- wall thickening in, differential diagnosis of, 1058b
- Colon cancer
- hematogenous spread of, 300b
- hemorrhage from, 228b
- metastases from
- liver, 1590-1591
- Colon cutoff sign, 1811-1812, 1812f, 2045
- Colonic interposition, 455-458, 458f
- Colonic stents, 1142, 1142f
- Colonography
- computed tomography, 905-927
- alternative protocols for, 911-912
- beam hardening in, 915, 915f
- bowel preparation for, 905-908, 907f, 912
- characterization of polyps in, 914-916, 914f
- colonic distention in, 908-910, 909f, 911f
- colon movement in, 915, 917f
- for colorectal cancer screening, 905, 921
- complications with, 922
- detection in, 911f, 912-914, 913f, 916f, 918f
- computer-aided, 918-919, 918f
- diagnostic indications for, 921-922
- extracolonic findings in, 923, 924f
- image acquisition in, 910-911
- indications for, 920-922

- Colonography (Continued)**
 interpretation of, 912-919
 computer-aided, 918-919
 literature reports on, 919-926
 polyp coating in, 907-908, 908f, 912
 radiation exposure in, 922-925
 reporting in, 918-919, 919f
 soft tissue and polyp differential in, 916-918
 for staging and surveillance, 922
 tagging in, 905-906, 906f, 912, 916, 917f
 technical components in, 905-912
magnetic resonance, 928-933
 accuracy of, 931
 bowel preparation for, 931-932
 contraindications to, 928
 data analysis in, 931
 guidelines for, 928
 indications for, 930
 multiplanar reformation mode in, 928
 patient acceptance of, 931-932
 prerequisites for, 928
 scar artifacts in, 928-929, 930f
 sequences in, 928, 929f, 929f, 931
 tagging agents in, 932, 932f
- Colonoscopy**
 accuracy of, 931
 on colonic ischemia, 1116
 colon polyp detection with, 1034f
 on colorectal cancer, 1030
 computed tomography colonography versus, 921-922
 ileocecal valve examinations in, 928
 ileocolonoscopy with computed tomography enterography, 692
 magnetic resonance colonography as adjunct to, 930
 with Peutz-Jeghers syndrome, 1093-1094
Colorectal cancer
 adenocarcinomas, 1035-1057
 circumferential resection margin for, 92-93
 complications with, 1036-1039
 computed tomography on, 1039-1050
 in inflammatory bowel disease, 1008-1009
 magnetic resonance imaging of, 90-91, 91f
 metastases of
 in the liver, 1720, 1720f
 tumor ablation of, 1508
 PET/CT of, 103-107, 104f-105f
 restaging and treatment response of, 105-107
 screening for
 computed tomography colonography in, 905, 921
 magnetic resonance colonography in, 930
 staging and surveillance of
 with computed tomography colonography, 922
 magnetic resonance colonography in, 929
 staging of, 92, 104-105
Colorectal transit studies, 1122, 1123f
Colostomy, 1133-1136, 1135f
 divided, and mucous fistula, 1135-1136, 1136f
 double-barreled, 1135
 double-contrast studies after, 887, 888f
 end-, 1135
 loop, 1135
 segmental resection with, 1133
Combined plane, 1903f, 1907f
Comb sign, 75, 75f, 744, 1004
Comet-tail artifacts, 1174, 1175f, 1383f
Common bile duct, 1283f. See also Biliary tract
 computed tomography of, 1779
 congenital abnormalities in, 1808
 cystic duct and, 1281-1282
 diameter of, 1305
 embryology of, 1797
Common bile duct (Continued)
 extrahepatic ducts and, 1283, 1283f
 normal anatomy of, 1304-1305
 strictures in, 1316f
 on ultrasound, 1288-1290
 ultrasound of, 1777-1778
Common hepatic duct, 1281-1282, 1283f, 1304
Common variable immunodeficiency, 763
Computed tomographic cholangiography (CTC), 13-14
Computed tomography (CT). See also Computed tomography angiography (CTA); Perfusion computed tomography
 3D reconstruction methods in, 828
 abdominal, 165-177
 of abdominal abscesses, 1255-1257, 1255f, 1257f-1258f
 on abdominal trauma, 2283
 bowel, 2287-2292
 image interpretation in, 2284
 imaging techniques and interpretation with, 2283-2284
 kidneys, 2285-2287, 2287f, 2288f
 liver and spleen, 2284-2285, 2285f, 2286f, 2287f
 mesentery, 2290, 2291f-2292f
 pancreas, 2285, 2286f, 2287f
 acute cholecystitis imaging in, 1355
 acalculous, 1361f, 1362
 gangrenous, 1364f-1365f
 after laparoscopic adjustable gastric band placement, 649
 after Roux-en-Y gastric bypass, 643
 after sleeve gastrectomy, 652, 652f
 angiography, 1164
 on appendicitis, 961-966, 962f-964f, 967f
 protocols for, 964-966
 with arterial portography, 1043-1047
 on ascites, 2029-2031, 2030f
 on biliary postoperative complications, 1450-1451
 biliary tract, 1290-1292, 1291f
 on cholangiocarcinomas, 1411-1413, 1412f-1414f
 of choledocholithiasis, 1371-1372, 1372f-1373f
 colon
 of benign polyps, 1035f
 cancer staging with, 1047-1050, 1048f-1049f, 1049f
 of carcinomas, 1039-1050
 mural thickening in, 1151f
 on obstructions, 1103-1104, 1104f
 polyp detection with, 1032-1035, 1035f
 postoperative, 1061-1062, 1061f-1062f
 on colonic ischemia, 1116, 1116f
 on Crohn's disease, 988f, 994f, 1002-1004, 1006f
 for diffuse esophageal spasm, 285
 of diffuse esophageal spasm, 287f
 on diverticulitis, 940-941, 941f-942f, 941f
 on diverticulosis, 937, 937f
 dosimetry and dose reduction in, 1158-1159
 dual-energy, 1157-1158, 1158f, 1166
 liver, 1486-1487, 1487f
 virtual noncontrast imaging, 1487
 of duodenal carcinoma, 565-566
 on echinococcal disease, 1934, 1934f
 in esophageal cancer staging, 380-382, 388f, 389
 of esophageal perforations, 417, 417f
 future of, 1166
 gallbladder, 1281, 1284-1286
 acute cholecystitis, 1359-1360, 1359f-1360f
 adenomyomatosis, 1384, 1384f-1385f
 on carcinomas, 1406-1408, 1407f
 in differential diagnosis, 1462
Computed tomography (CT) (Continued)
 on mural thickening, 1405f, 1406
 porcelain, 1350, 1352f
 gallstones, 1377-1379
 Mercedes-Benz sign, 1350, 1351, 1353f
 on gastric varices, 604, 606f
 of gastroduodenal lymphomas, 585, 585f
 gastrointestinal
 contrast agents for, 11-12
 multidetector-row, 67-78
 helical
 liver, 1482
 on hepatopulmonary syndrome, 433
 image-guided percutaneous tissue acquisition, 1242-1243, 1242f
 image postprocessing in, 1161-1162
 on imperforate anus, 2115-2116, 2116f
 interpretation principles in, 1161
 on intussusceptions, 1109, 1110f
 liver, 1489
 on AIDS-related disorders, 1653
 on alcoholic hepatitis, 1639
 on amebic abscesses, 1612, 1614f
 angiography and portography, 1484
 on angiosarcomas, 1586
 on bacterial (pyogenic) abscesses, 1610, 1611f
 biphasic helical, 1483, 1483f
 on Budd-Chiari syndrome, 1683-1684, 1685f
 on cirrhosis, 1660-1662, 1663f
 contrast-enhanced, 1481-1484, 1482f
 on cystadenomas and cystadenocarcinomas, 1383
 delayed iodine scanning, 1483-1484, 1483f
 differential diagnosis in, 1761
 dual-energy, 1486-1487
 on echinococcal disease, 1618-1619, 1619f, 1621f
 on fibrolamellar carcinoma, 1575, 1576f
 on focal nodular hyperplasias, 1539, 1540f
 on glycogen storage disease, 1645, 1645f
 helical portal venous phase, 1483
 of hemangiomas, 1532-1533, 1533f
 on hemochromatosis, 1642-1643, 1642f
 on hepatic congestion, 1689, 1689f
 on hepatoblastomas, 1578-1579, 1579f
 on hepatocellular adenomas, 1544, 1544f-1545f
 on hepatocellular carcinomas, 1564-1567, 1566f-1567f
 on infantile hemangioendothelioma, 1554, 1555f
 on intrahepatic cholangiocarcinomas, 1580, 1581f
 on lipomas, 1549-1550, 1549f-1550f
 of mesenchymal hamartomas, 1555, 1556f
 on metastases, 1595-1598, 1596f-1597f, 1597f
 of nodular regenerative hyperplasia, 1549
 noise reduction techniques for, 1485, 1485f
 perfusion imaging, 1485-1486, 1486f
 on portal vein thrombosis, 1692-1693, 1693f-1694f
 protocol optimization, 1484-1485
 of radiation-induced disease, 1640-1641
 on schistosomiasis, 1625, 1625f
 on steatosis, 1633, 1634f
 on trauma, 1709f-1710f
 on undifferentiated (embryonal) sarcomas, 1587
 unenhanced, 1481, 1481f
 of viral hepatitis, 1638, 1638f
 omentum, 2049
 pancreas, 1778-1779, 1778f
 on annular pancreas, 1805
 hypoperfusion complex in, 2218-2219, 2219f

- Computed tomography (CT) (*Continued*)
- on pancreas divisum, 1803
 - on pancreatitis, 1814f
 - acute, 1813-1819
 - chronic, 1826-1828, 1826f
 - pediatric, 2216
 - on trauma, 2217-2218, 2217f-2218f
 - postoperative, 1862-1863
 - post-transplant, 1874, 1876f
 - on trauma, 1857-1858, 1857f-1859f, 1858b
 - in percutaneous catheter drainage, 1264
 - perfusion, 1166, 1230-1238
 - pitch in, 1156, 1156f
 - on portal hypertension, 1668-1670, 1669f
 - portography, 1164
 - postoperative gastric and duodenal, 631
 - on primary sclerosing cholangitis, 1429-1431, 1430f
 - principles of contrast agents in, 1159-1161, 1159f-1160f
 - for small bowel evaluation, 682
 - of small bowel obstructions, 808-809, 809f
 - on small intestine vascular disorders, 827-828, 828f
 - of solid abdominal organs, 1155-1168
 - abdominopelvic survey in, 1162, 1162f
 - dual-energy, 1157-1158, 1158f
 - helical, 1156-1157, 1156f-1157f
 - historical perspective on, 1155
 - image creation in, 1155-1156
 - data acquisition for, 1155, 1156f
 - image display in, 1155-1156
 - image reconstruction in, 1155
 - liver, 1162-1164, 1163f
 - multidetector, 1157, 1157f
 - pancreas, 1164-1166
 - scanning protocols in, 1162-1166, 1162f
 - spleen, 1924
 - on accessory spleen, 1915, 1915f
 - anatomy in, 1901-1902, 1902f
 - on angiosarcomas, 1947, 1948f-1949f
 - differential diagnosis of, 1978
 - on hamartomas, 1928, 1929f
 - on hemangiomas, 1927, 1927f
 - on infarctions, 1941f-1942f, 1942
 - on lymphangiomas, 1930
 - on lymphomas, 1951-1952, 1951f-1952f
 - on metastatic disease, 1956, 1957f
 - pediatric, 2228
 - on pyogenic abscesses, 1940, 1940f
 - on trauma, 1968f-1970f, 1969
 - wandering, 1914, 1914f
 - on ulcerative colitis, 992, 994b, 994f
 - Whipplegram, 700-701, 702f
- Computed tomography angiography (CTA)
- abdominal, 135-148
 - of the abdominal aorta, 136f, 138-141
 - anatomy in, 135-137
 - on aortic aneurysms, 139-141, 140f
 - clinical applications of, 138-145
 - computed tomography enterography compared with, 684
 - contrast bolus monitoring in, 137f
 - image processing in, 137
 - of the kidneys, 141-142, 142f
 - of the liver, 143f
 - of mesenteric vasculature, 142-145, 143f-145f
 - of the pancreas, 141, 141f
 - technical considerations in, 135-137
- Computed tomography arterial portography (CTAP), 1484
- Computed tomography cholangiography (CTC), 1292, 1292f
- Computed tomography colonography (CTC), 905-927
- alternative protocols for, 911-912
 - beam hardening in, 915, 915f
 - bowel preparation for, 905-908, 907f, 912
 - characterization of polyps in, 914-916, 914f
 - colonic distention in, 908-910, 909f, 911f
 - colon movement in, 915, 917f
 - for colorectal cancer screening, 905, 921
 - complications with, 922
 - detection in, 911f, 912-914, 913f, 916f, 918f
 - computer-aided, 918-919, 918f
 - diagnostic indications for, 921-922
 - extracolonic findings in, 923, 924f
 - image acquisition in, 910-911
 - indications for, 920-922
 - interpretation of, 912-919
 - computer-aided, 918-919
 - literature reports on, 919-920
 - polyp coating in, 907-908, 908f, 912
 - radiation exposure in, 922-923
 - reporting in, 918-919, 919f
 - soft tissue and polyp differential in, 916-918
 - for staging and surveillance, 922
 - tagging in, 905-906, 906f, 912, 916, 917f
 - technical components in, 905-912
- Computed tomography enteroclysis (CTE), 694-709
- historical background of, 694-695
 - indications for and comparisons with other imaging methods, 695-704
 - for Crohn's disease, 695-697, 696f
 - miscellaneous, 701-704, 702f-704f
 - for small bowel neoplasms, 697-699, 697f-698f
 - for small bowel obstructions, 699-701, 699f-701f
 - on small bowel obstructions, 811
 - summary on, 705
 - technical problems and limitations in, 704-705
- Computed tomography enterography (CTE), 684-693
- carcinoid tumors on, 689, 690f
 - on Crohn's disease
 - luminal narrowing and stricture formation, 741-742
 - nomenclature for disease findings in, 738f
 - ulcers and sinus tracts, 742-743, 743f
 - vasa recta distention in, 744, 747f
 - wall findings, 739f-742f
 - difference of from routine abdominal CT, 684
 - differential diagnosis with
 - of segmental small bowel mural hyperenhancement, 687f
 - for gastrointestinal bleeding, 688-690, 689f
 - indications for, 684
 - common examinations by, 685f
 - technique adaptations with, 684
 - integration of with other tests, 692
 - interpretation of images in, 685-691
 - neuroendocrine tumors on, 689, 690f
 - nomenclature for Crohn's disease findings in, 737-752
 - normal images in, 686f
 - obstructions on, low-grade, 690-691
 - radiation dose in, 691-692
 - for suspected Crohn's disease, 686-688, 687f-688f
 - technique in, 684-685
 - vascular lesions on, 689-690, 691f
- Concretions, 198-199
- Conduit wall calcifications, 199-200, 199f
- Condylomas
- colonic squamous cell carcinoma from, 1081f
- Congenital esophageal stenosis, 425-426, 427f
- differential diagnosis of, 464f
- Congenital hepatic fibrosis, 1553-1554, 1553f, 2201
- Congenital tracheobiliary fistula, 1342
- Congestive heart failure
- hepatic congestion in, 1688-1689
 - periportal low density in, 1710
- Constipation
- chronic, 1122-1123
 - in diabetes, 1124
 - functional imaging for, 901
 - gastrointestinal causes of, 1111b
 - general, systemic, and psychological causes of, 1111b
 - presenting symptoms of, 890
 - with sigmoidoceles, 897
- Constrictor stripping wave, 223
- Contraceptives, oral
- focal nodular hyperplasia and, 1536
 - gallstones with, 1346
 - peliosis hepatis associated with, 1660
- Contractile rings. *See* Muscular rings, esophageal
- Contrast agents, 3-22. *See also* Barium studies with abdominal abscesses, 1257f
- administration routes for, 82
 - in appendix imaging, 964-966
 - barium sulfate, 7
 - adverse reactions to, 12-13
 - in magnetic resonance colonography, 932
 - in magnetic resonance enterography, 711
 - in magnetic resonance imaging, 81-82
 - for bile leak detection, 1444
 - biphasic enteral, 711, 711f
 - blood pool, 1186, 1490, 1331-1332
 - cholangiographic, 13-14
 - combined, 1186
 - in computed tomography
 - liver, 1481-1484, 1482f
 - pancreas, 1164-1165
 - principles of, 1159-1161, 1159f-1160f
 - for small intestine vascular disorders, 827-828
- in computed tomography enterography, 684-685
- dose of
 - for computed tomography, 1160
- enhancement phases with, 1159-1160, 1159f-1160f
- extracellular, 1186
- gadonate disodium, 1443
- gas, 68, 69f
- gastrointestinal, 7-13, 15-16
 - adverse reactions to, 12-13
 - anticholinergic, 19
 - for barium enemas, 9-10
 - barium sulfate, 7
 - for computed tomography, 11-12
 - negative, 10-11
 - pharyngographic, 7-8
 - for small bowel studies, 9
 - for upper gastrointestinal tract studies, 8-9
 - water-soluble, 10, 12-13
- for gastrointestinal multidetector-row computed tomography, 67-68
- hepatobiliary, 1186, 1190-1192
- injection of, 1180
- intraluminal, 80-82, 81f
- intravascular, 3-6, 14-15
 - blood pool, 15
 - gadolinium chelates, 14
 - reticuloendothelial, 14
- iodinated oil, 6-7
- iodinated water-soluble, 3-6
 - acute adverse reactions to, 4-6
 - basic properties of, 3
 - ionic, 3-4
 - nonionic, 4
 - pharmacokinetics of, 4

Contrast agents (Continued)

- IV
 - in computed tomography enterography, 684-685
 - in magnetic resonance
 - cholangiopancreatography, 1794
 - for magnetic resonance enterography, 710-711
 - magnetic resonance imaging
 - blood pool, 1490
 - extracellular fluid, 1489-1490
 - hepatobiliary-specific, 1490
 - liver, 1489-1490
 - reticuloendothelial, 1490
 - for magnetic resonance imaging, 14-16
 - gastrointestinal, 15-16
 - intravascular, 14-15
 - in magnetic resonance imaging, 1184-1186
 - with benign liver tumors, 1529
 - in MDCT, 357, 359
 - negative contrast enteral, 710-711
 - neutral, 67-68, 68f
 - oral
 - in computed tomography enterography, 684
 - patient-dependent factors with, 1161
 - pharmacologic, 16-21
 - hypotonia-producing, 17-19
 - mixed action, 20
 - that increase bowel motility, 19-20
 - vasoconstrictors, 16
 - vasodilators, 16-17
 - in pharyngeal radiographs, 218
 - positive, 67, 68f
 - positive contrast enteral, 710
 - for postoperative gastric and duodenal examinations, 631
 - saline chasers with, 1161
 - scan delay and, 1183-1186
 - in ultrasonography, 1173
 - liver, 1480-1481
 - for liver hemangiomas, 1532
 - water-soluble
 - with caustic esophagitis, 332
 - disadvantages of, 416-417
 - for esophageal perforation studies, 415-417
 - in small bowel studies, 675-676
- Cornelia de Lange's syndrome, 1151t
- Corticosteroids
- for autoimmune chronic pancreatitis, 1832-1833
 - for Crohn's disease, 1007
 - diverticulitis and, 938-939
 - hepatotoxicity of, 1639
 - peliosis hepatis associated with, 1690
 - for ulcerative colitis, 996
- Cowden's disease, 530, 794, 1093, 1095
- differential diagnosis of, 463t
 - with hamartomas, 360-361, 361f
 - small bowel, differential diagnosis of, 874t
- C-RADS reporting system, 918-919, 919t, 923
- Crescent sign, 1106, 2267f
- Cricopharyngeus
- esophageal distention and, 230
 - opening of, 225-226, 226f
- CRM. See Circumferential resection margin (CRM)
- Crohn's disease, 997-1007, 2046. *See also* Inflammatory bowel disease (IBD)
- abscesses in, 1004
 - computed tomography enterography on, 746
 - magnetic resonance enterography on, 719, 719f, 746
 - magnetic resonance imaging of, 1238f
 - percutaneous drainage of, 1235
 - active inflammatory, 748-749
 - activity of, 82-84, 83f-84f

Crohn's disease (Continued)

- activity index (AIS) scores, 752
- magnetic resonance index of activity (MaRIA) scores, 752
- acute abdomen from, 1265-1266
- acute ileitis in, 62f
- acute small bowel bleeding in, 841
- adenocarcinomas associated with, 798-799, 798f
- adenopathy in, 746
- adhesions in, 717
- advanced, barium studies on, 729-730
- amyloidosis with, 783
- angiography of, 121
- anorectal complications in, 1002
- antral narrowing in, 560
- aphthoid lesions in, 496, 497f
- aphthoid ulcers in, 507f, 669f, 1000-1001
- magnetic resonance enterography on, 714, 714f
- appendix involvement in, 970f, 971-972, 974f
- barium contrast examinations on, 727-733
- barium enema findings on, 999-1002, 1000f
- bezoars with, 867
- burnt-out, 873t
- bypass surgery for, 1133
- capsule endoscopy on, 726-727
- carcinoma associated with, 752
- classification of and therapy for, 725-726
- clinical considerations in, 725
- clinical findings in, 507, 998-999
- cobblestone mucosa in, 62f, 729-730, 729f, 1001, 1002f
- comb sign in, 75, 75f
- complications of, 85-86
- computed tomography enteroclysis on, 695-697, 696f, 704
- computed tomography enterography for
 - enteric phase demonstration of, 684-685
 - image interpretation of, 685-686
 - management decisions based on, 691-692
 - nomenclature for findings in, 737-752
 - radiation dose in, 685
 - suspected disease, 684, 685t, 686-688, 687f-688f
- computed tomography on, 1002-1004, 1006f
- ulcerative colitis versus, 988f, 994b
- diagnostic tools for, 726-737
- differential diagnosis of, 510, 768-769, 1012-1013, 1012t
 - appendicitis and, 969
- differentiated from gastric lymphomas, 586
- differentiated from intestinal tuberculosis, 761
- differentiated from ulcerative colitis, 1005, 1012-1013, 1013t
- distribution of, 1002
- drug therapy for, 1007
- duodenal carcinoma with, 565
- duodenal involvement in, 508-510
- duodenitis with, 519
- early disease
 - barium studies on, 727-728
 - magnetic resonance enterography on, 714, 714f
- endoscopic findings in, 999
- on enteroclysis, 674, 675f, 678f
- epidemiology of, 998, 998b
- erosions caused by, 499
- differential diagnosis of, 657t
- erosive gastritis caused, 496
- esophageal, 335-336
- differential diagnosis of, 462t
 - with intramural tracks, 336, 337f
 - with strictures, 336, 337f
 - ulceration with, 302, 336f

Crohn's disease (Continued)

- extraintestinal findings in, 746-748
- false-positive diagnoses of, 496
- fat wrapping in, 63
- fibrofatty proliferation in, 744, 747f, 1003-1004
- magnetic resonance enterography on, 717-719
- fibrostenotic
 - barium studies on, 730-731, 732f-733f
 - computed tomographic/magnetic resonance enterography on, 750-751
 - computed tomography enterography on, 743f
 - magnetic resonance enterography on, 717, 717f
 - ultrasound on, 736f
- fissures in, 1002, 1003f
- fistulas in, 1002, 1003f
 - barium studies on, 729-731, 730f
 - computed tomography enterography on, 743-744
 - magnetic resonance enterography on, 717, 718f
 - simple versus complex, 743-744, 745f-747f
 - ultrasound on, 733, 736f
- galstones with, 1010, 1348
- gastric involvement in, 507-508, 507f-508f
- gastric narrowing from, 659t
- gastric outlet obstruction from, 613, 613f
- gastroduodenal, 507-508, 508f
- historical perspective on, 997
- hypoalbuminemia with, 867
- ileal pouch-anal anastomosis in, 1139
- ileal reservoirs with, 855
- ileocecal valve involvement in, 1079
- ileocolonoscopy on, 726-727, 727f-728f
- ileostomy enemas and, 677
- inflammatory pseudopolyps in, 988
- intermediate
 - barium studies on, 728-729
- jejunoileitis in, 752
- locoregional lymphadenopathy in, 63
- luminal narrowing in, 741-742, 742f, 1002
- lymphoid hyperplasia in, 999-1000
- magnetic resonance colonography on, 930, 931f
- magnetic resonance enterography on
 - pulse sequences and disease type in, 715t
 - techniques for, 712-719
- magnetic resonance imaging for, 82-86, 710
- magnetic resonance imaging of, 1006-1007
- Marshak's principles on, 727
- Meckel's diverticula with, 2092
- medical management of, 1007
- mesenteric adenitis in, 969, 969f
- mesenteric fat in, 76
- mesenteric involvement of, 1003
- mesenteric lymphadenopathy in, 2240
- mesenteric lymph node enlargement in, 76
- mixed fibrostenotic and inflammatory
 - computed tomography enterography on, 749, 750f
- monitoring response to treatment of, 84-85, 85f
- mucosal inflammation
 - computed tomography enterography of, 686, 687f, 692
- multidetector computed tomography on, 736-737
- multiple duodenal ulcers with, 484
- oral stratification in, 687-688
- magnetic resonance enterography on, 715
- mural thickening in, 1002
- narrowing of terminal ileum in, 671f
- pathogenesis and causes of, 998
- pediatric, 2182, 2183f
- penetrating, 63, 63f, 688
- barium studies on, 731

Crohn's disease (Continued)

- computed tomographic/magnetic resonance enterography on, 750
- ultrasound on, 736f
- perienteric edema and inflammation in, 744-746, 747f
- on peroral pneumocolon, 679f
- PET/CT scanning of, 103f
- phlegmon and abscesses in, 87f
- prevalence of, 61, 996
- prognosis with, 1007
- pseudopolyps in
 - magnetic resonance enterography on, 743f
- quiescent
 - barium studies on, 730
 - computed tomography enterography on, 749, 749f
- radiation dose in, 737, 1257-1258
- radiographic findings in, 507-510, 999, 999f
- recurrence of, 86f
 - barium enema demonstration of, 676, 676f
- reparative or regenerative
 - magnetic resonance enterography on, 717, 718f
- sacculations in, 1002, 1004f
- on barium studies, 730, 731f
- segmental mural hyperenhancement in, 714
- sinus tracts in, 1002, 1003f
 - computed tomography enterography on, 742-743
 - magnetic resonance enterography on, 717, 742-743, 744f
- small bowel, 725-755
 - classification and therapy, 725-726
 - clinical considerations in, 725
 - diagnostic tools for, 726-737
 - barium contrast examinations, 727-733, 729f
 - ileocolonoscopy, 726-727, 717f-728f
 - video capsule endoscopy, 720-727
 - differential diagnosis of, 875t
 - evaluation of, 682t, 692
 - luminal narrowing in, 873t
 - micronodularity in, 871t
 - mucosal fold tethering in, 875t
 - obstructions in, 691, 818, 820f
- small bowel transplantation for, 858
- sonographic evaluation of, 61-63
- strictures from, 1002
 - on barium studies, 730-731
 - on computed tomography angiography, 691
 - computed tomography enterography on, 741-742, 742f
 - differential diagnosis of, 464t
 - magnetic resonance enterography on, 741-742, 742f
 - metoclopramide for visualization of, 671, 671f
 - ultrasound on, 735
- stricturing, 63
- superior mesenteric root syndrome caused by, 614
- surgical management of, 1007
- therapy for, 1007
- thickened folds in, 508-509, 509f, 2046f
 - differential diagnosis of, 659t, 661t
- toxic megacolon with, 1009
- transrectal ultrasonography on, 1004-1006
- ulcers in
 - barium studies on, 729-730, 729f-731f
 - computed tomography enterography on, 742-743, 743f
 - fixating, 1001-1002, 1002f
 - magnetic resonance enterography on, 715-717, 742-743, 743f-745f
 - small bowel site predilection of, 875t
 - ultrasound on, 736f

Crohn's disease (Continued)

- ultrasound on, 733, 735f-736f
- upper GI involvement, 506-512
- vasa recta distention in, 744
- wall hyperenhancement in, 737-739, 739f-742f
- wall thickening in
 - computed tomography enterography on, 739-741, 742f
 - magnetic resonance enterography on, 715, 739-741
 - ultrasound on, 733f
- Crohn's Disease Activity Index (CDAI), 731-733
- Cronkhite-Canada syndrome, 530, 530f, 794, 1093, 1096-1097
- clinical features of, 1097f
- differential diagnosis of, 874t
- ectodermal changes in, 1096
- Cross-sectional imaging
 - of appendiceal mucocoeles, 975
- colon
 - benign epithelial polyps, 1032-1035
 - on cancer, 1057-1058
 - polyp detection with, 1032-1035
 - postoperative, 1060-1067
 - on colorectal cancer, 1030-1031
 - of the liver, 1175
- Cruveilhier-Baumgarten syndrome, 1670f
- Cryoablation, 1506
- Cryosurgery, liver, 1723-1724, 1729
- Crypt abscesses, in ulcerative colitis, 988, 989f
- Cryptococcus
 - biliary spread of, 2008
 - hematogenous spread of, 2007
 - splenic infection with, 1936
- Cryptorchidism, 2244
- Cryptosporidiosis, 512-513
 - small bowel, 766, 766f
 - site predilection of, 875t
 - thickened duodenal folds from, 661t
- Cryptosporidium
 - biliary spread of, 2008
 - cholangiopathy with, 1356
 - esophagitis caused by, 322
- Cryptosporidium parvum, 766
- CT. See Computed tomography (CT)
- CTA. See Computed tomography angiography (CTA)
- CT severity index (CTSI), 1817-1818
- Callen's sign, 1811
- Carrarino triad, 2117-2118, 2118f
- Curved planar reformations, 1161
- Cyclooxygenase 1 (COX-2), 467
- Crypts of Lieberkühn, 988
- Cystadenocarcinomas, 1421
 - biliary, 1190, 1190f
 - biliary tract, 1421, 1423f
 - frequency of, 1422
 - incidence and clinical presentation of, 1582-1583
 - mucinous appendiceal, 975-977, 978f
 - pancreatic
 - differential diagnosis of, 1895t
 - pathologic findings on, 1581-1582, 1582f
 - radiologic findings on, 1583-1584, 1585f
 - surgery for, 1861
- Cystadenomas
 - biliary tract, 1421, 1423f
 - incidence and clinical presentation of, 1582-1583
 - liver, 1554
 - pancreatic
 - differential diagnosis of, 1895t
 - pathologic findings on, 1581-1582
 - radiologic findings on, 1583f-1584f
- Cystadenomas, biliary, 1190, 1190f, 1421, 1423f
- Cystic calcifications, 200, 200f

Cystic duct, 1261-1282, 1283f

- on endoscopic retrograde
 - cholangiopancreatography, 1310, 1312f
- in hepatoduodenal ligament, 1996
- normal anatomy of, 1304, 1304f
- Cystic fibrosis
 - biliary tract involvement of
 - pediatric, 2195
 - duodenal changes in, 627, 628f, 2155
 - fibrosing colonopathy with, 2176
 - liver involvement in, 2213
 - malabsorption in, 785-786, 786f
 - malabsorption related to, 774
 - meconium ileus equivalent syndrome in, 1110
 - pancreas involvement in, 2221-2222, 2222f-2223f
 - small bowel obstruction in, 822
- Cystic fibrosis transmembrane conductance
 - regulator (CFTR) gene, 2221-2222
- Cystic lesions
 - differentiated from leiomyomas, 354
 - pancreatic, 1195-1196, 1196f
- Cystoceles, 901
- Cystogastrotomy
 - ulcer scars differentiated from scars from, 486
- Cysts. See also Pseudocysts
 - biliary, 1190
 - branchial cleft, 238-239
 - choledochal, 1343-1345, 1422
 - cholangiocarcinomas with, 1419, 1422f
 - classification of, 1343f-1345f
 - magnetic resonance
 - cholangiopancreatography on, 1330, 1332f
 - widening of the duodenal sweep caused by, 618, 618f
 - duplication
 - gastroduodenal, 541-542, 543f
 - esophageal, 361-363
 - duplication, 361-363, 362f
 - retention, 363, 363f
 - liver, 1550-1554
 - bile duct hamartomas, 1551-1553, 1552f
 - cystadenomas, 1554
 - hepatic fibrosis and polycystic liver disease, 1548, 1553f
 - pediatric, 2202, 2202f
 - simple, 1550-1551, 1551f-1552f
 - mesenteric, 2049, 2049f, 2091
 - pediatric, 2246-2248, 2247f-2248f
 - omental, 2088
 - pediatric, 2246-2248
 - omphalomesenteric, 861
 - pancreas
 - congenital, 1899
 - pseudocysts, 576, 578f, 1321
 - after trauma, 1858
 - with pancreatitis, 1810
 - retention, 247f
 - appendiceal, 976f-977f
 - esophageal, 362f, 363, 464t
 - spleen, 1931-1935, 1931f
 - alcohol ablation of, 1908, 1908f
 - congenital, 1953-1955
 - pediatric, 2251-2253
 - tracheal, 2070-2071
- Cytomegalovirus (CMV)
 - after small bowel transplantation, 859
 - with AIDS, 1652
 - colitis, 1019-1020, 1019f
 - differentiated from gastric lymphomas, 586
 - duodenitis, 512, 513f
 - esophagitis, 318-319, 321f
 - differential diagnosis of, 462t
 - HIV ulcers distinguished from, 319-320

- Cytomegalovirus (CMV) (*Continued*)
 in graft-versus-host disease, 764
 infections
 gastric erosions caused by, 499, 512-513
 gastric narrowing from, 639f
 multiple duodenal ulcers from, 484
 in ulcerative colitis, 985
- D**
- Dacarbazine, hepatotoxicity of, 1630
- Defecography. *See* Evacuation proctography
- Delayed arterial phase of contrast
 in pancreas CT, 1165
- Dependent viscera sign of hernia, 813, 819f
- Depressed lesions, double-contrast studies of, 47-52
- Dermatomyositis, 288
 calcifications in, 2074
 gastric dilation caused by, 615
 malabsorption in, 776b
- Dermoids, mobility of ovarian, 202, 203f
- Descending perineum syndrome, 900
- Desmoid tumors, 793, 2036-2037, 2057f-2058f
 abdominal wall, 2072-2073
 pediatric, 2249, 2250f
- Desmoplastic small round cell tumors, 2041-2042, 2041f, 2249, 2250f
- Diabetes mellitus
 bezoar formation in, 619-620
 chronic gastric dilation caused by, 615
 chronic mesenteric ischemia with, 837
 colonic involvement of, 1124
 esophageal motility disorders with, 289
 fatty infiltration of liver in, 1478
 gastric distention with, 2154
 malabsorption in, 776b, 785
 necrotizing fasciitis with, 2072
 peliosis hepatis with, 1690
- Diaphragm
 antral mucosal, 2141, 2142f
 embryology of, 2080-2081
- Diaphragmatic crura, 174
- Diaphragmatic hernias, 2053, 2067-2069, 2067f
 pediatric, 2099-2100, 2100f-2101f
- Diaphragms
 antral, 611f
 duodenal, 610-611
- Diaphragm sign of ascites, 2031
- Diarrhea, 1127-1128. *See also* Ulcerative colitis
 bloody, 2271-2272
 computed tomography enterography and, 684
 due to small bowel mucosal damage, 775-776
 Hippocrates on, 984
 inflammatory, 1128
 major causes of acute, 1127b
 major causes of chronic, 1128b
 malabsorption conditions and, 774
 osmotic, 1127-1128
 pediatric causes of, 2167-2168
 secretory, 1128
- Diatrizoate, 907, 908f
- Diet, gastric carcinoma links to, 546-547
- Dieulafoy lesions, 688-689, 2278, 2278f
- Diffuse esophageal spasm (DES), 284-286, 285f-287f
 pulsion diverticula with, 424f
- Diffusion-weighted magnetic resonance imaging
 abdominal, 1215-1229
 artifacts in, 1220, 1220f-1221f
 b values for, 1219
 clinical application of, 1221-1226
 diagnostic pitfalls in, 1220-1221, 1221f
 diffusion coefficient values in, 1219
 future of, 1226-1227
 gallbladder, 1223
 Diffusion-weighted magnetic resonance imaging (*Continued*)
 gastrointestinal tract, 1224-1226
 image interpretation in, 1219-1221
 artifacts and, 1220
 qualitative, 1219
 quantitative, 1219-1221
 liver, 1221-1223, 1222f
 lymph nodes, 1223-1224
 optimizations for, 1218f
 pancreas, 1223
 peritoneum, 1224
 scan parameters for, 1218
 spleen, 1223
 treatment response assessment with, 1225
 artifacts in, 1220, 1221f
 of colorectal cancer, 911, 92f
 on Crohn's disease, 712-713
 in gastric cancer staging, 564, 564f
 image acquisition and sequence optimization in, 1216-1217
 intravoxel incoherent motion model of, 1216, 1218f
 liver metastases, 1599
 magnetic resonance colonography
 accuracy of, 931
 pancreas, 1781, 1781f
 physiologic motion in, 1217-1220
 principles of, 1215-1216
 sequences in, 1184
 Stejskal-Tanner sequence in, 1216f
 technical considerations in, 1216-1219
 in tumor response monitoring, 2364
 water diffusion measurement with, 1215-1216, 1216f-1217f
- Digestion. *See* Malabsorption conditions
- Digital subtraction angiography, 113, 113f
- Displaced crus sign of ascites, 2031
- Dissection sign of intussusception, 2173, 2173f
- Diversion colitis, 1125-1126
- Diverticula. *See also* Pseudodiverticula
 biliary tract
 in primary sclerosing cholangitis, 1428
 colon
 differentiated from polyps, 1032
 hemorrhage from, 2279-2280, 2280f
 with diffuse esophageal spasm, 285
 duodenal, 607-610
 filling defects in, 608, 609f
 intraluminal, 610, 610f
 lateral, 608f
 pseudo, 609-610, 609f
 true, 607-609, 608f
 epiphrenic, 285, 286f, 424-425, 425f
 esophageal, 423-425
 pediatric, 2125, 2127f
 in esophageal intramural pseudodiverticulosis, 343-346, 345f-346f
 gallbladder, 1341
 gastric, 607, 607f, 2084
 intramural, 607, 608f
 lateral cervical esophageal, 241
 Meckel's
 GI bleeding from, 688-690
 pharyngeal, 237, 238f
 pulsion, 423-424, 424f
 small bowel, 667-668, 667f
 sonographic features of, 61
 traction, 423-424, 425f
 vesicourachal, 2070-2071
- Diverticular abscesses, 1274-1275, 1275f
- Diverticular diseases. *See also* Diverticulitis
 carcinoma detection with, 1036
 colon, 934-934
- Diverticular diseases (*Continued*)
 diverticulitis, 937-949
 diverticulosis, 934-937
 diverticular hemorrhage, 951, 951f-952f
 giant sigmoid diverticulum, 952, 952f
 [Diverticulitis, 2045, 2046f]
 abscesses in, 1254, 1274-1275
 acute abdomen caused by, 2258-2259, 2258f-2259f
 angiography of, 121
 appendiceal, 973
 cecal, 946
 chronic, 944, 946f
 classification of, 943t
 colon carcinomas with, 1039f
 colonic, 937-949
 clinical findings in, 938-939, 938f
 epidemiology of, 937-938
 pathophysiology of, 938
 complications in, 947-949
 fistulas and sinuses tracts, 947-948, 948f
 pyelophlebitis and liver abscess, 949, 950f
 differential diagnosis of, 944-946, 1105t
 differentiated from appendicitis, 970, 971f
 differentiation of from carcinoma, 943-944, 945f
 epiploic appendagitis differentiated from, 946, 946f
 liver abscesses from, 1508-1509
 mesenteric adenitis in, 969
 pericolic abscesses with, 1036-1039
 radiologic findings on, 939-941
 sigmoid, carcinoma versus, 1105, 1105f
 sigmoid mesocolon in spread of, 2020
 small bowel
 acute abdomen from, 2266, 2266f
 differential diagnosis of, 875t
 small bowel obstruction from, 816
 sonographic features of, 61
 staging of, 943
 ultrasound of, 60-61, 61f
- Diverticulosis
 colon, 934-937
 caliber and haustral abnormalities in, 937, 937f
 causative factors of, 935, 935f
 clinical findings in, 935
 distinguishing features of polyps and diverticula, 935, 937f
 epidemiology of, 934-937
 pathophysiology of, 934-935, 936f
 radiologic findings in, 935-937
 computed tomography on, 937, 937f
 differential diagnosis of, 944-946
 diverticulitis in, 937-938
 esophageal intramural pseudodiverticulosis, 343-346, 345f-346f
 hemorrhage from, 2279
 intramural, 1381, 1385, 1385f-1385f
 jejunoileal, 776-777, 777f
 small bowel
 site predilection of, 875t
- Diverticulum of Kommerell, 1124
- Divided oostomy, 1135-1136
- DIXON sequence, 1184, 1186f
 on hepatic steatosis, 1189
- Dumperidone
 gastrointestinal effects of, 19
- Doppler imaging, 1173-1173
 of acute cholecystitis, 1356-1359, 1359f
 of the appendix, 966
 color, 1172, 1172f
 of Crohn's disease, 1005-1006
 on Crohn's disease, 733, 735f
 of hepatic vasculature, 1176-1177, 1177f

Doppler imaging (*Continued*)

- power, 117f
- pulsed-wave, (1172-1173), 1173f
- Dose-length product (mGy-cm), 1158
- Double-balloon enteroscopy (DBE), 688-690
- Double-barreled colonoscopy, 1135
- Double-channel pylorus, 489, 490f
- Double-contrast studies, 40-55. *See also* Barium studies: double-contrast
 - angulation in, 54f, 55
 - of annular lesions, 47, 49f
 - of aphthoid ulcers, 47-51, 51f
 - of carpet lesions, 47, 49f
 - cobblestoning in, 42, 43f
 - coil spring sign in, 43, 44f
 - of collar button ulcers, 51, 52f
 - colon, 879
 - colonic
 - on diverticulosis, 935-937, 936f
 - of contour abnormalities, 52-53
 - of contour defects, 45, 47f
 - of depressed lesions, 47-52
 - for duodenal ulcers, 479-480
 - of erosions, 47, 51f
 - esophageal
 - on drug-induced esophagitis, 327
 - of squamous cell carcinoma, 371
 - of squamous cell carcinoma of, 369-374, 369f-370f
- esophagography
 - artifacts in, 300-301
 - of Barrett's esophagus, 306-307
 - for GERD, 291
 - on herpes esophagitis, 317
- of exoenteric masses, 51-52, 52f
- of filling defects, 45, 46f
- flow technique in, 469, 469f
- fold patterns in, 42-45
- of gastric cardia, 439, 439f
- of gastroesophageal junction abnormalities, 438
- granularity in, 40-41, 42f
- of linitis plastica, 53, 53f
- nodularity in, 41, 42f
- for peptic ulcers, 469, 469f
- of the pharynx, interpretation of, 216-217
- of plaque, 47, 49f
- pleating in, 45, 46f
- pliability in, 47, 50f
- polypoid folds in, 43, 44f
- of polyps, 45-47, 48f
- postoperative gastric and duodenal, 631
- of protruding lesions, 45-47
- radiating folds in, 43, 44f
- reticular pattern in, 40, 41f
- sacculization in, 53-55, 54f
- serpentine folds in, 40, 45f
- shaggy pattern in, 41, 42f
- spiculation in, 54f, 55
- stack of coins appearance in, 45, 45f
- striae pattern in, 42, 43f
- of submucosal masses, 47, 50f
- surface patterns in, 40-42
- of tapering, 52, 53f
- of target lesions, 47, 50f
- tethering in, 45, 46f
- thumbprinting in, 53, 53f
- tracking in, 52, 52f
- of ulcerated masses, 47, 49f
- of ulcer niches, 51, 51f
- villous pattern in, 40, 41f
- web pattern in, 43, 43f

Doxorubicin, 1510

Doxycycline

- drug-induced esophagitis from, 326-327

Dragstedt ulcers, 468

- Drug-eluting bead chemoembolization (DEB-TACE), 1313
- Drug-induced disorders. *See also* Nonsteroidal anti-inflammatory drugs (NSAIDs)
 - colonic obstruction, 1110
 - disorders
 - esophagitis, 326-328, 328f-330f, 334f
 - differential diagnosis of, 462f
 - liver, 1639, 1640
 - with AIDS, 1653
 - malabsorption, 776b
 - small bowel, 762-763, 762b
 - angioedema, 845-846
- Dual-energy computed tomography (DECT), 1157-1158, 1158f, 1166
- liver, 1486-1487, 1487f
- virtual noncontrast imaging, 1487
- Duct of Santorini, 1773
 - congenital abnormalities in, 1806
 - embryology of, 2086
 - in pancreas divisum, (1800-1801)
- Duct of Wirsung, 1773
 - embryology of, 1797, 2086
 - in pancreas divisum, 1800
 - on ultrasound, 1777
- Ductopenic rejection, 1752
- Duke's classification, 1047-1050, 1048f
- Dumbbell lesions, 531
- Dumping syndrome, 637, 654
- Duodenal polyps, 527-528, 528f
- Duodenal ulcers, 479-483
 - bulbar, 480
 - differential diagnosis of, 484-486
 - examination technique for, 479-480
 - giant, 483, 485f
 - healing and scarring of, 483, 486f
 - linear, 481f
 - location of, 480, 481f
 - morphologic features of, 480-483
 - multiple, 483
 - obstructions from, 487
 - postbulbar, 480-483, 482f-485f
 - pyloric channel, 483-484
 - ring shadows with, 482f
 - shape of, 480, 481f
 - size of, 480
- Duodenitis, 518-519, 518f-519f
 - in celiac disease, 759f, 762
 - differential diagnosis of, 661f
 - with bubbly bulb, 519, 519f
- Duodenocolic fistulas, 490-491, 624-626
- Duodenocolic ligament, 2019
- Duodenojejunal intussusceptions, 624
- Duodenojejunal junction, 667-668
- Duodenojejunal junction, in intestinal malrotation, 864-865
- Duodenorenal fistulas, 491
- Duodenum
 - abnormal extrinsic masses in, 615-617
 - benign tumors of, 525-545
 - carcinomas of, 565-566, 565f-566f
 - ampullary, 566, 567f
 - periampullary, 566, 566f
 - caustic ingestion and, 515-516, 516f-517f
 - cystic fibrosis involvement in, 627, 628f
 - descending, 277f
 - differential diagnosis for, 657
 - diverticula, 607-610
 - filling defects in, 608, 609f
 - intraluminal, 610, 610f
 - lateral, 608f
 - pseudo, 609-610, 609f
 - true, 607-609, 608f
 - embryology of, 1797, 2084-2085
 - emphysematous gastritis in, 514-515

Duodenum (*Continued*)

- eosinophilic gastritis in, 513-514, 514f
- extrinsic impressions on, 615, 616f
- familial adenomatous polyposis syndrome in, 1091
- filling defects in, 660f
- fistulas in, 624-626, 624f
 - cholecystoduodenal, 625, 625f
- foreign bodies in, 620
- gallstones in, 621
- gastric lymphoma spread into, 586f
- GISTs in, 405
 - malignant, 591, 594f
- hematomas in, 620-621, 623f
- inflammatory conditions of, 496-522
 - atrophic gastritis, 504-506
 - differential diagnosis of, 504
 - erosive gastritis, 496-499
 - granulomatous, 506-512
 - hypertrophic gastritis, 503, 503f
 - Ménétrier's disease, 504, 505f
- intussusceptions, 624
- lymphomas of, 587, 587f-588f
 - spread from gastric lymphomas, 581
- megaduodenum, 508-509, 509f
- neoplasms
 - surgery for, 631
- normal anatomy of, 173, 273, 276f
- obstructions
 - in superior mesenteric root syndrome, 614f
- obstructions in, 613-614
 - in superior mesenteric root syndrome, 613-614, 613f
- pancreas in relation to, 1772, 1773f
- pancreatic diseases affecting, 620f
- pediatric disorders of, 2141-2157
 - acquired, 2146-2153
 - distention, 2154-2155, 2154f
 - foreign bodies, 2148-2149, 2151f
 - gastric perforations, 2146-2147
 - hematomas, 2148, 2150f
 - inflammatory disorders, 2152-2154, 2153f-2154f
 - neoplasms, 2150-2152, 2151f-2152f
 - peptic ulcer disease, 2152
 - pyloric stenosis, 2147-2148, 2147f-2150f
 - congenital, 2141-2146
 - antral mucosal diaphragm, 2141, 2142f
 - duodenal atresia and stenosis, 2141-2143, 2142f-2143f
 - duplication cysts, 2143-2144, 2144f
 - malrotation, 2144-2146, 2145f-2146f
 - microgastria, 2141, 2142f
 - pyloric and antral atresias, 2141
- perforations of, 626-627
 - postoperative, 630-636
 - complications in, 640-641
 - diagnostic evaluation of, 630-631
 - prolapsed antral mucosa in, 527-528, 528f
 - pseudolesions, 529f
 - radiation injuries in, 516-517
 - stenosis of, 2084
 - surgery for masses in, 640
 - varices in, 606-607, 606f
 - webs and diaphragms in, 610-611, 611f, 2085
 - widening of the duodenal sweep, 617-619, 617f
- Duplication cysts
 - differential diagnosis of, 658f
 - esophageal, 361-363, 362f
 - differential diagnosis of, 463f
 - differentiated from leiomyomas, 354
 - gastroduodenal, 541-542, 543f
 - pediatric, 2143-2144, 2144f
 - mesenteric, 2049, 2049f
 - midgut, 861-862, 863f

Duplications, midgut, 861-862, 863f
 Dynamic contrast-enhanced MR imaging, 1226-1227, 1235, 1204
 Dynamic cystocolporectography, 891
 Dyskinesia, gallbladder, 2194
 Dysphagia
 with achalasia, 284
 after radiation therapy, 230
 aging and, 230-231
 from alkaline reflux esophagitis, 340
 with *Candida* esophagitis, 312
 from caustic esophagitis, 331
 in chronic graft-versus-host disease, 342
 with eosinophilic esophagitis, 334
 with epidermolysis bullosa dystrophica, 337
 from epiphrenic diverticula, 424-425
 from esophageal metastases, 394
 with fibrovascular polyps, 358
 with idiopathic muscular hypertrophy, 356
 from leiomyosarcomas, 405
 with leiomyosarcomas, 403
 from nasogastric intubation, 339-340
 neurologic disease and, 231-232
 pediatric, 2125, 2128f
 with pemphigoid, 338
 postoperative, 449
 with Schatzki rings, 441
 with scleroderma, 288-289
 with spindle cell carcinoma, 402
 Dysplastic hepatocellular nodules, 1190-1192

E

Eagle-Barrett syndrome. *See* Prune-belly syndrome
 Early arterial phase of contrast, 1159-1160, 1159f
 in liver CT, 1164
 in pancreas CT, 1165
 EASL criteria. *See* European Association for the Study of the Liver (EASL) tumor response criteria
 Echinococcal disease
 cholangitis, 1440
 hepatic, 1614-1621
 clinical findings on, 1615-1616
 complications with, 1619-1620
 epidemiology of, 1614
 pathology of, 1615, 1616f-1617f
 pathophysiology of, 1614-1615
 radiologic findings on, 1616-1619, 1618f-1621f
 treatment of, 1620-1621
 spleen, 2232
Echinococcus granulosus, 1440
 epidemiology and pathogenesis of, 1932-1933
 in hepatic disease, 1614-1621
 life cycle of, 1616f-1617f
 splenic disease, 1932-1933, 1934f
 classification of, 1933-1934, 1934f
 clinical findings on, 1935
 differential diagnosis of, 1935
 epidemiology and pathogenesis of, 1932-1933
 pathology of, 1933
 radiologic imaging of, 1934, 1935
 WHO classification of cysts from, 1934
Echinococcus multilocularis, 1440
 in hepatic disease, 1614-1621
 life cycle of, 1616f-1617f
 Echo planar imaging artifacts, 1220
 Ectopic gastric mucosa, 425, 426f
 Ectopic liver, 1522
 Ectopic pancreatic rests, 538-539, 539f, 2087
 differential diagnosis of, 658t

Ectopic pancreatic rests (*Continued*)
 differentiated from GISTs, 532-533
 myoepithelial hamartomas differentiated from, 793
 Ectopic spleen, 1110, 1912-1915, 1925-1926
 Eddy current artifacts, 1218t, 1220, 1220f
 Edema
 colonic, differential diagnosis of, 1145t
 intestinal, small bowel, 866-867, 867f
 mesenteric, 2048-2049
 mosaic-submucosal pattern of, 1145t
 postoperative wrap, 452f
 in ulcerative colitis, 992-993, 995f
 Effective dose (mSv), 1158
 Effervescent agents, 269
 for esophageal foreign body removal, 419
 mucosal plaques simulated by, 315, 318f
 in small bowel follow-through, 669
 Ehlers-Danlos syndrome, 2074, 2125
 Elastography, liver, 1491
 Electrolyte imbalances
 chronic gastric dilation caused by, 615, 616f
 malabsorption and, 774
 Electromyography, 902
 Embolic metastases, colonic, 1086
 Embolization
 chemoembolization
 of hepatocellular carcinomas, 1740
 of liver tumors, 1725-1726, 1728-1729
 radiofrequency ablation with, 1726
 transarterial, 1505-1506, 1510-1513, 1512f
 ablation with, 1515
 drug-eluting bead, 1513
 radioembolization
 of hepatocellular carcinomas, 1740
 of liver metastases, 1206, 1729
 complications with, 1731f
 radiologic appearance after, 1731f
 transarterial, 1514f
 of liver tumors, 1726-1727, 1727f
 transarterial, 1513-1515
 Embryology
 abdominal wall, 2241
 ampulla of Vater, 1797
 appendix, 955-956, 956f
 biliary tract, 1340
 colon, 1985, 1985f
 common bile duct, 1797
 diaphragm, 2080-2081
 duct of Santorini, 2086
 duct of Wirsung, 1797, 2086
 duodenum, 1797, 2084-2085
 foramen of Winslow, 2087-2088
 gallbladder, 1340
 gastrointestinal tract
 early development, 2079-2080, 2080f
 esophagus, 2083-2084
 intraembryonic celom division and diaphragm formation, 2080-2081, 2081f
 midgut rotation and fixation in, 2089-2091, 2089f-2090f
 abnormalities in, 2091-2092
 stomach, duodenum, and lesser omentum, 2084-2085, 2084f
 kidneys, 1985-1986, 1988-1989
 liver, 201-202, 1520, 1521f, 1983, 1985, 2081-2082
 abnormal development of, 202
 of bare area of, 1983, 1984f
 subperitoneal spread and, 1998f
 lungs, 2080
 mesentery, 2085f
 omentum, 1984, 2084, 2087-2088, 2087f

Embryology (*Continued*)
 pancreas, 1797, 1798f, 1983-1984, 2085-2086, 2086f
 abnormal development of, 2086-2087
 peritoneal cavity, 1983-1986, 1984f-1986f
 spleen, 1912, 1913f, 1983-1984, 2088
 stomach, 2084-2085, 2084f
 urinary tract, 1985-1986
 Embryonal rhabdomyosarcomas, 1422
 Emphysema
 benign gastric, 627, 627f
 subcutaneous, with esophageal perforation, 415, 415f
 Emphysematous cholecystitis, 1193
 Emphysematous gastritis, 514-515, 515f
 Emphysematous cholecystitis, 1365-1367, 1366f-1367f
 End-colostomy, 1135
 Endocrine tumors. *See* Carcinoid tumors
 Endoluminal ultrasonography, on colon cancer, 1055-1058
 Endometriomas, 919f, 1111
 Endometriosis, 1112f
 of the appendix, 972-973
 colonic involvement of, 1111
 GI tract sites of, 972
 magnetic resonance colonography on, 930
 small bowel, 865-866, 867f, 875f
 Endoscopic heater probe therapy, 496, 499f
 Endoscopic retrograde cholangiopancreatography (ERCP), 1184, 1281, 1297, 1297f, 1303-1324
 on AIDS-related disorders, 1634
 on biliary postoperative complications, 1451-1452
 biliary tract infection and inflammation in, 1311-1320
 biliary tract neoplasias in, 1306-1311
 of Caroli's disease, 606-607, 606f
 on choledochal cysts, 1345
 of choledocholithiasis, 1371
 in common duct stone removal, 1308
 complications of, 1321-1322
 cost per correct diagnosis of, 1335
 indications for, 1781
 liver, on cystadenomas and cystadenocarcinomas, 1583, 1583f
 magnetic resonance cholangiopancreatography compared with, 1323
 normal anatomy in, 1304f
 biliary tract, 1303-1306, 1304f
 pancreatic duct, 1305-1306, 1306f
 pancreas
 on annular pancreas, 1805
 examination techniques in, 1781
 inflammation in, 1321, 1321f
 neoplasias in, 1187-1189
 on pancreas divisum, 1801-1802
 pancreatic duct strictures, 1891
 on pancreatitis, acute, 1812
 on pancreatitis, chronic, 1823-1826
 on trauma, 1859-1860
 pancreatitis from, 1815f
 pediatric, 2180, 2216
 percutaneous transhepatic cholangiography versus, 1295-1296
 on primary sclerosing cholangitis, 1428, 1429f
 technique for, 1303
 Endoscopic sclerotherapy, 431-432, 460
 Endoscopic studies
 on Barrett's esophagus, 305, 377
 on *Candida* esophagitis, 312-313
 capsule

Endoscopic studies (Continued)

- on acute small bowel bleeding, 841
- computed tomography enterography with, 684
- on gastrointestinal hemorrhage, 2272-2273
- integration of with computed tomography enterography, 692
- small bowel neoplasms on, 689
- esophageal, with epidermolysis bullosa dystrophica, 337-338
- esophageal perforation from, 413-414, 415f
- for gastrointestinal hemorrhage, 2272
- glutaraldehyde-induced injuries from, 342-343, 344f
- on herpes esophagitis, 316-317
- on Kaposi's sarcoma, 592
- on MALT lymphomas, 581
- for peptic ulcer diagnosis, 477-479
- postoperative gastric and duodenal, 631
- treatment of ulcers with, 486-487
- video capsule, 726-727, 728f

Endoscopic ultrasound (EUS)

- in esophageal cancer staging, 380-381, 383-385
- of esophageal leiomyosarcomas, 405
- of gastric carcinoma, 562-565, 563f
- of gastric carcinomas, 562-565, 563f-564f
- in gastric lymphoma staging, 585-586
- of gastroduodenal lymphomas, 585-586
- linear array, 1802
- of lymph node metastasis, 387f
- normal esophageal, 386f
- pancreas
 - on ductal adenocarcinomas, 1882
 - on pancreatitis, chronic, 1825
 - surgery and, 1863
- on pancreas divisum, 1802
- staging criteria in, 384-385
- technique, 383

Endovascular intra-arterial therapies

- drug-eluting bead chemoembolization, 1513
- for liver malignancies, 1510-1513
- transarterial chemoembolization, 1510-1513, 1512f

Endovascular transcatheter embolization, 1909-1910

Entamoeba histolytica, 1773

- hematogenous spread of, 2021
- life cycle of, 1613f
- liver abscesses from, 1611-1614

Enteral access for alimentation, 130-134

Enterectomy, small bowel, 852-855

Enteric duplications, small bowel obstruction by, 817

Enteritis

- acute infectious, 757f
- chemotherapy-related, 763
- HIV, 765
- mesenteric adenitis in, 969
- neutropenic, 765, 765f
- radiation, 843-845, 845f

Enterocoles, 896-898, 897f-898f

- with rectocele and intussusception, 899f
- with sigmoidocele, 899f

Enterocystitis, 9-10, 27-30, 670-672, 676f

- air-contrast, 672-673, 673f, 675f
- anesthesia in, 671
- on appendiceal mucocoeles, 975, 976f
- on appendicitis, 960-961, 961f-962f
- on celiac disease, 762
- chronic diarrhea and, 678

colon

- adenocarcinomas on, 1035-1039, 1035f-1036f
- benign epithelial polyps, 1032-1035, 1034f
- ischemia in, 1114-1116, 1115f
- on obstructions, 1103
- polyp detection with, 1052, 1034f
- postoperative follow-up in, 1029, 1059f

Enterodysia (Continued)

- on colorectal cancer, 1029-1030, 1030f
- postoperative follow-up with, 1058-1060, 1059f
- complications in, 886, 887f
- computed tomography, 694-709
 - historical background of, 694-695
 - indications for and comparisons with other imaging methods, 695-704
 - for Crohn's disease, 695-697, 696f
 - miscellaneous, 701-704, 702f-704f
 - for small bowel neoplasms, 697-699, 697f-698f
 - for small bowel obstructions, 699-701, 699f-701f
- summary on, 705
- technical problems and limitations in, 704-705

disadvantages of, 677-678

diverticulitis findings in, 939, 939f

diverticulosis and, 885

double-contrast, 879-884

- correct preparation in, 882f
- lymphoid follicular pattern on, 883-884, 884f
- materials and equipment for, 880-884
- patient preparation for, 879-880
- routine, 880-883, 880f, 881f-883f

filling of the entire colon in, 886

giant sigmoid diverticulum on, 952, 952f

with granulomatous colitis, 510

hypotonic duodenography, 674-675, 676f

intubation in, 671-672, 672f

on intussusceptions, 1109, 1109f

on Meckel's diverticulum, 861

methylcellulose-contrast, 673-674, 674f-675f

metoclopramide in, 671, 671f

normal small bowel parameters for, 870f

pancreas examination with, 1776

poor preparation for, 882f, 884, 885f

preparation for, 670-671

in salmonellosis, 1017-1018

single-contrast, 672, 674f, 884

on small bowel obstructions, 810-811, 811f

closed loop, 813, 813f

magnetic resonance, 722, 722f

technical problems in, 884-886

technique variations in, 886-887

toxic megacolon from, 1009

on ulcerative colitis, 987-992, 987b

water-soluble contrast agents in, 675-676, 676f

Enterocolitis

acute abdomen from, 2265, 2265f

infectious, 64-65

Enterocolitis

appendicitis differentiated from, 969

mesenteric adenitis in, 969

necrotizing, 1124-1125, 2098, 2103-2106, 2104f-2105f

small bowel transplantation for, 858

Enterocytozoan bienersi, 767

Enterography. See Computed tomography enterography (CTE); Magnetic resonance enterography (MRE)

Enteroliths

obstruction by, 1110

small bowel, 867, 868f

Enteropathy-associated T-cell lymphomas (EATLs), 720

Enteroscopy

- deep, on gastrointestinal hemorrhage, 688-690
- push, on acute small bowel bleeding, 841

Enterostomy, 855

Enterotoxins, 1128

Enzyme-linked immunosorbent assay (ELISA) test, 762

Eosinophilic cholangitis, 1432

Eosinophilic enteritis, 782-783, 783f, 786

Eosinophilic esophagitis, 333-335, 335f

eosinophilic gastroenteritis differentiated from, 313

pediatric, 2132-2133, 2133f

strictures from, 464f

Eosinophilic gastritis, 659f, 1021, 2152

Eosinophilic gastroenteritis, 513-514, 514f, 2152

Eovist, 1715

Epidermoid cysts. See Sebaceous cysts

Epidermolysis bullosa, 336-338, 338f, 2074

differential diagnosis of, 462t

pyloric atresia with, 2138, 2141

strictures from, 464f

Epigastric abscesses, 1276

Epiglottic tilt, 225

Epiglottitis, squamous cell carcinoma of, 249f-250f

Epiploic appendagitis

acute abdomen from, 2263, 2263f

differentiated from appendicitis, 969, 970f

differentiated from diverticulitis, 946, 946f

Epithelial cysts, spleen, 2232

Epithelial hemangioendotheliomas, 1588, 2205-2206

Epithelioid leiomyomas, 534

Epithelium, in Barrett's esophagus, 375

Epstein-Barr virus infection, 777-778, 1753

Erosions, double-contrast studies of, 47, 51f

See also Ulcers

Erosive gastritis, 496-499, 497f-498f

Erythema multiforme major, 338-339

Erythromycin, gastrointestinal effects of, 20

Escherichia coli

with biliary obstruction, 1297

colitis caused by, 1018, 1019f

in emphysematous gastritis, 514-515

in hemolytic uremic syndrome, 2168

in liver abscesses, 1608-1609, 1609f

in obstructive cholangitis, 1134-1135

pyogenic abscesses with, 1272-1273

Esophageal-airway fistulas, 420, 421f

Esophageal bronchus, 2125, 2126f

Esophageal bypass, 389

Esophageal devascularization, 460

Esophageal intramural pseudodiverticulosis, 343-346, 345f-346f

Esophageal papillomatosis, 350, 352f, 463t

Esophageal retraction, 428-429, 428f

Esophageal stents, palliative placement of, 458-459

Esophageal webs, 300

in chronic graft-versus-host disease, 342

differentiated from Schatzki rings, 443

Esophagectomy, 403

Esophagitis. See also Herpes esophagitis

acute alcohol-induced, 341-342, 342f

alkaline reflux, 340-341, 341f

caustic, 330-333, 332f-333f

cytomegalovirus, 318-319, 320f-321f

differential diagnosis of, 462t, 464t

drug-induced, 326-328, 328f-330f, 334t

eosinophilic, 333-335, 335f

eosinophilic gastroenteritis differentiated from, 513

pediatric, 2132-2133, 2133f

strictures from, 464f

focal contact, 317-318

HIV, 319-320, 321f

idiopathic eosinophilic, 333-335, 335f

infectious, 312-325

nasogastric intubation, 339-340, 340f-341f

radiation, 328-330, 330f

rare causes of, 322

reflux (See Reflux esophagitis)

tuberculous, 320-322, 322f-323f

viral, 312

- Esophagogastrectomy, 453-455
 complications with, 454-455
 for leiomyosarcomas, 403
 obstructions after, 451, 451f, 455f
 strictures after, 456f
 transhiatal-transcervical approach in, 454
 transthoracic approach in, 453, 455f
 tumor recurrence after, 454-455, 457f
- Esophagogastric mucosal prolapses, 446, 447f
- Esophagogram, 442f
- Esophagography
 double-contrast, 291
 for esophageal perforations, 415-417
 for GERD, 291
 single-contrast, 25
 of squamous cell carcinoma, 371
- Esophageojunostomy, anastomotic leaks after, 640, 640f
- Esophagopericardial fistulas, 422-423, 424f
- Esophagopleural fistulas, 420-421, 421f
- Esophagus
 abnormal development of, 2083-2084
 adenocarcinoma of, 374-378
 clinical aspects of, 378
 epidemiology and pathogenesis of, 374-377
 pathology of, 377
 radiographic findings of, 378, 378f-379f
 routes of spread of, 377
 arterial anatomy of, 113
 barium studies, 269-278
 Behçet's disease in, 343, 344f
 benign tumors of, 350-365
 cancer, 394-411
 differential diagnosis of, 379-380
 Kaposi's sarcoma, 407, 407f
 leiomyosarcoma, 403-405, 406f
 lymphoma, 400-401, 402f-403f
 malignant melanoma, 405-407, 407f
 metastases in, 394-396
 miscellaneous tumors, 408
 restaging and treatment response in, 99-100
 secondary achalasia, 396-399
 staging algorithm for, 389
 staging in, 98-99, 380-389
 treatment of, 389
 carcinoma of, 366-393
 gastroduodenal metastases from, 576
 small cell, 407-408, 408f
 spindle cell, 402-403
 surgery on, 453-459
 chronic graft-versus-host disease in, 342, 343f
 congenital short, 2084
 congenital stenosis of, 425-426
 Crohn's disease in, 335-336, 336f
 differential diagnosis of, 462
 diverticula in, 423-425
 duplication of, 2083-2084
 ectopic gastric mucosa in, 425, 426f
 embryology of, 2083-2084
 epidermolysis bullosa dystrophica in, 336-338, 338f
 esophageal bronchus, 2084
 extrinsic impressions on
 abnormal, 428, 428f
 esophageal retraction, 428-429, 428f
 normal, 426-429, 427f
 fistulas in, 420-423
 aorto-esophageal, 421-422, 423f
 esophageal-airway, 420, 421f
 esophagopericardial, 422-423, 424f
 esophagopleural, 420-421, 421f
 foreign body impactions in, 418-419, 418f-419f
 gastric cardia carcinoma involvement in, 556-557
- Esophagus (Continued)
 glutaraldehyde-induced injuries in, 342-343, 344f
 glycogenic acanthosis of, 273f
 hematomas in, 412-413, 413f-414f
 leukemia involvement of, 408, 408f-409f
 longitudinal lymphatics of, 382f
 Mallory-Weiss tears, 412, 413f
 metastases in, 394-396, 395f-397f
 motility disorders of the, 279-290
 nonspecific, 286-287, 288f
 primary, 281-286
 secondary, 287-289
 mucosal lesions, 350-353
 mucosal rings, 440, 440f
 muscular ring in, 438, 440-441
 normal anatomy of, 271, 272f, 279
 normal physiology of, 279
 normal radiographic appearance of, 438-441
 normal walls of, 69
 pediatric disorders of, 2123-2140
 achalasia, 2133
 acquired anomalies, 2129-2138
 congenital anomalies, 2125-2127
 overview of, 2125
 swallowing disorders, 2125-2127, 2128f
 eosinophilic esophagitis, 2132-2133, 2133f
 varices, 2133, 2134f
 pemphigoid, 338, 339f
 perforation of, 413-417
 cervical, 413-415
 from foreign body impaction, 419, 420f
 from intubation, 459
 pathogenesis of, 413-414
 from pneumatic dilation, 459-460
 postoperative, 450-451
 radiographic findings on, 415-417
 spontaneous, 414, 417f
 thoracic, 414-415
 PET/CT of, 98-100, 99f
 postoperative, 449-461
 benign strictures, 451-453
 complications in, 450b
 gastroesophageal reflux and hiatal hernia, 450-451
 general principles on, 449-450
 palliative intubation in, 458-459
 pushed versus pulled, 428-429, 429f
 radiation therapy damage to, 328-330, 330f, 367, 2138, 2138f
 radiographic evaluation of, 279-281
 ringed, 334-335
 sigmoid, 282-284, 283f
 squamous cell carcinoma of, 366-374
 advanced, 371-373, 371f-373f
 associated conditions with, 373-374
 clinical aspects of, 369
 early, 369-371, 369f-370f
 endoscopic findings with, 369
 epidemiology of, 366
 metastases of, 374f
 pathology of, 368
 predisposing conditions and, 366-367
 radiographic findings with, 369-374, 369f
 routes of spread of, 368
 stenosis of, 2084
 submucosal lesions, benign, 353-363, 658t
 varices of, 275
 downhill, 432-433, 434f
 idiopathic, 433, 434f
 with reflux esophagitis, 302
 treatment of, 431-432, 432f-433f
 uphill, 429-432, 430f
 varicoid carcinoma and, 431, 431f
- Estrogen replacement therapy, gallstones with, 1346
- European Association for the Study of the Liver (EASL) tumor response criteria, 2299-2300
- Evacuation proctography
 anal canal length in, 895-896
 anorectal angle in, 895, 895f
 anorectal junction level in, 896
 on chronic constipation, 1123
 logistics of, 891-892
 measurements in, 894f
 normal pelvic anatomy and, 890-892, 891f-892f
 normal results in, 894f
 normal variations in, 902
 pathology in, 896-901
 anterior mucosal prolapse, 900, 901f
 anterior mucosal wall prolapse, 898
 constipation and incontinence, 901
 cystoceles, 901
 enteroceles and sigmoidoceles, 896-898, 896f-899f
 pelvic floor dyssynergy, 899-900, 900f
 peritonocoeles, 897-898, 898f
 posterior-lateral rectal pouches, 899
 rectal intussusception, 898-899, 899f
 rectoceles, 895, 895f, 897f, 899f
 with anterior mucosal wall prolapse, 898
 solitary rectal ulcer syndrome, 890, 899
 uterine and vaginal vault prolapse, 900
 preprocedure preparation for, 892
 supplies for, 893, 893f
 technique in, 896-901
- Eventration, 2081
- Exoenteric masses, double-contrast studies of, 51-52, 52f
- Extrahepatic ducts, 1283, 1283f. *See also* Biliary tract on computed tomography, 1291f
 normal anatomy of, 1308
 on ultrasound, 1388-1390
- Extraluminal leaks after Roux-en-Y gastric bypass, 643-644
- Extramedullary hematopoiesis, 2038
- Exudates, 2025
- F**
 Facial trichilemmomas, 1095
 Falciform ligament, 1994, 1998f, 2009, 2010f
 disease spread through, 2020
 Familial adenomatous polyposis syndrome (FAPS), 523, 530, 793, 793f, 1089-1093
 adenocarcinoma associated with, 798
 attenuated, 1089
 colonic manifestations of, 1089-1090, 1090f-1091f
 colorectal cancer and, 1029
 differential diagnosis of, 874t
 extracolonic gastrointestinal manifestations of, 1090-1091
 extraintestinal manifestations of, 1091-1093, 1092f
 Familial dysautonomia, 232
 Familial Mediterranean fever, 783
 Familial polyposis coli, 1089, 1578. *See also* Familial adenomatous polyposis syndrome (FAPS)
 Fasciitis, necrotizing, 2072
 Fasciola hepatica, 1621, 1622f
 Fascioliasis, 1621
 Fast imaging with steady-state precession (FISP), 712
 on Crohn's disease, 735
 magnetic resonance colonography
 accuracy of, 931
 in magnetic resonance colonography, 928-929

- East low-angle shot (FLASH) imaging, 931, 933f
 FAST protocol. *See* Focused assessment with sonography in trauma (FAST) protocol
 Fat digestion and absorption, 774
 Fat halo pattern, 72-73, 74f
 Fat pads, retroperitoneal, 1986-1987
 Fat ring sign, 2047
 Fatty infiltration
 ileocecal valve, 1078-1079, 1079f
 liver, 1763f
 pancreas, 2085-2086
 imaging of, 1777, 1777f
 normal variants of, 1797-1799, 1799f
 Fat wrapping, 63
Fasciola hepatica, 1440
 FDG PET/CT. *See* F-fluorodeoxyglucose (FDG)-positron emission tomography (PET)/CT
 Fecal immunochemical test, 1029
 Fecal impaction, 1110, 1123-1124
 Fecaliths, 957-958
 Fecal occult blood test (FOBT), 1029
 Feline esophagus, 302
 Femoral hernias, 2064-2065, 2066f
 Femoral sheath hematomas, 2071
 Fibroepithelial polyps. *See* Fibrovascular polyps
 Fibrofatty proliferation, in Crohn's disease, 717-719, 744, 747f, 1003-1004
 Fibrolamellar carcinomas (FLC), 1573-1577
 differential diagnosis of, 1577, 1578f
 incidence and clinical presentation of, 1575
 pathologic findings in, 1573-1575, 1574f, 1575f
 radiologic findings on, 1575, 1575f-1577f
 Fibrolamellar hepatocellular carcinomas, 1187, 1188f
 Fibrolipomas. *See* Fibrovascular polyps
 Fibromas. *See* Fibrovascular polyps
 Fibromatosis, aggressive. *See* Desmoid tumors
 Fibromyxomas. *See* Fibrovascular polyps
 Fibropolycystic diseases, 2201-2202, 2201f
 Fibrosarcomas
 gastroduodenal, 598
 peritoneal, 2043f
 Fibrosing colonopathy, 2176
 Fibrosis
 after sleeve gastrectomy, 652-654
 congenital hepatic, 1553-1554, 1553f
 liver (*See also* Cirrhosis)
 diagnosis of with diffusion-weighted MRI, 1223
 image-guided biopsy of, 1240
 Fibrous histiocytomas
 malignant, 1580
 Fibrous histiocytomas, malignant
 liver, 1580
 peritoneal, 2043
 Fibrous mesotheliomas, 1556
 Fibrovascular polyps, 358f-359f
 esophageal, 354, 358-359
 in familial adenomatous polyposis syndrome, 1092, 1092f
 liver, mesotheliomas, 1556
 omental, 2050
 polypoid lesions with, 379
 FIESTA (free induction echo-stimulated acquisition), 712
 Filling defects
 after colorectal cancer, 1058-1059, 1059f
 biliary tract, 1506
 differential diagnosis of, 1463f
 postoperative, 1312
 with primary sclerosing cholangitis, 1432
 cecal, differential diagnosis of, 1148f
 colonic, differential diagnosis of, 1145t, 1148f
 double-contrast studies of, 45, 46f
 duodenal, differential diagnosis of, 660f
 from esophagogastric mucosal prolapses, 446
 filling defects (*Continued*)
 gallbladder, differential diagnosis of, 1460f
 intraluminal, 684
 Fine-needle aspiration. *See also* Percutaneous tissue acquisition techniques
 adrenal gland, 1249
 liver, 1247-1248
 Finney pyloroplasty, 632
 FISP. *See* Fast imaging with steady-state precession (FISP)
 Fissures
 in Crohn's disease, 1002, 1003f
 liver, accessory/pseudoaccessory, 1520, 1521f-1522f
 Fistulas
 abdominal abscesses with, 1272, 1272f
 aortoduodenal, 625-626, 626f
 aorto-esophageal, 421-422, 423f
 biliary tract
 after laparoscopic cholecystectomy, 1453
 differential diagnosis of, 1461f
 bilioenteric, 1193
 branchial cleft, 238-239
 cholecystenteric, 1348, 1377-1379, 1381f
 cholecystocholedochal, 1377
 colonic
 carcinomas causing, 1040f
 differential diagnosis of, 1149f
 in diverticulitis, 941, 947-948, 948f
 with diverticulitis, 939
 from radiation colitis, 1117
 congenital tracheobiliary, 1342
 in Crohn's disease, 63, 63f, 508, 1002, 1003f
 duodenal, 509-510, 510f
 esophageal, 420-423
 after esophagogastric resection, 454-455
 with cancer, 372-373, 374f
 from foreign body ingestion, 2134, 2137f
 postoperative, 456f
 esophagopericardial, 373
 gallbladder, differential diagnosis of, 1461f
 gastrocolic and duodenocolic, 624-626, 624f-625f
 with HIV esophagitis, 320
 liver
 arterioportal, 2209
 arteriovenous, 1713f
 mucous, divided colostomy and, 1135-1136, 1136f
 pancreatic, post-transplant, 1879-1880, 1880f-1881f
 from peptic ulcers, 489-491
 choledochoduodenal, 491, 491f
 duodenocolic, 490-491
 duodenorenal, 491
 gastrocolic, 489-490, 491f
 gastroduodenal, 489
 gastropericardial, 491
 rectovaginal, 1137f
 small bowel
 on computed tomography enterography, 688
 computed tomography enterography on, 685
 on small bowel follow-through, 678, 679f
 tracheoesophageal, 2083
 urinary tract, 1011
 Fistulotomy procedures, 1007
 Flank stripes, 173, 173f, 193
 FLASH. *See* Fast low-angle shot (FLASH) imaging
 Fleischner's sign, 1019
 Flip-flop pattern of contrast enhancement, 1683-1684, 1685f
 Flow cytometry, 1008
 Flow technique, 271, 271f, 469, 469f
 Floxuridine cholangitis, 1437
 Floxuridine toxicity, 517-518, 517f
 differential diagnosis of, 659f
 Floxuridine toxicity (*Continued*)
 duodenitis from, 519
 small bowel effects of, 762-763, 763f
 Fluid aspiration, bowel, 127
 Flukes, 759
 biliary tract, 1437-1440
 blood (*See* Schistosomiasis)
 Fasciola hepatica, 1621
 liver, 1410-1411, 1622f
 Fluorescent in situ hybridization, 1599
 Fluorinated antipyrimidines, 762-763
 F-fluorodeoxyglucose (FDG)-positron emission tomography (PET)/CT
 avidity of esophageal GISTs in, 355-356, 356f
 in gastric cancer staging, 560-561, 564, 564f
 18F-labeled
 of the adrenal glands, 1210-1211
 of biliary tract, 1202-1204
 of cholangiocarcinomas, 1202-1203, 1203f
 of colorectal cancer, 1056-1057
 of the gallbladder, 1202-1204
 carcinomas, 1203-1204, 1204f
 of the liver, 1204-1207
 on liver metastases, 1591-1592
 of malignant GISTs, 590
 of MALT lymphomas, 581-582
 of the pancreas, 1208-1210
 of the spleen, 1207-1208, 1207f-1208f
 of ulcerative colitis, 995-996
 pancreas, postoperative, 1863
 spleen, 1923-1924
 anatomy in, 1899
 on lymphomas, 1952-1953
 on metastatic disease, 1957, 1958f
 Fluoroscopic examinations
 of abdominal abscesses, 1254-1255, 1255f
 after Roux-en-Y gastric bypass, 642-643
 of esophageal perforations, 415-417
 of esophageal peristalsis, 280
 image-guided percutaneous tissue acquisition, 1241-1242
 postoperative gastric and duodenal, 630-631
 on primary sclerosing cholangitis, 1428, 1429f
 small bowel
 integration of with computed tomography enterography, 692
 Focal nodular hyperplasia (FNH), 1187, 1188f, 1535-1543, 1603
 angiography on, 1539
 computed tomography on, 1539, 1540f
 differential diagnosis of, 1578t, 1768t
 hepatocellular adenoma differentiated from, 1545
 imaging findings on, 1768t
 incidence and clinical presentation of, 1530
 liver, hepatocellular carcinomas differentiated from, 1573
 magnetic resonance imaging on, 1539-1542, 1541f-1542f
 nuclear medicine on, 1536-1537
 pathologic findings on, 1535-1536, 1538f, 1538t
 pediatric, 2210, 2211f
 plain radiographic findings on, 1536
 telangiectatic, 1187-1189, 1542-1543
 ultrasound on, 1537-1539, 1539f
 Focused assessment with sonography in trauma (FAST) protocol, 1173, 1712, 1971-1972
 Fold patterns
 in celiac disease, 762
 in double-contrast studies, 42-45
 Folds of Kerckring, 665, 666f
 Fonkalsrud pouches, 1139, 1139f
 Football sign, 187
 Foramen of Bochdalek hernias, 2068, 2068f
 pediatric, 2099-2100, 2100f-2101f

Foramen of Morgagni hernias, 200, 2068, 2068f
 pediatric, 2100
 Foramen of Winslow, 2003E, 2009
 embryology of, 2087-2088
 hernias, 2057, 2058f
 lesser sac connected to, 2087-2088
 Foreign body impactions
 esophageal, 418-419, 418f-420f
 perforations from, 419, 420f
 pediatric, 2133-2136, 2135f-2137f, 2148-2149, 2151f
 small bowel impactions by, 822
 Fossa masses, gallbladder, 1406-1408, 1407f
 Fossa of Landzert, 865, 2092
 Fossa of Waldeyer, 865
 Foveolar metaplasia, 862
 Free induction echo-stimulated acquisition (FIESTA), 712
 Free intraperitoneal perforations, 948, 949f
 Frey procedure, 1864, 1866f
 Frostberg, inverted 3 sign of, 618-619, 619f
 5-FUDR. *See* Floxuridine toxicity
 Fundic gland polyposis, 523, 525f, 1090-1091
 Fundic gland polyps, 523
 Fundoplication
 breakdown of, 453f
 complications with, 2132, 2132f
 normal appearance after, 450, 451f
 obstructions after, 452f
 secondary achalasia from, 396-397
 Fungal infections
 colonic
 histoplasmosis, 1021
 mucormycosis, 1021
 gastroduodenal, 512
 histoplasmosis, 762
 intra-abdominal abscesses from, 1271-1272
 spleen, 1036-1037

G

Gadobenate dimeglumine (Gd-BOPTA), 1186, 1294
 in benign liver tumor imaging, 1530, 1530f
 in liver metastases, 1599
 with liver trauma, 1715
 Gadofosveset trisodium, 1490
 Gadolinium
 for acute cholecystitis imaging, 1192, 1193
 in appendix imaging, 968-969
 in benign liver tumor imaging, 1530, 1530f
 in diffusion-weighted MRI, 1224
 fetal risks from, 968
 in liver MRI, 1489-1490, 1490f
 on hepatocellular carcinomas, 1569
 in pancreas imaging, 1780f
 Gadolinium chelate
 contrast agents, 14
 in magnetic resonance colonography, 928
 in magnetic resonance enterography, 712-713
 Gadopentetate dimeglumine, 1186
 in liver MRI, 1489-1490
 Gadoteridol, 1489-1490
 Gadotetate disodium (Gd-EOB-DTPA)
 for bile leak detection, 1444
 in liver imaging
 benign neoplasms, 1530, 1530f, 1534-1535
 on hepatocellular adenomas, 1533f, 1545
 on hepatocellular carcinomas, 1569-1570, 1572f
 on metastases, 1599
 on trauma, 1715
 Gadoxetic acid, 1186, 1294
 Gallbladder
 accessory, 1541
 agenesis of, 1540
 avulsion of, 1456, 1457f
 in biliary atresia, 2186, 2186f
 biliary calculi in, 198, 198f
 biliary sludge in, 1352, 1355f
 carcinomas of, 1402-1410
 biliary tract involvement in, 1307, 1312f
 classification and staging of, 1402-1403, 1404f
 clinical findings on, 1403
 differential diagnosis of, 1408
 epidemiology of, 1402
 etiology of, 1402
 fossa masses, 1406-1408, 1407f
 gastroduodenal metastases from, 577, 579f
 pathologic findings in, 1402-1403
 pathways of spread in, 1408-1409
 polypoid masses, 1406, 1407f
 radiographic findings on, 1403-1409, 1404f-1405f
 treatment and prognosis of, 1409-1410
 cholecystoduodenal fistulas in, 625, 625f
 cholecystomegaly, 1342
 congenital anomalies of, 1330-1332
 delayed visualization of, 1462f
 differential diagnosis of, 1460-1467
 diffusion-weighted MRI of, 1223
 diverticulum, 1341
 duodenal impressions by, 661f
 duplication of, 1341
 pediatric, 2180-2181, 2181f
 ectopic, 1341-1342, 1342f
 embryology of, 1340
 examination techniques for, 1283-1287
 cholescintigraphy, 1286, 1287f
 computed tomography, 1284-1286, 1286f
 magnetic resonance imaging, 1286-1287, 1287f
 ultrasound, 1284, 1285f
 filling defects in, 1460f
 fistulas in, 1461f
 gas in, differential diagnosis of, 1461f
 hydrops, 1385, 1386f, 2194f
 differential diagnosis of, 1461f
 pediatric, 2194
 post-traumatic, 1456-1457
 hyperplastic cholecystoses of, 1379-1385
 cholesterosis, 1379-1380, 1382f
 image-guided biopsy of, 1244-1245
 interventional radiology in, 1392-1401
 percutaneous cholecystostomy, 1392-1394
 percutaneous gallbladder aspiration, 1394
 preprocedural management for, 1392
 magnetic resonance cholangiopancreatography on, 1325-1326, 1326f, 1336
 magnetic resonance imaging of, 1192-1194, 1194f
 carcinomas, 1194, 1194f
 cholecystitis, acute, 1192-1193, 1193f
 cholelithiasis and choledocholithiasis, 1192, 1193f
 micro-, 1342
 multiseptate, 1341, 1461f
 neoplasms, 1402-1426
 benign, 1410
 carcinomas, 1402-1410
 normal anatomy of, 169, 170f, 1281, 1282f
 on computed tomography, 1285-1286, 1286f
 on magnetic resonance imaging, 1287, 1288f
 on ultrasound, 1284
 variations in, 1340-1347
 pediatric disorders of
 acalculous cholecystitis, 2193-2194, 2194f
 cholelithiasis, 2193, 2193f
 Gallbladder (Continued)
 dyskinesia, 2194
 hydrops, 2194, 2194f
 imaging modalities for, 2180
 neonatal jaundice and, 2182
 normal appearance of, 2180-2181, 2181f
 percutaneous cholecystostomy of, 130f
 perforation of, 1367-1369, 1368f-1369f
 pericholecystic fluid, differential diagnosis of, 1461f
 PET/CT of, 1202-1204
 carcinomas, 1203-1204, 1204f
 cholangiocarcinomas, 1202-1203, 1203f
 pitfalls in, 1204
 phrygian cap, 1282f, 1341
 porcelain, 1350, 1352f
 carcinoma associated with, 1402
 position anomalies of, 1341-1342
 postoperative lesions, 1442
 shape anomalies of, 1341
 size abnormalities, 1342, 2180
 small, differential diagnosis of, 1461f
 torsion of, 1341
 trauma to, 1456-1457, 1456f-1457f
 traversal of in percutaneous drainage, 1264
 ultrasonography on, 1178-1180, 1178f-1179f, 1284, 1285f
 wall thickening in, 1179, 1179f
 with acute cholecystitis, 1356, 1358f
 in carcinomas, 1403-1406, 1405f
 computed tomography on, 1359
 differential diagnosis of, 1461f
 with viral hepatitis, 1638
 wandering, 1341
 Gallium Ga 67, 1258
 Gallstones. *See* Cholelithiasis
 Gamma-Gandy bodies, 1665, 1939, 1939f
 Ganciclovir, 512
 Ganglioneuromas, 792, 2168
 Gangrenous cholecystitis, 1193, 1362-1364, 1363f
 on computed tomography, 1364f-1365f
 Murphy sign in, 1356
 on ultrasound, 1363f
 Gardner's syndrome, 1089. *See also* Familial adenomatous polyposis syndrome (FAPS)
 duodenal carcinoma with, 565
 extraintestinal manifestations of, 1091
 Gas
 abnormal bowel patterns of, 179-184
 with appendicitis, 185
 hepatic arterial, 190
 intramural, 190-191, 190f
 normal bowel patterns of, 178, 179f
 pneumobilia, 188-189, 189f
 portal venous, 189-190, 190f
 Gastrectomy
 alkaline reflux esophagitis after, 340-341
 bile reflux gastritis after, 638-639, 639f
 dumping after, 633
 for gastric masses, 632
 partial, 275, 277f
 bezoar formation after, 619-620, 622f, 637
 carcinoma recurrence after, 641
 for caustic ingestion, 515
 gastric carcinomas after, 547
 gastric resection in, 633-639
 for ulcer treatment, 469
 vertical sleeve, 630
 in Zollinger-Ellison syndrome, 492
 Gastric arteries, 1899-1900
 Gastric banding. *See* Laparoscopic adjustable gastric band placement (LAGB)

- Gastric bypass procedures
 bezoar formation after, 620
 Roux-en-Y, 630, 642-646, 643f
 abdominal wall hernias after, 646
 assessing for postoperative complications
 with, 642-643
 communication with excluded stomach after,
 644, 644f
 complications after, 643-646
 internal hernias after, 645-646
 intussusception after, 646, 647f
 marginal ulcers after, 644-645
 obstruction after, 645, 645f-646f
 stomal stenosis after, 645f, 646
- Gastric cancer. *See* Cancer: gastroduodenal
- Gastric cardia
 carcinoma of, 446, 446f
 carcinomas of, 555-557, 556f
 esophageal adenocarcinoma in, 378
 metastases to, 575f
 normal radiographic appearance of, 439, 439f
- Gastric dilation, 614-615, 615f
- Gastric outlet obstruction, 179, 275, 611-613
 after gastric resection, 636-637, 636f
 after sleeve gastrectomy, 652-654
 from caustic ingestion, 515
 differential diagnosis of, 660
 with eosinophilic gastritis, 513-514
 gastric dilation without, 614-615
 from gastric volvulus, 623, 623f
 from granulomatous disease, 613, 613f
 as indication for surgery, 631
 from villous tumors, 528-529
- Gastric pneumatosis, 515
- Gastric remnant neoplasms, 639
- Gastric resection, 630, 634-639
- Gastric stasis
 after gastric resection, 636
 ulcers caused by, 468
- Gastric surgery. *See also* Gastric bypass procedures
 afferent loop obstruction, 851-852, 852f
 small bowel after, 851-852
- Gastric ulcers, 469-479
 differential diagnosis of, 484-486
 examination technique for, 469
 healing and scarring of, 486
 location of, 471
 prone compression views with, 469, 470f
 shapes of, 470, 470f
 size of, 470-471, 471f
- Gastric volvulus, 622-623, 623f
- Gastrinomas
 pancreatic, 1850, 1851f
 surgery for, 1861-1862
 in Zollinger-Ellison syndrome, 491-492
- Gastrinoma triangle, 1850
- Gastritis
 antral, 499-500, 500f
 atrophic, 504-506, 506f
 gastric carcinoma linked to, 547
 bile reflux, 638-639, 639f
 chronic remnant, 638-639
 cytomegalovirus, 512-513
 differential diagnosis of, 504, 657f
 emphysematous, 514-515, 515f
 eosinophilic, 513-514, 514f
 erosive, 496-499
 gastric narrowing from, 659f
H. pylori, 500-503, 501f-502f
 gastric carcinoma and, 546-547
 hereditary factors in, 547
 hypertrophic, 502-503, 503f
- Gastrocolic fistulas, 489-490, 491f, 624-626,
 624f
- Gastrocolic ligament, 1083, 1935f
 disease spread through, 2016, 2016f
- Gastroduodenal fistulas, 489, 490f
- Gastroduodenal intussusceptions, 624
- Gastroduodenostomy, 630, 634-635
- Gastroenteritis, eosinophilic, 513-514, 514f
 pediatric, 2152
- Gastroenteropancreatic neuroendocrine tumors,
 799. *See also* Carcinoid tumors
- Gastroenterostomy, 515, 640
- Gastroesophageal junction abnormalities, 438-448
 carcinoma of the cardia, 446, 446f
 normal radiographic appearance and, 438-441
 prolapsed esophagogastric mucosa, 446, 447f
 radiographic technique for, 438
- Gastroesophageal reflux (GER)
 after achalasia treatment, 284
 after esophagogastric resection, 454-455
 after sleeve gastrectomy, 652-654
 diagnosis of, 292
 Garrett's esophagus with, 303
 hiatal hernias and, 291-292
 inflammatory esophagogastric polyps with,
 359-360
 postoperative, 449
 recurrent after surgery, 451
 surgery for, 450-451
- Gastroesophageal reflux disease (GERD),
 291-311
 actinomyces, 322, 323f
 Barrett's esophagus and, 303-308
 cytomegalovirus esophagitis and, 318-319
 esophageal dysmotility with, 288
 herpes esophagitis and, 316-318
 HIV esophagitis and, 319-320
 pediatric, 2129-2132, 2131f-2132f
 reflux esophagitis, 291-303
 tuberculosis and, 320-322
- Gastrohepatic ligament, 1994-1996, 1998f
- Gastrohepatic recess, 2001, 2001f
- Gastrointestinal hemorrhage, 2271-2281
 acute small bowel, 841-842, 843f
 from angiodysplasia, 1076-1077
 causes of, 2272
 clinical presentation and evaluation of,
 2271-2272
 computed tomography on
 in diagnosis, 842, 842f
 enteroclysis, 701-704, 704f
 enterography, 684, 685f, 688-690, 689f
 diagnostic and therapeutic procedures for,
 2272-2275
 angiography, 2275
 barium studies, 2275
 capsule endoscopy, 2272-2273
 deep enteroscopy, 2273
 endoscopy, 2272
 multidetector computed tomography, 2273,
 2274f
 nuclear scintigraphy, 2273-2275, 2274f
 from diverticular hemorrhage, 951,
 951f-952f
 etiology of, 2271
 from hemangiomas, colonic, 1075-1076
 lower, 2279-2280
 from colon neoplasms, 2280
 from diverticular hemorrhage, 2279-2280,
 2280f
 midgut, 2277-2279
 from small bowel neoplasms, 2279
 from small bowel ulcers, 2278-2279
 from small bowel vascular lesions, 2277-2278,
 2278f
 upper, 2275-2277
 from esophageal varices, 2276
 from gastritis, 2276
 from Mallory-Weiss tears, 2276-2277
 from peptic ulcers, 2275-2276
- Gastrointestinal radiology
 contrast agents for, 16-21
 hypotonia-producing agents in, 17-19
- Gastrointestinal stromal tumors (GISTs), 533f
 benign, 532f-533f
 calcifications in, 531, 532f
 chemotherapy for, 800, 802f
 classification of, 587-588
 clinical findings with, 531
 colonic, 1079-1080, 1081f, 1106, 1108f
 differential diagnosis of, 532-533, 658f
 differentiated from adenomatous polyps, 526
 differentiated from duodenal polyps, 527-528
 differentiated from ectopic pancreatic rests, 539
 differentiated from gastric lymphomas, 586-587
 differentiated from leiomyoblastomas, 478
 esophageal, 355-356, 355f-356f
 ulceration of, 354
 intussusceptions from, 1106, 1108f
 malignant, 407-408, 587-591
 calcification in, 590f
 clinical findings on, 588-589
 differential diagnosis of, 658f
 duodenal, 405
 exogastric, 590f
 pathology of, 587-588
 radiographic features of, 589-590, 589f
 small bowel, 799-801, 800f-801f
 as solitary lesions, 579
 pathology of, 531
 prevalence of, 530-531
 radiographic features of, 403
 radiographic findings on, 531-532
 small bowel benign, 790, 791f
 treatment of, 480
 ulcerated, 474-477, 477f
 ulcers differentiated from, 484
- Gastrointestinal tract. *See also* Appendix:
 Esophagus; Stomach
 acute gastrointestinal bleeding, 122-123
 acute mesenteric ischemia, 123-126
 angiography of, 120-123
 barium studies of the upper, 269-278
 catheter and needle placement in, 126-127
 diffusion-weighted MRI of, 123f-1226
 embryology of, 2079-2094
 early development, 2079-2080, 2080f
 esophagus, 2083
 intraembryonic celom division and
 diaphragm formation, 2080-2081, 2081f
 midgut rotation and fixation in, 2089-2091,
 2090f-2090f
 abnormalities in, 2091-2092
 stomach, duodenum, and lesser omentum,
 2084-2085, 2084f
 image-guided biopsy of, 1244-1245
 inflammatory disorders of, angiography of,
 121
 magnetic resonance imaging of, 79-95
 malignancies, 89-93
 multidetector-row computed tomography of,
 67-78
 mural thickening in, classification scheme for,
 72f
 neonatal radiology on, 2095-2124
 postoperative, magnetic resonance
 cholangiopancreatography on, 1332-1334
 primary vascular disease of, 120-121
 tumors of, angiography of, 121
 upper
 bleeding in
 from erosive gastritis, 497
 from lipomas, 535
 from ulcers, 468-469, 487, 487f
 postoperative examinations of, 630-631
 vascular disorders of, 122

- Gastrojejunocolic fistulas, 624, 625f
 Gastrojejunostomy, 630
 afferent loop syndrome after, 638
 Billroth II procedure, 633
 gastric carcinoma linked to, 547
 identification of anatomy after, 634-635
 Roux-en-Y, 630, 633-634, 635f
 small bowel fold thickening after, 872t
 Gastroparesis
 in bezoar formation, 619-620
 chronic gastric dilation and, 615
 ulcers caused by, 468
 Gastropathy, portal hypertensive, 607, 607f
 Gastropericardial fistulas, 491
 Gastropleural fistulas, 421, 422f
 Gastroschisis, 2097-2098, 2241-2245, 2243f
 Gastrosplenic ligament, 1996, 2016
 disease spread through, 2019, 2019f
 embryology of, 1984
 subperitoneal spread into, 1999f
 Gastrotomy
 percutaneous, 130-134, 131f-133f
 ulcer scars differentiated from scars from, 486
 Gaucher's disease, 1647, 1905, 1946f
 pediatric, 2215, 2213f, 2238
 Gd-BOPTA. *See* Gadobenate dimeglumine (Gd-BOPTA)
 Gd-EOB-DTPA. *See* Gadoxetate disodium (Gd-EOB-DTPA)
 GERD. *See* Gastroesophageal reflux disease (GERD)
 Geriatric ulcers, 471
 Giant cell arteritis, 838-839
 Giant sigmoid diverticulum, 952
 Giardiasis
 fold enlargement in, 786
 immunodeficiency and, 763
 magnetic resonance enterography on, 721
 pediatric, 2133
 small bowel
 site predilection of, 875t
 small bowel infestations of, 759, 759f
 GISTs. *See* Gastrointestinal stromal tumors (GISTs)
 Gliadin fraction, 778
 Glioblastoma multiforme, 1092
 Glisson's capsule, 1678, 1688, 2001f
 acute abdomen from, 2200-2207
 disease spread through, 2018-2019
 Glomus tumors, 536-537, 536f, 658t
 Glucagon
 in computed tomography colonography, 910
 as contrast agent, 17-18
 administration of for enteroclysis, 880
 contraindications and side effects of, 18-19
 preferred imaging modality with, 18
 spasmolytic effect of, 171
 for esophageal foreign body removal, 419
 gastric hypotonia induced by, 469
 for postoperative gastric and duodenal examinations, 631
 Glucagonomas, 1224f
 Glucose transporters (GLUTs), 96
 Glutaraldehyde
 caustic colitis from, 1023
 esophageal injuries caused by, 342-343, 344f
 strictures from, 464t
 Gluteus maximus, 175
 Glycogenic acanthosis, 273f, 351-353, 353f
 with Cowden's disease, 1095, 1096f
 differential diagnosis of, 463t
 distinguished from *Candida* esophagitis, 315
 Glycogen storage diseases, 1022, 1644-1645, 1645f
 pediatric, 2213
 Goiters, 1095
 Gonads
 embryogenesis of, 1985-1986
 splenic fusion with, 1916, 2088-2089
 Graded compression, 59
 Gradient recalled images (GRE), 932
 Graft-versus-host disease
 chronic, esophagitis in, 342, 343f
 colonic, 1021, 1022f
 differential diagnosis of, 768
 small bowel, 764, 764f-765f
 luminal narrowing in, 873t
 small bowel fold thickening in, 872t
 strictures from, 464t
 Granular cell renal cell carcinomas, 1198-1199
 Granular cell tumors, 537-538, 538f
 biliary tract, 1311, 1314f, 1424
 esophageal, 354, 359-360, 360f
 differential diagnosis of, 463t-464t
 gastroduodenal, differential diagnosis of, 658t
 Granularity, in double-contrast studies, 40-41, 42f
 Granulomas, hepatic, with AIDS, 1653
 Granulomatous conditions, 506-512.
 See also Crohn's disease
 chronic granulomatous disease of childhood, 1022
 fungal diseases, 512
 gastric syphilis, 512
 sarcoidosis, 510-511, 511f
 tuberculosis, 511
 Gray attenuation pattern, 72, 73f
 Gray units, 1158
 Grey Turner's sign, 1811, 1986-1987, 2013-2014
 Groove pancreatitis, 1829-1830, 1830f-1831f
 Ground-glass appearance of abdominal radiographs, 194, 1543-1544
- H**
Haemophilus influenzae, sickle cell disease and susceptibility to, 1944
 Half-Fourier acquisition single-shot turbo spin-echo (HASTE) sequence, 1325
 liver, 1488
 on pancreas divisum, 1803
 Half-Fourier RARE technique
 on Crohn's disease, 734-735
 on the gallbladder and bile ducts, 1287
 in magnetic resonance enterography, 712-713
 Halo sign, 2047
 Hamartomas. *See also* Bannayan-Riley-Ruvalcaba syndrome (BRRS); Cowden's disease
 bile duct, 1551-1553, 1552f
 biliary tract, 1190, 1424, 1649f, 1649f
 pediatric, 2202
 Brunner gland, 539-541, 540f
 esophageal, 360-361, 361f
 mesenchymal, 1555-1556, 1556f
 pediatric, 2207-2210, 2209f
 myoepithelial
 small bowel, 793
 Peutz-Jeghers, 1093-1095
 spleen, 1928-1929, 1929f
 pediatric, 2233-2234
 ultrasound on, 1181
 Hamartomatous polyposis syndromes. *See* Bannayan-Riley-Ruvalcaba syndrome (BRRS); Cowden's disease; Cronkhite-Canada syndrome; Juvenile polyposis; Peutz-Jeghers syndrome
 Hamoudi tumors, 1848-1849, 1849f
 Hampton's line, 471-472
 Hartmann procedures, 1138, 1138f
 Hashimoto's thyroiditis, with primary biliary cirrhosis, 1649, 1650
 HASTE sequence. *See* Half-Fourier acquisition single-shot turbo spin-echo (HASTE) sequence
 Haustra
 blunting and loss of in ulcerative colitis, 990, 991f-992f
 in salmonellosis, 1017
 Haustral clefts, 937
 in ulcerative colitis, 987, 995
 Heineke-Mikulicz pyloroplasty, 632
 Helical computed tomography, 1156-1157, 1156f-1157f
 image postprocessing in, 1161-1162
Helicobacter jejuni, mesenteric adenitis from, 2268
Helicobacter pylori
 antral gastritis caused by, 499
 atrophic gastritis associated with, 505-506
 in duodenitis, 518
 in gastric carcinomas, 500-501, 546-547
 gastritis, 500-503, 501f-502f
 differential diagnosis of, 504, 659t
 enlarged areae gastricae with, 586
 hereditary factors in, 547
 gastrointestinal hemorrhage with, 2271
 MALDs and, 580, 582
 in pediatric disease, 2152
 peptic ulcers caused by, 467, 657t
 treatment of, 631
 treatment of ulcers with, 469, 486-487
 Heller myotomy, 284, 284f, 460, 460f
 Hellmer's sign, 193
 HELLP syndrome. *See* Hemolysis, elevated liver enzymes, low platelets (HELLP) syndrome
 Hemangioendotheliomas
 epithelioid, 2205-2206
 gastroduodenal, 598
 infantile, 2206-2208, 2207f-2208f
 liver transplantation for, 1737
 Hemangiomas
 capillary, 1076
 cavernous, 1076
 colonic, 1075-1076, 1076f
 differentiated from leiomyomas, 354
 esophageal, 360
 differential diagnosis of, 463t-464t
 gastroduodenal, 536
 differential diagnosis of, 658t
 giant, 1531
 liver, 1530-1535
 angiography on, 1533
 cavernous, 1186-1187, 1187f
 evaluation of, 1603
 image-guided biopsy of, 1248
 mesenteric, 2042, 2042f
 omental, 2050
 small bowel
 benign, 791-792, 792f
 vascular disorders from, 846-848, 848f
 spleen, 1926-1928, 1927f
 splenic
 pediatric, 2233
 ultrasound on, 1181
 THADs and THIDs from, 1679f
 Hemangiomas, 1926
 Hemangiopericytomas, 598
 Hematemesis, 2271-2272, 2279
 Hematochezia, 2271-2272, 2279
 Hematogenous metastases, 2006-2007, 2007f
 esophageal, 394, 399f
 differential diagnosis of, 464t
 squamous cell carcinomas, 368

- Hematogenous metastases (*Continued*)
 from gastric carcinoma, 548
 gastroduodenal, 571-574
 small bowel
 differential diagnosis of, 874f
 site predilection of, 875f
- Hematomas
 anterior abdominal wall, 2071, 2071f
 duodenal, 620-621, 623f
 esophageal, 412-413, 413f-414f
 gallbladder, differential diagnosis of, 1408
 gastroduodenal
 pediatric, 2148, 2150f
 liver
 after transplantation, 1753
 from biopsies, 1706
 from trauma, 1709, 1710f, 1714f
 pancreatic, after percutaneous catheter drainage, 1791, 1792f
 retroperitoneal, 1988-1989
 small bowel intussusceptions by, 823-824
 spleen, subcapsular, 1966-1967, 1967f-1968f
- Hemihypertrophy, 1578
- Hemobilia, 1706
- Hemochromatosis, 1185f, 1192, 1641-1644
 clinical findings on, 1641
 hemosiderosis with, 1945-1946
 with hepatocellular carcinomas, 1567
 hereditary, liver transplantation for, 1738
 imaging findings on, 1642-1644, 1642f, 1706a
 pathologic findings on, 1641-1642, 1642f
- Hemolysis, elevated liver enzymes, low platelets (HELLP) syndrome, 1698-1699, 1699f
 spontaneous liver rupture in, 1721-1722
 subcapsular hematomas with, 1714f
- Hemolytic uremic syndrome (HUS), 2166-2169, 2168f
- Hemoperitoneum, 1971
- Hemophagocytic lymphohistiocytosis, 2238
- Hemorrhage. *See also* Gastrointestinal hemorrhage
 acute abdomen from, 2266
 ascites with, 2025, 2026f
 colonic diverticular, 951, 951f-952f
 gastrointestinal, 2271-2281
 mesenteric, 2048
 pararenal space spread of, 2013-2014, 2013f
- Hemorrhoids, internal, 1117-1118, 1118f
- Hemosiderosis, 1641-1644, 1945-1946, 1946f
- Hennekam syndrome, 2160
- Henoch-Schönlein purpura, 823-824, 838-840, 840f
 pediatric, 2152, 2161
- Hepatectomy, for echinococcal disease, 1621
- Hepatic artery, 1173
 anatomy of, 1899-1900
 aneurysms, 1699-1700
 Doppler ultrasound in, 1470-1480
 gas in, 190
 in hepatoduodenal ligament, 1996
 liver transplantation and
 complications involving, 1745-1746
 hepatic artery thrombosis, 1744-1745, 1745f
 pseudoaneurysm, 1745-1746, 1747f
 stenosis, 1745, 1745f
 normal postoperative Doppler findings on, 1744, 1744f
 preoperative imaging of, 1740
 normal anatomy of, 1471-1472
 in pancreatic blood supply, 1773
 stenosis, 1745, 1746f
 thrombosis, 1744-1745, 1745f
 ultrasound evaluation of, 1477
- Hepatic duct, 1175
 anomalies in, 1342-1345, 1342f
- Hepatic flexure obstructions, 1104
- Hepatic hydrothorax, 413-414
- Hepatic infarction, 1698
- Hepaticojejunosomy, 1442
 bile leaks after, 1455
 strictures after, 1455-1456
- Hepatic parenchymal phase of enhancement, 1159-1160
- Hepatic resection
 for benign lesions, 1720
 complications with, 1728-1729
 indications for, 1718, 1720-1721
 left lateral segmentectomy, 1722
 left lobectomy, 1722
 left trisegmentectomy, 1722
 minimally invasive, 1722
 patient selection for, 1720-1721
 postoperative radiologic findings on, 1727-1728, 1727f
 radiology in planning, 1718
 right lobectomy, 1721
 right posterior segmentectomy, 1722
 right trisegmentectomy, 1721-1722
 subsegmentectomy, 1721
 types of, 1721-1722, 1722f-1723f
 ultrasound during, 1718, 1719f
 wedge excision, 1721
- Hepatic sarcoidosis, 1432
- Hepatic veins
 assessment of for living donor liver transplantation, 1743
 dilation of, differential diagnosis of, 1759f
 Doppler ultrasound in, 1480
 Doppler ultrasound of, 1479-1480, 1480f
 lacerations of, 1710
 liver lobe agenesis and, 1525
 liver transplantation complications involving, 1747-1749, 1749f-1750f
 normal anatomy of, 1472-1473
- Hepatic veno-occlusive disease. *See* Sinusoidal obstruction syndrome
- Hepatic venous phase of enhancement, 1159-1160
- Hepatic venous pressure gradient (HVPG), 1502-1503
- Hepatitis, 1636-1639
 with AIDS, 1652, 1652f
 alcoholic, 1638-1639
 autoimmune, 1649-1650, 1658
 cirrhosis with, 1190
 clinical findings on, 1636
 gallbladder wall thickening in, 1356
 nonalcoholic steatohepatitis, 1630, 1633
 pathologic findings on, 1636
 with primary sclerosing cholangitis, 1427
 radiation, 1640-1641
 radiologic findings on
 viral, 1636-1637, 1637f-1638f
 viral, 1636-1638
 imaging findings on, 1765f
 lymphatic spread of, 2008
- Hepatobiliary contrast agents, 14-15
 with liver metastases, 1599
- in MRI on hepatocellular carcinomas, 1569-1570
- in work-up of liver masses, 1603
- Hepatoblastomas, 1577-1579
 incidence and clinical presentation of, 1578
 liver transplantation for, 1737
 pathologic findings on, 1577-1578, 1578f
 pediatric, 2202-2203, 2203f
 radiologic findings on, 1578-1579, 1579f
- Hepatocellular adenomas (HCA)
 angiography of, 1544
 classification of, 1529, 1543
 computed tomography of, 1544, 1544f-1545f
 differential diagnosis of, 1766f
 imaging findings on, 1766f
 incidence and clinical presentation of, 1543
- Hepatocellular adenomas (HCA) (*Continued*)
 magnetic resonance angiography of, 1545-1546, 1546f-1547f
 multiple, 1547
 nuclear medicine on, 1544
 pathology of, 1543f
 plain radiographic findings on, 1543-1544
 radiologic-pathologic features of, 1543f
- Hepatocellular carcinomas (HCC), 1561-1573
 ablation of, 1508
 chemical, 1506
 results of, 1509
 biliary involvement in, 1311
 with cirrhosis, 1655
 differential diagnosis of, 1767f
 diffusion-weighted MRI of, 1222
 encapsulated, 1561-1562, 1562f
 fibrolamellar, focal nodular hyperplasia differentiated from, 1187
 gallbladder, 1408
 with hemochromatosis, 1641
 image-guided biopsy of, 1248
 image-guided percutaneous biopsy of, 1499-1501, 1500f
 imaging findings on, 1767f
 incidence and clinical presentation of, 1563-1564
 intraoperative ultrasound of, 1479f
 liver transplantation and
 locoregional bridging therapy for, 1740
 MELD score and, 1739, 1739f
 Milan score and, 1738
 preoperative imaging for, 1739, 1739f-1740f
 recurrence after, 1753
 liver transplantation for, 1737
 patient evaluation for, 1738
 magnetic resonance imaging of, 1189-1192, 1191f
 metastatic, 1410, 2008
 mRECIST criteria on, 2300, 2301f
 pathologic findings on, 1561-1563, 1562f
 perfusion CT on, 1232-1233, 1234f
 perfusion MRI on, 1236, 1236f
 PET/CT of, 1204-1205
 radiologic findings on, 1564-1573
 regenerative versus dysplastic nodules in, 1570-1572, 1574f
 steatosis with, 1630
 transarterial chemoembolization of, 1510-1513, 1512f
 transarterial radioembolization of, 1513-1515
 with viral hepatitis, 1637-1638
- Hepatoduodenal ligament, 1179-1180, 1179f, 1291-1292, 1994-1996, 2016f
 disease spread through, 2019
 embryology of, 1983-1984
- Hepatolithiasis, 1720
- Hepatomas
 chemoembolization of, 1725-1726
 radioembolization of, 1726-1727, 1731f
- Hepatomegaly
 in Budd-Chiari syndrome, 1682-1683
 differential diagnosis of, 1757f
 diffuse, 1757f
 duodenal displacement from, 616
 focal enlargement, 1757f
 with gallbladder carcinoma metastasis, 1403
 in hemochromatosis, 1641
 in neonates, 1757f
 with steatosis, 1631
 in viral hepatitis, 1637
- Hepatopulmonary syndrome (HPS), 413-414, 1702, 1703f
- Hepatorenal space, 2002
- Hepatorenal syndrome, 413-414
- Hereditary hemorrhagic telangiectasia. *See* Osler-Weber-Rendu syndrome

- Hereditary nonpolyposis colorectal cancer (HNPCC), 798, 1074
- Turcot syndrome and, 1092
- Hernias**
- abdominal, 2054f
 - classification of, 2053, 2054b
 - external, 2053
 - internal, 2053-2060
 - after Roux-en-Y gastric bypass, 645-646
 - clinical and imaging findings for, 2055f
 - foramen of Winslow, 2057, 2058f
 - intersigmoid, 2058, 2059f
 - paraduodenal, 2054-2057, 2056f
 - periceal, 2057, 2059f
 - retroastomotic, 2059-2060, 2061f
 - transmesenteric, 2058-2059, 2060f
 - transomental, 2059, 2060f
 - intramesosigmoid, 2058
 - midgut, 2092
 - obstructions from, 1110
 - oburator, 174-175, 176f, 815-816
 - omentum, 2050
 - paraesophageal, 445-446, 445f
 - postoperative, 454f
 - parastomal, 855, 855f
 - pelvis and groin, 2063-2067
 - femoral, 2064-2065, 2066f
 - inguinal, 2063-2064, 2063f
 - Littre's, 2064
 - oburator, 2065-2067, 2067f
 - Richter's, 815, 816f, 2064
 - sciatic, 817f, 822-824
 - small bowel
 - from Meckel's diverticulum, 861
 - paraduodenal, 865, 865f-866f
 - with small bowel obstructions, 814-816, 814f
 - strangulated, 815f
 - transmesosigmoid, 2058
 - umbilical or paraumbilical, 814, 815f
 - abdominal wall, 2061-2063, 2061f
 - after Roux-en-Y gastric bypass, 646
 - incisional, 2063, 2063f-2064f
 - lumbar, 2062, 2063f
 - parastomal, 2063, 2064f
 - spigelian, 815, 816f, 2062, 2062f
 - umbilical, 2061
 - ventral, 2061, 2062f
 - afferent loop, 2060
 - colon
 - after colectomy, 1135, 1135f
 - parastomal, 1135f
 - complications of, 814
 - diaphragmatic, 2053, 2067-2069, 2067f, 2068f
 - foramen of Bochdalek, 2068, 2068f
 - pediatric, 2099-2100, 2100f-2101f
 - foramen of Morgagni, 200, 2068, 2068f
 - pediatric, 2100, 2102f
 - pediatric, 2099-2100, 2100f-2101f
 - traumatic, 2068-2069, 2069f
 - epigastric, 815
 - in gastroschisis, 2097-2098
 - hiatal, 443-446
 - after sleeve gastrectomy, 652-654
 - axial, 443-444, 444f, 446f
 - with floppy fundus, 444, 445f
 - gastric ulcers in, 471
 - in GERD, 291
 - invaginated, as pseudotumors, 446, 447f
 - postoperative, 450-451
 - recurrent, 451, 453f-454f
 - with reflux esophagitis, 291-292
 - with reflux ulcers, 443-444, 444f
 - with scleroderma, 289f
 - surgery for, 450-451
- Hernias (Continued)**
- incisional, 817f
 - inguinal, 814, 815f
- Herpes esophagitis, 301-302, 316-318**
- clinical findings in, 316
 - differential diagnosis of, 317-318, 462t
 - distinguished from Behçet's disease, 343
 - distinguished from drug-induced esophagitis, 327-328
 - distinguished from radiation esophagitis, 330
 - endoscopic findings in, 316-317
 - odynophagia caused by, 319
 - pathogenesis of, 316
 - plaques and nodules caused by, 315, 317f
 - radiographic findings in, 317, 317f
 - ulceration in, 319f-320f
- Herpes simplex, colonic involvement of, 1113**
- Herpes zoster, mosaic-submucosal edema pattern in, 1145t**
- Heterotaxy syndromes**
- malformations associated with, 1920b
 - polysplenia syndrome, 1918-1919, 1918f-1920f, 1919b
- Heterotopic gastric mucosa, 541, 541f, 795, 862-863**
- Highly active antiretroviral therapy (HAART), 1948-1949**
- Highly selective vagotomy (HSV), 632**
- Hilar cholangiocarcinomas, 1415-1417, 1416f-1418f**
- cholangiography of, 1416-1417, 1419f
 - magnetic resonance cholangiopancreatography on, 1329-1330, 1420f
 - surgical resectability of, 1416, 1418f
- Hirschsprung's disease, 1110, 2092**
- anorectal manometry on, 1122
 - anterior anus and, 2164
 - meconium plug with, 2119, 2120f
 - microcolon in, 1151t
 - pediatric, 2165-2167, 2166f-2167f
- Histamine-2 blockers (H2 blockers), for pelvic ulcer disease, 631**
- Histiocytic syndromes, 2238**
- Histoplasma capsulatum, 762, 1956**
- Histoplasmosis, 762, 871t, 1021**
- Histoplasmosis, gastric, 512, 721**
- HIV (human immunodeficiency virus)**
- colonic squamous cell carcinomas with, 1080-1081
 - enteritis, 765
 - Enterocytozoon bienersi infections with, 767
 - esophagitis, 319-320, 321f
 - differential diagnosis of, 462t
 - hepatic steatosis in, 1629-1630
 - squamous cell carcinoma with, 1080-1081
 - tuberculosis with, 760
- Hong Kong disease. See Pyogenic cholangitis; recurrent**
- Hookworms, 757-758**
- Hourglass stomach, 476-477, 478f, 813**
- with gastric syphilis, 512
- Howel-Evans syndrome. See Tylosis**
- Human leukocyte antigen (HLA) phenotypes, 985**
- Human papillomavirus (HPV), esophageal carcinoma and, 366**
- Humira, 996, 1007**
- Hydatid disease. See Echinococcus granulosus; Echinococcus multilocularis**
- Hydrocolonic ultrasonography, 1005**
- Hydrodissection**
- in guided-image biopsy, 1246f
 - in percutaneous abscess drainage, 126b, 1268f
- Hydronephrosis, with inflammatory bowel disease, 1011**
- Hyoid elevation, 224-225**
- Hyperamylasemia, 811, 1857**
- Hyperchlorhydria, 539**
- Hypergastrinemia, 596-598**
- Hyperplastic polyps, 523-525, 524f-526f**
- differential diagnosis of, 658t
- Hypersensitivity reactions, 338-339**
- Hypersplenism, 1909**
- Hypertension, portal. See Portal hypertension**
- Hypertensive lower esophageal sphincter, 287**
- Hypertriglyceridemia, 1348**
- Hypertrophic gastritis, 502-503, 503f**
- differential diagnosis of, 659t
- Hypertrophic osteoarthropathy, 353-354**
- Hypertrophic pyloric stenosis, 611, 612f**
- Hypoalbuminemia, 866-867, 1356**
- Hypoparathyroidism, 776b**
- Hypoperfusion complex, 2218-2219, 2219b**
- Hypothyroidism, 776b**
- Hypotonia, contrast agents that produce, 17-19**
- Hypotonic agents, 269**
- Hypotonic duodenography, 529, 566**
- I**
- Iatrogenic injuries. See also Radiation therapy**
- abdominal wall, from laparoscopy, 2074, 2074f
 - biliary tract, after laparoscopic cholecystectomy, 1445-1448, 1445f-1448f
 - glutaraldehyde-induced, 342-343, 344f
 - from intubation, differential diagnosis of, 462t
 - liver, 170b
- Idiopathic achalasia. See Achalasia; primary**
- Idiopathic eosinophilic esophagitis, 333-335, 335f**
- Idiopathic intestinal pseudo-obstruction, 289**
- Idiopathic muscular hypertrophy, esophageal, 356-358, 357f**
- Ileal dysgenesis, 863**
- Ileal pouch-anal anastomoses, 1139-1142, 1139f**
- Ileal reservoirs, 855-858**
- continent ileostomy, 856, 856f
 - ileoanal pouches, 856-858, 857f, 997, 997f
- Ileitis**
- acute infectious, 757f
 - backwash, in ulcerative colitis, 990, 992f
 - in Crohn's disease, 62f
 - magnetic resonance imaging of, 87f
 - small bowel, site predilection of, 875t
- Ileoanal pouches, 856-858, 857f, 997, 997f**
- Ileocecal valve**
- differential diagnosis of enlarged, 1148t
 - fatty infiltration of, 1078-1079, 1079f
 - large bowel obstruction evaluation and, 1103f
 - obstructions near, 1105
- Ileocectis, infectious, 64-65**
- Ileocecum, tuberculosis in, 65, 65f, 760-761**
- Ileocolonoscopy**
- on Crohn's disease, 726-727, 727f-728f
 - integration of with computed tomography enterography, 692
- Ileostomy, 855, 855f**
- Brooke, 996
 - continent reservoirs with, 856-858, 856f, 996
 - segmental resection with, 1133
 - for ulcerative colitis, 996-997
- Ileostomy enemas, 677, 677f**
- Ileum. See also Small bowel**
- atresia and stenosis of, 2110-2112, 2111f-2112f
 - carcinoid tumors in, 1077
 - computed tomography enterography of, 692
 - diverticulitis in, differentiated from appendicitis, 970, 971f

- Ileum (*Continued*)
 endometriosis in, 865-866, 866f-867f
 familial adenomatous polyposis syndrome in, 1091
 fold thickening in, differential diagnosis of, 873f
 lymphoid hyperplasia of, 667f
 normal anatomy of, 665
 vascular jejunalization of, 1004
- Ileus
 duodenal, megaduodenum in, 661f
 gallstone, 1348, 1377-1379, 1380f-1381f
 meconium, 2118-2119, 2119f
- Imatinib, 477-478, 800-801
- Iminodiacetic acid (IDA), 1355
- Immune system
 small bowel in, 756-757
 spleen in, 1898, 1972
 in ulcerative colitis, 985
- Immunodeficiency diseases. *See also* AIDS
 (acquired immune deficiency syndrome); HIV
 (human immunodeficiency virus)
 actinomycosis, 768
 common variable, 763
 cryptosporidiosis, 766
 cytomegalovirus infections, 765-766, 766f
 graft-versus-host disease, 764, 764f-765f
 isosporiasis and other intracellular protozoans, 766-767
 lymphomas with, 1948-1949
Mycobacterium avium-intracellulare complex, 767-768, 767f
 selective immunoglobulin A, 763
 small bowel inflammatory disease in, 763-768
 typhilitis, 765, 765f, 971, 972f, 1023-1024, 1023f, 2170-2172
- Immunoglobulin A
 in celiac disease, 778
 selective immunodeficiency in, 763
- Immunoglobulin G, 1258
- Immunoglobulin G4 (IgG4)-related sclerosing cholangitis, 1417, 1420f
- Immunoproliferative small intestinal disease (IPSID), 786, 872f
- Immunoscintigraphy with monoclonal antibodies (MoAb), 1056, 1058, 1066f
 postoperative, 1066
- Immunosuppressive therapy, sinusoidal obstruction syndrome from, 1680
- Imperforate anus, 2113-2117
 anterior anus and, 2164
 classification of, 2114f
 radiologic findings on, 2113-2117, 2115f-2117f
 treatment of, 2114-2115
 variants of, 2117
- Incidentalomas, adrenal, 1210
- Incisional hernias, 2063, 2063f-2064f
- Incontinence
 fecal, prevalence of, 890
 functional imaging for, 901
- Indium In 111, 1258
- Indium-labeled leukocyte scans, 1764f
- Infantile hemangioendothelioma (IHE), 1554-1555, 1555f, 2206-2208, 2207f-2208f
- Infarctions
 acute abdomen from, 2267-2268, 2267f
 with HELLIP, 1698
 hepatic, 1698, 1698f
 omental, appendicitis differentiated from, 969, 971f
 omentum, 2050
 spleen, 1941-1943, 1941b, 1941c-1942f
 with pancreatitis, 1944-1945
 pediatric, 2236
 from trauma, 1969
- Infections. *See also* specific infectious agents
 biliary spread of, 2008
 hematogenous spread of, 2007
 lymphatic spread of, 2008
 peritoneal spread of, 2009
 in pouch of Douglas, 2009, 2011f
 small bowel
 magnetic resonance enterography on, 721, 721f
 spleen, pediatric, 2235-2236
 Infectious mononucleosis, 2236
 Inferior epigastric arteries, 2004
 Inferior lumbar triangle, 1986-1987, 1988f
 Inferior mesenteric artery (IMA), 828
 Inferior mesenteric vein (IMV), 1696-1697, 1774
 Inferior vena cava
 anatomy of, 1986
 image-guided biopsy and, 1245-1246
 lacerations of, 1710
 liver transplantation and
 preoperative imaging of, 1740
 liver transplantation complications involving, 1747-1749, 1749f-1750f
 magnetic resonance angiography of, 160
 varices that drain into, 1656
- Inflammatory bowel disease (IBD), 61-63. *See also* Colitis; Crohn's disease
 abscesses in, 1254
 acute abdomen from, 2265-2266
 bowel wall thickening in, 61-62
 carcinomas with, 1008-1009
 causes of, 985
 cholelithiasis with, 1010
 colorectal cancer with, 1028-1029
 complications with
 hepatobiliary, 1009-1010
 intestinal, 1008-1009, 1008f
 musculoskeletal, 1011-1012
 pancreatic, 1010-1011
 pulmonary, 1012
 urinary tract, 1011
 computed tomography enterography in
 management of, 691-692
 differential diagnosis of, 1012-1013, 1012f
 diffusion-weighted MRI on, 1225-1226
 extraintestinal complications of, 1009-1012
 fat wrapping in, 63
 gut signature alterations in, 62
 hepatic steatosis with, 1010
 liver abscesses with, 1010
 magnetic resonance colonography in diagnosis
 and assessment of, 930, 931f
 magnetic resonance imaging of, 82-86
 mimics of, 64
 pediatric, 2167
 primary sclerosing cholangitis with, 1010
 sonographic evaluation of, 61-63
 toxic megacolon with, 1009, 1009f
 treat response monitoring in, 84-85, 85f
 vascular changes in, 63
- Inflammatory disorders. *See also* Colitis;
 Inflammatory bowel disease (IBD)
 biliary tract, 1427-1441
 AIDS-related cholangitis, 1436-1437, 1437f
 echinococcal cholangitis, 1440
 floxuridine cholangitis, 1437
 obstructive cholangitis, 1434-1435, 1436f
 parasitic infestations, 1437-1440, 1438f
 primary biliary cirrhosis, 1432-1434, 1433f, 1435f
 primary sclerosing cholangitis, 1010, 1011f, 1427-1432
 pyogenic cholangitis
 recurrent, 1376f, 1435-1436, 1436f
 lymphatic spread of, 2008
 pediatric, 2152-2154
- Inflammatory esophagogastric polyps, 351, 352f
 Inflammatory fibroid polyps, 538, 538f
 gastroduodenal, differential diagnosis of, 658f
 small bowel, 792-793
 Inflammatory pseudopolyps, 988, 990f, 992, 994f
 Inflammatory pseudotumors
 liver, 1556-1557, 1557f
 pediatric, 2151
 spleen, 1930
 Informed consent for biopsy, 1241
 Infradiaphragmatic bursa, 2088
 Inframesocolic compartment, 2000, 2008-2009, 2027
 Inframesocolic space, 2002-2004
 Infrapancreatic lymphatic chain, 1775
 Inguinal fossae, 2004, 2004f
 Inguinal hernias, 2063-2064, 2065f
 Injection granulomas, 2074
 Inspissated bile syndrome, 2193
 Insulinomas, 1165f, 1847f, 1849-1850
 imaging, 1850-1851
 surgery for, 1861, 1862
 Interfascial spread, 1986, 1987f
 Intersigmoid hernias, 2058, 2059f
 Interstitial cells of Cajal, 1079-1080
 Interstitial edematous pancreatitis, 1810
 Interventional radiology
 on abdominal abscesses, 1258-1276
 catheter fixation, 1263
 combined modality approach in, 1264-1266, 1267f
 diagnostic aspiration, 1259, 1259f
 gantry angulation, 1264, 1265f
 hydrodissection, 1266, 1268f
 organ traversal, 1263-1264, 1265f
 percutaneous drainage, advantages and disadvantages of, 1261f
 percutaneous drainage, clinical considerations in, 1259-1261
 percutaneous drainage, technique in, 1261, 1263, 1261f-1262f
 Seldinger technique, 1263, 1263f
 surgical drains and, 1264, 1266f
 applications of, 112
 liver, 1498-1519
 combination interstitial and endovascular therapy, 1513
 drug-eluting bead chemoembolization, 1513
 endovascular intra-arterial therapies, 1510-1515
 transarterial chemoembolization, 1510-1513
 transarterial radioembolization, 1513-1515
 tumor ablation, 1506-1510, 1509f, 1511f
 pancreas, 1785-1796
 in acute necrotizing pancreatitis management, 1788-1793
 background on, 1785
 biopsy indications in, 1785-1787, 1786f-1787f
 complications with, 1789
 diagnostic effectiveness of, 1788-1789
 in pancreatic pseudocyst management, 1793-1794, 1794f
 technical considerations in, 1787-1788
 spleen, 1905-1911
 alcohol ablation in, 1908f
 catheter drainage, 1907-1908, 1907f
 image-guided biopsy, 1905-1907, 1906f
 complications with, 1908
 patient preparation for, 1905
 radiofrequency ablation, 1908
 Intestinal myopathy, 1123
 Intestinal perforation, 167f
 Intestinal rotation and fixation abnormalities in, 2091-2092, 2091f-2092f
 clinical findings on, 2096

- Intestinal rotation and fixation (*Continued*)
 gastroschisis, 2097-2098, 2098f
 radiographic findings on, 2095-2097, 2096f-2097f
 embryology of, 2088-2091, 2089f-2090f, 2095-2096
 hyperrotation, 864, 2092
 malrotation, 863-865, 865f, 2144-2146
 clinical findings on, 2144
 colon volvulus with, 2174-2175
 congenital syndromes associated with, 1151t
 imaging findings on, 2144-2146, 2145f-2146f
 small bowel, 863-865, 865f
 nonrotation, 863-864, 864f
- Intracellular agents. See Hepatobiliary contrast agents
- Intraductal papillary mucinous neoplasms (IPMNs), 1196, 1197f, 1320-1321, 1845, 1845f-1846f, 1847-1848
 magnetic resonance cholangiopancreatography on, 1330, 1331f
 main duct, 1848f
- Intraembryonic celom, 2080-2081, 2080f
- Intraepithelial lymphocytes, 756-757
- Intrahepatic ducts, 1282-1283. *See also* Biliary tract
 dilation of, 1289
 normal anatomy of, 1303-1304
- Intraluminal stasis, 775
- Intramesosigmoid hernias, 2038
- Intramural gas, 190-191, 190f
- Intraperitoneal abscesses, 1275-1276
- Intraperitoneal fluid, 170f
 flow of, 1085f
 spread of disease through, 2006-2009
- Intraperitoneal seeding
 after image-guided biopsy, 1250
 colonic, 1084-1086, 1085f
 from gastric carcinoma, 548
 of ovarian carcinoma, 1112-1113
- Intraperitoneal spaces, 171-172
- Intravoxel incoherent motion model (IVIM), 1216, 1218f
- Intubation
 in enteroclysis, 671-672, 672f
 palliative, 458-459
 ulceration from, differential diagnosis of, 462t
- Intussusception
 after colostomy, 1135
 after Roux-en-Y gastric bypass, 646, 647f
 appendiceal, 962f, 973-974
 colon
 from colorectal cancer, 1036
 dissection sign of, 2173, 2173f
 pediatric, 2172-2174, 2173f-2174f
 from rectal mucosal prolapse, 1119
 gastroduodenal and duodenojejunal, 624
 with glucagon contrast agents, 18
 jejunojejunal, 637-638, 638f
 obstruction from, 1106-1109, 1108f
 rectal, 898-899, 899f
 small bowel, 822-824
 with Meckel's diverticulum, 2158
 in Peutz-Jeghers syndrome, 823-824, 1093
 transient, 720
- Inverted diverticulum, 2085
- Inverted 3 sign of Frostberg, 618-619, 619f
- Iodine
 in contrast agents, 3-6
 contrast concentrations, 1160
 liver enhancement with, 1161
 in computed tomography, 1481-1482
 delayed scanning, 1483-1484, 1483f
 tagging agents, 907-908
- IPMNs. *See* Intraductal papillary mucinous neoplasms (IPMNs)
- Iron depositional disease, 1192
- Iron overload diseases. *See* Hemochromatosis
- Irritable bowel syndrome (IBS), 1120-1124
 clinical findings on, 1120
 computed tomography enteroclysis on, 704
 diagnostic procedures for, 1121
 epidemiology of, 1120
 pathophysiology of, 1120-1121
- Ischemia
 acute abdomen from, 2262-2263, 2263f
 acute mesenteric, 828-835, 830f-831f
 chronic mesenteric, 835-838, 837f
 colonic, 1114-1116, 1114f-1115f
 mosaic-submucosal edema pattern in, 1145t
 risk factors for, 1110b
 small bowel
 differential diagnosis of, 875t
 differentiated from appendicitis, 971, 973f
 drug-induced, 762b
 magnetic resonance enterography on, 721
 segmental mural hyperenhancement in, 686, 687t
 in systemic lupus erythematosus, 840
- Ischemic bowel, 64, 64f, 88
- Ischemic colitis, 89f, 1114
 hemorrhage from, 2279
 toxic megacolon with, 1009
- Ischiorectal fossa, 175, 175f
- Islet cell tumors, 1596, 1849
- Islets of Langerhans
 embryology of, 1797, 2086
 histiocytic syndromes of, 2238
- Isopora belli*, 766-767
- Isosporiasis, 766-767
- Iterative reconstruction, 737
- Iterative reconstruction in image space (IRIS), 1485
- J**
- Jaboulay pyloroplasty, 632
- Jaundice
 biliary dilation without, differential diagnosis of, 1464t
 with cholangiocarcinomas, 1411-1413
 contrast agents with, 1452
 neonatal, 2182, 2212
 obstructive
 with choledochal cysts, 1344
 with neoplasms, 2196, 2196f
 in primary sclerosing cholangitis, 1427
 with villous tumors, 529
- Jejunum. *See also* Small bowel
 atresia and stenosis of, 2110-2112, 2111f-2112f
 on computed tomography enterography, 684, 686, 692
 Crohn's disease in, 687f
 diverticula in, 667f
 familial adenomatous polyposis syndrome in, 1091
- Jejunointerposition, 455-458
- Jejunogastric intussusception, 637-638, 638f
- Jejunioileal bypass surgery, 642
- Jejunioileal diverticulosis, 776-777, 777f
- Jejunointeritis
 in celiac disease, 763, 764f
 Crohn's-related, 752
 fold enlargement in, 786
 ulcerative, 763, 764f
 small bowel fold thickening in, 872t
- Jejunostomy, 855, 872t
- Jejunum. *See also* Small bowel
 atresia and stenosis of, 2110-2112, 2111f-2112f
 on computed tomography enterography, 684, 686, 692
 Crohn's disease in, 687f
 diverticula in, 667f
 familial adenomatous polyposis syndrome in, 1091
- Jejunum (*Continued*)
 GISTs in, 799-800
 normal anatomy of, 665
- J-pouch anastomoses, 1137, 1137f-1139f, 1139
- Juvenile polyposis, 530, 1093, 1095
- Juvenile polyps, 2175-2176
- K**
- Kaposi's sarcoma, 252
 after liver transplantation, 1733
 with AIDS, 407, 1629
 colonic involvement of, 1077
 differential diagnosis of, 407-408
 esophageal, 407, 407f
 differential diagnosis of, 464t
 gastric narrowing from, 659t
 gastroduodenal, 405
 clinical findings in, 407
 differential diagnosis of, 658t
 pathologic and endoscopic findings in, 407
 radiographic findings on, 407
 small bowel, differential diagnosis of, 874t
 ultrasound on, 1653
- Kasabach-Merritt syndrome, 1926
- Kasai procedure, 2183-2184, 2188
- Kawasaki's disease, 2168
- Kehr's sign, 1965
- Kidneys
 carcinomas of
 gastroduodenal metastases from, 576
 metastases from, 979
 renal cell, 1198-1199, 1199f
 transitional cell, 1199, 1199f
 CTA of, 141-142, 142f
 duodenal displacement from, 616, 617f
 duodenal impressions by, 661t
 embryology of, 1985-1988, 1988f, 1989
 failure of, 661t
 fistulas in, 626
 image-guided biopsy of, 1247
 magnetic resonance imaging of, 1198-1199, 1198f-1199f
 angiomyolipomas, 1198, 1198f
 carcinomas, 1198-1199, 1199f
 oncocytomas, 1198
 renal cysts, 1198
 normal anatomy of, 175f
 pancreas in relation to, 1779
 polycystic disease of, 1190
 size estimation of, 192
 transplantation of, 938-939
 trauma to, 2285-2287, 2287f, 2288f
- Killian-Jamieson diverticula, 241, 242f
- Klatskin's tumors, 1415, 1416f, 1419f
- Klebsiella pneumoniae*
 with biliary obstruction, 1297
 esophagitis caused by, 322
 pyogenic abscesses with, 1272-1273
- Klippel-Trenaunay-Weber syndrome, 846-848
 colonic hemangiomas in, 1076
 hemangiomas in, 1926
 intestinal lymphangiectasia in, 2160t
 venous angiomas in, 2278
- Kock pouches, 856, 856f, 996
- Kulchitsky cells, 407-408
- Kupffer cells, 1340
 in hematogenous spread of metastases, 2006
 superparamagnetic iron oxide take-up by, 1529-1530
 in viral hepatitis, 1836-1837

L

- Lactobacillus acidophilus*, esophagitis caused by, 322
- Lactose intolerance, 2168
- Lactose-phlorizin hydrolase deficiency, 775
- Ladd's bands, 863-864, 2096, 2097f
- Ladd's procedure, 2146, 2146f
- Langerhans cell histiocytosis, 2238
- Laparoscopic adjustable gastric band placement (LAGB), 630, 646-651, 648f
- band adjustment after, 649
- complications after, 649-651
- device-related, 651
- intragastric erosion and band migration, 651, 651f
- pouch dilation, 649, 649f-650f
- pouch dilation with band slippage, 649-651, 650f
- imaging after, 647-651
- Laparoscopic surgery, anterior abdominal wall injuries from, 2074, 2074f. *See also* Laparoscopic adjustable gastric band placement (LAGB)
- Laparoscopy, pancreas, 1863
- Large bowel
- obstructions, 948, 950f
- traversal of in percutaneous drainage, 1264
- Laryngoceles, 237-238
- Laryngotracheal cleft, 2110
- Larynx, 224-225, 228f
- Late arterial phase of enhancement, 1159-1160, 1164
- Lateroconal fascia, 173f
- Lateroconal plane, 1990-1991, 1990f-1992f
- Lead poisoning, 615, 776b
- Lecithin, 774
- Leiomyoblastomas. *See* Gastrointestinal stromal tumors (GISTs), 534-535, 534f
- differential diagnosis of, 658f
- pediatric, 2150
- Leiomyomas
- calcified, 201, 201f
- colonic, 1079-1080
- differentiated from GISTs, 355
- esophageal, 353-354, 354f-355f, 357f
- differential diagnosis of, 463f-464f
- pediatric intramural, 2125, 2127f
- liver, 1536
- Leiomyomatosis, 356-358, 204f
- Leiomyosarcomas
- colonic, 1079-1080
- esophageal, 354, 403-405, 406f
- liver, 1536
- Lesser sac, 172f, 2002, 2004f
- embryology of, 2087-2088
- Leukemia
- candidiasis infection with, 1622
- esophageal involvement in, 408, 408f-409f
- differential diagnosis of, 464f
- gastric involvement in, 598
- differential diagnosis of, 658f
- hepatosplenic fungal infections with, 1936
- splenic involvement in, 1953-1954
- pediatric, 2234
- Leukoplakia, 301, 463f
- Leukotriene inhibitors, 996
- Levovist, 148f
- Lhermitte-Duclos disease, 1095
- Lichen planus, 464f
- Ligamentum teres, 2020
- Light bulb sign, 1198
- Limb defect syndrome, 1916
- Linitis plastica
- appearance of in breast cancer metastases, 572-573, 573f
- caused by gastric carcinoma, 560
- Linitis plastica (*Continued*)
- differentiated from atrophic gastritis, 506
- differentiated from Crohn's disease, 510
- in double-contrast studies, 53, 53f
- double-contrast studies of, 53, 53f
- gastric, 529f, 550, 551f, 554-555, 555f-556f
- gastric metastases resembling, 573f-574f
- gastric narrowing from, 659f
- scirrhous carcinoma and, 554, 554f
- Lipohyperplasia. *See* Fatty infiltration
- Lipomas. *See also* Fibrovascular polyps
- biliary tract, 1424
- colonic, 1077-1078, 1078f-1079f
- differential diagnosis of, 463f, 658f
- differentiated from GISTs, 532-533
- differentiated from leiomyomas, 354
- esophageal, 360, 361f, 463f
- gastroduodenal, 535-536, 535f, 658f
- ileocecal valve, 1079, 1080f
- liver, 1549-1550, 1549f-1550f
- mesenteric, 2042
- omental, 2050
- small bowel
- benign, 790-791, 791f
- intussusceptions by, 823-824, 824f
- Lipomatosis, pancreatic, 1890f
- Lipomatous infiltration. *See* Fatty infiltration
- Liposarcomas
- colonic, 1077-1078
- gastroduodenal, 598
- mesenteric, 2042, 2042f
- Littre's hernias, 2064
- Liver
- abscesses, 1272-1273, 1273f
- amebic, 1273, 1611-1614
- aspiration and drainage of, 1501-1502, 1502f
- epidemiology and symptoms of, 1501
- pyogenic, 1272-1273, 1608-1611
- aspiration and drainage of, 939f, 1501-1502
- clinical findings on, 1609
- from diverticulitis, 939f, 948-949
- hematogenous spread of, 2007
- incidence of, 1608
- with inflammatory bowel disease, 1010
- pathogenesis of, 1608-1609, 1609f
- radiologic findings on, 1609-1610, 1609f-1611f
- treatment of, 1610-1611
- accessory/pseudoaccessory fissures, 1520, 1521f-1522f
- acute cholecystitis involvement in, 1359, 1360f
- anatomic anomalies of, 1521-1525
- agenesis and hypoplasia
- left lobe, 1525, 1526f
- right lobe, 1522-1525, 1524f-1525f
- pedunculated accessory lobes, 1522, 1524f
- Riedel's lobe, 1521-1522, 1523f
- aspiration and drainage, 1501-1502, 1502f
- bare area of, 199f, 199f, 2016f
- ascites and, 2031
- embryology of, 1983, 1984f
- benign tumors of, 1528-1560, 1529b
- cysts, 1550-1554
- focal nodular hyperplasia, 1545-1543
- imaging evaluation of, 1528-1530
- imaging techniques in, 1529b
- infantile hemangioendothelioma, 1554-1555, 1555f
- lipomatous, 1549-1550, 1549f-1550f
- mesenchymal hamartoma, 1555-1556, 1556f
- miscellaneous, 1556-1557
- nodular regenerative hyperplasia, 1548-1549, 1548f
- surgery for, 1720
- bile duct anatomy and, 1282-1283, 1287f
- blood supply to, 1676, 1677f-1678f
- Liver (*Continued*)
- bright, 1759f
- carcinomas
- fibrolamellar hepatocellular, 1187, 1188f
- gallbladder carcinoma metastases, 1408-1409
- computed tomography of, 1162-1164, 1163f, 1489
- contrast enhancement phases in, 1159-1160
- CTA of, 142, 143f
- cystic calcifications in the, 200f
- differential diagnosis of, 1756-1768
- acoustic shadowing, 1760f
- anechoic masses, 1760f
- with arteriography, 1764
- atrophy, 1758f
- biliary tract gas, 1759f
- Budd-Chiari syndrome, 1766f
- calcification, 1758f
- cavernous hemangioma, 1767f
- central scars in primary tumors, 1763f
- cirrhosis and portal hypertension, 1765f
- complex masses, 1760f
- with computed tomography, 1761
- decreased uptake, 1764f
- diffusely decreased liver intensity, 1763f
- diffusely dense liver, 1761f
- early/increased flow to the liver, 1763f
- fat-containing masses, 1762f
- fatty infiltration, 1765f
- fluid-fluid levels in focal lesions, 1762f
- focal enlargement, 1757f
- focal hyperdense lesions, 1762f
- focal hypodense lesions, 1761f-1762f
- focally decreased flow, 1764f
- focal nodular hyperplasia, 1768f
- focal uptake, 1764f
- halo sign, 1764f
- hemochromatosis, 1766f
- hepatic capsular retraction, 1758f
- hepatic vein dilation, 1759f
- hepatic vein Doppler waveform dampening, 1761f
- hepatocellular adenoma, 1766f
- hepatocellular carcinoma, 1767f
- hepatomegaly, 1757f
- hyperechoic masses, 1760f
- hyperperfusion abnormalities of liver, 1762f
- hyperplastic hepatocellular conditions, 1547f
- hypoechoic or anechoic focal masses, 1760f
- hypointense masses, 1763f
- increased periportal signal intensity, 1763f
- lesions, 1764f
- lesions with circumferential rim, 1763f
- liver rim sign, 1764f
- with magnetic resonance, 1763
- metastases, ultrasound echo patterns of, 1761f
- multiseptate cystic masses, 1760f
- neonatal liver calcification, 1758f
- nonvisualization of liver and, 1764f
- with nuclear scintigraphy, 1763
- patchy hepatograms, 1762f
- periportal lucency, 1762f
- porta hepatis masses, 1762f
- portal venous gas, 1758f
- prominent periportal echoes, 1760f
- pseudolesions, 1759f
- with scintigraphy, 1763
- TIPS malfunction, 1761f
- with ultrasound, 1759
- ultrasound echogenicity changes, 1759f
- vascular lesions, 1764f
- vascular "scar" tumors, 1762f
- viral hepatitis, 1765f
- wedge-shaped signal alterations, 1763f
- diffuse diseases of, 1628-1675
- AIDS, 1651-1654
- amyloidosis, 1645-1646

Liver (Continued)

- biliary hamartomas, 1649, 1649f
- cirrhosis, 1654-1670
 - Gaucher's disease, 1647
 - glycogen storage disease, 1644-1645
 - hemosiderosis and hemochromatosis, 1641-1644
 - hepatitis, 1636-1639
 - primary biliary cirrhosis, 1649-1650, 1649f
 - radiation-induced, 1640-1641
 - sarcoidosis, 1647-1648, 1648f
 - steatosis, 1629-1636, 1630t
 - toxin- and drug-induced, 1639-1640
 - Wilson's disease, 1646-1647, 1647f
- diffusion-weighted MRI of, 1221-1223
 - fibrosis and cirrhosis diagnosis with, 1223
 - lesion characterization in, 1222-1223
 - lesion detection in, 1221-1222
 - tumor treatment response assessment in, 1223
- duodenal displacement from, 616
- duodenal impressions by, 661t
- ectopic, 1522
- embryology of, 1520, 1521f, 1983, 1985, 2081-2082
 - abnormal development of, 202
 - subperitoneal spread and, 1998f
- familial adenomatous polyposis syndrome
 - manifestations in, 1092-1093
- focal infections of, 1608-1628
 - amebic abscesses, 1611-1614
 - bacterial (pyogenic) abscesses, 1608-1611
 - candidiasis and fungal, 1622-1623, 1622f
 - echinococcal disease, 1614-1621
 - Fasciola hepatica*, 1621
 - Pneumocystis carinii*, 1625
 - tuberculosis, 1625
- Hellmer's sign with, 193
- hemangiomas, 1530-1533
 - angiography on, 1533
 - computed tomography on, 1532-1533, 1533f
 - diagnostic work-up of, 1535
 - incidence and clinical presentation of, 1531
 - magnetic resonance imaging of, 1534-1535, 1534f, 1536f-1537f
 - nuclear medicine imaging of, 1531, 1531f
 - pathologic findings on, 1530-1531, 1530f, 1531t
 - plain radiographic findings on, 1531
 - ultrasound of, 1531-1532, 1532f
- hepatomegaly of, 192f
 - in Budd-Chiari syndrome, 1682-1683
 - differential diagnosis of, 1757t
 - diffuse, 1757t
 - duodenal displacement from, 616
 - focal enlargement, 1757t
 - with gallbladder carcinoma metastasis, 1403
 - in hemochromatosis, 1641
 - in neonates, 1757t
 - with steatosis, 1651
 - in viral hepatitis, 1657
- image-guided biopsy of, 1244-1248, 1248f
- incidental masses, differential diagnosis of, 1600
- infarctions of, 2267
- inflammatory bowel disease complications in, 1009-1010, 1010b
- interventional radiology of, 1498-1519
 - biopsies, 1498-1501
 - percutaneous, 1498-1501, 1499f-1500f
 - combination interstitial and endovascular therapy, 1513
 - endovascular intra-arterial therapies, 1510-1515, 1512f
 - hepatic venous pressure gradient, 1502-1503
 - preoperative portal vein embolization, 1505-1506, 1507f

Liver (Continued)

- transjugular intrahepatic portosystemic shunts, 416f, 418-419, 1503-1505
 - portal hypertension and, 1503
 - for varices, 460
- tumor ablation, 1506-1510, 1509f, 1511f
- lacerations, intraperitoneal fluid and, 170f
- lobar atrophy of with cholangiocarcinomas, 1416
- magnetic resonance imaging of, 1487-1492, 1488f
 - cavernous hemangiomas, 1186-1187, 1187f
 - cholangiocellular origin lesions, 1190, 1190f
 - choledocholithiasis and cholelithiasis, 1192, 1193f
- cirrhosis, 1190-1192
- colonography, 929
- contrast agents in, 1186
- focal nodular hyperplasia, 1187, 1188f
- hepatic adenomas, 1187-1189, 1189f
- hepatocellular carcinoma, 1190-1192, 1191f
- iron depositional disease, 1192
- malabsorption related to, 774, 775t
- malignant tumors of, 1561-1607, 1562b
 - angiosarcoma, 1584-1586
 - cystadenoma and cystadenocarcinoma, 1581-1584
 - differential diagnosis of, 1600
 - epithelial hemangioendotheliomas, 1588
 - fibrolamellar carcinoma, 1573-1577
 - hepatoblastoma, 1577-1579
 - hepatocellular carcinoma, 1561-1573
 - imaging techniques for, 1563b
 - intrahepatic cholangiocarcinoma, 1579-1581
 - lymphomas, 1588-1589, 1589f
 - metastases, 1589-1600, 1590t
 - practical approach to, 1600-1603
 - surgery for, 1720
 - of undifferentiated (embryonal) sarcomas, 1586-1588
- mesenchymal sarcomas, 1588
- metastases in
 - in carcinoid syndrome, 799
 - from colon, 1047f
 - from colon cancer, 1043, 1047, 1047f
 - from gallbladder carcinomas, 1408-1409
 - hematogenous spread of, 2006
 - pediatric, 2206, 2206f
- normal anatomy of, 168, 170f, 1175, 1471-1476, 1472f
 - anomalies and, 1521-1525
 - bile ducts, 1476, 1477f
 - blood supply, 1471-1473, 1472f-1473f
 - lobar and segmental, 1473-1475, 1474f-1476f
 - lymphatics, 1476, 1477f
 - nerve supply, 1476
 - porta hepatis, 1475-1476, 1476f
 - portal vein, 1471
 - variations in, 1520-1521
- obliteration of edge of with ascites, 193, 193f
- papillary process of the caudate lobe, 1521, 1523f
- pediatric disorders of, 2200-2215
 - benign neoplasms, 2206-2210
 - adenomas, 2210, 2210f
 - focal nodular hyperplasias, 2210, 2211f
 - mesenchymal hamartomas, 2209-2210, 2209f
 - vascular lesions, 2206-2209
- cirrhosis and diffuse disorders, 2212-2213, 2213f
- congenital, 2200-2202
- fibropolycystic, 2201-2202, 2201f
- hepatic cysts, 2202, 2202f
- malformations and hernias, 2200-2201

Liver (Continued)

- focal inflammatory-infectious lesions, 2211-2212, 2211f-2212f
- imaging of, 2210
- lymphoproliferative disorders, 2210
- malignant neoplasms, 2202-2206
 - angiosarcomas, 2205, 2205f
 - hepatoblastomas, 2202-2203, 2203f
 - hepatocellular carcinomas, 2204, 2204f
 - primary, 2202-2206
 - secondary, 2206
 - undifferentiated embryonal sarcomas, 2204-2205, 2205f
- neonatal jaundice, 2212
- vascular lesions, 2206-2209
 - arterioportal fistula, 2209
 - arteriovenous malformations, 2208-2209, 2208f
 - infantile hemangioendothelioma, 2206-2208, 2207f-2208f
 - portosystemic shunts, 2209
- PET/CT of, 1204-1207
 - hepatocellular carcinomas, 1204-1205
 - lymphomas, 1207, 1207f
 - metastatic disease, 1205-1207, 1205f
- primary sclerosing cholangitis in, 1427
- radiologic techniques on, 1476-1492
 - plain radiography, 1476-1477
 - selecting appropriate, 1492
- segments of, 1175, 1176f, 1717f
 - abnormal development of, 202
- size estimation of, 192, 1477
- ultrasound for, 1477-1478
- sliver of, 1520-1521, 1522f
- steatosis of, 1010, 1184, 1185f
- surgery on, 1717-1722
 - for benign lesions, 1720
 - complications with, 1728-1729, 1728f
 - indications for, 1718t, 1720-1721
 - for malignant lesions, 1720
 - patient selection for, 1720-1721
 - postoperative radiologic findings on, 1727-1729, 1727f
 - radiology in planning, 1718
 - types of resection, 1721-1722
 - ultrasound during, 1718, 1718f
- transplantation, 1737-1755
 - allograft rejection after, 1432
 - bile leakage after, 1455
 - biliary complications after, 1311-1314, 1315f
 - combined small bowel and, 858
 - for hepatopulmonary syndrome, 433
 - indications for, 1738t
 - HCC, 1205
 - living donor, 1741-1743, 1743f-1744f
 - locoregional bridging therapy before, 1740
 - patient evaluation for, 1738-1739
 - periportal low density in, 1710
 - postoperative complications with, 1743-1753
 - biliary, 1749-1752, 1750f-1752f
 - fluid collections, 1753
 - hepatic arterial, 1743-1746, 1744f-1747f
 - hepatic vein and inferior vena cava, 1747-1749, 1749f-1750f
 - portal venous, 1746-1747, 1747f-1748f
 - post-transplantation malignant disease, 1753
 - rejection, 1752-1753
 - postoperative imaging of, 1332-1334
 - preoperative imaging for, 1739-1740, 1739f-1740f
 - splenic arterial steal syndrome after, 1910

Liver (Continued)

- surgical technique for, 1740-1741, 1741E-1742f
- transarterial chemoembolization before, 1510-1511
- trauma to, 1706-1717, 2284-2285, 2285f, 2286f, 2287f
 - blunt, 1707, 1709f
 - classification of, 1712f
 - clinical findings on, 1706
 - complications with, 1716-1717
 - biliary tract, 1717
 - bleeding, 1716
 - infection, 1716
 - epidemiology of, 1706
 - iatrogenic injuries, 1708
 - pathophysiology of, 1707-1708
 - penetrating injuries, 1707, 1708f-1709f
 - radiologic findings on, 1708-1716
 - angiography, 1715-1716
 - computed tomography, 1708-1712, 1708f-1711f, 1713f
 - magnetic resonance imaging, 1715, 1715f
 - plain radiographs, 1716
 - scintigraphy, 1714-1715, 1714f
 - ultrasound, 1712-1715, 1714f
 - spontaneous rupture, 1721-1722
 - surgery types for, 1722f
 - treatment of, 1716
 - traversal of in percutaneous drainage, 1264
 - tumor response monitoring, 1487
 - ultrasound of, 1173-1178
 - Doppler, 1173f
 - on size and structure, 1477-1478
 - vascular disorders of, 1676-1705
 - acute abdomen from, 2266-2268
 - Budd-Chiari syndrome, 1680-1688
 - cardiac disease and, 1688-1689
 - cavernous transformation of the portal vein, 1695
 - hemolysis, elevated liver enzymes, low platelets syndrome, 1698-1699
 - hepatic infarction, 1698
 - hepatopulmonary syndrome, 413-414, 1702, 1703f
 - Osler-Weber-Rendu syndrome, 1701, 1702f
 - peliosis hepatis, 1689-1690
 - portal vein thrombosis, 1690-1695
 - sinusoidal obstruction syndrome, 1680-1688
 - splanchnic vein aneurysms, 1701, 1701f
 - splenic vein and inferior mesenteric vein thrombosis, 1696-1697
 - superior mesenteric vein thrombosis, 1696
 - transient hepatic attenuation/intensity differences, 1676-1680
 - visceral artery aneurysms, 1699-1701
- Liver-directed therapy, 1723-1728
 - chemoembolization, 1725-1726, 1728-1729
 - combination chemoembolization and radiofrequency ablation, 1726
 - cryosurgery, 1723-1724, 1729
 - postoperative radiologic findings on, 1727-1728, 1727f
 - radioembolization, 1726-1727, 1727f, 1729, 1729f
 - radiofrequency ablation, 1724, 1724f-1725f
- Liver flukes, 1410-1411
 - biliary infestations of, 1437-1440, 1438f
 - Fasciola hepatica*, 1621, 1622f
- Liver Imaging Reporting and Data System (LI-RADS), 1499
- Living donor liver transplantation (LDLT), 1741-1743, 1743f
- Locoregional bridging therapies, 1740
- Locust bean gum, 82, 684

- Loop colostomy, 1135
- Lou Gehrig's disease. *See* Amyotrophic lateral sclerosis
- Low anterior resection, colonic, 1136-1137, 1137f
- Lower esophageal sphincter (LES), 279
 - in achalasia, 281-284
 - diffuse esophageal spasm and, 284-285, 286f
 - in GERD, 291
 - hypertensive, 287
 - postoperative disruption of, 449
 - scleroderma in, 288-289, 288f
 - in swallowing, 279
- Lumbar hernias, 2062, 2063f
- Lungs
 - cancer of
 - image-guided biopsy of, 1246f-1247f
 - metastases from
 - adrenal glands, 1210, 1210f
 - appendiceal, 979
 - colonic, 1086
 - liver, 1591f
 - pancreatic, 1851, 1851f
 - carcinoid tumors in, 1077
 - carcinoma of
 - esophageal compression from, 397f
 - esophageal metastases from, 394, 395f
 - secondary achalasia from, 397-398
 - embryology of, 2080
 - gallstone migration to, 1433
 - image-guided biopsy of, 1244-1245, 1245f-1247f
- Lupus vasculitis, 838-839
- Lye ingestion, 246f, 330-331. *See also* Caustic ingestion
 - squamous cell carcinoma associated with, 367
 - strictures from, 373, 455
- Lymphangiectasia, 785f
- Lymphangiomas, splenic, 1929-1930, 1930f
- Lymphadenopathy
 - hilar, 1417
 - mesenteric
 - pediatric, 2248-2249, 2249f
 - small bowel intussusceptions by, 823-824
 - peritoneal, pediatric, 2248-2249
 - small bowel
 - in celiac disease, 760f
 - in differential diagnosis, 769
 - in Whipple's disease, 782
- Lymphangiectasia
 - hypoalbuminemia with, 867
 - micronodularity in, 871f
 - pediatric intestinal, 2160-2161
 - small bowel fold thickening in, 872f
- Lymphangiomas
 - colonic, 1076
 - gastrointestinal, 536
 - differential diagnosis of, 658f
 - mesenteric, 2042, 2042f, 2246-2248
 - omental, 2246-2248
 - splenic, 2232-2233, 2233f
- Lymphangiomatosis, 1556, 1929, 1930f
- Lymphatic metastases, 2007-2008, 2008f
 - in esophageal cancer staging, 382, 383f
 - cervical, 385-389, 387f
 - with esophageal squamous cell carcinomas, 368, 374f, 381
 - from gallbladder carcinoma, 1409
 - from gastric carcinoma, 548
- Lymphatic obstruction, malabsorption due to, 784-785
- Lymph nodes
 - accessory spleens differentiated from, 1181
 - calcifications in, 201, 201f
 - cavitary mesenteric syndrome of, 761f, 762-763
 - cervical, in esophageal cancer staging, 385-389
 - diffusion-weighted MRI of, 1223-1224
 - hepatic, normal anatomy of, 1476, 1477f

Lymph nodes (Continued)

- image-guided biopsy of, 1250
- magnetic resonance colonography, 929
- magnetic resonance imaging of, 1183-1184
- mesenteric, enhancement of, 84
- mesenteric and omental, 76-77
- metastatic disease in
 - from colorectal cancer, 1047
 - mediastinal, 395, 398f
- pancreatic, 1774-1775, 1775f
- prominent, in Crohn's disease, 733
- splenic malformations in, pediatric, 2232-2233
- Lymphogranuloma venereum, 1113, 1113f
- Lymphoid follicular pattern, 2164, 2165f
- Lymphoid hyperplasia, 243-244, 244f
 - benign gastroduodenal, 541, 541f
 - differentiated from Brunner gland hyperplasia, 541, 541f
 - with *H. pylori* gastritis, 501-503, 502f-503f
 - with immunodeficiency, 763, 764f
 - pediatric colon, 2164, 2165f
- Lymphomas
 - adrenal gland, 1202-1203, 1211f
 - appendiceal, 979
 - biliary tract, 1311, 1314f, 1422
 - pediatric, 2196
 - Burkitt's, 1950f
 - pediatric, 2206, 2206f, 2225, 2225f
 - colonic, 1074-1075, 1075f
 - enteropathy-associated T-cell, 720
 - esophageal, 400-401, 401f, 403f
 - Hodgkin's, 400-401
 - non-Hodgkin's, 403f-404f
 - thickened folds in, 464f
 - gallbladder, 1410
 - gastrointestinal, 580-587
 - advanced, 583-584
 - clinical findings in, 581
 - differential diagnosis of, 586-587, 659f
 - endoscopic findings in, 581
 - forms of, 583f
 - imaging modalities for, 585-586
 - MALT, 582, 582f
 - pathology of, 581
 - pediatric, 2150-2151
 - radiographic findings on, 582-586
 - response to chemotherapy, 584f-585f
 - thickened duodenal folds from, 661f
 - treatment and prognosis of, 581-582
 - ulcerated, 585f
 - Hodgkin's, 319-320
 - gastric narrowing from, 659f
 - image-guided biopsy of, 1250
 - H. pylori* gastritis differentiated from, 502-503
 - ileocecal, 681f
 - ileocecal valve, 1079
 - image-guided biopsy of, 1250
 - liver, 1588-1589, 1589f
 - with AIDS, 1629, 1633
 - candidiasis infection with, 1622
 - pediatric, 2206f
 - PET/CT on, 1207, 1207f
 - MALT, 503, 503f
 - mantle cell, 873f-874f
 - small bowel luminal narrowing in, 873f
 - Mediterranean
 - small bowel fold thickening in, 872f
 - mesenteric, 2044f, 2045f
 - pediatric, 2249
 - multiple duodenal ulcers with, 484
 - non-Hodgkin's
 - gastric narrowing from, 659f
 - small bowel obstruction by, 817, 818f
 - omentum, 2050
 - pancreatic

Lymphomas (Continued)

- gastrointestinal metastases from, 574-575
- pediatric, 2196
- pharyngeal, 250
- small bowel, 801-804, 803f
 - in celiac disease, 760f, 762-763, 763f
 - computed tomography enteroclysis on, 697-699
 - Crohn's associated, 752
 - differentiated from Crohn's disease, 688
 - intussusceptions from, 823-824
 - luminal narrowing in, 873t
 - magnetic resonance enterography on, 720-721
 - malabsorption due to, 786, 786f
 - mantle cell, 769f
 - obstruction by, 818, 818f
- spleen, 1939, 1946-1950
 - clinical findings on, 1950
 - epidemiology and pathogenesis of, 1948-1950
 - mantle cell, 1954f
 - pathology of, 1950
 - pediatric, 2234, 2234f
 - PET/CT on, 1207, 1207f-1208f
 - radiologic findings on, 1950-1953
 - computed tomography, 1951-1952, 1951f-1953f
 - radiography, 1950
 - ultrasound, 1950-1951
 - ultrasound on, 1181
 - staging, 1950
 - T-cell, 872t
 - thickened gastric folds with, differential diagnosis of, 504
- Lymphomatosis, peritoneal, 2044
- Lymphoproliferative disorders, 2210, 2211f

M

- Macrocephaly, 1095, 1097
- Macroglobulinemia, 871t
- Macrophage dysfunction, 1022
- Maffucci's syndrome, 846-848
- Magnesium citrate, 906-907
- Magnetic field-based electronic guidance systems, 1243
- Magnetic resonance angiography (MRA), 149-162
 - abdominal, clinical applications of, 154-160
 - on chronic mesenteric ischemia, 154-157, 158f, 837-838
 - for diseases of the inferior vena cava, 160
 - gallbladder, 1384-1385
 - for hepatic vasculature evaluation, 159-160, 159f
 - image postprocessing and display in, 153-154
 - maximum intensity projection technique, 154
 - multiplanar reformat technique for, 154
 - shaded surface display, 154
 - subtraction technique for, 153-154
 - volume rendering for, 154
 - liver, on hepatocellular adenomas, 1545-1546, 1546f-1547f
 - for magnetic resonance portography, 160, 160f
 - of median arcuate ligament syndrome, 157-158
 - pitfalls in, 160-161
 - of segmental arterial mediolysis, 159
 - for small bowel evaluation, 682
 - in splanchnic artery dissection, 158
 - techniques in, 149-153
 - contrast-enhanced, 150-153
 - nonenhanced, 149-150
 - of visceral artery aneurysms, 159

Magnetic resonance cholangiopancreatography

- (MRCP), 1183, 1281, 1288f, 1292-1295, 1293f, 1325-1339
 - on acute cholecystitis, 1360
 - on AIDS-related disorders, 1654
 - on bile duct calculi, 1326-1328, 1327f-1328f
 - for bile leak detection, 1444
 - on biliary atresia, 2188, 2188f
 - of Caroli's disease, 607, 607f
 - on choledochal cysts, 1345
 - clinical applications of, 1326-1332
 - on congenital anomalies, 1330-1332
 - contrast-enhanced, 1294
 - enhanced 3D, 1295f
 - on gallbladder diseases, 1336
 - liver, on hepatocellular carcinomas, 1567
 - on neoplasms, 1328-1330
 - normal anatomy in, 1294-1295, 1326f
 - pancreas, 1779-1781, 1780f-1781f
 - differential diagnosis with, 1890
 - on pancreatic duct strictures, 1891t
 - on pancreas divisum, 1802f, 1803
 - on pancreatic duct strictures, 1891t
 - surgery and, 1863
 - on pancreas divisum, 1802
 - on pancreatitis
 - acute, 1812
 - chronic, 1826
 - pediatric, 2216
 - percutaneous transhepatic biliary drainage with, 1395-1396
 - on primary sclerosing cholangitis, 1334-1335, 1334f-1335f, 1430-1431
 - secretin-enhanced, 1332, 1336
 - technique in, 1293-1294, 1294f, 1325-1326
 - on trauma, 1859, 1859f

Magnetic resonance colonography (MRC), 928-933

- accuracy of, 931
- bowel preparation for, 931-932
- contraindications to, 928
- data analysis in, 931
- guidelines for, 928
- indications for, 930
- multiplanar reformation mode in, 928
- patient acceptance of, 931-932
- prerequisites for, 928
- scar artifacts in, 928-929, 930f
- sequences in, 928, 929f, 929t, 931
- tagging agents in, 932, 932f

Magnetic resonance enteroclysis

- bowel distention in, 710-711
- on small bowel obstruction, 722, 722f
- on small bowel obstructions, 811

Magnetic resonance enterography (MRE), 710-724

- bowel distention in, 734
- clinical applications of, 713-722
 - bowel ischemia and vasculitis, 721
 - celiac disease, 720-721
 - Crohn's disease, 714f-717f, 715t
 - with abscess formation, 717, 719, 719f
 - fibrostenotic, 713-719
 - in fistulas in, 717, 718f
 - regenerative or reparative, 717
 - infections, 721, 721f
 - small bowel neoplasms, 719-720, 719f
 - small bowel obstruction, 721-722, 722f
- on Crohn's disease, 734
 - luminal narrowing and stricture formation, 741-742
 - ulcers and sinus tracts, 742-743
 - vasa recta distention in, 747f
- image interpretation, 713
- integration of with computed tomography enterography, 692

Magnetic resonance enterography (MRE)

- (Continued)
- normal findings in, 711f
- technical considerations in, 710-713
 - contrast agents for, 710-711
 - protocol and pulse sequences in, 712-713, 712t
 - technique for, 711
- Magnetic resonance imaging (MRI). *See also* Diffusion-weighted magnetic resonance imaging; Perfusion magnetic resonance imaging
 - of abdominal abscesses, 1255t, 1257-1258, 1258f
 - acute cholecystitis imaging in, 1355
 - acalculous, 1362, 1362f
 - of the appendix, 967-969
 - on ascites, 2031, 2032f
 - on cholangiocarcinomas, 1413-1414, 1414f
 - delayed contrast enhancement in, 1415-1416, 1416f
 - of choledocholithiasis, 1372-1374, 1373f
 - coil selection for, 80
 - colon
 - of adenocarcinoma, 1051f
 - of benign polyps, 1035
 - on cancer, 1050-1054, 1050f
 - endoluminal, 1051-1052, 1055-1056
 - ischemia in, 1116
 - mural thickening in, 1151t
 - on obstructions, 1104
 - computed tomography enteroclysis compared with, 698
 - contrast agents in, 14-16, 80-82, 1184-1186
 - on Crohn's disease, 733-736, 1006-1007
 - nomenclature for disease findings in, 737-752, 738t
 - diffusion-weighted, 84
 - on diverticulitis, 940, 940f
 - dynamic
 - on anorectal and pelvic floor dysfunction, 891-892, 901-902
 - contrast-enhanced, 1226-1227, 1235, 2304
 - contrast-enhanced 3D, 1184
 - on echinococcal disease, 1934-1935
 - of esophageal leiomyosarcomas, 405, 406f
 - fetal risks in, 968
 - field strength in, 1183
 - free-breathing navigator-triggered, 1184
 - gallbladder, 1283, 1286-1287, 1287f-1288f
 - acute cholecystitis, 1360, 1361f
 - biliary sludge in, 1352, 1355f
 - on carcinomas, 1406, 1407f, 1408
 - on mural thickening, 1405f, 1406
 - gallstones on, 1351, 1354f
 - in gastric cancer staging, 564, 564f
 - of gastrointestinal malignancies, 89-93
 - gastrointestinal tract, 79-95
 - GISTs in, 800
 - in image-guided percutaneous tissue acquisition, 1243, 1243f
 - on imperforate anus, 2116, 2117f
 - of infectious bowel disease, 86-88
 - of ischemic bowel disease, 88
 - liver, 1487-1492, 1491f
 - on AIDS-related disorders, 1654
 - on alcoholic hepatitis, 1639
 - on amebic abscesses, 1612, 1615f
 - on angiosarcomas, 1586, 1586f
 - artifact minimization in, 1492
 - on bacterial (pyogenic) abscesses, 1610, 1610f
 - benign liver tumors, 1529
 - on Budd-Chiari syndrome, 1684-1686, 1685f-1686f
 - on cirrhosis, 1659f, 1662-1665, 1664f

Magnetic resonance imaging (MRI) (*Continued*)
 contrast agents, 1489-1490
 on cystadenomas and cystadenocarcinomas, 1584, 1585f-1586f
 differential diagnosis in, 1763
 diffusion-weighted, 1490-1491
 on echinococcal disease, 1619, 1620f-1621f
 elastography, 1491
 fat suppression techniques, 1489
 on fibrolamellar carcinoma, 1573, 1577f
 on focal nodular hyperplasias, 1539-1542, 1541f-1542f
 on glycogen storage disease, 1643
 of hemangiomas, 1534-1535, 1534f-1535f
 on hemochromatosis, 1643-1644, 1643f-1644f
 on hepatic congestion, 1689
 on hepatoblastomas, 1579
 on hepatocellular carcinomas, 1564, 1567-1573, 1568f-1569f
 on infantile hemangioendothelioma, 1534, 1535f
 on intrahepatic cholangiocarcinomas, 1580-1581, 1581f-1582f
 on lipomas, 1549-1550
 of mesenchymal hamartomas, 1555-1556, 1556f
 of metastases, 1598-1599, 1598f-1600f, 1602f
 on metastases, 1601f
 of nodular regenerative hyperplasia, 1549
 perfusion, 1492
 on portal vein thrombosis, 1693-1694, 1694f-1695f
 of radiation-induced disease, 1641
 on schistosomiasis, 1625
 on steatosis, 1633-1636, 1635f
 T1-weighted, 1488, 1488f
 T2-weighted, 1488-1489, 1489f
 in treatment response monitoring, 1729, 1730f
 on undifferentiated (embryonal) sarcomas, 1597f, 1598
 magnetic susceptibility artifacts in, 1287
 pancreas, 1779-1780, 1779f-1780f
 on annular pancreas, 1805, 1805f
 on neuroendocrine tumors, 1850-1851
 on pancreatitis, 1813-1819
 pediatric, 2216
 post-transplant, 1874, 1876f
 surgery and, 1863
 patient preparation for, 80-82
 of pelvic floor, 891-892
 on primary sclerosing cholangitis, 1430-1431
 protocols for gastrointestinal tract imaging, 79-80, 81t
 rectal cancer staging with, 1052f, 1052t
 sequences in, 1183-1184
 signal-to-noise ratio in, 1183
 of solid parenchymal organs, 1183-1201
 adrenal glands, 1197-1198, 1197f
 biliary tract, 1190, 1190f, 1192-1194, 1193f, 1195f
 gallbladder, 1192-1194, 1194f
 kidneys, 1198-1199, 1198f-1199f
 liver, 1186-1192, 1187f-1189f, 1195f
 pancreas, 1194-1197, 1196f-1197f
 technique for, 1183-1186
 spleen, 1924
 on accessory spleen, 1915, 1916f
 on accessory spleens, 1925, 1926f
 anatomy in, 1902-1903, 1903f
 on angiosarcomas, 1947, 1949f
 differential diagnosis with, 1978
 on hamartomas, 1928
 on hemangiomas, 1927-1928, 1927f
 on infarctions, 1942-1943, 1942f
 on lymphangiomas, 1930

Magnetic resonance imaging (MRI) (*Continued*)
 on lymphomas, 1952-1953, 1953f
 on metastatic disease, 1956-1957
 pediatric, 2228, 2229f-2230f
 on pyogenic abscesses, 1940
 wandering, 1914
 surface coils in, 1183
 in tumor response monitoring, 2304
 on ulcerative colitis, 993
 Magnetic resonance index of activity (MRIA) scores, 752
 Magnetic resonance portography, 160, 160f
 Magnetic susceptibility artifacts, 1287
 MAI complex. *See* *Mycobacterium avium-intracellulare* (MAI) complex
 Main pancreatic duct (MPD), 1305-1306, 1306f
See also Biliary tract
 Main portal vein (MPV), 1176-1178
 Malabsorption conditions, 773-788. *See also* Celiac disease
 after gastric and duodenal surgery, 640-641
 anatomic classification of, 774-776, 775t
 bacterial overgrowth in, 775-778
 barium study choice for, 682t
 blind loop syndrome, 854-855
 clinical perspective on, 776
 differential diagnosis of fold enlargement in, 786, 786f
 digestion and absorption and
 fat digestion and absorption, 774
 fluid and electrolytes in, 774
 protein digestion and absorption, 774
 drug-induced, 762b
 epithelial cell damage in, 778-784
 HIV enteritis, 765
 lymphatic obstruction and lymphangiectasia, 784-785, 785f
 multifactorial, 785
 nonformation of chylomicrons in, 784, 784f
 Malacoplakia, 1022
 Malignant autonomic nerve tumors, 598
 Malignant peritoneal mesothelioma (MPM), 2037-2039, 2039f-2040f
 Malignant ulcers. *See* Carcinomas; gastric
 Mallory bodies, 1562, 1638
 Mallory-Weiss tears, 412, 413f
 MALT lymphomas. *See* Mucosa-associated lymphoid tissue lymphomas
 Marfanoid trisodium, 1490
 Mannitol, in magnetic resonance imaging, 82
 Mantle cell lymphomas, 873t-874t
 Marfan's syndrome, 1151t
 Marginal artery of Drummond, 837, 838f
 Marshak's principles on Crohn's disease, 727
 Mastocytosis, 786, 872t
 Maximum intensity projection (MIP) imaging, 828, 1281, 1325
 renderings in, 1161
 McBurney's point, 959-960, 2024
 MDCT. *See* Multidetector computed tomography (MDCT)
 Meckel's diverticulum, 862f, 2071, 2092, 2092f
 acute abdomen from, 2266f
 differentiated from appendicitis, 970, 972f
 giant, 2158, 2159f
 GI bleeding from, 688-690
 inverted, 861, 862f
 omphalocele with, 2098
 pediatric, 2158-2160, 2159f-2160f
 scintigraphy on, 2161f
 segmental dilation with, 863
 small bowel
 intussusceptions by, 823-824, 824f
 site predilection of, 875f
 Meconium ileus, 2118-2119, 2119f
 Meconium ileus equivalent syndrome, 1110

Meconium peritonitis, 2111-2113, 2112f
 Meconium plug syndrome, 2119-2120, 2120f
 Medial umbilical folds, 2004
 Median arcuate ligament syndrome, 846, 847f-848f
 Mediastinum
 esophageal cancer staging, 381-382
 inflammatory reactions to barium in, 415-416
 leiomyomas in, 354
 lymph node metastases, 395, 398f
 lymphomas
 esophageal compression from, 401, 402f
 Medusa's head appearance of varices, 1636
 Megacolon
 nonobstructive, 1123
 toxic, 185-186, 186f
 differential diagnosis of, 1148t
 with inflammatory bowel disease, 1009, 1009f
 pathologic findings in, 1009
 pediatric, 2167
 in pseudomembranous colitis, 1024
 radiologic findings in, 1009
 Megacystis-microcolon-intestinal hypoperistalsis (MMIH) syndrome, 2120-2121, 2120f
 Megaduodenum, 508-509, 509f
 pediatric, 2154-2155
 with strongyloidiasis, 513
 Melanomas, malignant
 esophageal, 405-407, 407f
 differential diagnosis of, 463t
 gastric metastases from, 548, 572f-573f
 image-guided biopsy of, 1247f
 metastatic
 to the colon, 1086
 on enteroclysis, 674f
 gallbladder, 1410
 differential diagnosis of, 1408
 image-guided biopsy of, 1242f, 1251f
 pancreatic, 1831, 1851f
 small bowel, differential diagnosis of, 874t-875t
 small bowel metastases in, 804
 small bowel intussusception associated with, 823
 Melena, 2271-2272
 Ménétrier's disease, 502-504, 505f
 differential diagnosis of, 504, 659t
 gastric carcinoma linked to, 547
 gastric carcinomas and, 547
 hypoalbuminemia with, 867
 pediatric, 2152
 Meniscus sign of malignant ulcer, 553
 Mercedes-Benz sign, 1350-1351, 1353f
 Mesalamine, for Crohn's disease, 1007
 Mesenchymal hamartomas, 1555-1556, 1556f
 pediatric, 2209-2210, 2209f
 Mesenchymal tumors, esophageal, 361
 Mesentericoparietal fossa, 865
 Mesenteric, retractile, 1021-1022
 Mesentery
 adenitis differentiated from appendicitis in, 969, 969f
 anatomy of, 2036
 cysts in, 2049, 2049f, 2091
 differential diagnosis on, 2048b
 embryology of, 2085f
 inflammatory and infiltrative diseases, 2045-2049
 amyloidosis, 2048
 Crohn's disease, 2046, 2046f
 cysts, 2049
 diverticulitis, 2045, 2046f
 edema, 2048-2049
 extramedullary hematopoiesis, 2048
 pancreatitis, 2045, 2046f
 panniculitis or sclerosing mesenteritis, 2047, 2047f

Mesentery (Continued)

- trauma and hemorrhage, 2046
 - Whipple's disease, 2046
 - ischemia in, 123-126, 124f-125f, 828-838
 - acute, 828-835, 830f-831f
 - chronic, 126, 835-838
 - MRA for, 154-157, 158f
 - thrombolytic therapy for, 125-126, 125f
 - lesions in, 2036-2052
 - malignant peritoneal mesothelioma, 2037-2039, 2039f-2040f
 - primary, 2036-2043, 2042f-2043f
 - adenomatoid tumors, 2042
 - desmoid tumors, 2036-2037, 2037f-2038f
 - desmoplastic small round cell tumors, 2041-2042, 2041f
 - malignant peritoneal mesothelioma, 2037-2039
 - multicystic mesothelioma, 2040-2041
 - peritoneal serous carcinoma, 2039-2040, 2040f
 - well-differentiated papillary mesothelioma, 2040, 2041f
 - secondary, 2043-2048
 - carcinoid, 2044, 2044f
 - lymphomas, 2044, 2045f
 - peritoneal carcinomatosis, 2043-2044, 2043f-2044f
 - mesenteric fat disease, 75-77
 - misty, 2048-2049, 2048b
 - pediatric disorders of, 2246-2248
 - stranding in, 84
 - trauma to, 2290, 2291f-2292f
 - vascular occlusions in, 125-126, 125f
- Mesocolic hernias. *See* Paraduodenal hernias
- Mesogastrium, 2087-2088, 2087f
- Mesorectal fascia, 93
- Mesotheliomas
 - fibrous, 1556
 - malignant peritoneal, 2037-2039, 2039f-2040f
 - multicystic peritoneal, 2040-2041
 - well-differentiated papillary, 2040, 2041f
- Metabolic infarcts, 1630
- Metabolic problems
 - after gastric and duodenal surgery, 640-641
 - after gastric resection, 635
- Metastatic disease
 - abdominal wall, 2073, 2073f
 - in adrenal glands, 1216, 1216f
 - appendiceal, 979
 - biliary tract, 1311, 1313f
 - from gallbladder carcinomas, 1203-1204
 - in spread of, 2008
 - colonic, 1082-1086, 1113-1114
 - from gynecologic malignancies, 1111-1113
 - downhill varices caused by, 432-433
 - embolic colonic, 1086
 - esophageal, 394-396, 395f-397f
 - differential diagnosis of, 464f
 - hematogenous, 394, 399f, 400-401
 - squamous cell carcinoma, 400f
 - gallbladder, 1410, 1410f
 - carcinomas, 1403, 1404f
 - pathways of spread in, 1408-1409
 - gastric, 571-580
 - carcinomas, 548, 560f-561f, 563f
 - clinical findings in, 571
 - differential diagnosis of, 578-580, 658f
 - esophageal squamous cell, 400f, 408
 - gastrosplenic ligament in spread of, 2019, 2019f
 - hematogenous, 571-574
 - from malignant melanomas, 550f
 - radiographic findings in, 571-578

Metastatic disease (Continued)

- from GISTs, 800-801, 802f
- gut, 2007
- hematogenous spread of, 2006-2007, 2007f
- liver
 - chemoembolization of, 1725-1726, 1726f
 - computed tomography of, 1486f
 - hepatic resection for, 1720
 - hypervascular, 1596, 1596f, 1597b
 - hypovascular, 1596, 1597f
 - incidence and clinical presentation of, 1590-1591, 1591f
 - incidence of at autopsy, 1720f
 - morphologic patterns of, 1590f
 - pathologic findings in, 1589-1590, 1590f
 - patient selection for surgery with, 1721
 - pediatric, 2206, 2206f
 - PET/CT on, 1205-1207, 1205f
 - radiologic findings on, 1591-1600, 1592f-1595f, 1596b
 - transarterial chemoembolization of, 1512
 - transarterial radioembolization of, 1513-1515, 1514f
 - ultrasound imaging of, 1761f
- lymphatic
 - with esophageal squamous cell carcinomas, 400, 400f
 - in gastric cancers, 574-576
 - spread of, 2007-2008
- needle track seeding, 1251
- omentum, 2050
- pancreas, 1851, 1851f
 - pediatric, 2225, 2225f
- perihaptic spaces, 2009
- peritoneal spread of, 2008-2009, 2010f
- pouch of Douglas, 2009
- retroperitoneal spread of, 2009-2014
- sigmoid mesocolon in spread of, 2020
- small bowel, 804, 804f
 - computed tomography enterography for, 684
 - differential diagnosis of, 874f
 - peritoneal spread of, 2009
 - site predilection of, 875f
 - with spindle cell carcinoma, 402
- spleen, 1935, 1939, 1954-1957
 - clinical findings on, 1956
 - epidemiology and pathogenesis of, 1934-1956, 1956f
 - pathology of, 1956
 - pediatric, 2234
 - PET/CT of, 1207, 1208f
 - radiologic findings on, 1956-1957
 - ultrasound on, 1181
- subperitoneal spread of, 2015-2021, 2019f
- tumor ablation of, 1508-1509

Methicillin-resistant *Staphylococcus aureus* (MRSA), splenic abscesses from, 1940f

- Methotrexate, hepatotoxicity of, 1639
- Methylcellulose, in small bowel follow-through, 665, 669-670, 673, 674f, 681

Metoclopramide

- in enteroclysis, 671, 671f
- gastrointestinal effects of, 19
- in small bowel follow-through, 669-670

Metronidazole, for Crohn's disease, 1007

Mexican hat sign, 526, 1032, 1034f

Microcystic serous cystadenoma. *See* Serous cystadenocarcinomas

Microgallbladder, 1342

Microgastria, 2141, 2142f

Microlithiasis. *See* Biliary sludge

Micronodularity, small bowel, 870, 871f

Microsomal triglyceride transport protein (MTTP), 784

Microsporidia, 766-767

Microwave ablation, 1508, 1509f, 1511f

Milan criteria, 1738-1739, 1739f

Milk allergy, 2168

Milk curd syndrome, 2119

Milk of calcium bile, 1385, 1386f

Minimum intensity projection renderings, 1161

Mirizzi syndrome, 1304, 1317f, 1377

gallstones with, 1348

imaging features of, 1379f

magnetic resonance cholangiopancreatography on, 1336

Mirror image artifacts, 1174, 1174f

Misoprostol, 469

Misty mesentery, 2048-2049, 2048b

Mithramycin, hepatotoxicity of, 1639

MMIH (megacystis-microcolon-intestinal hypoperistalsis) syndrome, 2120-2121, 2120f

Model-based iterative reconstruction (MBIR), 1485

Model for End-Stage Liver Disease (MELD), 1504, 1738-1739

Molybdenum, esophageal carcinoma and, 366

Morrison's pouch, 187, 2009

abscesses in, 2009

ascites in, 2027

Morphine, as contrast agent, 20

Morphology, attenuation, size, and structure (MASS) criteria, 2300, 2301f, 2302f

Mosaic-submucosal edema pattern, 1145f

MRECI criteria, 2300, 2301f

Mucinous cystadenocarcinomas, 1846-1847, 1847f, 1893f

Mucinous cystadenomas, 975-977, 978f, 1196, 1196f, 1223, 1846-1847

Mucinous gastric adenocarcinomas, 548, 558, 558f

Mucocoeles. *See* Retention cysts

Mucocutaneous cystadenomas, 1081

Mucormycosis, gastric, 512

Mucosa-associated lymphoid tissue lymphomas, 503, 503f

clinical findings on, 581

differential diagnosis of, 586

endoscopic findings on, 581

gastroduodenal, 582, 582f

lymphomas arising from, 580

pathology of, 581

radiographic findings on, 582

treatment and prognosis of, 581-582

Mucosal lesions

gastroduodenal, 523-530

adenomatous polyps, 526-527, 527f

differential diagnosis of, 658f

duodenal polyps, 527-528, 528f

hyperplastic polyps, 523-525, 524f-526f

polyposis syndromes, 530, 530f

villous tumors, 528-530, 529f-530f

Mucosal rests, biliary tract, 1424

Mucous fistulas, 1135-1136, 1136f, 1138

Multidetector computed tomography (MDCT), 1157. *See also* Computed tomography (CT)

of abdominal solid organs, 1159-1160, 1160f

biliary tract, 1290-1292

on cholangiocarcinomas, 1411-1413

on hilar cholangiocarcinomas, 1415-1416, 1418f

on postoperative complications, 1430-1451

of blood vessels, 75

of bowel wall pathologic changes, 70

of calcifications, 77, 77f

channel/row differentiation in, 1157, 1157f

clinical applications of, 82-93

colon, 911

on carcinomas, 1039-1050, 1041f-1042f

Multidetector computed tomography (MDCT)
(*Continued*)
on colorectal cancer, 1029-1031
contrast agents for, 67-68, 68f-69f
on Crohn's disease, 82-86, 733, 736-737
on diverticulitis, 940-941, 941f-942f, 941i
on duodenal carcinoma, 566, 566f
gallbladder, 1283
in gastric cancer staging, 564, 564f
of gastric carcinomas, 557-559, 557f-559f, 561-562, 562f
gastrointestinal tract, 67-78
hemorrhage, 686f, 690-691
liver, 1302
of benign liver tumors, 1529
on hepatocellular carcinomas, 1564-1566
on trauma, 1708-1712
lumen opacification in, 67-68
of lymph nodes, 76-77
of mesenteric and omental fat disease, 75-77
normal bowel wall in, 69-70
pancreas, 1164-1166
on neuroendocrine tumors, 1850-1851
on pancreatitis, 1813-1819, 1813f
chronic, 1826f-1827f
spatial resolution of, 719
vascular opacification in, 68
MultiHance, 1715
Multi-parametric imaging, 1226-1227
Multiplanar reformation (MPR) mode, 928, 1281
Multiple endocrine neoplasia (MEN-1) syndrome, 596, 1849
Multiple hamartoma syndrome, *See* Cowden's disease
Multiple myelomas, gastric involvement in, 598
differential diagnosis of, 658t
Multiple sclerosis, 231, 776b
Mural inflammation in Crohn's disease, 686
Mural thickening
classification scheme for, 72f
colonic, radiographic findings on, 1151t
in Crohn's disease, 82-86, 83f, 1002
on computed tomography endoscopy, 686-687
degree of, 71t
length of, 72t
multidetector computed tomography of, 71-73
patterns of, 71t
symmetry of, 72t
Murphy's sign, 1284, 1354, 1366
Muscular dystrophy, 615, 776b
Muscular rings, esophageal, 440-441
MUTYH gene, 1089
Mycobacterium avium-intracellulare (MAI)
complex, 320
with AIDS, 1652
differential diagnosis of, 769
lymphadenopathy in, 782
micronodularity in, 871t
in the small bowel, 767-768, 767f (*See also* Tuberculosis)
splenic infection with, 1933-1938, 1937f
Mycobacterium tuberculosis, 320. *See also* Tuberculosis
Myelolipomas, 1198
Myeloproliferative disorders, 1696, 1953-1954
Myochosis, colonic, 937f
Myoepithelial hamartomas, 793
Myxoglobulosis, 975

N

Narcotics
bezoar formation and, 619-620
chronic gastric dilation caused by, 615

NASH. *See* Nonalcoholic steatohepatitis (NASH)
Nasogastric intubation esophagitis, 339-340, 340f-341f
Nasopharyngeal reflux, 2125, 2128f
National Organ Transplant Act, 1737
National Trauma Data Bank, 1706
Necator americanus, 757
Necrotizing enterocolitis, 1124-1125, 2098, 2103-2106, 2104f-2105f
Necrotizing fasciitis, 2072
Needle biopsies. *See* Percutaneous tissue acquisition techniques
Needle track seeding, 1249, 1251
after tumor ablation, 1509-1510
from liver biopsies, 1499-1500, 1500f
Neisseria gonorrhoeae, 1113
NEMD. *See* Nonspecific esophageal motility disorder (NEMD)
Neonatal ascites, 2026
Neonatal jaundice, 2182
Neostigmine, 20
Nephrolithiasis, 746-748, 1011
Nephropathy, contrast-induced, 6
Nesidioblastosis, 2223
Neuroendocrine tumors
chemoembolization of, 1725-1726
on computed tomography enterography, 689, 690f
Crohn's associated, 752
gastroduodenal, 537, 537f
pancreatic, 1197, 1849-1851, 1850f
gastrinomas, 1850, 1851f
imaging, 1850-1851
insulinomas, 1847f, 1849-1850
nonfunctioning, 1850, 1850f
surgery for, 1861-1862
small bowel, 689, 690f
Neurofibromas
differentiated from leiomyomas, 354
duodenal, 537f
gastric, 537, 537f
pediatric, 2151-2152
gastroduodenal, differential diagnosis of, 658f
mesenteric, 2042-2043, 2043f
pediatric, 2151-2152
small bowel
benign, 792, 793f
differential diagnosis of, 874t
Neurofibromatosis
colonic, 1080
duodenal carcinoma with, 565
Neurofibrosarcomas, gastroduodenal, 598
Neuromas, biliary tract, 1424
Neutropenic colitis. *See* Typhilitis
Neutropenic enterocolitis, 765, 765f
Neutrophil dysfunction, 1022
Nissen fundoplication
complications with, 2132, 2132f
normal appearance after, 450, 451f
obstructions after, 452f
secondary achalasia from, 396-397
Nitrates, gastric carcinoma linked to, 546-547
Nodular duodenitis, 541
Nodular hyperplasia. *See* Hamartomas: spleen
Nodularity
with acanthosis nigricans, 301
in double-contrast studies, 41, 42f
liver surface, in cirrhosis, 1176
mucosal
granular pattern in ulcerative colitis, 987-988, 988f
mucosal
differential diagnosis of, 463t
in sarcoidosis, 511, 511f
small bowel, differential diagnosis of, 870, 871t

Nodularity (*Continued*)
mucosal, with esophageal carcinomas, 301
small bowel, 871t
Nodular regenerative hyperplasia (NRH), 1348-1349, 1548f
Nonalcoholic fatty liver disease, 1630
with AIDS, 1653
Nonalcoholic steatohepatitis (NASH), 1630, 1633, 1655
liver transplantation for, 1738
Nonobstructive megacolon, 1123
Nonperistaltic contractions (NPCs), 279, 280f
with achalasia, 282-283
with diffuse esophageal spasm, 285
GERD and, 288
Nonspecific colonic ulcer, 1021
Nonspecific esophageal motility disorder (NEMD), 286-287, 287f
Nonsteroidal anti-inflammatory drugs (NSAIDs)
antral flattening caused by, 499f
colorectal cancer associated with, 1029
diverticular hemorrhage caused by, 951
drug-induced esophagitis from, 327
enteropathy from
computed tomography enteroclysis for, 701-704
GI bleeding from, 688-690
segmental small bowel mural hyperenhancement in, 687t
erosive gastritis caused by, 496-499, 498f
air-contrast enteroclysis for, 682
gastric band erosion caused by, 651
gastrocolic and duodenocolic fistulas caused by, 624
in peptic ulcer disease, 631
peptic ulcers caused by, 467-469, 471
differential diagnosis of, 657t
equivocal appearance of, 478
gastrocolic fistulas from, 489-490, 491f
greater curvature, 472-473, 473f
small bowel obstructions caused by, 822f
differential diagnosis of, 874t
small bowel ulcers and stenosis related to, 762
Noonan syndrome, 2160
NSAIDs. *See* Nonsteroidal anti-inflammatory drugs (NSAIDs)
Nuclear medicine
liver
on angiosarcomas, 1585-1586
on fibrolamellar carcinoma, 1579
on hepatoblastomas, 1578
on hepatocellular carcinomas, 1564
on intrahepatic cholangiocarcinomas, 1580
on metastases, 1591-1597
of nodular regenerative hyperplasia, 1348-1349
on undifferentiated (embryonal) sarcomas, 1587
postoperative gastric and duodenal examinations, 631
Nutcracker esophagus, 286, 287f
Nutritional problems after gastric and duodenal surgery, 640-641, 649
Nyquist ghosting, 1218i, 1220, 1220f

O

Oat cell carcinomas, 1589-1590
Obesity, 641
bariatric surgery for, 641-654
colorectal cancer and, 1028-1029
esophageal carcinoma and, 366
fatty infiltration of the ileocecal valve with, 1078-1079
gallstones with, 1348
hepatic steatosis with, 1629-1630
small bowel bypass surgery for, 1133

Obstructions

- after esophagogastrectomy, 455f
- after Roux-en-Y gastric bypass, 645
- from appendicitis, 960, 961f, 965f
- appendicitis caused by, 957-958
- biliary tract, 1290, 1310 (*See also* Mirizzi syndrome)
 - after laparoscopic cholecystectomy, 1453
 - after liver transplantation, 1749-1750
 - with cholangiocarcinomas, 1411-1413
 - differential diagnosis of, 14630-14641
 - magnetic resonance
 - cholangiopancreatography on, 1328
 - in obstructive cholangitis, 1434-1435, 1436f
 - secondary biliary cirrhosis due to, 1650-1651, 1651f
- bowel
 - acute abdomen from, 2259-2260, 2260f
 - after biliopancreatic diversion with duodenal switch, 654
 - meconium ileus, 2118-2119, 2119f
 - meconium plug syndrome, 2119-2120, 2120f
 - with necrotizing enterocolitis, 2105-2106
 - in neonates and children, 2101, 2103f
- colon, 1102-1110
 - from adhesions, 1109-1110
 - from angiodysplasia, 1076-1077
 - cancer causing, 1039f
 - cancer staging and, 1049f
 - causes of mechanical, 1103t
 - clinical findings on, 1103
 - with colonic ischemia, 1115-1116
 - from colorectal cancer, 1036, 1039f
 - computed tomography on, 1103-1104, 1104f
 - contrast enemas on, 1103
 - differential diagnosis of, 1146-1147f
 - from diverticulitis, 1105, 1105f, 1105t
 - from hernias, 1110
 - incidence of by cause, 1103t
 - magnetic resonance imaging on, 1104
 - major types of, 1104-1110
 - in newborns, 1147t
 - obstruction, 1110
 - pathophysiology of, 1102
 - in postneonatal children, 1147t
 - pseudo-, 1147t
 - from radiation colitis, 1117
 - radiography on, 1103, 1103f
 - radiologic approach to suspected, 1103-1104
 - ultrasonography on, 1104
 - from volvulus, 1105
- from diverticulitis, 948-949, 950f
- duodenal, 613-614
 - megaduodenum in, 661t
 - from metastases, 576f
 - in superior mesenteric root syndrome, 613-614, 613f-614f
- esophageal
 - after esophagogastrectomy, 454
 - postoperative, 449, 451, 451f-452f
- gastric
 - in afferent loop syndrome, 638, 639f
 - after gastric and duodenal surgery, 640-641
 - after gastric resection, 636-637, 636f
 - after laparoscopic adjustable gastric band placement, 649
 - after Roux-en-Y gastric bypass, 645, 645f-646f
 - ulcers caused by, 468
- gastric outlet, 179, 275, 611-613, 612f
 - after gastric resection, 636-637, 636f
 - after sleeve gastrectomy, 652-654
 - from caustic ingestion, 515
 - differential diagnosis of, 660t
 - with eosinophilic gastritis, 513-514

Obstructions (*Continued*)

- gastric dilation without, 614-615
- from gastric volvulus, 623, 623f
- from granulomatous disease, 613, 613f
- as indication for surgery, 631
- from villous tumors, 528-529
- idiopathic intestinal pseudo-, 289
- from intussusception, 1106-1109
- liver, sinusoidal obstruction syndrome, 1680-1688
- lymphatic, 784-785, 2007
- obturator, 1110
- pancreas
 - with pancreas divisum, 1801
 - surgery for, 1861
- in peptic ulcer disease, 631
- from peptic ulcers, 487, 488f
- small bowel
 - acute mesenteric ischemia caused by, 829, 835
 - afferent loop, 851-852, 852f
 - barium studies on, 676, 682t
 - classification of, 811-824
 - closed loop and strangulation, 812-813, 813f
 - computed tomography enteroclysis on, 703f
 - on computed tomography enterography, 685t, 690-691
 - differential diagnosis of, 874t
 - extrinsic, 811-817
 - extrinsic tumors in, 816-817
 - hernias with, 814-816, 814f
 - magnetic resonance enterography on, 721-722, 722f
 - from Meckel's diverticulum, 861
 - strangulated, 703f
 - splenic vein, gastric varices and, 603-604, 606f
- Obstructive cholangitis, 1434-1435, 1436f
- Obturator obstructions, 1110
- Obturator hernias, 2065-2067, 2067f
- Obturator internus muscle, 174-175, 175f
- Obturator sign, 959-960
- Occult blood, 2271-2272
- Odynophagia
 - in caustic esophagitis, 331
 - in chronic graft-versus-host disease, 342
 - with drug-induced esophagitis, 327
 - with epidermolysis bullosa dystrophica, 337
 - in radiation esophagitis, 330
- Ogilvie's syndrome, 1147t
- Ohi classification system of biliary atresia, 2183, 2183t
- Omental cakes, 577-578, 1086, 1086f, 1996, 2050f
 - gastric narrowing from, 659t
- Omental fat disease, 75-77
- Omental infarctions, 969, 971f
- Omentum
 - after hepatic resection, 1728
 - anatomy of, 2036, 2037f
 - carcinomas of, gastroduodenal metastases from, 577-578, 580f
 - cysts in, 2088
 - embryology of, 1984, 2084, 2087-2088, 2087f
 - greater, 1996, 1999f
 - disease spread through, 2018f
 - lesions in, 2049-2050, 2050f
 - metastases in, 1084f, 1086, 1086f
 - pediatric disorders of, 2246-2248
 - torsion-infarction of, 2050, 2263-2264, 2264f
- Omphaloceles, 2098-2099, 2099f, 2241-2243, 2242f-2243f
 - segmental dilation with, 863
- Omphalomesenteric bands, 2158, 2159f
- Omphalomesenteric cysts, 861
- Omphalomesenteric duct abnormalities, 2071
- Oncocytomas, 1198

- Opisthorchis felinus*, 1440
- Opisthorchis viverrini*, 1440
- Opposed-phase gradient-echo imaging, 1633-1635
- Organic anion-transporting polypeptides 1B3 (OATP1B3), 1570
- Organ Injury Scaling Committee, 1707, 1970
- Organoaxial gastric volvulus, 444
- Organ Procurement and Transplantation Network (OPTN), 1737
 - criteria, 1499, 1738-1739, 1739t
- Organ traversal technique of percutaneous drainage, 1263-1264, 1263f
- Oriental cholangiohepatitis. *See* Pyogenic cholangitis
- Ortner's syndrome, 1812
- O sign, 650
- Osler-Weber-Rendu syndrome, 846-848, 1701, 1702f
- Osmotic diarrhea, 1127-1128
- Osteomas, in familial adenomatous polyposis syndrome, 1091-1092, 1092f
- Osteomyelitis, 783, 1012
- Osteonecrosis, 1011
- Osteoporosis, with inflammatory bowel disease, 1012
- Ovarian cancer
 - diffusion-weighted MRI on, 1225f
 - gastroduodenal metastases from, 580f
 - metastases from
 - appendiceal, 979
 - broad ligament in, 2020
 - colonic, 1083-1084, 1084f, 1111-1113, 1112f
 - intraabdominal seeding of, 1085f
 - omental, 577-578, 1086f, 2050, 2050f
 - peritoneal spread of, 2009
 - with Peutz-Jeghers syndrome, 1093
- Ovaries
 - benign tumors of, 1113
 - mobility of calcifications in, 202, 203f
 - traversal of in percutaneous drainage, 1264
- Overwhelming postsplenectomy sepsis syndrome, 1972

P

- PACS. *See* Picture archiving and communications system (PACS)
- Palate, 222-223, 248f
- Pancolitis, 1008. *See also* Pancreatitis
- Pancreas. *See also* Pancreatic cancer; Pancreatitis
 - adenocarcinomas, 1320
 - accuracy of imaging of, 1842-1844
 - cystic, 1840-1842, 1842f
 - endoscopic ultrasound on, 1842-1844
 - goals of imaging, 1839, 1839f
 - magnetic resonance imaging findings on, 1841-1844, 1843f
 - magnetic resonance imaging protocols on, 1840
 - multidetector CT findings on, 1840-1844, 1840f-1842f
 - multidetector CT protocols on, 1839-1840
 - other imaging modalities on, 1844-1845
 - pancreatic duct changes with, 1844, 1844f
 - ultrasound on, 1181
 - anatomy of, 173, 1771-1776, 1813f
 - arterial supply, 1773, 1774f
 - common bile duct entry into, 1772, 1773f
 - congenital anomalies in, 1800-1806
 - lymphatics, 1774-1775, 1775f
 - nerve supply, 1776, 1776f
 - pancreatic duct, 1773
 - topography of, 1771-1772, 1772f
 - in transplantation, 1872-1874

Pancreas (Continued)

- variants of normal, 1797-1800, 1798f-1800f, 2086-2087
- venous drainage, 1773-1774, 1775f
- annular, 1803-1805, 1803f-1805f, 2079
- ascites in, 2026
- calcifications in, 174f
- carcinomas of
 - biliary involvement in, 1307
 - biliary strictures from, 1307, 1308f
 - intraoperative ultrasound for, 1863
 - metastases from
 - appendiceal, 979
 - colonic, 1083-1084, 1084f
 - gastroduodenal, 576, 577f-578f
- computed tomography of, 1164-1166, 1165f
- in confined perforations, 488-489
- congenital anomalies of, 1800-1806
 - agenesis, hypoplasia, hyperplasia, 1800
 - annular and semiannular, 1803-1805, 1803f-1805f
 - cysts, 1806
 - ductal, 1806
 - ectopic, 1805-1806, 1806f
 - pancreas divisum, 1800-1803, 1802f
- contrast agents affecting, 20-21
- CTA of, 141, 141f
- cystic neoplasms in, 608, 609f, 1845-1849, 1845f
 - congenital, 1806
 - differential diagnosis of, 1890f, 1893-1894f
 - incidental, 1894f
 - pediatric, 2225-2226, 2225f-2226f
 - percutaneous biopsy of, 1786-1787, 1787f
 - pseudocysts, 576, 578f, 1321
 - serous cystadenomas, 1845-1846
- differential diagnosis of, 1889-1894
 - acute pancreatitis, 1892f
 - calcifications, 1889f
 - with cholangiography, 1891
 - chronic pancreatitis, 1892f
 - cystic neoplasms, 1893f
 - focal lesions, 1891f
 - focal masses, 1889f
 - focal shadowing masses, 1890f
 - hypervascular masses, 1890f
 - hypochoic masses, 1890f
 - incidental cystic lesions, 1894f
 - lipomatosis, 1890f
 - with magnetic resonance imaging, 1890
 - masses with pseudocysts, 1890f
 - pancreatic duct adenocarcinomas, 1893f
 - pancreatic duct dilation, 1890f
 - pancreatic duct gas, 1890f
 - pancreatic duct strictures, 1891f
 - pseudocysts versus neoplasms, 1890f
 - with ultrasound, 1890
 - with computed tomography, 1890
- diffusion-weighted MRI of, 1223, 1224f
- diseases of affecting the stomach and duodenum, 618-619, 619f
- divisum, 2079
- duodenal impressions by, 661f
- ectopic, 538-539, 539f, 862-863, 863f, 2087
 - differential diagnosis of, 658f
 - differentiated from GISTs, 532-533
 - myoepithelial hamartomas differentiated from, 793
- embryology of, 1797, 1798f, 1883-1884, 2085-2086, 2086f
 - abnormal development of, 2086-2087
 - subperitoneal spread and, 1998f
- familial adenomatous polyposis syndrome
 - manifestations in, 1092-1093
- fatty infiltration of, 1777, 1777f
 - normal variants in, 1793-1799, 1799f

Pancreas (Continued)

- historical perspective on, 1771
- image-guided biopsy of, 1244-1247, 1245f-1246f, 1249-1250, 1249f
- inflammation of, 1321, 1321f
- inflammatory bowel disease complications in, 1010-1011
- insulinomas in, 1165f
- interventional radiology of, 1785-1796
 - in acute necrotizing pancreatitis management, 1789-1793
 - ancillary procedures with, 1792-1793
 - background on, 1789
 - catheter, 1793f
 - catheter care in, 1791-1792
 - complications with, 1791, 1792f
 - image-guided catheter drainage for, 1789-1790, 1790f
 - infected, 1790-1791, 1791f
 - sterile, 1790
 - in neoplasm management, 1785-1789
 - background on, 1785
 - biopsy indications with, 1785-1787, 1787f
 - complications with, 1789
 - diagnostic effectiveness of, 1788-1789
 - technical considerations in, 1787-1788, 1788f
 - in pseudocyst management, 1793-1794, 1794f
- intraductal papillary mucinous neoplasms, 1330, 1331f
- magnetic resonance imaging of, 1194-1197, 1196f
 - acute pancreatitis, 1194-1195
 - adenocarcinomas, 1197
 - cystic lesions, 1195-1196, 1196f
 - neuroendocrine neoplasms, 1197
 - pseudopapillary neoplasms, 1197
 - solid lesions, 1196-1197, 1197f
- malabsorption related to, 774, 775f
- metastatic disease in, 1851, 1851f
- neoplasias, 1187-1189
- neoplasms, 1838-1855
 - background on, 1793-1794
 - cystic, 1845-1849, 1845f
 - mucinous, 1845f, 1846-1847
 - other, 1848-1849
 - serous cystadenomas, 1845-1846
 - ductal adenocarcinomas, 1838-1845
 - multiple solid, percutaneous biopsy of, 1787, 1788f
 - neuroendocrine tumors, 1849-1851
 - gastrinomas, 1850, 1851f
 - imaging, 1850-1851
 - insulinomas, 1849-1850
 - nonfunctioning, 1850, 1850f
 - with pancreas divisum, 1801
 - secondary, 1851
- normal orientation and appearances of, 1772f
- normal shapes and size of, 1776-1779
- pediatric disorders of, 2216-2227
 - autosomal dominant polycystic kidney disease, 2226, 2226f
 - Beckwith-Wiedemann syndrome, 2225-2226, 2226f
 - congenital cysts, 2223-2224
 - cystic fibrosis, 2221-2222, 2222f-2223f
 - imaging of, 2216, 2217f
 - masses, 2223-2225
 - metastatic disease, 2225
 - neoplasms, 2224-2225, 2224f
 - nesidioblastosis, 2223
 - pancreatitis, 2219-2221, 2220f-2221f
 - Schwachman-Diamond syndrome, 2223, 2223f
 - trauma, 2216-2219, 2217f-2218f
 - von Hippel-Lindau disease, 2225, 2225f-2226f

Pancreas (Continued)

- PET/CT of, 1208-1210, 1209f-1210f
- adenocarcinomas, 1208-1209
- cystic neoplasms, 1209
- in protein digestion and absorption, 774
- pseudocysts in
 - compression or displacement by, 580
 - gastroduodenal involvement from, 576, 578f, 621f
- percutaneous catheter drainage of, 1793-1794, 1794f
- radiologic examination techniques for, 1776-1781
 - computed tomography, 1778-1779, 1778f
 - contrast studies, 1776
 - endoscopic retrograde
 - cholangiopancreatography, 1781
 - magnetic resonance
 - cholangiopancreatography, 1780-1781, 1780f-1781f
 - magnetic resonance imaging, 1779-1780, 1779f-1780f
 - plain radiographs, 1776
 - ultrasound, 1776-1778, 1777f
- size of, 1800
- surgery on, 1860-1868
 - Beger procedure, 1864, 1866f
 - bypass procedures, 1868
 - central pancreatectomy, 1864
 - Frey procedure, 1864, 1866f
 - indications for, 1860-1862
 - benign disease, 1860-1861
 - malignant disease, 1861-1862
 - postoperative complications with, 1867f, 1868
 - postoperative radiologic findings on, 1864-1868
 - Puestow procedure, 1864, 1865f
- radiology in, 1862-1863
 - computed tomography, 1862-1863
 - FDG PET/CT, 1863
 - intraoperative ultrasound, 1863, 1864f
 - magnetic resonance imaging, 1863
- sphincterotomy, 1864
- types of, 1864-1868
- Whipple procedure, 1864-1868, 1867f
- transplantation, 1872-1888
 - anatomy in, 1872-1874, 1873f, 1875f
 - arterial supply to, 1872-1873, 1873f
 - complications with, 1874-1886
 - bowel, 1882-1884, 1885f-1886f
 - graft pancreatitis, 1881-1882, 1884f
 - graft rejection, 1880-1881, 1881f-1882f
 - graft stenosis, 1877-1879, 1879f
 - graft thrombosis, 1875-1877, 1877f-1879f
 - hemorrhage, 1882
 - intra-abdominal fluid collections, 1884-1885, 1886f-1887f
 - lymphoproliferative disease, 1885-1886, 1887f
 - pseudoaneurysms and fistulas, 1879-1880, 1880f-1881f
 - vascular, 1875-1880
 - exocrine secretions to, 1873-1874
 - graft rejection, 1880-1881, 1881f
 - normal radiographic findings on, 1874
 - postoperative complications with, 1874-1886
 - procurement for, 1872-1874
 - types of, 1872
 - venous drainage to, 1873
- trauma to, 1856-1860, 2285, 2286f, 2287f
- clinical findings on, 1857
- epidemiology and pathophysiology of, 1856-1857
- radiologic findings on, 1857-1860

Pancreas (Continued)

- computed tomography, 1857-1858, 1857f-1859f, 1858b
- endoscopic retrograde pancreatography, 1859-1860
- gastrointestinal studies, 1860
- magnetic resonance pancreatography, 1859, 1859f
- ultrasound, 1859
- surgical classification of, 1857, 1857b
- treatment of, 1860
- traversal of in percutaneous drainage, 1264
- ultrasonography on, 1180-1181, 1180f-1181f
- walled-off necrosis in, 1810-1811, 1815, 1818f, 1860-1861
- widening of the duodenal sweep caused by, 603, 618f
- Pancreas divisum, 1332, 1333f, 1800-1803
 - clinical findings on, 1800-1801
 - pancreatitis with, 1809-1810
 - radiologic findings on, 1801-1803, 1802f
- Pancreatotomy, central, 1864
- Pancreatic cancer
 - biliary tract, 1307, 1308f
 - gastrointestinal metastases from, 574-575
 - hematogenous spread of, 2006
 - magnetic resonance cholangiopancreatography on, 1328, 1329f
 - diagnostic sensitivity of, 1816-1817, 1817f-1818f
 - metastases from, 1591f
 - pancreatitis differentiated from, 1814-1815, 1817f
 - percutaneous biopsies on, 1785
 - indications for, 1785-1787
 - percutaneous biopsy for, 1786
 - with Peutz-Jeghers syndrome, 1093
 - subperitoneal spread of, 1999f
 - unresectable, imaging findings suggesting, 1785-1786, 1786f
- Pancreatic ducts, 1283, 1283f
 - adenocarcinomas and changes in, 1844, 1844f, 1893f
 - anatomy of, 1773, 1773f
 - bifid, 1800, 1801f
 - computed tomography of, 1779
 - congenital abnormalities in, 1806
 - differential diagnosis of, 1890f, 1893f
 - dilated, 1890f
 - embryology of, 1797
 - endoscopic retrograde
 - cholangiopancreatography on, 1781
 - gas in, 1890f
 - leaks, 1321, 1322f
 - normal anatomy of, 1305-1306, 1306f
 - ultrasound of, 1777
- Pancreatic heterotopia, 1536
- Pancreatic lithiasis, 201-202, 202f
- Pancreaticobiliary duct junction, 1402
- Pancreaticoduodenal arteries, 837
- Pancreaticoduodenal veins, 1773-1774, 1775f
- Pancreaticoduodenectomy. *See* Whipple procedure
- Pancreatitis, 1809-1837, 2043, 2046f
 - abscesses with, 1811
 - acute, 1321, 1809-1824
 - clinical findings on, 1811
 - complications with, 1819-1824
 - fluid collections and pseudocysts, 1820-1821, 1820f-1822f
 - hemorrhage, 1822-1824
 - infected pseudocysts, 1822
 - necrosis, 1821-1822, 1822f
 - pseudoaneurysm, 1822-1824, 1823f-1824f

Pancreatitis (Continued)

- definitions on, 1810-1811
- diagnosis of, 1810, 1814-1817
- diagnostic sensitivity on, 1816
- differential diagnosis of, 1892f
- etiology of, 1809
- grading, 1817-1818
- interstitial edematous, 1810
- magnetic resonance
 - cholangiopancreatography on, 1335, 1335f
- magnetic resonance imaging of, 1194-1195
- necrosis in
 - delineation of, 1819f
 - infected, 1823f
 - necrotic collection in, 1810, 1819f
 - necrotizing, 1815, 1817f, 1819f-1820f
 - nonsevere interstitial edematous, 1811
 - pathophysiology of, 1809-1810
 - pediatric, 2219-2221, 2220f
 - from percutaneous biopsy, 1789
 - radiologic findings on, 1811-1819
 - severe, 1811
 - staging, 1817
 - necrotizing
 - definition of, 1810
 - infected, 1790-1791, 1791f, 1819f
 - interventional radiology in management of, 1789-1793, 1791f-1792f
 - sterile, 1790, 1790f
 - walled-off, 1815, 1818f
- radiologic findings on
 - abdominal plain films, 1811-1812
 - angiography, 1812
 - barium studies, 1812
 - chest films, 1812
 - cholangiography, 1812
 - computed tomography, 1813-1819, 1814f, 1816f-1818f
 - magnetic resonance imaging, 1813-1819, 1815f, 1817f
 - ultrasonography, 1812-1815
- acute abdomen from, 2261-2262, 2262f
- after image-guided biopsy, 1246-1247, 1250-1251, 1788
- after magnetic resonance
 - cholangiopancreatography, 1332
- alcoholic, 1809
- ascites in, 2026
- autoimmune, 1831-1833, 1831f-1832f
- biliary strictures from, 1314, 1316f
- chronic, 1321, 1321f, 1824-1833
 - autoimmune, 1831-1833, 1831f-1832f
 - clinical findings on, 1824
 - computed tomography of, 1826-1828, 1826f
 - differential diagnosis of, 1892f
 - magnetic resonance
 - cholangiopancreatography on, 1335-1336, 1336f
 - magnetic resonance imaging on, 1826-1828
 - pediatric, 2221, 2221f-2222f
 - percutaneous biopsy on, 1786
 - radiologic findings on, 1824-1833
 - endoscopic retrograde
 - cholangiopancreatography, 1825-1826
 - endoscopic ultrasound, 1825
 - plain films, 1824, 1825f
 - ultrasonography, 1824-1825
- classification of, 1809-1811
- colonic involvement of, 1113
- compression or displacement by, 580
- differential diagnosis of, 661t, 1892f
- diffusion-weighted MRI of, 1223
- duodenitis and, 519

Pancreatitis (Continued)

- from endoscopic retrograde
 - cholangiopancreatography, 1321
- endoscopic retrograde
 - cholangiopancreatography on, 1321, 1322f
- gallstones with, 1348
- gastric outlet obstruction from, 613
- gastrointestinal involvement from, 619, 620f
- graft, 1881-1882, 1884f
- groove, 1829-1830, 1830f-1831f
- hemorrhagic, 1986-1987
- idiopathic, 1321
- from inflammatory bowel disease, 1010-1011
- magnetic resonance cholangiopancreatography on, 1335-1336, 1335f-1336f
- malabsorption related to, 774
- omental, 2050
- pancreas divisum with, 1332, 1800
- pancreatic pseudocysts with, 1810
- pancreaticopleural fistulas in, 1828-1829, 1829f
- pediatric, 2219-2221, 2219f
- peripancratic abscesses with, 1273-1274
- peripancratic fluid collection in, 1810, 1814-1816, 1815f-1816f
- phlegmon with, 1811
- pseudoaneurysms with, 1811
- retroperitoneal spread of, 1989, 1989f
- in root of the mesentery, 1996
- small bowel, 875t
- splenic involvement in, 1944-1945, 1972
- splenic vein thrombosis with, 1697
- splenorenal ligament in spread of, 2019-2020, 2020f
- spread of through retroperitoneal fat pads, 1986-1987
- subperitoneal spread of, 2016
- superior mesenteric root syndrome caused by, 614
- surgery for
 - indications for, 1860-1861
 - intraoperative ultrasound in, 1863
 - ultrasound on, 1180-1181
 - walled-off necrosis in, 1810-1811, 1818f
- Pancreaticopleural fistulas, 1828-1829, 1829f
- Pancreatoduodenectomy. *See* Whipple procedure
- Panniculitis, 2047, 2050
- Papillary cholangiocarcinomas, 1307, 1309f-1310f
- Papillary gastric carcinomas, 548
- Papillary process of the caudate lobe, 1521, 1523f
- Papillary renal cell carcinomas, 1198-1199
- Papillitis, AIDS-related, 1436-1437, 1437f
- Papillomas, benign esophageal, 350, 351f, 463t
- Papillomatosis, 1307, 1310f
- Paracetosis, 1813-1816, 2024
- Paracolic gutters, 170f-171f, 2002-2004
 - ascites in, 2027
 - spread of disease through, 2008-2009
- Paraduodenal hernias, 865, 865f-866f, 2054-2057, 2056f
- Paraesophageal hernias, 445-446, 445f
- Parallel acquisition techniques (PATs), 931
- Parallel-channel sign, 1289
- Parasitic infestations. *See also* Amebiasis;
 - Anisakiasis; Chagas' disease; Giardiasis; Schistosomiasis; Strongyloidiasis
- benign ductal diseases from, 1432
- biliary spread of, 2008
- biliary tract, 1457-1440, 2008
- colon, 1020-1021
 - amebiasis, 1020
 - anisakiasis, 1020
 - schistosomiasis, 1020
 - strongyloidiasis, 1020

Parasitic infestations (*Continued*)

- hematogenous spread of, 2007
- liver
 - amebic, 1612-1614
 - echinococcal, 1614-1621
 - schistosomiasis, 1623-1625
- pediatric, 2153, 2153f
- in recurrent pyogenic cholangitis, 1435-1436
- small bowel, 757-760
 - anisakiasis, 758-759
 - ascariasis, 758f
 - giardiasis, 759, 759f
 - hookworms, 757-758
 - strongyloidiasis, 758f
 - tapeworms, 759
 - trematodes, 759
 - trypanosomiasis, 760
- thickened duodenal folds from, 661t
- Parastomal hernias, 2063, 2064f
- Parenchymal phase of contrast, 1165t
- Parietal cell vagotomy. *See* Highly selective vagotomy (HSV)
- Parkinson's disease, malabsorption in, 776b
- Patent urachus, 2070
- Paterson-Kelly syndrome, 367
- Pathognomonic crescent sign, 1106
- Pearl necklace sign, 1337f
- Pediatric disorders
 - abdominal masses, 2101-2103
 - clinical findings on, 2101-2102
 - radiologic findings on, 2102-2103, 2104f
 - abdominal wall, peritoneum, and mesentery, 2241-2251
 - anterior abdominal wall defects, 2241-2245
 - bladder exstrophy, 2245
 - gastroschisis, 2243-2245, 2243f-2245f
 - omphalocele, 2241-2243, 2242f-2243f
 - pentology of Cantrell, 2241
 - embryology of, 2241
 - lymphadenopathy and neoplasms, 2248-2249, 2249f-2250f
 - mesenteric and omental cysts, 2241, 2246-2248, 2247f
 - peritonitis, 2246, 2247f
 - prune-belly syndrome, 1151t, 1917, 2071, 2245-2246, 2245f-2246f
 - caudal regression, 2117
 - cloacal malformation, 2117
 - colon, 2164-2179
 - anterior anus, 2164, 2165f
 - appendicitis, 2169-2170, 2169f
 - carcinoma, 2176
 - colitides and causes of diarrhea, 2167-2168
 - fibrosing colonopathy, 2176
 - hemolytic uremic syndrome, 2168-2169, 2168f
 - Hirschsprung's disease, 2165-2167, 2166f-2167f
 - inflammatory bowel disease, 2167
 - intussusception, 2172-2174, 2173f-2174f
 - juvenile polyps, 2175-2176
 - lymphoid follicular pattern and hyperplasia, 2164, 2165f
 - typhlitis, 2170-2172
 - volvulus, 2174-2175, 2175f
 - colonic atresia, 2113
 - Currarino triad, 2117-2118, 2118f
 - diaphragmatic hernia, 2099-2100, 2100f-2101f
 - esophagus, 2125-2140
 - achalasia, 2133
 - acquired anomalies of, 2129-2138
 - gastroesophageal reflux disease, 2129-2132, 2131f-2132f
 - atresia of, 2106-2110, 2106f
 - general considerations in, 2106-2107
 - radiologic findings on, 2107-2110, 2107f-2110f

Pediatric disorders (*Continued*)

- congenital anomalies of, 2125-2127
 - overview of, 2125
 - swallowing disorders, 2125-2127, 2128f
- eosinophilic esophagitis, 2132-2133, 2133f
- foreign body and caustic ingestion, 2133-2136, 2135f-2137f
- varices, 2133, 2134f
- gallbladder and biliary tract, 2180-2199
 - acalculous cholecystitis, 2193-2194, 2194f
 - Alagille's syndrome, 2188-2189, 2189f
 - bile plug and inspissated bile syndromes, 2193
 - biliary atresia, 2182-2188, 2183f-2185f, 2187f-2188f
 - Caroli's disease, 2191-2193, 2193f
 - choledochal malformations, 2190-2191, 2190f-2192f
 - choledocholithiasis, 2194-2195, 2195f
 - cholelithiasis, 2193, 2193f
 - cholestasis, 2183f
 - cystic fibrosis, 2195
 - gallbladder dyskinesia, 2194
 - gallbladder hydrops, 2194, 2194f
 - imaging modalities on, 2180
 - neonatal jaundice, 2182
 - neoplasms, 2196, 2196f-2197f
 - normal anatomy and, 2180-2182, 2181f-2182f
 - primary sclerosing cholangitis, 2195, 2196f
 - progressive familial intrahepatic cholestasis, 2189-2190
- gastrointestinal embryology and, 2079-2094
- imperforate anus, 2113-2117, 2116f-2117f
- jejunal and ileal stenosis and atresia, 2110-2112, 2111f
 - radiologic findings on, 2111-2112, 2111f-2112f
- laryngotracheal cleft, 2110
- liver, 2200-2215
 - benign neoplasms, 2206-2210
 - adenomas, 2210, 2210f
 - focal nodular hyperplasias, 2210, 2211f
 - mesenchymal hamartomas, 2209-2210, 2209f
 - vascular lesions, 2206-2209
 - cirrhosis and diffuse disorders, 2212-2213, 2213f
 - congenital, 2200-2202
 - fibropolycystic, 2201-2202, 2201f
 - hepatic cysts, 2202, 2202f
 - malformations and hernias, 2200-2201
 - focal inflammatory-infectious lesions, 2211-2212, 2211f-2212f
 - imaging of, 2210
 - lymphoproliferative disorders, 2210
 - malignant neoplasms, 2202-2206
 - angiosarcomas, 2205, 2205f
 - hepatoblastomas, 2202-2203, 2203f
 - hepatocellular carcinomas, 2204, 2204f
 - primary, 2202-2206
 - secondary, 2206
 - undifferentiated embryonal sarcomas, 2204-2205, 2205f
 - neonatal jaundice, 2212
 - vascular lesions, 2206-2209
 - arteriportal fistula, 2209
 - arteriovenous malformations, 2208-2209, 2208f
 - infantile hemangioendothelioma, 2206-2208, 2207f-2208f
 - portosystemic shunts, 2209
- low obstructive lesions, 2118-2121
 - meconium ileus, 2118-2119, 2119f
 - meconium peritonitis, 2112-2113
 - meconium plug syndrome, 2119-2120, 2120f
- megacystis-microcolon-intestinal hypoperistalsis syndrome, 2120-2121

Pediatric disorders (*Continued*)

- necrotizing enterocolitis, 2103-2106, 2104f-2105f
- neonatal gas, normal and abnormal, 2101, 2103f
- neonatal gastrointestinal radiology on, 2095-2124
- omphaloceles, 863, 2098-2099, 2099f
- pancreas, 2216-2227
 - autosomal dominant polycystic kidney disease, 2226, 2226f
 - Beckwith-Wiedemann syndrome, 2225-2226, 2226f
 - congenital cysts, 2223-2224
 - cystic fibrosis, 2221-2222, 2222f-2223f
 - imaging of, 2216, 2217f
 - masses, 2223-2225
 - metastatic disease, 2225
 - neoplasms, 2224-2225, 2224f
 - nesidioblastosis, 2223
 - pancreatitis, 2219-2221, 2220f-2221f
 - Schwachman-Diamond syndrome, 2223, 2223f
 - trauma, 2216-2219, 2217f-2218f
 - von Hippel-Lindau disease, 2225, 2225f-2226f
- small bowel, 2158-2163
 - Henoch-Schönlein purpura, 2161, 2162f
 - intestinal lymphangiectasia, 2160-2161
 - Meckel's diverticulum, 2158-2160, 2159f-2160f
- spleen, 2228-2240
 - benign neoplasms, 2233-2234
 - congenital abnormalities
 - polysplenia and asplenia, 2230, 2231f
 - splenogonadal fusion, 2231
 - splenules, 2229-2230, 2230f
 - wandering spleen, 2231, 2231f-2232f
 - cystic lesions, 2231-2233
 - lymphatic malformations, 2232-2233, 2233f
 - true cysts and pseudocysts, 2231-2232, 2232f
 - Gaucher's disease, 2238
 - histiocytic syndromes, 2238
 - infarction, 2236, 2237f
 - infections, 2235-2236, 2236f
 - malignant neoplasms, 2233, 2234f
 - normal histology and function of, 2228-2229, 2229f-2230f
 - peliosis, 2238, 2238f
 - sickle cell disease, 2236-2237, 2237f-2238f
 - size of, 2229, 2230f
 - trauma, 2234-2235, 2235f
- stomach and duodenum, 2141-2157
 - acquired, 2146-2155
 - distention, 2154-2155, 2154f
 - foreign bodies, 2148-2149, 2151f
 - gastric perforations, 2146-2147
 - hematomas, 2148, 2150f
 - inflammatory disorders, 2152-2154, 2153f-2154f
 - neoplasms, 2150-2152, 2151f-2152f
 - peptic ulcer disease, 2152
 - pyloric stenosis, 2147-2148, 2147f-2150f
 - congenital, 2141-2146
 - antral mucosal diaphragm, 2141, 2142f
 - duodenal atresia and stenosis, 2141-2143, 2142f-2143f
 - duplication cysts, 2143-2144, 2144f
 - malrotation, 2144-2146, 2145f-2146f
 - microgastria, 2141, 2142f
 - pyloric and antral atresias, 2141
- Peliosis, splenic, 1930
- Peliosis hepatis, 1689-1690, 2238, 2238f
- Pelvic floor dysfunction, 890-904
 - imaging methods on, 901-902
 - imaging preprocedure preparation, 892
 - imaging technique for, 892-895
 - measurements on, 895-896

- Pelvic floor dysfunction (Continued)**
 normal anatomy and, 890-892, 891f
 normal variations and, 902
 pathologies in, 896-901
 presenting symptoms of, 890
- Pelvic floor dyssynergy**, 899-900, 900f
- Pelvic inflammatory disease**, 1113
- Pelvic lipomatosis**, 1110
- Pelvis**
 abscesses in, 1274
 extraperitoneal spaces and planes in, 1994f, 1994f-1995f
 fluid accumulation in, 193-194
 functional imaging of, 890-904
 normal anatomy of, 174-176, 890-892, 891f
 pathways of disease spread in, 2006-2023
 biliary, 2006
 hematogenous, 2006-2007
 lymphatic, 2008
 peritoneal, 2009
 in pouch of Douglas, 2006, 2011f
 peritoneal spaces in, 2004, 2004f
 visceral radiographs, 175-176
- Pemphigoid**, 338, 339f, 462f
- Penetrating injuries**
 liver, 1707, 1708f, 1712f-1713f
 spleen, 1969
- Pentology of Cantrell**, 224f
- Peptic strictures**, 283-284
 caused by Zollinger-Ellison syndrome, 300, 304f
 with esophageal pseudodiverticulosis, 297-298, 304f
 with hiatal hernia, 298-300
 Schatzki rings and, 300
 with scleroderma, 288-289, 289f
- Peptic ulcer disease (PUD)**, 630
 acute abdomen from, 226f, 226f
 differential diagnosis of, 660f
 gastric narrowing from, 659f
 neoplasms after surgery for, 639
 pediatric, 2152
 surgical considerations for, 631-632
 surgical procedures for, 632
- Peptic ulcers**, 467-495
 anterior wall, 473, 474f-475f
 antral narrowing from, 560
 benign versus malignant, 477-479, 479f-480f
 clinical findings in, 468-469
 complications with, 487-491
 fistulas, 489-491, 491f
 obstructions, 487, 488f
 perforations, 487-491, 489f-490f
 upper GI bleeding, 487, 487f
 differential diagnosis of, 484-486
 duodenal, 479-483
 epidemiology and pathogenesis of, 467-468
 gastric, 469-479
 gastric outlet obstruction caused by, 611-612, 612f
 gastroduodenal and duodenocolic fistulas with, 624
 greater curvature, 471-473, 473f
 healing and scarring of, 474-477, 475f-478f
 lesser curvature, 471-472, 472f
 linear, 474-475, 475f
 location of, 471, 472f-473f
 morphologic features of, 471-473
 multiple, 474
 perforated, pneumoperitoneum caused by, 626-627
 posterior wall, 473, 473f-474f
 ring shadows with, 473, 474f
 radiographic findings on, 469-484
 shapes of, 470, 470f
 size of, 470-471, 471f
- Peptic ulcers (Continued)**
 superior mesenteric root syndrome caused by, 614
 treatment approaches to, 486-487
 treatment of, 469
 in Zollinger-Ellison syndrome, 491-492
- Percutaneous catheter drainage of abdominal abscesses**, 1258-1276
 of amebic abscesses, 1614
 antibiotics in, 1260
 appendicular, 1275
 catheter blockage and positioning in, 1269-1270, 1270f
 catheter drainage surface area in, 1270-1271, 1270f
 catheter management after, 1266-1270, 1269f-1270f
 catheter selection for, 1260
 causes of unsuccessful, 1269f
 clinical consideration in, 1265f
 in Crohn's disease, 1275
 diagnostic, 1259, 1259f
 diverticular, 1274-1275, 1275f
 echinococcal, 1620
 enteric, 1274-1275
 factors affecting outcome in, 1269, 1269f
 with fistulous communication, 1272, 1272f
 of fungal abscesses, 1271-1272
 indications for, 1259-1260
 intraperitoneal, 1275-1276
 liver, 1272-1273, 1273f, 1610-1611
 outcome improvement tips for, 1269-1272
 pancreatic
 acute necrotizing pancreatitis, 1789-1790, 1790f
 pseudocysts, 1793-1794, 1794f, 1820
 patient positioning for, 1260
 patient preparation for, 1260-1261
 pelvic, 1274, 1275f
 peripancreatic, 1273-1274, 1274f
 preprocedure work-up for, 1260
 retroperitoneal, 1274
 splenic, 1273, 1907-1908, 1907f
 techniques for, 1261-1263
 advantages and disadvantages of, 1261f
 catheter fixation, 1263
 combined modality approach, 1264-1266, 1267f
 CT gantry angulation, 1264, 1265f
 hydrodissection, 1266, 1268f
 organ traversal, 1263-1264, 1265f
 Seldinger, 1261f, 1263, 1263f-1264f
 surgical drains in, 1264, 1266f
 trocar, 1261-1263, 1261f-1262f, 1261f
 thrombolytic agents in, 1271, 1271f
 tumor, 1276
- Percutaneous cholecystectomy**, 1392-1394, 1394f
- Percutaneous cholecystolithotomy**, 1398
- Percutaneous gallbladder aspiration**, 1394
- Percutaneous tissue acquisition techniques**, 1239-1253
 for the adrenal glands, 1249
 anticoagulant/antiplatelet agent management for, 1240-1241, 1241f
 attached needle guide, 1242
 for the bowel, 1250
 complications with, 1250-1251
 freehand, 1242
 hematologic and coagulation parameters for interventions in, 1240-1241, 1240f
 image guidance modality choice for, 1241-1243
 for the liver, 1247-1248, 1248f
 biopsies, 1498-1501
- Percutaneous tissue acquisition techniques (Continued)**
 for fat quantification, 1635-1636
 image-guided, 1499-1501
 preprocedure evaluation and
 contraindications for, 1498-1499
 random, 1498-1499, 1499f
 technique for, 1498-1499
 needle biopsies, 1603
 for lymph nodes, 1250
 needle choice for, 1243-1244, 1244f, 1787-1788
 for the pancreas, 1249-1250, 1249f
 biopsies, 1785-1789
 background on, 1785
 complications with, 1789
 diagnostic effectiveness of, 1788-1789
 indications for, 1785-1787, 1786f-1788f
 technical considerations in, 1787-1788
 perioperative thromboembolism, risk stratification for, 1240-1241, 1240f
 planning, 1244-1247, 1245f-1246f
 preprocedure evaluation for, 1239-1241
 routes to avoid in, 1246-1247, 1247f
 for the spleen, 1250, 1251f, 1924
 angiosarcoma biopsy, 1947
 biopsies, 1905-1907, 1906f-1907f, 1906f
- Percutaneous transhepatic biliary drainage (PTBD)**, 1395f, 2180
- Percutaneous transhepatic cholangiography (PTC)**, 1281, 1296-1297, 1296f, 1395-1396
 biliary drainage with, 1395f
 on biliary postoperative complications, 145f
 complications from, 1332-1334
 endoscopic retrograde
 cholangiopancreatography versus, 1295-1296
- Perforations**
 acute abdomen from, 226f, 226f
 appendiceal, 956-957 (See also Appendix: appendicitis)
 bowel
 after guided biopsy, 1250-1251
 with necrotizing enterocolitis, 2104-2105, 2104f-2105f
 colonic
 with carcinoma obstructions, 1104
 carcinomas causing, 1040f, 1048f
 from colorectal cancer, 1036-1039
 with computed tomography colonography, 922
 of giant sigmoid diverticulum, 952
 in salmonellosis, 1017
 suspected, barium studies for, 886-887, 887f
 in diverticulitis, 938, 938f, 941
 duodenal, 626-627
 from endoscopic retrograde
 cholangiopancreatography, 1321-1322
 esophageal, from foreign body ingestion, 2134
 free intraperitoneal, in diverticulitis, 948, 949f
 gallbladder, 1193, 1367-1369, 1368f-1369f
 magnetic resonance
 cholangiopancreatography on, 1336
 gastric, 626-627
 from caustic ingestion, 515-516
 pediatric, 2146-2147
 intramural duodenal hematomas and, 621
 in peptic ulcer disease, 631
 from peptic ulcers, 487-491
 confined, 488-489
 free, 487-488, 489f
 small bowel, 802-804, 803f
- Perfusion computed tomography**, 1166, 1230-1233
 analytical methods and parameters for, 1231f
 basic principles of, 1230

- Perfusion computed tomography (*Continued*)
 clinical applications of, 1232-1233
 risk stratification and staging, 1233
 treatment response monitoring, 1233, 1234f
 in tumor biology, 1232-1233
 postprocessing in, 1232
 protocols for, 1231-1232
 technical parameters for, 1232f
 technical principles of, 1230-1231
 tissue perfusion terminology in, 1232f
- Perfusion lung scanning, 432-433
- Perfusion magnetic resonance imaging
 abdominal, 1235-1236, 1236f
 basic principles of, 1230
 clinical applications of, 1236, 1236f
 data analysis in, 1235
 liver, 1492
 protocols for, 1235
 technical principles in, 1235
- Periapillary carcinomas, 566, 566f, 1307, 1310-1311, 1313f, 1419-1421
- Periarteritis nodosa, 776b
- Peribiliary cysts, 1190, 1190f
- Pericardium, esophageal cancer in, 382, 384f-386f
- Pericecal hernias, 2057, 2059f
- Pericholangitis, 1427. *See also* Primary sclerosing cholangitis
- Pericholecystic fluid, 1359-1360, 1461f
- Perihepatic space, 2001, 2001f, 2009, 2012f
- Perinephric space, 1989, 1990f
- Perineum, descending perineum syndrome, 900
- Periodically rotated overlapping parallel lines with enhanced reconstruction (PROPELLER) sequence, 1183-1184
- Peripancratic abscesses, 1273-1274, 1274f
- Peripancratic lymphadenopathy, 574-575, 661f
- Peripancratic pseudocysts, 132f
- Periportal low density, 1710
- Perirenal space, 172
 anatomy of, 1987-1989
 anterior, 173
 disease spread through, 2014
 posterior, 173
- Peristalsis
 diffusion-weighted MRI on, 1219
 esophageal
 achalasia and, 397-398
 in diffuse esophageal spasm, 285
 normal physiology in, 279
 secondary, 279
 interstitial cells of Cajal in, 1080
 normal primary, 281f
- Peritoneal cavity
 anatomy of, 168-172, 1983-2003
 retroperitoneal planes, 1990-1994
 retroperitoneal spaces, 1986-1990
 subperitoneal spaces, 1994-2000
 upper abdomen peritoneal spaces, 175
 ascites in, 2024-2035
 embryology of, 1983-1986, 1984f-1986f
 mesenteric and omental lesions, 2036-2052
 primary neoplasms, 2036-2043
 mesentery and omental lesions
 malignant peritoneal mesothelioma, 2037-2039, 2039f-2040f
 primary
 adenomatoid tumors, 2042
 desmoplastic small round cell tumors, 2041-2042, 2041f
 malignant peritoneal mesothelioma, 2037-2039
 multicystic mesothelioma, 2040-2041
 peritoneal serous carcinoma, 2039-2040, 2040f
 well-differentiated papillary mesothelioma, 2040, 2041f
 secondary, 2043-2044
 carcinoid, 2044, 2044f
 lymphomas, 2044, 2045f
 peritoneal carcinomatosis, 2043-2044, 2043f-2044f
 pediatric disorders of, 2246
 serous carcinomas of, 2039-2040, 2040f
- Peritonitis
 after guided biopsy, 1250
 meconium, 2111-2113, 2112f
 pediatric, 2246, 2247f
 from pseudomembranous colitis, 1024
 superior mesenteric vein thrombosis with, 1696
 tuberculous, 2044
- Perivesical fat, 175-176, 176f
- Peroral pneumocolon, 670, 670f, 887, 888f
- Persistent hyperinsulinemic hypoglycemia, 2223
- Petit's triangle, 1986-1987, 1988f
- Peritoneal cavity (*Continued*)
 secondary, 2043-2044
 carcinoid, 2044, 2044f
 lymphomas, 2044, 2045f
 peritoneal carcinomatosis, 2043-2044, 2043f-2044f
 pathways of disease spread in, 2006-2023, 2010f
 biliary, 2008
 gastrosplenic ligament, 2019, 2019f
 gut, 2007
 hematogenous, 2006-2007, 2007f
 lymphatic, 2007-2008
 perihaptic spaces, 2009
 retroperitoneal, 2009-2014
 sigmoid mesocolon, 2020
 small bowel, 2009
 subperitoneal, 2015-2021, 2019f
- Peritoneal lavage, diagnostic, 1706-1707, 1712-1714
- Peritoneal spaces
 lower abdomen and pelvis, 2002-2004
 pelvic, 2004, 2004f
 upper abdomen, 2000-2002, 2001f
 left-sided, 2001-2002
 right-sided, 2002, 2002f
- Peritoneoceles, 897-898, 898f
- Peritoneum. *See also* Peritoneal cavity
 anatomy, 2000-2002, 2001f
 differential diagnosis on, 2048b
 diffusion-weighted MRI of, 1224
 disease pathways in, 2008-2009
 inflammatory and infiltrative diseases, 2045-2049
 amyloidosis, 2048
 Crohn's disease, 2046, 2046f
 cysts, 2049
 diverticulitis, 2045, 2046f
 edema, 2048-2049
 extramedullary hematopoiesis, 2048
 pancreatitis, 2045, 2046f
 panniculitis or sclerosing mesenteritis, 2047, 2047f
 trauma and hemorrhage, 2048
 Whipple's disease, 2048
 lesions in, 2036-2052
 malignant peritoneal mesothelioma, 2037-2039, 2039f-2040f
 primary, 2036-2043, 2042f-2043f
 adenomatoid tumors, 2042
 desmoid tumors, 2036-2037, 2037f-2038f
 desmoplastic small round cell tumors, 2041-2042, 2041f
 malignant peritoneal mesothelioma, 2037-2039
 multicystic mesothelioma, 2040-2041
 peritoneal serous carcinoma, 2039-2040, 2040f
 well-differentiated papillary mesothelioma, 2040, 2041f
 secondary, 2043-2044
 carcinoid, 2044, 2044f
 lymphomas, 2044, 2045f
 peritoneal carcinomatosis, 2043-2044, 2043f-2044f
 pediatric disorders of, 2246
 serous carcinomas of, 2039-2040, 2040f
- Peutz-Jeghers syndrome, 530, 793-794, 794f, 1093-1095
 cavernous hemangiomas in, 1076
 computed tomography enteroclysis on, 698f
 computed tomography on, 1094f
 fluoroscopic features of, 1094f
 mucocutaneous pigmentation in, 1093, 1093f
 pediatric, 2151, 2152f
 small bowel
 differential diagnosis of, 874f
 intussusception associated with, 823-824
- Peyer's patches, 756
 in salmonellosis, 761, 1017
 in yersiniosis, 761
- Pharyngeal pouches, 237-241, 238f
- Pharyngeal webs, 241-242
- Pharyngoepiglottic folds, 211f
- Pharyngoesophagogram, 216f
- Pharyngographic contrast agents, 7-8
- Pharynx
 benign tumors of, 244
 in compensatory swallowing techniques, 219-220
 divisions of, 209
 functional abnormalities in, 222-236
 inflammatory lesions of, 243-244
 larynx relationship to, 210f
 location of, 207
 malignant tumors of, 244-252
 motility examinations, 218
 motor function of, 215f
 muscles of, 209-214, 214f-215f
 neurologic disease and the, 231-232
 normal anatomy of, 207-214
 pharyngoepiglottic folds in, 211f
 pharyngoesophagograms, 216f
 postcricoid "defect" in, 213f
 radiographic techniques for, 214-220
 contrast agents and, 218
 double-contrast interpretation, 216-217
 patient positioning, 218
 patient preparation, 214
 routine examination components, 214-215
 in therapeutic examinations, 219-220
 salpingopharyngeal fold of, 210f
 structural abnormalities of, 237-263
 structures and mucosal patterns of, 207-209, 208f-209f, 212f
 in swallowing, 223
 therapeutic techniques with, 220
 tonsillar fossa in, 212f
 valleculae in, 210f
 Zenker's diverticulum and, 214f, 228-230, 239-241, 240f
- Pheochromocytomas, 1198, 1202-1204, 1240
- Phleboliths, 199, 199f
 acute abdomen from, 2268
 with gastric lipomas, 536
 with hemangiomas, 1076
- Phlegmons
 abdominal wall, 2072
 in diverticulitis, 941, 942f
 mesenteric, in Crohn's disease, 1003
 in pancreatitis, 1813
 small bowel, 688
- Phosphate nephropathy, 907
- Phospholipids, 774
- Photodynamic therapy (PDT), 1400
- Phrenicocolic ligament, 2016f, 2020
- Phrenoesophageal membrane, 439
- Phrygian cap, 1282f, 1341
- Phytobezoars, 619
- Picture archiving and communications system (PACS), 558, 1169
- Piriformis muscle, 174, 175f
- Pitch, in computed tomography, 1156, 1156f

- Plain film radiography
 of abdominal abscesses, 1254-1255
 on appendiceal mucocoeles, 975
 on appendicitis, 960
 on ascites, 2027
 of benign liver tumors, 1529
 biliary tract, 1288
 gallbladder, 1284
 on imperforate anus, 2115, 2115f
 liver, 1476-1477
 on angiosarcomas, 1585
 on echinococcal disease, 1616
 on fibrolamellar carcinoma, 1575
 hemangiomas, 1531
 on hemochromatosis, 1642
 on hepatoblastomas, 1578
 hepatocellular adenomas, 1543-1544
 on hepatocellular carcinomas, 1564
 on intrahepatic cholangiocarcinomas, 1580
 of mesenchymal hamartomas, 1555
 on metastases, 1591
 of nodular regenerative hyperplasia, 1548
 on portal vein thrombosis, 1692
 on steatosis, 1631
 on undifferentiated (embryonal) sarcomas, 1587
 omentum, 2049
 pancreas
 on acute pancreatitis, 1811-1812, 1812f
 on annular pancreas, 1804-1805, 1804f
 on chronic pancreatitis, 1824, 1825f
 examination techniques, 1776-1781
 spleen
 anatomy on, 1899, 1899f
 on lymphangiomatosis, 1929
 splenomegaly in, 1923-1924
 wandering, 1915
 on ulcerative colitis, 986-987, 986f
 Planar image reformations, 1161
 Plaque, double-contrast studies of, 47, 49f
 Plasmacytomas gastroduodenal, 598
 Pleating, in double-contrast studies, 45, 46f
 Pleural effusions
 with esophageal perforation, 415
 with esophagopleural fistulas, 421, 421f
 Pliability, in double-contrast studies, 47, 50f
 Plummer-Vinson syndrome, 367
 Pneumatic dilation, 459-460
 Pneumatosis, 190-191, 190f
 in acute mesenteric ischemia, 834, 835f
 coli, 190-191, 191f
 in computed tomography colonography, 922, 923f
 cystoides coli, differential diagnosis of, 1148
 cystoides intestinalis, 190-191, 777
 gastric, 515
 intestinalis, 836f, 1124-1125
 primary, 1124, 1125f
 secondary, 1124-1125, 1125f
 with superior mesenteric vein thrombosis, 1696
 with necrotizing enterocolitis, 2104, 2104f
 Pneumobilia, 188-189, 1342
 Pneumocolon
 double-contrast studies of, 888f
 peroral, 670, 670f, 887, 888f
Pneumocystis carinii. See *Pneumocystis jirovecii*
Pneumocystis jirovecii
 with AIDS, 1652
 hematogenous spread of, 2007
 liver infection with, 1625
 splenic infection with, 1938
 Pneumomediastinum
 with esophageal perforation, 414, 416f
 postoperative, 450-451
 Pneumonecrosis, esophagopleural fistulas after, 421-422, 422f
 Pneumoperitoneum, 168f, 186-187
 abdominal radiographs of, 166, 168f
 benign colonic, 1124
 from perforated ulcers, 626-627
 signs of on radiographs, 187f-188f
 Pneumoretroperitoneum, 187-188
 Pneumothorax, 450-451, 1250-1251
 Polyarteritis nodosa (PAN), 839-840, 839f, 1812
 Polycystic kidney disease, 1190
 Polycystic liver disease, 1553-1554, 1553f
 Polyethylene glycol
 in computed tomography colonography, 906-907
 in computed tomography enterography, 684
 in magnetic resonance enterography, 711, 713
 Polymyositis, 288, 615, 776b
 Polypectomy, endoscopic, 1032f
 Polypoid carcinomas, gastric, 547, 551, 551f-552f
 differentiated from adenomatous polyps, 526, 527f
 of the gastric cardia, 555
 Polypoid folds, in double-contrast studies, 43, 44f
 Polyposis syndromes, 530, 530f, 1089-1101. See also Familial adenomatous polyposis syndrome (FAPS)
 computed tomography enterography for, 684, 685f
 Cowden's disease, 530, 794, 1093, 1095
 differential diagnosis of, 463t
 with hamartomas, 360-361, 361f
 small bowel, differential diagnosis of, 874t
 Cronkrite-Canada syndrome, 530, 530f, 794, 1093, 1096-1097
 clinical features of, 1097f
 differential diagnosis of, 874t
 ectodermal changes in, 1096
 differential diagnosis of, 658t
 familial adenomatous polyposis syndrome, 523, 530, 793, 793f, 1089-1093
 adenocarcinoma associated with, 798
 attenuated, 1089
 colorectal cancer and, 1029
 differential diagnosis of, 874t
 extracolonic gastrointestinal manifestations of, 1090-1091
 fundic gland polyposis, 523, 525f
 hamartomatous, 1093-1097
 Peutz-Jeghers, 530, 793-794, 794f, 1093-1095, 1093f
 cavernous hemangiomas in, 1076
 computed tomography enteroclysis on, 698f
 computed tomography on, 1094f
 fluoroscopic features of, 1094f
 mucocutaneous pigmentation in, 1093, 1093f
 pediatric, 2151, 2152f
 small bowel
 differential diagnosis of, 874t
 intussusception associated with, 823-824
 small bowel, 793-794, 874t
 Polyps
 adenomatous, 523, 526-527, 527f
 cholesterol, 1406, 1408, 1410
 colon
 benign epithelial, 1031-1035, 1031f-1032f
 detection of, 1032-1035
 intussusceptions from, 1106
 sentinel, 1036
 double-contrast studies of, 45-47, 48f
 duodenal, 527-528, 528f
 Polyps (Continued)
 esophageal
 differential diagnosis of, 463t
 fibrovascular, 463t
 esophagogastric, inflammatory, 351, 352f
 fibrovascular, 354, 358-359, 358f-359f
 filiform, in Crohn's disease, 507-508, 508f
 gallbladder, risk stratification of, 1204
 gastric
 gastric carcinoma linked to, 547
 gastroduodenal inflammatory fibroid, 338, 338f
 hyperplastic, 523-525, 524f-526f
 inflammatory esophagogastric, 296, 298f
 juvenile, 2175-2176
 pseudopolyps
 inflammatory, 988, 990f, 992, 994f
 postinflammatory, 988, 991f, 992
 small bowel
 multiple, differential diagnosis of, 874t
 solitary, differential diagnosis of, 873t
 in ulcerative colitis, 988-990
 Polysplenias, 1151t, 2088, 2089f
 Pediatric, 2250, 2251f
 Polysplenia syndrome, 1912, 1918f
 Porphyria, 615
 Porta hepatis, 1175
 hepatoduodenal ligament and, 1996, 2019
 image-guided biopsy of, 1244-1245
 low-density masses in, 1762t
 normal anatomy of, 1475-1476, 1476f
 Portal hypertension
 with cirrhosis, 1655-1656
 classification of, 1655t
 computed tomography on, 1688-1670, 1669f
 gastric varices and, 603
 gastropathy caused by, 607, 607f
 hypersplenism in, 1909
 imaging findings on, 1765f
 interventional radiology on, 1502-1503
 magnetic resonance imaging on, 1670, 1670f
 splenic embolization in management of, 1909
 with splenic vein occlusion, 1696-1697
 superior mesenteric vein thrombosis with, 1696
 transjugular intrahepatic portosystemic shunts for, 1670, 1670f
 ultrasound on, 1665-1668, 1665f-1667f
 Portal inflow phase of enhancement, 1159-1160
 Portal vein
 assessment of for living donor liver transplantation, 1743
 cavernous transformation of, 1695, 1695f-1696f
 Doppler ultrasound in, 1480
 embolization, preoperative, 1505-1506, 1507f
 gas in, 189-190, 190f
 gas in, differential diagnosis of, 1758t
 in hematogenous spread of infections, 2007
 in hepatoduodenal ligament, 1996
 lacerations of, 1710
 liver lobe agenesis and, 1525
 liver transplantation and
 complications involving, 1746-1747
 normal postoperative Doppler findings and, 1746-1747, 1747f
 preoperative imaging for, 1739-1740
 stenosis and thrombosis with, 1747, 1748t
 normal anatomy of, 1471, 1472f
 in pancreas blood supply, 1774
 thrombosis, 1690-1695
 acute abdomen from, 2267
 causes of, 1691b
 clinical findings on, 1691
 pathophysiology of, 1691-1692
 radiologic findings on, 1692-1694, 1692f-1694f

- Portal vein (*Continued*)
 THADs and THIDs from, 1680f
 treatment of, 1693
 ultrasound of, 1777f
- Portal venous phase of contrast, 1159-1160
 in liver CT, 1164
 in pancreas CT, 1166
- Portography, CT, 1164
- Portomesenteric venous gas, 834
- Portosystemic shunts
 congenital, 2209
 preoperative imaging of, 1740
- Positron emission tomography (PET)
 carcinoid detection in, 799
 on colon cancer, 1056-1057, 1057f, 1066-1067, 1067f
 on Crohn's disease, 752
- liver
 benign tumors, 1529
 decreased uptake in, 1764f
 on focal nodular hyperplasias, 1536-1537
 focal uptake in, 1764f
 of hepatocellular adenomas, 1541
 on hepatocellular carcinomas, 1564
- spleen
 anatomy in, 1899, 1900f
 on lymphomas, 1955f
 on ulcerative colitis, 995-996, 996f
- Positron emission tomography/computed tomography (PET/CT), 96-111
 on colon cancer, 1067-1068, 1068f
 on Crohn's disease, 752
 disease staging with, 98-99
 esophageal cancer staging with, 380-381, 385, 387f-388f
 of esophageal GISTs, 355-356
 of the esophagus, 98-100, 99f
 liver, on metastases, 1591-1592, 1592f-1593f
 pancreas, in carcinoma staging, 1781
 patient preparation for, 97
 protocol for, 97
 restaging and treatment response in, 99-100
 of the small bowel, 102-103, 102f
 of solid parenchymal organs, 1202-1214
 adrenal glands, 1210-1211, 1210f-1211f
 gallbladder and biliary tract, 1202-1204
 liver, 1204-1207, 1205f-1206f
 pancreas, 1208-1210, 1209f-1210f
 spleen, 1207-1208, 1208f
 spleen, on metastatic disease, 1957, 1958f
 stomach, 100-102
- Positron emission tomography/magnetic resonance imaging, 752, 1593f
- Positron Emission Tomography Response Criteria in Solid Tumors (PERCIST), 2301-2302, 2302f, 2303f
- Postablation syndrome, 1510
- Postcricoid "defect", 213f
- Postembolization syndrome, 1512-1513
- Posterior pararenal space, 2014
- Postinflammatory pseudopolyps, 988-990, 991f, 992
- Postprandial gastrocolic reflex, 1124
- Post-transplantation lymphoproliferative disorder (PTLD), 859-860
 after liver transplantation, 1735, 1753f
 after pancreas transplantation, 1885-1886, 1887f
- Post-transplantation malignant disease, 1753
- Potassium chloride, drug-induced esophagitis from, 327
- Pouchitis, 858, 1140
- Pouch of Douglas, 1085, 1111, 2008-2009
 abscesses in, 2011f
 ascites in, 2027
 metastatic disease in, 2009, 2011f
- Praziquantel, 1625
- Predoduodenal portal vein, 614
- Pregnancy
 appendicitis in, 967-968
 HELLP in, 1698-1699, 1699f
- Presacral space, widened, 984, 993f, 1150f
- Presbyesophagus, 279, 286-287
- Presbyphagia, 230-231
- Primary biliary cirrhosis, 1432-1434, 1433f, 1435f, 1649-1650
 with AIDS, 1653
 differential diagnosis of, 1465f
 liver transplantation for, 1738
 pathologic findings in, 1649-1650, 1649f
 radiographic findings on, 1433-1434, 1434f, 1650, 1650f
- Primary sclerosing cholangitis, 746-748, 1011f, 1427-1432
 with AIDS, 1653
 benign ductal diseases differentiated from, 1432
 cholangiocarcinomas with, 1202-1203, 1431-1432
 computed tomography on, 1429-1431, 1430f
 differential diagnosis of, 1431-1432
 epidemiology and clinical findings in, 1427
 fluoroscopic cholangiography on, 1428, 1429f
 with inflammatory bowel disease, 1010
 interventional radiology for, 1399
 liver transplantation for, 1738
 magnetic resonance cholangiopancreatography on, 1334-1335, 1334f-1335f, 1430-1431
 magnetic resonance imaging on, 1430-1431, 1431f
 pathology of, 1427-1428, 1428f
 pediatric, 2195, 2196f
 with primary biliary cirrhosis, 1649-1650
 radiographic findings on, 1428
 secondary biliary cirrhosis due to, 1650-1651, 1651f-1652f
 strictures from, 1751
 ultrasound on, 1429-1431, 1429f
- Primary vascular disease, 120-121
- Pringle maneuver, 1726
- Proctectomy, 1137-1138, 1137f
- Proctitis, 992
- Proctocolectomy, 996
- Proctosigmoiditis, 1117
- Progressive familial intrahepatic cholestasis (PFIC), 2189-2190
- Prolapses
 colonic, after colostomy, 1135
 esophagogastric mucosal, 446, 447f
 rectal mucosal prolapse syndromes, 1119-1120
 uterine and vaginal vault, 900
- Prone compression views
 for duodenal ulcers, 479-480, 480f
 for gastric ulcers, 469, 470f
 anterior wall, 473
- PROPELLER (periodically rotated overlapping parallel lines with enhanced reconstruction) sequence, 1183-1184
- Prostaglandins, 467, 469
- Prostate gland
 cancer
 metastases from, 979, 1082-1083, 1083f
 multi-parametric imaging of, 1226-1227
 traversal of in percutaneous drainage, 1264
- Protein digestion and absorption, 774
- Proteus-like syndrome, 1095
- Proteus syndrome, 1095
- Proteus vulgaris*, 514-515
- Proton chemical shift imaging, 1633-1635
- Proton pump inhibitors
 for *H. pylori* gastritis treatment, 501
 MALT treatment with, 582
- Proton pump inhibitors (*Continued*)
 for pancreatic lesions, 1861-1862
 for pelvic ulcer disease, 631
- Protozoan infections, 766-767
- Protruding lesions, double-contrast studies of, 45-47
- Proximal gastric vagotomy. *See* Highly selective vagotomy (HSV)
- Prune-belly syndrome, 1151f, 1912, 2071, 2245-2246, 2245f-2246f
- Pseudoaccessory fissures, liver, 1520, 1521f-1522f
- Pseudochalasia. *See* Achalasia: secondary
- Pseudoaneurysms
 hepatic arterial, 1745-1746, 1747f
 liver, 1710, 1712
 pancreatic, 1793
 with pancreatitis, 1811, 1822-1824, 1823f
 post-transplant, 1879-1880, 1880f
 surgery for, 1861
 splanchnic artery, 1909-1910
- Pseudocalculus sign, 1305, 1306f
- Pseudocysts
 mesenteric, 2049, 2049f
 pancreatic
 after trauma, 1858
 differential diagnosis of, 1890f
 interventional radiologic management of, 1793-1794, 1794f
 with pancreatitis, 1810, 1820-1821, 1820f-1822f
 pediatric, 2221, 2221f
 surgery for, 1861
- splenic
 congenital, 1931-1932, 1932f-1933f
 with pancreatitis, 1945, 1945f
 pediatric, 2231-2233
- Pseudodiverticula
 with *Candida* esophagitis, 314
 with peptic strictures, 300, 304f
 pyloric channel ulcers differentiated from, 483-484
- Pseudolipomas, 1550
- Pseudolymphomas, 580
- Pseudomembranous colitis (PMC), 64, 65f, 1024, 1024f
- Pseudomyxoma peritonei, 975, 977f, 1084, 1954-1955
 ascites, 2026
 in peritoneal carcinomatosis, 2043-2044
- Pseudopapillary neoplasms, 1197, 1848-1849, 1849f
- Pseudo-prune-belly syndrome, 2245
- Pseudotumors
 esophagogastric mucosa prolapse as, 447f
 inflammatory, liver, 1536-1557, 1557f
 invaginated hiatal hernias as, 447f
- Psoas abscess, 1012
- Psoas muscle, 173-174, 174f
- Psoas sign, 959-960
- Psyllium fiber, as contrast agent, 82
- Puestow procedure, 1664, 1865f
- Pulmonary slings, 2130f
- Pulsed-wave Doppler imaging, 1172-1173, 1173f
- Pus, 2025
- Pyelonephritis, 626, 2268f
- Pylephlebitis, 949, 950f, 1608-1609
- Pyloric channel ulcers, 483-484, 486f
- Pyloric stenosis
 adult hypertrophic, 611, 612f
 pediatric, 2147-2148, 2147f-2150f
- Pyloroplasty
 Finney, 632
 Heineke-Mikulicz, 632
 Jaboulay, 632
 for peptic ulcer disease, 632
 for ulcer treatment, 469

- Pyogenic abscesses
liver, pediatric, 221f
spleen, 1939-1941, 1940f
- Pyogenic cholangitis
recurrent, 1376f, 1415-1416, 1416f
- Pyogenic infections, splenic, 1935
- Q**
- Quadratus lumborum muscle, 174
- Quinidine, drug-induced esophagitis from, 327
- R**
- Radiating folds, in double-contrast studies, 43, 44f
- Radiation dose. *See also* Thorotrast
for abdominal and pelvic malignancies, 1116
absorbed, 1158
in computed tomography, 1158-1159
colonography, 922-923
enterography, 685, 691-692
liver, 1484-1485
multidetector, 737
Crohn's disease and, 737, 1257-1258
in CT fluoroscopy, 1243
in defecography, 901-902
effective dose in, 1158
- Radiation-induced disorders
enteritis
malabsorption in, 776b
segmental small bowel mural
hyperenhancement in, 686, 687f
small intestinal, 843-845, 845f
enteropathy, small bowel
differential diagnosis of, 875f
obstruction from, 819-820, 820f-821f
esophagitis, differential diagnosis of,
462f-463f
liver disease, 1640-1641, 1640f
strictures, 804
- Radiation therapy
colitis from, 1116-1117, 1117f
dysphagia after, 230
for esophageal cancer, 389, 390f
esophageal narrowing from, 2138, 2138f
esophageal squamous cell carcinoma associated
with, 367
esophagitis from, 328-330, 330f
for gastric lymphomas, 584
gastric narrowing from, 659f
gastrointestinal injuries from, 516-517
for GISTs, 800
for leiomyosarcomas, 403
mechanisms of injury from, 1116
pharyngeal damage from, 252-253
sinusoidal obstruction syndrome in, 1680
small bowel disorders from, 871f
obstructions, 819-820, 820f-821f
spleen, transarterial irradiation of, 1970
thickened gastric folds from
differential diagnosis of, 659f
- Radioembolization
of hepatocellular carcinomas, 1740
of liver metastases, 1206, 1729
complications with, 1731f
radiologic appearance after, 1331f
transarterial, 1514f
of liver tumors, 1726-1727, 1727f
transarterial, 1513-1515
- Radiofrequency ablation (RFA), 1507-1508
with chemoembolization, 1726
for liver tumors, 1724, 1724f-1725f
spleen, 1908
- Radiographic studies. *See also* Interventional
radiology; Plain film radiography
after laparoscopic adjustable gastric band
placement, 647, 648f
on Barrett's esophagus, 305-308
on diverticulitis, 939
on portal hypertensive gastropathy, 607
spleen, on lymphomas, 1950
- Radiology, interventional
gallbladder and biliary tract, 1392-1401
for bile duct injury, 1398-1399, 1399f
for biliary strictures, 1396-1398, 1397f
for common duct stone removal, 1398
percutaneous cholecystostomy, 1392-1394
percutaneous gallbladder aspiration, 1394
preprocedural management for, 1392
for primary sclerosing cholangitis, 1399
- Reactive inflammation, colonic, 1022
- Reconstruction increments, 1156, 1157f
- Rectal cancer, 91f
diffusion-weighted imaging of, 91f, 92f
diffusion-weighted MRI on, 1225
magnetic resonance imaging of, 90-93, 91f,
1043-1047, 1045f, 1053f
metastatic
from colon, 1045f-1046f, 1048f
to lymph nodes, 1047
staging of, 1052f, 1053-1054, 1054f
treatment response monitoring, 1233, 1234f,
1236, 1236f
- Rectal mucosal prolapse syndromes, 1119-1120,
1122f
- Rectal valve abnormalities, 992
- Rectal varices, 1118-1119, 1119f
- Rectal water contrast agents, 82
- Rectoceles, 896, 897f, 898, 900
- Rectosigmoid junction, anterior indentation on
the, 1151f
- Rectum. *See also* Colon
angiography of, 116-119
carcinoid tumors in, 1077
caudal regression in, 2117
Currarino triad in, 2117-2118
embryology of, 1985-1986
endocrine cell tumors of, 1077
intussusception of, 898-899, 899f
normal anatomy of, 890-891, 891f-892f
PET/CT of, 103-107
posterior-lateral rectal pouches, 899
solitary rectal ulcer syndrome, 899
traversal of in percutaneous drainage, 1264
ulcerative colitis in, 992, 993f
widened presacral space and, 984, 993f, 1150f
- Rectus sheath hematomas, 2071
- Reed-Sternberg cells, 1588-1589
- Reflux esophagitis, 291-303
after esophagogastric anastomosis, 456f
Barrett's esophagus with, 375
chronic gastroesophageal reflux leading to,
454-455
clinical findings of, 292
diagnosis of, 292-293
differential diagnosis of, 300-303, 462f-463f
differentiated from adenocarcinoma, 381f
distinguished from *Candida* esophagus, 315
distinguished from drug-induced esophagitis,
328
esophagopericardial fistulas from, 424f
Garrett's esophagus with, 303
hiatal hernia, gastroesophageal reflux, and,
291-292
mucosal nodularity with, 301, 463f
pathogenesis of, 291
with pseudomembranes, 293, 294f, 381f
- Reflux esophagitis (Continued)
radiographic findings with, 293-300, 293f
scarring and strictures in, 296-300
with thickened folds, 294-296, 297f-298f
with ulceration, 293-294, 294f, 296f
ulceration in, 301-302
- Regenerative hepatocellular nodules, 1190-1191
- Remicade, 996, 1007
- Renal artery, 1989
- Renal cell carcinomas, 1198-1199, 1199f
with Cowden's disease, 1095
gastrointestinal metastases from, 576
MASS criteria on response to therapy, 2300,
2301f, 2302f
metastases from
colonic, 1083
pancreatic, 185f
- Renal colic, 2266
- Renal cysts, 1198
- Renal failure, 518, 518f
- Renal vein, 1989
- Response Evaluation Criteria in Solid Tumors
(RECIST) 1.0, 800-801, 1208, 2295
comparison of with RECIST 1.1, 2297f
comparison of with WHO criteria, 2295, 2296f
hepatic surgery and, 1728-1729
modified, 2300
in treatment response monitoring, 1233
- Response Evaluation Criteria in Solid Tumors
(RECIST) 1.1, 2295-2299, 2297f, 2299f
- Rests. *See* Ectopic pancreatic rests; Mucosal rests,
biliary tract
- Retention cysts, 247f
appendiceal, 976f-977f
esophageal, 362f, 363, 464f
- Reticular pattern, in double-contrast studies, 40,
41f
- Reticuloendothelial contrast agents, 14
- Retinal lesions, in familial adenomatous polyposis
syndrome, 1092
- Retractile mesenteritis, 1021-1022, 1110
- Retroanastomotic hernias, 2059-2060, 2061f
- Retromesenteric plane, 1991f-1993f
- Retroperitoneum. *See also* Peritoneal cavity
abscesses in, 1274
adenopathy in, 575-576, 575f
anatomy of, 2014f
planes in, 1990-1994
pelvic extraperitoneal, 1994, 1994f-1995f
retromesenteric and laterocaval, 1990-1991,
1991f-1992f
retrorenal, 1991-1994, 1993f
spaces in, 1986-1990
anterior pararenal, 1990f, 1992f
great vessel, 1986, 1988f
perirenal, 1987-1989, 1989f
posterior fat pads, 1986-1987, 1988f
transversalis fascia, 1986
disease spread through, 2009-2014
anterior pararenal space, 2013-2014, 2015f
perirenal space, 2014
posterior pararenal space, 2014
fibrosis in, 1110
layers and fluid distribution in, 1987f
normal anatomy of, 174f
- Retrorenal plane, 1991-1994, 1993f
- Reverberation artifacts, 1382-1384, 1384f
- Rhabdomyosarcomas, 1422, 2196, 2197f
- Richter's hernias, 815, 816f, 2064
- Riedel's lobe, 1521, 1522, 1523f
- Rigler's sign, 187, 187f
- Rigler's triad, 821, 1377-1379
- Riley-Smith syndrome. *See* Bamayan-Riley-
Ruvalcaba syndrome (BRRS)

Rim sign, 1463f, 1597, 1597f, 1764f
 Ring-down artifacts, 1174, 1175f
 Ring shadows
 with duodenal polyps, 328f
 with duodenal ulcers, 482f
 with gastric ulcers, 473, 474f-475f
 with pyloric channel ulcers, 483-484
 Rituximab, 802-804
 Rokitsky-Aschoff sinuses, 1257, 1337f, 1381-1383, 1383f, 1408
 Roux-en-Y procedures
 computed tomography enteroclysis on, 700-701
 esophagojejunostomy
 afferent loop obstruction after, 852f
 alkaline reflux esophagitis after, 340
 for gastric masses, 640
 gastric bypass, 630, 642-646, 643f
 abdominal wall hernias after, 646
 assessing for postoperative complications with, 642-643
 communication with excluded stomach after, 644, 644f
 complications after, 643-646
 internal hernias after, 645-646
 intussusception after, 646, 647f
 marginal ulcers after, 644-645
 obstruction after, 645, 645f-646f
 stomal stenosis after, 645f, 646
 gastrojejunostomy, 630, 633-634, 635f, 639
 jejunostomy, 855
 leaks after, 635, 644f
 Roux syndrome after, 636
 Roux syndrome, 636
 Rovsing's sign, 959-960
 Ruvalcaba-Myhre-Smith syndrome. *See* Bannayan-Riley-Ruvalcaba syndrome (BRRS)

S

Sacculations
 in Crohn's disease, 1002, 1004f
 in double-contrast studies, 53-55, 54f
 in reflux esophagitis, 296-297, 299f-300f
 Sacrocolopexy procedures, 897
 Sacroiliitis, 746-748, 748f
 Sacroiliitis-spondylitis, 1011
 Sacrospinous ligament, 175, 175f
 Saline chasers, 116f
 Salivary gland carcinomas, 250-251
Salmonella, 1017-1018, 1948
 Salmonellosis, 761, 873t, 1017-1018
 Salpingopharyngeal fold, 210f
 Sandifer's syndrome, 2131
 Sandlike patterns. *See* Micronodularity, small bowel
 Sarcoidosis
 antral narrowing in, 560
 gastric, 510-511, 511f
 gastric narrowing from, 639t
 gastric outlet obstruction from, 613
 hepatic, 1432
 liver, 1647-1648, 1648f
 multiple duodenal ulcers with, 484
 splenic, 1938, 1938f
 thickened folds in, 659t
 Sarcomas. *See also* Kaposi's sarcoma
 abdominal wall, 2071-2073
 gallbladder, 1410
 liver mesenchymal, 1588
 peritoneal, 2043, 2043f
 pharyngeal, 251-252
 small bowel, 697-699
 synovial, 408
 undifferentiated embryonal, 1586-1588, 2204-2205, 2205f
 Sarcomatoid renal cell carcinomas, 1198-1199
 Satisfaction of search, 2292
 Scan delay, 1160-1161
 Schatzki rings, 300, 441-443, 441f
 clinical findings of, 441
 differential diagnosis of, 443
 foreign body impactions with, 419, 419f
 overlap phenomenon with, 441-443, 442f
 pathogenesis of, 441
 radiographic findings on, 441-443
 Schistosoma spp., 759, 1020, 1623-1625
 Schistosomiasis
 clinical findings on, 1623
 colonic, 1020
 squamous cell carcinoma with, 1080-1081
 epidemiology of, 1623
 life cycle of, 1623, 1624f
 liver, 1623-1625
 pathology of, 1623
 pathophysiology of, 1623, 1624f
 portal hypertension from, 1636
 radiologic findings on, 1623-1625
 treatment of, 1625
 Schwachman-Diamond syndrome, 2223, 2223f
 Schwann cells, 537
 Scientific Registry of Transplant Recipients, 1737
 Scintigraphic studies
 of abdominal abscesses, 1258
 biliary tract, 1281, 1288, 1299-1300, 1299f
 on bile leaks, 1455
 of biliary atresia, 2186-2188, 2187f
 on colorectal cancer, 1030-1031, 1056, 1058
 gallbladder, 1462, 1462t
 on gastroesophageal reflux disease, 2131
 on gastrointestinal hemorrhage, 691-692
 liver
 on amebic abscesses, 1612
 on bacterial (pyogenic) abscesses, 1610
 on biliary postoperative complications, 1451
 on bilomas, 1734
 differential diagnosis in, 1763
 on focal nodular hyperplasias, 1536-1537
 hemangiomas, 1531, 1531f
 of hepatocellular adenomas, 1544
 on Meckel's diverticulum, 2159, 2161f
 pancreas, 1850-1851
 pediatric, 2180
 postoperative gastric and duodenal, 631
 spleen
 on accessory spleens, 1925
 anatomy in, 1899, 1899f
 on hamartomas, 1928-1929
 on hemangiomas, 1928
 on infarctions, 1943
 on lymphomas, 1933
 on metastatic disease, 1957
 pediatric, 2228-2229
 on pyogenic abscesses, 1940
 on trauma, 1972
 wandering, 1915, 1915f
 on ulcerative colitis, 995-996, 995f
 Scirrhous carcinoma. *See* Linitis plastica
 Scleroderma
 Barrett's esophagus and adenocarcinoma and, 377
 with *Candida* esophagitis, 314, 316f
 colonic involvement in, 1124
 esophageal, 288-289, 288f-289f
 gastric dilation caused by, 615
 malabsorption in, 777-778, 777f
 megaduodenum in, 661t
 with primary biliary cirrhosis, 1649-1650
 superior mesenteric root syndrome caused by, 614, 614f

Sclerosing cholangitis
 cholangiocarcinomas with, 1421f
 colorectal cancer with, 1029
 differential diagnosis of, 1465j
 immunoglobulin G4-related, 1317, 1420f
 primary, 1317f
 THADs and THIDs from, 1679f
 Sclerosing mesenteritis, 2047, 2047f
 Sclerotherapy for esophageal varices, 431-432, 432f
 Scolecidal agents, 1620-1621
 Scoliosis, 185
 Seat belt sign, 1862-1863
 Sebaceous cysts
 in familial adenomatous polyposis syndrome, 1091
 spleen, pediatric, 2232, 2232f
 Secondary biliary cirrhosis, 1650-1651, 1652f
 Secretin-enhanced magnetic resonance cholangiopancreatography, 1832, 1836, 1781, 1803, 1826
 Secretin test, sonographic, 1802
 Segmental arterial mediolysis (SAM), 159
 Segmental dilation, 863, 864f
 Segmental resection, colonic, 1133, 1134f
 Segmental small bowel mural hyperenhancement, 687t
 Segmentectomy, 1722, 1723f
 Seldinger technique of percutaneous drainage, 1261j, 1263, 1263f-1265f
 Selective immunoglobulin A immunodeficiency, 763
 Seminomas, 1589
 Senile antrum, 560
 Sentinel clots, 1708-1709, 1709f, 1967-1969, 1969f
 Sentinel loops, 2219f
 Sepsis, 1716, 2263
 Septic arthritis, 1012
 Septicemia, liver abscesses from, 1608
 Sequestration, acute splenic, 2236-2237
 Seromas, 1753
 Serosal fat density, 75-76
 Serotonin, 1077
 Serous carcinomas, peritoneal, 2039-2040, 2040f
 Serous cystadenocarcinomas, 197, 198f
 differential diagnosis of, 1893j
 diffusion-weighted MRI of, 1223
 surgery for, 1861
 Serous cystadenomas, pancreatic, 1195-1196, 1196f, 1845-1846, 1845f
 Serpentine folds, in double-contrast studies, 40, 45f
 Sertoli cell tumors, 1093
 Serum amylase levels, in pancreatitis, 1811
 Serum lipase levels, in pancreatitis, 1811
 Sex cord tumor with annular tubules (SCTAT), 1093
 Sexually transmitted diseases, colonic involvement of, 1113, 1113f. *See also* AIDS (acquired immune deficiency syndrome); HIV (human immunodeficiency virus); Syphilis
 Shaggy pattern, in double-contrast studies, 41, 42f
Shigella, 1018
 Shigellosis, 1018
 Shine-through, T2, 1220
 Shock bowel complex, 843, 844f
 Short gut syndrome, 783-784, 784f
 Short tau inversion recovery (STIR) sequences, 1488-1489
 Sicca complex, 1649-1650
 Sickle cell disease, 1943-1947, 1944f, 2211, 2212f, 2236-2237
 Siderotic hepatocellular nodules, 1191
 Side-to-side enterocolic anastomosis, 1133, 1134f
 Sigmoid colon
 disease spread through, 1996-2000, 2009, 2020
 obstructions in, 1104
 volvulus in, 183, 183f, 1105, 1106f, 1108f

- Sigmoidocele, 897-898, 897f, 899f
Sigmoidopexy procedures, 897
Sigmoidoscopy in ulcerative colitis, 986
Signal-to-noise ratio, 1153, 1218
Signet ring cell carcinomas, 548
Sincalide, 1207f
Single-balloon enteroscopy, 688-690
Single-contrast studies, 23-30
 barium enema, 28-30
 barium suspensions for, 24
 colon, 879
 diagnostic principles in, 23
 enteroclysis, 672
 equipment for, 23-24
 esophagography, 25
 quality controls in, 24-25
 small bowel, 26-27
 upper gastrointestinal series, 25-26
Single photon emission CT (SPECT) of liver hemangiomas, 1531
 spleen, 1899f, 1915
Single-shot fast spin-echo technique on acute cholecystitis, 1360
 on Crohn's disease, 734-735
 in magnetic resonance enterography, 712
Single-shot fat-suppressed spin-echo echo planar imaging (SS-EPI), 1216-1217
Sinogram-affirmed iterative reconstruction (SAFIRE), 1485
Sinusoidal obstruction syndrome, 1689-1698, 1683f, 1687f. *See also* Budd-Chiari syndrome
Sinus tracts, 688, 941, 1002, 1003f
SIR-spheres, 1513-1514
Situs ambiguus, 1917-1918, 1918f, 1920f
Skin cancer, nonmelanoma, 1753
 See also Melanomas, malignant
Skip lesions, 972
Sleeve gastrectomy, 651-654, 652f-653f
Sliver of the liver, 1520-1521, 1522f
Small bowel. *See also* Mesentery
 abnormalities of, 861-869
 bezoars, 867
 developmental, 861-865
 Meckel's diverticulum, 861, 862f
 edema, 866-867, 867f
 endometriosis, 865-866, 866f
 enteroliths, 867
 heterotopic tissue, 862-863, 863f
 malrotation, 863-865, 865f
 midgut duplications, 861-862, 863f
 paraduodenal hernias, 865, 865f
 segmental dilation, 863, 864f
 anatomy of, 665-666
 angiography of the, 115-116, 116f
 annular lesions in, 874t-875t
 aphthoid ulcers in, 667-668, 669f
 ascites in, 1027
 bacterial infections, 760-762
 bacterial overgrowth in, 775
 barium examinations of, 665-683
 enteroclysis, 670-675
 fluoroscopic examination method choices in, 677-682, 682t
 for abdominal pain, 679-680
 for chronic diarrhea, 678
 for malabsorption, 681
 for obstructions, 679, 680f
 for suspected perforation, 680-681
 for unexplained gastrointestinal bleeding, 681-682
Small bowel (Continued)
 follow-through, 668-670, 669f-670f, 677-678, 678f, 682f
 carcinoid tumors sensitivity of, 799
 computed tomography enteroclysis compared with, 695-697
 normal, 666f
 normal parameters for enteroclysis and small bowel follow-through, 666f
 peroral pneumocolon, 670, 670f
 retrograde, 676-677
 barium enemas, 676-677, 676f
 ileostomy enema, 677, 677f
 water-soluble contrast agents in, 675-676, 676f
 barium studies of, 26-27
 benign tumors of, 789-795
 adenomas, 790, 790f
 clinical considerations with, 789
 GISTs, 790, 791f
 hemangiomas, 791-792, 792f
 imaging considerations with, 789
 lipomas, 790-791, 791f
 uncommon, 792-793, 793f
 cancers
 computed tomography enteroclysis on, 697-699
 hematogenous spread of, 2006
 spread of in, 2009
 carcinoid tumors in, 668f
 computed tomography enteroclysis, 694-709
 historical background of, 694-695
 indications for and comparisons with other imaging methods
 for Crohn's disease, 695-697, 696f
 miscellaneous, 701-704, 702f-704f
 for neoplasms, 697-699, 697f-698f
 for obstructions, 699-701, 699f-701f
 summary on, 705
 technical problems and limitations in, 704-705
 computed tomography enterography of, 684-693
 contrast agents for studies of, 9
 Crohn's disease in, 725-755
 classification and therapy, 725-726
 clinical considerations in, 725
 diagnostic tools for, 726-737
 differential diagnosis of, 870-876
 digestion and absorption in, 773-774
 dilation, differential diagnosis of, 871t
 drug-induced disorders of, 762-763
 enterocele, 896-898, 896f, 898f
 enteroclysis of, 5
 exocentric cavity lesions in, 875t
 fold changes
 differential diagnosis of, 786, 870t
 irregular thickening in, diffuse, 872t
 irregular thickening in, distal ileum, 873t
 irregular thickening in, proximal, 872t
 mass effects with tethering, 875t
 micronodularity, 870, 871t
 normal parameters and, 870t
 smooth, straight, thickened folds, 871t
 follow-through
 normal parameters for, 870t
 on obstructions, 810-811, 810f-811f
 hemorrhages involving, 2277-2279
 hypomotility, drug-induced, 762b
 as immunologic organ, 756-757
 inflammatory disorders of, 756-772 (*See also* Crohn's disease)
 bacterial infections, 760-762, 760f-761f
 differential diagnosis of, 768-769
 drug-induced, 762-763, 762b, 763f
Small bowel (Continued)
 fungal infections, 762
 immunodeficiency and, 763-768
 immunologic function and, 756-757
 parasitic infestations, 757-760, 757f
 viral infections, 762
 intussusceptions, 822-824, 822f-823f
 ischemia, drug-induced, 762, 762b
 loop separation without tethering, 875t
 lymphoid hyperplasia of, 667f
 magnetic resonance enterography, 710-724
 malabsorption in, 773-788
 malignant tumors of, 796-805
 adenocarcinomas, 798-799, 798f
 carcinoid, 799, 799f-800f
 GISTs, 799-801, 801f-802f
 imaging, 796-798
 imaging features of, 797t
 metastases from, 804, 804f
 mesenteric attachments of, 578f
 multiple target lesions in, 874t
 neoplasms, magnetic resonance enterography on, 719-720, 719f
 normal parameters of, 870t
 normal villi in, 667f
 normal walls of, 70, 70f
 obstructions, 167f, 806-826
 acute mesenteric ischemia caused by, 829
 barium enemas and, 676
 barium study choice for, 821
 classification of, 811-824
 closed loop, 812-813, 813f
 computed tomography enteroclysis on, 703f
 computed tomography enterography on, 685t, 690-691
 from diverticulitis, 948-949, 950f
 extrinsic, 811-817
 extrinsic tumors in, 816-817
 gas patterns with, 180-181, 180f
 hernias with, 814-816, 814f
 magnetic resonance enterography on, 721-722, 722f
 from obturator hernia, 176f
 pathophysiology of, 806-807, 807b
 radiologic imaging of, 808-811
 barium studies, 810-811, 810f-811f
 computed tomography, 808-809, 809f
 plain radiographs of the abdomen, 808, 808f-809f
 strangulated, 703f, 813f
 symptoms of, 807
 terms used to describe, 806, 807f
 pancreas in relation to, 1772, 1773f
 parasitic infections, 757-760
 pediatric disorders of, 2158-2163
 Henoch-Schönlein purpura, 2161, 2162f
 intestinal lymphangiectasia, 2160-2161
 Meckel's diverticulum, 2158-2160, 2159f-2160f
 PET/CT of, 102-103, 102f
 postoperative, 851-860
 after enterectomy and anastomosis, 852-855, 853f
 after enterostomy, 855
 after gastric surgery, 851-852, 852f
 after ileal reservoirs, 855-858
 after transplantation, 858-860, 859f
 segmental mural hyperenhancement in, 687t
 site predilection of diseases in, 875t
 transplantation, 856, 859f
 traversal of in percutaneous drainage, 1263
 tubular, differential diagnosis of, 873t
 vascular disorders of, 827-850

Small cell carcinomas, 407-408, 408f
 Small for size syndrome, 174f
 Small intestine
 malabsorption related to, 775f
 malignancies of, 90
 normal anatomy of, 171
 Soap bubble appearance of villous tumors, 529-530, 529f
 Sodium phosphate, 907
 Soft palate, 215f
 Solid pseudopapillary neoplasms, 1197
 Solitary rectal ulcer syndrome, 890, 899, 1119, 1122f
 Somatostatin-receptor scintigraphy, 1850-1851
 Sonazoid, 1481
 SonoVue, 1481
 Sorbitol, 711
 SPACE (sampling perfection with application-optimized contrast with different flip-angle evolutions) sequence, 1183-1184
 Spasmolytics, 910, 928
 Spectroscopy, liver, 1491-1482
 Sphincterectomy, 1272
 Sphincter of Oddi, 1179-1180, 1205
 normal anatomy of, 1305, 1305f
 postoperative complications involving, 1311
 scintigraphy on, 1299-1300
 spasm in, 1299
 Sphincterotomy, 1322, 1864
 Spiculation, 54f, 55
 Spigelian hernias, 815, 816f, 2062, 2062f
 Spigos technique, 1909
 Spindle cell carcinomas, 402-403, 405f, 407, 463t, 1079-1080
 Spine, caudal regression of, 2117
 SPIOs. *See* Superparamagnetic iron oxides (SPIOs)
 Spiral CT. *See* Helical computed tomography
 Spiral enteroscopy, 688-690
 Spiral valves of Heister, 1281-1282, 1282f
 Spleen
 abscesses, 1273
 accessory, 1181, 1800, 1801f, 1915, 1926f, 2088
 pediatric, 2229-2230, 2230f
 acute abdomen from, 2266-2268
 alcohol ablation in, 1908
 anatomy, 1897-1904, 1898f
 on angiography, 1899-1900
 arterial, 1966f
 clefts, lobulations, bands, 1912, 1971f
 on computed tomography, 1901-1902, 1902f
 gross and microscopic, 1897
 heterotaxy syndromes, 1917-1919
 malformations associated with, 1920b
 on magnetic resonance imaging, 1902-1903, 1903f
 on plain film radiography, 1899, 1899f
 on position emission tomography, 1899, 1900f
 radiologic, 1899-1903
 on scintigraphy, 1899, 1899f
 on ultrasound, 1900-1901, 1901f
 variations in, 1912-1922
 arterial embolization in, 1908-1910
 of aneurysms or pseudoaneurysms, 1909-1910
 in hypersplenism, 1909
 in portal hypertension, 1909
 in splenic arterial steal syndrome, 1910
 in trauma, 1908-1909, 1909f
 asplenia, 2088
 asplenia syndrome, 1917-1918, 1917b, 1917f-1918f
 atrophy of in celiac disease, 762
 bare area of, 2002
 calcifications in, 1924b, 1952, 1954f
 in confined perforations, 489
 differential diagnosis of, 1977-1980

Spleen (Continued)
 on angiosarcomas, 1947-1948
 calcifications, 1979t
 with computed tomography, 1978
 congenital syndromes with splenomegaly, 1977b
 cystic masses, 1935
 decreased diffuse echogenicity, 1977b
 echogenic masses, 1977b
 focal hyperdense lesions, 1978b
 focal hypodense lesions, 1978b
 increased density, 1978b
 increased diffuse echogenicity, 1977b
 with magnetic resonance imaging, 1978
 multifocal hypoechoic masses, 1977b
 multiple hyperintensities, 1979b
 multiple hypointensities, 1978b
 small spleen, 1977b
 splenomegaly, 1978b, 1979f
 of supernumerary spleens, 1925-1926
 with ultrasound, 1977
 diffusion-weighted MRI of, 1223
 ectopic, 1110, 1912-1915, 1925-1926
 embryology of, 1912, 1913f, 1983-1984, 2088
 fractured, 1966, 1967f
 gastric lymphoma invasion of, 586f
 Gaucher's disease, 1647, 1945, 1946f
 gonadal fusion with, 1916, 2088-2089
 hemosiderosis, 1641-1644, 1945-1946, 1946f
 hypersplenism, 1909
 image-guided biopsy of, 1247, 1250, 1251f
 infarctions, 1941-1943, 1941b, 1941f-1942f
 acute abdomen from, 2267-2268, 2267f
 interventional radiology of, 1905-1911
 alcohol ablation in, 1908f
 catheter drainage, 1907-1908, 1907f
 image-guided biopsy, 1905-1907, 1906f
 complications with, 1906f
 patient preparation for, 1905
 radiofrequency ablation, 1908
 lesions, 1923-1964
 calcification sources and, 1924b
 cystic, 1931-1935, 1931f
 congenital, 1931-1932, 1932f-1933f
 differential diagnosis of, 1935
 hydatid disease, 1932-1935
 differential diagnosis of, 1979f
 hamartomas, 1928-1929, 1929f
 hemangiomas, 1926-1928, 1927f
 in infection and inflammatory disease, 1935-1941
 cat-scratch disease, 1938
 fungal, 1936-1937, 1936f
 Gamma-Gandy bodies, 1939, 1939f
 lymphomas or metastatic disease, 1939
 Mycobacterium avium complex, 1937-1938, 1937f
 nodular disease, 1935-1936
 P. jiroveci, 1938, 1938f
 pyogenic abscesses, 1939-1941, 1940f
 sarcoidosis, 1938, 1938f
 tuberculosis, 1937, 1937f
 inflammatory pseudotumor, 1930
 lymphangiomas, 1929-1930, 1930f
 malignant, 1947-1948
 angiosarcomas, 1947, 1948f
 lymphomas, 1948-1953
 metastatic, 1954-1957, 1955f-1958f
 secondary, 1948-1957
 nodular, 1935-1936, 1935b
 parenchymal patterns of involvement with, 1924b
 peliosis, 1930
 splenunculi, splenic ectopia, and splenosis, 1925-1926, 1926f

Spleen (Continued)
 neoplasms, radiofrequency ablation of, 1908
 nontraumatic rupture of, 1943, 1943b, 1943f
 normal anatomy of, 169, 170f
 in pancreatitis, 1944-1945
 parenchymal disease patterns of involvement, 1924b
 pediatric disorders of, 2228-2240
 benign neoplasms, 2233-2234
 congenital abnormalities
 polysplenia and asplenia, 2230, 2231f
 splenogonadal fusion, 2231
 splenules, 2229-2230, 2230f
 wandering spleen, 2231, 2231f-2232f
 cystic lesions, 2231-2233
 lymphatic malformations, 2232-2233, 2233f
 true cysts and pseudocysts, 2231-2232, 2232f
 Gaucher's disease, 2238
 histiocytic syndromes, 2238
 infarction, 2236, 2237f
 infections, 2235-2236, 2236f
 malignant neoplasms, 2233, 2234f
 normal histology and function of, 2228-2229, 2229f-2230f
 peliosis, 2238, 2238f
 sickle cell disease, 2236-2237, 2237f-2238f
 size of, 2229, 2230f
 trauma, 2234-2235, 2235f
 PET/CT of, 1207-1208, 1208f
 physiology of, 1897-1898
 polysplenia syndrome, 1918f, 2088
 rupture of, 1953-1954, 1969, 1969f
 shattered, 1967, 1968f
 sickle cell disease in, 1943-1947, 1944f
 size estimation of, 192, 193f, 1897, 1899
 pediatric, 2229
 splenomegaly and, 1943
 on ultrasound, 1900
 surgery, 1925-1926, 1972-1973
 Thorotrast effects on, 1946-1947
 torsion of, 2231, 2232f
 transarterial irradiation of, 1910
 trauma to, 1965-1973, 2284-2285, 2285f, 2286f, 2287f
 classification of, 1970-1971, 1971f
 clinical findings on, 1965
 complications with, 1972
 embolization in, 1908-1909, 1909f
 epidemiology of, 1965
 pathophysiology of, 1965-1966
 radiologic findings on, 1966-1972
 computed tomography, 1966-1971, 1967f
 ultrasound, 1971-1972
 splenectomy for, 1973
 treatment of, 1973
 ultrasound imaging of, 1971-1972, 1972f
 traversal of in percutaneous drainage, 1264
 ultrasonography on, 1181
 wandering, 1110, 1912-1915, 2088
 clinical findings on, 1912-1913
 diagnostic approach and therapy for, 1914-1915
 radiologic findings on, 1913-1914
 angiography, 1914
 computed tomography and magnetic resonance imaging, 1914, 1914f
 conventional radiography, 1913
 scintigraphic studies, 1913, 1913f
 ultrasound, 1913-1914, 1914f
 Splenectomy, immune function after, 1972
 Splenic arterial steal syndrome, 1910
 Splenic artery
 anatomy of, 1897, 1899-1900
 aneurysms, 1699-1700, 1699f

- Splenic artery (Continued)**
aneurysms and pseudoaneurysms, embolization of, 1909-1910
dissection, 158
embolization of
after trauma, 1908-1909, 1909f, 1971
in splenic arterial steal syndrome, 1910
in pancreatic blood supply, 1773
tortuous, 1777
- Splenic flexure, 184, 1104-1105**
- Splenic-portal fusion, 1916, 1925f, 2088-2089, 2231**
- Splenic vein**
aneurysms, 1701, 1701f
in pancreas blood supply, 1774
pancreas in relation to, 1799-1800
thrombosis, 1696-1697, 1697f
with trauma, 1972, 1972f
- Splenomegaly, 193f, 1943**
causes of diffuse, 1935b
classification of, 1935b
in common variable immunodeficiency, 763
differential diagnosis
congenital syndromes with, 1977b
hyperechoic pattern, 1978b
hypoechoic pattern, 1978b
with magnetic resonance imaging, 1979f
normal echogenicity, 1978b
in hemochromatosis, 1641
imaging of, 1923-1924
with lymphoma, 1952
platelet sequestration in, 1897-1898
in salmonellosis, 1017
in schistosomiasis, 1623
ultrasound on, 1181, 1181f
in viral hepatitis, 1637
- Splenopexy, 1915**
- Splenorenal ligament, 1984, 1996, 2004, 2019-2020, 2020f**
- Splenosis, 1923-1924, 1926f, 1972, 2235**
- Splenunculi. See Spleen; accessory**
- Spoke wheel pattern, 571, 572f, 1579**
- S pouches, 1139, 1139f**
- Squamocolumnar mucosal junction, 439-440**
- Squamous cell carcinoma**
colonic, 1080-1081, 1081f
esophageal, 366-374
advanced, 379-380
conditions associated with, 373-374
differential diagnosis of, 4631
early, 379
gastric metastases from, 574, 575f
lymphatic metastases with, 400, 400f, 574
gastric, 574, 575f, 598
hematogenous metastases of, 400-401
liver metastases, 1589
of the pharynx, 245-250, 248f, 251f
of the sinus, 251f
- Squamous papillomatosis, 301**
- Stack of coins appearance, in double-contrast studies, 45, 45f**
- Stalactites, 484**
- Standardized uptake value (SUV), 2301-2302**
- Staphylococcus, 1608-1609**
- Staphylococcus aureus, 322, 514-515**
- Starry sky appearance, 1637**
- Steady-state free precession (SSFP) technique, 713**
- Steatorrhea, 776, 778, 785, 1491-1492**
- Steatosis, hepatic, 1010, 1629-1636**
causes of, 1630f
chemotherapy-induced, 1639
clinical findings in, 1630
focal versus diffuse, 1189
imaging findings on, 1705f
- Steatosis, hepatic (Continued)**
magnetic resonance imaging of, 1189
pathologic findings in, 1630-1631, 1631f
radiologic findings on, 1631-1636
- Stenosis**
congenital esophageal, 425-426, 427f
duodenal, 2084, 2141-2143, 2143f
esophagus, 2084
gastric outlet obstruction from, 660f
hepatic artery, 1745, 1746f
hypertrophic pyloric, 611, 612f
mesenteric ischemia and, 837-838, 838f
pancreatic graft, 1877-1879, 1879f
portal vein, after liver transplantation, 1747, 1748f
small bowel, drug-induced, 762
stomal, after Roux-en-Y gastric bypass, 645f, 646
ultrasound on, 837-838
- Steroids, 468, 513**
- Stevens-Johnson syndrome, 338-339, 2138**
- Stierlin sign, 1019**
- Stitch granulomas, 1058-1059, 1059f**
- Stomach. See also Gastric outlet obstruction**
abnormal extrinsic masses in, 615, 616f
amyloidosis in, 627, 627f
anatomy of, 170, 170f, 272-273, 274f
anterior wall examination, 277f
antral webs and diaphragms in, 610, 611f, 2084, 2085f
gastric narrowing from, 659f
arterial anatomy of gut, 114-115
barium studies of, 272-273, 277f
benign gastric emphysema in, 627, 627f
benign tumors of, 523-545
mucosal lesions, 523-530
submucosal lesions, 530-542, 658f
bezoars in, 622f
carcinoma of
esophageal metastases from, 394-395, 396f-397f
recurrence of after gastrectomy, 641
secondary achalasia from, 396-399, 399f-400f
caustic ingestion and, 515-516, 516f-517f
differential diagnosis of, 657
dilation of without gastric outlet obstruction, 614-615, 615f
diverticula in, 607-610, 607f
duplication of, 2084
embryology of, 2084-2085, 2084f
emphysematous gastritis in, 514-515
eosinophilic gastroenteritis in, 513-514
esophageal squamous cell metastases to, 372, 374f
familial adenomatous polyposis syndrome in, 1091
fat digestion and absorption in, 774
fistulas in, 624-626, 624f
foreign bodies in, 620
gallstones in, 621
gastric narrowing, differential diagnosis of, 659f
GISTs in, 799-800
hematomas in, 620-621
hourglass, 476-477, 477f, 512
image-guided biopsy of, 1246f
inflammatory conditions of, 496-522
antral gastritis, 499-500
atrophic gastritis, 504-506
differential diagnosis of, 504
erosive gastritis, 496-499, 498f-499f
granulomatous, 506-512
H. pylori gastritis, 500-503
hypertrophic gastritis, 503, 503f
Ménétrier's disease, 504, 505f
- Stomach (Continued)**
intussusceptions, 624
lymphoid hyperplasia in, 501-502
lymphomas, 400-401, 401f
malignancies, magnetic resonance imaging of, 89-93, 90f
mesenteric attachments of, 578f
neoplasms, surgery for, 631
normal walls of, 69-70, 70f
organoaxial gastric volvulus, 444
pancreatic diseases affecting, 618-621
paraesophageal herniation of, 445-446, 445f-446f
partial gastrectomy of, 275, 277f
pediatric disorders of, 2181-2187
acquired, 2146-2155
distention, 2154-2155, 2154f
foreign bodies, 2148-2149, 2151f
gastric perforations, 2146-2147
hematomas, 2146, 2150f
inflammatory disorders, 2152-2154, 2153f-2154f
neoplasms, 2150-2152, 2151f-2152f
peptic ulcer disease, 2152
pyloric stenosis, 2147-2148, 2147f-2150f
congenital, 2141-2146
antral mucosal diaphragm, 2141, 2142f
duodenal atresia and stenosis, 2141-2143, 2142f-2143f
duplication cysts, 2143-2144, 2144f
malrotation, 2144-2146, 2145f-2146f
microgastria, 2141, 2142f
pyloric and antral atresias, 2141
perforations of, 626-627
PET/CT of, 100-102
portal hypertensive gastropathy, 607, 607f
postoperative, 630-636
afferent loop syndrome in, 638
after bariatric surgery, 641-654
after gastric resection, 630, 633-639
after neoplasm resection, 631
bile reflux and chronic remnant gastritis in, 638-639, 639f
complications in, 640-641
diagnostic evaluation of, 630-631
dumping syndrome in, 637
identification of anatomy in, 634-635
neoplasms growth in, 639
stomal and anastomotic ulceration in, 637
in protein digestion and absorption, 774
radiation injuries in, 516-517
thickened folds in, differential diagnosis of, 659f
traversal of in percutaneous drainage, 1268
varices, 603-606
volvulus of, 622-623, 623f
- Stool antigen tests, 501**
- Strasberg classification system, 1399**
- Streptococcus, 322, 1941**
- Stress, 468, 496**
- Striae pattern, in double-contrast studies, 42, 43f**
- Strictureplasty, 1007**
- Strictures**
after colonic interposition, 455-458, 458f
after esophagogastrectomy, 454-455
biliary tract, 1306-1311, 1307h, 1308f-1309f
after liver transplantation, 1750-1752, 1751f
from benign ductal diseases, 1432
differential diagnosis of, 1463f
liver abscesses from, 1608-1609
magnetic resonance
cholangiopancreatography on, 1532-1534, 1533f
from pancreatitis, 1516f
postoperative, 1311-1320, 1315f

Strictures (*Continued*)

- after biliary-enteric anastomosis, 1453-1456
- after laparoscopic cholecystectomy, 1449-1452, 1450f
- in primary sclerosing cholangitis, 1428
- with primary sclerosing cholangitis, 1432
- bowel, with necrotizing enterocolitis, 2109-2106, 2105f
- from chronic gastroesophageal reflux, 454-455
- colonic
 - in colonic ischemia, 1115
 - obstruction from, 1110
 - risk factors for, 1110b
 - in ulcerative colitis, 992
- in Crohn's disease, 1002
- on barium studies, 730-731
- duodenal, 508-509, 509f
- surgical management of, 1007
- esophageal
 - from alkaline reflux esophagitis, 340-341, 341f
 - in Barrett's esophagus, 305-307, 306f, 308f
 - benign, surgery for, 451-453
 - with *Candida* esophagitis, 314, 316f
 - from caustic esophagitis, 331-332, 333f-334f, 367, 373
 - from caustic ingestion, 2134-2135
 - differential diagnosis of, 464t
 - from drug-induced esophagitis, 327
 - with eosinophilic esophagitis, 334
 - with epidermolysis bullosa dystrophica, 338, 338f
 - foreign body impactions from, 419
 - lye, 455
 - from metastatic disease, 396
 - mid-esophageal, 308f
 - from nasogastric intubation, 339-340, 341f
 - with pemphigoid, 338
 - in pseudodiverticulosis, 345
 - in radiation esophagitis, 329-330, 330f
 - in reflux esophagitis, 296-300, 299f
 - squamous cell carcinoma associated with, 373, 374f
 - surgical treatment of, 453
- gastric, after sleeve gastrectomy, 652-654, 653f
- peptic, 283-284
- caused by Zollinger-Ellison syndrome, 300, 304f
- with esophageal pseudodiverticulosis, 297-298, 304f
- with hiatal hernia, 298-300
- Schatzki rings and, 300
- with scleroderma, 288-289, 289f
- radiation-induced, 804
- ringlike peptic, 443
- String of pearls sign, 1335f
- Stromal tumors
 - colonic, 1079-1080
 - gastrointestinal
 - Choi criteria on response to treatment in, 2299f, 2301t, 2302f
 - on computed tomography angiography, 689-690
 - pediatric, 2130-2131, 2131f
- Strongyloides stercoralis*, 513, 758, 2153
- See also Strongyloidiasis
- Strongyloidiasis, 513, 514f
- colonic, 1020
- duodenitis from, 519
- megaduodenum in, 661t
- small bowel changes in, 758, 758f, 872t-873t
- thickened duodenal folds from, 661t
- Subcapsular fluid, 2032
- Subdiaphragmatic space, 2002, 2002f
- Subhepatic space, 2008-2009

- Submucosal lesions, gastroduodenal, 530-542
- Brunner gland hyperplasias, 539-541, 540f
- differential diagnosis of, 658t
- duplication cysts, 541-542, 543f
- ectopic pancreatic rests, 538-539, 539f
- gastrointestinal stromal tumors, 532f-533f
- glomus tumors, 536-537, 536f
- granular cell tumors, 537-538, 538f
- hemangiomas, 536
- inflammatory fibroid polyps, 538, 538f
- leiomyoblastomas, 534-535, 534f
- lipomas, 535-536, 535f
- lymphangiomas, 536
- neural tumors, 537, 537f
- Submucosal masses, 47, 50f
- Subperitoneal fat density, 75-76
- Subperitoneal space, 2015-2021
- duodenocolic ligament, 2002-2004
- gastrocolic ligament and greater omentum, 2002
- gastrohepatic ligament, 1995f, 2002
- gastrosplenic ligament, 2002-2004
- hepatoduodenal ligament, 2002
- small bowel mesentery, 1997f
- splenorenal ligament, 2004
- spread of disease through, 1986, 1987t, 2015-2021
- transverse mesocolon, 2002
- Subperitoneum, 1994-2000. See also Peritoneal cavity
- Subphrenic abscesses, 1276, 2000
- Subphrenic space, 2002, 2009, 2013f, 2027
- Subsegmentectomy, 1721
- Sucralate, 469
- Sulfasalazine, 996
- Sulfur hexafluoride, 1173
- Sunitinib therapy, 1236, 1236f
- Superior mesenteric artery (SMA)
 - acute mesenteric ischemia in, 828-829, 831f-832f
 - computer tomography visualization of, 828
 - dissection of, 842-843, 843f-844f
 - in pancreatic blood supply, 1773
 - SMA syndrome, 2154
 - superior mesenteric ganglia and plexus around, 1776
- Superior mesenteric ganglia and plexus, 1776
- Superior mesenteric root syndrome, 613-614, 613f-614f, 661t
- Superior mesenteric vein (SMV)
 - in pancreas drainage, 1774
 - thrombosis, 1696, 1697f
- Superior vena cava, 1656, 1681f
- Superparamagnetic iron oxides (SPIOs), 710-711
- with benign liver tumors, 1529-1530, 1534
- in liver metastases, 1599, 1601f
- in MRI on hepatocellular carcinomas, 1569
- Suprahepatic space, spread of disease through, 2008-2009
- Supramesocolic compartment, 2008, 2001f, 2008-2009
- Suprapancreatic lymphatic chain, 1775
- Susceptibility artifacts, 1164, 1185f, 1220
- Swallowing. See also Dysphagia
 - adaptation, compensation, and decompensations in, 225f, 227-228, 227f-229f
 - aging and, 230-231
 - aspiration prevention in, 226-227
 - criopharyngeal opening in, 225-226
 - epiglottic tilt in, 225
 - esophageal distention and, 230
 - esophageal peristalsis in, 279, 280f
 - functional aspects of, 222-226, 223f-224f
 - functional components of, 222-226
 - infections affecting, 201f
 - laryngeal dynamics and hyoid elevation in, 224-225
 - neurophysiologic control of, 222

Swallowing (*Continued*)

- oropharyngeal phase of, 222-223
 - pediatric disorders in, 2125, 2128t
 - radiation therapy and functional changes in, 230
 - reflexes related to, 230
 - Zenker's diverticulum in, 228-230, 229f, 239-241, 240f
 - Swiss cheese spleen, 1930
 - Synovial sarcomas, 408
 - Syphilis
 - antral narrowing in, 560
 - colonic involvement of, 1113
 - differentiated from gastric lymphomas, 586
 - gastric, 512, 512f
 - gastric narrowing from, 659t
 - gastric outlet obstruction from, 613
 - multiple duodenal ulcers with, 484
 - Systemic lupus erythematosus, 776b, 840, 841f
 - colonic involvement of, 1124
 - pancreatitis with, 1812
 - with primary biliary cirrhosis, 1649-1650
- T**
- T1-weighted MRI. See also Magnetic resonance imaging (MRI)
 - in colonography, 928-929, 929f
 - in magnetic resonance enterography, 712
 - sequences in, 1188
 - T2 shine-through, 1230
 - T2-weighted MRI. See also Magnetic resonance imaging (MRI)
 - on Crohn's disease, 734-735
 - in magnetic resonance enterography, 712
 - sequences in, 1183-1184
 - TACE. See Transarterial chemoembolization (TACE)
 - Tagging agents
 - for computed tomography colonography, 907-908
 - in magnetic resonance colonography, 932, 932f
 - polyp coating properties of, 912
 - Takayasu's arteritis, 838-839
 - Tamoxifen, peliosis hepatis associated with, 1690
 - Tapering, in double-contrast studies, 52, 53f
 - Tapeworms, 759, 1440, 1614-1621
 - Target lesions. See Bull's-eye lesions
 - Target sign, in Crohn's disease, 687-688
 - TALUS. See Transabdominal ultrasound (TAUS)
 - Technetium 99m iminodiacetic acid, 1287f
 - Technetium 99m-labeled heat-damaged red blood cell scintigraphy (^{99m}Tc-HDRBC), 1913, 1916f, 1925
 - Technetium 99m-labeled red blood cell scans, 841-842, 2279
 - in benign liver tumor imaging, 1529
 - on gastrointestinal hemorrhage, 687f, 691-692
 - Technetium-tagged iminodiacetic acid (TIDA)
 - in acute cholecystitis imaging, 1355
 - Technetium Tc 99m HMPAO-labeled white blood cells, 1258
 - Technetium Tc 99m pertechnetate scintigraphy
 - for esophageal duplication cysts, 362-363
 - on gastrointestinal hemorrhage, 691-692
 - on Meckel's diverticulum, 861
 - no Meckel's diverticulum, 2159, 2161f
 - Technetium Tc 99m sulfur colloid scans, 691-692, 1869, 1899f, 1972
 - Telangiectasia, GI hemangiomas associated with, 536
 - Telangiectatic adenomas, 1187-1189
 - Telangiectatic focal nodular hyperplasia, 1187-1189, 1342-1343
 - Teratomas, 2049-2050, 2150
 - Tertiary contractions. See Nonperistaltic contractions (NPCs)

- Testes, Sertoli cell tumors of, 1093
 Testicular carcinoma, 548, 782
 Tethering of mucosal folds, in double-contrast studies, 45, 46f
 Tetracycline, 326-327, 1908
 Tetralogy of Fallot, 2114
 THADs. *See* Transient hepatic attenuation differences (THADs)
 Thalassemia, 1946f
 Theraspheres, 1513-1514
 Thermal ablation, 1506-1508
 Thiabendazole, 1432
 THIDs. *See* Transient hepatic intensity differences (THIDs)
 Thoracic duct, 449
 Thoracoabdominal wall defects, 1151f
 Thorax, gallstone migration to, 1453
 Thorotrast, 1584-1586, 1946-1947
 Thromboembolisms, in image-guided biopsy, 1240-1241, 1240f
 Thrombolytic agents, 125-126, 125f, 127f, 127f
 Thrombosis
 with acute pancreatitis, 1195
 with Crohn's disease, 746-748
 graft, after pancreas transplantation, 1875-1877, 1877f
 hepatic artery, 1744-1745, 1745f
 inferior mesenteric vein, 1696-1697
 portal vein, 1690-1695
 after liver transplantation, 1747, 1748f
 causes of, 1691b
 clinical findings on, 1691
 pathophysiology of, 1691-1692
 radiologic findings on, 1692-1694, 1692f-1694f
 THADs and THIDs from, 1680f
 treatment of, 1695
 splenic vein, 1696-1697, 1697f
 superior mesenteric vein, 1696, 1697f
 Thumbprinting
 in caustic colitis, 1022-1023
 in colonic ischemia, 1115, 1115f
 in double-contrast studies, 53, 53f
 Thyroid
 cancer
 Cowden's syndrome associated with, 794
 with familial adenomatous polyposis syndrome, 1092
 gastric metastases from, 548
 Cowden's disease and, 1095
 Tissue harmonic imaging, 1172, 1480, 1813
 Tissue plasminogen activator (tPA), 1271, 1271f
 Tobacco use, 366, 468, 985
 Todani type V choledochal malformation. *See* Caroli's disease; Choledochal malformations
 Tokyo Guidelines, 1354
 Tongue
 motor function of, 215f
 squamous cell carcinoma of, 247
 in swallowing, 222-223
 Tonsillar fossa, 212f
 Tonsils, 243-244, 247, 249f
Torulopsis glabrata, 322
 Total mesorectal excision (TME), 1051, 1053, 1062
 Total parenteral nutrition, 858, 1007, 1352
 Toxic megacolon, 185-186, 186f
 differential diagnosis of, 1148t
 with inflammatory bowel disease, 1009, 1009f
 pathologic findings in, 1009
 pediatric, 2167
 in pseudomembranous colitis, 1024
 radiologic findings in, 1009
 Toxic shock syndrome, 1637
 Toxin-induced disorders, liver, 1639-1640
 Toxoplasmosis, 512
 Trachea
 agenesis of, 2126f
 esophageal cancer invasion of, 381-382, 383f
 vascular rings of, 2125-2127, 2128f-2129f
 Tracheoesophageal fistula, 2083
 Transabdominal ultrasound (TAUS), 56-66
 abnormal bowel findings in, 56-58
 alteration of gut signature in, 62
 altered blood flow in, 57
 on Crohn's disease, 1004-1006
 extramural and mesenteric changes in, 57-58
 graded compression in, 59
 of infectious enterocolitides, 64-65
 of ischemic bowel, 64, 64f
 normal bowel features and, 56
 of peritoneal, mesenteric, omental abnormalities, 59-65
 plasticity, mobility, peristalsis in, 56-57
 ultrasound features of normal bowel in, 56
 ultrasound findings of abnormal bowel in, 56-58
 Transarterial chemoembolization (TACE), 1510-1513, 1512f, 1513
 Transarterial radioembolization, 1513-1515
 Transcholecystic cholangiography, 1297
 Transgluteal drainage of abscesses, 1274, 1275f
 Transhepatic cholangioscopy, 1398
 Transient hepatic attenuation differences (THADs), 1532-1533
 benign causes of, 1679f
 differential diagnosis of, 1762f
 from hemangioma, 1679f
 malignant causes of, 1680f-1681f
 with mass lesions, 1676-1678
 not associated with mass lesions, 1678-1680
 origin of, 1678f
 Transient hepatic intensity differences (THIDs), 1676-1680
 benign causes of, 1679f
 from hemangioma, 1679f
 malignant causes of, 1680f
 with mass lesions, 1676-1678
 not associated with mass lesions, 1678-1680
 origin of, 1678f
 Transitional cell carcinomas, 1081, 1199, 1199f
 Transition zone, colon, 2167
 Transjugular intrahepatic portosystemic shunts (TIPS), 416f, 418-419, 1503-1505
 Budd-Chiari syndrome and, 1687-1688
 for cirrhosis-related portal hypertension, 1670, 1671f
 complications with, 1504, 1505f
 contraindications for, 1503
 follow-up and revision of, 1505
 malfunction differential diagnosis, 1761f
 portal hypertension and, 1503
 rationale and indications for, 1503
 results from, 1504
 technique for, 1503-1504
 variceal bleeding with, 1668
 for varices, 460
 Transjugular liver biopsies, 1501
 Transmesenteric hernias, 2058-2059, 2060f
 Transmesosigmoid hernias, 2058
 Transomental hernias, 2059, 2060f
 Transplantation. *See also* Graft-versus-host disease
 diverticulitis and, 938-939
 liver, 1737-1755
 allograft rejection after, 1432
 HCC as indication for, 1205
 HCC diagnosis and, 1191-1192
 hepatic artery ultrasound on, 1480
 for hepatopulmonary syndrome, 433
 pancreas, 1872-1888
 periportal low density in, 1710
 splenic arterial steal syndrome after, 1910
 pancreas, 1872-1888
 anatomy in, 1872-1874, 1873f, 1875f
 arterial supply to, 1872-1873, 1873f
 complications with, 1874-1886
 bowel, 1882-1884, 1885f-1886f
 graft pancreatitis, 1881-1882, 1884f
 graft rejection, 1880-1881, 1881f-1882f
 graft stenosis, 1877-1879, 1879f
 graft thrombosis, 1875-1877, 1877f-1879f
 hemorrhage, 1882
 intra-abdominal fluid collections, 1884-1885, 1886f-1887f
 lymphoproliferative disease, 1885-1886, 1887f
 pseudocystic aneurysms and fistulas, 1879-1880, 1880f-1881f
 vascular, 1875-1880
 exocrine secretions to, 1873-1874
 postoperative complications with, 1874-1886
 procurement for, 1872-1874
 radiographic findings on, normal, 1874
 types of, 1872
 venous drainage to, 1873
 small bowel, 856, 859f
 rejection of, 859, 859f
 Transrectal ultrasonography (TRUS), 1004, 1054-1056, 1055f, 1065
 Transudates, 2025
 Transvaginal drainage of abscesses, 1274
 Transversalis fascia, 1966
 Transverse colon, 184, 1773f, 1985f
 Transverse mesocolon, 1996, 2000f
 disease spread through, 2016, 2017f
 embryology of, 1984, 2008
 inframesocolic compartment in, 2000
 supramesocolic compartment in, 2000, 2001f
 Trapezoid scans, 1170, 1170f-1171f
 See also Ultrasound
 Trauma
 abdominal, 2282-2294
 computed tomography on, 2283
 bowel, 2287-2292
 image interpretation in, 2284
 imaging techniques and interpretation with, 2283-2284
 kidneys, 2285-2287, 2287f, 2288f
 liver and spleen, 2284-2285, 2285f, 2286f, 2287f
 mesentery, 2290, 2291f-2292f
 pancreas, 2285, 2286f, 2287f
 diagnostic techniques for, 2283
 mechanisms of injury in, 2282-2283
 biliary tract, 1442
 FAST protocol with, 1173
 gallbladder, 1456-1457
 hernias from, 2068-2069, 2069f
 liver, 1706-1717
 abscesses from, 1608
 blunt, 1707, 1709f
 classification of, 1712f
 classification of, 1707, 1707f, 1712f
 clinical findings on, 1706
 complications with, 1716-1717
 biliary tract, 1717
 bleeding, 1716
 infection, 1716
 epidemiology of, 1706
 iatrogenic injuries, 1708
 pathophysiology of, 1707-1708

Trauma (Continued)

- penetrating injuries, 1707, 1708f-1709f
- radiologic findings on, 1708-1716
 - angiography, 1715-1716
 - computed tomography, 1708-1712, 1708f-1711f, 1713f
 - magnetic resonance imaging, 1715, 1715f
 - plain radiographs, 1716
 - scintigraphy, 1714-1715, 1714f
 - ultrasound, 1712-1715, 1714f
- spontaneous rupture, 1721-1722
- surgery types for, 1722f
- treatment of, 1716
- mesenteric, 2048
- omentum, 2050
- pancreas, 1856-1860
 - clinical findings on, 1857
 - epidemiology and pathophysiology of, 1856-1857
 - pediatric, 2216-2219, 2217f-2218f
 - radiologic findings on, 1857-1860
 - computed tomography, 1857-1858, 1857f-1859f, 1858b
 - endoscopic retrograde pancreatography, 1859-1860
 - gastrointestinal studies, 1860
 - magnetic resonance pancreatography, 1859, 1859f
 - ultrasound, 1859
 - surgical classification of, 1857, 1857b
 - treatment of, 1860
- small bowel vascular disorders due to, 843, 844f
- spleen, 1965-1973
 - classification of, 1970-1971, 1971f
 - clinical findings on, 1965
 - complications with, 1972
 - embolization in, 1908-1909, 1909f
 - epidemiology of, 1965
 - pathophysiology of, 1965-1966
 - pediatric, 2234-2235
 - radiologic findings on, 1966-1972
 - computed tomography, 1966-1971, 1967f
 - ultrasound, 1971-1972
 - splenectomy for, 1973
 - splenosis after, 1925-1926, 1926f
 - treatment of, 1973
 - ultrasound imaging of, 1971, 1971-1972, 1972f
- Trematodes, 759
- Treponema pallidum*, 512. *See also* Syphilis
- Triad syndrome. *See* Prune-belly syndrome
- Triangular cord sign, 2185-2186, 2186f
- Trichobezoars, 619, 2148, 2151f
- Trichuriasis, 1020-1021
- Tricuspid regurgitation, 1688
- Triglycerides, 774
- Trisegmentectomy, 1721-1722, 1723f
- Trisomy 21, 1151t
- Trocar technique of percutaneous catheter drainage, 1261-1263, 1261f-1262f, 1261t
- Tropheryma whippelii*, 763, 2048. *See also* Whipple's disease
- Tropical sprue, 764f, 766, 872t
- Truncal vagotomy, 632
- Trypanosoma cruzi*, 289, 614. *See also* Chagas' disease
- Trypanosomiasis, 760
- Tuberculosis (Continued)
 - esophagitis with, 320-322, 322f-323f, 462t
 - gastric narrowing from, 659t
 - gastric outlet obstruction from, 613
 - gastroduodenal involvement in, 511
 - hypertrophic, 760
 - intestinal, 65, 65f
 - liver involvement in, 1625
 - magnetic resonance enterography on, 721
 - multiple duodenal ulcers with, 484
 - Mycobacterium avium-intracellulare* complex, 767-768, 767f
 - omental, 2050
 - peliosis hepatis with, 1690
 - peritonitis in, 2044, 2047-2048
 - pyelonephritis in, 626
 - small bowel, 760-761, 760f, 818-819, 873t
 - splenic infection with, 1937, 1937f
 - thickened gastric folds in, 659t
 - ulcerative, 760
 - ulcerohypertrophic, 760

Tuberculosis (Continued)

- Tubo-ovarian abscesses, 1113
- Tubular carcinomas, 548
- Tufts, 1898
- Tumor, node, metastases (TNM) classification system, 1047-1049, 1048t-1049t, 1049f, 1055
- for gallbladder carcinomas, 1402-1403, 1403b
- of pancreatic adenocarcinomas, 1838
- Tumors. *See also* specific organs and types of tumors
 - abscess of, 1276
 - benign esophageal, 350-365
 - mucosal lesions, 350-353
 - submucosal lesions, 353-363, 658t
 - benign gastroduodenal, 523-545
 - mucosal lesions, 523-530
 - submucosal lesions, 530-542, 658t
 - benign pharyngeal, 244
 - gastric masses, surgery for, 632
 - gastroduodenal carcinoid, 408
 - head and neck, 367
 - liver
 - benign, 1528-1560
 - blood supply to, CT and, 1162, 1163f
 - malignant pharyngeal, 244-252
 - perfusion computed tomography on, 1232-1233
 - response to therapy, 2295-2305
 - Choi criteria on response to treatment in, 2299f, 2300, 2301t, 2302f
 - in colorectal cancer, 105-107
 - diffusion-weighted magnetic resonance imaging on, 1225, 2304
 - EASL criteria on, 2299-2300
 - MASS criteria on, 2300, 2301t, 2302f
 - monitoring with dynamic contrast-enhanced MRI, 2304
 - mRECIST criteria on, 2300, 2301f
 - PERCIST criteria on, 2301-2302, 2302t, 2303f
 - RECIST 1.0 criteria on, 2295, 2296t-2297t
 - RECIST 1.1 criteria on, 2295-2299, 2297t, 2299f
 - WHO classification of, 2295, 2296f
 - risk stratification and staging of, 1233
 - small bowel benign, 789-795
 - villous gastrointestinal, 528-530, 529f-530f
- Turcot syndrome, 1092
- Turner's syndrome, 1076, 2160
- Tylosis, 367, 373-374
- Typhlitis, 765, 765f, 1023-1024, 1023f
 - acute abdomen from, 2265f, 2265f
 - differentiated from appendicitis, 971, 974-975
 - pediatric, 2170-2172
- Typhoid fever, 761
- Tyrosine kinase, 1080
- Tyrosine kinase inhibitors, 800
- Tyrosinemia, 2212-2213, 2213f

U

- Ulcerated masses, double-contrast studies of, 47, 49f
- Ulcerative colitis, 984-997
 - angiography of, 121
 - of the appendix, 972, 974f
 - backwash ileitis in, 990, 992f
 - barium enema findings on, 987-992, 987b
 - clinical findings on, 986
 - collar button ulcers in, 988, 989f
 - colon diameter in, 987
 - colonic fecal residue in, 986-987, 986f
 - computed tomography on, 992
 - differential diagnosis of, 1012-1013, 1012t
 - differentiated from Crohn's disease, 1005
 - distribution of, 992
 - endoscopic findings on, 986
 - epidemiology of, 984-985, 985b
 - granular pattern in, 987-988, 988f
 - historical perspective on, 984
 - on magnetic resonance imaging, 993, 995f
 - magnetic resonance imaging of, 86
 - medical management of, 996
 - mucosal abnormalities in, 987, 987f, 992, 994f
 - mucosal stippling in, 988, 989f
 - mural thickness in, 987
 - pathogenesis and causative factors of, 985-986
 - polyps in, 988-990
 - prognosis for, 997
 - radiologic findings on, 986-987, 986f
 - rectal valve abnormalities in, 992
 - scintigraphy on, 992-993, 995-996, 995f
 - shigellosis in, 1018
 - squamous cell carcinoma with, 1080-1081
 - strictures in, 992
 - surgery for, 996-997
 - therapy for, 996-997
 - widened presacral space in, 984, 993f
- Ulcer collars, 471-473
- Ulcer wounds, 471-473
- Ulcers
 - aphthoid, in Crohn's disease, 507-508, 507f, 509f, 510
 - collar button, 51, 52f, 988, 989f
 - colonic, 1021, 1115
 - in cytomegalovirus esophagitis, 320f
 - Dragstedt, 468
 - duodenal, 540
 - esophageal
 - in Behçet's disease, 343, 344f
 - in caustic esophagitis, 332, 332f-333f
 - with Crohn's disease, 336, 336f
 - differential diagnosis of, 462t
 - from drug-induced esophagitis, 326-328, 329f
 - from foreign body ingestion, 2134
 - from nasogastric intubation, 340, 340f
 - esophageal pseudodiverticula distinguished from, 546
 - gastric, 469-479
 - after Roux-en-Y gastric bypass, 644-645
 - differential diagnosis of, 657t
 - gastrocolic and duodenocolic fistulas caused by, 624, 624f
 - postoperative stomal and anastomotic, 637
 - gastric carcinoma, 547
 - geriatric, 471
 - with GISTs, 531
 - in herpes esophagitis, 317, 319f
 - in HIV esophagitis, 319-320, 321f
 - niche, 51, 51f
 - peptic, 467-495
 - anterior wall, 473, 474f-475f
 - atrial narrowing from, 360
 - benign versus malignant, 477-479, 479f-480f
 - clinical findings in, 468-469
 - complications with, 487-491

Ulcers (Continued)

- fistulas, 489-491, 491f
 - obstructions, 487, 488f
 - perforations, 487-491, 489f-490f
 - upper GI bleeding, 487, 487f
 - differential diagnosis of, 484-486
 - duodenal, 479-483
 - epidemiology and pathogenesis of, 467-468
 - gastric, 469-479
 - gastric outlet obstruction caused by, 611-612, 612f
 - gastrocolic and duodenocolic fistulas with, 624
 - greater curvature, 471-473, 473f
 - healing and scarring of, 474-477, 475f-478f
 - lesser curvature, 471-472, 472f
 - linear, 474-475, 475f
 - location of, 471, 472f-473f
 - morphologic features of, 471-473
 - multiple, 474
 - pediatric, 2152
 - perforated, pneumoperitoneum caused by, 626-627
 - posterior wall, 473, 473f-474f
 - radiographic findings on, 469-484
 - shapes of, 470, 470f
 - size of, 470-471, 471f
 - superior mesenteric root syndrome caused by, 614
 - treatment approaches to, 486-487
 - treatment of, 469
 - in Zollinger-Ellison syndrome, 491-492
 - rectal, in solitary rectal ulcer syndrome, 899
 - riding, 443-444, 444f
 - small bowel, 678f, 762
- Ultrasound.** See also Transabdominal ultrasound (TAUS)
- 3D, 1172
 - 4D, 1172
 - of abdominal abscesses, 1255, 1255f, 1256f
 - acute cholecystitis imaging in, 1355-1359, 1358f
 - acalculous, 1361-1362, 1361f-1362f
 - gangrenous, 1363f
 - appendix imaging, 966-967, 966f-967f
 - on ascites, 2028-2029, 2028f
 - basic physics of, 1169-1171
 - on biliary postoperative complications, 1450-1451
 - biliary tract, 1288-1290
 - of biliary atresia, 2184-2185, 2184f-2186f
 - on cholangiocarcinomas, 1411-1413, 1413f
 - normal anatomy in, 1289
 - on primary sclerosing cholangitis, 1429-1431, 1429f
 - technique in, 1289, 1289f
 - bowel
 - features of abnormal, 56-58
 - features of normal, 61-63
 - peritoneal, mesenteric, omental abnormalities in, 59-65
 - strategic place for, 65
 - technique for, 58-59
 - of choledocholithiasis, 1371, 1371f
 - cholelithiasis on, 1349-1350
 - colon
 - on intussusceptions, 1105, 1109
 - on ischemia, 1116
 - mural thickening in, 1151t
 - on obstructions, 1104
 - on Crohn's disease, 733, 733f, 995b, 1006f
 - curvilinear arrays in, 1170
 - on diverticulitis, 940, 940f
 - Doppler, 1172-1173

Ultrasound (Continued)

- color, 1172f
- on gallstones, 1349
- of hepatic vasculature, 1177, 1177f
- of the liver, 1176-1177
- duplex, on chronic mesenteric ischemia, 837-838
- on echinococcal disease, 1934
- endoscopic
 - in esophageal cancer staging, 380-381, 383-385
 - of esophageal leiomyosarcomas, 405
 - of gastric carcinoma, 562-565, 563f
 - of gastric carcinomas, 562-565, 563f-564f
 - in gastric lymphoma staging, 585-586
 - of gastroduodenal lymphomas, 585-586
 - linear array, 1802
 - of lymph node metastasis, 387f
 - normal esophageal, 386f
 - pancreas
 - on ductal adenocarcinomas, 1842
 - on pancreatitis, chronic, 1825
 - surgery and, 1863
 - on pancreas divisum, 1802
 - staging criteria in, 384-385
 - technique, 383
 - esophageal cancer staging with, 385-389
- gallbladder, 1281, 1283-1284, 1285f
 - biliary sludge in, 1352, 1354f, 1356f
 - on carcinomas, 1407f
 - in differential diagnosis, 1461
 - hyperechoic foci in, 1462t
 - nonvisualization in, 1462t
 - shadowing and nonshadowing reflectors, 1461t-1462t
 - structures that mimic, 1462t
 - on gallstones, 1349-1350, 1350f
 - on gastroesophageal reflux disease, 2131
 - hemangiomas on, 1186-1187
 - historical perspective on, 1169
 - hydrocolonic, 1005
 - in image-guided percutaneous tissue acquisition, 1242, 1249-1250
 - on imperforate anus, 2115-2116, 2116f
 - intraoperative, 1718, 1719f
 - linear arrays in, 1170, 1170f
 - liver, 1477-1481
 - on alcoholic hepatitis, 1638-1639
 - on amebic abscesses, 1612, 1614f
 - on angiosarcomas, 1586
 - artifacts in, 1478
 - on bacterial (pyogenic) abscesses, 1609-1610, 1609f
 - of benign liver tumors, 1529
 - on Budd-Chiari syndrome, 1682-1683, 1684f
 - on cirrhosis, 1659-1660, 1661f-1662f, 1663-1668
 - contrast agents in, 1480-1481
 - on cystadenomas and cystadenocarcinomas, 1583, 1583f
 - differential diagnosis with, 1759
 - Doppler, 1479-1480, 1480f
 - on echinococcal disease, 1616-1618
 - echogenicity of normal, 1478, 1478f
 - evaluation techniques for, 1477
 - on fibrolamellar carcinoma, 1575, 1573f
 - on glycogen storage disease, 1644-1645
 - of hemangiomas, 1531-1532, 1532f
 - on hemochromatosis, 1642
 - on hepatic congestion, 1688-1689, 1689f
 - on hepatitis, 1637-1638, 1637f
 - on hepatoblastomas, 1578
 - on hepatocellular adenomas, 1544, 1544f
 - on hepatocellular carcinomas, 1564, 1563f
 - on infantile hemangioendothelioma, 1553

Ultrasound (Continued)

- on intrahepatic cholangiocarcinomas, 1580
- intraoperative, 1478-1479, 1479f
- on metastases, 1592-1595, 1595f, 1596b
- bull's-eye pattern in, 1593
- calcified, 1594
- cystic, 1593-1594
- diffuse infiltration of, 1594-1595
- hyperechoic, 1593
- hypoechoic, 1593
- of nodular regenerative hyperplasia, 1549
- on portal vein thrombosis, 1692, 1692f
- of radiation-induced disease, 1640
- on schistosomiasis, 1623-1625, 1625f
- on steatosis, 1631-1633, 1632f
- tissue harmonic imaging, 1480
- on undifferentiated (embryonal) sarcomas, 1587
- omentum, 2049
- pancreas, 1776-1778
 - on annular pancreas, 1805
 - endoscopic, 1778
 - examination techniques, 1776, 1777f
 - intraoperative, 1778, 1863, 1864f
 - normal findings in, 1776-1778
 - on pancreas divisum, 1802
 - on pancreatitis, acute, 1812-1813
 - on pancreatitis, chronic, 1824-1825
 - pediatric, 2216, 2217f
 - post-transplant, 1874, 1875f
 - on trauma, 1859
- on portal hypertension, 1665-1668, 1665f-1667f
- real-time, 1171-1172
- recent developments in, 1171-1172
- on small bowel obstructions, 811
- of solid abdominal viscera, 1169-1182
 - Doppler, 1172-1173, 1172f
 - gallbladder and biliary tract, 1178-1180, 1179f
 - liver, 1173-1178, 1178f
 - pancreas, 1180-1181, 1180f-1181f
 - spleen, 1181, 1181f
- specular versus nonspecular echoes in, 1171, 1171f
- spleen
 - on accessory spleens, 1915, 1925
 - anatomy in, 1900-1901, 1902f
 - on angiosarcomas, 1947, 1948f-1949f
 - differential diagnosis with, 1977
 - decreased diffuse echogenicity, 1977b
 - echogenic masses, 1977b
 - increased diffuse echogenicity, 1977b
 - multifocal hypoechoic masses, 1977b
 - solid heterogeneous masses, 1978b
 - splenomegaly, 1978b
 - on hamartomas, 1928, 1929f
 - on hemangiomas, 1927, 1927f
 - on infarctions, 1941-1942
 - on lymphangiomas, 1929-1930, 1930f
 - on lymphomas, 1950-1951
 - on metastatic disease, 1956-1957, 1957f
 - pediatric, 2228, 2229f
 - on pyogenic abscesses, 1940
 - on trauma, 1971-1972, 1972f
 - wandering, 1913-1914, 1914f
- tissue harmonic imaging in, 1172
- transabdominal, on Crohn's disease, 1004-1006
- transducers in, 1169-1170
- transrectal, 1004
- trapezoidal scanning in, 1170, 1170f-1171f
- on ulcerative colitis, 992-993, 995b
- Umbilical hernias, 2061
- Umbilical veins, 1178f
- Uncinate process, 1779

- Undifferentiated embryonal sarcomas, 1586-1588, 2205
- United Network for Organ Sharing (UNOS), 1499, 1737
- University of Wisconsin protocols, 905-908, 907f, 910, 911f
- Upper esophageal sphincter (UES), 279
- Upper gastrointestinal examinations (UGI)
after laparoscopic adjustable gastric band placement, 647-649, 648f
after Roux-en-Y gastric bypass, 643-644
after sleeve gastrectomy, 652
in neonates and children, 2097
before small bowel follow-through, 668-669
- Urachus, 2070-2071, 2073
- Urea breath test, 501, 504
- Ureteroceles, 1345
- Ureterolithiasis, 2268, 2268f
- Ureters, 202, 203f, 1989
- Urinary bladder, 175-176, 176f
exstrophy of, 2245
neck hypermobility in, 901, 901f
in pelvic extraperitoneum, 1994
rupture of, 2071-2072
transitional cell carcinomas of, 1199f
traversal of in percutaneous drainage, 1264
- Urinary tract
caudal regression in, 2117
cloacal malformation and, 2117
embryology of, 1985-1986
inflammatory bowel disease complications in, 1011
- Urine ascites, 2026-2027
- Urinomas, 1988-1989, 2026-2027, 2071-2072
- Urogenital sinus, embryology of, 1985-1986
- Urticaria, colonic involvement of, 1126-1127, 1127f, 1145f
- Uterus
calcifications in, 201, 201f
cancer
adenoma malignum, 1093
metastatic, from colon, 1046f
cloacal malformation and, 2117
traversal of in percutaneous drainage, 1264
vault prolapse, 900

V

- VACTERL (vertebral, anorectal, cardiac, tracheoesophageal, renal, and limb) anomalies, 2114, 2117, 2141, 2142f
- Vagina
cloacal malformation and, 2117
opacification of for imaging, 893
peritoneoceles, 897-898, 898f
traversal of in percutaneous drainage, 1264
vault prolapse, 900
- Vagotomy, 469, 631-632, 661f
- Vagus nerve, 1776
- Valleculae, folds of the, 210f
- Valsalva maneuver, pharyngeal distention with modified, 217, 217f
- Varices
with cirrhosis, 1656
duodenal, 606-607, 606f, 661f
endoscopic sclerotherapy for, 431-432, 460
esophageal, 275, 429-433
differential diagnosis of, 463f-464f
downhill, 432-433, 434f
from echinococcal disease, 1620
idiopathic, 433, 434f
pediatric, 2133, 2134f
postoperative, 460
with reflux esophagitis, 502
treatment of, 431-432, 432f-433f

- Varices (Continued)
uphill, 429-432, 430f
varicoid carcinoma and, 431, 431f
gastric, 603-606
clinical findings on, 604
differential diagnosis of, 606, 658f-659f
nonfundal, 605f
pathophysiology of, 603-604
radiographic findings on, 604-606, 604f
treatment of, 606
tumorous, 604, 605f
- GI bleeding from, 688-689
ligation of, 432, 433f
liver transplantation and, 1740
rectal, 1118-1119, 1119f
- Vasa recta
distention of, 744
diverticular hemorrhages, 951, 951f-952f
- Vascular disorders
computed tomography on, 827-828, 828f
lesions
anterior abdominal wall, 2073
liver
differential diagnosis of, 1764f
pediatric, 2206-2209
"scar" tumors, 1762f
small bowel
on computed tomography angiography, 690
on computed tomography enterography, 689-690, 691f
hemorrhage from, 2277-2278
- liver, 1676-1705
Budd-Chiari syndrome, 1680-1688
cardiac disease and, 1688-1689
cavernous transformation of the portal vein, 1695
hemolysis, elevated liver enzymes, low-platelets syndrome, 1698, 1699
hepatic infarction, 1698
hepatopulmonary syndrome, 1702, 1703f
Osler-Weber-Rendu syndrome, 1701, 1702f
peliosis hepatis, 1689-1690
portal vein thrombosis, 1690-1695
sinusoidal obstruction syndrome, 1680-1688
splanchnic vein aneurysms, 1701, 1701f
splenic vein and inferior mesenteric vein thrombosis, 1696-1697
superior mesenteric vein thrombosis, 1696
transient hepatic attenuation/intensity differences, 1676-1680
visceral artery aneurysms, 1699-1701
- small intestine, 827-850
computed tomography of, 827-828, 829f
drug-induced small bowel angioedema, 845-846
from hemangiomas, 846-848, 848f
median arcuate ligament syndrome, 846, 847f-848f
mesenteric ischemia, 828-838
radiation enteritis, 843-845
splanchnic artery aneurysms, 845
superior mesenteric artery dissection, 842-843, 843f
from trauma, 843, 844f
vasculitis, 838-842
spleen, pediatric, 2235
vascular rings, 2125-2127, 2128f-2129f
vascular slings, 2126, 2128f, 2130f
- Vascular grafts, 2073
- Vascular jejunitis of the ileum, 1004
- Vascular slings, 2130f
- Vasculitis
large vessel, 839
medium vessel, 839-840
pancreatitis with, 1812

- Vasculitis (Continued)
segmental small bowel mural hyperenhancement in, 686, 687f
small bowel, 721, 838-842
small vessel, 840-842
- Vasoactive intestinal polypeptide (VIP), 985
- Vasoconstrictors, 16
- Vasodilators, 16-17
- Venous thrombosis, 746-748, 1195. *See also* Thrombosis
- Ventral hernias, 2061, 2062f
- Ventriculoperitoneal shunts, ascites with, 2027
- Vermiform appendix. *See* Appendix
- Vertical banded gastroplasty (VBG), 642
- Vesicourachal diverticulum, 2070-2073
- Video capsule endoscopy, 726-727, 728f
- Villous pattern, in double-contrast studies, 40, 41f
- Villous tumors
colon, 1032-1035, 1033f
differential diagnosis of, 658f
gastrointestinal, 528-530, 529f-530f
polypoid carcinomas arising from, 563
- Viral infections, 762, 1019-1020, 1019f. *See also* HIV (human immunodeficiency virus)
- Virtual noncontrast imaging of liver, 1487
- Visceral artery aneurysms, 1699-1701
- Visceral neuropathies, 777-778
- Vocal cord paralysis, 449
- Volume CT dose index (mGy), 1138
- VoLumen, 82
- Volume rendering (VR), 1161-1162
- Volumetry, 1162
- Volvulus, 182-184, 1106f
cecal, 183-184, 184f, 1105, 1107f
mosaic-submucosal edema pattern in, 1145f
colonic
from giant sigmoid diverticulum, 952
obstruction from, 1105
pediatric, 2174-2175, 2175f
predisposing factors for, 1105
gastric, 622-623, 623f
distention in predisposition for, 2154
gastric outlet obstruction from, 660f
organoaxial, 444
major sites of, 1106f
midgut, 863, 2096-2097, 2097f
organoaxial gastric, 444, 623, 623f
sigmoid, 183, 183f, 1106f, 1108f
small bowel transplantation for, 858
splenic flexure, 184, 1105
- Von Gierke's disease, 1644, 1645f
- Von Hippel-Lindau disease, 2225-2226, 2225f-2226f
- Von Hippel-Lindau syndrome, 1845-1846, 1849
- Von Meyenburg complexes, 1190, 1551-1554, 1552f-1553f
- Von Recklinghausen's disease, 2151-2152, 2180

W

- Waldmann's disease, 2160
- Wall-echo-shadow pattern, 1178-1179, 1179f, 1330-1331
- Wandering gallbladder, 134f
- Wandering spleen, 1110, 1912-1913, 2088
clinical findings on, 1912-1913
diagnostic approach and therapy for, 1914-1915
pediatric, 2231, 2231f-2232f
radiologic findings on, 1913-1914
angiography, 1914
computed tomography, 1914, 1914f
conventional radiography, 1913
magnetic resonance imaging, 1913
scintigraphic studies, 1913, 1913f
ultrasound, 1913-1914, 1914f

Water halo pattern, 72, 74f
 Water lily sign, 1616
 Web pattern, in double-contrast studies, 43, 43f
 Webs
 antral, 610
 duodenal, 610-611, 611f, 2085
 esophageal, pediatric, 2125, 2127f
 gastroduodenal, pediatric, 2142f-2143f
 Wedge excision, 1721
 Wegener's granulomatosis, 838-839
 Wheel-within-a-wheel appearance, 1936-1937
 Whipplegrams, 700-701, 702f
 Whipple procedure, 640, 1866f
 afferent loop obstruction after, 1867f
 computed tomography enteroclysis in, 700-701, 702f
 duodenum in, 1862
 follow-up imaging after, 1867f
 Whipple's disease
 fold enlargement in, 786
 lymphadenopathy in, 770f
 malabsorption in, 765f, 767-768
 mesenteric involvement in, 2048
 micronodularity in, 8711
 small bowel, 875t
 White attenuation pattern, 71-72, 73f
 Wilms' tumors, 1578
 Wilson's disease, 1646-1647, 1647f, 1685, 1788

Windsock deformity, 2085
 World Health Organization (WHO)
 echinococcosis classification, 1933, 1934t
 lymphoma classification system, 1948
 pancreatic neoplasm classification system, 1838, 1845-1846, 1849
 tumor response classification system, 1728-1729, 2295, 2296t

X

Xanthogranulomatous cholecystitis, 1369-1370, 1371f, 1408

Y

Yersinia enterocolitica, 761
 enterocolitis, 1018, 2170, 2172f
 mesenteric adenitis from, 2264
 in ulcerative colitis, 985
Yersinia pseudotuberculosis, 2264
 Yersiniosis, 761, 761f
 colonic, mosaic-submucosal edema pattern in, 1145t
 differential diagnosis of, 768-769
 small bowel involvement in, 818-819, 873t
 Yttrium 90, 1640, 1726-1727, 1729, 1729f

Z

Zenker's diverticulum, 228-230, 229f, 239-241, 240f
 pseudo-, 241, 241f
 Z line, 439-440, 440f
 Zollinger-Ellison syndrome, 291, 300, 304f
 carcinoid tumors in, 596
 clinical aspects of, 492
 differential diagnosis of, 464t, 492, 659t, 661t
 differentiated from gastric lymphomas, 586
 gastrinomas in, 1850, 1851f
 malabsorption in, 775t
 megaduodenum in, 661t
 multiple duodenal ulcers in, 483-484, 510
 pediatric, 2152
 peptic ulcers in, 491-492, 657t
 radiographic findings in, 492
 small bowel involvement in, 872t, 875t
 thickened folds in, 492, 493f

